Russian Journal of Applied Chemistry, Vol. 78, No. 1, 2005, pp. 1–18. Translated from Zhurnal Prikladnoi Khimii, Vol. 78, No. 1, 2005, pp. 3–20.
Original Russian Text Copyright © 2005 by Kolosnitsyn, Dukhanin, Dumler, Novakov.

REVIEWS

Lithium-Conducting Polymer Electrolytes for Chemical Power Sources

V. S. Kolosnitsyn, G. P. Dukhanin, S. A. Dumler, and I. A. Novakov

Institute of Organic Chemistry, Ufa Scientific Center, Russian Academy of Sciences, Ufa, Bashkortostan, Russia

Volgograd State Technical University, Volgograd, Russia

Received November 2, 2004

Abstract—Polymer electrolytes for lithium and lithium–ion chemical power sources are described.

INTRODUCTION

Lithium chemical power sources (CPSs) have high specific electrical characterisitcs and show promise for power supply to diverse autonomous objects [1–4]. The use of Li, which has a high negative potential and a low electrochemical equivalent (0.259 g A^{-1} h^{-1}), allowed an increase in the working voltage and specific energy of such power sources.

Success in development of lithium CPSs was stimulated by a suggestion to use melts of lithium-containing salts and solutions of lithium salts in aprotic dipolar organic solvents (ADSs) as electrolytes. However, power sources with a lithium-based anode and a molten electrolyte have not found wide use because of problems with structural materials, design, and service. At the same time, lithium power sources (and later lithium–ion batteries) with a nonaqueous (aprotic) electrolyte, despite certain drawbacks, became commercially available. The most widely used organic solvents in such electrolytes are propylene carbonate (PC), ethylene carbonate (EC), diethyl carbonate (DEC), dimethyl carbonate (DMC), or their mixtures; as lithium salts are used perchlorate ($LiClO_4$), hexafluorophosphate ($LiPF_6$), hexafluoroarsenate ($LiAsF_6$), and tetrafluoroborate ($LiBF_4$). The electrical conductivity of the nonaqueous electrolytes is within 10^{-2}–10^{-3} S cm^{-1}.

Comparative analysis of the characteristics of various electrochemical systems [5] demonstrates advantages of the new generation of batteries: lithium–ion batteries with liquid (Li–IB) and polymer solid or thickened electrolyte (PLi–IB). Such systems provide voltages of 2.7–3.7 V and have a specific energy of 150–200 W h^{-1} kg^{-1}, which is 2–2.5 times higher compared to the well-known nickel–cadmium and nickel–metal hydride batteries.

Experts engaged in development and production of lithium–ion batteries believe that, by 2010, virtually all the autonomous power sources used in military equipment will be based on the technology of a lithium–ion battery [5].

Studies aimed at development of new and improvement of existing working bodies for lithium power sources are being performed during the whole period since the development of the first lithium voltaic cell (more than three decades).

One of promising lines in improvement of lithium and lithium–ion CPSs is the use of polymer electrolytes (PEs), which allows improvement of their energy and service characteristics and simplification of the production process. Studies of PEs are being performed since 1970s, and today the electrochemistry of polymer electrolytes is one of the most actively developing fields of the modern electrochemistry [6]. Polymer electrolytes to be used in lithium CPSs should exhibit good physicomechanical properties, high ionic and low electronic conductivity, and wide range of electrochemical stability; they should be inert toward the electrode materials.

Polymer electrolytes are subdivided into two large groups with respect to the component composition. The first group includes PEs that contain no low-molecular-weight solvent; they contain a high-molecular-weight polymer, a lithium salt, and (in some cases) finely dispersed inorganic fillers. Polymer electrolytes of this type are termed polymer solid electrolytes (PSEs). The second group includes electrolytes containing, along with polymers, lithium salts, and fillers, also low-molecular-weight solvents. Electrolytes of

1070-4272/05/7801-0001 © 2005 Pleiades Publishing, Inc.

this group are further subdivided into microporous, gel, and plasticized polymer electrolytes [7].

Microporous PEs are microporous polymer films prepared from chemically resistant polymers (e.g., polyethylene or polypropylene) and impregnated with solutions of lithium salts in dipolar aprotic solvents. These electrolytes exhibit good mechanical properties and high ionic conductivity approaching that of liquid nonaqueous electrolytes (10^{-2}–10^{-3} S cm^{-1}).

Gel PEs (GPEs) are multicomponent systems consisting, at least, of a film-forming polymer, an aprotic dipolar solvent, and a lithium salt. The solution of the salt in ADS is distributed in a three-dimensional GPE network formed by macromolecules or their aggregates. These electrolyte systems have a relatively high ionic conductivity (up to 10^{-3}–10^{-4} S cm^{-1}) and, in some cases, also fairly good mechanical properties.

The solvent content in plasticized polymer electrolytes is considerably lower than in gel polyelectrolytes; their electrical conductivity, as a rule, is also appreciably lower.

An essential disadvantage of PEs containing a low-molecular-weight solvent (except microporous PEs) is the possible thermodynamic instability of their phase composition. Also, a common drawback of PEs of the second group is the possibility of solvent evaporation during storage and service of CPSs. Finally, the presence of a solvent is responsible for the drawbacks characteristic of liquid nonaqueous electrolytes: chemical activity toward lithium and the possibility of undesirable cointercalation of solvent molecules into the cathode matherial. All these processes may result in degradation of electrode materials and deterioration of the characteristics of CPSs based on such polymer electrolytes.

From the viewpoint of safety and convenience in production and service, PSEs in lithium CPSs are preferable. However, certain problems restrict today the use of PSEs. First, they have low ionic conductivity at common temperatures (10^{-5}–10^{-8} S cm^{-1}); second, not only lithium ions but also anions participate in the charge transfer, which may lead to concentration polarization; third, similarly to liquid electrolytes, PSEs can form a transition layer with a high resistance in contact with electrode (both cathode and anode) materials [7–9].

Therefore, development of lithium-conducting polymer electrolytes exhibiting high electrical conductivity in a wide temperature range, chemical and electrochemical stability, and good physicomechanical properties remain an urgent problem.

POLYMER SOLID ELECTROLYTES

Interactions in Polymer–Lithium Salt Systems

Organic polymers used for preparing PEs are dielectrics. Their low conductivity (10^{-12}–10^{-10} S cm^{-1}) is due, as a rule, to the presence of impurities. Therefore, fairly good polymer ionic conductors can be obtained by introducing ionogenic or ionophoric groups into the polymer molecule, or ionophores into the polymer system as a whole. Ionization of ionogens and ionophores is possible in the case if the polymer system exhibits sufficiently high dielectric permittivity and solvating power toward various ions. Such properties are exhibited by systems based on functional polymers, i.e., polymers whose molecules contain electron-donor or electron-acceptor groups. Interaction of macromolecules with low-molecular-weight ionophores (e.g., lithium salts) is possible owing to solvation of cations, anions, or both with functional groups of the polymers.

Anions are usually solvated by hydrogen bonding with relatively "acidic" hydrogen atoms, i.e., with hydrogen atoms directly bonded to electronegative atoms of the polymer molecule, e.g., with oxygen atoms in polyalcohols or hydrogen atoms in polyamides. However, the interchain interaction in such polymers is relatively strong, resulting in high cohesion energy. Therefore, such polymers are unfavorable media for diffusion of ions in the absence of protic solvents having high dielectric permittivity (water). Furthermore, the mobile hydrogen atom may be electroactive in a wide range of chemical potentials, which excludes the use of such polymers in lithium power sources. Anions can also be solvated by Lewis acids, e.g., by organoboron compounds R_3B, but stable macromolecules containing such fragments are unknown [10].

It should also be noted that one of the major problems in development of lithium-conducting polymer electrolytes is elimination of the undesirable contribution of the anionic conductivity [11, 12]. Because of binding of the cations with polar groups of the polymer molecule, the anion makes a significant contribution to the conductivity. The mobility of the anions usually decreases with an increase in their size. The undesirable anionic conductivity can also be eliminated by using polyelectrolytes, i.e., polymers in which the negative ion is chemically bound to macromolecules. The electrical conductivity of such systems usually does not exceed 10^{-5} S cm^{-1}.

The cations are solvated via interaction with lone electron pairs of heteroatoms in functional groups of

the polymer molecules [13]. The most typical functional groups are ether (–O–), sulfide (–S–), amino (–N<), phosphino (–P<), carbonyl (>C=O), and cyano (–C≡N) groups.

According to Pearson's concept of hard and soft acids and bases, the electron-donor properties of heavy heteroatoms (S, P) are realized most efficiently in the presence of soft acids, i.e., cations with polarizable *d* orbitals (e.g., Ag^+, Pb^{2+}) [14]. Cations of alkali and alkaline-earth metals strongly interact with oxygen and nitrogen atoms.

The possibility of polymer–salt complexation depends on the cohesion energy of the polymer and crystal lattice energy of the salt [15, 16]. Complexes with the above-mentioned types of macromolecules are formed only by salts with a low lattice energy. Such salts generally contain large anions with the delocalized charge.

Polyethers [in particular, poly(ethylene oxide), PEO] were the first macromolecular compounds considered as candidate materials for PSEs [17, 18]. In particular, Papke *et al.* [19] showed that with PEOs, indeed, the crystal lattice energy of the salt determines the possibility of the polymer–salt complexation. The complexation of PEO with lithium salts $LiClO_4$, $LiPF_6$, $LiBF_4$, and others was proved in [20–22]. Robitaille and Fauteux [23], based on the conductivity and X-ray diffraction data, confirmed the results obtained for the system PEO–$LiCF_3SO_3$ and constructed the phase diagrams for the systems PEO–X, where X = LiI, $LiAsF_6$, and $LiClO_4$. In the latter case, also, at least one crystalline complex is formed, $(PEO)_6$–$LiClO_4$. Poly(ethylene oxide) forms mixed crystals of the pure polymer and complex at temperatures below T_m, and above T_m the salt-containing melt (elastomer) is in an equilibrium with the complex. For the majority of crystalline polymers, the crystalline phase, as a rule, occupies only about 70–85% of the volume of the polymer body because of entanglement of the polymer chains. The remaining volume is occupied by the amorphous phase. Such phase equilibria govern the properties of such polymers as poly(ethylene succinate) $(–C_2H_4–O–CO–C_2H_4–COO–)_n$, polyaziridine $(–CH_2–CH_2–NH–)_n$, poly(ethylene adipate) $(–C_2H_4–O–CO–C_4H_8–COO–)_n$, and polypropiolactone $(–C_2H_4–COO–)_n$ [10].

The DSC and NMR studies made by Berthier *et al.* [24, 25] showed that the crystalline phase of the complex (three monomer units per mole of salt) starts to dissolve in PEO at temperatures above T_m of PEO. It is assumed that the crystalline phase of the complex has a helical structure with the cations located inside, and the ion motion occurs in the elastomer phase, with the crystalline complex acting only as a salt reservoir.

Armand [10] summarized data on interaction of PEO and poly(propylene oxide) (PPO) with the most commonly used alkali metal salts. It was noted that the complexing power of PEO considerably exceeds that of PPO, despite the fact that the electron-donor properties (*DN*) of both polymers are comparable. A decrease in the stability of polymer–salt complexes is due to steric hindrance caused by the methyl groups in PPO. In amorphous polymers above their glass transition points and in polymers incapable of crystallization because of structural disordering, the salts bound in a complex form continuous solutions up to saturation.

When studying ionic association of PPO–$LiClO_4$ complexes, Schantz [26] noted that the amount of the dissociated ions remained constant with variation of the polymer/salt ratio from 1000 to 30 [26]. With an increase in the salt concentration in PPO, the intensity of ion pair formation decreased. The major contribution to an increase in the PE conductivity at low $LiClO_4$ concentrations is made by an increase in the number of dissociating ions, rather than in their mobility. The IR and polarized Raman spectra of the PPO–$LiCF_3SO_3$ complexes suggest existence of three types of associates: two differently coordinated ion pairs and a ternary ion. Manning and Frech [27] state that the free ions which were believed previously to exist in these polymer–salt complexes are actually the cation–anion pairs in which the cation weakly interacts with the terminal CF_3 group of the anion.

It was found that polymers with the crystalline structure, tending to form crystalline complexes with dissolved lithium salts, do not ensure the electrical conductivity acceptable for PSEs. The conductivity of PSEs, including those based on PEO, can be increased by decreasing the crystallinity of the polymer, because the high ionic conductivity is mainly provided by the amorphous part of the polymer electrolyte.

Therefore, the majority of studies involve choosing amorphous polymers for PSEs, forming the network structure (cross-linking), and introducing additives that render the system amorphous.

Polymer Solid Electrolytes Based on PEO and Its Modifications

As a rule, solid inorganic electrolytes have a unipolar conductivity. It was initially expected that PSEs would also exhibit unipolar conductivity. Indeed, the

preliminary results were encouraging: For the PSE based on $LiCF_3SO_3$, the lithium transport number was ~0.8 [28]. However, it was found soon that the transport numbers of the positive ions t^+ for the majority of salts in PSEs are within 0.3–0.5.

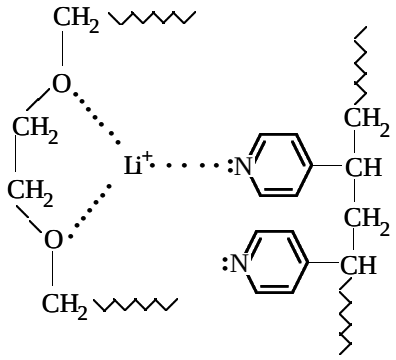
The transport numbers in PSEs are usually determined by impedance spectroscopy [29, 30], Tubandt method [31], dc electrolysis [32], potentiometry [33], and NMR spectroscopy [34]. For the lithium salts with such anions as SCN^-, ClO_4^-, and BF_4^-, all these methods give similar values characteristic of these salts in liquid electrolytes. An apparent exception is the $CF_3SO_3^-$ ion for which independent measurements give $t^- \approx 0.3–0.4$ [33, 34]. Presumably, synthesis of polymer electrolytes with unipolar lithium conductivity will lead to a considerable progress in this field.

Bruce and Vincent [35] studied by the emf method the ion transport in amorphous complexes PEO–$LiClO_4$ of various compositions. In potentiostatic polarization, the steady-state current was attained in several hours and was determined by the mobility of both Li^+ and ClO_4^- ions, and at high salt concentrations, also by the mobility of the ion pairs [36]. According to [37], at a given temperature the conductivity depends on the lithium perchlorate concentration in a complex manner. At low concentrations, with an increase in the salt content, the specific molar conductivity σ rapidly decreases. Then, as the salt concentration is increased further, σ increases, reaches a maximum (whose position depends on temperature), and then decreases again. The shape of the dependences of σ on the temperature and lithium perchlorate concentration suggests the transfer of the electricity not only by the simple ions Li^+ and ClO_4^-, but also by ion clusters $Li(ClO_4)_2^-$ and $Li_2(ClO_4)^+$.

Studies by Brillouin and photon-correlation spectroscopy [38] showed that the cooperative motion of approximately 20 monomeric units of the polymer is required for the ionic transport. At $n > 4$, short-lived ion–polymer cross-links arise in the electrolyte, limiting the mobility of polymer segments. The density of the cross-links abruptly decreases with increasing temperature because of formation of ion pairs exerting a plasticizing effect of PSE.

Arumugam *et al.* [39] determined the diffusion coefficients of Li^+ and PF_6^- in the amorphous electrolyte PEO–$LiPF_6$ by ^7Li and ^{31}P NMR spectroscopy with pulse field gradient in a wide temperature range (25–100°C) at a salt concentration of up to 0.25 mol dm^{-3}. Their results suggest different mechanisms of transfer of the cation and anion at low and high concentrations of the salt. The diffusion coefficients of the cation appeared to be weakly sensitive to the salt concentration; the system showed a deviation from the Nernst–Einstein relationship. To interpret the results obtained, Arumugam *et al.* suggested hopping of the cation between ion clusters and diffusion of neutral ion pairs.

Blending of two or several polymers is widely used to decrease the crystallinity of polymer electrolytes. Li and Khan [40] studied an interesting type of polymer electrolytes with a conductivity of 10^{-5} S cm^{-1} at 25°C. The electrolytes were prepared by blending PEO with poly(2-vinylpyridine) (P2VP) or poly(4-vinylpyridine) (P4VP) with $LiClO_4$ in solution. In these composite electrolytes, $LiClO_4$ behaves as agent improving the compatibility of the polymers, as it was shown previously that PEO and P4VP are immiscible and PEO–P2VP (40/60 by weight) blends are only slightly miscible [41], as indicated by independence of T_m of PEO and T_g of P2VP from the blend composition. Ueda *et al.* [41] believe that increased miscibility in the PEO–polyvinylpyridine system is most probably due to the fact that the lithium ion interacts simultaneously with the PEO oxygen atoms and nitrogen atom of the pyridyl unit. The probable structure of the complexes formed by this type of ion–dipole interactions is shown below:

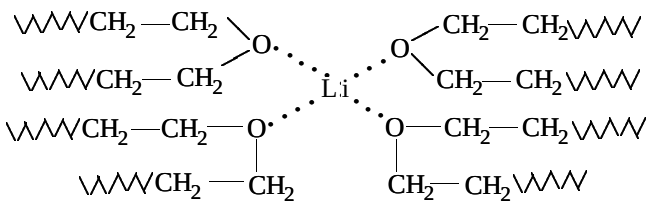


It was shown that the ion–dipole interactions improve the miscibility of polystyrene ionomers with poly(alkylene oxide) systems [42] and of polyamide-6 with lithium or sodium salts of sulfonated polystyrene [43, 44]; $LiCF_3SO_3$ improves the miscibility of poly(methyl methacrylate) and poly(propylene glycol) [45]. The increased miscibility is explained by simultaneous interaction of Li^+ with the carbonyl oxygen atoms of poly(methyl methacrylate) and ether oxygen atoms of poly(propylene glycol). Furthermore, it was shown that the blends have a phase-segregated structure with $LiCF_3SO_3$ acting as an emulsifier stabilizing the two-phase microstructure [46].

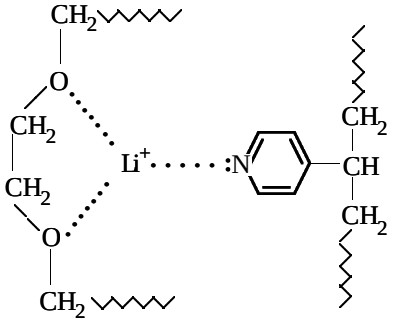
Mani *et al.* [46] explained the conductivity and

thermal transitions assuming the existence of three different types of ion–dipole complexes:

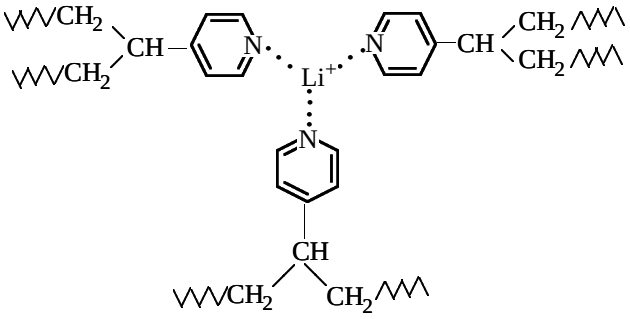
Complex of type 1



Complex of type 2



Complex of type 3



Complexes of type 1 are present in the pure PEO phase, and complexes of type 3, in the pure P2VP or P4VP phase. Complexes of type 2 stabilize the two-phase microstructure and are present at the phase boundary. Mani *et al.* suggested that the ions incorporated in complexes of types 1 and 2 are mobile and hence participate in the ionic transport. Complexes of type 3 form a rigid phase with a low segmental mobility at room temperature. Therefore, the ions in these phases are mostly immobile and do not make a significant contribution to the ionic conductivity. Preferential formation of complexes of types 1 and 2 increases the amount of charge carriers, increasing the ionic conductivity. However, the larger the amount of complexes of type 1, the weaker the segmental motion and the higher T_g [47]. As the segmental motion becomes less intense, the mobility of charge carriers and hence the ionic conductivity decrease. Wintersgill *et al.* showed that the amplitude of segmental motion plays an important role in the ion transport in polymer–salt complexes [48].

Zhukovskii *et al.* [49] blended two polymers to prepare an electrolyte based on PEO and amorphous poly(vinyl acetate) (PVA). The PEO crystallinity decreased with increasing PVA content and fully disappeared at a PVA content of about 30 wt %. The highest conductivity at room temperature was 10^{-5} S cm^{-1} at 10–20% PVA content.

Carre and Hamaid [50] succeeded in suppressing PE crystallization by adding to PEO an elastomer (butadiene–acrylonitrile copolymer) and a macromonomer derived from styrene. The polymer electrolyte consisting of a blend of a poly[bis(methoxyethoxyethoxidophosphazene)] complex salt (I) and PEO (II), doped with $LiCF_3SO_3$ or $LiClO_4$, was cast from a solution of I + II in acetonitrile and vacuum-dried at 100°C [51]. At a I : II ratio of 1 : 1, the specific conductivity of the electrolyte was 2×10^{-4} (at 20°C) and 5×10^{-2} S cm^{-1} (at 100°C).

Sehlenoff *et al.* [52] suggested a PE based on poly(*p*-phenylenevinylene) (PPV). Films were prepared from a mixture of aqueous solutions of the polymers, a PPV precursor (water-soluble sulfonium salt) and a water-soluble polymer such as PEO, methyl cellulose, or hydroxypropyl cellulose, taken in 1 : 1 ratio. To prepare PPV, the salt precursor was subjected to heat treatment. The best results were obtained with PPV–PEO blends doped with $LiClO_4$. Such blends are resistant to thermal degradation (up to 225°C) and have good mechanical properties.

Bannister *et al.* [53] reported on the conducting properties of PEO alloys with a polymer containing sulfonate or perfluorocarboxylate groups. The conductivity obtained was relatively low ($\sigma = 10^{-5}$ S cm^{-1} at 100°C), probably because the initial monomeric salts either were insoluble or dissociated only slightly in the polyether phase.

In [54], the polymer matrix was PEO in which each monomeric unit of the backbone contained a pendant $-(CH_2-CH_2-O)_x-R$ chain ($1 < x < 20$, R is alkyl). The backbone and pendant chains in the polymer were linked via ether groups. The molecular weight (MW) of the backbone was 10^4–5×10^6, and that of the pendant chain, 50–2000. Such a PSE has a high conductivity at 20°C and can be used in lithium batteries.

PEs derived from PEO can be modified by introducing lithium salts of various fluorinated monobasic acids. The complex of PEO with $LiCF_3SO_3$ shows the highest conductivity among the complexes studied

($\sigma = 4 \times 10^{-4}$ S cm^{-1} at 100°C). With an increase in the size of the anion in these salts, the conductivity decreases, which is attributable to changes in the interaction and mobility of the ions. With a mixture of $LiCF_3SO_3$ and NaI, the electrical conductivity of a PE based on PEO substantially increases, and the microviscosity decreases [55]. Presumably, this effect is associated with a considerable increase in the content of the amorphous elastomer phase and to nonuniform distribution of different cations and anions in different phases.

Zapol'skikh *et al.* [56] studied the properties of PSEs based on poly[poly(ethylene glycol) dimethacrylate] (PPEGDM) and lithium salts of fluorinated sulfonic acids CF_3SO_3Li and $CF_3CF_2CF_2SO_3Li$. They found that the anion does not participate actively in the salt–polymer intermolecular interaction. The structure of the anion affects the solubility and degree of dissociation of the salt in cross-linked PPEGDM and exerts no direct influence on the flexibility of the polymer chains and mobility of the cations. As the anion size increases, the salt solubility decreases, but the electrical conductivity of the PSE increases.

To enhance the ionic conductivity of polymer electrolytes and improve the service characteristics of power sources based on them, many researchers [57–62] introduced into PSEs organic and inorganic additives decreasing the degree of crystallinity of the formulations. Chervakov *et al.* [62] synthesized and tested as additives certain nitrogen-containing compounds. Organosilicon derivatives of 4,4'-bipyridine appeared to be among the best additives; they increased the PE conductivity by a factor of 2.

Relatively high conductivity and good mechanical properties are exhibited by PSEs of the composition $(PEO)_8LiClO_4$ filled with finely divided (<5 μm) β-Al_2O_3 by mixing with a solution of PEO and $LiClO_4$ in acetonitrile [57]. Addition of Al_2O_3 [58] and $LiAlO_2$ ceramic microspheres 1 μm in diameter [59] (to 10–30% content) positively affects the mechanical properties and conductivity of PSEs. The conductivity increases by an order of magnitude on adding to PEO-based PEs such fillers as β-Al_2O_3, Li_2O–B_2O_3–SiO_2 ionic glasses, and ion-exchange resins in the lithium form [60, 61]. Assuming that the relationship between the preexponential term in the conductivity equation and the activation energy obeys the Meyer–Neldel rule in the entire range of the filler concentrations, Wieczorek and Florjanczyk [60, 61] concluded that the ionically conducting fillers do not participate in the charge transport through the solid electrolyte; their only role is that they make the composite more amorphous.

An increase in the PE conductivity on mixing with Al_2O_3 powder was reported in numerous papers. Such PEs were studied by impedance spectroscopy, X-ray diffraction, and NMR. It was shown that the conductivity of the PEO–NaI polymer electrolyte increases on mixing with Al_2O_3, exceeding 10^{-5} S cm^{-1} at room temperature [63].

One more method for preventing crystallization of amorphous polymers is cross-linking, e.g., cross-linking of PEO induced by irradiation with γ-rays or an electron beam [64]. The PEs thus obtained have increased lithium ion conductivity at low temperatures. The mechanisms of radiation-induced degradation and cross-linking of PEO in the solid state and in aqueous solution were studied by ESR [65]. A decrease in the crystallinity of cross-linked polymer materials and enhancement of their mechanical properties and conductivity at 20°C show that γ-irradiation is a simple and efficient procedure for preparing highly conducting and mechanically stable PEs. However, Kronfli *et al.* [66] have not confirmed the effect exerted by γ-irradiation of PE samples based on PEO and lithium salts ($LiClO_4$, $LiCF_3SO_3$).

Cross-linking of PEO containing the terminal groups CO–CH=CH–C_6H_4R (R = NO_2, Cl, OCH_3), CO–CH=CH–CH=CH–C_6H_5, CO–C(CN)=CH–C_6H_5, and CO–C(CN)=CH–CH=CH–C_6H_5 was described in [67]. The cross-linking occurs under irradiation with accelerated electrons or UV light. A thin-film PE sample (in a mixture with lithium salts) with 90% degree of cross-linking was obtained; its ionic conductivity was 1.7×10^{-4} S cm^{-1} at 20°C.

A polymer solid electrolyte with good mechanical properties and fairly high electrical conductivity, 5×10^{-5} S cm^{-1} at 25°C, was prepared from lithium perchlorate and cross-linked PPEGDM with a low cross-linking density [68]. The behavior of the boundary between the lithium electrode and PSE based on PPEGDM and lithium perchlorate was studied by impedance Fourier spectroscopy [69, 70]. It was shown that the behavior of a passivating film on the lithium electrode at anodic and cathodic polarization is unsymmetrical. A dc polarization decreases the resistance of the electrode|PSE boundaries, probably owing to enrichment of the passivating film with charge carriers.

Methods for chemical cross-linking of the polymer matrix were described in [71–73]. For example, a film PE with satisfactory conductivity at 30°C [71] and a

strong and elastic PE with $\sigma = 6 \times 10^{-5}$ S cm^{-1} at 25°C [72] were prepared by mixing of a product of copolymerization of polyglycerol with ethylene oxide, or of a mixture of ethylene and propylene oxides, with a polyfunctional cross-linking agent (polyisocyanate) at 50–200°C and $P > 10$ atm. Procedures for preparing PEs based on lithium salts and poly(ethylene glycols) cross-linked with siloxane tetraisocyanate were described in [73].

Hu and Wright [74] reported on cross-linking of PEO-based resins with vinyl monomers. Lithium perchlorate was added to PEO-400 maleate isophthalate resins prior to cross-linking with styrene (I), vinylpyrrolidone (II), or vinylpyridine (III). At the ratio [PEO]/[Li^+] = 50, the conductivity of the resulting PEs increased in the order III < II < I, inversely correlating with the strength of Li^+ binding, which increases in going to more polar comonomers.

Wieczorek *et al.* [75] prepared composite electrolytes from amorphous PEO copolymer cross-linked with oxymethylene groups (OMPEO), with additions of poly(*N*,*N*-dimethylacrylamide) (NNPAAM); these electrolytes showed a room-temperature conductivity of 4×10^{-4}–10^{-5} S cm^{-1}. There is no hydrogen bonding in such systems, which allowed the interactions of both polymers with the Li^+ ions to be studied in a wide range of temperatures and NNPAAM concentrations. Three types of complexes were revealed in the OMPEO–NNPAAM–$LiClO_4$ system: polyether–Li^+–polyether (type 1), polyether–Li^+–NNPAAM (type 2), and NNPAAM–Li^+–NNPAAM (type 3). Wieczorek *et al.* suggest that, above T_g, the ion motion is associated with the segmental motions of polymeric chains. Below T_g, the ion motion is a result of activated hoppings and is associated with the segmental motion of chains to a minor extent.

In parallel with the attempts to reduce the crystallinity of known PSE matrices, some researchers chose another approach: preparation of polymers with intrinsic amorphous structure by copolymerization of different monomers, one of which, as a rule, was oxirane [76]. In particular, amorphous single-phase solid electrolyte with enhanced ionic conductivity, no crystallinity, and good elasticity at 20°C was prepared by copolymerization of ethylene oxide and other oxides of the type –CH_2–CH(R)–O–, where R is alkyl, alkenyl, or alkynyl group containing 1 to 12 carbon atoms, or –CH_2–O–R'–R, where R' is a polyether –$(CH_2$–CH_2–O–$)_p$ (p is an integer from the range 0–10) or a cyclic ether containing more than three carbon atoms in the ring [77]. The oxides are chosen from the group of tetrahydrofuran, dioxolane, and their derivatives. Short cross-links in the electrolyte are provided by additions of silicon, cadmium, boron, titanium, zinc, magnesium, or tin compounds. The polymer electrolyte contained 1.5 to 25 wt % $LiClO_4$ or $LiCF_3SO_3$. A PE with $LiClO_4$ was prepared from an amorphous copolymer of ethylene and propylene oxides and alkyl glycidyl ether (98% amorphous phase). Its maximal conductivity at 25°C was 7.5×10^{-5} S cm^{-1} at a lithium to oxygen ratio of 0.05 [78].

It was suggested in [79, 80] to use as a base of a polymer electrolyte for a lithium battery a cross-linked copolymer of ethylene and propylene oxides. In a combination with a lithium salt, such a PE ensures the specific conductivity of the order of 10^{-5} S cm^{-1} at 25°C. The product of the copolymerization of the vinyl ether R(O–$CH_2CH_2)_n$–O–CH=CH_2 (R = Me or Et, n = 1–16) with the divinyl ether CH_2=CH–(O–$CH_2CH_2)_n$–CH=CH_2 (n = 1–16) is a cross-linked polyether with a glass transition point of about 60–80°C; this polymer was used as a matrix for preparing solid PE.

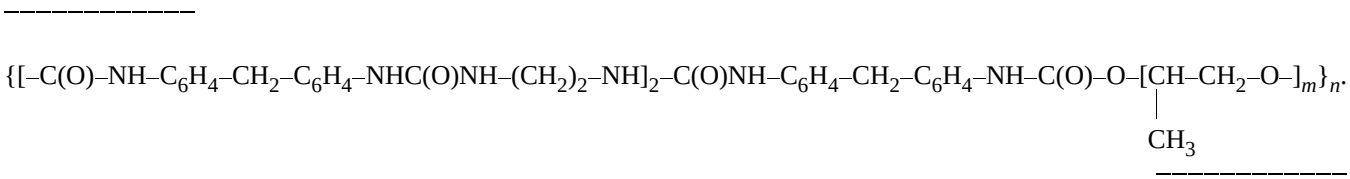
A procedure for preparing PE by mechanical mixing of acrylic poly(alkylene oxide) and a lithium salt with polyurethane (PU) or polyurethane–urea in a solvent at room temperature, followed by a heat treatment of the resulting mixture, was suggested in [81]. The resulting solid electrolyte had a conductivity of 1.5×10^{-5} S cm^{-1} and satisfactory mechanical properties. On adding $LiClO_4$ to PU, the ionic conductivity at 20°C increased to $\sigma = 4 \times 10^{-4}$ S cm^{-1} at PU : $LiClO_4$ = 8 : 1 [82]. At a high $LiClO_4$ content, the conductivity decreased because of growing viscosity. The difference between the conductivities of the PEs based on PU and PEO is especially significant below 80°C, since, as the temperature is decreased, the conductivity of PEO drastically (by a factor of about 10) decreases because of structural rearrangement. Experiments with lithium electrodes showed that the transport numbers of lithium cations at 50–100°C were 0.5–0.8. To prevent deterioration of the PE in prolonged storage, it was suggested to use as a polymer matrix a urethane-like polymer with the hydrogen atoms substituted by alkali or alkaline-earth metal atoms [83].

A polymer electrolyte having the structure of a modified polyurethane network was prepared from poly(dimethylsiloxane) with grafted PEO, cross-linked with an aliphatic diisocyanate and containing 10 wt % $LiClO_4$. Its ionic conductivity was 10^{-5} S cm^{-1} at 30°C. This electrolyte was used in solid-state lithium batteries. The voltammetric data showed that, after the completion of the formation of the polyurethane net-

work, the unchanged cross-linking agent can prevent the diffusion of lithium ions at the electrode–electrolyte phase boundary. The limiting currents were determined from the cathodic branches of the voltammogram. The internal resistance of the RuO_2/Li battery with the PE, 5 kΩ, was determined from the discharge curves taken at 60–80°C. After two discharge cycles with 95 and 73% degree of discharge, the adhesion of the PE film on RuO_2 and on Li remained unchanged [84].

The morphology and physical properties of the electrolytes from linear segmented polyurethanes based on PEG and alkali metal salts are described in [85]. Systems based on siloxane polymers can be prepared by mixing in a common solvent lithium salts and organopolysiloxane containing more than two COOH groups [86]. The conductivity of such PE at 25°C is 5.6×10^{-5} S cm^{-1}.

Another way to retain PE in the amorphous state is formation of segmented block copolymers in which the chain order is distorted and hence the crystallization is hindered. Watanabe *et al.* [87, 88] studied a series of materials in which this principle is followed, especially the system with segmented polyether–urethane–urea as primary crystal. This substance has an $(A–B)_n$ structure, where A is a rigid polyurethane–urea segment (~30 wt %) and B is a flexible polyether segment:



The polyurethane–urea segments tend to aggregate by hydrogen bonding with the formation of a two-phase microstructure, which imparts to the electrolyte excellent mechanical properties. Salts such as $LiClO_4$ selectively dissolve in the polyether. The relationships between the morphology, dynamic and mechanical properties, and ionic conductivity of these materials are given in [88, 89].

Liu *et al.* [90] suggested a related matrix polymer, polyurethane–urea (PUU) derived from 4,4'-methylenebis(phenyl isocyanate), ethylene diamine, and poly(ethylene glycol). The molecular weight of the flexible (polyether) segment was 1000, the weight fraction of the rigid (polyurethane–urea) segment, 35, and the melting point of the polymer, 180°C. A film prepared from the complex of a lithium salt with polyurethane–urea had the ionic conductivity $\sigma = 10^{-5}$ S cm^{-1} at 33°C; its mechanical strength was sufficiently high. To extend the assortment of polymer matrices, oligo(ethyleneoxy)polyphosphazene (OPP) containing alkyl groups was prepared in [91]. The procedure involved transformation of hexachlorotriphosphonitrile into dichlorophosphonitrile followed by its reaction with appropriate alcoholates. Up to 5 wt % $LiClO_4$ is introduced into OPP in the course of the synthesis, which ensures sufficiently high lithium ion conductivity of the PE.

Nagaoka *et al.* [92] prepared polymers with a very low glass transition point by polycondensation of dimethyldichlorosilane with poly(ethylene glycol):

$$[–Si(CH_3)_2–O–(CH_2–CH_2–O–)_n]_m.$$

The high flexibility of the backbone and the absence of crystallinity (because of irregular chain structure) provide relatively high conductivity of such polymers: 10^{-4}–10^{-5} S cm^{-1} (considerably higher than that of MEEP, see below).

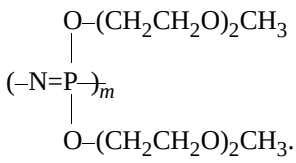
Zapol'skikh *et al.* [93] studied the PSEs based on poly(ethylene glycols) of various molecular weights, cross-linked with methyl- and phenyltrichlorosilanes. The polymers were transparent elastic heat-resistant materials. The highest room-temperature conductivity, 5×10^{-5} S cm^{-1}, was shown by the PSE prepared by cross-linking of PEG-300 with methyltrichlorosilane. However, the use of such systems is restricted by high susceptibility of siloxanes to hydrolysis.

Polymer Solid Electrolytes Based on Other Polymer Matrices

Numerous attempts to improve PSEs based on the traditional poly(ethylene oxide) matrix failed, which stimulated search for new polymer materials with low crystallinity and low glass transition point. Such properties are exhibited, e.g., by comb-shaped branched polymers.

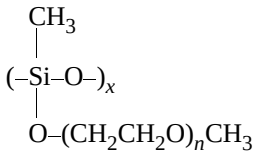
Flexible comb-shaped branched systems can be prepared from polymers whose backbone has a low

glass transition point [94]. With the aim to prepare such PEs, Allcock *et al.* [95–97] studied systems based on phosphazene and siloxane polymers. One of the best polymers for PEs was prepared by replacement of chlorine atoms in poly(dichlorophosphazene) with alkoxy groups under the action of sodium 2(2-methoxyethoxy)ethylate in the presence of tetra-*n*-butylammonium bromide to obtain the compound



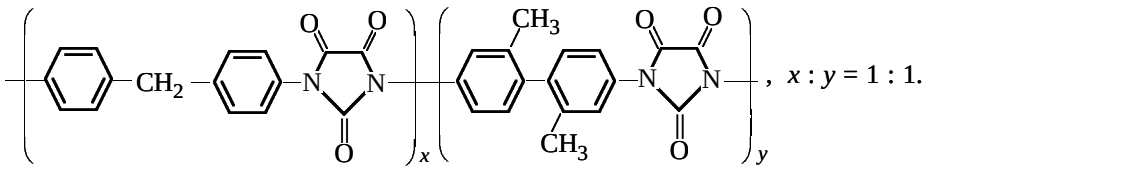
This polymer, poly[bis(methoxyethoxyethoxy)-phosphazene] (MEEP), forms single-phase amorphous electrolytes with salts of various uni-, bi-, and trivalent metals [95]. The complexes of some lithium salts with this inorganic polymer are PEs with a high conductivity. For example, the room-temperature conductivity of MEEP–$(LiBF_4)_{0.25}$ is 2×10^{-5} S cm^{-1}. However, the mechanical properties of these electrolytes are unsatisfactory, and they cannot be cast as free films to be used in solid-state lithium CPSs. Several approaches are used to enhance the mechanical stability of MEEP-based electrolytes [98]. One of them is blending of MEEP with PEO, PPO, polyvinylpyrrolidone, or poly(tetraethylene glycol diacrylate). The resulting composite electrolytes can be cast as free films. Their conductivity is somewhat lower than that of MEEP–$(LiX)_n$ but considerably higher than that of PEO–$(LiX)_n$. The dependences of the ionic conductivity of solid-phase polymer complexes of the oligo(ethylene oxide)–polyphosphazene graft copolymer on the temperature and salt concentration were studied by Hara [99]. The highest conductivity ($\sigma_{max} = 10^{-4}$ S cm^{-1}) of the complexes was observed at 25°C and 15 wt % content of $LiClO_4$. For the complexes of $LiClO_4$ (7.5 wt % salt content) with polyphosphazene modified by grafting of oligooxyethylene with the degree of oligomerization of 7, σ was as high as 3.5×10^{-4} S cm^{-1}. For the systems of polycyclotriphosphazene of a complex structure with $LiClO_4$, $\sigma = 1.2 \times 10^{-4}$ S cm^{-1} (at 90°C); with increasing temperature, the conductivity maximum shifted toward higher salt concentrations [100].

It was shown in [101] that liquid comb-shaped branched polymers of the structure



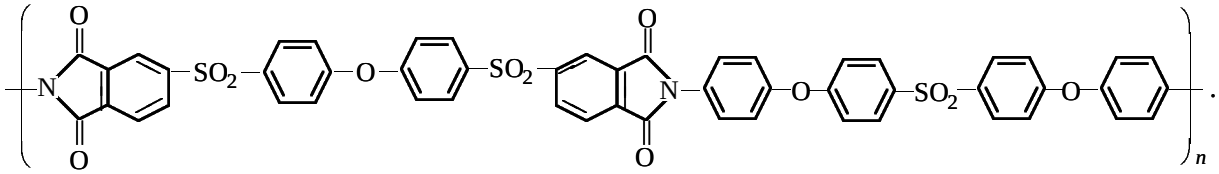
can be additionally cross-linked by heating to 150°C (to obtain rubber-like films). The length of the pendant chain in this case affects the conductivity insignificantly. For the PE containing $LiClO_4$ as an ionic additive, the conductivity was 10^{-4} S cm^{-1} at 25°C. Liquid curable organosiloxanooxyalkylene copolymer formulations with acrylate functional groups, containing $LiCF_3SO_3$ and azobis(isobutyronitrile), were patented. After curing at 85–90°C for 30 min, 1-mm-thick elastic films with a conductivity of 1.6×10^{-5} S cm^{-1} were obtained.

Yamamoto *et al.* prepared and studied polymer solid electrolytes based on polyvinyl alcohol (PVAl, MW 25 000, degree of saponification 88%) and heat-resistant polyarylene(1,3-imidazolidine-2,4,5-trione-1,3-diyl) (polyparabanic acid, PPA) [102]. These polymers dissolve large amounts of alkali metal salts such as $LiCF_3SO_3$, $LiBF_4$, $LiClO_4$, and $NaBF_4$ (1–1.5 g g^{-1} polymer) to form homogeneous films. Dissolution of lithium salts renders the polymers amorphous.



A DSC study of the pure polymers and polymer–salt compounds showed that T_g and T_m decreased on introducing salts into the polymer matrix. This contradicts the usually observed trend that formation of polymer electrolytes from commonly used polymers causes T_g and T_m to increase. Yamamoto *et al.* attribute a decrease in T_g and T_m to decreased degree of crysrtallinity and, correspondingly, to facilitated micromotions of the chain. It was suggested that a decrease in T_g facilitates motion of ions in polymer solid electrolytes. These results indicate that low T_g is important for migration of ions in a polymer electrolyte.

At the same time, ions can also migrate even in a polymer matrix containing relatively rigid domains. A polymer electrolyte can consist of amorphous domains with a high concentration of a lithium salt and domains with a relatively rigid structure and lower salt concentration; the ions mainly migrate through amorphous domains. Yamamoto *et al.* also examined the possibility of using as polymer electrolyte water-soluble and highly heat-resistant polysulfone–ether–imide (PSEI, $[\nu] = 0.5$ g dl^{-1}):



In contrast to PPA, this polymer gave only heterogeneous and brittle films on introducing $LiCF_3SO_3$ (0.16–0.5 g g^{-1} PSEI), despite the presence of a large amount of electron-donor atoms theoretically capable of solvating Li^+ cations.

Zapol'skikh *et al.* [103] studied the properties of PSEs based on poly(piperylene sulfone) and lithium perchlorate. They found that the room-temperature electrical conductivity of the PSE was 10^{-6} S cm^{-1} and explained this relatively high value by the presence of residual solvent, which could not be fully removed upon preparation of the films from a solution of the polymer and salt in dimethylformamide. An IR study showed that the lithium ion was coordinated with three oxygen atoms of sulfone groups and nitrogen atom of dimethylformamide. This results in displacement of the perchlorate ion from the inner coordination sphere of the lithium ion and thus in higher degree of electrolytic dissociation of the salt in the polymer matrix.

The goal of Smirnov *et al.* [104] was to develop new highly conducting PEs free of aprotic solvent. The formulation for preparing a PE consisted of an amorphous rigid-chain polymer (polyheteroarylene) and a lithium salt ($LiClO_4$ or $LiBF_4$). The polymer solid electrolytes exhibited high elasticity, mechanical strength, and acceptable adhesion to the electrode materials. Their conductivity at 20–60°C reached about 10^{-3} S cm^{-1}. The polarization at the PSE|Li phase boundary was 30–60 mV, and it gradually decreased in the course of charging–discharge, which was due to mutual adjustment of the components of the Li–PSE system. The photomicrographs of the surface of the lithium foil before and after the cycling revealed no significant changes.

Studies of the structure and mechanisms of the ion transfer in PE showed that the required set of transport properties can be attained in PSEs based on noncrystallizing polymer matrices, acrylonitrile–butadiene copolymers. Lirova *et al.* [105] used a 40 : 60 acrylonitrile–butadiene copolymer (SKN-40 rubber) containing highly polar CN groups capable of coordination interaction with the metal salts. The electrolyte films 40–120 μm thick were prepared by a modified casting procedure, with introduction of $LiClO_4$, $LiCF_3SO_3$, or $LiAsF_6$. The interaction of the lithium ions with the CN groups was studied by IR spectroscopy. By analogy with the well-studied interaction of Li^+ with acetonitrile, it was found that the solvation of the cations in SKN-40 is due to formation of coordination bonds with the cyano groups: $-C\equiv N^{\delta-}\cdots Li^+$. Lirova *et al.* [105] conclude that the solvation of the cation with the polar groups of the polymer is the factor ensuring solubility of the salt both in the low-molecular-weight solvent and in the chemically related polymer, and formation of a macromolecular ionic solution ensures high ionic conductivity of the electrolytes.

As a continuation of these studies, Dusheiko [106] prepared films from copolymers of acrylonitrile with styrene and vinyl acetate as PSEs. The solid electrolyte films prepared with these polymer matrices showed a conductivity of 10^{-5}–10^{-6} S cm^{-1} and high physicomechanical properties. Bushkova *et al.* systematically studied the ion solvation in PSEs in wide temperature and concentration ranges. As polymer matrices they used amorphous acrylonitrile copolymers (SKN-40, SKN-26, SKN-50) and polyacrylonitrile, into which $LiClO_4$, $LiAsF_6$, and $LiCF_3SO_3$ were introduced. The measurements of the temperature and concentration dependences of the PSE conductivity suggested that, in the range of maximally high salt concentrations, a specific mechanism of ion transport is realized, involving higher ionic associates.

In some cases, the conductivity of such electrolytes reached about 10^{-3} S cm^{-1}. However, stabilization of the highly conducting structure in the concentrated electrolytes was not yet attained.

Amorphous polymer electrolytes can be obtained from a copolymer of acrylonitrile with sulfoalkyl methacrylate [109]. The conductivity of various salt species of PE varies in the order Li salts > Na salts > K salts and increases as the oxygen to lithium ratio is increased from 20 to 100. The new PEs based on copolymers with polyvinyl alcohol, PVA, and polyacrylamide exhibit high heat resistance at fairly high conductivity [110].

Novakov *et al.* [9] tested as polymer matrices aliphatic polycarbonates: poly(ethylene carbonate) (PEC) and poly(propylene carbonate) (PPC), with lithium perchlorate introduced in various molar ratios. The electrical conductivity of the best formulations varied from 10^{-6}–10^{-5} at 293 K to 10^{-3} S cm^{-1} at 393 K. *Ab initio* quantum-chemical calculations of the PEC–$LiClO_4$ and PPC–$LiClO_4$ system showed that the lithium ion preferentially coordinates with the carbonyl oxygen atom, in agreement with the IR data.

Dusheiko *et al.* [111] used as PEs copolymers of acrylonitrile with butyl methacrylate (1 : 1), vinylpyridine (1 : 1), and vinyl fluoride (2.3 : 1). The copolymers were amorphous white nonhygroscopic powders. From their solutions, elastic transparent films 30–60 μm thick, doped with lithium perchlorate, were prepared. The highest conductivity, with preservation of the required physicomechanical properties, was attained at a $LiClO_4$ content of 15–20 wt %.

PLASTICIZED POLYMER ELECTROLYTES

Attempts to develop PSEs based on polymer–lithium salt systems, exhibiting acceptable electrochemical characteristics (in particular, room-temperature conductivity), were yet unsuccessful. Despite the optimism expressed in [104, 108, 112, 113], the results obtained with true PSEs are mainly inferior to those obtained with plasticized PEs. Therefore, much efforts were focused in the recent years on the development of plasticized or gel-polymer electrolytes (GPEs) containing, along with a polymer and a lithium salt, also plasticizers (solvents) and other components. The requirements to the plasticized PEs are mainly the same as those to PSEs: high electrical conductivity, satisfactory physicomechanical properties, chemical stability toward electrode materials, and wide range of electrochemical stability. However, in development of plasticized PEs, it is necessary to take into account also other factors: compatibility of the polymer matrix with the organic solvent, necessary for retention of the solvent in GPE; phase stability and efficiency in a wide temperature range. Otherwise, the GPE film can lose the solvent and the mechanical strength.

The above properties are largely determined by the kind of the polymer, composition of the plasticized PE, and temperature. Complex physicochemical processes involving the components and governing the characteristics of plasticized PEs occur in the system. The mechanisms of these processes are not fully understood. Presumably, donor–acceptor, ionic, and van der Waals interactions occur in the system [114].

The problem of enhancing the conductivity of PEO-based polymer electrolytes was solved in [115–119] by introducing crown ethers. Measurements of the electrical and electrochemical properties of PE films consisting of PEO and $LiCF_3SO_3$, $LiBF_4$, or $LiClO_4$ and containing 12-crown-4 (12C4) or free of it showed that, with each salt, the conductivity at a given temperature depends on the crown ether concentration and reaches a maximum at [12C4] : [Li] = 0.003 [116].

Eyring [117] studied the kinetics of complexation of alkali metal cations with macrocyclic ligands: 12-crown-4, 18-crown-6, and 15-crown-5. The crown ether groups (16-crown-5) were also introduced into polyphosphazenes (PPs) as pendant groups [120, 121]. The temperature dependence of the conductivity of such PEs containing $LiClO_4$ or $NaClO_4$ was studied. The $\log\sigma$–T^{-1} dependence was linearized using the VTF equation. The highest conductivity was attained in the system PP–$NaClO_4$, which was due to higher degree of ionization of the salt bound by the macrocyclic moiety of the polyphosphazene.

Introduction of 12-crown-4 both into a solid PE consisting of PEO and $LiBF_4$ and into the cathodic formulation enhances the ionic conductivity [119]. The electrolyte has a very low leakage current. Addition of the crown ether improves the cell performance, decreases the resistance to charge transport, increases the current, and makes the cell operation more reversible (with CoO_2 and TiS_2 cathodes). Along with crown ethers, a suitable additive is cryptand, a bicyclic compound also forming a complex with lithium ions [122].

Yarmolenko *et al.* [123] prepared and studied a series of new polymeric electrolytes based on $LiClO_4$ and PEO with additions of finely divided β-$LiAlO_2$,

γ-$LiAlO_2$, or Al_2O_3 powder and of 2,4-dioxo-16-crown-5. Measurements by impedance spectroscopy showed that the room-temperature conductivity of the samples was as high as 10^{-4}–10^{-5} S cm^{-1}; the compatibility with the cathodes based on thermally crosslinked polyacrylonitrile (TCPAN) and lithium anode was good. Introduction of 2,4-dioxo-16-crown-5 into PEO-based PSE improved its parameters owing to complexation of the lithium salt with the crown ether. In a later work [124], Yarmolenko *et al.* studied a series of new PSEs based on $LiClO_4$ and PEO with additions of 15-crown-5, benzo-15-crown-5, and 2,4-dioxo-16-crown-5. A series of the samples obtained exhibited high (10^{-4}–10^{-3} S cm^{-1}) room-temperature conductivity, good compatibility with the lithium anode, and stability in prolonged storage. Yarmolenko *et al.* found that introduction of 15-crown-5 and 2,4-dioxo-16-crown-5 into PEO-based PSE enhances its conductivity by two orders of magnitude, whereas introduction of benzo-15-crown-5 exerts no effect on the conductivity of this electrolyte.

Additions of 15-crown-5 and benzo-15-crown-5 to polymer electrolytes based on polyacrylonitrile, lithium perchlorate, and propylene carbonate allowed preparation of PEs with the conductivity at 20°C as high as 10^{-3} S cm^{-1} [118].

To enhance the electrical conductivity of films based on acrylonitrile copolymers, Clericuzio and Parket [125] added a mixture of propylene carbonate and dimethoxyethane as plasticizer; their content in the copolymer did not exceed 10 wt %. The conductivity of the PEs obtained was within 10^{-6}–10^{-4} S cm^{-1}.

Addition of low-molecular-weight plasticizers such as ethylene and propylene carbonate to electrolytes based on PEO [126, 127], polyacrylonitrile (PAN), poly(tetraethylene glycol diacrylate), or polyvinylpyrrolidone [128], and also to hybrid films based on poly(methyl methacrylate), polystyrene, poly(vinyl chloride) (PVC), PVA, PAN, and poly(vinylidene fluoride) in amounts of up to 30 mol % increased the electrical conductivity to 10^{-5}–10^{-3} S cm^{-1} [129]. The stable voltage of a Li|PE|MnO_2 voltaic cell, which operated for more than 70 h without electrolyte degradation, shows that hybrid films are suitable as PEs for solid-state batteries. The possibility of plasticizing PEO-based compounds by adding poly(propylene glycols) of various molecular weights was examined in [130, 131]. Such plasticization enhances the conductivity owing to an increase in the content of the amorphous phase in the electrolyte, with a simultaneous increase in the salt concentration in this phase.

The properties of gel polymer electrolytes based on PVC and solutions of lithium salts in sulfolane were studied in [132, 133]. An electrolyte solution in a polymer matrix acts as an intra- and interstructural plasticizer. The distribution of an electrolyte solution in a polymer matrix is determined by the kind and concentration of the electrolyte salts. In some cases, structural nonuniformity of GPEs results in dendrite formation in the course of prolonged dc polarization [134].

To obtain an amorphous polymer with PVC as a PE matrix, Chervakov *et al.* [135] performed a chemical modification by chlorination. As a result, the chlorine content increased from 56.8 (initial PVC) to 65%. The other electrolyte components were a salt and a plasticizer (aprotic solvent).

Polishchuk *et al.* [112] studied the system Li|Li^+|PE|FeS_2. The polymer matrix for the electrolyte was modified PVC. The modification of the polymer electrolyte was performed by additional chlorination, which afforded a more amorphous material. The conductivity of the polymer electrolytes prepared by this procedure was as high as 10^{-3} S cm^{-1}; it depended on the kind of the low-molecular-weight plasticizer and lithium salt.

The problem of development of a GPE based on PVC, which is insoluble in EC and PC, was solved by using tetrahydrofuran as solvent, in which all the components (PVC, EC, PC, $LiClO_4$) are soluble. Films with a conductivity of 1.2×10^{-3} S cm^{-1} at 20°C were prepared by casting [136].

A procedure for preparing new plasticized and microporous PEs based on poly(vinylidene fluoride) and chlorinated poly(vinyl chloride), with a room-temperature conductivity of 10^{-4}–10^{-3} S cm^{-1} and electrochemical stability in the range from 0.5 to 4.5 V (vs. lithium electrode), was suggested by Chervakov *et al.* [137]. A characteristic feature of the procedure developed is the possibility of preparing a polymer matrix with the required pore structure morphology and specific interaction with solutions of lithium salts in aprotic solvents. This is attained by a proper choice of a plasticizing system and a process for forming PE. It was shown that the nature and composition of the plasticizing system for PE essentially influence the formation of passivating films on metallic lithium and graphite anode and govern the specific characteristics of the cathode materials, stability in cycling, and self-discharge of the electrochemical systems. A process for preparing PEs for the systems Li|PE|$LiCoO_2$ and Li–MnO_2 involves preparation of a microporous polymer material and its subsequent

activation with a solution of a lithium salt in an aprotic solvent.

Kelly and Owen [138–140] enhanced the low-temperature conductivity of the systems PEO–$LiClO_4$ and PEO–$LiCF_3SO_3$ by adding low-molecular-weight polyethers $CH_3(OCH_2CH_2)_nOCH_3$. The materials obtained behaved similarly to solutions of the salts in poly(ethylene glycol) dimethyl ether ($\sigma = 10^{-4}$ S cm^{-1} at 40°C); however, the mechanical properties of the products appeared to be unsatisfactory.

An X-ray diffraction study showed that the unit cell of the PEO crystal remained monoclinic on adding the elastomer and macromonomer. The diffraction patterns and conductivities remained unchanged during a period of 15 months. The conductivity was also stabilized by partial replacement of PEO by oligo(ethylene oxide) with terminal styrene groups, with the weight ratio of ethylene oxide units to Li^+ kept unchanged [141]. The best results ($\sigma = 2 \times 10^{-4}$ S cm^{-1}) were obtained with $LiCF_3SO_3$ on adding 20 to 50% low-molecular-weight oligo(ethylene oxide) with MW 550.

Xia *et al.* [142] studied how the conductivity of solid polyelectrolyte complexes of alkali metal salts NaSCN, $NaCF_3SO_3$, and $LiCF_3SO_3$ with polymers derived from methoxypoly(ethylene glycol) methacrylate $CH_2{=}C(CH_3)COO(CH_2–CH_2O)_nCH_3$ [n = 8 (PMG-8) and n = 22 (PMG-22)] depend on the temperature and salt concentration. The systems based on copolymers of PMG-22 with polystyrene, like the systems plasticized with propylene carbonate, showed considerably higher conductivity than the systems based on the homopolymers. A highly conducting formulation based on a blend of alkylacrylate (alkyl C_1–C_8) and/or alkoxyacrylate (alkoxy C_2–C_5) polymer with 5–100% (relative to the weight of the acrylate polymer) of $LiClO_4$ or a lithium salt of a polymeric acid (polystyrenesulfonic, polyethylenesulfonic) was described in [143] as a thin-film electrolyte. The plasticizer and solvent was an organic solvent with a high dielectric permittivity.

Polymers derived from phosphazene with various alkyl ether and alkoxy pendant groups were prepared. The room-temperature ionic conductivity of the electrolytes consisting of such polymers and $LiCF_3SO_3$ was 10^{-4}–10^{-3} S cm^{-1} [144]. Villarreu [145] studied the behavior of polymer electrolytes formed by a blend of PEO and perfluorinated polyphosphazene and filled with γ-$LiAlO_2$ or propylene carbonate. It was found that the filler appreciably increases the ionic conductivity of the polyelectrolyte, whereas propylene carbonate decreases it; these effects were attributed to structural changes in the formulation.

Kicheev *et al.* [146] suggested aromatic polymers as the polymeric components, in view of the high thermal, chemical, and electrochemical stability of these polymers. As plasticizer they used a 1 M solution of $LiClO_4$ in a mixture of propylene carbonate and dimethoxyethane. The best of the polyelectrolytes studied showed the conductivity of 2.25×10^{-2} S cm^{-1} (298 K). An XPES study of the lithium anode showed that the polyelectrolyte was chemically inert.

Siling *et al.* [147] suggested a highly conducting gel-polymer electrolyte for lithium power sources, based on poly(phenylene oxide) prepared by a special procedure. The gel-polymer electrolytes were prepared by impregnation of the polymer with a solution of $LiClO_4$ in a mixed solvent. The electrical conductivity of the GPE was $(1.25–7) \times 10^{-2}$ S cm^{-1} at room temperature and $(4.1–7) \times 10^{-3}$ S cm^{-1} at 30°C; it was chiefly determined by the conditions of the synthesis of the polymeric component.

No oxide film is formed on lithium in the course of operation of Li–MnO_2 and Li–LiV_3O_8 cells with the GPE developed. No dendrites are formed either.

Yarmolenko and Efimov [148] found that oligo(urethane–methacrylates) derived from polytetrahydrofuran of molecular weight 1400–1600 (SKU–PFL) and poly(ethylene glycol monomethacrylate) (PPMBE) of molecular weight 370 can be used for preparing gel-polymer electrolytes for lithium batteries by introduction of liquid organic electrolytes (e.g., 1 M $LiClO_4$ in a 1 : 1 mixture of propylene carbonate and dimethoxyethane) into the oligomer, followed by film forming and photochemical or thermal curing. The conductivity of the film electrolytes is increased by formation of a branched network copolymer with a methacrylic comonomer in combination with addition of organic solvents for alkali metal salts; these solvents also act as plasticizers. Gel-polymer electrolytes based on SKU–PFL + PPMBE (1 : 1 by weight) and 1 M solution of $LiPF_6$ in EC + dimethyl carbonate (volume ratio 1 : 1) showed a conductivity of 2.5×10^{-3} S cm^{-1} (at 20 wt % content of the polymer in the system). The resulting thin-film electrolyte was a structured gel rather than a monolithic film. Therefore, a special procedure was developed to enhance the mechanical stability of PE. It involved introduction of the electrolyte formulation into a porous polypropylene separator, followed by photocuring. The highest conductivity (2.8×10^{-4} S cm^{-1}) was attained with the GPE containing 20 wt % SKU–PFL + PPMBE (1 : 1) and 80 wt % organic electrolyte (1 M $LiClO_4$ in γ-butyrolactone), applied to a fibrous polypropylene separator (99% porosity).

Gel-polymer electrolytes can also be prepared on the basis of anion- and cation-exchange polyelectrolytes [149–151]. Such electrolytes exhibit fairly high electrical conductivity (10^{-4}–10^{-3} S cm^{-1}) and selectivity with respect to the transported ion.

Papers concerning development of solid and plasticized polymer electrolytes show that it is very promising to search for nontraditional ways to improve the electrochemical and service properties of PEs. Among such ways are synthesis and use of new lithium salts with hyperlarge anions and chemical modification of electrolytes of lithium power sources with the aim to optimize the current transport in liquid and solid polymer media [5, 137, 152].

In particular, Chervakov *et al.* [137] develop procedures for preparing new lithium salts of *N,N'*-disubstituted alkyliminosulfinic acid amides. These resinous substances are readily soluble in aprotic solvents and are electrochemically stable in the range 1.1–4.6 V. By optimizing the structure of the anion, Chervakov *et al.* prepared lithium salts acting in PE not only as conducting additives but also as plasticizers. The following ionic salts with large anions were involved recently in PE studies: lithium tris(trifluoromethanesulfonyl)methide $LiC(CF_3SO_2)_3$, lithium bis(trifluoromethanesulfonyl)imide $LiN(CF_3SO_2)_2$, and lithium bis(perfluoroethanesulfonyl)imide $LiN\cdot(C_2F_5SO_2)_2$ [5].

CONCLUSION

Although a large body of data have been accumulated on lithium-containing polymer composites, search for new formulations of polymer electrolytes for lithium and lithium–ion batteries is being continued. The interest in basic and applied research in the field of development of new polymer electrolytes and high-capacity CPSs based on them undoubtedly grows.

REFERENCES

1. Skundin, A.M., *Elektrokhim. Energet.*, 2001, vol. 1, nos. 1–2, pp. 5–16.
2. Skundin, A.M., Efimov, O.N., and Yarmolenko, O.V., *Usp. Khim.*, 2002, vol. 71, no. 4, pp. 378–398.
3. Afanas'ev, V.N. and Grechin, A.G., *Usp. Khim.*, 2002, vol. 71, no. 9, p. 878.
4. Syromyatnikov, V.G., Paskal', L.P., and Mashkin, O.A., *Usp. Khim.*, 1995, vol. 64, no. 3, pp. 265–274.
5. Kedrinskii, I.A. and Yakovlev, V.G., *Litii-ionnye akkumulyatory* (Lithium–Ion Batteries), Krasnoyarsk: Platina, 2002.
6. Kolosnitsyn, V.S., Abstracts of Papers, *VI Mezhdunarodnaya konferentsiya "Litievye istochniki toka"* (VI Int. Conf. "Lithium Power Sources"), Novocherkassk, September 19–21, 2000, Novocherkassk: Nabla, 2000, p. 117.
7. Zhukovskii, V.M., Bushkova, O.V., Lirova, B.I., *et al.*, *Ross. Khim. Zh.*, 2001, vol. 45, no. 4, pp. 35–41.
8. Novakov, I.A., Dukhanin, G.P., Dumler, S.A., *et al.*, Abstracts of Papers, *VI Traditsionnaya nauchno-tekhnicheskaya konferentsiya stran SNG "Protsessy i oborudovanie ekologicheskikh proizvodstv"* (VI Traditional Scientific and Technical Conf. of CIS Countries "Processes and Equipment for Environmentally Clean Enterprises"), Volgograd, November 25–27, 2002, pp. 91–92.
9. Novakov, I.A., Dumler, S.A., and Dukhanin, G.P., Abstracts of Papers, *VII Mezhdunarodnaya konferentsiya "Fundamental'nye problemy preobrazovaniya energii v litievykh elektrokhimicheskikh sistemakh"* (VII Int. Conf. "Basic Problems of Energy Conversion in Lithium Electrochemical Systems"), Saratov, June 24–28, 2002, pp. 122–124.
10. Armand, M.B., *Ann. Rev. Mater. Sci.*, 1986, vol. 16, pp. 245–261.
11. Bruce, P.G., *Solid State Electrochemistry*, Cambridge Univ. Press, 1995.
12. Scrosati, B., *Applications of Electroactive Polymers*, New York: Chapman and Hall, 1993.
13. Dukhanin, G.P., Dumler, S.A., Novakov, I.A., and Shatalin, Yu.V., in *Khimiya i tekhnologiya elementoorganicheskikh monomerov i polimernykh materialov: Mezhvuzovskii sbornik nauchnykh trudov* (Chemistry and Technology of Organoelemental Monomers and Polymeric Materials: Intercollegiate Coll. of Scientific Works), Volgograd: Volgograd. Gos. Tekh. Univ., 2002, pp. 179–185.
14. Gutmann, V., *Coordination Chemistry in Non-Aqueous Solutions*, Vienna: Springer, 1968.
15. Van Krevelen, D.W. and Hoftyzer, R.J., *Properties of Polymers*, New York: Elsevier, 1976.
16. Vijh, A.K., *Appl. Phys. Commun.*, 1982–1983, vol. 2, no. 4, pp. 283–293.
17. Armand, M.B., Chabagno, J.M., and Duclot, M., Abstracts of Papers, *The Second Int. Meet. on Solid Electrolytes*, New York, March 5–9, 1979, New York: Elsevier, 1979, p. 131.
18. Armand, M.B., Abstracts of Papers, *The Second Int. Meet. on Lithium Batteries*, Paris, May 18–23, 1984, pp. 14–15.
19. Papke, B.L., Ratner, M.A., and Shriver, D.F., *J. Electrochem. Soc.*, 1982, vol. 129, no. 8, pp. 1694–1701.

20. Gray, F.M., *Polymer Electrolytes*, Cambridge: Royal Society of Chemistry, 1997.
21. Andreev, Y.G. and Bruce, P.G., *Electrochim. Acta*, 2000, vol. 45, pp. 1417–1421.
22. Tonge, J.S. and Shriver, D.F., *J. Electrochem. Soc.*, 1987, vol. 134, pp. 269–274.
23. Robitaille, C.D. and Fauteux, D., *J. Electrochem. Soc.*, 1986, vol. 133, pp. 307–311.
24. Berthier, C., Gorecki, W., Minier, M., *et al.*, *Solid State Ionics*, 1983, vol. 11, no. 1, pp. 91–95.
25. Minier, M., Berthier, C., and Gorecki, W., *J. Phys. Paris*, 1984, vol. 45, pp. 739–745.
26. Schantz, S., *J. Chem. Phys.*, 1991, vol. 94, pp. 6296–6300.
27. Manning, Y. and Frech, R., *Polymer*, 1992, vol. 33, pp. 3487–3490.
28. Armand, M.B., Chabagno, J.M., and Duclot, J.M., Abstracts of Papers, *The 2nd Int. Meet. on Solid Electrolytes*, St. Andrews (Scotland), January 11–16, 1978, Glasgow, 1978, p. 651.
29. Sorensen, P.R. and Jacobsen, T., *Electrochim. Acta*, 1982, vol. 27, no. 12, pp. 1671–1675.
30. Weston, J.E. and Steele, B.C.H., *Solid State Ionics*, 1982, vol. 7, no. 1, pp. 81–88.
31. Leveque, M., Le Nest, J.F., Gandini, A., and Cheradame, H., *J. Power Sources*, 1985, vol. 14, nos. 1–3, pp. 27–30.
32. Clancy, S. and Shriver, D.F., Abstracts of Papers, *Electrochemical Society Fall Meet.*, New Orleans, October 2–8, 1984, Pennington, NJ, 1984, p. 911.
33. Bouridah, A., Dalard, F., Deroo, D., and Armand, M.B., *Solid State Ionics*, 1986, vols. 18–19, pp. 287–291.
34. Gorecki, W., Andreani, R., Berthier, C., *et al.*, *Solid State Ionics*, 1986, vol. 20, pp. 402–405.
35. Bruce, P.G. and Vincent, C.A., *Solid State Ionics*, 1990, vols. 40–41, pp. 607–610.
36. Bruce, P.G., *Synth. Met.*, 1991, vol. 45, pp. 267–271.
37. Gray, F.M., *Solid State Ionics*, 1990, vols. 40–41, pp. 637–641.
38. Torell, L.M., Jacobsson, P., Sidebottom, D., and Petersen, G., *Solid State Ionics*, 1992, vols. 53–56, pp. 1037–1043.
39. Arumugam, S., Shi, J., Tunstall, D.P., and Vincent, C.A., *J. Phys. Condens. Matter*, 1993, vol. 5, pp. 153–157.
40. Li, J. and Khan, I.M., *Macromolecules*, 1993, vol. 26, no. 17, pp. 4544–4550.
41. Ueda, E., Graham, H., Qin, C., and Belfiore, L.A., *Polym. Mater. Sci. Eng.*, 1991, vol. 65, pp. 226–230.
42. Hara, M. and Eisenberg, A., *Macromolecules*, 1984, vol. 17, no. 7, pp. 1335–1340.
43. Molnar, A. and Eisenberg, A., *Macromolecules*, 1992, vol. 25, pp. 5774–5778.
44. Gao, Z., Molnar, A., Morrin, F.G., and Eisenberg, A., *Macromolecules*, 1992, vol. 25, pp. 6460–6463.
45. Mani, T. and Stevens, J.R., *Polymer*, 1992, vol. 33, pp. 834–840.
46. Mani, R., Mani, T., and Stevens, J.R., *J. Polym. Sci., Polym. Chem. Ed.*, 1992, vol. 94, pp. 2025–2030.
47. Fish, D., Khan, I.M., and Smid, J., *Macromol. Chem. Rapid Commun.*, 1986, vol. 7, pp. 115–121.
48. Wintersgill, M.C., Fontanella, J.J., Smith, M.K., *et al.*, *Polymer*, 1987, vol. 28, pp. 633–640.
49. Zhukovskii, V.M., Animitsa, I.E., and Volosentseva, L.I., in *Trudy XVI Mendeleevskogo s"ezda po obshchei i prikladnoi khimii* (Proc. XVI Mendeleev Congr. on General and Applied Chemistry), Moscow, February 14–19, 1988, vol. 2, p. 570.
50. Carre, C. and Hamaid, T., *Br. Polym. J.*, 1988, vol. 20, pp. 269–274.
51. Abraham, K.M., Alamgir, M., and Perrotti, S.J., *J. Electrochem. Soc.*, 1988, vol. 135, pp. 535–542.
52. Sehlenoff, J.B., Machado, J.M., and Glatkouski, P.J., *J. Polym. Sci., Part B*, 1988, vol. 26, pp. 2247–2250.
53. Bannister, D.J., Davies, G.R., Ward, I.M., and McIntyre, J.E., *Polymer*, 1984, vol. 25, no. 9, pp. 1291–1296.
54. JPN Patent 63–193954.
55. Tunstall, D.P., Tomlin, A.S., Gray, P.M., and Vincent, C.A., *J. Phys. Condens. Matter*, 1989, no. 1, pp. 4035–4041.
56. Zapol'skikh, V.V., Kolosnitsyn, V.S., and Leplyanin, G.V., *Elektrokhimiya*, 1992, vol. 28, no. 7, pp. 995–999.
57. Croce, F.J., *J. Power Sources*, 1990, vol. 32, pp. 381–387.
58. Wieczorek, W., Such, K., Przyluski, J., and Florjanczyk, Z., *Synth. Met.*, 1991, vol. 45, pp. 373–378.
59. Capuano, F., Croce, F.J., and Scrosati, B., *J. Electrochem. Soc.*, 1991, vol. 138, pp. 1918–1922.
60. Wieczorek, W., *Mater. Sci. Eng. B*, 1992, vol. 15, pp. 108–111.
61. Florjanczyk, Z. and Wieczorek, W., *Polym. Tworz. Wielkoczast.*, 1992, vol. 37, pp. 318–322.
62. Chervakov, O.V., Shembel', E.M., Globa, N.I., *et al.*, Abstracts of Papers, *VI Mezhdunarodnaya konferentsiya "Litievye istochniki toka"* (VI Int. Conf. "Lithium Power Sources"), Novocherkassk, September 19–21, 2000, Novocherkassk: Nabla, 2000, p. 89.
63. Plocharski, J. and Wieczorek, W., *Appl. Phys. A*, 1989, vol. 49, pp. 55–59.
64. UK Patent 2207547.

65. Ferloni, P., Magistris, A., Chiodelli, G., *et al.*, *Radiat. Phys. Chem.*, 1991, vol. 37, pp. 615–620.
66. Kronfli, E., Lovell, K.V., and Hooper, A., *Br. Polym. J.*, 1988, vol. 20, pp. 275–279.
67. JPN Patent 63–195117.
68. Zapol'skikh, V.V., Kolosnitsyn, V.S., and Leplyanin, G.V., *Vysokomol. Soedin., Ser. B*, 1991, vol. 32, no. 5, pp. 337–339.
69. Mochalov, S.E., Zapol'skikh, V.V., and Kolosnitsyn, V.S., *Elektrokhimiya*, 1993, vol. 29, no. 6, pp. 712–715.
70. Mochalov, S.E. and Kolosnitsyn, V.S., *Elektrokhimiya*, 1997, vol. 33, no. 4, pp. 402–408.
71. JPN Patent 63–189323.
72. JPN Patent Appl. 234661.
73. Xia, D.W. and Smid, J., *Polym. Prepr. Am. Chem. Soc.*, 1991, vol. 32, pp. 168–171.
74. Hu, C.P. and Wright, P.V., *Br. Polym. J.*, 1989, vol. 21, pp. 421–425.
75. Wieczorek, W., Such, K., Florjanczyk, Z., and Stevens, R., *Electrochim. Acta*, 1995, vol. 40, nos. 13–14, pp. 2417–2420.
76. Ballard, P.G.H., Cheshire, P., Mann, T.S., and Przeworski, J.E., Abstracts of Papers, *The 33rd IUPAC Int. Symp. on Macromolecules*, Montreal, September 7–11, 1990, p. 147.
77. US Patent 4758483.
78. Xiong, J., Zhang, Y., Zhao, X., and Wang, F., *Acta Polym. Sci.*, 1991, no. 1, pp. 7–13.
79. JPN Patent 63–175535.
80. EEC Patent 312160.
81. JPN Patent 1–169879.
82. McLennaghan, A.W., Hooper, A., and Pethrick, R.A., *Eur. Polym. J.*, 1989, vol. 25, pp. 1297–1303.
83. JPN Patent 1–197974.
84. Bouridah, A., Dalard, F., Deroo, D., *et al.*, *Solid State Ionics*, 1985, vol. 15, no. 3, pp. 233–240.
85. McLennaghan, A.W. and Pethrick, R.A., *Eur. Polym. J.*, 1988, vol. 24, pp. 1063–1067.
86. JPN Patent Appl. 280462.
87. Watanabe, M. and Ohashi, S., *Macromolecules*, 1985, vol. 18, pp. 1945–1953.
88. Watanabe, M., Sanui, K., and Ogata, N., *Macromolecules*, 1986, vol. 19, no. 3, pp. 815–819.
89. Watanabe, M. and Ogata, N., *Polymer Electrolyte Reviews*, MacCallum, J.R. and Vincent, C.A., Eds., London: Elsevier, 1987, vol. 1.
90. Liu, L., Gu, Q., and Mo, T., Abstracts of Papers, *The 5th Int. Meet. on Lithium Batteries*, Beijing (China), April 15–19, 1990, p. 200.
91. US Patent 4840856.
92. Nagaoka, K., Naruse, H., and Watanabe, M., *J. Polym. Sci., Polym. Lett.*, 1984, vol. 24, pp. 699–709.
93. Zapol'skikh, V.V., Kolosnitsyn, V.S., and Leplyanin, G.V., *Zh. Fiz. Khim.*, 1991, vol. 65, no. 2, pp. 518–521.
94. Smid, L., Fish, D., Zhou, G.B., and Xia, D.W., Abstracts of Papers, *The 33rd IUPAC Int. Symp. on Macromolecules*, Montreal, September 7–11, 1990, p. 108.
95. Blonsky, P.M., Shriver, D.F., Austin, P., and Allcock, H.R., *Solid State Ionics*, 1986, vols. 18–19, pp. 258–266.
96. Blonsky, P.M., Shriver, D.F., Austin, P., and Allcock, H.R., *J. Am. Chem. Soc.*, 1984, vol. 106, no. 22, pp. 6854–6855.
97. Allcock, H.R., Austin, P.E., Neenan, T.X., *et al.*, *Macromolecules*, 1986, vol. 19, pp. 1508–1512.
98. Abraham, K.M., Alamgir, M., and Moulton, R.D., in *Proc. 34th Int. Power Sources Symp.*, Cherry Hill, NJ, June 25–28, 1990, New York, 1990, pp. 81–83.
99. Hara, M., *Synth. Met.*, 1987, vol. 18, pp. 731–739.
100. Inoue, K., Nishikawa, Y., and Tanigaki, T., *Macromolecules*, 1991, vol. 24, pp. 3464–3472.
101. US Patent 4906718.
102. Yamamoto, T., Inami, M., and Kanbara, T., *Chem. Mater.*, 1994, vol. 6, pp. 44–50.
103. Zapol'skikh, V.V., Kolosnitsyn, V.S., Kurochkin, A.V., and Leplyanin, G.V., *Vysokomol. Soedin., Ser. A*, 1990, vol. 32, no. 7, pp. 1431–1436.
104. Smirnov, S.E., Agafonov, N.I., Morgunov, D.A., *et al.*, Abstracts of Papers, *VII Mezhdunarodnaya konferentsiya "Fundamental'nye problemy preobrazovaniya energii v litievykh elektrokhimicheskikh sistemakh"* (VII Int. Conf. "Basic Problems of Energy Conversion in Lithium Electrochemical Systems"), Saratov, June 24–28, 2002, pp. 164–165.
105. Lirova, B.I., Zhukovskii, V.M., and Bushkova, O.V., Abstracts of Papers, *V Mezhdunarodnaya konferentsiya "Fundamental'nye problemy preobrazovaniya energii v litievykh elektrokhimicheskikh sistemakh"* (V Int. Conf. "Basic Problems of Energy Conversion in Lithium Electrochemical Systems"), St. Petersburg, May 25–28, 1998, p. 86.
106. Dusheiko, V.A., Abstracts of Papers, *VI Mezhdunarodnaya konferentsiya "Litievye istochniki toka"* (VI Int. Conf. "Lithium Power Sources"), Novocherkassk, September 19–21, 2000, Novocherkassk: Nabla, 2000, p. 58.
107. Bushkova, O.V., Zhukovskii, V.M., and Lirova, B.I., Abstracts of Papers, *VI Mezhdunarodnaya konferentsiya "Litievye istochniki toka"* (VI Int. Conf. "Lithium Power Sources"), Novocherkassk, September 19–21, 2000, Novocherkassk: Nabla, 2000, p. 113.

108. Bushkova, O.V., Zhukovskii, V.M., Lirova, B.I., and Pivovarova, N.V., Abstracts of Papers, *VII Mezhdunarodnaya konferentsiya "Fundamental'nye problemy preobrazovaniya energii v litievykh elektrokhimicheskikh sistemakh"* (VII Int. Conf. "Basic Problems of Energy Conversion in Lithium Electrochemical Systems"), Saratov, June 24–28, 2002, p. 31.
109. Zhang, S., *Polym. J.*, 1991, vol. 23, pp. 73–78.
110. Przyluski, J. and Wieczorek, W., *Solid State Ionics*, 1992, vols. 53–56, pp. 1071–1076.
111. Dusheiko, V.A., Paskal', Ya.P., Rodchenko, V.V., and Parkhomenko, N.G., Abstracts of Papers, *V Mezhdunarodnaya konferentsiya "Fundamental'nye problemy preobrazovaniya energii v litievykh elektrokhimicheskikh sistemakh"* (V Int. Conf. "Basic Problems of Energy Conversion in Lithium Electrochemical Systems"), St. Petersburg, May 25–28, 1998, p. 83.
112. Polishchuk, E.V., Shembel', E.M., Neduzhko, L.I., *et al.*, Abstracts of Papers, *VII Mezhdunarodnaya konferentsiya "Fundamental'nye problemy preobrazovaniya energii v litievykh elektrokhimicheskikh sistemakh"* (VII Int. Conf. "Basic Problems of Energy Conversion in Lithium Electrochemical Systems"), Saratov, June 24–28, 2002, p. 136.
113. Angell, C.A., Liu, C., and Sanchez, E., *Nature*, 1993, vol. 137, pp. 362–366.
114. Korovin, N.V., Abstracts of Papers, *VI Mezhdunarodnaya konferentsiya "Litievye istochniki toka"* (VI Int. Conf. "Lithium Power Sources"), Novocherkassk, September 19–21, 2000, Novocherkassk: Nabla, 2000, p. 54.
115. Zhou, G., Khan, I.M., and Smid, J., Abstracts of Papers, *The 197th ACS Nat. Meet.*, Washington, DC, August 3–9, 1989, Washington, DC: Am. Chem. Soc., 1989, p. 879.
116. Nagasubramanian, G. and Di Stefano, S., *J. Electrochem. Soc.*, 1990, vol. 137, pp. 3830–3835.
117. Eyring, E.M., *Pure Appl. Chem.*, 1990, vol. 62, pp. 2237–2243.
118. Yarmolenko, O.V., Belov, D.G., and Efimov, O.N., *Elektrokhimiya*, 2001, vol. 37, pp. 321–327.
119. Nagasubramanian, G., Attia, A.I., and Halpert, G., *J. Electrochem. Soc.*, 1992, vol. 139, pp. 3043–3049.
120. Cowie, J.M.G., *Macromol. Chem. Rapid Commun.*, 1988, vol. 2, pp. 387–392.
121. Cowie, J.M.G., *Macromol. Chem. Macromol. Symp.*, 1992, vol. 53, pp. 43–46.
122. JPN Patent 63–14467.
123. Yarmolenko, O.V., Ukshe, A.E., Movchan, T.I., *et al.*, *Elektrokhimiya*, 1995, vol. 31, no. 4, pp. 388–393.
124. Yarmolenko, O.V., Ukshe, A.E., Yakushchenko, I.K., *et al.*, *Elektrokhimiya*, 1996, vol. 32, no. 4, pp. 508–511.
125. Clericuzio, M. and Parket, W.D., *Solid State Ionics*, 1995, vol. 82, pp. 179–185.
126. UK Patent 2201287.
127. Yu, D., Quin, W., Liu, Q., *et al.*, *Synth. Met.*, 1992, vol. 47, pp. 1–7.
128. Abraham, K.M. and Alamgir, M., *J. Electrochem. Soc.*, 1990, vol. 137, pp. 1657–1662.
129. Watanabe, M., Kanda, M., Matsuda, H., *et al.*, *Macromol. Chem. Rapid Commun.*, 1981, vol. 2, pp. 741–745.
130. Tsuchida, E., *Solid State Ionics*, 1983, vol. 11, pp. 227–231.
131. Conghua, W., Qingguo, L., Qijuan, C., *et al.*, *Solid State Ionics*, 1992, vols. 53–56, pp. 1106–1112.
132. Kolosnitsyn, V.S., Yakovleva, A.A., and Nikitin, Yu.E., *Zh. Prikl. Khim.*, 1990, vol. 63, no. 11, pp. 2523–2527.
133. Yakovleva, A.A. and Kolosnitsyn, V.S., *Elektrokhimiya*, 1991, vol. 27, no. 6, pp. 772–774.
134. Mochalov, S.E., Yakovleva, A.A., and Kolosnitsyn, V.S., *Elektrokhimiya*, 1989, vol. 25, no. 6, pp. 1404–1406.
135. Chervakov, O.V., Shembel', E.M., and Neduzhko, L.I., Abstracts of Papers, *V Mezhdunarodnaya konferentsiya "Fundamental'nye problemy preobrazovaniya energii v litievykh elektrokhimicheskikh sistemakh"* (V Int. Conf. "Basic Problems of Energy Conversion in Lithium Electrochemical Systems"), St. Petersburg, May 25–28, 1998, p. 84.
136. Abraham, K.M. and Alamgir, M., *J. Electrochem. Soc.*, 1993, vol. 140, pp. 535–540.
137. Chervakov, O.V., Shembel', E.M., Globa, N.I., *et al.*, Abstracts of Papers, *VII Mezhdunarodnaya konferentsiya "Fundamental'nye problemy preobrazovaniya energii v litievykh elektrokhimicheskikh sistemakh"* (VII Int. Conf. "Basic Problems of Energy Conversion in Lithium Electrochemical Systems"), Saratov, June 24–28, 2002, p. 177.
138. Kelly, I. and Owen, J.R., Abstracts of Papers, *The 2nd Int. Meet. on Lithium Batteries*, Paris, May 18–23, 1984, pp. 16–18.
139. Kelly, I. and Owen, J.R., *J. Electroanal. Chem. Interfacial Electrochem.*, 1984, vol. 168, pp. 467–472.
140. Kelly, I. and Owen, J.R., *J. Power Sources*, 1985, vol. 14, nos. 1–3, pp. 13–17.
141. Le Mehaute, A., *Polym. Bull.*, 1985, vol. 14, pp. 233–240.
142. Xia, D.W., Soltz, D., and Smid, J., *Solid State Ionics*, 1984, vol. 14, no. 3, pp. 221–224.

143. JPN Patent 1–249 851.

144. Allcock, H.R. and Austin, P.E., *Electrochim. Acta*, 1998, vol. 43, nos. 10–11, pp. 1145–1149.

145. Villarreu, E., *Angew. Makromol. Chem.*, 1999, vol. 266, pp. 24–28.

146. Kicheev, A.G., Smirnov, S.E., Komkov, V.A., *et al.*, Abstracts of Papers, *VI Mezhdunarodnaya konferentsiya "Litievye istochniki toka"* (VI Int. Conf. "Lithium Power Sources"), Novocherkassk, September 19–21, 2000, Novocherkassk: Nabla, 2000, p. 61.

147. Siling, S.A., Shamshin, S.V., and Smirnov, S.E., Abstracts of Papers, *VII Mezhdunarodnaya konferentsiya "Fundamental'nye problemy preobrazovaniya energii v litievykh elektrokhimicheskikh sistemakh"* (VII Int. Conf. "Basic Problems of Energy Conversion in Lithium Electrochemical Systems"), Saratov, June 24–28, 2002, p. 161.

148. Yarmolenko, O.V. and Efimov, O.N., Abstracts of Papers, *VII Mezhdunarodnaya konferentsiya "Fundamental'nye problemy preobrazovaniya energii v litievykh elektrokhimicheskikh sistemakh"* (VII Int. Conf. "Basic Problems of Energy Conversion in Lithium Electrochemical Systems"), Saratov, June 24–28, 2002, p. 185.

149. Kolosnitsyn, V.S., Yakovleva, A.A., and Nikitin, Yu.E., *Elektrokhimiya*, 1989, vol. 25, no. 3, pp. 99–101.

150. Kolosnitsyn, V.S. and Yakovleva, A.A., *Elektrokhimiya*, 1989, vol. 25, no. 3, pp. 544–546.

151. Kolosnitsyn, V.S., Yakovleva, A.A., and Nikitin, Yu.E., *Elektrokhimiya*, 1989, vol. 25, no. 3, pp. 546–547.

152. Grechin, A.G. and Afanas'ev, V.N., Abstracts of Papers, *VII Mezhdunarodnaya konferentsiya "Fundamental'nye problemy preobrazovaniya energii v litievykh elektrokhimicheskikh sistemakh"* (VII Int. Conf. "Basic Problems of Energy Conversion in Lithium Electrochemical Systems"), Saratov, June 24–28, 2002, p. 39.

Russian Journal of Applied Chemistry, Vol. 78, No. 1, 2005, pp. 19–22. Translated from Zhurnal Prikladnoi Khimii, Vol. 78, No. 1, 2005, pp. 21–24.
Original Russian Text Copyright © 2005 by Masloboeva, Tikhomirova, Masloboev, Arutyunyan.

INORGANIC SYNTHESIS AND INDUSTRIAL INORGANIC CHEMISTRY

Reaction of Lithium Tantalate (Niobate) with Lithium Carbonate

S. M. Masloboeva, E. L. Tikhomirova, V. A. Masloboev, and L. G. Arutyunyan

Institute of Chemistry and Technology of Rare Elements and Mineral Raw Materials, Kola Scientific Center, Russian Academy of Sciences, Apatity, Murmansk oblast, Russia

Received February 10, 2004

Abstract—Reactions of crushed wastes from lithium tantalate (niobate) production with lithium carbonate were studied by thermal and X-ray analyses. Conditions for their most complete conversion into lithium orthotantalate (orthoniobate) were determined.

In modern production of lithium metatantalate (metaniobate) single crystals, which are widely used in electronics, large amounts (70–80% in many cases) of the rare metals pass into wastes. Because of shortage and high cost of tantalum and niobium raw materials, and also of a substantial demand for the products of their conversion, development of the methods for the waste regeneration is an urgent problem.

Lithium metatantalate and metaniobate are very stable compounds, and their breakdown is a complex problem. In contrast to $LiNbO_3$, lithium orthoniobate was found [1] to react easily with H_2SO_4, HCl, and HNO_3; in the process, lithium passes into a solution and niobium is converted to complex compounds. Their calcination yields amorphous niobium pentoxide. However, the degree of Li_3NbO_4 decomposition depends not only on the acid in use, but also on the degree of $LiNbO_3$ conversion into Li_3NbO_4 by the reaction of $LiNbO_3$ with Li_2CO_3. At present, procedures for preparing lithium orthotantalate and its properties have not been adequately studied. At the same time, this problem is important for the technology of compound production and waste processing.

In this work we studied of the mechanism of the solid-state reaction between lithium tantalate (niobate) and lithium carbonate with the aim to find conditions of their most complete conversion into other less stable compounds.

We studied the Li_2CO_3–$LiTaO_3$ and Li_2CO_3–$LiNbO_3$ systems by differential thermal (DTA), differential thermal gravimetric (DTG), and thermal gravimetric analyses (TG), and also by X-ray diffraction and crystal-optics methods.

We studied the sintering process on an MOM Q-1500D derivatograph (Hungary) in platinum crucibles. We used calcined Al_2O_3 as a reference. The temperature was measured with a platinum/platinum–rhodium thermocouple. The heating rate was 10 and 20 deg min^{-1}.

We performed the X-ray analysis of the reaction products on a DRON-2 diffractometer with CuK_α radiation.

As starting substances we used predried ultrapure grade lithium carbonate; crushed wastes of $LiNbO_3$ and $LiTaO_3$ with particle size less than 160 μm (d > 50 μm, 40%; d < 50 μm, 60%), and also the 30–60-μm fractions.

The melting points of Li_2CO_3 reported by numerous researchers are inconsistent, because in the vicinity of the melting point of the compound (or simultaneously with melting) it starts to dissociate to give Li_2O. The following melting points are given for Li_2CO_3 in different papers: 618, 699, 710, 720, and 723°C. Plyushchev and Stepin [2] believe that these results are underestimated and the value of 735°C recommended in the handbook [3] and confirmed in numerous studies is the most reliable. The data characterizing the range of temperatures at which the dissociation of Li_2CO_3 starts and becomes noticeable are not always consistent either: 580–1000, 610–1010, and 777–1113 °C [2]. In this range, the CO_2 pressure increases from 1 mm Hg at 610°C to the atmospheric pressure (760 mm Hg) at 1270°C.

The experimental derivatogram of Li_2CO_3 is given in Fig. 1. It shows that the weight loss (the TG curve) starts at a temperature higher than 678°C. We assign this temperature to the onset of the stepwise dissociation of lithium carbonate. A sharp endothermic effect is observed in the DTA curve at 730°C; we assign it to the onset of Li_2CO_3 melting. The most reliable

1070-4272/05/7801-0019 © 2005 Pleiades Publishing, Inc.

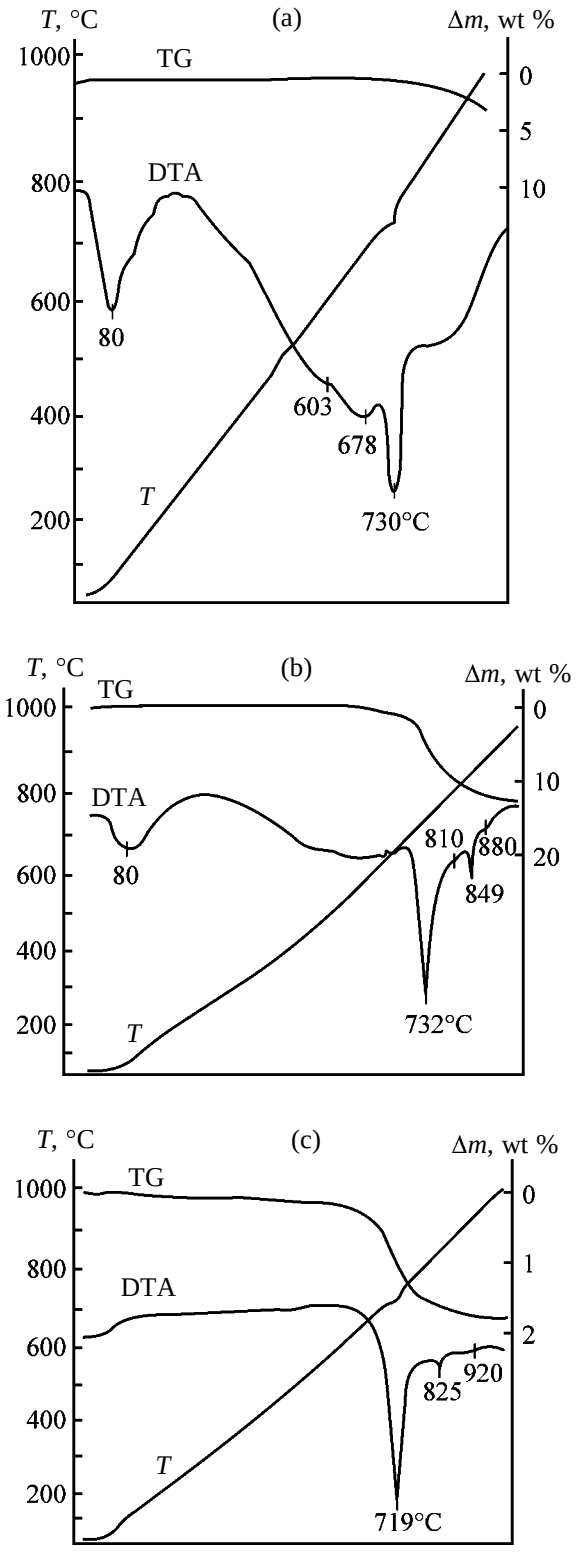


Fig. 1. Derivatograms of (a) Li_2CO_3, (b) mixtures $LiTaO_3 : Li_2CO_3 = 1 : 1$, and (c) mixture $LiNbO_3 : Li_2CO_3 = 1 : 1$, recorded in the dynamic mode. (*T*) temperature and (Δm) weight loss.

results can be obtained by visual polythermal analysis.

Reaction of Li_2CO_3 with $LiTaO_3$. The formation of lithium metatantalate in the Li_2CO_3–Ta_2O_5 system has been thoroughly studied in the literature. No clear steps can be distinguished in the reaction. In the DTA curve, one endothermic effect is always observed at different heating rates [4]. This effect coincides in temperature with the Li_2CO_3 melting. Starting from 550–600°C, lithium metatantalate appears to be the main reaction product at the ratio $Li_2CO_3 : Ta_2O_5 = 1 : 1$. Other possible phases are found only in trace amounts in definite temperature ranges: $LiTa_3O_8$, after annealing the mixture at 600°C; Li_7TaO_6, at 700°C; and α-Li_3TaO_4, at 900°C. However, the X-ray phase analysis shows that $LiTaO_3$ actively reacts with Li_2CO_3 even at 550°C. In this case, up to 700°C, the first and main product of the reaction is $LiTa_3O_8$, and only at 800°C β-Li_3TaO_4 appears, which transforms into α-Li_3TaO_4 at 900°C. At 1000°C, α-Li_3TaO_4 is the main phase. In turn, $LiTa_3O_8$ and α-Li_3TaO_4 react considerably less actively with Li_2CO_3, Ta_2O_5, and each other. According to the IR spectra, a certain amount of Li_2CO_3 is retained in the reaction mixture up to at least 900°C, which is also proved by a certain minor weight loss above 900°C.

We have recorded the derivatograms of sintering in the Li_2CO_3–$LiTaO_3$ system (Fig. 1b). The weight of a portion of jointly ground Li_2CO_3 and $LiTaO_3$ (<160 μm) was $m = 0.4988$, and their molar ratio was 1 : 1. The weight of the resulting cake was 0.4254 g. It follows from the DTA curve that at 732°C lithium carbonate melts. The endothermic effect at $T \sim 810$°C corresponds to the formation of a phase which we failed to identify by X-ray phase analysis. The next endothermic effect observed at $T \sim 850$°C can be assigned to the formation of the low-temperature β-phase of lithium orthotantalate Li_3TaO_4, which begins to transform into α-Li_3TaO_4 at $T \sim 880$°C. Figure 2b gives the X-ray diffraction pattern of the reaction products corresponding to the final state of the $LiTaO_3$–Li_2CO_3 system at 1000°C. The peaks of the high-temperature modification of Li_3TaO_4 in the X-ray pattern were assigned according to [5]. The weight loss in the TG curve ceases at the temperatures higher than 900°C, with the theoretical and experimental weight losses being in good agreement. Hence, we can believe that in the range 900–1000°C, when the Li_2CO_3 dissociation is completed, the α-phase of lithium orthotantalate is formed by the following reactions occurring simultaneously:

$$Li_2CO_3 = Li_2O + CO_2\uparrow, \quad (1)$$

$$Li_2O + LiTaO_3 = Li_3TaO_4. \quad (2)$$

Thus, the complex thermal analysis shows that sufficiently complete conversion of lithium metatantalate to orthotantalate by sintering with lithium carbonate requires the temperature of 900–1000°C. Further trials showed that this process should be carried out for 1–2 h. When studying the sintering of lithium tantalate and carbonate at the $LiTaO_3$ particle size of 30–60 μm, we obtained similar results.

Reaction of Li_2CO_3 with $LiNbO_3$. It follows from the total phase diagram of the Li_2O–Nb_2O_5 system [6] that there exist four lithium niobates: $Li_2Nb_{28}O_{71}$, $LiNb_3O_8$, $LiNbO_3$, and Li_3NbO_4. At 700–730°C, lithium metaniobate reacts with lithium carbonate to give Li_3NbO_4 [7]. At higher temperatures (higher than 1000°C), Li_3NbO_4 decomposes to $LiNbO_3$ and Li_2O, the latter evaporating.

The shapes of CO_2 pressure polytherms and DTA curves and the data of the X-ray phase analysis given in [4] suggest stepwise reaction between lithium carbonate and niobium compounds. We can choose temperature ranges corresponding predominantly to the reactions with gas evolution and without it. At 680–730°C, Li_3NbO_4 starts to appear in the mixture. As it is accumulated, the reaction with CO_2 evolution somewhat decelerates and the reactions without gas evolution starts to dominate. As a result of these reactions, of lithium carbonate melting, and of increasing temperature, the possibility of more active chemical reaction with CO_2 evolution appears again. Recrystallization of the products of this reaction, which occurs in the range 775–805°C, results in a strong increase in the amount of lithium orthoniobate. The IR data [4] point to the presence of lithium carbonate in the mixture up to at least 780°C.

Lithium orthoniobate was first described in [8] as an individual phase with the congruent melting point of 1408°C. Kulifeev *et al.* [1, 8] prepared Li_3NbO_4 by the reactions

$$3Li_2CO_3 + Nb_2O_5 = 2Li_3NbO_4 + 3CO_2, \quad (3)$$

$$Li_2CO_3 + LiNbO_3 = Li_3NbO_4 + CO_2 \quad (4)$$

and studied its thermodynamic characteristics and resistance to various acids.

The derivatogram of sintering in the Li_2CO_3–$LiNbO_3$ system is shown in Fig. 1c. The weight of jointly crushed Li_2CO_3 and $LiNbO_3$ (<160 μm) was m = 0.4806, and the weight of the resulting cake was 0.3856 g. The Li_2CO_3 : $LiNbO_3$ molar ratio was 1 : 1. An endothermic effect in the DTA curve is observed at T ~ 825 °C. This temperature may correspond to

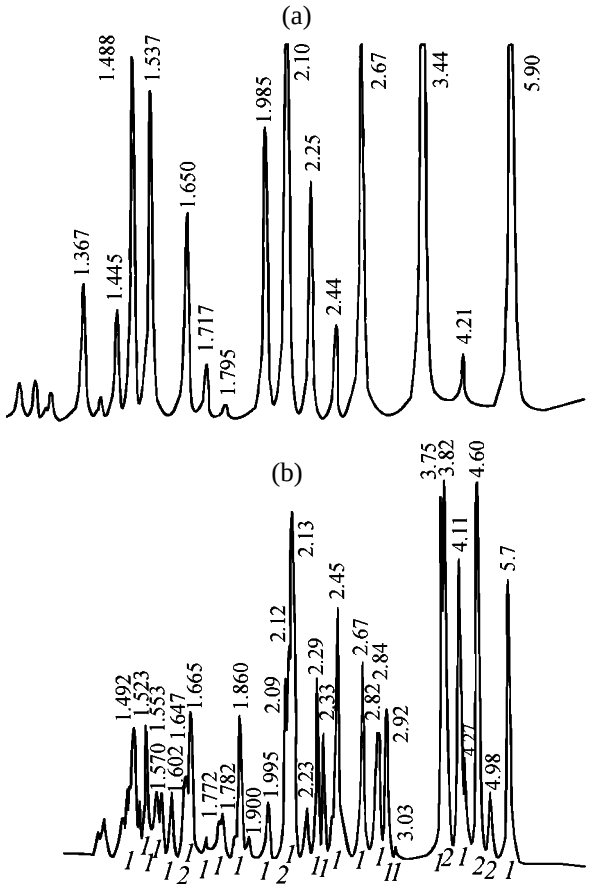


Fig. 2. X-ray diffraction patterns of the reaction products formed in the mixtures (a) $LiNbO_3$–Li_2CO_3 and (b) $LiTaO_3$–Li_2CO_3. Synthesis temperature, °C: (a) 950 and (b) 1000. Peak assignment: (*1*) Li_3TaO_4, high-temperature modification; (*2*) low-temperature modification. Interplanar spacings are given in Å.

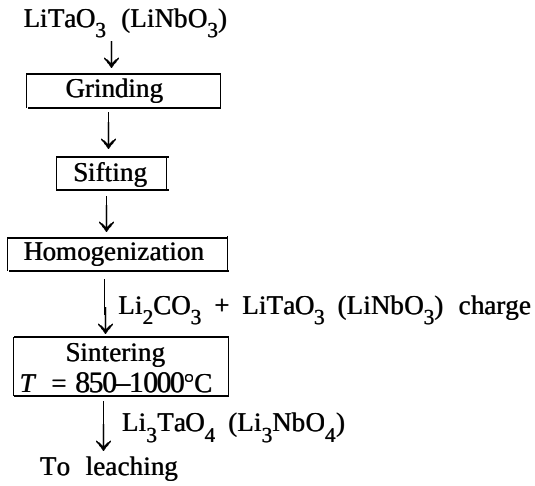
stepwise dissociation of lithium carbonate. However, by analogy with endothermic effects in the tantalum system, the peak at 825°C can be assigned to the formation of the ortho compound, the more so since, according to the X-ray diffraction data, sintering for 1–2 h under these conditions gives two phases, one of which corresponds to lithium orthoniobate and the other, to lithium niobate. The second endothermic effect is in the region of 920°C. Since at this temperature the weight loss is still observed, we can suggest that the formation of lithium orthoniobate is complete at T ~ 950 °C. For simplicity sake, the process may be considered to follow Eq. (4). This result is confirmed by the X-ray diffraction data (Fig. 2a) indicative of the presence of the single Li_3NbO_4 phase.

Thus, according to the results of the complex thermal analysis, it was found that sufficiently complete conversion of lithium metaniobate to orthoniobate by

sintering with lithium carbonate requires a temperature of 950°C.

Based on these studies, a process scheme was suggested for the conversion of lithium metatantalate (metaniobate) to lithium orthotantalate (orthoniobate). The scheme includes grinding of the wastes on a vibrational mill, their sifting through a sieve to obtain particles with $d < 160$ μm, homogenization of Li_3TaO_4 (Li_3NbO_4) with a 2–10% excess of Li_2CO_3, and subsequent fusion of the resulting charge at 900–1000°C for 1–2 h.

Scheme of production of lithium orthotantalate (orthoniobate)



The lower limit of the temperature range was chosen from the thermographic data, and the higher was specified with regard to the operating characteristics of thermal equipment and also to the kinetic (diffusion) limitations and decrease in the sintering time. The synthesis of tantalum (niobium) compounds can be carried out on standard equipment used in the production of $LiTaO_3$ ($LiNbO_3$) single crystals.

CONCLUSIONS

(1) The reactions of $LiTaO_3$ ($LiNbO_3$) with lithium carbonate were studied by complex thermal analysis, and the temperatures of their most complete conversion into orthotantalate (orthoniobate) were determined.

(2) A process scheme was proposed for the conversion of wastes from the production of $LiTaO_3$ ($LiNbO_3$) single crystals into compounds readily decomposing under the action of acids (HCl and H_2SO_4).

REFERENCES

1. Kulifeev, V.K., Myakisheva, L.V., and Derevyanko, A.D., *Izv. Vyssh. Uchebn. Zaved., Tsvetn. Metall*., 1999, no. 4, pp. 19–22.
2. Plyushchev, V.E. and Stepin, B.D., *Khimiya i tekhnologiya soedinenii litiya, rubidiya i tseziya* (Chemistry and Technology of Lithium, Cesium, and Rubidium Compounds), Moscow: Khimiya, 1970.
3. *Rare Metals Handbook*, Hampel, C.A., Ed., New York: Reinhold, 1961. Translated under the title *Spravochnik po redkim metallam*, Plyushchev, V.E., Ed., Moscow: Mir, 1965, pp. 343–383.
4. Palatnikov, M.N., Sidorov, N.V., and Kalinnikov, V.T., *Segnetoelektricheskie tverdye rastvory na osnove oksidnykh soedinenii niobiya i tantala* (Ferroelectric Solid Solutions Based on Niobium and Tantalum Oxide Compounds), St. Petersburg: Nauka, 2001.
5. Grenier, *Bull. Soc. Fr. Mineral. Cristallogr*., 1964, vol. 87, p. 316.
6. Shapiro, Z.I., Trunov, V.K., and Shishov, V.V., *Metody polucheniya niobatov shchelochnykh metallov* (Methods for Preparing Alkali Metal Niobates), Moscow: NIITEKh, 1978.
7. Agulyanskaya, L.A., Physicochemical Principles of the Synthesis of Lithium Metaniobate and Metaniobate, *Cand. Sci. (Chem.) Dissertation*, Moscow, 1986.
8. Kulifeev, V.K., Myakisheva, L.V., and Derevyanko, A.D., in *Trudy IV Mezhdunarodnoi konferentsii "Kristally: rost, svoistva, real'naya struktura, primenenie"* (Proc. IV Int. Conf. "Crystals: Growth, Properties, Actual Structure, Applications") Moscow, VNIISIMS, 1999, p. 297.

Russian Journal of Applied Chemistry, Vol. 78, No. 1, 2005, pp. 23–25. Translated from Zhurnal Prikladnoi Khimii, Vol. 78, No. 1, 2005, pp. 25–27.
Original Russian Text Copyright © 2005 by Khamaganova, Khrushcheva.

INORGANIC SYNTHESIS AND INDUSTRIAL INORGANIC CHEMISTRY

Synthesis and Properties of Scandium and Alkaline-Earth Double Borates $M_3Sc(BO_3)_3$

T. N. Khamaganova and N. M. Khrushcheva

Baikal Institute of Nature Management, Siberian Division, Russian Academy of Sciences, Ulan-Ude, Buryatia, Russia
Buryat State University, Buryatia, Ulan-Ude, Russia

Received March 18, 2004

Abstract—Compounds $M_3Sc(BO_3)_3$ (M = Ba, Sr) were prepared by solid-phase reactions and studied by X-ray diffraction (XRD) analysis and IR spectroscopy. The structural type of the compounds was determined and their unit cell parameters were refined.

Mixed borates $M_3RE(BO_3)_3$ (M = Ba, Sr; RE = rare-earth elements) are promising as laser, luminescence, and nonlinear-optical materials [1, 2]. Double borates $M_3RE(BO_3)_3$ (M = Ba, Sr; RE = La–Lu) were prepared previously [2–5] using $MO–RE_2O_3–B_2O_3$ three-components systems, and their crystal structure and some physicochemical properties were determined.

Published data on similar double borates with scandium concern preparation of single crystals and determination of their crystal structures. Centrosymmetrical $Sr_3Sc(BO_3)_3$ crystallizes in the trigonal system (space group $R\bar{3}$, Z 6) [1]. This structure is built of two types of scandium octahedra forming chains along the c axis; in turn, these chains are linked through nonahedra of Sr atoms to form a rhombohedral framework. The octahedra of Sc atoms are strongly distorted depending on the type of junction with the oxygen polyhedra of the Sr cations. For example, Sc octahedra linked with Sr nonahedra are trigonally extended, whereas the octahedra sharing triangular faces with Sr polyhedra are trigonally compressed. The BO_3 groups are isolated and arranged along the threefold axis. The isomorphic substitution of Sr cations by larger Ba cations destabilizes the rhombohedral framework to form the compound of a new structural type.

As seen from XRD data and results obtained by the second-harmonic generation (SHG) procedure, $Ba_3Sc(BO_3)_3$ crystals contain no center of symmetry [6]. Double borate $Ba_3Sc(BO_3)_3$ crystallizes in the hexagonal system (space group $P6_3cm$, Z 6). This cell contains two structurally independent Sc atoms occurring in distorted octahedral environment, and Ba atoms of four types occupy nonahedra. Boron cations of three types have trigonal planar oxygen surrounding. Large Ba cations form alternating layers in the (001) plane and each of these layers contains the atoms of similar type. These layers are linked in a three-dimensional framework through Sc octahedra and discrete BO_3 groups arranged perpendicularly to the c axis.

The aim of this work was to study the synthesis of $M_3Sc(BO_3)_3$ compounds and to determine their XRD characteristics.

EXPERIMENTAL

The compounds $M_3Sc(BO_3)_3$ (M = Sr, Ba) were prepared by annealing of the stoichiometric amounts of ultrapure grade $BaCO_3$, analytically pure grade $SrCO_3$, and chemically pure grade H_3BO_3 and Sc_2O_3 at 600–1000°C for 60 h.

The reaction completeness was checked with a DRON-UM-1 diffractometer (CuK_α radiation). The individual phases were identified by XRD analysis and IR spectrometry. The intensity data were collected on an FR-552 focusing camera-monochromator (CuK_α radiation, Ge internal reference). The unit cell parameters were refined by the least-squares method. The IR spectra were recorded on a UR-20 spectrometer in the 1500–400 cm^{-1} range using KBr pellets.

The XRD patterns showed that barium scandium double borate crystallizes in the hexagonal system (space group $P6_3cm$), whereas in the case of strontium the trigonal unit cell is formed (space group $R\bar{3}$).

The experimental data on the powder XRD patterns of these compounds are listed in Table 1. The unit cell

1070-4272/05/7801-0023 © 2005 Pleiades Publishing, Inc.

Table 1. Indexing of the powder diffraction patterns of $Ba_3Sc(BO_3)_3$ and $Sr_3Sc(BO_3)_3$

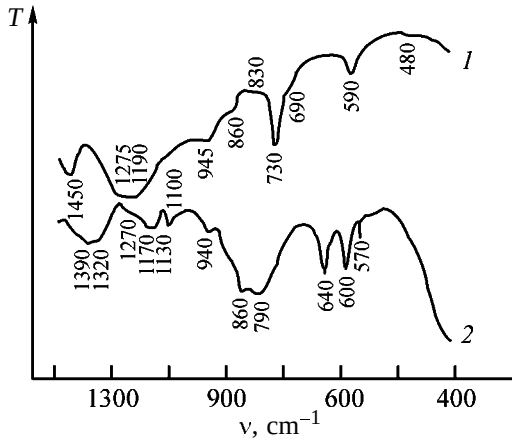
I/I_0	d, Å	$10^4/d^2_{exp}$	hkl	$10^4/d^2_{calc}$	I/I_0	d, Å	$10^4/d^2_{exp}$	hkl	$10^4/d^2_{calc}$
$Ba_3Sc(BO_3)_3$ (space group $P6_3cm$, z = 6)					$Sr_3Sc(BO_3)$ (space group $R\bar{3}$, z = 6)				
3	8.55	137	002	136	3	6.93	208	101	209
1	5.87	290	012	291	5	6.07	271	110	271
80	4.47	500	111	501	20	4.56	481	021	481
1	4.29	544	004	545	25	4.21	565	012	565
8	4.08	602	112	603	100	3.644	753	211	753
3	3.78	702	014	702	90	3.456	837	202	837
3	3.634	757	022	758	80	3.061	1067	003	1068
70	3.600	772	113	772	50	3.035	1086	220	1086
100	3.146	1011	114	1012	100	3.003	1109	122	1109
1	2.928	1167	024	1170	90	2.776	1298	131	1297
8	2.856	1226	122	1226	70	2.732	1340	113	1340
80	2.755	1317	115	1316	50	2.525	1568	401	1568
90	2.674	1399	123	1400	100	2.460	1653	312	1652
10	2.553	1535	032	1537	80	2.331	1840	321	1840
1	2.478	1629	124	1630	3	2.304	1883	303	1884
<1	2.329	1844	026	1845	50	2.293	1902	410	1902
15	2.270	1938	125	1938	10	2.279	1925	042	1924
30	2.237	1998	222	2000	10	2.242	1989	104	1989
15	2.165	2134	117	2136	70	2.154	2155	223	2155
40	2.148	2168	132	2169	50	2.133	2197	232	2196
3	2.083	2308	126	2310	3	2.102	2263	024	2261
<1	2.072	2330	018, 133	2331	25	2.048	2384	051	2384
100	2.039	2406	224	2407	80	1.986	2535	214	2533
1	1.945	2644	118	2644	5	1.941	2654	241	2654
1	1.891	2796	028	2796	8	1.910	2742	502	2741
3	1.762	3219	119	3218	50	1.847	2930	511	2928
20	1.744	3289	140	3288	50	1.834	2972	413,143	2970
3	1.684	3527	227	3528	8	1.821	3015	422	3012
40	1.673	3571	038, 143	3571	40	1.745	3283	152	3284
1	1.609	3864	1110	3864	40	1.733	3329	205	3329
					50	1.697	3471	431	3472
					40	1.683	3532	520	3530
					10	1.666	3602	125	3602

Table 2. Unit cell parameters of $M_3Sc(BO_3)_3$

M	a	c	V/z, Å^3	Crystal system
	Å			
Ba	9.232(1)	17.132(3)	210.7(1)	Hexagonal
Sr	12.134(5)	9.180(1)	194.9(1)	Trigonal

parameters (Table 2) agree with the experimental data recorded for single crystals [1, 6].

Only one type of coordination was found in these structures for boron atoms. The IR spectra of the compounds showed 10 and 12 bands (see figure). In the spectral region studied, we observed the expected characteristic vibrations of the isolated oxygen triangles (D_{3h} symmetry) (Table 3). The intense narrow band at 730 cm^{-1} in the spectrum of barium scandium borate corresponding to the out-of-plane bending vib-



IR spectra of (*1*) $Ba_3Sc(BO_3)_3$ and (*2*) $Sr_3Sc(BO_3)_3$. (*T*) Transmission and (ν) wave number.

Table 3. Vibration bands of BO_3^{3-} anion in the IR spectra of $M_3Sc(BO_3)_3$

ν, cm^{-1}		Assignment
BaSc	SrSc	
1450	1390	$\nu_3BO_3^{3-}$
	1320	
1275	1270	
1190	1170	
	1150	
	1100	
945	940	$\nu_1BO_3^{3-}$
860	860	
830	790	$\nu_2BO_3^{3-}$
730		
690	640	$\nu_4BO_3^{3-}$
590	600	
480	570	

ration ν_2 of the borate anion splits in two bands at 860 and 790 cm^{-1} for the strontium compound. Similar splitting of the band at 590 cm^{-1} into three components at 640, 600, and 570 cm^{-1} is observed for the in-plane bending vibrations ν_4. The IR spectrum of $Sr_3Sc(BO_3)_3$ also showed rather complex splitting of the stretching absorption bands of the B–O bonds. This splitting is probably due to a decrease in the symmetry of the boron environment on passing from barium to strontium borate.

CONCLUSIONS

(1) With the aid of XRD analysis of the intermediate and final products, the conditions of formation of double borates $M_3Sc(BO_3)_3$ (M = Sr, Ba) from the initial carbonates, scandium oxide, and boric acid were determined.

(2) The powder XRD patterns showed that $Ba_3Sc(BO_3)_3$ and $Sr_3Sc(BO_3)_3$ crystallize in hexagonal (space group $P6_3cm$) and trigonal (space group $R\bar{3}$) systems, respectively.

REFERENCES

1. Tompson, P.D. and Keszler, D.A., *Chem. Mater*, 1989, no. 1, pp. 292–294.
2. Stefanovich, S.Yu. and Khamaganova, T.N., *Izv. Ross. Akad. Nauk, Neorg. Mater.*, 2002, vol. 38, no. 1, pp. 78–80.
3. Khamaganova, T.N. and Trunov, V.K., *Zh. Neorg. Khim.*, 1997, vol. 42, no. 1, pp. 26–28.
4. Khamaganova, T.N., Kuperman, N.M., and Bazarova, Zh.G., *Zh. Neorg. Khim.*, 1998, vol. 43, no. 7, pp. 1000–1001.
5. Khamaganova, T.N., Kuperman, N.M., and Bazarova, Zh.G., *Solid State Chem.*, 1999, vol. 145, pp. 33–36.
6. Cox, J.R., Keszler, D.A., and Huang, J., *Chem. Mater.*, 1994, vol. 6, pp. 2008–2013.

Russian Journal of Applied Chemistry, Vol. 78, No. 1, 2005, pp. 26–32. Translated from Zhurnal Prikladnoi Khimii, Vol. 78, No. 1, 2005, pp. 28–35.
Original Russian Text Copyright © 2005 by Golubeva, Korytkova, Gusarov.

INORGANIC SYNTHESIS AND INDUSTRIAL INORGANIC CHEMISTRY

Hydrothermal Synthesis of Magnesium Silicate Montmorillonite for Polymer–Clay Nanocomposites

O. Yu. Golubeva, E. N. Korytkova, and V. V. Gusarov

Grebenshchikov Institute for Silicate Chemistry, Russian Academy of Sciences, St. Petersburg, Russia

Received September 7, 2004

Abstract—Conditions of hydrothermal synthesis of magnesium silicate montmorillonite $Mg_3Si_4O_{10}(OH)_2 \cdot nH_2O$ with a particle size of 50–100 nm are optimized, including the temperature, initial chemicals, reaction medium, and run duration.

At present, synthesis of hybrid polymer–inorganic nanocomposites appears to be one of the most effective ways in developing novel structural materials. A steadily growing interest in nanocomposites is stimulated by their improved physical and mechanical characteristics as compared to micro- and macrocomposites containing the same or even larger amounts of an inorganic filler.

Interest in polymer–inorganic nanocomposites based on layered silicates has quickened since 1987, when a series of works on Nylon–clay hybrids were published by the Toyota Research Center [1]. It was demonstrated that small additions of layered minerals, particularly montmorillonite, significantly enhance the thermal resistance and mechanical characteristics of the polymer.

Later on polymeric nanocomposites with layered silicates as fillers were intensively studied [2–6]. Polymer–silicate nanocomposites were found to be characterized by increased strength, thermal and chemical resistance, and ionic conductivity and by lower thermal expansion coefficient and gas permeability as compared to the initial polymer. Several characteristics were also improved, such as the flame propagation resistance and barrier action, which could not be realized with any other filler [7]. It is significant that such improvements of properties were not accompanied by noticeable increase in the density or decrease in the light transmission [8].

The possibility of improvement of a series of performance characteristics stimulated more extensive applications of polymer–inorganic materials in such areas as motor-car construction, light industry, electronics, and aerospace industry [9].

In the works devoted to synthesis and characterization of polymer–inorganic nanocomposites, such polymers as polyester, polyurethane, polystyrene, polypropylene, polyethylene, polybutadiene resin, polyaniline, and many others were used [10]. However, in all cases, practically the only material, montmorillonite, representing a layered silicate, was used a filler.

Layered silicates are very convenient materials for fabrication of nanocomposites (nanocomposite is a composite material in which a filler dispersed in the polymer matrix has at least one dimension of nanometer size). Silicate layers, being about 1 nm thick and 100–1000 nm wide, have highly developed surface capable of interacting with the polymer matrix. The particle size distribution and interaction of the silicate layers with the polymer matrix control the performance characteristics of the resulting composite. Minerals belonging to the montmorillonite group, in their turn (by virtue of their structural features), are the most suitable layered silicates for nanocomposites.

Montmorillonites are natural clay minerals with the general formula $(Na, Ca, K)_{x+y}(Si_{y-x}Al_x)(Al_{2-y}Mg_y) \cdot O_{10}(OH)_2$, $x = 0.05–0.45$; $y = 0.05–0.65$. The montmorillonite group includes about 20 different minerals, among them the title mineral, montmorillonite, being the most abundant. The crystal structure of these minerals is characterized by layered arrangement of cations and anions (Fig. 1). Montmorillonite stacks have a plane of symmetry. They are faced to each other by similarly charged oxygen layers, thus stabilizing the aluminum(magnesium)–oxygen–hydroxo layers by the van der Waals forces.

Water and other polar liquids can easily penetrate into the interlayer space of the montmorillonite lattice, expanding the layers to the extent depending on the

1070-4272/05/7801-0026© 2005 Pleiades Publishing, Inc.

amount of absorbed liquid. This structural feature promotes the use of montmorillonite as a filler for nanocomposites, since, to attain the required characteristics, a layered filler should be totally exfoliated in the polymer matrix.

At the same time, natural montmorillonite as a filler for polymer–inorganic nanocomposites demonstrates some drawbacks. For example, natural clay minerals represent mostly a mixture of several natural compounds, being, therefore, inhomogeneous in the chemical, phase, and disperse compositions. This makes the task of directed synthesis of functionalized nanocomposites more complicated.

To our best knowledge, in all the works on polymer–clay nanocomposites with montmorillonite as a filler, natural clay minerals were used, and the authors mostly gave no indication of their composition, rarely specifying the particle size. This does not allow establishment of the relationship between the composition and particle size of the filler and the properties of the resulting nanocomposite on the basis of published data. Establishment of such a relationship appears to be even more significant in view of the fact that no concept has been offered by now to explain the observed abrupt changes in characteristics of the polymers occurring with even small (2–3%) additions of montmorillonite.

Therefore, synthesis of montmorillonite of a fixed composition with a narrow particle size distribution is of considerable scientific and practical interest in view of its application as a filler in polymer–inorganic nanocomposites.

EXPERIMENTAL

The goal of this work was hydrothermal synthesis of magnesium silicate montmorillonite $Mg_3Si_4O_{10}\cdot(OH)_2\cdot nH_2O$ (analog of natural saponite) with a particle size of about 100 nm.

Optimization of the synthetic procedure was aimed at preparation of a single-phase product of a fixed composition with a narrow particle size distribution. Therefore, we studied the effects of such factors as the temperature, initial chemicals, reaction medium, and run duration on the yield and quality of the product.

As starting materials for the synthesis we used dry and ground silica gel $SiO_2\cdot nH_2O$, MgO, and $Mg(OH)_2$ precipitated from a $MgCl_2$ solution.

A stoichiometric mixture of the starting chemicals was treated with NaOH solutions of various concentrations under hydrothermal conditions (250–350°C, 70 MPa) for 0.5–7 h.

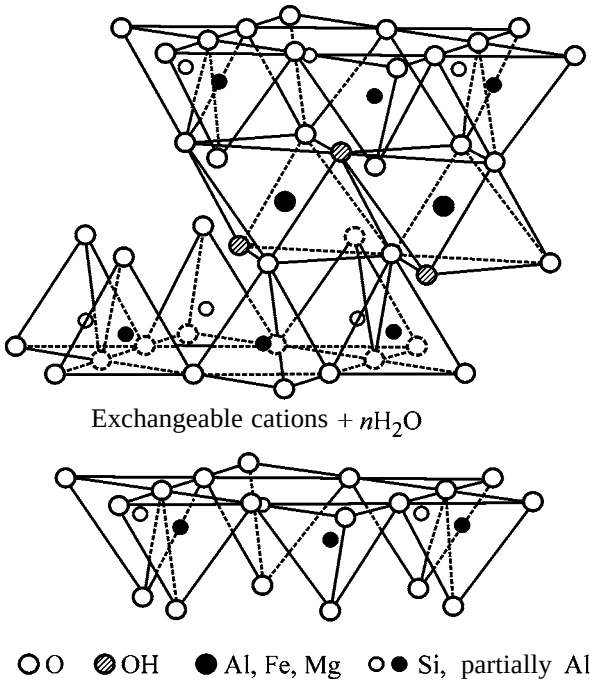


Fig. 1. Crystal structure of montmorillonite.

The resulting products were examined by X-ray diffraction (DRON-3 diffractometer, CuK_α radiation), crystal optics (MIN-8 microscope), and transmission electron microscopy (EM-125 electron microscope; U_{acc} = 75 kV).

The synthesis conditions and characteristics of the resulting products are summarized in the table.

The results show that, in hydrothermal synthesis of montmorillonite, brucite $Mg(OH)_2$ is the major impurity phase. Under certain conditions, the final product contains also other impurities such as magnesium oxide, quartz, and chrysotile (Fig. 2).

At 250 and 300°C, increasing alkalinity of the hydrothermal solution results initially in decrease in the montmorillonite content in the final product and increase in the brucite content (see table, experiment nos. 2, 3, and 7–9), and, with further increase, in a change montmorillonite/brucite ratio in the direction of increasing montmorillonite fraction (experiments nos. 4 and 5). In experiment no. 15 (350°C; 1 wt % NaOH), the product also contains MgO, which was not the case in experiment no. 14 performed with 3 wt % NaOH, all other conditions being equal. MgO was also found in the products obtained with 2.5 wt % NaOH at 250 and 300°C, but at a run time of 2 h (experiment nos. 1 and 6). Synthesis under the same

Synthesis conditions and characteristics of products (P = 70 MPa)

Experiment no.	Starting chemicals		T, °C	τ, h	Product	I_{MMT}/I_{br}*	Particle size**
	solids	c_{NaOH}, wt %, in hydrothermal solution					
1	$MgO + SiO_2$	2.5	250	2	MMT + brucite + MgO		Coarse particles (up to 0.2–0.3 mm)
2	$MgO + SiO_2$	2.5	250	4	MMT + brucite	1.2	
3	$MgO + SiO_2$	3.0	250	4	MMT + brucite	0.7	
4	$MgO + SiO_2$	3.5	250	4	MMT + brucite	0.75	
5	$MgO + SiO_2$	4.0	250	4	MMT + brucite	1.1	
6	$MgO + SiO_2$	2.5	300	2	MMT + brucite + MgO	–	
7	$MgO + SiO_2$	2	300	4	MMT + brucite	1.7	
8	$MgO + SiO_2$	2.5	300	4	MMT	–	
9	$MgO + SiO_2$	4.0	300	4	MMT + brucite	0.8	Broad particle size distribution, the coarsest particles are up to 0.25 mm
10	$MgO + SiO_2$	4.0	300	5	MMT + chrysotile + traces of brucite	–	Large amount of impurity phase
11	$MgO + SiO_2$	3.0	300	7	MMT + brucite	1.9	Finely dispersed fraction dominates as separate particles and conglomerates (70–90%). Coarse plate-like particles are also present
12	$MgO + SiO_2$	3.0	350	0.5	MMT + brucite + SiO_2	–	
13	$MgO + SiO_2$	3.0	350	0.75	MMT + brucite + SiO_2	–	
14	$MgO + SiO_2$	3.0	350	1	MMT + brucite	0.7	
15	$MgO + SiO_2$	1.0	350	1	MMT + brucite + MgO	–	
16	$MgO + SiO_2$	2.0	350	1	MMT + brucite	0.8	
17	$Mg(OH)_2 + SiO_2$	2.5	300	2	MMT + brucite	0.5	Broad particle size distribution, the coarsest particles are 0.2–0.3 mm in size
18	$Mg(OH)_2 + SiO_2$	3.0	300	1	MMT + brucite	0.7	

* (I_{MMT}/I_{br}) Montmorillonite (MMT) to brucite (br) ratio in the products. It was estimated from the X-ray diffraction data as the intensity ratio of the characteristic peaks of montmirillonite (2θ = 60.5°, I_{rel} = 100%) and brucite (2θ = 38°, I_{rel} = 100%).
** Characteristics of as-prepared (not subjected to acid treatment) products, determined by the crystallooptical method.

conditions, but for 4 h produces only montmorillonite and brucite (experiment nos. 2, 8). The use of more alkaline solutions (4 wt % NaOH) results in formation of brucite in considerable amount, and with increasing run time to 5 h, chrysotile is also formed (experiment no. 10).

According to the thermodynamic data (IVTAN–THERMO), magnesium hydroxide is stable over the experimental temperature and pressure ranges. Therefore, MgO that was found in the reaction products can be considered, most likely, as an unreacted initial component, but not as a decomposition product of brucite formed in the reaction.

It is known [11, 12] that the solubility of silica in a hydrothermal solution strongly increases in the presence of an alkali metal oxide, i.e., increase in the solution pH results in transfer of a considerable part of SiO_2 into the liquid phase. Dissolution of silica in the system Na_2O–SiO_2–H_2O may produce three phases: quartz, sodium silicate solution, and aqueous silicic acid. The latter two phases are liquids, and their compositions are temperature- and pressure-dependent [11]. Therefore, in performing the synthesis in alkaline solutions, the solid phase may be silica-deficient (relative to the fixed stoichiometry of montmorillonite). As a result, in addition to montmorillonite, other solid phases with a lower SiO_2 content can be formed, e. g., chrysotile (see table, experiment no. 10), and the final product will contain unreacted brucite.

According to the known classification of layered silicates [13] based on the layer structure, two major groups of minerals belong to the 1 : 1 and 2 : 1 types. In layered silicates of the 1 : 1 type, e.g., in chrysotile, a two-dimensional network built by SiO_4 tetrahedra is jointed to a two-dimensional network of MgO_6 octa-

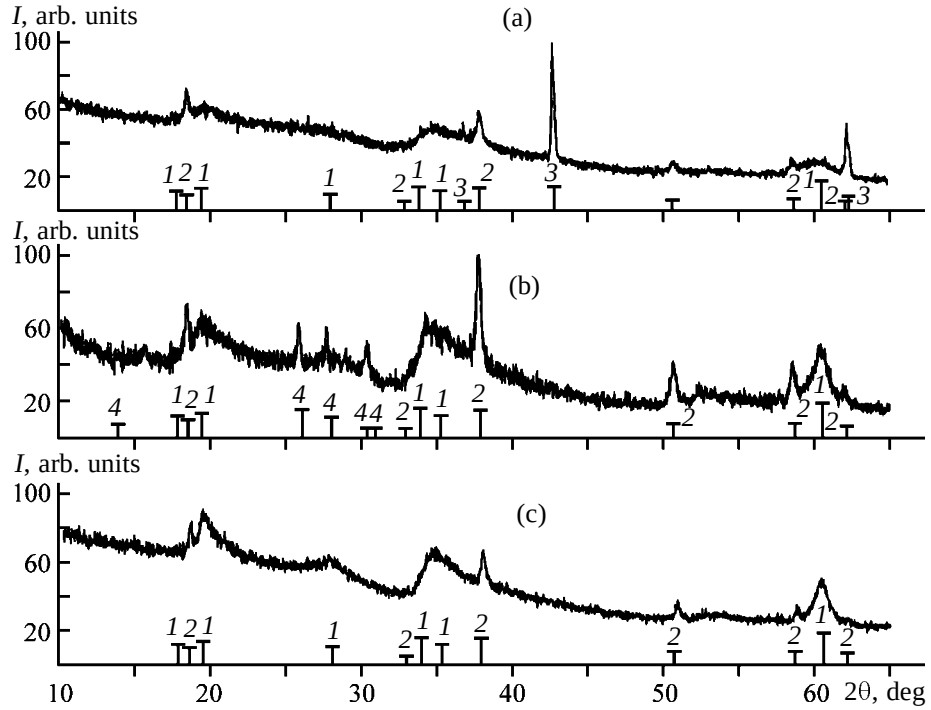


Fig. 2. X-ray diffraction patterns of montmorillonite samples obtained under different synthetic conditions together with XRD data for reference compounds. (*I*) Intensity and (2θ) Bragg angle; the same for Figs. 3, 5, and 6. (a) 250°C, 2 h, 2.5% NaOH; (b) 350°C, 0.5 h, 3.0% NaOH; and (c) 300°C, 4 h, 3.5% NaOH. (*1*) $Mg_3Si_4O_{10}(OH)_2 \cdot nH_2O$, (*2*) $Mg(OH)_2$, (*3*) MgO, and (*4*) SiO_2.

hedra. Montmorillonite is classed with layered silicates of the 2 : 1 type. In its structure, the octahedral layer is arranged between two tetrahedral layers (Fig. 1). Therefore, partial dissolution of silica may promote formation of chrysotile $Mg_3Si_2O_5(OH)_4$ whose structure contains smaller amount of SiO_2 than in montmorillonite $Mg_3Si_4O_{10}(OH)_2$.

Analysis of the effect of the alkalinity of the hydrothermal solution on crystallization of montmorillonite shows that increase in the NaOH concentration, first, increases the solubility of SiO_2, resulting in formation of chrysotile and brucite. At the same time, after formation of the nucleation centers, e.g., magnesium–oxygen octahedra in brucite, crystallization of montmorillonite is controlled by SiO_2 transfer to the reaction zone. Therefore, increase in the NaOH concentration and the corresponding increase in the solubility of SiO_2 in the hydrothermal solution should enhance the mass transfer of SiO_2 and, therefore, the montmorillonite formation rate.

Furthermore, increasing alkalinity of the solution produces silicates with highly associated silicon–oxygen complex polyanions such as $[SiO_3]^{2-}$ and $[Si_2O_5]^{2-}$ [11]. Entering the reaction, these silicates promote formation of silicates with infinite silicon–oxygen radicals, i.e., of layered silicates. This trend is supported by the data on the effect of the NaOH concentration in the hydrothermal solution: the yield of montmorillonite decreases on passing from 2.5 to 3.5 wt % NaOH (250°C; run time 4 h; see table, experiment nos. 2–4), and then increases as the NaOH concentration increases to 4 wt % (experiment no. 5; 4 wt % NaOH).

Finally, in low-alkaline solutions (1–2.5 wt % NaOH) and at small run time (2 h), the reaction between the starting components is incomplete. Increasing alkalinity to 3–4 wt % may result in stabilization of chrysotile. The maximal yield of montmorillonite was obtained at an alkalinity of 2–2.5 wt % NaOH at 350°C and run time of 2 h.

Increasing temperature from 250 to 300°C (4 h; experiment nos. 5 and 9) slightly increases the yield of montmorillonite and decreases the fraction of $Mg(OH)_2$ in the final product. Therefore, increasing temperature activates reactions between the initial components, promoting initially formation of brucite and then, of montmorillonite.

Similar trend was observed with respect to the run time. Increasing run time from 2 to 4 h at 250 and 300°C (2.5 wt % NaOH; experiment nos. 1, 2, 6,

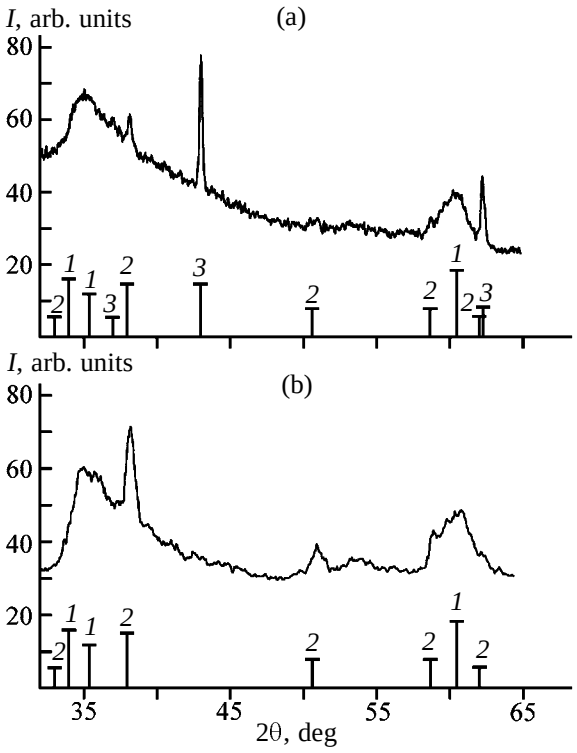


Fig. 3. XRD patterns of montmorillonite samples synthesized using (a) MgO and (b) $Mg(OH)_2$ (experiment nos. 6 and 17). T = 300°C, τ = 2 h, and c_{NaOH} = 2.5 wt %. (*1*) Montmorillonite $Mg_3Si_4O_{10}(OH)_2 \cdot nH_2O$, (*2*) $Mg(OH)_2$, and (*3*) MgO.

and 8) increases the yield of montmorillonite and decreases the fraction of $Mg(OH)_2$ in the product with formation of single-phase montmorillonite (experiment no. 8; 300°C; 2.5 wt % NaOH; 4 h).

The following conclusions could be made on the formation mechanism of montmorillonite under hydrothermal conditions. In alkaline solutions, initial stages of the process involve hydration of MgO with formation of brucite and partial dissolution of SiO_2. In the next stage, $Mg(OH)_2$ reacts with silica with formation of magnesium hydrosilicates, particularly, montmorillonite. Thus, the formation of $Mg(OH)_2$ precedes the formation of montmorillonite, which can be attributed to structural effects. Brucite has layered structure with the layers representing a magnesium–oxygen network [13]. Structurally these layers are similar to the magnesium–oxygen octahedral network arranged between the tetrahedral layers in the structure of montmorillonite. Evidently, $Mg(OH)_2$ plays a role of a nucleating center in crystallization of montmorillonite, which can be thought as formation of silicon–oxygen layers between still existing brucite layers through deposition of the silicon-containing component from the hydrothermal solution onto the layers of magnesium–oxygen octahedra.

Increasing run time, on the one hand, results in decreasing brucite fraction in the product, and, on the other hand, in increasing particle size.

Insofar as the goal of the work was synthesis of montmorillonite not of only the desired composition, but also with the optimal particle size distribution, we performed a series of experiments at higher temperature (350°C) and shorter run times (0.5–1 h) in hydrothermal solutions of various concentrations. Analysis of the resulting products revealed that synthesis in 3 wt % NaOH (experiment nos. 12, 13) affords products containing two impurity phases, $Mg(OH)_2$ and SiO_2. According to the XRD data, the latter product represents a labile intermediate phase SiO_2–X_2. It is known [14, 15] that hydrothermal crystallization of amorphous silica into quartz is a complex process involving formation of a series of intermediate phases. Introduction of a sufficient amount of the alkali into the reaction medium causes formation of intermediate phases representing cation-filled polymorphs of silica (SiO_2–X, kenyaite, SiO_2–Y, and magadiite). Further hydrothermal treatment converts the intermediate crystalline phases to quartz.

When performing the synthesis in 2 wt % NaOH (350°C; 1 h), we obtained montmorillonite with the minimal content of $Mg(OH)_2$ and dominating finely disperse fraction (up to 90%). This result is well consistent with the above considerations on the effects of the NaOH concentration in the hydrothermal solution, temperature, and run time on the characteristics of the resulting montmorillonite.

As mentioned above, brucite serves as a nucleation center in crystallization of montmorillonite. Therefore, it appeared desirable to use $Mg(OH)_2$ instead of MgO as an initial component, to increase the yield of the final product and also to accelerate the process (experiment nos. 17 and 18). The crystallooptical data show that the samples prepared using $Mg(OH)_2$ contain relatively larger amount of the coarse fraction even at a shorter run time (1 h, experiment no. 18), which can be attributed to agglomeration of the initial $Mg(OH)_2$ particles. This conclusion is supported by the mean size of $Mg(OH)_2$ particles in the product, estimated from the XRD data by the Scherrer equation [16]. For the sample obtained in experiment no. 17 (2.5 wt % NaOH, 300°C, 2 h), the mean size of $Mg(OH)_2$ particles was estimated to be 46 nm. In conducting the reaction under the same conditions, but using MgO as a starting reagent (experiment no. 6), we obtained $Mg(OH)_2$ particles with a mean size of 90 nm, i.e., twice that obtained in the experiment with MgO. Figure 3 shows the XRD patterns of montmoril-

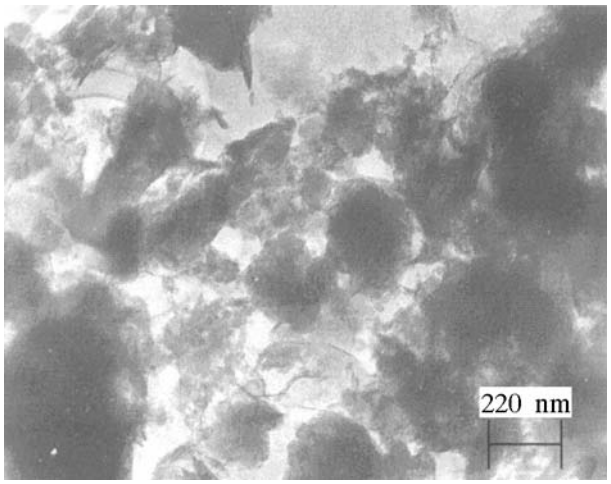


Fig. 4. Electron micrograph of montmorillonite prepared by hydrothermal synthesis.

lonite samples obtained from MgO and $Mg(OH)_2$.

To obtain single-phase finely dispersed montmorillonite, the samples were treated with 1 M HCl. Such a treatment allows removal of impurity phases, if they formed. At the same time, it is known [17] that acid treatment decreases the mechanical strength of clays through weakening the interparticle interactions and also interlayer interactions in the structure of clay minerals, realized with participation of the adsorbed water molecules. Such a disaggregation of the particles favors their dispersion in the polymer matrix in preparation of nanocomposites.

Using acid treatment of montmorillonite samples prepared under different conditions, we obtained single-phase samples of magnesium silicate montmorillonite with a particle size of 50–100 nm (Fig. 4).

As mentioned above, the authors of studies devoted to preparation and characterization of polymer–inorganic nanocomposites used either natural montmorillonite or modified clay materials [2–10]. In both cases, the starting materials represented mixtures of several natural compounds.

Figures 5 and 6 show XRD patterns of natural montmorillonite, of MMT–Na^+ modified montmorillonite (Southern Clay Products, Inc.), which is most often used in preparation of nanocomposites [4, 5], and also of the samples synthesized in this work (Figs. 5b, 6). Comparison of the XRD patterns (Figs. 5, 6) reveals that synthetic montmorillonite differs advantageously from its natural analogs in that it contains no impurity phases. Furthermore, it follows from electron microscopic data that the particles of

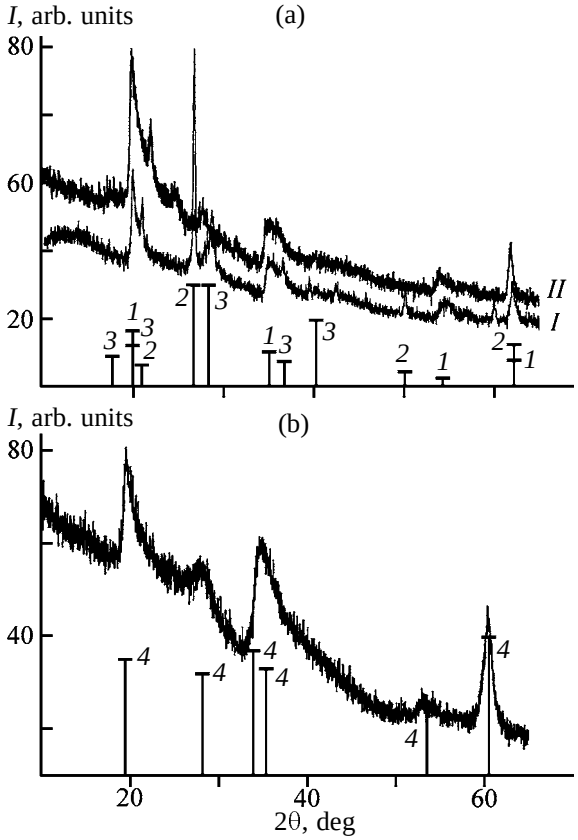


Fig. 5. XRD patterns: (a) (*I*) natural montmorillonite and (*II*) modified montmorillonite MMT-Na^+; (b) synthetic montmorillonite (see table, experiment no. 8). (*1*) Montmorillonite $Na_{0.3}(Al,Mg)_2Si_4O_{10}(OH)_2 \cdot 8H_2O$, (*2*) SiO_2 (quartz), (*3*) rectorite $K_{1.2}Al_4Si_8O_{20}(OH)_4 \cdot 4H_2O$, and (*4*) montmorillonite $Mg_3Si_4O_{10}(OH)_2 \cdot nH_2O$.

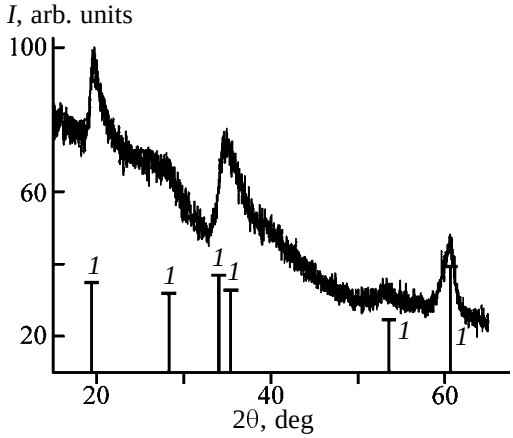


Fig. 6. XRD pattern of synthetic montmorillonite (experiment no. 12) after acid treatment. (*1*) $Mg_3Si_4O_{10}(OH)_2 \cdot nH_2O$.

synthetic montmorillonite are from 50 to 100 nm in size, whereas natural montmorillonite is characterized by broader particle size distribution (from 50 to 250 nm and more) (Figs. 4, 7).

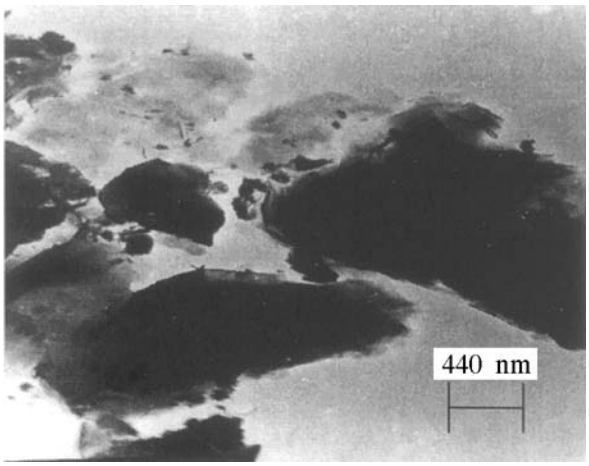


Fig. 7. Electron micrograph of natural montmorillonite.

CONCLUSIONS

(1) Synthesis of magnesium–silicate montmorillonite in alkaline solutions proceeds through the stage of formation of brucite [$Mg(OH)_2$], which may be considered as a nucleation phase in the formation of montmorillonite layers.

(2) The montmorillonite formation rate is controlled by the NaOH concentration in the hydrothermal solution. Increase in the NaOH concentration and correspondingly in the solubility of SiO_2 in the hydrothermal solution increases the montmorillonite formation rate. At the same time, increase in the SiO_2 concentration in the solution may distort the fixed stoichiometry of montmorillonite, resulting in formation of chrysotile and brucite. The optimal NaOH concentration providing the maximal yield of montmorillonite is 2–2.5 wt %.

(3) Increasing temperature activates reactions of the initial components, promoting, first, formation of brucite and then, montmorillonite.

(4) The optimal parameters of hydrothermal synthesis of magnesium silicate montmorillonite with the desired composition and grain size are as follows: c_{NaOH} = 2.5–3.0 wt %; temperature 300–350°C; and run duration 0.5–1 h, followed by treatment of the reaction products with 1 M HCl.

ACKNOWLEDGMENTS

The work was financially supported by the Russian Foundation for Basic Research (project 04-03-81005-Bel2004-a), Grant Program for Young Candidates of Science from St. Petersburg (PD04-1.3-24), and Foundation for Assistance to the Russian Science.

REFERENCES

1. Okada, A. and Kamasumi, M., *Polym. Prepr.*, 1987, vol. 28, pp. 447–448.
2. Abdalla, M.O., Dean, D.D., and Campbell, S., *Polymer*, 2002, vol. 43, pp. 5887–5893.
3. Tyan, H., Wu, C., and Wei, K., *J. Appl. Polym. Sci.*, 2001, vol. 81, pp. 1742–1747.
4. Wang, Z.M., Chung, T.C., Gilman, J.W., and Manias, E., *J. Polym. Sci.*, 2003, vol. 41, pp. 3173–3187.
5. Delozier, D.M., Orwoll, R.A., Cahoon, J.F., *et al.*, *Polymer*, 2002, vol. 43, pp. 813–822.
6. Manias, E., Touny, L., Strawhecker, K., *et al.*, *Chem. Mater.*, 2001, vol. 13, pp. 3516–3523.
7. Strawhecker, K. and Manias, E., *Chem. Mater.*, 2000, vol. 12, pp. 1943–1946.
8. Vaia, R.A., Polymer Melt Intercalation in Mica-Type Layered Silicates, *PhD Thesis*, USA: Cornell Univ., 1995.
9. Ranade, A., D'Souza, N.A., and Gnade, B., *Polymer*, 2002, vol. 43, pp. 3759–3766.
10. Sur, G.S., Sun, H.L., Lyu, S.G., and Mark, J.E., *Polymer*, 2001, vol. 43, pp. 9793–9789.
11. Litvin, B.N. and Popolitov, V.I., *Gidrotermal'nyi sintez neorganicheskikh soedinenii* (Hydrothermal Synthesis of Inorganic Compounds), Moscow: Nauka, 1984.
12. Korytkova, E.N., Chepik, L.F., Mashchenko, I.A., *et al.*, *Izv. Ross. Akad. Nauk, Neorg. Mater.*, 2002, vol. 38, no. 3, pp. 1–10.
13. Tarasevich, Yu.I., *Stroenie i khimiya poverkhnosti sloistykh silikatov* (Structure and Surface Chemistry of Layered Silicates), Kiev: Naukova Dumka, 1988.
14. Mitsyuk, B.M. and Gorogotskaya, L.I., *Fiziko-khimicheskie prevrashcheniya kremnezema v usloviyakh metamorfizma* (Physicochemical Transformations in Silica under Metamorphic Conditions), Kiev: Naukova Dumka, 1980.
15. Mitsyuk, B.M., *Vzaimodeistvie kremnezema s vodoi v gidrotermal'nykh usloviyakh* (Interaction of Silica with Water under Hydrothermal Conditions), Kiev: Naukova Dumka, 1974.
16. Rusakov, V.V., *Rentgenografiya metallov* (X-ray Diffraction Analysis of Metals), Moscow: Atomizdat, 1977.
17. Komarov, V.S., *Adsorbtsionno-strukturnye, fiziko-khimicheskie i kataliticheskie svoistva glin Belorussii* (Adsorption-Structural, Physicochemical, and Catalytic Properties of Clays of Belorussia), Minsk: Nauka i Tekhnika, 1970.

Russian Journal of Applied Chemistry, Vol. 78, No. 1, 2005, pp. 33–37. Translated from Zhurnal Prikladnoi Khimii, Vol. 78, No. 1, 2005, pp. 36–40.
Original Russian Text Copyright © 2005 by Dudkin, Loukhina, Isupov, Avvakumov.

INORGANIC SYNTHESIS AND INDUSTRIAL INORGANIC CHEMISTRY

Mechanical Activation of Kaolinite in the Presence of Concentrated Sulfuric Acid

B. N. Dudkin, I. V. Loukhina, V. P. Isupov, and E. G. Avvakumov

Institute of Chemistry, Komi Scientific Center, Ural Division, Russian Academy of Sciences, Syktyvkar, Komi Republic, Russia

Institute of Solid State Chemistry and Mechanochemistry, Siberian Division, Russian Academy of Sciences, Novosibirsk, Russia

Received August 17, 2004

Abstract—Physicochemical processes that occur in mechanical activation of kaolinite in centrifugal-planetary mills in the presence of concentrated sulfuric acid were studied. A scheme of formation of aluminum sulfate in the course of acid activation was analyzed.

The constant rise in the consumption of metallic aluminum, alumina, and other products formed in processing of aluminum-containing raw materials results in an increase in the share of unconventional, secondary, and technological kinds of raw materials involved in the processing procedures [1]. Kaolinites have long attracted the researchers' attention as a promising raw material, which can be successfully processed with mineral acids and, in particular, sulfuric acid [2].

Sulfuric acid methods for processing of layered aluminum-containing silicates have been intensively developed since the middle of the last century as a promising area of research. The common feature of various kinds of these techniques is the stage of preliminary activation of a raw material, which is performed in autoclaves or by a thermal or thermochemical method.

In the course of a thermal activation, kaolinite loses the most part of its structural water and passes into a metastable state, which makes it possible to extract Al(III) with hot H_2SO_4 solutions. The thermochemical activation of kaolinite is performed by its treatment with sulfuric acid at elevated temperatures, which leads to disintegration of the structure of the mineral and to formation of $Al_2(SO_4)_3$ crystal hydrates [3].

The elevated pressures and temperatures used in these kinds of activation are technologically and environmentally dangerous, impose strict requirements to the equipment employed, and lead to an increase in the number of process procedures and, in the end, to a higher cost of the product [4, 5].

The mechanical activation of kaolinite in centrifugal-planetary mills with high specific energy supplied to a substance being activated has demonstrated a high efficiency. This method yields, at a short time of activation, a product with a high reactivity, whose processing with acid solutions under moderate heating results in virtually complete recovery of Al(III) in the form of a sulfate [6].

Previously, a method has been suggested for mechanochemical activation of kaolinite in AGO mills in the presence of concentrated H_2SO_4 [7, 8]. The method provides virtually complete extraction of Al(III) from the product in the form of a sulfate with water without heating. This technique ensures environmental safety of processing of the raw materials because the amount of solid products formed is at a minimum and the acidity of wastewater is low.

In this work we studied physicochemical processes occurring in dry mechanical activation of kaolinite and its combined mechanochemical activation in the presence of concentrated H_2SO_4.

EXPERIMENTAL

White kaolinite from the Puzla deposit, Komi Republic, was used in the study. According to the results of elemental analysis, the kaolinite contains the following components (wt %): 37.2 Al_2O_3, 43.4 SiO_2, 2.5 TiO_2, 0.56 Fe_2O_3, 0.04 FeO, 0.17 MgO, 0.28 CaO, 0.16 Na_2O, 0.03 K_2O; calcination loss 14.47. The composition of the mineral is close to the empirical formula of aluminum silicate $Al_2O_3 \cdot 2SiO_2 \cdot 2H_2O$.

1070-4272/05/7801-0033 © 2005 Pleiades Publishing, Inc.

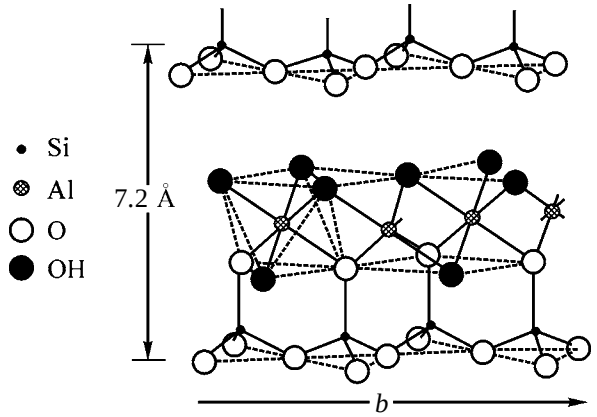


Fig. 1. Schematic structure of the kaolinite stack including a kaolinite layer and the interlayer space [21].

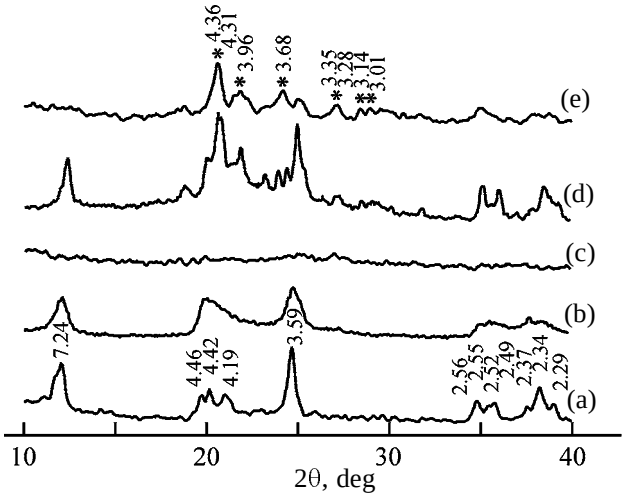


Fig. 2. X-ray diffraction patterns of (a) starting kaolinite; products formed upon mechanical activation of kaolinite for (b) 60 and (c) 390 s; and products of mechanochemical activation of kaolinite for (d) 60 and (e) 390 s in the presence of H_2SO_4. (2θ) Bragg angle.

The mechanical activation of the kaolinite was performed in AGO-2 centrifugal-planetary mills [9] with a ball diameter of 8 mm, the mass ratio of balls and weighed portion of kaolinite was 20 : 1, and the time of activation was varied within the range 0.5–10 min. The mechanochemical activation was carried out after preliminary mixing of kaolinite with a certain amount of concentrated H_2SO_4.

The structure of the starting kaolinite was studied by X-ray phase analysis (XPA) on a DRON-3M instrument with CuK_α radiation. IR absorption spectra were recorded on a Specord M-80 spectrometer in the range 4000–400 cm^{-1} in a thin layer of Vaseline oil on a KBr substrate.

Similarly to most of layered silicates, kaolinites have been sufficiently well studied [10–13]. The structural unit of minerals belonging to the group of kaolinites is the kaolinite layer (Fig. 1). There are no water molecules or metal cations in the interstack space, with the result that kaolinite shows no swelling and has a low exchange capacity.

The X-ray diffraction pattern of the starting kaolinite used in the study (Fig. 2a) is typical of the typomorphic varieties of the mineral. The X-ray diffraction pattern of the starting kaolinite contains high-intensity lines at Bragg angles 2θ of 12°, 20°, 25°, 34°–36°, and 38°–40°. The Hinckley crystallinity index of the starting kaolinite is 1.10, which characterizes it as a structurally ordered typomorphic variety [14]. The IR spectrum of kaolinite (Fig. 3, curve *1*) contains a set of absorption bands associated with the stretching vibrations of surface OH groups (3708, 3688, and 3668 cm^{-1}) and internal OH groups (3636 cm^{-1}) bound by weak hydrogen bonds. The spectral index of kaolinite is 3.5, which corresponds to its medium-ordered typomorphic variety [15]. The discrepancy in the estimates of the degree of ordering of the structure of the starting kaolinite is due to the fact that the evaluation procedures are based on different criteria.

The X-ray diffraction pattern of the product formed in dry mechanical activation of kaolinite shows broadened diffraction lines with a significantly lower intensity already after 60 s of treatment (Fig. 2b). Extending the treatment duration to 390 s leads to complete disappearance of lines from the diffraction pattern, which may be due either to a small size of kaolinite particles produced by intensive mechanical treatment or to complete disordering of the initial structure of kaolinite, in agreement with the results of [6].

Analysis of the IR spectra of the products formed in dry mechanical activation of kaolinite confirms the results of XPA. The IR spectra clearly demonstrate a change in the intensities of the absorption bands in the spectral range associated with stretching vibrations of surface and internal OH groups. As a result of activation for 60 s (Fig. 3, curve *2*), the bands at 3688 and 3668 cm^{-1} disappear and the intensity of the bands at 3708 and 3636 cm^{-1} decreases. Extending the time of activation to 390 s (Fig. 3, curve *4*) results in that the above bands merge into a broad band at 3700–2800 cm^{-1}, shifted to longer wavelengths, i.e., into the range of stretching vibrations of molecular water. Simultaneously, bands at 968 and 920 cm^{-1} decrease in intensity and then completely disappear. These bands are associated with bending vibrations of structural OH groups bound to the aluminum atom from the octahedral network of the kaolinite layer. A

similar behavior is exhibited by the band at 548 cm^{-1}, associated with mixed bending vibrations of Si–O and Al(III)–O. The disordering of bonds between the tetrahedral and octahedral networks of the kaolinite layer leads to merging of a doublet band of stretching vibrations of Si–O– (1038, 1012 cm^{-1}) into a broad unresolved peak [16].

The disordering of the structure of surface and internal OH groups of kaolinite and their condensation yield molecular water, which is confirmed by the fact that a broad low-intensity band peaked at 1630 cm^{-1} appears in the spectrum of the product formed upon activation for 180 s (Fig. 3, curve *3*). This band is associated with bending vibrations of H_2O in the polymer hydrate form. With increasing time of activation, the intensity of this band grows and its peak is shifted to shorter wavelengths (1660 cm^{-1}). A theoretical calculation demonstrated that absorption associated with bending vibrations of the H_3O^+ ion must be observed in this spectral range [17, 18]. The shift of the peak of the band under consideration to shorter wavelengths indicates that H_3O^+ ions are present in the product formed upon mechanical activation of kaolinite. Thus, it can be stated that the disordering of the structure of OH groups in kaolinite under intensive mechanical activation is accompanied by the appearance of water and hydroxonium ions in the activation product.

The appearance of protons in the course of mechanical activation of layered silicates of various types has been termed prototropy [19]. In the course of dry grinding, free protons appear through rupture of the O–H bond in structural OH groups in the octahedral network of the kaolinite layer. Recombination of protons in the structural OH groups leads to additional structural disordering.

The influence of protons on the disordering of the structure of kaolinite is well manifested in mechanical activation of kaolinite in the presence of concentrated H_2SO_4, when H_3O^+ ions are introduced into the system with the acid from the very beginning. The X-ray diffraction patterns of products formed under this kind of activation reflect not only the strong disordering of the initial structure of kaolinite, which is indicated by the disappearance of the diffraction lines at 2θ 12°, 45°–50°, and 54°–60° and by a decrease in the intensity of broad lines at 2θ 25°, 34°–36°, and 38°–40°. Also, new diffraction lines appear at 2θ 20°–22°, 24°, and 26°–29° (Figs. 2d, 2e), which confirms that the "alunogen" phase [$Al_2(SO_4)_3$ crystal hydrate] is formed in the course of activation.

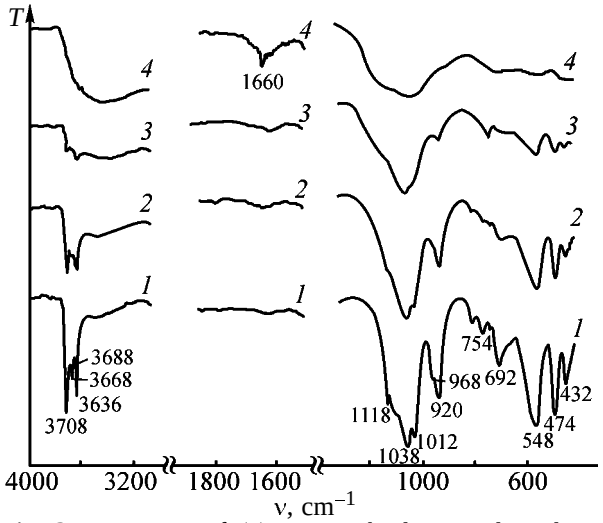


Fig. 3. IR spectra of (*1*) starting kaolinite and products formed upon mechanical activation of kaolinite for (*2*) 60, (*3*) 180, and (*4*) 390 s. (*T*) Transmission and (ν) wave number: the same for Fig. 4.

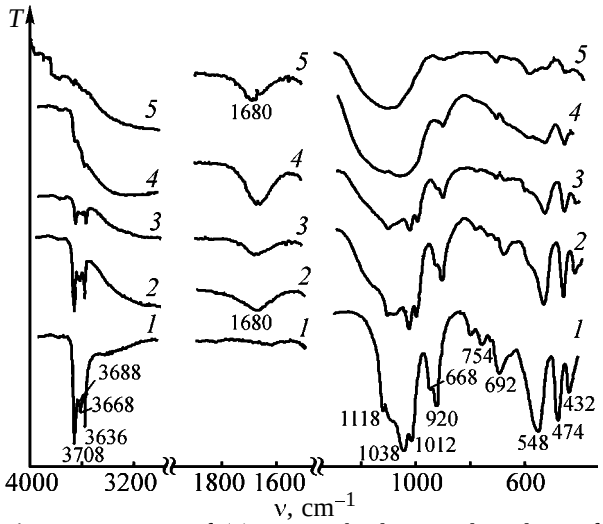


Fig. 4. IR spectra of (*1*) starting kaolinite and products of mechanochemical activation of kaolinite in the presence of sulfuric acid for (*2*) 60, (*3*) 150, and (*4*) 390 s and (*5*) in the presence of a stoichiometric amount of H_2SO_4 for 390 s.

The IR spectra of products formed in mechanochemical activation of kaolinite (Fig. 4, curves *2–5*) are similar in the set and positions of absorption bands to the spectra of products formed in dry mechanical activation. In the spectra of the products formed in mechanochemical activation, the absorption bands associated with structural OH groups completely disappear in the short-wavelength region when the activation time is made longer. The set and positions of the absorption bands at 1200–400 cm^{-1} are identical to those in the spectra of the products formed upon mechanical activation, which is due to the presence of SiO_2 in both types of products. However, the ab-

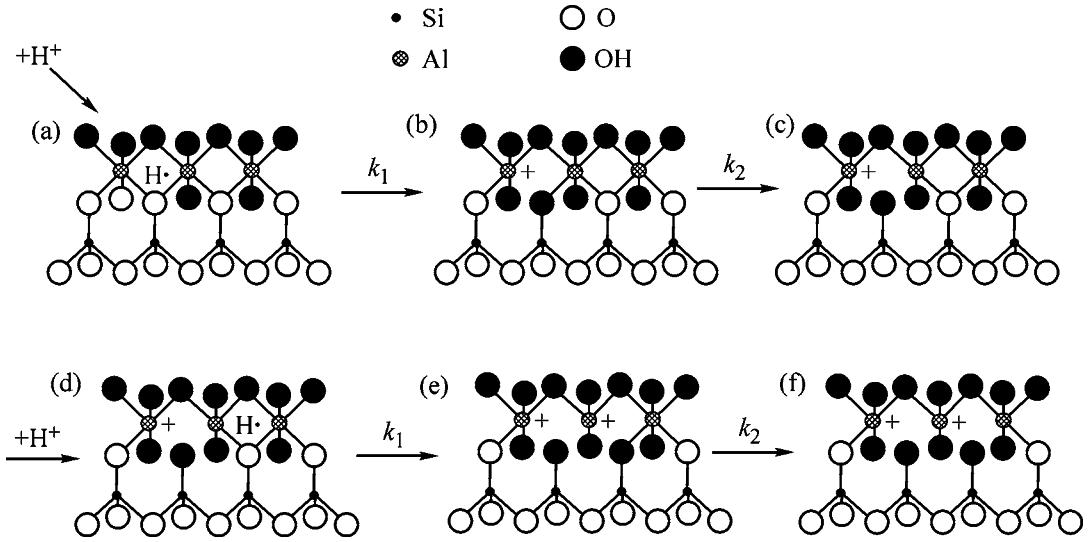


Fig. 5. Scheme of interaction of a proton with the structure of kaolinite [21].

sorption bands in the spectra of products formed in mechanochemical activation are markedly broadened in this spectral range, which gives no way of resolving the absorption bands associated with the sulfate ion. In addition, a clearly pronounced band peaked at 1680 cm^{-1} is present in all spectra of products formed upon mechanochemical activation. In the spectra obtained upon mechanical activation, this band appears after activation for 3 min and more.

The intensity of this band grows in the first stages of activation (Fig. 4, curves *2–4*), which indicates that the concentration of protons increases in the course of activation of kaolinite. The degree of structural disordering of kaolinite in the course of mechanochemical activation grows in proportion to the content of acid (protons) in a mixture being activated, which confirms that protons are strongly involved in the process of structural disordering of the mineral. It is noteworthy that the IR spectra of concentrated H_2SO_4 and an unactivated mixture of kaolinite and concentrated H_2SO_4 also contain a broad band at 1800–1600 cm^{-1} without any pronounced peak. This band is presumably due to the presence of H_2SO_4 hydrates [20].

A possible scheme of the structural disordering of kaolinite by protons was reported by Ganor *et al.* [21], who studied the dissolution of kaolinite in $HClO_4$ solutions. It was assumed that a hydrated proton penetrates into the octahedral network and, stage-by-stage, polarizes and ruptures bonds between the octahedral and tetrahedral networks of the kaolinite layer (Fig. 5).

In the case of activation of kaolinite in energy-intensive mills in the presence of concentrated H_2SO_4, ideal conditions are created for intercalation of protons into the crystal lattice of the mineral. Recombination of protons at bonds disrupts the structure of the kaolinite layer, which must lead to formation of amorphous aluminum and silicon oxides.

The capacity of sulfate ions for specific adsorption on the surface of aluminum and silicon oxides containing silanol and aluminol groups [22] leads to quantitative synthesis of alunogen in deformation-induced agitation of the mixture in the course of activation. The final products of mechanochemical activation of kaolinite in the presence of concentrated H_2SO_4 are $Al_2(SO_4)_3$ and a solid residue of the composition $ySiO_2 \cdot xH_2O$, which is low-temperature hydrated X-ray amorphous silicon dioxide.

CONCLUSION

A study of the mechanical and mechanochemical activation of kaolinite in the presence of sulfuric acid made it possible to substantiate and confirm the involvement of protons of the acid in physicochemical processes of structural disordering of the kaolinite layer and the formation of aluminum sulfate and X-ray amorphous hydrated silicon dioxide.

REFERENCES

1. Lainer, Yu.A. and Reznichenko, V.A., *Khim. Tekhnol.*, 2000, no. 2, pp. 22–28.
2. Lainer, Yu.A., *Kompleksnaya pererabotka alyuminii-soderzhashchego syr'ya kislotnymi sposobami* (Integrated Processing of Aluminum-Containing Raw Materials by Acid Methods), Moscow: Nauka, 1982.

3. Zapol'skii, A.K., *Sernokislotnaya pererabotka vysokokremnistogo alyuminievogo syr'ya* (Sulfuric Acid Processing of High-Silica Aluminum Raw Materials), Kiev: Naukova Dumka, 1981.
4. Zakharov, V.I., Kalinnikov, V.T., Matveev, V.A., and Maiorov, D.V., *Khimiko-tekhnologicheskie osnovy i razrabotka novykh napravlenii kompleksnoi pererabotki i ispol'zovaniya shchelochnykh alyumosilikatov* (Chemical and Technological Foundations and Development of New Areas of Integrated Processing and Use of Alkaline Aluminosilicates), part 1: *Kratkaya kharakteristika syr'evoi bazy: Obzor sposobov pererabotki: Azotnokislotnye metody* (Brief Characterization of Resources: Review of Processing Techniques: Nitric Acid Methods), Apatity: Ross. Akad. Nauk, 1995.
5. Gitis, E.B. and Safiullin, N.Sh., in *Tekhnologiya koagulyantov* (Technology of Coagulants), Leningrad: Khimiya, 1974, pp. 71–76.
6. Lapteva, E.S., Yusupov, T.S., and Berger, A.S., *Fiziko-khimicheskie izmeneniya sloistykh silikatov v protsesse mekhanicheskoi aktivatsii* (Physicochemical Changes in Layered Silicates in the Course of Mechanical Activation), Novosibirsk: Nauka, 1981, issue 493.
7. Dudkin, B.N., Loukhina, I.V., Isupov, V.P., and Avvakumov, E.G., *Khim. Inter. Ustoich. Razv.*, 2004, vol. 12, pp. 327–330.
8. Loukhina, I.V., Dudkin, B.N., Isupov, V.P., and Avvakumov, E.G., *INCOME 2003: Fourth Int. Conf. on Mechanochemistry and Mechanical Alloying: Program, Abstracts, List of Delegates*, Braunschweig, 2003, p. 111.
9. USSR Inventor's Certificate no. 975 068, *Byull. Izobret.*, 1982, no. 43.
10. Penkala, T., *Zarys Krystalochemii*, Warsaw: Naukowe, 1972, 2nd ed.
11. Bragg, W.L. and Claringbool, G.F., *Crystal Structures of Minerals*, Ithaca, NY: Cornell Univ. Press, 1965.
12. Toropov, N.A. and Bulak, L.N., *Kristallografiya i mineralogiya* (Crystallography and Mineralogy), Leningrad: Izd. Literatury po Stroitel'stvu, 1972.
13. Tarasevich, Yu.I., *Stroenie i khimiya poverkhnosti sloistykh silikatov* (Structure and Chemistry of the Surface of Layered Silicates), Kiev: Naukova Dumka, 1988.
14. *Rentgenografiya osnovnykh tipov porodoobrazuyushchikh mineralov (sloistye i karkasnye silikaty)* (X-Ray Diffraction Analysis of Main Types of Rock-Forming Minerals (Layered and Framework Silicates)), Frank-Kamenetskii, V.A., Ed., Leningrad: Nedra, 1983.
15. Gribina, I.A., Tarasevich, Yu.I., Plyusnina, I.I., and Belov, N.V., *Vestn. Mosk. Gos. Univ.*, 1972, no. 6, pp. 32–39.
16. Lazarev, A.N., *Kolebatel'nye spektry i stroenie silikatov* (Vibration Spectra and Structure of Silicates), Leningrad: Nauka, 1968.
17. Plyusnina, I.I., *Infrakrasnye spektry silikatov* (IR Spectra of Silicates), Moscow: Mosk. Gos. Univ., 1976.
18. Karyakin, A.V. and Kriventsova, G.A., *Sostoyanie vody v organicheskikh i neorganicheskikh soedineniyakh (po infrakrasnym spektram pogloshcheniya)* (State of Water in Organic and Inorganic Compounds (as Indicated by IR Absorption Spectra)), Moscow: Nauka, 1972.
19. Mendelovici, E., *J. Mater. Sci. Lett.*, 2001, vol. 20, pp. 81–83.
20. *Khimiya: Spravochoe rukovodstvo* (Handbook of Chemistry), Gavryuchenkov, F.G., Kurochkina, M.I., Potekhin, A.A., and Rabinovich, V.A., Eds., Leningrad: Khimiya, 1975.
21. Ganor, J., Mogollon, J.L., and Lasaga, A.C., *Geochim. Cosmochim. Acta*, 1995, vol. 59, no. 6, pp. 1037–1052.
22. Makarov, S.A., An Experimental and Theoretical Study of the Fundamental Aspects of Synthesis and Stability of Sols of Aluminum, Silicon, and Titanium Oxides, *Cand. Sci. Dissertation*, Syktyvkar, 2004.

Russian Journal of Applied Chemistry, Vol. 78, No. 1, 2005, pp. 38–41. Translated from Zhurnal Prikladnoi Khimii, Vol. 78, No. 1, 2005, pp. 41–44.
Original Russian Text Copyright © 2005 by Vasekha, Motov.

INORGANIC SYNTHESIS AND INDUSTRIAL INORGANIC CHEMISTRY

Redox Equilibria in the System $Fe(OH)_3(H_2SO_4)$–Na_2SO_3–H_2O Involving Precipitation of Iron(II) Sulfite as a Fe_2O_3 Precursor

M. V. Vasekha and D. L. Motov

Murmansk State Technical University, Murmansk, Russia
Tananaev Institute of Chemistry and Technology of Rare Elements and Mineral Raw Materials, Kola Scientific Center, Russian Academy of Sciences, Apatity, Murmansk oblast, Russia

Received March 30, 2004

Abstract—Experimental data on the equilibria Fe^{2+}/Fe^{3+} and SO_3^{2-}/SO_4^{2-} in the system $Fe(OH)_3(H_2SO_4)$–Na_2SO_3–H_2O are presented. The quantitative relations between the reduction of Fe(III) and the precipitation of $FeSO_3 \cdot 2.5H_2O$ as a Fe_2O_3 precursor have considered graphically.

An urgent problem for hydrometallurgical enterprises is the utilization of ferriferous dump cake, which is formed when solutions are purified to remove iron. The problem consists in recycling of valuable components coprecipitated with iron and in production of commercial iron oxide.

Ferriferous cake, which precipitates from industrial solutions as pH is increased, is amorphous iron(III) hydroxide resistant toward acids and alkalis [1]. Its mother liquor contains ions of impurity components, which cannot be removed by multiple repulpation. An efficient procedure of iron cake utilization is based on transformation of iron(III) hydroxide into another compound, e.g., into slightly soluble iron(II) sulfite, by its sulfitization, i.e., by treatment of $Fe(OH)_3$ with sodium sulfite followed by thermolysis of the suspension and preparation of hydrated iron(II) oxide. In the course of filtration and washing, $FeO \cdot nH_2O$ is separated from impurity components, and upon subsequent oxidation in air it is converted to Fe_2O_3, which is a commercial product (e.g., in the form of red iron oxide pigment).

The aim of this work was to study Fe^{2+}/Fe^{3+} and SO_3^{2-}/SO_4^{2-} redox equilibria in the system $Fe(OH)_3 \cdot (H_2SO_4)$–Na_2SO_3–H_2O with graphic representation of the precipitation of iron(II) sulfite from the aqueous solution as a phase capable of transforming to iron(II) oxide and then to iron(III) oxide, i.e., as a precursor of Fe_2O_3.

EXPERIMENTAL

The system $Fe(OH)_3(H_2SO_4)$–Na_2SO_3–H_2O was studied at 25°C. Ferriferous cake was used as the $Fe(OH)_3$ component. It was activated by sulfuric acid and transformed to the lyosol form by a treatment with a $FeCl_3$ solution as a peptizing agent, which was added to the cake at the molar ratio $FeCl_3 : Fe(OH)_3 = 1 : 30$. Sulfuric acid was added in the amount required for $Fe(OH)_3$ activation [molar ratio $H_2SO_4 : Fe(OH)_3 = 1 : 1.56$]. Chemically pure grade sodium sulfite was used in the form of aqueous solution. Its concentration was varied from 0.5 M to saturated solution (2.17 M) at 0.25 M intervals. The thermal hydrolysis of the suspension after the precipitation of iron(II) sulfite was carried out by boiling at a residual pressure of 30.4 kPa. Hydrated iron(II) oxide was separated from the mother liquor by filtration with washing and then was kept at 400°C in air.

The system was studied in eight sections, each corresponding to a certain sodium sulfite concentration and including 10 points in the pH range of 1.8–3.6 at the interval of 0.2 unit.

Iron(III) hydroxide peptization was accompanied by the formation of micelles and liquefaction of the amorphous precipitate by the reaction

$$n\mathrm{Fe(OH)_3} + \mathrm{FeCl_3} \rightarrow \{[\mathrm{Fe(OH)_3}]_n \cdot \mathrm{Fe^{3+}} \cdot (3 - x)\mathrm{Cl^-}\}^{x+} \cdot x\mathrm{Cl^-}.$$

It was shown experimentally that n is within the range 25–45 and x varies from 0.2 to 2.8.

In the course of the reaction with $Fe(OH)_3$, a part of sodium sulfite is consumed for the Fe(III) reduction and the other part, for the formation of the precursor, namely, of iron(II) sulfite precipitate. To reveal the redox equilibria accompanying the precipitation of iron(II) sulfite, we processed the experimental data

1070-4272/05/7801-0038 © 2005 Pleiades Publishing, Inc.

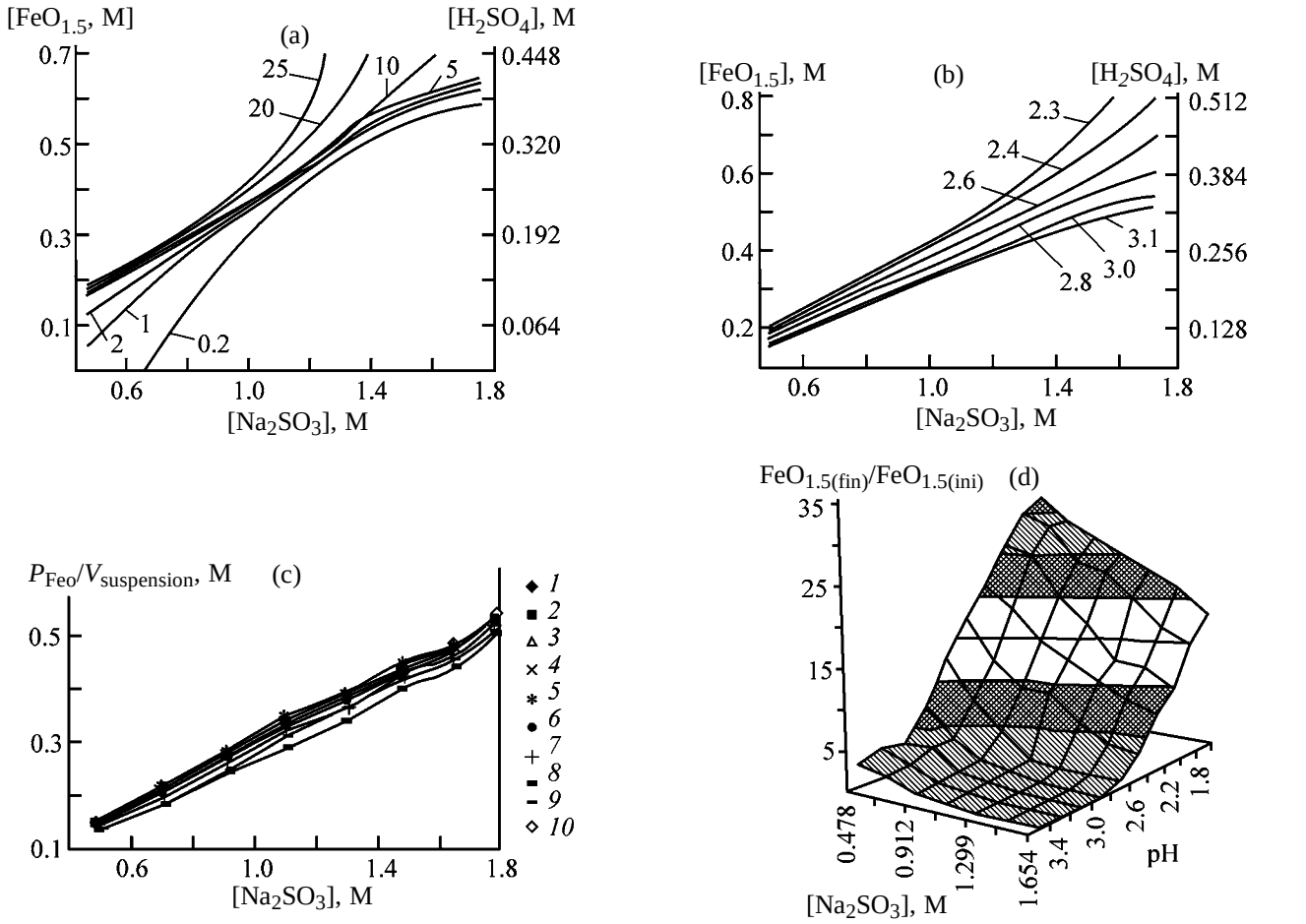


Fig. 1. Iron(III) reduction in the system $Fe(OH)_3(H_2SO_4)$–Na_2SO_3–H_2O at 25°C at various ratios of $FeO_{1.5}$, Na_2SO_3, and H_2SO_4 concentrations (M). (a) Isoreducts $FeO_{1.5(fin)}/FeO_{1.5(ini)}$; (b) isorelates $Na_2SO_3/Fe(OH)_3$; (c) specific yield $P_{FeO}/V_{suspension}$; and (d) dependence of the degree of iron(III) reduction $FeO_{1.5(fin)}/FeO_{1.5(ini)}$ on the sodium sulfite concentration and suspension pH. (c) pH: (*1*) 3.6, (*2*) 3.4, (*3*) 3.2, (*4*) 3.0, (*5*) 2.8, (*6*) 2.6, (*7*) 2.4, (*8*) 2.2, (*9*) 2.0, and (*10*) 1.8.

according to [2]. The system was presented graphically by two response functions: lines of equal degree of reduction $FeO_{1.5(fin)}/FeO_{1.5(ini)}$ (%) (isoreducts) (Fig. 1a) and lines reflecting the molar ratio of the reacting components $Na_2SO_3/FeO_{1.5}$ (isorelates) (Fig. 1b). The isorelates allowed us to determine the ratio of components in the system corresponding to the sufficient extent of the redox process. A combination of both isolines allowed us to suggest a mechanism of the reaction between sulfite ions and Fe(III) and to find the operation range corresponding to a high degree of iron(III) reduction at the optimal concentrations of the reacting components.

It follows from Fig. 1 that three molecules of Na_2SO_3 react in the system with one molecule of $Fe(OH)_3$ to provide almost complete precipitation of Fe(II) sulfite. The reaction can be expressed by the scheme [3]

$$Fe(OH)_3 + 3HSO_3^- \rightarrow [Fe(SO_3)_3]^{3-} + 3H_2O,$$

$$[Fe(SO_3)_3]^{3-} \xrightarrow{h\nu} [Fe(SO_3)_2]^{2-} + \dot{S}O_3^-,$$

$$[Fe(SO_3)_2]^{2-} \rightarrow FeSO_3\downarrow + SO_3^{2-}.$$

Iron sulfite is precipitated in the form of $FeSO_3 \cdot 2.5H_2O$, whereas sulfite radicals form $S_2O_6^{2-}$ dimers, i.e., the anions of dithionic acid.

The maximal yield of iron(II) sulfitization per unit volume of the suspension (Fig. 1c) corresponds to the pH range 3.0–2.8. Addition of excessive sulfuric acid suspension of $Fe(OH)_3$ results in decreased pH and increased iron(III) content.

The three-dimensional representation of the $Fe(OH)_3(H_2SO_4)$–Na_2SO_3–H_2O system (Fig. 1d), which shows the dependence of the Fe(II) content after sulfitization on both the concentration of sodium

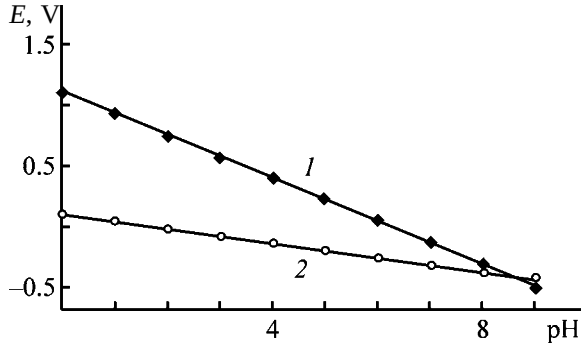


Fig. 2. *E*–pH dependence for the sulfitization process. Line numbers correspond to equation numbers.

sulfite and the pH of suspension, allows us to determine the boundary of the working region, which corresponds to the onset of ascent from the flat part of the diagram.

The redox equilibrium $Fe^{2+} : Fe^{3+}$ in the system can be described using the Nernst equation

$$E = E^0 + \frac{RT}{F}\ln(a_{Fe^{3+}}/a_{Fe^{2+}}).$$

Iron(III) ions are hydrolyzed in weakly acidic solutions; therefore, $a_{Fe^{3+}}$ is determined by the solubility of $Fe(OH)_3$. Taking the solubility product under standard conditions to be $K^0_{S[Fe(OH)_3]} = a_{Fe^{3+}}a^3_{OH^-} = 10^{-37.4}$, we find

$$a_{Fe^{3+}} = \frac{K^0_S[Fe(OH)_3]}{a^3_{OH^-}} = \frac{K^0_S[Fe(OH)_3]a^3_{H^+}}{K^3_w} = 10^{4.59}a^3_{H^+}.$$

Substituting the $a_{Fe^{3+}}$ values in the Nernst equation, we obtain

$$E = E^0 + \frac{RT}{F}\ln\frac{10^{4.59}a^3_{H^+}}{a_{Fe^{2+}}}.$$

At 298 K, the equation takes the form

$$E = 1.044 - 0.178\text{pH} - 0.059\log a_{Fe^{2+}}.$$

For $a_{Fe^{2+}} = 0.1$ M, we obtain the expression

$$E = 1.103 - 0.178\text{pH}. \quad (1)$$

Sulfite ions are oxidized according to the equation

$$SO_3^{2-} + H_2O - 2e \rightarrow SO_4^{2-} + 2H^+,\ E^0 = 0.104\ \text{V},$$

and the Nernst equation for the equilibrium SO_3^{2-}/SO_4^{2-} takes the form

$$E = E^0 + \frac{RT}{2F}\ln\frac{a_{SO_4^{2-}}a^2_{H^+}}{a_{SO_3^{2-}}}.$$

The dependence of the potential on pH for an aqueous solution with $a_{SO_3^{2-}} = a_{SO_4^{2-}} = 0.1$ M is described by the equation

$$E = 0.104 - 0.059\text{pH}. \quad (2)$$

The plots of $E = f(\text{pH})$ are expressed as the Pourbaix diagram (Fig. 2), which shows that the difference of the redox potentials decreases as pH increases, and consequently, the reducing power of sulfite ions decreases. The maximal yield of iron(II) and $\Delta E = 0.64$–0.67 V are observed in the pH range 3.0–2.8; in this range, sulfitization occurs spontaneously.

A single solid phase, $FeSO_3 \cdot 2.5H_2O$, is precipitated in the redox reaction of sulfite ion with $Fe(OH)_3$. Its solubility in water was determined by direct conductometric technique at 298–328 K [4]. At 298 K, the solubility is 1.87×10^{-3} M.

If the solubility product $K^0_{S(FeSO_3 \cdot 2.5H_2O)}$ is considered as a heterogeneous equilibrium constant, we can determine the pH corresponding to the onset of the $FeSO_3 \cdot 2.5H_2O$ precipitation at various concentrations of reactants in the solution:

$$\text{pH} = -\log a_{Fe^{2+}} + \log K^0_{S(FeSO_3)} - \log a_{HSO_3^-} - \log K_{2(HSO_3^-)}.$$

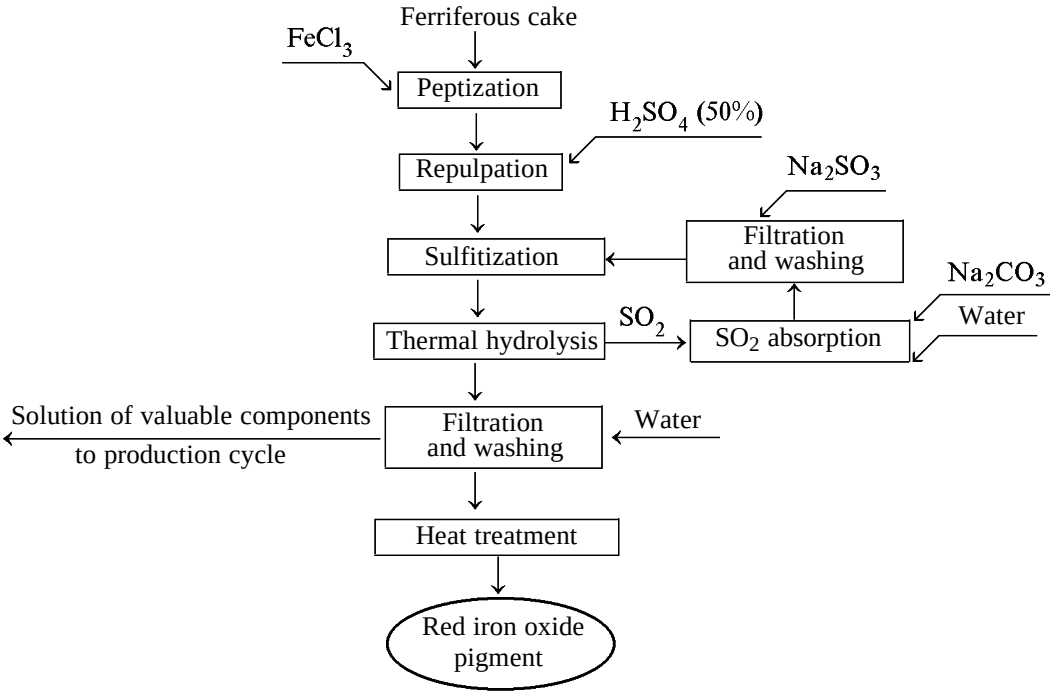
The pH of precipitation decreases as the concentrations of reactants increase. The substitution of the constant of the second ionization step of sulfurous acid $K_{2(HSO_3^-)}$ and the solubility product of iron(II) sulfite $K^0_{S(FeSO_3)}$ leads to the dependence

$$\text{pH} = 1.71 - \log a_{Fe^{2+}} - \log a_{HSO_3^-}.$$

The working region of the sulfitization process is limited, on the one hand, by the pH value of the onset of $FeSO_3 \cdot 2.5H_2O$ precipitation, and on other hand, by the difference of redox potentials, which tends to zero on reaching pH 8.39.

Within the estimated pH range, iron(II) sulfite can undergo thermal hydrolysis with the evolution of SO_2 and formation of crystalline iron(II) hydroxide, which can be readily filtered off, allowing high degree of recycling of valuable components into the solution. The liberated sulfur dioxide is absorbed by a sodium

Flowsheet of ferriferous cake processing



carbonate solution to recycle sodium sulfite to the sulfitization stage. The subsequent heat treatment of iron(II) oxide results in its oxidation with the formation of finely dispersed product utilizable as red iron oxide pigment.

The developed flowsheet involving iron(II) sulfite as precursor includes the following stages: peptization with iron(III) chloride, cake repulpation in a sulfuric acid solution, and sulfitization with the conversion of $Fe(OH)_3$ to $FeSO_3 \cdot 2.5H_2O$. This precursor is converted to Fe_2O_3 by thermal hydrolysis of the suspension, filtration and washing of hydrated iron(II) oxide, and its subsequent thermal treatment to obtain iron(III) oxide as a commercial product used as red iron oxide pigment.

CONCLUSIONS

(1) Graphic representation of the multicomponent system $Fe(OH)_3(H_2SO_4)$–Na_2SO_3–H_2O revealed a relationship between the redox processes occurring in this system and the concentration ratio of the reacting components.

(2) Joint plotting of isoreducts and isorelates in the same coordinates made it possible to suggest a redox reaction mechanism and to find optimal conditions for the precipitation of $FeSO_3 \cdot 2.5H_2O$ in the process of the conversion of ferriferous cake to iron sulfite, a precursor of Fe_2O_3, which, in turn, is used as red iron oxide pigment.

ACKNOWLEDGMENTS

This work was financially supported by the Leading Scientific Schools Program (project no. NSh-1616-2003.3).

REFERENCES

1. Zavarzina, M.A., *Stroit. Mater.*, 1999, no. 1, p. 48.
2. Motov, D.L., *Fizikokhimiya i sul'fatnaya tekhnologiya titano-redkometall'nogo syr'ya* (Physical Chemistry and Sulfate Technology of Titanium–Rare Metal Raw Materials), Apatity: Kol'sk. Nauchn. Tsentr, Ross. Akad. Nauk, 2002.
3. Ell-Wakil, A.M., Soliman, M.S., and Farag, A.B., *Z. Naturforsch. (b)*, 1983, vol. 38, pp. 858–860.
4. Vasekha, M.V. and Shibanov, V.N., *Vestn. Murmansk. Gos. Tekh. Univ.*, 2003, vol. 6, no. 1, pp. 93–96.

Russian Journal of Applied Chemistry, Vol. 78, No. 1, 2005, pp. 42–48. Translated from Zhurnal Prikladnoi Khimii, Vol. 78, No. 1, 2005, pp. 45–51.
Original Russian Text Copyright © 2005 by Stekhanova, Yatsenko, Milovidova, Sidorkin, Rogazinskaya.

INORGANIC SYNTHESIS AND INDUSTRIAL INORGANIC CHEMISTRY

Properties of Triglycine Sulfate Crystals Grown from Aqueous Solutions

Zh. D. Stekhanova, O. B. Yatsenko, S. D. Milovidova, A. S. Sidorkin, and O. V. Rogazinskaya

Voronezh State University, Voronezh, Russia

Received November 4, 2004

Abstract—A dielectric study of triglycine sulfate crystals was carried out and the phase transition temperatures were determined for samples grown at temperatures below 0°C. The influence exerted by a single-crystal silicon substrate treated by various methods on the shape of triglycine sulfate crystals was examined.

Crystals of triglycine sulfate, $(NH_2CH_2COOH)_3 \cdot H_2SO_4$ (TGS), are primarily known as classical ferroelectrics [1, 2]. Their ferroelectric properties are mainly determined by hydrogen bonds between atoms of nitrogen, hydrogen, and oxygen [1, 3].

Commonly these crystals are grown from aqueous solutions at temperatures of 20–60°C. The Curie point (T_c) of crystals of this kind (49°C) in a certain way characterizes the strength and rigidity of those bonds, which, undergoing transformations under the action of external factors (electric field, temperature), lead to formation and transformations of the domain structure of the crystals. Pyro-, piezoelectric, and other electrical properties of TGS crystals, which determine their practical importance and possible applications, depend on hydrogen bonds. Studies of the composition, structure, and properties of TGS crystals, which contain an amino acid (glycine), in relation to methods and conditions of their synthesis, with TGS used as a model material, yield valuable information about properties of various amino acids and their compounds. At the same time, it is of interest to study the possibility of directed modification of the properties of these TGS crystals in order to expand the area of their practical application. As an example, mention can be made of investigations devoted to doping of these crystals with various organic and inorganic components [1] and to their radiation treatment.

The properties of TGS crystals largely depend on the state of water both in their synthesis and growth and under the action of various external factors. With account of this fact, the range of variation of these factors was significantly expanded, primarily via a shift of the temperature range of crystal growth to below 0°C, where water can undergo phase transformations together with TGS. Simultaneously, it was decided to examine the effect of water vapor on the properties of the crystals. Finally, a study of TGS crystals grown on the surface of silicon single crystals pretreated by various methods was commenced with account of the fact that silicon is the basic material of solid-state electronics.

To find the conditions for growth of TGS crystals from aqueous solutions below 0°C, the eutectic point was determined in the phase diagrams of the systems water–glycine and water–TGS [4]. For this purpose, a method based on analysis of the kinetics of fractional melting of ice ingots crystallized from aqueous solutions with different initial concentrations has been developed [5] in view of the fact that attainment of a thermodynamic equilibrium in aqueous solutions at $T < 0$°C is hindered and requires a long time. The temperature and concentration of components at the eutectic point of the systems under study was found by determining the time necessary for the onset of melting of an ingot upon its heating from the temperature of complete crystallization of the solution and finding the type of distribution of the substance dissolved in water among fractions of the melt. A comparison of the eutectic points determined using the method developed with published data obtained for systems studied by the classical techniques, e.g., for water–salt systems [6], demonstrated good agreement.

The method of fractional melting is convenient for aqueous systems with a complex ionic-molecular composition, such as aqueous solutions of amino acids and their compounds. The data furnished by this

1070-4272/05/7801-0042 © 2005 Pleiades Publishing, Inc.

method make it possible to find the optimal conditions of synthesis and growth of single crystals of these substances and, simultaneously, to reveal specific features and fundamental aspects of their properties governed by interaction with water. The method of fractional melting was used to determine the eutectic points in the systems mentioned above, as well as in systems constituted by water and lysine and by water and lysine hydrochloride. This, on the one hand, made it possible to develop methods for low-temperature growth of crystals of these amino acids and their compounds, and on the other, confirmed the efficiency of the fractional melting in growth of crystals with varied nature of chemical bonding and different properties.

A study of the electrical properties of TGS crystals grown at $T < 0$°C revealed that their most important dielectric parameter, Curie point, shifts to higher temperatures [7], with the entire set of their electrical properties significantly changing.

In this work we further studied the dielectric properties of the crystals prepared and the influence exerted by properties of the silicon surface on the conditions of nucleation and growth of TGS crystals and on their properties. Also we report the results of X-ray phase analysis of these crystals.

EXPERIMENTAL

TGS crystals were grown from aqueous solutions saturated at different temperatures. Two methods were used: (i) lowering of the temperature of a saturated solution and (ii) slow evaporation of the solvent (water).

In the "classical" temperature range 20–50°C, "standard" crystals were grown and their properties were compared with those of crystals grown by the original technique at $T < 0$°C. The crystals were grown in Petri dishes without any special seeds. In parallel, crystals were grown in Petri dishes on whose bottom were placed standard wafers of single-crystal silicon, 76 mm in diameter and 400 μm thick, used in the planar silicon technology: KEF-20 (*n*-Si : P) (100), KEF-0.8 (111), and KDB-10 (*p*-Si : B) (111). The diameter of the silicon wafers was somewhat smaller than that of the Petri dishes. Before the experiments, the surface of single-crystal wafers was pretreated by various methods. Some of the wafers remained coated only with a layer of silicon oxide SiO_2 of thickness about 3 nm, which is commonly formed on the surface of silicon single crystals stored in air. Other wafers were coated with a SiO_2 layer with a thickness of about 300 nm, purposefully formed by thermal oxidation (thermal SiO_2) or pyrolytically by the standard procedures of silicon microelectronics. In addition, part of the wafers was coated with layers of specially deposited polycrystalline silicon of thickness ~100 nm and (separately) layers of metallic Ti (~100 nm); finally, layers of porous silicon were formed on the surface of part of the wafers [8].

It is known that the state of the silicon surface predetermines the type of its interaction with water. The surface of a clean single crystal is hydrophobic; its oxidation makes it hydrophilic; formation of a polycrystalline or porous structure on the surface changes its sorption properties. At the same time, lowering the temperature of water and aqueous solutions to below 0°C also significantly changes their structure and properties and, consequently, the type of interaction between the components of aqueous systems. A combination of these two, surface- and volume-related factors may make it possible to control the nucleation and growth of crystals of widely diverse substances (TGS, in the case in question) with prescribed properties.

Crystals with growth faces characteristic of TGS were chosen. The dimensions along the *X*, *Y*, and *Z* axes were the same as those for the standard TGS crystal and did not exceed 14, 17, and 6 mm, respectively. The samples prepared for study were in the form of rectangular wafers of polar *Y*-cut (thickness of about 1 mm and area of 3×5 mm^2). A conducting layer was deposited on these samples by vacuum evaporation of silver. The capacitance of the samples studied was measured with a Tesla-VM-484 semiautomatic bridge at a frequency of 1.59 kHz and amplitude of the measuring field of about 3 V cm^{-1}. Dielectric hysteresis loops were measured using the standard Sawyer–Tower scheme at a frequency of 1 kHz. Pyroelectric measurements were carried out in the quasistatic mode with a UT-6801A coulometer with a current sensitivity of 10^{-17} A, and temperature measurements, with a UTU-4 universal thermostat. The temperature was monitored with a mercury thermometer with an accuracy of ± 0.05°.

An X-ray diffraction analysis of the crystals on a DRON-4 diffractometer (CuK_α radiation, λ = 1.54178 Å) revealed a noticeable shift of reflections and a pronounced change in their intensity, compared with an ordinary TGS crystal as a control (Fig. 1). Preliminary calculations of the lattice constants demonstrated that the lattice constants *b* and *c* remain unchanged and the parameter *a* tends to increase. To analyze the influence exerted by low growth tempera-

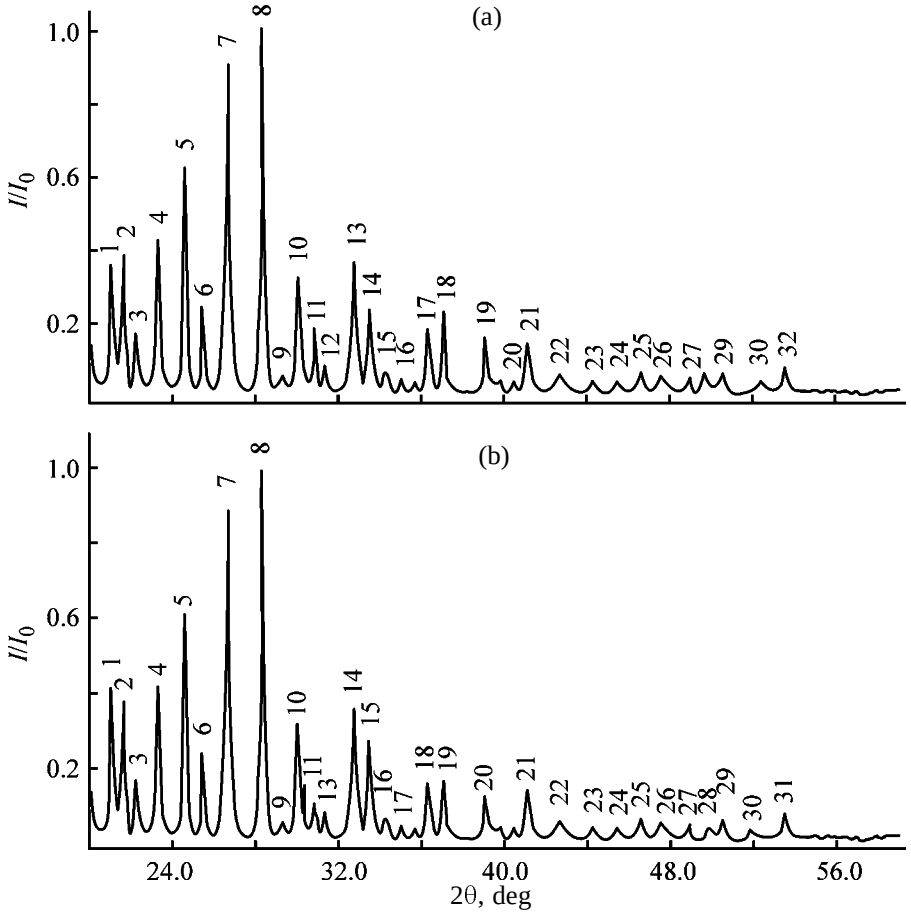


Fig. 1. X-ray diffraction patterns of (a) ordinary TGS crystal and (b) TGS crystal grown at $T_{gr} < 0$°C. (I/I_0) Relative intensity and (2θ) Bragg angle; the same for Fig. 5.

tures on the properties of TGS crystals, their main ferroelectric properties were studied.

The dielectric studies performed demonstrated that the phase transition temperature T_c increases for TGS samples grown at temperatures lower than 0°C by 0.5–0.7°C. For an ordinary TGS crystal, T_c is 49°C,

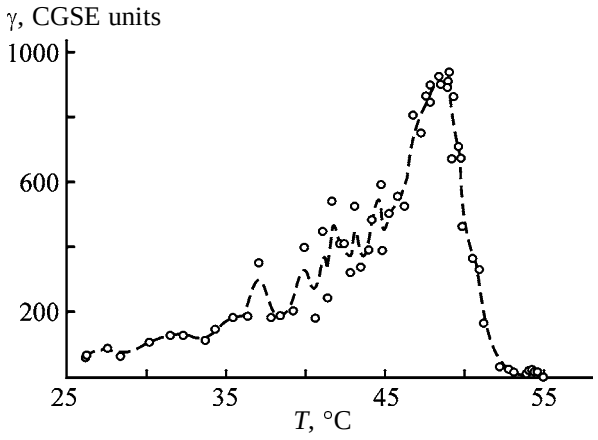


Fig. 2. Pyroelectric coefficient γ vs. temperature T for a TGS crystal grown below 0°C.

and the maximum values of the dielectric constant ε are as high as 50 000. TGS crystals grown at temperature lower than 0°C show a certain broadening of the phase transition; the maximum values of ε for different crystals are in the range from 800 to 2000. However, the type of the phase transition remains unchanged: both the "pair" and Curie–Weiss law are observed.

Pyroelectric studies of TGS crystals grown below 0°C demonstrated rather high values of the pyroelectric coefficient both at room temperature ($\gamma \cong 70$–100 CGSE units for different crystals) and at the maximum ($\gamma \approx 600$–1000 CGSE units). A specific feature of these crystals is that the pyroelectric effect vanishes at temperatures exceeding the Curie point of ordinary TGS crystals by 2–3°C (Fig. 2). The values of the macroscopic polarization P, calculated from the pyroelectric data ($P \approx 1.7$–2.3 μC cm^{-2}), are close to values of spontaneous polarization, found from dielectric hysteresis loops.

Figure 3 shows the temperature dependence of the

macroscopic polarization, determined from the results of pyroelectric measurements for one of the low-temperature samples. It is noteworthy that the polarization extends into the paraelectric phase. Commonly, such a behavior is observed for heavily doped crystals, whereas in the case in question, the TGS crystal is nominally undoped, but is grown at negative (on the centigrade scale) temperatures.

The dielectric hysteresis loops have a common shape with a minor bias field of 10 to 100 V cm^{-1} for different crystals. It should be noted that the hysteresis loops disappear at 50°C, which exceeds the phase transition temperature for ordinary TGS crystals (49°C). The hysteresis loops are saturated in sufficiently strong fields (~2–3 kV cm^{-1}). The coercive fields are about 400 V cm^{-1}.

The extension of the pyroelectric effect into the paraelectric phase and high values of coercive fields indicate that the domain structure of TGS crystals grown below 0°C is rigid.

The results obtained may be due to changes in the structure of water at 0°C. At this temperature, the network of hydrogen bonds in water and aqueous solutions becomes more rigid and the number of unruptured hydrogen bonds increases, which leads to fixing of domains and, consequently, to an increase in T_c.

The properties of TS crystals grown on the surface of silicon single crystals preliminarily subjected to various treatments were studied. The influence exerted by a single-crystal silicon wafer placed in the starting aqueous solution on the general characteristics of the crystallization process (shape and size of crystals, their number and distribution in the solution bulk) was determined. Under the same conditions, TS crystals were grown in a Petri dish in the absence of silicon and on the surface of single-crystal silicon coated with a layer of thermal SiO_2.

If a silicon wafer occupies part of the bottom of a Petri dish, the majority of the TGS crystals are formed beyond the bounds of the wafer or on its periphery (it is known that the number of ruptured bonds in the covalent silicon crystal is large in this region) [9]. Crystals formed on the surface of the wafer are arranged on it nonuniformly and have a more regular shape (rhombohedral crystals); all the crystals grown have approximately the same dimensions, shape, and crystallographic orientation and differ from those formed on the bottom of a Petri dish without a silicon wafer.

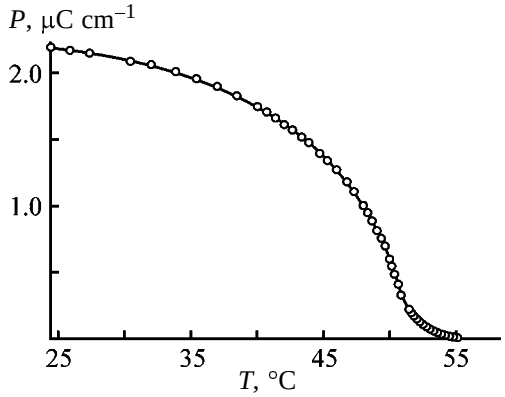


Fig. 3. Macroscopic polarization P vs. temperature T for a TS crystal grown below 0°C.

The dimensions of the crystals grown without silicon, as well as their shapes and orientations, differ more widely as compared to crystals grown in the presence of silicon. The coarsest crystals grow on the surface of single-crystal silicon, whereas the finest crystals are formed in a vessel without silicon. Thus, the very presence of single-crystal silicon in solution noticeably affects the growth of TGS crystals.

Similar results were obtained for TGS crystals grown at a temperature lower than 0°C on polished single-crystal wafers of KDB-10 (111) silicon.

Further, the patterns of TGS crystallization on the surface of identical single crystals of silicon, coated with thermal or pyrolytic silicon oxide, polycrystalline silicon, or having no coating, were compared. The crystals grown are shown in photographs in Figs. 4a–4d. It can be seen that the coarsest crystals are obtained on the surface of silicon coated with pyrolytic SiO_2 (Fig. 4c), with their dimensions varying from 7–8 to 4–5 mm. The crystals most frequently have the shape of a parallelepiped. Similar, but finer (6–5 to 4–5 mm) crystals were grown on the surface of silicon coated with thermal SiO_2 (Fig. 4b). The smallest number of TGS crystals was formed on the surface of silicon coated with polycrystalline silicon (crystals were mostly formed in the Petri dish beyond the bounds of the silicon wafer). The number of TGS crystals having the shape of rhombohedra and parallelepipeds is about the same. It can be seen that silicon treated in various ways affects the shape of TGS crystals by predetermining a predominant growth of crystals along some crystallographic direction.

It was established that the orienting effect of silicon varies with the type of a coating, but not disappears completely. This means that it is "translated" across the layer of amorphous SiO_2 or polycrystalline silicon.

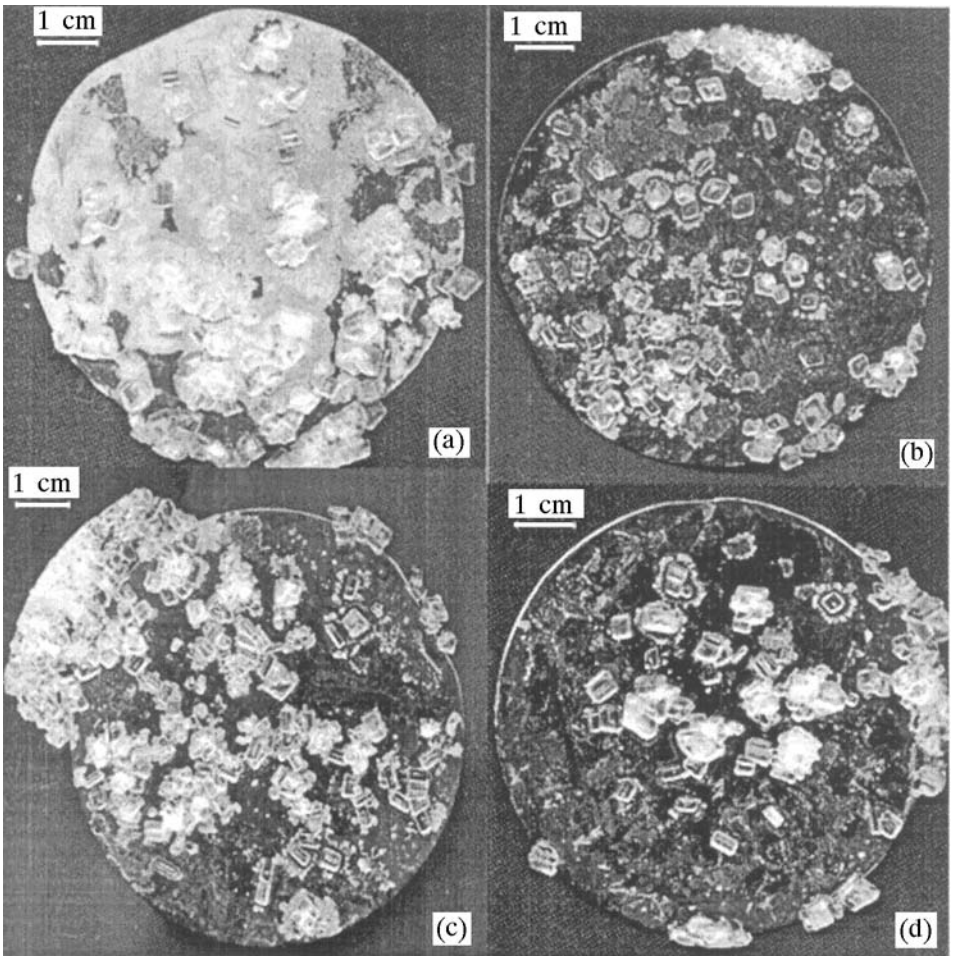


Fig. 4. Photographs of TGS crystals grown on single-crystal wafers: (a) KEF-20-500 (100), d = 380 nm; and (b–c) KDB-10 (111) silicon coated with: (b) thermal SiO_2, d = 85 μm; (c) pyrolytic SiO_2; and (d) layer of polysilicon.

Characteristically, this influence regularly varies along the surface of a silicon wafer from its center toward periphery. It is also important that, at this stage of the study, there is no reason to speak about any epitaxial relationships between single crystals of silicon and TGS, which are commonly expressed in term of crystal lattice parameters.

When speaking about the orienting influence of silicon single crystals on the growth of TGS crystals in the experiments in question, it is, in all probability, necessary to keep in mind the effect of silicon on the state of that initial medium (aqueous solution) in which TGS crystals nucleate and grow. For example, the predominant growth of crystals on the periphery of a silicon wafer can be attributed to the fact that the "long-range" field of silicon (gradient of the crystal-lattice potential) is the strongest at the edge of the wafer. In this region, the orienting influence of silicon first leads to a change in the structure of water and the aqueous solution, which, in turn, favors homogeneous nucleation of TGS crystals. Closer to the wafer center, the effect of silicon has another nature. The strict periodicity of the crystal field of silicon makes lower the contribution of the homogeneous, bulk component to the nucleation process, which leads to a decrease in the number of TGS crystals growing on its surface, but makes higher the probability of predominant orientation of these crystals. To confirm the results obtained, the crystals were subjected to X-ray phase analysis.

It was found that part of the crystals grown on KEF-20-500 (100) Si are single crystals with a [101] orientation (Fig. 5a). The rhombohedral crystals grown on silicon coated with thermal (Fig. 5b) or pyrolytic SiO_2 (Fig. 5c) have a polycrystalline structure with a clearly pronounced texture in the [101]

direction. Crystals grown under the same conditions in the form of a parallelepiped on polycrystalline silicon or on silicon coated with pyrolytic SiO_2 have also a polycrystalline structure, but with a [041] texture (Fig. 5d). This is, in all probability, accounted for by the orienting effect of polysilicon on the growth of TGS crystals.

Particularly noteworthy is the nature of TGS crystal growth on porous silicon (Fig. 6a), whose initial layer was grown of KEF-0.8 (111) Si by means of electrochemical etching [8]. Some of the wafers with such a layer were subjected to additional treatment: (a) additional anodic etching for 10 min (J = 15 mA cm^{-2}, pore size 10 μm), (b) etching in HCl (c = 30%, τ_{et} = 5 min), and (c) etching in HF (c = 20%, τ_{et} = 5 min). For comparison, ground silicon wafers were used (Fig. 6f).

The wafers were kept at 20°C in a saturated TGS solution for 12 days. Micrographs of TGS structures formed on the silicon surface are shown in Figs. 6b–6f. The crystals grown on the surface of porous silicon are coarser and have a more regular shape (Fig. 6c) than those formed on the surface of ground silicon (Fig. 6f). No coarse TGS crystals are formed on the surface of porous silicon subjected to additional anodic etching (Fig. 6c) or etching in HCl (Fig. 6d) or HF (Fig. 6e). The surface of silicon is decorated with microcrystals of TGS. Experiments show that the effect of silicon on the nucleation and growth of TGS crystals depends on the dispersity of its surface.

IR reflection spectra of these structures virtually coincide with one another and with the reference IR reflection spectrum of a single crystal of TGS. The characteristic lines of OH and NH_3^+ groups are somewhat shifted to longer wavelengths as the concentration of the initial solutions of TGS, brought in contact with silicon, becomes higher.

The results obtained make it possible to assess the prospects for further studies with the use of recent achievements of the planar silicon technology. It is known that, to fabricate microelectronic devices and solid-state integrated circuits, complex heterostructures containing layers and regions of single- and polycrystalline silicon, silicon oxide, and various metals and their compounds with silicon (titanium silicide being one of these) are created on the surface of silicon. The layers having a strictly prescribed shape and dimensions are formed in strictly specified order. We found how each of these layers affects the

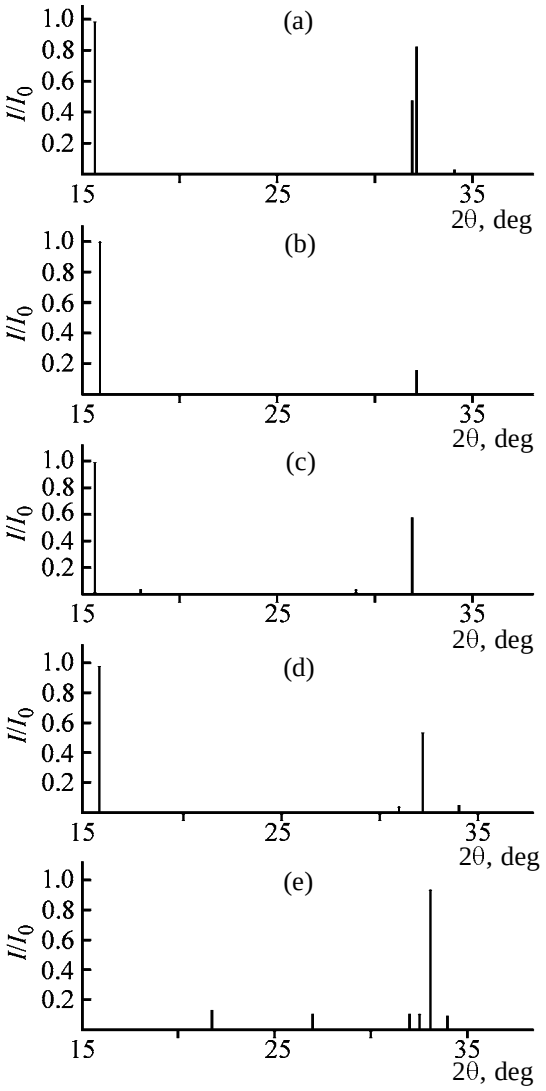


Fig. 5. X-ray diffraction patterns of TGS crystals (a) grown without silicon and those obtained on the surface (b) of KEF-20-500 (100) Si, and (c–e) of KDB-10 (111) Si coated with (c) thermal SiO_2, (d) pyrolytic SiO_2, and (e) polysilicon.

conditions of nucleation and growth of TGS crystals as a model material containing simultaneously organic (amino acid) and inorganic (sulfo groups) components. It is hoped that a prescribed "technological" pattern formed, e.g., by photolithography (a method widely used in microelectronics) on the silicon surface will make it possible to "array," e.g., various amino acids or their compounds on separate micro- or even nanoelements of solid-state circuits. Thereby, complex structures, including those of biological origin, will be formed with the use of the latest achievements of solid-state electronics and incorporated into solid-state electronic circuits.

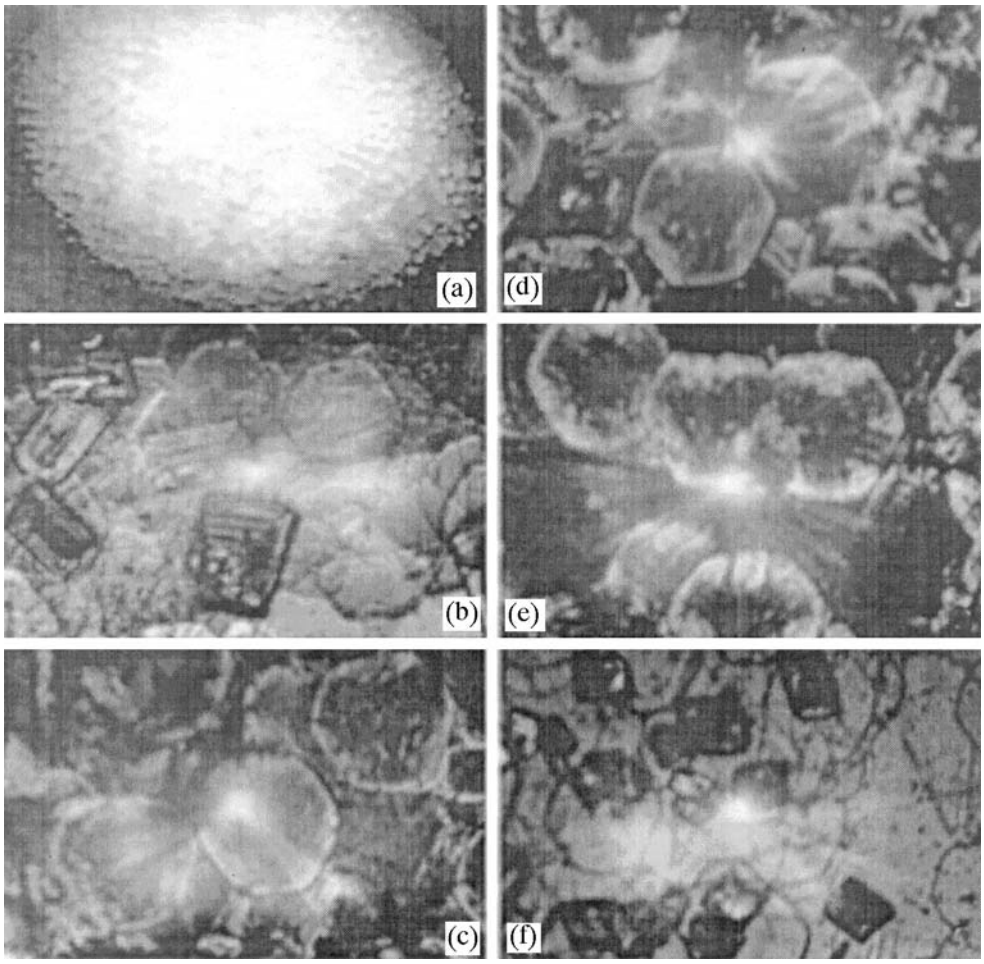


Fig. 6. Micrographs of crystalline structures on the surface of silicon: (a) porous Si, (b) porous Si + TGS, (c) porous Si + anodic etching + TGS, (d) porous Si + etching in HCl + TGS, (e) porous Si + etching in HF + TGS, and (f) ground Si + TGS.

CONCLUSIONS

(1) The extension of the pyroelectric effect into the paraelectric phase and the high coercive fields indicate that the triglycine sulfate crystals grown below 0°C have a rigid domain structure. The results obtained may be due to changes in the structure of water at 0°C: the network of hydrogen bonds becomes more rigid and the number of unruptured hydrogen bonds increases, which fixes the domains and, as a consequence, leads to an increase in T_c.

(2) Silicon affects the conditions of nucleation and growth of triglycine sulfate crystals in aqueous solutions because a silicon wafer present in a solution changes the number of triglycine sulfate crystals, their dimensions, and type of their arrangement in the bulk of the solution.

(3) Silicon treated in different ways affects the shape of triglycine sulfate crystals by predetermining a predominant growth of the crystals along some crystallographic direction.

REFERENCES

1. Tsedrik, M.S., *Fizicheskie svoistva kristallov semeistva triglitsinsul'fata (v zavisimosti ot uslovii vyrashchivaniya)* (Physical Properties of Crystals Belonging to the Family of Triglycine Sulfate (Depending on Growth Conditions)), Minsk: Nauka i Tekhnika, 1986.
2. Lemanov,V.V., Popov,S.N., and Pankova, G.A., *Fiz. Tverd. Tela*, 2002, vol. 44, no. 10, pp. 1840–1846.
3. Zheludev, I.S., *Osnovy segnetoelektrichestva* (Fundamentals of Ferroelectricity), Moscow: Atomizdat, 1973.
4. Chudotvortsev, I.G., Popova, I.A., Fedorets, A.A., and Yatsenko, O.B., *Trudy VIII Regional'noi konferentsii "Problemy khimii i khimicheskoi tekhnologii"* (Proc. VIII Regional Conf. "Problems of Chemistry and

Chemical Technology"), Voronezh, September 21–22, 2000, pp. 230–233.

5. Yatsenko, O.B. and Chudotvortsev, I.G., *Izv. Ross. Akad. Nauk, Neorg. Mater*., 2002, vol. 38, no. 9, pp. 1079–1086.
6. Lur'e, Yu.Yu., *Spravochnik po analiticheskoi khimii* (Handbook of Analytical Chemistry), Moscow: Khimiya, 1989.
7. Yatsenko, O.B., Chudotvortsev, I.G., Popova, I.A., *et al*., in *Fourth Int. Conf. on Single Crystal Growth and Heat Mass Transfer*, Obninsk, 2001, vol. 1, pp. 183–188.
8. Gavrilov, C.A., Belogorokhov, A.I., and Belogorokhova, L.I., *Fiz. Tekh. Poluprovodn*., 2002, vol. 36, pp. 104–107.
9. Anokhin, V.Z., *Kinetika i mekhanizm termicheskogo okisleniya kremniya* (Kinetics and Mechanism of Thermal Oxidation of Silicon), Voronezh: Voronezh. Gos. Univ., 1983.

Russian Journal of Applied Chemistry, Vol. 78, No. 1, 2005, pp. 50–52. Translated from Zhurnal Prikladnoi Khimii, Vol. 78, No. 1, 2005, pp. 52–54.
Original Russian Text Copyright © 2005 by Egorova, Radishevskaya, Bykonya, Shul'pekov.

INORGANIC SYNTHESIS AND INDUSTRIAL INORGANIC CHEMISTRY

Reaction of Cobalt Phosphomolybdate with Alcoholic Solutions of Tetraethoxysilane and Zirconium(IV) Oxychloride

L. A. Egorova, N. I. Radishevskaya, N. V. Bykonya, and A. M. Shul'pekov

Tomsk State University, Tomsk, Russia
Department of Structural Macrokinetics, Tomsk Scientific Center, Siberian Division, Russian Academy of Sciences, Tomsk, Russia

Received November 4, 2004

Abstract—Alcoholic solution of tetraethoxysilane was studied IR-spectroscopically. The compositions with various ratios of a binder and thermochromic substance were prepared, and their structure and thermal stability were studied. Mixtures of cobalt phosphomolybdate with tetraethoxysilane alcoholic solutions show promise for obtaining thermochromic compositions with the range of the working temperatures 350–400°C.

Phosphomolybdates of iron-like metals are materials for obtaining thermochromic compositions used for visual temperature monitoring of out-of-the-way places of devices, furnaces, etc., working at high temperatures. As a rule, thermochromic substances are applied onto the monitored surface as the compositions with various organic binders. However, the organic component rapidly loses its performance under the periodical impact of high temperatures. The binders based on inorganic compounds are more promising. In this work, we propose to use alcoholic solutions of Group IV element compounds as binders. Thermolysis of such compounds gives thermostable oxides as a matrix in which the thermochromic component is distributed.

In this work, we studied alcoholic solutions of tetraethoxysilane (TES) and oxyzirconium chloride as binders for obtaining thermochromic materials based on cobalt phosphomolybdate.

Cobalt phosphomolybdate was prepared from chloride solutions by the method described in [1]. The quantitative ratio of the initial components and the solution pH (pH < 1) were strictly controlled, which ensured formation of compounds with the Keggin structure. The crystalline form was prepared by the prolonged evaporation of the mother liquor. Cobalt phosphomolybdate obtained is a yellow powder readily soluble in water and ethanol. Phosphomolybdate and its compositions were identified by chemical, X-ray phase (a DRON-UM1 diffractometer, filtered Co radiation), and thermal (a Q-1500 derivatograph, MOM, Hungary) analyses and IR spectroscopy within the 4000–400 cm^{-1} range (a Specord M-80 spectrometer; samples were prepared as KBr pellets). Color transitions were determined visually at heating of the compositions in a furnace; the temperature was monitored with a Chromel–Copel thermocouple. The alcoholic solutions of tetraethoxysilane (20 vol % TES) and zirconium(IV) oxychloride (0.4 M) were used as binders [2]. The contents of the components were selected so that the solutions could be used for a long time. The compositions were prepared by mixing of the heteropoly compound (HPC) and the correspond-

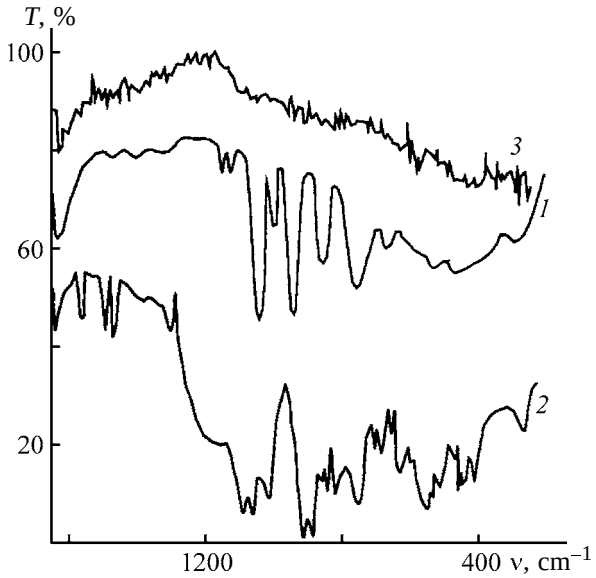


Fig. 1. IR spectra of (*1*) cobalt phosphomolybdate and its compositions with alcoholic solutions of (*2*) tetraethoxysilane and (*3*) zirconium oxychloride. (*T*) Transmittance and (ν) wavenumber.

1070-4272/05/7801-0050 © 2005 Pleiades Publishing, Inc.

ing alcoholic solutions in various ratios. During mixing of the cobalt 12-phosphomolybdate powder with an alcoholic solution of TES or zirconium(IV) oxychloride, the solution–gel transition was observed, which favored formation of a handy spread. This spread was applied onto glass supports by a thick-film method using a template and dried in air, with the subsequent heat treatment at 400°C. The minimal HPC content in the composition amounted to approximately 0.5 wt % and was determined by the threshold of visual determination of the color transition. The HPC content higher than 10 wt % favors accelerated gelation, which makes difficult applying the spread onto the support.

The structure of the initial cobalt 12-phosphomolybdate was determined IR-spectroscopically (Fig. 1). The IR spectrum of cobalt 12-phosphomolybdate, $CoH[PMo_{12}O_{40}]\cdot nH_2O$, contained the absorption bands characteristic of Keggin structures with stretching ν(P–O), ν(Mo=O), and ν(Mo–O–Mo) vibrations at 1080, 980, and 890 cm^{-1}, respectively, and bending δ(P–O) vibrations at 530 cm^{-1}. Vibrations of the bridging oxygen (–O–) lie at 800 cm^{-1}. Vibrations ν(OH) at 3680 cm^{-1} and δ(OH) at 1430 and 1030 cm^{-1} of the OH groups bound with the cation (Co) [3, 4] were also observed. A broad absorption band at 400–600 cm^{-1} indicates that the substance contains an impurity of cobalt chloride or hydrophosphate, which is caused by their coprecipitation at evaporation of the mother liquor. Weak bands at 1170 and 1260 cm^{-1} are assigned to vibrations of $[HPO_4]^{2-}$ groups. Absorption at 3200–3600 cm^{-1} (broad band) and 1640 cm^{-1} belongs to stretching and bending vibrations of water molecules, respectively [5, 6].

During mixing cobalt 12-phosphomolybdate with the TES solution (pH 4–5), the color changes from yellow to light blue, which is caused by conversion of $[PMo_{12}O_{40}]^{3-}$ into $[H_xPMo_{11}O_{39}]^{7-x}$ by the scheme

$$[PMo_{12}O_{40}]^{3-} + (5 - x)OH^- \rightleftarrows [H_xPMo_{11}O_{39}]^{7-x} + HMoO_4^- + (2 - x)H_2O.$$

In the process, the ν(P–O) band at 1080 cm^{-1} characteristic of HPC with the Keggin structure splits into two components at 1085 and 1060 cm^{-1}, suggesting formation of lacunary phosphomolybdate structure, $[H_xPMo_{11}O_{39}]^{7-x}$ [7]. In addition, a broad shoulder at 1250–1150 cm^{-1} caused by ν(SiO) vibrations and bands at 1100 and 720 cm^{-1} belonging to vibrations of the bridging Si–O–Si bonds [5, 7–9] appear. Absorption bands at 1580 and 1330 cm^{-1} suggest formation of the ethoxy groups $Me–OC_2H_5$ [10].

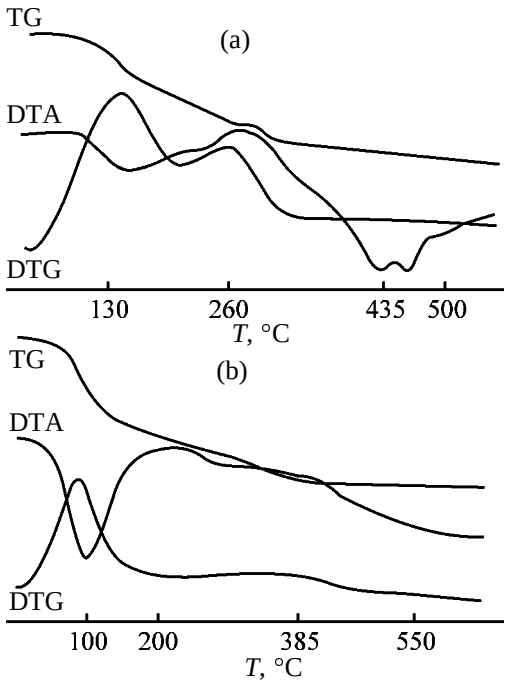


Fig. 2. Thermograms of decomposition of the spreads containing solutions of (a) tetraethoxysilane and (b) zirconium oxychloride. (*T*) Temperature.

To provide stability of zirconium oxychloride, pH 1–2 is required, which is reached at salt dissolution in ethanol. At mixing cobalt phosphomolybdate with an alcoholic solution of zirconium oxychloride, the color of the composition changes from yellow to green. The IR spectrum of the latter contains no bands of the phosphomolybdate ion (Fig. 1).

Processes in zirconium oxychloride solutions are less studied. The initial zirconium oxychloride is a tetramer with the composition $[Zr_4(OH)_8(H_2O)_{16}]Cl_8\cdot 12H_2O$ [11]. On dissolution, the initial salt dissociates with formation of a cyclic zirconium tetramer containing Zr–O–Zr bonds [12]. Ethanol converts into acetates on these groups [10, 13]. The IR spectra of the dried binders contain characteristic bands of the acetate groups. Introduction of HPC prevents formation of acetate on the zirconium ion, owing to decomposition of the heteropoly anion with the release of protons, molybdate, and phosphate ions. The reaction proceeds by the acid–base mechanism between the heteropoly anion and complex hydroxy cation exhibiting amphoteric properties. Water formation promotes hydrolysis and HPC decomposition.

To form thermochromic materials, the spread was subjected to the heat treatment. To study thermolysis, we measured thermograms of both the initial components and spreads within the 20–600°C range. The results showed (Fig. 2a) that the thermal decomposi-

tion of the spreads based on TES is accompanied by complex processes connected with the presence of HPC structures. In the course of the thermolysis, the weight of the spread decreases, suggesting formation of the silicon oxide framework. The thermal decomposition of cobalt phosphomolybdate starts above 430°C. The derivatograms of spreads based on TES show heat effects caused by structural changes in HPC, described previously [14]. This confirms once again the existence of the lacunary structure in these compositions. The X-ray phase analysis of the samples annealed at 600°C shows that the compositions studied are multiphase systems. The most intense reflections in the powder patterns belong to molybdenum, silicon, and cobalt oxide phases.

The composition containing zirconium oxychloride decomposes in two stages, which is characteristic of the thermal decomposition of the products of zirconium oxychloride hydrolysis (Fig. 2b).

The compositions prepared were tested for the thermochromism. The color of the composition based on TES changes at 375–380°C from light blue to dark blue. The thermogravimetric studies showed that, to obtain a thick-film thermochromic material based on silicon, the sample heating for 90–120 min at 400°C is required.

CONCLUSIONS

(1) The alcoholic solutions of tetraethoxysilane can be used as a binder for preparing thermochromic materials based on cobalt phosphomolybdates. In the reaction of the heteropoly compound with an alcoholic solution of tetraethoxysilane, $[PMo_{12}O_{40}]^{3-}$ transforms into the lacunary structure, $[H_xPMo_{11}O_{39}]^{7-x}$. The hydrolysis in the compositions including zirconium oxychloride prevents stabilization of the structure of the heteropoly compound responsible for the thermochromic color transitions.

(2) The optimal procedure for obtaining thick-film thermochromic materials is heating of the spread for 90–120 min at 400°C.

REFERENCES

1. Radishevskaya,N.I., Egorova, L.A., and Kozik, V.V., *Zh. Prikl. Khim.*, 2000, vol. 73, no. 7, pp. 1066–1068.
2. Suikovskaya, N.V., *Khimicheskie metody polucheniya tonkikh prozrachnykh plenok* (Chemical Methods of Preparing Thin Transparent Films), Leningrad: Khimiya, 1971.
3. Bielanski, A., Matecka, A., and Kubelkova, L., *J. Chem. Soc., Faraday Trans., 1*, 1989, vol. 85, no. 9, pp. 2847–2856.
4. Kazanskii, L.P., Ol'gin-Kin'ones, S., and Ivanov-Emin, B.N., *Zh. Neorg. Khim.*, 1979, vol. 24, no. 4, pp. 958–963.
5. Nakamoto, K., *Infrared and Raman Spectra of Inorganic and Coordination Compounds*, New York: Wiley, 1986.
6. Balicheva, T.G. and Lobaneva, O.A., *Elektronnye i kolebatel'nye spektry neorganicheskikh i koordinatsionnykh soedinenii* (Electronic and Vibrational Spectra of Inorganic and Coordination Compounds), Leningrad: Leningr. Gos. Univ., 1983.
7. Pope, M.T., *Heteropoly and Isopoly Oxometalates*, Berlin: Springer, 1983.
8. Rodtsevich, S.P., Eliseev, Yu.S., and Lukashevich, G.F., *Steklo Keram.*, 2001, no. 8, pp. 27–28.
9. Melamud, S.G., Yur'ev, B.P., and Bruk, L.B., *Metally*, 2001, no. 6, pp. 3–9.
10. Little, L.H., *Infrared Spectra of Adsorbed Species*, London: Academic, 1966.
11. Burkov, K.A., Kozhevnikova, G.V., Lilich, L.S., and Myund, L.A., *Zh. Neorg. Khim.*, 1982, vol. 27, no. 6, pp. 1427–1431.
12. Panda, C.R., Chakravortty, V., and Dash, K.S., *Indian J. Chem.*, 1987, vol. 26A, November, pp. 914–918.
13. Kiselev, A.V. and Lygin, V.I., *Infrakrasnye spektry poverkhnostnykh soedinenii* (Infrared Spectra of Surface Compounds), Moscow: Nauka, 1972.
14. Maksimovskaya, R.I., Bondareva, V.M., and Litvak, G.S., *Zh. Neorg. Khim.*, 1996, vol. 41, no. 7, pp. 1173–1180.

Russian Journal of Applied Chemistry, Vol. 78, No. 1, 2005, pp. 53–56. Translated from Zhurnal Prikladnoi Khimii, Vol. 78, No. 1, 2005, pp. 55–58.
Original Russian Text Copyright © 2005 by Petrov, Belen'kii.

PHYSICOCHEMICAL STUDIES OF SYSTEMS AND PROCESSES

Interactions in the Silver Selenide–Water System

G. V. Petrov and A. M. Belen'kii

Plekhanov State Mining Institute, St Petersburg, Russia

Received May 26, 2004

Abstract—Interactions in the Ag_2Se–H_2O system in the whole pH range was studied by thermodynamic calculations and polarization measurements. Refined Pourbaix diagrams at 25 and 80°C were constructed.

Chemical reactions in aqueous solutions find expanding application in metallurgy and chemical industry. An important process of this type is hydrochemical oxidation of chalcogens (sulfur, selenium, and tellurium) and their most stable compounds, metal chalcogenides. These reactions are involved in formation of natural minerals, in particular, in secondary transformations of earth's crust. The processes for recovering chalcogenides and non-ferrous and noble metals from both natural ores and various intermediate reprocessing products are usually based on these reactions. Development and industrial application of hydrometallurgical processing of copper electrolytic refining slimes containing noble metals substantially depends on the behavior of silver and gold chalcogenides in various solutions.

It is known that Ag_2Se is oxidized in alkaline solutions to selenate anion which is highly stable and can be reduced to elemental selenium only at a high pressure. Selenium(VI) is reduced with HCl only at elevated temperatures and high acid concentrations. In addition, liberation of Cl_2 complicates the industrial application of this process. Selenium(VI) can be reduced in acidic solution at room temperature in the presence of a catalyst (e.g., titanium salts). The catalytic reduction expands the possibility of oxidative acid breakdown of chalcogen-containing materials, but the problem of selenium recovery from alkaline solutions remains unsolved [1–3].

To develop new methods for breakdown of chalcogen-containing materials enriched with noble metals, we studied in this work the interactions in the Ag_2Se–H_2O system in the whole pH range by thermodynamic calculations (construction of Pourbaix diagrams) and potentiostatic measurements.

EXPERIMENTAL

Polarization curves were recorded on a P-5827 potentiostat using a KSP-4 electronic potentiometer and a three-electrode cell with separated electrode compartments. A silver plate coated with Ag_2Se by immersion in a sodium polyselenide solution immediately prior to the measurements was used as the working electrode. Platinum and silver chloride electrodes were used as auxiliary and reference electrodes, respectively. The polarization curves were recorded at a current sweeping rate of 75 A m^{-2} min^{-1} and the time providing attainment of the stationary potentials. The current density was varied in the range 1.0–1500 A m^{-2}.

In the examined system, silver can be formed by both the reduction and oxidation of Ag_2Se. The Pourbaix diagram for the Ag_2Se–H_2O system at pH < 6 and $\varphi > 0.4$ [2] shows that Ag_2Se is oxidized directly to selenate ions. However, this conclusion is not quite correct, since the solubility of Ag_2SeO_4 (SP = 5.6×10^{-8}) in acidic and neutral solutions [$K_2(H_2SeO_4) = 8.9 \times 10^{-3}$] was not taken into account. We calculated and constructed the refined φ–pH diagram for the Ag_2Se–H_2O system at 25 and 80°C (Figs. 1a, 1b).

The activity of all components except for hydrogen ions were taken as 1.

The stability region of Ag_2Se in the diagram of the Ag_2Se–H_2O system at 25°C (Fig. 1a) in the whole pH range (except for pH < 1) is bounded from the top by lines *1–3* corresponding to the equilibrium potential of reduction of Ag^+ to Ag^0 and oxidation of Se^{2-} to SeO_3^{2-}. The stability region of SeO_3^{2-} is narrow: Se(IV) can be oxidized to Se(VI) at the overvoltage as low as 0.1–0.2 V. At pH 1, Ag^+ is not reduced to Ag^0 and goes into the solution as Ag^+ cation. Above lines *7–11*, silver is mainly in the ionic or oxide form. On heating to 80°C, the Pourbaix diagrams of the Ag_2Se–H_2O system insignificantly changes (Fig. 1b). Thus, the electrochemical behavior of Ag_2Se is almost independent of temperature in the whole pH range.

The anodic polarization curves of Ag_2Se oxidation in an alkaline solution (NaOH concentration 80–

1070-4272/05/7801-0053© 2005 Pleiades Publishing, Inc.

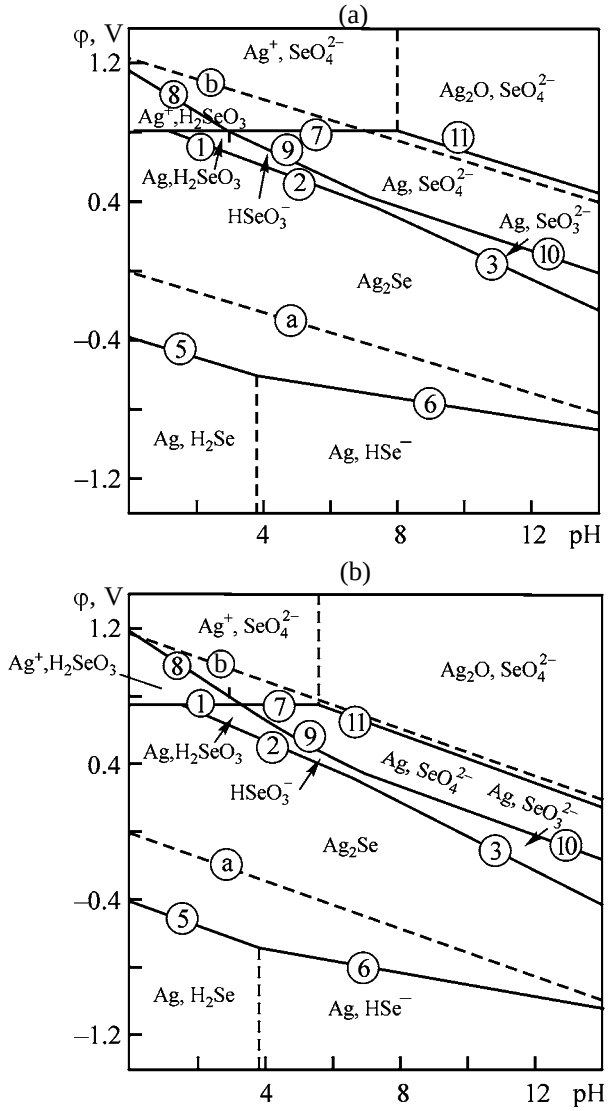


Fig. 1. Refined Pourbaix diagrams for the Ag_2Se–H_2O system at (a) 25 and (b) 85°C. (φ) Potential.

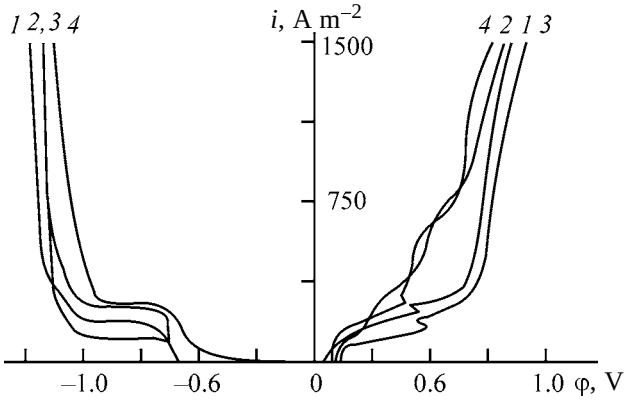


Fig. 2. Polarization curve of Ag_2Se at NaOH concentration of (*1*) 80, (*2*) 120, (*3*) 160, and (*4*) 200 g l^{-1} and the current sweeping rate of 75 A m^{-2} min^{-1}. (*i*) Current density and (φ) potential; the same for Fig. 4.

200 g l^{-1}) contain three typical waves (Fig. 2). The first wave appears at 0.3 V and the current density of 170 A m^{-2}. In accordance with the Pourbaix diagram (Fig. 1b), this wave is due to formation of Ag and SeO_3^{2-}. The second wave is observed in the potential range 0.4–0.5 V and is assigned to oxidation of SeO_3^{2-} to SeO_4^{2-}. The third wave at 0.55–0.6 V is due to oxidation of Ag^0 to silver oxide. At higher potentials, both hydroxide and selenium-containing anions are discharged to form O_2. Hence, to prevent formation of stable SeO_4^{2-} anions, the electrolysis should be performed at low current densities (Fig. 2).

As seen from the Pourbaix diagrams, Ag_2Se is reduced to elemental silver and Se^{2-} anions in the potential ranges from –0.4 to –0.8 (25°C) and from –0.5 to –0.9 V (80°C). Liberation of H_2Se from the solution with pH <4.0 (25°C) or 2.5 (80°C) is possible. At higher pH, hydrogen selenide is not liberated from solutions.

The hydrogen overvoltage decreases with increasing temperature (the boundary of H_2Se existence is moved away from the region of water stability), which complicates the reaction

$$HSe^- + 2Ag \rightleftarrows Ag_2Se + H^+ + 2e. \quad (1)$$

However, since the hydrogen overvoltage on silver is high, Ag_2Se can be reduced to elemental Ag and Se^{2-} in a wide temperature range at pH substantially lower than 14.

To transfer selenium into the gas phase, the electrolysis should be performed in acidic solution (pH < 3.8), and to transfer selenium into the solution, the process should be performed in neutral or weakly acidic solution (pH > 4).

The cathodic polarization curves of Ag_2Se in alkaline solution have several inflection points (Fig. 2). In the course of polarization the solution in the electrode compartment turns brown-red owing to formation of selenide and polyselenide anions. The color of the cathodically polarized electrode is grayish-metal owing to deposition of metallic silver. The standard potential of one of the potential-determining cathodic reactions,

$$Ag_2Se + 2e \rightleftarrows Se^{2-} + 2Ag, \quad (2)$$

is –1.06 V at 80°C. However, the other cathodic reactions yielding polyselenide ions are possible:

$$2Ag_2Se + 2e \rightleftarrows Se_2^{2-} + 4Ag, \quad \varphi^0 = -0.54 \text{ V}; \quad (3)$$

$$4Ag_2Se + 2e \rightleftarrows Se_4^{2-} + 8Ag, \quad \varphi^0 = -0.44 \text{ V}. \quad (4)$$

At high overvoltage observed in the range of saturation currents, hydrogen can be formed:

$$2H_2O + 2e \rightleftarrows H_2 + 2OH^-, \quad \varphi^0 = -0.83 \text{ V}. \quad (5)$$

Taking into account the calculated standard potentials and the polarization shift of the cathodic potential to the negative region, we suggest that various selenium oxide films adsorbed on the cathode in the course of synthesis of the initial Ag_2Se (Fig. 2) are reduced at the current densities of up to 30 A m^{-2} and cathodic potential of up to –0.6 V. The section of the cathodic curves at current densities from 30 to 60 A m^{-2} is characterized by constant potential of –0.65 V caused by cathodic reactions (3) and (4) yielding polyselenide ions.

The stationary cathodic potential at low current densities is affected by a low concentration of selenide ions in the solution. At the current density of 100 A m^{-2}, the cathodic potential reaches –0.95 V and is in the range of formation and existence of sodium monoselenide [reaction (2)]. As the current density increases to the maximal value (1300 A m^{-2}), the cathodic potential slightly changes to the value from –1.0 to –1.1 V. Under these conditions, the main electrode process is reaction (2).

The cathodic reaction not involving hydroxyl ions is independent of the alkaline concentration varied from 80 to 200 g l^{-1}. Since the polarization curves measured in these solutions at the stationary potentials virtually coincide, selenide ions are not hydrolyzed in this concentration range. When the potential sweeping is lower than the stationary potentials, the cathodic polarization is slightly higher and increases with increasing alkali concentration (Fig. 2). The calculated apparent activation energy E^* of the cathodic process at 20–80°C is 6.28 kJ mol^{-1}. The fact that the activation energy is independent of the redox potential suggests diffusion overvoltage of the electrode reaction (Fig. 3).

Since chalcogens and metal chalcogenides are hydrophobic, we studied cathodic polarization of Ag_2Se in alkaline solutions containing surfactants. In the presence of Na_2S, the shape of the polarization curve does not change (Fig. 4) except for the initial section. In this step, the reduction starts at more negative potentials since oxidized selenium films adsorbed on the electrode are probably reduced with sulfide ions. Formation of monosulfo- and disulfoselenides along

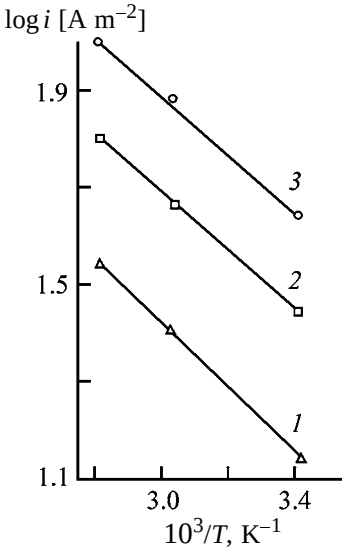


Fig. 3. Rate of cathodic reduction of Ag_2Se at φ (*1*) –0.7, (*2*) –0.8, and (*3*) –0.9 V in alkaline solution as a function of temperature *T*. (*i*) Current density.

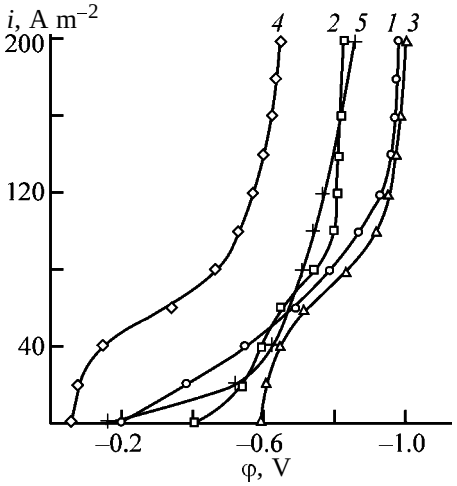


Fig. 4. Cathodic polarization curves of Ag_2Se in alkaline solution (80 g l^{-1} NaOH) at 80°C (*1*) without surfactant; in the presence of surfactant (g l^{-1}): Na_2S (*2*) 5 and (*3*) 100; C_2H_5OH (*4*) 5 and (*5*) 100.

with selenide ions is also possible:

$$2Ag_2Se + S^{2-} + 2e \rightleftarrows SSe^{2-} + Se^{2-} + 4Ag, \ \varphi^0 = -0.6 \text{ V}; \quad (6)$$

$$4Ag_2Se + S^{2-} + 4e \rightleftarrows SSe_2^{2-} + 2Se^{2-} + 8Ag, \quad \varphi^0 = -0.63 \text{ V}. \quad (7)$$

Ethanol, unlike Na_2S, strongly affects the cathodic polarization (Fig. 4). All typical inflection points in the cathodic curves are shifted to the positive potentials, which is due to stabilization of polyselenide

ions. In other words, introduction of ethanol decreases the reduction potential of Ag_2Se.

Thus, about 95–98% of selenium can be converted into water-soluble polyselenide species by electrochemical decomposition or hydrochemical reduction of deleaded copper slime in alkaline solution containing surfactant.

CONCLUSIONS

(1) In oxidation of silver selenide in the whole pH range, selenide ions exist in a narrow potential range. Extremely stable selenate anion, which can be reduced to elemental selenium only at elevated pressure or in the presence of catalyst, is formed at the redox potentials slightly exceeding this range.

(2) In the presence of surfactants (sodium sulfide or ethanol), reduction of silver selenide is accelerated and polyselenide anions are stabilized, which shifts the cathodic potential to the electropositive range and suppresses hydrogen liberation.

(3) Introduction of surfactants in electrochemical breakdown or chemical reduction of chalogenide-containing materials enriched with noble metals provides almost quantitative transfer of selenium into an alkaline solution.

REFERENCES

1. Belen'kii, A.M., Petrov, G.V., Plekhanov, K.A., *et al*., *Tsvetn. Met*., 1999, no. 1, pp. 43–45.
2. Buketov, E.A. and Ugorets, M.Z., *Gidrokhimicheskoe okislenie khal'kogenov i khal'kogenidov* (Hydrochemical Oxidations of Chalcogens and Chalcogenides), Alma-Ata: Nauka Kaz. SSR, 1975.
3. Greiver, T.N., Zaitseva, I.G., and Kosover, V.M., *Selen i tellur* (Selenium and Tellurium), Moscow: Metallurgiya, 1977.

Russian Journal of Applied Chemistry, Vol. 78, No. 1, 2005, pp. 57–63. Translated from Zhurnal Prikladnoi Khimii, Vol. 78, No. 1, 2005, pp. 59–65.
Original Russian Text Copyright © 2005 by Morachevskii, Tsymbulov, Kolosova, Tsemekhman.

PHYSICOCHEMICAL STUDIES OF SYSTEMS AND PROCESSES

Thermodynamic Properties of Liquid Alloys of the System Nickel–Copper–Cobalt

A. G. Morachevskii, L. B. Tsymbulov, E. Yu. Kolosova, and L. Sh. Tsemekhman

St. Petersburg State Polytechnic University, St. Petersburg, Russia
Gipronikel' Institute, Joint-Stock Company, St. Petersburg, Russia

Received December 8, 2004

Abstract—The integral thermodynamic characteristics and copper activity in liquid alloys of the system nickel–copper–cobalt at 1600°C were calculated by various methods from data on boundary binary systems.

For analysis of systems and processes involved in the main pyrometallurgical procedures in nickel and copper production, it is necessary to know the thermodynamic properties of various combinations of elements constituting the complex system Cu–Ni–Co–Fe–S–O at high temperatures. It is impossible today to estimate the thermodynamic characteristics of formation of a liquid alloy from pure components from data on their properties even for binary systems, to say nothing of more complex systems. The use of phase diagrams requires, as a rule, certain assumptions for calculating the thermodynamic characteristics of the system does not always affords reliable thermodynamic data. At the same time, a variety of pure geometrical and analytical models allow integral and partial thermodynamic characteristics of ternary and more complex systems to be estimated sufficiently reliably using only data on the corresponding properties of the boundary binary systems.

The suitability and reliability of the calculation methods, depending on the features of interactions in a particular multicomponent system, was confirmed for a great variety of liquid metallic systems, which are relatively fusible and convenient for experimental study [1–11]. For ternary and more complex systems formed by the above components, fairly reliable and comprehensive data are virtually lacking. In such cases, the extent to which the calculation results are close to true thermodynamic characteristics of mixing can be largely judged from the coincidence of the integral thermodynamic characteristics of ternary and more complex system calculated using different geometrical models (6–8 versions are possible) and polynomial methods, Redlich–Kister polynomials [12] in particular. The partial molar properties, activities, and activity coefficients of components in ternary system can be estimated both from the calculated integral characteristics and directly from the corresponding partial molar characteristics of binary systems. The second way seems more preferable, since it does not require to differentiate the equation expressing the dependence of the corresponding integral property on the composition of a ternary system along one or another section.

The choice of appropriate values for binary systems, based on detailed analysis of data available from the original literature, is important in calculating the thermodynamic properties of ternary and more complex systems. Presently, the thermodynamic characteristics (component activities, Gibbs energies, enthalpies and entropies of formation from elements) are available for a large number of binary metallic systems and systems metal–sulfur. They were obtained by different methods and different authors and are far from being consistent in all cases. Practical thermodynamic calculations require reliable and consistent values of thermodynamic functions, and choosing them is sometimes a problem of no less importance than obtaining new results. First of all, the preliminary expertise of thermodynamic functions should be based on the laws of chemical thermodynamics. Also, it should take into account the regular trends or dependences reliably established for more or less wide classes of systems and involve the assessment of the reliability of the applied experimental method and of the skill and experience of a specific experimental team, as well as of the results obtained by this team in studying other systems [13]. Such expertise can be also useful for characterizing the reliability of single thermodynamic data.

Previously, we used data on boundary binary systems to calculate the thermodynamic characteristics of

1070-4272/05/7801-0057 © 2005 Pleiades Publishing, Inc.

Table 1. Integral thermodynamic characteristics of the boundary binary systems at 1600°C accepted for calculating thermodynamic properties of the ternary system Ni–Cu–Co*

x_2**	Ni–Cu		Cu–Co		Ni–Co	
	ΔG^{ex}	ΔH	ΔG^{ex}	ΔH	ΔG^{ex}	ΔH
	kJ mol^{-1}					
0.1	1.33	1.50	3.01	3.42	–0.22	0.17
0.2	2.68	2.63	5.04	5.76	–0.40	0.30
0.3	3.69	3.38	6.30	7.30	–0.52	0.38
0.4	4.39	3.79	6.95	8.22	–0.60	0.42
0.5	4.73	3.87	7.07	8.61	–0,63	0.42
0.6	4.67	3.64	6.68	8.48	–0.61	0.39
0.7	4.20	3.11	5.81	7.76	–0.53	0.33
0.8	3.33	2.31	4.41	6.29	–0.41	0.24
0.9	2.04	1.30	2.49	3.82	–0.23	0.13

* Standard state: pure liquid metals.
** (x_2) Mole fraction of the component indicated second.

liquid alloys of the systems Ni–Cu–Fe [14, 15] and Fe–Ni–Co [16]. As noted above, quite satisfactory agreement of the results obtained in calculation of the integral molar excess Gibbs energies ΔG and enthalpies of mixing ΔH of ternary systems by various geometrical models and analytical Redlich–Kister equation gives grounds to consider that they are described rather reliably. The calculation was preceded by the detailed analysis of the available experimental data on thermodynamic properties of boundary binary systems.

The thermodynamic properties of liquid alloys of the system Ni–Cu were repeatedly studied by various methods, such as the emf measurements with molten or solid electrolyte, the saturated vapor pressure measurement by the transfer method and with a Knudsen's cell as a source of the molecular beam, and the high-temperature calorimetry. According to a calorimetric study [17], the enthalpy of mixing is positive over the entire composition range (1480°C), its maximum value does not exceed 2.5 kJ mol^{-1}, and the curve maximum is slightly shifted to the nickel-rich region of compositions. Kulkarni and Johnson [18] studied the system by the emf method with solid anion-conducting electrolyte (ZrO_2 + MgO) at 1400°C ($0.0 \le x_{Ni} \le 0.77$, where x is the mole fraction of nickel in the alloy). In calculation of the thermodynamic functions, nickel in the solid state and copper in the liquid state were standard states. According to [18], the isotherms of component activities in the system Ni–Cu exhibit moderate positive deviations from the ideality over the composition range studied.

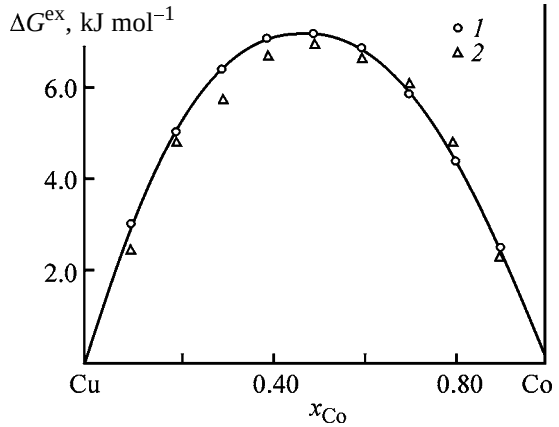


Fig. 1. Integral molar excess Gibbs energy ΔG^{ex} vs. Co mole fraction in liquid alloys in the system Cu–Co. References: (*1*) [27] (1600°C, extrapolation) and (*2*) [26] (1550°C).

The thermodynamic properties of liquid alloys of the system Ni–Cu were studied, analyzed, and optimized in a number of other studies [19–23]. Based on the comparison of the whole set of the experimental data used for calculating the thermodynamic properties of the ternary system Ni–Cu–Co at 1600°C, we have taken as input data the results from [21, 23]. The same data are recommended for the system Ni–Cu in a reference book [24]. The values accepted for calculation are validated in more detail in [25].

The interaction between the components in liquid alloys of the system Cu–Co has been studied less extensively. Timberg *et al*. [26] used the mass spectrometry with a Knudsen's cell as a source of the molecular beam ($0.060 \le x_{Co} \le 0.949$, 1422–1597°C) to study the thermodynamic properties of liquid alloys of copper with cobalt. The standard state was the liquid state of pure components. The copper and cobalt activities were calculated from the values of the ion currents at 1550°C. The system shows considerable positive deviations from the ideal behavior. The close results were obtained by Taskinen [27] who studied the thermodynamic properties of the Cu–Co system by the emf method with a solid oxygen-containing electrolyte ZrO_2 + MgO ($0.030 \le x_{Co} \le 0.700$, 1097–1457°C). The cobalt activity was determined directly from the results of the emf measurements. The calorimetric study and calculation of the phase diagram from the thermodynamic data of [28–30] were also performed. The ΔG^{ex} and ΔH values obtained by different authors for the Cu–Co system are compared in Figs. 1 and 2. The data on the copper alloys with cobalt in the liquid state, accepted as input data for thermodynamic calculation of the ternary sys-

Table 2. Results of calculation of ΔG^{ex} and ΔH in the ternary system Ni–Cu–Co at 1600°C

x_{Cu}, mole fraction	$x_{Ni} : x_{Co} = 3 : 1$		$x_{Ni} : x_{Co} = 1 : 1$		$x_{Ni} : x_{Co} = 1 : 3$	
	ΔG^{ex}	ΔH	ΔG^{ex}	ΔH	ΔG^{ex}	ΔH
	kJ mol^{-1}					
0.1	1.33 ± 0.06	2.24 ± 0.06	1.48 ± 0.05	2.84 ± 0.09	1.87 ± 0.03	3.33 ± 0.10
0.2	2.91 ± 0,05	3.61 ± 0.08	3.25 ± 0.05	4.50 ± 0.11	3.75 ± 0.04	5.36 ± 0.10
0.3	4.12 ± 0.06	4.54 ± 0.08	4.58 ± 0.07	5.59 ± 0.10	5.14 ± 0.05	6.63 ± 0.09
0.4	4.95 ± 0.08	5.05 ± 0.03	5.48 ± 0.07	6.16 ± 0.08	6.05 ± 0.06	7.28 ± 0.07
0.5	5.36 ± 0.08	5.15 ± 0.03	5.92 ± 0.09	6.31 ± 0.04	6.50 ± 0.07	7.44 ± 0.04
0.6	5.31 ± 0.08	4.87 ± 0.05	5.89 ± 0.09	6.02 ± 0.03	6.45 ± 0.08	7.12 ± 0.01
0.7	4.81 ± 0.07	4.24 ± 0.04	5.37 ± 0.07	5.31 ± 0.04	5.88 ± 0.08	6.32 ± 0.03
0.8	3.83 ± 0.05	3.23 ± 0.03	4.30 ± 0.07	4.12 ± 0.04	4.70 ± 0.05	4.96 ± 0.03
0.9	2.31 ± 0.02	1.85 ± 0.01	2.57 ± 0.03	2.39 ± 0.02	2.80 ± 0.02	2.91 ± 0.01

tem (Table 1), are based on the results of [26, 27].

Cobalt and nickel show unlimited mutual solubility in both liquid and solid states. The liquidus and solidus temperatures are so close that virtually merge into one line. Data on the thermodynamic properties of liquid Co–Ni alloys have been considered previously [16].

Table 1 summarizes the data on the integral molar excess Gibbs energy and enthalpy of mixing in liquid binary alloys, which were used for calculating the corresponding integral characteristics of the ternary system Ni–Cu–Co. The calculation of ΔG^{ex} and ΔH for the ternary system involves a number of geometrical models, which were analyzed in detail in a monograph [12] and applied in previous studies [14–16]. The symmetric geometrical models (Kohler's and Muggiani's methods and various versions of Colinet's method) and asymmetric models (Toop's method and two versions of Hillert's method) yield reasonably consistent results. For all the 27 considered compositions of the ternary system, the values calculated by the four main models (Toop, Kohler, Muggiani, and Colinet's methods) commonly deviate from the average value by no more than 1.5%, the deviation attaining 3% only in some cases. The average results of the ΔG^{ex} and ΔH calculation are presented in Table 2. The lines of the equal values of these functions are plotted in Figs. 3 and 4. The degree of consistency of the results obtained using various simple geometrical models is to a certain extent a criterion of reliability in description of the thermodynamic property of a ternary system.

The problem of expressing analytically the concentration dependence of integral thermodynamic functions of binary alloys is important for estimating the

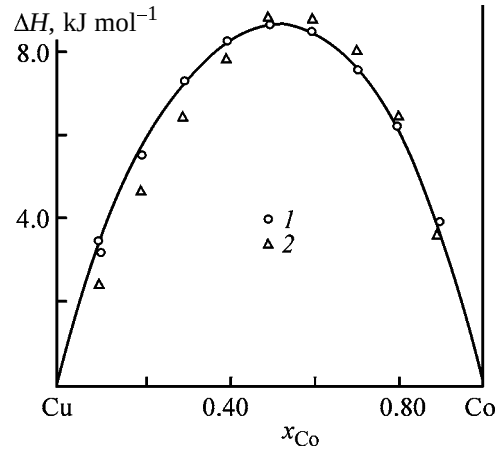


Fig. 2. Integral molar enthalpy of mixing ΔH vs. Co mole fraction in liquid alloys in the system Cu–Co. References: (*1*) [27] (1600°C) and (*2*) [26] (1550°C).

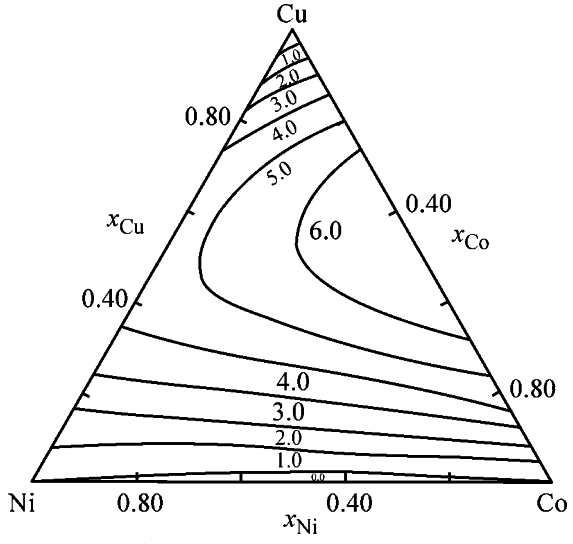


Fig. 3. Lines of equal integral molar excess Gibbs energies ΔG^{ex} (kJ mol^{-1}) for liquid alloys in the system Ni–Cu–Co at 1600°C.

Table 3. ΔG^{ex} and ΔH values for the ternary system Ni–Cu–Co at 1600°C, calculated by polynomial equations

x_{Cu}	$x_{Ni} : x_{Co} = 3 : 1$		$x_{Ni} : x_{Co} = 1 : 1$		$x_{Ni} : x_{Co} = 1 : 3$	
	ΔG^{ex}	ΔH	ΔG^{ex}	ΔH	ΔG^{ex}	ΔH
	kJ mol^{-1}					
0.2	2.92	3.52	3.27	4.50	3.76	5.24
0.4	4.96	4.98	5.52	6.16	6.08	7.24
0.6	5.36	4.87	5.94	6.02	6.48	7.12
0.8	3.82	3.23	4.12	4.11	4.66	4.95

integral thermodynamic characteristics of ternary system without using geometrical models. As in study of other ternary systems [14–16], we applied the Redlich–Kister method [12, 25]. In this method, the analytical expression of the ΔG^{ex} (kJ mol^{-1}) and ΔH (kJ mol^{-1}) dependences on the composition in ternary system involves the polynomials

$$\Delta G^{ex} = x_1(1 - x_1)[b + c(2x_1 - 1) + d(2x_1 - 1)^2], \quad (1)$$

$$\Delta H = x_1(1 - x_1)[b' + c'(2x_1 - 1) + d'(2x_1 - 1)^2]. \quad (2)$$

It was shown previously [31] that it is unnecessary for liquid metallic systems to use higher degrees of polynomials. For the binary systems discussed here, the following coefficients were obtained:

	Ni–Cu	Cu–Co	Co–Ni
b	18.8829	28.2676	–2.5158
c	–3.5732	3.2043	–0.0500
d	–0.3147	3.5208	0.0122
b'	15.4828	34.4250	1.6717
c'	1.6414	–2.7500	–0.2934
d'	–0.1771	9.0240	–0.0074

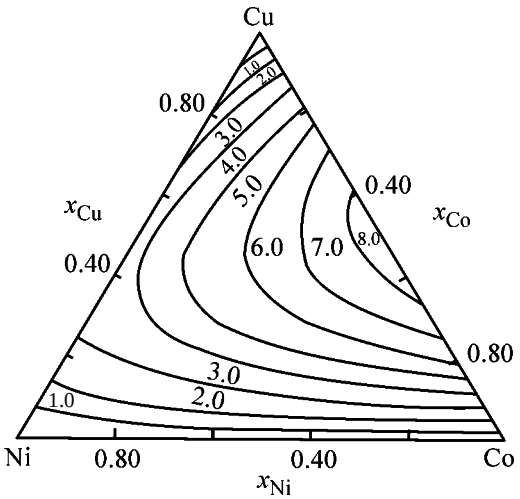


Fig. 4. Lines of equal integral molar enthalpies of mixing ΔH (kJ mol^{-1}) for liquid alloys of the system Ni–Cu–Co at 1600°C.

Table 4. Partial molar excess Gibbs energies of copper ΔG^{ex}_{Cu}, activity coefficients of copper γ_{Cu}, and copper activities a_{Cu} in liquid alloys of the system Ni–Cu–Co at 1600°C (Toop's method)

x_{Cu}	ΔG^{ex}_{Cu}, kJ mol^{-1}	$\ln\gamma_{Cu}$	γ_{Cu}	a_{Cu}
Section $x_{Ni} : x_{Cu} = 3 : 1$				
0.1	16.04	1.030	2.80	0.280
0.2	13.38	0.859	2.36	0.472
0.3	10.86	0.697	2.01	0.603
0.4	8.49	0.545	1.72	0.690
0.5	6.29	0.404	1.50	0.749
0.6	4.30	0.276	1.32	0.791
0.7	2.59	0.166	1.18	0.827
0.8	1.23	0.079	1.08	0.866
0.9	0.33	0.021	1.02	0.919
Section $x_{Ni} : x_{Cu} = 1 : 1$				
0.1	18.52	1.189	3.28	0.328
0.2	14.95	0.960	2.61	0.522
0.3	11.95	0.767	2.15	0.645
0.4	9.29	0.597	1.82	0.726
0.5	6.91	0.444	1.56	0.779
0.6	4.77	0.306	1.36	0.815
0.7	2.92	0.188	1.21	0.844
0.8	1.41	0.091	1.09	0.876
0.9	0.39	0,025	1.03	0.923
Section $x_{Ni} : x_{Cu} = 1 : 3$				
0.1	20.47	1.314	3.72	0.372
0.2	16.29	1.046	2.85	0.569
0.3	12.87	0.826	2.28	0.685
0.4	9.96	0.640	1.90	0.758
0.5	7.43	0.477	1.61	0.805
0.6	5.18	0.333	1.39	0.837
0.7	3.21	0.206	1.23	0.860
0.8	1.58	0.101	1.11	0.885
0.9	0.44	0.028	1.03	0.926

In Eqs. (1), (2), x_1 corresponds to the component indicated first for all the three binary systems. As noted previously [14, 16], the polynomial dependences for boundary binary systems allow the integral molar excess Gibbs energy and enthalpy of mixing to be calculated with reasonably simple expressions:

$$\Delta G^{ex} = x_1x_2[b_{12} + c_{12}(x_1 - x_2) + d_{12}(x_1 - x_2)^2] + x_2x_3[b_{23} + c_{23}(x_2 - x_3) + d_{23}(x_2 - x_3)^2] + x_3x_1[b_{31} + c_{31}(x_3 - x_1) + d_{31}(x_3 - x_1)^2], \quad (3)$$

$$\Delta H = x_1x_2[b'_{12} + c'_{12}(x_1 - x_2) + d'_{12}(x_1 - x_2)^2] + x_2x_3[b'_{23} + c'_{23}(x_2 - x_3) + d'_{23}(x_2 - x_3)^2] + x_3x_1[b'_{31} + c'_{31}(x_3 - x_1) + d'_{31}(x_3 - x_1)^2], \quad (4)$$

where x_1–x_3 characterize the composition of a ternary system ($x_1 + x_2 + x_3 = 1$); the subscripts 12, 23, and 31 in the polynomial coefficients refer to the binary systems Ni–Cu (1–2), Cu–Co (2–3), and Co–Ni (3–1), respectively.

The results of a calculation by Eqs. (3) and (4) are presented in Table 3 for a number of compositions of the ternary system. The calculated ΔG^{ex} and ΔH values reasonably agree with the results obtained using the geometrical models (Table 2).

A characteristic feature of the ternary system considered is that liquid alloys in the system Co–Ni show quasi-regular behavior and those in the system Ni–Cu and, especially, in the Cu–Co system exhibit rather significant positive deviations from the ideal behavior. The copper content in liquid alloys of the given ternary system determines the value of its integral and partial thermodynamic functions. Based on this fact, the thermodynamic functions of copper (ΔG^{ex}_{Cu}, γ_{Cu}, and α_{Cu}) were chosen to verify various methods used for direct estimation of the partial molar functions of a component from data on boundary binary systems.

The following dependence can be derived from Toop's equation [32–34]:

$$G_2^{ex} = [x_1(1 - x_2)^{-1}\Delta G^{ex}_{2(1)} + x_3(1 - x_2)^{-1}\Delta G^{ex}_{2(3)}]_{x_2} - (1 - x_2)^2[\Delta G^{ex}_{13}]_{x_1/x_3}, \quad (5)$$

where ΔG_2^{ex} is the partial molar excess Gibbs energy of component 2 in the ternary alloy of a composition determined by mole fractions of the components x_1–x_3; $\Delta G^{ex}_{2(1)}$ and $\Delta G^{ex}_{2(3)}$ are the partial molar excess Gibbs energies of component 2 in the boundary binary systems 1–2 and 2–3 at a given x_2; and ΔG^{ex}_{13} is the integral molar excess Gibbs energy of the system 1–3 at a given $x_1 : x_3$ ratio.

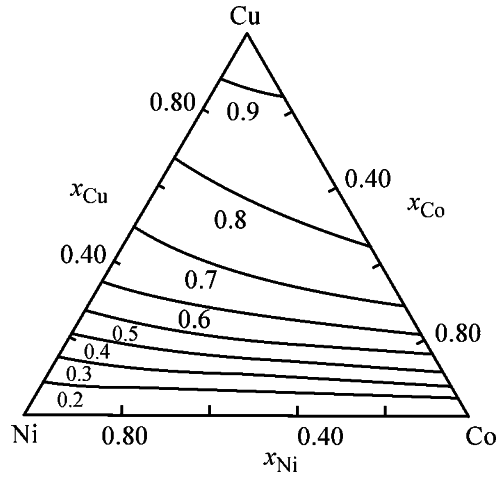


Fig. 5. Lines of equal copper activities in liquid alloys of the system Ni–Cu–Co at 1600°C.

In the given case, as in the subsequent expressions, components 1, 2, and 3 are nickel, copper, and cobalt, respectively. The results of the calculation are given in Table 4. The lines of the equal activities of copper in the concentration triangle are plotted in Fig. 5. The reliability of the results obtained was verified by taking Darken's integral [12] along one of sections of the ternary system ($x_1 : x_3 = 3 : 1$).

$$\Delta G^{ex} = (1 - x_2)\left\{\int_0^{x_2} [\Delta G_2^{ex}/(1 - x_2)^2]dx_2 + \Delta G^{ex}_{x_2=0}\right\}_{x_1/x_3}. \quad (6)$$

The integrand includes the ΔG_2^{ex} function along the section considered and the integral molar excess Gibbs energy $\Delta G^{ex}_{x_2=0}$ of the system 1–3 at a given $x_1 : x_3$ ratio, which were calculated by the above-indicated method. To the left, the integral molar excess Gibbs energy of the ternary system corresponding to the values calculated by Toop's method should be obtained. The integrand vs. composition is a continuous dependence without any singularities, which ensures highly accurate graphical integration. For a number of compositions, the ΔG^{ex} values obtained by the integration are compared below with the previously calculated values (Toop's method, $x_{Ni:Co} = 3 : 1$; ΔG^{ex}, kJ mol^{-1}, 1600°C).

x_{Cu}	$\Delta G^{ex}_{(i)}$*	$\Delta G^{ex}_{(T)}$*
0.2	2.80	2.82
0.4	4.77	4.79
0.6	5.13	5.16
0.8	3.71	3.73

* $\Delta G^{ex}_{(i)}$ was obtained by integration of Eq. (5), and $\Delta G^{ex}_{(T)}$ was calculated by Toop's method.

Table 5. Partial molar excess Gibbs energies, activity coefficients, and activities of copper in liquid alloys of the system Ni–Cu–Co at 1600°C

Composition, mole fraction			ΔG_{Cu}^{ex}, kJ mol^{-1}	$\ln\gamma_{Cu}$	γ_{Cu}	a_{Cu}
x_{Cu}	x_{Ni}	x_{Co}				
0.200	0.600	0.200	13.38*/14.09	0.859/0.905	2.36/2.47	0.472/0.494
0.500	0.375	0.125	6.29/6.85	0.404/0.440	1.50/1.55	0.750/0.775
0.600	0.300	0.100	4.30/4.51	0.276/0.290	1.32/1.34	0.791/0.802
0.600	0.100	0.300	5.18/5.35	0.333/0.344	1.39/1.41	0.837/0.846
0.800	0.100	0.100	1.41/1.50	0.091/0.096	1.09/1.10	0.876/0.881

Note: Numerator and denominator correspond to calculations by Toop's and Kohler's equations, respectively.

The dependence allowing calculation of ΔG_2^{ex} from data on boundary binary systems (component numbering is the same) can also be obtained from the main equation of Kohler's method [33, 35]:

$$G_2^{ex} = [(1 - x_1)\Delta G_{2(3)}^{ex} + x_1(1 - x_1)\Delta G_{2(3)}^{ex}]_{x_2/x_3} + [(1 - x_3)\Delta G_{2(1)}^{ex} + x_3(1 - x_3)\Delta G_{1(2)}^{ex}]_{x_2/x_1} - (1 - x_2)^2[\Delta G_{13}^{ex}]_{x_1/x_3}.$$

The partial molar excess Gibbs energies of copper, obtained by the two above methods, and the corresponding copper activities and activity coefficients of copper are compared in Table 5 for a number of compositions of the ternary system. For such kind of thermodynamic estimations, the observed deviation lies within the admissible limits.

CONCLUSIONS

(1) Calculations of the integral molar excess Gibbs energy and enthalpy of mixing in liquid alloys of the system nickel–copper–cobalt at 1600°C, using a number of geometrical models and Redlich–Kister polynomials, yield the consistent results.

(2) The copper activity in liquid Ni–Cu–Co alloys at 1600°C was calculated. The positive deviations of the copper activity from Raoult's law continuously increase as nickel is replaced by cobalt at the constant content of copper.

REFERENCES

1. Morachevskii, A.G., *Zh. Fiz. Khim.*, 1968, vol. 42, no. 3, pp. 573–583.
2. Morachevskii, A.G., *Zh. Fiz. Khim.*, 1968, vol. 42, no. 1, pp. 40–45.
3. Spenser, R.G., Hayes, F.H., and Kubaschewski, O., *Rev. Chim. Miner.*, 1972, vol. 49, no. 1, pp. 13–29.
4. Pool, M.G., Arpshofen, I., Predel, B., and Schultheiß, E., *Z. Metallkunde*, 1979, vol. 70, no. 11, pp. 726–731.
5. Gregorczyk, Z., and Jurzuk, E., *J. Chem. Thermodyn.*, 1984, vol. 16, pp. 551–559.
6. Ptak, W., Mozer, Z., and Zakulski, W., *Arch. Metall.*, 1988, vol. 33, no. 3, pp. 333–354.
7. Hoch, M., and Mozer, Z., *Arch. Metall.*, 1992, vol. 37, no. 3, pp. 283–296.
8. Mekhtsiev, I.G., Thermodynamic Functions and Analysis of the Phase Diagram of the Cd–Bi–Pb–Sn System, *Cand. Sci. Dissertation*, Baku, 1992.
9. Hassam, S., Gambino, M., and Bros, J.P., *Z. Metallkunde*, 1994, vol. 85, no. 7, pp. 460–471.
10. Mamedov, A.N., Mekhtsiev, I.G., Dzhakhandrov, Sh.D., and Agaeva, S.A., *Zh. Fiz. Khim.*, 1995, vol. 69, no. 4, pp. 742–744.
11. Florani, J.M., Naguet, Ch., Hertz, J., *et al.*, *Z. Metallkunde*, 1997, vol. 88, no. 9, pp. 711–716.
12. Morachevskii, A.G., Voronin, G.F., Geiderikh, V.A., and Kutsenok, I.B., *Elektrokhimicheskie metody issledovaniya v termodinamike metallicheskikh sistem* (Electrochemical Methods in Studying the Thermodynamics of Metallic Systems), Moscow: Akademkniga, 2003.
13. Lukashenko, G.M., in *Stabil'nye i metastabil'nye fazy v materialakh* (Stable and Metastable Phases in Materials), Kiev: IPM, 1987, pp. 10–29.
14. Morachevskii, A.G., Fedorova, N.A., Tsymbulov, L.B., and Tsemekhman, L.Sh., *Zh. Prikl. Khim.*, 2002, vol. 75, no. 11, pp. 1801–1805.
15. Morachevskii, A.G., Tsymbulov, L.B., and Kolosova, E.Yu., *Zh. Prikl. Khim.*, 2004, vol. 77, no. 9, pp. 1438–1441.
16. Morachevskii, A.G., Tsemekhman, L.Sh., Tsymbulov, L.B., and Fedorova, N.A., *Zh. Prikl. Khim.*, 2003, vol. 76, no. 11, pp. 1779–1784.

17. Predel, B., and Mohs, R., *Arch. Eisenhuttenwes.*, 1971, vol. 42, no. 8, pp. 575–579.
18. Kulkarni, A.D., and Johnson, R.E., *Met. Trans.*, 1973, vol. 4, July, pp. 1723–1727.
19. Tomiska, J. and Neckel, A., *Int. J. Mass Spectrom. Ion Phys.*, 1983, vol. 47, pp. 223–226.
20. Mey, S.A., *Z. Metallkunde*, 1987, vol. 78, no. 7, pp. 502–505.
21. Berezutskii, V.V., and Lukashenko, G.M., *Ukr. Khim. Zh.*, 1987, vol. 53, no. 10, pp. 1029–1032.
22. Srikanth, S., and Jacob, K.T., *Mater. Sci. Technol.*, 1989, vol. 5, May, pp. 427–431.
23. Turchanin, M.A., Porokhnya, S.V., Belevtsov, L.V., and Kokhan, A.V., *Rasplavy*, 1994, no. 4, pp. 8–12.
24. Belousov, A.A., Bakhvalov, S.G., Aleshina, S.N., *et al*., *Fiziko-khimicheskie svoistva zhidkoi medi i ee splavov: Spravochnik* (Physicochemical Properties of Liquid Copper and Its Alloys. Reference Book), Yekaterinburg: Inst. Metallurgii, Ural'sk. Otd., Ross. Akad. Nauk, 1997.
25. Morachevskii, A.G., Ryabko, A.G., and Tsemekhman, L.Sh., *Termodinamika zhidkikh splavov sistemy nikel'–med'–zhelezo* (Thermodynamics of Liquid Alloys of the System Nickel–Copper–Iron), St. Petersburg: Sankt-Peterb. Gos. Tekh. Univ., 2002.
26. Timberg, L., Toguri, J.M., and Azakami, T., *Met. Trans. B*, 1981, vol. 12, June, pp. 275–279.
27. Taskinen, P., *Z. Metallkunde*, 1982, vol. 73, no. 7, pp. 445–450.
28. Turchanin, M.A., and Nikolaenko, I.V., *Rasplavy*, 1989, no. 5, pp. 80–82.
29. Kaufman, L., *CALPHAD*, 1978, vol. 2, no. 2, pp. 117–146.
30. Hasebe, M., and Nishizawa, T., *CALPHAD*, 1980, vol. 4, no. 2, pp. 83–89.
31. Morachevskii, A.G., and Erofeev, K.B., *Zh. Prikl. Khim.*, 2000, vol. 73, no. 6, pp. 1032–1034.
32. Olson, N.J., and Toop, G.W., *Trans. Met. Soc. AIME*, 1966, vol. 256, April, pp. 590–592.
33. Jacob, K.T., and Fitzner, K., *Thermochim. Acta*, 1977, vol. 18, pp. 197–206.
34. Jiran, E., and Jacob, K.T., *Met. Trans. A*, 1986, vol. 17, June, pp. 1102–1104.
35. Kohler, F., and Findenegg, G.H., *Monatsh. Chem.*, 1965, vol. 96, no. 4, pp. 1228–1251.

Russian Journal of Applied Chemistry, Vol. 78, No. 1, 2005, pp. 64–70. Translated from Zhurnal Prikladnoi Khimii, Vol. 78, No. 1, 2005, pp. 66–72.
Original Russian Text Copyright © 2005 by Ivanenko, Lokshin, Vladimirova, Avsaragov.

SORPTION AND ION-EXCHANGE PROCESSES

Preparation of Titanium Phosphate Sorbents from Products of Processing Sphene Concentrate and Properties of These Sorbents

V. I. Ivanenko, E. P. Lokshin, V. V. Vladimirova, and Kh. B. Avsaragov

Institute of Chemistry and Technology of Rare Elements and Mineral Raw Materials, Kola Scientific Center, Russian Academy of Sciences, Apatity, Murmansk oblast, Russia

Received March 1, 2004

Abstract—Procedures for the preparation and granulation of sorbents based on $TiO(HPO_4)\cdot nH_2O$ from the products of processing of sphene concentrate were developed. The sorption and hydrodynamic characteristics of the sorbents were determined.

Titanium(IV) phosphates are of a great interest as sorption materials. Depending on synthesis conditions they can have the composition $TiO(OH)_{2x}(HPO_4)_{1-x}\cdot nH_2O$, $TiO(HPO_4)\cdot nH_2O$, or $Ti(HPO_4)_2\cdot nH_2O$, with $TiO(HPO_4)\cdot nH_2O$ being prepared more easily. Hydrated oxotitanium hydrophosphate can be produced both as a fine amorphous powder and as a granulated product. It was shown in numerous studies that this sorbent efficiently absorbs cations of radionuclides [1–8] and also of nonferrous metals and iron [9–14] from very dilute aqueous solutions. This sorbent can be used for efficient decontamination of liquid radioactive wastes, which are aqueous solutions with a high content (the studies covered concentrations of up to 32 g l^{-1}) of salts present in seawater [15–17]. Known procedures for preparing granulated sorbents are complicated and expensive [7, 18].

The developed technology of processing sphene concentrate for the synthesis of titanium phosphate sorbent (see scheme) can use titanium sulfate process solutions containing, g l^{-1}: TiO_2 160–340, H_2SO_4 280–570, CaO 1.6–5.6, F 4.4–7.7, Fe_2O_3 1.7–7.4, SiO_2 <0.05, and TR_2O_3 <0.20 (solution after sulfatization in the scheme); titanium–silica product (TSP) containing, wt %: TiO_2 48, SiO_2 37, CaO 0.56–3.00, Ln_2O_3 <0.018, Fe_2O_3 <0.64, Al_2O_3 <0.25, F <2.2, and NO_3^- 3.60; and hydrolytic sulfuric acid containing, g l^{-1}: TiO_2 12–13.5, Fe_2O_3 up to 7.4, and F 4.4–7.7.

In this work we studied the conditions of the synthesis of powdery titanium-phosphate sorbents based on $TiO(HPO_4)\cdot nH_2O$ from titanium-containing products obtained in processing of sphene concentrate using simple granulation procedures, and also the sorption and hydrodynamic characteristics of these sorbents.

EXPERIMENTAL

Titanium(IV) was precipitated from titanium sulfate process solutions by a stoichiometric amount of orthophosphoric acid according to the reaction

$$TiOSO_4 + H_3PO_4 + nH_2O = TiO(H_2PO_4)(HSO_4)\cdot nH_2O. \quad (1)$$

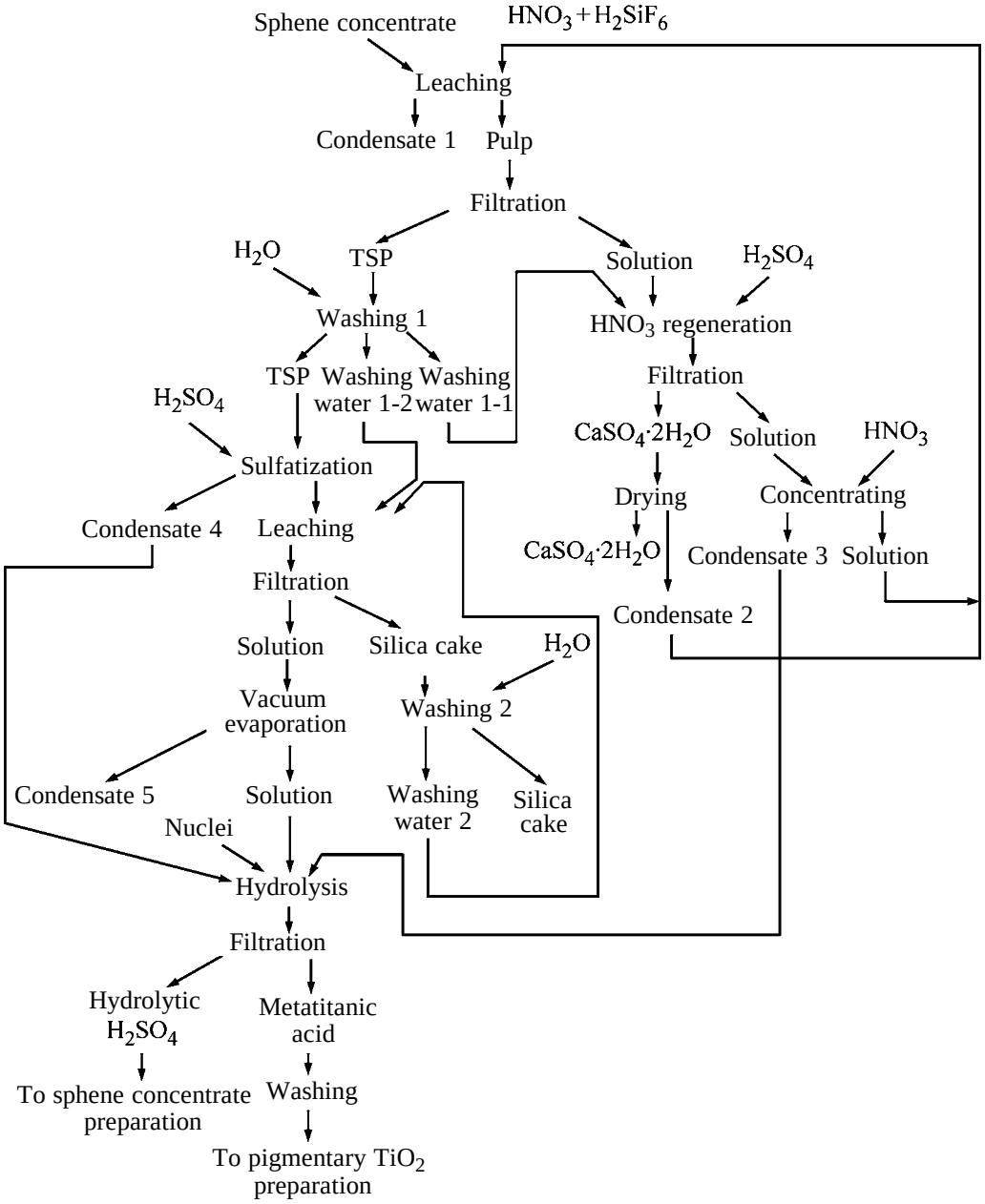
The further washing with water yields the desired product:

$$TiO(H_2PO_4)(HSO_4)\cdot nH_2O = TiO(HPO_4)\cdot nH_2O + H_2SO_4. \quad (2)$$

The product (sorbent 1) contains 45–46.7 wt % water, which corresponds to $n = 6.60 \pm 0.25$. A comparison with sorbents synthesized from Ti(IV) sulfate solutions in the absence of fluoride ions shows that their presence in the titanium sulfate solution had no effect on the composition and properties of the product, because fluoride ions remained in the highly acidic mother liquor.

A sort of such sorbent is the product obtained by the precipitation of residual Ti(IV) present in hydrolytic H_2SO_4 after thermohydrolytic isolation of hydrated Ti(IV) oxohydroxide. After adding a stoichiometric amount of H_3PO_4 with respect to Ti(IV) and heating the resulting solution to 90°C, more than 98% of Ti(IV) contained in the solution passes into

1070-4272/05/7801-0064 © 2005 Pleiades Publishing, Inc.



Flowsheet of processing sphene concentrate into titanium dioxide pigment.

this product. The resulting precipitate trapped the mother liquor (moisture content up to 84%), but after washing with water its moisture content decreased to 39% (sorbent 1-1).

To prepare titanium phosphate sorbent, we used also a titanium–silica product forming as an intermediate in processing of sphene concentrate. The titanium–silica product is synthetic leucoxene with a particle size of 0.07–0.15 mm, in which TiO_2 (about 47 wt % in the titanium–silica product) is uniformly dispersed in SiO_2 in an approximately equimolar proportion. It differs from natural leucoxene by the following features: TiO_2 is present there as anatase, whereas in natural leucoxene it is in the form of rutile; SiO_2 is hydrated (15–18 wt % of water is removed at high-temperature calcination of the product); chemically stable minerals, such as aegirines and feldspars, are present in it as impurities (5–10 wt %).

The interest in the sorbent based on a titanium–silica product is due to the fact that, in spite of the presence of "ballast" silica and sorption-inactive extrinsic minerals in it, its preparation does not

require preliminary sulfuric acid breakdown of the titanium–silica product, which can decrease the cost of the sorbent.

In this work we prepared the sorbent by the reaction of a titanium–silica product with H_3PO_4 at 140–150°C according to the reaction

$$TiO_2 + 2H_3PO_4 + (n - 2)H_2O = Ti(HPO_4)_2 \cdot nH_2O. \quad (3)$$

Then the forming titanium(IV) hydrophosphate was hydrolyzed by washing in water according to the reaction

$$Ti(HPO_4)_2 \cdot nH_2O + H_2O = TiO(HPO_4) \cdot nH_2O + H_3PO_4. \quad (4)$$

The resulting sorbent (sorbent 2) was $TiOHPO_4$ uniformly distributed in a matrix of hydrated silica. The particle size of such product substantially depended on the particle size of the sphene concentrate.

Granulated sorbents were prepared by two procedures. According to the first procedure, a titanium sulfate process solution was added dropwise to an H_3PO_4 solution, the mixture was held for 1–2 h, and the resulting granules were separated and washed with water. The product obtained consisted of hollow lenticular particles with a typical size of 3–5 mm. The granules were separated from the solution and subjected to heat treatment at various temperatures. We have found heat treatment conditions providing the preparation of granules stable in an aqueous medium (sorbent 3). According to the second procedure, the granulated sorbent was prepared from sorbent 1. Finely divided $TiO(HPO_4) \cdot nH_2O$ powder was separated from the solution by filtration and was then dried, also at various temperatures. The "monolithic" product was crushed and sieved into classes (sorbent 4). It was found that, depending on the heat treatment conditions, we can obtain both particles of the required coarseness that are stable in an aqueous medium, exhibit sufficient strength, and are not destroyed in solution, and particles that are broken down to the finest powder, which, however, preserved the sorption activity.

Finally, we made experiments aimed to obtain coarser particles of sorbent 2. When studying the possibility for coarsening of particles of phosphate-containing titanium sorbent based on silica, we also considered two approaches: preliminary coarsening of particles of titanium–silica product in both alkaline and acid media, followed by treatment of the solid phase with orthophosphoric acid; and direct treatment of the titanium–silica product with phosphoric acid followed by coarsening of particles.

An increase in particle size was observed in both cases. However, the sorbent aggregation in the acid solution was more intense than in alkaline solution.

The possibility for coarsening of product particles with the formation of granules stable in an aqueous medium can be associated with polymerization processes and can be rationalized on the following basis.

When $TiOHPO_4$ is formed, we should expect formation of oxo or phosphate bridging bonds between Ti(IV) atoms of different particles. The polymerization of Ti(IV) compounds in aqueous media with the formation of oxo-bridged compounds results from successive processes of hydroxylation, olation, and oxolation [19–21]. In the coarsening of particles based on TSP, it is not improbable that similar oxygen bridging bonds can also be formed between Si(IV) atoms. Interparticle oxotitanium or oxosilicon bonds are hardly formed through interaction between separate surface TiOH or SiOH groups of the approaching particles. Most likely, the primary stage consists in the activation of the particle surface (its hydroxylation) and in the formation of interparticle hydrogen bonds with more or less uniform distribution of Ti(IV) and Si(IV) oxohydroxides in the intermicellar liquid.

The formation of particles of Ti(IV) and Si(IV) oxohydroxides with activated surface can promote the formation of fairly large fragments of the solid phase. As Ti(IV) and Si(IV) in oxide compounds have vacant 3*d* orbitals and oxygen atoms have lone pairs of 2*p* electrons at oxygen, the dehydroxylation and polymerization process can yield oxotitanium or oxosilicon groups owing to the increased bond flexibility and the occurrence of d_π–p_π interaction [22]. Unlike p_π–p_π bonds with *p* orbitals having a rigid orientation relativen to σ bonds, d_π–p_π bonds are less sensitive to the deviations of the molecular geometry from planarity, owing to specific features of the symmetry of *d* orbitals. Therefore, even in nonplanar systems 3*d* orbitals can appreciably overlap with adjacent 2*p* orbitals. The increased flexibility of Ti–O–Ti and Si–O–Si bonds allows formation of diverse types of packing of titanium–oxygen octahedra and silicon–oxygen tetrahedra. Such d_π–p_π interaction of Ti(IV) or Si(IV) atoms with oxygen should result in increased bond multiplicity and additional strengthening of particles.

In near-neutral solutions, the mechanism of particle coarsening based on the amphoteric character of Ti(IV) oxohydroxide is the most probable. In this

case, different hydroxy groups of the same molecule or of different molecules of Ti(IV) oxohydroxide can exhibit both basic and acidic properties.

In acid solutions, a proton can add to a lone pair of oxygen electrons in OH groups of a part of Ti(IV) oxohydroxide molecules, increasing the positive charge and electrophilic power of titanium. The interaction of protonated and nonprotonated $TiO(OH)_2$ by the donor–acceptor mechanism results in particle coarsening. In the presence of electron–donor acido ligands of orthophosphoric acid in an aqueous medium, the particles should be coarsened more efficiently because of possible formation of bridging phosphate groups.

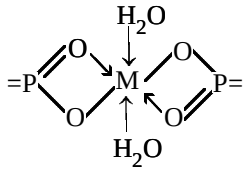
The results obtained may be due to the fact that the coarsening of sorbent particles and their mutual linking occurs through multiple repetition of the formation of oxo or phosphate bonds between Ti(IV) atoms, which requires time and can take place if the sample is dehydrated slowly. At fast drying, the amount of forming oxo-bridging bonds between various particles seems to be insufficient. It should be noted that the strength of particles increased with an increase in the acidity of the solution in which the particles were formed, which may be due to an increase in the rate of particle aggregation.

The synthesized sorbents were tested for chemical stability. All of them are stable in acid and neutral media. In the alkaline medium, partial hydrolysis of the titanium phosphate sorbent takes place to deplete it of phosphate groups and to convert a part of $TiHPO_4$ to $TiO(OH)_2$. At pH 9–10, a part of phosphate ions is "washed out" from oxotitanium hydrophosphate $TiO(HPO_4)\cdot nH_2O$ (Ti : P = 1 : 1), which is stable in acid and neutral solutions, and a solid phase with a Ti : P ratio close to 3 : 2 is formed. Such composition probably corresponds to the compound $(TiO)_3(HPO_4)_2(OH)_2\cdot nH_2O$. It is possible also that the solid phase formed by the hydrolysis is a hydroxide–phosphate matrix of variable composition. The further increase in the pH of the medium results in even greater depletion of the solid phase in phosphate groups. Apparently, the hydrolysis in alkaline solutions can be prevented or reduced by adding phosphate ions competing with hydroxide ions in heterogeneous anion exchange.

The heterogeneous sorption of alkali metal ions (M^+) in oxotitanium hydrophosphate can be presented by the reaction

$$TiOHPO_4\cdot nH_2O + M^+ \rightleftarrows TiOMPO\cdot nH_2O + H^+. \quad (5)$$

It was shown [11] that, in the course of the sorption, a double-charged metal ion combines with two hydrophosphate functional groups to form preferably chelates of the type



The sorption of double-charged metal ions (M^{2+}) is described by the reaction

$$2(TiOHPO_4\cdot nH_2O) + M^{2+} \rightleftarrows (TiOPO_4\cdot nH_2O)_2M + 2H^+. \quad (6)$$

We determined the static exchange capacity (SEC) of the samples at 20°C. A weighed portion of a sorbent was added to a 1 M solution of chloride of the corresponding metal, which was stirred to reach an equilibrium. The concentration of hydrogen ions, which were released by substitution with metal cations, was adjusted by potentiometric titration to pH 6. The pH was measured with an I-130.2M.1 ion meter with an accuracy of ± 0.02, and its values that did not change in time were considered as equilibrium values. As an indicator electrode we used a proton-selective ESL-43-07 electrode with the coordinates of the isopotential point pH_i 7 ± 0.3, and as an auxiliary electrode, an EVL-1M3 silver chloride electrode (Ag|AgCl, saturated KCl solution) with the potential of 202 ± 2 mV at 20°C relative to normal hydrogen electrode.

The experimental SEC values for various sorbents with respect to cations of some alkali and alkaline-earth metals, and also to Co^{2+} cations measured in solutions with pH 6 are given in Table 1.

The theoretically possible static exchange capacity of $TiO(HPO_4)\cdot nH_2O$ containing 45–46.7 wt % water (sorbent 1) is 3.33–3.44 mg-equiv g^{-1}. It is seen from Table 1 that SEC of sorbent 1 was no less than 85% of the theoretically possible value for cations of light (Na^+, Ca^{2+}), and 92–98%, for those of heavy (Cs^+, Sr^{2+}) alkali and alkaline-earth elements. The static exchange capacity for Co^{2+} ions appeared to be much lower. This may be due to the fact that, at pH 6, cobalt(II) salts are apparently hydrolyzed to form a poorly sorbable cobalt cation of a complicated composition [23]. In fact, when pH was reduced to 4.93, SEC of sorbent 1 with respect to Co^{2+} increased to 2.46 mg-equiv g^{-1}, though, according to reaction (6), the increase in the solution acidity should make the sorption worse.

Table 1. Static exchange capacity of sorbents at pH 6

Cation	Sorbent SEC, mg-equiv g^{-1}						Ratio of SECs of sorbents 2 and 1
	1	1-1	2	3	4		
					+0.7–2.0 mm	+0.2–0.7 mm	
Na^+	2.9	1.75	1.93	2.63	1.74	2.24	0.652
Cs^+	3.37	N/d*	2.14	3.02	2.24	N/d	0.635
Ca^{2+}	2.98	N/d	1.83	2.76	1.65	N/d	0.614
Sr^{2+}	3.17	N/d	2.08	2.93	2.11	2.36	0.656
Co^{2+}	1.89	N/d	1.52	1.67	1.26	N/d	0.804

* (N/d) Not determined.

The static exchange capacity of sorbent 1-1 with respect to Na^+ ions appeared to be much lower than the theoretical value, which may be due to capture of iron ions, which are present in hydrolytic H_2SO_4 in a concentration comparable with that of Ti(IV) and can be sorbed even at pH <1 [13]. However, the reached SEC of sorbent 1-1 is sufficient for some applications, especially if we take into account that it is obtained using Ti(IV) irrevocably lost in hydrolytic H_2SO_4.

For the majority of the cations under study, the SEC of sorbent 2 obtained on the basis of the titanium–silica product corresponded to the content of oxotitanium hydrophosphate in it, and for Co^{2+} it appeared to be even higher. Presumably, hydrated SiO_2, being a support of oxotitanium hydrophosphate, does not participate appreciably in the sorption of cations of alkali and alkaline-earth elements.

The static exchange capacity of granulated sorbent 3 is lower by only 7.6–11.6% than that of the powdery sorbent, whereas in the case of sorbent 4 it decreases to the level of sorbent 2. This is caused by diffusion limitations which inhibit penetration of sorbed cations into the depth of particles and release of protons from sorbent particles into the solution. In fact, the reduction in the sorbent particle size to 0.2–0.7 mm noticeably increased SEC with respect to Na^+ and Sr^{2+} ions.

Table 2. Distribution coefficients of radionuclides (α = 60) for sorbents 1 and 2

Radionuclide	K_d, $cm^3\ g^{-1}$, for indicated sorbent	
	1	2
^{134}Cs	1256	3080
^{90}Sr	1422	300
^{60}Co	332	128

The distribution coefficients K_d of cesium, strontium, and cobalt radionuclides in suspensions containing sorbents 1–3 are given in Tables 2 and 3. The distribution coefficients of the cations were determined by the formula

$$K_d = A_s/(A_{sol}\alpha), \quad (7)$$

where A_s is the fraction of metal ions sorbed by the solid phase; A_{sol}, fraction of metal ions remaining in the solution; and α, ratio of the sorbent weight (g) to the solution volume (cm^3).

The starting solutions contained (Bq kg^{-1}) ^{134}Cs 1×10^5, ^{90}Sr 2.2×10^4, and ^{60}Co 1×10^4. In the experiments, the ratio of the solution volume to the weight of the air-dry sorbent α was 60. The specific activity was measured in integral and differential modes on certified instrumentation: a Progress-G γ-ray spectrometer with a scintillation detecting block; PSO2-08 and DRG-01 T radiometers. The processing of spectra and the calculation of the activity and errors were carried out with a Progress software package. The exposure time was up to 1800 s depending on the activity of samples and their weight. The error of the determination of radionuclides for the confidence level of 0.95 was 11% on average. The β-radioactivity was determined on a UMF-1500D low-background installation.

Sorbent 3-1 was preliminarily heat-treated under optimal conditions; and the resulting granules, as noted above, were not destroyed in solutions, whereas sorbents 3-2 and 3-3 got dispersed on stirring in solutions.

As seen from Table 2, finely dispersed sorbents 1 and 2 were characterized by fairly high K_d values for

Table 3. Distribution coefficients and sorption percentages of radionuclides (α = 60) for sorbent 3 heat-treated at various temperatures

Radionuclide	Sorbent 3-1		Sorbent 3-2		Sorbent 3-3	
	K_d, $cm^3\ g^{-1}$	sorption, %	K_d, $cm^3\ g^{-1}$	sorption, %	K_d, $cm^3\ g^{-1}$	sorption, %
^{134}Cs	848	94.3	17026	99.7	7160	99.3
^{90}Sr	64	56	111	79	54	48
^{60}Co	9.4	15	14.9	12.4	14.4	21

Table 4. Interrelation between the filtration rate V and resistance to flow ΔP in the course of filtration. Sorbent bed height H_b = 10 cm, d_c = 1 cm

Sorbent 2		Sorbent 3		Sorbent 4 (+0.7–1.0 mm)	
ΔP, Pa	V, m h^{-1}	ΔP, Pa	V, m h^{-1}	ΔP, Pa	V, m h^{-1}
3180	0.074	562	49.0	264.1	0.255
5970	0.144	336	23.0	335.3	0.344
9060	0.234	265	12.7	406.6	0.421
190000	5.0	200*	5.0	4830**	5.0

* Obtained by interpolation of experimental data.
** Obtained by extrapolation of experimental data.

all the radionuclides under study. The distribution coefficients of ^{134}Cs and ^{90}Sr for sorbent 1 were close to each other. Higher K_d for ^{134}Cs in the case of sorbent 2 as compared to sorbent 1 cannot be satisfactorily accounted for at present, as the sorption of ^{134}Cs by hydrated silica contained in sorbent 2 is improbable [in this case the static exchange capacity of sorbent 2 with respect to ^{134}Cs should be higher (Table 2)]. Probably, this is associated with the breakdown of the sorbent particles during sorption with the formation of active centers, as it took place in the case of sorbent 3 (samples 3-2 and 3-3 showed very high K_d values for ^{134}Cs).

As the size of sorbent granules increases, K_d for all the radionuclides under study decreases, which is especially noticeable in the case of double-charged cations. This can be accounted for as follows. First, large granules of sorbents can trap acidic mother liquor, and it is practically impossible to wash it out completely. As pH of solutions was not determined and adjusted when determining K_d, the increase in the solution acidity resulted in the K_d reduction. This can be overcome by maintaining the optimal pH value [15, 16]. Second, when the size of sorbent particles increases, diffusion limitations arise.

As crystallographic radii of Cs^+, Sr^{2+}, and Co^{2+} ions are 1.69, 1.13, and 0.74 Å, respectively [24], lower K_d values for Sr^{2+} and Co^{2+} ions are attributable to a higher charge and a smaller ionic radius of these latter, which results in the appearance of a developed hydration shell. It should be expected that the activity of the sorbents under consideration toward Sr^{2+} and Co^{2+} cations will increase upon partial hydrolysis of the sorbent in alkaline solutions, resulting in an increase in the hydroxide component exhibiting the high affinity for hydrated cations [13].

To determine the hydrodynamic resistance ΔP of the sorbent, we measured the volume of water passing through the sorbent in a specified time interval at various fixed heights of the liquid column above the sorbent. The experiment has shown that the amount of the passing liquid linearly correlates with the height (pressure) of the column, which allows us to extrapolate or interpolate experimental data to determine the pressure (which is equal to the hydrodynamic resistance of the sorbent bed) ensuring a specified rate of the liquid flow through the sorbent bed. The experiments were carried out at the sorbent bed height H_b = 100 mm and the ratio of the sorbent bed height to its diameter H_b/d_c = 10.

Experimental data on the filtration rate and hydrodynamic resistance for the filtration through samples of sorbents 2–4 are given in Table 4. The bulk weight of the sorbents was 0.826, 0.484, and 0.784 g cm^{-3}, respectively.

The hydrodynamic resistance of sorbent 2, which is

the most finely dispersed among the sorbents under study, substantially increased (by a factor of 2–3) when it came in contact with water during the first 0.5 h owing to spontaneous compaction of the sorbent bed.

The particles of the sorbent based on the titanium–silica product were made coarser by pretreatment in an alkaline medium followed by interaction of the titanium silicate matrix with phosphoric acid. We have found that the sorbent resistance to filtration can be thus reduced by a factor of 1.4–1.7 as compared to sorbent 2, and pretreatment in an acid medium (HCl or H_2SO_4) ensures the 1.9–2.4-fold reduction. The filtration characteristics remain poor in spite of appreciable coarsening of particles of the titanium phosphate sorbent prepared on the basis of the titanium–silica product.

Table 4 shows that sorbents 3 and 4 have low hydrodynamic resistance and can be considered promising for the use in sorption columns. Sorbent 2 and, the more so, sorbent 1 have high hydrodynamic resistance and are promising for the use in batch processes.

CONCLUSIONS

(1) Sorbents based on $TiO(HPO_4)\cdot nH_2O$ can be obtained from products of sphene concentrate processing using simple granulation procedures.

(2) The sorbents obtained are chemically stable in acid and neutral media, but in an alkaline medium (pH ≥ 9) they gradually lose a part of phosphate groups.

(3) The static exchange capacity of powdery materials based on oxotitanium hydrophosphate obtained from sphene concentrate processing solutions is close to the theoretically possible capacity corresponding to the content of hydrophosphate groups in the sorbent.

(4) Simple granulating techniques ensure the preparation of a material with a low hydrodynamic resistance, suitable for use in columns. Powdery sorbents can be recommended for wide use in batch processes.

ACKNOWLEDGMENTS

This work was financially supported by the Leading Scientific Schools Program (project no. NSh-1616-2003.03).

REFERENCES

1. Sharygin, L.M., Muromskii, A.Yu., Moiseev, V.E., and Tsekh, A.R., *Zh. Prkl. Khim.*, 1996, vol. 69, no. 12, pp. 2009–2013.
2. US Patent 3 730 886.
3. RF Patent 2 090 944.
4. Sharygin, L.M., Moiseev, V.E., Shtin, A.P., *et al.*, *Radiokhimiya*, 1984, vol. 26, no. 2, pp. 156–161.
5. Sharygin, L.M., Gonchar, V.F., and Moiseev, V.E., in *Ionnyi obmen i ionometriya* (Ion Exchange and Ionometry), Leningrad: Leningr. Gos. Univ., 1986, issue 5, pp. 9–29.
6. Sukharev, Yu.I., *Sintez i primenenie oksigidratnykh sorbentov* (Synthesis and Application of Oxyhydrate Sorbents), Moscow: Energoatomizdat, 1987.
7. Sharygin, L.M., Moiseev, V.E., Pyshkin, V.P., *et al.*, *Izv. Akad. Nauk SSSR, Neorg. Mater.*, 1983, vol. 19, no. 11, pp. 1899–1902.
8. Komarevskii, V.M. and Kremlyakova, N.Yu., *Radiokhimiya*, 1995, vol. 37, no. 6, pp. 554–556.
9. Belyakov, V.N., Strelko, V.V., Bortun, A.I., *et al.*, *Ukr. Khim. Zh.*, 1984, vol. 50, no. 1, pp. 43–47.
10. Mitchenko, T.E. and Belyakov, V.N., *Vysokochist. Veshch.*, 1989, no. 2, pp. 110–113.
11. Bortun, A.I. and Kvashenko, A.P., *Zh. Fiz. Khim.*, 1990, vol. 64, no. 7, pp. 1963–1966.
12. Belyakov V.N., Dzyaz'ko, Yu.S., and Kazdobin, K.A., *Ukr. Khim. Zh.*, 1996, vol. 62, no. 3, pp. 18–21.
13. Laskorin, B.N., Goldobina, V.A., and Kopanev, A.M., *Tsvetn. Met.*, 1973, no. 1, pp. 22–24.
14. Laskorin, B.N., Goldobina, V.A., and Kopanev, A.M., *Tsvetn. Met.*, 1973, no. 2, pp. 21–22.
15. Lokshin, E.P., Ivanenko, V.I., Avsagarov, Kh.-M.B., *et al.*, *At. Energ.*, 2002, vol. 92, no. 2, pp. 118–123.
16. RF Patent 2 200 994.
17. Lokshin, E.P., Ivanenko, V.I., Udalova, I.A., and Kalinnikov, V.T., *Radiokhimiya*, 2003, vol. 45, no. 4, pp. 357–361.
18. Ukrainian Patent 40 389.
19. Griffith, W.P. and Wickins, T.D., *J. Chem. Soc.*, 1967, no. 4, pp. 675–679.
20. Nabivanets, B.I. and Kudritskaya, L.N., *Zh. Neorg. Khim.*, 1967, vol. 12, no. 5, pp. 1165–1170.
22. Biryuk, L.I. and Goroshchenko, Ya.G., *Zh. Neorg. Khim.*, 1977, vol. 21, no. 3, pp. 602–605.
22. Huheey, J.E., *Inorganic Chemistry. Principles of Structure and Reactivity*, New York: Harper and Row, 1983, 3rd ed.
23. Smirnov, V.I., Tseidler, A.A., Khudyakov, I.F., and Tikhonov, A.I., *Metallurgiya nikelya i kobal'ta* (Metallurgy of Nickel and Cobalt), Moscow: Metallurgiya, 1966.
24. Bragg, W.L. and Claringbool, G.F., *Crystal Structures of Minerals*, Ithaca, NY: Cornell Univ. Press, 1965.

Russian Journal of Applied Chemistry, Vol. 78, No. 1, 2005, pp. 71–76. Translated from Zhurnal Prikladnoi Khimii, Vol. 78, No. 1, 2005, pp. 73–78.
Original Russian Text Copyright © 2005 by Korneev, Kholin.

SORPTION AND ION-EXCHANGE PROCESSES

Physicochemical and Sorption Properties of Silica Gel with Immobilized Xylenol Orange Surface Groups

S. V. Korneev and Yu. V. Kholin

Karazin National University, Kharkov, Ukraine

Received October 22, 2004

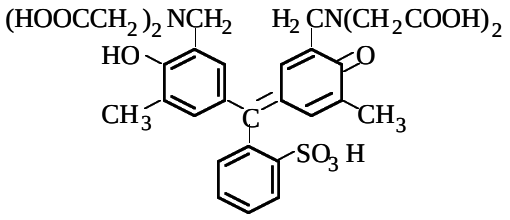
Abstract—Organomineral sorbents were prepared by sorption immobilization of Xylenol Orange on the surface of two different samples of silica gel from aqueous solutions with pH 1.68 under static conditions. The diffusion coefficients of Xylenol Organe in the near-surface layer of silica gel and the equilibrium sorption constants were determined. Wash-out of the dye from the sorbent was studied. Sorption of Cu(II), Zn(II), and Pb(II) on the sorbents from aqueous solutions with pH 5.8 was studied.

Organomineral materials combining the complexing properties of the organic ligand with the mechanical and morphological properties of the inorganic matrix are being intensively developed. These materials find expanding application in sorption, solid-phase extraction, and prompt analysis. Sorption immobilization of an organic compound on the silica surface, usually in the presence of a surfactant [1–3], is the simplest procedure for preparing organomineral materials. To determine the best conditions of synthesis and application of these materials, the sorption kinetics, sorption equilibria, and physicochemical and analytical properties of the sorbents should be studied.

In this work we studied sorption modification of silica with Xylenol Orange dye (XO) and sorption of some metal cations on the resulting materials. Since XO forms strong intensely colored complexes with metal cations, we used this compound to modify the silica surface with the aim of preparing new sorbents for solid-state spectrophotometric and prompt visual analysis of the sum of heavy metals.

EXPERIMENTAL

Xylenol Orange [3,3'-bis-*N*,*N*-di(carboxymethyl)-aminomethyl]-*o*-cresol sulfophthalein, H_6L (XO) (Table 1)



(analytically pure grade, Voikov Plant of Chemicals, Moscow) was purified by the procedure in [5]. The purity of distilled water was assessed by its electrical conductivity. The presence of impurity metals in the metal salts was checked by X-ray fluorescence spectroscopy. Acetate buffer was prepared from CH_3COONa (analytically pure grade) and CH_3COOH (chemically pure grade) [6]. The stock XO solutions were prepared by dissolving an accurately weighed portion of the dye in the buffer with pH 1.68 [GOST (State Standard) 8.135–74] and the stock solutions of $Cu(NO_3)_2$ (chemically pure grade), $Zn(NO_3)_2$ (ultrapure grade), and $Pb(NO_3)_2$ (chemically pure grade), by dissolving accurately weighed portions of these salts in an acetate buffer (pH 5.8). The metal concentrations in the initial solutions were determined by titration with EDTA [7]. A 0.01 M EDTA solution was prepared from the reference solution and standardized with metallic bismuth [7]. All working solutions were prepared by dilution of the stock solution with the same buffer.

Table 1. Logarithms of the constants of step protonation of XO [4]

Protonation step i	$\log K_{H_i}$ (I = 0.1 M)	Functional group
1	12.61	$\equiv NH^+$
2	9.68	$\equiv NH^+$
3	7.34	–OH
4	3.56	–COOH
5	2.16	–COOH
6	2.06	–COOH

1070-4272/05/7801-0071 © 2005 Pleiades Publishing, Inc.

Table 2. Morphological properties of silica gels

Sample	Specific surface area, S_{sp}, $m^2\ g^{-1}$	Pore volume, V_{pore}, $cm^3\ g^{-1}$
SG I(450)	117 ± 6*	0.87 ± 0.01
SG II(450)	510 ± 12	1.64 ± 0.05
SG II(900)	444 ± 9	1.29 ± 0.02

* Here and hereinafter, the confidence level of the measurements is 95%.

Silica gel SG I prepared from hydrogel of methyl silicate (Sorbi Research and Production Association, registry no. P.05.99/00646) was washed with 0.01 M HCl and water to the negative reaction for chloride ions and dried at 120°C. We also used commercial silica gel L 5/40 (Chemapol, Czech Republic) (SG II). To activate the silica gel surface, SG I was calcined at 450°C for 3 h [SG I(450)], and SG II was calcined at 450°C for 3 h [SG II(450)] and at 900°C for 2 h [SG II(900)]. The specific surface area of the samples was determined by thermal desorption of argon in accordance with GOST 23401–90. The specific pore volume of the sorbents was calculated from the true density which, in turn, was determined pycnometrically [8]. The morphological properties of the samples are summarized in Table 2. We recorded IR spectra of the samples pressed in conventional micropellets. The XO sorption was studied under the static conditions. Flasks containing accurately weighed portions of the sorbents (0.03–0.09 g) were filled with 25–50 ml of 4.0×10^{-5} to 2.8×10^{-4} M XO solutions. The current XO concentration was measured spectrophotometrically by the absorption at 432 nm (pH 1.68).

Modified silica gel (MSG) was separated from the solution by centrifuging, washed with water to the negative reaction for oxalate anions (pH of wash waters is 5.5–5.8), and dried at 105°C for 12 h. To determine the wash-out of XO from MSG, suspensions of accurately weighed portions of the samples (0.1–0.15 g) in 25 ml of hydrochloric acid (pH 1.0–3.0) or acetate buffer (pH 4.0–6.0) were mechanically stirred. The XO concentration in the solutions was determined at regular intervals by the absorption at 432 nm. The XO concentration became constant after stirring for 30–45-min.

Sorption of metal ions on MSGs from aqueous solutions was studied under the static conditions. Preliminary experiments on the determination of the best conditions of sorption of Cu(II), Zn(II), and Pb(II) showed that the sorption equilibrium was attained within 15 min and the optimal pH range for sorption of Cu(II) and Zn(II) and Pb(II) was 5.6–6.0 and 5.3–5.8, respectively. Therefore, the sorption experiments were performed at pH 5.8. Working solutions of the metal salts were placed in flasks containing precisely weighed portions of the samples (0.07–0.08 g). The initial metal concentration ranged from 6 to 300 μM. After the sorption completion, the sorbent was separated from the solution and dried at 105°C for 12 h. The diffuse reflectance spectra of the resulting materials were recorded. The equilibrium metal concentration in the solution was determined by the atomic absorption spectroscopy. The measurements were performed on an AAC-3 spectrophotometer (Carl Zeiss, Jena, Germany) using a conventional lamp with hollow cathode. The nonspecific absorption was compensated with a deuterium lamp. All measurements were performed with acetylene–air flame [9].

All sorption experiments were performed at 20 ± 1°C. The sorbent was separated from the solution by centrifuging at 7000 rpm for 5 min on an MLW centrifuge (Germany). The IR spectra were recorded on a Specord M-80 spectrophotometer (Carl Zeiss, Jena, Germany). The absorption spectra of XO solutions were recorded on a Specord M-40 spectrophotometer (Carl Zeiss, Jena, Germany).

The diffuse reflectance spectra were recorded on a Specord M-40 spectrophotometer with a $R\ 8°/d$ unit. The MgO reflection was used as the reference. The Kubelka–Munk function was calculated from the reflection intensities by the equation

$$F(R) = (1 - R)^2/2R.$$

The sorption kinetics was described in terms of the model of the sorption from a semi-infinite solution [10]. The initial sorption steps are described by the equation

$$c(\tau) = c(0)(1 - 2b\tau^{1/2}), \quad (1)$$

where $c(0)$ is the initial concentration of the adsorbate in the solution and $c(\tau)$ is the concentration of the adsorbate in time τ (s):

$$b = g[\rho D\pi^{-1}(1 + \beta)]^{1/2}.$$

Then

$$D = \frac{b^2\pi}{g^2\rho(1 + \beta)}, \quad (2)$$

where g is the geometrical factor [11]; ρ, porosity coefficient; β, constant of the sorption equilibrium; and

D, diffusion coefficient of the adsorbate in the near-surface layer.

The dye adsorption was determined from the difference between its initial n_a (mol) and equilibrium n_s (mol) amounts in the solution:

$$N_f = (n_a - n_s)/m,$$

where N_f is the adsorption (mol g^{-1}) and m is the sorbent weight (g).

The sorption isotherms were described by the Langmuir equation[1]

$$N_f = t\frac{\beta[X]}{1 + \beta[X]}, \quad (3)$$

where t is the concentration of the sorption sites (mol g^{-1}) and [X] is the equilibrium concentration of the adsorbate (XO or metal ion) in the solution (M).

The Langmuir isotherm can be readily transformed into the linear equation (4)

$$\frac{1}{K} = \frac{1}{N_f} = \frac{1}{\beta t} + \frac{[X]}{t}, \quad (4)$$

where K is the distribution coefficient (l g^{-1}).

Both the equilibrium constant β and the concentration of the sorption sites t can be determined by the mathematical treatment of the K^{-1} vs [X] dependence.

The estimation of these parameters by the linearized Langmuir equation (4) violates two principles of the least-squares (LS) method: (a) the lack of correlation of the independent variables and responses and (b) the absence of the random errors of the independent variables.

Estimation by the nonlinear weighted LS method is more precise. The parameters of the sorption equilibria were estimated by this method from the composition–property dependences. The criterial function

$$\chi^2_{exp} = \sum_{k=1}^{n} w_k \xi_k^2,$$

where $\xi = [X]_k^{calc} - [X]_k^{exp}$ and w_k is the statistical weight of the kth measurement, was minimized by the CLINP 2.1 program [10].

The statistical weights were set as $w_k = 1/\sigma_k^2$, where

[1] This equation is valid for ideal monolayer adsorption on the energetically uniform surface.

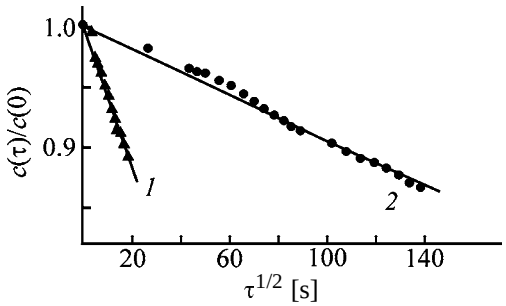


Fig. 1. Initial sections of the $c(\tau)/c(0)$ vs. $\tau^{1/2}$ dependence for adsorption of XO on (*1*) SG I(450) and (*2*) SG II(900).

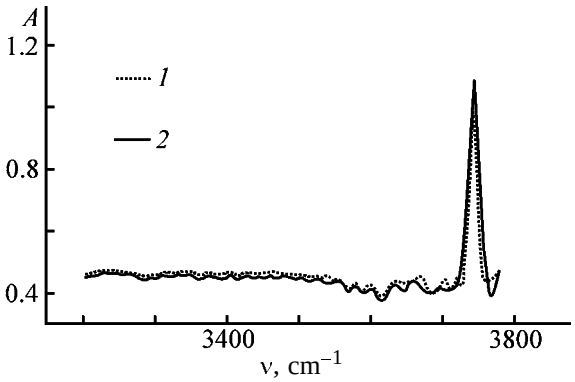


Fig. 2. IR spectra of (*1*) SG II(900) and (*2*) SG II(450). (*A*) Absorption and (ν) wave number.

$\sigma_k = [X]_k^{exp}\sigma_r$, σ_k is the random error of $[X]_k^{exp}$, σ_r is the relative error taken as 0.05.

Coefficient b was determined by linear LS treatment of the initial sections of the dependences plotted in the coordinates of Eq. (1) (Fig. 1). The diffusion coefficients of XO in the near-surface layer of SG I(450) and SG II(900), calculated by Eq. (2), were $(6 \pm 2) \times 10^{-9}$ and $(1.1 \pm 0.7) \times 10^{-9}$ $m^2\ s^{-1}$, respectively. The diffusion coefficients of XO are less by several orders of magnitude than those of H^+ and Cu^{2+} in the near-surface layer of slilicas containing amino groups [11, 12]. Clearly, the mobility of large XO molecules in both solution and sorbent pores is low. As determined by IR spectroscopy, physically sorbed water molecules are almost completely removed (the absence of broad band at 3450–3680 cm^{-1}) and the strong band of stretching vibrations of free silanol groups appears at 3742 cm^{-1} (Fig. 2) after activation of the surface of SG I and SG II at 450°C for 3 h [13]. However, the XO sorption on SG II is so low (~10^{-7} mol g^{-1}) that the sample becomes only light yellow after the sorption. Activation of SG II at 900°C increases its sorption capacity for XO to 2.8×10^{-5} mol g^{-1}. The modified samples are light orange. Activation at higher temperatures decreases the specific surface area and the pore volume. This is probably

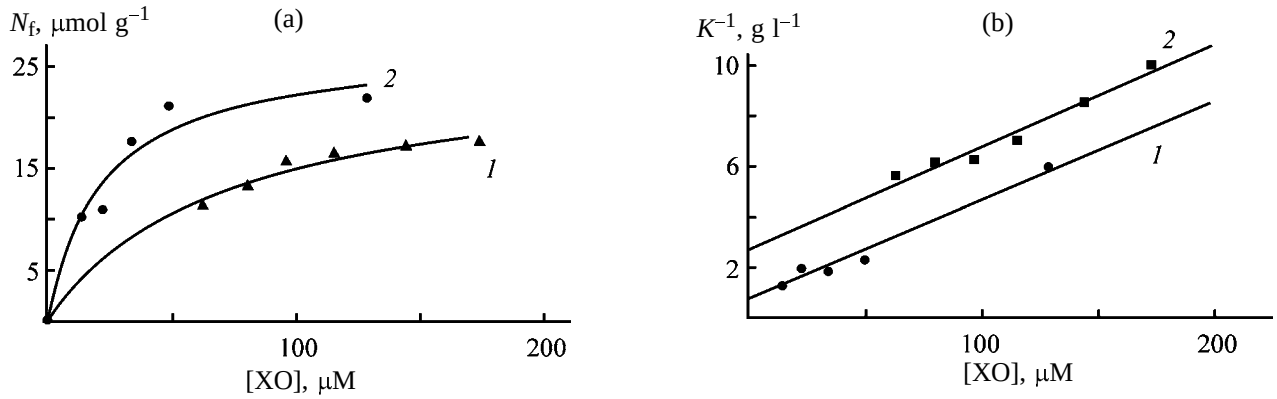


Fig. 3. (a) Sorption isotherms and (b) linearized sorption isotherms of XO on the surface of (*1*) SG II(900) and (*2*) SG I(450). (N_f) Adsorption, (K) distribution coefficient, and ([XO]) equilibrium XO concentration in the solution.

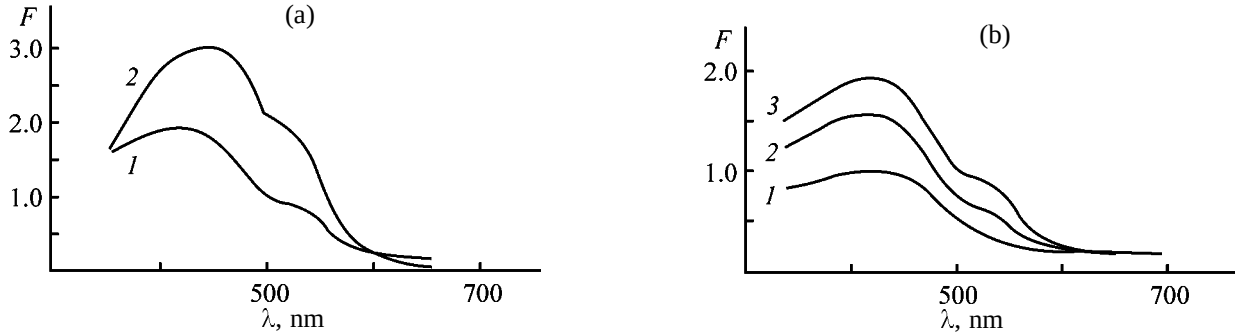


Fig. 4. Absorption spectra of (a) (*1*) MSG I(450) and (*2*) MSG II(900) and (b) MSG I(450). XO concentration (mol g^{-1}): (*1*) 1.3×10^{-5}, (*2*) 1.5×10^{-5}, and (*3*) 1.7×10^{-5}. (F) Kubelka–Munk function and (λ) wavelength; the same for Fig. 6.

due to enlargement of pores by dehydroxylation of the surface. As a result, the XO diffusion is simplified. It should be noted that the structure of silica surface subjected to high-temperature dehydroxylation and subsequent rehydroxylation differs from that of both initial and thermally dehydroxylated surface [14]. Although the intensity of the band at 3742 cm^{-1} decreases with increasing the activation temperature because of partial dehydroxylation of the surface, the concentration of the surface silanol groups remains high.

Table 3. Parameters of equilibrium sorption of XO

Sample	$t \times 10^{-5}$, mol g^{-1}	log β	r*	χ^2_{exp} ($\chi^2_{f=n-1}$)**
Eq. (4), linear LS treatment				
SG I(450)	2.5 ± 0.2	4.2 ± 0.2	0.97	–
SG II(900)	2.7 ± 0.2	4.6 ± 0.6	0.98	–
Eq. (3), weighted nonlinear LS treatment				
SG I(450)	2.5 ± 0.2	4.1 ± 0.3	–	4.6 (12.6)
SG II(900)	2.7 ± 0.2	4.65 ± 0.14	–	5.7 (11.1)

* (r) Correlation coefficient.
** 5% distribution point of χ^2 with $f = n - 1$ degrees of freedom.

The results of the linear LS treatment of the linearized sorption isotherms [Eq. (3)] and those of weighted nonlinear LS treatment of the isotherms of XO sorption on SG I(450) and SG II(900) (Fig. 3) are presented in Table 3. The fact that K^{-1} vs. [XO] dependence is almost linear and the results presented in Table 3 suggest that XO sorption on the surface of both samples is ideal, the lateral interactions are absent, and the surface sorption centers are energetically uniform.

We studied wash-out of XO from the modified SGs. In the pH range 1.0–6.0, no more than 10% of the dye is washed out depending on its concentration in the sample. Hence, unlike the previous opinion [1, 3], materials highly stable to wash-out of the organic modifier can be obtained without introduction of surfactants.

The Kubelka–Munk functions for the modified silica gels with different XO concentrations are shown in Fig. 4. The single broad absorption band at 415 nm

is observed at the XO concentration lower than 1.3×10^{-5} mol g^{-1}. Clearly, in this case the dye is sorbed in the form of H_3L^{3-} prevailing in the solution at pH 4.5–6.5. The absorption maximum of H_3L^{3-} and H_4L^{2-} species in aqueous solution is observed at 432–435 nm [5]. As the surface concentration of XO increases, a shoulder appears at 525–540 nm. Resolution of the spectra into the Gaussian components shows the presence of two bands. The first band is located at 405–415 nm in the spectrum of MSG I(450) and at 425–430 nm in the spectrum of MSG II(900). The second band in the spectra of both materials has a maximum at 520–525 nm. This band is tentatively assigned to H_4L^{2-} which absorbs in aqueous solutions at 578–580 nm [5]. The strong shift of the band to the short waves is due to formation of hydrogen bonds with surface groups of the silica gel. The appearance of the H_4L^{2-} band suggests partial neutralization of the silanol groups in the course of the dye sorption. The intensity of this band is maximal in the spectrum of SG II(900) in which the XO concentration is the highest. The fact that spectra of the sorbents prepared from silica gels with different morphological properties and activated at different temperatures are similar (Fig. 4) suggests similar mechanism of XO immobilization.

Since XO forms stable complexes with a number of transition metals, it is widely used in analytical chemistry [7]. We studied sorption of metal ions on MSG II(900). The XO concentration in this sorbent is the highest (2.8×10^{-5} mol g^{-1}). The sorption isotherms of Cu(II), Zn(II), and Pb(II) are shown in Fig. 5. The results of mathematical treatment of the sorption equilibrium are presented in Table 4. The sorption of metal ions is described well by the Langmuir equation, i.e., it is ideal as in the case of XO. The color of the sorbent brought into the contact with solutions of the metal salts changes within 3–5 min to purple-red. After the sorption, a strong band at ~600 nm appears in the spectrum (Fig. 6). The concentration of metal ions is stabilized in 10–15 min, i.e., the sorption kinetics is fast. Resolution of the absorption spectra into the Gaussian components gives two bands at 425–430 and 576–582 nm. As the metal sorption increases, the first band is weakened and the absorption at 576–582 nm increases (Fig. 6). This is probably due to a decrease in the concentration of free dye molecules and an increase in the concentration of the metal complexes on the surface. In aqueous XO solutions containing Cu(II), Zn(II), or Pb(II) cations (pH 5.0–7.0), the MH_3L^- complex prevails [15, 16]. These complexes absorb at 580, 570, and 580 nm, respectively.

Table 4. Parameters of equilibrium complexation, obtained by mathematical modeling

Metal ion	$t \times 10^{-6}$, mol g^{-1}	$\log \beta$	r	χ^2_{exp} ($\chi^2_{f=n-1}$)
Linear LS treatment, Eq. (4)				
Cu(II)	7.1 ± 0.6	4.36 ± 1.4	0.99	–
Zn(II)	3.7 ± 0.7	4.71 ± 1.4	0.99	–
Pb(II)	0.50 ± 0.03	4.7 ± 1.2	0.97	–
Weighted nonlinear LS treatment, Eq. (3)				
Cu(II)	7.1 ± 0.6	4.42 ± 0.20	–	3.8 (12.6)
Zn(II)	3.7 ± 0.7	4.65 ± 0.20	–	4.3 (12.6)
Pb(II)	0.50 ± 0.03	4.72 ± 0.18	–	4.0 (12.6)

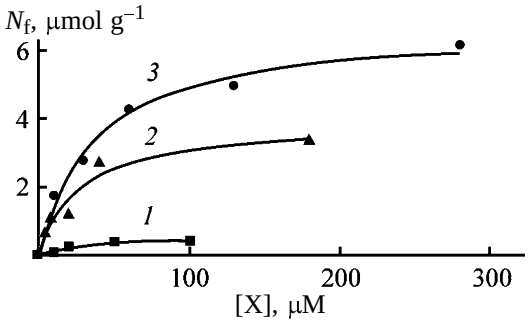


Fig. 5. Sorption isotherms of (*1*) Pb(II), (*2*) Zn(II), and (*3*) Cu(II) on SG II(900). (N_f) Metal adsorption and ([X]) equilibrium concentration of the metal ion in the solution.

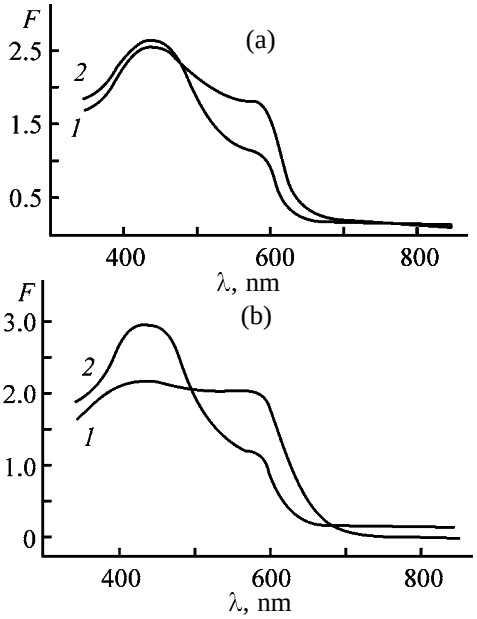


Fig. 6. Absorption spectra of MSG II(900) containing (a) Zn(II), and (b) Cu(II) and Pb(II). Metal concentration (mol g^{-1}): (a) (*1*) 3.4×10^{-6} and (*2*) 1.2×10^{-6}; (b) (*1*) 6.2×10^{-6} and (*2*) 4.2×10^{-7}.

High affinity of the sorbents for Cu(II), Zn(II), and Pb(II) ions, good sorption kinetics, and contrast color change in formation of the surface metal complexes make these sorbents promising for visual prompt analysis.

ACKNOWLEDGMENTS

The authors are grateful to N.V. Borisenko (Institute of Surface Chemistry, National Academy of Science of Ukraine) for measuring specific surface area of the silica gel.

CONCLUSIONS

(1) New organomineral materials were prepared by sorption immobilization of Xylenol Orange dye on the surface of two silica gel samples activated at different temperatures and having different morphological properties. No more than 10% of the dye is washed out from the sorbents at pH 1.0 – 6.0 under the static conditions.

(2) The initial steps of Xylenol Orange sorption on the silica gel surface can be described in terms of the sorption from a semi-infinite solution; the maximal diffusion coefficient of Xylenol Orange in the near-surface layer is $(6 \pm 2) \times 10^{-9}$ $m^2 s^{-1}$.

(3) The modified silica gel has high affinity for Cu(II), Zn(II), and Pb(II) in aqueous solutions. The complexes of these ions with immobilized dye absorb in the range 576–582 nm.

(4) The sorption equilibria of Xylenol Orange on silica gel and those of the metal cations on the modified silica gel surface are described well by the Langmuir equation, which suggests the ideal monolayer sorption on the energetically uniform surface.

REFERENCES

1. Zaporozhets, O.A. and Tsykalo, L.Ye., *Talanta*, 2002, vol. 58, pp. 861–868.
2. Zaporozhets, O.A., Petroniock, N., Bessarabova, O., and Sukhan, V., *Talanta*, 1999, vol. 49, pp. 899–906.
3. Kocjan, R. and Garbacka, M., *Talanta*, 1994, vol. 41, pp. 131–133.
4. Ghjlivand, M.B., Bamdad, F., and Chasemi, J., *Talanta*, 1998, vol. 46, pp. 875–894.
5. Murakami, M., Yoshino, T., and Harasawa, S., *Talanta*, 1967, vol. 4, pp. 1295–1303.
6. Korostylev, P.P., *Laboratornaya tekhnika khimicheskogo analiza* (Laboratory Procedure of Chemical Analysis), Moscow: Khimiya, 1981.
7. Umland, F., Janssen, A., Thierig, D., und Wünsch, G., *Theorie und praktische Anwendung von Komplexbildnern*, Frankfurt am Main: Akademische, 1971.
8. Voskresenskii, P.I., *Tekhnika laboratornykh rabot* (Laboratory Manual), Moscow: Khimiya, 1967.
9. Price, W.J., *Analytical Atomic Absorption Spectrometry*, London: Heyden, 1974.
10. Kholin, Yu.V., *Kolichestvennyi fiziko-khimicheskii analiz kompleksoobrazovaniya v rastvorakh i na poverkhnosti modifitsirovannykh kremnezemov: soderzhatel'nye modeli, matematicheskie metody i ikh prilozheniya* (Quantitative Physicochemical Analysis of Complexation in Solutions and on the Surface of Chemically Modified Silicas: Models, Mathematical Methods, and Their Application), Kharkov: Folio, 2000.
11. Zhmud, B., Pecheniy, A.B., and Golub, A.A., *Funct. Mater.*, 1995, vol. 2, no. 1, pp. 44 – 49.
12. Sevast'yanova, O.B., Zhmud', B.V., and Golub, O.A., *Visn. Kiivs'k. Univ., Khim.*, 1997, no. 34, pp. 89–95.
13. Kiselev, A.V. and Lygin, V.I., *Infrakrasnye spektry poverkhnostnykh soedinenii* (IR Spectra of Surface Compounds), Moscow: Nauka, 1972.
14. Lygin, V.I., *Ross. Khim. Zh. (Zh. Ross. Khim. O–va. im. D.I. Mendeleeva)*, 2002, vol. 46, no. 3, pp. 12–18.
15. Sato, H., Yokohama, Y., and Momoki, K., *Anal. Chim. Acta*, 1997, vol. 94, pp. 212–217.
16. Bulatov, M.I., *Zh. Neorg. Khim.*, 1968, vol. 13, pp. 3002–3005.

Russian Journal of Applied Chemistry, Vol. 78, No. 1, 2005, pp. 77–81. Translated from Zhurnal Prikladnoi Khimii, Vol. 78, No. 1, 2005, pp. 79–82.
Original Russian Text Copyright © 2005 by Korenman, Gubin, Sukhanov.

SORPTION AND ION-EXCHANGE PROCESSES

Extraction of Aromatic Sulfonic Acids in the Presence of a Surfactant

Ya. I. Korenman, A. S. Gubin, and P. T. Sukhanov

Voronezh State Technological Academy, Voronezh, Russia

Received July 19, 2004

Abstract—Extraction of phenol- and naphtholsulfonic acids from aqueous salt solutions in the presence of a surfactant, *N*-cetylpyridinium chloride, with hexane, ethylbenzene, and acetone–diacetone alcohol is studied.

Determination of carcinogenic organic substances, particularly, naphthols, phenol, and their derivatives is of a great significance in analysis of waters. Occurring in trace amounts, they cannot be detected by the existing methods. Determination of trace amounts of aromatic compounds involves preconcentration, for example, by liquid extraction.

The most efficient extractants for naphthol- and phenolsulfonic acids are hydrophilic solvents and their binary mixtures; in the presence of a salting-out agent they provide practically quantitative (95%) recovery [1, 2].

To increase the efficiency of extraction of naphthol- and phenolsulfonic acids, we suggested to use hydrophobic (hexane, ethylbenzene) and mixed hydrophilic (acetone–diacetone alcohol) solvents in the presence of a cationic surfactant, *N*-cetylpyridinium chloride, at 37°C.

In this work we studied the extraction of napthol-sulfonic [1-naphthol-4-sulfonic acid (1N4SA), 1-naphthol-5-sulfonic acid (1N5SA), 2-naphthol-6-sulfonic acid (2N6SA), 1-naphthol-3,8-disulfonic acid (1N38SA), and 2-naphthol-6,8-disulfonic acid (2N68SA)], phenolsulfonic [phenol-2-sulfonic acid (Ph2SA), phenol-4-sulfonic acid (Ph4SA), phenol-2,4-disulfonic acid (Ph24SA), phenol-2,4,6-trisulfonic acid (Ph246SA), 2-methylphenol-5-sulfonic acid (2MPh5SA), 4-methylphenol-5-sulfonic acid (4MPh5SA), and 2-ethylphenol-4-sulfonic acid (2EPh4SA)], aminophenol- and naphtholsulfonic [1-amino-2-naphthol-4-sulfonic acid (1A2N4SA), 2-aminophenol-4-sulfonic acid (2APh4SA), 2-amino-4-chlorophenol-6-sulfonic acid (2A4ClPh6SA), 1-amino-8-naphthol-2,4-disulfonic acid (1A8N24SA), 1-amino-8-naphthol-3,6-disulfonic acid (1A8N36SA), and 1-amino-8-naphthol-4,6-disulfonic acid (1A8N46SA)], and carboxy-substituted phenolsulfonic acids [sulfosalicylic acid (SSA) and 5-aminosulfosalicylic acid (5ASSA)].

EXPERIMENTAL

Naphthol- and phenolsulfonic acids in aqueous solutions were determined photometrically: naphtholsulfonic acids (except for 1N38SA and 1A2N4SA) by the reaction with diazotized sulfanilic acid; phenolsulfonic acids, with the same reagent in the presence of Na_2CO_3; 1N38SA, with 4-aminoantipyrine in the ammonia buffer solution in the presence of an oxidant, ammonium persulfate [3]; 1A2N4SA, by diazotization in the presence of Cu^{2+} [4, 5]; and SSA and 5ASSA, by the reaction with $FeCl_3$. The calibration curves were linear over the concentration ranges (M): $10^{-3.4}$–$10^{-6.7}$ for 1N38SA, $10^{-3.0}$–$10^{-5.5}$ for 1A2N4SA, and $10^{-2.8}$–$10^{-5.8}$ for other acids. The optical density was measured on a KFK-2MP photoelectric colorimeter.

To determine the distribution coefficients, to 10 ml of 10^{-4} M sulfonic acid solution we added *N*-cetylpyridinium chloride to obtain a $(1.0-4.0)\times10^{-4}$ M concentration, ammonium sulfate to obtain a saturated solution, and 1 ml of the acetone–diacetone alcohol mixture or of a hydrophobic solvent, hexane or ethylbenzene. Extraction was carried out with a mixture of the hydrophilic solvents at 20–37°C or with the hydrophobic solvents at 20°C; pH was varied from 0 to 12 by adding HCl or aqueous ammonia solutions. After extraction on a vibroshaker for 7–10 min, the extract was separated, and the optical density of the aqueous phase was measured at 400 nm (except for 1N38SA, SSA, and 5ASSA). The path length was 0.5 and 5 cm for the samples before and after extraction, respectively. In the case of 1N38SA, the measure-

1070-4272/05/7801-0077 © 2005 Pleiades Publishing, Inc.

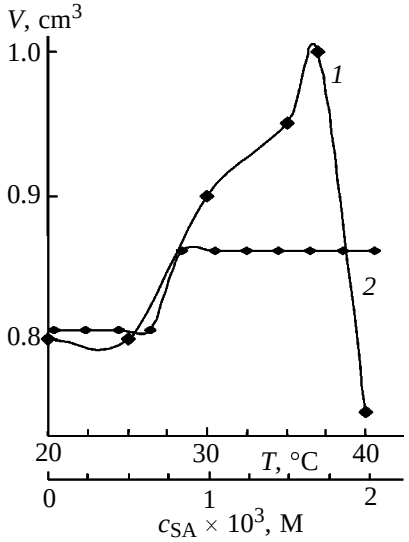


Fig. 1. Effects of (*1*) surfactant concentration c_{SA} and (*2*) temperature T on the efficiency of separation of the organic phase V in the system acetone–diacetone alcohol.

ments were performed at 540 nm, and with SSA and 5ASSA, at 490 nm.

The distribution coefficients D were estimated by Eq. (1):

$$D = [(A - A_{eq})/A_{eq}](V_w/V_o), \quad (1)$$

where A and A_{eq} are the optical densities of the solutions before and after extraction; and V_o and V_w, equilibrium volumes of the organic and aqueous phases (ml).

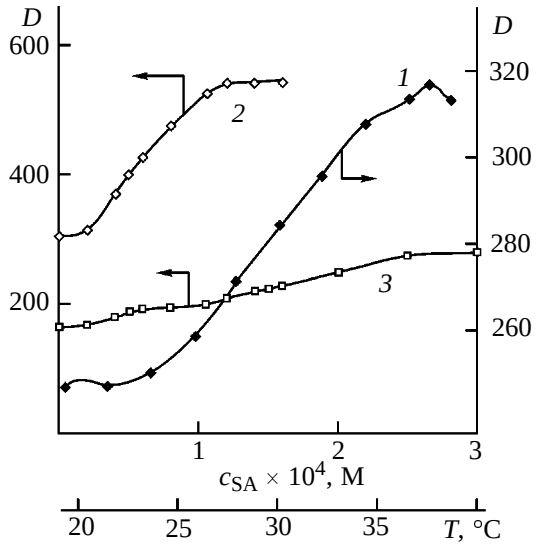


Fig. 2. Distribution coefficient D of naphtholsulfonic acids in the acetone–diacetone alcohol system as a function of the temperature T (*1*) in the absence and (*2, 3*) in the presence of the surfactant at 37°C: (*1, 2*) 1-naphthol-4-sulfonic acid and (*3*) 1-naphthol-3,8-disulfonic acid. pH: (*2*) 4 and (*3*) 7.

We studied extraction in the presence of *N*-cetylpyridinium chloride (NCPC) of twenty sulfonic acids with acetone–diacetone alcohol mixtures and of four sulfonic acids, with hexane and ethylbenzene.

In extraction with the hydrophilic extractants, the surfactant does not significantly influence the completeness of separation of the organic phase (Fig. 1). In the systems with hydrophobic solvents, at an NCPC concentration above $10^{-3.5}$ M, emulsions were formed, which could not be separated by centrifugation.

It is known that some hydrophilic solvents can form an equilibrium phase at a temperature increased to 35–40°C [3]. Acetone forms an individual phase at 37°C (Fig. 1). In extraction with acetone–diacetone alcohol mixtures, this allows an increase in the distribution coefficient of, for example, 1N4SA from 250 at 20°C to 310 at 37°C (Fig. 2).

Combination of these two factors, temperature and the presence of a surfactant in the aqueous solution, produces considerable increase in the distribution coefficient.

The effect of the number of the sulfonate group in a sulfonic acid on the distribution coefficient in the presence of NCPC suggests the formation of ion associates (Figs. 2, 3): the efficiency of extraction of monosulfonic acids is maximal at an NCPC concentration of $(1.2–1.5) \times 10^{-4}$ M; that of disulfonic acids, at 2.5×10^{-4} M; and that of trisulfonic acids and acids containing other ionic groups, at up to 4.0×10^{-4} M.

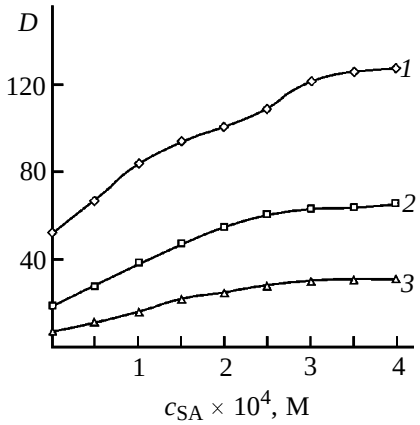


Fig. 3. Distribution coefficient D of (*1*) 5-aminosulfosalicylic, (*2*) sulfosalicylic, and (*3*) phenol-2,4,6-trisulfonic acids as a function of the surfactant concentration c_{SA} in extraction with acetone–diacetone alcohol mixtures.

In routine use, in extraction of ion associates, hydrophobic solvents (benzene, toluene, and, more rarely, hexane) are used in the presence of associate-forming agents such as positively or negatively charged dye species [6]. In this work, we used NCPC as an associate-forming agent.

In the presence of NCPC, the distribution coefficients of sulfonic acids between a hydrophobic solvent and water increased by a factor of 15 and more as compared to extraction in the absence of the surfactant (Table 1). To interpret the experimental results, we suggest the following extraction mechanism. A nonpolar hydrocarbon radical (hydrophobic fragment) of the surfactant, displaced from the polar phase (water), is oriented in the direction of the less polar phase (hexane or ethylbenzene). The extraction proceeds through absorption of ion associates on the surface of the hydrophobic solvent by van der Waals interaction.

In extraction with the hydrophilic solvents in the presence of NCPC, the organic phase is enriched with water. The extraction proceeds primarily through H bonding between the solvent and a sulfonic acid. The increased distribution coefficients are caused by higher hydrophobicity of the ion associates as compared to the sulfonic acids, which favors their transfer to the organic phase.

We studied the effect of pH on the extraction of sulfonic acids in the presence of NCPC (Figs. 4, 5). Based on the results obtained, the sulfonic acids studied can be divided in three groups as follows.

(1) Naphtholmono- and disulfonic acids; phenolmono-, di-, and trisulfonic acids; and alkylphenolsulfonic acids. The distribution coefficients of these acids remain unchanged over a wide pH range. Increasing pH from 0 to 8 has practically no effect on the degree of ionization of the hydroxy and sulfonate groups. In the pH range 8–11, the OH groups ionize, and the distribution coefficients of the sulfonic acids gradually decrease. At pH >11, D abruptly decreases, which is a resultant of two factors, practically full ionization of the OH groups and impossibility of formation of ion associates because of decreased solubility of NCPC in strongly alkaline solutions.

(2) Aminosulfonic acids. The highest distribution coefficients are obtained in neutral and weakly alkaline solutions (pH 7–8) (Figs. 4, 5). In acidic solutions, the NH_2 group of the acid is protonated and, therefore, it cannot be involved in H bonding. As pH increases from 1 to 7, the distribution coefficients strongly increase, reaching a maximum at pH 7–8,

Table 1. Extraction of sulfonic acids in the presence and absence of *N*-cetylpyridinium chloride (20°C, n = 3, P = 0.95)

Acid	Distribution coefficient	
	without NCPC	with NCPC
	Ethylbenzene	
1N5SA	0.55 ± 0.04	71.2 ± 3.4
1A2N4SA	1.35 ± 0.09	94.0 ± 55.2
1A8N36SA	0.35 ± 0.02	65.3 ± 4.0
	Hexane	
1N5SA	~0	53.0 ± 3.0
1A2N4SA	0.50 ± 0.04	68.0 ± 4.1
1A8N36SA	~0	47.2 ± 2.0

which is caused by deprotonation of the NH_2 group, making H bonding with the extractant possible.

The distribution coefficients of the aminosulfonic acids remain practically constant as pH increases to 11. In this case, the NH_2 group forms H bonds, and the ionized OH group is involved in formation of an ion associate with NCPC.

(3) Sulfosalicylic and 5-aminosulfosalicylic acids. These acids are efficiently extracted in a narrow pH range. At pH 3–4, the sulfonate groups are fully ionized, and the carboxy groups are partially ionized, so that ion associates with NCPC are formed, and the distribution coefficients increase. The maximal D values are observed at pH 7. In this case, a combined extraction mechanism is realized: the ionized

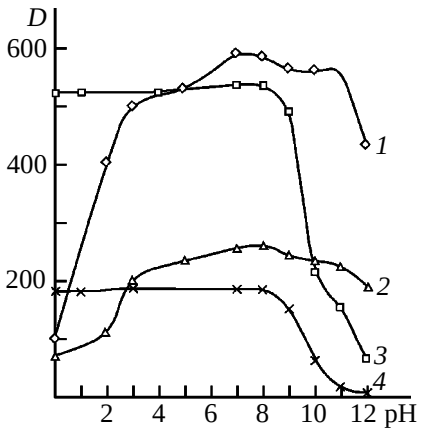


Fig. 4. Distribution coefficients of naphtholsulfonic acids as functions of pH of the aqueous phase in extraction with the acetone–diacetone alcohol mixture: (*1*) aminonaphtholmonosulfonic acid, (*2*) naphtholmonosulfonic acid, (*3*) aminonaphtholdisulfonic acid, and (*4*) naphtholdisulfonic acid. $C_{SA} \times 10^4$ (M): (*1*, *2*) 1.5 and (*3*, *4*) 2.5.

Table 2. Distribution coefficients (numerator) and their increase factors *b* (denominator) in extraction of sulfonic acids with acetone–diacetone alcohol mixture (n = 3, P = 0.95)

Acid	Distribution coefficient/*b*			
	without surfactant, 20°C	with surfactant, 20°C	without surfactant, 37°C	with surfactant, 37°C
1N4SA	250 ± 11/–	312 ± 12/1.25	310 ± 11/1.25	540 ± 21/2.16
1N38SA	120 ± 6.3/–	157 ± 8/1.30	165 ± 8.5/1.38	272 ± 11/2.27
Ph2SA	47.5 ± 4.1/–	77.2 ± 4.3/1.62	81.5 ± 4.3/1.72	125 ± 6/2.63
1A2N4SA	321 ± 12/–	382 ± 17/1.19	387 ± 18/1.21	594 ± 28/1.85
1A8N36SA	138 ± 5/–	187 ± 6/1.36	194 ± 9/1.41	270 ± 11/1.95
SSA	16.1 ± 1.8/–	22.8 ± 1.8/1.42	25.5 ± 3.1/1.58	55.1 ± 2.8/3.42
5ASSA	50.9 ± 2.1/–	77.0 ± 2.8/1.51	78.0 ± 2.5/1.53	110 ± 4/2.16

carboxy groups form ion associates with NCPC, and the nonionized OH and (or) NH_2 groups form H bonds with the extractant.

The equilibria in 5ASSA solutions can be described by the scheme shown below.

Table 2 shows the distribution coefficients of the sulfonic acids in extraction with the acetone–diacetone alcohol mixture and also the factors of their increase on passing from 20 to 37°C and in the presence of the cationic surfactant.

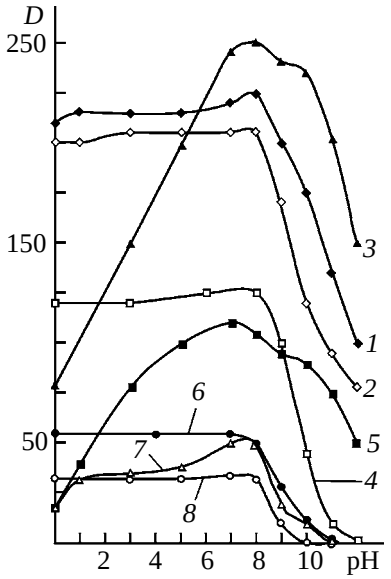
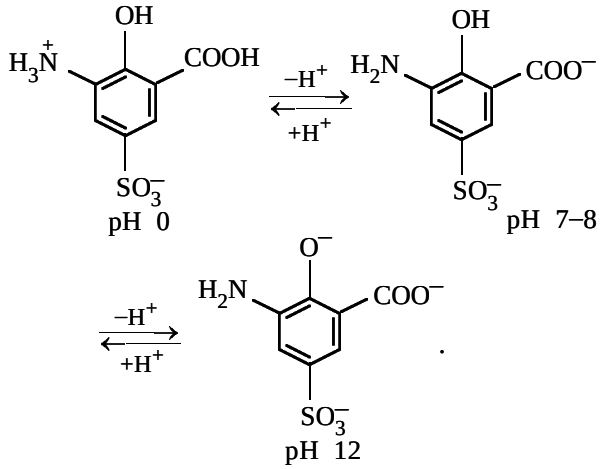


Fig. 5. Distribution coefficients *D* of phenolsulfonic acids as functions of pH of the aqueous phase in extraction with acetone–diacetone alcohol mixtures (37°C): (*1*) ethylphenolsulfonic acid, (*2*) cresolsulfonic acid, (*3*) 2-aminophenol-4-sulfonic acid, (*4*) phenolsulfonic acid, (*5*) 5-aminosulfosalicylic acid, (*6*) phenol-2,4-disulfonic acid, (*7*) sulfosalicylic acid, and (*8*) phenol-2,4,6-trisulfonic acid. $C_{SA} \times 10^4$ (M): (*1–4*) 1.5, (*5, 7, 8*) 4, and (*6*) 2.5.



Simultaneous increase in the temperature and addition of CNPC to the aqueous phase result in increasing *D* of the naphtholsulfonic acids by a factor of 2–3. The increase factor increases in the order aminonaphtholsulfonic acids < aminonaphtholdisulfonic acids < naphtholmonosulfonic acids = aminosulfosalicylic acid < naphtholdisulfonic acids < phenolsulfonic acid < sulfosalicylic acid. This order corresponds to the hydrophilicity order in the series of the sulfonic acids studied.

CONCLUSION

Extraction of 20 aromatic sulfonic acids from saturated ammonium sulfate solutions in the presence of *N*-cetylpyridinium chloride with hydrophobic solvents (hexane, ethylbenzene) and acetone–diacetone mixtures at 20–37°C is studied. Effects of the surfactant concentration, pH of the aqueous phase, and nature of the acids on the characteristics of the extraction systems are analyzed. Increasing temperature to 37°C and addition of the surfactant significantly increase

the distribution coefficients of strongly hydrated aromatic sulfonic acids.

REFERENCES

1. Zvarova, T.I., Shkinev, V.M., Spivakov, B.Ya., and Zolotov, Yu.A., *Dokl. Akad. Nauk SSSR*, 1983, vol. 273, pp. 107–110.
2. Ermolaeva, T.N., Extraction of Mono- and Polyfunctional Aromatic Compounds with Hydrophilic Solvents: General Trends and Electrochemical Analysis of Nonaqueous Concentrates, *Doctoral Dissertation*, Moscow: 1999.
3. Korenman, Ya.I., *Fotometricheskii analiz. Medody opredeleniya organicheskikh soedinenii* (Photometric Analysis. Methods for Determination of Organic Compounds), Moscow: Khimiya, 1975.
4. *Khimicheskaya entsiklopediya* (Chemical Encyclopedia), Moscow: Bol'shaya Ross. Entsiklopediya, 1998, vol. 1.
5. Dakar, G.M., *Zh. Fiz. Khim.*, 1996, vol. 70, no. 12, pp. 2177–2179.
6. Korenman, Ya.I., *Ekstraktsiya organicheskikh veshchestv* (Extraction of Organic Compounds), Gor'kii: Gor'k. Gos. Univ., 1973.

Russian Journal of Applied Chemistry, Vol. 78, No. 1, 2005, pp. 82–84. Translated from Zhurnal Prikladnoi Khimii, Vol. 78, No. 1, 2005, pp. 83–85.
Original Russian Text Copyright © 2005 by Makarov, Prusov, Lebedeva.

APPLIED ELECTROCHEMISTRY AND CORROSION PROTECTION OF METALS

Electroless Deposition of Nickel Coatings with High Phosphorus Content

V. F. Makarov, Yu. V. Prusov, and I. O. Lebedeva

Nizhni Novgorod State Technical University, Nizhni Novgorod, Russia

Received March 22, 2004

Abstract—Acid hypophosphite solution for electroless deposition of a Ni–P alloy containing up to 12 wt % phosphorus was developed and recommended for practical use. The possibility of repeated use of the solution developed was examined.

Nickel–phosphorus coatings formed by electroless deposition exhibit important functional and high protective properties. Among them, coatings deposited from acid solutions have the highest corrosion resistance [1], owing to increased phosphorus content and considerably lower porosity [2]. The melting point of the alloy containing 7.9 wt % P is 890°C and that of pure Ni, 1455°C, i.e., it decreases with increasing phosphorus content in the alloy [3]. This result is important for welding, soldering, and other operations with nickel–phosphorus coatings, which are widely used in electronic engineering [3]. The freshly deposited nickel–phosphorus alloys containing more than 8 wt % P are virtually resistant to magnetization [4]. The single use of a nickel-plating solution, with discharge of a large amount of hazardous and often rather valuable substances, is inadmissible from both the environmental and economical standpoints. Therefore, the subject of this study is rather urgent.

The coatings were deposited onto Cr18Ni10Ti steel plates in a temperature-controlled cell with a load of 1 $dm^2\ l^{-1}$ at 90°C for 1 h. Prior to coating deposition, the samples were subjected to the standard pretreatment. The deposition rate was calculated from the gain in the sample mass. The P content in the coatings was determined analytically [5]. The solutions were analyzed for the content of phosphite and hypophosphite ions and for the nickel content by the methods described in [6]. The pH value of nickel-plating solutions was measured with a pH-121 ionometer. All solutions were prepared from chemically pure and analytically pure grade chemicals. The automated correction was performed in a lab model of an AkNAR automated electroless nickel-plating installation [7].

The hypophosphite nickel-plating solutions used today contain organic ligands and buffer additives in relatively high concentrations [8], which increases the cost of these solutions and makes them more environmentally hazardous. Therefore, in development of a hypophosphite solution, attempts were made to avoid, as far as possible, the use of various organic compounds. The starting solution contained (g l^{-1}) $NiSO_4$ 20–30, $(NH_4)_2SO_4$ 20–30, NaH_2PO_2 20–30, and $NaNO_2$ (stabilizer) 0.02–0.03. The temperature was 80–85°C. The required pH of the solution was adjusted with 30% ammonia.

The P content in the coatings deposited from such solution varied from 18.4 to 14.5 wt %, depending on solution pH (Fig. 1). However, the deposition rate of the coatings was inadmissibly low (2.3–3.4 μm h^{-1} depending on solution pH). This is probably due to the fact that the buffer effect exerted by the above solution lies at pH ~ 3.4, which can be judged from the solution pH after coating deposition (Fig. 1). As known [9], at such pH values the coating deposition

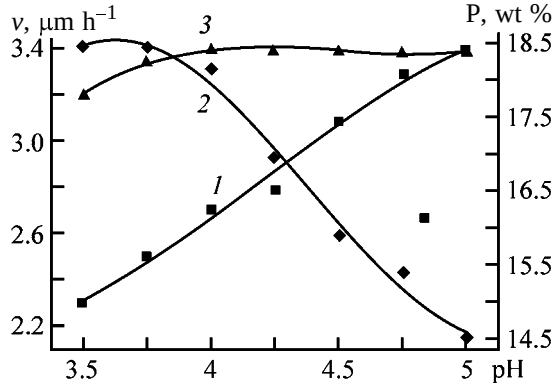


Fig. 1. Influence of pH of the initial electroless nickel-plating solution on the (*1*) coating deposition rate *v*, (*2*) P content in the coating, and (*3*) solution pH after the coating deposition.

1070-4272/05/7801-0082 © 2005 Pleiades Publishing, Inc.

virtually does not occur. Furthermore, in the course of the deposition, sparingly soluble nickel phosphite precipitated from the solution, making it turbid.

To avoid the above drawbacks, a part of the solution was modified. For example, to shift the region where the solution exerts the buffer effect toward necessary pH values and to increase the buffer capacity of the solution, the $(NH_4)_2SO_4$ concentration was increased to 50 g l^{-1} and acetic acid (20 ml l^{-1}) was added into the solution. Moreover, this prevents the nickel phosphite precipitation owing to its binding into the ammonia complex. The pH of the given solution was adjusted by varying NH_4OH concentration. In the pH range studied here (4.8–5.6), quality lustrous coatings containing 12.5–8.5 wt % P were deposited from the solution at a rate of 12–23 μm h^{-1} (Fig. 2). Both before and after the coating deposition, the solution was always stable and transparent.

Thus, the phosphorus content in the coating, and, consequently, its functional properties can be controlled using the dependences shown in Fig. 2. It was established that the pH range 5.0–5.2 (12–15 ml l^{-1} NH_4OH) is optimal. In this case, the rate of the coating deposition and the P content are fairly high, 15–18 μm h^{-1} and 12–11 wt %, respectively.

The suggested nickel-plating solution was used repeatedly under laboratory conditions. The solution was corrected nine times (ten deposition runs). The content of the main solution components (nickel salt and sodium hypophosphite) was adjusted according to the results of the analysis. The solution pH was adjusted to the initial value with 25% NH_4OH. The results are given in Table 1.

The results obtained made it possible to calculate the average consumption of the main components of a nickel-plating solution in one deposition run. In calculations, allowance was made for the consumption of components for coating deposition, their entrainment by parts, and evaporation. The component consumption in one deposition run was the following (g l^{-1}): $NiSO_4 \cdot 7H_2O$ 5.5, $(NH_4)_2SO_4$ 0.05, $NaH_2PO_2 \cdot H_2O$ 7.0, and $NaNO_2$ 0.015; CH_3COOH 1.0 and NH_4OH 4.0 ml l^{-1}. These values served as basis for the development of correcting solutions.

In an AKhNAR installation, the pH of the coating solution was adjusted automatically by adding equal portions of correcting solutions. Therefore, the ratio of the component concentrations in the correcting solutions must correspond to the given condition and their values must be reasonably large to prevent dilution of the coating solution. Moreover, the composition of the correcting solutions must ensure their prolonged stability. Taking into account these facts, we tested the correcting solutions containing $NiSO_4 \cdot 7H_2O$ 550 g l^{-1}, (solution no. 1); $NaH_2PO_2 \cdot H_2O$ 700 g l^{-1} and $NaNO_2$ 1.5 g l^{-1} (solution no. 2); $(NH_4)_2SO_4$ 5.0 g l^{-1}, NH_4OH 400 ml l^{-1}, and CH_3COOH 100.0 ml l^{-1} (solution no. 3).

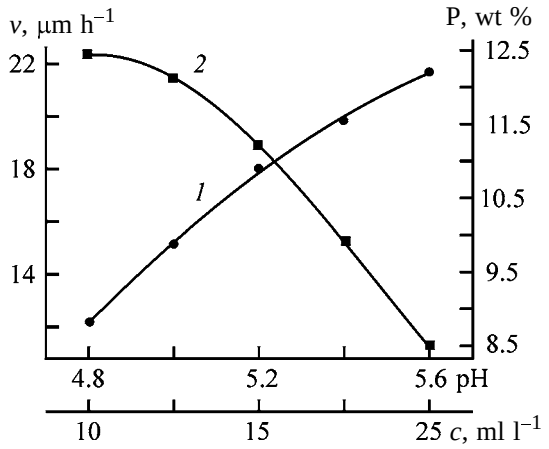


Fig. 2. Influence of pH of the modified electroless nickel-plating solution and NH_4OH concentration *c* on the (*1*) deposition rate *v* and (*2*) phosphorus content in the coating.

These solutions were tested for the correction of the developed nickel-plating solution in an automated AKhNAR installation. The results are given in Table 2.

The solution was stable and transparent over the entire working time (ten deposition runs). The deposited coatings were smooth, lustrous, and strongly adherent to the support. The deposition rate and the P content in the coatings varied within 15–18 μm h^{-1} and 12–14 wt %, respectively.

Table 1. Results of repeated use of electroless nickel-plating solution. pH of the solution before loading 5.0

Run no.	Solution pH after loading	Coating thickness, μm	P content, %
1	4.95	15.5	11.8
2	4.9	16.8	12.7
3	4.95	13.7	12.7
4	4.9	14.7	12.7
5	4.7	13.8	13.7
6	4.85	15.7	13.5
7	4.9	15.2	12.8
8	4.8	16.3	12.8
9	4.9	14.4	12.7
10	4.9	15.6	12.8

Table 2. Results of repeated use of electroless nickel-plating solution in automated mode

Run no.	Solution pH		Coating thickness, μm	P content, %
	before loading	after loading		
1	5.0	4.9	18.1	–
2	5.0	4.9	14.9	11.9
3	4.95	4.85	14.6	–
4	5.0	4.9	17.1	–
5	5.05	4.95	16.1	–
6	5.05	4.9	14.7	12.7
7	5.1	4.95	14.9	–
8	5.15	5.05	15.3	–
9	5.1	5.05	14.9	12.3
10	5.15	5	15	–

Manual correction of the suggested solutions is also possible. This involves addition of solution no. 3 after each deposition run to adjust pH of the coating solution, followed by addition of the same volumes of solution nos. 1 and 2 into the coating solution.

CONCLUSION

A process for electroless deposition of nickel–phosphorus coatings with a high phopshorus content was developed. The nickel-plating solution containis (g l^{-1}) $NiSO_4 \cdot 7H_2O$ 20, $NaH_2PO_2 \cdot H_2O$ 25, $(NH_4)_2SO_4$ 50, $NaNO_2$ 0.03; CH_3COOH 20 ml l^{-1}; NH_4OH 12–15 ml l^{-1}; pH 5.0–5.2. It withstands at least ten deposition runs with intermediate corrections in automated or manual mode.

REFERENCES

1. De Minjer, C.H. and Brenner, A., *Plating*, 1957, vol. 44, no. 12, pp. 1297–1305.
2. Jhuzlow, K.P., in *Conf. on Recent Developments and Use of Electrodeposition Technology and Coatings*, London, September 1983, pp. 1–6.
3. Colin, R., *Galvanotechnik*, 1966, vol. 57, no. 3, pp. 158–167.
4. Saubestre, E., *Met. Finish.*, 1962, vol. 60, no. 9, pp. 59–64.
5. Bogenschütz, A.F., and George, U., *Legierungsüberzuge und Legierungsbäder*, Sauglau/Würtemberg: Leuze, 1975.
6. Nikandrova, L.I., *Khimicheskie sposoby osazhdeniya metallicheskikh pokrytii* (Electroless Deposition of Metal Coatings), Leningrad: Mashinostroenie, 1971.
7. Makarov, V.F., Prusov, Yu.V., and Flerov, V.N., *Zashch. Met.*, 1980, vol. 16, no. 3, pp. 360–362.
8. Prusov, Yu.V., Makarov, V.F., and Flerov, V.N., *Izv. Vyssh. Uchebn. Zaved., Khim. Khim. Tekhnol.*, 1992, vol. 35, no. 2, pp. 3–19.
9. Gorbunova, K.M., and Ivanov, M.V., *Zh. Vses. Khim. O–va. im. D.I. Mendeleeva*, 1988, vol. 33, no. 2, pp. 157–164.

Russian Journal of Applied Chemistry, Vol. 78, No. 1, 2005, pp. 85–88. Translated from Zhurnal Prikladnoi Khimii, Vol. 78, No. 1, 2005, pp. 86–89.
Original Russian Text Copyright © 2005 by Shvab, Gur'yanova, Omel'chuk.

APPLIED ELECTROCHEMISTRY AND CORROSION PROTECTION OF METALS

Kinetics and Mechanism of Reactions Occurring in Electrodeposition of Silver from Thiosulfate Solutions

N. A. Shvab, I. A. Gur'yanova, and A. A. Omel'chuk

Vernadsky Institute of General and Inorganic Chemistry, Ukrainian National Academy of Sciences, Kiev, Ukraine

Received June 23, 2004

Abstract—The kinetics and mechanism of processes occurring in reduction of silver thiosulfate complexes on stationary and rotating disc electrodes and on fluidized glass-bead electrode were studied voltammetrically.

Owing to depletion of natural resources of nonferrous and noble metals, their recovery from various wastes acquires growing importance. Utilization of production waste is necessary not only from the standpoint of saving raw materials but also from the environmental standpoint. Among wastes contaminating the environment are spent thiosulfate fixing solutions from treatment of X-ray films and photographic materials used in printing industry. These solutions contain a considerable amount of silver (to 9–10 g l^{-1}) and sulfur compounds (up to 250 g l^{-1}). Only in the United States, up to 1/3 of the total industrial consumption of silver is spent for preparation of photographic materials [1], with approximately 1000 t of silver passing annually to fixing solutions. The spent fixing solutions, even those free of silver, are environmentally hazardous, since in water reservoirs they decompose with the release of toxic sulfur compounds.

Silver is present in spent fixing solutions mainly in the form of a complex compound $Na_3Ag(S_2O_3)_2$, whose instability constant is $K = 3.5 \times 10^{-14}$ [2]. The standard potential of the silver electroreduction from this complex is 0.017 V [3].

Various chemical and electrochemical methods of silver recovery from spent fixing solutions are known [1, 4–8]. Nevertheless, silver recovery from fixing solution has not received wide acceptance. The traditional electrolysis methods are suitable for recovery of pure silver only at very low current densities, hardly acceptable for commercial processes. Silver sulfide, which is reduced to silver with high specific consumption of chemicals and electric power, is deposited on the cathode at higher current densities. In this case, the electrochemical processing of silver-containing thiosulfate solutions is, in essence, a combination of the electrochemical and electroless methods. Also, the electroless methods do not allow recovery of pure silver in one stage and are labor-consuming.

The lack of data on the features of the cathodic reduction of silver thiosulfate complexes does not allow purposeful control of this process, optimization of the electrolysis conditions, and development of the corresponding processes. Therefore, study of the reactions proceeding on the cathode during electrolysis of silver-containing thiosulfate solutions is an urgent scientific and practical problem.

In this work we studied the reduction of a silver thiosulfate complex on stationary and rotating disc electrodes and in a fluidized bed of glass beads.

EXPERIMENTAL

The processes occurring on the cathode in reduction of silver thiosulfate complexes under the static conditions without stirring the electrolyte and with active transfer of electroactive species toward the cathode and removal of intermediate reduction products from the cathode surface were studied in a universal cell with a fluidized bed of glass beads [9]. The cathode and anode compartments of a poly(methyl methacrylate) cell had rectangular shape and were separated with a semitransparent diaphragm made of thermally densified Khlorin fabric. A 4 cm^2 platinum plate coated with silver and pressed into a flat poly(methyl methacrylate) holder, which was arranged normally in the cathode space using guiding slots, was the working electrode. Silver chloride reference electrode was fed closely to the surface of the working electrode using a Haber capillary. An electrolyte-flow distributor made of stacked polyethylene grids with

1070-4272/05/7801-0085 © 2005 Pleiades Publishing, Inc.

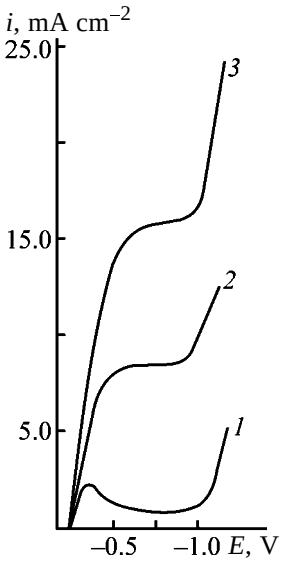


Fig. 1. Volt-ampere curves of reduction of the silver thiosulfate complex on silver electrode under different conditions. Silver concentration in solution 5.0 g l^{-1}. (*i*) Current density and (*E*) potential. Electrode: (*1*) Stationary without stirring electrolyte, (*2*) fluidized bed of glass beads, and (*3*) rotating (1000 rpm) disc electrode; the same for Fig. 2.

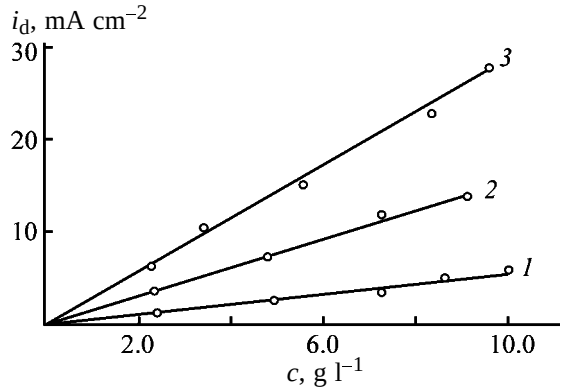


Fig. 2. Limiting current density i_d in reduction of the silver thiosulfate complex as a function of its concentration *c* under different conditions.

small windows was located on the bottom of the cathode space. The platinum anode was mounted in the anode space in the vertical direction after the semitransparent diaphragm. The cell contained an additional reservoir with the solution and was equipped with a centrifugal pump, which ensured fluidization of spherical glass beads 0.08–0.1 cm in diameter by electrolyte circulation through the electrode spaces [10]. The cathodic processes under the steady-state conditions were studied in this cell without electrolyte circulation and without addition of glass beads.

The additional information on the cathodic processes was obtained on an installation equipped with a rotating silver disc electrode of 1.9 cm^2 area. The rate of the electrode rotation was controlled with an ATT-6001 digital tachometer. The volt–ampere curves were taken with a PI-50-1 potentiostat and a two-coordinate self-recorder. The potential scan rate was 10 mV s^{-1}. The study was performed at 20–23°C. As test object was chosen a 1 M sodium thiosulfate solution containing varied amounts of silver in the form of the thiosulfate complex, which was obtained by addition of freshly prepared silver chloride to this solution. All the chemicals used were of chemically pure grade.

The study showed that only one wave is always recorded in the voltammograms of reduction of the silver thiosulfate complex (Fig. 1), with the characteristic current peak revealed on the stationary electrode without stirring the electrolyte. The current densities at a potential of –0.33 V are maximal and linearly increase with increasing silver concentration in the solution (Fig. 2, line *1*). The voltammograms show that the current sharply increases again at potentials more negative than –1.0 V.

The analysis of the cathodic deposits showed that the light gray silver deposit is formed with a 100% current efficiency at current densities not exceeding the maximum value. Further cathodic shift of the potential results in darkening of the silver deposit, which turns black at potentials from –0.8 to –0.9 V. At potentials more negative than –1 V, the deposition is accompanied by hydrogen evolution. Figure 3 shows how the composition of the electrolysis products on the cathode varies with the current density. The results obtained show that, at current densities corresponding to the maximum values, the silver thiosulfate complex and thiosulfate ions start to discharge jointly, since the difference of the standard potentials of these redox systems is as small as ~23 mV [3].

The rate of electroreduction of the anions is controlled by the slow discharge stage; it depends on the zero-charge potential of the electrode and is not controlled by transport limitations [11]. Data on the reduction of thiosulfate ions are lacking; it may be suggested that the rate of their electroreduction is also controlled by the slow discharge stage and is potential-dependent. Owing to the fact that the discharge of the silver thiosulfate complex occurs at the limiting diffusion current, the concentration of the silver ions on the electrode surface is equal to zero. The sulfide ions formed upon reduction of thiosulfate ions are accumulated in the near-electrode space and interact with the silver ions to form sparingly soluble silver sulfide. As a result, the concentration of the silver

ions in the near-electrode space decreases. The low electrical conductivity of silver sulfide (owing to blocking of a part of the cathode surface) and a decrease in the silver concentration in the near-electrode space are responsible for the appearance of a maximum in the discharge wave of $[Ag(S_2O_3)_2]^{3-}$ ions on the stationary electrode.

Taking into account the fact that the silver thiosulfate complex is moderately stable (instability constant is $K = 3.5 \times 10^{-14}$ [2]), the shape of the voltammograms, and the fact that the maximum current density is a linear function of the concentration of the complex in the solution, we may state that the discharge of the complex is accompanied by the concentration polarization and that the maximum current densities correspond to the limiting diffusion currents.

The above suggestion on the limiting diffusion currents of reduction of the silver thiosulfate complex is confirmed by the results of studying the cathodic process in a fluidized bed of glass beads and on a rotating disc electrode.

In this case, there is no current peak on the wave of reduction of the complex silver anions (Fig. 1, curves *2*, *3*). Low-conducting silver sulfide is not deposited on the cathode under the given hydrodynamic conditions. This ensures more intense delivery of the silver-containing ions toward the cathode. The limiting current densities are directly proportional to the concentration of the complex silver ions in the solution (Fig. 2) and to the square root of the electrode rotation rate (Fig. 4). These results show that the currents are limited by diffusion.

Thus, the mechanism of the reduction of silver thiosulfate complexes can be presented as follows. Depending on the current density, different processes occur at the cathode. At low current densities, not exceeding the limiting values, the silver thiosulfate complex is reduced at the cathode with the deposition of pure silver.

$$[Ag(S_2O_3)_2]^{3-} + e = Ag + 2(S_2O_3)^{2-}. \quad (1)$$

After the limiting current is attained, the simultaneous discharge of thiosulfate ions starts:

$$S_2O_3^{2-} + 2e = S^{2-} + SO_3^{2-}, \quad (2)$$

which is followed by the chemical deposition of silver sulfide:

$$2[Ag(S_2O_3)_2]^{3-} + S^{2-} \rightarrow Ag_2S + 4S_2O_3^{2-}. \quad (3)$$

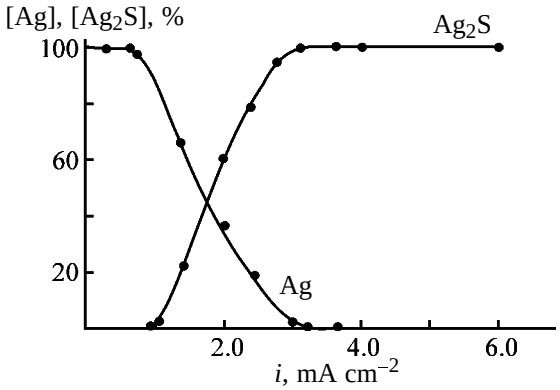


Fig. 3. Influence of the cathodic current density i on the composition of the deposit formed on stationary electrode without stirring the electrolyte. ([Ag], [AgS]) Contents of the components in the deposit.

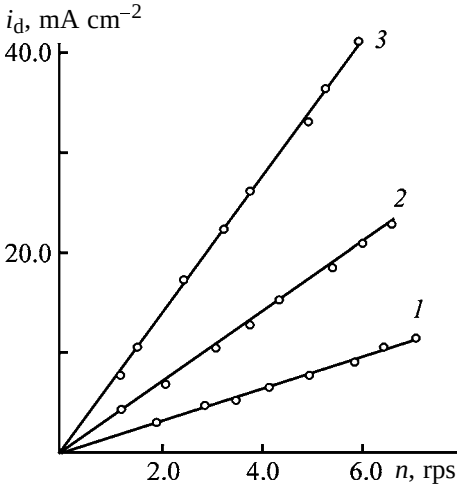


Fig. 4. Limiting current density i_d in reduction of the silver thiosulfate complex on a disc electrode vs. rotation rate n at various concentrations of the complex in the solution. Concentration of the silver complex (g l^{-1}): (*1*) 2.3, (*2*) 5.4, and (*3*) 9.6.

Thus, the reduction of the silver thiosulfate complex is a diffusion-controlled process. Pure silver can be obtained solely at the current densities not exceeding the limiting values. To increase the electrolysis intensity, it is necessary to make the diffusion limitations weaker. The electrolysis in a fluidized bed of glass beads is the best suited for this purpose [10]. A fluidized bed of glass beads not only increases the electrolysis rate, but also improves the quality of the cathodic deposit, even when the electrolysis current is close to the limiting diffusion currents. The latter is very important in selective recovery of silver. This electrolysis method is the best suited for recovery of metals from the solutions of arbitrary concentration and, from the economic standpoint, is more efficient than other electrolysis methods [12]. To use the elec-

trolysis in a fluidized bed of glass beads in selective recovery of silver from thiosulfate solutions, it is necessary to know the limiting diffusion currents, which would allow development of a program for controlling the current with time. From the data obtained, the necessary calculations can be done.

Study of the silver electrodeposition from thiosulfate solutions during electrolysis in a fluidized bed of glass beadse showed [13] that light gray finely crystalline silver deposits can be obtained at current densities exceeding by an order of magnitude those used in traditional electrolysis.

CONCLUSIONS

(1) A study of processes occurring in electrolysis of silver-containing thiosulfate solutions showed that the rate of the electroreduction of the silver thiosulfate complex is described by the laws of diffusion kinetics. At the current densities not exceeding the limiting values, pure silver is deposited on the cathode at a current efficiency close to the theoretically predicted value. At higher current densities, the joint discharge of $[Ag(S_2O_3)_2]^{3-}$ and $(S_2O_3)^{2-}$ ions, followed by the chemical reaction to yield silver sulfide, takes place.

(2) The composition of the reduction products as a function of the current density was determined. When the transport limitations for the delivery of discharging particles to the cathode and removal of intermediate reduction products (sulfite ions) are eliminated, the current density range ensuring deposition of pure silver can be extended. These conditions can be realized either in an electrolyzer with a fluidized bed of glass beads or on a rotating disc electrode.

REFERENCES

1. Sittig, M., *Metal and Inorganic Waste Reclaiming Encyclopedia*, New Jersey: Noyes Data, 1980.
2. Yatsimirskii, K.B. and Vasil'ev, V.P., *Konstanty nestoikosti kompleksnykh soedinenii* (Instability Constants of Complex Compounds), Moscow: Akad. Nauk SSSR, 1959.
3. *Spravochnik po elektrokhimii* (Handbook on Electrochemistry), Sukhotin, A.M., Ed., Leningrad: Khimiya, 1981.
4. US Patent 497433.
5. US Patent 506466.
6. JPN Patent Appl. 327493.
7. Australian Patent 623621.
8. Cuiling, Zh. and Shixiang, Yu., *Zhongnan Kuangye Zubao* (J. Cent. S. Inst. Min. Met.), 1992, vol. 23, no. 4, pp. 482–486.
9. Shvab, N.A., and Litovchenko, V.D., *Ukr. Khim. Zh.*, 2000, vol. 66, no. 7, pp. 37–39.
10. Shvab, N.A., *Ukr. Khim. Zh.*, 1999, vol. 65, no. 8, pp. 117–122.
11. Frumkin, A.N., Fedorovich, N.V., and Kulakovskaya, S.I., *Elektrokhimiya*, 1974, vol. 10, no. 2, pp. 330–334.
12. Stankovic, V.D., and Janes, D., *Inst. Chem. Eng. Symp. Ser.*, 1986, no. 51, pp. 269–279.
13. Gur'yanova, I.A., Litovchenko, V.D., Omel'chuk, A.A., and Kozin, V.F., *Ukr. Khim. Zh.*, 2003, vol. 69, no. 3, pp. 59–62.

Russian Journal of Applied Chemistry, Vol. 78, No. 1, 2005, pp. 89–95. Translated from Zhurnal Prikladnoi Khimii, Vol. 78, No. 1, 2005, pp. 90–96.
Original Russian Text Copyright © 2005 by A. Legin, Rudnitskaya, K. Legin, Ipatov, Vlasov.

APPLIED ELECTROCHEMISTRY AND CORROSION PROTECTION OF METALS

Methods for Multivariate Calibrations for Processing of the Dynamic Response of a Flow-Injection Multiple-Sensor System

A. V. Legin, A. M. Rudnitskaya, K. A. Legin, A. V. Ipatov, and Yu. G. Vlasov

St. Petersburg State University, St. Petersburg, Russia

Received November 15, 2004

Abstract—Application of chemometric methods to processing of the dynamic response of a flow-injection multiple-sensor system of the "electronic tongue" type is described. A through flow-injection multiple-sensor system of a new type is developed. The data processing is carried out using the method of projection to latent structures and the *n*-variate method of projection to latent structures (in processing of three-dimensional data). The results obtained in determining ions of lead and zinc in the case of their simultaneous presence in solution and comparative characteristics of various calibration models are presented.

Chemometrics is widely used at present in processing of experimental data obtained with various analytical instruments [1, 2]. In particular, chemometric methods are used to process signals produced by multiple-sensor systems in analyzers of the "electronic nose" and "electronic tongue" types [3, 4]. Multiple-sensor systems of this kind have been developed using organization principles of sensor systems, and primarily the sense of smell in mammals. By analogy with their biological prototypes, electronic tongues and noses include a large number of weakly selective or cross-selective sensors that can respond to several components of a multicomponent medium simultaneously, with the sensor signals processed by means of chemometric methods. Because the response of cross-sensitive sensors contains information about several components of a solution, use of chemometric methods to obtain analytical information from results of measurements with multiple-sensor systems is necessary and highly important.

Various chemometric methods have been suggested for processing of results of measurements with multiple-sensor systems, including the electronic tongue [4–6]. The choice of a particular method is primarily determined by an analytical task, as well as by the structure of the data obtained. In particular, principal component analysis (PCA) has been used for study of the structure of data and for recognition, and the self-consistent projection method of classification (SIMCA), as follows from its name, for classification. The multiple linear regression analysis (MLRA) and principal component regression analysis (PCRA), as well as the method of projection to latent structures (PLS) (other names can also be found in the literature: fractional or partial least squares), can be used both in multivariate regression analysis and in classification, and various types of artificial neural networks (ANN), for all of the above-mentioned purposes.

Previously, multiple-sensor systems of two types: static and flow-injection, have been developed and used to solve various analytical problems [4, 7]. In static systems, measurements are carried out similarly to those with separate sensors: sensors are submerged in a liquid being analyzed and the equilibrium potential of each sensor relative to a reference electrode is recorded. In flow-injection systems, sensors are brought in contact with a liquid being analyzed when flowing through a measurement cell, and the difference between the sensor signals in a background solution and the solution being analyzed serves as an analytical signal. Data obtained using both methods have been processed using the same techniques, despite the difference in how the analytical signal was obtained. It may be assumed that, in the flow-injection system, useful information can be contained not only in the difference between responses in a background solution and that being analyzed, but also in the temporal, or dynamic response of sensors.

In this study, an attempt was made to apply various chemometric methods to processing of the dynamic response of a flow-injection multiple-sensor system of the type of electronic tongue for the example of

1070-4272/05/7801-0089© 2005 Pleiades Publishing, Inc.

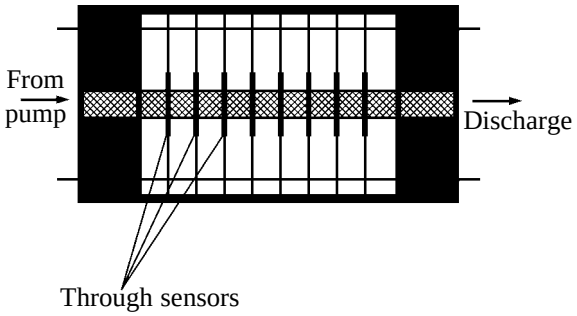


Fig. 1. Schematic of a flow-through cell.

determining the content of zinc and lead in mixed solutions.

EXPERIMENTAL

Measurements were performed using a flow-injection multiple-sensor system with a through cell. The flow-through cell is constituted by a set of poly(methyl methacrylate) discs, between which polymeric membranes are squeezed in the course of assembly. Each membrane has an aperture 3 mm in diameter at its center. These apertures form a channel along which a solution flows. All the membranes were fabricated with a solid inner contact. A silver chloride reference electrode was placed directly downstream of the cell. The flow-through cell is shown schematically in Fig. 1.

The array comprised seven sensors with plasticized polyvinyl chloride membranes of three different types. Sensors sensitive to both lead and zinc ions and having a low sensitivity were chosen for measurements. This choice was based on experimental data previously obtained in laboratory. The compositions of membranes in the sensors used, as well as data on their sensitivity and selectivity toward cations of transition metals were published in [8, 9].

Table 1. Compositions of mixed solutions containing simultaneously lead and zinc nitrates

Solution no.	*c*, M	
	Zn(II)	Pb(II)
1	10^{-5}	5×10^{-6}
2	10^{-4}	10^{-4}
3	10^{-5}	10^{-5}
4	10^{-4}	5×10^{-6}
5	5×10^{-6}	5×10^{-6}
6	10^{-5}	10^{-4}
7	5×10^{-6}	10^{-5}
8	10^{-4}	10^{-5}
9	5×10^{-6}	10^{-4}

Potentiometric measurements with the array of sensors were carried out using a multichannel voltmeter with a high input resistance. The process of measurements was controlled and data files were recorded with a personal computer. The sensor responses were measured at 4-s intervals during 2 min after injection of a sample into the system. Thus, 30 potentials were obtained for each sensor in each solution being analyzed. The sample volume was 500 μl, and the flow rate, 1.44 ml min^{-1}.

Preliminarily, calibration measurements were performed with an array of sensors in individual solutions of lead and zinc nitrates in the concentration range 10^{-7}–10^{-3} M. Then, measurements were carried out is solutions simultaneously containing cations of lead and zinc in the concentration range 5×10^{-6}–10^{-4} M. Nine mixed solutions with compositions listed in Table 1 were prepared. A 0.1 M solution of potassium nitrate served as a background. The calibration solutions of lead and zinc nitrates, both individual and mixed, were also prepared with 0.1 M potassium nitrate as background. All the solutions were prepared with double-distilled water.

The data processing consisted in a multivariate calibration and prognostication of lead and zinc concentrations. The PLS method was used for multidimensional calibration, and *n*-variate PLS, for modeling of 3D data. The calibration models were verified using test data, i.e., data not used for calculating the calibration model. The Unscrambler v.7.8 software was used for calculations by the PLS method, and Multiway matlab toolbox, for calculations by the *n*-vector PLS method [10].

The analytical signal in static measurements with potentiometric chemical sensors (ion-selective electrodes) is the equilibrium potential of a sensor, measured relative to a reference electrode in a solution being analyzed. Apparently, the result of measurements with an array of potentiometric sensors for a set of samples is a 2D matrix of data of dimension equal to the number of samples multiplied by the number of sensors. In this matrix, each row is formed by responses of each of the sensors of the array for a sample. The flow-injection system assumes that the dynamic response of a sensor is measured continuously: in the background solution, when passing a sample through the cell, and in washing of sensors and returning of the sensor potentials to the base line. A typical

form and basic parameters of the response of a sensor in the flow-injection system are shown in Fig. 2.

Traditionally, only a single parameter, the peak height H or the maximum difference between the sensor potentials in the background solutions before injecting a sample and in the sample, is used as an analytical signal (Fig. 2). However, the shape of the response of a sensor in the flow-through system may bear additional information. It is known from experiments that the time in which the potential of the sensor returns to the base line and the peak shape depend both on the concentration and on the nature of a component in a sample. This is due to differences in the interaction of the sensitive membrane of the sensor with ions of varied nature. It may also be assumed that the additional information contained in the dynamic response of the sensor will be of particular interest in measurements with an array of cross-sensitive sensors in multicomponent solutions.

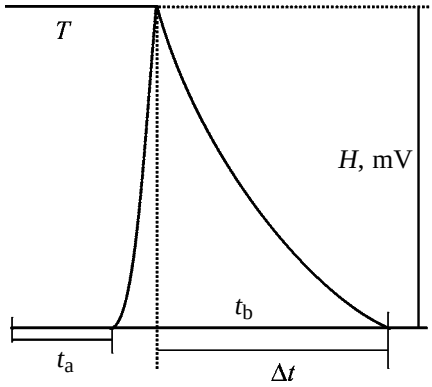


Fig. 2. Typical shape and parameters of the response of a sensor in a flow-injection system. (t_a) Time elapsed from the instant of injection of a sample into the system till its entry into the measuring cell, (T) time of residence of a sample in the flow-through cell, (t_b) width of the peak base, (Δt) time in which the sensor response returns to the base line, and (H) peak height.

The result of measurements with a flow-injection multiple-sensor systems is a 3D data array of dimension equal to the number of samples multiplied by the number of sensors and by the measurement time ($T + \Delta t$). Various methods for analyzing data arrays of dimension exceeding two have been described in the literature. One approach consists in the reduction of a multidimensional data array into a 2D array. In particular, the reduction of data obtained with a multiple-sensor flow-injection system yields a matrix of dimension equal to the number of samples multiplied by the number of sensors and measurement time. After that, any multivariate regression method, e.g., multiple linear regression analysis, PCRA, PLS [1, 2], neural networks [11], etc., can be used in data processing and analysis.

An alternative approach consists in that the initial dimension of the data array is preserved and the so-called multilinear statistical methods are used for their processing. By now, quite a number of methods of this kind have been suggested, including PARAFAC, Tucker model, trilinear PLS, etc. [12–14]. Although some of these methods started to be developed as far back as the 1960s [15], their application to mathematical processing of the results of chemical analysis was commenced only in recent years [16–18]. An advantage of application of multilinear methods to processing of high-dimension data consists in that the thus obtained calibration models are simpler, including the simplicity of interpretation, and more stable to presence of noise and, consequently, to overtraining. This is accounted for by the smaller number of parameters to be evaluated in the calibration model when using undeveloped data and multilinear processing methods, which can be illustrated by the following example.

Let us assume that experimental data form an array of dimension $2 \times 10 \times 100$. The reduction of such a data array yields a matrix of dimension 2×1000. In this case, the load vector of dimension 1000 is to be calculated for two samples. Apparently, such a solution cannot be stable; moreover, the increase in the number of variables makes rather complicated assessment of their contribution to the model. Two hundred samples are accessible if data undeveloped in the second dimension are used for calculating a load vector of dimension 10, and 20 samples in the case of data undeveloped in the third dimension and a load vector of dimension 100.

In this study, the multilinear PLS was used for mathematical processing of a 3D data array obtained in measurements with a flow-injection multiple-sensor system. This method was chosen among other multilinear methods because it takes into account (as also does the ordinary PLS), in data modeling, the covariance between the independent and dependent variables. As the aim of data processing in this study was to obtain a multivariate calibration model, this property of PLS may be of value. In addition, algorithms of other multilinear methods are rather slow and calculations take a long time even when carried out on modern computers.

Let us consider the basic principles of the trilinear PLS-1 algorithm used for data processing in this study. Here, the notion "trilinear" means that the method is used to process 3D data, and the index 1

refers to the number of dependent variables (component concentrations). As the algorithm of the multilinear PLS, suggested in [12], is an extension of the ordinary PLS algorithm to a larger number of dimensions, we first consider a bilinear PLS. In what follows, we use the following designations: X, matrix of independent variables (instrumental responses) of dimension $I \times J$ or $I \times J \times K$ for the 2D and 3D cases, respectively; y, vector of dependent variables (concentrations) of dimension $I \times 1$; T and W, matrices of markers and weights X, respectively; and A, number of components. The bilinear PLS consists in decomposition of the input data into a "model" and an "error," with the modeling performed with two matrices of markers and weights, which are also named bilinear factors. The model X has the following form for each of the components:

$$\hat{x}_{ij} = t_i w_j. \quad (1)$$

The algorithm of the bilinear PLS consists of two main parts. First, a new component (new variable) is calculated for X and y, and then the resulting model is subtracted from the input data and the remainder is used to calculate the next component, etc. If the weight vector w is known and has a unity length, markers t_i are calculated by the least-squares method, i.e., by projection of X to w:

$$t = Xw \text{ or } t_i = \sum_{j=1}^{J} x_{ij} w_j, \quad (2)$$

The problem consists in that it is necessary to find a vector w that would maximize the covariance between the markers t and the dependent variable y:

$$\max_w \left[\operatorname{cov}(t, y) = \sum_{j=1}^{J} x_{ij} w_j \Lambda \, |w|_A^2 = 1 \right]. \quad (3)$$

For centered data, the covariance between t and y can be expressed as a sum:

$$\max_w \left[\sum_{i=1}^{I} t_i y_i = \sum_{j=1}^{J} x_{ij} w_j \Lambda \, |w|_A^2 = 1 \right]. \quad (4)$$

In Eq. (4), the number of degrees of freedom is dropped, but it is constant and thus does not affect maximization. Combining the expressions for calculation of the covariance (4) and for least-squares calculation of loads (2), we obtain

$$\max_w \left[\sum_{i=1}^{I} \sum_{j=1}^{J} y_i x_{ij} w_j \Lambda \, |w|_A^2 = 1 \right]. \quad (5)$$

As X and y are known beforehand, a preliminary summation over i can be performed. This summation yields a vector z of dimension $J \times 1$:

$$\max_w \left[\sum_{j=1}^{y} z_j w_j \Lambda \, |w|_A^2 = 1 \right]. \quad (6)$$

As the weight vector w is normalized to unit length, expression (6) is maximized if w is a unit vector with the same direction as z. Thus, the weight vector can be calculated using the following equation:

$$w = \frac{z}{\|z\|} = \frac{X'y}{\|X'y\|}. \quad (7)$$

As in the case of the bilinear PLS, the aim of the algorithm of the trilinear PLS is to decompose the initial 3D data matrix X into "triads," which are analogs of bilinear factors in the ordinary PLS. A triad is constituted by a marker vector t and two weight or load vectors w^J and w^K for the second and third dimensions, respectively. Thus, the model X has, for each component, the form:

$$x_{ijk} = t_i w_j^J w_k^K. \quad (8)$$

Using (8), we can calculate markers t:

$$t_i = \sum_{j=1}^{J} \sum_{k=1}^{K} x_{ijk} w_j^J w_k^K. \quad (9)$$

As also in the case of the bilinear PLS, the problem consists in finding a set of unit weight vectors w^J and w^K that would maximize the covariance between the markers t and the dependent variable y. The expression for optimization has the following form

$$\max_{w^J w^K} \left[\sum_{i=1}^{I} t_i y_i = \sum_{j=1}^{J} \sum_{k=1}^{K} x_{ijk} w_j^J w_k^K \right]$$

$$= \max_{w^J w^K} \left[\sum_{i=1}^{I} \sum_{j=1}^{J} \sum_{k=1}^{K} y_i x_{ijk} w_j^J w_k^K \right] = \max_{w^J w^K} \left[\sum_{j=1}^{J} \sum_{k=1}^{K} z_{jk} w_j^J w_k^K \right]. \quad (10)$$

In the given case, Z is a matrix of dimension $J \times K$, rather than a vector. The weight vectors can be found by means of a singular decomposition:

$$\max_{w^J, w^K} [(w^J) Z w^K] \longrightarrow (w^J, s, w^K) = SVD(Z, 1). \quad (11)$$

A more detailed description of the algorithm of multilinear PLS was given in [12].

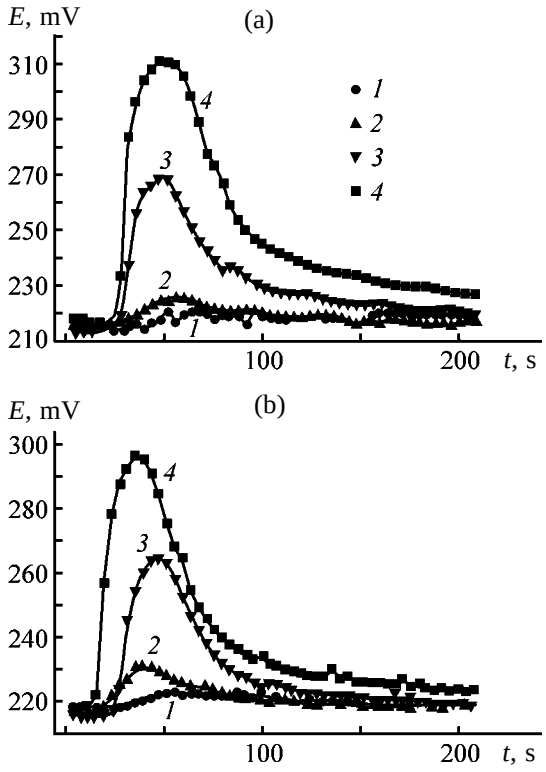


Fig. 3. Response of a sensor of the flow-injection system in individual solutions of ions of (a) lead and (b) zinc. (*E*) Potential and (*t*) time; the same for Fig. 4. pM: (*1*) 6, (*2*) 5, (*3*) 4, and (*4*) 3.

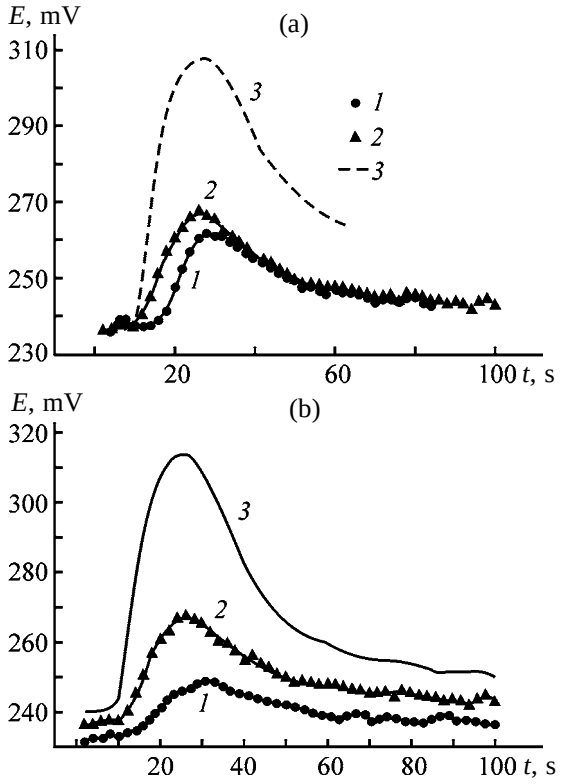


Fig. 4. Response of a sensor in the flow-injection multiple-sensor systems in mixed solutions. Response: (a) to zinc ions in the presence of a constant concentration of lead (pZn = 5) and (b) to lead ions in the presence of a constant concentration of zinc (pPb = 5). pM: (*1*) 5.3, (*2*) 5, and (*3*) 4.

Prior to measurements in mixed solutions, the sensitivity of sensors of the flow-injection multiple-sensor system to lead and zinc ions was studied in their individual solutions. The response of a sensor of the array to lead and zinc ions is shown in Fig. 3. It was established that the sensors of the array are sensitive to lead and zinc in the concentration range 10^{-6}–10^{-3} M, with the slope of the electrode function equal to 42 ± 1 and 33 ± 2 mV/pM, respectively. These results are in agreement with the data previously obtained in static measurements with sensors for these compositions. Interestingly, not only the magnitude, but also the shape of response of the sensor depends on concentration in the flow-injection system (Fig. 3).

Measurements with a flow-injection multiple-sensor system were carried out in mixed solutions containing simultaneously lead and zinc ions. The compositions of the solutions are listed in Table 1. A typical response of a sensor of the array in mixed solutions is shown in Fig. 4. The response of the sensor contains information about both cations. As also in the case of measurements in individual solutions, not only the magnitude, but also the shape of

Table 2. Determinations of lead and zinc concentrations in mixed solutions using three types of data*

Measurement	Slope	Offset	Correlation	rms error	Type of data
		Zinc			
Calibration	0.81	0.87	0.90	0.27	I
Test	0.65	1.75	0.92	0.23	
Calibration	0.88	0.58	0.94	0.19	II
Test	0.78	0.97	0.99	0.12	
Calibration	0.87	0.60	0.93	0.20	III
Test	0.78	1.03	0.99	0.13	
		Lead			
Calibration	0.91	0.43	0.95	0.19	I
Test	0.77	1.11	0.95	0.17	
Calibration	0.99	0.06	0.99	0.06	II
Test	1.03	–0.17	0.97	0.14	
Calibration	0.94	0.30	0.97	0.14	III
Test	0.94	0.32	0.97	0.13	

* (I) Only peak height, (II) developed dynamic data, (III) 3D dynamic data: parameters of the introduced/found curve (slope, offset, and correlation) for the calibration and test data arrays.

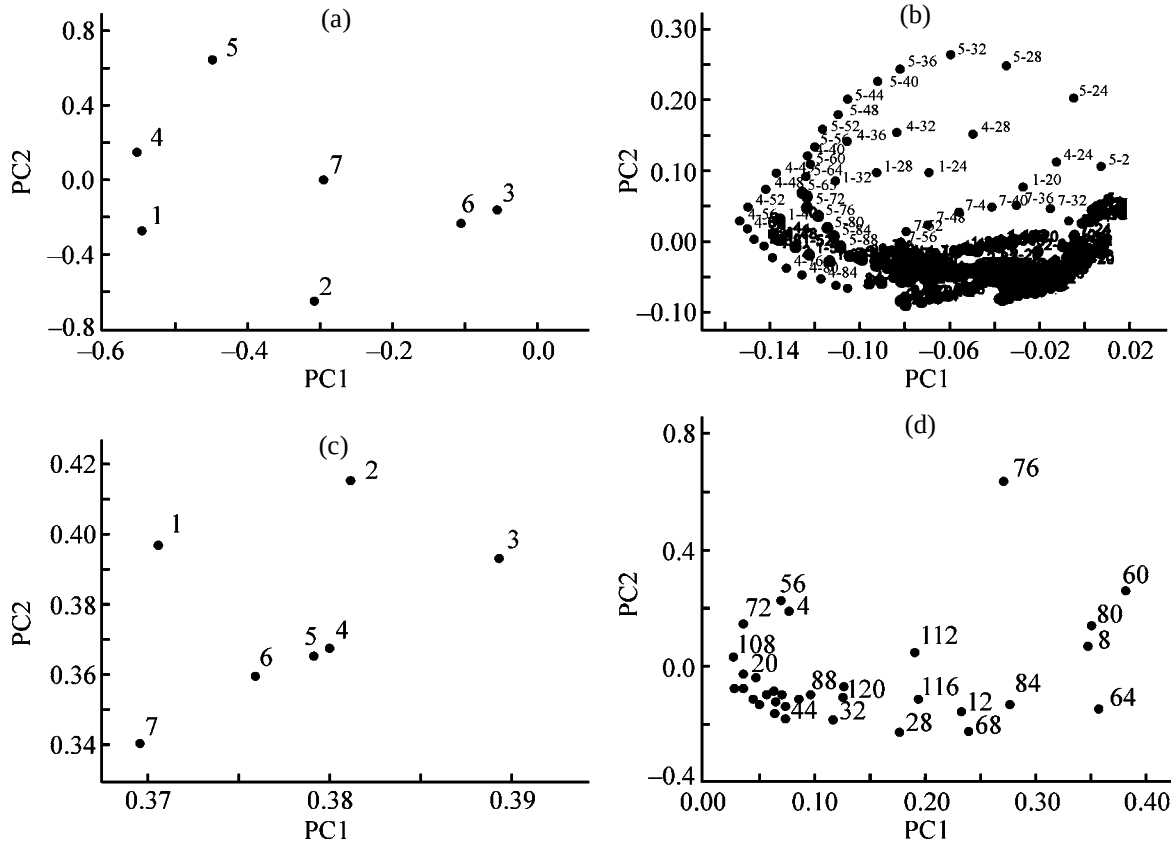


Fig. 5. Load plots for different types of data files. (a) Only peak height, (b) developed dynamic data, (c) 3D dynamic data in the direction of sensors, and (d) 3D dynamic data in the direction of time. Result of analysis for principal components in the form of load plots: PC1 and PC2 are the first and second principal components, respectively [principal components are new variables obtained in data processing in the form of a linear combination of the input variables, i.e., sensor potentials; the first two of these new variables, principal components, contain a major part of information about the system (account for the most part of variance in the data)]. Digits at points: (a, c) sensor number and (b) sensor number–time (s), and (d) time (s).

the dynamic response of the sensors varies with concentration. In particular, Fig. 4a can be regarded as an illustration of the fact that the dynamic response of sensors in the flow-injection system contains additional information about the solution components. Three types of data were used in calculations, and, accordingly, three multivariate calibrations were obtained for determining the concentrations of lead and zinc. The data array constituted by values of the maximum response H (I) and a "dimension-reduced" array of dynamic responses of the sensors (II) were processed using the ordinary PLS regression analysis. The 3D array of dynamic responses of the sensors (III) was processed using a trilinear PLS regression analysis. The parameters of the introduced/found curve for all the types of data for the calibration and test array are listed in Table 2. Apparently, in the ideal case, the slope and the correlation factor must be unity, and the offset, zero.

It follows from the results presented that using the dynamic response makes it possible to improve the accuracy of determination of transition metal cations in their simultaneous presence in solution, compared to the case when only the peak height serves as analytical signal. At the same time, no significant difference was observed between the calibration models obtained for 2D developed and 3D data, which is, on the whole, in agreement with published data [12, 16–18].

As already noted, use of multilinear methods for data processing makes it possible to obtain simpler and more noise- and overtraining-resistant calibration models. Also, the smaller number of parameters is to be evaluated, the smaller number of samples is necessary for obtaining a stable calibration model. The simplicity of a calibration model is determined by the number of parameters evaluated in calibration, i.e., by the number of variables. Let us consider as an example the load plots obtained for different types of data (Figs. 5a–5d). The load plots describe the con-

tributions of the input variables to the calibration model and are, as a rule, used to choose the most informative variables and to optimize the calibration model. When only the peak height is used as analytical signal, seven parameters are evaluated for the sensors used (as there are seven sensors). The resulting model is sufficiently simple, and the load plot is easy to interpret (Fig. 5a). However, as shown above, the prognosticating capacity of such a calibration model is poor. When a 2D reduced array of dynamic responses of an array of sensors is used, the number of variables is 210. The resulting load plot has the form of a cloud of points (Fig. 5b), which is rather difficult to analyze. When 3D dynamic data are used in calculations, two sets of loads are evaluated: those in the directions of sensors and time, a total of 37 parameters. The load plots in the direction of sensors (Fig. 5c) and in that of time (Fig. 5d) are sufficiently simple for interpretation.

CONCLUSIONS

(1) Using the calibration dependence of the dynamic response of a flow-injection multiple-sensor system makes it possible to improve the accuracy of determination of lead and zinc cations simultaneously present in solution, compared with the case when only the maximum response (peak height) is employed.

(2) Using a 3D data array and the trilinear method of projection to latent structures for the processing of this array yields a simpler calibration model, compared to the case of reduced 2D data.

REFERENCES

1. Sharaf, M.A., Illman, D.L., and Kowalski, B.R., *Chemometrics*, New York: Wiley–Interscience, 1986.
2. Esbensen, K., *Multivariate Analysis in Practice*, Norway, Oslo: Camo ASA/CAMO Process AS, 2001, 5th ed.
3. Gardner, J.W. and Bartlett, P.N., *Sensors Actuators B*, 1994, vols. 18–19, pp. 211–220.
4. Legin, A., Rudnitskaya, A., and Vlasov, Yu., *Integrated Analytical Systems, Comprehensive Analytical Chemistry*, Alegret, S., Ed., Amsterdam: Elsevier, 2003, vol. 39, pp. 437–486.
5. Toko, K., *Integrated Analytical Systems, Comprehensive Analytical Chemistry*, Alegret, S., Ed., Amsterdam: Elsevier, 2003, vol. 39, p. 487.
6. Krantz-Rülcker, C., Stenberg, M., Winquist, F., and Lundström, I., *Anal. Chim. Acta*, 2001, vol. 426, pp. 217–226.
7. Mortensen, J., Legin, A.V., Ipatov, A.V., *et al*., *Zh. Prikl. Khim*., 1999, vol. 72, no. 4, pp. 633–636.
8. Vlasov, Yu.G., Legin, A.V., and Rudnitskaya, A.M., *Zh. Anal. Khim*., 1997, vol. 52, no. 8, pp. 837–843.
9. Vlasov, Yu.G., Legin, A.V., Rudnitskaya, A.M., *et al*., *Zh. Anal. Khim*., 1997, vol. 52, no. 11, pp. 1214–1220.
10. Andersson, C.A. and Bro, R., *Chemom. Intell. Lab. Syst*., 2000, vol. 52, no. 1, pp. 1–4.
11. Despagne, F. and Massart, D.L., *Analyst*, 1998, vol. 123, p. 157.
12. Bro, R., *J. Chemom*., 1996, vol. 10, pp. 47–61.
13. Kroonenberg, P.M., *Stat. Appl*., 1992, vol. 4, pp. 619–633.
14. Bro, R., *Chemom. Intell. Lab. Syst*., 1997, vol. 38, pp. 149–171.
15. Tucker, L., *Psychometrica*, 1966, vol. 31, pp. 279–311.
16. Espinosa-Mansilla, A., Pena, A.M. de la, Goicoechea, T.C., and Olivieri, A.C., *Appl. Spectrosc*., 2004, vol. 58, no. 1, pp. 83–90.
17. Garcia, I., Sarabia, L.A., and Ortiz, M.C., *Anal. Chim. Acta*, 2004, vol. 501, no. 2, pp. 193–203.
18. Kourti, T., *J. Chemom*., 2003, vol. 17, no. 1, pp. 93–109.

Russian Journal of Applied Chemistry, Vol. 78, No. 1, 2005, pp. 96–100. Translated from Zhurnal Prikladnoi Khimii, Vol. 78, No. 1, 2005, pp. 97–101.
Original Russian Text Copyright © 2005 by Kuz'mina, Liventsev, Sevost'yanov, Dogadina.

CATALYSIS

Modification of the Alumina-Supported Platinum Catalyst of Reforming

R. I. Kuz'mina, V. T. Liventsev, V. P. Sevost'yanov, and N. V. Dogadina

Chernyshevsky Saratov State University, Saratov, Russia
Saratov Oil Refinery, Open Joint-Stock Company, Saratov, Russia

Received June 1, 2004

Abstract—The catalytic activity of alumina-supported platinum catalysts modified with rare earth metal (samarium, europium, gadolinium, ytterbium, yttrium) complexes in C_6 hydrocarbon reforming was studied.

Production of aromatic hydrocarbons, in particular, benzene, which is a raw material for chemical industry, is an important direction of the catalytic reforming, since the production of polyamide, polyester, and other fibers and, in addition, some types of plastics and specialty rubbers is based on conversion of benzene and its nearest homologs.

Alumina-supported platinum catalysts, which were for many years the main catalysts of hydrocarbon aromatization, now give place to the catalytic systems with a low platinum content, containing other metals (iridium, rhenium, germanium, tin) as modifiers [1].

Modifying additives introduced into the platinum catalyst can affect the properties of both active metal itself and a support. With regard to bifunctionality of the alumina-supported platinum catalyst, whose platinum catalyzes hydrogenation and dehydrogenation, while alumina catalyzes paraffin isomerization and hydrocracking, we took rare-earth metals (REMs) differing in the dehydrogenation and dehydrocyclization power as modifying additives [2]. It was interesting to find how the initial REM compound affects the catalyst activity.

EXPERIMENTAL

The catalyst properties were studied with a flow-type laboratory device within 440–540°C in a hydrogen atmosphere. *n*-Hexane was used as a feed in reforming.

To study the influence of REMs on the alumina-supported platinum catalyst and to develop a high-performance catalyst with a low platinum content, a series of catalysts containing 0.25 wt % platinum and 0.1–0.4 wt % samarium, europium, gadolinium, ytterbium, or yttrium were considered. The activity of the catalysts was evaluated by the content of benzene (aromatization) and C_1–C_5 hydrocarbons (hydrocracking) in the catalyzate. We found that the catalytic activity of the modified catalysts decreases in the order Gd > Y > Eu > Sm > Yb (Table 1).

The catalysts that were more active in aromatization also showed the elevated selectivity. Taking this into account, we studied the properties of the gadolinium-containing catalyst in the *n*-hexane conversion in more detail and found that, in the presence of the catalyst with gadolinium additives (0.1–0.4 wt %), the yield of benzene is higher than in the case of the REM–free alumina-supported platinum catalyst (Figs. 1, 2). Although the Gd-modified alumina-supported platinum catalyst is characterized by the elevated activity in hydrocracking, the ratio of the benzene concentration to the total concentration of C_1–C_5 hydrocarbons $[C_6H_6]/\Sigma(C_1–C_5)$ on the gadolinium-modified alumina-supported platinum catalyst is also higher than on the unmodified alumina-supported platinum catalyst, which indicates higher selectivity of the former in the aromatization.

Table 1. Influence of REMs on catalytic properties of the alumina-supported platinum catalyst at 500°C

REM	Composition of reaction product, wt %				
	ΣC_1–C_5	*iso*-C_6H_{14}	MCP*	C_6H_6	$C_6H_6/\Sigma C_1$–C_5
Sm	10.1	20.1	17.5	5.5	0.5
Eu	12.2	20.3	19.9	10.6	0.9
Yb	9.8	17.7	21.6	3.6	0.4
Gd	22.0	28.7	8.1	30.4	1.4
Y	20.0	28.1	10.1	15.2	0.7

* Methylcyclopentane.

1070-4272/05/7801-0096© 2005 Pleiades Publishing, Inc.

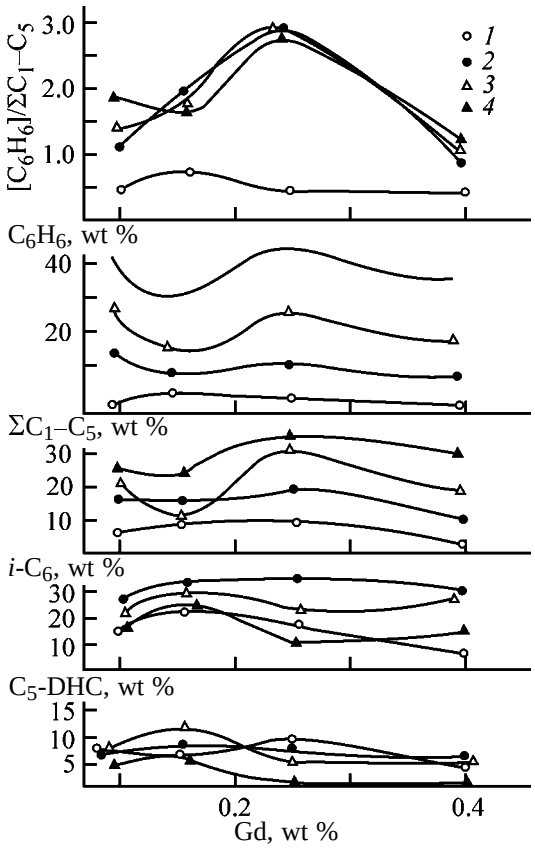


Fig. 1. Influence of the Gd content on the distribution of the products of *n*-hexane conversion on the modified alumina-supported platinum catalyst with the platinum content of 0.25 wt %. Temperature (°C): (*1*) 460, (*2*) 500, (*3*) 520, and (*4*) 540.

It should be noted that an increase in the Gd content to 0.25 wt % increases the aromatization activity of the catalyst. However, at a further increase in the Gd content, the benzene yield decreases (Fig. 1). The effect of the temperature on *n*-hexane conversion on the modified catalysts is shown in Fig. 3. As seen, the Gd content weakly affects the temperature dependence of the product yield. The benzene and $\Sigma(C_1–C_5)$ content increases with temperature; at 520–540°C, the degree of aromatization substantially exceeds the degree of hydrocracking. The temperature dependence of the content of isohexane (i-C_6) and C_5 dehydrocylization (C_5-DHC) products has a maximum at 460–520°C. The catalyst selectivity with respect to aromatization increases with temperature (Fig. 3).

To study the effect of Gd additives on the activity of the alumina-supported platinum catalyst, gadolinium was introduced into the catalyst with a gadolinium metanilate solution. A series of catalysts with the platinum content from 0.1 to 0.4 wt % and Pt : Gd ratio from 1 : 4 to 4 : 1 was prepared. As a whole,

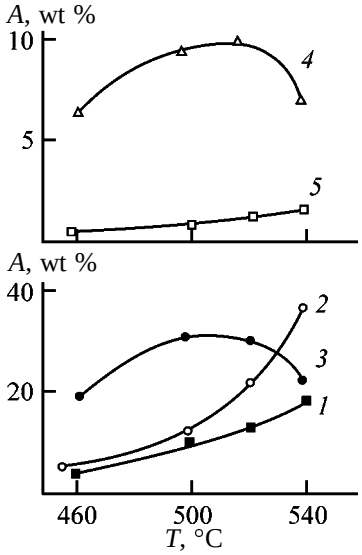


Fig. 2. Temperature dependence of the content of the products of *n*-hexane conversion, *A*, on the Pt/Al_2O_3 catalyst. Platinum content 0.25 wt %; the same for Figs. 3 and 5. (*1*) $\Sigma(C_1–C_5)$, (*2*) benzene, (*3*) isohexanes, (*4*) products of C_5-DHC, and $[C_6H_6]/\Sigma(C_1–C_5)$; the same for Fig. 3.

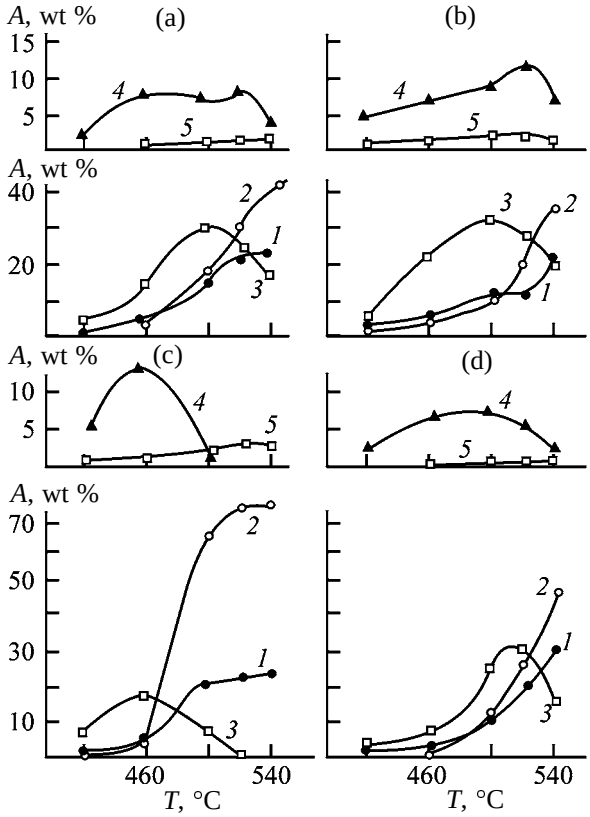


Fig. 3. Temperature dependence of the contents of the products of *n*-hexane conversion, *A*, on the alumina-supported platinum catalysts modified with gadolinium. Gadolinium content (wt %): (a) 0.1, (b) 0.15, (c) 0.25, and (d) 0.4.

Table 2. Conversion of *n*-hexane on the Gd-modified alumina-supported platinum catalysts

Catalyst, wt %	*T*, °C	Product composition, wt %				
		ΣC_1–C_5	*iso*-C_6H_{14}	MCP	benzene	$C_6H_6/\Sigma C_1$–C_5
0.1Pt + 0.1Gd	520	9.1	27.8	11.5	9.5	1.0
0.4Pt + 0.4Gd	520	27.9	25.9	8.8	23.7	0.7
0.25Pt + 0.25Gd	500	20.2	5.0	2.7	61.0	3.0
	520	23.5	–	–	72.5	3.0
	540	21.4	–	–	72.6	3.0
0.25Pt + 0.1Gd	520	32.4	4.3	0.6	62.5	1.9
0.25Pt + 0.5Gd	520	16.3	23.2	10.8	13.7	0.8
0.25Pt + 0.05Gd	520	7.3	15.8	10.5	17.1	2.3
0.4Pt + 0.1Gd	520	45.9	13.8	2.6	33.3	0.7
0.1Pt + 0.4Gd	520	20.7	8.4	8.4	23.2	1.0

the Gd added increases the activity and selectivity of the catalyst in the *n*-hexane aromatization.

The effect of the Pt : Gd ratio (wt %) on the catalyst activity in various directions of *n*-hexane conversion (0.1 Pt : 0.4 Gd, 1 : 4; 0.25 Pt : 0.5 Gd, 1 : 2; 0.25 Pt : 0.25 Gd, 1 : 1; 0.4 Pt : 0.1 Gd, 4 : 1) is shown in Fig. 4. The benzene yield grows with increasing Pt : Gd ratio to 1 : 1 at a slight increase in the yield of C_1–C_5 products (Fig. 4, curves *1*, *2*). The catalyst containing 0.25 wt % Pt and 0.25 wt % Gd showed the highest activity. The yield of the target product on this catalyst at 540°C and contact time of 0.6 s reaches 72.6 wt %. The selectivity in aromatization at 500–540°C is 3. At Pt : Gd > 1, the yield of hydrocracking products exceeds the yield of benzene. The decrease in the selectivity of the aromatization at increasing Pt : Gd ratio and a maximum in the benzene yield at 540°C show that the Pt : Gd ratio of 1 : 1 is optimal for the catalyst modification in the *n*-hexane conversion.

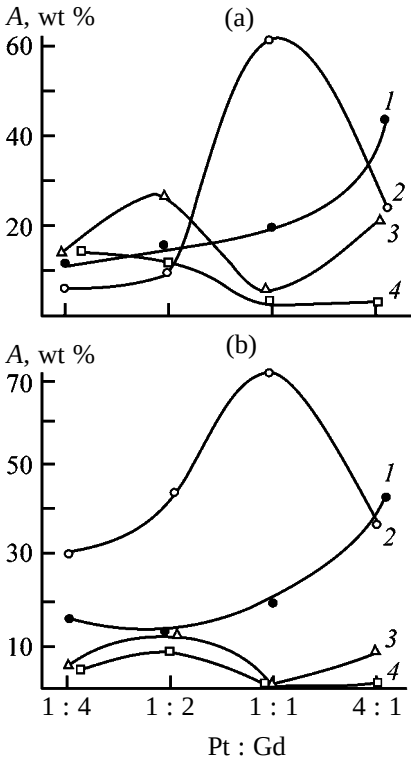


Fig. 4. Influence of the Pt : Gd ratio on the composition of the products of *n*-hexane conversion, *A*, at (a) 540 and (b) 500°C. Contact time 0.24 s. (*1*) $\Sigma(C_1$–C_5, (*2*) benzene, (*3*) isohexanes, and (*4*) products of C_5-DHC.

At the same Pt : Gd ratio, the content of the active components affects the catalyst activity. At the Pt : Gd ratio of 1 : 1, the aromatizing activity increases with increasing platinum and gadolinium content up to 0.25 wt %. Further increase in the Pt and Gd content is accompanied by a decrease in the catalyst activity. Thus, the catalyst sample containing 0.25 wt % Pt and 0.25 wt % Gd is the most active (Table 2).

The experimental data were treated with the Bassett–Habgood equation for first-order heterogeneous catalytic reactions [3]:

$$kK = \frac{F_0}{273Rm} \ln[1/(1-x)],$$

where *k* is the rate constant (s^{-1}); *K*, adsorption equilibrium constant; F_0, carrier gas flow rate recalculated to the normal conditions (ml s^{-1}); *x*, degree of conversion; and *m*, catalyst amount (g).

From the $\log(1/m)\ln[1/(1-x)]$–$1/T$ dependence, we calculated E_{app} of *n*-hexane aromatization. The *n*-hexane aromatization on the industrial alumima-sup-

ported platinum catalyst proceeds mainly through the C_5-DHC with the subsequent methylcyclopentane dehydroisomerization. The apparent activation energy of the *n*-hexane aromatization amounts to 134 kJ mol^{-1}. On the base-modified industrial alumina-supported platinum catalyst, when methylcyclopentane dehydroisomerization is suppressed because of blocking of acid centers, the *n*-hexane aromatization proceeds through the C_6-DHC. In this case, the apparent activation energy of the *n*-hexane aromatization is equal to 164 kJ mol^{-1} [4].

E_{app} on a Gd-modified alumina-supported platinum catalyst is 163 kJ mol^{-1}, i.e., coincides with E_{app} of the *n*-hexane aromatization on base-modified alumina-supported platinum catalyst (Fig. 5). Hence, modifying Al_2O_3 with the Gd compounds blocks active centers responsible for isomerization in the stage of methylcyclopentane isomerizatrion, which causes aromatization through the C_6-DHC [5, 6].

Thus, modifying the alumina-supported platinum catalyst with REM (samarium, europium, gadolinium, ytterbium, yttrium) increases its aromatization activity in the *n*-hexane conversion. Among the REMs studied, gadolinium is the most active.

Modifying alumina-supported platinum catalyst with REM suppresses the acid function of the support, which is accompanied by a decrease in the contribution of the C_5-DHC reaction in favor of benzene formation by successive dehydrogenation. In the REM series, the dimensions of atom and ion decrease with increasing atomic number, which decreases the basicity of REM oxides. Although the chemical properties of all the lanthanides(III) are similar, they regularly change from La to Lu. Yttrium has an ionic radius intermediate between those of Dy and Ho, which causes its similarity with lanthanides. The basicity of gadolinium oxide is higher than that of ytterbium oxide, which is manifested in their different influence on the support acidity.

To confirm this suggestion, we studied the IR spectra of the catalyst modified with Gd and Yb, which occupy the first and the last place, respectively, in the order of the activity of the modified alumina-supported platinum catalysts in the *n*-hexane aromatization. After the interaction with pyridine, the bands at 1630, 1580, 1490, and 1440 cm^{-1} appear in the IR spectrum of Al_2O_3 (Fig. 6). In accordance with the published data [7, 8], the bands at 1630 and 1490 cm^{-1} belong to vibrations of pyridine molecule coordinated to Lewis acid centers of the alumina surface, while the bands at 1580 and 1440 cm^{-1} correspond to physically adsorbed pyridine molecules.

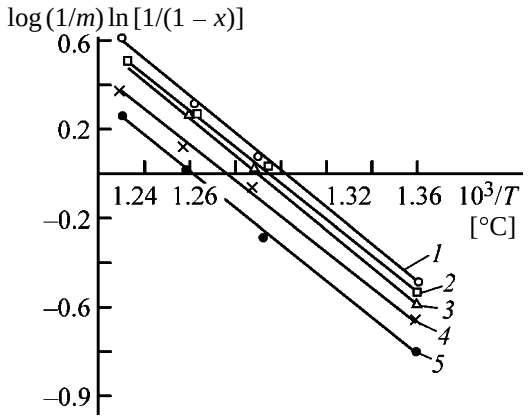


Fig. 5. The $\log(1/m)\ln[1/(1-x)]$–$1/T$ dependence for *n*-hexane aromatization on (*1*–*4*) Gd-modified alumina-supported platinum and (*5*) alumina-supported platinum catalysts. Gadolinium content (wt %): (*1*) 0.1, (*2*) 0.15, (*3*) 0.25, and (*4*) 0.4.

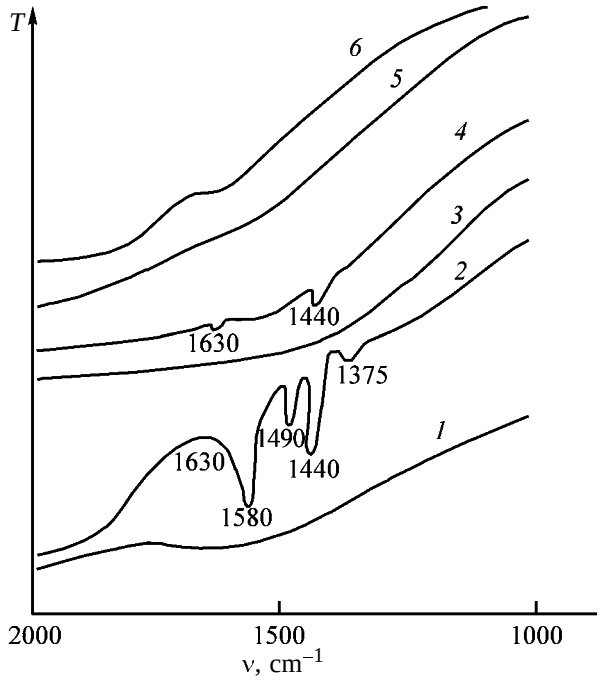


Fig. 6. IR spectra of (*1*, *2*) Al_2O_3, (*3*, *4*) Yb/Al_2O_3, and (*5*, *6*) Gd/Al_2O_3. (*T*) Transmittance and (ν) wave number. (*1*, *3*, *5*) Initial samples and (*2*, *4*, *5*) after pyridine adsorption.

Under the action of ytterbium as a modifying additive, the relative power of the active surface centers substantially changes. Although the bands at 1630 (Lewis acid centers) and 1440 cm^{-1} (physically adsorbed pyridine) are present in the IR spectrum of the catalytic system with sorbed pyridine, their intensities are substantially lower than after pyridine adsorption on the initial aluminum oxide, suggesting a substantial decrease in the surface acidity due to modification with ytterbium. It follows from the

IR spectrum that aluminum oxide modified with gadolinium contains almost no acid centers. Indeed, after slight evacuation, the bands of free and physically adsorbed pyridine completely disappear, bands characteristic for pyridinium ion are not observed, and the band at 1630 cm^{-1} assigned to pyridine molecules coordinated to Lewis acid centers is very weak. Thus, these data show different influence of REMs on the support acid function, which is manifested in the different catalytic activity of the modified alumina-supported platinum catalysts.

The apparent activation energy of the *n*-hexane conversion on the Gd-modified alumina-supported platinum catalyst, coinciding with E_{app} on the base-modified alumina-supported platinum catalyst, which is characterized by consecutive mechanism of the *n*-paraffin aromatization, confirms the REM influence on the acid properties of the support.

CONCLUSIONS

(1) An order of the activity and selectivity of modifying REMs in the *n*-hexane aromatization was determined: in the series Gd > Y > Eu > Sm > Yb; the catalyst modified with gadolinium is the most active.

(2) The optimal composition of the Gd-modified alumina-supported platinum catalytic system was found for the *n*-hexane aromatization.

(3) On the basis of the study of physicochemical and catalytic properties, the mechanism of the influence of the modifying additives on the activity and selectivity of the catalysts studied was suggested. Modification of the alumina-supported catalyst with rare-earth metals suppresses the acid centers of the support responsible for isomerization of hydrocarbons and, as a result, aromatization of *n*-paraffins proceeds through their successive dehydrogenation.

REFERENCES

1. *Kataliticheskii reforming uglevodorodov* (Catalytic Reforming of Hydrocarbons), Kuz'mina, R.I., Ed., Saratov: SYuI MVD Rossii, 2002.
2. Nikitina, A.M., Sen'kov, G.M., and Kozlov, N.S., *Vestsi Akad. Navuk Bel. SSR, Ser. Khim. Navuk*, 1986, no. 2, pp. 12–15.
3. Kuz'mina, R.I., Dogadina, N.V., Karyakin, V.A., and Sevost'yanov, V.P., Abstracts of Papers, *VI Rossiiskaya konferentsiya "Mekhanizmy kataliticheskikh reaktsii"* (VI Russian Conf. "Mechanisms of Catalytic Reactions"), Novosibirsk, 2002, vol. 2, pp. 199–200.
4. Dogadina, N.V. and Kuz'mina, R.I., in *Problemy analiticheskoi khimii: III Cherkesovskie chteniya* (Problems of Analytical Chemistry: III Cherkesov's Readings), Saratov: Slovo, 2002, pp. 177–179.
5. Kuz'mina, R.I., *Izv. Vyssh. Uchebn. Zaved., Khim. Khim. Tekhnol.*, 1999, vol. 42, no. 5, pp. 131–135.
6. Usov, Yu.N., Zubanova, L.G., and Kuvshinova, N.I., *Neftekhimiya*, 1977, vol. 17, no. 1, pp. 69–75.
7. Kiselev, A.V. and Lygin, V.I., *IK spektry poverkhnostnykh soedinenii* (IR Spectra of Surface Compounds), Moscow: Nauka, 1972.
8. Smith, A.L., *Applied Infrared Spectroscopy: Fundamentals, Techniques, and Analytical Problem-Solving*, New York: Wiley, 1979.

Russian Journal of Applied Chemistry, Vol. 78, No. 1, 2005, pp. 101–107. Translated from Zhurnal Prikladnoi Khimii, Vol. 78, No. 1, 2005, pp. 102–107.
Original Russian Text Copyright © 2005 by Pisarevsky, Polozova, Hockridge.

ENVIRONMENTAL PROBLEMS OF CHEMISTRY AND TECHNOLOGY

Chemical Oxygen Demand

A. M. Pisarevsky, I. P. Polozova, and P. M. Hockridge

Research Institute of Chemistry, St. Petersburg State University, St. Petersburg, Russia
Virginia Commonwealth University, Richmond, the United States

Received November 28, 2003

Abstract—New instrumental methods and tendencies of development of direct potentiometric determination of the chemical oxygen demand in the framework of the standard technique are considered.

In view of the increasing contamination of water, both the number of analyses made and that of studies of the analytical capacity of methods for determining the quality of water of various kinds are steadily growing [1–4]. The main parameter in the case in question is the oxygen concentration maintaining the normal ecological situation in water reservoirs. However, it is insufficient to determine only this parameter. The main task consists in monitoring the concentrations of substances (reducing agents of mostly organic nature) that can disturb the oxygen balance of water reservoirs, which leads to environmental disasters [1–4]. This problem has been solved by developing two integrated techniques for determining the parameters "biological oxygen demand" (BOD) and "chemical oxygen demand" (COD): in both cases, the total concentration of substances that can be oxidized, biologically or chemically, to inorganic final products is determined [3–6].

In the COD method, the results obtained are recalculated to the oxygen concentration (oxidizing agent, mg O_2 per liter).

Determination of BOD is a complicated analytical procedure requiring a high skill of analysts.[1] Two main difficulties have been noted [2, 5]: the necessity for introduction of a bacterial microflora and biogenic elements into a sample and the long duration of analysis. In practice, results obtained after incubation for five days (BOD_5) are most frequently used, but complete biochemical oxidation by oxygen may require 20–25 days. Even with substances chosen as reference for determination of BOD, the deviation from the calculated values is ±5 rel. %, and the reproducibility in the case of real wastewater is ±15–20 rel. % [5].

The introduction of such a parameter as COD into the analytical practice made it possible to obviate the above difficulties. The standard procedure involves boiling of a sample (2 h) in an 8 M H_2SO_4 solution, with introduction of $K_2Cr_2O_7$ and Ag_2SO_4 as catalysts and mercury salts for binding of chlorides. The unreacted $Cr_2O_7^{2-}$ is removed by titration with Mohr's salt. The standard procedure for determining COD makes it possible to achieve in many cases the required extent of oxidation, e.g., in analyses of household sewage (90–100% relative to the theoretically calculated values). In some cases, however, it is inefficient, which is primarily determined by the composition of water being studied. The COD method is inapplicable to water containing (upon dilution) more than 2 g l^{-1} chlorides.

Some countries use their own conditions of COD determination. For example, Japanese scientists believe that it sufficient to make analysis only for easily oxidizable components, which represent an immediate danger to the state of water reservoirs [2]. In this approach, $KMnO_4$ is chosen as an oxidizing agent and the conditions of analysis (temperature, acidity, and duration) are considerably milder. It is noteworthy that use of integral parameters is always rather difficult, because not only general principles are to be standardized, but also all details of the analytical procedure.

The method of direct potentiometric determination of COD (without sample titration) and the necessary apparatus were suggested in [7–9].[2]

The aim of this study was to reveal the most important issues associated with application of direct po-

[1] The parameter BOD corresponds to a greater extent to the natural conditions of oxidation of organic substances in water (according to the commonly accepted procedure, its determination resembles the process used in aerotanks in treatment of wastewater with activated sludge).

[2] Carried out at the Research Institute of Chemistry, St. Petersburg State University; the manufacture of the corresponding analyzers has been commenced in Russia.

1070-4272/05/7801-0101 © 2005 Pleiades Publishing, Inc.

Table 1. Potentiometric determination of COD in solutions of oxalic, tartaric, and phthalic acids

COD_{preset}, mg O_2/l	ΔE_{calc}, mV	COD_{exp}, mg O_2/l	Δ,* %
60	6.0	68	+13.3
120	11.3	116	–3.3
400	30.9	408	+2.0
600	41.9	584	–2.7
1200	69.4	1188	–1.0

* $\Delta = [(COD_{exp} - COD_{preset})/COD_{preset}] \times 100\%$.

tentiometry to determination of COD and to analyze the tendencies of development of new instrumental techniques for COD monitoring.

The voltaic cell developed in [7–9] can be represented as follows:

Glass pH electrode	Working solution	Glass redox electrode EO-021	(I)
	7.5 M H_2SO_4, $K_2Cr_2O_7$, $Ce(SO_4)_2$, $Ce_2(SO_4)_3$, Ag_2SO_4, $MnSO_4$		

The potentiometric determination of COD was made possible by use of new electrode systems. In voltaic cell I, having no liquid interface, the glass pH electrode is used as a reference [10], because the concentration of H_2SO_4 is high and constant, the electrochemically reversible metallic contact to the inner side of the glass membrane (LiSn alloy) ensures stable operation of the electrode at temperatures higher than 100°C, and the internal resistance of the electrode at 130°C does not exceed 300 kΩ.

The choice of a glass redox electrode (membrane made of electron-conducting titanosilicate glass) as an indicator, instead of the traditional platinum, gold, or iridium electrode, is due to the high selectivity of such electrode to the redox system $Ce^{4+/3+}$ (compared to components of other systems present in the working solution). The electrochemical reversibility of the voltaic cell as a whole made it possible to calculate the concentration dependence of the electromotive force on the solution composition in accordance with the Nernst equation. Severe difficulties in the development of cell I were encountered in choosing the composition of the working solution, because the system $Cr^{6+/3+}$ is not reversible on the known redox electrodes, including glass electrodes of the EO-021 type, owing to low exchange currents. This difficulty could be overcome by introducing the components of the $Ce^{4+/3+}$ redox system and minor amounts of $MnSO_4$ (catalyst of homo- and heterogeneous reactions of electron exchange) into the working solution.

The potentiometric COD analyzer comprises the following three basic units [7–9]: cell made of a heat-resistant glass (equipped with a reflux condenser), in which an indicator electrode, a reference, and a heater in a quartz sheath are placed; measuring unit[3]; and power source.

The range of COD measurements was from 30 to 1300 mg l^{-1}. The following formula was used in calculations (mg l^{-1}):

$$[COD_{pot}] = \frac{(A-1)[Ce^{4+}][Ce^{3+}] \times 8 \times 10^6}{A[Ce^{3+}] + [Ce^{4+}]V_s}, \qquad (1)$$

where $A = 10^{(E_1 - E_2)/\theta}$; $E_1 - E_2$, difference of the successive values of the electromotive force (mV) of cell I before and after introduction of a sample under study into the working solution; $\theta = 2.3RT/F = 79.2$ mV at 128°C; V_s, sample volume commonly equal to 5 or 10 ml.

The concentrations $[Ce^{3+}]$ and $[Ce^{4+}]$ (g-equiv l^{-1}) were found by calibrating the working solution. Oxalic acid or, as recommended in the standard method, potassium biphthalate was used in calibration [6, 7].

The principal results of the study performed are as follows.

(1) The conditions of COD determination close to those in the standard method as regards the concentration of $K_2Cr_2O_7$ and H_2SO_4 (and, consequently, as regards the boiling point of the working solution, too) could be created in the working solution. It proved to be possible to diminish by an order of magnitude the concentration of silver, $[Ag^+]$ [8, 9]. The concentration of cerium(IV, III) sulfates was chosen in such a way that just these system determined the redox buffer capacity of the working solution. The initial [Ce(IV)] : [Ce(III)] ratio in the working solution was $3.5 \times 10^{-3} : 0.5 \times 10^{-3}$. The correctness and accuracy of potentiometric determinations of COD in the range 60–1200 mg O_2/l are shown in Table 1 for model solutions of oxalic, tartaric, and phthalic acids. It is known that these acids are 100% oxidized to CO_2 and H_2O in the standard method.

(2) The formal potential of the $Ce^{4+/3+}$ system is approximately 120 mV higher than that of the $Cr^{6+/3+}$

[3] As measuring devices can be used digital voltmeters, pH-meters–millivoltmeters, or specially developed automated microprocessor devices (manufactured by LEK, Ekoniks, Ekoniks-Ekspert, etc.).

system. Such a difference is sufficient for ensuring virtually complete oxidation of chromium(III) with cerium(IV). From the standpoint of thermodynamics, it is easier to achieve complete oxidation of organic substances with the cerium system, and this system should be preferred in monitoring of COD. However, the specific features of oxidation reactions and of their kinetics were found to be the key factor. It was shown on model solutions that both a faster rate and a higher extent of oxidation can be achieved with $Cr_2O_7^{2-}$ (combined with a catalyst common in these cases, Ag^+). Therefore, the suggested mixture of oxidizing agents played an important part and provided close agreement between the results furnished by chemical and potentiometric methods for determining COD [7, 8] (Table 2).

The mechanism of oxidation of the total organic substance (Org) can be written as

$$Cr_2O_7^{2-} + Org \rightarrow 2Cr^{3+} + CO_2 + H_2O$$

$$Ce^{4+} + Org \rightarrow Ce^{3+} + CO_2 + H_2O \qquad (2)$$

$$Ce^{4+} + 2Cr^{3+} + H_2O \rightarrow Ce^{3+} + Cr_2O_7^{2-} + H^+$$

$$Ce^{4+} + Org \rightarrow Ce^{3+} + CO_2 + H_2O$$

System of equations (2) illustrates the assertion that only Ce(IV) is consumed in the course of the oxidation, irrespective of the actual relative amounts in which Ce(IV) and $Cr_2O_7^{2-}$ are involved in oxidation.

(3) The potentiometric technique obviates the problem of strict regulation of the analysis duration (more than 2 h in the standard method). After a sample is introduced into the working solution and boiling starts (2–3 min), it becomes possible to record the variation of the emf of the voltaic cell and, consequently, to monitor the oxidation rate. Figure 1 shows the dependences E–τ, measured both in the calibration of the working solution (successive introduction of two equal amounts of oxalic acid) and in experiments with model (working) solutions containing phenol, soluble cellulose, or isoamyl alcohol. In the latter case, no 100% oxidation is observed, and making the determination time any longer has no effect on the result obtained. On the whole, the determination time decreases dramatically in potentiometric determination of COD. For example, an analysis for COD of water before and after biological treatment took 50 an 20 min, respectively, at a water treatment plant[4] and 20 and 10 min at sewage treatment works.[5]

[4] Belyi Island, St. Petersburg.

[5] Sarov, Nizhni Novgorod oblast.

Table 2. COD values in wastewater. Standard and potentiometric methods

Wastewater	Sample no.	COD_{stand}	COD_{potent}	Δ,* %
		mg O_2/l		
Industrial before treatment	1	150	140	–7
	2	170	170	0
	3	420	400	–5
	4	600	600	0
Household (St. Petersburg) before treatment	5	325	265	–18
	6	285	295	4
	7	180	155	–14
	8	220	215	–2
after treatment	9	43	36	–16
	10	41	52	27
	11	45	57	27

* $\Delta = [(COD_{potent} - COD_{stand})/COD_{stand}] \times 100\%$.

In both cases, the COD of water delivered to treatment was 180–400 mg l^{-1}. Permanent control measurements by the standard method demonstrated that the difference between the COD values obtained by the two methods (standard and potentiometric) does not exceed, on the average, 8 rel. % in the range in question [11, 12].

(4) The possibility of monitoring of the kinetic parameters of the oxidation in analysis for COD is largely associated with the correct choice of the EO-021 electrode as indicator in cell I. The difference in behavior between these and platinum electrodes was the most clearly manifested in those cases when samples contained chlorides and bromides, but it was also

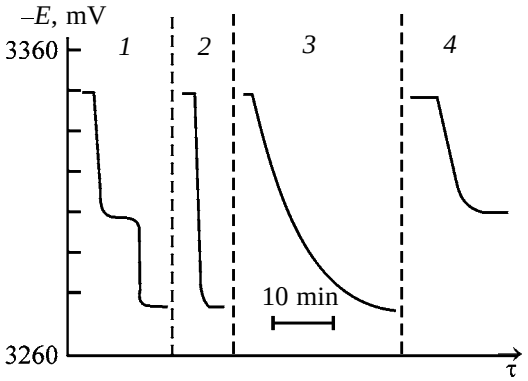


Fig. 1. Kinetic curves of oxidation of various organic substances in the working solution. (E) Potential and (τ) time; the same for Fig. 2. (*1*) Oxalic acid (calibration), (*2*) phenol, (*3*) cellulose (soluble), and (*4*) isoamyl alcohol.

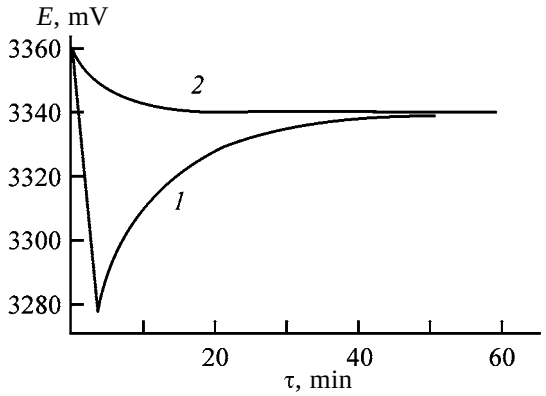


Fig. 2. Comparison of the selectivities of (*1*) Pt and (*2*) glass redoxmetric electrodes in oxidation of a mixture of chlorides and bromides in the working solution.

observed for solutions exhibiting a noticeable electrochemical activity on platinum. Figure 2 illustrates the difference in the properties of the indicator electrodes. Among the large number of determinations performed with cell (I), not a single case of violation of the reversibility of glass redox electrodes was recorded, which confirms their high selectivity toward the $Ce^{4+/3+}$ system [9, 12].

The possibility of differentiation of the contribution from difficultly and readily oxidizable substances to the COD value is an important advantage of the potentiometric method. The interpretation of kinetic dependences is strongly facilitated by the fact that the concentration of $Cr_2O_7^{2-}$ remains constant in the course of analysis (see paragraph 2).

(5) For particular cases,[6] the existence of a stable correlation between BOD_5 and COD_{potent} was established.

In the last 15 years, more than a hundred reports and patents reflecting the tendencies of development of the generalized COD parameter have been published. These publications emphasize the importance of using this parameter for monitoring of the composition of potable, natural, process, and wastewater and for control over industrial processes for which COD is a key parameter. Conventionally, the main areas of research, most important in the authors' opinion, can be formulated as follows: choice of oxidizing agents, new methods and apparatus, and relationship between COD and other parameters that characterize the quality of water.

Choice of an oxidizing agent. In view of the important role of cerium salts in the above-discussed "cocktail" for potentiometric determination of COD, the studies [13–16] in which use of cerium salts was continued should be mentioned first. Ce(IV) was used as an oxidizing agent in analyses of river water and industrial sewage under comparatively mild conditions as regards the concentration of the acid and temperature, i.e., in determination of readily oxidizable components that present an immediate hazard to the state of water reservoirs. According to Japanese regulations [13, 14], the procedures suggested can compete with the permanganate method. The main advantage of the cerimetric technique for determination of COD consists in its insensitivity to presence of very high concentrations of chlorides (up to 30 000 mg l^{-1}) in the samples, which eliminates the necessity of using mercury [13, 14]. The capabilities of the direct potentiometry were not used in these studies, and the loss of cerium(IV) in the course of oxidation was monitored spectrophotometrically.

At the same time, manganese salts started to be used extensively in new techniques as catalysts for homogeneous oxidation with potassium dichromate, instead of silver sulfate in the standard procedure [17]. An even more important step in the improvement of parameters of COD determination was made in [18]: it was suggested to replace $K_2Cr_2O_7$ as oxidizing agent with Mn(III), with no silver salt required in this case as catalyst. Also, the problem of elimination of mercury from the process was solved by preliminary removal of chlorides by treating a sample with sodium bismuthate. It was established for model solutions and wastewater of varied origin that the time of determination of COD at 150°C does not exceed 60 min. The procedure for removal of chlorides by preliminary treatment of a sample with sodium bismuthate (or, more precisely, with an adsorbent based on this compound) was also studied in [19].

Noteworthy among other solutions of interest are use of granulated titanium and Fenton's reagent as oxidation catalyst and coulometric determination of COD in an alkaline medium with a copper anode [20]. Coulometric generation of oxidizing agents [Ce(IV), Cl_2, BrO^-] for COD determination was also studied in [21].

New methods and apparatus. The aim of studies in this field has been to make the analysis time shorter and the determination threshold lower as compared to the standard method. Studies employing the microwave technology for sample heating and new analytical techniques based on flow-through and flow-injection methods (FIM) of analysis have been the focus of attention in recent years.

[6] Household sewage in St. Petersburg and Kharkov, wastewater of a poultry plant and a brewery.

Microwave heaters have been used in experiments devoted to COD determination under nearly standard conditions [22–25]. Water samples were placed both in sealed and in open cells. In all cases, it was possible to substantially diminish the time of analysis both by raising the temperature of the oxidation and by using spectrophotometric techniques to determine the loss of Cr(IV) or gain of Cr(III). For sealed Teflon cells with a sample volume of 0.5–2.0 ml and microwave heating, the analysis time decreased to 7 min at a COD of the samples of less than 1000 mg l^{-1} [25]. It may be assumed that application of the microwave technology in analysis for COD will be developing fast in the future.

The use of modern technology was excellently demonstrated in a study of Beltra *et al*. [26], who employed microwave heating, spectrophotometric determination of the reaction rate from the accumulation of Cr(III) (absorption at λ = 590 nm), and automated computer processing of the results obtained. Such parameters as the concentrations of an acid and silver and determination time were varied by a specially designed program. Analyzers of this kind will extend the field of research and will make it possible to find the optimal modes of analysis for samples of particular compositions.

Versions of flow-through and flow-injection methods (FIM) have been used under mild conditions of COD determination at a relatively low acidity and temperature [with $KMnO_4$ and Ce(IV) as oxidizing agents] [15, 27–31]. Only in [29], COD could be determined by FIM under standard conditions. It was also possible, in all of these studies, to diminish the determination time to 10 min and avoid introduction of Hg(II) to mask chlorides in samples. At present, it is difficult to assess the extent to which FIM-based analyzers can be widely used in determining COD.

The new approach to COD determination was also implemented in [30, 31], where a thin-layer flow-through electrochemical cell was used in combination with coulometric generation of reagents. The adequacy of analyses was achieved [30] owing to formation of highly active ozone or $OH^{\bullet}$ radicals. A lead dioxide electrode served as an anode, and a platinum or titanium plate, as a cathode. Ozone was also used as an oxidizing agent in [32, 33]. The indubitable interest in these studies is due to use of ozone chemiluminescence in monitoring the sample composition.

The enhanced capabilities of the relatively fast and reliable instrumental determinations of COD and the accumulation of data obtained by various methods promoted investigations aimed to gain deeper insight into the contribution of various substances and processes to the COD values of water of various kinds, and primarily wastewater. The interest in distinguishing the contributions of readily and difficultly oxidizable components, obtaining the kinetic data as an advantage of the potentiometric determination of COD, and different approaches to the choice of standard techniques were already mentioned above. The contributions of different kinds of substances and the approach to modeling of water-treatment processes were the subject of [34–37]. The closest attention is focused on gaining insight into the process of biological purification of wastewater [35]. The problem was analyzed from the seemingly opposite standpoint, by calculating the COD values from parameters of UV absorption spectra of organic compounds [38].

Relationship between COD and other parameters. Directly to in-depth studies of the problem are adjacent investigations in which relationships between parameters characterizing the extent of contamination of water are analyzed. In [39, 40], correlations between the total organic carbon (TOC) and COD were discussed; in [40], [TOC]/[COD] ratios of 0.91 were obtained for some kinds of wastewater. Of particular interest for paper-making is the paper by Bristol *et al*. [41]. Although empirical ratios [TOC]/[COD] or [COD]/[BOD] are known for wastewater of this industry, the [TOC]/[COD] ratio was very important both by itself and as regards its fluctuations, which made it possible to use this ratio as a contamination indicator. A classification of wastewater by the [TOC]/[COD] ratio has been suggested.

The existence of a stable correlation between COD and BOD has long been known in food industries, with the preference given to the first of these parameters in analyses of wastewater [42]. Now, the number of studies of this kind is growing because the main substances contained in sewage and process features of various industries became known. Of interest are the data reported in [43]: the [BOD]/[COD] ratio in wastewater formed in manufacture of various compounds is 0.97 for glucose and phthalate, 0.87 for near beer and ice-cream, and 0.93 in processing of fruits and vegetables. It is noteworthy that use of COD as a process parameter requires another approach to the problem of standardization of determinations.

CONCLUSIONS

(1) The standard chemical method for determining the chemical oxygen demand has become poorly applicable to monitoring the contamination of water,

primarily because of the toxicity of the reagents involved and due to the comparatively long time of determination. The steep rise in the number of analyses performed made this problem more acute.

(2) Analysis of tendencies in the development of new techniques and analyzers of the chemical oxygen demand, operating on electrochemical and spectrophotometric principles, including flow-through and flow-injection variants, made it possible to conclude that new devices will provide in the nearest future analysis durations shorter than 15 min and a detection limit of 10 mg l^{-1}.

(3) The results obtained in the last decade when studying the kinetics of oxidation with oxygen of substances dissolved in water revealed the key role of the chemical oxygen demand. This quantity is already being used as a parameter of new technologies in biological treatment of wastewater; in food, pulp-and-paper, and other industries; and in environmental monitoring.

ACKNOWLEDGMENTS

The study was financially supported by the Federal Target Program "Universities of Russia" (project no. UR.05.01.031) and National Science Foundation (grant no. CHE-9 419 539).

REFERENCES

1. Laitinen, G.A. and Harris, W.E., *Chemical Analysis*, New York; McGraw-Hill, 1975, 2nd ed.
2. Leithe, W., *Die Analyse der organischen Verunreinigungen in Trink-, Brauch-, und Abwassern*, Stuttgart: Wissenschaftliche, 1972.
3. Lur'e, Yu.Yu., *Analiticheskaya khimiya promyshlennykh stochnykh vod* (Analytical Chemistry of Industrial Wastewater), Moscow: Khimiya, 1984.
4. Posylaiko, V.I., Kozyreva, N.A., and Logacheva, Yu.P., *Khimicheskie metody analiza* (Chemical Methods of Analysis), Moscow: Vysshaya Shkola, 1989.
5. Golovatyi, E.I., *Instrumental'nye metody kontrolya BPK stochnykh vod mikrobiologicheskoi promyshlennosti: Obzornaya informatsiya* (Instrumental Methods for Monitoring BOD of Wastewater from Microbiological Industries: Review), Moscow: ONTITEI Mikrobioprom, 1982.
6. SO 6060–86: *Quality of Water: Determination of Chemical Oxygen Demand*.
7. RF Patent 1 223 123.
8. Dugin, G.V., Pisarevsky, A.M., and Polozova, I.P., *Khim. Tekhnol. Vody*, 1985, vol. 5, no. 4, pp. 51–53.
9. Dugin, G.V., Pisarevsky, A.M., Polozova, I.P., and Shul'ts, M.M., *Zh. Prikl. Khim.*, 1986, vol. 59, no. 1, pp. 22–27.
10. Beliustin, A.A., Pisarevsky, A.M., Lepnev, G.P., *et al.*, *Sensors Actuators B*, 1992, vol. 10, pp. 61–66.
11. *Kolichestvennyi khimicheskii analiz vod: Metodika vypolneniya izmerenii massovoi kontsentratsii khimicheski potreblyaemogo kisloroda v probakh prirodnykh i stochnykh vod bikhromatopotentsiometricheskim metodom. Minprirody Rossii* (Quantitative Chemical Analysis of Water: Procedure for Determining Chemical Oxygen Demand (Mass Concentration) in Samples of Natural and Waste Water by Bichromatopotentiometric Method, Ministry of Environment of the Russian Federation), PND F 14.1:2.19–95, Moscow, 1995.
12. Antsyshkina, N.D., Dugin, G.V., Pisarevsky, A.M., *et al.*, Abstracts of Papers, *Third International Congr. "Water: Ecology and Technology,"* Moscow. 1998, pp. 341–342.
13. JPN Appl. 09 311 130 A2.
14. JPN Appl. 06 341 981 A2.
15. Korenaga, T., Zhon, X., Okada, K., *et al.*, *Anal. Chim. Acta*, 1993, vol. 272, no. 2, pp. 237–244.
16. Simal, J., Lage, M.A., and Iglesias, I., *An. Bromatol.*, 1986, vol. 37, no. 1, pp. 125–142.
17. Zhang, S., Li, W., and Wang, H., *Huagong Huanbao* (China), 2001, vol. 21, no. 3, pp. 171–173.
18. Miller, D.G., Brayton, S.V., and Boyles, W.T., *Water Environ. Res.*, 2001, vol. 73, no. 1, pp. 63–71.
19. Vaidya, B., Watson, S.W., Coldiron, S.J., *et al.*, *Anal. Chim. Acta*, 1997, vol. 357, no. 12, pp. 167–175.
20. Lee, K.-H., Ishikawa, T., McNiven, S.J., *et al.*, *Anal. Chim. Acta*, 1999, vol. 398, nos. 2–3, pp. 161–171.
21. Abdullin, I.F., Dement'enko, A.A., Budnikov, G.K., *et al.*, *Zavod. Lab., Diagnost. Mater.*, 2001, vol. 67, no. 1, pp. 15–17.
22. Chinese Patent 1 128 352 A.
23. Chen, S.-Ch., Tzeng, J.-H., *et al.*, *Anal. Sci.* (Taiwan), 2001, vol. 17, no. 4, pp. 551–553.
24. Rustioni, M., Cassani, G., Faccetti, E., Nucci, G., *et al.*, in *4th World Surfactants Congr.*, Barcelona, 1996, vol. 1, pp. 474–488.
25. Jardin, W.F. and Rohwedder, J.J., *Water Res.*, 1989, vol. 23, no. 8, pp. 1069–1071.
26. Beltra, A.P., Iniesta, J., Gras, L., *et al.*, *Instr. Sci. Technol.*, 2003, vol. 31, no. 3, pp. 249–259.
27. Chen, H., An, T.-C., Fang, Y.-J., *et al.*, *Yankuany Ceshi* (China), 1999, vol. 18, no. 3, pp. 185–188.

28. Vallejo-Pecharroman, B., Izquierdo-Reina, A., and Castro, L. de, *Analyst*, 1999, vol. 124, no. 8., pp. 1261–1264.
29. Schmitz, A., Eberhardt, R., Spohn, U., *et al.*, *DECHEMA Biotechnol. Conf.*, 1992, vol. 5, part B, pp. 1117–1120.
30. FRG Patent 3 707 815 A1.
31. Lee, K.-H., Ishikawa, T., Sasaki, S., *et al.*, *Electroanalysis*, 1999, vol. 11, no. 16, pp. 1172–1179.
32. Vorontsov, A.M., Nikanorova, M.N., and Melent'ev, K.V., Abstracts of Papers, *Vserossiiskaya konferentsiya "Sensor-2000"* (Russian Conf. "Sensor-2000"), St. Petersburg, June 21–23, 2000, p. 21.
33. Vorontsov, A.M., Nikanorova, M.N., and Melent'ev, K.V., *Vodnye ob'ekty Sankt-Peterburga* (Water Bodies of St. Petersburg), Kondrat'ev, S.A. and Frumin, G.T., Eds., St. Petersburg, 2002, pp. 73–78.
34. Orhon, D. and Cokgor, E.U., *J. Chem. Technol. Biotechnol.*, 1997, vol. 68, no. 3, pp. 283–293.
35. Vestner, R.I. and Gunthert, F.W., *GWF, Wasser, Abwasser*, 2001, vol. 142, no. 9, pp. 635–644.
36. Sperandio, M., Urbain, V., Ginestet, P., *et al.*, *Water Sci. Technol.*, 2001, vol. 43, part 1, pp. 181–190.
37. Gorgun, E., Cokgor, E.U., Ohron, D., *et al.*, *Water Sci. Technol.*, 1995, vol. 32, no. 12, pp. 43–52.
38. Kato, Y., Kumagai, T., Nishioka, H., *et al.*, *Oriental J. Chem.*, 2001, vol. 17, no. 1, pp. 1–8.
39. Unmarino, G. and Russo, A., *Mater. Conc.* (Italy), 1996, vol. 72, no. 1, pp. 51–52.
40. Aisaka, K. and Mikashima, H., *Examination of COD Testing Methods for Waters from Industrial Final Disposal Sites*, Kenkyusho Nenpo (Japan), 1994, pp. 177–178.
41. Bristol, P., Civiello, J., Harp, D., *et al.*, *Water Environment Federation Annual Conf.*, Atlanta, 2001, vol. 74, pp. 5436–5449.
42. Belen'kaya, S.L., Popova, Yu.I., and Kalitvyanskaya, V.I., *Ferment. Spirt. Prom–st.*, 1987, no. 4, pp. 13–14.
43. Amarasinghe, H., Anusha, U., Gunavardena, H.D., *et al.*, *J. Nat. Sci. Council Sri Lanka*, 1993, vol. 21, no. 2, pp. 259–266.

Russian Journal of Applied Chemistry, Vol. 78, No. 1, 2005, pp. 108–112. Translated from Zhurnal Prikladnoi Khimii, Vol. 78, No. 1, 2005, pp. 108–113.
Original Russian Text Copyright © 2005 by Malyshev, Zolotnikov, Bomshtein, Sedov, Kruglik.

PROCESSES AND EQUIPMENT OF CHEMICAL INDUSTRY

A Method for Studying Kinetics of Crystallization from Solution in a Flow-Through Mixing Cell

R. M. Malyshev, A. N. Zolotnikov, V. E. Bomshtein, A. A. Sedov, and A. E. Kruglik

Institute of Chemicals and Ultrapure Chemical Substances, Federal State Unitary Enterprise, Moscow, Russia

Received July 12, 2004

Abstract—A method for determining the kinetic parameters of crystallization in a flow-through mixing cell using a mathematical model that takes into account the nonideality of agitation and the possible dependence of the growth rate of crystals on their size is suggested.

The kinetics of crystallization from solutions is mainly characterized by the nucleation function density and crystal growth rate, which depend on the composition, physicochemical and thermodynamic properties of the medium, and the hydrodynamics and fundamental aspects of mass transfer at the fluid–solid interface. The values of these parameters are commonly determined using indirect methods based on measuring in the course of an experiment some parameters related by known expressions to the crystallization kinetics. In one of methods used for determining kinetic parameters, the nucleation function density and the crystal growth rate are found from the theoretical dependence of the density of the crystal size distribution function (CSDF), which describes the CSDF at the outlet of a flow-through cell of ideal mixing, by minimizing the discrepancy between the results of calculation by the theoretical expression from the experimental CSDF [1]. This method is used in kinetic studies of crystallization on the assumption that the growth rate of crystals is independent of their size (McCabe's rule) and the hydrodynamic mode completely corresponds to that of ideal agitation. However, these assumptions are not always in agreement with the experimental conditions in actual practice. In an experimental study of the kinetics of crystallization in a flow-through mixing cell, it is difficult to choose *a priori* the working parameters of the stirrer and the drive power that would ensure uniform suspension of a polydispersed mass of the forming crystals at the originally unknown size distribution of crystals and their growth rate.

Particles are commonly suspended in a fluid in the turbulent mode in an apparatus equipped with a stirrer, with the parameters of the particle transport depending on the power consumed for agitation, flow structure, and characteristics of the apparatus and stirrer. If the energy supplied is insufficient for complete suspension of particles in the fluid, axial and radial nonuniformity of distribution of solid particles in the fluid is observed. However, even at a sufficient energy, the flow structure may differ from that in the ideal agitation mode [2].

Assuming that the main factor governing the hydrodynamics of motion of the suspension in the mixing cell is energy dissipation in the unit volume of the suspension agitated with a stirrer, let us evaluate the limiting size of growing crystals starting to settle down to the bottom of the flow-through mixing cell. The condition for the ascent of crystals of nominal size r in a turbulent flow from the sediment at the bottom follows from the inequality [3]

$$V'_a \geq [2r(\rho_s - \rho_f)g\varphi_0/\rho_f]^{1/2}, \quad (1)$$

where V'_a is the lifting component of the pulsation velocity at the bottom; ρ_s, ρ_f, densities of a solid particle and the fluid; and φ_0, volume fraction of particles contained in the sediment at the bottom.

The relationship between the thickness of a viscous sublayer, δ_0, and the normal component of the averaged pulsation velocity V'_0 on the scale δ_0 is known [4]:

$$\mathrm{Re}_{\delta_0} \sim \frac{V'_0\delta_0}{\nu_{\delta_0}} = 11.6, \quad (2)$$

where Re_{δ_0}, ν_{δ_0} are the Reynolds number and kinematic viscosity for a thickness δ_0.

1070-4272/05/7801-0108© 2005 Pleiades Publishing, Inc.

The quantity V'_0 on the scale of the thickness of the viscous sublayer (δ_0), regarded as a function of energy dissipation ε_0 (i.e., the power consumed per unit volume of a suspension volume agitated), is given by [4, 5]

$$V'_0 \sim (\varepsilon_0\delta_0)^{1/3}. \quad (3)$$

From Eqs. (1)–(3), we can find the size r_p of a solid particle in relation to the maximum radius r_{max} observed in crystallization. Particles of size $r < r_p$ are partly or completely suspended in the turbulent flow:

$$r_p \sim \frac{11.6k_f \nu_{\delta_0} \varepsilon_0 \rho_f^2}{[2(\rho_s - \rho_f)g\varphi_0]^2} < r_{max}, \quad (4)$$

where k_f is the ratio of the longitudinal component of the pulsation velocity of ascent of particles at the bottom, V'_{la}, to the normal component of the pulsation velocity V'_0 (according to [3], $k_f \approx 0.8$ and $\varphi_0 \approx 0.65$–0.68 for $r \geq r_p$ in the sediment [6]).

Knowing how the thickness of the viscous sublayer depends on the minimum characteristic rate of pulsations, we can use the density of the diffusion flow to find the mass-transfer rate and determine the range of crystal sizes in which the crystal growth rate is independent of the particle size [2, 3].

The crystallization process may be kinetically or diffusion-controlled; in the latter case, the crystal growth rate can also be strongly affected by parameters of the pulsation velocities V_0 on the scale of the thickness of the viscous sublayer, δ_0. In the case of a turbulent flow and large Peclet (Pe) and Reynolds (Re) numbers (Pe $\gg$ 1, Re $\gg$ 1), it follows from the equations for the diffusion flow density that, with account of relations (1) and (3), the mass-transfer rate is independent of the particle size r and the mass-transfer coefficient k_L is applicable to particles of size $r > (\lambda_0 < \delta_0)$, where λ_0 is the internal scale of turbulence [4]. For particles of smaller size in a turbulent flow (Pe $\gg$ 1, Re < 1), i.e., for $r < (\lambda_0 < \delta_0)$, the mass-transfer coefficient is determined by the velocity of the relative motion of a particle in the fluid and is inversely proportional to the particle size r raised to the power m. For the Stokes mode of a fluid flow around a particle and for Re < 1 [4], but with account taken of the natural convection around the particle [7], and for the fluid at rest [8], the mass-transfer coefficient is inversely proportional to the particle size r raised to the power $m = 0.25$ in the case of a natural convection or $m = 1$ for a fluid at rest.

As further development of the method for studying the crystallization kinetics in a flow-through cell with ideal mixing [1], we suggest a procedure for studying the crystallization kinetics in a flow-through cell with nonideal mixing and any crystallization mode, which is described by a mathematical model based on parameters of the structure of the flows of phases, determined preliminarily in experiments with the same mixing cell. Further, crystallization is performed, and kinetic parameters of the process are found from the densities of CSDF by minimizing the disagreement between the results of calculation and the experimental values at the outlet of the mixing cell.

In a flow-through mixing cell with a stirrer (300 rpm) and mass volume $V_c = (0.5–0.8) \times 10^{-3}$ m^3, the structure of the flow of phases was studied by means of pulsed introduction of tracers into the flow. An aqueous solution of sodium chloride was used as a tracer for the fluid phase, and sand composed of four fractions with a prescribed size of particles and the same number of particles in each fraction, as a solid phase in pulsed introduction. The concentration of sodium chloride at the outlet was measured conductometrically, and the composition of the solid phase at the outlet was found by sampling and subsequent determination of the number of particles in each fraction. The initial content of the solid phase in the pulsed introduction mode, recalculated to the volume of the mass in the cell, did not exceed 8 vol %, which is commonly sufficient for kinetic studies in a flow-through cell. The elution curves were processed using the method of moments. The measurement results and values of moments M_i for some experiments are listed in the table.

As seen from the table, the agitation in the fluid phase deviates only slightly from the ideal agitation mode (variance $\sigma^2 > 0.7–0.8$). The energy dissipation ε_0 is 1.8 W. A loose sediment was observed at the bottom of the mixing cell, with the minimum diameter of the sedimented particles $r_p \approx 0.16 \times 10^{-3}$ m. The average residence time of particles, τ^j, where j is the fraction number equal to the dimensional first moment M_1^j, varies approximately in proportion to the ratio of the average concentration of the solid phase in the bulk to its concentration at the outlet of the mixing cell. Turbulent transfer of solid particles is characterized by the second dimensionless moment M_2^j or by variance σ_j^2.The latter is considerably smaller than unity, which points to nonideality of agitation of the solid phase in the flow-through mixing cell.

The structure of flows can be approximated with a

Structure of the flow of phases in a mixing cell*

Moment	$Q \times 10^3$, $m^3\ h^{-1}/c_0^s$, vol %		
	1.0/3.1	0.77/6.5	0.43/8/05
Fluid phase			
M_1, min	33.1	44.1	77.5
$M_2 = \sigma^2$	0.82	0.75	0.78
Solid phase			
0.025–0.063-mm fraction:			
M_1, min	39.8	53.3	115
$M_2 = \sigma^2$	0.26	0.28	0.245
0.063–0.14-mm fraction:			
M_1, min	36.8	43.8	87.8
$M_2 = \sigma^2$	0.3	0.31	0.265
0.14–0.28-mm fraction:			
M_1, min	30.4	28.1	67.5
$M_2 = \sigma^2$	0.35	0.34	0.33
0.28–0.45-mm fraction:			
M_1, min	23.1	25.5	57.8
$M_2 = \sigma^2$	0.38	0.31	0.31

* Q, flow rate at the cell outlet; c_0^s, initial content of the solid phase.

typical cell model. Taking into account the relationship between the variance σ^2 and the number of cells, N, $\sigma^2 = 1/N$, it is allowable to describe the balance of substance in the fluid with a single cell. For describing the balance of the density of CSDF in the case when N is noninteger or more than integer, equations are written for $N - 1$ cells of equal volume, with an additional equation for a cell of smaller volume. For the steady state, the balance equations for the substance and the number of crystals take the form

$$\gamma c_0 - c = \sum_M \int_N \tau_{1,2} \rho_s \eta(r, \Delta c) \times 0.5\pi r^2 \, dr, \qquad (5)$$

$$\left.\begin{aligned}
&\frac{d[f_1^j \eta_1^j(r, \Delta c)]}{dr} = -\frac{1}{\tau_1^j} f_1^j, \\
&\cdots\cdots\cdots\cdots \\
&\frac{d[f_i^j \eta_i^j(r, \Delta c)]}{dr} + \frac{1}{\tau_1^j} f_{i+1}^j = \frac{1}{\tau_1^j} f_i^j, \\
&\frac{d[f_{N-1}^j \eta_{N-1}^j(r, \Delta c)]}{dr} + \frac{1}{\tau_1^j} f_{N-1}^j = \frac{1}{\tau_1^j} f_{N-2}^j, \\
&\frac{d[f_N^j \eta_N^j(r, \Delta c)]}{dr} + \frac{1}{\tau_2^j} f_N^j = \frac{1}{\tau_1^j} f_{N-1}^j,
\end{aligned}\right\} \qquad (6)$$

where τ_1^j, τ_2^j are the average residence times in cells of equal volume and in a cell of smaller volume, respectively; γ, ratio of the solution flow rate at the inlet to that of the suspension at the outlet; η, crystal growth rate; f_i^j, density of CSDF, $i = 1, \ldots, N$ and $j = 1, \ldots, M$, where M is the number of fractions; Δc, supersaturation of the crystallizing solution.

As Δc and temperature are virtually constant in the flow-through mixing cell under study, the crystal growth rate η_i remains unchanged in going from one cell to another for all jth fractions at $r > (\lambda_0 < \delta_0)$ and may depend on the crystal size r for fractions with $r < (\lambda_0 < \delta_0)$. It is assumed that nucleation occurs at the inlet into the flow-through mixing cell at the interface with a fresh supersaturated solution, i.e., only at the inlet of the first cell of the CSDF model. The density of CSDF is found by solving system of equations (6), and then parameters of the crystal growth rate η, $\eta(r)$, and density of the nucleation function, f_0, are determined by comparing the results of calculation and experimental data from the coincidences of the CSDF densities. Equation (5) is used to verify the material balance for the substance that passed from solution into crystals. For the general case of a model comprising $N - 1$ cells of equal volume, supplemented with a cell of smaller volume, for which the growth rate of crystals depends on their size and crystal size varies from that of a nucleus, r_{nuc}, to r_n, where $r_n \approx r_{\lambda_0}$, the solution to model (6) is as follows:

$$f_N(r) = (1/k\tau_1)^{n-1} \frac{f_0}{r_{nuc}^m} \frac{r^m}{(m+1)^{n-1}} \left\{ [(-1)^n r^{(m+1)} r_{nuc}^{n(m+1)} D_1 \right.$$

$$+ (-1)^{(n+1)} n r^{2(m+1)} r_{nuc}^{(n-1)(m+1)} D_2 + (-1)^{(n+2)} n(n-1)(2!)^{-1}$$

$$\times r^{3(m+1)} r_{nuc}^{(n-2)(m+1)} D_3 + \ldots + (-1)^N \frac{n(n-1)\ldots(n-N+3)}{(N-2)!}$$

$$\left. \times r^{(N-2)} r_{nuc}^{(n-N+2)(m+1)} D_{N-1}] - (-1)^{(n+1)} r_{nuc}^{(n+1)} \left[D_{0(N-1)} \right.\right.$$

$$\left.\left. - \sum_{l=1}^{N-1} (-1)^l D_{0l} \right] \right\} \exp\left[-\frac{1}{k\tau_2} \frac{r^{(m+1)}}{(m+1)} + \frac{1}{k\tau_1} \frac{r_{nuc}^{(m+1)}}{(m+1)} \right],$$

$$n = N - 2, \; i = 1, 2, \ldots N - 1; \qquad (7)$$

$$D_i = \left(1 + \frac{A^2 r^{(m+1)}}{1!(i+1)} + \frac{A r^{(m+1)^2}}{2![i + (m+1)]} + \frac{A^3 r^{(m+1)^3}}{3![i + (m+1)^2]} + \ldots \right),$$

$$D_{0i} = D_i \text{ at } r = r_{nuc};$$

$$A = (m+1)^{-1}(-1/k\tau_1 + 1/k\tau_2),$$

where k is a function of the mass-transfer coefficient in the region in which the crystallization rate depends on the crystal size, found from equations for Nusselt numbers [2, 4, 7].

For N cells of equal volume and a growth rate of crystals dependent on their size in the range from r_{nuc} to r_n, solution of model (6) gives for the density of CSDF

$$f_N(r) = \frac{1}{n!}(1/k\tau_1)^n \frac{f_0}{r_{nuc}^m}\frac{r^m}{(1+m)}(r^{m+1} - r_{nuc}^{m+1})^n \times \exp\left[-\frac{1}{k\tau_1(m+1)}(r^{m+1} - r_{nuc}^{m+1})\right], \quad (8)$$

where $n = N - 1$.

At $r > r_n$, the growth rate of crystals is independent of their size, and the solution to model equation (6) for the density of CSDF for $N - 1$ cells of equal volume, supplemented with a smaller cell at $f_i^0 = f_i(r_n)$, where i is the cell number, takes the form

$$f_N = \sum_{i=1}^{N-1}\left\{\frac{1}{(n+1-i)!}(\eta\tau_1)^{i-n-2} f_i^0 \{[(r - r_n)^{n+1-i}B^{-1} - (n+1-i)(r-r_n)^{n-i}B^{-2} - (n+1-i)(n-i)(r-r_n)^{n-1-i} \times B^{-1} \ldots + (-1)^{n-i}(n+1-i)!(r-r_n)B^{i-n-1} - (-1)^{n-i}(n+1-i)!B^{i-n-2}]\exp[-(\eta\tau_1)^{-1}(r-r_n)] - (-1)^{n+1-i}(n+1-i)!B^{i-n-2}\exp[-(\eta\tau_2)^{-1}(r-r_n)]\}\right\} + f_N^0 \exp[-(\eta\tau_2)^{-1}(r-r_n)], \quad (9)$$

where $n = N - 2$, $B = 1/(\eta\tau_1) + 1/(\eta\tau_2)$, and f_i^0 are the CSDF densities found from Eqs. (7) and (8).

For N cells of equal volume, Eq. (9) can be brought to the form

$$f_N = \sum_{i=1}^{N}\left[\frac{1}{(n-i)!}(\eta\tau_1)^{i-n} f_i^0 (r - r_n)^{n-i}\right] \times \exp[-(\eta\tau_1)^{-1}(r-r_n)], \quad (10)$$

where $n = N$.

The size of crystal nuclei, r_{nuc}, can be evaluated by comparing the CSDF density calculated by Eqs. (7)–(10) with the experimental CSDF density at known hydrodynamic conditions of agitation in the flow-through mixing cell and hydrodynamic and mass-transfer parameters at the phase boundary. If the influence of only the nonideality of agitation on the crystal growth rate and density of the nucleation function in the flow-through mixing cell is assumed in the model (6), then Eqs. (7)–(10) are brought, in passing to the limits $r_{nuc} \to 0$, $r_n \to 0$, $f_1 \to f_0$, $f_{i+1}(r_n) \to 0$, to the following form:

$$f_N = \frac{1}{n!}(\eta\tau_1)^{-(n+1)}\{[r^n B^{-1} - nr^{n-1}B^{-2} + \ldots + (-1)^{n-1}n!rB^{-n} + (-1)^n n!B^{-(n+1)}] - (-1)^n n!\exp(Br)\} f_0 \exp(-r/\eta\tau_1), \quad n = N - 2, \quad (11)$$

for $N - 1$ cells of equal volume, supplemented with a smaller cell ($N \geq 2$); and

$$f_N = \frac{1}{(n-1)!}(\eta\tau_1)^{-n} r^n f_0 \exp(-r/\eta\tau_1), \quad n = N - 1, \quad (12)$$

for N cells of equal volume ($N \geq 1$).

The method for studying the kinetics of mass crystallization from solution was tested for the example of a well-studied process, isothermal crystallization of sodium chloride [9]. In accordance with the technique suggested, the structural parameters of the flow of phases were determined, isothermal crystallization of sodium chloride was performed, the CSDF density was found experimentally for sodium chloride, and kinetic parameters of crystallization were determined by comparing the experimental CSDF density with the calculated value. Equations (5)–(12) were solved numerically for prescribed input and output parameters of the process and hydrodynamic characteristics for each jth fraction, and the sought-for parameters were varied, with the hydrodynamic and mass-transfer parameters adjusted, to give their optimal values at the minimum rms deviation of the results of calculation from the experimental data. In calculating the CSDF density by Eqs. (7)–(10), the exponent was taken to be equal to the average value $m = 0.5$ for the region in which the growth rate of crystals depends on their size, and parameter k was taken to be equal to the average value for calculation in the range from between r_{nuc} and r_n.

Figure 1a shows the experimental and calculated CSDF densities for a mode of crystallization of sodium chloride. The disagreement between the calculation and the experiment did not exceed ±9%. The calculated CSDF density was used to find the nucleation function density $f_0 = 1.9 \times 10^{13}$ m^{-1} m^{-3} and the crys-

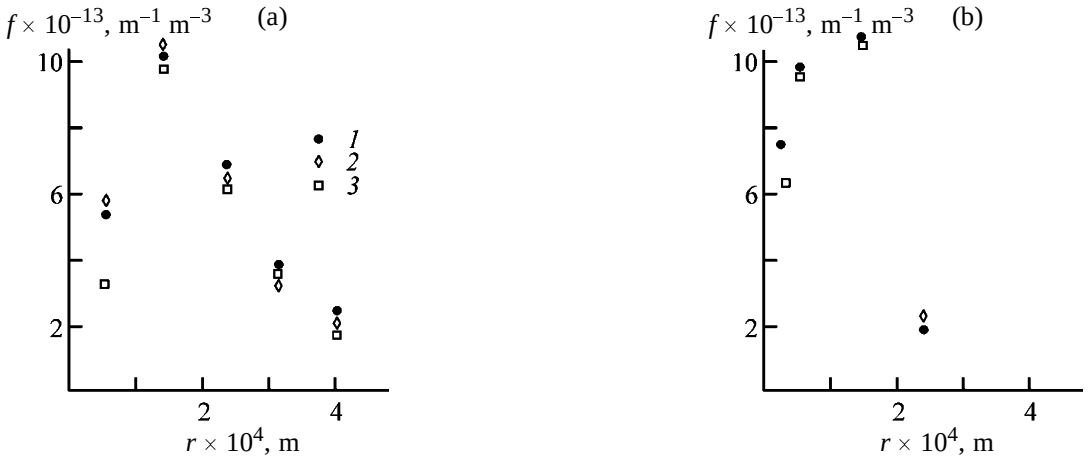


Fig. 1. Density of the distribution function f of crystals over size r in isothermal crystallization of (a) sodium chloride and (b) calcium formate. Crystallization modes for sodium chloride and potassium formate, respectively: suspension flow rate at the outlet, 0.43×10^{-3} and 1.0×10^{-3} m^3 h^{-1}; γ, 1.44 and 1.4; pressure, 0.009 and 0.017 MPa; temperature difference between the heat-exchange wall and the mass in crystallization, 15 and 12°C; and water evaporation rate, 0.19×10^{-3} and 0.25×10^{-3} m^3 h^{-1}. (*1*) Experiment; calculation by Eqs. (*2*) (7)–(10) and (*3*) (11) and (12).

tal growth rate $\eta = 8.1 \times 10^{-8}$ m s^{-1}. These values are close to published data [9], which indicates that the method and model are adequate. If the kinetic parameters are calculated by Eqs. (11) and (12) with the region in which the growth rate of crystals depends on their size disregarded, then, as follows from Fig. 1a, the disagreement between the calculation and the experiment for the fraction $r < \sim 0.1 \times 10^{-3}$ m grows, with the calculated density of the nucleation function increasing by an order of magnitude. However, taking into account the relatively insignificant contribution from the size of these crystals to the overall balance, solutions (11) and (12) to the model of CSDF can be used to make the calculations simpler.

The method was applied to a study of the kinetics of crystallization in manufacture of ultrapure calcium formate, which is used in electronics, radio engineering, and instrument making. Figure 1b shows as an example the experimental and calculated dependences of the CSDF density for a mode of crystallization of calcium formate. The disagreement between the experiment and the calculation did not exceed ±8.9%.

The kinetic parameters for this mode of crystallization of calcium formate are as follows: nucleation function density $f_0 = 2.5 \times 10^{13}$ m^{-1} m^{-3}, crystal growth rate $\eta = 0.12 \times 10^{-7}$ m s^{-1}.

CONCLUSIONS

(1) A cell model of the process of crystallization in a flow-through cell with nonideal mixing was constructed. The equations of the model for the density of the crystal size distribution function were solved for any crystal size, including the region at Re < 1, in which the crystal growth rate may depend on the crystal size.

(2) The method was tested in a study of the kinetics of mass crystallization from solutions of sodium chloride and calcium formate.

REFERENCES

1. Randolph, A.D. and Larson, M.A., *Am. Inst. Chem. Eng. J.*, 1962, vol. 8, no. 5, pp. 639–645.
2. Braginskii, L.N., Begachev, V.I., and Barabash, V.M., *Peremeshivanie v zhidkikh sredakh* (Agitation of Liquid Media), Leningrad: Khimiya, 1984.
3. Barabash, V.M. and Zelenskii, V.E., *Teor. Osn. Khim. Tekhnol.*, 1997, vol. 31, no. 5, pp. 465–471.
4. Levich, V.G., *Fiziko-khimicheskaya gidrodinamika* (Physicochemical Hydrodynamics), Moscow: Fizmatgiz, 1959.
5. Kolmogorov, A.N., *Dokl. Akad. Nauk SSSR*, 1941, vol. 32, no. 1, pp. 19–25.
6. Aerov, M.E. and Todes, O.M., *Gidravlicheskie i teplovye osnovy raboty apparatov so statsionarnym i kipyashchim sloem* (Hydraulic and Thermal Foundations of the Operation of Apparatus with Fixed and Fluidized Bed), Leningrad: Khimiya, 1968.
7. Aksel'rud, G.A., *Massoobmen v sisteme tverdoe telo–zhidkost'* (Mass Exchange in the Soid–Fluid System), Lvov: L'vov. Univ., 1970.
8. Brian, P.L.T. and Hales, H.B., *Am. Inst. Chem. Eng. J.*, 1969, vol. 15, pp. 419–423.
9. Todes, O.M., Seballo, V.A., and Gol'tsiker, A.D., *Massovaya kristallizatsiya iz rastvorov* (Bulk Crystallization from Solutions), Leningrad: Khimiya, 1984.

Russian Journal of Applied Chemistry, Vol. 78, No. 1, 2005, pp. 113–119. Translated from Zhurnal Prikladnoi Khimii, Vol. 78, No. 1, 2005, pp. 114–121.
Original Russian Text Copyright © 2005 by Kondrat'ev, Ivanchev.

PROCESSES AND EQUIPMENT OF CHEMICAL INDUSTRY

Optimization of Polymerization in Autoclave and Tubular Reactors

Yu. N. Kondrat'ev and S. S. Ivanchev

Central Research Institute of All-Round Automation, Joint-Stock Company, St. Petersburg, Russia
St. Petersburg Branch, Boreskov Institute of Catalysis, Siberian Division, Russian Academy of Sciences, St. Petersburg, Russia

Received May 14, 2004

Abstract—The possibilities of improving operation of one-zone autoclave and tubular reactors using appropriate initiating systems without changes in the reactor design and process scheme were analyzed and experimentally tested on pilot and industrial installations for high-pressure polymerization of ethylene.

Despite rapid development of processes for catalytic polymerization of ethylene at low pressures in the gas phase and solution, high-pressure polymerization of ethylene is still of industrial importance. At present, nearly 25% (~22 million tons per year) of the total production volume of polyolefins (~84 million tons) is produced using high-pressure autoclave and tubular reactors. Thus, the improvement of operation of reactors for high-pressure polymerization of ethylene, especially without changes in the reactor design and process scheme, is an urgent problem.

In this paper we analyzed the possibility of improving the operation of high-pressure autoclave and tubular reactors without changes in the reactor design and process scheme, on the basis of the analysis of the operation conditions and mechanism of polymerization as influenced by various initiating systems (peroxides and their mixtures, and mixtures of peroxides and oxygen).

The structure of peroxide initiator determines its important properties and feasibility of its use [1–3]. The later notion involves: (1) kinetic characteristics, operation temperature range, and performance; (2) solubility in oils (hydrocarbons) and thus simplicity of supply into the reactor; (3) absence of corrosion effect on the installation; (4) safe use and storage; and (5) hygienic, sanitary, and toxicological properties.

These requirements were used in selection of peroxides recommended for high-pressure polymerization of ethylene by the producer of peroxides, Akzo Nobel Company [3].

However, even for this group of reagents the operation parameters and conditions providing the most efficient use of peroxide, taking into account the specific consumption and quality (amount of extractable impurities) and assortment of the products, should be tested experimentally. This especially concerns the use of peroxide mixtures in autoclave reactors and mixtures of peroxides and oxygen in tubular reactors.

The data on the optimal use of peroxides in one- and two-zone industrial reactors of autoclave type (ideal mixing reactors) with production capacity from 16 to 20 thousand tons per year are given below.

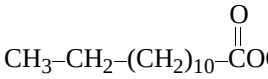
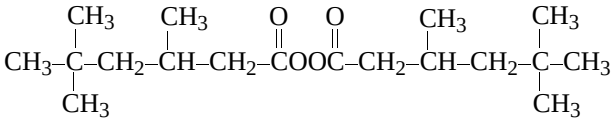
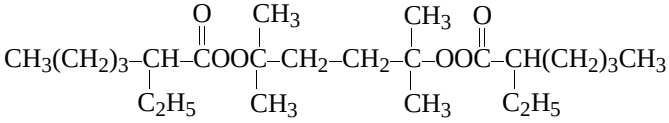
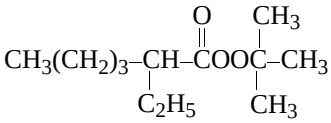
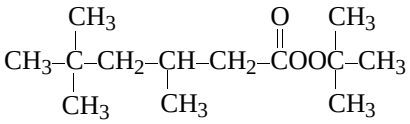
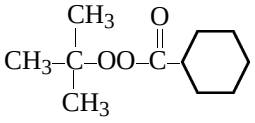
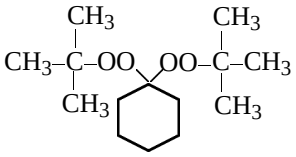
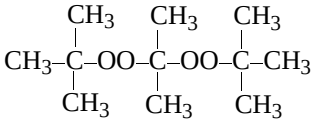
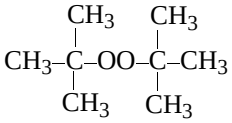
AUTOCLAVE REACTORS

Initiator performance. In our work we tested nine peroxy initiators; data on their initiation power are listed in Table 1.

As seen, the specific consumption of initiators decreases on passing from low-temperature (Tr-36) to high-temperature (Tr-B) peroxides. Only two peroxides do not obey the general trend toward a decrease in the specific consumption with increasing temperature: Tr-D initiator with very high performance in the corresponding temperature range and Tr-C initiator with increased specific consumption, which is due to its use in industrial reactors at temperatures higher then the optimum to provide the process stability. With increasing temperature of the reaction mixture, the generation of heat decreases and the temperature in the reaction zone begins to decrease, i.e., the process passes to the self-control mode. Specifically this operation mode is used with Tr-C initiator (240–255°C).

1070-4272/05/7801-0113© 2005 Pleiades Publishing, Inc.

Table 1. Specific consumption of peroxides per ton of polyethylene (PE) in industrial and pilot installations, as influenced by their structure

Initiator brand	Structure	Specific consumption per ton of polyethylene	
		kg	mol
Laurox		5–6	12.5–15.0
Trigonox-36 (Tr-36)		2.5	8.0
Trigonox-141* (Tr-141)		2.4	5.5
Trigonox-21 (Tr-21)		0.6	2.8
Trigonox-42 (Tr-42)		0.4	1.7
Trigonox-C (Tr-C)		0.35–0.5	1.8–2.5
Trigonox-22* (Tr-22)		0.47	1.8
Trigonox-D* (Tr-D)		0.14–0.24	0.6–1.0
Trigonox-B (Tr-B)		0.10–0.15	0.65–1.03

* Bifunctional peroxide.

Low activity of Laurox is due to its poor solubility. As a result, this initiator is only rarely used in reactors for ethylene polymerization.

We analyzed the operation of various autoclave installations for production of polyethylene with a melt flow index (MFI) of 2 g/10 min with the most widely used and available Tr-C initiator.

Amount of extractable impurities in polyethylene as influenced by Trigonox-C peroxy initiator. The data on the amount of extractable impurities in

Table 2. Amount of extractable impurities* and specific consumption of initiators and solvents in production of polyethylene with MFI of 2 g/10 min

Run no.	Initiating system**	Extractable impurities, wt %	Specific consumption, kg per ton PE	
			oil (solvent for initiator)	initiating system
1	Tr-C/Tr-C	1.0	4.5	0.49
2	Tr-C/(Tr-C + Tr-B)	0.78	4.1	0.32
3	(Tr-C + Tr-42)/(Tr-C + Tr-B)	0.8–0.9	6.3	0.17
4	Tr-C/Tr-B	0.82	3.2	0.36
5	Tr-C/Tr-B	0.86	5.8	0.26
6	Tr-C/Tr-B	0.9	6.0	0.27
7	(Tr-C + Tr-42)/Tr-B	0.9–0.7	6.2	0.165
8	(Tr-C + Tr-42)/Tr-B	0.58	5.8	0.125
9	(Tr-C + Tr-B)/(Tr-C + Tr-B	0.7	3.7	0.24
10	(Tr-C + Tr-42)/Tr-C	0.8	5.8	0.32

* Low-molecular-weight impurities (such as oil or oligomers) remaining in polyethylene.
** Peroxide added into the top/bottom section of the reactor.

polyethylene prepared in a one-zone industrial autoclave reactor at various initiating modes using Tr-C, Tr-B, and Tr-42 are listed in Table 2.

In some experiments, the oil (solvent for initiator) was replaced by isododecane (IDD) to exclude the transfer of oil-solvent into the extractable impurities, because IDD dissolves in ethylene in the low-pressure separator and does not remain in the polymer. In this case, the fraction of oil in the total amount of extractable impurities is about 30% of its specific consumption.

The correlation of the specific consumption of Tr-C initiator X and the residual content of extractable impurities in polyethylene A, which was calculated as the difference between the total content of extractable compounds E and amount of extractable compounds originating from the oil solvent ($0.3G$) is shown in Fig. 1.

As seen from Fig. 1, the residual content of extractable impurities linearly depends on the specific consumption of Tr-C initiator, and with a change in the specific consumption of Tr-C initiator by 0.1 kg per ton polymer the content of extractable impurities changes by 0.1 wt %. When the consumption of Tr-C initiator is close to 0, the content of extractable impurities decreases to 0.25–0.30 wt %, which is probably due to the contamination of the polymer with oil from compressors.

Table 2 shows that the Tr-C + Tr-42/Tr-C + Tr-B and Tr-C + Tr-42/Tr-B (run nos. 3, 8) systems provide the greatest increase in the process efficiency with simultaneous decrease in the content of extractable impurities.

Process improvement and increase in the product assortment using one-zone industrial autoclave reactor. The one-zone autoclave allows synthesis of polyethylene with MFI > 1 g/10 min, whereas preparation of polyethylene with MFI < 1 g/10 min requires a two-zone autoclave reactor with low operation temperature in the upper zone (<200°C) in which low-temperature peroxide initiators of Tr-36 type are used.

To make possible preparation of polyethylene with MFI < 1 g/10 min in a one-zone autoclave, the temperature in the top section of the reactor should be decreased, i.e., a relatively low-temperature peroxide should be used in this section. However, due to the rapid temperature increase along the reactor profile in the top section of the reactor, this peroxide will lose

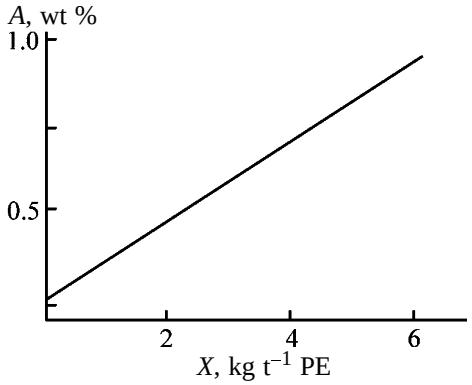


Fig. 1. Content of extractable impurities in polyethylene A as influenced by the specific consumption of Tr-C initiator X.

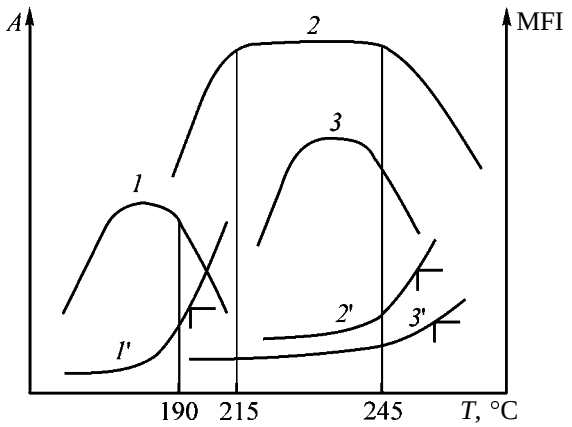


Fig. 2. (*1–3*) Polyethylene yield *A* and (*1'–3'*) MFI as influenced by temperature *T*. (*1, 1'*) Tr-36, (*2, 2'*) Tr-D, and (*3, 3'*) Tr-C.

the performance and decrease the molecular weight of the resulting polyethylene, i.e., will increase its MFI.

This process is schematically shown in Fig. 2 presenting the temperature dependences of MFI and specific consumption, determined for three peroxides.

In general, the use of each peroxide in the temperature range providing the highest yield of polyethylene seems to be optimal. However, monoperoxides are characterized by very narrow temperature range of the maximal polyethylene yield, and industrial operation in such a narrow range is very difficult and fraught with the loss of the temperature stability of the process. The loss of the temperature stability is related to the fact that, with changes in temperature in the reaction zone, the specific yield will always decrease [4, 5].

With decreasing temperature of the reaction medium, the rates of polymerization and heat release both decrease, and the temperature of the reaction zone also decreases. As a result, further decrease in the heat release and temperature are observed, which can cause the process termination (heat "removal" from the reaction zone by flow of cold ethylene supplied into this section of the reactor).

The temperature dependences of the PE yield and MFI (Fig. 2) show that bifunctional peroxide Trigonox-D allows preparation of polyethylene with low MFI and maximal specific yield in a fairly wide temperature range. Thus, Trigonox-D can be used in the top section of the one-zone reactor for process initiation at temperatures from 215–218 to 240–245°C to prepare polyethylene with a low MFI and the highest yield in this reactor section. As a result, the assortment of polyolefins prepared in the one-zone reactor can be expanded up to production of polyethylene with MFI of 0.2–0.3 g/10 min.

The experimental results obtained using industrial one-zone reactors are as follows.

(1) The use of polymerization initiator Tr-D provides easy start of the process, stability of its operation, and production of polyethylene with MFI from 0.3 to 2.0 g/10 min.

(2) When preparing polyethylene with MFI of 2 g/10 min, replacement of Tr-C by Tr-D initiator decreases the consumption of the initiating system (recalculated to 100% initiator) by a factor of 1.6 with preservation of all the operation parameters.

(3) Replacement of Tr-C + Tr-B by Tr-D + Tr-B mixture in the top and bottom sections of the reactor decreases the specific consumption of Tr-D peroxide by a factor of 2.1–2.6 as compared to Tr-C initiator; simultaneously, the specific consumption of Tr-B initiator decreases by a factor of 1.5.

(4) The use of Tr-D initiator in the top section and Tr-D peroxide or Tr-D + Tr-B mixture in the bottom section allows the pressure in the reactor to be decreased from 1440–1470 to 1290 kgf cm^{-2}, i.e., by 150–180 kgf cm^{-2}.

(5) The use of Tr-D + Tr-B and Tr-C + Tr-B mixtures in the top and bottom sections of the reactor increases the conversion, which (due to the temperature decrease in the top section and its increase in the bottom section) increases by 15 rel % the installation capacity in production of 10 803-020 brand polyethylene with MFI of 2.0 g/10 min.

The results obtained in comparative analysis of mono- and bifunctional peroxides showed that Tr-D peroxide is a promising initiator, providing lower specific consumption in wider ranges of initiation temperatures (in comparison with kinetically similar monoperoxides) and allowing preparation of polymers with a higher molecular weight. These data were confirmed experimentally using pilot setup and industrial installations with one-zone autoclave reactors.

TUBULAR REACTORS

The use of oxygen as initiator is well known. The disadvantages of the oxygen initiation are as follows.

(1) The use of oxygen as polymerization initiator almost excludes the possibility of control of the reaction temperature. Only maximal temperatures can be corrected, because of long dead time (7–15 min) for

oxygen transport from the dosing unit to the active zone of the reactor.

(2) Since preheating of the reaction mixture to relatively high temperatures (190–205°C) is necessary for the oxygen initiation of polymerization, fairly long sections are required for heating of the reaction mixture, with partial pressure loss in these sections. In this case, heating of the mixture to 150–180°C proceeds at low initiating activity of oxygen with formation of small amounts of the polymer with very high molecular weight, which condenses on the colder walls of the reactor. This decreases the heating rate of the reaction mixture and, as a rule, decreases the quality of the final product.

(3) Maintenance of the prescribed temperature ranges of the reaction mixture in various sections of the multizone reactor requires a complex system to control the oxygen concentration in the system of interconnected sections of the reactor, when any change in the oxygen concentration in a certain section requires the corresponding correction both in the total amount of oxygen supplied and in its distribution in the reactor zones.

(4) Relatively high temperature for initiation "start" decreases possible conversion and, thus, performance characteristics of the process.

Temperature profile of the reaction medium along a tubular reactor at oxygen initiation. Polymerization in a tubular reactor can proceed at variation of certain process parameters, including the temperature of the heating water.

In Fig. 3 we show the temperature profiles in the first zone of a tubular reactor differing in the temperature of the heating water: (*1*) 217–220°C, mode 1; (*2*) 205°C, mode 2; and (*3*) 195°C, mode 3.

As seen, heating of the reaction mixture to temperatures lower than 190°C proceeds linearly, i.e., the temperature of the reaction mixture is determined by the temperature of the heating water. This fact suggests very low rate of oxygen initiation at temperatures lower than 190–195°C. If in this temperature range the reaction mixture still receives sufficiently much heat from the heating water (mode 1), then the sum of this quantity with the heat of polymerization is sufficient to provide significant increase in the polymerization rate.

However, if the temperature of the heating water is close to the above temperature range (modes 2 and 3), then the amount of heat received from the heating water becomes insignificant, and further heating of the reaction mixture is due only to the heat of polymerization. We can conclude that the temperature at which the polymerization rate starts to increase (start temperature) is inversely proportional to the temperature of the heating water.

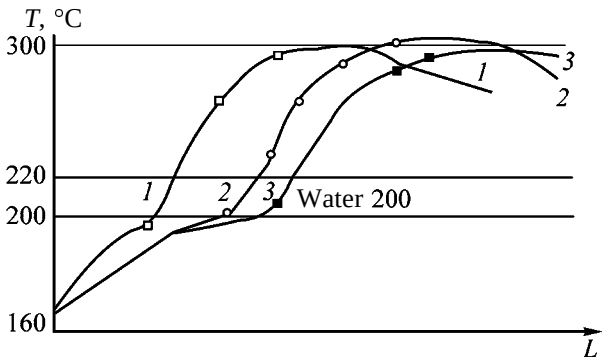


Fig. 3. Temperature profile of the reaction mixture *T* along the tubular reactor length *L* as influenced by the temperature of the heating water; pure oxygen initiation. Heating water temperature, °C: (*1*) 217–220, (*2*) 205–207, and (*3*) 195–197.

Further analysis of the temperature dependences (Fig. 3) shows that, after reaching the start temperatures in all of the above experimental modes, the polymerization rate and temperature of the reaction mixture sharply increase, and the rate of temperature increase is independent of the start temperature.

To decrease the length of the section for preheating of the reaction mixture to the temperatures of the oxygen initiation start and to eliminate the negative effect of hot water in the temperature range from 155–160°C to 225°C, additional heat supply using peroxy initiation systems is required.

In contrast to the oxygen dosing, solutions of peroxy compounds can be supplied in required amounts independently of the ethylene supply directly in any section of the reactor with very short dead time (several seconds). Various low-viscosity hydrocarbons from isododecane to oils of Risella-17 type are used as solvents for peroxides.

A feature of using peroxy initiators in tubular reactors is relatively narrow temperature range of efficient initiation, i.e., the temperature interval where the specific consumption of the given peroxide is minimal.

The specific consumption of peroxides in ethylene polymerization in autoclave and tubular reactors at operation in the temperature ranges of efficient initiation are listed in Table 3.

Table 3. Specific consumption of peroxides at optimal temperatures of initiation of ethylene polymerization

Initiator	*T*, °C	Specific consumption per ton polyethylene					
		autoclave reactor			tubular reactor		
		kg	mole	available O_2	kg	mole	available O_2
Trigonox-36	168	2.2	7.0	35	2.8	9.0	45
Trigonox-21	190	0.63	2.9	20			
Trigonox-42	215	0.44	1.9	15			
Trigonox-C	230	0.39	2.0	15	0.7	3.0	20
Trigonox-B	255	0.15	1.0	10			

Polymerization of ethylene with oxygen and peroxide initiation. The combined oxygen and peroxide initiation allows improvement of polyethylene polymerization in tubular reactors.

The use of low-temperature peroxy initiator at temperatures at which the initiating activity of oxygen is very low does not noticeably affect the efficiency of oxygen initiation, but the temperature profile will shift toward the zone start due to more rapid heating of the reaction mixture to the temperatures of the start of the oxygen initiation. This assumption was confirmed experimentally on an industrial tubular reactor using various systems of initiation of the ethylene polymerization in the first and second zones of the reactor. The temperature profiles of three modes of initiation studied are shown in Fig. 4.

Profile *1* in the first and second zones of the tubular reactor corresponds to the conditions of initiation using only oxygen in each section. The maxima of the temperature profiles are shifted to the end of each zone. Owing to the restrictions on the temperature of the reaction mixture at the outlet from the second zone, the temperature at the inlet of this second zone is increased to 225°C; as a result, the maximum of the temperature profile still more shifts toward the zone end and the temperature at the outlet exceeds the permissible range. Under the process conditions corresponding to profile *1*, conversion reaches only 19%.

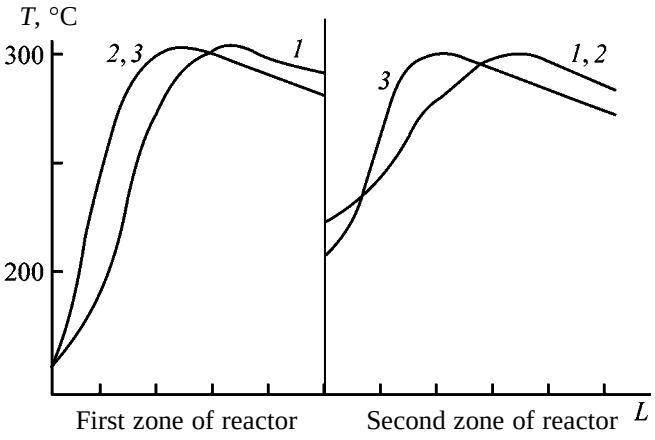


Fig. 4. Temperature of the reaction mixture *T* along the tubular reactor length *L* as influenced by initiation system. (*1*) Pure oxygen initiation in both zones, (*2*) Tr-36 and oxygen in the first zone and only oxygen in the second zone, and (*3*) Tr-C + Tr-36 and oxygen in the first zone and Tr-C and oxygen in the second zone.

Profile *2* was recorded at initiation using oxygen and Trigonox-36 peroxide in the first zone and only oxygen initiation in the second zone. In this case, the amount of oxygen supplied into the first and second zones of the reactor is similar to that used at pure oxygen initiation (profile *1*). In the first zone, the maximum in the temperature profile shifts to the zone start by 80–100 m, and the temperature at the first zone outlet decreases by 10°C. To maintain the required temperature at the inlet into the second zone, 225°C, the temperature of the ethylene flow supplied into the second zone should be increased to 150°C. Under these conditions, maximal temperatures in the first and second zones of the reactor are close to those observed at pure oxygen initiation (profile *1*).

As a result, te conversion increased by 2% and reached 21%. The consumption of Tr-36 per ton PE was about 2.6 kg.

Thus, a combination of low-temperature peroxide and oxygen initiation shifts the temperature profile toward the zone start, increases the polymer yield in the low-temperature initiation region (conversion increases by ~ 1%), and allows the polymerization to be performed locally in the low-temperature section without affecting the temperature of the reaction mixture in the remaining volume.

The use of a single low-temperature peroxide in the

first zone of the tubular reactor is a necessary but insufficient condition at low temperature of heating water (180–185°C). This water temperature allows the temperature difference between the reaction mixture and heat carrier to be increased by 20–30°C, thus enhancing the heat removal and increasing the conversion by ~1.5%. Efficient initiation should also be provided in the temperature range from 180 to 215–240°C, and this problem can be solved with peroxy initiators of Tr-21, Tr-C, and Tr-D types.

Temperature profiles *3* correspond to the combined use of oxygen and peroxide initiation in both reactor zones. In our case, along with oxygen we used Tr-36 + Tr-C mixture and Tr-C peroxide in the first and second zones of the reactor, respectively.

To provide similar temperature range in all the modes studied, in this process mode the oxygen supply in each section was decreased by 20%.

The temperature profile in the first zone remained unchanged in comparison with the process using a combination of Tr-36 and oxygen (profile *2*), i.e., Tr-C initiated polymerization and partially replaced oxygen initiation at relatively low temperatures (up to 25°C).

The use of Tr-C in the second zone allowed a decrease both in the oxygen supply and in the temperature at the inlet in the second zone (from 225 to 213°C), thus shifting the maximum in the temperature profile toward the start of this zone by almost 200 m.

In this case (profile *3*), the conversion was about 23%, i.e., 4% greater than at oxygen initiation (profile *1*).

The consumption of Tr-C per ton of additionally prepared PE was 1.0–1.2 kg.

Thus, the use of mixtures of Trigonox-21 and Trigonox-36 type peroxides in the first zone of a tubular reactor at a relatively low temperature (180–185°C) of heating water provides optimal operation conditions of the tubular reactor with simultaneous increase in the absolute capacity with respect to polyethylene by more than 5 abs. %.

CONCLUSION

Theoretical assumptions and experimental data show that the correct selection of the peroxy initiator significantly improves the efficiency of both autoclave and tubular reactors in production of polyethylene at high pressures.

REFERENCES

1. Ivanchev, S.S., *Radikal'naya polimerizatsiya* (Radical Polymerization), Leningrad: Khimiya, 1985.
2. Ivanchev, S.S. and Kondrat'ev, Yu.N., *Zh. Prikl. Khim.*, 1999, vol. 72, no. 4, pp. 682–687.
3. *Akzo Chemie Nederland bv. Noury Initiators. Delivery Program Polymerization Initiators. 1990. Akzo-Nobel Initiators for Polymer Production. Product Catalog*, 1990, pp. 10–18.
4. Vol'ter, B.V., Sal'nikov, I.V., and Sofiev, A.E., in *Materialy konferentsii po khimicheskim reaktoram* (Proc. Conf. on Chemical Reactors), Novosibirsk: Sib. Otd. Ross. Akad. Nauk, 1965, pp. 201–214.
5. Kafarov, V.V., Sofiev, A.E., and Trakhtenberg, A.M., *Dokl. Akad. Nauk SSSR*, 1985, vol. 268, no. 1, pp. 137–142.

Russian Journal of Applied Chemistry, Vol. 78, No. 1, 2005, pp. 120–124. Translated from Zhurnal Prikladnoi Khimii, Vol. 78, No. 1, 2005, pp. 122–126.
Original Russian Text Copyright © 2005 by Dikusar, Vyglazov, Moiseichuk, Zhukovskaya, Kozlov.

ORGANIC SYNTHESIS AND INDUSTRIAL ORGANIC CHEMISTRY

Preparative Synthesis of Vanillin and Vanillal Alkanoates

E. A. Dikusar, O. G. Vyglazov, K. L. Moiseichuk, N. A. Zhukovskaya, and N. G. Kozlov

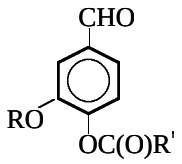
Institute of Physical Organic Chemistry, Belarussian National Academy of Sciences, Minsk, Belarus
Tereza Inter Limited Liability Company, Moscow, Russia

Received June 16, 2004

Abstract—Procedures for preparing vanillin and vanillal alkanoates were developed.

Vanillin (4-hydroxy-3-methoxybenzaldehyde, **Ia**) and its homolog, vanillal (4-hydroxy-3-ethoxybenzaldehyde, **Ib**) are widely used in food and perfume industries [1–3]. Vanillin can also be used as a synthetic precursor of biologically active substances [4, 5]. However, new processes in food industry demand new aroma chemicals that would have vanilla smell but be more heat-resistant than vanillin and stable in a wide range of pH in the presence of enzymes. These requirements stimulate chemists to prepare new vanillin and vanillal derivatives; many of them appeared to exhibit stronger vanilla smell, compared to the initial compounds, with diverse tints.

Here we report convenient synthetic routes to vanillin (**IIa**–**IIm**) and vanillal (**IIIa**–**IIIg**) esters.



II a–m, III a–g

II, R = Me, R' = H (**a**), Me (**b**), Et (**c**), Pr (**d**), Me_2CH (**e**), Bu (**f**), Me_2CHCH_2 (**g**), C_5H_{11} (**h**), C_6H_{13} (**i**), C_7H_{15} (**j**), $C_{12}H_{25}$ (**k**), CH_2Cl (**l**), 4-$MeC_6H_4O(CH_2)_2$ (**m**); **III**, R = Et, R' = H (**a**), Me (**b**), Et (**c**), Pr (**d**), Me_2CH (**e**), Bu (**f**), Me_2CHCH_2 (**g**).

Some of them were characterized [6–13], but the lack of some esters in the homologous series of the vanillin and vanillal derivatives and incompleteness of the available physicochemical data for the previously described compounds stimulated us to make this study, aimed to develop new flavor additives derived from vanillin and vanillal.

The formates were prepared by the reactions of vanillin **Ia** and vanillal **Ib** with formic acid in the presence of dicyclohexylcarbodiimide [14], which is a simpler procedure compared to the known routes [11]. The other esters **IIb**–**IIm** and **IIIb**–**IIIg** were prepared by reactions of **Ia** and **Ib** with alkanecarboxylic acid chlorides in the presence of pyridine [15, 16]. To simplify the production process and improve the purity of the target products for their use in formulations for perfume and food industry, the esters were also prepared by the Schotten–Baumann reaction [9, 17]. The resulting esters **IIb**–**IIe** and **IIIb**–**IIIe** (Tables 1, 2) do not require additional purification. They are free of benzene and pyridine impurities and can be directly used in the perfume industry.

The organoleptic assessment of the scents of **IIa**–**IIg** and **IIIa**–**IIIg** was made by the Tasting Council at the Accredited Checkout and Analytical Laboratory of the Tereza Inter Limited Liability Company (Moscow, Russia). Esters **IIa**–**IIg** and **IIIa**–**IIIg** have pronounced vanilla smell with various intense tints (Table 3). Esters **IIh**–**IIm** have no odor.

EXPERIMENTAL

The IR spectra of the compounds were recorded on a Protege-460 IR Fourier spectrometer (Nicolet) from the samples prepared as thin films or KBr pellets; the UV spectra, on a Specord UV-Vis spectrophotometer from 1×10^{-4} M solutions in 1-butanol; the ^1H NMR spectra, on a BS-587A spectrometer (100 MHz, Tesla) from 5% solutions in $CDCl_3$, with octamethyltetracyclosiloxane as internal reference; and the mass spectra, on a Chrommas GC/MS Hewlett–Packard 5890/5972 gas chromatograph–mass spectrometer equipped with an HP-5MS column, at an ionizing electron energy of 70 eV.

Alkanecarboxylic acid chlorides were prepared by refluxing the corresponding carboxylic acids with a 1.5-fold excess of $SOCl_2$ in benzene.

1070-4272/05/7801-0120© 2005 Pleiades Publishing, Inc.

Table 1. Properties of esters **IIa**–**IIm** and **IIIa**–**IIIg**

Ester	Yield, %	T_m, °C	Found, %		Formula	Calculated, %		*M*	
			C	H		C	H	found	calculated
IIa	70	54–55	60.08	4.43	$C_9H_8O_4$	60.00	4.48	180	180.2
IIb	92	78–79	62.05	5.43	$C_{10}H_{10}O_4$	61.85	5.19	194	194.2
IIc	79	35–36	63.64	5.79	$C_{11}H_{12}O_4$	63.46	5.77	208	208.2
IId*	81	–	65.12	6.42	$C_{12}H_{14}O_4$	64.86	6.31	222	222.2
IIe	89	29–30	65.07	6.46	$C_{12}H_{14}O_4$	64.86	6.31	222	222.2
IIf*	84	–	66.29	7.02	$C_{13}H_{16}O_4$	66.09	6.83	236	236.3
IIg*	84	–	66.27	7.04	$C_{13}H_{16}O_4$	66.09	6.83	236	236.3
IIh*	85	–	67.39	7.41	$C_{14}H_{18}O_4$	67.18	7.25	250	250.3
IIi*	82	–	68.45	7.80	$C_{15}H_{20}O_4$	68.16	7.63	264	264.3
IIj*	77	–	69.18	8.03	$C_{16}H_{22}O_4$	69.04	7.91	278	278.3
IIk	75	–	72.54	9.37	$C_{21}H_{32}O_4$	72.38	9.26	348	348.5
IIl*	78	–	52.63	4.08	$C_{10}H_9ClO_4$	52.53	3.97	228	228.6
IIm	76	63–64	69.02	5.97	$C_{18}H_{18}O_5$	68.78	5.77	314	314.3
IIIa	73	47–48	62.03	5.28	$C_{10}H_{10}O_4$	61.85	5.19	194	194.2
IIIb	87	33–34	63.72	5.84	$C_{11}H_{12}O_4$	63.46	5.77	208	208.2
IIIc	84	45–47	65.07	6.44	$C_{12}H_{14}O_4$	64.86	6.31	222	222.2
IIId*	92	–	66.34	7.07	$C_{13}H_{16}O_4$	66.09	6.83	236	236.3
IIIe	93	45–46	66.29	7.01	$C_{13}H_{16}O_4$	66.09	6.83	236	236.3
IIIf*	92	–	67.41	7.45	$C_{14}H_{18}O_4$	67.18	7.25	250	250.3
IIIg*	82	–	67.49	7.41	$C_{14}H_{18}O_4$	67.18	7.25	250	250.3

* T_m, °C (p, mm Hg), d_{20}^{20}, n_D^{20}: 137–138 (0.5), 1.2101, 1.5281 (**IId**); 129–130 (**I**), 1.1807, 1.5273 (**IIf**); 129–130 (0.5), 1.1825, 1.5235 (**IIg**); 155–156 (0.5), 1.1228, 1.5068 (**IIh**); 163–164 (0.5), 1.1033, 1.5092 (**IIi**); 170–171 (0.5), 1.0949, 1.5079 (**IIj**); 145–146 (0.5), 1.2009, 1.5272 (**IIId**); 150–151 (0.5), 1.1129, 1.5213 (**IIIf**); 132–133 (0.5), 1.0954, 1.5180 (**IIIg**).

** Cl, %: found 15.39, calculated 15.51 (**IIl**).

Table 2. ^{1}H, IR, and UV spectra of esters **IIa**–**IIm** and **IIIa**–**IIIg**

Ester	^{1}H NMR spectrum, δ, ppm	IR spectrum, ν, cm^{-1}	UV spectrum, λ_{max}, nm (ε)
IIa	3.91 s (3H, MeO), 7.20–7.57 m (3H, C_6H_3), 8.27 s [1H, OC(O)H], 9.95 s (1H, CHO)	3110, 3077, 3060, 3045, 3020, 2995, 2960, 2928, 2847, 2805, 2749, 1757, 1685, 1801, 1473, 1455, 1426, 1392, 1275, 1204, 1197, 1154, 1124, 1097, 1029, 962, 875, 867, 821, 733, 679, 632, 590, 574	205 (9000), 223 (14000), 260 (8000), 308 (3000)
IIb	2.32 s (3H, Me), 3.92 s (3H, MeO), 7.18 d, 7.48 m (3H, C_6H_3), 9.92 s (1H, CHO)	3090, 3070, 3055, 3017, 2965, 2945, 2920, 2848, 2805, 2755, 1758, 1690, 1599, 1507, 1471, 1427, 1396, 1377, 1280, 1220, 1209, 1155, 1126, 1033, 1014, 907, 862, 830, 739, 680, 600, 580	206 (8000), 224 (15000), 261 (8000), 309 (3000)
IIc	1.25 t (3H, $MeCH_2$), 2.52 q (2H, CH_2), 3.84 s (3H, MeO), 7.13 d, 7.42 m (3H, C_6H_3), 9.88 s (1H, CHO)	3115, 3070, 3017, 2968, 2940, 2875, 2855, 2800, 2745, 1766, 1700, 1602, 1504, 1466, 1423, 1393, 1275, 1180, 1182, 1145, 1120, 1032, 912, 870, 40, 780, 733, 645, 580	205 (8000), 223 (14000), 260 (8000), 310 (3000)
IId	1.02 t (3H, Me), 1.63 m (2H, CH_2), 2.51 t (2H, CH_2), 3.84 s (3H, MeO), 7.15 d, 7.40 m (3H, C_6H_3), 9.90 (1H, CHO)	3117, 3071, 3015, 2968, 2939, 2874, 2853, 2800, 2743, 1765, 1701, 1601, 1503, 1465, 1423, 1391,1272, 1181, 1145, 1120, 1031, 913, 865, 840, 780, 733, 647, 582	206 (8000), 224 (15000), 260 (7000), 310 (3000)

Table 2. (Contd.)

Ester	^{1}H NMR spectrum, δ, ppm	IR spectrum, ν, cm^{-1}	UV spectrum, λ_{max}, nm (ε)
IIe	1.30 s, 1.40 s, 2.88 s, 2.88 m (7H, *i*-Pr), 3.90 s (3H, MeO), 7.21 d, 7.50 m (3H, C_6H_3), 9.96 s (1H, CHO)	3115, 3075, 3015, 2976, 2940, 2878, 2845, 2800, 2745, 1763, 1701, 1601, 1503, 1468, 1423, 1389, 1270, 1202, 1180, 1150, 1121, 1191, 1033, 960, 914, 865, 815, 780, 734, 650, 580, 550	206 (9000), 223 (15000), 261 (7000), 311 (3000)
IIf	0.96 t (3H, Me), 1.20–1.90 m [4H, $(CH_2)_2$], 2.62 t (2H, CH_2), 3.96 s (3H, OMe), 7.15 d, 7.38 m (3H, C_6H_3), 9.90 s (1H, CHO)	3074, 3012, 2962, 2936, 2874, 2860, 2736, 1764, 1701, 1601, 1503, 1466, 1423, 1391, 1371, 1322, 1284, 1272, 1198, 1181, 1149, 1119, 1092, 1082, 1032, 964, 913, 866, 835, 781, 733, 645, 585, 548	206 (7000), 224 (14000), 261 (7000), 310 (3000)
IIg	1.06 d (6H, Me_2C), 1.35–2.90 m (3H, CH and CH_2), 3.96 s (3H, OMe), 7.12 d, 7.42 m (3H, C_6H_3), 9.91 s (1H, CHO)	3117, 3070, 3010, 2957, 2934, 2870, 2855, 2743, 1766, 1704, 1601, 1503, 1466, 1424, 1390, 1322, 1272, 1200, 1145, 1120, 1032, 965, 915, 866, 835, 780, 735, 645, 585, 545	206 (8000), 223 (14000), 260 (7000), 310 (3000)
IIh	0.90 t (3H, Me), 1.12–1.90 m [6H, $(CH_2)_3$], 2.58 m (2H, CH_2), 3.88 s (3H, OMe), 7.13 d, 7.44 m (3H, C_6H_3), 9.95 s (1H, CHO)	3110, 3070, 3010, 2958, 2935, 2872, 2856, 2743, 1765, 1704, 1602, 1503, 1465, 1424, 1392, 1321, 1271, 1200, 1144, 1120, 1033, 965, 915, 867, 835, 781, 736, 645, 585, 544	207 (8000), 223 (14000), 260 (7000), 311 (3000)
IIi	0.96 t (3H, Me), 1.15–1.88 m [8H, $(CH_2)_4$], 2.51 m (2H, CH_2), 3.86 s (3H, OMe), 7.12 d, 7.45 m (3H, C_6H_3), 9.91 s (1H, CHO)	3109, 3070, 3015, 2958, 2936, 2872, 2857, 2744, 1764, 1704, 1601, 1503, 1464, 1424, 1390, 1322, 1271, 1201, 1144, 1120, 1032, 965, 914, 867, 835, 782, 736, 644, 585, 545	207 (7000), 224 (14000), 261 (7000), 310 (3000)
IIj	0.92 t (3H, Me), 1.32 m [8H, $(CH_2)_4$], 1.79 m (2H, CH_2), 2.60 m (2H, CH_2), 3.88 s (3H, OMe), 7.14 d, 7.47 m (3H, C_6H_3), 9.90 s (1H, CHO)	3108, 3070, 3016, 2957, 2935, 2872, 2856, 2746, 1763, 1703, 1602, 1504, 1464, 1424, 1391, 1323, 1271, 1202, 1145, 1120, 1031, 965, 915, 867, 834, 782, 735, 644, 585, 544	208 (7000), 224 (14000), 262 (7000), 310 (3000)
IIk	0.89 t (3H, Me), 1.30 m [18H, $(CH_2)_9$], 1.75 m (2H, CH_2), 2.59 m (2H, CH_2), 3.87 s (3H, OMe), 7.16 d, 7.41 m (3H, C_6H_3), 9.91 s (1H, CHO)	3115, 3072, 3015, 2955, 2935, 2870, 2855, 2741, 1766, 1703, 1601, 1503, 1466, 1422, 1390, 1325, 1272, 1199, 1145, 1120, 1032, 964, 915, 866, 835, 780, 734, 645, 585	206 (7000), 223 (14000), 260 (7000), 310 (3000)
IIl	3.88 s (3H, MeO, 4.39 s (2H, CH_2), 7.24 d, 7.50 m (3H, C_6H_3), 9.89 s (1H, CHO)	3095, 3070, 3050, 3015, 2970, 2942, 2922, 2845, 2805, 2755, 1770, 1692, 1600, 1507, 1471, 1427, 1396, 1377, 1280, 1220, 1209, 1155, 1126, 1033, 1014, 908, 862, 830, 739, 680, 600, 580	208 (8000), 224 (16000), 261 (7000), 310 (3000)
IIm	2.28 s (3H, Me), 3.06 t (2H, CH_2O), 3.86 s (3H, OMe), 4.35 t (2H, CH_2C=O), 6.63–7.52 m (7H, C_6H_3 and C_6H_4), 9.90 s (1H, CHO)	3120, 3085, 3032, 3015, 2995, 2933, 2882, 2857, 2831, 2817, 2790, 2729, 1773, 1704, 1599, 1511, 1462, 1396, 1376, 1327, 1290, 1248, 1209, 1179, 1131, 1042, 1028, 955, 910, 890, 880, 850, 827, 818, 781, 731, 590, 514	204 (15000), 221 (20000), 260 (7000), 306 (3000)
IIIa	1.46 t (3H, Me), 4.18 q (2H, CH_2), 7.22 d, 7.51 m (3H, C_6H_3), 8.32 s [1H, OC(O)H], 9.97 s (1H, CHO)	3110, 3081, 3015, 2988, 2940, 2840, 2813, 2744, 1733, 1698, 1599, 1505, 1439, 1391, 1276, 1197, 1160, 1138, 1098, 1040, 895, 868, 851, 824, 800, 745, 618, 590	205 (8000), 222 (15000), 261 (8000), 308 (3000)
IIIb	1.41 t (3H, $MeCH_2$), 2.32 s [3H, MeC(O)], 4.11 q (2H, CH_2), 7.20 d, 7.45 m (3H, C_6H_3), 9.92 s (1H, CHO)	3080, 2982, 2934, 2907, 2880, 2850, 2830, 2736, 1768, 1694, 1600, 1592, 1509, 1479, 1441, 1392, 1370, 1320, 1288, 1273, 1210, 1197, 1156, 1040, 1011, 973, 900, 870, 832, 800, 786, 745, 726, 667, 632, 586, 528	204 (8000), 224 (15000), 261 (8000), 309 (3000)

Table 2. (Contd.)

Ester	^{1}H NMR spectrum, δ, ppm	IR spectrum, ν, cm^{-1}	UV spectrum, λ_{max}, nm (ε)
IIIc	1.35 m (6H, 2MeCH_2), 2.65 q (2H, CH_2C=O), 4.13 q (2H, CH_2O), 7.16 q, 7.45 m (3H, C_6H_3), 9.91 s (1H, CHO)	3115, 3080, 3055, 2985, 2942, 2890, 2875, 2840, 2795, 2740, 1760, 1697, 1601, 1589, 1508, 1480, 1465, 1435, 1401, 1380, 1353, 1353, 1324, 1288, 1264, 1206, 1161, 1140, 1115, 1075, 1040, 1007, 973, 890, 872, 826, 800, 784, 585	205 (8000), 224 (14000), 261 (8000), 310 (3000)
IIId	1.03 t (3H, Me), 1.42 t (3H, MeCH_2O), 1.64 m (2H, CH_2), 2.52 t (2H, CH_2), 4.12 q (2H, MeCH_2O), 7.17 d, 7.44 m (3H, C_6H_3), 9.92 s (1H, CHO)	3114, 3077, 3055, 2983, 2941, 2890, 2875, 2843, 2795, 2740, 1761, 1698, 1600, 1589, 1506, 1480, 1465, 1440, 1400, 1381, 1353, 1325, 1288, 1264, 1206, 1160, 1140, 1113, 1075, 1040, 1006, 973, 890, 872, 826, 800, 784, 585	206 (8000), 223 (15000), 261 (8000), 310 (3000)
IIIe	1.27 d (6H, Me_2C), 1.38 t (3H, Me), 2.78 m (1H, CH), 4.08 q (2H, CH_2), 7.10 d, 7.40 m (3H, C_6H_3), 9.91 s (1H, CHO)	3120, 3080, 3055, 2990, 2975, 2939, 2895, 2880, 2842, 2790, 2740, 1752, 1697, 1600, 1586, 1508, 1420, 1435, 1400, 1385, 1320, 1288, 1262, 1160, 1117, 1099, 1033, 974, 916, 870, 821, 800, 785, 751, 655, 580	204 (8000), 223 (14000), 261 (7000), 310 (3000)
IIIf	1.00 t (3H, Me), 1.20–1.90 m [4H, $(CH_2)_2$], 1.42 t (3H, MeCH_2O), 2.61 t (2H, CH_2C=O), 4.12 q (2H, MeCH_2O), 7.16 d, 7.43 m (3H, C_6H_3), 9.92 s (1H, CHO)	3110, 3076, 3055, 2984, 2941, 2891, 2875, 2845, 2795, 2740, 1763, 1698, 1602, 1589, 1506, 1480, 1465, 1441, 1402, 1381, 353, 1325, 1288, 1264, 1206, 1161, 1140, 1113, 1075, 1040, 1006, 975, 890, 873, 826, 801, 784, 584	205 (8000), 223 (15000), 261 (8000), 310 (3000)
IIIg	1.08 d (6H, Me_2C), 1.40 t (3H, MeCH_2O), 1.40–2.85 m (3H, CH and CH_2), 4.11 q (2H, MeCH_2O), 7.12 d, 7.42 m (3H, C_6H_3), 9.91 s (1H, CHO)	3118, 3070, 3050, 3020, 2963, 2936, 2874, 2834, 2785, 2737, 1764, 1699, 1600, 1503, 1467, 1434, 1391, 1370, 1321, 1280, 1272, 1180, 1150, 1119, 1092, 1041, 973, 915, 897, 869, 830, 786, 744, 730, 650, 580	206 (7000), 224 (15000), 261 (8000), 310 (3000)

Vanillin and vanillal formates IIa and IIIa. A 0.12-mol portion of 99% formic acid was added to a solution of 0.1 mol of **Ia** or **Ib** and 0.1 mol of dicyclohexylcarbodiimide in 500 ml of absolute benzene. The mixture was stirred and kept at 20–23°C for 24–36 h. The dicyclohexylurea precipitate was filtered off and washed with 100 ml of benzene; the filtrate was washed with water and saturated aqueous $NaHCO_3$. The benzene solution was dried over $CaCl_2$, the solvent was distilled off, and the residue was recrystallized from methanol.

Vanillin and vanillal alkanoates IIb–IIm and IIIb–IIIg. A 0.25-mol portion of anhydrous pyridine was added to a solution of 0.2 mol of vanillin **Ia** or vanillal **Ib** in 500 ml of anhydrous CH_2Cl_2, and 0.2 mol of appropriate alkanecarboxylic acid chloride was added in small portions, with stirring by shaking the reaction flask. The mixture was refluxed for 1 h, the solvent was distilled off by heating on a water

Table 3. Results of organoleptic assessment of the smell of esters **IIa–IIg** and **IIIa–IIIg**

Ester	Smell
IIa	Vanilla, wood, with powder tint
IIb	Vanilla-wood, with clove-spicy tint
IIc	Vanilla, honey
IId	Cream-milk, vanilla
IIe	Chocolate-vanilla, cream
IIf	Vanilla-rum, with cream tint
IIg	Vanilla-rum, with fruit tint
IIIa	Wood, vanilla, with spicy tint
IIIb	Vanilla-flower, with honey tint
IIIc	Vanilla-honey, with wood tint
IIId	Cream-vanilla, with baked milk tint
IIIe	Vanilla-cream, with white chocolate tint
IIIf	Vanilla-rum, with cream chocolate tint
IIIg	Vanilla-fruit, with cream-clove tint

bath, and the residue was dissolved in 500 ml of benzene, washed three times with water and three times with 5% aqueous $NaHCO_3$, and dried over $CaCl_2$. The solvent was distilled off, and the residue was distilled in a vacuum (**IId**, **IIf**–**IIj**, **IIId**, **IIIf**, **IIIg**) or recrystallized from benzene–hexane (**IIb**, **IIc**, **IIe**, **IIm**, **IIIb**, **IIIc**, **IIIe**). In the case of **IIk** and **IIl**, the residue was a noncrystallizing greasy substance.

The solvents CH_2Cl_2 and C_6H_6 distilled from the reaction mixture can be reused after distillation from P_2O_5 on a Vigreux column.

Vanillin and vanillal alkanoates IIb–IIg and IIIb–IIIg. A 1-mol portion of appropriate alkanecarboxylic acid anhydride was added in small portions with vigorous stirring to a solution of 1 mol of vanillin **Ia** or vanillal **Ib** in 1.1 l of 1 N aqueous KOH. The mixture was stirred for 3–5 h and allowed to stand for 10–15 h at 20–23°C. Compounds **IIb**–**IIg** and **IIIb**–**IIIg** were isolated by filtration or decanting, washed with water, and dried in air.

CONCLUSION

A procedure was developed for preparing vanillin and vanillal alkanoates in 70–96% yield. These compounds are of interest as components of flavor food additives with popular chocolate, caramel, and milk-cream smells.

ACKNOWLEDGMENTS

The study was financially supported by the Belarussian Republican Foundation for Basic Research (project no. Kh 03–079).

REFERENCES

1. Shulov, L.M. and Kheifits, L.A., *Dushistye veshchestva i poluprodukty parfyumerno-kosmeticheskogo proizvodstva: Spravochnik* (Fragrant Substances and Intermediates in Production of Perfumes and Cosmetics: Handbook), Moscow: Agropromizdat, 1990.
2. Shaikh, Y., *Specialty Aroma Chemicals in Flavors and Fragrance*, Carol Stream, Illinois: Allured, 2002.
3. Voitkevich, S.A. and Kheifits, L.A., *Ot drevnikh blagovonii k sovremennym parfyumerii i kosmetike* (From Ancient Fragrances to Modern Perfumes and Cosmetics), Moscow: Pishchevaya Prom–st., 1997.
4. Kozlov, N.G. and Basalaeva, L.I., *Zh. Org. Khim.*, 2003, vol. 39, no. 5, pp. 765–769.
5. Plemenkov, V.V., *Vvedenie v khimiyu prirodnykh soedinenii* (Introduction to Chemistry of Natural Compounds), Kazan, 2001, p. 374.
6. Shoenberg, A. and Heck, R.F., *J. Am. Chem. Soc.*, 1974, vol. 96, no. 25, pp. 7761–7764.
7. King, H., *J. Chem. Soc.*, 1939, nos. 7–9, pp. 1165–1168.
8. Burger, A.P.N., Brandt, E.V., and Koux, D.G., *Phytochemistry*, 1983, vol. 22, no. 12, pp. 2813–2817.
9. Pisovschi, I.J., *Chem. Ber.*, 1910, vol. 43, no. 8, pp. 2137–2144.
10. Russel, A., *J. Am. Chem. Soc.*, 1948, vol. 70, no. 3, pp. 1060–1064.
11. Ziegler, G. and Kantlehner, W., *Z. Naturforsch. (b)*, 2001, vol. 56, no. 11, pp. 1172–1177.
12. Grenier, J.L., Cotelle, N., Cattean, J.P., and Cotelle, P., *J. Phys. Org. Chem.*, 2000, vol. 13, no. 9, pp. 511–517.
13. Bohlmann, F. and Zdero, C., *Chem. Ber.*, 1968, vol. 101, no. 9, pp. 3243–3254.
14. Yuvchenko, A.P., Dikusar, E.A., Zhukovskaya, N.A., *et al.*, *Zh. Obshch. Khim.*, 1992, vol. 62, no. 1, pp. 204–212.
15. Kozlov, N.G., Dikusar, E.A., and Potkin, V.I., *Zh. Prikl. Khim.*, 2003, vol. 76, no. 1, pp. 107–110.
16. Dikusar, E.A., Nechai, N.I., Potkin, V.I., *et al.*, *Khim. Prirodn. Soedin.*, 2003, vol. 39, no. 2, pp. 186–190.
17. Buehler, C.A. and Pearson, D.E., *Survey of Organic Synthesis*, New York: Wiley–Interscience, 1970. Translated under the title *Organicheskie sintezy*, Moscow: Mir, 1973, part 2, pp. 290–292.

Russian Journal of Applied Chemistry, Vol. 78, No. 1, 2005, pp. 125–129. Translated from Zhurnal Prikladnoi Khimii, Vol. 78, No. 1, 2005, pp. 127–131.
Original Russian Text Copyright © 2005 by Shorina, Kosyakov, Bogolitsyn.

ORGANIC SYNTHESIS AND INDUSTRIAL ORGANIC CHEMISTRY

Acidity of Guaiacol Derivatives in Water–Acetone Mixtures

N. V. Shorina, D. S. Kosyakov, and K. G. Bogolitsyn

Arkhangelsk State Technical University, Arkhangelsk, Russia

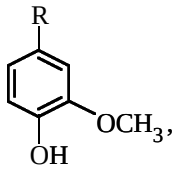
Received April 7, 2004

Abstract—Acid ionization constants of the phenolic hydroxy groups of guaiacol derivatives in water–acetone mixtures were determined. The acidity of these phenols was analyzed in relation to both the acetone content in the mixed solvent and kind of *para*-substituent.

Neat acetone and water–acetone mixtures are promising solvents for cooking of wood and modification of commercial lignin [1–3]. However, the solvent effect on the protolytic properties of phenol-containing structural units of lignin, mainly governing their reactivity, is poorly understood. In order to characterize the lignin reactivity, data on the acidity of its separate structural fragments in aqueous and aqueous–organic media are required [4].

In this work we studied the acidity of phenolic hydroxy groups of a series of guaiacol derivatives in water–acetone mixtures. The most reliable data on protolytic equilibria in solutions can be obtained by potentiometric titration with a glass electrode and by UV spectrophotometry [1, 3, 5–7]. However, the spectrophotometric determination of pK_a of phenols in water–acetone mixtures is impossible since the absorption bands of phenols and acetone (<300 nm) overlap [8]. Therefore, in this work pK_a of phenolic hydroxy groups was determined by potentiometric titration with an aqueous base using a glass electrode [11].

In this work we studied the acidity of nine guaiacol derivatives modeling certain structural fragments of coniferous lignin containing substituent R in α-position to the propane chain in the lignin structure:



where R = H (guaiacol), CH_3 (creosol), COH (vanillin), $COCH_3$ (acetovanillone), CH=CHCH (isoeugenol), $CH_2CH=CH_2$ (eugenol), CH=CHCOOH (ferulic acid), COOH (vanillic acid), and CH_2OH (vanillic alcohol).

All the guaiacol derivatives were of pure grade (Aldrich). Acetone, chemically pure grade (Ekros), was used without additional purification.

In our experiments, the acidity of guaiacol derivatives was studied using their 0.01 M solutions in water–acetone mixtures. 20% aqueous tetraethylammonium hydroxide (Merck) was used as titrant. The potentiometric titration of aqueous-acetone solutions of guaiacol derivatives was carried out under argon with continuous stirring in a temperature-controlled glass cell at 25 ± 0.1 °C. pH was measured on an Ekspert-001 (Ekoniks–Ekspert, Moscow) pH-ionometer equipped with an ESL-63-07 glass electrode and an EVL-1-M3 silver chloride electrode. This device was calibrated relative to aqueous reference solutions immediately before measurements. pK_a was determined in each point of the titration curve by the equation

$$pK_a = pH + \log[(V_e - V)/V],$$

where pH is the measured pH value in each point along the titration curve up to an equivalent point; V_e, equivlent volume of titrant; and V, added titrant volume.

The averaged experimental pH values of aqueous-acetone solutions of guaiacol derivatives were recalculated to the negative logarithm of the proton activity pa_{H^+} relative to the proton activity in the infinitely dilute aqueous-acetone solution as standard state. This recalculation was carried out using the correction factor δ [12] taking into account both the interface electrochemical potential at the boundary between aqueous and nonaqueous solutions and the free energy of proton transfer from aqueous to aqueous-acetone solution:

$$pa_{H^+} = pH - \delta.$$

The curves of potentiometric titration of weakly acidic phenols have a smeared equivalence point due to strong hydrolysis of the phenolate anions. This fact hinders the determination of the acid ionization constants of phenols. Therefore, for eugenol, vanillic

1070-4272/05/7801-0125 © 2005 Pleiades Publishing, Inc.

Table 1. pK_a of carboxy and phenolic groups of guaiacol derivatives in water–acetone mixtures at 25 ± 0.1°C

Guaiacol derivative	pK_a at indicated acetone content, wt %							
	10	20	30	40	50	60	70	80
Vanillin	7.57*/7.86	7.78/8.03	8.12/8.28	8.51/8.56	8.95/8.95	9.41/9.39	9.97/9.92	10.64/10.84
Vanillic acid:								
COOH	4.75/4.96	5.12/5.27	5.57/5.67	6.06/5.11	6.57/6.64	7.14/7.23	7.82/7.92	8.53/8.76
OH_{phen}	9.75/9.80	10.15/10.22	10.56/10.64	11.05/11.10	11.58/11.65	12.16/12.26	12.79/12.96	13.51/13.84
Ferulic acid:								
COOH	4.86/4.71	5.22/5.02	5.59/5.41	5.98/5.88	6.47/6.43	7.02/7.05	7.65/7.75	8.68/8.53
OH_{phen}	9.62/9.46	9.98/9.81	10.35/10.20	10.73/10.68	11.22/11.23	11.77/11.85	12.41/12.54	13.44/13.29
Acetovanillone	8.08/8.28	8.38/8.50	8.74/8.81	9.16/9.15	9.64/9.59	10.18/10.09	10.79/10.68	11.45/11.66
Vanillic alcohol	10.08/10.26	10.45/10.64	11.83/11.01	11.32/11.40	11.85/11.89	12.39/12.45	13.06/13.09	13.85/14.03
Isoeugenol	10.24/10.43	10.62/10.70	10.99/11.06	11.48/11.46	12.01/11.95	12.56/12.50	13.25/13.19	14.02/14.17
Guaiacol	10.33/10.45	10.72/10.73	11.08/11.09	11.57/11.49	12.12/11.98	12.69/12.54	13.35/13.18	14.16/14.22
Eugenol	10.43/10.69	10.79/10.97	11.28/11.33	11.71/11.73	12.21/12.23	12.75/12.79	13.39/13.48	14.42/14.47
Creosol	10.54/10.77	10.97/11.06	11.45/11.43	11.93/11.84	12.38/12.35	12.91/12.93	13.57/13.62	14.54/14.62
Benzoic acid	4.45	4.78	5.19	5.58	6.08	6.67	7.44	8.31

* Numerator refers to experimental pK_a, and denominator, to pK_a calculated by the Henderson equation.

alcohol, isoeugenol, guaiacol, and creosol, the equivalent titrant volume was determined by calculation. The pH values were calculated from the results of no less than 2–3 replicate determinations. The determination error did not exceed 0.05 pK_a unit.

To determine K_a more reliably, this factor was independently calculated by Henderson's method [13] based on comparative determination of the acidity of the substance under consideration and some reference substance:

$$pK_{a(X)} = pK_{a(HBz)} + (E_{1/2(X)} - E_{1/2(HBz)})/0.059 = pK_{a(HBz)} + pH_{1/2(X)} - pH_{1/2(HBz)},$$

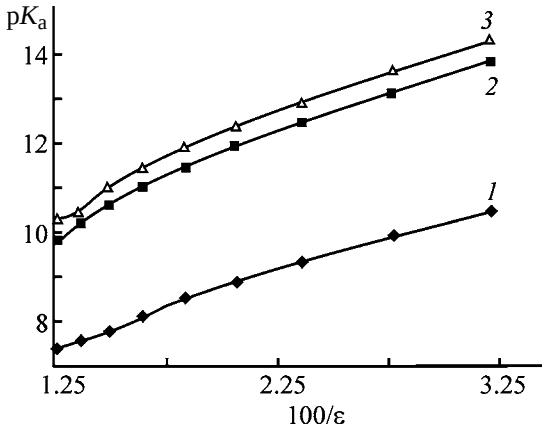


Fig. 1. Plot of pK_a of the phenolic hydroxy groups of guaiacol derivatives vs. the reciprocal permittivity ε of water–acetone mixtures: (*1*) vanillin, (*2*) vanillic alcohol, and (*3*) creosol. The same for Figs. 2 and 3.

where $E_{1/2}$ and $pH_{1/2}$ are the electrode potentials and pH of half-neutralization of the compound X being studied and the reference compound (benzoic acid HBz in our case) in water–acetone mixture.

The pK_a of benzoic acid within the entire range of acetone concentrations was calculated by the Harned–Robinson equation using the coefficients reported in [14].

EXPERIMENTAL

The pK_a values of the guaiacol derivatives in their aqueous-acetone solutions, obtained in our experiments, are listed in Table 1. The maximal difference between the experimental and calculated pK_a was 0.2.

Table 1 shows that, with an increase in the acetone mole fraction in aqueous-acetone solution, the acidity of guaiacol derivatives decreases (acid ionization constants decrease by 3–4 orders of magnitude). This is caused by a change in the free energy of solvation of both the nondissociated guaiacol derivatives and their ionized species in going from aqueous to aqueous-acetone solutions.

In order to elucidate how guaiacol derivatives are solvated in aqueous-acetone solutions, pK_a of phenolic hydroxy groups and carboxy groups was analyzed in relation to physicochemical parameters of water–acetone solvent characterizing its specific and nonspecific interactions with the solute. Figure 1 shows the dependence of pK_a of the phenolic hydroxy groups

of three guaiacol derivatives on reciprocal permittivity of water–acetone solvent. The guaiacol derivatives used in this experiment differ in the kind of substituents located *para* to the phenolic hydroxy group and are typical of the lignin molecular structure [15, 16].

According to the Brønstedt theory [17, 18], the effect of solvent on pK_a of acid is completely determined by electrostatic characteristics of acid molecule irrespective of its chemical composition. Therefore, in the absence of specific interaction between the acid and solvent, pK_a should be a linear function of 1/ε [18]. However, we found that the linear correlation between pK_a of phenolic hydroxy groups of the guaiacol derivatives in their aqueous-acetone solutions and 1/ε is observed only within a limited range of acetone content. This fact shows that the specific interactions of phenols with the solvent contribute to solvation. Therefore, in analysis of the influence of mixed water–acetone solvent on the acidity of phenolic hydroxy groups, the chemical features of the solvent components should be taken into account.

Figure 2 shows the plot of pK_a of the phenolic hydroxy groups of guaiacol derivatives vs. the Dimroth–Reichardt parameter E_T^N reflecting the electron-acceptor power (acidity) of water–acetone mixture. Figure 3 shows the plot of pK_a vs. B_{KT} parameter characterizing the electron-donor power (basicity) of water–acetone solvent [19].

These plots show that, with increasing E_T^N, the acid ionization constants of phenols increase nonlinearly (Fig. 2), and at the acetone content exceeding 60% the correlation between pK_a and B_{KT} is lacking (Fig. 3).

These results suggest that phenolic groups of the guaiacol derivatives are solvated in water–acetone mixtures due to both specific and nonspecific interactions with the solvent molecules. The similar pattern was observed for DMF and DMSO in water–aprotic solvent mixtures [10].

This multimode solvation of the guiacol derivatives in water–acetone mixtures is confirmed by the fact that pK_a of phenolic hydroxy groups of these model compounds is a linear function of the acetone mole fraction in water–acetone mixture (correlation factor 0.97–0.99) (Fig. 4). This correlation shows that the phenols under consideration are similarly solvated with water and acetone molecules in water–acetone mixtures [20].

We found that the effect of nonaqueous solvents on the acidity of guaiacol derivatives depends on the kind of *para*-substituent. The pK_a values of guaiacol derivatives containing nonolar *para*-substituent (eugenol, guaiacol, creosol) are the most sensitive to the composition of water–acetone solvent. The minimal effect of solvent composition on pK_a is observed with electron-acceptor substituents (vanillin, acetovanillone).

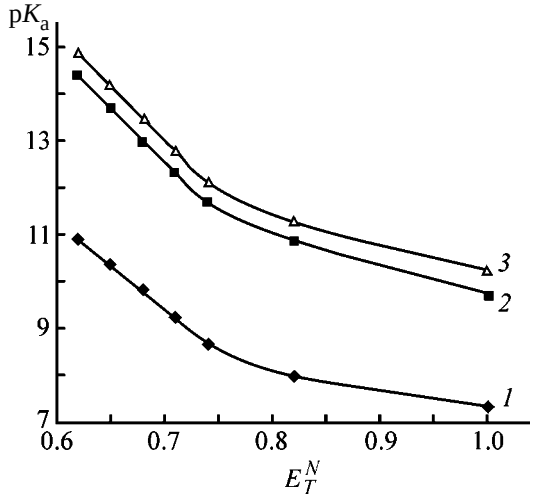


Fig. 2. Plot of pK_a of the phenolic hydroxy groups of guaiacol derivatives vs. the Dimroth–Reichardt parameter E_T^N of water–acetone mixtures.

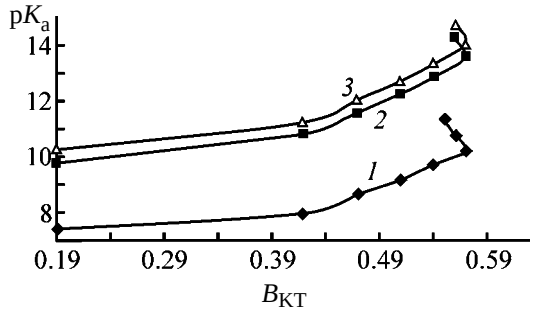


Fig. 3. Plot of pK_a of the phenolic hydroxy groups of guaiacol derivatives vs. the basicity parameter B_{KT} in aqueous-acetone mixtures.

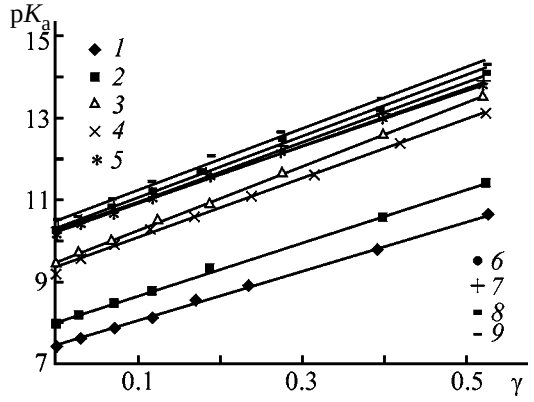


Fig. 4. Plot of pK_a of the phenolic hydroxy groups of guaiacol derivatives vs. the acetone mole fraction γ in water–acetone mixtures: (*1*) vanillin, (*2*) acetovanillone, (*3*) vanillic acid, (*4*) ferulic acid, (*5*) vanillic alcohol, (*6*) isoeugenol, (*7*) guaiacol, (*8*) eugenol, and (*9*) creosol.

Table 2. Factors *a* and *b* in the empirical equation correlating pK_a of phenolic group of guaiacol derivatives in water–acetone mixtures and their pK_a in aqueous solution (n = 9)*

Acetone content, wt %	pK_a(OH_{phen})	
	a	*b*
10	1.03	–0.03
20	1.08	–0.18
30	1.11	–0.02
40	1.15	0.14
50	1.17	0.46
60	1.18	0.88
70	1.21	1.18
80	1.30	1.20

* (*n*) Nubmer of tested guaiacol derivatives; the correlation factors are in the range 0.97–0.99.

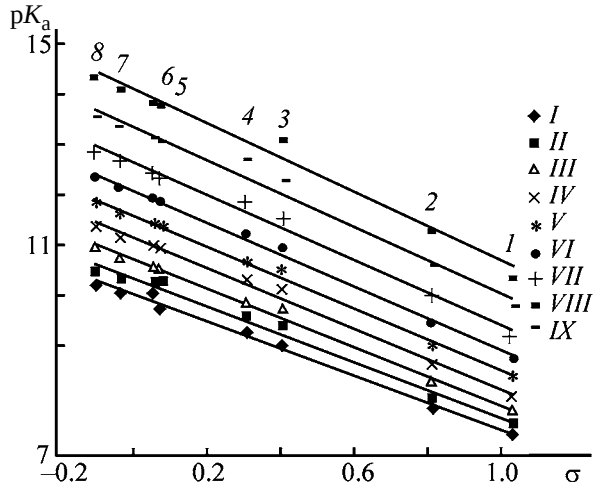


Fig. 5. Plots of pK_a in water–acetone mixtures of phenolic hydroxy groups of guaiacol derivatives vs. Hammett σ constant of their *para*-substituents: (*1*) vanillin, (*2*) acetovanillone, (*3*) ferulic acid (OH_{phen}), (*4*), vanillic acid (OH_{phen}), (*5*) vanillic alcohol, (*6*) isoeugenol, (*7*) eugenol, and (*8*) creosol. Acetone content, wt %: (*I*) 0, (*II*) 10, (*III*) 20, (*IV*) 30, (*V*) 40, (*VI*) 50, (*VII*) 60, (*VIII*) 70, and (*IX*) 80.

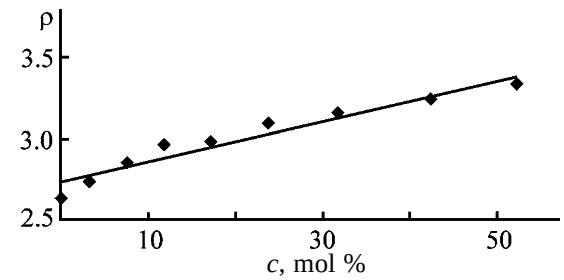


Fig. 6. Plot of the the sensitivity factor ρ vs. acetone content *c* in water–acetone mixtures at 25°C.

It is known that the slope of the plot of pK_a of acid in nonaqueous solvent (S) vs. pK_a of the same acid in aqueous solution characterizes the differentiating effect of the solvent on the acid strength: the larger the slope, the stronger the differentiating effect of the solvent [1].

By analysis of data on acid ionization constants of phenols in water–acetone mixtures and those in aqueous solutions [21], Ermakova *et al*. found that these data can be correlated by an empirical equation pK_a(S) = apK_a(H_2O) + b [22, 23]. This equation allows calculation of pK_a of phenol in nonaqueous solvent if its pK_a in aqueous solution is known. We can also determine pK_a of any water-insoluble phenol through its pK_a in nonaqueous solvent. Furthermore, the coefficients *a* and *b* in this equation allow quantitative characterization of the differentiating effect of aprotic solvents and their aqueous mixtures on acidity in some series of phenols [24] (Table 2).

Figure 5 shows that, within the limits of the determination accuracy, pK_a of all guaiacol derivatives under consideration is a linear function of the Hammett σ constant of their *para*-substituents [10, 25]. This correlation reflects the well-known effect of *para*-substituents on ionization of phenolic hydroxy groups described by the Hammett equation [20]

$$pK_a = pK_a^g - \rho\sigma_p,$$

where σ_p is the Hammett constant of a *para*-substituent; ρ, factor characterizing sensitivity of a given reaction to the substituent properties, and pK_a^g, ionization constant of phenolic hydroxy group of nonsubstituted quaiacol.

The sensitivity factors ρ of the phenolic hydroxy groups of guaiacol derivatives were calculated from the slope of the linear plots of pK_a vs. σ (Fig. 5). As seen from Fig. 6, the reaction factor ρ is a linear function (correlation factor 0.98) of the acetone content in water–acetone mixtures.

We believe that this correlation is caused by the following factors: (1) variation in the permittivity of mixed solvent influencing the contribution of the inductive effect of *para*-substituent to protonation of the phenolic hydroxy group; (2) change in solvation of *para*-substituents in the mixed solvents, affecting their Hammett constants [19].

CONCLUSIONS

(1) Acid ioniztion constants of phenolic hydroxy and carboxy groups of guaiacol derivatives in water–

acetone solvent were determined by potentiometric titration.

(2) pK_a of the phenolic group of guaiacol derivatives is a linear function of the acetone mole fraction in water–acetone mixtures at widely varied acetone content.

(3) pK_a of the phenolic groups of guaiacol derivatives in water–acetone mixtures is a linear function of their pK_a in aqueous solutions.

ACKNOWLEDGMENTS

This work was financially supported by the Russian Foundation for Basic Research and Administration of Arkhangelsk oblast (project no. 05-03-97504-r-sever-a).

REFERENCES

1. Kreshkov, A.P., Bykova, L.N., and Kazaryan, N.A., *Kislotno-osnovnoe titrovanie v nevodnykh rastvorakh* (Acid–Base Titration in Nonaqueous Solutions), Moscow: Khimiya, 1967.
2. Deineko, I.P., Chemical Transformations of Lignin in Delignification of Wood with Oxygen, *Doctoral Dissertation*, Leningrad: 1990.
3. Fialkov, Yu.Ya., Zhitomirskii, A.N., and Tarasenko, Yu.A., *Fizicheskaya khimiya nevodnykh rastvorov* (Physical Chemistry of Nonaqueous Solutions), Leningrad: Khimiya, 1973.
4. Zarubin, M.Ya., Kiryushina, M.F., Troitskii, V.V., *et al.*, *Khim. Drev.*, 1983, no. 5, pp. 3–16.
5. Bogolitsyn, K.G., Kosyakov, D.S., and Gorbova, N.S., *Zh. Fiz. Khim.*, 2003, vol. 77, no. 11, pp. 1943–1945.
6. Bates, R.G., *Determination of pH. Theory and Practice*, New York: Wiley, 1964.
7. Bogolitsyn, K.G., Kosyakov, D.S., and Gorbova, N.S., *Zh. Fiz. Khim.*, 2003, vol. 77, no. 4, pp. 667–671.
8. Gordon, A.J. and Ford, R.A., *The Chemist's Companion. A Handbook of Practical Data, Techniques, and References*, New York: Wiley, 1972.
9. Bogolitsyn, K.G., *Zh. Prikl. Spektrosk.*, 1987, vol. 46, no. 6, p. 1024.
10. Gorbova, N.S., Acid–Base Properties of Phenols Related to Lignin Phenols in the System Water–Aprotic Solvent, *Cand. Sci. Dissertation*, Arkhangelsk, 2002.
11. Shorina, N.V., Bogolitsyn, K.G., and Kosyakov, D.S., *Izv. Vysh. Uchebn. Zaved., Lesn. Zh.*, 2003, no. 6, pp. 89–94.
12. Aleksandrov, V.V., *Kislotnost' nevodnykh rastvorov* (Acidity of Nonaqueous Solutions), Kharkov: Vishcha Shkola, 1981.
13. Kreshkov, A.P., *Osnovy analiticheskoi khimii* (Fundamentals of Analytical Chemistry), Moscow: Khimiya; 1970, vol. 3.
14. Kovzhoga, A., Termodynamic Characteristics of Solvation of Ions and Molecules of Acetic and Benzoic Acids in Mixed Water–Acetone Solvents, *Cand. Sci. Dissertation*, Kharkov, 1988.
15. Åkerlöf, C., *J. Am. Chem. Soc.*, 1932, vol. 54, no. 11, p. 4125.
16. Mchedlov-Petrosyan, N.O. and Lyubchenko, I.N., *Zh. Obshch. Khim.*, 1987, vol. 57, no. 6, p. 1372–1378.
17. Brønsted, I.N., *Z. Phys. Chem. A*, 1934, vol. 32, p. 169.
18. Izmailov, N.A., *Zh. Fiz. Khim.*, 1950, vol. 24, no. 3, pp. 321–337.
19. Krygowski, T.M., Wrona, P.K., Zielkowska, U., and Reichardt, C., *Tetrahedron*, 1985, vol. 41, no. 20, pp. 4519–4527.
20. Palm, V.A., *Osnovy kolichestvennoi teorii organicheskikh reaktsii* (Fundamentals of Quantitative Theory of Organic Reactions), Leningrad: Khimiya, 1977.
21. Ragnar, M., Lindgren, C.T., and Nilvebrant, N.-O., *J. Wood Chem. Technol.*, 2000, vol. 20, no. 3, pp. 277–305.
22. Ermakova, M.I., Kiryushina, M.F., and Zarubin, M.Ya., *Khim. Drev.*, 1984, no. 5, pp. 23–29.
23. Ermakova, M.I., Kiryushina, M.F., and Zarubin, M.Ya., *Khim. Drev.*, 1985, no. 6, pp. 61–64.
24. Molchanova, N.R., *Vopr. Khim. Khim. Tekhnol.* (Kharkov), 1980, issue 59, pp. 75–76.
25. Barlin, D.B. and Perren, D.D., *Usp. Khim.*, 1968, vol. 37, no. 7, pp. 1303–1326.

Russian Journal of Applied Chemistry, Vol. 78, No. 1, 2005, pp. 130–136. Translated from Zhurnal Prikladnoi Khimii, Vol. 78, No. 1, 2005, pp. 132–138.
Original Russian Text Copyright © 2005 by Pavlov, Nazarova, Ebel, Mikhailova, Zaitseva, Bokov, Litvinova, Afanas'eva, Korneeva, Panarin.

MACROMOLECULAR CHEMISTRY AND POLYMERIC MATERIALS

Molecular Characteristics of Star-Like Polyvinylpyrrolidone with Fullerene C_{60} as the Branching Site in Dilute Solutions

G. M. Pavlov, O. V. Nazarova, C. Ebel, N. A. Mikhailova, I. I. Zaitseva, S. N. Bokov, L. S. Litvinova, E. V. Afanas'eva, E. V. Korneeva, and E. F. Panarin

Fock Research Institute of Physics, St. Petersburg State University, St. Petersburg, Russia
Institute of Macromolecular Compounds, Russian Academy of Sciences, St. Petersburg, Russia
Laboratoire de Biophysique Moleculaire, Institut de Biologie Structurale, Grenoble, France

Received September 24, 2004

Abstract—Star-like water-soluble macromolecules with fullerene as the branching site were synthesized by the reaction of fullerene C_{60} with polyvinylpyrrolidone whose molecules contain one terminal primary amino group. The initial and C_{60}-containing polymers were studied by UV spectroscopy, thin-layer chromatography, centrifugal sedimentation, translation diffusion, and viscometry in aqueous buffer solutions. Diffusion–sedimentation and sedimentation two-detector analyses of the initial and fullerene-containing samples were performed. The molecular weights of the polymers were estimated by the Svedberg equation. The proportion of the fullerene-containing segment in the samples synthesized was determined, and the number of the branches in the fullerene-containing macromolecules was estimated.

Fullerenes have recently become a subject of active studies in macromolecular chemistry. The specific features of the chemistry of fullerenes are determined by their aromatic nature and a high symmetry. Both fullerene-containing polymers with covalently bound fullerenes and fullerene-based noncovalent complexes were synthesized [1–3]. Fullerenes and their derivatives exhibit a spectrum of biological properties. They are capable of penetrating lipid membranes and exhibit antioxidative, antimicrobial, and antiviral activities and immunomodulating properties [4–7].

The biological properties of fullerenes should be studied with their water-soluble derivatives. There are published data on water-soluble derivatives of fullerene based on hydrophilic polymers such as poly(ethylene oxide) and polyvinylpyrrolidone (PVP), prepared by radical or anionic polymerization of the corresponding monomers in the presence of fullerene [8–10], as well as on noncovalent complexes of fullerene with PVP [11, 12]. Water-soluble compounds of fullerene based on polyalkylenimines and polyoxyethylene were synthesized by polymer-analogous transformations [13, 14]. Reactions of amine-containing polymers with fullerenes represent a convenient method of synthesis of their polymeric derivatives, since primary aliphatic amino groups under mild conditions easily react with fullerenes. This procedure was used for synthesizing compounds based on polyalkylenimines, polyallylamine, and allylamine copolymers with styrene, methyl methacrylate, and hydroxypropyl methacrylate [15, 16]. The reactions of fullerenes with polymers containing one terminal amino group should yield star-like derivatives, as revealed for polystyrene, polyoxyethylene, and polyoxypropylene [17, 18].

In this work, we studied reactions of fullerene C_{60} with a water-soluble polymer, poly-*N*-vinylpyrrolidone containing a terminal amino group (PVP-NH_2). We studied the fullerene-containing and initial PVP samples by molecular hydrodynamics methods (centrifugal sedimentation, translational diffusion, and viscometry) in aqueous buffer solutions.

EXPERIMENTAL

The initial polymers PVP-NH_2 (PVP-1 and PVP-2) were synthesized as described previously in [19]. We took advantage of the capability for chain propagation in radical processes, characteristic of thiols. We subjected *N*-vinylpyrrolidone to radical polymerization in the presence of an amine-containing thiol, cysteamine hydrochloride.

Reactions of fullerene with PVP-1 and PVP-2 were carried out at room temperature in a mixed solvent (dimethylformamide–toluene) for 24 h at the $[NH_2]:[C_{60}]$ molar ratio of 1 : 1 in the case of PVP-1 and 6 : 1 in the case of PVP-2. Next, the reaction mix-

1070-4272/05/7801-0130 © 2005 Pleiades Publishing, Inc.

ture was filtered, and the solvent was removed in a vacuum. The dry residue was dried to constant weight and dissolved in water, whereupon the resulting aqueous solution was filtered. The reaction products were isolated by freeze drying.

The UV spectra were taken in chloroform on a Specord M-40 spectrophotometer.

The adsorption thin-layer chromatography (TLC) variance was carried out on Alugram Sil G/UV$_{254}$ (Macherey-Nagel, Germany) silica gel plates with toluene, chloroform, or carbon tetrachloride as eluent.

The translation diffusion coefficients were determined by recording the time dependence of the variance of the diffusion boundary of the solution with the concentration $c = 0.07 \times 10^{-2}$ g cm^{-3} on a Tsvetkov diffusometer [20] (Fig. 1). The resulting values were taken as equal to those extrapolated to zero concentration. The refractive index increments $\Delta n/\Delta c$ were determined from the area enclosed by the interference curve.

Centrifugal sedimentation was studied on MOM-3170 and Beckman XLI analytical ultracentrifuges. The sedimentation coefficient was determined in cells in which the boundary was artificially formed by depositing a layer of the solvent onto the solution with the concentration $c = 0.3 \times 10^{-2}$ g cm^{-3} at the rotor rotation rate n = 40 000 rpm (Fig. 2). The resulting values were reduced to those corresponding to zero concentration, using the relationship

$$s^{-1} = s_0^{-1}(1 + k_s c) = s_0^{-1}\{1 + (k_s/[\eta])[\eta]c\}.$$

The dimensionless parameter $k_s/[\eta]$ was taken equal to that known for flexible-chain polymers, namely, ≈1.7 [21]. In all cases, the sedimentation boundaries preserved their unimodal nature throughout the experiment (~90 min). The primary experimental data were processed using well-known procedures [20, 22, 23]. The experiments on the Beckman XLI analytical ultracentrifuge were carried out at the rotor rotation rate n = 55 000 rpm using both interference and absorption optical devices (at the light wavelength λ = 250 nm) at the concentration $c = 0.03 \times 10^{-2}$ g cm^{-3}. The data were processed using the Sedfit routine [24].

In independent experiments we determined the density increments $\Delta\rho/\Delta c$ of the initial and fullerene-containing samples (Fig. 3). The measurements were carried out on a Kratky densitometer [25] (A. Paar, Austria) at 20°C. Since the $\Delta\rho/\Delta c$ parameters for the initial and fullerene-containing PVPs are virtually

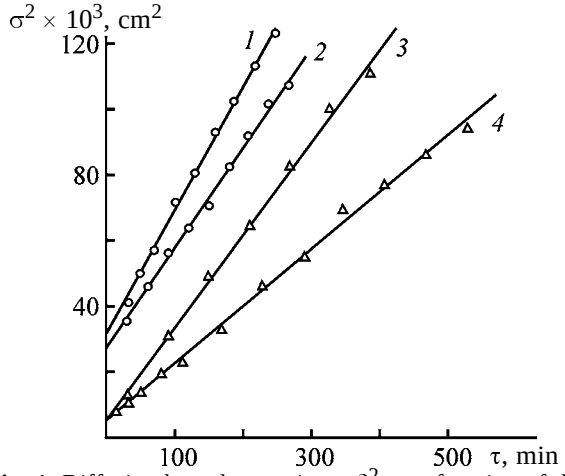


Fig. 1. Diffusion boundary variance δ^2 as a function of the diffusion time τ for the initial and fullerene-containing samples. Digits at curves corresponds to sample nos. in Table 1; the same for Fig. 2.

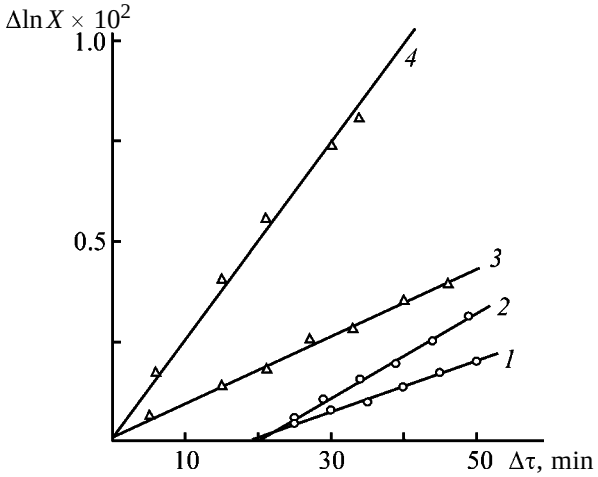


Fig. 2. Shift $\Delta\ln X$ of the sedimentation peaks obtained on a polarization interferometer (MOM 3180) as a function of the time $\Delta\tau$ for the initial and fullerene-containing samples. The sedimentation coefficient was calculated using the slope $s = \Delta\ln X/\omega^2\Delta\tau$, where $\omega = 2\pi n$.

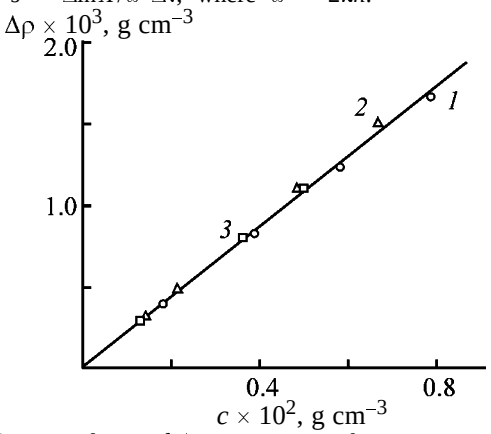


Fig. 3. Dependence of $\Delta\rho = \rho - \rho_0$ on the concentration of solution c for (*1*) the initial PVP and (*2, 3*) fullerene-containing PVPs. ρ and ρ_0 are densities, g cm^{-3}, of the solution and solvent, respectively.

Table 1. Hydrodynamic and molecular characteristics of the initial and fullerene-containing polymers in 0.1 M solution of sodium acetate at 25°C. Solvent viscosity η_0 = 0.92 cP, density ρ_0 = 1.002 g cm^{-3}, and specific partial volume of PVP $v = 0.782 \pm 0.006$ cm^3 g^{-1}

Sample no.	Polymer	$s_0 \times 10^{13}$, s	$D_0 \times 10^7$, cm^2 s^{-1}	$\Delta n/\Delta c$, cm^3 g^{-1}	$[\eta]$, cm^3 g^{-1}	k'	$M_{sD} \times 10^{-3}$	$A_0 \times 10^{10}$	M_2/M_1
1	PVP-1	0.65	15.5	0.19	6.5	0.75	4.6	3.19	–
2	PVP-1–C_{60}	1.1	12.6	0.18	5.6	1.50	9.7	3.17	2.1
3	PVP-2	0.8	11.7	0.17	9.5	0.70	7.7	3.26	–
4	PVP-2–C_{60}	2.3	7.25	0.18	12	0.65	35.7	3.64	4.6

identical, we used an average value $\Delta\rho/\Delta c = 1 - v\rho_0 = 0.22 \pm 0.01$ for further estimations.

The viscometric measurements were carried out on an Ostwald viscometer. The intrinsic viscosities $[\eta]$ and the Huggins parameters k' are listed in Table 1.

Reactions of PVP–NH_2 with fullerene C_{60} yielded water-soluble products PVP-1–C_{60} and PVP-2–C_{60}, which were colored, unlike the initial polymers. These products are characterized by intense absorption at 250–350 nm. However, by contrast to free C_{60} and its complexes with PVP, the UV spectra of PVP-1–C_{60} and PVP-2–C_{60} did not contain bands with λ_{max} = 260 and λ_{max} = 330 nm. The spectra are, essentially, monotonically descending curves with minor inflections near 260 nm, characteristics of covalently bound C_{60} [6, 8, 9].

The covalent nature of the polymer–fullerene bonding in the resulting derivatives is confirmed by the adsorption TLC analysis using toluene, chloroform, or carbon tetrachloride as eluent. When chromatograms are recorded on silica gel, free C_{60} moves together with the solvent front (Fig. 4, spot *1*). Out of the noncovalent complex of C_{60} with PVP, specially prepared for comparison, fullerene is also washed out (Fig. 4, spot *6*), like free C_{60}, moving together with the front, while PVP is adsorbed irreversibly (Fig. 4, spots *2* and *3*). When chromatograms of PVP-1–C_{60} and PVP-2–C_{60} are taken under identical conditions, C_{60} is not washed out (Fig. 4, spots *3* and *5*). After the PVP-1–C_{60} and PVP-2–C_{60} samples are eluted, a light brown spot remains at the start. This spot is also detected from UV absorption at 254 nm and from dark brown fluorescence at 366 nm, which is not typical for the initial PVP–NH_2 samples and can be due to the presence of covalently bound C_{60} only.

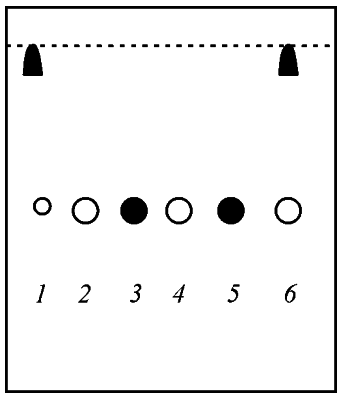


Fig. 4. TLC of (*1*) fullerene C_{60}, (*2*) PVP-1, (*3*) PVP-1–C_{60}, (*4*) PVP-2, and (*5*) PVP-2–C_{60} samples, and (*6*) PVP–C_{60} complex. Adsorbent silica gel, eluent toluene.

The initial and fullerene-modified polymers were studied by molecular hydrodynamic methods. As the main hydrodynamic characteristics served the centrifugal sedimentation coefficients s_0 and translation diffusion coefficients D_0, as well as intrinsic viscosities $[\eta]$.

The measurements of the refractive indices and density increments showed that both the $\Delta n/\Delta c$ and $\Delta\rho/\Delta c = 1 - v\rho_0$ parameters are virtually identical for the initial and fullerene-containing macromolecular systems, which is due to a relatively low content of the fullerene.

The specific partial volumes v were used for calculating by the Svedberg procedure [20]

$$M_{sD} = [RT/(1 - v\rho_0)]s_0/D_0,$$

the net molecular weights (see Table 1). This table also contains the M_2/M_1 ratio, where M_1 is the molecular weight of the initial polymer, and M_2, the corresponding weight of the polymer that reacted with C_{60}. The M_2/M_1 ratio is over unity, which suggests formation of new polymer structures incorporating fullerene molecules.

Also, we calculated the hydrodynamic invariant A_0 by the formula $A_0 = (R[D]^2[s][\eta])^{1/3}$, where $[D] = D\eta_0/T$, $[s] = s\eta_0/(1 - v\rho_0)$. The A_0 values have a

usual order, confirming consistency between the three independent experimental parameters s_0, D_0, and [η].

The sedimentation data obtained on a Beckman XLI analytical ultracentrifuge were processed using the Sedfit routine [24]. This routine allows the solution of the general Lamm equation for centrifugal sedimentation of a dilute solution of an ensemble of specifically noninteracting particles (molecules) that affords the best fit of the experimental and calculated profiles of the sedimentation boundary. The sum of the discrepancies between the experimental and calculated profiles of the sedimentation boundary is minimized using the regularization procedure based on the CONTIN routine [26]. The Sedfit routine allows the use of the mass-spectrometric potential of the centrifugal sedimentation method at a new level and furnishes additional molecular information about the samples under study (Fig. 5).

First, the data obtained with the use of interference optical devices show that the samples of the initial PVP are unimodal and are characterized by one narrow peak near 0.6 and 0.8 Sv for PVP-1 and PVP-2, respectively. These sedimentation coefficients are virtually identical to those yielded by analysis of migration of the sedimentation boundary (Fig. 2, Tables 1 and 2). Such comparison of the sedimentation coefficients yielded by various experimental data processing algorithms also serves as a test of the suitability of the Sedfit routine for estimating the centrifugal sedimentation coefficients of nonglobular macromolecules.

Second, the functions of distribution with respect to the sedimentation coefficients of the fullerene-containing samples contain peaks for which the sedimentation coefficients are virtually identical to those of the initial PVP samples. This means that the fullerene-containing samples comprise a part of the initial polymer that did not react with the fullerene. By comparing the distribution functions, we estimated the proportion of the fullerene-containing PVP macromolecules at ca. 40% for PVP-1–C_{60} and PVP-2–C_{60} (Fig. 5). This allows estimation of the average number of the polymer molecules corresponding to one fullerene molecule.

In view of the additivity of the weights, we can take, to a first approximation, the molecular weight of the fullerene itself negligible compared to that of the initial polymer molecule. Then, taking into account virtual identity of the density increments of the initial and fullerene-containing molecules (Fig. 3), we will change from the molecular weights to the ratio of the sedimentation coefficient to the translation diffusion coefficient:

$$M_{sD} = [RT/(\Delta\rho/\Delta c)]s_0/D_0 \sim s_0/D_0.$$

Hence,

$$s_0/D_0 = (s_0/D_0)_1 w_1 + (s_0/D_0)_2 w_2,$$

where s_0/D_0 is the net ratio yielded by the sedimentation diffusion analysis of the fullerene-containing sample; $(s_0/D_0)_1$, ratio yielded by the sedimentation diffusion analysis of the initial sample (without fullerene); w_1, proportion of unchanged initial sample in the fullerene-containing sample; w_2, proportion of the fullerene-containing segment of the sample (in the fullerene-containing sample); and $(s_0/D_0)_2$, desired average ratio for the fullerene-containing segment of the sample.

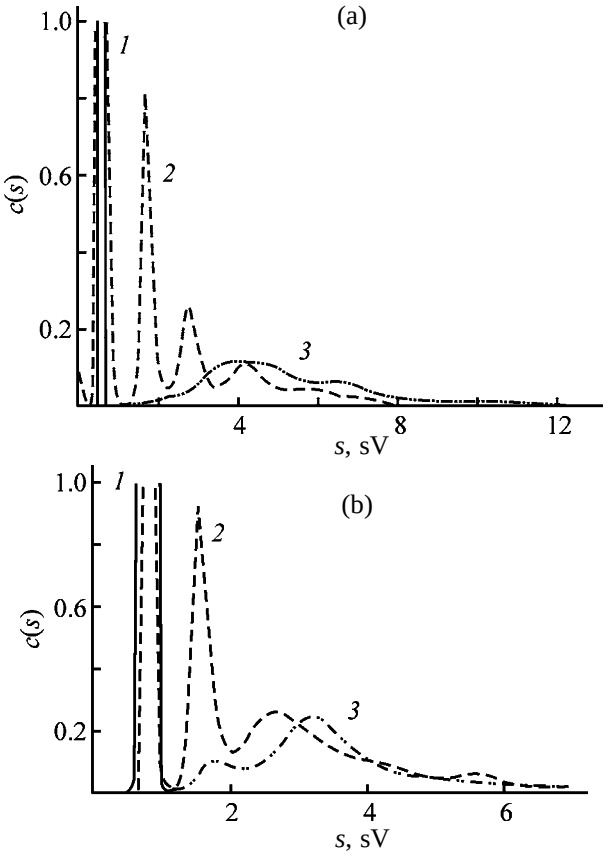


Fig. 5. Distribution $c(s)$ of the (*1*) initial and (*2, 3*) fullerene-containing samples with respect to the sedimentation coefficients s obtained by processing (*1, 2*) interference and (*3*) absorption scans (Beckman XLI analytical ultracentrifuge) by the Sedfit routine [24]. Concentration c of the initial PVP and fullerene-containing PVP–C_{60} polymers 0.10×10^{-2} and 0.02×10^{-2} g cm^{-3}, respectively. (a) PVP-1–C_{60} and (*2*) PVP-2–C_{60}.

Table 2. Sedimentation coefficients s and number of branches f in star-like polymers.* Solvent viscosity η_0 = 1.016 cP, density ρ_0 = 1.0069 g cm^{-3}

Sample/Fraction	Interference		Absorption		f
	$s \times 10^{13}$, s	fraction content, %	$s \times 10^{13}$, s	fraction content, %	
PVP-1	0.56	100	–	–	–
PVP-1-C_{60}/1	0.62	60	–	–	–
PVP-1–C_{60}/2	1.9	18	2.0	5	7
PVP-1–C_{60}/3	2.9	10	–	–	11
PVP-1–C_{60}/4	4.4	10	4.3	57	17
PVP-1–C_{60}/5	7	~2	6.8	24	29
PVP-1–C_{60}fr	4.5	75	4.7	78	19
PVP-2	0.71	100	–	–	–
PVP-2–C_{60}/1	0.79	58	–	–	–
PVP-2–C_{60}/2	1.8	15	1.7	12	4
PVP-2–C_{60}/3	2.9	15	3.3	59	9
PVP-2–C_{60}/4	4.2	11	5.4	10	15
PVP-2–C_{60}/5	–	–	8	10	26

* The measurements were carried out in 0.2 M NaCl solution at 20°C.

Evidently, $w_1 + w_2 = 1$, and the average number of the polymer molecules n, corresponding to one C_{60} molecule, will be equal to

$$n = (s_0/D_0)_2/(s_0/D_0)_1.$$

Then, the average number of the PVP molecules corresponding to one C_{60} molecule is equal to 4 for PVP-1–C_{60} and 10 for PVP-2–C_{60}; the larger the initial $[NH_2] : [C_{60}]$ ratio, the larger the number of the branches in the resulting star-like derivative.

The interference system of sedimentation recording (Beckman XLI) furnishes information about distribution with respect to the sedimentation coefficients for the entire sample, while the absorption system, only about the fullerene-containing segments of the sample, since fullerene is specifically responsible for the UV absorption. Comparison of the sedimentograms obtained with both recording systems suggests that the absorption optical devices record large sedimentation coefficients, which directly confirms formation of bulkier fullerene-based molecules compared to the initial polymers. Also, we revealed a molecular inhomogeneity of the fullerene-containing samples in the region of sedimentation coefficients larger than that of the initial PVP.

Since the initial polymers had one terminal amino group, it is reasonable to assume a star-like structure of the fullerene-containing macromolecules. Star-like polymer molecules are smaller in size than the corresponding linear macromolecules with identical molecular weight. For regular stars built up of chains of random wanderings of sufficient length, the following analytical expression for the ratio of the rms inertia radii g of the star-like and linear molecules was obtained [27]:

$$g = \langle R^2\rangle_{star}/\langle R^2\rangle_{lin} = (3f - 2)/f^2,$$

where f is the number of the branches in a regular star-like macromolecule.

A decrease in the size decreases the intrinsic viscosity, the translation friction coefficient, and, correspondingly, increases the sedimentation and diffusion coefficients of the star-like molecule relative to the linear molecule with identical molecular weight. Taking into account the decrease in size and the Kirkwood–Reisman hydrodynamic interactions of star-like molecules and using the model applied in [27], Stockmayer and Fixman [28] obtained the relationship

$$h = (s_0)_{lin}/(s_0)_{star} = 2.414f^{1/2}/(f + 2^{1/2}). \quad (1)$$

The theoretically calculated parameters h are slightly smaller than the corresponding $g^{1/2}$ parameters. This is due to strengthening of the hydrodynamic interaction in a star-like molecule, since $h = (P_{star}/P_{lin})g^{1/2}$, where P_{star} and P_{lin} are the hydrodynamic Flory parameters for the star-like and linear molecules, respectively. We calculated the molecular

weights of the macromolecules as $M_f = fM_1$ by expressions like the Kuhn–Mark–Houwink relationship, which we previously obtained for the linear homologous series of PVP [29, 30], and then calculated the $(s_0)_{lin}$ parameters corresponding to different M_f parameters. Next, using the h parameters calculated by formula (1), we estimated possible theoretical sedimentation coefficients of star-like PVP molecules at different numbers of branches, i.e., plotted the corresponding $s_{star} = s_{star}(f)$ nomograms for different M_1 parameters. By comparing the theoretical and experimental parameters s, we estimated the number of the branches in various fractions of the fullerene-containing samples. The results are presented in Table 2.

To test the possibility of separating the fullerene-containing segment out of the overall sample, we fractionated PVP-1–C_{60} on a column packed with a Sephadex G-200 gel (45×2 cm, eluent H_2O) and took the PVP-1–C_{60}fr fraction absorbing at 260 nm. Sedimentation analysis of this part of the sample shows that all its characteristics correspond to the PVP-1–C_{60}/4 fraction (Table 2), responsible for the maximal absorption in PVP-1–C_{60}. Thus, we isolated the fraction containing most of the covalently bound fullerene.

The occurrence in the fullerene-containing samples of fractions characterized by large sedimentation coefficients (high molecular weights) can be due to formation of more complex structures such as, e.g., stable clusters based on primary star-like macromolecules, which retain the macromolecular order both in size and weight. The solutions remain transparent and are not colloidal. Notably, cluster formation in fullerene-containing PVPs was also observed in studies of the same samples by small-angle neutron scattering [31].

CONCLUSION

Sedimentation and diffusion analysis allowed direct detection of formation of bulky fullerene-containing polyvinylpyrrolidone-based macromolecules. The primary fullerene-containing macromolecules have presumably a star-like structure with $n \leq 10$ arms. Simultaneously, fullerene-containing samples comprise bulkier water-soluble molecular structures.

REFERENCES

1. Karaulova, E.N. and Bagrii, E.I., *Usp. Khim.*, 1999, vol. 68, no. 11, pp. 979–989.
2. Prato, M., *Top. Curr. Chem., Fullerene Mater*., 1999, vol. 1999, pp. 174–187.
3. Budtov, V.P., Vinogradova, L.V., and Lebedev, V.T., *Panorama sovremennoi khimii Rossii: Sintez i modifikatisya polimerov* (Panorama of the Present-Day Russian Chemistry: Synthesis and Modification of Polymers), Monakov, Yu.B., Ed., Moscow: Khimiya, 2003, pp. 194–224.
4. Kotelnikova, R.A., Kotelnikov, A.I., Bogdanov, G.N., *et al*., *FEBS Lett*., 1996, vol. 389, no. 2, pp. 111–114.
5. Kiselev, O.I., Kozeletskaya, K.N., Melenevskaya, E.Yu., *et al*., *Dokl. Ross. Akad. Nauk*, 1998, vol. 361, no. 4, pp. 547–550.
6. Da Ros, T., Spalluto, G., and Prato, M., *Croat. Chem. Acta*, 2001, vol. 74, no. 4, pp. 743–755.
7. Andreev, S.M., Babakhin, A.A., Petrukhina, A.O., *et al*., *Dokl. Ross. Akad. Nauk*, 2000, vol. 370, no. 2, pp. 261–264.
8. Zgonnik, V.N., Vinogradova, L.V., Melenevskaya, E.Yu., *et al*., *Zh. Prikl Khim*., 1997, vol. 70, no. 9, pp. 1538–1542.
9. Vinogradova, L.V., Melenevskaya, E.Yu., Kever, E.E., *et al*., *Vysokomol. Soedin., Ser. A*, 1997, vol. 39, no. 11, pp. 1733–1739.
10. Karpacheva, G.P., *Vysokomol. Soedin., Ser. C*, 2000, vol. 42, no. 11, pp. 1974–1999.
11. Yamakoshi, Y.N., Yagami, T., Fucuhara, K., *et al*., *J. Chem. Soc., Chem. Commun*., 1994, no. 4, pp. 517–519.
12. Vinogradova, L.V., Melenevskaya, E.Yu., Khachaturov, A.S., *et al*., *Vysokomol. Soedin*., *Ser. A*, 1998, vol. 40, no. 11, pp. 1854–1862.
13. Sun, Y.P., Liu, B., and Morton, D.K., *J. Chem. Soc., Chem. Commun*., 1996, no. 24, pp. 2699–2670.
14. Song, T., Goh, S.H., and Lee, S.Y., *Macromolecules*, 2002, vol. 35, no. 10, pp. 4133–4137.
15. Geckeler, K.E. and Hirsch, A., *J. Am. Chem. Soc*., 1993, vol. 115, no. 9, pp. 3850–3851.
16. Li, F.-M., *Macromol. Symp*., 1996, vol. 101, pp. 227–236.
17. Weis, C. Friedrich, C., Muelhaupt, R., and Frey, H., *Macromolecules*, 1995, vol. 28, no. 1, pp. 403–405.
18. Manolova, N., Rashkov, I., Beguin, F., and van Damme, H., *J. Chem. Soc., Chem. Commun*., 1993, no. 23, pp. 1725–1727.
19. Nazarova, O.V., Afanas'eva, E.V., Panarin, E.F., and Ivanova, N.P., *Zh. Prikl. Khim*., 2000, vol. 73, no. 12, pp. 2060–2062.
20. Tsvetkov, V.N., Eskin, V.E., and Frenkel, S.Ya., *Struktura makromolekul v rastvorakh* (Structure of Macromolecules in Solutions), Moscow: Nauka, 1964.

21. Wales, M. and van Holde, K., *J. Polym. Sci*., 1954, vol. 14, no. 73, pp. 81–86.
22. Tsvetkov, V.N., *Zhestkotsepnye polimernye molekuly* (Rigid-Chain Polymer Molecules), Leningrad: Nauka, 1986.
23. Pavlov, G.M., Selyunin, S.G., Shil'dyaeva, N.A., *et al*., *Vysokomol. Soedin., Ser. A*, 1985, vol. 27, no. 8, pp. 1627–1632.
24. Schuck, P., *Biophys. J*., 2000, vol. 78, no. 3, pp. 1606–1619.
25. Kratky, O., Leopold, H., and Stabinger, H., *Meth. Enzymol*., 1973, vol. 27, pp. 98–110.
26. Provencher, S.W., *Comp. Phys. Comm*., 1982, vol. 27, no. 2, pp. 229–242.
27. Zimm, B., and Stockmayer, W.J., *Chem. Phys*., 1949, vol. 17, no. 12, pp. 1301–1306.
28. Stockmayer, W. and Fixman, M., *Ann. N.Y. Acad. Sci*., 1953, vol. 57, no. 4, pp. 332–337.
29. Pavlov, G.M., Panarin, E.F., Korneeva, E.V., *et al*., *Vysokomol. Soedin., Ser. A*, 1990, vol. 32, no. 6, pp. 1190–1196.
30. Pavlov, G.N., Panarin, E.F., Korneeva, E.V., *et al*., *Makromol. Chem*., 1990, vol. 191, pp. 2889–2899.
31. Lebedev, V.T., Torok, D., Klyubin, V.V., *et al*., *Vysokomol. Soedin*., 2004, vol. 46, no. 5, pp. 875–881.

Russian Journal of Applied Chemistry, Vol. 78, No. 1, 2005, pp. 137–143. Translated from Zhurnal Prikladnoi Khimii, Vol. 78, No. 1, 2005, pp. 139–145.
Original Russian Text Copyright © 2005 by Evlampieva, Lopatin, Yakimanskii, Nazarova, Melenevskaya, Dmitrieva, Belyaev, Litvinova, Lavrenko.

MACROMOLECULAR CHEMISTRY AND POLYMERIC MATERIALS

Electrooptical and Molecular Properties of Fullerene-Containing Poly(Methyl Methacrylates) Prepared by Introducing Fullerenes C_{60} and C_{70} into the Polymer Structure by Different Methods

N. P. Evlampieva, M. A. Lopatin, A. V. Yakimanskii, O. V. Nazarova, E. Yu. Melenevskaya, T. A. Dmitrieva, N. V. Belyaev, L. S. Litvinova, and P. N. Lavrenko

Fock Research Institute of Physics, St. Petersburg State University, St. Petersburg, Russia
Institute of Organometallic Chemistry, Russian Academy of Sciences, Nizhni Novgorod, Russia
Institute of Macromolecular Compounds, Russian Academy of Sciences, St. Petersburg, Russia

Received September 28, 2004

Abstract—Poly(methyl methacrylate) samples and their analogs containing covalently bound fullerenes C_{60} and C_{70} were prepared under varied synthesis conditions. The molecular weights and the electrooptical characteristics of the polymers in solutions were determined. The influence of the fullerenes on the molecular properties of poly(methyl methacrylate) was elucidated, and the most efficient method of its modification with fullerenes was proposed.

Fullerenes C_{60} and C_{70}, like other representatives of the family of framework carbon species, including nanotubes, have electronic properties making them promising for diversified applications to microelectronics and photon engineering [1–4]. In particular, the nonlinear optical properties of fullerenes and their derivatives make materials thereof suitable as limiters of laser radiation intensity, optical modulators, and carriers and accumulators of optically recorded information, as well as for other optoelectronic applications [2–4]. One of the problems faced by modern materials science, related to application of fullerenes, is their introduction into polymers. This makes it possible, first, to exploit the properties of fullerenes spread in thin polymer films and, second, to usefully modify the polymer support itself, e.g., to increase its electrical conductivity [5] or to impart to it nonlinear optical properties [6]. Our previous studies of C_{60} derivatives [7, 8] and published data on hybrid polymeric compounds with various types of chemical bonding of fullerenes [1–6, 9] suggest that the outcome of modification of the polymer depends on the method of introducing fullerene into its composition. Even relatively small weight fractions of fullerenes in some cases significantly affect the initial polymer. For example, covalent bonding of the fullerene C_{60} as a site of branching of the macromolecules of polyvinylpyrrolidone (PVP) [7] and polystyrene (PS) [6] of a star-like structure significantly modifies the optical, dielectric, and electrooptical properties of PVP and PS, when the C_{60} fraction is ca. 1 wt %. At the same time, when C_{60} is introduced into PVP by complexing, there are no such changes [8].

Troitskii *et al*. [10] and Lu *et al*. [11] already attempted modification of poly(methyl methacrylate) (PMMA) with fullerenes. In particular, Lu *et al*. [11] showed that PMMA can be endowed with nonlinear optical properties via copolymerizarion of its monomer, methyl methacrylate (MMA), with an amino derivative of C_{60}, benzylaminofullerene. However, these authors failed to enhance the nonlinear optical properties of the amino derivative of C_{60} when bound with PMMA in such a mode.

In this work, we tested various methods of introducing C_{60} and C_{70} into the PMMA structure. We set a task of determining the molecular characteristics of hybrid polymers of PMMA with C_{60} and PMMA with C_{70} and comparing them with the related characteristics of the PMMA samples prepared under identical conditions but in the absence of the fullerenes. To this end, we carried out viscometric studies of the polymer solutions in benzene, determined their molecular weights M, and studied their electrooptical properties by the method of the Kerr effect in a pulsed electric field [12]. We chose the Kerr effect for this study, since it is highly sensitive to any changes due to structural transformations in the polymer chain, as well as

1070-4272/05/7801-0137 © 2005 Pleiades Publishing, Inc.

Table 1. Synthesis conditions, fullerene content, molecular weight M_η, intrinsic viscosity [η], and electrooptical specific Kerr constants K of the fullerene-containing PMMA samples and their initial analogs

Synthesis procedure	Sample	Catalyst	Fullerene content, wt %	$M_\eta \times 10^{-3}$	$[\eta] \times 10^{-2}$, $cm^3\ g^{-1}$, benzene, 25°C	$K \times 10^{10}$, $cm^5\ g^{-1}\ (300\ V)^{-2}$, benzene, 21°C
1	PMMA-1	DCHPC + TBB	0	470	1.09	0.11
	PMMA-1–C_{60}	DCHPC + TBB	0.05	760	1.58	0.11
			0.09	540	1.22	0.11
			0.17	910	1.81	0.12
	PMMA-1–C_{70}	DCHPC + TBB	0.03	910	1.82	0.11
			0.11	600	1.31	0.11
2	PMMA-2	AIBN	0	3420	5.03	0.10
	PMMA-2–C_{60}	AIBN	0.5	1500	2.71	0.11
3	PMMA-3	AIBN	0	13.0	0.07	0.10
	PMMA-3–C_{60}	–	0.2	45.0	0.18	0.25
4	PMMA-4	DCHPC + TBB	0	470	1.09	0.11
	PMMA-4–C_{60}		0.04	1030	2.02	0.70
	PMMA-4–C_{70}		0.01	1670	2.88	0.45

since it already demonstrated its suitability for detecting the changes in the properties of fullerene-containing compounds relative to the initial analogs [7, 8]. The Kerr effect depends on the optical polarizability, which is also contributed by hyperpolarizability responsible for the occurrence of nonlinear optical properties of the molecules [13], and on the polarity of the covalently bound nanoparticles, fullerene derivatives, in the composition of the polymer. Thus, the change in the equilibrium electrooptical properties of PMMA–C_{60} (C_{70}) relative to the polymer support is suitable as a criterion of the efficiency of various methods of modification of PMMA with fullerenes [7, 8. 14].

EXPERIMENTAL

Samples of PMMA-1–C_{60} and PMMA-1–C_{70} were prepared by radical polymerization using the dicyclohexyl percarbonate–tri-*n*-butylboron (DCHPC–TNBB) initiating system, with the fullerenes introduced into the reaction mixture in varied weight proportions (Table 1). It should be emphasized that the procedure of synthesizing these samples took advantage of a limited solubility of the fullerenes in the monomer. Polymerization was run at 30°C in a sealed glass ampule for 24 h. The fullerene was introduced into MMA until complete dissolution, whereupon DCHPC was introduced, and the solution was degassed. Next, TNBB was introduced from another evacuated ampule, whereupon the ampule that served as reactor was sealed. The ratio (mol %) of DCHPC : TNBB = 0.17 : 0.80 to the total volume of the reaction mixture was identical for all the samples, and varied was only the content of C_{60} (C_{70}) in the reaction mixture. The UV and IR spectra of these samples in chloroform confirmed the absence of chemically unbound fullerenes in PMMA-1–C_{60} and PMMA-1–C_{70}.

The PMMA-2–C_{60} sample was synthesized using another initiator, azobis(isobutyronitrile) (AIBN). Polymerization was run at 60°C for 24 h. Before adding the initiator, the solution of C_{60} in MMA was ultrasonically treated for 1 h to convert the fullerene into a dispersed state, since its concentration much exceeded the limiting concentration (Table 1). We found experimentally that, at 60°C, no more than 0.11×10^{-2} g of fullerene C_{60} can be dissolved in 1 cm^3 of MMA.

The PMMA-3–C_{60} sample was synthesized by adding to the fullerene the PMMA whose macromolecules contained one terminal amino group. The initial PMMA–NH_2 was prepared by radical polymerization of the monomer in the presence of AIBN as the initiator and cysteamine hydrochloride (an amine-containing mercaptan) as the chain-terminating agent. The ethanolic solution of cysteamine hydrochloride was added to a benzene solution of the monomer and initiator. Polymerization was run for 24 h at 60°C in sealed ampules purged with argon. The polymer was isolated by precipitation into diethyl ether and reprecipitated many times. The reaction between fullerene and PMMA–NH_2 was run in a toluene solution by adding dropwise, with stirring, the polymer solution to the C_{60} solution. After 72 h, the mixture was filtered, and the solvent was removed on a rotary

evaporator. The product was dissolved in chloroform, filtered off, and precipitated into diethyl ether. Thin-layer chromatography on SiO_2 plates showed that the product contained the fullerene convalently bound to the polymer, as well as free fullerene from which the product was separated by reprecipitation from chloroform. A similar reaction between fullerene C_{60} and polyvinylpyrrolidone bearing a terminal $–NH_2$ group yielded a product containing 60 wt % homopolymer [15]. This suggests that PMMA-3–C_{60} contains the initial polymer which is difficult to separate from the overall product. The content of the bound fullerene in PMMA-3–C_{60} was estimated as the difference between the amounts of the initial and unchanged C_{60} (Table 1).

The PMMA-4–C_{60} and PMMA-4–C_{70} samples were synthesized similarly to PMMA-1–C_{60} (C_{70}), except that the fullerenes were introduced into the reaction mixture as a solution in *ortho*-dichlorobenzene, in which the fullerenes are strongly solvated at 30°C and form charge-transfer complexes [16]. At the instant when the C_{60}/C_{70} solution was combined with MMA, a finely ground suspension was formed, but after 5-min stirring the reaction mixture turned transparent again.

The fullerene-containing samples of PMMA were readily soluble in benzene, toluene, ethyl acetate, and chloroform, i.e., were identical in solubility to the initial PMMA. Therefore, the procedure for preparation of solutions in benzene, in which all the measurements were carried out, was identical for all the subjects of investigation: The samples were dissolved during 5 days at room temperature. The choice of the solvent in this case was dictated by reliable published data concerning the ratio of the intrinsic viscosity and molecular weight determined by light scattering method for a homologous series of PMMA in benzene [17], as well as by the tasks of electooptical measurements, where a nonpolar solvent (in our case, benzene) is always preferred. Benzene at 25°C had the following characteristics: density $\rho_0 = 0.873$ g cm^{-3}, viscosity $\eta_0 = 0.59$ cP, refractive index $n = 1.4979$, and dielectric permittivity $\varepsilon_0 = 2.252$.

The intrinsic viscosity [η] of the samples was measured at 25°C in an Ostwald capillary viscometer; the time of the solvent outflow was 119.9 ± 0.1 s. Figure 1 presents the concentration dependences of the specific viscosity $\eta_{sp}/c = (\eta - \eta_0)/(\eta_0 c)$, where η and η_0 are the viscosities of the solution and solvent, respectively, and c, solution concentration.

The intrinsic viscosities [η] were determined as the limits of the experimental dependence of $\eta_{sp}/c = f(c)$ at $c \to 0$. Using the resulting [η] values (Table 1), we estimated the molecular weight M of the samples by the Kuhn–Mark–Houwink relationship [17] $[\eta] = 4.68 \times 10^{-5} M^{0.77}$.

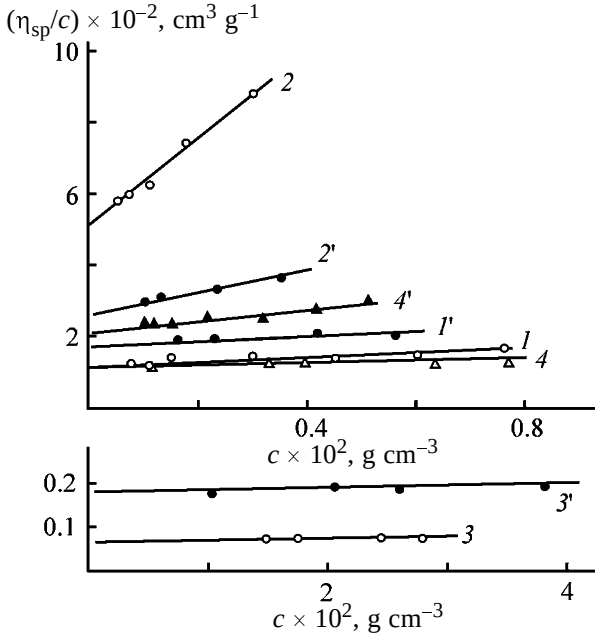


Fig. 1 Specific viscosity η_{sp}/c as a function of the concentration c of benzene solutions of (*1*) PMMA-1, (*1'*) PMMA-1–C_{60} (0.17 wt % C_{60}), (*2*) PMMA-2, (*2'*) PMMA-2–C_{60}, (*3*) PMMA-3, (*3'*) PMMA-3–C_{60}, (*4*) PMMA-4, and (*4'*) PMMA-4–C_{60} samples.

In [18], we substantiated the suitability of the scaling relationships, established for ordinary nonstereoregular PMMA, for estimating the molecular weights M of hybrid fullerene-containing PMMAs. We showed that, when fullerenes C_{60} (C_{70}) are introduced into PMMA during initiation of polymerization, the degree of branching of PMMA–C_{60} (C_{70}) does not markedly increase relative to the PMMA samples synthesized in a similar way by bulk polymerization.

The electrooptical Kerr effect, or birefringence under exposure to an external electric field, depends on the optical and dielectric susceptibilities of the molecular objects studied in solution or, more specifically, on their polar and anisotropic optical properties [12]. In this work, we studied the equilibrium electrooptical effect in the rectangular-pulsed electric field, where birefringence can be measured under conditions when it is independent of the duration and frequency of the pulses fed to the measurement cell. The electrooptical effect was characterized by the specific Kerr constant K defined by the relationship

$$K = \lim_{\substack{E \to 0 \\ c \to 0}} [(\Delta n - \Delta n_0)/E^2 c], \quad (1)$$

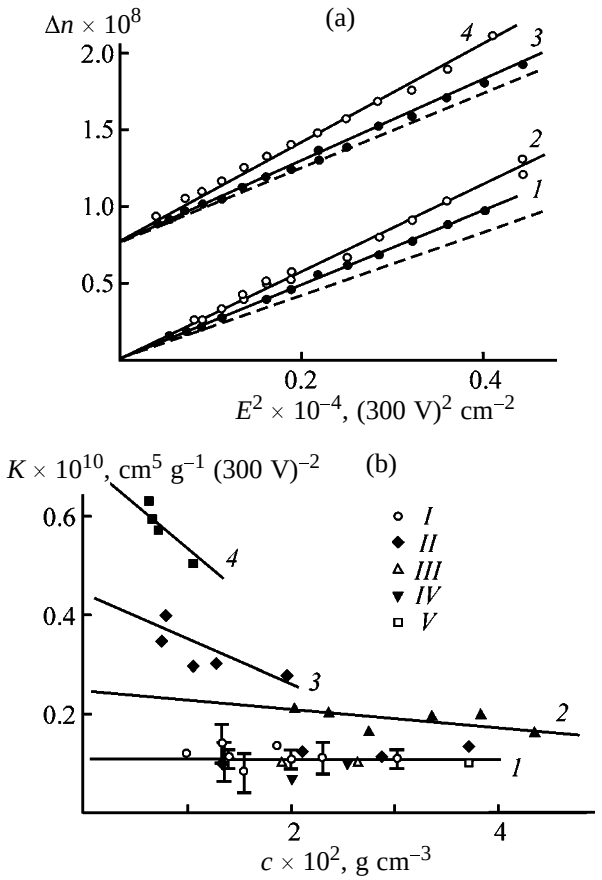


Fig. 2. (a) Birefringence Δn as a function of the squared electrical field intensity E^2 for (*1, 2*) PMMA-1–C_{70} (0.03%) and (*3, 4*) PMMA-3–C_{60} and (b) specific Kerr constant K as a function of the concentration of solutions in benzene c for fullerene-containing samples identical in the properties to (*1*) PMMA-1, (*2*) PMMA-3–C_{60}, (*3*) PMMA-4–C_{70}, and (*4*) PMMA-4–C_{60}. (a) Solution concentration, g cm^{-3}: (*1*) 2.14, (*2*) 3.79×10^{-2}, (*3*) 1.09, and (*4*) 3.83×10^{-2}. (Dashed line) The same dependence for the solvent, benzene. (b) (*I*) PMMA-1, (*II*) PMMA-1–C_{60} (0.09%), (*III*) PMMA-1–C_{60} (0.17%), (*IV*) PMMA-2–C_{60}, and (*V*) PMMA-1–C_{70} (0.11%).

where $\Delta n - \Delta n_0$ is the difference between the birefringences arising under field exposure of a solution of the substance studied at the concentration c and of the solvent, respectively, and E, electric field intensity.

We employed a standard compensation procedure of measuring the Kerr effect in weak electric fields using low-frequency light modulation [12]. The measurements were carried out in a 1.2 cm^3 cylindrical quartz cell. The voltage was supplied to the parallel-plane titanium electrodes soldered into the cell, which were separated by 0.05 cm; the cell length along the light beam path was 2 cm. The light source was a low-power He–Ne laser (1.5 mW cm^{-2}, λ = 632.8 nm). This excluded manifestation of laser-excited nonlinear optical effects in the solutions under study. A thin mica plate with an intrinsic phase shift of $0.01 \times 2\pi$ served as the compensator.

Electrooptical effect in solutions of flexible-chain polymers from the vinyl series, in particular, PMMA, is due to a small-scale, virtually free, orientation of their side groups when exposed to an electric field. The mono unit of PMMA is weakly polar with a dipole moment of 1.2 D [12, 19]. Therefore, PMMA in solutions exhibits a small electrooptical effect (Fig. 2) and has a low specific Kerr constant $K = (+0.11 \pm 0.04) \times 10^{-10}$ cm^5 g^{-1} (300 V)$^{-2}$.

As already mentioned, the synthesis of the PMMA-1–C_{60} (C_{70}), PMMA-2–C_{60}, and PMMA-4–C_{60} (C_{70}) samples was distinguished by the preliminary dissolution of the fullerenes in MMA. As known, radical bulk polymerization of MMA can be carried out with various initiators, which, along with their primary functions, can also affect the properties of the polymerization product [20–22]. For example, Dodonov *et al*. [21] showed that, when the MMA polymerization is initiated by DCHPC in the presence of TNBB and α,β-unsaturated carbonyl compounds, PMMA acquires an enhanced resistance to thermal oxidation, and the films of the PMMA synthesized in the presence of phthalides exhibit fluorescent properties [22]. Dodonov *et al*. [21] and Puzin *et al*. [22] modified the properties of PMMA by introducing special additives into the compound initiating polymerization of MMA and elucidated how these additives affect the polymerization rate and the molecular weight of the final product. Also, these authors found that, when added to the polymerization initiator, fullerenes affect the molecular weight of PMMA.

Studies of the PMMA-1, PMMA-2, and PMMA-4 samples in comparison with similarly prepared fullerene-containing samples of PMMA-1–C_{60}, PMMA-2–C_{60}, and PMMA-4–C_{60} showed that the effect exerted by the fullerenes in the reaction mixture on the properties of the final product of bulk polymerization varies with the type of the initiator. Table 1 lists the molecular weights of the samples studied, which were estimated from the [η] parameters measured in benzene at 25°C. These molecular weights agree well with those of the same samples, determined by the diffusion sedimentation analysis [17]. The intrinsic viscosity [η] and the molecular weight of the PMMA-1–C_{60} (C_{70}) and PMMA4–C_{60} (C_{70}) samples prepared using DCHPC–TNBB exceed those of the initial PMMA-1 and PMMA-4 samples (Table 1), while

Table 2. Dipole moments μ, optical polarizability anisotropies Δ*b*, molecular weights *M*, and molar Kerr constants K_M of the model molecules of butylamino adducts of C_{60} with different numbers of addends *m*, calculated by the PM3 quantum chemical method

*m**	$-\Delta H$, kJ mol^{-1}	*M*	μ, D	$\Delta b \times 10^{24}$, cm^3	$K_M^{**} \times 10^{10}$ cm^5 (300 V)$^{-2}$
1	3195.74	793	2.44	10.06	55.96
2-1	2996.29	866	0.0008	20.50	17.40
2-2	2994.28		3.37	10.36	53.99
3-1	2793.61	939	2.32	18.15	16.15
3-2	2791.27		4.00	1.63	26.66
4-1	2693.03	1012	0.001	21.43	19.01
4-2	2589.52		3.12	10.74	66.41
5	2386.97	1085	2.12	11.06	52.11
6	2183.09	1158	0.003	2.37	2.33

* The designations 2-1, 2-2, 3-1, etc. correspond to conformers with identical numbers of the addition sites *m* allowed by the regioselective scheme of addition to C_{60} [25] and close in the heats of formation ΔH.

** The molar Kerr constants were calculated by the formula $K_M = 2\pi N_A(\theta_1 + \theta_2)$, where $\theta_1 = (45kT)^{-1}[(b_1 - b_2)^2 + (b_2 - b_3)^2 + (b_3 - b_1)^2]$, $\theta_2 = (45k^2T^2)^{-1}[(\mu_1^2 - \mu_2^2)(b_1 - b_2) + (\mu_2^2 - \mu_3^2)(b_2 - b_3) + (\mu_3^2 - \mu_1^2)(b_3 - b_1)]$; b_i are the main values of the linear optical polarizability tensor; μ_i, projections of the dipole moment on the main axes of polarizability of the molecule; *k*, Boltzmann constant; N_A, Avogadro number; and *T*, absolute temperature.

with AIBN as initiator the molecular weight *M* of PMMA-2–C_{60} is smaller than that of PMMA-2.

We found no systematic variation of the molecular weight *M* of the PMMA-1–C_{60} (C_{70}) samples with varying concentrations of the fullerenes introduced (Table 1). In view of the above-mentioned dependence of the molecular weight of the fullerene-containing PMMAs on the specific initiator–fullerene system, we can suggest that, most probably, fullerene introduced into MMA during polymerization initiation participates in interaction with the initiator. Hence, the interaction of fullerene with the propagating polymer chains depends on the initiating system, i.e., on the polymerization mechanism. This holds for synthesis procedure nos. 1, 2, and 4.

By contrast to the PMMA-1, PMMA-2–C_{60}, and PMMA-4–C_{60} samples, for which we revealed no enhanced degree of branching of the chains [18], the PMMA-3–C_{60} macromolecules were branched, as predetermined by the synthesis conditions, at which reactions of C_{60} with amino derivatives yield star-like adducts of fullerene with a random number of addition sites [15, 23]. This is confirmed by an increase in the molecular weight of PMMA-3–C_{60} by a factor of 3.5 relative to that of PMMA-3. Thus, the synthesis procedure and the structure of this fullerene-containing sample radically differed from those of other samples.

Electrooptical studies of solutions of fullerene-containing PMMAs were highly representative and demonstrated how the method of introduction of the fullerene affects the polymer properties. First, the electrooptical properties of PMMA-1–C_{60} (C_{70}) and PMMA-2–C_{60} (C_{70}), on the one hand, and of the initial PMMA-1 and PMMA-2 samples, on the other, were identical (Table 1). This suggests a similar (absolutely neutral) state of the fullerenes in these polymers, whatever their content. Fullerenes C_{60} and C_{70} in these polymers behave similarly, namely, do not affect the electrooptical properties of PMMA when their content is varied from 0.03 to 0.48 wt %. Thus, when introduced into MMA directly during polymerization initiation, the fullerenes do not markedly change the electrooptical properties of PMMAs. Hence, this method is unsuitable for stimulating new properties of this polymer by the fullerenes. This is not true, however, of the two other methods of introduction of the fullerenes into PMMA.

Branched PMMA-3–C_{60}, prepared by adding a terminal amino group of the polymer to the fullerene, is characterized by a specific Kerr constant that is more than twice that of the initial PMMA. Such a change in the properties of PMMA-3–C_{60} is related to its specific structure.

Addition of primary amines to C_{60} yields compounds with random distribution with respect to the number of amino groups added [23]. Table 2 presents the polarity characteristics (dipole moment μ) and optical polarizability anisotropy Δ*b* of the model adducts of fullerene C_{60} with 1 to 6 arms. Table 2 shows how the properties of the butylamino adducts

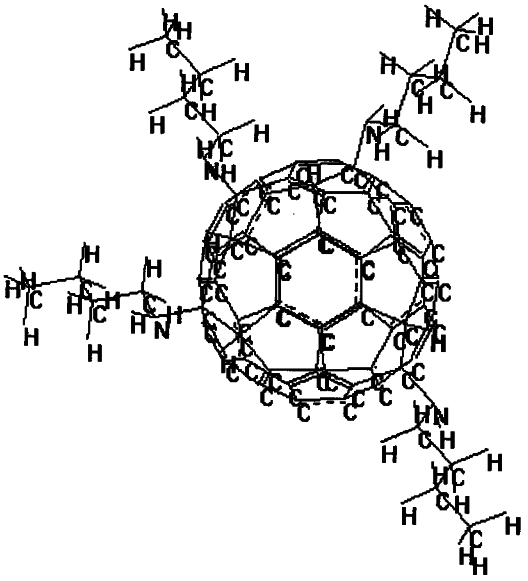


Fig. 3. Structure of butylaminofullerene C_{60} with $m = 4$ addition sites (an analog of the core of the star-like PMMA-3–C_{60} molecules), optimized by the PM3 method.

of C_{60} vary with the number of the addition sites allowed by the regioselective scheme [25]. The fullerene inclusions in branched PMMA-3–C_{60} correspond to the structure of the cores of the model molecules of the amino adducts of C_{60} (Fig. 3). Table 2 suggests that the fullerene-containing branching sites of the PMMA-3–C_{60} macromolecules with 1, 3, or 5 branches will have a dipole moment and exhibit an optical polarizability anisotropy and, thus, will make a noticeable positive contribution to the total electric birefringence observed experimentally in the PMMA-3–C_{60} solutions. The molar Kerr constant, i.e., that corresponding to a mole of the substance (by contrast to the previously introduced specific Kerr constant corresponding to a unit mass) exhibits additivity in solutions [12]. Therefore, assuming that the contributions from PMMA and the amino derivative of the fullerene in PMMA-3–C_{60} are independent, we can use the experimental molar Kerr constant $K_{M(\text{exp})}$ of PMMA-3–C_{60} for estimating the average number of the addition sites of the PMMA branches to C_{60} in the hybrid sample by comparison with the calculated data:

$$K_{M(\text{exp})} = K_{M_1} w_1 + K_{M_2} w_2, \qquad (2)$$

where K_{M_1} and K_{M_2} are the molar Kerr constants for free PMMA and branched PMMA with the C_{60} core, respectively, and w_1 and w_2, their mole fractions in solution.

The molar K_M and specific K Kerr constants are interrelated by the expression

$$K_M = [6n_0 K/(n_0^2 + 2)^2(\varepsilon_0 + 2)^2]M. \qquad (3)$$

For PMMA, $K_{M_1} = 2.3 \times 10^{-10}$, since its monomeric unit with the molecular weight $M_0 = 100$ is a polymer chain fragment, independently orienting in the electric field. According to Table 1, the experimental value for PMMA-3–C_{60} exceeds by a factor of 2.5 that for PMMA-3, $K_{M(\text{exp})} = 5.7 \times 10^{-10}$. By recalculating the weight fraction of the fullerene in PMMA-3–C_{60} (Table 1) into mole fraction, we will obtain $w_1 = 0.89$ and $w_2 = 0.11$, respectively. By substituting K_M, K_{M_1}, w_1, and w_2 into formula (2), we obtain $K_{M_2} = 33.2 \times 10^{10}$, which is close to the average of the nine calculated molar Kerr constants of 34.51×10^{10} (Table 2). This confirms, on the whole, an equally probable (from 1 to 6) number of the possible addition sites of the amino groups to the fullerene. Earlier [26] we studied the properties of the PVP–C_{60} prepared, similarly to PMMA-3–C_{60}, by adding the PVP branches to C_{60} via the terminal amino group of the polymer and showed that, because of a large positive contribution to the electrooptical effect from the PVP–C_{60} core, the negative electrooptical constant of the initial PVP changes to positive [26].

Six-arm adducts C_{60} (Table 2), like the fullerene proper, are characterized by a high symmetry (symmetry group S_6) and, thus, are virtually nonpolar and optically anisotropic compounds. It is known that reactions between C_{60} and free radicals yield predominantly hexa adducts [25]. Thus, it can be assumed that the reaction of C_{60} with an excess of various radicals during synthesis of PMMA-1–C_{60} (C_{70}) and PMMA-2–C_{60} (C_{70}) involves specifically such "neutralization" (saturation) of the fullerene. Thus, the resulting adducts of C_{60} do not contribute to the electroopticl properties of the fullerene-containing PMMA prepared by procedure nos. 1 and 2.

The electrooptical properties of PMMA-4–C_{60} (C_{70}) differ most profoundly from those of the initial polymer (Table 1). It should be reminded that, in this case, by contrast to PMMA-1–C_{60} (C_{70}) and PMMA-2–C_{60} (C_{70}), the fullerene was introduced into MMA in an *ortho*-dichlorobenzene solution, with which it forms crystal solvates and charge-transfer complexes [16]. The role of *ortho*-dichlorobenzene in the synthesis of PMMA-4–C_{60} (C_{70}) can only be hypothesized in the present stage of investigation. For example, we can assume that formation of very stable complexes between C_{60} and *ortho*-dichlorobenzene

prevents synthesis of symmetrical, nonpolar, and optically isotropic star-like PMMA with a C_{60} core. In any case, it is evident that the state of the fullerenes during polymerization and in PMMA-4–C_{60} (C_{70}) differs from that in PMMA-1–C_{60} (C_{70}) and PMMA-2–C_{60} (C_{70}). This is evidenced not only by a manyfold change of the electrooptical specific Kerr constant, but also by a more significant increase in the molecular weight of the PMMA-4–C_{60} (C_{70}) samples compared to the initial PMMA-4 and the PMMA-1–C_{60} (C_{70}) samples prepared using the same initiator (Table 1).

CONCLUSIONS

(1) Electrooptical properties of hybrid poly(methyl methacylates) are governed by the state of the fullerene in these polymers, which, in turn, is determined by the mode of its introduction into the polymer chains.

(2) The electrooptical properties of the product of bulk polymerization of methyl methacrylate changed most profoundly in the case when very small amounts of the fullerene (0.04 wt % C_{60} and 0.0053 wt % C_{70}) were introduced into the reaction mixture in the initiation stage as a complex with *ortho*-dichlorobenzene. This mode seems to be the least labor-consuming and the most suitable for stimulating new electrooptical properties of poly(methyl methacrylate) via introducing fullerenes into its structure.

REFERENCES

1. *Molecular Nanostructures*, Kuzmany, H., Fink, J., Mehring, M., and Roth, S., Eds., *AIP Proc.* (New York), 2003, vol. 685.
2. Belousov, V.P., Belousova, I.M., Gavronskaya, E.A., *et al.*, *Opt. Zh.*, 1999, vol. 66, no. 8, pp. 50–56.
3. Kamanina, N.V. and Sheka, E.F., *Opt. Spektrosk.*, 2004, vol. 96, no. 4, pp. 659–673.
4. Kamanina, N.V., Sizov, V.N., and Stasel'ko, D.I., *Opt. Spektrosk.*, 2001, vol. 90, no. 1, pp. 5–7.
5. Wang, Y. and Suna, A., *J. Phys. Chem. B*, 1997, vol. 101, pp. 5627–5638.
6. Koudoumas, E.M., Konstantaki, M., Mavromanolakis, A., *et al.*, *Chem. Phys. Lett.*, 2001, vol. 335, pp. 533–538.
7. Ryumtsev, E.I., Evlampieva, N.P., Nazarova, O.V., *et al.*, *Dokl. Ross. Akad. Nauk*, 2003, vol. 392, no. 2, pp. 212–216.
8. Evlampieva, N.P., Lavrenko, P.N., Zaitseva, I.I., *et al.*, *Vysokomol. Soedin., Ser. A*, 2002, vol. 44, no. 9, pp. 1564–1570.
9. Kapracheva, G.P., *Vysokomol. Soedin., Ser. C*, 2000, vol. 42, no. 11, pp. 1974–1999.
10. Troitskii, B.B., Domrachev, G.A., Khokhlova, L.V., and Anikina, L.I., *Vysokomol. Soedin., Ser. C*, 2001, vol. 43, no. 9, pp. 1540–1550.
11. Lu, Zh., Goh, S.H., Lee, S.Y., *et al.*, *Polymer*, 1999, vol. 40, pp. 2863–2867.
12. Tsvetkov, V.N., *Zhestkotsepnye polimernye molekuly* (Rigid-Chain Polymer Molecules), Leningrad: Nauka, 1986.
13. Vuks, M.F., *Elektricheskie i opticheskie svoistva molekul i kondensirovannykh sred* (Electrical and Optical Properties of Molecules and Condensed Media), Leningrad: Leningr. Gos. Univ., 1984.
14. Lavrenko, P.N., Evlampieva, N.P., Lekhner, M.D., *et al.*, *Vysokomol. Soedin.*, 2004, vol. 46, no. 10, pp. 1743–1753.
15. Nazarova, O.V., Pavlov, G.M., and Bokov, S.N., *Dokl. Ross. Akad. Nauk*, 2003, vol. 391, no. 2, pp. 212–214.
16. Doome, R.J., Dermaut, S., Fonseca, A., *et al.*, *Fullerene Sci. Technol.*, 1997, vol. 5, no. 7, pp. 1593–1606.
17. Tsvetkov, V.N., Skazka, V.S., and Krivoruchko, N.M., *Vysokomol. Soedin., Ser. A*, 1960, vol. 2, no. 7, p. 1045.
18. Evlampieva, N.P., Lopatin, M.A., Nazarova, O.V., *et al.*, Abstracts of Papers, *3 Mezhdunarodnaya konferentsiya "Uglerod: fundamental'nye problemy nauki, materialovedenie, tekhnologiya"* (3 Int. Conf. "Carbon: Fundamental Problems of Science, Materials Science, Technology), Moscow, October 13–15, 2004, p. 99.
19. Kobeko, P.P., *Amorfnye veshchestva* (Amorphous Substances), Moscow: Akad. Nauk SSSR, 1952.
20. Ivanchev, S.S, *Radikal'naya polimerizatsiya* (Radical Polymerization), Leningrad: Khimiya, 1985.
21. Dodonov, V.A., Garusova, Zh.V., Starostina, T.I., and Begantseva, Yu.E., *Vysokomol. Soedin., Ser. A*, 2000, vol. 42, no. 9, pp. 1483–1488.
22. Puzin, Yu.I., Egorov, A.E., Khatchenko, E.A., *et al.*, *Vysokomol. Soed., Ser. A*, 2000, vol. 42, no. 9, pp. 1461–1471.
23. Yevlampieva, N., Nazarova, O., Bokov, S., *et al.*, *Fullerenes, Nanotubes, Carbon Nanostruct.*, 2004, vol. 12, no. 1, pp. 369–375.
24. Stewart, J.J.P., *J. Computer-Aided Mol. Des.*, 1990, vol. 4, pp. 1–105.
25. Hirsch, A. and Vostrowsky, O., *Eur. J. Org. Chem.*, 2001, vol. 5, pp. 829–848.
26. Evlampieva, N.P., Nazarova, O.V., Bokov, S.N., *et al.*, *Vysokomol. Soedin.*, 2004, vol. 46, no. 5, pp. 822–829.

Russian Journal of Applied Chemistry, Vol. 78, No. 1, 2005, pp. 144–148. Translated from Zhurnal Prikladnoi Khimii, Vol. 78, No. 1, 2005, pp. 146–150.
Original Russian Text Copyright © 2005 by Ergozhin, Chalov, Kovrigina, Iskakova.

MACROMOLECULAR CHEMISTRY AND POLYMERIC MATERIALS

Ion-Exchange Polymers Based on Dihydroxydiphenylpropane Diglycidyl Ether, Allyl Halides, and Amines

E. E. Ergozhin, T. K. Chalov, T. V. Kovrigina, and R. A. Iskakova

Bekturov Institute of Chemical Problems, Ministry of Education and Science of Kazakhstan Republic, Almaty, Kazakhstan

Received June 15, 2004

Abstract—Polycondensation of dihydroxydiphenylpropane diglycidyl ether and allyl halides in the presence of some polyamines was studied. The optimal conditions of formation of ion-exchange polymers with three-dimensional structure, their composition and structure, and also physicochemical characteristics were determined.

The use of dihydroxydiphenylpropane diglycidyl ether (ED-20) as initial monomer for synthesis of ion-exchange resins and membranes provides formation of ordered structures improving the main physicochemical, optical, and strength characteristics of the resulting polymers [1, 2]. Introduction of allyl compounds into the reaction mixture improves the performance of the materials [3]. Therefore, in this work we used allyl halides [allyl bromide (AB) and allyl chloride (AC)] as comonomers. The choice of the above compounds is caused by the fact that these compounds readily react with homolytic rupture of the C–X bond (where X is Br, Cl, I, and F) due to conjugation with the C=C bond [4].

The aim of this work is development of methods for synthesis and study of characteristics of ion exchangers based on industrial epoxy resin, allyl halides (AHs), and some aromatic and aliphatic polyamines.

EXPERIMENTAL

Condensation of allyl halides with dihydroxydiphenylpropane diglycidyl ether and amines was carried out at 18–25°C for 1–2 h with subsequent curing of the prepolymer at 80–100°C. The gel was milled and dispersed and the fraction with a grain size of 0.25 mm was selected [5, 6].

Pretreatment and determination of the main physicochemical characteristics were performed by the procedures described previously [7].

The IR spectra of the initial, intermediate, and final products prepared as thin layers and KBr pellets (1 mg substance + 200 mg KBr) were recorded on a Specord M80/M85 spectrophotometer.

The potentiometric titration was carried out by the method of individual weighed portions. A weighed portion of air-dry anion exchanger (0.20–0.25 g) was brought into contact with various amounts of 0.1 N nitric acid (from 0.5 to 50 ml). The ionic strength of the solution (approximately 1 M) was supported by adding the corresponding amount of potassium nitrate. After the equilibrium was reached (7–10 days), the pH of the solution was measured on a DL-55 titrator.

With the aim to find the optimum conditions of synthesis of ion exchangers based on AHs, ED-20, and amines, we studied how the ratio of the initial components, the kind of AH, prepolymerization temperature, and curing conditions affect some characteristics of the anion exchangers (Tables 1 and 2) [8]. A decrease in the amine concentration results in a decrease in the static exchange capacity (SEC) from 9.5 to 6.3 in the case of polyethylenimine (PEI) and from 3.9 to 2.7 mg-equiv g^{-1} in the case of poly-2-methyl-5-vinylpyridine (PMVP). At the same time, its increase significantly hampers curing of the gel, which results in deterioration of the mechanical strength. The kind of allyl compound does not significantly affect the SEC. The presence of pyridine group assists to an increase in the exchange capacity with respect to highly basic groups.

In condensation of polyfunctional monomers, unchanged functional groups remain in the resulting macromolecules, which is caused by their different reactivity an also by steric and concentration factors. The presence of double bonds in allyl compounds

1070-4272/05/7801-0144© 2005 Pleiades Publishing, Inc.

Table 1. Influence of the ratio of the initial monomers on physicochemical characteristics of anion exchangers

Ratio of initial components, wt parts	SEC, mg-equiv g^{-1}		Swelling, ml g^{-1}
	for 0.1 N HCl	for 0.1 N NaCl	
ED-20 : AB : PEI = 1.5 : 1.0 : 3.0	9.5	0.2	3.4
ED-20 : AB : PEI = 1.5 : 1.0 : 2.0	7.5	0.1	3.0
ED-20 : AB : PEI = 1.5 : 1.0 : 1.0	6.3	0.1	2.9
ED-20 : AC : PEI = 1.5 : 1.0 : 3.0	9.2	0.1	3.1
ED-20 : AB : PMVP = 1.5 : 1.0 : 2.0	3.9	0.8	2.6
ED-20 : AB : PMVP = 1.5 : 1.0 : 1.0	3.1	0.6	2.3
ED-20 : AB : PMVP = 1.5 : 1.0 : 0.5	2.7	0.5	1.9
ED-20 : AC : PMVP = 1.5 : 1.0 : 2.0	3.5	0.7	2.9

Table 2. Influence of prepolymerization temperature on the main characteristics of sorbents

T, °C	ED-20 : AB : PEI		ED-20 : AB : PMVP	
	SEC_{HCl}, mg-equiv g^{-1}	swelling, mg g^{-1}	SEC_{HCl}, mg-equiv g^{-1}	swelling, mg g^{-1}
Prepolymerization:				
13	5.6	2.6	2.2	1.4
18	8.4	3.1	3.3	2.3
25	9.5	3.4	3.9	2.6
Curing:				
80	9.5	3.4	3.9	2.6
100	8.2	3.0	3.1	2.2
120	7.5	2.9	2.4	1.6

plays a certain part in formation of cross-linked structures. The probability of their scission under the action of atmospheric oxygen in aftercuring increases. In this connection, we determined the optimum temperature at which all functional groups enter into the reaction and the degree of scission of double bonds is maximal.

The influence exerted by prepolymerization temperature and curing conditions on SEC and swelling of the resulting ion-exchangers is illustrated by Table 2. With increasing prepolymerization temperature from 13 to 25°C, the sorption capacity of the ion exchanger significantly increases, from 5.6 to 9.5 mg-equiv g^{-1} in the case of PEI and from 2.2 to 3.9 mg-equiv g^{-1} in the case of PMVP. The increase in curing temperature from 80 to 120°C results in decreasing SEC of anion exchangers and correspondingly in decreasing swelling, which is caused by significant compaction of the copolymer structure during the reaction.

We found that the yield of the copolymer with the three-dimensional structure depends on the reaction temperature and duration (Fig. 1). With increasing temperature, the yield of the final product increases. The maximum yield of the anion exchanger based on ED-20, AB, and PMVP (80%) is reached in 120 min at 13°C, 90 min at 18°C (88%), and 60 min at 25°C. With PEI, the reaction proceeds at a higher rate and with a higher yield (96% in 40 min at 25°C).

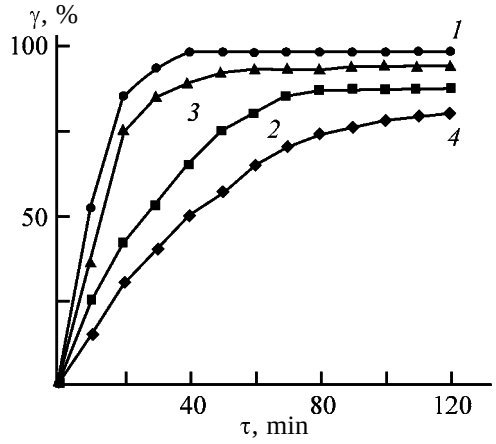


Fig. 1. Yield of the polymer γ as a function of the reaction duration τ. (*1–3*) ED-20 : AB : PMVP and (*4*) ED-20 : AB : PEI. *T*, °C: (*1*) 13, (*2*) 18, and (*3, 4*) 25.

Table 3. Chemical and thermal stability of the synthesized anion exchangers

Anion exchanger	SEC_{HCl} before treatment, mg-equiv g^{-1}	SEC_{HCl} after treatment, mg-equiv g^{-1} (loss, %)						
		chemical			thermal			
		5 N H_2SO_4	5 N NaOH	10% H_2O_2	3 h	5 h	7 h	12 h
ED-20 : AB : PEI	9.5	9.1 (4)	9.1 (4)	8.1 (15)	9.3 (2)	9.3 (2)	9.1 (4)	8.9 (6)
ED-20 : AC : PEI	9.2	8.4 (9)	8.7 (5)	7.6 (17)	8.8 (4)	8.7 (5)	8.9 (7)	8.5 (8)
ED-20 : AB : PMVP	3.9	3.8 (2)	3.8 (2)	3.6 (7)	3.8 (2)	3.8 (2)	3.8 (2)	3.8 (3)
ED-20 : AC : PMVP	3.5	3.4 (4)	3.4 (3)	3.2 (8)	3.4 (3)	3.4 (3)	3.4 (4)	3.4 (4)
ED-10P	8.0	7.9 (1.2)	7.9 (1.2)	3.3 (58.7)	7.4 (9.2)	7.1 (9)	6.3 (8)	6.3 (8)

The results of studying chemical resistance and thermal stability (Table 3) show that anion exchangers based on PEI are less resistant to solutions of acids, alkalis, and oxidants, since an increase in the fraction of tertiary amines decreases the thermal stability of the copolymer. In this case, the loss of the capacity does not exceed 17%, while under the same conditions ED-10P commercial ion exchanger loses 58.7% of its capacity [9]. The study of thermal stability of the synthesized ion exchangers in water in the range 80–100°C for 12 h (Table 3) shows that the loss in capacity does not exceed 8%. The most stable are anion exchangers based on PVMP.

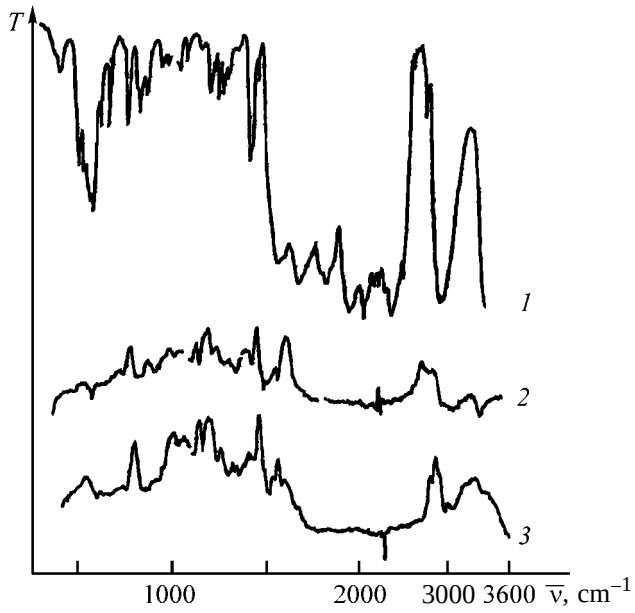


Fig. 2. IR spectra of ED-20 and anion exchangers based on it. (*T*) Absorption and ($\bar{\nu}$) wave number. (*1*) ED-20, (*2*) ED-20 : AB : PEI, and (*3*) ED-20 : AB : PMVP.

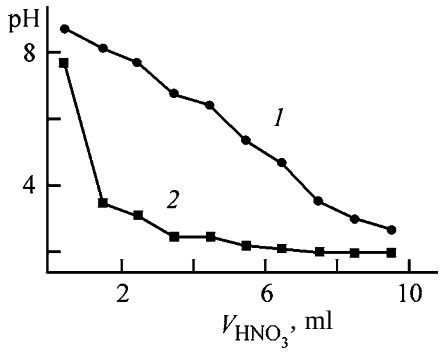


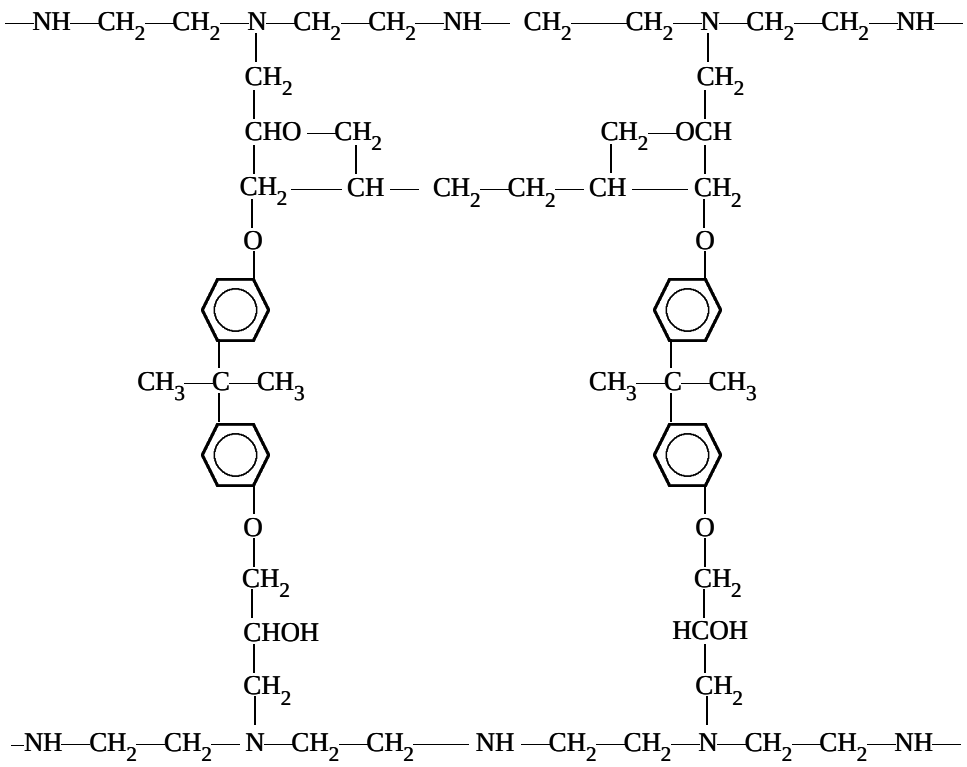
Fig. 3. Potentiometric titration curves of anion exchangers based on ED-20, AB, and polyamines (*1*) PEI and (*2*) PMVP. (V_{HNO_3}) volume of 0.1 N HNO_3.

Thus, the optimal conditions of synthesis of polyfunctional anion exchangers based on the above monomers are 25°C, 1–2 h, and weight ratios ED-20 : AB : PEI = 1.5 : 1.0 : 3.0 and ED-20 : AB : PMVP = 1.5 : 1.0 : 2.0.

The structures of the initial and final products were studied by IR spectroscopy (Fig. 2). The epoxy groups in ED-20 give rise to the absorption bands at 832, 916, 1240, and 3056 cm^{-1}. In the spectra of the synthesized anion exchangers, these bands are absent, which suggests chemical transformation of epoxy groups. The absorption bands corresponding to the stretching modes of amino groups appear in the range 3600–3300 cm^{-1}, and the bands characteristic of bending modes, in the range 1650–1550 cm^{-1}. Stretching modes of the C–N bonds are manifested in the range 1360–1250 cm^{-1}. The presence of absorption bands at 832 cm^{-1} and in the range 1600–1500 cm^{-1} confirms the presence of aromatic fragments. The spectra of the synthesized polyelectrolytes contain bands at 1075–1020 cm^{-1} of the in-plane bending modes of the C–H bonds in the benzene ring. The band at 1470–1460 cm^{-1} corresponds to the CH_2 group, at 1350–1300 cm^{-1}, to the CH_3 group, and at 1200–1180 cm^{-1}, to the quaternary carbon atom. The absorption bands of the stretching modes of the CH bonds (at 3070–3020 cm^{-1}) and the C=C and C=N bonds of pyridine ring (1660, 1560, and 1460 cm^{-1}) undergo certain changes. In the spectrum of the anion exchanger based

on PEI, there is a broad band in the range 1664 cm^{-1} characteristic of the C–N bond.

Thus, the structure of the elementary unit of the three-dimensional polyfunctional anion exchanger prepared using PEI can be schematically presented in the form



In the reaction of ED-20 with allyl halides and amines, nucleophilic attack of the epoxy ring with the nitrogen atom causes the ring opening. As a result, OH groups, which can enter into the reaction with allyl halides, are formed. The resulting allyl ether is apparently oxidized with atmospheric oxygen. In this case, isomerization of allyl radical takes place to form hydroperoxide of substituted vinyl ether, in which the double bond is activated by conjugation with an unshared pair of the ether oxygen atom; this enhances its capability for polymerization.

The functionality and basicity of the synthesized anion exchangers with the three-dimensional structure was studied by potentiometric titration. The negative logarithm of the acid dissociation constant of the ionogenic groups of the polymer pK_a and empirical coefficient m considering interunit interaction were determined by graphic method (Figs. 3, 4) from the Henderson–Hasselbach equation [10]. The pK_a value of the polyelectrolyte based on PEI is 7.0, of that based on PMVP, 3.6, and m is 2.5 and 2.3, respectively.

The shape of the potentiometric titration curve of the polyelectrolyte based on PMVP (Fig. 3) and also lower values of pK_a suggest its increased basicity in comparison with anion exchangers based on PEI.

It is evident that higher values of the empirical co-

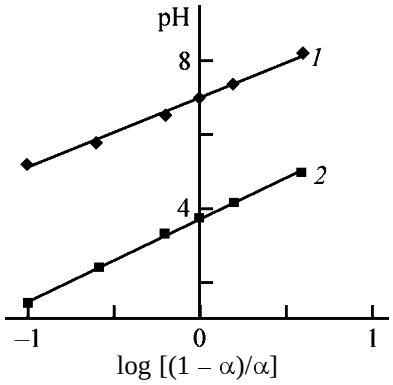


Fig. 4. Dependence of pH of the equilibrium solution on log[(1 – α)/α]. (α) Degree of protonation of functional groups of the ion exchanger. (*1*) ED-20 : AB : PEI and (*2*) ED-20 : AB : PMVP.

efficient *m* characterizing the electrostatic interaction of functional groups in the polymer can be explained by high concentration of ionogenic groups [11].

CONCLUSIONS

(1) Procedures were developed for synthesis of highly permeable polyfunctional anion exchangers based on dihydroxydiphenylpropane diglycidyl ether, allyl halides, and some polyamines. The resins are chemically resistant to solutions of acids, alkalis, and oxidizing agents.

(2) The acid dissociation constants of ionogenic groups of the polymer and the empirical coefficients considering interunit interaction suggest formation of weakly basic anion exchangers in the case of polyethylenimine and of highly basic anion exchangers in the case of poly-2-methyl-5-vinylpyridine.

(3) The synthesized anion exchangers are recommended for development of a sorption procedure for separation of transition and noble metal ions.

REFERENCES

1. Ergozhin, E.E. and Menligaziev, E.Zh., *Polifunktsional'nye ionoobmenniki* (Polyfunctional Ion Exchangers), Almaty: Nauka, 1986.
2. Paquin, A.M., *Epoxydverbindungen und Epoxydharze*, Berlin: Springer, 1958.
3. Vorob'eva, A.I., Prochukhan, Yu.A., and Monakov, Yu.B., *Vysokomol. Soedin., Ser. C*, 2003, vol. 45, no. 12, pp. 2118–2136.
4. Nesmeyanov, A.N. and Nesmeyanov, N.A., *Nachala organicheskoi khimii* (Principles of Organic Chemistry), Moscow: Khimiya, 1969, vol. 1.
5. Ergozhin, E.E., Chalov, A.K., Iskakova, R.A., and Kovrigina, T.V., *Zh. Prikl. Khim.*, 2004, vol. 77, no. 3, pp. 465–469.
6. Ergozhin, E.E., Chalov, A.K., Iskakova, R.A., *et al.*, *Zh. Prikl. Khim.*, 2002, vol. 75, no. 11, pp. 1826–1829.
7. *GOSTs* (State Standards) *10898–84, 10898.2–74, and 10898.5-84: Ion Exchangers: Procedures of Physicochemical Testing.*
8. Kazakhstan Prepatent no. 14674.
9. Zarkhina, T.S., Zarkhin, L.S., and Zelenetskii, A.N., *Vysokomol. Soedin., Ser. A*, 1982, vol. 24, no. 11, pp. 2429–2442.
10. Saldadze, K.M. and Kopylova-Valova, V.D., *Kompleksoobrazuyushchie ionity (kompleksity)* (Complex-Forming Ion Exchangers (Complexites)), Moscow: Khimiya, 1980.
11. Grissbach, R., *Austauschadsorption in Theorie und Praxis*, Berlin: Akademie, 1957.

Russian Journal of Applied Chemistry, Vol. 78, No. 1, 2005, pp. 149–152. Translated from Zhurnal Prikladnoi Khimii, Vol. 78, No. 1, 2005, pp. 151–154.
Original Russian Text Copyright © 2005 by Ergozhin, Mukhitdinova, Shoinbekova, Nikitina, Nuranbaeva, Zhunusova.

MACROMOLECULAR CHEMISTRY AND POLYMERIC MATERIALS

Derivatives of *ortho*- and *para*-Naphthoquinones and Monoethanolamine Vinyl Ether in Radical Copolymerization with Acrylic Acid

E. E. Ergozhin, B. A. Mukhitdinova, S. A. Shoinbekova, A. I. Nikitina, B. M. Nuranbaeva, and G. N. Zhunusova

Bekturov Institute of Chemical Problems, Ministry of Education and Science of Kazakhstan Republic, Almaty, Kazakhstan

Received May 11, 2004

Abstract—Radical copolymerization of new redox monomers based on derivatives of monoethanolamine vinyl ether and naphthoquinones with acrylic acid was studied.

With the aim to extend the set of monomers suitable for synthesis of redox polymers, new redox monomers based on monoethanolamine vinyl ether (MEAVE) and quinones [1] were prepared, and radical homo- and copolymerization of some of these monomers was studied [2–7]. It was found that quinoid derivatives of MEAVE fairly readily enter into homo- and copolymerization, contrary to the initial ether, which practically does not form polymers [8], and to quinones being polymerization inhibitors.

In this work we studied the influence of chemical structure of naphthoquinones on the reactivity of redox monomers in radical copolymerization with acrylic acid (AA).

EXPERIMENTAL

Redox monomers based on MEAVE and 1,2-naphthoquinone (MEAVE–1,2-NQ), MEAVE and 1,4-naphthoquinone (MEAVE–1,4-NQ), and dichloro-1,4-naphthoquinone (MEAVE–DC-1,4-NQ) were synthesized by the procedure described in [1]. Azobis(isobutyronitrile) (AIBN) was recrystallized from dry methanol; mp 102–103°C.

Copolymerization of redox monomers with AA was carried out in hermetically sealed tubes in DMF at 68°C in the presence of 6 wt % AIBN for 0.5 h. Conversion of monomers was judged from variation of their concentration, which was determined by the polarographic method (redox monomers) and titration (AA).

The polarographic curves were recorded in a temperature-controlled cell at 25 ± 0.5°C on a PU-1 polarograph (mercury dripping electrode with the capillary characteristic at open circuit $m^{2/3}\tau^{1/6} = 4.38\ mg^{2/3}s^{-1/2}$ [m is the weight of mercury outlowing from the capillary in 1 s and τ is the period of mercury dropping (s)] with phosphate buffer solution (pH 7.4) with DMF content of 25 wt % as supporting electrolyte. The reference electrode was a saturated calomel electrode. Oxygen was removed from the solutions used for polarography by bubbling with argon.

Determination of the constants of relative activity of monomers r_1 and r_2 is an important problem both in direct study of copolymerization and for establishment of the relation between the chemical structure of unsaturated compounds and their reactivity.

Copolymerization of MEAVE derivatives and various naphthoquinones (M_1) with AA (M_2) was studied in DMF solutions in the presence of AIBN. The composition of the copolymers was evaluated from data listed in Table 1. As seen from Table 1 and Fig. 1, none of the systems forms an azeotropic copolymer. In the case of joint polymerization of MEAVE–1,2-NQ and MEAVE–1,4-NQ with AA ($r_1 > 1$, $r_2 < 1$), the composition curves are located above the azeotropic line, i.e., at all the ratios of the initial compounds, the copolymers are significantly enriched with redox monomer units. For the monomer pair MEAVE–DC-1,4-NQ and AA ($r_1 < 1$, $r_2 > 1$), the composition curve is located below the azeotropic line and the copolymer is enriched with AA units.

The copolymerization constants were evaluated by the Mayo–Lewis integral equation of copolymer composition [9]. The parameter p in this equation was

1070-4272/05/7801-0149 © 2005 Pleiades Publishing, Inc.

Table 1. Composition of the initial mixtures of monomers and copolymers

Composition of the initial mixture				Concentration of monomers after 5 min, M		Copolymer composition, mol %	
mol %		M					
M_1^0	M_2^0	M_1^0	M_2^0	M_1	M_2	m_1	m_2
MEAVE–1,2-NQ : AA							
80	20	0.103	0.026	0.099	0.025	91.70	8.30
63	36	0.103	0.058	0.099	0.057	86.83	13.17
50	50	0.103	0.104	0.095	0.100	59.86	40.14
35	65	0.103	0.189	0.097	0.183	46.55	53.48
19	81	0.103	0.447	0.095	0.430	29.56	70.44
MEAVE–1,4-NQ : AA							
80	20	0.082	0.021	0.079	0.020	85.18	14.82
60	40	0.082	0.055	0.079	0.054	73.40	26.60
50	50	0.082	0.082	0.078	0.080	67.52	32.48
40	60	0.082	0.124	0.078	0.122	61.24	38.76
20	80	0.082	0.330	0.078	0.324	36.92	63.08
MEAVE–DC-1,4-NQ : AA							
79	21	0.072	0.019	0.071	0.018	72.98	17.02
60	40	0.072	0.048	0.070	0.046	48.25	51.75
47	53	0.072	0.080	0.070	0.077	33.69	66.31
39	61	0.072	0.115	0.070	0.110	24.47	75.53
15	85	0.072	0.397	0.070	0.382	9.89	90.11

Table 2. Constants of copolymerization, resonance stabilization, and polarity for system redox monomer (M_1) : AA (M_2)

Monomer (M_1)	p	r_1	r_2	r_1r_2	$1/r_1$	$1/r_2$	Q_1	e	Δe
MEAVE–1,2-NQ	–2.15	2.04	0.52	1.061	0.49	1.92	2.14	0.67	0.10
MEAVE–1,4-NQ	–0.57	1.48	0.16	0.237	0.68	6.25	2.85	–0.43	1.20
MEAVE–DC-1,4-NQ	–0.90	0.59	1.46	0.861	1.70	0.68	0.59	0.38	0.39

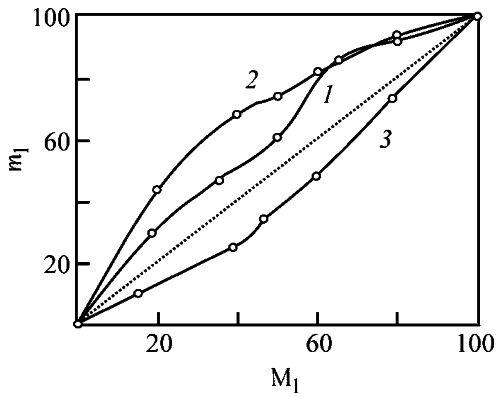


Fig. 1. Diagram of monomer–copolymer composition for the systems (*1*) MEAVE–1,2-NQ : AA, (*2*) MEAVE–1,4-NQ : AA, and (*3*) MEAVE–DC-1,4-NQ : AA. Mole fraction of redox monomers: (M_1) in the mixture of monomers and (m_1) in copolymers.

selected by the Shtraikhman graphic analytical method [10]. The polymerization constants and the Alfrey–Price parameters of resonance stabilization Q_1 and polarity e_1 for new redox monomers are given in Table 2. For AA, Q_2 = 1.15 and e_2 = 0.77 were taken from [11].

Table 2 shows that the monomer MEAVE–1,2-NQ is the most active, and the radical formed from this monomer is less reactive with respect to the monomer MEAVE–1,2-NQ. The radical MEAVE–1,4-NQ exhibits the highest activity in the reaction with the polymer radical AA; this is apparently caused by the influence of the polarity factor *e*, whose value in this case is negative. The greater the difference in the polarity of the two monomers Δe and the smaller the product r_1r_2, the stronger the tendency to alternation of the monomers in the copolymer [9]. For the system

Table 3. Probability of formation of various diads and block lengths in copolymerization of MEAVE–naphthoquinone derivatives (M_1) with AA (M_2)

M_1^0	M_2^0	M_1/M_2	$f_{M_1M_1}$		$f_{M_1M_2}$		$f_{M_2M_2}$		L_{M_1}	L_{M_2}
mol %			fraction	%	fraction	%	fraction	%		
MEAVE–1,2-NQ : AA (r_1 = 2.04, r_2 = 0.52)										
80	20	3.882	0.788	87.46	0.100	11.10	0.013	1.44	8.88	1.13
64	36	1.737	0.606	73.19	0.171	20.65	0.051	6.16	4.54	1.30
50	50	0.955	0.434	55.78	0.223	28.66	0.121	15.56	2.95	1.54
35	65	0.532	0.267	35.41	0.246	32.63	0.241	31.96	2.08	1.98
19	81	0.221	0.094	11.88	0.208	26.30	0.489	61.82	1.45	3.35
MEAVE–1,4-NQ : AA (r_1 = 1.48, r_2 = 0.16)										
80	20	3.854	0.736	84.60	0.129	14.83	0.005	0.58	6.70	1.04
60	40	1.463	0.507	66.10	0.234	30.51	0.026	3.39	3.17	1.11
50	50	0.975	0.400	55.40	0.277	38.36	0.045	6.23	2.44	1.16
40	60	0.642	0.297	43.17	0.313	45.49	0.078	11.34	1.95	1.25
20	80	0.241	0.118	17.64	0.331	49.48	0.220	32.88	1.36	1.66
MEAVE–DC-1,4-NQ : AA (r_1 = 0.59, r_2 = 1.46)										
79	21	3.838	0.488	62.17	0.215	27.39	0.082	10.44	3.27	1.38
60	40	1.515	0.232	31.31	0.259	34.95	0.250	33.74	1.90	1.96
47	53	0.909	0.130	17.13	0.241	31.75	0.388	51.12	1.54	2.61
39	61	0.639	0.081	10.32	0.214	27.26	0.490	62.42	1.38	3.29
15	85	0.183	0.011	1.22	0.099	10.99	0.791	87.79	1.11	8.99

MEAVE–1,4-NQ : AA, the lowest product r_1r_2 and the highest Δe suggest a strongest tendency to cross coupling of the monomers. For the other two monomer systems, the product r_1r_2 is close to 1, i.e., the copolymerization is "ideal": the monomer molecules randomly add to the polymer chain and the tendency to alternation of the monomer units is low. Short blocks of one monomer following blocks of the other monomer are more frequent in the copolymer. For MEAVE–DC-1,4-NQ, the lowest value of Q corresponds to the lowest activity of this monomer. Comparing the parameters Q of redox monomers, one can expect that MEAVE–1,4-NQ should be the most reactive; however, actually, MEAVE–1,2-NQ is the most active.

It is well-known [11] that the activity of radical governs the rate of homopolymerization. However, in other cases the governing factor is the activity of molecules rather than of the polymer radical. In the series of structurally related compounds, the homopolymerization rate varies in parallel with the activity of monomer molecules. The kinetic curves (Fig. 2) and also data listed in Table 2 show that the monomers can be ranked in the following order with respect to their reactivity: MEAVE–1,2-NQ : AA > MEAVE–1,4-NQ : AA > MEAVE–DC-1,4-NQ : AA. Apparently, for the systems studied the factor governing the main kinetic parameters of copolymerization is the activity of the monomer rather than of the polymer radical. The results obtained show that the reactivity of redox monomers depends on the chemical structure of naphthoquinones used for modification of MEAVE. The presence of a substituent (chlorine atom) and the

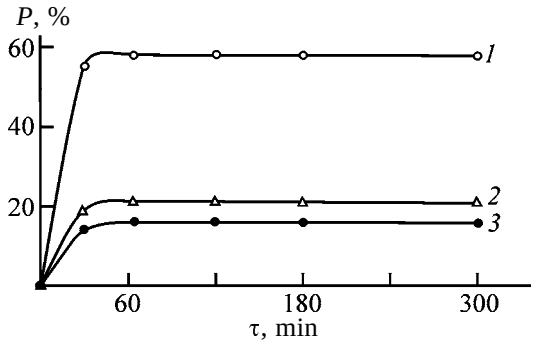


Fig. 2. Kinetic curves of copolymerization of systems redox monomer (M_1) : AA (M_2). (P) Yield of copolymers and (τ) time. M_1: (*1*) MEAVE–1,2-NQ, (*2*) MEAVE–1,4-NQ, and (*3*) MEAVE–DC-1,4-NQ.

ortho and *para* positions of carbonyl groups in the quinoid ring affect the donor–acceptor characteristics, which results in different electron density distribution in the molecules of these monomers and different polarization of the double bond. Since redox monomers (M_1) and AA (M_2) have different activity, in the systems at various monomer ratios different diads are formed: M_1M_1, M_1M_2, and M_2M_2. The probability of formation of these diads in the chain f and average statistical lengths of monomer blocks L_{M_1} and L_{M_2} were evaluated by the equations given in [13, 14] (Table 3).

At different ratios of the initial monomers, copolymers with different compositions are formed. It is seen from Table 3 that, at the composition of monomer mixture from 80 : 20 to 50 : 50, the derivatives MEAVE–1,2-NQ and MEAVE–1,4-NQ are more actively combined with "own" radicals to form mainly M_1M_1 and M_1M_2 diads. The higher the content of these monomers in the initial mixture, the larger the block length L_{M_1}. For the monomer systems studied, copolymers with more regular structure are obtained at the following ratios of the initial monomers: MEAVE–1,2-NQ : AA = 35 : 65, MEAVE–1,4-NQ : AA = 20 : 80–50 : 50, and MEAVE–DC-1,4-NQ : AA = 60 : 40.

CONCLUSIONS

(1) Radical polymerization of derivatives of monoethanolamine vinyl ether and naphthoquinones with acrylic acid was studied. As a result of this radical polymerization, macromolecular compounds having, along with redox characteristics, also adsorption and ion-exchange power are formed.

(2) The constants of the relative activity of monomers and the parameters of resonance stabilization and polarity of the new redox monomers were evaluated. The microstructure of the copolymers was determined.

ACKNOWLEDGMENTS

These studies are supported by ISTC (International Science and Technology Center) (Russia, USA, Canada, Japan, and Germany), grant no. K-604.

REFERENCES

1. Kazakhstan Patent 8813.
2. Shoinbekova, S.A., Nikitina, A.I., Mukhitdinova, B.A., and Ergozhin, E.E., *Zh. Prikl. Khim.*, 2001, vol. 74, no. 11, pp. 1847–1849.
3. Ergozhin, E.E., Mukhitdinova, B.A., Shoinbekova, S.A., *et al.*, *Zh. Prikl. Khim.*, 2003, vol. 76, no. 3, pp. 475–478.
4. Nuranbaeva, B.M., Shoinbekova, S.A., Nikitina, A.I., *et al.*, *Izv. Min. Obraz. Nauki Resp. Kaz., Ser. Khim.*, 2002, no. 3, pp. 111–115.
5. Nuranbaeva, B.M., Shoinbekova, S.A., Nikitina, A.I., *et al.*, *Izv. Min. Obraz. Nauki Resp. Kaz., Ser. Khim.*, 2002, no. 4, pp. 91–99.
6. Ergozhin, E.E., Mukhitdinova, B.A., Shoinbekova, S.A., *et al.*, *Izv. Min. Obraz. Nauki Resp. Kaz., Ser. Khim.*, 2002, no. 2, pp. 108–114.
7. Shoinbekova, S.A., Nikitina, A.I., Nuranbaeva, B.M., *et al.*, *Izv. Min. Obraz. Nauki Resp. Kaz., Ser. Khim.*, 2002, no. 5, pp. 51–57.
8. Shostakovskii, M.F., *Prostye vinilovye efiry* (Vinyl Ethers), Moscow: Izd. Akad. Nauk SSSR, 1952.
9. Teiji, T., *Reaktsii polucheniya sinteticheskikh polimerov* (Reactions Yielding Synthetic Polymers), Moscow: Goskhimizdat, 1963.
10. Shtraikhman, G.A., Vanshteidt, A.A., and Petrova, G.A., *Zh. Fiz. Khim.*, 1958, vol. 32, no. 3, pp. 512–519.
11. Ham, G.E., *Copolymerization*, New York, Interscience, 1964.
12. Chernobai, A.V., *Vysokomol. Soedin., Ser. A*, 1968, vol. 10, no. 8, pp. 1716–1720.
13. Gindin, L., Abkin, A., and Medvedev, S., *Zh. Fiz. Khim.*, 1947, vol. 21, no. 11, pp. 1269–1287.
14. Abkin, A. and Medvedev, S., *Dokl. Akad. Nauk SSSR*, 1947, vol. 56, no. 2, pp. 177–182.

Russian Journal of Applied Chemistry, Vol. 78, No. 1, 2005, pp. 153–158. Translated from Zhurnal Prikladnoi Khimii, Vol. 78, No. 1, 2005, pp. 155–160.
Original Russian Text Copyright © 2005 by Sashina, Novoselov, Heinemann.

MACROMOLECULAR CHEMISTRY AND POLYMERIC MATERIALS

Properties of Solutions and Films of Fibroin–Poly-3-Hydroxybutyrate Polymer Blends

E. S. Sashina, N. P. Novoselov, and K. Heinemann

St. Petersburg State University of Technology and Design, St. Petersburg, Russia
Thuringian Institute of Textile and Plastics, Germany

Received April 12, 2004

Abstract—Solutions of fibroin–poly-3-hydroxybutyrate polymer blends in hexafluoro-2-propanol and films obtained after removal of the solvent are experimentally studied at various polymer ratios.

Bombyx mori silk fibroin is a biopolymer with unique chemical, physical, and mechanical characteristics [1]. Silk is of a great interest not only as a textile material. It can also be used for biotechnological and biomedical purposes in manufacture of suture materials, contact lenses, biosensors, etc. Silk fibroin is used as fibers, gels, powders, and porous membranes. However, a significant drawback of films and other goods from regenerated fibroin is their brittleness. The mechanical characteristics of fibroin may be improved through blending with other natural or synthetic polymers [2–8]. Blends are prepared by simultaneous dissolution of polymers in an appropriate solvent or by grinding.

Dissolution of a polymer mixture in a single solvent to obtain a compatible blend in the form of a film appeared to be a very difficult problem because of phase segregation. The major factor causing incompatibility of polymers is a small gain in the entropy in mixing [9, 10]. The effect of this factor could be reduced through interpolymer interaction, e.g., hydrogen or ionic bonding [11]. Therefore, solution of the problem is reduced to selection of such compositions of a polymer blend in which interpolymer interaction is realized.

Keeping in mind the fact that fibroin has many hydrophobic sites in its structure, being, therefore, capable of forming hydrophobic bonds, we studied solutions and films of mixtures of fibroin with a hydrophobic polymer, poly-3-hydroxybutyrate (P3HB). This optically active biodegradable thermoplastic product containing (*R*)-3-hydroxybutyric acid units is synthesized by *Alcaligenes eutrophus*, *Pseudomonas oleovorants*, *P. Putida*, and *Phodospillium rubrum*. Poly-3-hydroxybutyrate is manufactured by ring-opening polymerization of β-butyrolactone racemic mixture in the presence of base catalysts containing Al, Zn, and other metals [12]. The (*R*) to (*S*) isomer ratio affects the melting point (it ranges from 58 to 180°C), crystallinity, and rate of enzyme-catalyzed hydrolysis of the product. High hydrophobicity of P3HB in combination with its biodegradability makes this polymer indispensable in biotechnology, food industry, and medicine. Also it can be used as a component of polymer blends [13–18].

The solubility of P3HB in a series of organic solvents, its mechanical characteristics, and biocompatibility and biodegradability are good reasons to consider this polymer as suitable for preparation of blends with fibroin. Fibroin is mostly dissolved in aqueous salt solutions with subsequent dialysis to remove salts, which confines the fibroin concentration in the solution because of gel formation in concentrated solutions after dialysis. Furthermore, P3HB is insoluble in aqueous salt solutions. Therefore, we selected hexafluoro-2-propanol (HFIP) as a solvent for fibroin–P3HB blends.

EXPERIMENTAL

Bombyx mori silk fibroin was pretreated prior to use to remove sericin and fatty, resinous, and mineral compounds, and then it was cut into short (3.6 mm) fibers 34.6 μm in diameter. In the work we used syndiotactic P3HB with MW 145 000 (M_w/M_n = 1.8), representing an 1 : 1 mixture of poly(*R*)- and poly(*S*)-3-hydroxybutyrate (mp 58.3–58.8°C; zero moisture content under normal conditions). As a solvent we used 1,1,1,3,3,3-hexafluoro-2-propanol (Merck) (main product content 99%, bp 58°C, d^{20} 1.615–1.618 g cm^{-3}).

1070-4272/05/7801-0153 © 2005 Pleiades Publishing, Inc.

Table 1. Properties of 1% fibroin–poly-3-hydroxybutyrate solutions in HFIP at 25°C

P3HB concentration, wt %	ρ, g cm^{-3}	η_{rel}	η_{ad}
0	1.60	5.0	–
20	1.61	8.6	12.1
40	1.52	13.3	19.3
60	1.59	19.1	26.5
80	1.64	29.0	33.6
100	1.58	40.8	–

Before dissolution in HFIP, fibroin was activated by dissolution in aqueous 6 M LiBr at 60°C, followed by dialysis through a semipermeable membrane [19]. Dialysis was carried out at room temperature with continuous stirring for a day with intermittent refreshment of water. This procedure provided complete removal of LiBr. The fibroin solution after dialysis was air-dried at room temperature to obtain a film, and then vacuum-dried at 40°C for 4–6 h. A weighed portion of thus activated fibroin was dissolved in HFIP at 25°C to obtain the desired concentration.

Poly-3-hyroxybutyrate was dissolved in HFIP at room temperature with stirring to obtain a clear solution of the desired concentration. Then estimated volumes of the equimolar solutions of both polymers were mixed with continuous stirring for an hour. As a result, stable clear solutions were obtained.

After filtration with a Büchner funnel, we measured the pycnometric density of the dilute solutions. The viscosity of the solutions η_{rel} was measured at 25°C with an Ubbelohde viscometer. The additive viscosity was estimated as

$$\eta_{ad} = \eta_1 c_1 + \eta_2 c_2,$$

where c_1 and c_2 are the concentrations of the first and second components in the mixture; and η_1 and η_2, exhaust times of the solutions of individual components.

The films were prepared by pouring the solutions onto foil plates, followed by removal of the solvent. The film thickness was 0.4–0.6 μm. Mechanical characteristics of the films were determined using an Instron tensile-testing machine in accordance with DIN EN ISO 527-3 standard. Swelling of the films in water was studied gravimetrically. The films were kept in distilled water at room temperature for 30 min (this time was demonstrated to be sufficient to reach the maximal swelling). The degree of swelling was estimated as

$$\Delta w = 100(w_1 - w_0)/w_0,$$

where Δw is the degree of swelling (%); w_1, weight of the swollen film (g); and w_0, weight of the dry film (g).

The density of the films was determined on an AccuPyc 1330 V2.01 He pycnometer. The film morphology was studied in a polarized light using an Olympus U-SMAD-2 BX-50 JVC microscope (magnification ×200). The infrared spectra of the films were recorded on an IFS25 spectrometer. Thermal analysis was carried out on a Mettler Toledo Star scanning calorimeter with heating from 25 to 350°C at a rate of 10 deg min^{-1} under nitrogen (N_2 flow rate 50 ml min^{-1}). The estimated enthalpies of melting were then used for determination of the degree of crystallinity (DC) of P3HB in the mixtures:

$$DC = \Delta H_{m.ap}/\Delta H_m^0,$$

where $\Delta H_{m.ap}$ is the apparent enthalpy of melting of P3HB in the mixture, as obtained from the DTA data; and ΔH_m^0, enthalpy of melting of fully crystalline P3HB (145 J g^{-1} [12]).

Based on comparative analysis of the rheological characteristics of dilute solutions of the individual polymers and their mixtures in HFIP, some conclusions could be made on the occurrence or lack of interaction between the fibroin and P3HB macromolecules.

The viscosity η and density ρ of the 1% solutions in HFIP, prepared at various fibroin to P3HB ratios, are given in Table 1. At a P3HB concentration in the mixture below 20 and above 80%, the density of mixed solutions in higher as compared to that of the solutions of the individual components, while at a P3HB concentration of 20–80%, the density decreases, reaching the minimum at a P3HB concentration of 40%.

The relative viscosity of mixed solutions η_{rel} is lower than the additive value η_{ad} estimated neglecting the interpolymer interaction. The negative deviation of the viscosity from the additive law suggests either the lack of interpolymer interaction in the solution or the formation of comb- or star-shaped intermolecular complexes [20]. Here we should keep in mind that the interpolymer interaction proceeds through local contacts caused by the presence of groups capable of a given type of interaction.

Straight fibroin films prepared from 4% solutions in HFIP are optically transparent. Films of polymer

blends are practically transparent too, except for the 40% P3HB blend. In the latter case, noticeable phase segregation was observed: the films appeared to be opalescent, suggesting the formation of agglomerates with a size comparable with the light wavelength.

The microscopic examination revealed that the film of straight fibroin is quite homogeneous with a clearly pronounced orientation of the fibrils (Fig. 1a). The film of straight P3HB consists of fine closely packed spherulites. Hardening of P3HB in the form of spherulites was also observed earlier [12, 14, 16, 18]. In the case of 20% P3HB, we observed microsegregation of the phases (Fig. 1b): irregular-shaped particles 1–4 μm in size, consisting of the finest P3HB spherulites, are surrounded by more hydrophilic fibroin representing a dispersion medium. At a P3HB concentration of 40%, the segregation is the most clearly pronounced: there are domains enriched with fibroin and P3HB-saturated domains (macrosegregation). With increasing P3HB concentration to 60%, the phase segregation decreases, and in the case of 80% P3HB, the most homogeneous structure of closely packed spherulites is realized (Fig. 1c). In this case, the size of spherulites is minimal.

Thus, microsegregation is found for all the samples, and macrosegregation, in the case of 40% P3HB. The microstructure of the polymer blend films can be easily controlled by changing the component ratio. In the case of microsegregation, a microdomain structure is formed, in which more energetically favorable contacts between the units of the same polymer are realized, as well as interactions between active groups of different polymers. At a P3HB concentration above 80%, the most homogeneous supramolecular structure is formed. Most likely, in this case, fibroin plays a role of a plasticizing agent, filling the interspherulite space.

The phase transition temperatures and thermal effects were studied in the range 25–500°C by scanning calorimetry for films of the individual polymers and their blends, prepared from 4% solutions in HFIP (Table 2). The DSC curve of regenerated fibroin shows an endothermic peak near 78°C, which is associated with removal of adsorbed water. The endothermic effect near 152°C is caused by glass transition of amorphous fibroin, which is followed by a weak exothermic effect due to transition of the amorphous phase into β-folded crystalline structure [21]. The exothermic peak at 246°C (not given in Table 2) reflects molecular motion in α-crystals of the polymer, which is observed only in the film of straight fibroin. Finally, the endothermic peak at 276°C is caused by thermal degradation of the disordered β-structure.

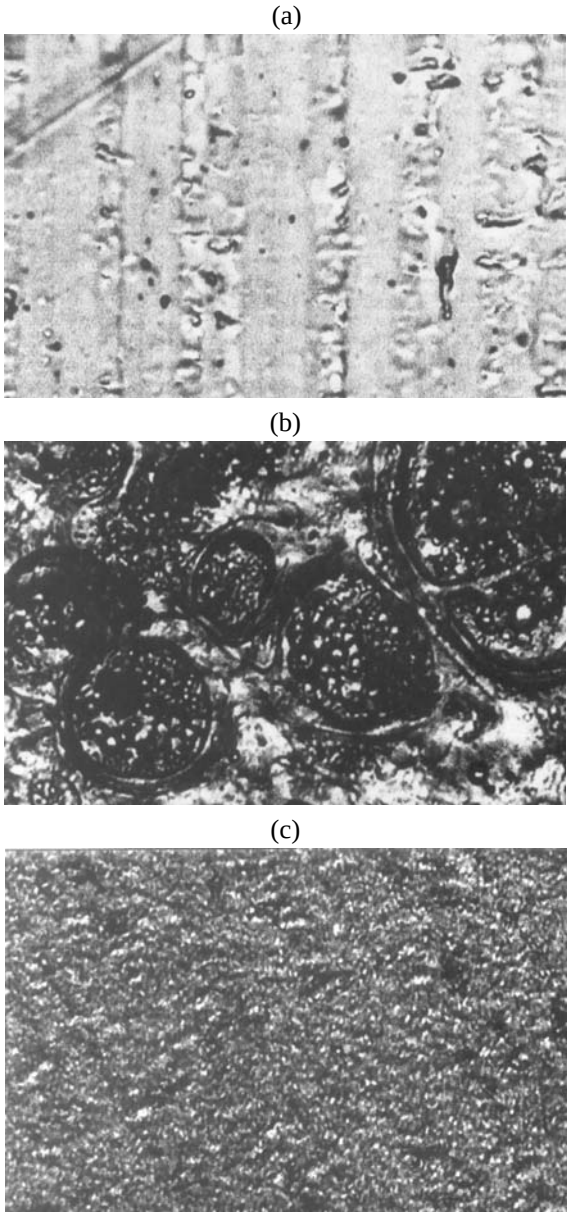


Fig. 1. Photomicrographs of films in a polarized light: (a) fibroin, (b) fibroin : P3HB = 80 : 20, and (c) fibroin : P3HB = 20 : 80.

The film of 100% P3HB demonstrates two endothermic peaks near 58 and 334°C. The former is associated with melting of the sample, and the latter, with onset of thermal degradation of the polymer. We found no glass transition of P3HB over the temperature range studied (it occurs at 3–7°C [12].

The blend films demonstrate the same set of endothermic peaks as for the individual compounds, but their temperatures and thermal effects change. For

Table 2. Temperatures and enthalpies of phase transitions of fibroin and P3HB in blends

Poly-3-hydroxybutyrate						Fibroin					
c, wt %	mp, °C	ΔH_m, J g^{-1}	T_{deg}, °C	ΔH_{deg}, J g^{-1}	DC, %	T_1, °C	ΔH_1, J g^{-1}	T_2, °C	ΔH_2, J g^{-1}	T_{deg}, °C	ΔH_{deg}, J g^{-1}
–	–	–	–	–	–	78.3	106.4	151.8	21.5	280.4	139.3
20	55.3	9.1	N. d*	N. d	6.3	~79	N. d	162.6	35.0	281.1	141.2
40	59.3	17.8	347.7	308.0	12.3	83.3	29.1	160.6	23.6	283.8	123.8
60	59.9	34.6	343.4	434.8	23.8	86.1	30.6	176.3	37.9	283.9	186.5
80	57.3	32.3	N. d	N. d	22.3	~92	N. d	178.4	21.1	281.7	56.5
100	58.3	42.7	334.1	540.1	29.4	–	–	–	–	–	–

* Not determined.

example, the endothermic peak due to removal of adsorbed water is found near 78°C for the film of straight fibroin; it is lacking at all in P3HB because of its hydrophobicity; and, in blend films, it shifts toward higher temperature (92°C for 80% P3HB), which can be attributed to the decreased crystallinity.

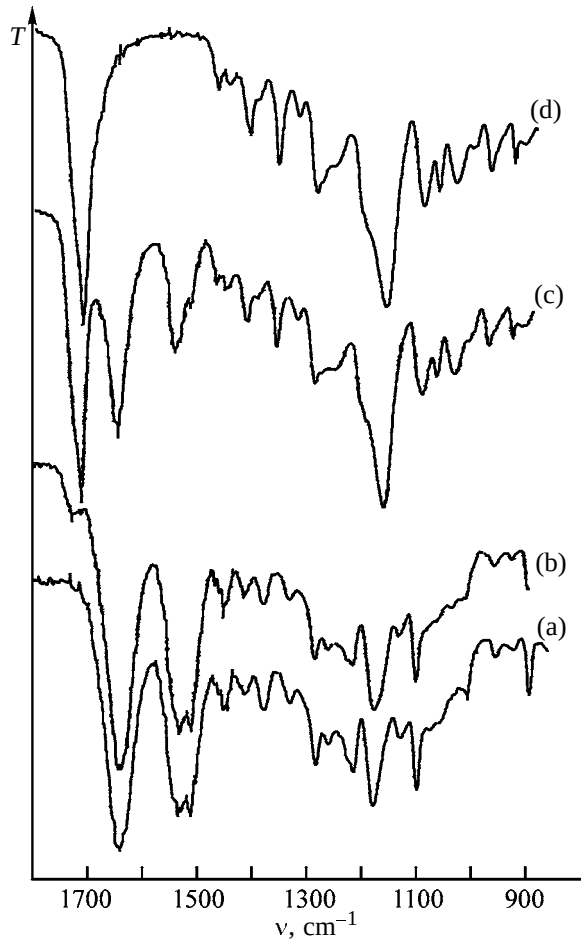


Fig. 2. IR spectra of polymer films: (a) fibroin, (b) fibroin : P3HB = 80 : 20, (c) fibroin : P3HB = 20 : 80, and (d) P3HB. (T) Transmission and (ν) wave number.

With increasing P3HB concentration, the endothermic effect due to glass transition in amorphous fibroin domains drifts towards higher temperature (from 151.8 to 178.4°C). The drift of the peaks in the presence of the second component suggests the possibility of intermolecular interaction with the second component in the amorphous fibroin domains and at the interface, which hinders the devitrification. At P3HB concentrations of 20 and 80%, its melting point in the blend decreases by 2–3°C, and at concentration of 40 and 60%, on the contrary, it increases by 1–2°C, i.e., in the presence of the second component, P3HB tends to melt more readily or vice versa, depending on the component ratio. The crystallinity of P3HB changes in parallel to its concentration in the blend. With decreasing P3HB concentration, the crystalline fraction decreases (from 29.4 for 100% P3HB to 6.3 for 20% P3HB). It may be concluded that the polymers plasticize each other, i.e., one affects crystallization of another, even though no cocrystallization occurs.

The IR spectra of the films of the individual components and their blends are presented in Fig. 2. The film of straight fibroin (Fig. 2a) shows a doublet at 1630 and 1642 cm^{-1} and a shoulder at 1660 cm^{-1}, which are assigned to absorption of the C=O groups [22, 23] in crystalline β-folded and α-spiral, and amorphous randomly globular conformations of the macromolecules, respectively. The absorption bands of the bound N–H and C–N groups at 1513, 1530, and 1540 cm^{-1} are assigned, respectively, to β-, α-, and amorphous conformations. With decreasing fibroin concentration to 80%, the intensity of the absorption band characteristic of α-spiral conformation increases, the band drifting to 1536 cm^{-1} (Fig. 2b). In the case of 20% fibroin, the spectrum shows only two absorption bands at 1650 and 1546 cm^{-1} corresponding

Table 3. Mechanical properties of fibroin–P3HB films

P3HB, wt %	G, N mm^{-2}	L, %	ρ, g cm^{-3}	Swellability, %	
				experiment	additive value
–	37.2	4.2	1.41	36.4	36.4
20	26.9	181.9	1.61	40.0	29.1
40	18.4	71.0	1.58	24.0	21.8
60	39.1	360.9	1.48	10.0	14.6
80	47.5	439.0	1.27	1.1	7.3
100	47.8	592.0	1.28	~0	~0

to the amorphous randomly globular conformation (Fig. 2c). Therefore, as the concentration of the second component increases, the crystallinity of fibroin in the blend decreases, and the β-folded conformation changes for α-spiral and then amorphous randomly globular conformations.

The spectrum of the film of straight P3HB (Fig. 2d) shows a strong peak at 1715 cm^{-1} due to absorption of the C=O groups characteristic of the crystalline domains, and also including absorption of the amorphous domains of the polymer [24]. In the spectrum of the blend with 80% P3HB (Fig. 2c), this strong peak is also found, but in the case of 20% P3HB (Fig. 2b), the corresponding band is shifted toward higher frequencies, suggesting practically total disappearance of crystalline domains of P3HB [24], i.e., in P3HB-rich blends crystalline domains occur along with amorphous ones, while at a P3HB concentration decreased to 20%, amorphous domains dominate.

The IR and DSC data show that, in mixing of fibroin with P3HB, a component dominating by the weight remains more crystalline, forming a polymer matrix, while small amount of the second component forms a dispersed phase. Interaction between different macromolecules can occur in amorphous domains and at the interface.

Films of straight fibroin demonstrate increased brittleness. In this case, the occurrence of a system of strong intermolecular bonds causes formation of a rigid, strained, and brittle structure. Films of straight P3HB are stronger and more elastic. Table 3 shows the mechanical characteristics of the films at various component ratios.

At a 40% concentration of P3HB, the breaking stress and elongation of the films are considerably lower as compared to the other samples, which can be attributed to the heterogeneity of the structure (macrosegregation) observed in this film. The swellability of this film is higher than that of the other samples including the film of straight fibroin. This is also caused by the heterogeneity, and occurrence of cavities at the interface, i.e., by the weakness of intermolecular interactions. For the film with 80% P3HB, the breaking stress is 47.5 N mm^{-2}, exceeding the additive value of 45.6 N mm^{-2} estimated neglecting interpolymer interaction. Evidently, this is a result of homogenization of the supramolecular structure, as was demonstrated by optical microscopy.

Finally, analyzing the results obtained, we may distinguish three ranges of the component compositions.

Range I covers P3HB concentrations below 20 wt %. In this range, fibroin is a more crystalline component forming a continuous polymer matrix with amorphous P3HB dispersed in it. Within this composition range, the swellability of the films exceeds the additive values, since amorphous P3HB domains loosen fairly hydrophilic fibroin. In this case, the fibroin structure remains crystalline, and P3HB plays a role of a plasticizing agent. Such films are characterized by higher elongation at break and increased density, which can be attributed to the interpolymer interaction at the interface. The occurrence of the interpolymer interaction is supported also by the increased density of the corresponding initial solution.

Range II covers compositions with a P3HB concentration from 20 to 80 wt %. In this range, two phases coexist, the interpolymer interaction being minimal. The films are characterized by the minimal breaking stress and by the swellability close to the additive values, i.e., two phases exist independently. The corresponding initial solutions have the lowest density.

Range III corresponds to compositions with a P3HB concentration above 80 wt %. Amorphous fibroin is dispersed in the continuous matrix of more crystalline P3HB. The swellability of the films is lower than the additive values, which is due to the fact

that the crystallites of hydrophobic P3HB hinder penetration of the liquid to the amorphous domains of hydrophilic fibroin. Interpolymer interaction can be realized at the interface. The density of the corresponding initial solutions is higher than that of the solutions of the individual components.

Generally, the fibroin and P3HB macromolecules in the blend solutions may interact through local contacts. On removing the solvent with formation of a film, macromolecules of the same sort tend to form a crystalline structure typical of the corresponding polymer, since the interaction energy in this case is higher than that between different macromolecules because of a smaller number of contacts. The crystallization depends on the component ratio in the blend. At a concentration of the second component below 20%, the macromolecules dominating in the quantity form a partially crystalline structure with inclusions of amorphous domains of the second component. If the components are taken in comparable concentrations, the structure appears to be loosened as a result of phase segregation. Since the polymers composing the blend crystallize separately, it may be suggested that, despite their incompatibility, intermolecular interactions with P3HB do affect the glass transition of fibroin in the blend, and that the presence of fibroin decreases the crystallinity of P3HB. The heterogeneity of the blend depends on the component ratio, controlling the mechanical properties of the resulting films.

CONCLUSIONS

(1) The compatibility of hydrophilic silk fibroin and hydrophobic poly-3-hydroxybutyrate in hexafluoro-2-propanol solutions and films prepared by removing the solvent is studied by IR spectroscopy, scanning calorimetry, viscometry, and optical microscopy.

(2) The indicated polymers are found to be incompatible at the molecular level, and no cocrystallization occurs after removal of the solvent.

(3) The microstructure of the films depends on the component ratio in the blend. When one of the components dominates, it forms a polymeric matrix with another polymer being dispersed in it. At comparable component ratio, macrosegregation occurs, thus deteriorating the mechanical characteristics of the films.

ACKNOWLEDGMENTS

The authors are grateful to R.-U. Bauer, Director of the Thuringian Institute of Textile and Plastics, for affording an opportunity to carry out experimental studies.

REFERENCES

1. *Silk Polymers: Materials Science and Technology*, Kaplan, D., Ed., Washington: Am. Chem. Soc., 1994.
2. Liang, C.X. and Hirabayashi, K., *J. Appl. Polym. Sci.*, 1992, vol. 45, pp. 1937–1943.
3. Freddi, G., Romano, M., Massafra, M.R., and Tsukada, M., *J. Appl. Polym. Sci.*, 1995, vol. 56, pp. 1537–1545.
4. Yang, G., Zhang, L., and Liu, Y., *J. Membrane Sci.*, 2000, vol. 177, pp. 153–161.
5. Noishiki, Y., Nishiyama, Y., Wada, M., *et al.*, *J. Appl. Polym. Sci.*, 2002, vol. 86, pp. 3425–3429.
6. Tsukada, M., Freddy, G., and Crighton, J.S., *J. Polym. Sci., Part B: Polym. Phys.*, 1994, vol. 32, pp. 243–248.
7. Gotoh, Y. and Tsukada, M., *Polymer*, 1997, vol. 38, no. 2, pp. 487–490.
8. Freddi, G., Tsukada, M., and Beretta, S., *J. Appl. Polym. Sci.*, 1999, vol. 71, no. 10, pp. 1563–1571.
9. Paul, D.R. and Newman, S., *Polymer Blends*, New York: Academic, 1978.
10. Olabisi, D., Robeson, L.M., and Shaw, M.T., *Polymer–Polymer Miscibility*, New York: Academic, 1979.
11. Filippova, O.E., Sitnikova, N.L., and Starodubtsev, S.G., *Vysokomol. Soedin., Ser. A*, 1995, vol. 37, no. 4, pp. 610–614.
12. Abe, H., Matsubara, I., and Doi, Y., *Macromolecules*, 1995, vol. 28, pp. 844–853.
13. Ikejima, T., Cao, A., Yoshie, N., and Inoue, Y., *Polym. Degrad. Stab.*, 1998, vol. 62, pp. 463–469.
14. Marand, H. and Collins, M., *Am. Chem. Soc. Div. Polym. Chem. Polym. Prepr.*, 1990, vol. 31, pp. 551–553.
15. Kumagai, Y. and Doi, Y., *Polym. Degrad. Stab.*, 1992, vol. 36, pp. 241–248.
16. Siciliano, A., Seves, A., De Marco, T., *et al.*, *Macromolecules*, 1995, vol. 28, pp. 8065–8072.
17. Koyama, N. and Doi, Y., *Polymer*, 1997, vol. 38, no. 7, pp. 1589–1593.
18. Avella, M. and Martuscelli, E., *Polymer*, 1988, vol. 29, pp. 1731–1737.
19. WO Patent 93/15244.
20. Bel'nikevich, N.G., Budtova, T.V., Ivanova, N.P., *et al.*, *Vysokomol. Soedin., Ser. A*, 1989, vol. 31, no. 8, pp. 1691–1696.
21. Motta, A., Fambri, L., and Migliaresi, C., *Macromol. Chem. Phys.*, 2002, vol. 203, pp. 1658–1665.
22. Miyazawa, T., Shimanouchi, T., and Mizuchima, S., *J. Chem. Phys.*, 1958, vol. 29, no. 3, pp. 611–616.
23. Asai, M., Tsuboi, M., Shimanouchi, T., and Mizushima, S., *J. Phys. Chem.*, 1955, vol. 59, pp. 322–325.
24. Ikejima, T., Yoshie, N., and Inoue, Y., *Macromol. Chem. Phys.*, 1996, vol. 197, pp. 869–880.

Russian Journal of Applied Chemistry, Vol. 78, No. 1, 2005, pp. 159–165. Translated from Zhurnal Prikladnoi Khimii, Vol. 78, No. 1, 2005, pp. 161–167.
Original Russian Text Copyright © 2005 by Men'shikova, Shabsel's, Evseeva, Shevchenko, Bilibin.

MACROMOLECULAR CHEMISTRY AND POLYMERIC MATERIALS

Synthesis of Carboxylated Monodisperse Latexes and Their Self-Organization in Thin Films

A. Yu. Men'shikova, B. M. Shabsel's, T. G. Evseeva, N. N. Shevchenko, and A. Yu. Bilibin

Institute of Macromolecular Compounds, Russian Academy of Sciences, St. Petersburg, Russia
St. Petersburg State University, St. Petersburg, Russia

Received July 15, 2004

Abstract—The capability of carboxylated latexes of poly(methyl methacrylate) and copolymers of styrene with glycidyl methacrylate or methacrylic acid for self-organization in thin films was studied in relation to the compositions of the dispersion medium and polymer and to the latex particle size.

Monodisperse polymer particles of submicrometer size can serve as basis for formation of photonic crystals (PCs), a new class of dielectric materials promising both for experimental and theoretical studies of nonlinear optical effects and for development of new devices for quantum electronics and telecommunications industry [1–5]. In the PC lattice, the dielectric permittivity modulates with a period of the order of the light wavelength. This fact accounts for the existence of the photonic band gap (PBG), an energy range in which the light propagation inside the crystal is suppressed [1]. Of particular interest are three-dimensional (3D) photonic crystals in which a high density of structural components can be attained.

Composites based on synthetic opals with a fcc lattice formed by close-packed submicrometer spheres of amorphous silica are considered as promising materials for obtaining the required photonic-crystal properties [6–8]. However, obtaining a perfect 3D lattice with these materials involves serious technological problems. The high density of SiO_2 results in particle sedimentation, giving rise to stresses and defects in the ordered structure. As a result, synthetic opals have a polydomain structure with a domain size of 30–100 μm. Furthermore, the surface nonuniformity of amorphous SiO_2 microspheres formed by aggregation of nanometer-sized particles results in considerably increased diffuse scattering of electromagnetic waves at the phase boundary and in suppressed photonic-crystal effects [8]. Methods of polymer chemistry allow preparation of monodisperse surface-uniform submicrometer-sized particles of a lower density compared to inorganic materials [9–12]. Development of 3D ordered structures based on polymer particles of various diameters and compositions would allow their optical properties (primarily the PBG position and width) to be varied in a wide range.

To reveal factors that act in the step of self-organization of the primary polymer matrix and affect the structure and optical characteristics of the forming PCs, it seems appropriate to study systematically how the structure of the polymer and the size and surface properties of the polymer particles affect their capability for formation of highly ordered 3D structures. For this purpose, we studied various kinds of latexes based on poly(methyl methacrylate) (PMMA) and copolymers of styrene with methacrylic acid (PSt–MAA) or glycidyl methacrylate (PSt–GMA).

To ensure monodisperse composition and stability of latexes, their polymer base was modified in the course of the synthesis with carboxy groups; their ionization imparts a surface charge to the particles. By varying the composition of the dispersion medium, it is possible to control this charge and hence the forces of electrostatic repulsion between the latex particles, and thus to optimize the conditions of formation of the ordered structures.

EXPERIMENTAL

Styrene (St) and dimethylformamide (DMF) were purified by distillation, following standard procedures. Glycidyl methacrylate (GMA), methacrylic acid (MAA, pure grade), and $K_2S_2O_8$, NaOH, HCl, and Na_2HPO_4 (chemically pure and analytically pure grade) were used without additional purification. The purification procedures and characteristics of

1070-4272/05/7801-0159 © 2005 Pleiades Publishing, Inc.

Table 1. Conditions of emulsion polymerization and characteristics of carboxylated latexes

Latex	T, °C	Monomer ratio, mol %	Monomer/H_2O, wt %	Initiator/H_2O, wt %	[NaOH] × 10^{-2}, M	pH*	D, nm	$M_\eta \times 10^{-4}$	[COOH], mg-equiv m^{-2}
I**	80	St : MAA = 92.7 : 7.3	5.3	$K_2S_2O_8$, 0.092	3.9	10.0	250	26.4	3.01
II**	80	〃	5.5	$K_2S_2O_8$, 0.092	5.6	11.5	250	20.0	1.49
III***	78	St : GMA = 92.5 : 7.5	10	ACVA, 0.2	1.9	10.2	300	Cross-linked	0.73
IV	75	MMA (100)	10	ACVA, 0.2	1.0	11.5	330	18.9	0.76

* Initial value.
** In the presence of a chain-terminating agent, diaminodiphenyl disulfide (DADPDS), 0.115 mol % relative to styrene.
*** In the presence of 4×10^{-2} M Na_2HPO_4.

Table 2. Conditions for formation of thin films and their characteristics

Latex	Film no.	Dry residue of latex, wt %	Medium	Support	Conditions of film formation	Film thickness		PBG,* nm
						μm	number of layers	
PSt–MAA, I	1	0.1	Ethanol	Glass	Drying (3 h)	5.4	25/26**	551
	2	0.1	Ethanol	Glass	Ultrasonic treatment, drying (24 h)	6.4	30/32	582
PSt–MAA, II	3	1.0	Ethanol	Glass	Drying (24 h)	5.5	26/26	580
	4	10	Water	Siliconized glass	Drying (24 h)	>1000	Bulk sample	590–620
PSt–GMA, III	5	1.0	Ethanol	Glass	Ultrasonic treatment, drying (24 h)	11.5	39/44	637
PMMA, IV	6	1.0	Water	Alkali-treated glass	Drying (24 h)	12.3	63/43	712

* Maximal PBG value.
** Numerator, calculation from the perfect fcc lattice structure and film thickness; denominator, examination of film chips by electron microscopy.

4,4'-azobis(4-cyanoisovaleric acid) (ACVA) are given elsewhere [9]. As dispersion medium we used double-distilled water. The latexes were prepared by emulsion polymerization without emulsifier [9–12]. The synthesis conditions and characteristics of the resulting particles are given in Table 1. The diameters of latex particles were measured by transmission electron microscopy (JEM 100 S JEOL microscope). For a set of more than 400 particles, the variance σ and polydispersity coefficient K were determined ($K = D_m/D_n$, where D_m and D_n are the weight-average and number-average diameters, respectively). The surface concentration of carboxy groups was determined by conductometric titration [13] after threefold washing of the latexes to remove water-soluble impurities by successive centrifugation and redispersion in double-distilled water. The intrinsic viscosities determined viscometrically in DMF were used to calculate the viscosity-average molecular weight of the polymers in the particles, M_η, by the Mark–Kuhn–Houwink equation $[\eta] = KM_\eta^{-\alpha}$ with the following parameters: for polystyrene, $K = 4.16 \times 10^{-5}$ and $\alpha = 0.788$; for PMMA, $K = 1.73 \times 10^{-4}$ and $\alpha = 0.645$ [14].

Thin films were prepared by self-organization of latex particles from their dispersions in water and ethanol (Table 2). Dispersion samples (40 μl) were applied to cover glasses which had been treated with CrO_3/H_2SO_4 and washed with double-distilled water. Aqueous dispersions formed a drop owing to surface tension forces; alcoholic dispersions, on the contrary, spilt over the whole support surface. After leaching of the glasses for 30 min in 30% NaOH followed by washing with double-distilled water, aqueous dispersions wetted the whole support surface also. Glasses with the applied dispersion were placed in desiccators in which the dispersion medium slowly evaporated. In the process, the polymeric particles formed a close-

packed fcc lattice. Some samples in the course of film forming were ultrasonically treated in a Unitra-Unima UM-4 ultrasonic bath. The structure of the thin films obtained was examined by optical and scanning electron microscopy (JEM 100 C JEOL micrioscope). For nondestructive monitoring of the structure of the ordered polymer matrices and evaluation of the photonic-crystal properties, we studied the spectra of Bragg light reflection from surface spots of a size corresponding to the characteristic monodomain size, 10–50 μm (in terms of the approach suggested in [15]). By this method we studied the spectra of mirror reflection from [111] growth surfaces of the thin films in the visible and IR ranges. The incidence angle θ was 10°.

To obtain monodisperse polymer particles which could act as structural elements of 3D ordered lattices exhibiting photonic-crystal properties, we performed emulsifier-free emulsion polymerization of MMA and copolymerization of St with GMA (ACVA initiator) or of St with MAA ($K_2S_2O_8$ initiator). Based on the previously revealed relationships between the polymerization parameters and characteristics of polymer particles (diameter, size distribution, surface properties) [10–12], we prepared series of latexes differing in the particle diameter and dispersity.

For preliminary examination of the influence exerted by the characteristics of monodisperse polymer particles on their capability for self-organization into a three-dimensional lattice of a photonic crystal, we chose four latexes with the narrowest particle size distribution (Table 1, Fig. 1). The diameters of particels of these latexes fell within a narrow range, 250–330 nm, which allowed us to study how the polymer base affects the capability of the particles for ordering and to find the optimal method for formation of the ordered structures from each latex.

We found that glass degreased with CrO_3/H_2SO_4 is the best support for obtaining highly ordered lattices from particles of copolymers of St with GMA and MAA. The alcoholic dispersions, whose drops spilt over the whole support surface, formed more uniform thin films with a smaller number of defects than water-based latexes. Thus, passing from an aqueous medium to an alcoholic medium decreases the surface tension forces in a drop of the polymer dispersion and favors its self-organization to a more ordered structure under the conditions close to equilibrium. On the contrary, with PMMA particles, which are less hydrophobic than those of St copolymers, the best thin films were obtained by applying aqueous dispersion on glass hydrophilized by alkali treatment.

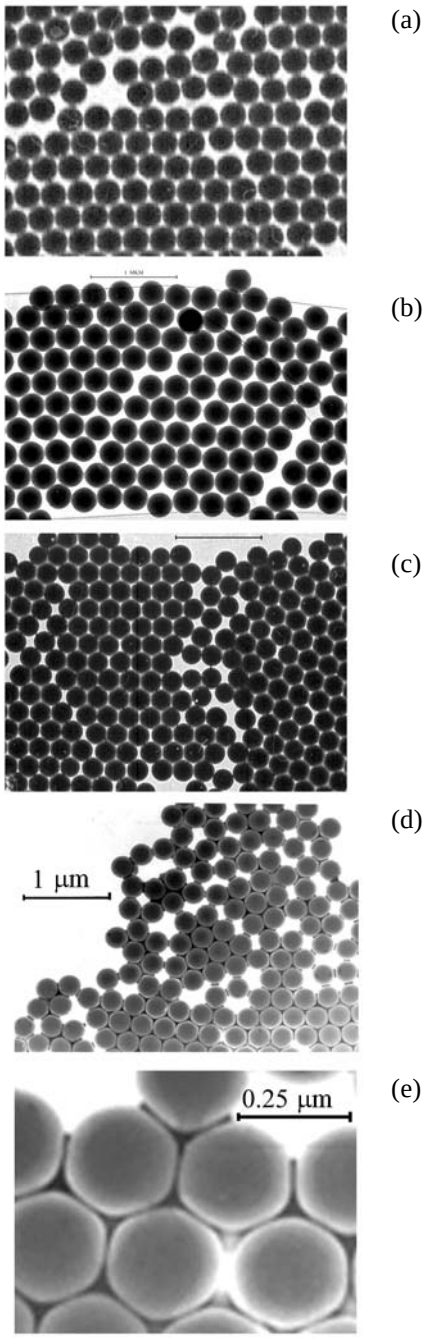


Fig. 1. Electron micrographs of latexes (a) IV, (b) III, (c) II, and (d, e) I.

Ultrasonic treatment of glasses in the course of self-organization of latex particles on them had no appreciable effect on the quality of the resulting thin film. The characteristics of the most ordered samples of the thin films obtained are given in Table 2. Examination by scanning electron microscopy showed that particles of all the latexes studied under the empirically chosen conditions form an fcc lattice with the

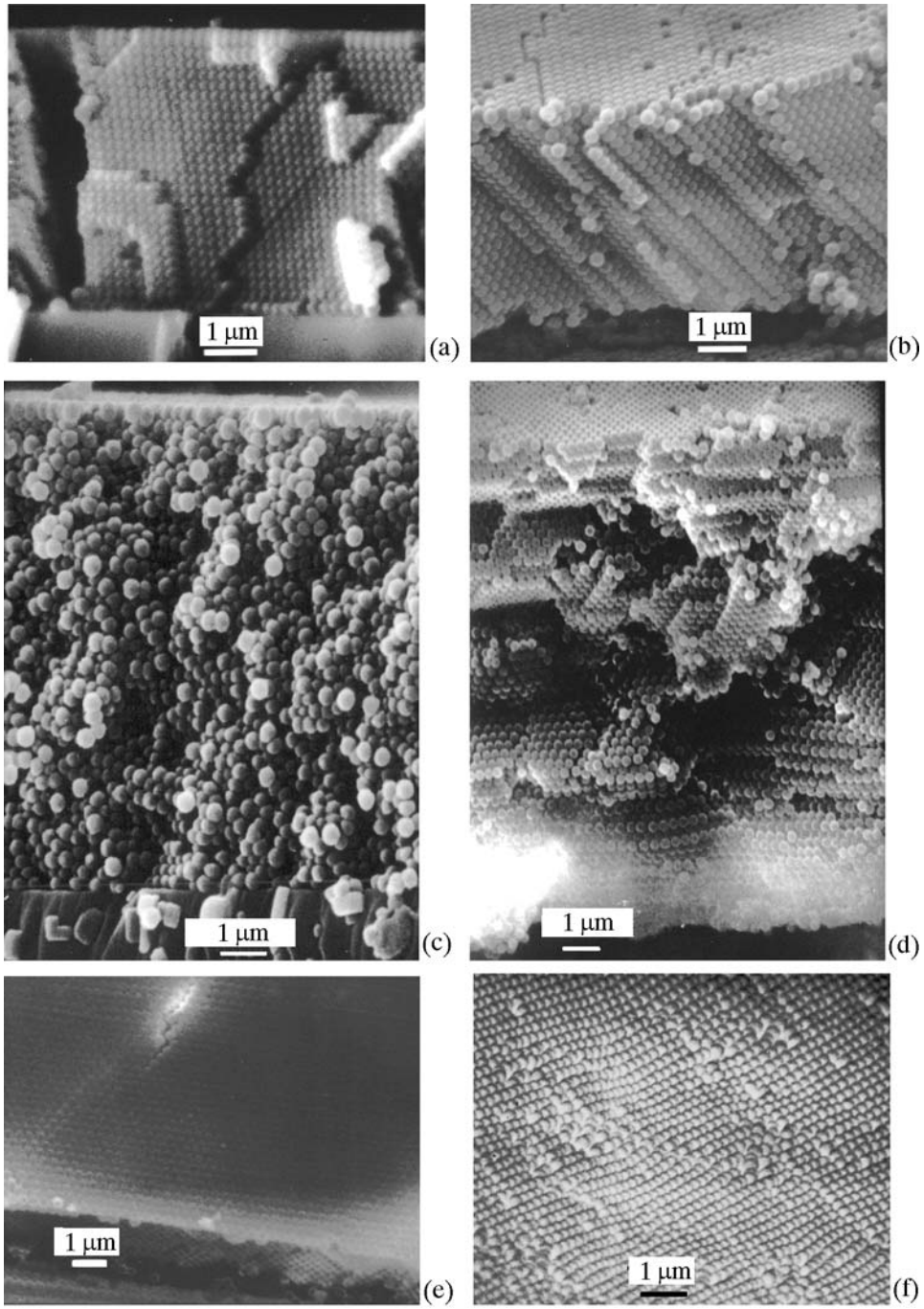


Fig. 2. Electron micrographs of thin films formed from particles of latexes (a, e) I, (b) II, (c) III, and (d, f) IV. (a–d) Side view and (e, f) top view.

structure thickness of up to 50–60 layers (Fig. 2). The quality of the thin films obtained (presence of point defects and breaks) depends on the composition of the dispersion medium (water, alcohol), rate of its evaporation, and also conditions of the preteatment of the glass supports. In particular, rough leached surface of the support in the case of PMMA (Figs. 2d, 2f) results in a shift of the layers relative to each other (corrugation effect), and particles based on copolymers of St with GMA, which is a bifunctional monomer and yields a cross-linked polymer matrix, get nonuniformly "crumpled" when forming a multilayered structure (Fig. 2c).

For the films prepared from PMMA and PSt–GMA particles, direct determination of the number of layers

in the film from electron micrographs and calculation of the number of layers from the film thickness (measured by optical microscopy) and particle diameter taking into account the fcc structure gave different results. The values obtained were close or coinciding only for the films formed from particles that had been obtained by copolymerization of St with MAA; this fact, along with the electron micrographs (Figs. 2a, 2b, 2e), suggests that their structure is the most perfect.

It is well known that emulsion copolymerization with water-soluble carboxyl-containing comonomers yields polymer particles whose surface layer is enriched in polymer chains with increased content of carboxyl-containing hydrophilic units [16]. Such a surface layer can change its volume depending on the salt composition and pH of the dispersion medium. For example, variation of the diameter of particles of latex I depending on pH of the dispersion medium was noticeable at an electrolyte concentration of 10^{-3} M (Fig. 3, curve *1*). The particle diameter appreciably increased in an alkaline medium, in parallel with an increase in the negative charge of the surface, inversely correlating with the electrophoretic mobility (Fig. 3, curve *2*). Swelling of the hydrophilic surface layer due to mutual repulsion of the ionized carboxy groups results not only in an increase in the particle diameter. Another consequence is that this surface layer can uniformly contract, with uniform shrinkage occurring upon particle packing and evaporation of the dispersion medium. In the process, the particles in the monolayer acquire hexagonal shape, similarly to honeycomb (Fig. 1e), and the structure of the multilayer fcc lattice formed from such particles is more perfect.

The structures obtained by self-organization of latex particles were examined by such a nondestructive method as spectral optical microscopy. The reflection spectra of all the synthesized films at inclined light incidence have a pronounced peak originating from the Bragg diffraction of electromagnetic waves on a large-scale periodic lattice. The photonic band gap appearing in the yellow–red range (Fig. 4) shows that the monodisperse latex particles self-organize to form a photonic crystal lattice. The structure of the polymer, along with the diameter of the monodisperse particles, significantly affects the PBG position (Fig. 4a). The long-range order of the periodic lattice based on St–MAA copolymer particles is confirmed most clearly by the reflection spectra of thick films, which, despite large thickness (several millimeters), show photonic-crystal properties (Fig. 4b).

Polymeric photonic crystals of millimeter size with

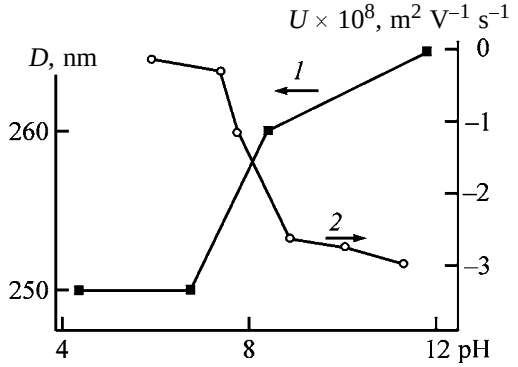


Fig. 3. Influence of the pH of the dispersion medium on the (*1*) diameter *D* and (*2*) electrophoretic mobility *U* of particles of latex I.

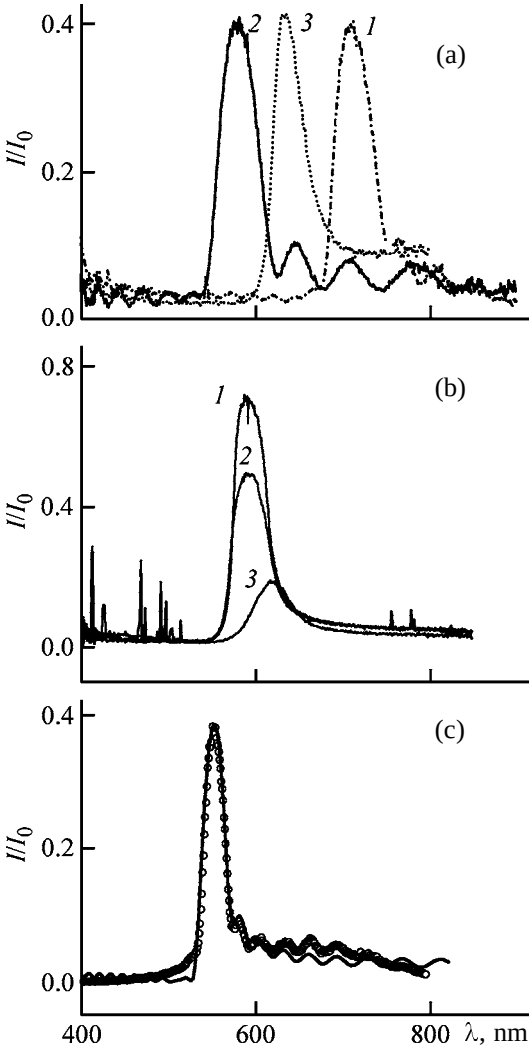


Fig. 4. Reflection spectra (a) of thin film nos. (*1*) 6, (*2*) 2, and (*3*) 5; (b) of bulk sample of latex IV of thickness (*1*) 1, (*2*) 2, and (*3*) 3 mm; and (c) of film no. 1. For the conditions of film preparation, see Table 2. (I/I_0) Intensity of the reflected light relative to the incident light; (λ) wavelength. (c) Points, experimental data; solid line, theoretical calculation.

a high degree of ordering and a period that can be varied in the submicrometer range by varying the particle size can be considered as reference objects for studying the interaction of light with a 3D regular structure of a photonic crystal. Experimental data obtained with the most perfect thin-film structures based on PSt–MAA particles can be used as a basis for constructing a theoretical model describing the specific features of photon propagation in a 3D large-scale (of the order of light wavelength) periodic lattice [17].

In the model developed, a 3D fcc lattice is approximated by a layered periodic system with the dielectric permittivity modulated along the [111] direction. The specific profile of the dielectric function was calculated with its averaging within the unit cell in the plane perpendicular to the [111] direction. The results of numerical calculations by the method of transfer matrices [17] appeared to be well consistent with the experimental reflection spectrum of a thin film obtained from latex I (Fig. 4c).

The theoretical calculations also allowed independent determination of the optical constants of the structures synthesized and of the geometric parameters of polymer particles in a film. The refractive index of the particles is similar to that of bulk polystyrene (1.59 at 20°C). The calculated particle diameter, 252.4 nm, is very close to the value determined by electron microscopy (250 nm). The calculated number of layers in the film (26) coincides with the results of electron-microscopic examination (Table 2). The model developed takes also into account the effects of contraction of latex particles, arising in the course of formation of the bulk material. The calculated shrinkage coefficient of particles in film no. 1 (Table 2) was 3%. As the latex particle diameter is 250 nm, their contraction in the film can amount to approximately 7.5 nm. This value seems quite reasonable, since it is comparable with the change in the particle diamater due to swelling of their hydrophilic surface layer (Fig. 4). Thus, the theoretical model is in good agreement with the experiment, which indicates that, on the one hand, the thin-film polymer periodic structures obtained are perfect and, on the other hand, these structures can be used as model objects in theoretical studies of interaction of light with the 3D lattice of photonic crystals.

CONCLUSIONS

(1) Procedures are optimized for preparing monodisperse latexes of poly(methyl methacrylate) and copolymers of styrene with glycidyl methacrylate and methacrylic acid and for obtaining highly ordered 3D lattices from these latexes. Dispersions of monodisperse polymer microspheres with the preset size and definite surface structure were prepared, and thin-film ordered lattices were obtained from them. The 3D periodicity of these lattices was proved by electron microscopy.

(2) In the examined objects, the electromagnetic waves strongly interact with the periodic lattice, and a photonic band gap arises. The photonic-crystal properties of thin films are significantly influenced by the structure of polymer particles from which they are prepared.

(3) Films based on particles of styrene–methacrylic acid copolymer form a more regular structure and are the most promising as structural elements for preparing 3D photonic crystals fully consisting of monodisperse polymer particles.

(4) The reflection spectra calculated within the framework of the theoretical model of light propagation in the synthesized structures, taking into account deformation of the monodisperse polymer particles, are well consistent with the experiment.

ACKNOWLEDGMENTS

The study was supported by the Scientific Program of the Presidium of the Russian Academy of Sciences "Nanostructures in Polymer Systems, Promising for Optoelectronics," by the Russian Foundation for Basic Research (project no. 04-03-33 080), and by the Scientific Program of the Division of Chemistry and Materials Science of the Russian Academy of Sciences "Development and Study of Macromolecules and Macromolecular Structures of New Generations."

The authors are grateful to A.B. Pevtsov and A.V. Sel'kin (Ioffe Physicotechnical Institute, Russian Academy of Sciences, St. Petersburg) for discussion of the results and assistance in measurements and theoretical treatment of the optical spectra.

REFERENCES

1. *Photonic Band Gap Materials*, Soukoulis, C.M., Ed., Dordrecht: Kluwer, 1996.
2. *Photonic Crystals and Light Localization in the 21st Century: Proc. NATO Advanced Studies Inst. on Photonic Crystals and Light Localization, Ser. C*, Soukoulis, C.M., Ed., Dordrecht: Kluwer, 2001, vol. 563.

3. Fleming, J.G., and Lin, Shawn-Yu, *Optics Lett.*, 1999, vol. 24, no. 1, pp. 49–51.
4. Yamamoto, Y. and Slusher, R.E., *Physics Today*, 1993, vol. 46, no. 1, pp. 66–73.
5. Kilin, S.Ya., *Usp. Fiz. Nauk*, 1999, vol. 169, no. 5, pp. 507–527.
6. Bogomolov, V.N., Feoktistov, N.A., Golubev, V.G., *et al.*, *J. Non-Cryst. Solids*, 2000, vols. 266–269, part 2, pp. 1021–1024.
7. Diaz-Guerra, C., Piqueras, J., Golubev, V.G., *et al.*, *Appl. Phys. Lett.*, 2000, vol. 77, no. 20, pp. 3194–3196.
8. Davydov, V.Yu., Dunin-Borkovski, R.E., Golubev, V.G., *et al.*, *Semicond. Sci. Technol.*, 2001, vol. 16, pp. L5–L7.
9. Lishanskii, I.S., Men'shikova, A.Yu., Evseeva, T.G., *et al.*, *Vysokomol. Soedin.*, 1991, vol. 33, no. 6, pp. 413–416.
10. Men'shikova, A.Yu., Evseeva, T.G., Shabsel's, B.M., *et al.*, *Kolloidn. Zh.*, 1997, vol. 59, no. 5, pp. 671–675.
11. Men'shikova, A.Yu., Evseeva, T.G., Ivanchev, S.S., *et al.*, *Vysokomol. Soedin., Ser. A*, 2001, vol. 43, no. 4, pp. 607–615.
12. Men'shikova, A.Yu., Evseeva, T.G., Chekina, N.A., *et al.*, *Zh. Prikl. Khim.*, 2001, vol. 74, no. 10, pp. 1677–1683.
13. *Praktikum po kolloidnoi khimii lateksov i PAV* (Practical Course of Colloid Chemistry of Latexes and Surfactants), Neiman, R.E., Ed., Moscow: Vysshaya Shkola, 1972.
14. *Polymer Handbook*, Brandrup, J., Immergut, E.H., and Grulke, E.A., Eds., New York: Wiley, 1999.
15. Vlasov, Yu.A., Deutsch, M., and Norris, D.J., *Appl. Phys. Lett.*, 2000, vol. 76, no. 12, pp. 1627–1629.
16. Eliseeva, V.I., *Polimernye dispersii* (Polymer Dispersions), Moscow: Khimiya, 1980.
17. Sel'kin, A.V., Abstracts of Papers, *12th Int. Symp. "Nanostructures: Physics and Technology,"* St. Petersburg (Russia): Ioffe Inst., June 21–25, 2004, pp. 111–112.

Russian Journal of Applied Chemistry, Vol. 78, No. 1, 2005, pp. 166–168. Translated from Zhurnal Prikladnoi Khimii, Vol. 78, No. 1, 2005, pp. 168–170.
Original Russian Text Copyright © 2005 by Morachevskii.

HISTORY OF CHEMISTRY AND CHEMICAL TECHNOLOGY

Theodor Grotthuss (to 220th Anniversary of His Birthday)

Theodor Grotthuss, a talented scientist, physicist, and chemist from the Baltic region, went down in history as the author of an original theory of electrolysis of aqueous solutions and of studies in the field of photochemistry and analytical chemistry. The theoretical ideas presented in his works largely foreshadowed the physical theory of solutions, concepts of electrolytic dissociation, and understanding of the phenomenon of luminescence and chemical action of light. Grotthuss made first observations in the field of electrochemistry of organic compounds. A major contribution to the study of the scientific legacy of Grotthuss and his life was made by J.P. Stradins, a known Latvian electrochemist and historian of science [1–5].

Baron Christian Johann Dietrich von Grotthuss, more known as Theodor Grotthuss, was born on January 24, 1785, in Leipzig, during a trip of his parents abroad. His family, belonging to an ancient house, owned a small estate Geduchi (Geduchai) in northern Lithuania, at the very border with Kurlandia. At this estate passed the youth and most part of the scientist's life. His father died soon after his birth, and Grotthuss was brought up by his mother and numerous teachers. Despite the humanitarian orientation of his home education and the obvious talent for music, the youth was strongly interested in natural sciences and self-educated using his father's library. In the spring of 1803, the eighteen-years-old Grotthuss first went to West Europe to be educated in natural sciences, and primarily in chemistry. The first stop was in Leipzig, but, at that time, the city was not yet among prominent centers of chemical science. Therefore, Grotthuss moved in the autumn of the same year to Paris, where he entered as an external student the Ecole Polytechnique, one of the best educational institutions of that time. Among Grotthuss's teachers are primarily named A.-F. de Fourcroy (1755–1809), a scientist, statesman, science popularizer, member of the Paris Academy of Sciences (since 1785), and an honorary foreign member of the St. Petersburg Academy of Sciences (since 1802); and also C.L. Berthollet (1748–1822) and L.N. Vauquelin (1763–1829), members of the Paris Academy of Sciences. Grotthuss



spent in Paris only a year, and the aggravation of relationships between France and Russia forced him, a Russian citizen, to move to Italy in September 1804.

After A. Volta (1745–1827), an Italian physicist, created the first chemical dc power cell (1799), scientists from many countries, and those from France and Italy in the first place, studied, with varied success, the electrolysis process. Grotthuss knew from lectures delivered by Fourcroy, Berthollet, and Vauquelin about difficulties encountered in explanation of electrochemical phenomena. Having acquired a power cell, Grotthuss carried out numerous experiments on electrochemical decomposition of aqueous solutions. He spent the whole year of 1805 in Naples and finished there his best-known study in September 1805. He, a twenty-years-old youth who had not received any systematic education, managed to be the first to give an interpretation of the electrolysis process and current transport in solutions. According to Grotthuss, electric energy is transferred through formation of chains of polar molecules in solutions. The decomposition of water at electrodes occurs via liberation of molecular fragments at places of direct contact between the chains and the electrodes [1, 2, 6–9]. This first study under the title "On Decomposition of Water and Substance Dissolved in It under the Action

1070-4272/05/7801-0166© 2005 Pleiades Publishing, Inc.

of Galvanic Electricity," published in French in Rome in the end of 1805, made him famous. Already in April 1806, Grotthuss's work was published in France in the journal *Annales de Chimie*; in the same year, it was published in British journals and, as a separate edition, in France in scientist's motherland at the town of Mitava (Elgava), the capital of Kurlandia. This work by Grotthuss was included, in Russian translation, into the collection of works [9]. Before that, the study had not been published in Russia, but Grotthuss's hypothesis was discussed in detail in the first Russia's textbook on physical chemistry [10].

From November 1805 till the end of 1806, Grotthuss lived in Rome and other Italian cities, improved his knowledge of Italian and mathematics, and commenced examination of bioluminescence. The young scientist spent nearly the whole year of 1807 in Paris, where he continued his scientific activities and, in particular, tried to reveal the role of galvanic electricity in formation of metallic dendrites. In addition, Grotthuss carried one of the first studies in organic electrochemistry. In 1807, Grotthuss was elected an honorary member of the Paris galvanic society. In the autumn of 1807, he left Paris and went home via Munich and Vienna. Since 1808, he never left Russia. As mentioned in Stradins's monograph [1], Grotthuss neither finished his education nor got scientific training or obtained a scientific degree. However, the talented young man was actively engaged in self-education, made acquaintance with a number of leading scientists of that time, comprehended the most topical problems in the fields of science he was interested in, and carried out investigations that got him a deserved fame. In 1814, Grotthuss was elected a corresponding member of the Munich Academy of Sciences.

Grotthuss lived without break at his mother's estate and encountered severe difficulties in obtaining scientific information, only being in correspondence with several scientists, and possessed only the simplest equipment. The only Grotthuss's far travel, to St. Petersburg for six months in 1812, occurred when he was compelled to go by the approaching French troops. During these months he made friends with A.I. Sherer (1772–1824), a professor of chemistry and later (since 1815) a member of the St. Petersburg Academy of Sciences. Sherer was the author of the first original textbook of chemistry in Russia, in which he, in particular, presented the oxygen theory developed by A.L. Lavoisier (1743–1794). A regular correspondence between Grotthuss and Sherer continued till the end of Grotthuss's life. A number of papers by Grotthuss were published in the journal published for a while by Sherer.

In 1817, Kurländiche Gesellschaft für Literatur und Kunst (Kurlandian Society of Literature and Fine Arts) was organized at Mitava. In conformity with its regulations, the society was to be engaged in historical-literature, scientific, and educational activities. During the first years of existence of the society, the natural-science area of these activities was predominant. Grotthuss became one of the most active members of the society. He repeatedly reported on his research activities at meetings of the society and published some of his works in the *Annual Report of the Society*. In particular, the most important of his investigations, "On the Chemical Action of Light and Electricity," was published in German in the first volume of this edition (1819). In this paper, occupying the central position in his scientific works, his ideas concerning the origin of photochemical and electrochemical phenomena were presented. Grotthuss was the first to establish that only absorbed light causes chemical transformations, he also noticed the proportionality of the photochemical effect to time. Important results of photochemical studies were also published by Grotthuss in one of his earlier papers "On an Absorbent of Light and Some General Considerations Concerning the Phosphorescence and Colors" (1815). Photochemical studies by Grotthuss have been analyzed by B.Ya. Dain [11] and Stradins [1].

The second in importance to Grotthuss's investigations in the field of electrochemistry, theory of light, and photochemistry are his studies of combustion of gas mixtures, carried out in 1809–1812. The widely diverse scientific activities of the Baltic scientist are discussed in ample detail in a monograph devoted to him [1]. Among prominent Grotthuss's publications, mention should be made of the collection of his physicochemical works [12] (only the first volume was published) and a separate volume, including works by Grotthuss, in the series of publications, *Klassiker der exacten Wissenschaften* (1906), founded by W. Ostwald. After this book was published, the attention of physical chemists and historians of science to Grotthuss's works became markedly closer. Grotthuss's activities were highly appreciated by Russian academician P.I. Walden (1863–1957). He believed that works by Grotthuss "...are exactly formulated predecessors of our modern molecular-kinetic and electrolytic theories" [13]. At the same time, Grotthus had to defend repeatedly, frequently without any good reason, his priority in separate issues.

Beginning at the age of 17, the scientist suffered from a severe hereditary abdomen illness, whose true nature remained unclear. On March 14, 1822, Grotthuss shot himself being in the state of a deep depres-

sion. He had virtually no disciples and followers. The interest in most of the problems Grotthuss studied arose only in the late XIX century, when physical chemistry formed as an independent scientific discipline. The list of Grotthuss's scientific works was given in the monograph [1], with some supplements made in [4]. The main publications by Grotthuss were listed in a reference bibliographic publication by Poggendorff [14]. The material concerning the life and scientific activities of Grotthuss is included, together with his scientific biography [1], in quite a number of reference publications [5, 15, 16] and monographs [6, 8, 17].

REFERENCES

1. Stradins, J.P., *Theodor Grotthuss*, Moscow: Nauka, 1966.
2. Stradins, J.P., *Izv. Akad. Nauk Latv. SSR*, 1958, no. 6, pp. 135–144.
3. Stradins, J.P., *Tr. Inst. Istor. Estestvozn. Tekh. Akad. Nauk SSSR*, 1962, vol. 39, pp. 49–65.
4. Stradins, J.P., in *Iz istorii estestvoznaniya i tekhniki Pribaltiki* (Essays on the History of Natural Science and Technology of the Baltic Region), 1972, vol. 4, pp. 15–35.
5. Stradins, J.P., *Dictionary of Scientific Biography*, Gillespie, Ch.S., Ed., New York: Ch. Scribner's Sons, 1981, vol. 5, pp. 558–559.
6. Ostwald, W., *Istoriya elektrokhimii* (History of Electrochemistry), St. Petersburg: Obrazovanie, 1911.
7. Solov'ev, Yu.I., *Zh. Fiz. Khim.*, 1955, vol. 29, no. 11, pp. 2097–2104.
8. Solov'ev, Yu.I., *Istoriya ucheniya o rastvorakh* (History of the Theory of Solutions), Moscow: Akad. Nauk SSSR, 1959.
9. Grotthuss, Th., *Izbrannye trudy po elektrichestvu* (Selected Works on Electricity), Moscow: Gostekhteorizdat, 1956, pp. 145–167.
10. Lyubavin, N.N., *Fizicheskaya khimiya* (Physical Chemistry), St. Petersburg, 1876, issue 1.
11. Dain, B.Ya., *Ukr. Khim. Zh.*, 1954, vol. 20, pp. 93–99.
12. Grotthuss, Th., *Physisch-Chemische Forschungen*, Nürnberg, 1820, vol. 1.
13. Walden, P.I., *Teoriya rastvorov v ikh istoricheskoi posledovatel'nosti* (Theories of Solutions in Their Historical Succession), Petrograd: Nauchn. Khim.-Tekh. Izd., 1921.
14. *G.C. Poggendorff's biographisch-literarisches Handwörterbuch der exakten Naturwissenschaften*, Leipzig, 1863, vol. 1, pp. 959–960.
15. Musabekov, Yu.S. and Chernyak, A.Ya., *Vydayushchiesya khimiki mira: Bibliograficheskii ukazatel'* (Outstanding Chemists of the World: Bibliographic Index), Moscow: Kniga, 1971.
16. Volkov, V.A. and Vonskii, E.V., *Vydayushchiesya khimiki mira: Biograficheskii spravochnik* (Outstanding Chemists of the World: Biographic Reference Book), Moscow: Vysshaya Shkola, 1991.
17. Solov'ev, Yu.I., *Ocherki po istorii fizicheskoi khimii* (Essays on the History of Physical Chemistry), Moscow: Nauka, 1964.

A. G. Morachevskii

Russian Journal of Applied Chemistry, Vol. 78, No. 1, 2005, p. 169. Translated from Zhurnal Prikladnoi Khimii, Vol. 78, No. 1, 2005, p. 171.
Original Russian Text Copyright © 2005 by Morachevskii.

INFORMATION

Fourth International Workshop "Intrachamber Processes, Combustion, and Gas-Dynamics of Dispersed Systems"

The Fourth International Workshop "Intrachamber Processes, Combustion, and Gas-Dynamics of Dispersed Systems" was held in St. Petersburg from June 28 to July 3, 2004. Similarly to the three preceding workshops devoted to this topic, the workshop in question was held under the auspices of the Ministry of Science and Education of the Russian Federation (Northwestern Division of the Scientific Council for Combustion and Explosion at the Presidium of the Russian Academy of Sciences) and Russian Academy of Rocket and Artillery Sciences (Northwestern Center). Among the main organizers of the workshop were the Voenmekh Baltic State Technical University and the Semenov Institute of Chemical Physics, Russian Academy of Sciences.

The international scientific committee of the workshop included, together with Russian scientists, representatives from the United States, Italy, Israel, France, Germany, India, Finland, and Ukraine. The workshop was one of the youth-oriented undertakings of the Integration Federal Target Program. Its main purpose was to satisfy the demand for scientific communication of scientists belonging to various generations. The youth had an opportunity to make direct scientific contacts with representatives of research centers of Russia and foreign countries. Fifty-three Russian and 8 foreign scientific institutions took part in the activities of the international workshop.

The reports submitted to the workshop were delivered at seven sections:

(1) Combustion of solid fuels and of their components.

(2) Gas dynamics, heat-and-mass exchange, and heat protection.

(3) Intrachamber processes, internal ballistics.

(4) Dynamics of gas–liquid heat-mechanic systems.

(5) Nonstationary combustion, explosion, impact, protection.

(6) Problems of ecology and safety.

(7) New computer technologies and means of computer simulation of intrachamber processes and related problems.

The program of the plenary meeting included the reports "Modern Problems of Internal Ballistics and of the Theory of Combustion" (A.M. Lipanov, Institute of Applied Mathematics, Ural Division, Russian Academy of Sciences, Izhevsk) and "Physics and Chemistry of Combustion of Gas Mixtures" (Yu.V. Polezhaev, Institute of High Temperatures, Russian Academy of Sciences, Moscow).

Staff members of the Voenmekh Baltic State Technical University (St. Petersburg) took the most active part in the workshop: they presented 28 out of 124 sectional and poster reports included in the program of the workshop. Among representatives of other scientific institutions of St. Petersburg, who delivered reports, were staff members of the Academy of Civil Aviation, Prikladnaya Khimiya Russian Scientific Center, Leninets Holding Company, and State University of Aerospace Instrument-Building. Representatives of higher-school institutions, institutions of the Russian Academy of Sciences, and other institutions from Moscow, Volgograd, Izhevsk, Kazan, Kemerovo, Novosibirsk, Perm, Tomsk, Tula, Chelyabinsk, Biisk, and Togliatti participated in the workshop.

The reports delivered were distributed among the sections as follows: 32 reports in Section 1, 29 in Section 2, 25 in Section 3, 21 in Section 4, 8 in Section 5, 6 in Section 6, and 3 in Section 7. The proceedings of the workshop were published as a collection of works in two volumes. The first of these (229 pp.) briefly describes the reports from the first and second sections, and the second (228 p.), the rest.

A. G. Morachevskii

1070-4272/05/7801-0169© 2005 Pleiades Publishing, Inc.

Russian Journal of Applied Chemistry, Vol. 78, No. 1, 2005, p. 170. Translated from Zhurnal Prikladnoi Khimii, Vol. 78, No. 1, 2005, p. 172.
Original Russian Text Copyright © 2005 by Morachevskii, Mamuilova.

INFORMATION

Fifth International Congress on Chemical Technologies

The Fifth International Congress on Chemical Technologies was held in St. Petersburg on October 12–14, 2004, in the framework of the traditional Week of Chemical Technologies. It was organized by the Ministry of Education and Science of the Russian Federation, Federal Atomic Energy Agency, St. Petersburg State Technological Institute (Technical University), St. Petersburg Scientific Center of the Russian Academy of Sciences, and Vystavki–Seminary–Biznes (Exhibitions–Seminars–Business) Ltd., with the active support by a number of other scientific institutions and enterprises.

The program of the plenary session devoted to "Chemical Industry in Russia, Prospects for Development" included three reports: "Promising Areas of Nanotechnology" (A.P. Alekhin and A.A. Malygin, St. Petersburg), "Strategy of SIBUR Joint-Stock Company in Solving the Problem of Doubling of the Gross National Product" (B.L. Baiburskii, Moscow), and "New Chemical Technologies for Processing of Liquid Radioactive Waste by Means of Nonstationary Membrane Processes" (M.A. Afonin and A.A. Kopyrin, St. Petersburg).

Three conferences: "Modern Inorganic and Organic Composites and Their Processing. Polymeric Materials: Technologies. Quality. Equipment," "Processing of Wastes. Materials and Technologies for Environment Conservation," and "Functional Coatings," were held in the framework of the Congress. The program of the first, second, and third of these conferences included 20, 33, and 14 reports, respectively. A rather high activity in the work of all the three conferences was exhibited by staff members of St. Petersburg Technological Institute (31 reports). Of other institutions, mention can be made of the Tananaev Institute of Chemistry and Technology of Rare Elements and Mineral Resources, Kola Scientific Center, Russian Academy of Sciences (Apatity) and the Khlopin Radium Institute (St. Petersburg). Specialists from Belarus and Estonia took part in the work of the Congress.

The reports were published in a special collection of works (V International Congress on Chemical Technologies, Proceedings, 2004, 96 pp.) The report by M.P. Fedorov and co-authors (St. Petersburg) "Processing of Wastes: the Most Important Environmental Issue of the XXI Century" discussed the necessity for a systematic and directed training at higher-school institutions of specialists in utilization of wastes with account of the recent advances in science and technology and in development and application of environmentally clean and low-waste technologies. To the problem of process waste were devoted the reports by L.A. Vaisberg (St. Petersburg) "Processing of Industrial and Household Wastes as a Basis for Global Resource Saving" and by D.A. Golubev and co-authors (St. Petersburg) "Organization of a Medical-Ecological Monitoring of the Environmental Safety at the Krasnyi Bor Site in Processing of Dangerous Industrial Wastes," and quite a number of other reports. The regulations concerning waste processing in the Russian Federation, new technologies for processing of the municipal waste, use of polymers for solidification of some radioactive wastes, transfer of toxic industrial wastes into a nontoxic product that can be used for a variety of purposes, and quite a number of other important environmental problems were considered.

A large group of reports was devoted to fabrication technology of new structural materials for various purposes and to protective coatings. To these reports belong those by S.S. Ordan'yan (St. Petersburg) "Physicochemical Foundations of Synthesis of Ceramic Composites Based on High-Melting Compounds," I.B. Panteleev and Ordan'yan "New Instrumental Hard Alloys Based on Tungsten Carbide," O.M. Merkushev and co-authors (St. Petersburg) "Sol–Gel Synthesis of Nanosize Electrochromic Films," V.Yu. Dolmatov (St. Petersburg) "Detonation-Synthesized Nanodiamonds as a Basis of a New Generation of Various Composite Coatings," and N.A. Zaitseva and A.V. Vasil'eva (St. Petersburg) "Electrodeposition of Metal Coatings onto Aluminum and Its Alloys."

The program of the Congress on chemical technologies was rather diverse and rich. A number of exhibitions were opened during the Week of chemical technologies. The Congress participants had an opportunity to visit some enterprises and scientific centers of St. Petersburg and Leningrad oblast. On October 14–16, 2004, a group of Congress participants went to southeastern Finland, where an out-of-town seminar "New Technologies for Processing and Storage of Household and Industrial Wastes" was held.

The next, Sixth International Congress on Chemical Technologies is to be held in October 2005.

A. G. Morachevskii and V. I. Manuilova

1070-4272/05/7801-0170 © 2005 Pleiades Publishing, Inc.

Russian Journal of Applied Chemistry, Vol. 78, No. 2, 2005, pp. 171–177. Translated from Zhurnal Prikladnoi Khimii, Vol. 78, No. 2, 2005, pp. 177–184.
Original Russian Text Copyright © 2005 by Lamberov, Aptikasheva, Egorova, Levin, Gil'manov.

INORGANIC SYNTHESIS AND INDUSTRIAL INORGANIC CHEMISTRY

Formation of the Morphology of Continuous-Precipitation Aluminum Hydroxides in the Course of Industrial Synthesis

A. A. Lamberov, A. G. Aptikasheva, S. R. Egorova, O. V. Levin, and Kh. Kh. Gil'manov

Kazan State University, Kazan, Tatarstan, Russia

Yukos RM Engineering Center Private Joint-Stock Company, Russia

Nizhnekamskneftekhim Open Joint-Stock Company, Nizhnekamsk, Russia

Received August 26, 2004

Abstract—X-ray phase and differential thermal analyses were used to study in detail how the morphology of aluminum hydroxides changes in separate stages of the technological process. The assumption that two pseudoboehmite modifications differing in crystallite dimensions and lattice constants can be formed in the course of precipitation was considered.

The effectiveness of catalytic systems based on γ-Al_2O_3 largely depends on their morphological structure, which affects a number of important characteristics of the support: specific surface area, porometric volume, pore size distribution, etc. [1]. Active alumina is for the most part industrially produced by thermal decomposition of aluminum hydroxide [2], which inherits the texture of the precursor because of the pseudomorphism in calcination. In turn, the texture of the precursor is determined by the conditions of precipitation and further technological procedures [3].

The influence exerted by the technological stages of industrial synthesis of aluminum hydroxide (AH) on the morphology of the active alumina obtained gas been insufficiently covered in the literature.

Previously, the transformation of the porous structure of AH synthesized under industrial conditions by the double-flow sulfate technology based on periodic precipitation upon mixing of low- and high-temperature hydroxides has been studied [4, 5]. It was established that the way in which the texture characteristics of the mixed hydroxide are formed is primarily determined by properties of individual hydroxides, type of interaction between particles, and transformation of the porous structure in all stages of the technological process.

It should also be noted that, in the course of industrial synthesis, AH passes a number of stages, each making its own contribution to the texturing of aluminum hydroxide in precipitation and of the resulting oxide in calcination [6]. At the same time, it was demonstrated in [7] that the texture of the system being synthesized is mainly formed in the precipitation stage. This texture can be controlled by varying the conditions in which the process occurs.

The aim of this study was to analyze in detail the influence exerted by factors associated with separate stages of synthesis on the formation of AH manufactured by continuous precipitation by the nitrate technology used at Novokuibyshev Plant of Catalysts Ltd.

EXPERIMENTAL

The object of study was AH synthesized by continuous reprecipitation of alumina trihydrate by the nitrate method. The samples to be examined were selected after the following stages of synthesis: (1) precipitation at 32°C and pH 8.6; (2) stabilization at 102°C, pH 5.0, τ = 90 min; (3) bringing the pH to 8.9, T = 80°C, τ = 130 min; (4) stabilization at 80°C, pH 8.8, τ = 4 h; (5) agitation; (6) pressing on a filter press; (7) repulpation; and (8) bringing the pH to 9.2.

Differential thermal analysis was performed with a Q-1500D derivatograph in air in the temperature range 20–1000°C at a heating rate of 10 deg min^{-1}; the sample mass was 200 mg. The accuracy of determining the loss of mass was ±0.5%.

X-ray diffraction patterns were measured on a DRON-2 instrument (Fe_{K_α} radiation, beta filter, 2θ = 5°–100°, 30 kV, 15 mA). Annealed copper foil was used as reference for determining the dimensions of

1070-4272/05/7802-0171 © 2005 Pleiades Publishing, Inc.

Table 1. Results of X-ray phase and diffraction analyses of AH

Sample no.	Composition, wt %		Lattice constant, Å					
	Pb_1	Pb_2	Pb_1			Pb_2		
			a	*b*	*c*	*a*	*b*	*c*
1*	57	3	3.74	12.19	2.88	3.86	13.42	2.82
2	98	2	3.69	12.14	2.83	3.33	12.38	2.67
3	98	2	3.69	12.18	2.83	3.33	12.38	2.67
4	98	2	3.69	12.14	2.84	3.33	12.38	2.67
5	97	3	3.69	12.14	2.84	3.33	12.33	2.62
6	97	3	3.69	12.14	2.84	3.33	12.33	2.62
8	97	3	3.69	12.19	2.84	3.33	12.33	2.62

Sample no.	Crystallite dimensions, Å						Defectiveness				*W*
	Pb_1			Pb_2			Pb_1**	Pb_2			
	b [020]	*a* [200]	*c* [002]	*b* [020]	*a* [200]	*c* [002]	[020]	[020]	[200]	[002]	
1*	35.98	48.95	68.60	948.60	998.83	978.66	7	3	1	–	8142
2	35.98	45.64	67.26	932.35	979.38	1001.94	3	3	1	–	5809
3	35.98	45.64	67.26	932.35	979.38	1001.94	3	3	1	–	5804
4	38.22	47.25	65.15	932.35	979.38	1001.94	2	3	1	–	5798
5	32.10	46.73	86.13	931.76	979.21	1010.72	2	6	7	–	3708
6	32.54	46.97	86.25	931.76	979.21	1010.72	2	6	–	1	5114
8	32.55	46.97	86.25	931.76	979.21	1010.72	2	6	1	2	4980

* Content of gibbsite in the starting sample no. 1, 40 wt %.

** No defectiveness of the crystal lattice on the [200] and [002] faces (Pb, pseudoboehmite).

crystallites (coherence domains) and microstrains. The interplanar spacings were found using the ASTM file. The accuracy of determining the lattice constants for samples of hydroxides was ±0.003 Å.

The results obtained in the X-ray phase (XPA) and diffraction analyses are listed in Table 1. The phase composition, lattice constants, and dimensions of the coherence domains were calculated using a special program package, Material Analysis Using Diffraction (MAUD). The content of particular crystalline forms in the samples obtained was evaluated by the ratio of the integral intensities of the lines characteristic of a given hydroxide form found in the mixture.

The X-ray diffraction pattern of a sample that passed the precipitation stage (Table 1, sample no. 1) shows narrow high-intensity characteristic reflections of gibbsite with interplanar spacings *d*/*l* of 4.856 and 4.373 Å at angles $2\theta \approx 17°–20°$, with a crystallite dimension of 300.54 Å. The content of the trihydrate present in a fresh precipitate because of the incomplete neutralization is 40 wt %.

The fact that the diffraction pattern contains low-intensity doublet peaks with asymmetric profiles, to which correspond interplanar spacings d/l_{020} = 6.056 and 6.709 Å at small angles ($2\theta \approx 10°–16°$), d/l_{120} = 2.364 and 2.522 Å at medium angles ($2\theta \approx 30°–60°$), and d/l_{200} = 1.871 and 1.925 Å and d/l_{002} = 1.441 and 1.378 Å at large angles ($2\theta \approx 70°–90°$) indicates that the pseudoboehmite phase is present in the precipitate.

The attempt to describe the X-ray diffraction pattern on the assumption that only gibbsite and one type of pseudoboehmite are present in the precipitate failed to produce any reliable result. The total rms deviation of this calculation, *W*, was 30304. Therefore, an assumption was made that the phase composition of the hydroxide is more complex. It was assumed, with account of the asymmetric profile of the pseudoboehmite peaks, that two pseudoboehmite modifications are present in the precipitate, together with gibbsite, and these modifications differ in the dimensions of crystallites (coherent domains). In this case, the experimental diffraction curve well coincides with that calculated with additive superposition of differential lines for separately taken components. The smallest value of *W* (8142) was obtained with this approach.

Table 2. Classification of AH

Criterion	Amorphous AH	Pseudoboehmite		Boehmite
		poorly crystallized	well-crystallized	
Specific surface area, $m^2 g^{-1}$	Not determined or <1	≥300	100–300	≤10
Number of H_2O moles per mole of Al_2O_3	≥1.7	2.0–1.2	1.2–0.9	<1.0
Interplanar spacing along the *b* axis, Å	–	13.0–12.5	12.5–12.3	<12.3
Defectiveness of the unit cell, %	–	>11	3–11	<3
Crystallite dimensions along the [020] face, Å	<13.0	13–20	>20	>35

Thus, the content of pseudoboehmite Pb_1 in a freshly precipitated hydroxide is 57 wt %, The crystallite dimensions are (Å) 35.89 × 48.95 × 68.60 along the planes [020] × [200] × [002], and the most defective crystallographic face is [020] (defectiveness 7%; Table 1, sample no. 1). In this case, the content of water in the interplanar space of the crystal lattice of the monohydroxide is 1.00 mol per mole of Al_2O_3 [6]. The pseudoboehmite Pb_2, simultaneously present in the precipitate in an amount of 3 wt %, has properties markedly different from those of Pb_1. First, the dimensions of primary particles along the corresponding cleavage planes ([020] × [200] × [002]) are (Å) 48.83 × 998.60 × 978.66, with the defectiveness of the structure on the [020] face being lower (~3%). Second, the significant expansion of the unit cell to 13.42 Å along the *b* axis indicates that an excess structural water is incorporated in an amount of 2.08 mol per mole of Al_2O_3.

The X-ray diffraction pattern of a hydroxide that passed the stabilization stage contains no lines of gibbsite. Calculations show that the fraction of Pb_1 increases by approximately 40 wt % (Table 1, sample no. 2), in agreement with published data [8], according to which large crystallites of trihydrate disintegrate in the course of time at relatively low pH values (4–6) to form pseudoboehmite particles about 30 Å in size. The dimensions of primary particles of the forming pseudoboehmite are virtually unchanged (Table 1) and the lattice constants *a*, *b*, and *c* remain constant. The defectiveness of the crystal lattice along the [020] face decreases by 4% to 3%. It is noteworthy that the amount of structural water between the cleavage planes along the [020] face also decreases only slightly, by 0.02 mol (0.98 mol H_2O/mole of Al_2O_3). The total rms deviation *W* for the given sample is 5809.

Similarly to the case of Pb_1, the dimensions of Pb_2 particles remain unchanged (Å): 932.35 × 979.38 × 1001.94 along the planes [020] × [200] × [002], with the lattice constants *a*, *b*, and *c* decreasing. It is of interest that, in contrast to the case of Pb_1, the lattice constant *b* of Pb_2 markedly decreases (to 12.38 Å) because the dehydroxylated layers become closer. This is due to removal of 0.92 mol of structural water (1.16 mol H_2O/mole of Al_2O_3) and the resulting approach of the dehydroxylated layers in the direction [020].

In the general case, crystallites of each pseudoboehmite modification have individual properties with isotropy along the crystallographic faces [020] × [200] × [002], and, as indicated by Table 1, can retain these properties in all stages of the technological process. The aforesaid is in agreement with the opinion [9] that the dimensions of primary particles formed in precipitation remain constant during the whole time of crystallization, because the structure is formed within the crystallites.

To discriminate more clearly between the pseudoboehmite phases described here by comparing the results obtained with published data [3, 10], the following criteria were suggested (Table 2).

The interpretation of the results of the X-ray phase analysis is in a good agreement with the data obtained by means of derivatography. For example, the thermal decomposition of the AH samples studied occurs in at least four stages with low- and high-temperature endothermic peaks recorded in DTA and DTG curves (Table 3).

In the initial stage of the thermal decomposition of a sample that passed the precipitation stage (Table 3, sample no. 1), unbound water is removed, which is accompanied by the appearance of an endothermic effect at 70–220°C, peaked at 145°C. The second complex endothermic effect is observed at 220–350°C. There is no commonly accepted opinion in the literature, concerning the genesis of the products formed

Table 3. Results of a differential thermal analysis of AH

Sample no.	Endothermic effects and loss of water in indicated temperature range, °C					
	70–240			240–300		
	I_{min}, °C	ΔG, 10^4 mol/%	n, mol H_2O/mol Al_2O_3	I_{min}, °C	ΔG, 10^4 mol/%	n, mol H_2O/mol Al_2O_3
1*	140	13.6/12	1.13	265; 290	9.2/8	0.77
2	135	11.9/11	0.85	275	3.0/3	0.24
3	145	12.2/11	0.87	265; 290	4.4/4	0.32
4	145	11.9/11	0.85	290	3.9/3	0.28
5	130	12.8/11	0.90	275	2.8/2	0.20
6	130	13.5/12	0.93	275	2.5/2	0.18
7	145	13.3/12	0.95	270	2.5/2	0.18
8	140	11.4/10	0.81	260	3.3/3	0.24

Sample no.	Endothermic effects and loss of water in indicated temperature range, °C							
	300–330			350–580			20–1000	
	III_{min}, °C	ΔG, 10^4 mol/%	n, mol H_2O/mol Al_2O_3	IV_{min}, °C	ΔG, 10^4 mol/%	n, mol H_2O/mol Al_2O_3	$\Sigma\,\Delta G$, 10^4 mol/%	$\Sigma\, n$, mol H_2O/mol Al_2O_3
1*	305	2.8/3	0.23	430	8.9/8	0.74	41.1/37	3.43
2	300	1.7/2	0.12	460	12.0/11	0.86	30.8/28	2.20
3	300	1.7/2	0.12	455	12.2/11	0.87	30.0/28	2.26
4	305	1.7/2	0.12	460	11.9/11	0.85	31.9/29	2.28
5	305	1.9/2	0.14	460	11.9/11	0.85	31.1/28	2.21
6	300	1.9/2	0.14	455	12.5/11	0.89	31.9/29	2.28
7	305	1.9/2	0.14	455	11.9/11	0.85	31.7/29	2.26
8	300	1.7/2	0.12	450	13.3/12	0.95	31.9/29	2.28

* Endothermic effect present at 870°C, with $\Delta G = 5.0 \times 10^{-4}$ mol (5 wt %) and $n = 0.42$ mol H_2O/mol Al_2O_3.

upon thermal decomposition in the given temperature interval. That is why a detailed phase analysis of the starting AH was performed by successive treatment of the sample in accordance with the thermal effects.

As indicated by X-ray phase analysis of a sample calcined at 270°C, the content of crystalline gibbsite markedly falls by the instant of a decrease in the mass of the sample, indicated by thermogravimetric curves (Table 3). This follows from a substantial decrease in the intensity of lines associated with trihydroxide in the diffraction pattern. A new aluminum oxide phase is formed in this sample in an amount of 39 wt %, as indicated by the appearance of peaks with d/l 2.330, 2.130, and 1.392 Å. This phase is χ-Al_2O_3, with the dimensions of primary particles along the [020] × [200] × [002] faces equal to 280.26 Å. At the same time, there is evidence [6, 11] that a minor amount of pseudoboehmite can be formed as an intermediate in dehydration of gibbsite at 250–360°C because of the creation of hydrothermal conditions in the bulk of particles. However, the dimensions of the coherent domains in the trihydrate must be no less than 680 Å in this case. An X-ray diffraction analysis of the systems under study demonstrated that the average size of gibbsite crystallites does not exceed 300 Å, and, therefore, thermal treatment of $Al(OH)_3$ leads directly to crystallization of the oxide χ-Al_2O_3 without formation of any intermediate phase.

It is noteworthy that the endothermic effect at 290°C in the DTA curves has a pre-effect at 265°C, which is probably associated with thermal decomposition of basic aluminum salts (the content of NO_3^- ions is 0.04–0.06 wt %, according to the results of an elemental analysis by the Kjoldahl method [12]). It was difficult to evaluate the contribution to the loss of mass (effect at 265°C) because of the closeness of

the temperature ranges of thermal decomposition. The presence of aluminum nitrate is confirmed by IR spectra (not given here), which contain an absorption band at 1385 cm^{-1}, associated with NO_3^- ions [13].

In addition, the X-ray diffraction pattern of a sample subjected to thermal treatment at 270°C shows a certain decrease in the intensity of pseudoboehmite peaks and the appearance of weak lines with *d*/*l* 1.827 and 1.409 Å. It is known [6] that pseudoboehmite, which is characterized as a hydroxide with a low crystallinity because of the presence in its structure of an excess amount of water, is converted to γ-Al_2O_3 at 280–330°C. This gives reason to believe that further removal of moisture at 305°C is due to thermal decomposition of Pb_2 containing 2.08 mol H_2O per mole of Al_2O_3. It was shown in [6, 14] that low temperatures of the phase transition pseudoboehmite $\rightarrow$ γ-Al_2O_3 are characteristic of fine and poorly crystallized hydroxides. The result obtained suggests that the phase transition temperature is determined largely by the crystallinity of pseudoboehmite, as well as by the size of crystallites. According to the results of calculations, the content of γ-Al_2O_3 (γ_2) formed in gradual dehydroxylation of Pb_2 in the given stage of thermal treatment is 1 wt %. Because of the pseudomorphism [1, 15], the dimensions of coherent domains in Pb_2 are comparable with those of its precursor (950.0 Å along the crystallographic planes [020] $\times$ [200] $\times$ [002]).

The absence of lines associated with gibbsite in the X-ray diffraction pattern of a sample calcined at 330°C indicates that it completely thermally decomposes into χ-Al_2O_3, whose content in the precipitate is 40 wt %. According to calculations, a certain increase in the intensity of peaks associated with γ_2-Al_2O_3 results from the completion of dehydration of Pb_2. The presence of broad bands associated with pseudoboehmite in the X-ray diffraction patterns indicates that the precipitate contains Pb_1 (~57 wt %).

The stage of dehydration of Pb_1 is observed in the DTA curves at 350–550°C, with a peak at 430°C. It is known [6, 16] that thermal decomposition of a pseudoboehmite with a high crystallinity occurs in this temperature range. According to [17], the temperature of dehydration of pseudoboehmite can be used to evaluate the dispersity of particles of the starting hydroxide. The dimensions of the coherent domains of Pb_1, which undergoes dehydration at around 430°C, do not exceed 100 Å (Table 1), in agreement with published data [15]. The presence of a high-temperature peak at 870°C indicates that there occurs a phase transformation χ-$Al_2O_3 \rightarrow$ *x*-Al_2O_3, with loss of 5% of mass.

The derivatogram of a hydroxide stabilized for 90 min shows the following changes (Table 3, sample no. 2). The endothermic peak associated with the dehydration of gibbsite is entirely absent in the DTA curves because of its phase transformation into pseudoboehmite [8], in agreement with the results of an X-ray phase analysis of the samples (Table 1, sample no. 2). It is of interest that the curves of thermal decomposition show, on the background of the disappearance of a broad peak at 290°C, a low-intensity peak at 275°C, with a loss of mass equal to 3%, which is due to thermal decomposition of basic aluminum salts.

The increase in the fraction of Pb_1 in this sample by approximately 40 wt % leads to a substantial loss of mass by the monohydroxide in the course of thermal decomposition, which is manifested in the DTA curves as an endothermic peak at 460°C (Table 3, sample no. 2). The observed shift of this peak by 30°C to higher temperatures is probably due to an increase in the crystallinity of the structure of Pb_1, which is indicated (according to XPA, by a decrease in the lattice constants (Table 1, sample no. 2). The high-temperature endothermic peak at 870°C, associated with the phase transition χ-$Al_2O_3 \rightarrow$ *x*-Al_2O_3, is not observed in the DTA curves because of the absence of gibbsite in the precipitate.

The derivatogram of a hydroxide that passed the stage in which the pH value is brought to 8.9 by adding a solution of sodium aluminate (Table 3, sample no. 3) shows an endothermic effect in the range 240–300°C, with a peak at 290°C and a pre-effect at 265°C. This is due to dehydroxylation of gibbsite formed in accordance with the scheme

$$NaAlO_2 + 2H_2O = Na^+ + Al(OH)_4^-,$$

$$Al(OH)_4^- \rightleftarrows Al(OH)_3 + OH^-,$$

in the first case, and to thermal decomposition of aluminum nitrate, in the second. The total loss of mass, associated with this effect, is 4 wt %.

The derivatogram of a hydroxide that passed the stage of stabilization for 4 h shows, in the range 240–300°C, only the effect of thermal decomposition of basic aluminum salts with a loss of mass equal to 3% (Table 3, sample no. 4). No changes are observed in other stages of dehydration of the given sample.

On the whole, the phase composition of the hydroxides does not change substantially in the subsequent stages of the technological process (Table 3), and, therefore, the pattern of thermal decomposition of sample nos. 5–8 is the same. It can be stated, on the

Table 4. Characteristics of samples obtained under the conditions of industrial synthesis

Sample no.	Synthesis conditions	Composition in accordance with XPA, wt %		DTA	
		Pb_1	Pb_2	endothermic effect*, °C	loss of mass, %
1	Freshly precipitated** (T = 32°C, pH 8.6)	57	3	Gibbsite → χ-Al_2O_3 (290°C)***	8
				Pb_2 → γ_2-Al_2O_3 (305°C)	3
				Pb_1 → γ_2-Al_2O_3 (430°C)	8
2	Stabilization (T = 102°C, pH 5.0, τ = 90 min)	98	2	Pb_2 → γ_2-Al_2O_3 (300°C)	2
				Pb_1 → γ_2-Al_2O_3 (460°C)	11
3	Bringing the pH to 8.9 (T = 102°C, τ = 130 min)	98	2	Pb_2 → γ_2-Al_2O_3 (300°C)	2
				Pb_1 → γ_2-Al_2O_3 (455°C)	11
4	Stabilization (T = 80°C, pH 8.8, τ = 4 h)	98	2	Pb_2 → γ_2-Al_2O_3 (305°C)	2
				Pb_1 → γ_2-Al_2O_3 (460°C)	11
5	Agitation	97	3	Pb_2 → γ_2-Al_2O_3 (305°C)	3
				Pb_1 → γ_2-Al_2O_3 (460°C)	11
6	Pressing on a filter press	97	3	Pb_2 → γ_2-Al_2O_3 (300°C)	2
				Pb_1 → γ_2-Al_2O_3 (455°C)	11
7	Repulpation (NH_4OH, pH 8.6)	97	3	Pb_2 → γ_2-Al_2O_3 (300°C)	2
				Pb_1 → γ_2-Al_2O_3 (450°C)	11
8	Bringing the pH to 9.2 (NH_4OH)	97	3	Pb_2 → γ_2-Al_2O_3 (300°C)	2
				Pb_1 → γ_2-Al_2O_3 (450°C)	12

* 130–140°C, removal of physically adsorbed water, loss of mass equal to 11–12 wt %; 260–275°C, thermal decomposition of basic aluminum salts, loss of mass equal to 2–3 wt %.

** Content of gibbsite in the starting sample no. 1 equal to 40 wt %.

*** Endothermic effect associated with the phase transition χ-Al_2O_3 → x-Al_2O_3 at 870°C, loss of mass equal to 5%.

basis of the whole set of XPA and DTA data, that the morphology of aluminum hydroxides obtained under the conditions of industrial synthesis is mostly formed in the stages of precipitation and stabilization. In the subsequent stages of the technological process, the phase composition of the samples does not change significantly (Table 4).

CONCLUSIONS

(1) It was suggested, on the basis of the results of X-ray phase and differential thermal analyses, that two pseudoboehmite phases are formed in the course of precipitation, Pb_1 and Pb_2. The dimensions of primary particles and the lattice constants of these two phases are strongly different.

(2) A thermal analysis demonstrated that Pb_2 undergoes thermal decomposition at low temperatures (300–330°C), and Pb_2, at high temperatures (350–580°C). The difference between the temperature ranges in which the phase transformations pseudoboehmite → γ-Al_2O_3 occur can be attributed to different degrees of crystallinity of the structure of Pb_1 and Pb_2.

(3) It was suggested to discriminate between the monohydroxide phases described (Pb_1 and Pb_2) on the basis of the lattice constant b of pseudoboehmite. For example, b does not exceed 12.19 Å for Pb_1, with 1.01–0.95 mol H_2O per mole of Al_2O_3 contained in the interlayer space, and 12.33 Å for Pb_2, with an excess amount of structural water (2.09–1.12 mol H_2O per mole of Al_2O_3).

(4) It was established that the morphology of aluminum hydroxides obtained under the conditions of industrial synthesis is formed in the stages of precipitation and stabilization. The other stages of the technological process have no effect on the composition of the phases and their relative amounts.

(5) An X-ray phase analysis revealed the following: the freshly precipitated hydroxide is a three-component system containing gibbsite and two modifications of pseudoboehmite (Pb_1 and Pb_2); no amorphous phase is formed; and stabilization leads to a complete phase transformation of gibbsite into Pb_1.

(6) Gibbsite contained in the freshly precipitated aluminum hydroxide undergoes a phase transition $Al(OH)_3$ → χ-Al_2O_3 in the course of thermal treatment, with no pseudoboehmite formed.

REFERENCES

1. Kefeli, L.M., *Kinet. Kataliz*, 1968, vol. 9, no. 6, pp. 1353–1357.
2. Ivanova, A.S., Litvak, G.S., Kryukova, G.N., *et al.*, *Kinet. Kataliz*, 2000, vol. 41, no. 1, pp. 137–141.
3. Dzis'ko, V.A., Karnaukhov, A.P., and Tarasova, D.V., *Fizikokhimicheskie osnovy sinteza oksidnykh katalizatorov* (Physicochemical Foundations of Synthesis of Oxide Catalysts), Novosibirsk: Nauka, 1978.
4. Lamberov, A.A., Levin, O.V., Egorova, S.R., *et al.*, *Zh. Prikl. Khim.*, 2003, vol. 76, no. 1, pp. 50–56.
5. Lamberov, A.A., Levin, O.V., Egorova, S.R., *et al.*, *Zh. Prikl. Khim.*, 2003, vol. 76, no. 3, pp. 365–372.
6. *Physical and Chemical Aspects of Adsorbents and Catalysts*, Linsen, B. G., Ed., London: Academic, 1970.
7. Dzis'ko, V.A., *Kinet. Kataliz*, 1979, vol. 20, no. 6, pp. 1526–1532.
8. Paramzin, S.M., Zolotovskii, B.P., Buyanov, R.A., *et al.*, *Sib. Khim. Zh.*, 1992, no. 2, pp. 130–132.
9. Buyanov, R.A. and Krivoruchko, O.P., *Izv. Sib. Otd. Akad. Nauk SSSR, Ser. Khim.*, 1982, no. 14, pp. 28–35.
10. Dzis'ko, V.A., *Osnovy metodov prigotovleniya katalizatorov* (Foundations of Methods for Catalyst Preparation), Novosibirsk: Nauka, 1983.
11. Zolotovskii, B.P., Shkarin, A.V., Krivoruchko, O.P., *et al.*, *Izv. Sib. Otd. Akad. Nauk SSSR, Ser. Khim.*, 1984, no. 17, pp. 36–38.
12. Alekseevskii, E.V., Gol'ts, R.K., and Musakin, A.P., *Kolichestvennyi analiz* (Quantitative Analysis), Leningrad: Goskhimizdat, 1955.
13. Chukin, G.D. and Seleznev, Yu.L., *Izv. Akad. Nauk SSSR, Ser. Neorg.*, 1987, vol. 23, no. 3, pp. 424–428.
14. Ivanova, A.S., Pugach, M.M., Moroz, E.M., *et al.*, *Izv. Akad. Nauk SSSR, Ser. Khim.*, 1989, no. 10, pp. 2169–2175.
15. Kvashonkin, V.I., Agievskii, D.A., and Pronin, V.A., *Kinet. Kataliz*, 1985, vol. 26, no. 5, pp. 1213–1219.
16. Vinnikova, T.S., Dzis'ko, V.A., Kefeli, L.M., *et al.*, *Kinet. Kataliz*, 1968, vol. 9, no. 6, pp. 1331–1341.
17. Levin, O.V., Sidel'kovskaya, V.G., Aliev, P.P., *et al.*, *Khim. Tekhnol. Topl. Masel*, 1977, no. 2, pp. 29–31.

Russian Journal of Applied Chemistry, Vol. 78, No. 2, 2005, pp. 178–183. Translated from Zhurnal Prikladnoi Khimii, Vol. 78, No. 2, 2005, pp. 185–190.
Original Russian Text Copyright © 2005 by Kshumaneva, Kasikov, Neradovskii.

INORGANIC SYNTHESIS AND INDUSTRIAL INORGANIC CHEMISTRY

Behavior of Sulfides of Nonferrous Metals in Hydrochloric-Acid Leaching of Residues Formed in Synthesis of Carbonyl Nickel

E. S. Kshumaneva, A. G. Kasikov, and Yu. N. Neradovskii

Tananaev Institute of Chemistry and Technology of Rare Elements and Mineral Raw Materials, Kola Scientific Center Russian Academy of Sciences, Apatity, Russia

Received November 2, 2004

Abstract—Specific features of hydrochloric-acid leaching of residues formed in synthesis of carbonyl nickel without removal and with forced removal of the gas phase were studied.

In producing metallic nickel by carbonylation of a nickel-containing raw material, residues substantially enriched with cobalt and platinum metals[1] are formed. However, the content of platinum group metals in these residues is approximately 10 times lower than that in anodic slimes, and, therefore, their joint processing to produce conditioned concentrates of platinum metals (PM) seems to be impossible. At present, residues of carbonyl nickel synthesis (RCS) are recycled, which leads to loss of non-ferrous and platinum metals and to the enrichment of the nickel raw material with copper. Removal of the carbonylation residues from the pyrometallurgical process to be subjected to a hydrometallurgical processing is a possible way to raise the recovery of both nonferrous and noble metals.

It is known [1, 2] that the specificity of synthesis of nickel tetracarbonyl is primarily associated with the reactivity of the material subjected to carbonylation, which is, in turn, proportional to its surface area accessible to the reaction with carbon oxide. The specific surface area of the material is most frequently raised through formation of sulfides at grain boundaries in metal phases, which leads to a spongy structure of the material. After the carbonylation is complete, with the main part of nickel and iron evaporated as the carbonyls $Ni(CO)_4$ and $Fe(CO)_5$, the impurities, namely copper, cobalt, noble metals, and sulfur, are concentrated in a solid residue.

[1] Severonikel' combine of Kola Mining and Smelting Co.

It is known that processing of RCS can be carried out by either a pyro- or a hydrometallurgical method, depending on their phase composition. The hydrometallurgical method for processing of RCS of the above-mentioned composition involves two-stage sulfatization, autoclave sulfuric-acid leaching, and ammonia-carbonate leaching [1, 3–7]. The low extraction of cobalt and platinum group metals is a disadvantage of the ammonia method [8], and leaching with sulfuric acid involves autoclave processes, which requires that expensive and power-consuming equipment should be used. Therefore, we tested several schemes of hydrochloride processing of these products [9–12]. These schemes use hydrochloric-acid solutions of iron(III) and gaseous chlorine and make it possible to process the material at atmospheric pressure, remove sulfur in the elementary form, and concentrate platinum metals in the final product.

As the acidity of the leaching solution strongly affects the phase transformations in the material under study, the initial stage of development of a hydrochloride technology for RCS processing consisted in a study of the behavior of separate phase components of the residues in their leaching with hydrochloric acid. The starting RCS samples, selected as the objects of study were decarbonylated by keeping them in a vacuum at the boiling point of nickel carbonyl (~43°C). They had the following composition (wt %): Ni 5.1–9.1, Co 12.0–18.0, Cu 29.0–43.2, Fe 3.8–7.9, S 18.9–21.4, and ΣPM 0.15–0.22.

1070-4272/05/7802-0178 © 2005 Pleiades Publishing, Inc.

The redox potentials of solutions in use were measured with a V7-34A voltmeter. Silver chloride and platinum electrodes served as a reference and an indicator electrode, respectively.

Two modes of leaching were used. In the first of these, reaction products were not removed from the reaction space before the process was complete, and in the second, they were forced from the gas-vapor phase (GVP). The effect of leaching parameters on the extraction of RCS components into solution was studied by analyzing samples of solid and liquid phases of the sludge. The concentrations of nickel, cobalt, iron, and copper in solutions and precipitates after their decomposition were determined by the atomic-absorption method, and that of platinum metals in solid products was found by X-ray fluorescence analysis. A comparison of the data for various samples of the starting material did not reveal any significant difference between them.

To study the main RCS phases and to determine their composition, we carried out mineralogical and X-ray phase analyses of the starting samples and products of their leaching. For the mineralogical analysis, we used preparations based on an epoxy resin, which were studied in reflected light under an Opton Ultarphot-3 microscope with a resolution of 0.2 μm. The main phases were analyzed by the X-ray fluorescence method on a Cameca MS-46 microprobe analyzer.

The mineralogical and electron-microprobe analyses demonstrated that the structure of characteristic particles of RCS is represented by spongy spherical aggregates with walls formed by a pentlandite-like phase (PP–M_9S_8, where M is Co, Ni, Fe, or Cu) and chalcosine (Cu_2S) in a tight and even accretion in a 50 : 50 (%) proportion. The pentlandite-like phase, in turn, consists of three sulfide components: nickel-rich $Ni_{3.18}Fe_{3.36}Cu_{2.25}Co_{0.21}S_8$ (~20%), copper $Cu_{7.13}Fe_{1.07}Ni_{0.48}Co_{0.35}S_8$ (~40%), and cobalt components $Co_{4.74}Fe_{2.06}Cu_{1.32}Ni_{0.84}S_8$ (~40%). A chalcosine mass is situated between sponge walls. The X-ray phase analysis revealed the presence of the main sulfide phases: $Cu_{1.96}S$, (Co, Ni, Fe)$_9S_8$, and Co_8FeS_8 (Fig. 1a).

The behavior of chalcosine and pentlandite in hydrochloric-acid leaching has been adequately described in the literature. For example, the dissolution of chalcosine in hydrochloric acid in the absence of oxidants proceeds in two stages [13–16]: in the first stage, a part of copper is extracted into solution as Cu^+, and CuS (covellite) is formed; in the second,

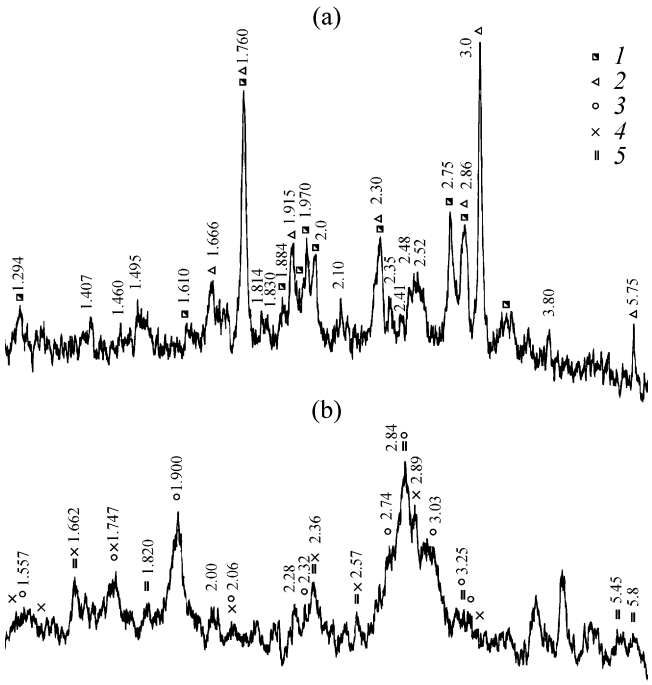


Fig. 1. X-ray diffraction pattern of a residue formed in synthesis of carbonyl nickel: (a) initial and (b) leached with 3.5 M HCl. (*1*) $Cu_{1.961}S$; (*2*) (Co, Ni, Fe)$_9S_8$, Co_8FeS_8; (*3*) CuS; (*4*) CuS_2; (*5*) Ni_2CoS_4, Co_3S_4.

CuS slowly dissolves as an intermediate phase with evolution of hydrogen sulfide. Presence of an oxidant leads to formation of sulfur in the second stage of decomposition.

It was shown in [17, 18] that the reaction of pentlandite (Fe, Ni)$_9S_8$, which contains a constant excess of metals over sulfur, with hydrochloric acid (1 M) proceeds mostly as the overall equation

$$M_9S_8 + 18HCl = 9MCl_2 + 8H_2S + H_2. \quad (1)$$

It involves reduction of hydrogen ions in the acid medium to the elementary state

$$2H^+ + 2e = H_{2(g)}$$

and oxidation of pentlandite

$$(Fe, Ni)_9S_{8(s)} + 16H^+_{(aq)} = 4.5Fe^2_{(aq)} + 4.5Ni^2_{(aq)} + 8H_2S + 2e.$$

If the potential of pentlandite increases under polarization with an external current or upon introduction of oxidants into the solution (e.g., $FeCl_3$), it decomposes to give an intermediate phase of violarite (Fe, Ni)$_3S_4$.

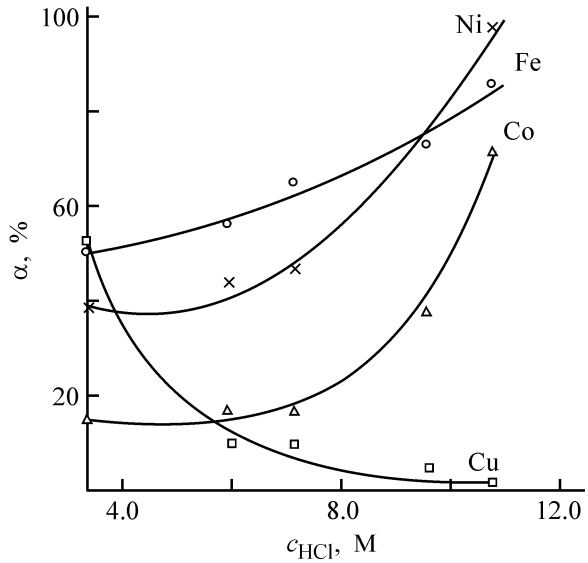


Fig. 2. Degree of extraction, α of nonferrous metals and iron from residues formed in synthesis of carbonyl nickel vs. the concentration of hydrochloric acid c_{HCl}, without removal of GVP. τ 5 h, s : l = 1 : 2, *T* 80°C.

Special experiments demonstrated that the redox potential of the solution, established in leaching of pentlandite (containing the main phase inan amount of about 95%) with hydrochloric acid (1 M) at 80°C is 0.04 V. When chalcosine (Cu content 76.5%) is leached under the same conditions, the potential is 0.20 V. The simultaneous presence of chalcosine and PP in the composition of RCS strongly affects the degree of extraction in the case of their decomposition with hydrochloric acid, with the HCl concentration being the key factor (Fig. 2). An examination of the results of the microscopic, X-ray fluorescence, and X-ray phase analyses revealed that leaching with the acid present in a concentration lower than 6 M in the atmosphere of evolving gases results in the decomposition of the pentlandite-like phase to give intermediate phases by the reactions

$$(Cu, M)_9S_8 + 8HCl = 4MCl_2 + M_3S_4 + Cu_2S + 3H_2S + H_2, \quad (2)$$

where M is Fe, Ni, or Co.

The M_3S_4 phase is represented by the sulfides Ni_2CoS_4, Co_3S_4, and $(Ni, Fe)_3S_4$, which have a trivalent cation in their lattice [17].

Chalcosine present in the starting material and formed via decomposition of PP to give covellite (CuS) dissolves in parallel to this reaction. The X-ray phase analysis also reveals the presence of CuS_2 (Fig. 1b). In this case the redox potential of the solution is 0.20 V, which corresponds to the potential of the equilibrium system Cu^{2+}/Cu^{+}, and tends to increase as the concentration decreases.

The dissolution of RCS PP in the acid with a concentration exceeding 6 M at 80°C mainly occurs by reaction (1). The redox potential of the solution is shifted in the negative direction to become lower than 0.04 V.

The results obtained show that the main part of RCS PP decomposes already within 2 h of leaching with 7.9 M hydrochloric acid, the degree of nickel, iron, and cobalt recovery being 80.5, 80.9, and 60.3 wt %, respectively. Making the process duration longer can raise the extent to which the above-mentioned metals pass into solution; however, a considerable part of cobalt (~30%) remains in the solid residue as linnaeite (Co_3S_4). Our earlier study [10] has shown that the presence of metallic nickel, which remains in RCS in the case of incomplete carbonylation, strongly lowers the redox potentials in the leaching solution, with no linnaeite formed and cobalt virtually completely (~97%) passing into solution. In a reducing atmosphere, copper passes into the solid residue as Cu_2S.

Thus, the data obtained indicate that the presence of chalcosine in RCS results in an increase in the redox potential of a leaching solution, which promotes formation of intermediate phases (and, in the end, linnaeite Co_3S_4) in PP decomposition. If a reducing atmosphere is created by raising the concentration of hydrochloric acid or by adding a reducing agent (e.g., metallic nickel), PP decomposition proceeds most completely, with copper concentrated in a residue ~80% composed of copper sulfide (Cu_2S).

Based on the results obtained, we suggested a scheme for RCS processing, which involves a two-stage leaching of a starting material. The selectivity and depth of nickel, cobalt, and iron recovery in the first stage was ensured by leaching with concentrated hydrochloric acid at an elevated temperature. The use of an iron(III) chloride solution in the second stage of leaching of the resulting copper residual allowed us to transfer 99% of copper into solution and to obtain a primary platinum concentrate containing ~1% platinum metals, which is suitable for processing together with anodic slimes. In this case, the residual concentration of platinum metals in solution was not higher than 0.1 mg l^{-1}. However, despite the possibility of the high level of metal recovery, concentration of platinum metals in the residue, and partial removal of sulfur in the elementary form, the scheme we developed has certain disadvantages. For example, use

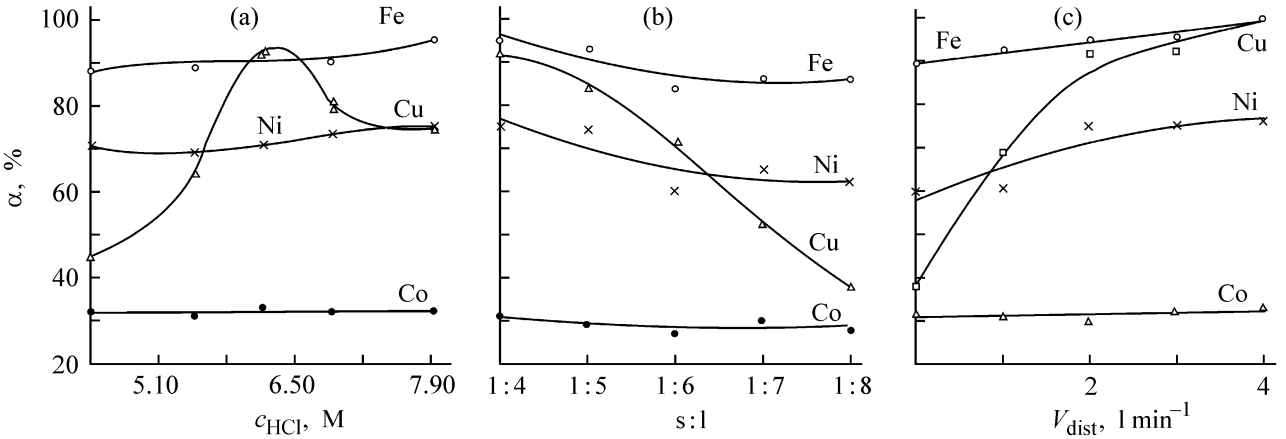


Fig. 3. Degree of extraction, α, of nonferrous metals and iron from residues formed in synthesis of carbonyl nickel with removal of GVP vs. (a) concentration of hydrochloric acid c_{HCl}, (b) solid-to-liquid ratio s : l, and (c) rate of removal of the gas-vapor phase, V_{dist}. τ = 4 h, T = 80°C. (a) s : l = 1 : 4, V_{dist} = 2 l min^{-1}; (b) c_{HCl} = 6 M, V_{dist} = 2 l min^{-1}; (c) c_{HCl} = 6 M, s:l = 1:4.

of concentrated hydrochloric acid imposes stringent requirements on the apparatus employed and on the working conditions.

To study the possibility of utilization of effluent gases and to achieve the most complete decomposition of the sulfides by shifting the equilibria of the occurring reactions on the basis of the Le Chatelier principle, we studied leaching of residues formed in nickel carbonylation in hydrochloric acid with a forced removal of a GVP. According to the Henry law, the concentration of hydrogen sulfide in solution is related to its partial pressure in the GVP by

$$[H_2S]_{aq} = fP_{H_2S}. \quad (3)$$

Here the coefficient f depends on temperature and salt composition of the solution and decreases as either of these factors increases [19].

Thus, we can change the concentration of hydrogen sulfide in solution by varying the composition of a GVP over the solution. Furthermore, it was of certain interest to compare the behavior of separate RCS phase components in acid leaching, with the reaction products removed by evaporation and bound during chlorination or in leaching with an iron(III) chloride solution [11] by the reactions

$$2FeCl_3 + H_2S \rightarrow 2FeCl_2 + S + 2HCl, \quad (4)$$

$$H_2S + Cl_2 \rightarrow S + 2HCl. \quad (5)$$

In these experiments, the GVP was removed from the reaction vessel through a system of absorption flasks, and the rate of the evaporation was measured with a rotameter. After a prescribed time of leaching, the sludge was filtered in a vacuum and the precipitate formed was washed with water and dried at 105°C. The influence exerted by the concentration of hydrochloric acid, solid : liquid ratio, and rate of removal of the gas-vapor mixture on the degree of recovery of the main components were studied. All the experiments were carried out at 80°C.

Preliminary experiments demonstrated (see table) that forced removal of GVP from the reaction space results in a virtually complete dissolution of chalcosine, and the pentlandite-like phases decompose to give intermediate compounds by reaction (2).

The dependence of the degree of copper extraction from RCS into a solution, with GVP removed from the reaction space, on the concentration of hydrochloric acid has a well pronounced maximum (Fig. 3a). In this case, the redox potential of the leaching solution is higher than 0.20 V in the range of acid concentrations used in the study. Raising the HCl concentration from 4.5 to 6 M leads to an increase in the degree of decomposition of copper sulfides, which becomes 92% at the removal rate of 2 l min^{-1}. Then, as the acid concentration is raised further, the degree of

Recovery of metals into solution in the case of a forced removal of the GVP in RCS leaching with hydrochloric acid (T = 80°C, c_{HCl} = 6 M, τ = 4 h, V_{dist} = 2 l min^{-1}, s : l = 1 : 4)

Leaching conditions	Extraction into solution, %			
	Ni	Co	Cu	Fe
Without evaporation	59.8	30.5	38.1	89.0
With evaporation	74.6	30.8	91.7	94.8

copper extraction decreases by 20%, with the transfer of nickel, iron, and cobalt into solution remaining virtually constant. The dependence observed can be explained if the arguments of the authors of [20] in favor of the possible oxidation of Fe^{2+} ions by Cu^{2+} ions are accepted. In this case, copper reduced to a monovalent state is incorporated into the lattice of solid covellite to form chalcosine.

The results of the experimental determination of the degree of copper, cobalt, nickel, and iron recovery in relation to the s : l ratio (Fig. 3b) indicate that the extent to which these components pass into solution falls as this ratio becomes lower, with the extraction of copper decreasing from 91.7 to 37.8% as the s : l ratio decreases from 1 : 4 to 1 : 8. It is most likely that the sharp decrease (by almost a factor of 2.4) in the copper extraction into solution is due to a change in the salt composition of the solution, which results, according to Eq. (3), in an increase in the content of hydrogen sulfide in the liquid phase.

The dependence of the degree of copper extraction into solution on the rate of GVP removal from the reaction vessel (Fig. 3c) conclusively shows that this parameter is one of main factors affecting the process. The recovery of copper is 38.1% without removal of the gas phase, but increases to 91.7% at a removal rate of 2 l min^{-1} and to almost 100% at a rate of 4 l min^{-1}. The extent to which cobalt and iron pass into solution varies within the indicated range of GVP removal rates insignificantly, being 32.0–33.4 and 88.5–99.3 wt %, respectively.

Thus, leaching of RCS with 6 M hydrochloric acid for 4 h, with GVP removed at a rate of 4 l min^{-1} at 80°C and an s : l ratio of 1 : 4, the degree of copper, nickel, and iron extraction into solution is 99.9, 77.0 and 99.3 wt %, respectively. The resulting solutions have the following composition (g l^{-1}): Cu 98.0, Ni 38.0, Co 12.0, and Fe 15.0. Cobalt is concentrated in the solid phase in the form of Co_3S_4. The content of copper in the residues obtained upon leaching is 2–3%.

CONCLUSIONS

(1) A study of the behavior of separate phase components of the residues formed in synthesis of carbonyl nickel by leaching with hydrochloric acid has shown that nickel, iron, and cobalt can be selectively leached, with copper isolated in a solid residue, when the process is carried out under atmospheric pressure without removal of the gas-vapor phase.

(2) It was found, when determining the optimal conditions of leaching, that the completeness of separation depends on the redox potential of the acid solution.

(3) The possibility of selective extraction of nickel, iron, and copper by leaching, with isolation of cobalt in a solid residue, was demonstrated for the case when the process is carried out with the gas-vapor phase removed from the reaction space.

(4) It was shown that the rate of removal of the gas-vapor phase and the solid-to-liquid ratio in leaching exert the decisive influence on the degree of copper recovery.

REFERENCES

1. Kipnis, A.J., Mikhailova, N.F., and Pevzner, G.R., *Karbonil'nyi sposob polucheniya nikelya* (Carbonyl Method of Nickel Production), Moscow: Tsvetmetinformatsiya, 1972.
2. Mnukhin, A.S., Verblovskii, A.M., and Vereshchagina, A.I., *O kharaktere razlichnykh nikel'soderzhashchikh materialov pri karbonolirovanii: Sbornik nauchnykh trudov instituta Gipronikel'* (On the Character of Various Nickel-Containing Materials in Carbonylation: Coll. of Sci. Works of Gipronikel' Institute), Leningrad, 1970, issue 49, pp. 60–65.
3. Zashchikhin, T.N., Beloglazov, I.K., and Danilova, O.M., *Gidrometallurgicheskie protsessy v tekhnologii nikelya i kobal'ta: Sbornik nauchnykh trudov* (Hydrometallurgical Processes in Nickel and Cobalt Technology: Coll. of Sci. Works), Leningrad, 1979, pp. 27–33.
4. Tyroler, P.M., Sanmiya, T.S., and Hodkin, E.W., Hydrometallurgical Processing of Inco's Carbonyl Residue: *17th Ann. Meet. Metall. Soc.*, Phoenix, Arizona, January 25–29, 1988.
5. Kabanova, E.V., Kondrashova, P.S., and Alekseeva, R.K., *Tsvetn. Met.*, 1983, no. 8, pp. 26–28.
6. Grewal, I., Dreisinger, D.B., Krueger, D., *et al.*, *Hydrometallurgy*, 1992, vol. 29, pp. 319–333.
7. Clement, C., Tyroler, P.M., Krause, E., and Nissen, N.C., *Hydrometallurgy*, 1992, vol. 29, pp. 335–356.
8. Reznik, I.D., Sobol', S.I., and Khudyakov, V.M., *Kobal't* (Cobalt), Moscow: Mashinostroenie, 1995, vol. 2.
9. Kshumaneva, E.S., Rtveladze, V.V., Bagrova, E.G., *et al.*, *Novye protsessy v metallurgii tsvetnykh, redkikh i blagorodnykh metallov* (New Processes in Metallurgy of Nonferrous, Rare, and Noble Metals), Apatity, 2001, p. 158.
10. Kasikov, A.G., Kshumaneva, E.S., Kuznetsov, V.Ya., and Neradovskii, Yu.N., Abstracts of Papers, *Nauchnaya konferentsiya "Pererabotka prirodnogo i tekhnogennogo syr'ya, soderzhashchego redkie, blagorodnye i tsvetnye metally"* (Sci. Conf. Processing of Natural and Technogenic Raw Materials Containing

Rare, Noble, and Nonferrous Metals), Apatity, 2003, p. 67.

11. Kasikov, A.G., Kshumaneva, E.S., Kuznetsov, V.Ya., and Neradovskii, Yu.N., Abstracts of Papers, *IV Kongress obogatitelei stran SNG* (IV Congress of Dressers of CIS Countries), Moscow, 2003, vol. 2, p. 57.
12. Kasikov, A.G., Kshumaneva, E.S., and Neradovskii, Yu.N., Abstracts of Papers, *Mezhdunarodnoe soveshchanie* (Inernational Conf.), Petrozavodsk, 2003, Moscow, 2003, p. 83.14.
13. Remy, H., *Lehrbuch der Anorganischen Chemie*, Bd. 2, Leipzig: Akademische, Geest and Portig K.-G., 1961.
14. Naboichenko, S.S. and Smirnov, V.I., *Gidrometallurgiya medi* (Hydrometallurgy of Copper), Moscow: Metallurgiya, 1974.
15. Karzhakov, N.A., Makatova, I.N., Beisembaev, B.B., *et al.*, *Kompl. Ispol'z. Miner. Syr'ya*, 1980, no. 6. pp. 17–21.
16. Naboichenko, S.S., Tsogtkhangai, D., and Dorzhpurev, M., *Izv. Vyssh. Uchebn. Zaved., Tsvetn. Metall.*, 1982, no. 5, pp. 18–20.
17. Vaughan, D.J. and Craig, J.R., *Mineral Chemistry of Metal Sulfides*, Cambridge: Cambridge Univ., 1978.
18. Warner, T.E., Rice N.M., and Taylor, N., *Hydrometallurgy*, 1992, vol. 31, pp. 55–90.
19. Reznik, I.D., Ermakov, G.P., and Shneerson, Ya.M., *Nikel'* (Nickel), Moscow: Nauka i Tekhnologii Ltd., 2003, vol. 3.
20. Chugaev, L.V., Berezkina, N.A., and Shneerson, Ya.M., *Khim. Tekhnol.*, 2003, no. 12, pp. 24–29.

Russian Journal of Applied Chemistry, Vol. 78, No. 2, 2005, pp. 184–187. Translated from Zhurnal Prikladnoi Khimii, Vol. 78, No. 2, 2005, pp. 191–194.
Original Russian Text Copyright © 2005 by Zhdanov, Ul'yanova, Ferapontov.

INORGANIC SYNTHESIS AND INDUSTRIAL INORGANIC CHEMISTRY

A Study of the Kinetics of Synthesis of Potassium Superoxide from an Alkaline Solution of Hydrogen Peroxide

D. V. Zhdanov, M. A. Ul'yanova, and Yu. A. Ferapontov

Tambov Research Institute of Chemistry Federal Unitary Enterprise, Tambov, Russia

Received April 20, 2004

Abstract—Kinetic aspects and the mechanism of shaping of particles of potassium superoxide in its synthesis from drops of an alkaline solution of hydrogen peroxide in a flow of a drying agent were studied.

The method for synthesis of potassium superoxide KO_2 is based on the fact that, being a weak acid, hydrogen peroxide enters, under certain conditions, into an exchange reaction with potassium hydroxide [Eq. (1a)] to give an intermediate adduct $K_2O_2 \cdot 2H_2O_2$ (potassium peroxide diperoxohydrate) [1]. This adduct disproportionates upon heating to above 40°C [Eq. (1b)] to give KO_2. The overall process of formation of potassium superoxide from the starting reagents is described by Eq. (1):

$$2KOH + 3H_2O_2 = K_2O_2 \cdot 2H_2O_2 + 2H_2O \quad (1a)$$

$$K_2O_2 \cdot 2H_2O_2 = 2KO_2 + 2H_2O \quad (1b)$$

$$2KOH + 3H_2O_2 = 2KO_2 \cdot 4H_2O. \quad (1)$$

Previously, this process has been carried out by spraying an alkaline solution of H_2O_2 onto the heated surface of a rotating drum blown over from the outside with an inert gas [2]. When the solution dries up, potassium superoxide is formed on the drum surface, cut-off with a blade, and discharged into the receiving bin.

However, this method has an important disadvantage: it is necessary to supply a saturated steam, which serves as a heat-transfer agent, into a rotating drum under elevated pressure and to remove the forming condensate from the drum. This impairs the reliability of the process and hinders its industrial application.

To eliminate these disadvantages, it is suggested to perform the process in a direct-flow spray reactor, with the synthesis of KO_2 and its drying in a dispersed state combined. The resulting powdered target product is separated from the drying agent in a cyclone and collected in a bin. Heated, dried, and purified (to remove CO_2) air or any inert gas can be used as a drying agent [3].

It is reasonable to assume that, under the experimental conditions, the disproportionation of $K_2O_2 \cdot 2H_2O_2$ may be accompanied by the following chemical side reactions:

$$2KO_2 + 3H_2O = 2(KOH \cdot H_2O) + 1.5O_2, \quad (2)$$

$$2KOH + CO_2 = K_2CO_3 + H_2O. \quad (3)$$

In the case of an intensive dehydration and low concentrations of H_2O and CO_2 vapor in the drying agent, the influence of these reactions can be neglected.

The rate of reaction (1) in a spray reactor depends on a number of factors (temperature, concentrations of the starting reagents, etc.). Therefore, determination and subsequent generalization of the fundamental kinetic aspects of this process and analysis of the shape of the forming grains is an obligatory stage in developing the scientific prerequisites for calculation of its performance and design parameters.

As shown by practical experience [4], the choice and substantiation of the optimal modes of synthesis of particular products should be primarily based on the information about the mechanism of internal processes and thermal characteristics of the substance being dried. It is the kinetics of heat-exchange processes in a separate particle that determines such important characteristics of the target product as dispersity, reactivity, bulk density of the powder, and its tendency toward caking.

1070-4272/05/7802-0184 © 2005 Pleiades Publishing, Inc.

Physicochemically, the process being considered consists in dispersion of an alkaline solution of hydrogen peroxide and its subsequent crystallization to give potassium superoxide under drying, with a simultaneous occurrence of chemical reactions.

In studying under laboratory conditions the kinetics of the internal heat-and-mass-exchange processes and the mechanism of shaping in a separate particle, this particle was regarded as a unit element of the whole dispersed system present in the chamber of the reactor. Therefore, the primary goal in studying the kinetics of the process in question was to examine just those external conditions that are experienced by a unit element of the system in a real apparatus. This refers, in the first place, to the basic characteristics of the drying agent: temperature, pressure, relative velocity, and chemical composition.

The information that can be directly obtained in an experiment with a single drop of the solution with a drying agent is a set of data on how its temperature, mass, size, and shape vary in the course of synthesis. Processing of the resulting experimental data enables a conclusion about the nature of the internal heat-and-mass-transfer processes in a particle under varied external conditions.

EXPERIMENTAL

The kinetics of synthesis of potassium superoxide from an alkaline solution of hydrogen peroxide in a flow of a drying agent was studied on an experimental stand shown schematically in Fig. 1.

The drying agent is delivered by a gas blower *1* through a flow control valve *2* into a psychrometer *3* and rheometer *4*, which measure the humidity and flow rate, respectively. Then the drying agent is delivered for heating into an electric air heater *5* and, further, discharged via pipe *6* into the atmosphere through a nozzle 17 mm in diameter. A thermocouple *7* is fixed on a special bracket *8* connected to a high-precision electronic microbalance *9*. The temperature and mass of a drop suspended on the junction of the thermocouple is recorded by self-recorders *10* and *11*. The temperature of the drying agent is determined from the reading of the recorder *10* in the absence of drop suspended on the thermocouple after the stand attains a steady state. A video camera *12* with a microattachment enables a continuous video recording of the drop in the course of synthesis.

To make lower the radiation heating of the drop, the pipe *6* has a 90° elbow. To diminish the heating

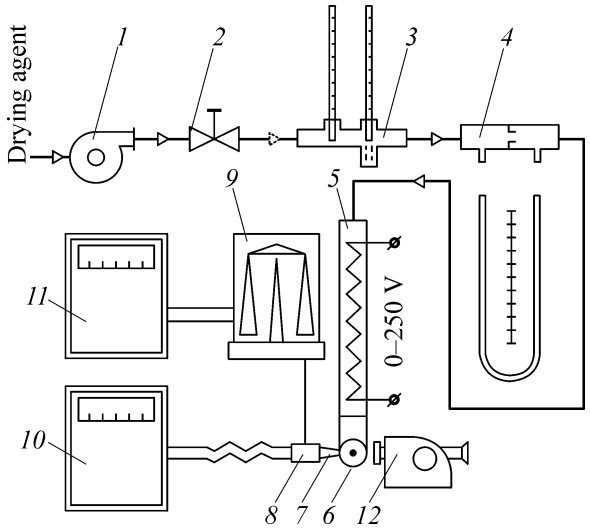


Fig. 1. Experimental stand for a study of the kinetics of synthesis of potassium superoxide from an alkaline solution of hydrogen peroxide in a flow of a drying agent.

of the drop via thermal conduction, the diameter of the wires of the thermocouple is chosen to be the minimum possible. In the case in question, this diameter is 50 μm. All this is done with the only objective, to ensure a mainly convective heat supply and to make the experimental conditions as close as possible to the real process of dehydration of solution drops in an industrial apparatus.

The alkaline solution of hydrogen peroxide to be used in the study was prepared by mixing 50% solutions of KOH and H_2O [5].

A drop of the resulting solution was suspended on the junction of the thermocouple and blown over with the drying agent (for its parameters, see table). The following parameters were recorded in the course of the experiment: temperatures T_{dr} and T_{moist} of dry and moistened thermometer, respectively; flow rate G_A; and temperature T_{DA} of the drying agent. As a result, curves describing how the temperature [$T_d = f(\tau)$], mass [$m_d = f(\tau)$], and diameter [$d_d = f(\tau)$] of a drop under study vary with the time τ of the process were obtained.

Experimental conditions (drying agent, atmospheric air purified to remove CO_2)

Sample no.	T_{dr}	T_{moist}	G_{DA}, l min^{-1}	T_{DA}, °C
	°C			
1	27.6	12.4	50	150
2	21.9	15.5	50	187
3	22.6	21.4	50	225

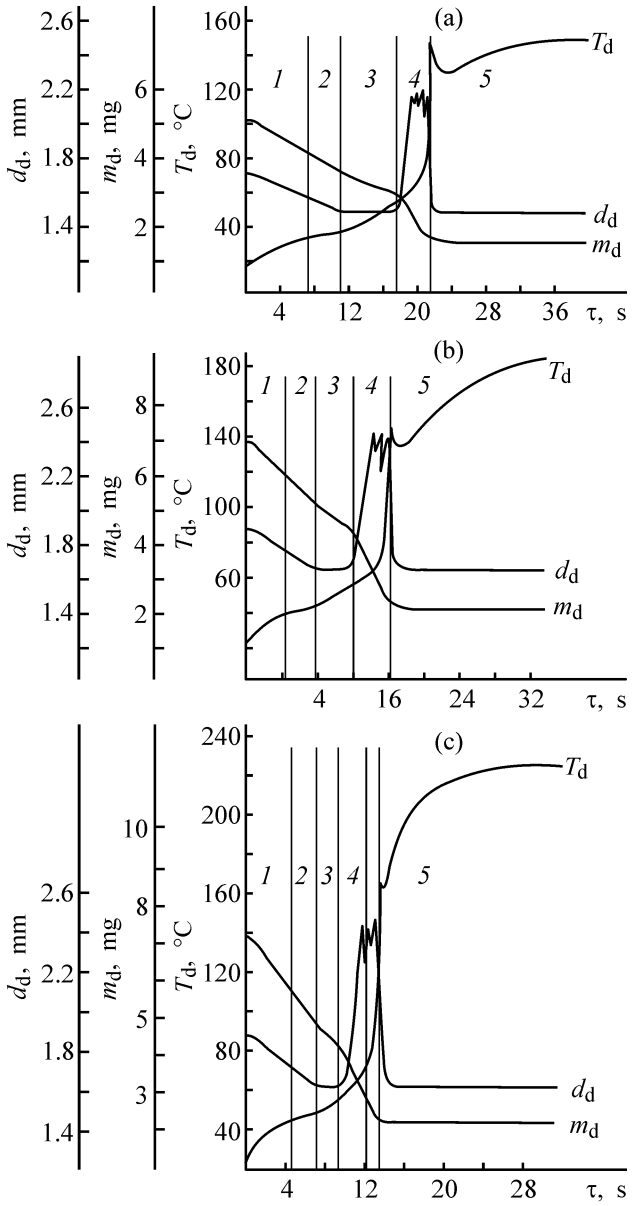


Fig. 2. Kinetic curves of synthesis of potassium superoxide for sample nos. (a) 1, (b) 2, and (c) 3. (d_d) Drop diameter, (m_d) drop mass, (T_d) drop temperature, and (τ) time. (*1*–*5*) Characteristic stages in synthesis of potassium superoxide.

The plots (Figs. 2a–2c) experimentally obtained at different temperatures and humidities of the drying agent make it possible to distinguish five characteristic stages in synthesis of potassium superoxide.

(1) The stage in which the drop is heated from the initial temperature T_0 to a temperature T_{eq}, which corresponds to the temperature of equilibrium evaporation of the solution at a given temperature and humidity of the heat-transfer agent.

(2) The stage of equilibrium evaporation, during which the moisture is intensively removed from the drop surface upon a slight increase in the temperature $T_{eq} = f(T_{DA}, \varphi_{DA}, c_s)$. The increase in the drop temperature at a fixed temperature T_{DA} and humidity φ_{DA} of the drying agent is due to a steady rise in the solution concentration c_s in the surface layer of the drop and to the resulting redistribution of heat flows in the heat exchange between the drop and the gaseous heat-transfer agent. During this period of time, the temperature of the drop at any given instant can be considered identical to the temperature of a moistened thermometer at the appropriate values of T_{DA} and φ_{DA}. The time of completion of this period is an important parameter of the kinetics of the internal processes, because it determines the instant of transition from the low-temperature stage of the process to the high-temperature stage.

(3) The stage of foam formation, which begins when the concentration of the dry substance reaches a value $c_s = 40–43\%$, and continues at a constant drop diameter. The process of moisture removal is accompanied by an inconsiderable release of oxygen in thermal decomposition of the excess amount of hydrogen peroxide. The release of oxygen leads to agitation of the substance in the drop. This gives reason to believe that the temperature and concentration gradients in the material of the drop are negligible, i.e., the assumption that the temperature $T_d(r, \tau) = T_s(\tau) = T_d(\tau)$ and concentration $c_d(r, \tau) = c_s(\tau) = c_d(\tau)$ are constant over the cross-section of the drop is not too exacting. This assumption is confirmed by the experimental curves $m_d = f(\tau)$: the rate of loss of mass by the drop changes by an exceedingly insignificant amount during the entire period. The increase in the temperature of the drop is due to a rise in the concentration of the solution (temperature depression) and to the exothermic nature of its decomposition. A hollow particle starts to be formed during this period.

(4) The stage of synthesis of KO_2 via formation of an intermediate adduct $K_2O_2 \cdot 2H_2O$. According to the dependences presented above, this period of time begins at a drop temperature $T_d = 53–57$°C.

The crystallization of $K_2O_2 \cdot 2H_2O$ from solution is accompanied by decomposition of an excess amount of hydrogen peroxide by the reaction

$$2H_2O_2 = 2H_2O + O_2. \quad (4)$$

This results in an intensive release of oxygen and an abrupt increase in the particle diameter, with an inflation coefficient $k_{in} = d_4/d_3 = 1.43–1.46$. The ab-

sence of a boiling stage characteristic of most of solutions subjected to spray drying suggests that there are no internal limitations to moisture transfer in the crystallization of the solution.

Further, $K_2O_2 \cdot 2H_2O_2$ disproportionates to give KO_2 and free water in accordance with the reaction equation (1b). In this case, a side reaction (2) of decomposition of the target product inevitably occurs and the oxygen released inflates the drop, thereby intensively agitating the reaction mass.

The completion of this period is visually determined from an abrupt contraction of the drop with a contraction coefficient $k_c = d_4/d_5 = 1.43–1.46$, to give a solid hollow particle of yellow-canary color virtually instantaneously. The completion of this period is the most clearly seen from the presence of an exothermic peak in thermograms.

(5) The stage of a decreasing rate of drying, which begins at the instant of time when the rate of moisture removal from the particle starts to be limited only by the rate of transition of water bound to the material into the free state. During this period, the intensity of dehydration noticeably falls, which can be attributed to a decrease in the amount of remaining water and its stronger binding to the material. However, the drop mass remains virtually unchanged during this period, and, therefore, this time can be excluded from consideration in calculating the reactor.

In the course of synthesis, the drop was transformed into a grain with an elastic crust. In all the experiments performed, the dried particles were hollow, with thin, nearly spherical shells.

The data obtained can be used as a basis in calculations of performance and design parameters of the process of synthesis of potassium superoxide from potassium hydroxide and hydrogen peroxide in a spray reactor.

CONCLUSIONS

(1) A study of the basic kinetic aspects of the physicochemical process of synthesis of potassium superoxide from an alkaline solution of hydrogen peroxide in a flow of a drying agent yielded thermograms, gravimetric curves, and video records and made it possible to distinguish five characteristic stages of the process.

(2) It was established that drying is the rate-determining stage in the synthesis of potassium superoxide by the method suggested.

(3) It was established experimentally that particles of the target product, formed by the technique suggested, are hollow spheres.

REFERENCES

1. Kazarnovskii, I.A., *Dokl. Akad. Nauk SSSR*, 1975, vol. 221, no. 2, pp. 353–356.
2. European Patent 0 086 138.
3. RF Patent 2 210 416.
4. Dolinskii, A.A. and Ivanitskii, G.K. *Optimizatsiya protsessov raspylitel'noi sushki* (Optimization of Spray Drying), Kiev: Naukova Dumka, 1984.
5. Gladyshev, N.F., Dvoretskii, S.I., Zhdanov, D.V. *et al.*, *Zh. Prikl. Khim.*, 2003, vol. 76, no. 11, pp. 1909–1910.

Russian Journal of Applied Chemistry, Vol. 78, No. 2, 2005, pp. 188–192. Translated from Zhurnal Prikladnoi Khimii, Vol. 78, No. 2, 2005, pp. 195–199.
Original Russian Text Copyright © 2005 by Zhilin, Ilyushin, Tselinskii, Nikitina, Kozlov, Shugalei.

INORGANIC SYNTHESIS AND INDUSTRIAL INORGANIC CHEMISTRY

Complex Energetic Perchlorates of Cobalt(III) Amminates, with Cyclopentamethylenetetrazole as Ligand

A. Yu. Zhilin, M. A. Ilyushin, I. V. Tselinskii, Yu. A. Nikitina, A. S. Kozlov, and I. V. Shugalei

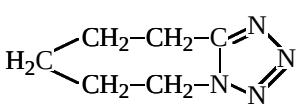
St. Petersburg State Technological Institute (Technical University), St. Petersburg, Russia

Received June 29, 2004

Abstract—Energetic metal complexes, pentammine(cyclopentamethylenetetrazole)cobalt(III) perchlorate and tetraammine-bis(cyclopentamethylenetetrazole)cobalt(III) perchlorate, were obtained by reaction of aquapentaamminecobalt(III) and diaquatetraamminecobalt(III) ions with cyclopentamethylenetetrazole. Microwave heating was used, together with the conventional convective heating, for thermal activation of the process. The thermal decomposition of the compounds synthesized was studied. The explosive characteristics and toxicity of the metal complexes were determined.

Worldwide, researchers try to find ecologically safe, low-toxic explosives (problem of development of "green" energetic materials) [1]. For example, perchlorates of Co(III) amminates with 5-substituted and 1,5-disubstituted tetrazoles are explosives, which have a short time of transition from combustion to detonation and are safer and less toxic than the standard priming explosives (mercuric fulminate, lead azide, and lead styphnate) [2, 3]. Lead is exceedingly hazardous for the environment, because it strongly enhances the toxicity of other transition metals when present together with these metals in ecosystems. Mercury is intensively transformed in the environment to give alkyl derivatives, which show a pronounced ability to be accumulated in living organisms [4]. The maximum permissible concentrations of these metals in a working zone (MPC_{wz}) are 0.01, 0.01, and 0.1 mg m^{-3} for Hg, Pb, and Co, respectively. Consequently, energy-saturated salts of cobalt are less toxic than the standard priming explosives [5]. Thus, synthesis of new compounds from the series of complex cobalt(III) perchlorates with tetrazole ligands and study of their properties are a matter of current interest.

Perchlorate penta- and tetraaminate complexes of Co(III) with cyclopentamethylenetetrazole [cyclo-$(CH_2)_5$Tetr] were synthesized:



The presence of four nitrogen atoms in the ring enhances the coordination capacity of this reagent as compared with the more extensively studied ligands, imidazoles and pyrazoles. Cyclopentamethylenetetrazole (corazol) is a medicine that has a stimulating ("wakening") action and is a human anti-anxiety agent. It is widely used as a reference in a search for, and study of, anticonvulsive and other neuro(phsycho)-tropic preparations [6].

In obtaining cobalt(III) tetrazolates, it is convenient to use water-containing cobalt(III) amminates (**I**, **II**). Water as a ligand in the system of ammonia complexes of cobalt(III) is less firmly bound to the central atom than the ammonia molecule and can be substituted with tetrazole derivatives [7].

It may be assumed that cyclopentamethylenetetrazole can substitute water in the inner sphere of complexes **I**, **II** and form compounds with a neutral ligand **III**, **IV** by the scheme below

$$[Co(NH_3)_{6-n}(H_2O)_n]^{3+}(ClO_4^-)_3 + n[\text{cyclo}(CH_2)_5\text{Tetr}]$$
$$\mathbf{I}\,(n = 1),\ \mathbf{II}\,(n = 2)$$

$$\rightarrow \{Co(NH_3)_{6-n}[\text{cyclo}(CH_2)_5\text{Tetr}]_n\}^{3+}(ClO_4^-)_3 + nH_2O.$$
$$\mathbf{III}\,(n = 1),\ \mathbf{IV}\,(n = 2)$$

The substitution reaction is commonly performed in a weakly acidic aqueous solution at 90–100°C in the course of 2–3 h [6]. Accordingly, the reactions of compounds **I** and **II** with cyclopentamethylenetetrazole were first performed at ~100°C (on a boiling water bath) in a 5% aqueous solution of hydrochloric acid in the course of 3 h. Already in 2 h,

1070-4272/05/7802-0188 © 2005 Pleiades Publishing, Inc.

the starting diaqua complexes are completely consumed and the expected products **III**, **IV** are contained in the reaction mass, and in the case of the tetraaminate complex, also compound **V**, which is a product of substitution of a water molecule in the inner sphere of the initial diaqua complex and has a structure $\{Co(NH_3)_4(H_2O)[cyclo(CH_2)_5Tetr]\}(ClO_4)_3$. In this way, pentammine(cyclopentamethylenetetrazole)cobalt(III) perchlorate and tetraammine-bis(cyclopentamethylenetetrazole)cobalt(III) perchlorate were obtained and also tetraammine(aqua)(cyclopentamethylenetetrazole)cobalt(III) perchlorate was isolated. It was established that the process first yields compound **V**, and only after its certain concentration in the reaction mass is reached, compound **VI** starts to be formed, i.e., the complexation is steplike in the given case.

Microwave heating accelerates the anionization reaction in ammine complexes of Co(III) [8]. For example, the same compounds were found in the case of tetraamminates after microwave heating for 1 h. However, their relative amounts substantially changed toward a higher content of compound **IV**. The yield of compound **IV** increased by 15% as compared with the conditions of conventional heating, which can only be in part accounted for by a difference in the temperature modes: in the case of the microwave heating, the reaction occurred with intensive boiling of the reaction mass (~102°C), whereas the conventional heating was on a boiling water bath. Thus, the microwave heating of the reactants raises the yield of compound **IV**, with the time of the complexation reaction considerably decreasing.

IR spectra of the compounds synthesized contain absorption bands of all the fragments: coordinated molecules of water and ammonia, pentamethylene and tetrazole rings, and perchlorate anions.

The electronic spectra of complexes **III** and **IV** in an aqueous solution are typical of the given class of compounds and are associated with the *d–d* transition ($^1T_{1g} \leftarrow {}^1A_{1g}$) at 462 nm with $\varepsilon = 42$ l cm^{-1} mol^{-1} and 456 nm with $\varepsilon = 71$ l cm^{-1} mol^{-1}, respectively. Another strong absorption band ($^1T_{2g} \leftarrow {}^1A_{1g}$) lies at 332 nm with $\varepsilon = 45$ l cm^{-1} mol^{-1} for compound **III** and 331 nm with $\varepsilon = 75$ l cm^{-1} mol^{-1} for compound **IV**. Apparently, the complexes obtained contain an octahedral chromophore CoN_6.

Cyclopentamethylenetetrazole occupies in the spectrochemical series of ligands the place between water and ammonia [10], which is confirmed in the case of the compounds synthesized by a calculation of the constant Δ of splitting of the d orbitals of the central atom under the action of the crystal field of the ligands: 21 930 cm^{-1} for compound **III** and 21 650 cm^{-1} for compound **IV**. These values do not exceed Δ of ammonium (22 886 cm^{-1}) for Co(III) hexaaminates [11].

The ^{1}H NMR spectra of complexes **III**–**V** show peaks at 3.4–4.4 ppm, which correspond to equatorial (in a weak field) and axial (in a strong field) molecules of ammonia. The difference in the positions of the peaks in these spectra is in an agreement with the fact of coordination of the heterocyclic ligands via a nitrogen atom [2], and their splitting in two in the case of compound **IV** points to nonequivalence of the related ammonia protons. This splitting is probably due to coordination of organic ligands to the metal ion by different N atoms of tetrazole rings. Previously, coordination of cyclopentamethylenetetrazole by N^3 or N^4 nitrogen atoms of the heteroring has been observed [13]. In all probability, bonding isomers are formed in this case, in agreement with [14], where the simultaneous N^3/N^4 coordination was confirmed by means of X-ray diffraction analysis for tetrammine-bis(1-methyl5-aminotetrazole)cobalt(III).

A study of the thermal decomposition of the products in nonisothermal conditions at a heating rate of 5 °C min^{-1} demonstrated that the cobalt(III) tetrazolate amminates synthesized are rather thermally stable, because the onset temperature of their intensive decomposition exceeds 230°C (Table 1).

In the first stage of decomposition of compound **III**, a broadened endothermic peak is observed at 95–245°C, with 14.7 wt % of a sample decomposing. Presumably, this stage involves elimination of four ammonia molecules from the inner sphere of the complex. Further, the sample starts to melt and at 245°C to thermally decompose, with a pronounced exothermic effect (250–350°C) and 71 wt % of the sample lost. It may be assumed that these are stages of melting and decomposition of the pentamethylenetetrazole ligand via rearrangement of the inner sphere of the complex and oxidation of the complex by outer-sphere anions. As a result of processes of additional oxidation, formation of cobalt oxide Co_2O_3, which is commonly produced in decomposition of cobalt(III) complexes in air [15], and its decomposition (14.1 wt % of the sample) are probable.

It was established in a study of the thermal decomposition that compound **IV** is less thermally stable than the compound containing a single tetrazole ligand. The onset temperature of its intensive decomposition is 235°C. A study of the decomposition of this complex demonstrated that molecules of coordi-

Table 1. Results of a derivatographic analysis of the complexes synthesized

Compound	Products of thermal decomposition	Temperature range °C	Residue		Peak temperature of an effect °C	Temperature range of an effect °C	Total content, %
			found	calculated			
III	$[Co(C_6H_{10}N_4)(NH_3)_5](ClO_4)_3$						100
		60–245			243	95–245	
	$Co(C_6H_{10}N_4)(ClO_4)_3$		85.0	85.3			
		245–360			275	250–280	
					295	280–300	
					320	300–350	
	$1/2Co_2O_3$	360–500	14.0	14.3			
IV	$[Co(C_6H_{10}N_4)_2(NH_3)_4](ClO_4)_3$						100
		60–235			233	95–235	
	$Co(C_6H_{10}N_4)_2(ClO_4)_3$		90.0	90.3			
		235–340			275	245–280	
					290	280–335	
	$Co(C_6H_{10}N_4)(ClO_4)$		42.0	42.3			
		340–365			345	342–360	
	$1/2Co_2O_3$	365–500	12.0	11.8			
V	$[Co(C_6H_{10}N_4)(H_2O)(NH_3)_4](ClO_4)_3$						100
		60–195			170	60–190	
	$Co(C_6H_{10}N_4)(ClO_4)_3$		85.0	85.2			
		195–425			310	220–380	
	$1/2Co_2O_3$	425–500	14.5	14.3			

nated ammonia are removed in the temperature range 95–235°C, with the loss of mass by a sample constituting 9.7 wt %. The strong overall exothermic effect (245–335°C) in the derivatogram of compound **IV** corresponds to decomposition of its organic constituent via oxidation by outer-sphere perchlorate anions, accompanied by a considerable loss of mass (48%).

This decomposition gradually gives way to the last exothermic effect, with the remaining organic part of a sample under study decomposing (30.5 wt %).

A study of the decomposition of complex **V** demonstrated that coordinated molecules of water and ammonia are removed in the first stage (60–195°C), with the loss of mass by a sample equal to 14.8%. To oxidation of the pentamethylenetetrazole ligand by perchlorate anions from the outer sphere, which occurs as a result of destruction of the inner sphere of the complex, and to their joint decomposition corresponds a strong exothermic effect (220–380°C) accompanied by a considerable loss of mass (71%). Presumably, Co_2O_3 is formed and decomposes in the final stage of decomposition of compounds **IV** and **V**.

The results obtained in examining compounds **III**, **IV**, **V** by thermogravimetric (TG) and differential-thermal (DTA) analyses are listed in Table 1.

The T–TG, T–DTG, and T–DTA curves were used to calculate the kinetic parameters of thermal decomposition for the compounds synthesized. Below are given for compounds **III**–**V** the onset temperature of intensive decomposition (°C), logarithm of the preexponential factor in the Arrhenius equation, activation energy of the process (kJ mol^{-1}), and the reaction order, all corresponding to the onset temperature of intensive decomposition: **III** 245, 8.6, 116, 1.0; **IV** 235, 9.3, 123, 1.0: **V** 220, 8.4, 114, 1.0. The reaction order equal to unity indicates that the decomposition does not involve diffusion.

Thus, the analysis of the thermal decomposition demonstrated that the complexes synthesized in this study decompose under nonisothermal conditions in several stages. In the first stage, there occurs deaquation and ammonia molecules are removed from the inner sphere of the complex, which leads to its destruction. Then, the tetrazole ligands undergo a steplike thermal decomposition, with the perchlorate ion involved in their oxidation in later stages of decomposition of the complex.

The aim of further studies was to reveal the explosive properties of the compounds obtained. The density and rate of detonation were calculated using the Kotomin method [16]. The impact sensitivity was determined in accordance with GOST (State Standard) 4545–88 (load mass 2 kg, H = 25 cm). The standard high explosive TEN has an impact sensitivity of 12%. The priming capacity of the metal complexes was

Table 2. Explosive properties of the complexes

Compound	Complex	Density ρ, g cm^{-1}	Oxygen factor α	Impact sensitivity measured on a K 44-II impact-testing machine	Minimum charge in terms of hexogen KD no. 8, g	Velocity of detonation, *D*, at ρ, km s^{-1}
III	$[Co(NH_3)_5(CH_2)_5–CN_4](ClO_4)_3$	1.82	0.55	16	0.4	6.98
IV	$[Co(NH_3)_4((CH_2)_5–CN_4)_2](ClO_4)_3$	1.80	0.34	16	>0.5	6.7

evaluated by their minimum charge in terms of hexogen [17]. The explosive properties of the compounds synthesized are illustrated by Table 2. Complex **III** is a priming explosive with a calculated velocity of detonation comparable with that of TNT and sensitivity to mechanical impact close to that of modern powerful high explosives.

The toxicity of corazol and complex **III** was experimentally determined on laboratory animals.[1] The experiments were performed with outbred males of white mice, with a mass of 26–30 g. It was established that the average lethal dose of corazol is, in the case of enteral introduction, ~70 mg kg^{-1} (0.0006 mol kg^{-1}) body mass. Complex **III** caused 50% loss of animals at a dose of ~300 mg kg^{-1} (0.0006 mol kg^{-1}), which indicates that the toxicities of these compounds are close and complex **III** can be tentatively placed in the third hazard class. Also, a tentative conclusion can be made that the coordination of corazol in an ammonia complex of Co(III) does not increase its toxicity as compared with the free ligand.

The average lethal dose of complex **III** in terms of pure metal is 35 mg kg^{-1}. Soluble salts of cobalt(II) and, in particular, cobalt(II) nitrate have LD_{50} of ~160 mg kg^{-1}, which equals 40 mg kg^{-1} in terms of pure metal [4]. Thus, the toxic effect of Co(III) is not enhanced by the complexation.

Consequently, the ammonia complex **III** is less toxic than the most widely occurring high explosive TNT, which belongs to the second hazard class [18, 19].

EXPERIMENTAL

The IR spectra were recorded on a Specord M-80 spectrophotometer in thin layer. The ^{1}H NMR spectra were obtained on a Bruker AC radiospectrometer with a working frequency of 300 MHz, with HMDS as internal reference. The UV spectra were recorded with a Perkin-Elmer LAMBDA 40 spectrometer in quartz cuvettes (l = 1 cm). The reaction course was monitored by means of thin-film chromatography on Silufol UV-254 plates, with a 3% aqueous solution of $NaClO_4$ as eluent.

As the device for microwave heating served a short-circuited 9 × 4.5-cm waveguide connected to a microwave generator (output power 600 W, working frequency 2450 MHz). The reaction vessel, a glass tube 35 mm in diameter (equipped with a thermometer and a reflux condenser), was introduced into the waveguide via a special opening.

The thermographic studies were carried out on a measuring and recording device (Derivatograph system: F. Paulik, J. Paulik, L. Erdey) at a heating rate of 5 °C min^{-1}.

Aquapentaamminecobalt(III) perchlorate **I** and tetrammine-bis(cyclopentamethylenetetrazole)cobalt(III) perchlorate **II** obtained by means of procedures described in [16] were used in further synthesis without their isolation from solution.

Pentaammine(cyclopentamethylenetetrazole)cobalt(III) perchlorate III and tetrammine-bis(cyclopentamethylenetetrazole)cobalt(III) perchlorate IV were obtained under the conditions described in [7] in 71 and 59% yield, respectively. Compound **III**: IR spectrum, ν, cm^{-1}, 1576 med, 1260 med (NH_3, Tetr), 1080 med (ClO_4), 1928 med, 1472 med (CH_2). ^{1}H NMR spectrum (DMSO–d_6), δ, ppm: 4.70 [CH_2 (N^1)]; 3.21 [CH_2 (C^5)]; 1.95, 1.82, 1.71 (CH_2–CH_2–CH_2); 3.75, 3.60 (15H, NH_3).

Found, %: C 12.3; H 4.4; N 21.4.
$C_6H_{25}Cl_3CoN_9O_{12}$.
Calculated, %: C 12.4; H 4.3; N 21.7.

Compound **IV**: IR spectrum, ν, cm^{-1}, 1560 med, 1264 med (NH_3, Tetr), 1072 med (ClO_4), 1948 med, 1480 med (CH_2). ^{1}H NMR spectrum (DMSO–d_6), δ,

[1] The tests were carried out under supervision of professor I.P. Lapin at the laboratory of psychopharmacology, Bekhterev Research Institute of Psychoneurology, St. Petersburg.

ppm: 4.71 [CH_2 (N^1)]; 3.20 [CH_2 (C^5)]; 1.92, 1.80, 1.69 (CH_2–CH_2–CH_2); 4.38, 4.18 (6H, NH_3 equat.); 4.32, 3.92 (6H, NH_3 ax.).

Found, %: C 20.3; H 5.1; N 23.6.

$C_{12}H_{32}Cl_3CoN_{12}O_{12}$.

Calculated, %: C 20.5; H 4.6; N 23.9.

Aquatetraammine(cyclopentamethylenetetrazole)cobalt(III) V. After isolation of complex **IV**, the mother liquor was evaporated to half-volume and the crystalline precipitate formed upon cooling was filtered off to give compound **V** in a 38% yield. IR spectrum, ν, cm^{-1}, 3312 med, 3152 med (H_2O), 1628 med, 1340 med (NH_3, Tetr), 1096 w (ClO_4), 1936 med, 1474 med (CH_2). ^1H NMR spectrum (DMSO–d_6), δ, ppm: 4.69 [CH_2 (N^1)]; 3.18 [CH_2 (C^5)]; 1.84, 1.80, 1.76 (CH_2–CH_2–CH_2); 3.95, 3.41 (12H, NH_3).

Found, %: C 12.8; H 4.6; N 19.5.

$C_6H_{24}Cl_3CoN_8O_{13}$.

Calculated, %: C 12.4; H 4.2; N 19.3.

CONCLUSIONS

(1) Two energetic coordination compounds, pentammine(cyclopentamethylenetetrazole)cobalt(III) perchlorate and tetraammine-bis(cyclopentamethylenetetrazole)cobalt(III) perchlorate, were synthesized by reaction of aquapentaamminecobalt(III) perchlorate **I** and diaquatetraamminecobalt(III) perchlorate **II** and studied.

(2) It was shown that, as judged from the whole set of its properties, compound **III** is a promising low-toxic priming explosive ("green" energetic material).

ACKNOWLEDGMENTS

The study was financially supported by the Ministry of Education of the Russian Federation, Intercollegiate program "Priority Areas of Development of Science and Technology."

REFERENCES

1. Zhoui, S., Liu, J., and Xie, G., *Theory and Practice of Energetic Materials*, Huang, P., Li, S., and Wang, Y., Eds., New York: Sci. Press, 2003, vol. 5, part A, pp. 183–185.
2. Danilov, Yu.N., Ilyushin, M.A., and Tselinskii, I.V., *Promyshlennye vzryvchatye veshchestva. Chast' 1. Initsiiruyushchie vzryvchatye veshchestva. Tekst lektsii* (Industrial Explosives, part 1, Priming Explosives: Course of Lectures), St. Petersburg: IK Sintez, 2004.
3. Ilyushin, M.A., Tselinsky, I.V., Zhilin, A.Yu., *et. al.*, *Hunneng Cailiao-Energ. Mater.*, 2004, vol. 12, no. 1, pp. 15–19.
4. Grushko, Ya.M., *Vrednye neorganicheskie soedineniya v promyshlennykh stochnykh vodakh* (Noxious Inorganic Substances in Industrial Wastewater), Moscow: Khimiya, 1989.
5. Bespamyatnov, G.P. and Krotov, Yu.A., *Predel'no-dopustimye kontsentratsii khimicheskikh veshchestv v okruzhayushchei srede* (Maximum Permissible Concentrations of Chemical Substances in the Environment), Leningrad: Khimiya. 1985.
6. Soldatenkov, A.T., Kolyadina, N.M., and Shendrik, I.V., *Osnovy organicheskoi khimii lekarstvennykh veshchestv* (Fundamentals of the Organic Chemistry of Pharmaceutical Substances), Moscow: Khimiya, 2001.
7. Zhilin, A.Yu., Ilyushin, M.A., and Tselinskii, I.V., *Zh. Obshch. Khim.*, 2001, vol. 71, no. 5, pp. 710–713.
8. Zhilin, A.Yu., Ilyushin, M.A., Tselinskii, I.V., and Brykov, A.S., *Zh. Prikl. Khim.*, 2001, vol. 74, no. 1, pp. 96–99.
9. Fronabarger, J., Schuman, A., Chapman, R.D., *et al.*, *Am. Inst. Aeronautics Astronautics Pap.*, 1995, no. 2858, pp. 1–7.
10. Moore, D.S. and Robinson, S.D., *Adv. Inorg. Chem.*, 1988, vol. 32, pp. 171–239.
11. Bramley, R., Brorson, M., Sargeson, A.M., and Schaffer, C.E., *J. Am. Chem. Soc.*, 1985, vol. 107, no. 9, pp. 2780–2787.
12. Sheng, D., Ma, F., Sun, F., and Lu, Q., *Hanneng Cailiao-Energ. Mater.*, 2000, vol. 8, no. 3, pp. 100–103.
13. Moore, D.S. and Robinson, S.D., *Adv. Inorg. Chem.*, 1988, vol. 32, pp. 171–239.
14. Zhilin, A.Yu., Ilyushin, M.A., Tselinskii, I.V., *et al.*, *Zh. Prikl. Khim.*, 2002, vol. 75, no. 11, pp. 1885–1888.
15. *Comprehensive Chemical Kinetics*, Bamford, C.H. and Tipper, C.F.H., Eds., vol. 22, *Reactions in the Solid State*, Brown, M.E., Dollimore, D., and Galwey, A.K., Eds., Amsterdam: Elsevier, 1980.
16. Ilyushin, M.A., Kotomin, A.A., Dushenok, S.A., *et al.*, *Sbornik nauchnykh trudov NPO im. S.A. Lavochkina* (Coll. Sci. Works, Lavochkin Research-and-Production Association), 2002, no. 4, pp. 87–96.
17. Avanesov, D.S., *Praktikum po fiziko-khimicheskim ispytaniyam vzryvchatykh veshchestv* (Manual of Physicochemical Tests of Explosives), Moscow: GIOP, 1959.
18. Novakovskii, M.S., *Laboratornye raboty po khimii kompleksnykh soedinenii* (Laboratory Practical Work on Chemistry of Complex Compounds), Kharkov: Kharkov Gos. Univ., 1972.
19. Generalov, M.B., *Osnovnye protsessy i apparaty tekhnologii promyshlennykh vzryvchatykh veshchestv* (Basic Processes and Apparatus in Technology of Industrial Explosives), Moscow: Akademkniga, 2004, p. 381.

Russian Journal of Applied Chemistry, Vol. 78, No. 2, 2005, pp. 193–196. Translated from Zhurnal Prikladnoi Khimii, Vol. 78, No. 2, 2005, pp. 200–203.
Original Russian Text Copyright © 2005 by Prusov, Makarov.

INORGANIC SYNTHESIS AND INDUSTRIAL INORGANIC CHEMISTRY

Some Properties of Chemically Deposited Ni–B Coatings

Yu. V. Prusov and V. F. Makarov

Nizhni Novgorod State Technical University, Nizhni Novgorod, Russia

Received June 3, 2004

Abstract—The influence exerted by impurities present in dimethylaminoborane and in solutions used for deposition of nickel–boron coatings on their properties was studied.

Nickel–boron alloy coatings exhibit increased microhardness and wear resistance, low contact resistance and resistivity, good solderability and microweldability, and satisfactory corrosion resistance. All these factors make these coatings competitors of gold and silver coatings for elements of microelectronic devices. Such deposits can be obtained chemically [1] or electrochemically [2] from aqueous solutions, with boron-containing substances as solutes.

Different fields of technology impose different requirements upon coatings. These requirements can be satisfied by depositing alloys with varied (8 to 0.1 wt %) content of boron. The alloy composition can be varied by changing the solution composition and deposition conditions. This requires that the mechanism of the process, which may depend on the composition of a boron-containing reducing agent [3] and on deposition conditions [4], should be known.

The aim of this study was to examine how the composition and some properties of Ni–B films depend on the composition of a reducing agent and deposition conditions. The Ni–B coatings were chemically deposited at 70°C in the course of 1 h onto pretreated steel, palladium, or nichrome samples from a weakly acidic solution of the following initial composition (g l^{-1}): $(NH_4)_2SO_4$ 60, sodium lauryl sulfate 0.03, $NaNO_2$ 0.003, NH_4OH 6.5, $NiSO_4 \cdot 7H_2O$ 30; pH 7.1. Dimethylaminoborane (DMAB) from different batches of the product was used as a reducing agent.[1] The coating deposition rate was calculated from the mass gain by a sample. The adhesion was measured from the loss of mass by a sample after making on its surface a grid of scratches with a step of 1 mm on an area of 1 cm^2. An exfoliated coating was removed with a brush, with the loss of mass recorded. The microhardness was measured using a PMT-3 device with an indenter load of 50 g. The solderability of the coatings was evaluated by the spreading coefficient of the POS-60 solder (with an FKDT flux) in conformity with GOST (State Standard) 9.302–79. The resistivity and contact resistance were measured using standard techniques described in [5].

Anodic polarization curves were obtained with a P-5848 potentiostat on the edge of a palladium rod embedded in fluorioplastic by compression. The amount of boron on the surface of the palladium sample was found from the quantity of electricity consumed for its oxidation, calculated on the assumption of three electrons per atom.

It is known that boron forms a series of hydrides, the simplest of which, monoborane BH_3, is unstable because of having an unsaturated coordination and actively tends to form coordination compounds with various radicals or species: amines, hydrazine, etc. Depending on the structure and composition, the forming compound will be more or less stable. The "longer" and more branched the chain of the molecule of an amine radical, the stronger the bonding between nitrogen and boron (N–B) and the weaker that between hydrogen and boron. This reflects, in particular, upon the susceptibility of boranes to hydrolysis, e.g.:

$$(CH_3)_2HN(BH_3) + 3H_2O = (CH_3)_2HN + H_3BO_3 + 3H_2. \quad (1)$$

In actual practice, DMAB, having the optimal relative strength of the N–B and B–H bonds, is frequently used as a reducing agent. This makes it sufficiently

[1] Commercially manufactured (in batches of several tons each) by Aviabor Joint-Stock Company (Dzerzhinsk, Nizhni Novgorod oblast).

1070-4272/05/7802-0193 © 2005 Pleiades Publishing, Inc.

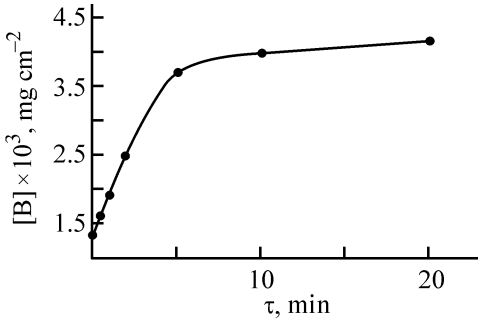


Fig. 1. Amount of boron, [B], formed on palladium vs. time τ of treatment in a solution. Solution composition (g l^{-1}): DMAB 3, $CH_3COONa \cdot 3H_2O$ 10, $Na_3C_6H_5O \cdot 5.5H_2O$ 10; pH 6, T = 70°C.

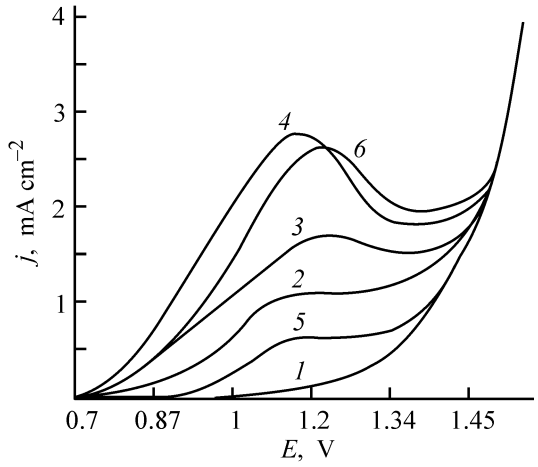


Fig. 2. Anodic polarization curves obtained on palladium treated in a DMAB-containing solution. (*j*) Current density and (*E*) potential. Treatment time (min): (*1*) 0, (*2*) 1, (*3*) 2, (*4–6*) 10. Keeping in air for (*1–4*) 10 min at 20°C, (*5*) 1 h at 150°C, and (*6*) 10 h at 20°C.

stable (in particular, against hydrolysis) and a rather strong reducing agent.

The deposition mechanism of the Ni–B alloy can be represented by the following scheme. The first stage of decomposition of the reducing agent is its dissociative adsorption onto the surface of a metal (Ni or Fe), with rupture of the H–B bond in the reducing agent:

$$(CH_3)_2HN(BH_3) + M = (CH_3)_2HN + M(BH_3)_{ads}. \quad (2)$$

The forming radical of borane BH_3 decomposes to give boron, firmly bound to the metal (by the coordination bond involving vacant *d*-orbitals of the metal) and hydrogen:

$$2M(BH_3)_{ads} = 2MB + 3H_2. \quad (3)$$

Surface layers of the metal are saturated with boron in the course of time, depending on the DMAB concentration in solution (Fig. 1). This process is accompanied by a competing reaction of hydrolysis of monoborane

$$M(BH_3)_{ads} + 3H_2O = M + H_3BO_3 + 3H_2. \quad (4)$$

After the surface layer of the metal is saturated with boron, B(M), other processes become possible, e.g., chemical or electrochemical oxidation of boron (Fig. 2) by the reaction

$$B(M) + 3H_2O = H_2BO_3^-(M) + 4H^+ + 3e, \quad (5)$$

whose equilibrium potential is described by the expression $E = -0.687 - 0.0788pH + 0.0197\log[H_2BO_3^-]$, or diffusion of boron deeper into the metal. The role of acceptors of electrons formed in oxidation of the surface boron by reaction (5) can be played by ions of hydrogen or metal, or other ions present in solution:

$$2H^+ + 2e = H_2, \quad (6)$$

$$M^{2+} + 2e = M. \quad (7)$$

Boron diffusing deeper into the metal enters into the composition of the alloy being deposited. The content of boron in the alloy is determined by the relative rates of reduction of metal ions and of the diffusion of boron into the alloy. In this way, a two-component alloy is formed. The electrons generated in reaction (5) can be consumed for reduction of ions of any metals present in solution, to give multicomponent alloys.

It is shown that elements belonging to Groups I, II, and III of the periodic system are codeposited in rather small amounts because of their strongly negative potential. The same is observed for elements that belong to the succeeding groups because of their increasing nonmetal properties (gallium, indium, thallium, tin, antimony, bismuth, selenium, and tellurium). The content of a third component can be raised by carrying out the process at a higher temperature, lowering the solution pH, and varying the composition of the buffer–complex–forming system. Commonly, the growth rate of a coating markedly decreases in the case of codeposition of these elements. For example, the deposition rate of nickel–iron–boron coatings decreases as the concentration of iron sulfate in solution increases, because Fe^{2+} ions affect the process of alloy formation as inhibitors of the reaction of reduction. This is due to the fact that iron has a much lower capacity for formation of coordination compounds

$M(BH_3)_{ads}$ than nickel. The content of iron in the alloy may be as high as 20 wt % at a deposition rate of up to 6 μm h^{-1}. In other cases, the deposition rate changes more significantly in obtaining alloys. This is due to the fact that poison-metals (bismuth, cadmium, tin, etc.) codeposited onto the surface of active nickel have high exchange currents and, therefore, being preferentially deposited (compared with nickel), enforce their potential to the surface, thereby shifting its potential in the negative or positive direction. The renewed surface is predominantly composed of the impurity metal, which has a low affinity for boron and does not form with it any coordination compound. As a result, the rate of reaction (5) occasionally decreases to zero. Nickel present in solution has a low exchange current and cannot compete with impurity metals in deposition onto the surface. This scheme is indirectly confirmed by a decrease in the boron content of the alloy [6].

Tin, arsenic, thallium, and other elements are frequently not revealed by X-ray diffraction analysis in three-component coatings containing these metals, despite their high content. Consequently, these elements form X-ray-amorphous solid solutions in the alloys.

Nonmetal elements can be incorporated into an alloy by another mechanism. If a catalytically active component (e.g., phosphorus in the form of a hypophosphite) is introduced into the solution, the deposition rate not only does not decrease, but may even increase [8]. These observations served as a basis for the method, developed by the authors, for deposition of a nickel–boron–phosphorus alloy with a high metallization rate. The deposit obtained has a low resistivity, high solderability (preserved in the course of time), and corrosion resistance.

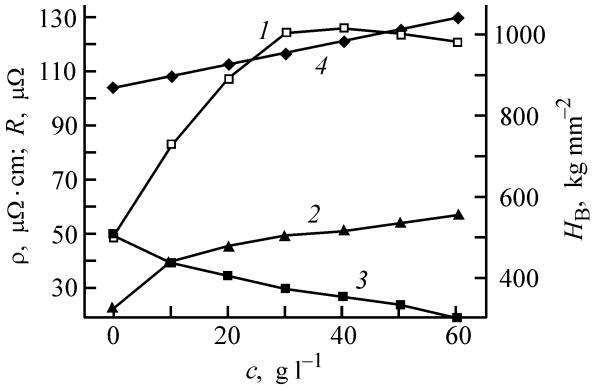


Fig. 3. (*1*) Resistivity ρ, (*2*) contact resistance *R*, and (*3*, *4*) microhardness H_B of coatings vs. caprolactam concentration *c*. (*3*) Without thermal treatment and (*4*) with thermal treatment at 350°C for 1 h.

Introduction of caprolactam into a solution for electroless nickel plating results in that the whole molecules of this compound or their fragments are incorporated into the resulting coatings. Deposits of this kind may contain up to 1.35 wt % carbon and 0.5 wt % hydrogen. The amount of nitrogen in the coating is small, which may indicate that the nitrogen-containing group is eliminated in adsorption and overgrowth of caprolactam with nickel. This leads to a significant decrease in the internal stresses and grain size, which is accompanied by an increase in the contact resistance and chemical activity (Fig. 3). Coatings

Effect of impurities in DMAB on coating properties*

Sample no.**	*v*, μm h^{-1}	Adhesion %	Solderability, K_{spr}	H_B, kg mm^{-2}	ρ, Ω mm^{-2} m^{-1}	Total content of impurities, %
1	7.5	0.9	0.71	303	0.41	0.65
2	6.4	2.4	0.86	315	0.4469	0.67
3	5.9	1.7	0.81	285	0.4864	0.69
4	6.8	4.1	0.84	280	0.3787	0.79
5	8.4	4.8	1.06	376	0.4505	0.79
6	7.1	3.2	0.76	337	0.4717	0.83
7	7.4	2.1	0.81	304	0.511	0.84
8	7.1	3.2	0.62	312	0.429	0.86
9	7.2	1.4	0.85	311	0.509	0.92
10	7.0	2.7	0.69	313	0.442	1.15
11	6.2	1.6	0.78	322	0.595	1.41
12	6.3	1.4	0.86	303	0.423	1.58
13	6.6	1.6	0.73	279	0.4	1.64
14	5.9	2.7	0.78	293	0.293	1.8
15	7.5	1.1	0.75	321	0.497	–

* *v*, coating deposition rate; H_B, microhardness; and ρ, resistivity.

** Type of DMAB: (nos. 1–10, recrystallized and purified; nos. 11–14, containing various products used in its manufacture; no. 5, reference manufactured by BAKER (Austria).

of this kind can be deposited onto aluminum without its special pretreatment, with a high adhesion.

It may be assumed that the properties of a nickel–boron coating can also be strongly affected by the composition of DMAB. Synthesis of the dimethylaminoborane complex from diborane and dimethylamine in a diethyl ether or other media yields as the final product a mixture of DMAB with mono- and trimethylaminoborane and other boron-containing compounds, which are rather difficult to separate because they are determined and calculated as DMAB in an analysis for boron. Even the amount of determinable impurities in commercial batches may be as high as 0.65 to 1.8 wt % (see table).

As it can be seen from the table, no influence of the impurities on the characteristics under study is revealed. All these characteristics are in the same ranges for DMAB manufactured by BAKER Co. and domestic samples. Consequently, further deep purification of commercial DMAB is inexpedient.

CONCLUSION

It was shown that nickel–boron coatings deposited from solutions whose composition includes dimethylaminoborane may contain carbon, nitrogen, hydrogen, sulfur, phosphorus, cadmium, and other alloying components, which can modify the functional properties of the coatings. Coatings composed of such alloys have properties valuable for microelectronics.

REFERENCES

1. Sviridov, V.A., Vorob'eva, T.N., Gaevskaya, T.V., and Stepanova, L.I., *Khimicheskoe osazhdenie metallov iz vodnykh rastvorov* (Chemical Deposition of Metals from Aqueous Solutions), Minsk: Universitetskoe, 1987.
2. Gaevskaya, T.V., Novotvortsev, I.G., and Tsybul'skaya, L.S., *Zh. Prikl. Khim.*, 1995, vol. 68, no. 4, pp. 587–592.
3. Matsuoka, M. and Hayashi, J. *Metal Finish. Soc. Japan*, 1978, vol. 46, no. 1, pp. 25–30.
4. Ivanov, M.I. and Gorbunova, K.M., *Sovremennye metody naneseniya gal'vanicheskikh i khimicheskikh pokrytii: Materialy seminara* (Modern Techniques for Deposition of Galvanic and Chemical Coatings: Proc. Symp.), Moscow, 1979, pp. 147–150.
5. Vyacheslavov, P.M. and Shmeleva, N.M., *Metody ispytanii elektroliticheskikh pokrytii* (Methods for Testing of Electroplated Coatings), Leningrad: Mashinostroenie, 1977.
6. Kostyanovskii, M.A., Prusov, Yu.V., Makarov, V.F., and Flerov, V.N., *Zh. Prikl. Khim.*, 1990, vol. 63, no. 6, pp. 1412–1414.

Russian Journal of Applied Chemistry, Vol. 78, No. 2, 2005, pp. 197–199. Translated from Zhurnal Prikladnoi Khimii, Vol. 78, No. 2, 2005, pp. 204–206.
Original Russian Text Copyright © 2005 by Ogenko, Dubrovina, Volkov.

INORGANIC SYNTHESIS AND INDUSTRIAL INORGANIC CHEMISTRY

Synthesis and Structure of Composites of Nanosize Silica Particles Modified with Glass Microspheres

V. M. Ogenko, L. V. Dubrovina, and S. V. Volkov

Vernadskii Institute of General and Inorganic Chemistry, National Academy of Sciences, Ukraine, Kiev

Received May 27, 2004

Abstract—A method for production of porous composites from pyrogenic silicas, whose surface is preliminarily modified with methyl and trimethyl siloxane groups, was developed. In order to diminish shrinkage, glass microspheres and organosilicon compounds were used as modifiers. The total porosity of the composites obtained was 0.28–0.55.

Porous materials are widely used as sorbents, catalyst supports, and membranes. The effectiveness of their various applications is mainly determined by the capacity and rate of sorption, which largely depend on the porous structure of a material. However, materials based on inorganic compounds do not have a rational porous structure, and, consequently, synthesis of complex composite structures with improved functional parameters is a matter of current interest [1–4].

Silica gel is a porous material of particular importance. The scale of its use exceeds that of any other oxide adsorbent and the fundamental aspects of formation of its porous structure have been studied in sufficient detail. Commonly, silica gels are obtained from silicates of alkaline metals by precipitation with an acid. Use of sols of silicic acid makes it possible to control the structure of the resulting silica gel, whose porosity depends on the size distribution of colloid particles [1–4]. Xerogels of varied porosity are also obtained by the sol-gel technique from silicon alcoxides. Monolithic samples of xerogels produced by any synthesis method undergo shrinkage and cracking in drying. This disadvantage can be eliminated by varying the composition of the dispersion medium, making longer the duration of drying, or using special additives [1–9].

The aim of this study was to obtain composites with an openwork structure constituted by silica nanoparticles and glass microspheres and to study the properties of these composites.

As structure-forming elements of the composites served pyrogenic silicon dioxides (aerosils) composed of 5–50-nm spherical particles of nonporous amorphous SiO_2. These primary particles form sufficiently stable 100–500-nm aggregates. These aggregates mostly disintegrate upon a short-time ultrasonic or mechanical treatment of suspensions [10]. When mixed with appropriate liquids, aerosils form gels, which are transformed into xerogels upon drying. This makes it possible to obtain nanostructure composites of varied porosity.

EXPERIMENTAL

As starting silica particles were taken pyrogenic silicon dioxides: hydrophobic aerosils (AD, with a surface modified with methyl groups, S_{sp} = 175 $m^2 g^{-1}$, and AO, with a surface modified with trimethylsiloxane groups, S_{sp} = 195 $m^2 g^{-1}$).

As the dispersion media served water, ethanol, and hexane. The composition of xerogels was modified with tetraethoxysilane (TES), whose hydrolysis gives silicon dioxide:

$$(C_2H_5O)_4Si + 2H_2O \rightarrow 4C_2H_5OH + SiO_2\downarrow.$$

Polydimethylsiloxane (PMS) and SIEL silicon rubber were also used for this purpose. SF glass microspheres, d = 10–40 μm (ρ = 30 kg m^{-3}), washed in hexane served as a filler.

In order to obtain xerogels, to the aerosil were added the dispersion medium (until fluidity appeared), modifying agents, and glass spheres, and the mixture was stirred. The gels formed were placed in Petri dishes and dried in air, first at room temperature (20 ± 2°C) and then at 160°C. Electron micrographs of composites dried on silicon supports were obtained with an REM-101 electron microscope.

1070-4272/05/7802-0197 © 2005 Pleiades Publishing, Inc.

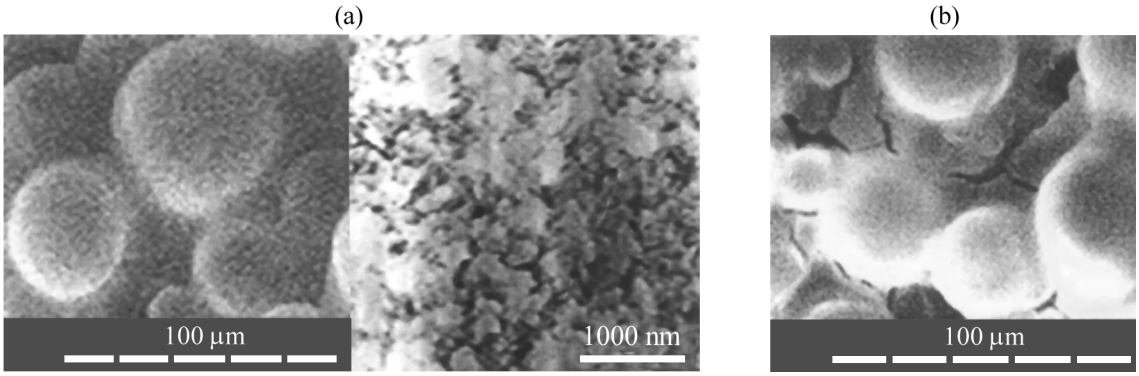


Fig. 1. Electron micrograph of a composite formed from aerosil and glass spheres. [SF] : [AD]: (a) 3.3 and (b) 2.6.

The total porosity *W* of the samples was determined by their impregnation with carbon tetrachloride [11]. The volume of the samples was calculated from their dimensions.

It was shown [12] that replacing quartz with glass makes lower the adhesion between a quartz plate and glass particles or a glass plate and quartz particles. Consequently, introduction of glass microspheres can give a three-dimensional (3*D*) structure of SiO_2 particles and glass spheres with coagulation contacts weakened as compared with a gel formed only from SiO_2 and make looser the aggregates formed.

SiO_2 particles of hydrophobic aerosil AD are wetted in ethanol via adsorption of alcohol molecules on the aerosil surface, with the C_2H_5 groups of these molecules facing the particle surface and the OH groups looking in the opposite direction. Glass spheres are wetted by both water and ethanol, with molecules of the latter adsorbed on their surface with the OH groups facing the surface. The C_2H_5 groups are turned away and can be adsorbed on the surface of aerosil particles. This may lead to binding of glass spheres, SiO_2 particles, and aggregates of these particles. In addition, since the reagent used was not absolute alcohol, its water molecules can bind particles and aggregates of aerosil with glass spheres via formation of hydrogen bonds with the OH groups of ethanol molecules adsorbed on the SiO_2 surface. As a result, a solid 3*D* structure can be formed from aggregated aerosil particles of various sizes, glass spheres, water, and ethanol, bound by a system of nonvalence interactions. Drying of these gels gives monolithic samples in the form of close-packed glass spheres, with the inter-sphere space filled with openwork structures constituted by aerosil particles (Fig. 1a). The composition and selected parameters of the composites obtained are listed in the table.

Parameters of composites obtained from AD aerosil and glass spheres

Sample no.	[SF] : [AD] mass ratio, modifier	Drying at *T*, °C				Weight loss after heating at 160°C, %
		20		160		
		d_{app}, g cm^{-3}	*W*	d_{app}, g cm^{-3}	*W*	
1	0.5	0.40	–	–	–	–
2	1.0	0.34	–	–	–	–
3	2.0	0.33	–	–	–	–
4	2.6	0.30	–	–	–	–
5	3.0	0.29	–	–	–	–
6	3.3	0.26	0.34	0.32	0.42	0.6
7	3.3, 5% TES	0.27	0.32	0.32	0.38	0.6
8	3.3, 5% PMS	0.27	0.31	0.28	0.35	0.5
9	3.3, 10% SIEL	0.28	0.28	0.29	0.37	0.6
10*	3.3	0.30	0.37	0.31	0.38	0.6
11**	3.3	0.23	–	0.25	0.55	0.4

* AO used instead of AD. ** Hexane as the dispersion medium.

Monolithic samples could not be obtained at [glass spheres] : [aerosil] ratios of up to 3.0. Shrinkage, cracking (Fig. 1b), and lamination of samples (upper layers were enriched in glass spheres) were observed in the course of drying. As can be seen from the table, the apparent sample density decreases as the concentration of glass spheres becomes higher. Composites with [SF] : [AD] = 3.3 have the best physicomechanical properties. Modification of the composite with TES, PMS, or SIEL affects the properties of the composite, although the nature of this influence varies. As already noted, hydrolysis of TES yields an additional amount of SiO_2, which makes the concentration of the dispersed phase higher, and the porosity of the resulting composite, lower. Macromolecules of PMS and SIEL adsorbed on the surface of aerosil particles bind the aggregates together and thereby diminish the looseness of the 3*D* network of the gel. This leads to a decrease in the porosity of the composite and an increase in its apparent density. The SIEL silicon rubber differs from PMS in a greater length of macromolecules, and, therefore, its effect is stronger.

The loss of weight by samples heated to 160°C to remove physically bound water [13] did not exceed 0.6%, i.e., the pores obtained are virtually empty even upon drying at room temperature. Such a heating can be to a certain extent compared with hydrothermal treatment of silica gels, which is confirmed by the data in the table. Samples of the composite samples have a higher density and porosity upon heating.

Replacement of AD with AO, which has a greater number of surface CH_3-groups per silicon atom, raises the porosity of the composite owing to formation of looser aggregates and, possibly, leads to a decrease in the pore size. If hexane is used as the dispersion medium, complete wetting of the surface of AD aerosil particles occurs, but it does not promote their binding into aggregates. At the same time, hexane does not wet glass spheres and favors their aggregation with coagulation contacts weaker than those in aerosil aggregates. Combined, these factors make it possible to produce a composite with a low density and the highest porosity among all the samples. The composite has a virtually zero mechanical strength and disintegrates in CCl_4.

CONCLUSIONS

(1) Monolithic samples of porous composites were obtained in the form of close-packed glass spheres with the inter-sphere space filled with structured nanosize particles of nonporous silica.

(2) The porosity and density of the composites can be controlled by modifying the surface of SiO_2 particles and varying the nature of the dispersion media, concentration of glass spheres and silicon dioxide, and temperature mode of drying.

REFERENCES

1. *Physical and Chemical Aspects of Adsorbents and Catalysts*, Linsen, B.G., Ed., London: Academic, 1970.
2. Neimark, I.E., *Sinteticheskie mineral'nye adsorbenty i nositeli katalizatorov* (Synthetic Mineral Adsorbents and Catalyst Supports), Kiev: Naukova Dumka, 1982.
3. Ermolenko, V.F. and Efros, M.D., *Regulirovanie poristoi struktury okisnykh adsorbentov i katalizatorov* (Control over the Porous Structure of Oxide Adsorbents and Catalysts), Minsk: Nauka i Tekhnika, 1971.
4. Iler, R.K., *The Chemistry of Silica*, New York: A Wiley-Interscience, John Wiley & Sons, 1979.
5. Dobruskin, V.Kh., Belotserkovskii, G.M., Karel'skaya, V.F., *et al.*, *Zh. Prikl. Khim.*, 1968, vol. 40, no. 11, pp. 2443–2448.
6. Airapetyan, S.S. and Khachatryan, A.G., *Zh. Prikl. Khim.*, 2003, vol. 76, no. 6, pp. 918–921.
7. Khimich, N.N., Venzel', B.I., Drozdova, I.A., *et al.*, *Zh. Prikl. Khim.*, 2002, vol. 75, no. 7, pp. 1125–1130.
8. Fenelonov, V.B., Tarasova D.V., and Gavrilov, V.Yu., *Izv. Sibirsk. Otd. Akad. Nauk SSSR, Ser. Khim. Nauk*, 1978, no. 9, issue 4, pp. 116–129.
9. Ur'ev, N.B. and Potanin, A.A., *Tekuchest' suspenzii i poroshkov* (Fluidity of Suspensions and Powders), Moscow: Khimiya, 1992.
10. *Khimiya poverkhnosti kremnezema* (Surface Chemistry of Silica), Chuiko, A.A., Ed., Kiev: Naukova Dumka, 2001, vol. 1, part 2.
11. Grigorov, O.N., Karpova, I.F., Koz'mina, Z.P., *et al.*, *Rukovodstvo k prakticheskim rabotam po kolloidnoi khimii* (Manual of Laboratory Works in Colloid Chemistry), Moscow: Khimiya, 1964.
12. Deryagin, B.V., Churaev, N.V., and Muller, V. M., *Poverkhnostnye sily* (Surface Forces). Moscow: Nauka, 1985.
13. *Modifitsirovannye kremnezemy v adsorbtsii, katalize i khromatografii* (Modified Silica in Adsorption, Catalysis, and Chromatography), Lisichkin, G.V., Ed., Moscow: Khimiya, 1986.

Russian Journal of Applied Chemistry, Vol. 78, No. 2, 2005, pp. 200–203. Translated from Zhurnal Prikladnoi Khimii, Vol. 78, No. 2, 2005, pp. 207–210.
Original Russian Text Copyright © 2005 by Kamaev, Archugov, Mikhailov.

PHYSICOCHEMICAL STUDIES OF SYSTEMS AND PROCESSES

Study and Thermodynamic Analysis of the ZrO_2–SiO_2 System

D. N. Kamaev, S. A. Archugov, and G. G. Mikhailov

South-Ural State University, Chelyabinsk, Russia

Received November 2, 2004; in final form, September 2004

Abstract—The system ZrO_2–SiO_2 was additionally studied by means of differential thermal analysis. The temperatures of the solid-state decomposition of zircon and the coordinates of the eutectic point were refined. A thermodynamic calculation of the system in terms of the theory of subregular ionic solutions was carried out on the basis of the experimental data obtained.

The positive effect of zirconium on steel properties [1] is caused by its vigorous reaction with oxygen, nitrogen, sulfur, and silicon to give stable chemical compounds [2]. In particular, zirconium additives make smaller the grain size, raise strength, improve weldability, and enhance oxidation and corrosion resistance. A thermodynamic analysis of how zirconium added to a steel interacts with oxygen dissolved in it is necessary for solving problems associated with steel alloying with zirconium in metallurgy. If silicon is present in a steel, information on the interaction of zirconium and silicon with oxygen can be obtained when precise data on the Fe–Zr–Si–O system are available. In an attempt to carry out a thermodynamic analysis, we found that published data on the phase diagram of the ZrO_2–SiO_2 system are ambiguous.

It has been shown [3–5] that heating of zircon ($ZrSiO_4$) to high temperatures leads to its dissociation into oxide components. There is an opinion [3] that zircon melts incongruently at 1775 ± 10°C, whereas its eutectic temperature is appreciably lower: 1675°C (94 mol % SiO_2). According to [4], the melting point of zircon is 1720 ± 20°C. The authors of [5] believe that $ZrSiO_4$ decomposes even in the solid phase at 1540°C.

According to experimental data on the high-temperature behavior of zircon [6], it decomposes into component oxides at 1676°C, and its eutectic point is 1687°C. These data are consistent with the results of [7], but differ from the data of [3]. However, the eutectic point was not determined in [7], and only the decomposition of zircon in the solid phase and the approximate eutectic composition (about 97 mol % SiO_2) were reported.

However, assessment [8] of the results obtained in a study of the zircon synthesis from ZrO_2 and SiO_2 [5] shows that zircon is thermodynamically stable approximately up to 1727°C, and the free energy of its dissociation into component oxides is zero at 1771°C. This value differs by only 4°C from the temperature reported in [3].

To eliminate these contradictions and to obtain a thermodynamic description of the system ZrO_2–SiO_2, we determined the temperature of zircon decomposition, its eutectic point, and eutectic composition.

EXPERIMENTAL

A modified installation for precision high-temperature thermal analysis [9] was used in the experiments. The addition of the third crucible with a reference substance with well-known properties [10] into the cell maked it possible to obtain data accurate to no less than ±10°C in the temperature range 1700–2100°C. Earlier, experimental data of high precision have been obtained on a similar installation [11, 12].

Samples for the experiments were prepared from analytically pure silicon and zirconium oxides. To remove moisture and adsorbed admixtures, the starting oxides were calcined in air at 1200°C for 3 h and immediately after that were placed in weighing bottles stored in a desiccator in dry air. The accuracy rating of the balance used to prepare weighed samples guarantied that the composition deviated from a calculated value by no more than 0.01 wt %.

Samples with the SiO_2 content varied in the range 80–100 mol % with a step of 2% and a sample containing 50 mol % SiO_2 were prepared. After being

1070-4272/05/7802-0200 © 2005 Pleiades Publishing, Inc.

mixed, the samples were compacted in a special hard-alloy press mold. The compacted samples were weighed and placed in a crucible of the thermographic installation. The weight of samples placed in the crucible was varied in the range 0.0500 – 0.0900 g.

Analytically pure aluminum oxide was used as a reference. The experiments were carried out in the atmosphere of argon at a pressure of 1 atm.

The following procedure was suggested for obtaining DTA curves: (1) heating of a sample to 1500°C at a rate of 60 deg min^{-1} with a subsequent cooling at the same rate to 800°C; (2) heating of the sample to 1400°C at a rate of 60 deg min^{-1} and annealing at this temperature for 3 min; (3) heating of the annealed sample to a temperature exceeding by 20–50°C the presumed eutectic point at a rate of 30 deg min^{-1} and its keeping at this temperature for 3 min with a subsequent heating to 2100°C at the same rate; (4) cooling of the sample to a temperature higher by 20–50°C than the presumed eutectic point at a rate of 60 deg min^{-1} and keeping it at this temperature for 3 min; (5) cooling of the sample to room temperature at a rate of 60 deg min^{-1}; and (6) heating of the sample to 2100°C at a rate 30–100 deg min^{-1}.

The first two stages were sufficient for synthesizing zircon from the starting components, which was confirmed by X-ray fluorescence spectroscopy: only zircon and silicon oxide were detected in the samples. The other stages were necessary for obtaining equilibrium compositions. Thermocouples were calibrated in stages 3 and 6 against the peak of Al_2O_3 melting in the reference crucible.

The most reliable DTA data were obtained in stage 6. Up to 12 samples of the same composition were studied to gather statistically significant data on each transformation.

An examination of the DTA curves of the samples under study (Fig. 1), measured with heating at different rates (30–100 deg min^{-1}), revealed the effect of heating rate on DTA curves and allowed us to extrapolate these data to zero heating rate. This made it possible to determine the dissociation temperature of zircon, its eutectic point, and the liquidus temperature for samples containing 80 to 100 mol % SiO_2 (Fig. 2).

Three successive peaks can be seen in the DTA curve. It was found that the first two peaks correspond to dissociation of zircon and its eutectic transformation, and the third peak, to melting of the solid phase formed upon the eutectic transformation (liquidus line). If the first peak corresponded to eutectic transformation, the formation of a liquid would be visually detected after terminating the heating and withdrawing the crucible with a sample.

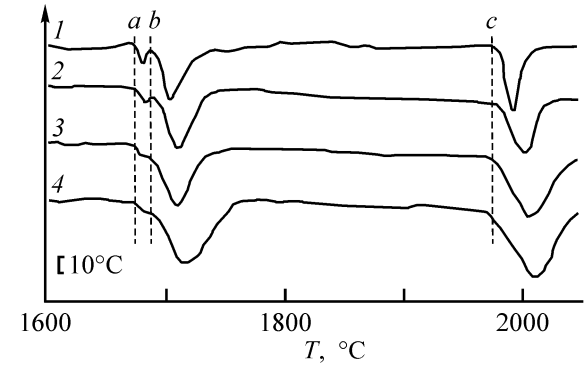


Fig. 1. DTA curves of a sample containing 90 mol % SiO_2. (*T*) Temperature. The temperature of (*a*) zircon decomposition, (*b*) eutectic transformation, and (*c*) liquidus was measured. Heating rate (deg min^{-1}): (*1*) 30, (*2*) 40, (*3*) 50, and (*4*) 60.

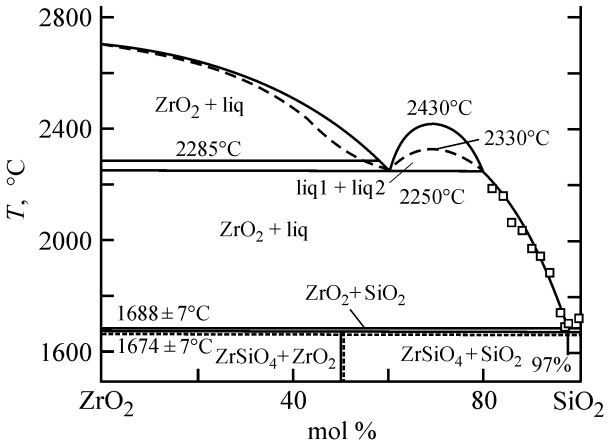


Fig. 2. Phase diagram of the ZrO_2–SiO_2 system, plotted using the data of [6] and the experimental and calculated data of the present study. *Points*, experimental data for the liquidus line; *dashed line*, calculation.

To confirm the decomposition of zircon in the solid phase and to determine the dissociation temperature, we heated the sample containing 50 mol % ZrO_2 and 50 mol % SiO_2 (initial composition for synthesis of zircon in stages 1 and 2). When the peak corresponding to a probable decomposition appeared in the thermogram, the sample was kept for a few minutes at a temperature higher than that at which the first peak appeared, but lower than that of the second peak. Then the sample was cooled to room temperature. After being removed, the sample retained its initial shape and exhibited no traces of melting. It should be also noted that the peaks corresponding to solid phase transformations are commonly lower than melting

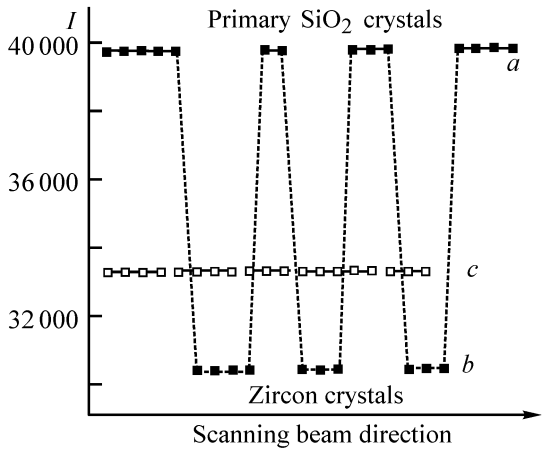


Fig. 3. Silicon distribution. (*I*) Intensity of characteristic pulses of Si. (*a*, *b*) Primary SiO_2 crystals and zircon (sample with 88 mol % SiO_2); (*c*) synthesized zircon (sample with 50 mol % SiO_2).

peaks. For comparison, a sample containing 88 mol % SiO_2 was subjected to the heating–cooling procedure in the same temperature mode, and similar results were obtained.

The distribution of silicon in grains of synthesized zircon with 50 mol % SiO_2 and of a sample with 88 mol % SiO_2 (primary SiO_2 crystals and zircon crystals) are shown in Fig. 3. This distribution was determined from the intensities of characteristic pulses in scanning in an X-ray microanalyzer. If the intensity of the characteristic radiation of silicon in scanning of synthesized zircon is constant, this means that the sample is homogeneous and zircon is stable at temperature below 1674°C.

The liquidus line constructed within the range of compositions under study (Fig. 2) is in a good agreement with other published data [6, 7].

The eutectic temperature was determined from all experimental temperatures corresponding to the liquidus line peaks. In the course of experiments, thermocouple readings were corrected against the peaks corresponding to melting of alumina and then against those associated with copper melting [13–15]. The eutectic composition was determined from the point of intersection between the experimental liquidus line and the conode at 1688°C.

As a result, it was found that the heating first leads to a solid-phase decomposition of zircon at 1674 ± 7°C and then to an eutectic transformation at 1688 ± 7°C. According to our estimates, the eutectic melt contains 97 mol % SiO_2.

Based on the experimental data obtained, we carried out a thermodynamic calculation of the phase diagram in terms of the theory of subregular ionic solutions [16]. According to this theory, the chemical potentials of components in a binary oxide system have the form

$$\mu_1 = \mu_1^0 + \nu_1[RT\ln x_1 + 3x_1^2x_2^2Q_{1112} + x_1x_2^2(2 - 3x_1)Q_{1122} + x_2^3(1 - 3x_1)Q_{1222}],$$

$$\mu_2 = \mu_2^0 + \nu_2[RT\ln x_2 + x_1^3(1 - 3x_2)Q_{1112} + x_1^2x_2(2 - 3x_2)Q_{1122} + 3x_1^2x_2^2Q_{1222}].$$

Then the equilibrium constant of zircon formation by the reaction

$$ZrO_2 + SiO_2 = ZrSiO_4$$

can be expressed as

$$\log K = -\frac{A}{B} + B = \frac{\nu_1[3x_1^2x_2^2Q_{1112} + x_1x_2^2(2 - 3x_1)Q_{1122} + x_2^3(1 - 3x_1)Q_{1222}]}{2.3RT} + \frac{\nu_2[x_1^3(1 - 3x_2)Q_{1112} + x_1^2x_2(2 - 3x_2)Q_{1122} + 3x_1^2x_2^2Q_{1222}]}{2.3RT} + \nu_1\log x_1 + \nu_2\log x_2.$$

Here R is the universal gas constant; T, absolute temperature; ν_i, number of cations in an oxide molecule; μ_i^0, standard chemical potential; Q_{1112}, Q_{1122}, and Q_{1222}, energy parameters of the interaction between components; x_i, molar fraction; K, equilibrium constant of the reaction of zircon formation; and A and B, numerical constants; subscripts 1 and 2 refer to ZrO_2 and SiO_2, respectively.

The following reference points were chosen for the calculations: experimental eutectic point (97 mol % and 1688°C), points corresponding to the composition of monotectic transformation at 2250°C (78 mol % SiO_2 and 60 mol % SiO_2) [6], and point of syntectic transformation (50 mol % SiO_2 at 1674°C). In the calculation, expressions for monotectic, syntectic, and eutectic equilibria were written, and the resulting set

of equations was solved. The thus found energy parameters are as follows: Q_{1112} = –15850, Q_{1122} = 86630, and Q_{1222} = 27600 J mol^{-1}. The constant of zircon formation from the starting oxides is given by

$$\log K = \frac{76\,026}{T} + 25.90.$$

Further, we calculated the whole phase diagram of the ZrO_2–SiO_2 system (Fig. 3), using the values obtained. There is a certain disagreement between the resulting calculated and experimental diagrams at temperatures above 2250°C. The most likely reason is that the effect of temperature on the interaction parameters was disregarded in the calculations and the parameters were averaged over a rather wide temperature range.

CONCLUSIONS

(1) The solid-phase decomposition of zircon was confirmed experimentally and the temperatures of this decomposition (1674 ± 7°C) and of the eutectic transformation (1688 ± 7°C) were refined. The eutectic composition was found to be 97 mol % SiO_2.

(2) The thermodynamic calculation confirmed the stratification of melts in the ZrO_2–SiO_2 system. The information obtained makes possible further thermodynamic analysis of the FeO–ZrO_2–SiO_2, Fe–Zr–Si–O, and other multicomponent systems containing zirconium and silicon, which, in turn, allows evaluation of parameters of the interactions between oxygen and zirconium added to a steel, in the presence of silicon and other elements. These data are of great importance for the theoretical metallurgy.

REFERENCES

1. Livshits, G.L. and Toropanova, G.A., *Redkie metally i splavy* (Rare Metals and Alloys), Moscow: Metallurgizdat, 1960, pp. 343–365.
2. *Bor, kal'tsii, niobii i tsirkonii v chugune i stali* (Boron, Calcium, Niobium, and Zirconium in Cast Iron and Steel), Moscow: Metallurgizdat, 1961.
3. Geller, R.F. and Lang, S.M., *J. Am. Ceram. Soc.*, 1949, vol. 32, no. 12, pp. 157–159.
4. Cocco, A. and Shromek, N., *La Ceramica* (Milan), 1957, vol. 12, no. 8, pp. 45–48.
5. Curtis, C.E. and Sowman, H.G., *J. Am. Ceram. Soc.*, 1953, vol. 36, no. 6, pp. 190–198.
6. Butterman, W.C. and Foster, W.R., *Am. Mineral.*, 1967, vol. 52, no. 5, pp. 880–885.
7. Toropov, N.A. and Galakhov, F.Ya., *Izv. Akad. Nauk SSSR, Otd. Khim. Nauk*, 1956, no. 2, pp. 158–161.
8. Berezhnoi, A.S., *Dokl. Akad. Nauk SSSR*, 1962, no. 1, pp. 65–67.
9. Kamaev, D.N., Archugov, S.A., and Mikhailov, G.G., *Izv. Vyssh. Uchebn. Zaved., Chern. Metall.*, 2003, no. 6, pp. 46–49.
10. Zherebtsov, D.A. and Mikhailov, G.G., *Prib. Tekh. Eksp.*, 2000, no. 5, pp. 140–148.
11. Jerebtsov, D.A., Mikhailov, G.G., and Sverdina, S.V., *Ceramics Int.*, 2000, vol. 26, pp. 821–823.
12. Jerebtsov, D.A. and Mikhailov, G.G., *Ceramics Int.*, 2001, vol. 27, pp. 247–250.
13. Wendlandt, W.Wm., *Thermal Methods of Analysis*, New York: Wiley Int. Science, 1974.
14. Berg, L.G. *Vvedenie v termografiju* (Introduction to Thermography), Moscow: Nauka, 1964, 2nd ed.
15. Bragin, B.K., *Trudy Vsesoyuznogo Nauchno-Issledovatel'skogo Instituta Metrologii im. D.I. Mendeleeva* (Proc. Mendeleev All-Union Research Institute), Gordov A.N., Ed., Moscow: Standartgiz, 1963, issue 71(131), pp. 97–100.
16. Mikhailov, G.G. and Povolotskii, D.Ya., *Termodinamika raskisleniya stali* (Thermodynamics of Steel Keeling), Moscow: Metallurgiya, 1993.

Russian Journal of Applied Chemistry, Vol. 78, No. 2, 2005, pp. 204–206. Translated from Zhurnal Prikladnoi Khimii, Vol. 78, No. 2, 2005, pp. 211–213.
Original Russian Text Copyright © 2005 by Poltoratskii, Osovskaya, Chumanov.

PHYSICOCHEMICAL STUDIES OF SYSTEMS AND PROCESSES

Temperature Dependences of HCl Activity Coefficients in Aqueous Solutions

G. M. Poltoratskii, I. I. Osovskaya, and S. V. Chumanov

St. Petersburg State Technological University of Phytopolymers, St. Petersburg, Russia

Received January 15, 2004

Abstract—Temperature coefficients of activity of the ionic fraction of HCl in water, calculated from tensimetric and calorimetric data, are compared. A correlation dependence is suggested for recalculating the activity coefficients of hydrochloric acid from 298 K to other temperatures.

It is commonly believed that solutions of HCl in water are sufficiently well studied, and, therefore, they are widely recommended for use as reference in calibration of various devices and, in particular, those intended for measuring electromotive forces and pH values [1]. At the same time, recent studies have revealed an inconsistency in published data, especially as regards the quantitative characteristics of ionic dissociation and the methods of their determination [2, 3].

It is known that the Guggenheim equation [4] makes it possible to correlate the temperature dependences of activity coefficients of an electrolyte in solution with the corresponding values found from experimental data on the heats of dilution.

Relative partial molal (r.p.m.) enthalpies of a solvent and an electrolyte in solution, $\bar{L}_1$ and $\bar{L}_2$ (subscripts 1 and 2 refer to the solvent and the electrolyte, respectively) are commonly calculated from the results of direct calorimetric measurements (integral heat of electrolyte dilution) [5, 6].

These data must coincide with the results of calculation of the same values from the temperature dependences of the activities of the corresponding solution components.

The activity coefficients of water are commonly recalculated into those of an electrolyte and back with the use of the known Bierrum's relation [5], from which follows an expression that makes possible a mutual recalculation of the temperature coefficients of the activities of a solvent and an electrolyte:

$$\left(\frac{\partial \ln \gamma}{\partial T^{-1}}\right)_m = -\frac{55.51}{\nu m}\left(\frac{\partial \ln a_w}{\partial T^{-1}}\right)_m. \quad (1)$$

Here a_w is the activity of a solvent (water, in particular); γ, average ionic activity coefficient of an electrolyte; ν, number of ions formed in dissociation of the electrolyte; and m, molality of the solution.

A comparison of the values of $\bar{L}_1$ and $\bar{L}_2$, calculated from calorimetric data, with the same values calculated using the derivatives $(\partial \ln a_w/\partial T^{-1})_m$ and $(\partial \ln \gamma/\partial T^{-1})_m$ for aqueous solutions of HCl demonstrated that detailed and repeatedly published data on the heats of dissolution and dilution are available only for 298 K [7]. For other temperatures, only results of fragmentary measurements can be found [8–11].

The overwhelming majority of authors and reference books indicate a linear, within the limits of errors declared by the authors, temperature dependence of the logarithms of the activity of water over the whole interval of compositions and temperatures studied. At the same time, both the linearity [12] and minor deviations from this behavior [13–16] have been observed for the logarithms of the average ionic activity coefficients in a limited range of compositions and temperatures. Such discrepancies primarily contradict Eq. (1). Moreover, the values of $R(\partial \ln \gamma/\partial T^{-1})_m$ and the r.p.m. enthalpies $\bar{L}_2$ are constant within the errors of determination of the initial values, i.e., they are independent of temperature.

To analyze this discrepancy, we decided to supplement with our own calorimetric measurements primarily that range of concentrations and temperatures in which deviations from the main body of data were observed.

We measured the heats of HCl dilution in water at 288, 298, and 308 K in a calorimeter with an iso-

1070-4272/05/7802-0204 © 2005 Pleiades Publishing, Inc.

Heat of dilution in water and r.p.m. enthalpies in comparison with temperature coefficients of average ionic activity coefficients

m	ΔH_m^0, kJ mol^{-1}			$\bar{L}_2$, kJ mol^{-1}			$2R(\partial \ln \gamma_\pm / \partial T^{-1})_m^*$		
	at indicated temperature, K								
	288	298	308	288	298	308	288	298	308
0.1	–0.38	–0.55	–0.49	0.61	0.82	0.80	0.6	0.8	0.8
0.2	–0.50	–0.77	–0.76	0.80	1.14	1.22	0.8	1.1	1.2
0.5	–0.87	–1.20	–1.21	1.41	1.79	1.95	1.4	1.8	2.0
1.0	–1.46	–1.71	–1.85	2.36	2.65	2.99	2.4	2.7	3.0
2.0	–2.44	–2.61	–2.89	3.93	4.37	4.66	3.9	4.4	4.7
3.0	–3.31	–3.50	–3.92	5.75	6.23	6.76	5.8	6.2	6.8
4.0	–4.22	–4.42	–4.96	7.50	8.12	8.74	7.5	8.1	8.7

* Calculation from the data of [13].

thermal jacket at an average measurement error of 0.5%. The results for 298 K are in a full agreement with the most reliable published data [7]. We did not find any systematized published data for 288 and 308 K. The design of the devices used and the measurement procedure have been described in detail earlier [17, 18]. The results of direct measurements of the dilution heats at three temperatures and r.p.m. enthalpies calculated on their basis are listed in the table.

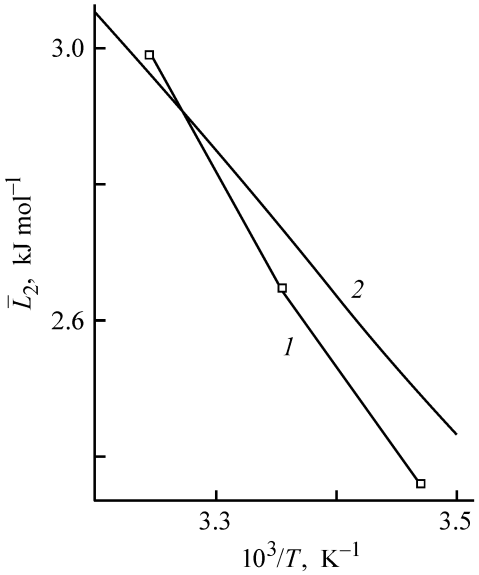
It can be seen that the variation of $\bar{L}_2$ with temperature is not so narrow as it would be expected, at least within the range from 288 to 308 K at molalities of 0.1 to 4 mol kg^{-1} of H_2O. Consequently, the temperature coefficients of the average ionic activity coefficients are not constant, but also depend on temperature. This fact contradicts the majority of published tabulated data on the activity coefficients for various temperatures. At the same time, $\bar{L}_1$ also depends on temperature, but deviates from constancy far beyond the errors of the majority of modern methods for measuring a_w (±5–10%) and derivatives $(\partial \ln a_w / \partial T^{-1})_m$. Therefore, in our opinion, Eq. (1) can be used for calculating the temperature dependence of the logarithm of the activity of water, but there is no sense in the reverse calculation.

Within the experimentally accessible ranges of concentrations and temperatures, $\bar{L}_2$ can be expressed as an empirical dependence $\bar{L}_2 = f(m, 1/T)$, which makes it possible to interpolate $\ln \gamma$ to any temperature with a substantially better accuracy, since it allows integration of Guggenheim the equation within the required limits:

$$\ln \gamma(T) = \ln \gamma(298) + \frac{1}{\nu R} \int_{298}^{T} \bar{L}_2 \, \mathrm{d}T^{-1}. \qquad (2)$$

The authors of [13] measured the electromotive force of the systems with a chloride electrode at temperatures of 298 to 353 K and concentrations m of 1 to 11 mol kg^{-1} of H_2O. They approximated the dependences of $\ln \gamma$ on $1/T$ with parabolas and calculated $\bar{L}_2$ from these parabolas to obtain a perfect agreement with published data [7] for 298 K.

As can be seen from the figure, the dependence of $\bar{L}_2$ on inverse temperature, obtained in direct calorimetric measurements at a molality m = 1 (curve *1*), is not linear. The linearity (curve *2*) results from differentiation of the parabolic approximation to the de-



Comparison of r.p.m. enthalpies $\bar{L}_2$ of HCl in an aqueous solution with a molality m = 1 mol kg^{-1} of H_2O, calculated from calorimetric and electrochemical data. (T) Temperature. (*1*) This study and (*2*) calculation from the data of [13].

pendence of $\ln\gamma$ on $1/T$ ($\ln\gamma = a + b/T + c/T^2$), obtained using the data of [13] with a standard deviation of 0.11% (average measurement error is 0.15% [13]).

The approximation of the same data with a straight line $\ln\gamma = a + b/T$ gives a standard deviation of 0.22%, a value that is not considerably higher than that in the case of a parabolic approximation. Differentiating the linear regression equation, we come to a constant value of $\bar{L}_2$ over the whole temperature range under study for each of the concentrations used. Consequently, the data obtained by most of authors can be reproduced with an error somewhat exceeding that in the majority of reports, using an equation based on the assumption that $\bar{L}_2$ is independent of temperature:

$$\ln\gamma(T) = \ln\gamma(298) + \frac{\bar{L}_{2(298)}}{\nu R}(T^{-1} - 298^{-1}). \quad (3)$$

CONCLUSIONS

(1) The temperature dependences of the logarithms of the activity coefficients of HCl in aqueous solutions, obtained from calorimetric experiments, were compared with published data. It was shown that calorimetry can give more accurate results.

(2) Equations (2) and (3) were suggested for recalculating the activity coefficients of HCl in aqueous solutions from 298 K to any other temperature within the existence limits of a solution, with varied error not exceeding the accuracy of the majority of published data.

(3) The possibility, in principle, of more accurate calculations by equation (2) requires additional labor-consuming calorimetric measurements.

ACKNOWLEDGMENTS

This study was financially supported by the Ministry of Education of the Russian Federation (grant no. E02-5.0-332).

REFERENCES

1. Bates, R.G., *Determination of pH. Theory and Practice*, New York: Wiley, 1964.
2. Albert, A. and Serjeant, E., *Ionization Constants of Acids and Bases. A Laboratory Manual*, New York: Wiley, 1962.
3. Poltoratskii, G.M., *Zh. Obshch. Khim.*, 2000, vol. 70, no. 11, pp. 1785–1789.
4. Guggenheim, E.A., *Modern Thermodynamics By the Methods of Willard Gibbs*, New York: Dutton, 1933.
5. Harned, H.S. and Owen, B.B., *The Physical Chemistry of Electrolytic Solutions*, New York: Reinhold, 1943.
6. Mishchenko, K.P. and Poltoratskii, G.M., *Termodinamika i stroenie vodnykh i nevodnykh rastvorov elektrolitov* (Thermodynamics and Structure of Aqueous and Nonaqueous Electrolyte Solutions), Leningrad: Khimiya, 1976.
7. Parker, V.B., Thermal Properties of Aqueous Uni-univalent Electrolytes, *Ed. NBS USA*, 1965.
8. Berthelot, M., *Ann. Chim. et Phis.*, 1875, vol. 4, no. 5, pp. 467–488.
9. Tucker, W.S., *Phil. Trans. Roy. Soc. London*, 1915, vol. A215, pp. 319–351.
10. Vrevskii, M.S. and Zavaritskii, N., *Z. Phys. Chem.*, 1924, vol. 112, pp. 90–96.
11. Tsvetkov, V.G., Ivanov, A.V., and Zueva, O.A., *Termodinamika solvatatsionnykh protsessov* (Thermodynamics of Solvation Processes), Ivanovo, 1983, pp. 75–79.
12. *Spravochnik khimika* (Chemist's Handbook), Nikol'skii, B.P., Ed., Moscow: Khimiya, 1964, vol. 3.
13. Cerquetti, A., Longni, P., and Mussini, T., *J. Chem. Eng. Data*, 1968, vol. 13, no. 4, pp. 458–461.
14. *Spravochnik po elektrokhimii* (Handbook of Electrochemistry), Sukhotin, A.M., Ed., Leningrad: Khimiya, 1981.
15. Voznesenskaya, I.E., *Voprosy fizicheskoi khimii rastvorov elektrolitov* (Physical Chemistry of Electrolyte Solutions), Leningrad: Khimiya, 1968, pp. 172–201.
16. Ryabin, V.A., Ostroumov, M.A., and Svift, T.F., *Termodinamicheskie svoistva veshchestv: Spravochnik* (Thermodynamic Properties of Substances: Reference Book), Leningrad: Khimiya, 1977.
17. Belogorodetskaya, N.N., Poltoratskii, G.M., and Shadskii, S.V., *Kontsentratsionnye zavisimosti integral'nykh teplot rastvoreniya iodida natriya v smeshannom vodno-organicheskom rastvoritele voda–atseton–izopropilovyi spirt razlichnogo sostava pri 298 K* (Concentration Dependences of Integral Heats of Dissolution of Sodium Iodide in Mixed Aqueous-Organic Water–Acetone–Isopropyl Alcohol Solvent of Varied Composition at 298 K), Available from ONIITEKhIM, Cherkassy, no. 894khp-D84.
18. Poltoratskii, G.M., Parfenova, L.N., and Bogolitsyn, K.G., *Sbornik statei po termokhimii i termodinamike* (Coll. of Papers on Thermochemistry and Thermodynamics), Moscow: Lit. izd. R. Elinina, 1991, p. 147.

Russian Journal of Applied Chemistry, Vol. 78, No. 2, 2005, pp. 207–211. Translated from Zhurnal Prikladnoi Khimii, Vol. 78, No. 2, 2005, pp. 214–218.
Original Russian Text Copyright © 2005 by I. Dobryakova, Yu. Dobryakov.

PHYSICOCHEMICAL STUDIES OF SYSTEMS AND PROCESSES

Limiting Activity Coefficients of Phenol in Hydrocarbons

I. E. Dobryakova and Yu. G. Dobryakov

Research Institute of Chemistry, St. Petersburg State University, St. Petersburg, Russia

Received November 29, 2004

Abstract—The activity coefficients of phenol in a number of hydrocarbons were determined from experimental data on phenol distribution between aqueous and hydrocarbon liquid phases, using data on the limiting activity coefficients of phenol in water. Ten systems containing saturated and aromatic hydrocarbons were examined in the temperature range 283–328 K.

The limiting activity coefficient γ^∞ is an important thermodynamic parameter, which characterizes the properties of a dissolved substance and is necessary for calculation of processes of impurity removal and substance separation. A knowledge of γ^∞ makes it possible to describe a liquid–vapor equilibrium at a small content of a dissolved component and to estimate the degree of nonideality of the system. The distribution coefficients between liquid and vapor phases can be readily determined from experimental values of γ^∞, which is especially important both for chromatography and for solution of various problems of analytical ecology, e.g., for determining trace amounts of toxic substances (including phenol) in the environment. The fact that the limiting activity coefficient is an important parameter for calculation of phase equilibria has been reported elsewhere [1–3]. It has been shown [4–6] that, with only binary data on the limiting activity coefficients used for estimating the energy characteristics of model systems, one can calculate characteristics of liquid–vapor and liquid–liquid–vapor equilibria in binary and multicomponent systems. For this reason, experimental γ^∞ values are thoroughly studied, systematized, and introduced into experimental databases and reference books [7, 8].

The goal of this study was to determine the limiting activity coefficients of a low-volatile component, phenol, in volatile hydrocarbons by an indirect method based on the previously obtained experimental data on the phenol distribution between liquid phases in the water–hydrocarbon system [9].

The distribution coefficient of a dissolved component between the organic and aqueous phases is related to the activity coefficients by

$$K_x = \frac{x_{org}}{x_{aq}} = \frac{\gamma_{org}}{\gamma_{aq}},$$

where x is the mole fraction, and γ, the activity coefficient of the solute in terms of a pure component.

At $x \to 0$, K_x takes a constant value (Berthelot–Nernst law):

$$K_x^\infty = \lim_{x \to 0} K_x = \frac{\gamma_{org}^\infty}{\gamma_{aq}^\infty},$$

where the superscript ∞ stands for an infinitely diluted solution.

Thus, if the distribution coefficient of a dissolved component between the aqueous–organic phases and the limiting activity coefficient of this component in either of the solvents are known, then the limiting activity coefficient of this component in another solvent can be readily estimated. This "indirect measurement method" [10] was applied, in particular, for determining γ^∞ for a number of organic substances in water. As reference was used the activity coefficient γ^∞ of a component under study in a heavy hydrocarbon (hexadecane), measured by dynamic gas–liquid chromatography [11].

The limiting activity coefficients of phenol in the organic solvent were calculated by the formula

$$\gamma_{org}^\infty = \frac{\gamma_{aq}^\infty}{K_x^\infty}. \quad (1)$$

The limiting activity coefficient of phenol in water at a given temperature, γ_{aq}^∞, was determined from the temperature dependence of the data obtained by ebullioscopy [12–15]. The dependence of the nat-

1070-4272/05/7802-0207 © 2005 Pleiades Publishing, Inc.

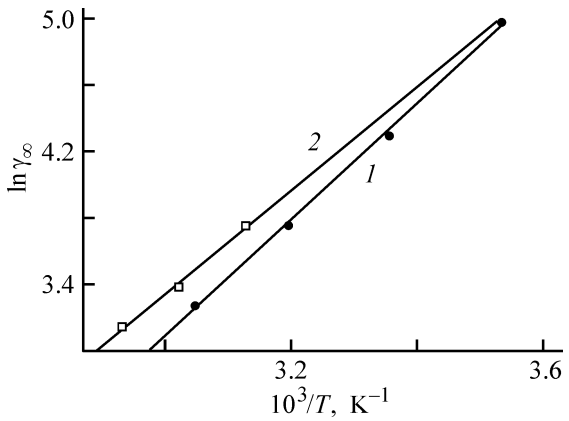


Fig. 1. Comparison of the limiting activity coefficients of phenol, γ^∞, in cyclohexane determined in (*1*) this study and (*2*) in [14]. (*T*) Temperature; the same for Fig. 2.

ural logarithm of γ_{aq}^∞ on the reciprocal temperature was linearly approximated with a straight line for all the available published data falling within a 5% range of deviations from the approximating line. The molar distribution coefficient (according to [9]) was recalculated to K_x by the formula:

$$K_x^\infty = K_c \frac{\rho_{org}}{\rho_{aq}} \frac{M_{org}}{M_{aq}}, \quad (2)$$

where K_c is the distribution coefficient of phenol between the aqueous and organic phases in terms of molar concentration; ρ_{aq} and ρ_{org}, densities of aqueous and organic phases, respectively; and M_{aq} and M_{org}, molecular weights of water and organic solvent, respectively.

As the organic substances used here are to a certain extent mutually soluble and the density of a liquid layer somewhat differs from that of a pure solvent, the layer densities were determined experimentally for each temperature studied. Since the ratio of densities of the liquid phases, rather than their absolute values, are necessary for calculation by formula (2), the Archimedean method of hydrostatic weighing is the optimal procedure for measurements.

We used an Ohaus Explorer electronic balance with an accuracy of 0.1 mg, a 50-ml glass cell thermostated with a Julabo F-32 thermostat (Germany), and a probing glass ball suspended by a thin metallic wire from an arm attached to the balance pan. The ratio of changes in the probe mass with respect to its initial value G_0 in two different liquids is proportional to the ratio of densities of these liquids.

$$\frac{\rho_{org}}{\rho_{aq}} = \frac{G_0 - G_{aq}}{G_0 - G_{org}}.$$

This method can be employed to determine the density of an organic phase that is in equilibrium with an aqueous phase at a given temperature, using pure water, whose density is known in a wide temperature interval, to calibrate the probe. In our study, the densities of organic phases were determined by this method with an accuracy of ± 0.0004 g cm^{-3}. The data obtained were compared with the densities of pure solvents [16] and with those calculated for the temperatures studied by Francis and Cibulka equation [17, 18]. We used in measurements a specially prepared double-distilled water. The density of water was taken for calibration from a reference book [19].

It was found that the densities of the organic phases under study differ only slightly from those of the corresponding pure solvents. The deviations are ± 0.0007 g cm^{-3}, on the average, which is close to the experimental error of the method used. As the experimental error in determining K_c is considerably larger than that in measuring the solvent density, the densities of pure solvents can be also used in calculations for hydrocarbon–water systems by formula (2). In our study, the experimentally determined density ratios of two phases were used in calculations.

Thus, we studied the temperature dependences of the limiting activity coefficients of phenol in hydrocarbons in 10 binary systems at four temperatures. For seven of these, data were obtained for the first time. The limiting activity coefficients are listed in the table.

The error of the indirect method used is largely determined by the reliability of data obtained for the standard system. If it is assumed that the accuracy of determining the limiting activity coefficients for the standard system is about 5% and that for the distribution coefficient in the liquid–liquid system, 3–5%, we have a value of 8–12% for the accuracy of γ_{org}^∞ determination by the distribution method. Presumably, the application field of this method is limited to systems in which the limiting activity coefficients are on the same order of magnitude and the distribution coefficients fall within the range $0.01 < K_c < 100$.

The only data available for the limiting activity coefficients of phenol in organic solutions have been obtained by differential ebullioscopy for systems containing *n*-hexane, benzene, cyclohexane, and tetrachloromethane [14]. However, the measurement error was large because of the low relative volatility of components, as also noted by the authors themselves. The limiting activity coefficients of phenol in cyclohexane are shown in Fig. 1 in comparison with those

determined by ebullioscopy in [14]. The discrepancy is 10–15% for this system and somewhat larger for other systems studied.

The dependence of the logarithm of the limiting activity coefficient of phenol in alkanes on the reciprocal temperature is shown in Fig. 2a, and that in aromatic hydrocarbons, in Figs. 2b and 2c.

It can be seen that the values for alkanes differ only slightly and become somewhat closer at higher temperatures. These systems exhibit a strong positive deviation from Raoult's law, especially pronounced at about 10°C (where the activity coefficient exceeds 100), which is responsible for the stratification of these solutions at medium concentrations. By contrast, deviations from ideality for phenol in arenes are smaller and the limiting activity coefficients do not exceed 20. Therefore, phenols exhibit, as a rule, a better solubility in aromatic hydrocarbons and are easily extracted with these compounds from aqueous solutions. Data for *m*- and *p*-xylenes virtually coincide within the experimental error.

The method for determining the limiting activity coefficients, considered in this study, can be used when direct methods are technologically difficult or fail to give satisfactory results. For systems with a low relative volatility of the constituent components, the present method is the optimal.

Using the limiting activity coefficients of phenol, we calculated by Eq. (3) the limiting coefficients of phenol distribution K_2^∞ for the liquid–vapor equilibrium at four temperatures (here and hereinafter, subscripts 1 and 2 refer to the solvent and solute, respectively).

$$K_2^\infty = \lim_{c_2 \to 0} \frac{c_2^{\text{liq}}}{c_2^{\text{vap}}} = \frac{RT\rho_1^{\text{org}}}{\gamma_2^\infty p_2^0 M_1^{\text{org}}}, \qquad (3)$$

where R is the universal gas constant, equal to 8.315 J K mol^{-1}; ρ_1^{org} and M_1^{org}, density (g cm^{-3}) and molecular weight (g mol^{-1}) of organic solvent, respectively; p_2^0, vapor pressure of pure phenol (MPa) at T (K); p_2^0 was calculated by Antoine's equation [20].

The values of K_2^∞, calculated by Eq. (3), are listed in the table. The solvation functions can be calculated from the temperature dependence of the distribution coefficient of a dissolved component between the liquid and vapor phases.

Solvation involves the whole set of energetic and structural changes in that occur in the system in the course of the vapor–liquid phase transformation to give a homogeneous solution of certain chemical composition and structure.

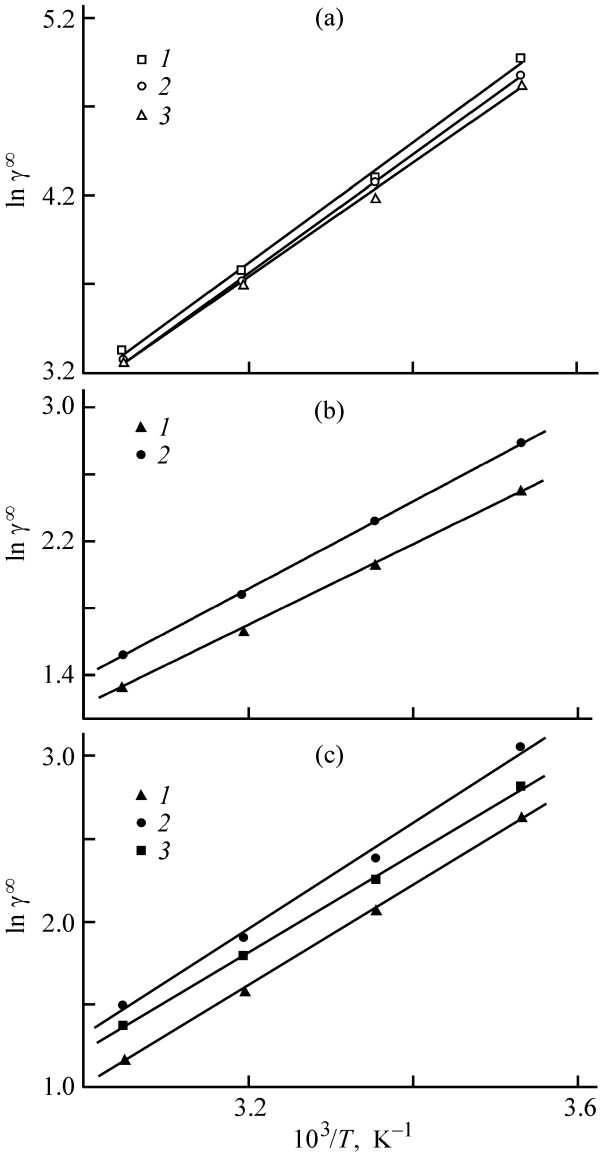


Fig. 2. Limiting activity coefficients of phenol, γ^∞, in (a) alkanes and (b, c) aromatic hydrocarbons. (a) (*1*) hexane, (*2*) heptane, and (*3*) octane; (b) (*1*) benzene and (*2*) toluene; (c) (*1*) benzene, (*2*) ethyl benzene, and (*3*) *para*- and *meta*-xylene.

The energetic changes that occur in solvation are largely determined by the enthalpy characteristics of solvation, and the structural changes, by its entropy characteristics. Both kinds of changes reflect the total changes in the Gibbs energy in the course of solvation and are determined by the chemical structure of a solution.

The quantity $\Delta G_{\text{sol}} = -RT\ln K_2^\infty$ is equal to the difference of the chemical potentials of phenol in solu-

Limiting activity coefficients, distribution coefficients, and solvation functions for phenol in organic solvents at various temperatures

Solvent	T, °C	γ_2^∞	K_2^∞	ΔG_{sol}, kJ mol^{-1}	ΔH_{sol}, kJ mol^{-1}	ΔS_{sol}, J mol^{-1} K^{-1}
Cyclohexane	10	147	10 700	–21.8	–29.7	–27.6
	25	74	5800	–21.5		
	40	43	3200	–21.0		
	55	27	1900	–20.6		
n-Hexane	10	146	8900	–21.4	–30.6	–32.6
	25	74	4700	–21.0		
	40	44	2600	–20.5		
	55	28	1500	–19.9		
n-Heptane	10	132	8800	–21.4	–31.2	–34.9
	25	72	4400	–20.8		
	40	41	2500	–20.3		
	55	26	1400	–19.3		
n-Octane	10	128	8100	–21.2	–32.0	–38.0
	25	66	4300	–20.7		
	40	40	2200	–20.1		
	55	26	1300	–19.5		
Benzene	10	12.2	155 000	–28.1	–38.8	–37.8
	25	7.9	66 000	–27.5		
	40	5.3	32 000	–27.0		
	55	3.8	16 000	–26.4		
Toluene	10	16.1	98 000	–27.1	–37.1	–35.4
	25	10.1	43 000	–26.4		
	40	6.6	21 000	–26.0		
	55	4.5	11 000	–25.5		
ortho-Xylene	10	12.6	110 000	–27.3	–39.2	–41.9
	25	8.1	47 000	–26.7		
	40	5.6	22 000	–26.0		
	55	4.0	11 000	–25.5		
para-Xylene	10	14.1	97 000	–27.0	–39.2	–42.9
	25	9.0	41 000	–26.3		
	40	6.3	19 000	–25.7		
	55	4.5	9900	–25.1		
meta-Xylene	10	–	–	–	–40.5	–47.2
	25	8.8	42 000	–26.4		
	40	6.2	19 000	–25.7		
	55	–	–	–		
Ethyl benzene	10	17.2	80 000	–26.6	–37.5	–38.4
	25	10.0	38 000	–26.1		
	40	6.8	18 000	–25.5		
	55	5.0	9100	–24.9		

tion and in the form of an ideal gas at equal bulk concentrations. This quantity is the contribution of intermolecular interactions to the chemical potential of phenol in a given solvent and a quantitative characteristic of the Gibbs energy of a dissolved substance in a given solvent.

As known from the literature, the free energy of solvation is frequently defined as $-RT\ln K_H$, where K_H is Henry's constant:

$$K_H = \lim \frac{p_2}{x_2^{liq}} = p_2^0\gamma_2^\infty = \frac{K_2^\infty M_1^{org}}{RT\rho_1^{org}}.$$

The enthalpy of solvation can be found from the temperature dependence of the distribution coefficient

$$\Delta H_{\text{solv}} = R\frac{\partial \ln K_2}{\partial(1/T)}.$$

The entropy of solvation was calculated by the relation:

$$\Delta S_{\text{solv}} = \frac{\Delta H_{\text{solv}} - \Delta G_{\text{solv}}}{T}.$$

The calculated thermodynamic characteristics of the solvation are listed in the table.

CONCLUSION

The limiting activity coefficients of phenol in cyclohexane, *n*-hexane, *n*-heptane, *n*-octane, benzene, toluene, ethyl benzene, and *ortho*-, *meta*- and *para*-xylene at 10, 25, 40, and 55°C were determined with an accuracy acceptable for an indirect method. The results obtained are in a satisfactory agreement with the scarce published data. The distribution coefficients of phenol between the liquid and vapor phases were calculated, and the solvation functions at infinite dilution were evaluated.

ACKNOWLEDGEMENTS

The authors thank N.A. Smirnova for helpful discussions.

The study was financially supported by the Federal Program for Leading Research Schools (project NSh-676.2003.3) and by the Russian Foundation for Basic Research (project 02-03-32 709).

REFERENCES

1. Pividal, K.A., Sandler, St., and Orbey, H., *Fluid Phase Equilibria*, 1992, vol. 72, pp. 227–250.
2. Kikic, I., Alessi, P., and Fermeglia, M., *Fluid Phase Equilibria*, 1983, vol. 14, pp. 363–372.
3. Prausnitz, J., Andersen, T., Grens, E., *et al.*, *Computer Calculation for Multicomponent Vapor-Liquid and Liquid–Liquid Equilibria*, New Jersey: Prentice-Hall, 1980.
4. Schreiber, L.B., and Eckert, C.A., *Ind. Eng. Chem. Process. Des. Dev.*, 1971, vol. 10, pp 572–576.
5. Nicolaides, G.L., and Eckert, C.A., *Ind. Eng. Chem. Fundam.*, 1978, vol. 17, pp. 331–340.
6. Bastos, J.C., Soares, M.E., and Medina, A.G., *Ind. End. Chem. Res.*, 1988, vol. 2, pp. 1269–1277.
7. Gmehling, J., Menke, J., and Schiller, M., *Activity Coefficients at Infinite Dilution. Dechema Data Series*, Frankfurt/Main: Dechema, 1994, vol. 9, part 3.
8. Morachevskii, A.G., Smirnova, N.A., Balashova, I.M., and Pukinskii, I.B., *Termodinamika rasplavlennykh rastvorov neelektrolitov* (Thermodynamics of Molten Solutions of Non-Electrolytes), Leningrad: Khimiya, 1982.
9. Dobryakova I.E., and Dobryakov, Yu.G., *Zh. Prikl. Khim.*, 2004, vol. 77, no. 11, pp. 1768–1771.
10. Sherman, S.R., Trampe, D.B., Bush, D.M., *et al.*, *Ind. Eng. Chem. Res.*, 1996, vol. 35, pp. 1044–1058.
11. Aarna, A.Ya., Melder, L.I., and Ebber, A.V., *Zh. Prikl. Khim.*, 1979, vol. 52, no. 7, pp. 1640–1642.
12. Moore, R.C., Jonah, D., Cohran, H.D., *et al.*, *Sep. Sci. Technol.*, 1995, vol. 30, pp. 1981–1996.
13. Tabai, S., Rogalski, M., Solimando, R., and Malanowski, S.K., *J. Chem. Eng. Data*, 1997, vol. 42, pp. 1147–1150.
14. Dobrjakov, Y.G., Balashova, I.M., and Maurer, G., *Fluid Phase Equilibria*, 2001, vol. 181, pp. 59–70.
15. Dohnal, V., and Fenclova, D., *J. Chem. Eng. Data*, 1995, vol. 40, pp. 478–483.
16. Weissberger, A., Proskauer, E.S., Riddick, J.A., and Toops, E.E., *Organic Solvents*, New York: Interscience, 1955.
17. Smith, B.D., and Srivastava, R., *Thermodynamic Data for Pure Compounds. Phys. Sciences Data 25*, Amsterdam: Elsevier, 1986, parts A + B.
18. Cibulka, I., *Fluid Phase Equilibria*, 1993, vol. 89, pp. 1–18.
19. *Spravochnik khimika* (Chemist's Handbook), Nikol'skii, B.P., Ed., Moscow: Goskhimizdat, 1962, part 2.
20. Stephenson, R.M., and Malanowski, S., *Handbook of the Thermodynamics of Organic Compounds*, New York: Elsevier, 1987.

Russian Journal of Applied Chemistry, Vol. 78, No. 2, 2005, pp. 212–216. Translated from Zhurnal Prikladnoi Khimii, Vol. 78, No. 2, 2005, pp. 219–223.
Original Russian Text Copyright © 2005 by Bibik.

PHYSICOCHEMICAL STUDIES OF SYSTEMS AND PROCESSES

Rheological Equations for Concentrated Suspensions

E. E. Bibik

St. Petersburg State Technological Institute, St. Petersburg, Russia

Received February 13, 2004

Abstract—The dependence of viscosity on stress in stable concentrated suspension is studied, the physical meaning of rheological constants in the rheological equation for these suspensions is revealed, and a method for experimental determination of these constants is described.

Concentrated suspensions (CS) are the most important element of the technology of manufacture of ceramic articles for various purposes, from large electric insulators and abrasive wheels to minute components of electronic devices. The quality and manufacturability of articles are largely determined by properties of suspensions from which these articles are formed. These are primarily the rheological properties, which characterize the ability of a suspension to be deformed, i.e., to acquire and retain the required shape of the article to be obtained. The rheological properties of a suspension, as also those of any other material, are described by rheological laws: dependence of the rate of deformation of a material, $\dot{\gamma}$, on the amount of stresses τ existing in the material. As a rule, these laws are not universal, being only applicable to materials (suspensions) with a certain prescribed structure.

It is known that the maximum concentration of a dispersed material can be only reached in well-stabilized suspensions [1]. In suspensions of this kind, the interaction between particles of the dispersed material is characterized by predominance of repulsion forces. Therefore, neighboring particles of the suspension lie at the maximum possible distance from one another. At identical sizes and regular shapes of particles, this leads to their fixation at sites of a regular crystal-like lattice. Such a structure has been named "periodic colloid structure" (PCS [2]) or quasi-crystalline structure. In the extent of spatial filling by the particles, such suspensions are similar to liquids and solids, and, therefore, the concepts of the activation mechanism of molecular motion [3] and deformation in these bodies were extended to these objects. The activation mechanism of flow was quantitatively expressed as Eyring's rheological law [4]

$$\dot{\gamma} = f_0 \sinh z, \quad (1)$$

where $\dot{\gamma}$ is the rate of shear deformation, and f_0 is a characteristic parameter having the meaning of the frequency of thermal oscillations of a particle at a lattice site.

Under the action of shear stresses τ, the amplitude of a certain part, $\sinh z$, of these oscillations reaches a value equal to the distance between neighboring stable positions of a particle, and, therefore, the particle jumps at a frequency $f = f_0 \sinh z$ in the direction of the force it experiences. The parameter $z = \tau/nkT$ is a dimensionless acting stress (stress related to the volume density nkT of the kinetic energy of particles); n, the concentration of particles; k, the Boltzmann constant; and T, temperature. At $z << 1$, $\sinh z = z$. Then, $\dot{\gamma} = f_0 \tau/nkT$ and, according to Newton's law of internal friction,

$$\tau = \eta\dot{\gamma}. \quad (2)$$

The viscosity of the suspension, $\eta = \tau/\dot{\gamma}$, is given by

$$\eta_0 = nkT/f_0. \quad (3)$$

The subscript "0" on the viscosity indicates that it characterizes the behavior of the liquid only at low stresses. For ordinary liquids, any stress of interest is low because of the high value of nkT. Therefore, the viscosity remains constant and equal to η_0 as the stress increases (i.e., the liquid is Newtonian).

1070-4272/05/7802-0212 © 2005 Pleiades Publishing, Inc.

The situation in suspensions is the opposite (even in those highly dispersed and concentrated, in which the number of particles in unit volume may be as large as 10^{18} m^{-3}). This means that, according to expression (1), the deformation rate will progressively grow with increasing stress, and the viscosity will accordingly decrease. Such a dependence of the deformation rate and viscosity on stress is qualitatively characterized as thixotropic.

The practical experience shows that a dilatant dependence of the shear rate on stress is more characteristic of stable concentrated suspensions. In this case, the increment in the shear rate lags behind that in the stress, and the more so, the higher the stress. At high stresses, the shear rate asymptotically approaches a constant value (limiting shear rate), and the viscosity, accordingly, tends to infinity.

The impossibility of shear deformation of a system of densely packed particles without an increase in the volume occupied by them has been regarded as the reason for the dilatant behavior. Such an explanation has become commonly accepted [5] and was fixed in the name of the phenomenon of "dilatancy," which consists in a disproportionately strong rise in resistance upon a minor increase in the deformation rate. It can be readily seen that the activation and dilatation models of deformation lead to fundamentally different laws of rheological behavior, even though these models refer to one and the same structural model of a material being deformed.

It was shown in [1] that the controversy between these two concepts is eliminated if the flow of these systems is adequately described quantitatively in terms of the Frenkel–Eyring activation mechanism. The changes that should be made in the classical theory are as follows.

(1) The shear rate is to be calculated by the formula

$$\dot{\gamma} = (c/n) fs/d \qquad (4)$$

instead of its classical variant $\dot{\gamma} = fs/d$. Here, c is the concentration of vacant sites in the CS lattice; s, the length of a single jump of a particle, equal to the distance s between CS lattice sites; d, the distance between a jumping particle and the nearest layer of immobile particles. It can be taken that d is also equal to the lattice constant s. Then the classical theory gives $\dot{\gamma} = f$, and its modernized variant,

$$\dot{\gamma} = (c/n) f, \qquad (5)$$

where $f = f_0 \sinh z$.

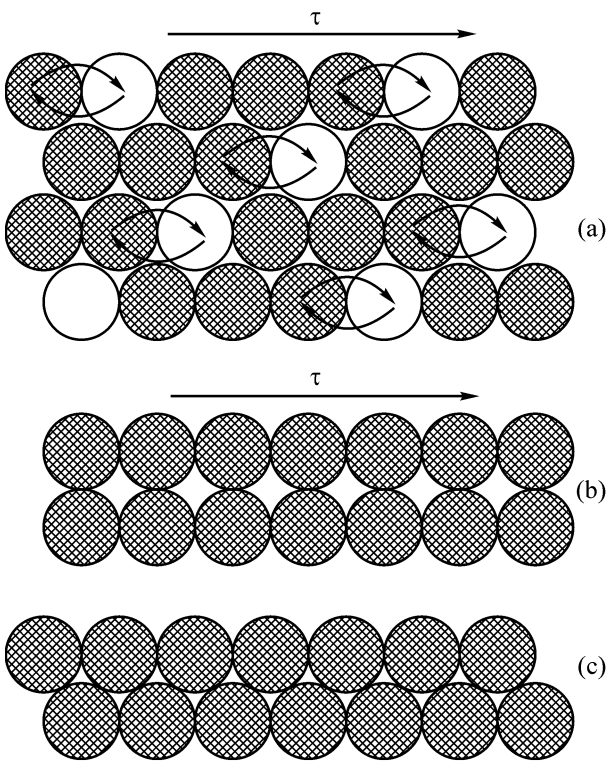


Fig. 1. Schematic of particle motion under the action of shear stress. (a) In the case of the activation mechanism, a group of three particles moves to a distance equal to a single lattice constant after all of them, by turns, move to this distance. In the case of a dilatation mechanism, stress cause a shift of all particles of a layer with respect to the neighboring one and leads to a change of particle packing from (c) denser to (b) looser one.

The physical substantiation of this modernization consists in that, to find the shear rate, i.e., the ratio between the motion velocity of a layer of particles and the distance from the mobile to immobile layer (or, more precisely, to the layer taken to be immobile), it is necessary, at least, to calculate this velocity. At the same time, the classical variant of the theory actually uses, instead of the layer motion velocity, the velocity of a local motion of a particle to a neighboring site. Apparently, for the whole layer of particles to be displaced to a distance s, equal to the lattice constant, all particles of this layer are to jump to the same distance in the necessary direction. This will require a time longer by a factor equal to the number of particles in a layer. In a defect-free lattice, the number of particles in a layer (or, more precisely, in a group of particles extended along the direction of motion) can be considered infinite, or, even if finite, then dependent on the geometry of the deforming device.

The situation changes if account is taken of the known fact, the imperfectness of real lattices, and its quantitative characteristic, concentration c of vacant lattice sites, is introduced. In this case, the length of the group of particles, which can move under the action of the deforming force, is determined by the number of particles along the line of their motion from one vacancy to another (Fig. 1a). The number of particles in such a group is n/c, and just this number appears in the correct formula for calculating the shear rate. In a defect-free lattice ($c = 0$), flow by the activation mechanism becomes impossible, but the deformation can be formed by the dilatation mechanism (Figs. 1b, 1c). The difference between these two cases is fundamental. In the first case, application of a stress results in that particles move by turns and, accordingly, the activation energy of flow is equal to the energy of displacement of a single particle, with the increase in the volume of the system being virtually zero. In the second case, only a simultaneous displacement of all the particles of a layer is possible, associated with a shear deformation of the lattice (change in the particle arrangement from the scheme in Fig. 1c to that in Fig. 1b), i.e., with a change of its crystallographic type and increase in its volume and energy. In this case, the activation energy of flow is orders of magnitude higher than that for the activation mechanism, and the resistance to deformation strongly depends on the opportunity to increase in volume, furnished by the experimental conditions. This means that, in the case of a purely dilatation mechanism of deformation, the rheological constants of suspensions depend on the geometrical conditions of the experiment, rather than being an invariant characteristic of a suspension.

(2) A defective structure can be regarded as a kind of an inhomogeneous mixture of two components: particles of the dispersed phase and voids. Deformation affects this mixture in the same way is it does for any inhomogeneous system: makes it more homogeneous. It is for this purpose that various kinds of suspensions are agitated. The higher the deformation rate, the more uniform the distribution of the components of the system (in the given case, spatial regions unoccupied by particles) over its volume. This circumstance is quantitatively manifested in a decrease in the concentration of vacancies and, in accordance with formula (4), in a decrease in the deformation rate. It is noteworthy that, at a concentration of vacancies comparable with that of particles, transition to their uniform distribution would actually lead to disintegration of the coagulation structure and to a decrease in the activation energy of flow to zero. In what follows, it is assumed that the concentration of vacancies is sufficiently low and their spreading over the interstitial spaces in the lattice has no effect on the activation energy of flow.

The dependence of the concentration of vacancies on the deformation rate can be obtained by introducing a formal parameter ϑ, relaxation time of vacancies, so that the rate of their generation will be $(c_0 - c)/\vartheta$, where c_0 is the initial concentration of vacancies. The parameter c_0 can be evaluated by the difference between the limiting theoretical concentration of particles, corresponding to a certain structural model, and the actual (prescribed) concentration of particles in the system. At the same time, vacancies disappear upon deformation. Each jump of a vacancy into a new position means that it disappears for a certain time, and, therefore, the disappearance rate of vacancies coincides with the number of their jumps, cf, in a unit volume of the dispersed system in unit time. In the steady state, the rates of generation and disappearance are equal, which gives

$$c = c_0/(1 + f\vartheta). \quad (6)$$

Combined with Eq. (5), this expression gives a new rheological law of shear deformation:

$$\dot{\gamma} = \left(\frac{c_0}{n}\right)\frac{f_0 \sinh z}{1 + \vartheta f_0 \sinh z}. \quad (7)$$

This expression contains two undetermined constants, f_0 and ϑ. They can be found using some model of particle motion over lattice sites [1]. However, more reliable in practical calculations are constants that can be determined experimentally. Therefore, it is desirable to transform the dependence (7) so that it would contain experimentally determinable rheological constants. One of these latter is the product ϑf_0, which is conveniently dimensionless and has a simple physical meaning: this is the ratio of the relaxation time of a vacancy to the period of particle oscillations in the lattice. In what follows, it is named the relaxation parameter and denoted by a symbol θ. For introducing the other rheological constant, it is convenient to represent expression (7) as a dependence of the viscosity on stress:

$$\eta = \left(\frac{n}{c_0 f_0}\right)\left[\frac{1}{\sinh z} + \theta\right]\tau. \quad (8)$$

If this expression is simplified for the case of low stresses, the combination $n^2kT/c_0 f_0$ of a number of quantities, to which the whole right-hand part of (8) is reduced, has the meaning of viscosity of a dispersed system at the minimum stress (initial viscosity η_0).

Hence follows the method of experimental determination of this constant. Further, it is denoted by the same symbol η_0 as the initial viscosity in the classical theory. However, it should be remembered that the latter is understated by a factor of n/c_0. With the new rheological constants introduced, dependence (8) takes the form

$$\eta = \eta_0\left[\frac{1}{\sinh z} + \theta\right]z. \qquad (8a)$$

Thus, to find out how the viscosity changes as the stress becomes higher, it suffices to analyze the expression

$$F = \left[\frac{1}{\sinh z} + \theta\right]z. \qquad (9)$$

which contains only a single unknown rheological constant θ. This expression gives the relative viscosity $F = \eta/\eta_0$ as a function of the dimensionless stress. The dependence is shown in Fig. 2 at different values of the relaxation parameter θ.

At $\theta = 0$, the dependence shows a steady decrease in viscosity as the stress increases, in conformity with the classical theory. At $\theta \geq 0.32$, the system exhibits a dilatant type of the dependence of viscosity on stress over the entire range of stresses and a more or less pronounced inflection at dimensionless stresses $z \leq 2$. At $0 < \theta < 0.32$, the dependence is of a mixed dilatant-thixotropic type. In a narrow range of low stresses ($z < 1$), the viscosity grows as the stress becomes higher. Then follows the range of medium stresses, in which the viscosity decreases. Finally, at sufficiently high stresses, it again starts to increase. Accordingly, the rheological viscosity–stress curves show a minimum and a maximum. The difference between their coordinates along both axes grows as the relaxation parameter θ decreases. Its value of 0.32 is critical: the maximum and minimum merge to give an inflection point, with the curve running horizontally in its vicinity. At $\theta > 0.32$, the inflection is preserved, but becomes less pronounced and the viscosity grows with increasing stress in the vicinity of the inflection.

The asymptotic dependence of F on z is described at large z by the equation

$$F = \theta z. \qquad (10)$$

Hence follows that the relaxation parameter θ is found experimentally as the slope of the asymptotic straight line, the ray running from the origin of coordinates and passing very close to the right-hand branch of the plot, but not intersecting it, even with account of its extrapolation to infinity.

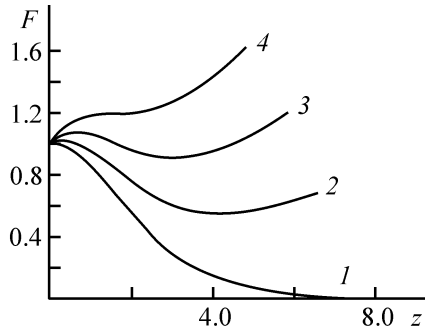


Fig. 2. Relative viscosity F vs. dimensionless stress z at different values of the relaxation parameter θ. θ: (*1*) 0, (*2*) 0.1, (*3*) 0.2, and (*4*) 0.32.

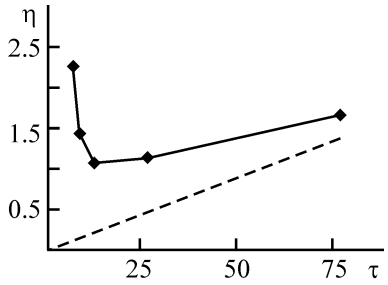


Fig. 3. Viscosity η of alundum suspended in a 0.5 wt % solution of starch vs. stress τ. Composition of suspension (wt %): Al_2O_3 60, liquid phase 30, components of binder the rest. *Dashed line*: asymptotic dependence at $\eta/\tau = 0.018$.

Because of the limited capabilities of instruments, experiments commonly cover only a certain relatively narrow range of stresses, so that it is only possible to observe a part of the full rheological curves in Fig. 2. Figure 3 shows as an example the results of measurements carried out with a suspension of alundum (Al_2O_3) on an RPM 1 rotation viscometer.

Noteworthy in the first place is the absence of the initial portion in the plot, which means that it is impossible to find the initial viscosity η_0 and then pass to its dimensionless value F. However, the asymptotics of the dependence of viscosity on stress remains the same:

$$\eta = (n/c_0)\vartheta\tau. \qquad (11)$$

This expression follows directly from Eq. (8) at $z >> 1$. The slope of the asymptotic straight line is 0.018 in the given case. The meaning of this value is clear from Eq. (11). The formulation of the suspension gives, to a certain extent conventionally, the ratio n/c_0. In the given case, this ratio was, probably, equal

to several dimensionless units, which gives a relaxation time of vacancies, ϑ, (time in which their number is restored by approximately 30% after total disappearance) of about 0.01 s.

Similar rheological properties were observed for other suspensions (based on silicon carbide and silicon carbide mixed with alundum) used to fabricate abrasive tools by slip casting.[1] The dispersed phase of these suspensions contained, in addition to Al_2O_3 and SiC, up to 10 wt % highly dispersed components intended for formation of a ceramic binder in calcination of half-finished articles.

A large body of dependences of this kind has been obtained by Pivinskii [6] on suspensions intended for fabrication of ceramic, refractory, and building articles. It is this abundance of experimental data that stimulated a study of the rheology of concentrated suspensions. It should be noted that the rheological law (7) itself was derived theoretically more than 20 years ago [1]. However, there was no representative experimental database at that time, which made impossible any conclusion about the typical nature of the thixotropic-dilatant flow or about the range and field of applicability of this law. It is clear now that curves with a minimum viscosity are typical of concentrated, aggregatively stable suspensions, which are widely used in technology. Moreover, the practical experience and prerequisites for derivation of this law suggest that the presence of a minimum is a criterion for a high quality of a suspension.

[1] Formulations developed with participation of E.A. Popova.

CONCLUSION

Experimental data for thixotropic-dilatant suspensions conform to the rheological pattern that is based on the activation mechanism of flow of a suspension with a crystal-like structure and takes into account the role of vacant sites in the lattice. The dependence of the viscosity of such suspensions on the shear stress is determined by two rheological constants: their initial viscosity and relaxation parameter. It is shown how these constants and the basic structural characteristic of the suspension, fraction of vacant sites in the lattice, can be found from experimental data.

REFERENCES

1. Bibik, E.E., *Reologiya dispersnykh sistem* (Rheology of Dispersed Systems), Leningrad: Len. Gos. Univ., 1981.
2. Efremov, I.F., *Periodicheskie kolloidnye struktury* (Periodic Colloid Structures), Leningrad: Khimiya, 1971.
3. Frenkel, Ya.I., *Sobranie izbrannykh trudov* (Coll. of Selected Works), Moscow: Akad. Nauk SSSR, 1958, vol. 2.
4. Vinogradov, G.V. and Malkin, A.Ya., *Reologiya polimerov* (Rheology of Polymers), Moscow: Khimiya, 1977.
5. *Colloid Science*, Kruyt, H.R., Ed., Amsterdam: Elsevier, 1952.
6. Pivinskii, Yu.E., *Keramicheskie vyazhushchie i keramobetony* (Ceramic Binders and Ceramic Concrete), Moscow: Metallurgiya, 1990.

Russian Journal of Applied Chemistry, Vol. 78, No. 2, 2005, pp. 217–221. Translated from Zhurnal Prikladnoi Khimii, Vol. 78, No. 2, 2005, pp. 224–228.
Original Russian Text Copyright © 2005 by Bibik.

PHYSICOCHEMICAL STUDIES OF SYSTEMS AND PROCESSES

Electrokinetic Potential of Particles in Suspensions and Donnan Equilibrium in a Thin Gel Film

E. E. Bibik

St. Petersburg State Technological Institute, St. Petersburg, Russia

Received February 13, 2004

Abstract—The influence exerted by the thickness of a gel layer on the difference of the electric potentials of phases and on the distribution of the potential near the phase boundary are considered in terms of the classical theory of the Donnan equilibrium in a two-phase system constituted by a gel and an electrolyte solution. The results obtained make it possible to explain a number of experimental facts.

The electrokinetic potential of the surface is the only electrical characteristic of a dispersed system that can be directly determined experimentally, irrespective of the aggregative state, chemical nature of particles, and topological features (structure) of dispersed systems. This predetermines the exceedingly important role of this potential as a guiding line in choosing and adjusting the ionic composition of the dispersion medium for industrially used dispersed systems: slurries for fabrication of ceramic articles, clayey solutions for well drilling, suspensions for hydroclassification and flotation dressing of minerals, etc. Some methods for medical diagnostics are also based on phenomena directly related to the electrokinetic potential of cell membranes in a living organism. The information obtained by measuring the electrokinetic potential can be used correctly only if the mechanism of the influence exerted by various factors on the potential is known. Below, some aspects of this mechanism are considered.

The surface of real solids differs from its representation as a smooth surface, which is frequently used in describing theoretically properties of solids and phenomena occurring on the surface of solids. This also refers to electrochemical properties of the surface, among which of fundamental importance are the equilibrium surface potential, thickness of the electric double layer (EDL), its capacitance (or surface charge), and electrokinetic potential. A number of experimental results cannot be explained in terms of the double-layer theory for smooth surfaces. To these results belong the following: an increase in the electrokinetic potential, observed in some electrochemical systems when the concentration of an indifferent electrolyte is raised at low concentrations [1]; an exceedingly high adsorption capacity of the EDL [2]; manifestations of liophility in typical liophobic colloids [3]; etc. Various reasons for such anomalies have been named, including the presence of a thin gel film or a porous layer of the substance itself on the surface of a solid.

Theories of the electric double layer on an uneven surface (rough, porous, covered with a gel layer) have been developed [4, 5]. However, these theories have not been brought to a level that enables a comparison of theoretical and experimental results related to the anomalies mentioned above. Most frequently, this is due to the fact that the formulation of the problem is a complicated task. Meanwhile, many features of uneven surfaces can be revealed without using the EDL theory. This can be done in terms of the Donnan equilibrium, which determines the difference between the electric potentials and ionic compositions of two phases, one of which is inaccessible to charge carriers of a certain type. This may be a gel whose structural units (colloid particles, polyelectrolyte molecules) can only be present in the gel phase.

The Donnan theory is based, as it is commonly emphasized in its presentation [1], on the concept of ideal electrolyte solutions. Therefore, we further represent phases 1 and 2 in a two-phase system as follows: phase 1, as a gel, a swollen, weakly dissociated, ionogenic polymer of the CP type; and phase 2, as a dilute solution of an ordinary CA electrolyte. Here, C stands for the cation common to the electrolyte and the gel; A is anion, and P, polyanion (or a negatively

1070-4272/05/7802-0217 © 2005 Pleiades Publishing, Inc.

charged colloid particle). The dilution is meant to be a way to make the solution ideal.

As the basic parameters describing the state of the two-phase system, we chose the concentration P of ionogenic groups in the gel (in equivalents) and the concentration A_1 of co-ion A in the gel. In the initial state, immediately after the two phases are brought in contact, the concentration A_1 is zero, and the concentration A_2 in phase 2 is equal to the initial concentration c_0 of the CA electrolyte in this phase. The concentration of the polyion remains unchanged and not equal to zero only in phase 1.

After the two phase are brought in contact, co-ion A starts to diffuse from phase 2 (solution) into phase 1 (gel), where it was absent originally. This gives rise to a potential difference Ψ_f associated with the fact that ions of only one sign pass from one phase into the other. Naturally, this also leads to transfer of counterions C in the same direction and in the same amount, so that both phases remain electrically neutral

$$C_2 = A_2, \quad C_1 = P + A_1, \tag{1}$$

where C_1 and C_2 are the concentrations of the common ion C in the first and second phases, respectively.

To these equations should be added the material balance equation for the co-ion. At equal volumes of the phases

$$c_0 = A_1 + A_2. \tag{2}$$

In the state of equilibrium, the difference between the ion concentrations in the two phases is maintained by the difference Ψ_f between the electric potentials of the phases and by the corresponding term $z_i F \Psi_f$ for the chemical potential of the ions, where z_i is the valence of ions of ith type. It is convenient to reckon the electric potentials from the potential of phase 2, which is, consequently, taken to be zero. From the equality of the chemical potentials in the phases brought in contact (at $z_1 = 1$) follows that [1]:

$$\begin{aligned} \Psi_f F + RT\ln(C_1/C_2) &= 0 \text{ for cations,} \\ -\Psi_f F + RT\ln(A_1/A_2) &= 0 \text{ for anions.} \end{aligned} \tag{3}$$

Summing up these expressions, we obtain that $\ln(C_1A_1/C_2A_2) = 0$ or

$$C_1A_1 = C_2A_2. \tag{4}$$

which gives, after substituting (1) and (2) and making some rearrangements

$$A_1 = c_0^2/(2c_0 + P). \tag{5}$$

Then, the concentrations of other ions in both phases can be readily calculated. It should be noted that A_1 is far from being small. Roughly speaking, near half of the electrolyte passes from phase 2 into phase 1 (exactly the half at equal volumes of the phases and $P = 0$, which goes without saying). The same refers to the counterion.

The Donnan potential Ψ_f is related in the standard way to the concentrations of the common ions in phases 1 and 2 by expressions (3). Replacing in these expressions the concentrations of ions (at $z = 1$) with the concentration of the electrolyte in the solution phase and that of ionogenic units in the gel phase with the use of formulas (2) and (5), we obtain

$$\Psi_f = -(RT/F)\ln(1 + P/c_0),$$

where c_0 is the initial concentration of the electrolyte in the solution phase. In equilibrium and equal volumes of the phases, $c_0 = A_1 + A_2$, and then

$$\Psi_f = -(RT/F)\ln[1 + P/(A_1 + A_2)]. \tag{6}$$

At small P/c_0, the concentrations of anions, A_1 and A_2, in both phases are approximately the same. In turn, A_2 is equal to the equilibrium concentration c of the electrolyte in the solution phase, and, therefore, we have, approximately, $A_1 + A_2 = 2c$. Under the same conditions, $\ln[1 + P/2c] \approx P/2c$ and then

$$\Psi_f \sim -PRT/2cF. \tag{7}$$

If the ratio between the volumes V_1 and V_2 of the solution and gel phases, respectively, is arbitrary, the only changes in the system of equations (1)–(4) are those in the material balance equation (2):

$$c_0V_2 = A_1V_1 + A_2V_2 \tag{8}$$

and in the expressions for the concentrations of ions in the solution phase, $A_2 = c_0 - rA_1$ and $C_2 = c_0 - rA_1$, where $r = V_1/V_2$. Their substitution in the equilibrium equation (4) yields the following algebraic equation

$$A_1^2(1 - r^2) + (2rc_0 + P)A_1 - c_0^2 = 0. \tag{9}$$

At $r \neq 1$, this equation gives

$$\begin{aligned} A_1 = &-(2rc_0 + P)/2(1 - r^2) \\ &+ \{[(2rc_0 + P)/2(1 - r^2)]^2 + c_0^2/(1 - r^2)\}^{1/2}. \end{aligned} \tag{10}$$

If there is a gel-like phase in the form of thin films on the surface of particles of the dispersed phase present in the electrolyte solution, then, apparently, $r \to 0$. In this case, only a negligible fraction of the electrolyte passes into the film, so that its equilibrium concentration c in solution is virtually equal to the initial concentration c_0. Therefore,

$$A_1 = -P/2 + \{P^2/4 + c^2\}^{1/2}. \quad (11)$$

In this case, however, the relationship between the film thickness g and the thickness δ of the electric double layer in the film becomes rather important. Relation (11) makes sense only for thick films ($g >> \delta$). Anyway, it is expedient to determine the law by which the potential varies near the phase boundary between the gel and electrolyte solution. Finding this law requires that the Poisson–Boltzmann equation should be solved for the gel phase. In the gel, the positions of the ionogenic groups P are fixed at units of the chain of the cross-linked polymer and, therefore, remain unchanged when the potential varies:

$$(d^2\Psi/dx^2) = [PF + 2cF\sinh(F\Psi/RT)]/\varepsilon\varepsilon_0, \quad (12)$$

where c is the equilibrium concentration of the 1–1 electrolyte in solution.

The coordinate x is directed from the gel phase into the solution phase perpendicularly to the phase boundary; the zero x is at this boundary, i.e., $x < 0$ in the gel phase.

The expression in the square brackets is, apparently, the volume density of charge in the gel, taken with the opposite sign. It is zero in a thick gel layer, far away from the phase boundary, and the potential difference Ψ between two regions of the two phases, which are remote from the phase boundary, must be equal to the Donnan potential Ψ_f, which gives an alternative method for calculation of this potential:

$$\Psi_f = -(RT/F)\,\mathrm{Arcsinh}(P/2c), \quad (13)$$

which, naturally, coincides with the previously obtained result (7) at $P/2c < 1$.

A thin film of the gel ($g < \delta$), bounded by the solid phase, substrate (Fig. 1, shaded band), on one side and by the electrolyte solution on the other, is not electrically neutral. Under the conditions specified above, it has a distributed negative charge and acts as the inner part of the electric double layer with respect to the adjacent electrolyte solution. The charge of the film is neutralized by the opposite charge of the outer part of the EDL, the diffuse layer in the solution phase occupying in Fig. 1 the whole space at $x > 0$. From the equality to zero of the total charge of the film and the diffusion layer in solution follows, in accordance with Gauss law, that the field strength at the inner side of the film (on its boundary with the substrate) is zero, i.e., $d\Psi/dx = 0$ at $x = -g$. In this case, the potential has a certain, highest in magnitude, value Ψ_g (Fig. 1) and is equivalent to the interphase potential difference of the classical EDL. This potential is the main electrochemical characteristic of a two-phase system in the case when a gel film is present at the phase boundary. The potential at the outer side of the film (at $x = 0$) has a value Ψ_0. In accordance with the existing concepts of the nature of electrokinetic phenomena, Ψ_0 can be taken equal to the electrokinetic potential of the surface.

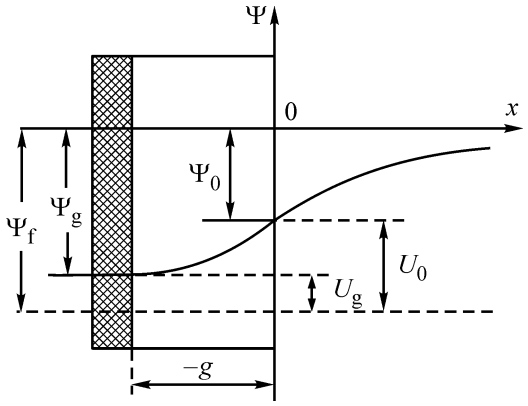


Fig. 1. Distribution of the potential Ψ at the interface between a gel film of thickness g with an electrolyte solution and characteristic potentials of this distribution.

At a low potential, $\sinh(F\Psi/RT) = F\Psi/RT$, which simplifies Eq. (12) and brings it to the form

$$(d^2\Psi/dx^2) = k^2(\Psi - \Psi_f). \quad (14)$$

Here, we take into account that $2cF^2/\varepsilon\varepsilon_0 RT = k^2$ and, according to expression (7), $PRT/2cF = -\Psi_f$. Integrating this equation, we obtain $(d\Psi/dx)^2 = k^2(\Psi - \Psi_f)^2 + C_1$. Using the above-mentioned conditions at the interface with the substrate ($d\Psi/dx = 0$ and $\Psi = \Psi_g$), we find the integration constant $C_1 = -k^2(\Psi_g - \Psi_f)^2$ and obtain a differential equation in the finished form:

$$(d\Psi/dx) = \pm k[(\Psi - \Psi_f)^2 - (\Psi_g - \Psi_f)^2]^{1/2}. \quad (15)$$

The outer boundary of the gel film is permeable, so that ions cannot be fixed there to create a surface charge, i.e., the dense part of the double layer, or cause other effects associated with the finite size of

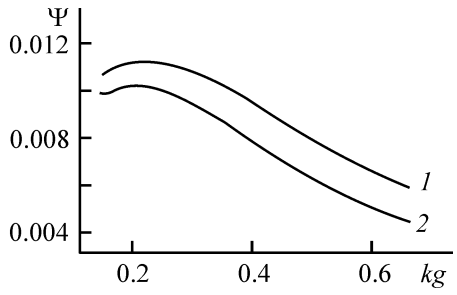


Fig. 2 Potentials Ψ_g and Ψ_0 of (*1*) inner and (*2*) outer sides of a gel layer of thickness $g = 2 \times 10^{-9}$ m at a concentration of ionogenic groups in the layer $P = 0.01$ kmol m^{-3} vs. the dimensionless layer thickness kg (at the electrolyte concentration increasing from 0.0005 to 0.01 kmol m^{-3}.

ions [6]. Therefore, the potential distribution in the solution phase is fully described by the classical Gouy–Chapman theory: $\Psi = \Psi_0 \exp(-kx)$. The potential distribution in the gel phase can be obtained by integrating Eq. (15) and making some rearrangements:

$$U + (U^2 - U_g^2)^{1/2} = H\exp(kx), \qquad (16)$$

where $U = \Psi - \Psi_f$, $U_g = \Psi_g - \Psi_f$, $U_0 = \Psi_0 - \Psi_f$ are potentials reckoned from the potential Ψ_f of the gel phase (Fig. 1); $H = U + (U_0^2 - U_g^2)^{1/2}$.

Equation (16) adequately describes how the potential Ψ depends on the distance x in the gel layer of arbitrary thickness g at any characteristic potential, which, however, should satisfy the condition $|\Psi_f| > |\Psi_g| > |\Psi_0|$, but do not give a unique solution to the problem. To obtain a unique solution, we have to find an additional equation that would relate these parameters. We can use as an equation of this kind the matching conditions for equations describing the potential distribution in both phases at the gel–solution interface. One of these conditions consists in that the potential Ψ_0 is a common value of the following functions at $x = 0$: dependence (16) of the potential on the distance x in the gel film and the dependence of the potential on distance in the solution phase. Another condition refers to the field strengths $-(d\Psi/dx)_0$ at the phase boundary on the gel and solution sides. As already noted, no concentrated charge can appear at the interface. In addition, the difference between the dielectric constants of the gel and solution phases can be neglected at a low concentration of the polymer. In this case, the derivative $(d\Psi/dx)_0$ will have the same value on the gel and solution sides. At a low potential Ψ_0 on the solution side, $(d\Psi/dx)_0 = -k\Psi_0$; on the gel side, $(d\Psi/dx)_0 = \pm k[(\Psi_0 - \Psi_f)^2] - [(\Psi_g - \Psi_f)^2]^{1/2}$ in accordance with Eq. (15). Hence, we find

$$\Psi_0 = \Psi_g[1 - (\Psi_g/\Psi_f)/2]. \qquad (17)$$

We can derive one more equation relating these same potentials from Eq. (16), provided that $U = U_g$ at $x = -g$ (g is the gel layer thickness):

$$U_0 = U_g\cosh(kg). \qquad (18)$$

Having solved the system of equations (17) and (18), we obtain

$$\Psi_g = \Psi_f\{[\cosh^2(kg) - 1]^{1/2} - \cosh(kg) + 1\}. \qquad (19)$$

According to Eq. (19), the potential difference Ψ_g between two extended phases, substrate and solution, separated by a thin gel layer, increases as the relative thickness kg of this layer grows, and approaches asymptotically the potential difference Ψ_g between the bulk phases of the gel and solution. The interphase potential difference Ψ_g can also increase with the electrolyte concentration in the solution phase (Fig. 2, upper plot). At a constant potential Ψ_g of the substrate surface, the potential Ψ_0 at the gel–solution interface will exponentially decrease with increasing concentration of the electrolyte, in accordance with Eq. (18). However, owing to a simultaneous increase in the potential Ψ_g of the substrate surface, the potential Ψ_0 of the outer side of the gel layer may vary nonmonotonically, first increasing and then decreasing as the concentration of the indifferent electrolyte increases (Fig. 2, lower plot), which is indeed occasionally observed experimentally.

It should be kept in mind that the presence of a gel layer at the interface between two phases may be not the only reason for the appearance of a potential difference between these phases. In this case, the dependence of the electrokinetic potential, whose role is played in such a situation by Ψ_0, on the electrolyte concentration will be a combination of the dependence presented above and the classical monotonic dependence. The occurrence of a maximum will then become even less clearly pronounced [1].

The energy of electrostatic repulsion between charged surfaces or colloid particles is determined by the distance between the localization planes of the surface charge [1]. Apparently, if this charge is actually spread within the gel layer, its effective plane of localization will lie in the gel layer at a distance comparable with the thickness of this layer from the surface of the solid phase. If the density of the gel is considerably lower than that of the solid phase on whose surface it is situated, then the energy of molecular

attraction between particles of the solid phase will be determined by the distance h between the solid–gel interfaces, which exceeds by $2g$ the distance between the charge localization planes. This circumstance may fundamentally change the relationship between the repulsion and attraction forces acting between dispersed particles in such a way that irreversible coagulation of dispersed systems at higher electrolyte concentrations will become impossible [7]. Such a behavior is characteristic of liophilic systems [8]. Thus, the liophilicity can be explained in terms of the same concepts as those underlying the theory of stability of liophobic colloids, if these concepts are supplemented with a point that is apparent by itself and is not necessarily associated with the presence of a gel layer. It consists in that the localization plane of the surface charge responsible for repulsion between particles does not necessarily coincide with the phase boundary determining the attraction forces between particles. The presence of a gel layer is a possible reason for noncoincidence of the charge localization planes and the phase boundary and, consequently, for the appearance of liophilic properties.

Apparently, the presence of a gel layer on the surface of the adsorbent or a microporosity of this surface, disregarded in determining the specific surface area of the adsorbent, make the actual exchange capacity of the adsorbent higher than its calculated value, and this may be the reason for the apparent superequivalent exchange of ions [2].

CONCLUSION

The electric potential of the outer boundary of a thin gel layer grows as the concentration of an indifferent electrolyte in solution becomes higher. This leads to an increase in the electrokinetic potential of the surface covered with a thin gel layer at low electrolyte concentrations and to appearance of liophilic properties in typical liophobic colloids at higher electrolyte concentrations. The latter can be predicted on the basis of the classical theory of stability of these colloids.

REFERENCES

1. *Colloid Science*, Kruyt, H.R., Ed., vol. 1, *Irreversible systems*, Amsterdam: Elsevier, 1952.
2. Urakova, I.N., *Cand. Sci. Dissertation*, St. Petersburg, 2002.
3. Lipson, G.A. and Kolodieva, T.S., *Kolloid. Zh.*, 1972, vol. 34, pp. 235–237.
4. Sidorova, M.P., Liklema, I., and Fridrikhsberg, D.A., *Kolloid. Zh.*, 1976, vol. 38, pp. 716–721.
5. Martynov, G.A., *Kolloid. Zh.*, 1978, vol. 40, pp. 1110–1117.
6. Bibik, E.E., *Zh. Prikl. Khim.*, 1999, vol. 72, no. 6, pp. 920–924.
7. Bibik, E.E., *Zh. Prikl. Khim.*, 1997, vol. 70, no. 8, pp. 1258–1262.
8. Shchukin, E.D., Pertsov, A.V., and Amelina, E.A., *Kolloidnaya khimiya* (Colloid Chemistry), Moscow: Mos. Gos. Univ., 1982.

Russian Journal of Applied Chemistry, Vol. 78, No. 2, 2005, pp. 222–228. Translated from Zhurnal Prikladnoi Khimii, Vol. 78, No. 2, 2005, pp. 229–234.
Original Russian Text Copyright © 2005 by Sharygin, Kalyagina, Borovkov.

SORPTION AND ION-EXCHANGE PROCESSES

Sol–Gel Technique for Production of Spherically Granulated Zirconium(IV) Phosphate

L. M. Sharygin, M. L. Kalyagina, and S. I. Borovkov

Termoksid Research-and-Production Company, Zarechnyi, Sverdlovsk oblast, Russia

Received May 12, 2004

Abstract—A sol–gel technique for production of spherically granulated zirconium(IV) phosphate of Termoksid-3A brand is described. The method includes the following main stages: electrolysis of a zirconium(IV) chloride solution to give a sol of zirconium(IV) hydroxide, drop dispersion of the sol into an ammonia solution, conversion of gel-spheres of zirconium(IV) hydroxide into zirconium(IV) phosphate, and washing and drying of gel-spheres. The physicochemical and ion-exchange properties of the product obtained were studied.

The physicochemical properties of zirconium(IV) phosphate, a promising inorganic adsorbent, cation-exchanger, and catalyst, obtained by the conventional precipitation method have been studied in sufficient detail [1–7]. The properties of the product strongly depend on the composition characterized by the atomic ratio $\overline{P}/\overline{Zr}$, conditions of gel preparation and dehydration, and degree of crystallinity. For the stoichiometric zirconium(IV) phosphate, $\overline{P}/\overline{Zr} = 2$ and the formula $Zr(HPO_4)_2 \cdot xH_2O$ is ascribed to this compound. Crystalline α-phosphate of zirconium α-$Zr(HPO_4)_2$[1] has exactly the above stoichiometric composition and a layered structure [2, 8]. The layers in α-$Zr(HPO_4)_2$ are composed of zirconium(IV) ions lying nearly in the same plane and bound via phosphate groups situated above and below the plane of zirconium atoms. The layers are packed into blocks in such a way that they constitute a structure in the form of a monoclinic lattice with lattice constants $a = 0.9097$, $b = 0.5307$, and $c = 1.6284$ nm; $\beta = 111.38°$. Most of zirconium phosphate gels have an amorphous or semicrystalline structure composed of fragments of crystalline α-$Zr(HPO_4)_2$.

A sol–gel method has been suggested for obtaining zirconium(IV) phosphate in the form of spherical grains with high mechanical strength [9–13]. This method consists of the following main stages: synthesis of a sol of zirconium(IV) hydroxide by electrolysis of a $ZrCl_4$ solution, drop dispersion of the sol into an ammonia solution to give gel-spheres of $Zr(OH)_4$, conversion of gel-spheres of $Zr(OH)_4$ into zirconium(IV) phosphate, and washing and drying of gel-spheres of zirconium(IV) phosphate.

This communication describes the sol–gel technique for production of zirconium(IV) phosphate and reports on a study of its physicochemical properties.

The basic stage of the method under consideration and of the sol–gel processes suggested by other authors [14, 15] is that of conversion or the stage of treatment of $Zr(OH)_4$ gel-spheres with a H_3PO_4 solution, which leads to transformation of gel-spheres of zirconium(IV) hydroxide into gel-spheres of zirconium(IV) phosphate. Carrying out the sol–gel process became at all possible because gel-spheres do not disintegrate in the conversion stage. This is due to the layered structure of zirconium(IV) phosphate and hydroxide. In accordance with the model of [2], zirconium(IV) hydroxide layers are formed by tetrameric ions bound together by hydroxide groups lying above and below the layer plane. As a result, each zirconium(IV) ion is surrounded by eight hydroxy groups forming a distorted cube. The hydroxy groups lying above and below the layer of zirconium(IV) ions are replaced with hydrophosphate ions without any significant change in the positions of zirconium(IV) ions in the layer, with the result that the integrity of the gel-spheres is retained. The conversion process can be regarded as an acid–base reaction described by the equation

$$Zr(OH)_4 + 2H_3PO_4 = Zr(HPO_4)_2 + 4H_2O.$$

[1] $Zr(HPO_4)_2$ is zirconium(IV) hydroorthophosphate, α-$Zr(HPO_4)_2$ is named here and hereinafter α-phosphate of zirconium.

1070-4272/05/7802-0222 © 2005 Pleiades Publishing, Inc.

The chemical composition of the product is commonly characterized, with the crystallization water disregarded, by the $\bar{r} = \bar{P}/\bar{Zr}$ ratio, where $\bar{P}$ and $\bar{Zr}$ are the numbers of moles of phosphate ions and zirconium(IV) ions in the product. The value of $\bar{r}$ for the reaction product primarily depends on the ratio of the reactants, i.e., on the atomic ratio r = P/Zr in the starting mixture, where P and Zr are the numbers of moles of phosphoric acid in solution and zirconium(IV) hydroxide in gel-spheres, respectively. Figure 1 shows the chemical composition of zirconium(IV) phosphate as a function of the P/Zr ratio in the starting mixture. The study was carried out with gel-spheres of zirconium(IV) hydroxide, obtained using the procedure described in [16] and having the following characteristics: zirconium(IV) hydroxide concentration 1.2 M, pH value of the mother liquor 5.5, grain diameter 0.6–1.5 mm, moisture content of grains 62 wt %. To a certain volume of gel-spheres was added the same volume (s : l = 1 : 1) of a H_3PO_4 solution in the presence of 0.4 M of HCl, with r varied from 1.0 to 2.0. The mixture was kept at 80–85°C for 4 h with agitation. It can be seen from Fig. 1 that H_3PO_4 virtually completely enters into the reaction and the composition of the final product is determined by that of the starting mixture. Even at r = 2, more than 99% of phosphoric acid enters into the reaction. As phosphate ions are present in zirconium(IV) phosphate as hydrophosphate HPO_4^{2-} [2] at any $\bar{r}$, the conversion process for $r < 2$ can be described by the expression

$$Zr(OH)_4 + xH_3PO_4 = Zr(OH)_{4-2x}(HPO_4)_x + 2xH_2O.$$

Varying the HCl concentration within the range 0.1–0.5 M has no effect on the chemical composition of the final product.

Figure 2 shows kinetic curves for conversion of $Zr(OH)_4$ gel-spheres at s : l = 1 : 1, r = 1.8, and HCl concentration of 0.4 M, under agitation to lift outer-sphere restrictions. The degree of conversion is plotted along the ordinate axis. This parameter is defined by $F = (c_t/c_0) \times 100$, where c_t and c_0 are the H_3PO_4 concentrations in solution at an instant of time t and in the initial solution. The reaction of $Zr(OH)_4$ with H_3PO_4 is fast. The time of half-conversion at 25°C is less than 3 min. The high rate of the reaction would be expected because gel-spheres are highly dispersed macroporous bodies with a moisture content of 60–70 wt %. However, the extent of the process strongly depends on temperature. The degree of conversion in 2.5 h is 99.97% at 85°C and only 93% at 25°C. At 25°C, the value of F was 96% even after keeping for 24 h.

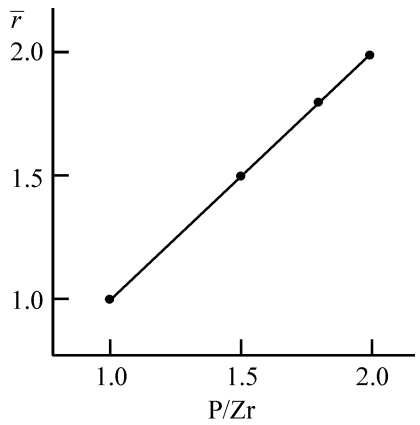


Fig. 1. Chemical composition of zirconium phosphate, $\bar{r}$, vs. the P/Zr ratio in the starting mixture.

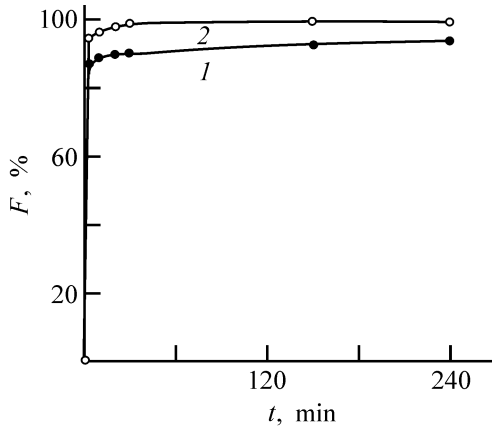


Fig. 2. Kinetic curves for conversion of gel-spheres of zirconium(IV) hydroxide at (*1*) 25 and (*2*) 85°C. (F) Degree of conversion and (t) time.

In [11], the influence exerted by the duration and temperature (25–90°C) of pretreatment of $Zr(OH)_4$ gel-spheres on their interaction with H_3PO_4. In aging, grains shrink and the reactivity of gel-spheres becomes lower, which is manifested in a decrease in the degree of hydroxide conversion into the phosphate, especially at low equilibrium concentrations of H_3PO_4. In aging of $Zr(OH)_4$, there occur ocolation chemical processes [2, 17] leading to conversion of diol bonds into oxo bonds with elimination of a water molecule by the reaction

$$\rangle Zr\langle^{OH}_{OH}Zr \langle \rightarrow \rangle Zr{-}O{-}Zr\langle + H_2O.$$

Being more stable, the oxo bond is less active in the interaction with H_3PO_4, and it is this fact that accounts for the lower reactivity of the aging product. Therefore, conversion of zirconium oxo hydroxide into zirconium phosphate can be represented as the reaction

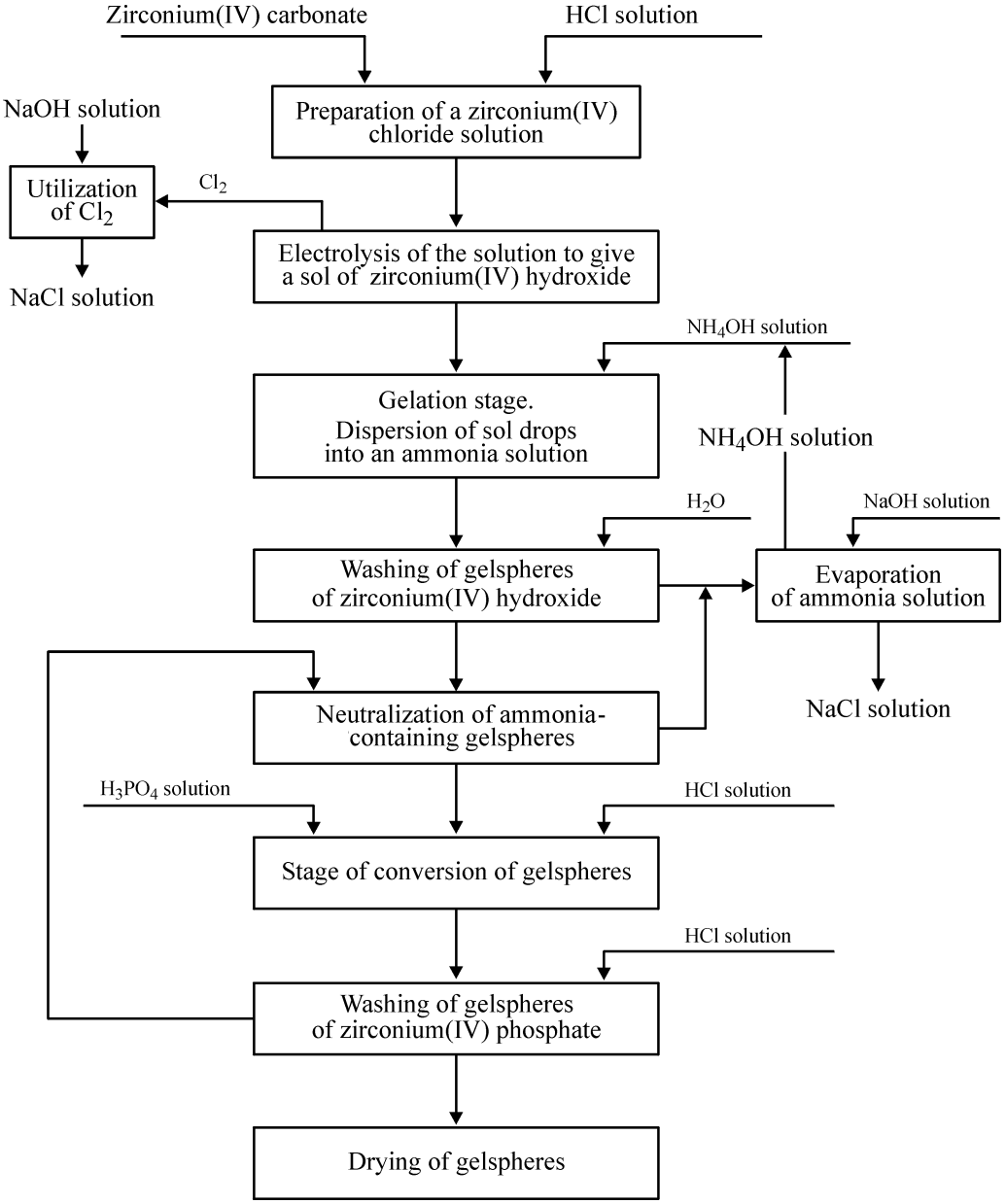
$$ZrO_x(OH)_{4-2x} + (2 - x)H_3PO_4 = ZrO_x(HPO_4)_{2-x} + (4 - 2x)H_2O.$$

However, as the equilibrium concentration of H_3PO_4 becomes higher, the reaction products have $r \le 2$, irrespective of the aging conditions of gel-spheres [11]. In this case, the oxo bonds formed as a result of aging are involved in the interaction with H_3PO_4 and the overall reaction can be represented as

$$ZrO_x(OH)_{4-2x} + 2H_3PO_4 = Zr(HPO_4)_2 + 4H_2O.$$

A similar effect is caused by raising the treatment temperature (Fig. 2). As this temperature increases, oxo bonds enter into the reaction with H_3PO_4.

The gel-spheres of zirconium(IV) phosphate, obtained after the conversion stage, have a moisture content of 60–70 wt %, which is found by drying a sample to constant weight at 100°C, and a pore volume of 1.5–2.3 $cm^3\ g^{-1}$ per 1 g of solid mass. This means that these gel-spheres are liquefied highly dispersed porous bodies. To improve their mechanical strength and optimize other characteristics, gel-spheres are subjected to drying. In the process, the grains shrink considerably, their mechanical strength in-



Technological flow diagram for manufacture of spherically granulated zirconium(IV) phosphate.

creases, porosity decreases, bulk mass becomes higher, and other physicochemical properties of the sorbent change [9, 12]. A xerogel of zirconium(IV) phosphate, obtained by drying of gel-spheres at 100°C, is a nonporous product that is impermeable to molecules of nitrogen, benzene, and helium, which restricts its use as an adsorbent in this form. However, the material slowly swells in the presence of water or in an aqueous solution, its moisture content increases to 25 wt %, and its pores become accessible to ion sorption.

In [18], the evolution of the structure of gel-spheres of zirconium(IV) phosphate with the changing content of water in the course of drying was studied by means of structural neutron diffraction analysis and small-angle neutron scattering. The starting gel-spheres and products formed in initial stages of drying are constituted by fragments of two-dimensional (2*D*) layers of α-zirconium phosphate. As the content of water decreases in the course of drying, blocks are formed from α-$Zr(HPO_4)_2$ layers without changes in the positions of zirconium(IV) ions in the layers. The blocks are 1.6–2.1-nm-thick, i.e., contain 2 to 3 layers, and have a lateral size of 5.0 ± 0.1 nm and no clearly delimited boundaries. Thus, gel-spheres with varied moisture content are constituted by branched fragments (layers, blocks) of α-zirconium(IV) phosphate.

According to the flow diagram for production of spherically granulated zirconium(IV) phosphate, presented below, the starting raw material for manufacture of the product is $Zr(CO_3)_2$, which is decomposed in a HCL solution to give a zirconium(IV) chloride solution with a concentration of 1.3–1.5 M in terms of zirconium(IV) and a Cl/Zr ratio of 1.4–2.0. It is possible to use zirconium(IV) oxochloride as a starting raw material. A solution of zirconium(IV) chloride is subjected to electrolysis to obtain a sol of zirconium(IV) hydroxide [16]. In the course of electrolysis, the HCl concentration in solution decreases because of the decomposition of the acid at electrodes into gaseous Cl_2 and H_2, the extent of hydrolysis and polymerization of zirconium(IV) ions increases, and a sol of zirconium(IV) hydroxide is formed with the following parameters: concentration in terms of zirconium(IV) 1.3–1.5 M, Cl/Zr = 0.15–0.3, pH 1.8–2.2, and viscosity 8–30 cSt. Gaseous Cl_2 evolved in electrolysis is caught with a NaOH solution to give sodium hypochlorite, which gradually decomposes into NaCl. The resulting sol of zirconium(IV) hydroxide is delivered to the gelation stage.

The gelation is performed by drop dispersion of the sol into aqueous ammonia. Diffusion of $NH_3 \cdot H_2O$ into a sol drop leads to neutralization of free HCl and chloride ions bound to colloid particles and to gelation of sol drops to give gel-spheres of $Zr(OH)_4$ with a mechanical strength sufficient for further operations.

Gel-spheres are washed to remove the excess amount of ammonia. The washing solutions are fed into evaporators to remove ammonium, which is recycled into the gelation stage as a solution of $NH_3 \cdot H_2O$.

Ammonia-containing gel-spheres show an alkaline reaction. They are neutralized with a hydrochloric solution formed in the conversion stage. The solutions formed in the stage of neutralization of gel-spheres are delivered to evaporation of the ammonia solution.

The conversion stage is carried out by treating gel-spheres of zirconium(IV) hydroxide with a H_3PO_4 solution at a P/Zr ratio of 1.8–2.0, HCl concentration in solution in the range 0.3–0.5 M, and temperature of 80–90°C in the course of 2–4 h. Gel-spheres of zirconium(IV) phosphate are washed to remove the excess amount of the acid and the washing solutions are delivered into the stage of neutralization of ammonia-containing gel-spheres.

To improve the mechanical strength and form the necessary porosity, gel-spheres of zirconium(IV) phosphate are dried in air to residual moisture content of 20–36 wt % and used as spherically granulated zirconium(IV) phosphate in the H^+ form. The sorbent can be transferred into the salt form, e.g., of sodium type, by treating the product with a Na_2CO_3 solution.

A pilot production of the product was set-up by the Termoksid research-and-production company. The spherically granulated zirconium(IV) phosphate manufactured by the so-gel method has a brand name Termoksid-3A. The main physicochemical parameters of the sorbent are listed below:

Chemical composition	
$Zr(OH)_{4-2x}(HPO_4)_x$	$x = 1.8$
	$x = 2.0$
Moisture content determined	30–36 wt %
by drying at 100°C	18–20 wt %
Grain shape	Spherical
Grain size	0.4–1.0 mm
Bulk mass	1.04–1.1 kg l^{-1}
Mechanical strength	150–300 kg cm^{-2}

The products are chemically, morphologically, and crystal-chemically homogeneous. The chemical homogeneity with respect to zirconium and phosphorus, evaluated as a scatter of the content of a macrocomponent relative to the average value, which is determined with an electron probe 2–3 μm in diameter,

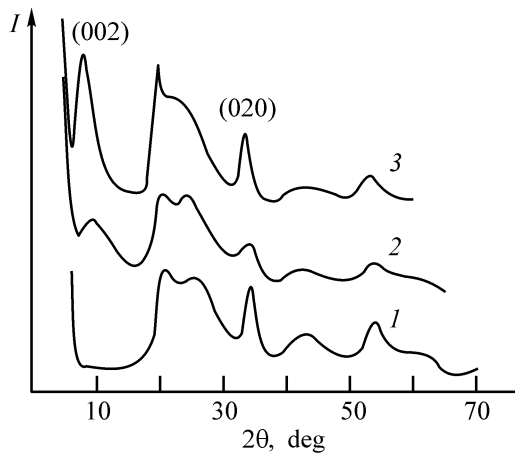


Fig. 3. X-ray diffraction patterns of Termoksid-3A samples. (*I*) Intensity and (2θ) Bragg angle. $\bar{r}$: (*1*, *2*) 1.8 and (*3*) 2.0. Moisture content (wt %): (*1*, *3*) 36 and (*2*) 20.

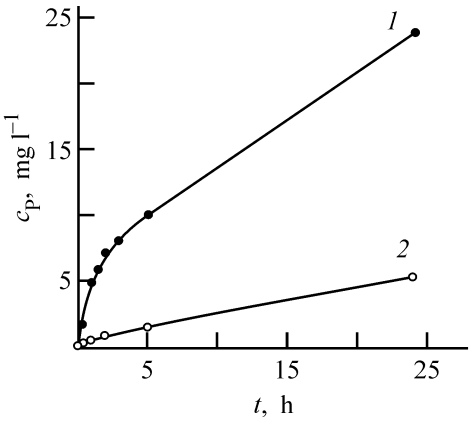


Fig. 4. Kinetic curves for hydrolysis of Termoksid-3A samples in the Na^+ form. (c_P) Concentration of phosphate ions in solution in terms of P and (*t*) time. Moisture content (wt %): (*1*) 36 and (*2*) 20.

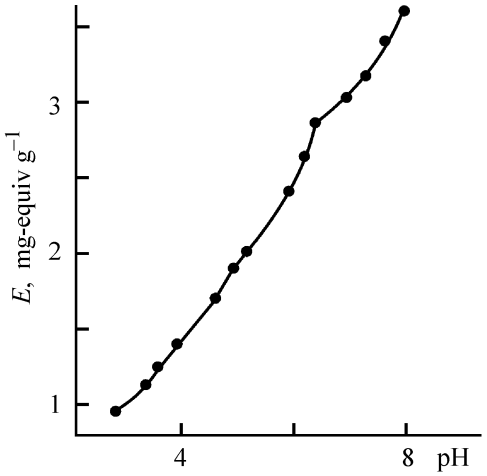


Fig. 5. Titration curve for a Termoksid-3A sample. Moisture content 36 wt %, $\bar{r}$ = 1.8. (*E*) Capacity.

does not exceed ±1.5 rel. % for a two-sided confidence probability of 0.99 [19]. Also, products with a varied degree of crystallinity are manufactured.

Figure 3 shows X-ray diffraction patterns of products in the H^+ form. Reflections genetically related to the corresponding Bragg reflections of crystalline α-$Zr(HPO_4)_2$ are indicated in the figure. In the X-ray diffraction pattern of Termoksid-3A sample no. 1, there is no reflection from the (002) plane. As the (002) reflection is related in crystalline α-zirconium phosphate to spacings between layers of zirconium(IV), the solid-phase skeleton of the ion-exchanger under consideration is constituted by fragments of 2*D* α-$Zr(HPO_4)_2$ layers about 6 nm in size. Therefore, this product has the lowest steric hindrance to cation exchange. The X-ray diffraction pattern of Termoksid-3A sample no. 2 contains a broad reflection from the (002) plane, which indicates that blocks composed of layers with an interplanar spacing of 1.05 nm are present in the system. Termoksid-3A sample no. 3 has a higher degree of crystallinity, its solid-phase structure is constituted by α-$Zr(HPO_4)_2$ blocks with an interplanar spacing of 1.05 nm. The blocks have dimensions in the (002) plane of about 4.5 nm, i.e., they are constituted by four layers, on the average. The dimensions in the (020) plane are, as for the first two samples, about 6.0 nm.

In aqueous solutions, zirconium(IV) phosphate is subject to hydrolysis [2, 7, 20], accompanied by replacement of hydrophosphate groups by hydroxy groups, which can be represented, e.g., for the H^+ form, as

$$Zr(HPO_4)_2 + xH_2O = Zr(OH)_x(HPO_4)_{2-x/2} + (x/2)H_3PO_4.$$

The resistance to hydrolysis increases when the degree of crystallinity becomes higher, and the $\overline{P}/\overline{Zr}$ ratio in the ion exchanger, decreases. In an alkaline medium, hydrolysis is enhanced, which hinders use of the material at pH > 8. Figure 4 shows kinetic curves for hydrolysis of Termoksid-3A samples ($\overline{P}/\overline{Zr}$ = 1.8, Na^+ form, content of Na^+ 2.4 mg-equiv g^{-1}), measured under static conditions at s : l = 5 g : 100 cm^3 and pH 7.4–7.5, with solution agitation. In the course of time, the hydrolysis rate decreases. Therefore, it is better to compare the hydrolytic stabilities of the samples with the use of the average hydrolysis rate, determined during the first 24 h of keeping, by the expression

$$\vartheta = \frac{c_P V}{m\tau},$$

where c_P is the concentration of phosphate ions in solution in terms of phosphorus; V, solution volume; m, sorbent mass; and τ, time of keeping, equal to 24 h.

The average hydrolysis rate for Termoksid-3A sample no. 1 during the first 24 h of keeping was 2×10^{-2} mg g^{-1} h^{-1}. For the Na^+ form of Termoksid-3A sample no. 3 ($\overline{P}/\overline{Zr}$ = 2.0), the hydrolysis rate has a close value. A higher hydrolytic stability is observed for Termoksid-3A sample no. 2, for which the hydrolysis rate is 5.8×10^{-3} mg g^{-1} h^{-1}. Thus, the hydrolysis rate depends on how a sorbent is prepared and treated.

Figure 5 shows as an example a typical titration curve for a Termoksid-3A sample ($\overline{P}/\overline{Zr}$ = 1.8, moisture content 36 wt %), measured with respect to the Na^+ cation under static conditions at an ionic strength of the solution of 0.1 M. The sorbent is a weakly acidic ion exchanger whose capacity strongly depends on the pH value of the solution. The titration curve has a shape typical of zirconium(IV) phosphate having and amorphous or semicrystalline structure [1–3, 6]. Some ion-exchange properties of Termoksid-3A were studied in [21–23]. The ion exchanger has perfect kinetic characteristics [24] and an increased selectivity toward cesium radionuclides, which made it possible to use this sorbent industrially to purify water from spent fuel storage reservoirs of the first and second reactor units of Beloyarskaya nuclear power station [25]. The use of the sorbent enabled elimination of a potentially dangerous radiochemical contamination. The ion-exchange properties of zirconium(IV) phosphate synthesized by the precipitation technique have been studied extensively and the main results obtained are summarized in reviews [1–3, 7]. The fundamental aspects of the ions exchange, revealed in these studies, can be extended to Termoksid-3A with account of its structure and the preparation method.

CONCLUSIONS

(1) The statics and kinetics of the interaction between gel-spheres of zirconium hydroxide and phosphoric acid were studied.

(2) A sol–gel method for synthesis of spherical zirconium phosphate was described.

(3) Physicochemical characteristics, phase composition, titration curve, and hydrolytic stability of zirconium(IV) phosphate of Termoksid-3A brand were presented.

REFERENCES

1. Amphlett, C.B., *Inorganic Ion Exchangers*, Amsterdam: Elsevier, 1964.
2. Clearfield, A., Nancollas, G.H., and Blessing, R.H., *Ion Exchange Solvent Extraction*, 1973, vol. 5, no. 1, pp. 1–20.
3. Clearfield, A. and Jahangir, L.M., *Recent Dev. Separ. Sci.*, Boco Raton (Fla), 1986, vol. 8, pp. 131–160.
4. Komarov, V.D. and Tikavyi, V.F., *Izv. Vyssh. Uchebn. Zaved., Khim. Khim. Tekhnol.*, 1971, vol. 14, no. 5, pp. 651–655.
5. Karaseva, T.A., Skripkin, Z.D., and Strelko, V.V., *Ukr. Zh.*, 1976, vol. 42, no. 5, pp. 479–483.
6. Chernorukov, N.G., Korshunov, I.A., and Shuklina, N.P., *Ionity i ionnyi obmen* (Ionites and Ion Exchange), Leningrad: Nauka, 1975, pp. 10–14.
7. Sukharev, Yu.N. and Egorov, Yu.V., *Neorganicheskie ionity tipa fosfata tsirkoniya* (Inorganic Ionites of Zirconium Phosphate Type), Moscow: Energoatomizdat, 1983.
8. Clearfield, A., *Ann. Rev. Mat. Sci*., 1984, vol. 14, pp. 205–207.
9. Sharygin, L.M., Moiseev, V.E., Pyshkin, V.P., *et al.*, *Izv. Akad. Nauk SSSR, Neorg. Mater.*, 1983, vol. 19, no. 11, pp. 1899–1902.
10. Sharygin, L.M., Gonchar, V.F., and Moiseev, V.E., *Ion. Obmen Ionometr.*, Leningrad: Len. Gos. Univ., 1986, no. 5, pp. 9–29.
11. Galkin, V.M., Sharygin, L.M., Moiseev, V.E., and Pyshkin, V.P., *Izv. Akad. Nauk SSSR, Neorg. Mater.*, 1983, vol. 19, no. 8, pp. 1337–1340.
12. Galkin, V.M., Sharygin, L.M., Moiseev, V.E., *et al., Zh. Prikl. Khim.*, 1986, vol. 62, no. 10, pp. 2207–2212.
13. RF Patent 2034645.
14. Caletka, R. and Tympl, M., *J. Inorg. Nucl. Chem.*, 1977, vol. 39, no. 4, pp. 669–678.
15. Timakov, V.P., Pospelov, A.A., and Krylov, V.N., *Neorganicheskie ionoobmennye materialy* (Inorganic Ion-Exchange Materials), Leningrad: Len. Gos. Univ., 1980, pp. 141–148.
16. Sharygin, L.M., *Zh. Prikl. Khim.*, 2002, vol. 23, no. 9, pp. 1442–1430.
17. Zaitsev, L.M. and Shubina, T.N., *Izv. Akad.*

Nauk SSSR, Neorg. Mater., 1966, vol. 2, no. 9, pp. 1952–1957.

18. Bogdanov, S.G., Valiev, E.Z., Dorofeev, Yu.A., *et al.*, *J. Phys. Condens. Mater.*, 1997, no. 9, pp. 4031–4039.
19. Vizzhachii, A.G., Moiseev, V.E., and Sharygin, L.M., *Izv. Akad. Nauk SSSR, Neorg. Mater.*, 1986, vol. 22, no. 3, pp. 460–463.
20. Blumenthal, W.B., *The Chemical Behavior of Zirconium*, New York: Van Nostrand, 1958.
21. Perekhozheva, T.N. and Sharygin, L.M., *Zh. Neorg. Khim.*, 1992, vol. 37, no. 2, pp. 280–286.
22. Sharygin, L.M., Borovkov, S.I., Moiseev, V.E., and Galkin, V.M., *Khim. Tekhnol. Vody*, 1993, nos. 11–12, pp. 785–788.
23. Sharygin, L.M., Moiseev, V.E., Muromskii, A.Yu., *et al.*, *Atom. Energ.*, 1994, vol. 77, no. 4, pp. 308–313.
24. Perekhozheva, T.N., Sharygin, L.M., and Albantova, G.P., *Izv. Akad. Nauk SSSR, Neorg. Mater.*, 1989, vol. 25, no. 9, pp. 1532–1537.
25. Sharygin, L.M., Muromskii, A.Yu., Saraev, O.M., *et al.*, *Atom. Energ.*, 2001, vol. 91, no. 2, pp. 126–130.

Russian Journal of Applied Chemistry, Vol. 78, No. 2, 2005, pp. 229–233. Translated from Zhurnal Prikladnoi Khimii, Vol. 78, No. 2, 2005, pp. 235–239.
Original Russian Text Copyright © 2005 by Borovkov, Sharygin.

SORPTION AND ION-EXCHANGE PROCESSES

A Study of the Competitive Equilibrium in Ion Exchange of Calcium(II) on Zirconium Phosphate in Multicomponent Salt Solutions

S. I. Borovkov and L. M. Sharygin

Termoksid Research-and Production Company, Zarechnyi, Sverdlovsk oblast, Russia

Received July 14, 2004

Abstract—A sorption technology for stabilization of multicomponent salt solutions (wines) subject to calcium clouding is being developed on the basis of an inorganic cation-exchanger of Termoksid-3A brand. In this connection the ion-exchange equilibrium on a zirconium(IV) phosphate of Termoksid-3A brand in multicomponent solutions at pH 2.5–3.0 was studied. The selectivity series of the sorbent were determined in relation to the solution composition.

A topical goal of wine industry is to ensure a reliable stability of finished wines, which become cloudy in the course of time [1]. Wine is a complex solution of salts of potassium, calcium, magnesium, sodium, and other cations [2, 3]. The high mass concentration of calcium(II) in wine, exceeding the solubility of calcium salts (calcium tartrate, mucate, oxalate) leads to formation of calcium-containing dregs. Wine can be stabilized by removing the excess amount of calcium(II). Development of a technique for wine stabilization is an exceedingly complicated task because of the influence exerted by a wide variety of factors both on the wine formation and on processes associated with removal of excess calcium(II) from wine materials [1].

It was shown in [4] that the sorption method can be, in principle, used for removing excess amounts of calcium(II) from wines with an inorganic spherically granulated zirconium phosphate cation-exchanger of the Termoksid-3A brand, $Zr(HPO_4)_2 \cdot nH_2O$. It has been noted [5] that the process of ion removal from solutions with ion-exchangers is strongly affected by the pH value of the medium and by the nature and concentration of competing ions. Mg^{2+}, K^+, and Na^+ cations present in wines in macroscopic amounts can exert a competing influence on the sorption of Ca^{2+} cations by the Termoksid-3A cation exchanger. However, the fundamental aspects of the competing influence of the above-mentioned cations on the sorption of Ca^{2+} by inorganic cations of this kind have not been studied in sufficient detail.

The aim of this study was to examine the ion exchange of Ca^{2+} on the inorganic sorbent Termoksid-3A in multicomponent salt systems at pH 2.0–3.5.

Termoksid-3A is the trademark of the known inorganic zirconium phosphate cation exchanger synthesized by the sol-gel method [6] in the form of spherical grains with a good mechanical strength. The main physicochemical characteristics of Termoksid-3A are as follows:

Granulometric composition	0.4–1.0 mm
Bulk mass	1.1 ± 0.1 kg cm^{-3}
Moisture content	32 ± 2 wt %
Crushing strength	15 ± 10 MPa

Termoksid-3A has, in outward appearance, the form of glass-like spherical grains with a semicrystalline structure. The product is chemically, morphologically, and crystal-chemically homogeneous. Termoksid-3A has good kinetic characteristics, which compare well with those of medium-linked organic sulfocation exchangers [7]. The sorbent is chemically stable in wine materials and does not exert any adverse influence on the organoleptic characteristics of processed wines.

Sorption experiments were carried out under dynamic conditions by passing metal chloride solutions with a certain pH value through a sorption column with an inner diameter of 6 mm and sorbent bed height of 70 mm until the pH values and metal concentrations at the inlet and outlet of the column became equal. The necessary pH value of the solution was

1070-4272/05/7802-0229 © 2005 Pleiades Publishing, Inc.

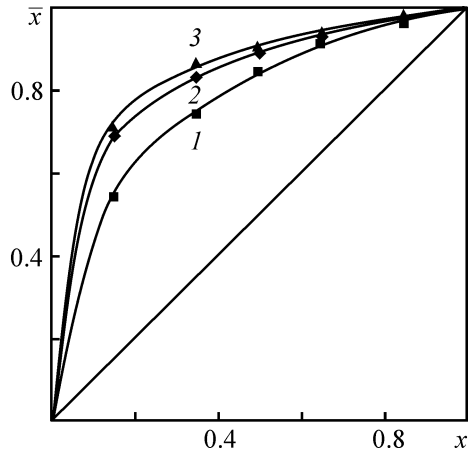


Fig. 1. Ion-exchange isotherms for the Ca^{2+}–Na^{+} system at different pH values. ($\bar{x}$) Equivalent fraction of Ca^{2+} in the sorbent and (x) equivalent fraction of Ca^{2+} in the solution; the same for Figs. 2–4. pH: (*1*) 2.5, (*2*) 3.0, and (*3*) 3.5.

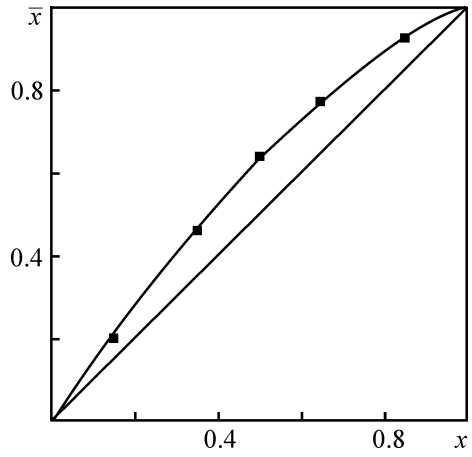


Fig. 2. Ion-exchange isotherm for the system Ca^{2+}–Mg^{2+} at pH 2.0–3.5.

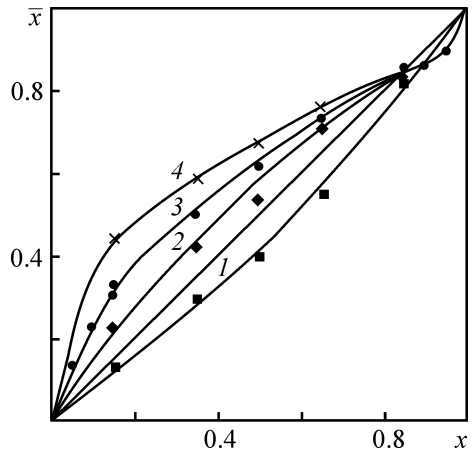


Fig. 3. Ion-exchange isotherms for the system Ca^{2+}–K^{+} at different pH values. pH: (*1*) 2.0, (*2*) 2.5, (*3*) 3.0, and (*4*) 3.5.

maintained by introducing hydrochloric acid. The rate of solution filtration was 30 column volumes per hour. The total concentration of metal cations in solution was 0.1 g-equiv l^{-1}. The column with the sorbent was washed with desalted water and cations sorbed were eluted with a 3M HCl solution. The content of calcium and magnesium ions in the initial solutions and eluates was determined by complexonometry with NaEDTA, and that of sodium and potassium, by flame photometry.

First, the ion-exchange equilibrium in binary systems Ca^{2+}–Mg^{2+}, Ca^{2+}–Na^{+}, and Ca^{2+}–K^{+} in the pH range 2.0–3.5.

The selectivity of the Termoksid-3A sorbent toward the Ca^{2+} ion can be formally characterized by the concentration constant of ion exchange, which is described, in accordance with the mass action law for a binary system, by the expression [8]:

$$\tilde{\tilde{K}}_{M}^{Ca} = \frac{\bar{x}_{Ca}^{1/2} x_{M}^{1/z}}{x_{Ca}^{1/2} \bar{x}_{M}^{1/z}}, \quad (1)$$

where $\bar{x}_{Ca}$ and $\bar{x}_{M}$ are the equivalent fractions of Ca^{2+} and the competing ion in the sorbent; x_{Ca} and x_{M}, equivalent fractions of Ca^{2+} and the competing ion in solution; and z, charge of the competing ion.

The equivalent fraction of calcium in the sorbent was determined using the formula

$$\bar{x}_{Ca} = \frac{\bar{c}_{Ca}}{\bar{c}_{Ca} + \bar{c}_{M}}, \quad (2)$$

where $\bar{c}_{Ca}$ and $\bar{c}_{M}$ are the concentrations of Ca^{2+} and the competing ion in the sorbent.

As Termoksid-3A is virtually not subject to swelling in aqueous solutions, it is more convenient to express the concentration in the solid phase in equivalents per unit volume or mass. For convenience of practical use, the results obtained in determining the capacity in this study are reduced to unit bulk volume of the sorbent. For practical purposes, it is more convenient to use as a quantitative characteristic of selectivity in describing the interphase distribution of ions the separation factor calculated by the formula [8]:

$$\alpha_{M}^{Ca} = \frac{\bar{x}_{Ca} x_{M}}{\bar{x}_{M} x_{Ca}}. \quad (3)$$

Figures 1–3 show ion-exchange isotherms for the systems under study at different pH values of solutions in the coordinates of the equivalent fraction of

Ca^{2+} in the sorbent against the equivalent fraction of the same ion in solution. As can be seen from Figs. 1 and 2, the ion-exchange isotherms for the systems Ca^{2+}–Na^{+} and Ca^{2+}–Mg^{2+} lie above the diagonal, which indicates that the Termoksid-3A sorbent is selective toward the Ca^{2+} ion in the entire range of pH values and compositions of the solution. For the Ca^{2+}–Na^{2+} system, the selectivity of the sorbent toward the Ca^{2+} ion increases in the entire range of solution compositions (Fig. 1). For example, the separation factor α_{Na}^{Ca} grows at x_{Ca} = 0.5 from 5.3 at pH 2.5 to 9.0 at pH 3.5. For the system Ca^{2+}–Mg^{2+} (Fig. 2), changing the solution pH from 2.0 to 3.5 does not affect the selectivity of the sorbent toward Ca^{2+} ions.

For the system Ca^{2+}–K^{+} (Fig. 3), the ion-exchange isotherms strongly vary with the solution pH. For example, the ion-exchange isotherm at pH 2.0 lies below the diagonal (curve *1*), which indicates that the selectivity of the sorbent toward K^{+} exceeds that for Ca^{2+} at this acidity in the entire range of solution compositions. As the pH value of the solution increases, the selectivity of the sorbent toward the Ca^{2+} ion grows, so that, already at pH 2.5 (curve *2*), the sorbent preferably absorbs Ca^{2+}, except at solution compositions with $x_{Ca} > 0.85$.

In the general case, the selectivity of cation exchangers depends on the charge, size, hydration, and hydrolysis of cations, as well as on polarization, specific interaction, sieve effect, and some other factors [5, 8, 9]. If the selectivity is regarded as a competition of the co-ions of a solution, fixed groups of the ion-exchanger, and water molecules for solvation of an ion being exchanged [9], then the inversion of selectivity on changing the pH value can be attributed to an enhancement of the solvating ability of phosphate groups of the sorbent toward the Ca^{2+} ion as a result of an increase in the degree of their dissociation upon a decrease in the concentration of H^{+} ions. The ion-exchange isotherms at pH 2.5, 3.0, and 3.5 (Fig. 3, curves *2*–*4*) are S-shaped.

At $x_{Ca} > 0.85$, i.e., at high degrees of filling of the sorbent capacity with Ca^{2+} ions, a selectivity inversion is observed. Ion-exchange isotherms of this kind are characteristic of inorganic ion exchangers with a rigid skeleton (zeolites, clayey materials, zirconium phosphate) in exchange of ions strongly differing in size, e.g., in ion exchange in the systems Cs^{+}–H^{+} and Rb^{+}–H^{+} on zirconium phosphate [10, 11]. On the whole, the selectivity of the sorbent toward the Ca^{2+} for the system Ca^{2+}–K becomes higher as the pH value increases, with the exception of solution compositions with $x_{Ca} > 0.85$. The separation factor α_{K}^{Ca} at x_{Ca} = 0.5 grows from 0.7 at pH 2.0 to 2.0 at pH 3.5.

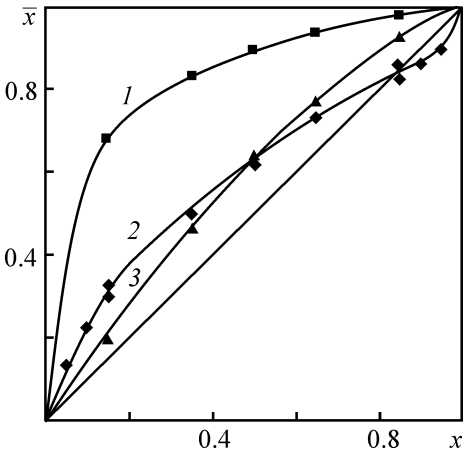


Fig. 4. Ion-exchange isotherms for the systems (*1*) Ca^{2+}–Na^{+}, (*2*) Ca^{2+}–K^{+}, and (*3*) Ca^{2+}–Mg^{2+} at pH 3.0.

Figure 4 shows ion-exchange isotherms for the systems Ca^{2+}–Na^{+}, Ca^{2+}–Mg^{2+}, and Ca^{2+}–K^{+} at constant pH value of the solution, equal to 3.0. Commonly, the equivalent fraction of Ca^{2+} relative to other cations in the solutions studied does not exceed 0.2. The separation factors calculated using the data of Fig. 4 for x_{Ca} = 0.2 have the following values: α_{Na}^{Ca} = 8.6, α_{Mg}^{Ca} = 1.4, and α_{K}^{Ca} = 2.4.

The results obtained indicate that Termoksid-3A has a higher selectivity toward Ca^{2+} ions, compared with other ions (Mg^{2+}, Na^{+}, and K^{+}). The order in which the selectivity of the sorbent toward the cations under consideration increases, which is determined by the order in which the separation factor grows, depends on the solution composition. For solutions with x_{Ca} in the range from 0 to 0.50, the selectivity series has the form $Ca^{2+} > Mg^{2+} > K^{+} > Na^{+}$.

Such an order of selectivity variation does not contradict the concept of electroselectivity [5] and corresponds to the selectivity series for amorphous zirconium phosphate toward ions of alkali and alkaline-earth elements [12].

At x_{Ca} of 0.50 to 0.85, the selectivity series changes to $Ca^{2+} > K^{+} > Mg^{2+} > Na^{+}$. Finally, the selectivity series for x_{Ca} ranging from 0.85 to 1.0 is as follows: $K^{+} > Ca^{2+} > Mg^{2+} > Na^{+}$.

The fact that the selectivity series varies with the solution composition is due to an increase in the selectivity of the sorbent toward K^{+} ions. As already noted, the ion-exchange isotherm for the system

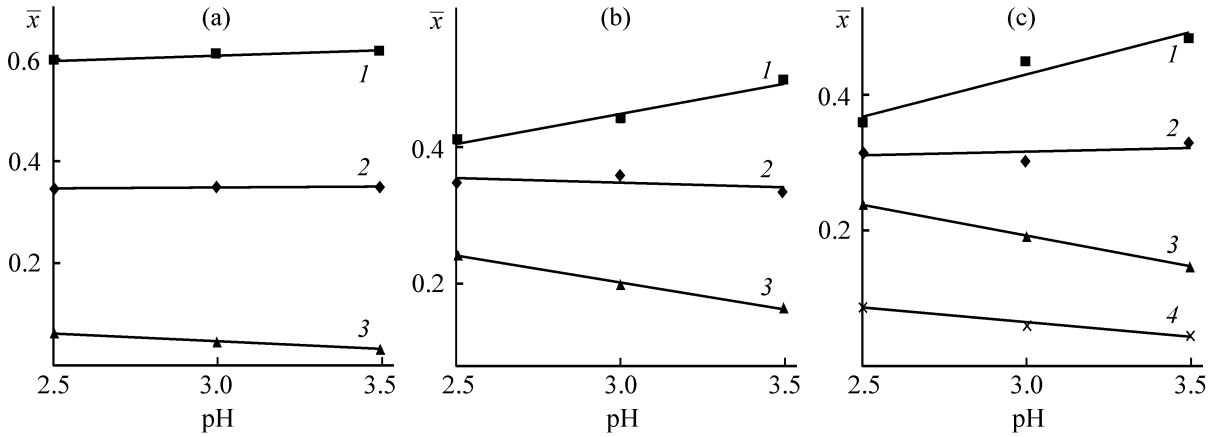


Fig. 5. Equivalent fraction of the metal ion in the sorbent, $\bar{x}$, vs. the solution pH for the systems (a) Ca^{2+}–Mg^{2+}–Na^+, (b) Ca^{2+}–Mg^{2+}–K^+, and (c) Ca^{2+}–Mg^{2+}–K^+–Na^+. (a) (*1*) Ca^{2+}, (*2*) Mg^{2+}, and (*3*) Na^+; (b) (*1*) Ca^{2+}, (*2*) Mg^{2+}, and (*3*) K^+; (c) (*1*) Ca^{2+}, (*2*) Mg^{2+}, (*3*) K^+, and (*4*) Na^+.

Ca^{2+}–K^+ is S-shaped, which results in a selectivity inversion at $x_{Ca} > 0.85$.

As the solutions studied contain simultaneously all the cation metals under consideration, the ion-exchange equilibrium was examined in the systems Ca^{2+}–Mg^{2+}–Na^+, Ca^{2+}–Mg^{2+}–K^+, and Ca^{2+}–Mg^{2+}–Na^+–K^+, which contain equal equivalent fractions of ions in equilibrium solutions. The total concentration of metal ions was 0.1 g-equiv l^{-1}, the acidity of the solutions was adjusted by introducing hydrochloric acid. The results obtained are shown in Figs. 5a–5c and listed in Tables 1 and 2. It can be seen that, if the cations are simultaneously present in solution in equal equivalent concentrations, the sorbent capacity for each cation corresponds to the above selectivity series $Ca^{2+} > Mg^{2+} > K^+ > Na^+$.

For the system Ca^{2+}–Mg^{2+}–Na^+ (Fig. 5a), the equivalent fraction of Ca^{2+} in the sorbent increases, the equivalent fraction of Na^+ decreases, and that of Mg^{2+} remains unchanged as the solution pH grows in the range 2.5–3.5. A similar behavior is observed for the system Ca^{2+}–Mg^{2+}–K^+ (Fig. 5b): an increase

Table 1. Ion-exchange equilibrium on a Termoksid-3A sorbent in three-component systems

pH	Exchange capacity of the sorbent, mequiv cm^{-3}, for indicated system							
	Ca^{2+}–Mg^{2+}–Na^+				Ca^{2+}–Mg^{2+}–K^+			
	Ca^{2+}	Mg^{2+}	Na^+	total	Ca^{2+}	Mg^{2+}	K^+	total
2.5	0.487	0.276	0.049	0.812	0.338	0.287	0.199	0.824
3.0	0.688	0.397	0.050	1.135	0.505	0.408	0.224	1.137
3.5	0.950	0.540	0.054	1.544	0.800	0.540	0.263	1.603

Table 2. Ion-exchange equilibrium on a Termoksid-3A sorbent in the system Ca^{2+}–Mg^{2+}–K^+–Na^+

pH	Exchange capacity of the sorbent, mequiv cm^{-3}				
	Ca^{2+}	Mg^{2+}	Na^+	K^+	total
2.5	0.288	0.255	0.192	0.070	0.805
3.0	0.508	0.342	0.218	0.070	1.138
3.5	0.750	0.510	0.231	0.070	1.561

in the equivalent fraction of Ca^{2+} and a decrease in that of K^+ in the sorbent are more clearly pronounced.

For the four-component system Ca^{2+}–Mg^{2+}–K^+–Na^+ (Fig. 5c), the equivalent fraction of Ca^{2+} in the sorbent increases, the equivalent fractions of K^+ and Na^+ decrease, and that of Mg^{2+} remains virtually unchanged as the solution pH grows.

The pattern revealed is associated with a rise in the sorbent selectivity toward Ca^{2+} as the solution pH increases. Comparison of Figs. 5a and 5b shows that replacing the Na^+ ion in a three-component solution with an equivalent amount of the K^+ ion, which has a higher selectivity toward the sorbent, leads to a noticeable decrease in the equivalent fraction of Ca^{2+} in the sorbent. It follows from Tables 1 and 2 that the total capacity of the sorbent for all the cations is virtually independent of the solution composition at a constant pH value of the solution. As the pH value increases, the total capacity of the sorbent grows, which is characteristic of zirconium phosphate, a bifunctional cation exchanger of medium strength [13, 14].

Thus, zirconium phosphate of the Termoksid-3A brand shows in ion exchange in the system Ca^{2+}–Mg^{2+}–K^+–Na^+ at pH 2.5–3.5 and low and medium filling of the sorption capacity with calcium the following selectivity series: $Ca^{2+} > Mg^{2+} > K^+ > Na^+$.

CONCLUSION

Termoksid-3A sorbent enables an effective decalcination in the column mode of solutions imitating the average macroscopic composition of wines in the content of mineral impurities at pH 3.0–3.2. The total capacity of the sorbent for all the cations at a constant pH value of a solution is virtually independent of its composition, being equal to 1.45 mequiv cm^{-3} at pH 3.2. The capacity of the sorbent for the Ca^+ ion strongly depends on the concentration of K^+ and Mg^{2+} ions, whereas that of Na^+ exerts a weak competitive influence.

REFERENCES

1. Valuiko, G.G., Zinchenko, V.I., and Mekhuzla, N.A., *Stabilizatsiya vinogradnykh vin* (Stabilization of Wines), Moscow: Agropromizdat, 1987.
2. Nilov, V.I. and Skurikhin, I.M., *Khimiya vinodeliya* (Chemistry of Wine-Making), Moscow: Pishchevaya Prom–st., 1967.
3. Schaper, H.-H. and Schwedt, G., *Dtsch. Lebensm. Rdsch.*, 1990, vol. 86, no. 6, pp. 178–182.
4. Zinchenko, V.I., Taran, N.G, Gnet'ko, L.V., *et al.*, *Sadovod., Vinogradar. Vinodel. Mold.*, 1992, no. 3–4, pp. 23–25.
5. Helfferich, F., *Ionenaustauscher*, Bd. 1, Weinheim: Chemie, 1959.
6. Sharygin, L.M., Moiseev, V.E., Pyshkin, V.P., *et al.*, *Izv. Akad. Nauk SSSR, Neorg. Mat.*, 1983, vol. 19, no. 11, pp. 1899–1902.
7. Perekhozheva, T.N., Sharygin, L.M., and Albantova, G.P., *Izv. Akad. Nauk SSSR, Neorg. Mat.*, 1989, vol. 25, no. 9, pp. 1532–1536.
8. Soldatov, V.S. and Bychkova, V.A., *Ionoobmennye ravnovesiya v mnogokomponentnykh sistemakh* (Ion-Exchange Equilibria in Multicomponent Systems), Minsk: Nauka Tekhnika, 1988.
9. Diamond, R.M. and Whitney, D.C. *Ion Exchange. A Series of Advances*, vol. 1, Marinsky, J.A., Ed., New York: Dekker, 1966. Translated under the title *Selektivnost' ionitov v razbavlennykh i kontsentrirovannykh vodnykh rastvorakh: Ionnyi obmen*, Moscow: Mir, 1968, pp. 174–280.
10. Amphlett, C.C., Eaton, P., McDonald, L.A., and Miller, A.J., *J. Inorg. Nucl. Chem.*, 1964, vol. 26, no. 2, pp. 297–304.
11. Harkin, J.P., Nancollas, G.H., and Paterson, R., J. *Inorg. Nucl. Chem.*, 1964, vol. 26, no. 2, pp. 305–310.
12. Clearfild, A., Nancollas, G.H., and Blessing, R.H., *Ion Exchange and Solvent Extraction*, Marinsky, J.A. and Marcus, Y., Eds., New York: Marcel Dekker, Inc., 1973, no. 5, pp. 1–119.
13. Ahrland, S., Albertsson, J., Johansson, L., *et al.*, *Acta Chem. Scand.*, 1964, no. 18, pp. 707–720.
14. Tikavyi, V.F. and Komarov, V.D., *Vestsi Akad. Nauk BelSSR, Ser. Khim. N.*, 1968, no. 1, pp. 41–45.

Russian Journal of Applied Chemistry, Vol. 78, No. 2, 2005, pp. 234–238. Translated from Zhurnal Prikladnoi Khimii, Vol. 78, No. 2, 2005, pp. 240–244.
Original Russian Text Copyright © 2005 by Prokof'ev, Il'in, Basova.

SORPTION AND ION-EXCHANGE PROCESSES

Influence of Surfactants on Structuring of Molding Blends Based on ZnO

V. Yu. Prokof'ev, A. P. Il'in, and T. V. Basova

Ivanovo State Chemical-Engineering University, Ivanovo, Russia

Received October 22, 2004

Abstract—The correlation between the surfactant sorption and structural mechanical properties of molding blends and granulated sorbents was studied.

ZnO is widely used a a chemisorbent foo removing impurities and, in particular, sulfur compounds [1], from process gases. Zinc oxide almost irreversibly sorbs hydrogen sulfide to form solid zinc sulfide, which allows almost complete removal of H_2S from the gas being treated. At the same time [1, 2], granulated sorbent should have not only a strongly developed microporous structure but also large pores for penetration of reagents deep into a granule.

Uzugi and Tamia found [3] that the sorption of hydrogen sulfide on zinc oxide depends not only on its specific surface area but also, to a great extent, on the pore size distribution. Zinc oxide having, along with micropores, coarse pores with radius larger than 100 nm exhibits the highest sorption activity. As follows from the stoichiometry of the reaction of ZnO with H_2S, the highest sorption capacity of zinc oxide for hydrogen sulfide is 39 wt%. The actual sorption capacity is lower than 20 wt%. Hence, the H_2S sorption strongly depends on its diffusion into the sorbent matrix. Under the industrial conditions, only the external surface of zinc oxide granules is converted into the sulfide, and the internal surface does not work.

It is known that pelletized granules have a nanoporous structure, whereas extruded granules contain broad transport pores, along with narrow pores. Preparation of extruded sorbents based on ZnO was examined in our previous study [4].

Surfactants are widely used to improve the moldability of blends (including those based on ZnO) to be extruded.

EXPERIMENTAL

We used ZnO powder with an almost 100% content of the main compound. The molding blends were prepared by addition of polyvinyl alcohol (PVA) or carboxymethyl cellulose (CMC) solutions of different concentrations to a ZnO powder. The mixture was stirred to obtain a homogeneous suspension.

The optimal water content in the blend, φ_{opt}, was determined on a conical Rebinder plastometer by the procedure described in [5]. The structural-mechanical constants (ultimate shear stress P_{k1} and maximum plastic viscosity η_1) and parameters (plasticity Ps and relaxation time Θ) were calculated using the Maxwell–Shvedov and Kelvin model. For this purpose, we used the time–strain curves measured on a D.M. Tolstoi's plastometer [6]. The complete rheological curves were measured on a Rheotest-2 rotary viscometer in the range of shear rates 2–4960 s^{-1}. The data obtained were processed by the procedure described in [6, 7]. We calculated the following rheological parameters: full power consumed for flow N, power for degradation of the coagulation structure ΔN, consistency constant η_0, and flow index n.

The butt crushing strength of the granules was measured on a hydraulic press [8]. The BET specific surface area was determined from low-temperature sorption of argon [9].

We studied the sorption of CMC and PVA on ZnO particles under different conditions. A maximum at a 1–2 wt % PVA concentration in the solution is observed in all the sorption curves (Fig. 1). The maxima in the sorption curves are due to structuring of more concentrated CMC and PVA solutions with the formation of aggregates. The sorption capacity of the solid phase in dispersed solutions is higher by a factor of 2 than that in the stirred solutions.

The sorption capacity depends on the hydrophilic shell on the surface and the size of oxide particles.

1070-4272/05/7802-0234 © 2005 Pleiades Publishing, Inc.

The ion-exchange sorption from 0.l N HCl shows that the ZnO surface is almost completely coated with OH groups. In addition, the particle size of zinc oxide decreases from 250 to 20 μm after dispersion in a high-speed homogenizer. It should also be noted that diffusion of a large polymeric molecule into a porous particle is virtually impossible. Thus, the polymer sorption depends mainly on the size and hydroxyl shell of zinc oxide particles, rather than on their specific surface area.

The influence of the surfactant concentration on the optimal water content in the blend, φ_{opt}, was studied for the example of the ZnO–CMC–water system. The φ_{opt} decreases from 31.6 to 29.9 wt % with the CMC concentration increasing to 2 mg g^{-1} ZnO (Fig. 2). As the CMC concentration increases further, the optimal water content in the blend monotonically increases to 30.9 wt %. The dependence of the plastic strength at φ_{opt} is similar. At a CMC concentration of 2 mg g^{-1}, $P_m|_{\varphi=\varphi_{opt}}$ decreases by a factor of 2 and then monotonically increases, virtually reaching the initial value.

Comparison of the dependences shown in Figs. 1 and 2 shows that a decrease in φ_{opt} and $P_m|_{\varphi=\varphi_{opt}}$ corresponds to an increase in the surfactant sorption, i.e., the maximum in the $A = f(c_{surfactant})$ curve corresponds to the minium in the $\varphi_{opt} = f(c_{surfactant})$ and $P_m|_{\varphi=\varphi_{opt}} = f(c_{surfactant})$ curves. Hence, the intermolecular bonds of sorbed CMC macromolecules that substitute water molecules in the solvation shells make an increasing contribution to the coagulation interactions with increasing sorption. This accounts for the fact that the optimal water content in the blend decreases at a surfactant concentration of up to 2 mg g^{-1}. At the same time, the strength of coagulation bonds between polymer macromolecules is lower than that of the bonds formed by the hydration shell of zinc oxide particles. As a result, the plastic strength of the molding blends decreases at the best water content in the blend. As noted above, the surfactant sorption decreases with a further increase in the CMC concentration in the system (Fig. 1). This results in the formation of additional hydration bonds between ZnO particles, and hence φ_{opt} and $P_m|_{\varphi=\varphi_{opt}}$ increase (Fig. 2). Thus, structuring in molding blends depends not only on the total surfactant content in the system, but also, and to a greater extent, on the surfactant sorption on the surface of dispersed particles.

Let us consider the influence of the surfactant concentration (for the example of PVA) on the properties of molding blends based on ZnO at the optimal water content in the blend. Our experimental results (Fig. 3a) show that the dependence of ultimate shear

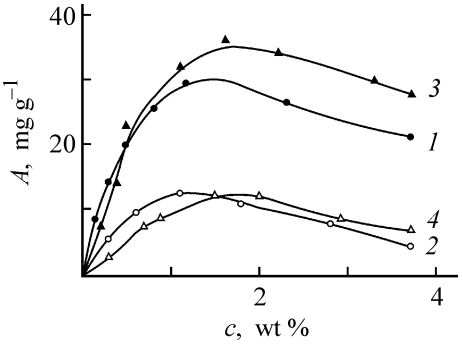


Fig. 1. Sorption *A* of (*1*, *2*) CMC and (*3*, *4*) PVA on ZnO at 25°C vs. the surfactant concentration in an aqueous solution *c*. Treatment conditions: (*1*, *3*) dispersion for 15 min; and (*2*, *4*) stirring for 2 h; s : l = 1 : 3.

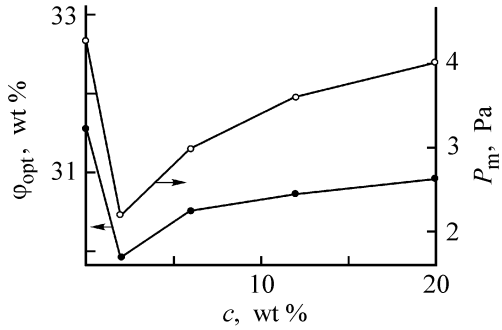


Fig. 2. Optimal water content in the blend, φ_{opt}, and the plastic strength P_m at $\varphi = \varphi_{opt}$ vs. the CMC content *c* in the molding blends based on ZnO.

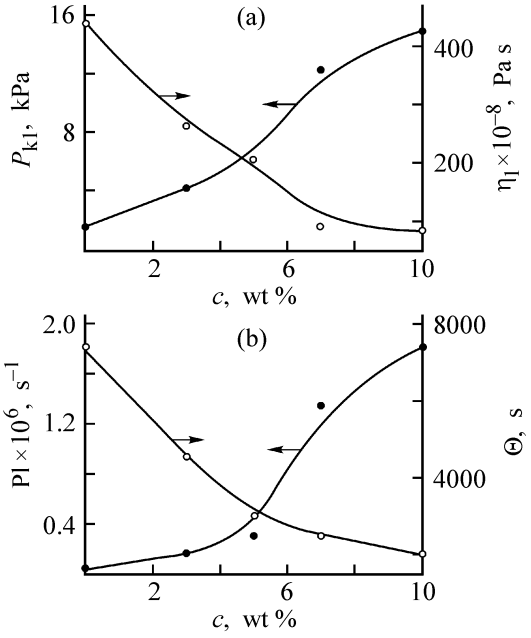


Fig. 3. (a) Ultimate shear stress P_{k1} and maximum plastic viscosity η_1 and (b) plasticity Pl and relaxation time Θ vs. the PVA content *c* in molding blends based on ZnO.

Rheological properties of molding blends based on zinc oxide

PVA content, wt %	N, MW m^{-3}	ΔN, MW m^{-3}	η_0, Pa s	n
0	22.7	3.1	228	0.501
3	23.6	4.7	194	0.476
5	25.6	5.2	178	0.471
7	25.8	6.2	133	0.459
10	26.1	6.3	128	0.414

stress on the PVA content is S-shaped, with the steepest portion of the curve corresponding to a PVA content of 5–7 wt %. The dependence of the maximum plastic viscosity on the surfactant concentration is initially exponential and then, at a PVA concentration higher than 7 wt %, flattens out. The dependence of the plasticity on the surfactant concentration is also S-shaped, and the dependence of the relaxation time is exponential (Fig. 3b).

These phenomena can be explained as follows. At a PVA content of up to 5–7 wt %, the polymolecular sorption layer is formed incompletely. Hence, a change in the surfactant concentration strongly affects the structuring processes in the system, namely, formation of coagulation bonds between solid particles. Structuring of the polymer solution starts to affect the structural-mechanical properties of the molding blends at PVA concentrations higher than 7 wt %, i.e., when the surfactant molecules cease to be sorbed on zinc oxide particles. Clearly, the influence of these structures on P_{k1} and η_1 and hence on Pl and Θ is lower than that of coagulation bonds between ZnO particles.

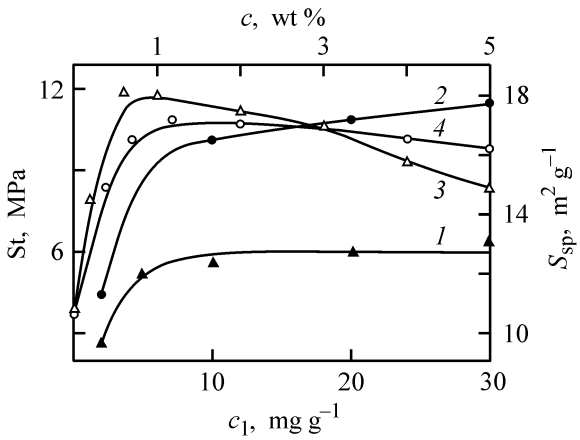


Fig. 4. (*1*, *2*) Mechanical strength St and (*3*, *4*) specific surface area S_{sp} of granulated sulfur adsorbent based on ZnO vs. the polymer content c and c_1. Surfactant: (*1*, *3*) CMC and (*2*, *4*) PVA.

It should be noted that the total power N consumed for flow of the blends remains unchanged, and the power for degradation of the coagulation structure ΔN increases by a factor of 2 (see table) with increasing PVA content. At the same time, the constant η_0 decreases by a factor of 2, and the flow index n only slightly varies in the range 0.4–0.5. It should be noted that the rheological parameters also noticeably change at the PVA concentrations lower than 7 wt %. This is also due to the processes occurring in sorption of PVA molecules on ZnO particles. These processes have the strongest effect on the structure of the system, i.e., on ΔN and η_0.

The mechanical strength and specific surface area of extruded articles strongly depend on the concentration and type of a surfactant. In our case, the strength of ZnO granules grows as the polymer concentration increases to 15–20 mg g^{-1} (Fig. 4). The strength is the highest at the surfactant concentration of about 5 wt %. Our calculations show that the sorbent prepared under these conditions contains about 1.5–2.0 wt % surfactant. As can be seen from Fig. 1, this surfactant content is close to the maximum sorption. Hence, the mechanical strength of the extrudate will be the highest when the surface of solid particles is completely covered with a polymer layer. It should be noted that the mechanical strength of the granules increases at high concentration of the polymeric adsorbate (PVA) in the extrudate.

The specific surface area of molded zinc oxide prepared from 0.5–0.2 wt % solutions of CMC or PVA increases from 12 to 18 m^2 g^{-1} (Fig. 4). At surfactant concentrations higher than 2 wt %, the specific surface area does not exceed 13–14 m^2 g^{-1} due to three-dimensional structuring of the polymer in the solution, which prevents dispersion and stirring of the system.

It is known that the properties of a ready extrudate depend not only on the physicochemical properties of the initial composition, but also on the extrusion conditions. We have shown previously [10] that the mechanical strength of extruded granules depends on the molding rate. These dependences may pass both through maxima and through minima. One of parameters depending both on the properties of the molding blend and on the extrusion conditions is the Weissenberg criterion [11].

The dependences of the mechanical strength and pore volume of ZnO sorbent on the Weissenberg criterion We are shown in Fig. 5. The dependence of the mechanical strength passes through a maximum, and the dependence of the pore volume, through a minimum. All the extrema appear at Weissenberg criteria of 200–300. The opposite course of these dependences is due to the fact that the strength of granules decreases with an increase in their porosity, all other conditions being the same.

Let us consider the factors responsible for appearance of the extrema. The relaxation time Θ entering into the equation for calculation of We characterizes the development of the plastic strain [6, 11]. When the extrusion is slow and, hence, We is low (up to 200), the plastic strain develops to a high extent and the sample is not ruptured. To increase the extrusion rate, the molding stress should be increased, which results in densification of the sample and, hence, in shortening of the interparticle distance. As result, the mechanical strength of the granules increases and their pore volume decreases.

At a higher extrusion rate, the strain of the molding charge at the extruder outlet is incomplete and fluctuations appear. The sorbent prepared under these conditions has a defective structure; its mechanical strength decreases and pore volume increases.

One more feature of the dependence of the pore volume on We is a strong influence of the extrusion rate on the volume of open pores (Fig. 5).

The total porosity strongly depends on the volume of open pores. This is probably due to the fact that, in accordance with Poiseuille's law, the flow rate of the molding charge at the center of a channel is substantially higher than that in the near-wall layer [7]. Hence, the defectiveness of the structure at the center of granules, where the flow rate is the highest, will be more pronounces than that at the periphery. The porosity of peripheral layers largely determines the volume of open pores.

Thus, PVA is a more effective surfactant, since it strengthens the interparticle interactions, whereas CMC promotes structuring of the dispersion medium. This is confirmed by the change in all the rheological properties of the suspensions. The influence of PVA on the rheological behavior of the ZnO suspension is stronger than that exerted by CMC.

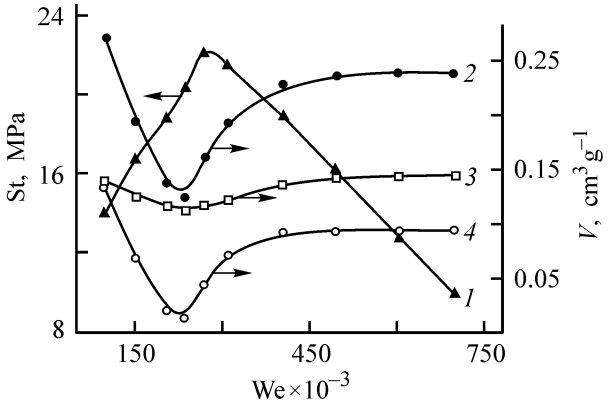


Fig. 5. (*1*) Mechanical strength St and (*2*) total pore volume, (*3*) volume of closed pores, and (*4*) volume of open pores, *V*, of ZnO sorbent vs. the Weissenberg criterion We.

CONCLUSIONS

(1) The curves of sorption of the surfactants from aqueous solutions on zinc oxide have maxima at a surfactant concentration of 1–2 wt %. This is due to structuring of the surfactants in the solution.

(2) The correlations between the surfactant sorption on ZnO particles and the structural-mechanical and rheological parameters of the molding formulation were revealed, as well as the correlation between the mechanical strength and the specific surface area of granules. All these phenomena are caused, on the one hand, by formation of sorption layer on the particle surface and, on the other, by structuring of the polymer solutions.

(3) The mechanical strength and pore structure of the granules are determined both by the properties of the molding blends and by the extrusion conditions. These parameters are related by the Weissenberg criterion. Hence, if the properties of a molding blend are known, the granules with required strength and porosity can be prepared by varying the extrusion rate and the die size.

REFERENCES

1. Ganz, S.N., *Ochistka promyshlennykh gazov* (Treatment of Industrial Gases), Dnepropetrovsk: Promin', 1977.
2. *Physical and Chemical Aspects of Adsorbents and Catalysts*, Linsen, B.G., Ed., London: Academic, 1970.
3. Uzugi, K. and Tamia, H., *J. Chem. Soc. Japan*, 1965, vol. 86, no. 7, pp. 699–704.
4. Shirokov, Yu.G., Ul'in, A.P., Kirillov, I.P., *et al.*, *Zn. Prikl. Khim.*, 1979, vol. 52, no. 6, pp. 1228–1233.

5. Il'in, A.P., Shirokov, Yu.G., and Titel'man, L.I., *Izv. Vyssh. Uchebn. Zaved., Khim. Khim. Tekhnol.*, 1984, vol. 27, issue 1, pp. 78–80.
6. Kruglitskii, N.N., *Osnovy fizikokhimicheskoi mekhaniki* (Foundations of Physicochemical Mechanics), Kiev: Vishcha Skola, 1975, part 1.
7. Prokof'ev, V.Yu., Il'in, A.P., Shirokov, Yu.G., and Yurchenko, E.N., *Zh. Prikl. Khim.*, 1995, vol. 68, no. 4, pp. 613–618.
8. Shchukin, E.D., Bessonov, A.I., and Paranskii, S.A., *Mekhanicheskie ispytaniya katalizatorov i sorbentov* (Mechanical Tests of Catalysts and Sorbents), Moscow: Nauka, 1971.
9. Buyanova, N.E., *Opredelenie udel'noi poverkhnosti katalizatorov* (Determination of the Specific Surface Area of Catalysts), Moscow: Khimiya, 1973.
10. Prokof'ev, V.Yu., Il'in, A.P., Shirokov, Yu.G., *et al.*, *Zh. Prikl. Khim.*, 1996, vol. 69, no. 10, pp. 1685–1690.
11. Il'in, A.P. and Prokof'ev, V.Yu., *Katal. Prom.*, 2002, no. 6, pp. 45–51.

Russian Journal of Applied Chemistry, Vol. 78, No. 2, 2005, pp. 239–242. Translated from Zhurnal Prikladnoi Khimii, Vol. 78, No. 2, 2005, pp. 245–248.
Original Russian Text Copyright © 2005 by Bondaletov, Troyan, Chernov, Bannikova, Dmitrieva.

SORPTION AND ION-EXCHANGE PROCESSES

Adsorption of Gaseous Hydrocarbons on the Surface of Modified Petroleum-Polymeric Resins

V. G. Bondaletov, A. A. Troyan, E. B. Chernov, E. V. Bannikova, and Z. T. Dmitrieva

Institute of Petroleum Chemistry, Siberian Division, Russian Academy of Sciences, Tomsk, Russia, Polytechnic University, Tomsk, Russia

Received July 23, 2004

Abstract—The kinetics of adsorption of model hydrocarbons (benzene, toluene, ethyl benzene, isopropyl benzene, cyclohexane) from the gas phase on the surface of ozonized and maleized petroleum-polymeric resins was studied. The dependences of the dynamic equilibrium capacity of the petroleum-polymeric resins and of the adsorption kinetic parameters on the composition of the adsorbent–adsorbate system were elucidated.

Physical adsorption is low-selective process governed by the ratio of the translation kinetic energy of sorbate molecules to the surface energy of the adsorbent. This predetermines the ways of improving the adsorption-structural parameters of the adsorbent. Along with the sorption power of porous materials, the selectivity of the adsorbent is also of importance. In this study, we examined modified (ozonized and maleized) petroleum-polymeric resins (PPR) as new adsorbents for adsorption of hydrocarbons from the gas phase.

EXPERIMENTAL

To prepare adsorbents based on modified PPR, the piperylene-amylene (C5), styrene-indene (SIF), and dicyclopentadiene (DCPDF) fractions of the liquid products of pyrolysis of straight-run naphtha were subjected to catalytic polymerization at 80°C for 3 h in the presence of the Ziegler–Natta catalytic system based on $TiCl_4$–$(C_2H_5)_3Al$ system at a 1 : 0.33 component molar ratio and $TiCl_4$ concentration of 2 wt % [1]. Crystalline, insoluble in hydrocarbons, PPRs ($OPPR_{C5}$, $OPPR_{SIF}$, $OPPR_{DCPDF}$) were prepared by ozonation of a 10% PPR solution in xylene with an air–ozone mixture (O_2–O_3 flow rate 38.5 l h^{-1}, O_3 concentration 2 vol %) in a bubbler at 5°C for 3 h [2]. The maleization was performed by the PPR reaction with 10 and 20 wt % maleic anhydride in the melt at 180°C for 4 h. The subsequent ozonation of maleized PPR gave modified PPRs ($OPPR_{SIFM10}$ and $OPPR_{SIFM20}$).

The samples of modified PPRs were ground into powders, and the 200–250-μm fraction was separated. Before experiment, the adsorbent samples were vacuum-treated for 5–8 h at 50–60°C and 0.133 Pa. The true and bulk densities of the adsorbent were found densimetrically [3].

Chemically and analytically pure benzene, toluene, ethyl benzene, isopropyl benzene, and cyclohexane were additionally distilled and stored in hermetically sealed vessels over freshly calcined NaA zeolite.

Adsorption of the model hydrocarbons from an air–gas mixture was performed at 20°C on a device equipped with a compressor, Drechsel bottle charged with the adsorbate, and a filter with the adsorbent. The adsorbent (2–5 g) was loaded into the filter as a continuous bed. An air–gas flow generated by the compressor was filtered through the adsorbent layer at the initial pressure of $(2–3) \times 10^4$ Pa. The rate of hydrocarbon feeding with the air–gas flow was 5–6 $cm^3 h^{-1}$. The weight of the adsorbed hydrocarbon was determined gravimetrically at 15–20 min intervals until the equilibrium was attained.

The process duration for each adsorbent–adsorbate system studied and the total weight of the adsorbed hydrocarbons at equilibrium were determined from the kinetic dependences of the hydrocarbon adsorption (Figs. 1a, 1b). From the total increase in the weight,

1070-4272/05/7802-0239 © 2005 Pleiades Publishing, Inc.

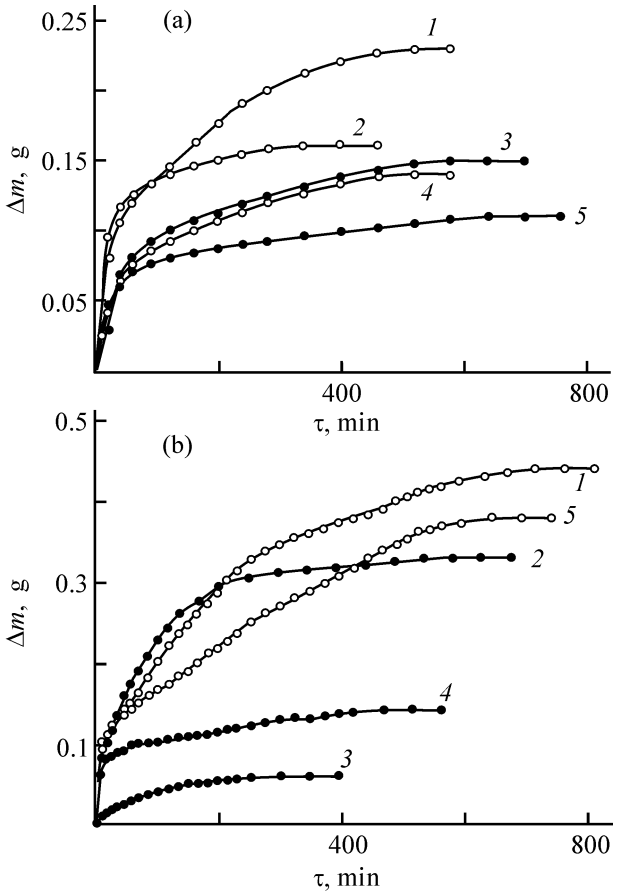


Fig. 1. Kinetics of (a) cyclohexane and (b) toluene adsorption. (Δm) Total weight of hydrocarbons adsorbed and (τ) process duration. Adsorbents: (*1*) $OPPR_{SIFM10}$, (*2*) $OPPR_{SIFM20}$, (*3*) $OPPR_{C5}$, (*4*) $OPPR_{DCPDF}$, and (*5*) $OPPR_{SIF}$.

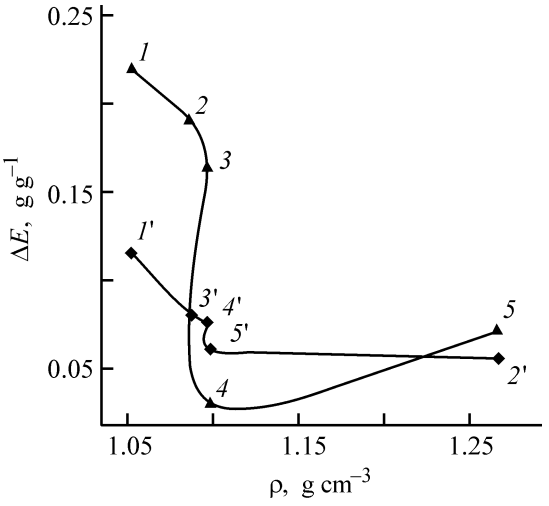


Fig. 2. OPPR capacity ΔE, in adsorption of (*1*–*5*) toluene and (*1*'–*5*') cyclohexane vs. adsorbent density ρ. (*1*, *1*') $OPPR_{SIFM10}$, (*2*, *2*') $OPPR_{SIF}$, (*3*, *3*') $OPPR_{SIFM20}$, (*4*, *4*') $OPPR_{C5}$, and (*5*, *5*') $OPPR_{DCPDF}$.

the equilibrium adsorbent capacity was calculated with respect to each adsorbate by the formula

$$\Delta E = (\Sigma \Delta m)/m,$$

where $\Sigma \Delta m$ is the weight gain due to the adsorbed hydrocarbon at equilibrium (g), and m, adsorbent weight in the filtering bed (g).

The adsorption of hydrocarbons from the gas phase on the resin surface is an equilibrium nonlinear process described by the equation

$$\Delta m_\tau = \Delta m_1(1 - e^{-k_1\tau}) + \Delta m_2(1 - e^{-k_2\tau}), \quad (1)$$

where Δm_τ is the total weight of the hydrocarbons adsorbed (g); Δm_1, weight of hydrocarbons adsorbed on the external surface (first-kind centers) (g); Δm_2, weight of hydrocarbons adsorbed on the internal surface (second-kind centers) (g); k_1, rate constant of hydrocarbon adsorption on the external surface (s^{-1}); k_2, rate constant of hydrocarbon adsorption on the internal surface (s^{-1}); and τ, duration of adsorption (s) (independent variable).

Equation (1) containing five parameters was solved by the unconstrained optimization method with the OPTIM software, including zeroth, first, and second optimization orders [4–6]. The zeroth order is a direct method for search and calculation of the function being optimized, the first order is the calculation of its first derivative, and the second order is the calculation of its first and second derivatives.

The rate constants k_a and k_d (s^{-1}), equilibrium constants K_{eq}, and Gibbs energies ΔG (kJ g^{-1} sorbate) of adsorption–desorption of hydrocarbons on the external and internal adsorbent surfaces were determined by Eq. (1) and equations $K_{eq} = k_a/k_d$ and $\Delta G = -RT \ln K_{eq}$, respectively, with an error of 0.1–0.3% (Table 1).

The OPPR surface was regenerated by forced displacement of adsorbed hydrocarbons with an air flow. The kinetic parameters of this procedure are listed in Table 2.

The time of equilibrium attainment (TEA) depends on the surface area of the adsorbent and kind of an adsorbate (Figs. 1a, 1b). On the surface of maleized $OPPR_{SIF}$ and $OPPR_{DCPDF}$, the equilibrium in the adsorbent–cyclohexane system is attained faster than on $OPPR_{C5}$ (Fig. 1a), and in adsorbent-toluene system, by contrast, TEA is shorter on $OPPR_{C5}$ (Fig. 1b). In contrast to TEA, the adsorption capacity of $OPPR_{SIF}$, $OPPR_{SIFM10}$ and $OPPR_{SIFM20}$ with respect to toluene increases by a factor of 2–3 as compared to cyclohexane (Fig. 2). On the surface of $OPPR_{DCPDF}$, and

Table 1. Kinetic parameters of hydrocarbon adsorption on the external and internal surface of OPPR

OPPR	Adsorbate	External surface					Internal surface				
		$k_a \times 10^4$, s^{-1}	$k_d \times 10^4$, s^{-1}	m, %	K_p	ΔG, kJ g^{-1}	$k_a \times 10^4$, s^{-1}	$k_d \times 10^4$, s^{-1}	m, %	K_p	ΔG, kJ g^{-1}
S5	Benzene	0.21	0.25	45.54	0.84	0.43	0.29	0.24	54.46	1.20	–0.44
	Toluene	0.94	2.19	29.93	0.43	2.06	2.22	0.95	70.07	2.34	–2.07
	Ethyl benzene	9.53	11.28	45.80	0.85	0.40	0.11	0.09	54.20	1.18	–0.40
	Cyclohexane	8.85	18.67	32.16	0.47	1.13	0.56	0.27	67.84	2.11	–1.13
DCPDF	Benzene	0.12	0.73	14.61	0.17	4.32	0.32	0.06	85.39	5.85	–4.30
	Toluene	0.48	0.53	47.36	0.90	0.26	30.13	27.11	52.64	1.11	–0.25
	Ethyl benzene	3.68	5.17	41.60	0.71	0.83	52.58	37.45	58.40	1.40	–0.82
	Cyclohexane	13.24	14.72	47.35	0.90	0.26	0.24	0.21	52.65	1.11	–0.25
SIF	Benzene	5.02	0.004	5.02	0.02	7.30	0.18	0.01	94.98	18.92	–7.16
	Toluene	16.56	0.13	16.56	0.13	3.92	0.40	0.08	83.44	5.04	–3.94
	Ethyl benzene	47.75	0.02	47.75	0.02	0.23	4.29	3.93	52.25	1.09	–0.21
	Cyclohexane	34.94	0.0003	34.94	0.02	1.50	27.03	14.51	65.06	1.86	–1.51
SIFM10	Benzene	29.11	0.41	29.11	0.41	2.17	2.10	0.86	70.89	2.44	–2.17
	Toluene	1.17	1.64	41.67	0.71	0.83	58.33	1.40	58.33	1.40	–0.82
	Ethyl benzene	31.82	102.64	23.66	0.31	2.85	76.34	3.23	76.34	3.23	–2.86
	Cyclohexane	42.16	110.62	27.59	0.38	2.36	72.41	2.62	72.41	2.62	–2.35
SIFM20	Benzene	2.11	2.17	49.21	0.97	0.07	50.79	1.03	50.79	1.03	–0.07
	Toluene	2.15	2.63	44.92	0.82	0.48	55.08	1.23	55.08	1.23	–0.50
	Ethyl benzene	19.18	45.35	29.72	0.42	2.11	70.28	2.36	70.28	2.36	–2.09
	Cyclohexane	43.94	0.78	43.94	0.78	0.61	48.52	38.03	56.06	1.28	–0.60

Table 2. Kinetics of adsorbent regeneration

OPPR	Adsorbate	External surface		Internal surface	
		$k_1 \times 10^4$, s^{-1}	m_1, %	$k_2 \times 10^4$, s^{-1}	m_2, %
S5	Benzene	557.89	63.77	9.64	36.23
	Toluene	1100.40	83.82	0.48	16.18
	Cyclohexane	6095.19	56.07	493.59	43.93
DCPDF	Benzene	2473.17	69.23	213.32	30.77
	Toluene	750.32	69.63	30.40	30.37
	Cyclohexane	1730.04	8.63	1672.26	91.37
SIF	Benzene	1252.61	70.64	57.77	29.36
	Toluene	373.11	87.99	30.26	12.01
	Cyclohexane	826.32	64.93	806.75	35.07
SIFM10	Benzene	700.25	75.36	18.60	24.64
	Toluene	339.15	81.52	14.68	18.48
	Cyclohexane	1350.60	59.34	58.55	40.66
SIFM20	Benzene	1672.95	62.36	200.04	37.64
	Toluene	2774.25	77.50	107.29	22.50
	Cyclohexane	5508.89	88.37	352.03	11.63

especially, $OPPR_{C5}$, the capacity with respect to cyclohexane is higher than with respect to toluene. The surfaces of $OPPR_{SIF}$ and its maleized modifications demonstrate selectivity with respect to aromatic hydrocarbons, and especially to benzene and toluene. The correlation between the adsorbent capacity and its density is noteworthy. The lower the OPPR density, the higher its adsorption capacity (Fig. 2). The decrease in the material density must lead to an increase in its porosity. As seen (Fig. 2), maleization

of $OPPR_{SIF}$ increases the adsorbent capacity due to an increase in its porosity (surface area). $OPPR_{SIFM10}$ has the highest capacity.

The kinetic parameters, similarly to the capacity and TEA, depend on the nature of a particular OPPR–hydrocarbon system. In adsorption of hydrocarbons on OPPR, the equilibrium of adsorption on the external surface is shifted toward desorption (K_{eq} is less than unity, ΔG is positive), and on the internal surface, toward adsorption (Table 1). The maleization of $OPPR_{SIF}$ causes a noticeable redistribution of the values of the kinetic parameters. In particular, k_d exceeds k_a by 1–2 orders of magnitude on the external surface of $OPPR_{SIFM10}$. At the same time, k_a increases and k_d decreases on the internal surface. In accordance with such a redistribution of the rate constants, the weight of hydrocarbons adsorbed on the OPPR internal surface increases, which agrees with the change in the adsorbent density and capacity, caused by $OPPR_{SIF}$ maleization (Fig. 2). The adsorbent capacity decreases and density increases with increasing degree of maleization. Hence, the surface porosity of petroleum-polymeric resins can be controlled by their modification and, in particular, by maleization. Along with structural changes, maleization increases the OPPR selectivity with respect to aromatic hydrocarbons.

In contrast to equilibrium adsorption-desorption of hydrocarbons on OPPR, the nonequilibrium process of OPPR regeneration is characterized by very high rate constants and short time of displacement of the adsorbed hydrocarbon from the polymer surface (Table 2). The rate constants of regeneration of the external surface increase and those of the internal surface area decrease with increasing degree of $OPPR_{SIF}$ maleization. This agrees with kinetic parameters of the equilibrium adsorption-desorption of hydrocarbons on the same surface of the maleized $OPPR_{SIF}$ (Table 1) and with the capacities and densities of the adsorbents.

CONCLUSIONS

(1) Ozonized and maleized petroleum-polymeric resins were tested as adsorbents of aliphatic and aromatic hydrocarbons from the gas phase. The equilibrium adsorption capacity and selectivity of the adsorbents depend on the degree of resin maleization and the composition of the adsorbent–adsorbate system.

(2) Maleization leads to an increase in the internal surface area of the ozonized petroleum-polymeric resins. This is manifested in a decreased resin density and an increased adsorption capacity.

(3) Maleization provides a thermodynamic stability of adsorbed hydrocarbons on the internal surface of the ozonized petroleum-polymeric resins. The adsorption of hydrocarbons on the internal surface of the resin is spontaneous: $K_{eq} > 1$ and $\Delta G < 0$.

REFERENCES

1. RF Patent 2079514.
2. Bondaletov, V.G., Bondaletova, L.I., and Troyan, A.A., *Izv. Vyssh. Uchebn. Zaved., Khim. Khim. Tekhnol.*, 2003, vol. 46, no. 2, pp. 43–45.
3. Pavlenko, Yu.P., Bilyushov, V.M., and Ovsyanik, V.D., *Laboratornyi praktikum po ulavlivaniyu utilizatsii pylei i gazov* (Laboratory Course of Suppression of Dusts and Gases), Moscow: Metallurgiya, 1996.
4. Ostrovskii, G.M. and Berezhinskii, T.A., *Optimizatsiya khimiko-tekhnologicheskikh protsessov. Teoriya i praktika* (Optimization of Chemical Processes. Theory and Practice), Moscow: Khimiya, 1984.
5. Reklaitis, G.V., Ravindran, A., and Ragsdell, K.M., *Engineering Optimization. Methods and Applications*, New York: John Wiley and Sons, 1983.
6. Dmitrieva, Z.T., Bondaletov, V.G., Antonov, I.G., and Chernov, E.B., *Zh. Prikl. Khim.*, 2002, vol. 75, no. 12, pp. 1988–1992.

Russian Journal of Applied Chemistry, Vol. 78, No. 2, 2005, pp. 243–246. Translated from Zhurnal Prikladnoi Khimii, Vol. 78, No. 2, 2005, pp. 249–252.
Original Russian Text Copyright © 2005 by Kuntyi, Olinets, Kalymon, Olenych.

APPLIED ELECTROCHEMISTRY AND CORROSION PROTECTION OF METALS

Synthesis of Dispersed System (CuO, ZnO) from Lump Braze with a Vertical Flow-through Electrolyzer

O. I. Kuntyi, V. T. Olinets, Ya. A. Kalymon, and R. R. Olenych

Lvivska Politekhnika National University, Lviv, Ukraine

Received July 26, 2004

Abstract—The electrochemical synthesis of a mixture of dispersed oxides (CuO and ZnO) from secondary lump braze was studied. The influence exerted by electrolysis parameters on the intensity of synthesis of the oxide mixture was investigated. The design of the electrolyzer and the flow diagram for synthesis of a mixture of oxides (CuO and ZnO) from lump braze was suggested.

The electrochemical synthesis of inorganic compounds of nonferrous metals: oxides [1, 2], hydroxides [3, 4], and salts [5, 6], is one of the areas of preparative chemistry that have been rapidly developing in the last decade. Use of electrolysis makes it possible to obtain not only pure target products, but also substances with certain physicochemical characteristics. For example, electrochemically obtained vanadium(V) oxide is distinguished by good performance as a cathode material for lithium batteries [7], and copper(II) oxide, by high dispersity and purity [8].

In this study, we continued a comprehensive study of the electrochemical synthesis of hydroxides, oxides [2], and salts [6] of nonferrous metals from secondary raw materials.

EXPERIMENTAL

Anodic polarization curves were measured in a standard thermostated electrochemical cell at a potential sweep rate of 5.0 mV s^{-1} with a PI-50-1.1 potentiostat. Platinum was used as the auxiliary electrode, and silver chloride, as reference. Zinc, copper, and braze (L63 brand, 63 wt % copper and 37 wt % zinc) in the form of rods 2-mm in diameter pressed into a fluoroplastic cartridge served as working electrodes. The samples were trimmed with a fine emery paper and washed with ethanol prior to each experiment. A 0.5 M solution of Na_2SO_4 was used as a working electrolyte.

The mixture of oxides CuO and ZnO was synthesized from lump braze in an electrolyzer schematically shown in Fig. 1.

The steel vessel of the electrolyzer is coated with nickel by means of electroless plating. The inner walls are lined with a dielectric film. Current is conveyed to the bulk anode through the bottom. The cross-sectional diameter of the bulk anode is 100 mm. As the cathode serves a copper disc 60 mm in diameter, closed from above and on sides with a polypropylene cap, so that only its lower part is working. The spacing between the cathode and bulk anode can be adjusted by moving the cathode. In the experiments, braze cuttings with a conventional diameter of 2–3 mm, length of 3–30 mm, and a bulk weight of 1.0–1.1 g cm^{-3}

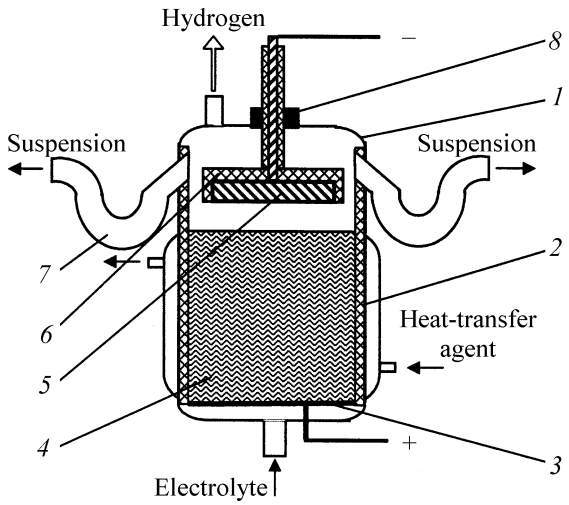


Fig. 1. Schematic of the electrolyzer used to synthese a mixture of CuO and ZnO from lump braze. (*1*) Metallic vessel, (*2*) vessel lining, (*3*) current lead, (*4*) bulk anode (cuttings), (*5*) copper cathode, (*6*) insulating cap, (*7*) hydraulic lock, and (*8*) seal.

1070-4272/05/7802-0243 © 2005 Pleiades Publishing, Inc.

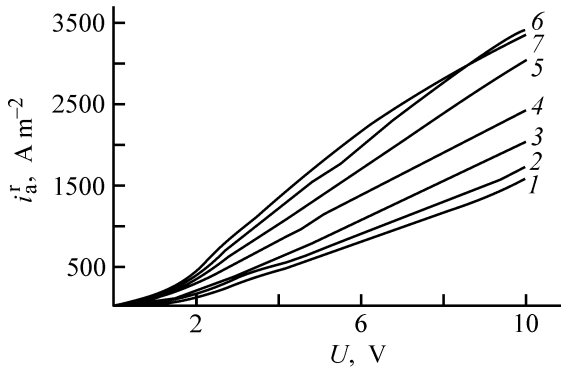


Fig. 2. Current–voltage curves measured in anodic dissolution of L63 braze in a 0.5 M Na_2SO_4 solution. (i_a^r) Current density and (U) voltage. Temperature (°C): (*1*) 20, (*2*) 30, (*3*) 40, (*4*) 50, (*5*) 60, (*6*) 70, and (*7*) 80.

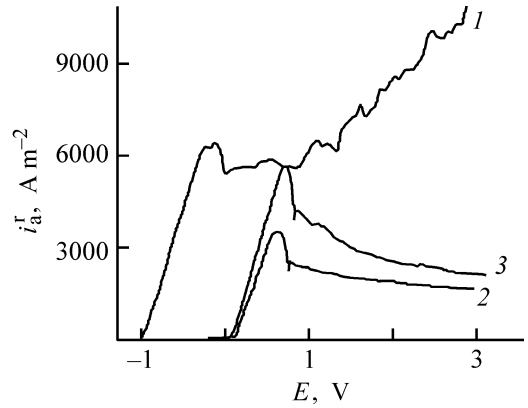


Fig. 3. Anodic polarization curves obtained under hydrostatic conditions for (*1*) zinc, (*2*) copper and (*3*) braze in a 0.5 M Na_2SO_4 solution at 60°C. (i_a^r) Current density and (E) voltage.

(copper 1.3–1.4 g cm^{-3}) were charged, after being degreased, into the electrolyzer to a height of 150 mm. The electrolysis was performed in the flow-through mode using a preheated 0.5 M solution of Na_2SO_4. The working temperature of the electrolyte was maintained by thermostating the electrolyzer. Current–voltage characteristics were recorded in the range 20–80°C, with voltage sweeping from 0 to 10 V in steps of 0.5 V and the system kept for 30 s at each point. The electrochemical synthesis was performed at U = const. The suspension passed through the electrolyzer was filtered immediately after that or upon being heated to the boiling point. Then it was allowed to settle, washed with water, and dried at 50°C in air. The pH value of the filtrate was adjusted when necessary and again fed into the electrolyzer. The CuO + ZnO content was determined by calcination of predried powders at 600°C.

The powders obtained were subjected to an X-ray phase analysis on a DRON-3M diffractometer (Cu_{K_α} radiation, θ–2θ scan angle, Bragg–Brentano technique), with a stepwise recording of diffraction patterns.

In a flow-through electrolyzer (Fig. 1), Zn^{2+} and Cu^{2+} ions formed in the near-anode space through anodic dissolution of braze are carried by the electrolyte into the interelectrode space and the near-cathode layer, where pH > 7 is established because of the occurrence of a cathodic reaction

$$2H_2O + 2e \rightarrow H_2 + 2OH^-. \quad (1)$$

Therefore, insoluble complexes $Zn(OH)_2$ and $Cu(OH)_2$ are formed in the interelectrode space and, in part, in the near-cathode space, which predetermines electrodeposition of copper and zinc onto the cathode.

As temperature increases (≥50°C), $Cu(OH)_2$ starts to decompose by the reaction

$$Cu(OH)_2 \rightarrow CuO + H_2O, \quad (2)$$

which is indicated by the fact that the deposit turns dark, to become virtually black at above 90°C, and by the results of the X-ray phase analysis.

The results of the study show that the reduced anodic current density i_a^r ($i_a^r = I/S$, where I is current strength, and S, surface area of the bulk anode) is proportional to the voltage across the electrolyzer and grows with increasing temperature (Fig. 2). Above 70°C, a decrease in the rate at which the i_a^r increases is observed.

The anodic currents of dissolution of lump braze are considerably higher than those of lump copper under the analogous conditions of electrolysis.

For example, at voltages of 5, 7, and 9 V and a temperature of 70°C, i_a^r is 1605, 2445, and 3159 A m^{-2}, respectively, for lump braze and 1120, 1745, and 2370 A m^{-2} for lump copper. This is due to the fact that the anodic dissolution currents of the main component of braze, zinc, are higher than those of copper (Fig. 3). In addition, the dissolution of braze is a selective process: first dissolves zinc, as a more electronegative metal, and only after that, copper [9]. The surface of braze becomes porous after the removal of zinc, which also facilitates the anodic dissolution.

The intensity of electrochemical synthesis of the oxide mixture may be governed by (1) electrolysis voltage, (2) concentration of a supporting electrolyte (Na_2SO_4), and (3) temperature.

As the voltage increases, the current density at the electrodes grows; however, the limiting anodic current density [10, 11], which increases for a bulk anode owing to the electrochemical inhomogeneity of the surface, is not reached even at 10 V.

The concentration of the supporting electrolyte is not the limiting factor, because, as shown in our study, the dissolution currents of braze in a 0.2–0.5 M Na_2SO_4 solution are virtually equal even at a voltage of 15 V.

With temperature raised by 10°C, the rate of electrochemical synthesis increases by 15–25% (table, Fig. 2). Apparently, this result can be accounted for by a decrease in the electrical resistance of the electrolyte and by the diffusion factor.

In addition, raising the temperature accelerates the coagulation of the deposit and leads to changes in its composition. For example, according to the results of an X-ray phase analysis, the deposit obtained below 50°C contains only the hydroxide $Cu(OH)_2$, and that formed at 60°C, also the oxide phase CuO. The content of the oxide phase grows with increasing temperature and, after the boiling temperature is reached, the suspension is virtually composed of a single phase, CuO. An X-ray phase analysis of powders obtained from the suspensions below 100°C revealed intermediate compounds of basic salts. For example, the powders synthesized below 50°C contain $6Zn(OH)_2 \cdot ZnSO_4 \cdot 4H_2O$.

The rate of removal of the products formed in the dissolution of the anode (braze) is determined by the flow rate of the electrolyte. Calculations show that, at a flow rate of the electrolyte in the electrolyzer equal to 1 $dm^3\ min^{-1}$, its flow velocity near the anode surface is about 1 $cm\ s^{-1}$. It was experimentally established that higher flow rates of the electrolyte (≥2–3 $dm^3\ min^{-1}$) lead to removal of fine metallic particles from the surface layer and to contamination of the oxides synthesized with these particles. In addition, these values are lower by one or two orders of magnitude than those in fast anodic dissolution of metals in electrochemical anodic sizing (EAS) [12]. Consequently, the electrolyte flow velocity is not an essential parameter in control over the rate of electrochemical synthesis of the oxides CuO and ZnO.

Thus, the main factors responsible for the intensification of the electrochemical synthesis of a mixture of oxides CuO and ZnO from lump braze in a vertical flow-through electrolyzer are the electrolyzer voltage and temperature. However, as the electrolyzer voltage increases, the specific electric power consumption W_{sp} ($W_{sp} = U/1.5CE_a$, where CE_a is anodic current efficiency) becomes higher. By assuming that CE_a is approximately 100% (electrochemical equivalent of the CuO and ZnO mixture is 1.5 $g\ A^{-1}\ h^{-1}$), a value of 3.33 $kW\ h\ kg^{-1}$ is obtained for the specific power consumption W_{sp} (CuO, ZnO) at 5 V, which increases by 0.67 $kW\ h\ kg^{-1}$ as the voltage is raised by 1 V.

Main parameters of electrochemical synthesis of a CuO and ZnO mixture from lump braze in a 0.5 M Na_2SO_4 solution at an electrolyte flow rate of 1 $dm^3\ min^{-1}$

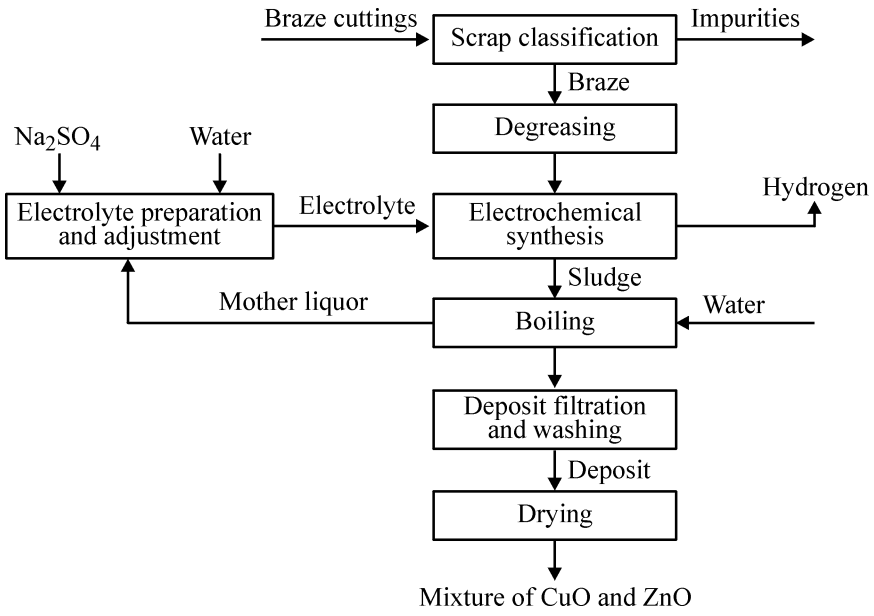
T, °C	U, V	Synthesis intensity CuO, ZnO,* $kg\ m^{-2}\ h^{-1}$
50	5	1.68
	7	2.50
	9	3.29
60	5	2.05
	7	3.07
	9	4.15
70	5	2.41
	7	3.67
	9	4.74
80	5	2.67
	7	3.82
	9	4.78

* In terms of anhydrous metal oxides CuO and ZnO.

Our study demonstrated that the interelectrode spacing is predetermined by the electrolysis rate. The higher i_a^r, the more vigorous is the gas evolution at the cathode. When interelectrode spacing is small, the resulting gaseous foam can reach the bulk anode, which results in the formation of hydroxides (oxides) and their adherence in the zone of the lump metal. It was found that, at an electrolyte flow velocity of 1 $cm\ s^{-1}$ and more and a reduced anodic current density of 2000, 3000, and 4000 $A\ m^{-2}$, the optimal interelectrode spacing is 15, 20, and 25 mm, respectively.

It was found that raising the electrolyte temperature to above 70°C is ineffective as regards the electrolysis intensification. However, with account of the necessity for boiling of the sludge of copper and zinc hydroxides in order to enhance the coagulation and, accordingly, the filterability of the deposit obtained, to prevent formation of basic salts, and to ensure complete transformation of oxides into hydroxides, the optimal temperature of the electrolysis should be 70–80°C.

Based on the results obtained, we suggested the following flow diagram of the electrochemical synthesis of a mixture of oxides CuO and ZnO from lump braze.



Flow diagram of synthesis of dispersed oxides.

In the stage of classification of the scrap, the impurities are removed from braze cuttings by a method dependent on the type and content of impurities. After that, the cuttings are degreased, if necessary.

The thus prepared cuttings are charged into the electrolyzer as a bulk anode. The electrolyte (Na_2SO_4 solution) is fed into the electrolyzer continuously, thus ensuring removal of the electrolysis products in the form of a sludge. The sludge is boiled to improve its filterability, separated from the electrolyte by filtration, and washed. The mother liquor is recycled into the stage of electrolyte preparation. The deposit obtained is dried at 150–200°C.

CONCLUSIONS

(1) It is suggested to perform the electrochemical synthesis of a mixture of oxides CuO and ZnO by anodic dissolution of lump braze in a flow-through vertical electrolyzer in a Na_2SO_4 solution.

(2) It is shown that the main factors important for raising the electrolysis rate are the temperature of the electrolyte and the electrolysis voltage. The intensity of electrochemical synthesis of oxides CuO and ZnO may be as high as 4.8 kg m^{-2} h^{-1} and more when the temperature and voltage have the optimal values.

(3) The flow diagram of electrochemical synthesis of a mixture of oxides CuO and ZnO from lump braze is suggested and tested in laboratory conditions.

REFERENCES

1. Stankovich, Z.D., Rajcic-Vajasinovic, M., Vucovic, M., *et al.*, *J. Appl. Electrochem.*, 1999, vol. 29, no. 1, pp. 81–85.
2. Kuntyi, O.I., Znak, Z.O., and Baranovich, Z.O., *Ekoteknol. Energosberezh.*, 2003, no. 5, pp. 21–25.
3. Jayashree, R.S. and Vishnu, K.P., *J. Appl. Electrochem.*, 1999, vol. 29, no. 4, pp. 449–454.
4. Kovalenko, V.A., Pinielle, I.D., Kotok, V.A., and Baskevich, A.S., *Vopr. Khim. Khim. Tekhnol.*, 2003, no. 5, pp. 130–131.
5. Aliev, Z.N., Vladimirov, M.V., Kharlamov, T.A., and Malofeev, A.S., *Zh. Prikl. Khim.*, 2002, vol. 75, no. 1, pp. 50–53.
6. Yavors'kii, V.T., Sribnui, V.M., Kuntii, O.I., *et al.*, *Ekoteknol. Energosberezh.*, 2001, no. 3, pp. 32–34.
7. Nagirnyi, V.M., Apostolova, R.D., and Shembel', E.M., *Zh. Prikl. Khim.*, 2001, vol. 74, no. 9, pp. 1429–1432.
8. USSR Inventor's Certificate, no. 523872.
9. Pokhmurskii, V., Kopylets, V., and Kornii, S., *Phys.-Chem. Mechanics of Materials*, 2004, no. 4, pp. 271–274.
10. Mirzoev, R.A., Davydov, A.D., and Kabanov, B.N., *Elektrokhimiya*, 1983, no. 10, pp. 1415–1418.
11. Davydov, A.D., *Elektrokhimiya*, 1991, no. 8, pp. 947–960.
12. Orlov, V.F., and Chugunov, B.I., *Elektrokhimicheskoe formoobrazovanie* (Electrochemical Shaping), Moscow: Mashinostroenie, 1990.

Russian Journal of Applied Chemistry, Vol. 78, No. 2, 2005, pp. 247–253. Translated from Zhurnal Prikladnoi Khimii, Vol. 78, No. 2, 2005, pp. 253–259.
Original Russian Text Copyright © 2005 by Boguta, Rudnev, Terleeva, Belevantsev, Slonova.

APPLIED ELECTROCHEMISTRY AND CORROSION PROTECTION OF METALS

Effect of ac Polarization on Characteristics of Coatings formed from Polyphosphate Electrolytes of Ni(II) and Zn(II)

D. L. Boguta, V. S. Rudnev, O. P. Terleeva, V. I. Belevantsev, and A. I. Slonova

Institute of Chemistry, Far-Eastern Division, Russian Academy of Sciences, Vladivostok, Russia

Institute of Inorganic Chemistry, Siberian Division, Russian Academy of Sciences, Novosibirsk, Russia

Received June 11, 2004

Abstract—Characteristics of microplasma-produced coatings formed on an aluminum alloy under anodic and combined anodic–cathodic polarizations in electrolytes with polyphosphate complexes of Ni(II) and Zn(II) are compared.

Two areas can be conventionally distinguished in research and development concerned with formation of anodic electrolytic coatings on aluminum and its alloys under the action of electric discharges giving rise to a large group of microplasma-assisted electrochemical processes [1].

The first of these is associated with the development of methods for implementation and monitoring of advantageous current (current–voltage) modes and analysis of how they affect the composition, structure, and properties of protective layers. Mostly simple aqueous electrolytes, acids, alkalis, silicate-alkaline solutions have been used in these studies [2–13]. It is within this area of research that a group of scientists from Novosibirsk was the first to establish that combining the anodic and cathodic polarizations may dramatically improve the quality of the coatings obtained (with diminished and even completely eliminated through porosity and increased adhesion, microhardness, wear resistance, corrosion resistance, etc.) [4, 14, 15]. This is mostly due to inclusion of high-temperature aluminum oxide phases (γ- and(or) α-Al_2O_3) in the microstructure of the composite layer adjacent to the substrate. It is quite natural that the development of these studies is aimed at a search for optimal current modes. It was possible to raise the growth rate of microplasma-produced layers, improve their operation parameters and diminish the energy intensity of the process as a whole by controlling the repetition frequency of cathodic and anodic current pulses and varying their widths and relative amplitudes [16–18]. It was shown in a generalizing analytical review that analysis of particular results and general patterns should take into account not only a specific current–voltage mode, but also the type (composition and state) of an electrolyte.

The second area of research is aimed to find electrolyte compositions that would make it possible to use microplasma-assisted processes to form on the surface of rectifying metals, including aluminum and its alloys, complex oxide structures in order to provide a wide variety of their properties. However, only anodic polarizations have been commonly employed. A considerable progress has also been made in this area, e.g., conditions have been developed in which layers containing oxides of transition metals [19, 20], spinels [21], phosphates [22–24], and perovskite structures [25, 26] can be obtained on aluminum alloys. These layers have found use or show promise in medicine and catalysis, as active elements of gas analyzers, layers resistant to hard ultraviolet and protecting from the action of corrosive media, and structures exhibiting bioinert or biocide properties.

It has been shown [22–24] that it is possible to form, in electrolytes with water-soluble polyphosphates and salts of M(II) and M(III), oxide structures containing, together with oxides of a metal being treated, also compounds of M(II) and M(III), including, under certain conditions, high-temperature phosphates of M(II) and M(III). The potential fields of application of coatings containing high-temperature metal phosphates are rather wide: catalysts and catalyst supports, sublayers under paint-and-varnish materials, anticorrosive colored decorative layers, and structures with bactericide or biocompatible properties.

1070-4272/05/7802-0247 © 2005 Pleiades Publishing, Inc.

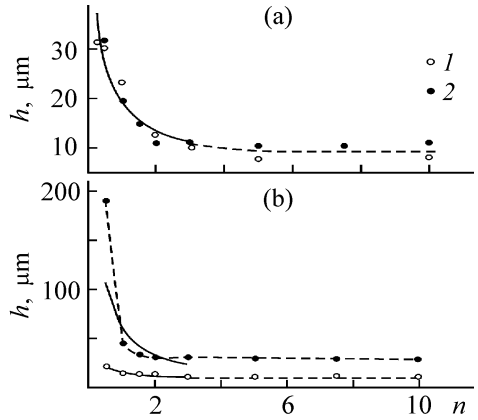


Fig. 1. Thickness h of coatings vs. the molar ratio n of the electrolyte components. (a) Coatings with nickel: (*1*) anodic and (*2*) anodic–cathodic modes, formation time 10 min; (b) coatings with zinc, anodic–cathodic mode, formation time: (*1*) 10 and (*2*) 60 min; the same for Figs. 3 and 4. *Solid line*, approximation with a power function at $n < 3$.

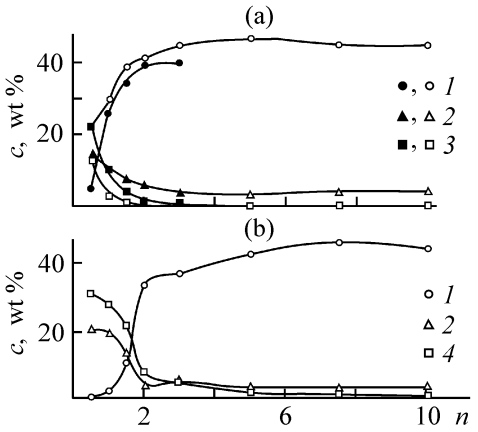


Fig. 2. Elemental composition c of coatings vs. the molar ratio n of the electrolyte components. Coating: (a) with zinc and (b) with nickel. Formation mode: anodic (*full symbols*) and AC + C (*open symbols*); formation time 10 min, oxygen concentration in the coatings undetermined. (*1*) Al, (*2*) P, (*3*) Zn, and (*4*) Ni.

It was of interest to find out whether the previously established patterns of influence exerted by the composition and state of electrolytes with polyphoshate complexes on certain characteristics of coatings formed on an aluminum alloy in the anodic mode are valid, if this mode is changed for the anodic–cathodic mode.

EXPERIMENTAL

The coatings were formed under anodic (mode A) and combined anodic–cathodic (mode AC) polarizations. In the first case, a TEP4-100/460 thyristor source of unipolar current was used, with an effective current density of galvanostatic formation j = 0.05 A cm^{-2}. In the second case, a capacitive power source providing alternating trains of anodic–cathodic and cathodic current pulses (mode AC + C) with a repetition frequency of 50 Hz was employed.[1] The effective current density in an anodic–cathodic train was j_{ac} = 0.05 A cm^{-2}, with equal cathodic and anodic components, and that in a cathodic train, j_c = 0.005 A cm^{-2}. The duration of the anodic–cathodic and cathodic pulse trains was 2 and 0.66 s, respectively.

The surface of a 10-l cylindrical stainless-steel bath was used as a counter electrode. The electrolyte was agitated by air bubbling. To cool the system, cold water was pumped through hollow walls of the bath. The solution temperature in the course of treatment did not exceed 45°C.

The electrolytes were prepared from sodium hexametaphosphate (HMP) of pure grade and $Ni(CH_3COO)_2 \cdot 4H_2O$ and $Zn(CH_3COO)_2 \cdot 4H_2O$ salts of chemically pure grade. First, 30 g l^{-1} of HMP was dissolved in distilled water and then a weighed portion of a salt was introduced into the solution to obtain the required molar ratio $n = [P_6O_{18}]/[M]$ in the bulk of the electrolyte.

The coatings were formed on preliminarily degreased $40 \times 10 \times 1$ and $40 \times 20 \times 1$ mm samples of an AMtsN alloy. Six samples with a total area of 62 cm^2 were placed in the bath simultaneously. The treatment duration was 10 or 60 min. Samples with a deposited coating were washed with distilled water and dried in air at 60–70°C.

The elemental composition of the coating surface was studied with a JXA-5A *n* electron-probe X-ray fluorescence microanalyzer, and the phase composition was judged from X-ray diffraction patterns obtained with a DRON-2.0 X-ray diffractometer (Cu_{K_α} radiation) for coatings on substrates. The coating thickness was determined with a VT-10NTs vortex thickness meter. The average thickness was calculated from the results of 20 measurements. The coating roughness was determined with a Kalibr profile meter with an accuracy of ±10%. The volume porosity of the coatings was calculated from data on oil absorption measured in conformity with GOST (State Standard) 9.302–88 with the use of a VM-1 vacuum oil.

Dependences of the thicknesses and elemental compositions of Ni- and Zn-containing coatings formed in the anodic and combined AC + C modes on the molar ratio n of components in the electrolyte are shown in Figs. 1 and 2. Similar dependences have been ob-

[1] Experiments with a unipolar pulsed thyristor unit were carried out at the Institute of Chemistry, Far-Eastern Division, Russian Academy of Sciences, and those with a combined anodic–cathodic power source, at the Institute of Inorganic Chemistry, Siberian Division, Russian Academy of Sciences.

Table 1. Constants h_0 and b and their standard deviations in the model of $h = f(n)$ dependences obtained for different modes of coating formation on the AMts alloy (effective current density of galvanostatic formation j = 0.05 A cm^{-2})

Electroyte	Mode	h_0, μm (±Δ, %)	b
$Na_6P_6O_{18}$ + $Zn(CH_3COO)_2 \cdot 4H_2O$	AC + C:		
	10 min	15.8 (±9)	0.33 ± 0.07
	60 min	60.3 (±22)	0.84 ± 0.31
$Na_6P_6O_{18}$ + $Ni(CH_3COO)_2 \cdot 4H_2O$	10 min	19.5 (±7)	0.62 ± 0.09
	60 min	81.3 (±9)	0.94 ± 0.12
	ac [30]	17.8 (±12)	0.46 ± 0.09
	Half-wave [30]	16.2 (±7)	0.31 ± 0.08
	dc [30]	17.0 (±3)	0.53 ± 0.02
	Pulsed	18.6 (±7)	0.49 ± 0.08

tained previously in electrolytes containing acetates of various metals (e.g., Mg^{2+}, Mn^{2+}, Pb^{2+}) and polyphosphates, using a thyristor power source with unipolar pulsed current [22–24, 27] or ac and half-wave sinusoidal current [28].

In all the current modes considered, two characteristic regions can be distinguished in the experimental curves (Figs. 1–4). In the first of these ($n > 3$), the coating thickness becomes virtually independent of n (Fig. 1), the content of electrolyte components in the coating is virtually zero (Fig. 2), the roughness remains virtually uchanged (Fig. 3), and the porosity varies without any clearly pronounced specific features (Fig. 4). It is also noteworthy that the initial electrolyte is a true solution at these values of n.

In the second region ($n < 3$), the thickness (Fig. 1) and composition of the coatings (Fig. 2) vary monotonically, and variation of other characteristics shows clearly pronounced specific features (Figs. 3, 4). As regards the state of the electrolyte, this region can be subdivided in two: metastable subregion with a colloid component ($1.5 \le n \le 3$) and a subregion ($0.25 \le n \le 1.5$) in which the "bulk" of the initial solution contains a suspension of dispersed phases or even a precipitate. Presumably, just the last factor tells on the way in which n affects the roughness (Fig. 3). Possibly, the position of the local porosity maximum at $n \approx 1.5$ (Fig. 4a) is also associated with differences in the above-described states of the initial electrolytes.

Making longer the time during which coatings are formed in an electrolyte with Zn polyphosphate in the AC + C mode (from 10 to 60 min) leads to a substantial increase in the coating thickness (Fig. 1b), which is especially noticeable for small n and low roughness (Fig. 3b). In this case, the generality of the type of the dependences observed is retained.

It has been shown previously [28, 29] that the effect of the molar ratio n on the thickness of coatings formed in electrolytes with polyphosphate complexes of metals on aluminum and titanium at different kinds of anodic polarization is well approximated with a power function $h(n) = h_0 n^{-b}$, where h_0 and b are fixed parameters of a model adequate for a certain range of n in the vicinity of $n = 1$. The dependences of the thickness of coatings formed in the AC + C mode at $0.25 \le n \le 3$ are also satisfactorily approximated with a similar function. The points for $n > 3$ were disregarded because the coating thickness is virtually constant at these values. It is noteworthy, in addition, that, in the range $n < 0.25$ not examined in this study, this approximation will undoubtedly be equally inadequate.

Table 1 lists estimates of the parameters h_0 and b, calculated by the least-squares method, and their standard

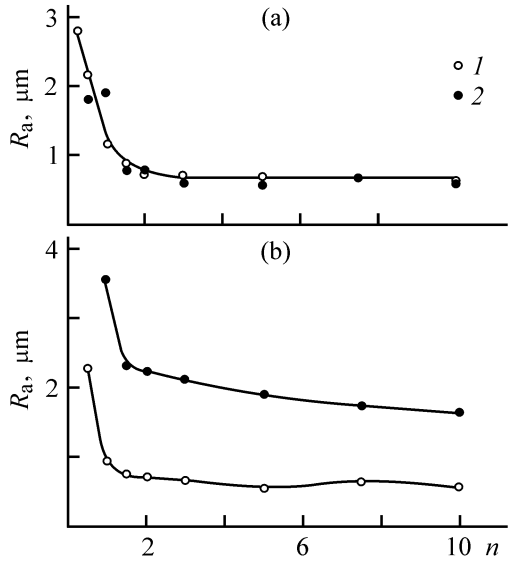


Fig. 3. Roughness R_a of the coatings vs. the molar ratio n of the electrolyte components.

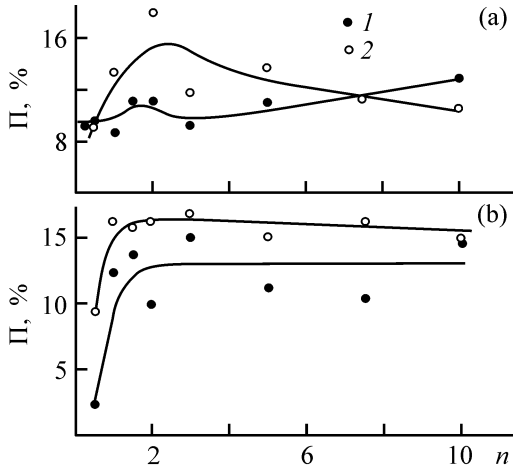


Fig. 4. Volume porosity П of the coatings vs. the molar ratio *n* of the electrolyte components.

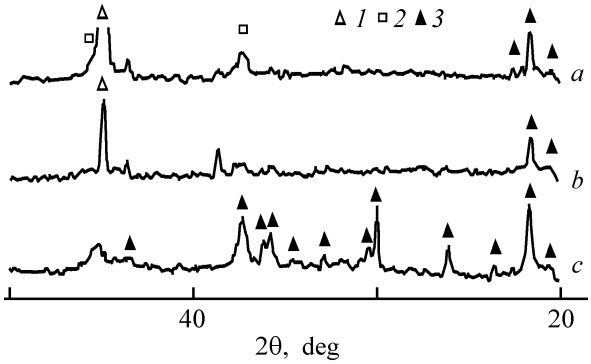


Fig. 5. X-ray diffraction patterns of nickel-containing coatings formed on substrates in an electrolyte with $[P_6O_{18}]/[Ni] = 1$ in different modes. (*a*) Anodic mode, formation time 10 min; (*b*) AC + C mode, formation time 10 min; and (*c*) AC + C mode, formation time 60 min. (*1*) Al, (*2*) γ-Al_2O_3, and (*3*) $AlPO_4$.

deviations for data obtained for $0.25 \le n \le 3$ in this study in the AC + C mode and, previously, in other (anodic) modes at equal quantities of electricity consumed in the process. It should be, first of all, noted that the standard relative deviations were 5–7% for the curves included in the processing, which exceeds by a factor of 2–3 the values expected on the basis of starting error model. It can be seen that, irrespective of the current mode, the approximation parameters have sufficiently close values and agree well with previously obtained data, including those for coatings formed in electrolytes with polyphosphate complexes of Mg(II), Mn(II), Pb(II), and Eu(II) and electrolytes with $Na_6P_6O_{18}$ replaced with $Na_5P_3O_{10}$ [29].

Introduction of a cathodic component in the forming current affects the phase composition of the oxide layers obtained (Fig. 5, Table 2). All other conditions being the same, coatings formed in the AC + C mode are better crystallized. In addition, introduction of a cathodic component of the current at $n > 1.5$ results in that high-temperature Al_2O_3 phases, including α-Al_2O_3, appear in the coatings. Making longer the time of AC + C formation leads to an increase in the crystallinity of the coatings and to appearance of $NiAl_2O_4$ spinel at $n = 1.5$ and α-$Zn_3(PO_4)_3$ at $n = 0.5$ in Ni- and Zn-containing electrolytes, respectively.

For coatings with nickel, it is necessary to note once more the presence of a clearly pronounced maximum in the dependences of the coating porosity on *n* in the region of transition from a metastable solution (colloid state) to a solution with a precipitate ($n \approx 1.5$) (Fig. 4a). The maximum is also observed in the anodic mode, but is less pronounced.

For electrolytes with $n > 1$, the porosity of AC + C coatings with zinc is comparable with that calculated for coatings with nickel (Fig. 4). At the same time, the porosity of coatings with zinc becomes substantially lower as *n* decreases to 0.5, for formation times of both 10 and 60 min. The coatings obtained in this case have the form of a partly fused glassy mass. On the whole, the volume porosity of the coatings formed

Table 2. Phase composition of coatings formed on AMts alloy in different modes

Electrolyte	Mode	Phase composition at *n*		
		10	1.5	0.5
$Na_6P_6O_{18} + Ni(CH_3COO)_2 \cdot 4H_2O$	A, 10 min	æ-Al_2O_3	γ-Al_2O_3, $AlPO_4$	γ-Al_2O_3, $AlPO_4$
	AC + C:			
	10 min	α,γ,η-Al_2O_3	γ-Al_2O_3, $AlPO_4$	$AlPO_4$
	60 min	α,γ,η-Al_2O_3	Al_2O_3, $AlPO_4$, $NiAl_2O_4$	$AlPO_4$
$Na_6P_6O_{18} + Zn(CH_3COO)_2 \cdot 4H_2O$	A, 10 min	X-ray amorphous	X-ray amorphous	$AlPO_4$
	AC + C:			
	10 min	α,γ-Al_2O_3	α-Al_2O_3	Al_2O_3, $AlPO_4$
	60 min	α,γ,η-Al_2O_3	α,γ,η-Al_2O_3	Al_2O_3, $AlPO_4$, α-$Zn_3(PO_4)_2$

in the AC + C mode somewhat exceeds that obtained in the anodic mode (Fig. 4).

The specific features of growth and the composition of microplasma-produced coatings formed on rectifying metals in the anodic mode in polyphosphate electrolytes were reported in [22–24, 28–30]. It was established that the composition and parameters of coatings of this kind depend in a certain way on the molar ratio of the electrolyte components (n = [polyphosphate]/[M]), which also determines the state of the electrolyte (true, metastable, or colloid solution, solution with an admixture of suspended dispersed phases or even with a precipitate). It was reasonable to relate these facts to a difference between "mechanisms of coating formation" in true ($n > 3$) and other ($n \le 3$) solutions. The whole set of data obtained [22–24, 28–30] indicates that a decrease in n (approach of the electrolyte to the state of precipitation leads to predominance of the "thermolytic formation mechanism," in which the mass of a coating increases mainly through thermally induced transformations of the colloid and dispersed fractions of polyphosphates in the vicinity of electric discharges. In the region of true polyphosphate electrolyte solutions, the "coating growth mechanism" predominates because of the formation of oxides from the components of the substrate.

The anodic–cathodic microplasma-assisted processes have been studied extensively [4, 13–18, 31–34]. During the cathodic half-period, defects that facilitate the process under the anodic polarization can be formed [31]. In the opinion of the authors of [32], stronger discharges that fuse the oxide layer occur during the periods of cathodic polarization. According to [33], the cathodic polarization leads to a decrease in the space charge in the oxide, which facilitates coating formation under the succeeding anodic polarization. Use of ac current not only limits the time of action of discharges during the anodic period, but is also accompanied by flow of currents associated with recharging of the metal–oxide–electrolyte system [13]. In addition, the hydrogen evolution during the cathodic period creates conditions under which gas bubbles are formed near the surface, and their breakdown affects the growth of oxide films. In any case, introduction of a cathodic component of the current leads to heating of the inner part of the oxide layer, which favors formation of high-temperature phases in this region [4, 13–18].

However, the data obtained in this study demonstrate that, all other conditions being the same, introduction of an additional cathodic component into the current at the accepted initial and boundary conditions does not exert any significant influence on the elemental composition, thickness, and roughness of coatings formed in electrolytes with polyphosphate complexes at $n \le 3$. This confirms the previously made conclusion about the thermolytic mechanism of formation of coatings in electrolytes of this kind. The assumption that the α-Al_2O_3 phase crystallizes in the coatings seems to be reasonable with account of the heating of their inner part. However, the absence of crystalline phases with phosphorus and nickel or zinc, despite the high content of these elements in the coatings, was rather unexpected in this case. The heating by the cathodic component of the current of the inner part of a growing coating favors formation of high-temperature phases of aluminum oxide, but does not lead to crystallization of nickel or zinc phosphates. The possible reason is that phases based on the electrolyte components are concentrated in the outer layer of a coating.

It is noteworthy that surface layers containing crystalline phosphates $Ni_2P_2O_7$ and $NaNiPO_4$ are obtained on aluminum in an electrolyte with polyphosphate complexes only if dc current is used (full-wave rectifier with a capacitance filter [28]). In other current modes, mainly X-ray-amorphous layers are formed, which crystallize upon a high-temperature heating (>500°C) in air [22–24]. Presumably, this is due to the following. In the course of a microplasma treatment with a dc current, a separate discharge passing all stages of its development exists for a comparatively long time and heats the adjacent layers of the oxide. In various pulsed modes, including that with an additional cathodic component of the current, higher working voltages can be achieved, but the discharge duration is limited to that of a single current pulse. The melt locally formed in the discharge zone is in contact with the electrolyte and, therefore, it cools fast, which favors formation of amorphous phases. It is noteworthy that synthesis of crystalline anhydrous phosphates, e.g., nickel pyrophosphate $Ni_2P_2O_7$, by thermal decomposition of nickel phosphates requires their prolonged (not pulsed) heating at a temperature exceeding 600°C [35, 36].

The volume porosity of the coatings strongly depends on the current mode. In the case of nickel-containing layers (Fig. 4a), the data obtained, combined with the results of [28], indicate the following. In the region of true solutions ($n > 3$), the porosities of the coatings formed in various pulsed modes are rather close (10–15%). At the same time, if the process is performed with a dc current, coatings with

an increased porosity (>20%) are obtained. This fact can also be attributed to different times of action of discharges in the dc case and in pulsed mode. For metastable solutions or those already containing a dispersed phase (at $n \leq 3$) the situation is different. The current modes can be arranged, with account of the data of [28], in order of increasing porosity of the resulting nickel-containing coatings as follows: half-wave current mode, pulsed mode (thyristor power source), ac current mode ($j_a = j_c$, 50 Hz), and ac current mode with an additional cathodic component.

Thus, the cathodic component of the current does not diminish the volume porosity of coatings deposited from dispersed polyphosphate electrolytes with nickel. The porosity of zinc-containing coatings formed from dispersed solutions (with *n* decreasing from 1–1.5 to 0.5, Fig. 5) is considerably lower, in contrast to that of nickel-containing coatings. This may be due to a poorer thermal stability of zinc polyphosphates, compared with nickel polyphosphates. The melting points of zinc polyphosphates are 830–1106°C, and those of nickel phosphates, 1200–1400°C [35]. In all probability, the discharge energy is sufficient for a Zn-containing coating to be fused and an amorphous layer with low porosity to be formed. Unfortunately, such characteristics as through porosity, adhesion, microhardness, corrosion resistance, and layer-by-layer wear resistance could not be subjected to an experimental analysis as yet. According to the available data, it is these characteristics, or part of them, that may prove significantly different for the anodic and AC + C modes.

CONCLUSIONS

(1) The main patterns concerning the variation of the thickness, elemental composition, and surface roughness, established for the case when microplasma-produced coatings are formed on aluminum alloys in electrolytes with polyphosphate metal complexes under anodic polarization are also valid in the case of anodic–cathodic formation conditions.

(2) The incorporation of components of polyphosphate electrolytes into the coatings is associated, for both the anodic and the ac anodic–cathodic polarizations, with thermolysis of the colloid and(or) dispersed components of the electrolyte in the vicinity of the zones affected by electric discharges.

(3) Compared with the anodic modes, the combined anodic–cathodic + cathodic mode leads to changes in the phase composition of the coatings and to a higher crystallinity of some of the phases.

ACKNOWLEDGMENTS

The study was financially supported by the Presidium of the Far-Eastern Division of the Russian Academy of Sciences (grant no. 04-2-0-00-021) and the Presidium of the Siberian of the Russian Academy of Sciences (grant no. 168).

REFERENCES

1. Belevantsev, V.I., Terleeva, O.P., Markov, G.A., *et al., Zash. Met.*, 1998, vol. 34, no. 5, pp. 469–484.
2. Nikolaev, A.V., Markov, G.A., and Peshchevitskii, B.I., *Izv. Sib. Otd. Akad. Nauk SSSR, Ser. Khim. Nauk*, 1977, no. 5, no. 12, pp. 32–33.
3. Markov, G.A., Tatarchuk, V.V., and Mironova, M.K., *Izv. Sib. Otd. Akad. Nauk SSSR, Ser. Khim. Nauk*, 1983, no. 3, no. 7, pp. 34–37.
4. Markov, G.A., Belevantsev, V.I., Terleeva, O.P., *et al., Trenie Iznos*, 1988, vol. 9, no. 2, pp. 286–289.
5. Timoshenko, A.V., Opara, B.K., Kovalev, A.F., *et al., Zashch. Met.*, 1991, vol. 27, no. 3, pp. 417–424.
6. Slonova, A.I., Terleeva, O.P., Shulepko, E.K., and Markov, G.A., *Elektrokhimiya*, 1992, vol. 28, no. 9, pp. 1280–1285.
7. Shulepko, E.K., Markov, G.A., and Slonova, A.I., *Elektrokhimiya*, 1993, vol. 29, no. 5, pp. 670–672.
8. Slonova, A.I., Markov, G.A., and Terleeva, O.P., *Zashch. Met.*, 1995, vol. 31, no. 5, pp. 532–534.
9. Voevodin, A.A., Yerokhin, A.L., Lyubimov, V.V., *et al., Surf. Coat. Technol.*, 1996, vols. 86–87, pp. 516–521.
10. Malyshev, V.N., Kalmakov, A.K., and Bunin, I.Zh., *Fiz. Khim. Obrab. Mat.*, 1997, no. 5, pp. 77–84.
11. Dearnley, H.A., Gummersbach, J., Weiss, H., *et al., Wear*, 1999, vols. 225–229, pp. 127–134.
12. Suminov, I.V., Epel'fel'd, A.V., Borisov, A.M., *et al., Izv. Ross. Akad. Nauk, Ser. Fiz.*, 2000, vol. 64, no. 4, pp. 763–766.
13. Yerokhin, A.L., Snizhko, L.O., Guverina, N.L., *et al., J. Phys. D: Appl. Phys.*, 2003, vol. 36, pp. 2110–2120.
14. Markov, G.A., Terleeva, O.P., and Shulepko, E.K., *Trudy Mosk. Inst. Neftekhim. Gaz. Prom–sti.*, Moscow, 1985, no. 185, pp. 54–64.
15. USSR Inventor's Certificate, no. 1200591.
16. Slonova, A.I., Terleeva, O.P., and Markov, G.A., *Zashch. Met.*, 1997, vol. 33, no. 2, pp. 208–212.
17. Markov, G.A., Clonova, A.I., and Terleeva, O.P., *Zashch. Met.*, 1997, vol. 33, no. 3, pp. 289–294.
18. Terleeva, O.P., Utkin, V.V., and Slonova, A.I., *Fiz. Khim. Obrab. Mat.*, 1999, no. 2, pp. 60–64.
19. Yarovaya, T.P., Gordienko, P.S., Rudnev, V.S., *et al., Elektrokhimiya*, 1994, vol. 30, no. 11, pp. 1395–1396.
20. Rudnev, V.S., Gordienko, P.S., Kon'shin, V.V.,

et al., *Elektrokhimiya*, 1996, vol. 32, no. 10, pp. 1242–1246.

21. Kurze P., Schrechenbach, J., Schwarz, Th., and Krysmann, W., *Metalloberfläche*, 1986, vol. 40, no. 12, pp. 539–540.
22. Rudnev, V.S., Yarovaya, T.P., Boguta, D.L., *et al.*, *J. Electroanal. Chem.*, 2001, vol. 497, nos. 1–2, pp. 150–158.
23. Tyrina, L.M., Rudnev, V.S., Abozina, E.A., *et al.*, *Zashch. Met.*, 2001, vol. 37, no. 4, pp. 366–369.
24. Boguta, D.L., Rudnev, V.S., Yarovaya, T.P., *et al.*, *Zh. Prikl. Khim.*, 2002, vol. 75, no. 10, pp. 1639–1642.
25. Schrechenbach, J., Schlottig, F., and Marx, G., *J. Mater. Res.*, 1999, vol. 14, no. 4, pp. 1437–1443.
26. Schlottig, F., Dietrich, D., Schrechenbach, J., and Marx, G., *Fresenius J. Anal. Chem.*, 1997, vol. 358, pp. 105–107.
27. Boguta, D.L., Rudnev, V.S., Yarovaya, T.P., *et al.*, *Zh. Prikl. Khim.*, 2000, vol. 73, no. 8, pp. 1296–1300.
28. Boguta, D.L., Rudnev, V.S., and Gordienko, P.S., *Zashch. Met.*, 2004, vol. 40, no. 3, pp. 299–303.
29. Rudnev, V.S., Boguta, D.L., and Gordienko, P.S., *Zashch. Met.*, 2003, vol. 39, no. 2, pp. 219–221.
30. Rudnev, V.S., Yarovaya, T.P., Boguta, D.L., *et al.*, *Elektrokhimiya*, 2000, vol. 36, no. 12, pp. 1457–1462.
31. Terleeva, O.P., Belevantsev, V.I., Markov, G.A., *et al.*, *Fiz. Khim. Obrab. Mat.*, 2000, no. 2, pp. 35–39.
32. Epel'fel'd, A.V., Lyudin, V.B., Dun'kin, O.N., and Nevskaya, O.S., *Izv. Ross. Akad. Nauk, Ser. Fiz.*, 2000, vol. 64, p. 759.
33. Magurova, Yu.V. and Timoshenko, A.V., *Zashch. Met.*, 1995, vol. 31, no. 4, pp. 414–418.
34. Snezhko, L.A., Tikhaya, L.S., Udovenko, Yu.E., and Chernenko, V.I., *Zashch. Met.*, 1991, vol. 27, no. 3, pp. 425–430.
35. Konstant, Z.A. and Dindune, A.P., *Fosfaty dvukhvalentnykh metallov* (Phosphates of Bivalent Metals), Riga: Zinatne, 1987.
36. Tananaev, I.V., *Zh. Neorg. Khim.*, 1984, vol. 29, no. 2, pp. 467–483.

Russian Journal of Applied Chemistry, Vol. 78, No. 2, 2005, pp. 254–258. Translated from Zhurnal Prikladnoi Khimii, Vol. 78, No. 2, 2005, pp. 260–264.
Original Russian Text Copyright © 2005 by Saltykov, Kornienko.

APPLIED ELECTROCHEMISTRY AND CORROSION PROTECTION OF METALS

Dependence of the Current Efficiency by Target Product of Electrosynthesis on Polarization

Yu. V. Saltykov and V. L. Kornienko

Institute of Chemistry and Chemical Technology, Siberian Division, Russian Academy of Sciences, Krasnoyarsk, Russia

Received October 6, 2004

Abstract—The known dependences of the current efficiency by target products of electrosynthesis on polarization are analyzed for the cases when the principle of independent occurrence of concurrent reactions is observed or not.

It is known that electrochemical methods for synthesis of chemical products are ecologically safer than the conventional chemical techniques. This is primarily due to the fact that electrochemical methods use electric current, which is ecologically clean, as an oxidizing or reducing agent. However, the rate of electrode transformations is rather low under ordinary conditions and limited by the interface between the electrolyte and an electrode. The electrode transformations in electrosynthesis are commonly intensified by using electrodes with a developed surface, e.g., porous hydrophobized [1–4], or by making stronger the polarization [5–8].

It is known that the current efficiency (CE) by the target product is frequently lower than 100%. This is due to the fact that, virtually in all cases, the target reaction is accompanied by competing concurrent or consecutive electrochemical reactions. The behavior of CE with polarization is largely determined by the extent to which the competing reactions affect one another. It is known that, in the case when the mutual influence of competing electrochemical reactions is insignificant, the principle of independence of concurrent reactions (PICR) can be used [9, 10]. According to this principle, each of the concurrent electrode reactions proceeds independently of the others, as if it were the only reaction occurring at the given electrode. It has been shown previously [11] that, when the PICR is applicable, the CE of the target products increases as the polarization becomes stronger if the ratio of the Tafel slopes of the target (b_1) and side (b_2) reactions is less than unity and, conversely, decreases at $b_1/b_2 > 1$. It may occur in electrosynthesis that the PICR is not observed. This is the case when the course of the electrode process is strongly affected by the starting reagents, intermediates, and final product. Naturally, the influence exerted by the target electrochemical reaction may vary: the side reaction may be virtually completely suppressed, as in dechlorination of 1,1,2-trichlorotrifluoroethane on zinc and cadmium hydrophobized electrodes (HPE) [2, 12]. Also possible is a comparatively weak influence, as, e.g., in electrochemical chlorination of alkanes [2, 13, 14].

In the simplest case, the influence exerted by the target reaction on the side process may consist in that the surface concentration of electrically active species involved in the rate-determining stage of the side reaction is diminished. It would be expected that this should lead to a decrease in the overall rate of the side process at an unchanged Tafel slope. Then, the behavior of CE with polarization should be the same as that in the case when the PICR is observed.

If the products of the target reaction strongly affect the side reaction, the mechanism of the latter may change. In this case, the pattern based on applicability of the PICR may be invalid when the CE by the target product changes as the polarization becomes stronger.

In this communication, the known experimental data on the polarization dependence of CE, obtained in electrosynthesis of various chemical substances in HPE in aqueous electrolytes are analyzed and compared with the theoretical dependence to be observed in the case when the PICR is valid.

EXPERIMENTAL

At present, the following electrosynthesis processes performed in HPE are known, for which the depen-

1070-4272/05/7802-0254 © 2005 Pleiades Publishing, Inc.

dence of the CE by the target product on potential has been determined [2].

(1) Reduction of carbon monoxide on Ni and other metals in a 3M solution of H_2SO_4 [2, 3, 15]. It was found that, as the polarization becomes stronger, the CE by the target products (ethane and other hydrocarbons) increases. The reaction proceeds on the background of a vigorous evolution of hydrogen, and the CE by the target products is several percent. In this case, it may be assumed that the PICR is observed.

The data of [16] show that the Tafel slope for the reaction of hydrogen evolution is close to 0.12 V in this case.

The authors of [2, 15] assume that the rate-determining stage of electroreduction of CO under the conditions studied is addition of a first electron to an adsorbed molecule of carbon monoxide. Then, the apparent transfer coefficient of the electrochemical reaction with a successive transfer of several electrons is equal to the true coefficient [10]. One of definitions of the transfer coefficient means that this coefficient accounts for the asymmetry of the forward and reverse processes [17], i.e., the reverse reaction is strongly hindered. It may be assumed, on the basis of this definition, that the transfer coefficient exceeds 0.5 in the case in question. Then the Tafel slope for the electrochemical reaction of CO reduction must be less than 0.12 V, and the ratio of the Tafel slopes of the forward and side reactions, less than unity. Then, the CE by the target product must grow with increasing polarization, and this is the case in actual practice.

(2) Reduction of carbon dioxide on Zn and Sn in $NaHCO_3$ solutions [2]. The current efficiency by the electrosynthesis product, formic acid, is virtually independent of the electrode potential. Hydrogen evolution is the competing reaction.

As in the case of CO, it may be assumed that the rate-determining stage is addition of a first electron to an adsorbed CO_2 molecule. In this case, the apparent transfer coefficient must be equal to the true one. A reverse reaction, oxidation of formic acid to CO_2, is known, and, therefore, it would be expected that the transfer coefficient is close to 0.5. Then the Tafel slope for the electrochemical reaction of CO_2 reduction to formic acid must be close to 0.12 V. It would be expected that the ratio of the Tafel slopes of the forward and side reactions should be close to unity and no significant change in CE must occur as the polarization becomes stronger.

(3) Electrochemical chlorination of *N*-alkanes on graphite in a 6 M solution of HCl [2, 13, 14]. The current efficiency by the products of electrosynthesis, monochloralkanes, markedly increases as polarization becomes stronger. The competing reaction is evolution of chlorine gas. The Tafel slope for chlorine evolution on graphite at comparatively strong polarizations is 0.12 V [18].

In evaluating the Tafel slope for the reaction of electrochemical chlorination of alkanes, the process of chlorination itself can be understood as the succeeding chemical rate-determining stage in which no electron is transferred. Naturally, the assumption that the chlorination process occurs in a single stage is rather incorrect, but has no effect on the substance of the matter. In this case, the apparent transfer coefficient is equal to the ratio between the number of preceding stages, *m*, and the stoichiometric number, which is unity for hydrogen evolution [10]. Consequently, the Tafel slope can be taken to be approximately 0.03 V for the process of electrochemical chlorination. Then the ratio of the Tafel slopes for the forward and reverse reactions is less than unity and the CE by monochloralkanes must increase as polarization becomes stronger, and this is the case in actual practice.

(4) Electroreduction of nitromethane to methylhydroxylamine in a 3 M solution of HCl [2, 19]. The competing reaction is electroreduction of nitromethane to methylamine. The current efficiency by methylhydroxylamine decreases as polarization becomes stronger.

According to the scheme of electrochemical reduction of nitroalkanes, presented in [20], methylhydroxylamine formed in four-electron reduction of nitromethane can undergo further two-electron reduction to methylamine.

It is known that, for electrochemical reactions with successive transfer of several electrons, there exists the relation [2]:

$$\alpha_{eff} = m/\nu + n\alpha, \quad (1)$$

where α_{eff} is the apparent transfer coefficient; *m*, number of stages preceding the rate-determining stage; ν, stoichiometric coefficient; α, true transfer coefficient; and *n*, number of electrons transferred in the rate-determining stage.

When successive reactions occur, different numbers of stages that precede the rate-determining stage correspond to formation of the first and second prod-

uct. This means that that the quantity m in Eq. (1) for the second stage increases by a certain amount p, which shows how far apart are the rate-determining stages of formation of the first and second product. In the simplest case, it can be taken that, in considering the succeeding reaction, ν, n, and α remain the same as those for the first reaction. Then, it can be written that

$$\alpha_{\text{eff}_2} = (m + p)/\nu + n\alpha. \quad (2)$$

Comparison of expressions (1) and (2) shows that the ratio of Tafel slopes for the first and second stages is less than unity, and, therefore, the rate of the second stage must grow as potential increases, and this is the case in the actual practice.

(5) Electroreduction of *ortho*-nitrophenol to *ortho*-aminophenol [2, 21] **on copper electrodes.** The competing reaction is formation of azoxyphenol and azophenol in an alkaline medium and evolution of hydrogen in an acid medium.

The formation of noticeable amounts of side products in reduction of *ortho*-nitrophenol in an alkaline medium can be accounted for by the fact that the rate-determining stage is the same for the target and side processes [8]. If a medium of another type is taken, the ratio of the rates of the target and side reactions substantially changes, with the result that *ortho*-aminophenol is mostly formed in an acid medium in the given case.

In an acid medium, the share of the side process, i.e., hydrogen evolution, is insignificant and it increases as polarization becomes stronger. Nevertheless, the potentials at which the process is performed are sufficiently high for hydrogen evolution to occur. Hence follows that, in the case in question, PICR is not observed and it is difficult to explain the polarization dependence of the CE.

(6) Electrooxidation of aliphatic alcohols in HPE under the conditions of formation of higher nickel oxides [2, 22]. The competing reactions are formation of higher nickel oxides and oxygen evolution.

As the electrode potential becomes higher, the current efficiency by carboxylic acids first increases and then falls. At low polarizations, the CE by carboxylic acids grows with increasing potential. This behavior can be readily understood if the reaction of higher nickel oxides with adsorbed alcohol molecules is taken to be the rate-determining stage. Then, according to EQ. (1), the Tafel slope for the reaction of electrooxidation of alcohols will be smaller than that for the reaction of formation of higher nickel oxides, and, consequently, a rise in the CE by carboxylic acids must be observed as the potential becomes higher. With the potential increasing further, O_2 evolution commences, i.e., there appears an extra competing reaction and, as a result, the CE by carboxylic acids starts to decrease.

(7) Dechlorination of 1,1,2-trichlorotrifluoroethane [2, 23–25]. The target electrochemical reaction occurs at potentials of hydrogen evolution, but the CE by the target product is close to 100%. This means that the electrochemical reaction of H_2 evolution is very strongly suppressed in dechlorination of 1,1,2-trichlotrifluroethane, and, consequently, application of PICR is not justified.

(8) Electrochemical reduction of oxygen to hydrogen peroxide [3, 26]. The target electrochemical reaction occurs with a sufficiently high current efficiency. The CE by hydrogen peroxide decreases as polarization becomes stronger.

In electrosynthesis of H_2O_2 from oxygen in hydrophobized carbon black electrodes, hydrogen evolution is not a competing reaction. The fact that the current efficiency is less than 100% in this case can be attributed to occurrence of processes involving H_2O_2, of both electrochemical and purely chemical nature. Therefore, it can be assumed that the sum of processes of H_2O_2 decomposition can be represented in a certain overall form and the Tafel slope of such an electrochemical dependence will be smaller than that of the reaction of H_2O_2 formation. Then, it would be expected that the CE should decrease with increasing polarization, and this is the case in actual practice.

It should be noted that the considerations concerning the possible Tafel slopes of the target and side reactions are rather simplified. Nevertheless, a slope ratio larger or smaller than unity can be used, with certain reservations, to make the necessary conclusions. For clarity, the results of discussions of the known polarization dependences of CE are summarized in the table.

In those cases when PICR is observed, the CE by the target product increases or decreases as polarization becomes stronger, depending on the ratio of the Tafel slopes of the target and side reactions. If this ratio is less than unity, the CE by the target product increases with polarization. Then, it is advisable to perform the process of electrosynthesis at strong polarizations. If, by contrast, this ratio exceeds unity, the CE by the target product decreases as polarization

Character of variation of the CE of the target reactions with increasing polarization and deviation of the ratio of the Tafel slopes of the target (b_1) and side (b_2) reactions from unity for some processes of electrosynthesis in HPE

Electrosynthesis process	Applicability of PICR	Presumed b_1/b_2 ratio	Behavior of CE with increasing polarization
$CO \rightarrow C_2H_6$	+	<1	Grows
$CO_2 \rightarrow HCO_2H$	+	≈1	No noticeable change
$HR \rightarrow ClR$	+	<1	Grows
$CH_3NO_2 \rightarrow CH_3NHOH$	+	>1	Decreases
ortho-Nitrophenol → *ortho*-aminiphenol:			
in alkaline medium	–	?	No noticeable change
in acid medium	–	?	≈100%, decreases
$RCH_2OH \rightarrow RCOOH$	+	<1	Grows
1,1,2-trichlorotrifluoroethane → chlorotrifluoroethylene	–	?	≈100%, decreases
$O_2 \rightarrow H_2O_2$	+	>1	Decreases

becomes stronger. Then, a high CE by the target product can be achieved if electrosynthesis is carried out at low polarizations.

A clearly pronounced noncompliance with the PICR in electrosynthesis is observed when the competing process is strongly suppressed by the products formed in the target reaction. In this case, the CE by the target process is, as a rule, high. The CE becomes considerably less than 100% when the rate-determining stages for the target and side processes coincide. In this case, the CE can be raised by creating conditions under which the rate of the side process becomes considerably lower than that of the target process.

CONCLUSIONS

(1) If the principle of independence of concurrent reactions is observed, the current efficiency of the target reaction depends on the ratio of the Tafel slopes of the target and side reactions. If this ratio is less than unity, the current efficiency by the target product increases with polarization. At a slope ratio exceeding unity, the current efficiency decreases.

(2) If the principle of independence of concurrent reactions is not observed, the competing process is strongly suppressed and a rather high current efficiency by the target product is observed.

(3) If the principle of independence of concurrent reactions is not observed and the limiting stages of the target and side processes coincide, the current efficiency may be considerably less than 100%.

REFERENCES

1. Chirkov, Yu.G., Kedrinskii, I.A., and Kornienko, V.L., *Itogi nauki: Elektrokhimiya* (Advances of Science: Electrochemistry), Moscow: VINITI, 1974, vol. 11, pp. 176–218.
2. Kornienko, V.L., Kolyagin, G.A., Kornienko, G.V., *et al.*, *Intensifikatsiya elektrokhimicheskikh protsessov* (Intensification of Electrochemical Processes), Moscow: Nauka, 1988, pp. 149–170.
3. Kornienko, V.L. and Saltykov, Yu.V., *Elektrokhimiya*, 1995, vol. 31, no. 7, pp. 675–694.
4. Kornienko, V.L., *Elektrokhimiya*, 1996, vol. 32, no. 1, pp. 85–103.
5. Torii, S., *Electrochim. Acta*, 1997, vol. 42, pp. 1933–1943.
6. Tomilov, A.P., Mairanovskii, S.G., Fioshin, M.Ya., and Smirnov, V.A., *Elektrokhimiya organicheskikh soedinenii* (Electrochemistry of Organic Compounds), Leningrad: Khimiya, 1968.
7. Tomilov, A.P., Fioshin, M.Ya., and Smirnov, V.A., *Elektrokhimicheskii sintez organicheskikh veshchestv* (Electrochemical Synthesis of Organic Substances), Leningrad: Khimiya, 1976.
8. *Organic Electrochemistry. An Introduction and a Guide*, Baizer, M.M., Ed., New York: Marcel Dekker, 1973.
9. Antropov, L.I., *Teoreticheskaya elektrokhimiya* (Theoretical Electrochemistry), Moscow: Vysshaya Shkola, 1984, 4th ed.
10. Damaskin, B.B.and Petrii, O.A., *Vvedenie v elektrokhimicheskuyu kinetiku* (Introduction to Electrochemical Kinetics), Moscow: Vysshaya Shkola, 1975.
11. Saltykov, Yu.V. and Kornienko, V.L., *Elektrokhimiya*, 2004, vol. 40, no. 7, pp. 798–803.
12. Kornienko, V.L., Kalinichenko, N.V., Kedrinskii, I.A., and Chirkov, Yu.G., *Zh. Prikl. Khim.*, 1986, vol. 59, p. 1179.
13. Saltykov, Yu.V., Kornienko, V.L., and Tomilov, A.P., *Zh. Prikl. Khim.*, 1987, vol. 60, no. 1, pp. 199–201.
14. Saltykov, Yu.V. and Kornienko, V.L., *Zh. Prikl. Khim.*, 1988, vol. 61, no. 8, pp. 1918–1921.

15. Kolyagin, G.A., Danilov, V.G., and Kornienko, V.L., *Elektrokhimiya*, 1985, vol. 21, no. 1, pp. 133–135.
16. *Spravochnik po elektrokhimii* (Handbook of Electrochemistry), Sukhotin, A.M., Ed., Leningrad: Khimiya, 1981.
17. Budnikov, G.N., Maistrenko, V.N., and Vyasilev, M.R., *Osnovy sovremennogo elektrokhimicheskogo analiza* (Fundamentals of Modern Electrochemical Analysis), Moscow: Mir, 2003.
18. Krishtalik, L.I., *Elektrodnye reaktsii: Mekhanizm elementarnogo akta* (Electrode Reactions: The Mechanism of an Elementary Event), Moscow: Nauka, 1979.
19. Kornienko, V.L. and Kornienko, G.V., *Elektrokhimiya*, 1981, vol. 17, no. 11, p. 1756.
20. Kokorekina, V.A., Petrosyan, V.A., and Feoktistov, L.G., *Elektrokhimicheskoe okislenie alifaticheskikh nitrosoedinenii: Elektrosintez monomerov: Progress elektrokhimii organicheskikh soedinenii* (Electrochemical Oxidation of Aliphatic Nitro Compounds: Electrosynthesis of Monomers: Advances in Electrochemistry of Organic Compounds), Moscow: Nauka, 1980, p. 83.
21. Kornienko, V.L., Tomilov, A.P., and Vakar, T.P., *Elektrokhimiya*, 1986, vol. 22, no. 5, pp. 666–669.
22. Chaenko, N.V., Kornienko, V.L., Avrutskaya, I.A., and Fioshin, M.Ya., *Zh. Prikl. Khim.*, 1987, vol. 60, no. 6, pp. 1339–1343.
23. Kornienko, V.L., Kalinichenko, N.V., Kedrinskii, I.A., and Chirkov, Yu.G., *Zh. Prikl. Khim.*, 1986, vol. 59, no. 5, pp. 1179–1182.
24. Kornienko, V.L., Kolyagin, G.A., Kornienko, G.V., and Saltykov, Yu.V., *Elektrokhimiya*, 1992, vol. 28, no. 4, pp. 507–516.
25. Kolyagin, G.A.and Kornienko, V.L., *Zh. Prikl. Khim.*, 1990, vol. 63, no. 7, pp. 1550–1553.
26. Kornienko, V.L., Kolyagin, G.A., and Saltykov, Yu.V., *Zh. Prikl. Khim.*, 1999, vol. 72, no. 3, pp. 353–361.

Russian Journal of Applied Chemistry, Vol. 78, No. 2, 2005, pp. 259–266. Translated from Zhurnal Prikladnoi Khimii, Vol. 78, No. 2, 2005, pp. 265–272.
Original Russian Text Copyright © 2005 by Turaeva, Pegova, Vasilevskii.

APPLIED ELECTROCHEMISTRY AND CORROSION PROTECTION OF METALS

Cyclic Voltammetry of a Fluoride-Selective Electrode in Contact with Metals

M. S. Turaeva, I. A. Pegova, and V. L. Vasilevskii

Research Institute of Agrophysics, Russian Academy of Agricultural Sciences, St. Petersburg, Russia

Prometei Central Research Institute of Structural Materials, St. Petersburg, Russia

Received July 14, 2004

Abstract—Electrochemical behavior of the interface between a $LaF_3 : Eu^{2+}$ single-crystal fluoride-selective membrane and Bi, Sn, Pb, Sb, and Cd metallic microelectrodes is considered with the aim to apply a fluoride-selective electrode in solid-state voltammetry. The ionization–discharge processes on the metals in air, involving mobile fluoride ions from the LaF_3 membrane, were studied by cyclic voltammetry.

Eu^{2+}- or Sr^{2+}-doped LaF_3 single crystals exhibit unique properties, of which the most important are the homopolar fluoride ionic conductivity and high chemical resistance in aqueous and nonaqueous solutions and in air. These features enabled application of fluoride-conducting solid electrolytes (FSELs) in various devices, such as fluoride-selective electrode (FSE) [1, 2], sensors for F and HF [3–5], oxygen and oxygen-containing gases [6–8], and chemical power sources [9, 10].

The aim of our studies is to apply FSELs to full-solid-state voltammetry with FSE. Previously, we have shown that anodic polarization of the interface between the LaF_3 (0.8 mol % Eu^{2+}) membrane of an FSE with metals produces an intermediate phase and modifies the interface to give $LaF_3 \mid MF_n \mid M$ electrodes. A stripping voltammetric (SVA) study of electrochemical processes involving mobile fluoride ions from FSEL revealed such trends as the dependence of the peak potential of cathodic curves on the nature of the metallic electrode and the dependence of the peak current of the cathodic curves on the potential sweep rate V and on the charge Q consumed for formation of MF_n [12–14]. These trends have been found for the interface between a metallic electrode and a membrane of FSE with an aqueous [12–14] or solid-state reference system [15]. We have also reported relationships between the peak current and the contact area of Bi [16] and Ag [17] with the membrane.

Here we report the results of further studies of the electrochemical behavior of the interface between $LaF_3 : Eu^{2+}$ single-crystal membrane of FSE and metallic electrodes in air in systems simulating trace contamination of a metallic surface (Ag foil) with such metals as Bi, Sn, Sb, Pb, and Cd. The possibility of simultaneous solid-phase determination of several metals on the surface of conducting solids was studied using cyclic voltammetry.

EXPERIMENTAL

In this study we used fluoride-selective electrodes with polished membranes (1–1.5 mm thick, 5 mm in diameter) prepared from single-crystal LaF_3 activated with Eu^{2+} (0.8 mol %). The internal reference system was built up using a large-area Ag/AgCl electrode and an aqueous solution with high fluoride and chloride concentrations. The use of the aqueous electrolyte allowed elimination of uncontrollable polarization effects at the junctions between the FSE membrane and the reference system in studying the processes at the FSEL | M interface.

The measurements were carried our in FSE | M two-electrode pressed-contact cells using a PU-1 polarograph, an LKD 4-003 *x–y* recorder, and an I-120 ion meter. The solid electrolyte and metal surfaces were pretreated as in [13, 14]. Experimental data were processed using the Microcal Origin v.7.0 software package.

To improve the data reproducibility, we tested fluoride-selective electrodes prior to use. The procedure involved (1) measurement of electromotive force of FSE as a function of the F^- activity in aqueous KF solutions (acetate buffer, pH 5) over

1070-4272/05/7802-0259 © 2005 Pleiades Publishing, Inc.

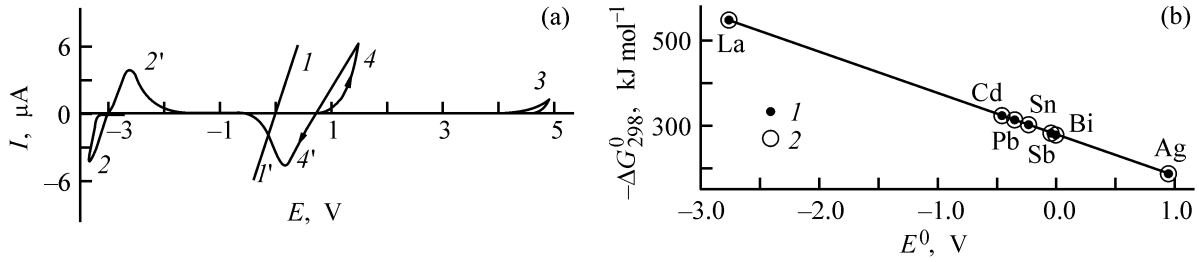


Fig. 1. Voltammograms *I–E* of the cells: (a) (*1*, *1*') Ag, AgCl | KCl 1 M, KF 1 M | $LaF_3 : Eu^{2+}$ | KF 1 M, KCl 1 M | AgCl, Ag (V = 0.002–0.05 V s^{-1}), (*2*, *2*', *3*) FSE | Y (V = 0.05 V s^{-1}), and (*4*, *4*') FSE | Ag (V = 0.05 V s^{-1}); and (b) (*1*) theoretical and (*2*) experimental potentials of fluorinated electrodes $E^0_{MF_n}$ with the standard Gibbs energy of formation of MF_n, ΔG^0_{298}; see text for details.

the pF range 1–5; (2) recording of current–voltage characteristics of the symmetric cell (Fig. 1a, curves *1*, *1*');

$$\text{Ag, AgCl} \,|\, \text{KCl 1 M, KF 1 M} \,|\, LaF_3 : Eu^{2+} \,|\, \text{KF 1 M, KCl 1 M} \,|\, \text{AgCl, Ag,} \quad (1)$$

and (3) recording of a voltammogram of the asymmetric cell (Fig. 1a, curves *2*, *2*').

$$\text{Ag, AgCl} \,|\, \text{KCl 1 M, KF 1 M} \,|\, LaF_3 : Eu^{2+} \,|\, \text{Y.} \quad (2)$$

We experimentally demonstrated the necessity for a preliminary control of the voltammetric and potentiometric responses of FSE. It was confirmed the quality of the surface of the FSE membrane to affects the electrode sensitivity and the response time in dilute fluoride solutions (pF ~ 5). Contamination of the membrane surface makes shorter the linear portion in the concentration dependence of the electromotive force and impairs the lower detection limit of the fluoride ion in aqueous solutions.

In the potentiometric mode, we found no effect of cleaning; however, voltammograms of cell (1) appeared to be more sensitive to this factor. The potentiodynamic curve allows detection of a contamination that remained unnoticed under the equilibrium conditions. The criteria of thorough cleaning of the membrane surface and readiness of FSE to be used in an experiment was the linearity of the *I–E* curve of cell (1) within ±3 V and also the independence from the sweep rate over the range 0.002–0.05 V s^{-1} (Fig. 1a, curves *1*, *1*'). The deviation of the *I–E* curve from linearity in the experimental potential range, hysteresis of the curve, which becomes more pronounced as the sweep rate V increases, and also the rise in the cell resistance, determined as the slope of the linear portion of the *I–E* curve of cell (1), as compared to the active component of the impedance at a frequency of 1 kHz, all these facts indicated that an additional cleaning of the membrane was necessary. The current–voltage characteristic of symmetric cell (1) was also used in choosing the potential sweep rate, estimating of the ohmic drop of the potential across the solid electrolyte, and selecting electrodes with a membrane resistance of no more than 50 kΩ.

A steady-state or dynamic current–voltage curve of asymmetric cell (2) (Fig. 1a, curves *2*, *2*', *3*) allowed estimation of the working potential range within which one could observe formation of fluorides of the metals in contact with the FSE membrane and also their reduction. In the cathodic range (Fig. 1a, curve *2*), at a potential more negative than E^0 = –2.94 V, the current is mostly caused by the reduction of the fixed cation of the membrane, whose anodic oxidation is reflected by curve *2*' in Fig. 1a [11]. An anodic polarization of the LaF_3 | Y interface from –1.5 V to E > +4.0 V produced a weak current, which decreased or even disappeared upon repeated polarization (Fig. 1a, curve *3*). Therefore, the reaction of the fluoride ion with yttrium as a working electrode was not detected, which can be attributed to the fact that fluorination of yttrium is hindered, and the electrochemical treatment of the interface results in inhibition of the reaction. Furthermore, the standard potential $E^0(Y, YF_3)$ = –2.81 V, estimated from $\Delta G^0_{298}(YF_3)$ = –1655.2 kJ mol^{-1}, is more negative than $E^0(La, LaF_3)$ = –2.76 V, estimated from $\Delta G^0_{298}(LaF_3)$ = –1643 kJ mol^{-1}, or that determined experimentally (–2.765 ± 0.005 V) [11]. Thus, the charge transfer at the ionic semiconductor–electronic conductor (LaF_3 | Y) heterojunction in cell (2) is blocked up to the potential corresponding to decomposition of the membrane by the reaction $La^{3+}_M + 3e \rightarrow La_M$, and the fluorine evolution $2F^- - 2e \rightarrow F_2\uparrow$ (E^0 = +2.87 V)

has a high overvoltage. Therefore, the current–voltage characteristic of the cell has a wide ideal polarizability range, and it could be regarded as a background curve in studying reactions between the fluoride ions from the FSE membrane and metals. Such an electrochemical stability of the membrane allows extension of the working potential range in solid-state voltammetry with FSE to 7 V.

An inadequate treatment of the $LaF_3 \mid Y$ interface is reflected in the voltammogram of cell (2) as overvoltage of La reduction with the current of the reaction appearing at a more negative potential than –3.0 V. In some cases, we observed in a cathodic potential sweep polarization at a more positive potential than –3.0 V. Presumably, this is caused by adsorption relaxation of the electrical double layer with participation of the cations of the membrane, as a result of hindered injection of electrons. We could eliminate the indicated undesirable effects, which make both the experiment and interpretation of the results more difficult, by mechanical or chemical treatment or by using electrochemical regeneration of the surface of the solid electrolyte in strongly acidic fluoride solutions [13, 14].

We studied the voltammetric response of the FSE membrane/metal interface in the cycling mode using cells (3)–(5), which gradually become more complex:

$$Ag, AgCl \mid KCl\ 1\,M,\ KF\ 1\,M \mid LaF_3 : Eu^{2+} \mid M_s, \quad (3)$$

$$Ag, AgCl \mid KCl\ 1\,M,\ KF\ 1\,M \mid LaF_3 : Eu^{2+} \mid M_1\ (M_s), \quad (4)$$

$$Ag, AgCl \mid KCl\ 1\,M,\ KF\ 1\,M \mid LaF_3 : Eu^{2+} \mid (M_1 + M_2)\ (M_s). \quad (5)$$

In cell (3), the metallic support M_s was used as a working electrode, while in cells (4) and (5), the working electrodes were microsamples of metals M_1 and M_2, with M_s serving as a support and a current lead. The fluoride-selective electrode operated as a counter electrode and a reference. As a support and current lead we used a 0.1 mm-thick high-purity silver foil pretreated by annealing at 300 – 400°C to refresh the surface. Silver was chosen because it has the highest positive potential of formation of the fluoride, $E^0(Ag \mid AgF) = 0.95$ V (Fig. 1b), which restricts the anodic potential range of cycling in cells (4) and (5). Another reason was the reversibility of this reaction. The working electrodes investigated were Sn, Bi, Pb, Cd, and Sb metals. The standard potentials of formation of the corresponding fluorides $E^0(M \mid MF_n)$ (SnF_2 –0.23, BiF_3 –0.01, SbF_3 –0.05, PbF_2 –0.34, and GdF_3 –0.45 V, respectively), determined from experimental data [12, 16] using stripping voltammetry, are shown in Fig. 1b. The area of metallic microsamples on the support ranged from 0.01 to 0.08 mm^2. The area was determined before the experiment, using an ocular micrometer of an MBS-1 microscope (magnification ×64). After the experiment, the contact spot area was determined similarly.

The experimental system was designed as a voltammetric sensor [16], providing mechanical contact of the metal with the FSE membrane and the support.

Microamounts of Bi, Sn + Bi, Pb + Sb, and Cd + Bi were arranged on Ag foil. Such a selection of the pairs is caused by the fact that the potentials at which the electrode reactions involving a metal and the fluoride ion from the solid electrolyte take place differ by more than 120/*n* mV, suggesting the possibility of simultaneous detection of the metals. Our previous studies of the $LaF_3 \mid M$ interface by stripping voltammetry [12, 13] revealed that the formation of Bi and Sn fluorides at the optimal generation potentials can be quasi-reversible, while Pb and Sb irreversibly react with the fluoride ion. Therefore, it was of interest to study the interface between the FSE membrane and Cd + Bi electrodes on the Ag support, i.e., the effect of electropositive elements on the cathodic signals of cadmium, in view of the fact that stripping voltammograms showed one reduction peak upon anodic polarization of the interface, and after repeated polarization, the cathodic current abruptly dropped and then disappeared at all [16].

$LaF_3 : Eu^{2+} \mid Ag$ interface. In order to specify the anodic limit of cycling in simulating contamination on a conducting substrate, we recorded the cyclic voltammogram of the cell

$$Ag,\ AgCl \mid KCl\ 1\ M,\ KF\ 1\ M \mid LaF_3 : Eu^{2+} \mid Ag \quad (6)$$
$$\text{or } FSE \mid Ag,$$

where the working electrode was an Ag foil. The current–voltage characteristic of the FSE membrane/Ag foil interface, recorded at $V = 0.05$ V s^{-1} in the ranges from 0 to +1.2 V and from +1.2 to –3.0 V, is shown in Fig. 1a (curves *2*, *2*', *4*, *4*'). As mentioned above, curves *2* and *2*' refer to the oxidation–reduction of lanthanum, and curves *4* and *4*', to oxidation–reduction of silver, which was observed at a potential of about 0.7 V. The anodic–cathodic curve of the FSE | Ag interface shows a hysteresis loop (Fig. 1a, curves *4*, *4*'), which suggests, in solutions, hindered crystallization [18, 19]. However, this does not contradict our previous potentiostatic data on the formation of metal fluorides at the unconditioned FSE | metal interface in air [14]. From curves *2*, *2*', *4*, and *4*' (Fig. 1a) we determined the anodic limit of the potential range in which

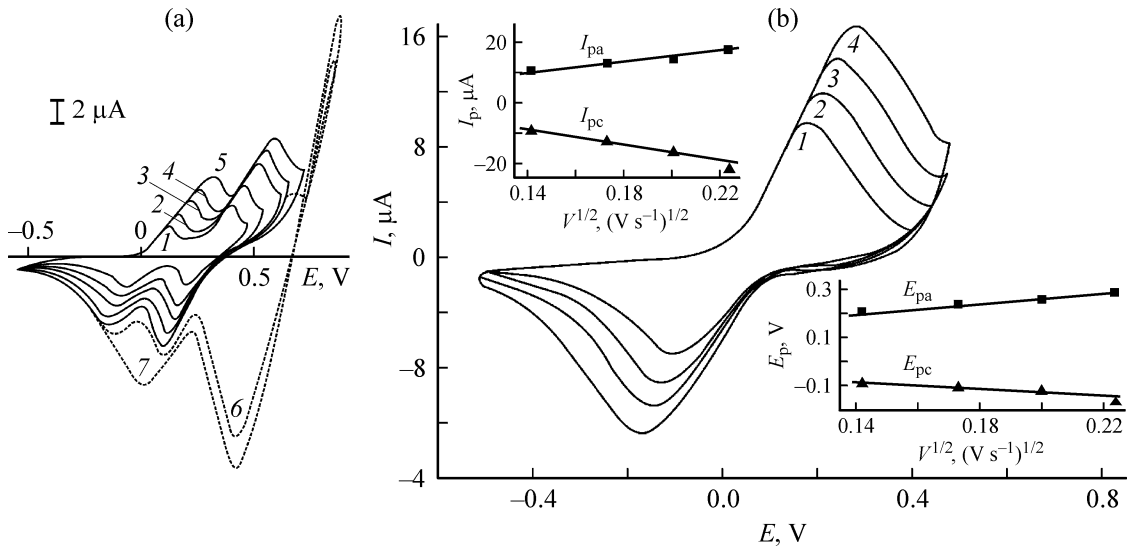


Fig. 2. Cyclic voltammograms *I*–*E* of the cell FSE | Bi | Ag, recorded at V = 0.01–0.05 V s^{-1} and the anodic polarization limit extended to (a) (*1*–*5*) 0.7 and (*6*, *7*) 0.9 V, and (b) at a potential of –0.5 to +0.5 V (first peak) and a sweep rate of (*1*) 0.02, (*2*) 0.03, (*3*) 0.04, and (*4*) 0.05 V. (b) Upper inset: the anodic peak current I_{pa} and cathodic peak current I_{pc} vs. $V^{1/2}$; lower inset: anodic peak potential E_{pa} and cathodic peak potential E_{pc} vs. $V^{1/2}$; for explanations, see text.

a voltammetric response from the microsamples on the Ag support (conducting matrix) could be detected.

LaF_3 : Eu^{2+} | Bi | Ag interface. In the cell

$$\text{FSE} \mid \text{Bi} \mid \text{Ag}, \qquad (7)$$

the FSE membrane was in contact with a microsample of Bi (S = 0.008 mm^2) and the Ag support. The potentiodynamic *I*, *E* response of the solid-phase interface, obtained in the potential range from –0.5 to +0.75 V at a sweep rate varied from 0.01 to 0.05 V s^{-1}, showed two anodic and one cathodic peaks corresponding to oxidation–reduction of Bi (Fig. 2a, curves *1*–*5*). Data presented in Fig. 2a were obtained after the 12th anodic–cathodic cycle. The extension of the anodic limit to +0.9 V and a reverse potential sweep resulted in occurrence of the third cathodic peak corresponding to the reduction of oxidized silver (Fig. 2a, curves *6*, *7*).

A more detailed examination of the first peak corresponding to oxidation of Bi is presented in Fig. 2b as an anodic–cathodic cyclic voltammogram (CVA) of the FSE|Bi interface on the Ag foil, obtained with a Bi microsample (S = 0.02 mm^2) in the potential range from –0.50 to +0.48 V at the sweep rate varied from 0.02 to 0.05 V s^{-1}. When recording the curve from –0.1 to +0.2 V and altering the sweep direction, we observed a typical hysteresis loop similar to that considered above for the FSE | Ag interface, suggesting hindered growth of a new phase with Bi. In the initial portion, the anodic curve is independent of *V*, which is indicative of hindered charge transfer.

The following trends were observed for the anodic and cathodic peaks. The dependences of log I_{pa1} and log I_{pc1} on log V are linear with a slope of 0.52 and 0.58, respectively. Therefore, I_{pa1} and I_{pc1} are linear functions of $V^{1/2}$ (Fig. 2b), confirming that the process is diffusion-controlled. The I_{pa1}/I_{pc1} ratio is close to unity (1.1–1.2) at a sweep rate from 0.02 to 0.04 V s^{-1}, which is one of the criteria of process reversibility. With increasing sweep rate (V > 0.06 V s^{-1}), the I_{pa1}/I_{pc1} ratio increases. The peak potentials E_{pa1} and E_{pc1} are linear functions of $V^{1/2}$ (Fig. 2b, lower inset). The dependence of the anodic peak potential T_{pa1} on the peak current I_{pa1} is linear over the entire experimental sweep rate range. The linear dependences of I_{pa} and E_{pa} on $V^{1/2}$ and also of E_{pa} on I_{pa} are typical of the growth of passivation films in electrolyte solutions, which is controlled by the electrolyte resistance in pores of the passivation layers [18, 20]. This suggests that the growth rate of the intermediate phase is controlled by the interfacial resistance R_c between the membrane and working electrode, allowing estimation of R_c from the slope of the E_{pa}–I_{pa} curve at $V \neq$ const. In the potentiodynamic experiments,

$$E(t) = E_s + Vt + R_c I(t), \qquad (8)$$

where E_s is the initial potential; V, sweep rate; and $I(t)$, current across the working electrode.

The peak potential E_{pa} is written as

$$E_{pa} = E_o + R_c I_{pa} + \eta_r, \qquad (9)$$

where E_o is the potential at which the reaction current appears; I_{pa}, anodic peak current; and η_r, overvoltage limiting the growth rate of the phase.

The parameter $A = E_o + \eta_r$ in the equation $E_{pa} = A + R_c I_{pa}$ is independent of the sweep rate up to 0.05 V s^{-1}. The potential difference of the first peak, corrected for the ohmic polarization of the contact, $E_{pc1} - E_{pa1} = 2.2RT/nF = 0.06$, corresponds to single-electron charge transfer.

The potential difference of the second peak is $E_{pc2} - E_{pa2} = 0.12$ V (Fig. 2a). The linear dependence of the current of the second cathodic peak on $V^{1/2}$ was observed until the 11th cycle over the sweep rate range 0.01–0.05 V s^{-1}. However, in the 12th anodic–cathodic cycle at $V = 0.05$ V s^{-1} the function deviated from linearity (Fig. 2a). The limitation of the process rate is probably due to a conjugated chemical reaction. The potentials E_{pa2} and E_{pc2} are linear functions of $V^{1/2}$ up to $V = 0.05$ V s^{-1}. The dependence of E_{pa2} on the peak current I_{pa2} is also linear, but its slope is lower than that for the E_{pa1}-vs.-I_{pa1} plot. The extension of the polarization range toward the more positive values and the delay at $E = 0.9$ V gave rise to the third cathodic peak associated with the reduction of AgF formed as a result of anodic polarization of the FSE | Ag interface, and also to an increase in the currents of the two peaks of step-by-step decomposition of BiF_3. An increase in the delay time at $E = 0.9$ V resulted in that the cathodic peaks corresponding to electrochemical transformations of the products of anodic oxidation of Bi merged.

After multiple cycling, we observed a finely dispersed black deposit at the FSE | Bi interface. At the same time, the shape of the curves, as well as the formal potential, remained unchanged.

The formation of BiF_3 involves several stages.

$$nF^-_{FSEL} \rightleftarrows nF^-_{sur}, \quad (10a)$$

$$Bi \rightleftarrows Bi_{ad}. \quad (10b)$$

Presumably, the fluoride ions play a role of an initiator for ionization of Bi. In this case, Bi adatoms can react with the fluoride ions of the solid electrolyte:

$$Bi_{ad} + nF^-_{sur} \rightleftarrows [BiF_n]^{n-}_{ad}, \quad (10c)$$

$$BiF^{n-}_{nad} \rightleftarrows BiF^{n-}_n. \quad (10d)$$

Since the adsorption of the reactants does not limit the reaction rate, and the potential difference of the first peak, corrected for the ohmic polarization of the contact, $E_{pc1} - E_{pa1} = 0.06$, the first peak can be assigned to the reaction

$$BiF^{n-}_n \rightleftarrows BiF^{(n-1)-}_n + e. \quad (10e)$$

The second peak corresponds to a reaction whose rate is lower as compared to the sweep rate of the polarization potential, e.g.,

$$BiF^{(n-1)-}_n \rightarrow BiF^{n-3}_n + 2e. \quad (10f)$$

If $n = 3$, the overall reaction can be written as

$$Bi + 3F^- \rightarrow BiF_3 + 3e.$$

The major distinctive features of the processes observed are the shift of the steady-state potential of the reaction $Bi \rightleftarrows Bi^{n+} + ne$ toward positive values and the two-peak nature of oxidation–reduction of Bi.

Previously, we observed in stripping voltammograms after anodic deposition at the FSE | Bi interface (without support or on a support made of an appropriate material) at optimal generation potential ($E_r = 0.4$ V), single-peak cathodic reduction curves of Bi [12]. The steady-state potential E_{st} of the product anodically generated under potentiostatic conditions, i.e., of the $LaF_3:Eu^{2+} | BiF_3 |$ Bi electrode formed at the $LaF_3 |$ Bi interface, was more negative [$E_{st}(Bi/BiF_3) = -0.23$ V] as compared to the product of anodic oxidation of Bi in the cycling mode ($E_{st} = 0.05$ V).

The shift of the deposition potential of metal atoms on a foreign metallic electrode toward a more positive value as compared to the reversible (Nernst) potential is known for electrocrystallization from aqueous and nonaqueous solutions and is actively discussed in the literature. This effect, known as underpotential deposition (ΔU_p), was studied using electrochemical, optical, and radiation-chemical methods. The effect is influenced by the surface conditions of the support (point and linear defects), surface energy, lattice constants of the substrate and deposited material, and also by the electrolyte composition, i.e., by the bulk and surface properties of the solids and components of the solution [21–24]. Lorenz *et al*. [25] interpreted the underpotential deposition of the product on single-crystal substrates as the formation of well-ordered two-dimensional metallic layers (superlattice structures). To explain the energy gain, ΔU_p was studied in relation to some physical characteristics of the system, such as the differences in electronegativities and in work functions of electron, W^e, between the substrate and active material [26]. With Bi as an active material and Ag as a substrate, the electronic work functions

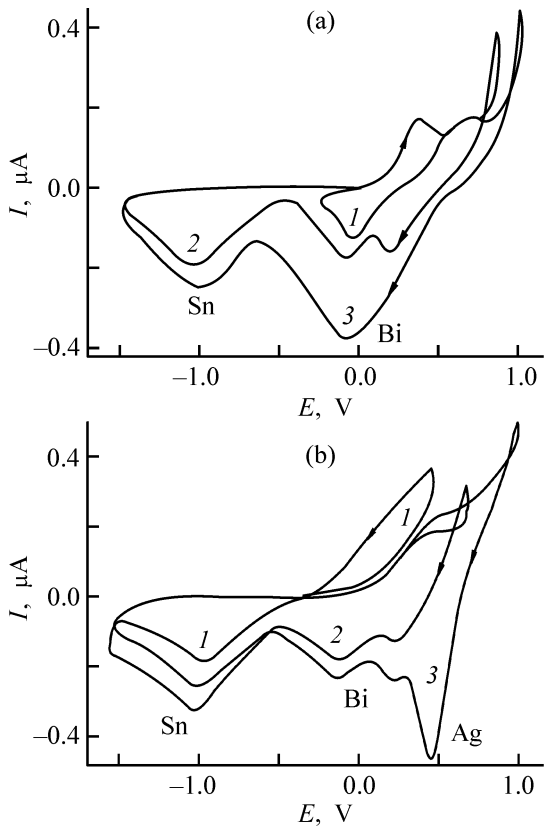


Fig. 3. Voltammogram *I*–*E* of the cell FSE | Bi + Sn | Ag (V = 0.05 V s^{-1}) with extension of the cycling limit and variation of the spot area ratio of the microsamples. (a) $S_{Sn} < S_{Bi}$ and (b) $S_{Sn} >> S_{Bi}$; for explanation, see text.

are quite similar (W^e_{Ag} = 4.3 and W^e_{Bi} = 4.4 eV [27]). A important parameter controlling the mechanism of formation of a new phase at a foreign solid-phase boundary is the binding energy of adatoms (or adions) of the active (deposited or ionized) metal to the substrate [28]. The formation of bismuth fluoride in air and the effect of the Ag support on this process can be accounted for by the fact that the binding between the Bi atoms is weaker than that between Bi and the Ag support. The more positive stationary potential can be attributed to a decreased thermodynamic activity and interaction of Bi with inert Ag support.

The effect of the support was confirmed in the experiments with a copper foil instead of a silver one. The standard potential $E^0(Cu|CuF_2)$ = 0.38 V is more positive than $E^0(Bi|BiF_3)$, but less positive than $E^0(Ag|AgF)$ = 0.95 V. However, after anodic polarization of the $LaF_3:Eu^{2+}|Bi$ (or Cu) interface, the estimated standard electrode potential $E^0(Bi|BiF_3)$ = –0.01 V well corresponded to that determined by SVA, and the reduction of anodically generated Bi was characterized by one broad peak. Evidently, in the case of the $LaF_3:Eu^{2+}|$ Bi (or Cu) interface, the Bi–Bi bonds are stronger than Bi–Cu bonds (W^e_{Cu} = 4.4 eV).

Effects similar to those found with the Ag support (splitting of Bi peaks and two-peak oxidation of Bi at a potential more positive than the equilibrium value) were observed in studying the deposition–ionization of Bi in aqueous solutions [29]. Also, a shift of the peak potential in the anodic curves in the presence of more electropositive components of the solution was reported [30].

$LaF_3:Eu^{2+}|(M_1 + M_2)|$Ag interface. Let us consider how introduction of one more impurity metal affects the voltammogram. After arrangement of Bi and Sn microsamples on the Ag support at a distance of 0.5–0.8 mm, the shape of the cyclic voltammograms of the cell

$$FSE|Sn + Bi|Ag \qquad (11)$$

depended on the spot area ratio of Sn and Bi microsamples. In the case when the Sn spot area was smaller than that of Sn ($S_{Sn} < S_{Bi}$), we observed after anode–cathode polarization from –1.0 to 0.5 V at V = 0.05 V s^{-1} a single-peak curve corresponding to oxidation–reduction of Bi (Fig. 3a, curve *1*), but we detected no reduction of Sn in the cathodic sweep. After an extension of the anodic sweep limit to E = 0.7 V, a delay at this potential, and a subsequent cathodic sweep, we obtained a two-peak Bi reduction curve and a single-peak curve (E_{pc} = 1.05 V) corresponding to reduction of Sn (Fig. 3a, curve *2*). The peak of Sn remained clearly pronounced after a delay at E = 0.9 V in the third cycle, although the overvoltage of Sn ionization increased again (Fig. 3a, curve *3*). To avoid a direct contact of the Ag support with the FSE membrane, the Ag foil was insulated with a Teflon film in this experiment.

In the case when $S_{Sn} >> S_{Bi}$, the shape of CVA somewhat changed (Fig. 3b). An anodic–cathodic sweep from –1.0 to –0.1 V showed oxidation (fluorination) of Sn and a cathodic peak of Sn (Fig. 3b, curve *1*). A repeated sweep with a delay at E = 0.7 V showed cathodic peaks of Bi and Sn (Fig. 3b, curve *2*). Raising the anodic polarization to +0.8 V (reverse sweep) allowed detection of an additional cathodic peak at 0.38 V reflecting the involvement of the Ag support in the reaction with the fluoride ions (Fig 3b, curve *3*) (in this case it was not insulated).

The specific features of the voltammetric response of the solid-phase interface in air are similar to those of anodic dissolution of alloys, when the potential of metal dissolution shifts toward the anodic range,

and, at certain component ratio, more electropositive components prevent or hinder selective dissolution of more electronegative components.

Figure 4 shows CVA of the cell

$$\text{FSE}\,|\,\text{Pb + Sb}\,|\,\text{Ag} \qquad (12)$$

recorded at $V = 0.05$ V s^{-1} with an extension of the anodic limit of cycling first to 0.7 V (Fig. 4, curve *1*) and then to 1.2 V (Fig. 4, curve *2*). The microsamples of Pb and Sb differed in their spot area ($S_{Pb} >> S_{Sb}$). Despite the fact that we used as model impurities metals tending to irreversibly form fluorides, the response of the LaF_3 : $Eu^{2+}\,|\,$Pb + Sb$\,|\,$Ag interface is similar to that observed for LaF_3:$Eu^{2+}\,|\,$Sn + Bi$\,|\,$Ag interface at the same component ratio. The cyclic voltammogram shows clearly pronounced peaks of Pb, Sb, and Ag. The occurrence of the second peak of Sb can be attributed to the fact that, as in the case of Bi, fluorination of Sb proceeds in two stages with step-by-step electron transfer. A repeated cycling of the FSE interface was accompanied by an increase in the overvoltage of the anodic reactions and, accordingly, by a decrease in the peak current of the cathodic curves, with the peak potentials shifted toward more negative values, which is associated with the limitation of the reaction rates by conjugated chemical reactions.

It is known that introduction of a third component frequently improves the sensitivity of voltammetry in aqueous solutions [31]. We observed a similar effect in recording a CVA of the cell with Cd and Bi microimpurities on an Ag support. Figure 5 shows the voltammogram of the FSE$\,|\,$Cd + Bi$\,|\,$Ag interface. After anodic polarization to 0.5 V, we observed in the cathodic sweep a reduction peak of fluorinated cadmium (Fig. 5, curve *1*). In the second cycle, with extension of the anodic polarization limit to 0.9 V, the cathodic curve shows three peaks corresponding to Cd, Bi, and Ag (Fig. 5, curve *2*). The cathodic peak current of reduction of anodically generated cadmium is slightly lower, being shifted toward the negative range. However, this peak is more clearly pronounced than that in the stripping voltammogram without an Ag support [16].

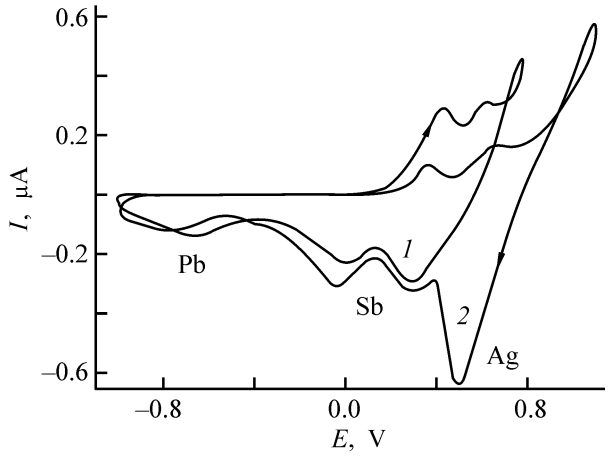


Fig. 4. Cyclic voltammogram *I–E* of the cell FSE$\,|\,$Pb + Sb$\,|\,$Ag ($V = 0.05$ V s^{-1}) for scans (*1*) from –0.9 to 0.7 V and (*2*) from –0.9 to 1.2 V.

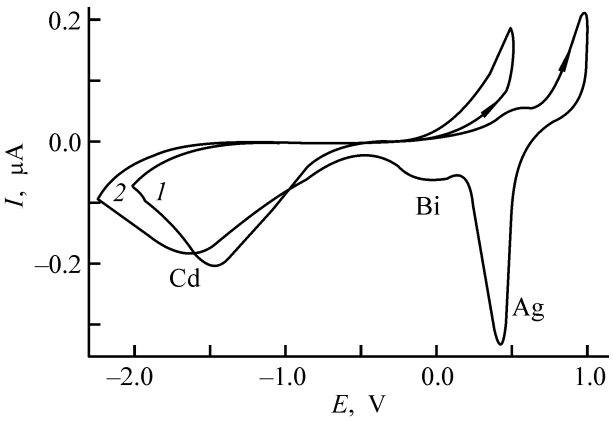


Fig. 5. Voltammogram *I–E* of the cell FSE$\,|\,$Bi + Cd$\,|\,$Ag ($V = 0.05$ V s^{-1}) with extension of the cycling limit to (*1*) 0.5 and (*2*) 0.9 V.

CONCLUSIONS

(1) Cyclic voltammetry of fluoride-selective electrode in contact with metallic microelectrodes allows simultaneous detection of electrochemical responses from several metals. Such a technique can be used for local determination of trace amounts of Bi, Sn, Pb, Sb, and Cd on a silver support in air.

(2) This is a reagent-free method of qualitative analysis, which is nondestructive with respect to both the LaF_3 membrane and a solid phase to be analyzed.

(3) In this method, the medium to be analyzed is a solid, rather than a liquid, and the working potential range (about 7 V) is significantly wider than that in aqueous and nonaqueous solutions with liquid and solid-state electrodes.

(4) The dependence of the voltammetric response of the fluoride-selective electrode on the relative amounts of impurity metals on the conducting support is established.

(5) Electropositive components (silver support) affect the formation of the output signal at the interface between a fluoride-conducting solid electrolyte and metallic electrodes.

REFERENCES

1. Koryta, J. and Štulik, K., *Iontove-selektivní elektrody*, Praha: Academia, 1984.
2. *Spravochnoe rukovodstvo po primeneniyu ionoselektivnykh elektrodov* (A Handbook on Applications of Ion-Selective Electrodes), Petrukhin, O.N., Ed., Moscow: Mir, 1986.
3. Yamazoe, N., Hisamoto, J., Miura, N., and Kuwata, S., *Sensors Actuators*, 1987, vol. 12, pp. 415–423.
4. Lukaszewicz, J.P., Miura, N., and Yamazoe, N., *Sensors Actuators, Ser. B*, 1990, vol. 1, nos. 1–6, pp. 195–198.
5. Harke, S., Wiemhofer, H.-D., and Gopel, W., *Sensors Actuators, Ser. B*, 1990, vol. 1, nos. 1–6, pp. 188–194.
6. Moritz, W., Krause, S., Vasiliev, A.A., *et al.*, *Sensors Actuators, Ser. B*, 1995, vol. 24, nos. 1–3, pp. 194–196.
7. Vasiliev, A.A., Moritz, W., Fillipov, V., *et al.*, *Sensors Actuators, Ser. B*, 1992, vol. 9, pp. 191–196.
8. Bartholomaus, L. and Moritz, W., *Solid State Ionics*, 2000, vol. 132, pp. 31–37.
9. Fergus, J.W., *Sensors Actuators, Ser. B*, 1997, vol. 42, no. 2, pp. 119–130.
10. UK Patent 1318713.
11. Lyalin, O.O., Turaeva, M.S., and Mogilevskii, B.M., *Elektrokhimiya*, 1977, vol. 13, no. 11, pp. 1716–1718.
12. Turaeva, M.S., Lyalin, O.O., and Vasilevskii, V.L., *Elektrokhimiya*, 1992, vol. 28, no. 10, pp. 1505–1511.
13. Turaeva, M.S., Pegova, I.A., and Vasilevskii, V.L., *Elektrokhimiya*, 1996, vol. 32, no. 4, pp. 491–497.
14. Turaeva, M.S., *Elektrokhimiya*, 1996, vol. 32, no. 4, pp. 498–502.
15. Turaeva, M.S., Kot, S.A., Glumov, O.V., and Murin, I.V., *Zh. Prikl. Khim.*, 2001, vol. 74, no. 4, pp. 579–585.
16. Turaeva, M.S., Pegova, I.A., Vasilevskii, V.L., and Grilikhes, M.S., *Zh. Prikl. Khim.*, 1996, vol. 69, no. 8, pp. 1321–1331.
17. Turaeva, M.S., Kot, S.A., Urchukova, M.M., and Murin, I.V., *Elektrokhimiya*, 2003, vol. 39, no. 5, pp. 633–638.
18. Macdonald, D.D., *Transient Techniques in Electrochemistry*, New York: Plenum, 1981.
19. Budevski, E., Staikov, G., and Lorenz, W.J., Electrochim. Acta, 2000, vol. 45, pp. 2259–2574.
20. Calandra, A.J., de Tacconi, N.R., Pereiro, R., and Arvia, A.J., *Electrochim. Acta*, 1974, vol. 19, pp. 901–905.
21. Leiva, E., *Electrochim. Acta*, 1996, vol. 41, no. 14, pp. 2185–2206.
22. El-Maksoud, S.A.A., Taguchi, S., Fukuda, T., and Aramata, A., *Electrochim. Acta*, 1996, vol. 41, no. 13, pp. 1947–1952.
23. Salgado, L., Sanchez, H., Cabrera, C.R., *et al.*, *J. Solid State Electrochem.*, 1998, vol. 2, no. 6, pp. 405–412.
24. Rasmussen, A.A., Jensen, J.A.D., Horsewell, A., and Somers, M.A.J., *Electrochim. Acta*, 2001, vol. 47, pp. 67–74.
25. Lorenz, W.J. and Staikov, G., *Surf. Sci.*, 1995, vol. 335, pp. 32–43.
26. Kolb, D.M., Przasnyski, M., and Gerischer, H., *J. Electroanal. Chem. Interfac. Electrochem.*, 1974, vol. 54, no. 1, pp. 25–38.
27. *Svoistva elementov: Spravochnik* (Properties of Elements: A Handbook), Drits, M.E., Ed., Moscow: Metallurgiya, 1985.
28. Sanchez, C. and Leiva, E.P.M., *Electrochim. Acta*, 1999, vol. 45, nos. 4–5, pp. 691–697.
29. Popov, G.N., Pnev, V.V., and Zakharov, M.S., *Zh. Anal. Khim.*, 1972, vol. 27, no. 7, pp. 1335–1339.
30. Moskovskikh, L.A., Pnev, V.V., and Zakharov, M.S., *Zh. Anal. Khim.*, 1972, vol. 27, no. 8, pp. 1624–1626.
31. Brainina, N.Z., Neiman, E.Ya., and Slepushkin, V.V., *Strippingnye elektroanaliticheskie metody* (Stripping Electroanalytical Methods), Moscow: Khimiya, 1988.

Russian Journal of Applied Chemistry, Vol. 78, No. 2, 2005, pp. 267–272. Translated from Zhurnal Prikladnoi Khimii, Vol. 78, No. 2, 2005, pp. 273–278.
Original Russian Text Copyright © 2005 by Chernysheva, Loginova, Bazilyanskaya.

APPLIED ELECTROCHEMISTRY AND CORROSION PROTECTION OF METALS

Metal Ion Buffer Systems for Ionometry in Water–Ethanol Mixtures and Micellar Medium of Sodium Dodecyl Sulfate

O. S. Chernysheva, L. P. Loginova, and V. D. Bazilyanskaya

Karazin National University, Kharkov, Ukraine

Received January 22, 2003; in final form, April 2004

Abstract—The concentration dissociation constants of nitrilotriacetic acid and the concentration stability constants of Cd(II) complexes with the nitrilotriacetic acid anion in water–ethanol mixtures and of Cu(II) and Cd(II) complexes with *o*-phenanthroline and 2,2'-bipyridine in micellar solutions of sodium dodecyl sulfate were determined potentiometrically. Based on the concentration constants determined, Cd^{2+} and Cu^{2+} buffer solutions were developed for calibration of a Cd^{2+}-selective electrode in water–ethanol mixtures and Cd^{2+} and Cu^{2+}-selective electrodes in micellar solutions of sodium dodecyl sulfate within the ranges pCu 9.7–13.5 and pCd 7.5–11.8.

Mixed, organic, or micellar solutions of surfactants can be an alternative to aqueous solutions for study of protolytic and complexing properties of bioactive substances that are poorly soluble in water by potentiometry with solid membrane electrodes [1].

Change of a medium is accompanied by the shift of the calibration characteristics of ion-selective electrodes (ISE), which should be considered when calibration solutions are prepared.

Electrolyte solutions prepared by successive dilution are suitable for ISE calibration at concentrations of the ion to be analyzed higher than 10^{-4}–10^{-5} M. In more dilute solutions, the actual concentration of the potential-determining ion differs from the calculated concentration because of the solution contamination or losses caused by adsorption, oxidation, etc. [2]. The ISE calibration dependences for dilute solutions deviate from linearity, with their slope decreasing [3], which corresponds to additional supply of the potential-determining ion into the solution, primarily from the membrane material. Iodide and sulfide-selective electrodes with more complex response in dilute solutions are an exception [4].

The stable low (less than 10^{-4}–10^{-5} M) concentrations of the potential-determining ion are provided by metal ion buffer systems based on chemical reactions, involving reactants in relatively high total concentrations. This idea, which is the basis of the calibration in the pH-metry, is used in making metal and anion-buffer systems. Already in early studies concerned with ISE, heterogeneous ion buffer systems containing silver halide and sulfide mixtures were used [5]. Still earlier, metal buffer systems as media for biological investigations were suggested [6, 7]. Metal buffer systems are also used in other analyses [8, 9]. Recently, they have been used in studying the effect of oxygen dissolved on Cu^{2+} ISE [10].

The known ion-buffer systems are mainly used for calibration of ISE with solid-phase membranes, for which transfer of the potential-determining ion from the membrane to the solution substantially exceeds the equilibrium solubility and is caused by the elution processes [4].

In this study, we applied the principle of Cd^{2+} and Cu^{2+}-selective electrode calibration with metal ion buffer solutions to new media: water–ethanol mixtures and media with a higher level of structuring, i.e., surfactant micellar solutions (sodium dodecyl sulfate, SDS).

The commonly used components of metal ion-buffer systems are the carboxyl-containing complexing agents: imidoacetic (H_2Ida), nitrilotriacetic (H_3Nta), and ethylenediaminetetraacetic (H_4Edta) acids, although metal ion-selective electrodes show in their presence an anomalous behaviorwhich becomes more pronounced $Ida^{2-} < Nta^{3-} < Edta^{4-}$ [11]. It has been shown earlier that Cu^{2+} buffer systems based on

1070-4272/05/7802-0267 © 2005 Pleiades Publishing, Inc.

Table 1. Concentration constants of stepwise complexation of Cd^{2+} with Nta^{3-}, I = 0.01 M ($LiNO_3$), titrant concentration 1.0×10^{-3} M

Version no.	Composition of titrated solution, M	Titrant	Property measured		$\log K_i$
			main	auxiliary	
1	Nta^{3-}, 1.5×10^{-3}	$Cd(NO_3)_2$	pCd	pH	$\log K_1 = 11.12 \pm 0.09$, $\log K_2 = 3.95 \pm 0.09$
2	H_2Nta^-, 1.0×10^{-3}	$Cd(NO_3)_2$	pH	pCd	$\log K_1 = 11.07 \pm 0.07$
3	$HNta^{2-}$, 5×10^{-4} $CdNta^-$, 5×10^{-4}	NaOH	pH	pCd	$\log K_2^* = 3.93 \pm 0.08$

* In $\log K_2$ calculation, $\log K_1 = 11.07$ was used.

Cu(II)–Ida^{2-} complexes are suitable for calibration of a Cu^{2+}-selective electrode in aqueous ethanol [12]. In this study, we took nitrilotriacetic acid anion as a ligand for cadmium-buffer systems. The Cd(II) complexes with Nta^{3-} are very stable, and the specific influence of Nta^{3-} on the membrane of the Cd^{2+}-selective electrode is weaker than that in the case of $Edta^{4-}$, at least in aqueous solutions.

The equilibrium constants of complexation and concomitant reactions are required to calculate the main characteristics of the metal-buffer systems. The experimentally found complexation constants are concentration constants. This allows the negative logarithm of the equilibrium concentration of free metal ions $pM = -\log[M^{2+}]$ to be regarded as the main characteristic of metal ion buffer solution [13].

The acid–base equilibria of the components of the cadmium buffer system were studied by pH-metric titration. The logarithms of the acid–base equilibrium constants in the water–ethanol mixture are presented below:

$H_2O \rightleftarrows H^+ + OH^-$, $\log K_w = -14.76 \pm 0.1$;

$H_3NTA \rightleftarrows H^+ + H_2NTA^-$, $\log K_{a1} = -3.24 \pm 0.08$;

$H_2NTA^- \rightleftarrows H^+ + HNTA^{2-}$, $\log K_{a2} = -3.82 \pm 0.08$;

$HNTA^{2-} \rightleftarrows H^+ + NTA^{3-}$, $\log K_{a3} = -8.13 \pm 0.03$;

$Cd^{2+} + 2OH^- \rightleftarrows Cd(OH)_2$, $\log \beta_{OH2} = 14.75$.

The pK_{a3} of nitrilotriacetic acid was calculated with high errors, probably, due to specific interaction of Nta^{3-} with a glass membrane [14]. The pK_{a3} was determined spectrophotometrically in a water–ethanol mixture with Bromocresol Red as an indicator with $pK_a = 7.53 \pm 0.04$ (λ_{max} of the base form 595 nm, and that of the acid form 425 nm).

Complexation of Cd^{2+} with Nta^{3-} should be studied by the method independent of Cd^{2+}-selective electrode. However, the usual method of the competitive pH-metry is inapplicable for determination of the $CdNta^-$ stability constant exceeding the Nta^{3-} protonation constant. At the same time, the result obtained with the Cd^{2+}-selective electrode may be distorted by specific influence of Nta^{3-} on ISE membrane. We applied three different approaches to make the experimental stability constants of the Cd^{2+} complexation with the Nta^{3-} ions more reliable. In each case, the titration conditions were chosen so that the ion determined potentiometrically had the lowest equilibrium concentration [15]. In the first case, it was the cadmium(II) ion and, in the second and third cases, the hydrogen ion. The use of additionally controllable property in the calculations allowed us to obtain a more precise information on the complex composition and constants. The well consistent results (Table 1) show that Nta^{3-} does not exert any specific influence on the Cd^{2+}-selective electrode membrane in aqueous ethanol and that the constants obtained are reliable.

The simple cadmium-buffer systems contain the highest complex $Cd(Nta)_2^{4-}$ and excess unbound ligand; the reaction

$$Cd(Nta)_2^{4-} \rightleftarrows Cd^{2+} + 2Nta^{3-} \quad (1)$$

provides buffer action with respect to Cd^{2+}.

In this case, the unbound Nta^{3-} anion can be involved in the competitive protolytic equilibria. Therefore, simple cadmium-buffer systems are pH-dependent [7]. Their equilibrium composition was calculated with regard to pH measured (Table 2, buffer solutions 1–3).

If there are no competitive protolytic reactions in metal buffer systems, the concentration of the un-

Table 2. Composition and characteristics of aqueous–ethanolic cadmium-buffer solutions, I = 0.01 M ($LiNO_3$)

Version no.	Total concentration, M	Reaction	pH	pCd_{calc}	pCd_{exp}	Buffer capacity, M
1	$Cd(NO_3)_2$, 2.3×10^{-4} H_3Nta, 1.15×10^{-3} NaOH, 3.45×10^{-3} $LiNO_3$, 4.19×10^{-3}	(1)	8.96	12.32	12.32	2.6×10^{-4}
2	$Cd(NO_3)_2$, 3.3×10^{-4} H_3Nta, 1.00×10^{-3} NaOH, 3.00×10^{-3} $LiNO_3$, 4.69×10^{-3}	(1)	8.47	11.58	11.56	2.6×10^{-4}
3	$Cd(NO_3)_2$, 5.0×10^{-4} H_3Nta, 7.5×10^{-4} NaOH, 2.25×10^{-3} $LiNO_3$, 5.51×10^{-3}	(1)	7.88	10.19	10.13	2.4×10^{-4}
4	$Cd(NO_3)_2$, 6.9×10^{-4} H_3Nta, 8.4×10^{-4} NaOH, 2.52×10^{-3} $LiNO_3$, 4.71×10^{-3}	(3) pH-independent	–	9.70	9.68 ± 0.09	1.9×10^{-4}

bound ligand and the system as a whole are pH-independent. To make pH-independent buffer systems, we used the fact that, in the region of coexistence of two complexes, the buffer capacity with respect to Nta^{3-} is determined by the equilibrium

$$Cd(Nta)_2^{4-} \rightleftarrows Nta^{3-} + CdNta^{-}. \quad (2)$$

Then, the buffer effect with respect to Cd^{2+} is described by the reaction

$$2Cd(Nta)^{-} \rightleftarrows Cd^{2+} + CdNta_2^{4-}. \quad (3)$$

An optimization of the cadmium-buffer system composition by methods described in [16] showed that, at a fixed ionic strength μ = 0.01 M, the solution containing 2.08×10^{-3} M $CdSO_4$, 2.54×10^{-3} M H_3Nta, and 7.62×10^{-3} M NaOH has the maximum buffer capacity. However, a precipitate was formed when the solution with such a composition was prepared directly. Therefore, the concentrations of the components of the buffer solution were decreased with their optimal ratio preserved (Table 2, buffer solution no. 4). In contrast to the first three buffer solutions, the pCd of solution no. 4 can be calculated without additional pH determination by the equation

$$pCd = 7.14 + \log(c_L - c_{Cd}) - 2\log(2c_{Cd} - c_L), \quad (4)$$

where c_L and c_{Cd} are the total molar concentrations of H_3Nta and $Cd(NO_3)_2$, respectively.

The good agreement of the calculated and experimental pCd values in the buffer solutions confirms linearity of the response of the Cd^{2+}-selective electrode in aqueous–ethanol up to pCd ~12.3.

o-Phenanthroline (phen) and 2,2'-bipyridine (bipy) are appropriate components of metal-buffer systems. They form stable complexes with Ag^{+}, Cu^{2+}, and Cd^{2+}, for which ISE have been developed, and with other ions. They can be auxiliary for the "second-kind buffers" [17]. As these ligands are relatively weak bases (Table 3), competitive protonation reactions affect the complexation insignificantly within a very wide pH range, and the pM of metal-buffer systems is independent of pH.

The published data on ligand protonation constants and stability constants of the complexes in aqueous solutions [17] refer to different experimental conditions. To reveal the effect of the micellar medium, we studied aqueous and micellar solutions under the same conditions. Complexation of Cd^{2+} and Cu^{2+} with phen and bipy in the micellar SDS solution was studied potentiometrically [18]. However, at the total reactant concentrations of approximately 10^{-4} M, we cannot determine the stability constants of the higher complexes CuL_3^{2+}, which should be taken into account when buffer properties of Cu-phen or Cu-bipy systems are estimated. The results of an additional study at the reactant concentrations of approximately 10^{-3} M are listed in Table 3.

Table 3. Logarithms of the concentration constants of ligand protonation and stepwise complexation of Cu^{2+} and Cd^{2+} with *o*-phenanthroline and 2,2'-bipyridine in aqueous and micellar solutions

Ligand	Parameter measured		Complex composition	log *K*, aqueous solutions		log *K* in 0.05 M SDS
	main	auxiliary		this work	data of [17]	
bipy	pH	–	HL^+	4.35 ± 0.03	4.4 (I = 0.1, KNO_3)	5.24 ± 0.03
phen	pH	–	HL^+	5.14 ± 0.03	4.96 (I = 0.1, KNO_3)	5.61 ± 0.03
bipy	pCu	pH	CuL^{2+}	7.24 ± 0.02	8.15	7.67 ± 0.10
			CuL_2^{2+}	5.65 ± 0.02	5.50 (I = 0.3, K_2SO_4)	6.51 ± 0.17
			CuL_3^{2+}	3.49 ± 0.03	3.30	4.09 ± 0.25
phen	pCu	pH	CuL^{2+}	–	8.82	8.87 ± 0.12
			CuL_2^{2+}	13.83 ± 0.06	6.57 (I = 0.3, K_2SO_4)	6.43 ± 0.12
			CuL_3^{2+}	4.66 ± 0.09		4.11 ± 0.17
bipy	pCd	pH	CdL^{2+}	–	4.28	–
			CdL_2^{2+}	8.32 ± 0.02	3.51 (I = 0.05, KNO_3)	10.13 ± 0.02
			CdL_3^{2+}	–	2.69	–
phen	pCd	pH	CdL^{2+}	–	5.17	6.44 ± 0.03
			CdL_2^{2+}	10.48 ± 0.02	4.83 (I = 0.1, KCl)	6.31 ± 0.02
			CdL_3^{2+}	–	4.26	3.65 ± 0.03

Table 4. Composition and characteristics of micellar cadmium-buffer (0.05 M SDS) solutions, I = 0.1 M ($NaNO_3$)

Solution no.	Total concentration, M	pCd_{calc}	pCd_{exp}	Buffer capacity, M
1	$Cd(NO_3)_2$, 1.01×10^{-3}; bipy, 3.7×10^{-3}	7.58	7.51	6.8×10^{-4}
2	$Cd(NO_3)_2$, 1.01×10^{-3}; phen, 6.20×10^{-3}	11.95	11.76	6.4×10^{-4}
3	$Cd(NO_3)_2$, 1.01×10^{-3}; phen, 6.35×10^{-3}	12.01	11.87	6.6×10^{-4}
4	$Cd(NO_3)_2$, 1.01×10^{-3}; phen, 4.72×10^{-3}	11.21	11.20	4.3×10^{-4}
5	$Cd(NO_3)_2$, 1.01×10^{-3}; phen, 3.46×10^{-3}	10.02	10.00	2.4×10^{-4}
6	$Cd(NO_3)_2$, 1.01×10^{-3}; phen, 4.06×10^{-3}	10.70	10.58	3.3×10^{-4}

Within the concentration range studied, formation of $Hphen^+$ species in aqueous solution at pH 5.4 [19] and self-association of phen and bipy molecules [20] are not confirmed.

Simple Cd^{2+} and Cu^{2+}-buffer systems contain higher complexes $Cd(bipy)_2^{2+}$, $Cd(phen)_3^{2+}$, $Cu(bipy)_2^{2+}$, or $Cu(phen)_3^{2+}$ and excess unbound ligand (Table 4, buffer solution nos. 1–6; Table 5, buffer solutions nos. 1, 3, 4). As compared to aqueous solutions, the range in which the $Cu(bipy)_2^{2+}$ complex prevails in the micellar media is wider (Table 3). This makes it possible to prepare a Cu^{2+} buffer system with a lower pCu by on the reaction

$$3Cu(dipy)_2^{2+} \rightleftarrows Cu^{2+} + 2Cu(dipy)_3^{2+}. \quad (5)$$

The involvement of the complexing agent in the exchange of counterions on the micelle surface, which can affect the properties of the reaction mixture, additionally restricts the choice of the initial composition of metal-buffer systems in a micellar medium of anionic surfactants. This effect is poorly understood; however, it is known that, when sodium counterions are replaced with double-charged cations, micelles acquire cylindrical shape [21]. In order to provide the constant micelle composition, we used the same total concentration of the complexing agent in the metal-buffer solutions as in determination of the stability

Table 5. Composition and characteristics of copper-buffer micellar (0.05 M SDS) solutions, I = 0.1 M ($NaNO_3$)

Solution no.	Total concentration, M	pCu_{calc}	pCu_{exp}	Buffer capacity, M
1	$Cu(NO_3)_2$, 9.99×10^{-4}; phen, 3.78×10^{-3}	13.26	13.57	2.3×10^{-4}
2	$Cu(NO_3)_2$, 1.01×10^{-3}; phen, 2.94×10^{-3}	11.43	11.59	1.2×10^{-4}
3	$Cu(NO_3)_2$, 1.0×10^{-3}; bipy, 4.66×10^{-3}	12.98	12.96	3.8×10^{-4}
4	$Cu(NO_3)_2$, 1.0×10^{-3}; bipy, 3.51×10^{-3}	11.71	11.19	1.9×10^{-4}
5	$Cu(NO_3)_2$, 1.0×10^{-3}; bipy, 2.48×10^{-3}	8.97	9.77	1.2×10^{-4}

constants (1×10^{-3} M). To stabilize the ionic strength of the metal-buffer solutions, we used $NaNO_3$; its total concentration was 4.70×10^{-3} M.

The pCd values measured with ISE in Cd^{2+}-buffer systems agree with the calculated values within the error of determination of the mass action law (MAL) constants. Buffer solution no. 1 is the best for practical purposes (Table 4). In the solutions containing excess ligand, the $Cd(bipy)_2^{2+}$ complex prevails, whereas the concentration of the 1 : 1 complex is negligible. This simplifies calculation of pCd at varied concentration of the buffer solution:

$$pCd = \log \beta_2 + 2\log(c_L - 2c_{Cd}) - \log c_{Cd}, \quad (6)$$

where c_L and c_{Cd} are the total molar concentrations of bipy and Cd(II), respectively.

After storage of the cadmium buffer solutions for 7 days, pCd changed by less than ± 0.03.

The pCu values measured with ISE (Table 5) are worse consistent with the calculated values than in the case of Cd^{2+}-buffer systems. During storage, the pCu values for Cu^{2+}-buffer solutions substantially changed: pCu increased by 0.6 in two weeks. The error of determination of the stability constants of the Cu^{2+} complexes with phen and bipy is higher compared to the corresponding Cd^{2+} complexes. This fact suggests that some unaccounted processes occur in the solution or at the interface between the solution and the Cu^{2+}-selective membrane. Therefore, we cannot recommend for use the Cu^{2+}-buffer systems listed in Table 5 without understanding of the nature of these processes.

The metal ion buffer systems suggested (except those listed in Table 5) can be useful for calibration ISEs used for studying complexation in the corresponding media. These metal-buffer solutions allow calibration at pM close to the values being determined, as in pH-metry, which improves the accuracy of determination of the MAL constants [15].

EXPERIMENTAL

A Cu^{2+}-selective solid-phase electrode based on chalcogenide glasses $Cu_xAg_{25-x}As_{37.5}Se_{37.5}$ [22], Orion 94-48 Cd^{2+}-selective electrode, ESL-63-07 glass electrode, and EVL-1M3 reference electrode were used for a potentiometric study of the equilibria. A potentiometric cell included a liquid junction of capillary type filled with 2 M KNO_3 aqueous solution. The electromotive force was measured with a compensating scheme (R 307 potentiometer and a pH-121 pH-meter as a null-indicating instrument); all measurements were performed at a constant temperature of 298.0 ± 0.1 K. Chemically pure grade reagents, SDS (Sigma) with the main substance content of no less than 99 wt %, and double-distilled water were used to prepare the solutions. The Cu(II) and Cd(II) content in the initial solutions was determined complexometrically [23]. The ionic strength of the aqueous–ethanol solutions (I = 0.01 M) was supported with $LiNO_3$, and that of micellar solutions (I = 0.1 M), with $NaNO_3$; the contribution of micelles to the ionic strength was disregarded. The Cd^{2+} buffer solutions in aqueous–ethanol were prepared from the component stock solutions and metal-buffer solutions in the SDS medium, using precisely weighed portions of phen or bipy and stock solutions of Cu(II) and Cd(II) salts and $NaNO_3$.

The potentiometric titration data were processed using the CLINP software, which enables calculation of the equilibrium constants and refinement of the complexation model [24]. The equilibrium compositions and buffer capacities of solutions with regard to all the competing reactions were calculated with the projecting method using an appropriate software.

CONCLUSIONS

The compositions of cadmium-buffer solution based on Cd(II) complexes with nitrilotriacetic acid in aqueous–ethanol solutions were developed for calibration of a Cd^{2+}-selective electrode within the pCd

range 9.7–12.3. To calibrate the Cd^{2+}-selective electrode in micellar solutions of sodium dodecyl sulfate, cadmium-buffer systems based on Cd(II) complexes with *o*-phenanthroline and 2,2'-bipyridine were suggested. Similar copper-buffer solutions are characterized by relatively poor repeatability and reproducibility of measured pCu.

REFERENCES

1. Shtykov, S.N., *Zh. Anal. Khim.*, 2000, vol. 55, no. 7, pp. 679–686.
2. Koryta, J. and Štulik, K., *Iontove-selektivn¸ elektrody*, Praha: Academia, 1984.
3. *Handbook of Electrode Technology*, Cambridge: Orion Research Inc., 1982.
4. Morf, W.E., *The Principles of Ion-selective Electrodes and Membrane Transport*, Budapest: Akad. Kiado, 1981.
5. *Ion-Selective Electrodes*, Durst, R.A., Ed., Washington: National Bureau of Standards, 1969.
6. Wolf, H.U., *Experientia*, 1973, vol. 29, no. 2, pp. 241–249.
7. Perrin, D.D. and Dempsly, B., *Buffers for pH and Metal ion Control*, London: Chapman and Hall, 1974.
8. Wada, H., Yuchi, A., and Nakagawa, G., *Anal. Chim. Acta*, 1983, vol. 149, pp. 291–296.
9. Ishibashi, N., Imato, T., and Tsukiji, K., *Anal. Chim. Acta*, 1986, vol. 190, no. 4, pp. 185–194.
10. Tani, Y., Soma, M., Harsanyi, E.G., and Umezawa, Y., *Anal. Chim. Acta*, 1999, vol. 395, pp. 53–63.
11. Neshkova, M. and Sheytanov, H., *Talanta*, 1985, vol. 32, no. 10, pp. 937–945.
12. Loginova, L.P. and Bazilyanskaya, V., *Anal. Chim. Acta*, 1995, vol. 315, pp. 55–61.
13. Skoog, D., West, D.M., and Holler, F.J., *Fundamentals of Analytical Chemistry*, Harcurt College, 2003.
14. Loginova, L.P.and Lycheva, O.S., *Khim. Fiz.*, 1996, vol. 15, no. 11, pp. 97–104.
15. Beck, M. T. and Nagypal, I., *Chemistry of Complex Equilibria*, Budapest: Akad. Kiado, 1989.
16. Bugaevskii, A.A., *Approximate Estimations of the Solution Equilibrium Composition*, Kharkov: Folio, 1996, Part 2.
17. Martell, A.E. and Smith, R.M., *Critical Stability Constants*, New York: Plenum, 1974–1976, vols. 1–4.
18. Loginova, L.P. and Chernysheva, O.S., *J. Mol. Liq.*, 2000, vol. 85, pp. 351–359.
19. Rund, J.V. and Keller, P.C., *J. Chem. Soc. A*, 1970, no. 17, pp. 2827–2829.
20. Mitchell, P.R., *J. Chem. Soc., Dalton Trans.*, 1980, no. 7, pp. 1079–1086.
21. Vakarelski, I.M. and Dushkin, C.D., *Colloids Surf., A*, 2000, vol. 63, nos. 2–3, pp. 177–190.
22. Vlasov, Yu.G., Bychkov, E.A., and Medvedev, A.M., *Anal. Chim. Acta*, 1986, vol. 185, pp. 137–158.
23. Umland, F., Janssen, A., Thierig, D., und Wünsch, G., *Theorie und praktische Anwendung von Komplexbildnern*, Frankfurt am Main: Akademische Verlagsgesellschaft, 1971.
24. Kholin, Yu.V., *Kolichestvennyi fiziko-khimicheskii analiz kompleksoobrazovaniya v rastvorakh i na poverkhnosti khimicheski modifitsitovannykh kremnezemov: soderzhatel'nye modeli, matematicheskie metody i ikh prilozheniya* (Quantitative Physicochemical Analysis of Complex Formation in Solutions and on the Surface of Chemically Modified Silica: Substantial Models, Mathematical Methods, and Their Applications), Kharkov: Folio, 2000.

Russian Journal of Applied Chemistry, Vol. 78, No. 2, 2005, pp. 273–277. Translated from Zhurnal Prikladnoi Khimii, Vol. 78, No. 2, 2005, pp. 279–283.
Original Russian Text Copyright © 2005 by Zakarina, Volkova, Shchukina, Khan.

CATALYSIS

Pillared Tagan Montmorrilonite in Cracking of Isopropylbenzene

N. A. Zakarina, L. D. Volkova, O. V. Shchukina, and Ch. G. Khan

Institute of Organic Catalysis and Electrochemistry, Ministry of Education and Science of the Republic of Kazakhstan, Almaty, Kazakhstan

Received September 10, 2004

Abstract—Tagan montmorillonite clay fixed with aluminum and zirconium oxides was prepared, and its catalytic (in cracking of isopropylbenzene), adsorption, and structural characteristics were studied.

It is known that the heat resistance of catalysts derived from clays is poor [1–4] because of the possible closure of the silicate layers at high temperatures. Intercalation of metal oxide clusters (pillars) into the interlayer space of montmorrilonite-type layered clays by cation exchange with inorganic polyoxo cations allows preparation of a new class of materials exhibiting the prescribed porosity, acidity, and heat resistance. Pillared clays attract researchers' attention as adsorbents and catalysts for cracking, isomerization, etc.

Preparation and use of intercalated clays have been discussed in numerous reviews [1–3]. The features of intercalation are specific to montmorillonites from different deposits.

In this study, we examined intercalation of natural Kazakhstan montmorrilonite from the Tagan deposit and tested pillared materials derived from it in cracking of hydrocarbons.

EXPERIMENTAL

Montmorrilonite clay from the Tagan deposit was used without isolation of the monomineral montmorillonite fraction. The initial clay was converted to the Na form by treatment with 1 M NaCl to raise its dispersity. The H form of Tagan montmorillonite was prepared by the standard procedure [4].

As fixing agents we tested oligomeric aluminum hydroxo cations of the presumed composition $[Al_{13}O_4(OH)_{24}(H_2O)_{12}]^{7+}$ (Al_{13}^{7+}) with a four-coordinate Al atom, which were prepared according to [5] at various synthesis temperatures, and aqueous solutions of $ZrOCl_2$, which were introduced into clay according to [6]. As reported in [7, 8], 70–80% of aluminum hydroxo cations have a Keggin structure. Oligomeric Al_{13}^{7+} is commonly prepared by hydrolysis of a 0.2 M $AlCl_3$ solution in 0.5 M NaOH at OH^-/Al^{3+} = 2.5 and final pH 4.1 with vigorous stirring. After aging for 24 h, the fixing agent (oligomeric Al_{13}^{7+}) was added dropwise into a 5% aqueous suspension of the clay. The oligomeric complex was prepared at room temperature [7] and at 353 K [8].

In the synthesized samples, the Al^{3+}/clay ratio was 2.5, 5.0, and 7.5 mmol g^{-1} clay. The resulting product, aluminum–fixed montmorillonite (Al–FM), was separated by centrifugation, washed to negative reaction for Cl^- ions, dried in a thin layer at 293 and 423 K, and calcined at 823 K.

Zirconium–fixed montmorrilonite (Zr–FM) was prepared by slow addition of a $ZrOCl_2$ solution of a given concentration to a 5% clay suspension. The activity of the resulting samples was studied in a micropulse installation in cracking of a model hydrocarbon, isopropylbenzene (IPB), in the temperature range 623–773 K (T_{cr}). The catalysts were preliminarily calcined at 823 and 1023 K (T_{tr}). An X-ray diffraction analysis was performed with a DRON-4.7 diffractometer (Co_{K_α} radiation). An electron-microscopic examination was performed with an EM-125K electron microscope using microdiffraction. The specific surface area, total pore volume, and pore size distribution were determined with an ACCUSORB device from the isotherms of low-temperature nitrogen adsorption.

The structural (first basal reflection in the diffraction patterns, d_{001}, and interlayer spacing Δd) and adsorption (pore volume V and specific surface area S_{sp}, determined from by BET low-temperature N_2 adsorption) characteristics of the samples are listed in Table 1, and the pore size distribution is shown in Fig. 1.

1070-4272/05/7802-0273 © 2005 Pleiades Publishing, Inc.

Table 1. Texture characteristics of the initial montmorillonite and pillared samples on its basis, calcined at 823 K

Sample	d_{001}, nm	Δd, nm	S_{sp}, $m^2\ g^{-1}$	V_{max}, $cm^3\ g^{-1}$	R_{eff}, nm
Na form	1.26	–	69	0.275	<5.0
Al–FM	1.76	0.5	232	0.335	5.0–8.0
Zr–FM	Not detected	–	176	0.325	5.0–8.0

Comparative analysis of data in Table 1 and Fig. 1 for the Na form of montmorrilonite, Al–FM, and Zr–FM shows that the material obtained differs from the initial form. Dealumination of the aluminosilicate layers of pillared clays results in that the mesopore range becomes wider (Fig. 1) and the specific surface area (Table 1) increases from 69 $m^2\ g^{-1}$ for the Na form to 232 for Al–FM and 176 $m^2\ g^{-1}$ for Zr–FM.

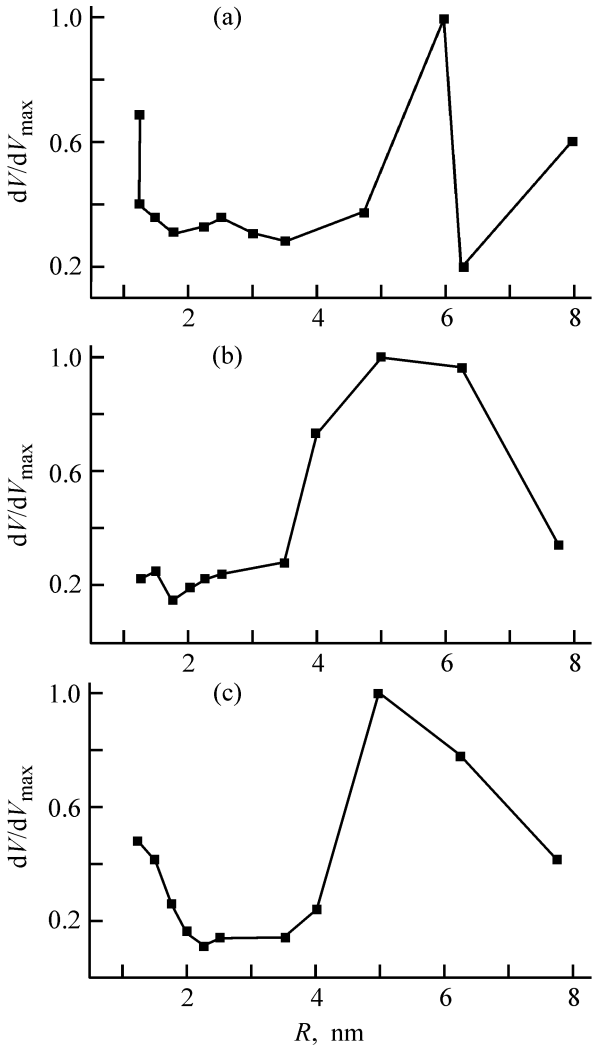


Fig. 1. Distribution of pores (dV/dV_{max}) with respect to effective radius R for samples heat-treated at 823 K. Sample: (a) Na-M, (b) Zr–FM (2.5), and (c) Al–FM (2.5).

The distance between the aluminosilicate layers in Al–FM reaches 0.5 nm.

The electron micrographs of a suspension sample of the initial clay, obtained in the transmission mode, exhibit basal reflections at the bends of montmorillonite lamellas with a set of interplanar spacings (19.10, 17.30, 10.53, 9.21, 8.64, 8.42 Å) corresponding to smectites. Examination of the profile of the aluminum-fixed clay reveals a fine-grained phase of aluminum oxide (particle size 500–1000 Å) on smooth montmorillonite lamellas.

X-ray phase analysis of Zr–FM reveals formation of an amorphous phase. This may be due to dealumination of the crystal lattice of montmorillonite [5].

According to the shape of the desorption branch of the isotherm of low-temperature nitrogen adsorption (76 K), the samples based on fixed montmorillonite belong to type B of IUPAC classification [9], i.e., to materials with slitlike pores [10, 11].

It is of interest to compare the activities of pillared clay samples in IPB cracking. The activities (evaluated as degrees of IPB conversion), apparent rate constants, and activation energies for Na-M and fixed pillared Al- and Zr-montmorillonite samples with various concentrations of fixing agents (mmol g^{-1} clay) in the range of cracking temperatures 623–773 K are given in Table 2 and Fig. 2.

As can be seen from these data, the conversion of IPB on Na-M is low at all the cracking temperatures, and it considerably decreases (by almost a factor of 4) as the pretreatment temperature is raised to 1023 K. Intercalation enhances the activity and heat resistance of the catalysts. With Al–FM (2.5) heat-treated at 823 and 1023 K, the conversion of IPB at T_{cr} = 723 K is 26.0 and 21.4%, respectively. It should be noted that the activity of the Al–FM sample prepared at 353 K is approximately a factor of 3 lower than that of the samples prepared at room temperature; this is apparently due to the formation at elevated temperatures of the cationic species $Al(H_2O)_6^{3+}$ differing from the hydroxylated product Al_{13}^{7+} [12]. The Al_{13}^{7+} species present in the catalyst apparently enhances its heat re-

Table 2. Effect of the nature of a fixing cation on the activity α, apparent rate constant of cracking K_{app}, and activation energy of cracking E for intercalated samples of Tagan montmorillonite in the Na^+ and H^+ forms

Catalyst	T_{cr}, K	T_{tr} = 823 K			T_{tr} = 1023 K		
		α, %	$K_{app} \times 10^5$, mol $g^{-1} s^{-1} atm^{-1}$	E, kJ mol^{-1}	α, %	$K_{app} \times 10^5$, mol $g^{-1} s^{-1} atm^{-1}$	E, kJ mol^{-1}
Na-M	623	1.2	0.13	33.9	0.0	–	58.2
	673	3.0	0.36		0.7	0.08	
	723	4.1	0.48		1.1	0.13	
	773	5.4	0.64		2.2	0.26	
Al–FM (2.5)	623	4.0	0.60	42.6	3.4	1.20	43.5
	673	14.5	1.90		11.5	1.40	
	723	26.0	3.50		21.4	2.80	
	773	36.5	5.30		32.3	4.50	
Al*–FM (2.5)*	623	3.5	0.41	42.3	1.8	0.21	41.0
	673	7.1	0.85		5.6	0.67	
	723	12.4	1.53		7.5	0.90	
	773	19.0	2.44		12.3	1.50	
Al–FM (5.0)	623	8.2	1.10	32.2	6.1	0.73	35.2
	673	13.1	1.60		10.4	1.30	
	723	20.0	2.60		18.5	2.40	
	773	27.0	3.60		24.3	3.22	
Al–FM (7.5)	623	8.0	0.96	23.3	6.5	2.10	26.4
	673	13.0	1.61		9.5	1.95	
	723	16.0	2.00		15.5	1.15	
	773	18.0	2.30		17.0	0.78	
Zr–FM (2.5)	623	2.0	0.23	51.9	2.0	0.23	45.6
	673	8.5	1.03		7.5	0.64	
	723	17.0	2.16		13.5	1.24	
	773	23.1	3.00		17.5	1.80	
Zr–FM (5.0)	623	16.5	2.37	33.5	15.0	2.02	37.7
	673	26.6	3.58		24.3	3.22	
	723	36.3	5.20		35.0	5.00	
	773	48.7	7.66		47.5	7.46	
Zr–FM (7.5)	623	8.0	0.96	34.0	4.5	0.53	21.4
	673	15.2	1.93		6.3	0.75	
	723	23.0	3.02		8.1	0.97	
	773	30.2	4.16		10.0	1.2	
Montmorillonite**	623	16.5	2.10	42.0	7.5	0.9	45.5
	673	33.4	4.70		22.6	2.96	
	723	49.3	7.86		36.6	5.27	
	773	65.3	12.20		52.0	8.49	
Al–FM** (2.5)	623	39.1	5.74	35.8	34.0	4.81	37.8
	673	52.4	8.59		50.2	8.07	
	723	66.0	12.49		64.4	11.95	
	773	81.1	19.28		80.0	18.63	
Zr–FM** (5.0)	623	33.2	4.67	21.4	28.4	3.87	22.0
	673	43.4	6.59		36.2	5.20	
	723	51.0	8.26		45.0	6.92	
	773	59.5	10.5		53.0	8.73	

* Intercalation at 353 K.

** Samples based on the H form of Tagan montmorillonite.

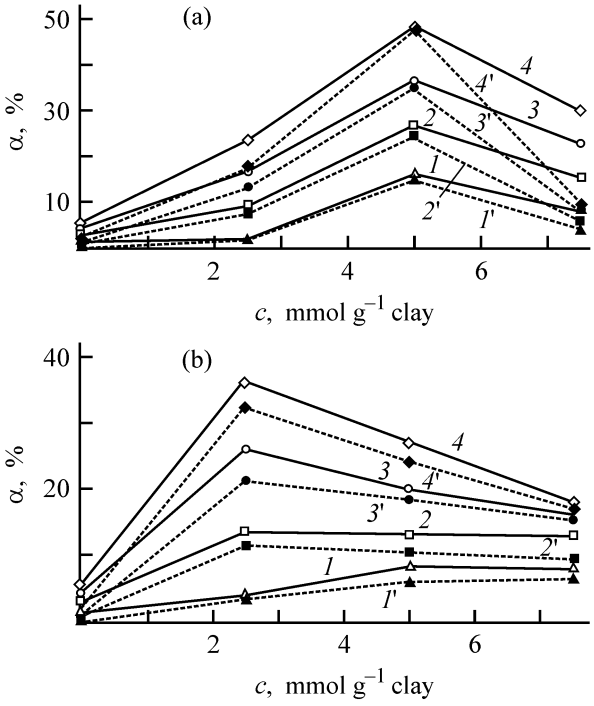


Fig. 2. Catalyst activity α vs. concentration *c* of the fixing agent. Catalyst: (a) Zr–FM and (b) Al–FM. Cracking temperature, K: (*1*) 623, (*2*) 673, (*3*) 723, and (*4*) 773. Pretreatment temperature, K: (*1*–*4*) 823 and (*1*'–*4*') 1023.

sistance. In particular, the activity of Al*–FM (2.5) heat-treated at 1023 K in cracking of IPB at 723 K amounts to 65% of the activity of the same catalyst heat-treated at 823 K, whereas with Al–FM (2.5) the related ratio is 88.5%. The activity of Al–FM (5.0) is somewhat lower than that of Al–FM (2.5) heat-treated at the same temperature (823 K), but its heat resistance is higher (the activity at T_{tr} = 1023 K is 92% of that at T_{tr} = 823 K at the same cracking temperature). As the concentration of the fixing agent is raised to 7.5 mmol g^{-1} clay, α at T_{tr} 823 and 1023 K further decreases to 16.0 and 15.5%, respectively, whereas the heat resistance of the catalyst grows.

With Zr–FM, the intercalation also exerts a positive effect, especially noticeable at the fixing agent content of 5.0 mmol g^{-1} clay. The conversion of IPB is 36.3 and 35.0% at heat treatment temperatures of 823 and 1023 K, respectively. These values of α are the best for the fixed clays examined, which are derived from the Na form of montmorillonite. At the optimal Zr content (5.0 mmol g^{-1} clay), the activity of the catalyst heat-treated at 1023 K is 92.0–98.1% of that of the catalyst heat-treated at 823 K at any cracking temperature in the range from 623 to 773 K. With an increase in the Zr concentration to 7.5 mmol g^{-1} clay, the activity and heat resistance decrease (Fig. 2, Table 2).

Figure 2 shows that the optimal concentration of Al in Al–FM is 2.5, and that of Zr in Zr–FM, 5.0 mmol g^{-1} clay. It is of interest that raising the pretreatment temperature to 1023 K does not appreciably alter the activity of Zr- and Al-fixed clays of the optimal composition, which is one of the most important requirements to hydrocarbon cracking catalysts.

To examine the effect of Al and Zr fixing agents on the activity of the montmorillonite clay in the H form, we prepared samples with the optimal concentrations of the Al^{3+} and Zr^{4+} ions (2.5 and 5.0 mmol g^{-1} clay, respectively). The dependences of the IPB conversion on the cracking temperature for the H form of the clay and samples fixed with Al and Zr and heat-treated at 823 and 1023 K are illustrated in Table 2. As the temperature of the pretreatment of the H form is raised to 1023 K, the activity in IPB cracking at temperatures within 623–773 K decreases by 9–12.7%. With Zr–FM, α decreases by 5.2–7.2, and with Al–FM, by 1.6–5.2%. Thus, the heat resistance of the intercalated samples prepared from the H form of the clay remains fairly high at all the cracking temperatures, being, however, somewhat lower than that of the samples prepared from the Na form (Table 2). The samples differ not only in the apparent rate constants but also in the activation energies. The activation energies are the highest with the Na and H forms of montmorillonite (58.2 and 45.5 kJ mol^{-1}, respectively) and decrease in going to the intercalated samples.

Comparison of the activities of samples of similar composition, prepared from the Na and H forms of montmorillonite, shows that the more active catalyst is obtained by pillaring the H form of natural montmorillonite. This catalyst approaches in the activity and heat resistance the NaHY zeolitic catalyst on clay [13] previously tested in IPB cracking.

CONCLUSIONS

(1) Substitution of the interlayer Na^+ cations with oligomeric aluminum and zirconium hydroxo cations allows control of the pore structure, activity, and acidity of the resulting catalysts.

(2) Intercalation of the H form of montmorillonite with zirconium and aluminum allows preparation of active and heat-resistant catalysts whose activity in isopropylbenzene cracking approaches that of NaHY-zeolitic catalyst on clay.

(3) Pillared Al- and Zr-montmorillonites can be used as hydrocarbon cracking catalysts.

REFERENCES

1. Rozengart, M.I., V'yunova, G.M., and Isagulyants, G.V., *Usp. Khim.*, 1988, vol. 57, no. 2, pp. 204–227.
2. Figueras, F., *Catal. Rev. – Sci. Eng.*, 1988, vol. 30, no. 3, pp. 457–490.
3. Gil, A. and Gandia, L.M., *Catal. Rev. – Sci. Eng.*, 2000, vol. 42, nos. 1–2, pp. 145–212.
4. Tarasevich, Yu.I. and Ovcharenko, F.D., *Adsorbtsiya na glinistykh mineralakh* (Adsorption on Clay Minerals), Kiev: Naukova Dumka, 1975.
5. Lahov, N. and Shani, U., *Clays Clay Miner.*, 1978, vol. 26, no. 2, pp. 107–113.
6. Figueras, F., Vattrod-Bashi, A., Fetter, G., and Thriezz, A., *J. Catal.*, 1989, vol. 119, pp. 91–96.
7. Schutz, A., Stone, W.E., Poncelet, Y., and Fripiat, J.J., *Clays Clay Miner.*, 1987, vol. 35, no. 4, pp. 251–261.
8. Del-Rey-Perez-Caballero, F. and Poncelet, G., *Microporous Mesoporous Mater.*, 2000, vol. 41, pp. 169–181.
9. Gregg, S.J., and Sing, K.S.W., *Adsorption, Surface Area, and Porosity*, New York: Academic, 1967.
10. Burch, R. and Warburton, C.J., *J. Catal.*, 1986, vol. 97, no. 2, pp. 503–510.
11. Tarasevich, Yu.I., Rak, V.S., Bondarenko, S.V., *et al.*, *Zh. Fiz. Khim.*, 1992, vol. 66, no. 12, pp. 3310–3315.
12. Akitt, J.W., Greenwood, N.N., Khandelwal, B.L., and Lester, Y.D., *J. Chem. Soc., Dalton Trans.*, 1972, no. 8, pp. 604–610.
13. Zakarina, N.A., Volkova, L.D., and Chshukina, O.V., *Euras. Chem.-Technol. J.*, 2000, no. 4, pp. 131–135.

Russian Journal of Applied Chemistry, Vol. 78, No. 2, 2005, pp. 278–280. Translated from Zhurnal Prikladnoi Khimii, Vol. 78, No. 2, 2005, pp. 284–286.
Original Russian Text Copyright © 2005 by Yutilov, Smolyar, Minkina.

ORGANIC SYNTHESIS AND INDUSTRIAL ORGANIC CHEMISTRY

Synthesis of 3-(3"-Aminobenzoylamido)-1-(2',4',6'-trichlorophenyl)pyrazol-5-one, an Intermediate in the Synthesis of the Purple Component of Color Photographic Materials

Yu. M. Yutilov, N. N. Smolyar, and L. V. Minkina

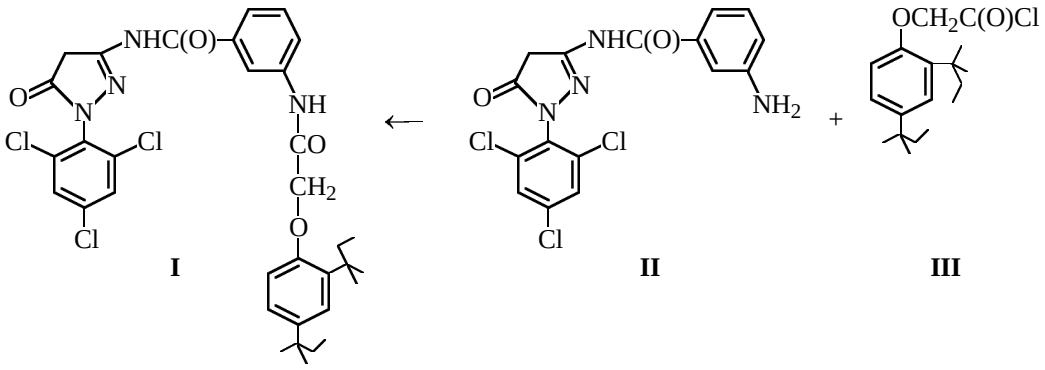
Litvinenko Institute of Physical Organic and Coal Chemistry, National Academy of Sciences of Ukraine, Donetsk, Ukraine

Received August 4, 2004

Abstract—Catalytic reduction of 3-(3"-nitrobenzoylamido)-1-(2',4',6'-trichlorophenyl)pyrazol-5-one with hydrogen and hydrazine hydrate to 3-(3"-aminobenzoylamido)-1-(2',4',6'-trichlorophenyl)pyrazol-5-one, the key intermediate in the synthesis of the purple component of color photographic and motion-picture materials, was studied.

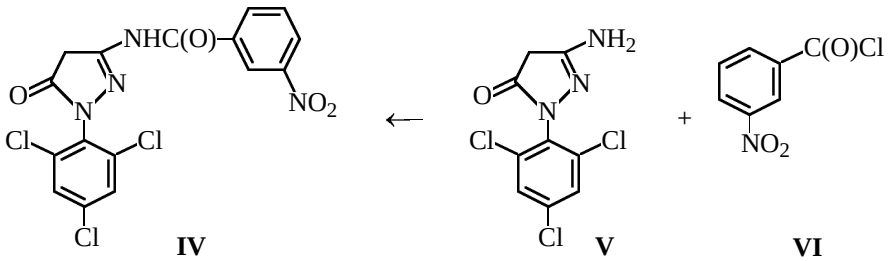
It is known that the protectable purple component, 3-[3-(2",4"-di-*tert*-pentyl)phenoxyacetamido]benzoylamido-1-(2',4',6'-trichlorophenyl)pyrazol-5-one **I**, shows high photographic properties [1, 2]. One of procedures for its synthesis is labor-consuming and involves use of difficultly available chemicals [3].

The most facile route to **I** is based on the reaction of 3-(3"-aminobenzoylamido)-1-(2',4',6'-trichlorophenyl)pyrazol-5-one **II** with 2,4-di(*tert*-pentyl)phenoxyacetyl chlolride **III**, with a 75% yield of the target product [4]:



I **II** **III**

Intermediate **II** is formed by reduction of 3-(3"-nitrobenzoylamido)-1-(2',4',6'-trichlorophenyl)pyrazol-5-one **IV**, which is, in turn, prepared by acylation of 3-amino-1-(2',4',6'trichlorophenyl)pyrazol-5-one **V** with *m*-nitrobenzoyl chloride **VI** in 80% yield [4]:



IV **V** **VI**

1070-4272/05/7802-0278 © 2005 Pleiades Publishing, Inc.

Yield and melting point of amino compound **II** prepared by catalytic reduction of **IV** under various conditions

Yield, %	mp,* °C	Reductant	Catalyst	T, °C	c_{NaOH}, wt %
94.5	297–299	H_2	Raney Ni	20	0.5
95.7	298–300	H_2	Raney Ni	20	2
95.1	298–300	H_2	5% Pd/C	20	2
94.9	297–300	H_2	5% $Pd/BaSO_4$	20	2
96.4	298–300	H_2	5% Pt/C	20	1
94.8	297–299	H_2	5% $Pt/BaSO_4$	20	1
96.8	297–299	H_2	5% Pt/C	20	3
95.0	296–298	$N_2H_4 \cdot H_2O$	Raney Ni	30	2
95.7	298–300	$N_2H_4 \cdot H_2O$	Raney Ni	40	2
92.5	285–287	$N_2H_4 \cdot H_2O$	Raney Ni	40	6
93.0	269–273	$N_2H_4 \cdot H_2O$	Raney Ni	50	0.5
96.2	296–298	$N_2H_4 \cdot H_2O$	5% Pd/C	40	2
97.03	296–298	$N_2H_4 \cdot H_2O$	5% $Pd/BaSO_4$	40	4
97.1	295–298	$N_2H_4 \cdot H_2O$	5% $Pt/BaSO_4$	40	6

* According to [6], the melting point of **II** is 297–300°C.

To diminish the corrosive effect of HCl released in the acylation of **II**, it is bound by adding triethylamine [5]; this also favors preparation of pure **I**.

Among the known procedures for reduction of **IV** to **II**, of particular interest is the hydrogenation on Raney nickel [6]. Some alternative reduction procedures are also feasible [6], e.g., those with iron in hydrochloric or acetic acid, with sodium or ammonium sulfide and with hydrogen in acetic acid in the presence of Pd/C. The last procedure allows preparation of amine **II** in a high yield without degradation processes such as, e.g., hydrolytic cleavage of the amide group occurring in other procedures. Other possible side processes are acetylation of the NH_2 group with acetic acid (when reduction of **IV** is performed in this medium) and formation of sulfur (in reduction of **IV** with sodium sulfide) negatively affecting the photographic properties of **II**. Being environmentally clean, reduction with hydrogen on Raney nickel has a drawback: The conditions of reduction of **IV** in alkaline alcoholic solution (1–20 wt % Raney nickel, 20–110°C, 1–20 atm of H_2) give rise to an explosion hazard.

To eliminate these drawbacks, we attempted to improve the procedure for reduction of **IV** with hydrogen. For this purpose, we performed the reduction under the normal conditions (H_2 pressure 1 atm, room temperature) in aqueous-alcoholic NaOH solutions. As catalysts, along with Raney nickel, we also tested 5% Pd/C, 5% Pt/C, 5% $Pd/BaSO_4$, and 5% $Pt/BaSO_4$.

In reduction of **IV** with hydrogen under normal conditions in homogeneous 0.5% and 2% aqueous NaOH solutions, the yield of **II** was 94.5 and 95.7%, respectively. In reduction of **IV** with hydrogen in 2% aqueous NaOH in the presence of 5% Pd/C and 5% $Pd/BaSO_4$, the yield of **II** was 95.1 and 94.9%.

The reduction of **IV** with hydrogen in 1% aqueous NaOH in the presence of 5% Pt/C and 5% $Pt/BaSO_4$ under the similar conditions affords **II** in 96.4 and 94.8% yield, respectively. At a higher (3%) NaOH concentration, the yield of **II** in reduction of **IV** in the presence of 5% Pt/C increased to 96.8%. The conditions of reduction of **IV** and the yield and melting point of **II** are listed in the table.

In view of the problems associated with the use of hydrogen, we attempted to replace it with hydrazine hydrate. In our experiments, we used the same catalysts as in the reduction with H_2. Along with the catalyst, we varied the reaction temperature and NaOH concentration.

Reduction of nitro compound **IV** with hydrazine hydrate in 2% aqueous NaOH at 30 and 40°C in the presence of Raney Ni affords **II** in 95 and 95.7% yield. When the reduction of **IV** with hydrazine hydrate is performed at 40°C in the presence of the same catalyst but in 6% aqueous NaOH, the yield of **II** decreases.

The yield of **II** increases, respectively, to 96.2 and 96.3% when compound **IV** is reduced with hydrazine hydrate at 40°C in the presence of Pd/C (in 2% aqueous NaOH) or $Pd/BaSO_4$ (in 4% aqueous NaOH).

Raney nickel appeared to be the most effective in aqueous NaOH at a 25-fold excess of hydrazine hydrate. In this case, the yield of **II** is the highest, and its melting point and chromatographic characteristics are identical to those of an authentic sample [7].

At a smaller (15-fold) excess of hydrazine hydrate, or with an alkaline alcoholic solution used, the reduction of **IV** to **II** is incomplete.

EXPERIMENTAL

The purity of **II** was checked by high-velocity microcolumn liquid chromatography on a Milikhrom device equipped with a UV detector. A 64 × 2-mm stainless steel column (≥3000 TP) was packed with Separon (particle diameter 4 μm). The best system for elution of **II** was acetone–water–hexane, 86 : 12 : 2 (by volume). The chromatographing conditions were as follows: sensitivity range 1.6, measurement time 0.15 s, wavelength λ in the STOP mode 280 nm, eluent feed rate 200 μl min^{-1}, and paper feed rate 1800 mm h^{-1}. The retention time of **II** under these conditions was 48 s.

Reduction of IV with hydrogen in 0.5–3.0% aqueous NaOH solutions at 20°C. A 10.0-g (23.4-mmol) portion of **IV** was dissolved in 200 ml of water containing 1–6 g (25–150 mmol) of NaOH and subjected to catalytic hydrogenation in the presence of a catalyst (Raney nickel, 5% Pd/C, 5% Pt/C, 5% $Pd/BaSO_4$, or 5% $Pt/BaSO_4$). To do this, the reaction vessel was first purged with nitrogen to remove air, and then nitrogen was replaced with hydrogen. The reduction was performed at 25°C and an H_2 pressure of 1 atm with continuous stirring until the hydrogen uptake ceased (200 ml). The catalyst was filtered off, and the filtrate was acidified with a solution of hydrochloric or acetic acid to pH 6. The precipitate was filtered off, washed with a small amount of water, and dried.

Reduction of IV with hydrazine hydrate in 0.5–6.0% aqueous NaOH solutions at 30–50°C. A 10.0-g (23.4-mmol) portion of **IV** was mixed with a solution of 0.5–6 g of NaOH in 100 ml of water, and 2.0 g of a catalyst (Raney nickel, 5% Pd/C. 5% Pt/C, 5% $Pd/BaSO_4$, or 5% $Pt/BaSO_4$) was added. Then 40 ml (0.8 mol) of 98–100% hydrazine hydrate was added in portions with vigorous stirring and heating to 30–50°C. After heating for 3–4 h under these conditions, the catalyst was filtered off, and the filtrate was acidified with 2% H_2SO_4 to pH 6. The precipitate was filtered off, washed with a small amount of water, and dried.

CONCLUSIONS

(1) Preparative procedures were suggested for the reduction of 3-(3''-nitrobenzoylamido)-1-(2', 4', 6'-trichlorophenyl)pyrazol-5-one with hydrogen or hydrazine hydrate in aqueous NaOH in the presence of Raney nickel, 5% Pd/C, 5% Pt/C, 5% $Pd/BaSO_4$, or 5% $Pt/BaSO_4$ to obtain 3-(3''-aminobenzoylamido)-1-(2', 4', 6'-trichlorophenyl)pyrazol-5-one.

(2) A procedure was developed for prompt analysis of the quality of the amine with a Milikhrom liquid chromatograph.

REFERENCES

1. Theys, R.D. and Sosnovsky, Y., *Chem. Rev.*, 1997, vol. 97, no. 1, pp. 83–132.
2. Arient, J. and Dostal, J., *Chem. Listy*, 1988, vol. 82, no. 12, pp. 1254–1281.
3. US Patent 3 812 145.
4. US Patent 2 600 788.
5. US Patent 3 823 156.
6. JPN Appl. 58-140 075.
7. USSR Inventor's Certificate, no. 1 441 734.

Russian Journal of Applied Chemistry, Vol. 78, No. 2, 2005, pp. 281–285. Translated from Zhurnal Prikladnoi Khimii, Vol. 78, No. 2, 2005, pp. 287–291.
Original Russian Text Copyright © 2005 by Titova, Nikol'skaya, Buyanov, Pudova, Karzhavina.

ORGANIC SYNTHESIS AND INDUSTRIAL ORGANIC CHEMISTRY

Decomposition in Prolonged Storage of $KF \cdot H_2O_2$ Stabilized with Carboxylic Acids

K. V. Titova, V. P. Nikol'skaya, V. V. Buyanov, O. B. Pudova, and G. P. Karzhavina

Institute of Problems of Chemical Physics, Russian Academy of Sciences, Chernogolovka, Moscow oblast, Russia

State Research Institute of Biological Instrument-Making, Federal State Unitary Enterprise, Moscow, Russia

Received November 15, 2004

Abstract—Decomposition of $KF \cdot H_2O_2$ stabilized with carboxylic acids (maleic, fumaric, succinic, adipic) in storage for more than three years at 20°C was studied. Rate constants of decomposition of stabilized $KF \cdot H_2O_2$ were determined in different time intervals. The chemical reactions in the system $KF–H_2O_2$–carboxylic acid in the stage of preparation of solid $KF \cdot H_2O_2$ stabilized with carboxylic acid and those during prolonged storage of the final product are discussed.

Hydrogen peroxide, is irrespective of its state (pure anhydrous substance, aqueous solutions, salt solvates with hydrogen peroxide), a chemically unstable compound prone to catalytic decomposition. The stability of hydrogen peroxide is raised by adding various stabilizers. As a rule, chemical interactions responsible for the stabilization of hydrogen peroxide are poorly understood [1, 2]. Various approaches to hydrogen peroxide stabilization have been developed. For example, a widely used commercial bleach based on sodium caronate solvate with hydrogen peroxide $Na_2CO_3 \cdot 1.5H_2O_2$ is stabilized by binding catalytic impurities into poorly soluble or inert species (salts, complexes) and by protecting this compound from moisture. It has also been repeatedly shown that hydrogen peroxide can be efficiently stabilized with additives incapable of binding catalytic impurities and protecting the compound from moisture [2].

It has been reported [3] that potassium fluoride solvates with H_2O_2 ($KF \cdot nH_2O_2$) can be stabilized using, along with other compounds, with acidic compounds, such as potassium hydrogen bifluoride and oxalic, citric, and boric acids. It was found that KHF_2 is the most efficient among these stabilizers. However, even minor additions of this compound to $KF \cdot nH_2O_2$ make it corrosion-active.

Modern disinfectants with a broad spectrum of antimicrobial effect are based on potassium fluoride solvate with H_2O_2 ($KF \cdot H_2O_2$) [4]. The stabilization of this compound to ensure its long-term storage at ambient temperature is a topical problem.

In this study, we examined $KF \cdot H_2O_2$ stabilization with carboxylic acids, which are less corrosive than KHF_2. The kinetics of decomposition of $KF \cdot H_2O_2$ stabilized with carboxylic acids in its storage for more than three years was studied at 20°C. We also attempted to elucidate the mechanisms of interaction of $KF \cdot H_2O_2$ with carboxylic acids in liquid systems $KF–H_2O_2$–carboxylic acid and in the solid stabilized solvate.

EXPERIMENTAL

All the compounds studied were prepared under conditions typical of their semicommercial production [4]. Maleic, fumaric, succinic, and adipic acids (pure grade) were added to $KF \cdot 2H_2O$ (analytically pure grade) in aqueous peroxide (30%) in an amount of 0.5–1.0 wt % relative to the mass of the final solid product at an H_2O_2 : KF molar ratio of 1 : 2. To isolate solid $KF \cdot H_2O_2$, the reaction mixture was placed in a metallic device equipped with a film rotary evaporator, and water and excess H_2O_2 were removed at 40–50°C.

The final product was stored in closed polymeric beakers at 20 ± 2°C. The content of hydrogen peroxide in the final product was determined permanganatometrically (at intervals of 10–15 days in the early

1070-4272/05/7802-0281 © 2005 Pleiades Publishing, Inc.

Table 1. Rate constants of decomposition of $KF \cdot H_2O_2$ stabilized with carboxylic acids in prolonged storage at 20 ± 2°C

Storage interval Δτ, days	H_2O_2 content (wt %) by the end of storage interval τ	$k \times 10^4$ (day^{-1}) averaged Δτ	Storage interval Δτ, days	H_2O_2 content (wt %) by the end of storage interval τ	$k \times 10^4$ (day^{-1}) averaged Δτ
Maleic acid, 0.5 wt %			Succinic acid, 0.5 wt %		
0	34.66	0	0	34.61	0
0–34	33.72	8.1 ± 1.1	0–43	34.67	0
34–129	32.79	2.6 ± 0.5	43–333	34.00	0.7 ± 0.1
129–1257	32.52	0.9 ± 0.3	333–1257	34.51	0
Maleic acid, 2.0 wt %			Succinic acid, 1.0 wt %		
0	33.99	0	0	34.21	0
0–62	31.85	5.6 ± 2.5	0–55	34.53	0
62–550	29.90	2.1 ± 0.8	55–502	32.71	1.2 ± 0.2
550–1257	31.03	0.4 ± 0.1	502–1257	32.47	0.1
Fumaric acid, 0.5 wt %			Adipic acid, 0.5 wt %		
0	35.44	0	0	35.35	0
0–35	34.33	9.1 ± 1.2	0–36	34.85	3.7 ± 1.6
35–315	34.21	0.1 ± 0.05	36–203	33.77	1.6 ± 0.3
315–1203	33.88	0.1 ± 0.04	203–1207	33.61	0.6 ± 0.2
Fumaric acid, 1.0 wt %			Adipic acid, 1.0 wt %		
0	34.65	0	0	35.75	0
0–38	33.54	8.6 ± 1.0	0–55	34.98	2.0 ± 0.4
38–370	33.05	0.4 ± 0.1	55–565	33.70	0.7 ± 0.2
370–627	32.92	0.1 ± 0.05	565–1207	33.60	0.4 ± 0.2
627–1198	32.90	0			

stage, and 2–3 months in the periods of later storage). The rate constants k of $KF \cdot H_2O_2$ decomposition were calculated by the equation

$$\ln c_0/c = k(\tau - \tau_0).$$

The IR spectra of the compounds prepared (mulls in Vaseline oil between KBr plates) were recorded in the range 400–4000 cm^{-1} on a UR-20 IR spectrometer.

We found that IR spectra of all the compounds do not change after prolonged storage. These spectra contain the following absorption bands of coordinated hydrogen peroxide (cm^{-1}): ν_3, O–O stretching (855 s, 885 s); ν_4, torsion (960 s); ν_6, OOH bending (1485 m); ν_2, OOH bending (1670 m); ν_5, OH stretching (2600–2800 s. br); and ν_1, OH stretching (3200 s. br) [3].

Analysis of the rate of $KF \cdot H_2O_2$ decomposition over the entire storage period shows that the total decomposition curve consists of separate portions with individual rate constants. The time intervals and average rate constants corresponding to different portions of the total decomposition curve are listed in Table 1.

These data show that, in the early storage period (τ from 0 to 30–60 days), the rate of decomposition of $KF \cdot H_2O_2$ stabilized with maleic, fumaric, and, to a lesser extent, adipic acid is relatively high ($k \times 10^4$ = 2.0–9.1 day^{-1}). The rate constant passes through a maximum in the storage time intervals from 30–60 to 200–500 days and then decreases to $k \times 10^4$ = 0.1–2.6. In the later storage stages (from 200–500 to 900–1257 days), the rate constant decreases to $k \times 10^4$ = 0–0.9.

$KF \cdot H_2O_2$ stabilized with succinic acid shows a different decomposition pattern. This compound does not lose oxygen in the early storage period (from 0 to 43–55 days) and then starts to slowly decompose. The maximal decomposition rate ($k \times 10^4$ = 0.7–1.2 day^{-1}) is reached after a long time (from 45–55 to 333–502 days) and then, during a long

time (1257 days), this compound decomposes either at low rate ($k \times 10^4 = 0.1$ day^{-1}) or is stored without decomposition.

Figure 1 shows the plot for k of $KF \cdot H_2O_2$ stabilized with maleic acid vs. storage time, which is typical of all the stabilizers under consideration except for succinic acid. This figure also shows the time dependence of k for $KF \cdot H_2O_2$ stabilized with succinic acid. These plots were built using the times and rate constants averaged over different portions of the total kinetic curve of $KF \cdot H_2O_2$ decomposition. Table 1 and Fig. 1 show that succinic acid is a more efficient stabilizer of $KF \cdot H_2O_2$ than the other carboxylic acids tested and that the time dependence of k for $KF \cdot H_2O_2$ stabilized with succinic acid considerably differs from that for $KF \cdot H_2O_2$ stabilized with the other carboxylic acids.

It is not improbable that the more efficient stabilization of $KF \cdot H_2O_2$ with succinic acid and the kinetic features of decomposition of $KF \cdot H_2O_2$ stabilized with this acid are caused by reactions of succinic acid with hydrogen peroxide, in particular, with excess hydrogen peroxide present in the initial reaction mixture. These reactions can produce of peroxy derivatives succinic acid, which may be more efficient stabilizers than succinic acid itself.

It was reported in [5] that, depending on conditions, succinic acid can react with hydrogen peroxide to form persuccinic, hydroxysuccinic, malonic, and maleic acids, and also succinic anhydride. No data have been reported on reactions of hydrogen peroxide with the other carboxylic acids that we tested.

We found that the IR spectra of individual carboxylic acids used in our experiments as stabilizers do not change after their treatment with hydrogen peroxide under the same conditions as in preparing KF solvate with hydrogen peroxide. For example, the IR spectra of adipic and succinic acids before and after treatment with aqueous hydrogen peroxide contain the following absorption bands (cm^{-1}). The initial adipic acid: 520 s, 690 s, 740 s, 960 s.br, 1200 s, 1280 s, 1380 s, 1425 s, 1460 vs, 1700 vs, 2800–3000 vs; adipic acid after treatment with aqueous hydrogen peroxide: 520 s, 690 s, 740 s, 930 s.br, 1200 s, 1280 s, 1380 s, 1420 s, 1460 vs, 1700 s, 2800–3000 s.br. The initial succinic acid: 550 s, 585 s, 640 s, 740 w, 810 narrow, 930 s.br, 1205 s, 1300 s, 1380 s, 1440 s, 1470 s, 1700 s.br, 2800–3000 s.br; succinic acid after treatment with aqueous hydrogen peroxide: 545 s, 585 s, 640 s, 745 m, 810 s.

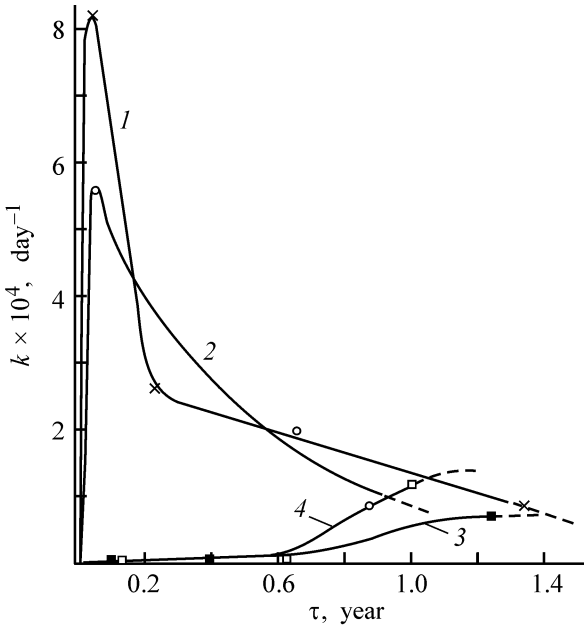


Fig. 1. Rate constants k of decomposition of $KF \cdot H_2O_2$ stabilized with carboxylic acids vs. storage time τ. (τ) average storage time in interval Δτ. Carboxylic acids: (*1*, *2*) maleic and (*3*, *4*) succinic. Acid concentration, wt%: (*1*, *3*) 0.5; (*2*) 2.0, and (*4*) 1.0

narrow, 930 s.br, 1205 s, 1310 s, 1385 s. narrow, 1460–1480 s.br, 1700 s.br, 2800–3000 s.br.

The IR spectra of maleic and fumaric acids also showed no significant changes after treatment with aqueous hydrogen peroxide.

Therefore, we believe that, in the systems under consideration, the exchange reaction between KF and carboxylic acid, yielding potassium carboxylate, is more probable:

$$2KF + (HOOC)_2R = (KOOC)_2R + 2HF. \quad (1)$$

This reaction is accompanied by several additional processes: formation of hydrogen bifluoride anions through association of hydrogen fluoride with fluoride anion

$$KF + HF = KHF_2, \quad (2)$$

solvation of potassium hydrogen bifluoride with hydrogen peroxide [6]

$$KHF_2 + H_2O_2 = KHF_2 \cdot H_2O_2, \quad (3)$$

breakdown of unstable potassium hydrogen bifluoride solvate with hydrogen peroxide

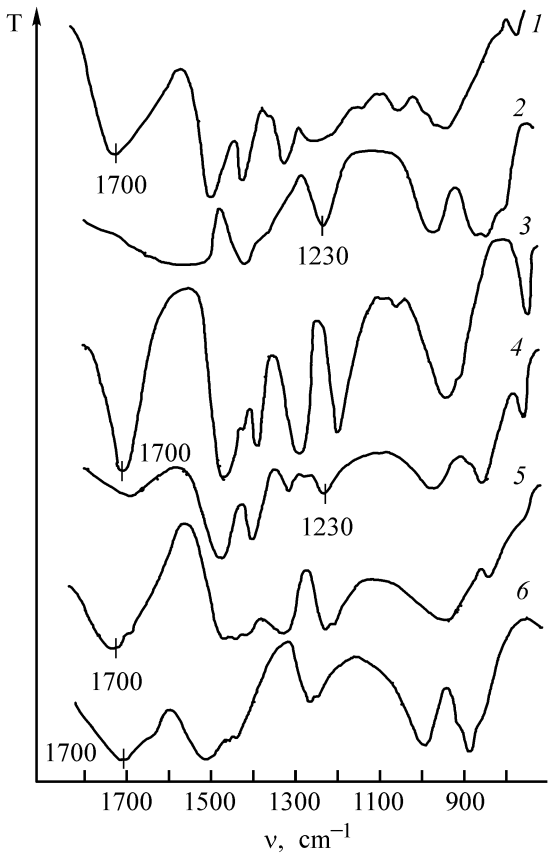


Fig. 2. IR spectra of carboxylic acids before and after their reaction with $KF \cdot H_2O_2$. (T) Transmission and (ν) wave number. Acids: (*1*, *2*) adipic, (*3*, *4*) fumaric, and (*5*, *6*) succinic.

$$KHF_2 \cdot H_2O_2 = KHF_2 + H_2O + 0.5O_2. \quad (4)$$

The formation of potassium carboxylate on treatment of $KF \cdot H_2O_2$ with carboxylic acid is manifested in the IR spectra as disappearance of the broad absorption band of protonated carboxy groups (1700 cm^{-1}) [7]. Potassium carboxylate should exhibit absorption bands of carboxylate anions (1550 and 1400 cm^{-1}). However, these bands are obscured by absorption by coordinated hydrogen peroxide and Vaseline oil.

The formation of potassium hydrogen bifluoride by reaction (2) is manifested in the IR spectrum as a sharp absorption band of bending vibrations of hydrogen bifluoride anions HF_2^- (1230 cm^{-1}) [6]. Thus, the IR spectra clearly show that, in the systems under consideration, potassium carboxylates and HF_2^- anions are formed.

We found that the above-noted spectral effects caused by addition of carboxylic acids (20 wt % of $KF \cdot H_2O_2$ amount) to $KF \cdot H_2O_2$ are clearly manifested with fumaric, and less clearly with adipic acid. At the same time, under these conditions, succinic acid is either completely inert to potassium fluoride or only slightly reacts with it. In this case, the IR spectrum contains an unchanged broad absorption band at 1700 cm^{-1}, and the absorption band at 1200 cm^{-1} only slightly broadens and shifts toward higher wave numbers. We do not rule out that admixture of HF_2^- may contribute to this spectroscopic effect (Fig. 2). Our spectroscopic data show that succinic acid, in contrast to other carboxylic acids tested, is not noticeably converted to the potassium salt by the exchange reaction with $KF \cdot H_2O_2$. We believe that this chemical inertness of succinic acid is responsible for the specific features of the time dependence of *k* for $KF \cdot H_2O_2$ stabilized with succinic acid.

We believe that the sharp increase in the rate of decomposition of $KF \cdot H_2O_2$ stabilized with maleic, fumaric, and, to a lesser extent, adipic acids in the early storage period is caused by successive reactions (1)–(3), followed by decomposition of low-stable potassium hydrogen bifluoride solvate with hydrogen peroxide by reaction (4). The content of KHF_2 solvate with hydrogen peroxide varies in proportion to the content of carboxylic acid in the reaction mixture and does not exceed 1–2 wt %. After decomposition of this unstable compound, the rate of $KF \cdot H_2O_2$ decomposition decreases first sharply and then gradually till the end of storage. We believe that, in the late storage periods, the stabilizing effect is caused not by carboxylic acid but by a mixture of potassium carboxylate with potassium hydrogen bifluoride.

Figure 1 shows that the initial sharp increase in *k* for stabilized $KF \cdot H_2O_2$, typical of carboxylic acids, is not observed for $KF \cdot H_2O_2$ stabilized with succinic acid. We believe that this feature of succinic acid is caused by the fact that, in preparing $KF \cdot H_2O_2$ stabilized with succinic acid, this acid does not react with potassium fluoride (or reacts to a small extent) and, therefore, is not involved in further reactions, including reaction (4) responsible for a sharp increase in rate constant of $KF \cdot H_2O_2$ decomposition.

However, the small positive slope in the plot of *k* for $KF \cdot H_2O_2$ stabilized with succinic acid vs. storage time (Fig. 1) shows that reactions (1)–(4) proceed slowly in prolonged storage of the final product. We found that the IR spectra of the sample prepared by thorough grinding of solid succinic acid and $KF \cdot H_2O_2$ contains a distinct absorption band of HF_2^- anions (1230 cm^{-1}) and no absorption band of

protonated carboxy groups at 1700 cm^{-1}. We believe that these spectroscopic effects are caused by the fact that succinic and, to a smaller extent, adipic acids are weaker ($k_1 = 6.89 \times 10^{-5}$ and $k_1 = 3.7 \times 10^{-5}$, respectively) than maleic and fumaric acids ($k_1 = 1.42 \times 10^{-2}$ and $k_1 = 9.30 \times 10^{-4}$, respectively) [8] and, therefore, they are less reactive (or even inert) with respect to potassium fluoride in preparing stabilized $KF \cdot H_2O_2$. However, in prolonged storage, succinic acid begins to react slightly with $KF \cdot H_2O_2$. In the early period of storage, this reaction is very slow and, after a certain period of time, it stops at all because of rupture of molecular contacts between the components of the system under consideration. Thus, succinic acid efficiently stabilizes $KF \cdot H_2O_2$, preventing its decomposition during prolonged storage.

The ratios of the rate constants of decomposition of the initial and stabilized $KF \cdot H_2O_2$ are listed in Table 2. These data show that the stabilizing power of succinic acid exceeds that of the other carboxylic acids by a factor of 2–5, and the stabilizing power of potassium hydrogen bifluoride, by a factor of 1.5. Thus, among the carboxylic acids tested, succinic acid is the most promising non-corrosive additive ensuring efficient stabilization of modern PFK disinfectants based on potassium fluoride solvate with H_2O_2.

CONCLUSIONS

(1) $KF \cdot H_2O_2$ stabilized with carboxylic acids, prepared under conditions typical of its semicommercial production shows stability in storage for more than 3 years. The H_2O_2 loss during this storage time varies from 1 to 5%.

(2) The rate constant of decomposition of $KF \cdot H_2O_2$ stabilized with carboxylic acids depends on a particular carboxylic acid and storage time.

(3) In the early period of storage of $KF \cdot H_2O_2$ stabilized with carboxylic acids, potassium carboxylate and KHF_2 are formed. In further storage, KHF_2 forms an unstable solvate responsible for H_2O_2 decomposition. Succinic acid is inert toward KF; therefore, its stabilizing efficiency exceeds that of the other carboxylic acids and also of potassium hydrogen bifluoride.

(4) Succinic acid can be used as a non-corrosive stabilizer of modern PFK disinfectants based on potassium fluoride solvate with H_2O_2.

Table 2. Relative performance of stabilizing agents* (storage time 3.4 years)

Stabilizing agent	Content, wt %	H_2O_2 loss, % from the initial amount	β, % day^{-1}	β^{unstab}/β
–	0	14.9	0.012	1
KHF_2	0.5	1.61	0.0013	9.3
Acid:				
maleic	0.5	4.84	0.0039	3.1
	2.0	4.59	0.0037	3.2
fumaric	0.5	1.86	0.0015	6.7
	1.0	4.34	0.0035	3.4
succinic	0.5	1.12	0.0009	13.3
	1.0	3.35	0.0027	4.6
adipic	0.5	4.22	0.0034	3.5
	1.0	3.35	0.0027	4.4

* β_{unstab} and β are the rate constants of the decomposition of the initial $KF \cdot H_2O_2$ and of $KF \cdot H_2O_2$ stabilized with carboxylic acids, respectively.

REFERENCES

1. Schumb, W.C., Satterfield, Ch. N., and Wentworth, R.L., *Hydrogen Peroxide*, New York: Chapman and Hall, 1955.
2. Titova, K.V., Kolmakova, E.I., and Rosolovskii, V.Ya., *Fizikokhimicheskie svoistva i sposoby stabilizatsii peroksogidrata karbonata natriya* $Na_2CO_3 \cdot 1.5H_2O_2$ (Physicochemical Properties and Stabilization Techniques of Sodium Carbonate Solvate with Hydrogen Peroxide $Na_2CO_3 \cdot 1.5H_2O_2$), Available from VINITI, 1984, Moscow, no. 1254–84.
3. Titova, K.V., Nikol'skaya, V.P., and Buyanov, V.V., *Koordinatsionnye soedineniya perekisi vodoroda* (Coordination Compounds of Hydrogen Peroxide), Chernogolovka: Inst. Probl. Khim. Fiz., Ross. Akad. Nauk, 2000.
4. Buyanov, V.V., Nikol'skaya, V.P., Pudova, O.B., *et al.*, *Peroksosol'vaty v dezinfektologii* (Peroxosolvates in Disinfectology), Chernogolovka: Inst. Probl. Khim. Fiz., Ross. Akad. Nauk, 2000.
5. *Khimicheskaya entsiklopediya* (Chemical Encyclopedia), Moscow: Bol'shaya Ross. Enciklopedia, 1998, vol. 5, p. 533.
6. Titova, K.V., Gelyuk, I.P., and Rosolovskii, V.Ya., *Zh. Neorg. Khim.*, 1988, vol. 34, no. 12, pp. 3212–3215.
7. Gordon, A.J. and Ford, R.A., *The Chemist's Companion. A Handbook of Practical Data, Techniques and References*, New York: Wiley, 1972.
8. *Spravochnik khimika* (Chemist's Handbook), Nikol'skii, B.P., Ed., Leningrad: Goskhimizdat, 1952, vol. 3, pp. 495–505.

Russian Journal of Applied Chemistry, Vol. 78, No. 2, 2005, pp. 286–290. Translated from Zhurnal Prikladnoi Khimii, Vol. 78, No. 2, 2005, pp. 292–296.
Original Russian Text Copyright © 2005 by A. Radbil', Ismagilov, B. Radbil'.

ORGANIC SYNTHESIS AND INDUSTRIAL ORGANIC CHEMISTRY

Thermally Curable Emulsion Binders for Mold Cores and Molds Based on Tall Pitch

A. B. Radbil', R. M. Ismagilov, and B. A. Radbil'

Lesma Research Innovation, Limited Liability Company, Nizhni Novgorod, Russia

Ural Wood-Chemical Plant, Joint-Stock Company, Neivo-Rudyanka urban village, Sverdlovsk oblast, Russia

Received July 28, 2004

Abstract—Preparation of thermally curable emulsion binders for mold cores and molds using tall pitch was studied. Preparation conditions, composition, and colloid-chemical properties of the resulting emulsions were investigated.

Thermally curable binders (TCBs) for preparing mold cores and molds should meet rather strict requirements. The compression and tensile strength of mold cores should be no less than 0.12–0.20 (wet state) and 12–20 kgf cm^{-2} (after drying), respectively. At the same time, the mixture should not adhere to casting patterns when preparing mold cores (and molds), especially with the so-called core-blowing procedure [1].

In [2, 3], we studied TCBs for sand and core stocks with a tall pitch (TP) binder, which is a by-product from production of cellulose by the sulfate procedure. One of these TCBs (TOP brand) is a solution of TP (50–90 wt %) in an organic solvent (10–50 wt %), namely, in a hydrocarbon, alcohol, ketone, acetic acid ester, or their mixture. However, aqueous solutions of lignosulfonates (LSs) should be added to the sand stock to provide the required strength and to improve the geometry of mold cores and molds, which somewhat complicates the process.

In [3], we studied a TCB based on equal amounts of a 60–65% TP solution in kerosene and a 50% aqueous solution of LS. However, this TCB fails the provide a stable quality of the resulting molds and cores because of the composition heterogeneity, mainly caused by the low aggregation stability of the emulsion based on the TCB component; it is unstable and separates into aqueous and organic layers during storage and use. Thus, development of stable emulsions containing TP and LS is of particular importance for both foundry and timber enterprises.

In this study, we analyzed formation of stable emulsions based on TP and various LSs and examined their colloid-chemical properties.

It is known that, depending on the composition (TP and LS ratio) and preparation conditions, we can obtain either oil-in-water (direct) or water-in-oil (reverse) emulsions. Due to the intense coloring and high viscosity of the resulting mixtures, their type was determined from the data on the electrical conductivity of the system and its components and from the wetting angles of the glass (θ_g, deg) and waxed (θ_w, deg) supports. In the case of the water-in-oil emulsions, the electrical capacitance reflecting the dielectric properties of the system was also recorded.

Oil-in-water emulsions (Table 1, nos. 1–5) were prepared using nonionic surfactants based on OP-10 polyoxyethylene alkylphenols and Reapon Pluronic with the index of the hydrophilic-lipophilic balance (HLB) equal to ~10. The electrical conductivity χ^{25} of emulsion nos. 1–5 is 1.26 ± 0.06 S m^{-1}, which is close to the conductivity of the aqueous solution (χ^{25} = 0.15 S m^{-1}) and differs from that of the tall pitch by more than three orders of magnitude ($\chi^{25} = 4.8 \times 10^{-4}$ S m^{-1}). These data show that emulsion nos. 1–5 belong to the oil-in-water type. This is also confirmed by the linear dependence of the electrical conductivity on the content of surfactant in the emulsion upon its dilution with water (dispersion medium), which is illustrated by the example for emulsion no. 4 (Fig. 1).

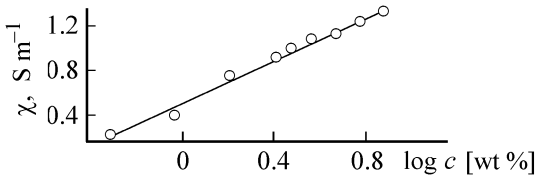


Fig. 1. Electrical conductivity χ of emulsion no. 4 vs. Reapon surfactant concentration c (at dilution of the emulsion with water).

1070-4272/05/7802-0286 © 2005 Pleiades Publishing, Inc.

Table 1. Composition and properties of the oil-in-water emulsions based on TP

Emulsion no.	Emulsion composition wt %					Emulsion properties		
	water				oil	A	θ_g, deg	η, s
	50 wt % LS in water	surfactant	hydrotrope	water	TP			
1	44.3	OP-10, 8.8	– –	17.7	29.2	Slight phase separation	66	440
2	41.7	OP-10, 8.3	Urea, 5.8	16.7	27.5	Stable	62	410
3	41.7	OP-10, 8.3	2-Propanol, 5.8	16.7	27.5	″	62	320
4	40.6	Reapon, 8.1	Glycerol, 8.1	16.4	26.8	″	50	300
5	43.5	Reapon, 8.7	Urea, 6.1	13.0	28.7	″	50	330

Table 2. Composition and properties of the water-in-oil emulsions based on TP

Emulsion no.	Emulsion composition, wt %						Emulsion properties		
	oil				water		A	θ_g, deg	η, s
	TP	kerosene	surfactant	cosolvent	50 wt % LS in water	water			
6	24.7	16.3	OP-4, 8.2	– –	42.7	8.1	Strong phase separation	24	
7	22.5	14.9	OP-4, 7.4	1-Heptanol, 9.0	38.8	7.4	Slight phase separation	20	
8	24.7	16.3	Ethox CO-5, 8.2	– –	42.7	8.1	Stable	15	250
9	22.5	14.9	Ethox CO-5, 7.4	1-Heptanol, 9.0	38.8	7.4	″	10	180
10	22.5	14.9	Ethox CO-5, 7.4	Glycerol, 9.0	38.8	7.4	″	10	200

As can be seen from Table 1, the aggregation stability A of oil-in water emulsions based on TP can be efficiently controlled by adding hydrotropes and cosolvents (e.g., 2-propanol, urea, and glycerol), which solubilize compounds sparingly or poorly soluble in water. In this case, no phase separation is observed and the limiting wetting angle on the glass support strongly decreases. Emulsion nos. 4 and 5 containing Reapon surfactant and urea and glycerol hydrotropes are the most stable (Table 1); simultaneously, the viscosity η of emulsions, evaluated from the outflow time, decreases to 300–330 s.

The water-in-oil emulsions (Table 2, nos. 6–10) were prepared using nonionic surfactants based on OP-4 polyoxyethylene alkylphenols and Ethox CO-5 polyoxyethylene ester of castor oil, with HLB ~4. Tall pitch was dissolved in a nonpolar solvent (kerosene); 1-heptanol and glycerol were used as cosolvents.

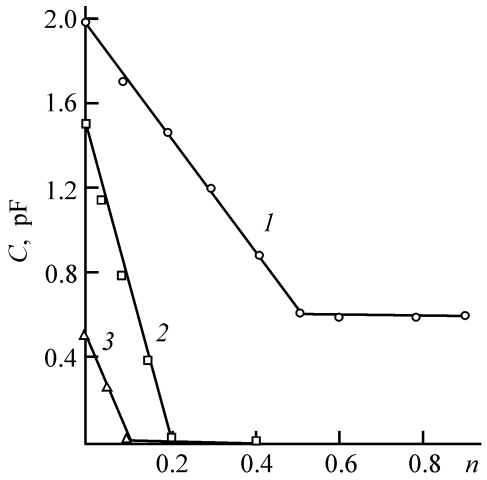


Fig. 2. Electrical capacitance of the emulsions as influenced by dilution with kerosene. Emulsion no.: (*1*) 8–10, (*2*) 7, and (*3*) 6. (*C*) Electrical capacitance and (*n*) dilution ratio [weight ratio of kerosene (dispersion medium) and emulsion].

The electrical capacitance of emulsion nos. 6–10 as influenced by dilution with kerosene is shown in Fig. 2. As seen, the electrical capacitance of emulsion no. 8 containing Ethox CO-5 is 2 pF before dilution. With dilution, the electrical capacitance first decreases linearly to 0.6 pF (0.5 dilution ratio) and then remains constant. It should be noted that addition of 1-hepanol and glycerol affects neither the initial electrical capacitance of the emulsions nor its changes upon dilution with kerosene.

Addition of kerosene does not affect the dependences of the electrical capacitance of emulsion nos. 6 and 7, prepared using OP-4 surfactant (Fig. 2, curves *2*, *3*), but addition of 1-heptanol strongly changes the dielectric properties of the emulsions. The initial electrical capacitance of emulsion no. 6 is 0.5 pF, whereas for emulsion no. 7 containing 1-heptanol it is higher by a factor of 3 (1.5 pF). The inflection points in the dependences of the electrical capacitance on the kerosene content are observed at dilution ratios of 0.1 and 0.2, respectively. In this case, in contrast to the emulsions prepared with Ethox CO-5, the electrical capacitance at the inflection point is 0.

These data, characterizing changes in the dielectric properties of emulsion nos. 6–10, indicate that they belong to the water-in-oil type. However, on adding kerosene to the emulsion up to the dilution ratio corresponding to the inflection point (Fig. 2), the emulsions break down. Thus, water-in-oil emulsions based on TP and LS belong to the limitedly dilutable dispersion systems, and the dilution ratio can be used as a criterion of the aggregation stability of the emulsion, *A*. Apparently, emulsion nos. 8–10 based on Ethox CO-5 (dilution ratio at the inflection point 0.5) are more stable than emulsion nos. 6 and 7 prepared using OP-4 (dilution ratio 0.1 and 0.2, respectively).

As can be seen from Table 2, Ethox CO-5 is preferable as compared to OP-4 surfactant, because in this case, the phase separation is fully absent and the limiting wetting angle on the waxed support decreases to 15°.

On adding 1-heptanol or glycerol, the aggregation stability of the emulsion with Ethox CO-5 increases, which is confirmed by a decrease in the limiting wetting angle to 10°; simultaneously their viscosity (outflow time) decreases to 180–200 s.

It should be noted that glycerol is a versatile component stabilizing both oil-in-water and water-in-oil emulsions based on TP and LS. It has been suggested [4] that the effect of hydrotropes may include three factors: breakdown of the native structure of water and weakening of hydrophobic interactions; complexation with molecules of poorly soluble compounds; and breakdown of the liquid-crystal order and formation

Table 3. Quality parameters of the mold cores and molds prepared using emulsion TCBs based on TP

TCB (emulsion no.)	TCB / sand, wt %	Strength, kgf cm^{-2}		Adhesion to casting patterns
		compression strength in the wet state	tensile strength after drying	
2	7	0.10	10	Weak
2	8	0.13	15	Strong
3	6	0.12	14	Weak
3	7	0.15	19	"
4	6	0.12	15	"
4	7	0.15	22	"
5	5.5	0.13	14	"
5	6.5	0.16	20	"
7	7	0.12	10	Absent
7	8	0.16	14	Weak
8	6	0.13	16	Absent
8	7	0.18	22	"
9	6.5	0.12	14	"
9	7.5	0.16	19	"
10	6.5	0.12	15	"
10	7.5	0.15	20	"

of mixed aggregates. In our case, the increase in the aggregation stability is probably due to an increase in the thermodynamic compatibility between water and molecules of nonionic surfactants and LSs.

Stable emulsions based on TP and LS, prepared in this study, were tested as TCBs for preparing mold cores and molds; their main performance parameters are listed in Table 3. As seen, our emulsion TCBs provide the required strength of the sand stocks in both wet and dry states, and no additional components are required. Moreover, stable water-in-oil emulsion nos. 8–10 completely suppress adhesion of the sand stock to the casting patterns, which makes them preferable over the existing TCBs.

Since preparation of emulsion TCBs does not require development of special installations, they were industrially produced at the Ural Wood-Chemical Plant, Joint-Stock Company (Neivo-Rudyanka urban village, Sverdlovsk oblast).

The use of emulsion binders for preparing mold cores and molds also does not require development of any special equipment, the process can be performed using available foundry facilities, which was confirmed by the results of their tests at the Nizhni Tagil Plant of Boilers and Radiators, Joint-Stock Company (Sverdlovsk oblast).

EXPERIMENTAL

In our study, we used tall pitch [TU (Technical Specifications) 13-0281078–84 with alternation no. 1 (Tall Pitch for Road Building)] with a softening point of 24°C and acid number of 55 mg KOH per gram of the product; A brand liquid lignosulfonates (TU 13-0281036-029–94) with the weight fraction of the dried compounds of 50%. Since the quality of the other components (surfactants, kerosene, and other chemicals) met the norms and regulations, they were used without additional purification.

The oil-in-water emulsions were prepared as follows. The required amounts of a 50% LS aqueous solution, surfactant, distilled water, and auxiliary component [hydrotrope or cosolvent] were stirred for 20 min at 20°C to complete homogenization, avoiding strong foaming; then the required amount of TP preheated to 100–110°C was slowly added to the reaction mixture with increasing stirring rate, and the mixture was stirred for 30–40 min at 50–60°C to obtain a stable emulsion.

The water-in-oil emulsions were prepared as follows. The required amounts of TP heated to 70–80°C, kerosene, surfactant, and auxiliary component were stirred at 20°C for 20 min to complete homogenization; then the required amount of a mixture of a 50% LS aqueous solution and distilled water, prepared in advance, was slowly added to the reaction mixture with increasing stirring rate, and the mixture was stirred for 30–40 min at 20°C to obtain a stable emulsion.

The aggregation stability of emulsions *A* was characterized by a change in the volume of the separated phases after heating of the emulsions at 70–80°C for 3 h and subsequent settling for 1 month.

The wetting angle on the waxed and glass supports, specific electrical conductivity, and electrical capacitance of the emulsions were measured by procedures given in [5].

The viscosity of the emulsions was evaluated with a VZ-4 viscometer (4 mm orifice diameter) according to the GOST (State Standard) 11503.

The performance of the emulsion systems was tested in accordance with [1]: 1KO-A quartz sand was mixed in a runner with the required amount of TCB, then the core was prepared and its compression strength in the wet state and adhesion to the casting pattern were determined. Then, the mold was dried for 1 h at 230–250°C and its tensile strengths in the dried state was determined.

CONCLUSIONS

(1) Stable oil-in-water (direct) and water-in-oil (reverse) emulsions based on tall pitch and lignosulfonates were prepared.

(2) Addition of hydrotropes (2-propanol, 1-heptanol, urea, and glycerol) increases the aggregation stability of the emulsions probably due to an increase in the thermodynamic compatibility between water and molecules of surfactants (in our case, nonionic surfactants and lignosulfonates). Glycerol stabilizes both oil-in-water and water-in-oil emulsions.

(3) The resulting emulsions are effective thermally curable binders for preparing mold cores and molds providing high compression and tensile strength of the cores: 0.12–0.18 and 14–22 kgf cm^{-2} in the wet and dried states, respectively. The mixture does not adhere to the casting patterns when preparing mold cores.

REFERENCES

1. *Formovochnye materialy i tekhnologiya liteinoi formy. Spravochnik* (Molding Materials and Mold Technology: handbook), Zhukovskii, S.S., Ed., Moscow: Mashinostroenie, 1993.
2. Ismagilov, R.M., Rabdil', B.A., and Rabdil', A.B., Abstracts of Papers, *Konferentsiya "Khimiya i tekhnologiya rastitel'nykh veshchestv"* (Conf. "Chemistry and Technology of Vegetable Substances"), Syktyvkar, September 25–30, 2000, Syktyvkar: Komi Nauchn. Tsentr, Ural. Otd. Ross. Akad. Nauk, 2000, p. 196.
3. Ismagilov, R.M., Rabdil', A.B., and Rabdil', B.A., Extended Abstracts, *Vserossiiskii seminar "Novye dostizheniya v khimii i khimicheskoi tekhnologii rastitel'nogo syr'ya"* (Russia Workshop "Modern Achievements in Chemistry and Chemical Technology of Vegetable Raw Materials"), Barnaul, March 28–29, 2002, Barnaul: Altai. Univ., 2002, pp. 209–211.
4. Pletnev, M.Yu., *Kosmetiko-gigienicheskie moyushchie sredstva* (Cosmetic and Hygienic Detergents), Moscow: Khimiya, 1990.
5. *Emulsion Science*, Sherman, P., Ed., London: Academic, 1968.

Russian Journal of Applied Chemistry, Vol. 78, No. 2, 2005, pp. 291–294. Translated from Zhurnal Prikladnoi Khimii, Vol. 78, No. 2, 2005, pp. 297–300.
Original Russian Text Copyright © 2005 by Yumagulova, Kolesov, Monakov.

MACROMOLECULAR CHEMISTRY AND POLYMERIC MATERIALS

Radical Copolymerization of Methyl Methacrylate and Styrene in the Presence of Metallocenes

R. Kh. Yumagulova, S. V. Kolesov, and Yu. B. Monakov

Institute of Organic Chemistry, Ufa Scientific Center, Russian Academy of Sciences, Ufa, Bashkortostan, Russia

Received October 5, 2004

Abstract—The effect of ferrocene and zirconocene dichloride on the rate and constants of copolymerization of methyl methacrylate with styrene was studied. The results obtained suggest that the metallocenes in the elementary steps of the reaction.

The main way to control the product composition in radical copolymerization is introduction of special additives (as a rule, protic and aprotic acids). These acids coordinate with the monomers and thus enhance their electron-acceptor properties, which allows preparation of alternating copolymers [1–3]. The major drawback of this approach is that the controlling additive is introduced in an amount comparable with that of the monomer, which results in contamination of the polymer product and impairs its properties. Purification of the products is very expensive; therefore, this method for controlling the composition and structure of macromolecular compounds is of limited use.

Organometallic compounds (OMCs) are free of this drawback, since their controlling effect on the chain propagation is manifested when the amounts of these compounds are comparable with that of the initiator. This fact indicates that, in contrast to Lewis acids, complexation of OMCs occurs with the macroradicals rather than monomers. For example, Grishin and Moikin [4] found, when studying the monomer system methyl methacrylate (MMA)–methacrylic acid (MAA), that addition of triethylantimony results in rigorous alternation of units in the copolymer, instead of enrichment of the copolymer with methacrylic acid as the more active monomer (r_{MAA} = 1.40, r_{MMA} = 0.08). They noted that the alternation of the units is associated with the increased rate of cross coupling as a result of formation of a cyclic reaction complex consisting of the coordination-unsaturated organometallic additive, macroradical, and monomer. However, addition of triethylantimony in copolymerization of MAA with an electron-donor monomer, styrene, considerably accelerates the reaction, but has virtually no effect on the composition of the copolymers and relative activities of the monomers [5].

There are indications in the literature that, in homopolymerization of styrene in the presence of various organometallic compounds of Groups II and III, the chain propagation occurs by the common radical mechanism without participation of the OMCs, since the OMCs do not interact with the propagating polystyrene radicals because of the effect of electronic and steric factors. Furthermore, some Group-III OMCs even inhibit the styrene polymerization [6]. Puzin *et al.* [7] reported that the carbonyl group of the monomer is involved coordination interaction with the organometallic compound in homopolymerization of MMA in the presence of metallocenes. It has also been found [8] that, in contrast to Group II–III OMCs, styrene is also involved in the coordination-radical polymerization in the presence of metallocenes.

In this study, we examined the effect of ferrocene and zirconocene dichloride on the radical copolymerization of methyl methacrylate with styrene.

EXPERIMENTAL

The monomers were purified by standard procedures [9]. Benzoyl peroxide was repeatedly recrystallized from methanol and dried at room temperature in a vacuum to constant weight; mp 108°C (dec.). Ferrocene and zirconocene dichloride (both of analytically pure grade) were used without additional purification.

The copolymerization was performed at 60°C in the metallocene concentration range 0.2×10^{-3}–

1070-4272/05/7802-0291 © 2005 Pleiades Publishing, Inc.

Effect of metallocenes on the rate (v) and constants (r_1, r_2) of copolymerization of methyl methacrylate (M_1) with styrene (M_2) at 60°C*

Metallocene, $c \times 10^3$, M	v, mol l^{-1} min^{-1}, at indicated $M_1 : M_2$			r_1	r_2	Metallocene, $c \times 10^3$, M	v, mol l^{-1} min^{-1}, at indicated $M_1 : M_2$			r_1	r_2
	2 : 1	1 : 1	1 : 2				2 : 1	1 : 1	1 : 2		
Ferrocene						Zirconocene dichloride					
0	0.72	0.55	0.82	0.52	0.46	0.2	0.83	0.73	0.33	0.41	0.34
0.2	2.24	2.03	2.62	0.38	0.36	0.5	1.01	0.98	0.47	0.57	0.48
0.5	2.98	2.48	3.80	0.23	0.28	1.0	0.65	0.43	1.08	0.53	0.42
1.0	2.30	2.30	2.04	0.18	0.3						

* The rate of homopolymerization of MMA and styrene in the absence of metallocenes is 5.89×10^{-3} and 0.95×10^{-3} mol l^{-1} min^{-1}, respectively.

1.0×10^{-3} M at a constant concentration of the initiator (benzoyl peroxide), 1×10^{-3} M.

The radical copolymerization in the bulk was performed in 5–7-ml molybdenum glass dilatometers. The reaction mixture consisting of the monomers, initiator, and metallocene was charged into the dilatometer in air. Then the contents were deoxygenated by three freeze–pump–thaw cycles (residual pressure 0.01 mm Hg), after which the dilatometer was sealed with a gas burner. Polymer samples were obtained at low conversions (≤5%), reprecipitated three times by adding benzene solutions into hexane, and dried in a vacuum to constant weight at 35°C.

The contraction factor required for calculating the degree of conversion of the monomers to the polymer was determined experimentally for each monomer ratio. The copolymerization constants were calculated by the Fineman–Ross method [10].

Addition of ferrocene increases the initial copolymerization rate by an order of magnitude at various monomer ratios. With zirconocene dichloride, the acceleration is insignificant, and at low concentrations of zirconocene dichloride and excess of styrene the copolymerization rate is even lower than that in the absence of the additive (see table).

In copolymerization of MMA and styrene in the absence of ferrocene and zirconocene dichloride, the copolymerization rate is lower than the rates of homopolymerization of these monomers (see table). The copolymerization rate has a minimum at the equimolar ratio of the monomers. These data correlate with the rate constants of addition of a monomer to a radical. It is known that, in the system styrene–MMA, each free radical reacts preferentially with the monomer of the other kind; therefore, the copolymerization rate is higher when one of the monomers is in excess [11].

The experimental data on copolymerization of methyl methacrylate with styrene at a fixed concentration of ferrocene show that the dependence of the copolymerization rate on the composition of the monomer mixture also passes through a minimum at the equimolar ratio of the monomers (Fig. 1a); also, the reaction decelerates with conversion. With zircono-

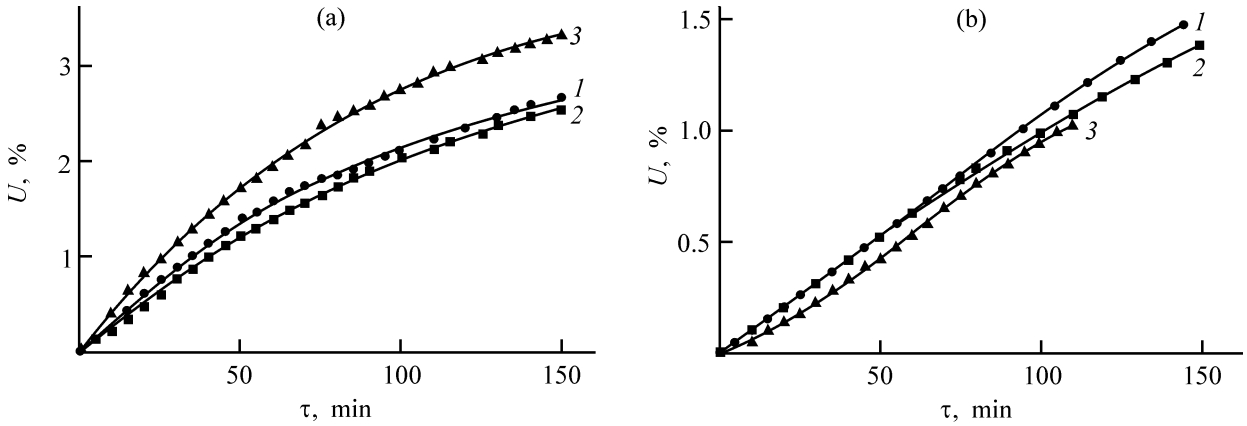


Fig. 1. Copolymerization of methyl methacrylate with styrene in the presence of 0.5×10^{-3} M (a) ferrocene and (b) zirconocene dichloride at 60°C. (U) Conversion and (τ) time; the same for Fig. 2. MMA : styrene ratio: (*1*) 2 : 1, (*2*) 1 : 1, and (*3*) 1 : 2.

cene dichloride, the copolymerization rate decreases with an increase in the styrene content (Fig. 1b).

As the ferrocene concentration increases at a fixed ratio of the monomers, the copolymerization rate grows, reaches a maximum at a ferrocene concentration of 0.5×10^{-3} M, and then decreases (Fig. 2a). With zirconocene dichloride, the reaction rate is the highest at a metallocene concentration of 1.0×10^{-3} M and a twofold excess of styrene (Fig. 2b).

In polymerization of monomers containing a polar substituent, the chain propagation occurs by two mechanisms: on free radicals and on a monomer radical coordination-bound to the metallocene [7]. Radicals of the second type significantly contribute to the polymerization. This fact apparently accounts for a decrease in the copolymerization rate with an increase in the degree of conversion, since the chain propagation mainly occurs on more stable reaction centers. In our case, these are complexes of metallocenes with methyl methacrylate, which are accumulated in the course of the process. Since PMMA radicals are coordinated with metallocene, an increase in the content of ferrocene and styrene is accompanied by an increase in the rate of addition of coordination-bound PMMA radicals to styrene, so that the copolymerization rate becomes higher. The dependences of the reaction rate on the ferrocene concentration and on the MMA : styrene ratio pass through a maximum and a minimum, respectively (in the latter case, at the equimolar ratio of the monomers).

The experimental copolymerization constants are listed in the table. It is seen that, with ferrocene, they tend to decrease with increasing concentration of metallocene. The relative activity of MMA varies to the greatest extent. With zirconocene dichloride, the copolymerization constants only slightly differ from those characteristic of free-radical copolymerization of MMA with styrene.

Our constants are, apparently, effective quantities averaged over two copolymerization pathways: free-radical and coordination-radical. A decrease in the relative activity of MMA in the presence of a metallocene may be due both to a decrease in K_{11} and to an increase in K_{12}, or to simultaneous variation of both constants. These trends may be caused by increased electron-withdrawing power of the poly(methyl methcarylate) radical coordinated with the metallocene. Apparently, with an increase in the electrophilicity of the macroradical, its reactivity toward the π bond of monomeric MMA with an electron-withdrawing substituent decreases, and that toward styrene (electron-donor monomer) increases.

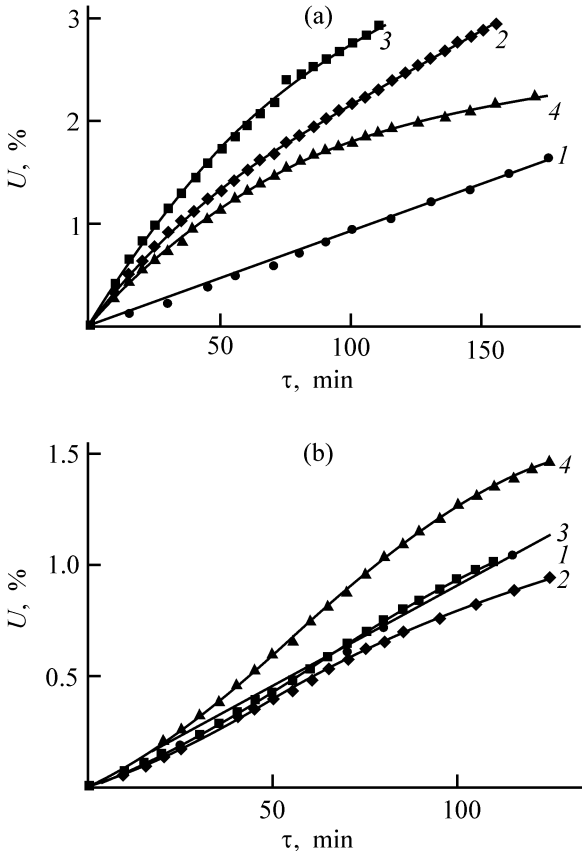


Fig. 2. Copolymerization of methyl methacrylate with styrene at the monomer ratio MMA : styrene = 1 : 2 at 60°C in the presence of (a) ferrocene and (b) zirconocene dichloride. Metallocene concentration $c \times 10^3$, M: (*1*) 0, (*2*) 0.2, (*3*) 0.5, and (*4*) 1.0.

With zirconocene dichloride, this trend is weakly pronounced. The reason is, apparently, the same as that for the weak effect on the copolymerization rate: low rate of formation and hence low concentration of the coordination complexes.

CONCLUSION

Our experimental data show that metallocenes are involved in the elementary events of copolymerization of methyl methacrylate with styrene.

REFERENCES

1. Kabanov, V.A., Zubov, V.P., and Semchikov, Yu.D., *Kompleksno-radikal'naya polimerizatsiya* (Coordination-Radical Polymerization), Moscow: Nauka, 1987.
2. *Novoe v chereduyushcheisya sopolimerizatsii* (New Data on Alternating Copolymerization), Krentsel', B.A., Ed., Leningrad: Inst. Neftekhim. Sinteza, Akad. Nauk SSSR, 1976.

3. Furukawa, J., *Vysokomol. Soedin., Ser. A*, 1979, vol. 21, no. 11, pp. 2591–2605.
4. Grishin, D.F. and Moikin, A.A., *Dokl. Ross. Akad. Nauk*, 1997, vol. 356, no. 6, p. 766.
5. Grishin, D.F. and Semenycheva, L.L., *Usp. Khim.*, 2001, vol. 70, no. 5, pp. 486–510.
6. Grishin, D.F. and Moikin, A.A., *Vysokomol. Soedin., Ser. B*, 1996, vol. 38, no. 11, pp. 1909–1912.
7. Puzin, Yu.I., Prokudina, E.M., Yumagulova, R.Kh., *et al.*, *Dokl. Ross. Akad. Nauk*, 2002, vol. 386, no. 1, p. 69.
8. Sigaeva, N.N., Kolesov, S.V., Prokudina, E.M., *et al.*, Abstracts of Papers, *XVII Mendeleevskii s"ezd po obshchei i prikladnoi khimii* (XVII Mendeleev Congr. on General and Applied Chemistry), Kazan, September 21–26, 2003, vol. 3, p. 481.
9. *Analytical Chemistry of Polymers*, part 1, *Analysis of Monomers and Polymeric Materials*, Kline, G.M., Ed., New York: Interscience, 1959.
10. Toroptseva, A.M., Belogorodskaya, K.V., and Bondarenko, V.M., *Laboratornyi praktikum po khimii i tekhnologii vysokomolekulyarnykh soedinenii* (Laboratory Manual on Chemistry and Technology of Macromolecular Compounds), Leningrad: Khimiya, 1972.
11. Gladyshev, G.P., *Polimerizatsiya vinil'nykh monomerov* (Polymerization of Vinyl Monomers), Alma-Ata, 1964.

Russian Journal of Applied Chemistry, Vol. 78, No. 2, 2005, pp. 295–300. Translated from Zhurnal Prikladnoi Khimii, Vol. 78, No. 2, 2005, pp. 301–305.
Original Russian Text Copyright © 2005 by Kurenkov, Zhelonkina, Kovalenko.

MACROMOLECULAR CHEMISTRY AND POLYMERIC MATERIALS

Concentration Effect in Copolymerization of Sodium 2-Acrylamido-2-methylpropanesulfonate with *N*-Vinylpyrrolidone in Aqueous Solutions

V. F. Kurenkov, T. A. Zhelonkina, and V. I. Kovalenko

Kazan State Technological University, Kazan, Tatarstan, Russia

Received September 21, 2004

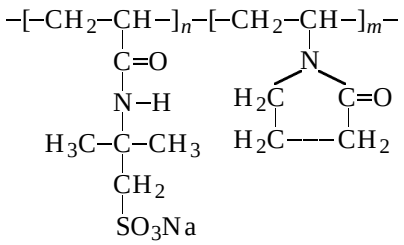
Abstract—The kinetics of copolymerization of sodium 2-acrylamido-2-methylpropanesulfonate with *N*-vinylpyrrolidone in aqueous solutions in the presence of potassium persulfate at 40–70°C and the molecular characteristics of the resulting complexes were studied, as influenced by the total concentration of the initial monomer mixture, comonomer ratio, temperature, and conversion. The kinetic data were explained taking into account the state of the ionic groups, electrostatic interactions between the reacting particles, and complexation of comonomers in the course of copolymerization.

Radical copolymerization in aqueous solutions is one of the main, but still insufficiently studied procedures for preparing water-soluble copolymers of sodium 2-acrylamido-2-methylpropanesulfonate (Na-AMS) with *N*-vinylpyrrolidone (VP), which exhibit high flocculation [1], adhesive and antistatic properties [2], and thickening and complexing power and show promise for various branches of industry and medicine. In this study, copolymerization of Na-AMS and VP was examined as influenced by concentration. Being unusual from the standpoint of the classical theory, this effect is due to specific features of copolymerization of ionic monomers [3] with, in particular, salts of unsaturated sulfonic acids [4, 5] and can be described as a dependence of the polymer composition on the total concentration of the comonomers in the course of copolymerization at fixed composition of the initial monomer mixture and conversion. The concentration effect in copolymerization of Na-AMS and VP has not been studied previously.

EXPERIMENTAL

The properties of the starting compounds and the experimental procedures used (copolymerization, dilatometric analysis of the reaction kinetics, etc.) were similar to those described in [6]. The initial rates of copolymerization, v_0, at low conversion (<4%) were determined from the kinetic curves obtained dilatometrically.

After copolymerization, the resulting polymers were precipitated from aqueous solutions with acetone, filtered off, washed with acetone, and dried to constant weight in a vacuum at 50°C. The yield of the copolymers was determined gravimetrically. The content of ionic units in the copolymer of Na-AMS and VP



was determined from the content of sulfur [7]. The molecular weight of copolymers (M) was calculated with the Mark–Houwink equation from the intrinsic viscosity [η] of their solutions, which was measured in a 0.5 M NaCl solution at 30°C on a VPZh-3 viscometer (d_c = 0.43 mm). The experimental dependence of the reduced viscosity η_{sp}/c_p on the copolymer concentration c_p was plotted. Then, using the linear dependence $\eta_{sp}/c_p = f(c_p)$, we determined

$$[\eta] = \lim(\eta_{sp}/c_p) \text{ at } c_p \to 0.$$

The IR spectra were recorded on an Avatar 360 Fourier spectrometer (ThermoNicolet, the United States) in the 4000–400 cm^{-1} range using VP and a solution of Na-AMS in VP (1 : 9 molar ratio) prepared by mixing of alcoholic monomer solutions

1070-4272/05/7802-0295 © 2005 Pleiades Publishing, Inc.

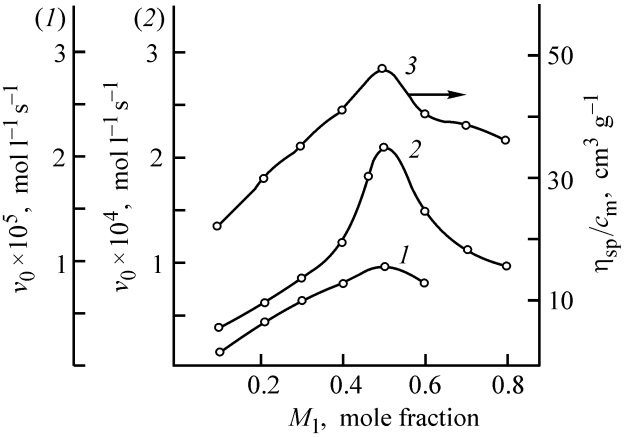


Fig. 1. (*1*, *2*) Initial copolymerization rate v_0 and (*3*) reduced viscosity of monomer solutions, η_{sp}/c_m, vs. the Na-AMS mole fraction in the initial monomer mixture, M_1. Concentration of the monomer mixture c_m = 0.25 g cm^{-3}. $[M_1]_0 + [M_2]_0$, (%): (*1*) 10 and (*2*) 30.

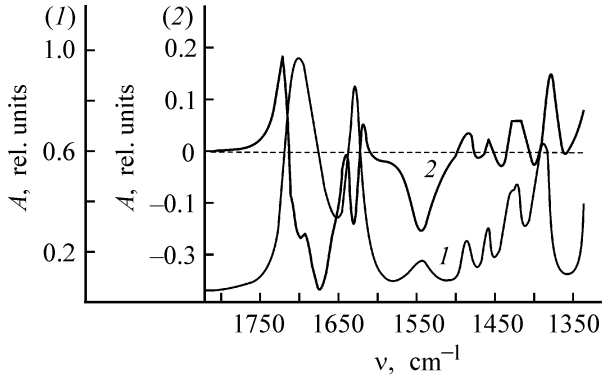


Fig. 2. IR spectrum of (*1*) Na-AMS solution in VP ($[M_1]_0/[M_2]_0$ = 9 : 1) and (*2*) differential spectrum obtained by subtraction of the VP spectrum from the spectrum of Na-AMS solution in VP (for additional explanations, see text). (*A*) Absorption and (ν) wave number.

with subsequent removal of the solvent. The spectra were processed using a KnowItAll software (v.3.0 Academic Edition Bio-Rad Laboratories, the United States).

Copolymerization of Na-AMS with VP was carried out in 10–30% aqueous solutions at 50°C and pH 9. The reaction was initiated by thermal decomposition of potassium persulfate ([PP] = 7.4 × 10^{-4} M). Maintaining pH 9 during copolymerization with PP [8] is necessary to provide fairly high and constant rates of initiation when the ionic strength μ [9] varies due to changes in the Na-AMS concentration in the initial solution and in the course of copolymerization, and also to prevent hydrolysis of Na-AMS [10] and VP [11]. In our experiments, copolymerization proceeded under homogeneous conditions, and no spontaneous formation of the copolymer was observed.

First, we studied the effect of the monomer ratio $[M_1]_0/[M_2]_0$ in the initial solution on the copolymerization, where $[M_1]_0$ and $[M_2]_0$ are the initial concentrations of Na-AMS and VP, respectively. The experiments were performed at the total concentration of comonomers of 10, 25, and 30%, the other experimental conditions being equal. The dependences of v_0 on the concentration of Na-AMS $[M_1]$ in the initial monomer mixture are shown in Fig. 1. As seen, the dependence $v_0 = f(M_1)$ passes through a maximum in the case of copolymerization in 10 and 30% solutions. These results agree with published data [6, 12] and suggest a donor–acceptor interaction between Na-AMS and VP, with Na-AMS being a moderate electron acceptor, and VP, a moderate electron donor.

As seen, the [η] values of the resulting copolymers of Na-AMS and VP vary in parallel with the dependence $v_0 = f(M_1)$, and v_0 and [η] are the highest at $[M_1]_0/[M_2]_0$ = 5 : 5, when the degree of complexation of Na-AMS and VP is the highest. The complexation of Na-AMS with VP is also confirmed by viscometry (Fig. 1, curve *3*). Thus, the dependence $\eta_{sp}/c_m = f(M_1)$ (c_m is the concentration of the monomer mixture) passes through a maximum at the equimolar component ratio corresponding to the highest concentration of Na-AMS–VP complexes.

The complexation in the system was also studied by IR spectroscopy. Due to the low solubility of Na-AMS in VP, we recorded only the IR spectrum of a 1 : 9 (mol/mol) Na-AMS solution in VP. At a large excess of VP, the resulting IR spectrum exhibited only a weak band of Na-AMS near 1545 cm^{-1}, which gave no way of monitoring the monomer interaction. This problem was solved by computer subtraction; the spectrum of pure VP was subtracted from the spectrum of Na-AMS solution (Fig. 2). In curve *2* (Fig. 2) the bands belonging to pure VP and Na-AMS solution in VP lie above and below the zero (dashed) line. Apparently, in the absence of interaction between the monomers, such a subtraction should give only the absorption bands belonging to Na-AMS and occurring below the zero line. As seen, the differential spectrum (Fig. 2, curve *2*) contains a single band at 1545 cm^{-1}, which belongs to Na-AMS and does not overlap with VP bands, and the amide I band near 1675 cm^{-1}, overlapping with the strong band at 1705 cm^{-1}. The occurrence of complexation in the system is confirmed by a shift of the absorption bands at 1705 and 1630 cm^{-1} belonging to vibrations of the pyrrolidone ring. The first of these, originating

from stretching vibrations of the C=O group in the pyrrolidone ring, shifts toward lower frequencies, whereas the band at 1630 cm^{-1} becomes narrower and shifts toward higher frequencies, which is clearly seen when comparing the peak and a higher-intensity low-frequency shoulder of this band, directed below and above the zero line, respectively.

With the total concentration of the comonomers increasing in the course of copolymerization at $[M_1]_0/[M_2]_0$ = const, i.e., on passing from curve *1* to curve *2* (Fig. 1), v_0 and [η] increase. This is probably due to the increasing molecular weight of the resulting copolymers, and the polymer with the highest molecular weight is formed in the course of copolymerization in 30% aqueous solutions.

The yield of Na-AMS–VP complexes increases as the Na-AMS content in the initial monomer mixture is raised from 23 to 58%.

The dependences of the current concentration of the Na-AMS–VP copolymer at low conversions (x < 3%) on the composition of the initial monomer mixture are shown in Fig. 3. In all the cases, the curves are S-shaped with the corresponding azeotropic points. From these data (Fig. 3), we calculated the effective copolymerization constants of the monomers $r_1 = k_{11}/k_{12}$ and $r_2 = k_{22}/k_{21}$ for Na-AMS and VP (see table). The values of r_1 and r_2 confirm that, in the system studied, both macroradicals react with a "foreign" monomer more readily than with their "own" monomer owing to the stabilization of the transition state by the donor–acceptor interaction between the macroradical and the monomer. This provides alternation of the monomer units in the chain ($r_1 r_2 < 1$). As can be seen from the table, $r_2 > r_1$ in all the cases, which confirms the higher copolymerization reactivity of VP as compared to Na-AMS.

As can be seen from Fig. 3, the content of Na-AMS units in the copolymer increases with increasing total concentration of comonomers (from curve *1* to curve *3*) in a wide range of compositions of the initial monomer mixture, which is due to the increase in r_1 and decrease in r_2, respectively (see table).

The above kinetic data on the copolymerization of Na-AMS and VP in aqueous solutions at various concentrations of the initial monomer mixture can be explained taking into account the equilibrium of the ionic groups in Na-AMS and its units in the macroradicals in aqueous salt solutions:

$$\underset{\mathbf{I}}{A^-X^+} \rightleftarrows \underset{\mathbf{II}}{A^- \| X^+} \rightleftarrows \underset{\mathbf{III}}{A^- + X^+},$$

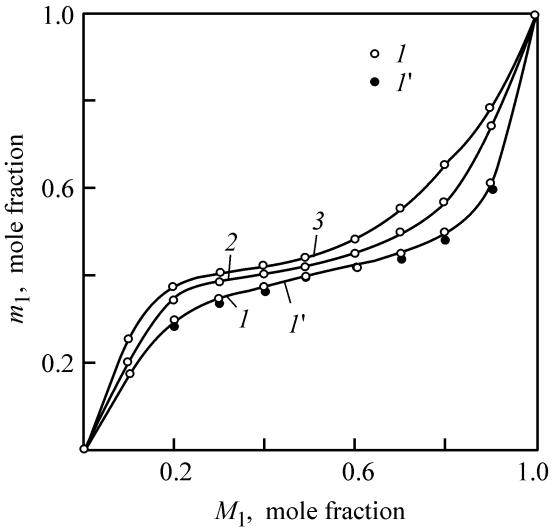


Fig. 3. Mole fraction of Na-AMS units in copolymer, m_1, at conversion x < 3% vs. the Na-AMS mole fraction in the initial monomer mixture, M_1. $[M_1]_0 + [M_2]_0$, %: (*1*, *1*') 10, (*2*) 25, and (*3*) 30. Temperature, °C: (*1*–*3*) 50 and (*1*') 70.

where A^- is the anion of the monomer or macroradical; X^+ is the cation; and **I**, **II**, and **III** are the contact ion pairs, ion pairs separated by a solvent, and free ions, respectively.

Changes in μ with the concentration of Na-AMS in the initial monomer mixture and in the course of copolymerization shift the ionization equilibrium of the ionic groups, thus changing the relative content in the reaction mixture of various ionic species differing in the reactivity. This changes the intra- and intermolecular electrostatic interactions and affects the conformation state of the growing macroradicals and, thus, affects the reactivity of ionic monomers in copolymerization (r_1, r_2). Due to the nonisoionic synthesis conditions, copolymerization of the ionic monomers in the ionizing media cannot be described using fixed copolymerization constants r_1 and r_2. It should be noted that, in copolymerization of Na-AMS and VP, changes in μ did not affect the reactivity of

Parameters of copolymerization of Na-AMS (M_1) and VP (M_2)

$[M_1]_0 + [M_2]_0$, %	r_1	r_2	$r_1 r_2$
10	0.01 ± 0.01	0.51 ± 0.05	0.01
25	0.11 ± 0.02	0.42 ± 0.10	0.05
30	0.17 ± 0.02	0.33 ± 0.08	0.06

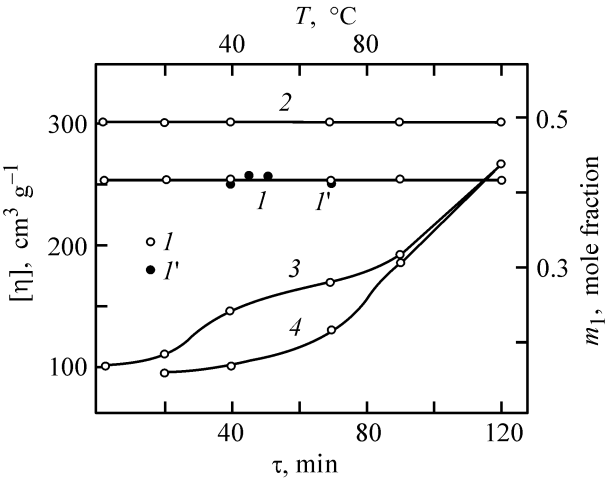


Fig. 4. (*1*, *1'*, *2*) Mole fraction of Na-AMS units, m_1, and (*3*, *4*) intrinsic viscosity [η] of Na-AMS–VP copolymer vs. the (*1–4*) copolymerization time τ and (*1'*) temperature *T* (*1'*). $[M_1]_0/[M_2]_0$; (*1*, *1'*, *4*) 5 : 5 and (*2*, *3*) 7 : 3.

VP and its macroradical, because the rate of VP polymerization did not change on adding low-molecular-weight salts [13].

In aqueous solutions, the ionic groups in Na-AMS and its units in copolymer are completely ionized, and the ionization equilibrium shifts to the left with increasing μ; this fact is confirmed by viscometry. At c_p = const, η_{sp}/c_p of Na-AMS–VP copolymer decreases with μ increasing upon addition of Na-AMS and NaCl. This is due to a decrease in the electrostatic repulsion between the sulfonate anions along the chain with an increase in their shielding by sodium counterions, which makes shorter the linear size of macromolecular polymer aggregates. In copolymerization of Na-AMS with VP, an increase in μ decreases the electrostatic repulsion between similarly charged particles in the events of chain propagation (in reaction of Na-AMS with a macroradical containing the terminal Na-AMS unit) or termination (in reaction between macroradicals with terminal Na-AMS units), and thus increases the constants of chain propagation k_p and termination k_t. As the concentration of the initial monomer mixture becomes higher, k_p (i.e., k_{11}) increases to a greater extent than k_t, which is confirmed by a rise in the molecular weight of the resulting copolymers and causes the increase in v_0. Moreover, a certain decrease in the charge of the growing chains with increasing μ makes higher the local concentrations of Na-AMS in the environment of the "own" active centers and thus also increases v_0.

To examine the effect of conversion on the molecular properties of the resulting copolymers of Na-AMS and VP, we performed copolymerization in 25% aqueous solutions at $[M_1]_0/[M_2]_0$ molar ratios of 5 : 5 and 7 : 3, the other experimental conditions being equal (Fig. 4). As seen, the copolymer composition does not change with increasing copolymerization time (Fig. 4, curves *1* and *2*). Apparently, in copolymerization in concentrated comonomer solutions, the main contribution to μ is made by changes in the concentration of Na-AMS in the initial monomer mixture, prevailing over the effect of binding of a certain fraction of Na^+ counterions with polyanions. The fact that the composition of the copolymer does not change with conversion agrees with the data on copolymerization of acrylamide with dimethylaminoethyl methacrylate sulfate in aqueous solution [14], which is due to the difference in the local concentration of the monomers near macroradicals as compared to the average concentration of the monomers in the reaction mixture, caused by hydrophobic interactions in the system.

The [η] values increase in the course of the reaction (Fig. 4, curves *3* and *4*), which agrees with the data on copolymerization of complex-bound monomers in other systems [15]. Apparently, the increase in the viscosity of the reaction mixture with conversion decreases the rate of mutual diffusion of the macroradicals and k_t, which promotes the increase in the molecular weight of the copolymer.

The effect of temperature on the copolymerization of Na-AMS and VP was studied at 40–70°C using 25% aqueous solutions ($[M_1]_0/[M_2]_0$ = 5 : 5), the other conditions being equal. As can be seen from Fig. 5a, v_0 increases with temperature. The experimental data give a linear plot in the Arrhenius coordinates (Fig. 5a) and correspond to the effective overall activation energy of copolymerization, E_{tot}, of 44.0 kJ mol^{-1}. The lower E_{tot} in the system studied (compared to common radical polymerization) is frequent in alternating copolymerization [15].

It should be noted that changes in the conformational state of the macroradicals of Na-AMS-VP copolymer with temperature can also affect v_0, which is confirmed by viscometry (Fig. 5b). As seen, η_{sp}/c_p in the solution of Na-AMS–VP copolymer at c_p = const decreases with increasing temperature.

This is caused by a decrease in the effective size of macromolecular aggregates with increasing temperature, which is due to weakening of the electrostatic

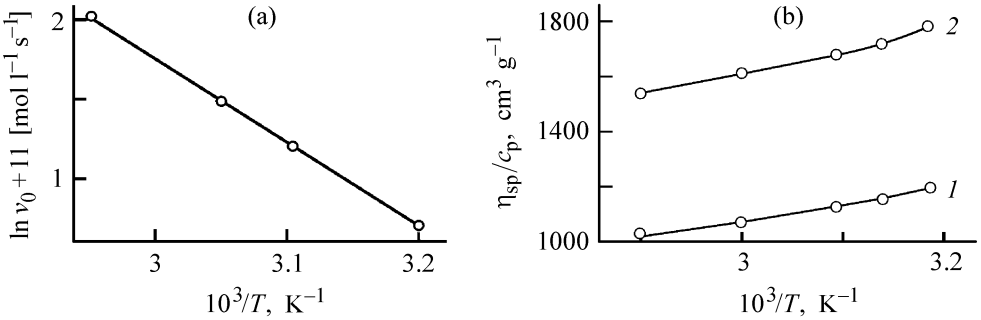


Fig. 5. (a) Initial rate of copolymerization, v_0, of VP with Na-AMS and (b) reduced viscosity η_{sp}/c_p of the aqueous solution of copolymer ([η] = 265 cm^3 g^{-1}, 48 mol % Na-AMS units) vs. temperature T. (a) $[M_1]_0/M_2]_0$ = 5 : 5; $[M_1 + M_2]_0$ = 25%. η_{sp}/c_p (b) $c_p \times 10^2$, g cm^{-3}: (*1*) 0.2 and (*2*) 0.5.

repulsion of the fixed charges along the chain with decreasing ionization of the ionic groups. This, in turn, results in that the local concentration of Na-AMS near the active centers (macroradicals with terminal Na-AMS groups) and, hence, v_0 increase with temperature.

Figure 3 shows the dependence of the copolymer composition on the initial composition of the monomer mixture at 50 (Fig. 3, curve *1*) and 70°C (Fig. 3, curve *1*'), and the temperature dependence of the polymer composition at $[M_1]_0/[M_2]_0$ = 5 : 5 is plotted in Fig. 4 (curve *1*'). These data show that the composition of the Na-AMS–VP copolymer is independent of the copolymerization temperature, which agrees with published data on copolymerization of acrylic and methacrylic acids in solvents capable of hydrogen bonding with the monomers [15]. Obviously, a decrease in the molecular weight of the copolymers due to an increase with temperature in the concentration of radicals generated by the initiator degradation agrees with common trends observed in radical copolymerization.

CONCLUSIONS

(1) The copolymerization rate v_0, molecular weight, and content of the sodium 2-acrylamido-2-methylpropanesulfonate units in the copolymer increase with the concentration of the initial monomer mixture due to the increasing effective relative activity r_1 (for sodium 2-acrylamido-2-methylpropanesulfonate) and decreasing r_2 (for *N*-vinylpyrrolidone).

(2) With increasing $[M_1]_0/[M_2]_0$ in the initial monomer mixture, the dependences of v_0 and molecular weight pass through a maximum at $[M_1]_0/[M_2]_0$ = 1 : 1 due to the formation of donor-acceptor complexes of the comonomers.

(3) With increasing conversion, the molecular weight of the copolymer grows and its composition remains unchanged, whereas with increasing temperature, v_0 becomes higher, molecular weight decreases, and the copolymer composition also remains unchanged.

ACKNOWLEDGMENTS

This study was financially supported by the Research-and-Development Foundation of the Republic of Tatarstan (project no. 07-7.1-104/2004).

REFERENCES

1. Kurenkov, V.F., Sharapova, Z.F., and Khairullin, M.R., *Zh. Prikl. Khim.*, 1999, vol. 72, no. 8, pp. 1374–1378.
2. Shevtsova, S.A., Barkhanova, T.A., Zhelonkina, T.A., and Kurenkov, V.F., in *Materialy konferentsii "III Kirpichnikovskie chteniya"* (Proc. Conf. "III Kirpichnikov Readings"), Kazan: Kazan. Gos. Tekhnol. Univ., 2003, pp. 308–311.
3. Kabanov, V.A. and Topchiev, D.A., *Polimerizatsiya ionizuyushchikhsya monomerov* (Polymerization of Ionizable Monomers), Moscow: Nauka, 1975.
4. Kurenkov, V.F. and Myagchenkov, V.A., *Eur. Polym. J.*, 1979, vol. 15, pp. 849–862.
5. Kurenkov, V.F. and Myagchenkov, V.A., *Zh. Prikl. Khim.*, 1999, vol. 72, no. 6, pp. 881–890.
6. Kurenkov, V.F., Sirotkin, R.O., Beryachkova, E.A., and Khairullin, M.R., *Zh. Prikl. Khim.*, 1999, vol. 72, no. 8, pp. 1533–1537.
7. Charlot, G., *Les methods de la chimie analytique. Analyse quantitative minerale*, Paris: Masson, 1961, 4th ed.
8. Kholodnova, L.V., Pavlyuchenko, V.N., Alekseeva, Z.M., and Andreeva, A.I., in *Kataliticheskie i initsiiruyushchie sistemy dlya sinteza i modifikatsii poli-*

merov (Catalytic and Initiating Systems for Synthesis and Modification of Polymers), Leningrad: Plastpolimer, 1984, pp. 90–104.

9. Kolthoff, I.M. and Miller, I.K., *J. Am. Chem. Soc.*, 1951, vol. 73, no. 7, pp. 3055–3059.
10. *2-Acrylamido-2-methylpropane Sulfonic Acid Monomer*, Wickliffe, Ohio (USA): Lubrizol, 1994, pp. 1–18.
11. Sidel'kovskaya, F.P., *Khimiya N-vinilpirrolidona i ego polymerov* (Chemistry of *N*-Vinylpyrrolidone and Its Polymers), Moscow: Nauka, 1970.
12. Schultz, D.N., Kitano, K., Danik, J.F., and Kaladas, J.J., *Polym. Mater. Sci. Eng.*, 1987, vol. 57, pp. 149–153.
13. Topchiev, D.A., Shakirov, R.Z., Kalinina, L.P., *et al.*, *Vysokomol. Soedin., Ser. A*, 1972, vol. 14, no. 3, pp. 581–586.
14. Gromov, V.F., Bogachev, Yu.S., Bune, E.V., *et al.*, *Vysokomol. Soedin.*, 1993, vol. 35, no. 1, pp. 7–12.
15. Kabanov, V.A., Zubov, V.P., and Semchikov, Yu.D., *Kompleksno-radikal'naya polimerizatsiya* (Coordination Radical Polymerization), Moscow: Khimiya, 1987.

Russian Journal of Applied Chemistry, Vol. 78, No. 2, 2005, pp. 301–304. Translated from Zhurnal Prikladnoi Khimii, Vol. 78, No. 2, 2005, pp. 306–309.
Original Russian Text Copyright © 2005 by Novikov, Varlamov, Mnatsakanov.

MACROMOLECULAR CHEMISTRY AND POLYMERIC MATERIALS

Cluster Structure of the Surface of Plasticized Cellulose Triacetate Films

D. V. Novikov, A. V. Varlamov, and S. S. Mnatsakanov

St. Petersburg State University of Motion Pictures and Television, St. Petersburg, Russia

Received December 5, 2003; in final form, October, 2004

Abstract—The influence of plasticizers, dibutyl phthalate and triphenyl phosphate, on the structure of the surface of cellulose triacetate films was studied. The parameters of an infinite cluster of the cellulose triacetate molecules on the film surface, the correlation radius ξ of the spatial distribution of density, the degree ρ_s of surface filling of the cluster, and the fractal dimensionality D, were calculated from the electron-microscopic data, using the cluster model.

Film bases for film-photographic materials are presently manufactured from partially hydrolyzed cellulose triacetate (CTA) with a degree of substitution equal to 2.75–2.95 [1]. Partially hydrolyzed CTA belongs to semirigid-chain polymers [2] whose macromolecules can form domain-type anisotropic aggregates in solution. The nature of aggregation of the CTA macromolecules in solution [3], at the solution–solid interface [4], and in transition of the polymer to the condensed state [5] is governed by the concentration and thermokinetic modes, as well as by the hydrodynamic volume of the macromolecules. The hydrodynamic volume strongly depends on the molecular weight, degree of substitution, distribution of the primary and secondary hydroxy groups in the macrochain, and solvent quality [3].

Krasovskii *et al.* [3] and Kharlampiev [5] used the cluster lattice model [6] in studies of the hydrodynamic behavior and the structure of the CTA samples in a series of proton-donating solvents; the samples differed in the distribution of the primary and secondary hydroxy groups in the macrochain. The formation of aggregates or clusters of macromolecules was revealed in going from dilute to semidilute CTA solutions. It was found that, with growing polymer concentration c in solution, the finite clusters tend to transform into an infinite (percolation) cluster, which is formed at c = 9–11 wt % and T = 293 K [5].

Our previous studies [7] suggest that the sites of the physical network of macromolecules in the CTA films obtained from polymer solution are represented by aggregates or clusters of the macromolecules, formed in solution. Such clusters have a fractal nature and exhibit an enhanced density of packing of the macromolecules, compared to the average density of the polymer. The topology of the spatial distribution of the cluster density determines the most important parameters of the physicomechanical and performance characteristics of films [8].

In Russia, the natural rigidity of CTA is commonly decreased by plasticization of polymer films with a mixture of triphenyl phosphate (TPP) and dibutyl phthalate (DBP) [1]. However, the influence of the plasticizer additions on the CTA cluster structure topology still remains to be elucidated. As known [9], the plasticizers introduced into the polymer film can modify the cluster topology by various mechanisms. In the case of true, or molecular, plasticization, the plasticizer molecules are incorporated into supramolecular CTA formations and loosen their structure. In the case of the structural plasticization, the plasticizer is localized along the cluster boundaries and in the intercluster space.

In this study, we examined the topology of the cluster structure of the CTA films containing commercial plasticizers, TPP and DBP, with the aim to elucidate the plasticization mechanisms and the influence of the plasticizers on the density of distribution of the supramolecular formations or clusters of the CTA macromolecules.

EXPERIMENTAL

We used a commercial sample of partially hydrolyzed CTA (Svema, Shostka, Ukraine) prepared

1070-4272/05/7802-0301 © 2005 Pleiades Publishing, Inc.

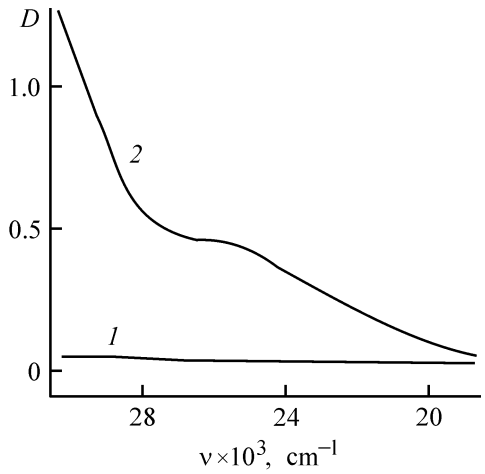


Fig. 1. Electronic absorption spectra of (*1*) initial and (*2*) bromine-activated CTA film. (*D*) Optical density and (ν) frequency.

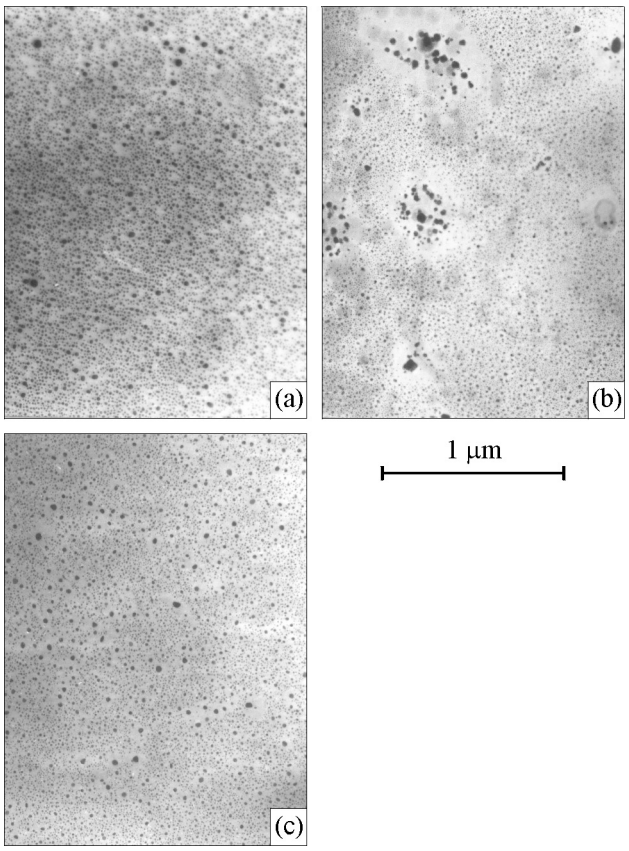


Fig. 2. Electron micrographs of the decorating gold particles on the bromine-activated surface of CTA film samples. Magnification × 25 000. Film: (a) Initial, (b) CTA–DBP, and (c) CTA–TPP.

by a heterogeneous procedure and having a degree of polymerization of 300, degree of substitution of 2.85, and random distribution of the hydroxy groups. Film samples with a thickness of ca. 100 μm were prepared by casting a 10 wt % polymer solution in a 9 : 1 methylene chloride–ethanol mixture onto a leveled mirror glass at 293 K. The amount of the plasticizers, TPP and DBP, was 10 wt % relative to CTA.

We studied the film surface formed at the film–air interface. The topology of the cluster structure of the polymer on the film surface was studied by electron microscopy with gold decoration and preactivation with bromine. This procedure was suggested for the first time in [10, 11] for studying the structure of the macromolecular aggregates on the surface of amorphous and partially crystalline polymers. Surface activation yields molecular complexes of bromine with electron-donating functional groups of the CTA macromolecules, the so-called "chemical labels," acting as $AuBr_3$ formation sites in decoration, which are potential nuclei for the decorating gold particles. The chemical activation of the surface was carried out in a 0.5 wt % aqueous solution of bromine for 30 s, which was followed by vacuum sputtering of gold to an effective layer thickness of 0.4 nm [7].

Figure 1 presents the electronic absorption spectra of the CTA film before and after activation with bromine. The bromine-activated CTA film was preliminarily kept in a vacuum for 30 min. The absorption band at $\nu = 25\,000$ cm^{-1} was assigned to chemisorbed bromine, since prolonged keeping of the film in a vacuum substantially decreases the band intensity.

Figure 2 presents the electron micrographs of carbon replicas with gold particles, taken from the bromine-activated CTA film surface. The spatial distribution of the decorating particles is nonuniform; the film surface contains areas with enhanced local density of particles. These areas correspond to the macromolecular clusters [7] between which larger gold particles are formed by the "point" particle coalescence mechanism. The surface of the CTA film containing TPP exhibits nonuniformly distributed extended areas, in which large decorating particles are localized (Fig. 2c). These areas can be assigned to discrete TPP inclusions constituting an individual phase.

The pattern of distribution of the decorating gold particles on the surface of the bromine-activated CTA film can be accounted for as follows. The degree of chemisorption of bromine on the polymer film surface depends on the local density of the polymer. Looser areas between the clusters of macromolecules bind a larger amount of bromine, which is responsible for the formation of larger gold particles.

In the presence of DBP, the relative proportion of the large fraction of the decorating particles and,

hence, the proportion of the intercluster space, tend to increase (Fig. 2b). This can be due to possible microphase segregation of the CTA–DBP system.

The topography of the gold particles on the surface of the film samples was studied on an EMV 100L electron microscope at the $\times 40\,000$ magnification and analyzed by the procedure described in [7, 10, 11]. The area of scanning of the micrographs with $\times 150\,000$ magnification, when processed on a PC, was 2–2.5 μm^2.

The agglomerations of the decorating gold particles on the film surface were represented as lattice clusters [6] on a two-dimensional lattice with the interpoint distance equal to the most probable distance r (see table) separating the particles and with the coordination number m corresponding to the average number of the nearest neighbors around an arbitrarily chosen particle [7]. The micrographs show that there is a single cluster of decorating particles on the film surface, and the topology of this duster corresponds to that of the infinite cluster of the CTA macromolecules. Using the procedure from [7], we calculated the correlation radius of the cluster, ξ, and the average lattice density ρ_s of the cluster (equal to the degree of the surface filling by the cluster at $R > \xi$), as well as the fractal dimensionality D of the cluster at $R < \xi$.

Figure 3 presents ρ_s-vs.-R plots (R is the radius of the circle centered at the lattice site occupied by a particle), constructed in the log–log coordinates for the initial and plasticized CTA films. The average lattice density ρ_s of the cluster decreases with increasing scale radius R as $\rho_s(R) \sim R^{D-2}$, and the corresponding log–log plots are straight lines (Fig. 3). The inflection point corresponds to the correlation radius ξ of the cluster or to the alternation period of the density fluctuation L (for the quadratic lattice with $m = 4$). For $R > \xi$, the fractal dimensionality of the infinite cluster is close to 2 (Fig. 3). At $R \le \xi$, D, in turn, determines the pattern of distribution of the density inside the cluster.

When DBP is introduced into the CTA film, the cluster density, and also D at $R \le \xi$, tend to decrease (see table and Fig. 3). This suggests that DBP loosens the structure of the supramolecular formations of CTA, which is typical of true plasticization at the molecular level [9]. The increase in the proportion of the intercluster space and in the correlation radius ξ may be due to possible microphase segregation of the CTA–DBP system.

On the whole, TPP additions do not modify the morphology of the infinite cluster of the CTA macromolecules at $R < \xi$, as suggested by the invariance of the fractal dimensionality D in going from the initial to the TPP-containing CTA film (see table and Fig. 3). This means that, in the presence of TPP, plasticization follows the structural mechanism implying a predominant distribution of the plasticizer between the supramolecular formations of the polymer. This decreases the proportion ρ_s of the surface occupied by the cluster and increases the correlation radius ξ of the density fluctuations. Partial egress of TPP into the microphase, revealed by electron microscopy, is due to a purely surface effect. Indeed, commercial manufacture of plasticized CTA films involves local egress of a port of TPP onto the film surface.

Parameters of distribution of the decorating gold particles and of the cluster structure of the polymer on the surface of the CTA film samples

Sample	r, nm	m	$\rho_s \pm 0.02$	ξ, nm	$D(R \le \xi) \pm 0.03$
CTA	15.5	3.8	0.59	42	1.85
CTA–DBP	12.4	3.7	0.43	51	1.74
CTA–TPP	13.4	4.2	0.54	53	1.83

The correlation radius ξ of the cluster structure of the CTA film surface is virtually independent of the nature of the plasticizer (see table and Fig. 3); it was estimated at ca. 53 nm for plasticized CTA films. Varlamov *et al.* [12] studied the dependence of the small-angle X-ray scattering intensity I for a commercial sample of a plasticized CTA film. The discrete maximum of I corresponds, according to the Bragg formula, to an alternation period of the electron density equal to 53 nm, which agrees well with the electron-microscopic data.

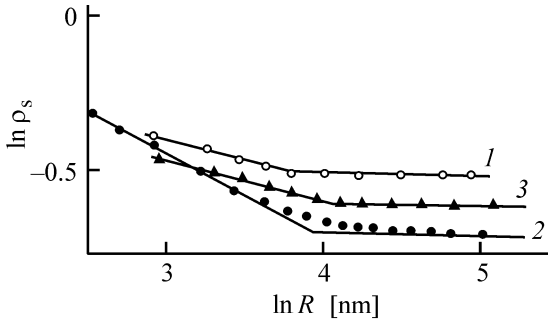


Fig. 3. log–log plot of the dependence of the lattice density ρ_s of distribution of the clusters of decorating gold particles on the radius scale R for (*1*) CTA, (*2*) CTA–DBP, and (*3*) CTA–TPP samples.

CONCLUSIONS

(1) A cluster structure was revealed for the surface of the cellulose triacetate film prepared from a 10 wt % polymer solution in a 9 : 1 methylene chloride–ethanol mixture. Supramolecular formations or aggregates of the cellulose triacetate macromolecules constitute an infinite cluster network.

(2) Introduction of plasticizers into the cellulose triacetate film decreases the proportion of the surface covered with a cluster of macromolecules and increases the alternation period of the cluster density. Dibutyl phthalate additions loosen the structure of the cluster and, hence, decrease its fractal dimensionality. By contrast, triphenyl phosphate additions do not affect the fractal dimensionality D and the cluster morphology. These results suggest the predominantly molecular mechanism of plasticization of cellulose triacetate with dibutyl phosphate and the structural mechanism of plasticization with triphenyl phosphate.

REFERENCES

1. Braginskii, G.I. and Kudrna, S.K., *Tekhnlogiya osnovy kinofotomaterialov i magnitnykh lent* (Technology of the Film-Photographic Material and Magnetic Tape Base), Leningrad: Khimiya, 1980.
2. Tsvetkov, V.N., *Zhestkotsepnye polimernye molekuly* (Rigid-Chain Polymer Molecules), Leningrad: Nauka, 1986.
3. Krasovskii, A.N., Polyakov, D.N., and Mnatsakanov, S.S., *Vysokomol. Soedin., Ser. A*, 1995, vol. 37, no. 9, pp. 1551–1557.
4. Polyakov, D.N., Krasovskii, A.N., and Odlyanitskii, L.A., *Kolloidn. Zh.*, 1993, vol. 55, no. 6, pp. 90–95.
5. Kharlampiev, A.A., Spectra of Optical Constants and Structure of Boundary (Surface) Layers of Polymers Intended for Photographic Purposes and Recording Media, *Cand. Sci. Dissertation*, St. Petersburg, 1999.
6. Feder, J., *Fractals*, New York: Plenum, 1988.
7. Novikov, D.V., Krasovskii, A.N., Filippov, V.N., *et al., Zh. Prikl. Khim.*, 2003, vol. 76, no. 7, pp. 1160–1166.
8. Perepechko, I.I., *Vvedenie v fiziku polimerov* (Introduction to Polymer Physics), Moscow: Khimiya, 1978.
9. Tager, A.A., *Fizikokhimiya polimerov* (Physical Chemistry of Polymers), Moscow: Khimiya, 1978.
10. Novikov, D.V., Varlamov, A.V., and Veselova, S.V., *Zh. Prikl. Khim.*, 1997, vol. 70, no. 7, pp. 1180–1185.
11. Novikov, D.V., Krasovskii, A.N., Andreeva, A.I., and Basov, S.V., *Kolloidn. Zh.*, 1999, vol. 61, no. 2, pp. 240–246.
12. Varlamov, A.V., Kenarov, A.V., Dyshlevskaya, O.S., and Mnatsakanov, S.S., in *Khimicheskaya tekhnologiya, svoistva i primenenie plastmass: Mezhvuz. sbornik* (Chemical Technology, Properties, and Application of Plastics: Intercollegiate Coll. of Works), St. Petersburg: Izd. Tekh. Univ., 1992, pp. 131–135.

Russian Journal of Applied Chemistry, Vol. 78, No. 2, 2005, pp. 305–310. Translated from Zhurnal Prikladnoi Khimii, Vol. 78, No. 2, 2005, pp. 310–315.
Original Russian Text Copyright © 2005 by Krivoguz, Pesetskii.

MACROMOLECULAR CHEMISTRY AND POLYMERIC MATERIALS

Free-Radical Grafting of Methylenebutanedioic Acid to Polypropylene–Polyethylene Blends and Rheological Properties of Melts

Yu. M. Krivoguz and S. S. Pesetskii

Belyi Institute of Mechanics of Metal-Polymer Systems, National Academy of Sciences of Belarus, Gomel, Belarus

Received June 3, 2004

Abstract—Specific features of grafting of methylenebutanedioic acid to polypropylene–polyethylene blends during reactive extrusion were studied. The ratio of the polymeric components exerts a certain influence on the yield of the grafted product and on the side processes accompanying the grafting reaction. The factors underlying this influence were analyzed.

Functionalization of polyolefins (POs), based on free-radical grafting of polar monomers to PO macromolecules, has been fairly comprehensively studied [1–3] but still remains topical. Of special importance are studies concerned with the reaction extrusion (RE) technology [1]. This method allows preparation of a number of technically valuable products suitable for divers applications, such as adhesives, compatibilizers of blends of incompatible polymers, and additives facilitating the processing of polymer waste and improving its quality [2, 3].

A large number of studies [2–8] have been devoted to elucidating the relationships in free-radical grafting of unsaturated polar monomers to macromolecules of some POs, including polyethylene (PE), polypropylene (PP), and ethylene–propylene copolymer (EPC). It has been found that the grafting reactions may be accompanied by a number of side processes, whose character is determined by the nature of the PO. For example, PE tends to undergo cross-linking [4, 5], and PP, degradation of the macromolecules during functionalization [6–8], whereas EPC exhibits both degradation and cross-linking of the macrochains [2, 9]. Published data suggest that free-radical grafting of polar monomers to PO blends will be accompanied by even more complex macromolecular transformations than those occurring in the course of grafting to homopolyolefins.

Though clearly topical, studies concerned with monomer grafting to PO blends in the course of RE are scarce [10]. Chaoqin *et al.* [10] considered specific features of grafting of maleic anhydride to a PE/PP blend at concentrations of the polymeric components varied within a comparatively narrow range of the component ratios (the PP content in the blend was 5–20 wt %). These authors confirmed that the degree of grafting and the rheological properties of the polymer melt depend on the PP and PE concentrations. However, these data do not disclose the mutual influence of the polymeric components on the main and side processes under varied component ratio throughout the concentration range studied [10].

In this study, we examined the specific features of grafting in the course of RE of unsaturated monomers in PO blends. To this end, we used methylenebutanedioic acid (MA) and a mixed PP/PE system, in which the ratio of the polymeric components was varied over a wide concentration range.

EXPERIMENTAL

In our study we used the following POs: Kaplen isotactic PP [01030 grade, TU (Technical Specifications) 2211-015-00203521–95, density 0.905 g cm^{-1}, mp 169°C (according to DSC data, at β = 16 deg min^{-1}), melt flow index 4.9 g/10 min at 190°C and a load of 5 kg] and low-density polyethylene (LDPE) [15803-020 grade, GOST (State Standard) 16337–77, density 0.92 g cm^{-3}, mp 106°C (according to DSC data, at β = 16 deg min^{-1}), melt

1070-4272/05/7802-0305 © 2005 Pleiades Publishing, Inc.

flow index 7.4 g/10 min at 190°C and a load of 5 kg]. Methylenebutanedioic acid available from Chemical Division Pfizer (US) (molecular weight 130.1 g mol^{-1}, mp 172°C) served as the monomer to be grafted. The grafting reaction was initiated by 2,5-dimethyl-2,5-di(*tert*-butylperoxy)hexane from Atofina Co. (France) under the L-101 trademark ($\tau_{0.5}$ = 0.6 min at 180°C; available active oxygen concentration 11.03%). Acetone (99.5% pure) and absolute ethanol (99.9% pure) served as solvents.

Methylenebutanedioic acid was grafted to PP/LDPE blends in an extrusion reactor based on a Brabender plastograph and equipped with a dynamic mixer [4], in the following modes: worm rotation rate 50 rpm at a shear rate of ca. 100 s^{-1}; temperature 160, 180, and 185°C in zones I, II–III, and IV, respectively. The reaction mixture remained in the reactor for ca. 4 min, on the average.

Prior to grafting, we prepared PP/LDPE blends with the PP : LDPE component ratios (wt %) of 100 : 0, 99 : 1, 95 : 5, 75 : 25, 50 : 50, 25 : 75. 5 : 95, 1 : 99, and 0 : 100, by coextrusion in melt at 200°C in a one-worm extruder (worm diameter 25 mm, $L : D$ = 25), followed by water cooling and granulation of the resulting formulations. Next, granulate of the PP/LDPE formulations was treated with L-101, dissolved in acetone, and with powdered MA. The concentrations of the MA and L-101 introduced into the PP/LDPE blends in all the experiments were constant, namely, 1.0 and 0.3 wt %, respectively. The resulting reaction mixture was passed through the extrusion reactor.

The end products of the grafting reaction were functionalized PP/LDPE ([PP/LDPE]-*graft*-MA) blends containing grafted and nongrafted MA. The nongrafted portion of MA could be removed from the samples by extraction in ethanol. This procedure served as a basis for evaluation of the grafting efficiency α, i.e., the ratio of the amount of the grafted monomer to its total amount introduced into PP/LDPE [4].

To determine the grafting efficiency, 40–50-μm film samples of the [PP/LDPE]-*graft*-MA blends, pressed on a laboratory press, were placed into a temperature-controlled vessel containing ethanol at 70°C, in which the nongrafted portion of MA was extracted. After being kept in ethanol for 18–20 h, the films were removed and analyzed by IR spectroscopy on a UR-20 spectrophotometer (Carl Zeiss, Jena, Germany).

As analytical band we used the absorption band near 1720 cm^{-1}, corresponding to absorption of carbonyl groups. To eliminate the influence of the film thickness fluctuations on the optical density of the absorption band, reduced this optical density to that of the internal reference. To this end, we used the absorption band at 1325 cm^{-1}, corresponding to the stretching vibrations of the C–C bonds [4]. The parameter α, %, was calculated by the formula

$$\alpha = \frac{D_\tau}{D_0} \times 100. \quad (1)$$

Here, D_τ and D_0 are the relative optical densities of the absorption band of carbonyls (ratio of the optical densities of the band analyzed and of the internal reference, ν_{C-C} = 1325 cm^{-1}) before and after extraction of the films in ethanol, respectively.

Taking into account the data from [11], we assumed that the extinction coefficient of the >C=O bonds in the carboxy groups remains unchanged upon grafting. The arithmetic mean grafting efficiency was calculated using the data for nine samples. The relative error of a single measurement was within 8%.

The viscosity of the molten materials was estimated from the melt flow index (MFI). The measurements were carried out on an IIRT-AM device at a load of 5 kg, capillary diameter of 2.095 ± 0.005 mm, and temperatures of 190 and 230°C. A granulated material was charged into the heated cylinder of the device and kept for 4 min. Five replicate measurements were made for each material. The relative error of the measurements was within 1% at a confidence level of 0.95.

Using the MFI values determined at two temperatures and identical loads, we calculated the activation energy E_a of viscous flow by the equation [12]

$$E_a = -R \ln k \frac{T_1 T_2}{T_2 - T_1}. \quad (2)$$

Here, R is the universal gas constant; T_1 and T_2, test temperatures ($T_1 < T_2$); and k, coefficient defined as

$$k = \mathrm{MFI}_{T_1}/\mathrm{MFI}_{T_2}. \quad (3)$$

Using the MFI values at the set temperature, we also determined the melt viscosity η, which is close to the Newtonian viscosity [12]

$$\eta = \frac{P r_c^4 \rho t_c}{2 D_p^2 (L_c + \nu r_c) \mathrm{MFI}}. \quad (4)$$

Here, P is load; t_c, time constant; r_c, capillary radius; L_c, capillary length; D_p, plunger diameter; ρ, melt density; and ν, input correction (eliminated from the calculations).

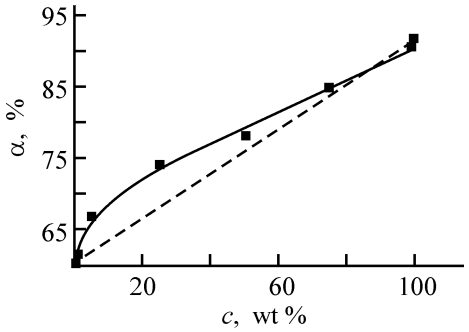


Fig. 1. MA grafting efficiency α vs. the LDPE concentration *c* in the PP/LDPE blend. (*Dashed line*) Additive values; the same for Figs. 2–3.

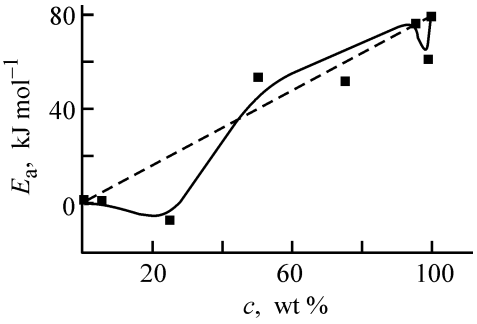


Fig. 2. Activation energy E_a of viscous flow of the [PP/LDPE]-*graft*-MA blends vs. the LDPE concentration *c*.

Figure 1 and the table illustrate the course of the reactions of MA grafting to PP, LDPE, and PP/LDPE blends. Among the materials studied, the lowest grafting efficiencies α were exhibited by the functionalized homopolymer PP (PP-*graft*-MA), and the highest, by LDPE-*graft*-MA. Machado *et al.* [7, 8] also reported a higher, compared to PP, yield of the grafted products in the case when polar monomers were grafted to LDPE. The PP-to-LDPE ratio in the initial reaction mixture strongly affects the parameter α. The grafting efficiency tends to grow with increasing LDPE concentration in the PP/LDPE blend. At relatively small LDPE additions (up to 25 wt %), α tends to grow more rapidly and nonlinearly with increasing LDPE content in the blend. In the 25–95% range, the concentration dependence of α is close to linear. In the 1–90% concentration range, the actual grafting efficiencies exceed the additive values.

On the whole, minor (up to 25 wt %) LDPE additions affect (raise) α more strongly than minor additions of PP affect (decrease) this parameter when MA is grafted to the PP/LDPE blend.

The melt flow index determined at 190°C and a load of 5 kg varies with the PP/LDPE blend composition in a more complex manner than the grafting efficiency (see table). Based on the tabulated data, three groups of blends can be distinguished, depending on their rheological behavior under varied PP-to-LDPE ratio.

For example, at 190°C, the [PP/LDPE]-*graft*-MA blends with the PP content within 99–75 wt % exhibit enhanced MFIs, close to that of PP-*graft*-MA; they are more than three times that of the initial PP. The maximum MFIs are exhibited by the [95PP/5LDPE]-*graft*-MA blend. Blends containing 99–75 wt % PP also exhibit a sharp decrease in the activation energy of viscous flow of their melts, down to negative values for the [75PP/25LDPE]-*graft*-MA blend (Fig. 2).

The 50 : 50 and 25 : 75 PP/LDPE blends exhibit a sharp increase in viscosity (a decrease in MFI). The MFI values for these blends are close to additive.

Further increase in the LDPE concentration (5 : 95 and 1 : 99 compositions) even more strongly decreases the MFI. This is accompanied by an increase in E_a. Notably, the [PP/LDPE]-*graft*-MA blends containing 1 and 5 wt % PP exhibit smaller MFIs than LDPE-*graft*-MA.

The pattern of variation of the MFI at 230°C and a load of 5 kg with the [PP/LDPE]-*graft*-MA blend composition differs from that at 190°C (see table). The primary distinguishing features are that enhanced MFIs, exceeding that of PP-*graft*-MA, are exhibited by a larger number of the formulations and that a sharp increase in viscosity is manifested only when the PP

Efficiency of MA grafting to PP–LDPE blends and rheological properties of the melts, depending on the ratio of the polymeric components

Material studied, wt %	α, %	MFI, g/10 min, at indicated *T*, °C	
		190	230
PP	–	4.9	11.4
PP-*graft*-MA	60.2	15.6	16.2
[99PP/1LDPE]-*graft*-MA	61.8	16.9	17.0
[95PP/5LDPE]-*graft*-MA	66.8	17.3	17.4
[75PP/25LDPE]-*graft*-MA	74.2	16.6	16.2
[50PP/50LDPE]-*graft*-MA	78.3	5.7	17.1
[25PP/75LDPE]-*graft*-MA	85.1	5.5	16.5
[5PP/95LDPE]-*graft*-MA	89.8	0.1	0.5
[1PP/99LDPE]-*graft*-MA	90.6	0.2	0.7
LDPE-*graft*-MA	91.8	0.3	1.6
LDPE	–	7.4	18.0

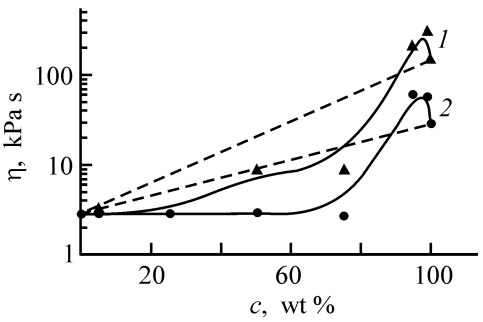
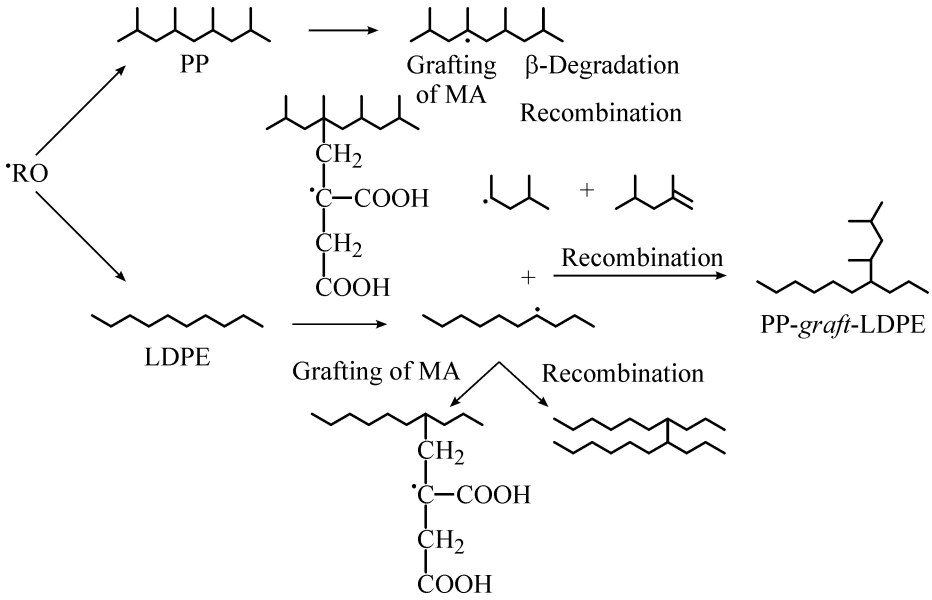


Fig. 3. Newtonian viscosity η of the [PP/LDPE]-*graft*-MA blends vs. the content of LDPE *c* at (*1*) 190 and (*2*) 230°C.

concentration is within 5 wt %. This may be due to major differences in the activation energies of viscous flow of the PP/LDPE blends under study (Fig. 2) because of the processes occurring in the course of free-radical grafting of MA [13]. The Newtonian viscosity of the melts studied and MFI vary in the opposite directions (Fig. 3).

The changes accompanying the MA grafting to the PP/LDPE blends can be explained in the context of the present-day views on the mechanism of the free-radical processes occurring in PP and LDPE melts, initiated by organic peroxides (see scheme). Studies performed in [1–8] suggest that a peroxy initiator forms macroradicals by abstraction of a hydrogen atom from the polymer substrate when reacting with the free radicals yielded by peroxide thermolysis. The resulting macroradicals can be involved in a number of subsequent chemical reactions, such as chemical grafting of the monomer, cross-linking of the macromolecules, their degradation, etc. The tendency of a macroradical toward participation in a reaction is determined by its chemical structure, as well as by the composition of the reaction medium and process factors.

The PP$^{\cdot}$ macroradicals are generated by reactions in which a hydrogen atom is abstracted mostly from the tertiary carbon atoms in the polymer chain [7–9]. Further, the macroradicals can be involved either in β-degradation, with breakdown of the macrochains, or in the monomer addition reactions (see scheme).



Scheme of possible chemical reactions at free-radical grafting of MA to PP/LDPE blends.

The relatively low grafting efficiencies typical of both the initial PP and PP/LDPE blends with a high PP content (from 99 to 75 wt %) may be due to the fact that β-degradation of the PP macromolecules is faster than the MA grafting [7, 8]. Intensive β-degradation is suggested by a major increase in MFI of PP-*graft*-MA and [PP/LDPE]-*graft*-MA relative to the initial PP, with the PP content increasing to 75%.

The methyl group CH_3, close to the reaction center, creates an additional steric hindrance to reactions between the monomer being grafted and the PP macroradicals [14]. This hinders grafting and facilitates β-degradation.

In the case of LDPE, there is no such hindrance for macroradicals formed with secondary carbon atoms involved. As a result, the efficiencies of the MA grafting to the LDPE macromolecules exceed those for PP and grow with increasing LDPE content in the blend. In addition to reactions with the monomer, the LDPE macroradicals are also involved in recombination reactions resulting in cross-linking, branching, or propagation of the macromolecules [2, 4–8]. This is suggested by an increase in the melt viscosity (decrease in MFI) for LDPE-*graft*-MA and a number of blends with increased LDPE concentrations.

The scheme suggests that β-degradation of the PP macromolecules yields new macroradicals at the secondary carbon atom. However, Machado *et al.* [7, 8] reported that these macroradicals rapidly decay and hence do not markedly affect grafting.

The β-degradation and recombination reactions of the macroradicals accompanying monomer grafting to PP and LDPE are side, frequently undesired, processes since they decrease the yield of the grafted product and can deteriorate the rheological and other properties of functionalized POs (FPOs). In view of the fact that PP and LDPE enter into oppositely directed side reactions in grafting (degradation and cross-linking), it can be assumed that the extent of macromolecular transformations and the rheological properties of polymer melts can be controlled by introducing minor additives of a component into the PP/LDPE blend. However, the table suggests that minor PP additives not only do not increase but even decrease the MFI of [PP/LDPE]-*graft*-MA relative to LDPE-*graft*-MA. Minor LDPE additives, in turn, increase the MFI of the FPO blends relative to PP-*graft*-MA, contrary to expectations. In our opinion, these facts are very important for comprehending the general pattern of the transformations of interest. Clearly, in blends with the LDPE concentrations of up to 25 wt %, degradation of the PP macrochains dominates over recombination of the macroradicals and is faster, compared to PP-*graft*-MA. This may be due to two factors. First, the rate of the reaction between the PP macromolecules and free radicals generated by degradation of the peroxy initiator may exceed that for LDPE. Since, in the case of PP, the hydrogen atom is abstracted from the tertiary, rather than secondary, carbon atom, as in the case of LDPE, the resulting radical will be more prone to β-degradation than to recombination. This can hinder formation of grafted copolymers like LDPE-*graft*-PP, which could affect the rheological parameters of the materials. Second, formation of the LDPE-*graft*-PP copolymers can be hindered, as indicated by Braun *et al*. [15], by the two-phase nature of the PP/LDPE blends, also characteristic of their melts. This means that each polymer should participate in free-radical processes independently. However, this would imply additive changes in the MFI.

Clearly, in the region of medium concentrations of the components (~1 : l ratio), their influence on the MFI is determined by the ratio of the degrees of conversion of the blend components.

In the case of minor PP additives, the MFI of [PP/LDPE]-*graft*-MA may decrease relative to that of LDPE-*graft*-MA because of an increase in the concentration of the LDPE macroradicals, whose formation can be promoted by the radical degradation products of the PP macromolecules. Also, in the presence of PP, formation of the LDPE macroradicals may become more probable due to mechanochemical reactions, also typical of reactive extrusion [1, 2].

Along with the above-mentioned factors, the rheological properties of the materials may additionally change during the MFI measurements.

The changes in the E_a are also due to the chemical processes occurring in the course of MA grafting to the PP/LDPE blends and are governed by their composition. Very small activation energies observed for high-index blends, containing 99–75 wt % PP, are, evidently, due to several factors. In particular, β-degradation makes the PP macromolecules less branched because of a decrease in the number of the side substituents (methyl groups), and a major amount of low-molecular-weight oligomers is accumulated in the polymer structure; owing to the plastisizing effect of LDPE, the macromolecules acquire an enhanced flexibility [16, 17]. The negative activation energies for the [75PP/25LDPE]-*graft*-MA blend are, evidently, due to an additional cross-linking of the material in the measuring cylinder of the IIRT-AM device, when the MFI is determined at an elevated temperature. As a result, in particular, the MFI at 230°C proved to be smaller than at 190°C. For compositions containing ≥50 wt % LDPE, E_a grows because of the predominance in these systems of macroradical recombination reactions. These are responsible for an increased number of side branches of the macrochains, which decrease their flexibility and hinder their conformational rearrangements in a flow [16, 17].

Thus, analysis of the rheological behavior of the [PP/LDPE]-*graft*-MA materials shows that the polymeric components affect in a complex manner

the course of the free-radical transformations of the macromolecules during reactive extrusion. Combined analysis of the concentration dependences of the grafting efficiency and MFI gives a better insight into the pathways of the proceeding reactions.

CONCLUSIONS

(1) The polymeric component ratio in polypropylene–low-density polyethylene blends strongly affects the course of the reaction of grafting of methylenebutanedioic acid and its accompanying macromolecular transformations (side reactions). The influence of the polypropylene additions on the monomer grafting is primarily manifested as a decrease in the yield of the grafted product with increasing concentration of this component in the blend.

(2) At relatively small additions of low-density polyethylene (up to 25 wt %), the efficiency of grafting of methylenebutanedione acid to the polypropylene–low-density polyethylene blend grows nonlinearly (exceeding the additive values). At polyethylene concentrations of 25–95 wt %, the dependence of the grafting efficiency on the composition is close to linear: The grafting efficiency α tends to monotonically increase with increasing polyethylene concentration.

(3) When minor additions of a polymeric component are introduced, the rheological properties of the molten blends change in a complex, somewhat unexpected manner. Addition of low-density polyethylene, prone to cross-linking under functionalization, in amounts of up to 25 wt % tends to increase the MFI (to decrease the viscosity) of the [PP/LDPE]-*graft*-MA melt relative to PP-*graft*-MA; additions of polypropylene, prone to degradation under functionalization, in amounts of up to 5 wt % tend to decrease the MFI (to increase the viscosity) of the [PP/LDPE]-*graft*-MA melt relative to PP/LDPE-*graft*-MA. Blends with polyethylene concentrations of up to 25% are characterized by an extremely low viscous flow activation energy, down to negative values for the [75PP/25LDPE]-*graft*-MA blend.

REFERENCES

1. Xanthos, M., *Reactive Extrusion: Principles and Practice*, Munich: Hanser, 1992.
2. Moad, G., *Prog. Polym. Sci.*, 1999, vol. 24, no. 1, pp. 81–142.
3. Chung, T.C., *Functionalization of Polyolefins*, San-Diego: Academic, 2002.
4. Pesetskii, S.S., Jurkowski, B., Krivoguz, Yu.M., and Urbanovicz, R., J. *Appl. Polym. Sci.*, 1997, vol. 65, no. 8, pp. 1493–1502.
5. Pesetskii, S.S., Jurkowski, B., Krivoguz, Yu.M., and Olkhov, Y.A., *J. Appl. Polym. Sci.*, 2001, vol. 81, no. 14, pp. 3439–3448.
6. Pesetskii, S.S., Jurkowski, B., and Makarenko, O.A., *J. Appl. Polym. Sci.*, 2002, vol. 86, no. 1, pp. 64–72.
7. Machado, A.V., Covas, J.A., and van Duin, M., *Polymer*, 2001, vol. 42, no. 8, pp. 3649–3655.
8. Machado, A.V., van Duin, M., and Covas, J.A., *J. Polymer Sci., Part A: Polym. Chem.*, 2000, vol. 38, no. 21, pp. 3919–3932.
9. Heinen, W., Rosenmoller, C.H., Wenzel. C.B., *et al.*, *Macromolecules*, 1996, vol. 29, p. 1151.
10. Chaoqin Li, Yong Zhang, and Yinxi Zhang, *Polym. Test.*, 2003, vol. 22, no. 2, pp. 191–195.
11. Fodor, Z.S., Iring, M., Tudos, F., and Kelen, T., *J. Polym. Sci., Part A: Polym. Chem.*, 1984, vol. 22, no. 10, pp. 2539–2550.
12. Kalinchev, E.L. and Sakovtseva, M.B., *Svoistva i pererabotka termoplastov* (Properties and Processing of Thermoplastics), Leningrad: Khimiya, 1983.
13. Severs, E.T., *Reologiya polimerov* (Polymer Rheology), Moscow: Khimiya, 1966.
14. Do, I.H., Yoon, L.K., Kim, B.K., and Jeong, H.M., *Eur. Polym. J.*, 1996, vol. 32, no. 12, pp. 1387–1393.
15. Braun, D., Richter, S., Hellmann, G.R., and Ratzsch, M., *J. Appl. Polym. Sci.*, 1998, vol. 68, no. 12, pp. 2019–2028.
16. Ivanyukov, D.V. and Fridman, M.L., *Polipropilen* (Polypropylene), Moscow: Khimiya, 1974.
17. Vinogradov, G.V. and Malkin, A.Ya., *Reologiya polimerov* (Polymer Rheology), Moscow: Khimiya, 1977.

Russian Journal of Applied Chemistry, Vol. 78, No. 2, 2005, pp. 311–314. Translated from Zhurnal Prikladnoi Khimii, Vol. 78, No. 2, 2005, pp. 316–319.
Original Russian Text Copyright © 2005 by K. Guliev, Ponomareva, A. Guliev.

MACROMOLECULAR CHEMISTRY AND POLYMERIC MATERIALS

Copolymerization of 2-Chloro-Substituted *p*-Cyclopropylstyrenes with Styrene and Properties of the Resulting Copolymers

K. G. Guliev, G. Z. Ponomareva, and A. M. Guliev

Institute of Polymeric Materials, National Academy of Sciences of Azerbaijan, Sumgait, Azerbaijan

Received July 14, 2004

Abstract—2,2-Dichloro- and 2-chloro-1-(*p*-vinylphenyl)cyclopropanes were prepared and brought into copolymerization with styrene. The effect of substituents on the reactivity of the monomers was examined. The physicomechanical properties of the copolymers were studied.

One of the ways to improve the physicomechanical, thermal, and optical properties and enhance the flame resistance of polystyrene plastics is copolymerization of styrene with other monomers. In so doing, it is possible to vary the properties of the copolymers in a wide range.

The copolymerization of styrene with substituted styrenes has been studied extensively [1–7].

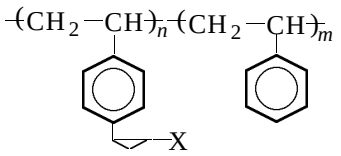
In this study, we prepared 2,2-dichloro- and 2-chloro-1-(*p*-vinylphenyl)cyclopropanes (**I**, **II**, respectively) and performed their copolymerization with styrene in the bulk and in solution; we also examined the effect of the chlorinated substituents on the reactivity of the monomers and on the properties of the resulting copolymers. We found that styrene smoothly copolymerizes with the monomers synthesized, without opening of the cyclopropane ring; the resulting copolymers are soluble.

The copolymerization under the conditions of our experiments occurred through opening of the double bond, yielding macromolecules with pendant phenyl groups (unsubstituted and those bearing chlorinated cyclopropane fragments). This is suggested by the spectra of the copolymers. The ratio of the monomeric units (**I** or **II** to styrene) in the copolymer was estimated from the chlorine content determined by elemental analysis.

The IR spectra of both the starting monomers and copolymers thereof contain characteristic bands belonging to vibrations of the C–Cl bond (675 cm^{-1}) and cyclopropane ring (1030–1040 cm^{-1}). The spectra of the copolymers also contain well-defined bands at 1450, 1500, 1585, and 1605 cm^{-1} belonging to vibrations of the benzene ring. Strong bands at 1213 and 1170 cm^{-1} and bands at 1110 and 1013 cm^{-1} are characteristic of 1,4-disubstituted benzenes and belong to the in-plane bending modes of the four hydrogen atoms of the benzene ring.

Changes in the intensities of the bands belonging to the main functional groups of **I** and **II** suggest changes in the composition of the monomeric units.

The IR data allow us to ascribe the following structure to the copolymers:



where X = 2Cl (**I**), Cl (**II**).

For this pair of monomers, we calculated the copolymerization constants and the Alfrey–Price parameeters *Q* and *e* [8]. To evaluate the distribution of units in the macromolecular chain, we calculated the microstructural parameters L_{M_1}, L_{M_2}, and *R* [9]. The results are listed in Table 1.

Table 1 shows that, at any ratio of the starting monomers, the copolymer is always enriched in units of mono- or gem-dichloro-substituted cyclopropylstyrenes, which is due to the higher reactivity of these monomers, caused by the presence of the substituted cyclopropane ring.

The chlorine atoms, which are present in **I** and **II** as substituents in the cyclopropane ring and are separated from the reaction center by the phenyl ring and a cy-

1070-4272/05/7802-0311 © 2005 Pleiades Publishing, Inc.

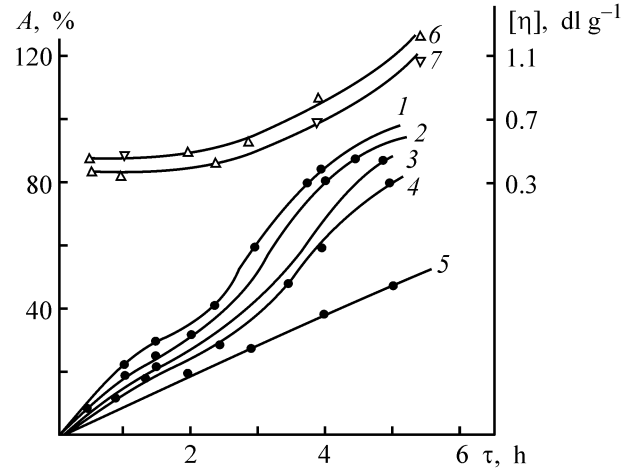
Table 1. Copolymerization of 2,2-dichloro- and 2-chlorocyclopropylstyrenes **I** and **II** (M_1) with styrene (M_2)

Starting mixture, mol %		Copolymer composition, mol %		Microstructure*			Parameters of copolymerization of **I** and **II** (M_1) with styrene (M_2)					
M_1	M_2	M_1	M_2	L_{M_1}	L_{M_2}	R	r_1	r_2	r_1r_2	Q_1	e_1	Cl, %
Cyclopropylstyrene (**I**)												
10	90	17.10	82.90	1.134	5.500	30.15						5.70
25	75	35.95	64.05	1.403	2.500	51.24						11.98
50	50	59.75	40.43	2.210	1.500	53.91	1.21 ± 0.06	0.50 ± 0.03	0.605	3.523	–1.508	19.86
75	25	79.87	20.19	4.630	1.167	34.50						26.62
90	10	91.85	8.15	11.890	1.056	15.45						30.62
Cyclopropylstyrene (**II**)												
10	90	16.66	83.34	1.13	5.68	29.37						3.31
25	75	35.07	64.93	1.4	2.56	50.5						6.98
50	50	59.13	40.87	2.2	1.52	53.76	1.20 ± 0.04	0.52 ± 0.02	0.624	2.77	–1.486	11.76
75	25	79.68	20.32	4.6	1.17	34.66						15.85
90	10	91.77	7.96	10.72	1.06	16.98						18.25

* (L_{M_1}, L_{M_2}) Mean lengths of blocks of the corresponding monomeric units; (R) harwood parameter of block structure.

clopropane fragment in the *p*-position relative to the styrene double bond, decrease the copolymerization constants relative to unsubstituted styrene. This is due to increased conjugation in the monomer molecule as a result of the effect of the substituents additionally stabilizing the forming radical. The copolymerization constants of **I** and **II** differ insignificantly.

The influence exerted by the chlorine atoms on the vinyl group through the three-membered carbon ring and phenyl ring leads to an increase in the extent of conjugation in the monomer molecule, but only slightly depends on the number of chlorine atoms. This is confirmed by the UV spectra of **I** and **II**, in which the absorption maxima are located at 295 and 292 nm, respectively.



Variation with time τ of the (*1*–*5*) yield *A* and (*6*, *7*) intrinsic viscosity [η] of 2,2-dichloro-1-(*p*-vinylphenyl)cyclopropane (**I**)–styrene copolymer. 70°C. Content of **I** in the starting mixture, %: (*1*, *7*) 100, (*2*) 90, (*3*) 80, (*4*, *6*) 70, and (*5*) 0.

To reveal regular trends in the polymerization and study the properties of the copolymers, we performed copolymerization of **I** and **II** with styrene in a wide range of ratios of the starting monomers.

The kinetic curves of initiated copolymerization of **I** with styrene at 70°C (see figure) show that, after 37–46% conversion of the monomers is reached, the copolymerization occurs with autoacceleration. The effect becomes more pronounced as the content of **I** in the mixture is increased. The molecular weight of the forming polymers appreciably increases at high conversions.

Experiments on thermal copolymerization at high temperatures (110–150°C) revealed no appreciable self-acceleration, and the intrinsic viscosity of the copolymers remained virtually constant at all the conversions. Some properties of the copolymers are given in Table 2.

Table 2 shows that introduction of chloro-substituted cyclopropylstyrene units into the polystyrene chain increases the Vicat softening point and enhances the optical and physicomechanical properties, compared to styrene homopolymer. Some of the copolymers obtained show self-extinguishing behavior. This property becomes more pronounced with an increase in the content of **I** in the copolymer.

Table 2. Physicomechanical characteristics of the copolymers prepared

Parameter	Polystyrene	Copolymers with indicated content of **I** or **II**, %			
		40		60	
		I	**II**	**I**	**II**
Intrinsic viscosity [η], dl g^{-1}	1.15	1.17	–	–	
Refractive index	1.5895	1.6010	1.5905	1.6040	1.6010
Vicat softening point, °C	103	119	116	128	126
Brinell hardness, kgf cm^{-2}	14	16	15	–	–
Ultimate tensile strength, MPa	39.0	34.8	35.0	35.0	
Relative elongation at break, %	1.7	1.5	–	1.5	–

Parameter	Polystyrene	Copolymers with indicated content of **I** or **II**, %					
		70		80		90	
		I	**II**	**I**	**II**	**I**	**II**
Intrinsic viscosity [η], dl g^{-1}	1.15	1.13	–	1.15	–	–	–
Refractive index	1.5895	1.6053	1.6038	1.610	1.6080	1.6115	1.6105
Vicat softening point, °C	103	132	130	139	–	148	136
Brinell hardness, kgf cm^{-2}	14	24	16	–	–	27	19
Ultimate tensile strength, MPa	39.0	–	–	45.0	47.0	46.8	48.7
Relative elongation at break, %	1.7	–	–	1.9	–	1.9	–

Thus, the properties of the copolymers derived from chloro-substituted cyclopropylstyrenes are governed by the substituent in the monomers, and the activity of the monomers in the copolymerization depends on the extent of conjugation of the vinyl π electrons with the substituent *p* electrons.

EXPERIMENTAL

The starting monomer, 2,2-dichloro-1-(*p*-vinylphenyl)cyclopropane **I**, was prepared as described in [6]. 2-Chloro-1-(*p*-vinylphenyl)cyclopropane **II** was prepared as follows. Sodium metal (0.1 mol, 2.3 g) was added in small pieces to a solution of **I** (0.2 mol, 42.6 g) in benzene, after which methanol was added dropwise with stirring and cooling on an ice bath. After the reaction was complete, distilled water was added, the organic layer was separated, and the aqueous layer was extracted with ether. The combined organic phases were evaporated, and the product was vacuum-distilled; bp 78–80°C/1 mm Hg. Yield 36% (12.85 g); n_D^{20} = 1.5630, d_4^{20} = 1.12, $MR_{D\text{calc}}/MR_{D\text{exp}}$ = 52.388/51.76. Analytical data:

Found, %: C 73.95, H 6.16, Cl 19.88.
Calculated, %: C 73.58, H 6.05, Cl 19.75.

The purity of the monomers was checked chromatographically; it was 99.9% in all the cases. The kinetics of the copolymerization of **I** and **II** with styrene was studied in ampules in a nitrogen atmosphere at various ratios of the starting monomers. To determine the copolymerization parameters, the reaction was stopped at ≤10% conversion. The compositions of the copolymers were determined by elemental analysis for chlorine, and their molecular weights were estimated from the intrinsic viscosity, determined with an Ubbelohde viscometer at 25°C in benzene. All the copolymers were reprecipitated from a benzene solution with methanol. The softening points of the copolymers were determined by the Vicat method. The physicomechanical parameters of the copolymers were determined with film samples prepared by casting from a benzene solution. The IR spectra were measured with a Specord M-80 spectrophotometer.

After appropriate purification and drying, all the copolymers were white powders soluble in aromatic and chlorinated hydrocarbons.

CONCLUSIONS

(1) New monomers, 2,2-dichloro- and 2-chloro-1-(*p*-vinylphenyl)cyclopropanes, were prepared, and

their copolymerization with styrene was performed. These monomers are more reactive than styrene in polymerization, owing to the presence of a substituted cyclopropane ring.

(2) The copolymerization constants and Alfrey–Price parameters of the cyclopropylstyrenes were calculated. The chlorine substituents in the cyclopropane ring make higher the relative reactivity constants and the specific activity of the monomers.

(3) The physicomechanical properties of the copolymers were determined. Introduction of chloro-substituted cyclopropylstyrene units into the polystyrene chain increases the softening point, refractive index, and hardness of the copolymers.

REFERENCES

1. Bylina, G.S., Burykina, L.K., and Ol'dekop, Yu.A., *Vysokomol. Soedin., Ser. B*, 1970, vol. 12, no. 10, pp. 739–742.
2. Kato, M., *J. Polym. Sci., Part A-1*, 1969, vol. 7, no. 8, pp. 2175–2184.
3. Rupyshev, V.G., Ivanko, T.P., Kozlova, G.I., *et al.*, *Plast. Massy*, 1983, no. 1, pp. 58–59.
4. Zaitsev, B.A. and Shtraikhman, G.A., *Vysokomol. Soedin., Ser. A*, 1968, vol. 10, no. 2, pp. 438–445.
5. Chernobai, A.V. and Zelichenko, Zh. Kh., *Vysokomol. Soedin., Ser. A*, 1969, vol. 11, no. 7, pp. 1631–1638.
6. Guliev, K.G., Nazaraliev, Kh.G., and Guliev, A.M., *Azerb. Khim. Zh.*, 1999, no. 1, pp. 87–90.
7. Guliev, K.G., Ponomareva, G.Z., Nazaraliev, Kh.G., and Guliev, A.M., *Azerb. Khim. Zh.*, 2002, no. 3, pp. 45–50.
8. *Copolymerization*, Ham, G.E., Ed., New York: Interscience, 1964.
9. Zil'berman, E.N., *Vysokomol. Soedin., Ser. B*, 1979, vol. 21, no. 1, pp. 33–36.

Russian Journal of Applied Chemistry, Vol. 78, No. 2, 2005, pp. 315–318. Translated from Zhurnal Prikladnoi Khimii, Vol. 78, No. 2, 2005, pp. 320–323.
Original Russian Text Copyright © 2005 by Klyuchnikov, Chachkov, Deberdeev, Zaikov.

MACROMOLECULAR CHEMISTRY AND POLYMERIC MATERIALS

Mechanism of Depolymerization of Polymeric *p*-Dinitrosobenzene in Vulcanization of Unsaturated Rubbers: A Quantum-Chemical Study

O. R. Klyuchnikov, D. V. Chachkov, R. Ya. Deberdeev, and G. E. Zaikov

Kazan State University of Power Engineering, Kazan, Tatarstan, Russia
Kazan State Technological University, Kazan, Tatarstan, Russia
Emanuel' Institute of Biochemical Physics, Russian Academy of Sciences, Moscow, Russia

Received June 1, 2004

Abstract—The mechanism of depolymerization of polymeric *p*-dinitrosobenzene in vulcanization of unsaturated rubbers is analyzed. The results obtained explain why the vulcanizing activity of *p*-dinitrosobenzene decreases in the course of its prolonged storage.

p-Dinitrosobenzene (DNB) is a component of rubber–substrate adhesion systems [1] and a low-temperature vulcanizing agent for stocks based on unsaturated rubbers [2]. DNB is a polymeric compound virtually insoluble under common conditions in any solvent [3].

The vulcanizing activity of DNB is known to change in the course of its storage [4, 5]; this fact calls for theoretical substantiation. Furthermore, data on the structure of polymeric *p*-dinitrosobenzene (poly-DNB) are contradictory, and nothing is known about the mechanism of its depolymerization in the course of addition to unsaturated compounds (in particular, in vulcanization of unsaturated rubbers).

In the papers concerning the kinetics and mechanism of addition of poly-DNB to unsaturated compounds [6, 7], the authors, as a rule, presented the monomeric DNB structure; some authors assumed the structure has a dimeric sandwich form (Fig. 1) [7–9], but this structure does not stand up to criticism.

It is known that IR spectra of poly-DNB contain a strong band at 1264 cm^{-1} [10, 11], characteristic of nitrosoarene trans dimers [10, 12], with a C–N–N angle in the sandwich structure close to 120°. At the same time, the C–N–N angle in the sandwich structure is close to 90°, and, therefore, this structure should be strained and thermodynamically unstable.

Experimental determination of the poly-DNB structure is complicated by its high dispersity and insolubility in all the solvents under common conditions. Therefore, to study the geometry of poly-DNB and energy effects of its reactions, we used quantum-chemical calculations. We chose the relatively reliable DFT B3LYP method with the 6-31G(d) basis set. The calculations were performed with a computer cluster of the Kazan State Technological University, using the GAUSSIAN 98 program package [13], with full geometry optimization. For the model structures, we calculated the force constants, vibration frequencies, thermodynamic quantities, and variation of the relative energy in extension of the (O)N–N'(O') bond of model structures. To reduce the number of basis functions, we used 2-butene and 2-pentene as structures modeling a fragment of an unsaturated rubber.

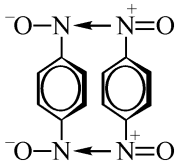


Fig. 1. Presumed dimeric sandwich structure of DNB.

1070-4272/05/7802-0315 © 2005 Pleiades Publishing, Inc.

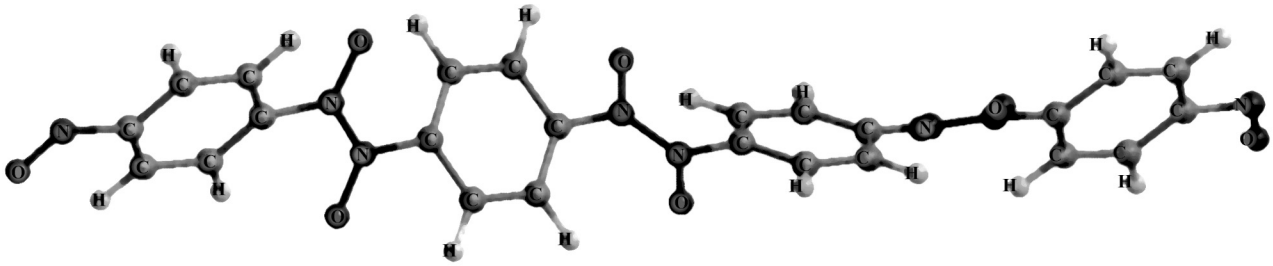


Fig. 2. Geometry of DNB tetramer.

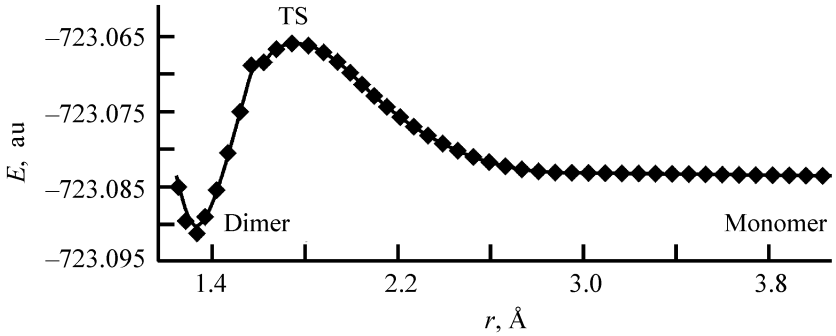


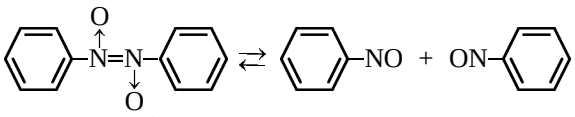
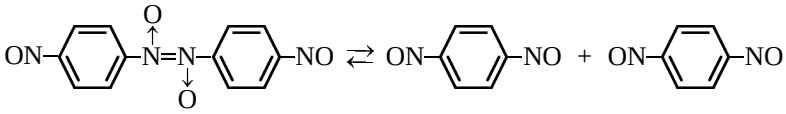
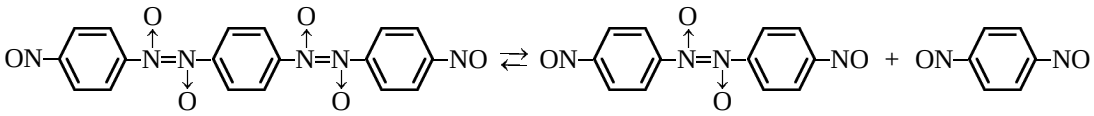
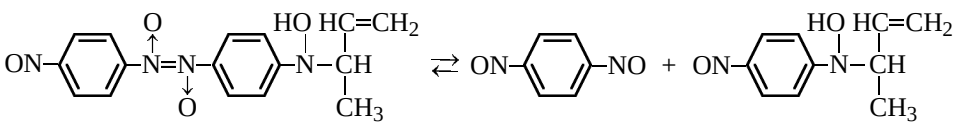
Fig. 3. Variation of the energy E (1 au = 2625 kJ) in extension of the N=N bond in nitrosobenzene dimer. (r) N=N distance; (TS) transition state.

Figure 2 shows the optimized geometry of DNB tetramer as a model of poly-DNB. The tetramer has a linear *trans*-azo-N,N'-dioxy-1,4-phenylene structure twisted in a spiral; the phenylene fragments are turned relative to each other by 45°. Attempts to optimize the geometry of the DNB dimer in the form of a sandwich failed, apparently because of the strain of the C–N–N–C bond system.

Calculations of the relative energy of the nitrosobenzene dimer at extension of the (O)N–N'(O') bond to 5 Å and at its contraction from 5 Å at a 0.05 Å step revealed maxima on the potential energy surface, corresponding to the transition states (TS) with the same geometries and activation enthalpies $\Delta H^{\neq}$ = 66.1 kJ mol^{-1} (Fig. 3). These calculations also showed that the nitrosobenzene dimer has a lower energy than the monomer.

The calculated activation enthalpy of dissociation of the nitrosobenzene dimer is reasonably consistent with the experimental activation energy of

Activation enthalpy of dissociation of the azo-*N*,*N*'-dioxy group to monomeric nitroso groups

Model reaction	$\Delta H^{\neq}$, kJ mol^{-1}
	66.1
	67.4
	66.9
	64.3

the process, determined in dichloromethane: $E^{\neq}$ = 86 kJ mol^{-1} [14].

Calculations of the potential energy surfaces in extension of the (O)N–N'(O') bond to separate nitroso groups in the DNB dimer, trimer, and product of addition of DNB dimer to 2-butene gave similar results (see table). These dissociation reactions are also endothermic.

The calculated activation enthalpy of dissociation of the DNB trimer is slightly lower than that of the DNB dimer. Addition of the DNB dimer to the alkene decreases the activation barrier of its subsequent dissociation across the (O)N–N'(O') bond by 3.1 kJ mol^{-1}.

The decrease in the activation parameters of dissociation of the (O)N–N'(O') bond in going from the DNB dimer to trimer can be accounted for by a weaker electron-withdrawing power of the azo-*N*,*N*'-dioxy group, compared to the nitroso group. In addition of DNB dimer to 2-butene, the hydroxylamine derivative can be regarded as a *p*-substituent of the first kind, which makes lower the activation energy of dissociation of the (O)N–N'(O') bond. It is known that, as the electron-donor power of *p*-substituents increases, the energy of dissociation of nitrosoarene dimers to monomers decreases, so that nitrosoanilines exist as stable monomers [12].

A study of the addition of the DNB dimer to 2-pentene showed that the reaction product is a secondary hydroxylamine. In this case, as also in that of the model reaction of addition of the DNB monomer to 2-pentene [15], a six-membered transition state is formed. This was confirmed by calculations involving forward and reverse descent from the transition state along the reaction coordinate to the reaction products and starting compounds.

The calculated thermal effects of the reactons of the DNB dimer with 2-pentene were as follows: activation

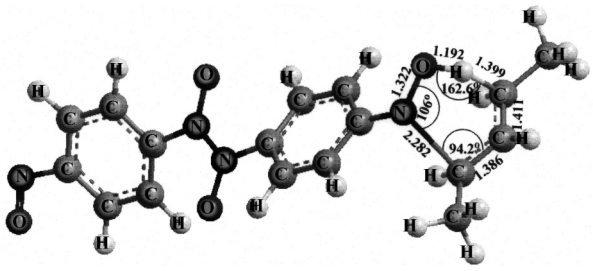


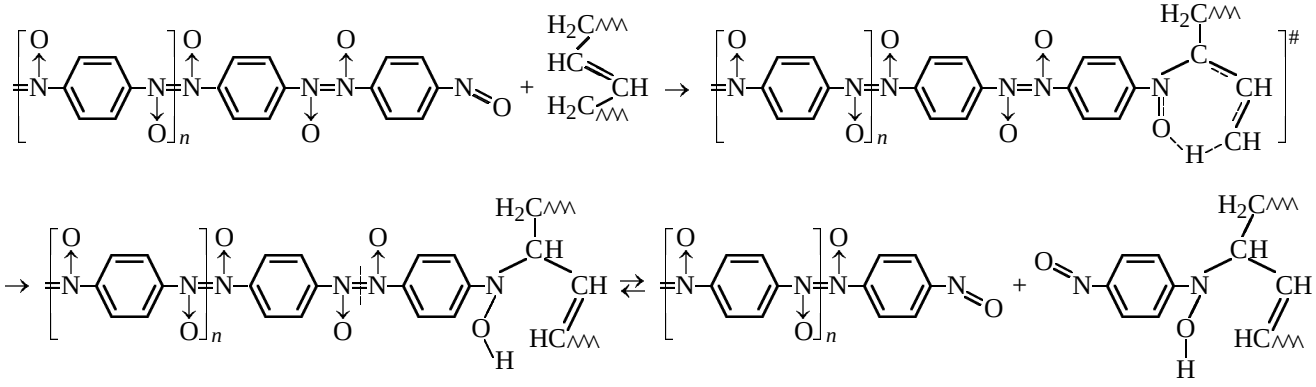
Fig. 4. Structure of the transition state of addition of the DNB dimer to 2-pentene.

enthalpy $\Delta H^{\neq}$ = 97 kJ mol^{-1}, enthalpy of the reaction ΔH = –48 kJ mol^{-1}, and Gibbs energy of the reaction ΔG = –24.7 kJ mol^{-1}. Thus, the reaction is exothermic and can occur spontaneously, which is confirmed by the occurrence of cold curing of unsaturated rubbers with poly-DNB.

The imaginary vibration frequency of the transition state, ν = 1201 cm^{-1}, in combination with the high imaginary vibration intensity, corresponds to the transfer of the methylene proton of 2-pentene to the oxygen atom of the nitroso group.

Figure 4 shows the structure of the transition state and its main geometric characteristics.

Our results suggest the following mechanism of depolymerization of poly-DNB in the course of vulcanization of stocks based on unsaturated rubbers. In the first step, a linear helical molecule of poly-DNB reacts with an alkene fragment of an unsaturated rubber to form a secondary hydroxylamine. The subsequent energetically most favorable step is reversible dissociation of the closest (and weakest) O(N)–N'(O') bond in the *p*-position relative to the hydroxylamine fragment formed by addition of the poly-DNB macromolecule to the unsaturated rubber:



The free nitroso groups subsequently add to other rubber macromolecules to form cross-links, with further fragmentary depolymerization of poly-DNB. Thus, the higher the degree of poly-DNB polymerization, the greater the number of elementary events of dissociation of the (O)N–N'(O') bonds and that of steps in the vulcanization as a whole.

Our results are consistent with the experimental evidence [4, 5] of a decrease in the vulcanizing activity of poly-DNB, caused by an increase in the degree of its polymerization and a decrease in the concentration of terminal nitroso groups during prolonged storage.

CONCLUSIONS

(1) According to the calculation results, polymeric *p*-dinitrosobenzene has a linear *trans*-azo-*N*,*N*'-dioxy-1,4-phenylene structure twisted in a spiral, with the phenyl rings turned relative to each other by 45°.

(2) The activation enthalpy of dissociation of the azo-*N*,*N*'-dioxy groups to monomeric nitroso groups in polymeric *p*-dinitrosobenzene is 64–68 kJ mol^{-1}.

(3) The depolymerization of polymeric *p*-dinitrosobenzene is endothermic.

(4) Changes in the vulcanizing activity of polymeric *p*-dinitrosobenzene in the course of storage are caused by polymerization processes.

ACKNOWLEDGMENTS

The calculations were supported by the Russian Foundation for Basic Research (project no. 03-07-90 092).

REFERENCES

1. Tikhonova, N.P., Ginzburg, L.V., and Dontsov, A.A., *Kauchuk Rezina*, 1987, no. 3, p. 13.
2. Gofman, V., *Vulkanizatsiya i vulkanizuyushchie agenty* (Vulcanization and Vulcanizing Agents), Moscow: Khimiya, 1968.
3. Rugli, P. and Bartusch, G., *Helv. Chim. Acta*, 1944, vol. 26, no. 6, pp. 1375–1378.
4. Klyuchnikov, O.R., Makarov, T.V., Vol'fson, S.I., *et al.*, *Izv. Vyssh. Uchebn. Zaved., Khim. Khim. Tekhnol.*, 2004, vol. 47, no. 2, pp. 22–25.
5. Zaikov, G.E., Klyuchnikov, O.R., Makarov, T.V., and Deberdeev, R.Ya., *Zh. Prikl. Khim.*, 2004, vol. 77, no. 10, pp. 1722–1724.
6. Gan, L.M. and Chew, C.H., *J. Appl. Polym. Sci.*, 1979, vol. 24, no. 2, pp. 371–383.
7. Kabina, T.S., Bugrov, V.P., Sokolov, A.V., and Spiridonova, G.N., *Sintez, svoistva i primenenie zhidkikh butilkauchukov i poliizobutilenov* (Synthesis, Properties, and Use of Liquid Butyl Rubbers and Polyisobutylenes), Moscow: TsNIITEI Neftepererabatyvayushchei i Neftekhimicheskoi Prom–sti., 1986.
8. Gan, L.M. and Chew, C.H., *Rubber Chem. Technol.*, 1983, vol. 56, no. 5, pp. 883–891.
9. Baldwin, E.P., *Rubber Chem. Technol.*, 1970, vol. 43, no. 3, pp. 522–544.
10. Klyuchnikov, O.R., Thermal Decomposition of Derivatives of *N*-Oxides and Aromatic *C*-Nitroso Compounds, *Cand. Sci. Dissertation*, Kazan, 1990.
11. Hacker, N.P., *Macromolecules*, 1993, vol. 26, pp. 5937–5942.
12. *The Chemistry of the Nitro and Nitroso Groups*, Feuer, H., Ed., New York: Interscience, 1969, part 1.
13. *GAUSSIAN 98*, Revision A.9, Pittsburgh (PA), 1998.
14. Azoulaym M. and Fischer, E., *J. Chem. Soc., Perkin Trans. 2*, 1982, no. 6, pp. 637–642.
15. Klyuchnikov, O.R., Deberdeev, R.Ya., and Berlin, A.A., *Dokl. Ross. Akad. Nauk*, 2004, vol. 398, no. 1, pp. 68–71.

Russian Journal of Applied Chemistry, Vol. 78, No. 2, 2005, pp. 319–323. Translated from Zhurnal Prikladnoi Khimii, Vol. 78, No. 2, 2005, pp. 324–328.
Original Russian Text Copyright © 2005 by Zemnukhova, Fedorishcheva, Egorov, Sergienko.

MACROMOLECULAR CHEMISTRY AND POLYMERIC MATERIALS

Recovery Conditions, Impurity Composition, and Characteristics of Amorphous Silicon Dioxide from Wastes Formed in Rice Production

L. A. Zemnukhova, G. A. Fedorishcheva, A. G. Egorov, and V. I. Sergienko

Institute of Chemistry, Far Eastern Division, Russian Academy of Sciences, Vladivostok, Russia

Received April 12, 2004

Abstract—The conditions of recovery of amorphous and crystalline silicon dioxide from husk and straw of rice cultivated in various regions were studied. The dependence of the impurity composition and characteristics of amorphous silica on the plant strain, waste type, and procedures of waste processing was established. The optimum conditions of production of high-purity silicon dioxide were determined, and its characteristics were compared with those of commercial products.

Amorphous silicon dioxide (silica) has a wide field of application, depending on its structure, purity, and physicochemical characteristics. It is used in food, pharmaceutical, fragrance, paint-and-varnish, chemical, metallurgical, construction, oil-refining, rubber-processing, porcelain, glass, textile, plastic, paper, and other branches of industry. Such forms of amorphous silicon dioxide as diatomite or diatomaceous earth, kieselguhr, tripoli powder, carbon white, Aerosil, and microsilica are used for production of modified silica, sorbents for various purposes, including those for filtration of water, beer, wine, oils, sugar, and other food substances and solvents [1–4].

Traditionally, the main sources of silica are mineral forms, whose resources in our country and in the world are rich. A great number of crystalline modifications of SiO_2 is known: they differ in the content of impurities. Impurity metals are incorporated into the crystal lattice of silica, forming strong bonds. Production of amorphous silica from crystalline SiO_2 involves a large expenditure for pretreatment of the initial raw materials and subsequent removal of concomitant impurities [5, 6]. Amorphous SiO_2 is more chemically active and, if required, it can be easily transformed into the crystalline form.

A promising raw material for production of amorphous SiO_2 is the hydrothermal heat carrier used in regions with operating geothermal power plants [7] and large-tonnage wastes from rice production: straw and fruit shells of corn (husk), in regions of rice cultivation [8–12].

The use of rice husk as a renewable raw material for production of high-quality amorphous SiO_2 is extremely promising, since the husk is concentrated in grain-cleaning plants and is a source for additional production of a number of organic compounds, e.g., furfural, xylose, and polysaccharides [8, 9, 12, 13]. However, until now, the main amounts of husk and straw have not been in industrial use because of the absence of integrated technologies taking into account the regional conditions. To develop an integrated scheme for processing of the waste from rice production, it is necessary to know the chemical composition of raw materials as influenced by the strain and area of plant vegetation, which have not been studied adequately.

This study continues the examination of the integrated processing of waste from rice production [12–14] and the conditions of production, impurity composition, and characteristics of amorphous SiO_2 prepared from rice husk and straw.

1070-4272/05/7802-0319 © 2005 Pleiades Publishing, Inc.

Table 1. Particle size distribution of rice husk (RH-1) and maximum content of SiO_2 in ash obtained from particles under the same conditions

Particle size, nm	Weight fraction of particles, %	SiO_2 content in ash, wt %	Particle size, nm	Weight fraction of particles, %	SiO_2 content in ash, wt %
0.5–2	13.4	> 99	0.1–0.16	10.5	< 90
0.25–0.5	45.4	< 99	0.05–0.1	5.9	< 90
0.16–0.25	18.1	~90	≤0.05	6.7	< 87

Table 2. Schemes of raw material processing and ash yield

Scheme	Processing conditions of rice husk and straw	Ash color	Ash yield, %	
			RH	RS
I	Thermolysis at 750°C	Black	36–44	14–28
II	Oxidative burning at 750°C	Dark	11–21	7–14
III	Extraction with H_2O, burning	Light	10–20	6–12
IV	Burning, leaching with 1 N HCl	″	10–20	6–12
V	Extraction with 0.1 N HCl, burning	White	10–20	6–12
VI	Threefold extraction with 0.1 N HCl, burning	″	10–20	6–12
VII	Extraction with 1 N HCl, burning	″	9–19	6–12

EXPERIMENTAL

The objects of study were samples of rice husk (RH) and rice straw (RS) taken in various regions.[1]

The samples of rice husk contained an admixture of corn and meal (product of corn grinding), which were fractionated with respect to the particle size (Table 1). The proportion of the 0.25–0.05-mm fraction varied between different batches of raw materials. Preliminary experiments showed that silica with the highest purity, containing more than 99% SiO_2, is recovered from the husk with a particle size of no less than 0.5 mm (Table 1). In this study, we examined husk samples with a particle size of 0.5 mm and samples of straw cut to 10-mm fragments. The samples were washed with water and dried in air to constant weight. Weighed portions of raw materials were 60–100 g in laboratory experiments and 5–9 kg in a pilot installation.

To recover SiO_2, the RH and RS samples were processed according to various schemes listed in Table 2 and used in [12, 15–18]. Water-soluble substances of RH and RS were extracted with hot water or HCl (analytically pure grade) solution. Thermolysis of the raw materials was carried out at 750°C with deficiency of air or in a helium flow. Oxidative burning was carried out in two stages. First, a weighed portion of a raw material was ashed in a quartz cup on a hot plate to remove volatiles at $T < 500$°C, then the residue was additionally burnt in a laboratory muffle in air at 750 ± 50°C to constant weight and analyzed by chemical, spectral (PGS-2 spectrometer), flame atomic absorption (AA-780 device, Nippon Jharrell Ash, Japan), IR spectroscopic (Specord spectrophotometer, 400–4000 cm^{-1}), X-ray diffraction

[1] The samples of rice husk and straw, locality and year of sampling, and rice strain were as follows: RH-1, Chernigovka, Primorskii Krai, 1995, Dal'nevostochnyi strain; RH-2, Krasnodar, 1999; RH-3–RH-6, Krasnodar, 2002, Kuban'-3, Izumrud, Rapan, and Regul strains, respectively; RH-7, Kiri-Kili, Astrakhan oblast, 1995; RH-8, Kiliya, Odessa oblast, Ukraine, 1993; RH-9, Harbin, China, 2000; RH-10, Shengyang, China, 2000; RH-11 Dunin, China, 2001; RH-12, South Vietnam, 2001; RH-13–RH-15, Novorossiisk, 2002, Slavyanskii, Poltavskii, and Angelinskii KKhP strains, respectively; RH-16, Novoshakhtinsk, Rostov oblast, 2002; RH-17, Timiryazevskii, Primorskii krai, 2000; Khankaiskii 429 strain; RH-18, Seoul, South Korea, 2001; RH-19, Taiwan, China, 2003; RS-1–RS-4, Timiryazevskii, Primorskii Krai, 2001, Darii-8, Dal'nevostochnyi, Khankaiskii 429, and Khankaiskii 52 strains, respectively; RS-5, the same locality, 2002, Darii-122 strain (numbering of the samples of raw materials from rice production wastes is given according to the collection of the Institute of Chemistry, Far-Eastern Division, Russian Academy of Sciences).

Table 3. Content of amorphous SiO_2 in ash from rice husk and straw in relation to the processing procedure

Raw material	SiO_2 content, wt %, for indicated processing scheme						
	I	II	III	IV	V	VI	VII
RH-1	77.50*	93.48	96.40	96.44	99.80	99.79	
RH-2	80.45*	91.71	95.83	98.05	99.27	99.80	99.83
RH-3	47.50	93.48	96.40	96.44	99.81	99.86	99.79
RH-4	44.70	93.56	95.64	97.60	99.89	99.83	99.53
RH-5	42.50	93.26	95.64	98.07	99.65	99.55	99.83
RH-6	44.12	92.73	95.71	98.36	99.86	99.99	99.98
RH-7	38.70	88.63	97.55	95.47	98.75	99.99	97.68
RH-8	38.05	87.58	91.45	94.34	97.32	99.99	98.43
RH-9	38.22	88.54	97.32	95.43	98.42	99.99	99.05
RH-10		88.20**			97.05	99.99	
RH-11	39.92	89.54	93.59	94.92	99.72	99.80	99.95
RH-12	39.56	92.70	96.05	95.53	97.64	99.00	99.10
RH-13	38.76	91.84	95.98	98.06	99.50	99.99	99.64
RH-14	42.44	91.74	95.92	98.60	99.72	99.87	99.88
RH-15	43.58	91.80	95.75	98.46	99.72	99.56	98.46
RH-16	43.05	92.85	96.02	98.76	99.72	99.78	98.76
RH-17	44.76	93.58	95.64	97.60	99.89	99.53	
RH-18	43.51	91.46	94.62	97.54	99.95	99.99	99.84
RH-19	35.48	92.43	96.07	95.61	99.88	99.99	99.90
RS-1	39.43	88.16	92.34	94.68	97.54	99.84	
RS-2					95.53	98.16	
RS-3	38.42	87.57	90.44	91.42	93.36	98.58	
RS-4					97.47	99.03	
RS-5	37.60	86.54	89.60	95.88	97.86	99.39	99.40

* Thermolysis in a helium flow.

** Burning in the pilot installation.

Table 4. Content of metal oxides in the samples of amorphous SiO_2 obtained from rice husk and straw

Raw material	Content, wt %							
	SiO_2	Na_2O	MgO	CaO	ZnO	Al_2O_3	MnO	Fe_2O_3
RH-3	96.40	0.03	0.33	0.35	0.008	0.043	0.09	0.027
	99.79	0.08	0.06	0.11	0.003	0.043	0.07	0.021
RH-6	92.73	0.02	0.46	0.87	0.013	0.062	0.20	0.06
	99.86	0.02	0.07	0.02	0.002	0.017	0.014	0.054
RS-1	97.54	0.15	0.08	0.08	0.002	0.07	0.05	0.16
	99.84	0.05	0.03	0.005	0.005	0.14	0.023	0.163
RS-3	93.36	0.09	0.86	0.50	0.025	0.08	0.15	0.26
	98.58	0.11	0.09	0.13	0.003	0.172	0.056	0.50

(DRON-2.0 diffractometer, Cu_{K_α} radiation), and thermal gravimetric (Q-1000 derivatograph, MOM, Hungary) methods by the standard procedures. The silicon content was found gravimetrically [19]. The content of free carbon was determined by the procedure described in [20], and that of phosphorus, photocolorimetrically [21]. The specific surface area of amorphous SiO_2 was measured by the procedure described in [22], with methylene blue. The substance density in toluene at 25°C, bulk weight, solubility in water, and solution pH were determined by the common procedures. The results of chemical analysis of ash and specific surface area of its particles are listed in Tables 3–5.

Table 5. Solubility of silica *s* (SiO_2 content >95%) and solution pH

Solution temperature, °C	Heating time, min	Solution pH	*s*, %
25	60	8.34	3.2
70	60	8.45	4.6
90	5	7.92	2.4

Table 6. Specific surface area of ash from rice husk and straw in relation to the preparation procedure

Processing scheme	S_{sp}, $m^2 g^{-1}$	
	RH	RS
I	142–459	
II	80–309	230–302
III	159–310	
IV	173–297	
V	270–300	291–309
VI	243–301	
VII	270–303	

All ash samples obtained from RH and RS by the procedures listed in Table 2 have the same powder X-ray patterns, typical of amorphous substances [12]; they contain a single diffuse peak in the range $2\theta = 18°–26°$. In pyrolysis of RH and RS samples in a helium flow or at air deficiency (Table 2, scheme I), a black amorphous product (black ash) is formed. The yield of this product is 14–28% from straw and 36–44% from husk. According to Table 3, the SiO_2 content in this product varies in the range 77–80% in helium flow and 39–88% at air deficiency. The carbon concentration in the black ash is 4–60°C, depending on the conditions of thermolysis and pretreatment of raw materials.

Oxidative burning of RH and RS in an air flow (Table 2, scheme II) is accompanied by formation of a dark grey ash; its yield is 7–14% from RS and 11–21% from RH. The content of amorphous SiO_2 in the ash varies in the range 86–88% for RS and 87–93% for RH.

Leaching of this ash with an acid (Table 2, scheme IV) gives a light finely dispersed amorphous substance with a SiO_2 content of 91–95% for RS and 94–98% for RH (Table 3).

Schemes III, V–VII (Table 2) involve extraction of water-soluble organic and inorganic substances from the raw material with hot water or an acid. The composition and content of the extractive substances depends on the type of a raw material and extraction conditions. Extracts with various compositions can be obtained depending on the goals of their subsequent treatment to recover biologically active polysaccharides [13], xylose [12], and other substances [9].

Oxidative burning of the residue of the raw material after extraction gives light (Table 2, scheme III) or white (schemes V–VII) ash consisting of pure amorphous SiO_2 (Table 3). The SiO_2 content in the product obtained after extraction of the raw material with water is 89–92% for RS and 91–97% for RH. The purest silica samples in which the SiO_2 content reaches 99.99% are obtained from the raw material pretreated with an acid. An increase in the acid concentration from 0.1 to 1 N does not appreciably affect the product quality.

Oxides of the following elements were found in the samples of amorphous silica: Na, K, Rb, Cu, Ag, Mg, Ca, Zn, Al, Mn, Fe, and P. The content of oxides depends on the SiO_2 purity and varies in the following ranges (wt %): Fe(III) 0.5–0.02, Al 0.4–0.02, Ca 0.3–0.005, Mg 0.8–0.03, Zn 0.02–0.003, Mn(II) 0.1–0.01, Cu 0.002–0.0007, and Ag less than 0.0005. Data on the content of the main concomitant oxides in some ash samples are listed in Table 4.

The calcination loss of silica obtained by schemes III and V–VII at 1000°C is 0.1–5%. According to an X-ray phase analysis, after heating all the substances studied transform from amorphous to crystalline state corresponding to α-cristobalite and tridymite.

The density of silica obtained from RH and RS containing no less than 95% SiO_2 was determined in toluene at 25°C to be 2.01 ± 0.05 g cm^{-3}. The bulk weight of the substance obtained from RH compacted under a pressure of 150 kgf cm^{-2} is 867, and that in the case of RS, approximately 600 g l^{-1}. The solubility and pH of the solution of amorphous silica vary with the solution temperature and heating duration (Table 5).

The specific surface area S_{sp} of ash depends on the type of a raw material and procedure of its processing (Table 6). The samples of black ash obtained by scheme I (Table 2) have the highest S_{sp}. This product containing silica and carbon is of independent interest for industries using carbon-silicon materials as fillers for industrial rubber items, in metallurgy, and as a sorbent. The other substances (products obtained by schemes II–VII) also have a large surface area; S_{sp} varies in the range 80–310 $m^2 g^{-1}$, depending on

the type of the raw material and preparation procedure. In crystallization of the substance, the S_{sp} decreases, on the average, to 8–10 $m^2 g^{-1}$.

Comparison of the characteristics of amorphous SiO_2 obtained from rice husk and straw with the main characteristics of some references for silicon dioxide recovered from mineral raw materials shows that the product meets the requirements of GOST (State Standard) 14922–77 and 9428–73. The concentration of concomitant impurities in the samples of silica obtained from rice husk and straw is lower.

Thus, the data obtained suggest that the wastes from rice production, RH and RS, are good raw materials for production of amorphous SiO_2 of varied quality. This product can be used first and foremost in branches using such forms of silica as diatomaceous earth, kieselguhr, tripoli powder, carbon white, Aerosil, microsilica, and carbonized silica.

CONCLUSIONS

(1) Sodium, potassium, rubidium, copper, silver, magnesium, calcium, zinc, manganese(II), aluminum, iron(III), and phosphorus oxides were found among concomitant impurities in samples of amorphous silica obtained from rice husk and straw.

(2) All silicon-containing products obtained in processing of rice husk and straw can be used in various branches of industry as carbon-silicon materials and as pure amorphous or crystalline silica.

ACKNOWLEDGMENTS

The study was financially supported by the Ministry of Industry and Science of the Russian Federation (project no. 02.42.9).

REFERENCES

1. Voronkov, M.G., Zelchan, G.I., and Lukevics, E.J., *Kremnii i zhizn'* (Silicon and Life), Riga: Zinatne, 1978.
2. Iler, R.K., *The Chemistry of Silica*, New York: Wiley, 1979.
3. *Modifitsirovannye kremnezemy v sorbtsii, katalize i khromatografii* (Modified Silicas in Sorption, Catalysis, and Chromatography), Lisichkin, G.V., Ed., Moscow: Khimiya, 1986.
4. *Meditsinskaya khimiya i klinicheskoe primrnenie dioksida kremniya* (Medical Chemistry and Clinical Applications of Silicon Dioxide), Chuiko, A.A., Ed., Kiev: Naukova Dumka, 2003.
5. *Poluchenie sinteticheskogo dioksida kremniya osoboi chistoty* (Production of Synthetic Silicon Dioxide of Ultrapure Grade), Moscow: NIITEKhim, 1979.
6. Krot, V.V., Zorya, L.N., Orlova, O.D., *et al.*, *Zh. Neorg. Khim.*, 1992, vol. 37, no. 6, pp. 1209–1213.
7. Potapov, V.V. and Kashura, V.N., *Khim. Tekhnologiya*, 2002, no. 9, pp. 2–9.
8. *Ris i ego kachestvo* (Rice and Its Quality), Koz'mina, E.P., Ed., Moscow: Kolos, 1976.
9. Govindorao Venneti, M.H., *J. Sci. Ind. Res.*, 1980, vol. 39, no. 9, pp. 495–515.
10. Saprykin, L.V. and Kiseleva, N.V., *Khim. Drev.*, 1990, nos. 3/7, pp. 119–126.
11. Nakata, Y., Suzuki, M., Okutani, T., *et al.*, *J. Ceram. Soc. Jpn. Int. Ed.*, 1989, vol. 97, no. 8, pp. 830–836.
12. Zemnukhova, L.A., Sergienko, V.I., Davidovich, R.L., *et al.*, *Vestn. Dal'nevost. Otd. Ross. Akad. Nauk*, 1996, no. 3, pp. 82–87.
13. Sergienko, V.I., Zemnukhova, L.A., Egorov, A.G., *et al.*, *Zh. Ross. Khim. O–va im. D.I. Mendeleeva*, 2004, vol. 48, no. 3, pp. 116–124.
14. Kolzunova, L.G., Zemnukhova, L.A., Fedorishcheva, G.A., *et al.*, *Zh. Prikl. Khim.*, 2000, vol. 73, no. 10, pp. 1644–1651.
15. RF Patent 2061656.
16. Chakraverty, A., Banerjiee, H.D., and Pandey, S.K., *Thermochim. Acta*, 1987, vol. 120, pp. 241–255.
17. USSR Inventor's Certificate, no. 1699918.
18. Saprykin, L.V., Kiselev, N.V., and Temerdashev, Z.A., *Khim. Drev.*, 1989, no. 2, pp. 80–82.
19. *GOST* (State Standard) *9428–73. Chemicals: Silicon(IV) Oxide*.
20. Klimova, V.A., *Osnovnye mikrometody analiza organicheskikh soedinenii* (The Main Methods of Analysis of Organic Compounds), Moscow: Khimiya, 1975.
21. *Khimicheskii analiz gornykh porod i mineralov* (Chemical Analysis of Rocks and Minerals), Moscow: Nedra, 1974.
22. Aivazov, B.V., *Praktikum po khimii poverkhnostnykh yavlenii i adsorbtsii* (Practical Guide on Chemistry of Surface Phenomena and Adsorption), Moscow: Vysshaya Shkola, 1973.

Russian Journal of Applied Chemistry, Vol. 78, No. 2, 2005, pp. 324–328. Translated from Zhurnal Prikladnoi Khimii, Vol. 78, No. 2, 2005, pp. 329–333.
Original Russian Text Copyright © 2005 by Zemnukhova, Shkorina, Fedorishcheva.

MACROMOLECULAR CHEMISTRY AND POLYMERIC MATERIALS

Composition of Inorganic Components of Buckwheat Husk and Straw

L. A. Zemnukhova, E. D. Shkorina, and G. A. Fedorishcheva

Institute of Chemistry, Far Eastern Division, Russian Academy of Sciences, Vladivostok, Russia

Received June 3, 2004

Abstract—The composition of inorganic components and content of soluble substances in wastes from processing of seed (ordinary) buckwheat were studied in relation to the plant strain, type of a raw material (straw or husk), and processing conditions.

The interest in renewable agricultural wastes as promising raw materials for production of a variety of chemicals has increased recently. Here we studied some characteristics of large-tonnage wastes from processing of buckwheat: straw and husk (fruit shells, shucks). Much less data on these wastes are available as compared to the related products of rice processing [1–4]. In comparison with rice wastes, buckwheat wastes contain more organic matter and significantly less inorganic matter. Among organic substances are compounds of the flavoid group, including rutin and quercetin [5], lipids, and biologically active polysaccharides [5–8]. There are data on recovery of polysaccharides [9–11], cellulose [12], dyes and food additives [13, 14], furfural [8], medicinals [15], antioxidants [16], and sorbents [17] from buckwheat wastes. However, until now, the main part of buckwheat wastes has not been used in chemical industry and is burnt in fields or used as a fuel for boilers, fillers for pillows, packing of fruits and fragile goods, and feed.

In this study, we examined inorganic components in ash and extracts of wastes from production of seed buckwheat in relation to the plant strain, type of raw materials (straw or husk), and processing conditions.

EXPERIMENTAL

We studied samples of buckwheat husk (BH) and straw (BS) taken in 1994–2002 in the Primorskii (BH-2, 3, 6–9, and BS-1–7) and Krasnodar (BH-10) krais, Amurskaya (BH-1) and Nobosibirsk (BH-9) oblasts, and China (BH-4).[1]

[1] The numbering of raw material samples is given according to the collection of the Institute of Chemistry, Far Eastern Division, Russian Academy of Sciences.

Husk was sifted through a sieve, and a fraction with a particle size of no less than 2 mm was selected for experiments. Straw was cut into fragments approximately 10 mm long. The initial raw material was washed with water and dried in air.

All the samples of raw materials were analyzed for the content of ash residue and soluble (extractable) substances. For this purpose, a weighed portion of a raw material (60 g) was carbonized in a quartz cup in air at approximately 300°C to remove volatiles and then burnt in a muffle at 650°C to constant weight to obtain an ash residue. Another weighed portion of the raw material was extracted at 80–90°C for 1 h with water or acid (HCl, H_2SO_4, HNO_3) or NaOH solutions (concentration of acids and alkali 0.1 and 1 N), or a mixture (1 : 3) of chloroform with ethanol. In all runs, the solid : liquid ratio was 1 : 10.

The resulting products (ash, extracts, and insoluble residue of raw materials) were subjected to chemical, spectral (a PGS-2 spectrometer), flame atomic absorption (an AA-780 Nippon Jharrell Ash device, Japan), IR spectroscopic (a Perkin–Elmer spectrophotometer, 400–4000 cm^{-1}), and X-ray phase (a DRON-2.0 diffractometer, Cu_{K_α} radiation) analyses by the standard procedures. The content of silicon was determined gravimetrically [18, 19], and that of phosphorus in the extracts, photocolometrically [20].

The results obtained in studying the ash obtained from buckwheat husk and straw are listed in Tables 1 and 2.

According to the X-ray diffraction analysis, the ash obtained from buckwheat husk and straw is, in contrast to that from rice husk and straw [21], in the crystalline state (Fig. 1). The yield of ash from buckwheat

1070-4272/05/7802-0324 © 2005 Pleiades Publishing, Inc.

Table 1. Yield of ash from buckwheat husk and straw and its composition

Characteristic	Content, wt %	
	BH-1–10	BS-1–7
Ash	2.00	2.80–11.10
Loss in ash calcination at 1000°C	10.34–19.55	14.62–22.22
Ion:		
K	9.12–16.16	9.98–17.86
Mg	8.08–10.09	2.85–4.52
P	0.94–6.84	0.88–1.46
Si	0.90–3.64	0.53–1.78
Ca	0.69–1.55	1.43–2.68
Fe	$(1.9–6.3)\times10^{-1}$	$(0.6–1.4)\times10^{-1}$
Na	$(1.5–3.7)\times10^{-1}$	$(5.5–9.3)\times10^{-2}$
Mn	$(0.2–3.8)\times10^{-1}$	$(3.6–9.3)\times10^{-2}$
Al	$(0.6–3.01)\times10^{-1}$	$(1.05–1.32)\times10^{-1}$
Zn	$(0.5–1.31)\times10^{-1}$	$(2.5–5.1)\times10^{-2}$
Cu	$(2.3–2.8)\times10^{-2}$	$(2.65–4.5)\times10^{-3}$
Ni	$(3.4–9.95)\times10^{-3}$	$(4.6–7.0)\times10^{-3}$
Cr	$(2.8–9.3)\times10^{-3}$	$(2.8–8.0)\times10^{-3}$
Ag	$(1.5–5.5)\times10^{-4}$	1.5×10^{-4}

Table 2. Chemical composition of ash obtained from buckwheat husk and straw and from rice husk and straw (RH, RS) under the same conditions

Oxide	Content, wt %			
	BH-1	RH-17	BS-3	RS-2
K_2O	21.98	4.27	43.03	7.27
MgO	16.73	0.56	6.19	0.43
SiO_2	4.01	91.71	1.75	95.54
CaO	0.97	0.99	2.9	0.18
Fe_2O_3	0.41	0.10	0.09	0.20
Al_2O_3	0.31	0.06	0.20	0.23
Na_2O	0.30	0.07	0.07	0.58
MnO	0.27	0.14	0.09	0.08
ZnO	0.12	0.03	0.06	0.01
CuO	0.032	0.001	0.004	0.002
Cr_2O_3	0.027	N/d*	0.016	N/d
Ni_2O	0.009	N/d	0.005	N/d
Ag_2O	0.0001	0.006	N/d	0.004
PbO	N/d	N/d	N/d	N/d
Ash yield	1.74	15.6	5.8	7.7

* Not detected by the atomic adsorption method.

husk is 1.5–2.3% and that from straw, 2.8–11.1%, depending on the plant strain.

In the ash residue of buckwheat husk and straw, we found the same set of elements (they are given in the order of decreasing content): potassium, magnesium, phosphorus, silicon, calcium, iron, sodium, manganese, aluminum, zinc, copper, nickel, chromium, and silver ions. Their concentration in ash depends on the plant strain and raw material type (husk and straw). The intervals of concentrations of the elements are given in Table 1.

Contrary to ash obtained from rice husk and straw, which contains mainly amorphous silica [21], the ash residues of BH and BS contain predominantly K ions, similarly to sunflower ash (ash yield 5–6%), in which the K^+ concentration is approximately 15% [22]. The ash obtained from buckwheat wastes (Table 1) contains a significant amount of Mg ions (especially that from husk, up to 10%) and also Cr and Ni ions, absent in the ash from rice wastes. The compositions of ashes obtained from buckwheat husk and straw and from rice husk and straw are compared in Table 2.

The silica content in BH ash is approximately 4%, and that in BS, up to 2%; this differentiates buckwheat wastes from the similar rice wastes, in whose ash the SiO_2 content is more than 90% (Table 2). An X-ray diffraction analysis of SiO_2 recovered from the BH and BS ashes showed that in contrast to the ash from rice wastes [21], this substance is not amorphous, but crystalline: in the form of α-quartz and cacholong, in the ash from BH; and in the form of α-quartz, cacholong, and tridymite, in the ash from BS. It should also be noted that, among the crystalline phases of SiO_2 from rice husk and straw, formed in heating of the amorphous substance to 1000°C, no cacholong phase was found. The calcination loss of ash samples from BH and BS at 1000°C is 10–22% (Table 1). After calcination, the blue-green

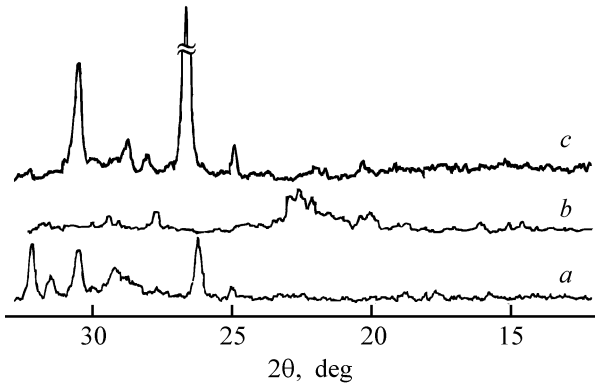


Fig. 1. Fragments of powder X-ray patterns of ash samples (*a*) obtained from buckwheat straw BS-7 at 650°C, (*b*) the same after heating to 1000°C, and (*c*) obtained from BS-1 at 650°C after preliminary extraction of the raw material with 0.1 N HCl. (2θ) Bragg angle.

Table 3. Influence of extractant on recovery of soluble substances from buckwheat husk and straw

Extractant, M	Raw materials and recovery of substances into solution, wt %								Solution color
	BH-1	BH-2	BH-3	BH-4	BH-5	BS-1	BS-2	BS-3	
H_2O	27	22	27	27	13	21	21	21	From light brown to dark brown
HCl:									
0.1	44	26	26	26	22	30	30	30	From light apricot to light red
1.0	57	48	48	48	35	34	34	34	
H_2SO_4:									
0.05	37	26	26	26	22	31	31	31	The same
0.5	58	50	50	50	35	18	18	18	Apricot
HNO_3:									
0.1	51	34	34	34	35	17	17	17	From light brown to light red
1.0	74	70	70	70	75	57	57	57	Bright yellow and yellow
NaOH:									
0.1	50	21	21	21	21	27	27	27	Dark reddish brown
1.0	51	12	12	12	35	1	1	1	Reddish brown
Chloroform + ethanol (1 : 3)	19.5	19.8	10.3	36.3	18.3	38.7		27.2	From light brown to brown

ash becomes grey-beige. Among crystalline compounds contained in the ash obtained at 650°C, K_2CO_3 and $MgCO_3$ were identified by X-ray phase analysis (Fig. 1a). After heating to 1000°C, metal oxides may be present in the ash along with carbonates (Fig. 1b).

The presence of carbonates is also confirmed by gas evolution in the reaction of the ash with an acid solution and by comparison of the IR spectra of the ash residue of the raw materials with the spectra of carbonates [23]. It is well known that the isolated CO_3^{2-} ion (point group D_{3h}) shows a set of IR-active frequencies of 1087 (ν_1), 874 (ν_2), 1432 (ν_3), and 706 cm^{-1} (ν_4). In the formation of coordination compounds or carbonates with a mixed composition, the characteristic absorption bands are split or shifted, which is observed in the IR spectra of the samples of BS and BH ash examined in this study.

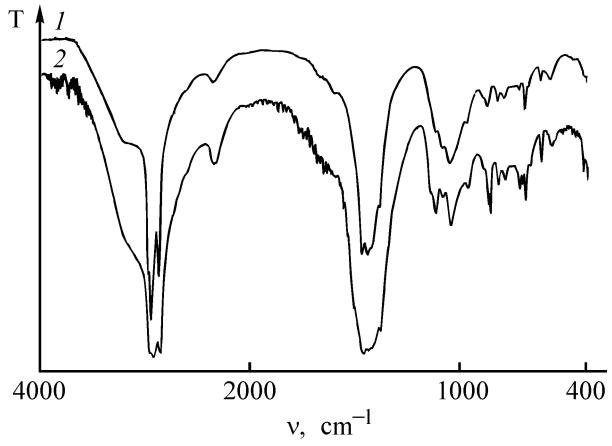


Fig. 2. IR spectra of samples of (*1*) BH-4 ash obtained at 690°C and (*2*) BS-3 obtained at 1000°C. (T) Transmission and (ν) wave number.

Our results show that the IR spectra of ash obtained from buckwheat husk and straw are independent of the plant strain and temperature of oxidative burning of raw materials (650 or 1000°C). However, the splitting pattern of the absorption bands (Fig. 2) is governed by the type of wastes (husk or straw). The absorption peaks (cm^{-1}) in the spectra of the ashes obtained from buckwheat husk and straw are as follows: ash from BH, 470–500 m.br, 620 w, 640 w, 670 w, 690 w, 830 w, 860 w, 1050 m.br, 1260 m, 1630 m, and 3100 w.br; ash from BS, 510 br.m, 560 w, 620 m, 680 w, 880 m, 1040 m.br, 1130 m, 1630 w.br, 1730 w, and 3100 w.br.

The strongest absorption band is in the range 900–1180 cm^{-1}; it is split to two components in the spectrum of BH ash.

The influence of the extractant on the yield of soluble substances from buckwheat husk and straw is demonstrated in Table 3. The yield of extractable substances from buckwheat wastes essentially depends on the extractant, its concentration, and type of a raw material (husk or straw). The content of soluble substances in buckwheat straw is independent of the plant strain and their recovery into the solution is governed by the extractant characteristics only. The recovery of substances from straw (57%) is the highest with 1 N

Table 4. Content of metal ions in extracts of buckwheat husk and straw and sunflower pedicles (SP)

Ion	Content in solution, mg l^{-1}		
	BH-1–10	BS-1–7	SP
K	$(0.4–2.4)\times10^{-1}$	$(2–9)\times10^{-1}$	$(1.45–2.7)\times10^{-1}$
Ca, Mg	$(0.3–7.8)\times10^{-2}$	$(0.3–9.9)\times10^{-2}$	$(0.1–7.5)\times10^{-2}$
Na	$(1.8–4.3)\times10^{-3}$	$(1.5–6.0)\times10^{-3}$	$(4.4–5.0)\times10^{-2}$
Fe	$(1.0–4.0)\times10^{-3}$	$(0.8–1.8)\times10^{-3}$	$(0.3–1.3)\times10^{-3}$
Mn	$(0.9–1.7)\times10^{-3}$	$(1.0–5.0)\times10^{-3}$	$(0.7–2.5)\times10^{-3}$
Zn, Al*	$(0.4–6.0)\times10^{-3}$	$(0.4–8.0)\times10^{-4}$	$(0.6–2.6)\times10^{-3}$
Cu	$(0.4–2.6)\times10^{-4}$	$(0.4–6.0)\times10^{-4}$	$(1.8–2.0)\times10^{-4}$
Ni	1.6×10^{-4}–9.9×10^{-3}	1.4×10^{-4}–4.6×10^{-3}	N/d*
Cr	3.5×10^{-4}–9.3×10^{-3}	2.5×10^{-4}–8×10^{-3}	N/d
Ag	2×10^{-5}–5.5×10^{-4}	1.5×10^{-4}	N/d

* Al, Ni, Cr, and Ag ions in extracts of sunflower pedicels were not detected by the atomic absorption method.

nitric acid and the lower (1%) with 1 N sodium hydroxide.

In contrast to straw, the composition of soluble substances in buckwheat husk depends on the plant strain and their recovery, on the solvent. For example, in treatment of BH with hot water, depending on the buckwheat strain, 13–27% of substances is extracted. The recovery of extractable substances from buckwheat husk with HNO_3 is the highest (Table 3).

The presence of pigments in soluble substances of buckwheat husk and straw results in different color of extractants. Although some flavonoid compounds from buckwheat flowers are used in medicine [5, 13], the chemical composition and content of pigments in processing wastes (husk and straw) are known insufficiently.

In extraction of buckwheat husk and straw, metal ions are recovered into solution along with organic substances. The concentration ranges of metal ions found in the extracts are listed in Table 4. The composition and content of metal ions in hydrolytic solutions from sunflower pedicles, obtained under the similar conditions, are given for comparison.

The residue of buckwheat husk and straw after extraction with water or acid, forms less than 0.8% ash. A fragment of the X-ray diffraction pattern of ash from a BS-1 sample extracted with an HCl solution is shown in Fig. 1c. Identification of the strongest lines in the X-ray pattern suggests the presence of KCl and MgO in this ash. The IR spectrum of this ash contains a strong band at 718 cm^{-1} characteristic of KCl [23].

CONCLUSIONS

(1) The yield of ash from buckwheat husk and straw only slightly depends on the plant strain and is 1.5–2.0%. This value differs from the yield of ash from buckwheat straw, which varies in the range 2.8–11.13%. The ash is crystalline and contains metal carbonates; among these, potassium (9–18%) and magnesium (3–10%) carbonates predominate. As shown by the X-ray phase analysis, silica, whose content in the ash from buckwheat husk does not exceed 4.5%, has three modifications: cacholong, tridymite, and α-quartz.

(2) Extraction of soluble substances from wastes formed in processing of buckwheat depends on the type of a raw material (husk or straw) and on the extractant. The content of soluble substances from husk depends on the plant strain and virtually does not affect the yield from straw.

REFERENCES

1. Sergienko, V.I., Zemnukhova, L.A., Egorov, A.G., *et al., Zh. Ross. Khim. O–va im. D.I. Mendeleeva*, 2004, vol. 48, no. 3, pp. 116–124.
2. Alekseva, E.S., *Selektsiya podol'skikh sortov grechikhi* (Selection of Podol'e Strains of Buckwheat), Chernovtsy: Ruta, 1999.
3. Vul'f, E.V., *Mirovye resursy poleznykh rastenii: Spravochnik* (World Resources of Useful Plants: A Handbook), Leningrad: Nauka, 1985.
4. Ikeda, S., Yamashita, Y., and Kreft, I., *Fagopyrum*, 1999, vol. 16, pp. 89–94.
5. Kiselev, V.E., Kovalenko, V.I., and Minaeva, B.G.,

Grechikha kak istochnik flavonoidov (Buckwheat as a Source of Flavonoids), Novosibirsk: Nauka, 1985.

6. Lubsandorzhieva, P.B., Dergacheva, T.D., Patudin, A.V., and Bodaev, A.B., *Rast. Resursy*, 1996, vol. 32, no. 3, pp. 92–96.
7. Gonskii, Ya.I., Kondratyuk, V.A., and Gusar, I.V., in *Genetika, selektsiya, semenovodstvo i vozdelyvanie krupyanykh kul'tur: Sbornik nauchnykh trudov* (Genetics, Selection, Seed Growing, and Cultivation of Cereals: Collection of Scientific Works), Cishinau, 1988, pp. 122–125.
8. Sharkov, V.I. and Kuibina, N.I., *Khimiya gemitsellyuloz* (Chemistry of Hemicelluloses), Moscow: Lesn. Prom–st., 1972.
9. Dudkin, M.S. and Ozolina, S.A., *Khim. Prirodn. Soedin.*, 1976, no. 4, pp. 417–419.
10. Ozolina, S.A. and Darmin'yan, P.M., *Pishch. Prom–st.*, 1977, no. 23, pp. 40–42.
11. Zemnukhova, L.A., Tomshich, S.V., Shkorina, E.D., and Klykov, A.G., *Zh. Prikl. Khim.*, 2004, vol. 77, no. 7, pp. 1192–1196.
12. Dudkin, M.S., Ozolina, S.A., and Shkantova, N.G., *Khim. Drev.*, 1980, no. 4, pp. 18–22.
13. Aleinikov, I.N., Sergeev, V.N., Rusakov, A.V., and Aganyan, V.E., *Pishch. Ingred.: Syr'e Dobavki*, 2001, no. 1, pp. 30–31.
14. Aleinikov, I.N. and Sergeev, V.N., *Pishch. Prom–st.*, 1998, no. 8, p. 43.
15. Kaputskii, F.N. and Yurkshtovich, T.L., *Lekarstvennye preparaty na osnove proizvodnykh tsellylozy* (Medicinals Based on Cellulose Derivatives), Minsk: Universitetskoe, 1989.
16. Watanabe, Mitsure, *J. Agric. Food*, 1998, vol. 46, no. 3, pp. 839–845.
17. Shchepakin, M.B., Mishulin, G.M., Gafarov, I.G., *et al., Ekologiya Prom–st. Ross.*, 2001, December, pp. 20–25.
18. *GOST* (State Standard) *9428–73: Chemicals: Silicon(IV) Oxide*.
19. *Analiz mineral'nogo syr'ya* (Analysis of Mineral Raw Materials), Knipovich, Yu.N. and Morachevskii, Yu.V., Eds., Leningrad: Lengoskhimizdat, 1956.
20. *Khimicheskii analiz gornykh porod I mineralov* (Chemical Analysis of Rocks and Minerals), Moscow: Nedra, 1974.
21. Zemnukhova, L.A., Sergienko, V.I., Davidovich, R.L., *et al., Vestn. Dal'nevost. Otd. Ross. Akad. Nauk*, 1996, no. 3, pp. 82–87.
22. Efanov, M.V. and Zabelina, A.V., *Khim. Prirodn. Soedin.*, 2002, no. 6, pp. 482–483.
23. Nyquist, R.A. and Kagel, R.O., *Infrared Spectra of Inorganic Compounds*, New York: Academic, 1971.

Russian Journal of Applied Chemistry, Vol. 78, No. 2, 2005, pp. 329–332. Translated from Zhurnal Prikladnoi Khimii, Vol. 78, No. 2, 2005, pp. 334–337.
Original Russian Text Copyright © 2005 by Sagdullaev.

MACROMOLECULAR CHEMISTRY AND POLYMERIC MATERIALS

Cleaning of Microfiltration Membranes for Filtration of Aqueous Extract of Marsh Mallow

B. T. Sagdullaev

Yunusov Institute of Chemistry of Vegetable Compounds, Academy of Sciences of the Republic of Uzbekistan, Tashkent, Uzbekistan

Received January 20, 2004

Abstract—Cleaning of a microfiltration membrane was studied using various chemicals. The activation energy and cleaning constant were estimated for alkaline cleaning.

Baromembrane filtration methods (microfiltration, ultrafiltration, nanofiltration, and reverse osmosis) are widely used in processing of synthetic and natural high-molecular-weight compounds for their concentration, desalination (removal of low-molecular-weight compounds from solutions of macromolecules), and fractionation [1].

Among the most important problems arising in using membrane filtration in biotechnology and food and pharmaceutical industries is that the membrane throughput decreases in the course of filtration [2–4], which is caused by such factors as increase in the concentration of components retained at the membrane surface [5, 6] and adsorption of colloids, microorganisms, and organic compounds on the surface and in the pores of the membrane [6, 7]. Both these factors reduce the effective pore size, thus increasing the resistance of the membrane to the flux [8].

The problems arising from membrane fouling started to be manifested in full measure upon accumulation of data on operation of industrial units [9]. Fouling with organic contaminants plays an especially significant role in filtration of macromolecular compounds, which can form a gel layer on the membrane surface [10]. Studies concerned with the problem of fouling are being conducted in various areas including development of cleaning methods [9]. Chemical cleaning involves treatment of filters with various agents, allowing regeneration of a membrane without disassembling of a membrane unit (cleaning-in-place) [11]. To optimize chemical cleaning, specific features of a given process and the type of the membrane used should be taken into account.

The goal of this study was to optimize the chemical cleaning of a membrane contaminated during microfiltration of the extract of marsh mallow.

EXPERIMENTAL

In the study we used an Alpma microfiltration system (Germany) (Fig. 1) equipped with two membrane units (Kerasep, France). Each unit consisted of nine cylindrical membranes fabricated from TiO_2 with the Al_2O_3/TiO_2 active layer (nominal pore size 0.2 μm). Membranes of this type are thermally and chemically resistant over the pH range 1–14 at 293–358 K.

The water flux across an unused membrane at a transmembrane pressure P_{TM} = 85 kPa was 1650 l m^{-2} h^{-1}, and the resistance, $R_m = 1.96 \times 10^{11}$ m^{-1}.

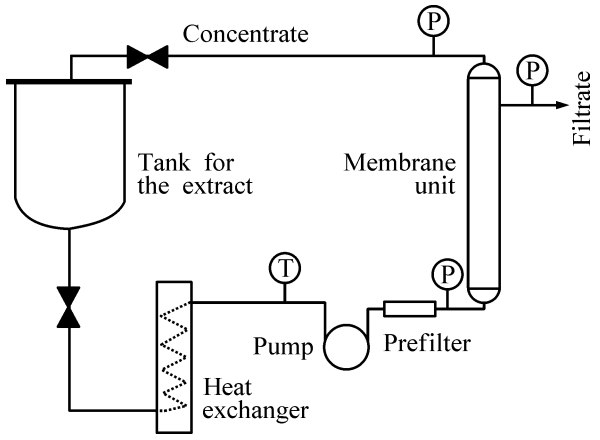


Fig. 1. Microfiltration flowsheet.

1070-4272/05/7802-0329 © 2005 Pleiades Publishing, Inc.

Table 1. Cleaning conditions

	c, wt %	*T*, K
NaOH	0.1, 0.3, 0.5, 1.0	295, 313, 333, 353
HNO_3	0.1, 0.3, 0.5, 1.0	295, 313, 333, 353
Ultrasil-11	0.3	295

Table 2. Cleaning efficiency for different chemicals

Agent	*c*, wt %	FR	t_c, min
NaOH	0.1	0.54	60
	0.3	0.63	60
	0.5	0.65	60
	1.0	0.65	60
HNO_3	0.1	0.36	80
	0.3	0.49	80
	0.5	0.50	80
	1.0	0.52	80
Ultrasil-11	0.3	0.54	60

We used in experiments an aqueous extract of marsh mallow prepared from roots of *Althaea armeniaca* by turbulent extraction. The total content of extractive substances in the solution was 1.65 wt % and the concentration of water-soluble polysaccharides in the extract, 0.8 wt %. The extract also contained sucrose, pigments, betaine, and mineral substances.

We used as cleaners three different chemicals (Table 1). Ultrasil-11 from Henkel Chemicals is sodium hydroxide with surfactant additives.

All the cleaning experiments were carried at a cross flow velocity of 1 m s^{-1}, low transmembrane pressure (85 kPa), and various temperatures. After filtration, the extract was removed, and the membrane was rinsed with distilled water at 295 K, which removed the residual concentrate from the membrane surface.

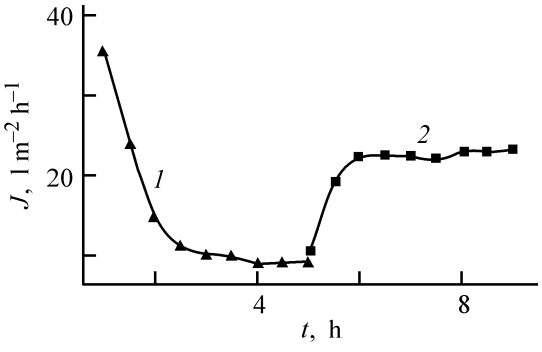


Fig. 2. Flux *J* vs. the time *t*: (*1*) extract of marsh mallow and (*2*) distilled water.

Cleaners were dissolved in distilled water at room temperature and heated to a desired temperature prior to use. After chemical treatment, the membrane was additionally cleaned with distilled water, to determine its permeability to water. To minimize pore plugging, the cleaning was carried out at low transmembrane pressure. To provide cleaning inside the pores of the membrane, the permeate line was switched on throughout the cleaning.

In all the experiments in which the solvent flux was measured, distilled water was used ($[Ca^{2+}] < 10$ mg l^{-1}).

To evaluate the cleaning efficiency, we used two major parameters, namely, (1) the flux recovery FR defined as the ratio of the water flux across the worked membrane after cleaning to that across the unused membrane, and (2) cleaning time t_c [12].

According to Darcy's law, the permeate flux *J* (l m^{-2} h^{-1}) is proportional to the transmembrane pressure P_{TM} (Pa):

$$J = \frac{P_{TM}}{\mu_p(R_m + R_f)}, \quad (1)$$

where μ_p is the permeate viscosity (g cm^{-1} s^{-1}); R_m, initial membrane resistance (m^{-1}); and R_f, resistance after fouling (m^{-1}).

The resistance that appears after fouling (R_f) can be estimated by rearranging (1) to the form of Eq. (2).

$$R_f = \frac{P_{TM}}{\mu_p J} - R_m. \quad (2)$$

R_f includes the resistance R_{ir} of a residual contamination after cleaning, which is due to irreversible adsorption of the molecules in the pores and on the surface of the membrane, and also the resistance R_r of reversible contamination caused by reversible deposition of the molecules on the membrane surface and also by concentration polarization [1], which can be removed by cleaning.

Upon a 5-h filtration of the extract of marsh mallow, the flux decreased to 9.3 l m^{-2} h^{-1} (Fig. 2). To evaluate the nature and amount of contamination, the membrane was first washed with distilled water. The procedure was carried out at P_{TM} = 85 kPa and T = 295 K. Washing with water could only remove the concentrate residue from the surface. As a result, the flux recovery was insignificant (water flux was 22.4 l m^{-2} h^{-1}.

The cleaning efficiencies of three different chemicals at 295 K are listed in Table 2, as influenced by their concentration. As seen, the flux recovery FR and the cleaning time t_c depend on the nature of chemicals

and their concentration. Sodium hydroxide showed the highest cleaning efficiency (0.65) among the chemicals studied. With HNO_3 and Ultrasil-11, the cleaning efficiency was found to be 0.52 and 0.54. Because of the high cost of the latter chemical, its use appears to be inadvisable in this case.

A study of the effect of the cleaner concentration (Table 2) showed that cleaning with NaOH provides the best result (FR = 0.63) at a concentration (0.3%) lower than that of NaOH (0.5%) used for cleaning of a ceramic membrane [12]. Raising the cleaner concentration to above 0.3% provided only an insignificant gain in the flux recovery.

The experiments with 0.3% NaOH showed that the temperature has a considerable effect on both the cleaning time and flux recovery (Fig. 3), the effect being more clearly pronounced at lower temperatures (<313 K). The flux recovery at 353 K was 17.1% higher than that at 295 K. Raising the temperature to above 313 K only insignificantly increases FR, allowing, however, a considerable reduction of the cleaning time (from 27 min at 313 K to 12 min at 353 K).

Bird *et al*. demonstrated [11] that the kinetic equation describing the cleaning can be written as

$$\frac{dR_f}{dt} = k_c R_f. \quad (3)$$

Integrating over the limits from $t = 0$ to t at k_c = const and assuming that R_f varies from R_{max} to R_{ir}, we obtain Eq. (4).

$$\ln(R_{max}/R_{ir}) = -k_c t, \quad (4)$$

where R_{max} is the maximum resistance of the contaminant layer and R_{ir}, residual resistance after cleaning for a time t_c.

In our experiments, the membrane was cleaned until a steady-state water flux was obtained.

The R_{max} depends only on the contamination of the membrane. After a 5-h operation of the microfiltration system, R_f was 3.48×10^{13} m^{-1}. For a given cleaner, R_{ir} varies with temperature (Table 3).

The temperature dependence of the cleaning rate constant can be derived from the Arrhenius equation:

$$k_c = k_{c0} e^{-E_c/RT}. \quad (5)$$

Substituting it into Eq. (4), we obtain

$$\ln(R_{max}/R_{ir})\frac{1}{t} = -k_{c0} e^{-E_c/RT}, \quad (6)$$

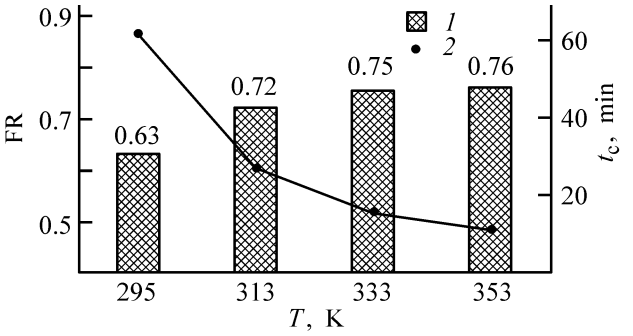


Fig. 3. (*1*) Flux recovery FR and (*2*) cleaning time t_c vs. the temperature T, with 0.3% NaOH as a cleaner.

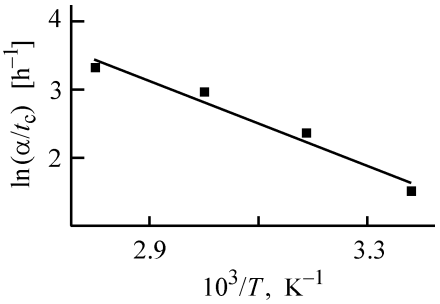


Fig. 4. $\ln(\alpha/t_c)$ vs. reciprocal temperature T.

where E_c is the activation energy of cleaning; k_{c0}, preexponential factor reflecting the cleaning capacity of a chosen cleaning method and membrane cleaning conditions.

Assuming $\alpha = \ln(R_{max}/R_{ir})$, $a = E_c/R$, and $b = \ln k_{c0}$ and rearranging Eq. (6), we obtain

$$\ln(\alpha/t_c) = b - a(1/T). \quad (7)$$

The temperature dependence of $\ln(\alpha/t_c)$ is shown in Fig. 4. A small change in R_{ir} with increasing temperature has no considerable effect on *a* and *b*, suggesting that R_{ir} is a temperature-independent parameter, i.e., the temperature influences the kinetics of cleaning, but not the maximum cleaning capacity of a given chemical.

Table 3. Residual resistance R_{ir} at various temperatures of cleaning with 0.3% NaOH

T, K	$R_{ir} \times 10^{11}$, m^{-1}	$\ln(R_{max}/R_{ir})$
295	3.11	4.72
313	2.72	4.85
333	2.61	4.89
353	2.57	4.91

The activation energy of cleaning, E_c, is the energy required for breaking the bonds between contaminant particles and the membrane. In the case of NaOH, the activation energy was estimated to be 25.4 kJ mol^{-1}. The other kinetic parameters are as follows: k_{c0} = 49.9 s^{-1}, $a = E_c/R$ = 3053, and $b = \ln k_{c0}$ = 12.1.

CONCLUSIONS

(1) It was foun that cleaning of a fouled membrane only with distilled water does not restore its performance.

(2) The effects of the temperature and cleaner concentration on the cleaning efficiency were studied. It was established that cleaning of the microfiltration membrane with 0.3% NaOH proceeds quite rapidly and efficiently: the flux is recovered to 76% of the initial value in 12 min at 353 K.

(3) The activation energy of alkaline cleaning E_c was estimated at 25.4 kJ mol^{-1}, and the preexponential factor of the Arrhenius equation k_{c0}, at 49.9 s^{-1}.

REFERENCES

1. Howell, J., Sanchez, V., and Field, R.W., *Membranes in Bioprocessing: Theory and Applications*, London: Blackie Academic Professional, 1993, p. 241.
2. Short, J.L., *Desalination*, 1988, vol. 70, nos. 1–3, pp. 341–352.
3. Berg, G.V., van der Smolders, C.A., *Desalination*, 1990, vol. 77, no. 1, pp. 101–133.
4. Horst, H.C. van der and Hanemaaijer, J.H., *Desalination*, 1990, vol. 77, no. 1, pp. 235–258.
5. Huisman, I., in *Crossflow Microfiltration of Particle Suspensions: The Influence of Hydrodynamics and Physicochemical Interactions*, Sweden: Lund Univ., 1998, p. 110.
6. Elysee-Collen, B. and Lencki, R.W., *J. Membr. Sci.*, 1997, vol. 129, pp. 115–124.
7. Dytnerskii, Yu.I., *Baromembrannye protsessy: Teoriya i raschet* (Baromembrane Processes: Theory and Calculation), Moscow: Khimiya, 1986.
8. Zhuzhikov, V.A., *Fil'trovanie: teoriya i praktika razdeleniya suspenzii* (Filtration: Theory and Practice of Separating Suspensions), Moscow: Khimiya, 1980.
9. Dytnerskii, Yu.I. and Kocharov, R.G., *Zh. Vses. Khim. O–va. im. D.I. Mendeleeva*, 1987, vol. 32, no. 6, pp. 607–614.
10. Chilukuri, V.V., Marshal, A.D., Munro, P.A., and Singh, H., *Chem. Eng. Process.*, 2001, vol. 40, no. 4, pp. 321–328.
11. Bird, M.R. and Barlett, M., *Trans. Inst. Chem. Eng.*, 1995, vol. 73, part C, pp. 63–70.
12. Sagdullaev, B.T., Safonova, E.V., and Khodzhaeva, M.A., *Zh. Prikl. Khim.*, 2003, vol. 76, no. 9, pp. 1518–1521.

Russian Journal of Applied Chemistry, Vol. 78, No. 2, 2005, pp. 333–335. Translated from Zhurnal Prikladnoi Khimii, Vol. 78, No. 2, 2005, pp. 338–340.
Original Russian Text Copyright © 2005 by Ordan'yan, Yurchenko, Vikhman.

BRIEF COMMUNICATIONS

Polythermic Section B_4C–LaB_6 in the Ternary System La–B–C

S. S. Ordan'yan, O. V. Yurchenko, and S. V. Vikhman

St. Petersburg State Technological Institute, St. Petersburg, Russia

Received July 13, 2004

Abstract—The interaction was studied and the polythermic section B_4C–LaB_6 was constructed for the ternary system La–B–C described by a eutectic phase diagram.

Covalent carbides, SiC and B_4C, find increasingly wide application in modern technology, from abrasives to materials for space and nuclear power engineering. Borides of *d*- and *f*-elements, e.g., M^dB_2 and M^fB_6 as substances possessing a complex of properties reflecting the strength of their chemical bonding (hardness, refractoriness, electrical conductivity, and effective thermionic emission), are also rather promising for technical applications. In the LnB_6 series, lanthanum hexaboride has the minimum work function [1]. In a number of cases, it is of interest to use, instead of single-phase LnB_6, composite materials containing this compound. Therefore, a problem arises of the chemical compatibility of the components intended to be used in a material being developed. It has been shown previously that LaB_6 coexists with M^dB_2 and their interaction is described by eutectic phase diagrams [2]. Analysis of the phase composition in the ternary systems M^d–B–C [3] and M^f–B–C [4] shows that the borides M^dB_2 and M^fB_6 coexist with B_4C. The fundamental aspects of their interaction in a quasibinary system B_4C–M^dB_2 were summarized in [3]. Data on the structure of polythermic sections in the systems M^f–B–C are virtually lacking. If obtained, these data will make it possible to differentiate the ternary systems B_4C–M^dB_2–M^fB_6 and to begin a systematic study of these systems as a basis for a large number of composites produced by the ceramic technology or by directed crystallization [5].

We used in this study B_4C and LaB_6 powders (both of pure grade) manufactured by Donetsk Plant of Chemical Reagents. The powders were ground in a vibration mill (TiB_2 milling bodies) to 5–10-μm particles, with the introduction of a milled substance of the milling bodies virtually eliminated, and then the compositions in the B_4C–LaB_6 system under study were prepared. The powders were used to produce mixtures in the entire concentration range by stirring in ethanol (see table). The dried powders were compacted to obtain $3 \times 3 \times 40$ mm prismatic samples and sintered at 1900°C in a high-purity argon. Holes

Melting point and microhardness of formulations in the B_4C–LaB_6* system

Content, mole fraction		Content, weight fraction		T_{mel}, °C	H_μ, GPa
B_4C	LaB_6	B_4C	LaB_6		
0.95	0.05	0.83	0.17	2400 ± 30	B_4C, 48.5 ± 2
0.85	0.15	0.62	0.38	2340 ± 30	–
0.82	0.18	0.55	0.45	2340 ± 30	–
0.78	0.22	0.50	0.50	2320 ± 20	–
0.75	0.26	0.44	0.56	2280 ± 20	–
0.70	0.30	0.40	0.60	2240 ± 20	34 ± 1 (eutectic) 38.8**
0.66	0.34	0.35	0.65	2260 ± 20	–
0.57	0.43	0.26	0.74	2300 ± 20	–
0.45	0.55	0.19	0.81	2320 ± 20	–
0.40	0.60	0.15	0.85	2330 ± 30	–
0.26	0.74	0.09	0.91	2480 ± 40	LaB_6, 26 ± 2

* Two phases present in all the formulations. ** Additive value.

1070-4272/05/7802-0333 © 2005 Pleiades Publishing, Inc.

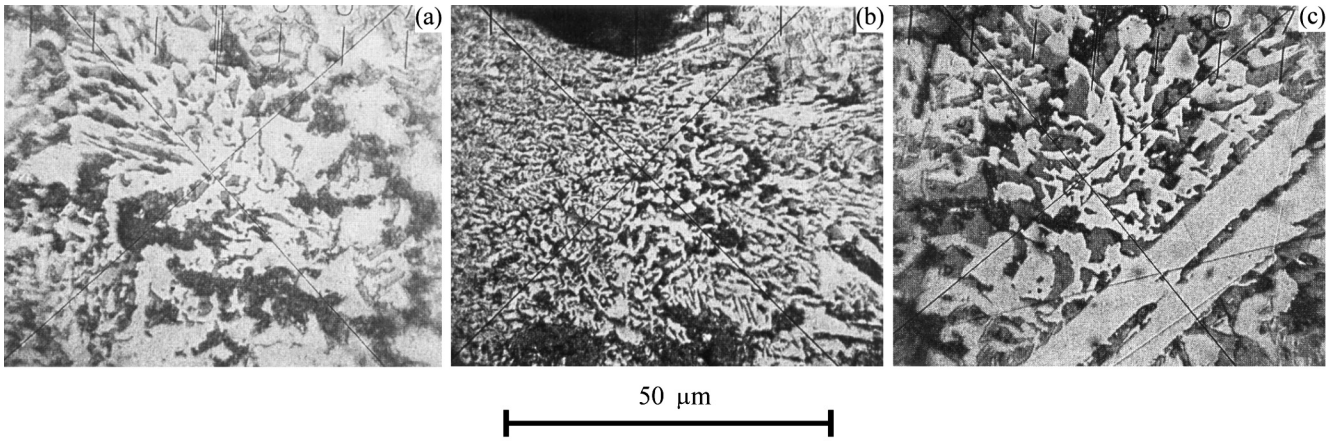


Fig. 1. Microstructure of fused samples in the B_4C–LaB_6 system. LaB_6 concentration (mol %): (a) 25, (b) 30, and (c) 55.

0.5 mm in diameter and 1.5 mm long were made at mid-length of the samples for optical measurements of their temperature with a micropyrometer (blackbody configuration). The melting point was determined with an indirect heating of samples placed within a tubular heater so as to preclude any contact of the samples with the material of the heater. Taking into account the optical absorption in a viewing window [6], we obtained close results, which were then averaged. Sintered, annealed, and fused samples were subjected to X-ray diffraction analysis, to determine the phase composition and the lattice constants and to metallographic analysis. Also the microhardness of the phase components was determined (see table).

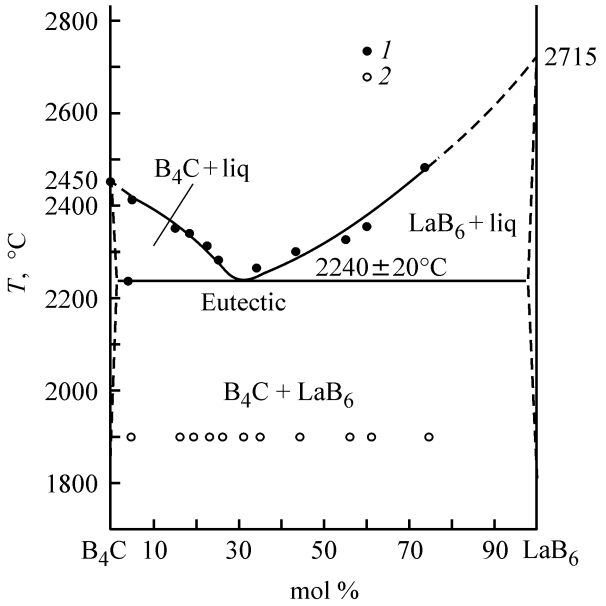


Fig. 2. Polythermic section of the system B_4C–LaB_6. (*T*) Temperature. (*1*) Fusion in indirect heating and (*2*) two-phase material.

As shown in [6], a sample is "ruptured" in direct heating by electric current upon the appearance of a certain amount of melt; therefore, $T_{rup} < T_{liq}$. In eutectic mixtures, $T_{eut} < T_{rup} < T_{liq}$ and direct heating by electric current makes it possible to determine the melting point of congruently melting components and eutectic. T_{liq} can be estimated by the temperature at which a drop appears on the sample in indirect heating.

The data obtained show that, in the B_4C–LaB_6 system, the concentration dependence of the melting point passes through a minimum. The structure typical of eutectic, hypoeutectic, and hypereutectic regions is recorded for samples that have been fused and then crystallized at T_{min} (Fig. 1). The microhardness of the constituent phases corresponds to that of pure components ($H_\mu = 49 \pm 1$ GPa for B_4C and $H_\mu = 26.8 \pm 1.1$ GPa for LaB_6 [7]); and in this system too, the microhardness of the eutectic is markedly lower than the additive value (see table).

The data obtained, as well as the fact that all the heat-treated samples have a two-phase composition, suggest that the polythermic section B_4C–LaB_6 in the ternary system La–B–C is described by an eutectic phase diagram (Fig. 2), with the eutectic composition containing 70 mol % B_4C and 30 mol % LaB_6 and having a melting point $T_{eut} = 2240 \pm 20$°C. This temperature is higher than T_{eut} in the SiC–LaB_6 system [8], although T_{mel} of B_4C < T_{mel} of SiC (2450 and 2760°C, respectively). The last result shows that B_4C has a higher resistance to contact interaction, as already noted in [9] when comparing T_{eut} in the B_4C–M^dB_2 and SiC–M^dB_2 systems, for which an analogous dependence also exists.

REFERENCES

1. Kresanov, V.S., Malakhov, N.P., Morozov, V.V., *et al.*, *Vysokoeffektivnyi emitter elektronov na osnove geksaborida lantana* (High-Efficiency Electron Emitter Based on Lanthanum Hexaboride), Moscow: Energoatomizdat, 1987.
2. Ordan'yan, S.S., *Izv. Akad. Nauk SSSR, Neorg. Mater.*, 1988, vol. 24, no. 2, pp. 235–238.
3. Ordan'yan, S.S., *Ogneupory*, 1993, no. 5, pp. 15–17.
4. Ivanovskii, A.L., Gusev, A.I., and Shveikin, G.P., *Kvantovaya khimiya v materialovedenii* (Quantum Chemistry in Materials Science), Yekaterinburg: Inst. Khim. Tverd. Tela, Ural Otd., Ross. Akad. Nauk, 1996.
5. Paderno, Yu.B., Paderno, V.N., Dyachenko, L.I., and Filippov, V.B., *Dokl. Ukr. Akad. Nauk*, 1992, no. 4, pp. 65–68.
6. Ordan'yan, S.S., Avgustinnik, A.I., and Vigdergauz, V.Sh., *Issledovaniya v oblasti khimii silikatov i okislov* (A Study in Chemistry of Silicates and Oxides), Moscow: Nauka, 1965, pp. 220–228.
7. Alekseev, A.G., Bovkun, G.A., Bolgar, G.A., Bolgar, A.S., *et al.*, *Svoistva, poluchenie i primenenie tugoplavkikh soedinenii. Spravochnik* (Properties, Preparation, and Application of Refractory Compounds: Reference Book), Kosolapova, T.Ya., Ed., Moscow: Metallurgiya, 1986.
8. Ordan'yan, S.S., Yurchenko, O.V., and Vikhman, S.V., *Neorg. Mater.*, 2004, vol. 40, no. 6, pp. 1–4.
9. Ordan'yan, S.S., *Zh. Prikl. Khim.*, 1993, vol. 66, no. 11, pp. 2439–2444.

Russian Journal of Applied Chemistry, Vol. 78, No. 2, 2005, pp. 336–338. Translated from Zhurnal Prikladnoi Khimii, Vol. 78, No. 2, 2005, pp. 341–343.
Original Russian Text Copyright © 2005 by Yakovlev, Ovchinnikov, Fokeeva.

BRIEF COMMUNICATIONS

Effect of Unpaired Electron in Thermochemical Description of the Dissociation Energy of Heteronuclear Diatomic Molecules

V. M. Yakovlev, D. V. Ovchinnikov, and I. G. Fokeeva

Samara State Railway Academy, Samara, Russia

Gipronikel Institute, Joint Stock Company, St. Petersburg, Russia

Received January 11, 2005

Abstract—The dissociation energy of heteronuclear diatomic molecules with polar covalent bonds was calculated by the modified Pauling procedure taking into account the presence of an unpaired electron on one of the atoms.

Spin polarization caused by the presence of an unpaired outer electron in a diatomic heteronuclear radical AB is believed [1, 2] to destabilize the chemical bond (CB). At first glance, this assumption is obvious because of a certain analogy with the homoatomic anion H_2^-, commonly regarded as a classical example of a system with an antibonding effect. A typical example of the antibonding effect in AB systems is beryllium monofluoride. In this compound and in its analogues, the unpaired *s* electron of Be repulsively interacts with the bonding electron pair [2]. This assumption is confirmed by the fact that the dissociation energies [D(AB)] of gaseous molecules of BeF (5.96 [1], 5.98 [3] eV) and LiF (5.94 [1], 5.98 [3] eV) are virtually equal [2]. In this comparison, noticeable shortening of the CB in going from LiF to BeF [2] was primarily taken into account, whereas the decrease in the ionic character of the bond was ignored. However, the tabulated dissociation energy taken from another source D(BeF) = 6.62 eV [4, 5] suggests strengthening of a BeF molecule, which casts doubt on the above reasoning.

In this paper, we show in what case and how the influence of an unpaired electron on D(AB) should be taken into account. The influence of unpaired electron localized on a metal atom differs from that of the electron localized on a nonmetal atom. Our analysis shows that formation of an antibonding electron pair is energetically favorable only when the electron is localized on the nonmetal atom.

In our calculations, we used the modified Pauling equation [6, 7] suitable for calculating D(AB) of majority of heteroatomic CB with any polarity, provided that at least one *p*-AO is involved in MO, which makes the bond directional and more localized

$$D(\mathrm{AB}) = [D(\mathrm{AB})] + (2c)^{1/2}\Delta\chi^2 \ (\mathrm{eV}), \qquad (1)$$

where $[D(\mathrm{AB})]$ is the geometric mean of D(A–A) and D(B–B) energies of homoatomic covalent bonds; $\Delta\chi$, difference in the Pauling electronegativities (EN) χ(A) and χ(B); and c, degree of covalence of CB, which is unambiguously related to the relative difference in EN (i.e., polarity) $p = \Delta\chi/\chi(\mathrm{B})$ [$\chi(\mathrm{A}) < \chi(\mathrm{B})$] by the equation $c = \exp(-3p^2)$.[1] In particular cases, when atoms of hydrogen and elements of the second row are present in the compound, corrections for donor–acceptor interactions (DAI) and antibonding contribution to CB, i.e., promotion of bonding electron density (ED) from the internuclear region to the metal atom [9], should be taken into account. The latter effect is caused by the difference in the valence ED of atoms in the molecule. The DAI is manifested in interactions of acceptor atoms (H, Li, Be, B, C) with donor atoms (N, O, F). This effect can be taken into account by introducting the electron affinity (EA, Eα) of the acceptor in Eq. (1). The weakening of CB is taken into account by subtracting EA of the metal atom exerting an antibonding effect on the CB from the right-hand part of Eq. (1). This correction is

[1] The effect of saturation of a heteropolar bond [7], mentioned in many reports (e.g. [8]), can be taken into account by introducing parameter c in to the equation of the ionic increment.

1070-4272/05/7802-0336 © 2005 Pleiades Publishing, Inc.

Table 1. Calculated dissociation energies of alkali and alkaline-earth metal monoxides*

A	χ(A), $eV^{1/2}$ [2, 5]	$E\alpha$(A), eV [2]	D(A–A), eV [2]	D(AB), eV	
				calculated	experimental
Li	0.98	0.618	1.14	3.62	3.64 [8]
Na	0.93	0.548	0.745	2.83	2.83 [4]
K	0.80	0.501	0.53	2.77	2.77 [4]
Rb	0.75	0.486	0.51	2.78	2.82 [8]
Be	1.45	1.02 [11]	(1.45)	4.66	4.64 [12]
Ca	1.10 [13]	0.63 [14]	0.90	4.18	4.38 [12]; 3.97 [3]
Sr	1.05	0.59 [14]	0.83	4.22	4.30 [3]

* We used χ(O) = 3.30 $eV^{1/2}$ [7] and D(O–O) = 1.86 eV [10] in the calculation. Average value of D(Be–Be) taken from [2, 15] is in parentheses. The electron affinities of Be, Ca, and Sr refer to valence states typical for monochalcogenides.

introduced when this metal atom interacts with a small nonmetal atom of the second row. Analysis of molecular systems [e.g., alkali metal (AM) halides or alkaline-earth metal (AEM) chalcogenide] confirms the validity of Eq. (1) supplemented with the above rules and shows why these corrections should be ignored in the case of monosulfides and monochlorides, but should be taken into account in the case of monoxides and monofluorides.

To analyze the reason for the different strengths of CBs in AB radicals, we assume that the unpaired electron on the metal atom virtually eliminates the antibonding effect. However, when this electron is localized on the nonmetal atom, it weakens the chemical bonds in proportion to EA of the nonmetal atom. Indeed, as can be seen from Table 1, to calculate D(AB) of AM monoxides, not only EA of the metal atom but also $E\alpha$(O) = 1.461 eV [2] should be subtracted from the results of the calculation by Eq. (1). In AEM oxides, in which all the valence electrons are paired, only the antibonding caused by transfer of the ED to the metal atom is observed. It should be noted that the antibonding effect is compensated by DAI in LiO and LiF (Table 2).

Thus, to calculate the dissociation energies of AM monofluorides and AEM monofluorides, the corrections can be introduced in Eq (1). However, the strengthening of CB due to DAI should be taken into account only in calculation of D(AB) of BeF. Since the unpaired electron in CaF, SrF, and BeF is localized on the metal atom, the antibonding effect in their molecules is compensated and D(AB) can be calculated by Eq. (1) without correction (Table 2). As can be seen from Tables 1 and 2, the drastic destabilization of alkali metal monoxides as compared to alkali metal monofluorides and other alkali metal halides can explained in the framework of our approach.

We did not consider Cs and Ba compounds since the relativistic effect observed in these compounds strongly weakens the antibonding influence of the metal atom. We also omitted data on Mg compounds since the strength of CB in these compounds decreases by $E\alpha$ of the Mg atom (in the valence state) owing to its abnormal electronic structure [8]. Presumably, this effect should be observed in all diatomic Mg compounds with any nonmetal atom, irrespective of the presence of an unpaired electron in the AB radical.

Thus, in most cases our approach allows the presence of unpaired electron to be taken into account in thermochemical calculations of the dissociation energies of diatomic heretonuclear molecules.

Table 2. Calculated dissociation energies of alkali and alkaline earth metal monofluorides*

A	D(AB), eV	
	calculation	experimental
Li	5.97	5.98
Na	5.19	(5.17)
K	5.12	5.13
Rb	5.12	5.09
Be	6.62	6.62
Ca	5.72	5.81
Sr	5.72	5.64

* We used $\chi(F)$ = 3.68 $eV^{1/2}$ [16] and D = 1.65 eV [2] and $E\alpha$ of AM and Be given in Table 1 in the calculation. The average of substantially different values tabulated in [3, 4] is in parentheses.

REFERENCES

1. Batsanov, S.S., *Eksperimental'nye osnovy strukturnoi khimii* (Experimetal Foundations of Structural Chemistry), Moscow: Standarty, 1986.
2. Batsanov, S.S., *Strukturnaya khimiya* (Structural Chemistry), Moscow: Dialog-Mosk. Gos. Univ., 2000.
3. C.R.C. H*andbook of Chemistry and Physics Boca Raton (FL)*: CRC, 1993–1994, 74th ed.
4. Barin I., *Thermochemical Data of Pure Substances*. Weinheim (Germany): VCH, 1995, 3rd ed.
5. Murphy, L.R., Meek, T.L. and Allen, L.C., *J. Phys. Chem. A*, 2000, vol. 104, no. 24, pp. 5867–5871.
6. Yakovlev, V.M., *Rasplavy*, 2002, no. 5, pp. 50–53.
7. Yakovlev, V.M., Anfilof'ev, I.N., and Korneev, I.N., *Zh. Obshch. Khim.*, 2004, vol. 74, no. 4, pp. 546–549.
8. Shchukarev, S.A., *Neorganicheskaya khimiya*, (Inorganic Chemistry), Moscow: Vysshaya Shkola, 1970, vol. 1.
9. Yakovlev, V.M., Vasil'chenko, L.M., and Chertykovtseva, N.V., in *Materialy tret'ei mezhdunarodnoi konferentsii "NBITT-21"* (Proc. Third Int. Conf. "NBITT-21"), Petrazovodsk: Petr. Gos. Univ., 2004, p. 65.
10. Dos Santos, R.M.B., Muralha, V.S.F., Correia, C.F., and Simoes, J.A.M., *J. Am. Chem. Soc.*, 2001, vol. 123, no. 50, pp. 12670–12674.
11. Bergmann, D. and Hinze J., *Angew. Chem. Int. Ed. Engl.*, 1996, vol. 35, no. 2, pp. 150–163.
12. Gurvich. L.V., Karachevtsev, G.V., Kondrat'ev, V.N., *et al.*, *Energiya razryva khimichekikh svyazei: Potentsialy ionizatsii i srodstvo k elektronu* (Dissociation Energy of Chemical Bonds: Ionization Potentials and Electron Affinity), Moscow: Nauka, 1974.
13. Urusov, V.S., *Energeticheskaya kristallokhimiya* (Energetic Crystal Chemistry), Moscow: Nauka, 1975.
14. Gagarin, S.G., *Zh. Fiz. Khim.*, 2001, vol. 75, no. 4, pp. 675–678.
15. Batsanov, S.S., *Izv. Ross. Akad. Nauk, Neorg. Mater.*, 1994, vol. 30, no. 7, pp. 999–1000.
16. Batsanov, S.S., *Izv. Akad. Nauk SSSR, Ser. Khim.*, 1989, no. 2, pp. 467–470.

Russian Journal of Applied Chemistry, Vol. 78, No. 2, 2005, p. 339. Translated from Zhurnal Prikladnoi Khimii, Vol. 78, No. 2, 2005, p. 344.
Original Russian Text Copyright © 2005 by Pashchenko.

BRIEF COMMUNICATIONS

Mechanochemical Changes in the Structure of Layered Silicates according to ^{27}Al and ^{29}Si NMR Data

E. A. Pashchenko

Kiev National University of Technology and Design, Kiev, Ukraine

Received July 20, 2004

Abstract—Mechanochemical structural changes in layered silicates were studied by ^{27}Al and ^{29}Si NMR spectroscopy.

Layered silicates and, in particular, pyrophyllite and montmorillonite, are widely used in manufacture of radio- and electroceramics [1] and as sorbents and various fillers [2]. Their use in some fields involves preliminary dispersion [3].

In this study, ^{27}Al and ^{29}Si NMR spectroscopy was used to examine changes in the coordination state of aluminum and silicon ions in pyrophyllite and montmorillonite upon a mechanical activation.

As objects of study served natural zeolites: mordenite and clinoptilolite. Air-dry samples were activated by dispersion in a mechanical agate mortar for 20–120 min. The ^{27}Al and ^{29}Si NMR spectra were obtained on a Bruker CXP-200 spectrometer with sample rotation at a magic angle to the external field at a frequency of ~3 kHz. The chemical shifts were measured relative to the $Al(H_2O)_6^{3+}$ ion and tetramethylsilane as external standards.

It was found that the mechanochemical activation of pyrophyllite causes a strong distortion of aluminum- and silicon-oxygen polyhedra, which leads to broadening of signals at δ 1 ppm (octahedral oxygen configuration) and 94 ppm (tetrahedral oxygen configuration), respectively, in ^{27}Al and ^{29}Si NMR spectra. However, the positions of the peaks in the spectra do not change noticeably even upon a mechanochemical treatment of a sample for 1 h. This means that the existing Si–O–Al bonds are for the most part preserved in the deformed structure of pyrophyllite.

The study demonstrated that the structure of montmorillonite more readily undergoes profound changes in the course of mechanical treatment, compared with that of pyrophyllite. For example, it was found that changes in the ^{29}Si NMR spectra are similar to those for pyrophyllite, but occur upon a more prolonged treatment. However, changes in the ^{27}Al NMR spectra have a different nature. For example, similarly to the spectra of the initial sample, spectra of activated montmorillonite show two signals with δ close to the initial values. The intensity of the signal at δ = 50 ppm in these spectra markedly increases upon activation, which points to a considerable transformation of the octahedral layer, accompanied by a decrease in the coordination of Al^{3+} ions to a tetrahedral coordination.

REFERENCES

1. Myagii, M.Ya., Samoson, A.V., Tarmak, M.Kh., *et al.*, *Dokl. Akad. Nauk SSSR*, 1981, vol. 261, no. 5, pp. 1169–1173.
2. Stepanov, V.G., Shubin, A.A., Ione, K.G., *et al.*, *Kinet. Kataliz*, 1984, vol. 25, no. 5, pp. 1225–1227.
3. Goncharuk, V.V., Kornilovich, B.Yu., Pavlenko, B.M., *et al.*, *Khim. Tekhnol. Vody*, 2001, vol. 23, no. 4, pp. 410–415.

1070-4272/05/7802-0339 © 2005 Pleiades Publishing, Inc.

Russian Journal of Applied Chemistry, Vol. 78, No. 2, 2005, pp. 340–341. Translated from Zhurnal Prikladnoi Khimii, Vol. 78, No. 2, 2005, pp. 345–346.
Original Russian Text Copyright © 2005 by Semenov, Arapov, Charykov, Nekrasov, Alekhin, Gerasimov, Seregin.

BRIEF COMMUNICATIONS

Sorption of Light Fullerenes (C_{60} and C_{70}) on Materials Prepared by Sublimation of Graphite Rods

K. N. Semenov, O. V. Arapov, N. A. Charykov, K. V. Nekrasov, O. S. Alekhin, V. I. Gerasimov, and V. I. Seregin

St. Petersburg State University, St. Petersburg, Russia

St. Petersburg State Technological Institute, St. Petersburg, Russia

Received September 9, 2004

Abstract—Sorption of fullerenes C_{60} and C_{70} from *o*-xylene, toluene, and *o*-dichlorobenzene solutions under static conditions on a sorbent prepared by sublimation of graphite rods was studied. The sorption isotherms of both fullerenes at 25°C were measured.

In this study, we examined sorption of fullerenes from *o*-xylene, toluene, and *o*-dichlorobenzene solutions on a sorbent prepared by sublimation of graphite rods. The research in this field is aimed at determining the conditions of chromatographic separation of fullerene mixtures [1–3]. This study continues our previous investigations concerned with sorption of light fullerenes on unmodified carbon materials [3]. It should be noted that the first works in this field in Russia were those by Samonin *et al.* [4, 5], which, however, disregarded the possibility of chromatographic separation and purification of light fullerenes.

We used fullerene C_{60} containing 99.9 wt % main compound (0.1 wt % C_{70}) and C_{70} containing 99 wt % main compound (1 wt % C_{60}) (ILIP Joint-Stock Company, St. Petersburg, Russia). *o*-Xylene, *o*-dichlorobenzene, and toluene were of analytically pure grade. The sorbent was prepared by sublimation of graphite rods [reactor graphite of ultrapure grade (>99.995 wt %)] at 2500 ± 50°C and a residual pressure of 2×10^{-3} mm Hg. The carbon vapor was condensed on a steel support water-cooled to temperatures below 70°C. The resulting carbon crust was ball-milled using steel balls. The powder was mechanically sieved into fractions. We used a fraction with the following particle size distribution: $d > 70$ μm less than 10 wt %, $d = 40$–70 μm 80–85 wt %, and $d < 40$ μm 5–10 wt %. Just before the experiment, the sorbent was heated in air at 200 ± 20°C for 1.5–2.0 h.

To study the sorption properties of the carbon, concentrated stock solutions of the fullerenes in the above solvents were prepared (taking into account their solubilities) by isothermal saturation at 25°C for 24 h. The concentration of C_{60} and C_{70} in *o*-xylene, toluene, and *o*-dichlorobenzene was 4.1 and 2,3, 1.3 and 0.46, and 26 and 3.3 g l^{-1}, respectively. Less concentrated solutions in all of these solvents were prepared by sequential dilutions.

To weighed portions of the carbon (1 g), 10-ml aliquots of the fullerene solutions of different concentrations were added. The mixture was stirred on a magnetic stirrer for 24 h at 25 ± 0.05°C. This time is required to attain an equilibrium in the carbon-solution system. The mixture was filtered through a Schott filter (porosity 16) to remove the sorbent, and the fullerene content in the resulting solution was determined.

The content of C_{60} and C_{70} in the solutions before and after the sorption was determined spectrophotometrically on an SF-46 spectrophotometer from the optical density at λ = 335.5 and 472.0 nm [6].

The concentrations were calculated by the following empirical equations:

$$c(C_{60}) = 13.10(D_{335} - 1.8080D_{472}), \quad (1)$$

$$c(C_{70}) = 42.51(D_{472} - 1.0081D_{335}), \quad (2)$$

where D_{335} and D_{472} are the optical densities of a 1-cm layer of the solution at the indicated wavelength; $c(C_{60})$ and $c(C_{70})$ are the fullerene concentrations (g l^{-1}).

1070-4272/05/7802-0340 © 2005 Pleiades Publishing, Inc.

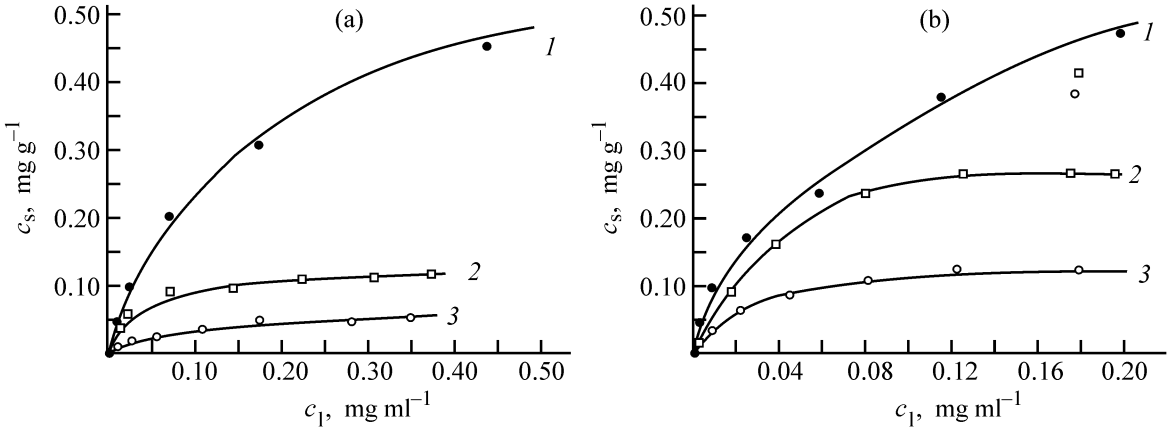


Fig. 1. Isotherms of adsorption of (a) C_{60} and (b) C_{70} from (*1*) *o*-dichlorobenzene, (*2*) *o*-xylene, and (*3*) toluene at 25°C on the unmodified carbon sorbent prepared by vacuum sublimation of graphite rods. Sorbent weight $m \sim 1$ g, solution volume $V \sim 10$ ml. (c_s, c_l) Fullerene concentrations in the solid and solution, respectively.

The sorption isotherms of fullerene are shown in Figs. 1a and 1b.

All the sorption isotherms measured in toluene and *o*-xylene are of Langmuir type. This is not the case for *o*-dichlorobenzene solutions. In this solvent, no saturation is reached in the concentration range examined.

The static sorption capacity of the sorbent in *o*-xylene, toluene, and *o*-dichlorobenzene for C_{60} and C_{70}, determined from the height of the plateau in the isotherms (Figs. 1a, 1b) is 0.10 and 0.24, 0.04 and 0.09, and 0.45 and more than 0.50 mg g^{-1} (the saturation is not reached), respectively.

As can be seen from Figs. 1a and 1b, the distribution coefficients of the fullerenes between the solid and liquid phases strongly depend on the solvent (isotherms measured in these solvents differ) and monotonically decrease for both fullerenes as their concentrations in both phases increase. Finally, the distribution coefficient of C_{70} is higher by a factor of 2–2.5 than that of C_{60}, which is favorable for chromatographic separation of the fullerenes. The only exception are *o*-dichlorobenzene solutions. In this solvent, the distribution coefficients of C_{60} and C_{70} are close, which makes their sorption separation ineffective.

ACKNOWLEDGMENTS

This study was financially supported by the Russian Ministry of Education, Grant for Basic Research in the Field of Natural Philosophy and Exact Science (project no. E02-5.0-227) and by the Russian Foundation for Basic Research (project no. 03-05-65164).

REFERENCES

1. Parker, D.H., Chatterjee, K., Wurz, P., *et al.*, *Carbon*, 1992, vol. 30, no. 8, pp. 1167–1182.
2. Lazukhina, E.E. and Bubnov, V.P., *Izv. Ross. Akad. Nauk, Ser. Khim.*, 1995, no. 7, pp. 1223–1226.
3. Semenov, K.N., Seregin, V.I., Arapov, O.V., and Charykov, N.A., *Zh. Prikl. Khim.*, 2004, vol. 77, no. 10, pp. 1638–1642.
4. Samonin, V.V. and Slutsker, E.M., *Zh. Fiz. Khim.*, 2003, vol. 77, no. 7, pp. 1287–1293.
5. Samonin, V.V. and Marakulina, E.A., *Zh. Fiz. Khim.*, 2002, vol. 76, no. 5, pp. 888–893.
6. Ponomarev, N., Yudovich, M.E., Charykov, N.A., *et al.*, *Opt. Spectrosc.*, 2000, vol. 88, no. 2, pp. 195–197.

Russian Journal of Applied Chemistry, Vol. 78, No. 2, 2005, pp. 342–343. Translated from Zhurnal Prikladnoi Khimii, Vol. 78, No. 2, 2005, pp. 347–348.
Original Russian Text Copyright © 2005 by Aslanov, Mamedli, Guliev.

BRIEF COMMUNICATIONS

Synthesis of Saccharindicarboxylic Acids and Their Derivatives

T. A. Aslanov, U. M. Mamedli, and A. M. Guliev

Institute of Polymeric Materials, National Academy of Sciences of Azerbaijan, Sumgait, Azerbaijan

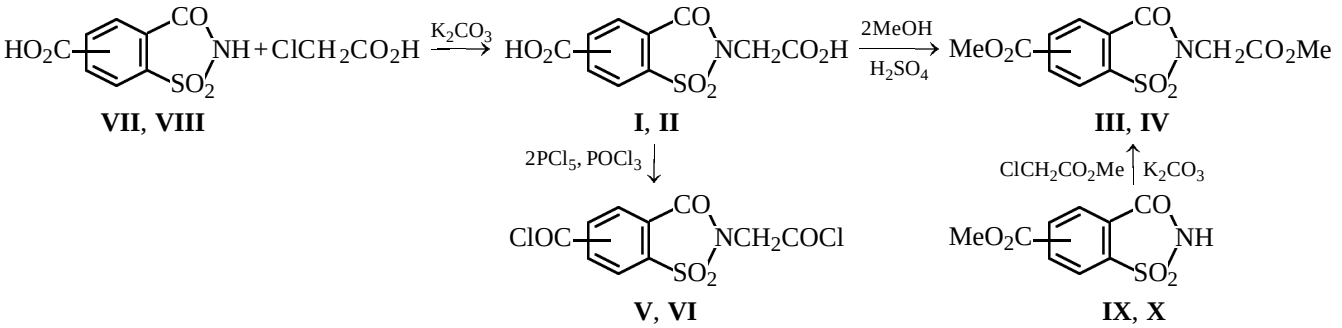
Received June 22, 2004

Abstract—Procedures were developed for preparing saccharindicarboxylic acids and their derivatives.

Imido dicarboxylic acids and their derivatives are used as monomers in synthesis of polyamido imides and polyester imides [1, 2]. Structurally related monomers with aliphatic and aromatic fragments were prepared in [3, 4].

In this study we prepared previously unknown saccharindicarboxylic acids **I** and **II**, their methyl esters **III** and **IV**, and chlorides **V** and **VI**, starting from saccharin-5-carboxylic acid **VII** and saccharin-6-carboxylic acid **VIII**, prepared as described in [4].

The reactions of acids **VII** and **VIII** with monochloroacetic acid were performed in dimethylacetamide (DMAA) in the presence of K_2CO_3:



where compounds **I**, **III**, and **V** are substituted in 5-position, and compounds **II**, **IV**, and **VI**, in 6-position.

The resulting saccharin-5- (**I**) and saccharin-6-carboxy-*N*-acetic (**II**) acids were recrystallized from hot distilled water. The isolated products are crystalline substances, mp 300 and 278°C, respectively.

The composition and structure of **I** and **II** were confirmed by elemental analysis and IR spectroscopy. The IR spectra contain bands at 1690–1700 (C=O of saccharin ring), 1180, and 1365 cm^{-1} (asymmetric SO_2 stretching vibrations in the saccharin ring). Also, the IR spectra of **I** and **II** contain a band at 3480–3600 cm^{-1}, characteristic of stretching vibrations of the O–H group in carboxylic acids [5].

Esters **III** and **IV** were prepared either by esterification of acids **I** and **II** with methanol or by condensation of methyl esters **IX** and **X** with methyl chloroacetate. Compounds **III** and **IV** are crystalline substances, mp 184 and 163°C, respectively, readily soluble in aprotic solvents.

The IR spectra of diesters **III** and **IV** contain absorption bands at 1730–1740 (C=O in ester group), 1370–1380, and 1460 cm^{-1} (CH_3); the band at 720–740 cm^{-1} belongs to the CH_2 group. The bands at 1320–1350 and 1140–1180 cm^{-1} belong to stretching vibrations of the SO_2N group.

Dichlorides **V** and **VI** were prepared by the reactions of acids **I** and **II** with PCl_5 in the presence of a minor amount of $POCl_3$ [6]. Compounds **V** and **VI**

1070-4272/05/7802-0342 © 2005 Pleiades Publishing, Inc.

Yields and elemental analyses of saccharindicarboxylic acids and their derivatives **I**–**VI**

Compound	Yield, %	Found, %				Formula	Calculated, %				*M*	
		C	H	N	S		C	H	N	S	found	calculated
I	70	43.44	2.60	5.26	12.12	$C_{10}H_7NO_7S$	42.1	2.45	4.91	11.22	293	285
III	80	47.05	3.48	4.38	11.14	$C_{12}H_{11}NO_7S$	46.0	3.51	4.47	10.22	320	313
V[*]	85	38.20	1.48	4.03	10.11	$C_{10}H_5Cl_2NO_5S$	37.2	1.55	4.34	9.93	318	322
II	68	44.01	2.55	5.15	12.00	$C_{10}H_7NO_7S$	42.1	2.45	4.91	11.22	289	285
IV	72	46.66	3.60	4.67	10.88	$C_{12}H_{11}NO_7S$	46.0	3.51	4.47	10.22	310	313
VI[*]	82	38.10	1.61	4.48	10.13	$C_{10}H_5Cl_2NO_5S$	37.2	1.55	4.34	9.93	325	322

[*] Found Cl, %: 23.24 (**V**), 21.33 (**VI**); calculaed Cl, %: 22.05 (**V**), 22.05 (**VI**).

are gray powders soluble in aprotic solvents; mp 166 and 145°C, respectively.

The IR spectrum of dichloride **V** contains, along with other bands, characteristic bands of the imide ring at 1136–1210, 1380, 1720, 1780, and 3220 cm^{-1}.

The characteristics of **I**–**VI** are given in the table.

EXPERIMENTAL

5-Carboxysaccharin-*N*-acetic acid I. To a solution of 11.36 g of **VII** in 130 ml of DMAA, we added 7 g of powdered potassium carbonate, 4.75 g of chloroacetic acid, and 50 g of KI; the mixture was refluxed for 6 h. After the reaction was complete, the mixture was cooled to room temperature, and the precipitate was filtered off and washed with two portions of DMF. The filtrate was evaporated to dryness and vacuum-dried to constant weight.

Acid **II** was prepared similarly.

***N*-Carboxymethylsaccharin-5-carboxylic acid dimethyl ester III.** (a) To a solution of 10 ml of concentrated H_2SO_4 in 250 ml of methanol, we added 14.25 g of acid **I** and refluxed the resulting mixture to obtain a homogeneous solution. Then this solution was mixed with 500 ml of cold distilled water, and the yellowish precipitate was filtered off, washed with distilled water to neutral reaction, and dried first in air and then in a vacuum.

Ester **IV** was prepared similarly.

(b) To a solution of 12.1 g of ester **IX** in 50 ml of DMF, we added 3.5 g of K_2CO_3 at 70°C and then 5.45 g of methyl chloroacetate and 0.5 g of KI; the mixture was heated at 125–130°C for 2 h. Then the mixture was poured into 200 ml of distilled water, and the precipitate was filtered off, recrystallized, and dried first in air and then in a vacuum at 60–70°C.

Diester **IV** was prepared from ester **II** similarly.

***N*-Carboxymethylsaccharin-5-carboxylic acid dichloride V.** Phosphorus pentachloride (2.1 g) and acid **I** (2.85 g) were mixed at room temperature. In so doing, the mixture spontaneously warmed up to 40–45°C. After the exothermic reaction was complete, the mixture was heated to 95–100°C and stirred at this temperature for 2 h. After the reaction was complete, the phosphorus oxychloride formed was distilled off in a water-jet-pump vacuum. The remaining oily product was successively washed with anhydrous chloroform and benzene and then recrystallized from anhydrous toluene.

Dichloride **VI** was prepared similarly.

CONCLUSION

Previously unknown *N*-carboxymethylsaccharin-5- and -saccharin-6-carboxylic acids, their methyl esters, and dichlorides, which are promising monomers for heat-resistant polyimides, were prepared in high yields (70–85%).

REFERENCES

1. Suvorov, B.V., Zhubanov, B.A., and Mashkevich, S.A., *Trimellitovaya kislota i polimery na ee osnove* (Trimellitic Acid and Polymers Derived from It), Alma-Ata: Nauka, 1975.
2. Aslanov, T.A., Salakhov, M.S., and Efendiev, A.A., *Vysokomol. Soedin., Ser. B*, 2004, vol. 46, no. 2, pp. 379–382.
3. Meserle, P.E., Musina, T.K., and Zhubanov, B.A., *Izv. Akad. Nauk Kaz. SSR, Ser. Khim.*, 1974, no. 1, pp. 56–62.
4. Aslanov, T.A., *Zh. Prikl. Khim.*, 2003, vol. 76, no. 2, pp. 340–341.
5. Kazitsyna, L.A. and Kupletskaya, N.B., *Primenenie UF, IK, YaMR i mass-spektroskopii v organicheskoi khimii* (Applications of UV, IR, NMR, and Mass Spectroscopy to Organic Chemistry), Moscow: Mosk. Gos. Univ., 1979.
6. Arkhipova, I.A., Zhubanov, B.A., Kim, L.V., and Ivashchenko, N.I., *Zh. Prikl. Khim.*, 1976, vol. 49, no. 6, pp. 1399–1402.

Russian Journal of Applied Chemistry, Vol. 78, No. 2, 2005, p. 344. Translated from Zhurnal Prikladnoi Khimii, Vol. 78, No. 2, 2005, pp. 349–350.
Original Russian Text Copyright © 2005 by Zaikov, Artsis.

========== **INFORMATION** ==========

The XI International Conference on Polymeric Materials: Properties, Processing, Modification, and Applications

The XI conference on polymeric materials was held on September 29 to October 1, 2004, at the Martin Luther University in Halle/Saale, Germany. The Conference Chair was H. Michler. The Conference Committee included such well-known German scientists as Jörg Kressler, Hans-Joachim Radusch, Rainer Schnabel, and others.

Amohg the conference participants were more than 450 scientists from 80 research centers of 33 countries including Algeria, Australia, Austria, Belgium, Brazil, Bulgaria, Canada, China, Croatia, Czech Republic, France, Germany, Greece, Hungary, India, Israel, Italy, Japan, the Netherlands, Poland, Portugal, Romania, Russia, Slovakia, Slovenia, Spain, Sri Lanka, Sweden, Switzerland, the United Kingdom, the United States, and Uzbekistan.

Primary attention was given at the conference to the following problems: structure and morphology; characterization and testing of polymers; modification of polymers; polymer processing; properties of polymers and applications; deformation and fracture processes; new polymeric materials, blends, and nanocomposites; biomedical materials; "green" (ecologically clean) polymers; and sustainable development of polymers and recycling.

The Conference Program included four plenary lectures. Then the Conference was held in the form of a series of minisymposia on five dedicated topics and two poster sessions.

The first plenary lecture [E.J. Balta-Calleja (Spain)] was devoted to micromechanical properties of polymers and polymer blends (nanostructure and morphology). P. Eyrer, R. Emmerich, and M. Kaiser (Germany) reviewed in their lecture processes used for manufacturing polymers with improved characteristics. V. Altstadt and J. Sandler (Germany) considered problems of synthesis and processing of nanocomposites. The main concern of the fourth lecture [K. Friedrich, F. Haupert, and Z. Zhang (Germany)] was the structure and properties of polymers reinforced with spherical nanoparticles.

Section A (Structure and Morphology. Polymer Characterization and Testing) included 30 presentations.

Section B (Modification of Polymers. Polymer Processing) included six presentations covering such topics as organic and inorganic fireproof polymeric materials; cryogenic mechanical milling of thermoplastic polymers and their blends; processing of PVA blends; properties of rubbers, fibers, and films; and use of plasma for modification of the surface of polymeric articles.

Section C (Properties of Polymers and Application. Deformation and Fracture Processes) included 34 presentations.

Section D [New Polymeric Materials, Blends and Nanocomposites, Biomedical Materials] also included 34 presentations.

Section E (Green Polymers. Sustainable Development of Polymers and Recycling) included 14 contributions devoted to synthesis and characterization of new green polymers based on natural products and, in particular, chitin and chitosan, cellulose, sugars, polysaccharides, lignin, starch, and also to the possibility of development of polymer hybrids.

The first poster session included about 80 presentations devoted to the structure, morphology, and properties of polymers.

The second poster session also included about 80 presentations on modification of polymers; polymer processing; new polymeric materials, blends, composites and nanocomposites; biomedical materials; and green polymers.

The conference was accompanied by an exhibition of new scientific instruments for study of properties and structure of polymers.

The conference revealed the steadily growing interest in polymers and polymeric materials. Presently, the world output of polymers (by volume, not by weight) is equal to that of steel, cast iron, rolled metal, and nonferrous metals combined.

Rapid growth of the polymer industry settles many problems, posing, in turn, new problems, which are being gradually solved.

The next XII conference is planned to be held at the Martin Luther University in 2006.

G.E. Zaikov and M.I. Artsis

1070-4272/05/7802-0344 © 2005 Pleiades Publishing, Inc.

Russian Journal of Applied Chemistry, Vol. 78, No. 2, 2005, p. 345. Translated from Zhurnal Prikladnoi Khimii, Vol. 78, No. 2, 2005, pp. 350–351.
Original Russian Text Copyright © 2005 by Zaikov.

INFORMATION

Symposium "Topical Problems of Chemistry and Physics of Functionalized and Mesophase Polymers"

Symposium "Topical Problems of Chemistry and Physics of Functionalized and Mesophase Polymers" was held on November 3, 2004. The symposium was organized by the Topchiev Institute of Petrochemical Synthesis (TIPS), Russian Academy of Sciences, and the Scientific Council for Macromolecular Compounds, Chemistry Division, Russian Academy of Sciences. The sponsors were the Corium International Co. (the United States) and TNO (Institute for Innovations in Power Engineering) (the Netherlands).

Amond the Symposium participants were about 150 scientists from 38 research centers of France, Germany, Italy, Kazakhstan, the Netherlands, Russia, Tajikistan, the United States, and Uzbekistan. In fact, the Symposium was dedicated to fifty-year research activities and seventieth birthday of Academician N.A. Plate, Vice President of the Russian Academy of Sciences, Director of the Topchiev Institute of Petrochemical Synthesis. The symposium included 17 presentations.

Known Russian scientists: N.A. Plate, V.A. Kabanov, I.A. Oreshkin, V.G. Kulichikhin, A.D. Litmanovich, L.I. Valuev, V.V. Volkov, G.F. Tereshchenko, and S.N. Khadzhiev, took part in the Opening Ceremony. A total of four sessions were held.

In the first session, four reports were presented. H. Finkelman (Germany) reviewed the history of research from mesophase polymers to mesophase elastomers. A group of authors [R.V. Tal'roze, V.N. Vasilets, and G.A. Shandryuk (Russia)] reported on development of novel mesophase polymeric brushes. The lecture given by E.M. Antipov (Russia) was devoted to preparation and characterization of superelastic fibers and nanocomposites based on biodegradable and biocompatible polyhydroxyalkanoates. V.P Shibaev (Russia) considered in his lecture new prospects for development, testing, and application of mesophase polymers.

The second session included five presentations. K. Matyjaszewski (the United States) reported on "well-organized" hybrid polymers as promising materials for the future. The lecture given by A. Jansen (the Netherlands) was devoted to use of membrane processes in oil and gas industry. The molecular design of functionalized polymeric membranes was discussed in the lecture presented by E. Drioli (Italy). A group of Russian researchers (V.V. Volkov, A.G. Fadeev, and G.N. Bondarenko) described the structure, molecular flexibility, and membrane properties of comb-shaped polymers containing perfluoro groups. D. Khalikov (Tajikistan) considered the physicochemical aspects of catalyzed degradation of a natural network polymer, plant-cell protopectin.

Four lectures were delivered in the third session. G. Cleary (the United States) described properties of ternary mixtures of hydrophilic polymers demonstrating adhesion to biological surfaces. The lecture given by L.I. Valuev (Russia) was devoted to synthesis and characterization of polymers having a lower critical temperature of mixing, which can be used as carriers for bioactive agents. D. Duchene (France) presented the results obtained with polymers adapted to targeted drug transportation. Z. Nurkeeva (Kazakhstan) considered new stimulus-sensitive vinyl ether polymers and their complexes.

The last fourth session included four presentations. The lecture given by Ya.V. Kudryavtsev and A.D. Litmanovich (Russia) was devoted to the theory of interchain exchange in polymer blends. V.G. Kulichikhin (Russia) described nanocomposite-based hydrocolloid systems for medical purposes. J. Kirsch (Germany) reported on recent RAS/Bayer collaboration programs. He outlined that the collaboration was enabled by N.A. Plate's activities. In the concluding remarks, N.A. Plate told about his research activities, particularly, in the field of polymer chemistry and physics.

Finally, the symposium revealed that problems of chemistry and physics of functionalized and mesophase polymers are being successfully solved. Russian scientists, primarily Academician Plate's scientific school, contribute significantly to their solution.

G. N. Zaikov

1070-4272/05/7802-0345 © 2005 Pleiades Publishing, Inc.

Russian Journal of Applied Chemistry, Vol. 78, No. 3, 2005, pp. 347–350. Translated from Zhurnal Prikladnoi Khimii, Vol. 78, No. 3, 2005, pp. 353–356.
Original Russian Text Copyright © 2005 by Kamaev, Archugov, Mikhailov.

INORGANIC SYNTHESIS AND INDUSTRIAL INORGANIC CHEMISTRY

Behavior of the Al_2O_3–ZrO_2 System at High Temperatures

D. N. Kamaev, S. A. Archugov, and G. G. Mikhailov

South-Ural State University, Chelyabinsk, Russia

Received September 17, 2004

Abstract—The system Al_2O_3–ZrO_2 at temperatures of up to 2100°C was studied by differential thermal analysis.

The oxide system Al_2O_3–ZrO_2 is of great practical interest. Data on its phase diagram are significant for the production of abrasive and structural materials operating at high temperatures. These materials are produced either by fusion of the components with their subsequent crystallization or by sintering of finely dispersed powders. The phase diagram furnishes information on the material crystallization, and the use of appropriate cooling mode makes it possible to control the product quality. However, the high liquidus temperature in the Al_2O_3–ZrO_2 system significantly complicates studying this system and obtaining reliable results. Therefore, data on this system are far from being exhaustive.

Most authors [1–7] believe that the system components form a simple eutectic and state that any intermediates are absent from the system. However, there is no agreement in the literature regarding the eutectic composition, its temperature, and shape of liquidus lines. In particular, according to the above-mentioned data, the temperature of the eutectic transition varies from 1710 to 1920°C, and the eutectic composition, from 30 to 55 wt % ZrO_2.

According to [5], the eutectic transition takes place at 1890°C, and the eutectic contains about 40 wt % ZrO_2. The eutectic composition was confirmed in [8] by the method of three-crucible thermal analysis, which makes it possible to obtain high-precision data [8–10]; however, the eutectic temperature was found to be 1866 ± 7°C. In addition, according to [8], the liquidus line has a complicated shape, suggesting the tendency of the system to phase separation at temperatures slightly exceeding those of the liquidus line.

Taking into account the importance of the phase diagram of the Al_2O_3–ZrO_2 system for the production of refractories and abrasives and also the ambiguous character of the previously obtained data, we have reexamined the phase diagram of this system.

EXPERIMENTAL

The experiment was carried out on a computer-controlled upgraded installation for high-temperature three-crucible differential thermal analysis, with data processing on a PC [12].

Analytically pure grade aluminum oxide (Al_2O_3) and zirconium nitrate $Zr(NO_3)_4 \cdot 5H_2O$ were used as starting reagents. According to thermographic analysis, zirconium nitrate loses water of crystallization at low temperatures and decomposes to the oxide at high temperatures. Therefore, it was annealed in air for 3 h at 1200°C. Before weighing, the starting oxides were additionally annealed for several hours to remove moisture and adsorbed impurities. Then they were immediately placed in weighing bottles, which were subsequently stored in a desiccator under dry air, which excluded the saturation of the oxides with water vapor and the corresponding weighing errors. The grade of accuracy of the balance in use warranted that the deviation of the obtained composition from the calculated composition did not exceed 0.01 wt %. Samples containing from 0 to 90 wt % ZrO_2 in 10 wt % steps were prepared. In the range from 40 to 60 wt % ZrO_2, the step was 2 wt %. After mixing, the samples were pressed in a special hard-alloy mold.

Despite the fact that ZrO_2 and Al_2O_3 practically do not react with atmospheric moisture and CO_2, the pressed samples were annealed once more at 1200°C under 1 atm of argon. To obtain data required for the subsequent calculations, the sample pellets were weighed before placing in a crucible of the thermographic installation.

The samples under study were homogenized by step-by-step annealing. In the first step, the sample was heated at a rate of 60 deg min^{-1} to 2100°C. In the second step, it was sharply cooled to 800–1000°C. In the third step, the sample was heated at a rate of

1070-4272/05/7803-0347 © 2005 Pleiades Publishing, Inc.

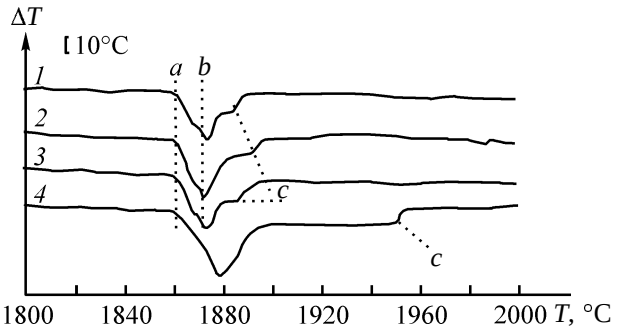


Fig. 1. Typical DTA curves recorded at a heating rate of 60 deg min^{-1}. (*T*) Temperature; the same for Fig. 2. Temperature measured: (*a*) solidus, (*b*) onset of phase separation, and (*c*) liquidus. ZrO_2 content in the sample (wt %): (*1*) 46, (*2*) 50, (*3*) 60, and (*4*) 30.

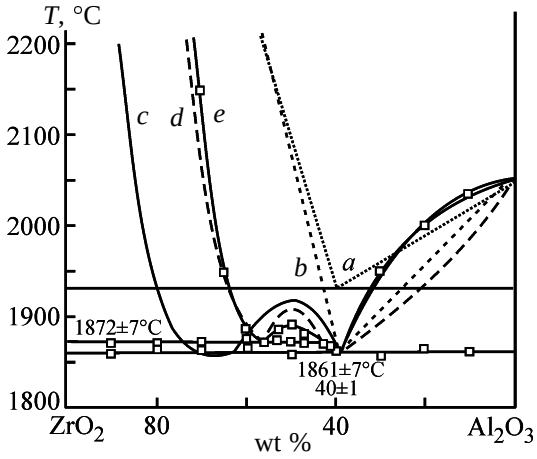


Fig. 2. Phase diagram of the Al_2O_3–ZrO_2 system. Experimental and calculated data: (*a*) model of perfect solutions, (*b*) model of regular solutions, (*c*, *d*) model of subregular ionic solutions, and (*e*) experimental points.

60 deg min^{-1} to a temperature higher by 100–200°C than the expected liquidus point. Finally, after keeping for 3–5 min at the maximal temperature, which provided complete homogenization of the sample, it was cooled at the same rate to the temperature 30–100°C lower than the eutectic point and kept at this temperature for 3–5 min. X-ray spectral microanalysis of the quenched alloys indicates that such a treatment is sufficient for the homogenization.

The resulting sample was subjected to thermal analysis. The sample was heated at a rate of 30 deg min^{-1} to 2100°C and then was cooled at the same rate to a temperature 30–100°C lower than the eutectic transition point. At this temperature, it was kept for 3–5 min. In the next step, the annealed sample was sharply cooled to room temperature. In the final step, the sample was heated at a rate of 20–60 deg min^{-1} to 2100°C and then cooled to room temperature.

Multistep heating and cooling allowed us to obtain highly reproducible results. To collect a statistically significant representative dataset, each sample after homogenization was subjected 7–13 times to the subsequent treatment steps. Thermocouple readings were corrected during an experiment by the Al_2O_3 melting point and further by the copper melting point [13].

The DTA curves of the samples heated at various rates (20–60 deg min^{-1}) demonstrate the effect of the heating rate and allow us to extrapolate the data obtained to the zero heating rate and finally to determine the equilibrium liquidus and eutectic lines in the phase diagram (Figs. 1, 2).

The shape of the experimental liquidus line suggests that either a chemical compound is formed in this system or it separates into layers.

To answer this question, we specially studied several samples containing 50 wt % ZrO_2. Each sample was heated to approximately 1900°C and kept at this temperature for 3 min. Then the temperature was decreased to 1890°C (according to the data obtained, this temperature corresponded to a point in the liquidus line) and the sample was kept at this temperature for 3 min. Then the temperature was further decreased by 10°C, and the sample was kept for about 10 min. If the sample actually separates into layers, such keeping at 1880°C must ensure efficient formation of separable liquids. Then the sample was sharply cooled by purging the furnace with cold argon. The further study has shown that such a sharp cooling conserved to room temperature the phase composition of the samples characteristic of 1880°C.

The quenched samples were studied by the X-ray diffraction analysis, which showed no formation of any chemical compounds in the sample containing 50 wt % ZrO_2.

The distribution of elements in the quenched sample with a total ZrO_2 content of 50 wt % was analyzed with a scanning electron microscope. Phase conglomerates with high and low Zr(IV) content and, correspondingly, with low and high Al(III) content were observed (Fig. 3). No primary crystals of either ZrO_2 or Al_2O_3 were found in this sample. Samples with a ZrO_2 concentration of 60 and 30 wt % kept at the same temperature (1880°C) were quenched for comparison.

Primary crystals of pure ZrO_2 and a phase with the composition corresponding to the melt in equilibrium with ZrO_2 were found in the quenched sample containing 60 wt % ZrO_2 (Fig. 4a). The distribution of elements in these phases was analyzed. In one phase

(quenched melt), the ratio of intensities of Al(III) and Zr(IV) characteristic radiation was invariable. In the other phase (primary ZrO_2 crystals), aluminum was not found at all, but the intensity of Zr(IV) radiation was much higher than in the phase of the quenched melt. The quenched sample containing 30 wt % ZrO_2 was also analyzed. In the quenched melt, the ratio of the intensities of Al(III) and Zr(IV) characteristic radiation was invariable. The other phase appeared to be primary corundum crystals without Zr(IV) (Figs. 4b).

The eutectic temperature was determined by well reproducible bases of the DTA peaks for all the experiments. It was estimated at 1861 ± 6°C. The eutectic composition was estimated at 40 wt % ZrO_2 by the interception point of the liquidus and solidus lines.

The detected invariant monotectic transition has the following parameters: temperature 1861 ± 6°C and melt compositions from 45 to 58 wt % ZrO_2.

Reliable experimental data obtained make it possible to calculate the phase diagram using various mathematical theories of oxide melts, such as theories of perfect, regular, and subregular ionic solutions.

The models of perfect and regular solutions [14, 15] failed to describe satisfactorily the liquidus line of the system (Fig. 2, *a*); therefore, we have attempted to calculate coordinates of the liquidus line within the framework of the theory of subregular ionic solutions [16]. According to this model, the chemical potential of a liquid solution in a binary system is

$$\mu_1 = \mu_1^0 + \nu_1[RT\ln x_1 + 3x_1^2x_2^2Q_{1112} + (2 - 3x_1)x_1x_2Q_{1122} + (1 - 3x_1)x_2^3Q_{1222}],$$

$$\mu_2 = \mu_2^0 + \nu_1[RT\ln x_2 + (1 - 3x_2)x_1^3Q_{1112} + (2 - 3x_2)x_1^2x_2Q_{1122} + 3x_1^2x_2^2Q_{1222}],$$

where R is the universal gas constant; ν_i, number of cations in an oxide molecule; μ_i^0, standard chemical potential; Q_{1112}, Q_{1122}, and Q_{1222}, energy parameters; and x_i, mole fraction, with index 1 referring to ZrO_2 and index 2, to Al_2O_3.

To construct liquidus lines, we choose the experimental reference points without taking into account separation into layers: 20, 40, and 60 wt % ZrO_2; then we wrote down the expressions for the equilibria in these points and solved the resulting system of equations. Using the parameters obtained, we calculated the liquidus line coordinates. The resulting liquidus line points to the separation of the system into layers

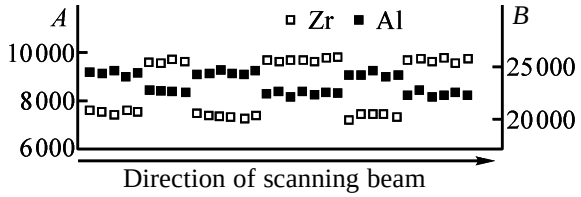


Fig. 3. Distribution of Zr(IV) and Al(III) in quenched samples containing 50 wt % ZrO_2. (*A*, *B*) Intensities of characteristic Zr(IV) and Al(III) radiation, respectively; the same for Fig. 4.

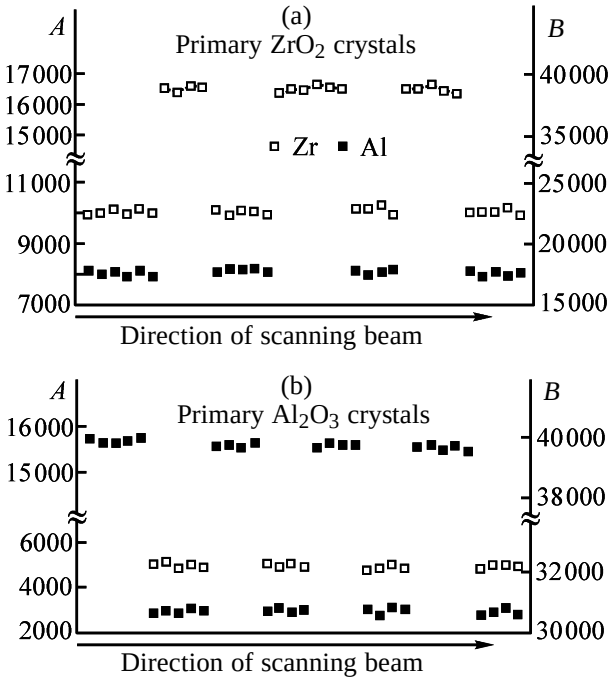


Fig. 4. Distribution of Zr(IV) and Al(III) in quenched samples containing (a) 60 wt % ZrO_2 and (b) 30 wt % ZrO_2: equilibrium of primary ZrO_2 crystals with a melt.

(Fig. 2, *c*), but it agrees with the experimental data insufficiently. Then we carried out calculations taking into account the separation into layers found experimentally. The following points were chosen: 40 wt % ZrO_2, 1861°C; 43 wt % ZrO_2, 1872°C; 56 wt % ZrO_2, 1872°C; and 60 wt % ZrO_2. For these points, we composed equilibrium expressions and solved the system of the resulting equations. The following energy parameters were found: Q_{1112} = 9897, Q_{1122} = 71 280, and Q_{1222} = 20 490 J mol^{-1}.

The liquidus line calculated with the parameters found is shown in Fig. 2, *d*. It differs to some extent from the experimental liquidus line, which may be due to the averaging of the calculated interaction parameters for a relatively wide temperature range.

Thus, the experimental study of the system Al_2O_3–

ZrO_2 and the application of the theory of subregular ionic solutions to this system suggest that the possibility of phase separation in the melt.

REFERENCES

1. Suzuki, H., Kimura, H., Yamada, S., and Yamauchi, T., *J. Ceram. Assoc. Jpn.*, 1961, vol. 69, no. 782 (2), p. 52.
2. Suzuki, H., Kimura, H., Yamada S., and Yamauchi, T., *J. Ceram. Assoc. Jpn.*, 1961, vol. 69, no. 790 (10), pp. 345–350.
3. Cevales, G., *Ber. Deutsch. Keram. Ges.*, 1968, vol. 45, no. 5, pp. 216–219.
4. Fisher, G.R., Manfredo, L.J., McNally R., and Doman, R.C., *J. Mater. Sci.*, 1981, vol. 16, no. 12, pp. 3447–3451.
5. Alper, A.M., *Science of Ceramics: Proc. Int. Conf.*, July 5–8, 1965, vol. 3, pp. 335–369.
6. Volkova, I.Yu., Semenov, S.S., Kravchik, A.E., *et al.*, *Izv. Akad. Nauk SSSR, Neorg. Mater.*, 1987, vol. 23, no. 3, pp. 448–451.
7. Wartenberg, H., Linde, H., and Jung, R., *Z. Anorg. Chem.*, 1928, vol. 176, p. 349.
8. Jerebtsov, D.A., Mikhailov, G.G., and Sverdina, S.V., *Ceram. Int.*, 2000, vol. 26, pp. 821–823.
9. Zherebtsov, D.A. and Mikhailov, G.G., *Prib. Tekh. Eksp.*, 2000, no. 5, pp. 140–148.
10. Jerebtsov, D.A. and Mikhailov, G.G., *Ceram. Int.*, 2001, vol. 27, pp. 25–28.
11. Jerebtsov, D.A. and Mikhailov, G.G., *Ceram. Int.*, 2001, vol. 27, pp. 247–250.
12. Kamaev, D.N., Archugov, S.A., and Mikhailov, G.G., *Izv. Vyssh. Uchebn. Zaved., Chern. Metall.*, 2003, no. 6, pp. 46–49.
13. Bragin, B.K., *Tr. Vses. Nauchno-Issled. Inst. Metrol. im. D.I. Mendeleeva*, 1963, issue 71 (131), pp. 97–100.
14. Kozheurov, V.A., *Statisticheskaya termodinamika* (Statistical Thermodynamics), Moscow: Metallurgiya, 1975.
15. Gerasimov, Ya.I. and Geiderikh, V.A., *Termodinamika rastvorov* (Thermodynamics of Solutions), Moscow: Mosk. Gos. Univ., 1980.
16. Mikhailov, G.G. and Povolotskii, D.Ya., *Termodinamika raskisleniya stali* (Steel Deoxidation Thermodynamics), Moscow: Metallurgiya, 1993.

Russian Journal of Applied Chemistry, Vol. 78, No. 3, 2005, pp. 351–355. Translated from Zhurnal Prikladnoi Khimii, Vol. 78, No. 3, 2005, pp. 357–361.
Original Russian Text Copyright © 2005 by Bashkirov, Kostyushko.

INORGANIC SYNTHESIS AND INDUSTRIAL INORGANIC CHEMISTRY

Formation of Ferrite–Chromites $BaFe_{10}Cr_2O_{19}$ and $SrFe_{10}Cr_2O_{19}$ in the Solid-Phase Reaction of Fe_2O_3 and Cr_2O_3 with Barium or Strontium Carbonate

L. A. Bashkirov and Yu. L. Kostyushko

Belarussian State Technological University, Minsk, Belarus

Received April 9, 2004; in final form, October 2004

Abstract—X-ray phase analysis and the thermomagnetic method were applied to study solid-phase reactions in mixtures of powders $5Fe_2O_3 + Cr_2O_3 + BaCO_3$ and $5Fe_2O_3 + Cr_2O_3 + SrCO_3$, yielding, respectively, barium and strontium ferrite–chromite solid solutions $BaFe_{10}Cr_2O_{19}$ and $SrFe_{10}Cr_2O_{19}$.

Substitution of Fe^{3+} ions in the crystal lattice of high-coercivity barium and strontium ferrites $BaFe_{12}O_{19}$ and $SrFe_{12}O_{19}$ with a structure of magnetoplumbite by Al^{3+}, Cr^{3+}, Ga^{3+}, Sc^{3+}, and In^{3+} ions significantly alters their magnetic properties, which is used in developing a magnetic material with a prescribed set of magnetic parameters [1].

Bertaut *et al.* [2, 3] found that substitution of Fe^{3+} ions in the ferrites $BaFe_{12}O_{19}$ and $SrFe_{12}O_{19}$ by Cr^{3+} ions yields a continuous series of $BaFe_{12-x}Cr_xO_{19}$ and $SrFe_{12-x}Cr_xO_{19}$ solid solutions. With an increase in the chromium(III) content in these solid solutions, their lattice constants become smaller, and the saturation magnetization and Curie point, lower.

The solid solutions $Ba(Sr)Fe_{12-x}M_xO_{19}$ (M^{3+} = Al^{3+}, Cr^{3+}, Ga^{3+}, In^{3+}, or Sc^{3+}) are commonly obtained using the ceramic method, i.e., they are synthesized by sintering at 1173–1573 K a mixture of powdered oxides Fe_2O_3, M_2O_3 and carbonates $BaCO_3$, $SrCO_3$. The kinetics and mechanism of formation of the ferrites $BaFe_{12}O_{19}$, $SrFe_{12}O_{19}$ have been studied in sufficient detail [4, 5]. They are synthesized by the reaction of iron oxide Fe_2O_3 with a carbonate, $BaCO_3$ or $SrCO_3$, via a step of formation of an intermediate compound, $BaFe_2O_4$ or $SrFeO_{3-x}$, respectively. The kinetics and mechanism of formation of solid solutions based on the ferrites $BaFe_{12}O_{19}$ and $SrFe_{12}O_{19}$ are virtually unknown. It was only found in [6] that ferrite–aluminate solid solutions $BaFe_{1.5}Al_{2.5}O_{19}$ and $SrFe_{1.5}Al_{2.5}O_{19}$ are synthesized via a number of steps and the intermediate phases, $BaFe_{12-x}Al_xO_{19}$ and $SrFe_{12-x}Al_xO_{19}$, formed in the process contain less aluminum(III) than the final product.

This study is concerned with solid-phase reactions of the oxides Fe_2O_3, Cr_2O_3 with the carbonates $BaCO_3$, $SrCO_3$ to give the ferrite–chromites $BaFe_{10} \cdot Cr_2O_{19}$, $SrFe_{10}Cr_2O_{19}$, which have been suggested, together with the ferrite–aluminates $BaFe_{9.5}Al_{2.5}O_{19}$, $SrFe_{9.5}Al_{2.5}O_{19}$, for use as additives to raise the energy product $(BH)_{max}$ of ceramic permanent magnets made of these ferrites.

EXPERIMENTAL

The formation of $BaFe_{10}Cr_2O_{19}$ and $SrFe_{10}Cr_2O_{19}$ was studied in isothermal heating for varied time of pellets compacted from mixtures of powdered iron oxide Fe_2O_3 of MM-2 brand, analytically pure grade chromium oxide Cr_2O_3, and pure grade carbonates of barium, $BaCO_3$, or strontium, $SrCO_3$, taken in a 5 : 1 : 1 molar ratio and thoroughly mixed in a vibration mill. The pellets prepared from the mixture $5Fe_2O_3 + Cr_2O_3 + BaCO_3$ were isothermally calcined in air at 1243, 1263, or 1293 K for a certain time and then rapidly cooled in air. The $5Fe_2O_3 + Cr_2O_3 + SrCO_3$ pellets were isothermally calcined at 1203, 1223, or 1253 K. The X-ray phase analysis of the initial mixtures and samples calcined at a certain temperature for a prescribed time was made on a DRON-3 diffractometer (CuK_α radiation) at the same operation modes of the apparatus. This allowed the changes in the quantitative content of phases in the course of the solid-phase reaction to be monitored by the height (intensity) of X-ray reflections.

The Curie point T_C of the ferromagnetic phase formed in the solid-phase reaction was found from the temperature dependence of the specific saturation

1070-4272/05/7803-0351 © 2005 Pleiades Publishing, Inc.

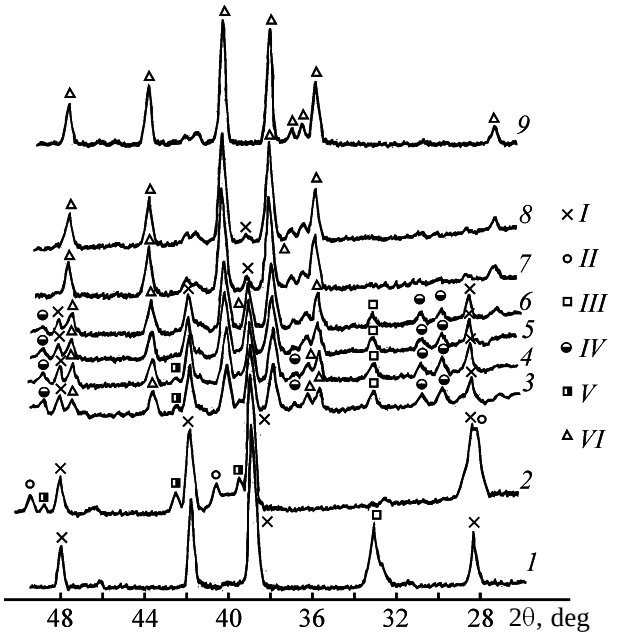


Fig. 1. X-ray diffraction patterns of (*1*) $4.75Fe_2O_3$ + $1.25Al_2O_3$ + $BaCO_3$ mixture calcined at 1173 K for 5 min and a $5Fe_2O_3$ + Cr_2O_3 + $BaCO_3$ mixture calcined at (*2*–*8*) 1293 and (*9*) 1573 K for varied time. (2θ) Bragg angle; the same for Fig. 3. Calcination time (min): (*2*) 0, (*3*) 5, (*4*) 10, (*5*) 15, (*6*) 30, (*7*) 120, (*8*) 480, and (*9*) 180. X-ray diffraction peak: (*I*) α-Fe_2O_3, (*II*) $BaCO_3$, (*III*) $BaFe_2O_4$, (*IV*) $BaCr_2O_4$, (*V*) Cr_2O_3, and (*VI*) $BaCr_xFe_{12-x}O_{19}$.

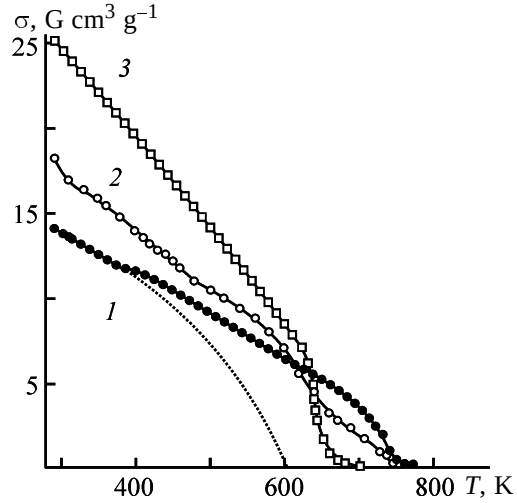


Fig. 2. Specific saturation magnetization σ of a $5Fe_2O_3$ + Cr_2O_3 + $BaCO_3$ mixture calcined at 1293 K for (*1*) 5 and (*2*) 240 min and (*3*) at 1573 K for 180 min vs. temperature *T*.

magnetization σ measured by the Faraday method in a magnetic field of 5 kOe. The run of the $\sigma = f(T)$ dependence and the Curie points, combined with published data on the dependence of T_C on the content of chromium(III) in ferrite–chromites, were used to assess the compositional homogeneity of the ferromagnetic phases formed. X-ray diffraction patterns of a mixture of powders $5Fe_2O_3$ + Cr_2O_3 + $BaCO_3$, calcined at 1293 K for varied time, are shown in Fig. 1. Comparison of the X-ray diffraction patterns of the initial mixture (pattern no. 2) and the mixture calcined for 3 min (pattern no. 3) shows that thermal treatment of this kind leads to formation of the magnetoplumbite phase and intermediates $BaFe_2O_4$, $BaCr_2O_4$. It should be noted here that the reflections associated with $BaCO_3$ are virtually absent in the X-ray diffraction pattern of a mixture calcined for 5 min, and the intensities of Cr_2O_3 lines are substantially lower. Longer calcination leads to an increase in the intensity of peaks of the magnetoplumbite phase $BaFe_{12-x}\cdot Cr_xO_{19}$ and to a decrease in the intensities of the peaks associated with Fe_2O_3 and Cr_2O_3.

The temperature dependence of the specific saturation magnetization shows that the intermediate product formed in calcination of the $5Fe_2O_3$ + Cr_2O_3 + $BaCO_3$ mixture is not magnetically homogeneous and contains phases with different Curie points. For example, a ferromagnetic phase with a lower temperature $T_C \approx 600$ K (Fig. 2, curve *1*) is present, in addition to an almost pure ferrite $BaFe_{12}O_{19}$ ($T_C = 750$ K), after the reaction for 5 min. This indicates that the minor amount of the hexagonal ferromagnetic phase formed contains Cr^{3+} ions, and it is their presence that depresses the Curie point of barium ferrite.

The Curie point of the solid solution $BaFe_{10}Cr_2\cdot O_{19}$, obtained at a calcination temperature of 1573 K, is 660 K (Fig. 2, curve *3*). The temperature dependence of the specific saturation magnetization of a mixture calcined at 1293 K for 240 min (Fig. 2, curve *2*) reveals formation of phases with Curie points of 750, ~680, and ~600 K, i.e., nearly pure barium ferrite and $BaFe_{12-x}Cr_xO_{19}$ solid solutions close in composition to $BaFe_{10}Cr_2O_{19}$ ($x \approx 2$, $T_C \approx 680$ K) and of those with an increased content of chromium(III) ($x > 2$, $T_C \approx 600$ K). The phase with a Curie point $T_C \approx 600$ K, which is 60 K lower than the Curie point of the final product $BaFe_{10}Cr_2O_{19}$, is probably formed through diffusion of iron(III) ions into barium chromite $BaCr_{12}O_{19}$ already formed in a minor amount. Diffusion of Cr^{3+} ions from the oxide Cr_2O_3 into $BaFe_{12}O_{19}$ leads to formation of a $BaFe_{12-x}\cdot Cr_xO_{19}$ solid solution ($x \approx 2$, $T_C \approx 680$ K), which is also formed by the reaction

$$BaCr_2O_4 + 5Fe_2O_3 = BaFe_{10}Cr_2O_{19}.$$

The kinetics of formation of the $BaFe_{10}Cr_2O_{19}$

solid solution in the reaction of $BaCr_2O_4$ and Fe_2O_3 powders taken in a 1 : 5 molar ratio was studied in [7]. It is not improbable that mutual dissolution of $BaFe_2O_4$ and $BaCr_2O_4$ to give the $BaFe_{2-x}Cr_xO_4$ solid solution occurs in addition to the above-mentioned solid-phase reactions. We confirmed this possibility in a study of the kinetics of mutual dissolution of $BaFe_2O_4$ and $BaCr_2O_4$ upon heating of a mixture of powders taken in a 1 : 1 molar ratio.

The lattice constants *a* and *c* of the crystalline hexagonal phase were calculated from the reflections (220) and (205). According to published data [8], the lattice constants *a* and *c* of barium ferrite $BaFe_{12}O_{19}$ are 5.887 and 23.192 Å, respectively. Close to these values are the lattice constants *a* and *c* of the hexagonal phase formed at 1293 K during the first 5 min of calcination, 5.891 and 23.222 Å, suggesting predominant formation of a phase of an almost pure barium ferrite $BaFe_{12}O_{19}$ [9]. This is in agreement with the temperature dependence of the specific saturation magnetization.

As the reaction time becomes longer, the lattice constants *a* and *c* of the hexagonal phase decrease to 5.882 and 23.066 Å, respectively. Raising the content of chromium(III) in the $BaFe_{12-x}Cr_xO_{19}$ solid solution leads to a linear decrease in the lattice constant [2]. Consequently, the decrease in the lattice constants *a* and *c*, observed with increasing calcination time, points to a gradual increase in the content of chromium(III) ions in the phase of the $BaFe_{12-x}Cr_xO_{19}$ solid solution through their diffusion from the crystal lattice of Cr_2O_3 or barium chromites $BaCr_2O_4$ and $BaCr_{12}O_{19}$ formed into the crystal lattice of $BaFe_{12}O_{19}$.

Substitution of Fe^{3+} ions in the crystal lattice of barium ferrite $BaFe_{12}O_{19}$ with Cr^{3+} ions leads to significant changes in the exchange interactions responsible for the ordering of the spin magnetic moments of Fe^{3+} ions. This allows the compositional inhomogeneity of $BaFe_{12-x}Cr_xO_{19}$ solid solutions to be revealed from the temperature dependence of the specific saturation magnetization.

Figure 3 shows X-ray diffraction patterns of a $5Fe_2O_3 + Cr_2O_3 + SrCO_3$ mixture calcined at 1253 K for varied time and of the same mixture in the initial state. Calcination at 1253 K for 5 min results in that the intensities of lines associated with α-Cr_2O_3 strongly decrease and lines of strontium chromate $SrCrO_4$ appear. The reflections at 2θ 30.10°, 30.90°, and 34.65°, present in the X-ray diffraction patterns of the mixtures calcined at 1253 K for 5 to 90 min, and

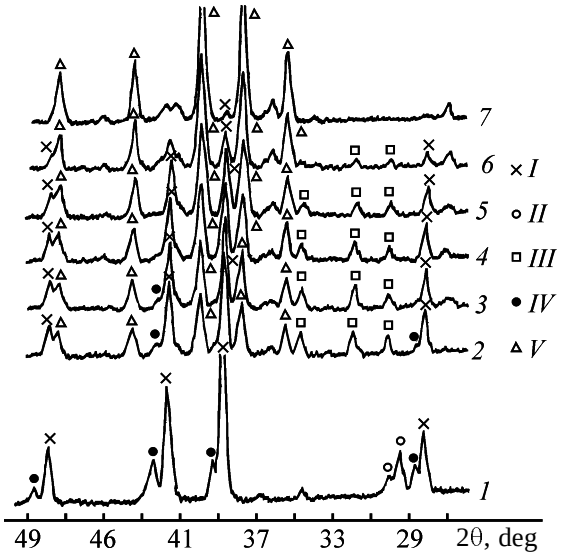


Fig. 3. X-ray diffraction patterns of the $5Fe_2O_3 + Cr_2O_3 + SrCO_3$ mixture calcined at 1253 K for (*1*) 0, (*2*) 5, (*3*) 10, (*4*) 15, (*5*) 60, (*6*) 90, and (*7*) 480 min. X-ray diffraction peak: (*I*) α-Fe_2O_3, (*II*) $SrCO_3$, (*III*) $SrCrO_4$, (*IV*) Cr_2O_3, and (*V*) $SrCr_xFe_{12-x}O_{19}$.

the interplanar spacings calculated from these reflections are in good agreement with published data for $SrCrO_4$ [10], rather than for $SrCrO_{3-x}$ [11]. The X-ray diffraction pattern of a $SrCO_3 + 0.5Cr_2O_3$ mixture calcined in air at 1423 K for 2 h is also in good agreement with published data for $SrCrO_4$, but not for $SrCrO_{3-x}$. The strongest X-ray diffraction line of the intermediate phase $SrFeO_{3-x}$ (2θ = 38.10°, *d* = 2.74 Å) was present only in the diffraction pattern of the $5Fe_2O_3 + Cr_2O_3 + SrCO_3$ mixture calcined at 1173 K for 30 min. In other X-ray diffraction patterns of the same mixture calcined at higher temperatures, this line of the $SrFeO_{3-x}$ phase was absent, suggesting a high reactivity of this intermediate phase.

It should be noted that the strongest lines of $SrCO_3$, present in the X-ray diffraction pattern of the initial mixture, are not observed in the pattern of the mixture calcined at 1253 K for 5 min. Longer heating of the mixture leads to a decrease in the intensity (height) of the X-ray diffraction lines of α-Fe_2O_3 and of the intermediate compound $SrCrO_4$, and to an increase in the intensity of the lines of the hexagonal phase $SrFe_{12-x}Cr_xO_{19}$ (Fig. 4). No shift of the diffraction peaks of α-Fe_2O_3 is observed in this case, which indicates that $Fe_{2-x}Cr_xO_3$ solid solutions are not formed.

The initial $5Fe_2O_3 + Cr_2O_3 + SrCO_3$ mixture is not ferromagnetic, but its calcination at 1253 K for 5 min leads to formation of a ferromagnetic phase and

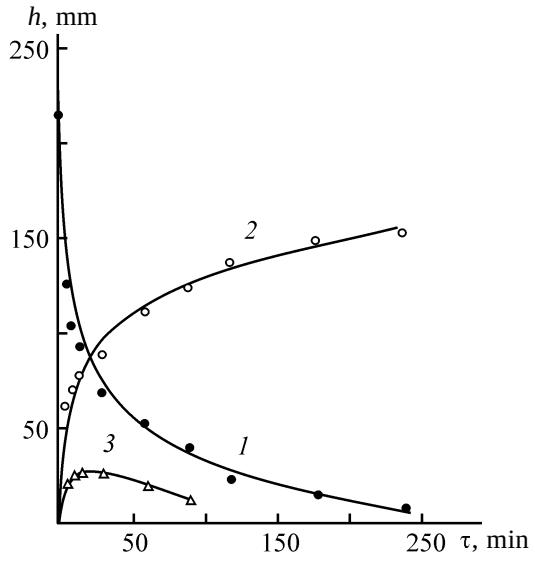


Fig. 4. Height h of X-ray diffraction peaks of (*1*) α-Fe_2O_3, (*2*) $SrFe_{12-x}Cr_xO_{19}$, and (*3*) $SrCrO_4$ vs. the calcination time τ of a $5Fe_2O_3 + Cr_2O_3 + SrCO_3$ mixture at 1253 K.

the specific saturation magnetization of the mixture becomes equal to 17.8 G cm^3 g^{-1}. The calcination for 60 min leads to only a minor increase in the saturation magnetization to 19.2 G cm^3 g^{-1} (Fig. 5, curve *1*). Longer calcination of this mixture at 1223 and 1203 K results in that the specific saturation magnetization first increases, then somewhat decreases, and after that starts to increase again. Such a complicated behavior of the magnetization indicates that the ferromagnetic phase formed in different stages of the process is inhomogeneous as regards the content of chromium(III).

Calculation of the lattice constants a and c of the hexagonal phase $SrFe_{12-x}Cr_xO_{19}$ formed in calcination of the $5Fe_2O_3 + Cr_2O_3 + SrCO_3$ mixture at 1253 K for varied time demonstrated that raising the calcination time to 480 min has virtually no effect on the lattice constant a (5.868–5.872 Å) and leads to a gradual decrease in the lattice constant c from 23.081 to 22.922 Å. The latter trend indicates that, in the course of synthesis, the forming solid solution $SrFe_{12-x}Cr_xO_{19}$ is gradually enriched with chromium(III) to its content in the final product $SrFe_{10}Cr_2O_{19}$.

The magnetic phase formed in $5Fe_2O_3 + Cr_2O_3 + SrCO_3$ mixtures in the initial stage of the reaction has a Curie point of 765 K (Fig. 6, curve *1*), which is close to the Curie point of strontium ferrite $SrFe_{12}O_{19}$ (T_C = 750 K) [4]. Mixtures calcined for a long time contain, in addition to this magnetic phase, a phase with a Curie point of about 680 K (Fig. 6, curve *2*), which is a $SrFe_{12-x}Cr_xO_{19}$ solid solution with a composition close to $SrFe_{11}CrO_{19}$. The Curie point of the final product $Fe_{10}Cr_2O_{19}$ is 600 K (Fig. 6, curve *3*). The results obtained demonstrate that, at the beginning of the solid-phase reaction, $SrCO_3$ is completely consumed for formation of the chromate $SrCrO_4$ and ferrite $SrFeO_{3-x}$, whose reaction with Fe_2O_3 gives the ferrite $SrFe_{12}O_{19}$. Strontium chromate $SrCrO_4$ reacts with Fe_2O_3 to give the solid solution $SrFe_{11}CrO_{19}$ by the reaction

$$SrCrO_4 + 5.5Fe_2O_3 \rightarrow SrFe_{11}CrO_{19} + 0.75O_2.$$

The final product $SrFe_{10}Cr_2O_{19}$ is mainly formed through diffusion of Cr^{3+} ions from Cr_2O_3 or $SrCrO_4$ into $SrFe_{12}O_{19}$ formed in the reaction of $SrCO_3$ and

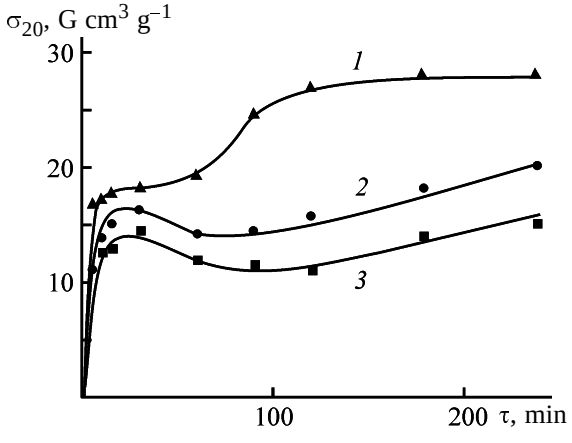


Fig. 5. Room-temperature specific saturation magnetization σ_{20} vs. calcination time τ of a $5Fe_2O_3 + Cr_2O_3 + SrCO_3$ mixture. Calcination time (K): (*1*) 1253, (*2*) 1223, and (*3*) 1203.

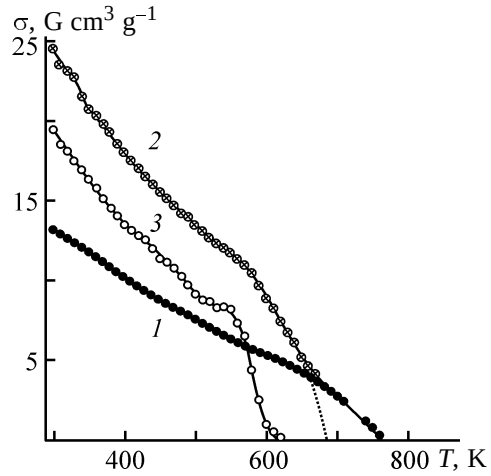


Fig. 6. Specific saturation magnetization σ of a $5Fe_2O_3 + Cr_2O_3 + SrCO_3$ mixture calcined at 1253 K for (*1*) 10 and (*2*) 480 min and (*3*) at 1523 K for 120 min vs. temperature T.

Fe_2O_3. This is the reason why the solid solution $SrFe_{12-x}Cr_xO_{19}$ formed in the course of the reaction is not compositionally homogeneous and has different magnetic characteristics.

CONCLUSIONS

(1) In the initial stage of heating of the mixture of powders $5Fe_2O_3 + Cr_2O_3 + BaCO_3$ at 1243–1293 K, intermediate nonmagnetic phases $BaFe_2O_4$ and $BaCr_2O_4$ and their solid solutions are formed together with a compositionally inhomogeneous ferromagnetic phase with a structure of magnetoplumbite, $BaFe_{12-x}Cr_xO_{19}$. Together with regions having a Curie point of 750 K, i.e., almost pure barium ferrite, there are minor regions with Curie points of 600 and 680 K, which contain, respectively, somewhat higher and somewhat lower amounts of chromium(III), compared to $BaFe_{10}Cr_2O_{19}$. In the concluding stage, there occurs diffusion equalization of the contents of chromium(III) in regions of $BaFe_{12-x}Cr_xO_{19}$ solid solutions with different values of the parameter x to the homogeneous composition of the final product $BaFe_{10}Cr_2O_{19}$, whose Curie point is 660 K.

(2) A study of solid-phase reactions occurring upon heating of the mixture of powders $5Fe_2O_3 + Cr_2O_3 + SrCO_3$ demonstrated that the solid solution $SrFe_{10}Cr_2O_{19}$ is synthesized with formation of intermediate compounds $SrCrO_4$ and $SrFeO_{3-x}$, which further react with Fe_2O_3 and Cr_2O_3 to give, first, almost pure strontium ferrite $SrFe_{12}O_{19}$ and then $SrFe_{12-x}Cr_xO_{19}$ solid solutions with $x \leq 2$.

REFERENCES

1. Yakovlev, Yu.M. and Gendelev, S.Sh., *Monokristally ferritov v radioelektronike* (Single Crystals of Ferrites in Radio Electronics), Moscow: Sovetskoe Radio, 1975.
2. Bertaut, F., Deschamps, A., Pauthenet, R., and Pikart, S., *J. Phys. Radium*, 1959, vol. 20, pp. 404–408.
3. Bertaut, F., Deschamps, A., and Pauthenet, R., *C. R. Acad. Sci. Paris*, 1958, vol. 246, pp. 2594–2597.
4. Aksel'rod, N.L., Barium and Strontium Ferrites: Phase Relationships, Properties, Kinetics, Mechanism, and Technology of Synthesis, *Cand. Sci. Dissertation*, Sverdlovsk, 1987.
5. Aksel'rod, N.L., Tkachenko, E.V., Buyanova, E.S., and Shapovalov, A.G., *Zh. Neorg. Khim.*, 1984, vol. 29, no. 11, pp. 2775–2779.
6. Bashkirov, L.A. and Kostyushko, Yu.L., *Izv. Ross. Akad. Nauk, Neorg. Mater.*, 2003, vol. 33, no. 4, pp. 476–482.
7. Bashkirov, L.A., But'ko, T.A., Dudchik, G.P., *et al.*, *Vestsi Nats. Akad. Navuk Bel., Ser. Khim. Navuk*, 1999, no. 2, pp. 5–9.
8. Collomb, A., Wolfers, P., and Obradors, X., *J. Magn. Magn. Mater.*, 1986, vol. 62, pp. 57–68.
9. Bashkirov, L.A. and Pan'kov, V.V., *Mekhanizm i kinetika obrazovaniya ferritov* (Mechanism and Kinetics of Formation of Ferrites), Minsk: Nauka i Tekhnika, 1988.
10. ICDD no. 15-368.
11. ICDD no. 20-1192.

Russian Journal of Applied Chemistry, Vol. 78, No. 3, 2005, pp. 356–359. Translated from Zhurnal Prikladnoi Khimii, Vol. 78, No. 3, 2005, pp. 362–366.
Original Russian Text Copyright © 2005 by Demidov, Krasovitskaya, Andreeva, Tolypin.

INORGANIC SYNTHESIS AND INDUSTRIAL INORGANIC CHEMISTRY

Obtaining Nickel Hydroxide from Half-Products of Hydrometallurgical Processing of Nickel–Iron Batteries

A. I. Demidov, O. A. Krasovitskaya, V. D. Andreeva, and E. S. Tolypin

St. Petersburg State Polytechnic University, St. Petersburg, Russia

Received January 19, 2005

Abstract—The possibility of obtaining nickel hydroxide from solutions produced in ammonia leaching of the active paste of positive electrodes of a nickel–iron battery was studied.

One of widely occurring kinds of secondary nickel-containing raw materials in Russia is constituted by spent positive electrodes of nickel–iron batteries, which are processed by pyrometallurgical or hydrometallurgical methods [1–3]. A possible scheme for processing of spent nickel–iron batteries includes treatment of the positive electrodes, based on the previously suggested [2] ammonia leaching to recover nickel without preliminary disassembly of lamellas. With the properly chosen processing conditions, the recovery of nickel into solution in this stage may be as high as 96–99%.

Nickel-containing process solutions can be used for further recovery of nickel and its compounds by various methods, e.g., by extraction with organic reagents, electrodeposition, hydrogen reduction, and crystallization in the form of neutral and double salts or nickel hydroxide [1].

In this study we examined the possibility of using ammonia leaching solutions to obtain pure nickel hydroxide, which is a valuable raw material for battery industry. Nickel(II) hydroxide was precipitated from ammonia leaching solutions containing sulfate ions [2] with a 4.85 M NaOH solution (density 1.18 g cm^{-1}). Preliminarily, a 100-ml portion of the solution was evaporated to a volume of approximately 25 ml, with a precipitate of a double complex salt of nickel formed at the end of evaporation. Then the volume was brought to 100 ml with water and the mixture was heated ($T \approx 70$°C), with the precipitate dissolving and the pH of the solution becoming 7. The resulting solution was placed in a buret, and the NaOH solution, in a microburet. The precipitation was performed under continuous agitation in a temperature-controlled ($T = 50$°C) 150-ml vessel. The alkali and ammonia solution were simultaneously introduced into the reaction volume (dropwise and as a flow, respectively), with their volume ratio maintained at 1 : (1–10) and the interval between addition of reagent portions (total volume of a portion 5–10 ml) equal to 10 min. After the last addition of alkali (pH 12), the reaction solution with a precipitate was kept with agitation for 90 min. The precipitate was allowed to settle for 120 min and filtered on a vacuum filter. Then the precipitate was washed with cold distilled water (~800 ml) and dried at 80°C for 120 min.

The precipitates obtained had light emerald to light green color, depending on the volume ratio of the reagent solutions added and on the uniformity of their introduction into the reaction volume. It was established that the optimal, as regards the filterability and homogeneity of the precipitates, ratio of the alkali and the ammonia solution is 1 : 5, with the best results obtained when this ratio is strictly maintained throughout the precipitation time. At the very beginning of the process, immediately after the addition of the first portions of the reagents, a finely dispersed well-agitated precipitate is formed in the reaction vessel. This precipitate can later be well filtered off; it has a light green color upon drying. If the volume ratio was shifted toward an excess (with respect to the optimal value) of an alkali, the precipitate became too dense and gave coarse clotted aggregates. At an excess of the ammonia solution, the precipitate dissolved and the solution acquired an emerald color and was poorly filterable; a dried precipitate had the form of shining crystalline scales of light emerald color. These specific features were the most pronounced in the initially made attempts to perform precipitation, when the ammonia solution was poured to an alkali solution or, in the opposite way, an alkali solution was poured to the ammonia solution. As already noted,

1070-4272/05/7803-0356 © 2005 Pleiades Publishing, Inc.

the optimal method is that of simultaneous mixing of the reagents in a prescribed volume ratio.

The X-ray diffraction pattern of the precipitate obtained from an ammonia–sulfate solution under the optimal conditions is shown in Fig. 1a. The peak positions are characteristic of nickel(II) hydroxide, which has a layered hexagonal crystal lattice of the CdI_2 type. It should be noted that the positions of the diffraction peaks and their relative intensities are in precise agreement with the tabulated data for pure nickel hydroxide, in contrast to those of the starting active paste (Figs. 1b, 1c), which also contain peaks corresponding to impurity phases. This fact confirms the efficiency of iron separation in the stage of nickel recovery by leaching from the spent active paste containing, on the average, 0.3–0.7 wt % Fe at 40–44 wt % Ni [2].

To assess the prospects for their possible utilization, the precipitates obtained from sulfate–ammonia leaching solutions were subjected to a comprehensive study.[1] The chemical analysis of the precipitates demonstrated that they contain (% relative to the initial mass): Ni 59–62, SO_4^{2-} 0.1–0.3, N <0.01, and Na <0.01. These data indicate that the precipitates contain only small amounts of water of crystallization and of main impurities. Figure 2 shows the results of an X-ray fluorescence microanalysis of the nickel hyroxide obtained. It can be seen that both the base elements (Ni and O) and trace impurities (Al, Si, S) are uniformly distributed over the precipitate particles. This indicates that the coagulation of particles in their nucleation and subsequent growth is uniform if the conditions specified above are satisfied. As the concentration of main impurities in the resulting nickel(II) hydroxide is low, it can be further used to obtain nickel salts.

An analysis of the size distribution of $Ni(OH)_2$ particles (Fig. 3a) demonstrated that particles of size 5–20 μm predominate in precipitates obtained under the optimal conditions. Precipitates of this kind have a specific surface area of about 1.6×10^3 $cm^2\ cm^{-3}$ and average pycnometric density of about 3.94 $g\ cm^{-3}$ (measured in a KOH solution of density 1.26 $g\ cm^{-3}$). Figure 3b shows an SEM pattern of nickel hydroxide particles. It follows from this figure that the precipitate is a dispersed system, with its separate particles having no pronounced crystal faceting and their shape being nearly spherical. These properties of the precipitates are of interest as regards their possible application as an electrode material for nickel–metal–hydride batteries in which spherical nickel hydroxide is widely used.

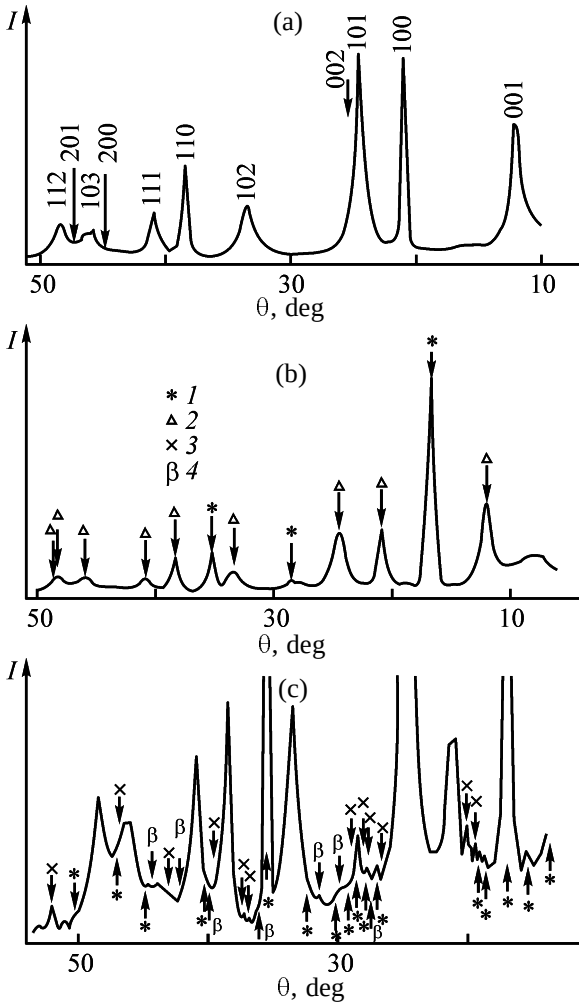


Fig. 1. X-ray diffraction patterns of (a) $Ni(OH)_2$ precipitate obtained upon addition of NaOH to sulfate–ammonia leaching solutions and (b, c) starting active paste of positive electrodes of nickel–iron batteries. FeK_α radiation. (θ) Bragg angle. Phase: (*1*) graphite, (*2*) $Ni(OH)_2$, (*3*) FeOOH, and (*4*) β-FeOOH.

The electrochemical properties of the material obtained were studied on electrodes fabricated by applying the paste on the current-carrying foamed-nickel support, with the subsequent drying and additional compaction. The substrate thickness before the additional compaction was 2.0 mm. The table lists the results obtained in measuring the discharge capacity of electrodes of this kind after the third charging–discharge cycle in comparison with the similar parameters of the electrodes fabricated from $Ni(OH)_2$ manufactured by OMG (Finland).

The data presented demonstrate that the nickel hydroxide precipitates obtained in this study compare

[1] Studied at the Gipronikel' Research Institute (St. Petersburg).

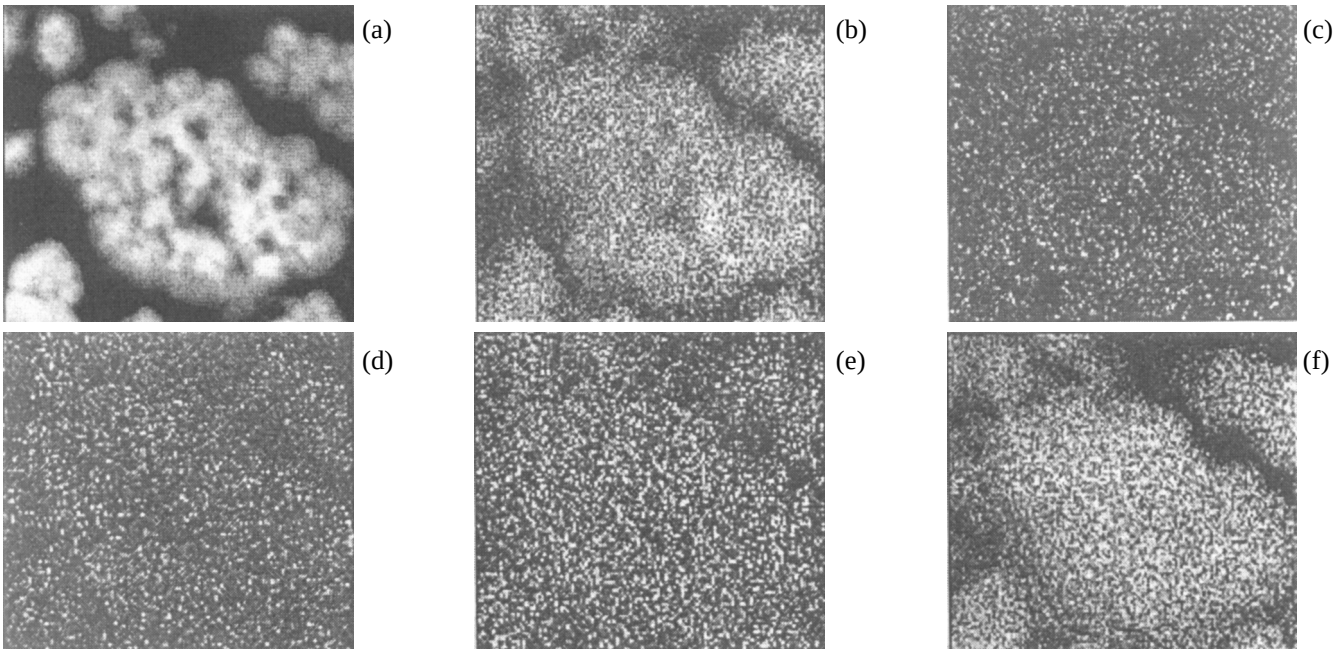


Fig. 2. Results of X-ray fluorescence microanalysis of the $Ni(OH)_2$ precipitate obtained by introduction of NaOH into sulfate–ammonia leaching solutions. (a) Image of a sample being analyzed; distribution of the intensity of the characteristic K_α radiation over this sample for (b) oxygen, (c) aluminum, (d) silicon, (e) sulfur, and (f) nickel.

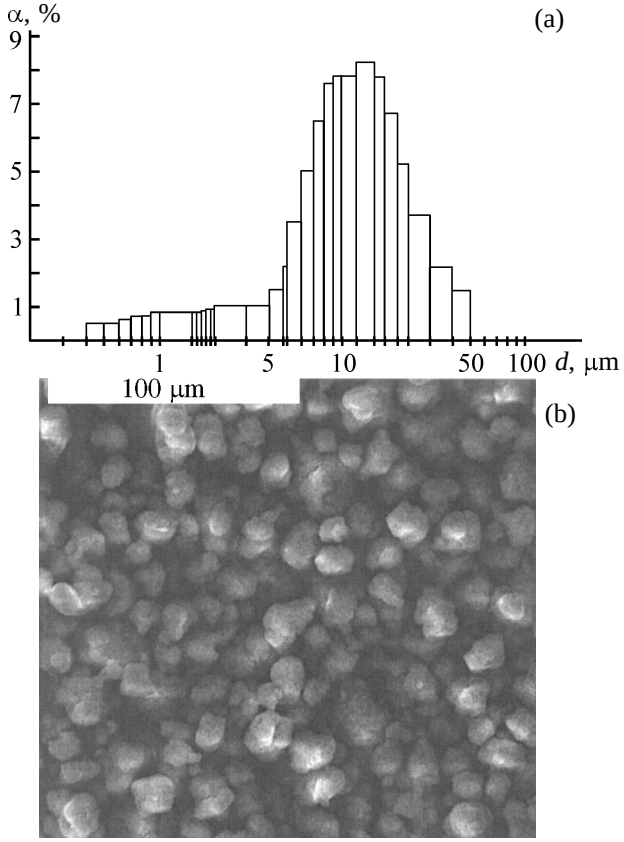


Fig. 3. (a) Size and (b) shape distribution *s* of $Ni(OH)_2$ particles obtained by introduction of NaOH into sulfate–ammonia leaching solutions. (α) Fraction of particles and (*d*) particle size.

well in their specific characteristics with the commercial material, being, however, looser, i.e., having a lower density, which leads to significant differences of the shape of the electrodes fabricated from these precipitates, compared to the presently existing samples. These facts suggest that, with the technology of $Ni(OH)_2$ precipitation from ammonia leaching solutions further optimized, it will be possible to improve the parameters of the precipitates obtained to values allowing their practical use.

CONCLUSIONS

(1) Pure nickel(II) hydroxide can be recovered from ammonia leaching solutions, which are half-products formed in hydrometallurgical processing of spent positive electrodes of nickel–iron batteries.

Electrochemical properties of electrodes based on OMG and $Ni(OH)_2$

Electrode material	Discharge capacity		Electrode thickness after additional compaction, mm	ρ_r,* g cm^{-1}
	A h g^{-1}	A h cm^{-3}		
OMG	0.22	0.55	~1.3	1.8
	0.24	0.57	~1.3	1.9
$Ni(OH)_2$	0.25	0.42	~0.47	0.7

* Density of rammed powder.

(2) Nickel(II) hydroxide obtained from ammonia leaching solutions containing sulfate ions can be used for subsequent production of pure nickel salts owing to the low content of the main impurities.

(3) Provided that the technology of its precipitation is further optimized, nickel(II) hydroxide obtained from ammonia–sulfate leaching solutions is of interest as a material for the active paste of electrodes of alkaline batteries.

REFERENCES

1. Demidov, A.I. and Krasovitskaya, O.A., *Nauch.-Tekhn. Ved. Sankt-Peterb. Gos. Tekh. Univ*., 2001, no. 1, pp. 112–123.
2. Demidov, A.I. and Krasovitskaya, O.A., *Zh. Prikl. Khim.*, 2000, vol. 73, no. 10, pp. 1656–1660.
3. Demidov, A.I. and Krasovitskaya, O.A., *Zh. Prikl. Khim.*, 2001, vol. 74, no. 5, pp. 717–721.

Russian Journal of Applied Chemistry, Vol. 78, No. 3, 2005, pp. 360–362. Translated from Zhurnal Prikladnoi Khimii, Vol. 78, No. 3, 2005, pp. 366–368.
Original Russian Text Copyright © 2005 by Yurkinskii, Firsova, Proskura.

INORGANIC SYNTHESIS AND INDUSTRIAL INORGANIC CHEMISTRY

Thermal Dissociation of Sodium Hydroxide upon Evacuation

V. P. Yurkinskii, E. G. Firsova, and S. A. Proskura

St. Petersburg State Polytechnic University, St. Petersburg, Russia

Received December 27, 2004

Abstract—Kinetics of dehydration of sodium hydroxide melt upon evacuation was studied in relation to the temperature. The kinetic parameters of thermal decomposition of NaOH were evaluated. Methods for dehydration of the hydroxide melt were suggested.

Sodium hydroxide melt and fusible mixtures based on it are widely used in production engineering. In particular, they are used as electrolytes in electrochemical purification of steel casts, electrolytic production of sodium, refining of lead and other heavy metals, and also in production of secondary lead [1–4].

As known [2–7], moisture significantly affects the physicochemical properties, electrochemical behavior, and corrosion activity of NaOH melt. However, there is no common opinion about the conditions of dehydration of sodium hydroxide and salt mixtures based on it [6, 7]. The main procedure for dehydration of NaOH melt is prolonged evacuation at 770–820 K for 2–8 h [6, 7].

In this study we examined the kinetics of dehydration of NaOH melt and thermal dissociation of sodium hydroxide upon evacuation at varied temperatures.

EXPERIMENTAL

Experiments were carried out in the temperature range 750–1023 K. Granular NaOH (chemically pure grade) was used. The experimental procedure was as follows. A 100-g sodium hydroxide sample was placed in a corundum beaker with a diameter of 40 and height of 100 mm. The beaker was placed in a quartz tube with a diameter of 50–60 and length of about 400 mm, which had been kept in a furnace at the required temperature. The quartz tube was hermetically sealed and connected to a vacuum system. The residual pressure in the system was 13.3 Pa. The moisture released from the NaOH melt was trapped in a U-shaped vessel which was packed with silica gel and cooled to 263±2 K. Silica gel of KSS no. 4 grade was dried before use at 373–393 K for 3 h. The rate of dehydration of the melt was evaluated by weighing the U-shaped vessel with the collected water at regular intervals of 0.5–2.0 h in the course of the experiment. To check the completeness of moisture recovery, the total mass of the water removed was determined by weighing the corundum beaker with sodium hydroxide before and after the experiment. The weights of water removed from the beaker and collected in the trap coincided within 5–7%.

The data on vacuum dehydration of NaOH melt at various temperatures are shown in Table 1 and Fig. 1.

As seen from Fig. 1, the mean rate v of vacuum dehydration of NaOH melt as a function of time τ at various temperatures is satisfactorily fitted by the empirical equation

$$v = A + B\exp(-\tau/C), \quad (1)$$

where A, B, and C are the temperature-dependent coefficients.

The coefficients A, B, and C were determined using Statgraphics package (Table 2). The correlation coefficient was 0.999.

Table 1. Mean rate v of dehydration of NaOH melt as a function of evacuation time τ and temperature

τ, h	v, g h^{-1}, at indicated temperature, K				
	750	773	823	873	906
1.5	–	–	–	–	0.602
2.0	0.404	0.451	0.547	0.575	–
2.5	–	–	–	–	0.206
3.0	0.195	0.208	0.203	0.183	–
3.5	–	–	–	–	0.203
4.0	0.111	0.124	0.147	0.180	–
4.5	–	–	–	–	0.205
5.0	0.095	0.105	0.138	0.177	–
6.0	0.091	0.103	0.138	0.179	–

1070-4272/05/7803-0360 © 2005 Pleiades Publishing, Inc.

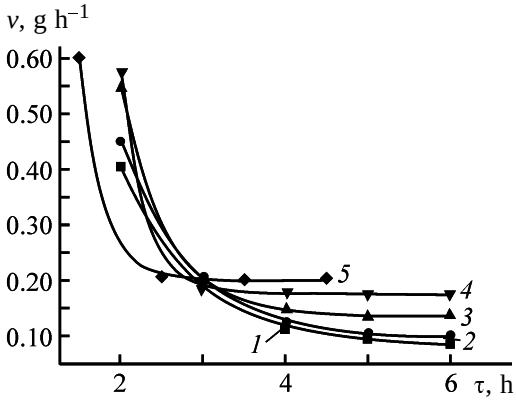


Fig. 1. Mean rate v of vacuum dehydration of NaOH melt as a function of time τ at (*1*) 750, (*2*) 773, (*3*) 823, (*4*) 873, and (*5*) 906 K.

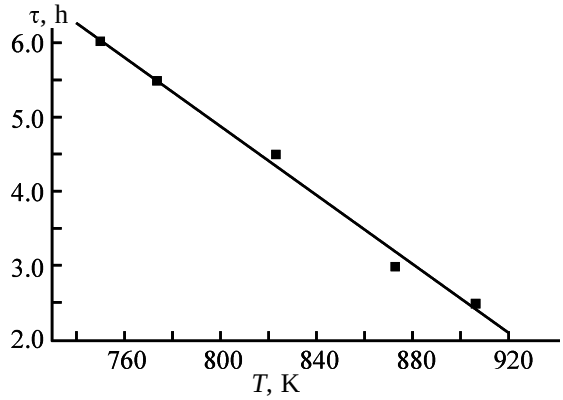


Fig. 2. Optimal time τ of vacuum dehydration of NaOH melt as a function of temperature T.

The v–τ dependences suggest that the vacuum dehydration of the hydroxide melt involves two conjugated processes: removal of crystallization or adsorbed water (2) and decomposition of hydroxide melt (3):

$$NaOH \cdot H_2O \rightarrow NaOH + H_2O, \quad (2)$$

$$2NaOH = Na_2O + H_2O. \quad (3)$$

As seen from Fig. 1, in the initial step of dehydration of NaOH melt processes (2) and (3) occur simultaneously. We believe that removal of crystallization and adsorbed water (2) is completed when the rate of water evaporation becomes constant. Further dehydration is associated solely with decomposition of the melt by reaction (3). From our results (Fig. 1), we determined the optimal time of vacuum dehydration of NaOH melt at various temperatures (Fig. 2).

Figure 2 shows that the dependence of time of NaOH melt dehydration τ (h) on temperature T (K) is linear:

$$\tau = (23.416 \pm 0.937) - (0.0232 \pm 0.0011)T, \quad (4)$$

with the correlation coefficient of 0.996 and variance of 0.149.

The degree of NaOH melt dehydration can be evaluated from its melting point [1–4]. According to published data [1, 2, 8], it is 593–596 K. The melting point of NaOH melt after the dehydration under the conditions found in this work was 594 ± 1 K, suggesting virtually complete dehydration of the melt.

The rate of NaOH decomposition v_{NaOH} within the temperature range studied was determined in accordance with the stoichiometry of reaction (3) from the rate of water removal (Table 1) in the time interval in which it was constant. The results are presented in Table 3.

It should be noted that, in our experiments, the thermal decomposition of NaOH (Table 3) at a given temperature was performed to low conversions (the weight loss of sodium hydroxide in the course of the experiment did not exceed 3.0%). Thus, the change in the composition of the NaOH melt could not affect

Table 2. Coefficients of Eq. (1)

T, K	A	B	C
750	0.083 ± 0.006	2.892 ± 0.477	0.9106 ± 0.0714
773	0.096 ± 0.004	3.793 ± 0.456	0.8448 ± 0.0044
823	0.137 ± 0.001	15.86 ± 0.47	0.5472 ± 0.0045
873	0.176 ± 0.004	308.0 ± 30.9	0.3007 ± 0.0046
906	0.201 ± 0.005	89.8 ± 11.2	0.2772 ± 0.064

Table 3. Mean rates of moisture removal v_{H_2O} and NaOH decomposition v_{NaOH} under evacuation at various temperatures

T, K	v_{H_2O}	v_{NaOH}
	g h−1	
750	0.091	0.404
773	0.104	0.462
823	0.138	0.613
873	0.178	0.791
893	0.200	0.889
906	0.205	0.911
926	0.225	1.00
971	0.260	1.155
1023	0.329	1.462

the rate of process (3) significantly.

In this case, the temperature dependence of the NaOH decomposition rate v_{NaOH} can be treated with the Arrhenius equation

$$\ln v_{NaOH} = A - B/T, \quad (5)$$

where A is a constant, $B = E/R$, E is the activation energy of reaction (3), and R is the universal gas constant (8.314 J mol^{-1} K).

From the mean rates of sodium hydroxide decomposition at various temperatures (Table 3), we determined the coefficients of Eq. (5): $A = 3.9211 \pm 0.0749$, $B = -3636.1 \pm 65.2$. The correlation coefficient was 0.998, and variance, 0.021. The calculated activation energy of thermal decomposition of molten sodium hydroxide, 30.23 kJ mol^{-1}, is indicative of the diffusion control of the process. Presumably, the limiting stage of NaOH thermal dissociation is diffusion of water molecules in a hydroxide melt or water evaporation from the melt surface.

CONCLUSIONS

(1) Dehydration of NaOH melt under evacuation involves simultaneous removal of adsorbed and crystallization water from NaOH and decomposition of NaOH.

(2) The optimal times for NaOH vacuum dehydration at various temperatures were suggested.

(3) The kinetic parameters of thermal decomposition of sodium hydroxide melt were determined. The process is diffusion-controlled. Its activation energy is 30.23 kJ mol^{-1}.

REFERENCES

1. *Natrii; Svoistva, proizvodstvo, primenenie* (Sodium; Properties, Production, and Applications), Morachevskii, A.G., Ed., St. Petersburg: Khimiya, 1992.
2. Morachevskii, A.G., Vaisgant, Z.I., and Demidov, A.I., *Pererabotka vtorichnogo svintsovogo syr'ya* (Reprocessing of Secondary Lead Resources), St. Petersburg: Khimiya, 1993.
3. Delimarskii, Yu.K. and Zarubitskii, O.G., *Elektroliticheskoe rafinirovanie tyazhelykh metallov v ionnykh rasplavakh* (Electrolytic Refining of Heavy Metals in Ionic Melts), Moscow: Metallurgiya, 1975.
4. Delimarskii, Yu.K., Fishman, I.R., and Zarubitskii, O.G., *Elektrokhimicheskaya ochistka otlivok v ionnykh rasplavakh* (Electrochemical Purification of Casts in Ionic Melts), Moscow: Mashinostroenie, 1976.
5. Galloway, R.C., *J. Electrochem. Soc*., 1987, vol. 134, no. 1, pp. 256–257.
6. Gerasimenko, L.N., Morachevskii, A.G., Yurkinskii, V.P., *et al*., *Zh. Prikl. Khim*., 1973, vol. 46, no. 10, pp. 2227–2229.
7. Demidov, A.I., Morachevskii, A.G., and Mit'kina, N.N., *Zh. Prikl. Khim*., 1979, vol. 52, no. 5, pp. 1193–1195.
8. *Spravochnik po rasplavlennym solyam* (Reference Book on Molten Salts), Morachevskii, A.G., Ed., Leningrad: Khimiya, 1971, vol. 1.

Russian Journal of Applied Chemistry, Vol. 78, No. 3, 2005, pp. 363–366. Translated from Zhurnal Prikladnoi Khimii, Vol. 78, No. 3, 2005, pp. 369–372.
Original Russian Text Copyright © 2005 by Voitenko, Zhilyak, Kopilevich.

INORGANIC SYNTHESIS AND INDUSTRIAL INORGANIC CHEMISTRY

Double Hydrated Cobalt(II) Copper(II) and Nickel(II) Copper(II) Ammine Diphosphates

L. V. Voitenko, I. D. Zhilyak, and V. A. Kopilevich

National Agricultural University, Kiev, Ukraine

Received December 22, 2004

Abstract—Synthesis of amorphous and crystalline double hydrated cobalt copper and nickel copper ammine diphosphates with a coordination structure is described.

Information about synthesis of double hydrated ammine diphosphates of bivalent transition metals is lacking [1–4]. In this context, the aim of our study was to isolate phosphates of this kind, which presumably exhibit a biological or catalytic activity [5–8] or can be used as luminophores or components of these [3], from their ammonia solutions.

EXPERIMENTAL

Double hydrated nickel(II) copper(II) ammine diphosphates were obtained by salting-out from an ammonia solution with an organic solvent [9]. As starting reagents were used a mechanical mixture, in a prescribed molar ratio, of nickel and copper diphosphates synthesized by the procedures described in [10, 11], concentrated aqueous ammonia (23–25 wt %), and acetone. The mechanical mixture of nickel and copper diphosphates with a prescribed Ni : Cu molar ratio was dissolved in concentrated aqueous ammonia. The solution obtained was poured into acetone. As a result, a bottom phase, intensely blue oily liquid, was separated. The mother liquor was separated and the bottom phase was kept in air at 15–25°C to complete hardening and to constant weight. The synthesis conditions and the compositions of the compounds obtained are listed in Table 1.

Double hydrated cobalt(II) copper(II) ammine diphosphates were obtained using a method similar to that for the synthesis of cobalt ammine monophosphate [12]. As starting reagents were used cobalt diphosphate $Co_2P_2O_7 \cdot 6H_2O$ and copper diphosphate $Cu_2P_2O_7 \cdot 5H_2O$, synthesized by the procedure described in [11, 13]. For this purpose, a mechanical mixture of powdered $Co_2P_2O_7 \cdot 6H_2O$ and $Cu_2P_2O_7 \cdot 5H_2O$, taken in prescribed molar ratios, was saturated with gaseous ammonia under static conditions at 15–25°C for 24–36 h, to complete dissolution of the substances. After being extracted from the ammonia atmosphere, the products were kept at 15–25°C in air to constant weight. The synthesis conditions and the compositions of the compounds obtained are listed in Table 2.

The content of Ni^{2+} and Co^{2+} was determined by EDTA titration [14] (with copper masked with thiosulfate); that of copper, iodometrically; P_2O_5, gravimetrically [15]; ammonia, by evaporation in a Seren'ev apparatus [16]; and the total content of water and ammonia, from the weight loss upon heating at 750°C for 2 h. The anionic composition of the synthesis products was analyzed by quantitative paper chromatography [1].

An X-ray diffraction analysis was performed on a DRON-UM1 diffractometer (CuK_α radiation). As a monochromator served a single crystal of graphite, inserted in the path of the diffracted beam. X-ray diffraction patterns were obtained by step scanning in the range 2θ 4°–80°. The scanning step was 0.05°, and the time of exposure at a point, 3–9 s. The experimental diffraction peaks were approximated with a pseudo-Voigt function, with the K_{α_1} component isolated. The IR spectra were recorded with a Specord 75-IR spectrophotometer. Samples for IR spectral measurements were prepared as KBr pellets with the substance content of 0.2–0.3 wt %.

An X-ray phase analysis demonstrated that, at a molar ratio of copper to nickel in the starting mixture exceeding 1.5 : 0.5, crystalline $Ni_{0.10}Cu_{1.90}P_2O_7 \cdot 3.0NH_3 \cdot 2.5H_2O$ and $Ni_{0.20}Cu_{1.80}P_2O_7 \cdot 3.0NH_3 \cdot 2.5H_2O$ are formed. These compounds are isostructural, but differ in the structure from hydrated copper ammine diphosphate, which is confirmed by their

1070-4272/05/7803-0363 © 2005 Pleiades Publishing, Inc.

Table 1. Synthesis conditions of solid hydrated double nickel copper ammine diphosphates

Molar ratio	Product composition, wt %					Anionic composition, rel. % P_2O_5		Salting-out product*
	NiO	CuO	P_2O_5	NH_3	H_2O	PO_4^{3-}	$P_2O_7^{4-}$	
0.1 : 1.9	1.9	38.1	35.8	12.9	11.3	6.5	93.5	$Ni_{0.10}Cu_{1.90}P_2O_7 \cdot 3.0NH_3 \cdot 2.5H_2O$
0.2 : 1.8	3.7	35.5	35.4	13.8	11.6	6.1	93.9	$Ni_{0.20}Cu_{1.80}P_2O_7 \cdot 3.0NH_3 \cdot 2.5H_2O$
0.5 : 1.5	7.6	28.4	32.3	12.0	19.7	6.0	94.0	$Ni_{0.45}Cu_{1.55}P_2O_7 \cdot 3.0NH_3 \cdot 5.0H_2O$
1.0 : 1.0	16.4	20.0	33.7	12.2	17.7	8.0	92.0	$Ni_{1.0}Cu_{1.0}P_2O_7 \cdot 3.0NH_3 \cdot 4.0H_2O$
1.5 : 0.5	24.1	11.5	33.0	9.6	21.8	9.5	90.5	$Ni_{1.40}Cu_{0.60}P_2O_7 \cdot 2.0NH_3 \cdot 5.0H_2O$

* Without account of the impurity of monophosphate PO_4^{3-} contained in the starting $Ni_2P_2O_7 \cdot 6H_2O$ and $Cu_2P_2O_7 \cdot 5H_2O$; the starting nickel and copper diphosphates contain an impurity of monophosphate PO_4^{3-} in an amount of 5.0 rel. % P_2O_5.

Table 2. Synthesis conditions of solid hydrated double cobalt copper ammine diphosphates

Molar ratio	Product composition, wt %					Anionic composition, rel. % P_2O_5		Salting-out product*
	NiO	CuO	P_2O_5	NH_3	H_2O	PO_4^{3-}	$P_2O_7^{4-}$	
0.5 : 1.5	9.0	28.5	33.5	13.1	15.9	9.5	90.5	$Co_{0.50}Cu_{1.50}P_2O_7 \cdot 3.0NH_3 \cdot 4.0H_2O$
1.0 : 1.0	17.5	19.4	34.1	13.0	16.1	8.0	92.0	$Co_{1.00}Cu_{1.00}P_2O_7 \cdot 3.0NH_3 \cdot 4.0H_2O$

* Without account of the impurity of monophosphate PO_4^{3-} contained in the starting $Cu_2P_2O_7 \cdot 5H_2O$ and $Co_2P_2O_7 \cdot 6H_2O$; the starting cobalt and copper diphosphates contain an impurity of monophosphate PO_4^{3-} in an amount of 5.4 rel. % P_2O_5.

X-ray diffraction patterns (Fig. 1). The reflections of these compounds are satisfactorily indexed in the rhombic crystal system with the unit cell parameters a = 8.455, b = 15.624, c = 18.327 Å, V = 2421.1 Å^3 for $Ni_{0.2}0Cu_{1.80}P_2O_7 \cdot 3.0NH_3 \cdot 2.5H_2O$ and a = 8.531, b = 15.720, c = 18.780 Å, V = 2518.3 Å^3 for $Ni_{0.10} \cdot Cu_{1.90}P_2O_7 \cdot 3.0NH_3 \cdot 2.5H_2O$.

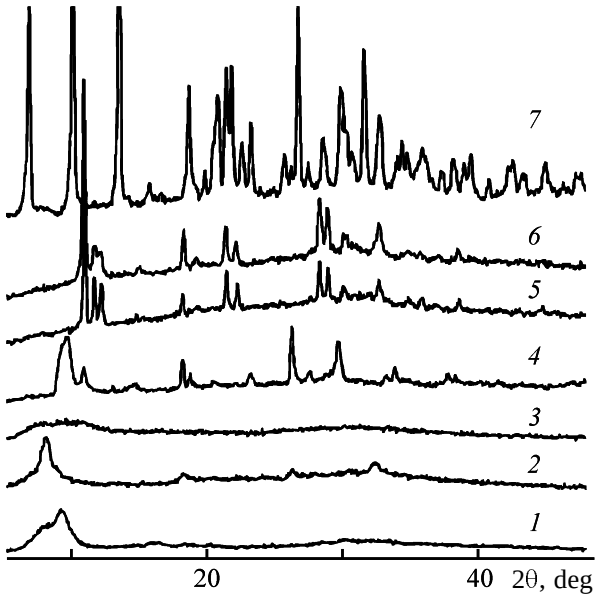


Fig. 1. X-ray diffraction patterns of (*1*) $Ni_2P_2O_7 \cdot 3.0NH_3 \cdot 6.0H_2O$, (*2*) $Ni_{1.40}Cu_{6.60}P_2O_7 \cdot 2.0NH_3 \cdot 5.0H_2O$, (*3*) $Ni_{1.0} \cdot Cu_{1.0}P_2O_7 \cdot 3.0NH_3 \cdot 4.0H_2O$, (*4*) $Ni_{0.45}Cu_{1.55}P_2O_7 \cdot 3.0NH_3 \cdot 5.0H_2O$, (*5*) $Ni_{0.20}Cu_{1.80}P_2O_7 \cdot 2.5H_2O$, (*6*) $Ni_{0.10} \cdot Cu_{1.90}P_2O_7 \cdot 2.5H_2O$, and (*7*) $Cu_2P_2O_7 \cdot 3.0NH_3 \cdot H_2O$. (2θ) Bragg angle; the same for Fig. 2.

According to the results of the X-ray phase analysis of cobalt- and copper-containing samples (Fig. 2), an individual compound is obtained at Co : Cu = 1 : 1. The reflections of the compound synthesized, $Co_{1.00} \cdot Cu_{1.00}P_2O_7 \cdot 3.0NH_3 \cdot 4.0H_2O$, are satisfactorily indexed in the monoclinic crystal system with the unit cell parameters a = 11.064, b = 12.675, c = 10.409 Å, γ = 103.73°, and V = 1417.9 Å^3. The starting $Ni_2P_2O_7 \cdot 6.0H_2O$ and $Cu_2P_2O_7 \cdot 5.0H_2O$ are crystalline, whereas the starting $Co_2P_2O_7 \cdot 6.0H_2O$ is, on the whole, X-ray amorphous, with a single clearly pronounced reflection at 2θ = 6.5° and a broad band peaked at 2θ = 19°–20°. Their X-ray diffraction patterns are in agreement with those reported in [10, 11, 17].

Table 3 lists the IR data for double cobalt copper and nickel copper ammine diphosphates. The spectra of all the compounds contain a strong absorption band associated with stretching vibrations of the NH and OH groups at 3500–2900 cm^{-1} and absorption bands associated with bending vibrations of water and asymmetric bending vibrations of ammonia in ammine complexes at 1650–1500 cm^{-1}. Thus, it is impossible to resolve vibrations of coordinated ammonia and water in these spectral ranges. At 1465–1410 cm^{-1}, the spectra of ammine diphosphates show the presence

Table 3. Peak frequencies (cm^{-1}) of the absorption bands in IR spectra*

$Ni_{0.20}Cu_{1.80}P_2O_7 \cdot 3.0NH_3 \cdot 2.5H_2O$	$Ni_{0.45}Cu_{1.55}P_2O_7 \cdot 3.0NH_3 \cdot 5.0H_2O$	$Ni_{1.0}Cu_{1.0}P_2O_7 \cdot NH_3 \cdot 4.0H_2O$	$Co_{0.50}Cu_{1.50}P_2O_7 \cdot 3.0NH_3 \cdot 4.0H_2O$	$Co_{1.00}Cu_{1.00}P_2O_7 \cdot 3.0NH_3 \cdot 4.0H_2O$	Assignment
500–2900 s.br	3400–3100 s.br	3400–3000 s.br	3400–2900 s.br	3400–3000 s.br	$\nu(H_2O)$, $\nu_{as}(NH_3)$
1605 m	1600 m	1650 sh	1650 sh	1670 w	$\delta(H_2O)$
1510 sh	1540 w	1610 m	1600 m	1610 m	$\delta_{as}(NH_3)$
1445 m	1450 m	1440 m	1455 m	1450 m	$\delta_s(NH_3)$
		1410 sh			
1240 w	1230 sh	1320 sh	1260 w	1220 sh	$\delta_s(NH_3)$
		1240 sh			
1135–1050 sh	1100 w	1130 w	1120 s	1120 sh	$\nu_{as}(PO_3)$
	1070 s	1080 s	1080 s	1080 s	$[P_2O_7]$
1000 sh	1025 w	1010 sh	1010 sh		
870 s	890 s	870 s	870 s	860 s	$\nu_s(PO_3)(PO)$
710 w	710 w	700 w	700 w	700 m	$\nu_{as}(POP)$
					$[P_2O_7]$
605 s.sh	680 w	600 w	600 sh		$\delta_{as}(OPO)$
405 m	540 s	540 m	540 sh	520 m	$\delta_s(OPO)$
510	500 sh		510 m		Me–N
460 sh	450 w	460 sh	460 sh	480 sh	Me–O

* s, strong; m, medium-intensity; w, weak; s.br, strong broad absorption band; sh, shoulder.

of ammonia, which forms a strong hydrogen bond with proton transfer between ammonia coordinated to metal ions and $P_2O_7^{4-}$. This is accompanied by averaging of the electron density over the whole chain of atoms forming the hydrogen bond [5, 6, 18]. The IR spectra of the same compounds contain at around 1325 cm^{-1} an absorption band associated with only bending vibrations of coordinated ammonia molecules [19]. Asymmetric and symmetric vibrations of the $P_2O_7^{4-}$ anion appear at 1135–800 cm^{-1} as strong absorption bands. Weak absorption bands at 700–540 cm^{-1} can be assigned to vibrations of P–O–P and O–P–O groups. Stretching vibrations of the Me–N and Me–O bonds appear in the spectra of the ammine diphosphates at 510–465 cm^{-1} [20, 21].

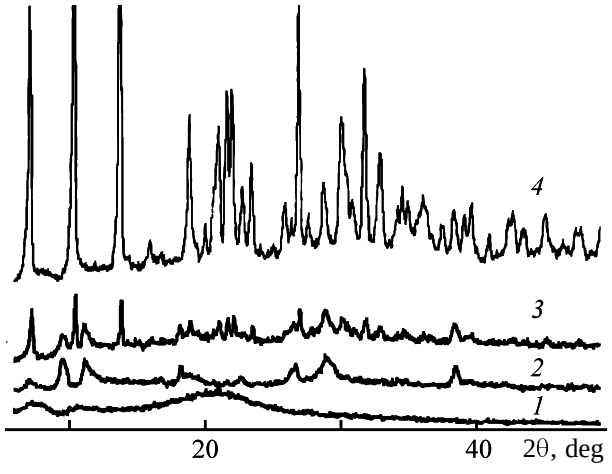


Fig. 2. X-ray diffraction patterns of (*1*) $Co_2P_2O_7 \cdot 3.0NH_3 \cdot 4.0H_2O$, (*2*) $Co_{1.00}Cu_{1.00}P_2O_7 \cdot 3.0NH_3 \cdot 4.0H_2O$, (*3*) $Co_{0.50} \cdot Cu_{1.50}P_2O_7 \cdot 3.0NH_3 \cdot NH_3 \cdot 4.0H_2O$, and (*4*) $Cu_2P_2O_7 \cdot 3.0NH_3 \cdot 2.5H_2O$.

Thus, the IR spectra suggest that double nickel copper and cobalt copper ammine diphosphates contain two different kinds of ammonia molecules: those interacting with metal atoms solely by the donor–acceptor mechanism and those additionally involved in a hydrogen bond with charge transfer.

CONCLUSION

Previously unknown individual solid double hydrated nickel copper and cobalt copper ammine diphosphates were prepared. The composition of the compounds synthesized was studied by IR spectroscopy, and their coordination structure was confirmed.

REFERENCES

1. Shchegrov, L.N., *Fosfaty dvukhvalentnykh metallov* (Phosphates of Bivalent Metals), Kiev: Naukova Dumka, 1987.
2. Konstant, Z.A. and Dindune, A.P., *Fosfaty dvukhvalentnykh metallov* (Phosphates of Bivalent Metals), Riga: Zinatne, 1987.

3. *Neorganicheskie fosfatnye meterialy* (Inorganic Phosphate Materials), Kanazawa, T., Ed., Kiev: Naukova Dumka, 1998.
4. Komisarova, L.N., *Usp. Khim.*, 2002, vol. 71, no. 8, pp. 707–740.
5. Voitenko, L.V., *Cand Sci. Dissertation*, Kiev, 1994.
6. Ukrainian Patent 13102.
7. Corbridge, D.E., *Phosphorus. An Outline of Its Chemistry, Biochemistry and Technology*, Amsterdam: Elsevier, 1980.
8. Kopilevich, V.A., Kokhan, S.S., and Voitenko, L.V., *11th World Fertilizer Congr. of CIEC: Proc.*, Ghent (Belgium), 1997, vol. 2, p. 296.
9. Ukrainian Patent 62782.
10. Lavrov, A.V., Bykanova, T.A., and Kessler, Yu.M., *Izv. Akad. Nauk SSSR, Neorg. Mater.*, 1976, vol. 12, no. 3, pp. 491–494.
11. Kokhanovskii, V.V. and Zemtsova, Z.N., *Vestsi Akad. Navuk Bel. SSR*, 1988, no. 5, pp. 5–9.
12. RF Patent 2032615.
13. Bassett, W.L., Bedwell, J.B., and Hutchinson, J.B., *J. Chem. Soc.*, 1936, no. 10, pp. 2883–2885.
14. Přibil, R., *Komplexony v chemicki analyse*, Prague: Ceskoslov. Akad., 1957.
15. *GOST* (State Standard) *20851–75. Mineral Fertilizers: Methods for Analysis*.
16. *Sovremennye metody khimicheskogo analiza pochv i rastenii: Metodicheskie ukazaniya* (Modern Techniques for Chemical Analysis of Soils and Plants: Methodological Recommendations), Kiev: Nauchno-Issled. Inst. Sakharnoi Svekly, 1984.
17. Kokhanovskii, V.V. and Prodan, E.A., *Zh. Neorg. Khim.*, 1988, vol. 33, pp. 761–765.
18. Shevchenko, Yu.N., *Doctoral Dissertation*, Moscow, 1991.
19. Nakamoto, K., *Infrared Spectra of Inorganic and Coordination Compounds*, New York: Wiley, 1963.
20. Voitenko, L.V., Shchegrov, L.N., and Kopilevich, V.A., *Ukr. Khim. Zh.*, 1992, vol. 58, no. 3, pp. 223–226.
21. *Atlas IK spektrov fosfatov: Dvoinye mono- i difosfaty* (IR Spectral Atlas for Phosphates: Double Mono- and Diphosphates), Pechkovskii, V.V., Ed., Moscow: Nauka, 1990.

Russian Journal of Applied Chemistry, Vol. 78, No. 3, 2005, pp. 367–374. Translated from Zhurnal Prikladnoi Khimii, Vol. 78, No. 3, 2005, pp. 373–379.
Original Russian Text Copyright © 2005 by Sosnov, Malkov, Malygin.

INORGANIC SYNTHESIS AND INDUSTRIAL INORGANIC CHEMISTRY

Calculation of the Stoichiometric Composition of Nanostructures Synthesized by Molecular Layer Deposition on the Surface of Solid Matrices

E. A. Sosnov, A. A. Malkov, and A. A. Malygin

St. Petersburg State Technological Institute, St. Petersburg, Russia

Received December 28, 2004

Abstract—Calculational formulas for determining from the results of chemical and thermogravimetric analyses the true relative contents of components in products formed in molecular layer deposition of nanostructures on the surface of solid matrices are suggested. The approaches considered are illustrated by the example of evaluation of the chemical composition of titanium oxide (nitrogen) and silicon–nitrogen nanolayers synthesized by molecular layer deposition on the silica surface.

Chemical modification of the surface of solid matrices is widely used in modern processes for production of materials and articles. Recent publications have shown convincingly that modern tendencies in the development of many areas of solid-phase materials science (micro- and nanoelectronics; development of luminophores, sorbents, and catalysts) are well matched by the method of molecular layer deposition (MLD), which yields nanostructures of a prescribed chemical composition on the surface of various solid matrices [1–5]. The method consists in that chemical reactions between low-molecular-weight reagents (LMWR) and functional groups (FG) of the starting matrix are performed under nonequilibrium conditions (to achieve the maximum filling of the surface).

In contrast to the conventional techniques for chemical modification of solid substances, the MLD method is a multistage cyclic process in which no more than a single monolayer of new structural units, functional groups, is formed on the surface in each cycle. In the process, the mass ratio of the starting solid matrix and the layer being grown changes after each synthesis stepe. The method used in preparative chemistry to determine the empirical chemical composition of the products obtained not only gives no way of finding the true relative contents of their components, but also hinders a correct comparative analysis of the stoichiometry of the surface nanostructures in various steps of the synthesis. To tackle with these problems, it has been suggested to relate data on the chemical composition of surface structures to unit mass of the starting solid matrix [2, 3]. Thus, the main step in a calculation of the stoichiometric composition of the products is reduced to a choice of a procedure for determining the share of the starting matrix in a unit mass of the sample synthesized.

The approaches suggested have been implemented for a number of particular systems, e.g., various element oxide layers grown on the surface of dispersed silicon dioxide. Previously, Kol'tsov has suggested a procedure [6] for calculating the content p_i of the silica matrix in titanium-containing silica obtained by the schemes

$$k(|\text{–Si–OH}) + \text{TiCl}_4 \rightarrow (|\text{–Si–O})_k\text{TiCl}_{4-k} + k\text{HCl}, \quad (1)$$

where k = 1–3;

$$(|\text{–Si–O})_k\text{TiCl}_{4-k} + \text{H}_2\text{O} \rightarrow (|\text{–Si–O})_k\text{Ti(OH)}_{4-k} + (4 - k)\text{HCl}, \text{ etc.} \quad (2)$$

where the symbol $|$ denotes the skeleton of the solid matrix on whose surface the FGs are situated.

$$p_i = \frac{4a_i + b_i - c_i}{4A_{i-1} + B'_{i-1} - C'_{i-1}}, \quad (3)$$

where a, b, c, and p are the contents of Ti^{4+} (mmol), OH^- (mmol), Cl^- (mmol), and SiO_2 (g) per gram of the product; A, amount of titanium(IV) per gram of SiO_2; B', C', amounts of OH^- and Cl^- per gram of SiO_2 in hydrolysis products; and i, number of an MLD cycle.

1070-4272/05/7803-0367 © 2005 Pleiades Publishing, Inc.

To calculate the stoichiometric composition, it was necessary to determine, on the basis of chemical analytical data, not only the content of the modifying element [Ti(IV) according to scheme (1)] in the product obtained and the amount of a halogen hydride released in vapor-phase hydrolysis of the chemisorbed structures. Also, the amount of newly formed FGs [OH groups, according to scheme (2)] was to be found. This involves certain experimental difficulties in chemical analysis of the silica surface for the content of OH groups by the known reaction with CH_3MgI [6]. Use of formula (3) requires a full elemental analysis of the samples obtained after each cycle of molecular layer deposiiton.

In [7], a simplified procedure for calculating the content of the starting matrix in the products synthesized was suggested for the example of a chromium-containing silica gel. The approach is based on recalculation of the experimental concentrations of elements or groups per gram of the product to the empirical composition in the form of oxides by the formula

$$\{SiO_2\} = 1000 - ([Cr^{6+}](M_{Cr} + 3M_O) + [Cr^{3+}](M_{Cr} + 3/2M_O) + 1/2M_{H_2O}[OH], \quad (4)$$

where $\{SiO_2\}$ is the mass (mg) of the starting matrix in 1 g of a sample synthesized in any stage of MLD; $[Cr^{6+}]$, content of chromium(VI) in terms of CrO_3 per gram of the product; $[Cr^{3+}]$, content of chromium(III) in terms of Cr_2O_3 per gram of the product; [OH], content of hydroxy groups (mmol) in terms of H_2O per gram of the product; and M_{Cr}, M_O, M_{H_2O}, atomic and molecular masses of Cr, O, and H_2O, respectively.

In the case of analysis of chlorine-containing products, the content of chlorine is recalculated to the corresponding oxychloride with account of the oxidation state of the elements involved. Taking into account the methodological difficulties encountered in evaluation of the concentration of OH groups in various stages of MLD, they can be disregarded in the calculation or a constant correction can be used as their concentration. Experiments demonstrated that, in this case, the deviations in calculation do not exceed the error of chemical analysis. Thus, the suggested simplified calculational procedure has a number of limitations associated with the fact that the possibility of an incomplete extent of processes involving, e.g., OH groups is neglected. Considerably more complicated is the calculation of the true composition and structure of surface formations of another chemical nature, when several types of FGs may appear in the course of synthesis on the surface (e.g., ≡N:, =NH, and $–NH_2$ groups can be formed in synthesis of nitrogen-containing structures [8]), when a compound of complex composition (e.g., SiN_xH_y) is formed on the surface, or on nonoxide matrices.

Taking into account the practical importance of obtaining true relative contents of the components on the surface of various solid matrices, we suggest a generalized procedure for calculating the chemical composition of products formed in chemical assembly of element-containing layers. This procedure is based on the results of a chemical analysis of a material in the stage of LMWR chemisorption. The results obtained are compared with the data furnished by calculations by formulas (3) and (4).

In developing the calculation procedure, we specified the following conditions for its applicability.

(1) There is no chemical reaction between LMWR and products of their interaction with the matrix and other, non-FG, active centers of the substrate (e.g., direct chlorination of the surface).

(2) The functional groups of the matrix enter into chemical reactions only with LMWR molecules, i.e., there are no interfunctional interactions of the initial FGs (e.g., de- or rehydroxylation of the matrix in the course of synthesis).

(3) The synthesis is performed under the conditions in hich the products of interaction of the LMWRs with the matrix form no sorption complexes at active centers of the substrate (e.g., by adsorption of HCl or NH_4Cl on the surface).

(4) Surface structures are formed in accordance with the law of multiple proportions (it is possible that redox reactions occur in the course of synthesis, without changes in the amount of the modifying element).

Let us consider the course of a chemical assembly of a single-component layer of prescribed thickness on the surface of a chalcogenide matrix having only a single type of reactive FGs (|–X–ZH, where H is hydrogen; X = C, Me, Si; Z = O, S) (e.g., SiO_2, Al_2O_3, ZnO, MgO, ZnS, CdS, etc.). As LMWRs can be used the following reagents: AE_n ($n \geq 3$), where A = M, MO, Si, B, P, PO; E = Hal, OR, and DH_m ($m \geq 2$), where D = O, S, N, P.

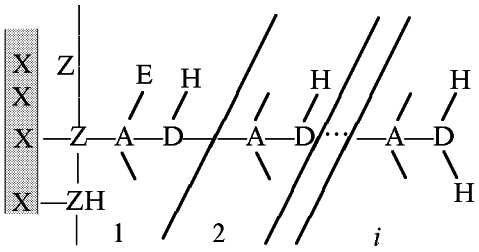
In alternating treatments of the starting matrix with the reagents by the MLD method, an element-containing layer can be formed on its surface by the schemes

$$k(|–X–ZH) + AE_n \rightarrow (|–X–Z)_kAE_{n-k} + kHE, \quad (5)$$

where $n \geq k + 1$;

$$(\mid\!\text{–X–Z})_k\text{AE}_{n-k} + \text{DH}_m \rightarrow (\mid\!\text{–X–Z})_k\text{AD}_{m-n-k}) + (n - k)\text{HE}, \text{ etc.} \quad (6)$$

Taking into account the probability of an incomplete substitution of functional groups in each stage of synthesis and assuming, for simplicity of calculations, that all the products of incomplete substitution of E atoms in $–\text{AE}_{n-k}$ groups are associated with the first monolayer, we can represent the structure of the layer synthesized as the following scheme:



(7)

In this case, the content of the starting matrix, {XZ}, in the product obtained after synthesis of *i*th layer can be expressed, with account of the fact that half of the atom Z in ZH groups belongs to the matrix, as

$$\{\text{XZ}\}_i = \{1000 - Z\text{H}_{\text{rem}}(M_\text{Z}/2 + 3M_\text{H}) - Z\text{H}_{\text{sp}}M_\text{Z}/2 - Y_{\text{rem}\,i}M_\text{E} - A_iM_\text{A} - D_iM_\text{D} - H_iM_\text{H} - \sum_{j-1}^{i-1} H_{\text{rem}\,i}M_\text{H}\}/1000, \quad (8)$$

where $\{XZ\}_i$ is the content of the starting matrix (g) in 1 g of the synthesis product; ZH_{sp}, ZH_{rem}, amounts of FGs of the matrix spent in the course of chemisorption of AE_n and remaining on the surface of the support (mmol g^{-1}); A_i, D_i, H_i, $E_{\text{rem}i}$, $H_{\text{rem}i}$, amounts of elements A, D, and hydrogen, and also of element E and hydrogen remaining deep within the *i*th layer (mmol g^{-1}); and M_Z, M_A, M_D, M_E, M_H, atomic masses of elements Z, A, D, E, and hydrogen, respectively.

Henceforth, the quantities expressed in mmol per gram of the matrix without FG (mmol g_0^{-1}) are given in square brackets, and those expressed in mmol per gram of the chemisorption product (mmol g^{-1}), without brackets. It should be noted that A_i, D_i, and $E_{\text{rem}i}$ are commonly determined in chemical analysis of products synthesized by the MLD method. {*XZ*} can be expressed in terms of the experimentally found quantities.

Let us calculate the amounts ZH_{sp} of FGs consumed in the chemical reaction with AE_n and ZH_{rem} of FGs that did not enter into the reaction, using the formulas

$$ZH_{\text{sp}} = [\Delta A]_1(n - ([E_{\text{el}}]_1 + [E_{\text{rem}}]_1)/[\Delta A]_1)\{XZ\}_i, \quad (9)$$

$$ZH_{\text{rem}} = ZH_{\text{st}} - ZH_{\text{sp}} = [ZH_{\text{st}}]\{XZ\}_i - [\Delta A]_1(n - ([E_{\text{el}}]_2 + [E_{\text{rem}}]_1)/[\Delta A]_1)\{XZ\}_i, \quad (10)$$

where $[E_{\text{el}}]_1$ is the amount of element *E* from the first monolayer, eliminated in the course of reaction (6) (mmol g_0^{-1}); and $[ZH_{\text{st}}]$, the amount of FGs on the surface of the starting matrix (mmol g_0^{-1}).

The quantity $[ZH_{\text{st}}]$, which reflects the actual composition of the FGs on the surface of the starting matrix under the synthesis conditions, can be determined by chemical analysis. Let us express the content of hydrogen in the $–\text{DH}_{m-(n-k)}$ structures formed on the surface of the matrix as follows:

$$H_j = [\Delta D]_j(m - [E_{\text{el}}]_i/[\Delta D]_j)\{XZ\}_i. \quad (11)$$

Taking into account that the amount of protons substituted in synthesis of the succeeding layer by the reaction with AE_n is given by

$$H_{\text{sp}_j} = [\Delta A]_{j+1}(n - [\Delta E_{\text{el}}]_{j+1}/[\Delta A]_{j+1})\{XZ\}_i, \quad (12)$$

we can express the number of the remaining protons as

$$H_{\text{rem}_j} = H_j - H_{\text{sp}_j}. \quad (13)$$

Substituting the resulting expressions (9)–(13) into the starting equation (8) and grouping like terms, we obtain

$$1000\{XZ\}_i = 1000 - [ZH_{\text{st}}]\{XZ\}_i(M_\text{Z}/2 + M_\text{H}) - A_i(M_\text{A} - nM_\text{H}) - D_i(M_\text{D} + mM_\text{H}) - [E_{\text{rem}}]_1\{XZ\}_iM_\text{H} - E_{\text{rem}\,i}M_\text{E}. \quad (14)$$

From expression (14), we derive formulas for calculating the content of the starting matrix in the product obtained for $i = 1$ (15) and $i > 1$ (16):

$$\{XZ\}_i = [1000 - A_i(M_\text{A} - nM_\text{H}) - D_i(M_\text{D} + mM_\text{H}) - E_{\text{rem}\,i}(M_\text{E} + M_\text{H})]\{1000 + [ZH_{\text{st}}](M_\text{Z}/2 + M_\text{H})\}^{-1}, \quad (15)$$

$$\{XZ\}_i = [1000 - A_i(M_A - nM_H) - D_i(M_D + mM_H) - E_{rem\,i}M_E]\{1000 + [ZH_{st}](M_Z/2 + M_H) + E_{rem\,i}M_H\}^{-1}, \quad (16)$$

In a chemical assembly of surface structures by the MLD method, two particular cases are possible, which can hinder the calculation of the stoichiometric composition of a layer synthesized: (1) modification of the matrix with a compound of the same class (Z = D) and (2) modification of the matrix with a compound of the same element (X = A). In the first case, we can, taking into account that element D is bivalent, determine its amount in each layer in the reaction of substitution of element E:

$$(|\text{–X–Z})_k\text{AE}_{n-k} + \text{DH}_2 \rightarrow (|\text{–X–Z})_k\text{A(DH)}_{n-k} + (n - k)\text{HE}. \quad (17)$$

It follows from scheme (17) that

$$\Delta D_i = H_i = E_{eli}, \quad (18)$$

$$D = \sum_{j=1}^{i} [E_{el}]_j\{XZ\}_i. \quad (19)$$

Substituting expressions (9), (10), (12), (13), (18), and (19) into the starting equation (8) and collecting like terms, we obtain

$$1000\{XZ\}_i = 1000 - [ZH_{st}]\{XZ\}_i(M_Z/2 + M_H) - A_i(M_A - nM_H) - [E_{rem}]_1\{XZ\}_iM_H - E_{rem_i}M_E - \sum_{j=1}^{i} [E_{el}]_j\{XZ\}_i(M_D + 2M_H). \quad (20)$$

Then we have at $i = 1$

$$\{XZ\}_i = [1000 - A_i(M_A - nM_H) - E_{el}(M_D + 2M_H) - E_{rem\,i}(M_E + M_H)]\{1000 + [ZH_{st}](M_Z/2 + M_H)\}^{-1}. \quad (21)$$

At $i > 1$, the calculation is to be performed using the recurrence formula

$$\{XZ\}_i = [1000 - A_i(M_A - nM_H) - E_{el\,i}(M_D + 2M_H) - E_{rem\,i}M_E]\{1000 + [ZX_{st}](M_Z/2 + M_H) + [E_{rem}]_1M_H + \sum_{j=1}^{i-1} [E_{el}]_j(M_D + 2M_H)\}^{-1}. \quad (22)$$

As a particular example, we present calculational formulas for titanium oxide structures on the surface of silica after single ($i = 1$) and multiple ($i > 1$) treatment of the starting matrix with vapors of $TiCl_4$ and H_2O:

$$\{SiO_2\}_1 = [1000 - Ti_1(M_{Ti} - 4M_H) - Cl_{el1}(M_O + 2M_H) - Cl_{rem\,i}(M_{Cl} + M_H)]\{1000 + [OH_{st}](M_O/2 + M_H)\}^{-1}, \quad (23)$$

$$\{SiO_2\}_i = [1000 - Ti_i(M_{Ti} - 4M_H) - Cl_{eli}(M_O + 2M_H) - Cl_{rem\,i}M_{Cl}]\{1000 + [OH_{st}](M_O/2 + M_H) + [Cl_{rem}]_iM_H + \sum_{j=1}^{i-1} [Cl_{el}]_j(M_O + 2M_H)\}^{-1}. \quad (24)$$

The results of calculations by formulas (23), (24) and Eqs. (3) and (4) earlier suggested in [6, 7] are listed in Table 1. As follows from these data, the discrepancy between the amounts of the starting matrix in 1 g of the product, determined using different methods, and those of the modifying element per gram of SiO_2 do not exceed 3%, which is close to the error in determining the content of the modifying element by chemical methods [10]. However, the fact that it is difficult to determine experimentally the content of OH groups on the sample surface, which is necessary in the procedure described in [6], hinders application of Eq. (3). At the same time, the recurrence formula for calculating the amount of the matrix material in a sample, which makes it possible to determine the chemical composition and structure of nanostructures obtained in any stage of synthesis, requires sampling in each cycle, which is possible in research or testing of the synthesis modes. It is the most appropriate to use the simplified procedure [Eq. (4)] suggested in [7] for evaluation monitoring of the stoichiometry of products in the course of an industrial synthesis. At the same time, this techniques gives no way of determining the structure of the layer synthesized, because it is impossible to find from the empirical formula the multiplicity of bonds of the modifying element and, in the case of multicomponent structures, the order of alternation of the monolayers formed and the chemical composition of a separate layer. Thus, the applicability of a method is determined by the task to be accomplished and by the set of the available experimental data.

In the case of modification of the matrix with a compound of the same element (X = A), the stoichiometric composition of the structures formed can be determined by performing the chemical assembly by the MLD method on a thermogravimetric setup with a spring McBain balance [11]. Experiments on

Table 1. Chemical composition of titanium oxide layers on the surface of dispersed silica

T_C, °C	MLD cycle no. i	Content determined by chemical analysis, mmol g^{-1}			$[OH_{st}]$,* mmol g_0^{-1}	Content of SiO_2 per gram of product, g, calculated by formulas		
		[Ti]	$[Cl_{el}]$	$[Cl_{rem}]$		(23), (24)	(3) from [6]	(4) from [7]
200	1	0.96	1.83	0,29	3.57	0.886	0.901	0.899
	2	1.56	1.68	0.18		0.837	0.813	0.855
	3	2.10	1.47	0.13		0.793	0.762	0.815
	4	2.56	1.21	0.18		0.755	0.730	0.780
400	1	0.70	1.26	0.00	2.51	0.925	0.924	0.933
	2	1.14	1.15	0.00		0.888	0.900	0.899
	3	1.57	1.08	0.00		0.852	0.858	0.865
	4	1.97	1.06	0.00		0.819	0.826	0.833
600	1	0.47	0.84	0.00	1.67	0.950	0.946	0.955
	2	0.86	0.87	0.00		0.918	0.915	0.923
	3	1.24	0.84	0.00		0.888	0.895	0.893
	4	1.56	0.71	0.00		0.863	0.872	0.869

* Content of OH groups in heat-treated silica gel [9].

synthesis of a titanium oxide monolayer on dispersed silica [11] showed good agreement between the changes in mass, experimentally determined in the stages of chemisorption and vapor-phase hydrolysis, and the data calculated from the results of a chemical analysis. This fact makes it possible to find from thermogravimetric data the chemical composition of the surface products synthesized. A typical curve describing the variation of the sample mass, Δm, in different stages of synthesis is shown in the figure. The sample mass gain $\Delta m_{ch.s}$, used in the calculations [formulas (25)–(29)], is determined after the stages of chemisorption of AE_n (figure, step *I*) and removal of physically sorbed gaseous products (step *II*). After the stages of treatment with a DH_m vapor (step *III*) and sample drying (step *IV*), the mass of the product decreases as a result of substitution of atoms of element E with lighter-weight FG, DH_{m-1}, by an amount Δm_G, which is used in further calculations [formulas (29) and (30)].

When the first monolayer ($i = 1$) is formed, the gain in mass, $\Delta m_{ch.s}$, in the course of chemisorption of AE_n can be expressed as

$$\Delta m_{ch.s1} = [A]_1 M_A + [E_{el}]_1 M_E + [E_{rem}]_1 M_E] - [ZH_{sp}]M_H, \quad (25)$$

where ΔA is the change in the amount of the modifying element in the stage of chemisorption of AE_n.

At $i > 1$,

$$\Delta m_{ch.s\,i} = [A]_i M_A + [E_{el}]_i M_E - [H_{sp}]_{i-1} M_H. \quad (26)$$

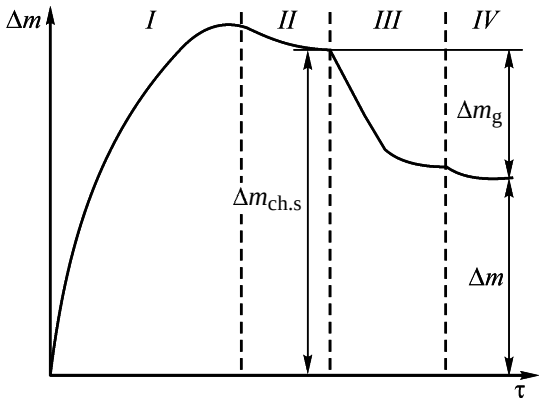
Then, with account of expressions (9) and (12), we obtain for $i = 1$ and $i > 1$, respectively,

$$[A]_1 = \frac{\Delta m_{ch.s1} - ([E_{el}]_1 + E_{rem\,i})(M_E + M_H)}{M_A - nM_H}, \quad (27)$$

$$[A]_i = \frac{\Delta m_{ch.s\,i} - [E_{el}]_i (M_E + M_H)}{M_A - nM_H}, \quad (28)$$

Similarly, the change in sample mass in the course of reaction (6), Δm_g, can be used to calculate the content of element D in each layer:

$$\Delta m_{g\,i} = [\Delta D]_i M_D + [H]_i M_H - [E_{el}]M_E, \quad (29)$$



Changes in sample mass, Δm, in synthesis by MLD, measured on a thermogravimetric setup with a spring McBain balance. (τ) Process duration. (*I*) Chemisorption of AE_n, (*II*) removal of excess reagent, (*III*) treatment with DH_m vapor, and (*IV*) removal of excess reagent.

Table 2. Chemical composition of titanium–nitrogen layers on the surface of dispersed silica

T_C, °C	MLD cycle no., i	Content determined by chemical analysis, mmol g^{-1}			$[OH_{st}]$,* mmol g_0^{-1}	Content of SiO_2 per gram of product, g, calculated by formulas	
		[Ti]	$[Cl_{el}]$	$[Cl_{rem}]$		(15), (16)	(35), (36) from [7]
400	1	0.76	0.48	0.25	2.51	0.929	0.924
	2	1.05	0.68	0.15		0.916	0.912
	3	1.33	0.89	0.15		0.901	0.894
	4	1.60	1.09	0.17		0.885	0.876
600	1	0.47	0.60	0.00	1.67	0.955	0.953
	2	0.75	0.95	0.00		0.937	0.935
	3	1.06	1.35	0.00		0.917	0.914
	4	1.33	1.72	0.00		0.899	0.896

* Content of OH groups in heat-treated silica gel [9].

whence follows

$$[\Delta D]_i = \frac{\Delta m_{g\,i} - [E_{el}]_i(M_E + M_H)}{M_D - mM_H}. \quad (30)$$

The resulting expressions (15), (16), (27), (28), and (30) were used to determine the true stoichiometric composition of the products formed in chemical assembly of titanium–nitrogen (by treatment with $TiCl_4$ vapor and NH_3) of silicon–nitrogen (by treatment with $SiCl_4$ vapor and NH_3) layers on the surface of silica. The synthesis was performed on a thermogravimetric setup with a McBain balance [11]. The concentration of elements in the samples was determined by chemical analysis and from the results of an *in situ* monitoring of the change in the mass of the products on a McBain balance.

Let us consider the applicability of previously developed procedures to analysis of titanium–nitrogen nanostructures on the surface of SiO_2 (Table 2). As the quantitative analysis of the whole spectrum of FG (–NH, ≡NH, and ≡N groups) was not performed after each MLD cycle, it is impossible to use the approach suggested in [6] for calculating the stoichiometric composition of the samples. At the same time, a certain modification of the procedure [7] for recalculation to an empirical composition in the form of titanium-containing compounds (Ti_3N_2, Ti_3N_4, TiO_2, $TiCl_4$) yields adequate results.

Let us present an example of calculation of the content of SiO_2, $\{SiO_2\}$, in 1 g of the product formed at T_s = 400°C. As the N/Ti ratio in the samples is close to 0.67, we can express the layer composition as Ti_3N_2. Then, in accordance with the procedure described in [7],

$$\{SiO_2\}_i = 1000 - (Ti'_i M_{Ti_3N_2}/3 + Ti''_i M''_{TiO_2} + Ti'''_i M'''_{TiCl_4} + [OH_{st}]M_{H_2O}/2), \quad (31)$$

where, judging from the formula composition of the presumed components,

$$Ti'_i = 3/2N_i, \quad (32)$$

$$Ti''_i = 1/4Cl_{rem}, \quad (33)$$

$$Ti'''_i = Ti'_i - Ti''_i = Ti_i - 3/2N_i - 1/4Cl_{rem\,i} = (4Ti_i - 6N_i - Cl_{rem\,i})/4. \quad (34)$$

From here we obtain, substituting expressions (32)–(34) into (31):

$$\{SiO_2\}_i = 1000 - [N_i M_{Ti_3N_2}/2 + (2Ti_i - 6N_i - Cl_{rem\,i})M_{TiO_2}/4 + Cl_{rem\,i}M_{TiCl_4}/4 + [OH_{st}]M_{H_2O}/2). \quad (35)$$

It should be noted that, if $Ti''_i \le 0$ as a result of the error in the chemical analysis, we take $Ti''_i = 0$.

Similar transformations performed for samples synthesized at 600°C yield the following formula:

$$\{SiO_2\}_i = 1000 - [N_i M_{Ti_3N_4}/4 + (4Ti_i - 3N_i - Cl_{rem\,i})M_{TiO_2}/4 + Cl_{rem\,i}M_{TiCl_4}/4 + [OH_{st}]M_{H_2O}/2). \quad (36)$$

The results of a calculation of $\{SiO_2\}$ in the samples synthesized are listed in Table 2. The discrepancy between the amounts of the starting oxide matrix, obtained with formulas (15), (16) and (35), (36), does

Table 3. Chemical composition of silicon–nitrogen layers on the surface of dispersed silica

T_C, °C	MLD cycle no., i	Change in mass, mg g^{-1}			Content, mmol g_0^{-1}						$[Cl_{el}]/[\Delta Si]$	[N]/[Si]
		$\Delta m_{ch.s}$	Δm_g	Δm	$[Cl_{el}]$	$[Cl_{rem}]$	[Si]	[ΔSi]	[N]	[ΔN]		
400	1	84.2	38.7	45.5	1.77	0.10	0.67	0.67	1.52	1.52	2.65	2.27
	2	51.0	29.2	21.8	1.09		1.14	0.47	2.14	0.62	2.32	1.87
	3	53.8	27.4	26.4	1.11		1.70	0.56	2.91	0.77	2.00	1.71
	4	54.3	26.9	27.4	1.13		2.24	0.54	3.75	0.84	2.07	1.67
	5	57.0	29.2	27.8	1.16		2.86	0.62	4.51	0.76	1.88	1.58
	6	52.9	29.7	23.2	1.13		3.34	0.48	5.19	0.68	2.32	1.55
	7	56.6	29.7	26.9	1.17		3.92	0.58	5.95	0.76	2.01	1.52
	8	60.3	30.2	30.1	1.25		4.54	0.62	6.86	0.91	2.04	1.51
600	1	65.1	35.2	29.9	1.33	0.07	0.59	0.59	0.78	0.78	2.27	1.33
	2	62.5	31.5	31.0	1.23		1.32	0.73	1.57	0.79	1.67	1.19
	3	66.8	30.9	35.9	1.32		2.10	0.78	2.58	1.01	1.70	1.23
	4	77.0	35.6	41.4	1.52		3.00	0.90	3.75	1.17	1.69	1.25
	5	81.8	35.5	46.3	1.64		3.91	0.91	5.18	1.43	1.79	1.32
	6	73.1	34.1	39.0	1.47		4.73	0.82	6.32	1.14	1.80	1.34
	7	72.3	32.3	40.0	1.45		5.54	0.81	7.53	1.21	1.79	1.37
	8	68.0	28.5	39.5	1.36		6.31	0.77	8.77	1.24	1.77	1.39

not exceed 1%, which indicates that the approach suggested in [7] is applicable to calculation of the stoichiometric composition of nonoxide nanostructures.

Table 3 shows that the procedure we suggested not only makes it possible to calculate the stoichiometric composition of the products synthesized, even in the case when it is impossible to perform a chemical analysis for the content of one or both components of a layer being synthesized, but also enables a study of the formation pattern of nanostructures in the course of MLD on the surface of a matrix (changes in $[\Delta A]_i$, $[\Delta D]_i$, $[E_{rem}]_i/[\Delta A]_i$, $[D]_i/[A]_i$ with increasing number of monolayers). It should be noted that the procedure described in [7] can also be used to determine the stoichiometric composition of the product in the case of titanium oxide structures on SiO_2 (Table 2). At the same time, the procedure we suggest in this communication is the only one applicable to calculation of the stoichiometric composition of surface structures in the case when it is impossible to determine the content of the layer components by chemical analysis (Table 3).

CONCLUSIONS

(1) Generalized formulas were suggested for calculating the change in the content of the starting matrix in products formed in synthesis of nanostructures on its surface by molecular layer deposition in relation to the number of cycles of treatment with low-molecular-weight reagents. The calculation is based on the results of a chemical analysis of the synthesis products for the content of the main grafted components, functional groups on the starting matrix, and takes into account the possibility of incomplete consumption of functional groups in different steps of molecular layer deposition.

(2) The approaches suggested are in good agreement with the previously developed procedures for performing similar calculations.

(3) A combination of the gravimetric methods for monitoring of synthesis by the MLD method and of the formulas suggested made it possible to determine the stoichiometry of surface nanostructures produced by MLD and having the same composition as the matrix, which cannot be done using the previously suggested techniques.

ACKNOWLEDGMENTS

The study was financially supported by a grant of the President of the Russian Federation for Support of the Leading Scientific Schools of Russia, Program "Chemistry of Highly Organized Substances" (project NSh 2236.2003.3), and, in part, by the Russian Foundation for Basic Research (project no. 04-03-32048) and programs of the Ministry of Science and Education of the Russian Federation.

REFERENCES

1. Aleskovskii, V.B., *Zh. Prikl. Khim.*, 1974, vol. 47, no. 10, pp. 2145–2157.
2. Kol'tsov, S.I., *Reaktsii molekulyarnogo naslaivaniya: Tekst lektsii* (Reactions of Molecular Layer Deposition: Lectures), St. Petersburg: Sankt-Peterb. Gos. Tekhnol. Inst., 1992.
3. Malygin, A.A., Malkov, A.A., and Dubrovenskii, S.D., *Adsorption on New and Modified Inorganic Sorbents*, Dabrowski A. and Tertykh, V.A., Eds., Amsterdam: Elsevier, 1996, vol. 99, pp. 213–236.
4. Malygin, A.A., *Zh. Prikl. Khim.*, 1996, vol. 69, no. 10, pp. 1585–1593.
5. Alekhin, A.P., *Elektron. Prom–st.*, 1990, no. 2, pp. 3–10.
6. Kol'tsov, S.I., *Zh. Prikl. Khim.*, 1969, vol. 42, no. 5, pp. 1023–1028.
7. Volkova. A.N., Malygin, A.A., Smirnov, V.M., *et al.*, *Zh. Obshch. Khim.*, 1972, vol. 42, no. 7, pp. 1431–1434.
8. Malkov, A.A., Malygin, A.A., Sosnov, E.A., and Zaporozhets, V.I., *Zh. Prikl. Khim.*, 1989, vol. 62, no. 7, pp. 1467–1471.
9. Kol'tsov, S.I., Volkova, A.N., and Aleskovskii, V.B., *Zh. Fiz. Khim.*, 1970, vol. 44, no. 9, pp. 2246–2249.
10. Sosnov, E.A., Malkov, A.A., and Malygin, A.A., *Zh. Prikl. Khim.*, 2000, vol. 73, no. 7, pp. 1074–1079.
11. Malkov, A.A., Sosnov, E.A., and Malygin, A.A., *Zh. Prikl. Khim.*, 2004, vol. 77, no. 8, pp. 1245–1248.

Russian Journal of Applied Chemistry, Vol. 78, No. 3, 2005, pp. 375–378. Translated from Zhurnal Prikladnoi Khimii, Vol. 78, No. 3, 2005, pp. 380–383.
Original Russian Text Copyright © 2005 by Sviderskii, Voronkov, S. Klimenko, V. Klimenko, and Skakun.

INORGANIC SYNTHESIS AND INDUSTRIAL INORGANIC CHEMISTRY

Effect of the Metal Salt Anion on Thermal Transformations of Plumbo- and Zincosiloxanes Prepared by the Sol–Gel Method

V. A. Sviderskii, M. G. Voronkov, S. V. Klimenko, V. S. Klimenko, and E. V. Skakun

Kiev Polytechnic Institute, National Technical University of Ukraine, Kiev, Ukraine
Irkutsk Institute of Chemistry, Siberian Division, Russian Academy of Sciences, Irkutsk, Russia

Received July 20, 2004

Abstract—The effect exerted by the anion of Pb and Zn salts on the thermal evolution of the structure of polymetallosiloxanes formed by base-catalyzed (NH_4OH) hydrolytic polycondensation of ethyl silicate with zinc(II) or lead(II) salts was studied.

In synthesis of polymetallosiloxanes by the sol–gel method, the anion of the starting salt determines the rate and depth of its hydrolytic polycondensation with ethyl silicate and also the composition, structure, and properties of the resulting metal–silica gels at common temperatures [1]. However, the effect of anions of metal salts on solid-state transformations of the resulting polymetallosiloxanes on their annealing was not studied. Such data would show how the heat treatment of the synthesized metal–silica gels and materials based on them, performed within a wide temperature range, affects their structure and properties.

EXPERIMENTAL

The starting chemicals were commercial ethyl silicate-40 (ES) (partially hydrolyzed tetraethoxysilane) and the lead and zinc salts $PbCl_2$, $Pb(NO_3)_2$, $Pb(OCOCH_3)_2 \cdot 3H_2O$, $ZnSO_4 \cdot 7H_2O$, $ZnCl_2$, $Zn(NO_3)_2 \cdot 6H_2O$, and $Zn(OCOCH_3)_2 \cdot 2H_2O$.

The choice of these salts was governed by the ability of lead(II) and zinc(II) salts to affect the crystallization of amorphous silica phases of polymetallosiloxanes at relatively low temperatures, as it was found earlier [2]. We used 2-propanol as an organic solvent. The molar ratio ES : H_2O : $(CH_3)_2CHOH$ was 1 : 8 : 4. The process was carried out as follows: A metal salt was dispersed in aqueous ammonia at 35.0 ± 0.5 °C within 1 h. The resulting dispersion was added to an ES solution in 2-propanol, also heated to 35.0 ± 0.5°C, with continuous stirring, and the mixture was stirred for an additional 1 h. For the gelation completion, the system was allowed to stand for a day at room temperature without stirring. The resulting products of hydrolytic polycondensation were thoroughly washed by decanting and dried to a xerogel state for 16 h at 120 ± 5°C. Then they were studied by X-ray diffraction analysis (DRON-3) and IR spectroscopy (a Specord IR-75 spectrophotometer, KBr pellets).

After heat treatment in air for 3.5 h at 900°C, the amorphous phase of plumbo- and zincosiloxanes actively crystallizes to form several modifications of silicon dioxide (Tables 1, 2). This is confirmed by the appearance of well-defined strong reflections cor-

Table 1. Changes in the intensity of the characteristic maxima I/I_0 in the X-ray patterns of plumbosiloxanes after heating at 900°C for 3.5 h

d, nm	Mineral*	I/I_0, %		
		$PbCl_2$	$Pb(NO_3)_2$	$Pb(OCOCH_3)_2$
0.430	γ-Tr	42.3/37.5**	19.8/17.6	23.4/20.9
0.403	β-Cr	100.0/43.2	64.3/60.9	67.0/27.3
0.381	γ-Tr	7.8/12.3	7.4/5.9	8.2/7.6
0.313	β-Cr	4.6/–	6.4/2.5	4.5/–
0.296	γ-Tr	1.4/3.2	–/–	5.6/2.1
0.283	β-Cr	5.8/1.8	7.8/3.1	6.6/1.1
0.248	β-Cr	14.2/7.4	16.3/9.2	14.1/5.9
0.201	β-Cr	1.6/–	2.1/–	1.5/–
0.192	β-Cr	2.8/–	3.4/1.4	3.4/–
0.186	β-Cr	2.5/–	3.1/1.7	2.9/–
0.168	β-Cr	1.3/–	1.5/–	1.7/–
0.160	β-Cr	2.5/–	2.8/1.4	2.7/–
0.153	β-Cr	1.8/–	1.8/1.1	1.7/–
0.149	β-Cr	1.6/–	1.4/–	1.5/–

* γ-Tr and β-Cr are γ-tridymite and β-cristobalite, respectively.
** Synthesis at pH 11.0/12.0; the same for Table 2.

1070-4272/05/7803-0375 © 2005 Pleiades Publishing, Inc.

Table 2. Changes in the intensity of characteristic maxima I/I_0 in the X-ray patterns of zincosiloxanes after heating at 900°C for 3.5 h

d, nm	Mineral	I/I_0, %			
		$ZnSO_4$	$ZnCl_2$	$Zn(NO_3)_2$	$Zn(OCOCH_3)_2$
0.430	γ-Tr	–/28.0	1.4/25.2	22.6/38.7	38.9/24.0
0.403	β-Cr	11.6/10.6	1.4/–	6.1/6.1	6.6/8.2
0.349	Zn_2SiO_4	7.9/22.2	3.1/16.3	9.9/16.3	18.4/14.9
0.321	γ-Tr	–/71.1	7.1/67.9	63.7/67.6	67.7/69.1
0.283	β-Cr	6.8/25.2	3.5/19.1	12.7/17.7	20.5/17.0
0.263	Zn_2SiO_4	5.4/25.5	3.2/17.0	11.7/17.9	21.2/15.7
0.246	β-Cr	–/10.6	–/10.9	8.5/11.9	9.6/9.9
0.232	Zn_2SiO_4	3.3/12.3	1.4/8.2	5.2/7.8	9.9/7.4
0.230	γ-Tr	–/9.9	–/7.5	6.4/–	11.2/7.8
0.228	α-Tr	–/4.8	–/3.3	3.5/10.6	–/–
0.211	β-Cr	–/7.4	–/6.8	5.8/8.4	8.5/6.5
0.195	α-Tr	–/4.4	–/3.5	–/–	5.2/3.4
0.186	β-Cr	2.5/9.8	–/5.9	3.7/6.1	7.8/6.0
0.184	γ-Tr	–/17.4	–/15.6	15.6/19.8	20.4/14.4
0.168	β-Cr	–/5.2	–/4.9	3.4/5.7	5.7/4.1
0.153	β-Cr	–/12.2	–/9.9	7.4/12.7	12.7/9.3
0.152	α-Tr	–/2.3	–/2.1	–/–	1.8/–
0.141	β-Cr	–/7.4	–/6.4	3.9/5.9	6.1/5.7
0.136	β-Cr	–/13.0	–/10.5	8.9/13.0	13.5/9.6

responding to β-cristobalite (interplanar spacings *d* 0.403, 0.313, 0.283, 0.248, 0.246, 0.211, 0.201, 0.192, 0.186, 0.168, 0.160, 0.153, 0.141, and 0.136 nm) and γ-tridymite (*d* 0.430, 0.381, 0.321, 0.296, 0.230, and 0.184 nm), which were identified by comparison with the reference data [3]. The lines corresponding to α-tridymite (*d* 0.228, 0.195, and 0.152 nm) and willemite (*d* 0.349, 0.263, and 0.232 nm) are also present in the X-ray patterns of zincosiloxanes. Willemite is formed by the thermal reaction of SiO_2 with ZnO (product of dissociation of the sorbed zinc salt) [2]. The formation of SiO_2 crystal modifications is apparently induced by lead(II) or zinc(II) atoms incorporated in the siloxane structure as Si–O–M–O–Si (M = Pb or Zn) fragments and also by salts of these metals sorbed in the polysiloxane matrix. As noted above, this is primarily determined by the nature of the introduced metal and by high molecular homogeneity of the resulting systems [2]. Highly dispersed lead(II) and zinc(II) oxides formed by thermal decomposition of the starting salts, being highly reactive in phase transformations (Hedwall effect), are also catalytically active.

The crystallization of the amorphous silica phase of polymetallosiloxanes also depends on the conditions of their synthesis (the cation and anion of the starting salt, pH of the reaction medium, and reaction temperature). This is confirmed by variations of the intensity I/I_0 of the characteristic maxima in the corresponding X-ray patterns of metallosiloxanes (Tables 1, 2).

The catalytic effect of lead salts at pH 11 of the reaction medium on the formation of the major phase (β-cristobalite) decreases in the order $PbCl_2$ (100%) > $Pb(OCOCH_3)_2$ (67.0%) > $Pb(NO_3)_2$ (64.3%), corresponding to a decrease in the thermal stability of the salts. This is proved by the reflection intensities I/I_0 calculated relative to the intensity of the major peak (*d* = 0.403 nm) in the X-ray pattern of plumbosiloxane obtained from $PbCl_2$, taken as 100% for all the systems. However, at pH 12 the catalytic effect of the salts decreases in another sequence: $Pb(NO_3)_2$ (100%) > $PbCl_2$ (70%) > $Pb(OCOCH_3)_2$ (44%). As a whole, plumbosiloxanes crystallize after annealing much more actively if the sol–gel process is carried out at pH 11.0 (Table 1).

When zinc(II) salts are used in the sol–gel process at pH 12.0, crystalline phases in zincosiloxane are formed more actively. After the synthesis at pH 11.0, zincosiloxanes show similar tendency to crystallize only when zinc nitrate and acetate are used (most readily dissociating on heating to form ZnO). With

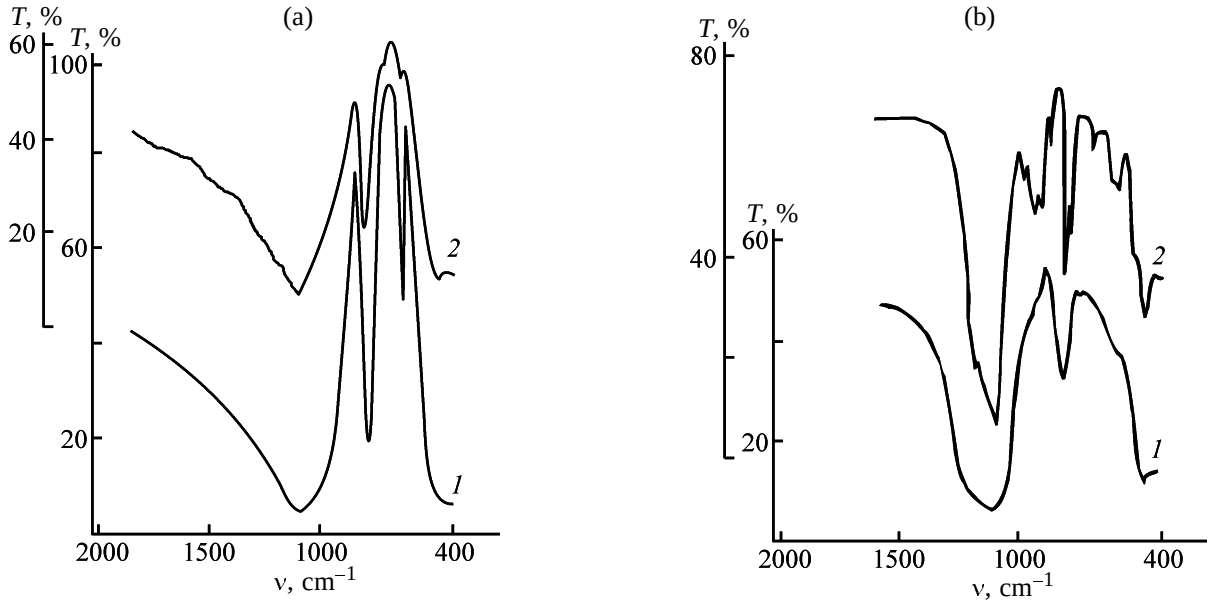


Fig. 1. IR absorption spectra of (a) plumbosiloxanes obtained from $PbCl_2$ and (b) zincosiloxanes obtained from $ZnCl_2$ after heating at 900°C for 3.5 h. (*T*) Transmission and (ν) wave number. pH: (*1*) 11 and (*2*) 12.

zinc sulfate and chloride (most stable thermally), the crystallization of the system is insignificant. With $ZnCl_2$ as the starting salt, β-cristobalite is not noticeably formed in the xerogel. Zincosiloxanes differ from plumbosiloxane by the higher content of crystalline phases. Except for β-cristobalite and γ-tridymite, these are α-tridymite and willemite (Zn_2SiO_4). The content of the major phases of γ-tridymite and willemite essentially depends on the conditions of the sol–gel synthesis (the zinc salt anion and pH of the reaction medium).

This conclusion is also supported by the IR data, in particular, by the fact that the typical spectra contain well-defined strong absorption bands at 969, 917, 890, 853, 790, 752, 677, 613, and 507 cm^{-1} (Figs. 1a, 1b). However, direct determination of the majority of the forming phases by IR spectroscopy is severely complicated by the overlap of the absorption bands characteristic for all high-temperature SiO_2 forms in the range 400–1200 cm^{-1}. In this connection, only cristobalite was identified in the IR spectra by the absorption band at 615 cm^{-1}, characteristic of only this SiO_2 modification [4]. Its content in the products of the sol–gel synthesis was estimated from the optical density *D* of this band in the maximum [4]. In the IR spectra of the plumbosiloxanes obtained, this band is somewhat shifted toward lower frequencies owing to a change in the spacial orientation of the silicon–oxygen tetrahedra of cristobalite in the presence of other crystalline phases. The value of *D* for this band is consistent with the results of the X-ray phase analysis demonstrating how the crystallization of the system depends on the anions of the starting lead and zinc salts and on pH of the reaction medium. Thus, the content of cristobalite in plumbosiloxanes after heat treatment is always higher if the synthesis was carried out at pH 11.0, and not 12.0, of the starting reaction medium. The content of all the crystalline phases after the heat treatment of the zincosiloxanes obtained from $ZnSO_4$ and $ZnCl_2$ (most thermally stable) at pH 11.0 is considerably lower.

This is confirmed also by variation of *D* for the absorption band in the region of 800 cm^{-1}, characteristic of practically all silica modifications [4, 5].

Table 3. Optical density *D* of the absorption bands at 615/800 cm^{-1} for plumbo- and zincosiloxanes after heating at 900°C for 3.5 h in relation to the conditions of their preparation

Starting salt	*D* at indicated pH of reaction medium during synthesis	
	11	12
$PbCl_2$	0.26/0.63	0.03/0.34
$Pb(NO_3)_2$	0.18/0.41	0.15/0.38
$Pb(OCOCH_3)_2$	0.19/0.43	0.02/0.26
$ZnCl_2$	–/0.23	0.06/0.28
$ZnSO_4$	0.01/0.46	0.09/0.71
$Zn(NO_3)_2$	0.12/0.42	0.15/0.55
$Zn(OCOCH_3)_2$	0.14/0.65	0.13/0.45

Depending on the structure of other crystalline phases formed, this band is shifted to 780–797 cm^{-1} in the spectra of zincosiloxanes and to 776–789 cm^{-1} in the spectra of plumbosiloxanes. The data obtained indicate that *D* of this band for plumbo- and zincosiloxanes is always higher in the case of more crystallized systems (Table 3). These data correlate with the I/I_0 ratios in the X-ray diffraction patterns.

Thus, by varying the anions of the starting lead(II) or zinc(II) salts and pH of the reaction medium during the sol–gel process, we can control the crystallization and phase composition of the basic amorphous polysiloxane matrix of metal–silica compounds.

CONCLUSIONS

(1) High-temperature crystal transformations of amorphous silica phases of plumbo- and zincosiloxanes (metal–silica compounds) obtained by a sol–gel method from ethyl silicate and a metal salt in 2-propanol in the presence of NH_4OH depend on the salt anion and pH of the medium.

(2) The major phases formed upon the heat treatment (900°C, 3.5 h) of metal–silica compounds are β-cristobalite in the case of plumbosiloxanes and γ-tridymite and willemite in the case of zincosiloxanes.

REFERENCES

1. Sviderskii, V.A., Voronkov, M.G., Klimenko, S.V., and Bystrov, D.N., *Zh. Prikl. Khim*., 2001, vol. 74, no. 12, pp. 2027–2030.
2. Sviderskii, V.A., Voronkov, M.G., Klimenko, S.V., and Klimenko, V.S., *Zh. Prikl. Khim*., 2001, vol. 74, no. 7, pp. 1137–1141.
3. Gorshkov, V.S., Timashev, V.V., and Savel'ev, V.G., *Metody fiziko-khimicheskogo analiza vyazhushchikh veshchestv* (Methods of Physicochemical Analysis of Binders), Moscow: Vysshaya Shkola, 1981.
4. Mtschedlow-Petrossian, O.P., Degtjerewa, L.L., Spirin, I.A., and Ugintsches, D.A., *Silikattechnik*, 1989, vol. 40, no. 5, p. 148.
5. *Infrakrasnye spektry shchelochnykh silikatov* (Infrared Spectra of Alkaline Silicates), Vlasov, A.A. and Florinskaya, V.A., Eds., Leningrad: Khimiya, 1970.

Russian Journal of Applied Chemistry, Vol. 78, No. 3, 2005, pp. 379–385. Translated from Zhurnal Prikladnoi Khimii, Vol. 78, No. 3, 2005, pp. 384–389.
Original Russian Text Copyright © 2005 by L'vov, Ugolkov.

PHYSICOCHEMICAL STUDIES OF SYSTEMS AND PROCESSES

Application of the Hertz–Langmuir Equation to Studying the Kinetics of Dehydration of Solid Compounds in Air

B. V. L'vov and V. L. Ugolkov

St. Petersburg State Polytechnic University, St. Petersburg, Russia
Institute of Silicate Chemistry, Russian Academy of Sciences, St. Petersburg, Russia

Received January 19, 2005

Abstract—A simple and reliable method was suggested for studying thermal dehydration of solid substances. The method is based on the application of the Hertz–Langmuir equation to determining the rate of decomposition in air and on the use of the third-law method for calculating the enthalpy of the process.

Two fundamentally different approaches to the interpretation of the exponential temperature dependence of the rate of thermal decomposition of solid substances are known. The first of them it based on the Arrhenius hypothesis, which assumes that only the active part of reagent molecules participate in a reaction. According to the Maxwell–Boltzmann distribution, this part is an exponential function of temperature. The second approach is based on classical studies by Hertz and Langmuir that revealed proportionality between the rate of evaporation and the equilibrium vapor pressure, which, in turn, depends exponentially on temperature.

It is well known [1] that the first approach was transferred to the theory of solid-phase reactions from the kinetics of homogeneous reactions without proper theoretical substantiation. As a result, the kinetic parameters of the Arrhenius equation (preexponential factor A and activation energy E) lost their physical sense. Attempts of use the simple Polanyi–Wigner equation followed by application of the transition state (or activated complex) theory developed by Eyring, Evans, and Polanyi were restricted only to rather approximate estimates of the preexponential factor [1]. Moreover, within the framework of this approach, the main relationships of decomposition reactions determining the mechanism of nucleation, autocatalytic development of the reactions, deceleration of the decomposition in the presence of gaseous products, low evaporation coefficients for many substances, Topley–Smith effect, and kinetic compensation effect remain without quantitative interpretation. The lack of the quantitative theory and the stagnation in this field have been admitted by leading experts [2].

Much greater success in solution of the above-listed problems has been reached by using the Hertz–Langmuir approach developed in [3–9]. The observation of dissociative evaporation of a number of metal nitrates [4, 5] by quadrupole mass spectroscopy gave impetus to the development of this ideology, widely applied earlier to comparative study of decomposition rates of solid substances by methods of Langmuir and Knudsen [10–12]. It has allowed extending this mechanism to all solid compounds. As a result, in view of two other assumptions, the developed concept [6, 8] is based on the following propositions: (1) the initial stage of thermal decomposition consists in congruent dissociative evaporation of the reagent; (2) initial components of the decomposition can differ from equilibrium products; (3) the energy liberated during condensation of the low-volatile product in the reaction zone partly reduces the enthalpy of the overall decomposition reaction (including the condensation stage) as compared to the enthalpy of the initial stage of the dissociative evaporation.

Of the above-listed assumptions, the first assumption provokes the greatest doubts or objections of opponents of this concept. The following reasons are usually advanced. What is the reason for the low-volatile product to pass into vapor, if it should be in the condensed state at a decomposition point according to its thermochemical characteristics? In this case, it is forgotten that the question is not the evaporation of the product, but the dissociative evaporation of the starting compound. Furthermore, it is silently assumed in this case that the starting reagent is allotted by the information on the thermochemical properties of the reaction system, which allows the thermodynamically optimal decomposition pathway to be selected. There-

1070-4272/05/7803-0379 © 2005 Pleiades Publishing, Inc.

fore, for example, when Ag_2O decomposes, silver atoms remain in their initial positions defined by the oxide crystal lattice, and Zn and Cd atoms pass into the gas phase in the cousre of the decomposition of ZnO and CdO. It is difficult to agree with these anthropomorphic notions. It is more logical to assume that solid decomposition products are formed by collisions and condensation of low-volatile particles (atoms and molecules) appearing in the free state in the gas phase as a result of the decomposition by a uniform mechanism of congruent dissociative evaporation.

One more argument against extending the mechanism of dissociative evaporation to thermal decomposition of any compounds is the supposedly low probability of the existence of rather complicated molecules in the gas phase, in particular, of molecules of many metal salts formed by the thermal decomposition of crystal hydrates. This reason is disproved by the data obtained recently by mass spectrometry. On the basis of systematization and generalization of the data published in Russia and other countries and of the results of own long-term studies of the composition of vapor of borates, aluminates, carbonates, silicates, nitrates, phosphates, sulfates, hydroxides, chromates, and other binary oxides, Kazenas [13] concluded: "...the discovery of molecules of new types has completely refuted the notion on the high-temperature vapor as a medium poor of molecular species. In particular, it was found that the molecular composition of vapor–gas phases of a number of chemical compounds and their mixtures is much more complicated and more manifold than it seemed earlier."

Nevertheless, verification (direct and indirect) of the dissociative evaporation as the first step of thermal decomposition of solid compounds remains an urgent problem on the pathway of the further development of the Hertz–Langmuir approach and its application to the kinetics of solid-phase reactions. This is the subject of our study. Also, we offer a simple and reliable method of studying dehydration reactions. It consists in the application of the Hertz–Langmuir equation to determining the dehydration rates in air and in the use of the third law for calculating the reaction enthalpy. To show experimentally the possibility of widely applying the method suggested, we chose hydrated compounds of different classes: $Li_2SO_4 \cdot H_2O$ and $3MgO \cdot 4SiO_2 \cdot H_2O$ (talc).

Let us consider some aspects of the theory used in this study. The third-law method is based on the application of the fundamental equation of chemical thermodynamics:

$$\Delta_r H_T^0 = T(\Delta_r S_T^0 - R\ln K_e), \quad (1)$$

where $\Delta_r H_T^0$ and $\Delta_r S_T^0$ are the enthalpy and entropy of the decomposition and K_e is the equilibrium constant.

If reagent R decomposes (according to the mechanism of dissociative evaporation) into gaseous products A and B with simultaneous condensation of low-volatile component A, i.e.,

$$R(s/l) \rightarrow aA(g)\downarrow + bB(g), \quad (2)$$

the equilibrium constant is

$$K_e = P_A^a P_B^b. \quad (3)$$

The equivalent partial pressure P_{eq} (bar) of product A can be found from the Hertz–Langmuir equation through the maximal decomposition rate J ($kg\,m^{-2}\,s^{-1}$):

$$P_{eq} = \frac{(2\pi\overline{M}RT)^{1/2} J}{\gamma M_B}, \quad (4)$$

where $\gamma = 10^5$ Pa bar^{-1} corresponds to the factor of recalculation of pressure from pascals to bars; $\overline{M}$ is the gometric mean of the molar weights of primary products

$$\overline{M} = (M_A^a M_B^b)^{1/(a+b)} = (M_A^a M_B^b)^{1/\nu}, \quad \nu = a + b. \quad (5)$$

Taking into account the stoichiometric coefficients of reaction (2), the equilibrium constant under high-vacuum conditions (equimolar decomposition mode) [6, 8] is described by Eq. (6):

$$K_e = P_A^a P_B^b = (b/a)^b P_{eq}^\nu. \quad (6)$$

In the presence of excess gaseous product B in the reactor (isobaric decomposition mode), we have

$$K_e = P_A^a P_B^b = P_{eq}^a P_B^b. \quad (7)$$

In the case of dissociative evaporation of a reagent, the parameter E in Arrhenius equation is related to the reaction enthalpy as follows [6, 8]: for the equimolar mode,

$$E^e = \Delta_r H_T^0/\nu = \Delta_r H_T^0/(a + b), \quad (8)$$

and for the isobaric mode,

$$E^i = \Delta_r H_T^0/(\nu - b) = \Delta_r H_T^0/a. \quad (9)$$

In the first case, the parameter E corresponds to the

reaction enthalpy per mole of primary products, i.e., to the molar enthalpy, and in the second case, to the reaction enthalpy per mole of the products except for the component present in excess.

The requirement of the maximal decomposition rate or, in other words, of the decomposition from the free surface in the equimolar mode means the absence of any diffusion limitations for the removal of the gaseous product (or products) from the surface of the decomposing reagent. In the case of dehydration, H_2O vapor is the only gaseous product. Other primary products (or product), being low-volatile, immediately condense. To eliminate diffusion limitations for the removal of H_2O vapor, it is necessary to use high vacuum in the reactor.

In the presence of excess H_2O vapor in the reactor (isobaric mode), the conditions of the removal of H_2O liberated during the decomposition are of no significance, as the external pressure of H_2O vapor is much higher than its equivalent pressure. This feature opens a remarkable possibility for the realization of the decomposition from the free surface (after Langmuir) in the presence of any foreign gas, in particular, in air. In fact, the presence of air should not affect the decomposition rate, as diffusion limitations for H_2O vapor removal under isobaric conditions are insignificant, as noted above, and all the low-volatile primary dehydration products instantaneously condense. This means that. in the presence of H_2O vapor in the reactor, the Hertz–Langmuir equation can be used to estimate the equivalent partial pressures of primary dehydration products not only in a vacuum or under low pressure, but also at atmospheric or even higher pressure of a foreign gas. Certainly, this conclusion is valid only under conditions of congruent dissociative evaporation of hydrates when, according to Eqs. (6) and (7), primary decomposition products are described by the laws of the equilibrium thermodynamics, in particular, by the law of mass action. If this is the case, the enthalpies determined by Eq. (6) for a high vacuum and by Eq. (7) for air should be equal.

It is evident from Eq. (1) that the determination of the enthalpy by the third-law method suggests the possibility of calculating the reaction entropy. At first sight, this can seriously restrict the application of this method. Fortunately, the situation in this field has considerably changed within the last 40 years. The standard entropies S^0_{298} and the corresponding temperature increments $S^0_T - S^0_{298}$ for the majority of substances were calculated and published in the tabulated form in several handbooks. Nevertheless, such data for several low-volatile molecules (in particular, of metal salts) in thegaseous state are lacking. The most common approach to the estimation of the reaction entropies in these cases is based on the similarity of the molar entropies $\Delta_r S^0_T/\nu$ for decomposition of various compounds. The recent analysis [8] revealed certain difference in $\Delta_r S^0_T/\nu$ for compounds decomposing to free metal atoms and to metal-containing molecules. The mean value of $\Delta_r S^0_T/\nu$ appeared to be 136 ± 9 J mol^{-1} K^{-1} in the first case and 160 ± 9 in the second. The uncertainty in $\Delta_r S^0_T/\nu$ (± 9 J mol^{-1} K^{-1}) results in an error in the enthalpy and parameter E of about 3%. Therefore, against the background of the total, random, and fixed errors, the effect of this factor is insignificant [9]. Furthermore, these values can be recalculated as soon as $\Delta_r S^0_T/\nu$ values are refined.

EXPERIMENTAL

The essence of the experiments consisted in determining the equilibrium constants of dehydration under high-vacuum conditions (in the absence of H_2O vapor in the reactor) and in air (in the presence of H_2O vapor in the reactor) with the aim of subsequently calculating reaction enthalpies. The sample weight loss per unit time $\Delta m/\Delta t$ and its temperature were measured with STA 429 and STA 449 Netzsch thermoanalyzers with TG and TG + DSC units, respectively. Open crucibles of internal diameter 5.7 mm and height 4.0 mm were used. The materials under study were $Li_2SO_4 \cdot H_2O$ (analytically pure grade) crystals grown at the laboratory and transparent pieces of talc mica (without inclusions) of thickness 0.2–0.5 mm. The composition of substances was preliminarily checked by the weight loss on heating. The surface area of samples S_0 was estimated with an MPB-2 ($\times 24$) microscope.

Experiments in a vacuum were carried out with an STA 429 analyzer. The chamber was evacuated up to a pressure of $n \times 10^{-8}$ bar with roughing and diffusion pumps. The measurements were carried out at continuous pumping under isothermal conditions. The experiments in air were carried out with both analyzers. The partial pressure of H_2O vapor was estimated by indications of a digital thermohygrometer (moisture percentage) and by H_2O saturated vapor pressure at room temperature.

The rate of heating the samples from room temperature to an intermediate temperature (5 K below the final temperature) was 4 deg min^{-1} for $Li_2SO_4 \cdot H_2O$ and 30 for talc. The heating rate from the intermediate

Table 1. Experimental conditions and the enthalpy of dehydration of $Li_2SO_4 \cdot H_2O$ and talc, calculated by the third-law method

P_{air}	P_{H_2O}	T, K	m_0, mg	S_0, mm^2	α_m	S_m,* mm^2	$\Delta m/\Delta t$, $\mu g\ s^{-1}$	J, $kg\ m^{-2}\ s^{-1}$	P_{eq}, bar	K_e,** bar^2, bar^8	$\Delta_r S_T^0/\nu$, $J\ mol^{-1}\ K^{-1}$	$\Delta_r H_T^0$, $kJ\ mol^{-1}$
bar												
Dehydration of $Li_2SO_4\ H_2O$												
5×10^{-7}	5×10^{-9}	326.9	10.4	27.9	0.12	25.6	0.052	2.03×10^{-6}	3.05×10^{-8}	9.30×10^{-16}	175.0	208.5
5×10^{-7}	5×10^{-9}	327.4	12.7	29.5	0.13	26.9	0.059	2.19×10^{-6}	3.29×10^{-8}	1.08×10^{-15}	175.0	208.4
1	1.1×10^{-2}	350.9	49.5	141	0.02	139	0.047	3.38×10^{-7}	5.27×10^{-9}	5.80×10^{-11}	174.1	191.0
1	9.4×10^{-3}	351.7	29.7	42.4	0.01	42.1	0.024	5.70×10^{-7}	8.89×10^{-9}	8.36×10^{-11}	174.1	190.3
1	9.9×10^{-3}	352.0	10.3	39.2	0.03	38.4	0.028	7.29×10^{-7}	1.14×10^{-8}	1.13×10^{-10}	174.1	189.6
1	1.1×10^{-2}	360.1	13.9	31.7	0.14	28.7	0.118	4.11×10^{-6}	6.49×10^{-8}	7.14×10^{-10}	173.9	188.3
1	8.9×10^{-3}	360.9	12.1	29.5	0.16	26.3	0.147	5.59×10^{-6}	8.83×10^{-8}	7.86×10^{-10}	173.8	188.4
1	1.4×10^{-2}	376.4	9.7	40.4	0.34	30.6	0.374	1.22×10^{-5}	1.99×10^{-7}	2.79×10^{-9}	173.3	192.1
1	1.3×10^{-2}	382.0	15.1	26.0	0.30	20.5	0.719	3.51×10^{-5}	5.72×10^{-7}	7.43×10^{-9}	173.1	191.7
Dehydration of talc												
8×10^{-8}	8×10^{-10}	1248.2	16.6	58.0	0.52	35.6	0.182	5.11×10^{-6}	1.51×10^{-7}	3.93×10^{-56}	–	2922
8×10^{-8}	8×10^{-10}	1258.8	15.0	55.3	0.55	32.5	0.184	5.66×10^{-6}	1.68×10^{-7}	8.89×10^{-56}	–	2938
1	1.4×10^{-2}	1220.7	6.01	37.2	0.35	27.9	0.053	1.90×10^{-6}	5.55×10^{-8}	2.27×10^{-53}	–	2793
1	1.2×10^{-2}	1220.7	8.03	47.1	0.33	36.1	0.070	1.94×10^{-6}	5.66×10^{-8}	2.24×10^{-53}	–	2793
1	9.9×10^{-3}	1250.5	13.3	49.3	0.41	34.7	0.099	2.85×10^{-6}	8.44×10^{-8}	3.03×10^{-52}	–	2834
1	1.3×10^{-2}	1250.7	5.88	34.6	0.46	22.9	0.063	2.75×10^{-6}	8.14×10^{-8}	3.08×10^{-52}	–	2834
1	1.1×10^{-2}	1250.7	6.66	42.2	0.53	25.5	0.076	2.98×10^{-6}	8.82×10^{-8}	4.57×10^{-52}	–	2830
1	9.9×10^{-3}	1275.0	10.8	35.8	0.37	26.3	0.462	1.76×10^{-5}	5.23×10^{-7}	1.07×10^{-46}	–	2754
1	1.1×10^{-2}	1275.0	12.9	39.2	0.34	29.7	0.584	1.97×10^{-5}	5.86×10^{-7}	2.61×10^{-46}	–	2745
1	8.9×10^{-3}	1294.8	15.2	69.8	0.16	62.2	1.63	2.62×10^{-5}	7.89×10^{-7}	1.69×10^{-45}	–	2767
1	8.4×10^{-3}	1294.8	13.8	73.7	0.30	58.1	1.23	2.12×10^{-5}	6.37×10^{-7}	3.57×10^{-46}	–	2784

* Surface area at the moment of measurement, calculated by the formula $S_m = S_0(1 - \alpha_m)^{2/3}$.

** Equilibrium constant K_e has the dimension bar^2 ($Li_2SO_4 \cdot H_2O$) and bar^8 (talc).

Table 2. Enthalpy of dehydration of $Li_2SO_4 \cdot H_2O$, calculated by the third-law method from the data of [14, 15]

P_{air}	P_{H_2O}	T, K	J, $kg\,m^{-2}\,s^{-1}$	P_{eq}, bar	K_e, bar^2	$\Delta_r S_T^0/\nu$, $J\,mol^{-1}\,K^{-1}$	$\Delta_r H_T^0$, $kJ\,mol^{-1}$	Reference
bar								
4×10^{-10}	6.0×10^{-12}	300	5.70×10^{-8}	8.66×10^{-10}	7.50×10^{-19}	351.8	209.6	[14]
4×10^{-10}	6.0×10^{-12}	348	2.73×10^{-5}	4.26×10^{-7}	1.81×10^{-13}	348.5	206.2	[15]

Table 3. Averaged enthalpies (measured in air) and parameters E for equimolar (1) and isobaric (2) dehydration conditions

Dehydration reaction (primary stage)	$\Delta_r H_T^0$, $kJ\,mol^{-1}$	E,* $kJ\,mol^{-1}$	
		1	2
$Li_2SO_4 \cdot H_2O(s) \rightarrow Li_2SO_4(g)\downarrow + H_2O$	190.2 ± 1.5	95.1 ± 0.8	190.2 ± 1.5
$3MgO_4 \cdot SiO_2 \cdot H_2O(s) \rightarrow 3MgO(g)\downarrow + 4SiO_2(g)\downarrow + H_2O$	2793 ± 34	349 ± 4	399 ± 5

* Calculated by formulas (8) and (9).

to the final temperature was 1 deg min^{-1}. The furnace was heated at a chosen temperature for 5–10 min until a steady-state decomposition rate was attained. The change in the surface area of samples was taken into account in the calculations. We have found experimentally that the relative decrease in the surface area is proportional to $(1 - \alpha_m)^{2/3}$), where α_m is the decomposition degree at the moment of measurement. This dependence can be attributed to decreasing size of crystals. All primary signals ($\Delta m/\Delta t$) were corrected for the idle signal (0.02–0.07 $\mu g\,s^{-1}$), which depended on temperature and pressure and was measured independently with an empty crucible. The temperature was measured with a Pt–Pt/10% Rh thermocouple placed under a crucible bottom. The temperature variations during the measurement (usually 15–30 min) did not exceed ±0.2 K.

The experimental conditions and calculated enthalpies for both compounds are given in Table 1, and the enthalpy calculated for $Li_2SO_4 \cdot H_2O$ from the data of [14, 15], in Table 2. The averaged enthalpies and parameters E for $Li_2SO_4 \cdot H_2O$ and talc are given in Table 3. The entropy of dehydration of $Li_2SO_4 \cdot H_2O$ was calculated using $\Delta_r S_{298}^0/\nu$ = 175.9 $J\,mol^{-1}\,K^{-1}$ determined in [7]. For talc, we used the approximate value $\Delta_r S_T^0/\nu$ = 160 $J\,mol^{-1}\,K^{-1}$, which is valid for compounds decomposing to molecular products. The number of moles of primary products of talc decomposition is eight; therefore, $\Delta_r S_T^0$ = 1280 $J\,mol^{-1}\,K^{-1}$. The results obtained allow the following conclusions.

The most significant fact is the closeness of $\Delta_r H_T^0$ values obtained in a vacuum and in air (Table 1); hence, the primary step of the dehydration corresponds to the following mechanism of dissociative evaporation

$$Li_2SO_4 \cdot H_2O(s) \rightarrow Li_2SO_4(g)\downarrow + H_2O(g), \quad (10)$$

$$3MgO \cdot 4SiO_2 \cdot H_2O(s) \rightarrow 3MgO(g)\downarrow + 4SiO_2(g)\downarrow + H_2O(g). \quad (11)$$

In the case of talc, the condensation products are enstatite ($MgSiO_3$) and amorphous SiO_2 form [16], which also agrees well with the mechanism of the decomposition by dissociative evaporation–condensation. It is difficult to imagine that enstatite and amorphous silicon dioxide can be formed otherwise than by vapor deposition. Somewhat higher $\Delta_r H_T^0$ values for vacuum result from sample self-cooling under the conditions when the only source of its heating is radiation of crucible walls. In the case of $Li_2SO_4 \cdot H_2O$ at 330–360 K, the difference in $\Delta_r H_T^0$ and correspondingly in the sample temperatures in a vacuum and in air attains 10%. When talc is decomposed at 1220–1290 K, the difference is only 5%, which is attributable to the difference in the radiation power, which is known to be proportional to temperature raised to the fourth power. The measured rate of the dehydration in air practically rules out the influence of self-cooling on the measured $\Delta_r H_T^0$ because of the preferential contribution of the gas thermal conductivity to the sample heating.

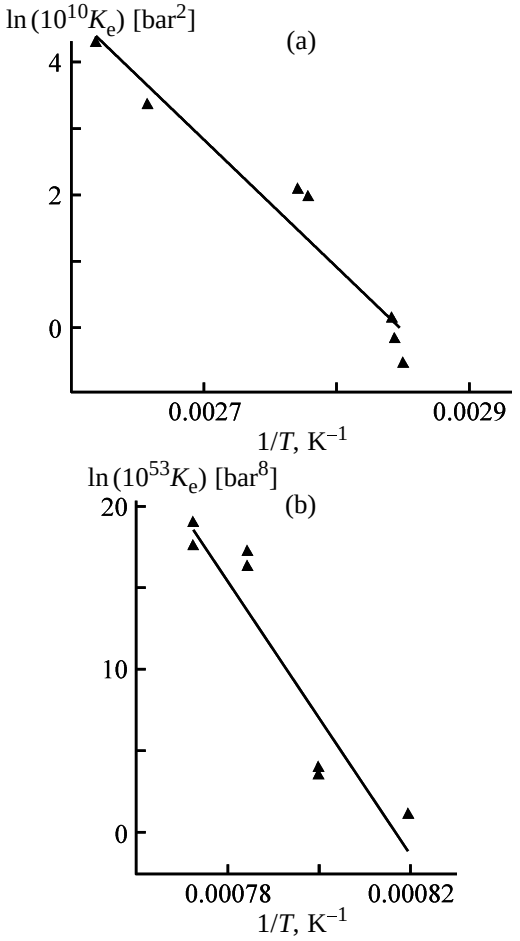


Fig. 1. Logarithm of the equilibrium constant K_e [(a) bar^2 and (b), bar^8] as a function of reciprocal temperature T for the decomposition of (a) $Li_2SO_4 \cdot H_2O$ and (b) talc in air.

The relative standard error in the determination of $\Delta_r H_T^0$ for both reagents is about 1% (Table 3). It confirms the high accuracy of the third-law method, which was theoretically justified earlier [8, 9]. In the case of the second-law method, the standard error is greater by more than an order of magnitude: $\Delta_4 H_T^0 = 160 \pm 27$ and 3500 ± 500 kJ mol^{-1} for $Li_2SO_4 \cdot H_2O$ and talc, respectively (Fig. 1). This difference agrees with the theoretical estimation. In fact, the difference in the accuracy of the results is determined by the ratio $T_{max}/(T_{max} - T_{min})$, where T_{max} and T_{min} are the maximal and minimal temperatures of the measurements. In the case of $Li_2SO_4 \cdot H_2O$ and talc, this ratio is 382/31 ≃ 12 and 1295/74 ≃ 17, respectively.

The enthalpy of $Li_2SO_4 \cdot H_2O$ dehydration in a vacuum, calculated by the third-law method from the data of [14, 15] (Table 2), practically coincides with our data for vacuum (Table 1). The average values are 208 and 209 kJ mol^{-1} K^{-1}, respectively. However, as mentioned above, both these results are overestimated owing to self-cooling. The only published value of E^i for talc dehydration [16] is 423 ± 17 kJ mol^{-1} (in Ar containing H_2O), which agrees well with the result of this study, E^i = 3995 kJ mol^{-1} (Table 3).

Unfortunately, the suggested method is inapplicable the decomposition of metal hydroxides. This is due to the presence of about 0.003% CO_2 in air, which reacts with metal oxides with partial formation of thermally stable carbonates. This conclusion was checked by the example of $Mg(OH)_2$ (brucite) dehydration. At 650 K, the apparent decomposition rate appeared to be 20–30 times less than the expected value (in the absence of CO_2 in reactor).

CONCLUSIONS

(1) A method was developed for determining the enthalpies of dehydration of various crystal hydrates (except for metal hydroxides). The method is simple, fast, precision, and free from errors caused by the self-cooling effect. It is based on the application of the Hertz–Langmuir equation to measuring the dehydration rates in air and of the third-law method to calculating the enthalpy. The values of $\Delta_r H_T^0$ found for $Li_2SO_4 \cdot H_2O$ and talc are 190.2 ± 1.5 and 2793 ± 34 kJ mol^{-1}, respectively.

(2) The equality of the enthalpies of $Li_2SO_4 \cdot H_2O$ and talc dehydration measured in a high vacuum (equimolar decomposition mode) and in air (isobaric mode) confirms the mechanism of dissociative evaporation of these compounds with simultaneous condensation of low-volatile products according to schemes (10) and (11).

ACKNOWLEDGMENTS

The authors are grateful to L.K. Polzik for useful remarks.

REFERENCES

1. Galwey, A.K. and Brown, M.E., *Thermal Decomposition of Ionic Solids*, Amsterdam: Elsevier, 1999.
2. Galwey, A.K. and Brown, M.E., *J. Therm. Anal. Calorim.*, 2000, vol. 60, pp. 863–877.
3. L'vov, B.V. and Ryabchuk, G.N., *Zh. Anal. Khim.*, 1981, vol. 36, pp. 2085–2096.
4. L'vov, B.V., *Zh. Anal. Khim.*, 1990, vol. 45, pp. 2144–2153.
5. L'vov, B.V. and Novichikhin, A.V., *Spectrochim. Acta, Part B*, 1995, vol. 50, pp. 1427–1448.

6. L'vov, B.V., *Thermochim. Acta*, 2001, vol. 373, pp. 97–124.
7. L'vov, B.V. and Ugolkov, V.L., *J. Therm. Anal. Calorim*., 2003, vol. 74, pp. 697–708.
8. L'vov, B.V., *Thermochim. Acta*, 2004, vol. 424, pp. 183–199.
9. L'vov, B.V., *J. Therm. Anal. Calorim*., 2005, vol. 79, pp. 151–156.
10. Margrave, J.L., *Physicochemical Measurements at High Temperatures*, London: Butterworths, 1959, pp. 225–246.
11. Inghram, M. and Drowart, J., *Proc. Int. Symp. on High Temperature Technologies (California)*, New York: McGraw-Hill, 1959, pp. 219–252.
12. Powell, E.K. and Searcy, A.W., *Met. Trans. B*, 1980, vol. 11, pp. 427–432.
13. Kazenas, E.K., *Termodinamika ispareniya dvoinykh oksidov* (Thermodynamics of the Evaporation of Double Oxides), Moscow: Nauka, 2004.
14. Okhotnikov, V.B., Yakobson, B.I., and Lyakhov N.Z., *React. Kinet. Catal. Lett*., 1983, vol. 23, pp. 125–130.
15. Modestov, A.N., Poplaukhin, P.V., and Lyakhov, N.Z., *J. Therm. Anal. Calorim*., 2001, vol. 65, pp. 121–130.
16. Ward, J.R., *Thermochim. Acta*, 1975, vol. 13, pp. 7–14.

Russian Journal of Applied Chemistry, Vol. 78, No. 3, 2005, pp. 386–389. Translated from Zhurnal Prikladnoi Khimii, Vol. 78, No. 3, 2005, pp. 390–393.
Original Russian Text Copyright © 2005 by Anufrikov, Fedicheva, Kuranov.

PHYSICOCHEMICAL STUDIES OF SYSTEMS AND PROCESSES

Solubility of Sodium Sulfate in a Mixed Solvent Water–Methyldiethanolamine at 25 and 35°C

Yu. A. Anufrikov, N. D. Fedicheva, and G. L. Kuranov

St. Petersburg State University, St. Petersburg, Russia

Received November 29, 2004

Abstract—The solubility of sodium sulfate in a mixed solvent water–methyldiethanolamine at 25 and 35°C was studied experimentally using the gravimetric method and gravimetric acid–base titration. The solubility diagrams obtained for the first time were compared with those of sodium sulfate in binary solvents monoethanolamine–water and diethanolamine–water.

Aqueous methyldiethanolamine (MDEA) solutions are widely used as sorbents of acid gases, such as hydrogen sulfide, carbon dioxide, and sulfur oxides. In industrial installations, the absorption of acid gases is frequently complicated by formation of strong electrolytes exerting the salting-out effect. For example, in a gas flow containing sulfur trioxide, the following process takes place in an aqueous MDEA solution:

$$SO_3 + H_2O + 2MDEA \rightarrow (MDEAH)_2SO_4.$$

The forming methyldiethanolammonium sulfate decreases the solubility of acid gases in an aqueous MDEA solution. The subsequent regeneration of the amine with a base yields sodium sulfate as by-product:

$$(MDEAH)_2SO_4 + 2NaOH \rightarrow 2MDEA + 2H_2O + Na_2SO_4.$$

This salt exerts the strong salting-out effect on acid gases [1, 2]. Therefore, when the content of Na_2SO_4 in an aqueous MDEA solution becomes high, this salt should be removed from the solution. In this context, it becomes necessary to know the Na_2SO_4 solubility in the MDEA–H_2O binary solvent. These data are of not only applied but also scientific importance, as giving new information on the phase equilibria in systems constituted by a salt and a mixed solvent.

In this study we determined the Na_2SO_4 solubility in the system at 25 and 35°C. The temperature of 35°C, at which the Na_2SO_4 solubility in water is maximal [3], was chosen as the upper temperature limit. The Na_2SO_4 solubility in the mixed solvent MDEA–H_2O was not measured previously.

EXPERIMENTAL

Anhydrous Na_2SO_4 (analytically purity grade), MDEA containing more than 99% main substance (Aldrich), chemically pure grade barium chloride and 5 wt % hydrochloric acid, $AgNO_3$ (pure grade), and Methyl Red indicator were used without additional purification. All solutions were prepared in freshly distilled water.

A mixture (about 50 ml) of Na_2SO_4 and MDEA was charged into a round-bottom flask and agitated in a temperature-controlled shaker to attain the thermodynamic equilibrium, i.e., to obtain a saturated solution of the salt in the binary solvent. To preset the overall composition of the mixture, each component was weighed with an accuracy of 0.1 mg. The equilibration time was determined in the course of the kinetic experiment by taking liquid phase samples at 12-h intervals and determining the content of Na_2SO_4 and MDEA in them. In solutions containing up to 30 wt % MDEA, the equilibration took 3 days; in those containing 30–50 wt % MDEA, 4 days; and in those with the amine concentration above 50 wt %, 5 days. The long equilibration time is due to the high viscosity of MDEA solutions.

The Na_2SO_4 concentration was determined gravimetrically. To do this, the sulfate ion was precipitated in the form of $BaSO_4$. The samples for the analysis were transferred into tightly closed weighing bottles with a pipet equipped with a finely porous filter on the tip to avoid ingress of small crystals of the bottom phase. Then, the bottles were weighed with an accuracy of 0.1 mg. The volume of the test samples was from 0.5 to 6 ml, depending on the Na_2SO_4 concentration. It corresponded to formation of 0.3 g of

1070-4272/05/7803-0386© 2005 Pleiades Publishing, Inc.

$BaSO_4$ and was estimated in a preliminarily experiment. The weighed samples were transferred into beakers, and their pH was adjusted with 10% HCl (1 ml). Then, they were heated to 70°C, and a 5% $BaCl_2$ solution was added dropwise with vigorous stirring. The precipitate obtained was kept for 3 h to mature, filtered through an ashless paper filter (blue tape), and repeatedly washed in warm water. The filters with the precipitate dried in air were placed into quartz crucibles, which were calcined to constant weight, ashed, and calcined in a muffle furnace at 900°C for 4 h. The calcination time was determined experimentally: longer calcination did not further change the weight of the crucibles and their contents.

The MDEA concentration was determined by the adapted procedure of the gravimetric acid–base titration. From 0.5 to 6 ml of the test solution was sampled into a conical flask with a ground-glass neck. To the weighed solution, 30 ml of water and Methyl Red indicator were added. After that, the test solution was titrated with an HCl solution (0.1 mol kg^{-1} H_2O). The volume of the test solution was chosen so that about 20 ml of the HCl solution was spent for the titration. This volume ensured sufficient experimental accuracy and was convenient to fix the color transition point (from yellow to crimson). The amount of the acid spent for titration was determined to within 0.1 mg by weighing. To standardize the titrant, the chloride ions were precipitated in the form of AgCl by the standard procedure [4] and determined gravimetrically.

The composition of the solid phase was determined by the Schreinemakers method. In the procedure used, Schreinemakers path was passed from the point of the liquid phase composition through the point of the overall composition preset in preparation of the three-component mixture.

Each concentration of Na_2SO_4, determined gravimetrically, and MDEA, determined titrimetrically, was an averaged result of three replicate measurements; the scatter of the results did not exceed 0.3 rel. %.

This method was checked by determining the Na_2SO_4 and MDEA concentrations in a ternary solution of a known composition. The preset and experimentally determined concentrations coincided within 0.2 rel. %.

Our experimental results are presented in Table 1, and the compositions of the saturated solutions, along with the overall compositions used in construction of the Schreinemakers paths, in Table 2. The solubility diagrams in the Na_2SO_4–MDEA–H_2O system, constructed from the data obtained, are shown in Fig. 1.

Table 1. Compositions of MDEA–Na_2SO_4–H_2O saturated solutions

Content, wt %			
MDEA	Na_2SO_4	MDEA	Na_2SO_4
T = 25°C		T = 35°C	
1.366	19.67	2.464	30.13
4.209	17.78	5.486	26.14
6.837	15.98	13.78	19.39
8.985	14.52	21.33	14.13
11.04	13.25	30.45	8.325
16.12	10.30	47.40	1.916
21.99	7.285	48.37	1.811
29.89	4.560	64.09	0.418
35.80	2.450		
44.03	1.719		
49.40	1.289		
59.96	0.552		

Table 2. Compositions of equilibrium phases, determined by the Schreinemakers method

T, °C	Content, wt %		Overall composition, wt %		Solid phase
	MDEA	Na_2SO_4	MDEA	Na_2SO_4	
25	11.04	13.25	9.624	16.43	$Na_2SO_4 \cdot 10H_2O$
	35.81	2.450	33.48	9.746	Na_2SO_4
	59.96	0.552	57.32	5.037	Na_2SO_4
35	21.33	14.13	18.79	20.75	Na_2SO_4
	30.45	8.325	27.37	17.66	Na_2SO_4
	48.37	1.811	44.36	9.979	Na_2SO_4
	64.09	0.418	59.44	8.264	Na_2SO_4

The saturated solution coexists with the crystal hydrate $Na_2SO_4 \cdot 10H_2O$ in the range of the MDEA concentrations below 15 wt % at 25°C. As the MDEA concentration is increased, the solid phase changes for anhydrous Na_2SO_4. At 35°C, the solid phase coexisting with the saturated solution over the entire range of the MDEA concentrations is anhydrous Na_2SO_4. The presence of the crystal hydrate at 25°C and its absence at 35°C is in agreement with the data on the $Na_2SO_4 \cdot H_2O$ binary system [3], according to which the saturated aqueous Na_2SO_4 solution coexists with the

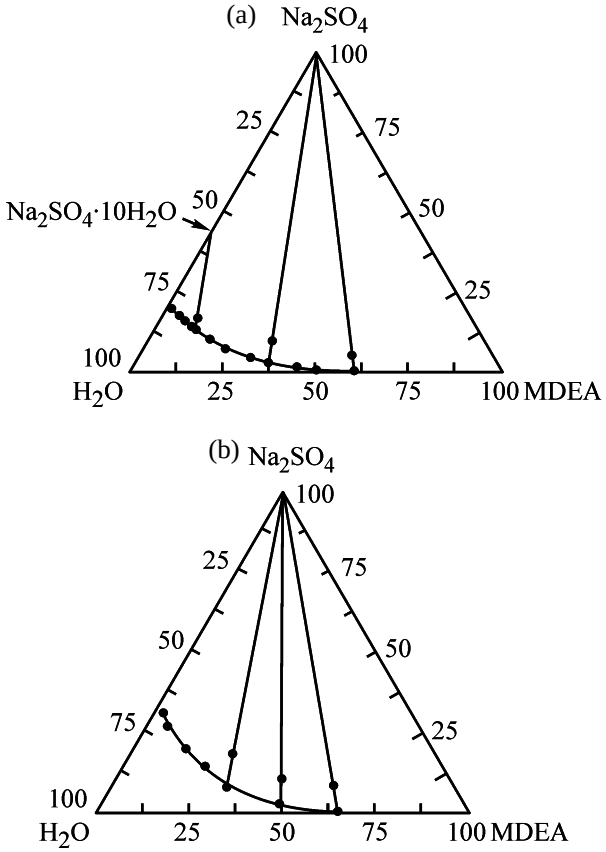


Fig. 1. Solubility diagrams (wt %) of the MDEA–Na_2SO_4–H_2O system. Temperature (°C): (a) 25 and (b) 35; the same for Fig. 2.

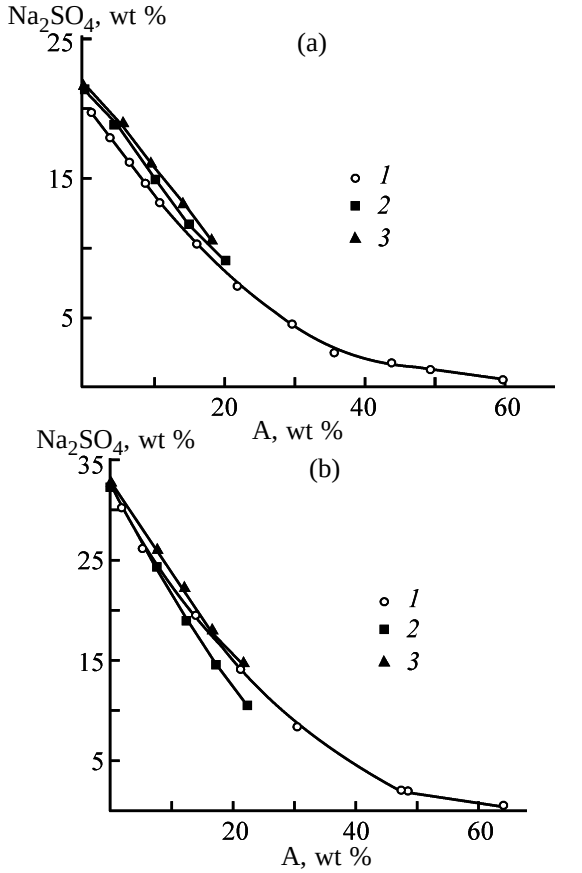


Fig. 2. Solubility isotherms of Na_2SO_4 in mixed solvents (*1*) MDEA–H_2O, (*2*) MEA–H_2O, and (*3*) DEA–H_2O. (A) amine.

$Na_2SO_4 \cdot 10H_2O$ solid phase up to 32.38°C; above this temperature, this crystal hydrate decomposes.

As noted above, published data on the solubility in the Na_2SO_4–MDEA–H_2O system are lacking. The solubility of Na_2SO_4 in aqueous solutions of monoethanolamine (MEA) and diethanolamine (DEA) was studied in [5, 6]. The experimental results of our study, along with the known data for the above systems, are plotted in Fig. 2. As seen, the Na_2SO_4 solubilities in the binary solvents MEA–H_2O and DEA–H_2O are close. The solubility of Na_2SO_4 in the mixed solvent MDEA–H_2O is lower than in both the above binary solvents. At 35°C, the solubility in the DEA–H_2O system is higher than in the MEA–H_2O system. The solubility isotherm of Na_2SO_4 in the mixed solvent MDEA–H_2O at 35°C lies between the isotherms taken in the other two systems and is closer to the Na_2SO_4 solubility curve in the DEA–H_2O solvent.

The comparison of the solubility diagrams at 25 and 35°C, obtained in this study, shows that, in the range of the MDEA concentrations 0–40 wt %, the Na_2SO_4 solubility at 35°C is considerably higher. As the amine concentration is increased, the solubility of the salt in the MDEA–H_2O binary solvent decreases and the temperature dependence of the solubility becomes less pronounced. At an MDEA concentration of about 50 wt %, the solubility curves for both temperatures virtually merge together, with the solubility in this region being about 1.5 wt % and tending to zero at higher MDEA concentrations. The low solubillity of Na_2SO_4 in concentrated MDEA solutions can be of interest for practice, since these solutions, as less corrosive than those of other alkanolamines, recently found use as sorbents of acid gases [7]. Probably, the low solubility of Na_2SO_4 in concentrated aqueous MDEA solutions will allow their use for sorption of acid gases without additional treatment to remove Na_2SO_4.

CONCLUSIONS

(1) Experimental data on the solubility of Na_2SO_4 in the MDEA–H_2O binary solvent at 25 and 35°C were obtained.

(2) The compositions of the solid phase coexisting with the saturated solution were determined by the Schreinemakers method.

(3) Qualitative trends in the influence of temperature on the solubility in the ternary system were revealed.

ACKNOWLEDGMENTS

This study was financially supported by the Russian Foundation for Basic Research (project nos. NSh-676.2003 and 02-03-32709).

The authors are grateful to N.A. Smirnova and A.G. Morachevskii for their attention to this study.

REFERENCES

1. Anufrikov, Yu., Perez-Salado Kamps, A., Kuranov, G., *et al.*, *Am. Inst. Chem. Eng. J.*, 2002, vol. 48, pp. 168–177.
2. Anufrikov, Yu., Perez-Salado Kamps, A., Kuranov, G., *et al.*, *Ind. Eng. Chem. Res.*, 2002, vol. 40, no. 10, pp. 2571–2578.
3. Williams, W.J., *Handbook of Anion Determination*, London: Butterworths, 1979.
4. *Spravochnik eksperimental'nykh dannykh po rastvorimosti solevykh sistem* (Handbook of Experimental Data on Solubility of Salt Systems), vol. 3: *Dvukhkomponentnye sistemy: Elementy I gruppy i ikh soedineniya* (Binary Systems: Group I Elements and Their Compounds), Vyazovov, V.V. and Pel'sh, A.D., Eds., Leningrad: Gos. Nauch.-Tekh. Izd. Khim. Lit., 1961.
5. Gorzelany, W., Wasag, T., and Trzesniowski, W., *Chem. Stosow.*, 1968, vol. 12, no. 3A, pp. 321.
6. Gorzelany, W., Wasag, T., and Trzesniowski, W., *Chem. Stosow.*, 1969, vol. 13, no. 1A, pp. 15.
7. Perez-Salado Kamps, A., Balaban, A., Joedecke, M., *et al.*, *Ind. Eng. Chem. Res.*, 2001, vol. 40, no. 2, pp. 696–706.

Russian Journal of Applied Chemistry, Vol. 78, No. 3, 2005, pp. 390–393. Translated from Zhurnal Prikladnoi Khimii, Vol. 78, No. 3, 2005, pp. 394–397
Original Russian Text Copyright © 2005 by Sinegubova, Il'in, Cherkasov.

PHYSICOCHEMICAL STUDIES OF SYSTEMS AND PROCESSES

Mutual Solubility of Components and Critical Solution Points in the System Water–Isopropyl Alcohol–*n*-Dodecane in the Temperature Range 5–120°C

S. I. Sinegubova, K. K. Il'in, and D. G. Cherkasov

Chernyshevskii Saratov State University, Saratov, Russia

Received June 30, 2004

Abstract—The mutual solubility of components and critical solution points in the ternary system water–isopropyl alcohol–*n*-dodecane were studied by a visual-polythermal technique at saturated vapor pressure in the temperature range 5–120 °C. The mixture composition in the critical solution point was studied in relation to temperature.

The mutual solubility of components in ternary systems water–aliphatic alcohol–*n*-alkane was studied by numerous researchers. In [1], the mutual solubility of components in 19 ternary systems was analyzed in relation to the molecular structure of particular components and features of intermolecular interactions. The isothermal and polythermal solubility diagrams of several systems of this kind were studied in detail in [2–5]. It was shown in these papers that the critical solution point is an important characteristic of the phase diagram, because its location reflects the mutual solubility of components and their interaction in the system. Therefore, in studying the mutual solubility of liquid compounds, the location of the critical solution point in the phase diagram and factors influencing the system composition in this point should be determined. The temperature effect on the mixture composition in the critical solution point at a constant pressure was studied only for a few ternary systems and in a narrow temperature range.

In this study we examined the influence of temperature on the mutual solubility of components and the composition of the critical point in the system water–isopropyl alcohol–*n*-dodecane at saturated vapor pressure in the temperature range 5–120°C. This system was not studied previously.

EXPERIMENTAL

All the compounds used in our experiments were thoroughly purified. Water was purified on a DEM-20 MERA-POLNA double-distiller. The initial isopropyl alcohol (chemically pure grade) containing 99.8% main compound was dried over calcined K_2CO_3 for a day, decanted, and then distilled on a 0.3-m Vigreux column, and the fraction with bp 82.2–82.4°C was collected. The purified isopropyl alcohol was stored over molecular sieves (4 Å). *n*-Dodecane (chemically pure grade) was dried over molecular sieves (4 Å) and used without further purification. All the liquids were identified by their boiling point, refractive index, and density. These characteristics were in good agreement with the reference data [6].

The temperature of the phase transition from a two-phase mixture ($l_1 + l_2$) to a homogeneous state (l) $l_1 + l_2 = l$ in the ternary systems was determined in sealed test tubes by the visual polythermal technique [7] with ±0.1°C accuracy. The required temperature was maintained with a Mechanic Medingen U-10 thermostat and was monitored with calibrated decimal mercury thermometers in the temperature ranges 0–50, 50–100, and 100–150°C. The relative accuracy of determining the composition of the coexisting equilibrium phases did not exceed ±0.5%.

The compositions of the ternary system in the critical solution points were determined by the phase volume ratio technique [8]. We chose such compositions of ternary mixtures water–isopropyl alcohol–*n*-dodecane at which the mixture exhibited the critical opalescence in the vicinity of the critical solution point (±0.1 C) and separated into two liquid phases of equal volume. The critical behavior of the systems under consideration was studied in sealed graduated test tubes. The phase volumes were determined with an accuracy of about 5%.

1070-4272/05/7803-0390© 2005 Pleiades Publishing, Inc.

The critical solution point was considered to be equilibrium if, in approaching from both the higher and lower temperatures, the equal values were obtained.

In studies of mutual solubility of components in the ternary system (Fig. 1), their trigonal phase diagrams were built with 15 sections as follows. Sections *I–III*: constant water to isopropyl alcohol weight ratio [(*I*) 80 : 20, (*II*) 50 : 50, and (*III*) 36 : 64] and varied *n*-dodecane content; sections *IV–XIII*: constant isopropyl alcohol to *n*-dodecane weight ratio [(*IV*) 80 : 20, (*V*) 75 : 25, (*VI*) 70 : 30, (*VII*) 60 : 40, (*VIII*) 55 : 45, (*IX*) 50 : 50, (*X*) 45 : 55, (*XI*) 40 : 60, (*XII*) 30 : 70, and (*XIII*) 20 : 80] and varied water content; sections *XIV* and *XV*: constant dodecane to water weight ratio [(*XIV*) 43 : 57 and (*XV*) 21 : 79] and varied isopropyl alcohol content.

The polytherms of the mutual solubility of the components in the ternary systems, built with fifteen sections of the phase diagrams, have similar shape: the solubility curve separates the field of homogeneous solutions from the field of separation into two liquid phases (not illustrated). Of particular interest are the polytherms of systems corresponding to sections *VI–XI* in which the critical solution points were determined. For systems located on these and several similar sections, the critical solution points and the corresponding system compositions were determined by the phase volume ratio technique. Figure 2 shows the water and *n*-dodecane content in the critical solution points in relation to temperature.

The curves in this plot are the orthogonal projections onto the composition–temperature planes of the critical solution curve located on the surface of the three-dimensional region of separation of the ternary systems into two phases in the prismatic phase diagram.

The mutual solubility of components and the system composition in the critical points were determined from the polythermal curves by graphic interpolation technique at 5.0, 10.0, 20.0, 25.0, 30.0, 40,0, 50.0, 60.0, 70.0, 80.0, 90.0, 100.0, 110.0, and 120.0°C. These data for 5.0, 25.0, 50.0, 80.0, and 120.0°C are presented in the table and Fig. 1. The isotherms of the mutual solubility of the components at these temperatures are shown in Fig. 1. The *CC* curve is the orthogonal projection of the critical solution curve of two-phase systems onto the base of the prismatic phase diagram. These results show that the mutual solubility of the components increases with increasing temperature.

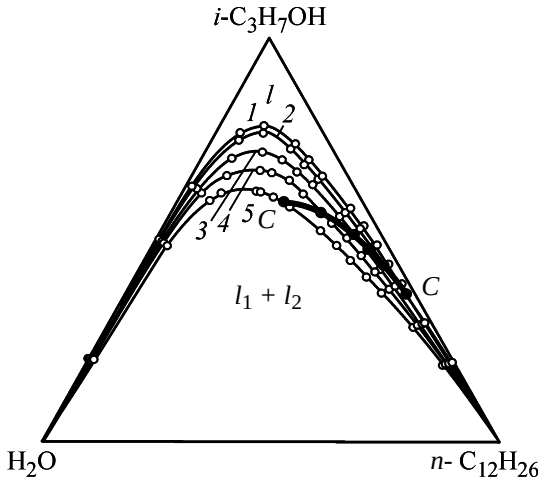


Fig. 1. Isotherms of mutual solubility of components in the system water–isopropyl alcohol–*n*-dodecane at (*1*) 5.0, (*2*) 25.0, (*3*) 50, (*4*) 80.0 and (*5*) 120.0 °C. (*CC*) critical solubility curve.

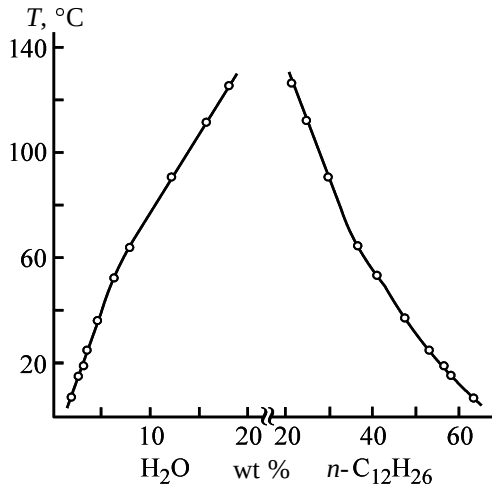


Fig. 2. Temperature dependence of the water and *n*-dodecane content in the critical solution points of the system water–isopropyl alcohol–*n*-dodecane.

Figure 2 shows that, with increasing temperature, the critical mixtures are enriched in water and depleted of dodecane. As a result, the critical solution points shift toward the maximum of the binodal curves (Fig. 1). At 5.0 and 25.0°C (curves *1, 2*), the critical points are located in the vicinity of the triangle side corresponding to the binary system *n*-$C_{12}H_{26}$–*i*-C_3H_7OH, virtually on the tangent to the binodal curve passing from the *n*-$C_{12}H_{26}$ apex. According to an approach to analysis of multiphase multicomponent systems developed by Mertslin [9], this kind of binodal curve shows that, in the ternary systems under consideration, the molecular interactions typical of the binary system water–isopropyl alcohol prevail.

Mutual solubility of components in the ternary system water–isopropyl alcohol–*n*-dodecane (wt %)

n-$C_{12}H_{26}$	H_2O	*i*-C_3H_7OH	*n*-$C_{12}H_{26}$	H_2O	*i*-C_3H_7OH	*n*-$C_{12}H_{26}$	H_2O	*i*-C_3H_7OH
				T = 5.0°C				
0.3	79.8	19.9	23.3	6.8	69.9	53.6	2.5	43.9
0.4	49.8	49.8	28.3	5.7	66.0	58.6	2.4	39.0
0.9	35.7	63.4	38.5	3.7	57.8	61.6*	2.0*	36.4*
5.1	18.7	76.2	43.6	3.1	53.3	68.7	1.8	29.5
9.5	12.6	77.9	48.6	2.8	48.6	79.4	0.8	19.8
18.4	7.8	73.8	–	–	–	–	–	–
				T = 25.0°C				
0.4	79.7	19.9	22.9	8.5	68.6	53.1*	3.6*	43.3*
0.6	49.7	49.7	27.9	7.0	65.1	53.1	3.5	43.4
1.3	35.5	63.2	37.9	5.2	56.9	58.3	2.8	38.9
5.3	19.9	74.8	43.1	4.2	52.7	68.3	2.4	29.3
10.2	13.4	76.4	48.2	3.6	48.2	79.2	1.1	19.7
18.1	9.5	72.4	–	–	–	–	–	–
				T = 50.0°C				
0.6	79.5	19.9	22.3	10.8	66.9	47.5	5.0	47.5
0.8	49.6	49.6	27.3	8.9	63.8	52.4	4.7	42.9
2.3	35.2	62.5	37.2	7.1	55.7	57.8	3.7	38.5
6.3	23.5	70.2	42.3	6.0	51.7	67.9	2.9	29.2
12.2	16.1	71.7	42.7*	6.0*	51.3*	78.9	1.3	19.8
17.5	12.7	69.8	–	–	–	–	–	–
				T = 80.0°C				
0.8	79.4	19.8	21.6	13.7	64.7	46.4	7.2	46.4
1.5	49.2	49.3	26.3	12.5	61.2	51.5	6.3	42.2
3.8	34.6	61.6	32.7*	10.5*	56.8*	57.0	5.0	38.0
7.2	27.0	65.8	36.2	9.6	54.2	67.5	3.6	28.9
14.1	18.8	67.1	41.3	8.2	50.5	78.6	1.8	19.6
16.7	16.7	66.6	–	–	–	–	–	–
				T = 120.0°C				
1.2	79.1	19.7	20.2	19.1	60.7	44.9	10.2	44.9
2.7	48.7	48.6	23.3*	17.3*	59.4*	50.3	8.5	41.2
6.4	33.7	59.9	25.0	16.7	58.3	55.7	7.2	37.1
8.1	30.5	61.4	34.8	13.1	52.1	66.8	4.6	28.6
15.5	22.4	62.1	39.9	11.4	48.7	77.8	2.7	19.5
16.5	21.6	61.9	–	–	–	–	–	–

* Critical solution point.

At the highest temperature (120°C), the critical solution point shifts to the maximum of the binodal curve (Fig. 1, curve *5*). According to the Mertslin approach, this means that, on heating of the ternary system from 5 to 120°C, the intermolecular interactions governing the phase behavior change from those typical of the binary system water–isopropyl alcohol to the interactions typical of the system *n*-dodecane–isopropyl alcohol. We believe that the shift of the critical solution points with increasing temperature is caused by breakdown of isopropyl alcohol hydrates with weakening of interactions between isopropyl alcohol and water molecules in the ternary system.

CONCLUSIONS

(1) The mutual solubility of components in the ternary system water–isopropyl alcohol–*n*-dodecane and the composition of this system in the critical solution point were determined in the temperature

range 5.0–120°C. The mutual solubility of the components increases with temperature.

(2) It was suggested that, in heating the system water–isopropyl alcohol–*n*-dodecane, the shift of both the critical solution point and the binodal maximum is caused by the replacement of the intermolecular interactions typical of the binary system water–isopropyl alcohol by those typical of the system *n*-dodecane–isopropyl alcohol, due to breakdown of isopropyl alcohol hydrates.

(3) The phase diagrams of the system water–isopropyl alcohol–*n*-dodecane in a wide temperature range can be used in extraction practice and as reference data.

ACKNOWLEDGMENTS

This work was financially supported by the Russian Foundation for Basic Research (project no. 03-03-33128).

REFERENCES

1. Zhurkina, A.I. and Karapet'yants, M.Kh., *Tr. Mosk. Khim.-Tekhnol. Inst. im. D.I. Mendeleeva*, 1968, no. 58, pp. 86–91.
2. Il'in, K.K. and Cherkasov, D.G., *Int. J. High Temp.–High Press.*, 1997, vol. 29, no. 3, pp. 345–348.
3. Il'in, K.K. and Cherkasov, D.G., *ELDATA: Int. Electron. J. Phys.-Chem. Data*, 1998, vol. 4, no. 1, pp. 11–20.
4. Il'in, K.K. and Cherkasov, D.G., *ELDATA: Int. Electron. J. Phys.-Chem. Data*, 1998, vol. 4, no. 2, pp. 99–104.
5. Il'in, K.K. and Cherkasov, D.G., *ELDATA: Int. Electron. J. Phys.-Chem. Data*, 1999, Vol. 5, no. 2, pp. 107–116.
6. *Khimicheskaya entsiklopediya* (Chemical Encyclopedia), Knunyants, I.L., Ed., Moscow: Sov. Entsiklopediya, 1988–1998, vols. 1–5.
7. Anosov, V.Ya., Ozerova, M.I., and Fialkov, Yu.Ya., *Osnovy fiziko-khimicheskogo analiza* (Foundations of Physicochemical Analysis), Moscow: Nauka, 1976.
8. Treybal, R.E., *Liquid Extraction*, New York: McGraw-Hill, 1963.
9. Nikurashina, N.I. and Mertslin, R.V., *Metod sechenii: Prilozhenie ego k izucheniyu mnogofaznogo sostoyaniya mnogokomponentnykh sistem* (Section Method: Its Application to Analysis of Multiphase State of Muplticomponent Systems), Saratov: Saratov. Univ., 1969.

Russian Journal of Applied Chemistry, Vol. 78, No. 3, 2005, pp. 394–398. Translated from Zhurnal Prikladnoi Khimii, Vol. 78, No. 3, 2005, pp. 398–402.
Original Russian Text Copyright © 2005 by Sinegubova, Cherkasov, Il'in.

PHYSICOCHEMICAL STUDIES OF SYSTEMS AND PROCESSES

Salting-Out of *n*-Propyl Alcohol with Potassium Nitrate from Aqueous Solutions

S. I. Sinegubova, D. G. Cherkasov, and K. K. Il'in

Chernyshevskii Saratov State University, Saratov, Russia

Received December 6, 2004

Abstract—The solubility of components and critical phenomena in the ternary system constituted by potassium nitrate, water, and *n*-propyl alcohol were studied by the visual polythermal method in the temperature range 25–80°C. The temperature of formaiton of the critical node of the monotectic equilibrium (critical solution–solid phase) and the solution compositions corresponding to the critical solution points at different temperatures were determined. The isothermal solubility diagrams of the system were constructed and the distribution coefficients of *n*-propyl alcohol at different temperatures were calculated. A comparative analysis of the salting-out effect exerted by potassium nitrate on aqueous solutions of *n*-propyl alcohol and isopropyl alcohol was done.

The salting-out of *n*-propyl alcohol from aqueous solutions with various salts has been studied by many researchers [1–4]. However, data on the influence of alkali metal nitrates on the phase separation of mixtures constituted by water and propanol are lacking. In this study we examined the phase equilibria and critical phenomena in the ternary system $KNaO_3$–H_2O–C_3H_7OH in the temperature range 25–80°C to reveal the temperature dependences of the salting-out effect.

EXPERIMENTAL

The phase equilibria in the ternary system KNO_3–H_2O–*n*-C_3H_7OH were studied by the visual polythermal method [5]. Experimental procedures and pretreatment of potassium nitrate and water have been described in detail in [6]. Chemically pure grade *n*-propyl alcohol (containing more than 99.5% main substance) was used without purification, since its constants (T_b = 97.4°C, n_D^{20} = 1.3850) coincided with the reference data [7]. KNO_3 and *n*-C_3H_7OH were stored over calcined $CaCl_2$ in desiccators protected from direct light.

The compositions of the component mixtures were varied along ten sections of the concentration triangle of the system under study. The component mixtures belonging to sections *I*–*VIII* had a varied content of KNO_3 and the constant weight ratio of *n*-propyl alcohol to water: (*I*) 10 : 90, (*II*) 24 : 76, (*III*) 37 : 63, (*IV*) 50 : 50, (*V*) 58 : 42, (*VI*) 71 : 29, (*VII*) 83 : 17, and (*VIII*) 90 : 10. The component mixtures belonging to section *IX* had the constant content of the salt (30.00 wt %) and the varied weight ratio of *n*-propyl alcohol to water, whereas the component mixtures along section *X* had the varied content of alcohol (up to 18 wt %) and the constant weight ratio of KNO_3 to water (65 : 35).

For all the sections, polytherms of the phase states of the system were plotted. The polytherms of sections *IX* and *X* allowed determination of the temperature at which the critical node of the monotectic equilibrium (critical solution–solid phase) is formed, which corresponds to the onset of phase separation in the system (Fig. 1). The polytherm of the phase states along section *IX* comprises four curves which converge to a common point and delimit four fields of phase states, those of unsaturated solutions *l*, saturated solutions $l + S$, phase separation $l_1 + l_2$ (l_1 is alcohol phase and l_2, aqueous phase), and monotectic equilibrium $l_1 + l_2 + S$. The solid phase is potassium nitrate. The polytherm of section *X* has two fields of phase states, $l + S$ and $l_1 + l_2 + S$. In going from the saturated into the monotectic state, critical phenomena in the system of two liquid phases were observed in both sections. The region of critical points corresponding to the compositions of the solution with a critical opalescence is encircled with a dashed line, and the critical point corresponding to a mixture with equal volumes of liquid phases is denoted by a large circle and letter *C*. Evidently, this point *C* corresponds to a mixture composition belonging to the critical node *CS* (critical solution–solid phase), which appears in

1070-4272/05/7803-0394© 2005 Pleiades Publishing, Inc.

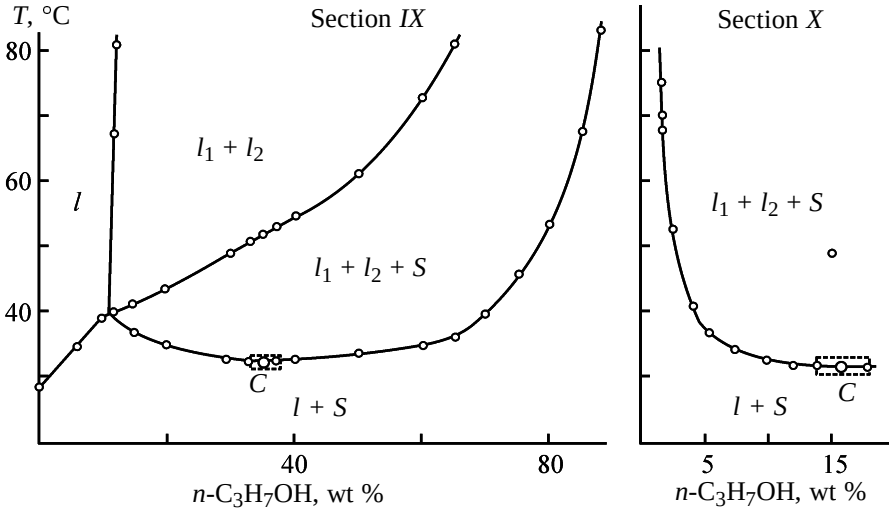


Fig. 1. Polytherms of the phase states in the KNO_3–H_2O–*n*-C_3H_7OH system in mixtures of the components along sections *IX* and *X* of the composition triangle. (*T*) Temperature.

Table 1. Solubility of the components in the ternary system KNO_3–H_2O–*n*-C_3H_7OH*

Composition of saturated solution, wt %								
KNO_3	H_2O	*n*-C_3H_7OH	KNO_3	H_2O	*n*-C_3H_7OH	KNO_3	H_2O	*n*-C_3H_7OH
				T = 25.0°C				
27.2	72.8	0.0	9.8[a]	56.8[a]	33.4[a]	1.6[a]	28.5[a]	69.9[a]
19.5[a]	72.4[a]	8.1[a]	6.0[a]	47.0[a]	47.0[a]	1.0[a]	16.9[a]	82.1[a]
13.8[a]	65.4[a]	20.8[a]	4.0[a]	40.3[a]	55.7[a]	0.1[a]	10.2[a]	89.7[a]
				T = 32.1°C				
32.4	67.6	0.0	13.8**	55.6**	30.6**	2.5[d]	28.3[d]	69.2[d]
30.0[b]	68.1[b]	1.9[b]	13.1[d]	54.8[d]	32.1[d]	0.4[d]	16.9[d]	82.7[d]
24.4[b]	68.0[b]	7.6[b]	7.9[d]	46.0[d]	46.1[d]	0.2[d]	10.0[d]	89.8[d]
17.8[b]	62.5[b]	19.7[b]	5.4[d]	39.7[d]	54.9[d]			
				T = 35.0°C				
34.8	65.2	0.0	13.3**	55.7**	31.0**	2.6[d]	28.2[d]	69.2[d]
30.0[b]	66.3[b]	3.7[b]	13.1[c]	54.7[c]	32.2[c]	1.0[d]	16.9[d]	82.1[d]
26.5[b]	66.2[b]	7.3[b]	8.0[c]	46.0[c]	46.0[c]	0.3[d]	10.0[d]	89.7[d]
18.1[c]	62.2[c]	19.7[c]	5.6[c]	39.6[c]	54.8[c]			
				T = 50.0°C				
44.0	56.0	0.0	13.9[c]	54.2[c]	31.9[c]	4.0[c]	28.0[c]	68.0[c]
33.0[c]	60.3[c]	6.7[c]	13.4**	54.0**	32.6**	0.8[d]	16.9[d]	82.3[d]
30.0[c]	62.0[c]	8.0[c]	8.3[c]	45.8[c]	45.9[c]	0.4[d]	10.0[d]	89.6[d]
18.3[c]	62.1[c]	19.6[c]	5.6[c]	39.6[c]	54.8[c]			
				T = 80.0°C				
62.8	37.2	0.0	15.0[c]	53.6[c]	31.4[c]	9.0[c]	26.4[c]	64.6[c]
35.3[c]	58.3[c]	6.4[c]	14.5**	52.4**	33.1**	1.5[c]	16.7[c]	81.8[c]
30.0[c]	61.3[c]	8.7[c]	11.5[c]	44.3[c]	44.2[c]	0.5[d]	10.0[d]	89.5[d]
19.5[c]	61.1[c]	19.4[c]	10.0[c]	37.8[c]	52.2[c]			

* [a] Phase transition $l \rightleftarrows l + S$, [b] phase transition $l \rightleftarrows l_2 + S$, [c] phase transition $l \rightleftarrows l_1 + l_2$, and [d] phase transition $l \rightleftarrows l_1 + S$.
** Critical solution point.

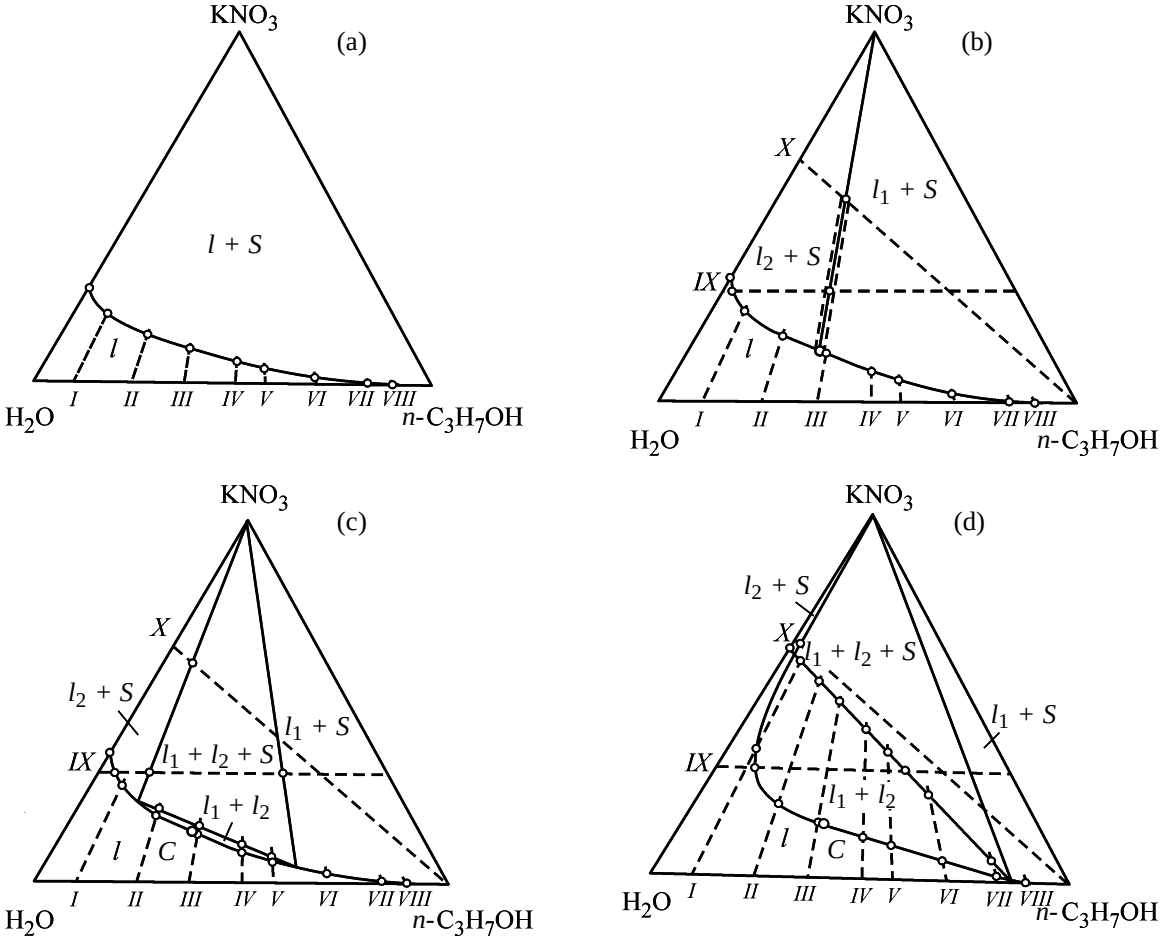


Fig. 2. Isotherms of the phase states of the KNO_3–H_2O–*n*-C_3H_7OH system at (a) 25.0, (b) 32.1, (c) 35.0, and (d) 80.0°C.

the field of saturated solutions at 32.1°C. This temperature corresponds to the onset of the phase separation in the system.

The temperature dependence of the solution composition corresponding to the critical solution point was found. For this purpose, we studied the component mixtures belonging to additional sections and having a varied content of KNO_3 and the constant weight ratio of water to the alcohol. We found that the composition of the critical solution changes only slightly with temperature (Table 1).

The polytherms and the temperature dependences of the composition of the critical solution were used to plot the isothermal phase diagrams of the system at 25.0, 32.1, 35.0, 50.0, and 80.0°C. At temperatures in the range from 25.0 to 32.1°C, a simple diagram of KNO_3 solubility in mixtures of water and *n*-propyl alcohol is observed. For example, at 25.0°C, there is a field of homogeneous solutions *l*, separated by a smooth curve of solubility from the field of saturated solutions $l + S$ (Fig. 2a). At 32.1°C, a critical point *C* appears on the solubility line (Fig. 2b). This point corresponds to a mixture in which two liquid phases, $l_1 + l_2$, have identical compositions and properties. As the critical liquid phase *C* is in equilibrium with the solid phase *S* (KNO_3), there appears a critical node *CS* of the monotectic equilibrium. The composition of the critical liquid phase *C* of the node *CS* was determined graphically in the concentration triangle from the point of interception of the critical node with the solubility line.

As the temperature is raised, the critical node transforms, as seen from the isotherm at 35.0°C (Fig. 2c), into a monotectic triangle $l_1 + l_2 + S$, with the adjacent field of phase separation $l_1 + l_2$ with the critical solution point *C* and the fields of saturated solutions $l_2 + S$ and $l_1 + S$. As the temperature is raised further, the isotherms of phase states do not change qualitatively, but the fields of the monotectic state and phase separation increase in size, and the fields of saturated solutions become narrower, as seen from the diagram at 80°C (Fig. 2d).

Table 2. Compositions of the liquid phases of the monotectic equilibrium and distribution coefficients K_d of *n*-propyl alcohol in the ternary system KNO_3–H_2O–*n*-C_3H_7OH

Composition of liquid phases in equilibrium with solid KNO_3, wt %						T, °C	K_d
aqueous phase			organic phase				
KNO_3	H_2O	*n*-C_3H_7OH	KNO_3	H_2O	*n*-C_3H_7OH		
13.8*	55.6*	30.6*	13.8*	55.6*	30.6*	32.1	1.0
22.2	64.6	13.2	4.0	34.9	61.1	35.0	4.6
39.5	56.6	3.9	2.2	21.2	76.6	50.0	19.6
61.0	37.5	1.5	1.3	14.5	84.2	80.0	56.1

* Composition of liquid phase in the critical node of the monotectic equilibrium (critical solution–solid phase).

The results obtained in determining the solubility of the system components are listed in Table 1. Data on the solubility of KNO_3 in water were taken from a reference book [8]. The compositions of the liquid phases of the monotectic equilibrium (Table 2) were found graphically by plotting the triangles of the monotectic equilibrium on the plane of the concentration triangle at different temperatures (Fig. 3). The dashed line *aCb* (Fig. 3), which reflects the variation of the compositions of the equilibrium liquid phases of the monotectic with temperature, consists of two branches. The composition of the aqueous phase l_2 varies along branch *Ca* and that of the organic phase, along branch *Cb*. As the temperature increases, the aqueous phase is enriched with the salt and depleted of the alcohol, and the organic phase is enriched with the alcohol and depleted of water and the salt.

The distribution coefficient K_d of the alcohol was calculated as the ratio of the concentrations of the alcohol in the organic and aqueous phases of the monotectic equilibrium (Table 2). The fact that the distribution coefficient grows with temperature indicates that the effect of salting-out of *n*-propyl alcohol with potassium nitrate from aqueous solutions is enhanced. Evidently, this is due to decomposition of alcohol hydrates [9, 10] and to a significant increase in the concentration of KNO_3 in the aqueous phase.

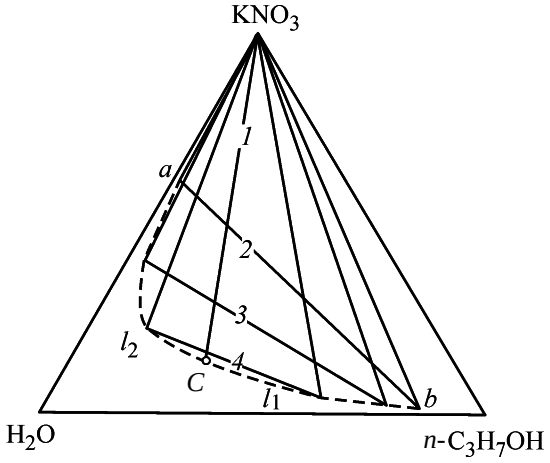


Fig. 3. Variation with temperature of the compositions of the liquid phases of the monotectic equilibrium and of the position of the monotectic triangle in the KNO_3–H_2O–*n*-C_3H_7OH system. T (°C): (*1*) 32.1, (*2*) 35.0, (*3*) 50.0, and (*4*) 80.0.

Comparison of the results obtained in the polythermal studies of phase equilibria in the KNO_3–H_2O–*n*-C_3H_7OH and KNO_3–H_2O–*i*-C_3H_7OH [6] systems revealed an analogy between the topological transformations of their phase diagrams with temperature. The difference is in the onset temperature of phase separation: 32.1°C in the system with *n*-propyl alcohol and 47.2°C in that with isopropyl alcohol. At equal temperatures and concentrations, the excess enthalpy of mixing in the H_2O–*n*-C_3H_7OH system at relatively low alcohol concentrations is less negative than in the H_2O–*i*-C_3H_7OH system [11]. This indicates that the interactions between H_2O and isopropyl alcohol are stronger. Apparently, this fact is responsible for a decrease in the onset temperature of phase sepaation and for a higher distribution coefficient of the alcohol in the KNO_3–H_2O–*n*-C_3H_7OH system compared to that in the KNO_3–H_2O–*i*-C_3H_7OH system (Table 3).

Table 3. Distribution coefficients K_d of alcohol and temperature of the onset of phase separation in the ternary systems H_2O–KNO_3–*n*-C_3H_7OH (*i*-C_3H_7OH)

Alcohol	K_d at indicated T, °C		T_{CS},* °C
	50.0	80.0	
n-C_3H_7OH	19.6	56.1	32.1
i-C_3H_7OH	5.5	33.6	47.2

* (T_{CS}) Temperature of formation of the critical node of the monotectic equilibrium.

CONCLUSIONS

(1) The phase equilibria in mixtures of components along ten sections in the composition triangle of the ternary system constituted by potassium nitrate, water, and *n*-propyl alcohol were studied in the temperature range 25–80°C by the visual polythermal method. The temperature corresponding to the onset of phase separation in the system is 32.1°C.

(2) The distribution coefficient of *n*-propyl alcohol between the liquid phases of the monotectic equilibrium increases with temperature.

(3) At equal temperatures in the range 50–80°C, the effect of salting-out of *n*-propyl alcohol from aqueous solutions with potassium nitrate is stronger than that of isopropyl alcohol. In the system with *n*-propyl alcohol, the temperature of formation of the critical node of the monotectic equilibrium is lower than in that with isopropyl alcohol.

ACKNOWLEDGMENTS

The study was financially supported by the Russian Foundation for Basic Research (project no. 03-03-33128).

REFERENCES

1. *Spravochnik po rastvorimosti: Troinye mnogokomponentnye sistemy* (Reference Book of Solubility: Ternary Multicomponent Systems), Kafarov, V.V., Ed., Moscow: Akad. Nauk SSSR, 1963, vol. 2, books 1, 2.
2. Bakeeva, M.I. and Akimova, I.P., *Tr. Khim.-Metall. Inst. Akad. Nauk Kaz. SSR* (Alma-Ata), 1969, no. 9, pp. 113–118.
3. Nikurashina, N.I. and Il'in, K.K., *Zh. Fiz. Khim.*, 1972, vol. 46, no. 3, pp. 660–666.
4. Kolker, A.M., Krestov, G.A., and Klopov, V.I., *Zh. Fiz. Khim.*, 1976, vol. 50, no. 9, pp. 2432–2433.
5. Anosov, V.Ya., Ozerova, M.I., and Fialkov, Yu.Ya., *Osnovy fiziko-khimicheskogo analiza* (Fundamentals of Physicochemical Analysis), Moscow: Nauka, 1976.
6. Sinegubova, S.I., Il'in, K.K., Cherkasov, D.G., *et al.*, *Zh. Prikl. Khim.*, 2004, vol. 77, no. 12, pp. 1945–1949.
7. *Khimicheskaya entsiklopediya* (Chemical Encyclopedia), Knunyants, I.L., Ed., Moscow: *Sovetskaya Entsiklopediya*, 1988–1998, vols. 1–5.
8. *Spravochnik po rastvorimosti: Binarnye sistemy* (Reference Book of Solubility: Binary Systems), Kafarov, V.V., Ed., Moscow: Akad. Nauk SSSR, 1961, vol. 1, book 1.
9. Krestov, G.A., *Termodinamika ionnykh protsessov v rastvorakh* (Thermodynamics of Ionic Processes in Solutions), Leningrad: Khimiya, 1984, p. 174.
10. Belgorodskaya, N.M., Shadskii, S.V., and Poltoratskii, G.M., Abstracts of Papers, *5-ya Respublikanskaya konferentsiya molodykh uchenykh-khimikov* (5th Republican Conf. of Young Chemists), Tallinn, 1983, p. 205.
11. Belousov, V.P. and Panov, M.Yu., *Termodinamika vodnykh rastvorov neelektrolitov* (Thermodynamics of Aqueous Solutions of Nonelectrolytes), Leningrad: Khimiya, 1983.

Russian Journal of Applied Chemistry, Vol. 78, No. 3, 2005, pp. 399–403. Translated from Zhurnal Prikladnoi Khimii, Vol. 78, No. 3, 2005, pp. 403–407.
Original Russian Text Copyright © 2005 by Prikhod'ko, Komarova, Gorelova, Gorlova, Bondaletov.

PHYSICOCHEMICAL STUDIES OF SYSTEMS AND PROCESSES

Liquid–Vapor Phase Equilibria in Binary and Ternary Subsystems Constituted by Pyrocondensate Components from the Pyrolysis of Straight-Run Naphtha

S. I. Prikhod'ko, L. F. Komarova, O. M. Gorelova, N. N. Gorlova, and V. G. Bondaletov

Polzunov Altai State Engineering University, Barnaul, Russia
Tomsk Polytechnic University, Tomsk, Russia

Received November 20, 2003; in final form, September 2004

Abstract—Liquid–vapor equilibrium in the binary subsystems of the ethylbenzene–*o*-xylene–α-methylstyrene–*p*-vinyltoluene–dicyclopentadiene–indene system was predicted using UNIFAC group model and studied experimentally. To assess the reliability of parameters, the liquid–vapor equilibrium was studied experimentally in the ternary systems and compared with the calculated data.

Petroleum polymeric resins (PPRs) are widely used as a rosin substitute and in production of paintwork materials, wooden fiberboards, adhesive solutions, and anticorrosive coatings. Waste and side products of petroleum-chemical production, and, first of all, liquid products of hydrocarbon pyrolysis are the raw materials for PPR production [1].

Unsaturated reactive hydrocarbons are the resin-forming components. Their content in the raw material should be no less than 30%. In addition, it may contain admixtures decreasing the quality of the polymers synthesized, which makes necessary appropriate pretreatment of the raw material.

The requirements to the raw material are determined by the properties of PPR formed, polymerization conditions, and catalytic systems used, which allows selection of the method of the raw material preparation. As a rule, distillation is used to separate pyrocondensate components.

Ethylene and propylene monomers are gaseous products of the pyrolysis of hydrocarbon raw material, in particular, straight-run naphtha. The residual (after ethylene or propylene separation) pyrocondensate contains a lot of components with unsaturated bonds, namely, styrene, α- and β-methylstyrenes, vinyltoluenes, allylbenzene, dicyclopentadiene, indene, and indan in a mixture with such solvents as toluene, xylene, ethylbenzene, propylbenzene, and cumene. High-molecular-weight resinous products can also be present. This pyrocondensate can be used to prepare PPRs (which are the components of varnishes and paints) after removal of solvents, dicyclopentadiene (DCPD), and tars.

Although DCPD is unsaturated hydrocarbon and hence a resin-forming component, its presence in the raw-material is undesirable. The point is that powdered aluminum chloride used as a catalytic system polymerizes DCPD to form insoluble in PPR cross-linked polymers, which is inadmissible. High content of DCPD favors formation of the intensely colored polymerizate, which is also undesirable.

With regard to the above facts, the raw material preparation includes distillation of highly resinous liquid products of the pyrolysis of straight-run naphtha with high content of oligomers and monomers.

To develop the process for distillation separation of the pyrocondensate, we have analyzed the known properties of substances comprising PPR [2, 3]. Many components of the mixture to be separated have close boiling point, which makes it impossible to solve the task by the elementary distillation. The mixture contains thermolabile components, capable of polymerization, which requires addition of polymerization inhibitors and reduced pressure in the distillation column.

Preliminarily, we reduced the dimension of the initial concentration space by discrimination of certain homologs, isomers, and components with low concentrations [4]. To develop the process for separation by distillation, the system ethylbenzene (EB)-*o*-xylene (*o*-X)–styrene (S)–α-methylstyrene (α-MS)–*p*-vinyl-

1070-4272/05/7803-0399© 2005 Pleiades Publishing, Inc.

Table 1. Liquid–vapor equilibrium in binary systems at P = 760 mm Hg

System	Mole fraction of component 1		bp, °C	System	Mole fraction of component 1		bp, °C
	X, in liquid	*Y*, in vapor (calcd.)			*X*, in liquid	*Y*, in vapor (calcd.)	
α-MS (1)–DCPD (2)	0.0500	0.0533	166.4	*o*-X (1)–I (2)	0.0500	0.1243	178.5
	0.1000	0.1062	166.3		0.1000	0.2303	175.6
	0.2000	0.2106	166.1		0.2000	0.4018	170.5
	0.3000	0.3131	165.8		0.3000	0.5349	165.9
	0.4000	0.4135	165.6		0.4000	0.6414	162.0
	0.5000	0.5120	165.4		0.5000	0.7286	158.4
	0.6000	0.6087	165.3		0.6000	0.8013	155.1
	0.7000	0.7043	165.2		0.7000	0.8628	152.1
	0.8000	0.7998	165.2		0.8000	0.9153	149.2
	0.9000	0.8972	165.2		0.9000	0.9606	146.6
α-MS (1)–I (2)	0.0500	0.0885	179.9	S (1)–α-MS (2)	0.0400	0.0681	164.4
	0.1000	0.1636	178.6		0.0600	0.1007	163.8
	0.2000	0.2914	176.4		0.1000	0.1631	162.8
	0.3000	0.4024	174.6		0.2000	0.3046	160.3
	0.4000	0.5038	173.0		0.3000	0.4281	158.0
	0.5000	0.5986	171.5		0.4000	0.5370	155.9
	0.6000	0.6880	170.2		0.5000	0.6337	153.9
	0.7000	0.7727	168.9		0.6000	0.7205	152.1
	0.8000	0.8528	167.7		0.7000	0.7991	150.3
	0.9000	0.9285	166.5		0.8000	0.8710	148.6
					0.9000	0.9376	147.1
α-MS (1)–*o*-X (2)	0.0500	0.0856	164.0	S (1)–DCPD (2)	0.0500	0.0850	165.2
	0.1000	0.1646	162.7		0.1000	0.1643	163.9
	0.2000	0.3062	160.2		0.2000	0.3075	161.7
	0.3000	0.4304	157.9		0.3000	0.4329	158.8
	0.4000	0.5406	155.6		0.4000	0.5430	156.6
	0.5000	0.6390	153.5		0.5000	0.6404	154.4
	0.6000	0.7272	151.5		0.6000	0.7269	152.4
	0.7000	0.8065	149.6		0.7000	0.8045	150.5
	0.8000	0.8778	147.7		0.8000	0.8748	148.8
	0.9000	0.9421	145.9		0.9000	0.9394	147.1
o-X (1)–DCPD (2)	0.0500	0.0820	165.3	S (1)–I (2)	0.0500	0.1456	177.5
	0.1000	0.1601	164.1		0.1000	0.2560	174.2
	0.2000	0.3047	161.5		0.2000	0.4184	168.9
	0.3000	0.4341	159.0		0.3000	0.5385	164.8
	0.4000	0.5490	156.6		0.4000	0.6350	161.2
	0.5000	0.6503	154.2		0.5000	0.7165	158.1
	0.6000	0.7390	151.9		0.6000	0.7872	155.2
	0.7000	0.8163	149.7		0.7000	0.8497	152.6
	0.8000	0.8838	147.7		0.8000	0.9053	150.1
	0.9000	0.9437	145.8		0.9000	0.9551	147.8

toluene (*p*-VT)–DCPD–indene (I) was taken as an initial system.

The development of a process for separation of the above mixture requires the information on the liquid–vapor equilibrium (LVE) in binary systems constituting the total system. For the initial seven-component mixture, the number of binary subsystems is 21. In the case of *o*-X–S and EB–S subsystems, the data on LVE are known [5, 6]. For certain systems, such data were obtained experimentally by the method described in [5] at P = 760 mm Hg; for the other subsystems, they were predicted using UNIFAC group model.

In the first stage of the experimental study, the initial substances were purified [7–9]. The purity was

checked by the boiling point, refractive index, and chromatographically on an LKhM-80 chromatograph, model 1, with a catharometer as a detector and with temperature programming. A Separon porous polymer was used as a chromatographic phase. The composition of the mixture analyzed was calculated by normalization of the peak areas with regard to correction factors [10].

The liquid–vapor equilibrium we studied as the dependence of the boiling point on the liquid–phase composition under the isobaric conditions (*X*–*P*–*T*) at 760 mm Hg using the Gillespie circulating device [5].

The binary systems were prepared gravimetrically with 10^{-4} g error at 100–120-g weight of samples. The boiling point was measured with a mercury thermometer with a 0.1°C error, with correction for the pressure and projecting mercury column [5, 9].

The results of the experiments on LVE are listed in Table 1.

For certain binary subsystems, the data on LVE were obtained using UNIFAC group model. Fragmentation of molecules into group components was standard and unambiguous; the parameters of group interaction were taken from [11].

To describe and predict the liquid–vapor equilibrium in binary and multicomponent systems and to calculate the distillation process, we examined the temperature dependence of the vapor pressure of the individual substances using the Antoine equation:

$$\log P_0 = A - B/(C + T),$$

where P_0 is the vapor pressure (mm Hg); *T*, temperature (°C); *A*, *B*, and *C*, constants of Antoine equation.

The Antoine equation constants were calculated using published data [12] within the 5–760 mm Hg range; their values are shown in Table 2.

All the seven binary systems are azeotropic, some of them are close to ideal, and the other systems approach the square diagonal at low or high concentrations of the low-boiling component. Typical dependences of the vapor composition on the liquid composition in the systems studied are shown in the figure.

The experimental, previously published, and predicted (UNIFAC) data on LVE in the binary systems we described by the Wilson equation [13] using the software developed at the Karpov Research Physicochemical Institute. The Wilson parameters obtained are so-called major dimensionless parameters.

Table 2. Constants of Antoine equation

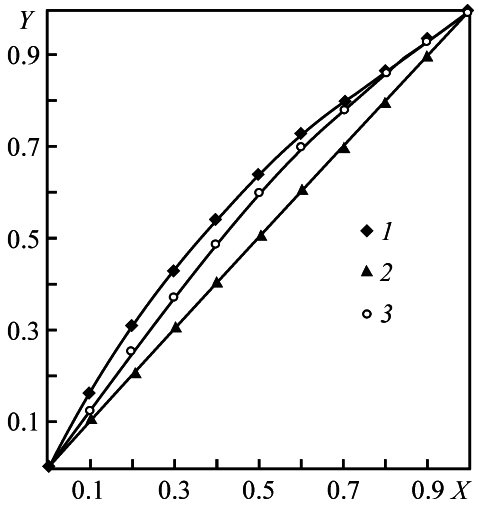
Substance	*A*	*B*	*C*
Styrene	7.512352	1840.9970	251.9218
o-Xylene	7.006800	1476.4478	213.6900
Ethylbenzene	7.029640	1469.6550	218.0385
Dicyclopentadiene	8.207209	2433.8280	290.3344
p-Vinyltoluene	7.401321	1844.3210	232.9937
Indene	8.109468	2428.2820	282.8192
α-Methylstyrene	8.700804	2819.1690	319.0038

A set of parameters of binary interaction lies in the basis of the mathematical model of the liquid–vapor phase area for the mixture studied; it is necessary for performing computer experiments on distillation. The parameters of binary interaction for binary subsystems of the mixture studied (λ_{12} and λ_{21}) and the average and maximal boiling point deviations are listed in Table 3.

As seen, the calculated data reasonably agree with the experimental and pseudo-experimental data, since the average and maximal deviations do not exceed 1% relative to the boiling point of the components.

The reliability of the parameters obtained can be assessed by simulation of LVE in the ternary systems and comparison of the results obtained with the experimental data.

The LVEs in the ternary subsystems were studied experimentally. For a limited number of points of the



The liquid–vapor equilibrium in binary systems at *P* = 760 mm Hg. (*X*, *Y*) composition (mole fraction scale) of vapor and liquid, respectively. System: (*1*) S–I, (*2*) α-MS–DCPD, and (*3*) DCPD.

Table 3. Data on mathematical description of LVE

System	Data	Wilson parameters		ΔT_{av}, °C	ΔT_{max}, °C
		λ_{12}	λ_{21}		
S–DCPD	Experimental	1.4830	0.5768	0.54	0.85
S–I	″	0.4237	1.5180	0.48	0.76
S–α-MS	″	1.1940	0.7671	0.52	0.84
S–*p*-VT	UNIFAC	1.2700	0.7425	0.21	0.46
o-X–EB	″	0.8046	1.2430	0.22	0.36
o-X–DCPD	Experimental	2.0300	0.3343	0.46	0.73
o-X–I	″	0.6214	1.3820	0.45	0.76
o-X–α-MS	″	1.5270	0.5617	0.42	0.85
o-X–*p*-VT	UNIFAC	0.6013	1.4050	0.12	0.64
EB–DCPD	″	2.0440	0.3075	0.15	0.70
EB–I	″	0.6782	1.3530	0.23	0.50
EB–α-MS	″	0.7638	1.1950	0.25	0.70
EB–*p*-VT	″	0.8400	1.0860	0.18	0.40
DCPD–I	Experimental	0.6446	1.6470	0.53	0.98
DCPD–α-MS	″	0.4932	1.6020	0.50	0.85
DCPD–*p*-VT	UNIFAC	0.5368	1.5930	0.33	0.60
α-MS–I	Experimental	0.3751	1.7440	0.46	0.80
p-VT–I	UNIFAC	0.3547	1.8860	0.18	0.33
α-MS–*p*-VT	″	0.7790	1.2470	0.35	0.68
o-X–S	[5, 6]	1.7150	0.5833	0.51	0.96
EB–S	[5, 6]	1.564	0.6937	0.44	0.87

Table 4. Equilibrium compositions of the liquid and vapor phases in the ternary systems at P = 760 mm Hg

System	Component content, mol %						T_b^{ex}, °C	T_b^c, °C
	in liquid			in vapor (calculated)				
	X_1	X_2	X_3	Y_1	Y_2	Y_3		
S (1)–DCPD (2)–I (3)	35.52	10.60	53.88	58.18	6.46	35.36	163.2	164.0
	31.70	20.21	48.09	52.83	15.17	32.00	164.8	165.2
	20.70	47.91	31.39	33.28	46.23	20.49	167.2	166.5
	20.00	78.00	2.00	27.66	71.26	1.08	163.5	163.1
	10.00	75.00	16.00	15.00	75.78	9.22	167.2	168.0
o-X (1)–α-MS (2)–I (3)	30.10	10.50	59.40	50.90	10.92	38.17	164.4	164.7
	87.50	6.00	6.50	93.77	3.65	2.58	146.8	147.4
	64.00	31.00	5.00	76.95	20.77	2.27	151.0	151.9
	80.12	1.32	18.56	91.29	0.87	7.83	149.1	149.9
	21.10	42.10	36.80	35.13	40.84	24.03	163.9	164.5
o-X (1)–S (2)–DCPD (3)	3.56	10.85	85.59	5.46	17.33	77.21	162.8	163.8
	67.34	6.22	26.44	77.37	6.39	16.24	149.4	150.1
	45.20	28.10	26.70	51.78	30.94	17.28	150.3	151.0
	33.10	35.33	31.57	38.40	40.60	21.00	151.3	152.0
	84.03	2.40	13.57	90.04	2.18	7.78	146.7	146.9
S (1)–α-MS (2)–I (3)	38.56	51.34	10.10	53.47	40.87	5.66	157.1	158.0
	5.61	45.22	49.17	11.28	51.21	37.51	149.6	150.0
	70.12	8.34	21.54	83.50	5.87	10.63	151.9	152.3
	12.33	56.21	31.46	21.84	56.38	21.78	165.5	165.2
	30.11	29.17	40.72	47.97	26.52	25.50	161.8	162.5

concentration field, we determined the dependences of the boiling points on the liquid phase composition by the above method. The results are listed in Table 4.

To simulate liquid–vapor equilibria in the ternary systems, we used a set of the parameters of the binary interaction in the Wilson equation (Table 3). The calculated boiling points in the ternary systems are listed in Table 4. As seen, the calculated boiling points reasonably agree with the experiment (the difference between them does not exceed of 1°C), confirming the reliability of the parameters of the binary interaction.

CONCLUSIONS

(1) The parameters of the Antoine equation for calculating the vapor pressure of the individual substances at various temperatures were determined.

(2) The mathematical description of the experimental and pseudo-experimental data was performed. The set of parameters of binary interaction between the components of the mixture studied was obtained, allowing simulation of the liquid–vapor equilibrium in multicomponent systems and realization of computer experiments on distillation.

(3) The reliability of the binary interaction parameters was confirmed by the comparison of the calculated and experimental values describing the equilibrium in the ternary systems.

REFERENCES

1. Dumskii, Yu.V., *Neftepolimernye smoly* (Petroleum Polymeric Resins), Moscow: Khimiya, 1988.
2. *Spravochnik khimika* (Chemist's Handbook), Nikol'skii, B.P. Ed., Moscow: Khimiya, 1963, vol. 2.
3. *Catalog Handbook of Fine Chemicals*, Aldrich, 1990.
4. Zharov, V.T. and Serafimov, L.A., *Fiziko-khimicheskie osnovy distillyatsii i rektifikatsii* (Physicochemical Principles of Distillation and Rectification), Leningrad: Khimiya, 1975.
5. Kogan, V.B., Fridman, V.M., and Kafarov, V.V., *Ravnovesie mezhdu zhidkost'yu i parom* (Liquid–Vapor Equilibrium), Moscow: Nauka, 1966, vols. 1, 2.
6. Lyudmirskaya, G.S., Barsukova, T.A., Bogomol'nyi, A.M., *et al*., *Ravnovesie zhidkost'–par* (Liquid–Vapor Equilibrium), Bogomol'nyi, A.M., Ed., Leningrad: Khimiya, 1987.
7. Gordon, A.J. and Ford, R.A., *The Chemist's Companion. A Handbook of Practical Data, Techniques, and References*, New York: Wiley–Interscience, 1972.
8. Becker, H., Berger, W., Domschke, G., *et al*., *Organikum. Organisch-chemisches Grundpraktikum*, Berlin: Wissenschaften, 1990, vols. 1, 2.
9. Weissberger, A. and Proskauer, E.S., *Organic Solvents. Physical Properties and Methods of Purification*, Riddick, J.A. and Toops, E.E., Eds., New York: Interscience, 1955.
10. Vyakhirev, D.A. and Shushunova, A.F., *Rukovodstvo po gazovoi khromatografii* (Guide on Gas Chromatography), Moscow: Vysshaya Shkola, 1987.
11. Wales, S.M., *Phase Equilibria in Chemical Engineering*, Boston: Butterworth, 1985.
12. Stull, D.R., Vapor Pressure of Pure Substances, *Ind. Eng. Chem.*, 1947, vol. 39, N 4, pp. 517–550.
13. Reid, R.G., Prausnitz, J.M., and Sherwood, T.K., *The Properties of Gases and Liquids*, New York: McGraw-Hill, 1977.

Russian Journal of Applied Chemistry, Vol. 78, No. 3, 2005, pp. 404–408. Translated from Zhurnal Prikladnoi Khimii, Vol. 78, No. 3, 2005, pp. 403–407.
Original Russian Text Copyright © 2005 by Gaivoronskii, Granzhan.

PHYSICOCHEMICAL STUDIES OF SYSTEMS AND PROCESSES

Solubility of Adipic Acid in Organic Solvents and Water

A. N. Gaivoronskii and V. A. Granzhan

Khimtekhnologiya State Research and Designing Institute of Chemical Engineering, Severodonetsk, Lugansk oblast, Ukraine

Received December 22, 2004

Abstract—The solubility of adipic acid in methanol, ethanol, propanol, isopropanol, *n*-butanol, *tert*-butanol, acetone, 1,4-dioxane, acetic acid, and water was measured within the 0–60°C temperature range. A sampler for determination of the temperature dependence of the solubility of solids in liquids by the isothermal method was suggested. The thermodynamic parameters of solution of adipic acid in the above solvents were calculated. The dependence of the solubility on the solvent and temperature was considered.

Adipic acid (AA) is a large-capacity product used mainly in fiber production. The solubility of solids in liquids is one of the most important process parameters and is of scientific interest for the development of the solution theory.

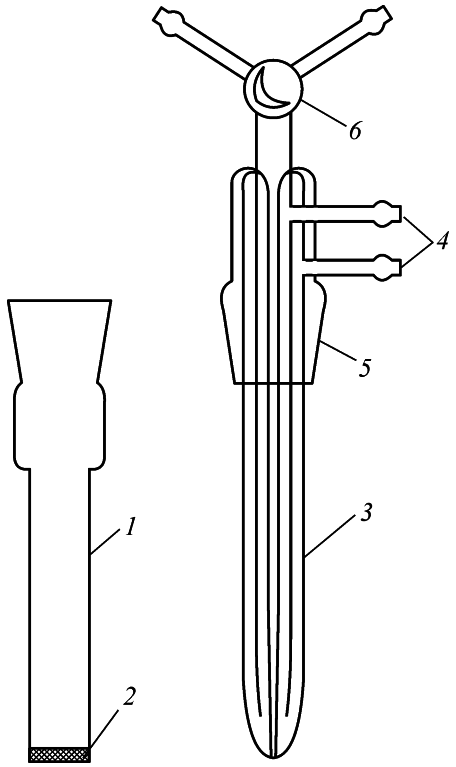
EXPERIMENTAL

Analytically pure grade adipic acid was recrystallized twice from water and dried at 120°C. Its melting point was 151.5±0.2°C, which agrees with the most reliable published data [1]. Chemically pure and analytically pure grade organic solvents were dried by standard procedures [2]. Acetone and alcohols were kept for a day over drierite and then distilled. 1,4-Dioxane was kept over KOH for two weeks, refluxed over sodium metal for a day, and then distilled. Acetic acid had mp 16.6°C after twofold freezing. The water content in solvents was no higher than (wt %): 0.04 in methanol, 0.08 in ethanol, 0.06 in propanol, 0.06 in isopropanol, 0.08 in *n*-butanol, 0.08 in *tert*-butanol, 0.02 in acetone, 0.02 in 1,4-dioxane, and 0.1 in acetic acid. The water content in acetic acid was determined using the melting point depression curve [3] and in the other solvents, by Fischer titration. Double-distilled water was used.

The AA solubility was determined by the isothermal method. The thermodynamic equilibrium between excess solid phase at the solvent was attained by continuous agitation and a constant temperature with a device consisting of a U-10 ultrathermostat and a mechanical stirrer. The stirrer was mounted on the thermostat lid.

To determine the solubility, adipic acid and a solvent were charged into 100–200-ml flasks with ground-glass stoppers. The flasks were fixed on a coupling rod and introduced into a thermostat. The flask contents were stirred by reciprocal motion of the flask, provided by a synchronous electric motor (e.g., SD-54 motor with 60 rpm rotation speed) equipped with a crank system. The temperature was kept constant to within ±0.1°C.

To measure the solubility by the isothermal method, solution samples should be taken for analysis in



Sampler: (*1*) tube, (*2*) glass frit. (*3*) temperature-controlled pipet, (*4*) connecting tubes, (*5*) conical ground-glass joint, and (*6*) stopcock.

1070-4272/05/7803-0404© 2005 Pleiades Publishing, Inc.

Table 1. Solubility of adipic acid in various solvents

Solvent	AA solubility at indicated temperature, °C					
	0	10	20	30	40	60
Water	0.000855	0.001396	0.00227	0.00377	0.00627	0.0208
Methanol	0.0218	0.0306	0.0422	0.0576	0.0775	–
Ethanol	0.01618	0.0212	0.0326	0.0453	0.0624	0.1146
Propanol	0.01014	0.01569	0.0232	0.0338	0.0485	0.0953
Isopropanol	0.01238	0.01913	0.0287	0.0422	0.0601	0.1125
Butanol	0.00861	0.01305	0.01934	0.0284	0.0411	0.0829
tert-Butanol	–	–	0.0503	0.0649	0.0825	0.1259
Acetone	0.00650	0.00941	0.01351	0.0193	0.0274	–
1,4-Dioxane	–	0.0242	0.0347	0.0487	0.0670	0.1215
Acetic acid	–	–	0.01731	0.0250	0.0362	0.0731
Ideal solubility	0.00376	0.00630	0.01009	0.01592	0.0245	0.0548

definite time intervals up to attaining the thermodynamic equilibrium (e.g., formation of the saturated solution). The solution is in contact with adipic acid crystals and should be filtered. This is done using various samplers equipped with a glass frit [4–6]. In addition, when the temperature of the solution exceeds the room temperature, it is necessary to prevent crystallization in the solution during sampling. Our sampler (see figure) solves both these problems.

The sampler consists of a tube *1* with a glass frit *2* and a temperature-controlled pipet *3*. Before sampling, tubes *4* are attached to a thermostat for attaining the temperature of the solution studied, and the pipet is inserted into tube *1* and fixed with a conical ground-glass joint *5*. After heating for 3–5 min, the sampler is introduced into the flask, and the saturated solution is sampled into the pipet through a stopcock *6* using a water-jet pump or rubber bulb. The sample is transferred into a beaker for weighing and the subsequent analysis.

The equilibrium between the solid and liquid phases in all cases was attained within less than 2 h, which follows from the constancy of AA concentration in several successively taken samples.

The concentration of AA in the saturated solution was determined gravimetrically. The volume of the solution samples was chosen so that the dry precipitate weight was 0.2–0.5 g [7]. After weighing the bottles with the solution samples, the solvent was removed by evaporation in two steps. Initially the weighing bottles were heated on a temperature-controlled plate in an exhaust hood at 50°C up to visual disappearance of the liquid. Then, AA was dried to constant weight at 80°C. Such a technique prevents the possible AA loss caused by spraying when the solution is boiled. Each solubility value is an average of three measurements. The maximal relative error in the solubility determination at a confidence probability of 0.95 is 0.5. The results of solubility determination are listed in Table 1. For comparison, the published data on the AA solubility in water are given in Table 2 [8–10].

The data on the AA ideal solubility calculated by the modified Schroeder equation [11] are listed in Table 1. As seen, the AA solubility in all the solvents studied except water exceeds the ideal solubility. The negative deviations from the ideality are substantial and may be caused by specific interactions between the solute and solvent. The enthalpies of AA solution were calculated from the temperature dependence of the solubility. The free energy of solution is

$$\Delta G = -RT\ln a. \quad (1)$$

Table 2. Solubility of adipic acid in water

T, °C	AA solubility, wt %			
	experimental	[10]	[8]	[9]
0	0.690 ± 0.003	0.79		
10	1.122 ± 0.006	0.99		
20	1.812 ± 0.009	1.87		
25	2.32 ± 0.01		2.335	
30	2.97 ± 0.01	2.91	2.974	
40	4.88 ± 0.02	4.76	4.912	4.87
50	8.31 ± 0.04			8.46
60	14.73 ± 0.07	15.25		14.96

Table 3. Activity coefficients of adipic acid in water

T, °C	AA content in water, mol per 1000 g	α	I	γ
0	0.0475	0.028	0.004	0.999
20	0.1263	0.017	0.006	0.998
40	0.351	0.010	0.010	0.997
60	1.182	0.006	0.020	0.996

Table 4. Coefficients of Eq. (3)

Solvent	A	B	C
Methanol	8.69	–0.0474	–0.00009
Ethanol	9.37	–0.0487	–0.00012
Propanol	10.36	–0.0574	–0.00011
Isopropanol	9.98	–0.0674	0.00003
Butanol	10.80	–0.0566	–0.00014
tert-Butanol	8.11	–0.0419	0.00004
Acetic acid	10.99	–0.0509	–0.00019
1,4-Dioxane	9.31	–0.0549	–0.0005
Acetone	11.44	–0.0430	–0.00022
Water	16.00	–0.0408	–0.00077

For poorly soluble, weakly dissociating substances, the activity a can be replaced by its mole fraction x [12], and then

$$\Delta G = -RT\ln x. \quad (2)$$

To check the validity of such substitution, we determined the degree of AA dissociation in water using the Ostwald dilution law. The AA dissociation constant in water was taken from Dobos handbook [13]. The α values obtained assuming the dissociation constant to be temperature-independent are given in Table 3. The solution ionic strengths I produced by the ionized fraction of AA are also listed in Table 3. The dependence of the AA activity coefficient on the solution ionic strength was determined in [14] from the solubility in water in the presence of electrolytes. The calculated activity coefficients γ are listed in Table 3. As seen, they only slightly differ from unity, and hence Eq. (2) can be used for calculating ΔG.

Since the AA dissociation constants in the chosen organic solvents should be substantially lower than in water, Eq. (2) is also applicable to the other solvents.

The temperature dependence of ΔG is approximated by a quadratic equation:

$$\Delta G = A + B(T - 273.15) + C(T - 273.15)^2. \quad (3)$$

The coefficients of Eq. (3) are listed in Table 4.

Then, using the known thermodynamic equations, we calculated ΔS and ΔH of solution (see Table 5). In all the cases, the enthalpies of solution are positive and hence the enthalpies of solvation do not exceed the enthalpies of the molecular crystal lattice. In the series of normal alcohols, the AA solubility decreases from methanol to butanol, and the enthalpy of solution increases. In other words, in the series of normal alcohols, the interaction of AA molecules with solvent molecules becomes weaker. For the most part of solvents studied, this interaction becomes weaker with increasing temperature. Thus, an interesting fact is observed: the enthalpy growth in one case is accompanied by a decrease in the solubility and in the other case, by its increase.

The enthalpy of solution characterizes only the energetic aspects of the solute–solvent interaction. However, the interaction between solvent molecules, determining the solvent structure, also changes upon dissolution; this factor also affects the dissolution. The joint analysis of the thermodynamic characteristics of AA dissolution shows that both the enthalpy and entropy components increase in the series of normal alcohols. The enthalpy component changes to a greater extent than the entropy component. As a result, the interaction between AA and alcohol molecules becomes weaker in this series. With increasing temperature, the entropy component increases faster than the enthalpy component, and ΔG decreases. Hence, the temperature affects more strongly the solution structure, whereas the alcohol molecule size affects more strongly the energy of intermolecular interactions.

For isopropyl and *tert*-butyl alcohols, the enthalpy component decreases with increasing temperature, while the entropy component increases, i.e., both components of the free energy favor dissolution, which explains their anomalous position in the alcohol series.

It should be noted that the entropy component increases to the greatest extent in water and acetone. The AA solubility in these solvents is the lowest as compared to the solubility in the other solvents studied. This means that the water and acetone structures are fairly stable at the temperatures studied and that AA dissolution actively breaks these structures. The structure of liquid *tert*-butyl alcohol is weak, and AA molecules weakly affect the level of its ordering.

Table 5. Thermodynamic characteristics of adipic acid solution in various solvents

Parameter	Temperature, °C					
	0	10	20	30	40	60
Methanol:						
ΔG, kJ mol^{-1}	8.7	8.2	7.7	7.2	6.7	–
ΔH, kJ mol^{-1}	21.6	22.1	22.6	23.1	23.6	–
$T\Delta S$, kJ mol^{-1}	12.9	13.9	14.9	15.9	17.0	–
Ethanol:						
ΔG, kJ mol^{-1}	9.4	8.9	8.3	7.8	7.2	6.0
ΔH, kJ mol^{-1}	22.7	23.4	24.0	24.8	25.5	27.1
$T\Delta S$, kJ mol^{-1}	13.3	14.5	15.7	17.0	18.3	21.1
Propanol:						
ΔG, kJ mol^{-1}	10.4	9.8	9.2	8.5	7.9	6.5
ΔH, kJ mol^{-1}	26.1	26.7	27.4	28.0	28.7	30.3
$T\Delta S$, kJ mol^{-1}	15.7	16.9	18.2	19.5	20.8	23.8
Isopropanol:						
ΔG, kJ mol^{-1}	10.0	9.3	8.7	8.0	7.3	6.1
ΔH, kJ mol^{-1}	28.4	28.2	28.1	27.9	27.6	27.2
$T\Delta S$, kJ mol^{-1}	18.4	18.9	19.4	19.9	20.3	21.1
n-Butanol:						
ΔG, kJ mol^{-1}	10.8	10.2	9.6	9.0	8.3	6.9
ΔH, kJ mol^{-1}	26.3	27.0	27.8	28.7	29.5	31.3
$T\Delta S$, kJ mol^{-1}	15.5	16.8	18.2	19.7	21.2	24.4
tert-Butanol:						
ΔG, kJ mol^{-1}	–	–	7.3	6.9	6.5	5.7
ΔH, kJ mol^{-1}	–	–	19.1	18.9	18.6	18.1
$T\Delta S$, kJ mol^{-1}	–	–	11.8	12.0	12.1	12.4
Acetic acid:						
ΔG, kJ mol^{-1}	–	–	9.9	9.3	8.6	7.3
ΔH, kJ mol^{-1}	–	–	27.1	28.2	29.3	31.9
$T\Delta S$, kJ mol^{-1}	–	–	17.2	18.9	20.7	24.6
1,4-Dioxane:						
ΔG, kJ mol^{-1}	–	8.8	8.2	7.6	7.0	5.8
ΔH, kJ mol^{-1}	–	24.6	24.9	25.2	25.4	26.1
$T\Delta S$, kJ mol^{-1}	–	15.8	16.7	17.6	18.4	20.3
Acetone:						
ΔG, kJ mol^{-1}	11.4	11.0	10.5	10.0	9.4	–
ΔH, kJ mol^{-1}	23.2	24.5	25.7	27.1	28.4	–
$T\Delta S$, kJ mol^{-1}	11.8	13.5	15.2	17.1	19.0	–
Water:						
ΔG, kJ mol^{-1}	16.0	15.5	14.9	14.1	13.1	10.8
ΔH, kJ mol^{-1}	27.1	31.4	35.9	40.5	45.2	55.2
$T\Delta S$, kJ mol^{-1}	11.1	15.9	21.0	26.4	32.1	44.4

CONCLUSIONS

(1) A sampler for studying the solubility of solids in liquids by isothermal method is developed.

(2) Solutions of adipic acid in organic solvents are characterized by negative deviation from the ideality, which suggests specific interactions between the solute and solvent.

(3) Thermodynamic characteristics of adipic acid solution depend on both the temperature and solvent.

REFERENCES

1. Babinkov, A.G., Nistratov, V.P., Larina, V.N., *et al.*, in *Termodinamika organicheskikh soedinenii, Mezhvuzovskii sbornik* (Thermodynamics of Organic Com-

pounds. Intercollegiate Collection), Gor'kii: Gor'k. Gos. Univ., 1979, no. 8, pp. 28–33.

2. Weissberger, A. and Proskauer, E.S., *Organic Solvents. Physical Properties and Methods of Purification*, Riddick, J.A. and Toops, E.E., Eds., New York: Interscience, 1955.
3. Gyenes, I., *Titration in Non-Aqueous Media*, Cohen, D., Ed., Budapest: Akademiai Kiado, 1967.
4. Polyanskaya N.L. and Polyanskii, N.G., *Zh. Fiz. Khim.*, 1982, vol. 56, no. 2, pp. 503–504.
5. Shvedov, V.P. and Zhurenkov, E.M., *Zh. Neorg. Khim.*, 1956, vol. 11, no. 7, pp. 1659–1661.
6. Gorodetskii, E.T., *Izv. Vyssh. Uchebn. Zaved., Khim. Khim. Tekhnol.*, 1980, vol. 33, no. 3, pp. 268–272.
7. Kreshkov, A.P., *Osnovy analiticheskoi khimii* (Fundamentals of Analytical Chemistry), Moscow: Khimiya, 1976, vol. 2.
8. Davies, M. and Griffithes, D.M., *Trans. Farad. Soc.*, 1953, vol. 49, no. 12, pp. 1405–1410.
9. *Spravochnik po rastvorimosti* (Handbook on Solubility), Kafarov, V.V., Ed., Moscow: Akad. Nauk SSSR, 1961, vol. 1, book 1.
10. Mullin, J.W., *Crystallization*, London: Butterworth, 1961.
11. Li, I.F., Semenov, L.V., Gaile, A.A., and Pul'tsin, M.N., *Zh. Fiz. Khim.*, 1984, vol. 58, no. 10, pp. 2435–2438.
12. Krestov, G.A. and Abrosimov, V.K., in *Termodinamika i stroenie rastvorov: Mezhvuzovskii sbornik* (Thermodynamics and Structure of Solutions: Intercollegiate Collection), Ivanovo: Ivanov. Khim.-Tekhnol. Inst., 1976, issue 3, pp. 13–28.
13. Dobos, D., *Electrochemical Data*, Budapest: Akademiai Kiado, 1978.
14. Mel'nik, V.V., Komar', N.P., Shcherban', S.N., and Slyshova, L.D., *Izv. Vyssh. Uchebn. Zaved., Khim. Khim. Tekhnol.*, 1973, vol. 26, no. 8, pp. 1186–1188.

Russian Journal of Applied Chemistry, Vol. 78, No. 3, 2005, pp. 409–413. Translated from Zhurnal Prikladnoi Khimii, Vol. 78, No. 3, 2005, pp. 413–417.
Original Russian Text Copyright © 2005 by Pestova, Myund, Khripun, Prigaro.

PHYSICOCHEMICAL STUDIES OF SYSTEMS AND PROCESSES

Polythermal Study of the Systems $M(ClO_4)_2$–H_2O (M^{2+} = Mg^{2+}, Ca^{2+}, Sr^{2+}, Ba^{2+})

O. N. Pestova, L. A. Myund, M. K. Khripun, and A. V. Prigaro

St. Petersburg State University, St. Petersburg, Russia

Received January 28, 2005

Abstract—The solubility polytherms in the systems for which the cryoscopic data are lacking were measured. The structural models of the electrolyte solutions were discussed on the basis of the solubility polytherms.

Unique properties of eutectic compositions of solutions and salt melts make them important for metallurgical applications. They are widely used in modern technology [1] to improve the quality of metal production and obtain materials with prescribed properties. The overwhelming majority of physicochemical studies concerning formation of natural salts is based on the thermodynamic principles and, as theoretical background, uses the phase diagrams of water–salt systems corresponding in the composition to natural brines [2, 3].

The solubility polytherm is the dependence of the freezing point of a solution on the solute concentration. In the certain range of the concentrations (dilute solution) it is described by the Raoult's law, which is valid for any binary system. However, as the solute concentration is increased, a deviation from the linearity followed by a change in the behavior of the curve above the eutectic concentrations is observed, i.e., the freezing point of a solution increases with the concentration. In addition, the supereutectic branch can have additional singularities, depending on how many (two or more) crystal hydrates of the salt are formed.

The solubility isotherm represents in the graphical form the Raoult's law and the deviations from it and reflects the dynamics of structural processes in a solution as its concentration increases. The developed structural models of aqueous electrolyte solutions are based on comparison of the character of changes in physicochemical properties with the solubility polytherm of the salt. With this approach, regions of the predominance of different structures corresponding to the structure of the solid phase crystallizing from the solution with dereasing temperature can be revealed over the entire concentration range of existence of the solution [4].

In the region of subeutectic concentrations, water as a major component determining the solution structure crystallizes from the solution upon cooling. On cooling of supereutectic solutions, the solute in the form of a crystal hydrate or anhydrous salt precipitates as the bottom phase. This means that in the supereutectic region a certain structural type of the associates termed cybotactic group [4, 5] dominates in a solution. Water becomes a solute and a component of this group. For some salts, the solubility polytherm, apart from the eutectic, contains one or several singularities (peritectics). They separate the region of the concentrated solution into the regions of predominance of the corresponding crystal hydrates.

The way of formation and the origin of the eutectic remain still an open question stimulating much interest. The whole set of the data obtained by many researchers shows the existence of two principal concepts. According to one of them, the eutectic is a mechanical mixture of solid components (in the case of an aqueous solution, these are crystals of salt and ice) having constant composition and melting point. According to this traditional concept, the eutectic is formed owing to the short-term local deviations from the average composition of the solution. According to the other concept, the eutectic is a chemical compound [1].

As known, the solution of eutectic composition (at 25°C) is characterized by the following specific properties.

(1) The isotherms of the viscosity and proton magnetic relaxation rate (which is the measure of the water mobility), taken for solutions of salts forming crystal hydrates, undergo an inversion in the region of eutectic concentrations, which is not the case for solutions of anhydrous salts [6, 7].

1070-4272/05/7803-0409© 2005 Pleiades Publishing, Inc.

(2) The isotherms of the specific electrical conductivity of electrolyte solutions pass through a maximum at a concentration coinciding within 1–2 wt % with the eutectic composition. The maximum is observed for solutions of salts forming crystal hydrates. The presence of the maximum is due to structural transformation of the surrounding medium, rather than to strengthening of the interaction between the ions moving in it. This is noted in all the relevant papers [1, 5].

(3) The X-ray diffractometry of salt solutions shows that the solution of eutectic concentration is the most disordered [8].

(4) It is significant that, at concentrations corresponding to the eutectic composition, the relative partial molal entropy of water passes through a maximum, which is a consequence of the strongest disordering [9, 10].

According to the results of this study, the probable cause of the behavior of all the characteristics (presence of singularity points in the curves) is the change in the kind of the prevailing structures in the solution in the eutectic point [11–14].

In this study, we determined the previously unknown solubility polytherms of the systems $M(ClO_4)_2$–H_2O, where M^{2+} is Mg^{2+}, Ca^{2+}, Sr^{2+}, or Ba^{2+}. We determined the eutectic concentrations of the solutions, the composition of the crystal hydrates, and the fraction of 'free water' (i.e., water not incorporated in crystal hydrate) in the eutectic. The correlation between the latter parameter and the water activity in the eutectic solution at 25°C is discussed.

The choice of the salts was dictated by the following reasons. As known, the perchlorate ion has a highly symmetrical (tetrahedral) structure, low electron-donor and proton-acceptor power, and relatively low polarizability; it is very stable in solution. Owing to these properties, the perchlorate ion does not form any acido complexes with the metal cations and is not involved in the protolytic reactions of water in the vicinity of perchlorate ion, which makes its salts convenient objects for study.

EXPERIMENTAL

The metal perchlorates were prepared from the corresponding analytically pure grade carbonates (Ca^{2+}, Sr^{2+}, Ba^{2+}, and Mg^{2+}) and 57% perchloric acid (chemically pure grade) and were recrystallized two times from distilled water. Concentrated solutions of the salts were prepared; these were analyzed for the content of metal cations and ClO_4^- anions.

The ClO_4^- content was determined by the ion-exchange chromatography with a KU-2 resin, followed by pH-metric titration of perchloric acid with a borax solution. The content of M^{2+} (M^{2+} is Ca^{2+}, Mg^{2+}) was determined by EDTA titration. The content of strontium and barium ions was determined gravimetrically after precipitation in the form of sulfates. The error in determining the concentrations did not exceed 0.5%. Less concentrated salt solutions were prepared by dilution of the concentrated stock solutions. The freezing point was determined by the visual polythermal method.

The reaction vessel was cooled with liquid nitrogen. The cooling rate was varied within 0.3–1 deg min^{-1}. The freezing points (as averaged results of three measurements) are listed in Table 1. The cryoscopic data at $T > 0$°C were taken from a reference book [15].

The composition of the crystal hydrates $Mg(ClO_4)_2 \cdot nH_2O$ and $Ca(ClO_4)_2 \cdot mH_2O$ formed from the above solutions was determined in the region of negative temperatures. Test solutions of the known concentration belonging to the supereutectic region were cooled until the formation of crystals, which were then filtered at a temperature from –18 to –20°C. After that, the sample was passed through an ion-exchange column packed with KU-2 resin and the content of the ions was determined by pH-metric titration with a borax solution. The analysis results were used to calculate the number of molecules in the crystal hydrate.

According to the polythermal measurements, all the solutions studied, except that of strontium perchlorate, form simple eutectic systems. Barium perchlorate has an eutectic at a higher temperature (–33°C) compared to the other salts (Table 2). Apparently, this is due to weak interaction of this salt with water.

The eutectic compositions of calcium, strontium, and barium perchlorate solutions are close (4.2, 4.0, and 4.02 mol/1000 g H_2O, respectively). Magnesium perchlorate differs from this group in that it forms an eutectic at m = 3.35 mol/1000 g H_2O, which is not surprising because of its stronger tendency to hydration. Then, at first glance, it would seem that the eutectic concentration depends on the cation. However, as will be shown below, the main attention must be paid to the number of water molecules incorporated in the crystal hydrate crystallizing in the supereutectic region.

Table 1. Freezing points of aqueous solutions T_f at different concentrations m

$Mg(ClO_4)_2$		$Ca(ClO_4)_2$		$Sr(ClO_4)_2$		$Ba(ClO_4)_2$	
m, mol/1000 g H_2O	T_f, °C	m, mol/1000 g H_2O	T_f, °C	m, mol/1000 g H_2O	T_f, °C	m, mol/1000 g H_2O	T_f, °C
0.65	–5.8	0.67	–5.4	0.80	–6.8	0.50	–5.7
0.76	–7.5	0.70	–6.2	1.17	–10.7	0.75	–7.4
1.32	–12.5	0.91	–6.6	1.38	–12.4	1.01	–10.1
1.55	–16	1.37	–10.8	1.58	–16	1.50	–13.7
1.76	–18.8	1.52	–12.9	1.66	–17.7	1.99	–17.1
1.99	–22.8	1.85	–17.5	1.95	–22	2.49	–21.2
2.20	–27	2.06	–20.6	2.11	–25	2.99	–25
2.28	–28.8	2.30	–25.7	2.33	–30.1	3.49	–27.6
2.40	–30.8	2.47	–27.1	2.50	–33.2	4.02	–33.6
2.51	–33.8	2.77	–32.7	3.00	–40.5	4.40	–23
2.70	–38	2.91	–34.0	3.50	–50.7	4.88	–8.9
2.78	–39.3	3.17	–38.5	4.00	–66.5	5.17	0.6
3.00	–46.2	3.23	–42.1	4.25	–62.5	5.47	13
3.25	–57	3.33	–45.4	4.50	–61.7	5.70	25
3.31	–60	3.70	–57.2	5.00	–60	5.90	30
3.48	–68.6	3.82	–61.6	5.50	–59.4	6.32	40
3.69	–42.3	4.03	–70.8	5.75	–57.9		
3.81	–28.4	4.20	–74.6	6.25	–35		
3.93	–11.4	4.47	–65.1	6.50	–30.3		
4.05	0	4.58	–62.8	7.23	–16.5		
4.13	10	4.77	–57.2	8.14	0		
4.57	25	5.02	–49.6	8.97	10		
4.75	40	5.50	–31.9	10.76	25		
		7.12	0	12.02	35		
		7.77	20				
		8.89	40				

The solubility polytherm of strontium perchlorate also has the specific features deserving more detailed discussion. Strontium perchlorate is one of the least studied perchlorates of Group II metals. The unusual property of this salt consists in its tendency to vitrify in the region of supereutectic concentrations. This is reflected by a dashed line drawn in the range from 5.50 to 6.25 mol/1000 g H_2O (Fig. 1). In this concentration region, the solution became thick on cooling and its viscosity grew until the onset of vitrification. Above 6.25 mol/1000 g H_2O, the solid crystal hydrate precipitated again as the bottom phase. Evidently, the 5.5 m solution corresponds to the peritectic composition.

There is an opinion in the literature that, in solutions of strontium perchlorate (capable of forming acido complexes), saturated with respect to tetrahydrate, the amount of water not involved in the coordination with Sr^{2+} is very small, and even this water is hardly free [16]. Latysheva [16] believes that this water, most probably, plays the role of bridges binding $Sr(H_2O)^{2+}$ and ClO_4^- ions into a continuous viscous structure, which is responsible for the tendency of solutions to high degree of supersaturation. James and Culter [17] studied the spectral properties of $Sr(ClO_4)_2$ and calculated the parameters of the perchlorate ion

Table 2. Eutectic concentrations m_{eut}, number of water molecules in crystal hydrate n, fraction of free water in the eutectic N_w, and water activity in the eutectic at 298 K for the systems studied

Substance	m_{eut}	n	N_w	$a_{w_{298}}$
$Mg(ClO_4)_2$	3.45	8	0.503	0.499
$Ca(ClO_4)_2$	4.20	6	0.546	0.520
$Sr(ClO_4)_2$	4.00	6	0.568	0.599
$Ba(ClO_4)_2$	4.02	4	0.710	0.691
$Zn(ClO_4)_2$	3.05	7	0.615	0.632
$Cd(ClO_4)_2$	3.40	6	0.630	0.607
$Hg(ClO_4)_2$	3.90	6	0.581	0.575
$HClO_4$	6.60	4	0.520	0.560

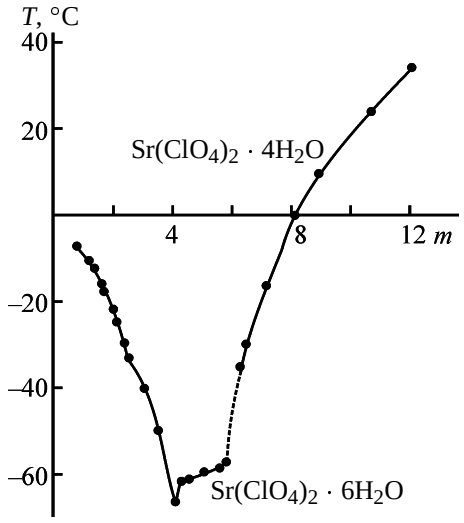


Fig. 1. Solubility polytherm of strontium perchlorate: (*T*) freezing point of solution and (*m*) molal concentration.

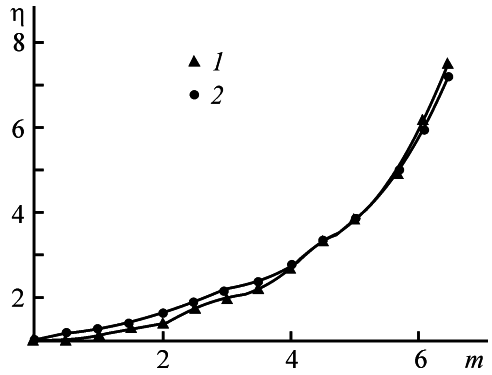


Fig. 2. Relative dynamic viscosity η of the strontium perchlorate–water system. (*m*) Molal concentration. Temperature (°C): (*1*) 25 and (*2*) 50.

from the data obtained. They came to the conclusion that contact ion pairs exist at concentrations above 5.5 mol/1000 g H_2O. As seen, the opinions of different authors about the speciation of this salt in solution are contradictory. However, the concentrations at which the specific effects are observed are the same.

We believe that complexes and ion pairs in concentrated strontium perchlorate solutions can be formed by the so-called structure-induced processes occurring owing to the solution microheterogeneity, rather than by the commonly accepted traditional mechanism [18]. From our viewpoint, the existence of two structural modifications, α-$Sr(ClO_4)_2$ and β-$Sr(ClO_4)_2$, of this salt, revealed by X-ray phase analysis, is the most probable origin of the vitrification. Though these are the modifications of the solid anhydrous salt, it may be suggested that the similar structural modifications exist for the crystal hydrate whose structure dominates in the vitrification region. This assumption can account for the observed vitrification. This phenomenon is also known for solutions of other salts, i.e., calcium chloride, which also have several structural modifications and is readily vitrified.

It is important that the difference between the eutectic and peritectic temperatures in the polytherm is small, i.e., there exists a fairly large region of the structural constancy in which the parameters and properties do not change. This assumption is also supported by Fig. 2 illustrating the dependences of the relative dynamic viscosity on the concentration of strontium perchlorate solutions within the range 0.5–6.5 mol/1000 g H_2O at 25 and 50°C. As seen, the two dependences corresponding to different temperatures are very close, i.e., increasing the temperature of the strontium perchlorate solution affects only slightly the relative dynamic viscosity. However, the curves show inversion, although it is observed in a certain region rather than point; the curves coincide in the region from 4 to 5.6 mol/1000 g H_2O, i.e., between the eutectic and the peritectic. Because the eutectic and peritectic solutions in the strontium perchlorate–water system considered here and in other similar systems tend to vitrify and have a low freezing point, determination of the bottom phase compositions becomes difficult.

The number of water molecules incorporated in the crystal hydrate is related to the fraction of free water N_w by

$$N_w = (55.51 - nm_e)/55.51,$$

where n is the number of water molecules in the crystal hydrate; m_e, eutectic concentration (mol/kg H_2O); and 55.51, the amount of water (moles) in 1 kg of the water.

In this study, the numbers n for magnesium and calcium perchlorates were determined to be 8 and 6, respectively. The published data [15] show that the obtained values are the common hydration numbers of the salts of these metals. For example, in calcium halides, chlorate, iodate, and nitrite $n = 6$, and in magnesium iodide, most closely resembling perchlorate, $n = 8$.

The calculated N_w values, 0.503 and 0.546 for magnesium and calcium perchlorates, respectively, are close to the water activities $a_{w_{298}}$ at 298 K, 0.499 and 0.525, respectively, obtained from the water vapor pressure in [19]. This similarity has been observed previously [20].

For barium and strontium perchlorates, the compositions of the bottom phases formed just above the eutectic concentration are unknown. The phase diagram of strontium perchlorate has a peritectic. We suggest that, in the range 4–5.5 mol/1000 g H_2O, the hexahydrate is the major structure. In such a case, $N_w = 0.570$, which is close to the corresponding value of the water activity at 298 K (0.599). In the barium perchlorate polytherm, there are no other singularities in the supereutectic region. Therefore, it may be suggested that, just as the concentration of 4 mol/1000 g H_2O is exceeded, the tetrahydrate becomes the major structure. Then, $N_w = 0.710$ and the corresponding value of the water activity is equal to 0.691.

The fraction of water not incorporated in the crystal hydrate (free water) in the eutectic is close to the value of water activity in the eutectic solution. Thus, N_w and $a_{w_{298}}$ in the eutectic solution at 25°C are interconnected through the number of water molecules *n* in the crystal hydrate precipitating into the bottom phase just above the eutectic concentration. This relationship is confirmed for the perchlorate solutions of zinc group metals and for perchloric acid. The results obtained are listed in Table 2.

CONCLUSION

In eutectic solutions, the fraction of water not incorporated in the crystal hydrate (free water) is close to the water activity in the eutectic solution at 298 K. This makes it possible, in particular, to estimate the composition of the crystal hydrate precipitated in the supereutectic region.

REFERENCES

1. Zalkin, V.M., *Priroda evtekticheskikh splavov i effekt kontaktnogo plavleniya* (Nature of Eutectic Alloys and Contact Melting Effect), Moscow: Metallurgiya, 1987.
2. Charykova, M.V., and Charykov, N.A., *Termodinamicheskoe modelirovanie protsessov evaporitovoi sedimentatsii* (Thermodynamic Modeling of Evaporite Sedimentation), St. Petersburg: Nauka, 2003.
3. Kurilenko, V.V., *Sovremennye basseiny evaporitovoi sedimentatsii* (Modern Basins of Evaporite Sedimentation), St. Petersburg: Sankt-Peterb. Gos. Univ., 1997.
4. Stewart, G.H., *Ind. J. Phys.*, 1932, vol. 7, pp. 603–615.
5. Khripun, M.K., Lilich, L.S., and Efimov, A.Yu., in *Problemy sovremennoi khimii koordinatsionnykh soedinenii* (Problems of Modern Coordination Chemistry), Leningrad: Leningr. Gos. Univ., 1983, issue 7, pp. 58–102.
6. Lilich, L.S., and Khripun, M.K., *Rastvory kak khimicheskie sistemy* (Solutions as Chemical Systems), St. Petersburg: Sankt-Peterb. Gos. Univ., 1994, p. 61.
7. Penkina, N.V., and Smaev, V.N., *Zh. Fiz. Khim.*, 1974, vol. 48, no. 3, pp. 637–640.
8. Petrun'kin, S.P., Trostin, V.N., and Krestov, G.A., *Izv. Vyssh. Uchebn. Zaved., Khim. Khim. Tekhnol.*, 1986, vol. 29, no. 6, pp. 15–19.
9. Khripun, M.K., Karavan, S.V., and Bulgakov, S.A., in *Problemy khimii koordinatsionnykh soedinenii* (Problems of Coordination Chemistry), Leningrad: Leningr. Gos. Univ., 1987, issue 8, pp. 123–141.
10. Puchkov, L.V., and Sargaev, P.M., *Zh. Prikl. Khim.*, 1973, vol. 46, no. 12, pp. 2637–2639.
11. Khripun, M.K., Myund, L.A., Baranova, G.I., *et al.*, *Zh. Obshch. Khim.*, 1998, vol. 68, no. 4, pp. 550–555.
12. Khripun, M.K., Chervonenko, K.Yu., Kiselev, A.A., and Khripun, A.V., *Zh. Obshch. Khim.*, 2001, vol. 71, no. 1, pp. 25–35.
13. Khripun, M.K., Chervonenko, K.Yu., Kiselev, A.A., and Petranovskii, V.P., *Zh. Obshch. Khim.*, 2002, vol. 72, no. 6, pp. 932–937.
14. Kiselev, A.A., Zubtsov, M.K., and Khripun, M.K., *Vestn. Sankt-Peterb. Gos. Univ., Ser. 4*, 2002, issue 3, pp. 51–54.
15. Kirgintsev, A.N., Trushnikova, L.N., and Lavrent'eva, V.G., *Rastvorimost' neorganicheskikh veshchestv v vode: Spravochnik* (Solubility of Inorganic Substances in Water: Handbook), Leningrad: Khimiya, 1972.
16. Latysheva, V.A., *Vodno-solevye rastvory, sistemnyi podkhod* (Water–Salt Solutions. A Systematic Approach), St. Petersburg: Sankt-Peterb. Gos. Univ., 1998.
17. James, D. and Culter, P., *New J. Chem.*, 1986, vol. 39, pp. 137–147.
18. Samoilov, O.Ya., *Struktura vodnykh rastvorov elektrolitov i gidratatsiya ionov* (Structure of Aqueous Solutions of Electrolytes and Ion Hydration), Moscow: Akad. Nauk SSSR, 1957.
19. Robinson, R.A., and Stokes, R.H., *Electrolyte Solutions. The Measurement and Interpretation of Conductance, Chemical Potential, and Diffusion in Solutions of Simple Electrolytes*, London: Butterworths, 1959.
20. Mikulin, A., *Voprosy fizicheskoi khimii rastvorov elektrolitov* (Problems of Physical Chemistry of Electrolyte Solutions), Leningrad: Khimiya, 1968, pp. 46–48.

Russian Journal of Applied Chemistry, Vol. 78, No. 3, 2005, pp. 414–421. Translated from Zhurnal Prikladnoi Khimii, Vol. 78, No. 3, 2005, pp. 418–424.
Original Russian Text Copyright © 2005 by Dzyaz'ko, Rozhdestvenskaya, Pal'chik.

SORPTION AND ION-EXCHANGE PROCESSES

Recovery of Nickel Ions from Dilute Solutions by Electrodialysis Combined with Ion Exchange

Yu. S. Dzyaz'ko, L. M. Rozhdestvenskaya, and A. V. Pal'chik

Vernadsky Institute of General and Inorganic Chemistry, National Academy of Sciences of the Ukraine, Kiev, Ukraine

Received April 14, 2004; in final form, December 2004

Abstract—The possibility of using inorganic ion exchangers based on zirconium hydrophosphate and a weakly cross-linked cation-exchange resin for continuous purification of dilute nickel-containing solution by a combined method of electrodialysis and ion exchange was studied.

A promising technique for recovery of Ni^{2+} ions from dilute solutions is a combined method of electrodialysis and ion exchange (electrodeionization), which enables continuous purification of a solution, simultaneously with reagent-free regeneration of the ion exchanger used [1–3]. Unfortunately, the use of this method is limited by the low mobility of Ni^{2+} in the ion exchanger phase [4] and by the possibility of formation of sparingly soluble hydroxo compounds on the surface of the ion-exchange materials [5]. In addition, presence of hardness ions markedly lowers the degree of recovery of heavy metal ions [6].

To overcome these difficulties, it is primarily necessary to choose an appropriate ion exchanger. The factors predetermining the performance of an ion-exchange material in electrodeionization processes are its high sorption capacity and selectivity, as well as a high mobility of absorbed ions. Among the known ion exchangers, the best in kinetic properties are weakly cross-linked sulfonic ion-exchange resins [7]. High sorption capacity and selectivity with respect to heavy metal ions are exhibited by inorganic ion exchangers such as, e.g., zirconium hydrophosphate (ZHP) [8].

The aim of this study was to assess the possibility of using these ion exchangers in electrodeionization purification of Ni^{2+}-containing solutions.

EXPERIMENTAL

ZHP samples with varied content of functional groups were synthesized for the study. The procedure used to obtain sample ZHP-1.1 included preparation of a hydrogel of zirconium dioxide by the reaction of a 1 M solution of $ZrOCl_2$ with an equal volume of a mixed solution containing glycerol (1.4 M), hexamethylenetetramine (2 M), and urea (2 M). The resulting hydrogel wax treated with 5 M H_3PO_4 at 373 K for 1 h. Sample ZHP-1.2 was prepared similarly, but with the concentration of urea in the solution used to precipitate zirconium dioxide equal to 6 M. In addition, the hydrogel was dried at 333 K prior to phosphatization.

The particles of the ion exchangers obtained were nearly spherical. The 0.2–0.5-mm fraction was taken for the study.

The elemental composition of the samples was determined by dissolving them in concentrated H_2SO_4, with the subsequent photometric analysis of the resulting solution [9]. The water content was found from the loss of mass by the ion exchanger after heating at 373 K for 2 h. The average pore diameter was calculated from nitrogen adsorption isotherms obtained with a Tristar 3000 adsorption analyzer [10]; the total cation-exchange capacity, concentration of cation-exchange groups, and pK of their dissociation were determined by potentiometric titration [11, 12].

The procedures described in [13] were used to study the Dowex 50WX-2 sulfonic ion exchanger (0.2–0.5-mm fraction) containing a cross-linking agent in an amount of 2%. Its total exchange capacity was determined by treating the resin with 0.1 M NaOH for 20 min with the subsequent titration of the excess alkali. The apparent volume of the H^+- and Ni^{2+}-substituted forms was determined volumetrically. The content of water in the resin was evaluated by the loss of mass upon drying over P_2O_5.

To study the kinetics of sorption of Ni^{2+} ions by

1070-4272/05/7803-0414 © 2005 Pleiades Publishing, Inc.

the "thin bed" method, a weighed portion of the sample was placed in the form of a single bed between two grids fixed at the end of a glass tube 1.5 cm in diameter, connected to a pump. Then, a 0.1 M solution of $NiSO_4$, acidified with H_2SO_4 to pH 3, was passed through the ion exchanger bed in the direct-flow mode for a certain time. The linear flow velocity of the solution was 0.14 m s^{-1}. After the required time elapsed, the ion exchanger was washed with deionized water and nickel(II) ions were eluted with an H_2SO_4 solution. The content of desorbed Ni^{2+} ions in the eluate was determined by the atomic-absorption method on a PUY UNICAM SP 9 spectrophotometer.

The sorption isotherms were obtained by treating the ion exchangers under static conditions with individual $NiSO_4$ and $CaCl_2$ solutions with initial concentrations of 1×10^{-4}–0.1 M. The ion exchanger : solution volume ratio was 1 : 100, and the time of contact, 24 h. After the equilibrium was established, the solution was separated from the ion exchanger and the concentration of the Ni^{2+} and Ca^{2+} in it was determined by the atomic-absorption method. The ion exchanger was treated with 2 M H_2SO_4 and the content of the ions in the eluate was found similarly.

The electrodeionization was studied on a setup comprising a three-chamber electrodialysis cell, three independent liquid circuits, current source, and measuring instruments (Fig. 1) [2]. Platinum electrodes were in the side compartments of the cell, and the ion exchanger bed, in the central compartment. The effective area of the membranes and electrodes was 24 cm^2 (1.5×6 cm), and the ion exchanger bed thickness, 1 cm. CMI-7000 cation-exchange and AMI-7001 anion-exchange heterogeneous membranes (Membrane International) or two Nafion-117 cation-exchange homogeneous membranes (Du Pont) were used.

To avoid a change in the volume of the organic ion exchanger in the course of electrodeionization, the resin was preliminarily converted into a partially nickel-substituted form by treatment with a 0.1 M solution of $NiSO_4$ at a 1 : 100 resin-to-solution volume ratio. The inorganic ion exchanger, whose volume remains unchanged upon conversion into the substituted form, was not treated preliminarily with a nickel-containing solution.

The $NiSO_4$ solution or a combined solution containing Ni^{2+}, Ca^{2+}, and Mg^{2+} ions was fed from the input vessel into the central compartment in the direct-flow mode. The forming solution was delivered into the output vessel. Acid solutions were circulated through the electrode compartments at a flow velocity of 1.67×10^{-2} m s^{-1}. The volume of the acid solution

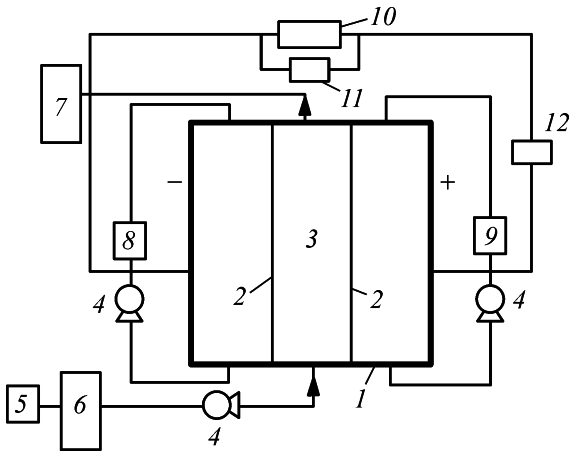


Fig. 1. Electrodeionization setup: (*1*) three-chamber cell, (*2*) ion-exchange membranes, (*3*) ion exchanger bed, (*4*) pumps, (*5*) thermostat, (*6*) vessel with the starting solution, (*7*) vessel with a purified solution, (*8*) vessel with the catholyte, (*9*) vessel with the anolyte, (*10*) current source, (*11*) voltmeter, and (*12*) ammeter.

in each compartment was 200 cm^3. In a separately specified case, the catholyte was additionally acidified in the course of the experiment in order to prevent formation of a sparingly soluble precipitate in the cathode compartment and on the membrane on the cathode side.

The electrodeionization purification of solutions was performed in the voltage stabilization mode. The solutions in the cathode and anode compartments and at the outlet of the central compartment were sampled at fixed intervals of time.

The sorption and electrodeionization were studied at 298 ± 0.05 K.

The parameters of the ion exchangers are listed in Table 1. It can be seen that the ZHP samples synthesized have a developed mesoporous structure. The total cation-exchange capacity of these materials considerably exceeds that of Dowex WX-2. At the same time, the content of water in the cation-exchange resin and inorganic ion exchangers is approximately the same. In contrast to the case of ZHP, conversion of the organic cation exchanger into the Ni^{2+}-substituted form is accompanied by a substantial decrease in its volume.

It should also be noted that ZHP-1.1 sample, which contains a certain amount of hydrophosphate ions in addition to dihydrophosphate ions, contains a larger amount of P(V) than ZHP-1.2. Nevertheless, the total cation-exchange capacity of ZHP-1.1 is substantially lower, and the p*K* value of functional groups, higher than those of ZHP-1.2.

Table 1. Parameters of ion exchanger samples

Parameter	ZHP-1.1	ZHP-2.2	Dowex 50WX-2
Zr : P molar ratio	0.53 : 1	0.92 : 1	–
Specific surface area, $m^2\ g^{-1}$	90	100	–
Average pore diameter, nm	24.1	11.5	–
Water content, wt %	67	65	70
Total cation-exchange capacity of the H^+ form for Na^+, mol m^{-3}	2900	3100	600
$H_2PO_4^-$ concentration, mol m^{-3}	1200	1500	–
HPO_4^{2-} concentration, mol m^{-3}	500	–	–
pK_1	2.2	2	1
pK_2	4.2	3.8	–
Loss of volume upon conversion of ion exchanger from H^+ into Ni^{2+}-substituted form, %	–	–	30

Table 2. Effective diffusion coefficients of Ni^{2+}

Ion exchanger	$\bar{c}_{Ni,\infty}$, mol m^{-3}	$\bar{d}$, m	$t_{0.5}$, s	$\bar{D}_{Ni}$, $m^2\ s^{-1}$
ZHP-1.1	1.18×10^3	1.75×10^{-4}	5.40×10^3	4.20×10^{-14}
ZHP-1.2	1.21×10^2	1.75×10^{-4}	4.78×10^2	4.80×10^{-13}
Dowex 50WX-2	3.00×10^2	3.10×10^{-4}	10.00	7.20×10^{-11}

The structural-sorption properties of ion exchangers determine the rate of ion exchange. Figure 2 shows kinetic curves of Ni^{2+} sorption, which have the form of the dependence of $\bar{c}_{Ni}/\bar{c}_{Ni,\infty}$ on the time of sorption t, where $\bar{c}_{Ni}$ and $\bar{c}_{Ni,\infty}$ are the contents of Ni^{2+} reached after a certain time and at $t = \infty$, respectively. Preliminarily, it was established that the rate of sorption from a 0.1 M solution of $NiSO_4$ is independent of the flow velocity. This suggests that the sorption rate at the given solution concentration is controlled by internal diffusion [12].

The effective diffusion coefficient $\bar{D}_{Ni}$ was calculated by the equation [12]

$$\bar{D}_{Ni} = 0.03\bar{d}/4t_{0.5}, \quad (1)$$

where $t_{0.5}$ is the exchange half-time, and $\bar{d}$ is the particle diameter.

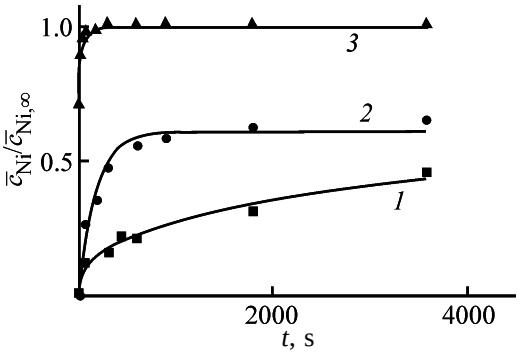


Fig. 2. Degree of completion of Ni^{2+} sorption, $\bar{c}_{Ni}/\bar{c}_{Ni,\infty}$, on (*1*) ZHP-1.1, (*2*) ZHP-1.2, and (*3*) Dowex 50WX-2 ion exchangers vs. time t.

The values of $\bar{c}_{Ni,\infty}$, $t_{0.5}$, and $\bar{d}$, as well as the effective diffusion coefficients of Ni^{2+}, calculated by Eq. (1), are listed in Table 2. The diameter of resin particles was evaluated taking into account the change in volume: in conversion into the Ni^{2+}-substituted form, a 30% decrease in volume corresponds to a decrease in the particle diameter by a factor of 1.13.

Table 2 shows that the mobility of Ni^{2+} in a weakly cross-linked ion-exchange resin considerably exceeds that in inorganic ion exchangers. This is due to the fact that water filling voids in resins of this kind retains a more or less liquid structure and absorbed ions can freely move in the liquid [12]. In ion exchangers of the ZHP type, water molecules are mostly associated with functional groups via hydrogen bonds [14]. In this case, the ions sorbed are transferred by hoppings from one group to another. The higher mobility of cations in ZHP-1.2 ion exchanger, compared to ZHP-1.1, is apparently associated with the higher acidity of the functional groups and, according-

ly, with a shorter distance between the dissociated groups.

Further studies were carried out with ion exchangers in which the mobility of Ni^{2+} is the highest: Dowex 50WX-2 and ZHP-1.2. Figure 3 shows Ni^{2+} and Ca^{2+} sorption isotherms in the form of dependences of the equivalent fraction of M metal ions in the ion exchanger phase, $\bar{\gamma}_M$, on the equivalent fraction of M in solution, γ_M. The quantity $\bar{\gamma}_M$ was calculated by the formula

$$\bar{\gamma}_M = \frac{z_M \bar{m}_M}{z_M m_M + z_H \bar{m}_H}, \quad (2)$$

where $\bar{m}$ is the molal concentration of cations in the ion exchanger; z, charge; and subscript H corresponds to hydrogen ions.

The concentration of H^+ in the ion exchanger was calculated from the total cation-exchange capacity (Dowex 50WX-2) or from the concentration of dissociated groups at certain pH values (ZHP-1.2). The equivalent fraction of metal ions in solution was determined using a formula similar to (2).

As seen from Fig. 3, the sorption isotherms for Dowex 50WX-2 are typical of strongly acidic ion exchangers: the $\bar{\gamma}_M$–γ_M curves steeply ascend at low solution concentrations. In the case of a moderately acidic ion exchanger ZHP-1.2, a significant increase in sorption is observed in more concentrated solutions. Nevertheless, the inorganic ion exchanger absorbs mostly Ni^{2+} in dilute solutions. For the ion-exchange resin, the differences in the sorbability of Ni^{2+} and Ca^{2+} become more pronounced as the solution concentration increases.

Also, we examined the possibility of electrodeionization purification of Ni^{2+}-containing solutions with ZHP-1.2 and Dowex 50WX-2 ion exchangers. In the first set of experiments, heterogeneous membranes (cation-exchange CMI-7000 and anion-exchange AMI-7001, Membrane International) were used to separate the cathode and anode spaces from the central compartment. A 3 M solution of HCl was circulated through the cathode compartment, and a 3 M solution of H_2SO_4, through the anode compartment. The solution being purified contained 0.17 or 1 mol m^{-3} of $NiSO_4$. The flow velocity of the solution was 1.46×10^{-3} m s^{-1}, and the cell voltage, 10 V.

The results obtained are listed in Table 3 and shown in Fig. 4, which illustrates the dependence of the amount of Ni^{2+} in the catholyte, $n_{Ni,c}$, on the time of electrodeionization. As seen from Fig. 4 and

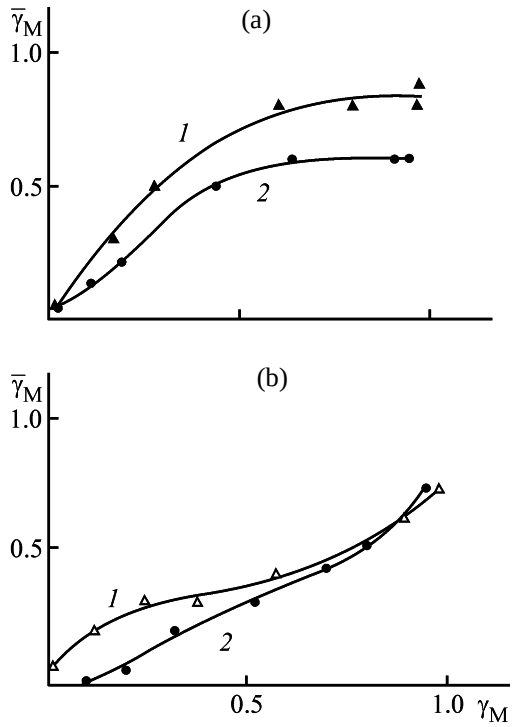


Fig. 3. Sorption isotherms of (*1*) Ni^{2+} and (*2*) Ca^{2+} from individual solutions for (a) Dowex 50WX-2 and (b) ZHP-1.2 ion exchangers. ($\bar{\gamma}_M$) Equivalent fraction of metal ions in the ion exchanger and (γ_M) equivalent fraction of metal ions in solution.

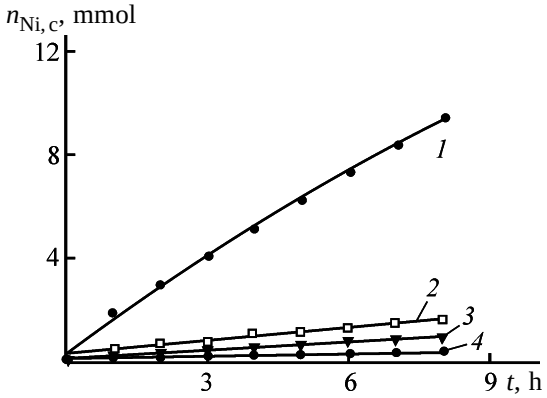


Fig. 4. Amount of Ni^{2+} in the catholyte, $n_{Ni,c}$, vs. time t of electrodeionization of individual solutions containing (*1*, *3*) 1 and (*2*, *4*) 0.17 mol m^{-3} of Ni^{2+}. Ion exchanger: (*1*, *2*) Dowex 50WX-2 and (*3*, *4*) ZHP-1.2.

Table 3, for the cation-exchange resin, the rate of transfer of Ni^{2+} into the cathode compartment somewhat decreased during the first 2 h, with the current simultaneously increasing. This was, apparently, due to a certain decrease in the concentration of metal ions in the ion exchanger phase. Further, the flux of Ni^{2+} into the catholyte and the current remained unchanged. No deposit was formed on the cation-exchange mem-

Table 3. Electrodeionization recovery of Ni^{2+} from solutions of various compositions

Parameter	ZHP-1.2		Dowex 50WX-2		
Initial content of ions in solution being purified, mol m^{-3}	Ni^{2+} 0.17	Ni^{2+} 1.00	Ni^{2+} 1.17	Ni^{2+} 1.00	Ni^{2+} 1.00, Ca^{2+} 1.00, Mg^{2+} 0.50
Linear flow velocity of solution being purified, m s^{-1}	1.46×10^{-3}	1.46×10^{-3}		1.46×10^{-3}	4.10×10^{-3}
Experiment duration, h	8	8	8	8	~48
Cell voltage, V	10	10		10	5
Current density, A m^{-2} (without additional acidification of catholyte)	16	Decreased from 66 to 37 V	Increased from 68 to 119 V in 2 h and then stabilized	Increased from 84 to 128 V in 2 h and then stabilized	Increased from 20 to 36 V in 2 h and then remained unchanged for 41 h, after which decreased to 6 V in 5 h
pH of dialyzate (without additional acidification of catholyte)	2.5	2.5	2.5	2.5	During the first 48 h remained equal to 4 and then increased to 9 in the course of 5 h
Degree of removal of Ni^{2+}, %	42	12	>99	92	12
Apparent current efficiency by Ni^{2+}, %	7.1	4.8	3.7	19.2	23.8
grad $\bar{E}$, V m^{-1}	820	820	820	820	320
c_{Ni}, mol m^{-3}	0.135	0.940	0.085	0.540	0.830
Theoretically calculated fluxes of Ni^{2+} through solution, mol m^{-2} s^{-1}:					
N_{Ni}^{migr}	5.52×10^{-6}	3.86×10^{-5}	3.48×10^{-6}	2.21×10^{-5}	1.32×10^{-5}
N_{Ni}^{dif}	3.08×10^{-6}	2.14×10^{-5}	1.94×10^{-6}	1.23×10^{-5}	3.79×10^{-5}

brane. An analysis of the material balance demonstrated that the amount of Ni^{2+} absorbed by the ion exchanger in unit time is equal to the amount of Ni^{2+} arriving at the cathode compartment. The acidification of the solution formed in the central compartment was due to diffusion of the acid across the anion-exchange membrane [2, 15].

In the case of the ZHP-1.2 ion exchanger and a $NiSO_4$ concentration of 1 mol m^{-3}, both the rate of Ni^{2+} transfer across the cation-exchange membrane and the current slightly decrease in the course of time. This is, apparently, due to conversion of the ion exchanger into the cation-substituted form, and also to formation of a deposit on the cation-exchange membrane. At a lower solution concentration, the flux of Ni^{2+} into the catholyte and the current remained virtually unchanged. In all cases, no reduction of Ni^{2+} at the cathode was observed.

As seen from Table 3, the most effective is the organic weakly cross-linked cation exchanger. With this resin, the highest degree of solution purification and the highest current efficiency are achieved. Therefore, we assessed the possibility of using this material for continuous recovery in a direct-flow mode of Ni^{2+} ions from a combined solution containing, in addition, hardness ions.

In these experiments, Nafion-117 cation-exchange membranes were placed between the central compartment and electrode chambers. The use of these membranes is due to the need to preclude the concentration polarization at low voltages and to provide a lower acidity of the solution being purified. A 1 M solution of HCl was circulated through the cathode chamber, and a 1 M solution of H_2SO_4, through the anode chamber. Every 20 h, a 10 cm^3 portion of concentrated HCl was added to the catholyte. The electrodeionization was performed continuously for 80 h at 5 V and a flow velocity of the solution being purified equal to 4.10×10^{-3} m s^{-1}. The efficiency of electrodeionization with ion-exchange resins increases with the flow velocity of the solution being purified [3]. In this connection, the solution flow velocity was

raised when passing from an individual solution to a combined solution.

Figure 5 shows how $n_{Ni,c}$ depends on the time of electrodeionization (solid lines). It can be seen that not only Ni^{2+} but also Ca^{2+} and Mg^{2+} arrived at the catholyte. No reduction of Ni^{2+} at the cathode or formation of a deposit in the central compartment was observed. The current density increased from 20 to 36 A m^{-2} during the first 2 h and then remained unchanged. The acidity of the dialyzate was constant during the experiment (pH 4).

If the catholyte was not additionally acidified, Ni^{2+} reduction commenced at the cathode after approximately 43 h because of the decrease in the concentration of the acid in the cathode compartment. In the process, the current decreased, and the pH of the solution in the central compartment increased dramatically (Table 3), which was accompanied by intensive formation of hydroxo compounds of Ni^{2+} on the membranes and ion exchanger particles. The amount of Ni^{2+} in the catholyte decreased because of the deposition of Ni^{2+} onto the cathode, and the rate of transfer of Ca^{2+} and Mg^{2+} into the cathode chamber diminished virtually to zero (Fig. 5, dotted lines).

The results obtained enable certain estimates of the transport of Ni^{2+} into the catholyte. Under conditions of forced convection, the flux of Ni^{2+} across the cation-exchange membrane, $\bar{\bar{N}}_{Ni}$, associated with the transport through the solution, is determined by migration of ions in the solution bulk, N_{Ni}^{migr}, and by diffusion across the layer of the solution at the membrane surface, N_{Ni}^{dif} [16]:

$$\bar{\bar{N}}_{Ni} = N_{Ni}^{migr} + N_{Ni}^{dif}. \quad (3)$$

The diffusion flux exceeds that associated with migration by a factor γ, where γ is the charge ratio of the cation and anion. In the case of a binary symmetric electrolyte $NiSO_4$, $\gamma = 1$ and, consequently, $\bar{\bar{N}}_{Ni} = 2N_{Ni}^{migr}$ (the current does not reach its limiting value) or $\bar{\bar{N}}_{Ni} = 2N_{Ni}^{dif}$ (limiting and "overlimiting" current). In turn,

$$N_{Ni}^{migr} = u_{Ni}\bar{\bar{c}}_{Ni}\,\mathrm{grad}\,\bar{E}, \quad (4)$$

$$N_{Ni}^{dif} = k_{Ni}(c_{Ni} - c_{Ni}^{0}), \quad (5)$$

where u_{Ni} and k_{Ni} are the mobility and mass-transfer coefficient of Ni^{2+}; c_{Ni} and c_{Ni}^{0}, concentrations of cations in the solution bulk and the near-membrane layer, respectively; and $\mathrm{grad}\,\bar{E}$, the voltage drop across the central compartment of the cell.

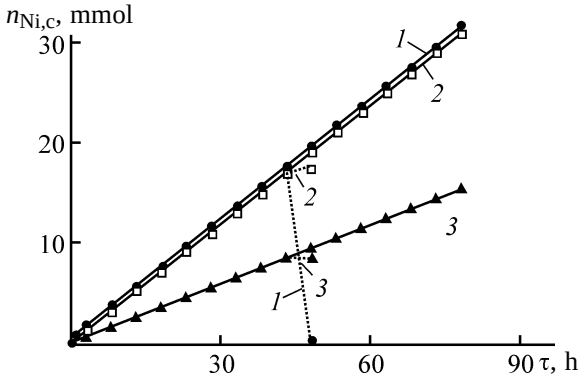


Fig. 5. Amount of metal ions in the catholyte, $n_{Ni,c}$, as a function of the time τ of electrodeionization of a combined solution with (solid lines) and without (dashed lines) additional purification. Dowex 50WX-2 resin. Cation: (*1*) Ni^{2+}, (*2*) Ca^{2+}, and (*3*) Mg^{2+}.

The value of $\mathrm{grad}\,\bar{E}$ was calculated by the formula

$$\mathrm{grad}\,\bar{E} = \frac{E(E_c - E_a)}{l}, \quad (6)$$

where E, E_c, and E_a are the cell voltage and potentials of the cathode and anode, respectively; and l, width of the central compartment.

In this calculation, the voltage drop in the rather concentrated solutions filling the compartments and in membranes whose thickness is considerably less than 1 mm was disregarded. As indicated by voltammetric measurements, $E_c + E_a$ is 1.8 V.

The thickness δ of the near-membrane layer can be found from an empirical relationship [12]

$$\delta = 0.05\,d^{0.16}(w/v)^{-0.84}, \quad (7)$$

where w and v are the linear flow velocity and viscosity of the solution. With account of the fact that $k_{Ni} = D_{Ni}/\delta$ (D_{Ni} is the diffusion coefficient of Ni^{2+} in solution), $D_{Ni} = 6.49 \times 10^{-10}$ $m^2\,s^{-2}$, $v = 8.99 \times 10^{-7}$ $m^2\,s^{-2}$ [18], the mass-transfer coefficients for Ni^{2+} are 2.28×10^{-5} ($w = 1.46 \times 10^{-3}$ m s^{-1}) and 5.50×10^{-5} m s^{-1} ($w = 4.10 \times 10^{-3}$ m s^{-1}).

The concentrations c_{Ni} were evaluated as average solution concentrations at the inlet and outlet of the central compartment (Table 3). The migration fluxes were calculated using Eq. (4), taking into account that $u_{Ni} = 4.99$ $m^2\,V^{-1}\,s^{-1}$ [18], and the diffusion fluxes corresponding to the limiting conditions were found

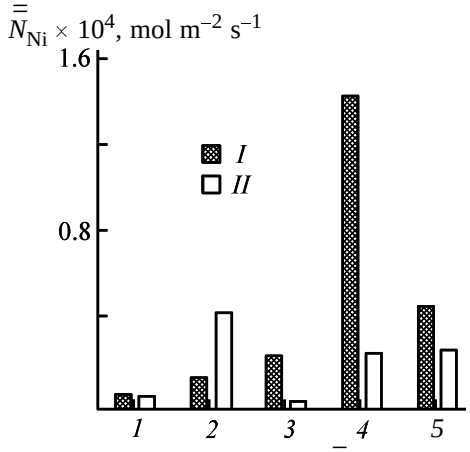


Fig. 6. Ni^{2+} flux into the catholyte, $\bar{\bar{N}}_{Ni}$, associated with transport (*I*) through ion exchanger–solution system and (*II*) through the solution. Ion exchanger: (*1, 2*) ZHP-1.2 and (*3, 5*) Dowex 50WX-2. Solution (mol m^{-3}): individual, containing (*1, 3*) 0.17 and (*2, 4*) 1 Ni^{2+}; and (*5*) a combined solution containing 1 Ni^{2+}, 1 Ca^{2+}, and 0.5 Mg^{2+}.

as $k_{Ni}c_{Ni}$. As follows from Table 3, the diffusion fluxes calculated for the case of electrodeionization at 10 V are smaller than the migration fluxes, and, consequently, the current exceeded the limiting values. At 5 V, $N_{Ni}^{dif} < N_{Ni}^{migr}$ and the electrodeionization mode corresponded to the "sublimiting" current.

The results obtained make it possible to calculate quantitatively the flux of Ni^{2+}, associated with their transport through the electrolyte across the membrane (Fig. 6). It can be seen from this figure that the calculated values of $\bar{\bar{N}}_{Ni}$, corresponding to fluxes through the solution, are somewhat lower than those obtained experimentally. At the same time, the flux through the ion exchanger–solution system, found experimentally for Dowex 50WX-2 resin, well exceeds that calculated theoretically. Hence follows that the use of ion exchangers based on zirconium hydrophosphates in electrodeionization purification of nickel-containing solutions is inexpedient, because ions are mostly transferred through solution as a result of the low mobility of Ni^{2+} in the ion exchanger phase.

The use of weakly cross-linked ion-exchange resin Dowex 50WX-2 markedly improves the efficiency of solution purification because of the possible ion transport in the ion exchanger. If the acidity of the catholyte is maintained constant, the purification in the direct-flow mode can be performed continuously. Acidification of the catholyte at regular intervals of time makes it possible to avoid formation of sparingly soluble nickel(II) hydroxo compounds on the surface of membranes and ion exchangere particles, observed in [3].

CONCLUSIONS

(1) The kinetic method was used to determine the mobility of nickel ions in a Dowex 50WX-2 weakly cross-linked cation-exchange resin and inorganic cation exchangers based on zirconium hydrophosphates. It was found that the highest diffusion coefficient of Ni^{2+} is achieved for the organic cation exchanger (7.20×10^{-11} m^2 s^{-1}), whereas for inorganic cation exchangers this parameter is 2–3 orders of magnitude lower.

(2) The sorption of Ni^{2+} and Ca^{2+} on ion exchangers was studied. It was shown that, in the case of weakly concentrated solutions, the inorganic ion exchanger mostly sorbs Ni^{2+}, whereas the ion-exchange resin equally effectively absorbs both Ni^{2+} and Ca^{2+}.

(3) The possibility of using ion exchangers for electrodeionization recovery of nickel(II) ions from solutions was assessed. It was established that, in the case of an inorganic ion exchanger, the transport of Ni^{2+} mostly occurs via solution. At the same time, the highest degree of solution purification and current efficiency are obtained with Dowex 50WX-2, which is due to predominant transport of Ni^{2+} via the ion exchanger. Thus, the main criterion to be used in selecting an ion-exchange material is the mobility of ions in its phase.

(4) Maintaining constant the acid concentration in the catholyte enables continuous electrodeionization purification of a solution and minimizes the probability of formation of sparingly soluble hydroxo compounds of Ni on the surface of ion-exchange materials.

(5) Foreign double-charged cations are transported, together with nickel(II) ions, across the bed of the Dowex 50WX-2 resin. Further development of a technique for purification of nickel-containing solutions should, apparently, be based on weakly cross-linked ion-exchange resins with a higher selectivity toward ions of this metal, compared to Dowex 50WX-2.

REFERENCES

1. Spoor, P.B., Koene, L., ter Veen, W.R., and Janssen, L.J.J., *J. Appl. Electrochem.*, 2002, vol. 32, no. 1, pp. 1–10.
2. Dzyazko, Yu.S. and Belyakov, V.N., *Desalination*, 2004, vol. 162, pp. 179–189.
3. Spoor, P.B., Koene, L., ter Veen, W.R., and Janssen, L.J.J., *Chem. Eng. J.*, 2001, vol. 85, nos. 2–3, pp. 127–135.

4. Spoor, P.B., Koene, L., and Janssen, L.J.J., *J. Appl. Electrochem.*, 2002, vol. 32, no. 4, pp. 369–377.
5. Spoor, P.B., ter Veen, W.R., and Janssen, L.J.J., *J. Appl. Electrochem.*, 2001, vol. 31, no. 5, pp. 523–530.
6. Vasilyuk, S.L., Maltseva, T.V., and Belyakov, V.N., *Desalination*, 2004, vol. 162, pp. 249–254.
7. Boyd, G.E. and Soldano, B.A., *J. Am. Chem. Soc.*, 1953, vol. 75, no. 10, pp. 6091–6099.
8. Sukharev, Yu.I. and Egorov, Yu.V., *Neorganicheskie ionity tipa fosfata tsirkoniya* (Inorganic Ion Exchangers of the Type of Zirconium Phosphate), Moscow: Energoatomizdat, 1983.
9. Charlot, G., *Les methods de la chimie analytique. Analyse quantitative minerale*, Paris: Masson, 1961, 4th ed.
10. Gregg, S.J. and Sing, K.S.W., *Adsorption, Surface Area and Porosity*, London: Academic, 1982.
11. Aivazov, B.V., *Praktikum po khimii poverkhnostnykh yavlenii i adsorbtsii* (Manual of Chemistry of Surface Phenomena and Adsorption), Moscow: Vysshaya shkola, 1973.
12. Helfferich, F., *Ionenaustauscher*, Weinheim: Chemie, 1959, vol. 1.
13. Marhol, M., *Ion Exchangers in Analytical Chemistry. Their Properties and Use in Inorganic Chemistry*, Prague: Academia, 1982.
14. Slearfield, A. and Kalnins, J.M., *J. Inorg. Nucl. Chem.*, 1978, vol. 40, no. 11, pp. 1933–1936.
15. Spoor, P.B., ter Veen, W.R., and Janssen, L.J.J., *J. Appl. Electrochem.*, 2001, vol. 31, no. 5, pp. 523–530.
16. Walsh, F., *A First Course in Electrochemical Engineering*, London: Alresford, 1993.
17. Koene, L. and Janssen, L.J.J., *Electrochim. Acta*, 2001, vol. 47, no. 5, pp. 695–703.
18. Parsons, R., *Handbook of Electrochemical Constants*, London: Butterworth Scientific, 1959.

Russian Journal of Applied Chemistry, Vol. 78, No. 3, 2005, pp. 422–424. Translated from Zhurnal Prikladnoi Khimii, Vol. 78, No. 3, 2005, pp. 425–427.
Original Russian Text Copyright © 2005 by Blokhin, Kaloshina, Lyubman, Murashkin.

SORPTION AND ION-EXCHANGE PROCESSES

Sorption Purification of Aqueous Ammonium Molybdate To Remove Tungsten Impurities with a Cation Exchanger Containing Pyrocatechol Functional Groups

A. A. Blokhin, L. G. Kaloshina, N. Ya. Lyubman, and Yu. V. Murashkin

St. Petersburg State Technological Institute, St. Petersburg, Russia

Received June 15, 2004

Abstract—The sorption of molybdenum(VI) and tungsten(VI) from weakly alkaline and neutral solutions with PK-S cation exchanger containing pyrocatechol functional groups was studied. The possibility of selective recovery of tungsten(VI) impurities from aqueous ammonium molybdate with PK-S resin was examined.

Tungsten impurities strongly affect the properties of metallic molybdenum. Among techniques commonly used for molybdenum purification to remove tungsten (extraction of molybdenum from its hydrogen chloride solutions [1], sublimation of molybdenum oxychloride [2], etc.), the simplest and the most efficient is ion-exchange sorption allowing the selective removal of tungsten impurities from aqueous ammonium molybdate (AM). For example, tungsten can be removed from aqueous molybdenum-containing solutions by sorption on hydrated polyvalent metal oxides [3] or on certain anion exchangers [4]. It is known that polyhydric phenols such as pyrocatechol coordinate with molybdenum(VI) and tungsten(VI) and that the tungsten(VI) complexes are stronger than those of molybdenum(VI) [5]. Therefore, PK-S cation exchanger of the condensation type containing pyrocatechol functional groups [6] shows promise for purification of aqueous molybdate solutions to remove tungsten impurities.

In this work we tested PK-S cation exchanger containing pyrocatechol functional groups for purification of aqueous ammonium molybdate to remove tungsten(VI) impurities.

EXPERIMENTAL

In our experiments we used PK-S cation exchanger in the H^+ form with the total cation-exchange capacity of 8.7 mg-equiv g^{-1}, prepared at the Kazmekhanobr Institute, Almaty. The sorption experiments were carried out under static and dynamic conditions. In the static experiments, the sorbent (g) to liquid phase (ml) ratio was 1 : 100. The sorption time was 5–7 days. The dynamic experiments were carried out in 20-ml glass columns with the height to diameter ratio of 15 : 1. In these experiments, aqueous molybdate solutions to be purified to remove tungsten were passed through the column at a rate of 0.7–1.0 column volume per hour. The molybdenum(VI) content in solutions was determined spectrophotometrically [6]. The pH was measured on an I-120 pH meter equipped with an ESL-47-07 glass electrode and an EVP-AM-3 silver chloride reference electrode. The ion-exchange sorption of tungsten(VI) was studied with tungsten-185 tracer added as aqueous sodium tungstate. The activity (count rate) was measured on a KRK-1-01A device equipped with a BDIB-01-1 counter and a PSO2-4 scaling unit.

The acidity is the main factor governing the state of molybdenum(VI) and tungsten(VI) in aqueous solutions. The dissociation of the phenolic functional groups of PK-S cation exchanger and their coordination with metals under consideration also strongly depend on the acidity. Therefore, we first studied how the ion-exchange sorption of molybdenum(VI) and tungsten(VI) from their 0.01 M solutions containing 1 M ammonium sulfate on PK-S cation exchanger depends on pH. Figure 1 shows that molybdenum(VI) and tungsten(VI) are sorbed on PK-S not only from acidic but also from alkaline solutions and their sorption decreases with increasing pH. It seen that the sorption of tungsten(VI) starts at a higher pH than that of molybdenum. These data suggest that, in the pH range corresponding to stronger sorption of tungsten(VI), tungsten(VI) impurities can be separated from large amounts of molybdenum(VI) with PK-S cation exchanger. To check this hypothesis, we studied

1070-4272/05/7803-0422 © 2005 Pleiades Publishing, Inc.

sorption of tungsten(VI) impurities (0.01 M) from 1 M aqueous ammonium molybdate.

Figure 2 shows that PK-S cation exchanger, indeed, sorbs tungsten(VI) from aqueous solutions containing large amounts of ammonium molybdate. The plot of the tungsten sorption vs. pH passes through a maximum at pH ~ 9.

It is known that at pH 9 both molybdenum and tungsten are present in aqueous solutions in the form of monomeric anions MoO_4^{2-} and WO_4^{2-}, respectively. We believe that these anions are sorbed on PK-S cation exchanger by the mechanism of complexation with the phenolic hydroxy groups in the *ortho* position relative to each other

$$Ar(OH)_2 + MO_4^{2-} + 2H^+ \rightleftarrows ArO_2MO_2 + 2H_2O, \quad (1)$$

where Ar is the benzene ring and M is molybdenum or tungsten.

It is known that tungsten and molybdenum form strong complexes with polyhydric phenols and the complexation occurs even in alkaline solutions [5]. The phenolic groups coordinate with tungsten(VI) more strongly than with molybdenum(VI) and the tungsten complexes start to form at higher pH. As a result, the sorption of tungsten(VI) on PK-S cation exchanger start at higher pH than the sorption of molybdenum(VI) (Fig. 1). Equation (1) shows that acidification of solutions should strengthen the coordination of phenolic groups with molybdenum(VI) and tungsten(VI). Therefore, with decreasing pH, the sorption capacity of the PK-S resin for tungsten increases. However, at certain pH, the pyrocatechol groups of the resin start to coordinate with molybdenum(VI) also. Because the molybdenum(VI) content in the solutions considerably exceeds the tungsten content, molybdenum starts to displace tungsten from the resin. Furthermore, in acidification of solutions containing molybdenum(VI) and tungsten(VI), mixed Mo(VI)–W(VI) polyanions are formed at pH < 8 [8].

The coordination of the phenolic groups of PK-S resin with tungsten(VI) is manifested in the IR spectra (Fig. 3). The IR spectra of all the samples of PK-S resin contain a strong broad absorption band of bending vibrations of water molecules and phenolic OH groups (~1620 cm^{-1}) and the absorption band of C=C stretching vibrations of the benzene ring (1520 cm^{-1}) [8]. The IR spectra of PK-S resin in the H^+ form contains an absorption band of the bending vibrations of the phenolic group (1440 cm^{-1}), a broad absorption band of C–O stretching vibrations of the phenolic groups (~1300 cm^{-1}), and an absorption band of

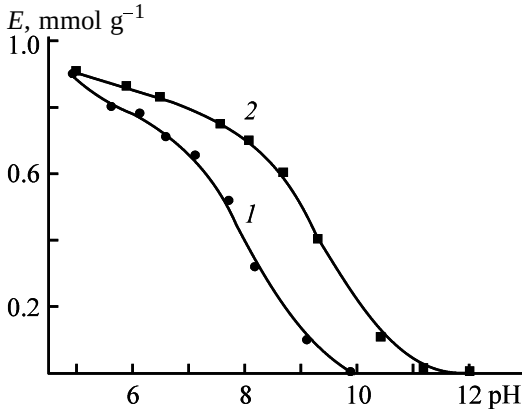


Fig. 1. Influence of pH on the sorption capacity *E* of PK-S cation exchanger for (*1*) molybdenum(VI) and (*2*) tungsten(VI) in sorption from their 0.01 M solutions containing 1 M Na_2SO_4.

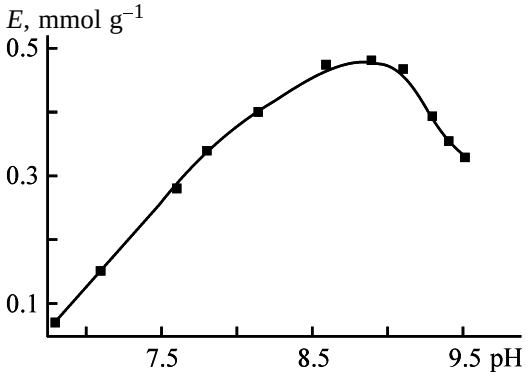


Fig. 2. Influence of pH on the sorption capacity of PK-S cation exchanger for tungsten(VI) in sorption from its 0.01 M solution containing 1 M $(NH_4)_2MoO_4$.

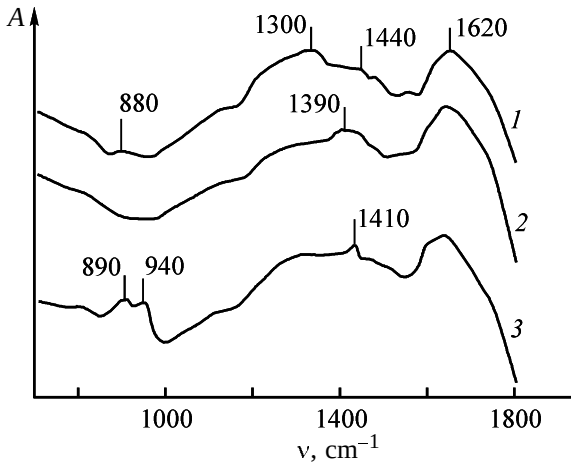


Fig. 3. IR spectra of PK-S cation exchanger in the (*1*) H^+ and (*2*) Na^+ forms, and (*3*) of PK-S resin saturated with tungsten(VI) from 0.05 M aqueous Na_2WO_4 at pH 9.0 to the sorption capacity of 1.4 mmol g^{-1}. (ν) Wave number and (*A*) absorption.

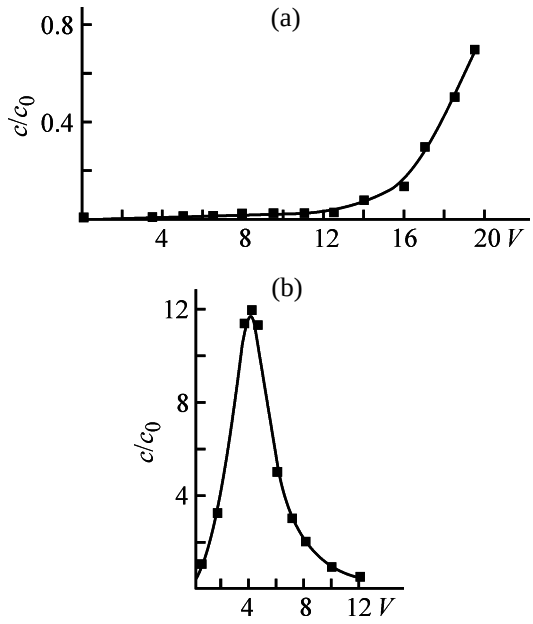


Fig. 4. (a) Breakthrough curves for tungsten(VI) sorption on PK-S resin from 1 M aqueous $(NH_4)_2MoO_4$ containing 0.1 g l^{-1} tungsten(VI) and (b) curve of tungsten(VI) desorption from PK-S with 0.5 M aqueous NaOH. (c/c_0) Ratio of the tungsten(VI) concentration at the column outlet and its concentration in the initial solution; (V) solution volume passed though the column (number of resin bed volumes).

the out-of-plane vibrations of the phenolic groups at ~880 cm^{-1}. The IR spectrum of PK-S resin in the Na^+ form contains no absorption bands at 1440, 1300 and 880 cm^{-1}, but a new absorption band of the ionized phenolic groups Ar–O^- appears at 1390 cm^{-1}. The IR spectrum of PK-S saturated with tungsten(VI) differs from that of the resin in the Na^+ form: the absorption band of vibrations of the ionized phenolic groups becomes narrower and shifts towards shorter waves by approximately 20 cm^{-1} (~1410 cm^{-1}), apparently due to coordination of the phenolic groups with tungsten. This spectrum contains also two new absorption bands of W–O vibrations at 890 and 940 cm^{-1} [10, 11].

Our dynamic sorption experiments showed that PK-S cation exchanger ensures efficient purification of concentrated aqueous ammonium molybdate to remove tungsten impurities. Figure 4 shows the breakthrough curve for tungsten sorption from aqueous solution containing 1 M $(NH_4)_2MoO_4$ (chemically pure grade) and tungsten impurities (0.1 wt % relative to molybdenum) and the curve of tungsten desorption with 0.5 M aqueous sodium alkali. The tungsten was desorbed with aqueous NaOH, since aqueous ammonia desorbs tungsten incompletely. We found that treatment of aqueous ammonium molybdate containing tungsten impurities with PK-S cation exchanger decreases the tungsten content by a factor of no less than 100. Unfortunately, PK-S cation exchanger as well as most of the other cation exchangers of the condensation type are poorly stable in alkaline solutions. As a result, in the course of desorption of tungsten from PK-S with aqueous NaOH, the resin degrades and the eluate becomes yellow-brown.

CONCLUSION

PK-S cation exchanger with the pyrocatechol functional groups selectively sorbs tungsten(VI) impurities from aqueous ammonium molybdate. The treatment of 1 M aqueous ammonium molybdate with this resin decreases the tungsten content in the solution by a factor of no less than 100.

REFERENCES

1. Sorokina, E.F. and Plyushcheva, S.V., *Tsvetn. Met.*, 1985, no. 5, pp. 67–69.
2. Kopetskii, N.F., Klimenko, G.L., and Plyushcheva, S.V., in *Poluchenie i analiz veshchestv osoboi chistoty* (Preparation and Analysis of Ultrapure Substances), Moscow: Nauka, 1973. pp. 120–126.
3. Semenov, M.I., Blokhin, A.A., Taushkanov, V.P., and Rumyantsev, V.K., *Zh. Prikl. Khim.*, 1984, vol. 57, no. 7, pp. 1501–1506.
4. Blokhin, A.A., Pak, V.I., Kopyrin, A.A., and Pirmatov, E.A., *Tsvetn. Met.*, 2000, no. 2, pp. 64–66.
5. Halmekowski, J., *Suomalaisen Tiedeakat Tormituks, Ser. AII*, 1959, no. 96, pp. 1–64.
6. Lyubman, M.Ya., Imangazieva, G.K., Makhmudova, A.U., and Simkin, E.A., *Tsvetn. Met.*, 1974, no. 10, pp. 26–30.
7. Busev, A.I., Tiptsova, V.G., and Ivanov, V.M., *Rukovodstvo po analiticheskoi khimii redkikh metallov* (Manual on Analytical Chemistry of Rare Metals), Moscow: Khimiya, 1978.
8. Pope, M.T., *Heteropoly and Isopoly Oxometalates*, Berlin: Springer, 1983.
9. Blokhin, A.A., Solodukhin, S.S., and Kopyrin, A.A., *Zh. Neorg. Khim.*, 2003, vol. 48, no. 3, pp. 505–508.
10. Bellamy, L.J., *Advances in Infrared Group Frequencies*, London: Methuen, 1968.
11. Kholmogorov, A.G., Mokhosoev, M.V., and Zonkhoeva, E.L., *Modifitsirovannye ionity v tekhnologii molibdena i vol'frama* (Modified Ion-Exchange Resins in Molybdenum and Tungsten Technology), Novosibirsk: Nauka, 1985.

Russian Journal of Applied Chemistry, Vol. 78, No. 3, 2005, pp. 425–429. Translated from Zhurnal Prikladnoi Khimii, Vol. 78, No. 3, 2005, pp. 428–432.
Original Russian Text Copyright © 2005 by Arkhangel'skaya, Krasnobryzhii, Kas'yan, Loginova, Vinogradova.

APPLIED ELECTROCHEMISTRY AND CORROSION PROTECTION OF METALS

Processes in a Nickel–Zinc Battery with a Negative Electrode Containing a Calcium Hydroxide Additive

Z. P. Arkhangel'skaya, A. V. Krasnobryzhii, T. B. Kas'yan, M. M. Loginova, and D. A. Vinogradova

Rigel' Open Joint-Stock Battery Company, St. Petersburg, Russia

Received October 12, 2004

Abstract—The influence exerted by a calcium hydroxide additive introduced into the negative electrode on the serviceability of a sealed nickel–zinc battery with a nickel oxide electrode fabricated from spherical nickel hydroxide on a foamed-nickel support was studied.

It was established in a study of processes governing the cycling life of a sealed nickel–zinc (SNZ) battery that the most important limitations are imposed by transport and incorporation of zinc into the structure of a nickel oxide electrode (NOE) in amounts leading to its gradual degradation and accelerated "loss of shape" by the zinc electrode.

The incorporation into nickel hydroxide of a part of zinc(II) transferred to the positive electrode leads to unbalance of migration and diffusion flows of $Zn[OH]_4^{2-}$ ions directed toward the NOE in charging and in the opposite direction in discharge. Therefore, to decelerate the accumulation of zinc in the NOE, the following is necessary. The fraction of $Zn[OH]_4^{2-}$ ions, which are involved, in parallel with OH^- ions, in current transport, is to be lowered and the gradient of their concentration, which appears in charging between the zones of the reactions in the negative and positive electrodes, is to be diminished to the maximum possible extent. Both these goals are achieved by lowering the equilibrium concentration of $Zn[OH]_4^{2-}$ in the electrolyte. However, of high importance in this case are physicochemical parameters of the NOE (porosity and structure of its pore space, electrical conductivity of the active paste), which determine the current distribution in the electrode and concentration changes in the electrolyte filling the pore space. These parameters affect the stability of the zincate complex and the rate of incorporation of zinc into the structure of nickel hydroxide. Zinc is incorporated into the layered structure of nickel hydroxide in the form of a cation in battery charging in the localized interlayer space, with hydrogen bonds [1] and covalent bonds [2] formed to give $Ni_{1-x}Zn_x(OH)_2$ or $Ni_{1-x}Zn_xOOH$ complexes.

In particular, the accumulation of incorporated zinc in pressed electrodes with a foamed-nickel (FN) support, which contain electrically conducting components, is 1.5–2 times slower than that in electrodes with a metal–ceramic support [1].

However, with nickel oxide electrodes of the FN type used in a battery and, simultaneously, the initial KOH concentration lowered from 7 to 6 M, it was impossible to make longer the cycling life of SNZ batteries. This was due to a decrease in the concentration of the electrolyte in the course of cycling to 3–3.5 M and the resulting deterioration of the serviceability of the electrodes [3, 4].

These results demonstrated that, to improve to an even greater extent the service life of a sealed nickel–zinc (NZ) battery, it is necessary to diminish the solubility of the zincate complex without any further decrease in the concentration of OH^- ions in the zone of the negative electrode, e.g., upon introduction of a $Ca(OH)_2$ additive into the zinc electrode.

The introduction of $Ca(OH)_2$ into the zinc electrode in order to make longer the service life (in cycling) of an NZ battery was first suggested by A.A. Zhulidov [5]. The battery developed by him for miner's lamps had a prolonged, by that time, cycling life of up to 250–300 cycles.

In recent years, it has been suggested to introduce a $Ca(OH)_2$ additive into the zinc electrode in the form of a sparingly soluble calcium zincate in order to make longer the cycling life of an NZ battery [6–8].

Calcium zincate is a complex compound, which is not stoichiometric [6], but in equilibrium with a 20% KOH solution has a definite composition: $Ca(OH)_2 \cdot 2Zn(OH)_2 \cdot 2H_2O$. The complex is formed upon mixing of $Ca(OH)_2$ with ZnO in an alkaline medium

1070-4272/05/7803-0425© 2005 Pleiades Publishing, Inc.

Table 1. Parameters of the NTsG-25 batteries under study

Battery	Composition of active paste of electrode, wt %		Theoretical capacity, A h		Capacity ratio (–)/(+)	Electrolyte composition, M; volume *V*, cm^3
	(–)	(+)	(–)	(+)		
1	ZnO 64.5, $Ca(OH)_2$ 22, PbO 6, fluoroplastic 3, PEO 0.5	$Ni(OH)_2$ 84.3, $Co(OH)_2$ 8.7, ZnO 3.7, fluoroplastic 1	64.8	50	1.3	KOH 6, LiOH 1.25; *V* = 90
2 (control)	Zn 13, ZnO 82.75, HgO 0.9, PbO 0.25, fluoroplastic 2.5, PEO 0.5	″ ″	98	50	1.96	KOH 6, LiOH 1.25; *V* = 95
3 (control)	Zn 13, ZnO 82.75, HgO 0.9, PbO 0.25, fluoroplastic 2.5, PEO 0.5	″ ″	98	50	1.96	KOH 7, LiOH 1; *V* = 95

and prolonged keeping in the absence [6] or in the presence [7] of catalysts. In an electrolyte with 0 to 30% KOH, the amount of ZnO that is in equilibrium with a solution of potassium zincate and calcium zincate is 2–3 times lower than that in the case of its equilibrium with KOH [6]. However, as the content of KOH and calcium zincate increases, the solubilities of ZnO in these compounds approach each other to become equal at a KOH concentration of 8 M (34 wt %).

A question arises in practical use of calcium zincate additives as to whether it is appropriate to use it in finished form or as separate components. This is because calcium zincate mostly decomposes in charging and is formed again in discharge only partially [8]. The amount of the material present as separate components depends on the discharge conditions and on the period of time during which the battery is in the discharged state.

In this study, a $Ca(OH)_2$ additive to ZnO was introduced in the form of separate components in amounts closely corresponding to the composition $Ca(OH)_2 \cdot 2Zn(OH)_2 \cdot 2H_2O$ (batteries 1). In parallel with the experimental batteries we tested control batteries containing no $Ca(OH)_2$ additive. The initial concentration of KOH in the electrolyte was 6 (batteries 1, 2) and 7 M (Table 1, batteries 3).

Table 2. Charging and discharge capacities of the NTsG-25 batteries under study

Cycle	Charging		Discharge	
	capacity, A h, for indicated battery			
	1	2, 3	1	2, 3
Forming:				
1st	15	54	4.5	18
2nd	5–6	70	2.5–2.7	35
3rd	32–33	–	25	–
4th	25	–	22.5–23	–
Working	26–23	26–23	25–22	25–22

EXPERIMENTAL

The basic parameters of the sealed nickel–zinc batteries are listed in Table 1.

The experimental and control batteries under study differed in the composition of the active pastes of the negative electrode and the capacity ratio of the negative and positive electrodes.

The active paste of the negative electrodes of all the batteries was fabricated with thorough mixing of the components. In batteries 1, the amount of $Ca(OH)_2$ in the mixture was 22 wt %. The mixture contained about 10 wt % excess of ZnO, relative to its content in calcium zincate. In all the variants, the pressed positive electrodes used were fabricated by pasting the active mass on the FN support and subsequent pressing.

The capacity ratio of the active pastes of the negative and positive electrodes in batteries 1, with a $Ca(OH)_2$ additive, is smaller than that in batteries 2 and 3. This is so because part of ZnO in the negative electrode of batteries 1 is replaced with $Ca(OH)_2$ (at a thickness equal to that of electrodes in batteries 2, with a HgO additive).

The batteries were formed in a ventilated state (with an opened low-pressure valve). The modes of charging and discharge of the batteries in the forming and subsequent cycles are listed in Table 2. The forming mode was chosen so that, at the beginning of the

subsequent cycling, the active paste contained no less than 20% oxidized phase in the charged state and 30–40% reduced phase, when discharged.

The charging current in forming was 3 A, and that in cycling, 5 A in the first stage and 1.5 A in the second. The final charging voltage was 2.05 V in forming, and 1.98 V for batteries 1 and 1.93 V for batteries 2 and 3, in cycling. The discharge current was 5 A in forming and 6 A in cycling. The final discharge voltage was 1.2 V.

As seen from Table 2, the forming of batteries 1 was hindered, which required two additional forming cycles.

Measurements demonstrated that the way in which potentials vary in forming of positive electrodes of the batteries is the same for all the batteries. The charging potential of negative electrodes with a $Ca(OH)_2$ additive in batteries 1 is higher and especially steeply increases when charging is commenced, which indicates that the ohmic component of the polarization is significant.

In further studies of sealed batteries (with pressure gages on cover), the charging and discharge voltages and the internal pressure associated with accumulation of oxygen and hydrogen were measured. In doing so, it was kept in mind that the difference in battery voltages in the initial period of cycling is due to specific features of processes occurring in the negative electrode and the battery capacity is determined by the positive electrode, which has a lower calculated capacity (Table 1).

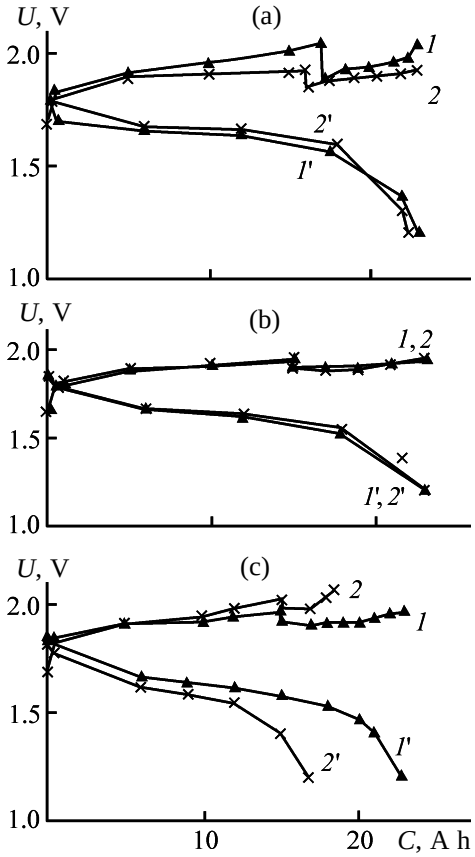


Fig. 1. Voltage U of NTsG-25 batteries (*1*, *1*') 1 and (*2*, *2*') 2 in (*1*, *2*) charging and (*1*', *2*') discharge in the course of cycling. (*C*) Discharge capacity. Cycle: (a) 35th, (b) 100th, and (c) 170th. Additive to the zinc electrode (%): (*1*, *1*') 22 $Ca(OH)_2$ and (*2*, *2*') 0.9 HgO + 0.25 PbO.

At the beginning of cycling, <30–40 cycles, the charging voltage of batteries 1 with a $Ca(OH)_2$ additive was higher than that in batteries 2 (Fig. 1a). At the instant when the current is switched on, the voltage increases abruptly. A stronger increase in voltage is also observed for batteries 1 in the final stage of charging, when a larger part of zinc(II) is reduced and further reduction of the remaining part of the oxidized phase (ZnO) is hindered because its contact with the current-carrying support may be disrupted in the presence of $Ca(OH)_2$. The charging and discharge voltages of batteries 1 and 2, respectively, become closer by the 50th cycle and virtually completely coincide by the 100th cycle (Fig. 1b).

However, the situation changes after 160–180 cycles. The manner in which the charging voltage and discharge capacity vary in batteries 1 remains the same, but in batteries 2 the voltage increases in the course of charging more steeply, which leads to a shorter time of their charging and to the resulting decrease in the discharge capacity (Fig. 1c). It has been established [2] that the deteriorating chargeability of batteries 2 results from the hindrance to the anodic process at the positive electrode, which arises during this stage of cycling.

The variation of the gas pressure in batteries 1 (Fig. 2) exhibited specific features characteristic of batteries with NOE fabricated from spherical nickel hydroxide [9]. The build-up of pressure in these batteries, preserved during the first 30–40 cycles, is due to predominant accumulation of hydrogen. This is associated with the low rate of its oxidation on the NOE, which originally has a smoothened and denser surface [9]. Beginning with 30th–40th cycle, the evolved H_2 is oxidized on the NOE virtually completely because of the loosening of the surface layer of the active paste, and the pressure within the batteries is due to the evolution of oxygen, being determined by the rate of its absorption at the zinc electrode. In further cycling, the pressure varies narrowly at around

Table 3. Content of KOH in the electrolyte and accumulation of zinc in the NOE of the NTsG-25 batteries under study in different cycles

Battery	Initial electrolyte concentration, M (g l^{-1})	Cycle	KOH concentration		Content of zinc	
			M	g l^{-1}	in electrolyte, g l^{-1}	in NOE, $[Zn/Ni(OH)_2]_2$, %
1	6 (336)	90th	2.9	163	4.6	5.2
		220th	2.8	158	–	–
2	6 (336)	70–90th	3.0	168	8.0	7.8
		218th	2.95	166	–	–
3	7 (392)	90th	4.8	269	12.6	9
		200th	–	–	–	10.6
		286th	4.5	250	12	11.6

0.6×10^2 kPa, which indicates that the zinc electrode containing a $Ca(OH)_2$ additive can actively react with oxygen evolved at the NOE.

The charging and discharge capacities of batteries 1 and 2 vary similarly in the initial stage of cycling (Fig. 3), although the time of their stabilization is longer in batteries 1. Probably, this is due to gradual formation of the calcium zincate phase. By the 40th–50th cycle, the charging capacities of both kinds of batteres attain the same level, whereas the discharge capacity of batteries 1 with a $Ca(OH)_2$ additive is higher, which is presumably due to the better chargeability of the positive electrode. This result can be attributed to an increased overvoltage of O_2 evolution in the presence of calcium(II) [10].

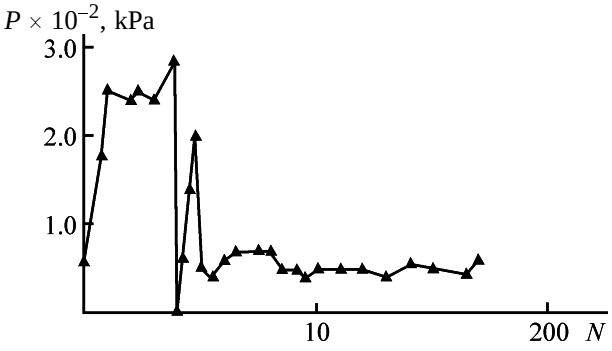


Fig. 2. Variation of the internal pressure in NTsG-25 battery 1 with a $Ca(OH)_2$ additive to the negative electrode. (*P*) Pressure and (*N*) number of cycles.

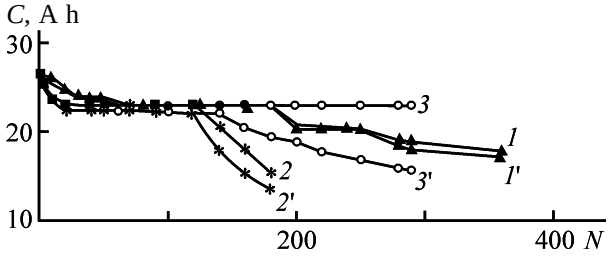


Fig. 3. Variation of (*1*–*3*) charging and (*1*'–*3*') charge capacity *C* of NTsG-25 batteries *1*–*3* with various additives to the negative electrode and at different concentrations of KOH in the electrolyte. (*N*) Number of cycles. Additive (%): (*1*, *1*') 22 $Ca(OH)_2$ and (*2*, *2*', *3*, *3*') 0.9 HgO + 0.25 PbO. Initial KOH concentration (M): (*1*, *2*) 6 and (*3*) 7.

The charging and discharge capacities first start to decrease in batteries 2 with a lowered initial concentration of KOH (6 M). Their service life does not exceed 200 cycles. At a higher initial concentration of KOH (7 M), the decrease in the battery capacity (to 0.6 C_{in}), observed in batteries 3 after 160–180 cycles, was slower and the service life was 300 cycles.

In batteries containing a $Ca(OH)_2$ additive, the capacity decreased only slightly in the course of cycling to 360 cycles at a change in the electrolyte composition similar to that in batteries 2.

These results can be understood on the basis of data on changes in the electrolyte composition in the batteries under study and on accumulation of zinc in the NOE (Table 3).

The concentration of KOH in the electrolyte in batteries 1 and 2 reaches a constant value by the 70th cycle and then varies only slightly. In batteries 3, it reaches a rather high level. The service life of this kind of batteries is limited by the accumulation of zinc in the NOE in amounts exceeding 10% $Zn/Ni(OH)_2$.

The decrease in the capacity of batteries 2 is due to the low steady-state concentration of hydroxide ions. At a similar, to batteries 2, change in the concentration of OH^- ions, batteries 1 retain a stable capacity because of the presence of $Ca(OH)_2$ and calcium zincate, which serve as an additional source of hydroxide

ions in the zone of the occurring reactions. The accumulation of zinc in the NOE of this kind of batteries is slow because of the lower concentration of $Zn(OH)_4^{2-}$ in the electrolyte, which results in that their service life is longer.

According to results of a chemical analysis, cycling leads to transfer of not only zinc(II), but also calcium(II), into the active paste of the NOE in batteries 1. At a very low content of calcium(II) in the electrolyte of a charged battery (0.07 g l^{-1}) by the 90th cycle, 0.112 g of calcium(II) was transferred into the active paste of the NOE, which corresponds to 0.37 g of calcium zincate. At such a low concentration of calcium(II) in the electrolyte, it transport may occur only via diffusion in the form of a complex and decomposition of this complex in the reaction of zinc with nickel hydroxide. It was found from the ratio of the transferred amounts of zinc(II) and calcium(II) that zinc is transferred into the NOE of batteries containing a $Ca(OH)_2$ additive mainly in the form of zincate ions at an insignificant fraction of its transport by calcium zincate formed in the course of cycling.

CONCLUSIONS

(1) Calcium hydroxide introduced into the negative electrode of a sealed nickel–zinc battery is an additional source of hydroxide ions in the zone of the occurring reactions. In the course of cycling, it reacts with zinc oxide and thereby gradually transforms into calcium zincate.

(2) The reduced phase of a zinc electrode containing calcium zincate actively reacts with oxygen evolved at the nickel oxide electrode, which results in that the internal pressure of oxygen in the sealed battery is not high.

(3) The transport of zinc(II) by $Zn(OH)_4^{2-}$ ions becomes slower in the presence of calcium zincate because of its lower equilibrium concentration in the electrolyte. Calcium zincate is involved in the transport of zinc(II) in the nickel oxide electrode as a result of its diffusion in the form of a complex.

REFERENCES

1. Ezhov, B.B., Egorova, S.A., and Goryainova, T.N., *Zh. Prikl. Khim.*, 1992, vol. 65, no. 1, pp. 11–15.
2. Tessier, C., Faure, C., Guerlou, L., *et al.*, *J. Electrochem. Soc.*, 2002, vol. 149, no. 9, pp. 1136–1145.
3. Arkhangel'skaya, Z.P., Kas'yan, T.B., and Loginova, M.M., *Zh. Prikl. Khim.*, 2003, vol. 76, no. 10, pp. 1648–1652.
4. Arkhangel'skaya, Z.P., Kas'yan, T.B., and Loginova, M.M., *Elektrokhim. Energet.*, 2003, vol. 3, no. 4, pp. 192–199.
5. USSR Inventor's Certificate no. 116812.
6. Ram A. Sharma, *J. Electrochem. Soc.*, 1986, vol. 133, no. 11, pp. 2215–2219.
7. US Patent 5460899.
8. Yu, J., Yang, H., Ai, X., and Lhy, X., *J. Power Sources*, 2001, vol. 103, pp. 93–97.
9. Arkhangel'skaya, Z.P., Kas'yan, T.B., Loginova, M.M., and Vinogradova, D.A., *Zh. Prikl. Khim.*, 2004, vol. 77, no. 1, pp. 70–74.
10. Yuan, A., Cheng, S., Zhang, J., and Cao, C., *J. Power Sources*, 1998, vol. 76, pp. 36–40.

Russian Journal of Applied Chemistry, Vol. 78, No. 3, 2005, pp. 430–434. Translated from Zhurnal Prikladnoi Khimii, Vol. 78, No. 3, 2005, pp. 433–437.
Original Russian Text Copyright © 2005 by Varentsova, Varentsov.

APPLIED ELECTROCHEMISTRY AND CORROSION PROTECTION OF METALS

Formation of Surface Oxides in Electrode Polarization of Fibrous Carbon Materials in a Sulfuric Acid Solution and Their Influence on Ion-Exchange and Electrochemical Properties of These Materials

V. I. Varentsova and V. K. Varentsov

Institute of Solid-State Chemistry and Mechanochemistry, Siberian Division, Russian Academy of Sciences, Novosibirsk, Russia

Received May 19, 2004

Abstract—Formation of surface oxides in the course of cathodic and anodic polarization of fibrous carbon materials in a 0.25 M sulfuric acid solution and their influence on the cation- and anion-exchange properties of fibrous carbon materials, steady-state electrode potential in a 0.1 M sodium sulfate solution, and electrodeposition of copper from a sulfuric acid solution were studied.

The use of fibrous carbon materials (FCMs) in technical electrochemistry has proved to be effective in manufacture of electric power sources, electrodeposition, recovery of noble, rare, and nonferrous metals from mineral and secondary raw materials, and deactivation of toxic compounds and liquid waste in various branches of industry [1–3]. In prolonged operation of FCM electrodes, problems necessarily arise, associated with the change of their properties in cyclic and nonstationary processes [1, 3, 4]. It has been shown previously that preliminary electrode treatment of some FCMs in acid and alkaline solutions leads to a significant change in the morphology of carbon fibers and in the mass, electrical conductivity, and steady-state electrode potential of FCMs. All these factors can strongly affect further use of FCMs in electrochemical processes [5–7].

Published data suggest that the change in the FCM properties is due to formation of oxide compounds on the surface of carbon compounds in the course of electrode treatment. The existence of oxide compounds on the surface of carbon materials has long been known, and a considerable attention is being given to a study of these materials because of their pronounced influence on the catalytic, ion-exchange, adsorption, and other properties of carbon materials [8–15].

Surface oxide compounds are produced in reaction of carbon materials with atmospheric oxygen without formation of an independent phase. Surface oxides are nonstoichiometric, but enter into chemical reactions characteristic of bulk compounds because of the presence of a chemical bond. A fruitful way to study surface compounds is to identify them with functional groups known from organic chemistry. Thanks to this approach, carboxy, phenol, carbonyl, and lactone surface oxides have been identified. The identification was the most reliable for carboxy and phenol groups [10, 11, 14, 15]. A distinctive feature of carbon materials is the possibility of widely varying the composition and relative concentrations of surface oxides, which leads to variation of their surface properties in a wide range. Depending on the conditions and method of treatment, carbon materials can adsorb from solutions both acids and alkalis; the steady-state electrode potential of carbon materials in electrolyte solutions varies by several hundreds of millivolts [11, 13].

The most flexible way to modify the surface properties of carbon materials is the electrochemical method [11, 13–15]. Data concerning the application of electrode treatment of FCMs for modification of their surface properties are scarce [14, 15]. It was shown in [14] that the surface properties of carbon fibers subjected to anodic and chemical treatment are identical. By contrast, it was found in [15] that the amount of phenol groups, involved in the esterfication reaction, on the surface of anodically oxidized fibers considerably exceeds that on the surface of chemically and thermally oxidized fibers.

1070-4272/05/7803-0430© 2005 Pleiades Publishing, Inc.

The goal of this study was to determine the composition of oxide compounds formed on the FCM surface in cathodic and anodic polarization in an H_2SO_4 solution and their influence on the ion-exchange and electrochemical properties of FCMs.

EXPERIMENTAL

As objects of the study we chose carbonized (graphite content ~85 wt %) woven (AMT, AUT, knitted fabric) and nonwoven (NT-1) fibrous carbon materials. The electrode polarization in the galvanostatic mode was carried out using a B5-49 dc power source, with the solution circulated by a pp-304 peristaltic pump through the electrode volume with an overall surface area of 2 cm^2 on a setup described schematically in [5]. A platinum wire served as an anode, and a perforated titanium or platinum plate, as a current lead. After treatment, the electrode was washed with distilled water to constant pH and dried at 80–100°C. The variation of the ion-exchange properties of FCMs was monitored by absorption of an acid or alkali from solutions, and that of electrochemical properties, by the change in the steady-state electrode potential and by the efficiency of electrodeposition of copper(II) from a sulfuric acid solution.

The steady-state electrode potential was measured in 0.1 M Na_2SO_4, without drying of the FCM, with an OP-265/1 pH-meter relative to a saturated silver chloride electrode and recalculated to the hydrogen scale. Copper(II) was electrodeposited from a solution of composition (g l^{-1}): copper(II) 0.15 and sulfuric acid 25, on the setup used for FCM treatment. The efficiency of the process was evaluated by the degree of copper(II) electrodeposition from solution, α,

$$\alpha = (c_0 - c_\tau)/c_0 \times 100,$$

where c_0 and c_τ are the initial and final concentrations of copper in solution, g l^{-1}.

The amount of surface oxides was determined using the neutralization reaction, by the procedure described in [16]. The method of separate determination of surface oxide groups [10, 11, 16] is based on the different activities of surface oxides with respect to bases with different strengths. NaOH is used to neutralize carboxy and phenol groups, and $NaHCO_3$, carboxy groups, with the amount of phenol groups found from the difference.

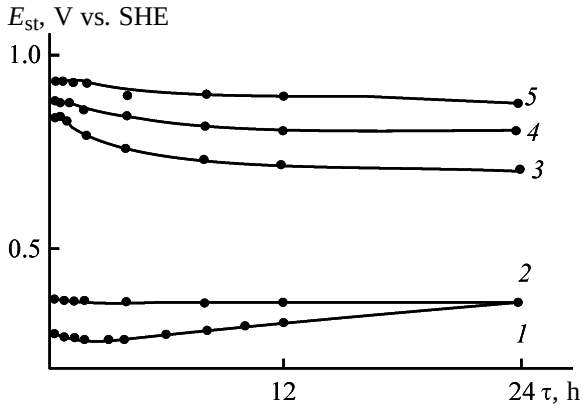
Table 1 lists the results obtained in measuring the amount of ion-exchange groups on the surface of carbon fibers after the anodic polarization of FCM. It can be seen that the amount of ion-exchange groups and the relative amounts of cation- and anion-exchange groups vary with the conditions of electrode treatment. As a result of anodic treatment under the conditions studied, FCMs acquire cation-exchange properties. Under the conditions of cathodic polarization, both cation- and anion-exchange groups can be found on the FCM surface.

Table 1. Amount n of anion- (a/e) and cation-exchange (c/e) groups on the FCM surface after an electrode treatment in a 0.25 M H_2SO_4 solution. Current density I = 500 A m^{-2}, electrolysis duration τ = 2 h

Material	n, mg-equiv g^{-1}	
	a/e	c/e
Anodic polarization		
AMT	None	0.700
AUT	″	1.369
Knitted fabric	″	1.609
NT-1	″	1.020
Cathodic polarization		
AMT	0.264	0.283
AUT	0.329	0.282
Knitted fabric	0.210	0.229
NT-1	0.200	0.280

The influence exerted by the conditions of electrode polarization on the composition and ratio (relative amounts) of cation-exchange groups (carboxy and phenol) on the surface of FCM fibers was studied with NT-1 as example. Table 2 shows that, by varying the conditions of electrode polarization, one can affect not only the amount of cation-exchange groups, but also the ratio of carboxy and phenol groups. In a cathodic treatment, the amount of carboxy groups remains unchanged and that of phenol groups decreases, with the extent of this decrease depending on the conditions of cathodic treatment. Changing the cathodic current density exerts a stronger influence than the duration of treatment. In anodic polarization, the amount of phenol groups increases by a factor of 1.5–2, and that of carboxy groups, by a factor of more than 8. As the current density increases, the amount of phenol groups grows by ~35%, and the amount of carboxy groups is independent of the conditions of anodic polarization. The ratio of phenol and carboxy groups varies from 0.75 to 4.3, depending on the conditions of electrode treatment.

It should be noted that the ability of an FCM sub-



Steady-state electrode potential E_{st} of an NT-1 FCM vs. time τ of keeping in a 1 M Na_2SO_4 solution after (*1*, *2*) cathodic and (*3*–*5*) anodic polarization of the FCM in an H_2SO_4 solution. Steady-state electrode potential of the initial NT-1 sample +0.37 V. Polarization current density (A m^{-2}): (*1*, *5*) 1000, (*2*, *4*) 500, and (*3*) 250. Polarization time (h): (*1*, *2*, *4*, *5*) 1–3 and (*3*) 1.

jected to electrode polarization to absorb alkali from solution remains virtually unchanged if, upon sorption of NaOH, the samples are neutralized with acid and washed with water, and alkali is again sorbed after that.

The state of the surface of FCM fibers strongly affects the steady-state electrode potential of FCM, E_{st}, and the extent to which it changes upon an electrode treatment [5–7]. In the presence of atmospheric oxygen at the interface between the carbon material and the aqueous electrolyte solution, E_{st} must be determined, depending on the solution pH, by the electrochemical equilibria

$$O_2 + 4H_3O^+ + 4e = 6H_2O \text{ (acid medium)},$$

$$O_2 + 2H_2O + 4e = 4OH^- \text{ (alkaline medium)}.$$

However, this is virtually not the case because carbon materials are not inert toward oxygen and suffer from corrosion to give surface oxides. The contribution from the formation of surface oxides to E_{st} can be evaluated by subjecting the FCM to preliminary cathodic or anodic polarization, thereby changing the amount and ratio of the surface oxides. The figure shows how E_{st} of NT-1 varies after a cathodic or anodic polarization of NT-1 in a 0.25 M H_2SO_4 solution.

The figure shows that cathodic treatment has a little effect on E_{st}, with only a slight negative shift of E_{st} observed at a treatment current density of 1000 A m^{-2}. On keeping an NT-1 sample in a solution for 24 h, E_{st} returns to its initial value. The negative shift of E_{st} is due to desorption of oxygen from the FCM surface in cathodic polarization, and its return to the initial value on keeping in a solution, to chemisorption of oxygen [5, 7, 11, 13]. After a cathodic treatment, the amount of acidic surface oxides decreases, with a pronounced decrease (by a factor of 2) observed for samples subjected to cathodic polarization at a current density of 1000 A m^{-2} (Table 2). On keeping such a sample in a 0.1 M Na_2SO_4 solution for 24 h, 0.3 mg-equiv g^{-1} of acidic complexes was found on its surface, which is close to the value characteristic of the initial NT-1 (Table 2). An anodic treatment of NT-1 in a sulfuric acid solution strongly shifts E_{st} in the positive direction from the value attained in 0.1 M Na_2SO_4, even at a low anodic current density. As the treatment current density increases, the positive shift of E_{st} becomes more pronounced, reaching a value of 0.68 V. It has been assumed that the shift of E_{st} upon anodic polarization of NT-1 results from formation of oxide compounds on the NT-1 surface [6]. The amount of surface oxides found after an anodic treatment of NT-1 confirms this assumption (Table 2).

Table 2. Amount *n* of cation-exchange groups on the NT-1 surface in relation to conditions of electrode treatment in a 0.25 M H_2SO_4 solution. Current density 500/1000 A m^{-2}

Cation-exchange surface groups	*n*, mg-equiv g^{-1}, during indicated treatment time, h		
	0	1	2
Cathodic polarization			
Total amount	0.32	0.31/0.15	0.28
Phenol	0.26	0.25/0.09	0.22
Carboxy	0.06	0.06/0.06	0.06
Anodic polarization			
Total amount	0.32	0.90/1.06	1.02
Phenol	0.26	0.39/0.53	0.50
Carboxy	0.06	0.51/0.53	0.52

Thus, it follows from the results obtained that the steady-state electrode potential attained by an FCM upon its electrode treatment in an aqueous electrolyte solution is largely determined by the presence of surface oxides on the surface of carbon fibers.

As noted previously [6], anodic treatment of FCM results in that their electrical conductivity decreases, with the parameters of metal recovery on electrodes of this kind markedly impaired. It can be seen from

Table 3. Change in the mass Δm and electrical conductivity χ of NT-1 and in the amount n of surface oxides upon an electrode polarization in a 0.25 M H_2SO_4 solution

Polarization	Δm, %	χ, S cm^{-1}	n, mg-equiv g^{-1}
Initial sample	–	0.041	0.32
Anodic	+14.5	0.011	0.90
Anodic, followed by cathodic	+25	0.040	0.50

Table 4. Degree α of electrolytic recovery of copper(II) from solution in relation to conditions of preliminary electrode treatment of NT-1 in a 0.25 M H_2SO_4 solution

Treatment	i, A m^{-2}	τ, h	α, %
Initial sample	–	–	56.0
Anodic	500	1	41.7
Cathodic	500	1	57.0

the data obtained that the reason for the decrease in the electrical conductivity of FCMs is formation of surface oxides. This is also manifested in a significant increase (by 15–19%) in the mass of FCM samples [6]. The data in Table 2 suggest that cathodic treatment of samples subjected to anodic polarization can regenerate the FCM properties.

Table 3 shows how successive anodic-cathodic treatment affects the NT-1 properties. The current density of anodic and cathodic polarization was 500 A m^{-2}, and the time of treatment at each polarization, 1 h. Table 3 shows that cathodic treatment of an anodically polarized FCM restores its electrical conductivity, the positive gain in mass decreases by more than 80%, and the amount of surface oxide groups becomes smaller.

The results of experiments on electrolytic recovery of copper(II) from a sulfuric acid solution on an electrode of this kind at a current density of 500 A m^{-2} are listed in Table 4. The electrolytic recovery of copper(II) was performed at a current density of 500 A m^{-2} in the course of 20 min, because, as shown in [17], the contribution of concurrent reduction of hydrogen ions was at a minimum under these conditions.

Table 4 shows that the degree of electrolytic recovery of copper(II) onto an FCM electrode regenerated by cathodic polarization in an H_2SO_4 solution reaches values characteristic of the initial FCM. This result is important for application of FCM electrodes to processes associated with electrolytic recovery of metals, their subsequent anodic dissolution, and repeated use of fibrous carbon electrodes.

CONCLUSIONS

(1) The amount of ion-exchange groups on the surface of the fibrous carbon materials studied depends on the conditions of electrode treatment; as a result of anodic polarization, the materials acquire cation-exchange properties.

(2) The amount of cation-exchange (phenol and carboxy) groups on the NT-1 surface was determined. Depending on the polarization conditions, their total amount varies within a factor of 2–3.5, and their ratio, from 0.75 to 4.3.

(3) The steady-state electrode potential of fibrous carbon materials depends on the composition and amount of oxide groups on their surface. An increase in the amount of acidic surface oxides leads to a shift of E_{st} by 0.68 V in the positive direction.

(4) Cathodic treatment of samples subjected to anodic polarization can regenerate the properties of fibrous carbon materials.

REFERENCES

1. Varentsov, V.K., *Intensifikatsiya elektrokhimicheskikh protsessov* (Intensification of Electrochemical Processes), Tomilov, A.P., Ed., Moscow: Nauka, 1988, pp. 94–118.
2. Bek, R.Yu., *Izv. Sib. Otd. Akad. Nauk SSSR, Ser. Khim. Nauk*, 1977, no. 14, pp. 11–17.
3. Varentsov, V.K., *Khim. Inter. Ustoich. Razv.*, 1977, vol. 5, no. 2, pp. 247–256.
4. Konkin, A.A., *Uglerodnye i drugie zharostoikie voloknistye materialy* (Carbon-Type and Other Heat-Resistant Fibrous Materials), Moscow: Khimiya, 1974.
5. Varentsov, V.K. and Varentsova, V.I., *Zh. Prikl. Khim.*, 1999, vol. 72, no. 4, pp. 605–609.
6. Varentsov, V.K. and Varentsova, V.I., *Zh. Prikl. Khim.*, 1999, vol. 72, no. 4, pp. 609–613.
7. Varentsov, V.K. and Varentsova, V.I., *Elektrokhimiya*, 2001, vol. 37, no. 7, pp. 811–820.
8. Lepin', L.K., *Usp. Khim.*, 1940, vol. 9, no. 5, pp. 533–549.
9. Dubinin, M.M., *Usp. Khim.*, 1955, vol. 24, no. 5, pp. 513–526.
10. Donnet, J.B., *Carbon*, 1968, vol. 6, no. 1, pp. 161–176.

11. Tarasevich, M.R., *Elektrokhimiya uglerodnykh materialov* (Electrochemistry of Carbon Materials), Moscow: Nauka, 1984.
12. Fialkov, A.S., *Uglerodnye mezhsloevye soedineniya i kompozity na ego osnove* (Carbon Intercalation Compounds and Composites Based on Them), Moscow: Aspekt, 1997.
13. Tarasevich, M.R., Gol'din, M.M., Luzhnikov, E.A., and Bogdanovskaya, V.A., *Itogi Nauki Tekh., Ser.: Elektrokhim.*, 1990, vol. 31, pp. 217–250.
14. Weinberg, N.L. and Reddy, T.B., *J. Appl. Electrochem.*, 1973, vol. 3, pp. 73–75.
15. Jannakoudakis, P. D., Jannakoudakis, A.D., Theodoridou, E., and Besenhard, J.O., *J. Appl. Electrochem.*, 1989, vol. 19, pp. 341–344.
16. Lezhnev, N.N., Terent'ev, A.P., Novikova, I.S., and Kobzeva, T.A., *Kauch. Rezina*, 1961, no. 11, pp. 21–27.
17. Varentsova, V.I. and Varentsov, V.K., *Zh. Prikl. Khim.*, 2000, vol. 73, no. 2, pp. 217–221.

Russian Journal of Applied Chemistry, Vol. 78, No. 3, 2005, pp. 435–437. Translated from Zhurnal Prikladnoi Khimii, Vol. 78, No. 3, 2005, pp. 438–440.
Original Russian Text Copyright © 2005 by Igumnov, Lekontseva, Shipigusev, Mukhametshin.

ORGANIC SYNTHESIS AND INDUSTRIAL ORGANIC CHEMISTRY

A New Procedure for Preparing Perfluoroalkoxypropanoic Acid Fluorides

S. M. Igumnov, G. I. Lekontseva, A. A. Shipigusev, and V. F. Mukhametshin

Perm Branch, Prikladnaya Khimiya Russian Scientific Center, Federal State Unitary Enterprise, Perm, Russia

Received September 15, 2004

Abstract—Condensation of perfluoro carboxylic acid fluorides with hexafluoropropene epoxide in the presence of *N,N,N',N'*-tetraalkyldiaminomethanes was studied.

Perfluoroalkoxypropanoic acid fluorides (PFPAFs) are starting compounds for preparing perfluoroalkyl vinyl ethers (monomers for fluoro rubbers, elastomers, vulcanizates with high heat, ozone, and weather resistance), emulsifiers, fluorinated surfactants, chemically and thermally stable liquids, lubricating oils, and polymeric materials [1].

Procedures for preparing PFPAFs are based on the reaction of hexafluoropropene epoxide (HFPE) with perfluoro carboxylic acid fluorides (PFAFs) in polar aprotic solvents in a wide temperature range (from –80 to 200°C) in the presence of various catalysts, e.g., alkali metal halides [2], quaternary ammonium salts [3], tris(dimethylamino)difluorophosphorane [4], sulfonium salts [5], tetraalkylurea [6], and *N,N,N',N'*-tetraalkyldiaminodifluoromethane [7].

As a rule, reactions with low-boiling PFAFs, e.g., with carbonyl fluoride, trifluoroacetyl fluoride, or pentafluoropropionyl fluoride, are performed at a pressure ranging from 0.7 to 24 atm. As solvents are used mixtures of polar aprotic solvents [dinitriles of saturated aliphatic dicarboxylic acids (C_5–C_8), dimethyl ethers of polyethylene glycols $CH_3O(CH_2CH_2O)_n \cdot CH_3$, n = 2–6] [8] or of polar aprotic (acetonitrile, diglyme) and nonpolar (pentane, hexane, cyclohexane, or a halogenated alkane, e.g., trifluorotrichloroethane) solvents [7]. The PFPAF yield in these procedures does not exceed 50%, being in some cases as low as 6–12%.

In this work, with the aim to increase the reaction selectivity, we studied the conditions of condensation of HFPE with PFAFs according to the scheme

$$R_F COF + CF_3CF\!-\!CF_2 \longrightarrow R_F CF_2OCFCOF,$$

(O bridge; CF$_3$ branch)

where R_F = F, CF_3, C_2F_5, $CF_3(CF_2)_3$, $HCF_2(CF_2)_3$, $CF_3(CF_2)_5$, $CF_3(CF_2)_7$, $BrCF_2$, or $C_2F_5OCF_2$.

In the process, we used new catalysts, *N,N,N',N'*-tetraalkyldiaminomethanes $R^1R^2NCH_2NR^3R^4$ (see table), where R^1–R^4 are linear or branched alkyls (C_1–C_6) or perfluoroalkyls (C_1–C_6), C_2H_4OH groups, or fragments forming with the nitrogen atom a heteroring containing one more nitrogen atom or an oxygen atom. Examples are bis(dimethylamino)methane, bis(diethylamino)methane, dipiperidinomethane, dimorpholinomethane, and bis[di(β-hydroxyethyl)amino]methane.

Condensation of HFPE with PFAF is performed in a polar aprotic solvent (acetonitrile or diglyme) in the presence of a nonpolar perfluorinated solvent (perfluoroheptane, perfluorooctane, perfluoromethylcyclohexane, perfluoroethylcyclohexane, perfluorodecalin, perfluoro-2-methyldecalin) acting as extractant for the forming PFPAF.

We found that the optimal catalyst concentration is 10–15 wt %; with its lower amounts, the yield of the target product decreases, and with larger amounts the PFPAF yield does not increase further.

The starting components, HFPE and PFAF, are taken in a molar ratio from 1 : 1 to 1 : 2. Under these conditions, the reaction mainly yields the monoaddition product, with a minor impurity (~1–3 wt %) of the HFPE isomerization product, pentafluoropropanoic acid fluoride.

The synthesis is performed in a stirred vessel at ambient pressure. The condensation product formed in the process is extracted with the organofluorine solvent. After the reaction completion, the PFPAF is distilled off from the extract, and the nonpolar organofluorine solvent is reused. The reaction products are

1070-4272/05/7803-0435 © 2005 Pleiades Publishing, Inc.

Preparation of PFPAFs [$R_FCF_2OCF(CF_3)COF$]

PFAF (amount, mol)	HFPE amount, mol	Catalyst (amount, mol)	Polar aprotic solvent, g	Nonpolar perfluorinated solvent, g	*T*, °C	PFPAF yield, %
FCOF (1.2)	0.75	Dipiperidinomethane (0.0769)	Acetonitrile, 25	Perfluoromethylcyclohexane, 210	–20	97
CF_3COF (0.8)	0.53	Bis(dimethylamino)methane (0.1078)	Acetonitrile, 25	Perfluorooctane, 200	–20	98
C_2F_5COF (0.63)	0.5	Bis(diethylamino)methane (0.0633)	Diglyme, 30	Perfluoroethylcyclohexane, 180	–15	98
$CF_3(CF_2)_3COF$ (0.53)	0.3	Dimorpholinomethane (0.0376)	Diglyme, 30	Perfluoro-2-methyldecalin, 180	15	98
$CF_3(CF_2)_3COF$ (0.4)	0.4	Bis(2-methylpiperidino)methane (0.0286)	Diglyme, 25	Perfluoro-2-methyldecalin, 150	20	98
$CF_3(CF_2)_7COF$ (0.3)	0.3	Bis[di(2-hydroxyethyl)amino]methane (0.0625)	Acetonitrile, 30	Perfluoroheptane, 200	25	99
$BrCF_2COF$ (0.5)	0.3	Dipiperidinomethane (0.0659)	Acetonitrile, 40	Perfluoro-2-methyldecalin, 200	–15	97
$C_2F_5OCF_2COF$ (0.5)	0.3	Bis(diethylamino)methane (0.0633)	Diglyme, 30	Perfluorodecalin, 150	–10 to –15	98
$HCF_2(CF_2)_3COF$ (0.4)	0.4	Dipiperidinomethane (0.0329)	Acetonitrile, 30	Perfluorodecalin, 200	15	97

identified by ^{19}F NMR spectroscopy. The yield of perfluoroalkoxypropanoic acid fluorides is 97–99% (see table).

Under these conditions, HFPE oligomers and products of addition of two or more HFPE molecules to PFAF are not formed.

The condensation of HFPE with PFAF in the presence of *N*,*N*,*N*',*N*'-tetraalkyldiaminomethanes involves intermediate formation of dialkylaminofluoromethane generating fluoride ion [9] which, in turn, initiates formation of perfluoroalkoxide anion by the reaction with PFAF. The perfluoroalkoxide anion reacts with HFPE as a nucleophilic agent to form the corresponding PFPAF:

$$R_FCOF + CH_2(NR_2)_2 \rightarrow R_FCONR_2 + R_2NCH_2F$$

$$\rightleftarrows R_2NCH_2^+ + F^-,$$

$$R_FCOF + F \rightleftarrows R_FCF_2O^-,$$

$$R_FCF_2O^- + CF_3\underset{\diagdown\,O\,\diagup}{CF}{-}CF_2 \longrightarrow R_FCF_2OCFCF_2O^-$$
$$\Big|$$
$$CF_3$$

$$\rightleftarrows R_FCF_2OCFCOF + F^-.$$
$$\Big|$$
$$CF_3$$

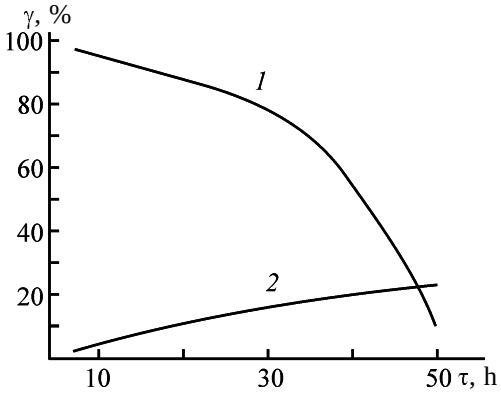
With the condensation of carbonyl fluoride with HFPE in the presence of bis(diethylamino)methane (BDEAM) as example [solvent acetonitrile, extractant perfluoro-2-methyldecalin (PFMD) or perfluorooctane (PFO)], we examined the dependence of the catalyst activity on the reaction time (see figure).

It is seen that the conversion of HFPE into perfluoromethoxypropanoic acid fluoride (curve *1*) decreases from 98 to 21% in the interval from 6 to 45 h, and after 50-h operation of the catalyst it does not exceed 2–3%. In the same period, the conversion of HFPE into pentafluoropropanoic acid fluoride increases from 2–3 to 20–21%.

These results show that the useful life of the catalyst in the system CH_3CN–PFMD–BDEAM is 37–40 h on the average. After 48.5 h, the catalyst activity appreciably decreases: The conversion of HFPE decreases to 40%.

It was also interesting to test the new catalyst in oligomerization of HFPE. The reaction is performed in the presence of bis(diethylamino)methane in a polar aprotic solvent (diglyme) at –40 to –30°C. The ^{19}F NMR spectra of the reaction products demonstrate selective formation of HFPE tetramer (n = 4).

The mechanism of HFPE oligomerization involves isomerization of HFPE by attack of the electrophilic carbon atom of HFPE with a lone electron pair of the nitrogen atom in tetrasubstituted bis(diethylamino)methane, resulting in cleavage of the C–O bond in the epoxy ring and rearrangement of the unstable intermediate perfluoroalkoxide anion into pentafluoropropion-



Catalyst activity as a function of the reaction time τ. (γ) Conversion of HFPE into (*1*) perfluoromethoxypropanoic and (*2*) pentafluoropropanoic acid fluorides.

yl fluoride. The latter reacts with HFPE to form addition products:

$$CF_3CF_2COF + n\,CF_3CF(O)CF_2 \xrightarrow{F^-} CF_3CF_2CF_2O(CFCF_2O)_{n-2}CFCOF.$$

EXPERIMENTAL

Bis(diethylamino)methane was synthesized in a 3-l three-necked flask equipped with a reflux condenser and a dropping funnel. The flask was charged with 200 g of paraform and approximately 700 ml of water; the mixture was stirred to obtain a unifom suspension and heated to 90°C to dissolve the paraform. After cooling to 30–40°C, 1.15 kg of diethylamine was added, the mixture was cooled to 20–25°C, and NaOH was added in portions. After stirring for 2–3 h, the mixture was distilled. Diethylamine and water were removed at 55–100°C, and bis(diethylamino)-methane was distilled at 110–112°C. The distilled product was dried over NaOH or KOH. Yield 1.75 kg (69%). The other catalysts were prepared similarly.

The condensation of HFPE with PFAF was performed in a three-necked flask equipped with a stirrer, a reflux condenser (cooled to –30°C), a dropping funnel, and a bubbler for feeding HFPE and gaseous PFAFs. The reactant amounts, reaction conditions, and yields of the target products are listed in the table.

The products were identified by ^{19}F NMR spectroscopy (Bruker WP-80 device, 80 MHz, internal reference hexafluorobenzene).

CONCLUSIONS

(1) A procedure was developed for selective preparation of perfluoroalkoxypropanoic acid fluorides in a quantitative yield. The procedure involves new catalysts, *N,N,N',N'*-tetraalkyldiaminomethanes, and extraction of the forming reaction products with nonpolar organofluorine solvents.

(2) Oligomerization of hexafluoropropene epoxide in the presence of *N,N,N',N'*-tetraalkyldiaminomethanes yields the hexafluoropropene epoxide tetramer as the major product.

REFERENCES

1. Ponomarenko, V.A., Krukovskii, S.P., and Alybina, A.Yu., *Ftorsoderzhashchie geterotsepnye polimery* (Fluorine-Containing Heterochain Polymers), Moscow: Khimiya, 1973, pp. 118–123.
2. US Patent 3 250 808.
3. PCT Patent 97/44 303.
4. FRG Patent 2 461 445.
5. US Patent 4 081 466.
6. JPN Patent 2-4733.
7. UK Patent 1 550 268.
8. US Patent 4 940 814.
9. Knunyants, I.L., Delyagina, N.I., and Igumnov, S.M., *Izv. Akad. Nauk SSSR, Ser. Khim.*, 1981, no. 4, pp. 857–859.

Russian Journal of Applied Chemistry, Vol. 78, No. 3, 2005, pp. 438–440. Translated from Zhurnal Prikladnoi Khimii, Vol. 78, No. 3, 2005, pp. 441–443.
Original Russian Text Copyright © 2005 by Gataullin, Ishberdina, Sotnikov, Abdrakhmanov.

ORGANIC SYNTHESIS AND INDUSTRIAL ORGANIC CHEMISTRY

Synthesis of 6-Methyl-4-(1-methyl-2-buten-1-yl)-2-(2-cyclohexen-1-yl)- and 6-Methyl-4-(1-methyl-2-buten-1-yl)-2-(1-cyclohexen-1-yl)anilines

R. R. Gataullin, R. R. Ishberdina, A. M. Sotnikov, and I. B. Abdrakhmanov

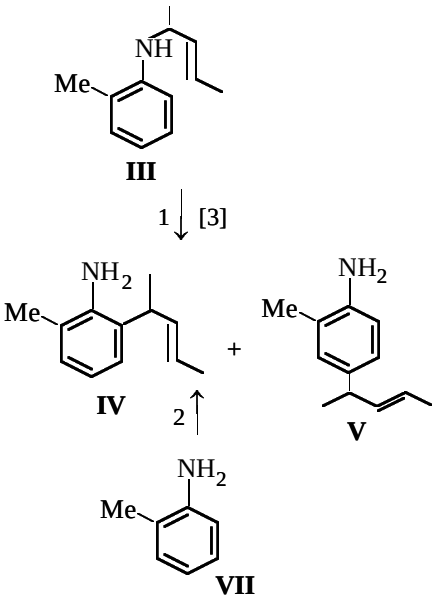
Institute of Organic Chemistry, Ufa Scientific Center, Russian Academy of Sciences, Ufa, Bashkortostan, Russia

Received July 2, 2004; in final form, December 2004

Abstract—Alkenylation of 6-methyl-2-(2-cyclohexen-1-yl)- and 2-(1-cyclohexen-1-yl)anilines with piperylene in the presence of $AlCl_3$ and transformation of the resulting cyclohexenylanilines into carbazole structures were studied.

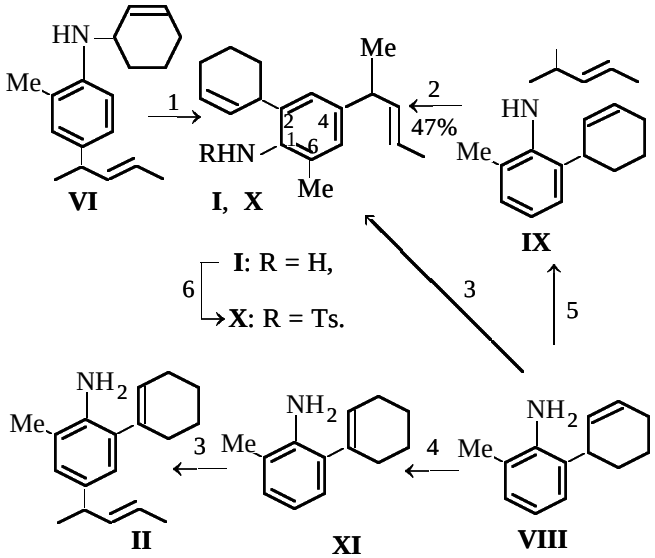
Major attention is given to synthesis of heterocyclic systems of the pyridocarbazole series, as such derivatives (e.g., ellipticine, olivacine, and their isomers) show antitumor activity. One of the main routes to such compounds involves as intermediates 6-substituted carbazoles or their partially hydrogenated analogs [1] prepared from 2-cyclohexenylanilines [2].

To develop a procedure for preparing amines **I** and **II**, which are key substances in the synthesis of olivacine and its isomers, we examined several routes. Aromatic Claisen amino rearrangement of **III** yields amines **IV** and **V** [3]:



Conditions and reagents: (1) HCl, then excess toluidine, 140°C; (2) piperylene, $AlCl_3$, benzene, 135°C, 3 h.

The ratio of the *ortho* and *para* isomers is approximately 85 : 15; therefore, cyclohexenylation of the minor *para* isomer **V** followed by the rearrangement of the resulting N-substituted product **VI** into the desired amine **I** is of little preparative use:



Conditions and reagents: (1) HCl, then excess **V** or *o*-xylene, 140°C; (2) HCl, then excess **VIII**, 165–170°C, 6 h; (3) piperylene, $AlCl_3$, benzene, 135°C, 3 h; (4) KOH, 300°C, 1 h; (5) 3-chloro-2-pentene; (6) TsCl, Py, 20°C.

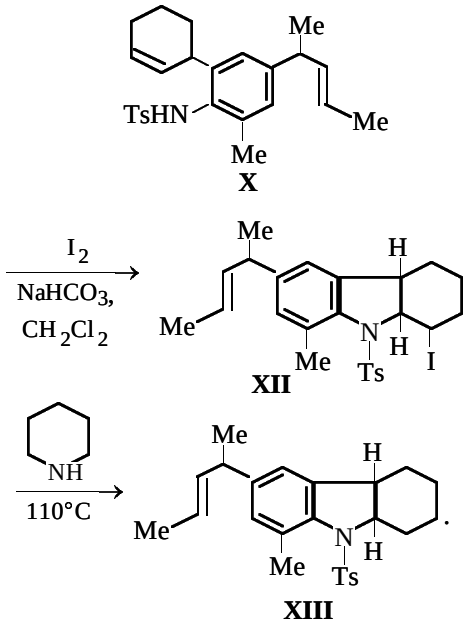
In alkenylation of toluidine **VII** with piperylene in the presence of excess $AlCl_3$, the isomer ratio **IV** : **V** becomes inverse (15 : 85), but the problem of their separation remains.

The reaction of cyclohexenyltoluidine **VIII** with 3-chloro-2-pentene yields *N*-pentenyl derivative **IX**.

1070-4272/05/7803-0438 © 2005 Pleiades Publishing, Inc.

Heating of the hydrochloride of **IX** at 170°C also gives dialkenylaniline **I** in 47% yield based on the reacted amine **VIII**. Alkenylation of **VIII** with piperylene in the presence of $AlCl_3$ appeared to be the most efficient; the yield of **I** was 88%. Cyclohexenylaniline derivatives with the vinyl location of the double bond can be successfully used for the synthesis of relatively complex heterocyclic systems of the carbazole series. Proceeding with such studies [5], we also performed alkenylation of aniline **XI** with piperylene in the presence of $AlCl_3$. The product is formed in 85% yield by heating of **VIII** with KOH at 300°C. The reaction of amine **XI** with piperylene gives compound **II** in 87% yield.

The reaction of amine **I** with TsCl in pyridine gives *N*-tosyl derivative **X**, which, when treated with electrophilic agents (in particular, with molecular iodine), yields hexahydrocarbazole system **XII**, with the double bond in the methylbutenyl moiety remaining intact. Refluxing of **XII** in piperidine results in *trans* elimination with the formation of tetrahydrocarbazole **XIII** in 90% yield:



The compositions and structures of the compounds prepared were proved by IR and NMR spectroscopy and by elemental analysis.

EXPERIMENTAL

The ^1H and ^{13}C NMR spectra were taken on a Bruker AM-300 spectrometer (operating frequencies 300 and 75 MHz, respectively; solvent $CDCl_3$; internal reference TMS), and the IR spectra, on a UR-20 spectrometer. The product purity was monitored on a Chrom-5 chromatograph (stationary phase SE-30 on Chromaton N-AW-DMCS, 1200 × 3-mm column, flame ionization detector, heating rate 12 deg min^{-1}, carrier gas He). Qualitative analysis was performed with Sorbfil UV 254 plates (Lyuminofor Private Company, Krasnodar, Russia), eluent CH_2Cl_2. A mixture of *cis* and *trans* isomers of piperylene (Kaustik plant, Sterlitamak, Bashkortostan, Russia) was used for alkenylation without additional purification.

6-Methyl-4-(1-methyl-2-buten-1-yl)-2-(2-cyclohexen-1-yl)aniline I. (a) A 17-ml pressure vessel was charged with 1 g of aniline **VIII**, 10 ml of benzene, 0.69 g of $AlCl_3$, and 0.68 g of piperylene. The mixture was heated on an oil bath at 135°C for 3 h and cooled to room temperature, after which 30 ml of 20% aqueous NaOH was added, the mixture was stirred, 30 ml of benzene was added, and the organic phase was separated and dried over KOH. The solvent was evaporated to a minimal volume (2–3 ml). Yield of amine **I** after chromatographic purification on a short (1 × 1 cm) silica gel column (eluent hexane) 1.2 g (88%).

(b) To 35 g of amine **VIII** was added 9.5 g of 3-chloro-2-pentene. After the condensation completion (GLC monitoring of reaction mixture samples treated with a NaOH solution), the mixture was heated on an oil bath at 160–170°C. The consumption of **IX** was monitored by GLC. After the rearrangement completion, the mixture was cooled and neutralized with 20% aqueous NaOH (50 ml); the organic layer was dried over KOH. Vacuum distillation gave 20 g of the unchanged amine **VIII** (42% conversion) and 9.6 g (47% based on the reacted amine **VIII**) of dialkenylated product **I**, bp 140–145°C (2 mm Hg).

(c) To 32.37 g of **V** was added 14.9 g of 3-bromo-1-cyclohexene. The mixture was heated on a water bath at 90°C for 1 h and cooled to room temperature; 50 ml of 20% aqueous NaOH was added, and the mixture was shaken in a separating funnel. The organic layer was dried over KOH, filtered, and saturated with gaseous HCl. The resulting hydrochloride of **VI** was heated in excess amine **V** or in *o*-xylene at 140°C until aniline **VI** disappeared (GLC monitoring of reaction mixture samples neutralized with a NaOH solution). After the isomerization completion, the mixture was cooled to room temperature, 100 ml of 20% aqueous NaOH was added, the mixture was shaken in a separatory funnel, and the organic phase was dried over KOH. Vacuum distillation gave 15 g of the unchanged amine **V** and 10.8 g (42% based on

the reacted amine **V**) of dialkenylaniline **I**, bp 140–145°C (2 mm Hg).

6-Methyl-4-(1-methyl-2-buten-1-yl)-2-(1-cyclohexen-1-yl)aniline II was prepared similarly to **I** by procedure (a) from 1 g of **XI**; yield 1.19 g (87%).

***N*-Tosyl-6-methyl-4-(1-methylbut-2-en-1-yl)-2-(2-cyclohexen-1-yl)aniline X.** To a solution of 1.27 g of amine **I** in 10 ml of pyridine was added 1.7 g of *p*-toluenesulfonyl chloride. The mixture was allowed to stand at room temperature for 24 h, 0.5 ml of H_2O was added, the mixture was stirred for 30 min, and the solvent was vacuum-evaporated. The residue was diluted with 5 ml of H_2O and 50 ml of CH_2Cl_2. The organic phase was separated, washed with 30 ml of 5% HCl and water (2 × 10 ml), and dried over $MgSO_4$. After vacuum evaporation of the solvent, 2 g of crude **X** was obtained; the product slowly solidified in air and was sufficiently pure for the subsequent syntheses. Recrystallization from EtOH gave 0.63 g of crystalline **X**, mp 124–126°C (from EtOH). An additional 0.4-g crop of **X** was obtained from the mother liquor after its prolonged storage; mp 126–130°C.

6-Methyl-2-(1-cyclohexen-1-yl)aniline XI. 6-Methyl-2-(2-cyclohexen-1-yl)aniline (10 g) [3] and KOH (10 g) were heated for 1 h on a silicone bath (300°C) in a steel test tube equipped with a reflux air condenser. After cooling, the product was decanted from KOH and vacuum-distilled. Yield 9.5 g (95%), bp 118–120°C (3 mm Hg).

***N*-Tosyl-1-iodo-6-(1-methyl-2-buten-1-yl)-1,2,3,-4,4a,9a-hexahydrocarbazole XII.** To a solution of 0.41 g of amide **X** in 20 ml of CH_2Cl_2, we added 0.85 g of $NaHCO_3$ and 0.51 g of I_2. After the complete consumption of the starting amide **X** (~6–7 h), the precipitate was filtered off, and the solution was washed with 10% aqueous $Na_2S_2O_3$ (2 × 20 ml) and water (2 × 10 ml) and dried over $MgSO_4$. The solvent was vacuum-evaporated. Compound **XII** was obtained as an amorphous mass; yield 0.51 g (95%), R_f 0.4 (eluent CH_2Cl_2).

***N*-Tosyl-6-(1-methyl-2-buten-1-yl)-3,4,4a,9a-tetrahydrocarbazole XIII.** A solution of 0.377 g of 1-iodohexahydrocarbazole **XII** in 3 ml of piperidine was heated at 110°C for 3 h. After the dehydroiodination completion, the solvent was vacuum-evaporated, and the residue was dissolved in 50 ml of CH_2Cl_2 and washed with water (2 × 20 ml). The organic phase was dried over Na_2SO_4, and the solvent was vacuum-evaporated; yield of **XIII** 0.26 g (90%), R_f 0.7 (eluent CH_2Cl_2).

CONCLUSIONS

(1) Alkenylation of 6-methyl-2-(2-cyclohexen-1-yl)- and -2-(1-cyclohexen-1-yl)anilines with piperylene in the presence of $AlCl_3$ gives the corresponding 4-(1-methyl-2-buten-1-yl)anilines in 87–88% yields.

(2) The reaction of the synthesized 6-methyl-2-(2-cyclohexen-1-yl)-4-(1-methyl-2-buten-1-yl)aniline with I_2 gave iodohexahydrocarbazole in 95% yield. On refluxing in piperidine, it transformed into the tetrahydrocarbazole in 90% yield.

REFERENCES

1. Narasimhan, N.S. and Gokhale, S.M., *J. Indian Inst. Sci.*, 2001, vol. 81, no. 2, pp. 135–138.
2. Mustafin, A.G., Khalilov, I.N., Sharafutdinov, V.M., *et al.*, *Izv. Ross. Akad. Nauk, Ser. Khim.*, 1997, no. 3, pp. 630–631.
3. Abdrakhmanov, I.B., Sharafutdinov, V.M., and Tolstikov, G.A., *Izv. Ross. Akad. Nauk, Ser. Khim.*, 1982, no. 9, pp. 2160–2162.
4. Abdrakhmanov, I.B., Mustafin, A.G., Tolstikov, G.A., *et al.*, *Zh. Org. Khim.*, 1986, vol. 22, pp. 613–618.
5. Gataullin, R.R., Sotnikov, A.M., Abdrakhmanov, I.B., and Tolstikov, G.A., *Mendeleev Commun.*, 2003, no. 5, pp. 235–236.

Russian Journal of Applied Chemistry, Vol. 78, No. 3, 2005, pp. 441–442. Translated from Zhurnal Prikladnoi Khimii, Vol. 78, No. 3, 2005, pp. 444–446.
Original Russian Text Copyright © 2005 by Aslanov, Mamedli, Guliev.

ORGANIC SYNTHESIS AND INDUSTRIAL ORGANIC CHEMISTRY

Synthesis of Diester Disulfimides from Saccharinmonocarboxylic Acids and Aromatic Diols

T. A. Aslanov, U. M. Mamedli, and A. M. Guliev

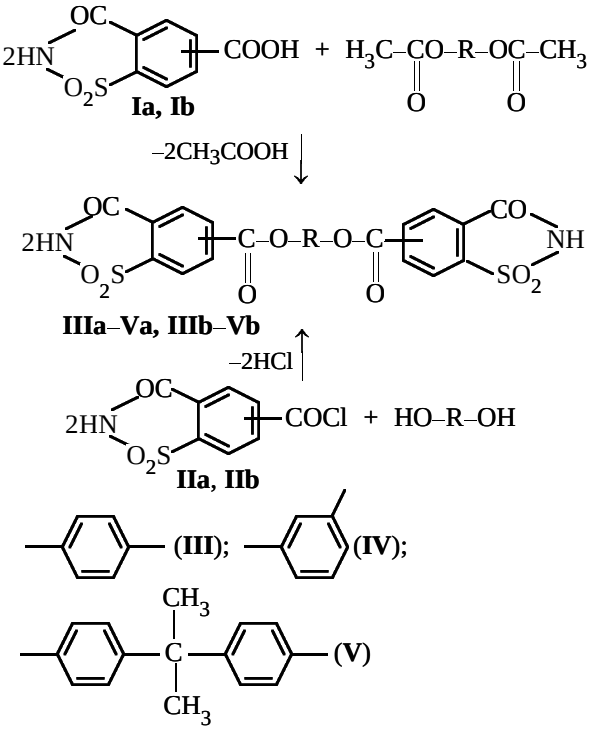
Institute of Polymeric Materials, National Academy of Sciences of Azerbaijan, Sumgait, Azerbaijan

Received January 13, 2005

Abstract—The reactions of saccharinmonocarboxylic acids with bisphenol acetates and of saccharinmonocarboxylic acid chlorides with bisphenols yielded the corresponding diester disulfimides.

Diester disulfimides are used as monomers for preparing poly(ester sulfimides) [1]. Diester diimides are usually prepared by ester interchange of trimellitimide methyl esters with glycols [2]. In particular, diester diimides containing aromatic fragments were prepared from trimellitic acid imide and bisphenol acetates [3]. Such products can also be prepared by reactions of trimellitimide chloride with aromatic diols.

Here we report on the synthesis of diester disulfimides **IIIa**–**Va** and **IIIb**–**Vb**. These compounds can be formed both by reactions of saccharin-5(or 6)-carboxylic acid **Ia** or **Ib** with bisphenol acetates [4] and by reactions of saccharin-5(or 6)-carboxylic acid chloride **IIa** or **IIb** with bisphenols:



Diester disulfimides **IIIa**–**Va** and **IIIb**–**Vb** prepared by both routes are identical, according to analytical data and spectra. Their characteristics are given in the table.

Synthesis of diester disulfimides **IIIa**–**Va** and **IIIb**–**Vb** from saccharinmonocarboxylic acid **Ia** or **Ib** and bisphenol acetates was performed in diphenyl ether at 270–280°C for 3 h until the release of acetic acid was complete. Yield of the target product 85–90%.

In the reactions with saccharinmonocarboxylic acid chlorides, triethylamine was added to the bisphenol solution (2 mol per mole of bisphenol) to bind the released HCl.

The composition and properties of **IIIa**–**Va** and **IIIb**–**Vb** were confirmed by elemental analysis and IR spectroscopy [5]. The IR spectra of **IIIa**–**Va** and **IIIb**–**Vb** contain absorption bands at 1760–1720 (C=O groups of saccharin ring); 1370–1300 and 1200–1180 (SO_2); 1300–1250 and 1120–1100 (ester C–O–C); and 3350–3310 cm^{-1} (NH).

Diester disulfimides **IIIa**–**Va** and **IIIb**–**Vb** are readily soluble in aprotic solvents (DMAA, DMSO, DMF, *N*-methylpyrrolidone).

EXPERIMENTAL

Diester disulfimides IIIa and IIIb derived from hydroquinone acetate III. A flask was charged with 22.7 g (0.1 mol) of saccharinmonocarboxylic acid **Ia** and 38.8 g (0.2 mol) of hydroquinone diacetate dissolved in 100 ml of diphenyl ether. The mixture was stirred at 270–275°C for 3 h. The released acetic acid was collected in a trap. The resulting mixture was dissolved in acetone, and the product was precipitated with distilled water. The gray crystalline powder

1070-4272/05/7803-0441 © 2005 Pleiades Publishing, Inc.

Characteristics of diester disulfimides **IIIa**–**Va** and **IIIb**–**Vb**

Compound	Yield, %	T_m, °C	Empirical formula	Found, %/Calculated, %				*M*
				C	H	N	S	
IIIa	88	285–287	$C_{22}H_{12}O_{10}N_2S_2$	51.10/50.0	2.38/2.27	5.28/5.30	13.01/12.12	528
IVa	87	263–265	$C_{22}H_{12}O_{10}N_2S_2$	51.08/50.0	2.35/2.27	5.30/5.30	13.04/12.12	528
Va	85	251–253	$C_3H_{22}O_{10}N_2S_2$	56.58/57.58	3.20/3.40	4.25/4.33	9.86/9.90	646
IIIb	90	290–292	$C_{22}H_{12}O_{10}N_2S_2$	51.12/50.0	2.35/2.27	5.30/5.30	13.10/12.12	528
IVb	88	271–273	$C_{22}H_{12}O_{10}N_2S_2$	51.1/50.0	2.30/2.27	5.35/5.30	23.01/12.12	528
Vb	87	259–261	$C_{31}H_{22}O_{10}N_2S_2$	56.70/57.58	2.25/3.40	4.30/4.354	9.90/9.90	646

obtained was dried at room temperature and then in a vacuum oven to constant weight.

Diester disulfides **IIIb**, **IVb**, and **Vb** were prepared similarly from resorcinol diacetate, diphenylolpropane diacetate, and saccharinmonocarboxylic acid **Ia** or **Ib**.

Saccharinmonocarboxylic acid chloride IIa and IIb. A mixture of 2.1 g (0.01 mol) of PCl_5 and 2.27 g (0.01 mol) of saccharinmonocarboxylic acid **Ia** or **Ib** was stirred. The mixture spontaneously warmed up to 40–45°C, after which it was heated at 90–95°C for 2 h. After adding dry benzene, the mixture was filtered, and the precipitate was washed with chloroform and benzene, recrystallized from a mixture of toluene and acetone, and dried in a desiccator. Yield 70–75%; T_m = 260°C; M = 245.5.

Found, %: C 39.42; H 1.68; N 5.61; S 14.00; Cl 15.05. $C_8H_4O_4NSCl$.
Calculated, %: C 39.10; H 1.63; N 5.70; S 13.03; Cl 14.46.

Preparation of diester disulfimides IIIa–Va and IIIb–Vb from saccharinmonocarboxylic acid chloride. A mixture of 24.5 g (0.1 mol) of saccharinmonocarboxylic acid chloride **IIa**, 22.8 g (0.05 mol) of diphenylolpropane, and 10.1 g (0.1 mol) of triethylamine in 50 ml of dry toluene was stirred at 25–30°C for 1.5–2 h. A dark product formed. After the reaction completion, 100 ml of distilled water was added, and the mixture was filtered through a glass frit. The product was dried at room temperature and then in a vacuum oven to constant weight. Yield of diester disulfimide **Va** 85%.

Diester disulfimides **IIIa**, **IVa**, and **IIIb**–**Vb** were prepared from saccharinmonocarboxylic acid chloride similarly.

The starting compounds were purified as described in [6].

CONCLUSION

Previously unknown diester disulfimides derived from saccharin-5(or 6)-carboxylic acid and aromatic diols (hydroquinone, resorcinol, diphenylolpropane) were prepared. These compounds can be used as monomers for preparing poly(ester imides).

REFERENCES

1. Aslanov, T.A., Salakhov, M.S., and Efendiev, A.A., *Vysokomol. Soedin., Ser. B*, 2004, vol. 46, no. 2, pp. 379–382.
2. Suvorov, B.V., Zhubanov, B.A., and Mashkevich, S.A., *Trimellitovaya kislota i polimery na ee osnove* (Trimellitic Acid and Polymers Derived from It), Alma-Ata: Nauka, 1975.
3. Arkhipova, I.A., Zhubanov, B.A., Kim, L.V., and Ivashchenko, N.I., *Zh. Prikl. Khim.*, 1976, vol. 49, no. 6, pp. 1399–1402.
4. Tagiev, B.A. and Aslanov, T.A., *Azerb. Khim. Zh.*, 1997, no. 1, p. 62.
5. Kazitsyna, L.A. and Kupletskaya, N.B., *Primenenie UF, IK, YaMR i mass-spektroskopii v organicheskoi khimii* (Applications of UV, IR, NMR, and Mass Spectroscopy to Organic Chemistry), Moscow: Mosk. Gos. Univ., 1979.
6. Gordon, A.J. and Ford, R.A., *The Chemist's Companion. A Handbook of Practical Data, Techniques, and References*, New York: Wiley, 1972.

Russian Journal of Applied Chemistry, Vol. 78, No. 3, 2005, pp. 443–447. Translated from Zhurnal Prikladnoi Khimii, Vol. 78, No. 3, 2005, pp. 447–451.
Original Russian Text Copyright © 2005 by Nosacheva, Revkov, Perkel'.

ORGANIC SYNTHESIS AND INDUSTRIAL ORGANIC CHEMISTRY

Ethylbenzene Oxidation in the Presence of Acetic Anhydride

I. M. Nosacheva, O. A. Revkov, and A. L. Perkel'

Kuzbass State Technical University, Kemerovo, Russia

Received May 28, 2004; in final form, December 2004

Abstract—The kinetics of formation and subsequent transformation of the products of ethylbenzene oxidation in the presence of acetic anhydride at 100°C was studied by solution of the inverse kinetic problem.

Secondary hydroperoxides are the main primary molecular intermediates of liquid-phase oxidation of saturated aliphatic, alicyclic, and some alkylaromatic hydrocarbons [1–4]. These intermediates can further react with carboxylic acid anhydrides (important products of oxidative degradation of saturated hydrocarbons and their oxygen derivatives) [4, 5].

Carboxylic acid anhydrides react with hydroperoxides to form peroxy esters [4–7]. Synthesis of peroxy esters of secondary hydroperoxides and their properties are poorly studied. This is probably due to the fact that peroxy esters of secondary hydroperoxides are substantially less stable than those of primary and especially tertiary hydroperoxides and decompose even at low temperatures [6, 7].

In this work we studied the kinetics of ethylbenzene (EB) oxidation in the presence of acetic anhydride (AA). 1-Phenylethyl hydroperoxide formed in EB oxidation reacts with AA to form 1-phenylethyl peroxyacetate. In this study we examined the main relationships in formation and subsequent reaction of 1-phenylethyl peroxyacetate.

EXPERIMENTAL

Ethylbenzene (pure grade) was treated with concentrated sulfuric acid to remove oxygen-containing compounds [8] and then was distilled in an argon flow. As determined by gas–liquid chromatography, the concentration of methylphenylcarbinol and acetophenone in the resulting product was lower than 0.003 and 0.005 wt %, respectively.

Acetic anhydride (analytically pure grade) was purified by distillation after conversion of the acetic acid impurity into methyl acetate by the reaction with diazomethane.

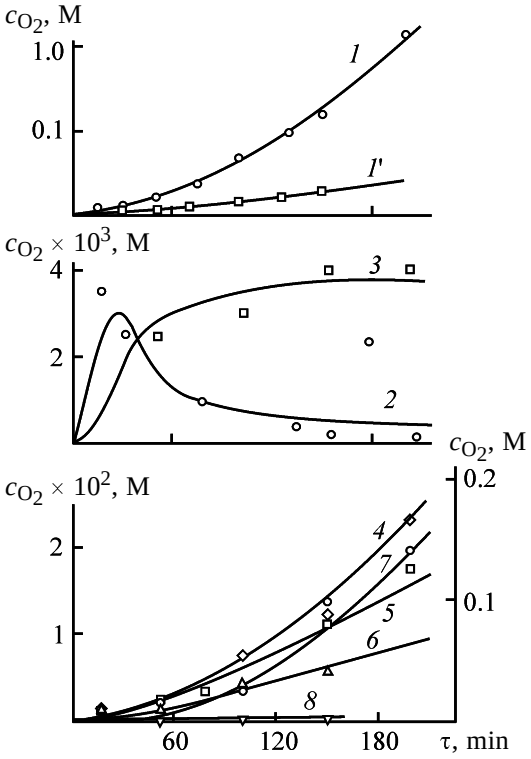
The total peroxide content in the EB oxidation products was determined colorimetrically after treatment of the sample with the reagent containing Fe^{2+} and *N*,*N*-dimethyl-*p*-phenylenediamine [9]. The content of 1-phenylethyl peroxyacetate (PEPA) was calculated as the difference between the content of 1-phenylethyl acetate (PEA) in the sample reduced with triphenylphosphine and in the oxidized sample. Acetic anhydride was decomposed with a methanol–pyridine mixture (1 : 1 v/v) immediately after the sampling. The content of 1-phenylethyl hydroperoxide (PEHP) was determined as the difference between the total peroxide content and the PEPA content. To determine the content of benzoic acid by GLC, it was converted into methyl benzoate by treatment with diazomethane. The GLC analysis of nonperoxide products of EB oxidation was performed at 140°C on a 2000 × 3-mm column; stationary phase 15% Carbowax-6000 on Chromaton N-AW-DMCS, internal reference nitrobenzene.

Ethylbenzene was oxidized in a manometric unit under the conditions of the kinetic control of the oxygen uptake.

The parameters of the kinetic equations were calculated by the least-squares procedure using the Delphi 5.5 program. A set of differential equations was solved in each step by the fourth-order Runge–Kutta method.

Peroxy esters of secondary hydroperoxides are thermally unstable and can be studied only under special conditions [6, 7] which substantially differ from the conditions of hydrocarbon oxidation. The general features of formation and subsequent transformations of peroxy esters of secondary hydroperoxides under the autooxidation conditions were studied with an example of PEPA. This compound was prepared *in situ* by reaction of AA introduced into the reaction

1070-4272/05/7803-0443 © 2005 Pleiades Publishing, Inc.



(*1*') Kinetic curves of oxygen uptake in EB oxidation at 100°C in the absence of AA and kinetic curves of (*1*) total accumulation of the products of EB oxidation at 100°C in the presence of AA and accumulation of (*2*) PEHP, (*3*) PEPA, (*4*) AP, (*5*) MPC, (*6*) BAl + BAc, (*7*) PEA, and (*8*) BAc. (C_{O_2}) concentration of absorbed oxygen and the oxidation products and (τ) time. (*1*–*7*) Calculated curves and (*1*', *8*) experimental curves.

mixture with PEHP formed in radical-chain oxidation of EB.

Ethylbenzene was oxidized with oxygen at 100°C in the absence of AA and in the presence of 1.1 M AA. The experimental kinetic curves of oxygen uptake (in the absence of AA), total accumulation of the EB oxidation products, and accumulation of PEHP, PEPA, methyphenylcarbinol (MPC), acetophenone (AP), PEA, benzaldehyde (BAl) + benzoic acid (BAc), and BAc are shown in the figure.

The rate of ethylbenzene oxidation to form PEHP at 100°C in the absence of AA is almost constant (see figure)

$$PhCH_2Me \xrightarrow{RO_2^*,\ O_2,\ RH} PhCH(OOH)Me\ (PEHP). \quad (1)$$

Clearly, PEHP decomposition under these conditions is slow and is initiated mainly by chain generation. The rate of radical-chain oxidation of EB is described by the equation [1, 2]

$$-d[RH]/d\tau = k_p(2k_t)^{-0.5}[RH](w_i^0)^{0.5}, \quad (2)$$

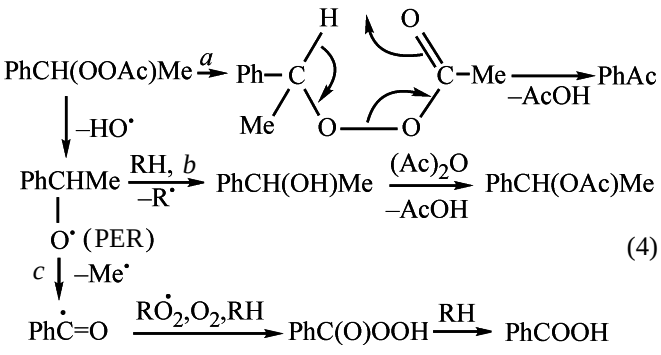
where k_p and $2k_t$ are the rate constants of chain propagation and termination, respectively; w_i^0 is the rate of initiation by chain generation.

Substitution of $k_p(2k_t)^{-0.5} = 22.2 \times 10^{-4}$ l mol$^{-0.5}$ s$^{-0.5}$ [2], the rate constant of radical-chain oxidation of EB in the absence of acetic anhydride ($w_{rc} = 3.9 \times 10^{-6}$ mol l^{-1} s^{-1}), and [RH] = 8.2 M into Eq. (2) gives $w_i^0 = 4.5 \times 10^{-8}$ mol l^{-1} s^{-1} at 100°C.

The kinetic curve of oxygen uptake in the presence of AA is more complex. In the first steps, the curve is typical of an autocatalytic process and then it becomes linear (see figure). Along with PEHP, PEPA is accumulated by acylation of PEHP with AA:

$$PhCH(OOH)Me \xrightarrow[-AcOH]{(Ac)_2O} PhCH(OOAc)Me\ (PEPA). \quad (3)$$

Acceleration of EB oxidation in the presence of AA is due to increasing contribution of degenerate branching caused by homolytic decomposition of PEPA. Probably, radical decomposition of PEPA in the course of BE oxidation is faster than that of the initial PEHP [5]. The main oxidation product of EB in the presence of AA is AP. Its yield is substantially higher than that in thermal oxidation of EB at 120°C in the absence of AA [2]. We suggest that AP is formed by pericyclic transformation of PEPA [scheme (4), pathway *a*]. The relative yield of MPC in the presence of AA (see figure) is substantially lower than that in the absence of AA [2]. Probably, methylphenylcarbinol is formed by the reaction of 1-phenylethoxy radical (PER) with EB and partially reacts with AA to form PEA [scheme (4), pathway *b*]. Clearly, homolytic decomposition of PEPA yields BAl which is further oxidized to BAc [scheme (4), pathway *c*].

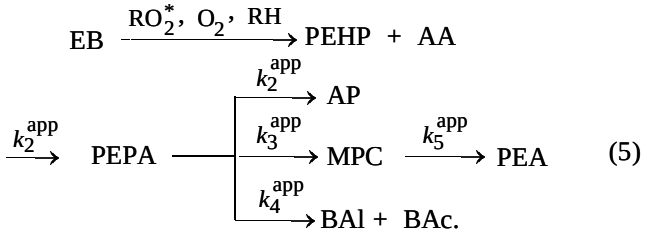


(4)

Calculated rate constants of formation and transformations of PEPA in EB oxidation in the presence of AA

i	$k_i \times 10^4$		$k_i' \times 10^2$		$(k_i'/k_i) \times 10^2$
	s^{-1}	$l\ mol^{-1}\ s^{-1}$	$l\ mol^{-1}\ s^{-1}$	$l^2\ mol^{-2}\ s^{-1}$	
0	10.00		0.19		1.90
1		9.57		16.68	174
2	32.5		0.76		2.34
3	6.13		0.22		3.59
4	2.52		0.0016		0.063
5		2.57		0.000	0.00

Thus, EB oxidation in the presence of AA can be described by the following kinetic scheme:



(5)

Kinetics of reactions (1), (3), and (4) can be described by the following set of equations:

$$-d[EB]/d\tau = k_p(2k_t)^{-0.5}[EB](w_i^0) + k_0^{app}[PEPA]^{-0.5}, \quad (6)$$

$$d[PEHP]/d\tau = k_p(2k_t)^{-0.5}[EB](w_i^0) + k_0^{app}[PEPA]^{-0.5} - k_1^{app}[PEPA][AA], \quad (7)$$

$$d[PEHP]/d\tau = -k_1^{app}[PEPA][AA] - (k_2^{app} + k_3^{app} + k_4^{app})[PEPA], \quad (8)$$

$$d[AP]/d\tau = k_2^{app}[PEPA], \quad (9)$$

$$d[MPC]/d\tau = k_3^{app}[PEPA] - k_5^{app}[MPC][AA], \quad (10)$$

$$d([BAl] + [BAc])/d\tau = k_4^{app}[PEPA], \quad (11)$$

$$d[PEA]/d\tau = k_5^{app}[MPC][AA], \quad (12)$$

$$-d[AA]/d\tau = k_1^{app}[PEHP][AA] + k_5^{app}[MPC][AA], \quad (13)$$

$$d[AA]/d\tau = k_1^{app}[PEHP][AA] + (k_2^{app} + k_3^{app} + k_4^{app})[PEPA] + k_5^{app}[MPC][AA], \quad (14)$$

$$\Delta[O_2] = [EB]_0 - [EB] = [PEHP] + [PEPA] + [AP] + [MPC] + [BAl] + [BAc] + [PEA], \quad (15)$$

where [X] is concentration of the reactants, M; $[O_2]$, amount of oxygen taken up, M; k_1^{app}–k_5^{app} are the apparent rate constants of the steps of reaction (5); and k_0^{app} is the apparent rate constant of initiation by PEPA decomposition.

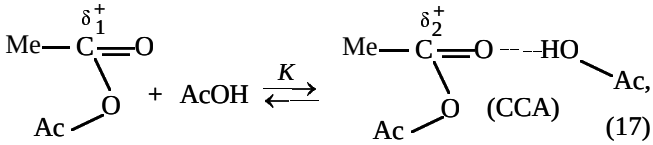
Since formation and subsequent transformations of 1-hydroxycyclohexyl peroxydodecanoate are acid-catalyzed [10, 11], we suggest that the corresponding apparent rate constants can depend on the acetic acid (AAc) concentration

$$k_i^{app} = k_i + k_i'[AAc], \quad (16)$$

where k_i is the autocatalytic constant.

The rate constants calculated by solution of the inverse kinetic problem are presented in the table, and the calculated kinetic curves are shown in the figure.

As seen from the figure, the calculated kinetic curves fit well the experimental results (the sum of squares of the deviations is 4.9×10^{-4}). Comparison of the rate constants shows that the conversion of PEPA into AP is about 75%. Although all k_i^{app}, except for k_5^{app}, depend on the AAc concentration, the autocatalytic contribution to reactions steps, as indicated by the k_i'/k_i ratio (see table), noticeably differ. The influence of AAc on acylation of PEHP with AA is the most pronounced. Clearly, the catalytic effect in this case is caused by formation of AAc–AA (CCA) complex which is more reactive than the free anhydride with respect to the nucleophilic attack of the hydroperoxide ($\delta_2^+ > \delta_1^+$):



(17)

$$(CCA) + PEHP \underset{}{\overset{k_2''}{\rightleftarrows}} PEPA + AAc, \quad (18)$$

where k_2'' is the rate constant of reaction of PEHP with CCA and K is the equilibrium constant of reaction (17).

Taking into account reactions (17) and (18), the PEHP consumption can be described by the kinetic equation of an autocatalytic reaction

$$-d[PEHP]_{cat}/d\tau = k_2'' K[AAc][AA][PEHP]$$

$$= k_2'[AAc][AA][PEHP]. \quad (19)$$

Hence, $k_2' = k_2'' K$.

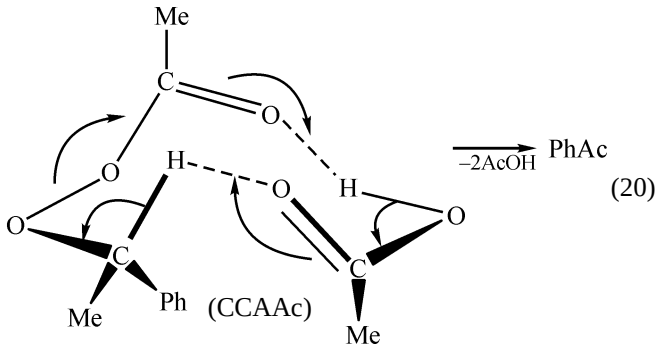
Acylation of MPC with AA should be seemingly also acid-catalyzed. However, our previous kinetic study of this reaction in chlorobenzene at 80–110°C [12] shows that AAc has no effect on this reaction. The k_5^{app} determined in this study (2.57×10^{-4} l mol^{-1} s^{-1}) is close to $k_5^{app} = 2.66 \times 10^{-4}$ l mol^{-1} s^{-1} calculated from the dependence $\ln k_0 = (10.9 \pm 2.9) - (59\,300 \pm 8900)/RT$ [12].

The reason of this distinction is not clear. We assume that it is due to the fact that the steric hindrance in the attack of the carbon atom of the carbonyl group in CCA by the hydroxy group of MPC is stronger than that in the reaction of CCA with the hydroperoxy group of PEHP.

The influence of AAc in the step of PEPA decomposition is weaker than that in the step of its formation. The ratio k_i'/k_i (table) shows that the contribution of the autocatalytic reaction to the overall process is substantially lower [particularly, in the case of reaction (4, pathway *c*)] than in the case of decomposition of 1-hydroxycyclohexyl peroxydodecanoate (intermediate of Baeyer–Villiger oxidation of cyclohexanone with peroxylauric acid) [10, 11]. The ratio of the constants for heterolytic rearrangement of 1-hydroxycyclohexyl peroxydodecanoate (α-hydroxy peroxy ester) into lactone (18°C) is 17.3, whereas for the homolytic decomposition it is 41.8 [11]. Probably, decomposition of the peroxy ester is less acid-sensitive than that of α-hydroxy peroxy ester owing to lower probability of the decomposition by the mechanism of relay proton transfer [10, 11].

We suggest that the decomposition mechanism of PEPA in the cyclic complex with AAc (CCAAc) to form AP (20) is similar.

The apparent rate constant of initiation by homolytic decomposition of PEPA (k_0^{app}) (see table) is almost independent of the presence of acetic acid.



(20)

This constant should be related, by definition, to the apparent rate constants of PEPA decomposition into MPC and BAl by the equation

$$k_0 + k_0'[AAc] = 2e(k_3 + k_3'[AAc]) + (k_4 + k_4'[AAc]), \quad (21)$$

where e is the coefficient of radical escape from the solvent cage.

At [AAc] = 0.2 M, substitution of the constants in Eq. (21) gives $e = 0.57$ which is close to the known value ($e = 0.6$) for aromatic solvents [13].

Thus, carboxylic acid anhydrides substantially catalyze decomposition of secondary hydroperoxides and change the decomposition mechanism. Contrary to the previous data [7], about 25% of the peroxy ester of the secondary hydroperoxide decomposes homolytically, i.e., this compound initiates the radical-chain oxidation but to a lesser extent as compared to peroxy esters of tertiary hydroperoxides [7, 14]. Since carboxylic acid anhydrides are consumed mainly by reactions with hydroperoxides [4], formation and decomposition of peroxy esters of secondary hydroperoxides can contribute significantly to both initiation of oxidation of organic compounds and formation of carbonyl-containing products.

CONCLUSIONS

(1) Acetic anhydride substantially catalyzes radical-chain oxidation of ethylbenzene at 100°C. The primary molecular product of ethylbenzene oxidation, 1-phenylethyl hydroperoxide, decomposes via 1-phenylethyl peroxyacetate formation to give mainly acetophenone by the pericyclic mechanism.

(2) Acceleration of ethylbenzene oxidation in the presence of acetic anhydride is due to homolytic decomposition of the peroxy ester into methylphenylcarbinol and benzaldehyde.

(3) Acetic acid formed in acylation of the hydroperoxide and peroxy ester decomposition catalyzes

both peroxy ester formation and, to a lesser extent, its decomposition.

REFERENCES

1. Emanuel', N.M., Denisov, E.T., and Maizus, Z.K., *Tsepnye reaktsii okisleniya uglevodorodov v zhidkoi faze* (Chain Reactions of Hydrocarbon Oxidation in the Liquid Phase), Moscow: Nauka, 1965.
2. Emanuel', N.M. and Gal, D., *Okislenie etilbenzola (model'naya reaktsiya)* (Ethylbenzene Oxidation (Model Reaction)), Moscow: Nauka, 1984.
3. Nazimok, V.F., Ovchinnikov, V.I., and Potekhin, V.M., *Zhidkofaznoe okislenie alkilaromaticheskikh uglevodorodov* (Liquid-Phase Oxidation of Alkylaromatic Hydrocarbons), Moscow: Khimiya, 1987.
4. Perkel', A.L., Voronina, S.G., and Freidin, B.G., *Usp. Khim.*, 1994, vol. 63, no. 9, pp. 793–809.
5. Nosacheva, I.M., Voronina, S.G., and Perkel', A.L., Abstracts of Papers, *XI Mezhdunarodnaya konferentsiya po khimii organicheskikh i elementoorganicheskikh peroksidov* (XI Int. Conf. on Chemistry of Organic and Oraganoelemental Peroxides), Moscow, June 24–26, 2003, pp. 256–257.
6. Durham, L.J., Glover, L., and Mosher, H.S., *J. Am. Chem. Soc*., 1960, vol. 82, no. 6, pp. 1508–1509.
7. Ryukhardt, S., *Usp. Khim*., 1968, vol. 37, no. 8, pp. 1402–1442.
8. Weissberger, A., Proskauer, E., Riddick, J.A., and Toops, E.E., Jr., *Organic Solvents. Physical Properties and Methods of Purification*, New York: Interscience, 1955.
9. Perkel', A.L., Voronina, S.G., and Perkel', R.L., *Zh. Anal. Khim*., 1991, vol. 46, no. 11, pp. 2283–2286.
10. Shumkina, T.F., Voronina, S.G., Krutskii, D.L., and Perkel', A.L., *Zh. Prikl. Khim*., 1995, vol. 68, no. 2, pp. 290–297.
11. Shumkina, T.F., Voronina, S.G., and Perkel', A.L., *Zh. Prikl. Khim*., 1996, vol. 69, no. 2, pp. 287–294.
12. Perkel', A.L., Nosacheva, I.M., and Revkov, O.A., *Vestn. Kuzbassk. Gos. Tekh. Univ*., 2004, no. 3, pp. 78–81.
13. Denisov, E.T. and Kovalev, G.I., *Okislenie i stabilizatsiya reaktivnykh topliv* (Oxidation and Stabilization of Jet Fuels), Moscow: Khimiya, 1983.
14. Antonovskii, V.L., *Organicheskie perekisnye initsiatory* (Organic Peroxy Initiators), Moscow: Khimiya, 1972.

Russian Journal of Applied Chemistry, Vol. 78, No. 3, 2005, pp. 448–452. Translated from Zhurnal Prikladnoi Khimii, Vol. 78, No. 3, 2005, pp. 452–456.
Original Russian Text Copyright © 2005 by Zhong, Krupei, Pleshkova, Popova, Zakharychev, Perevalov.

ORGANIC SYNTHESIS AND INDUSTRIAL ORGANIC CHEMISTRY

Modification of *L*-α-Polyglutamic Acid with Xanthene Dyes via γ-Carboxy Groups of Amino Acid Residues

Xu Zhong, I. I. Krupei, N. V. Pleshkova, G. V. Popova, V. V. Zakharychev, and V. P. Perevalov

Mendeleev Russian University of Chemical Engineering, Moscow, Russia

Received September 14, 2004; in final form, January 2005

Abstract—Modification of *L*-α-glutamic acid with xanthene dyes (rhodamine and fluorescein) and the optical properties of the incorporated luminophores were studied.

Photosensitive natural proteins, as a rule, are photosensors and energy converters. Light absorption with dye fragments in proteins results in transfer of the electronic excitation energy, which is modeled well by interaction of a donor–acceptor pair upon irradiation of a simple protein [1, 2].

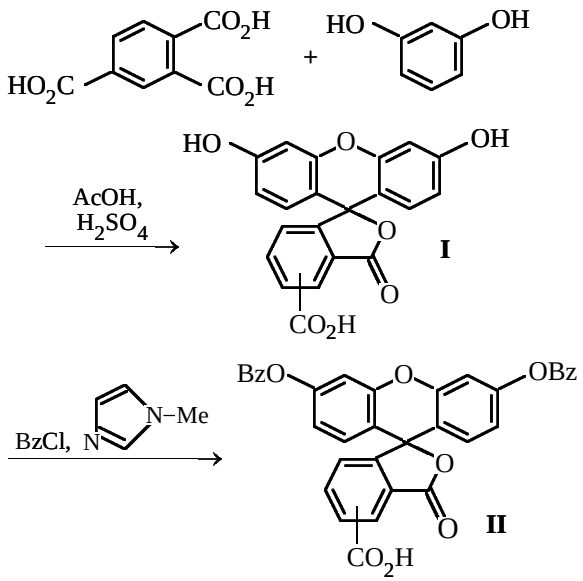
The researchers' interest was focused on photochromic and photosensitive polypeptides; this was reflected in a number of reviews and summarizing papers [3–5]. Polyamino acids are similar in properties to natural peptides; they can change conformation under the influence of even a weak external action, which results in changes in the physicochemical, physical, and mechanical properties of the macromolecule as a whole [3].

Previous luminescence studies demonstrated the possibility of nonradiative energy transfer between 9-aminoacridine (radiation donor) and 4-amino-*N*-phenylnaphthimide (radiation acceptor) in a polymer matrix upon laser irradiation [6]. Proceeding with these studies, we prepared in this work a model of an α-helical biopolymer, suitable for studying the migration of the energy of electronic excitation of the luminescing groups in the macromolecule, the changes in the chain conformation occurring under external impacts, and the formation of intra- and intermolecular contacts.

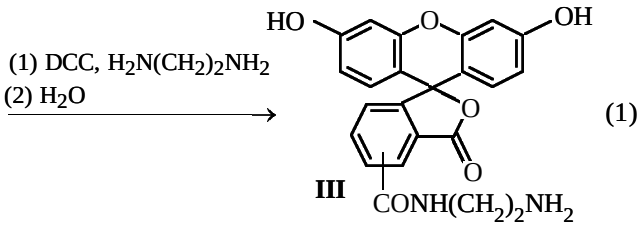
Polyglutamic acid (PGA) is a comprehensively studied protein model. It contains free γ-carboxy groups capable of polymer-analogous transformations; therefore, it can be a convenient biopolymer matrix for modification with dyes. For our experiments, we chose xanthene dyes: fluorescein (Fl) and rhodamine (Rh), taking into account the fact that the luminescence maximum of Fl (radiation donor) corresponds to the absorption maximum of Rh (radiation acceptor) [7].

Modification of γ-carboxy groups of PGA with luminophores was performed by formation of an amide bond. To this end, it was necessary to introduce primary amino groups into Fl and Rh. To preserve the optical properties of the luminophores, the functional group was separated from the dye core by an aliphatic hydrocarbon spacer.

5(6)-Carboxyfluorescein **I** was prepared by condensation of trimellitic acid with resorcinol. To protect the hydroxy groups, compound **I** was converted into 3',6'-dibenzoyl-5(6)-carboxyfluorescein **II**, whose reaction with dicyclohexylcarbodiimide (DCC) and ethylenediamine gave 5(6)-(2-aminoethylcarbamoyl)-fluorescein **III**:

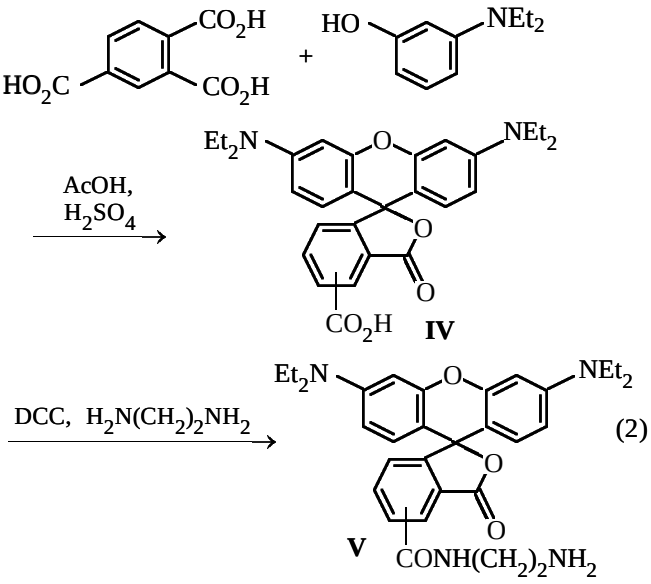


1070-4272/05/7803-0448 © 2005 Pleiades Publishing, Inc.



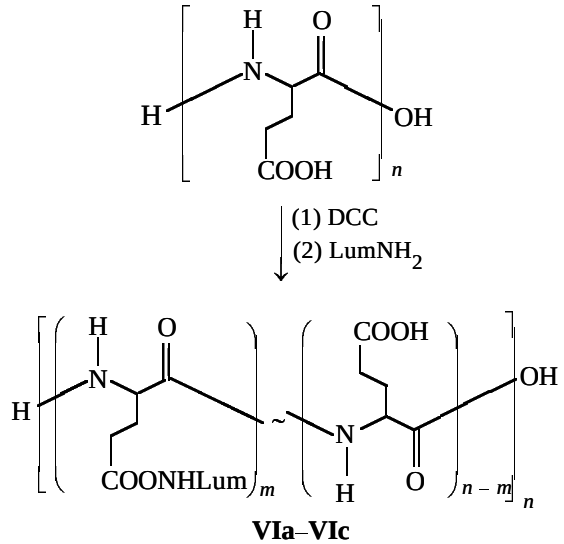
(1)

5(6)-Carboxy-*N*,*N*,*N*',*N*'-tetraethylrhodamine **IV** was prepared from trimellitic acid and 3-(diethylamino)phenol. Its subsequent reaction with DCC and ethylenediamine gave 5(6)-(2-aminoethylcarbamoyl)-*N*,*N*,*N*',*N*'-tetraethylrhodamine **V**:

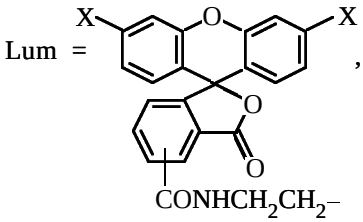


(2)

Taking into account our experience in introducing various dyes into PGA [8, 9], we performed the polymer-analogous transformations of the PGA γ-carboxy groups using dicyclohexylcarbodiimide:



VIa–**VIc**



(3)

where X = OH, $m \approx 13$ (**a**); X = NEt_2, $m \approx 10$ (**b**); X = OH or NEt_2, $m \approx 10$ (**c**); $n \approx 40$.

In all the reactions we used *L*-α-polyglutamic acid of molecular weight 5200 ($n \approx 40$) [8]. The regular structure of the modified macromolecule could be attained at the maximal degree of the polymer modification with the dye. For this purpose, we initially performed computer simulation (GAMESS program) of the target molecules: amides derived from PGA and modified Fl **III** and Rh **V**. We found that the content and arrangement of the dyes in the polypeptide chain are governed by steric factors. The maximal content of Fl in the polypeptide corresponds to modification of every third amino acid molecule with the dye. The bulkier Rh derivative can be introduced only in every fourth amino acid fragment. Taking into account these results, we chose appropriate component ratios.

We also prepared the polyamino acid containing both dyes in the chain simultaneously (compound **VIc**). Successive addition of the dyes to the γ-carboxy group of PGA resulted in a random, virtually uncontrollable distribution of the dyes in the polymer matrix. Therefore, our choice was to introduce **III** and **V** simultaneously. Since Rh contains bulkier diethylamino substituents, we expected that alternation of the Rh and Fl substituents separated by at least two free amino acid units would be sterically favorable and chose the corresponding component ratio. The reaction progress was monitored by TLC and indirectly by formation of the reaction by-product, dicyclohexylurea (DCHU). Its total amount corresponded to the complete conversion of the dyes. Comparison of the chromatograms of the reactants, product, and reaction mixture showed the absence of residual amounts of unchanged dyes **III** and **V**.

To obtain the same yield of the modified polymer (~60%), the reaction of PGA with **V** (60 h) took longer time, compared to the reaction with **III** (36 h).

The content of the chromophores in PGA was determined by ^1H NMR and electronic spectroscopy. In the first case, we compared the integral intensities of the signals of the aromatic protons (7.6–8.1 ppm) of the dyes and methylene (β-CH_2, 2.25 ppm; γ-CH_2,

Electronic absorption and fluorescence spectra of compounds in a 10% solution of triethylamine in DMSO

Compound	λ_{max}^{abs}, nm (log ε)	λ_{max}^{fl}, nm
III	521.5 (4.07)	565
V	558 (4.05)	587
VIa	523 (4.06)	552
VIb	566 (4.05)	605
VIc	531 (4.06), 587 (4.00)	563, 612

2.65 ppm) protons of PGA [9]. Using the optical method of successive dilutions, we estimated the dye content in the polymer from variation of the solution absorption at λ_{max}. The results obtained by both methods were consistent and corresponded to 33 mol % content of Fl and 25 mol % of Rh in PGA. The total content of Fl and Rh in **VIc** was 26 mol %. The absorption spectra of the compounds recorded at different concentrations show that the content of the fragments of the two dyes in the polymer is approximately equal.

The electronic absorption and luminescence spectra of **III**, **V**, and **VIa**–**VIc** were recorded in ethanol, DMSO, and DMSO–triethylamine mixture (10 wt %) (see table). In the absence of a base, the Fl derivatives lose the capability for the luminescence. This feature can be used in subsequent studies of the behavior of luminescing biopolymers in media with different pH values. The parameters of the electronic absorption and luminescence spectra of the compounds are given in the table.

In binding of the dyes with PGA, the long-wave absorption maxima of Fl and Rh are shifted bathochromically by 1.5 and 8 nm, respectively. The emission maximum of Fl is shifted hypsochromically by 13 nm, and that of Rh, bathochromically by 18 nm. As a result, the Stokes shift of Fl after the reaction with PGA decreased by 15 nm, and that of Rh increased by 10 nm. Thus, compounds **VIa** and **VIb** preserve the properties of the donor–acceptor pair: The emission maximum of the Fl derivative (radiation donor, 552 nm) is close to the absorption maximum of the Rh derivative (radiation acceptor, 566 nm).

EXPERIMENTAL

The IR spectra were recorded on a UR-20 spectrophotometer (mulls in mineral oil), and the ^{1}H NMR spectra, on a Bruker WP-400SY spectrometer (400 MHz, reference TMS). The electronic absorption spectra were taken on a Jasco videc 510 spectrophotometer, and the luminescence spectra, on an Edinbourgh Injfr. 549 spectrofluorimeter with the time-resolved photon counting in the pulse mode; the mass spectrum was taken on a Kratos MS 50 TS spectrometer (chemical ionization, 3 eV). The reaction progress and the homogeneity of the products were monitored by TLC on UV-254 plates (UV development).

Polyglutamic acid (M ~5200, n = 40) was prepared by the *N*-carboxy anhydride method from *N*-benzoyloxycarbonyl-*L*-glutamic acid γ-methyl ester (Sigma) [10].

5(6)-Carboxyfluorescein I. A mixture of trimellitic acid (5.0 g, 23.8 mmol), resorcinol (5.4 g, 47.6 mmol), and glacial acetic acid (1.4 ml) was heated with stirring at 185°C for 15 min, 1.0 g of concentrated H_2SO_4 was added dropwise, and the mixture was heated to 210°C and stirred at this temperature for 30 min. Then the mixture was cooled, crushed, and boiled with 20 ml of water for 10 min. The precipitate was filtered off, washed with water, and recrystallized from ethanol; yield of **I** 4.64 g (52%), R_f = 0.70 (EtOH–$CHCl_3$, 1 : 50). Electronic absorption spectrum (EtOH): λ_{max} = 492 nm (log ε = 4.40).

3',6'-Dibenzoyl-5(6)-carboxyfluorescein II. To a solution of **I** (4.0 g, 10.6 mmol) in 30 ml of dry pyridine, we added dropwise with stirring 1-methylimidazole (0.9 g, 10.6 mmol) and benzoyl chloride (6.6 g, 47.2 mmol). The mixture was stirred for 1 h, evaporated to a volume of 10 ml, and diluted with 100 ml of 1 M HCl. The light yellow precipitate was filtered off, washed on the filter with 1 M HCl (2 × 30 ml) and cold water, and dried in air. Yield of **II** after recrystallization from glacial acetic acid 6.8 g (60%), R_f = 0.80 (EtOH–$CHCl_3$, 1 : 25).

5(6)-(2-Aminoethylcarbamoyl)fluorescein III. Compound **II** (3.0 g, 5.43 mmol) and dicyclohexylcarbodiimide (1.0 g, 5.43 mmol) were dissolved in DMF (20 ml); the solution was stirred for 5 min. The resulting solution was added in portions with stirring to a solution of ethylenediamine (0.64 g, 8.15 mmol) in DMF (10 ml). The mixture was stirred for 1 h, the DCHU precipitate was filtered off, and the solvent was distilled off in a vacuum. A solution of NaOH (0.43 g, 10.8 mmol) in water (10 ml) was added, the mixture was refluxed for 30 min, and the precipitate was filtered off, washed on the filter with water, and dried in air. Yield of **III** 1.66 g (73%), R_f = 0.75 (AcOH–water, 3 : 1). Electronic absorption spectrum (EtOH): λ_{max} = 500 nm (log ε = 4.10).

^{1}H NMR spectrum (δ, ppm, $CDCl_3$): 2.89–3.02 br.d (2H, NH_2), 3.23–3.65 m (2H, C$H_2$$NH_2$), 3.75–

4.00 m (2H, CONHCH_2), 6.12 br.s (2H, OH), 7.27–8.68 m (9H, arom. CH), 9.02 br.d (1H, CONH).

Found, %: C 66.18, 66.10; H 4.08, 4.14; N 6.62, 6.65. $C_{23}H_{18}N_2O_6$.
Calculated, %: C 66.02; H 4.33; N 6.69; *M* = 418.405.

5(6)-Carboxy-*N,N,N',N'*-tetraethylrhodamine IV. Trimellitic acid (2.0 g, 9.5 mmol), 3-(diethylamino)phenol (3.1 g, 19.0 mmol), and glacial acetic acid (3.2 ml) were mixed and heated in a heat-resistant test tube at 185°C for 15 min with stirring, after which concentrated H_2SO_4 (0.4 ml) was added dropwise, and the mixture was heated to 210°C and stirred at this temperature for 30 min. The resulting mixture was cooled, ground, and boiled for 10 min with 20 ml of water, after which 10% NaOH was added to neutral reaction, and the precipitate was filtered off, washed with water, and recrystallized from ethanol–water (2 : 1). Yield of **IV** (red-violet crystals) 3.01 g (65%), R_f = 0.30 (AcOH–water, 1 : 4). Electronic absorption spectrum (EtOH): λ_{max} = 541 nm ($\log\varepsilon$ = 4.64).

5(6)-(2-Aminoethylcarbamoyl)-*N,N,N',N'*-tetraethylrhodamine V. Compound **IV** (3.0 g, 6.16 mmol) and dicyclohexylcarbodiimide (1.14 g, 6.16 mmol) were dissolved in DMF (20 ml); the mixture was stirred for 5 min. The resulting solution was added in portions with stirring to a solution of ethylenediamine (0.72 g, 9.25 mmol) in DMF (10 ml). The mixture was stirred for 1 h, the DCHU precipitate was filtered off, and the solvent was distilled off in a vacuum. The residue was triturated with 10 ml of 25% ammonia, and the resulting crystals were filtered off, washed with water, and dried in air. Yield of **V** 2.28 g (70%), R_f = 0.40 (AcOH–water, 1 : 3). Electronic absorption spectrum (EtOH): λ_{max} = 547 nm ($\log\varepsilon$ = 4.58). Mass spectrum (*m*/*z*): 529 $[M + 1]^+$ (100%).

Found, %: C 70.16, 70.21; H 6.92, 6.98; N 10.50, 10.45. $C_{31}H_{36}N_4O_4$.
Calculated, %: C 70.43; H 6.86; N 10.60; *M* = 528.653.

γ-Amide of *L*-α-polyglutamic acid and 5(6)-(2-aminoethylcarbamoyl)fluorescein VIa. Polyglutamic acid (3.9 g, 0.03 mol of monomeric units) was dissolved in DMF (15 ml); a solution of **III** (4.6 g, 0.011 mol) in DMF (15 ml), dicyclohexylcarbodiimide (2.27 g, 0.011 mol), and pyridine (1 drop) were added, and the mixture was kept at 0°C for 2 h and then was allowed to stand at room temperature. The reaction progress was monitored by TLC. After the reaction completion (36 h), the DCHU precipitate was filtered off, and the solvent was distilled off in a vacuum. The residue was dissolved in ethyl acetate, the solution was filtered, and the filtrate was vacuum-evaporated. The residue was reprecipitated from chloroform with diethyl ether and dried in a vacuum. Yield of **VIa** 4.7 g (60%), R_f = 0.13 (BuOH–AcOH–water, 4 : 1 : 1). IR spectrum (ν, cm^{-1}): 3100–2700 br, 3340 br (OH, NH), 1700 (C=O), 1670 (amide I), 1620 (C=C), 1550 (amide II).

γ-Amide of *L*-α-polyglutamic acid and 5(6)-(2-aminoethylcarbamoyl)-*N,N,N',N'*-tetraethylrhodamine VIb was prepared similarly from PGA (3.9 g, 0.03 mol of monomeric units), **V** (4.4 g, 0.008 mol), and dicyclohexylcarbodiimide (1.65 g, 0.008 mol). The reaction was complete in 60 h; yield 4.9 g (60%); R_f = 0.10 (BuOH–AcOH–water, 4 : 1 : 1). IR spectrum (ν, cm^{-1}): 3100–2700 br, 3340 br (OH, NH), 1700 (C=O), 1670 (amide I), 1620 (C=C), 1550 (amide II).

Mixed γ-amide of *L*-α-polyglutamic acid and 5(6)-(2-aminoethylcarbamoyl)fluorescein and 5(6)-(2-aminoethylcarbamoyl)-*N,N,N',N'*-tetraethylrhodamine VIc was prepared similarly from PGA (3.9 g, 0.03 mol of monomeric units), **III** (2.09 g, 0.005 mol), **V** (2.64 g, 0.005 mol), and dicyclohexylcarbodiimide (2.27 g, 0.011 mol). Yield of **VIc** 4.1 g; R_f = 0.30 (BuOH–AcOH–water, 4 : 1 : 1). IR spectrum (ν, cm^{-1}): 3370, 3000–2600 (NH, OH), 1700 (C=O), 1670 (amide I), 1620 (C=C), 1540 (amide II).

CONCLUSIONS

(1) *L*-α-Polyglutamic acid was modified with covalently bound xanthene dyes, rhodamine and fluorescein, containing primary amino groups; the degree of substitution of the pendant γ-carboxy groups of the substrate depends on the steric factors.

(2) Luminophores linked via amide bond to *L*-α-polyglutamic acid preserve their optical properties; the emission maximum of fluorescein (552 nm) virtually corresponds to the absorption maximum of rhodamine.

ACKNOWLEDGMENTS

The study was performed within the framework of the Multifunctional Smart Polymers project, New Chemical Materials and Products program of the RF Ministry of Education and within the framework of B0025 UNTs project (Supramolecular Chemistry and High Technologies for Preparing New Materials) of the Integration Federal Target Program.

REFERENCES

1. *Recombinant Photoproteins in the Design and Binding Assay*, Low, W.I., Akmal, N., and Usmani, A.M., Eds., New York: Marceil Dekker, 2002, pp. 259–270.
2. Deo, S.K. and Dounert, S., *Fresenius J. Anal. Chem.*, 2001, vol. 369, special issue, pp. 258–266.
3. Pieroni, O., Fissi, A., and Popova, G., *Prog. Polym. Sci.*, 1998, vol. 23, pp. 81–122.
4. Cooper, T., Natarajan, L., and Crane, R., *Trends Polym. Sci.*, 1993, no. 12, pp. 400–406.
5. Willner, I. and Rubin, S., *Angew. Chem. Int. Ed.*, 1996, no. 35, pp. 367–375.
6. Popova, G.V., Korigodski, A.R., Manaev, Ya.A., *et al.*, *Phys. Scripta*, 1995, no. 5, pp. 231–235.
7. Krichevskii, G.E., *Fotokhimicheskie prevrashcheniya krasitelei i stabilizatsiya okrashennykh materialov* (Photochemical Transformations of Dyes and Stabilization of Dyed Materials), Moscow: Khimiya, 1986.
8. Khalid, M., Eliseeva, E.N., Popova, G.V., and Yudin, S.G., *Polym. Sci.*, 1994, vol. 13, no. 36, pp. 425–428.
9. Xu Zhong, Popova, G., and Kireev, V., *Polym. Sci. A*, 2003, vol. 45, no. 5, pp. 430–435.
10. Suvorov, N.N., Popova, G.V., and Nekhlyudov, A.D., *Zh. Obshch. Khim.*, 1981, vol. 52, no. 10, pp. 2337–2340.

Russian Journal of Applied Chemistry, Vol. 78, No. 3, 2005, pp. 453–455. Translated from Zhurnal Prikladnoi Khimii, Vol. 78, No. 3, 2005, pp. 457–460.
Original Russian Text Copyright © 2005 by Vazhev, Aldabergenov.

ORGANIC SYNTHESIS AND INDUSTRIAL ORGANIC CHEMISTRY

The Use of IR Spectra for Estimating the Boiling Points and Molecular Weights of Monohydric Aliphatic Alcohols

V. V. Vazhev and M. K. Aldabergenov

Kostanai State Teacher's Training College, Kostanai, Kazakhstan

Received December 9, 2004

Abstract—The use of transformed IR spectra as descriptors of molecular structure in estimating the boiling points and molecular weights of alcohols was studied. No additional data on molecular structure are required for the estimation.

The boiling point T_b is a fundamental characteristic of organic compounds; therefore, development of methods of its theoretical estimation attracts much attention for a long time. Numerous additive methods for estimation of T_b were suggested, but the most widely used is the QSPR (Quantitative Structure–Property Relationships) method, whose current status can be judged from published reviews [1, 2]. The majority of studies on estimating T_b concerns hydrocarbons or heterogeneous systems containing hydrocarbons and other low-polarity molecules. Much less attention was given to simulation and estimation of T_b of highly polar substances. This is apparently caused by the fact that the traditionally used descriptors of molecular structure (mainly topological indices) insufficiently adequately reflect the structural features of molecules responsible for formation of hydrogen bonds in solutions. In particular, the QSPR studies of T_b of alcohols were made only in a few papers [3–9]. The model constructed in [3] for a small set of 37 monohydric alcohols was characterized by the correlation coefficient between experimental and evaluated boiling points R = 0.978 and standard deviation S = 7.4988. For the same subjects, Yang *et al*. in a later study [4] obtained R = 0.9837 and S = 6.35. For the set of 29 alcohols Galvez *et al*. obtained R = 0.979 and S = 3.63 [5]. Recently [6] it was found that, for a small set of 54 saturated alcohols, R = 0.9945 and S = 4.26. For 58 alcohols, Randic and Basak [7] constructed a series of models, the best of which had R = 0.9943 and S = 3.891. For 106 monohydric alcohols, Cao and coworkers [8] constructed a model with R = 0.9899 and S = 4.5727. The highest quality of estimation with R = 0.9960 and S = 3.814 was reached by Ren for 108 alcohols [9].

Here we studied the possibility of estimating T_b and molecular weight of monohydric alcohols using their IR spectra as descriptors of molecular structure. Previously the IR spectra were successfully used in estimating chromatographic retention indices of a set of substances of various classes, among them alcohols [10], and normal boiling points of alkanes [11]. The possibility of determining the molecular weights of compounds from the IR spectra was not considered previously.

EXPERIMENTAL

We used the IR transmission spectra in the gas phase and the boiling points of monohydric aliphatic alcohols with the number of carbon atoms from 2 to 12, available from the server of the National Institute of Standards (NIST, USA) [12]. The training sample contained 60 substances, and the control sample, 40. Before the calculations, the spectra were normalized by the formula

$$d_{ij} = h_{ij}\left(\sum_{k=1}^{k=n} h_{ik}\right)^{-1}, \quad (1)$$

where d_{ij} are operating values of descriptors used in calculations; n, number of points in the IR spectrum; and h_{ij}, transmission in the spectrum of substance i in point j.

A part of spectra in the range 550–3798 cm^{-1} was used; in this range, the spectrum was interpolated linearly with a step of 4 cm^{-1}; the number of points in the spectrum n = 813. Elements d_{ij} form a matrix of descriptors D in which submatrices of training sample A and control sample C can be distinguished. In our case, the number of descriptors (813) exceeds the number of substances in the training sample (60) and the problem of choice of the least correlated descriptors, well-known in estimation, arises. A new

1070-4272/05/7803-0453 © 2005 Pleiades Publishing, Inc.

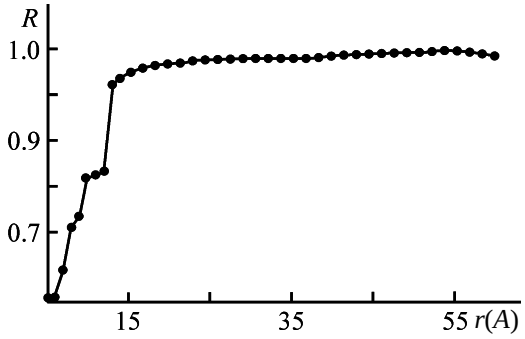


Fig. 1. Correlation coefficient R for the whole set of substances as a function of the estimated rank of descriptor matrix $r(A)$.

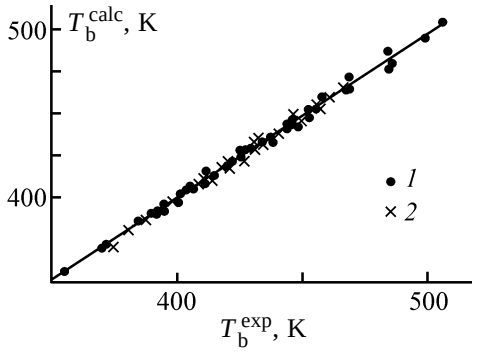


Fig. 2. Correlation between experimental boiling points of alcohols (T_b^{exp}) and those estimated from the IR spectra (T_b^{calc}). Sample: (*1*) training and (*2*) control; the same for Fig. 3.

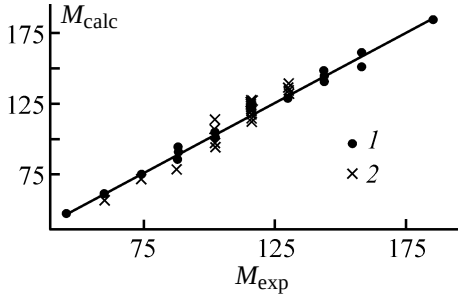


Fig. 3. Correlation between the experimental molecular weight M_{exp} and that estimated from the IR spectra (M_{calc}).

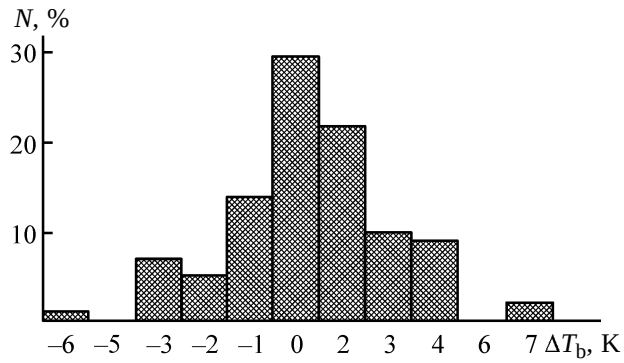


Fig. 4. Error distribution histogram for estimation of T_b of alcohols. (*N*) Incidence.

Table 1. Indexes of correlation between the experimental and calculated boiling points and molecular weights of alcohols

Characteristic	Index of correlation	Whole set	Sample	
			training	control
T_b	R	0.9972	0.9976	0.9963
	S	2.268	2.324	2.129
M	R	0.9896	0.9974	0.9693
	S	3.441	1.929	4.751

approach to solving of this problem was suggested in [13]. Here we present the expression used for the calculations:

$$p = CV_r\Gamma_r^{-1}U_r^T b, \quad (2)$$

where p is the sought-for vector consisting of characteristics of the control sample; b, vector consisting of characteristics of the training sample of substances; U, matrix consisting of eigenvectors of matrix AA^T; V, matrix consisting of eigenvectors of matrix A^TA; and Γ, diagonal matrix of nonzero singular numbers coinciding for both matrix products.

The subscript is the estimated rank of the descriptor matrix $r(A)$; it denotes that r highest eigenvalues and the corresponding eigenvectors are used. For comparison of the results obtained with published data, the submatrix of descriptors in Eq. (2) was completed with the submatrix of training sample A and, correspondingly, vector b was completed with vector p. This procedure is equivalent to constructing a correlation model from the training sample and estimating the characteristics of both control and training samples. Calculations were performed using the PROGROC software (PROGram RObustness Calculation) developed by us [13]. The quality of estimation was characterized by the correlation coefficient R between the estimated and experimental values and by the standard deviation S.

The dependence of the correlation coefficient for T_b of the whole set of substances on the estimated rank of the matrix of descriptors is shown in Fig. 1.

The maximum $R = 0.9972$ for T_b is reached at $r = 54$, standard deviation $S = 2.268$. The results of estimation of T_b and molecular weight at this rank are shown in Figs. 2 and 3.

The quantitative characteristics of the corresponding correlation dependences are listed in Table 1.

A part of the results obtained in estimating T_b

Table 2. Experimental and estimated from the IR spectra boiling points of alcohols (K) for the control sample

Substance	T_b, K		Difference
	experiment	calculation	
2-Ethyl-1-pentanol	439.15	436.24	2.91
5-Methyl-3-hexanol	420.15	422.75	–2.60
5-Methyl-1-heptanol	455.65	454.30	1.35
2,3-Dimethyl-1-butanol	417.70	419.19	–1.49
2-Hexanol	411.00	412.53	–1.53
2,5-Dimethyl-2-hexanol	426.65	423.05	3.60
4-Methyl-2-ethyl-1-pentanol	449.65	445.96	3.69
2,2,3-Trimethyl-3-pentanol	426.65	423.38	3.27
4-Methyl-2-hexanol	421.15	420.35	0.80
2-Methy-1-propanol	380.80	381.25	–0.45
2,3-Dimethyl-3-pentanol	412.90	413.27	–0.37
2,3-Dimethyl-3-heptanol	446.15	450.46	–4.31
2-Ethyl-1-butanol	421.00	420.47	0.53
4-Methyl-3-hexanol	422.65	422.27	0.38
3-Pentanol	388.00	387.47	0.53
3-Hexanol	407.00	407.30	–0.30
6-Methyl-2-heptanol	445.00	447.16	–2.16
3-Heptanol	425.15	424.67	0.48
6-Methyl-1-heptanol	460.15	461.47	–1.32
3-Methyl-1-pentanol	426.00	425.32	0.68
2-Methyl-3-pentanol	398.00	397.93	0.01
4-Nonanol	465.65	466.18	–0.53
2-Methyl-2-butanol	375.10	370.98	4.12
5-Methyl-1-hexanol	440.65	439.31	1.34
2-Heptanol	432.00	436.49	–4.49
4-Methyl-4-heptanol	434.20	433.14	1.06
5-Methyl-2-hexanol	422.20	419.67	2.53
3-Methyl-3-hexanol	414.00	412.34	1.66
2-Methyl-2-hexanol	414.00	414.44	–0.41
Isopropanol	355.00	349.16	5.84
2-Methyl-2-heptanol	432.00	431.50	0.50
1-Hexanol	430.00	433.69	–3.69
2,2-Dimethyl-3-pentanol	409.00	409.50	–0.57
2-Methyl-3-ethyl-3-pentanol	432.15	432.70	–0.55
2-Ethyl-1-hexanol	456.00	456.11	–0.11
3-Methyl-2-pentanol	407.00	405.50	1.50
2,5-Dimethyl-3-hexanol	431.00	430.33	0.67
2-Octanol	453.00	454.14	–1.14
2,3-Dimethyl-2-pentanol	410.65	411.42	–0.77
4-Methyl-1-heptanol	455.85	454.04	1.81

of alcohols, related to the control sample only, are presented in Table 2.

The maximal error is observed for isopropanol and reaches 5.84 K. The error distribution for T_b of alcohols (Fig. 4) is close to the normal distribution, which confirms the reliability of the model; 71% of deviations of the calculated boiling points are in a narrow range (±2 K).

The above data show that our estimation of T_b of alcohols is better than the best published results obtained with the commonly used statistical characteristics.

CONCLUSIONS

(1) The use of normalized IR spectra as descriptors of molecular structure allows simultaneous estimation of the boiling point and molecular weight of alcohols in one numerical experiment.

(2) The quality of estimation is characterized by the correlation coefficient between the experimental and estimated boiling points $R = 0.9972$ and standard error of the estimate $S = 2.268$. For the molecular weight, $R = 0.9896$ and $S = 3.441$.

(3) The important feature of the suggested approach is the possibility of estimating the characteristics of unknown compounds without identification, using only their IR spectra.

REFERENCES

1. Katritzky, A.R., Maran, U., Lobanov, V.S., and Karelson, M., *J. Chem. Inf. Comput. Sci.*, 2000, vol. 40, no. 1, pp. 1–18.
2. Taskinen, J. and Yliruusi, J., *Adv. Drug Delivery Rev.*, 2003, vol. 55, pp. 1163–1183.
3. Yao, Y., Xu, L., Yang, Y., and Yuan, X., *J. Chem. Inf. Comput. Sci.*, 1993, vol. 33, no. 4, pp. 590–594.
4. Yang, Y.-O., Xu, L., and Hu, C.-Y., *J. Chem. Inf. Comput. Sci.*, 1994, vol. 34, no. 5, pp. 1140–1145.
5. Galvez, J., Garcia, R., Salabert, M.T., and Soler, R., *J. Chem. Inf. Comput. Sci.*, 1994, vol. 34, no. 3, pp. 520–525.
6. Kompany-Zareh, M., *Acta Chim. Slov.*, 2003, vol. 50, pp. 259–273.
7. Randic, M. and Basak, S.C., *J. Chem. Inf. Comput. Sci.*, 1999, vol. 39, no. 2, pp. 261–266.
8. Cao, C., Liu, S., and Li, Z., *J. Chem. Inf. Comput. Sci.*, 1999, vol. 39, no. 6, pp. 1105–1111.
9. Ren, B., *Comput. Chem.*, 2002, vol. 26, pp. 223–235.
10. Vazhev, V.V., *Vestn. Kaz. Nats. Univ. im. Al'Farabi* (Almaty), 2003, no. 3 (31), pp. 86–91.
11. Vazhev, V.V., *Neft' Gaz* (Almaty), 2003, no. 4, pp. 74–82.
12. *NIST Chemistry WebBook: NIST Standard Reference Data-base*, November 1998 Release, no. 69. http://webbook.nist.gov/chemistry/
13. Vazhev, V.V., *Ispol'zovanie IK- i mass-spektrov v QSAR/QSPR-issledovaniyakh* (The Use of IR and Mass Spectra in QSAR/QSPR Studies), Kostanai: Kost. Gos. Univ., 2003.

Russian Journal of Applied Chemistry, Vol. 78, No. 3, 2005, pp. 456–460. Translated from Zhurnal Prikladnoi Khimii, Vol. 78, No. 3, 2005, pp. 461–465.
Original Russian Text Copyright © 2005 by Vazhev, Aldabergenov.

ORGANIC SYNTHESIS AND INDUSTRIAL ORGANIC CHEMISTRY

The Use of Mass Spectra for Estimating the Melting Points of Esters

V. V. Vazhev and M. K. Aldabergenov

Kostanai State Teacher's Training College, Kostanai, Kazakhstan

Received December 9, 2004

Abstract—The possibility of using low-resolution mass spectra as descriptors of molecular structure in estimating the melting points of 79 esters was studied.

The melting point T_m is one of the most important characteristics of organic compounds. In synthesis of new compounds it is determined first among other physicochemical characteristics, since it is used for identifying the compound and checking its purity. Experimental determination of T_m requires fairly large amounts of high-purity sample and in many cases is complicated by low thermal stability of substances. In this connection, approximate estimation of T_m is an urgent problem.

A recognized leader in estimation of various physicochemical characteristics is the QSPR (Quantitative Structure–Property Relationships) method based on a search for correlation equations relating the target characteristic and certain molecular characteristics (topological, electronic, etc.) of the compounds from a training sample. The resulting equations are used for further estimation of characteristics of other compounds. The topological indices, which are the invariants of the matrix of the graph reflecting the molecular structure, are mainly used as molecular characteristics. The estimation quality is characterized by the correlation coefficient R between the estimated and experimental values and standard deviations S. Published reviews [1, 2] show that the estimation accuracy in many characteristics already approaches the experimental accuracy. The melting point, whose estimation quality should be considered up to now as insufficient, is among a few exceptions (Table 1) [3–12].

A low accuracy of the models is caused in some cases by poor accuracy of experimental values used in training samples. In particular, sometimes the presence of small impurities can significantly decrease T_m. The other reason is that, as compared to, e.g., the boiling point, T_m is governed by additional factors related to the features of the crystal lattice. Although T_m is a function of the structure, up to now there are no fairly general and accurate methods for its estimation on the basis of molecular structure. The commonly used characteristics of molecular structure cannot reflect numerous factors governing T_m.

Here we studied the possibility of estimating T_m of esters from the mass spectra. Previously it was shown that the mass spectra can be successfully used to estimate the chromatographic retention indices of a set of substances of various classes, among them esters [13], and standard boiling points of alkanes [14].

We used low-resolution mass spectra of 79 esters with the number of carbon atoms from 2 to 15, available from the server of the National Institute of Stan-

Table 1. Results of estimating the melting points of various substances from published data

Substance class	Number of substances	R	S	References
Aniline derivatives	42	0.941	24.6	[3]
Alkanes	90	0.977	16.0	[4]
Alkanes	366	0.9584	17.9	[5]
Benzene derivatives	443	0.9150	30.19	[6]
Polychlorobiphenyls	209	0.9055	–	[7]
Alkanes	74	0.7632	22.14	[8]
Bromides of pyridine derivatives	126	0.888	–	[9]
Bromides of imidazole derivatives	104	0.9712	–	[10]
Organic sulfides	150	0.9381	21.93	[11]
Sulfonates	226	0.8911	23.66	[11]
1,2,3-Diazaborine derivatives	72	0.9257	16.78	[12]

1070-4272/05/7803-0456© 2005 Pleiades Publishing, Inc.

dards (NIST, USA) [15]. The T_m values were taken from the site of the University of Akron (USA) [16] and PhysProp database [17]. The training sample contained 55 substances and the control sample, 24 substances. Among all the mass spectra of the set used, there are 189 nonzero vectors of peak intensities in the range of the ratios *m*/*z* from 2 to 244. To obtain operating values of descriptors, before calculations, the mass spectra were preliminarily transformed by the formula

$$d_{ij} = h_{ij} m_{ij} \left(\sum_{k=1}^{k=n} h_{ik} m_{ik} \right)^{-1}, \quad (1)$$

where d_{ij} are the operating values of the descriptors used in calculations; *n*, number of peaks; h_{ij}, their relative intensities; *I*, substance number; *j*, peak number; and m_{ik}, ratio of the weight of *k*th ion to its charge in the *i*th molecule.

Elements d_{ij} form the matrix of descriptors *D* consisting of submatrices of training *A* and control *C* samples. For estimatoin, we used the matrix equation suggested in [18]:

$$p = CV_r \Gamma_r^{-1} U_r^T b, \quad (2)$$

where *p* is the sought-for vector of characteristic values of the control sample; *b*, vector of characteristics values of the training sample of substances; *U*, matrix consisting of the eigenvectors of matrix AA^T; *V*, matrix consisting of the eigenvectors of matrix A^TA; and Γ, diagonal matrix of nonzero singular numbers coinciding for both matrix products.

The subscript is the estimated rank of the descriptor matrix *r*(*A*); it denotes that *r* largest eigenvalues and the corresponding eigenvectors are used. For comparison of the results obtained with published data, the submatrix of descriptors in Eq. (2) was completed with the submatrix of training sample *A* and, correspondingly, vector *b* was completed with vector *p*. This procedure is equivalent to construction of a correlation model from the training sample and estimation of the characteristics of both control and training samples. The calculations were carried out using the PROGROC (PROGram RObustness Calculation) software [18].

The dependence of the correlation coefficient between the experimental and calculated T_m values for the overall set of substances on *r*(*A*) (estimated rank of descriptor submatrix) is presented in Fig. 1.

The maximum value $R = 0.986$ is reached at *r*(*A*) = 52. The results of estimating T_m of esters at this rank are presented in Table 2 and Fig. 2.

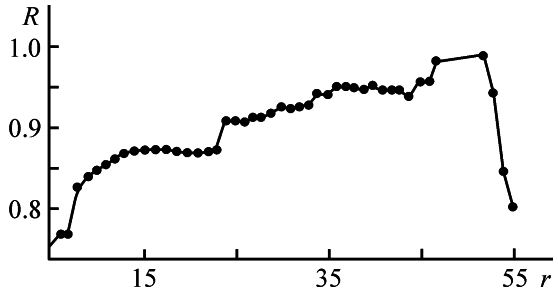


Fig. 1. Correlation coefficient *R* between experimental and calculated T_m as a function of estimated rank of descriptor submatrix *r*(*A*).

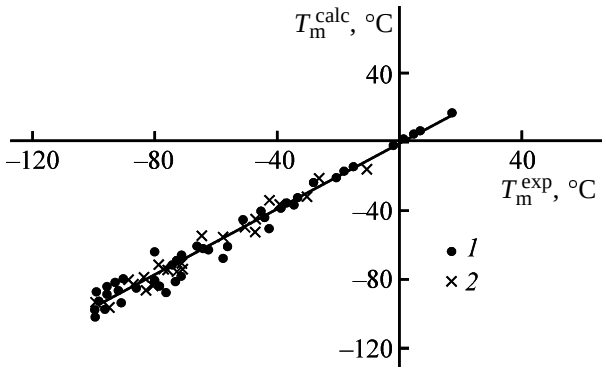


Fig. 2. Correlation between experimental (T_m^{exp}) and calculated from the mass spectra (T_m^{calc}) melting points of esters. Sample: (*1*) training and (*2*) control.

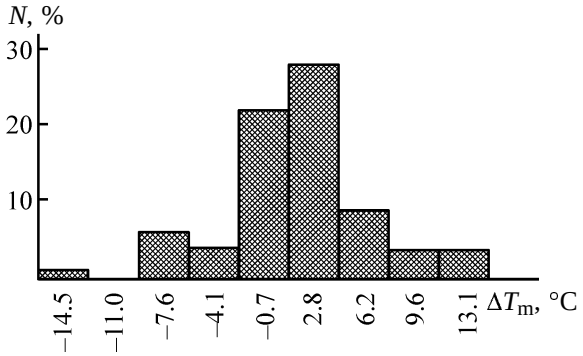


Fig. 3. Error distribution histogram for estimating the melting point T_m of esters. (*N*) Incidence.

The error distribution histogram for the estimation, shown in Fig. 3, is close to the normal distribution.

The quantitative characteristics of correlations between the experimental and calculated T_m values are listed in Table 3.

It should be noted that the accuracy of the results obtained in estimating the melting points of esters

Table 2. Experimental [16, 17] and calculated from mass spectra melting points of esters (°C)

Compound no.	Compound	T_m, °C		Difference	References
		experimental	calculated		
1	2-Ethylhexyl acetate	–45.0	–40.9	–4.1	[16]
2	Ethyl heptanoate	–66.0	–62.3	–3.7	[16]
3	Propyl pentanoate	–70.7	–71.9	1.2	[17]
4	Ethyl 2,2-dimethylpropionate	–89.6	–89.0	–0.6	[16]
5	Ethyl propionate	–74.0	–72.8	–1.2	[16]
6	Pentyl formate	–73.0	–7.1	2.1	[16]
7	Methyl 2-methylpropionate	–85.0	–87.0	2.0	[16]
8	Methyl hexanoate	–71.0	–67.6	–3.4	[17]
9	*n*-Heptyl hexanoate	–34.4	–38.2	3.8	[17]
10	3-Methyl-1-butyl acetate	–78.0	–85.5	7.5	[16]
11	Hexyl propionate	–57.5	–68.9	11.4	[16]
12	Methyl pentanoate	–56.0	–62.8	6.8	[16]
13	Butyl pentanoate	–92.8	–83.3	–9.5	[17]
14	*n*-Propyl acetate	–95.0	–90.4	–4.6	[16]
15	Hexyl formate	–62.6	–64.6	2.0	[16]
16	3-Methyl-1-butyl formate	–93.5	–83.3	–10.2	[17]
17	1-Methylpropyl acetate	–98.9	–89.4	–9.6	[16]
18	Ethyl decanoate	–20.0	–20.8	0.8	[16]
19	1,1-Dimethylethyl acetate	–90.0	–89.6	–0.4	[16]
20	Ethyl formate	–79.6	–82.1	2.5	[17]
21	Pentyl propionate	–73.1	–70.5	–2.6	[17]
22	Butyl acetate	–76.0	–89.1	13.1	[16]
23	Methyl formate	–99.0	–99.1	0.1	[17]
24	Pentyl nonanoate	–27.0	–24.9	–2.1	[17]
25	Butyl propionate	–90.0	–81.7	–8.3	[16]
26	Heptyl propionate	–50.9	–47.0	–4.0	[17]
27	Methyl tetradecanoate	18.0	17.5	0.5	[16]
28	Ethyl pentanoate	–91.0	–95.5	4.5	[16]
29	Propyl butyrate	–95.2	–86.4	–8.8	[16]
30	Ethyl dodecanoate	–2.0	–1.1	–0.9	[16]
31	Butyl nonanoate	–38.0	–38.6	0.6	[17]
32	Methyl pentanoate	–91.0	–89.0	–2.0	[16]
33	Butyl formate	–92.0	–91.1	–0.9	[16]
34	Octyl hexanoate	–28.0	–25.0	–3.0	[17]
35	2-Methylpropyl formate	–95.8	–98.2	–2.4	[16]
36	Ethyl butyrate	–92.0	–88.9	–3.1	[16]
37	2-Methylpropyl propionate	–71.0	–79.6	8.6	[16]
38	*n*-Dodecyl acetate	1.3	0.9	0.4	[17]
39	Methyl tridecanoate	6.5	6.6	–0.1	[17]
40	Octyl formate	–39.1	–39.6	–0.5	[17]
41	Hexyl acetate	–80.0	–65.5	–14.5	[16]
42	Methyl decanoate	–18.0	–17.3	–0.7	[16]
43	4-Methyl-2-pentyl acetate	–63.8	–63.2	–0.7	[16]
44	Ethyl nonanoate	–44.0	–45.6	1.6	[16]
45	Propyl formate	–93.0	–92.4	–0.6	[16]
46	Heptyl heptanoate	–33.0	–33.4	–0.4	[17]
47	Methyl acetate	–98.0	–94.2	–3.8	[16]
48	Methyl octanoate	–36.7	–37.1	–0.4	[16]
49	1-Methylethyl acetate	–73.0	–77.9	–4.9	[16]
50	2-Methylpropyl acetate	–99.0	–103.7	4.7	[16]

Table 2. (*Contd.*)

Compound no.	Compound	T_m, °C		Difference	References
		experimental	calculated		
51	Methyl dodecanoate	4.5	3.2	1.3	[16]
52	Pentyl butyrate	–73.2	–82.9	–9.7	[16]
53	Octyl pentanoate	–42.3	–52.3	–10.0	[17]
54	Decyl acetate	–15.0	–15.1	–0.1	[17]
55	Propyl octanoate	–46.2	–46.2	0.0	[17]
56	Ethyl octanoate	–47.0	–53.4	6.4	[16]
57	3-Methylbutyl butyrate	–73.2	–78.8	5.6	[16]
58	Hexyl butyrate	–78.0	–75.0	–3.0	[17]
59	Methyl butyrate	–84.0	–80.4	–3.6	[16]
60	Heptyl caprylate	–10.6	–16.5	5.9	[17]
61	Octyl propionate	–42.6	–35.4	–7.2	[17]
62	Butyl hexanoate	–64.3	–55.5	–8.8	[17]
63	Methyl propionate	–87.0	–85.2	–1.8	[16]
64	Butyl butyrate	–91.5	–89.8	–1.7	[16]
65	Octyl acetate	–38.5	–37.7	–0.8	[16]
66	Ethyl 3-methylbutyrate	–99.0	–95.2	–3.8	[16]
67	Ethyl 2-methylpropionate	–88.0	–81.7	–6.3	[16]
68	Hexyl octanoate	–30.6	–32.8	2.2	[17]
69	Heptyl butyrate	–57.5	–55.9	–1.6	[17]
70	Ethyl acetate	–83.0	–87.2	–4.2	[16]
71	Nonyl acetate	–26.0	–22.3	–3.7	[16]
72	Pentyl hexanoate	–47.0	–45.1	–1.9	[17]
73	2-Pentyl acetate	–70.8	–71.3	0.5	[16]
74	Pentyl acetate	–71.0	–76.1	5.1	[16]
75	Propyl propionate	–75.9	–75.4	–0.5	[17]
76	1-Methylethyl butyrate	–95.0	–97.6	2.6	[16]
77	Pentyl pentanoate	–78.8	–73.3	–5.5	[17]
78	2-Methylpropyl 2-methylpropionate	–80.7	–84.2	–3.6	[16]
79	Heptyl acetate	–50.2	–50.7	–0.5	[16]

Notes: Substances nos. from 1 to 55 form training sample, and those from 56 to 79, control sample.

exceeds the accuracy of estimating the T_m for compounds of different classes.

CONCLUSIONS

(1) The use of normalized mass spectra as descriptors of molecular structure allows estimation of melting points of esters with the correlation coefficient $R = 0.986$ between the experimental and estimated melting points and standard deviation $S = 5.01$.

(2) The advantage of the approach developed is that, for estimating a substance characteristic, it is sufficient to have only the mass spectrum of the substance.

Table 3. Characteristics of correlation between experimental and calculated melting points of esters

Characteristic of correlation	Whole set	Sample	
		training	control
R	0.986	0.9860	0.983
S	5.01	5.34	4.37
Average standard deviation	3.7	3.8	3.6

REFERENCES

1. Katritzky, A.R., Maran, U., Lobanov, V.S., and Karelson, M., *J. Chem. Inf. Comput. Sci.*, 2000, vol. 40, no. 1, pp. 1–18.
2. Taskinen, J. and Yliruusi, J., *Adv. Drug Delivery Rev.*, 2003, vol. 55, pp. 1163–1183.
3. Dearden, J.C., *J. Sci. Total. Environ.*, 1991, vols. 109–110, pp. 59–68.
4. Baskin, I.I., Palyulin, V.A., and Zefirov, N.S., *Dokl. Akad. Nauk SSSR*, 1993, vol. 332, no. 6, pp. 713–716.

5. Charton, M. and Charton, B., *J. Phys. Org. Chem.*, 1994, no. 7, pp. 196–206.
6. Katritzky, A.R., Maran, U., Karelson, M., and Lobanov, V.S., *J. Chem. Inf. Comput. Sci.*, 1997, vol. 37, pp. 913–919.
7. Gramatica, P., Navas, N., and Todeschini, R., *Chemometr. Intell. Lab.*, 1998, vol. 40, pp. 53–63.
8. Lucic, B., Milicevic, A., Nikolic, S., and Trinajstic, N., *Chroat. Chem. Acta*, 2002, vol. 75, no. 4, pp. 847–868.
9. Katritzky, A.R., Lomaka, A., Petrukhin, R., *et al.*, *J. Chem. Inf. Comput. Sci.*, 2002, vol. 42, no. 1, pp. 71–74.
10. Katritzky, A.R., Jain, R., Lomaka, A., *et al.*, *J. Chem. Inf. Comput. Sci.*, 2002, vol. 42, no. 2, pp. 225–231.
11. Koziol, J., *Internet Electron J. Mol. Des.*, 2002, no. 1, pp. 80–93.
12. Johnson-Restrepo, B., Pacheco-Londono, L., and Olivero-Verbel, J., *J. Chem. Inf. Comput. Sci.*, 2003, vol. 43, no. 5, pp. 1513–1519.
13. Vazhev, V.V., *Vestn. Kaz. Nats. Univ. im. Al'-Farabi* (Almaty), 2003, no. 3 (31), pp. 86–91.
14. Vazhev, V.V., *Neft' Gaz* (Almaty), 2003, no. 4, pp. 74–82.
15. *NIST Chemical WebBook: NIST Standard Reference Database*, November 1998 Release, no. 69. http://webbook.nist.gov/chemistry/
16. http://ull.chemistry.uakron.edu/erd/index.html
17. http://esc.syrres.com/interkow/physdemo.htm
18. Vazhev, V.V., *Ispol'zovanie IK- i mass-spektrov v QSAR/QSPR-issledovaniyakh* (The Use of IR and Mass Spectra in QSAR/QSPR Studies), Kostanai: Kost. Gos. Univ., 2003.

Russian Journal of Applied Chemistry, Vol. 78, No. 3, 2005, pp. 461–464. Translated from Zhurnal Prikladnoi Khimii, Vol. 78, No. 3, 2005, pp. 466–469.
Original Russian Text Copyright © 2005 by Zevatskii.

ORGANIC SYNTHESIS AND INDUSTRIAL ORGANIC CHEMISTRY

Relationship between the Relative Permittivity of Nonpolar Gases and Ionization Potential of Molecules

Yu. E. Zevatskii

St. Petersburg State Technological Institute, St. Petersburg, Russia

Received December 6, 2004

Abstract—A method is suggested for relating the relative permittivity, ionization potential, polarizability, and linear dimensions of nonpolar molecules. This was demonstrated for the example of inert gases, some spherical- and symmetric-top molecules, and linear molecules.

Taking into account the polarizability of organic molecules and ions is important when describing quantitatively the mechanisms and rates of nonradical reactions. The energy of intermolecular dispersion interaction is directly related to the polarizabilities of molecules under consideration. The influence of the dispersion interaction on the reactivity was analyzed in [1–6]. The polarizabilities are commonly determined by extrapolation methods from the refractive index (using the Lorentz–Lorenz formula) and from the relative permittivities of substances. The most accurate values of the molecular polarizability can be obtained from the above parameters determined for the gaseous state, i.e., the case in which the contribution of intermolecular interactions can be neglected.

In analysis of models of the molecular polarizability, attention is attracted by the fact that the influence exerted by the field of the induced dipole on the atomic polarization is disregarded in the literature concerned with nonpolar molecules. An attempt to consider this factor was made in [7]. However, an important point is that the field of the induced dipole is considered in a superposition with that of the permanent dipole for polar molecules. Atoms are regarded as isotropically polarized points, and the induced dipole moment of a molecule is represented as

$$\mu_i = A_i\left[E_i - \sum_{\substack{j=1\\ i\neq j}}^{N} T_{ij}\mu_j\right], \qquad (1)$$

where A_i is the polarizability tensor of ith atom, and T_{ij} is the tensor of a field created by the induced dipole, which can be written in the matrix form as

$$T_{ij} = -\frac{3}{r^5}\begin{bmatrix} x^2 - r^2/3 & xy & xz \\ xy & y^2 - r^2/3 & yz \\ xz & yz & z^2 - r^2/3 \end{bmatrix}, \qquad (2)$$

where r is the distance between ith and jth atoms; x, y, z, components of the vector running from point i to point j in the Cartesian coordinates. The expression in the brackets reflects the total field at ith atom, constituted by the externally applied field and the field of all induced dipoles of the system. However, this model gave a good (within 10%) agreement with experiment for medium polarizabilities and an unsatisfactory agreement for the main components of polarizability and anisotropy. This concept was further developed in [8], with anisotropic effects included, and then in [9], where the repulsion of electrons was taken into account.

Further complication and modification of the model, made in [10, 11], failed to improve significantly the agreement between the quantities mentioned. The last study employing this model and some of its preceding modifications was performed in 1999. The average and principal components of polarizability, calculated in this study for amino acids and peptides, coincided with the expected values only within an order of magnitude. This is natural, because the field of the induced dipole for polar molecules is three orders of magnitude lower than the field of the permanent dipole. Therefore, the model of polarizability of nonpolar molecules, suggested here, does not use tensor quantities, but is based on the relationship between the polarizability and the ionization potential. The idea of establishing such a relationship has been reflected in the literature [13–16]. However, this rela-

1070-4272/05/7803-0461 © 2005 Pleiades Publishing, Inc.

tionship has not been substantiated theoretically and only empirical relations between the experimental and calculated ionization potentials U and polarizabilities α have been obtained in the forms

$$\alpha = a/U^3 + b \quad (3)$$

and

$$\alpha = c/U^\gamma, \quad (4)$$

where a, b, c, and γ are variable parameters. The degree of the correlation was not specified in [15] and was found to be 0.98 in [13, 14, 16]. It was mentioned in [13, 14] that the degree of the correlation strongly depends on the set of atomic radii, used in the calculations. The dependences were constructed using the commonly known relationship between the polarizability of a charged sphere and its volume (radius) and the apparent dependence of the ionization energy on the atomic radius. The existence of a relationship between the polarizability and volume was shown for molecules only in [17].

The aim of this study was to establish a relationship between the polarizability and the ionization potential of nonpolar molecules. The calculation was performed by taking into account the mutual influence of the fields of the induced charges within a molecule. The induced dipole moment of a unit volume of an insulator placed in a uniform external electric field E is given by

$$P = \alpha\varepsilon_0 n_0 E, \quad (5)$$

where α is the polarizability coefficient; m_0, volume concentration of molecules; and ε_0, permittivity of free space. The polarizability coefficient is related to the relative permittivity ε of a nonpolar gas by the Clausius–Mosotti formula

$$\alpha = \frac{3}{n_0}\frac{\varepsilon - 1}{\varepsilon + 2} \approx \frac{\varepsilon - 1}{n_0}. \quad (6)$$

The induced dipole moment per molecule is equal to

$$\mu = \alpha\varepsilon_0 E. \quad (7)$$

Let us represent this dipole as two equal charges q with opposite signs, spaced by a distance l not exceeding the linear dimensions of the molecule. The electric field strength at positions of the induced charges will be changed by the presence of a field associated with the charge of the opposite sign:

$$E_q = \frac{E}{\varepsilon} - \frac{q}{4\pi\varepsilon_0 l^2}. \quad (8)$$

As the field strength increases from zero to E, the work of forces associated with the external field

$$\int_{l(E)}^{l(E)} q E_q \,\mathrm{d}l = \alpha\varepsilon_0 \int_0^E \frac{E^2}{l}(1/\varepsilon - \alpha/4\pi l^3)\frac{\mathrm{d}l}{\mathrm{d}E}\,\mathrm{d}E \quad (9)$$

is at a minimum at

$$\alpha\varepsilon = 4\pi l^3, \quad (10)$$

or if

$$\mathrm{d}l/\mathrm{d}E = 0. \quad (11)$$

Let us assume that, in the case of ionization in a constant electric field, the induced dipole moment of the molecule reaches the value

$$\mu_\mathrm{i} = el, \quad (12)$$

where e is elementary charge, and the field strength in ionization is proportional to the ionization potential U related to the molecular size, i.e., the maximum distance by which the induced charges can be spaced,

$$E_\mathrm{i} = fU/l. \quad (13)$$

Then, if the condition (10) is satisfied, the proportionality factor f can be found from

$$f = (e/\varepsilon_0 U)^{1/2}[n_0/16\pi^2(\varepsilon - 1)]^{1/6}. \quad (14)$$

Analysis of values of f for various substances shows that it is close to unity only for the helium atom and hydrogen molecule. For other nonpolar substances, this factor is within the range from 0.8 for benzene to 1.3 for carbon tetrachloride. This means that formulas (10) and (14) are inadequate as applied to a calculation of the properties of nonpolar substances. If the condition (11) is satisfied, the factor f can be found from the equation

$$f = (4e/\pi\varepsilon_0 Ul)^{1/2}\{1 + [1 + 2(\varepsilon - 1)/\pi n_0 l^3]^{1/2}\}^{-1}, \quad (15)$$

to be in the range from 0.91 to 1.17 for inert gases, a number of linear molecules, and spherical- and symmetric-top molecules. Thus, taking into account the influence exerted by the field of the induced charge

Relative permittivity $\varepsilon - 1$ and volume concentration n_0 at a temperature T, density ρ under normal conditions, linear size l, ionization potential U, and factor f for selected nonpolar substances

Substance	ρ, kg m^{-3}	T, K	$n_0 \times 10^{-25}$, m^{-3}	$l \times 10^{10}$, m	U, V	$(\varepsilon - 1) \times 10^4$	f
He	178	273	2.680	1.22	24.58	0.68	1.17
Ne	900	273	2.710	1.60	21.56	1.27	1.12
Ar	1784	273	2.688	1.92	15.75	5.54	1.03
Ar	1784	298	2.460	1.92	15.75	5.04	1.03
Kr	3708	298	2.435	1.98	14.00	7.68	1.00
Xe	5857	298	2.464	2.18	12.13	12.38	0.98
CH_4	717	293	2.514	2.06	12.99	8.04	1.04
CF_4	3893	298	2.441	2.80	17.8	6.00	0.93
CCl_4	5158	383	2.028	3.87	10.47	30.0	0.91
H_2	89.88	273	2.706	1.02	15.43	2.72	1.05
H_2	89.88	298	2.479	1.02	15.43	2.52	1.04
N_2	1251	273	2.691	1.79	15.51	5.80	1.01
N_2	1251	293	2.507	1.79	15.51	5.28	1.02
O_2	1429	273	2.689	1.87	14.01	5.30	1.09
CO_2	1977	273	2.706	2.99	13.79	9.90	1.00
CS_2	3393	424	1.731	4.16	10.08	20.6	0.96
C_2H_2	1171	196	3.778	3.33	11.41	18.9	1.04
C_2H_2	1171	298	2.485	3.33	11.41	12.17	1.04
C_2H_4	1260	237	3.122	2.70	10.51	16.8	1.07
C_2H_4	1260	298	2.483	2.70	10.51	13.28	1.07
C_2H_6	1356	200	3.715	2.78	11.65	20.6	1.02
C_2H_6	1356	298	2.494	2.78	11.65	13.8	1.02
C_6H_6	2699	373	2.084	5.24	9.25	2.74	1.07

with the opposite sign in Eq. (8) makes it possible to relate the ionization potential, linear dimensions of molecules, and relative permittivity of nonpolar gases by a dimensionless coefficient close to unity.

Below is given the table that lists the experimental values of the linear sizes of a number of molecules, relative permittivities, and ionization potentials. Also given are proportionality factors found by formula (15). The atomic radius for inert gases and the maximum internuclear distance plus the atomic radius of the terminal atom for molecules of various types served as a linear size of molecules. Data on the density, relative permittivity, internuclear distances, atomic radii, and ionization potentials were taken, for the sake of uniformity, from a single source [18]. The only exception is CF_4, for which the density and relative permittivity were taken from [19]. The densities of carbon tetrachloride, carbon disulfide, and benzene were found by the van der Waals equation at a given temperature, with the use of critical parameters.

These data suggest the following. For inert gases, the relative deviation of the factor f from the average value is at a maximum (10%). This deviation is <7% for spherical-top molecules, 4% for diatomic and linear molecules, and ≤3% for symmetric-top molecules. This gives reason to use formula (15) for calculating the ionization potential of nonpolar molecules at a known relative permittivity and, vice versa, to find the relative permittivity (and, consequently, the polarization too) from the ionization potential. The second opportunity is of practical importance, because different experimental values of the ionization potentials of molecules, found in the literature, are commonly in good agreement. Further, we intend to extend the applicability domain of formula (15) to calculation of the polarizability of ions with a symmetric electronic configuration ensuring the absence of a dipole moment. It is necessary to use, instead of the ionization potential, the electron affinity for anions and the second ionization potential of a neutral molecule for cations.

REFERENCES

1. Rubio, M., Torrens, F., and Sanchez-Marin, J., *J. Comput. Chem.*, 1993, vol. 14, pp. 647–654.
2. Fraga, S., *J. Comput. Chem.*, 1982, vol. 3, p. 329.
3. Fraga, S., *Comput. Phys. Commun.*, 1983, vol. 29, pp. 351–359.

4. Torrens, F. and Sanchez-Marin, J., *Comput. Phys. Commun.*, 1991, vol. 66, p. 341.
5. Torrens, F., Orten, E., and Sanchez-Marin, J., *J. Mol. Graph.*, 1991, vol. 9, p. 254.
6. Gerwens, H. and Jug, K., *Int. J. Quantum Chem.*, 1995, vol. 56, p. 563.
7. Applequist, J., Carl, J.R., and Fung, K.K., *J. Am. Chem. Soc.*, 1972, vol. 94, pp. 2952–2960.
8. Birge, R.R., *J. Chem. Phys.*, 1980, vol. 72, no. 10, pp. 5312–5319.
9. Thole, B.T., *Chem. Phys.*, 1981, vol. 59, pp. 341–350.
10. Olson, M.L. and Sundberg, K.R., *J. Chem. Phys.* 1978, vol. 69, no. 12, pp. 5400–5404.
11. Applequist, J., *Chem. Phys.*, 1993, vol. 97, pp. 6016–6023.
12. Torrens, F., Sanchez-Marin, J., and Nebot-Gil, I., *J. Mol. Struct. (THEOCHEM)*, 1999, vol. 463, pp. 27–39.
13. Politzer, P., Jin, P., and Murray, J.S., *J. Chem. Phys.*, 2002, vol. 117, no. 18, pp. 8197–8202.
14. Politzer, P., Murray, J.S., Grice, M.E., *et al.*, *J. Chem. Phys.*, 1991, vol. 95, pp. 6699–6704.
15. Fricke, B., *J. Chem. Phys.*, 1986, vol. 84, pp. 862–866.
16. Dmitrieva, K. and Plindov, G.I., *Phys. Scripta*, 1983, vol. 27, pp. 402–406.
17. Gough, K.M., *J. Chem. Phys.*, 1989, vol. 91, pp. 2424–2432.
18. *Spravochnik khimika* (Chemist's Handbook), Nikol'skii, B.P., Ed., Leningrad: Khimiya, 1971, vol. 1.
19. Maksimov, B.N., Barabanov, V.G., *et al.*, *Promyshlennye ftororganicheskie produkty* (Industrial Organofluorine Products), St. Petersburg: Khimiya, 1996, p. 23.

Russian Journal of Applied Chemistry, Vol. 78, No. 3, 2005, pp. 465–468. Translated from Zhurnal Prikladnoi Khimii, Vol. 78, No. 3, 2005, pp. 470–473.
Original Russian Text Copyright © 2005 by Baranov, Tsypin, Malin, Laskin.

ORGANIC SYNTHESIS AND INDUSTRIAL ORGANIC CHEMISTRY

Nucleophilic Substitution of Chlorine with Hydrazine, Methylhydrazine, and 1,1-Dimethylhydrazine in 5-Aryl-2-chloromethyl-1,3,4-oxadiazoles

A. B. Baranov, V. G. Tsypin, A. S. Malin, and B. M. Laskin

Prikladnaya Khimiya Russian Scientific Center, St. Petersburg, Russia

Received November 2, 2004

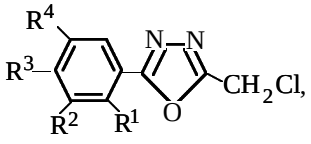
Abstract—The reactions of 1,1-dimethylhydrazine, methylhydrazine, and hydrazine hydrate with 5-aryl-2-chloromethyl-1,3,4-oxadiazoles were studied. The structures and compositions of the final products were confirmed by ^{1}H NMR spectroscopy and elemental analysis.

Hydrazine and its derivatives attract great interest of researchers [1] owing to wide use of these compounds in medicine (antitubercular, antitumor, and other drugs), agriculture (plant growth regulators and stimulants), and industry (production of synthetic fibers, films, coatings, etc.) [2–5].

5-Aryl-2-chloromethyl-1,3,4-oxadiazoles, aromatic five-membered heterocycles, are key fragments of various drugs (antiviral agents, antidepressants, etc.) [6]. At the same time, introduction of a hydrazine fragment may enhance their biological activity.

Our goal was synthesis of previously unknown 5-aryl-2-hydrazinomethyl-1,3,4-oxadiazoles, 5-aryl-2-(1-methylhydrazino)methyl-1,3,4-oxadiazoles, and 5-aryl-2-(1,1-dimethylhydrazinio)methyl-1,3,4-oxadiazole chlorides, which are of interest as potentially bioactive substances and agents for further fine organic synthesis.

Accessible 1,3,4-oxadiazole substrates for nucleophilic substitution of chlorine by hydrazine, methylhydrazine, and 1,1-dimethylhydrazine fragments are 2-chloromethyl-5-phenyl-1,3,4-oxadiazole **I**, 2-chloromethyl-5-(2,4-dimethoxyphenyl)-1,3,4-oxadiazole **II**, 2-chloromethyl-5-(2-chlorophenyl)-1,3,4-oxadiazole **III**, and 2-chloromethyl-5-(3,4,5-trimethoxyphenyl)-1,3,4-oxadiazole **IV** [7–9]:

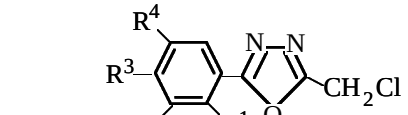


I–**IV**

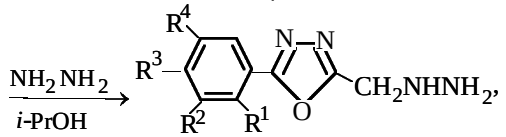
where $R^1 = R^2 = R^3 = R^4 = H$ (**I**); $R^2 = R^4 = H$, $R^1 = R^3 = MeO$ (**II**); $R^1 = Cl$, $R^2 = R^3 = R^4 = H$ (**III**); $R^2 = R^3 = R^4 = MeO$, $R^1 = H$ (**IV**).

It is known that 5-aryl-2-chloromethyl-1,3,4-oxadiazoles react with amines and methylmercaptoacetyl derivatives selectively with the replacement of Cl in the 2-chloromethyl group [8, 9].

We found that compounds **I**–**IV** react with hydrazine hydrate in 2-propanol at 55–65°C strictly selectively to give 2-hydrazinomethyl-5-phenyl-1,3,4-oxadiazole **V**, 2-hydrazinomethyl-5-(2,4-dimethoxyphenyl)-1,3,4-oxadiazole **VI**, 2-hydrazinomethyl-5-(2-chlorophenyl)-1,3,4-oxadiazole **VII**, and 2-hydrazinomethyl-5-(3,4,5-trimethoxyphenyl)-1,3,4-oxadiazole **VIII** in 67, 23, 25, and 75% yields, respectively.[1] Note that compounds **I**–**IV** react with hydrazine hydrates at different rates depending on substituents in the aromatic ring. The reactions of hydrazine hydrate with **I**–**IV** take 5, 6, 4, and 3 h, respectively. Compounds **V**–**VIII** are isolated as poorly crystallizing hygroscopic crystals.



I–**IV**



V–**VIII**

[1] The synthesis conditions and yields of **V**–**XVI** are given in Table 1; the melting points and analytical data, in Table 2; and the ^{1}H NMR data, in Table 3.

1070-4272/05/7803-0465 © 2005 Pleiades Publishing, Inc.

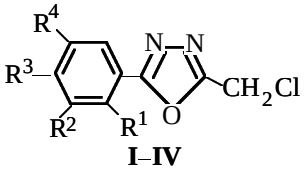
Table 1. Conditions, yields, and products of reactions of **I**–**IV** with hydrazine hydrate, methylhydrazine, and 1,1-dimethylhydrazine

Compound	Ratio*	*T*, °C	τ, h	Product	Yield, %
I	1/2.5[a]	55–65	5	**V**	67
II	1/2.5[a]	55–65	6	**VI**	23
III	1/2.5[a]	55–65	4	**VII**	25
IV	1/2.5[a]	55–65	3	**VIII**	75
I	1/2.5[b]	80–83	5	**IX**	55
II	1/2.5[b]	50–60	5	**X**	45
III	1/2.5[b]	80–83	4	**XI**	56
IV	1/2.5[b]	50–60	4	**XII**	85
I	1/1.2[c]	55–60	5	**XIII**	68
II	1/1.2[c]	55–60	6	**XIV**	84
III	1/1.2[c]	55–60	18	**XV**	71
IV	1/1.2[c]	55–60	7	**XVI**	80

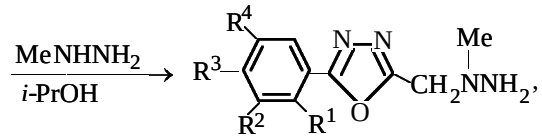
* Component indicated in the denominator: [a] hydrazine, [b] methylhydrazine. and [c] 1,1-dimethylhydrazine.

where $R^1 = R^2 = R^3 = R^4 = H$ (**I**, **V**); $R^2 = R^4 = H$, $R^1 = R^3 = MeO$ (**II**, **VI**); $R^1 = Cl$, $R^2 = R^3 = R^4 = H$ (**III**, **VII**); $R^2 = R^3 = R^4 = MeO$, $R^1 = H$ (**IV**, **VIII**).

The reactions of **I**–**IV** with methylhydrazine were performed in 2-propanol at 50–60 or 80–83°C. The reactions gave 2-(1-methylhydrazino)methyl-5-phenyl-1,3,4-oxadiazole **IX**, 2-(1-methylhydrazino)methyl-5-(2,4-dimethoxyphenyl)-1,3,4-oxadiazole **X**, 2-(1-methylhydrazino)methyl-5-(2-chlorophenyl)-1,3,4-oxadiazole **XI**, and 2-(1-methylhydrazino)methyl-5-(3,4,5-trimethoxyphenyl)-1,3,4-oxadiazole **XII** in 55, 45, 56, and 85% yields, respectively. With **I** and **III**, 1-methylhydrazine reacts at 80–83°C within 5 and 4 h, and with **II** and **IV**, at 50–60°C within 5 and 4 h, respectively. Compounds **IX**–**XII** are noncrystallizable hygroscopic oils:



I–**IV**



IX–**XII**

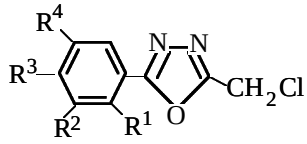
where $R^1 = R^2 = R^3 = R^4 = H$ (**I**, **IX**); $R^2 = R^4 = H$, $R^1 = R^3 = MeO$ (**II**, **X**); $R^1 = Cl$, $R^2 = R^3 = R^4 = H$ (**III**, **XI**); $R^2 = R^3 = R^4 = MeO$, $R^1 = H$ (**IV**, **XII**).

The analytical data (Table 2) for **V**–**XII** unambiguously show that hydrazine and methylhydrazine react with **I**–**IV** along the monoalkylation pathway, i.e., the starting compounds react in an equimolar ratio.

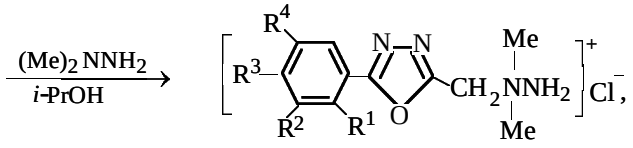
The occurrence of monoalkylation is provided by a 2.5-fold excess of hydrazine hydrate and methylhydrazine in the mixture of the starting components (Table 1). A broadened signal of amine protons at 4.62–4.68 ppm (2H) in the ^{1}H NMR spectra of **IX**–**XII** is an unambiguous evidence of the regioselective alkylation of monomethylhydrazine at the methyl-substituted nitrogen atom (Table 3).

It is known that 1,1-dimethylhydrazine reacts with aliphatic and aromatic chlorides strictly at the N^1 atom to form quaternary ammonium salts [10].

The reactions of **I**–**IV** with 1,1-dimethylhydrazine occurred selectively as nucleophilic substitution of the chlorine atom. The reactions were performed in 2-propanol and gave the corresponding quaternary hydrazinium salts 2-(1,1-dimethylhydrazinio)methyl-5-phenyl-1,3,4-oxadiazole chloride **XIII**, 2-(1,1-dimethylhydrazinio)methyl-5-(2,4-dimethoxyphenyl)-1,3,4-oxadiazole chloride **XIV**, 2-(1,1-dimethylhydrazinio)methyl-5-(2-chlorophenyl)-1,3,4-oxadiazole chloride **XV**, and 2-(1,1-dimethylhydrazinio)methyl-5-(3,4,5-trimethoxyphenyl)-1,3,4-oxadiazole chloride **XVI** in 68, 84, 71, and 80% yields, respectively. All the salts **XIII**–**XVI** are hygroscopic and water-soluble:



I–**IV**



XIII–**XVI**

where $R^1 = R^2 = R^3 = R^4 = H$ (**I**, **XIII**); $R^2 = R^4 = H$, $R^1 = R^3 = MeO$ (**II**, **XIV**); $R^1 = Cl$, $R^2 = R^3 = R^4 = H$ (**III**, **XV**); $R^2 = R^3 = R^4 = MeO$, $R^1 = H$ (**IV**, **XVI**).

The ~2-ppm downfield shift of the amine proton signal (2H) to 6.65–6.82 ppm in the ^{1}H NMR spectra of **XIII**–**XVI** relative to **V**–**VIII** (4.88–4.97 ppm) and **IX**–**XII** (4.62–4.68 ppm) indicates that the positive charge is localized on the dimethyl-substituted nitrogen atom, i.e., a quaternary hydrazinium salt is formed (Table 3).

Table 2. Melting points and elemental analyses of **V**–**XVI**

Compound no.	T_m, °C	Found, %				Formula	Calculated, %			
		Cl*	C	H	N		Cl*	C	H	N
V	71–73		56.12	5.19	50.98	$C_9H_{10}N_4O$		56.84	5.26	51.38
VI	53–55		53.22	5.51	22.21	$C_{11}H_{14}N_4O_3$		52.80	5.60	22.40
VII	96–98		48.46	4.05	24.43	$C_9H_9ClN_4O$		48.11	4.01	24.64
VIII	52–54		51.17	5.64	19.84	$C_{12}H_{16}N_4O_4$		51.43	5.71	20.00
IX	Oil		58.53	5.76	27.33	$C_{10}H_{12}N_4O$		58.82	5.88	27.45
X	Oil		54.69	6.13	21.19	$C_{12}H_{16}N_4O_3$		54.54	6.06	21.21
XI	Oil		50.04	4.57	23.12	$C_{10}H_{11}ClN_4O$		50.31	4.61	23.28
XII	Oil		52.87	6.05	18.88	$C_{13}H_{18}N_4O_4$		53.0	6.12	19.05
XIII	183–185	13.9	51.8	5.82	21.95	$C_{11}H_{15}ClN_4O$	13.9	51.9	5.89	22.00
XIV	198–199	11.3	49.5	6.01	17.73	$C_{13}H_{19}ClN_4O_3$	11.3	49.6	6.04	17.81
XV	191–192	11.8	45.5	4.78	19.31	$C_{11}H_{14}ClN_4O$	11.9	45.7	4.84	19.38
XVI	216–218	10.4	48.6	6.05	16.21	$C_{14}H_{21}ClN_4O_4$	10.3	48.8	6.10	16.25

* The content of chloride ions in **XIII**–**XVI** was determined by mercurimetric titration.

Table 3. ^{1}H NMR data for **V**–**XVI** (solvent DMSO-d_6)

Compound	^{1}H NMR spectrum, δ, ppm
V	4.12 s (2H, CH_2); 7.37–7.57, 7.98–8.06 m ($5H_{arom}$); 4.88 s (2H, NH_2); 10.10 s (1H, NH)
VI	4.22 s (2H, CH_2); 6.89–7.06, 7.35–7.55 m ($3H_{arom}$); 4.97 s (2H, NH_2); 10.07 s (2H, NH); 3.79 s (6H, 2MeO)
VII	4.30 s (2H, CH_2); 7.31–7.38, 7.86–7.92 m ($4H_{arom}$); 4.95 s (2H, NH_2); 9.97 s (1H, NH)
VIII	4.33 s (2H, CH_2); 7.17–7.27 m ($2H_{arom}$); 4.92 s (2H, NH_2); 10.06 s (1H, NH); 3.88 s (6H, 2MeO); 3.76 s (3H, MeO)
IX	4.68 s (2H, CH_2); 7.83–8.01, 7.39–7.55 m ($5H_{arom}$); 2.61 s (3H, Me); 4.68 s (2H, NH_2)
X	4.31 s (2H, CH_2); 6.86–7.09, 7.40–7.60 m ($3H_{arom}$); 2.62 s (3H, Me); 4.62 s (2H, NH_2); 3.85 s (6H, 2MeO)
XI	4.40 s (2H, CH_2); 7.70–7.91, 7.16–7.36 m ($4H_{arom}$); 2.61 s (3H, Me); 4.65 s (2H, NH_2)
XII	4.41 s (2H, CH_2); 7.17–7.26 m ($2H_{arom}$); 3.88 s (6H, 2MeO); 3.76 s (3H, MeO); 4.64 s (2H, NH_2); 2.62 s (3H, Me)
XIII	5.41 s (2H, CH_2); 8.63–8.25, 7.57–7.63 m ($5H_{arom}$); 6.75 s (2H, NH_2); 3.59 s (6H, 2Me)
XIV	5.31 s (2H, CH_2); 7.08–7.13, 7.50–7.63 m ($3H_{arom}$); 6.66 s (2H, NH_2); 3.88 s (6H, 2 MeO); 3.54 s (6H, 2Me)
XV	5.45 s (2H, CH_2); 7.85–7.97, 7.31–7.40 m ($4H_{arom}$); 6.82 s (2H,NH_2); 3.62 s (6H, 2Me)
XVI	5.30 s (2H, CH_2); 7.23–7.31 m ($2H_{arom}$); 6.65 s (2H, NH_2); 3.53 s (6H, 2Me); 3.78 s (3H, MeO); 3.90 s (6H, 2MeO)

Thus, compounds **I**–**IV** readily undergo nucleophilic substitution and are convenient starting compounds for preparing various hydrazine-containing compounds. All the hydrazine derivatives prepared are potenitally bioactive and can be brought into further transformations.

EXPERIMENTAL

The ^{1}H NMR spectra were taken on a DPX-300 spectrometer (300 MHz, DMSO-d_6, internal reference TMS). The elemental analysis was performed on a Hewlett–Packard automatic C, H, N analyzer. The melting points were determined with a PTP device. The TLC analysis was performed on Silufol UV-254 plates (eluent chloroform–methanol, 9 : 1, development under UV light or with iodine vapor).

5-Aryl-2-hydrazinomethyl-1,3,4-oxadiazoles V–VIII (general procedure). A solution of 1.5 g of 100% hydrazine hydrate in 10 ml of 2-propanol was added with stirring to a solution of 2 g of **I**–**IV** in 40 ml of 3-propanol. The reaction temperatures and times are given in Table 1. The resulting mixture was cooled, excess 2-propanol was distilled off, and the precipitate was filtered off and dried in a desiccator.

5-Aryl-2-(1-methylhydrazino)methyl-1,3,4-oxadiazoles IX–XII (general procedure). A solution of 1 g of methylhydrazine in 10 ml of 2-propanol was added with stirring to a solution of 2 g of **I**–**IV** in 3 ml of 2-propanol. The reaction temperatures and times are given in Table 1. The resulting mixture was cooled, excess 2-propanol was distilled off, and the remaining oily liquid was dried in a desiccator.

5-Aryl-2-(1,1-dimethylhydrazinio)methyl-1,3,4-oxadiazole chlorides XIII–XVI (general procedure). A solution of 1 g of 1,1-dimethylhydrazine in 10 ml of 2-propanol was added with stirring to a solution of 3 g of **I**–**IV** in 40 ml of 2-propanol. The reaction temperatures and times are given in Table 1. The resulting mixture was cooled, excess 2-propanol was distilled off, and the precipitate was filtered off and dried in a desiccator.

CONCLUSIONS

(1) Hydrazine and methylhydrazine react with 5-aryl-2-chloromethyl-1,3,4-oxadiazoles with the substitution of chlorine to form the corresponding hydrazino and methylhydrazino derivatives.

(2) 1,1-Dimethylhydrazine reacts with 5-aryl-2-chloromethyl-1,3,4-oxadiazoles with the substitution of chlorine to form the corresponding quaternary hydrazinium salts.

REFERENCES

1. Baranov, A.B., Tsypin, V.G., Malin, A.S., and Laskin, B.M., *Zh. Prikl. Khim.*, 2004, vol. 77, no. 12, pp. 2021–2024.
2. Grekov, A.P., *Organicheskaya khimiya gidrazina* (Organic Chemistry of Hydrazine), Kiev: Tekhnika, 1966.
3. Soldatenkov, A.T., Kolyadina, N.M., and Shendrik, I.V., *Osnovy organicheskoi khimii lekarstvennykh veshchestv* (Fundamentals of the Organic Chemistry of Drugs), Moscow: Khimiya, 2001.
4. Mel'nikov, N.N., *Khimiya i tekhnologiya pestitsidov* (Chemistry and Technology of Pesticides), Moscow: Khimiya, 1974.
5. Kolla, V.E. and Berdinskii, I.S., *Farmakologiya i khimiya proizvodnykh gidrazina* (Pharmacology and Chemistry of Hydrazine Derivatives), Ioshkar-Ola: Mariiskoe Knizhnoe, 1976.
6. Hill, J., *Comp. Heterocyclic Chem.*, 1984, vol. 6, pp. 427–446.
7. Kristinsson, H., *Synthesis*, 1979, no. 2, pp. 102–103.
8. Cojocariu, I., Cojocariu, Z., and Nistor, C., *Rev. Chim.* (Bucharest), 1977, vol. 28, no. 1, pp. 15–18.
9. Vakula, T.R. and Srinivasan, V.R., *Indian J. Chem.*, 1973, vol. 11, no. 8, pp. 732–734.
10. Ioffe, B.V., Kuznetsov, M.A., and Potekhin, A.A., *Khimiya organicheskikh proizvodnykh gidrazina* (Chemistry of Organic Hydrazine Derivatives), Leningrad: Khimiya, 1979.

Russian Journal of Applied Chemistry, Vol. 78, No. 3, 2005, pp. 469–473. Translated from Zhurnal Prikladnoi Khimii, Vol. 78, No. 3, 2005, pp. 474–478.
Original Russian Text Copyright © 2005 by Kalinina, Silinskaya, Sklizkova, Kozhurnikova, Filippov, Kudryavtsev.

MACROMOLECULAR CHEMISTRY AND POLYMERIC MATERIALS

Structure of Solutions of Polyamido Acid Salts in a Mixed Solvent

N. A. Kalinina, I. G. Silinskaya, V. P. Sklizkova, N. D. Kozhurnikova, A. P. Filippov, and V. V. Kudryavtsev

Institute of Macromolecular Compounds, Russian Academy of Sciences, St. Petersburg, Russia

Received December 28, 2004

Abstract—The changes in the structural organization of solutions of *N,N*-dimethylhexadecylammonium salt of the polyamido acid based on 3,3',4,4'-diphenyltetracarboxylic dianhydride and *o*-tolidine in a dimethylacetamide–dioxane mixed solvent during 24-h keeping at room temperature were studied by polarized light scattering. The stability of the salt solutions was studied as influenced by the composition of the mixed solvent, chemical nature of its components, and molecular weight of the polymer.

In our previous work [1] we carried out light-scattering and viscometric studies of the structure formation and revealed supramolecular associative structures in dilute solutions of comb-shaped *N,N*-dimethylhexadecylammonium salt PAA–C_{16} of polyamido acid based on 3,3',4,4'-diphenyltetracarboxylic dianhydride and *o*-tolidine (PAA DP-T) in a mixed dimethylacetamide (DMAA)–benzene solvent. The PAA–C_{16} solutions at the 50 : 50 solvent : precipitant volume ratio and the concentration of 1 mM are used for preparing ultrathin polyimide (PI) films by the Langmuir–Blodgett (LB) technique [2]. As known, solutions of salts obtained by PAA neutralization with a long-chain tertiary amine are prepared immediately before formation of LB films [3], since even within several hours their performance characteristics get deteriorated: Films thereof are strongly defective and heterogeneous. We showed that keeping 0.5% solutions of PAA–C_{16} in a 50 : 50 DMAA–benzene mixture significantly modifies their supramolecular structure, namely, their microheterogeneity and microordering [1] tend to increase. It seemed reasonable to study how variations of the structure of the PAA–C_{16} solutions during 24-h keeping depend on the composition of the mixed solvent, chemical nature of its components, and molecular weight M of the polymer.

As known, the consumers' properties of the polyimide macrofilms formed from PAAs are virtually unaffected by the molecular weights M within 50 000–200 000. However, films prepared from PAAs with $M < 50\,000$ do not exhibit the required physicomechanical characteristics [4], but, at the same time, these salts do not form a supramolecular structure in dilute solutions, as demonstrated by our control tests. Therefore, we chose solutions (0.4 g dl^{-1}) of salts based on a PAA with a comparatively high molecular weight M = 135 000 (sample 1) and on a low-molecular-weight PAA with M = 50 000 (sample 2). The ratio γ of the components of the DMAA–dioxane mixed solvent was varied around practically used compositions: 55 : 45, 50 : 50, and 48.4 : 51.6.

EXPERIMENTAL

Polyamido acid DP-T was synthesized as a 10% solution in DMAA by the standard procedure [4]. The monomers for synthesis of PAA and *N,N*-dimethylhexadecylamine were purified by vacuum distillation. Solvents DMAA and dioxane were dried over calcium hydride and distilled. The PAA salts were prepared in two steps. First, 1% solutions of PAA and the tertiary amine in the DMAA–dioxane mixture of the desired composition were prepared separately. Then, immediately before the experiment, they were mixed in the amounts corresponding to 1 : 2 molar ratio of the PAA unit to amine; the resulting solution was diluted to the desired concentration by the solvent of the same composition. After 30 min, an equilibrium was established, and the solution was placed into a measuring cell and kept at a constant temperature for 20 min. The intensities of the polarized V_V and depolarized H_V components of the light scattered by the PAA–C_{16} solutions at the scattering angles θ of 40°–140° were measured on an FPS-3M photoelectric light-scattering instrument at the wavelength λ = 578 nm. Benzene was used for calibration. For nonpolarized light at

1070-4272/05/7803-0469© 2005 Pleiades Publishing, Inc.

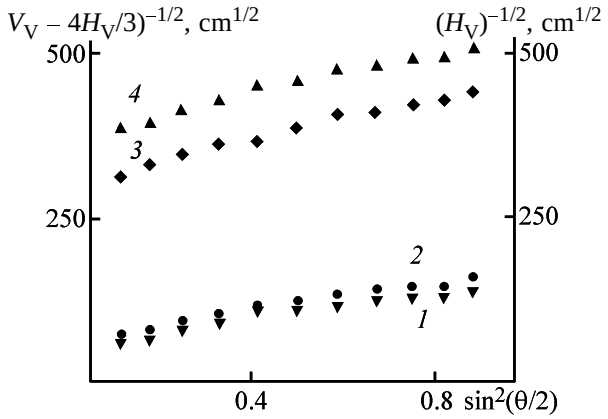
Table 1. Intrinsic viscosity of DP-T polyamido acid and its salt PAA–C_{16} as influenced by the mixed solvent composition

DMAA : dioxane volume ratio	Intrinsic viscosity, dl g^{-1}	
	DP-T	PAA–C_{16}
100 : 0	3.00	2.15
55 : 45	2.50	1.65
50 : 50	2.40	1.50
48.4 : 51.6	2.25	1.35

this wavelength, the Rayleigh ratio for benzene was 13.06×10^{-6} cm^{-1}. The intrinsic viscosity [η] of the polymer macromolecules was determined in a capillary Ubbelohde viscometer at 20°C. The time of outflow of the mixed solvent was 90–100 s. Table 1 lists the intrinsic viscosities of PAA and the PAA salt in the mixed solvent of different compositions. The molecular weight of the samples of the initial PAA in DMAA was determined by the light scattering method at the angle of 90°. The supramolecular structure of the solutions was quantitatively analyzed by the polarized light scattering method in terms of the Debye–Stein statistical theory [5].

The Debye–Stein statistical theory connects the experimentally determined Rayleigh ratios for the vertically R_V and horizontally R_H polarized components of the scattered light and the structural characteristics of the scattering polymeric medium by the relationships

$$R_V - \frac{4}{3}R_H = 4\pi K_0^4 \langle \eta \rangle \int_0^\infty \gamma(r) \frac{\sin(2KrS)}{2KrS} r^2 \, dr, \quad (1)$$



Angular plots of (*1*, *2*) $(V_V - 4H_V/3)^{-1/2}$ and (*3*, *4*) $(H_V)^{-1/2}$ for the PAA–C_{16} salt sample in the DMAA–dioxane mixed solvent at γ = 55 : 45. (*1*, *3*) Initial samples and (*2*, *4*) samples kept for 24 h.

$$R_H = \frac{4}{15} 4\pi K_0^4 \langle \delta^2 \rangle \int_0^\infty f(r) \frac{\sin(2KrS)}{2KrS} r^2 \, dr, \quad (2)$$

where $K = K_0 n$; n, refractive index of the medium; $K_0 = 2\pi/\lambda$; r, distance between two elementary scattering volumes; $S = \sin^2(\theta/2)$; $\gamma(r)$, correlation function of the polarizability fluctuation; $f(r)$, correlation function of the mutual orientation of the optical axes of the elementary scattering volumes.

Using the exponential correlation functions $\gamma(r) = \exp(-r a_V)$ and $f(r) = \exp(-r/a_H)$, it is possible to obtain the following parameters of the scattering medium: a_V and a_H, correlation radii of the polarizability fluctuation and orientation, respectively; $\langle \eta^2 \rangle$, mean squared polarizability fluctuation, and $\langle \delta^2 \rangle$, mean squared optical anisotropy density. Since the exponential correlation function of the orientation is related to the angle θ_{ij} between the optical axes of two arbitrarily chosen optical elements, it is possible to determine the factor of local orientation F within the areas confined by the radius $r = a_V$ [6]:

$$F = (\cos^2 \theta_{ij}) a_V = [1 + 2\exp(-a_V/a_H)]/3. \quad (3)$$

Thus, the isotropic parameters $\langle \eta^2 \rangle$ and a_V characterize the degree of the density heterogeneity of the system and the correlation size of the microheterogeneities, and anisotropic parameters $\langle \delta^2 \rangle$ and a_H, the degree of ordering of the system and sizes of the ordered areas.

For all the tested solutions of the PAA–C_{16} salt samples in a mixed solvent, we obtained the experimental plots of $(H_V)^{-1/2}$ and $(V_V - 4H_V/3)^{-1/2}$ vs. $\sin^2(\theta/2)$ (see figure). From the slopes of the approximating straight lines and the intercepts, we calculated four statistical structural parameters of the scattering system [5] and the local orientation factor F [6], using the exponential correlation function. Table 2 lists the statistical parameters characterizing the structure of the solutions of the two samples of the PAA–C_{16} salt with different molecular weighs M in the DMAA–dioxane mixtures. Also, Table 2 lists the molecular weights M of the initial PAAs that were used for preparing the PAA–C_{16} salts studied.

We showed previously [1] that PAA DP-T forming the backbone of the salt dissolves completely and that amide solvents are thermodynamically good for *o*-tolidine-based PAA macromolecules. Upon addition of dioxane to the solution, the thermodynamic quality of the solvents is deteriorated, and the macromolecular globule gets contracted, which decreases [η] for

Table 2. Structural characteristics of the PAA–C_{16} salt solutions in the DMAA–dioxane mixed solvent at c = 0.4 g dl^{-1}

Sample	M (initial PAA)	γ	Time of keeping, h	$\langle\eta^2\rangle \times 10^9$	a_V, nm	$\langle\delta^2\rangle \times 10^9$	a_H, nm	F
1	135 000	55/45	0	10.8	45	4.1	22	0.42
			24	8.8	40	2.9	22	0.42
		50/50	0	12.8	48	6.9	19	0.39
			24	12.0	46	5.8	19	0.39
		48.4/51.6	0	17.8	56	5.5	27	0.42
			24	8.7	56	5.8	19	0.37
2	50 000	50/50	0	9.5	35	10.9	12	0.36
			24	13.9	25	2.1	18	0.50

both PAA and the PAA–C_{16} salt (Table 1). However, when dissolved, comb-shaped PAA–C_{16} salts prepared from PAA form molecular-dispersed solutions neither in amide solvents nor in their mixtures with benzene or dioxane, which suggests that these are associated systems [7]. Intermolecular association may be realized via long side aliphatic chains of the tertiary amine.

Table 2 shows that the difference between the statistical parameters characterizing the structural organization of the PAA salt solutions in mixed solvents with close compositions substantially exceeds the measurement inaccuracy.

It is known that, with deteriorating thermodynamic quality of the solvent, the polymer–polymer interactions are enhanced, which is responsible for contraction of the macromolecular globule and an increase in the segment density [8]. It was found experimentally that, with increasing proportion of the precipitant, the structural changes in solutions of associated macromolecules are manifested in an increase in the microheterogeneity of the solution, i.e., in the mean squared density of the optical polarizability $\langle\eta^2\rangle$ in parallel with a decrease in the size of the associative formations a_V. Such a behavior was revealed for PAA solutions in mixed solvents [9].

In dilute PAA–C_{16} salt solutions, the parameter $\langle\eta^2\rangle$ also increased with increasing proportion of precipitant (dioxane) in the mixed solvent, but this was accompanied by an increase in a_V (Table 2). Increase in the proportion of dioxane results in contraction of the backbone of PAA–C_{16} for which dioxane is precipitant [10]. This is responsible for increases in the optical density of the macromolecular globule and in the corresponding $\langle\eta^2\rangle$ parameter. Evidently, contraction of the globule enhances interaction between the long side aliphatic branches of the tertiary amine. This favors association in solution, which increases a_V.

We found that all the PAA–C_{16} salt solutions that we studied exhibit microanisotropic properties. The calculated anisotropic structural parameters, the mean squared density of the optical anisotropy $\langle\delta^2\rangle$ and the mean correlation radius of orientation of the scattering elements of the volume a_H, vary insignificantly with the mixed solvent composition. The local order factor F fluctuates around 0.4, which is typical for dilute polymer solutions [6].

Since the PAA salt solutions in mixed solvents of close compositions differ substantially in the structural organization, it can be expected that, during keeping, these solutions will behave differently as well. Table 2 shows that, during 24-h keeping at room temperature, the statistical parameters characterizing the supramolecular structure of the PAA–C_{16} salt solutions significantly vary, whatever the composition of the mixed solvent studied, with the solvent composition and the molecular weight M of the initial PAA.

For the solution of the high-molecular-weight sample no. 1 in the mixed solvent at the DMAA : dioxane ratio γ of 55 : 45 and 50 : 50, all the structural parameters tend to decrease within 24 h, and the mean correlation radius of orientation of the scattering elements of volume a_H remains virtually unchanged. This suggests homogenization of the solution. The local orientation factor F remains virtually unchanged. For the system with a maximal amount of the precipitant (γ = 48.4 : 51.6), when the polymer still occurs in solution, the mean squared polarizability fluctuation $\langle\eta^2\rangle$ decreases by a half within 24 h, and the parameter a_V remains unchanged within the accuracy. Thus, the size a_V of the associative formations remains unchanged with time, but their density decreases, that is, the solution becomes more homogeneous. The correlation size of the ordered areas a_H noticeably decreases and, therefore, the degree of ordering of the

associative formations, characterized by the factor *F*, decreases.

As the system approaches the precipitation point (γ = 48.4 : 51.6), the instability of the structural organization of the solutions is manifested stronger than for the other systems: The parameter $\langle\eta^2\rangle$ decreases almost by a half, and a_H also significantly decreases. Thus, not only homogenization but also disordering of the structure of the associative formations take place, probably owing to a decrease in the degree of mutual orientation of the side fragments of the macromolecules.

Studies of the structural organization of solutions of mesogenic PAA in amide solvents showed that, in the course of keeping, the diamine and dianhydride components of the monomeric unit undergo mutual ordering, which increases the optical anisotropy density [10]. In the PAA–C_{16} salt solution at γ of 55 : 45 and 50 : 50, the development of this process is precluded by side aliphatic chains which create steric hindrance to mutual approach of the PAA backbone segments. However, as the system approaches the precipitation point, the polymer–polymer interaction is strengthened, and this favors mutual approach of the monomeric units, thus enhancing the order at the microlevel. This can be responsible for a certain increase in the parameter $\langle\delta^2\rangle$ during keeping of the solutions of sample no. 1 of the PAA–C_{16} salt in the solvent with γ = 48.4 : 51.6.

We showed previously [9] that the structural organization of the systems studied, quantitatively characterized by statistical parameters, depends on the molecular weight *M* of the polyamido acid. In view of the fact that the solutions of polymers with different molecular weights *M* strongly differ in the structural features at identical concentrations, it is important to compare the supramolecular organizations of the solutions for which the polymer concentrations are identical and molecular weights *M* differ. This is the more important, since, in practice, Langmuir–Blodgett films are usually prepared from solutions with one, fixed, polymer concentration.

To elucidate how the structural organization of the PAA–C_{16} salt solutions is influenced by the molecular weight *M*, we compared the characteristics of two samples in mixed solvents of the same concentration (γ = 50 : 50). For the high-molecular-weight sample no. 1 within 24 h of keeping, both isotropic ($\langle\eta^2\rangle$ and a_V) and anisotropic ($\langle\delta^2\rangle$ and a_H) parameters decrease insignificantly, i.e., the solutions become more homogeneous in density and more disordered (Table 2). In contrast to sample no. 1, a low-molecular-weight sample no. 2 exhibits a qualitatively different pattern of variation of the structural parameters on keeping: The parameters $\langle\eta^2\rangle$ and a_H tend to significantly increase, while the two other parameters, to significantly decrease (Table 2). An increase in $\langle\eta^2\rangle$ suggests that the heterogeneity of the solution of sample no. 2 tends to increase with time, which can be due to an increase in the density of the monomeric units inside the associative formations. Increase in the correlation size of the ordered areas a_H suggests an increase in the degree of ordering in system 2 with time. For a low-molecular-weight sample, a lower mean density of the monomeric units in the molecular globule and a more unfolded chain can create more favorable conditions for the mutual ordering of the side aliphatic chains [11] of the polymer and solvent molecules, incorporated into the associative formation. This is manifested in an increase in the orientation correlation radius a_H and local orientation factor *F*. Ordering of long side chains, in turn, results in a decrease in the equilibrium flexibility of the macromolecules [11], which can be manifested experimentally in an increase in the microheterogeneity $\langle\eta^2\rangle$.

Comparative analysis of the behavior of the PAA–C_{16} solutions suggests that solutions of low-molecular-weight salts have a less stable structure than high-molecular-weight samples. This should be taken into account when applying solutions of low-molecular-weight PAA–C_{16} salts in formation of Langmuir–Blodgett films.

Comparison of the changes in the structural organization of the PAA–C_{16} salt solution in DMAA–benzene and DMAA–dioxane mixtures revealed a marked difference in their supramolecular organization and stability. In particular, within 24 h of keeping, solutions of the high-molecular-weight salt in the DMAA–benzene mixture undergo substantial structural changes, which are manifested in increases in $\langle\eta^2\rangle$ and a_H by a factor of 1.5–2. By contrast, in solutions of the high-molecular-weight salt in the DMAA–dioxane mixture the structural characteristics slightly decrease. Morphological changes in time, similar to those in the PAA–C_{16}–DMAA–benzene system, are exhibited in the DMAA–dioxane system only by the low-molecular-weight sample.

CONCLUSIONS

(1) A comparative analysis of the structural organization was carried out for solutions of high-molecular-weight samples of PAA–C_{16} in mixed dimethyl-

acetamide–dioxane solutions of various compositions. The homogeneity of these solutions is the higher, the smaller the proportion in them of the precipitant, dioxane. The mean density of the associative formations and their statistical size tend to decrease with time, like the mean squared anisotropy density and the size of the ordered areas. This means that solutions of high-molecular-weight PAA–C_{16} become more homogeneous and disordered.

(2) The structural organization and behavior with time, exhibited by the PAA–C_{16} salt solutions in solvents with identical compositions, depend on the molecular weight M of the PAA: Solutions of the low-molecular-weight sample of the comb-shaped salt become more heterogeneous and microordered with time.

(3) In the case of the high-molecular-weight PAA–C_{16} salt and the mixed solvent with a composition close to that corresponding to precipitation of the polysalt, the dimethylacetamide–dioxane system can be more advantageous than the dimethylacetamide–benzene system from the viewpoint of the stability of solutions. This should be taken into account in preparing Langmuir–Blodgett films.

ACKNOWLEDGMENTS

This work was financially supported by the Russian Foundation for Basic Research (project no. 02-03-32 683).

REFERENCES

1. Kalinina, N.A., Sklizkova, V.P., Silinskaya, I.G., *et al.*, *Vysokomol. Soedin., Ser. A*, 2001, vol. 43, no. 4, pp. 707–712.
2. Kudryavtsev, V.V., Sklizkova, V.P., Baklagina, Yu.G., *et al.*, *Vysokomol. Soedin., Ser. A*, 2001, vol. 43, no. 7, pp. 1211–1216.
3. Arslanov, A.A., *Usp. Khim.*, 1994, vol. 64, no. 1, pp. 3–28.
4. Bessonov, M.I., Koton, M.M., Kudryavtsev, V.V., and Laius, L.A., *Poliamidy – klass termostoikikh polimerov* (Polyamides: A Class of Heat-Resistant Polymers), Leningrad: Nauka, 1983.
5. Stein, P., *Polymer Blends*, Paul, D.R. and Newman, S., Eds., New York: Academic, 1978, vol. 1, ch. 1, p. 339.
6. Kallistov, O.V. and Silinskaya, I.G., *Vysokomol. Soedin., Ser. A*, 1992, vol. 34, no. 7, pp. 3–5.
7. Silinskaya, I.G., Sklizkova, V.P., Kalinina, N.A., *et al.*, *Vysokomol. Soedin., Ser. A*, 2003, vol. 45, no. 10, pp. 1725–1731.
8. Tsvetkov, V.N., *Zhestkotsepnye polimernye molekuly* (Rigid-Chain Polymer Molecules), Leningrad: Nauka, 1986.
9. Silinskaya, I.G., Kalinina, N.A., Sklizkova, V.P., *et al.*, *Vysokomol. Soedin., Ser. A*, 2003, vol. 45, no. 2, pp. 292–297.
10. Kalinina, N.A., Silinskaya, I.G., Kallistov, O.V., *et al.*, *Vysokomol. Soedin., Ser. B*, 1995, vol. 37, no. 5, pp. 850–853.
11. *Zhidkokristallicheskie polimery* (Mesomorphic Polymers), Plate, N.A., Ed., Moscow: Khimiya, 1988, ch. 3, p. 73.

Russian Journal of Applied Chemistry, Vol. 78, No. 3, 2005, pp. 474–477. Translated from Zhurnal Prikladnoi Khimii, Vol. 78, No. 3, 2005, pp. 479–483.
Original Russian Text Copyright © 2005 by Shevchenko, Voloshanovskii, Petrova, Berbat.

MACROMOLECULAR CHEMISTRY AND POLYMERIC MATERIALS

Preparation of Branched Poly(Methyl Methacrylate) Using a Macroinitiator Based on Cobalt(II) 3-Allylpentane-2,4-dionate

O. V. Shevchenko, I. S. Voloshanovskii, E. V. Petrova, and T. I. Berbat

Mechnikov Odessa National University, Odessa, Ukraine

Received November 25, 2004

Abstract—Cobalt(II) 2-allylpentane-2,4-dionate, when used as an initiator of methyl methacrylate polymerization, yields a polymer containing metal chelate groups and exhibiting the properties of a macroinitiator capable of initiating secondary polymerization with the formation of branched high-molecular-weight methyl methacrylate polymers with a low polydispersity.

Polymers containing functional groups in the chain can be used in various processes [1]. Recently we suggested a procedure for preparing functional polymers starting from transition metal vinyl β-diketonates [2]. The presence of a double bond in these compounds allows their copolymerization with vinyl monomers, and the radical-generating metal chelate ring exhibits initiating power. Initiation with transition metal β-diketonates has been described in sufficient detail in [3]; however, no data are available on initiation with polymers containing β-diketonate fragments in pendant chains. Macroinitiators based on peroxides were reported in [4, 5]. They are of interest for preparation of branched and graft polymers and for cross-linking and modification of polymers [6].

In this work we studied polymerization of methyl methacrylate (MMA) initiated with a cobalt(II) vinyl β-diketonate and some characteristics of the resulting polymers.

EXPERIMENTAL

As initiator we used cobalt(II) 3-allylpentane-2,4-dionate [APD-Co(II)] [7]. Polymerization was performed in a solution of dimethylformamide (DMF) and dimethyl sulfoxide (DMSO) at 70°C. In these solvents, the attainable concentration of the chelate is higher than in bulk polymerization. Furthermore, donor solvents should exert an activating effect on the polymerization. The monomer concentration was 5.32 M in all the experiments. The initiator concentration in DMF solutions was 1 wt %, and in DMSO solutions, 2 wt % based on the monomer. The polymerization was performed in ampules. The reaction kinetics was studied by the method of dry residue.

To calculate the content and length of the grafted chains, the polymerization was performed in two steps. In the first step, we isolated polymers formed at incomplete conversion (from 13.0 to 19.9%). Since initiation and copolymerization with the chelates occurred simultaneously, we obtained an MMA polymer containing metal chelate groups in the pendant chains. The polymers were reprecipitated two times with a tenfold excess of ethanol. For the samples obtained, we determined the cobalt(II) content and the molecular-weight characteristics.

In the second step, the polymers obtained were used as macroinitiators (MIs) in MMA polymerization. We determined the molecular-weight characteristics of the resulting graft polymers. The content and mean length of the grafted chains were determined by comparison of the matrix polymer prepared in the first step with the graft polymer formed in the second step. The cobalt(II) content was determined with a Saturn atomic absorption spectrometer equipped with an LSP-1 lamp (analytical line of Co 240.7 nm). The molecular weights of the polymers were determined by gel permeation chromatography on a Waters-200 chromatograph using Waters monodisperse polystyrene references. The branched PMMA was subjected to fractional precipitation in the benzene–petroleum ether system at 20°C. The molecular weights of the fractions were estimated from their intrinsic viscosities [η].

The polymerization of MMA initiated with APD-Co(II) was performed at 70°C to various conversions (Table 1). In DMF solutions at a chelate concentration of 1 wt %, the polymerization rate is fairly high (the rate of thermal polymerization in the bulk was 1.1%

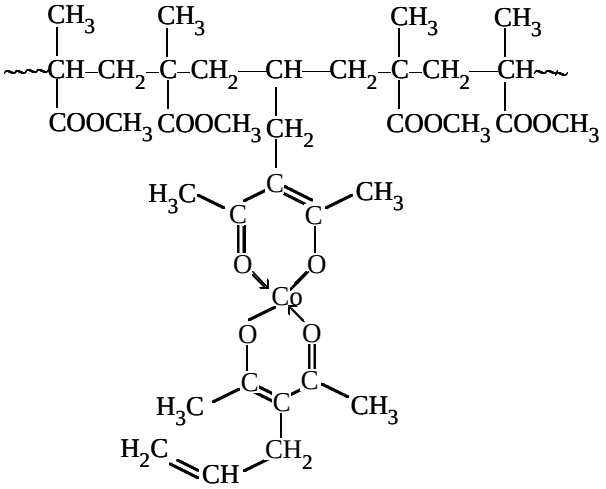
1070-4272/05/7803-0474© 2005 Pleiades Publishing, Inc.

Table 1. Some parameters of copolymerization of cobalt(II) 3-allylpentane-2,4-dionate with MMA* (70°C, [M] = 5.32 M)

Solvent	c_{chel}, wt %	τ, h	S, %	V_{av}, % h^{-1}	c_{Co}, wt %	$M_n \times 10^{-5}$	$M_w \times 10^{-5}$	M_w/M_n	N_{Co}	MI
DMSO	2.0	0.5	13.5	27.0	0.98	–	–	–	–	MI-1
	2.0	1.0	17.4	17.4	0.23	–	–	–	–	MI-2
	2.0	1.5	18.4	12.3						CLP**
DMF	1.0	1.5	13.0	8.68	0.28	–	–	–	–	MI-3
	1.0	2.0	14.5	7.25	0.17	1.35	6.83	5.06	20	MI-4
	1.0	2.5	18.1	7.24	0.16	2.47	8.24	3.33	22	MI-5
	1.0	3.0	19.9	6.64	0.14	1.81	7.45	4.12	18	MI-6

* (C_{Co}) Co(II) content in the copolymer; (N_{Co}) number of cobalt atoms per macromolecule; (M_n, M_w) number-average and weight-average molecular weights of the products; (M_w/M_n) degree of polydispersity; (S) conversion.
** A cross-linked polymer is formed.

per hour). The cobalt(II) content in the polymer substantially decreases with increasing conversion, which may be due to exhaustion of the polymer in the course of the polymerization. Therefore, the polymer samples taken at low conversions contain more metals and hence are more active as macroinitiators. Copolymerization of the initiator with MMA yields a copolymer with metal chelate groups.



Since APD-Co(II) contains two ligands, each with a C=C bond, it is a diene monomer. Therefore, the copolymerization can be accompanied by cross-linking through unchanged double bonds. The metal atoms present in the monomer can also effect cross-linking [8]. The chelate groups incorporated in the copolymer form active centers behaving as branching centers. The branches can also contain chelate groups and undergo further branching. Therefore, the polymers listed in Table 1 will contain two types of chelate groups: converted groups which formed branches and unchanged groups which can act as initiation centers after isolation of the polymers. The degree of the polydispersity of the polymers is high. One of the polymers contained a small (1.5%) low-molecular-weight fraction (M_n = 2800, M_w = 3500, M_w/M_n = 1.28) whose formation may be associated with the inhibiting effect of β-diketonates [2].

The polymerization in DMSO shows similar trends. However, in this case the mean reaction rates were very high, and the Co(II) content in the polymer reached 1 wt %. Furthermore, a cross-linked product was obtained when the polymerization was performed for 1.5 h. Additional experiments showed that the cross-linked polymer was always formed in both solvents at the chelate concentration of 2 wt %, polymerization time of >1.5 h, and temperature of 70°C. From the cobalt(II) content in the polymer and M_w of the polymers, we calculated the cobalt content per macromolecule N_{Co}; the results confirm the participation of the chelate in the copolymerization with MMA as comonomer.

The polymers prepared by the above procedure were used as initiators of graft polymerization of MMA (Table 2), which was performed in the bulk.

Table 2. Parameters of graft polymerization of MMA, initiated with MI (70°C, c_{MI} = 2 wt %, 7 h)

MI	S, %	V_{av}, % h^{-1}	$M_n \times 10^{-6}$	$M_w \times 10^{-6}$	M_w/M_n
MI-1	42.3	6.0	1.7	4.8	2.85
MI-2	30.2	4.3	2.2	6.1	2.77
MI-3*	51.7	4.4	2.3	7.2	3.12
MI-4	53.8	7.7	3.0	8.0	2.66
MI-5	34.9	5.0	2.4	7.0	2.91
MI-6	32.0	4.6	1.8	5.3	2.94

* With MI-3, the graft polymer contained 20% cross-linked fraction.

Table 3. Comparison of the molecular-weight characteristics of macroinitiators and graft polymers*

MI	Macroinitiator				Graft polymer					
	$M_n \times 10^{-5}$	$M_w \times 10^{-5}$	M_w/M_n	N_{Co}	$M_n \times 10^{-6}$	$M_w \times 10^{-6}$	M_w/M_n	n	$M_{t.gr} \times 10^{-6}$	$\overline{M}_{gr} \times 10^{-5}$
MI-4	1.35	6.83	5.06	20	3.0	8.0	2.66	20	7.32	3.66
MI-5	2.47	8.24	3.33	22	2.4	7.0	2.91	22	6.18	2.81
MI-6	1.81	7.45	4.12	18	1.8	5.3	2.94	18	4.56	2.53

* (n) Number of grafting sites, ($\overline{M}_{gr}$) mean molecular weight of grafted chains, and ($M_{t.gr}$) total molecular weight of grafted chains.

As already noted, a part of the metal chelate groups incorporated in the macroinitiator formed branchings even in the step of its preparation. Such groups will not initiate secondary polymerization. This is indicated by the fact that a high cobalt(II) content in MI (Table 1) does not always ensure higher rate of secondary polymerization. A similar phenomenon was observed previously with MIs containing peroxy groups of the same thermal stability. Nevertheless, the reaction rates are fairly high in all the cases. It is interesting that a cross-linked fraction formed in the MI sample with the highest Co content (DMF solution). The molecular weights of the graft polymers exceeded those of the initial macroinitiators by more than an order of magnitude, suggesting high degree of grafting. It should be emphasized that the degree of polydispersity of the graft polymers is relatively low (<3) and in all the cases lower than that of the initial MIs. This may be due to weaker inhibiting effect of the β-diketonate groups incorporated in the polymer, which is caused by steric factors and diffusion limitations. Therefore, the chain termination on an MI will be weaker than on the monomeric chelate; as a result, the polydispersity will decrease. In the case of peroxy MIs, the degree of polydispersity was more than 10 [4]. This fact demonstrates an advantage of MIs based on β-diketonates.

Comparison of data from Tables 1 and 2 allows determination of the content and length of the grafted chains. Considering the mechanism of initiation with monomeric cobalt(II) vinyl β-diketonates, we can expect that the metal chelate groups incorporated in the polymer will initiate graft polymerization. Then the amount of the cobalt atoms in the macromolecule (Table 1) will determine the limiting amount of the grafting sites (Table 3). The exceptions are the metal chelate groups that already formed graftings in the step of MI preparation. However, the amount of such groups can be reduced to a minimum by decreasing the time and temperature of MI preparation. From data in Table 3, we calculated the total and mean molecular weights of the grafted chains in the macromolecule. Thus, MIs prepared under similar conditions but at different conversions (from 14.5 to 19.9%) only slightly differ in the number of grafting sites (from 18 to 22). The mean molecular weight of the grafted chains is (2.53–3.66) × 10^5, which amounts to 34–54% of the molecular weight of the macroinitiator. Thus, comb-shaped polymers with a high molecular weight of the grafted chains were obtained. The total weight of the grafted chains is many times higher than the weight of the macroinitiator.

It is known that grafting of monomers onto a polymer matrix containing a peroxy fragment yields, along with the graft product, also the thermopolymer and the homopolymer (owing to participation in the polymerization of a small radical formed by cleavage of the peroxy bond) [4]. The presence of large amounts of these polymers appreciably impairs the properties of the graft products. The mechanism suggested previously in [9] does not involve formation of a small radical in initiation with MIs based on cobalt(II) β-diketonates; therefore, the graft product should be mainly contaminated with the thermopolymer. To confirm this assumption, we fractionated the graft polymer obtained on MI-2. The results are listed in Table 4.

The sample was separated into three fractions, and the intrinsic viscosity [η] and molecular weight of each fraction were determined. For the nonfractionated sample, [η] = 6.04. Calculation of the intrinsic viscosity of this sample from [η] of separate fractions and their relative content (by weight) gave [η] = 6.17. Thermal polymerization of MMA at 70°C occurs at a rate of 1.1% h^{-1}, and the intrinsic viscosity of the resulting polymer is 5.81. If the rate of the polymerization initiated with MI-2 is 4.3% h^{-1} (Table 2), then the relative content of the thermopolymer in the sample should be 25.6%. The same conclusion follows from the results of the gravimetric analysis. Comparison of these data with the characteristics of fraction II shows that it is the thermopolymer. Hence, fraction I of the highest molecular weight is the graft polymer. Fraction III remains unidentified. Presumably, this

Table 4. Results of fractionation of the secondary polymer obtained on MI-2

Fraction	$[\eta]$, dl g^{-1}	$M_\eta \times 10^{-6}$	Content of fraction, %	Molecular weight		
				$M_n \times 10^{-6}$	$M_w \times 10^{-6}$	M_w/M_n
I	7.39	6.00	58.0	–	–	–
II	5.34	3.83	26.0	–	–	–
III	3.09	1.81	16.0	–	–	–
Nonfractionated sample	6.04	4.54	–	2.2	6.1	2.77

lowest-molecular-weight fraction is formed by termination of the propagating chains on MI chelate fragments. Thus, the graft polymer does not contain MMA homopolymer, which confirms the initiation mechanism suggested in [9]. The high degree of polydispersity (>10) of the graft polymers prepared with MIs of peroxy type may be due to the presence of the homopolymer.

Table 4 also shows that the molecular weight of fraction I (graft polymer) is 33% higher than that of the nonfractionated sample. The calculations of the lengths of the grafted chains were based on data for nonfractionated samples, and even in this case the molecular weight of the grafted chains reached 54% of that of MI. Thus, actually the molecular weight of the grafted chains is, apparently, almost equal to that of the polymer.

CONCLUSIONS

(1) Branched methyl methacrylate polymers were obtained with macroinitiators containing cobalt(II) diketonate fragments in the pendant chains.

(2) The number and mean molecular weight of the grafted chains were calculated. The polymers obtained are comb-shaped with the molecular weight of the grafted chains close to that of the macroinitiator and have a low degree of polydispersity.

(3) Examination of the fractional composition of the graft polymer showed that the polymer blend contained no homopolymer that could form by secondary polymerization. This fact furnishes additional information on the mechanism of initiation with cobalt β-diketonates.

REFERENCES

1. Sherrington, D., *Usp. Khim.*, 1991, vol. 60, no. 7, pp. 1494–1512.
2. Shevchenko, O.V., Voloshanovskii, I.S., Berbat, T.I., and Zakhariya, A.I., *Vopr. Khim. Khim. Tekhnol.*, 2003, no. 6, pp. 111–115.
3. Nizel'skii, Yu.K., *Kataliticheskie svoistva β-diketonatov metallov* (Catalytic Properties of Metal β-Diketonates), Kiev: Naukova Dumka, 1983.
4. Ivanchev, S.S., Budtov, V.P., Romantsova, O.I., *et al.*, *Vysokomol. Soedin., Ser. A*, 1976, vol. 18, no. 5, pp. 1005–1011.
5. Mesh, A.M., Ivanchev, S.S., Ratsch, M., *et al.*, *Vysokomol. Soedin., Ser. B*, 2001, vol. 43, no. 9, pp. 1591–1594.
6. Dmitrenko, A.V., Mesh, A.M., and Agapitov, A.P., *Vysokomol. Soedin., Ser. B*, 1990, vol. 32, no. 3, pp. 523–528.
7. Voloshanovskii, I.S., Shevchenko, O.V., Berezhnitskaya, A.S., and Krasnova, E.A., *Ukr. Khim. Zh.*, 2001, vol. 67, no. 5, pp. 5–10.
8. Movchan, T.I., Voloshanovskii, I.S., and Pomogailo, A.D., *Izv. Ross. Akad. Nauk, Ser. Khim.*, 1993, no. 12, pp. 2060–2064.
9. Voloshanovskii, I.S. and Shevchenko, O.V., *Kompoz. Polim. Mater.*, 2000, vol. 22, no. 2, pp. 108–113.

Russian Journal of Applied Chemistry, Vol. 78, No. 3, 2005, pp. 478–483. Translated from Zhurnal Prikladnoi Khimii, Vol. 78, No. 3, 2005, pp. 484–489.
Original Russian Text Copyright © 2005 by Kuryndin, Mokreva, Terlemezyan, Sidorovich, Praslova, Elyashevich.

MACROMOLECULAR CHEMISTRY AND POLYMERIC MATERIALS

Electrophysical Properties and Thermal-Deformation Stability of Composites Containing Polyaniline Layers Deposited on Porous Polyethylene Films

I. S. Kuryndin, P. Mokreva, T. Terlemezyan, A. V. Sidorovich, O. E. Praslova, and G. K. Elyashevich

Institute of Macromolecular Compounds, Russian Academy of Sciences, St. Petersburg, Russia
Institute of Polymers, Bulgarian Academy of Sciences, Sofia, Bulgaria

Received December 16, 2004

Abstract—The conducting properties of composites prepared by deposition of polyaniline layers on the surface of porous polyethylene films from dispersions and by polymerization *in situ* were studied.

Conducting polymers such as polyacetylene, polyaniline (PANI), polypyrrole, polythiophene, and their derivatives are novel promising materials attracting researchers' attention [1, 2]. They are used in membrane processes, electric batteries, and new types of electronic and optoelectronic devices, and also as sensitive elements in modern sensor systems, antistatic agents, and microwave absorbers. Due to relatively high intrinsic conductivity and chemical stability, and also to diverse and simple preparation procedures, polyaniline is the most promising conducting polymer [3, 4]. However, low strength, brittleness, and very poor solubility hinder utilization and treatment of PANI. These disadvantages can be effectively overcome by preparing composites containing PANI as conducting component [5, 6]. Development of methods for preparing composites consisting of conducting layers on various supports is an urgent problem. When the composites are used as membranes, the resistance of the supports to the mass transfer should be minimal, and porous materials containing through channels meet this requirement.

In this work we used porous polyethylene (PE) supports, because they exhibit good mechanical properties and high chemical resistance with respect to organic solvents, acids, and alkalis.

We studied the electrical and mechanical properties of composites consisting of PANI layers deposited on porous PE film supports. Since in service these composites can be exposed to thermal treatment, we also studied their thermal-deformation behavior and structural transformations.

EXPERIMENTAL

The required porous films were prepared from high-density polyethylene (M_w 1.4×10^5, M_w/M_n 6–8, and mp 132°C). The porous structure was formed by uniaxial extension of the film prepared by extrusion of the melt with subsequent annealing [7]. The total porosity of the resulting 20-μm films was 40%. These porous films contained through channels (180–360 nm in diameter) [7, 8] and had developed rough surface [9, 10] providing high adhesion of the films to the layers deposited.

The PE/PANI composites were prepared by two procedures: by chemical oxidative polymerization from aniline solutions directly on the porous film surface [PE/PANI(*in situ*)] and by deposition of a polyaniline dispersion on the film surface [PE/PANI (disp.)].

To prepare the PE/PANI(*in situ*) systems, the porous PE film was immersed into the reaction mixture containing aniline hydrochloride (0.2 M), ammonium peroxodisulfate (0.25 M), and excess hydrochloric acid (1 M). The polymerization time was varied from 8 min to 2 days. Then, the resulting film was dried in a vacuum at room temperature. The polymerization was carried out at 5 and 20°C.

The colloidal PANI dispersion was prepared as follows. To a solution of dodecylbenzenesulfonic acid (0.1 M, 100 ml), we successively added aniline (0.01 mol) and a solution of ammonium peroxodisulfate (0.01 mol) in deionized water (5 ml). The polymerization was carried out at room temperature for

1070-4272/05/7803-0478© 2005 Pleiades Publishing, Inc.

Table 1. Electrical conductivity of the PE/PANI composites (thickness of the porous PE support 20 μm)

Sample	Thickness, μm	PANI content, %	Conductivity, S cm^{-1}	
			surface	through
PE/PANI(*in situ*), T_p,* °C:				
20	21	23	1	1×10^{-6}
5	21	25	6	8×10^{-6}
PE/PANI(disp.)	26	70	5	7×10^{-6}

* (T_p) Polymerization temperature.

4 h. The size of the PANI particles was 5–30 nm [11]. To prepare the PE/PANI(disp.) system, the porous PE film was placed in the colloidal dispersion for 4 h and then dried at room temperature. The PANI content in the samples was determined gravimetrically.

The surface electrical conductivity of the composites (conductivity in the direction parallel to the film surface) was measured by the standard four-point method, and the through conductivity (conductivity from one film surface to the other), by the two-disc procedure.

The mechanical properties of the porous PE films and composites were studied on an R-5 tensile-testing machine. The strength, elastic modulus, and relative elongation at break were calculated from the stress–strain curves recorded at uniaxial extension of the samples (2×30 mm) at a rate of 100% min^{-1}. The strength was determined as the maximal (breaking) force related to the initial cross-section of the sample. The elastic modulus was determined at 0.5% strain. The mechanical properties of the porous PE films and composites were determined in directions parallel and perpendicular to the direction of extension of the porous support.

The thermomechanical properties were studied at uniaxial extension of the films at a heating rate of 10 deg min^{-1}. These tests were carried out in a vacuum to exclude oxidation of the films.

The heat of melting and melting point of the films were determined by differential scanning calorimetry on a DSM-2 microcalorimeter at a heating rate of 16 deg min^{-1}.

Kinetics of formation of polyaniline layers on the surface of porous PE films. The samples with various content of PANI were prepared by polymerization *in situ* at 20°C. Formation of the PANI film on the porous support surface is described by the kinetic dependence shown in Fig. 1. As seen, after certain induction period (~5 min), PANI is formed fairly rapidly in the first ~0.5 h, then the formation rate sharply decreases and the content of PANI in the composite changes insignificantly with increasing polymerization time. The thickness of the PANI layer at a polymerization time of 48 h was about 1 μm.

Electrical conductivity of porous PE supports with polyaniline layers. The porous structure of PE films is formed under the conditions of complex effects, and, as a result, they exhibit pronounced anisotropy [12, 13]. Therefore, we studied how the surface conductivity of the composites depends on the direction with respect to the orientation axis of the film. Our experimental results showed no dependence of the surface conductivity on the film orientation, i.e., the resulting PANI layers are uniform.

An electron-microscopic study showed that, when the monomer polymerization procedure is used, the PANI layer appears not only on the PE film surface but also on the pore walls, forming conducting bridges between the surfaces of the composite and thus providing the through conductivity of the sample. As seen from Table 1, the through conductivity is lower than the surface conductivity by several orders of

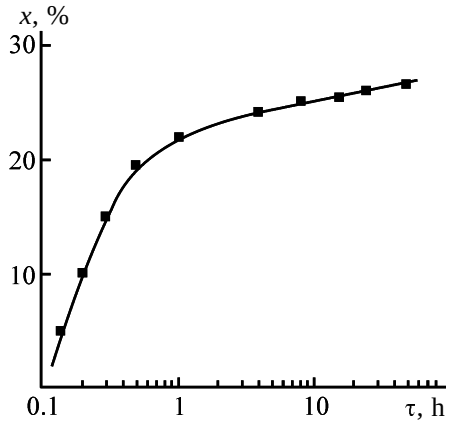


Fig. 1. Content of PANI x in the composite as a function of the polymerization time τ; polymerization *in situ* at 20°C.

Table 2. Mechanical properties of porous PE films and PE/PANI composites

Sample	Breaking stress	Elastic modulus	Relative elongation at break, %
	MPa		
Porous PE film	110/11*	650/700	60/5.0
PE/PANI(*in situ*), T_p, °C:			
20	109/11	750/800	58/4.8
5	107/10	800/950	55/4.5

* Data recorded in direction parallel/perpendicular to the support extension axis.

magnitude, which can be explained by the complex structure and tortuosity of the through channels.

The conductivity of the PE/PANI(*in situ*) systems prepared at 20°C is plotted in Fig. 2 vs. PANI content. With increasing content of PANI, the surface conductivity of the samples first increases and then becomes constant at a PANI content of ~20%. The flattering-out of this dependence suggests formation of the conducting uniform surface layer. When the content of PANI is below 5%, the conducting polymer does not form a continuous coating, and the conductivity of this sample is close to that of the PE film support.

As in the case of the surface conductivity, the dependence of the through conductivity on the content of PANI flattens out at a PANI content of ~20%. This is due to the fact that, with a further increase in the PANI content, the thickness of the surface layer increases, whereas the structure of the conducting phase in the porous support bulk remains unchanged.

It is known [14, 15] that lower polymerization temperatures favor formation of PANI with more ordered structure and, as a result, with a higher conductivity. Indeed, polymerization at 5°C allows preparation of the PE/PANI systems with higher conductivities than that of the systems prepared at 20°C (Table 1).

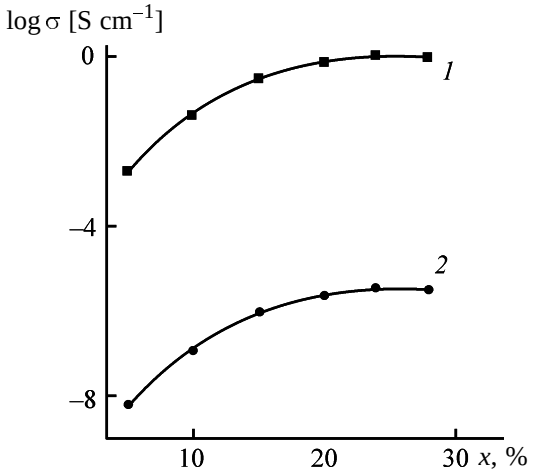


Fig. 2. (*1*) Surface and (*2*) through conductivity σ of the PE/PANI composites prepared by polymerization *in situ* at 20°C as functions of the PANI content *x*.

Our results show (Table 1) that the conductivities of the composites prepared by deposition of the PANI dispersions are comparable with those of the composites prepared by polymerization, despite considerably higher content of PANI.

Thus, polymerization *in situ* and deposition of the dispersion on the support surface yield the composites with the surface conductivity close to that of the free PANI films (1–40 S cm^{-1} [2]), which suggests that the PANI layers formed by these procedures are defect-free and uniform.

Mechanical properties of the porous PE films coated with polyaniline layers. Our study of the mechanical properties of supports and composites showed that the oriented structure of the porous PE films causes anisotropy of mechanical properties, which is retained in the composites on their base. As seen from Table 2, the strength and relative elongation at break in the direction of the film extension are greater by an order of magnitude than the corresponding values measured in the direction perpendicular to the extension axis.

After the polymerization deposition of the PANI layers, the strength and elasticity of the porous PE films (both in the extension direction and perpendicularly to it) slightly decrease, whereas the elastic modulus increases (Table 2). These systems are characterized by high adhesion of the PANI layers to the porous support, and no exfoliation was observed even at the sample break. From our viewpoint, this fact suggests that the monomer penetrates not only into the support pores, but also in the intercrystallite space, and polymerization provides formation of the continuous phase of the conducting polymer both on the support surface and in its bulk.

In extension of the composites containing layers prepared from PANI dispersion, exfoliation of the layers was observed even at low strains, i.e., the composites lost their uniformity. In this case, low adhesion of the layers to the porous support is due to the fact that dispersion particles, whose size is greater than that of the monomer molecules, cannot penetrate into the pores and no continuous skeleton of the conducting polymer in the porous support bulk is formed.

Thus, only polymerization *in situ* as a procedure for preparing PANI layers on porous PE supports yields the composites combining high electrical properties of the conducting polymer with high mechanical stability of the support polymer.

Thermomechanical properties of porous PE films coated with polyaniline layers. Since the structure of the PE films is oriented, they exhibit shrinkage in the orientation direction. It was found [9, 16] that the thermal-deformation stability of porous films increases after deposition of polyaniline layers; as a result, shrinkage of these systems starts at higher temperatures and the degree of shrinkage in the entire temperature range is significantly smaller as compared to the porous supports. In this work we studied the deformation behavior of porous PE supports with PANI layers under a load in the course of heating.

The thermomechanical curves for porous materials (Fig. 3, curve *1*) and composites PE/PANI(*in situ*) and PE/PANI(disp.) (Fig. 3, curves *2*–*4*) were recorded under a tensile load of 0.2 MPa. The behavior of all the samples under this load is typical for ordered systems containing flexible-chain polymers: the shrinkage is maximal at temperatures close to the melting point of PE (T_m^{PE}), and at heating above this temperature sharp elongation followed by the break is observed. As seen from Fig. 3, shrinkage of the composite materials in the entire temperature range is smaller than that of the porous supports. This suggests that PANI layers stabilize the structure of the PE supports.

Higher thermal-deformation stability of the PE–PANI(*in situ*) systems as compared to PE/PANI(disp.) composites is due to the fact that, in contrast to the supports coated with PANI dispersion, in the first case a more rigid PANI skeleton strongly fixed on the support surface is formed.

The thermal-deformation stability of the samples prepared by PANI polymerization at 5°C is higher as compared to the samples formed at 20°C, because a more compact and ordered PANI layer is formed at the lower temperature; this fact is confirmed by higher conductivity of this layer.

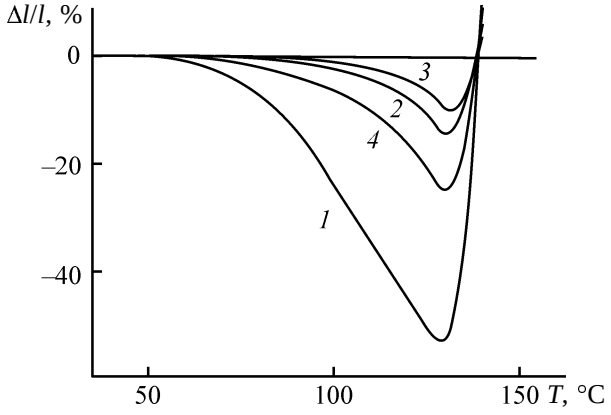


Fig. 3. Relative elongation $\Delta l/l$ of the (*1*) porous films, PE/PANI(*in situ*) systems polymerized at (*2*) 20 and (*3*) 5°C, and (*4*) PE/PANI(disp.) composites under a tensile load of 0.2 MPa as a function of temperature *T*.

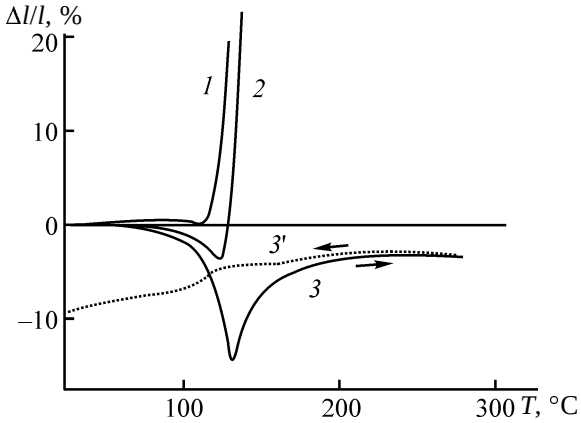


Fig. 4. Relative elongation $\Delta l/l$ of the PE/PANI(*in situ*) systems polymerized at 5°C under a load of (*1*) 1.0, (*2*) 0.5, and (*3*, *3*') 0.05 MPa as a function of temperature *T*.

The thermomechanical curves of PE/PANI(*in situ*) composites recorded under various tensile loads are shown in Fig. 4. Under medium loads (in the experimental range studied) of 0.1–1.0 MPa, shrinkage of the PE/PANI(*in situ*) sample up to the break is observed upon heating to T_m^{PE} (Fig. 4, curve *2*). It should be noted that the shrinkage decreases with increasing tensile load, and no shrinkage of the sample and even small elongation was observed under a tensile load of 1 MPa (Fig. 4, curve *1*). The behavior of the composite upon heating under a tensile load of 0.05 MPa (Fig. 4, curve *3*'), and less was quite different: the samples stand the load and do not change their size in a wide temperature range above T_m^{PE}. The plateau in the thermomechanical curves in the 180–300°C range confirms this. Preservation of the sample integrity

Table 3. Thermal characteristics of the porous PE supports and the PE/PANI composites

Sample	T_m^{PE}, °C	ΔH, J g^{-1}
Porous PE support	132	180
PE/PANI(*in situ*), T_p, °C:		
20	133	166
5	134	158
PE/PANI(disp.)	132	180

in this temperature range (where PE is already molten) is due to the fact that the load acts on the three-dimensional skeleton of the rigid-chain PANI polymer spreading, according to the electron microscopic data, through the bulk of the PE support. The section of thermomechanical stability is observed only for PE/PANI(*in situ*) composites polymerized at 5 and 20°C, and no effect was observed for PE/PANI(disp.) systems.

The data on mechanical relaxation [17] showed that, when PANI is heated to 200°C, the mobility of the polymer chains decreases, which, in the authors' opinion, is due to the formation of weakly cross-linked structures. With PE samples [18], no thermal effects except melting at ~130°C were observed in the TGA curves recorded upon heating to 300°C in a vacuum. Hence, the mechanical stability of the PE/PANI(*in situ*) composites in the 180–300°C range is due to the cross-linking of PANI. Irreversible changes in the PANI layer structure are confirmed by the curve of the sample cooling (Fig. 4, curve *3*'). The run of this curve is essentially different from that registered upon heating, and its shape is typical for cross-linked systems. At repeating of the heating–cooling cycles, the shape of curve *3*' (Fig. 4) remains unchanged. This fact indicates that the irreversible changes caused by cross-linking of the PANI polymer occur at first heating of the system.

Structural transformations of the porous supports coated with PANI layers upon heating. Since the PE/PANI(*in situ*) composites do not melt and preserve their integrity upon heating to the temperatures above T_m^{PE}, their structural transformations were studied by DSC.

Our experimental results showed (Table 3) that the heat of PE melting ΔH in the PE/PANI(*in situ*) composites is lower than that of the PE support (these values were calculated taking into account the weight fraction of PE in the composite). Moreover, after formation of the PANI layer, the melting peak shifts toward higher temperatures by 1–2°C. Since the PE film is oriented, we suggest that heating of the PE/PANI(*in situ*) composites does not cause formation of an isotropic melt and certain orientation of the polymer is preserved owing to fixation of the PE chains by the rigid PANI skeleton. Specifically these structural features in the course of melting hinder passing of the PE chains into the equilibrium state, decreasing the heat and increasing the temperature of PE melting in the PE/PANI(*in situ*) composites. Our assumption is confirmed by the data of wide-angle X-ray scattering [16], which showed that the PE/PANI(*in situ*) samples exhibit the oriented structure after their heating to the temperatures higher than T_m^{PE} by several tens of degrees and subsequent cooling to room temperature.

As seen from Table 3, these effects (decrease in the heat of melting and increase in the melting point) are more pronounced for the systems polymerized at 5°C than for those prepared at 20°C, i.e., the PE chains are more strongly fixed in the PANI skeleton in the course of the low-temperature process.

It should be noted that the heat and temperature of melting of PE in the PE/PANI(disp.) systems correspond to those determined for the uncoated porous PE films. This fact confirms that no PANI skeleton is formed in this case, and the PANI layer prepared from a dispersion does not affect the characteristics of PE melting.

CONCLUSIONS

(1) Polymerization *in situ* of the polyethylene–polyaniline systems yields a continuous three-dimensional phase of the conducting polymer both on the surface and in the bulk of the porous support, providing surface and through conductivity of the composites.

(2) The resulting polymers combine the electrical properties of the conducting polymer and high mechanical properties of the porous support.

(3) Formation of the rigid polyaniline skeleton strongly increases the thermal-deformation stability of the polyethylene/polyaniline systems prepared by polymerization *in situ* as compared to the porous support.

ACKNOWLEDGMENTS

This work was financially supported by the Russian Foundation for Basic Research (project nos. 01-03-32290 and 04-03-32229) and the Program for

Basic Research of the Chemistry and Materials Science Division, Russian Academy of Sciences, project "Synthesis and Study of New Polymeric Systems Containing Polyconjugated Polymers and Exhibiting Semiconducting and Conducting Properties," direction "Conducting and Electroactive Polymers."

REFERENCES

1. MacDiarmid, A.G., *Synth. Met.*, 2002, vol. 125, p. 11–22.
2. *Handbook of Organic Conductive Molecules and Polymers*, Nalwa, H.S., Ed., New York: Willey, 1987, vol. 2.
3. Nicolas-Debarnot, D. and Poncin-Epaillard, F., *Anal. Chim. Acta*, 2003, vol. 475, pp. 1–15.
4. Ruil, A., Jr., Galardo Soto, A.M., Mello, S.V., *et al*., *Synth. Met*., 2003, vol. 132, pp. 109–116.
5. Strumpler, R. and Glatz-Reichenbach, J., *J. Electroceramics*, 1999, vols. 3–4, pp. 329–346.
6. Malinnauskas, A., *Polymer*, 2001, vol. 42, pp. 3957–3972.
7. Elyashevich, G.K., Karpov, E.A., and Kozlov, A.G., *Mechanical Behavior of Polymeric Materials*, Kahovec, J., Ed., *Macromol. Symp*., 1999, vol. 147, pp. 91–101.
8. Elyashevich, G.K., Kozlov, A.G., and Rozova, E.Yu., *Vysokomol. Soedin., Ser. A*, 1998, vol. 40, no. 6, pp. 956–958.
9. Elyashevich, G.K. and Kuryndin, I.S., *Polym. Adv. Techn*., 2002, vol. 13, pp. 725–736.
10. Elyashevich, G.K., Kalyuzhnaya, L.M., Rozova, E.Yu., and Wolinska-Grabczyk, A., *Vysokomol. Soedin., Ser. A*., 2003, vol. 45, no. 10, pp. 1653–1658.
11. Gospodinova, N., Mokreva, P., Tsanov, T., and Terlemezyan, L., *Polymer*, 1997, vol. 38, pp. 743–746.
12. Elyashevich, G.K., Kozlov, A.G., and Moneva, I.T., *Vysokomol. Soedin., Ser. B*, 1998, vol. 40, no. 3, pp. 483–486.
13. Raab, M., Scudla, J., Kozlov, A.G., *et al*., *J. Appl. Polym. Sci*., 2001, vol. 80, pp. 214–222.
14. Ayad, M.M., Salahuddin, N., and Sheneshin, M.A., *Synth. Met*., 2003, vol. 132, pp. 185–190.
15. Stejskal, J., Riede, A., Hlavata, D., *et al*., *Synth. Met*., 1998, vol. 96, pp. 55–61.
16. Elyashevich, G.K., Terlemezyan, L., Sazanov, Yu.N., *et al*., *Zh. Prikl. Khim*., 2002, vol. 73, no. 7, pp. 1164–1169.
17. Rodrigues, P.C., de Souza, G.P., Da Motta Neto, J.D., and Akcelrud, L., *Polymer*, 2002, vol. 43, pp. 5493–5499.
18. Sazanov, Yu.N., Ugolkov, V.L., Praslova, O.E., *et al*., *Zh. Prikl. Khim*., 2003, vol. 76, no. 7, pp. 1167–1171.

Russian Journal of Applied Chemistry, Vol. 78, No. 3, 2005, pp. 484–486. Translated from Zhurnal Prikladnoi Khimii, Vol. 78, No. 3, 2005, pp. 490–492.
Original Russian Text Copyright © 2005 by Kulish, Gerchikov, Kolesov, Zaikov.

MACROMOLECULAR CHEMISTRY AND POLYMERIC MATERIALS

Supramolecular Effect in Initiated Oxidation of Polyisoprene and Polyisoprene–Polybutadiene Blends in Chlorobenzene Solution

E. I. Kulish, A. Ya. Gerchikov, S. V. Kolesov, and G. E. Zaikov

Bashkir State University, Ufa, Bashkortostan, Russia
Institute of Biochemical Physics, Russian Academy of Sciences, Moscow, Russia

Received December 9, 2004

Abstract—Specific features of initiated oxidation of polyisoprene and polyisoprene–polybutadiene blends in chlorobenzene solution were studied in relation to the supramolecular state of the polymer in solution.

Available data [1–5] show that the mechanisms of oxidation of low- and high-molecular-weight compounds have much in common. Nevertheless, there are certain differences associated primarily with the structural features of the polymers and their state in solution. Polymer solutions are nonuniform, and conditions of diffusion of oxygen molecules into a macromolecular globule are different, which gives rise to supramolecular effect in oxidation of polymers and polymer blends in solution.

EXPERIMENTAL

Polyisoprene (PI) and polybutadiene (PB) were purified by double reprecipitation with ethanol from solution in chlorobenzene (CB). Chlorobenzene was purified as described in [2]. The initiator, dicyclohexyl peroxydicarbonate (DCPDC), was recrystallized from toluene. The polymer solution was prepared at 40°C for 4 h with inert gas bubbling. Solutions of polymer blends were prepared by mixing the solutions of the individual polymers of equal concentration in the required proportion. The initiator was added just before the kinetic experiment. The initiation rate constant k_i for dicyclohexyl peroxydicarbonate was taken from [6].

The rate of initiated oxidation of the polymers was determined in a manometric unit from the oxygen uptake. The solution in the reaction vessel was stirred at 60°C with a magnetic stirrer (200 rpm). No apparent oxidation of CB at 60°C was observed (no oxygen uptake), which allows us to neglect the solvent oxidation in the experiments on initiated oxidation of PI and PI–PB blends in solution.

The kinetic curve of oxygen uptake with PI in CB is linear and is independent of the liquid phase volume and of the stirring rate, which indicates that the oxidation is kinetically controlled.

Viscometric studies of solutions of the polymers and their blends were performed with an Ubbelohde viscometer by the standard procedure [6].

The dependence of the PI oxidation rate on the PI content in solution is plotted in Fig. 1a. As seen, with increasing content of the polymer the oxidation rate grows nonlinearly. A similar pattern was observed previously in [2] for initiated oxidation of PE and PP and in [7] for oxidation of PB in CB.

By plotting the experimental data in the ln–ln coordinates, we determined the reaction order with respect to the polymer, $n = 0.32$. The order with respect to the polymer of the previously studied liquid-phase oxidation of PB in CB was 0.35.

The observed trends can be explained taking into account the structural changes occurring in the polymer solution. Viscometric studies of solutions of PI in CB, performed at the same temperature as that of the oxidation runs, show that the transition (crossover) from a dilute solution containing discrete macromolecular globules which do not interact with each other to a semidilute solution occurs for PI at a concentration $c^* = 1$ g dl^{-1} (Fig. 1b). Thus, as for the previously studied PB, in a dilute polymer solution, when the sequence of oxidation events occurs within one globule, the oxidation rate appreciably grows with an increase in the total polymer content in the solution (Fig. 1a, portion *1*).

1070-4272/05/7803-0484© 2005 Pleiades Publishing, Inc.

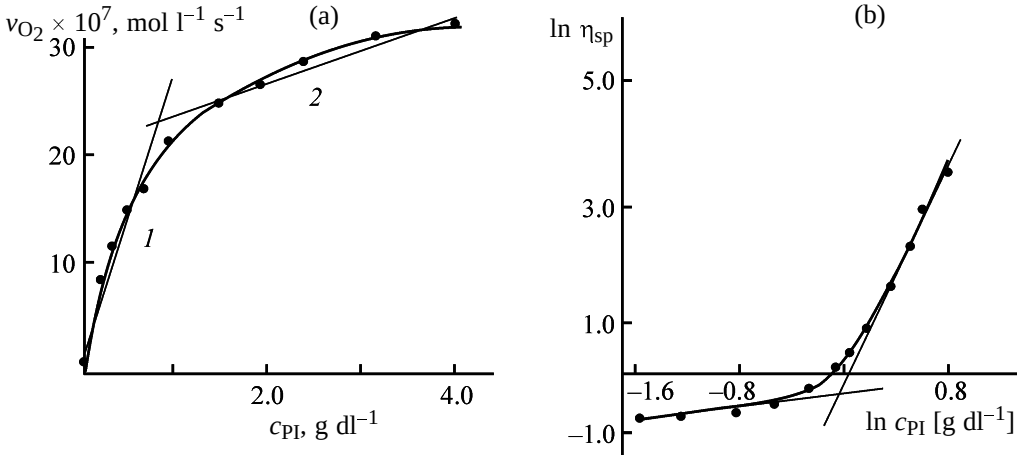


Fig. 1. (a) Oxidation rate v_{O_2} and (b) specific viscosity η_{sp} as functions of the PI concentration in chlorobenzene c_{PI}.

On passing beyond the crossover range, areas with local densification of units arise, hindering the diffusion of oxygen into the system. As a result, the influence of the solution concentration on the rate of PI oxidation becomes substantially weaker (Fig. 1a, portion *2*).

The dependence of the rate of PI oxidation in CB solution on the initiator concentration, as in the case of PB solutions, is indicative of the linear termination (Fig. 2) occurring, apparently, on the solvent molecules.

Thus, the transition from a dilute to a semidilute solution, accompanied by the development of reversible aggregation of macromolecules at PI concentrations $c > c^*$, is manifested as a change in the slope of the dependence of the PI oxidation rate on the PI concentration in CB solution.

In solutions of polymer blends, different kinds of supramolecular structures can form, depending on what contacts are preferable: polymer 1–polymer 1 and polymer 2–polymer 2 (homoaggregates), or polymer 1–polymer 2 (heteroaggregates). The type of the aggregates, if they form, will be one of the decisive factors (along with the general characteristics of the conformational and supramolecular state of the polymers in solution) affecting the physicochemical properties of the system.

There are indications in the literature that the kind of the forming aggregates can be judged from the deviations of the viscosity of a polymer blend solution from the additive values [8]. As a rule, positive deviations suggest formation of heteroaggregates, and negative deviations, formation of homoaggregates. Figure 3a shows that only dilute solutions of PI–PB blends show no deviations of the relative viscosity from the additive values.

In going to semidilute solutions (beyond the crossover point), the relative viscosities of the polymer blends become lower than the additive values. These facts suggest that, whereas in dilute solutions PI and PB, showing a low thermodynamic affinity, do not noticeably interact with each other, in semidilute solutions PB and PI form homoaggregates.

This change in the supramolecular structure of the polymer blend is manifested in the dependence of the rate of initiated oxidation of the blend. Figure 3b shows that only in a dilute solution the oxidation rate is an additive function of the relative content of the polymers. In going to semidilute solutions containing interacting, aggregated polymer globules, the oxidation rate becomes a nonadditive function of the blend composition. The higher the concentration of the polymers, i.e., the stronger the tendenct to form homo-

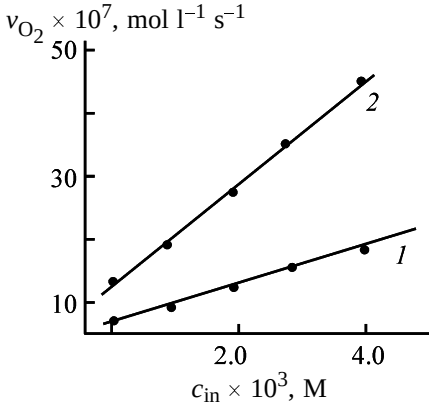


Fig. 2. Rate v_{O_2} of PI oxidation in (*1*) 0.2 and (*2*) 2.5 g dl^{-1} solutions in chlorobenzene as a function of initiator concentration c_{in}.

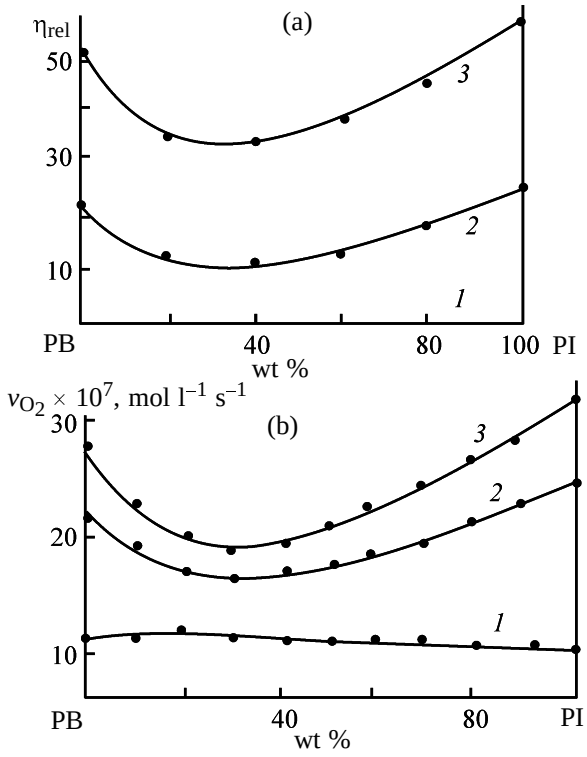


Fig. 3. (a) Relative viscosity η_{rel} of solutions and (b) oxidation rate v_{O_2} of solutions of PB–PI blends as functions of the polymer ratio in solution. Total polymer concentration, g dl^{-1}: (*1*) 0.2, (*2*) 2.0, and (*3*) 3.0.

aggregates, the larger the deviations of the oxidation rate from the additive values. The fact that the rate of the initiated oxidation of a polymer blend in the region of aggregated solutions is appreciably lower compared to the solutions of the individual polymers is apparently due to increased density of packing of the macromolecular segments in the homoaggregates forming in the blend. This, in turn, causes significantly hinders the duffusion of oxygen to macromolecular units.

Thus, our results show that the rate of oxidation of polymers and polymer blends in solution is largely determined by the supramolecular structure of the solution.

REFERENCES

1. Shilov, Yu.B. and Denisov, E.T., *Vysokomol. Soedin., Ser. A*, 1972, vol. 14, no. 11, p. 2385.
2. Shilov, Yu.B. and Denisov, E.T., *Kinet. Katal.*, 1973, vol. 14, no. 2, p. 306.
3. Denisov, E.T., *Vysokomol. Soedin., Ser. A*, 1977, vol. 19, no. 11, p. 2513.
4. Denisov, E.T., *Usp. Khim.*, 1978, vol. 47, no. 6, p. 1090.
5. Denisov, E.T., *Konstanty skorosti gomoliticheskikh zhidkofaznykh reaktsii* (Rate Constants of Homolytic Liquid-Phase Reactions), Moscow: Nauka, 1971.
6. Rafikov, S.R., Budtov, V.P., and Monakov, Yu.B., *Vvedenie v fiziko-khimiyu rastvorov polimerov* (Introduction to Physical Chemistry of Polymer Solutions), Moscow: Nauka, 1978.
7. Kulish, E.I., Gerchikov, A.Ya., Chirko, K.S., *et al.*, *Vysokomol. Soedin., Ser. B*, 2004, vol. 46, no. 2, p. 349.
8. Mukhina, V.R., Pastukhova, N.V., Semchikov, Yu.D., *et al.*, *Vysokomol. Soedin., Ser. A*, 2001, vol. 43, no. 10, p. 1797.

Russian Journal of Applied Chemistry, Vol. 78, No. 3, 2005, pp. 487–491. Translated from Zhurnal Prikladnoi Khimii, Vol. 78, No. 3, 2005, pp. 493–497.
Original Russian Text Copyright © 2005 by Sashina, Novoselov.

MACROMOLECULAR CHEMISTRY AND POLYMERIC MATERIALS

Polyelectrolyte Complexes of Fibroin with Chitosan

E. S. Sashina and N. P. Novoselov

St. Petersburg State University of Technology and Design, St. Petersburg, Russia

Received September 23, 2004

Abstract—Fibroin–chitosan polyelectrolyte complexes are studied by X-ray diffraction, IR spectroscopy, and scanning calorimetry. Mechanical characteristics and the swellability of the blend films at various pHs are examined.

The polysaccharide chitosan is a chitin deacetylation product exhibiting fungicidal and bactericidal activities [1]. Blends of chitosan with uncharged polymers such as polyvinyl alcohol and polyesters, and also polyelectrolyte complexes with carboxymethyl cellulose, alginate, carboxymethyl chitin, and other polyelectrolytes were studied [2–7]. In these complexes, chitosan behaves as a weak polymeric base (pK_a 6.3 [6]).

At present, polymer blends of chitosan with fibroin are being studied. Fibroin is a weak polymeric acid (isoelectric point at pH 4.0–5.0) [8]. When mixing dialyzed aqueous salt solutions of fibroin with chitosan solutions in dilute acids [9, 10], pH-sensitive polymeric complexes are formed, which can be used in the form of films or gels as separating membranes, microcapsules, medicinal implants, and catalysts.

In this work we studied synthesis and properties of chitosan–fibroin blend films prepared from hexafluoro-2-propanol solutions.

EXPERIMENTAL

In the work we used *Bombyx mori* silk fibroin pretreated to remove sericin and fatty, waxy, and mineral compounds, and cut into short fibers 3.6 mm long and 34.6 μm in diameter. The fibers were dissolved in aqueous 6 M LiBr at 60°C and dialyzed across a semipermeable membrane. The dialyzed fibroin solution was dried at room temperature to obtain a film and then allowed to stand in a vacuum at 40°C for 4–6 h.

Chitosan was purchased from Dalwoo-Chitosan Co. Ltd. (Korea) (degree of deacetylation 95%; moisture content 7.5%; viscosity at 25°C of 2% solution in 2% acetic acid 30.8 mP).

As a solvent we used 1,1,1,3,3,3-hexafluoro-2-propanol (HFP) from Merck (main product content 99%; bp 58°C; ρ_4^{20} 1.615–1.618 g cm^{-3}).

The polymers were dissolved in HFP at room temperature to obtain a clear solution of the desired concentration. The resulting solution was then vacuum-filtered (Buchner funnel) through a glass filter no. 1. Equimolar polymer solutions were mixed for 1 h with continuous stirring to obtain the desired polymer weight ratio. As a result, stable clear solutions were formed.

Films were prepared by pouring the solutions onto a foil, which was followed by removing the solvent. The resulting films were 0.4–0.6 μm thick. Some of the films were treated with methanol for 30 min and then air-dried. Mechanical characteristics of the films were determined using an Instron tensile-testing machine in accordance with DIN EN ISO 527-3 standard. Swelling of the films in distilled water and buffer solutions at pH 2.0 and 4.0 was studied gravimetrically. The films were kept in solution at room temperature for 30 min (this time was demonstrated to be sufficient to reach the maximal swelling). The degree of swelling Δw (%) was estimated as

$$\Delta w = (w_1 - w_0)/w_0 \times 100,$$

where w_0 and w_1 are the weights of the film before and after swelling (g).

The density of the films was measured on an AccuPyc 1330 V2.01 He pycnometer (the United States). The film morphology was examined in a polarized light using an Olympus U-SMAD-2 BX-50 JVC microscope (magnification ×200). The infrared spectra of the films were recorded on an IFS25 spectrometer (Bruker). Thermal analysis was carried out on a

1070-4272/05/7803-0487 © 2005 Pleiades Publishing, Inc.

Table 1. Scanning calorimetry data for fibroin, chitosan, and their blends

Chitosan content, wt %	T_{df}	T_{1ch}	ΔH_1, J g^{-1}	T_{2f}	T_{2ch}	ΔH_2, J g^{-1}	$T_{\alpha f}$	$T_{f.deg}$	$T_{ch.deg}$
	°C			°C			°C		
–	78.2	–	106.3	151.7	–	21.5	246.4	280	–
20	79.4	79.4	134.9	147.6	147.6	16.6	241 very weak	280	280
30	88.3	88.3	119.2	143.2	143.2	5.5	–	277	277
40	78.9	78.9	124.5	144.0	144.0	13.4	–	276	276
60	96.8	96.8	236.1	164.2	164.2	22.9	–	275	275
80	81.7	81.7	267.5	156.7	156.7	39.8	–	268	268
100	–	101.0	109.3	–	165.5	26.1	–	–	262

Table 2. Interplanar spacings in crystallites

Sample	2θ, deg	*d*, Å
Fibroin	20.4	4.33
1 : 1 Blend	10.2	8.73
	15.6	5.71
	19.7	4.51
Chitosan	10.0	8.92
	19.5	4.58

Mettler Toledo Star scanning calorimeter with heating from 25 to 350°C at a rate of 10 deg min^{-1} under nitrogen (N_2 flow rate 50 ml min^{-1}). X-ray diffraction patterns were obtained on a Bruker D8 Advance diffractometer.

Scanning calorimetry is widely used for studying interpolymer interactions in blends. For incompatible polymers, two glass transition points, characteristic of individual components, are observed in blends, whereas blends formed by compatible polymers are characterized by single glass transition point (T_{gt}), depending on the component ratio. This point can be estimated by the Fox equation [11]:

$$1/T_{gt} = w_1/T_{gt1} + w_2/T_{gt2},$$

where T_{gt}, T_{gt1}, and T_{gt2} are the glass transition points of the blend, polymer 1, and polymer 2, respectively; and w_1 and w_2, weight fractions of the components in the blend.

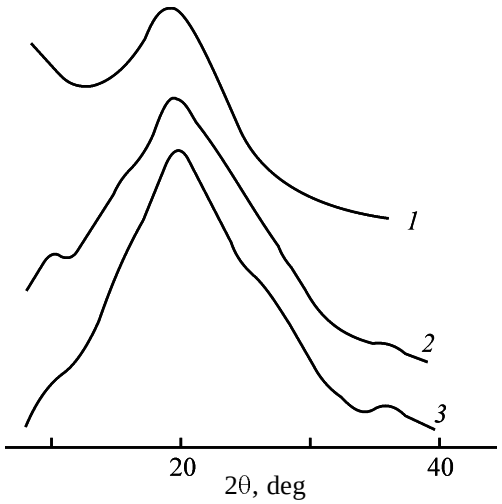


Fig. 1. X-ray diffraction patterns of the films: (*1*) fibroin, (*2*) 1 : 1 blend, and (*3*) chitosan. (2θ) Bragg angle.

The results of thermal analysis of fibroin, chitosan, and their blends are given in Table 1. The DSC curve of straight fibroin shows an endothermic peak near 78°C (T_{1f}), which is associated with removal of adsorbed water. The endothermic effect near 152°C (T_{2f}) is caused by glass transition of amorphous fibroin, which is followed by a weak exothermic effect due to transition of the amorphous phase into β-folded crystalline structure [12]. The endothermic peak at 246°C reflects molecular motion in α-crystals of the polymer, which is observed only for straight fibroin and for the blend containing 80% fibroin. Finally, the endothermic peak at 280°C ($T_{f.deg}$) is caused by thermal degradation of the disordered β-structure.

The DSC curve of chitosan shows endothermic peaks associated with removal of adsorbed water (T_{1ch} = 101°C), devitrification (T_{2ch} = 165°C), and onset of thermal degradation at 262°C ($T_{ch.deg}$).

The blend films demonstrate common thermal effects T_1, T_2, and T_{deg}, suggesting compatibility of the components. The deviation of the experimental glass transition points T_{gt} from those estimated by the Fox equation was within 15%. On passing to the blends with a chitosan content of 20 to 40%, T_{gt} and glass transition enthalpy decrease, which can attributed to decreased size of amorphous domains between the crystallites as a result of formation of a more homo-

Table 3. Swellability of fibroin–chitosan blend films

pH	Chitosan content, wt %						
	–	20	30	40	60	80	100
	Untreated films						
2.0	68	465	623	Soluble films			
4.0	53	227	215	252	315	360	415
7.0	59	157	129	180	212	281	357
	Methanol-modified films						
2.0	25	119	218	303	644	1090	Soluble films
4.0	10	86	78	121	174	189	310
7.0	14	45	40	67	107	166	233

geneous structure at the indicated component ratio.

The formation of a more homogeneous and, presumably, more ordered structure is demonstrated by X-ray diffraction patterns of the films obtained from chitosan, fibroin, and 1 : 1 mixed solutions (Fig. 1). The interplanar spacings in the crystal lattices of the polymers are given in Table 2. The X-ray diffraction pattern of 100% fibroin shows only a halo at 2θ 20.4°. The film of 100% chitosan shows a typical pattern with weak peaks at 2θ 19.5° and 10°. For the blend film, we observed an increased peak at 2θ 10° and a very weak peak at 2θ 15.6°, suggesting formation of a modification of chitosan with more closely packed straightened chains.

The pH dependence of the swellability of the fibroin, chitosan, and blend films is given in Table 3. The measurements were carried out with the untreated films and those modified by treatment with methanol. As seen, the swellability increases in parallel to the chitosan content in the films, depending on pH: the maximal swellability was observed at pH 2.0; at a chitosan content above 40 wt % and pH 2.0, the films become soluble. The increase in the swellability is caused by protonation of the amino groups of chitosan in acidic solutions, resulting in weakened intermolecular interaction. The swellability of straight fibroin depends on pH insignificantly. It slightly decreases at pH 4.0, i.e., near the isoelectric point. The minimal swellability in the system was observed at a chitosan content of 30 wt %. At this component ratio, one may suggest the strongest intermolecular interaction causing formation of a more homogeneous structure.

Modification of the films with methanol decreases the swellability by a factor of about three at all the experimental pHs, which is probably due to formation of the β-folded crystalline structure of fibroin [13] and hydrogen bonding between chitosan and fibroin. Analysis of the published data [14–16] shows that the α- and β-conformations can be easily distinguished by their characteristic absorptions in the IR spectra. The spectrum of fibroin shows characteristic Amide I (C=O), Amide II (bound N–H, C–N), Amide III (C–N, bound N–H, CH_3–C), Amide IV, and Amide V bands. On passing from the α-spiral to β-folded structure, the frequencies of the Amide I and II bands generally decrease by 10–30 cm^{-1}, and those of Amide III and V, on the contrary, increase. It is more difficult to distinguish α- and randomly globular conformations by IR spectra. Table 4 shows the Amide I and II absorption bands in the IR spectra of blend films before and after methanol treatment.

The observed shift of the Amide I and II bands of fibroin toward lower frequencies after methanol treat-

Table 4. Amide I and II absorption bands in the IR spectra of fibroin–chitosan blend films before and after methanol treatment

Chitosan content, wt %	Absorption, cm^{-1}, before/after treatment	
	Amide I	Amide II
–	1649/1619	1536/1513
20	1643/1620	1536/1513
30	1649/1619	1536/1513
40	1649/1619	1536/1518
60	1649/1619	1536/1518
80	– / –	1536/1536
100	– / –	1536, 1555*/1536, 1555

* Absorption of the amide groups of chitosan.

Table 5. Mechanical properties of fibroin–chitosan films

Chitosan content, wt %	Breaking stress, N mm^{-2}	Elongation at break, %	Density, g cm^{-3}
–	37.2	4.1	1.37
21	40.3	6.9	1.53
32	43.7	5.6	1.55
53	39.7	7.7	1.39
100	41.0	7.5	1.42

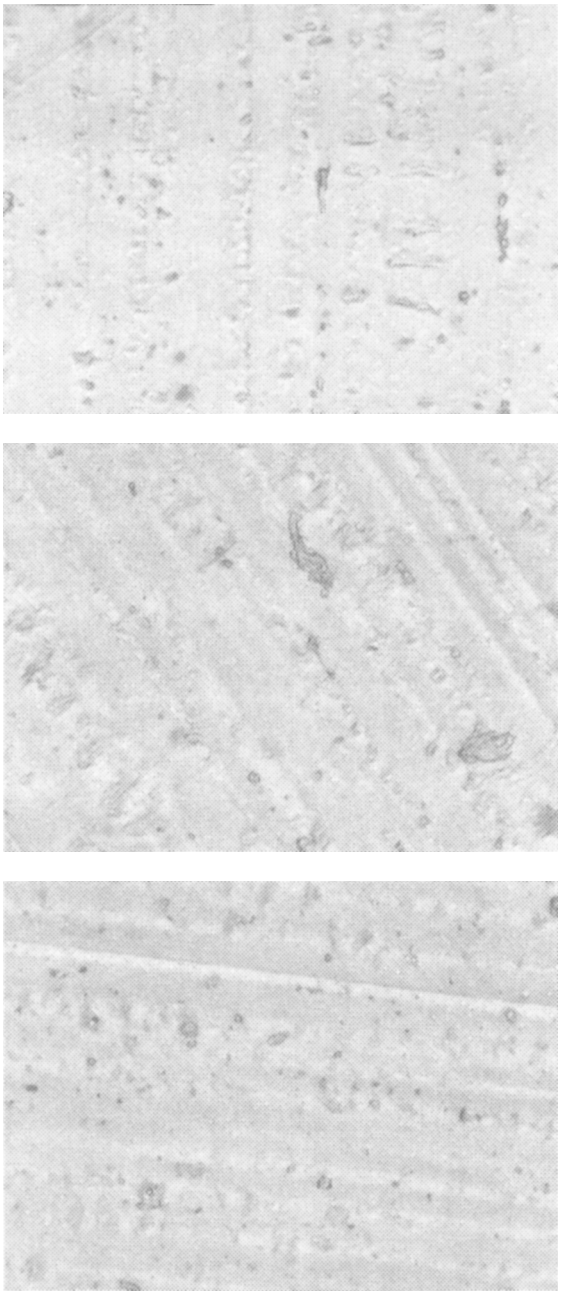


Fig. 2. Photomicrographs of films: (a) fibroin, (b) 1 : 1 blend, and (c) chitosan.

ment confirms the transformation into the β-folded structure.

The mechanical characteristics of the fibroin–chitosan films at various component ratios are given in Table 5. The increase in the density and strength of the films at a chitosan content of about 30 wt % supports the hypothesis stated earlier that this composition is characterized by the strongest intermolecular interaction.

Figure 2 shows the photomicrographs of fibroin, chitosan, and 1 : 1 fibroin–chitosan blend films. As seen, the blend film is quite homogeneous with no coarse particles dispersed throughout the bulk and no noticeable phase separation.

CONCLUSIONS

(1) Fibroin–chitosan blends exhibit common glass transition point, suggesting compatibility of these polymers. Interpolymer interaction initiates formation of more ordered structures, which is the most pronounced at a chitosan content of 20–40 wt %.

(2) Methanol treatment of the films initiates formation of the β-folded conformation of fibroin and interpolymer H-bonding, which is reflected in reduced swellability.

ACKNOWLEDGMENTS

The authors are grateful to Dr. R.-U. Bauer, Director of the Thuringian Institute of Textile and Plastics, for affording an opportunity to carry out experimental studies.

REFERENCES

1. *Chitin and Chitosan Sources, Chemistry, Biochemistry, Physical Properties, and Applications*, Skjak-Braen, G., Anthonsen, T., and Sanford, P., Eds., London: Elsevier, 1989.
2. Mukhina, V.P., Pastukhov, N.V., Semchikov, Yu.D., *et al.*, *Vysokomol. Soedin., Ser. A*, 2001, vol. 43, no. 10, pp. 1797–1804.
3. Nishio, Y., Koide, H., Miyashita, Y., *et al.*, *J. Polym. Sci.: Polym. Phys.*, 1999, vol. 37, pp. 1533–1538.
4. Ratajska, M. and Boryniec, S., *Polym. Adv. Technol.*, 1999, vol. 10, no. 10, pp. 625–633.
5. Alekseev, V.L., Kel'berg, E.A., Bronnikov, S.V., and Evmenenko, G.A., *Vysokomol. Soedin., Ser. B*, 2001, vol. 43, no. 10, pp. 1856–1860.
6. Skorikova, E.E., Vikhoreva, G.A., Kalyuzhnaya, R.I.,

et al., *Vysokomol. Soedin., Ser. A*, 1988, vol. 30, no. 1, pp. 44–49.

7. Ageev, E.P., Vikhoreva, G.A., Gal'braikh, L.S., *et al*., *Vysokomol. Soedin., Ser. A*, 1990, vol. 40, no. 7, pp. 1198–1204.
8. Arijama, T. and Shimura, K., *Protein Chemistry*, Japan: Asakura, 1950.
9. Chen, X., Li, W., Shao, Z., *et al*., *J. Appl. Polym. Sci*., 1999, vol. 73, pp. 975–980.
10. Kweon, H., Ha, H.C., Um, I., and Park, Y.H., *J. Appl. Polym. Sci*., 2001, vol. 80, pp. 928–934.
11. Fox, T.G., *Bull. Am. Phys. Soc*., 1956, no. 1, p. 123.
12. *Silk Polymers: Material Science and Biotechnology*, Kaplan, D. *et al*., Eds., Washington: Am. Chem. Soc., 1994.
13. Miyazawa, T., Shimanouchi, T., and Mizushima, S., *J. Chem. Phys*., 1958, vol. 29, no. 3, pp. 611–616.
14. Asai, M., Tsuboi, M., Shimanouchi, T., and Mizushima, S., *J. Phys. Chem*., 1955, vol. 59, pp. 322–325.
15. Venyaminov, S.Yu. and Kalnin, N.N., *Biopolymers*, 1990, vol. 30, pp. 1259–1271.
16. Motta, A., Fambri, L., and Migliaresi, C., *Macromol. Chem. Phys*., 2002, vol. 203, pp. 1658–1665.

Russian Journal of Applied Chemistry, Vol. 78, No. 3, 2005, pp. 492–495. Translated from Zhurnal Prikladnoi Khimii, Vol. 78, No. 3, 2005, pp. 498–501.
Original Russian Text Copyright © 2005 by Bronnikov, Dem'yantseva.

MACROMOLECULAR CHEMISTRY AND POLYMERIC MATERIALS

Particle-Size Distribution of Wood Resin and Sulfate Lignin in Aqueous Alkaline Solution

S. V. Bronnikov and E. Yu. Dem'yantseva

Institute of Macromolecular Compounds, Russian Academy of Sciences, St. Petersburg, Russia
St. Petersburg State Technological University of Plant Polymers, St. Petersburg, Russia

Received December 27, 2004

Abstract—Particle-size distribution of wood resin, sulfate lignin, and their mixtures in aqueous alkaline solutions (pH 12.7) at 293–333 K was described in the framework of the thermodynamic model. The increase in the average particle size and the broadening of the distribution are caused by an increase in the energy of thermodynamic fluctuations.

To develop a theory of sulfate delignification of wood and to solve applied urgent problems of pulp and paper industry, we studied previously colloidal chemical properties of aqueous alkaline solutions of sulfate lignin, wood resin, and their mixtures [1–3]. We found that the systems are heterogeneous, containing mainly nanoparticles, and tend to aggregate with changing temperature. We also proved formation of coagulation compounds in solutions containing sulfate lignin and wood resin [3]. These compounds are unstable not only at temperature changes but also in the presence of electrolytes [4].

Here we continue our study of particle-size distribution of wood resin, sulfate lignin, and their mixture in colloidal aqueous alkaline solution. The aim of this study is to describe statistically the particle-size distribution of these substances and their mixtures in strongly alkaline solutions (pH 12.7) at 293–333 K.

EXPERIMENTAL

Solutions of sulfate lignin and wood resin were prepared as follows. Sulfate lignin and wood resin were extracted from birch chips with dioxane and diethyl ether, respectively. The extracts were dried to constant weight and treated by the conventional procedure of sulfate cooking. Sulfate lignin was recovered from the solution with sulfuric acid and the resin was extracted with dichloroethane. The samples were dried again to constant weight by evacuation at 323 K and dissolved in aqueous solutions of sodium hydroxide (pH 12.7) at 363 K. The concentration of birch resin and sulfate lignin was 0.27 and 2.5 wt %, respectively.

The particle-size distribution of the dispersions at 293, 313, and 333 K was studied by dynamic light scattering. The measurements were performed on a Coulter Nr. 4 correlator of dynamic light scattering (Coultronic, France). Operation of the device and calculation of the size of diffusing particles were described in our previous papers [1–3]. Based on the results obtained, the particle-size distribution curves (Fig. 1) were constructed. The distribution was simulated using the reversible aggregation model [5–7].

The model of reversible aggregation suggests formation of steady-state microstructures by aggregation of identical particles into metastable clusters (aggregates). In the liquid state, these aggregates are closely packed and are characterized by definite lifetime, i.e., aggregates form and decompose with time (reversibility conditions). Thus, the composition of aggregate ensembles fluctuates steadily. In instantaneously frozen liquid, we will have only one of numerous thermodynamically equivalent configurations. In the framework of this model, using the thermodynamic principles, we suggested to describe the relative distribution of aggregates $n(y)$ by the following equation [5–7]:

$$h(y) = ay^q \exp(-y\Delta u_0/kT), \quad (1)$$

where a is the normalization factor; q, dimension of space where particles aggregate; $y\Delta u^0$, aggregation energy defined as the product of the aggregate size and the standard aggregation energy Δu^0; k, Boltzmann constant; and T, absolute temperature. Equation (1) is the canonical Gibbs distribution [8] modified on the assumption that the aggregation energy depends on the aggregate size. This equation is known as the Γ-distribution [8]. As seen from Eq. (1), ag-

1070-4272/05/7803-0492 © 2005 Pleiades Publishing, Inc.

Parameters of Eq. (1)–(6) describing particle-size distribution of wood resin, sulfate lignin, and their mixtures at different temperatures

T, K, for particles	a_1, nm^{-3}	Δu_{01}, J nm^{-1}	$(Dy_1)^{1/2}$, nm	My_1, nm	a_2, nm^{-3}	Δu_{02}, J nm^{-1}	$(Dy_2)^{1/2}$, nm	My_2, nm
Resin:								
298	1.50	3.63	1.34	2.68	–	–	–	–
313	1.08	3.63	1.43	2.86	–	–	–	–
333	1.27	3.63	1.51	3.05	–	–	–	–
Lignin:								
298	6.3×10^{-3}	0.73	6.65	13.3	6.3×10^{-7}	0.104	46.5	93
313	6.8×10^{-3}	0.73	7.10	14.2	1.3×10^{-6}	0.104	51.5	103
333	7.4×10^{-3}	0.73	7.58	15.2	2.3×10^{-6}	0.104	54.0	108
Mixture:								
298	3.0×10^{-4}	0.26	18.2	36.4	1.2×10^{-7}	0.0285	171	342
313	4.9×10^{-4}	0.26	18.9	37.7	1.1×10^{-7}	0.0285	182	364
333	5.0×10^{-4}	0.26	21.1	42.1	1.8×10^{-7}	0.0285	1.94	388

gregation is initiated by thermal fluctuations with energy kT.

Previously the model of reversible aggregation was successfully used to describe statistical ensembles of colloidal particles of carbon black and their clusters in compounded rubber [6], ordered liquid crystal phase in the course of transition of isotropic liquid to the nematic phase [9–11], and microdomains of glassy polymers in chemical reactions [12–15].

The particle-size distribution of wood resin particles at 293 K is shown in Fig. 1a as a dotted curve. As seen from Fig. 1a, the particles form a statistical ensemble described by Eq. (1) (continuous line) at $q = 3$ (three-dimensional space). The other parameters (a, Δu_0) of the distribution are presented in the table. The experimental particle-size distributions of wood resin at 313 and 333 K were treated similarly. The distribution parameters at the indicated temperatures are given in the table. As seen from the table, the particle-size distributions at different temperatures are described by Eq. (1) at constant standard aggregation energy.

As follows from Eq. (1), the most probable (average) particle size in the statistical ensemble can be expressed as the normalized population mean of the distribution My

$$My = \frac{\int_0^\infty yh(y)\mathrm{d}y}{\int_0^\infty h(y)\mathrm{d}y} = \frac{(q+1)kT}{\Delta u_0} = 4kT/\Delta u_0, \quad (2)$$

and the distribution width (rms deviation from the average) can be expressed as $(Dy)^{1/2}$, where Dy is the normalized variance:

$$(Dy)^{1/2} = [M(y^2) - (My)^2]^{1/2} = [(q+1)^{1/2}kT]/\Delta u_0 = 2kT/\Delta u_0. \quad (3)$$

According to Eqs. (2) and (3), My and $(Dy)^{1/2}$ are inversely proportional to $\Delta u_0/kT$. If Δu^0 is constant, the increase in the average particle size of the resin and the broadening of the distribution with increasing temperature (see table) will be due to an increase in the energy of thermal fluctuations (parameter kT) governing formation of a statistical ensemble.

The particle-size distribution of sulfate lignin at 293 K is shown in Fig. 1b. In this case, the particles form two partially overlapped statistical ensembles. This distribution is described by Eq. (1) modified for the case of polynomial distribution [11, 14, 15].

$$h(y) = \sum_i^{i=N} a_i y_i^q \exp(-y_i \Delta u_{0i}/kT), \quad (4)$$

where $N = 2$ is the number of statistical ensembles. The average particle size in each ensemble is described by Eq. (5) derived from Eq. (2):

$$My_i = 4kT/\Delta u_0, \quad (5)$$

and the distribution width is described by Eq. (6) derived from Eq. (3):

$$(Dy_i)^{1/2} = 2kT/\Delta u_{0i}. \quad (6)$$

The distribution calculated by Eq. (4) is shown in

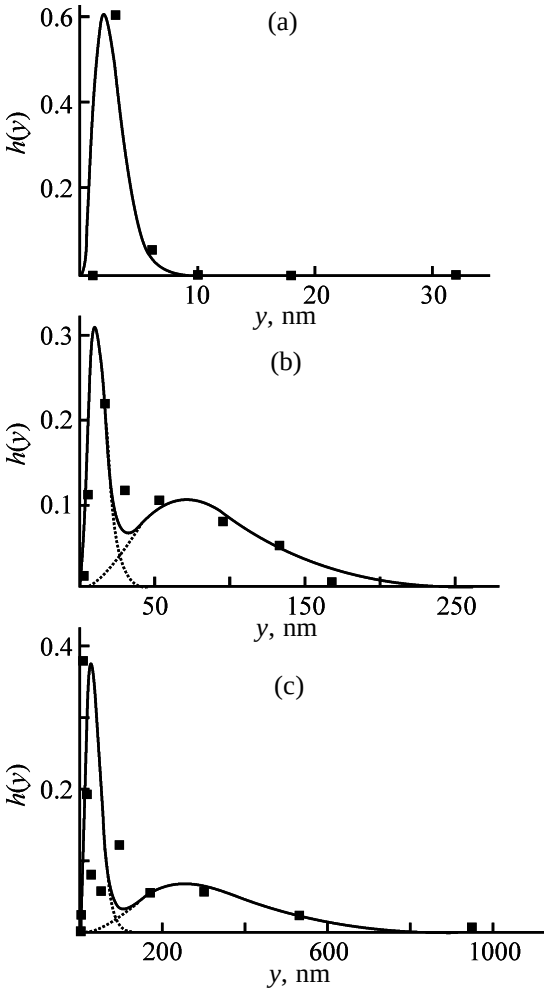


Fig. 1. Experimental particle-size (y) distribution $h(y)$ of (a) birch resin, (b) sulfate lignin, and (c) their mixture in aqueous alkaline solution (pH 12.7) at T = 293 K and the distribution simulated by Eqs. (1) and (4).

Fig. 1b as a continuous line; the distributions of separate ensembles are shown by the dotted lines. Both ensembles have the common starting point on the abscissa (y = 0). Hence, the second ensemble (with larger average particle size) is based on the statistical elements of the first ensemble (with smaller average particle size), i.e., these is a hierarchical system of two statistical ensembles of lignin particles.

The statistical parameters of the distribution, the distribution width, and the average particle size in the ensembles, calculated, respectively, form Eqs. (5) and (6) and simulating the experimental particle size distribution of lignin at 293, 313, and 333 K, are presented in the table. As in the case of the resin, the distribution of statistical ensembles of lignin particles is broadened and the average particle size in each ensemble increases with temperature owing to intensification of thermal fluctuations (see table). It should be noted that, at all temperatures, the average particle size of lignin in the first ensemble is larger by almost an order of magnitude than that of the resin particles. This indicates that the supramolecular structures (clusters) of the polymer (lignin) are larger than those of the oligomer (resin).

In the third part of this work we described the particle size distribution in a solution containing the resin and sulfate lignin in a 1 : 9 ratio. The experimental particle size distribution in this system (dotted line) and the results of its simulation by Eq. (4) are shown in Fig. 1c. As in the previous case, the particles of this mixture form two hierarchic statistical ensembles. The distribution parameters of these ensembles and their average particle size are presented in the table together with the results of statistical treatment of the experimental data for this mixture at 313 and 333 K.

As in the case of resin and lignin particles aggregated in ensembles, the statistical ensembles of particles of their mixtures are broadened and their average size increases with temperature (see table). It should be noted that, in the examined temperature range, the average particle size of ensembles formed in the mixture is substantially larger than the sum of the average sizes of resin and lignin particles. This is likely due to thermal coagulation of particles in the mixture, which increases with temperature.

CONCLUSIONS

(1) Particle size distribution of birch resin, sulfate lignin, and their mixtures (1 : 9) in aqueous alkaline solutions (pH 12.7) at 293, 313, and 333 K was studied by dynamic light scattering.

(2) Resin particles form a single statistical ensemble, and particles of lignin and its mixture with the resin form two statistical ensembles which can be described in the framework of the model of reversible aggregation.

(3) The fact that the distribution is broadened and the average particle size increases with temperature is caused by an increase in the energy of thermal fluctuation governing formation of statistical ensembles.

REFERENCES

1. Dem'yantseva, E.Yu., Lysogorskaya, N.P., Klyubin, V.V., and Zaitseva, S.V., *Zh. Prikl. Khim.*, 2002, vol. 75, no. 1, pp. 149–152.

2. Lysogorskaya, N.P., Dem'yantseva, E.Yu., and Klyubin, V.V., *Kolloidn. Zh.*, 2002, vol. 64, no. 3, pp. 427–431.
3. Dem'yantseva, E.Yu. and Lysogorskaya, N.P., *Zh. Prikl. Khim.*, 2002, vol. 75, no. 7, pp. 1193–1196.
4. Krugovskaya, T.I., Dem'yantseva, E.Yu., Kozlova, O.A., and Rakitina, G.V., Abstracts of Papers, *XIV Mezdunarodnaya mezhotraslevaya konferentsiya "Organizatsiya sistemy upravleniya prirodnymi resursami i povyshenie effektivnosti ekologicheskoi bezopasnosti"* (XIV Interdisciplinary Conf. "Organization of Management of Natural Resources and Improvement of Environmental Safety"), St. Petersburg, 2004, p. 264.
5. Kilian, H.G., Metzler, R., and Zink, B., *J. Chem. Phys.*, 1997, vol. 107, pp. 8697–8704.
6. Kilian, H.G., Koepf, M., and Vettergen, V.I., *Prog. Colloid Polym. Sci.*, 2001, vol. 117, pp. 172–181.
7. Kilian, H.G., Bronnikov, S., and Sukhanova, T., *J. Phys. Chem. B*, 2003, vol. 107, pp. 13575–13582.
8. Lavenda, B.H., *Statistical Physics. A Probabilistic Approach*, New York: Wiley, 1991.
9. Zuev, V.V. and Bronnikov, S.V., *Zh. Fiz. Khim.*, 2003, vol. 77, no. 6, pp. 974–977.
10. Zuev, V. and Bronnikov, S., *Liquid Crystals*, 2002, vol. 29, pp. 1279–1281.
11. Bronnikov, S. and Dierking, I., *Phys. Chem. Chem. Phys.*, 2004, vol. 6, pp. 1745–1749.
12. Bronnikov, S.V., Sukhanova, T.E., and Laius, L.A., *Vysokomol. Soedin., Ser. A*, 2002, vol. 44, no. 6, pp. 940–946.
13. Bronnikov, S.V., Sukhanova, T.E., Meleshko, T.K., *et al.*, *Zh. Prikl. Khim.*, 2003, vol. 76, no. 5, pp. 829–832.
14. Bronnikov, S.V., Sukhanova, T.E., and Goikhman, M.Ya., *Zh. Prikl. Khim.*, 2003, vol. 76, no. 6, pp. 995–999.
15. Bronnikov, S. and Sukhanova, T., *Phys. Chem. Chem. Phys.*, 2003, vol. 5, pp. 4252–4257.

Russian Journal of Applied Chemistry, Vol. 78, No. 3, 2005, pp. 496–499. Translated from Zhurnal Prikladnoi Khimii, Vol. 78, No. 3, 2005, pp. 502–505.
Original Russian Text Copyright © 2005 by Galikhanov, Deberdeev.

MACROMOLECULAR CHEMISTRY AND POLYMERIC MATERIALS

Corona-Poled Electrets Based on Vinyl Chloride/Vinyl Acetate Copolymer–Zinc White Composites

M. F. Galikhanov and R. Ya. Deberdeev

Kazan State Technological University, Kazan, Tatarstan, Russia

Received April 28, 2004; in final form, December 2004

Abstract—Electret properties of vinyl chloride/vinyl acetate copolymer and its composites with zinc oxide are studied.

Diverse engineering applications of electrets (electrical analogs of permanent magnets) [1–4] stimulate searching for novel electret materials and developing electrets with stable characteristics. In this respect, the most promising are composite materials consisting of two or more chemically dissimilar materials with an interface between them, which are capable of Maxwell–Wagner polarization. However, the trends in electrical polarization of plastics are not thoroughly understood even for some comparatively simple binary systems. In this connection, it is of interest to study the features of electrical polarization in filled polymers.

It is a standard technique of electret charging to inject charge carriers generated in a corona discharge. Among the advantages of this method are technical simplicity and fairly high process rate. The mechanism of such a polarization involves injection of charge carriers (electrons, ions) into a polymeric dielectric and their trapping by impurities and structural defects [1, 2]. Corona-discharge polarization is used for nonpolar polymers to obtain high-performance electrets.

On the contrary, electret charging in polar polymers proceeds through dipolar-group and dipolar-segmental polarization [4].

Previously we demonstrated with an example of ethylene/vinyl acetate copolymers that the stability of corona-poled electrets decreases with increasing polarity of the polymer [5], which is caused by migration of the charge carriers from the surface of a polymeric material and by relaxation. The degree of depolarization is controlled by the specific volume conductivity of the material γ_V, which is the lower, the higher the content of polar groups in the polymer. However, the initial surface charge density σ_{eff} in corona-poled electrets based on polar polymers is higher compared to nonpolar polymers. As the polarity of the copolymer increases, the starting σ_{eff} initially increases and then slightly decreases. In [5], our interpretation was that, when entering the surface layer of a polymer sample, the charge carriers polarize the nearest dipoles (polar groups), initiating orientation of the dipoles in the field of the injected charge. The oriented dipoles are traps for the injected charges, attracting and retaining them by Coulombic forces. The higher the content of polar (acetate) groups in a polymer, the higher the content of the traps and the initial surface charge density. Liberation of the charge carriers from the surface traps occurs more intensively than from the bulk traps, which is due to increased charge carrier concentration in the surface layer and, therefore, higher conductivity of the polymer [5]. This mechanism is supported by data of [6] that the major part of charge carriers injected to a polar polymer is localized in the surface layer, so that their concentration in the bulk is negligible.

Earlier we have patented a process for manufacturing a coating based on a corona-poled electret prepared from vinyl chloride/vinyl acetate copolymer (VCVAC), having stable high charge [7]. In this work we studied the electret effect in filled VCVAC.

EXPERIMENTAL

In the work we used A-15-0 random VCVAC (weight fraction of chlorine 52.5%) [TU (Technical Specifications) 6-01-1181–87] and ZnO with a particle size of 2–4 μm and specific surface area of 3–4 $m^2 g^{-1}$.

The polymer with mixed with the filler at 135 ± 5°C for 3 min using a laboratory roll mill. Samples in the form of 0.8–1.2-mm-thick plates were fabricated by

1070-4272/05/7803-0496© 2005 Pleiades Publishing, Inc.

pressing at 170 ± 5°C according to GOST (State Standard) 12 019–66. The samples were polarized by corona charging using an electrode with 196 pointed needles uniformly arranged on a 7 × 7-cm square. The distance between the sample and electrode was 20 mm; polarizing voltage, 35 kV; and polarization time, 90 s. The samples were preheated at 90°C for 10 min in an oven prior to polarization.

The surface potential of the electrets U_e was measured at 24-h intervals by the contactless induction method using a vibrating electrode according to GOST 25 209–82. The observation time was 1 year. The time elapsed since the onset of polarization to the first measurement was 1 h. The electrets were stored at room temperature in the nonshorted state. The effective surface charge density σ_{eff} was estimated [2] as

$$\sigma_{eff} = U_c \varepsilon \varepsilon_0 / \delta,$$

where U_c is the compensating voltage (V); ε, permittivity of the composite; ε_0, dielectric constant equal to 8.854×10^{-12} F m^{-1}; and δ, sample thickness (m).

The charge relaxation time τ was determined as the time in which the surface potential of the samples decreased by a factor of *e* (~2.71).

After 1-year storage, we recorded the thermally stimulated current (TSC) spectra of the samples at a heating rate of 5 deg min^{-1} using a specially designed cell equipped with blocking electrodes and Teflon spacer [3, 4].

The TSC data were then compared with the results of DTA analysis (Q-1500 D derivatograph; samples 150 ± 50 mg; heating rate 5 deg min^{-1}).

The dependence of the surface potential of the VCVAC corona-poled electret on the storage time is a curve with a minimum (Fig. 1, curve *1*). The initial decline of the surface potential is due to charge relaxation.

Evidently, the observed abrupt decline of the potential in the period from the 80th to 160th day is caused by shielding of the electret charge by the water molecules adsorbed from air on the surface. In the course of the experiment, the indicated period fell on the season of the maximal humidity. As the humidity decreased, a considerable fraction of water desorbed from the surface of the electret, and surface potential increased after 300 days of storage. The decrease in the charge with increasing humidity and its subsequent restoration is typical of the conventional electrets [8]. At the same time, the charge relaxation rate

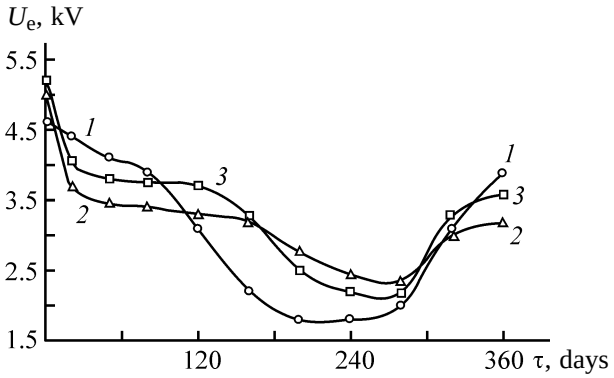


Fig. 1. Variation with storage time τ of the surface potential U_e of (*1*) VCVAC corona-poled electret and (*2, 3*) composites with ZnO. ZnO content (vol %): (*2*) 4 and (*3*) 8.

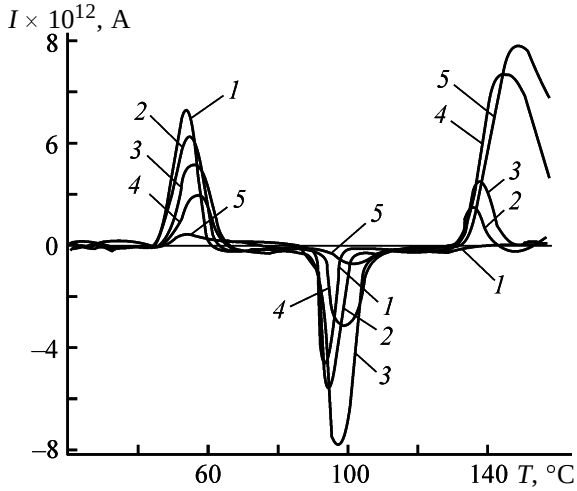


Fig. 2. Thermally stimulated depolarization current spectra of corona-poled electrets: (*1*) VCVAC and (*2–5*) VCVAC–ZnO composites. (*I*) Current and (*T*) temperature. ZnO content (vol %): (*2*) 2, (*3*) 4, (*4*) 6, and (*5*) 8.

at increased humidity increases, which can be attributed to an increase in the surface conductivity of the polymeric samples and preferential relaxation of the homocharge in the surface and near-surface layers of the electret [9, 10].

Analysis of the TSC spectra of the copolymer (Fig. 2, curve *1*) revealed two levels of trapping. The first-level traps are destroyed at 60–65°C, which corresponds to the glass transition point as determined by DTA. Presumably, at this temperature, the hindrances to rotation of dipolar groups are overcome, which results in the decay of the dipolar-group or dipolar-segmental polarization [3]. The activation energy of charge relaxation W_a corresponding to this peak was estimated by the Garlick–Gibson method [2] to be about 0.70 eV.

The presence of a negative current peak suggests that the second trapping level decays at 95–105°C,

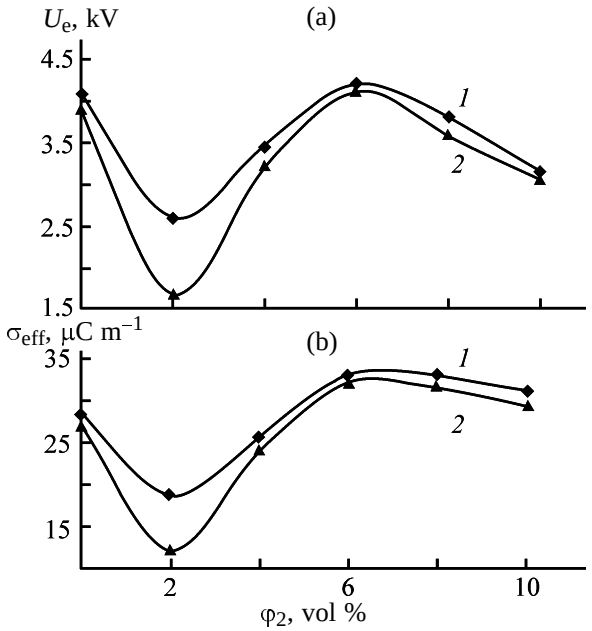


Fig. 3. (a) Surface potential U_e and (b) effective surface charge density σ_{eff} in ZnO-filled VCVAC as functions of the filler content φ after (*1*) 50 and (*2*) 350 days of storage.

which corresponds to the viscous-flow transition observed in the DTA curve. At these temperatures, the intermolecular physical and hydrogen bonds are broken, which results in liberation of the injected charge. The W_a of this process is about 1.30 eV, which suggests that the charge carriers are localized in deep wells, thus imparting stable high surface potential to the polymer.

The TSC data show that the observed stable high charge on the corona-poled VCVAC electrets is caused by the external and dipolar-group types of polarization, the polarization by virtue of the injected charge controlling the quantity of the charge, and the dipolar polarization, its stability. Preheating the polymer to 90°C prior to corona charging transfers it into the hyperelastic state, when the dipolar groups become capable to be oriented in the polarizing field, and on cooling, to be frozen with formation of a heterocharge.

In polarization of filled VCVAC in the corona discharge field, charge carriers are trapped at the interfaces. According to the Maxwell–Wagner effect, accumulation of charges on the interfaces is caused by different conductivities of the phases in heterogeneous samples. Let us analyze the mechanism of polarization in VCVAC–ZnO composites from this standpoint.

It was demonstrated in the previous studies of the effect of a conducting filler on the electret properties in polar polymers [4, 11–13] that increasing filler loading initially increases and then decreases the electret effect. Pinchuk *et al*. [14] observed only a decrease in TSC on adding 0.5 wt % of ultradisperse sialon-like particles in butyral resin.

Our experiments showed that filling with ZnO affects the electret properties of VCVAC: with increasing ZnO content in the copolymer, the surface potential (Fig. 3a) and effective surface charge density of the electrets (Fig. 3b) seccessively pass through a minimum and a maximum.

The initial decrease in the surface potential is probably due to perfection of the supramolecular VCVAC structure at low ZnO loading. Filling of polymers always alters the supramolecular structure, i.e., the size, shape, and size distribution of structural blocks, as well as the packing density of macromolecules. Being in low concentration, finely dispersed solid fillers may serve as nucleating agents [15]. Furthermore, fillers significantly affect the flexibility of kinetic units of macromolecules and their relaxation time.

The subsequent increase in U_e and σ_{eff} is probably due to changing type and depth of the energy traps for the injected charges with filling. In the presence of reactive fillers, carboxy, carbonyl, and other groups could be generated in the macromolecules, primarily at the polymer–filler interface. Furthermore, mechanochemical activation of the material in the course of composite preparation could generate free radicals [16], also capable to serve as energy traps for the charges.

Starting from the ZnO content of 6 vol %, the observed deterioration of the electret characteristics of the composites can be attributed to increase in their conductivity, which controls the decay rate of the electret surface potential.

To check these hypotheses for consistency, we analyzed the TSC spectra of the filled composites. The spectra show changes in the intensity and position of the TSC peaks relative to those typical of straight VCVAC and also the appearance of a new high-temperature peak at 130–150°C. At small ZnO content (2 vol %) we observed a decrease in W_a of the energy traps to 0.65 and 0.7 eV for the first and second types of the traps, respectively, which is caused by decreasing flexibility of the macromolecules in the presence of the filler and, as a result, by hindered rotation of the dipolar groups (Fig. 2, curve *2*). Presumably, this is due to adsorption of the copolymer macromolecules on the filler particles with formation of interfacial layers characterized by decreased flexibility of structural units of the copolymer. Furthermore, the presence of the filler intensifies mechanical degradation of the copolymer in the course of composite preparation,

which could decrease the amount of groups capable of serving as traps for the injected charges and, at the same time, intensifies trapping of the injected charges in the traps formed in the course of mechanically activated degradation.

The formation of new types of traps at the copolymer–filler interface, associated with manifestation of the Maxwell–Wagner effect, increases the fraction of charge carriers in high-energy traps, as demonstrated by the occurrence of a new level of trapping of the injected charge carriers, whose decay is observed at 130–150°C (Fig. 2). The activation energy of charge relaxation from traps of this type increases, depending on the ZnO content, from about 0.55 (2 vol % ZnO) to 1.90 eV (10 vol % ZnO), thus improving the electret characteristics of the composites (Fig. 3).

The appearance of a new peak in the TSC spectra, caused by filling, is well known. For example, in polyamide–fiber glass composites, the appearance of a low-temperature thermally stimulated depolarization current peak was observed at about 55°C [17]. This peak was assigned to charging of defects on the fiber glass surface or at the polymer–filler interface.

Nevertheless, low W_a of traps in the initial VCVAC limits the polarization in highly loaded composites. Without question, this is favored also by increased conductivity of such composites.

CONCLUSIONS

(1) Vinyl chloride/vinyl acetate copolymer exhibits high initial surface charge density.

(2) Filling with zinc oxide imparts stability to the polarized state of the polymer, typical of the Maxwell–Wagner polarization.

ACKNOWLEDGMENTS

The authors are grateful to L.S. Pinchuk (Institute of Mechanics of Metal–Polymer Systems, National Academy of Sciences of Belarus, Gomel) for valuable discussions.

REFERENCES

1. *Electrets*, Sessler, G., Ed., Berlin: Springer, 1987.
2. Lushcheikin, G.A., *Polimernye elektrety* (Polymeric Electrets), Moscow: Khimiya, 1984.
3. Kestelman, V.N., Pinchuk, L.S., and Goldade, V.A., *Electrets in Engineering: Fundamentals and Applications*, Boston: Dordrecht, 2000.
4. Pinchuk, L.S., and Gol'dade, V.A., *Elektretnye materially v mashinostroenii* (Electret Materials in Mechanical Engineering), Gomel: Infotribo, 1998.
5. Galikhanov, M.F. and Budarina, L.A., *Plast. Massy*, 2002, no. 1, pp. 40–42.
6. Boev, S.G., Lopatkin, S.A., and Ushakov, V.Ya., in *Elektretnyi effect i elektricheskaya relaksatsiya v tverdykh dielektrikakh: Mezhvuzovskii sbornik* (Electret Effect and Electrical Relaxation in Solid Dielectrics: Intercollegiate Collection), Moscow: MIEM, 1988, pp. 71–73.
7. RF Patent 2066890.
8. Gubkin, A.N., *Elektrety* (Electrets), Moscow: Nauka, 1978.
9. Shuvaev, V.P., Turyshev, B.I., Romanovskaya, O.S., *et al.*, *Vysokomol. Soedin., Ser. A*, 1977, vol. 19, no. 3, pp. 603–606.
10. Klassov, V.N. and Osipov, K.A., in *Neravnovesnye protsessy v dielektricheskikh materialakh: Mezhvuzovskii sbornik nauchnykh trudov* (Nonequilibrium Processes in Dielectric Materials: Intercollegiate Collection of Scientific Works), Moscow: MIREA, 1983, pp. 93–98.
11. Vertyachikh, I.M., Development of Polymeric Composite Materials with Electret Components for Mechanical Engineering, *Cand. Sci. Dissertation*, Gomel, 1990.
12. Vertyachikh, I.M., Pinchuk, L.S., and Tsvetkova, E.A., *Vysokomol. Soedin., Ser. B*, 1987, vol. 29, no. 6, pp. 460–463.
13. Snezhkov, V.V., Gol'dade, V.A., Gromyko, Yu.V., and Pinchuk, L.S., *Dokl. Akad. Nauk Bel. SSR*, 1988, vol. 32, no. 9, pp. 810–813.
14. Pinchuk, L.S., Zotov, S.V., Gol'dade, V.A., *et al.*, *Zh. Tekh. Fiz.*, 2000, vol. 70, no. 2, pp. 38–42.
15. Lipatov, Yu.S., *Fizicheskaya khimiya napolnennykh polimerov* (Physical Chemistry of Filled Polymers), Moscow: Khimiya, 1977.
16. Baramboim, N.K., *Mekhanokhimiya vysokomolekulyarnykh soedinenii* (Mechanochemistry of Macromolecular Compounds), Moscow: Khimiya, 1978.
17. Sviridenok, A.I., Kovalevskaya, T.I., Kravtsov, A.G., and Bernatskaya, Zh.I., *Dokl. Akad. Nauk Bel.*, 2000, vol. 44, no. 5, pp. 119–122.

Russian Journal of Applied Chemistry, Vol. 78, No. 3, 2005, pp. 500–505. Translated from Zhurnal Prikladnoi Khimii, Vol. 78, No. 3, 2005, pp. 506–511.
Original Russian Text Copyright © 2005 by Myagchenkov, Chichkanov, Yakovenko.

CHEMISTRY OF FOSSIL FUEL

Toms Effect in Direct Crude Oil Emulsions as Influenced by the Stream Velocity and Concentration of Anionic Copolymers of Acrylamide

V. A. Myagchenkov, S. V. Chichkanov, and D. F. Yakovenko

Kazan State Technological University, Kazan, Tatarstan, Russia

Received June 2, 2004; in final form, December 2004

Abstract—The major relationships in the Toms effect in direct crude oil emulsions differing in the dispersed phase concentration were studied on a modified turbulent rheometer with anionic copolymer of acrylamide as the polymer additive. The Toms effect was studied as influenced by the polymeric additive concentration and shear stress.

One of the most important and urgent problems currently faced by the oil extraction industry is development of efficient, scientifically sound power-saving technologies accelerating high-speed pipeline transportation of hydrocarbon raw materials [1, 2]. Unlike laboratory experiments, real processes yield a water-rich end product, which creates additional problems. In view of the fact that the water enrichment of the extracted crude oil tends to increase with increasing time of exploitation of wells [3], this necessitates a search for new methods of intensifying the transportation of hydrocarbon raw materials. This concerns not only dehydrated but also water-enriched oil-containing dispersed systems with a complex composition, above all, direct (oil-in-water) and reverse (water-in-oil) emulsions [4, 5].

In this situation, much promise is offered by polymeric additives (PAs) introduced into the dispersion medium in minor amounts in order to reduce the hydraulic resistance in turbulent streams of disperse systems (Toms effect). The Toms effect was most successfully applied to dehydrated oil [6, 7]. Good performance of PAs can be illustrated by the results of the tests on the 125-km long Tikhoretsk–Novorossiisk main crude oil pipeline with the internal diameter of the pipe of 0.8 m [8]. With nonpolar high-molecular-weight polyhexene in the concentration of 8 g cm^{-3} as additive, the oil transportation was considerably accelerated owing to a 20% decrease in the friction loss.

Good performance of polyolefin-based nonpolar polymeric additives as turbulence "quenchers" in oil streams was also confirmed by experiments on pumping dehydrated oil through the Aleksandrovskoe–Anzhero–Sudzhensk main pipeline (oil density 850 kg m^{-3}; kinematic viscosity 5×10^{-6} m^2 s^{-1}; Reynolds number Re = 3.5×10^5 at shear stress of 3 Pa) [9].

The promise of ionic and nonionic water-soluble (co)polymers for decreasing the hydrodynamic resistance in oil-containing disperse systems is understood to a much lesser extent. There are only fragmentary data confirming the suitability for this purpose of water-soluble polymer additives [10] whose essential properties need to be characterized more precisely [11]. At the same time, development of technologies of high-speed transportation of oil streams using water-soluble PAs is well justified: They showed the best performance in development and application of industrial technologies intensifying high-speed transportation of water streams [12, 13].

Here, we continue our previous studies [14] by quantitatively analyzing the Toms effect as influenced by the concentration of water-soluble PAs (anionic copolymers of acrylamide) and by the velocity of the turbulent streams of direct oil emulsions.

EXPERIMENTAL

Crude oil from Novosheshminsk site (Tatarstan) served as the main component of the dispersed phase of the emulsions. At 20°C, the oil had the kinematic viscosity $\nu = 210 \times 10^{-6}$ m^2 s^{-1} and density $\rho_4^{20} =$ 910 kg m^{-3}. The viscosity of oil was decreased by preliminary dilution with kerosene [Volgograd Refin-

1070-4272/05/7803-0500© 2005 Pleiades Publishing, Inc.

ery, Technical Specifications (TU) 3840158-10–90] to the 3 : 1 volume ratio. Diluted oil in all the experiments was characterized by $\nu = 23.5 \times 10^{-6}$ m^2 s^{-1} and density $\rho_4^{20} = 880$ kg m^{-3}. A water-soluble anionic surfactant, sodium alkylbenzenesulfonate (Sulfonol), served as stabilizer of direct emulsions. Direct emulsions with different compositions were prepared by the following procedure. The calculated amounts of distilled water, oil, and stabilizer (2% of the volume of dispersed phase, oil) were thoroughly stirred with a magnetic stirrer until formation of the primary emulsion. The resulting emulsion was additionally stabilized by ultrasonication with a UZDN-1 ultrasonic disperser (working frequency 22 kHz, total time of ultrasonication 15 min).

The size of the dispersed phase particles in the emulsions, as estimated by optical microscopy, did not exceed 1.5×10^{-6} m. This made the resulting emulsions fairly resistant to aggregation and sedimentation.

An anionic copolymer of acrylamide with sodium acrylate (Alcoflood 1175 A), available from Allied Colloids, the United Kingdom, with the molecular weight $M = 10.8 \times 10^6$ and 21.5% content of ionic units served as the polymeric additive.

The Toms effect was studied on a modified turbulent rheometer with a glass capillary (1.66×10^{-3} m in diameter and 0.6 m long). Figure 1 shows the schematic of the setup. The experiment consisted in the following. Thick-walled steel 350 cm^3 reservoir *1* was filled with 300 cm^3 of the liquid under study. Using gas cylinder *2* with valve *3* and reducer *4*, an excess pressure was created in receivers *5* and was monitored by manometer *6*. At the preset time, electric drive of valve *7* was switched on, which, in turn, opened valve *8*. The liquid flew via capillary *9* from reservoir *1* into receiver *10* under pressure. After 2 s, the valve closed automatically. The amount of the liquid that flew out of reservoir *16* was measured with an A&D (Japan) electronic balance *11*.

The Toms effect T was calculated by the relationship

$$T = (m - m_0)/m_0,$$

where m and m_0 are the masses of the consumed emulsion with and without PA additive, respectively [15, 16].

The reduced Toms effect T/c was calculated by the formula [16]

$$T/c = (m - m_0)/m_0 c,$$

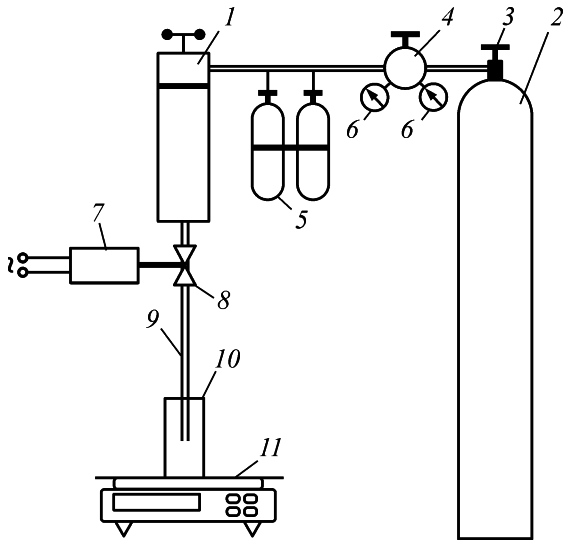


Fig. 1. Schematic of the setup for studying the Toms effect. For comments, see text.

where c is the PA concentration.

The polymer adsorption A was estimated from the difference in the concentrations of the copolymer before (c) and after (c_x) its contact with the dispersed phase particles, using the calibration plot of the specific viscosity vs. the concentration $\eta_{sp} = f(c)$. The copolymer concentration in the aqueous phase of the emulsion was determined viscometrically after the oil was separated on an OPN-8 centrifuge at 8000 rpm. To correctly measure the viscosity when plotting the calibration curve, we used as the aqueous medium the aqueous mother liquor yielded by centrifugation of the emulsion. The reason was that the aqueous phase of the emulsions contains a relatively large amount of the ionic stabilizer, anionic surfactant, able of markedly affecting the size of the macromolecules of anionic copolymer of acrylamide and, thus, the viscosity numbers n_{sp}/c of the copolymer solutions analyzed. With the aqueous mother liquor as the aqueous medium, in all the reference aqueous solutions of the copolymer the concentration of the surfactant not bound with the dispersed phase was identical to that in the oil emulsion analyzed. This precluded possible complications in the viscosity analysis due to the difference in the surfactant concentrations in the reference [used for plotting the $\eta_{sp} = f(c)$ calibration curve] solutions of copolymers and in the aqueous phase of the emulsion.

Viscometric studies were carried out in an Ubbelohde viscometer with the capillary diameter of 0.54×10^{-3} m.

The macroscopic Toms effect is determined by a

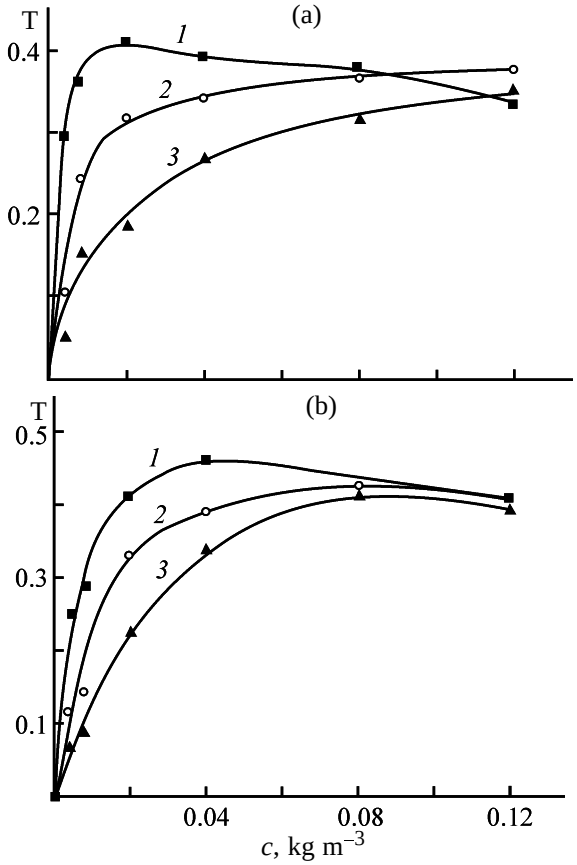


Fig. 2. Toms effect T as a function of the polymeric additive concentration *c* for (a) 15% direct oil emulsion and (b) water at the pressure *p* of (*1*) 5, (*2*) 10, and (*3*) 15 atm.

large number of active parameters of the system, governed primarily by the nature of the PA, polymeric medium, and hydrodynamic features of the turbulent stream of the liquid [12, 13]. Principal complications in quantitative analysis of the experimental data and, especially, in judging the detailed mechanism of this phenomenon arise in changing from true solutions to multicomponent heterophase systems exhibiting synergistic and antagonistic effects [15]. In this study, we examined how the Toms effect T in direct oil emulsions differing in the content of the dispersed phase (5, 10, 15, and 20 vol %) varies with the stream velocity and concentration of the water-soluble PA. Figure 2a illustrates the concentration dependence of T, as well as the interrelation between T and external pressure *p*, when the emulsion is pumped through the capillary (we will note that *p* is proportional to the shear stress τ), with the 15% oil emulsion as an example. For oil emulsions with other compositions, the T = $f(c)$ and T = $f(p)$ dependences were similar. Table 1 lists the main hydrodynamic characteristics of the direct oil emulsions in the presence of various amounts of PA.

It should be noted that, for the systems of interest, the Reynolds numbers Re significantly exceed the critical value of 2.3×10^3, which suggests the turbulent flow regime in the emulsions analyzed. Figure 2a and Table 1 show that, at high concentrations, T flattens out. This suggests that, with increasing PA concentrations, the contribution to the resulting Toms effect from the successively added portions of the polymer tends to decrease. This is clearly illustrated by a decrease in the parameter T/*c* with increasing polymer concentration (Table 1). The pattern is similar not only for direct oil emulsions but also for aqueous solutions of the copolymer (Fig. 2b). This can be due to the existence of a certain optimal concentration of the macromolecules c_{opt} in the stream zone occurring in the immediate vicinity of the internal surface of the capillary. Further increase in the copolymer concentration above 0.002–0.004 wt % is not accompanied by an increase in c_{opt} and only markedly increases the dynamic viscosity of the aqueous dispersion medium, which, naturally, decreases T and T/*c*. It is clear from Figs. 2a and 2b and Table 1 that T tends to decrease with increasing p within a wide range of the PA concentrations.

The influence of the external pressure on the capability of PA to decrease the hydraulic resistance of turbulent streams of direct oil emulsions can be understood most clearly from comparison of the dependences of T/*c* (for fixed *c* and *p*) on the composition of the emulsion (Fig. 3). There is no significant difference in the dependences of the parameters T and T/*c* on the external pressure *p* in purely aqueous media and in direct oil emulsions differing in the dispersed phase composition. Thus, the empirically established interrelation between T and *p* is not directly related to the heterophase nature of the system.

Another factor responsible for a decrease in T with increasing *p* may be mechanical degradation of the macromolecules of the copolymers in turbulent streams and direct oil emulsions. Mechanical degradation accompanied by rupture of the C–C bonds of the macromolecules decreases the average molecular weight *M* of the copolymer. This, naturally, decreases the effective size of the macromolecular globules. Under mechanical degradation, this should be accompanied by decreases in such macroscopic parameters as T and T/*c* [16] to the greater extent, the higher the pressure *p* in the turbulent rheometer. Special experiments showed that the viscosity numbers of the aqueous solutions of the copolymer before and after passing through the capillary of the rheometer at the

Table 1. Hydrodynamic characteristics of the 20% direct oil emulsion in the presence of PA in different concentrations*

System	$\eta \times 10^3$, Pa s	p, atm	$\gamma \times 10^5$ m^3 s^{-1}	v, m s^{-1}	$\mathrm{Re} \times 10^{-3}$	T	T/c, m^3 kg^{-1}
Water	1.006	5	1.76	8.14	13.41	–	–
		10	3.02	13.94	22.98	–	–
		15	3.88	17.91	29.53	–	–
Emulsion	1.756	5	1.62	7.49	6.97	–	–
		10	2.80	12.94	12.04	–	–
		15	3.66	16.91	15.73	–	–
Emulsion + PA, wt%:							
0.0004	1.798	5	1.92	8.88	8.07	0.185	46.23
		10	3.10	14.33	13.02	0.107	26.76
		15	3.92	18.11	16.45	0.070	17.70
0.0008	1.820	5	2.04	9.42	8.45	0.257	32.13
		10	3.22	14.87	13.34	0.148	18.60
		15	4.03	18.65	16.73	0.102	12.84
0.002	1.880	5	2.26	10.47	9.10	0.398	19.90
		10	3.58	16.57	14.41	0.281	14.06
		15	4.51	20.84	18.12	0.233	11.66
0.004	1.983	5	2.33	10.77	8.88	0.438	10.97
		10	3.96	18.33	15.11	0.417	10.43
		15	4.77	22.04	18.17	0.304	7.60
0.008	2.145	5	2.19	10.13	7.72	0.354	4.42
		10	4.07	18.81	14.34	0.455	5.69
		15	5.34	24.67	18.81	0.461	5.76
0.012	2.217	5	2.17	10.05	7.42	0.343	2.86
		10	4.03	18.61	13.74	0.441	3.67
		15	5.43	25.11	18.53	0.487	4.06

* η is dynamic viscosity; γ, liquid flow rate; and v, flow velocity.

pressures of 5, 10, and 15 atm differed by no more than 3%.

Thus, under the actual conditions, mechanical degradation of the macromolecules in the turbulent stream cannot be primarily responsible for a decrease in T with increasing p.

The experimental $T = f(p)$ dependence can with a good reason be accounted for by the specific features of the mass transfer and of the conformation of the macromolecules in turbulent streams, especially in view of the fact that these features are common for aqueous solutions and oil emulsions. A specific feature of the mass transfer in turbulent streams is formation in close proximity of the capillary walls of a special parietal zone of stream (extending by no more than several tens of micrometers). In this zone, the concentration of the PA macromolecules (as well as of the dispersed phase particles) can markedly differ from the concentration in the bulk [12, 15]. Certainly, the rheology of the turbulent streams of direct oil emulsions is also strongly affected by the conformation of the macromolecules. This is manifested, above all, in a significant difference in the size and shape of the macromolecular globules in the laminar and turbulent streams, especially in view of the velocity gradient in the transverse and longitudinal directions in turbulent streams [17, 18]. Under the experimental conditions, another factor affecting the conformation

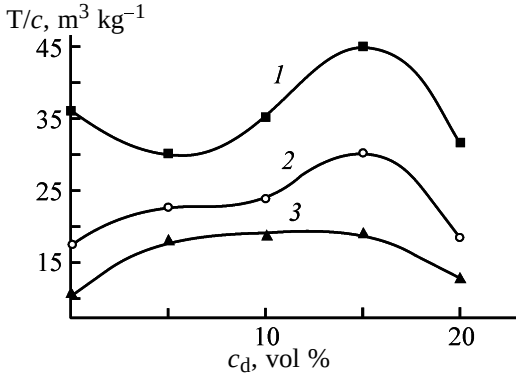


Fig. 3. Reduced Toms effect T/c as a function of the content of the dispersed phase in the direct oil emulsion c_d at the pressure p of (*1*) 5, (*2*) 10, and (*3*) 15 atm. Polymeric additive concentration 8×10^{-4} wt %.

Table 2. Selected data on adsorption of PA on the particles of the 10% oil emulsion

c, wt %	η_{sp} of aqueous solutions of PA		c_x, wt %	$c - c_x$, wt %	A, mg g^{-1} of oil
	initial	after contact with the oil			
0.002	0.055	0.044	0.00173	0.00027	0.028
0.004	0.216	0.200	0.00374	0.00026	0.027
0.012	0.620	0.583	0.01153	0.00047	0.049

of the macromolecules of the copolymer is a fairly high thermodynamic and kinetic flexibility of the units in the macromolecules of the acrylamide copolymers [19].

Common knowledge suggests that the hydrodynamic characteristics of the oil emulsions are also markedly affected by the specific features of the structure of the dispersed phase particles (Fig. 4). This is primarily due to the specific aggregation state (liquid) of these particles, as well as to the occurrence in their structure of complex structural units (CSUs) (Fig. 4), comprised of a solid core and an adsorption–solvation layer [14].

The aggregate of the dispersed phase particles is surrounded by an electrical double layer (EDL) consisting of adsorption layer *II* of the potential-determining ions (anions of the stabilizer) and adsorption *III* and diffusion *IV* layer of counterions (primarily Na^+ cations). Because of the transverse-longitudinal velocity gradients in the turbulent streams, the changes in the oil emulsions are observed not only in the diffusion part *IV* of the EDL. Complex deformation of the aggregate *I* is due to transition from a sphere to, e.g., an ellipse, disk, or cylinder. Evidently, the change in the shape of the aggregate is accompanied by relaxation changes in structural elements *II* and *III*. These changes are accompanied by charge density redistribution on the surface of the dispersed phase particles, which affects, in particular, the electrokinetic potential. Such rearrangement of the structural elements of the dispersed phase particles is accompanied by a change in the balance of the potential energies of attraction U_{att} and repulsion U_{rep} both between the dispersed phase particles and in their interaction with the charged internal surface of the capillary. Naturally, the changes in the shape of the dispersed phase particles and in the balance of the forces U_{att} and U_{rep} should substantially affect such macroscopic parameters as T and T/c. The current knowledge of the inherent relationships in the turbulent flow processes in direct oil emulsions allows us to speculate only about some correlations rather than about rigorous quantitative relationships in the heterophase systems under consideration.

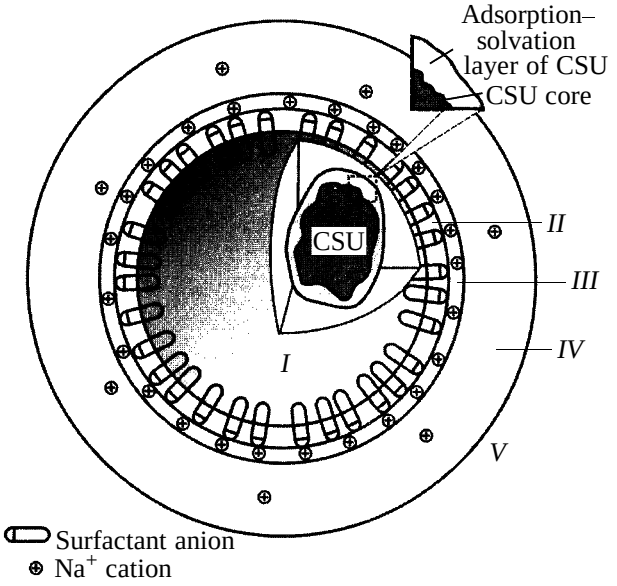


Fig. 4. Schematic picture of the oil particle in direct emulsion: (*I*) dispersed phase aggregate, (*II*) adsorption layer of the potential-determining ions, (*III*) adsorption layer of the counterions, (*IV*) diffusion layer of the counterions, and (*V*) dispersion medium (aqueous solutions of surfactants and electrolytes).

More rigorous conclusions about the relationships in the turbulent flow of direct oil emulsions in the presence of PA requires, in the first stage of analysis, knowledge of the effective concentrations of the PA in the dispersion (aqueous) medium and on the surface of the dispersed phase particles and, hence, data on adsorption of the macromolecules on the dispersed phase particles [20]. Table 2 presents selected data concerning adsorption in the 10% direct oil emulsion. Compared to adsorption of anionic copolymers of acrylamide on solid model adsorbents like ocher and kaolin with negatively charged dispersed phase particles [21], the coefficient A of adsorption of close in composition anionic copolymers of acryalmide on the oil particles is much smaller. This is due to two

factors, namely, a high density of the negative charge on the dispersed phase particles, generated by the anions of the stabilizer, and the already mentioned specific features of the interface surface (liquid state of aggregation), which creates additional problems with fixing negatively charged macroions of the polymeric additive on the oil particle surface [20].

CONCLUSIONS

(1) Water-soluble anionic copolymers of acrylamide, introduced into direct oil emulsions, sharply (by up to 50%) decrease the hydraulic resistance of turbulent streams.

(2) The influence of the polymeric additive concentration and the turbulent stream velocity of direct oil emulsions on the Toms effect was analyzed quantitatively. Reduced Toms effect is only weakly dependent on the composition of direct oil emulsions and is close to that of purely aqueous media.

REFERENCES

1. Zvereva, T.V., Chelintsev, S.N., and Yakovlev, E.I., in *Modelirovanie truboprovodnogo transporta neftekhimicheskikh proizvodstv* (Simulation of Pipeline Transportation in Petrochemical Productions), Moscow: Khimiya, 1987.
2. Brezitskii, S.V., Medvedev, A.P., *et al*., *Neft. Khoz*., 2002, no. 12, pp. 106–110.
3. Tronov, V.P., *Promyslovaya podgotovka nefti* (Pretreatment of Oil at Oil Fields), Kazan: Fen, 2000.
4. Tumanyan, B.P., *Nauchnye i prikladnye aspekty teorii neftyanykh dispersnykh sistem* (Scientific and Applied Aspects of the Theory of Crude Oil Dispersed Systems), Moscow: Tekhnika, 2000.
5. Syunyaev, Z.I., Syunyaev, R.Z., and Safieva, R.Z., in *Neftyanye dispersnye sistemy* (Oil Dispersed Systems), Moscow: Khimiya, 1990.
6. Movsumzade, E.M., Mastobaev, B.N., Dmitrieva, T.V., and Zorina, S.R., *Proizv. Ispol'z. Elastom.*, 2000, no. 5, pp. 22–25.
7. Small, S.R., *Neft', Gaz Neftekhim. Rubezhom*, 1986, no. 7, pp. 60–63.
8. Nesyn, G.V., Manzhai, V.N., and Ilyushnikov, A.V., *Inzh.-Fiz. Zh.*, 2003, vol. 76, no. 3, pp. 142–146.
9. Gareev, M.M., Nesyn, G.V., and Manzhai, V.N., *Neft. Khoz.*, 1992, no. 10, pp. 30–33.
10. Myagchenkov, V.A and Chichkanov, S.V., *Neft. Khoz.*, 2004, no. 1, pp. 93–95.
11. Poraiko, I.N., *Primenenie poliakrilamida v tekhnologicheskikh protsessakh, svyazannykh s dobychei nefti: tematicheskii nauchno-tekhnicheskii obzor* (Application of Polyacrylamide to Processes Involved in Oil Extraction: a Topical Scientific and Technical Review), Moscow: VNIIOENG, 1974.
12. Virk, P.S., Merril, E.W., Mickley, H.S, *et al*., *J. Fluid Mech.*, 1967, vol. 30, pp. 305–328.
13. Min, T., Yoo, J.Y., Choi, H., and Joseph, D.D., *J. Fluid Mech.*, 2003, vol. 486, pp. 213–238.
14. Myagchenkov, V.A. and Chichkanov, S.V., *Zh. Prikl. Khim.*, 2003, vol. 76, no. 11, pp. 1901–1905.
15. Mjagchenkov, V.A., Chichkanov, S.V., Proskurina, V.E., and Krupin, S.V., *Georesources*, 2002, no. 6, pp. 19–23.
16. Myagchenkov, V.A., Chichkanov, S.V., Proskurina, V.E., and Myagchenkov, A.V., *Zh. Prikl. Khim.*, 2002, vol. 75, no. 9, pp. 1517–1520.
17. Brestkin, Yu.V., Frenkel, S.Ya., Zoolshoev, Z.F., *et al*., *Vysokomol. Soedin., Ser. A, B*, 1994, vol. 36, no. 8, pp. 1281–1286.
18. Pogrebnyak, V.G. and Naumchuk, N.V., *Inzh.-Fiz. Zh.*, 1995, vol. 68, no. 1, pp. 146–148.
19. Abramova, L.I., Baiburdov, T.A., Grigoryan, E.P., *et al*., *Poliakrilamid* (Polyacrylamide), Moscow: Khimiya, 1992.
20. Lipatov, Yu.S. and Sergeeva, L.M., in *Adsorptsiya polimerov* (Polymer Adsorption), Kiev: Naukova Dumka, 1984.
21. Myagchenkov, V.A., Baran', Sh., Bekturov, E.A., and Bulidorova, G.V., *Poliakrilamidnye flokulyanty* (Polyacrylamide Flocculants), Kazan: Kazan. Gos. Tekhnol. Univ., 1998.

Russian Journal of Applied Chemistry, Vol. 78, No. 3, 2005, pp. 506–510. Translated from Zhurnal Prikladnoi Khimii, Vol. 78, No. 3, 2005, pp. 512–516.
Original Russian Text Copyright © 2005 by Ivanov, Savel'eva, Yudina, Lomovskii.

CHEMISTRY OF FOSSIL FUEL

Evolution of Composition and Properties of Lipids of Peat in Mechanochemical Treatment

A. A. Ivanov, A. V. Savel'eva, N. V. Yudina, and O. I. Lomovskii

Institute of Petroleum Chemistry, Siberian Division, Russian Academy of Sciences, Tomsk, Russia
Institute of Solid State Chemistry and Mechanochemistry, Siberian Division, Russian Academy of Sciences, Novosibirsk, Russia

Received November 15, 2004

Abstract—Effects of mechanical abrasion and applied shock in the presence of cellulolytic enzyme and NaOH on the yield and properties of peat lipids are studied.

Plant raw materials, among them peat, are structured composites containing fat- and water-soluble compounds, and their specific features should be taken into account in developing efficient processes for recovering bioactive components. Cell walls of plants consist essentially of lipids. To destoy and dissolve spacer lipid structures, solvent extraction is mostly used.

Mechanical treatment also promotes degradation of the lipid structures, thus facilitating subsequent recovery of water-soluble components. Mechanochemical treatment not only initiates degradation of the lipid structures, but also provides transportation of a chemical just into cells [1, 2]. Study of the evolution in the composition and properties of lipids in the course of such a treatment is of particular interest in view of their applications as a source of bioactive substances and development of physiological action preparations [3–5].

In this study we examined the effect of mechanochemical treatment on the composition and properties of lipids from high-moor and valley peats.

EXPERIMENTAL

As raw material we used peat of two kinds: high-moor peat of the Temnoe deposit (Tomsk oblast) classified with the peat-moss group with low degree of degradation (5 wt %) and low ash content (4 wt %), and valley wood peat of the Taganskoe deposit (Tomsk oblast) with high degree of degradation (30 wt %) and high ash content (25 wt %).

Mechanochemical treatment of peat was carried out in mill activators of two types: VTsM-10 flow vibratory vapart mill activator and APF-4 planetary mill with 10-mm steel balls in both cases. In the VTsM-10 mill activator, the ball acceleration was 180 m s^{-2} and treatment time, 2 min, and in the APF-4 planetary mill, 200 m s^{-2} and 2 min. These apparatuses differ in the nature (abrasion and applied shock, respectively) and intensity of action. Peat sample preparation was performed under various conditions: no mechanical treatment; mechanical activation, but no chemicals; and mechanical activation in the presence of chemicals [cellulolytic enzyme celloviridine (CV) or solid alkali].

Lipids were extracted from the initial activated peat samples with chloroform under stirring for 1 h. Then the solvent was removed in a rotary evaporator at 30°C and a residual pressure of 0.5 Pa [6].

The content of antioxidants c_{AO} and inhibiting rate constants k_7 were determined from the data on the kinetics of oxidation of cumene at 60°C and constant initiation rate $W_i = 6.8 \times 10^{-8}$ mol l^{-1} s^{-1}. As an initiator we used azobis(isobutyronitrile). The experiments were carried out on an automated gasometric system for measuring microconsumption of oxygen. The bubble volume was constant (10 ± 0.2 μl) throughout the experiment. The time dependence of the amount of oxygen consumed was processed using a specially designed computer program and was represented as an integral kinetic curve (Fig. 1) divided into linear sections: (1) linear circuit break and (2) uninhibited oxidation. In semilogarithmic coordinates, the first section represents a straight line characterized by specific induction period τ. The AO concentration (mol kg^{-1}) was calculated from the relationship

$$c_{AO} = W_i\tau/P,$$

1070-4272/05/7803-0506© 2005 Pleiades Publishing, Inc.

Table 1. Yield and antioxidant properties of lipids

Peat	c_l, wt %	$c_{AO} \times 10^2$, mol kg^{-1}		$K \times 10^4$, l mol^{-1} s^{-1}		W,* ml min^{-1}
		AO_1	AO_2	$^1k_7$	$^2k_7$	
High-moor peat (VTsM)						
Initial	2.8	24.1	14.9	0.69	0.55	98
Activated in the presence of an additive:						
none	1.9	31.0	15.0	1.75	0.82	125
0.5 wt % CV	1.9	29.2	22.8	0.78	0.31	115
3.0 wt % NaOH	0.6	28.3	19.7	1.41	0.55	108
High-moor peat (APF)						
Activated in the presence of an additive:						
none	1.2	29.2	37.8	0.53	0.40	90
0.5 wt % CV	3.5	28.0	40.0	0.77	0.50	85
3.0 wt % NaOH	2.1	37.5	37.5	0.70	0.45	90
Valley peat (VTsM)						
Initial	0.8	27.5	30.5	0.81	0.60	112
Activated in the presence of an additive:						
none	0.6	39.4	17.2	0.78	0.42	123
0.5 wt % CV	0.6	31.1	18.3	1.25	0.45	120
3.0 wt % NaOH	0.5	30.2	17.0	1.25	1.09	123
Valley peat (APF)						
Activated in the presence of an additive:						
none	0.5	30.5	31.7	0.85	0.52	106
0.5 wt % CV	1.0	29.2	33.1	1.05	0.57	98
3.0 wt % NaOH	0.4	31.4	20.2	0.95	0.75	102

* Rate of initiated oxidation of cumene (reference) 100 ml min^{-1}.

where W_i is the initiation rate (mol l^{-1} s^{-1}); τ, experimental induction period (s); and P, concentration of the sample to be analyzed (kg l^{-1}).

The inhibition rate constants $^1k_7$ and $^2k_7$ were estimated from the parameters of the corresponding linear sections of the kinetic curve [7–9].

The composition of normal and isoprene hydrocarbons was studied by TLC on Silufol plates and also by GLC (24-m capillary column, SE-54 stationary phase, programmed heating from 100°C at a rate of 3 deg min^{-1}).

Mechanical activation, particularly in the presence of chemicals (NaOH and CV), affected the yield and characteristics of the major components of peat. Previously we studied the effect of abrasion action on the group and fraction composition of peat and catalytic properties of water-soluble and humic preparations [10, 11]. It was demonstrated that mechanochemical activation increases the yield and catalytic activity of humics. The extent and direction of transformations in lipids in relation to the kind of peat and conditions of mechanical activation can be judged from the changes occurring in the composition of liposoluble components and their antioxidant properties.

Our results reveal that the yield of lipids strongly depends on the activation conditions of peat (Table 1).

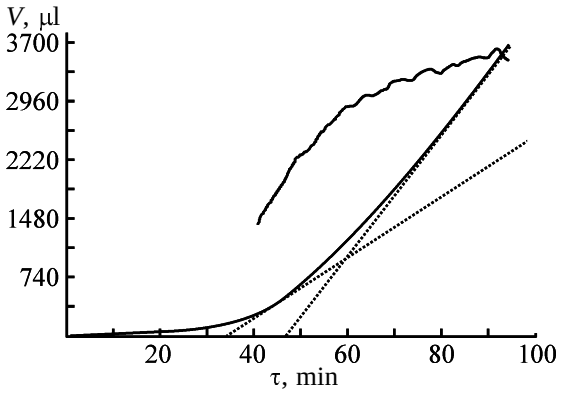


Fig. 1. Kinetic curve of initiated oxidation of cumene in the presence of lipids from high-moor peat. (*V*) Volume of oxygen consumed and (τ) treatment time.

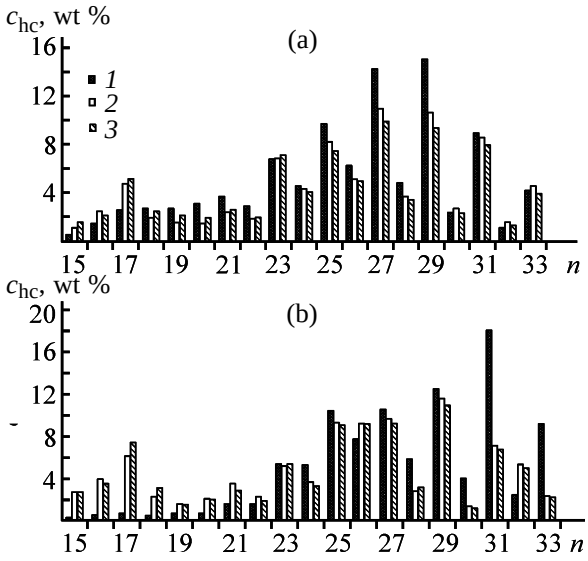


Fig. 2. Chain-length distribution of normal hydrocarbons in lipids of (a) high-moor and (b) valley peat activated in VTsM-10. (c_{hc}) Hydrocarbon concentration and (*n*) number of carbon atoms. Peat: (*1*) initial, (*2*) mechanically activated (no chemicals), and (*3*) activated in the presence of the enzyme.

Activation of high-moor and valley peat in VTsM decreased the yield of lipids c_l, the trend being more pronounced for high-moor peat. Valley wood peat is characterized by low content of liposoluble components; their yield slightly decreases upon activation, depending on the activation conditions. The increase in the yield of lipids after shock activation in APF-4 in the presence of CV can be attributed to degradation of the base cellulose and hemicellulose network in the initial raw material and also to facilitated interaction with the solvent. Activation of both high-moor and valley peat in the presence of NaOH decreases the total yield of liposoluble components by virtue of formation and removal of water-soluble compounds. This phenomenon can be explained taking into account the structure of lipid molecules representing glycoglycerolipids. On the one hand, they consist of long-chain hydrophobic hydrocarbon fragments and, on the other hand, of more compact hydrophilic fragments related to alcohols, carbohydrates, acids, and phenols. Such amphiphilic molecules form associates whose degradation depends on the kind of chemicals and mechanical activation.

Mechanical activation primarily affects long hydrocarbon chains of lipids as the most thermodynamically unstable fragments of the indicated associates [12]. Gas–liquid chromatographic analysis of peat lipids revealed the presence of normal alkanes C_{15}–C_{33} with dominating odd hydrocarbons over the range C_{23}–C_{33}. Isoprene hydrocarbons are represented essentially by pristane (*i*-C_{19}) and phytane (*i*-C_{20}). The relative concentrations of hydrocarbons c_{hc} and their chain-length distribution in lipids depend on the kind of peat and activation procedure. Figure 2 clearly shows that, for the samples obtained from activated peat, the concentration maximum in the distribution curve is shifted toward shorter-chain hydrocarbons, and a second maximum appears near C_{17}. These alkanes are formed as a result of cleavage of C–C bonds in long aliphatic chains. Changes in the composition of hydrocarbons during activation can be characterized by the parameters given in Table 2. A decrease in the odd index K_{odd} and C_{17}/C_{27} ratio and an increase in the concentration of normal alkanes C_{15}–C_{17} characterize the extent of mechanochemical degradation [13, 14]. In valley peat, the maximal degradation is observed for paraffins C_{31}–C_{33}, resulting in a considerable increase in the yield of alkanes C_{15}–C_{17}. Activation of valley peat in the presence of NaOH resulted in considerable transformation of hydrocarbons (Table 2). The content of alkanes C_{15}–C_{17} and C_{17}/C_{27} ratio increased by a factor of 10. The parameters *n*-C_{17}/*i*-C_{19} and *n*-C_{18}/*i*-C_{20} decreased in the activated peat samples, suggesting increase in the content of pristane and especially of phytane as a result of isomerization.

Lipids are characterized by high content of antioxidants inherited from peat-forming plants and transformed as a result of biochemical reactions occurring in peat deposit. The antioxidant activity in lipids is exhibited by compounds with labile hydrogen atom (phenols, carotinoids, and amino acids). In lipids separated from both kinds of peat, we found two groups of antioxidants (AO_1 and AO_2) different in their reactivity, which is typical of natural compounds. Table 1 includes the inhibition rate constants ${}^1k_7$ and ${}^2k_7$ determined to within 10% and characterizing the reactivity of AO_1 and AO_2. The data on the antioxidant activity show that, in lipids separated from untreated peat, AO_1 and AO_2 exhibit similar ${}^1k_7$ and ${}^2k_7$. In all the samples activated in VTsM-10, the amount of AO_1 and ${}^1k_7$ increased, whereas the AO_2 content and reactivity mostly decreased (Table 2).

Activation of peat in APF-4 strongly increased the total content of antioxidants, primarily by virtue of increasing AO_2 content (Table 1). The reactivity of antioxidants was found to be lower than in the case of activation in VTsM, as demonstrated by lower ${}^1k_7$ and ${}^2k_7$. The maximal content of antioxidants was found in lipids separated from peat activated in the presence

Table 2. Evolution of the composition of alkanes in lipids in the course of activation of peat

Peat	n-C_{17}/n-C_{27}	ΣC_{15}–C_{17}	n-C_{17}/i-C_{19}	n-C_{18}/i-C_{20}	K_{odd}
High-moor peat					
Initial	0.17	4.2	1.66	1.09	3.14
Activated in the presence of an additive:					
none	0.43	8.4	1.33	0.80	2.87
0.5 wt % CV	0.51	8.8	1.25	0.80	2.80
3.0 wt % NaOH	0.60	8.9	1.14	0.75	2.73
Valley peat					
Initial	0.06	1.5	2.54	4.20	2.70
Activated in the presence of additives:					
none	0.62	12.8	1.56	0.73	1.94
0.5 wt % CV	0.79	13.7	1.49	0.85	1.88
3.0 wt % NaOH	0.83	13.9	1.36	0.80	1.51

of NaOH. The final rate of uninhibited oxidation of cumene changed after full consumption of antioxidants. Most of the peat lipids decreased the oxidation rate after completion of the induction period [5]. Activation of both kinds of peat in VTsM imparts additional antioxidant capacity to lipids. Table 1 shows that the final oxidation rate amounts to 108–125 ml min^{-1}. Lipids from peat activated in APF reduce the final oxidation rate, suggesting that, depending on the conditions, activation results in degradation of terminal alkyl radicals in the lipid associates with formation of new associates different in their antioxidant characteristics.

CONCLUSIONS

(1) The yield and composition of lipids depend on the conditions of mechanical activation of peat. The yield slightly increases in the presence of celloviridine under shock activation and decreases in all other cases.

(2) Mechanochemical activation results in degradation of high-molecular-weight n-alkanes C_{27}–C_{33} in lipids of high-moor and valley peat with formation of shorter-chain hydrocarbons (C_{15}–C_{17}).

(3) Mechanochemical activation of high-moor and valley peat increases the total antioxidant content in lipids. Activation in the vibratory vapart mill increases the amount of antioxidants of higher reactivity, whereas shock activation produces antioxidants of lower reactivity.

ACKNOWLEDGMENTS

The work was supported by the grants from the Siberian Division, Russian Academy of Sciences (Integrated Project no. 35) and Civilian Research and Development Foundation (project no. 3H455-04).

REFERENCES

1. Bel'kevich, P.I., Gaiduk, K.A., Zuev, T.T., *et al.*, *Torfyanoi vosk i soputstvuyushchie produkty* (Peat Wax and Concomitant Products), Minsk: Nauka i Tekhnika, 1977.
2. Bel'kevich, P.I., Golovanov, N.G., and Dolidovich, E.F., *Khimiya ekstraktivnykh smol torfa i burogo uglya* (Chemistry of Extractive Resins from Peat and Brown Coal), Minsk: Nauka i Tekhnika, 1985.
3. Yudina, N.V., Pisareva, S.I., and Saratikov, A.S., *Mezhdunarodnaya konferentsiya "Poisk, razrabotka i vnedrenie novykh lekarstvennykh sredstv"* (Int. Conf. "Searching for, Developing, and Introducing Novel Medicines), Tomsk, June 27–29, 2000, Tomsk: Tomsk. Tsentr Nauchno-Tekh. Inf., 2000, pp. 72–74.
4. *Torf v narodnom khozyaistve* (Peat in National Economy), Sokolov, L.B., Ed., Moscow: Nedra, 1988.
5. Naumova, G.V., Raitsina, G.I., and Lyakh, V.V., *Primenenie torfa i produktov ego khimicheskoi pererabotki v narodnom khozyaistve* (Applications of Peat and Its Chemical Processing Products in National Economy), Kaliningrad: Kaliningrad Univ., 1980.
6. Kates, M., *Techniques of Lipidology, Isolation, Analysis, and Identification of Lipids*, New York: North-Holland, 1972.

7. Tsepalov, V.F., Kharitonova, A.A., Gladyshev, G.P., *et al*., *Kinet. Katal*., 1977, vol. 18, no. 5, pp. 1261–1266.
8. Roginskii, V.A., *Fenol'nye antioxidanty* (Phenolic Antioxidants), Moscow: Nauka, 1988.
9. Burkova, V.N., Pisareva, S.I., and Yudina, N.V., *Geokhimiya*, 1998, no. 11, pp. 1164–1171.
10. Yudina, N.V., Zvereva, A.V., and Lomovskii, O.I., *Khim. Tverd. Topl*., 2002, no. 5, pp. 3–10.
11. Yudina, N.V., Savel'eva, A,V., Ivanov, A.A., Lomovskii, O.I., *Zh. Prikl. Khim*., 2004, vol. 77, no. 1, pp. 48–53.
12. Ovchinnikov, Yu.A., *Bioorganicheskaya khimiya* (Bioorganic Chemistry), Moscow: Prosveshchenie, 1987.
13. Tissot, B.P. and Welte, D.H., *Petroleum Formation and Occurrence: A New Approach to Oil and Gas Exploration*, Berlin: Springer, 1978.
14. Petrov, A.A., *Uglevodorody nefti* (Petroleum Hydrocarbons), Moscow: Nauka, 1984.

Russian Journal of Applied Chemistry, Vol. 78, No. 3, 2005, pp. 511–513. Translated from Zhurnal Prikladnoi Khimii, Vol. 78, No. 3, 2005, pp. 517–519.
Original Russian Text Copyright © 2005 by Yurchenko, Ivashchenko, Pilipenko, Pogrebova.

BRIEF COMMUNICATIONS

Pyridinium Halides and Their Mixtures as Inhibitors of Steel Corrosion in Sulfuric Acid Solutions

R. I. Yurchenko, S. V. Ivashchenko, T. N. Pilipenko, and I. S. Pogrebova

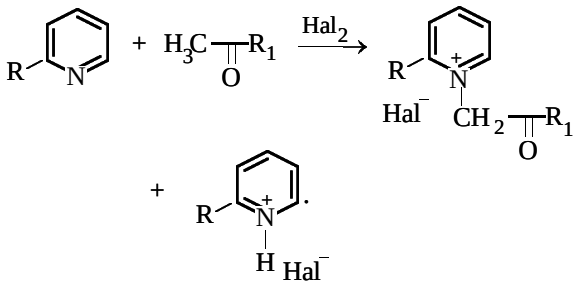
Kiev Polytechnic Institute, National Technical University of Ukraine, Kiev, Ukraine

Received October 15, 2004

Abstract—Mixtures of 1-acylmethylpyridinium halides with equimolar amounts of pyridinium halides were prepared by the Ortoleva–King reaction. The inhibiting effect of various pyridinium halides and their mixtures on corrosion of steel in sulfuric acid solutions was studied.

Previously we found [1, 2] that some of 1-phenacylmethylpyridinium bromides are relatively effective inhibitors of the acid corrosion of steel, especially at elevated temperatures. These compounds were prepared by alkylation of appropriate pyridine derivatives with ω-bromoacetophenones.

Corrosion inhibitors of this type can be prepared by the Ortoleva–King reaction [3], i.e., the reaction of pyridine derivatives, iodine, and compounds containing labile hydrogen atoms. Since pyridine and its derivatives act as both reagents and acceptors of the forming hydrogen halide, this reaction gives, along with the desired pyridinium salts, also the corresponding pyridinium halides. For example, the reaction of pyridine, acetophenone, and bromine yields an equimolar mixture of 1-phenacylmethylpyridinium bromide and pyridinium bromide:



When the solubility of the resulting salts is strongly different, they can be separated to prepare individual 1-acylmethylpyridinium halides. For example, treatment with alcohol of the salt mixture formed in the reaction of pyridine or 2-methylpyridine with acetophenone in the presence of bromine or iodine allows preparation of the corresponding 1-phenacylmethylpyridinium bromides and iodides with high yields. In many cases, the Ortoleva–King reaction strongly simplifies synthesis of 1-acylmethylpyridinium halides: it can be performed in one step without using halomethyl ketones (lacrimators) and allows preparation of pyridinium salts that cannot be obtained by common methods. Moreover, this reaction yields acylmethylpyridinium halides in mixtures with pyridinium halides, which can enhance their corrosion-protective effect [4].

EXPERIMENTAL

The synthesis was performed according to the procedure described in [3]. The corrosion-protective effect of the compounds prepared was evaluated using the coefficients of corrosion deceleration γ and degree of corrosion protection Z, calculated from the weight loss of 08KP steel samples in 3 M sulfuric acid at 20 and 60°C and inhibitor concentration of 1×10^{-2} M (see table).

The coefficient of corrosion inhibition of 1-phenacylmethylpyridinium bromide (I-1) at 20°C is 11.3 [1]. This compound is formed by the Ortoleva–King reaction from pyridine, acetophenone, and bromine in a mixture with pyridinium bromide and the coefficient of corrosion inhibition of this mixture (inhibitor I-1a) is as high as 18.0. In the case of iodine, the reaction yields 1-phenacylmethylpyridinium iodide (I-2) and pyridinium iodide; the first compound, when isolated pure, exhibits the coefficient of inhibition of 17.7 at 20°C. The coefficient of corrosion inhibition of the resulting mixture (I-2a) is 24.3. In the case of 1-phenacylmethyl-2-methylpyridinium bromide (I-3), the coefficients of corrosion inhibition are 15.5 and 209.1 [1], and for its mixture with

1070-4272/05/7803-0511 © 2005 Pleiades Publishing, Inc.

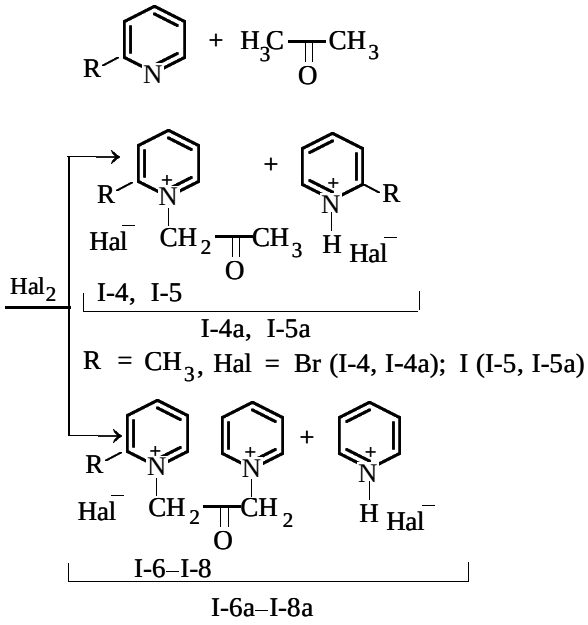
Coefficients of corrosion inhibition γ and degree of corrosion protection *Z* of 08KP steel in 3 M H_2SO_4 in the presence of acylmethylpyridinium halides (I-1–I-8) and their mixtures with the corresponding pyridinium halides (I-1a–I-8a)

Inhibitor	20°C		60°C		Inhibitor	20°C		60°C	
	γ	*Z*, %	γ	*Z*, %		γ	*Z*, %	γ	*Z*, %
I-1	11.7	91.45	–	–	I-1a	18.0	94.44	–	–
I-2	17.7	94.35	–	–	I-2a	24.3	95.88	–	–
I-3	15.5	93.55	209.1	99.52	I-3a	21.4	95.33	237.8	99.58
I-4	19.6	94.90	223.9	99.55	I-4a	22.5	95.56	250.3	99.60
I-5	–	–	–	–	I-5a	23.1	95.67	594.6	99.83
I-6	–	–	–	–	I-6a	22.0	95.45	237.9	99.58
I-7	21.4	95.33	333.8	99.70	I-7a	23.1	95.67	464.0	99.78
I-8	–	–	–	–	I-8a	25.0	96.00	864.9	99.88

2-methylpyridinium bromide, 21.4 and 237.9 at 20 and 60°C, respectively.

The reaction with acetone can be performed through one or two methyl groups. The reaction of 2-methylpyridine, acetone, and bromine or iodine in a 2 : 1 : 1 ratio yields the corresponding 1-acetylmethylpyridinium bromide (I-4) or iodide (I-5) in a mixture with 2-methylpyridinium bromide or iodide (I-4a and I-5a). We failed to isolate pure compounds I-4 and I-5 because of their close solubilities with the corresponding pyridinium salts. Pure I-4 was prepared by a common procedure, i.e., by alkylation of 2-methylpyridine with α-bromoacetone. The reaction of pyridine or 2-methylpyridine, acetone, and bromine or iodine (4 : 1 : 2 molar ratio) yields bis-salts (I-6–I-8) in the form of mixtures with the corresponding pyridinium salts (inhibitors 1-6a–I-8a, respectively). Pure I-7 was prepared by treatment of the reaction mixture with alcohol. As seen from the table, the corrosion-protective power of I-7a is higher than that of individual compound I-7 by a factor of 1.5.

Our experimental results show that the corrosion-protective effect of 1-phenacylmethylpyridinium halides increases in the presence of equimolar amounts of the corresponding pyridinium halides and on passing from bromine to iodine. This trend is the most pronounced at elevated temperatures. The products of reaction of pyridine or 2-methylpyridine with acetone and iodine (I-5a, I-7a, and I-8a) are the most effective inhibitors exhibiting at 60°C the coefficients of corrosion inhibition of 594.6, 464.0, and 864.9 and the degrees of corrosion protection of 99.83, 99.48, and 99.88%, respectively:



R = CH_3, Hal = Br (I-4, I-4a); I (I-5, I-5a)

R = H, Hal = Br (I-6, I-6a), I (I-7, I-7a)

R = CH_3, Hal = I (I-8, I-8a)

CONCLUSIONS

(1) The Ortoleva–King reaction essentially simplifies synthesis of 1-acylmethylpyridinium halides exhibiting corrosion-protective properties and allows preparation of pyridinium salts that are difficultly accessible by common procedures.

(2) The inhibiting effect of the mixtures of pyridinium salts formed by the Ortoleva–King reaction is stronger than that of the individual acylmethylpyridinium halides. The best inhibitors at a concentration of 1×10^{-2} provide the coefficients of corrosion

inhibition and the degrees of corrosion protection of 08 KP steel at 60°C in 3 M sulfuric acid of 464.0–864.9 and 99.58–99.88%, respectively.

REFERENCES

1. Yurchenko, R.I., Pogrebova, I.S., Pilipenko, T.N., and Kras'ko, E.M., *Zh. Prikl. Khim.*, 2003, vol. 76, no. 11, pp. 1814–1818.
2. Yurchenko, R.I., Pogrebova, I.S., Pilipenko, T.N., and Shubina, T.E., *Zh. Prikl. Khim.*, 2004, vol. 77, no. 7, pp. 1132–1136.
3. Yurchenko, R.I. and Vizir, T.A., *Zh. Org. Khim.*, 1979, vol. 15, no. 7, pp. 1525–1532.
4. Podobaev, N.I., Khar'kovskaya, N.L., Korotkikh, E.V., and Ustinskii, E.N., *Zashch. Met.*, 1980, vol. 16, no. 1, pp. 73–75.

Russian Journal of Applied Chemistry, Vol. 78, No. 3, 2005, pp. 514–515. Translated from Zhurnal Prikladnoi Khimii, Vol. 78, No. 3, 2005, pp. 520–521.
Original Russian Text Copyright © 2005 by Kasimova, Mnatsakanov, Sirota.

BRIEF COMMUNICATIONS

Degradation of Cellulose Triacetate upon Irradiation with Accelerated Electrons

V. Yu. Kasimova, S. S. Mnatsakanov, and A. G. Sirota

St. Petersburg State University of Movie and Television, St. Petersburg, Russia

Received December 9, 2004

Abstract—The radiation-chemical yield G of degradation of cellulose triacetate was calculated from the viscometric data. The radiation dose providing formation of cellulose triacetate with the modified structure and with the desired reactivity was determined.

The properties of irradiated cellulose and its derivatives were extensively studied [1–8], as these polymers are of principal importance in industry, medicine, and agriculture. Owing to high content of oxygen, cellulose has low radiation resistance. Breakdown of the polymer chain (degradation) is the main result of irradiation of cellulose and its derivatives, which decreases the degree of polymerization and changes structural and mechanical properties, solubility, and reactivity.

In contrast to other cellulose esters and ethers, the effect of irradiation on cellulose acetates (CAs) is poorly studied [7, 8]. At the same time, irradiation of CA can yield an ideally compatible modifier and plasticizer of the acetate film. Insignificant amounts of the irradiated polymer, when added to the film-forming CA solution, can change the supramolecular polymer structure and, in particular, the packing density of macromolecules in the films.

EXPERIMENTAL

In our work we used cellulose triacetate (CT) prepared by the heterogeneous procedure (Svema). Before irradiation, the polymer was dried at 105°C. The cellulose samples were irradiated in air on an ILU-6 installation with accelerated electrons (1.9 MeV) at a dose rate of 0.18 kGy s^{-1}. The sample thickness was 2.5 mm. The samples were irradiated to doses D of 40, 70, and 150 kGy. The viscometric measurements were carried out at 25°C with an Ubbelohde viscometer according to the procedure given in [9] using trichloromethane; the outflow time of the pure solvent was t_0 = 53.7 s. The intrinsic viscosities [η] of the samples are given below:

D, kGy	[η], dl g^{-1}
–	1.83
40	0.80
70	0.56
150	0.29

The polymer degradation can be described using the statistical method [1, 10, 11]. The radiation-chemical yield G of degradation can be calculated from the dependence of the number-average molecular weight of the polymer $\overline{M}_n$ on the absorbed radiation dose [1]:

$$(\overline{M}_n)^{-1} - (\overline{M}_n^0)^{-1} = \frac{GD}{10^2 N_A}, \quad (1)$$

where $\overline{M}_n^0$ is the initial number-average molecular weight of the polymer, D is the radiation dose (eV), and N_A is the Avogadro number.

In this work, all the molecular weights of the CT

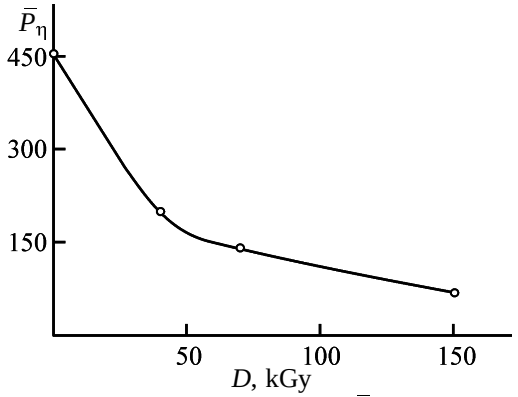


Fig. 1. Degree of CT polymerization $\bar{P}_\eta$ as a function of the radiation dose D.

1070-4272/05/7803-0514© 2005 Pleiades Publishing, Inc.

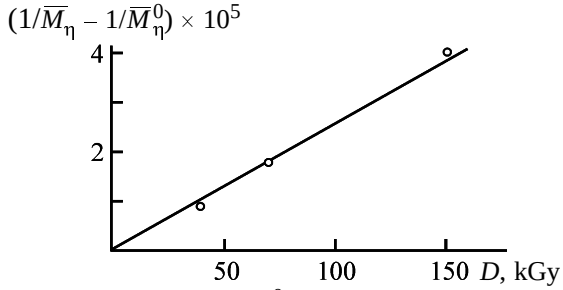


Fig. 2. Plot of $1/\overline{M}_\eta - 1/\overline{M}_\eta^0$ vs. the absorbed radiation dose D.

samples were determined from the viscosity of the dilute solutions. For CT in trichloromethane, the coefficient K in the Mark–Kuhn–Houwink equation and coefficient α are 1.4×10^{-5} and 1 [12], respectively. The dependence of the viscosity-average degree of CT polymerization $\overline{P}_\eta$ on the radiation dose is shown in Fig. 1.

The viscosity-average molecular weight $\overline{M}_\eta$ can be determined using $\overline{M}_n$ from the following equation [11]:

$$\overline{M}_\eta = \overline{M}_n[(\alpha + 1)\Gamma(\alpha + 1)]^{1/\alpha}. \quad (2)$$

At $\alpha = 1$, $\Gamma(\alpha + 1) = 1$ and $\overline{M}_\eta = 2\overline{M}_n$. Then the yield of degradation G can be calculated as follows:

$$(\overline{M}_\eta)^{-1} - (\overline{M}_\eta^0)^{-1} = \frac{GD}{2 \times 10^2 N_A}, \quad (3)$$

where $\overline{M}_\eta^0$ is the viscosity-average molecular weight of the polymer.

The dependence of $1/\overline{M}_\eta - 1/\overline{M}_\eta^0$ on the absorbed radiation dose is shown in Fig. 2. As in the case of cellulose [1], this dependence is linear. The degradation yield calculated from the curve tangent is 4.7 break events per 100 eV. As expected, this value is smaller than that in the case of cellulose, because the acetyl groups decelerate the polymer degradation.

CONCLUSIONS

(1) The radiation-chemical yield of degradation of cellulose triacetate is relatively high, and its radiation modification is feasible.

(2) Since relatively low-molecular-weight polymers are used to prepare film materials, 40-kGy dose seems to be sufficient. Irradiation of cellulose triacetate to higher doses is undesirable, because it can change moisture absorption and mechanical properties of the resulting material.

REFERENCES

1. Ershov, B.G., *Usp. Khim.*, 1998, vol. 67, no. 4, pp. 353–375.
2. Komarov, V.B., Gordeev, A.V., Samuilova, S.D., *et al.*, *Khim. Vys. Energ.*, 1999, vol. 33, no. 3, pp. 189–193.
3. Sharpatyi, V.A., Shapilov, A.A., and Pintelin, S.N., *Khim. Fiz.*, 2001, vol. 20, no. 12, pp. 19–24.
4. Muratov, A., Vakhidov, N., Razikov, K.Kh., *et al.*, *Vysokomol. Soedin.*, 1975, vol. 17, no. 8, pp. 819–824.
5. Kaputskii, F.N., Kaputskii, V.E., Mortina, T.P., *et al.*, *Zh. Prikl. Khim.*, 1975, vol. 48, no. 9, pp. 2045–2050.
6. Wach, R.A., Mitomo, H., Yoshii, F., and Kume, Y., in *Proc. Takasaki Symp. on Radiation Application of Natural Polymers in Asia*, October 1–2, 2001, Takasaki (Japan): JAERI, 2002, pp. 72–82.
7. Pasal'skii, B.K., Moshkovskii, N.S., Staren'kii, A.G., and Lavrentovich, Ya.I., *Khim. Vys. Energ.*, 1977, vol. 11, no. 5, pp. 363–364.
8. Timofeeva, V.G., Senyukov, V.D., Borisenko, I.V., *et al.*, *Vysokomol. Soedin.*, 1979, vol. 21, no. 8, pp. 586–591.
9. Rafikov, S.R., *Metody opredeleniya molekulyarnykh vesov i polidispersnosti vysokomolekulyarnykh soedinenii* (Methods for Determining Molecular Weights and Polydispersity of Macromolecular Compounds), Moscow: Akad. Nauk SSSR, 1963.
10. Frenkel', S.Ya., *Vvedenie v statisticheskuyu teoriyu polimerizatsii* (Introduction to Statistical Theory of Polymerization), Moscow: Nauka, 1965.
11. Charlesby, A., *Atomic Radiation and Polymers*, New York: Pergamon, 1960.
12. Krasovskii, A.N., Polyakov, D.N., and Mnatsakanov, S.S., *Vysokomol. Soedin., Ser. A.*, 1995, vol. 37, no. 9, pp. 1551–1560.

Russian Journal of Applied Chemistry, Vol. 78, No. 3, 2005, p. 516. Translated from Zhurnal Prikladnoi Khimii, Vol. 78, No. 3, 2005, p. 522.
Original Russian Text Copyright © 2005 by Vetyukov, Lebedev, Morachevskii.

OBITUARIES

Nikolai Andreevich Kaluzhskii (1925–2005)

Nikolai Andreevich Kaluzhskii, one of the most prominent organizers of the domestic aluminum industry, honored science worker, doctor of technical science, and professor, died of a severe illness on January 9, 2005, at the age of 79. He had headed for many years the All-Union Research and Design Institute of Aluminum, Magnesium, and Electrode Industries (VAMI).

Kaluzhskii was born on November 15, 1925, at Smorodino village (Kursk oblast) into an office workers' family. He started to work in the war years at the age of sixteen. From January 1943 till March 1944 he served in the Soviet Army and took part in action. After being severely wounded, he was demobilized and continued his education.

In 1951, Kaluzhskii graduated with a first-class honors degree from Leningrad Polytechnic Institute as an engineer-metallurgist. During the following three years, he worked his way up from a foreman to production manager at the electrolysis shop of the aluminum plant in Novokuznetsk. Kaluzhskii took part in starting-up the Nadvoitsy aluminum plant (Karelia) in 1954 and became its director in 1956.

From 1960 till 1966 Kaluzhskii occupied executive positions in the Council of Ministers of the Republic of Karelia and in the regional committee of the communist party. Beginning in 1966, and for more than 25 years, Kaluzhskii had been director of VAMI in Leningrad. Designs were made and production facilities were put in service at virtually all aluminum plants constructed in our country in the post-war years under his supervision and with his direct involvement. A particular pronounced contribution was made by Kaluzhskii to the development of theoretical foundations of aluminum manufacture with the use of high-power electrolyzers with burnt anodes. In his doctoral dissertation defended in 1976, Kaluzhskii thoroughly substantiated the feasibility of application of elec-



trolyzers with burnt anodes, operating at currents of up to 260 kA, in the aluminum industry. Kaluzhskii's achievements in equipping with high-performance process apparatus, designing, and putting in operation the Bratsk, Krasnoyarsk, Tajik, and Sayany aluminum plants are remarkable.

Kaluzhskii was a prominent scientist in the field of chemical technology, electrochemistry of melts, powder metallurgy, and composites. He was the author of more than 100 scientific publications, made 95 inventions, and obtained a large number of patents in various countries.

Kaluzhskii was decorated for his research, production, and organizational achievements with high state awards and prizes of the Council of Ministers of the USSR and Government of Russia.

M. M. Vetyukov, O. A. Lebedev, and A. G. Morachevskii

1070-4272/05/7803-0516© 2005 Pleiades Publishing, Inc.

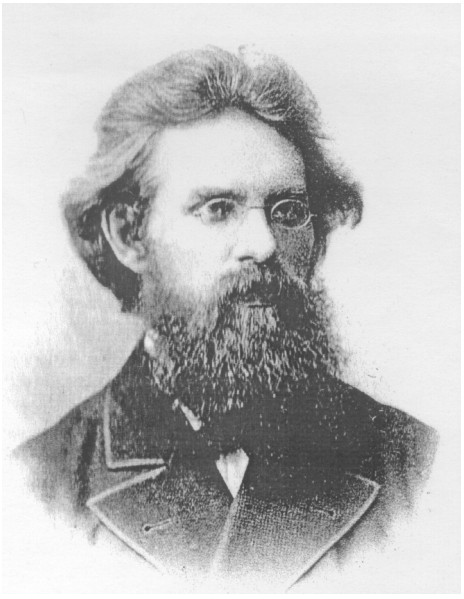
Russian Journal of Applied Chemistry, Vol. 78, No. 3, 2005, pp. 517–518. Translated from Zhurnal Prikladnoi Khimii, Vol. 78, No. 3, 2005, pp. 523–524.
Original Russian Text Copyright © 2005 by Morachevskii.

HISTORY OF CHEMISTRY AND CHEMICAL TECHNOLOGY

Professor Aleksei Lavrent'evich Potylitsyn (to 160th Anniversary of His Birthday)

A.L. Potylitsyn, one of the closest disciples and followers of D.I. Mendeleev, professor of Warsaw University, and later professor, director, and honorary member of Novaya Aleksandriya Institute of Agriculture and Forestry, devoted his research to solution of one of the most important problems of physical chemistry in the second half of the XIX century, that of the driving force of chemical reactions, i.e., chemical affinity, and ways to measure this quantity.

Aleksei Lavrent'evich Potylitsyn was born on March 16 (28), 1845, in Krasnoyarsk into the family of a junior officer of the Yenisei Cossack regiment. The youth received his primary education at Irkutsk military college (military pre-gymnasium), which did not give its graduates the right to enter higher-school institutions. Having graduated from the college, Potylitsyn remained there as a teacher and started to prepare, on his own, for a full gymnasium course examination. In July 1865, at the age of 20, he went to St. Petersburg and, in August of the same year, successfully passed the entrance examination at Larin gymnasium, one of the best male gymnasia of the city. In September 1865, Potylitsyn became a student of Medical-Surgery (later, Military-Medical) Academy. However, he soon went to the natural department of the physicomathematical faculty of St. Petersburg University. At those years, among the teachers of chemical disciplines were A.A. Voskresenskii (1809–1880), N.N. Sokolov (1826–1877), and D.I. Mendeleev (1834–1907), and N.A. Menshutkin (1842–1907) just commenced his pedagogical activities. A.M. Butlerov (1828–1886) became a professor of the University in 1868. As noted by F.F. Selivanov, the author of the only sufficiently full biographical essay about Potylitsyn's life [1], Mendeleev became the favorite teacher of Aleksei Lavrent'evich. The area of Potylitsyn's research was determined already in his student years. At the end of 1872, he graduated from the University and continued studies of the mutual displacement of substances in chemical reactions at Mendeleev's laboratory. In September 1873, Potylitsyn became a staff member (laboratory assistant) at Menshutkin's laboratory, but continued the already commenced studies in his free time. In the autumn of



1876, the young scientist was sent to France, because he was in the state of acute tuberculosis, for treatment and familiarization with works of French chemists. The most favorable impression was produced on Potylitsyn by his acquaintance with A.E. Saint-Clair Deville (1818–1881), a rather well known chemist and member of the Paris Academy of Sciences. In the late summer of 1878, Potylitsyn returned to Russia and resumed his interrupted service and research activities. Together with working at the University, he taught chemistry at the Pavel military college and wrote a textbook on chemistry for higher military educational institutions, which later ran into eight editions.

In December 1879, at the VI Congress of Russian natural scientists and physicians in St. Petersburg, Potylitsyn delivered a report "On the Action of Hydrogen on Halide Salts of Silver and on the Maximum Work Rule," which was of considerable interest for such well-known chemists as Mendeleev, Menshutkin, and G.G. Gustavson (1843–1908). In 1880, after Potylitsyn successfully defended the dissertation "On Methods for Measuring the Chemical Affinity" at St. Petersburg University, a master's degree in chemistry was conferred on him. As was customary in

1070-4272/05/7803-0517 © 2005 Pleiades Publishing, Inc.

those years, the full text of the dissertation was published as a separate edition (St. Petersburg, 1880, 155 pp.). In the same year, he made, together with Mendeleev, a trip to the Caucasus, to familiarize himself with oil fields. As a result of this, and two later (1884 and 1891) trips, Potylitsyn carried out a number of studies concerned with oil and its by-products.

In January 1881, Potylitsyn was appointed a professor of the Institute of Agriculture and Forestry at Novaya Alaksandriya (Lublin province, Poland), and already in July 1882, he was transferred to Warsaw University as an extraordinary professor of chemistry. During his work in Warsaw (1882–1895), Potylitsyn delivered lectures and carried out a large number of studies. In 1886, after Potylitsyn defended his dissertation "On the Importance of the Heat of Salt Formation for Double-Decomposition Reactions" at St. Petersburg University, the degree of a doctor of chemistry was conferred on him. The text of the dissertation was also published (Warsaw, 1888, 101 pp.) In the same year, Potylitsyn becomes an ordinary professor. However, he was appointed director of the Novo-Aleksandriya Institute in September 1895.

In 1900, in view of the difficulties with his family and deterioration of his health, Potylitsyn retired and went to live first to Warsaw and then to St. Petersburg.

The principal area of Potylitsyn's research was, in fact, formulated in his master's dissertation: methods for measuring the chemical affinity. The list of Potylitsyn's scientific publications can be found in [1]. His research activities were analyzed in sufficient detail in the monographs [2–5] and papers by B.Ya. Rozen [6] and R.B. Dobrotin [7]. The main, but far from being the only, objects of Potylitsyn's research were reactions of mutual displacement of halogens from halo derivatives of a number of metals. He studied in detail the reactions of mutual displacement of chlorine and bromine from their compounds with metals. The principal experimental result was that the percentage of displacement of one halogen by another under the experimental conditions was determined. The analysis of the results obtained was based on the position of an element under consideration in Mendeleev's periodic table.

Potylitsyn's experiments convincingly confirmed, among other things, that the reactions occurring with heat release do not go to completion. Thus, it was demonstrated experimentally that the maximum-work principle formulated by M. Berthelot (1827–1907) requires a better definiteness and has applicability limits. It is inapplicable to, in the first place, reactions occurring with consumption of heat.

As noted by Dobrotin [7], the importance of Potylitsyn's experimental studies is not limited to restrictions of the maximum-work principle. A major achievement of the scientist was wide use of data obtained in analysis of reaction equilibria for finding a rational measure of the chemical affinity. Potylitsyn also formulated the concept of the influence exerted by temperature on the direction in which the equilibrium is shifted. This was done before J. van't Hoff (1852–1911) published his studies in this area [1, 8].

Potylitsyn was a strong supporter of Mendeleev's standpoint concerning the principal problems of chemistry at that time and, in particular, the hydrate theory of solutions. It is noted in Potylitsyn's biography [1] that he was keenly interested not only in science, but also in literature and arts (and primarily fine arts).

Potylitsyn died of tuberculosis on February 25 (March 10), 1905, in St. Petersburg. In an article devoted to the death of his disciple, Mendeleev wrote that the name of Aleksei Lavrent'evich Potylitsyn as a chemist-researcher and pedagogue should be preserved in Russian memory. Of particular importance, in Mendeleev's opinion, are Potylitsyn's investigations concerned with the limits to chemical reactions, displacement of one halogen with another, and influence exerted by heats of formation on the course of chemical transformations.

REFERENCES

1. Selivanov, F.F., *Zh. Russk. Fiz.-Khim. O–va., Ch. Chim.*, 1908, vol. 40, no. 7, pp. 1149–1182.
2. Kipnis, A.Ya., *Razvitie khimicheskoi termodinamiki v Rossii* (The Development of Chemical Thermodynamics in Russia), Moscow: Nauka, 1964.
3. Solov'ev, Yu.I., *Ocherki po istorii fizicheskoi khimii* (Essays on the History of Physical Chemistry), Moscow: Nauka, 1964.
4. *Istoriya ucheniya o khimicheskom protsesse: Vseobshchaya istoriya khimii* (History of the Theory of a Chemical Process: General History of Chemistry), Moscow: Nauka, 1981.
5. Solov'ev, Yu.I., *Istoriya khimii v Rossii* (The History of Chemistry in Russia), Moscow: Nauka, 1985.
6. Rozen, B.Ya., *Zh. Fiz. Khim.*, 1954, vol. 28, no. 10, pp. 1854–1858.
7. Dobrotin, R.B., *Vestn. Leningr. Gos. Univ., Ser. Fiz. Khim.*, 1957, no. 16, no. 3, pp. 148–155.
8. Akhumov, E.I. and Rozen, B.Ya., *Zh. Fiz. Khim.*, 1952, vol. 26, no. 9, pp. 1711–1712.

A. G. Morachevskii

Russian Journal of Applied Chemistry, Vol. 78, No. 3, 2005, p. 519.
Original Russian Text Copyright © 2005 by the Editorial Board.

==========

Errata

The authors made the following corrections to the article published in *Zh. Prikl. Khim.*, 2003, vol. 76, no. 11, pp. 1901–1905 (*Russ. J. Appl. Chem.*, 2003, vol. 76, no. 11, pp. 1850–1854).

In formula (7), ω_i/M_i should be replaced by $\omega_i M_i$.

The conclusion should be formulated as follows.

CONCLUSION

The reduced Toms effect in direct oil emulsions in media differing in the ionic strength depends on the molecular weight polydispersity in a complex manner, passing through extrema. This is due to nonadditivity of the contributions from the samples of the copolymer with different molecular weights to the resulting macroscopic Toms effect.

In *Russ. J. Appl. Chem.*, 2005, vol. 78, no. 1, p. 101 and Contents, the name of one of the authors was erroneously given as P. M. Hockridge. Correct is F. M. Hawkridge.

1070-4272/05/7803-0519© 2005 Pleiades Publishing, Inc.

Russian Journal of Applied Chemistry, Vol. 78, No. 4, 2005, pp. 521–537. Translated from Zhurnal Prikladnoi Khimii, Vol. 78, No. 4, 2005, pp. 529–544.
Original Russian Text Copyright © 2005 by Myagchenkov, Chichkanov.

REVIEWS

Toms Effect in Model and Real Systems

V. A. Myagchenkov and S. V. Chichkanov

Kazan State Technological University, Kazan, Tatarstan, Russia

Received November 25, 2004

Abstract—Selected data on use of macromolecular compounds (polymers) as additives that diminish the hydraulic resistance of turbulent fluid flows (Toms effect) are presented. Theoretical and applied (concerning mainly oil production) aspects of the phenomenon are considered.

General evidence concerning the Toms effect. Polymers have played the key role in the development of numerous branches of industry; they can be rightfully named among the motive forces of the technological progress [1]. One of interesting and, at the same time, insufficiently studied phenomena associated with the successful application of polymers is the Toms effect: decrease in the hydraulic resistance of turbulent fluid flows upon introduction of small amounts of macromolecular polymers (on the order of 10^{-3}–10^{-4} wt %) [2, 3]. As a consequence, the flow rate increases at a constant pressure or the pumping pressure decreases at a constant flow rate of the fluid. This phenomenon has been named the Toms effect by the name of the scientist who was the first to study it systematically. This effect, which can be manifested in both aqueous and organic media, is of a particular importance in those branches of industry, in which it is necessary to transport large volumes of fluids, e.g., in oil production in pumping of water, oil, oil products, and oil emulsions (of both direct and reverse types).

History of discovery. A minor amount of guar (polymer of vegetable origin, a variety of caoutchouc) accidentally found its way into a fluid flow in oil pumping through a pipe at an oil refinery in the United States [4]. After that, the maintenance staff noticed that the pumps transporting the oil started to work with a reduced load. Naturally, this phenomenon attracted interest. Primarily, all the events exhibiting any even remote analogy were analyzed. It was found that, occasionally, the speed of ships unexpectedly increased, at a constant driving power, in sea regions with large amounts of plankton of animal or vegetable origin and, after a certain time, returned to its original value. A similar behavior was observed in experiment tanks in tests with rapidly moving ship models, when, in a repeated test with the same model after a certain interval of time, its resistance changed significantly.

The first scientist to commence a serious study of the enigmatic phenomenon was an English chemist B.A. Toms, who reported in 1948 the results of his experiments with dilute solutions of macromolecular polymers with a linear structure of molecules. In these experiments, the friction resistance in a turbulent flow decreased by 50–80% [5].

A comprehensive analysis of the set of experiments carried out by Toms revealed the reason for the dramatic increase in the speed of ships in regions with a high content of plankton. It was found that seaweeds and microorganisms excrete macromolecular compounds (biopolymers), which, when present in water even at low concentrations, markedly reduce the resistance to a body moving in it at a high speed. Subsequent studies revealed that a strong effect is observed not only for biopolymers, but also for polyoxyethylene (POE) and a number of other synthetic water-soluble polymers. It was found experimentally that, in particular, the resistance of water containing even an exceedingly low amount of POE (~0.002% and less) to a rapidly moving body decreased by 30–40%.

This phenomenon primarily attracted the interest of scientists and engineers working in areas of military technology, associated with hydrodynamics. For example, according to by no means complete data, more than 30 foreign scientific institutions were engaged in studies of the influence exerted by polymer additives on the turbulent fluid flow already in 1970. At present, the researchers' interest in this largely enigmatic phenomenon remains keen. A great success in studies of the Toms effect has been achieved by Russian and foreign research teams. The Toms

1070-4272/05/7804-0521 © 2005 Pleiades Publishing, Inc.

effect has found a wide application in oil-production and oil-refining industries, fire engineering, and medicine.

Main hypotheses for the mechanism of the effect. The issues associated with the mechanism of the Toms effect still give rise to heated discussions. Several tens of hypotheses for the possible mechanism have been suggested. These hypotheses for the most part interpret rather one-sidedly only separate aspects of the phenomenon, whereas a theory that would describe in a unified way the mechanism of the Toms effect has not been developed yet.

Let us consider further the most interesting and important studies of the Toms effect, aimed to establish its fundamental aspects.

The rheodynamics of a flow of dilute solutions of POE through thin capillaries has been studied by Naumchuk by methods of laminar and turbulent rheometry with the use of images of fluid flow lines in various radial zones of the flow [6]. On the basis of the experimental results obtained, an original model of the turbulent flow of polymer solutions was suggested. A flow without polymer additives is turbulized by strong outbreaks of a fluid from the laminarized boundary sublayer of a fluid, situated near the wall, into the center of the flow. Introduction of a polymer into the flow results in that strong outbreaks from the "viscous" boundary layer become simply unfavorable for purely energetic reasons. As a result, turbulent momentum transfer in a macroscopic fluid flow becomes less probable, and this leads to a decrease in the hydrodynamic resistance. To confirm the assumptions made, the author presents data obtained in studying the profiles of longitudinal velocity gradients and the dynamic birefringence appearing near the wall surface. A comprehensive analysis of the information obtained shows with certainty that macromolecules undergo conformational changes under the action of longitudinal velocity gradients arising in fluid flows.

It has been established in a study of the influence exerted by polymer additives (POE and guar resin) on the frequency characteristics of near-wall pressure pulsations arising in a flow around rough surfaces that the hydraulic resistance becomes lower because of the decrease in the frequency levels of near-wall pressure pulsations [7, 8].

The turbulent flow of dilute polymer solutions has been the subject of [9]. Based on modern concepts of turbulence and diffusion and on his own experimental data, the author of this study suggested an integrated method for calculation of parameters of a turbulent boundary layer with polymer additives. This method makes it possible to calculate the longitudinal distributions of the friction characteristics, characteristic values of the flow thickness, and effective concentration of the polymer additive.

It was shown that polymer additives strongly rearrange the flow in the inner region of the boundary layer, thereby making thicker the viscous sublayer. In addition, the calculation methods suggested make it possible, in the author's opinion, to give certain recommendations concerning the introduction mode of a polymer additive into the flow and to prognosticate the magnitude and nature of the decrease in the hydraulic resistance in engineering calculations and in interpretation of the results of model experiments.

Also of interest and original in their goal are studies by Kulik [10]. He examined, in addition to individual polymers, the influence exerted by damping coatings (based on organosilicon rubbers) on the magnitude of the decrease in the hydraulic resistance of a turbulent flow. It was established that, depending on the properties of a material chosen, a monolayer damping coating may either reduce or raise the hydraulic resistance coefficient. It was shown that the decrease in the hydraulic resistance is due to scattering of the limiting contour of "turbulent energy" by the wall and to a decrease in the density of pressure pulsations at the wall. Kulik gave a new, but in certain respects disputable interpretation of the results obtained in experiments with polymer additives (POE). He analyzed in ample detail the mechanism of action of damping coatings, which is based on damping of pressure pulsations just in the near-wall zone of the turbulent flow. Having done so, he made, when passing to polymer additives, an insufficiently reasonable assumption that hypothetical spatial structures exist in the polymer solution. Structured polymers disintegrate in the field of shear and pulsating stresses, thereby making larger the number of actively working macromolecules. To advantages of Kulik's works should be referred that he was the first to perform a systematic study of the joint action of damping coatings and polymer additives, which makes lower the hydraulic resistance of turbulent flows. It was, in particular, shown that the effects are additive at low polymer doses, whereas at high doses, the magnitude of the decrease in friction becomes considerably larger than the sum of the effects caused by separate use of a coating and a polymer additive.

An important contribution to studies of the mechanism of the Toms effect has been made by foreign scientists. For example, Tiederman and Reischman

developed a computer model of propagation of the velocity profile in a turbulent polymer flow [11]. Virk and Suraiya [12] calculated, based on their own experimental data obtained by means of spectrophotometry, the thickness of the near-wall diffusion (elastic) layer, which reduces the turbulent friction. The studies by Lumley [13] and Hinch [14] have also been devoted to a theoretical substantiation of the Toms effect. In addition to the theoretical studies by Tiederman and Reischman, interesting experimental data on the distribution of the velocity profile in a turbulent flow with polymer additives have been obtained by the photographic method and Doppler anemometry [15, 16].

In [17], the influence exerted by the polymer additive on the coefficient of turbulent diffusion, which is a positive factor in interpretation of experimental data obtained in analyzing the Toms effect in other studies. Finally, an important stage in the development of the theory of the influence exerted by polymers on the near-wall turbulence is the publication by Ayyash and McComb [18], who could form a layer of adsorbed polymer on the inner surface of a tube.

Proceeding from the structural inhomogeneity of the medium, Kalashnikov [19] correlated the decrease in the hydraulic resistance with the presence of polymer associates in any solution. In this case, a polymer solution is regarded as a suspension (even comparative data for real suspensions and polymer solutions are given), and the decrease in the hydraulic resistance depends on the concentration, size, and structure of associates. This statement is also confirmed by the fact that the size of the associates is well comparable with the maximum transverse size of near-wall vortices. This enables the associates to dissipate the energy of vortices and thereby to reduce the turbulent friction [20]. The author maintains that it is owing to the formation of macromolecular associates in solution that the Toms effect starts to be manifested only after the critical molecular weight of $(0.2–0.3) \times 10^6$ and more is reached. The point is that polymers with a lower molecular weight cannot form associates in solution and, consequently, do not serve as hydrodynamically active additives. In the author's opinion, which is far from being indisputable, data of his experiments indicate that "anomalous" effects arising in a flow of solutions of polymers with a high molecular weight are due to aggregation of macromolecules.

Brestkin [21] analyzed dynamic phase transitions in a flow of polymer solutions and experimentally confirmed that a strong asymmetry appears in coils of macromolecules of a flexible-chain polymer with $M = 10^6$ and more when a longitudinal hydrodynamic field is generated in a dilute solution. Similar experiments were carried out by de Gene in a study of the conformation of macromolecules in solution in the case of a turbulent flow [22]. He established that macromolecules undergo a transition from a coil to an unrolled conformation of the type of a strongly straightened macromolecule.

Povkh and Stupin [23] suggested their own interpretation of the mechanism by which the hydraulic resistance is reduced via resonance absorption of the turbulent energy by polymer macromolecules. They modeled the macromolecule with a formation composed of N statistical segments. Upon introduction of external perturbations, the macromolecule shows a set of relaxation times (or intrinsic absorption frequencies). In the case of a turbulent flow of fluids, turbulent pulsations of a certain frequency arise in the fluids. These pulsations are characterized by the so-called spectrum of turbulent perturbations. At a certain instant of time, when the frequency of turbulent perturbations becomes equal to the first intrinsic frequency of the macromolecule, macromolecules start to exhibit resonance absorption of the turbulent energy, with the result that the intensity of velocity pulsations decreases. The authors planned and carried out experiments on heat exchange in a flow of water and dilute polymer solutions. Originally, they assumed that, if macromolecules suppress perturbations (breakouts) from the near-wall region, then the heat-transfer coefficient must also decrease. Their experiments with aqueous solutions of polyacrylamide (PAA) confirmed, on the whole, the assumption made.

The influence exerted by polymer additives on heat-exchange processes has been studied by Khabakhpasheva [24]. She also concluded that, when a polymer additive finds its way into the immediate vicinity of the tube wall, the intensity of pulsations of the velocity component perpendicular to the wall strongly decreases. As a result, the thickness of the transition layer increases and, therefore, its thermal resistance becomes higher.

Among theoretical studies of the turbulent mass exchange in the presence of polymer additives, mention should be made of that by Mikhailu [25]. When calculating the parameters of a mass exchange in aqueous solutions of macromolecular polymers, he came to conclusions similar to those reported in [24].

Factors that affect the magnitude of the Toms effect. Despite the differences in the interpretation of the mechanism of the phenomenon, all researchers

emphasize that the Toms effect starts to be manifested already at Reynolds numbers Re $(2–4) \times 10^3$, i.e., in the boundary region in a transition from the laminar flow mode to the turbulent one. It will be recalled that

$$\mathrm{Re} = \rho v d/\eta,$$

where ρ and η are the density and viscosity of the fluid; v, flow velocity; and d, inner diameter of the tube (capillary) [26].

As the Reynolds number increases, the efficiency of a polymer additive in making lower the hydraulic resistance of the flow becomes higher, but only up to a certain value of Re. It was shown in [27] that, for laminar flows of polymer solutions (PAA; Re $\le 2.3 \times 10^3$), the magnitude T of the Toms effect is either zero or negative, i.e., polymer additives lead to an increase in the effective viscosity and, naturally, do not act as agents reducing the resistance to the flow. At Re > $(3–5) \times 10^3$, the Toms effect comes into play and, as Re increases, the magnitude of the Toms effect grows until Re becomes equal to Re_{cr}. At Re > Re_{cr}, T is constant (and even somewhat decreases), i.e., the effect is the strongest at Re_{cr}.

Prior to passing to a detailed analysis of the factors that affect the magnitude of the Toms effect, it should be noted that this magnitude can be evaluated in different ways and, therefore, severe difficulties are encountered in making comparative estimates. The most frequent was use of methods based on measuring the flow rate of a fluid that passed through a capillary (or a tube) [28–31] or on determining the resistance factor for a cylinder rotating within another cylinder on standard instruments of the Reotest type [32]. Also, measurements of the Toms effect by unconventional techniques have been reported. For example, this effect can be evaluated by comparing the maximum distances to a target in its "shooting" with a fluid jet in the presence of a polymer and without it [33]. Upon introduction of a polymer additive, this distance increased because of the "spreading" of the water jet. Abroad, methods based on measuring the parameters of a flow around bodies of various shapes [34, 35] and the resistance forces in rotation of flat discs relative to each other (with the fluid in between) [36] are used to characterize the effect. The fluid flow lines are commonly visualized by "dyeing" the flow with various dyes, with subsequent photographing of its certain zones [37], and by laser anemometry, which yields a real pattern of velocity profiles in any part of the flow [38]. In medicine and physiology, experiments are performed *in vivo*, i.e., on animals. The blood circulatory system of rats, dogs, or cats is used as a model "setup" that is far from being standard [39]. In these experiments, a manifestation of the Toms effect is judged from an increase in the rate of blood circulation or from a decrease in the arterial blood pressure.

Despite the wide variety of methods used to study the Toms effect, most of researchers prefer to analyze the rheological properties of aqueous polymer solutions by modeling the pipeline transport of a fluid with tubes or capillaries. In this case, either the fluid flow rate or the pressure difference between the tube ends is fixed or the flow parameters are used to calculate the coefficient of the hydraulic resistance to the flow [31, 40–44]. Such an experimental procedure is preferable to another technique, which measures the effective viscosity of polymer solutions at high shear stresses on instruments of the "cylinder-in-cylinder" type [45]. The reason is that there are no convenient criteria for a comparative assessment of the mass-transfer process and the subsequent processing and interpretation of the data obtained are inevitably complicated in the case of a viscometric monitoring of the process.

The decrease in the hydraulic resistance of a turbulent flow becomes noticeable when the molecular weight of the polymer introduced reaches a value $M \sim 10^4$.

Studies of the influence exerted by the molecular weight M of PAA [46–49] lead to the same conclusion: the Toms effect is the more pronounced, the higher the molecular weight of the polymer introduced. For the overwhelming majority of water-soluble polymers, the Toms effect is negligible or lacking at all at $M < 1 \times 10^4$.

In studying the influence exerted by the molecular properties of a polymer additive on the extent to which the hydraulic resistance of turbulent flows is reduced, the effect of such an important parameter of the polymer as its molecular weight polydispersity remained virtually unexamined [50].

In comparative analysis of the efficiency of various polymers in lowering the hydraulic resistance of a flow, it is advisable to use the reduced Toms effect, $\gamma = \mathrm{T}/c$. Here c is the polymer concentration; T, magnitude of the Toms effect, evaluated by comparing the mass flow rates of the fluid in its flow through a capillary in the turbulent mode:

$$\mathrm{T} = (m - m_0)/m_0,$$

m_0, mass flow rate of pure water; and m, mass flow rate of water with a polymer additive [31, 50]. A cor-

rect analysis of the dependences $\gamma = f(F)$ was performed for the example of ionogenic (cationic) statistical copolymers of acrylamide in the absence of complications associated with the inconstancy of the composition α of the copolymers, with the conditions $\overline{M}$ = const and $\bar{\alpha}$ = const satisfied (Fig. 1). As a quantitative characteristic of the M polydispersity was used the Schultz parameter F [51]:

$$F = \overline{M}_m/\overline{M}_n - 1,$$

where $\overline{M}_m$ and $\overline{M}_n$ are the mass-average and number-average molecular weights, respectively.

The complex, extremal nature of the $\gamma = f(F)$ dependences for the acrylamide copolymers studied is due to nonadditivity of the contributions of separate fractions to the resulting effect, which is favored by ionogenic (acrylate) main-chain links preset in the polymer additive.

Important results have been obtained in this field by Berman [52, 53]. Berman used in his studies narrow (with respect to molecular weight) fractions of a polymer (POE), obtained by gel-chromatography. He particularly emphasized that nonfractionated polymer samples with an unknown molecular-weight distribution were used in most of his experiments when studying the hydraulic resistance. This is an additional complicating factor in making an adequate estimate of the influence exerted by the molecular weight on the magnitude of the Toms effect. In Berman's opinion, it is important to trace in experiments of this kind the contribution of a separate macromolecule (or a group of macromolecules with the same molecular parameters) to the total reduction of the hydraulic resistance. It was shown in his experiments that the magnitudes of the Toms effect for fractionated and nonfractionated samples with the same average molecular weight may differ significantly. Having made a thorough analysis of the experimental data obtained, Berman concluded that, in the case of a nonfractionated polymer, the major contribution to the reduction of the hydraulic resistance is made by minor amounts of fractions with the largest molecular weight.

It can be well seen from the very concept of the Toms effect that its magnitude also strongly depends on the concentration of the polymer additive. It is virtually a common opinion of all researchers that the efficiency of a polymer as an agent reducing the hydraulic resistance of a turbulent flow increases as its concentration becomes higher. The efficiency of the polymer additive increases until a certain critical concentration is reached, after which the magnitude of the Toms effect starts to decrease gradually.

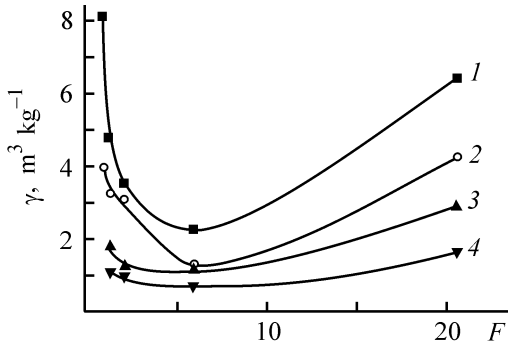


Fig. 1. Reduced Toms effect γ vs. the Schultz parameter F for mixtures of copolymers with $\overline{M} = 6.1 \times 10^5$. $c \times 10^3$ (kg m^{-3}): (*1*) 5, (*2*) 10, (*3*) 50, and (*4*) 100.

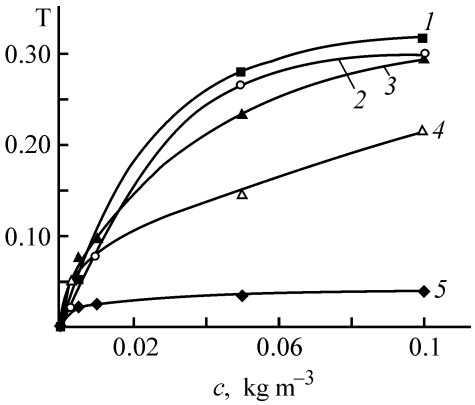


Fig. 2. Magnitude T of the Toms effect vs. the concentration c of water-soluble (co)polymers. (*1*) PAA, (*2*) cationic copolymer of acrylamide with dimethylaminoethyl methacrylate hydrochloride, (*3*) anionic copolymer of acrylamide with sodium acrylate, (*4*) POE, and (*5*) Na-CMC.

Figure 2 shows as an example a typical concentration dependence of the magnitude of the Toms effect for aqueous solutions of watersoluble (co)polymers of varied nature [54].

Pokryvailo and Gol'bina [7] studied the influence exerted by polymer additives on the intensity and frequency spectrum of pressure pulsations in a turbulent flow. Samples of POE, sodium carboxymethyl cellulose (Na-CMC), and guar resin were used in their experiments. An analysis of the results of the experiments demonstrated that for each polymer there is an optimal concentration at which the pressure pulsations are quenched to the greatest extent. The most effective among the polymers studied were solutions of POE and guar resin. Na-CMC solutions did not reduce the friction and even raised the flow resistance in some cases.

The conclusion that there exists an optimal polymer concentration c_{opt} in solution was also made by Manzhai *et al.* [55] in a study of the hydrodynamic

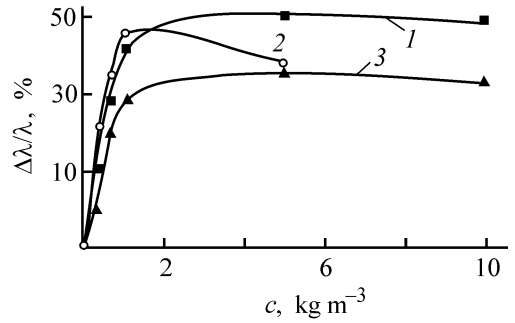


Fig. 3. Decrease in the hydraulic resistance, $\Delta\lambda/\lambda$ vs. the concentration c of natural caoutchouc in oil. Molecular weight $M \times 10^5$: (*1*, *3*) 2.4 and (*2*) 5.5. Shear stress (Pa): (*1*) 240 and (*2*, *3*) 120.

efficiency of polyisoprene samples in a turbulent flow of dry oil. On carrying out a set of experiments with polyisoprene samples of varied molecular weight introduced into and oil-containing dispersed system, the authors revealed a dependence of the optimal concentration on the molecular weight of the polymer additive. After c_{opt} is reached, the efficiency of the polymer additive "damping" the turbulence of the flow decreases (Fig. 3).

In some cases, practical application of polymers to reduce the resistance encounters difficulties associated with the fact that macromolecular polymers undergo mechanical destruction under certain conditions. In the case of a developed turbulent flow, the destruction is the most intensive [56], which automatically leads to a pronounced decrease in the magnitude of the Toms effect. Therefore, it is, in some cases, advisable to use polymers in closed-circulation systems, especially at a fast turbulent flow of fluids with large Reynolds number ($Re > 10^4$) [2].

An important contribution to investigation of dynamic processes of destruction of polymer solutions in a turbulent flow has been made Frenkel and Brestkin [21, 57]. A special emphasis was placed in these studies on analysis of the dynamics of conformational transitions in macromolecules in a longitudinal mode of solution flow. A study of the destruction products by means of chromatography led to a conclusion that, despite the decrease in the molecular weight in the course of destruction, the Schultz parameter characterizing the polydispersity in molecular weight does change significantly.

Data on destruction of polymers in a turbulent flow have also been reported by Makogon *et al.* [58, 59]. PAA and POE solutions were passed through a capillary and the resulting solutions were studied by the light-scattering method and sedimentation-diffusion analysis. The author concluded that, in addition to a simple decrease in the molecular weight of samples in solution, there also occur processes in which intra- and intermolecular cross-links are formed under the action of the hydrodynamic field. This leads to a decrease in the thermodynamic flexibility and effective dimensions of macromolecules and, consequently, their efficiency as turbulent flow "dampers" becomes lower.

In a study of the destruction of a solution of polyisobutylene in oil on a setup of the "cylinder-in-cylinder" type, Patterson *et al.* [60] made the following generalizations: (1) the extent of destruction is the greater, the higher the shear rate and (2) the strongest destruction is observed at comparatively low temperatures.

It is known that the resistance of a polymer additive to mechanical destruction is closely associated with the chemical structure of a polymer. Layec-Raphalen [61] made an attempt to reveal this relationship in experiments on circulation of a number of flexible-, moderately flexible (PAA and POE), and rigid-chain (xanthane) polymers in a system of pipelines and made a conclusion that rigid-chain polymers (xanthane) are more stable against destruction than POE and PAA.

Undoubtedly, a more in-depth and comprehensive analysis of the fundamental aspects of the destruction of polymer additives in a turbulent fluid flow will contribute to elimination of difficulties in practical application of polymer additives in industrial processes of high-rate transportation of fluids (e.g., in circulation systems).

The existence of a strong dependence of the hydrodynamic resistance of turbulent flows on the size $(\bar{h}^2)^{0.5}$ of macromolecular coils has been demonstrated on a vast body of experimental data. Therefore, it would be expected that, with water-soluble polymer additives used, the parameters T and $\gamma = T/c$ should depend on the pH value and ionic strength of the medium, and on the content of active components (surfactants, electrolytes, etc.) in it. This assumption has been confirmed by a large number of experiments with model and real systems.

There is no commonly accepted opinion concerning the influence exerted by the pH value. Some researchers have noted a pronounced enhancement of the Toms effect with increasing pH of the medium [47, 48, 62, 63]. This occurs if an increase in the pH value is accompanied by a simultaneous rise in the size $(\bar{h}^2)^{0.5}$ of macromolecular coils of the polymer. A sufficiently versatile and well-reasoned standpoint can be noted for another group of researchers, who believe that the maximum magnitude of the Toms

effect is observed in a neutral or weakly alkaline aqueous medium [64–66].

A considerable attention to the influence exerted by the pH value on the magnitude of the Toms effect has been given by Makogon, Klenin, and Povkh [45, 58, 59, 67]. They carried out a comparative study of the structure and thermodynamic activity of aqueous PAA solutions with different degrees of hydrolysis and various pH values and noted that the viscosity numbers of nonhydrolyzed PAA remained virtually unchanged in the pH range 2–10. No experiments have been carried out at pH > 10, because, in this case, PAA hydrolyzes already in the stage of solution preparation. The strong dependence of the reduced viscosity on the pH value was observed for samples of hydrolyzed PAA. It was found that macrocoils have the smallest size in an acid medium because of the presence of hydrogen bonds between un-ionized carboxy groups. At pH 8, the coils of macromolecules were the largest owing to an increase in the degree of ionization and to appearance of electrostatic repulsion forces between acrylate ions along the chain of the copolymer macromolecule. In an alkali medium, the size of macrocoils starts to decrease again because of the shielding of charged carboxy groups by sodium counterions, and, as a result, the repulsion forces between negatively charged main-chain links become weaker. Data on the conformational states of the macromolecules were compared with hydrodynamic parameters of turbulent flows in media with varied pH values. For those pH values at which the macromolecules of hydrolyzed PAA became smaller, a decrease in the magnitude of the Toms effect was observe; in distilled water, the reduction of the hydraulic resistance was at a maximum (Fig. 4).

In [68], the relationship between the magnitude of the Toms effect and the conformational state of macromolecules of cationic copolymer of acrylamide in neutral, acid, and alkaline aqueous media was subjected to a quantitative comparative analysis.

To summarize this series of investigations, it may be stated that the dependence of the size $(\bar{h}^2)^{0.5}$ of macromolecular coils (and, consequently, also that of the magnitude of the Toms effect) on the pH value of the solutions is largely determined by the chemical nature of (co)polymers being analyzed and invites a more detailed study for each class of polymers, separately.

As the ionic strength I of a solution increases, the Toms effect becomes less pronounced [30, 32]. In [69, 70], the influence exerted by the ionic strength of a solution (with respect to NaCl) on the magnitude of the Toms effect for hydrolyzed PAA was

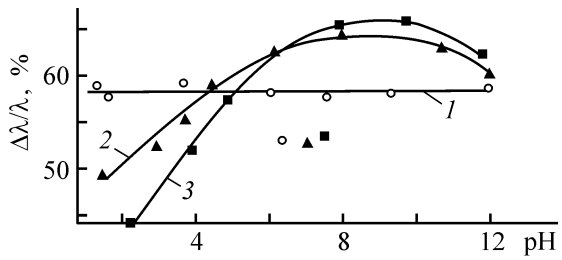


Fig. 4. Reduction of the hydrodynamic resistance, $\Delta\lambda/\lambda$, vs. pH value. c = 0.004 kg m^{-3}, $M = 6 \times 10^6$, shear stress 33 Pa. (*1*) Nonhydrolyzed PAA, (*2*) HPAA (α = 12.5%), and (*3*) HPAA (α = 16.8%).

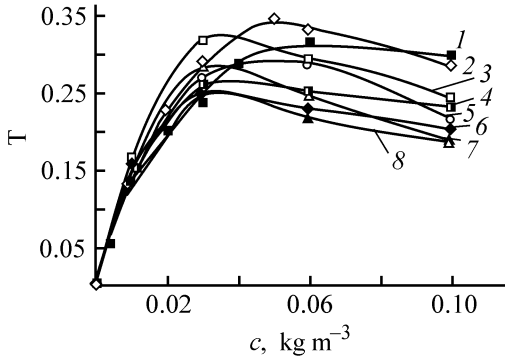


Fig. 5. The magnitude T of the Toms effect vs. the concentration c of (*1*, *3–8*) anionic copolymers of acrylamide with various degrees of hydrolysis and (*2*) Alcoflood 1175-A reference sample (α = 21.5 mol %, $M = 10.8 \times 10^6$). Degree of hydrolysis (mol %): (*1*) 1.50, (*3*) 47.93, (*4*) 10.33, (*5*) 63.70, (*6*) 41.02, (*7*) 36.20, and (*8*) 22.20.

studied at varied shear strength. It was shown that the magnitude of the Toms effect depends on the size $(\bar{h}^2)^{0.5}$ of macromolecules. The authors call special attention to the correlation between the dependences of the parameters T and $(\bar{h}^2)^{0.5}$ on the electrolyte concentration. It is also noted that introduction of salts changed the conformational state of macromolecules not only in the inner regions of the fluid flow, but also in a thin fluid layer at the phase boundary, which, naturally, reflected upon the magnitude of the resultant macroscopic Toms effect [70, 71].

In some cases, the key contribution to the dependence of the magnitude of the Toms effect on I is made not only by the conformational state of the copolymer macromolecules, but also by parameters of the near-wall layer at the inner wall of a capillary or a tube along which the fluid flows [72, 73].

Studies of the concentration dependences of the magnitude of the Toms effect for samples of hydrolyzed polyacrylamide (HPAA) with different degrees of hydrolysis, α, revealed a complex, ambiguous type of $T = f(\alpha)$ dependences [73] (Fig. 5). One more distinctive feature of the curves in Fig. 5 is that they

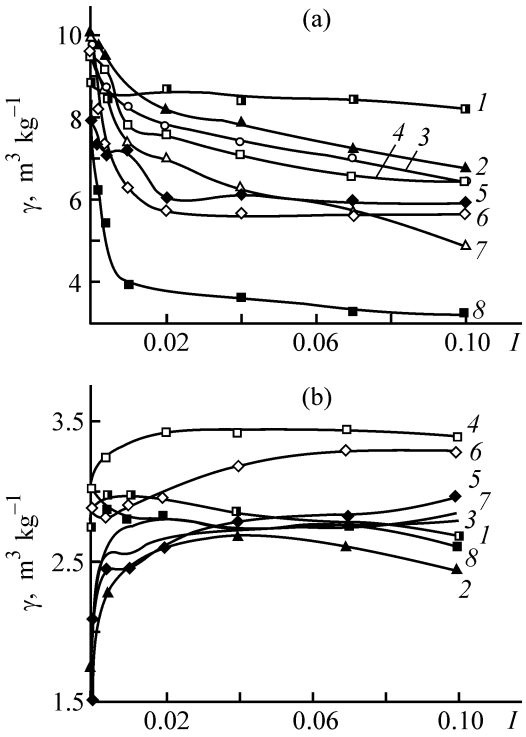


Fig. 6. Reduced Toms effect γ vs. the ionic strength *I* for (*1–5*, *7*, *8*) anionic copolymers of acrylamide with various degrees of hydrolysis and (*6*) Alcoflood 1175-A reference sample (α = 21.5 mol %, $M = 10.8 \times 10^6$). Copolymer concentration *c* (kg m^{-3}): (a) 0.03 and (b) 0.1. Degree of hydrolysis (mol %): (*1*) 10.33, (*2*) 22.20, (*3*) 63.70, (*4*) 47.93, (*5*) 41.02, (*7*) 36.20, (*8*) 1.50.

exhibit a clearly pronounced peak. This is attributed by the authors primarily to processes involving macroanions in the zone of the most effective damping of the arising turbulence waves, which is, specifically, the local volume of the fluid flow in the immediate vicinity of the capillary walls. With account of the type of fluid motion in this zone, the local concentration of macroanions and the size and shape of macromolecular coils are significantly different from those in the initial solution, in the absence of a turbulent fluid flow. It is this concept of the turbulent flow of a polymer solution that may logically lead to such notion as the optimal concentration ("saturation" concentration) c_{opt} of the polymer in the near-wall zone of the flow. Raising the polymer concentration to above a certain critical value (which was about 0.003% for the polymers studied) makes higher the dynamic viscosity in the flow, rather than c_{opt}, with the result that the efficiency of the polymer component in damping the turbulence of a solution decreases (as also does the magnitude of the Toms effect).

To illustrate the important role of the processes occurring in the near-wall zone of the capillary, the $\gamma = f(I)$ dependences were analyzed for two concentration "sections" in Figs. 6a, 6b. For this purpose, two polymer concentrations $c = c_{cr} = 0.003\%$ and $c = 0.01\%$ were chosen on the assumption that differences in the influence exerted by the electrolyte dose on the magnitude of the Toms effect are the most pronounced just at these concentrations. Indeed, the types of the dependences for the copolymer concentrations of 0.003 and 0.01% are fundamentally different. A steady decrease in the first case (Fig. 6a) and, contrariwise, an increase in the reduced Toms effect, $\gamma = T/c$, (and, consequently in the parameter T [54], too, because c = const in this set of experiments), in the second (Fig. 6b) were observed as the ionic strength became higher. It should be noted that, for all the systems studied, the dependence of the dynamic viscosity on the ionic strength of the solution was of the type characteristic of flexible-chain polymers, i.e., the viscosity decreased as the ionic force became higher.

One of the most probable reasons why the reduced Toms effect is more pronounced for systems with $c = 0.01\%$ may be associated with a decrease in $(\overline{h}^2)^{0.5}$ and dynamic viscosity at higher *I* and with a local increase in the intensity of transition of a part of macromolecules from the regions of the solution that are remote from the walls of the limiting contour into the near-wall region, which makes c_{opt} higher.

The magnitude of the Toms effect is affected not only by the ionic strength of the solution, but also by the nature of the electrolyte, which was clearly demonstrated in [72]. This study was concerned with the influence of multicharged ions on the magnitude of the Toms effect, with anionic and cationic copolymers of acrylamide used as polymers. It was found that the magnitude of the Toms effect is affected not only by the electrolyte concentration, but also, strongly, by the nature of a multicharged ion. For example, the magnitude of the Toms effect dramatically decreased for the cationic copolymer of acrylamide as the concentration of the electrolyte with a multicharged anion ($K_4[Fe(CN)_6]$) became higher, and decreased stepwise for anionic copolymers of AA as the concentration of $FeCl_3$ increased. The source of the experimentally observed strong antagonistic effects for the above-mentioned binary formulations constituted by an ionogenic copolymer and a polyvalent electrolyte is the selective electrostatic interaction of charged parts of macroanions (macrocations)

with polyvalent cations Fe^{3+} ($[Fe(CN)_6]^{-4}$ anions). This interaction leads to a dramatic decrease in the root-mean-square size of macromolecular coils and to their subsequent globulization.

The joint influence of the pH value and the ionic strength of a solution on the magnitude of the Toms effect was analyzed. Polyacrylic acid was used as a polymer object, and the ionic strength of the solution was adjusted with NaCl and $MgCl_2$ salts. Mainly the range of low pH values was studied. It was found that addition of small amounts of NaCl (up to 10^{-2} M) has virtually no effect on the extent to which the hydraulic resistance decreased in the whole range of pH values. At the same time, replacing the electrolyte with $MgCl_2$ led, all other conditions being the same, to a significant decrease in hydraulic resistance, especially at high pH values. A possible reason for the behavior observed, mentioned by researchers, is interaction of double-charged ions of magnesium with macromolecules of polyacrylic acid, which results in a substantial decrease in electrostatic repulsion forces between separate negatively charged groups of a macromolecule. This makes smaller the macromolecular coils and, consequently, reduces the magnitude of the Toms effect.

It is noteworthy that the above data on the influence exerted by the pH value and the ionic strength of a solution on the magnitude of the Toms effect are particularly important for the oil industry, which has, more and more frequently, to deal with highly mineralized formation water (with a mineralization as high as 200–300 g l^{-1}), which may have widely varying pH values and contain salts of varied nature [75]. Therefore, knowledge of the salt composition and pH value of the formation water is necessary even for a semiquantitative prognostication of the macroscopic effect produced by a particular polymer reagent.

In most cases, real dispersed objects are complex, multicomponent systems, whose various components may affect in a certain way the resulting macroscopic effect. Among components of this kind are surfactants, which can exert a strong influence both on the physicochemical parameters of fluids and on the conformational state of macromolecules. Despite that this area of research is a matter of particular current interest, the number of reports on systematic studies of this problem is insufficient.

In [31, 76–80], the influence exerted by the nature and concentration c_s of a surfactant in the dispersion medium on the resultant Toms effect was evaluated and the main conditions for the appearance in systems

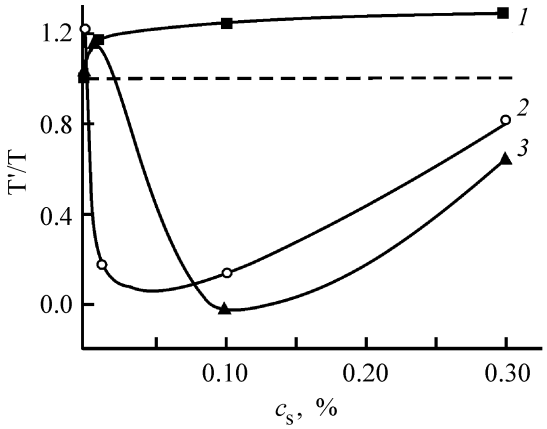


Fig. 7. Parameter T'/T vs. the surfactant concentration c_s for the binary mixtures (*1*) HPA + nonionogenic surfactant, (*2*) C + anionic surfactant, and (*3*) HPAA + cationic surfactant.

of this kind of a synergism and antagonism in the action of the components of binary polymer–surfactant mixtures were analyzed. The occurrence of these effects is indicated by the data in Fig. 7. A binary formulation composed of HPAA and a nonionogenic surfactant exhibits a weakly pronounced synergism, and those constituted by a cationic copolymer (C) and an anionic surfactant and by HPAA and a cationic surfactant, an antagonism in the action of the components. With account of the presence of two active components, HPAA and a surfactant, are contained in the system being analyzed, the magnitudes T' of the Toms effect for the binary formulations polymer–surfactant were calculated by the formula

$$T' = (m' - m_0)/m'_0.$$

In the expression, the prime means that the corresponding parameter was determined in an aqueous solution of a surfactant (for each fixed concentration of the surfactant).

The experimentally observed steep fall in the values of the parameter T'/T at surfactant concentrations of 0.05–0.1% is due not only to a decrease in the size of macromolecular coils as a result of selective interactions between an anion and a cation of a cationic surfactant or between a cation and an anion of an anionic surfactant. It also results from formation of dense globular associates composed of macromolecules with immobilized molecules or micelles of the surfactant. The visually observed, or indicated by results of optical measurements, strong turbidization of solutions of ionogenic copolymers of acrylamide in the presence

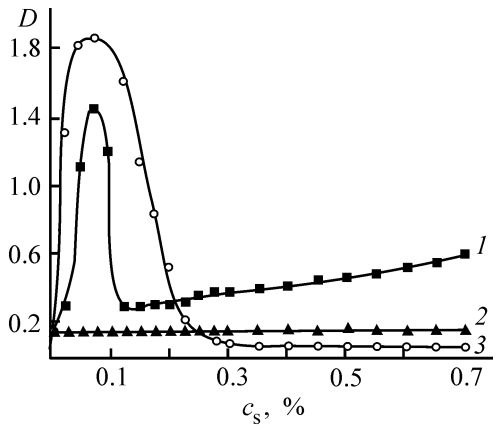


Fig. 8. Optical density D vs. the surfactant concentration c_s for binary mixtures constituted by (*1*) HPAA + cationic surfactant, (*2*) HPAA + nonionogenic surfactant, and (*3*) C + anionic surfactant. (Co)polymer concentration $c = 0.1$ kg m^{-3}, wavelength 400 nm.

of minor amounts of a surfactant (Fig. 8, curvers *1* and *2*) confirms that compact globular structures composed of macromolecules of the polymer and a surfactant are formed in the system.

Of indubitable practical interest are the results of studies [29, 81, 82] in which the resistance to the flow decreased when a surfactant with a concentration exceeding the critical micelle concentration (CMC) was introduced into a solution. For example, rod-like micelles were observed in solution when a surfactant was used as an additive [82]. It was noted that the flow structure was nearly laminar upon addition of the surfactant.

Of theoretical and practical importance are studies in which binary polymer formulations were used as additives. Data on the reduction of the hydraulic resistance of a flow with binary polymer formulations composed of polymers of varied nature were reported in [54, 78, 83, 84]. It was noted that both synergism and antagonism in the action of the components may arise in the general case in formulations of this type. The highest efficiency in the "quenching" of the turbulence of a flow is observed for the POE–HPAA and POE–C mixtures, and the lowest, for the HPAA–C mixture. The manifestation of antagonism in the action of the components of the last binary mixture can be accounted for by formation of a dense, compact, and hydrodynamically inactive interpolymer complex.

Model binary polymer formulations composed of samples of the same polymer but having different molecular weights have been studied [50, 68]. The authors call attention to the nonadditive contributions from separate fractions of the polymer to the resultant effect of reduction of the hydraulic resistance of aqueous flows.

The turbulent outflow of solutions of CMC, PAA, and xanthane polymer and of their mixtures has been studied [28]. Primary attention was given to the relationship between their rheological properties and the Reynolds number. In [85], experimental data on joint use of formulations with POE and a surfactant were reported, but, unfortunately, no attempt was made to evaluate the efficiency of action of separate components in order to determine whether or not there is a synergism (or an antagonism) in the system.

Application of the Toms effect in petroleum engineering. In the development of new industrial technologies, polymers have found wide use in virtually each stage of production, transportation, and treatment of oil [40]. One of the most original, unexpected, and effective ways to use polymers in oil production has been their application as agents that quench turbulence in a fluid flow in aqueous, organic, and aqueous-organic media. The use of the Toms effect made it possible to reduce the time of well-boring and make lower the power consumption by pumps maintaining the seam pressure at a prescribed level, and markedly diminish the expenditure for transportation of oil and oil products [3].

At present the following polymers are the most frequently used to quench turbulence in aqueous media in oil production: (1) (co)polymers of acrylamide (cationic, anionic, nonionogenic), (2) cellulose and its derivatives (carboxymethyl cellulose, oxyethyl cellulose, etc.), (3) POE, etc.

Among the polymers listed above, the highest efficiency is observed for polyacrylamide and POE. The technological advantage of polyacrylamide over POE is due to its higher resistance to destruction in quenching of the flow turbulence and to the fact that the amount of its industrial manufacture exceeds that of POE, and its cost is lower. Therefore, polyacrylamide have found the widest use, both in our country and in the rest of the world, as an agent reducing the hydraulic resistance of aqueous turbulent flows [2, 3].

Natural cellulose-based polymers are also commonly accepted as active agents for reduction of the hydraulic resistance of water, but their efficiency is not as high as that of POE and polyacrylamide. However, their use in those cases when they serve several purposes simultaneously is justified if account is taken of the difference between their cost and that of polyacrylamide (and POE). For example, use of cellulose esters to stabilize drilling agents in oil and gas pro-

duction makes it possible to raise simultaneously the drilling rate and the flow rate of solutions without any increase in the power of the apparatus used [2, 40].

In addition to aqueous media, the Toms effect is also widely used in hydrocarbon media. Its application made it possible to solve an important problem of making higher the rate of transportation of fluids in transfer of oil, oil emulsions, and commercial oil products. The most widely used as effective turbulence-quenching agents for these systems are such polymers as polyethylene and copolymers of ethylene (in particular, a copolymer of ethylene and vinyl acetate: Sevilen), polybutadiene, polyisoprene, and polystyrene and its derivatives [86–88].

It is necessary to distinguish additives lowering the turbulence of a flow and those of the depressor type among the large number of reagents that intensify transportation of oil and oil products via pipes, because the mechanisms of their action are different.

Polymer additives were first used industrially to reduce the hydraulic resistance when transporting low-viscosity oils via the Trans-Alaska pipeline in 1979. This was the CDR additive, a solution of polyolefins in a hydrocarbon solvent, manufactured by Conoco Speciality Products, Inc. [86]. In 1991, the first domestic additive acting as turbulence-quenching agent was manufactured at Tomsk Petrochemical Combine (VIOL, 10% solution of a copolymer of α-olefin in heptane) [89].

The problem of the mechanism of the Toms effect in hydrocarbon media is rather ambiguous. In particular, studies by scientists from Ufa, Movsumadze and Mastobaev, are known in Russia [90, 91]. They believe that the polymer is adsorbed on particles of oil and thereby stabilizes its flow by reducing the internal friction. Of certain interest are their generalizing papers devoted to separate aspects of application of reagents differing in the functionality of action and chemical nature (surfactants, polymers and formulations on their basis) in pipeline transport of oil and oil products [92, 93].

Studies by Chelintsev and co-authors are known in Russia and abroad [88]. They reported not only experimental data on application of various reagents, but also the most important aspects of the mathematical modeling of the pipeline transport of oil and oil products containing these reagents.

The most important characteristics of polybutylene as a turbulence-quenching agent were analyzed in [94]. In particular, the main parameters that affect

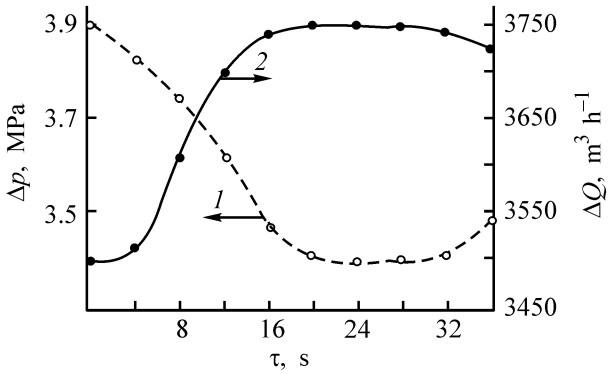


Fig. 9. Variation with time τ of (*1*) pressure drop Δ*p* and (*2*) volumetric flow rate Δ*Q* of oil at a part of the Tikhoretsk–Novorossiisk pipeline in the case of a continuous introduction of a polymer additive into the oil being transported.

the Toms effect: the molecular weight of a polymer, its concentration, and the nature of a solvent, were studied.

In [95, 96], the reduction of friction of a turbulent flow in hydrocarbon media with various polymer additives, with the decrease in friction being as large as 40% and more, was briefly reviewed.

The influence exerted by the concentration and molecular weight of polyhexene-1 on the magnitude of the Toms effect in real and model hydrocarbon media was considered in [41, 42]. The authors analyzed the main reasons for the frequent inconsistency of results obtained in laboratory and in industrial tests and present the necessary criteria to be used in a scientifically substantiated choice of a polymer additive in order to achieve the strongest effect. To confirm their theoretical concepts, the authors of these publications performed a successful experiment on reducing the energy expenditure in transfer of oil via the Tikhoretsk–Novorossiisk pipeline with a total length of 125 km (pipe diameter 0.8 m), which is clearly illustrated by Fig. 9.

At present, the quality of oil obtained from wells that have worked for a long time steadily decreases. In particular, this is manifested in the increased watering of oil [97]. Most frequently, an emulsion of oil with formation water is obtained from a well instead of oil. This emulsion has a high sedimentation and aggregative stability. Therefore, the negative tendency toward an increase in the water content of oil in the course of the service life of wells is combined with another, even more complicated problem of separating water from oil. Oil emulsions are separated at special stations for integrated treatment of oil (UKPN), as

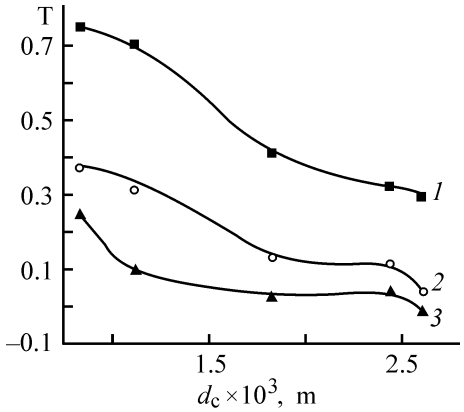


Fig. 10. Parameter T vs. capillary diameter d_c at a pressure P of 15 atm in the rheometer tank. Capillary length L (m): (*1*) 0.6, (*2*) 0.15, and (*3*) 0.075.

well as in intermediate stages of collection and transportation of the product obtained from wells to UKPN [98]. In this context, the question of how the transportation of oil emulsions can be accelerated is rather acute, because the viscosity of these emulsions is very high and distances to which they are to be transported may be as long as several tens of kilometers. Therefore, studies of the conditions for the most rational use of the Toms effect in high-speed transportation of reverse and direct emulsions of oil are of current interest and, undoubtedly, their results will be in demand in the near future. However, information about reduction of the hydraulic resistance of a flow in reverse oil emulsions is still exceedingly scarce and contradictory. For example, it was noted in [40], without describing the experimental procedure, that the hydraulic resistance to a turbulent flow of watery oil can be reduced by introducing minor amounts of aqueous solutions of polyacrylamide, with a dispersing agent (surfactant) added to achieve a homogeneous distribution of the aqueous phase (with the polymer additive) in the hydrocarbon medium.

In the USSR, experiments of pipeline transfer of high-solidifying oil on the industrial scale were performed. It was found that continuous introduction of a 0.2–0.5% solution of polyacrylamide (1.5–3.0 g of dry substance per 1 ton of oil) raises the throughput of an oil pipeline by 20%, with the amount of paraffin deposits on the inner surface of pipes simultaneously reduced [99].

Recently, separate publications have appeared in which a method for transportation of heavy oil in the form of a direct emulsion stabilized with an aqueous solution of a surfactant has been suggested [100–103]. In some cases, it is recommended to transfer high-solidifying crude oil in a rather original way, with continuous supply of water into the annular space near the pipeline wall [100]. Thereby there occurs layer transportation of oil on a water substrate. As a result, the expenditure for transfer of crude oil in this way is considerably lower than that for transfer of oils in the pure form. Despite that the transportation of oil in a mixture with an aqueous phase is seemingly complicated, the methods suggested are promising because introduction of rather small (relative to the target product) amounts of a polymer into the aqueous phase will further reduce the expenditure for transportation.

With account of the fact that transportation of crude oil and oil products in the form of direct and reverse emulsions is undoubtedly promising in economical and ecological regards, rheological aspects of a turbulent flow of direct oil emulsions with water-soluble polymers as additives [104–109]. It was noted that the manner in which the most important parameters of both the polymer additive (chemical nature of repeated links, molecular weight, concentration, molecular-weight and compositional polydispersity) and the dispersion medium (ionic strength, pH value, presence of active components of the type of surfactants) for unconcentrated direct oil emulsions (10–25%) is similar to that of the aqueous medium in some respects. However, the presence of particles of the dispersed phase, oil, in the aqueous medium leads to a number of interesting features. The most important of these is that the magnitude of the Toms effect decreased as the concentration of the dispersed phase became higher. This was attributed by the authors to the occurrence of adsorption processes on the surface of particles of the dispersed phase, which lead to a certain decrease in the concentration of the polymer in the dispersion medium. This effect is more pronounced for POE, which exhibits a high surface activity, and less so for (co)polymers of acrylamide. In addition to the factors mentioned above, the influence exerted by the flow velocity of the oil emulsion on the magnitude of the Toms effect was also studied [109]. A certain decrease in the magnitude of the Toms effect at higher transfer rates was observed experimentally. This can be attributed to a possible distortion of the spherical shape of particles of the dispersed phase (and, consequently, to a change in other parameters of particles of the dispersed phase) [110] upon a transition from the laminar mode of flow of direct oil emulsions to a turbulent mode.

Undoubtedly, not only the properties of a polymer additive and dispersion medium, but also the velocity of the turbulent flow and geometric parameters of the limiting contour affect the magnitude of the Toms

effect. The influence exerted by these factors on the Toms effect in direct oil emulsions and in a purely aqueous medium was studied in [109, 111]. Experiments were carried out on a modified turbulent rheometer with replaceable glass capillaries, which made it possible to vary widely their length and diameter. Based on the experimental data obtained with a set of glass capillaries, the authors made a conclusion that the parameters T and γ increase as the capillary becomes longer, and its diameter, smaller (Fig. 10).

It should be especially noted that, irrespective of the length and diameter of the capillaries, the manner in which the magnitude of the Toms effect depends on the active parameters of the system remained unchanged, with only the "scaling factor" (for T and γ) varied.

Other areas of manifestation of the Toms effect. In addition to the oil-producing industry, the Toms effect has found use in other areas: in fire extinguishing, for making longer the range of water jets from water cannons; in stone cutting, for intensifying the water-jet cutting of marble and granite flagstones; in shipbuilding, for raising the velocity of ships and submarines; and in biology and medicine [2–4].

The question of the possible manifestation of the Toms effect in living organisms has long escaped the attention of researchers. Only in the early 1970s, there appeared first experimental studies devoted to application of macromolecular polymers in experimental medicine and physiology. It was found that a natural biopolymer with a high molecular mass, C26, which is contained in blood, can lower the hydrodynamic resistance in a flow of blood [112]. Erythrocytes of blood also contain a macromolecular component that can be involved in the reduction of the resistance to a blood flow. In addition to natural polymers, synthetic polymers have also been used to diminish the resistance to a blood flow. Low-toxic water-soluble polymers (POE, polyacrylamide, and polyvinylpyrrolidone) was employed for this purpose [113].

Despite the comprehensive studies in this field, the issue of manifestation of the Toms effect in living organisms remains open to question and is far from being clear. The principal feature of application of polymers is that, in most cases, the turbulent flow does not virtually occur in its pure form in the circulatory system of animals (the Reynolds number in large arteries in the human circulatory system is, on average, as small as 100–1000, which, according to formal criteria, corresponds to a laminar flow mode [114]). Many physiologists note that the blood flow in the circulatory system is pulsating, rather than stationary. In the strongly branched network of resistive (resistance-creating) vessels, deviations from the laminar flow mode appear in the zone of branching (in the so-called initial portions) and constriction of blood vessels. These deviations give rise to local hydraulic resistances in the blood stream. In addition, the size of erythrocytes contained in blood are comparable with the diameter of the smallest vessels, which introduces additional "perturbations" into the flow in chaotic motion of erythrocytes in these vessels. Just these conditions have led physiologists to a conclusion that the Toms effect can be manifested in the circulatory system of animals.

However, the question as to whether or not the Toms effect does exist in living organisms, or the above-described effect caused by introduction of a polymer occur for some other reasons remains disputable. One thing is apparent, a more in-depth study of the fundamental aspects of this phenomenon in the field of biomedicine will favor development of new effective ways to control the dynamics of blood circulation and unconventional methods for improving the efficiency of the presently existing and new medicinal agents.

CONCLUSION

A sufficiently large number of experimental and theoretical studies have been devoted to various aspects of investigation and application of the Toms effect in aqueous and hydrocarbon media. Despite this circumstance, the influence exerted on the Toms effect by such most important parameters of copolymers as their molecular weight and compositional dispersity remain insufficiently studied and open to question. The same applies to the active parameters of a dispersion medium (nature of solvent, which is more important for organic media; nature and concentration of surfactants; ionic strength; pH value; and presence of impurities). The information about the influence exerted on the resultant macroscopic effect by binary formulations of the polymer–polymer, polymer–surfactant, and polymer–electrolyte types is scarce. This is so despite that just binary additives of this kind exhibit both synergism and antagonism, which is particularly important in passing from modeling to real systems. Most of researchers use model systems, distilled water, individual hydrocarbons, or organic fluids, as "convenient" objects of study. However, real objects (e.g., direct and reverse emulsions) are more complex multicomponent mixtures whose separate ingredients can strongly affect the resultant Toms effect, which is unclear and unpredictable in-

most cases. Therefore, studies of these problems are of indisputable practical interest and their results will find use, and some of these, in the nearest future. These issues become particularly important in development of industrial technologies for fast transportation of dispersed oil systems, including their direct and reverse emulsions, via pipelines.

REFERENCES

1. Shur, A.M., *Vysokomolekulyarnye soedineniya* (Macromolecular Compounds), Moscow: Vysshaya Shkola, 1981.
2. Nikolaev, A.F. and Okhrimenko, G.I., *Vodorastvorimye polimery* (Water-soluble Polymers), Leningrad: Khimiya, 1979.
3. Abramova, L.I., Baiburdov, T.A., Grigoryan, E.P., *et al.*, *Poliakrilamid* (Polyacrylamide), Moscow: Khimiya, 1992.
4. Shapiro, L.S., *Samye nelegkie puti k Neptunu* (Most Difficult Ways to Neptune), Leningrad: Sudostroenie, 1987.
5. Toms, B.A., *1st Internat. Congr. Rheol.*, Amsterdam, 1949, vol. 2, pp. 135–141.
6. Naumchuk, N.V., Hydrodynamic Activity of Aqueous Solutions of Polymers in Flows with Expansion, *Cand. Sci. Dissertation*, Perm, 1990.
7. Pokryvailo, N.A. and Gol'bina, I.I., Abstracts of Papers, *VIII Vsesoyuznyi simpozium po reologii "Reologiya polimernykh i dispersnykh sistem i reofizika", Gomel, 27–31 maya 1974 g.* (VIII All-Union Symp. On Rheology "Rheology of Polymer and Dispersed Systems and Rheophysics," Gomel, May 27–31, 1974), Minsk: Inst. Tepl. Massoobmena, Akad. Nauk BSSR, 1975, pp. 28–34.
8. Greshilov, E.M., Evtushenko, A.V., Lyamshev, L.M., and Shirokova, N.L., *Inzh. Fiz. Zh.*, 1975, vol. 25, no. 6, pp. 999–1005.
9. Mashkov, S.L., Diffusion in a Turbulent Boundary Layer in Concentrated and Distributed Feed of Polymer Additives, *Cand. Sci. Dissertation*, Moscow, 1991.
10. Kulik, V.M., Joint and Separate Actiion of the Viscoelastic Boundary and Polymer Additives on the Near-Wall Turbulence, *Cand. Sci. Dissertation*, Novosibirsk, 1988.
11. Donohue, G.L., Tiederman, W.G., and Reischman, M.M., *J. Fluid Mech.*, 1972, vol. 56, pp. 559–575.
12. Virk, P.S. and Suraiya, T., *2nd Int. Conf. Drag Reduction, Cranfield, 31 Aug.–2 Sept. 1977*, Cranfield, 1977, pp. G341–G356.
13. Lumley, J.L., *J. Polym. Sci., Macromol. Revs.*, 1973, vol. 7, pp. 263–290.
14. Hinch, E.J., *Colloques Internationaux du C.N.R.S*, no. 233, *Polymeres et Lubrification*, Paris, 1975, pp. 241–247.
15. Scrivener, O., *Colloques Internationaux du C.N.R.S*, no. 233, *Polymeres et Lubrification*, Paris, 1975, pp. 315–324.
16. Dancey, C.L., Balakrishnan, M., Diplas, P., and Papanicolaou, A.N., Exp. Fluids, 2000, vol. 29, pp. 402–410.
17. Sellin, R.H.J., *Colloques Internationaux du C.N.R.S*, no. 233, *Polymeres et Lubrification*, Paris, 1975, pp. 331–340.
18. Ayyash, S. and McComb, W.D., *Chem. Eng. Sci.*, 1976, no. 31, pp. 169–170.
19. Kalashnikov, V.N., *Trudy Vsesoyuznoi shkoly po reologii "Reologiya (Polimery i neft')"* [Proc. All-Union Symp on Rheology "Rheology (Polymers and Oil)"], Novosibirsk: Inst. Teplofiz., 1977, pp. 80–92.
20. Belokon', V.S., Vlasov, S.A., and Kalashnikov, V.N., *Inzh. Fiz. Zh.*, 1971, vol. 21, no. 5, pp. 892–897.
21. Brestkin, Yu.V., Dynamic Phase Transitions in a Flow of Polymer Fluids, *Doctoral Dissertation*, Leningrad, 1990.
22. de Gennes, P.-G., *Scaling Concepts in Polymer Physics*, Ithaca: Cornell Univ., 1979.
23. Povkh, I.L. and Stupin, A.B., *Trudy XVIII Sibirskogo teplofizicheskogo seminara "Pristennoe turbulentnoe techenie,"* (Proc. XVIII Siberian Thermal-Physic Seminar "Near-Wall Turbulent Flow"), Novosibirsk: Inst. Teplofiz., 1975, pp. 224–231.
24. Khabakhpasheva, E.M., *Trudy Vsesoyuznoi shkoly po reologii "Reologiya (Polimery i neft')"* [Proc. All-Union Symp on Rheology "Rheology (Polymers and Oil)"], Novosibirsk: Inst. Teplofiz., 1977, pp. 93–111.
25. Mikhailu, A.G., Diffusion and Heat Exchange in a Flow of a Fluid with Additives Diminishing the Turbulent Friction, *Cand. Sci. Dissertation*, Moscow, 1984.
26. Rabinovich, E.Z., *Gidravlika* (Hydraulics), Moscow: Nedra, 1980.
27. Hou, H., *3rd Int. Conf. Drag Reduction, Bristol, 2–5 July 1984*, Bristol, 1984, pp. C21–C26.
28. Escudier, M.P., Presti, F., and Smith, S., *J. Non-Newton. Fluid Mech.*, 1999, vol. 81, no. 3, pp. 197–213.
29. De Guzman, Manuel R., Takashi, S., Hiromoto, U., and Tatsuo, N., *J. Chem. Eng. Jap.*, 1999, vol. 32, no. 4, pp. 402–408.
30. Seo Young Hyo, Park O Ok, and Chun Miung-Suk, J. *Chem. Eng. Jap.*, 1996, vol. 29, no. 4, pp. 611–619.
31. Mjagchenkov, V.A., Chichkanov, S.V., Proskurina, V.E., and Krupin, S.V., *Georesources*, 2002, no. 6, pp. 19–23.
32. Brestkin, Yu.V., Frenkel, S.Ya., Zoolshoev, Z.F., *et al.*, *Vysokomol. Soedin.*, 1994, vol. 36A–B, no. 8, pp. 1281–1286.
33. Pogrebnyak, V.G. and Naumchuk, N.V., *Inzh. Fiz. Zh.*, 1995, vol. 68, no. 1, pp. 7–11.

34. Breder, C.M., *Fishery Bulletin*, 1976, no. 74, pp. 471–502.
35. Hoyt, J.W., *Swimming and Flying in Nature*, New York: Plenum, 1975, pp. 653–672.
36. Mashelkar, R.A., Kale, D.D., and Ulbrecht, *J. Transactions Inst. Chem. Eng.*, 1975, no. 53, pp. 143–153.
37. Oldaker, D.K. and Tiederman, W.G., *Phys. Fluids*, 1977, vol. 20, pp. S133–S144.
38. McLaughlin, D.K. and Tiederman, W.G., *Phys. Fluids*, 1973, vol. 6, pp. 2083–2088.
39. Grigoryan, S.S., Sokolova, I.A., and Shakhnazarov, A.A., *Usp. Fiziol. Nauk*, 1995, vol. 26, no. 2, pp. 31–43.
40. Poraiko, I.N., *Primenenie poliakrilamida v tekhnologicheskikh protsessakh, svyazannykh s dobychei nefti: Tematicheskii nauchno-tekhnicheskii obzor* (Use of Polyacrylamide in Technological Processes Associated with Oil Production: Sci.-Tekh. Subject Review), Moscow: VNIIOENG, 1974.
41. Nesyn, G.V., Manzhai, V.N., and Ilyushnikov, A.V., *Inzh. Fiz. Zh.*, 2003, vol. 76, no. 3, pp. 142–146.
42. Malkin, A.Ya., Nesyn, G.V., Manzhai, V.N., and Ilyushnikov, A.V., *Vysokomol. Soedin.*, 2000, vol. 42B, no. 2, pp. 377–384.
43. Povkh, I.L. and Chernyuk, V.V., *Inzh. Fiz. Zh.*, 1986, vol. 51, no. 3, pp. 357–361.
44. Kulik, V.M., *Inzh. Fiz. Zh.*, 1998, vol. 71, no. 3, pp. 491–495.
45. Makogon, B.P., Pavelko, M.M., Bondarenko, T.A., *et al., Inzh. Fiz. Zh.*, 1986, vol. 51, no. 1, pp. 47–52.
46. Martischius, F. and Heide, W., *3rd Int. Conf. Drag Reduction, Bristol, 2–5 July 1984*, Bristol, 1984, pp. D91–D93.
47. Si Qin, Xia Qing, Liu Qingpu, and Ha Runhua, *Petrochem. Technol.*, 1994, vol. 23, no. 8, pp. 523–526.
48. Mumick, Pavneet S., Hester, Roger D., and McCormick, Charles L., *Polym. Eng. Sci.*, 1994, vol. 34, no. 18, pp. 1429–1439.
49. Myagchenkov, V.A., Chichkanov, S.V., and Krupin, S.V., *Vserossiiskii simpozium "Khimiya: fundamental'nye i prikladnye issledovaniya, obrazovanie," Khabarovsk, 24–27 iyunya 2002 g.* (All-Russia Symp. "Chemistry: Basic and Applied Research, Education," Khabarovsk, June 24–27, 2002), Khabarovsk: Dal'nauka, 2002, vol. 1, pp. 78–80.
50. Myagchenkov, V.A., Chichkanov, S.V., Proskurina, V.E., and Myagchenkov, A.V., *Zh. Prikl. Khim.*, 2002, vol. 75, no. 9, pp. 1517–1520.
51. Tsvetkov, V.N., Eskin, V.E., and Frenkel, S.Ya., *Struktura makromolekul v rastvorakh* (Structure of Macromolecules in Solutions), Moscow: Nauka, 1964.
52. Berman, N.S. and George, W.K., *Proc. Heat Transfer and Fluid Mechanics Institute*, Davis, L.R. and Wilson, R.E., Eds., Stanford: Stanford Univ., 1974, pp. 348–364.
53. Berman, N.S. and Yuen, J., *2nd Int. Conf. Drag Reduction, Cranfield, 31 Aug.–2 Sept. 1977*, Cranfield, 1977, pp. C11–C110.
54. Myagchenkov, V.A., Chichkanov, S.V., and Krupin, S.V., *Neft. Khoz.*, 2002, no. 12, pp. 118–119.
55. Manzhai, V.N., Echevskaya, L.G., Ilyushnikov, A.V., *et al., Zh. Prikl. Khim.*, 2004, vol. 77, no. 3, pp. 456–460.
56. Baramboim, N.K., *Mekhanokhimiya vysokomolekulyarnykh soedinenii* (Mechanochemistry of Macromolecular Compounds), Moscow: Khimiya, 1971.
57. Brestkin, Yu.V., Frenkel, S.Ya., Chubarova, E.V., *et al., Vysokomol. Soedin.*, 1989, vol. 31B, no. 7, pp. 506–510.
58. Makogon, B.P., Structure, Hydrodynamic Efficiency, and Instability of Aqueous Solutions of Polyethylene Oxide and Polyacrylamide, *Cand. Sci. Dissertation*, Leningrad, 1989.
59. Makogon, B.P., Bykova, E.N., Bezrukova, M.A., *et al., Inzh. Fiz. Zh.*, 1985, vol. 48, no. 3, pp. 378–384.
60. Patterson, G.K., Shen, A.-M., and Chen, I.-M., *3rd Int. Conf. Drag Reduction, Bristol, 2–5 July 1984*, Bristol, 1984, pp. E41–E46.
61. Layec-Raphalen, M.N., *3rd Int. Conf. Drag Reduction, Bristol, 2–5 July 1984*, Bristol, 1984, pp. E21–E25.
62. Balakrischnan, C. and Gordon, R.J., *J. Appl. Polym. Sci.*, 1975, vol. 19, no. 3, pp. 909–913.
63. Hand, J.H. and Williams, M.C., *J. Appl. Polym. Sci.*, 1969, vol. 13, no. 11, pp. 2499–2503.
64. Parker, C.A. and Hegley, A.H., *Nature Physical Sci.*, 1972, vol. 236, no. 65, pp. 61–62.
65. White, D. and Gordon, R.J., *Am. Inst. Chem. Eng. J.*, 1975, vol. 21, no. 5, pp. 1027–1029.
66. Virk, P.S., *Am. Inst. Chem. Eng. J.*, 1975, vol. 21, no. 4, pp. 625–656.
67. Makogon, B.P., Pavelko, M.M., Toryanik, A.I., *et al.*, Abstracts of Papers, *III Vsesoyuznaya konferentsiya po mekhanike anomal'nykh sistem* (III All-Union Conf. on Mechanics of Anomalous Systems), Baku: Azineftekhim, 1982, p. 66.
68. Myagchenkov, V.A., Chichkanov, S.V., Krupin, S.V., and Proskurina, V.E., *Khim. Tekhnol. Vody*, 2003, vol. 25, no. 3, pp. 281–288.
69. Ait-Cady, A., Carreau, P., and Chauveteau, G., *J. Reol.*, 1987, vol. 31, no. 7, pp. 537–561.
70. Kulichke, W. and Grager, H., *3rd Int. Conf. Drag Reduction, Bristol, 2–5 July 1984*, Bristol, 1984, pp. A51–A52.
71. Mjagchenkov, V.A., Chichkanov, S.V., and Mjagchenkov, A.V., *Georesources*, 2004, no. 1, pp. 27–31.
72. Myagchenkov, V.A. and Chichkanov, S.V., *Zh. Prikl. Khim.*, 2003, vol. 76, no. 5, pp. 842–846.
73. Myagchenkov, V.A., Chichkanov, S.V., Krupin, S.V.,

and Proskurina, V.E., *Vestn. Kaz. Tekhnol. Univ.*, 2003, nos. 1–2, pp. 121–130.

74. Sellin, R.H.J. and Loeffler, E.J., *2nd Int. Conf. Drag Reduction, Cranfield, 31 Aug.–2 Sept. 1977*, Cranfield, 1977, pp. C211–C220.
75. Tronov, V.P. and Tronov, A.V., *Ochistka vod razlichnykh tipov dlya ispol'zovaniya v sisteme PPD* (Purification of Water of Various Kinds for Use in the PPD System), Kazan: Fen, 2001.
76. Myagchenkov, V.A., Chichkanov, S.V., and Krupin, S.V., *Neft. Khoz.*, 2003, no. 11, pp. 82–84.
77. Chichkanov, S.V., Myagchenkov, V.A., and Krupin, S.V., *12-i Evropeiskii simpozium "Povyshenie nefteotdachi plastov," Kazan, 8–10 sentyabrya 2003 g.* (12th Eur. Symp. "Raising the Oil Recovery from Oil Pools," Kazan, September 8–10, 2003), Kazan: Idel-Press, 2003, pp. 244–249.
78. Myagchenkov, V.A., Chichkanov, S.V., Proskurina, V.E., and Lebukhov, V.I., *Mezhdunarodnaya nauchnaya konferentsiya "Aziatsko-Tikhookeanskii region v global'noi politike, ekonomike i kul'ture XXI veka," Khabarovsk, 22–23 oktyabrya 2002 g.* (Int. Sci. Conf. Asian Pacific Region in Globasl Politics, economy, and Culture of the XXI Century," October 22–23, 2002), Khabarovsk: Khab. Gos. Ped. Univ., 2002, vol. 4, pp. 85–93.
79. Chichkanov, S.V., Krupin, S.V., and Myagchenkov, V.A., *IV Vserossiiskaya konferentsiya molodykh uchenykh "Sovremennye problemy teoreticheskoi i eksperimental'noi khimii," Saratov, 23–25 iyunya 2003 g.* (IV All-Russia Conf. of Young. Scientists "Modern Problems of Theoretical and Experimental Chemistry," Saratov, June 23–25, 2003), Saratov: Yul, 2003, pp. 218.
80. Myagchenkov, V.A., Chichkanov, S.V., Proskurina, V.E., and Krupin, S.V., *Georesursy*, 2003, no. 1, pp. 7–12.
81. Bewersdorff, H.-W., *Progr. Colloid. Polym. Sci.*, 1990, vol. 81, pp. 248–249.
82. Samuilov, V.O., *Protsessy teplomassoobmena v energeticheskikh ustanovkakh* (Heat-and-Mass Transfer in Power Installations), Minsk, 1990, pp. 21–25.
83. Chichkanov, S.V. and Myagchenkov, V.A., *Nauchno-metodicheskaya konferentsiya "III Kirpichnikovskie chteniya," Kazan, 25–28 marta 2003 g.* (Sci.-Methodol. Conf. "III Kirpichnikov Reading," Kazan, March 25–28, 2003, Kazan: Kazan. Gos. Tekh. Univ., 2003, pp. 285–286.
84. Chichkanov, S.V. and Myagchenkov, V.A., *Nauchnaya sessiya Kazanskogo Gosudarstvennogo Tekhnicheskogo Univesiteta, Kazan, 4–8 fevralya 2002 g.* (Scientific Session of Kazan State Technical University, Kazan, February 4–8, 2002), Kazan: Kazan. Gos. Tekh. Univ., 2002, p. 17.
85. Kurbanbaev, M., Gershtanskii, O.S., and Bulina, I.G., *Razrabotka neftegazovykh mestorozhdenii: Nauchno-Tekhicheskii Sovet Instituta KazNIPIneft'* (Development of Oil and Gas Fields: Sci.-Techn. Council of KazNIPIneft'), Moscow: VNIIOENG, 1993, issue 1, no. 1, pp. 63–67.
86. Smoll, S.R., *Neft', Gaz Netekhim. za Rubezh.*, 1986, no. 7, pp. 60–63.
87. Movsumzade, E.M., Mastobaev, B.N., Dmitrieva, T.V., and Zorina, S.R., *Neft' Ross.*, 2000, no. 8, pp. 21–27.
88. Zvereva, T.V., Chelintsev, S.N., and Yakovlev, E.I., *Modelirovanie truboprovodnogo transporta neftekhimicheskikh proizvodstv* (Modeling of the Pipeline Transport at Petrochemical Plants), Moscow: Khimiya, 1987.
89. Gareev, M.M., Nesyn, G.V., and Manzhai, V.N., *Neft. Khoz.*, 1992, no. 10, pp. 30–33.
90. Mastobaev, B.N., Dmitrieva, T.V., and Movsumzade, E.M., *Neft. Khoz.*, 2000, no. 11, pp. 107–108.
91. Movsumzade, E.M, Mastobaev, B.N., Dmitrieva, T.V., and Zorina, S.R., *Proizv. Ispol'z. Elastomer.*, 2000, no. 5, pp. 22–25.
92. Mastobaev, B.N. and Dmitrieva, T.V., *Bashk. Khim. Zh.*, 1999, vol. 6, no. 4, pp. 51–53.
93. Mastobaev, B.N. and Dmitrieva, T.V., *12-ya Mezhdunarodnaya konferentsiya "Khimicheskie reaktivy, reagenty i protsessy malotonnazhnoi khimii," Ufa, 7–9 sent. 1999 g.* (12th Int. Conf. "Chemicals, Reagents, and Processes of Low-Tonnage Chemistry," Ufa, September 7–9, 1999), Ufa, 1999, pp. 213–214.
94. Choi, H.J., Kim, C.A., and Jhon, M.S., *Polymer*, 1999, vol. 40, no. 16, pp. 4527–4530.
95. *Reibungsverminderer beim Mineraloiltransport in Pipelines Erdol–Erdgas–Kohle*, 1993, vol. 109, no. 11, pp. 458–465.
96. Katsyutsevich, E.V., Gostev, N.M., and Belousov, E.P., *Neftepererab. Neftekhim.*, 1990, no. 2, pp. 47–50.
97. Pozdnyshev, G.N., *Stabilizatsiya i razrushenie neftyanykh emul'sii* (Stabilization and Destruction of Oil Emulsions), Moscow: Nedra, 1982.
98. Tronov, V.P., *Promyslovaya podgotovka nefti* (Field Processing of Oil), Kazan: Fen, 2000.
99. *Itogi nauki i tekhniki, Ser. "Truboprovodnyi transport"* (Advances of Science and Technology, Ser. "Pipeline Transport"), Moscow: VINITI, 1976, vol. 6.
100. Gubin, V.E. and Gubin, V.V., *Truboprovodnyi transport nefti i nefteproduktov* (Pipeline Transport of Crude Oil and Oil Products), Moscow: Nedra, 1982.
101. Poraiko, I.N. and Vasilenko, S.N., *Transp. Khranen.-Nefti Nefteprodukt.*, 1975, no. 7, pp. 3–5.
102. Abuzova, F.F., Aliev, R.A., Novoselov, V.F., *et al.*, *Tekhnika i tekhnologiya transporta i khraneniya nefti i gaza* (Technology of Transport and Storage of Oil and Gas), Moscow: Nedra, 1992.
103. US Patent 4153575.
104. *Khimiya okruzhayushchei sredy* (Chemistry of

the Environment), Bokris, D.M., Ed., Moscow: Khimiya, 1982.

105. Myagchenkov, V.A. and Chichkanov, S.V., *Zh. Prikl. Khim.*, 2003, vol. 76, no. 11, pp. 1901–1905.
106. Chichkanov, S.V. and Myagchenkov, V.A., *Vestn. Kazan. Tekhnol. Univ.*, Kazan: Kazan. Gos. Tekh. Univ., 2003, nos. 1–2, pp. 322–334.
107. Myagchenkov, V.A. and Chichkanov, S.V., *Neft. Khoz.*, 2004, no. 1, pp. 93–95.
108. Chichkanov, S.V. and Myagchenkov, V.A., *Neftepromysl. Delo*, 2004, no. 11, pp. 42–46.
109. Chichkanov, S.V., Krupin, S.V., and Myagchenkov, V.A., *Interval*, 2004, no. 6, pp. 29–32.
110. Syunyaev, Z.I., Syunyaev, R.Z., and Safieva, R.Z., *Neftyanye dispersnye sistemy* (Dispersed Oil Systems), Moscow: Khimiya, 1990.
111. Chichkanov, S.V. and Myagchenkov, V.A., *Zh. Prikl. Khim.*, 2005, vol. 78, no. 4, pp. 669–672.
112. Grigoryan, S.S., Kameneva, M.V., and Shakhnazarov, A.A., *Dokl. Akad. Nauk SSSR*, 1976, vol. 231, no. 5, pp. 1070–1073.
113. Grigoryan, S.S., Sokolova, I.A., and Shakhnazarov, A.A., *Dokl. Ross. Akad. Nauk*, 1998, vol. 358, no. 6, pp. 842–843.
114. Levtov, V.A., Regirer, S.A., and Shadrina, N.Kh., *Reologiya krovi* (Rheology of Blood), Moscow: Meditsina, 1982.

Russian Journal of Applied Chemistry, Vol. 78, No. 4, 2005, pp. 538–540. Translated from Zhurnal Prikladnoi Khimii, Vol. 78, No. 4, 2005, pp. 545–547.
Original Russian Text Copyright © 2005 by Kolosov, Miroshnichenko, Orlov, Prokhorova.

INORGANIC SYNTHESIS AND INDUSTRIAL INORGANIC CHEMISTRY

Potassium-Reduced Tantalum Powders

V. N. Kolosov, M. N. Miroshnichenko, V. M. Orlov, and T. Yu. Prokhorova

Tananaev Institute of Chemistry and Technology of Rare Elements and Mineral Raw Materials, Kola Scientific Center, Russian Academy of Sciences, Apatity, Russia

Received December 21, 2004

Abstract—Properties of powders produced by potassium-reduction of tantalum from K_2TaF_7 were studied.

High-purity tantalum powders with a developed surface, which are necessary for manufacture of high-capacitance volume-porous capacitors, are mostly produced by metallothermic reduction from potassium heptafluorotantalate (K_2TaF_7). The role of the reducing metal is, as a rule, played by sodium:

$$K_2TaF_7(l) + 5Na(l) = Ta(s) + 5NaF(l) + 2KF(l). \quad (1)$$

Reaction (1) gives NaF (5 mol), which has a low solubility. Of interest is use of potassium as a reducing agent:

$$K_2TaF_7(l) + 5K(l) = Ta(s) + 7KF(l), \quad (2)$$

because only KF having a very high solubility is formed in reduction by reaction (2) in addition to powdered Ta. This would make it possible to decrease by more than an order of magnitude the amount of water necessary for removing salts from the reaction mass and favor their utilization [1]. In addition, this would facilitate production of powders with an exceedingly low content of sodium ($c_{Na} \le 2 \times 10^{-4}$ wt %), which is important for making lower the leakage current [2], one of the most important quality characteristics of capacitors.

The aim of this study was to examine properties of tantalum powders obtained with potassium used as a reducing metal.

EXPERIMENTAL

Tantalum(V) was reduced by reaction (2) by delivering liquid potassium and a flux to the surface of a K_2TaF_7 melt (liquid-phase reduction) [3]. Potassium heptafluorotantalate with a content of metallic impurities of less than 0.001 wt % for each impurity was used. Chemically pure KCl served as a flux for varying the concentration of K_2TaF_7 in the melt and lowering the melting point. It should be noted that use of other halides is undesirable in the given case. Use of KF as the flux would lead to a high melting point of the final melt, and addition of NaCl would result in formation of a sparingly soluble NaF in the melt via an exchange reaction with KF.

The experimental setup is shown schematically in Fig. 1. The stock composed of K_2TaF_7 and a flux was charged into a nickel vessel *1* and placed in the retort-reactor *2*. Potassium was available in an amount necessary for the reduction in a container *3*. After being assembled, the retort was placed in a furnace and

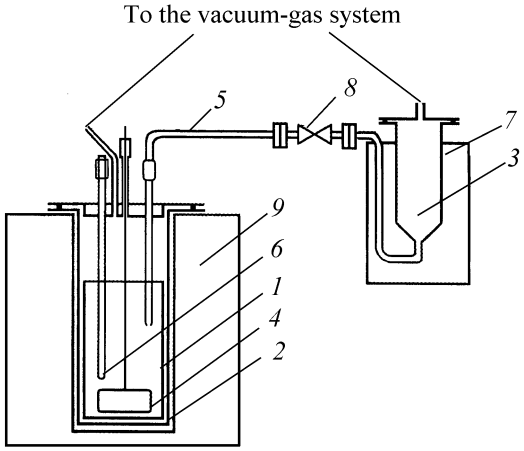


Fig. 1. Schematic of the experimental setup: (*1*) reaction vessel, (*2*) retort-reactor, (*3*) container with potassium, (*4*) rabble, (*5*) pipe, (*6*) thermocouple sheath, (*7*) electric heater of the container, (*8*) valve, and (*9*) electric heater of the reactor.

1070-4272/05/7804-0538 © 2005 Pleiades Publishing, Inc.

heated in a vacuum, with the temperature of the stock gradually raised. When the residual pressure decreased to approximately 5 Pa, the temperature was raised to melt the salts, the rabble *4* was lowered, and the melt was agitated until the melt was homogenized. Then, liquid potassium was delivered into the reactor via a pipe *5* under continuous agitation. The process was performed in the temperature range 750–850°C. After the reduction was complete, the reactor was cooled to room temperature. The tantalum powder formed was separated from the reaction products by hydrometallurgical treatment [1].

The specific surface area of the powders obtained was determined by the BET static adsorption method on a FlowSorb II 2300 installation. A morphological analysis of the powders was made with a SEM LEO-420 electron microscope. Anodes fabricated from the powders were sintered at 1650°C for 30 min. The anodes were oxidized at 80°C in a 1% H_3PO_4 solution to a voltage of 70 V and kept at this voltage for 3 h. The characteristics of the anodes were measured using the commonly accepted procedure.

The study was performed at a molar ratio K_2TaF_7 : KCl in the stock equal to 1, 2, and 3. The initial melting point of mixtures of this kind was in the range 725–775°C, and that after the completion of reduction was 730–820°C, depending on the content of KCl. Accordingly, the reduction process was performed in the temperature range 750–850°C. The results obtained indicate that replacing sodium with potassium as a reducing metal leads to a significant change in the granulometric composition of the resulting powders. With potassium used, up to 30% of the tantalum obtained was in the form of spongy mass with agglomerates more than 200 μm in size (Fig. 2a). At the same time, agglomerates of this kind are virtually absent upon reduction with sodium, irrespective of the process conditions. Finer particles of the powders had the same morphology as those of the powder produced by sodium reduction: equiaxed dendrite-like particles (Fig. 2b).

The formation of a spongy mass in reduction of Ta and Nb was observed by the authors of [4, 5], who developed the theory of electron-assisted reduction reactions [6]. According to this theory, metallothermic reduction involves not only electron transfer resulting from a direct physical contact between the reactants (see scheme). Also possible is an indirect electron transfer via an external circuit, without any direct contact (pathway b). In the authors' opinion, just mechanism b leads to formation of a spongy mass. However, such an explanation is hardly valid in the case

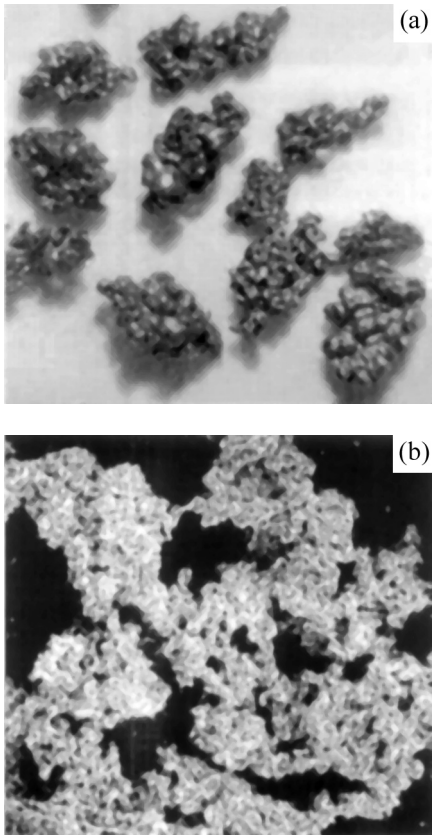
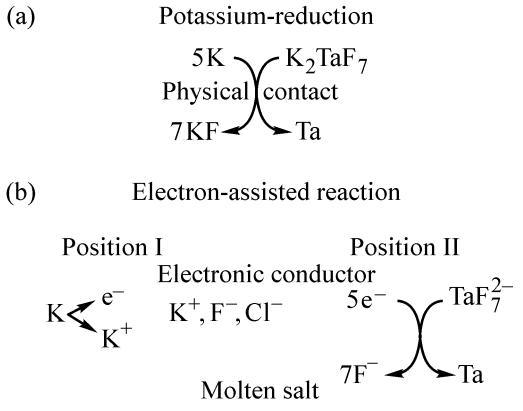


Fig. 2. Morphology of potassium-reduced tantalum powders. (a) Spongy mass, 20× magnification; (b) dendrite-like particles, 1000× magnification.

in question, because the spongy mass was formed in the solution bulk, rather than at reactor walls, in the case of a liquid-phase reduction with agitation.



Scheme of possible reaction pathways in metallothermic reduction.

It is more probable that the aggregative state of the reducing metal was the factor affecting the morphology of the product formed. The heat effect of reactions (1) and (2) involving Na and K in the liquid

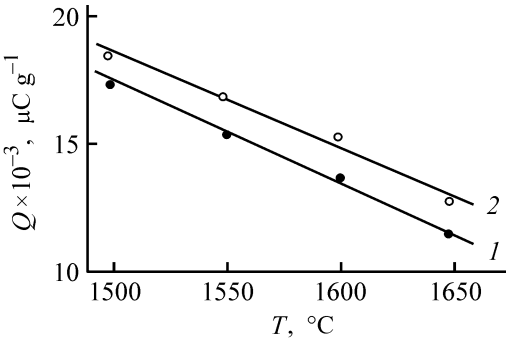


Fig. 3. Specific charge Q of the anodes vs. the sintering temperature T. Powders produced by reduction with (*1*) potassium and (*2*) sodium from a melt composed of KCl and 14 mol % K_2TaF_7.

state is about 1240 and 110 kJ kg^{-1} stock, respectively. As the potassium-induced reduction occurred at a temperature exceeding the boiling point of potassium (760°C), it may be assumed that the potassium vapor is involved in the reaction. In this case, the heat effect of reaction (2) is considerably higher (about 1850 kJ kg^{-1} stock). This may result in a substantial local overheating of the zone of powder particle formation, which favors growth of coarser and better faceted particles and their sintering. To minimize the involvement of the potassium vapor in the reaction, experiments with a stock with K_2TaF_7 : KCl : NaF = 1 : 4 : 2 and K_2TaF_7 : KCl = 1 : 6 molar ratios were carried out. This made it possible to perform reduction at a temperature of about 750°C, i.e., below the boiling point of potassium. The reduction carried out under these conditions resulted in a significant change in the properties of the Ta powder formed. Despite that the bulk density of the powder decreased by a factor of 2–2.5, the surface area remained virtually unchanged and was smaller than that of sodium-reduced powders obtained under the identical conditions. Accordingly, the specific charge of the anodes was lower, too (Fig. 3). A positive factor was that the leakage current of the anodes decreased by a factor of 1.5–2. A morphological analysis demonstrated that the >100-μm fraction of the powder obtained under these conditions is virtually completely composed of lamellate scaly particles. In the case of reduction in a melt containing NaF, which leads to an increase in the surface tension, the amount of this fraction was about 40%, of which 11% were more than 200 μm in size. As established previously, particles of this shape result from the formation of a metallic film on the surface of the melt [7]. In the case in question, the bath temperature measured in the bulk exceeded the freezing point of the melt only slightly. With account of thermal radiation, the temperature of the melt surface was even lower, which reflected upon the surface tension. The higher surface tension could favor formation of a considerable amount of scaly particles [8].

Thus, the study demonstrated that use of potassium as a reducing agent for obtaining tantalum powders from K_2TaF_7 makes it possible to simplify washing of the metal to remove salts, to diminish the content of Na in the powders, and to lower the leakage current of anodes. However, a considerable part of the powder formed is represented by a fraction unsuitable for capacitor anodes. Use of potassium as a reducing agent may be feasible if this part of the powder serves to produce a compact metal.

CONCLUSIONS

(1) It was found that replacing sodium as a reducing metal with potassium strongly affects the granulometric composition and morphology of the powders obtained. The potassium-reduction produced a considerable amount of spongy aggregates and resulted in a decrease in the yield of a powder suitable for fabrication of capacitor anodes.

(2) Reduction with potassium led, all other conditions being the same, to a decrease in the specific surface area of the powders obtained and resulted in that the anode capacitance became lower by 5–10% and the leakage current of the capacitor anodes decreased by a factor of 1.5–2.

REFERENCES

1. Belyaev, K.Yu., Orlov, V.M., Prokhorova, T. Yu., and Savotkina, M.N., *Tekhnologiya mineral'nogo syr'ya i svoistva soedinenii redkikh metallov* (Technology of Mineral Raw Materials and Properties of Compounds of Rare Metals), Apatity: Kola Nauchn. Tsentr Ross. Akad. Nauk, 1997, pp. 24–33.
2. Tripp, T.B., *Tantalum and Niobium, Proc. Int. Symp., 24–28th September 1995*, Goslar, Germany, 1995, pp. 219–226.
3. Tripp, T.B., Naito, H., and Anderson, K., *TIC Bull.*, 1995, no. 82, pp. 4–7.
4. Okabe, T.H., Park, Il, Jacob, K.T., and Waseda, Y., *J. Alloys Compd.*, 1999, vol. 288, pp. 200–210.
5. Park, Il, Okabe, T.H., and Waseda, Y., *J. Alloys Compd.*, 1998, vol. 280, pp. 265–272.
6. Okabe, T.H. and Sadoway, D.R., *J. Mater. Res.*, 1998, vol. 13, no. 12, pp. 3372–3377.
7. Orlov, V.M., Belyaev, K.Yu., Prokhorova, T.Yu., *et al.*, *Persp. Mater.*, 2002, no. 3, pp. 74–78.
8. Kolosov, V.N., Orlov, V.M., Prokhorova, T.Yu., and Belyaevskii, A.T., *Rasplavy*, 2003, no. 2, pp. 57–60.

Russian Journal of Applied Chemistry, Vol. 78, No. 4, 2005, pp. 541–545. Translated from Zhurnal Prikladnoi Khimii, Vol. 78, No. 4, 2005, pp. 548–552.
Original Russian Text Copyright © 2005 by Sizeneva, Kondrashova, Val'tsifer.

INORGANIC SYNTHESIS AND INDUSTRIAL INORGANIC CHEMISTRY

Spontaneous Decomposition of Industrially Manufactured Sodium Hypochlorite Solutions

I. P. Sizeneva, N. B. Kondrashova, and V. A. Val'tsifer

Institute of Technical Chemistry, Ural Division, Russian Academy of Sciences, Perm, Russia

Received December 16, 2004; in final form, November 2004

Abstract—Spontaneous decomposition of industrially manufactured aqueous solutions of sodium hypochlorite was studied. The rate constants of the decomposition reactions were calculated for different pH values.

In view of the exceedingly high toxicity and volatility of metallic mercury (MPC for habitats 0.0003 mg m^{-3}) [1] and its wide use, the problem of efficient salvation in tackling with possible mercury spillage events remains a matter of current interest. For this purpose, new demercurization methods are being developed and the already existing techniques are being improved. At present, the most widely used methods are those in which mercury is oxidized with strong oxidizing agents [2, 3]. In developing a demercurizer, with industrially manufactured sodium hypochlorite (HC) solutions as an oxidizing agent, it became necessary to assess the stability of solutions of this kind in storage and to study the oxidizing activity of these industrial solutions at various pH values.

HC solutions are nonequilibrium systems that undergo spontaneous decomposition. The problem of spontaneous decomposition of HC solutions has been extensively studied. The influence exerted by the concentration, temperature, and acidity on decomposition processes has been analyzed and the possible mechanisms and kinetic characteristics of decomposition have been reported [4–8]. In the known studies, solutions of both calcium and sodium HC were examined. Model solutions have been mostly studied, with the HC solutions having low concentrations: 0.01–0.20 M in terms of active chlorine.

The aim of this study was to assess the stability of industrially manufactured concentrated HC solutions in order to determine the maximum shelf life of solutions of this kind. Another goal was to determine the kinetic characteristics of real solutions used to prepare the demercurizing agent.

The choice in developing the demercurizer was made in favor of sodium HC, taking into account its availability as a solution, high content of active chlorine, and high stability against decomposition in an alkaline medium (compared with calcium HC) [9]. The behavior of the solutions was analyzed at two temperatures, 25 and 35°C, in view of the regional climatic conditions (the maximum summer temperature is not, as a rule, higher than 35°C).

EXPERIMENTAL

As object of study served industrially manufactured (Berezniki Soda Plant Open Joint-Stock Company) sodium HC solution with a concentration of 180–200 g l^{-1} in terms of active chlorine. Model solutions were prepared by passing at (0–5°C) Cl_2 obtained by reacting chemically pure hydrochloric acid with $KMnO_4$ through a NaOH solution containing no carbonates. The excess amount of the alkali was about 20 g l^{-1}. The reaction vessel was cooled with a mixture of NaCl and ice. The pH values of the solutions were measured with an EV-74 ionometer with glass and silver chloride electrodes.

In stability studies, the alkaline (pH 13.5) HC solutions under study were thermostated in hermetically sealed polyethylene jars for 3 months. The pH value of the solutions remained virtually constant, irrespective of the duration and temperature of experiments, because of the presence of an excess amount of NaOH in the HC solutions.

The dependence of the degree of HC decomposition on the pH value was studied at 25 and 30°C.

1070-4272/05/7804-0541 © 2005 Pleiades Publishing, Inc.

Table 1. Decomposition of industrially manufactured sodium HC in solutions of different concentrations at 25 and 35°C

T, °C	t, h	Variation of c in storage, M	k, mol l^{-1} h^{-1}	Variation of c in storage, M	k, mol l^{-1} h^{-1}
25	0	c_{in} = 5.20 M		c_{in} = 2.10 M	
	144	5.10	0.2618×10^{-4}	2.09	0.2060×10^{-4}
	216	4.86	0.6229×10^{-4}	2.08	0.2120×10^{-4}
	312	4.50	0.9588×10^{-4}	2.07	0.4579×10^{-4}
	384	4.39	0.9240×10^{-4}	2.00	0.6200×10^{-4}
	480	4.19	0.9658×10^{-4}	1.97	0.6547×10^{-4}
	696	3.90	0.9210×10^{-4}	1.92	0.6414×10^{-4}
	1272	3.20	0.9449×10^{-4}	1.80	0.6239×10^{-4}
	2040	2.70	0.9078×10^{-4}	1.64	0.6253×10^{-4}
k_{av} (312–2040 h) = $(0.9371 \pm 0.0225) \times 10^{-4}$				k_{av} (384–2040 h) = $(0.6296 \pm 0.0155) \times 10^{-4}$	
35	0	c_{in} = 5.20 M		c_{in} = 2.10 M	
	144	4.50	0.2077×10^{-4}	2.00	0.1653×10^{-4}
	216	4.20	0.2119×10^{-3}	1.95	0.1695×10^{-3}
	312	3.65	0.2617×10^{-3}	1.89	0.1696×10^{-4}
	384	3.45	0.2540×10^{-3}	1.85	0.1676×10^{-3}
	480	3.23	0.2444×10^{-3}	1.80	0.1653×10^{-3}
	696	2.76	0.2443×10^{-3}	1.69	0.1660×10^{-3}
	960	2.12	0.2910×10^{-3}	1.58	0.1633×10^{-3}
	1272	1.84	0.2761×10^{-3}	1.46	0.1641×10^{-3}
	2136	1.30	0.2649×10^{-3}	1.20	0.1672×10^{-3}
k_{av} = $(0.2507 \pm 0.0266) \times 10^{-3}$				k_{av} (384–2040 h) = $(0.1668 \pm 0.021) \times 10^{-3}$	

The experiments were performed with solutions containing the same amounts of active chlorine (1.24, 1.29 M) at a virtually constant pH value, which was continuously monitored during the experiments. The acidity of the medium was adjusted by adding an H_2SO_4 solution. The degree of decomposition was determined after 10 min.

To study the kinetics of decomposition at different acidities, HC solutions were placed in hermetically sealable glass jars, with the required acidity adjusted by introduction of an HCl solution. Changes in the acidity of the medium and in the concentration were determined at regular intervals of time. In all the experiments, the variation of the HC concentration was monitored iodometrically.

The experiments in which the stability of sodium HC solutions was studied were carried out with industrial and model solutions of close concentrations. The data obtained were used to calculate the order of the reaction by which the alkaline solution of sodium HC decomposes, using the known Van't Hoff formula

$$n = \frac{w_1/w_2}{\log(c_1/c_2)}.$$

This formula makes it possible to determine the reaction order n from the initial rates w_1 and w_2, i.e., from the reaction rates at different initial concentrations c_1 and c_2 of the starting HC.

The calculations demonstrated that spontaneous decomposition of sodium HC in alkaline solutions occurs as a second-order reaction at both 25 and 35°C. The second reaction order was also obtained by graphical differentiation from the slope of the dependence of the rate of HC decomposition on the logarithm of the concentration, $\log(-\Delta c/\Delta t) - \log c$. The rate constants of the decomposition reaction were calculated using second-order kinetic equations

$$k = 1/t \frac{c_0 - c}{c_0 c}.$$

The results obtained are listed in Table 1.

The second order of the reactions and the formal rate constants of decomposition were obtained using

the above-described procedures for a model HC solution with a concentration of 2.26 M at two temperatures: $k_{av} = 0.2060 \times 10^{-4}$ M at 25°C and $k_{av} = 0.1064 \times 10^{-3}$ M at 35°C.

The activation energies calculated using the Arrhenius equation

$$E = \frac{\log (k_2/k_1)}{(T_2 - T_1)/T_2T_1},$$

were 82.33 kJ mol^{-1} (19.67 kcal mol^{-1}) for a sodium HC solution with a concentration of 5.2 M and 79.53 kJ mol^{-1} (19.00 kcal mol^{-1}) for that with a concentration of 2.1 M. The results obtained are in an agreement with published data for alkaline HC solutions [10].

The decomposition of HC consists of two concurrent processes, oxygen and chlorate decompositions, which can be expressed by the following reactions

$$ClO^- + ClO^- = 2Cl^- + O_2, \quad \text{(I)}$$

$$ClO^- + ClO^- = ClO_2^- + Cl^-, \quad \text{(II)}$$

$$ClO_2^- + ClO^- = ClO_3^- + Cl^-. \quad \text{(III)}$$

The rate-determining reactions are (I) and (II), whereas reaction (III) is considerably faster than the first two [11].

As can be seen in Table 1, a certain deviation from the average kinetic parameters (reaction orders, reaction rate constants) is observed in the initial stage of the process (~216 h) at 25°C, which can be attributed to predominance of the oxygen decomposition [11]. At 35°C, the process is considerably faster: the chlorate decomposition predominates. The model solutions decompose in a similar way.

The experimental data were used to compare the decomposition rates of sodium HC in industrially manufactured and model solutions at 25 and 35°C. Figures 1 and 2 show kinetic curves that describe the self-decomposition of alkaline solutions of sodium HC. It can be seen that that the processes of spontaneous decomposition are autocatalytic at 25°C, with the process rates dependent on the initial concentration. The calculated rate constants of HC decomposition were used to compare the decomposition rates of HC in solutions with different concentrations at this temperature.

For example, sodium HC decomposes at 25°C in the solution with a concentration of 5.2 M approximately 1.5 times faster than in that with a concentration of 2.1 M. The temperature dependence of the decomposition rate is particularly strong. The decomposition is approximately 2.8 times faster at 35°C, compared with 25°C, for the solution with a sodium HC concentration of 5.2 M, and 2.65 times faster at a concentration of 2.1 M.

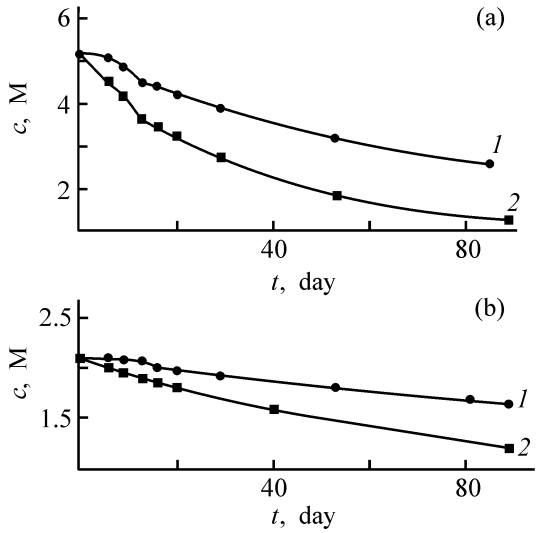


Fig. 1. Stability of industrially manufactured sodium hypochlorite solutions with a concentration of (a) 5.2 and (b) 2.1 M. (*c*) Concentration and (*t*) time; the same for Fig. 2. Temperature (°C): (*1*) 25 and (*2*) 35.

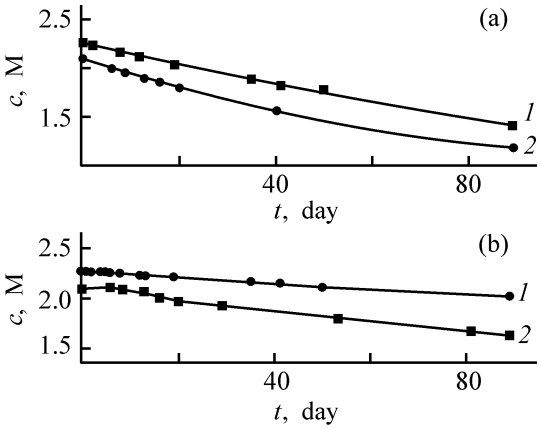


Fig. 2. Stability of (*1*) model sodium hypochlorite solutions with a concentration of 2.26 M and (*2*) industrially manufactured sodium hypochlorite solutions with a concentration of 2.1 M at (a) 35 and (b) 25°C.

Comparison with model solutions shows that decomposition of a diluted industrially manufactured sodium HC solution with a concentration of 2.1 M at 25°C is approximately 3 times faster than that of a model solution with a close concentration (c = 2.26 M). This can be attributed to presence in the industrial solution of mostly colloid particles of iron

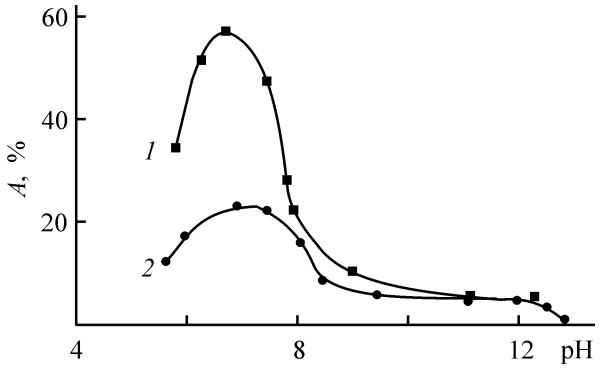


Fig. 3. Degree of sodium hypochlorite decomposition, *A*, vs. the pH value. (*A*) Ratio of the number of decomposed moles of HClO + ClO^- to their initial number. c_0 (M): (*1*) 1.24 and (*2*) 1.29. Temperature (°C): (*1*) 30 and (*2*) 25.

hydroxide $Fe(OH)_3$. These particles have an excess energy and accelerate the decomposition of HC, with the catalytic action of $Fe(OH)_3$ becoming less pronounced in the course of time, which is commonly accounted for by a decrease in dispersity, named "aging" [12]. At 35°C, the decomposition rate of the industrial solution exceeds that of the model solution only by approximately a factor of 1.5, because the accelerating effect of temperature equally tells upon the decomposition of both HC solutions. At the same time, the catalytic action of $Fe(OH)_3$ on the decomposition of the industrial becomes less pronounced as temperature increases, because a higher temperature favors coagulation, i.e., leads to coarsening of colloid particles and, consequently, to a decrease in their total surface area and excess energy.

The stability and oxidizing power of sodium HC solutions are strongly dependent on the activity of hydrogen ions in solution. Figure 3 shows how the degree of HC decomposition depends on the pH value at 25 and 30°C. It can be seen that the maximum degree of HC decomposition is observed at pH close to 7.

Table 2. Dynamics of variation of the pH value and concentration of sodium HC solutions

Solution no.	*t*, h	*c*, M	pH
1	0	1.188	8.06
	0.5	0.689	7.84
	1.0	0.437	7.52
	2.0	0.255	6.09
	3.0	0.207	6.05
	4.0	0.185	6.45
2	0	0.941	4.83
	96	0.323	5.01
	168	0.182	5.30
	384	0.132	5.25
	528	0.105	5.22

It is known that not only the mechanisms of HC decomposition in alkaline, neutral, and acid media, but also the rates of this process are different: the decomposition rate is at a minimum in a strongly acidic medium (pH < 1), increases with the pH value to reach a maximum in a nearly neutral medium, and then again decreases in an alkaline medium. Thus, the activity of hydrogen ions is one of the key factors affecting the composition and stability of HC solutions and, consequently, their oxidizing power [13–15].

The decomposition kinetics of industrial sodium HC solutions was studied at pH 6.5–8.0 (solution no. 1, c_0 = 1.188 M) and pH 4.8 (solution no. 2, c_0 = 0.941 M) at room temperature (21–22°C). A fast change in both the pH of the medium and the HC concentration was observed at pH 6.5–8.0. The experimental data obtained are listed in Table 2.

The order of the reaction of HC decomposition was determined from the variation of the HC concentration with time, and the rate constants of the reaction were calculated. The reaction order was found using the graphical variety of the method of substitution of experimental data (HC concentrations at different instants of time in the course of the reaction) into first-, second-, and third-order kinetic equations. For this purpose, time dependences of various functions of concentration were constructed. Each kinetic equation gives a straight line only in the appropriate coordinates [16]. Both for pH 6.5–8.0 and for pH 4.8, a linear plot was obtained for the $1/c$–t dependence, i.e., for a second-order kinetic equation. The reaction order was confirmed, as in the case of an alkaline medium, by graphical differentiation. The rate constants were calculated for a second-order kinetic equation:

pH	k, $l^{-1}\ mol^{-1}\ h^{-1}$
4.80	$(2.12 \pm 0.60) \times 10^{-2}$
8.0–6.5	1.34 ± 0.20
13.5	$(0.63 \pm 0.02) \times 10^{-4}$

It was noted in [8] that the reaction at pH 6.0–8.0 is so fast that the rate of self-decomposition increases by several orders of magnitude to become comparable with that of fast reactions.

The same dependence was observed in the present study.

The decomposition of sodium HC solutions at pH < 4.8 was not considered because preparation of solutions of this kind is accompanied by vigorous evolution of Cl_2, which leads to its waste and inefficient use of HC.

CONCLUSIONS

(1) An assessment of the stability of industrially manufactured sodium hypochlorite solutions revealed that dilute sodium hypochlorite solutions are the most stable in storage at temperatures not exceeding 25°C. It was shown that model hypochlorite solutions prepared with distilled water are more stable in storage than the industrially manufactured solutions.

(2) It was demonstrated that the spontaneous decomposition of industrial sodium hypochlorite solutions in a wide range of pH values (4.8–13.5) is a second-order reaction. The rate constants of the decomposition process, calculated at different pH values, confirmed the extremal type of the dependence of the decomposition rate on the pH value. It was shown that the decomposition pattern of dilute hypochlorite solutions is also valid for concentrated solutions.

REFERENCES

1. Trakhtenberg, I.M. and Korshun, M.N., *Rtut' i ee soedineniya v okruzhayushchei srede* (Gigienicheskie i ekologicheskie aspekty) [Mercury and Its Compounds in the Environment (Hygienic and Ecological Aspects)], Kiev: Vysshaya Shkola, 1990.
2. Mel'nikov, S.M., *Tekhnika bezopasnosti v metallurgii rtuti* (Safety Measures in Metallurgy of Mercury), Moscow: Metallurgiya, 1974.
3. Zakharov, L.N., *Tekhnika bezopasnosti v khimicheskikh laboratoriyakh* (Sfety Measures in Chemical Laboratories), Leningrad: Khimiya, 1985.
4. Flis, I.E. and Bynyaeva, M.K., *Zh. Prikl. Khim.*, 1957, vol. 30, no. 3, pp. 339–345.
5. Flis, I.E., *Zh. Prikl. Khim.*, 1963, vol. 36, no. 8, pp. 1669–1675.
6. Grigor, T.T., Tumanova, T.A., Mishchenko, K.P., and Shalanki, L., *Zh. Prikl. Khim.*, 1967, vol. 40, no. 9, pp. 2039–2044.
7. Nikol'skii, B.P., Krunchak, V.G., L'vova, T.V., *et al.*, *Dokl. Akad. Nauk SSSR*, 1970, vol. 191, no. 6, pp. 1324–1326.
8. Nikol'skii, B.P., Krunchak, V.G., Pal'chevskii, V.V., and Sosnovskii, R.I., *Dokl. Akad. Nauk SSSR*, 1971, vol. 197, no. 1, pp. 140–142.
9. Krunchak, V.G., *Zh. Prikl. Khim.*, 1974, vol. 47, no. 9, pp. 2112–2113.
10. Perel'man, F.M. and Zvorykin, A.Ya., *Zh. Fiz. Khim.*, 1955, vol. 29, no. 6, pp. 980–982.
11. Prokopchik, A.Yu., *Zh. Fiz. Khim.*, 1955, vol. 29, no. 6, pp. 1020–1026.
12. Prokopchik, A.Yu. and Yanitskii, I.V., *Zh. Fiz. Khim.*, 1954, vol. 28, no. 11, pp. 1999–2005.
13. Nikol'skii, B.P. and Flis, I.E., *Trudy Len. Tekhnol. Inst.*, 1949, no. 1, pp. 61–90.
14. Nikol'skii, B.P. and Flis, I.E., *Zh. Obshch. Khim.*, 1952, vol. 22, no. 8, pp. 1298–1307.
15. Flis, I.E., *Zh. Prikl. Khim.*, 1958, vol. 31, no. 8, pp. 1194–1201.
16. Stromberg, A.G. and Semchenko, D.P., *Fizicheskaya khimiya* (Physical Chemistry), Moscow: Vysshaya Shkola, 1973.

Russian Journal of Applied Chemistry, Vol. 78, No. 4, 2005, pp. 546–548. Translated from Zhurnal Prikladnoi Khimii, Vol. 78, No. 4, 2005, pp. 553–555.
Original Russian Text Copyright © 2005 by Sizeneva, Val'tsifer, Strel'nikov.

INORGANIC SYNTHESIS AND INDUSTRIAL INORGANIC CHEMISTRY

A Study of Mercury Dissolution in Aqueous Solutions of Sodium Hypochlorite

I. P. Sizeneva, V. A. Val'tsifer, and V. N. Strel'nikov

Institute of Technical Chemistry, Ural Division, Russian Academy of Sciences, Perm, Russia

Received December 16, 2004

Abstract—Dissolution of mercury in aqueous solutions of sodium hypochlorite at pH 5.9–8.5, the corresponding reaction order, and the mechanism of this process were studied. The ratio of the rates of mercury oxidation and sodium hypochlorite decomposition was analyzed.

Salts of hypochlorous acid, hypochlorites, find wide application as strong oxidizing agents, their oxidizing power being largely determined by the acidity of the medium.

The aim of this study was to assess the possibility of using a sodium hypochlorite (NaClO) solution at pH 5.9–8.5 for oxidation of mercury and to determine the rate constants of mercury dissolution via its oxidation to Hg^{2+} ions in the above-mentioned acidity range.

EXPERIMENTAL

Mercury was oxidized with an aqueous solution of NaClO at pH 5.9, 6.5, 6.9, and 8.5 and temperatures of 25 and 50°C; the concentration in terms of active chlorine was 0.3–0.8 M. The required acidity was created with a buffer phosphate solution obtained by adding orthophosphoric acid, potassium dihydrophosphate, and sodium hydrophosphate to the NaClO solution. The pH value was monitored with an EV-74 ionometer with glass and silver chloride electrodes.

The NaClO solution was produced by passing chlorine through a carbonate-free solution of sodium hydroxide at a temperature of –5…0°C. The reaction vessel was cooled with a mixture of sodium chloride and ice. Chlorine was obtained by reacting chemically pure hydrochloric acid with potassium permanganate. The concentration of the hypochlorite was determined iodometricaly.

A mercury drop of mass 0.05–0.15 g was placed in a hermetically sealable glass jars thermostated at 25 and 50°C, and 50 ml of a sodium hypochlorite solution with certain acidity was added. The Hg^{2+} concentration was determined at regular intervals of time by a selective spectrophotometric technique with dithizone [1]. The optical density of the solutions was determined with a KFK-2 photoelectric colorimeter.

Mercury is a metal that is liquid at room temperature. The high surface tension allows even comparatively large mercury drops to take the shape of a sphere, the body with the smallest relative surface area. Dissolution of mercury is a heterogeneous process that occurs at the interface and depends on the area and state of the surface. Kinetic characteristics of the process of mercury dissolution in sodium hypochlorite solutions were determined using the formula established experimentally by A.N. Shchukarev for the rate of dissolution of a solid body in a liquid [2, 3]. This formula made it possible to calculate the rate constant k of mercury dissolution:

$$w = kS(c_s - c),$$

where w is the dissolution rate; S, area of contact between the solid and liquid; c, concentration of the substance being dissolved in the bulk of the liquid; c_s, concentration of a saturated solution; and k, constant for the given experimental conditions.

As the concentration of a saturated solution was taken the maximum possible concentration of Hg^{2+} ions. The latter was determined from the mass of the mercury drop and the volume of the hypochlorite solution in which it dissolved. The rate of mercury dissolution was found from the concentration of mercury(II) at certain instants of time. The contact area was calculated from the mass of a spherical drop of mercury and its density [4] at a given temperature.

1070-4272/05/7804-0546 © 2005 Pleiades Publishing, Inc.

The order of the dissolution reaction was determined for two mercury drops with different masses by the Van't Hoff formula

$$n = (\log w_1 - \log w_2)/(\log c_1 - \log c_2),$$

which includes reaction rates for two concentrations of the starting substance.

The parameters of the reaction of mercury dissolution at pH 5.9–8.5 are listed in the table. The kinetic curves plotted as the Hg^{2+} concentration c vs. time t (Fig. 1a) and $\log c$ vs. t (Fig. 1b) confirm the first reaction order obtained by calculation, because the time dependence of the concentration of Hg^{2+} ions is exponential, and that of $\log c$, linear (see Fig. 1). The activation energies were calculated using the Arrhenius equation from the dissolution rate constants for 25 and 50°C. The results obtained are listed in the table.

The dissolution of mercury is a heterogeneous process in which a kinetic region, with the process rate determined by the chemical reaction, and a diffusion region, with the process rate determined by diffusion, can be distinguished. As a rule, the reaction occurs in the kinetic mode at low temperatures. As the temperature is raised, the rate constant of the chemical process rapidly increases and, at a certain temperature at which the rate constant of the chemical reaction becomes higher than that of diffusion, the heterogeneous process passes from the kinetic to the diffusion region. It has been noted in the literature [2] that, if the activation energy is 5–20 kJ mol^{-1}, the process can be identified as occurring in the diffusion mode. If the activation energy is 50–200 kJ mol^{-1}, then the heterogeneous process occurs in the kinetic region. In the intermediate region, the rate of the heterogeneous process is determined both by diffusion and by the chemical process at the phase boundary. The calculated activation energies suggest that the dissolution of mercury proceeds in the intermediate region, with its rate determined both by the rate of the chemical reaction and by the diffusion process.

The temperature dependence of the reaction rate is characterized by the temperature coefficient defined as the amount by which the rate increases on raising the temperature by 10°C. The temperature coefficients are 2–4 for the rate of the chemical reaction, $\gamma_{ch} = (k_{ch})_{T+10}/(k_{ch})_T$, and 1.1–1.4 for that of the diffusion process, $\gamma_D = (k_D)_{T+10}/(k_D)_T$, [2]. According to this rule, an increase in the reaction rate by at least a factor of 6 would be observed on raising the temperature by 25°C if the dissolution of mercury preferentially occurred in the kinetic region. However, the reaction rate actually increases by only a factor of 2.6–4, which points to a substantial influence exerted by the diffusion process on the dissolution of mercury. The same is indicated by the temperature coefficients of mercury dissolution, calculated for different pH values. The range pH 6–7 corresponds to the maximum decomposition rate of hypochlorite and, as a result, to a high rate of mercury oxidation by active chlorine evolved in the decomposition. Therefore, the key role in the dissolution process is played in the given case by diffusion. On passing to the alkaline region, the rate of hypochlorite decomposition markedly decreases and the chemical reaction of oxidation starts to exert a noticeable influence on the process at pH 8.5. The observed increase in the dissolution rate on raising the temperature to 50°C is small as compared with that expected. This is probably accounted for by a rise in the instability of the hypochlorite solution with increasing temperature, which is accompanied by a decrease in the concentra-

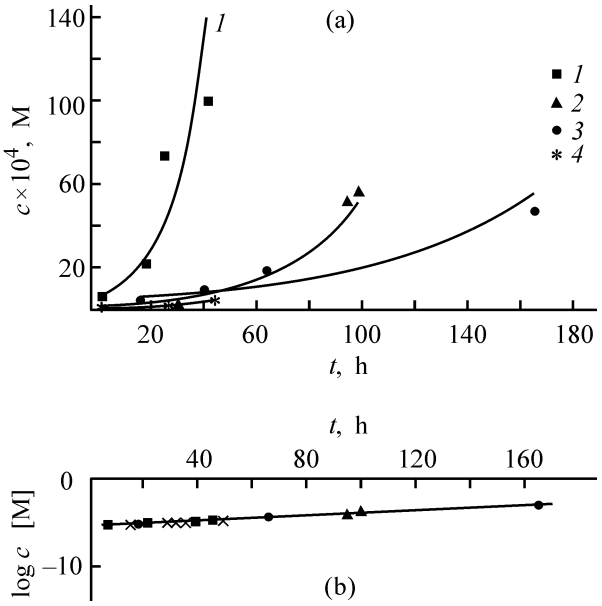


Fig. 1. Kinetic curves of mercury dissolution at 25°C. (c) Concentration of Hg^{2+} ions and (t) time. Variation of the Hg^{2+} concentration at pH: (*1*) 6.5, (*2*) 6.9, (*3*) 5.9, and (*4*) 8.5.

Parameters of the reaction of mercury dissolution

pH	k, cm^{-1} h^{-1}		γ^*	E, kJ mol^{-1}	Reaction order
	25°C	50°C			
5.90	2.17×10^{-3}	–			1.003
6.50	1.18×10^{-3}	3.65×10^{-2}	1.24	36.15	1.008
6.90	2.07×10^{-2}	5.38×10^{-2}	1.04	30.58	1.010
8.50	6.75×10^{-3}	2.68×10^{-3}	4.00	44.15	–

* γ, temperature coefficient of the dissolution process.

tion of active chlorine and the resulting decline in the oxidizing power.

It was established experimentally that the reaction of self-decomposition of hypochlorite occurs at the maximum rate at pH 6–8.5 and is first-order with respect to the concentration of hydrogen ions, i.e., the self-decomposition rate changes by a factor of 10 upon a unity change in the pH value. Therefore, the self-decomposition rate increases at pH 6–8.5 by several orders of magnitude, to become comparable with the rate of fast reactions [5–7]. The maximum rate of mercury dissolution is observed at pH 6.5–6.9, which correlates well with published data for the maximum rate of hypochlorite decomposition (pH ~7) [8]. The rate constant of mercury dissolution at pH 5.9–8.5 is $(0.2–2.0) \times 10^{-2}$, i.e., the decomposition rate of the hypochlorite is many times that of mercury oxidation. Therefore, in the authors' opinion, use of sodium hypochlorite for oxidation of mercury in this pH range is inadvisable because most part of active chlorine is wasted without having enough time for entering into the reaction.

CONCLUSIONS

(1) The rate constants of mercury dissolution in hypochlorite solutions at pH 5.9–8.5 were calculated. It was shown that the maximum rate of mercury dissolution is observed at pH 6.5–6.9.

(2) It was established that the reaction of mercury dissolution is first-order. The apparent activation energies of 30–44 kJ mol^{-1} indicate that the heterogeneous dissolution occurs in the intermediate region, in which both the chemical reaction and diffusion affect this process.

(3) It was found that the rate of mercury oxidation by sodium hypochlorite at pH 5.9–8.5 is considerably lower than the decomposition rate of the hypochlorite itself.

REFERENCES

1. *Unifitsirovannye metody analiza vod* (Unified Methods for Analysis of Water), Lur'e, Yu.Yu., Ed., Moscow: Khimiya, 1973.
2. Stromberg, A.G. and Semchenko, D.P., *Fizicheskaya khimiya* (Physical Chemistry), Moscow: Vysshaya Shkola, 1973.
3. Golikov, G.A., *Rukovodstvo po fizicheskoi khimii* (Manual of Physical Chemistry), Moscow: Vysshaya Shkola, 1988.
4. Mel'nikov, S.M., *Metallurgiya rtuti* (Metallurgy of Mercury), Moscow: Metallurgiya, 1971.
5. Nikol'skii, B.P., Krunchak, V.G., Pal'chevskii, V.V., and Sosnovskii, R.I., *Dokl. Akad. Nauk SSSR*, 1971, vol. 197, no. 1, pp. 140–142.
6. Nepenin, N.N., *Tekhnologiya tsellyulozy* (Technology of Cellulose), Moscow: Goslesbumizdat, 1956.
7. Pozin, M.E., *Tekhnologiya mineral'nykh solei* (Technology of Mineral Salts), Moscow: Goskhimizdat, 1961.
8. Nikol'skii, B.P. and Flis, I.E., *Zh. Obshch. Khim.*, 1952, vol. 22, no. 8, pp. 1298–1307.

Russian Journal of Applied Chemistry, Vol. 78, No. 4, 2005, pp. 549–551. Translated from Zhurnal Prikladnoi Khimii, Vol. 78, No. 4, 2005, pp. 556–558.
Original Russian Text Copyright © 2005 by Zhernovoi, Naumov.

INORGANIC SYNTHESIS AND INDUSTRIAL INORGANIC CHEMISTRY

A New Method for Study of Magnetic Suspensions

A. I. Zhernovoi and V. N. Naumov

St. Petersburg State Technological Institute, St. Petersburg, Russia

Received October 13, 2004

Abstract—A procedure for determining the magnetization of a ferrofluid from the shift of ^{1}H NMR signal of the solvent by rotating a sample having the shape of an oblate ellipsoid is suggested. The possibility of using the NMR spectroscopy for evaluating the size of magnetite particles and for examining the distribution of the local magnetization of the ferrofluid in a magnetic field is analyzed. The NMR method is compared with the classical Gouy technique.

Magnetic fluids (colloid solutions of magnetite particles), which have found a wide application in various fields of technology, medicine, and chemical technology, have been attracting a considerable interest in recent years. The possibility of controlling the shape and structure of the surface of a magnetic fluid make it a promising technological medium for mass-exchange apparatus. The important part in the behavior of a magnetic fluid in a magnetic field is played by the size of magnetic particles and their distribution in the bulk. Control over these parameters, which is necessary in manufacture and application of magnetic fluids, is hindered by the lack of methods that can be used to measure them in sufficiently small volumes of a fluid. This control is enabled by measuring the shift of the ^{1}H NMR signal.

When placed in a magnetic field, a ferrofluid with a volume magnetite concentration c_0 acquires a magnetization

$$J_0 = c_0 (J_m - J_s) + J_s, \quad (1)$$

where J_m and J_s are the magnetizations of magnetite and the fluid substrate (solvent).

Commonly, a concentrated ferrofluid has $c_0 \approx 2$–4 vol %. At this magnetite concentration, it is difficult to record a ^{1}H NMR signal because of the too large line width, and, therefore, the ferrofluid should be diluted with the solvent to a volume magnetite concentration $c \approx 0.01$–0.02 vol %. The magnetization of a diluted ferrofluid placed in a magnetic field can be expressed as

$$J(c) = (J_m - J_s) + J_s. \quad (2)$$

From Eqs. (1) and (2) follows a relationship between the magnetization of the initial ferrofluid, J_0, and that of a diluted ferrofluid, $J(c)$, measured by the NMR method:

$$J_0 = KJ(c) - J_s(K - 1), \quad (3)$$

where $K = c_0/c$ is the dilution factor.

When a sample of a ferrofluid with a concentration c is placed in a magnetic field of the NMR spectrometer, the effective magnetic field strength H experienced by solvent molecules differs from the field strength H_0 of the magnet [1–3]:

$$H = H_0 + \left(\frac{1}{3} - N + q\right) J(c), \quad (4)$$

where N is the demagnetization factor of the sample surface, and q is a coefficient introduced by Dickinson [1] to characterize the additional shift of the NMR signal in paramagnetic solutions, caused by their magnetic anisotropy.

According to Eq. (4), the difference of the field strengths H in samples with demagnetization factors N_1 and N_2 is given by

$$H(N_2) - H(N_1) = (N_1 - N_2)J(c), \quad (5)$$

whence follows that

$$J(c) = \frac{H(N_2) - H(N_1)}{N_1 - N_2}. \quad (6)$$

The difference of the field strengths in the numerator of expression (6) is found from the shift of the peak

1070-4272/05/7804-0549 © 2005 Pleiades Publishing, Inc.

NMR signal from the ferrofluid, measured on an NMR spectrometer with a uniform field at different demagnetization factors N of the sample surface. The demagnetization factor can be varied by using samples with different shapes. For example, $N = 1/3$ for a sphere, 1/2 for a cylinder with axis perpendicular to H_0, 1 for a cylinder with axis parallel to H_0, 1 for a thin disc with axis perpendicular to H_0 and 0 for a thin disc with axis parallel to H_0.

With the experimental value of $J(c)$ determined using formula (6) and substituted into Eq. (3), we can find the magnetization J_0 of the initial ferrofluid. The solvent magnetization $J_s = \chi_s H_0$, where χ_s is the volume magnetic susceptibility. If χ_s is unknown, the solvent magnetization can be found experimentally from the shift of the NMR signal, using a formula similar to (6):

$$J_s = \frac{H_s(N_2) - H_s(N_1)}{N_1 - N_2}, \quad (7)$$

where the numerator is the difference of resonance fields of the NMR signal of a pure solvent at two demagnetization factors of a sample.

If our samples have ideal shapes of ellipsoids of revolution, we can calculate their dipole moments [4]. Otherwise, the difference $N_1 - N_2$ can be determined experimentally by measuring the shift of the NMR signal of a certain reference substance whose magnetic susceptibility χ_r is known. In this case, by analogy with formulas (6) and (7), we have

$$N_1 - N_2 = \frac{H_r(N_2) - H_r(N_1)}{\chi_r H_0}, \quad (8)$$

where $H_r(N_2) - H_r(N_1)$ is the shift of the NMR signal from the reference sample on changing the sample shape.

Substituting formula (8) into (6) and (7), we obtain an expression for determining $J(c)$ and J_s at unknown demagnetization factors N_1 and N_2:

$$J(c) = \frac{H(N_2) - H(N_1)}{H_r(N_2) - H_r(N_1)}\chi_r H_0,$$
$$J_s = \frac{H_s(N_2) - H_s(N_1)}{H_s(N_2) - H_r(N_1)}\chi_r H_0. \quad (9)$$

For an experimental study, we took a colloid magnetite solution in water with a particle size of about 10 nm, a concentration $c_0 = 2.7$ vol %, and a stabilizer based on oleic acid. To record the NMR signal, we diluted the solution with water to a concentration $c = 0.0135$ vol % (dilution factor $K = 200$). We measured the shift of the ^{1}H NMR signal with a high-resolution spectrometer operating at 40 MHz (with a magnetic field strength $H_0 = 7.46 \times 10^5$ A m^{-1}). As a probe with a varied demagnetization factor of a sample served an oblate thin-walled glass spheroid (disc) 2 mm thick and 8 mm in diameter, filled with a fluid under study via a thin glass pipe.

We determined $J(c)$ by the method with a reference substance (water).

With the probe filled with the ferrofluid, turning the disc axis from the direction perpendicular to H_0 ($N_1 \approx 0$) to that parallel to H_0 ($N_2 \approx 1$) resulted in that the resonance frequency changed by –508 Hz, which corresponds to a change in the magnetic field strength, $H(N_2) - H(N_1) = -9.5$ A m^{-1}.

With the probe filled with water, a similar turning of the disc axis led to a change in the resonance NMR frequency by 143 Hz, which corresponds to a change in the magnetic field strength $H_r(N_2) - H_r(N_1) \approx 2.68$ A m^{-1}. Substituting the values obtained for the change in H(N), χ_r equal to the magnetic susceptibility of water $\chi_{H_2O} = -9.0 \times 10^{-6}$, and $H_0 = 7.46 \times 10^5$ A m^{-1} into expression (9), we obtain $J(c) = 25.2$ A m^{-1}. Substituting this value of $J(c)$, $K = 200$, and $J_s = \chi_{H_2O} H_0 = -7.1$ A m^{-1} into (3), we find the magnetization of the initial ferrofluid, $J_0 = 6.5$ kA m^{-1}.

The theoretical value of J_0 can be calculated by the formula

$$J_{0th} = J_m c_0 P_m, \quad (10)$$

where P_m is the volume fraction of a solid possessing magnetic properties, and J_m is the magnetization of magnetite.

The values of P_m, taken from [5], and the theoretical values of J_{0th}, calculated from these P_m by formula (10) for three presumed particle sizes d are listed in the table.

We can obtain by means of interpolation that the experimental value $J_0 = 6.5$ kA m^{-1} coincides with the theoretical value at $d = 6$ nm. As d decreases or increases, the theoretical values become lower or higher than the experimental value, respectively. This circumstance can be used for evaluating the particle size.

To measure the magnetization by the Gouy method, we suspended a test tube with the fluid under study from an arm of a beam balance and measured the ponderomotive force F appearing under the action

of a magnet that was mounted below the test tube and created a field gradient directed along its axis. Theoretically, the force F is given by the expression

$$F = S\int_{B_1}^{B_2} J(B)\mathrm{d}B, \quad (11)$$

where S is the inner cross-sectional area of the test tube; and B_1, B_2 are the magnetic inductions at the upper and lower boundaries of the fluid.

The dependence of the magnetization J on induction B is given by the Langevin formula, which can be represented at $B > 0.05$ T as [6]:

$$J(B) = J_0 - \frac{nKT}{B}, \quad (12)$$

where n is the concentration of colloid particles; K, Boltzmann constant; and T, temperature.

Substituting formula (12) into (11) and integrating, we obtain

$$F = S\left[J_0(B_2 - B_1) - nKT\ln\frac{B_2}{B_1}\right], \quad (13)$$

whence follows

$$J_0 = \frac{\frac{F}{S} + nKT\ln\frac{B_2}{B_1}}{B_2 - B_1}. \quad (14)$$

In an experimental setup, $S = 27.3 \times 10^{-6}$ m, $KT = 4 \times 10^{-2}$ J, $B_1 = 0.05$ T, and $B_2 = 0.25$ T. The particle concentration n is related to the volume concentration c of magnetite and particle size d by

$$n = \frac{6c}{3\pi d^3}.$$

From Eq. (14) follows a formula for the experimental value of the magnetization, obtained using the Gouy method at $c = c_0$:

$$J_{0G} = 1.8 \times 10^5 F + \frac{6.1 \times 10^{-20} c_0}{d^3}. \quad (15)$$

In an experiment performed at $c_0 = 0.027$, we obtained $F = 0.096$ H. Substitution of this value into (15) gives

$$J_{0G} = 1.98 \times 10^4 + \frac{1.6 \times 10^{-21}}{d^3}. \quad (16)$$

The values of J_{0G}, obtained using formula (16) at various d, are listed in the table. It can be seen that all the experimental values exceeds those yielded by the theory. This can be attributed to magnitophoresis resulting in a rise in the particle concentration at high field gradients. This assumption can be verified by measuring the local magnetization of the ferrofluid by the NMR method.

P_m and ferrofluid magnetizations J_{0th} and J_{0G} in relation to particle size d

d_0, nm	P_m (S) [5]	J_{0th}^*	J_{0G}^{**}
		kA m^{-1}	
5	0.5	6.05	32.4
10	0.67	8.11	20.2
15	0.8	9.68	20.07

* Obtained using the theoretical formula (10).

** Obtained using the experimental calculational formula (16) at $c = 2.7$ vol %.

The results obtained open up new opportunities for study of the structure of a ferrofluid placed in a gradient magnetic field. This is of practical interest in design of magnetic seals and other devices that employ ferrofluids.

ACKNOWLEDGMENTS

The study was supported by the Ministry of Education of the Russian Federation (grant E02-3.5-129).

REFERENCES

1. Dickinson, W.C., *Phys. Rev.*, 1951, vol. 81, no. 5, pp. 717–731.
2. Losche, A., *Kerninduktion*, Berlin: Deutscher Verlag der Wissenschaften, 1957.
3. Mank, V.V. and Lebovka, N.I., *Spektroskopiya YaMR vody v geterogennykh sistemakh* (NMR Spectroscopy of Water in Heterogeneous Systems), Kiev: Naukova dumka, 1988.
4. Arnol'd, R.R., *Raschet i proektirovanie sistem s postoyannymi magnitami* (Calculation and Design of Systems with Permanent Magnets), Moscow: Energiya, 1969.
5. Berkovskii, B.M., Medvedev, V.F., and Krakov, M.S., *Magnitnye zhidkosti* (Magnetic Fluids), Moscow: Khimiya, 1989.
6. Taketomi, S. and Tikatzumi, S., *Magnitnye zhidkosti* (Magnetic Fluids), Moscow: Mir, 1993.

Russian Journal of Applied Chemistry, Vol. 78, No. 4, 2005, pp. 552–555. Translated from Zhurnal Prikladnoi Khimii, Vol. 78, No. 4, 2005, pp. 559–562.
Original Russian Text Copyright © 2005 by Kiryushov, Skvortsova.

INORGANIC SYNTHESIS AND INDUSTRIAL INORGANIC CHEMISTRY

Optimal Conditions for Masking of Sulfite Anions with Formaldehyde in Iodometric Titration of Photographic Fixing Solutions

V. N. Kiryushov and L. I. Skvortsova

Institute of Solid State and Mechanochemistry, Siberian Division, Russian Academy of Sciences, Novosibirsk, Russia

Received October 22, 2004

Abstract—The iodometric titration of photographic fixing solutions can be simplified by masking sulfite anions with 3% aqueous formaldehyde in a weakly acidic medium, instead of their standard masking with concentrated aqueous formaldehyde in weakly alkaline solutions.

The concentrations of sodium thiosulfate and sodium sulfite in photographic fixing solutions are commonly determined by iodometric titration. In this method, two identical aliquots of a fixer are titrated with iodine. In the first aliquot, the sum of $S_2O_3^{2-}$ and SO_3^{2-} anions is determined. The second aliquot is titrated in the presence of an agent masking SO_3^{2-} anions to determine the content of $S_2O_3^{2-}$ anions. The sulfite anions can be masked with formaldehyde [1–5] or acetone [4, 6], or by precipitating poorly soluble strontium sulfite [7, 8]. The accuracy of sodium thiosulfate and sodium sulfite determination depends on the reliability of masking sulfite anions.

As a rule, acetone is not used for masking of sulfite anions because of its volatility and inflammability. Futuremore, in iodometric titration in water–acetone mixture, the color of the iodine-sensitive indicator is strongly weakened and the color transition at the equivalent point is puurly defined.

The precipitation of sulfite anions is expedient only if other interfering components of the fixer are coprecipitated. For example, in determination of sodium thiosulfate in bleaching fixers, the precipitation of strontium sulfite is apparently accompanied by coprecipitation of thiourea interfering with the thiosulfate titration.

As a rule, in iodometric titration of fixers, sulfite anions are masked with formaldehyde. Formaldehyde is bound with sulfite anions to form a complex unoxidizable with iodine. The formation of this complex is described by reaction (1) in an acidic medium [9] and by reaction (2) in a neutral or weakly alkaline medium [10]:

$$CH_2O + SO_3^{2-} + H^+ \rightarrow CH_2OHSO_3^-, \quad (1)$$

$$Na_2SO_3 + CH_2O + H_2O \rightarrow H_2COHSO_3Na + NaOH. \quad (2)$$

In iodometric titration of photographic fixers, sulfite anions are commonly masked in an alkaline medium. The initial aqueous solution of the fixer is diluted with water and alkalized to pH 8–10, with phenolphthalein as indicator. Thereafter, 37% aqueous formaldehyde is added, and the resulting mixture is allowed to stand for several minutes. This mixture is acidified with 10% aqueous acetic acid (10 ml), and a standard solution of iodine is added. The amount of formaldehyde, recommended for masking of sulfite anions (ml of formaldehyde solution per ml of fixer), varies over a wide range: 1.0 [2], 2.0 [3], 2.5 [1], 5 [5], and even 10 ml [4, 11]. It has also been reported [5] that sulfite anions can be masked in a weakly acidified fixer (pH 3–4) by adding a large excess of 37% aqueous formaldehyde.

Published data on masking of sulfite anions with formaldehyde in iodometric titration of fixers show that the recommended formaldehyde additions significantly exceed its stoichiometric amount required for complexation of sulfite anions by reactions (1) and (2). These reactions show that 1 mol of formaldehyde is bound with 1 mol of sulfite anions. The maximum content of sodium sulfite in the fixers does not exceed 40 g l^{-1} (0.32 M). Therefore, to mask sulfite anions present in 1 ml of this fixer, 0.027 ml of 37% (11.6 M) aqueous formaldehyde is required. In practice, the formalehyde addition exceeds its stoichiometric amount by a factor of 40–400.

1070-4272/05/7804-0552 © 2005 Pleiades Publishing, Inc.

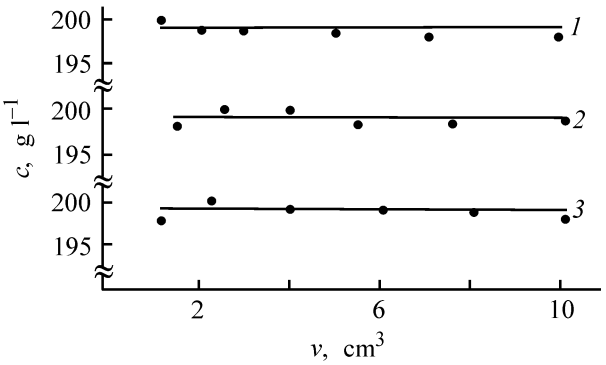
It is known [12] that the complex of formaldehyde with sulfite anion is the most stable in weakly acidic solutions (pH 3–5). Therefore, we can suggest that sulfite anions can be masked in weakly acidic media with a smaller amount of formaldehyde than in commonly used alkaline solutions. The masking of sulfite anions in acidic medium could significantly simplify iodometric analysis of fixers.

In this study, we improved iodometric titration of fixers by masking sulfite anions with formaldehyde in weakly acidic solutions.

EXPERIMENTAL

The search for the optimal conditions of masking sulfite anions with formaldehyde was carried out with a fixer containing $Na_2S_2O_3 \cdot 5H_2O$ (199.5 g l^{-1}), Na_2SO_3 (20 g l^{-1}), and sulfuric acid. In our experiments sodium thiosulfate and sodium sulfite were determined by iodometric back-titration of 1-ml aliquots of the fixer. The first aliquot was diluted with distilled water (10 ml), and a 15 ml 0.1 N reference solution of iodine was added. The excess iodine was titrated with 0.1 aqueous thiosulfate in the presence of starch as indicator, and the iodine solution volume v consumed for oxidation of the sum of $S_2O_3^{2-}$ and SO_3^{2-} was determined. The second aliquot of the fixer was diluted with distilled water (10 ml) and alkalized to pH 9–10 with phenolphtalein as indicator, and then formaldehyde was gradually added, starting with a 1-ml portion, to its total volume equal to 10 ml. Along with commonly used 37% aqueous formaldehyde, we tested 14% and 10% aqueous formaldehyde. After adding each portion of formaldehyde, the mixture was kept for 5 min, and acidified with 10% aqueous acetic acid (5 ml), and a standard solution of iodine (15 ml) was added. Excess iodine was titrated with 0.1 M aqueous thiosulfate in the presence of starch, and the iodine solution volume v_1 consumed for oxidation of $S_2O_3^{2-}$ was determined. The iodine solution volume v_2 consumed for oxidation of SO_3^{2-} was determined as the difference $v - v_1 = v_2$.

In order to elucidate how the fixer acidity influences the efficiency of masking of sulfite anions with formaldehyde, the fixing solutions with different formaldehyde contents were iodometrically titrated at various pH. The fixing solutions were prepared by standard procedures [13, 14]. The reference solutions of iodine and sodium thiosulfate (0.1 N) were prepared from the reference samples. As indicator served 0.5% aqueous starch. All the solutions used in our experiments were prepared from chemicals analytically or chemically pure grades.



$Na_2S_2O_3$ content in a weakly acidic fixer, determined by iodometric back-titraition, vs. the formaldehyde volume added, v. Fixer: $Na_2S_2O_3 \cdot 5H_2O$ 200.0 g l^{-1}, Na_2SO_3 20 g l^{-1}, and H_2SO_4. (*c*) Sodium thiosulfate concentration. Formaldehyde concentration, %: (*1*) 37, (*2*) 14, and (*3*) 10.

The accuracy and reproducibility of sodium thiosulfate determination in fixers depend on the reliability of masking of sulfite anions. The figure shows how the iodometric determination of sodium thiosulfate in the fixer depends on the formaldehyde amount added. As seen from the figure (curve *1*), in masking of sulfite anions by successively adding 37% aqueous formaldehyde, starting with 1-ml portion to its total volume equal to 10 ml, the difference between the actual thiosulfate content and that determined iodometrically does not exceed 2 g l^{-1} (1%) within the entire range of formaldehyde volumes. Approximately the same difference between the actual and iodometrically determined thiosulfate content was obtained upon addition of 14% and 10% aqueous formaldehyde, starting with a 1.5-ml portion to the total volume of 10 ml (figure, curve *2*) and starting with a 2-ml portion to the total volume of addition 10 ml (figure, curve *3*). In masking of sulfite anions with 1 ml of 10% aqueous formaldehyde, the thiosulfate content was under-estimated by approximately 4%.

We found that small formaldehyde additions (1 ml of 37% aqueous formaldehyde or 1.5–2 ml of 10% aqueous formaldehyde) to 1 ml of the fixer completely mask sulfite anions. Thus, we can reliably mask sulfite anions in weakly acidified fixing solution by adding 5 ml of 3% aqueous formaldehyde to 1 ml of the fixing solution (see, e.g., the second point in curve *3* of the figure). Dilute solutions of formaldehyde are more stable and safer in handling in the course of analysis.

Our experiments showed that a 3% solution of formaldehyde in 10% aqueous acetic acid is the optimal masking mixture. Owing to the simultaneous presence of both the fixing and acidifying agents in a masking solution, this mixture is convenient in

Determination of sodium thiosulfate and sodium sulfite in various fixing solutions by (A) direct [OST (All Union Standard) 19-1–83] and (B) back iodometric titration as suggested in this study (n = 5, P = 0.95)

Kind of fixer	Titration procedure	$Na_2S_2O_3 \cdot 5H_2O$, g l^{-1}			Na_2SO_3, g l^{-1}		
		added	found	S_r	added	found	S_r
Simple	A	206.8	207 ± 1	0.004	–	–	–
	B		206.8 ± 0.7	0.003	–	–	–
Quick, containing NH_4Cl	A	247.0	248.8 ± 1.2	0.003	–	–	–
	B		246.9 ± 0.5	0.002	–	–	–
Quick, containing NH_4SCN and Na_2SO_3	B	329.4	327 ± 4	0.01	9.95	9.5 ± 0.5	0.04
Acidic, containing $Na_2S_2O_5$ (30 g l^{-1})	A	248.4	251 ± 1	0.003	–	33.7 ± 0.5	0.008
	B		250.1 ± 1.7	0.005	–	33.4 ± 0.7	0.017
Tanning, containing potash alum	A	255.3	254.5 ± 1.9	0.006	14.85	15.3 ± 0.6	0.03
	B		255.2 ± 1.8	0.006		14.8 ± 0.2	0.012
Tanning, containing chromium alum	A	242.4	238.7 ± 1.5	0.005	15.6	14.7 ± 1.2	0.012
	B		241.8 ± 0.5	0.002		15.1 ± 0.3	0.016
Bleaching, containing thiourea (2 g l^{-1})	A	164.3	167.4 ± 1.3	0.006	2.08	1.9 ± 0.3	0.12
	B		168.3 ± 0.7	0.003		4.2 ± 0.4	0.09
	B*		166.3 ± 0.9	0.004		2.0 ± 0.3	0.13
Bleaching, containing KSCN (10 g l^{-1})	A	160.6	161.2 ± 0.5	0.003	2.16	2.3 ± 0.3	0.11
	B		161.8 ± 0.9	0.004		3.3 ± 0.3	0.07
	B*		161.8 ± 0.9	0.004		2.2 ± 0.2	0.04

* (B*) Back-titration of a sum of thiosulfate and sulfite anions in a 1-ml aliquote of the fixer, acidified with 10% aqueous acetic acid (5 cm^3).

use. It should be noted that the possibility of reliable masking of sulfite anions with formaldehyde in weakly acidic media [Eq. (1)] follows from previous data [5, 12]. The adduct has been reported to be resistant to atmospheric oxygen in acidic media. The above-described masking of sulfite anions in weakly acidic solutions can be used in both direct and back iodometric titration of sodium thiosulfate in fixers.

Procedure for iodometric back-titration of sodium thiosulfate in fixer. A 1-ml portion of the fixer was placed in a 150-ml beaker, and distilled water (10 ml) and the masking solution (3% solution of formaldehyde in 10% aqueous acetic acid, 5 ml) were added. The resulting mixture was stirred, and right after that (without keeping for 5 min as prescribed by the standard protocol) a precisely measured volume of a reference 0.1 N solution of iodine (from 10 to 15 ml) was added. This mixture was stirred, and the excess iodine was titrated with a reference solution of thiosulfate in the presence of starch as indicator. The sodium thiosulfate concentration in the initial fixing solution was calculated by multiplying the iodine solution volume v_1 consumed for the oxidation of thiosulfate by 24.8.

In order to determine the content of the sulfite anion in the fixer, its 1-ml aliquot was placed in a 150-ml beaker and titrated with a standard iodine solution as described above, without masking of sulfite anions with formaldehyde. Under these conditions, the total volume of iodine solution v consumed for oxidation of $Na_2S_2O_3$ and Na_2SO_3 was determined. The iodine solution volume consumed for oxidation of sulfite anions was determined as the difference $v - v_1 = v_2$. The sodium sulfite content was determined by multiplying v_2 by 6.3.

A series of available fixers was analyzed by the above-described iodometric back-titration technique. In these experiments, the $Na_2S_2O_3$ and Na_2SO_3 content in the fixers, determined by our method, was compared with that determined by direct titration of these fixers in a weakly alkaline medium with masking of sulfite anions with 37% aqueous formaldehyde (10 ml) [11]. The amount of iodine consumed for oxidation of the sum of $Na_2S_2O_3$ and Na_2SO_3 was determined by titration of the fixer acidified with 10% aqueous acetic acid, without adding formaldehyde.

The results of determination of sodium thiosulfate and sodium sulfite in various fixers by the standard direct iodometric titration technique [11] and by the iodometric back-titration developed in this study are listed in the table. These data show that the standard method ensures correct determination of sodium sul-

fite in all the fixers tested. The sodium thiosulfate is correctly determined in all the fixers except the bleaching fixer containing thiourea, in which sodium thiosulfate is determined with a fixed error caused by the reaction of iodine with thiourea.

Our technique of iodometric back-titration in a weakly acidic medium also ensures a correct determination of sodium thiosulfate in all the fixers under consideration, except those containing thiourea. Both our and the standard [11] methods ensure correct determination of sodium sulfite for all the kinds of fixers except those containing bleaching agents. We found that, in determination of the sum of sodium thiosulfate and sodium sulfate in the acidified initial fixer (B^*), the back-titration of Na_2SO_3 is carried out without a fixed error. Under these conditions, the results obtained by our method have better reproducibility than those obtained by the standard direct titration [OST (Branch Standard) 19-1–83].

Thus, with masking of sulfite anions in a weakly acidified fixer with a dilute (3%) solution of formaldehyde, the accuracy of iodometric determination of sodium thiosulfate and sodium sulfite is not inferior to that ensured by standard iodometric titration (OST 19-1–83).

CONCLUSION

In iodometric titration of photographic fixers, sulfite anions can be masked with a 3% solution of formaldehyde in 10% aqueous acetic acid. Titration in an acidic medium simplifies the analytical procedures and improves the safety of handling formaldehyde. Under these conditions, the reproducibility and accuracy of sodium thiosulfate and sodium sulfite determination are not inferior to those ensured by the standard titration.

REFERENCES

1. Atkinson, R.B. and Shaner, V.C., *J. Soc. Motion Picture Eng.*, 1940, vol. 34, no. 15, pp. 485–523.
2. Russel, G., *Chemical Analysis in Photography*, London: Focal, 1965.
3. Greyf, S. and Rossens, L., *Photo Korrespondenz*, 1971, vol. 107, no. 1, pp. 5–10.
4. Novitskaya, T.A., Filippova, N.I., and Shakhnazarova, A.S., *Metody kolichestvennogo analiza obrabatyvayushcikh rastvorov* (Technique for Quantitative Analysis of Treating Solutions), Leningrad: Leningr. Inst. Kinoinzhenerov, 1978.
5. Abramkina, I.V., Gas'kova, E.A., and Danilova, N.E., *Analiticheskaya khimiya veshchestv, ispol'zuemykh v fotografii* (Analytical Chemistry of Compounds Used in Photography), Leningrad: Leningr. Inst. Kinoinzhenerov, 1979.
6. Zolotnitskii, D.M., *Kontrol' protsessov obrabotki kinoplenki* (Monitoring of Movie Film Processing), Moscow: Iskusstvo, 1986.
7. Kieser, K. and Rhein, B., *Phot. Ind.*, 1934, vol. 32, no. 24, pp. 696–698.
8. Grigor'eva, E.L., Oreshkina, G.N., and Strel'nikova, A.P., *Tekh. Kino Televid.*, 1985, no. 10, pp. 10–13.
9. Szekeres, L., *Talanta*, 1974, vol. 211, no. 1, pp. 1–44.
10. *Inorganic Sulfur Chemistry*, Nickless, G., Ed., Amsterdam: Elsevier, 1968.
11. *OST* (Branch Standard) *19-1–83*.
12. Hansen, L.D., Ruther, B.E., and Rollins, D.K., *et al.*, *Anal. Chem.*, 1979, vol. 5, no. 6, pp. 633–637.
13. Zaks, M.I., *Fotomaterialy i ikh obrabotka: Spravochnoe posobie* (Photomaterials and Their Treatment: Handbook). Moscow: Legprombytizdat, 1993.
14. *Fotoretsepturnyi spravochnik cherno-beloi i tsvetnoi obrabotki* (Photographic Formulation Handbook for Black-and-White and Color Treatment), Moscow: Tsentr. Bibl. Nauchno-Tekh. Inf., 1991.

Russian Journal of Applied Chemistry, Vol. 78, No. 4, 2005, pp. 556–558. Translated from Zhurnal Prikladnoi Khimii, Vol. 78, No. 4, 2005, pp. 563–565.
Original Russian Text Copyright © 2005 by Kuntyi, Olenych.

APPLIED ELECTROCHEMISTRY AND CORROSION PROTECTION OF METALS

Electrochemical Precipitation of Dispersed Ni–Ag Powders in Ammonia Electrolytes

O. I. Kuntyi and R. R. Olenych

Lvivska Politekhnika National University, Lviv, Ukraine

Received September 20, 2004; in final form, January 2005

Abstract—The electrochemical precipitation of a dispersed Ni–Ag powder from aqueous systems $[Ni(NH_3)_6]^{2+}$–$[Ag(NH_3)_2]^{+}$–$(NH_4)_2SO_4$–$NH_3 \cdot H_2O$ was studied.

Electrochemical codeposition of metals is widely used for obtaining compact coatings [1–3]. Separation of two-component dispersed powders M(1)–M(2) has been little studied. The first attempt to generalize data of few studies devoted to the cathodic codeposition of dispersed metals has been made for the example of copper alloys [4]. The accelerating development of power metallurgy [5] stimulates design of new multicomponent formulations, increase in the dispersity and homogeneity of dispersed powder systems, and decrease in their cost. Mostly mechanical agitation is used to homogenize dispersed powder systems, with the homogeneity of their components not always attained [6]. For this reason, chemical, physicochemical, and electrochemical processes are also used to prepare a homogeneous multicomponent stock. The last method is used in two modifications: cladding of dispersed powders by electrolysis [7–9] and cathodic codeposition of metals in the form of dispersed precipitates [4]. Use of secondary raw materials [8, 10–12] is a promising way for decreasing the cost of powder systems. The present study continues an integrated investigation of the electrochemical precipitation of dispersed bimetal powders with the use of secondary raw material [8, 9].

EXPERIMENTAL

The electrolysis was performed at 30°C in ammonia electrolytes based on complexes of nickel(II) and silver(I) complexes [or only nickel(II)] at the following concentrations of the components (M): $NiSO_4$ ($NiCl_2$) 0.1–0.5, $AgNO_3$ 0.01–0.05 (or 0), $(NH_4)_2SO_4$ 0.5, and $NH_3 \cdot H_2O$ added to adjust pH to 10. The nickel and Ni–Ag powders were deposited onto cylindrical aluminum cathodes (diameter 10 mm and surface area 15 cm^2) in a 1-dm^3 electrolyzer (Fig. 1).

At the beginning of electrolysis the current I was set on the basis of the current density i_c and then electroprecipitation was performed at a constant potential in the laminar agitation mode. After 10–20 min the cathode with a deposit was removed from the electrolyzer and placed in a vessel filled with an ammonia solution. To make shorter the time of contact silver deposition onto the surface of a dispersed nickel-containing deposit, the current was not switched off in the process. The deposit was scraped from the cathode, washed with an ammonia solution, water, and ethanol under agitation, and dried in a vacuum. To study the morphology of the deposit, it was obtained on the edge of a cylindrical cathode with a fully insulated lateral surface and examined with a Tesla-BS-300 scanning electron microscope (Fig. 1, *1'*). After the electrolysis was complete,

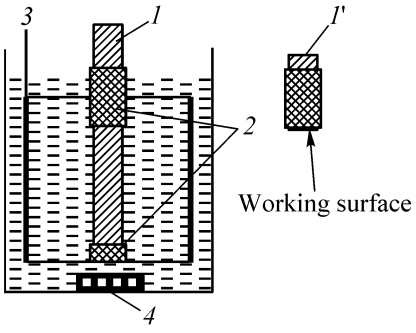


Fig. 1. Schematic of an electrolyzer for cathodic deposition of Ni–Ag alloy. (*1, 1'*) cylindrical cathodes, (*2*) hermetic fluoroplastic screens, (*3*) current lead to a concentric nickel anode, and (*4*) magnetic stirrer.

1070-4272/05/7804-0556 © 2005 Pleiades Publishing, Inc.

the powders, not removed from the support, were washed, dried (as described above), and mounted into the scanning microscope.

The powders obtained were analyzed on a DRON-3M diffractometer (Cu_{K_α} radiation, θ–2θ scanning mode, Bragg–Brentano method), with a stepwise recording of a diffraction pattern.

Solutions containing ammonia complexes of nickel(II) and ammonium salts are formed in processing of secondary raw materials [12] and can be used to prepare electrolytes for deposition of dispersed nickel and nickel alloys. The following reactions occur in the course of the electrolysis in the system $[Ni(NH_3)_6]^{2+}$–NH_4^+–NH_3 at the cathode and in the near-cathode layer:

$$[Ni(NH_3)_x]^{2+} + 2e \rightarrow Ni + xNH_3, \quad (1)$$

$$2H_2O + 2e \rightarrow H_2 + 2OH^-, \quad (2)$$

$$NH_4^+ + OH^- \rightarrow NH_4OH \rightarrow NH_3 \cdot H_2O. \quad (3)$$

The electrochemical reactions, the main reaction (1) directly and the conjugate reaction (2) indirectly via the chemical reaction (3), yield free ammonia and lead to its local concentration in the near-cathode layer. This prevents a considerable "alkalization" of the catholyte and deposition of $Ni(OH)_2$, which makes it possible to obtain pure dispersed powders without any admixture of nickel(II) hydroxide even at high current densities. Similarly, the components NH_4^+ and NH_3 favor precipitation of pure dispersed silver {Ag^+ forms $[Ag(NH_3)_2]^+$} complex and, accordingly, a dispersed nickel–silver deposit).

The silver concentration in the dispersed deposit depends nonlinearly on the concentrations of the $[Ni(NH_3)_6]^{2+}$ and $[Ag(NH_3)_2]^+$ ions (Fig. 2). It should be noted that, in electrolytes with a higher concentration of nickel(II), the composition of the dispersed deposit is less sensitive to the concentration of the silver salt. For example, the Ag concentration in the deposit depends nearly linearly on the $[Ag(NH_3)_2]^+$ concentration in 0.3–0.5 M solutions of $[Ni(NH_3)_6]^{2+}$ at $[Ag(NH_3)_2]^+$ concentrations of 0.01–0.05 M (Fig. 2a).

The coprecipitation of silver leads to a significant change in the morphology of the dispersed deposit and to an increase in its dispersity, compared with the dispersed nickel obtained in the ammonia electrolyte (Fig. 3).

The current density i_c in precipitation of dispersed deposit is a conventional value. It has a physical

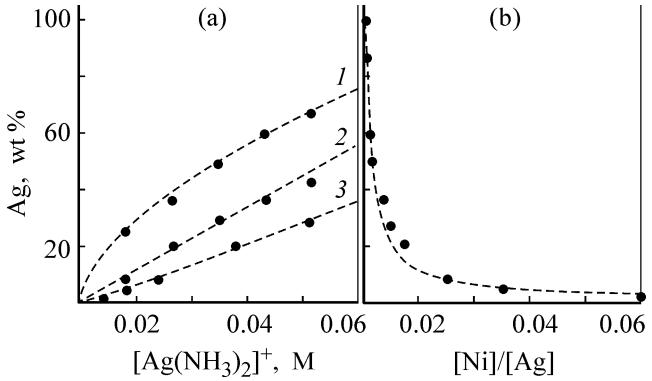


Fig. 2. Composition of dispersed cathodic Ni–Ag deposit vs. (a) $[Ag(NH_3)_2]^+$ concentration (M) and (b) [Ni]/[Ag] molar ratio in ammonia electrolyte. Temperature 30°C, i_c =20 A dm^{-2}, deposition duration 10 min. (Ag) Ag content in the deposit. $[Ni(NH_3)_6]^{2+}$ concentration (M): (*1*) 0.1, (*2*) 0.3, and (*3*) 0.5.

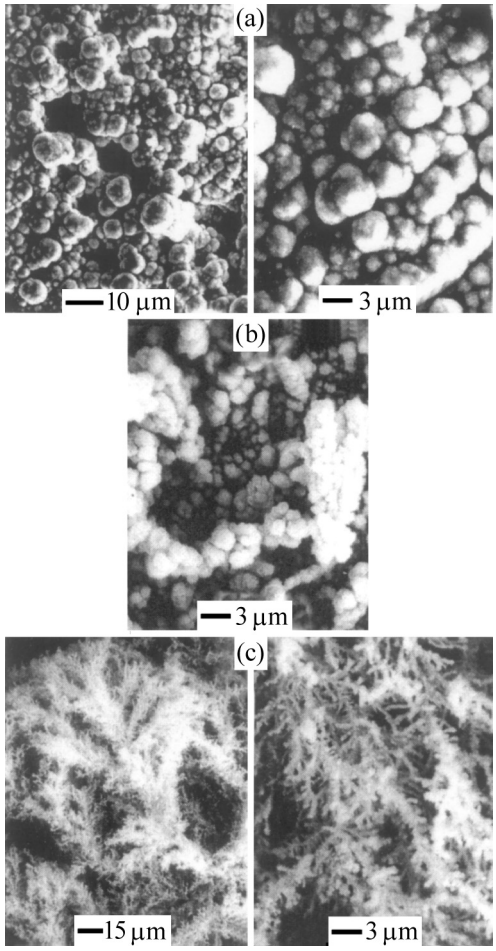


Fig. 3. Micrographs of dispersed cathodic deposits of (a, b) nickel and (c) Ni–Ag alloys obtained in electrolytes containing 0.5 M $(NH_4)_2SO_4$ and $NH_3 \cdot H_2O$ (up to pH 10) at T = 30°C. $NiSO_4$ concentration (M): (a) 0.5 and (b, c) 0.1; $AgNO_3$ concentration (M): (c) 0.02. i_c (A dm^{-2}): (a, c) 20 and (b) 100.

meaning only at the beginning of the electrolysis, since a kind of a "coat" is formed on the cathode in several minutes, and its electrochemically active area rapidly increases with time. Accordingly, the cathodic current at a constant potential increases. For example, in an electrolyte containing 0.1 M $[Ni(NH_3)_6]^{2+}$ and 0.02 M $[Ag(NH_3)_2]^+$ at the initial value i_c = 20 A dm^{-2} (U = const = 4.2 V), I increases virtually linearly from 3 to 7.5 A in 20 min. Thus, it may be concluded that, in electrochemical precipitation tion of a dispersed deposit at U = const, i_c stabilizes to a certain extent owing to an increase in the cathodic current. This electrolysis mode provides more favorable conditions for formation of a monodisperse deposit than that at I = const.

According to the results of an X-ray phase analysis, only nickel and silver are present in the cathodic deposits obtained. It is known [13] that nickel and silver form no intermetallic compounds and virtually no solutions with each other. As can be seen, the electrochemical codeposition of these metals in the form of dispersed deposits is not an exception. Therefore, the formation of a cathodic deposit can be regarded as a continuous formation of 3D nuclei of nickel and silver on the intrinsic and foreign bases. Taking into account that $E^0_{[Ni(NH_3)_6]^{2+}/Ni}$ and $E^0_{Ag(NH_2)]^+/Ag}$ = +0.373 V [14], it would be expected that the silver nucleation is faster in alternate deposition of nickel and silver. At the same time, a high concentration and diffusion overvoltage is observed for silver at high cathodic current densities and low concentrations of the $[Ag(NH_3)_2]^+$ complexes. Therefore, nucleation process dominates over the process of nucleus growth. This, in turn, also hinders growth of nickel nuclei, which results in the formation of an ultradispersed cathodic Ni–Ag deposit.

CONCLUSIONS

(1) It was established that coprecipitation of silver in ammonia electrolytes strongly affects the morphology of the Ni–Ag cathodic deposit, leading to its dispersion and formation of ultradispersed powders.

(2) The main parameter that can be used to control the composition of dispersed Ni–Ag deposit in ammonia electrolytes is the concentration of salts of these metals.

REFERENCES

1. Vyacheslavov, P.M., *Elektroliticheskoe osazhdenie splavov* (Electrolytic Deposition of Alloys), Leningrad: Mashinostroenie, 1980.
2. Povetkin, V.V., Kovenskii, I.M., and Ustinovshchikov, Yu.I., *Struktura i svoistva elektroliticheskikh splavov* (Structure and Properties of Electrolytic Alloys), Moscow: Nauka, 1992.
3. Gamburg, Yu.D., *Elektrokhimiya*, 2001, vol. 37, no. 6, pp. 686–692.
4. Nechiporenko, O.S., Pomosov, A.V., and Naboichenko, S.S., *Poroshki medi i ee splavov* (Copper and Copper-Alloy Powders), Moscow: Metallurgiya, 1988.
5. Levina, D.A., and Chernyshev, L.I., *Poroshk. Metall.*, 2001, nos. 3/4, pp. 124–126.
6. Andrievskii, R.A., *Poroshkovoe materialovedenie* (Materials Science for Powders), Moscow: Materialovedenie, 1991.
7. Kurvyakova, L.M., Zhbanov, A.M., and Zakharova, E.P., *Poroshk. Metall.*, 1979, no. 12, pp. 4–17.
8. Kuntyi, O.I., Minakova, R.V., Kozak, S.I., *et al.*, *Fiz.-Khim. Mekhan. Mater.*, 2004, vol. 40, no. 1, pp. 122–124.
9. Kunty, O.I., Sribny, V.M., Minakova, R.V., and Kozak, S.I., *Proc. Int. Conf.* "*Science for Materials in the Frontier of Centuries: Advantages and Challenges,*" Kyiv, 2002, pp. 349–350.
10. Babutina, T.E., Uvarova, I.V., Konchalovskaya, L.D., and Kuz'menko, L.N., *Poroshk. Metall.*, 2004, nos. 3/4, pp. 1–38.
11. Maslyuk, V.A., Panasyuk, O.A., and Vlasova, O.V., *Poroshk. Metall.*, 2003, nos. 9/10, pp. 114–118.
12. Demidov, A.I. and Krasovitskaya, O.A., *Zh. Prikl. Khim.*, 2000, vol. 73, no. 10, pp. 1656–1660.
13. Vol, A.E., *Stroenie i svoistva dvoinykh metallicheskikh sistem* (Structure and Properties of Binary Metal Systems), Moscow: Fizmatgiz, 1962, vol. 2.
14. Dobos, D., *Electrochemical Data. A Handbook for Electrochemists in Industry and Universities*, Budapest: Akad. Kiado, 1975.

Russian Journal of Applied Chemistry, Vol. 78, No. 4, 2005, pp. 559–564. Translated from Zhurnal Prikladnoi Khimii, Vol. 78, No. 4, 2005, pp. 566–571.
Original Russian Text Copyright © 2005 by Kuz'min, Borovkov, Kolker, Brazhyunas.

APPLIED ELECTROCHEMISTRY AND CORROSION PROTECTION OF METALS

Synthesis of Metallofullerenes by Electric-Arc Method with a Surface-Modified Electrode

S. M. Kuz'min, N. Yu. Borovkov, A. M. Kolker, and V. L. Brazhyunas

Institute of Chemistry of Solutions, Russian Academy of Sciences, Ivanovo, Russia

Ivanovo State University of Chemical Technology, Ivanovo, Russia

Received September 30, 2004; in final form, February 2005

Abstract—A method for synthesis of metallofullerenes by electric-arc sputtering of graphite, in which lanthanum compounds are deposited on the surface of a graphite electrode, was suggested. The influence exerted by the amount of deposited lanthanum on the yield of lanthanum was studied.

At present, endohedral complexes of fullerenes [1] and higher fullerenes attract researchers' attention as potential objects of nanotechnologies [2], which possess nonlinear optical characteristics [3] and unique physicochemical properties [4]. Synthesis and identification of new forms of endofullerenes (various isomers, bi- and trinuclear complexes in encapsulation of the whole variety of the available elements in the void in the fullerene molecule) have been extensively studied [5–18]. The known methods for synthesis of metallofullerenes consist in bombardment of a fullerene-containing substrate with metal ions [19] or in evaporation of a metal–carbon composite in the atmosphere of an inert gas [16–23]. The composites are evaporated with lasers [21, 22] or by electric-arc sputtering [16, 22, 23].

Commonly, the composite is prepared as follows. A hole bored in a graphite rod is filled with a mixture of a metal oxide, powdered graphite, and binder resins. Then the rod (electrode) is annealed in a vacuum at a temperature of about 2000°C. As a result, the carbide of the starting metal is formed and fixed in the bulk of the electrode.

It should be noted that C_{60} and C_{70} are formed in synthesis of metallofullerenes. There is evidence [16, 21, 23] that the amount of a metal oxide introduced into the electrode affects the total yield of fullerenes. The ratio of yields of hollow fullerenes and metallofullerenes [16, 21, 24] suggests that the formation of an endocomplex is, in fact, the side process in synthesis of hollow fullerenes.

Use of a combined electrode results in that metal atoms are introduced into the discharge zone in sputtering of the electrode. Having a low ionization potential, metal atoms markedly change the discharge parameters, and, primarily, make lower the temperature of electrons in the arc and of the gas [25]. Using a combined electrode, as a rule, leads to a decrease in the yield of fullerenes [16, 25, 26].

The yield of metallofullerenes in synthesis is low and the procedure for preparing a composite is prolonged and complicated. This results in that the problem of obtaining industrial samples of metallofullerenes remains unsolved. The efficiency of synthesis of metallofullerenes is raised by varying the composition of the composite [22] and by improving the design of the reactors used for this purpose [23].

The aim of this study was to examine specific features of synthesis of metallofullerenes with a surface-modified electrode.

EXPERIMENTAL

The experimental installation for synthesis of fullerenes by electric-arc sputtering of graphite is shown schematically in Fig. 1. A combined electrode was fabricated from 10-cm-long rectangular graphite rods with a cross-section of 2×4 to 4×6 mm. The electrode was prepared by depositing an aqueous suspension of lanthanum carbonate on its surface. The deposited layer was dried in air to constant mass and then the electrode mounted into the reactor was an-

1070-4272/05/7804-0559 © 2005 Pleiades Publishing, Inc.

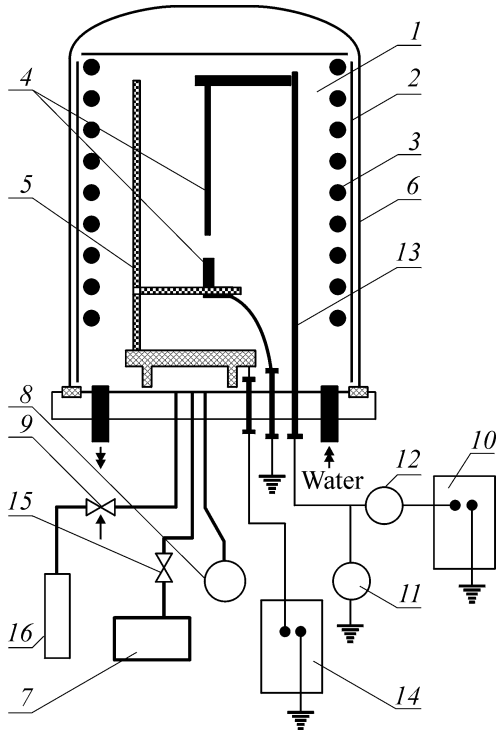


Fig. 1. Schematic of the experimental installation for electricarc synthesis of fullerenes: (*1*) reactor, (*2*) reflector, (*3*) cooling circuit, (*4*) graphite rods, (*5*) microlift, (*6*) bell-jar, (*7*) vacuum station, (*8*) vacuum gage, (*9*) leak valve, (*10*) discharge feeding unit, (*11*) voltmeter, (*12*) ammeter, (*13*) current-carrying bar, (*14*) microlift-feeding unit, (*15*) vacuum cock, and (*16*) cylinder with helium.

nealed by passing a dc current of 50–70 A through short-circuited electrodes at a residual pressure in the reactor of 10^{-2} Pa or in the atmosphere of helium.

The cycle of reactor preparation to synthesis included the following stages: (1) mounting of graphite electrodes in the reactor, with their mass preliminarily determined; (2) evacuation of the reactor to a pressure of about 10^{-3} Pa; (3) heating of the electrode by passing an electric current; (4) filling of the reactor with helium to the working pressure and heating of the electrodes in this atmosphere; (5) repeated evacuation of the reactor to a pressure of 10^{-3} Pa; and (6) letting-in helium to a working pressure of 2×10^4 Pa.

The working pressure in synthesis of metallofullerenes has been experimentally determined previously [27]. This pressure corresponds to the maximum yield of hollow fullerenes.

To sputter the combined electrode, a voltage sufficient for arc initiation was applied across the electrodes and microlift displacement at a preliminarily adjusted velocity was switched on. In the course of sputtering, the arc current was 100–150 A at a voltage across the discharge gap equal to 20–25 V. The completion of the sputtering process was judged by visual inspection.

After the sputtering of the electrode, the carbon black obtained in the course of synthesis was collected and its mass was determined. Also weighed were the residue of the electrode being sputtered and the cathode deposit (carbon layer formed on the cathode in synthesis).

The fullerenes contained in the carbon black were extracted with *ortho*-xylene at a temperature of 40°C under agitation for 24 h. Then the solution was filtered on a glass filter and the carbon black was additionally washed with *ortho*-xylene to a colorless extract. The resulting filtrate was brought to a mark of 100 ml in the volumetric flask with *ortho*-xylene.

The concentration of individual fullerenes in solution was analyzed by HPLC and spectrophotometry. Chromatograms were obtained on a LIQUOCHROME 2010 chromatograph with a UV detector (analytical wavelength 330 nm), with hexane as eluent (residual content of water $\leq 6 \times 10^{-3}$%) and a column packed with SGX Separon adsorbent (grain size 7 μm). The chromatograms of reference solutions and those being analyzed were processed using Multichrom 1.5 software. The spectra were recorded with a Hitachi U2001 spectrometer.

A theoretical description of the synthesis of fullerenes has resulted in model concepts of the assembly of a carbon skeleton [28–31]. Also represented in the literature are the results of quantum-chemical calculations of the stability of various endocomplexes [32, 33]. An analysis of published data made it possible to maintain that both the C_{60} fullerene and the endocomplex are formed in the jet of a carbon vapor produced by sputtering in the electric-arc synthesis of fullerenes [30].

It is known that [34], in synthesis of the fullerene, the ions bombarding the cathode do not sputter it, but, conversely, are incorporated into its structure to give a cathode deposit. In this case, both the amount of the deposit formed and its structural features depend on the composition and energy of ions bombarding the cathode. Under the conditions of the synthesis performed, three sources are responsible for the composition of the near-cathode layer of plasma: buffer gas, sputtered graphite, and sputtered lanthanum. The lower the ionization energy, the larger the fraction of an ionized component. The ionization energy of helium is 24.587 eV [35]; that for components of the carbon vapor: C 11.260, C_2 12.10, C_3 11.65, and C_4 11.28 eV [36]; the energies of successive ionization

for lanthanum ions are 5.577, 11.06, and 19.17 eV [35]. It should be noted that the existence of high-energy metastable states of helium leads to ionization of easily ionized components of plasma by the Penning mechanism [36]:

$$A^* + B \rightarrow A + B^+ + e,$$

where A^* stands for helium in excited state, and B, for the easily ionized component.

Thus, it would be expected that the ionic composition of plasma is mainly represented by C_n^+ and La^+ ions. As the discharge current in the cathode region is carried by positive ions, the mass of the deposit is proportional to the quantity of electricity consumed in the process and to the accommodation coefficient of the incident ion. The amount of graphite being evaporated is also proportional to the charge passed [37]. As a result, the ratio of the mass of sputtered graphite to that of the deposit can be used to characterize an experiment.

The shape of the deposit obtained in the experiment (Figs. 2a and 2b) corresponds to that of the electrode being sputtered. The cross-section of the cathode deposit exceeds that of the initial electrode and a crater is always present in the central part of the cathode deposit. Use of both graphite and surface-modified electrodes leads to the same distribution of sputtered graphite among the fullerene black and the cathode deposit (Fig. 3). The lanthanum being evaporated does not change the nature of the ion flow toward the cathode surface and, consequently, does not enter into the near-cathode zone of the discharge. In the authors' opinion, this is an indication of the separate evaporation of graphite and lanthanum.

The decrease in the amount of the cathode deposit with respect to the amount of sputtered graphite on making smaller the cross-section of the electrode is understandable. There exists a considerable temperature gradient at the cathode from the axis of the arc toward its periphery, as well as a temperature gradient in the gas phase [37, 38]. As a result, the gas phase contains larger carbon clusters in the peripheral parts of the near-cathode region; the lower surface temperature leads to a higher accommodation coefficient, compared with that in the central parts of the cathode. Apparently, the area of the peripheral regions of the electrodes increases in proportion to a squared characteristic size (equivalent electrode diameter). The factors mentioned lead to an increase in the fraction of the cathode deposit on raising the cross-section area of the electrode being sputtered and provide the observed shape of the cathode deposit.

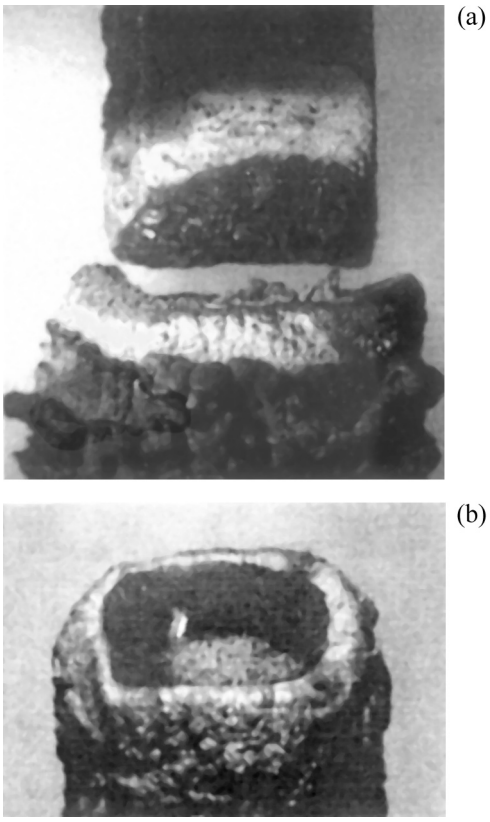


Fig. 2. Photographs of a typical cathode deposit upon completion of the synthesis. (a) Correspondence between the electrode being sputtered and the deposit formed, and (b) characteristic crater at the center of the deposit.

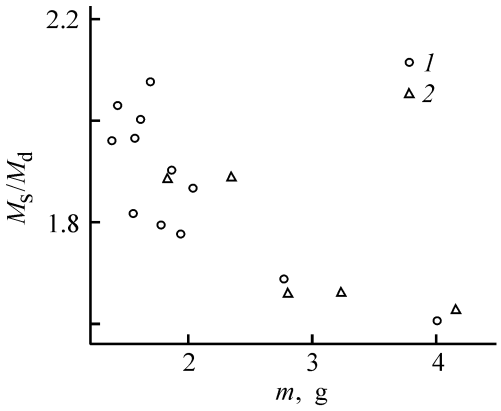


Fig. 3. Influence exerted by the mass m of the electrode being sputtered on the ratio M_s/M_d of the mass of the sputtered graphite to that of the cathode deposit for (*1*) graphite and (*2*) combined electrodes.

The flow of evaporated lanthanum is virtually not involved in the formation of the plasma composition in the arc, but affects the synthesis of fullerenes in the carbon vapor jet. This influence is primarily manifested in a change in the composition of the

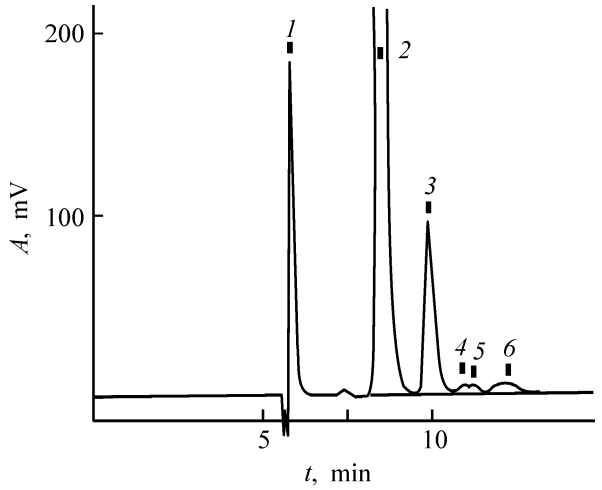


Fig. 4. Typical chromatogram of an extract of the carbon black synthesized. (*A*) Signal from the UV detector and (*t*) time. Peak assignment: (*1*) *ortho*-xylene, (*2*) C_{60}, (*3*) C_{70}, (*4*, *5*) C_{72}–C_{86}, and (*6*) La@C_n.

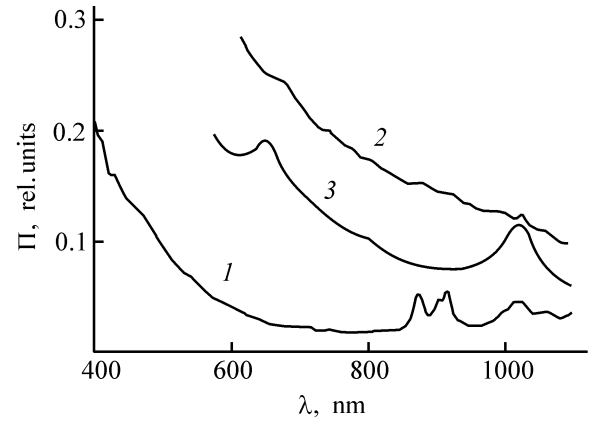


Fig. 5. Typical absorption spectrum of the extract. (П) Absorption and (λ) wavelength. Extraction with (*1*) *ortho*-xylene and (*2*) DMFA; (*3*) published La@C_{82} spectrum.

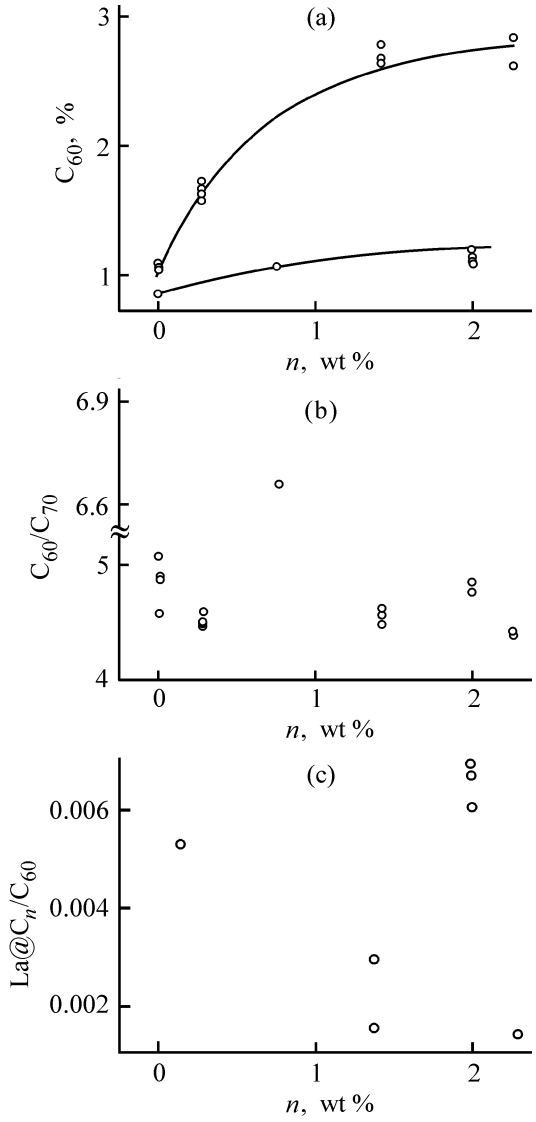


Fig. 6. Effect of the content *n* of lanthanum carbonate in the electrode on (a) yield of C_{60} and yield ratios, (b) C_{60}/C_{70}, and (c) La@C_n/C_{60}.

carbon black being synthesized and extracts obtained (Figs. 4–6).

A typical chromatogram of an extract of the carbon black obtained using the combined electrode under study differs from chromatograms of samples obtained with a graphite electrode in that peak *6* appears (Fig. 4). The spectrum of the extract obtained with the combined electrode contains absorption bands coinciding with the characteristic absorption bands of metallofullerenes [39] (Fig. 5). The yields of the substance (Fig. 6c), calculated from the absorption band at around 1000 nm and from peak *6* of the chromatogram (Fig. 4) are in a good agreement for all syntheses, which makes it possible to attribute peak *6* in the chromatogram to metallofullerenes. The shapes of the chromatographic peak *6* and optical absorption peak at around 1000 nm indicate that several forms of endohedral fullerenes exist in the substrate synthesized.

The yield of the fullerene C_{60} increases as the fraction of lanthanum in the combined electrode becomes higher (Fig. 6a). It is noteworthy that a similar tendency has been observed previously in synthesis of metallofullerenes by electric-arc sputtering of a combined electrode [24]. The maximum total yield of fullerenes was observed at a C/La ratio in the combined electrode equal to 50. Surprisingly, the maximum yield of La@C_{82} has been observed at the same C/La

ratio in synthesis of metallofullerenes by laser evaporation of a combined electrode [21], although the influence exerted by lanthanum-doping of the electrode on the yield of hollow fullerenes was quite the opposite. It may be assumed that this is due to the existence of a temperature gradient in the carbon vapor jet. It has been shown in a study of how the synthesis temperature affects the yield of fullerenes that the yield of $La@C_{82}$ is the highest at 1200 K, whereas the maximum yield of C_{60} is obtained at lower temperatures. Apparently, the optimal conditions for stabilization of a certain structure of the carbon cluster can be satisfied in an expanding carbon vapor jet only locally.

The relative yield of C_{60} (Fig. 6b) remained virtually unchanged in a set of experiments, with the exception of that with a mass fraction of lanthanum carbonate equal to 0.75% (C_{60}/C_{70} of about 6.6). At the same time, the yield of metallofullerenes shows a significant scatter (Fig. 6c). This scatter is possibly due, as mentioned above, to presence of a mixture of various forms of metallofullerenes in a sample being analyzed, with the concentration of any particular form of metallofullerenes in the extract being low.

Experiments with a mass fraction of lanthanum carbonate equal to 0.75 and 2% (Fig. 6) cannot be explained in the same way as other experiments. Of a similar nature are the data of [16, 21, 23]. The possible reason for this phenomenon is that different steady states of the arc and structures of the gas-dynamic flows in the reactor are possible in the course of synthesis, even if the synthesis procedure is strictly observed. In the case under study, there exist at least two different dependences of the yield of fullerenes on the mass fraction of lanthanum in the combined electrode (Fig. 6a).

Apparently, it is necessary to take into account, in determining the yield of fullerenes and in comparing the results obtained with published experimental data, that studies of extracts provide only a limited knowledge of the structure and composition of the carbon black. It is known that the carbon substrate obtained by electric-arc sputtering of graphite contains a large amount of fullerene-like fragments [40]. In the course of extraction, the imperfect carbon structures are separated from the fullerenes synthesized. The aggregation susceptibility of fullerenes, including that with incomplete fullerene fragments, hinders extraction of fullerenes from the substrate. Therefore, the yield of the target product can be raised severalfold by changing the solvent used for extraction and the method for recovery of fullerenes from the substrate [42, 43].

CONCLUSIONS

(1) Use of a surface-modified electrode simplifies the electrode preparation procedure and makes it possible to synthesize by electric-arc sputtering a mixture of metallofullerenes in amounts comparable with those reported by other authors.

(2) Raising the amount of lanthanum carbonate contained in the electrode does not change the C_{60}/C_{70} ratio in the samples synthesized and leads to an increase in the total amount of fullerenes obtained at a mass fraction of lanthanum within the range studied. In addition, use of the electrodes suggested leaves unchanged the amount of graphite utilized into the cathode deposit. This fact supports the assumption that lanthanum and carbon evaporate separately in the case when surface-modified electrodes are used.

REFERENCES

1. Chai, Y., Guo, T., Jin, C., *et al.*, *J. Phys. Chem.*, 1991, vol. 95, pp. 7560–7564.
2. Neeb, M., Klingeler, R., Bechthold, P.S., *et al.*, *Appl. Phys. A*, 2001, vol. 72, pp. 289–295.
3. Gu, G., Huang, H., Yang, S., *et al.*, *Chem. Phys. Lett.*, 1998, vol. 289, pp. 167–173.
4. Liu, S. and Sun, S., *J. Organomet. Chem.*, 2000, vol. 599, pp. 74–86.
5. Wang, C.R., Inakuma, M., and Shinohara, H., *Chem. Phys. Lett.*, 1999, vol. 300, pp. 379–384.
6. Nishibori, E., Takata, M., Inakuma, M., and Shinohara, H., *Chem. Phys. Lett.*, 1998, vol. 298, pp. 79–84.
7. Wang, C.R., Kai, T., Tomiyama, T., *et al.*, *Nature*, 2000, vol. 408, pp. 426–427.
8. Takata, M., Nishibori, E., Sakata, M., *et al.*, *Phys. Rev. Lett.*, 1999, vol. 83, pp. 2214–2216.
9. Yamamoto, K., Saunders, M., Khong, A., *et al.*, *J. Am. Chem. Soc.*, 1999, vol. 121, pp. 1591–1603.
10. Murphy, T.A., Pawlik, T., Weidinger, A., *et al.*, *Phys. Rev. Lett.*, 1996, vol. 77, pp. 1075–1078.
11. Knapp, C., Dinse, K.-P., Piezak, B., *et al.*, *Chem. Phys. Lett.*, 1997, vol. 272, pp. 433–437.
12. Stevenson, S., Rice, G., Glass, T., *et al.*, *Nature*, 1999, vol. 401, pp. 55–57.
13. Olmstead, M.M., de Bettencourt-Dias, A., Duchamp, J.C., *et al.*, *J. Am. Chem. Soc.*, 2000, vol. 122, pp. 12 200–12 206.
14. Olmstead, M.M., de Bettencourt-Dias, A., Duchamp, J.C., *et al.*, *Angew. Chem. Int. Ed.*, 2001, vol. 40, pp. 1223–1225.
15. Wang, C.R., Kai, T., Tomiyama, T., *et al.*, *Angew. Chem. Int. Ed.*, 2001, vol. 40, pp. 397–399.

16. Bubnov, V.P., Kol'tover, V.K., Laukhina, E.E., *et al.*, *Izv. Akad. Nauk, Ser. Khim.*, 1997, no. 2, pp. 254–258.
17. Tagmatarchis, N., Aslanis, E., Shinohara, H., and Prassides, K., *J. Phys. Chem. B*, 2000, vol. 104, pp. 11 010–11 012.
18. Okazaki, T., Lian, Y., Gu, Z., *et al.*, *Chem. Phys. Lett.*, 2000, vol. 320, pp. 435–440.
19. Hirata, T., Otomo, Y., and Hatakeyama, R., *Thin Solid Films*, 2002, vol. 407, pp. 32–37.
20. Ying, Z.C., Jin, C., Hettich, R.L., *et al.*, *Fullerenes: Recent Advances in the Chemistry and Physics of Fullerenes and Related Materials*, vol. 1, Kadish, K. and Ruoff, R., Eds., Pennington: Electrochem. Soc., 1994, pp. 1402–1412.
21. Suganuma, T., Kasuya, D., Ishigaki, T., *et al.*, *Eur. Phys. J. D*, 1999, vol. 9, pp. 373–376.
22. Lian, Y.F., Shi, Z.J., Zhou, X.H., *et al.*, *J. Phys. Chem. Solids*, 2000, vol. 61, pp. 1037–1040.
23. Tran, N.E. and Lagowski, J.J., *Carbon*, 2002, vol. 40, pp. 939–948.
24. Sueki, K., Kikuchi, K., Akiyama, K., *et al.*, *Chem. Phys. Lett.*, 1999, vol. 300, pp. 140–144.
25. Lange, H., Huczko, A., Byszewski, P., *et al.*, *Chem. Phys. Lett.*, 1998, vol. 289, pp. 174–180.
26. Wilson, M.A., Moy, A., Rose, H., *et al.*, *Fuel*, 2000, vol. 79, pp. 47–56.
27. Kuz'min, S.M., Kozlov, A.V., and Leonov, A.A., Abstracts of Papers, *VII Mezhdunarodnaya konferentsiya "Problemy sol'vatatsii i kompleksoobrazovaniya v rastvorakh" Ivanovo, 8–11 okt. 2001 g*, (VII Int. Conf. "Problems of Solvation and Complexation in Solutions," Ivanovo, October 8–11, 2001), p. 185.
28. Yamaguchi, Y. and Maruyama, S., *Chem. Phys. Lett.*, 1998, vol. 286, pp. 336–342.
29. Gao, X. and Gao, J., *J. Phys. Chem. B*, 1994, vol. 98, pp. 5618–5620.
30. Krestinin, A.V., Moravskii, A.P., and Tesner, P.A., *Khim. Fiz.*, 1998, vol. 17, no. 9, pp. 70–84.
31. Churilov, G.N., Novikov, P.V., Tarabanko, V.E., *et al.*, *Carbon*, 2002, vol. 40, pp. 891–896.
32. Mandziuk, M. and Bacic, Z., *J. Phys. Chem. B*, 1994, vol. 101, pp. 2126–2140.
33. Kobayashi, K., Nagase, S., and Akasaka, T., *Chem. Phys. Lett.*, 1996, vol. 261, pp. 502–506.
34. Ellacott, M.V., Pang, L.S.K., and Prochazka, L., *Carbon*, 1994, vol. 32, pp. 542–544.
35. *Fizicheskaya entsiklopediya* (Physical Encyclopedia), Prokhorov, A.M., Ed., Moscow: Bol'sh Sov. Entsikl., 1988, vol. 1; 1990, vol. 2.
36. Egorov, V.S., Tolmachev, V.A., Klyucharev, A.N., *et al.*, *Spravochnik konstant elementarnykh protsessov s uchastiem atomov, ionov, elektronov, fotonov* (Reference Book og Constants of Elementary Processes Involving Atoms, Ions, Electrons and Phonons), Zhiglinskii, A.G., Ed., St. Petersburg: SPb. Gos. Univ., 1994.
37. Byszewski, P., Lange, H., Huczko, A., and Behnke, J., *J. Phys. Chem. Solids*, 1997, vol. 58, pp. 1679–1683.
38. Lange, H., Huczko, A., and Starski, A., *J. Phys. Chem. A.*, 1997, vol. 101, pp. 1267–1269.
39. Shinohara, H., *Rep. Prog. Phys.*, 2000, vol. 63, pp. 843–892.
40. Kanowski, M., Vieth, H.-M., Luders, K., *et al.*, *Carbon*, 1997, vol. 35, pp. 685–695.
41. Nath, S., Pal, H., and Sapre, A.V., *Chem. Phys. Lett.*, 2000, vol. 327, pp. 143–148.
42. Sun, D., Liu, Z., Guo, X., *et al.*, *J. Phys. Chem. B*, 1997, vol. 101, pp. 3927–3930.
43. Sun, B., Feng, L., Shi, Z., and Gu, Z., *Carbon*, 2002, vol. 40, pp. 1591–1595.

Russian Journal of Applied Chemistry, Vol. 78, No. 4, 2005, pp. 565–567. Translated from Zhurnal Prikladnoi Khimii, Vol. 78, No. 4, 2005, pp. 572–574.
Original Russian Text Copyright © 2005 by Binkauskene.

APPLIED ELECTROCHEMISTRY AND CORROSION PROTECTION OF METALS

Influence of the Composition of Dilute Nickel-Plating Electrolytes on the Physicomechanical Properties of Electroplated Coatings

E. Binkauskene

Institute of Chemistry, Vilnius, Lithuania

Received June 23, 2004

Abstract—The influence of the composition of dilute nickel-plating electrolyte containing luster-forming additives on the leveling, plasticity, and internal stresses of coatings being electroplated was studied. The possibility of combining nickel sulfate, sodium chloride, and boric acid as the main composition of a dilute nickel-plating electrolyte was analyzed.

Technological solutions that would make lower the expenditure of nonferrous metals, such as nickel, tin, copper, and their alloys, are sought for in order to further develop the galvanic industries. Compositions of bright-nickel-plating electrolytes ensuring a common plating rate of 0.8–1.2 μm min^{-1} at the concentrations of salts of a metal being deposited lowered by a factor of 2–2.5 (with a total nickel concentration of up to 30–35 g l^{-1}) have been suggested [1–4]. The rate of nickel plating depends not only on the anionic composition of an electrolyte [5], but also on the luster-forming formulations used. The nature and cathodic behavior of luster-forming additives may lead to a redistribution of the rates of nickel deposition and hydrogen evolution in favor of the latter process. In this case, formation of nickel hydroxide compounds in a near-cathode layer and their inhibiting effect on nickel electrodeposition become more likely, and the microstructure of the resulting coatings is changed. The considerable increase in the hydrogenation of the deposits deteriorates the physicomechanical properties of the coatings obtained [6–8]. To improve the main characteristics of the bright-nickel-plating process, acetylene compounds are used in combination with ethylene and organosulfur additives [9].

The aim of this study, was to assess the influence exerted by the composition of a dilute nickel-plating electrolyte containing luster-forming additives based on β-oxyethyl cinnamide (OECAM) on the physicomechanical properties of the coatings being deposited.

EXPERIMENTAL

The study was performed in nickel-plating electrolytes containing (g l^{-1}): no. 1: 140 $NiSO_4 \cdot 7H_2O$, 30 $NiCl_2 \cdot 6H_2O$, and 30 H_3BO_3; no. 2: 33 $NiSO_4 \cdot 7H_2O$, 120 $NiCl_2 \cdot 6H_2O$, and 30 H_3BO_3; no. 3: 150 $NiSO_4 \cdot 7H_2O$, 50 NaCl, and 30 H_3BO_3. The electrolytes prepared were subjected to selective purification. Chemically and analytically pure reagents were used in the experiments. OECAM was synthesized and purified[1] mp 87°C. 2-butyne-1,4-diol (YN) was twice recrystallized from chloroform, mp 58°C; 2-butene-1,4-diol (EN) was purified chromatographically, mp 113°C at a pressure of 5 mm Hg. Saccharin was recrystallized from ethanol, mp 225–226°C. The temperature of the experiment was 50°C and pH 4.0. The pH value of the electrolytes was measured with an LPU-01 pH-meter and adjusted with hydrochloric acid or sodium hydroxide.

The microleveling power was determined by measuring profilograms of a titanium substrate with triangular grooves cut to a depth of about 4 μm (angle 120°). The microleveling factor B (%) was calculated from data on the average depth of the grooves before and after the nickel plating with the use of the formula:

$$B = \frac{h_1 - h_2}{h_1} \times 100, \quad (1)$$

where h_1 and h_2 are the depths of the substrate grooves (μm) before and after the deposition of a coating, respectively.

The plasticity of the coatings was evaluated by their ultimate tensile elongation, measured with a spiral elastometer.[2] Plates with coatings (170 × 10 mm in size and 1 mm thick) were placed on the elastometer having the form of a spiral template with a step-

[1] At the Department of Organic Chemistry, Vilnius University.

[2] Designed at the Institute of Chemistry.

1070-4272/05/7804-0565 © 2005 Pleiades Publishing, Inc.

Limiting current density i_c in a Hull cell for various nickel plating electrolytes for bright nickel plating

Electrolyte	Electrolyte no.	Luster-forming additive, g l^{-1}	i_c, A dm^{-2}
Sulfate	1	Saccharin, 1.5; OECAM, 0.5; YN, 0.05	1.9
Chloride	2	The same	2.8
	3	"	2.0
	2	Saccharin, 1.5; YN, 0.08; EN, 0.16	3.2

wise changing radius of curvature. The critical elongation, at which coatings cracked, was determined with a special paste containing *o*-phenanthroline chloride indicator, which could reveal an uncoated steel substrate.

The elongation l (%) was calculated by the formula

$$l = [d/(2r + d)] \times 100, \quad (2)$$

where d is the thickness of a plate with a coating (mm), and r, the radius of curvature at the critical point of the spiral surface.

The internal stresses (IS) in the nickel coatings were measured by the method of a flexible cathode with a device that could measure the cathode curvature after its being coated in a stirred electrolyte [10].

It is known that chloride nickel-plating electrolytes ensure a higher rate of nickel deposition, compared with sulfate electrolytes [5]. Introduction of sodium salts as supporting additives, which are used to improve the throwing power of nickel-plating electrolytes [6], makes lower the electrodeposition rate. The table lists the electrolyte formulations and estimates of the nickel-plating rates, found by the fast method [5] with a Hull cell. The formulation suggested is similar to the technological solution of [9], which consists in that small concentrations of YN are used in combination with an ethylene compound, EN, with the key role played by the competition of acetylene and ethylene groups in hydrogenation. β-Oxyethyl cinnamide is described by the formula $C_6H_5CH{=}CH{-}CONHCH_2CH_2OH$ and, unlike EN, contains a phenyl radical and nitrogen. A comparative study of the known bright-nickel-plating electrolyte based on a mixture of YN and EN [9] in an untypical formulation of a dilute electrolyte no. 2 demonstrated that the rates of metal plating in a dilute chloride solution differ only slightly for the additives used.

The coatings obtained in a chloride electrolyte have a factor of 1.5–2.0 lower internal compression stresses over the entire range of the current densities i_c (Fig. 1a).

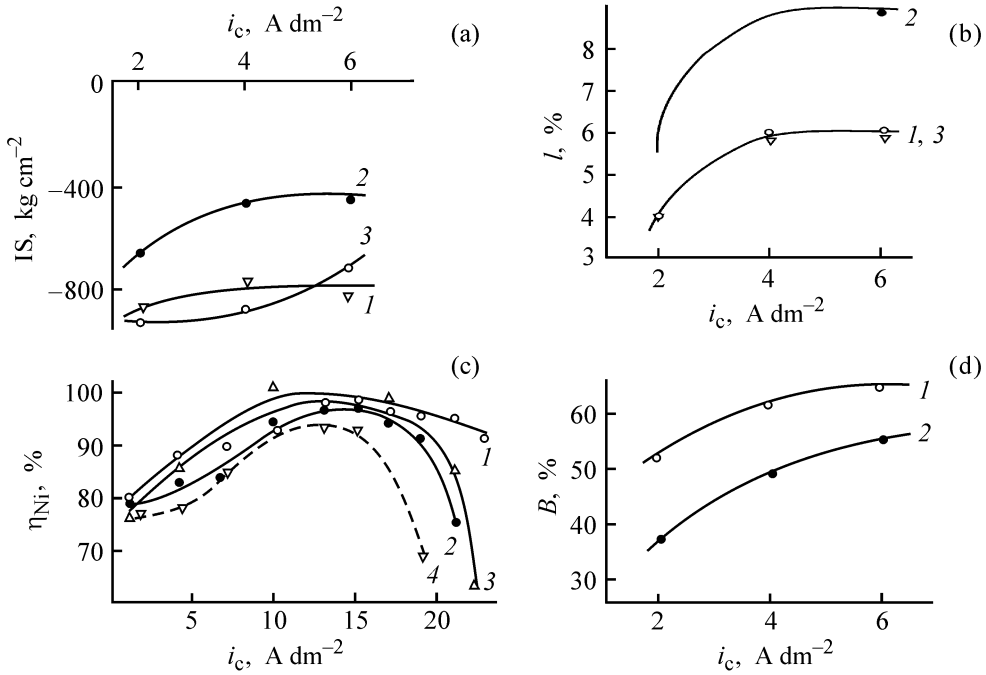


Fig. 1. (a) Internal stresses IS, (b) plasticity l, (c) current efficiency η_{Ni}, and (d) microleveling factor B vs. the current density i_c in various nickel-plating electrolytes. Temperature 50°C and pH 4.0. (a, b, d) Digits at curves are the electrolyte numbers; Additive to the electrolytes (g l^{-1}): saccharin 1.5, OECAM 0.5, and YN 0.05. (c) Electrolyte (g l^{-1}): (*1*) no. 2; (*2*) no. 2 + saccharin, 1.5; (*3*) $NiCl_2 \cdot 6H_2O$, 27; Na_2SO_4, 70; H_3BO_3, 30; and (*4*) no. 1 + saccharin, 1.5.

The plasticity of a lustrous nickel coating formed under the same conditions reaches a value of 9% (Fig. 1b), which is very high, compared with that obtained previously (up to 6%) for the technological solutions suggested in [9]. It should be noted that sufficiently plastic deposits (6%) are also obtained from dilute nickel-plating electrolyte nos. 1 and 3 (Fig. 1b). Presumably, the possible reason for the smaller elongation is the lower current efficiency by nickel in sulfate electrolytes, compared with chloride electrolytes. A similar effect is produced by sodium ions (Fig. 1c). In this case, a stronger alkalization of the near-cathode space is observed and the amount of impurities incorporated into the nickel deposit is larger. The best leveling power is observed for sulfate electrolyte no. 1 (Fig. 1d). This may be due to different catalytic activities of the renewed nickel surface in reactions of cathodic conversion of ethylene and acetylene compounds. Therefore, the choice of the electrolyte composition depends on whether a higher plasticity or leveling is required for a particular coating.

The data in the table indicate that the rates of nickel plating in dilute nickel-plating electrolytes, sulfate electrolyte no. 1 and chloride electrolyte no. 3, are nearly the same and the coatings obtained from these electrolytes have the same internal stresses and plasticities (Figs. 1a, 1b). This shows that nickel sulfate, sodium chloride, and boric acid can be combined in the formulation of a dilute nickel-plating electrolyte based on OECAM if nickel chloride is completely replaced with sodium chloride.

CONCLUSION

A study of the influence exerted by the composition of a dilute nickel-plating electrolyte containing β-oxyethyl cinnamide as luster-forming additive on the physicomechanical properties of the coatings deposited demonstrated that nickel sulfate, sodium chloride, and boric acid can be used in combination in the formulation of a dilute nickel-plating electrolyte.

REFERENCES

1. Baker, E.A., Hemsley, S., and House, J.R., *Trans. Inst. Metal Finish.*, 1977, vol. 55, no. 3, pp. 129–135.
2. Duchene, J.R., *Plating Surf. Finish.*, 1980, vol. 67, no. 9, pp. 37–39.
3. Jayakrishnan, S., Pushpavanam, M., Raman, V., and Shenoi, B.A., *Metal Finish.*, 1984, vol. 82, no. 7, pp. 65–69.
4. Binkauskene, E. and Vegys, J., *Inorg. Chem. Technol.*, Kaunas, 1997, pp. 32–35.
5. Binkauskene, E., *Zh. Prikl. Khim.*, 2002, vol. 75, no. 5, pp. 869–870.
6. *Blestyashchie elektroliticheskie pokrytiya* (Lustrous Electroplated Coatings), Matulis, Yu.Yu., Ed., Vilnius: Mintis, 1969.
7. Binkauskene, E., *Khimiya*, 1996, no. 2, pp. 33–36.
8. Monev, M., Baumgartner, M.E., Loebich, O., and Raub, Ch.J., *Metalloberflache*, 1991, vol. 45, no. 2, pp. 77–85.
9. Binkauskiene, E., *J. Chem. Technol. Biotechnol.*, 1997, vol. 70, no. 5, pp. 106–110.
10. Bodnevas, A.I., and Matulis, Yu.Yu., *Tr. Akad Nauk LitSSR*, 1963, vol. 1(32)B, pp. 49–60.

Russian Journal of Applied Chemistry, Vol. 78, No. 4, 2005, pp. 568–573. Translated from Zhurnal Prikladnoi Khimii, Vol. 78, No. 4, 2005, pp. 575–580.
Original Russian Text Copyright © 2005 by Kirsanov, Legin, Babain, Vlasov.

APPLIED ELECTROCHEMISTRY AND CORROSION PROTECTION OF METALS

Polymeric Sensors Based on Extraction Systems for Determination of Rare-Earth Metals

D. O. Kirsanov, A. V. Legin, V. A. Babain, and Yu. G. Vlasov

St. Petersburg State University, St. Petersburg, Russia
Khlopin Institute of Radium, St. Petersburg, Russia

Received February 14, 2005

Abstract—New polymeric sensors based on bidentate neutral organophosphorus compounds of varied structure with addition of chlorinated cobalt dicarbollide, which are highly sensitive to Fe^{3+}, Y^{3+}, La^{3+}, Pr^{3+}, Nd^{3+}, and Eu^{3+} cations in a wide range of concentrations at pH 2, were suggested. The selectivity, detection limits, and pH-dependence of the potential of the sensors developed were studied. The influence of chlorinated cobalt dicarbollide on the electrochemical characteristics of the sensors was demonstrated.

At present, the areas of analytical chemistry associated with design of chemical sensors of various types are being intensively developed. A particular place is occupied by studies concerned with such sensors as ion-selective electrodes (ISE), which are very convenient in measurements, do not require any complex and expensive apparatus, and can be used in field conditions. Film-type ISEs with a matrix of plasticized polyvinyl chloride (PVC) open up wide opportunities for variation of their sensor properties by modifying the chemical structure of the active substance of the membrane (ionophore), by changing the concentration ratio between the ionophore and the ion-exchange additive, and by using various solvents-plasticizers. A particularly topical task is to create sensors for determining stable isotopes of metals in liquid radioactive wastes. This is so because sensors of this kind can be used to create systems that enable on-line monitoring without direct involvement of an operator, which diminishes the health hazard for the personnel working with sources of ionizing radiation.

A rather large number of potentiometric sensors reversible to ions of cesium, barium, and other elements present in liquid radioactive waste have been developed. However, a considerably smaller number of studies have been devoted to development of film-type ISEs sensitive to triple-charged metal cations. Film-type ISEs reversible to the cations La^{3+}, Ce^{3+}, Nd^{3+}, Sm^{3+}, etc. have been created [1–6]. As a rule, macrocyclic organic compounds with various heteroatoms are used as membrane-active components in sensors of this kind. The sensitivity of such sensors is commonly close to the theoretical value of 19 mV decade^{-1}; however, the working pH range lies above pH 3 for most of the ISEs described, which is an important limitation in analyses for rare-earth elements (REE). At higher proton concentrations, the sensitivity markedly decreases, which gives no way of using sensors of this kind in strongly acidic solutions. In addition, the detection limits for most of the ISEs developed are rather high (4.5–5.5 pM^{3+}), which makes markedly narrower the variety of possible practical applications of sensors of this kind.

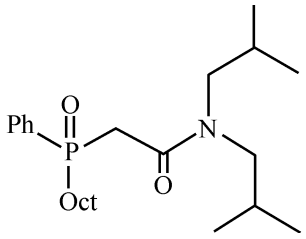
A possible way to overcome these difficulties is to search for new active compounds that can form strong complexes with multicharged metal cations.

The authors' approach to development of polymeric sensors sensitive to triple-charged metal cations consists in that various bifunctional neutral organophosphorus compounds (BNOPC) and the anion of chlorinated cobalt dicarbollide (CCD) are used as active substances. Compounds of this kind and their synergetic mixtures with CCD are used with success in extraction for separating and concentrating rare-earth elements from a strongly acidic radioactive waste formed from spent nuclear fuel [7–9]. Carboranes and substituted carboranes have been suggested as membrane components for ISEs sensitive to cesium [10, 11]. Carboranes and, in particular, CCD have the form of a large lipophilic anion and act in extraction systems as a cation-exchanger, similarly to potassium tetra(*p*-chlorophenyl)borate (PTCPB) conventionally used in ionometry. However, CCD is a con-

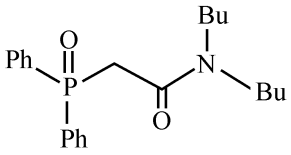
1070-4272/05/7804-0568 © 2005 Pleiades Publishing, Inc.

siderably stronger acid than PTPB and is stable against acid hydrolysis. Consequently, CCD is more stable when used with acid solutions. In addition, CCD shows a high radiation-hardness, which enables its effective use in extraction of various radioactive elements.

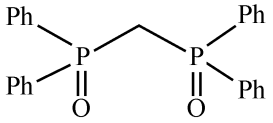
The aim of this study was to develop, on the basis of BNOPC and CCD, new polymeric sensors reversible to triple-charged metal cations. The working characteristics of the sensors, such as sensitivity, detection limits, selectivity, and pH-dependence of the potential, were examined. On the basis of extraction data, the following BNOPC were chosen as membrane-active substances: octylphenyl-*N*,*N*-di-isobutylcarbamoylmethylphosphine oxide (**I**), diphenyl-*N*,*N*-di-*p*-butylcarbamoylmethylphosphine oxide (**II**), tetraphenylmethylenediphosphine dioxide (**III**), and CCD:



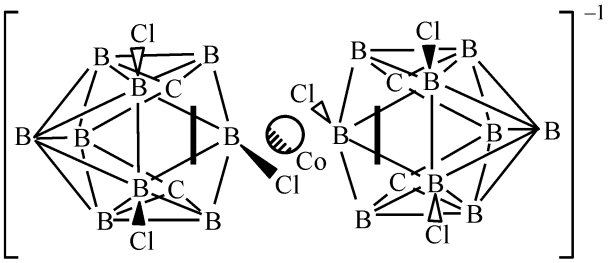
I



II



III



CCD

EXPERIMENTAL

PVC and *o*-nitrophenyloctyl ester (NPOE) manufactured by Fluka (Switzerland) were used in the study.

Table 1. Compositions of sensor membranes

Sensor no.	Mass of indicated components, g				BNOPC structure
	PVC	NPOE	CCD	BNOPC	
1	0.066	0.130	–	0.0041	**I**
2	0.066	0.130	–	0.0037	**II**
3	0.066	0.130	–	0.0042	**III**
4	0.066	0.130	0.018	0.0041	**I**
5	0.066	0.130	0.018	0.0037	**II**
6	0.066	0.130	0.018	0.0042	**III**
7	0.066	0.130	0.18	0.0041	**I**
8	0.066	0.130	0.18	0.0037	**II**
9	0.066	0.130	0.18	0.0042	**III**
10	0.066	0.130	0.18	–	–

Octylphenyl-*N*,*N*-diisobutylcarbamoylmethylphosphine oxide, diphenyl-*N*,*N*-di-*p*-butylcarbamoylmethylphosphine oxide, and tetraphenylmethylenediphosphine dioxide were synthesized at the Institute of Chemical Reagents and Special-Purity Chemical Substances (IREA, Moscow). The cesium salt of CCD was purchased from Katchem (Czech Republic) and converted into the H^+ form prior to use in a membrane. Yttrium, praseodymium, neodymium, and europium nitrates were provided by the Khlopin Institute of Radium in the form of 0.5 M solutions in 0.1 M nitric acid. Other inorganic salts and organic solvents of chemically pure grade were purchased from Reaktiv Co. (St. Petersburg). All the solutions were prepared using twice-distilled water.

The compositions of the polymeric sensor membranes studied are listed in Table 1. Composition nos. 1–3 contained BNOPC in a concentration of 50 mmol kg^{-1} membrane; composition nos. 4–6, BNOPC in the same concentration and CCD (10 mmol kg^{-1} membrane); composition nos. 7–9, CCD in a concentration of 100 mmol kg^{-1} membrane; and composition no. 10, no BNOPC and only CCD in a concentration of 100 mmol kg^{-1} membrane. These relative concentrations of the active substances of the membranes were chosen on the basis of the following considerations: a considerable excess of the concentration of a neutral ligand over that of an ion-exchange additive is traditionally used in developing the composition of a membrane in inonometry [12], with the particular ratio of the concentrations chosen in accordance with the stoichiometry of the complex constituted by the ligand and the target ion. It has been established in studies of extraction that the maximum

extracting capacity for rare-earth elements is observed for 1 : 2 mixtures of BNOPC and CCD [13]. The membrane composition nos. 1–3, 10 were prepared for determining the individual contributions of the active components to the electrode characteristics of the sensors.

The sensor membranes were fabricated using the standard procedure. Weighed portions of the membrane components were poured over with tetrahydrofuran (THF) and the mixture was agitated with a magnetic stirrer to complete dissolution of the components. The resulting cocktail was poured into a Teflon weighing bottle with a flat bottom and allowed to stay to complete evaporation of THF (~24 h). Discs 7 mm in diameter were cut from the membrane obtained and glued into electrode cases. Three sensors with a membrane of each type were fabricated. The numerical values of various parameters of the electrodes, presented below, were obtained by averaging over sensors of the same type.

Potentiometric measurements were performed with the following galvanic cell

Ag | AgCl, KCl_{sat} | Solution under study | Membrane | 0.01 M NaCl | AgCl, KCl_{sat} | Ag

The readings were taken with a high-input-resistance multichannel digital voltmeter connected to a personal computer for data acquisition and processing. An EVL 1M 3.1 silver chloride reference electrode was used. The sensitivity of the sensors was studied at metal cation concentrations in the range 10^{-7}–10^{-2} M. At least four calibrations were made in solutions of each cation. The slopes of the linear portions of the electrode functions were calculated for the concentration range 10^{-5}–10^{-3} M. The cation concentrations were not recalculated into activities because of the deficiency of comparable data on the activity coefficients of triple-charged metals. For all the triple-charged metals studied the pH value of the calibration solutions was adjusted by addition of nitric acid to pH 2 in order to suppress hydrolysis.

The pH values of the solutions were monitored using an ESL 43-07 glass pH-electrode.

Table 2. Electrode sensitivity of sensors in solutions of triple-charged metal cations at fixed pH 2

Sensor no.	Electrode sensitivity, mV decade^{-1}					
	Fe^{3+}	Y^{3+}	La^{3+}	Pr^{3+}	Nd^{3+}	Eu^{3+}
1	12 ± 1	9 ± 1	26 ± 1	24 ± 3	24 ± 2	22 ± 2
2	6 ± 2	13 ± 1	11 ± 1	17 ± 2	15 ± 1	11 ± 2
3	17 ± 1	16 ± 1	17 ± 1	20 ± 3	18 ± 1	15 ± 2
4	15 ± 2	18 ± 1	22 ± 1	26 ± 1	22 ± 1	21 ± 1
5	32 ± 1	25 ± 1	26 ± 3	32 ± 1	23 ± 2	23 ± 2
6	34 ± 1	16 ± 3	24 ± 2	28 ± 2	18 ± 1	18 ± 2
7	11 ± 1	10 ± 2	5 ± 2	6 ± 1	8 ± 2	6 ± 1
8	10 ± 1	10 ± 1	5 ± 1	7 ± 1	8 ± 1	7 ± 1
9	10 ± 2	7 ± 2	2 ± 1	7 ± 2	7 ± 1	5 ± 1
10	7 ± 1	5 ± 1	2 ± 1	6 ± 2	5 ± 2	3 ± 1

The selectivity of the sensors was studied by the method of mixed solutions at a fixed concentration of La^{3+} ions (interfering ions) and a constant pH value of 2.

The pH dependence of the potential of the sensors was determined in two ways: (i) in a 0.01 M solution of tris(hydroxymethyl)aminomethane (TRIS), with gradual addition of nitric acid (pH 1.5–9), and (ii) in a 0.0001 M solution of lanthanum nitrate, also with gradual addition of nitric acid (pH 1.5–6).

The sensors fabricated were calibrated against solutions of the cations Fe^{3+}, Y^{3+}, La^{3+}, Pr^{3+}, Nd^{3+}, and Eu^{3+} at a fixed pH 2, and the slopes of the linear portions of the electrode functions of the sensors were calculated. The data obtained are listed in Table 2. The major attention is attracted by the high electrode sensitivities of most of the sensors, which exceed in some cases the theoretical value of 19.7 mV/pM^{3+} for triple-charged cations. For example, sensor nos. 5 and 6, which are based on diphenyl-*N*,*N*-di-*p*-butylcarbamoylmethylphosphine oxide, and tetraphenylmethylenediphosphine dioxide with addition of CCD with a molar ratio BNOPC : CCD = 5 : 1, exhibit a super-Nernst sensitivity to Fe^{3+}, La^{3+}, and Pr^{3+} cations, with the slope ratios of the electrode functions close to the theoretical values for double-charged cations (29.5 mV decade^{-1}). Sensor nos. 1 and 4 also exhibit a super-Nernst response for some cations. The closeness of the sensor sensitivities in M^{3+} solutions to the theoretical values for M^{2+} is presumably due to the following: compounds of the type $M(X)_n^{m+}$ (where X is an inorganic anion, NO_3^- in the given case), with a formal charge of +2, rather than M^{3+} cations, enter into the reaction of complexation with BNOPC. This is indirectly confirmed by electro-

spray-mass-spectrometric experiments in systems constituted by BNOPC and an aqueous solution of an REE nitrate [14].

The influence exerted by the CCD concentration in a sensor membrane on the sensor sensitivity is clearly seen. Membrane nos. 1–3, based on BNOPC without CCD additive, possess, on the whole, lower sensitivities to all of the cations studied, compared with membrane nos. 4–6. The increase in sensitivity upon addition of CCD is the most clearly pronounced for composition nos. 5 and 6. Further increase in the CCD concentration from 10 to 100 mmol kg^{-1} leads to the opposite effect and composition nos. 7–9 exhibit only an insignificant sensitivity to the triple-charged cations studied. Composition no. 10 also shows very low slope rates of the electrode functions. Composition nos. 7–10 were excluded from further consideration.

In addition to the cations listed in Table 2, the sensor responses were studied in solutions of Al^{3+}, Cr^{3+}, Cu^{2+}, Ba^{2+}, and Pb^{2+}. It was found that the sensors developed show no sensitivity to these cations at pH 2. The only exception is sensor no. 1, based on octylphenyl-*N*,*N*-diisobutylcarbamoylmethylphosphine oxide, which has a response of 29 ± 1 mV $decade^{-1}$ with a detection limit of 6 pM^{2+} in lead solutions and a response of 20 ± 1 mV $decade^{-1}$ with a detection limit of 4 pM^{2+} in barium solutions.

The detection limits of the sensors are listed in Table 3. La^{3+} can be determined with the lowest detection limits for all of the sensors studied. Compared with those reported in [5, 6], the sensors developed in the present study open up wider opportunities of practical application. For example, it was established in [5] that electrodes with polymeric membranes containing monoaza-12-crown-4 as a neutral ligand can be used to determine La^{3+} cations at concentrations exceeding 3×10^{-5} M (4.5 pLa^{3+}) and satisfactorily work in the pH range 3–7. A detection limit of 6.3 pLa^{3+} was reported in [6] for sensors based on dicyclohexano-18-crown-6, which can be used in the pH range 4–9. The developed composition nos. 2 and 6 have lower detection limits and are applicable to determination of La^{3+} in acid media with pH 2. This is an important practical conclusion, because the elements to be determined exist in the ionic form only at low pH values. The detection limits of a number of the sensors developed for the cations Pr^{3+}, Nd^{3+}, and Eu^{3+} are also significantly lower than any of the previously known values.

The results obtained in determining the sensitivity of the sensors by the method of mixed solutions are presented in Fig. 1. Most of the sensors developed are more selective toward lanthanum cations. For composition nos. 2 and 3, the selectivity coefficients measured in Fe^{3+}/La^{3+} and Y^{3+}/La^{3+} solutions exceed 4. Introduction of CCD additive makes lower the sensitivity of the sensors to La^{3+} (composition nos. 4–6), and in the case of composition no. 4, there even occurs sensitivity reversal in favor of Nd^{3+} and Pr^{3+} and equalization of the sensitivities in the pair Eu^{3+}/La^{3+}. The most discriminated for all the sensors studied is the iron ion Fe^{3+}.

Table 3. Detection limits of sensors

Sensor no.	Detection limit, ±0.1 pM^{3+}					
	Fe^{3+}	Y^{3+}	La^{3+}	Pr^{3+}	Nd^{3+}	Eu^{3+}
1	5.1	4.0	6.3	5.4	5.4	5.0
2	6.9	5.0	7.0	5.5	5.8	5.2
3	5.5	5.1	6.1	5.6	5.7	5.7
4	3.8	5.2	6.4	6.3	5.8	6.2
5	4.9	5.1	6.5	5.7	5.9	5.6
6	4.7	4.9	6.6	6.2	5.2	6.2

Figure 2a shows the results obtained in determining the pH-dependence of the sensor potential in the absence of lanthanum ions in solution, with the response of a standard glass pH-electrode presented for comparison. For sensors with composition nos. 2, 3, and 6, the pH response in an acid medium becomes of the Nernst type, and composition no. 5 exhibits a considerable pH sensitivity in the alkaline region. On pass-

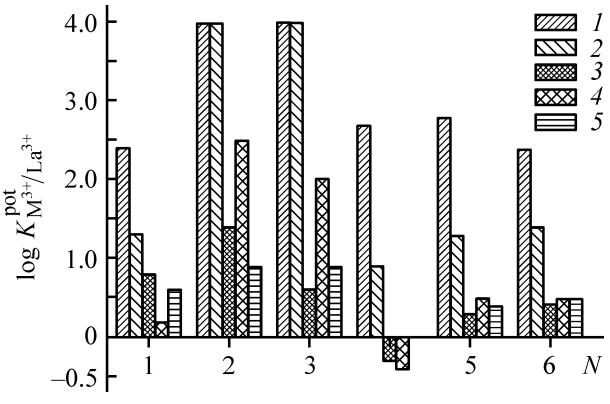


Fig. 1. Logarithms of the selectivity coefficients of the sensors, $\log K^{pot}_{M^{3+}/La^{3+}}$, determined by the method of mixed solutions. Typical determination error $\pm 0.1 \log K^{pot}_{M^{3+}/La^{3+}}$. (*N*) Sensor number. (*1*) Fe^{3+}, (*2*) Y^{3+}, (*3*) Pr^{3+}, (*4*) Nd^{3+}, and (*5*) Eu^{3+}.

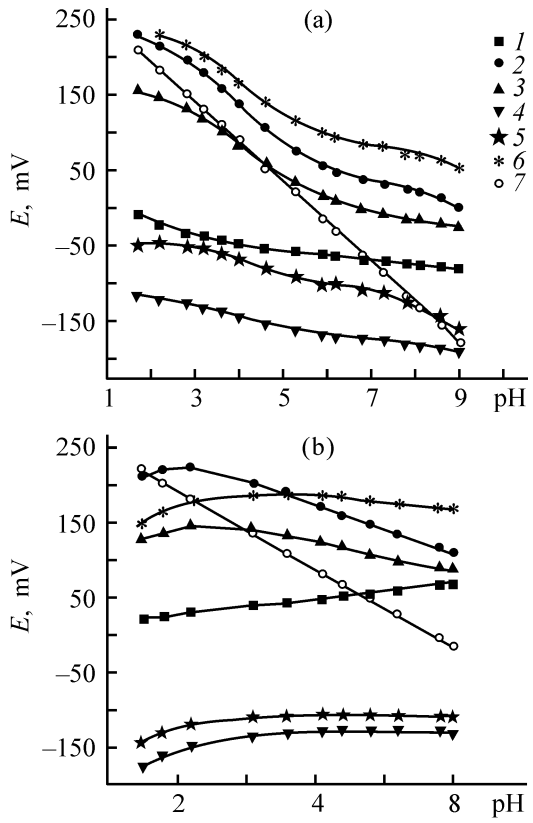


Fig. 2. Type of the pH-dependence of the potential E of (*1–6*) sensor nos. 1–6 (a) in the absence of metal cations in solution and (b) in a 0.0001 M solution of lanthanum nitrate. (*7*) Response of a standard glass pH-electrode.

ing to lanthanum-containing solutions, the type of the pH-dependence of the sensor potential changes significantly (Fig. 2b). At pH 2–6, the dependence for sensor nos. 4–6, which contain BNOPC and CCD in a concentration ratio of 5 : 1, virtually vanishes, which points to a high (>10) value of the selectivity coefficient $K^{pot}_{H^+/La^{3+}}$.

The published data [1–6] for the lower limit of the pH range in which polymeric sensor membranes reversible to triple-charged metal cation can successfully operate is no less than pH 3–4. At pH < 3, the influence exerted by protons on the electrode function becomes unacceptably strong and the sensitivity of the sensors to metals in acid solutions falls dramatically. It should be particularly noted that the sensors developed can be used to determine the concentrations of triple-charged metal cations at pH 2, which lifts a number of restrictions on practical application of such sensors, e.g., in analysis of solutions and wastes in radiochemical industry.

Of particular interest as regards possible analytical applications in analysis of liquid radioactive wastes are, in the authors' opinion, sensors with composition nos. 4–6, based on a mixture of BNOPC and CCD. Sensors of this kind, studied for the first time, surpass all the existing analogues in the whole set of their electrochemical characteristics.

CONCLUSIONS

(1) New polymeric sensors based on bidentate neutral organophosphorus compounds of varied structure, with addition of a chlorinated cobalt dicarbollide, were developed. It was established that the new sensors have a high sensitivity to Fe^{3+}, Y^{3+}, La^{3+}, Pr^{3+}, Nd^{3+}, and Eu^{3+} cations in a wide range of concentrations at pH 2.

(2) The detection limits of the sensors were determined, which lie below 6 pM^{3+} for La^{3+}, Pr^{3+}, and Eu^{3+} cations for a number of sensor compositions.

(3) It was established that, in the presence of the triple-charged metal cations under study, most of the membrane formulations are selective toward lanthanum cations. It was shown that addition of a chlorinated cobalt dicarbollide affects various electrochemical properties of the sensors.

(4) It was found that high H^+ concentrations do not interfere with determination of triple-charged cations.

(5) The efficiency of the approach suggested for sensor development was confirmed. This approach can be used to create convenient analytical instruments for practical monitoring of liquid radioactive wastes.

ACKNOWLEDGMENT

The authors thank N.A. Bondarenko (Institute of Chemical Reagents and Special-Purity Substances, IREA, Moscow) for synthesis and purification of octylphenyl-*N*,*N*-diisobutylcarbamoylmethylphosphine oxide, diphenyl-*N*,*N*-di-*p*-butylcarbamoylmethylphosphine oxide, and tetraphenylmethylenediphosphine dioxide.

REFERENCES

1. Akhond, M., Najafi, M.B., and Tashkhourian, *J., Sens. Actuators B*, 2004, vol. 99, pp. 410–415.
2. Ganjali, M.R., Pourjavid, M.R., *et al., Sens. Actuators B*, 2003, vol. 89, pp. 21–26.
3. Ganjali, M.R., Naji, L., *et al., Anal. Chim. Acta*, 2003, vol. 475, pp. 59–66.
4. Choudhury, D.A., Ogata, T., and Kamata, S., *Anal. Chem.*, 1996, vol. 68, pp. 366–370.

5. Gupta, V.K., Jain, S., and Chandra, S., *Anal. Chim. Acta*, 2003, vol. 486, pp. 199–207.
6. Mittal, S.K., Ashok Kumar, S.K., and Sharma, H.K., *Talanta*, 2004, vol. 62, pp. 801–805.
7. Romanovsky, V., Smirnov, I., Babain, V., *et al.*, *Solv. Extr. Ion Exchange*, 2001, vol. 19, no. 1, pp. 1–21.
8. Horwitz, E.P., *Solv. Extr. Ion Exchange*, 1986, vol. 4, pp. 449–494.
9. Chmutova, M.K., Kochetkova, N.E., and Myasoedov, B.F., *Radiokhimiya*, 1978, vol. 20, no. 5, pp. 713–718.
10. Peper, S., Telting-Diaz, M., *et al.*, *Anal. Chem.*, 2002, vol. 74, pp. 1327–1332.
11. Vin, C., Gomez, S., *et al.*, *J. Organometal. Chem.*, 1999, vol. 581, pp. 188–193.
12. Bakker, E., Buhlmann, P., and Pretsch, E., *Chem. Rev.*, 1997, vol. 97, pp. 3083–3132.
13. Rais, J., Tachimori, S., *et al.*, *Separation Sci. Tech.*, 1994, vol. 29, no. 2, pp. 261–274.
14. Gall', L.N., Chuprikov, A.V., *et al.*, *Dokl. Akad. Nauk*, 1992, vol. 325, no.3, pp. 514.

Russian Journal of Applied Chemistry, Vol. 78, No. 4, 2005, pp. 574–578. Translated from Zhurnal Prikladnoi Khimii, Vol. 78, No. 4, 2005, pp. 581–585.
Original Russian Text Copyright © 2005 by Sadyrbaeva.

APPLIED ELECTROCHEMISTRY AND CORROSION PROTECTION OF METALS

Electrodialysis Separation of Copper(II) and Platinum(IV) with Liquid Membranes Based on Di(2-Ethylhexyl)Phosphoric Acid

T. Zh. Sadyrbaeva

Institute of Inorganic Chemistry, Riga Technical University, Salaspils, Latvia

Received November 25, 2004

Abstract—Separation of copper(II) and platinum(IV) in extraction from binary acid chloride solutions with liquid membranes containing technical-grade di(2-ethylhexyl)phosphoric acid with addition of tri-*n*-octyl amine in 1,2-dichloroethane under the conditions of the galvanostatic electrodialysis was studied. The influence exerted by the current density and composition of aqueous solutions and liquid membranes on the rate and selectivity of copper(II) extraction was analyzed. The optimal conditions of metal separation were determined.

Membrane extraction is a promising technology for extraction and separation of metal ions. Acid organophosphorus reagents and, in particular, di(2-ethylhexyl)phosphoric acid (D2EHPA), are widely used for extraction of copper(II) ions from neutral and weakly acid solutions with impregnated and emulsion-type liquid membranes [1]. The membrane extraction is performed by the scheme of a counterflow transport of Cu^{2+} and H^+ ions and involves the interphase cation-exchange reaction

$$Cu^{2+}_{(a)} + 2HA_{(o)} \rightleftarrows CuA_{2(o)} + 2H^{+}_{(a)}, \qquad (1)$$

where HA stands for D2EHPA; (a), for the aqueous phase; and (o), for the organic phase.

The re-extraction of copper(II) from the organic phase is provided by the high acidity of the receiving solution. On applying a dc electric field, the transport of copper(II) ions across liquid D2EHPA-containing membranes occurs in the same direction as that of hydrogen ions. Under the conditions of electrodialysis, the transport of ions across bulk liquid membranes is intensified and extraction of metals into weakly acid solutions of mineral acids becomes possible [2]. Previously, electrodialysis extraction of copper(II) with liquid membranes containing pure and technical-grade D2EHPA in 1,2-dichloroethane has been studied [3, 4]. It was shown that, upon introduction of a tri-*n*-octyl amine (TOA) additive to raise their electrical conductivity, membranes of this kind provide an effective purification of dilute acid sulfate solutions to remove copper(II) and enable a thorough separation of copper(II) and palladium(II) in extraction from binary acid chloride mixtures.

The aim of this study was to examine the electrodialysis extraction of copper(II) from acid chloride solutions containing platinum(IV) with liquid membranes based on technical-grade D2EHPA with TOA additives and to determine the optimal conditions of metal ion separation.

EXPERIMENTAL

The electrodialysis transport of metal ions was studied using a five-compartment cell with a liquid membrane confined between vertical cellophane films in the system

(+) Pt, H_2SO_4	$CuCl_2$ H_2PtCl_6	D2EHPA TOA	HCl	H_2SO_4, Pt (–)
	MA		MA	

A dc current was passed across planar platinum electrodes in the galvanostatic mode. The volume of the liquid membrane was 2 cm^3, its thickness was 0.2 cm, and the phase contact area, 7.1 cm^2. The cellophane films confining the liquid membrane were preliminarily soaked in water.

The electrode compartments filled with a 0.15 M H_2SO_4 solution (17 cm^3) were separated from the compartments filled with a donating and receiving solution (13 cm^3) with MA-40 solid anion-exchange membranes.

1070-4272/05/7804-0574 © 2005 Pleiades Publishing, Inc.

As liquid membranes served 1,2-dichloroethane solutions of technical-grade D2EHPA (containing about 63% main substance) with addition of pure grade tri-*n*-octyl amine (containing 95% main substance). The donating solution, which, as a rule, contained 0.04 M copper(II) and 0.018 M platinum(IV), was prepared by dissolving hydrogen hexachloroplatinate hexahydrate $H_2PtCl_6 \cdot 6H_2O$ (pure grade) and a salt $CuCl_2 \cdot 2H_2O$ (analytically pure grade) in a 0.01 M hydrochloric acid. In most cases, 0.1 M HCl was used as receiving solution. The concentration of metal ions in the aqueous solutions was determined spectrophotometrically: copper(II), with NH_4OH [5], and platinum(IV), with tin chloride [6]. The optical density was measured on an SF-46 spectrophotometer.

In organic solutions of D2EHPA, an ionic pair is formed in the presence of tri-*n*-octyl amine (R_3N). This pair comprises an organic cation and organic anion, i.e., a binary extractant is formed [7].

$$R_3N_{(o)} + HA_{(o)} \rightleftarrows R_3NH^+A^-_{(o)}. \quad (2)$$

Copper(II) ions are extracted into the phase of the liquid membrane by the cation-exchange mechanism:

$$Cu^{2+}_{(a)} + 2Cl^-_{(a)} + 2R_3NH^+A_{(o)} \rightleftarrows CuA_{2(o)} + 2R_3NHCl_{(o)}. \quad (3)$$

The CuA_2 complex being extracted is transferred across the organic layer, to be decomposed at the interface with the receiving solution under the action of the electric field via a reaction reverse to reaction (3). The transport of Cu^{2+} ions across liquid D2EHPA membranes in the zero-current mode is virtually absent, since the receiving solution of 0.1 M hydrochloric acid does not provide copper(II) re-extraction from the organic phase. Platinum(IV) is present in the acid chloride solutions mainly in the form of an anionic chlorocomplex $PtCl_6^{2-}$ [6] and is extracted with tri-*n*-octyl amine by the interphase anion-exchange mechanism [8]:

$$H^+_{(a)} + Cl^-_{(a)} + R_3N_{(o)} \rightleftarrows R_3NHCl_{(o)}, \quad (4)$$

$$2R_3NHCl_{(o)} + PtCl^{2-}_{6(a)} \rightleftarrows [(R_3NH)_2PtCl_6]_{(o)} + 2Cl^-_{(a)}. \quad (5)$$

The effect of the current density on the rate of transmembrane transfer of the metal ions was studied with liquid membranes containing 20 vol % D2EHPA and 0.1 M TOA in dichloroethane. The flow rate of copper(II) ions is directly proportional to the current density in the range 4.2–10.6 mA cm^{-2} (Fig. 1).

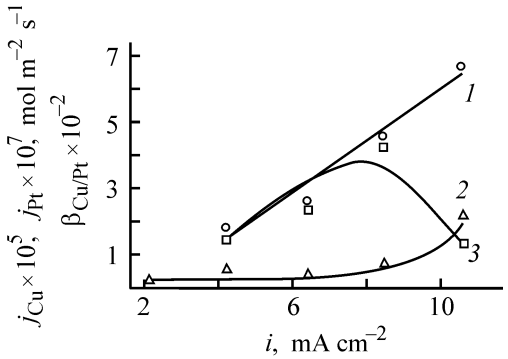


Fig. 1. Transfer rate of (*1*) copper(II) J_{Cu} and (*2*) platinum(IV) J_{Pt} and (*3*) separation coefficient $\beta_{Cu/Pt}$ vs. the current density i. c_{D2EHPA} = 20 vol %, c_{TOA} = 0.1 M, and τ = 60 min.

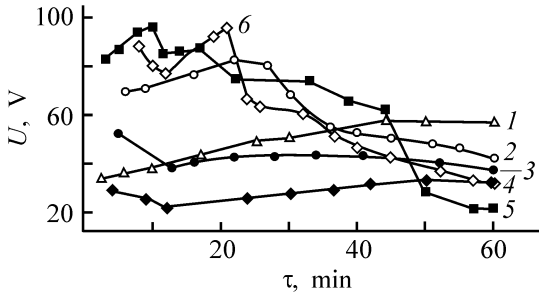


Fig. 2. Variation of the voltage U with time τ at different current densities and concentrations of TOA additive. i (mA cm^{-2}): (*1*) 4.2, (*2–5*) 8.5, and (*6*) 10.6. c_{TOA} (M): (*1, 2, 6*) 0.1, (*3*) 0.15, (*4*) 0.2, and (*5*) 0.05.

The current efficiency by Cu^{2+} during 1 h of electrodialysis in the given system is <13%. The current is mainly carried across the liquid membrane by hydrogen and chloride ions. The re-extraction of platinum(IV) from tri-*n*-octyl amine solutions is hindered by the high stability of the forming compounds [8]. In addition, the flow of $PtCl_6^{2-}$ anions through the membrane is impeded by the polarity of an electric current applied in the experiments. For this reason, metal ions are effectively separated in the course of electrodialysis. The degree of platinum(IV) extraction into the receiving solution is, as a rule, <0.1%. At the same time, the transfer of copper(II) during 1 h of electrodialysis at the highest current density is about 33%. The separation coefficient of metal ions is as high as 430 at a current density of 8.5 mA cm^{-2} (Fig. 1, curve *3*). Therefore, further experiments were performed at this current density.

In the course of the galvanostatic electrodialysis, a peak or a gradual increase in voltage is observed in the kinetic curves describing how the voltage varies at different current densities and compositions of the liquid membrane (Fig. 2). The rise in voltage is

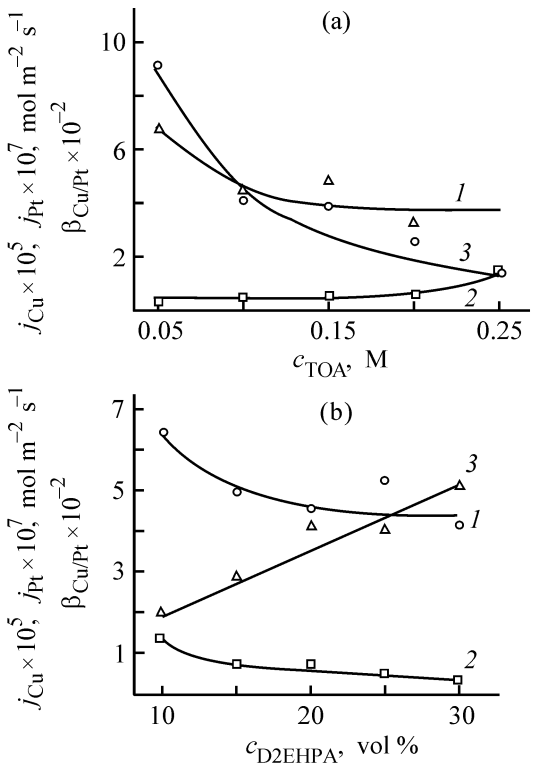


Fig. 3. Transfer rates of (*1*) copper(II) J_{Cu} and (*2*) platinum(IV) J_{Pt} and (*3*) separation coefficient of metals $\beta_{Cu/Pt}$ vs. the concentrations of (a) additive, c_{TOA}, and (b) transferring agent, c_{D2EHPA}. i = 8.5 mA cm^{-2}, and τ = 60 min.

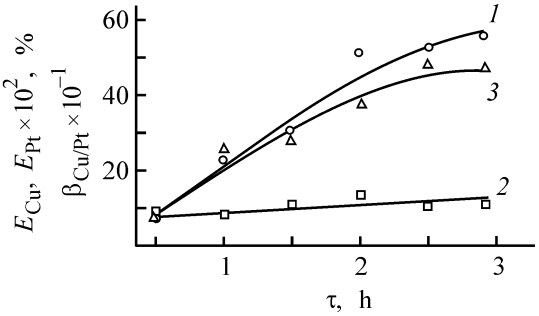


Fig. 4. Degree of extraction of (*1*) copper(II) E_{Cu} and (*2*) platinum(IV) E_{Pt}, and (*3*) separation coefficient $\beta_{Cu/Pt}$ vs. the process duration τ. i = 8.5 mA cm^{-2}, $c_{Cu} = 4.0 \times 10^{-2}$ M, $c_{Pt} = 1.8 \times 10^{-2}$ M in a 0.01 M HCl solution.

presumably due to formation of a deposit at the phase boundary between the donating solution and the liquid membrane in the interaction of Cu^{2+} with D2EHPA. Such a light blue deposit, containing copper(II), was observed on a cellophane film on the side of the organic phase. The decrease in voltage, following its increase, is due to accumulation of water in the liquid membrane. In some cases, the voltage decreases in steps, i.e., an "electric breakdown" is observed (Fig. 2, curve *5*). It has been suggested [2] that the reason for electric breakdowns in the liquid membrane is supersaturation of the organic phase with water to form through aqueous channels. The electrical conductivity of the membrane system is largely determined by the concentration of the tri-*n*-octyl amine additive and grows as its concentration increases (Fig. 2). Solutions of technical-grade D2EHPA in dichloroethane have a low electrical conductivity and cannot be used in electrodialysis extraction without additives, because it is impossible to maintain high current densities in these solutions.

Raising the TOA concentration in the liquid membrane somewhat decreases the rate of copper(II) transfer and increases that of platinum(IV) (Fig. 3a). Probably, this is associated with enhancement of the flow of chloride ions across the liquid membrane, which leads to a decrease in the current efficiency by copper(II). The maximum separation coefficient of the metal ions in the system containing 0.05 M TOA exceeds 900 and considerably decreases as the concentration of the amine additive becomes higher. However, the voltage is insufficiently stable in electrodialysis at the minimum concentration of TOA in the liquid membrane (Fig. 2, curve *5*), and it is more convenient to use D2EHPA solutions containing 0.1 M amine when studying the fundamental aspects of the membrane extraction of copper(II).

During 3 h of electrodialysis at a current density of 8.5 mA cm^{-2}, more than 55% of copper(II) is transferred across the liquid membrane from a solution containing 0.04 M $CuCl_2$ and 0.018 M H_2PtCl_6 (Fig. 4). Cu^{2+} ions are extracted at the highest rate during the first 2 h of process, after which the kinetic curve levels off. The content of platinum(IV) in the receiving solution is about 0.1% and remains virtually unchanged in the course of time in the interval 0.5–3 h. The highest separation coefficient of copper(II) and platinum(IV) is reached after 2.5 h of electrodialysis ($\beta_{Cu/Pt}$ ~500).

The influence exerted by the D2EHPA concentration on the rates of copper(II) and platinum(IV) extraction across the liquid membrane is demonstrated in Fig. 3b (curve *1*). Raising the concentration of the transport agent in the organic phase within the range 10–30 vol % lowers the transmembrane flows of both metal ions and improves the selectivity of Cu^{2+} extraction. The adverse influence exerted by excess D2EHPA on the electrodialysis extraction of copper(II) with liquid membranes is due to competition of copper and hydrogen ions in current transport

Table 1. Influence of the composition of the receiving solution on the electrodialysis transport and separation of metals* (c_{D2EHPA} = 20 vol %, c_{TOA} = 0.1 M, i = 8.5 mA cm^{-2}, τ = 60 min)

Receiving solution	E_{Cu}	E_{Pt}	$\beta_{Cu/Pt}$	$J_{Cu} \times 10^5$	$J_{Pt} \times 10^8$
	%			mol m^{-2} s^{-1}	
0.1 M HCl	25.4	0.084	302	5.19	7.7
0.1 M H_2SO_4	19.8	0.055	363	4.05	4.99
0.1 M HNO_3	27.4	0.42	65	5.6	38.4
0.1 M $HClO_4$	13	0.036	357	2.66	3.32
H_2O	22.6	0.08	283	4.62	7.27

* E, degree of extraction; $\beta_{Cu/Pt}$, separation coefficient.

Table 2. Influence of the copper(II) concentration J_{Cu} in the donating solution on the transfer rate, degree of extraction E, and current efficiency W (c_{D2EHPA} = 20 vol %, c_{TOA} = 0.1 M, i = 8.5 mA cm^{-2})

c_{Cu}, M	τ, min	J_{Cu}, mol m^{-2} s^{-1}	E	W	c_{Cu}, M	τ, min	J_{Cu}, mol m^{-2} s^{-1}	E	W
			%					%	
0.02	49	0.81	64.4	18.3	0.7	60	1.14	32	26
0.04	57	1.4	64.5	31.8	0.1	60	1.25	24.4	28.3

across the interface between the liquid membrane and the receiving solution. Raising the concentration of the transport agent, which acts as the supporting electrolyte, hinders the stage of copper(II) re-extraction from the organic phase.

Under the action of an electric field, the nature of an acid in the receiving solution does not, as a rule, affect to any significant extent the transmembrane flow of the component being extracted (Table 1). Copper(II) is extracted at approximately equal rates into dilute solutions of hydrochloric, sulfuric, nitric, and perchloric acids and into water. In all these cases, with the exception of HNO_3, a thorough separation of copper(II) from platinum(IV) is reached. HNO_3 solutions can re-extract platinum(IV) from organic solutions of salts of tertiary amines [8]. When 0.1 M HNO_3 is used as the receiving solution, the rate of copper(II) extraction is virtually the same as that with the other systems studied. However, the rate of platinum(IV) extraction increases and the separation coefficient of the metal ions decreases dramatically.

The influence exerted by the copper(II) concentration in the initial solution on the rate of transmembrane transfer of Cu^{2+} ions was studied using individual solutions of $CuCl_2$ in water. At copper(II) concentrations less than 0.07 M, the voltage across the membrane system steeply increases in the course of electrodialysis at a current density of 8.5 mA cm^{-2} (Fig. 5). Hypothetically, the drop in the electrical conductivity is due to desalting of the donating solution through extraction of copper(II) into a liquid membrane and to transfer of Cl^- ions across a solid anion-exchange membrane into the anode compartment.

At higher concentrations of copper(II) in the donating solution, the degree of extraction into the receiving solution is about 65% and independent of the concentration of metal ions within the range 0.02–0.04 M. At the same time, the transmembrane flow of copper(II) and the current efficiency proportionally increase under these conditions (Table 2). At higher $CuCl_2$ concentrations, the rate of copper(II) trans-

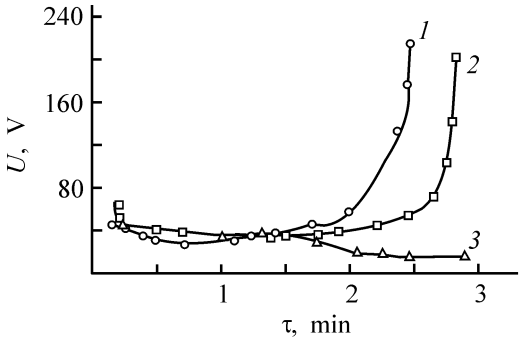


Fig. 5. Variation of the voltage U with the process duration τ at different copper(II) concentrations in the donating solution. i = 8.5 mA cm^{-2}, c_{D2EHPA} = 20 vol %, c_{TOA} = 0.1 M. c_{Cu} (M): (*1*) 0.02, (*2*) 0.04, and (*3*) 0.07.

fer into the cathode compartment somewhat decreases, which may be due to enhancement of copper(II) extraction with tri-*n*-octyl amine to form a complex containing $CuCl_4^{2-}$ anions [9].

CONCLUSIONS

(1) Liquid membranes based on technical-grade di(2-ethylhexyl)phosphoric acid in 1,2-dichloroethane ensure extraction of Cu^{2+} into dilute solutions of mineral acids and provide a single-stage separation of copper(II) from platinum(IV) in extraction from binary acid chloride mixtures under the conditions of the galvanostatic electrodialysis.

(2) The rate of transmembrane transfer of copper(II) is determined by the current density of electrodialysis, concentrations of transport agent and tri-*n*-octyl amine additive in the liquid membrane, and copper(II) concentration in the donating solution, and is virtually independent of the composition of the receiving solution.

(3) The selectivity of the copper(II) extraction from binary solutions is improved as the current density, duration of electrodialysis, and concentration of di(2-ethylhexyl)phosphoric acid become higher and the concentration of tri-*n*-octyl amine in the liquid membrane is lowered. Under the optimal conditions, the separation coefficient of the metals exceeds 900.

REFERENCES

1. Ivakhno, S.Yu. and Yurtov, E.V., *Membrannaya ekstraktsiya. Itogi nauki i tekhniki: Neorganicheskaya khimiya* (Membrane Extraction. Advances of Science and Technology: Inorganic Chemistry), Moscow: VINITI, 1990, vol. 18.
2. Purin, B.A., *Proc. Int. Symp. on Solvent Extraction*, Moscow, 1998, pp. 234–241.
3. Sadyrbaeva, T.Zh. and Purin, B.A., *Khim. Tekhnol.*, 2000, no. 11, pp. 23–27.
4. Sadyrbaeva, T.Zh. and Purin, B.A., *Khim. Tekhnol.*, 2001, no. 10, pp. 17–22.
5. Malkina, T.G. and Podchainova, V.N., *Zh. Anal. Khim.*, 1964, vol. 19, no. 6, pp. 668–670.
6. Ginzburg, S.I., Ezerskaya, N.A., Prokof'eva, I.V., *et al.*, *Analiticheskaya khimiya platinovykh metallov* (Analytical Chemistry of Platinum Metals), Moscow: Nauka, 1972.
7. Khol'kin, A.I., Belova, V.V., Pashkov, G.L., *et al.*, *Sovremennye problemy khimii i tekhnologii ekstraktsii* (Present-Day Problems of Chemistry and Technology of Extraction), Moscow, 1999, vol. 1, pp. 112–135.
8. Gindin, L.M., *Ekstraktsionnye protsessy i ikh primenenie* (Extraction Processes and Their Application), Moscow: Nauka, 1984.
9. Sato, T. and Kato, T., *J. Inorg. Nucl. Chem.*, 1977, vol. 39, no. 7, pp. 1205–1208.

Russian Journal of Applied Chemistry, Vol. 78, No. 4, 2005, pp. 579–583. Translated from Zhurnal Prikladnoi Khimii, Vol. 78, No. 4, 2005, pp. 586–590.
Original Russian Text Copyright © 2005 by Turaev, Kruglikov.

APPLIED ELECTROCHEMISTRY AND CORROSION PROTECTION OF METALS

Regeneration of a Solution for Electroless Copper Plating

D. Yu. Turaev and S. S. Kruglikov

Mendeleev Russian University of Chemical Technology, Moscow, Russia

Received September 15, 2004; in final form, February 2005

Abstract—The possibility of electrochemical regeneration of a solution for electroless copper plating by membrane electrolysis was studied. The conditions of anodic dissolution of copper in a spent solution for electroless copper plating, under which the concentration of copper ions increases at a rate exceeding by an order of magnitude that of their deposition in the course of electroless copper plating, were examined. A scheme for regeneration of spent solutions for electroless copper plating was suggested.

Metals are commonly deposited from aqueous solutions to obtain metal coatings with various functional properties by the electrochemical method. However, the method of chemical reduction is used in some cases (electrically nonconducting support, intricate shape of articles). An electrically conducting sublayer for subsequent electrodeposition of metals and alloys is most frequently deposited by electroless copper plating. When in use, solutions for electroless copper plating accumulate reaction products and this restricts their service life. In this study, the method of membrane electrolysis was used to develop a process for complete regeneration of a tartrate-formaldehyde solution for electroless copper plating, widely used in Russia.

The reduction of copper ions is described by the equation

$$Cu^{2+} + 2HCOH + 4OH^- = Cu^0 + 2HCOO^- + H_2 + 2H_2O. \quad (1)$$

Equation (1) expresses the overall result of the conjugated cathodic and anodic reactions:

$$[CuT_4]^{6-} + 2e = Cu^0 + 4T^{2-}, \quad (2)$$

$$2HCOH + 4OH^- = 2HCOO^- + 2H_2O + H_2 + 2e, \quad (3)$$

where T^{2-} stands for the tartrate ion $C_4H_4O_6^{2-}$.

The equilibrium potential of reaction (3) depends on the solution pH:

$$E = 0.372 - 0.118\,\mathrm{pH}. \quad (4)$$

It was shown in [1] that the anodic reaction (3) occurs in a number of stages to form unstable intermediates. A side reaction in electroless copper plating is the disproportionation of formaldehyde (Cannizzaro reaction) [2, 3]:

$$2HCOH + OH^- = HCOO^- + CH_3OH. \quad (5)$$

When in use, the solution is to be adjusted at regular intervals of time by addition of copper sulfate, alkali, and formaldehyde, in order to compensate for the consumption of these components. However, SO_4^{2-}, $HCOO^-$, and CO_3^{2-} ions are simultaneously accumulated, which impairs the plasticity of the copper films obtained. For example, additional introduction of 0.28 M SO_4^{2-} into the working solution leads to a decrease in the relative elongation at break of a copper film by a factor of 6–12 [4]. Therefore, the incapacitation of solutions for electroless copper plating is due to accumulation of reaction products, rather than to consumption of the starting reagents.

In [5], a method for regeneration of solutions for electroless copper plating with a three-chamber electrolyzer having two anion-exchange membranes was described. The middle chamber of the electrolyzer contains a solution to be regenerated, and the cathode and anode chambers, a sodium hydroxide solution and dilute sulfuric acid, respectively.

In the present study, copper ions were introduced into a solution for electroless copper plating by anodic dissolution of copper, which yields solutions containing the minimum amount of copper sulfate.

EXPERIMENTAL

Two- and three-compartment cells with cation- and anion-exchange membranes, working volume of each compartment equal to 25–30 ml, and working surface area of each membrane of 16 cm^2 were used in

1070-4272/05/7804-0579 © 2005 Pleiades Publishing, Inc.

Table 1. Characteristics of the process of anodic dissolution of copper in tartrate-alkaline solutions*

c_{NaOH}, M	E_{st}, V	E_{po}, V	i_{po}, A m^{-2}	E_{cp}, V	i_{cp}, A m^{-2}	E_{rp}, V	ΔE, V
0.40	–0.10	0.07	40	0.31	0.25	0.59	0.27
0.75	–0.11	0.09	75	0.32	0.90	0.58	0.26
0.975	–0.12	0.10	112	0.34	1.5	0.56	0.22
2.0	–0.13	0.11	180	0.36	3.6	0.55	0.19

* E_{st}, stationary potential; E_{po} and i_{po}, potential and current density of passivation onset; E_{cp} and i_{cp}, potential and current of complete passivation; E_{rp}, repassivation potential; and ΔE, interval of passivation potentials.

the study. Nickel served as the cathode, and copper and platinum-plated titanium (PTA), as the anode. The solutions were analyzed for the content of copper and alkali by titrimetry. The current efficiency by copper was determined gravimetrically and titrimetrically. Polarization curves in the solutions under study were measured with a PI-50-1 potentiostat. All the potentials are given relative to a standard hydrogen electrode. The study was carried with model solutions containing $CuSO_4 \cdot 5H_2O$, $KNaC_4H_4O_6 \cdot 4H_2O$, and NaOH.

The rate of electroless copper plating in tartrate-formaldehyde solutions is about 1 μm h^{-1}, which is equivalent to a cathode current density of 7.5 A m^{-2}. Therefore, it is necessary to choose such conditions of anodic copper dissolution at which the rate of copper dissolution will exceed that of electroless copper plating by no less than an order of magnitude. The results obtained in studying the anodic dissolution of copper in solutions containing 0.28 M $KNaC_4H_4O_6$ and 0.4–2.0 M NaOH are presented in Fig. 1a and Table 1.

It follows from Fig. 1 and data of Table 1 that, at a constant concentration of tartrate ions, the current density of passivation onset strongly depends on the concentration of free alkali: 40 A m^{-2} at 0.4 M and 180 A m^{-2} at 2.0 M.

The increase in the current density of passivation onset, observed as the alkali concentration becomes higher, may be due both to involvement of OH^- ions in the anodic reaction and to formation of complex compounds with two ligands, hydroxy and tartrate ions:

$$Cu + T^{2-} + 2OH^- - 2e \rightarrow [Cu(OH)_2T]^{2-}. \quad (6)$$

Presence of sulfate and chloride ions in minor concentrations (0.1 M) has no significant effect on

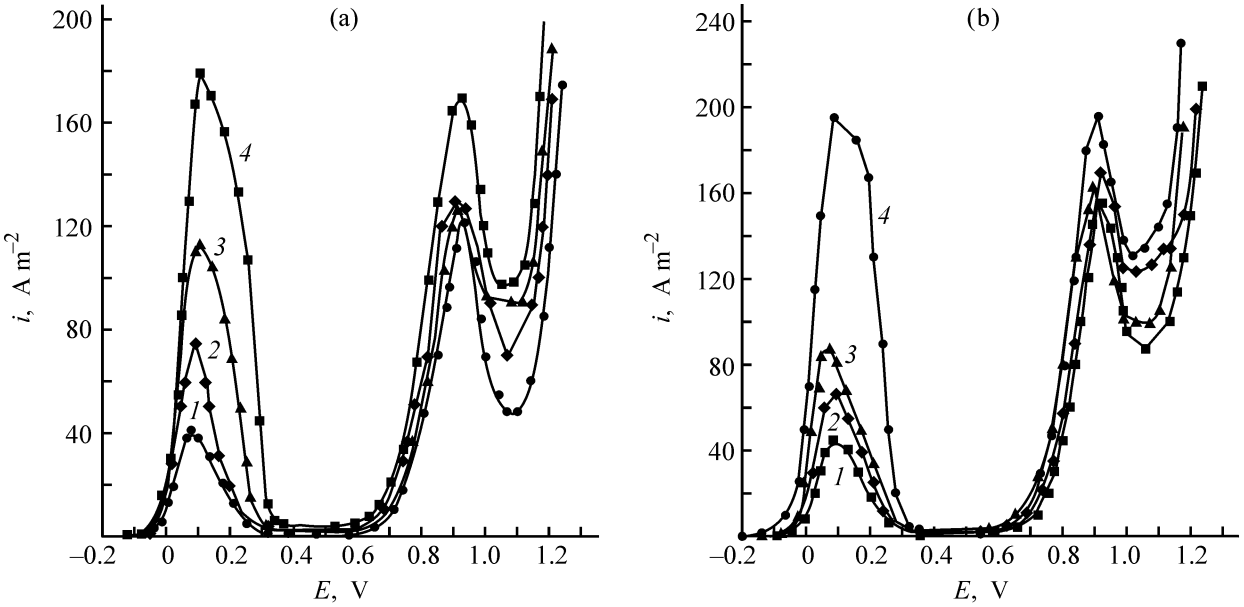


Fig. 1. Anodic potentiodynamic polarization curves obtained on copper in a tartrate-alkaline solution containing (a) 0.283 and (b) 0.566 M of $KNaC_4H_4O_6$. Potential sweep rate 1 mV s^{-1}. (*i*) Current density and (*E*) potential. NaOH concentration (M): (*1*) 0.4, (*2*) 0.75, (*3*) 0.975, and (*4*) 2.0.

Table 2. Anodic current efficiency CE by copper at different potentials and current densities in a tartrate-alkaline solution

E, V	CE, %	*E*, V	CE, %	*E*, V	CE, %	*E*, V	CE, %	*E*, V	CE, %	*E*, V	CE, %
–0.03	98 (20)*	0.01	99 (60)	0.08	99 (70)	0.15	97 (40)	0.66	3 (20)	0.75	1 (60)
0	101 (40)	0.04	98 (70)	0.10	98 (60)	0.17	98 (20)	0.70	3 (40)	0.77	0.7 (70)

* Steady-state current density i (A m^{-2}) at indicated value of E is given in parentheses.

Table 3. Concentration of NaOH and H_2SO_4 in the near-electrode and middle compartments of a three-chamber cell and the transport numbers upon passing a quantity of electricity Q (initial concentrations of sodium hydroxide and formate in spent solution 0.775 and 2.0 M, respectively; Ni cathode and PTA anode)

Run no.	Concentration, M					Transport number, %		Q, A h l^{-1}
	NaOH			H_2SO_4, anolyte		t_{Na^+}	t_{HCOO^-}	
	catholyte		middle compartment					
	initial	final		initial	final*			
1**	0.78	1.15		0.5	1.35		22.8	43.9
2	1.10	1.18	0.94	0.48	1.15	12.5	28.75	26.8
3	1.01	1.29	1.03	0.98	2.34	16.9	32.6	43.9
4	1.01	1.26	0.94	1.5	3.13	18.3	30.1	36.8

* $c_{\Sigma H^+}$, determined by sulfuric and formic acids.

** Performed in a two-chamber cell with an anion-exchange membrane in a spent solution in the cathode chamber.

the rate of anodic dissolution of copper. These ions are already contained in a freshly prepared solution for electroless copper plating, because this solution is obtained using copper sulfate or (more rarely) copper chloride.

Formate ions can be accumulated in a solution for electroless copper plating in considerably greater amounts via reactions (1), (3), and (5). To study the influence exerted by the concentration of formate ions on the rate of anodic dissolution of copper in a tartrate-alkaline solution, these ions were introduced, from the very beginning, in a high concentration (2 M) in the form of sodium formate into a solution containing 0.75 M NaOH and 0.28 M $KNaC_4H_4O_6$. It was found that presence of an excess amount of formate ions in a solution results in that the current density of the passivation onset of copper increases only slightly.

Also, the influence exerted by a change in the concentration of tartrate ions on the rate of anodic dissolution of copper was studied. Figure 1b shows anodic polarization curves obtained under the conditions similar to those for the curves in Fig. 1a, but at a higher concentration of tartrate ions (0.57 M). Comparison of the curves in Figs. 1a and 1b shows that raising the concentration of the ligand did not lead to any significant decrease in the current density of passivation onset.

It follows from the polarization curves that copper may be passivated in the solutions under study. Therefore, it is necessary to determine the current efficiency of the target reaction, anodic dissolution of copper, for various portions of the anodic polarization curve (Table 2).

The data of Table 2 were obtained under potentiostatic conditions with control over the current strength in a solution containing 0.283 M $KNaC_4H_4O_6$ and 0.75 M NaOH.

The results obtained demonstrate that the current efficiency by copper is close to 100% only in the regions of active dissolution and active-passive transition. In the repassivation region, the current efficiency by copper decreases dramatically (to 3% at 20 A m^{-2}), with the current efficiency by copper decreasing as the current density becomes higher (to 0.7% at 70 A m^{-2}).

To determine the rates of transfer of formate and tartrate ions from a solution for electroless copper plating into the anode chamber, experiments were carried out in a two-chamber cell with an anion-exchange membrane and a three-chamber cell with two anion-exchange membranes (Tables 3, 4). The spent

Table 4. Variation of the concentration of NaOH and H_2SO_4 in the near-electrode compartments of a two-chamber cell with an anion-exchange membrane [catholyte, solution under study (sodium hydroxide + potassium sodium tartrate with an initial concentration of 0.28 M); anolyte, sulfuric acid solution; Ni cathode, PTA anode]

Run no.	Concentration, M			Transport number $t_{C_4H_4O_6^{2-}}$,* %	Q of catholyte, A h l^{-1}
	NaOH, catholyte		H_2SO_4, anolyte, initial		
	initial	final			
1	0.78	0.78	0.5	0	59.9
2	0.61	0.63	0.48	2.81	14.3
3	0.61	0.64	0.48	2.68	30
4	0.79	0.85	1.0	5.53	30.5
5	0.75	0.76	1.5	1.0	33.5

* Transport number for the tartrate ion, calculation for catholyte.

Table 5. Variation of the concentrations of NaOH and copper ions in the anode compartment of a two-chamber cell with an anion-exchange membrane

Run no.	Concentration, M				i, A m^{-2}	CE, %	Q of anolyte, A h l^{-1}
	NaOH		$CuSO_4$, initial	Cu^{2+}, final			
	initial	final					
1	0.61	0.65	0.075	0.21	20	100	7.24
2	0.78	0.76	0	0.09	20	100	4.94
3	0.78	0.76	0	0.09	20	97	5.0
4	0.78	0.77	0	0.085	40	99	4.60
5	0.53	0.56	0.005	0.11	40	103	5.46
6	0.34	0.19	0.005	0.08		91	4.40
7	0.35	0.39	0	0.075	20	91	4.41

solution was placed in the cathode chamber in the first case, and in the middle chamber in the second; a sulfuric acid solution served as catholyte in both cases. An alkali solution served as catholyte in experiments with a three-chamber cell.

It can be seen from Tables 3, 4 that the rate of transfer of formate ions into the anolyte is several times higher than that of formate ions.

Under industrial conditions, it is more difficult to control the anode potential of the electrode than to maintain a certain anode current density. Therefore, the possibility of introducing copper ions by anodic dissolution of copper in a solution based on sodium hydroxide and Rochelle salt (0.28 M) at a constant current strength (density) was analyzed in this study. To preclude deposition of copper at the cathode, it was separated from the solution for electroless copper plating by an anion-exchange membrane, with the process carried out in a two-chamber cell. A 0.1 M NaOH solution was used as the catholyte. The results of the experiments are listed in Table 5.

It was found that, after electrolysis, the catholyte contains no compounds of bivalent copper and no copper is deposited at the cathode, which points to a negative charge of complex compounds of the tartrate ion with the Cu^{2+} ion. Copper is dissolved anodically with a current efficiency of 91–100% at a low (20–40 A m^{-2}) current density both in the presence and in the absence of sulfate ions.

The results obtained served as a basis for the development of a technological scheme (Fig. 2) of operation of a regeneration unit.

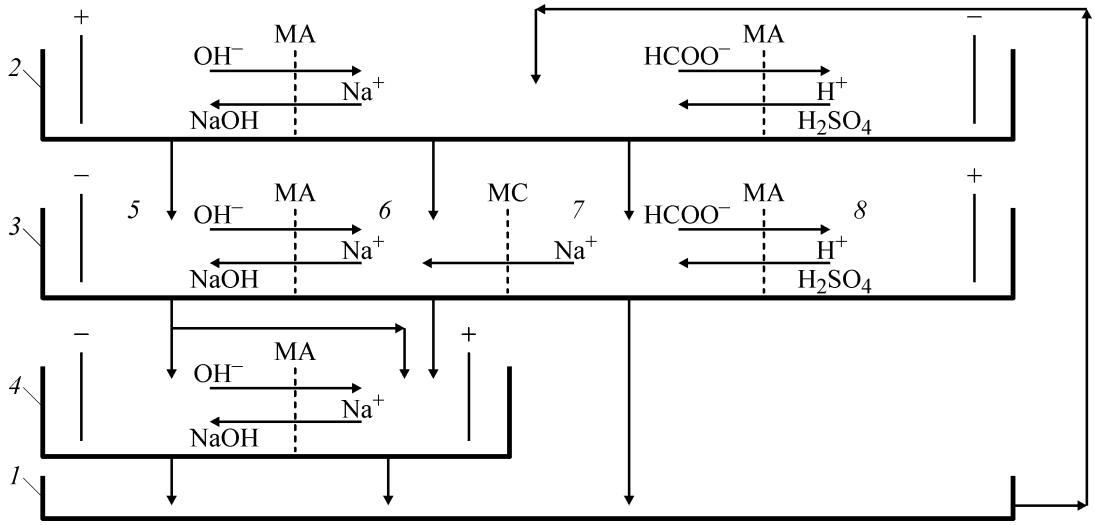


Fig. 2. Scheme of regeneration of a spent solution for electroless copper plating: (*1*) working bath; (*2*) three-chamber cell with two anion-exchange membranes; (*3*) four-chamber cell with two anion-exchange and one cation-exchange membranes; (*4*) two-chamber cell with an anion-exchange membrane; (*5*, *8*, *6*, *7*) cathode, anode, and auxiliary compartments of cell *3*.

CONCLUSIONS

(1) A technology for regeneration of a spent solution for electroless copper plating was developed on the basis of the experiments performed.

(2) A scheme of a membrane electrolysis unit for regeneration of a spent solution for electroless copper plating was suggested.

REFERENCES

1. Golovchanskaya, R.G., Kruglikov, S.S., and Morozova, M.A., *Elektroosazhdenie metallov i splavov: Sbornik nauchnykh trudov Mos. Khim.-Tekhnol. Inst.* (Electrodeposition of Metals and Alloys: Coll. of Works of Moscow Chim.-Technol. Inst.), Moscow, 1991, pp. 31–49.
2. Rozovskii, G.I. and Vashkyalis, A.I., *Khimicheskoe mednenie* (Electroless Copper Plating), Vilnius: Resp. Inst. Nauch.-Tekh. Inform. Propagandy, 1966.
3. Vashkyalis, A.I., *Khimicheskaya metallizatsiya plastmass* (Chemical Metallization of Plastics), Leningrad: Khimiya, 1985, 3rd ed.
4. Sviridov, V.V., *Khimicheskoe osazhdenie metallov iz vodnykh rastvorov* (Chemical Deposition of Metals from Aqueous Solutions), Minsk: Universitetskoe, 1987.
5. Horn, R.E., *Plating Surf. Finish.*, 1981, October, pp. 50–52.

Russian Journal of Applied Chemistry, Vol. 78, No. 4, 2005, pp. 584–587. Translated from Zhurnal Prikladnoi Khimii, Vol. 78, No. 4, 2005, pp. 591–594.
Original Russian Text Copyright © 2005 by Astaf'eva, Sidoikin, Krichevskii, Kagarlitskii.

APPLIED ELECTROCHEMISTRY AND CORROSION PROTECTION OF METALS

Electrocatalytic Hydrogenation of Nicotine

Z. M. Astaf'eva, P. B. Sidoikin, L. A. Krichevskii, and A. D. Kagarlitskii

Institute of Phytochemistry, Ministry of Education and Science of the Republic of Kazakhstan, Karaganda, Kazakhstan

Received November 10, 2004; in final form, January 2005

Abstract—Electrocatalytic reduction of the nicotine alkaloid in the presence of skeletal nickel catalysts was studied.

Natural nicotine, the main alkaloid contained in tobacco (2–10 wt % in a plant), is an (*S*)-isomer [1] and acts as an exceedingly strong poison upon the peripheral and central nervous systems. For this reason, it does not find any wide use, even in the form of a sulfate, as an insecticide for pest control in agriculture and for curing parasitic skin diseases in veterinary medicine. An attempt to apply this alkaloid in curing Alzheimer [2] or Parkinson diseases [3] proved to be unsuccessful because of the strong side effects [4].

The discovery of the bactericide and pesticide activity of synthetic analogues of nicotine and products of its reductive transformations [5] attracted the attention of researchers to development of methods for synthesis of compounds of this kind. However, nicotine itself was not was used for synthetic purposes. This was done using not nicotine itself, but a product of its metabolism in mammal organisms, the cotinine alkaloid whose skeleton transforms to the structure of the corresponding nicotine derivative [6–9]. In this context, it may be assumed that hydrogenated and partly hydrogenated nicotine derivatives are of interest as syntons for obtaining new physiologically active compounds. As for sources of nicotine, it should be emphasized that it is important to utilize wastes from the tobacco industry, whose stock may be as large as tens of thousands of tons, with this alkaloid and its analogues contained in an amount of 2–3 wt %.

It is well known that hydrogenation of pyridine bases requires noble metal catalysts and rather severe conditions: high temperature and hydrogen pressure [10, 11]. A fully hydrogenated nicotine, hexahydronicotine, can be obtained either by reduction of nicotine with metallic sodium or catalytically, by hydrogenation in the presence of platinum black [12], Adams catalyst in acetic acid [13], or skeletal nickel [14]. The yield of hexahydronicotine under these conditions is as high as 23–25%.

Undoubtedly advantageous in reduction of the pyridine ring is the reaction of electrocatalytic hydrogenation. It proceeds on a skeletal nickel catalyst under atmospheric pressure at low temperature [15, 16].

For this reason, the electrocatalytic reduction of nicotine on a skeletal nickel catalyst under conditions closely similar to those in reduction of pyridine bases was studied in order to develop a technique for synthesis of hexahydronicotine.

EXPERIMENTAL

The skeletal nickel catalyst was obtained by the Rayney method from a 50 : 50 alloy of nickel and aluminum [15].

Experiments on reduction of nicotine were carried out in a thermostated electrocatalytic diaphragm cell. As the cathode served a stainless steel disc with a surface area of 0.05 dm^2, which was closely adjacent to the cell bottom. A skeletal nickel catalyst was placed on the cathode and kept in the reaction zone by the field of a permanent magnet. A stainless steel plate was used as the anode. An MA-40 anion-exchange membrane served as the diaphragm. The anolyte was a 20% solution of sodium hydroxide; the alkali concentration in the catholyte was selected experimentally. The gases evolved were collected into graduated burettes.

Nicotine well dissolves in aqueous solutions of sodium hydroxide in the temperature conditions studied. Therefore the electrolytic hydrogenation was performed without agitation.

The composition of the reduction products was determined by gas–liquid chromatography with marker

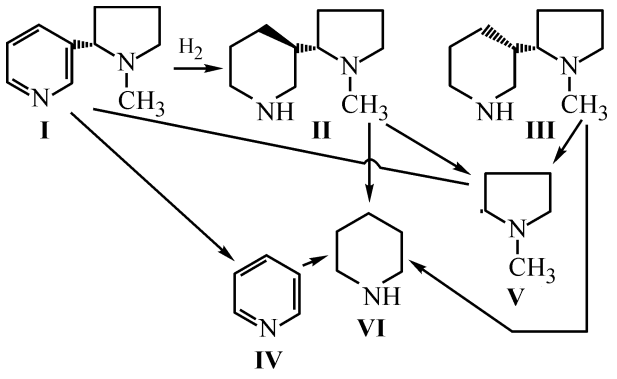
1070-4272/05/7804-0584 © 2005 Pleiades Publishing, Inc.

Table 1. Results of hydrogenation of nicotine **I**

Catalyst	Amount of absorbed H_2, ml	Total yield, %		Unchanged nicotine, %
		of hexahydronicotine isomers	of side products	
Ni_{skel}	200	57	0.8	40
Pd/Ni, 5% Pd	110	42	1.8	54
Pt/Ni, 5% Pt	60	Trace amounts	Trace amounts	98
Re/Ni, 5% Re	40	″	″	99
Mo/Ni, 5% Mo	110	42	1.6	55
V/Ni, 5% V	230	62	0.8	36

substances [Chrom-5 chromatograph; flame-ionization detector; 3.5-m-long stainless steel column with an inner diameter of 3.0 mm, packed with Chromaton NAW-HMDS with a grain size of 0.315–0.400 mm, supporting an SE-30 silicone elastomer (5 wt %)]. The temperature of the column, detector, and evaporator was 200, 240, and 240°C, respectively; the flow rate of the carrier-gas (argon) was 40 ml min^{-1}. An analysis of the catalyzates formed on skeletal nickel demonstrated that the main reduction product of nicotine (**I**) is hexahydronicotine in the form of two 2*S*,3*S*'- (**II**) and 2*S*,3*R*'-diastereomers (**III**).

The electrocatalytic reduction is accompanied by hydrogenolysis leading to decomposition of compound **I** and to formation of pyridine (**IV**) and *N*-methylpyrrolidine (**V**). Also, piperidine (**VI**) was found, which could be formed both via hydrogenation of nicotine **I** and via hydrogenolysis of hexahydronicotine **II** and **III**:



Diastereoisomers obtained in hydrogenation of compound **I** were isolated from the catalyzates by extraction with diethyl ether and separated on a column packed with Al_2O_3 (II degree of activity), with successive elution with petroleum ether and chloroform. The constants of these compounds were in an agreement with published data [14]; however, the ratio of diastereoisomers **II** and **III** was 5.1 : 1 in the case in question, as opposed to the 4 : 1 ratio in [14]. The total yield of side reaction products (pyridine, piperidine, methylpyrrolidine) did not exceed 1–3%.

The rate of electrocatalytic reduction of substance **I** increases with its concentration, reaching the highest value of 1.3 mol H_2/min at a content of alkaloid of 0.185 M in the catholyte. The highest utilization coefficient of hydrogen is observed at the same concentration. Raising further the concentration of nicotine **I** does not change the process rate and the coefficient of hydrogen utilization. However, an analysis of the catalyzates by gas–liquid chromatography demonstrated that this leads to an increase in the content of side products of hydrogenolysis of the starting molecule. For example, as the concentration of substance **I** increases from 0.185 to 0.250 M, the yield of pyridine grows from 0.8 to 3.0%.

The optimal hydrogenation parameters are as follows: temperature, within the range 20–30°C; the current density, 20 A dm^{-2}; alkali concentration in the catholyte, 1–2 wt %; and alkaloid **I** : catalyst ratio, 1.5 : 1.0. The total yield of diastereoisomers of hexahydronicotine **II** and **III** under these conditions is 57%.

It is known that promotion of a skeletal nickel catalyst with other metals favors occurrence of many difficultly performable reactions [17]. Therefore, it seemed reasonable to use, in order to raise the activity and selectivity of skeletal nickel, binary skeletal catalysts containing, in addition to nickel, such metals as Pt, Pd, Re, mo, and V, which are themselves used in hydrogenation processes as catalysts. Platinum and palladium were deposited onto a nickel catalyst by cementation; rhenium, molybdenum, and vanadium were introduced in the form of salts NH_4ReO_4, K_2MoO_4, and NH_4VO_3, respectively, into a 20% aqueous solution of sodium hydroxide intended for leaching of the Ni–Al alloy. The concentration of the salts corresponded to a 5% content of a metal added, relative to the mass of nickel in the catalyst.

The experimental results listed in Table 1 indicate that of particular interest among the six skeletal nickel

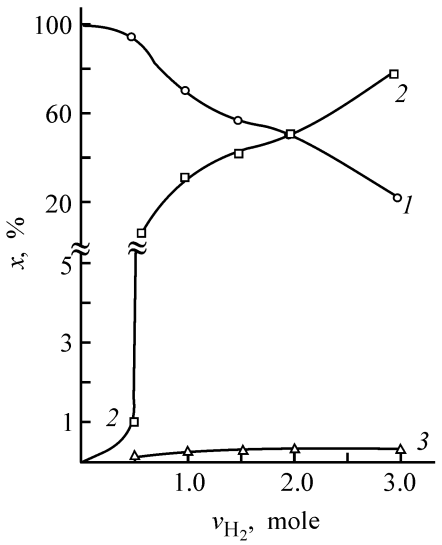
Table 2. Yield of the sum of hexahydronicotine isomers **II** and **III** in relation to the content of vanadium in the catalyst

V content, wt %	Yield, %		Unchanged nicotine, %	V content, wt %	Yield, %		Unchanged nicotine, %
	of the final product	of side products			of the final product	of side products	
–	57	0.8	40	15	70	0.9	27
5	62	0.8	36	20	76	0.8	22
10	65	0.9	32	25	65	0.8	32

catalysts studied under comparable conditions is the nickel-vanadium catalyst in whose presence 62% of alkaloid **I** was converted into hexahydronicotine **II** and **III**.

A study of how the yield of a sum of hexahydronicotine isomers **II** and **III** depends on the amount of ammonium *meta*-vanadate added in preparing a skeletal nickel catalyst (Table 2) demonstrated the following. As the content of vanadium in solution increases from 5 to 20 wt %, the yield grows from 57 to 76%, whereas the amount of side products in the catalyzate remains virtually unchanged.

Possibly, the mechanism of promotion of the skeletal nickel catalyst consists in formation of phase surface vanadium oxides with lower degrees of oxidation, which have high isosteric heat of adsorption, Q_{M-H}. Such oxidized forms can be formed on the cathode components of the initial nickel-aluminum alloys, where the anion VO_3^- is reduced. For example, it is known that a saltlike product is deposited at the cathode in electrolysis of alkaline solutions of vanadates. The cation of this product contains V^{4+}, and its anion, V^{5+} [17].



Catholyte composition x vs. amount v_{H_2} of hydrogen absorbed in electrocatalytic reduction of nicotine **I** on a nickel catalyst promoted with the VO_3^- anion. (*1*) Nicotine, (*2*) 2*S*,3*R*-hexahydronicotine, and (*3*) 2*S*',3*S*-hexahydronicotine.

The figure shows the dependence of the catholyte composition on the amount of hydrogen absorbed in electrocatalytic reduction of nicotine **I** on a nickel catalyst promoted with the VO_3^- anion. The concentration of nicotine (curve *1*) steadily decreases to become 24% upon absorption of 3 mol of hydrogen. Simultaneously, a sum of hexahydronicotine isomers **II** and **III** is accumulated (curves *2* and *3*). Only the yield of isomer **II** increases with the amount of absorbed hydrogen (curve *2*), whereas the content of 2*S*,3*R*'-isomer **III** remains virtually unchanged (curve *3*), so that their ratio becomes 26 : 1 by the end of the process.

The results of the study also demonstrated that the promotion of a skeletal nickel catalyst with vanadium not only raises its activity, but also leads to a nearly twofold increase in its service life, from 40 to 72 h.

CONCLUSIONS

(1) It was established that hexahydronicotine is formed in electrocatalytic reduction of nicotine on an unpromoted skeletal nickel catalyst and that promoted with various metals.

(2) The best results are obtained with a Ni-skeletal catalyst promoted with ammonium *meta*-vanadate, in whose presence the selectivity of the process grows and the yield of a sum of hexahydronicotine diastereoisomers increases from 57 to 76%. The yield of the 2*S*',3*S*-isomer is 75%, and the service life of the catalyst increases from 40 to 72 h.

REFERENCES

1. Berkman, C.E., Park, S.B., and Wrighton, S.A., *Biochem. Pharmacology*, 1995, vol. 50, no. 4, pp. 565–570.
2. Newhouse, P.A., Sunderland, T., and Tariot, P.N., *Psychopharmacology*, 1988, vol. 95, no. 1, pp. 171–173.
3. Prasad, C., Ikegami, H., Shimizu, I., and Onaivi, E.S., *Life Sci.*, 1994, vol. 54, no. 5, pp. 1169–1172.
4. Haass, M. and Kübler, N., *Cardiovascular Drugs Therapy*, 1996, vol. 10, no. 2, pp. 657–665.
5. US Patent 5015741.
6. US Patent 4442292.
7. Mahboodi, S. and Wiegrebe, W., *Arch. Pharm.*, 1988, vol. 321, no. 3, pp. 175–177.
8. Edwards, W.B., Glenn, D.F., and Green, F., *J. Labelled Compounds Radiopharm.*, 1978, vol. 2, no. 2, pp. 255–261.
9. Shibagaki, M., Matsushita, H., and Kaneko, H., *Heterocycles*, 1985, vol. 23, no. 7, pp. 1681–1684.
10. Sokol'skii, D.V., Dembitskii, A.D., and Ualikhanova, A., *Zh. Prikl. Khim.*, 1985, vol. 58, no. 2, pp. 322–325.
11. Ualikhanova, A., Dembitskii, A.D., Sokol'skii, D.V., *et al.*, *Izv. Akad. Nauk KazSSR, Ser. Khim.*, 1989, no. 5, pp. 55–58.
12. Shmuk, A.A., *Khimiya tabaka i makhorki* (Chemistry of Tobacco and Makhorka), Moscow: Gos. Izd. Khim. Lit., 1948.
13. Hubert-Brierre, Y., Herlem, D., and Khuong-Huu, F., *Tetrahedron*, 1975, vol. 31, no. 24, pp. 3049–3055.
14. Shibagaki, M., Matsushita, H., and Kaneko, H., *Heterocycles*, 1985, vol. 23, no. 9, pp. 2351–2356.
15. Kirilyus, I.V., *Elektrokataliticheskoe gidrirovanie* (Electrocatalytic Hydrogenation), Alma-Ata: Nauka KazSSR, 1981.
16. Kirilyus, I.V., Murzatova, G.K., and Malikov, Zh.A., *Trudy Kar. Gos. Univ.*, Karaganda, 1979, no. 5, pp. 68–72.
17. Fasman, A.B. and Sokol'skii, D.V., *Struktura i fiziko-khimicheskie svoistva skeletnykh katalizatorov* (Structure and Phyasicochemical Properties of Skeletal Catalysts), AlmaAta: Nauka KazSSR, 1960.

Russian Journal of Applied Chemistry, Vol. 78, No. 4, 2005, pp. 588–591. Translated from Zhurnal Prikladnoi Khimii, Vol. 78, No. 4, 2005, pp. 595–598.
Original Russian Text Copyright © 2005 by Shul'pekov, Lyamina, Rybakov, Kirdyashkin, Maksimov.

APPLIED ELECTROCHEMISTRY AND CORROSION PROTECTION OF METALS

Structure and Properties of a Compound Based on a Copper Powder and Polysiloxane

A. M. Shul'pekov, G. V. Lyamina, A. N. Rybakov, A. I. Kirdyashkin, and Yu. M. Maksimov

Department of Structural Macrokinetics, Tomsk Scientific Center, Siberian Division, Russian Academy of Sciences, Tomsk, Russia

Tomsk State University, Tomsk, Russia

Received November 29, 2004

Abstract—The phase composition, thermal stability, and electrical conductivity of a compound formed by a polymethylsiloxane lacquer and copper were studied in relation to the temperature of formation of a coating on its basis.

At present, development of heating elements with a large heating surface area and high efficiency is a topical task. The most effective solution to this problem is deposition of an electrically conducting coating onto the surface of an article to be heated. A coating of this kind can be created in the simplest way by depositing a suspension based on an electrically conducting powder and a polymer binder by the paint-and-varnish technology. The electrical conductivity of such composite coatings (compounds) is provided by the contact between particles of the conducting phase [1]. Apparently, the electrical conductivity of a compound is affected both by the nature of particles and the phase composition of their surface and by the properties of the polymeric matrix.

As an electrically conducting phase was used powdered copper of the PM 1 brand. It is known that a considerable oxidation of copper starts at 180–200°C, depending on the dispersity of the metal. However, it may be assumed, based on the data of [1], that incorporation of the metal into the polymeric matrix should prevent its oxidation.

Compounds based on most of organic polymers have a low working temperature (not higher than 150°C) because of the destruction of macromolecules. It has been suggested to use as a binder for the electrically conducting compound an organosilicon polymer stable against oxidation up to 400°C [3].

The present study is concerned with properties (electrical conductivity, thermal resistance, phase composition) of the system constituted by a polysiloxane lacquer and copper.

EXPERIMENTAL

The compound was prepared by mixing a toluene solution of the polymer (15 wt %) with powdered copper in a 2 : 1 ratio (by weight). The mixture was ground in a porcelain mortar and applied on glass plates, the resulting coatings were dried at 50–350°C for 1 h. The thermal destruction of the compound was studied by differential thermal analysis (DTA) on a Q-1500 instrument.

The phase composition of the metal in the compound was determined by X-ray phase analysis (DRON-UM1, Co_{K_α} radiation) and voltammetric (VA) analysis with a carbon paste (CP) electrode in the cyclic voltammetry (CVA) mode [4].

The coating surface was analyzed by a nondestructive VA method with an all-in-one sampling and indicator electrode (Hg and HgNa) [5–7]. The voltammograms were recorded in the differential mode of potential variation on a PU-1 polarograph. The phase composition of the surface and bulk of the compound was studied using two methods of solid-phase voltammetry (see table).

The electrical conductivity of a coating largely depends on the particle packing density and the uniformity of distribution of Cu particles in the bulk. Mechanical grinding of a Cu powder in a solvent,

1070-4272/05/7804-0588 © 2005 Pleiades Publishing, Inc.

Methods of solid-phase voltammetry

VA method	Type of electrode	Electrochemical process	Application field
CVA	CP	Reduction of oxidized forms of the metal from the bulk of the composite and oxidation of the reduced metal into the solution	Identification of the phase composition in the bulk of the composite and determination of ratio between the elementary and oxidized forms of the metal
VA	Hg	Oxidation of the metal that formed an amalgam when brought in contact with the surface	Determination of the elementary form of the metal on the surface
	HgNa	The same (with account of the phase exchange)	Determination of the bulk content of the elementary and oxidized forms of the metal

with its subsequent mixing with a polymer, makes it possible to obtain a lower electrical resistance of the coating. It can be seen in micrographs obtained with an MIM-8 optical microscope at a magnification of 400 that, in this case, the distribution of Cu in the coating is more uniform and the number of agglomerates of Cu particles is smaller.

The dependence of the resistance of formulations on the formation temperature is shown in Fig. 1. The resistance remains virtually unchanged in the range 100–200°C, and decreases to 10–20 Ω at 200–250°C. As the formation temperature increases, the resistance becomes higher.

To identify the phase composition of the conducting component (copper), X-ray phase and VA analyses of samples formed at temperatures of 100 to 300°C were made. The results of a VA analysis of the surface of the polysiloxane–copper compound with mercury and amalgam electrodes are shown in Fig. 2. The error in determining the metal on the surface was too large in most cases for evaluating the phase composition of the surface. However, comparison of the signals obtained by means of VA (semi-quantitative approach) suggests that the content of copper on the surface of the samples studied increases with temperature. This is due to the following. As the temperature becomes higher, the polymeric matrix contracts because of the evaporation of the solvent and cross-linking of polysiloxane, and, therefore, part of Cu atoms "emerge" to the surface. The currents of Cu oxidation, obtained on the mercury and amalgam electrodes brought in contact with the surface of the compound differ only slightly. Consequently, mainly the elementary form of Cu is present on the surface. The differences in the currents obtained after bringing the electrodes in contact with the surface of compounds formed at different temperatures are insignificant. Consequently, the polymeric matrix "retains" copper particles rather firmly and is an appropriate binder.

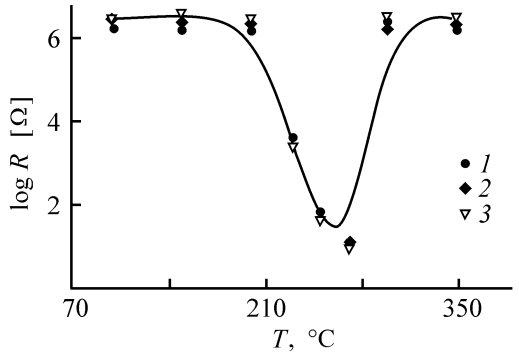


Fig. 1. Effect of the formation temperature *T* of the compound on its resistance *R*. (*1*–*3*) Parallel runs.

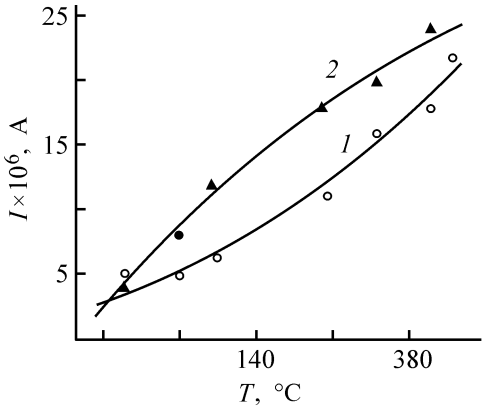


Fig. 2. Copper oxidation currents *I* obtained on (*1*) mercury and (*2*) amalgam electrodes brought in contact with the surface of polymethylsiloxane–copper samples formed at a temperature *T*.

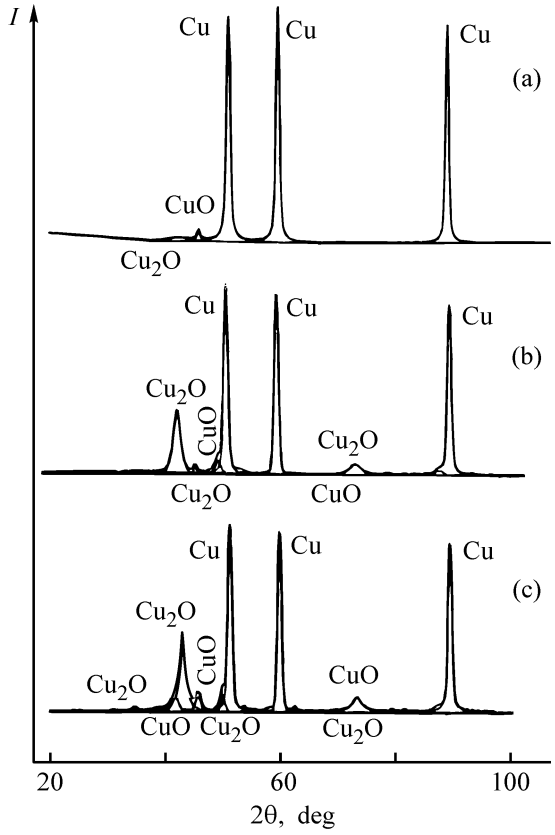


Fig. 3. X-ray diffraction patterns of a polyorganosiloxane–copper compound formed at a temperature *T*. (*I*) Intensity and (2θ) Bragg angle. Temperature (°C): (a) 70, (b) 250, and (c) 300.

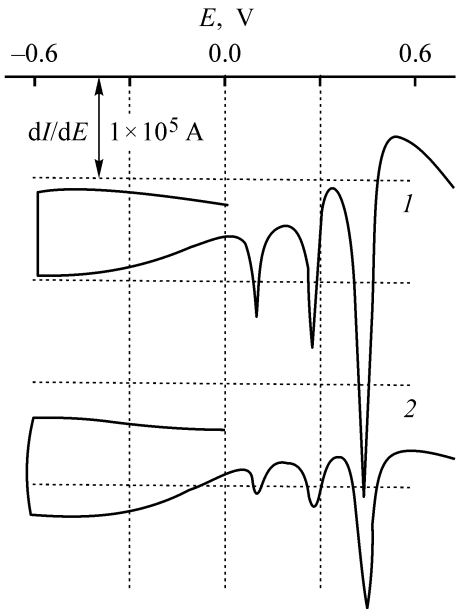


Fig. 4. CVA curves for a CP electrode containing samples formed at (*1*) 250 and (*2*) 100°C. (*E*) Potential.

The X-ray diffraction patterns of samples obtained at 70–200°C are similar; noticeable changes begin at above 250°C (Fig. 3). It can be seen that Cu is the main phase below 300°C. The weak reflections associated with Cu(I) and Cu(II) oxides can be only attributed to phases on the surface of copper particles. As the temperature is raised to 250°C, the content of the Cu(I) oxide phase starts to grow and a Cu(II) oxide phase appears at 300°C. For comparison, the initial Cu powder was analyzed. It was found that, in this case, a considerable amount of the Cu_2O phase is present at 250°C.

The cyclic voltammograms of the CP electrode containing samples formed at different temperatures do not differ in the spectra of the signals obtained (Fig. 4). The anodic curve shows three peaks at 0.06, 0.28, and 0.40 V, which correspond to oxidation of copper from the surface annd bulk layers of the compound. The difference in the oxidation current can be attributed to different electrical conductivities of compounds formed at 100 and 250°C. The absence of signals in the cathodic curve (reduction current) can be attributed to the fact that the content of oxidized forms of copper in the compound is less than 5%. The data obtained using CVA with a CP electrode confirm the results of the X-ray phase analysis.

To elucidate the mechanism of coating formation, the compound and the starting components, polysiloxane and copper powder, were subjected to a thermal analysis (Fig. 5). Analysis of the initial copper powder shows that the oxidation of Cu begins at around 200°C and occurs in several successive stages. Thermolysis of polymethylsiloxane also occurs in a number of stages: the polymer is cross-linked at 130–450°C to form a three-dimensional network structure and then (at 450–700°C) side groups burn-out, with the process accompanied by strong exothermic effects. A mass gain corresponding to oxidation of Cu contained in the composite is observed at above 400°C, with the nature of this process coinciding with that of oxidation of the copper powder.

Thus, the run of the dependence of the electrical resistance of the coating on the thermal treatment temperature can be explained as follows. In the temperature range 100–200°C, the resistance remains constant until the cross-linking of polymethylsiloxane begins. In the process, the matrix contracts and Cu particles come in direct contact with one another to form a continuous conducting "network," with the resistance of the composite decreasing. As the heating temperature is raised to above 300°C, the resistance again increases, which is due to oxidation of the surface of copper particles.

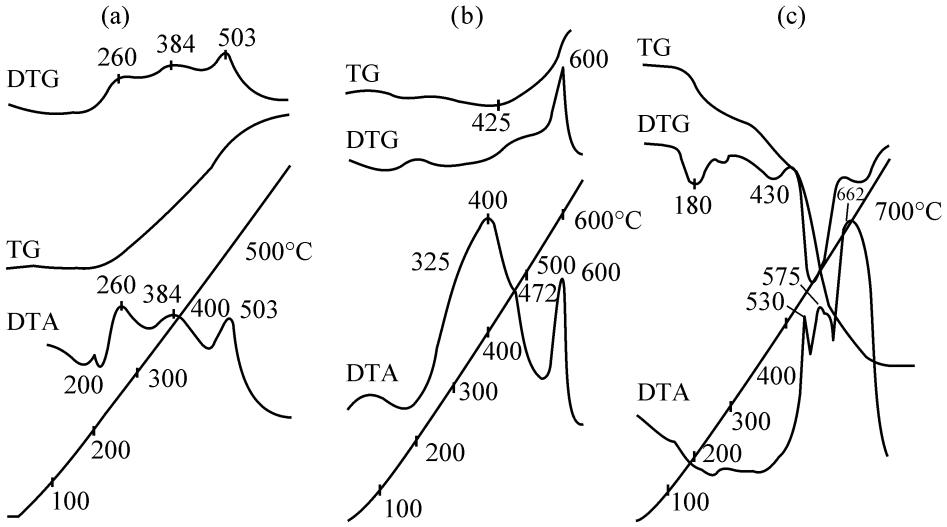


Fig. 5. Thermograms of (a) copper powder, (b) compound, and (c) polyorganosiloxane.

CONCLUSIONS

(1) It was found, using voltammetry and X-ray phase and termogravimetric analyses, that polymethylsiloxane prevents oxidation of copper at temperatures of up to 250°C.

(2) It was demonstrated that the optimal formation temperature of a polymethylsiloxane–copper coating is 250°C.

(3) It was shown that the compound can be used to develop heating elements with a large heating surface area and high efficiency.

REFERENCES

1. Svenchanskii, A.D. and Malyshev, S.A., *Nizkotemperaturnye nagrevatel'nye elementy* (Low-Temperature Heating Elements), Moscow: Nauka, 1964.
2. Kubashevskii, O. and Gopkins, B., *Okislenie metallov i splavov* (Oxidation of Metals and Alloys), Moscow: Metallurgiya, 1965.
3. Andrianov, K.A. and Khananashvili, L.M., *Tekhnologiya elementoorganicheskikh monomerov i polimerov* (Technology of Organoelement Monomers and Polymers), Moscow: Khimiya, 1973.
4. Brainina, Kh.Z., Neiman, E.Ya., and Slepushkin, V.V., *Inversionnye elektroanaliticheskie metody* (Inversion Electroanalytical Methods), Moscow: Khimiya, 1988.
5. Mokrousov, G.M., Knyazeva, E.P., Volkova, V.N., and Alifanova, I.A., *Zh. Anal. Khim.*, 1994, vol. 49, no. C, pp. 1013–1016.
6. Mokrousov, G.M., Knyazeva, E.P., and Volkova, V.N., *Zavod. Lab.*, 1995, no. 3, pp. 7–10.
7. Lyamina, G.V., Rybakov, A.N., Shul'pekov, A.M., *et al.*, *Vestn. KazNU., Ser. Khim.*, 2003, pp. 213–216.

Russian Journal of Applied Chemistry, Vol. 78, No. 4, 2005, pp. 592–598. Translated from Zhurnal Prikladnoi Khimii, Vol. 78, No. 4, 2005, pp. 599–605.
Original Russian Text Copyright © 2005 by Chirkst, Cheremisina, Ivanov, Chistyakov.

ENVIRONMENTAL PROBLEMS OF CHEMISTRY AND TECHNOLOGY

Sorption of Iron(II) on Ferromanganese Nodules

D. E. Chirkst, O. V. Cheremisina, M. V. Ivanov, and A. A. Chistyakov

St. Petersburg State Mining Institute, St. Petersburg, Russia

Received May 26, 2004; in final form, October 2004

Abstract—The dynamic capacity, specific surface area, grindability, and wearability of filter materials based on pyrolusite were determined. The dynamic capacity of ferromanganese nodules was compared with the capacity of imported filter materials.

Treatment of wastewater from many metallurgical plants to remove various iron species and removal of iron(II) ions, which are not precipitated in a neutral medium, from artesian water are important environmental problems.

Owing to the low pH of hydrate formation at neutralization, iron(III) ions present in water are precipitated as $Fe(OH)_3$. Iron(II) is precipitated in the form of low-soluble hydroxide to a residual concentration corresponding to the maximum permissible concentration (MPC) (0.1 mg ml^{-1}, MPC for fish breeding reservoirs) only at pH 9.5, which is confirmed by the following calculation:

$$Fe(OH)_2 \rightleftarrows Fe^{2+} + 2OH^-,$$

$$L = [Fe^{2+}][OH^-]^2 = 1.6 \times 10^{-15} \quad [1],$$

where $[Fe^{2+}] = MPC = 1.79 \times 10^{-6}$ M.

Hence, $[OH^-] = 3 \times 10^{-5}$, pH 9.5. This result explains why Fe^{2+} ions remain in solution. Hence, Fe^{2+} should be converted to Fe^{3+} with oxidants (e.g., ozone or chlorine), but the oxidation procedures are rather expensive [2, 3].

The aim of the treatment procedures is to decompose pollutants and remove decomposition products, which requires additional material costs.

Various ion-exchanging resins provide a high degree of purification of water, but the required sorbents are rather expensive and, thus, the cost of this procedure is very high [4]. For this purpose, inorganic filter materials are promising. These materials, exhibiting high thermal, chemical, and radiation stability, allow treatment of hot solutions and wastewater from radiochemical plants [5]. At present, treatment of wastewater to remove Fe(II) is frequently performed using imported pyrolusite-containing sorbents, such as Aquamandix filler for bulk filters, which is a crushed material with a particle size of 0.5–1.0 mm (78–80% MnO_2 content, 3.5–4.0 g cm^{-3} density, and 2.0 g cm^{-3} bulk density). Pyrolusite oxidizes Fe(II) to Fe(III), and then iron(III) hydroxide precipitates even from weakly acidic solutions. The oxidative effect of the sorbent is described by the reaction

$$MnO_2 + 2Fe^{2+} + 5H_2O \rightarrow MnO + 2Fe(OH)_3\downarrow + 4H^+.$$

It should be noted that there are no pyrolusite deposits in Russia. Because of the high cost of the imported sorbent, it is advisable to substitute it with a domestic analog. The use of ferromanganese nodules (FMNs) as sorbents for Fe(II) ions seems to be promising.

The FMN deposits are rather widespread in the Gulf of Finland of the Baltic Sea, occurring predominantly on the bottom surface. Search for new deposits available for mining is actively performed [6].

The deposits in this region can be subdivided into two types. Deposits of the first type occur in the southern and northern parts of the Gulf of Finland at a depth of about 60 m. Nodules of this type are spherical particles 1–2 to 30 mm in size [1–16 mm predominant diameter, 100 kPa (1 kg cm^{-2}) strength, and 1.6 g cm^{-3} density). The resources of ferromanganese nodules in these regions are tentatively estimated as 25–30 million tons, which corresponds to a continental deposit of a medium profitability [7].

Another deposit lies in the Luga Bay and Kopor'e Bay at a smaller depth (25–30 m). The predominant particle size in this deposit is 3–5 mm, with nodules

1070-4272/05/7804-0592 © 2005 Pleiades Publishing, Inc.

of size 15–30 mm being rare. In 2000, the first 2500 tons of the nodule-containing material were uplifted in prospecting of the Kopor'e Bay[1] from a depth of 30 m.

The nodules can be separated from silt ashore, using a conical hydraulic screen, which allows separation of a gravel with a particle size exceeding 20 mm and nodule particles 2–20 mm in size. The chemical composition of the nodules from the Kopor'e Bay is given in Table 1 [9]; they contain todorokite $(Mn^{2+}, Ca, Mg)Mn_3^{4+}O_7 \cdot H_2O$ and vernadite $MnO_2 \cdot H_2O$ and minor amounts of pyrolusite MnO_2, psilomelane $(M, Mn)O \cdot mH_2O$ (where M = K, Ca, Ba, Ni, etc.), and rancieite $(Ca, Mn^{2+})Mn_4^{4+}O_8 \cdot 3H_2O$ [10]. The parameters of selected minerals are listed in Table 2.

Iron predominantly occurs as hydrated goethite FeO(OH) and double silicates with aluminum of ferrihydrite type $Fe_5Al_2(Al_2Si_6O_{22})(OH)_2$ [10].

A study of the FMN composition [10] demonstrated that the main ore fraction is constituted by iron and manganese hydroxides, and non-ferrous metals are isomorphically bound with manganese and iron minerals. Owing to strongly developed surface area (porosity of up to 58%), the FMN material is highly hygroscopic. The environmentally safe FMN material is a finished granulated material with round particles and particle-size distribution suitable for bulk filters.

The total content of manganese in various forms is shown in Table 1; data on the oxidation states of manganese in these forms are lacking. We assume that the average content of MnO_2 in the nodules, minus MnO inactive in water treatment, is nearly 20%, which is lower than that in pyrolusite Aquamandix sorbent by a factor of 4. However, the significantly larger surface area of the nodules compensates for the lower content of MnO_2 on the surface as compared to the pyrolusite sorbent.

The strength of FMNs can be raised by their grinding, mixing with bentonite (colloidal clays), and subsequent granulation.

The dynamic capacity, specific surface area, and strength were studied to compare the properties of the filter materials.

The dynamic capacity of the sorbents for Fe(II) was determined by the procedure similar to that given in [11]. A sorbent sample was placed in a column (300 mm bed height and 16 mm diameter); the elution rate was 0.5–1.0 ml min^{-1}. All the sorbents were preliminarily washed with distilled water (5 l). We studied the following samples: FMN (1.0–1.6 mm) washed with 2 l of 0.01 M oxalic acid (FMN 1), FMN without washing (FMN 2), Aquamandix sorbent (Aqu.), and Chinese sorbent based on pyrolusite (Pyr.). An aqueous NaOH solution was added to the ini-

Table 1. Chemical compositions of nodules from the Kopor'e Bay [9]*

Component	Average content	Content range
	wt %	
SiO_2	17.87	9.91–26.43
TiO_2	0.28	0.21–0.36
Total Mn recalculated to MnO_2	33.80 (35.87)	15.51–53.43
Al_2O_3	4.49	1.63–6.39
Fe_2O_3	20.19 (36.23)	10.31–33.98
MgO	1.59	0.94–2.14
CaO	1.41	0.93–2.21
Na_2O	1.43	1.11–1.77
K_2O	1.92	1.29–3.13
P_2O_5	2.70	1.42–4.88
Ba	0.328	0.1–1.0
Sr	0.0027 (0.263)	0.0005–0.0050
V	0.0076	0.0030–0.0120
Co	0.0067	0.0030–0.0120
Cr	0.0016	0.0012–0.0025
Ni	0.0134	0.0010–0.0500
Y	0.0015	0.0005–0.0025
Mo	0.0070	0.0020–0.0150
Cu	0.0034 (0.339)	0.0020–0.0080
Pb	0.0034 (0.449)	0.0001–0.0200
Zn	0.0057 (0.074)	0.0005–0.0150

* The weight fractions of elements determined in this study by X-ray fluorescence analysis are given in parentheses.

Table 2. Properties of selected minerals contained in nodules

Mineral	Density, g cm^{-3}	Moos hardness	mp, °C	Total content of Mn, %
Todorokite	3.3–3.8	1.5	660–800	47–64
Vernadite	1.8–3.3	2.0–3.0*		44–52
Pyrolusite	4.7–5.0	4.0–6.0	1050	63.19
Psilomelane		2.0–4.0	1000	37–51
Rancieite	2.8–3.3	2–3		43–50

* Similar to that of gypsum and calcite.

[1] The prospecting was performed with a Leningradskii-1 hydraulic dredge equipped with an slit-like suction pipe taking a 10–15-cm soil layer in operation on sandy and clayey bottom sediments [7, 8].

Table 3. Dynamic capacity to breakthrough of 0.1 mg l^{-1} Fe(II) solution and total dynamic capacity of sorbents (60 ml sorbent volume)

Sorbent	Sorbent weight, g	DC		TDC	
		equiv l^{-1}	equiv kg^{-1}	equiv l^{-1}	equiv kg^{-1}
Aqu.	67.3	0.13	0.12	1.12	1.00
Pyr.	40.3	0.50	0.74	0.89	1.33
FMN I	21.0	0.85	2.41	1.12	3.19
FMN II	21.0	0.89	2.54	1.23	3.51

Table 4. Preparation conditions of modified sorbents based on FMNs

Sample no.	Temperature of drying or annealing, °C	Fraction, mm	Binder	Sample no.	Temperature of drying or annealing, °C	Fraction, mm	Binder
1	150	1.0–2.0	–	11	400	1.0–2.0	Water glass
2	150	2.0–3.2	–	12	900	1.0–2.0	〃
3	400	1.0–2.0	–	13	150	1.0–2.0	PVA
4	400	2.0–3.2	–	14	150	<0.1	Water glass
5	25	0.3–1.0	–	15	400	<0.1	〃
6	25	1.0–2.0	–	16	25	1.0–2.0	〃
7	25	2.0–3.2	–	17	25	1.0–2.0	PVA
8	900	1.0–2.0	–	18	25	3.2–5.0	Water glass
9	900	2.0–3.2	–	19	25	<0.1	〃
10	150	1.0–2.0	Water glass	20	25	<0.1	Bentonite
				21	25	<0.1	〃

tial solution of $(NH_4)_2Fe(SO_4)_2 \cdot 6H_2O$ with a Fe^{2+} concentration of 0.7–7.5 mg l^{-1}, to attain pH 7–8. The dynamic capacity to breakthrough (DC) of the 0.1 mg l^{-1} Fe(II) solution (3.57 mg-equiv l^{-1}, i.e., MPC for fish breeding reservoirs) and the total dynamic capacity (TDC) with respect to Fe(II) were determined by analyzing 50-ml aliquots taken at the column outlet. The total content of Fe(II) and Fe(III) in the samples was determined spectrophotometrically with KSCN by absorption at λ 420 nm, and the content of Fe(III), at λ 536–540 nm with sulfosalicylic acid in an acidic medium. The content of Fe(II) was determined as the difference between the total content of iron and that of Fe(III). The dynamic capacity to breakthrough of the Fe(II) solution with a concentration of 0.1 mg l^{-1} and the total dynamic capacity of the sorbents, evaluated as the amount of Fe(II) ions adsorbed by unit weight or unit volume of the air-dried sorbent, are listed in Table 3. The initial concentrations of Fe(II) at the column inlet in the course of determination of DC and TDC were 0.026 and 0.134 equiv l^{-1}, or 0.728 and 7.504 g l^{-1}, respectively.

The model solutions sampled at the column outlet in the course of DC determination contained only Fe(II) ions, because no reaction was observed between Fe(III) ions and sulfosalicylic acid in the acidic medium.

The experimental results showed that the FMN capacity is higher than that of the imported fillers owing to its higher porosity and lower bulk density.

With the aim to enhance the FMN strength, we studied the modified nodules from the Gulf of Finland, prepared by granulation with bentonite clays, polyvinyl acetate glue (PVA), or water glass at various component ratios and temperatures (Table 4).

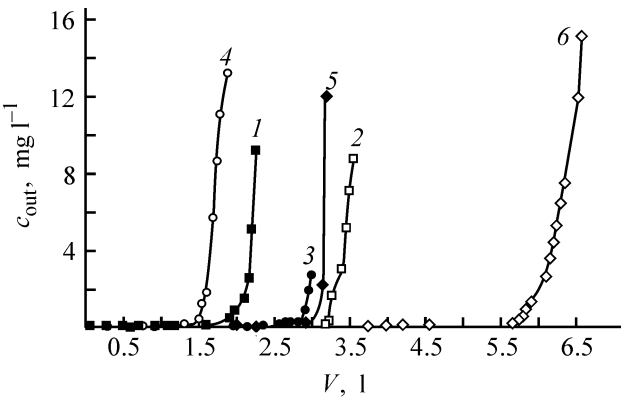
The mechanical strength was studied using the procedure given in [12]. First the particle-size distribution was determined and the major fraction was separated ($-d_1$; $+d_2$), where d is the side of the sieve mesh. Then the sample of the selected material was washed with distilled water, dried at 110°C, placed in a 250-ml conical flask, and poured over with distilled water. The flask was sealed and shaken for 24 h. After this procedure, the solutions were transferred

Table 5. Strength characteristics of modified FMNs

Sample no.	Fraction weight			Strength, %		Major fraction ($-d_1$; $+d_2$)
	($-d_1$; $+d_2$)	($-d_2$; $+d_2/2$)	($-d_2/2$; +0)	grindability	wearability	
1	100.34	4.02	1.27	4.01	1.27	(–2.0; +1.0)
2	78.00	0.18	1.46	0.23	1.87	(–2.5; +0.63)
3	95.56	2.91	0.74	3.04	0.78	(–2.0; +1.0)
4	100.30	7.27	1.95	7.25	1.94	(–3.0; +2.0)
5	109.05	7.36	1.75	6.75	1.60	(–1.0; +0.5)
6	107.15	0.28	1.22	0.26	1.14	(–2.5; +0.63)
7	107.59	0.16	1.39	0.15	1.29	(–2.5; +0.63)
10	77.02	0.37	0.89	0.48	1.16	(–2.5; +0.63)
11	56.94	2.90	0.25	5.09	0.43	(–2.0; +1.0)
12	48.51	1.01	0.15	2.08	0.31	(–1.0; +0.5)
13	91.64	0.64	1.31	0.70	1.43	(–2.5; +0.63)
14	27.07	3.25	1.68	12.02	6.20	(–1.0; +0.5)
15	16.48	0.76	1.53	4.64	9.30	(–1.0; +0.5)
16	92.81	0.54	0.91	0.58	0.98	(–2.5; +0.63)
17	100.19	0.27	0.06	2.85	0.35	(–2.5; +0.63)
18	82.30	0.37	0.66	0.45	0.80	(–2.0; +1.0)
20	105.27	3.97	0.30	3.76	0.30	(–1.0; +0.5)
21	70.52	2.73	0.15	3.87	0.21	(–2.5; +0.63)

Table 6. Dynamic capacity of modified ferromanganese nodules

Sample no.	c_{ini} of Fe(III), g l^{-1}	Volume to breakthrough of 0.1 mg l^{-1}, l	DC			
			equiv l^{-1}	equiv kg^{-1}	g kg^{-1}	g l^{-1}
1	0.90	1.63	1.66	0.87	46.34	24.47
2	0.90	0.73	0.66	0.39	18.51	10.92
3	1.37	1.75	2.81	1.42	78.65	39.84
4	0.90	1.63	1.01	0.87	28.14	24.47
5	0.90	1.89	1.63	1.01	45.56	28.25
6	0.97	1.38	1.41	0.79	37.69	21.03
7	0.97	0.28	0.27	0.16	7.67	4.42
8	1.45	0.08	0.11	0.07	2.91	1.82
9	1.45	0.08	0.06	0.07	1.76	1.82
10	0.96	1.78	1.39	1.02	37.21	27.16
11	1.37	3.15	3.63	2.56	101.72	71.71
12	1.37	1.70	1.50	1.38	41.94	38.70
13	0.92	2.55	2.16	1.39	60.48	39.00
14	1.40	1.23	1.85	1.02	51.77	28.59
15	1.40	1.60	2.00	1.33	54.57	37.32
16	1.45	1.45	1.70	1.25	47.52	34.92
17	1.45	1.45	2.00	1.25	56.03	34.92
18	0.94	0.28	0.27	0.15	7.45	4.31
19	0.94	0.08	0.08	0.04	2.18	1.18
20	1.40	3.98	4.15	3.31	116.17	92.76
21	0.94	5.73	4.41	3.21	123.56	89.90



Curves of saturation with Fe(II) of sorbent nos. 3, 11, 13, 17, 20, and 21, which exhibit the highest dynamic capacity. (c_{out}) Concentration of Fe(II) at the column outlet and (V) volume of eluate passed through the column. Sorbent no.: (*1*) 3, (*2*) 11, (*3*) 13, (*4*) 17, (*5*) 20, and (*6*) 21.

into porcelain dishes, water was evaporated, and the samples were dried at 110°C in air. The dried samples were successively sifted on sieves (d_2 and $d_2/2$) at a shaking frequency of 50 Hz for 10 min. The weight of the material that passed through sieve d_2 (percentage relative to the total weight of the material sample) characterizes the material grindability, and the weight of the material that passed through sieve $d_2/2$, its wearability. The strength characteristics of modified FMN samples are listed in Table 5.

As can be seen, the strength properties of several samples meet the requirements of GOST (State Standard) [12], according to which the grindability and wearability should not exceed 4.0 and 0.5%, respectively.

The dynamic capacity of the modified nodules to breakthrough of 0.1 mg l^{-1} Fe(II), determined as the content of Fe(II) ions adsorbed by unit weight or unit volume of the air-dried sorbent, is given in Table 6 (300 mm bed height and 16 mm diameter, 0.5–1.0 ml min^{-1} elution rate).

As can be seen from the experimental results, the capacity of the majority of the modified sorbents is higher than that of unmodified FMN samples by a factor of 2–3. This is apparently due to an increase in the specific surface area in the course of grinding and granulation with the binder. The saturation curves of sorbents exhibiting the highest dynamic capacity are shown in the figure.

Table 7. Specific surface area of ferromanganese nodules and Aquamandix sorbent (5-g samples)

Sorbent	MB concentration, equiv l^{-1}		S, m^2 g^{-1}
	initial	equilibrium	
FMN	0.01	2.341×10^{-3}	43.809
Aquamandix	0.002	1.665×10^{-3}	1.915

To understand the origin of high dynamic capacity of the sorbents, we evaluated their specific surface area by sorption of Methylene Blue (MB) from solution. A weighed portion of an air-dried sorbent (5 g) was placed in a 100-ml conical flask, and a 50-ml portion of a 0.001–0.01 M solution of MB was added. The flask was shaken, and the dispersion was stored for 12–14 h.

Then, the colored suspension was filtered twice through a "blue band" paper filter. The first two filtrate fractions (~10 ml) were rejected because of the MB sorption on the filter. Aliquots of the resulting filtrate and initial solution (1 ml) were diluted with water to 100 ml, and their optical density was measured at λ 665 nm. The MB concentration in the filtrate was calculated by the equation

$$c_f = c_{ini} D_f / D_{ini},$$

where D_f and D_{ini}, and c_f and c_{ini} are the optical densities and concentrations of the filtrate and initial solution, respectively.

The capacity (equiv g^{-1}) was calculated with an accuracy of up to 0.1 mg-equiv. from the following equation:

$$E = \Delta c V \times 10^{-3}/m, \quad (1)$$

where Δc is the difference between the concentrations of the initial and equilibrium MB solution (equiv l^{-1}); V, volume of the initial MB solution (cm^3); and m, weight of the sorbent sample.

From the exchange capacity, we calculated the specific surface area. According to X-ray diffraction analysis [13], the area occupied by a single MB molecule is 95.6×10^{-20} m^2. If we assume that the maximum amount of MB sorbed on the sample surface forms a monomolecular layer, then the specific surface area S (m^2 g^{-1}) can be calculated as

$$S = E N_A W_0, \quad (2)$$

where E is the sorbent capacity for MB (equiv g^{-1}); N_A, Avogadro constant; and W_0, area occupied by a single MB molecule.

Data on the specific surface area of FMNs and Aquamandix sorbent are listed in Table 7.

Table 8. Dynamic capacity to breakthrough of 0.1 mg l^{-1} of Fe(II) and mechanical strength of pyrolusite-containing filter materials

Sample no.	Bulk density, kg dm^{-3}	DC				Strength, %	
		equiv l^{-1}	equiv kg^{-1}	g kg^{-1}	g l^{-1}	grindability	wearability
1	0.53	1.66	0.87	46.34	24.47	4.01	1.27
3	0.51	2.81	1.42	78.65	39.84	3.04	0.78
11	0.70	3.63	2.56	101.72	71.71	5.09	0.43
12	0.92	1.50	1.38	41.94	38.70	2.08	0.31
14	0.55	1.85	1.02	51.77	28.59	12.02	6.20
17	0.62	2.00	1.25	56.03	34.92	2.85	0.35
20	0.80	4.15	3.31	116.17	92.76	3.76	0.30
21	0.73	4.41	3.21	123.56	89.80	3.87	0.21
Pyr.	0.61	0.74	0.45	20.66	12.57	<4	<0.5
Aqu.	1.08	0.12	0.13	3.35	3.63	<4	<0.5
FMN I	0.35	2.41	0.85	67.30	23.74	7.4–9.8	1.3–1.4
FMN II	0.35	2.54	0.89	70.93	24.85	7.4–9.8	1.3–1.4

As can be seen, the specific surface area of FMNs exceeds that of Aquamandix by more than a factor of 20. Hence, although the content of pyrolusite in FMNs is lower by a factor of 3–4, the large specific surface area compensates for the low content of MnO_2 on the nodule surface as compared to the imported pyrolusite-containing sorbent. The presence of goethite and other iron-containing minerals, which act as nucleation centers for precipitation of iron(III) hydroxide, is also an important factor.

Data on the capacity and mechanical strength of some pyrolusite-containing filter materials are summarized in Table 8.

As can be seen from Table 8, the capacity for Fe(II) of all the FMN samples is higher than that of the imported pyrolusite-containing sorbents. In general, the strength properties of the FMN samples do not meet the requirement of GOST. Sample no. 17 has the highest mechanical strength, and its capacity is close to that of the natural unmodified nodules. Sample nos. 3,11,12, 20, and 21 also have a satisfactory strength and a high capacity. These samples were prepared by granulation of ground nodules with appropriate binders (Table 4). Our experimental data suggest that the FMNs from the Gulf of Finland allow preparation of a filter material with a high capacity for Fe(II), meeting the requirements of GOST [12]. The low bulk density, developed porosity, and large specific surface area are the advantages of this environmentally safe material exhibiting sufficient strength, which can be controlled by grinding and mixing with bentonite. In this context, the low content of manganese oxides cannot be regarded as an essential disadvantage. For sorbents, it is advisable to use the fine fraction of nodules with a size of 1–3 mm, which are less valuable for metallurgy. The low cost of these inorganic sorbents makes them attractive for use.

The process for FMN recovery was developed by V.B. Dobretsov at the St. Petersburg Mining Institute [14]. The possibility of utilization of spent nodules is being examined [14, 15]. This utilization can be performed by means of pyrometallurgy at metallurgical plants, using a procedure that can recover nonferrous metals, such as manganese, copper, cobalt, and nickel [16].

CONCLUSIONS

(1) Treatment of wastewater to remove Fe(II) with ferromanganese nodules was studied.

(2) The dynamic capacity of the nodules for Fe(II) to breakthrough of 0.1 mg l^{-1} exceeds that of the imported pyrolusite-containing filter materials by a factor of 12–36. The high sorption capacity of ferromanganese nodules is determined by their large specific surface area, which is greater than the specific surface area of Aquamandix sorbent by a factor 20, and by the presence of goethite and iron-containing minerals on the sample surface, which act as nucleation centers for the precipitation of iron(III) hydroxide.

(3) Grinding and granulation of ferromanganese nodules with binders increases their capacity by a factor of 2–3 and enhances their strength characteristics to the level prescribed by the GOST.

ACKNOWLEDGMENTS

This study was supported by subprogram 207 "Ecology and Efficient Nature Management" of the Scientific and Technical Program of the Federal Agency of Education "Scientific Research at the Higher School in the Priority Areas of Science and Engineering."

REFERENCES

1. Kirgintsev, L.A., Trushnikova, L.N., and Lavrent'eva, V.G., in *Rastvorimost' neorganicheskikh veshchestv v vode: Spravochnik* (Solubility of Inorganic Compounds in Water: Reference Book), Leningrad: Khimiya, 1972, pp. 24–25.
2. Chelishchev, N.F., and Berenshtein, B.G., *Metody ochistki stochnykh vod i gazovykh vybrosov s primeneniem prirodnykh sorbentov* (Procedures for Treatment of Wastewaters and Gas Exhausts Using Natural Sorbents), Moscow: Mir, 1979.
3. Vakhler, B.L., *Vodosnabzhenie i vodootvedenie na metallurgicheskikh predpriyatiyakh* (Water Supply and Water Drainage at Metallurgical Plants), Moscow: Metallurgiya, 1977.
4. Romankova, P.G. and Nikol'skii, B.P., *Ionity v khimicheskoi tekhnologii* (Ion Exchangers in Chemical Engineering), Leningrad: Khimiya, 1982.
5. Vol'khin, V.V., Abstracts of Papers, *2 Vsesoyuznaya konferentsiya po neorganicheskim ionoobmennym materialam* (2nd All-Union Conf. on Inorganic Ion-Exchange Materials), Perm, June 14, 1980, pp. 3–7.
6. *Sovremennoe sostoyanie i perspektivy razvitiya tekhnicheskikh sredstv dlya osvoeniya mineral'nykh resursov okeana: Trudy Tsentral'nogo naucno-issledovatel'skogo institute im. A.N. Krylova* (Modern State and Prospects of the Facilities for the Development of the Ocean Mineral Resources: Proc. Krylov Central Research Instuitute), Orlov, O.P., Ed., Leningrad: Sudostroenie, 1972.
7. Rogalev, V.A., Dobretsov, V.B., and Evdokimenko, V.S., in *Sbornik nauchnykh dokladov na VI mezhdunarodnoi konferentsii "Ekologiya i razvitie Severo-Zapada Rossii"* (Coll. of Reports at VI Int. Conf. "Ecology and Development of the North-West of Russia"), St. Peterburg, July 11–16, 2001, St. Petersburg: MANEB, 2001, pp. 116–122.
8. Dobretsov, V.B., Chirkst, D.E., Kuleshov, A.A., and Glazov, A.N., *Gorn. Zh.*, 2002, no. 8, pp. 636–650.
9. Zaritskii, P.V., in *Konkretsii i konkretsionnyi analiz: Sbornik statei* (Nodules and Nodule Analysis: Coll. of Papers), Moscow: Nauka, 1977, pp. 79–84.
10. Chelishchev, N.F., Gribanov, N.K., and Novikov, G.V., *Sorbtsionnye svoistvs okeanicheskikh zhelezomargantsevykh konkretsii i korok* (Sorption Properties of the Oceanic Ferromanganese Nodules and Crusts), Moscow: Nedra, 1992.
11. *GOST* (State Standard) *20255.2–89: Ion Exchangers. Procedures to Determine the Dynamic Exchange Capacity*.
12. *GOST* (State Standard) *R 51641–2000: Granular Filter Materials: General Technical Specifications*.
13. *Metodicheski rekomandatsii po opredeleniyu fiziko-khimicheskikh svoistv glinisytykh gruntov* (Technical Recommendations on Analysis of Physicochemical Properties of Clay Soils), Kul'chinskii, L.I., Moscow: Vsesoyuz. Nauchn.-Issled. Inst. Gidrolog. Inzh. Geolog., 1979.
14. Teplyakov, N.M. and Fedorov, I.A., Abstracts of Papers, *Gornoe oborudovanie, pererabotka mineral'nogo syr'ya, novye technologii, ekologiya: V Mezhdunarodnyi Gorno-geologicheskii forum "Mineral'no-syr'evye resursy stran SNG"* (Mining Equipment, Processing of Mineral Resources, New Processes, Ecology: V Int. Mining-Geological Meet. "Mineral Resources of the CIS Countries"), St. Petersburg, October 7–10, 1997, ST. Petersburg: Sankt-Peterb. Gos. Gorn. Inst., 1997, pp. 27–28.
15. Teplyakov, N.M. and Dar'in, A.A., Abstracts of Papers, *Mezhdunarodnaya konferentsiya "Metallurgicheskie tekhnologii i ekologiya"* (Int. Conf. "Metallurgical Processes and Ecology"), St. Petersburg, April 25, 2003, St. Petersburg, 2003, pp. 84–86.
16. Teplyakov, N.M., *Teoriya i praktika izvlecheniya blagorodnykh metallov pri kompleksnoi pererabotke rud s primeneniem agregatsionnogo i sul'fatiziruyushchego obzhigov* (Theory and Practice of Recovery of Noble Metals in Complex Treatment of Ores Using Aggregation and Sulfatizing Roasting), St. Petersburg: Sankt-Peterb. Gos. Gorn. Inst., 2000.

Russian Journal of Applied Chemistry, Vol. 78, No. 4, 2005, pp. 599–601. Translated from Zhurnal Prikladnoi Khimii, Vol. 78, No. 4, 2005, pp. 606–608.
Original Russian Text Copyright © 2005 by Grekov.

ENVIRONMENTAL PROBLEMS OF CHEMISTRY AND TECHNOLOGY

Application of the Nanofiltration Method in Systems for Recycling of Washing Water in Photographic Development of Motion-Picture Films

K. B. Grekov

St. Petersburg State University of Cinema and Television, St. Petersburg, Russia

Received April 26, 2004; in final form, February 2005

Abstract—The possibility of using the nanofiltration method for purification of washing water in photographic development of professional motion-picture films is analyzed. Characteristics of domestic membranes, OPMN-K of nanofiltration type and OFAM-KN of low-pressure reverse-osmosis type, obtained in desalting of silver-containing washing water, are presented.

The amount of wastewater produced at motion picture and photolaboratories is small as compared with that formed at plants of other industries, but their complex composition necessitates development of techniques for their detoxication [1, 2]. According to some estimates, photographic development is a process with rather high water consumption because it exceeds in this regard (per unit mass of manufactured products) even such industries as tanneries, manufacture and rolling of steel, etc.

As shown by an analysis of published data and by the results of the author's own studies, the ecological problems of the technology of photographic development of motion picture and photographic materials can be solved in an integrated way virtually only by the membrane techniques, which can be used to create a closed-loop recirculation system of water consumption.

The most widely used among membrane methods are baromembrane techniques, whose main parameters are listed in Table 1. However, the boundaries between various baromembrane processes are rather conditional, and, in some cases, their applicability regions may overlap in practice.

The reverse osmosis method is applicable to purification of various kinds of thiosulfate-containing washing water, formed in fixation procedures. It is recommended to maintain the working pressure at 6 MPa and more, and the permissible $Na_2S_2O_3$ concentrations in the initial solution depend on the scheme of a reverse-osmosis installation used and vary within the range 10^{-3}–1.0 M [2].

The nanofiltration method occupies an intermediate position between ultrafiltration and reverse osmosis (Table 1). The applicability regions of nanofiltration and low-pressure reverse osmosis partly overlap and, occasionally, these two terms are used as synonyms [3].

Recently, a publication "Nanofiltration in Professional Cinematography" has appeared. This paper is

Table 1. Comparison of applicability regions of baromembrane methods*

Method	*d*, nm	*M*, DA	*P*, MPa
Microfiltration	10^2–10^4	–	0.01–0.1
Ultrafiltration	$(0.03–1) \times 10^2$	10^3–10^6	0.1–1.0
Nanofiltration	<3	$(0.5–1) \times 10^3$	0.5–1.5
Reverse osmosis, including its low-pressure variant	<3	$<5 \times 10^2$	2.5–25.0 1.5–2.5

* *d*, average pore size of the membrane; *M*, molecular mass of retained substances.

1070-4272/05/7804-0599 © 2005 Pleiades Publishing, Inc.

Table 2. Nanofiltration of the model solutions (P = 0.8 MPa)

$Na_2S_2O_3$		Ag^+,	Π,*	RC, %	
g l^{-1}	M	g l^{-1}	l m^{-2} h^{-1}	for $Na_2S_2O_3$	for Ag^+
1.74	0.007	–	22.5–23.5	63–68	–
3.5	0.014	0.07	21–23	61–64	75
19.8	0.08	0.13	5–10	25–40	54
42.7	0.17	–	3.5–5.5	4–12	–

* Π, membrane throughput.

Table 3. Nanofiltration of the model solutions at different working pressures

P, MPa	Concentration, g l^{-1}		RC, %		Π, l m^{-2} h^{-1}
	$Na_2S_2O_3$	Ag^+	for $Na_2S_2O_3$	for Ag^+	
0.8	3.5	0.07	66	75	21
	18.5	0.13	32	54	5
1.4	3.5	0.07	72	80	41
	18.5	0.13	58	71	12

Table 4. Effect of gelatin additives on the parameters of the nanofiltration process (P = 1.4 MPa)

Concentration, g l^{-1}			Π, l m^{-2} h^{-1}	RC, %	
$Na_2S_2O_3$	Ag^+	gelatin		for $Na_2S_2O_3$	for Ag^+
3.5	0.07	–	41	72	80
3.5	0.07	0.15	19.5	80	87
17.9	0.17	0.15	11.3	58	71

devoted to the possibility of application of this membrane technique for desalting of washing and wastewater discharged in photographic development of negative and positive color films (ECN-2 and ECP-2 processes).[1] The experimental data presented have been obtained by TECHNO-MEMBRANES Co. In performing the tests, a membrane installation equipped with nanofiltration units (MPSW-11 brand) was used; each of the three stages of the unit had a filtrate throughput of up to 0.5 m^3 h^{-1}. It was shown that the retention capacity (RC) of nanofiltration membranes for various components (with the exception of chloride and bromide ions) was 80% and more, and the concentration of Ag^+ in the filtrate did not exceed 2 and 0.1 mg l^{-1} for the ECN-2 and ECP-2 processes, respectively.

Analogous data for nanofiltration membranes of domestic manufacture cannot be found in the literature. Therefore, model thiosulfate- and silver-containing solutions, as well as the industrial silver-containing washing water produced in the fixation procedure, were chosen as the main object for preliminary studies. The concentration of $Na_2S_2O_3$ in the model solutions were in the range from 0.007 to 0.8 M. It was shown in preliminary experiments performed at a working pressure P = 0.5 MPa in an FM-02-200 laboratory cell that the RC of the OPMN-K domestic nanofiltration membrane is too low for effective desalting at $Na_2S_2O_3$ concentrations in solution exceeding 0.17 M.

The next set of experiments was carried out in a flow-through flat-chamber cell with a working surface area of the membrane equal to 38 cm^2, at a temperature of 18–20°C. It was found (Table 2) that the RC and specific throughput of the membrane start to decrease substantially when the $Na_2S_2O_3$ concentration becomes higher than 0.14 M. The dependence of the same type for reverse-osmosis membranes is qualitatively similar to a certain extent, but there still are rather significant differences due, on the one hand, to the large pore size in the nanofiltration membrane and, on the other, to the enhanced role of electrochemical factors (negative charge of the membrane and the ion being retained) in the retention mechanism. The higher RC for Ag^+ (in the form of thiosulfate complexes) is due to both steric and electrochemical factors.

Raising the working pressure from 0.8 to 1.4 MPa makes the RC higher and leads to a substantial increase (by approximately a factor of 2) in throughput (Table 3).

If a linear approximation similar to that used for reverse-osmosis membranes is applied to a nanofiltration membrane, the constants b_1 and b_2 can be found to be 31 and 85.4, respectively, for a solution with $Na_2S_2O_3$ concentration of 0.014 M, and 7.8 and 28.4 for that with 0.08 M.

In addition, the experimental results obtained demonstrated that the RC (for $Na_2S_2O_3$ and Ag^+) falls dramatically when the transmembrane volumetric flow rate decreases to 8–10 l m^{-2} h^{-1}, which also makes it possible to evaluate the applicability limits of the nanofiltration method.

The data in Table 4 also show that introduction of gelatin into the model solution leads to an increase in

[1] Internet site of KODAK Co. (www.kodak.com).

Table 5. Desalting of silver-containing solutions with membranes for nanofiltration and low-pressure reverse osmosis (P = 1.4 MPa)

Membrane	Concentration, g l^{-1}		Π, l m^{-2} h^{-1}	RC, %	
	$Na_2S_2O_3$	Ag^+		for $Na_2S_2O_3$	for Ag^+
OPMN-K	30	0.1	15	32	52
OFAM-KN	30	0.1	2.1	70	82
	5.1	0.0043	5.4	79	88

the RC of the membrane, which is accompanied by a considerable (by more than a factor of 2) decrease in its throughput, caused by the formation of a gel-like layer on the membrane surface [2].

Also, experiments on desalting of silver-containing spent solutions taken from a 40P3 developing machine processing an MZ-3 positive black-and-white film were carried out. In these experiments, the already studied OPMN-K nanofiltration membrane and an OFAM-KN membrane for low-pressure reverse osmosis were tested (Table 5).

CONCLUSION

Domestic nanofiltration membranes can be used in industrial units for desalting of washing water. However, they fail to provide a high degree of solution concentration. At the same time, their indisputable advantage is that, in contrast to reverse-osmosis membranes, they can effectively work at pressures of up to 1.5 MPa.

REFERENCES

1. Bober, T.W., Dagon, T.J., and Fowler, H.E., *Handbook of Industrial Waste Treatment*, Wang, L.K., and Mu Hao Sung Wang, Eds., New York: Marcel Dekker, 1992, vol. 1, pp. 173–227.
2. Grekov, K.B. and Tsapyuk, E.A., *Zh. Prikl. Khim.*, 1984, vol. 57, no. 6, pp. 1291–1294.
3. Bon, A.I., Dzyubenko, V.G., Saburova, M.V., and Shishova, I.I., *Materialy II Respublikanskoi konferentsii po membranam i membrannoi tekhnologii* (Proc. II Resp. Conf. on Membranes and Membrane Technology), Kiev: UkrgiproNIIneft', 1991, pp. 55–56.

Russian Journal of Applied Chemistry, Vol. 78, No. 4, 2005, pp. 602–605. Translated from Zhurnal Prikladnoi Khimii, Vol. 78, No. 4, 2005, pp. 609–612.
Original Russian Text Copyright © 2005 by Zykova, Panov.

ENVIRONMENTAL PROBLEMS OF CHEMISTRY AND TECHNOLOGY

Recovery of Heavy Metals from Excess Active Sludges with Aeration

I. V. Zykova and V. P. Panov

St. Petersburg State University of Technology and Design, St. Petersburg, Russia

Received December 9, 2004

Abstract—The fundamental aspects of recovery of heavy metal ions from excess active sludges produced at biological treatment plants with the use of various calcium-containing materials (chemically pure, of natural and technological origin) upon introduction of biogenic elements with aeration were studied.

Previously, it has been shown that the problem of detoxication of excess active sludges to remove heavy metal ions (HMI) and utilization of these sludges in agriculture as fertilizers are matters of current interest and new engineering solutions have been suggested as an alternative to deposition or burning of sludges [1–3].

Introduction of sparingly soluble compounds containing Ca(II) into a humid excess sludge leads to immobilization of microorganisms from the sludge on solid surfaces and adsorption of humic acids, amino acids, proteins, and vitamins. In this case, HMI are desorbed by the ion-exchange mechanism from the cell surface, extracted from the cytoplasm of bacterial cells, and replaced by Ca(II) ions in humates. The immobilization of microorganisms on the surface of calcium-containing materials intensifies physical and biochemical processes leading to replacement of HMI in sludge components by Ca(II) ions. Aeration of the system and introduction of phosphate ions, which are necessary for stimulation of the vital functions of microorganisms, may favor a deeper extraction of HMI from sludges [4]. It would be expected that the recovery of HMI should be also more complete when calcium-containing materials containing phosphate components, e.g., phosphogypsum and phosphorite ores, are used.

HMI were recovered from samples of excess sludges from the biological treatment plant (BTP) (Velikii Novgorod) with the use of Kingissep phosphorite, technical-grade $Ca_3(PO_4)_2$, natural gypsum, phosphogypsum, and conversion chalk. To study the influence exerted by phosphate ions on the process, $CaHPO_4$ or NaH_2PO_4 was introduced into the excess sludge before its being mixed with a calcium-containing material in order to create PO_4^{3-} ions in a concentration of 1–100 mg l^{-1}. The volumetric flow rate of air supply was 16 h^{-1}. The concentration of HMI was analyzed on a Perkin–Elmer spectrophotometer by the procedure described in [5].

If the system is agitated with air, the surface of the calcium-containing material becomes more accessible for immobilization of microorganisms and adsorption of organic substances and enzymes. Presence of oxygen in the system leads to partial oxidation of organic compounds, including that occurring via development of an aerobic microflora, which decomposes compound complex substances [6, 7]. As a result, the degree of recovery of HMI from sludges into the aqueous phase increases by 10– 30%, compared with that in the case of mechanical agitation (Table 1).

In the case of aeration, HMI are recovered at a high rate during 1 h, with further agitation (for up to 3 h) having virtually no effect on the completeness of recovery.

Introduction of phosphate ions into the system in a concentration of up to 50 mg l^{-1} at an agitation duration of 3 h and a concentration of the calcium-containing material of no less than 25 g l^{-1} leads to a 10–50% increase in the degree of recovery of Cu(II), Pb(II), Ni(II), Cr(III), and Zn(II) ions from the "solid" phase of the sludge into the "aqueous" phase (includ-

1070-4272/05/7804-0602 © 2005 Pleiades Publishing, Inc.

Table 1. Concentration of heavy metal ions in the treated sludge (T = 20°C, τ = 1 h)

Material, g l^{-1}	Concentrations of indicated metal ions in the sludge, mg kg^{-1} dry mass							
	Pb_{tot}		Ni_{tot}		Cd_{tot}		Cr_{tot}	
	A*	M	A	M	A	M	A	M
Starting sludge	510		315		165		475	
Natural gypsum:								
25	189	330	142	174	99	99	240	260
17	230	350	158	180	105	110	250	273
Phosphogypsum:								
25	163	290	126	164	56	72	190	250
12.5	173	300	158	179	58	73	199	276

* Agitation: A, with air; M, mechanical.

Table 2. Concentration of heavy metal ions in the sludge treated under mechanical agitation

Material, g l^{-1}	PO_4^{3-}, mg l^{-1}	τ, h	Concentrations of indicated metal ions in the sludge, mg kg^{-1}		
			Zn_{tot}	Cu_{tot}	Pb_{tot}
Sludge before thickening	–	0	1800	1200	400
Gypsum, 25	0	3	990	550	150
	50	3	648	444	128
	100	3	666	444	116
$Ca_3(PO_4)_2$, 45	0	2.5	820	450	140
	50	2.5	510	341	54
Phosphorite, 12.5	0	3	1390	530	121
	50	3	1350	516	104
Permissible concentration of metal ions in an excess sludge being utilized, mg kg^{-1}		EEC GOST (State Standard) R 17.4.3.07–2001	250–4000 1750 (group I) 3500 (group II)	1000–1750 750 (group I) 1500 (group II)	750–1200 250 (group I) 500 (group II)

ing that in the form of colloids) under mechanical agitation (Table 2).

According to experimental data, aeration of the system and introduction of phosphate ions markedly accelerate the replacement of HMI by Ca(II) ions in the solid phase of the sludge. Residual HMI concentrations in the treated sludge (per unit mass of dry sludge) that are below the standard concentrations established by GOST (State Standard) R 17.4.3.07–2001 [8] for group-I sediments, which are allowed for use as fertilizers in agriculture, can be reached by agitating the system for 1 h. The data obtained served as a basis for the method suggested for intensifying the process of sludge detoxication [9].

The intensification of HMI recovery from components of the active sludge is also favored by presence of phosphate ions in the starting calcium-containing material. With most of the above-mentioned calcium-containing materials used, the rate of HMI recovery from the sludge is higher during the first 30 min of a process performed with mechanical agitation, compared with that in the case of aeration. However, already 1 h of agitation of systems by aeration results in that the total rate and the degree of recovery exceed (and remain at this level for 3 h) the parameters obtained with mechanical agitation.

Any calcium-containing material introduced into a sludge changes the pH of the medium. For example, the pH of the medium changes, depending on the dose, by 0.7–0.9, 0.5–0.7, 0.5–0.8, and 0.7–0.8 upon introduction of $CaCO_3$, phosphogypsum, natural gypsum, and phosphorite, respectively. Attracting ions of

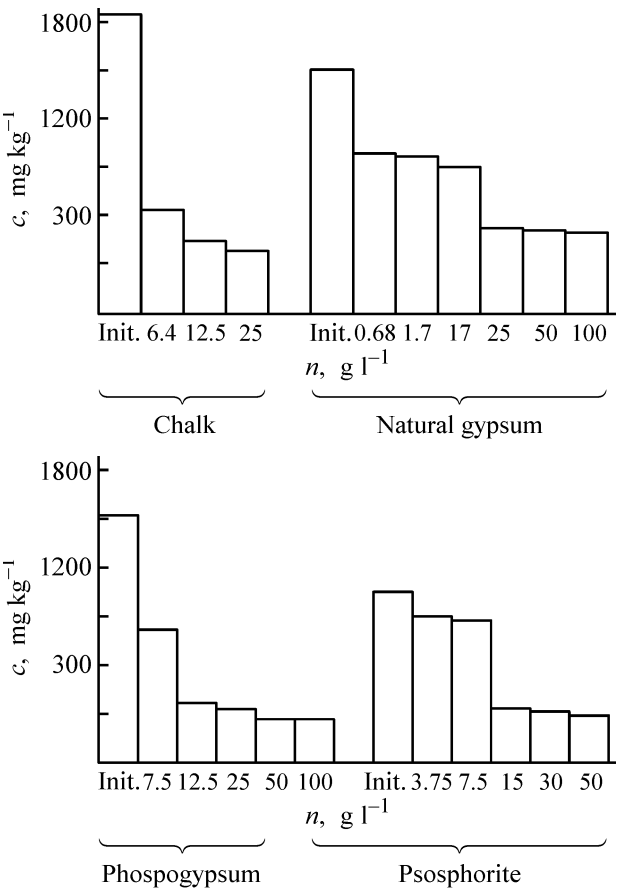


Fig. 1. Comparison of the residual concentrations c of copper ions in the sludge at various doses n of calcium-containing materials. T = 22–25°C, pH 6.8, aeration duration 1 h.

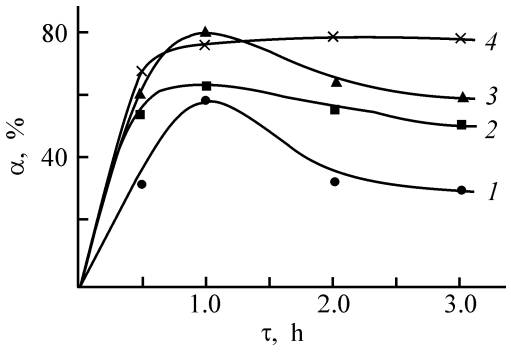


Fig. 2. Degree of copper ion recovery, α, vs. the process duration τ with (*1*, *3*) phosphorite and (*2*, *4*) phosphogypsum used in doses of 15 and 12.5 g l^{-1} of sludge, respectively. T = 22–25°C, pH 6.8. Agitation: (*1*, *2*) mechanical and (*3*, *4*) with air.

the opposite sign from solution, the charged surface of the calcium-containing material changes the conditions of occurrence and the rate of surface reactions. At the interface between the positively charged surface of the material and the liquid medium, the pH may increase by 0.5–2.0 to become 8.5–9.0, which changes the stability of humus complexes [6] and the possibility of replacement of HMI in these complexes and other organic substances by Ca(II) ions.

According to experimental data, the residual concentration of, e.g., copper(II) ions in a dehydrated sludge is the lowest, all other conditions being the same, when phosphogypsum and phosphorite are used as a calcium-containing material (Fig. 1). Some differences are observed when the process is performed using phosphorite and phosphogypsum under mechanical agitation or phosphorite under aeration (Fig. 2). The maximum degree of recovery is observed after 1 h of agitation. If the process duration is made longer, the degree of recovery decreases, This is due to the presence of a considerable amount of fluoride ions in phosphorite, which may lead to loss of microorganisms, with the resulting, after a certain time, biosorption of HMI by "dead" microorganisms and a decrease in the degree of recovery. Phosphogypsum also contains an admixture of fluoride ions, but in a lower concentration and in the form of complex silicofluorides, which results in that its action on microorganisms is not so fatal.

The results of this study demonstrate the possibility of effective detoxication of active sludges from biological treatment plants to remove HMI with the use of various sparingly soluble calcium-containing materials of natural and technological origin. If the process is carried out under certain physicochemical conditions (pH value, temperature, dose of calcium-containing materials, aeration of the system, introduction of biogenic materials, duration of agitation of a system constituted by the sludge and a calcium-containing material), the residual concentration of HMI in a dehydrated sludge can be brought to a standard level that permits use of sludges and sediments from wastewater as fertilizers.

CONCLUSIONS

(1) Introduction of phosphate ions into a system constituted by an excess active sludge and a calcium-containing material and agitation of the heterogeneous system with air intensify the extraction of heavy metals and substantially diminish their residual concentrations.

(2) The rate of replacement of heavy metal ions by calcium ions depends on the composition of the calcium-containing materials used, presence of impurities, and pH value at the phase boundary.

(3) The residual concentrations in the active sludge from biological treatment plants can be brought, by using the method suggested, to a level permissible in utilization of the excess sludge as an organomineral fertilizer in agriculture.

ACKNOWLEDGMENTS

The study was financially supported by the Ministry of Education of the Russian Federation (grant for basic research in technical sciences, T02-11.3-3399).

REFERENCES

1. Zykova, I.V., Alekseeva, E.A., and Panov, V.P., *Zh. Prikl. Khim.*, 2000, vol. 74, no. 11, pp. 1901–1903.
2. RF Patent 2133231.
3. Zykova, I.V., Makashova, T.G., and Panov, V.P., *Sbornik nauchnykh trudov SPGUTD* (Coll. of Sci. Works of St. Petersburg State Univ. of Technol. Design), St. Petersburg, 2002, no. 4, pp. 88–95.
4. Golubovskaya, E.K., *Biologicheskie osnovy ochistki vody* (Biological Foundations of Water Purification), Moscow: Vysshaya Shkola, 1978.
5. Lur'e, Yu.Yu., *Analiticheskaya khimiya promyshlennykh stochnykh vod* (Analytical Chemistry of Industrial Wastewater), Moscow: Khimiya, 1984.
6. Zvyagintsev, D.G., *Vzaimodeistvie mikroorganizmov s tverdymi poverkhnostyami* (Interaction between Microorganisms and Solid Surfaces), Moscow: Nauka, 1973.
7. Orlov, D.S., *Guminovye kisloty pochv i obshchaya teoriya gumifikatsii* (Humic Acids in Soils and General Theory of Humification), Moscow: Mos. Gos. Univ., 1990.
8. *GOST* (State Standard) *R 17.4.3.07–2001: Nature protection. Soils: Requirements to the properties of sediments from wastewater in their use as fertilizers*, 2001.
9. RF Patent 2174964.

Russian Journal of Applied Chemistry, Vol. 78, No. 4, 2005, pp. 606–608. Translated from Zhurnal Prikladnoi Khimii, Vol. 78, No. 4, 2005, pp. 613–615.
Original Russian Text Copyright © 2005 by Alekseev, Nersesova, Khalyapina.

ORGANIC SYNTHESIS AND INDUSTRIAL ORGANIC CHEMISTRY

Determination of Benzylpenicillin, Ampicillin, and Carbenicillin by Paper Chromatography

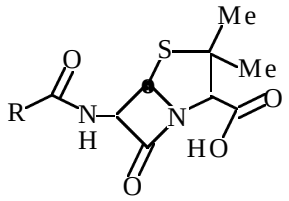
V. G. Alekseev, A. F. Nersesova, and Ya. M. Khalyapina

Tver State University, Tver, Russia

Received June 16, 2004

Abstract—A mobile phase was developed for selective determination of benzylpenicillin, carbenicillin, and ampicillin in drugs by paper chromatography.

Antibiotics of the penicillin group are widely used in the medical practice for treatment of infectious diseases. Numerous agents of this group are used today [1, 2]. The molecular structures of penicillins are as follows [3, 4]:



where R = $PhCH_2$ (benzylpenicillin), $PhCH(CO_2H)$ (carbenicillin), or $PhCH(NH_2)$ (ampicillin).

These antibiotics significantly differ in performance, spectrum of the antimicrobial effect, and price. In particular, carbenicillin (CC) differing from benzylpenicillin (BP) only in the presence of one more carboxy group is 9–10 times more expensive than BP. Thus, a risk arises that an expensive drug can be adulterated by replacement with a cheaper drug of the same group. In this case, the drug identification is of crucial importance [5, 6]. Therefore, an urgent problem is the development of selective methods for analysis of antibiotics, as their adulteration is more frequent [7]. Titrimetric [8, 9], spectrophotometric [10–13], and ionometric (with membrane ion-selective electrodes [14, 15] and biosensors [16]) methods, as well as flow injection analysis [17], can be successfully used for quantitative determination of penicillin of a known chemical structure, but are unsuitable for identification of particular penicillins. According to recent studies, high-performance liquid chromatography (HPLC) can be successfully used for selective determination of penicillins [18, 19]. However, this procedure requires expensive apparatus. Thin-layer chromatography (TLC) and paper chromatography (PC) are simpler but also efficient methods; they are widely used in the analytical chemistry of drugs [20].

The possibility of using TLC and PC for the determination of penicillins was examined in numerous studies [21–29]. As eluents were used alcohols, ethers, esters, ketones, and their mixtures with addition of acetic or formic acid, or of aqueous buffer solutions (phosphate, carbonate, citrate). It should be noted, however, that many studies were performed with outdated drugs (heptylpenicillin, propionylpenicillin, ethylmercaptomethylpenicillin, etc.). Furthermore, the results obtained by different authors are inconsistent and sometimes even contradictory.

The goal of this study was to develop a procedure for qualitative determination of three penicillin drugs widely used today: BP, ampicillin (AP), and CC, using such a simple and cheap method as paper chromatography.

EXPERIMENTAL

Experiments were performed with antibiotics in the form of powders in vials: benzylpenicillin sodium salt (Biokhimik, Saransk, Mordovia, Russia), ampicillin sodium salt (Krasfarma, Krasnoyarsk, Russia), and carbenicillin disodium salt (Ferane, Moscow, Russia). Acetone, ethanol, 2-propanol, 1-butanol, diethyl ether, ethyl acetate, carbon tetrachloride, chloroacetic acid, and crystalline iodine were of analyticaly pure grade. Borate buffer solution (pH 9.18), a 0.01 M solution of sodium tetraborate, was prepared from a reference sample.

1070-4272/05/7804-0606 © 2005 Pleiades Publishing, Inc.

In the first step, we examined the possibility of separation of BP, AP, and CC on filter paper using several solvent systems [20, 26]: acetone–ethanol (1 : 1), 1-butanol–ethanol–water (4 : 1 : 5), 1-butanol–acetic acid–water (4 : 1 : 5), 2-propanol–ethanol (3 : 7), and diethyl ether.

The development of the chromatograms with the Bouchard and Dragendorff reagents [26] failed. Better results were obtained with an iodine vapor; the antibiotics always gave dark orange spots against a light yellow background. Unfortunatelly, the R_f values obtained significantly differed from published data. The results are listed in the table.

It is seen that all the mobile phases tested are unsuitable for determination of BP, AP, and CC because of very low R_f. Therefore, we decided to use a denser material, SvetoCopy office paper (80 g m^{-2}, Svetogorsk Joint-Stock Company, Russia), on which the eluent front moved more slowly. The R_f values were the same, but the chromatograms became clearer. However, foreign spots appeared, apparently originating from wash-out of certain components from the paper with the eluent. Therefore, the SvetoCopy paper was preliminarily washed with the eluent to be used for chromatographing. Paper strips (200 × 25 mm) were placed in a chromatographic chamber with an eluent and kept for 8 h. Then the paper was removed and dried in air.

We performed two series of experiments: (1) separation of penicillins in the form of anions, using a mixture of an organic solvent and aqueous borate buffer solution (pH 9.18), volume ratio 95 : 5; (2) separation of penicillins in the form of acids, with addition of chloroacetic acid (5 wt %) to the solvent system.

The choice of chloroacetic acid was governed by its good solubility in organic solvents and sufficiently strong acidity for converting the antibiotics into the acid form: for chloroacetic acid pK_a 2.87 [30], whereas for the carboxy group of penicillins pK_a 3.04 (BP), 2.79 (CC), and 2.96 (AP) [31].

Freshly prepared 5 mg ml^{-1} solutions of the antibiotics were applied to the start line on the pretreated paper with a glass capillary. The paper was dried and placed in a chromatographic chamber for 6 h. The eluent front moved in this time by 75–85 mm. The resulting chromatogram was dried in air and developed in iodine vapor by placing it for a few minutes in a closed vessel containing crystalline iodine on the bottom. The developed chromatogram contains spots ~8 mm in diameter of almost regular round shape.

Chromatographic mobility (R_f) of penicillins

Mobile phase	AP	BP	CC
Acetone–ethanol (1 : 1)	0.05	0.04	0.06
1-Butanol–ethanol–water (4 : 1 : 5)	0.09	0.10	0.09
1-Butanol–acetic acid–water (4 : 1 : 5)	0.43	0.44	0.45
2-Propanol–ethanol (3 : 7)	0.44	0	0
Diethyl ether	0.08	0.09	0.08
CCl_4–chloroacetic acid (95 : 5)	0.16	0.18	0.20
Diethyl ether–chloroacetic acid (95 : 5)	0.10	0.08	0
Ethyl acetate–chloroacetic acid (95 : 5)	0.13	0.19	0.17
Acetone–chloroacetic acid (95 : 5)	0.07	0.10	0.09
Ethanol–chloroacetic acid (95 : 5)	0.89	0.87	0.93
Ethyl acetate–CCl_4–chloroacetic acid (47.5 : 47.5 : 5)	0.15	0.18	0.19
Ethanol–CCl_4–chloroacetic acid (47.5 : 47.5 : 5)	0.18	0.18	0.21
Ethanol–ethyl acetate–chloroacetic acid (47.5 : 47.5 : 5)	0.16	0.18	0.20
Ethanol–water–chloroacetic acid:			
20 : 75 : 5	0.61	0.62	0.55
35 : 60 : 5	0.65	0.67	0.59
47.5 : 47.5 : 5	0.69	0.71	0.61
60 : 35 : 5	0.71	0.72	0.63
75 : 20 : 5	0.83	0.75	0.70

We tested the following individual organic solvents: CCl_4, diethyl ether, ethyl acetate, acetone, and ethanol. With the borate buffer solution, the results were unsuccessful; R_f was zero in all the cases. Separation of the antibiotics was attained in acidic mobile phases (see table). The best results were obtained with the ethanol–chloroacetic acid (95 : 5) system. The use of mixed organic solvents afforded no significant advantages, compared to the individual solvents. We tested the following systems: ethyl acetate–CCl_4–chloroacetic acid (47.5 : 47.5 : 5), ethanol–CCl_4–chloroacetic acid (47.5 : 47.5 : 5), and ethanol–ethyl acetate–chloroacetic acid (47.5 : 47.5 : 5). The larger difference between BP, AP, and CC in R_f was attained only with the ethanol–water–chloroacetic acid system. The best component ratio is 75 : 20 : 5.

CONCLUSION

Penicillins are better separated by paper chromatography in the form of acids rather than anions. A procedure was developed for selective determination of benzylpenicillin, ampicillin, and carbenicillin by paper chromatography.

REFERENCES

1. Belousov, F.B., Moiseev, V.S., and Lepakhin, V.K., *Klinicheskaya farmakologiya i farmakoterapiya: Rukovodstvo dlya vrachei* (Clinical Pharmacology and Pharmacotherapy: A Guide for Physicians), Moscow: Universum, 1997.
2. Demain, A.L. and Elander, R.P., *Antonie van Leeuwenhoek*, 1999, vol. 75, pp. 5–19.
3. *Comprehensive Organic Chemistry. The Synthesis and Reactions of Organic Compounds*, Barton, D. and Ollis, W.D., Eds., Oxford: Pergamon, 1979. Translated under the title *Obshchaya organicheskaya khimiya*, Moscow: Khimiya, 1983, vol. 10, pp. 336–344.
4. Soldatenkov, A.T., Kolyadina, N.M., and Shendrik, I.V., *Osnovy organicheskoi khimii lekarstvennykh veshchestv* (Fundamentals of the Organic Chemistry of Drugs), Moscow: Mir, 2003.
5. Zolotov, Yu.A., *Zh. Anal. Khim.*, 2001, vol. 56, no. 11, p. 1125.
6. Degterev, E.V., *Ross. Khim. Zh.*, 2002, vol. 46, no. 4, pp. 43–51.
7. Arzamastsev, A.P., Dorofeev, V.L., Konovalov, A.A., *et al.*, *Khim.-Farm. Zh.*, 2004, vol. 38, no. 3, pp. 48–51.
8. Ashworth, M.R.F., *Titrimetric Organic Analysis*, New York: Interscience, 1964–1965.
9. Pohloudek-Fabini, R. and Beyrich, Th., *Organische Analyse*, Leipzig: Geest und Portig, 1975.
10. Amin, A.S., *Farmaco*, 2001, vol. 56, no. 3, pp. 211–218.
11. Belikov, V.G., *Ross. Khim. Zh.*, 2002, vol. 46, no. 4, pp. 52–56.
12. Krasnikova, A.V. and Iozep, A.A., *Khim.-Farm. Zh.*, 2003, vol. 37, no. 9, pp. 40–51.
13. Ahmad, A.S., Rahman, N., and Islam, F., *Zh. Anal. Khim.*, 2004, vol. 59, no. 2, pp. 138–142.
14. Shvedene, N.V. and Borovskaya, S.V., *Zh. Anal. Khim.*, 2003, vol. 58, no. 11, pp. 1208–1213.
15. Kulapina, E.G., Baraguzina, V.V., and Kulapina, O.I., *Zh. Anal. Khim.*, 2004, vol. 54, no. 9, pp. 971–975.
16. Pogossian, A., Schöning, M.J., Schroth, P., *et al.*, *Sensors Actuators*, 2001, vol. B76, pp. 519–526.
17. Evgen'ev, M.I., Garmonov, S.Yu., and Shakirova, L. Sh., *Zh. Anal. Khim.*, 2001, vol. 56, no. 6, pp. 642–646.
18. Skudar, K., Brüggemann, O., Wittelsberger, A., *et al.*, *Anal. Commun.*, 1999, vol. 36, pp. 327–331.
19. Sokolova, L.I. and Chernyaev, A.P., *Zh. Anal. Khim.*, 2001, vol. 56, no. 11, pp. 1177–1180.
20. Sarsünová, M., Schwarz, V., and Michalec, Č., *Chromatografia na Tenkych Vrstvách vo Farmácii a v Klinekey Biochemii*, Bratilava: Osveta, 1977.
21. Bjadzhi, F.J. and Nelson, D.B., *J. Am. Chem. Soc.*, 1970, vol. 92, pp. 333–342.
22. Phuks, A. and Mattok, H., *Antimicrob. Agents Chemother.*, 1974, vol. 4, pp. 24–32.
23. Nicolaus, R., *J. Chromatogr.*, 1975, vol. 52, pp. 111–117.
24. Berdt, L. and Marshall, J., *J. Antibiot.*, 1979, vol. 22, pp. 233–236.
25. O'Nill, G., *Antimicrob. Agents Chemother.*, 1981, vol. 6, pp. 637–643.
26. Blinov, N.O. and Khokhlov, A.S., *Bumazhnaya khromatografiya antibiotikov* (Paper Chromatography of Antibiotics), Moscow: Nauka, 1970.
27. Serova, L.I., Kotova, N.I., Tomashchik, A.D., *et al.*, *Antibiotiki*, 1975, vol. 20, no. 2, pp. 106–110.
28. Serova, L.I. and Korchagin, V.B., *Antibiotiki*, 1976, vol. 21, no. 1, pp. 84–88.
29. Bystrova, L.V. and Serova, L.I., *Antibiotiki*, 1982, vol. 27, no. 8, pp. 14–16.
30. Gordon, A.J. and Ford, R.A., *The Chemist's Companion. A Handbook of Practical Data, Techniques, and References*, New York: Wiley, 1972.
31. Alekseev, V.G. and Volkova, I.A., *Zh. Obshch. Khim.*, 2003, vol. 73, no. 10, pp. 1709–1711.

Russian Journal of Applied Chemistry, Vol. 78, No. 4, 2005, pp. 609–612. Translated from Zhurnal Prikladnoi Khimii, Vol. 78, No. 4, 2005, pp. 616–618.
Original Russian Text Copyright © 2005 by Petrova, Grebennikov, Burinskaya.

ORGANIC SYNTHESIS AND INDUSTRIAL ORGANIC CHEMISTRY

Changes in the Structure of Wool Fiber in Dyeing in a Redox Medium

O. V. Petrova, S. F. Grebennikov, and A. A. Burinskaya

St. Petersburg State University of Technology and Design, St. Petersburg, Russia

Received December 29, 2004

Abstract—The suitability of redox systems for wool dyeing with acid and active dyes at temperatures below the boiling point of the dyeing solutions was studied. The influence of the hydrogen peroxide–reductant (glucose, ethylene glycol, 1,2,3-propanetriol, polyoxymethylene, and hexamethylenetetramine) systems on the surface of wool roving was elucidated.

Finishing of wool fiber fabrics governs to a significant extent the quality and competitiveness of ready-for-use textile articles. As is known, wool preliminarily damaged by dyeing, light exposure, and high temperatures, as well as by alkalis, chlorine, and oxidants, is especially sensitive to mechanical loads (pressure, twisting, shear). Mechanical treatment of wool fibers causes various transverse and longitudinal cracks, depending on the moisture content of the fibers. These cracks are responsible for dust formation upon degradation of the cuticle when treated on fast rotating machines, which poses risks on human health. Most of the wool lint is formed in the yarn production stage. However, wool dyeing causes respiratory tract diseases more often than other jobs do, because dyed yarn exceeds undyed yarn in the dust content [1].

Wool is traditionally dyed at the boiling temperature of the dyeing solution, which may lead to inefficient use of raw materials and energy. Therefore, it is of great practical importance to develop processes for low-temperature dyeing of wool, which damage the fiber and contaminate the environment to a lesser extent and are more energy-efficient. Low-temperature dyeing can be performed with the use of redox systems, tems, which allows the temperature at which the wool fiber is dyed with acid and active dyes to be lowered from the boiling point of the solution to 80°C, and the treatment time, to be made a factor of 1.5–2 shorter [2].

In this study, we took as dyeing intensifiers hydrogen peroxide–reductant systems with glucose (system no. 1), ethylene glycol (system no. 2), 1,2,3-propanetriol (system no. 3), polyoxymethylene (system no. 4), and hexamethylenetetramine (system no. 5) as reductants.

When introduced into a dye bath, reagents with high redox potentials cause degradation of the wool fiber and, possibly, of the chromophore system of the dyes. In this context, we studied how the above systems affect the structure of the wool substrate. To determine the optimal oxidant : reducer ratio in the systems, we estimated the redox potentials of a number of intensifiers. The optimal concentration of the reductant, favoring the maximum sorption of acid and active dyes, is 0.0075–0.015 M [3]. The figure shows the electrochemical potentials at the actual concentrations of hydrogen peroxide and the reductant.

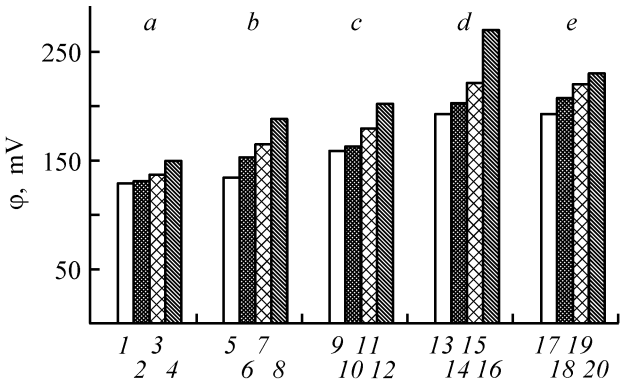


Fig. 1. Redox potential φ of system nos. (*a*) 1, (*b*) 2, (*c*) 3, (*d*) 4, and (*e*) 5. H_2O_2–reductant concentrations, M: (*1*) 0.0075–0.0075, (*2*) 0.015–0.015, (*3*) 0.03–0.03, (*4*) 0.15–0.15, (*5*) 0.03–0.0075, (*6*) 0.06–0.015, (*7*) 0.12–0.03, (*8*) 0.6–0.15, (*9*) 0.03–0.0075, (*10*) 0.06–0.015, (*11*) 0.12–0.03, (*12*) 0.6–0.15, (*13*) 0.022–0.0075, (*14*) 0.045–0.015, (*15*) 0.09–0.03, (*16*) 0.45–0.15, (*17*) 0.022–0.0075, (*18*) 0.045–0.015, (*19*) 0.09–0.03, and (*20*) 0.45–0.15.

1070-4272/05/7804-0609 © 2005 Pleiades Publishing, Inc.

Table 1. Sorption a of benzene vapor (P/P_0 = 0.98) by the wool fiber

Dyeing conditions	a, $cm^{-3}\ g^{-1}$	
	Acid Bordeaux	Active Scarlet 4ZhT
Without intensifiers, by boiling	0.0147	0.0103
At 80°C with indicated intensifier:		
1	0.0018	0.0001
2	0.0021	0.0014
3	0.0042	0.0019
4	0.0051	0.0086
5	0.0126	0.0097
Undyed sample	0.0163	

Table 2. Sorption a of the water vapor (P/P_0 = 0.98) by the dyed wool fiber

Dyeing conditions	a, mmol g^{-1}			
	φ = 31%		φ = 98%	
	Acid Bordeaux	Active Scarlet 4ZhT	Acid Bordeaux	Active Scarlet 4ZhT
Without intensifiers, by boiling	10.00	9.44	14.67	15..11
At 80°C with indicated intensifier:				
1	7.22	5.00	11.67	11.11
2	7.59	5.81	11.96	11.53
3	8.33	6.11	12.78	12.22
4	8.89	7.22	12.78	12.78
5	8.89	8.33	13.89	13.33
Undyed sample	15.55			

The concentrations of the components in the systems constituted by hydrogen peroxide and a reducing agent correspond to the stoichiometric ratios in the equations of the redox reactions at the initial H_2O_2 concentrations of 0.0075 (system no. 1), 0.03 (system nos. 2 and 3), and 0.022 M (system nos. 4 and 5). The optimal concentration of the reductant in the redox systems corresponds to the electrochemical potential of 129–210 mV.

We studied by sorption methods (sorption of benzene and water vapors, as well as of iodine from a 0.2 wt % solution) how the redox systems affect the surface properties of the wool fiber [4]. The choice of specifically these substances was dictated by the fact that benzene is an inert sorbate for wool [5], characterizing the total volume of micro- and mesopores. Water causes wool to swell, and the sorption at a relative pressure P/P_0 = 0.3–0.4 is proportional to the amount of active (polar) centers in the free volume of the wool. At $P/P_0 \to 1$, like in the case of aqueous solutions in dyeing, swelling is accompanied by cleavage of intermolecular physical bonds, and the sorption value characterizes the total amount of polar groups in the amorphous domains of the polymer [6]. Tables 1 and 2 present the measured sorption of benzene and water vapor by the wool fiber dyed with Acid Bordeaux and Active Scarlet 4ZhT dyes at 80°C using the redox systems and by boiling of dyeing solutions without intensifiers.

The data in the tables show that, in the presence of the intensifiers, sorption of benzene vapor by the wool fiber dyed at 80°C with acid and active dyes is lower than that in the case of samples dyed with the same dyes by boiling the solution without intensifying ad-

Table 3. Sorption *a* of iodine by the wool fiber

Samples	*a*, %		
	undyed fiber	Acid Bordeaux	Active Scarlet 4ZhT
Untreated	14.00	11.56	12.03
Treated with indicated intensifier:			
1	29.82	6.92	7.24
2	19.26	8.78	9.13
3	18.63	9.65	10.01
4	16.45	10.43	10.34
5	16.38	10.88	10.6

ditives. This suggests strengthening of the surface of the wool fiber dyed in the presence of the redox systems, since the dye and the intensifier have filled a significant pore volume. The redox systems act, presumably, via generation of free radicals in the reaction of the reductant with hydrogen peroxide, which detach labile hydrogen atoms from the amine and carboxy groups of the polymer substrate and dye molecules. Recombination of the macroradicals on the wool fiber surface strongly increases its activity, and the dye sorption by the fiber tends to grow. This is supported by the results of our previous studies [3].

A decrease in the water sorption by the dyed wool fiber, compared to the undyed fiber, suggests that the dye and the intensifiers penetrate into the polymer bulk. They block polar groups, both those occurring in the free volume of the polymer and "released" by the wool fiber swelling. It is also possible that, in the presence of the redox systems, the hydrophobic scaly layer (exocuticle) of the wool fiber partly degrades (as it occurs under the action of a low-temperature plasma [7]), which leads to an increase in the size of the hydrophilically bound segments on the fiber. The diffusion barrier for dye molecules is mainly due to the hydrophobic nature of the exocuticle, resulting from the presence of a large number of disulfide bridges, and to the lipid material {isodipeptide bonds [ε-(γ-glutamyl)lysine]} whose degradation allows spreading of dye molecules and their retention on the fiber surface, which can also be responsible for the enhanced sorption and diffusion of the dyes into the fiber.

The possible degradation of the scaly layer is suggested by the value of iodine sorption from a 0.2% solution by the undyed wool fiber pretreated with the redox systems and dyed in the presence of these systems (Table 3).

The enhanced iodine sorption by the undyed wool fiber pretreated with the redox systems, compared to the untreated fiber, also confirms the influence of the intensifiers on the polymer, which causes its swelling. A decrease in the iodine sorption by the wool fiber dyed at 80°C in the presence of the redox systems, compared to the fiber treated by the conventional procedure (boiling of the dyeing solution without intensifiers), suggests that additional active centers in the wool fiber and new bonds are formed. The performance of the intensifiers tends to improve in the series H_2O_2–hexamethylenetetramine < H_2O_2–polyoxymethylene < H_2O_2–1,2,3-propanetriol < H_2O_2–ethylene glycol < H_2O_2–glucose. However, the strength properties of the wool fiber do not decrease, compared to that treated at the boiling temperature of the dyeing solution. This is due to the fact that the radicals yielded by the reaction between the reductant and oxidant favor formation of new cross-links both within the fiber and with the dye molecules, as confirmed by our previous studies [8, 9].

CONCLUSION

The redox systems studied, taken in the revealed optimal concentrations, intensify wool dyeing and allow the wool to be dyed with acid and active dyes at temperatures below the boiling temperature of the dyeing solution, with the fiber strength preserved.

REFERENCES

1. Pustyl'nik, Ya.I., *Katalog v mire oborudovaniya* (A Catalog in the World of Equipment), Moscow: Legprombiznes, 2002, no. 5, p. 28.
2. Petrova, O.V., Burinskaya, A.A., and Kotetskii, V.V., *Zh. Prikl. Khim.*, 2004, vol. 77, no. 5, pp. 866–867.

3. Petrova, O.V., Burinskaya, A.A., and Zhukova, A.N., *Izv. Vyssh. Uchebn. Zaved., Tekhnol. Teksil. Prom–sti*, Ivanovo, 2002, no. 6, pp. 57–60.
4. Fenelonov, V.B., *Vvedenie v fizicheskuyu khimiyu formirovaniya supramolekulyarnoi struktury adsorbentov i katalizatorov* (Introduction to Physical Chemistry of Formation of the Supramolecular Structure of Adsorbents and Catalysts), Novosibirsk, Sib. Otd. Ross. Akad. Nauk, 2002.
5. Grebennikov, S.F. and Kynin, A.T., *Zh. Prikl. Khim.*, 1982, vol. 55, no. 10, pp. 2299–2303.
6. Klyuev, L.E. and Grebennikov, S.F., *Zh. Prikl. Khim.*, 1996, vol. 70, no. 11, pp. 2053–2958.
7. Novoradovskaya, T.S. and Sadova, S.F., *Khimiya i khimicheskaya tekhnologiya shersti* (Chemistry and Chemical Technology of Wool), Moscow: Legprombytizdat, 1986.
8. Petrova, O.V., Petrova, L.N., and Burinskaya, A.A., *Izv. Vyssh. Uchebn. Zaved., Tekhnol. Tekstil. Prom–sti*, Ivanovo, 2003, no. 4, pp. 52–55.
9. RF Patent 2212665.

Russian Journal of Applied Chemistry, Vol. 78, No. 4, 2005, pp. 613–616. Translated from Zhurnal Prikladnoi Khimii, Vol. 78, No. 4, 2005, pp. 619–622.
Original Russian Text Copyright © 2005 by Nikolaeva, Osadchev.

MACROMOLECULAR CHEMISTRY AND POLYMERIC MATERIALS

Supramolecular Structure of the Polyamidine–Bisphenol System

M. N. Nikolaeva and A. Yu. Osadchev

Institute of Macromolecular Compounds, Russian Academy of Sciences, St. Petersburg, Russia

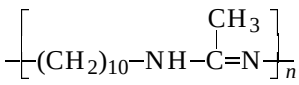
Received December 9, 2004

Abstract—Supramolecular organization of poly-1,10-decamethyleneacetamidine complexes with low-molecular-weight bisphenols was studied by the ^{1}H nuclear magnetic relaxation and UV spectroscopy.

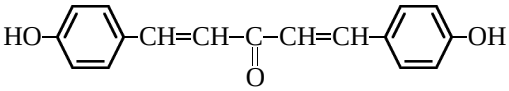
Noncovalent bonded networks are promising materials for development of new type polymer systems exhibiting nonlinear optical properties [1]. It is known that hydrogen-bonded polymer networks formed in the interaction of polymers of the polyamidine type with dyes of the bisphenol type can also exhibit nonlinear optical properties [2]. Therefore, a study of the supramolecular structure of these polymer systems is of particular interest. It is known [3, 4] that the hydrogen bond is formed between polyamidine molecules and also between polyamidine and bisphenol (**II**) molecules both through the peripheral hydroxo group of the dye and through the lateral hydroxo group of the quinoid form of the dye or keto group of its main form [5] (structural formulas **IIa** and **IIb**). However, the mobility and strength of interchain interactions of the polyamidine are mainly governed by the interactions of the peripheral hydroxy groups of bisphenols.

EXPERIMENTAL

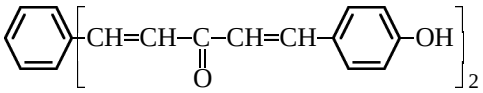
We studied the interaction of poly-1,10-decamethyleneacetamidine (hereinafter, polyamidine)



with the following low-molecular-weight additives: phenol (**I**), bis-(4-hydroxybenzylidene)acetone (**II**)



and 1,4-bis[5-(4-hydroxyphenyl)-3-oxopenta-1,4-dien-1-yl]benzene (**III**)



Synthesis and characteristics of poly-1,10-decamethyleneacetamidine were described in [6].

The degree of polymerization of the polyamidine n = 50; glass transition point 4°C; melting point approximately 60°C [3]. The melting points of phenol **I**, bisphenol **II**, and bisphenol **III** are 43, 220, and 169°C, respectively.

We used the NMR relaxation method, which allows estimation of the mobility of polymer chains with proton-containing groups. Introduction of new compounds into the polymer composition alters the mobility of macromolecules and, hence, the NMR relaxation time. The relaxation data offer information on how the interaction of polymer chains changes [7]. Here, we studied the spin–spin relaxation time of polyamidine and its mixtures with low-molecular-weight additives. Bisphenols dissolve in the polyamidine melt. Poly-1,10-decamethyleneacetamidine and its mixtures with bisphenols and phenol were heated to 180°C and allowed to stand at this temperature for 15 min; then the samples were cooled to the melting point of polyamidine and the measurements began.

The mole fraction of the bisphenols in the mixture with the polyamidine was varied from 0.05 to 0.35. At these concentrations, the bisphenols are compatible with the polymer.

The spin–spin relaxation times of protons T_2 for polyamidine and a mixture of polyamidine with addition of low-molecular-weight bisphenols were measured in melts on an RRP-1 relaxometer in the temperature range 70–140°C. Each measurement was made

1070-4272/05/7804-0613 © 2005 Pleiades Publishing, Inc.

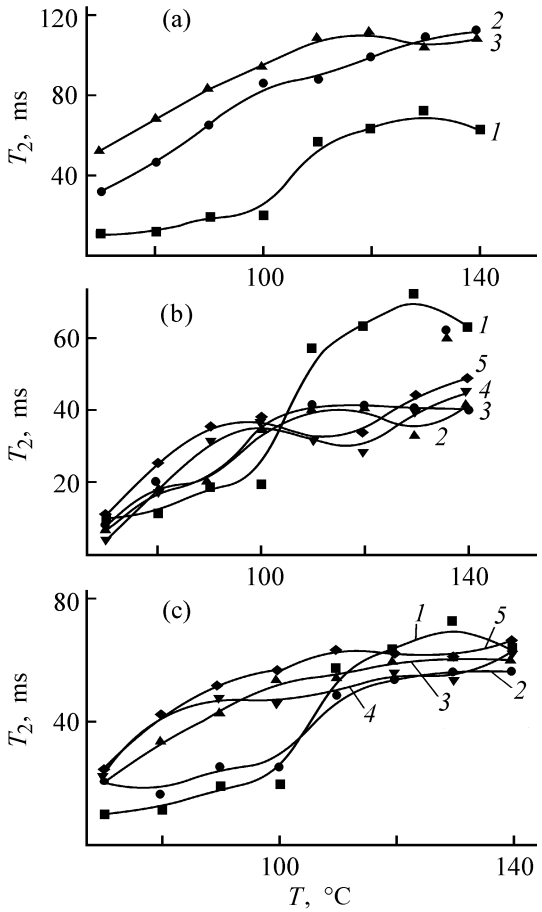


Fig. 1. Spin–spin relaxation time T_2 for mixtures of poly-1,10-decamethyleneacetamidine with (a) phenol **I**, (b) bisphenol **II**, and (c) bisphenol **III** vs. temperature T. (a) Mole fraction of phenol **I**: (*1*) 0, (*2*) 0.15, and (*3*) 0.3. (b) Mole fraction of bisphenol **II**: (*1*) 0, (*2*) 0.1, (*3*) 0.2, (*4*) 0.3, and (*5*) 0.35. (c) Mole fraction of bisphenol **III**: (*1*) 0, (*2*) 0.05, (*3*) 0.1, (*4*) 0.15, and (*5*) 0.2.

after a sample was kept at a given temperature for 15 min. The measurement error did not exceed 10%.

The spin–spin relaxation time T_2 was found from the decrease in magnetization after the action of a train of RF pulses $(\pi/2–\pi)_n$. The decrease in magnetization is usually described by one or two exponentials:

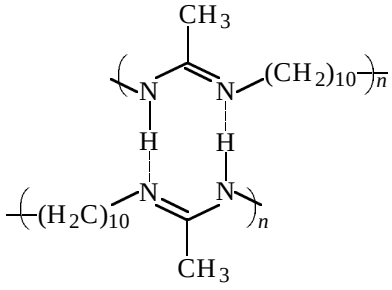
$$A(t) = A_1 \exp(-t/T_{2(1)}) + A_2 \exp(-t/T_{2(2)}),$$

where $A_{1,2}$ are the initial amplitudes of the NMR signal and $A(t)$ is the amplitude of the NMR signal at instant of time t.

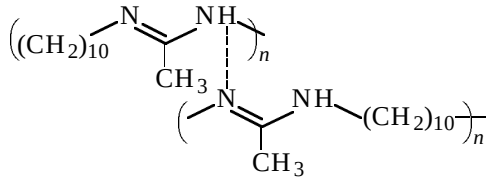
When the relaxation curve is described by one exponent, the medium is homogeneous in molecular mobility. Superposition of two exponents suggests the appearance of a component with a different molecular mobility [6].

The UV spectrum was obtained on an SF-2000-01 spectrophotometer.

It is well known [7] that polyamidine forms interchain hydrogen bonds in *E-syn* (**a**) and *E-anti* (**b**) conformations of the amidine groups:



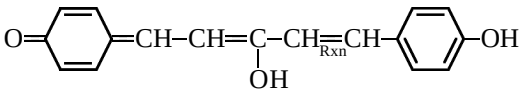
(**a**)



(**b**)

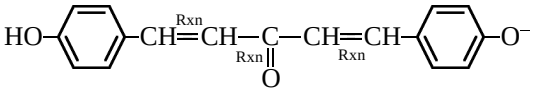
In the solid state, polyamidine has predominantly the *trans* conformation (**b**) [7].

For bisphenol **II**, the quinoid structure is



IIa

The deprotonated nonquinoid structure is



IIb

To estimate the influence of interchain hydrogen bonds in straight polyamidine on the spin–spin relaxation time, polyamidine was modified with phenol. Because of the presence of a hydroxy group, phenol can compete with interchain hydrogen bonds of polyamidine for formation of new hydrogen bonds. As a result of this interaction, comb-shaped polymer structures are formed. Addition of phenol to the melt decreases the viscosity of the polymer blend and the correlation time decreases. This is indicated by an increased relaxation time T_2 for polyamidine with addition of phenol as compared to straight polyamidine (Fig. 1a). Hence, a decrease in the spin–spin relaxation time for the straight polyamidine at a temperature above 130°C (Fig. 1a) suggests most likely a change

in the polyamidine conformation from *trans* to *cis*, since the prototropic tautomerism characteristic of the *cis* conformation [6] can accelerate the proton relaxation and, correspondingly, decrease T_2. The prototropic tautomerism is characterized by fast hoppings of proton through two bonds, and in the case of the polyamidine studied, from one nitrogen atom in the amidine group to another. On addition of phenol **I** (Fig. 1a) and bisphenols **II** and **III** to a polyamidine melt (Figs. 1b, 1c), a decrease in T_2 above 130°C was not observed or was insignificant, since it is likely that molecules of low-molecular-weight compounds, forming comb-shaped polymers and network structures, prevent mutual approach of the polyamidine polymer chains.

Rigid linear molecules of bisphenols in the polyamidine melt alter the strength of noncovalent interchain interactions in the polymer and thus the stability of the resulting network structure. These changes depend on the molecular weight of bisphenols. For example, with the molecular weight of bisphenol increasing from 274 (bisphenol **II**) to 422 (bisphenol **III**) (molecular weight of monomeric unit of polyamidine, 196), the relaxation time T_2 increases (Figs. 1b, 1c), since long molecules of bisphenol **III** can strongly separate the polymer chains. As shown previously [8], the relaxation time increases also upon addition of dihydroxydiphenyl, whose molecular weight is lower than that of bisphenol **II**. In this case, addition to the polymer of dihydroxydiphenyl, which has a lower acidity constant in comparison with polyimidine, so that only one group can be deprotonated, favors formation of comb-shaped structures rather than of a hydrogen-bonded polymer network.

The estimation of the thermodynamic compatibility of polyamidine with the bisphenols by the procedure described in [9] showed a high degree of compatibility of bisphenol **II** with polyamidine. The Hildebrand solubility parameter δ was calculated by the formula

$$\delta = \rho \Sigma F_i / M,$$

where ρ is the polymer density; M, molecular weight of the monomeric unit; and ΣF_i, sum of all molecular constants of attraction of chemical groups in the monomeric unit.

The calculated difference in solubility parameters δ for bisphenols **II** and **III** in polyamidine was approximately 7% (the solubility of bisphenol **II** is higher). The parameter of interaction, χ, of polyamidine with bisphenol **II** is 0.0027, which corresponds to the compatibility of the compounds at their ratio of 1 : 1 up to the degree of polymerization of approximately 750.

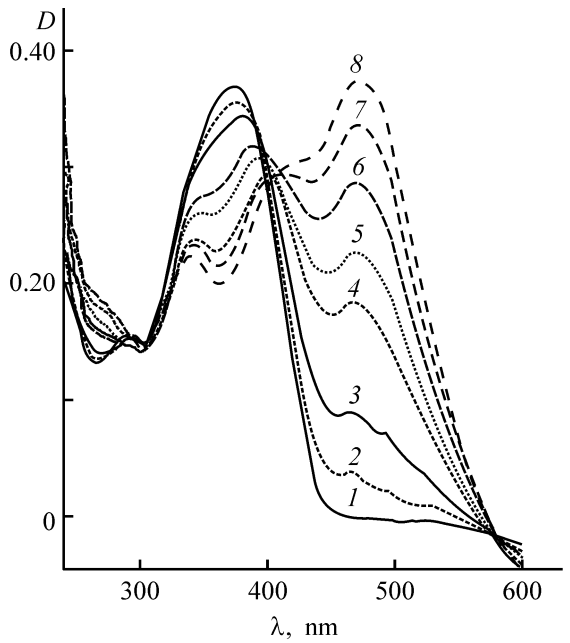


Fig. 2. Electronic spectra of bis(4-hydroxybenzylidene)-acetone in ethanol at various contents of poly-1,10-decamethyleneacetamidine. Concentration of bis(4-hydroxybenzylidene)acetone 1.97×10^{-7} M. (*D*) Optical density and (λ) wavelength. Molar ratio of hydroxy and amidine groups: (*1*) 1.9 : 0, (*2*) 1 : 2.6, (*3*) 1 : 5.2, (*4*) 1 : 7.8, (*5*) 1 : 10.4, (*6*) 1 : 13, (*7*) 1 : 15, and (*8*) 1 : 18.2.

Since the degree of polymerization of one of the components in the system is 50 and the second component is a monomer, the calculated value should differ from the true value. The presence of hydrogen bonds in the system complicated evaluation of the thermodynamic compatibility; therefore dynamic methods were to be used for its estimation. Here we used as such method NMR relaxation. Variation of the shape of the relaxation curve, with a second component appearing as the content of bisphenols in the polymer blend becomes higher suggests that phase segregation of the mixture occurs. This critical concentration (mole fraction) in polyamide is 0.3 for bisphenol **II**, and 0.2 for bisphenol **III**, i.e., the solubility of bisphenol **III** in the polymer is lower, which agrees with the calculation. The differences found can be caused by different molecular weights of the low-molecular-weight dyes, since they are closely related in their structure. The T_2 relaxation time was measured under the conditions of a thermodynamic compatibility of the components. Thus, an increase in the relaxation time T_2 upon addition of bisphenol **III** to polyamidine to a mole fraction of 0.20 is not caused by formation of the individual phase of dye, but is most likely due to an increase in the distance between the polymer chains.

The measured relaxation time is a quantity averaged over all the proton-containing groups in the sample, since the method is nonselective. Therefore, to elucidate the nature of interaction of bisphenols molecules with polyamidine, we used UV spectroscopy, with bisphenol **II** as an example. As shown previously [10], there are two absorption peaks at a 10^{-5} M concentration of dye **II** in an ethanol solution: the first with a maximum at 380 nm is due to absorption by free bisphenol **II**, and the second, to formation of a complex of polyamidine with the quinoid form of the dye. The spectra obtained in a dilute solution contain two peaks in the absorption band of bisphenol **II** (Fig. 2). One of these peaks is assigned to free dye molecules (330 nm), and the second, to monodeprotonated dye molecules of nonquinoid form bonded to the polymer (390 nm). This assignment of the resulting bands is quite reasonable, since the energy difference between these states (approximately 4.5 kcal mol^{-1}) is sufficiently large for a new intermolecular complex to be formed. In addition, it is known [7] that the content of the quinoid form of the dye in deuterated methanol at a sufficiently high concentration of the polyamidine is only 10%. Thus, the interaction of polyamidine and low-molecular-weight bisphenol in solution results in the formation of both comb-shaped polymers and network structures. Most likely, the similar structures should also exist in melts of polyamidine with bisphenols.

CONCLUSIONS

(1) The interaction of polyamidine and low-molecular-weight bisphenols in solutions and melts results in the formation of both comb-shaped polymers and network structures.

(2) The molecular sizes of rigid linear bisphenols are responsible for the differences in molecular mobility between the resulting network hydrogen-bonded polymer structures. The most stable hydrogen-bonded network of polyamidine is formed upon addition of bis-(4-hydroxybenzylidene)acetone to its melt. Addition of bisphenols with a higher {1,4-bis[5-(4- hydroxyphen-1-yl)-3-oxopenta-1,4-dienyl]benzene} or lower (dihydroxydiphenyl) molecular weight results in weakening of hydrogen bonds between the polymer chains and thus in lower stability of the resulting network structure.

ACKNOWLEDGMENTS

The authors are grateful to A.V. Ten'kovtsev (Institute of Macromolecular Compounds, Russian Academy of Sciences) for providing poly-1,10-decamethyleneacetamidine.

REFERENCES

1. Böhme, F., Häubler, L., Tenkovtsev, A.V., and Yakimansky, A.V., *Polym. Prep.*, 1999, vol. 40, no. 2, pp. 1140–1141.
2. Ten'kovtsev, A.V., Yakimanskii, A.V., Lukoshkin, V.N., *et al.*, *Fiz. Tverd. Tela*, 2000, vol. 42, no. 11, pp. 2099–2102.
3. Bohme, F., Klinger, C., Komber, H., *et al.*, *J. Polym. Sci., Part A: Polym. Chem.*, 1998, vol. 36, pp. 929–938.
4. Bohme, F., Kunert, C., Klinger, C., and Komber, H., *Macromol. Symp.*, 1998, vol. 128, pp. 183–185.
5. Bohme, F., Tenkovtsev, A.V., Haussler, L., and Komber, H., *Macromol. Symp.*, 1998, vol. 128, p. 102.
6. Kamber, H., Klinger, C., and Bohme, F., *Macromolecules*, 1997, vol. 30, pp. 8066–8068.
7. Chizhik, V.I., *Yadernaya magnitnaya relaksatsiya* (Nuclear Magnetic Relaxation), Leningrad: Leningr. Gos. Univ., 1991.
8. Bobashova, A.B., Dudkina, M.M., and Nikolaeva, M.N., *Zh. Prikl. Khim.*, 2002, vol. 75, no. 9, pp. 5533–5535.
9. *Polymer Blends*, Paul, D.R. and Newman, S., Eds., New York: Academic, 1978, vol. 1.
10. Tenkovtsev, A.V., Yakimansky, A.V., Dudkina, M.M., *et al.*, *Macromolecules*, 2001, vol. 34, no. 20, pp. 7100–7107.

Russian Journal of Applied Chemistry, Vol. 78, No. 4, 2005, pp. 623–627. Translated from Zhurnal Prikladnoi Khimii, Vol. 78, No. 4, 2005, pp. 629–633.
Original Russian Text Copyright © 2005 by Khimich, Tennikova.

MACROMOLECULAR CHEMISTRY AND POLYMERIC MATERIALS

Use of an Acrylic Dendron-containing Monomer in the Synthesis of a Macroporous Polymeric Material

G. N. Khimich and T. B. Tennikova

Institute of Macromolecular Compounds, Russian Academy of Sciences, St. Petersburg, Russia

Received July 26, 2004; in final form, December 2004

Abstract—A procedure was developed for preparing a monolithic macroporous material by photoinitiated copolymerization of glycidyl methacrylate, ethylene glycol dimethacrylate, and an acrylic comonomer containing a dendron with protected terminal amino groups. The macropore formation is provided by a blowing agent.

Dendrimers and superbranched polymers were synthesized in the late 1980s. Active efforts are made today to find applications for dendrimers. For this purpose, numerous modified dendrons and dendrimers have been synthesized. The use of dendritic monomers as building blocks, along with linear monomers, substantially expanded the possibilities of macromolecular design and led to macromolecules of unusual architecture [1]. Incorporation of bulky dendrons into the polymer structure is of both basic and applied interest. The high degree of functional substitution of such polymers opens virtually unlimited opportunities for further transformations, which can lead to novel materials. Modification of the surface of macromolecules, with the aim to impart to them pronounced lyophilic or lyophobic properties, is also possible.

Dendron-containing polymers of several types have been synthesized: monodendrons with a polymer chain in the focal point [2]; dumbbell-like hybrids containing a polymer chain between two monodendrons [3, 4]; and dendron-containing polymers prepared by polymerization of dendron-containing monomers [5, 6].

The interest in dendron-containing polymers is due to the possibility of obtaining new speciality materials and using them in biology, medicine, and medical diagnostics [7, 8]. In particular, dendrimers are used for detecting oligonucleotides in DNA diagnostics [9, 10], and polynucleotide dendrimers with fluorescent markers, in microchip DNA diagnostics [11]. Dendritic polyvalent ions can be used to bind proteins [12].

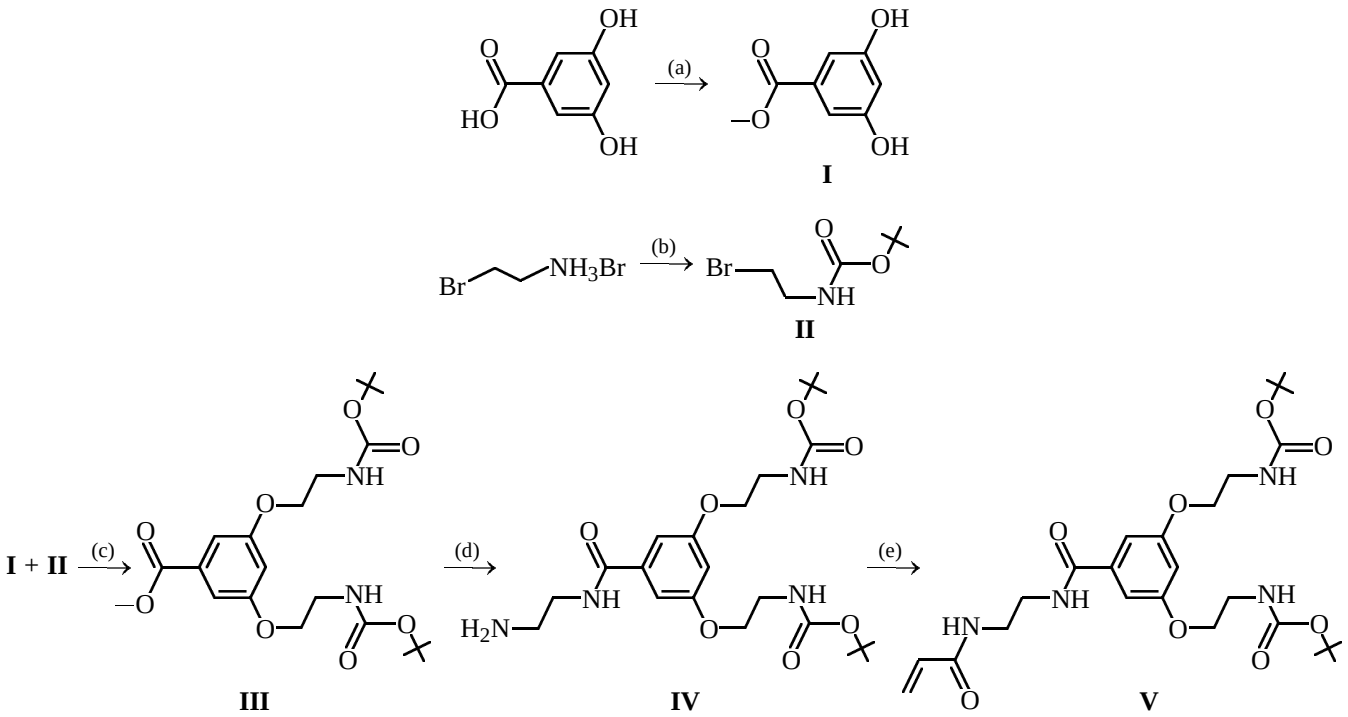
However, only very few studies have been concerned with the possibility of using dendrimers and dendron-containing monomers for preparing modified sorbents [13, 14]. In particular, aliphatic highly branched poly alcohols were used for preparing polymeric chiral stationary phases by postmodification of a macroporous copolymer [13].

The use of vinyl monomers linked through spacers to dendrons containing various terminal groups may be a promising route to adsorption-active macroporous polymers.

Monolithic sorbents, a new generation of stationary phases, are prepared by copolymerization of monomers containing active groups whose high reactivity provides for easy functionalization of the internal surface of the sorbent [15, 16]. Macroporous flow-through layers based on a monolithic copolymer of glycidyl methacrylate (GMA) and ethylene glycol dimethacrylate (EDMA) were developed in the late 1980s–early 1990s [17–21]. Dendron-containing monomers seem promising for preparing functionalized macroporous polymers, since addition of even a small amount of a dendron-containing monomer allows the content of functional groups in the sorbent to be sharply increased. By varying the level of generation and the chemical nature of substituents on the external surface of a dendron molecule, and also by varying the length of a spacer linking the dendron to the acryloyl group, it is possible to control the characteristics of the resulting sorbents.

In the first step, we prepared an acrylic derivative of a dendron containing Boc-protected amino groups by controllable multistep synthesis:

1070-4272/05/7804-0623 © 2005 Pleiades Publishing, Inc.



Steps: (a) MeOH, H^+; (b) Boc_2O; (c) $KHCO_3$, DMF; (d) $NH_2(CH_2)_2NH_2$; and (e) CH_2=CHCOCl, NEt_3.

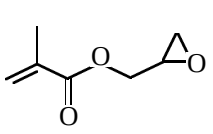
Methyl 3,5-di(2-*tert*-butoxycarbonylaminoethoxy)-benzoate **III** was prepared by alkylation of methyl 3,5-dihydroxybenzoate **I** with 2-(*tert*-butoxycarbonyl-amino)ethyl bromide **II**. It is known that compound **III** can be prepared in the presence of various catalysts [15, 16, 22, 23]. We performed alkylation in the presence of potassium carbonate, with DMF as solvent [15]. The reaction occurs at 40°C within 16 h; yield about 80%.

The starting compounds, methyl 3,5-dihydroxybenzoate **I** and 2-(*tert*-butoxycarbonylamino)ethyl bromide **II**, were prepared as follows: **I**, by esterification of 3,5-dihydroxybenzoic acid with methanol in acid solution [15]; **II**, by protection of the amino group of 2-bromoethylamine hydrobromide with di-*tert*-butyl pyrocarbonate [16].

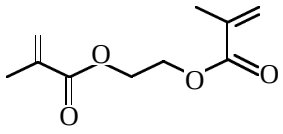
We prepared previously unknown dendron of the first generation **IV** with the amino group at the focal point and terminal Boc-amino groups. To do this, methyl 3,5-di(2-*tert*-butoxycarbonylaminoethoxy)benzoate was treated with excess ethylenediamine at room temperature. The subsequent acylation of the NH_2 group in **IV** with acryloyl chloride in anhydrous methylene chloride in the presence of triethylamine at low temperature yielded dendritic monomer **V**. The structures of the compounds prepared were confirmed by ^{1}H NMR spectroscopy.

The porosity of monolithic sorbents depends on the monomer ratio, blowing agents used, and polymerization conditions [18]. Therefore, the participation of a dendron-containing monomer in copolymerization can affect the pore structure of the resulting material and, in particular, cause its ordering.

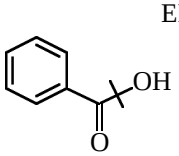
Monolithic macroporous polymers were prepared by radical photoinitiated copolymerization of EDMA, GMA, and acrylic comonomer **V** containing a dendron of the first generation. The reaction was performed in cyclohexanol (a solvent acting as blowing agent [19]) using 2,2-dimethyl-2-hydroxyacetophenone (Darocure 1173) as initiator of radical polymerization [24, 25]:



GMA



EDMA

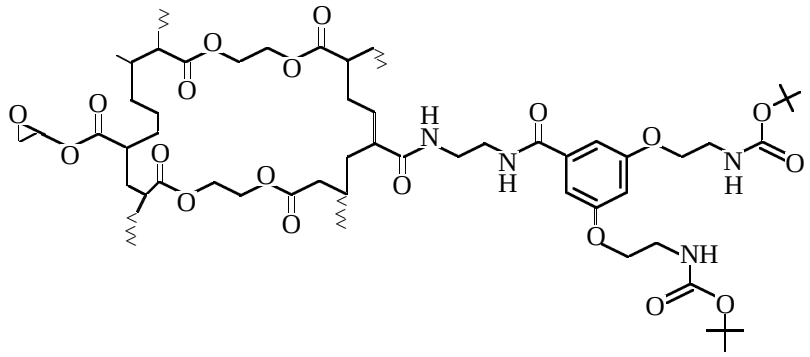


Darocure 1173

We prepared the copolymers containing 10 and 20 mol % **V**.

The IR spectrum confirmed the involvement of the acrylic dendron-containing monomer in the copolymerization. The IR spectrum of the hybrid material contains absorption bands of the N–H (3340 cm^{-1}) and CO (1690 cm^{-1}, amide I; 1520 cm^{-1}, amide II) bonds.

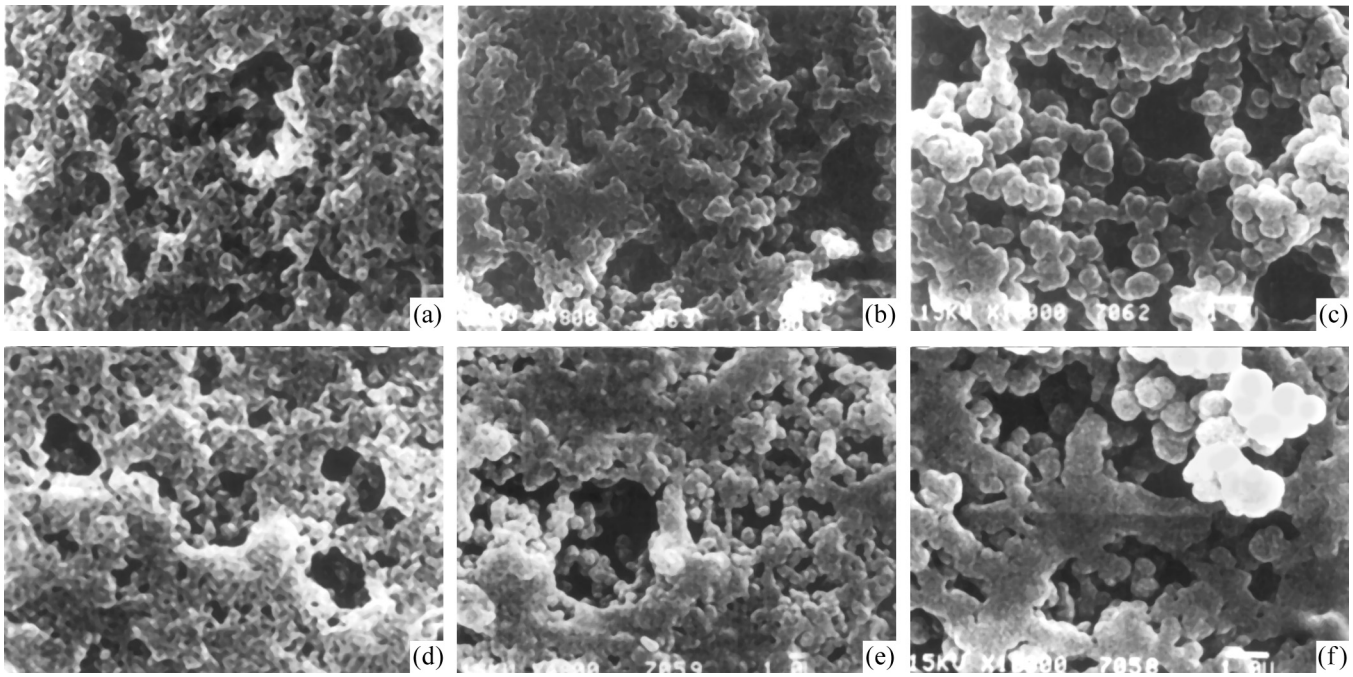
A fragment of the assumed chemical structure of the resulting macroporous polymer is shown below:



The pore structure of the materials obtained was examined by electron microscopy. The polymer layers have a homogeneous internal morphology of the pores. Figure shows plane and cross-sectional electron micrographs of the samples. The polymer containing 10 wt % dendritic monomer has a looser structure. The time required for formation of such monolythic macroporous materials is longer than that for synthesis of GMA–EDMA polymers.

EXPERIMENTAL

GMA was purchased from Fluka (Switzerland); 2,2-dimethyl-2-hydroxyacetophenone, from Merck–Schuchard (Germany); EDMA, cyclohexanol, 3,5-dihydroxybenzoic acid, (2-bromoethyl)amine hydrobromide, and di-*tert*-butyl pyrocarbonate, from Sigma–Aldrich (Germany); and acryloyl chloride, from Reakhim (Russia).



Electron micrographs of microporous monolithic layers prepared by ternary copolymerization of GMA, EDMA, and acrylic monomer. Acrylic monomer content, wt %: (a–c) 10 and (d–f) 20. (a, d) Planar and (b, c, e, f) cross-sectional. Magnification: (a, b, d, e) ×4800 and (c, f) ×10000.

The ^{1}H NMR spectra were recorded on a Bruker AC300 spectrometer (300 MHz), with deuterated acetone as solvent.

The structural homogeneity of the monoliths was examined by scanning electron microscopy using a JSM-35CF device with cathodic sputtering of a 50–100-Å gold layer.

The IR spectra were measured with a Bruker IFS 88 spectrophotometer (KBr pellets). UV irradiation was performed with a 125-W mercury lamp having a broad radiation spectrum and constant intensity.

Methyl 3,5-di(2-*tert*-butoxycarbonylaminoethoxy)benzoate III. A mixture of 2.82 g (0.017 mol) of methyl 3,5-dihydroxybenzoate, 10.0 g (0.045 mol) of 2-(*tert*-butoxycarbonylamino)ethyl bromide, 10.58 g (0.0765 mol) of potassium carbonate, and 25 ml of DMF was stirred at 80°C for 4 h and left overnight. The precipitate was filtered off, and the solution was concentrated. The product was purified by preparative adsorption column chromatography. Yield 5.08 g (81.5%); colorless crystalline substance. ^{1}H NMR spectrum (acetone-d_6), δ, ppm: 1.47 s [18H, 2C(C$\underline{H}_3$)$_3$], 3.47 m (4H, 2C$\underline{H}_2$NH), 3.86 s (3H, CO$_2$C$\underline{H}_3$), 4.10 m (4H, 2OC$\underline{H}_2$), 6.25 br.s (1H, N$\underline{H}$Boc), 6.76 t (1H, Ar–H), 7.13 d (2H, Ar–H).

Found, %: C 57.98, H 7.81, N 6.21.

$C_{22}H_{34}N_2O_8$.

Calculated, %: C 58.14, H 7.54, N 6.16.

Dendron IV. A solution of 1.5 g (3.28 mmol) of methyl 3,5-di(2-*tert*-butoxycarbonylaminoethoxy)benzoate **III** in 15 ml of methanol was slowly added dropwise to 20 ml of ethylenediamine. The mixture was kept in the dark at room temperature for 3 days, after which the solvent and excess ethylenediamine were distilled off in a vacuum. The residue was dissolved in chloroform, washed with water, dried with sodium sulfate, and concentrated. Yield 1.06 g (67%); oily substance. ^{1}H NMR spectrum (acetone-d_6), δ, ppm: 1.45 s [18H, 2C(C$\underline{H}_3$)$_3$], 3.42 (6H, 2C$\underline{H}_2$NH), 3.60 m (2H, 2CH$_2$NH$\underline{H}_2$), 4.04 t (4H, 2OC$\underline{H}_2$), 6.64 t (1H, Ar–H), 7.05 d (2H, Ar–H).

Found, %: C 57.51, H 8.03, N 11.47.

$C_{23}H_{38}N_4O_7$.

Calculated, %: C 57.24, H 7.94, N 11.61.

Acrylic monomer V. To a solution of 0.31 g (0.64 mmol) of dendron **IV** in 5 ml of anhydrous methylene chloride, we added 0.073 g (0.72 mmol) of triethylamine and then, slowly with cooling to 0°C, 0.06 ml (0.66 mmol) of acryloyl chloride. The mixture was stirred for 30 min at 0°C and then for 3 h at room temperature. The reaction course was monitored by TLC. After the reaction was complete, 5 ml of methylene chloride was added, and the mixture was washed with water, dried over sodium sulfate, and concentrated; 0.151 g (44%) of **V** was obtained. ^{1}H NMR spectrum (acetone-d_6), δ, ppm: 1.45 s [18H, 2C(C$\underline{H}_3$)$_3$], 3.46 t (4H, 2C$\underline{H}_2$NH), 3.60 m (2H, 2CH$_2$NH$\underline{H}_2$), 3.82 s (4H, NHC$\underline{H}_2$C$\underline{H}_2$NH), 4.07 t (4H, 2OC$\underline{H}_2$), 5.52 d.d (1H, C$\underline{H}_2$=CH), 5.88 d.d (1H, CH$_2$=C$\underline{H}$), 6.3 d.d (1H, C$\underline{H}_2$=CH), 6.62 t (1H, Ar–H), 7.05 d (2H, Ar–H).

Found, %: C 58.23, H 7.68, N 10.27.

$C_{26}H_{40}N_4O_8$.

Calculated, %: C 58.19, H 7.51, N 10.44.

The radical polymerization of GMA, EDMA, and acrylic monomer (molar ratios 5.4 : 4 : 0.6 and 4.8 : 4 : 1.2) in cyclohexane in the presence of 0.5% Darocure 1173 was performed under the photoinitiation conditions for 1 h. After the reaction was complete, the polymers obtained were washed with ethanol and dried at 100°C.

CONCLUSIONS

(1) A procedure was developed for preparing dendron of the first generation with the amino group at the focal point and terminal Boc-amino groups and an acrylic monomer derived from it.

(2) A monolithic material can be prepared by photoinitiated ternary copolymerization of glycidyl methacrylate, ethylene glycol dimethacrylate, and an acrylic dendron-containing monomer in the presence of Darocure in a cyclohexanol solution.

(3) Scanning electron microscopy shows that the layers obtained have a homogeneous internal morphologhy of pores.

REFERENCES

1. Zhang, A., Shu, L., Bo, Z., and Schlüter, A.D., *Macromol. Chem. Phys.*, 2003, vol. 204, no. 2, pp. 328–339.
2. Zhang, G.A., Vetter, S., and Schlüter, A.D., *Macromol. Chem. Phys.*, 2001, vol. 202, no. 17, pp. 3301–3315.
3. Toby, M., Chapman, T.M., Hillyer, G.L., *et al.*, *J. Am. Chem. Soc.*, 1994, vol. 116, no. 24, pp. 11 195–11 196.
4. Hest, J.C.M. van and Delnoye, D.A.P., *Science*, 1995, vol. 268, no. 5217, pp. 1592–1595.

5. Wetter, S., Koch, S., and Schlüter, A.D., *J. Polym. Sci. A, Polym. Chem.*, 2001, vol. 39, no. 11, pp. 1940–1954.
6. Shu, L., Gsosl, I., Rabe, J.P., and Schluter, A.D., *Macromol. Chem. Phys.*, 2002, vol. 203, no. 18, pp. 2540–2550.
7. Stiriba, S.-E., Frey, H., and Haag, R., *Angew. Chem.*, 2002, vol. 114, no. 8, pp. 1385–1390.
8. Ong, K.K., Jenkins, A.L., Cheng, R., *et al.*, *Anal. Chim. Acta*, 2001, vol. 444, no. 1, pp. 143–148.
9. Hudson, R.H.E. and Damha, M.J., *J. Am. Chem. Soc.*, 1993, vol. 115, no. 6, pp. 2119–2124.
10. Nilsen, T.W., Grayzel, J., and Prensky, W., *J. Theor. Biol.*, 1997, vol. 187, no. 2, pp. 273–284.
11. Stears, R.L., Getts, R.C., and Gullans, R.S., *Physiol. Genomics*, 2000, vol. 3, no. 1, pp. 93–99.
12. Thoma, G., Katopodis, A.G., Voelcker, N., *et al.*, *Angew. Chem.*, 2002, vol. 114, no. 17, pp. 3327–3330.
13. Liu, Y., Juneau, K.N., Frantisek, S., and Frechet, J.M.J., *Polym. Bull.*, 1998, vol. 41, no. 1, pp. 183–189.
14. Newkome, G.R., Yoo, K.S., Kabir, A., and Malik, A., *Tetrahedron Lett.*, 2001, vol. 42, no. 43, pp. 7537–7541.
15. Brouwer, A.J., Mulders, J.E., and Liskamp, R.M.J., *Eur. J. Org. Chem.*, 2001, no. 10, pp. 1903–1915.
16. Zeng, F., Zimmerman, S.C., Kolotuchin, S.V., *et al.*, *Tetrahedron*, 2002, vol. 58, no. 4, pp. 825–843.
17. US Patent 4889632.
18. Svec, F., Tennikova, T.B., and Deyl, Z., in *Monolithic Materials: Preparation, Properties and Applications*, Amsterdam: Elsevier, 2003, vol. 67, p. 457.
19. Štrancar, A., Barut, M., Podgornik, A., *et al.*, *LC–GC Int.*, 1998, vol. 11, no. 11, pp. 660–664.
20. Tennikova, T.B. and Freitag, R., *J. High Resol. Chromatogr.*, 2000, vol. 23, no. 1, pp. 27–38.
21. Giovannini, R., Freitag, R., and Tennikova, T., *Anal. Chem.*, 1998, vol. 70, no. 16, pp. 3348–3357.
22. Zhang, J., Drugeon, G., and L'hermite, N., *Tetrahedron Lett.*, 2001, vol. 42, no. 21, pp. 3599–3601.
23. Mulders, S.J.E., Brouwer, A.J., Meer, P.G.J. van der, and Liskamp, R.M.J., *Tetrahedron Lett.*, 1997, vol. 38, no. 4, pp. 631–634.
24. Lecamp, L., Youssef, B., Bunel, C., and Lebandy, P., *Polymer*, 1999, vol. 40, no. 6, pp. 1403–1409.
25. Xu Dong-Mei, Zhang Ke-Da, and Zhu Xiu-Lin, *J. Appl. Polym. Sci.*, 2004, vol. 92, no. 2, pp. 1018–1022.

Russian Journal of Applied Chemistry, Vol. 78, No. 4, 2005, pp. 628–632. Translated from Zhurnal Prikladnoi Khimii, Vol. 78, No. 4, 2005, pp. 634–638.
Original Russian Text Copyright © 2005 by Vilenskii, Gritsai, Shtompel', Goncharenko.

MACROMOLECULAR CHEMISTRY AND POLYMERIC MATERIALS

Epoxy Composites Modified with Polyvinylidene Fluoride

V. A. Vilenskii, S. I. Gritsai, V. I. Shtompel', and L. A. Goncharenko

Institute of Macromolecular Chemistry, Ukrainian National Academy of Sciences, Kiev, Ukraine

Received July 12, 2004; in final form, February 2005

Abstract—Microheterogeneous structure and morphology of epoxy-based polymeric composites modified with polyvinylidene fluoride were studied.

Epoxy resins (ERs) are widely used as adhesives, structural materials, and coatings [1–8]. To accomplish the desired performance characteristics, both ER blends [8–11] and epoxy hardener mixtures [12–15] are used, with low- and high-molecular-weight organic and inorganic compounds as fillers [1, 3, 16–18]. Because of the broadening application area of such polymeric composites, more stringent requirements are imposed on their hardening conditions, physicochemical and mechanical properties, and, first of all, environmental safety. The latter is of particular importance for coatings and, specifically, for self-leveling floor finishes [16–20], which are used in immediate contact with humans.

Here we report on a study of composites based on blends of ERs of the epoxy-diphenylolpropane and aliphatic nature, which can be used as self-leveling floor finishes [18]. We studied the microheterogeneous structure and morphology of cured polymeric composites (PCs) modified with polyvinylidene fluoride (PVDF).

EXPERIMENTAL

In the study, we examined the epoxy resin blend composed of ED-20 (100 wt parts), DEG-1 (20 wt parts), and Oksilin (7 wt parts) (Ufakhimprom, Russia). Polyethylenepolyamine (PEPA) (RIAP, Ukraine) was used as an epoxy hardener (ER : PEPA = 1.0 : 0.17). The epoxy resin and hardener were used without further purification. Polyvinylidene fluoride (Aldrich) was added to the epoxy resin as a 10% solution in DMF, and the resulting mixture was stirred for 1 h. Then PEPA was added dropwise and the mixture was stirred for additional 30 min. The mixture was cast onto a Teflon support and cured for 72 h. The PVDF concentration in the system varied from 0.1 to 10 wt % (see table).

The microheterogeneous structure of the initial and PVDF-modified composites as $1.0 \times 0.50 \times 0.02$ cm plates was studied by small-angle X-ray scattering, using a KRM-1 camera with a collimating system meeting the condition of the infinite height of the primary beam [21, 22]. The measurements were carried out with monochromated Cu_{K_α} radiation (Ni foil filter), using a Kratky slit collimator [21]. The diffraction pattern was recorded with a scintillation detector in the automatic step-by-step scan mode. The measured scattering intensity was corrected for the primary beam attenuation factor for the test sample, which was followed by subtraction of the background scattering of the collimating system. Finally, the intensity thus

Composition of polymeric composites and heterogeneity of their structure*

Sample no.	Composition	Coherence length l_c, nm
1	Initial composite (IC)	3.0
2	IC + PVDF, wt %:	3.1
3	0.2	3.4
4	0.5	3.1
5	0.75	3.5
6	1.0	3.2
7	1.5	3.7
8	1.75	3.4
9	2.0	3.7
10	4.0	4.7
11	6.0	5.1
12	8.0	5.5
13	10.0	6.1

* Heterogeneity range l_g, nm: 12.6 (sample no. 10), 13.2 (no. 11), 13.7 (no. 12), and 14.2 (no. 13).

1070-4272/05/7804-0628 © 2005 Pleiades Publishing, Inc.

obtained was normalized to the scattering volume. The scattering profiles were then reduced to the point collimation by the Schmidt method [23, 24].

The surface morphology of the samples was studied on an REMMA-102 scanning electron microscope (X-ray electron probe microanalyzer) in the secondary electron emission mode (accelerating potential 15 kV; normal excitation of the condenser; horizontal arrangement of the sample; magnification in the range from 1000 to 10 000). The SEM micrographs were recorded in the format 512 × 512 pixels (512 scans per point), which provided optimal signal filtering and high-quality imaging.

Sample preparation for a morphological examination included pouring-over with a binder so that the sample face could be seen at the base of the washer thus obtained. Then the washer base was ground with emery-papers of progressively decreasing grain size and polished on opal glass and silk. The resulting "disturbed" surface layer of the composite was converted into the vapor phase by plasma ablation in a JEOL JFC-1100 device operating at 1.2 keV. The ablation products were removed from the surface during 2 h. The samples were etched for 1 h in a plasma with a low concentration of high-energy particles.

The sample surface was coated with a 30–50-nm gold layer (99.99 wt % purity) by cathode sputtering to enhance the contrast of the surface and also to remove the surface charge.

Figure 1 shows that the small-angle X-ray scattering intensity grows with increasing PVDF concentration in the composites, which is probably due to transition from the network structure of the polymer to the microheterogeneous structure of the composite. In this case, the nature of the polymeric composite changes from a strongly cross-linked polymer to a semi-interpenetrating polymer network (s-IPN), in which fragments of the PVDF macrochains penetrate into the network formed by the epoxy resins.

Generally, the microheterogeneity of the structure of the composites under study can be assessed by comparison of the scattering invariants Q (arb. units) of the initial and PVDF-modified composites, using Eq. (1) [25].

$$Q = \int_0^\infty q^2 I(q)\,\mathrm{d}q, \qquad (1)$$

where $q = (4\pi/\lambda)\sin\theta$ is the scattering vector (nm^{-1}); λ, X-ray wavelength (nm); 2θ, scattering angle (deg); and I, scattering intensity in the case of a point collimation of the primary beam (arb. units).

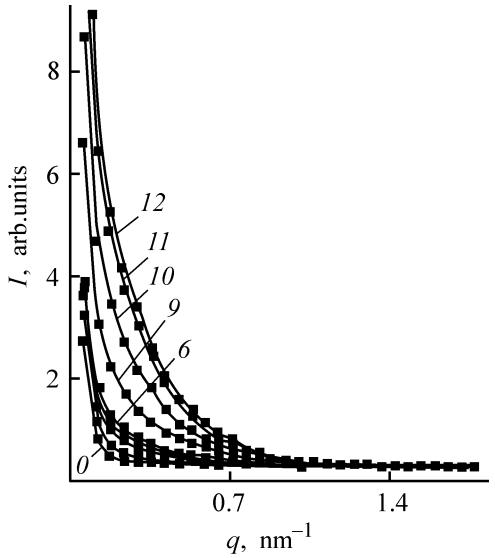


Fig. 1. Small-angle X-ray diffraction patterns of polymeric composites. (I) Scattering intensity and (q) scattering vector. *The numerals at the curves* correspond to the sample numbers in the table.

It is known that the parameter Q characterizes the scattering capacity of an object, being directly dependent on the mean-square fluctuation of the electron density $\overline{\Delta\rho^2}$, $(\mathrm{e\,nm^{-3}})^2$, in the bulk of two-phase systems, such as s-IPN.

$$Q = 2\pi^2 I_e V \overline{\Delta\rho^2}, \qquad (2)$$

where V is the scattering volume of the sample (nm^3); I_e, X-ray scattering intensity on single electron (nm^2); and $\overline{\Delta\rho}$, the parameter determined by Eq. (3).

$$\overline{\Delta\rho^2} = \varphi_1\varphi_2(\rho_1 - \rho_2)^2, \qquad (3)$$

where φ_i and ρ_i are the volume fraction ($\varphi_1 \le 1$) and electron density ($\mathrm{e\,nm^{-3}}$) of the ith phase [8].

The calculated concentration dependences of Q_i are shown in Fig. 2. The heterogeneity of the polymeric composites increases starting from the PVDF concentration in the matrix of 0.5 wt % and reaches the first maximum (Q_I) at 1.5 wt %. A decrease in the heterogeneity of the composites containing 1.75–2 wt % PVDF can be attributed to the onset of microphase segregation between the network and the foreign linear polymer.

At the same time, the lack of the interference peak in the scattering profiles of s-IPNs characterized by clearly pronounced steady rise in the heterogeneity for the composites containing 2.5–10 wt % PVDF sug-

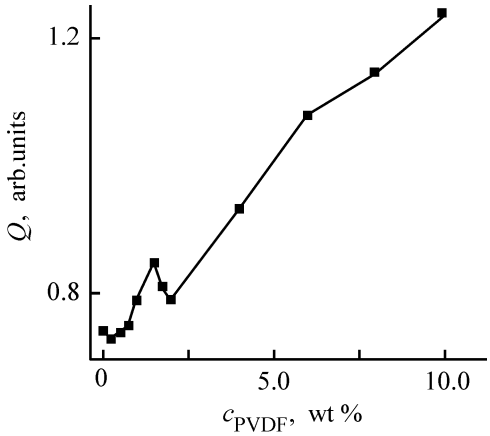


Fig. 2. Concentration dependence of the heterogeneity of the polymeric composites expressed via parameter *Q*. (c_{PVDF}) PVDF concentration in the composite.

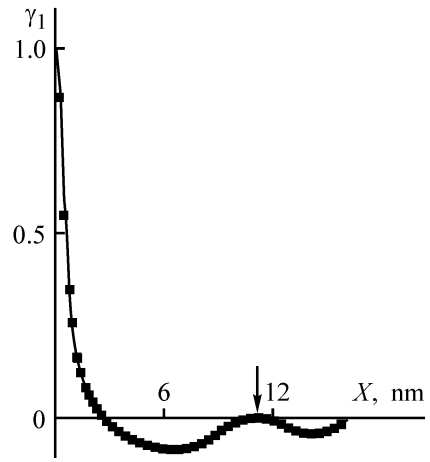


Fig. 3. One-dimensional correlation function γ_1 of the sample with 10 wt % PVDF. (*X*) Projection of the vector *r* in the real space onto the *x* axis.

gests a topological distribution of microheterogeneous domains in the bulk of the composites. Since PVDF is a partially crystalline polymer, and it can crystallize under microphase segregation conditions to form an individual phase, the lack of the diffuse peak in the scattering curve of the polymeric composites was somewhat surprising. However, this result can be accounted for by the plane anisotropy of PVDF crystallites. In this case, the 2*D* order controlled by the crystallization conditions in the network structure could give no peak in the small-angle scattering curve.

We analyzed the structure of the s-IPN with the optimally high level of heterogeneity (in accordance with Fig. 2 and table, this is sample no. 13 containing 10 wt % PVDF) using the one-dimensional correlation function for the electron density γ_1 [26]:

$$\gamma_1(x) = \frac{\int_0^\infty q^2 I(q)\cos(Xq)\,dq}{\int_0^\infty q^2 I(q)\,dq}, \quad (4)$$

where *X* is the projection of the vector *r* in the real space onto the *x* axis.

Figure 3 shows the one-dimensional correlation function of sample no. 13 (10 wt % PVDF). The lack of the positive maximum suggests no 1*D* order in arrangement of the domains of heterogeneity. However, the occurrence of the maximum with a peak value lying on the *x* axis at $X \sim 12$ (marked with an arrow in Fig. 3) shows that the most probable one-dimensional distance d_{1D} between the microdomains of heterogeneity amounts to 12 nm.

The size of the heterogeneity microdomains were estimated using two different approaches. First of all we determined the coherence length l_c (nm) from Eq. (5) [25]:

$$l_c = \frac{1}{\pi}\frac{\int_0^\infty \tilde{I}(q)\,dq}{\int_0^\infty q\tilde{I}(q)\,dq}, \quad (5)$$

where $\tilde{I}(q)$ is the intensity of primary beam scattering (arb. u.) for the slit collimation.

It follows from the table that l_c increases in parallel with the PVDF concentration in the composite.

The second parameter characterizing the microheterogeneous structure of the polymeric composites is the heterogeneity range l_g (nm), which is directly related to the mean diameter of the heterogeneity microdomains with different electron densities via Eq. (6) [25, 27]:

$$l_g = \varphi_2\langle l_1\rangle = \varphi_1\langle l_2\rangle, \quad (6)$$

where φ_1, φ_2 and l_1, l_2 (nm) are the volume fractions and sizes of the heterogeneity microdomains of the first and second kinds.

The parameter l_g was estimated by the method described in [27]. It also follows from the estimated l_g for s-IPNs containing 4–10 wt % PVDF (see table) that the size of the heterogeneous microdomains with increasing fraction of the linear polymer.

It is well known that curing of polyepoxides is front-propagating after the system reaches the gelation point [28]. It is clear that, after a time, the abruptly increasing viscosity of the 3*D* network starts to decel-

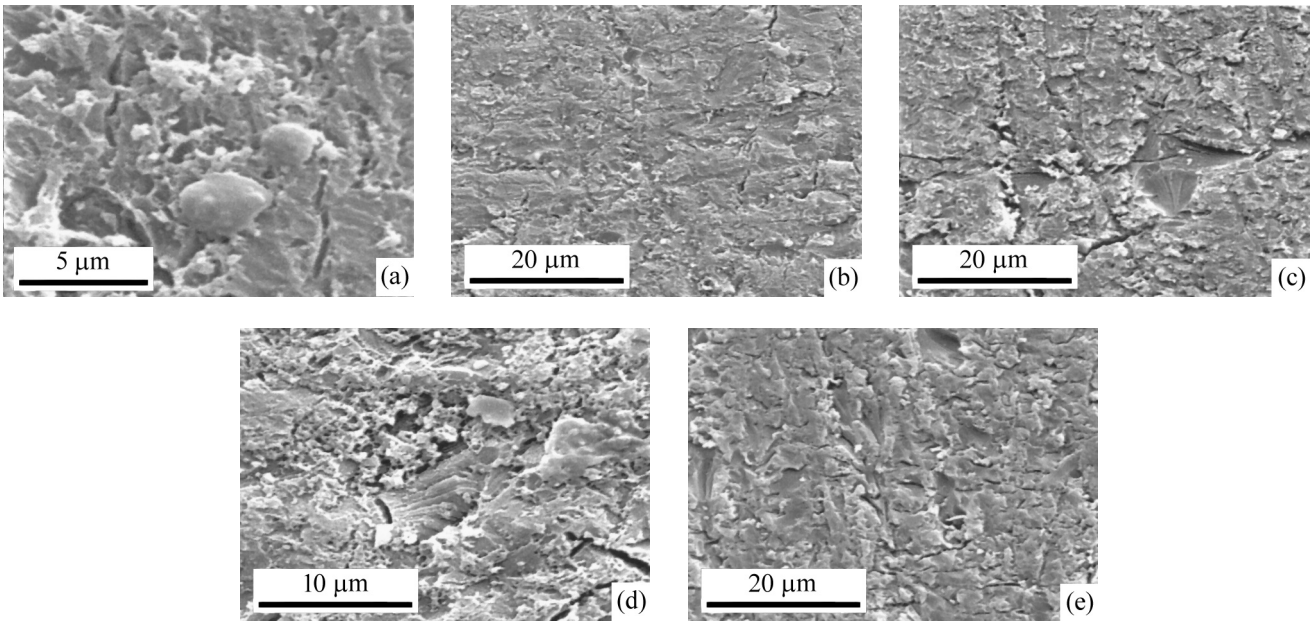


Fig. 4. Micrographs of polymeric composites. PVDF concentration (wt %): (a) 0, (b) 1.5, (c) 2, (d) 6, and (e) 8.

erate the polyaddition reaction between the diamines and polyepoxides, and, unless additional measures are taken, the reaction stops at a conversion level of about 69 mol %. Here two points should be taken into account. First, the high reactivity of the epoxy groups and aliphatic amines can warm the reaction mass up to 200°C in the initial stage [28], which will result in build up of stresses in the cured composite and in microcracking. This is illustrated by Fig. 4a, in which microcracks are clearly seen on the surface of the initial composite. Analysis of the morphology of the composites shows that its structure is inhomogeneous. This conclusion is supported by the second fact manifested in the course of propagation of the gelation front: the front of addition polymerization by passes some regions, which remain in the sol state, i.e., uncured. The size of the sol domains is about 4 μm (Fig. 4a).

Figure 4b shows the surface morphology of sample no. 5. It is seen that the structure of this composite includes not only the epoxy matrix, but also ordered regions and dips of various sizes and shapes. The ordered domains can be identified as PVDF inclusions. The dips most likely correspond to uncured zones of the epoxy resin, which is consistent with the conclusions drawn in [29] that, in the first 48–72 h, the conversion of epoxy resins based on Bisphenol A diglycidyl ether with aliphatic diamines does not exceed 60–70% recalculated to the amount of reactive group. It may be also suggested that some of the elements of the morphological profile are composed of the PVDF phase, which is confirmed by the X-ray diffraction data. This conclusion is also supported by the fact that the constituents of the composite, epoxy resin and PVDF, are strongly different in their molecular weight (MW 400 – 600 and 7×10^4, respectively), and, being thermodynamically incompatible [30], tend to undergo microphase seqregation, which is illustrated by Fig. 4c (2 wt % PVDF).

The microdomains of the PVDF phase in the 3*D* network of the epoxy resin are clearly seen in the micrograph of the sample with 6 wt % PVDF (Fig. 4d). In this case, the morphological elements have an individual structure in the form of divergent lamellas (× 3000). At a larger magnification (× 6000), it is seen that the inclusion is formed by scalene trapezia delimited from one side by the boundary (crack) between incompatible microphases.

Comparison of the micrographs presented in Figs. 4e and 4b shows how an increase in the PVDF concentration in the epoxy matrix to 8 wt % fundamentally changes the composite surface. First of all, it is seen that, with increasing PVDF concentration, its microphases are fused and run to the surface, forming layers and healing the microcracks in the polymer matrix.

CONCLUSIONS

(1) A steady increase in the polyvinylidene fluoride concentration in the epoxy matrix from 0.1 to 10 wt % is accompanied by an abrupt change in

the degree of heterogeneity in the concentration range 1–1.75 wt %, which is probably due to incompatibility of the 3*D* chemical network with the linear high-molecular-weight polymer.

(2) Further increase in the polyvinylidene fluoride fraction in the matrix is accompanied by a rise in the heterogeneity of the polymeric composite material as a result of transition from the network polymer, having a typical homogeneous structure, to a polymeric composite with clearly pronounced microheterogeneity.

(3) Fragments of the polyvinylidene fluoride chains displaced by the network elements can fill up cracks in the epoxy matrix, thus forming a microphase. In this case, a distortion of the network structure will result not in degradation, but in healing of its defects, as demonstrated by the morphological data.

REFERENCES

1. Rennenberg, H. and Schneider, W., *Plastics for Chemical Engineering: Materials, Construction, Welding Technologies, Quality Control*, Dusseldorf: Schweiben und Verwandte Verfahren, 1998.
2. Wegmann, A. and Vogel, T., *Surf. Coat. Int.*, 1998, vol. 81, no. 7, pp. 342–347.
3. Kunze, S., Lesch, G., Klett, H., and Oechsner, W., *Farbe Lack*, 1997, vol. 103, no. 12, pp. 36–38.
4. Amin, K.G., Patel, K.J., and Patel, R.G., *Iran Polym. J.*, 1997, vol. 6, no. 4, pp. 227–233.
5. Maltese, P., *Mater. Plast. Elastom.*, 1993, vol. 1, no. 2, pp. 34–50.
6. Ghaemy, M. and Riahi, M.H., *Iran Polym. J.*, 1996, vol. 5, no. 2, pp. 119–126.
7. *Farbe Lack*, 1996, vol. 102, no. 5, p. 22.
8. Ishida, H. and Zimmerman, D.A., *Polym. Compos.*, 1994, vol. 15, no. 2, pp. 93–100.
9. Anand, M. and Srivatsaava, A.K., *Macromol. Rep., Ser. A*, 1993, vol. 30, no. 5, pp. 435–446.
10. Thakkar, J.R., *Macromol. Rep., Ser. A*, 1995, vol. 32, no. 8, pp. 1171–1179.
11. Sue, H.-J., Earls, J.D., Hefner, R.E., Jr., *et al.*, *Polymer*, 1998, vol. 39, no. 20, pp. 4707–4714.
12. Gimenez, V., Mantecon, A., Ronda, J.C., and Cadiz, V., *J. Appl. Polym. Sci.*, 1997, vol. 65, no. 8, pp. 1643–1651.
13. Miasik, G.M., *Surf. Coat. Int.*, 1996, vol. 79, no. 6, pp. 258–267.
14. Matynia, T., Ksiezopolski, J., and Pawlowska, E., *J. Appl. Polym. Sci.*, 1998, vol. 68, no. 9, pp. 1423–1429.
15. Gutierrez, C., Martinez-Ruvalcaba, A., Michel-Valdivia, E., and Gonzalez-Romero, V.M., *Ann. Tech. Conf. Soc. Plast. Eng.*, 1996, pp. 900–904.
16. Pethrick, R.A., *Plast. Rubber Compos. Process. Appl.*, 1995, vol. 24, no. 4, pp. 167–173.
17. Hale, J.M., Gibson, A.G., and Speake, S.D., *J. Compos. Mater.*, 1998, vol. 32, no. 10, pp. 969–986.
18. Rosenqvist, R. and Frederix, A., *Surf. Coat. Int.*, 1998, vol. 81, no. 1, pp. 26–29.
19. UA Patent no. 33017A.
20. UA Patent Appl. no. 003054102.
21. Kratky, O., Pilz, I., and Schmitz, P.J., *J. Colloid Interface Sci.*, 1966, vol. 21, no. 1, pp. 24–34.
22. Lipatov, Yu.S., Shilov, V.V., Gomza, Yu.P., and Kruglyak, N.E., *Rentgenograficheskie metody issledovaniya polymerov* (X-ray Diffraction Methods for Studying Polymers), Kiev: Naukova Dumka, 1982.
23. Schmidt, P.W. and Hight, R.J., *Appl. Crystallogr.*, 1960, vol. 13, no. 4, pp. 480–483.
24. Chu, B. and Tan Greti, D.M., *Appl. Crystallogr.*, 1965, vol. 18, no. 5, pp. 1083–1084.
25. Guinier, A. and Fourner, G., *Small-Angle Scattering of X-rays*, New York: Wiley, 1955.
26. Vonk, C.G., *J. Appl. Crystallogr.*, 1973, vol. 6, no. 1, p. 81.
27. Perret, R. and Ruland, W., *Kolloid Z.–Z. Polym.*, 1971, vol. 247, pp. 835–843.
28. Chernin, I.Z., Smekhov, F.M., and Zherdev, Yu.V., *Epoksidnye polimery i kompozitsii* (Epoxy Polymers and Composites), Moscow: Khimiya, 1982.
29. Zaitsev, Yu.S., Kochergin, Yu.S., Pakter, M.K., and Kucher, R.V., *Epoksidnye oligomery i kleevye kompozitsii* (Epoxy Oligomers and Adhesive Composites), Kiev: Naukova Dumka, 1990.
30. Weber, T. and Helfand, E., *Macromolecules*, 1976, vol. 9, no. 2, pp. 311–316.

Russian Journal of Applied Chemistry, Vol. 78, No. 4, 2005, pp. 633–635. Translated from Zhurnal Prikladnoi Khimii, Vol. 78, No. 4, 2005, pp. 639–641.
Original Russian Text Copyright © 2005 by Imankulova, Kondrashev, Val'tsifer.

MACROMOLECULAR CHEMISTRY AND POLYMERIC MATERIALS

Curing of Epoxy-containing Oligomers with Oxidized Carbon Black

S. A. Imankulova, N. B. Kondrashev, and V. A. Val'tsifer

Institute of Technical Chemistry, Ural Division, Russian Academy of Sciences, Perm, Russia

Received October 5, 2004; in final form, February 2005

Abstract—The physical properties of polymeric composites based on polydieneurethane-diepoxide and filled with particles of carbon black of various degrees of oxidation were studied.

Modern composite materials are not only multiphase in the polymeric composition but also contain mineral fillers, which determines nonuniformity of the polymer–inorganic phase boundary. Thus, filled composites can be regarded as a micrononuniform and microheterophase system.

The activity of a filler depends on its specific surface area, morphology, and chemical and energy characteristics of the surface; the interphase interaction with the polymer is determined by the specific surface area.

Since carbon black (CB) is widely used as highly active filler of polymeric materials [1–3], it seemed advisable to study the mechanical properties of the polymer as influenced by the acidity and content of oxygen-containing groups on the CB surface. Certain parts of the CB particle surface can be occupied by various functional groups appearing in the course of oxidation of the filler surface by atmospheric oxygen; just these parts can form strong chemical bonds with polymers. The chemical principles of formation of highly filled materials are poorly understood yet.

The goal of this study was to prepare epoxy-containing polymeric composites cured with surface functional groups of the filler (e.g., carbon black). This is a particular case of such a fundamental problem as study of processes in complex dispersion systems with a high content of the solid phase.

EXPERIMENTAL

The CB samples with similar particle-size distributions, but different degrees of the surface oxidation were prepared from low-active furnace carbon black (P-803 brand) prepared by thermal oxidative decomposition of liquid hydrocarbon raw materials. The CB samples were supplied by the Temp Scientific and Technical Center (Yaroslavl, Russia).

By varying the time of thermal oxidation of the initial CB by atmospheric oxygen at 500°C, we prepared samples with varied oxygen content (CB-1)–(CB-6).

The procedure for determining the content of oxygen-containing groups on the CB surface was based on the difference in their chemical activity. The total content of surface oxygen-containing acidic groups was determined by potentiometric titration with a strong (hydrochloric) acid of a CB suspension with an aqueous NaOH solution, and the content of carboxy groups, by titration of the CB suspension with an aqueous Na_2CO_3 solution, using an EV-74 pH-meter.

The mechanical tests were carried out with oligodiene-urethane–diepoxide (M 5000), which was mixed with a CB filler (30 wt %) and stirred for 30 min at 50°C under reduced pressure. The composition was cured for 10 days at 80°C, with no additional curing agents used.

The mechanical properties (elongation at break and strength) of the filled CB composites based on polydiene-urethane–diepoxide were determined on an R-5 2099 tensile-testing machine at various temperatures, with the measurement error of 5% according to GOST (State Standard) 270–75.

The degree of oxidation of the CB particle surface stongly affects the surface (sorption) properties and the structuring power of the CB [4]. The strength of the CB particles depends both on the micromosaic structure of the oxidized particle surface and on the

1070-4272/05/7804-0633 © 2005 Pleiades Publishing, Inc.

Degree of CB surface oxidation as influenced by annealing time τ

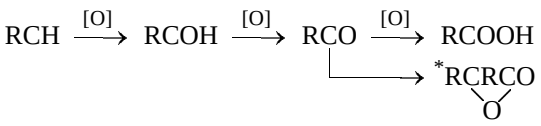
Sample	τ, h	OH, COOH,* %
CB-1	0	0
CB-2	1	0.084
CB-3	2	0.320
CB-4	3	0.430
CB-5	4	0.554
CB-6	5	0.880

* Total acidity.

content of the initial aggregates formed by unchanged CB particles [4].

The surface layer of a CB particle can contain various chemical groups affecting its properties [5]. The chemical properties are determined by functional groups containing oxygen, hydrogen, and sulfur. The chemical composition of the surface is often characterized by the total content of oxygen and some individual oxygen-containing groups. Oxygen on the CB surface can occur in carboxy, phenol, quinoid, and lactone groups.

As can be seen from the table, the moderate CB oxidation increases the content of all the oxygen-containing groups. Further, more profound oxidation first increases the content of carboxy groups to 0.24% (CB-6), but then causes breakdown to CO and CO_2, which agrees with the following scheme of CB oxidation [6]



* Hydrocarbon radical from another molecule.

Our experimental data show that the strength of epoxy composites cured with CB depends on both the total acidity and the content of carboxy groups on the CB particle surface.

The dependences of the strength and strain of the cured epoxy samples on the total surface acidity are shown in Figs. 1a and 1b. As seen, the strength of cured composites is rather high, which suggests a chemical interaction between the functional surface groups on the CB particle surface and active functional groups of the oligomer to give a three-dimensional (3*D*) network of chemical bonds in the resulting material.

As can be seen from Fig. 1a, the strength of all the samples filled with CB particles is appreciable. However, the data on the swellability of the polydiene-urethane–diepoxide samples filled with unoxidized CB particles (CB-1) in various solvents show that they rapidly swell and dissolve in 3 days at room temperature. This fact indicates that there is no chemical interaction between unoxidized CB particles and epoxy oligomer, and the strength of these samples is probably due to their structuring caused by physical interactions.

The samples filled with CB particles with a total surface acidity of about 0.1% contain 3*D* networks of chemical bonds and show limited swelling in various solvents (the equilibrium swelling in toluene is 280%). Slight changes in the mechanical properties of the samples as influenced by the degree of surface oxidation agree with the insignificant changes in their swellability (from 270 to 290%). This fact confirms that the total acidity of 0.1% is sufficient to provide formation of a network of chemical bonds in the cured polymer, and its further increase does not affect noticeably the composite strength, i.e., only some frac-

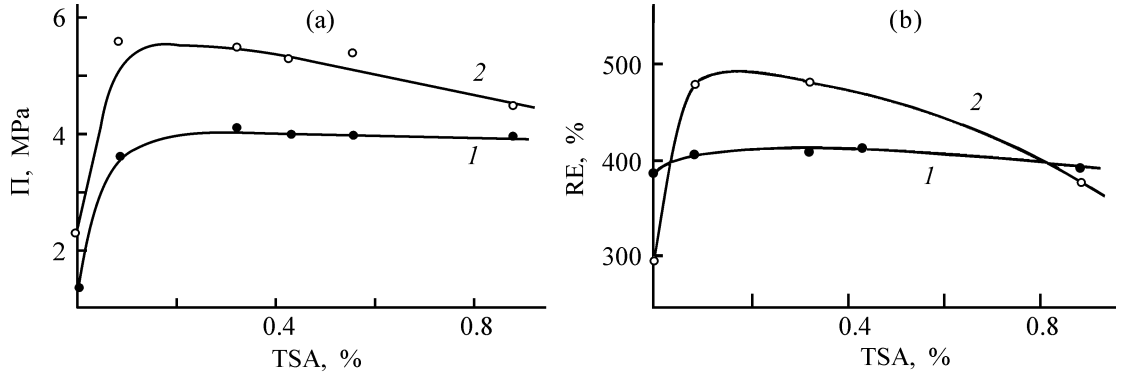
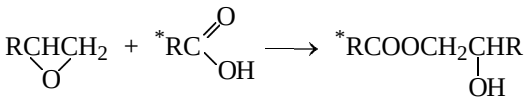


Fig. 1. (a) Strength Π and (b) relative elongation RE of cured epoxy oligomer filled with CB particles vs. the total surface acidity TSA at (*1*) 25 and (*2*) 40°C.

tion of the CB functional groups are involved in the formation of the 3*D* network in the polymer.

Most probably, the oligomer is cured by the reaction of the carboxy groups on the CB surface with epoxy groups of the oligomer [7, 8]



* Hydrocarbon radical from another molecule.

Thus, it is feasible to prepare filled epoxy composites cured only by functional groups present on the CB particle surface (without any other curing agents).

CONCLUSIONS

(1) Samples of carbon black with various degrees of surface oxidation were prepared by thermal oxidation with atmospheric oxygen.

(2) Functional groups formed on the surface of the carbon black affect curing of epoxy composites without addition of other curing agents.

REFERENCES

1. *Entsiklopediya polimerov* (Encyclopedia of Polymers), Kabanov, V.A., Ed., Moscow: Sov. Entsiklopediya, 1977, vol. 2.
2. Tarkovskaya, I.A., *Sto "professii" uglya* (A Hundred Jobs of Coal), Kiev: Naukova Dumka, 1990.
3. Tarkovskaya, I.A., *Okislennyi ugol'* (Oxidized Coal), Kiev: Naukova Dumka, 1981.
4. Izhik, A.P. and Ur'ev, N.B., *Kolloidn. Zh.*, 2002, vol. 64, no. 5, pp. 623–627.
5. Zuev, V.P. and Mikhailov, V.V., *Proizvodstvo sazhi* (Production of Carbon Black), Moscow: Khimiya, 1970.
6. Pechkovskaya, K.A., *Sazha kak usilitel' kauchuka* (Carbon Black as a Rubber Reinforcing Agent), Moscow: Khimiya, 1968.
7. Onishchenko, Z.V., Zorina, V.B., Zamkovaya, V.V., and Kutyanina, V.S., *Kauchuk Rezina*, 1982, no. 1, pp. 20–23.
8. Saunders, J.H. and Frish, K.C., *Polyurethanes. Chemistry and Technology*, New York: Interscience, 1962.

Russian Journal of Applied Chemistry, Vol. 78, No. 4, 2005, pp. 636–640. Translated from Zhurnal Prikladnoi Khimii, Vol. 78, No. 4, 2005, pp. 642–646.
Original Russian Text Copyright © 2005 by Solovskii, Tarabukina, Shpyrkov, Denisov, Vlasova, Korchagin.

MACROMOLECULAR CHEMISTRY AND POLYMERIC MATERIALS

Synthesis and Properties of Soluble Copolymers of *N*-Vinyl-2-pyrrolidone with 2-Hydroxyethyl Methacrylate

M. V. Solovskii, E. B. Tarabukina, A. A. Shpyrkov, V. M. Denisov, E. N. Vlasova, and A. M. Korchagin

Institute of Macromolecular Compounds, Russian Academy of Sciences, St. Petersburg, Russia

Received December 29, 2004

Abstract—Features of radical copolymerization of *N*-vinyl-2-pyrrolidone with 2-hydroxyethyl methacrylate in the presence of azobis(isobutyronitrile) were studied. The copolymerization constants of these monomers were calculated. The structure of the resulting copolymer was confirmed. The composition, microstructure, and molecular-weight parameters of the copolymers were determined.

Polymeric *N*-vinylpyrrolidone (VP), polyvinylpyrrolidone, is widely used in medicine as detoxicant [1] and modifier of morphine, iodine [2], and silver [3]. VP copolymers are studied as carriers for antimicrobial [4], hormone-containing [5], and other pharmaceuticals [6] and haptens [7]. At the same time, poly-(2-hydroxyethyl methacrylate) (HEMA) exhibits a number of valuable medical and biological properties: its hydrogels can be used to immobilize various pharmaceuticals [8] and to produce contact lenses [9].

VP–HEMA copolymers with a combination of VP and HEMA units can be used as carriers of biologically active compounds since they are hydrophilic, low toxic, and biocompatible with blood and tissues of a living body. These properties are provided by primary hydroxy groups in the side unit of the copolymers.

At the same time, features of copolymerization of VP and HEMA and the microstructure and molecular-weight parameters of VP–HEMA copolymers are poorly understood. Here we studied these issues.

As can be seen from Fig. 1a, the copolymerization rate strongly depends on the initial concentration of the monomer mixture. The higher this concentration, the faster the copolymerization. The copolymerization of VP with HEMA in isopropanol (Fig. 1b) also accelerates as the HEMA concentration $[M_2]$ in the initial mixture becomes higher, which indicates that HEMA (M_2) is more reactive than VP in copolymerization.

In the first copolymerization steps, the concentration of HEMA (M_2) units in the copolymer is substantially higher than the HEMA concentration in the initial mixture. In the course of copolymerization, this

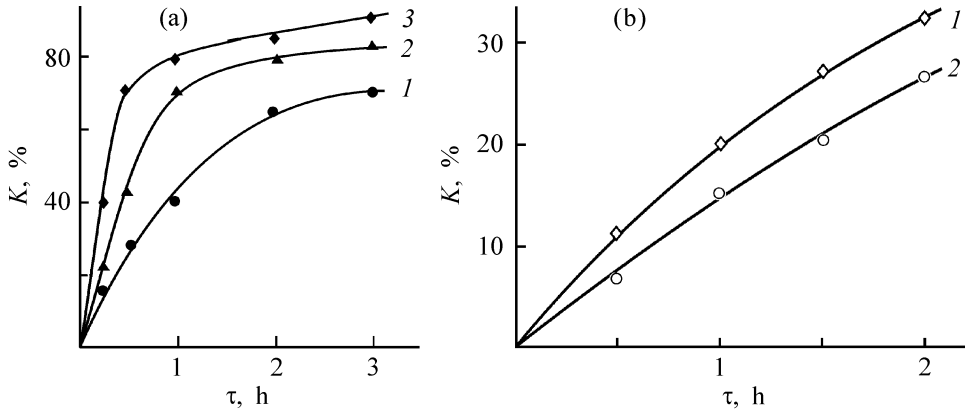


Fig. 1. Monomer conversion *K* in copolymerization of VP with HEMA in isopropanol at 60°C vs. time τ. (a) [AIBN] = 4.5 wt %, $[M_1^0] : [M_2^0]$ = 80 : 20 mol %. $[M_1^0] + [M_2^0]$ (wt %): (*1*) 10, (*2*) 20, and (*3*) 30. (b) [AIBN] = 1.5 wt %, $[M_1^0] + [M_2^0]$ = 20 wt %. $[M_1^0] : [M_2^0]$ (mol %): (*1*) 75 : 25 and (*2*) 80 : 20.

1070-4272/05/7804-0636 © 2005 Pleiades Publishing, Inc.

Table 1. Copolymerization of VP with 2-HEMA in isopropanol and the properties of VP–HEMA copolymers (T = 60°C and [AIBN] 4.5 wt %)

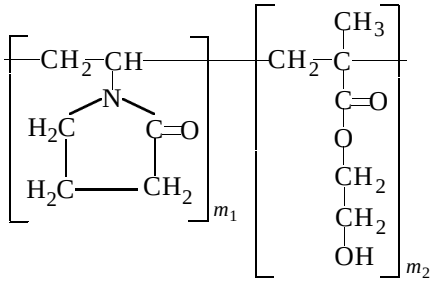
$[M_1^0]$	$[M_2^0]$	$[M_1^0 + M_2^0]$, wt %	Copolymer	Yield, % in 24 h	N content in copolymer, %	m_2, mol %	$[\eta]$, dl g^{-1}	M_{SD}
mol %								
95	5	10	**Ia**	83.2	10.41	15.5	0.17	50 000
90	10	10	**Ib**	86.2	8.90	26.1	0.17	49 000
80	20	10	**Ic**	65.0*	8.92	25.8	0.13	31 000
80	20	20	**Id**	88.2	7.92	33.6	0.22	67 000
75	25	20	**Ie****	88.9	7.06	40.2	0.25	93 000

* In 2 h. ** Insoluble in water.

difference sharply decreases, which is typical of copolymerization of monomers strongly differing in polymerization activity (Fig. 2). The copolymers isolated at high conversions (83–88%) are enriched in HEMA units (Table 1). As can be seen from Fig. 2, the intrinsic viscosity of the copolymers increases with the monomer conversion. This is probably due to deceleration of unit termination at high viscosity of the reaction mixture. Water-soluble VP–HEMA copolymers containing 15.5 to 33.6 mol % HEMA (M_2) units can be obtained by varying the molar ratio of the monomer in the initial mixture (Table 1).

The copolymer structure was confirmed by IR and ^{1}H NMR spectroscopy. The IR spectrum of copolymer **Id** contains a strong absorption band of stretching vibrations of the carbonyl group of the pyrrolidone ring of VP units at 1674 cm^{-1} and the band of the C=O group of HEMA units at 1722 cm^{-1}. The bands of asymmetric and symmetric stretching vibrations of the ether $-\overset{|}{C}-O-\overset{|}{C}-$ group of HEMA units appear at 1079 and 1167 cm^{-1}, respectively. The broad band at 3411 cm^{-1} is due to stretching vibrations of the associated hydroxy group.

The ^{1}H NMR spectrum of copolymer **Ia** contains of both VP and HEMA units. The signals at 0.95 and 1.25 ppm are assigned to the methyl protons of HEMA units. A characteristic doublet at 2.0 and 2.5 ppm is due to protons of the $-CH_2-\overset{\|}{C}O-$ group of VP units. Strong signals at 3.2 and 3.65 ppm are assigned to the H_2C and $-CH-$ groups of VP units, respectively. The signal of the methylene protons of HEMA units is observed at 4.4 ppm. These data allow us to assign the following structure to the VP–HEMA copolymer



where m_1 = 66.4–84.5 and m_2 = 15.5–33.6 mol %.

At high conversions, M_{SD} of the copolymers containing up to 25–30 mol % HEMA is about 50 000 (Table 1). As the HEMA content increases to 40 mol %, MW grows by a factor of 2. This is due to the higher copolymerization activity of HEMA as compared to that of VP. When polymerization was terminated in 2 h, M_{SS} of the copolymer with a fairly high HEMA content (25.8 mol %) was 31 000. This molecular weight does not exceed the threshold molecular weight

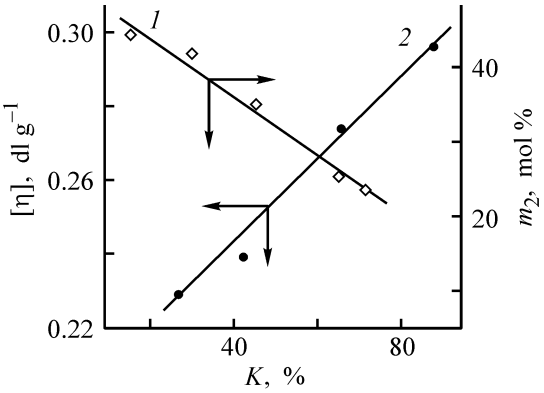


Fig. 2. (*1*) Content m_2 (mol %) of HEMA units in copolymer **Id** and (*2*) intrinsic viscosity of **Id** η vs. conversion K.

Table 2. Initial parameters for calculation of the copolymerization constants of VP (M_1) with HEMA (M_2) in isopropanol at 60°C ([AIBN] = 1.0 wt %, $[M_1^0 + M_2^0]$ = 10 wt %)

$[M_1^0]$	$[M_2^0]$	$[M_1^0 + M_2^0]$, wt %	K, %	N content in copolymer, %	Copolymer composition, mol %	
mol %					m_1	m_2
95	5	10	5.8	10.21	83.04	16.96
90	10	10	6.7	8.05	67.39	32.61
85	15	10	6.4	6.49	55.78	44.22
80	20	20	7.9	5.12	44.58	55.42

Table 3. Copolymerization constants of VP (M_1) with 2-HEMA (M_2) in isopropanol at 60°C, calculated taking into account the influence of the terminal unit

r_1	r_2	r_2/r_1	$1/r_2$	$1/r_1$	r_1r_2	Determination method*
0.30 ± 0.02	6.72 ± 0.34	22.4	0.149	3.33	2.02	Calculation [10], r_K = 0.999
0.29 ± 0.01	6.68 ± 0.37	23.0	0.149	3.49	1.93	Fineman–Ross, r_K = 0.998 [11]
0.29 ± 0.02	6.66 ± 0.01	22.9	0.150	3.49	1.93	Kelen–Tudos, r_K = 0.998 [12]

* r_K is the linear correlation coefficient.

Table 4. Probability of formation of structures M_1–M_1 (f_{11}), M_1–M_2 = M_2–M_1 ($f_{12} = f_{21}$), and M_2–M_2 (f_{22}) and average length of blocks consisting of M_1 and M_2 units in VP (M_1)–HEMA (M_2) copolymers, calculated taking into account the influence of the terminal unit

$[M_1^0] : [M_2^0]$, mol %	f_{11}	$f_{12} = f_{21}$	f_{22}	$\bar{L}_1$	$\bar{L}_2$
90 : 10	0.480	0.191	0.135	3.51	1.70
80 : 20	0.237	0.212	0.337	2.11	2.59
65 : 35	0.090	0.161	0.585	1.56	4.66
50 : 50	0.033	0.111	0.740	1.29	7.67
40 : 60	0.016	0.082	0.821	1.19	11.00
25 : 75	0.004	0.045	0.907	1.09	21.1
10 : 90	0.0005	0.016	0.967	1.03	62.01

(40 000) of polymers used as carriers of biologically active compounds (BAC). The intrinsic viscosity of the copolymers prepared by 24-h copolymerization (Table 1) grows from 0.17 to 0.25 dl g^{-1}, in parallel with MW, with increasing the HEMA content.

The initial parameters for calculation of the copolymerization constants of VP (M_1) with HEMA (M_2) in isopropanol at 60°C, $[M_1^0 + M_2^0]$ = 10 wt % and [AIBN] = 1.0 wt % are listed in Table 2.

The copolymerization constants were calculated by Naio-Lewis differential equation [10] and by Fineman-Ross [11] and Kelen-Tudos [12] procedures. In the last two cases, the linear regression was computed by the least-squares method. In all cases, the calculated linear correlation coefficients were 0.998–0.999.

The copolymerization constants calculated taking into account the influence of the terminal unit are close in all the three cases (Table 3). These constants confirm that HEMA is more reactive than VP. The rate constant of the reaction of HEMA macroradical with HEMA monomer is approximately a factor of 23 higher than that of the reaction of VP macroradical with VP monomer. The parameter $1/r_1$, ehich characterized the ratio of the reactivity of HEMA to that of VP macroradical, shows that the reaction of HEMA with VP macroradical is faster than that with HEMA macroradical. The high values of the product r_1r_2 (Table 3) suggest that M_1 and M_2 units in the macromolecule do not tend to alternate (Table 4). By contrast, the probability of formation of HEMA microblocks separated by single VP units is high. This

assumption is confirmed by a calculation [13] of the probability of formation of the M_1–M_1, M_1–M_2, M_2–M_1, and M_2–M_2 structures in the polymeric unit at low conversion and of the average lengths $\bar{L}_1$ and $\bar{L}_2$ of the blocks consisting of M_1 and M_2, respectively. The results of these calculations are listed in Table 4. It can be seen that the probability of formation of the M_1–M_1 diad at $[M_1^0] : M_2^0] > [50] : [50]$ mol % sharply decreases, and $\bar{L}_1$ approaches unity. The probability of formation of M_2–M_2 diads sharply increases at the indicated molar ratio of the monomers and so does $\bar{L}_2$. At $[M_1^0] : M_2^0] = [10] : [90]$ mol %, $\bar{L}_2$ is 62. Analysis of the structure and composition of the copolymers reveals their compositional nonuniformity.

EXPERIMENTAL

N-Vinylpyrrolidone was three times distilled in a vacuum from KOH. HEMA (Fluka) was double-distilled from molecular sieves in the presence of hydroquinone. Monomers of chromatographically pure grade were used. A gas-chromatographic analysis of the monomers was performed by the procedure described in [14]. Azobis(isobutyronitrile) was three times recrystallized form a chloroform–ethanol (1 : 5) mixture at temperatures lower than 40°C (mp 103°C).

VP–HEMA copolymer was prepared as follows. Weighed portions of the initiator, VP, HEMA, and isopropanol were loaded in a glass ampule pretreated with live steam. The ampule was purged with argon, sealed, and placed in a thermostat. The copolymerization was performed at 60°C. Then the ampule was cooled and opened. The viscous copolymer solution was poured dropwise into diethyl ether (200 ml). The precipitated copolymer was collected on a Schott filter and dried in a vacuum to constant weight. The yield and composition of the copolymer were determined. The composition was calculated from the nitrogen content, which, in turn, was determined on a Perkin–Elmer analyzer. When the conversion-vs.-time dependence was studied (Figs. 1, 2), the copolymerization was monitored gravimetrically.

The ^{1}H NMR spectrum of copolymer **Ia** was recorded in $CDCl_3$ on a Bruker AC-200 spectrometer. The IR spectrum of copolymer **Id** in a chloroform film was recorded on a JFS spectrometer.

The molecular properties of the copolymer in DMF solutions were studied by methods of molecular hydrodynamics. The intrinsic viscosity was measured on an Ostwald viscometer. Centrifugal sedimentation was performed on an MOM 3180 analytical ultracentrifuge (Hungary) at 45 000 rpm, using a refractometric registration system. The sedimentation boundary was produced by layering of a solvent onto the solution. The sedimentation coefficient was determined from the time dependence of the average shift of the sedimentation curves. The diffusion experiments were performed in a Tsvetkov diffusometer equipped with a polarization optical system. The diffusion coefficient D was calculated by the methods of areas and maximal ordinates. The molecular weights were calculated by the Svedberg equation [15]

$$M_{SD} = \frac{kT}{1 - \bar{\nu}\rho_0}\frac{S_0}{D},$$

where S_0 is the sedimentation constant; T, temperature; k, Boltzmann constant; ρ_0, solvent density; and $\bar{\nu}$, partial specific volume of the polymer.

The partial specific volume of copolymers, measured pycnometrically, was independent of the copolymer composition within the experimental error. The average partial specific volume ($\bar{\nu} = 0.84 \pm 0.06$ cm^3 g^{-1}) was close to that of PVP in various solvents [16].

CONCLUSIONS

(1) A copolymer of *N*-vinylpyrrolidone (M_1) with 2-hydroxyethyl methacrylate (M_2), prepared in isopropanol at 60°C in the presence of azobis(isobutyronitrile), is enriched in M_2 units.

(2) The constants of copolymerization of M_1 with M_2, determined by three methods, are as follows: $r_1 = 0.30 \pm 0.02$, $r_2 = 6.72 \pm 0.34$; $r_1 = 0.29 \pm 0.01$, $r_2 = 6.68 \pm 0.37$; $r_1 = 0.29 \pm 0.02$, $r_2 = 6.66 \pm 0.01$.

(3) The compositions, molecular weights, and microstructure of the copolymer confirm their compositional nonuniformity.

ACKNOWLEDGMENTS

The authors are grateful to B.M. Shabsel's for participation in the study. This study was financially supported by the Research School Program (project no. NSh-1823.2003.3).

REFERENCES

1. Sidel'kovskaya, V.P., *Khimiya N-vinilpirrolidon i ego polimerov* (Chemistry of *N*-Vinylpyrrolidone and Its Polymers), Moscow: Nauka, 1970.
2. Kirsh, Yu.E., *Poli-N-vinilpirrolidon i drugie poli-N-vinilamidy* (Poly-*N*-vinylpyrrolidone and Other Poly-*N*-vinylamides), Moscow: Nauka, 1998.

3. Kopeikin, V.V. and Panarin, E.F., *Dokl. Ross. Akad. Nauk*, 1998, vol. 380, no. 4, pp. 497–500.
4. Afinogenov, G.E. and Panarin, E.F., *Antimikrobnye polimery* (Antimicrobial Polymers), St. Petersburg: Gippokrat, 1993.
5. Kropachev, V.A., Shchukovskaya, L.L., Bolotina, I.A., *et al.*, *Mol. Biol.*, 1972, vol. 6, no. 2, pp. 727–736.
6. Plate, N.A. and Vasil'ev, A.E., *Fiziologicheski aktivnye polimery* (Physiologically Active Polimers), Moscow: Khimiya, 1986.
7. Solovskij, M.V., Nazarova, O.V., Panarin, E.F., *et al.*, *Biomed. Sci.*, 1991, vol. 2, no. 4, pp. 420–424.
8. Zaks, I.N. and Perkins, R.Ya., *Izv. Akad. Nauk Latv. SSR, Ser. Khim.*, 1988, no. 4, pp. 436–440.
9. Lavrov, N.A. and Nikolaev, A.F., *Plast. Massy*, 1986, no. 8, pp. 55–57.
10. Zi'lberman, E.N. and Navolokina, R.A., *Primery i zadachi po khimii vysokomolekulyarnykh soedinenii* (Examples and Problems on Chemistry of Macromolecular Compounds), Moscow: Vysshaya Shkola, 1984.
11. Alfrei, A., Borer, Dzh., and Mark, G., *Sopolimerizatsiya* (Copolymerization), Korshak, V.V., Ed., Moscow: Inostrannaya Literatura, 1953.
12. Tudos, F. Kelen, T., Foldes-Berezhnykh, T., *et al.*, *React. Kinet. Catal. Lett.*, 1975, vol. 2, no. 4, pp. 439–447.
13. Gindin, L.M., Abkin, A.D., and Medvedev, S.S., *Dokl. Akad. Nauk SSSR*, 1947, vol. 56, no. 2, pp. 177–180.
14. Solovskii, M.V., Ushakova, V.N., Panarin, E.F., *et al.*, *Khim. Vys. Energ.*, 1987, no. 2, pp. 143–147.
15. Tsvetkov, V.N., Eskin, V.E., and Frenkel', S.Ya., *Struktura makromolekul v rastvorakh* (Structure of Macromolecules in Solutions), Moscow: Nauka, 1964.
16. *Polymer Handbook*, Brandrupt, J. and Immergut, E.H., Eds., New York: Wiley, 1975.

Russian Journal of Applied Chemistry, Vol. 78, No. 4, 2005, pp. 641–645. Translated from Zhurnal Prikladnoi Khimii, Vol. 78, No. 4, 2005, pp. 647–651.
Original Russian Text Copyright © 2005 by Shaglaeva, Lebedeva, Sultangareev, Trofimova.

MACROMOLECULAR CHEMISTRY AND POLYMERIC MATERIALS

Synthesis and Properties of Copolymers Based on Vinyl Chloride

N. S. Shaglaeva, O. V. Lebedeva, R. G. Sultangareev, and K. S. Trofimova

Favorskii Irkutsk Institute of Chemistry, Siberian Division, Russian Academy of Sciences, Irkutsk, Russia
Irkutsk State Technical University, Irkutsk, Russia

Received September 30, 2004; in final form, January 2005

Abstract—Radical copolymerization of 1-vinylazoles with vinyl chloride and the composition and properties of the resulting copolymers were studied.

Polyvinyl chloride (PVC) and its copolymers (CPVCs) are among the most important macromolecular compounds. They are widely used for preparing plastic items, insulating materials, flexible films, pipes, and sheets. Copolymers of PVC with vinyl acetate and other monomers are starting substances for production of varnishes and adhesives [1, 2].

The applications and performance of copolymers are largely determined by their chemical nature. In particular, it is known that introduction of nitrogen-containing monomeric units into the PVC macromolecule improves the adhesive properties [3, 4]. Furthermore, nitrogen-containing monomeric units, as a rule, are internal plasticizers and are readily cross-linked at elevated temperatures, enhancing the cohesion of the material, which is particularly important for pasty formulations. At the same time, nitrogen-containing compounds can promote dehydrochlorination of PVC [1, 5]. Nevertheless, no special studies have been performed up to now to elucidate the influence exerted by the chemical nature of a comonomer on the degree of dehydrochlorination in the course of copolymerization.

In this study, we examined how the structure of the azole ring in 1-vinylazoles (VAZs) and the compositions of the starting mixture and the copolymer affect the dehydrochlorination in the course of copolymerization of vinyl chloride (VC) with 1-vinyl imidazole (VIM), 1-vinylbenzimidazole (VBI), 1-vinyl-1,2,4-triazole (VTA), and 1-vinylpyrazole (VPA).

EXPERIMENTAL

Copolymerization of the monomers in the bulk and in dimethylformamide (DMF) was performed in sealed ampules at 60°C in the presence of azobis(isobutyronitrile) (AIBN) under argon. After the polymerization was complete, the mixture was dissolved in DMF, and the copolymer was precipitated with ice-cold water. The reprecipitation was repeated twice. The copolymer composition was determined by elemental analysis, following the standard procedure [4].

The IR spectra were taken on a Specord IR-75 spectrometer in KBr and in mineral oil. The ^{13}C NMR spectra of copolymer samples were recorded on a Varian VXR-500S spectrometer (working frequency 125.5 MHz, relaxation delay 2.5 s, 90° pulse, solvent DMSO-d_6). As relaxant we used 0.02 M chromium tris(acetylacetonate). The relative error in quantitative determination of the comonomer content by NMR and elemental analysis of the copolymers did not exceed 6.7%.

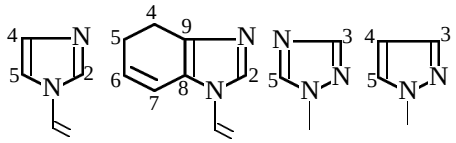
The TG curves were taken on an MOM derivatograph (Hungary) in air at a heating rate of 5 deg min^{-1}. The maximum temperature was 700°C, and the DTA sensitivity, 1/5–1/10.

The IR spectra of the CPVCs contain stretching vibration bands of the azole rings and C–Cl bond (1480–1500 and 680 cm^{-1}, respectively); the bands of the VAZ vinyl fragments are absent. In the ^{13}C NMR spectra of the CPVCs, the signals of the vinyl groups of VAZs and VC are absent, but there are broadened signals assignable to the carbon atoms of the azole ring and the >CHCl, >N–CH_2–, and >CH_2 fragments. The chemical shifts of the carbon atoms in the VAZ and VC units of CPVCs are listed in Table 1.

The occurrence of dehydrochlorination in the course of the copolymerization was judged from the group of signals of the ~CH=CH~ fragment (128.03–127.58 ppm) in the ^{13}C NMR spectra of the samples.

1070-4272/05/7804-0641 © 2005 Pleiades Publishing, Inc.

Table 1. ^{13}C NMR spectra of CPVCs



VIM VBI VTA VPA

Carbon atom	δ, ppm			
	VIM	VBI	VTA	VPA
C^2	136.6	140.5–146.0*	–	–
C^3	–	–	151.1–152.3	128.5–131.5
C^4	129.9	120.3	–	105.3
C^5	116.9	122.7	143.0–145.0	139.5
C^6	–	123.2	–	–
C^7	–	110.0–112.5	–	–
C^8	–	140.5–146.0*	–	–
C^9	–	133.6	–	–
>NCH	48.0–52.0	50.4–53.2	52.2–55.0	55.5–57.5
$>CH_2$	N/d**	41.5–44.4	40.3–43.2	40.0–45.0
$>CH_2BX$	N/d	44.4–47.6	43.2–46.2	45.0–46.8
–CHCl	55.0–58.0	56.2–60.0	55.0–59.0	56.7–60.0

* The C^2 and C^8 signals of VBI and CPVC overlap.

** (N/d) Not determined, because the CH_2 carbon signals in the spectra of VIM and VC are obscured by a strong signal of the solvent, DMSO-d_6.

Table 2. Copolymerization of VAZ (M_1) with VC (M_2) in DMF ([AIBN] 0.5 wt %, 60°C)

Run no.	Composition of starting mixture, mole fractions		Copolymer composition from ^{13}C NMR data, mole fractions			Z, %
	M_1	M_2	m_1	m_2	CH=CH	
			VIM–VC			
1	0.80	0.20	0.9296	0.0353	0.0351	49.9
2	0.60	0.40	0.8437	0.0871	0.0692	44.3
3	0.40	0.60	0.6850	0.2365	0.0785	25.0
4	0.20	0.80	0.5002	0.4113	0.0885	17.7
			VBI–VC			
1	0.80	0.20	0.8753	0.0767	0.0480	38.5
2	0.50	0.50	0.8045	0.1429	0.0526	26.9
3	0.30	0.70	0.5845	0.3850	0.0305	7.3
4	0.20	0.80	0.4658	0.5342	–	–
			VTA–VC			
1	0.80	0.20	0.8295	0.1223	0.0482	28.1
2	0.65	0.35	0.7987	0.1851	0.0162	8.1
3	0.30	0.70	0.4672	0.5328	–	–
4	0.20	0.80	0.3846	0.6154	–	–
			VPA–VC			
1	0.80	0.20	0.8421	0.1579	–	–
2	0.50	0.50	0.7855	0.2145	–	–
3	0.30	0.70	0.6090	0.3910	–	–
4	0.20	0.80	0.3490	0.6510	–	–

The degree of dehydrochlorination Z is defined as follows [3]:

$$Z = A/(B + A),$$

where A is the content of the ~CH=CH~ units, and B, content of VC units.

The content of VC and ~CH=CH~ units in CPVCs was determined by quantitative ^{13}C NMR analysis (spectra, Table 1; anaytical data, Table 2).

Table 2 shows that the dehydrochlorination occurs in the copolymerization of VC with VIM and VBI. In the copolymerization of VC with VTA, HCl is eliminated only at a high content of the azole comonomer. The copolymerization of VC with VPA involves no side processes; in the ^{13}C NMR spectrum of the reaction products, the group of signals of the ~CH=CH~ fragment is absent. Thus, the occurrence of the dehydrochlorination depends on the nature of the comonomer (VAZ), specifically, on its basicity [4, 6].

Since VIM is the most basic (pK_{BH^+} 7.52) among the VAZs studied, the degree of dehydrochlorination in the VIM–VC system is the highest. Apparently, the dehydrochlorination occurs via formation of an intermediate complex in the macromolecular chain (for the scheme, see [3]). As the basicity of the pyridine-like nitrogen atom in VAZ increases, the hydrogen atom of the CH_2 group in VC becomes more labile, and the HCl elimination is facilitated.

It should be noted that the degree of dehydrochlorination in the systems of VC with VIM, VBI, and VTA (Table 2, run nos. 1, 2) grows as the VAZ content (both in the starting mixture and in the copolymer) increases.

1-Vinylpyrazole is the weakest base (pK_{BH^+} 1.70); therefore, the pyridine-like nitrogen atom of the pyrazole ring does not promote the HCl elimination. The absence of dehydrochlorination in the copolymerization of VPA and VTA (Table 2, run nos. 3 and 4) with VC indicates that DMF does not promote dehydrochlorination. At the same time, DMF is a polar aprotic solvent with appreciable basic properties, which should not be disregarded. Available data show that the dehydrochlorination of PVC in DMF is due to the presence in DMF of amine impurities (dimethylamine, ammonium formate) and to accumulation of the reaction products (HCl, Cl^-) in solution [5, 7]. Release of HCl is observed at high temperatures (>90°C). Freshly distilled DMF contains only minor amounts of dimethylamine and dimethylammonium formate (10^{-3}–10^{-2} M) [7]. In our experiments, we used freshly distilled DMF, and, apparently, minor amounts of these impurities did not promote the dehydrochlorination. Also, the copolymerization was performed at a lower temperature (60°C) than in [5, 7]. Examination of the composition of the VBI–VC copolymer showed that the eliminated HCl is fully bound to the pyridine-like nitrogen atom [3]. In the VTA–VC copolymers, HCl is also fully trapped by the heterocycle, with the formation of quaternized VTA units. This conclusion is based on a comparison of the copolymer compositions determined by chemical analysis (run no. 1, Table 2, found, %: C 48.85, H 5.81, N 39.74, Cl 5.60; run no. 2, Table 2, found, %: C 50.32, H 6.40, N 37.18, Cl 5.80) and by ^{13}C NMR spectroscopy on the assumption of complete binding of the eliminated HCl with the triazole ring (run no. 1, found, %: C 49.44, H 5.22, N 40.25, Cl 5.09; run no. 2, found, %: C 52.09, H 4.99, N 37.02, Cl 5.90).

Thus, experiments on radical copolymerization of VAZs with VC showed that the degree of dehydrochlorination depends on a particular VAZ, and with VPA the copolymers contain no polyene structures, i.e., ~CH=CH~; the eliminated HCl is fully trapped by the pyridine-like nitrogen atom in the heterocycle, which excludes the autocatalytic effect of HCl on the dehydrochlorination and is important for processing and use of VC-based copolymers.

To evaluate the modifying effect of VAZs on the properties of polyvinyl chloride materials, we studied some physicochemical and mechanical characteristics of the CPVCs prepared.

Introduction of units containing bulky heterocyclic substituents increases the distance between the main polymer chains and thus decreases the rigidity and the temperature of transition to the viscous-flow state; the solubility grows owing to distortion of the intermolecular interactions of the polar C–Cl groups.

Copolymerization of VAZs with VC in DMF yielded powdered products soluble in dimethyl sulfoxide (DMSO), DMF, C_6H_6, cyclohexanone, and a 1 : 2 : 3 (by volume) mixture of acetone, butyl acetate, and toluene. These polymers can be processed under milder conditions, compared to VC and vinylidene chloride homopolymers.

It is known that PVC and polyvinylidene chloride (PVDC) can form only dilute solutions (≤5 wt %) [1]. The limited solubility of these polymers makes their solutions unsuitable for preparing varnish coatings. The new CPVCs dissolve in a wider range of solvents and can form 50 wt % solutions, which meets the requirements to paint-and-varnish materials.

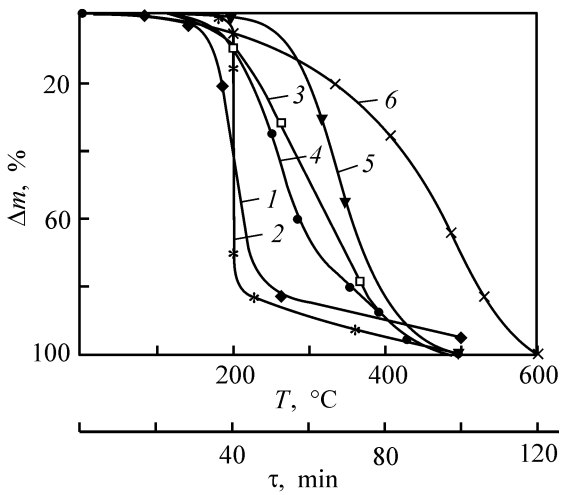
Table 3. Properties of coatings based on VC–VAZ copolymers

VAZ mole fraction in copolymer	Impact strength, kg cm	Bending strength, mm	Adhesion (notching method), points	
			grid	parallel
VTA–VC				
0.25	50	4	1	1
0.45	40	1	1	1
0.75	35	1	1	2
VPA–VC				
0.61	45	1	1	1
0.73	50	2	1	1
0.84	50	2	1	2

The varnish coaatings based on VTA–VC, VPA–VC, VBI–VC, and VIM–VC copolymers were tested for the strength and adhesion properties by standard procedures [8].

The best results, which are or practical interest, were obtained with coatings prepared from solutions of VTA–VC and VPA–VC copolymers. These coatings show good strength and adhesion properties (Table 3). Their impact strength is 40–50 kg cm, and bending strength, 1–2 mm. The adhesive properties of the varnish coatings were evaluated in points by the method of grid and parallel notchings.

Table 3 shows that the best results are obtained at the VTA mole fraction in VTA–VC copolymer of 0.25–0.45 and at the VPA mole fraction in VPA–VC copolymer of 0.61–0.73. The adhesion of the varnish coatings (method of parallel notchings) was 1 point, i.e., the copolymer coatings have high adhesion to metal surfaces.



Weight loss Δm by CPVCs. (T) Temperature and (τ) time. (*1*) PVC, (*2*) VBI–VC, (*3*) VTA–VC, (*4*) VPA–VC, (*5*) VIM–VC, and (*6*) VTGI–VC.

One of the most significant disadvantages of PVC is its instability at temperatures required for normal reprocessing. Degradation of PVC involves a set of different chemical processes occurring simultaneously in several directions. The main reaction is the intramolecular elimination of HCl resulting in formation of polyene systems, altering the color and impairing the performance of PVC.

The initial step of degradation of PVC and VC copolymers is autocatalytic elimination of HCl. Therefore, it becomes necessary to stabilize PVC with toxic agents (compounds of lead, cadmium, barium) belonging to hazard class 1, which is undesirable from the environmental viewpoint.

Raskulova *et al.* [9] studied the heat resistance of copolymers of VC with butyl vinyl ether (BVE). Despite the fact that BVE contains no functional groups that could bind the eliminated HCl, the heat resistance of VC–BVE copolymers appeared to be higher than that of suspension PVC (decomposition point 162.5°C). Raskulova et al. believe that the enhanced heat resistance of VC–BVE copolymers is exclusively due to the structural features (short VC blocks are separated by single units of the comonomer); this phenomenon was termed structural stabilization.

The presence in the copolymer of functional groups that can bind the released HCl should enhance its heat resistance. This was demonstrated by the example of VC copolymers with unsaturated glycidyl ethers [9]. The epoxy groups trap HCl, and the decomposition point of the copolymer is as high as 252°C.

The thermograms (see figure) show that the heat resistance of CPVCs is higher than that of suspension PVC. This is indicated by both the higher decomposition point of CPVCs (up to 193–217°C) and lower rate of their degradation. The cross-linked VIM–VC copolymer prepared in the bulk is thermally stable up to 290°C. For comparison, we also show the TG curve for a copolymer of VC with *N*-vinyl-4,5,6,7-tetrahydroindole (VTHI).

The enhanced heat resistance of the copolymers, compared to PVC, is apparently due to both internal and structural stabilization. It is known [4, 9] that the HCl elimination rate decreases with shortening of VC blocks. The internal stabilization is due to the pres-

ence of a nitrogen-containing heterocycle efficiently trapping HCl.

CONCLUSIONS

(1) Copolymers of vinyl chloride with 1-vinylazoles were prepared. The activity of the monomers in copolymerization with vinyl chloride increases in the order 1-vinylpyrazole, 1-vinylimidazole, 1-vinylbenzimidazole, 1-vinyl-1,2,4-triazole, as the polarity of the vinyl group, which depends on the number and mutual arrangement of the nitrogen atoms in the heteroring, becomes higher.

(2) Formation of the copolymers is accompanied by dehydrochlorination; its degree grows in parallel with an increase in the content of a 1-vinylazole and in its basicity. The released HCl reacts with the pyridine-like nitrogen atoms to form quaternized products, which suppresses the autocatalytic pathway of dehydrochlorination.

(3) The copolymers prepared surpass commercial polyvinyl chloride in heat resistance and solubility in organic solvents. Varnish coatings based on these copolymers exhibit good adhesion to metal surfaces and high strength.

REFERENCES

1. *Poluchenie i svoistva polivinilkhlorida* (Production and Properties of Polyvinyl Chloride), Zil'berman, E.N., Ed., Moscow: Khimiya, 1968.
2. Minsker, K.S. and Fedoseev, G.G., *Destruktsiya i stabilizatsiya polivinilkhlorida* (Degradation and Stabilization of Polyvinyl Chloride), Moscow: Khimiya, 1972.
3. Shaglaeva, N.S., Lebedeva, O.V., Pirogova, G.A., *et al.*, *Vysokomol. Soedin., Ser. B*, 2003, vol. 45, no. 10, pp. 1769–1773.
4. Lebedeva, O.V., *Cand. Sci. Dissertation*, Irkutsk, 2001.
5. Vaiman, E.Ya., Pakshver, A.B., and Fikhman, V.D., *Vysokomol. Soedin., Ser. A*, 1972, vol. 14, no. 1, pp. 90–95.
6. Baikalova, L.V., Domnina, E.S., Kashik, T.V., *et al.*, *Zh. Obshch. Khim.*, 1998, vol. 68, no. 5, pp. 842–846.
7. Evsyukov, S.E., Kudryavtsev, Yu.P., and Korshak, Yu.V., *Usp. Khim.*, 1991, vol. 60, no. 4, pp. 764–798.
8. Karyakina, M.I., *Laboratornyi praktikum po ispytaniyu lakokrasochnykh materialov i pokrytii* (Laboratory Manual on Testing of Paint-and-Varnish Materials and Coatings), Moscow: Khimiya, 1977.
9. Raskulova, T.V., Volkova, L.I., Salaurov, V.N., *et al.*, *Zh. Prikl. Khim.*, 1998, vol. 71, no. 7, pp. 2184–2188.

Russian Journal of Applied Chemistry, Vol. 78, No. 4, 2005, pp. 646–648. Translated from Zhurnal Prikladnoi Khimii, Vol. 78, No. 4, 2005, pp. 652–654.
Original Russian Text Copyright © 2005 by Sazanov, Kutsenko, Novoselova.

MACROMOLECULAR CHEMISTRY AND POLYMERIC MATERIALS

Thermochemical Analysis of Cyanoethyl Ethers of Cellulose Blended with Polyacrylonitrile

Yu. N. Sazanov, L. I. Kutsenko, and A. V. Novoselova

Institute of Macromolecular Compounds, Russian Academy of Sciences, St. Petersburg, Russia

Received January 11, 2005

Abstract—Thermochemical reactions of cyanoethyl ethers of cellulose with polyacrylonitrile in the temperature range of its cyclization were studied.

It is well known that polyacrylonitrile (PAN) is a unique polymer allowing production of carbon materials with a high coke number (CN) and shows by a high reactivity in polymer-analogous transformations in combinations with other macromolecular compounds. This feature has been noted in studying thermochemical reactions of PAN blended with nitrogen-containing polysaccharides (chitin, chitosan) and in a series of graft copolymers with cellulose ethers [1–5]. The above studies revealed the leading role of cyano groups in the formation of a carbon skeleton in the temperature range of increased reactivity of these groups, in which a series of occurring heterogeneous reactions initiate formation of a precursor of the carbonized network structure. The well-known procedures of directional cross-linking of the reaction mixture of copolymers and intermediates of thermal degradation allow the initial structures of carbonizates to be fixed and the yield of low-molecular-weight products to be minimized. Thus, real prerequisites arise for a noticeable increase in CN, for a decrease in the temperature and energy barrier of carbonizate formation, and for use of the potential of nitrogen atoms which, as shown previously [6–8], play a decisive role in formation of aromatic carbonizates from heteropolymers.

With the aim to raise the thermal stability of cellulose derivatives and also to produce carbonization products therefrom with specific characteristics and increased CN, we considered thermochemical reactions of cyanoethyl ethers of cellulose (CEC) and their blends with PAN. For this purpose, we used PAN synthesized in the presence of catalysts of the radical type and cyanoethyl derivatives of cellulose, synthesized by the well-known procedure [9] involving the reaction of viscose fiber CEC_1 [degree of substitution (DS) 2.8, degree of polymerization (DP) 300], CEC_2 (DS 2.3, DP 300), and finely crystalline cellulose with acrylonitrile.

Initially, to reveal the influence of cyano group on thermochemical transformations of cellulose, we used its cyanoethyl derivatives. As shown by TGA and DTA [10, 11] under conditions of heating of the sample (50 mg) at a constant rate of 10 deg min^{-1} in the self-generated medium (SGM), up to 225–250°C there is only insignificant weight loss (approximately 1.5–2.5%) caused by removal of adsorbed volatiles. Above these temperatures, thermal degradation starts, and its rate abruptly increases with heating. In this stage, we observed avalanche-like release of low-molecular-weight degradation products whose amount reached 70–75% of the total weight of the sample. Above 360–370°C, the residue gets carbonized, and this stage proceeds with a low and constant rate of weight loss until complete burning-out of the sample at approximately 800°C (Fig. 1a). For CEC_1 and CEC_2 samples, which differ in the degree of substitution with cyanoethyl groups, we observed small deviations from the above temperature-weight characteristics of the process, which did not noticeably affect the kinetics of CEC thermal degradation. Thermal effects for CEC_1 and CEC_2 samples in the range of 400–500°C can be assigned to melting of separate ordered fragments of the precarbonizate formed by transformations of the sample residue after completion of the oxidative reactions at 295–355°C. The reasons for its appearance should be looked for in studying spectral characteristics of these products in the initial stage of carbonization.

1070-4272/05/7804-0646 © 2005 Pleiades Publishing, Inc.

Returning to the problem of cocarbonization of CEC with PAN, we should note that, according to the DTA and TG curves of both polymers, the most favorable temperature range of these reactions is the range of intense degradation of the main chains of CEC and cyclization of PAN at 200–300°C. A blend of powdered CEC and PAN in a weight ratio of 1 : 1 (sample 1) and films prepared from mixed solutions at CEC : PAN weight ratios of 0.25 : 0.75 and 1 : 1 (sample nos. 2–4) were thermally treated under the same dynamic conditions. The TG and DTA curves of the blends recorded during heating in SGM are shown in Figs. 1a and 1b. It is seen that, in thermal degradation of the blends, there are stages of weight loss typical of both components of the blend. However, depending on the composition and aggregative state of the samples, the kinetics of their thermal degradation show significant differences, compared to the initial polymers. For example, the difference in CN for PAN and CEC at 800°C is almost 50%, and, for the blends at the CEC : PAN ratio of 1 : 1, CN varies from 40 to 30% (samples nos. 2–4). This difference indicates that PAN reacts with CEC during thermal cocarbonization and the degree of substitution of CEC strongly affects the process. In addition, the blends in the form of a powder and a film show a noticeable difference both in CN and in the weight loss Δm in the first stage of thermal degradation. Δm is 35% for sample no. 2, 14% for sample no. 3, and almost 40% for sample 4; this can be caused by differences in the procedure of preparation of the samples obtained by precipitation of a CEC–PAN blend from the solution (powdered precipitate) and by dry forming of a composite film from the dimethylformamide solution. In the thermochemical characteristics, sample no.1 is similar to PAN, since the weight fraction of CEC in this sample is 0.25; however, the influence of CEC is noticeable only in the first stage of thermal degradation (there is no abrupt weight loss at 200°C). In the subsequent stages of cocarbonization, the kinetics of weight loss (beginning at 300°C) almost exactly coincide with the kinetics of carbonization of PAN, and CN at 800°C even exceeds CN for PAN by 4%, i.e., for this sample the CEC structure is completely realized in the carbonized residue with PAN.

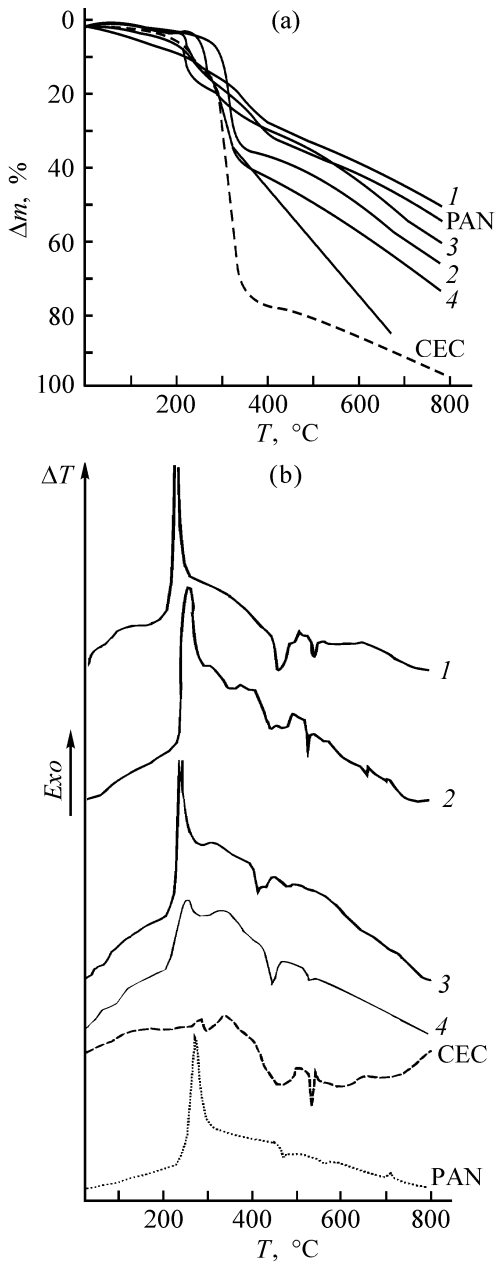


Fig. 1. (a) TG and (b) DTA curves for samples of CEC–PAN blends at component ratios of (*1*) 0.25 : 0.75 and (*2–4*) 1 : 1. (Δm) Weight loss by the sample and (T) temperature; the same for Fig. 2. Samples: (*1*, *3*, *4*) films and (*2*) powder. Degree of substitution of CEC: (*1–3*) 2.3 and (*4*) 2.8. (*Dotted line*) CEC and (*dashed line*) PAN.

When analyzing the thermal effects accompanying thermal transformations of CEC, PAN, and their mixtures in the range 20–800°C (Fig. 1b), we can note the following features of behavior of mixed compositions: (1) For all the samples, the exothermic peaks of PAN cyclization are observed at temperatures lower by 50–60°C than those for pure PAN; (2) the absolute values of this effect (kcal mol^{-1}) differ insignificantly, except for sample no. 4; (3) in the carbonization stage (above 400°C), the endothermic effects are significant; these effects can be assigned to formation of carbonizate with various degrees of ordering.

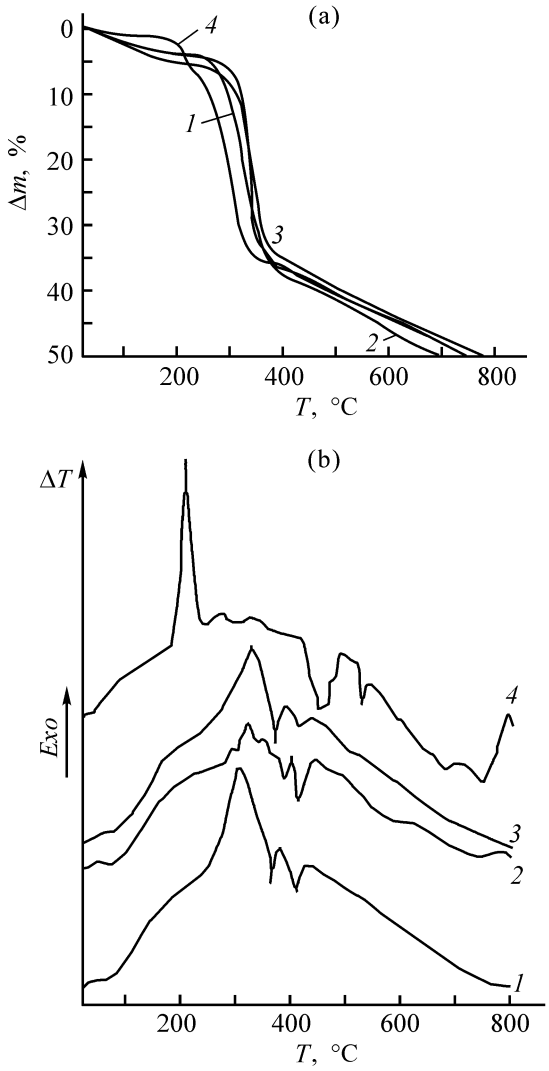


Fig. 2. (a) TG and (b) DTA curves of the samples of (*1*) long staple cotton, (*2*) cotton linter, (*3*) flax fiber, and (*4*) cyanoethyl nitrocellulose (DS 2.3 with respect to cyanoethyl groups and 0.7 with respect to nitro groups).

The modifying role of PAN, which not only favors a significant increase in CN of its blends with CEC but also noticeably enhances their thermal stability, is illustrated by Figs. 2a and 2b. The TG and DTA curves of long staple cotton, cotton linter, and flax fiber show that the kinetics of thermal degradation involves two major stages, similar to CEC. After an insignificant weight loss below 250°C, thermal rearrangements of the main chain of the polymers start in the range 250–360°C. This stage is characterized by a significant rate of release of volatiles in the amount of 60–65% of the initial weight of the sample and by a noticeable exothermic effect. Furthermore, in the carbonization stage, the residue gradually burnts out and the sample is completely evaporated at 700–800°C. An attempt to introduce additional nitrogen-containing groups (cyanoethyl group, nitro group, or both) into cellulose or its ethers did not noticeably affect the carbonization of the polymers examined.

Thus, it can be concluded that PAN is a certain reinforcing skeleton, around which, under favorable carbonization conditions (as mentioned above) the carbonizate of concomitant heterostructures is formed by intermolecular and intramolecular layering.

CONCLUSIONS

(1) In combined thermal treatment of polyacrylonitrile and cyanoethyl ethers of cellulose, cyclyzation of polyacrylonitrile noticeably decreases (by 50–60°C).

(2) Cocarbonization of the polymers studied results in a noticeable increase in the coke number of the blends as compared to the homopolymers of cellulose ethers.

REFERENCES

1. Spirina, T.N., Sazanov, Yu.N., Novoselova, A.V., and Zgonnik, V.N., *J. Polym. Sci.*, 1992, vol. 34, no. 5, pp. 395–398.
2. Sazanov, Yu.N., Simanovich, I.E., Szekely, T., and Blazo, M., Abstracts of Papers, *Polykondensation: XII Int. Mikrosimp. Polykondensation*, Schwerin (Germany), 1989, p. 61.
3. Sazanov, Yu.N., *J. Thermal Anal.*, 1990, vol. 36, no. 2, pp. 361–367.
4. Sazanov, Yu.N., Nud'ga, L.A., Novoselova, V.A., *et al.*, *Zh. Prikl. Khim.*, 2004, vol. 77, no. 4, pp. 643–648.
5. Sazanov, Yu.N., Nud'ga, L.A., Petrova, V.A., *et al.*, *Zh. Prikl. Khim.*, 2004, vol. 77, no. 8, pp. 1366–1369.
6. Gribanov, A.V. and Sazanov, Yu.N., *Zh. Prikl. Khim.*, 2000, vol. 73, no. 3, pp. 465–469.
7. Gribanov, A.V. and Sazanov, Yu.N., *Zh. Prikl. Khim.*, 2000, vol. 73, no. 6, pp. 897–901.
8. Gribanov, A.V. and Sazanov, Yu.N., *Zh. Prikl. Khim.*, 2000, vol. 73, no. 10, pp. 1705–1709.
9. MacGregor, J.H., *J. Soc. Dyers Colour.*, 1957, vol. 67, p. 66.
10. Sasanov, Yu.N. and Sysoev, V.A., *Eur. Polym. J.*, 1974, vol. 10, pp. 867–869.
11. Gribanov, A.V., Sazanov, Yu.N., Beloborodova, U.V., *et al.*, *Zh. Prikl. Khim.*, 1999, vol. 72, no. 3, pp. 467–473.

Russian Journal of Applied Chemistry, Vol. 78, No. 4, 2005, pp. 649–651. Translated from Zhurnal Prikladnoi Khimii, Vol. 78, No. 4, 2005, pp. 655–657.
Original Russian Text Copyright © 2005 by Ivanova, Averko-Antonovich.

MACROMOLECULAR CHEMISTRY AND POLYMERIC MATERIALS

Use of Amines as Complex-Action Additives to Butadiene–Vinylidene Chloride Latex

A. A. Ivanova and I. Yu. Averko-Antonovich

Kazan State Technological University, Kazan, Tatarstan, Russia

Received July 26, 2004; in final form, December 2004

Abstract—The suitability of amines with different structures for modifying ready-for-use butadiene–vinylidene chloride latexes was examined. The influence of the amines on the main physicochemical properties of the latexes was elucidated.

Butadiene–vinylidene chloride latexes have been manufactured for more than 60 years; their synthesis technology is streamlined, and the raw materials for their production are readily available. The currently produced commercial[1] butadiene–vinylidene chloride latexes are DVKhB-70 [TU (Technical Specifications) 38.303-04-03–90] and DVKhB-Sh (TU 2294-049-05 766 764–02).

The polymer of the DVKhB-70 latex (butadiene : vinylidene chloride 30 : 70) contains a large amount (35–37 wt %) of bound chlorine imparting to it a set of valuable properties [1]. However, application of the polymer is substantially restricted by the inadequate aggregative stability of the latex, as well as by the low stability upon introduction of fillers and the possible dehydrochlorination of the polymer in the latex stage. Elimination of these drawbacks will make DVKhB-70-based compositions suitable for application in building industry as adhesives, coatings, building materials, etc. [2].

The manufacture of the DVKhB-Sh latex (butadiene : vinylidene chloride 90 : 10) with 7.3 wt % bound chlorine, intended for tire cord impregnation, was commenced only recently.

The specific features of emulsion polymerization do not allow efficient use of additives of modifying chemical reagents in synthesis of the latex. It seems more reasonable to introduce them into latex with particles already coated with a protective surface layer [3].

As complex-action additives can serve amines with various structures, used previously for preparation of synthetic latexes [4]. Many of these amines are surfactants and, moreover, affect structuring of aqueous solutions.

In this context, we examined here the suitability of additives of some amines for improving the colloidal chemical characteristics of butadiene–vinylidene chloride latexes and elucidated how the structure of the amine affects its performance in modification of ready-for-use latexes.

EXPERIMENTAL

The latexes under study were liquids with a specific odor, dark brown in the case of DVKhB-70 and light in the case of DVKhB-Sh. Selected parameters of the latexes are listed in the table.

As additives for DVKhB-70 and DVKhB-Sh latexes we used a number of readily available amines: diethanolamine, ethanolamine, and diethylamine. Ethanolamine and diethanolamine are viscous hygroscop-

Physicochemical properties of DVKhB-Sh and DVKhB-70 latexes [emulsifier, potassium soap of synthetic fatty acids, C_{13}–C_{15} (4 wt parts)]

Parameter	DVKhB-70	DVKhB-Sh
Weight fraction, % of:		
dry substance	27.6	32.0
chlorine in rubber (within)	35.6	6.1
Average diameter of latex particles, nm	110	150

[1] Kazan Synthetic Rubber Plant, Open Joint-Stock Company.

1070-4272/05/7804-0649 © 2005 Pleiades Publishing, Inc.

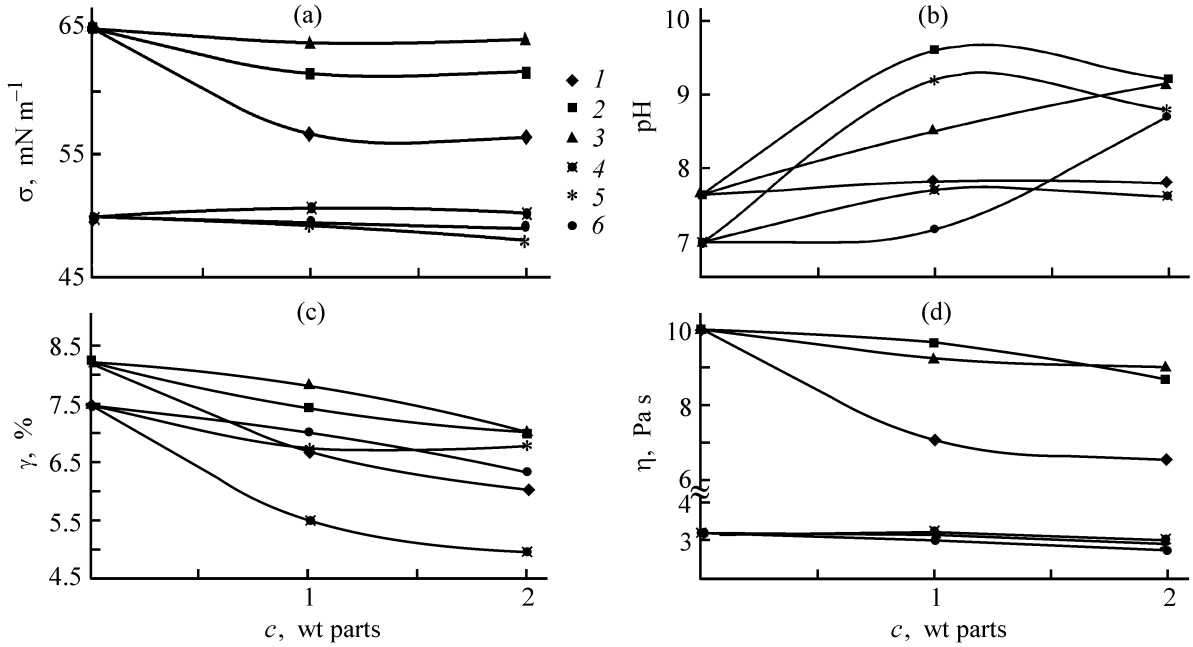


Fig. 1. (a) Surface tension σ, (b) pH, (c) mechanical stability γ, and (d) Hoeppler viscosity η of (*1–3*) DVKhB-Sh and (*4–6*) DVKhB-70 latexes vs. the amine content *c*. (*1*, *4*) Diethanolamine, (*2*, *5*) ethanolamine, and (*3*, *6*) diethylamine.

ic liquids, well soluble in water, ethanol, and chloroform; these are weak bases combining the properties of amines and alcohols. By contrast, diethylamine is a strong base ($K_b = 9.6 \times 10^{-4}$) with the properties of amines solely.

The amines were introduced at room temperature into a commercial butadiene–vinylidene chloride latex in various amounts. The resulting mixture was stirred; after the adsorption equilibrium was established, we studied by the known procedures [5] how the amines affect the properties of the latexes.

The surface tension was determined by the Du Nouy ring method [GOST (State Standard) 20216–74]. The surface tension σ characterizes the degree of saturation of the adsorption shells of the rubber globules in the latex and, hence, the stability of the latex, as well as its wetting power with respect to hydrophilic surfaces. The results of replicate measurements agreed within 0.2 mN m^{-1}.

Viscosity is an important characteristic of latexes, which are colloid systems. It depends on the properties of the protective layers on the surface of a rubber particle in the latex, all other conditions being the same. The viscosity was determined on a Hoeppler rheoviscometer. The results of replicate measurement agreed within 0.3 s.

The mechanical stability of the latexes was tested on a Maron instrument.

As is known, the low stability of butadiene–vinylidene chloride latex is due to the elimination of HCl from the latex polymer macromolecules with time. This changes the pH, thereby destabilizing the latex. The pH of the latexes was measured on a pH-meter with glass electrodes. The results of replicate measurements agreed within 0.2.

The surface tension of the DVKhB-Sh latex is much, lower compared to DVKhB-70, and this parameter for the latexes differently varies with increasing amount of the amines introduced (Fig. 1a). Since both latexes were synthesized in the presence of the same emulsifier taken in identical amounts, the difference in the surface tension can be due to the latex polymer composition only. Evidently, more polar (because of a high content of bound chlorine in the polymer) surface of the DVKhB-70 latex particles absorbs the emulsifier less effectively than do the hydrophobic particles of DVKhB-Sh. This increases the amount of the emulsifier dissolved in the aqueous phase and decreases the surface tension of the latex.

The same factor is the reason why the surface tension of the DVKhB-70 latex remains virtually unchanged upon introduction of various amines (Fig. 1a, curves *4–6*). The surface tension of the DVKhB-Sh latex in the presence of the amines tends to decrease (Fig. 1a, curves *1–3*). The influence of the amines on the surface tension decreases in the order diethanolamine > ethanolamine > diethylamine. This suggests,

first, that the amines are differently adsorbed on the latex particle surface and, second, that not only the nitrogen atom, but also the alcoholic functional group are involved in the latex modification. Indeed, the behavior of ethanolamine in the butadiene–vinylidene chloride latex is similar to that of diethanolamine, but is manifested more weakly. Diethylamine contains no OH groups and exhibits no prominent surface activity, which is responsible for a minor decrease in the surface tension of the latex with increasing amount of diethylamine.

Also, the surface tension of the latex can be affected by formation of a new surfactant via the reaction of the alcoholic groups of the amine with the free carboxylic acid yielded by hydrolysis of the emulsifier, potassium soap of synthetic fatty acids. As is known, salts of diethanolamine and carboxylic acids are much more effective emulsifiers than potassium or ammonium soaps of the corresponding acids. Formation of a more effective emulsifier decreases the surface tension of the latex; diethanolamine is more actively involved in the formation of a soap with synthetic fatty acids, and the resulting surfactant is more effective.

During synthesis, storage, and processing of the latex, HCl can be spontaneously eliminated from the polymer macromolecules and can dissolve in the aqueous phase of the latex, thus decreasing its pH. Therefore, DVKhB-70 latex with a fivefold, compared to DVKhB-Sh, amount of bound chlorine has a smaller pH (Fig. 1b). Amines are capable of binding free HCl into quaternary ammonium salts with an enhanced surface activity, compared to the initial amines. Upon introduction of ethanolamine and diethylamine, pH of the DVKhB-Sh and DVKhB-70 latexes tends to increase (Fig. 1b, curves *2*, *3*, *5*, *6*). Evidently, binding of the eliminated HCl intensifies dehydrochlorination; the relative change in the pH is 0.15 and 0.63 pH units for DVKhB-Sh and DVKhB-70 latexes, respectively, which is almost four times that for DVKhB-Sh and suggests binding of a larger amount of free HCl. Diethanolamine virtually does not affect the pH of the latex, which suggests its reduced activity in binding of HCl.

The above-described processes should be responsible for the enhanced stability of the latexes. Indeed, adding the amines of interest in amounts of 1 and 2 wt parts per 100 wt parts of dry substance of the latex increases its mechanical stability (leads to a decrease in the percentage of coagulum) (Fig. 1c). The maximum enhancement of the mechanical stability is observed for diethanolamine-modified latexes (both DVKhB-Sh and DVKhB-70).

Additional adsorption of the amines on the latex particle surface, formation of new surfactants of different types in the system, increase in the pH of the latexes, and the known effect of the amines on the water structure will necessarily affect the viscosity of the latexes. The Hoeppler viscosity depends both on the type of the latex and on the nature and amount of the amine introduced (Fig. 1d). The viscosity of the DVKhB-70 latex remains virtually unchanged on introducing any type of amine (Fig. 1d, curves *4*–*6*). At the same time, the viscosity of the DVKhB-Sh latex decreases most significantly upon addition of diethanolamine in amounts exceeding 1 wt part per 100 wt parts of the dry latex.

CONCLUSIONS

(1) Introduction of amines into a ready-for-use butadiene–vinylidene chloride latex can improve its characteristics.

(2) Diethanolamine is the best modifier for DVKhB-70 and DVKhB-Sh latexes; ethanolamine and diethylamine improve the properties of these latexes to a smaller extent. The optimal amount of the modifier introduced is not larger than 1 wt part per 100 wt parts of the latex polymer. The amine-modified latexes exhibit reduced surface tension, as well as increased pH and improved mechanical stability.

REFERENCES

1. Averko-Antonovich, I.Yu. and Kalinina, I.E., *Sintez i ispol'zovanie lateksov polimerov i sopolimerov vinilidenkhlorida: tematicheskii obzor* (Synthesis and Use of Latexes of Polymers and Vinylidene Copolymers: A Topical Review), Moscow: TsNIITEneftekhim, 1995, issue 2.
2. Galimullin, A.I., Banderov, V.N., Averko-Antonovich, I.Yu., *et al.*, Abstracts of Papers, *VII Rossiiskaya nauchno-prakticheskaya konferentsiya rezinshchikov "Syr'e i materialy dlya rezinovoi promyshlennosti"* (VII Russian Conf. of Rubber Engineers "Resources and Materials for Rubber Industry"), Moscow: 2000, pp. 134–135.
3. Averko-Antonovich, I.Yu., *Vestn. Kazan. Tekhnol. Univ.*, Kazan, 2001, pp. 3–15.
4. Averko-Antonovich, I.Yu. and Averko-Antonovich, L.A., *Zh. Prikl. Khim.*, 1991, vol. 64, no. 7, pp. 1595–1597.
5. Reikhsfel'd, V.O., Erkova, L.N., and Ruban, V.L., *Laboratornyi praktikum po sinteticheskim kauchukam* (Laboratory Practical Guide on Synthetic Rubbers), Leningrad: Khimiya, 1967.

Russian Journal of Applied Chemistry, Vol. 78, No. 4, 2005, pp. 652–655. Translated from Zhurnal Prikladnoi Khimii, Vol. 78, No. 4, 2005, pp. 658–661.
Original Russian Text Copyright © 2005 by Mironovich, Nikozyat', Ivashchenko.

MACROMOLECULAR CHEMISTRY AND POLYMERIC MATERIALS

Curing of Divinyl Triethylene Glycol Bis-*o*-phthalate Films in the Presence of Photoinitiators

L. M. Mironovich, Yu. B. Nikozyat', and E. D. Ivashchenko

Sumy State University, Sumy, Ukraine

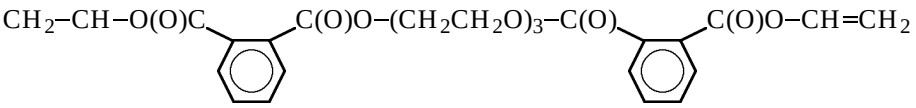
Poltava University of Ukrainian Consumers' Cooperative Societies, Poltava, Ukraine

Received January 13, 2005

Abstract—The film-forming properties of divinyl triethylene glycol bis-*o*-phthalate in air in the presence of a redox system and β-diketonates of transition metals were studied.

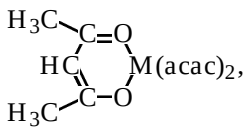
Oligoether acrylates are widely used in production of homopolymer and composite materials. Much attention is given today to photopolymerization of oligomers containing double bonds, because of the possibility of combining the polymerization and curing in a single process cycle and of using such compounds in production of optical disks, in protective and adhesive coatings, in polygraphy, and in stomatology [1, 2]. Promising photoinitiators (PIs) are transition metal β-diketonates because of their availability and high stability in storage [3]. There are virtually no data on the use of these photoinitiators for curing of films of vinyl oligomers.

In this study, we examined the photopolymerization of divinyl triethylene glycol bis-*o*-phthalate (DPT) in the presence of transition metal β-diketonates, with the aim to search for new applications of this vinyl oligomer.



DPT was prepared by the reaction of ethylene chlorohydrin with phthalic anhydride, followed by dehydrochlorination of the resulting monoester in the presence of alkali. The monovinyl *o*-phthalate thus obtained was brought into the reaction with triethylene glycol, which was performed by the azeotropic method in the presence of catalytic amounts of H_2SO_4. The properties of DPT agreed with those described in [4].

As PIs we used Co(III) and Fe(III) acetylacetonates



where M = Fe^{3+}, Co^{3+}.

The properties of the transition metal acetylacetonates agreed with those described in [5, 6]. The choice of these PIs was governed by their absorbing power, examined in [7].

Films (15–35 μm thick) were applied by casting a toluene solution onto quartz glass plates. Initially the samples were kept at 298–343 K and UV-irradiated with a DRT-400 quartz lamp, placed at a distance of 10 cm from the film surface, for 300 s at 298–343 K. To eliminate the inhibiting effect of atmospheric oxygen in the surface layer of DPT films, the films to be irradiated were covered with quartz glass (thickness ≤0.1 μm).

For comparison, we studied polymerization of DPT films in air at 353 K in the presence of a redox system consisting of 0.55% cyclohexanone hydroperoxide

1070-4272/05/7804-0652 © 2005 Pleiades Publishing, Inc.

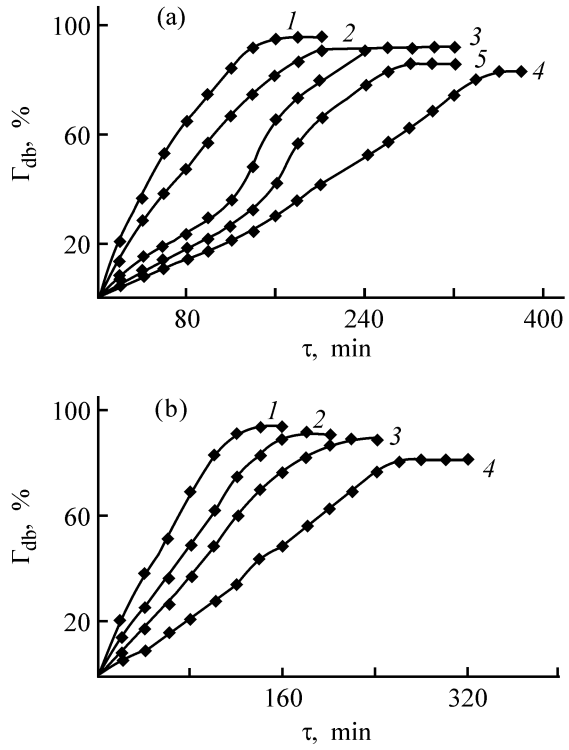


Fig. 1. Curing of DPT films at 353 K as influenced by the film thickness and concentrations of (a) iron(III) and (b) cobalt(III) acetylacetonates. Exposure time 300 s; photoinitiation temperature 298 K. (Γ_{db}) Conversion of double bonds and (τ) time; the same for Fig. 2. Film thickness, μm: (a) 15 and (b) 35. M(III) concentration, %: (*1*) 5, (*2*) 4, (*3*) 3, and (*4*) 2.5; (*5*) redox system 0.55% CHP + 0.1% CN.

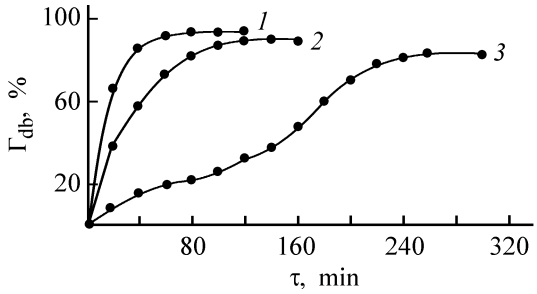


Fig. 2. Curing of DPT at 353 K in 35-μm films as influenced by the kind of photoinitiator. Exposure time 300 s, photoinitiation temperature 343 K, photoinitiator concentration 3%. Photoinitiator: (*1*) cobalt(III) acetylacetonate, (*2*) iron(III) acetylacetonate, and (*3*) redox system 0.55% CHP + 0.1% CN.

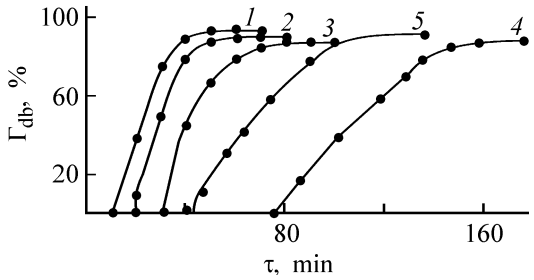


Fig. 3. Yield of three-dimensional polymer Γ_{td} in photopolymerization of DPT in 35-μm films vs. time τ. Exposure time 300 s, photoinitiator concentration 3%, drying at 353 K. Photoinitiation temperature, K: (*1, 2*) 343 and (*4, 5*) 298. Photoinitiator: (*1, 5*) cobalt(III) acetylacetonate, (*2, 4*) iron(III) acetylacetonate, and (*3*) redox system 0.55% CHP + 0.1% CN.

(CHP) and 0.1% cobalt naphthenate (CN) in terms of metal.

The conversion of double bonds in the films, Γ_{db}, was determined bromatometrically. The content of the three-dimensional polymer, Γ_{td}, was determined gravimetrically after extraction with boiling acetone for 6 h. The samples were dried at 353 K. The results are shown in Figs. 1–3.

The curing of DPT in films, irrespective of the initiation mode, photoinitiation temperature, and film thickness, occurs without any induction period (Figs. 1 and 2). The absence of the induction period in curing of DPT in the presence of the redox system in air (Fig. 1a, curve *5*; Fig. 2, curve *3*) is due to the free air access. Starting from the lowest conversions, double bonds are consumed under the conditions of film curing not only in the reactions $HO_2^{\bullet} + M \rightarrow MOOH$, but also in destructive oxidative transformations. The high conversion of the double bonds can be accounted for by the plasticizing effect of the –O–O– groups in the three-dimensional polymer formed in air.

The limiting degrees of film curing are close, 92–96% (Figs. 1a, 1b, curves *1–3*; Fig. 2, curves *1*, *2*) and exceed Γ_{db} in DPT polymerization in the presence of the redox system in air (Fig. 1, curve *5*; Fig. 2, curve *3*), irrespective of the film thickness and photoinitiation temperature, except in the experiments at the lowest PO concentration, 2.5 wt % (Figs. 1a, 1b, curves *4*).

The film curing rate grows with an increase in the PI concentration, irrespective of its nature, film thickness, and photoinitiation temperature.

The curing time is the shortest at a PI concentration of 5 wt % (Figs. 1a, 1b, curves *1*), but the physicomechanical characteristics of the resulting films are worse (Table 1). The photocuring of DPT film in the presence of $Co(acac)_3$ occurs faster (Fig. 2, curve *1*; the limiting Γ_{db} is attained in 80 min) than that in the presence of $Fe(acac)_3$ (Fig. 2, curve *2*; the limiting Γ_{db} is attained in 110 min).

Table 1. Physicochemical characteristics of DPT coatings (photoinitiation temperature 298 K, film thickness 15 μm)

$Fe(acac)_3$ content, wt %	Curing time at 353 K, min	Aging time at 298 K, h	Γ_{db}, %	Bending strength, mm	Impact strength, N m	Relative hardness
2.5	360	24	84	4	4.5	0.66
		168	88	4	4.5	0.65
		720	89	3	4.0	0.65
3	240	24	93	5	4.5	0.66
		168	94	5	5.0	0.66
		720	95	4	5.0	0.67
4	200	24	92	3	4.0	0.53
		168	94	3	4.0	0.55
		720	95	4	3.5	0.55
5	150	24	96	3	3.5	0.50
		168	97	3	3.5	0.53
		720	97	4	3.5	0.55

Table. 2. Physicochemical characteristics of DPT coatings (photoinitiation temperature 298 K, film thickness 35 μm)

Photo-initiator	Curing time at 353 K, min	Aging time at 298 K, h	Γ_{db}, %	Bending strength, mm	Impact strength, N m	Relative hardness
$Co(acac)_3$	220	24	92	5	5.0	0.66
		168	93	5	5.0	0.68
		720	95	5	5.0	0.68
$Fe(acac)_3$	260	24	92	5	5.0	0.66
		168	93	5	5.0	0.66
		720	93	5	4.5	0.67
Redox system	240	24	90	5	5.0	0.66
		168	90	5	4.0	0.66
		720	92	5	4.0	0.68

As can be seen from Table 1, the impact strength and relative hardness of the films decrease with an increase in the content of $Fe(acac)_3$. The film elasticity decreases in the course of thermal aging. The curing time decreases by a factor of 2.4 (from 360 to 150 min) with an increase in the PI concentration by a factor of 2. The coatings obtained at a PI concentration of 3 wt % meet the requirements to paint-and-varnish materials (Γ_{db} 94%, bending strength 5 mm, impact strength 5.0 N m, relative hardness 0.66 at a curing time of 240 min and aging time of 168 h); similar parameters are attained when a DPT film is cured in the presence of the redox system).

We examined the DPT film curing at a PI concentration of 3 wt %, photoinitiation temperature of 343 K, and film thickness of 35 μm. Figure 2 (curves *1*, *2*) shows that the general trends in the film curing are preserved, irrespective of the photoinitiation temperature and film thickness. The physicomechanical characteristics of the films cured at the optimal PI concentration of 3 wt % are listed in Table 2. It is seen that the films have a bending strength of 5 mm and a relative hardness of 0.66–0.68, irrespective of the initiation procedure. The impact strength of the photocured DPT films (4.5–5 N m) exceeds that of DPT films cured in the presence of the redox system (4–5 N m) and meets the requirements to protective coatings. Comparison of Tables 1 and 2 shows that, in photocuring of DPT films of different thicknesses in the presence of $Fe(acac)_3$, the curing time at the same photoinitiation temperature is longer in thicker films: 35 μm, 260 min; 15 μm, 240 min.

An important characteristic of curing is the kinetics of accumulation of the three-dimensional polymer. Figure 3 shows that the induction period of the three-dimensional polymerization is observed in all the cases,

irrespective of the initiation procedure. It is believed that, during the induction period, intermediate soluble polymers are formed, and the viscosity of the film-forming material increases. The induction period of the three-dimensional polymerization depends on the photoinitiation temperature. As the photoinitiation temperature is raised, the induction period becomes shorter. In particular, with $Co(acac)_3$, the induction period is 38 min at the photoinitiation temperature of 298 K and as short as 10 min at 343 K (Fig. 3, curves *1*, *5*). The same trend is observed with $Fe(acac)_3$ (Fig. 3, curves *2*, *4*). The induction period depends on the initiation procedure and kind of PI; at the photoinitiation temperature of 343 K, it increases in the order $Co(acac)_3 < Fe(acac)_3 <$ redox system.

The rate of the three-dimensional polymerization at a photoinitiation temperature of 343 K in the presence of $Co(acac)_3$ and $Fe(acac)_3$ (Fig. 3, curves *1*, *2*) is higher than the rate of the three-dimensional polymerization of DPT initiated with the redox system (Fig. 3, curve *3*), but at 298 K the rate is considerably lower (Fig. 3, curves *4*, *5*). The limiting degrees of conversion in the DPT photopolymerization (92–95%) differ insignificantly from those attained with the redox system.

The DPT photocured in the presence of $Fe(acac)_3$ has found use as a film-forming material in preparation of dentures by compression molding.

CONCLUSION

The rate of curing of divinyl triethylene glycol bis-*o*-phthalate films largely depends on the kind and concentration of the photoinitiator. As the photoinitiator concentration is increased, the physicomechanical characteristics of coatings based on divinyl triethylene glycol bis-*o*-phthalate get worse. The optimal photoinitiator concentration for the photopolymerization of divinyl triethylene glycol bis-*o*-phthalate is 3 wt %. The photocuring of divinyl triethylene glycol bis-*o*-phthalate is more efficient at elevated photoinitiation temperatures.

REFERENCES

1. Maslyuk, A.F. and Khranovskii, V.A., *Fotokhimiya polimerizatsionnosposobnykh oligomerov* (Photochemistry of Polymerizable Oligomers), Kiev: Naukova Dumka, 1989.
2. Shibanov, V.V., Mizyuk, V.L., and Milyashkevich, P.E., *Zh. Org. Khim.*, 1982, vol. 18, no. 5, pp. 1113–1117.
3. Nizel'skii, Yu.N., *Kataliticheskie svoistva β-diketonatov metallov* (Catalytic Properties of Metal β-Diketonates), Kiev: Naukova Dumka, 1983.
4. Salistyi, S.M., Mironovich, L.M., and Ivashchenko, E.D., *Zh. Prikl. Khim.*, 1999, vol. 72, no. 6, pp. 1094–1096.
5. Petrova, L.A., Borisov, A.P., Aleshin, V.V., and Makhaev, V.D., *Zh. Neorg. Khim.*, 2000, vol. 45, no. 3, pp. 390–394.
6. Brauer, G., *Handbuch der Präparativen anorganischen Chemie*, Stuttgart: Ferdinand Enke, 1954. Translated under the title *Rukovodstvo po neorganicheskomu sintezu*, Moscow: Mir, 1986, vol. 5, pp. 1510–1864.
7. Ustinov, A.Yu., *Zh. Fiz. Khim.*, 1995, vol. 69, no. 7, pp. 1268–1273.

Russian Journal of Applied Chemistry, Vol. 78, No. 4, 2005, pp. 656–662. Translated from Zhurnal Prikladnoi Khimii, Vol. 78, No. 4, 2005, pp. 662–668.
Original Russian Text Copyright © 2005 by Zagorskii, Kalnin'sh, Toropov.

MACROMOLECULAR CHEMISTRY AND POLYMERIC MATERIALS

Structure and Absorption Spectra of Polyhydroquinones

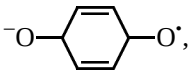
A. L. Zagorskii, K. K. Kalnin'sh, and D. K. Toropov

EKOTEK Research and Production Group of Companies, St. Petersburg, Russia
Institute of Macromolecular Compounds, Russian Academy of Sciences, St. Petersburg, Russia
Research Institute of Ultrapure Biopreparations, St. Petersburg, Russia

Received February 18, 2005

Abstract—Radical polymerization of hydroquinone was studied in an aqueous medium. Black polymers of low molecular weight (up to 1500 Da), poorly soluble in water and alcohols, are formed. *Ab initio* calculations of the steric and electronic structure and vibrational and electronic spectra of molecules containing 1 to 5 hydroquinone units were performed.

It is known that polymerization of hydroquinone under the action of alkali or atmospheric oxygen in alkaline medium gives low-molecular-weight oligohydro- and oligooxyhydroquinones [1, 2]. As compared to phenol and naphthol, hydroquinone is more reactive [3], which is caused by the mutual influence of two hydroxy groups. It has been shown [2] that oligomerization of hydroquinone yields semiquinone radical ions



which are further involved in recombination dimerization followed by hydrogen transfer from the core to carbonyl groups. Molecules of the reaction product consist of hydroquinone units in-series connected by C–C bonds. The structural studies performed did not confirm formation of the polymers in which adjacent aromatic rings are bound by C–O–C bridges [1].

Polyhydroquinones and polyphenols substantially differ in their properties from monomeric analogues; in particular, they show acidic properties [4] and exist as stable semiquinone-type polyradicals. It is believed that the unusual properties of the polymers are caused by conjugation in the polymeric chain, strong intra- and intermolecular bonds, and high local concentration of the hydroxy groups. Polymeric products with unusual black color are heat-resistant nonvolatile compounds, whose electrical properties can widely range and exhib biological activity.

It is interesting that the similar products can be prepared by *p*-benzoquinone polymerization [5–8]. Both the starting monomers, hydroquinone and *p*-benzoquinone, exist in equilibrium with each other in water or an organic solvent [9]. Crystalline quinone–hydroquinone complexes (so-called quinhydrone) undergo redox transformations with an increase in the difference between the hydroquinone ionization potential and quinone electron affinity [10]. It has been shown that transfer of two hydrogen atoms from hydroquinone to quinone occurs in the electron-excited state of quinhydrone [11].

p-Benzoquinone polymerizes under the action of an alkali or acid, and also under the action of Lewis acids, e.g., anhydrous $AlCl_3$ [7, 8]. Black oligomeric products (M_n = 810–1120) are well soluble in acetone and ethanol and melt at low temperatures (85–120°C). A study of *p*-benzoquinone polymerization products in all the cases revealed hydroquinone structure of units [6, 8] with *o*-substitution in the aromatic ring.

In this study, we performed radical polymerization of hydroquinone in an aqueous solution and examined the steric and electronic structure of polyhydroquinone by molecular spectroscopy and *ab initio* quantum-chemical calculations.

EXPERIMENTAL

The ESR spectra of polyhydroquinones were recorded on a BER-418 spectrometer both in the solid

1070-4272/05/7804-0656 © 2005 Pleiades Publishing, Inc.

state and as an aqueous solution (Fig. 1). The concentration of unpaired electrons (spins) was determined with a known reference, diphenylpicrylhydrazyl, which was taken as a mixture with an inert matrix; the concentration was 5×10^{18} per gram of substance. As compared to solids, the intensity of the ESR signal decreases in solution by approximately a factor of 10. In both cases, the signal is a single line with a 5-G width without resolved hyperfine structure, which is indicative of a complete delocalization of the unpaired electron and the lack of its magnetic interaction with protons.

The molecular weights of the polymer were determined by liquid exclusion chromatography in dimethylformamide with addition of trifluoroacetic acid (TFAA) and sodium trifluoroacetate (STFA) on a GMA Gel G-5 column (Fig. 2). Two fractions were studied. One of them (major) is limitedly (40 g l^{-1}) soluble in water, and its retention time τ = 45.5 min corresponds to a molecular weight of 650–700 Da. The second fraction is a water-insoluble precipitate; it is precipitated with water from the polymer solution in dimethylformamide and has shorter τ = 43.5 min corresponding to the molecular weight of 1500 Da (calibration against polystyrene).

Quantum-chemical calculations of the structure of molecules in the singlet S_0 and triplet T_1 states were performed with GAMESS software within RHF, ROHF/6-31G*, and SBK schemes. The electronic absorption spectra were calculated by the CNDO/S or ZINDO/S methods (HyperChem soft-ware); for *ab initio* calculations of the vibrational spectra, we used the GAMESS software. The theory and methods of quantum-chemical calculations were considered in more detail in [12].

Polymerization of hydroquinone under the action of a radical initiator is essentially nonequilibrium, which is apparently responsible for the polymer nonuniformity in molecular weights. The IR spectra of both isolated fractions in the solid state (Fig. 3) are similar, suggesting similar structures of the molecules.

The strong low-frequency shift of the bands of ν_{OH} stretching vibrations (2600 and 2300 cm^{-1}) indicates a very strong intrachain hydrogen bond OH…OH (Fig. 3, spectrum *2*). In the IR spectrum of the water-soluble fraction, these bands are less intense, probably, due to a shorter conjugated chain (Fig. 3, spectrum *1*). The band at 3380 cm^{-1} belongs to ν_{OH} stretching vibrations of absorbed water, which is always present in air-dry polyhydroquinone. The band at 3300 cm^{-1} belongs to hydroxy groups involved in moderately strong intrachain and intermolecular hydrogen bonding, O–H…OH.

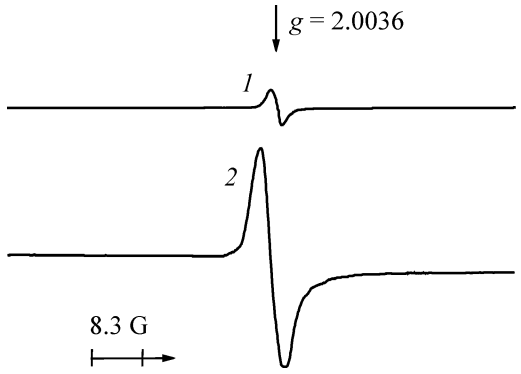


Fig. 1. ESR spectra of solid (*1*) diphenylpicrylhydrazyl and (*2*) polyhydroquinone.

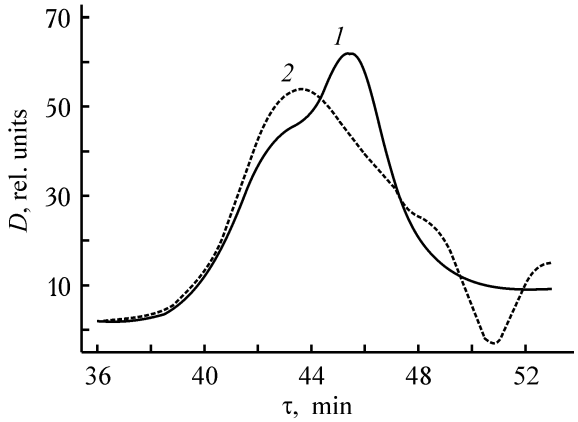


Fig. 2. Chromatogram of polyhydroquinone in DMF + 0.05 M STFA + 0.005 M TFAA on a GMA Gel G-5 column. (*D*) Optical density and (τ) time. (*1*) Fraction soluble in water and (*2*) precipitate; the same for Fig. 3.

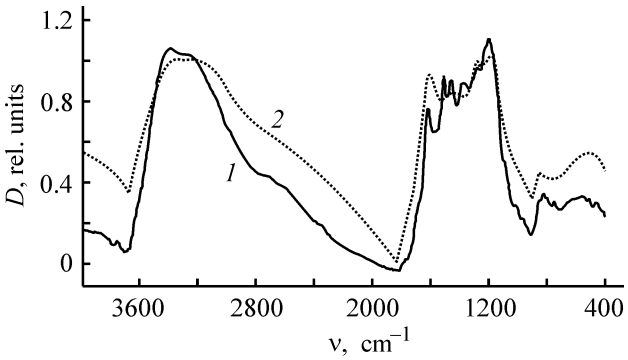


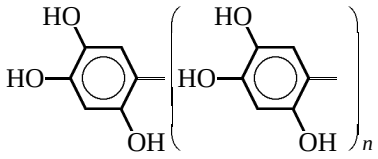
Fig. 3. IR spectra of polyhydroquinone in KBr pellets: (*D*) optical density and (ν) wavenumber; the same for Fig. 4.

A strong band at 1600 cm^{-1} should be assigned to the stretching, so-called breathing C–C vibrations of the aromatic ring. For unconjugated compounds, this band is weak, but its intensity sharply increases with increasing number of aromatic rings in the conjugated

Table 1. Calculated (RHF/SBK) frequencies ν and intensities *I* ($D^2/Å^2$) of polyhydroquinones [scheme (I)] (scaling factor for frequencies is 0.9)

Number of units, *n*	(ν, cm^{-1})/(*I*, rel. units) for indicated thransition							
	no. 1	no. 2	no. 3	no. 4	no. 5	no. 6	no. 7	no. 8
1	1644 / 0.18	1633 / 1.47						
2	1655 / 1.73	1630 / 0.36	1619 / 2.12	1604 / 0.59				
3	1655 / 2.45	1643 / 0.05	1630 / 0.53	1619 / 2.29	1607 / 0.03	1579 / 0.30		
1	1656 / 2.75	1646 / 0.02	1638 / 0.01	1628 / 0.57	1620 / 2.29	1607 / 0.01	1589 / 0.24	1571 / 0.13

chain. This conclusion is confirmed by *ab initio* calculations of the vibrational spectrum of the first members of the polyhydoquinone series (Table 1):



$n = 0–4.$ (I)

Table 1 shows that the calculated intensities of IR transitions related to stretching $\nu_{C=C}$ vibrations at 1600 cm^{-1} increase with lengthening of the polymeric chain. Values of *I* in Table 1 are comparable with *I* for the most intense transitions in the IR spectra, such as, e.g., $\nu_{C=O}$ stretching vibrations. The calculated data confirm the assignment of the broad and intense band at 1600 cm^{-1} to $\nu_{C=C}$ stretching vibrations of the conjugated aromatic rings.

Bands at 1530 and 1470 cm^{-1} are also associated with $\nu_{C=C}$ stretching vibrations. The high-frequency shoulder at 1730 cm^{-1} of the 1640 cm^{-1} band can be assigned to $\nu_{C=O}$ stretching vibrations of the terminal units of the polyhydroquinone molecules bearing an unpaired electron. The strongest band at 1200 cm^{-1} belongs to $\nu_{C–OH}$ stretching vibrations of the polymer. The structured band at 825 cm^{-1}, belonging to out-of-plane bending vibrations of C–H bonds of aromatic rings, should also be noted.

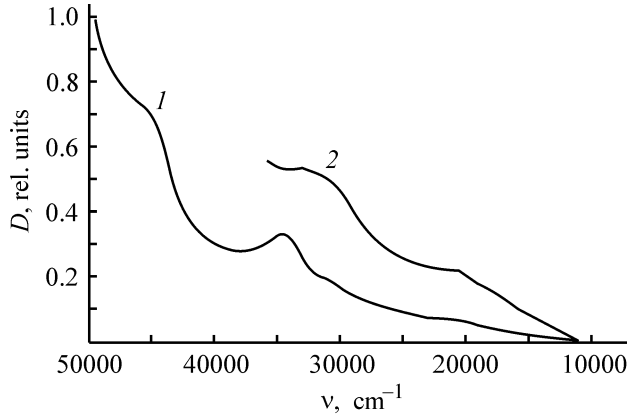


Fig. 4. Absorption spectra of polyhydroquinone: (*1*) solution in water and (*2*) precipitate from aqueous solution in dimethylformamide.

In the electronic absorption spectrum of polyhydroquinone in the UV–VIS region, several broad bands are observed (Fig. 4). The black (brown in dilute solution) color of the polymer is caused by a broad band ($\pi–\pi^*$ transition) peaked at 34500 cm^{-1}, which extends throughout the visible region of the spectrum (Fig. 4, spectrum *1*). At least two bands at 30700 and 28000 cm^{-1}, probably assigned to minor components of polyhydroquinone, are seen on the low-frequency wind of this broad band. Finally, a structured band at 20000 cm^{-1} is observed. In the high-molecular-weight fraction studied in dimethylformamide (Fig. 4, spectrum *2*), these bands are shifted to lower frequencies, to 30000, 28000 and less than 28000 cm^{-1}. This shift is caused in part by the specific effect of dimethyformamide as a solvent, but the main reason is the lengthening of the polyhydroquinone polymeric chain.

Generally, the ^1H and ^{13}C NMR spectra furnish the most complete information on the polymer structure. However, NMR spectra cannot be measured in the case in question because of the presence of paramagnetic particles, which broaden the signal and the spectrum. Therefore, we used quantum-chemical calculations to gain insight into three structural characteristics: (1) mode of binding of the adjacent aromatic rings, C–C or C–O–C; (2) intrachain conjugation be-

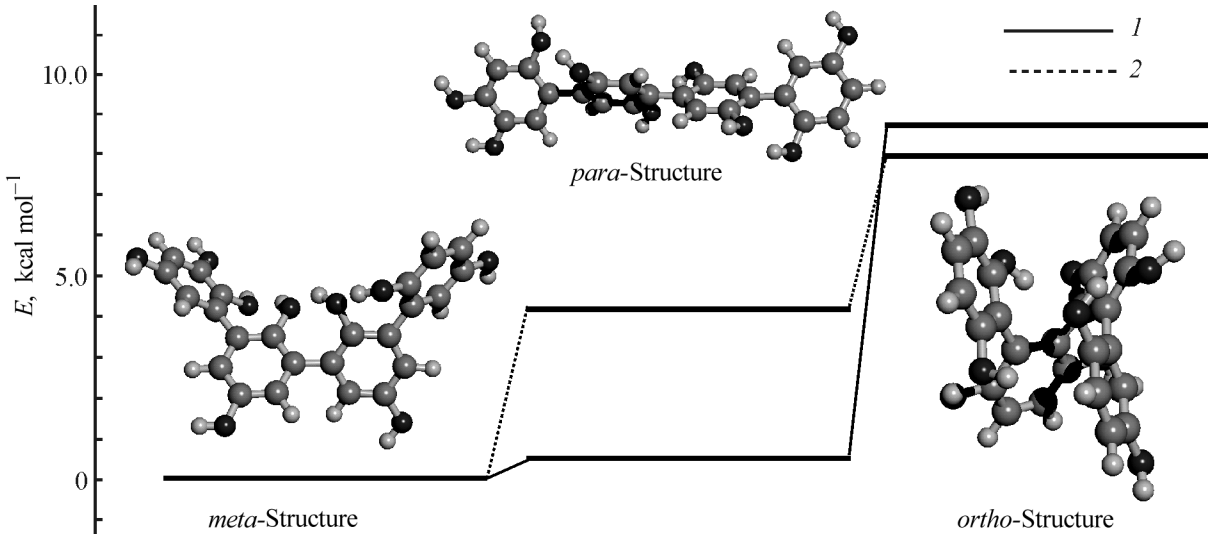


Fig. 5. Relative energies *E* of model polyhydroquinone molecules consisting of four units in *ortho*, *meta*, and *para* configurations, according to (*1*) PM3 and (*2*) RHF/SBK calculations.

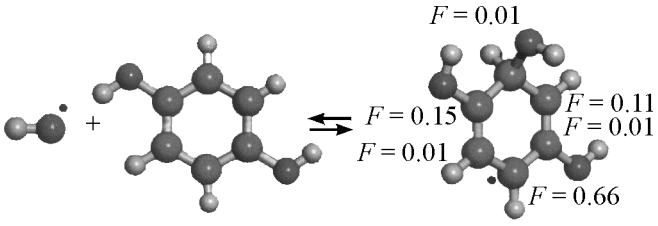
tween adjacent units; and (3) mechanism of chain termination during polymerization. The last item is directly associated with the nature of the paramagnetic species. Elucidation of these questions is necessary for understanding of both the polymerization mechanism and the structure and properties of the polymerization product.

Assuming that the monomeric units in polyhydroquinone are bound with each other by the C–C bonds, let us consider three probable kinds of binding of two adjacent rings: 1) *ortho*, 2) *meta*, and 3) *para* (Fig. 5). In the first case, a compact spiral structure of the polymeric chain with close contacts (< 3 Å) between the atoms of the distant rings is formed. Such a strained structure is the least favorable energetically, being inferior to the *para* structure by 3.76 kcal mol^{-1} and to the *meta* structure at n = 4 by 7.94 kcal mol^{-1} (RHF/SBK calculation). A semiempirical PM3 calculation gives somewhat different relative energies (Fig. 5): the *ortho* structure lies higher than the most stable *meta* structure by 8.73 kcal mol^{-1}, and the *para* and *meta* structures are close to in energy.

In the *ortho* structure, the distance between the adjacent hydroxy groups OH…OH is the longest: 1.9–2.2 Å. This value corresponds to a weak H bond. Conjugation along the molecular chain is characterized by the dihedral angle γ, which determines the mutual orientation of the adjacent aromatic rings. In this parameter, the *ortho* structure is also less favorable than the other two structures: γ = 57°–70°. These results allow us to rule out an *ortho* addition as a way of junction of adjacent aromatic rings in polyhydroquinone.

The *para* structure is characterized by a moderately strong intrachain H bond OH…O ($R_{OH...O}$ = 1.83–1.85 Å); dihedral angles γ are 49.2°–49.8°. For the most stable *meta* structure, we obtained by RHF/SBK method the shortest, and hence the strongest, H bonds OH…H ($R_{OH...O}$ = 1.76–1.82 Å). According to the available data, *ab initio* RHF/SBK method may overestimate the contribution of H bond to the total energy of the molecule, which may be responsible for the lower (by 4.18 kcal mol^{-1}) energy of *meta* structure, compared to *para* structure. When calculated by the semiempirical PM3 method, which is usually used for theoretical estimation of the H bond strength, both structures have close energies and the same lengths of the H bond, 1.83 Å (Fig. 5).

Along with the energetic criterion, the probability of formation of a chemical compound is determined by the spin population, or by indices of free valence on the atoms of the reaction structure. Equation (1) reflects the initial step of polymerization of hydroquinone in which the OH• radical adds to the carbon atom of the aromatic ring to give a radical-type σ complex:

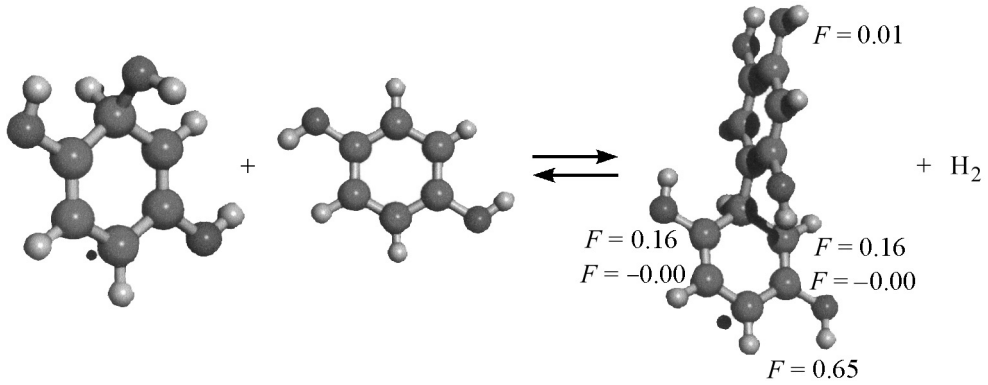


Scheme 1.

The enthalpy ΔH of reaction (1) is negative and equal to –2.2 kcal mol^{-1} (RHF and ROHF/6-31G* calculations), i.e., the initiation is thermodynamically feasible. The spin populations or indices of free valence in Scheme (1) reveal the reactive carbon atoms of the σ complex. The C_{para} atom (F = 0.66) is the most active, and the hydroquinone molecule should be attacked just through this atom to give a dimeric product.

The unsubstituted C_{ortho} atom is less reactive (F = 0.11), while the C_{meta} atom with the zero index of free valence is inactive. Hence, in the radical polymerization of hydroquinone, addition to the *meta*-carbon atom is forbidden by the spin control principle.

The next step of the reaction, addition of the hydroquinone molecule to the primary radical σ complex, is shown in Scheme (2):



Scheme 2.

This step yields a dimeric radical σ complex and a hydrogen molecule. The distibution of the indices of free valence is the same as that for the primary complex: the carbon atom in the *para* position (F = 0.65) is the most reactive; addition to it of the next hydroquinone molecule should give the trimeric σ complex. As in the case of the monomeric σ complex, the carbon atom in the *ortho* position is less reactive (F = 0.16). Hence, propagation of the polymeric chain through this center is unlikely. In addition, the *ortho* structure is, as already mentioned, energetically less favorable relative to the other two structures. The C_{meta} carbon atom in the dimeric complex is characterized by a zero index of free valence and is inactive in addition. The propagation of the polymeric chain stops in the stage of chain termination, which is probably caused by the substantial decrease in the reactivity of the radical center. The polymerization of hydroquinone stops in a rather early stage, after addition of only 10–15 units. In this context, a question arises concerning the termination mechanism of polymerization.

We believe that the propagation of the polymeric chain stops because of the rapid increase in degree of conjugation along the polyhydroquinone chain with its lengthening in the initial step of the reaction, which results in delocalization of the unpaired electron and its stabilization with loss of reactivity of the propagating radical center. The degree of conjugation can be characterized by the frequency and intensity of the low-frequency electronic transition.

The calculated electronic spectra of the series of molecules differing in chain length and kind of junction between the monomeric units are listed in Table 2. The number of π–π^* transitions in the low-frequency region of the spectrum is equal to the number of aromatic rings, but the lowest (in energy) transition is delocalized and related to the whole molecule. It can be seen that, in the case of *para* junction, the frequency of the lowest transition monotonically decreases, and its intensity sharply increases at the expense of high-frequency transitions, reaching a value that is limiting for ZINDO/S at a chain length of five units. For molecules containing five and more units, this transition lies in the visible region and, because of the very high intensity, should impart dark color to the substance.

The *ortho* substitution does not produce any conjugation in the molecular chain or in the system of H bonds. In this case, the spectrum of the spectrum should be similar to the spectrum of the initial hydroquinone, i.e., a substance with such a chain structure should be colorless. As can be seen from Table 2, the *meta* substitution also cannot be responsible for the observed deep color of polyhydroquinone because of the low intensity of low-frequency transitions. In

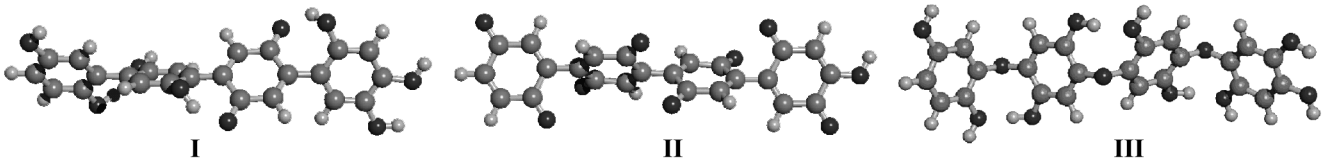
Table 2. Calculated (ZINDO/S) absorption spectra of polyhydroquinones [scheme (I)] containing different numbers of hydroquinone (*n*) and quinoid (*m*) units with different junction modes (ν, frequency, cm^{-1} and *f*, oscillator strength)

Number of units, *n*	(ν, cm^{-1})/*f* for indicated thransition				
	no. 1	no. 2	no. 3	no. 4	no. 5
			C–C_{para}		
1	34682 / 0.046				
2	32973 / 0.252	33619 / 0.096			
3	32873 / 0.154	32951 / 0.129	33491 / 0.107		
4	32435 / 0.715	32832 / 0.000	33220 / 0.040	33690 / 0.084	
n = 3, *m* = 1 (Fig. 6, *I*)	25646 / 0.312	23671 / 0.000	21520 / 0.000	21136 / 0.000	
n = 0, *m* = 4 (Fig. 6, *II*)	36778 / 1.007	32867 / 0.038	32214 / 0.016	31461 / 0.004	30230 / 0.014
5	32030 / 1.040	32743 / 0.052	32970 / 0.001	33124 / 0.025	33720 / 0.100
			C–C_{ortho}		
4	32671 / 0.008	33019 / 0.026	33293 / 0.027	33827 / 0.034	
			C–C_{meta}		
4	32742 / 0.017	32946 / 0.115	33215 / 0.089	33728 / 0.094	
			C–O–C_{para}		
3	33530 / 0.061	33641 / 0.003	34172 / 0.044		
4	33307 / 0.135	33469 / 0.013	33628 / 0.015	34422 / 0.027	

addition, as noted above, formation of the *meta* structure is forbidden by the spin control principle.

After oxidation of polyhydroquinone and substitution of one of the four units of the *para* structure by the quinoid unit (Fig. 6, structure **I**), a substantial long-wave shift of the intense electronic transition at 32435 (0.715) cm^{-1} is observed (Table 2), with its intensity somewhat decreasing. The appearance of the absorption at 25000 cm^{-1} should impart dark color to the substance. At the same time, polybenzoquinone (which is the product of complete polyhydroquinone oxidation) (Fig. 6, structure **II**) should have, in accordance with the calculated absorption spectrum, a weak yellow color, similarly to *para* benzoquinone. Probably, in partially oxidized polyhydroquinone, inclusion of the quinoid ring in the conjugation chain provides more efficient interaction of the monomeric units than in the initial polymer.

Thus, the above analysis showed that the oxidation of polyhydroquinone and conversion of a certain amount of hydroquinone units into quinoid units is accompanied by a shift of intense π–π^* transitions into



I **II** **III**

Fig. 6. Optimized (RHF/SBK) structure of the model molecules: (**I**) partially oxidized polyhydroquinone (*n* = 3, *m* = 1), (**II**) polybenzoquinone (*n* = 0, *m* = 4), and (**III**) polyhydroquinone with an ether bond between units (*n* = 4).

the visible region, which can account for the experimentally observed black color of the polymer.

Table 2 can clarify the question being discussed in the literature, concerning the possibility of formation of ether bonds C–O–C in the polyhydroquinone chain. For instance, Anderson *et al.* [1], based on the ESR spectra, suggest formation of a dimeric product with the ether bond between the rings during oxidation of fluoro- and chloro-substituted hydroquinones. We calculated the structure and absorption spectra of polyhydroquinones with an ether bond between the units (Fig. 6, structure **III**; Table 2). In agreement with the later published results, the calculated data do not confirm the existence of any substantial amounts of units bound by ether bridges. In such structures, the electronic transitions should have low intensity and lie in the UV region; they cannot be responsible for the experimentally observed black color of the polymer.

CONCLUSIONS

(1) Black polyhydroquinones with a molecular weight less than 1500 Da, weakly soluble in water and alcohols, were prepared by polymerization of hydroquinone in water under the action of a radical initiating system.

(2) Polyhydroquinones are characterized by long-lived paramagnetism (existing for no less than a year). In the solid state and in water, the ESR signal is a single line with a 5-G width and without resolved hyperfine structure.

(3) *Ab initio* quantum-chemical calculations of polyhydroquinone molecules with a chain length of up to six units with *ortho*, *meta*, and *para* substitution in the aromatic ring were performed. The *para* structure with the single C–C bond between the hydroquinone rings is the most probable configuration of the polymeric chain.

(4) Termination of the chain propagation in the early stage of polymerization of hydroquinone is probably caused by a sharp decrease in the reactivity of the propagating radical center because of the delocalization of the unpaired electron in the polyconjugated molecular chain.

REFERENCES

1. Anderson, D.U., Frank, P.J., and Gutowsky, N.S., *J. Chem. Phys.*, 1960, vol. 32, no. 1, pp. 196–204.
2. Ragimov, A.V., Mamedov, B.A., Guseinov, S.A., and Liogon'kii, B.I., *Vysokomol. Soedin.*, 1982, vol. 24, no 10, pp. 2125–2129.
3. Ragimov, A.V., Mamedov, B.A., Guseinov, S.A., *et al.*, *Vysokomol. Soedin.*, 1983, vol. 25, no 4, pp. 776–780.
4. Ragimov, A.V., Sadykh-Zade, S.I., Suleimanov, S.S., and Liogon'kii, B.I., *Vysokomol. Soedin.*, 1974, vol. 16, no. 6, pp. 1222–1227.
5. Liogon'kii, B.I., Ragimov, A.V., Bektashi, F.T., and Nagiev, A.Yu., *Dokl. Akad. Nauk, SSSR*, 1982, vol. 266, no. 4, pp. 903–907.
6. Sadykh-Zade, S.I., Ragimov, A.V., Suleimanov, S.S., and Liogon'kii, B.I., *Vysokomol. Soedin.*, 1972, vol. 14, no 6, pp. 1248–1255.
7. Berlin, A.A., Ragimov, A.V., Sadykh-Zade, S.I., and Gadzhiev, T.A., *Vysokomol. Soedin.*, 1973, vol. 15, no 6, pp. 788–791.
8. Medvedev, Yu.V., Sidorkina, N.V., Kol'tsov, A.I., *et al.*, *Vysokomol. Soedin.*, 1975, vol. 17, no 3, pp. 557–563.
9. Kalninsh, K.K., *J. Chem. Soc., Faraday Trans. 2*, 1982, vol. 78, pp. 327–337.
10. Kalninsh, K.K., *Elektronnoe vozbuzhdenie v khimii* (Electronic Excitation in Chemistry), St. Petersburg: Sankt Peterb. Gos. Univ. Tekhnol. Dizaina, 1998.
11. Kalninsh, K.K., *J. Chem. Soc., Faraday Trans. 2*, 1984, vol. 80, pp. 1529–1538.
12. Kalnin'sh, K.K. and Semenov, S.G., *Zh. Prikl. Khim.*, 2003, vol. 76, no. 10, pp. 1585–1600.

Russian Journal of Applied Chemistry, Vol. 78, No. 4, 2005, pp. 663–666. Translated from Zhurnal Prikladnoi Khimii, Vol. 78, No. 4, 2005, pp. 669–672.
Original Russian Text Copyright © 2005 by Chichkanov, Myagchenkov.

MACROMOLECULAR CHEMISTRY AND POLYMERIC MATERIALS

Toms Effect as Influenced by the Glass Capillary Length and Diameter

S. V. Chichkanov and V. A. Myagchenkov

Kazan State Technological University, Kazan, Tatarstan, Russia

Received September 16, 2004; in final form, February 2005

Abstract—The degree of reduction of the hydraulic resistance was studied as influenced by the concentration of the anionic copolymer of acrylamide, geometric parameters of the contour, and turbulent flow velocity.

High-speed transportation of oil-containing dispersed systems via main pipelines with the use of polymeric additives, such as, e.g., polyolefins, for reducing the hydraulic resistance of turbulent oil streams (Toms effect) has recently demonstrated a high economic efficiency [1–4].

The prospects for use of water-soluble polar polymers, e.g., (co)polymers of acrylamide, for intensifying the mass transfer of oil-containing dispersed system still remain to be elucidated more precisely. The use of water-soluble (co)polymers for reducing the hydraulic resistance of oil streams under turbulent flow mode is especially urgent in view of the fact that the water content of the extracted crude oil tends to increase [5]. For real objects, the dispersion media are mostly complex systems with variable parameters, including pH, ionic strength, concentration of active components, etc. All this affects the resulting macroscopic Toms effect. Quantitative studies of the Toms effect as influenced by various factors (parameters of the medium and of the restricting contour and characteristics of the polymeric additive) become increasingly important.

We have demonstrated earlier [6–9] that the Toms effect is strongly dependent on the chemical nature, molecular parameters, and concentration of the polymeric additives, pH, ionic strength of the medium, and the content of active components (polymers, surfactants, electrolytes) in it. We assumed that, near the inner surface of the capillary, there is a special near-wall zone of the stream [6, 9], in which the optimal concentration of the polymeric additive is created, preventing the spread of turbulent waves from the wall to the core of the stream. A rather thin electrical double layer (EDL) is formed on the inner wall of the tubes (capillaries), whose parameters strongly affect the resulting balance of the attraction and repulsion forces between the charged macroions of the polymer and the capillary wall. Changes in such parameters of the medium as pH or ionic strength affect the conformation and size of the polymer macromolecules, as well as the ratio between the sizes of the near-wall layer and EDL, thus affecting the Toms effect.

Also, the performance of polymeric additives in reducing the hydraulic resistance of turbulent streams is governed by the diameter, length, and the degree of branching of the pipeline network. Clearly, conducting numerous experiments on real pipelines is a difficult and, in most cases, impossible task. Theoretical studies of the transportation of crude oil via pipelines have not received wide acceptance, since they are suitable only for selected special cases and require some simplifying prerequisites and assumptions. Now, hydraulic processes are being studied fairly successfully by the experimental method based on the similarity theory: A pipeline is simulated in a reduced, compared to the original, scale, so that the process of interest is reproduced "in miniature," with all the relationships being preserved. Specifically this approach was taken in developing the experimental procedure in this study.

Here, we examined how the concentration of acrylamide (co)polymers and the geometric parameters of the contour (capillary diameter and length) affect the degree of reduction of the hydraulic resistance of turbulent water streams. The experiments were run in a modified turbulent rheometer.

1070-4272/05/7804-0663 © 2005 Pleiades Publishing, Inc.

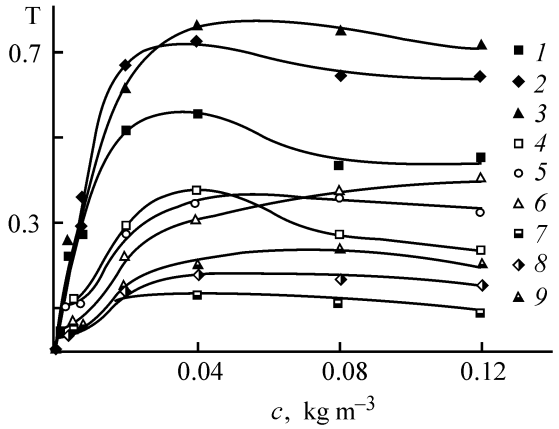


Fig. 1. Variation of the Toms effect T with the copolymer concentration c for a capillary with a fixed diameter $d_c = 0.84 \times 10^{-3}$ m. l_c, m: (*1–3*) 0.6, (*4–6*) 0.15, and (*7–9*) 0.075. p, atm: (*1*, *4*, *7*) 5, (*2*, *5*, *8*) 10, and (*3*, *6*, *9*) 15.

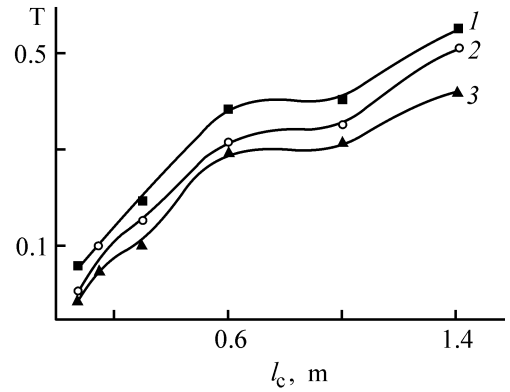


Fig. 2. Variation of the Toms effect T with the capillary length l_c at $c = 0.08$ kg m^{-3}. $d_c = 0.84 \times 10^{-3}$ m. p, atm: (*1*) 5, (*2*) 10, and (*3*) 15.

EXPERIMENTAL

In experiments on studying the direct-current turbulent flow of aqueous media with polymeric additives, we used Alcoflood 1175A acrylamide–sodium acrylate anionic copolymer available from Allied Colloids, the United Kingdom, with the molecular weight $M = 10.8 \times 10^6$ and 21.5 wt % of ionic (acrylate) units.

The experimental setup (modified turbulent rheometer) consisted of a thick-walled reservoir, into which the liquid under study was poured, and a glass capillary connected to the reservoir. Under excess pressure of a gas (nitrogen) in the reservoir, the liquid flowed via the capillary into the receiver which was weighed on a one-arm electronic balance (for details, see [10]). An advantage offered by this setup is operation with a set of separate glass capillaries, which allowed the capillary length and diameter to be easily varied within the desired range. During the experiment, the capillary length l_c was widely varied from 0.075 to 1.410 m, and the diameter d_c, from 0.84×10^{-3} to 2.61×10^{-3} m.

The Toms effect was estimated by the formula

$$T = (m - m_0)/m_0,$$

where m_0 and m are the gravimetric flow rates of the liquid without and with a polymeric additive, respectively [6].

Let us consider the dependence of T on the polymer concentration c (Fig. 1) for capillaries with a fixed diameter $d_c = 0.84 \times 10^{-3}$ m and different lengths l_c of 0.075, 0.15 and 0.60 m.

Figure 1 shows that, first, the concentration dependences of T are virtually identical for all the capillary lengths and differ only in the scale (magnitude of T). The fact that the $T = f(c)$ dependences are similar has been noted by the majority of researchers [1, 11]. With increasing polymer concentration, T initially tends to increase and then, upon achieving certain optimal concentration, approaches a constant value or begins to smoothly decrease. Second, T clearly tends to decrease with increasing pressure (at constant l_c and d_c) and with decreasing l_c.

To get a more specific and clearer insight into the dependence of the Toms effect on l_c, we carried out a special series of experiments, taking the capillary with the diameter $d_c = 2.61 \times 10^{-3}$ m and initial length $l_c = 1.41$ m as the initial capillary. After the experiment, we prepared from this capillary other capillaries with smaller l_c. We gradually reduced the capillary length and thus obtained a set of experimental data on how the Toms effect T is influenced by l_c. This excluded complications caused by the use of different capillaries, associated, above all, with different surface characteristics.

Figure 2 shows how the Toms effect T varies with l_c at $c = 0.08$ kg m^{-3}. It is seen that, with increasing l_c, the polymeric additive tends to perform better. Such a run of the curves is fairly unusual and even paradoxical. With increasing length and unchanged diameter of the capillary, the liquid flow rate tends to decrease, since the pressure loss by turbulent friction of the stream tends to grow with increasing l_c. This is also confirmed by our experimental data: The Reynolds number (Re) for water tends to decrease with increasing l_c (see table).

The Reynolds number of water for various capillary lengths l_c and pressures p ($d_c = 2.61 \times 10^{-3}$ m)

l_c, m	Re at indicated p, atm			l_c, m	Re at indicated p, atm		
	5	10	15		5	10	15
0.075	33980	56290	68600	0.60	21770	37040	47420
0.15	32100	50710	63420	1.00	12190	21210	27250
0.30	27730	46500	57840	1.41	16920	29140	37770

As to the rheological relationships revealed in this study for aqueous solutions of the polymers, there is an essential difference in the T-vs.-Re and T-vs.-l_c experimental dependences obtained by different authors [12, 13]. Kulik carried out the most systematic study in this field [13] and, taking polyoxyethylene as an example, showed that the degree of reduction of the hydraulic resistance of a turbulent stream tends to grow with increasing l_c.

We qualitatively explain the results presented in Fig. 2 on the basis of the fundamental concepts of hydraulics. From this viewpoint, the reservoir–glass capillary joint can be regarded as a kind of a local hydraulic resistance of the "internal nozzle" type, when the liquid outflows under pressure [14] (Fig. 3).

When coming out of the reservoir into the capillary with diameter d_c, a liquid jet is first compressed, then gradually expands, and at a certain length once again fills the entire cross section of the capillary. The jet can be compressed by 20 % [15]. The higher the flow rate of the liquid, the longer the section with the length l_1 within which the jet is compressed. In the zone of compression of the jet, an area with vortical movement of the liquid is formed (Fig. 3, zone *A*). However, after passing the section with length l_1, the stream of the liquid is not yet in equilibrium, since the hydraulics of turbulent streams should also take into account the length of the straight section of the pipe l_2, within which the local resistance ceases to exert a disturbing impact on the stream. The length of this section depends on the type of local resistance, Re, l_c, and roughness and generally can reach (20–50)d_c [15]. Thus, the near-wall zone of a turbulent stream with stable characteristics is formed only after this section with the length l_2 is passed, and in capillary sections 1 and 2 (Fig. 3) the polymer either does not act at all as a turbulence quencher or executes this function only partially.

For the pressures p of interest (5, 10 and 15 atm), we tentatively estimated at 0.05–0.13 m the length of the section where the local resistance is important. This suggests that, in 0.075-and 0.15-m-long capillaries, the Toms effect should either be small or completely lacking, which is really the case, as can be seen from Fig. 2. Naturally, the lengths of the unstable zones of stream l_1 and l_2 tend to become shorter with decreasing flow velocity (and Re), most prominently near the transition area from turbulent to laminar mode of the liquid flow. With increasing l_c, the relative length of the stable section, where the polymer performs at full power, tends to increase, thus improving the performance of the polymeric additive. Figure 2 shows that, already at $l_c = 0.30$ m, the Toms effect T begins to increase and becomes appreciable. This can also account for the nature of the dependence of T on p: The Toms effect naturally decreases with increasing p.

This assumption is also confirmed by the results reported by Gnativ [16], who analyzed how polymeric additives affect the local hydraulic resistances, for which abrupt expansions and constrictions of the pipeline are responsible. He showed that the capability of the additives to reduce the hydraulic friction resistance, lacking (or weakly manifested) when a polymer solution flows through local resistance, is restored downstream.

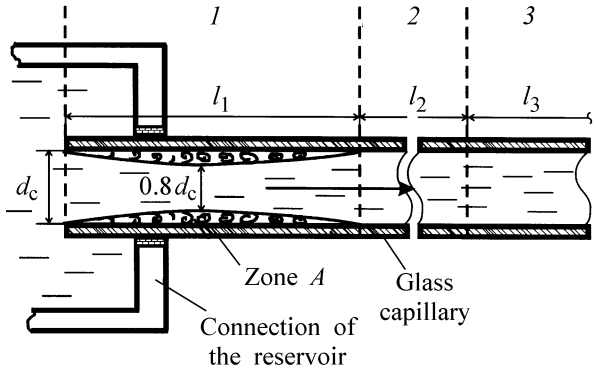


Fig. 3. Schematic structure of the turbulent stream in a capillary. Section: (*1*) compression of jet, (*2*) stabilization of the flow mode, and (*3*) working section.

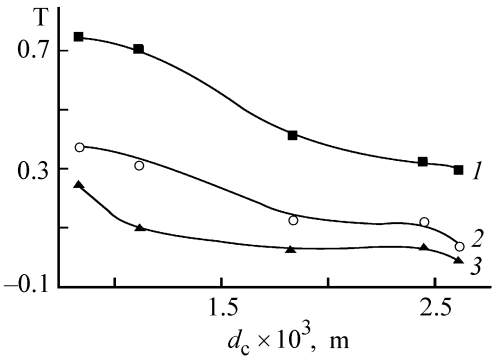


Fig. 4. Variation of T with the capillary diameter d_c at the pressure in the reservoir p = 15 atm. l_c, m: (*1*) 0.6, (*2*) 0.15, and (*3*) 0.075.

This is also validated indirectly by our studies of the Toms effect T as influenced by d_c (Fig. 4). For all the three capillary lengths studied, T clearly tends to decrease with increasing d_c (i.e., with decreasing l_c/d_c), especially in the initial segments of the curves. Common knowledge suggests that, with increasing d_c, the length of the capillary sections characterized by unstable mode of the liquid flow will also increase (Fig. 3, sections *1* and *2*). As a result, the polymeric additive performs worse in reducing the hydraulic resistance of a turbulent stream of liquid throughout the capillary length ($l_1 + l_2 + l_3$), which eventually decreases the Toms effect T.

CONCLUSIONS

(1) The degree of reduction of the hydraulic resistance of turbulent water streams was studied on a modified turbulent rheometer as dependent on the concentration of a polymeric additive and the geometric parameters of the contour (capillary diameter and length). For all the capillary diameters and lengths studied, these dependences are virtually identical, with the only difference in the scale.

(2) A probable reason for the rise in the Toms effect with increasing length and decreasing diameter of the capillary is the instability of the turbulent stream of the liquid in the initial section of the capillary.

REFERENCES

1. Manzhai, V.N., Echevskaya, L.G., Ilyushnikov, A.V., *et al.*, *Zh. Prikl. Khim.*, 2004, vol. 77, no. 3, pp. 456–460.
2. Malkin, A.Ya., Nesyn G.V., Manzhai V.N., and Ilyushnikov, A.V., *Vysokomol. Soedin., Ser. B*, 2000, vol. 42, no. 2, pp. 377–384.
3. Nesyn, G.V., Manzhai, V.N., and Ilyushnikov, A.V., *Inzh.-Fiz. Zh.*, 2003, vol. 76, no. 3, pp. 142–146.
4. Zvereva, T.V., Chelintsev, S.N., and Yakovlev, E.I., in *Modelirovanie truboprovodnogo transporta neftekhimicheskikh proizvodstv* (Simulation of Pipeline Transportation in Petrochemical Productions), Moscow: Khimiya, 1987.
5. Tronov, V.P., *Promyslovaya podgotovka nefti* (Pretreatment of Oil at Oil Fields), Kazan: Fen, 2000.
6. Mjagchenkov, V.A., Chichkanov, S.V., Proskurina, V.E., and Krupin, S.V., *Georesources*, 2002, no. 6, pp. 19–23.
7. Myagchenkov, V.A., Chichkanov, S.V., Krupin, S.V., and Proskurina, V.E., *Khim. Tekhnol. Vody*, 2003, no. 3, pp. 281–288.
8. Myagchenkov, V.A., Chichkanov, S.V., Proskurina, V.E., and Myagchenkov, A.V., *Zh. Prikl. Khim.*, 2002, vol. 75, no. 9, pp. 1517–1520.
9. Myagchenkov, V.A. and Chichkanov, S.V., *Zh. Prikl. Khim.*, 2003. vol. 76, no. 5, pp. 842–846.
10. Myagchenkov, V.A., Chichkanov, S.V., and Yakovenko, D.F., *Zh. Prikl. Khim.*, 2005, vol. 78, no. 3, pp. 506–511.
11. Pokryvailo, N.A and Gol'bina, I.I., *Materialy VIII Vsesoyuznogo simpoziuma po reologii "Reologiya polimernykh i dispersnykh system i reofizika"* (Proc., All-Union Symp. on Rheology "Rheology of Polymeric and Disperse Systems and Rheophysics"), Gomel, May 27–31, 1974, Minsk: Inst. Teplo- i Massoobmena, Akad. Nauk Bel. SSR, 1975, pp. 28–34.
12. Hou, H., *Drag Reduct. 3rd Int. Conf., Bristol, July 2–5, 1984*, Bristol, 1984, pp. C2/1–C2/6.
13. Kulik, V.M., *Inzh.-Fiz. Zh.*, 1992, vol. 62, no. 2, pp. 228–234.
14. Al'tshul', A.D., *Gidravlicheskie soprotivleniya* (Hydraulic Resistances), Moscow: Nedra, 1982.
15. Rabinovich, E.Z., *Gidravlika* (Hydraulics), Moscow: Nedra, 1980.
16. Gnativ, R.M., Influence of the Geometric Characteristics of Local Resistances in Pipelines on the Toms Effect, *Cand. Sci. Dissertation*, Moscow, 1991.

Russian Journal of Applied Chemistry, Vol. 78, No. 4, 2005, pp. 667–669. Translated from Zhurnal Prikladnoi Khimii, Vol. 78, No. 4, 2005, pp. 673–676.
Original Russian Text Copyright © 2005 by Glazkov, Biryukova.

MACROMOLECULAR CHEMISTRY AND POLYMERIC MATERIALS

Simulation of Wood Impregnation with Oligomer Solutions

S. S. Glazkov and I. P. Biryukova

Voronezh State Academy of Forestry Engineering, Voronezh, Russia

Received January 26, 2004; in final form, February 2005

Abstract—An adequate model is developed for the impregnant distribution along the fibers of a small-dimension crosscut end under conditions of isothermal diffusion impregnation with oligomer solutions.

Synthetic materials are widely used for modification of wood and wooden articles [1, 2]. The properties of the resulting material are controlled by the nature of wood, type and content of impregnant, impregnant distribution in the matrix of the capillary-porous body of wood, and compatibility with wood material. In turn, the impregnant distribution is determined by various factors and process parameters. Capillary-diffusion impregnation of wood remains practical for goods with high end surface fraction, particularly, for friction assembly bushings, compressed-wood frictionless bearings, and end face parquet and wall panels [3–5]. In accomplishing a specific task of impregnation, it is advisable to develop an adequate mathematical model for the impregnant distribution along the fibers of a sample, as influenced by the process time and characteristics of the impregnant.

EXPERIMENTAL

To describe the impregnant distribution in a wood sample with thickness h, which is small compared to the sample length and width, the second Fick's law for 1D diffusion along the x axis is used:

$$\frac{\partial c}{\partial t} = D_M \frac{\partial^2 c}{\partial x^2}, \quad (1)$$

where D_M is the effective mass-transfer coefficient along the x axis; t, impregnation time; and c, impregnant concentration per unit volume (or weight) of the sample.

Assume that at $t = 0$ the material contains no impregnant and the impregnant concentration in solution is constant.

In the study, we used Eq. (1) at the following initial and boundary conditions: at $t = 0$ $c(x, 0) = 0$, $c(\pm h/2, t) = c^*$. In this case, we obtain

$$c(x, t) = c^* \left[1 - \sum_{n=1}^{\infty} \frac{2}{\mu_n}(-1)^{n+1} \cos \mu_n \frac{x}{R_2} \exp(-\mu_n^2 F_0)\right], \quad (2)$$

where $\mu_n = (2n - 1)\pi/2$ are the characteristic series roots; n is a natural number; R_2, half-width of the sample; $F_0 = D_M t/R_2^2$, Fourier criterion (dimensionless time); $c(x, t)$, current impregnant concentration in the wood (%); and c, equilibrium impregnant concentration in the wood (%).

Let us apply Eq. (2) to estimate the effective mass transfer coefficient. At a sufficiently long impregnation time ($t > 80$ min), we can take only the first term of the series, which introduces a relative error of no more than 1%.

We denote the impregnant content in the wood sample by $c(0, t) = A_m$ (mg g^{-1}); the maximal impregnant content in the sample, by $c^* = A_\infty$ (mg g^{-1}); and the degree of process completeness, by $F = A_m/A_\infty$. Then we obtain for D_M

$$D_M = -\frac{[0.24 + \ln(1 - F)]h^2}{\pi^2 t}. \quad (3)$$

In the study, we used samples of birch, pinetree, and oak with dimensions $a \times b \times h = 40 \times 40 \times 1.5$ mm, which corresponds to the infinite board model.

The current sorption was estimated by Eq. (4).

$$A(t) = \frac{m_0(t) - m_0}{m_0}, \quad (4)$$

where m_0 is the weight of the initial absolutely dry sample (g), and $m(t)$, current weight of the impregnated sample dried to constant weight (g).

In the study, we used synthetic oligomers of 4-vinylcyclohexene (VCH) with styrene [SKT-70 (numeral

1070-4272/05/7804-0667 © 2005 Pleiades Publishing, Inc.

Table 1. Characteristics of oligomers and their solutions*

Oligomer	$\overline{M}_n$, amu	c_s, wt %	σ, mN m^{-1}	θ, deg	η, Pa s
SKT-70	4000	32	30.4 ± 7.0	17	16
OBMMA-15	4750	27	27.1 ± 0.1	9	19
OBMA-6	1200	28	27.9 ± 0.8	13	12
OBS-50	1050	30	36.8 ± 0.8	5	10
SKOP	11 000	31	25.6 ± 1.7	27	23
Drying oil	2300	30	26.3 ± 1.3	7	14

* (c_s) Impregnant concentration (solvent xylene), (σ) surface tension, (θ) contact angle, and (η) dynamic viscosity.

Table 2. Effective mass-transfer coefficient of oligomeric impregnants for various sorts of wood*

Oligomer	$D_M \times 10^{-9}$, m^2 s^{-1}					
	birch		pine-tree		oak	
	$\overline{X}$	σ	$\overline{X}$	σ	$\overline{X}$	σ
SKOP	1.78	0.07	1.21	0.05	0.76	0.03
Drying oil	2.30	0.11	2.00	0.08	1.24	0.06
SKT-70	3.30	0.13	2.64	0.10	1.90	0.09
OBMA-6	3.90	0.17	3.10	0.12	2.20	0.11
OBS-50	4.60	0.21	3.80	0.13	2.70	0.04

* ($\overline{X}$) Arithmetic mean and (σ) standard deviation.

denotes the bound comonomer content)], methyl methacrylate (OBMMA-15), maleic anhydride (OBMA-6), and sulfur (OBS-50), obtained using still bottoms from production of butadiene rubber. Characteristics of the oligomers and their solutions are summarized in Table 1.

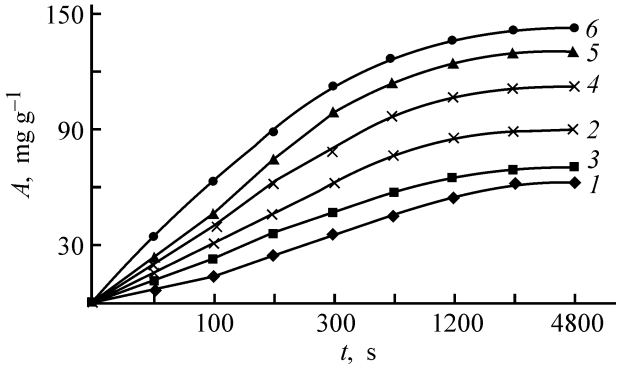


Fig. 1. Kinetic curves of impregnation of pine-tree with (*1*) SKOP, (*2*) drying oil, (*3*) OBMMA-15, (*4*) SKT-70, (*5*) OBMA-6, and (*6*) OBS-50. (*A*) Current absorption, and (*t*) time.

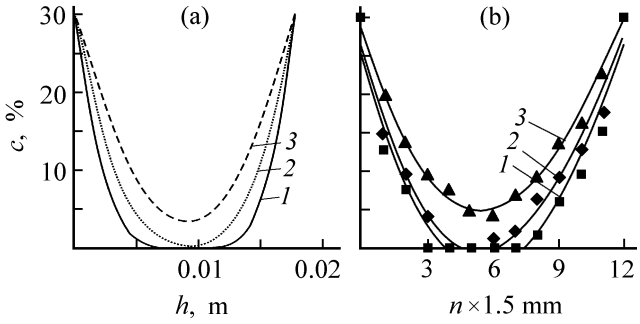


Fig. 2. (a) Theoretical and (b) experimental distribution of OBMA-6 impregnant across the sample. (*h*) Penetration depth and (*n*) number of 1.5-mm layers. Impregnation time (min): (*1*) 20, (*2*) 40, and (*3*) 80.

We experimentally verified the mass transfer model of essentially end-type impregnation for consistency. Test samples were prepared by successive cutting with a milling machine to obtain cuts 40 × 40 × 1.5 mm in size (mill cut thickness was 0.2 mm). Then the end cuts were closely jointed together in the initial order and fastened with a Teflon tape at the side faces. After impregnation the cuts were disjointed and weighed. The initial samples were dried to constant weight at 105 ± 3°C and stored in a desiccator over calcined $CaCl_2$.

Figure 1 shows the kinetic curves of impregnation of pine-tree, which correlate with the molecular weights of the cooligomers used and physical properties of their solutions (Table 1).

From the absorption data obtained at a sufficiently long impregnation time we estimated the effective mass-transfer coefficients by Eq. (3). The coefficients (Table 2) regularly change depending on the sort of wood and molecular and structural features of the oligomers used. D_M decreases in the order birch > pine-tree > oak and also with increasing molecular weight of the oligomers.

Let us use Eq. (2), which is a solution to Eq. (1), for the cases of two-end impregnation mode and fully immersed sample at the above-specified initial and boundary conditions. The distribution of OBMA-6 across the birch sample, estimated by Eq. (2) for various impregnation times (Fig. 2a), is well consistent with the experimental data (Fig. 2b). The theoretical data adequately reproduce the observed increase in the impregnant penetration to the center of the sample.

It should be pointed out that the model demonstrates sufficient adequacy only for thin end cuts

Table 3. Characteristics of end cuts of birch after bulk diffusion impregnation

Impregnant	Concentration in wood, %		Density, kg m^{-3}		W_{24}, %		h_v^{24}, %	
	$\bar{X}$	σ	$\bar{X}$	σ	$\bar{X}$	σ	$\bar{X}$	σ
Reference	0	0	523	10	95.6	2.3	17.8	0.7
SKOP	19.0	1.4	556	11	47.2	1.7	12.4	0.4
OBMMA-15	23.2	0.9	564	7	45.2	3.1	11.2	0.6
OBMA-6	28.7	0.8	577	9	41.1	2.4	8.2	0.6
OBS-50	35.7	0.3	630	6	27.4	3.7	4.7	0.3
SKT-70	25.1	0.5	561	7	43.8	1.5	10.6	0.5

and the two-end impregnation mode, when the sample thickness h is small as compared to its length and width, and the side-edge diffusion is comparable with the experimental error.

In the cases of the two-end impregnation mode and full immersion of the sample, the amount of one-side open pores, for which the capillary effect is negligible, increase as compared to the case of one-end impregnation.

Analysis of properties of the impregnated wood shows that raising the impregnant concentration in the wood increases the density of the resulting composite material and improves its water resistance (Table 3). The density demonstrates more pronounced tendency to increase with decreasing molecular weight of the impregnant, which is evidently caused by the ability of small macromolecules to be more closely packed in the porous matrix of wood.

The water resistance changes in proportion to the packing density of the macromolecules. At a relatively low impregnant concentration in the wood, the water absorption index W can be decreased by a factor of 2.0–2.5, and the volume swelling index, by a factor of 2–3 (Table 3). The best performance characteristics were obtained after impregnation with the sulfur-containing impregnant OBS-50 having the minimum molecular weight and a heterochain structure with labile sulfur atoms capable of structural rearrangement.

CONCLUSIONS

(1) An analytical solution of the differential equation for the mass transfer in the course of impregnation of thin end cuts of wood provided a relationship for estimating the effective diffusion coefficients.

(2) The impregnation kinetics was studied and the effective diffusion coefficients were determined for various oligomer solutions.

(3) It was found the theoretical and experimental effective diffusion coefficients correlate with the chemical and structural features of oligomers, as well as with the characteristics of the porous structure of wood.

(4) It was astablished that the mass-transfer model suggested reproduces well the experimental data on the distribution of oligomers across the wood fibers, allowing prediction of the impregnation kinetics and performance characteristics of the impregnated wood.

REFERENCES

1. Lavnichek, M., *Derevoobrab. Prom–st.*, 1977, no. 7, pp. 29–31.
2. Zoldners, Yu.A., Abstracts of Papers, *Vsesoyuznaya nauchnaya konferentsiya "Teoreticheskie osnovy modifikatsii drevesiny"* (All-Union Scientific Conf. "Foundations of Wood Impregnation"), Riga, May 21–23, 1983, pp. 23–26.
3. Shutov, G.M., *Modifitsirovanie drevesiny termokhimicheskim sposobom* (Thermochemical Modification of Wood), Moscow: Ekologiya, 1991.
4. Glazkov, S.S., Nikulin, S.S., Tarasova, A.I., and Malikov, B.F., *Izv. Vyssh. Uchebn. Zaved., Stroitel'stvo*, 1996, no. 2, pp. 58–61.
5. RF Patent 2096171.

Russian Journal of Applied Chemistry, Vol. 78, No. 4, 2005, pp. 670–673. Translated from Zhurnal Prikladnoi Khimii, Vol. 78, No. 4, 2005, pp. 677–680.
Original Russian Text Copyright © 2005 by Glazkov.

MACROMOLECULAR CHEMISTRY AND POLYMERIC MATERIALS

Model of a Polymeric Stabilizer and Optimization of Its Compatibility with Wood

S. S. Glazkov

Voronezh State Academy of Forestry Engineering, Voronezh, Russia

Received February 10, 2004

Abstract—The structure and functionality of a reactive oligomer are characterized in terms of the adhesion, cohesion, and diffusion theories. The dimensions and chain-length distribution of the stabilizer are calculated using the fundamental aspects of adsorption of macromolecules on porous supports and result of an analysis of the capillary-pore system of wood. The statistical model obtained adequately reproduces the properties of stabilized wood over the investigated ranges of the process parameters.

Stabilization of the dimensions of wood materials at varying humidity is, without question, a topical problem. The present-day Russian market of impregnants for wood is saturated with materials of this kind, which are mostly imported. These impregnants, even being highly effective, are, as a rule, expensive, and their use by Russian consumers is occasionally limited by specific process conditions [1]. Therefore, it is an urgent task to extend the range of impregnants for wood through synthesis of new materials from petrochemistry waste products and to characterize these materials [2, 3].

In this study, we developed a model for a thermoplastic polymeric impregnant produced from monomers of still bottoms from synthetic rubber production.

The basic concept of the model is the ability of a polymeric impregnant to penetrate the capillaries of the cell wall and to be involved in structural transformations via functional groups, residual moisture, and the siccative complex in the course of thermal treatment.

Let us consider the model of a macromolecule of a polymeric impregnant, including its structure, functionality, and molecular-weight distribution, which would be best suited for the problem in hand, i.e., would impart hydrophobicity to wood and provide the desired stability of shape.

In interaction of a solid (wood) with an impregnant solution, the adhesion F (N cm^{-1}) is described, as for two solids, by Eq. (1) [4]

$$F_{ad}(W_{ad}) = f(N_0,\ R_0,\ k,\ S_{eff},\ h,\ D), \qquad (1)$$

where N_0 (N) and R_0 (J) are the interaction strength and energy, referred to a single contact point; k is the number of contact points per unit effective contact surface area (per 1 cm^2); S_{eff}, effective contact surface area (cm^2); h, distance between the contact points (cm); and D, dielectric constant.

Impregnation of wood with a polymeric impregnant bearing polar oxygen-containing groups (carboxy groups at best) is strongly affected by the residual moisture contained in a sample (moisture promotes deprotonation of the carboxy groups).

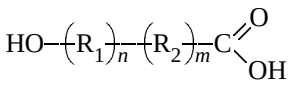
Interaction of metal cations from the siccative with the anions of the acid residues of the hydrophobic polymeric fragments of the impregnant may result in formation of chemical bonds providing very high adhesion between the interacting bodies. This process is facilitated by raising the temperature in the stages of solvent removal and thermal hardening when an elevated temperature provides a closer contact between macromolecules of the polymeric impregnant.

The proportion between the aliphatic (hydrophobic) part of the macromolecule and the amount of functional groups of the hydrophilic part may vary with the kind of a wood article and purposes of processing. However, it is clear that, to improve the hydrophobicity of an article, it is necessary to minimize the amount of oxygen-containing functional groups, right up to

1070-4272/05/7804-0670 © 2005 Pleiades Publishing, Inc.

bifunctional macromolecules with terminal functional groups. These groups can be readily introduced at the stage of polymerization of vinyl compounds under the action of radical initiators of the peroxy and hydroperoxy types.

The structure of the model impregnant can be schematically represented as



where R_1 and R_2 are structural units of one or different types of vinyl monomers.

The chemical nature and composition of vinyl monomers will control the film-forming capacity of the polymeric impregnant and physicochemical properties of the resulting film.

The optimal molecular-weight distribution or the degree of polymerization P, and the parameters n and m in the general formula of the impregnant are determined, on the one hand, by the desired level of cohesion and, on the other, by the minimal pore space, which limits the permeability to macromolecules with a high molecular weight.

According to one of the known hypotheses, the macromolecules are arranged on the surface in the whole-chain contact mode. Therefore, the packing becomes the closest after the limiting adsorption is reached. However, this is the case only at a very high adsorption. The thickness of a molecule adsorbed on a plane surface D_a (Å) can be approximately estimated by the De Gennes equation [5]:

$$D_a \cong a_u \delta^{-3/2}, \quad (2)$$

where a_u is the averaged unit length in vinyl compounds (3.08 Å), and δ, dimensionless parameter (equation is exactly valid at $1 \ll \delta \ll P^{-2/5}$).

In simulating the structure, composition, and functionality of the polymeric impregnant, let us proceed from the basic cross dimensions of the conducting system at the macro- and microlevels (Table 1) [6].

Table 1 shows that the macro- and microstructures of the capillary-pore structure of both softwood and hardwood are considerably different in their pore diameter. The pore system of the cell wall and intercellular channels are smaller, primarily in their cross dimensions, by several orders of magnitude (by up to a factor of 10^5) as compared to the base conducting system. It is known [6] that changes in the linear dimensions of wood are primarily controlled by characteristics of the cell wall, whose dimensions are sensitive to the humidity. Therefore, only delivery of a polymeric impregnant to cell walls, specifically, to hydrophilic and amorphous parts of the cellulose and hemicellulose fibrils can provide a high stability of shape of wood articles.

Table 1. Cross dimensions of the major conducting elements in various sorts of wood [6]*

Conducting element	Inner diameter, Å		
	pine-tree	birch	oak
Micro level:			
tracheids	2.4×10^5	–	
vessels	–	7×10^5	$\frac{3 \times 10^6}{0.35 \times 10^6}$
fibers	–	1.6×10^5	5×10^4
Micro level:			
micropores in matrix	$\frac{300–400}{50–60}$	2.8×10^5	6×10^5
interfibrillar spacings	50–100	0.32	–
intercellular membrane channels	200	–	

* Averaged data obtained from the wood permeability; data for summerwood and latewood zones are given in the numerator and denominator, respectively.

Let us now approximately calculate the size of macromolecules of a polymeric impregnant that would be capable to reach the indicated structures of wood by comparison with the pore size of the wood conducting system (Table 1). Rearrangement of Eq. (2) gives Eq. (3) [5].

$$R_F \approx a_u P^{3/5}, \quad (3)$$

where P is the degree of polymerization, and R_F, size of the polymeric globule (Å) R_F is taken equal to approximately half the corresponding pore diameter, i.e., $R_F \approx D_a/2$). Then we obtain

$$P = \left(\frac{D_u}{2a_u}\right)^{5/3}. \quad (4)$$

As a simplified model we take an outstretched chain of the macromolecule of the polymeric impregnant, whose length (Å) is written as

$$L_{mol} = a_u P. \quad (5)$$

Table 2. Estimated molecular and thermodynamic characteristics of impregnant macromolecules capable of penetrating the micropores in pine-tree wood

Conducting element	P	L_{mol}, Å	ΔG_a, kJ mol^{-1}
Micropores in matrix	817* 37	2.5×10^3 117	2.7 2.4
Interfibrillar spacings	32 102	99 315	2.5 2.6
Intercellular membrane channels	323	994	2.5

* Data for summerwood and latewood are given in the numerator and denominator, respectively.

Table 3. Characteristics of oligomers and their solutions*

Polymer	$\overline{M}_n$, amu	c, wt %	σ, mN m^{-1}	θ, deg	η, Pa s
SKT-70	4000	32	30.4 ± 7.0	17	16
OBMMA-15	4750	27	27.1 ± 0.1	9	19
OBMA-6	1200	28	27.9 ± 0.8	13	12
OBS-50	1050	30	36.8 ± 0.8	5	10
SKOP	11000	31	25.6 ± 1.7	27	23
Drying oil	2300	30	26.3 ± 1.3	7	14

* (c) Impregnant concentration (solvent xylene), (σ) surface tension, (θ) contact angle, and (η) dynamic viscosity.

The calculated data for the intercellular and cell-wall capillary systems of pine-tree are given in Table 2.

Table 2 shows that the interfibrillar spacings having the narrowest pores show the lowest permeability to the impregnant. At the same time, these regions are responsible for the absorbed moisture content and, correspondingly, for the stability of shape of the cell wall and of a wood article as a whole. The free energy changes ΔG_a reflecting the changes in the flexibility of macromolecules vary slightly (Table 2), which can be attributed to both rough estimates and close sizes of the cellular micropores.

Turning back to the structure of the model polymeric impregnant, it may be suggested that the desired degree of polymerization $P = n + m$ ranges from 32 to 102 structural units.

Taking into account the indicated optimal range of the degree of polymerization and accepting the molecular weight of 4-vinylcyclohexen (MW 108) as the molecular weight of the basic structural unit, we obtain the average statistical molecular weight of the impregnant macromolecule of 3500–11 000.

EXPERIMENTAL

In the study, we used copolymers of VCH with styrene SKT-70 (numeral denotes the content of the bound comonomer), methyl methacrylate (OBMMA-15), maleic anhydride (OBMA-6), and sulfur (OBS-50), obtained using still bottoms from production of butadiene rubber [7]. The characteristics of the oligomers and their solutions are summarized in Table 3.

For OBMA-6 containing 6% MA units ($\overline{M}_n$ 900–1500), the degree of polymerization ($P = n + m$) is 8.4–14.1, which corresponds to the size of linear macromolecule of 2.6–4.2 nm.

Impregnated wood was prepared as follows. Pine-tree samples (20 × 20 × 30 mm; density 540 kg m^{-3}; moisture content 5–7%) were immersed in an impregnant solution with fixed impregnant and siccative concentrations. The samples were allowed to stand at room temperature and then were dried in an oven at 105–135°C for 1–2.5 h.

After statistical processing, we obtained the following regression equations (confidence probability $p < 0.05$) for the water absorption in 24 h, W_{24} (%):

$$Y_1 = 133.5 - 0.55X_1 - 5.75X_2 - 0.575X_3 - 6.625X_4 + 0.033X_2X_3,$$

for volume swelling in 24 h, h_v^{24} (%):

$$Y_2 = 56.57 - 0.25X_1 - 2.12X_2 - 0.35X_3 - 9.48X_4 + 0.04X_1X_4 + 0.01X_2X_3 + 0.22X_2X_4 + 0.06X_3X_4,$$

for the ultimate strength at break along the fibers, σ (MPa)

$$Y_3 = -16.59 + 0.56X_1 + 1.88X_2 + 0.61X_3 + 6.13X_4 + 0.81X_3X_4,$$

and for the oligomer concentration in wood c_{ol}^w (%):

$$Y_4 = -22.29 - 0.35X_1 - 1.11X_2 + 0.17X_3 + 3.16X_4 + 0.019X_1X_2 + 0.005X_1X_3 + 0.22X_2X_4 + 0.081X_1X_4.$$

The regression equations were tested for an extremum by the Fiacco–McCormick method [8] under the following constrictions: oligomer concentration in impregnating solution $20 \le A \le 40\%$; impregnation time $4 \le B \le 8$ h; temperature of the impregnating solution $60 \le C \le 90$°C; and siccative concentration $2 \le D \le 4\%$.

Optimization with the indicated ranges was performed using the internal penalty function method.

Comparison of the optimization data allowed determination of the optimal process conditions: oligomer concentration 40%, impregnation time 6 h, temperature 90°C, and siccative concentration 3%.

CONCLUSIONS

(1) A statistical model of a polymeric impregnant was experimentally verified for polymeric products obtained from still bottoms from synthetic rubber production.

(2) The wood stabilization process was optimized in a full factorial experiment 2^4. The resulting system of regression equations was tested for an extremum, and the optimal operation mode was found.

(3) For wood impregnated under the optimized conditions, the water absorption and volume swelling decreased by a factor of 5–7, and the ultimate strength at break along the fibers increases by a factor of 2.0–2.5, with all the other mechanical characteristics remaining no worse the before the impregnation.

REFERENCES

1. Sakano Koichi, *J. Appl. Polym. Sci.*, 1992, no. 48, p. 224.
2. Beketov, V.D., *Tendentsii i prognozy razvitiya proizvodstva listovykh drevesnykh materialov* (Trends in Production of Sheet Wood Materials and Prediction of Its Progress), Moscow: VNIPIEIlesprom, 1990.
3. Glazkov, S.S., Enyutina, M.V., Semenova, L.K., and Shut, N.I., *Mekh. Kompoz. Mater. Konstr.*, 2003, vol. 9, no. 1, pp. 96–103.
4. Moskvitin, N.I., *Fiziko-khimicheskie osnovy protsessov skleivaniya i prilipaniya* (Physicochemical Principles of Agglutination and Adhesion), Moscow: Lesnaya Prom–st., 1964.
5. Entelis, S.G., *Reaktsionnosposobnye oligomery* (Reactive Oligomers), Moscow: Khimiya, 1985.
6. Fengel, D. and Wegener, G., *Wood: Chemistry Ultrastructure, Reactions*, Berlin: Walter de Gruyter, 1984.
7. Glazkov, S.S., Panyushkin, N.N., Levykin, E.N., and Panyushkin, A.N., *Proizv. Ispol'z. Elastom.*, 2002, no. 6, pp. 11–13.
8. Bandi, B., *Metody optimizatsii: Vvodnyi kurs* (Optimization Methods: Introductory Course), Moscow: Radio i Svyaz', 1988.

Russian Journal of Applied Chemistry, Vol. 78, No. 4, 2005, pp. 674–676. Translated from Zhurnal Prikladnoi Khimii, Vol. 78, No. 4, 2005, pp. 681–683.
Original Russian Text Copyright © 2005 by S. Sokol'skii, Fedosov, A. Sokol'skii, Barulin.

BRIEF COMMUNICATIONS

Thermal Treatment and Hydrophobization of Components of Fire-Extinguishing Powders

S. A. Sokol'skii, S. V. Fedosov, A. I. Sokol'skii, and E. P. Barulin

Ivanovo State Academy of Architecture and Building, Ivanovo, Russia

Ivanovo State University of Chemical Engineering, Ivanovo, Russia

Received October 28, 2004; in final form, January, 2005

Abstract—Experimental data on the thermal treatment and hydrophobization of components of fire-extinguishing powdered formulations in an apparatus with active hydrodynamics of a two-phase flow are presented.

Fire-extinguishing formulations have the form of a powdered mixture of various inorganic salts and dopants. Depending on the fire-extinguishing capacity of their components, the mixtures can contain ammonium sulfate, ammophos, carbon white, nepheline, talcum, sodium hydrocarbonate, aerosil, potassium chloride, sodium chloride, etc. The main active components of fire-extinguishing powdered mixtures are ammophos and ammonium sulfate, which form a fusion cake at 160–200°C and thereby screen an inflammation site from interaction with atmospheric oxygen. The rest of the additives, such as talcum and carbon white, impart fluidity to the fire-extinguishing powder and protect it from caking. The moisture content of the components of fire-extinguishing mixtures should not exceed 0.5 wt %.

To prevent caking and to raise the fluidity of powders, a mixture is hydrophobized. Such organosilicon liquids as GKZh-94, Penta-804, MN-15, *et al.* are used as water repellents [1]. Most frequently, either main active components or additives introduced into the formulation are subjected to hydrophobization [2]. In the industry, the components are dehydrated in various drying apparatus, and then some of the dried-up substances are subjected to hydrophobization. To save expensive water-repellent agents, that component of the mixture is treated, which has the highest capacity for moisture absorption under normal atmospheric conditions. It would be the most expedient to combine the processes of thermal treatment of a component and its hydrophobization. Such combined processes can be carried out effectively in vortex apparatus in a high-temperature heat carrier under conditions of a high relative velocity of the interacting phases, which provide an intensive removal of moisture from the material and a high degree of polymerization of a water repellent.

EXPERIMENTAL

The components of fire-extinguishing powdered formulation were heat treated and hydrophobized in an installation shown schematically in Fig. 1. The installation contained the following units: whirlpool

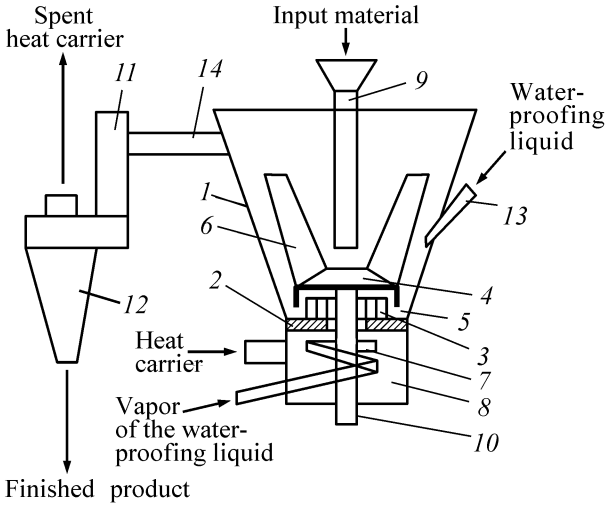


Fig. 1. Schematic of the experimental installation.

1070-4272/05/7804-0674 © 2005 Pleiades Publishing, Inc.

chamber *1*, end plate *2*, turbine section *3*, turbulator *4* in the form of a truncated cone with downwards-directed rim beaters *5* mounted on the periphery of its base, blades *6* attached to the conic surface, evaporator *7*, gas-intake box *8*, feed spout *9*, driving shaft *10*, ventilator *11*, cyclone discharger *12*, droppers *13*, and output fitting pipe *14*.

The device works as follows. The input product is conveyed by a feeder through a gutter *9* into the whirlpool chamber *1* onto the rotating turbulator *4* having blades *6* on its conic surface. When the turbulator rotates with such a rate that its peripheral velocity is equal to, or exceeds the flow velocity of the heat carrier leaving the turbine section *3*, a highly turbulized twirled gas-dispersion flow is formed in the whirlpool chamber. The agglomerates present in the input product are disintegrated by blades and then thrown by the centrifugal force to the periphery into the working zone of beaters *5*, to be partly crushed there. The heat carrier moves from the gas-intake box *8* through a central outlet in the end plate *2* into the turbine section *3*. The blades of the turbine section are arranged so as to ensure the tangential inflow of the heat carrier into the whirlpool chamber in the direction coinciding with the direction of rotation of the turbulator mounted on the driving shaft *10*. As a result, the material is crushed and heat-treated. Under the action of the whirling flow of the heat carrier and of the centrifugal force created by rotating blades of the turbulator, the material is dispersed and ascends to the top part of the whirlpool chamber along a spiral path, wherefrom it is delivered via an outlet fitting pipe *14* and a ventilator *11* into a cyclone discharger *12*. The gas-suspension is separated in the cyclone into a finished product and spent heat carrier, which is then delivered into a bag filter for additional purification. The waterproofing liquid can be fed into the evaporator *7*, where its vapor is formed and mixed with the heat carrier in the gas-intake box, or it is delivered in the form of a liquid through droppers directly into the layer of a material under treatment.

Crushed ammophos was hydrophobized and thermally treated in the experimental installation described above. The effect of heat carrier temperature on the moisture absorption by the finished product was studied. The consumed concentration of the solid phase, μ, was 0.04 kg kg^{-1}; the amount of waterproofing liquid was 3.5% relative to the mass of the solid phase; and the heat carrier temperature was varied within the range 100–150°C.

The curve of moisture absorption by the active component, shown in Fig. 2, was obtained using

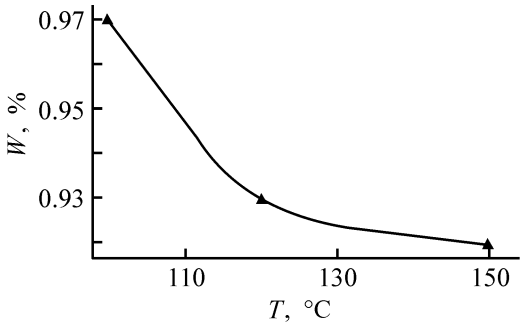


Fig. 2. Moisture absorption by the active component *W* vs. the heat carrier temperature *T*.

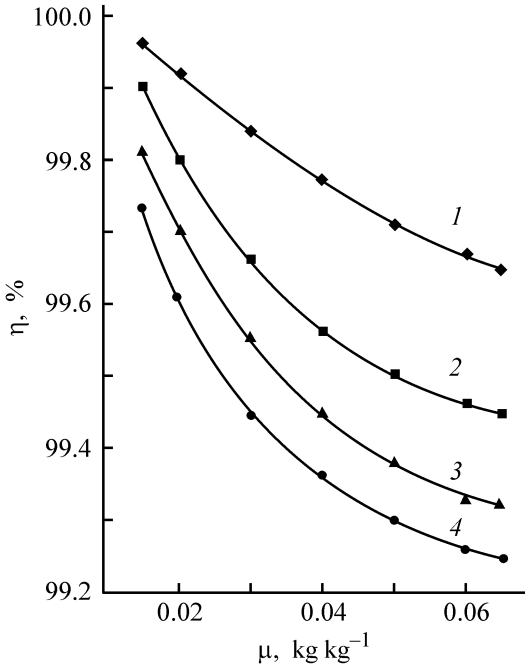


Fig. 3. Degree of silicon dioxide hydrophobization, ν, vs. the consumed concentration of the solid phase, μ. Temperature (°C): (*1*, *2*) 250, (*3*) 200, and (*4*) 150. Water repellent expenditure (kg kg^{-1} of a solid phase): (*1*, *3*) 0.96, (*2*) 0.7, and (*4*) 0.47.

a standard procedure after a treatment of the component in an apparatus with an active hydrodynamics of a two-phase flow. An analysis of the curve shows that the moisture absorption by the powder at a heat carrier temperature of 150°C is 0.92 wt %. As the temperature of the heat carrier decreases, the moisture absorption increases, which points to an incomplete polymerization of the waterproofing liquid. The humidity of the powder fed into the apparatus was 1 wt %. The permissible moisture absorption should not exceed 2 wt %.

Figure 3 shows how the degree of hydrophobization of a highly dispersed silicon dioxide depends on

the consumed concentration of the solid phase at various flow rates of the water repellent and heat carrier temperatures. The heat carrier flow rate L = 11.5 kg h^{-1}. Analysis of the curves in Fig. 3 shows that, as the temperature of the heat carrier increases, the hydrophobicity of the material being treated grows, whereas an increase in the consumed concentration of the solid phase leads to a decrease in the degree of powder hydrophobization.

Our calculations show that 0.028 kg of the waterproofing liquid is consumed for hydrophobization of 1 kg of the active component, which is contained in a powdered formulation in an amount of up to 80 wt %. When a highly dispersed hydrophobized silicon dioxide is introduced into a powdered mixture as a dusting additive in an amount of 2 wt %, 30 to 60% of the waterproofing liquid is saved, which considerably reduces the production costs at the same quality of a fire-extinguishing formulation [2].

CONCLUSIONS

(1) It was found experimentally that 0.035 kg of a water repellent per 1 kg of a solid phase is required to achieve a high hydrophobicity of the active component of a powdered formulation.

(2) The expenditure of the water repellent should be varied within the range 0.47–0.96 kg kg^{-1} of a solid phase for hydrophobization of a highly dispersed silicon dioxide. In this case, the hydrophobicity of the powder is 99.22–99.88%.

(3) If a highly dispersed hydrophobized silicon dioxide is introduced into a powdered fire-extinguishing formulation in an amount of 2 wt %, 30–60% of the water repellent can be saved.

REFERENCES

1. *Kremniiorganicheskie produkty, vypuskaemye v SSSR: Katalog-spravochnik* (Organosilicon Products Manufactured in the USSR: Catalogue and Reference Book), Gorbunov, A.I., Ed., Moscow: Khimiya, 1975.
2. Moshkovskii, N.S., Selenyuk, D.V., Onishchenko, A.I., and Tychkina, O.N., *Ognetushashchie poroshkovye sredstva: Sbornik nauchnykh trudov* (Fire-Extinguishing Powdered Agents, Proc. Scientific Works), Moscow: VNIIPO of the Ministry of Internal Affairs of the USSR, 1982, pp. 105–110.
3. Sokol'skii, A.I., Barullin, E.P., Kruchinin, M.I., and Sokol'skii, S.A., *Materialy mezhdunarodnoi nauchnoi konferentsii "Energosberegayushchie tekhnologii i oborudovanie, ekologicheski bezopasnye proizvodstva"* (Proc. Int. Scientific Conf. "Energy-Efficient Technologies and Equipment, Ecologically Safe Industries") Ivanovo, 2004, p. 33.

Russian Journal of Applied Chemistry, Vol. 78, No. 4, 2005, pp. 677–679. Translated from Zhurnal Prikladnoi Khimii, Vol. 78, No. 4, 2005, pp. 684–686.
Original Russian Text Copyright © 2005 by Akhrimenko.

BRIEF COMMUNICATIONS

On Raising the Corrosion Stability of Cement Stone

V. E. Akhrimenko

Kuban State Agrarian University, Krasnodar, Russia

Received June 21, 2004

Abstract—A water–paraffin slurry formulation was elaborated and sedimentation-stable cement mortars with low filter output were obtained on its basis.

Development of a quantitative theory of corrosion processes occurring in a cement stone placed in a corrosive liquid and the forecast of its longevity have been the subject of numerous studies [1–5].

The effect of salt additives on the corrosion stability of the cement stone has been considered earlier [6]. It was shown that addition of salts to a cement paste improves the corrosion stability of a cement stone against a salt aggression and that the main reason for destruction of a cement stone in a sodium sulfate solution is its reaction with unreacted tricalcium aluminate $3CaO \cdot Al_2O_3$ and calcium hydroxide $[Ca(OH)_2]$ to give calcium hydrosulfoaluminate (ettringite) $3CaO \cdot Al_2O_3 \cdot 3CaSO_4 \cdot 31H_2O$) which increases in volume upon its crystallization and destroys the cement stone.

Under conditions of polymineral aggression in the presence of hydrogen sulfide, cement stone samples reinforced with asbestine and basalt fibers are the most corrosion-resistant [7]. Cement stone is hydrated to a greater extent in the contact layer with filler fibers, newly formed particles in it are packed more densely, and filler fibers grow into its structure, making lower the overall permeability of the stone. As a result of an intensive clogging of the porous structure, an aggressive liquid cannot freely penetrate into a stone and initiate destruction corrosion processes in it.

The permeability of a cement stone can be diminished by lowering the water-to-cement ratio (w/c), which makes the crystal structure of the stone more dense and depresses diffusion processes occurring in the cement stone and leading to its corrosion. However, the decrease in the water-to-cement ratio changes the rheological characteristics and cementation time. Therefore, development of a formulation of a manufacturable grouting mortar hardening to form a strong corrosion-resistant stone is an important item in the general problem of building of concrete constructions and well casing.

EXPERIMENTAL

In this study, the effect of mudding of the porous structure of a forming cement stone on its permeability and corrosion resistance was examined. We used paraffin as a mudding agent, which was introduced into a cement mortar together with a tempering liquid having the form of a water–paraffin dispersion.

The water–paraffin dispersion was prepared by intensive stirring of paraffin fused in hot water. To stabilize the water–paraffin dispersion, we added to it high-molecular substances and surfactants of the type of oxoethylated alkyl phenols. To obtain a water–paraffin dispersion, we used a paraffin with a melting point of 50–55°C. Cement was tempered with the water–paraffin dispersion prepared (w/c=0.5), thoroughly stirred, and the resulting cement mortar [8] and the stone based on it were tested using the standard procedures (see table).

The resulting cement stone was tested for permeability and corrosion resistance. The permeability of the cement stone was estimated by the filtration coefficient K_f calculated by the formula

$$K_f = Q/S\tau.$$

Here Q is the amount of water filtered through a cement stone (g); τ, filtration time (s); and S, cross-section area of the cement stone (mm^2).

To determine the permeability of the cement stone, we poured the cement mortar under study into a 20-cm^3

1070-4272/05/7804-0677 © 2005 Pleiades Publishing, Inc.

Properties of cement mortar and stone based on a water–paraffin dispersion (w/c = 0.5, t = 22°C)

Sample no.	Additive, %			W, %	S, cm	Cementation time, h–min		σ_{comp}, MPa	$K_f \times 10^{-10}$, m s^{-1}	Δm, g	K_{destr}
	PVA	Surfactant	Paraffin			beginning	end				
1	–	–	–	5.3	23	6–40	8–15	13.76	0.58	5.84	0.13
2	0.33	0.16	–	0.5	22	7–00	8–50	13.86	0.37	5.63	0.12
3	0.33	0.17	1.0	0.2	20	6–50	9–15	12.20	0.11	2.87	0.08
4	0.33	0.32	1.5	0.1	17	7–10	9–30	10.67	0.08	2.14	0.05
5	0.33	0.32	3.3	0.06	14	7–40	9–50	7.12	0.06	1.08	0.02

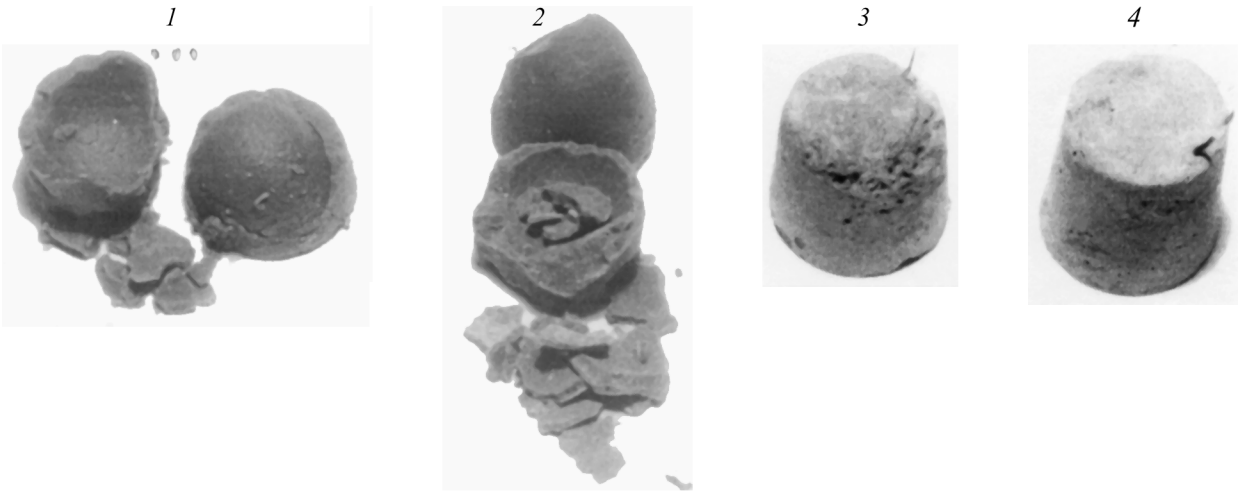
* W, dehydration; S, spreading; σ_{comp}, stone strength after 7 days; Δm, loss of mass after 3 days; and K_{destr}, corrosive destruction coefficient.

medical syringe to a height of 1 cm and left it to harden. After the hardening of the cement stone for 3 days, distilled water was poured into the syringe and forced through the cement stone under a certain pressure created by placing a set of weights on the piston. The permeability of the cement stone was estimated by the volume of water passing through the stone sample in a certain time.

It follows from the table that addition of paraffin to a cement mortar makes it sedimentation-stable; dehydration of such a solution is 2–4 times less as compared with a paraffin-free solution. As to the filtration coefficient, it is an order of magnitude smaller in the case of a paraffin-containing cement stone.

The corrosion stability of the cement stone was estimated using the express gravitational procedure. For this purpose, the cement stone sample under study was kept for 1 h in distilled water, then immersed in a vessel with water, and weighed on an electronic balance. After weighing, the stone sample was placed in a 10 wt % solution of hydrochloric acid. After a certain time, the sample was taken from the acid, placed in a vessel with water, and weighed again. The loss of mass was determined from the difference of sample masses before and after immersion in the acid solution, and the corrosive destruction coefficient K_{destr} was calculated from this loss. The corrosive destruction coefficient is defined as the ratio of the mass of the dissolved stone to the initial mass of the stone (see table).

It follows from the table and figure that sample no. 1 of pure portland cement is subject to strong destruction in an acid medium, as well as cement stone sample no. 2 with an addition of polyvinyl alcohol (PVA) and a surfactant, and their corrosive destruction coefficients are 0.13 and 0.12, respectively. As to the cement stone samples containing paraffin (sample nos. 3 and 4), they were found to be corro-



Changes in cement stone samples. (*1*) Pure portland cement; portland cement with an additive: (*2*) PVA and surfactant, (*3*) 1.0% paraffin, and (*4*) 1.5% paraffin.

sion-resistant, their corrosive destruction coefficients are 0.08 and 0.05, respectively. Thus, our study demonstrated that finely dispersed paraffin contained in a tempering liquid leads to mudding of the porous structure of the forming cement stone and makes it low-permeable and corrosion-resistant.

CONCLUSIONS

(1) A novel water–paraffin tempering liquid was developed.

(2) It was shown that the water–paraffin tempering liquid affects rheological characteristics of a cement mortar.

(3) It was found that introduction of paraffin into a cement mortar leads to mudding of the porous structure of the resulting stone and makes it low-permeable and corrosion-resistant.

ACKNOWLEDGMENTS

The study was financially supported by the Russian Foundation for Basic Research (project no. 00-05-960-17).

REFERENCES

1. Kind, V.V., *Korroziya tsementov i betonov v gidrotekhnicheskikh sooruzheniyakh* (Corrosion of Cements and Concretes in Hydraulic Works), Moscow: Nedra, 1990.
2. Sheikin, A.E., *Struktura, prochnost' i treshcinostoikost' tsementnogo kamnya* (Structure, Strength, and Crack Resistance of Cement Stone), Moscow: Stroiizdat, 1997.
3. Moskvin, V.M., Ivanov, F.M., and Alekseev, S.N., *Korroziya betona i zhelezobetona, metody ikh zashchity* (Corrosion of Concrete and Ferro-Concrete, Methods of Their Protection), Moscow: Stroiizdat, 1980.
4. Tikhomirov, M.F. and Vlasicheva, L.G., *Beton Zhelezobeton*, 1990, no. 11, p. 40.
5. Arutyunov, A.A., *Trudy VNIIKR Nefti*, Krasnodar, 1986.
6. Akhrimenko, V.E., Akhrimenko, Z.M., and Korol', O.E., *NTE Stroitel'stvo Neft. Gaz. Skvazh. Sushe More* (Construction of Oil and Gas Wells on Land and at Sea), 1999, nos. 1–2, p. 34.
7. Akhrimenko, V.E., Gagai, G.I., Parinov, P.F., and Ryabova, L.I., *Trudy VNIIKR Nefti*, Krasnodar, 1986, p. 72.
8. RF Patent 2204012.

Russian Journal of Applied Chemistry, Vol. 78, No. 4, 2005, pp. 680–682. Translated from Zhurnal Prikladnoi Khimii, Vol. 78, No. 4, 2005, pp. 687–689.
Original Russian Text Copyright © 2005 by Danov, Kolesnikov, Efremov, Mezhenin.

BRIEF COMMUNICATIONS

Kinetic Aspects of Dimethylamine Hydroxyethylation in the Presence of Water

S. M. Danov, V. A. Kolesnikov, R. V. Efremov, and D. Yu. Mezhenin

Nizhni Novgorod State Technical University, Dzerzhinsk Branch, Dzerzhinsk, Nizhni Novgorod oblast, Russia

Received June 30, 2004; in final form, January 2005

Abstract—The kinetics of dimethylamine hydroxyethylation at an ethylene oxide : dimethylamine : water molar ratio of 1 : 3 : (0.1–0.5) was studied in the temperature range 20–50°C. A kinetic model of the reaction, which adequately describes the experimental data, was suggested.

Dimethylethanolamine (DMEA) is produced industrially by hydroxyethylation of dimethylamine (DMA) with ethylene oxide (EO) in the liquid phase. At one of the existing plants, the synthesis is carried out in a "tube-in-tube" reactor at 80–175°C, pressure of 5–6 MPA, and DMA : EO molar ratio of 3 : 1 in the presence of water (6% relative to the total weight of the starting reagents).

Previously, the kinetic aspects of DMA hydroxyethylation in the absence of water have been studied [1]. It was shown that the reaction is autocatalytic and accelerated by DMEA. The parameters of the Arrhenius equation for noncatalytic and autocatalytic reactions were found.

It is known from published data that the reaction is accelerated by proton donors (water, alcohols, phenols, and acids) [2–6]. Therefore, the aim of the present study was to examine previously unstudied kinetic aspects of DMA hydroxyethylation in the presence of water. The data obtained can be further used in choosing the optimal equipment and operation mode of a reaction unit. As to other amines, the kinetics of aniline hydroxyethylation in the presence of water was studied in [3]. It was shown that the reaction is first-order with respect to water, and the rate constant of the catalytic reaction at 100°C and water concentration of 0.5 M is 4.7×10^{-4} l mol^{-1} s^{-1}.

It is also known that dimethylaminoethoxyethanol (DMAEE) is formed as a by-product, in addition to DMEA, in hydroxyethylation of DMA, with EO isomerized to give acetaldehyde and also dimerized and polymerized [7]. Furthermore, glycols can be formed in an alkaline medium in the presence of water [8]. The products obtained can undergo further transformations. Preliminary studies have shown that the side reactions proceed to an insignificant extent at 20–60°C, DMA : EO molar ratio of 3 : 1, and low water content. The synthesis in industrial reactors is carried out at the same ratio, and, therefore, the kinetics of DMA hydroxyethylation in the presence of water was studied under the same conditions.

The reaction rate was monitored by the accumulation of DMEA in the reaction mass, with the concentration of DMEA determined by gas–liquid chromatography.

In developing the kinetic model, the reaction orders with respect to EO, DMA, and DMEA were taken to be unity in accordance with the authors' [1] and published [3–6] data. The reaction order with respect to water was calculated from the experimental data obtained. Thus, the rates of noncatalytic (r_1), autocatalytic (r_2), and catalytic (r_3) reactions were described by the following equations

$$r_1 = k_1 c_1 c_2,\ r_2 = k_2 c_3 c_1 c_2,\ r_3 = k_3 c_4^n c_1 c_2.$$

Here k_1, k_2, and k_3 are the rate constants of the noncatalytic, autocatalytic, and catalytic reactions, respectively; c_i, molar concentration of ith component (1, EO; 2, DMA; 3, DMEA; and 4, water); and n, reaction order with respect to water.

The reaction proceeds with a decrease in the number of moles of reagents, which becomes 12% at a complete EO conversion. Therefore, the material balance equations for each component

$$\mathrm{d}(Vc_i)/\mathrm{d}\tau = \nu_i V(r_1 + r_2 + r_3),\ i = 1, 2, 3, 4$$

[where V is the volume of the reaction mass; τ, time; and ν_i, stoichiometric coefficient of ith component

1070-4272/05/7804-0680 © 2005 Pleiades Publishing, Inc.

($\nu_1 = -1$, $\nu_2 = -1$, $\nu_3 = 1$, $\nu_4 = 0$)] were solved simultaneously with the equation describing the change in the volume in the course of the reaction:

$$dV/d\tau = \sum_{i=1}^{4} \nu_i V(r_1 + r_2 + r_3)/\rho_i.$$

Here ρ is the molar density of a component.

The order of the catalytic reaction with respect to water was estimated using the kinetic curves obtained at various initial concentrations of water in the reaction mass (Fig. 1a). The system of equations was numerically integrated by the fourth-order Runge–Kutta method. In the integration of the system, the values of k_1 and k_2 were fixed and corresponded to the previously obtained values of the coefficients A and E (J mol^{-1}) of the Arrhenius equation [1]: k_1 9.25×10^5, 58 800; k_2 1.75×10^5, 49 800. The reaction order n with respect to water and the constant k_3 of the catalytic reaction at 30°C were calculated from the condition that the sum of squared deviations F of the calculated DMEA yields b_i^c from the experimental values b_i^e at each point i is at a minimum for all the kinetic curves, with account of the weighting factors w_i (T = 30°C):

$$\min_{n,\,k_3} F = \sum_{i=1}^{N} w_i (b_i^c - b_i^e)^2.$$

Here N is the number of experimental points.

The minimum of the function F was found using the modified gradient method.

The following values of the sought-for parameters were obtained: n = 1.62 and k_3 = 4.58×10^{-4} $l^{2.62}\,mol^{-2.62}\,min^{-1}$. As can be seen from Fig. 1a, the calculated and experimental values of the yield are in a good agreement.

The kinetic curves of DMEA formation at various temperatures and equal initial water concentrations are shown in Fig. 1b.

The parameters A_3 and E_3 (J mol^{-1}) of the temperature dependence of rate constant of the catalytic reaction [$k_3 = A_3 \exp(-E_3/RT)$] were calculated from the condition that the sum of squared deviations F of the experimental DMEA yields from the calculated values for all the experimental points shown in Fig. 1b is at a minimum:

$$\min_{A_3,\,E_3} F = \sum_{i=1}^{N} w_i (b_i^c - b_i^e)^2, \quad T \ 20, 30, 40, 50°C.$$

For a water-catalyzed reaction (k_3), the following parameters of the Arrhenius equation were obtained: A_3 13.79×10^5 and E_3 54 700 J mol^{-1}.

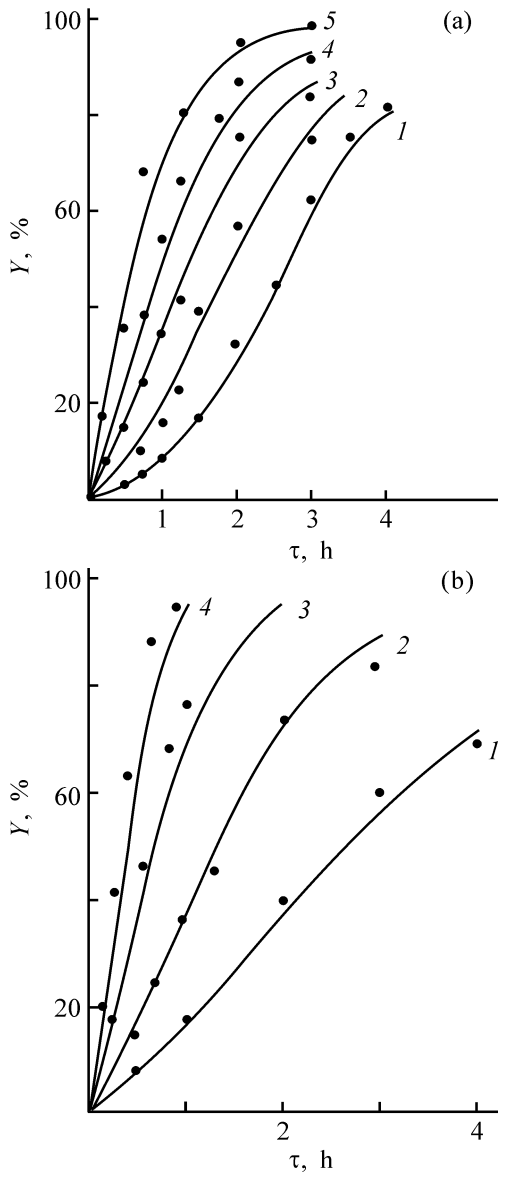


Fig. 1. Kinetic curves of DMEA formation at the EO : DMA : water molar ratio of (a) 1 : 3 : (0–0.5) and (b) 1 : 3 : 0.2 and temperature of (a) 30°C and (b) (*1*) 20, (*2*) 30, (*3*) 40, and (*4*) 50°C. (*Y*) DMEA yield, (τ) time, and (q^0) initial amount of a reagent. (a) $q^0_{EO} \times 10^4$ (mol): (*1*) 431.5, (*2*) 332.1, (*3*) 345.8, (*4*) 339.6, (*5*) 330.5. $q^0_{DMA} \times 10^4$ (mol): (*1*) 1264.3, (*2*) 929.9, (*3*) 1006.3, (*4*) 1018.8, (*5*) 978.3. $q^0_{water} \times 10^4$ (mol): (*1*) 0, (*2*) 33.0, (*3*) 69.1, (*4*) 102.3, (*5*) 166.2. (b) $q^0_{EO} \times 10^4$ (mol): (*1*) 430.5, (*2*) 345.8, (*3*) 462.8, (*4*) 431.2. $q^0_{DMA} \times 10^4$ (mol): (*1*) 1321.6, (*2*) 1006.3, (*3*) 1346.7, (*4*) 1302.2. $q^0_{water} \times 10^4$ (mol): (*1*) 89.0, (*2*) 69.1, (*3*) 92.0, (*4*) 87.4. *Points*, experiment; *lines*, calculation.

Thus, the experimental data are well described in terms of the kinetic model suggested, which can be used to optimize a reaction unit for DMEA production.

EXPERIMENTAL

In the experiments, EO [GOST (State Standard) 7568–88] and DMA (GOST 9967–74) without additional purification and twice-distilled water were used. The experimental procedure and the method of analysis are similar to those described earlier [1].

REFERENCES

1. Danov, S.M., Kolesnikov, V.A., Efremov, R.V., and Mezhenin, D.Yu., *Zh. Prikl. Khim.*, 2004, vol. 77, no. 3, pp. 434–436.
2. Shenfeld, N., *Poverkhnostno-aktivnye veshchestva na osnove oksida etilena* (Surfactants Based on Ethylene Oxide), Moscow: Khimiya, 1982.
3. Lebedev, N.N. and Smirnova, M.M., *Izv. Vyssh. Uchebn. Zaved., Khim. Khim. Tekhnol.*, 1960, vol. 3, no. 1, pp. 104–108.
4. Lebedev, N.N. and Smirnova, M.M., *Kinet. Katal.*, 1961, vol. 2, no. 3, pp. 519–524.
5. Lebedev, N.N. and Smirnova, M.M., *Kinet. Katal.*, 1965, vol. 6, no. 3, pp. 457–465.
6. Lebedev, N.N. and Smirnova, M.M., *Zh. Obshch. Khim.*, 1969, vol. 39, no. 12, pp. 2732–2737.
7. Zimakov, P.V., *Okis' etilena* (Ethylene oxide), Moscow: Goskhimizdat, 1946.
8. Dyment, O.N., Kazanskii, K.S., and Miroshnikov, A.M., *Glikoli i drugie proizvodnye okisei etilena i propilena* (Glycols and Other Derivatives of Ethylene and Propylene Oxides), Moscow: Chemistry, 1976.

Russian Journal of Applied Chemistry, Vol. 78, No. 4, 2005, pp. 683–684. Translated from Zhurnal Prikladnoi Khimii, Vol. 78, No. 4, 2005, pp. 690–691.
Original Russian Text Copyright © 2005 by Agaev, Madatzade.

BRIEF COMMUNICATIONS

Catalytic Activity of a Mordenite Catalyst in Alkylation of Xylenols with Methanol

A. A. Agaev and K. M. Madatzade

Sumgait State University, Sumgait, Azerbaijan

Received July 26, 2004; in final form, February 2005

Abstract—The catalytic activity of a palladium-containing mordenite catalyst in alkylation of 2,6-, 2,4-, 2,5-, 2,3-, 3,4-, and 3,5-xylenols with methanol was studied. The main and by-products of catalysis and the activity of the catalyst in synthesis of individual trimethylphenols were determined.

Methyl derivatives of phenol are consumed in considerable amounts because of their being the most important half-products of small- and medium-tonnage chemistry. However, the last decade exhibited not only an absolute increase in the amount of their manufacture, but also, and to a greater extent, an expansion of their assortment [1].

Catalytic alkylation of phenols with methanol, which is employed with success in manufacture of *ortho*-cresol and 2,6-xylenol [2–4] or recommended for use in synthesis of other isomers of mono- and dimethyl derivatives of phenol, virtually has not been systematically studied in synthesis of individual trimethylphenols.

The aim of this study was to examine the catalytic activity of a mordenite catalyst in alkylation of isomeric xylenols with methanol.

EXPERIMENTAL

Experiments on alkylation were performed in a laboratory reactor under stationary conditions with a fixed catalyst bed of volume 10 cm^3. Synthetic mordenites (SiO_2 : Al_2O_3 molar ratio x = 25), containing Pd-H-mordenite, served as catalysts. The mordenites were obtained by treating a Na-mordenite (x = 10) with a 1 N NH_4Cl solution, with the subsequent washing and drying. Palladium was introduced in an amount of 1.0 wt % into grains of a mixture of a zeolite and γ-aluminum oxide with an aqueous solution of $[Pd(NH_3)_4]Cl_2$. Before delivering the raw material, the catalysts were calcined at 450°C in a flow of dry air (1 h, 1000 h^{-1}) and then kept for 1 h in a flow of hydrogen (1000 h^{-1}) at 410°C and a pressure of 0.1 MPa. The products formed were condensed in a refrigerator-separator and analyzed by gas-liquid chromatography on a Khrom-5 chromatograph with a column (3.6 m × 4 mm) packed with dimenthylphthalate (18 wt %) on Chromocorb W and catharometer as detector. Dimenthylphthalate was synthesized using an accelerated procedure from menthol and phthalic anhydride.

To reveal the role of noncatalytic transformations, preliminary experiments were performed under the reaction conditions, but without a catalyst. In this case, more than 98% of methanol and 100% of isomeric xylenols (virtually all the isomers) were recovered in an unreacted state, which indicated that there was no reaction in the after-catalyst space [6]. In addition, it was established that isomeric xylenols are isomerized and disproportioned over the Pd-H-mordenite catalyst under the conditions studied (350°, 0.8 h^{-1}) to only a slight extent, because a study of transformations of 2,6-, 2,4-, 2,5-, and 3,5-xylenols in the presence of Pd-H-mordenite without methanol demonstrated that their conversion does not exceed 3.2%.

Analysis of the results obtained in alkylation of isomeric xylenols with methanol shows that this reaction occurs by the concurrent-consecutive mechanism. In this case, the alkylation of isomeric xylenols at the carbon atom of the benzene ring is far ahead of the methylation at the hydroxy group of a particular xylenol. Formation of trimethylphenols via intramolecular conversion of the resulting methyl esters of the respective xylenols is unlikely at the given temperature. According to the previously obtained data [5, 7], such a scheme of formation of methyl homologues of phenol in the presence of mordenite and other zeolite catalysts is accompanied by a low selectivity with respect to the target isomers.

It can be seen from the table that trimethylphenols are formed rather selectively with respect to some of the isomers. For example, 2,4,6-trimethylphenol is

1070-4272/05/7804-0683 © 2005 Pleiades Publishing, Inc.

Alkylation of xylenols with methanol in the presence of a Pd-containing mordenite (T = 350°C, v = 0.8 h^{-1}, xylenol : methanol molar ratio 2 : 1)

Xylenol–methanol	Conversion of xylenol, %	Yield of trimethylphenol in terms of a xylenol taken, %	Yield of reaction products in terms of reacted xylenol, %							
			dimethylanisole	2,4,6-trimethylphenol	2,3,6-trimethylphenol	2,4,5-trimethylphenol	2,3,4-trimethylphenol	2,3,5-trimethylphenol	3,4,5-trimethylphenol	tetramethylphenols
Xylenol:										
2,6-	35	28	2	80	8	–	–	–	–	8
2,4-	48	35	0.5	73	–	13	–	–	–	11
2,5-	40	32	–	–	79	3	–	–	–	13
2,3-	51	41	–	–	80	–	5	5	–	7
3,4-	53	45	–	–	–	40	45	–	1	10
3,5-	58	40	1	–	–	–	–	70	6	17

the main reaction product in methylation of 2,4- and 2,6-xylenols, mainly 2,4,6-trimethylphenol is formed in methylation of 2,5- and 2,3-xylenols, and predominant formation of 2,3,6-trimethylphenol is observed in the catalytic system constituted by 3,5-xylenol and methanol. In contrast to other xylenols, the 3,4-isometer is methylated less selectively on the mordenite catalyst. Methylation of 3,4-xylenol yields two isomers, 2,4,5- and 2,3,4-trimethylphenols in a virtually equimolar ratio. However, the total yield of these isomers in terms of reacted 3,4-xylenol is rather high (95%), and the conversion of 3,4-xylenol in a single pass is practically important (53%).

It can also be seen in the table that the Pd-containing mordenite exhibits a sufficiently high selectivity in methylation of isomeric xylenols. The highest selectivity of the reaction with respect to the target trimethylphenols is observed in the case of methylation of 2,6- and 2,3-xylenols (80%), and the lowest (70%), in the case of a 3,5-xylenol. It should be noted that the yield of trimethylphenols in terms of reacted methanol is also high (74–88%).

In addition to the main isomers listed above, other trimethylphenols are also formed under the reaction conditions, but in a considerably lower yield. The concentration of the main trimethylphenol in the mixture of its isomers varies rather widely (47–82%).

The composition of the tetramethylphenols obtained is not complex and depends on the starting xylenol only slightly. The 2,3,5,6-isomer predominates in the tetramethylphenol fraction obtained in the case of 3,5-xylenol, and mostly 2,3,4,6-tetramethylphenol is formed in other cases.

A comparison of the yields of the main reaction products (trimethylphenols) in terms of a xylenol taken demonstrated that, on the whole, the catalytic activity of the Pd-containing mordenite decreases in the following order: 3,4-xylenol > 2,3-xylenol > 3,5-xylenol > 2,4-xylenol > 2.5-xylenol > 2.6-xylenol.

Under the conditions of catalysis, methanol is transformed only slightly: it undergoes dehydration, dehydrogenation, decarbonylation, and decomposition. Methyl ether, CO, CO_2, and trace amounts of formaldehyde and ethylene were found in the gaseous reaction products.

CONCLUSIONS

(1) A sufficiently high catalytic activity of a Pd-containing zeolite catalyst in synthesis of individual trimethylphenols and their mixtures from xylene isomers and methanol was demonstrated.

(2) It was shown that, under the conditions studied, the conversion of xylenols is 35–57% and the yield of the main trimethylphenol in terms of a reacted xylenol, 70–80%.

REFERENCES

1. Maravek, J., *Eur. Chem. News*, 1998, vol. 69, no. 18, p. 10.
2. Novikova, Yu.A., *Khim. Prom–st. Rubezh.*, 1979, no. 9, pp. 47–61.
3. Kharlampovich, G.D. and Churkin, Yu.V., *Fenoly* (Phenols), Moscow: Khimiya, 1974.
4. Jpn Patent Application 1148040.
5. Agaev, A.A., Methylation of Phenols on Oxide and Zeoite Catalysts, *Doctoral Dissertation*, Baku, 1992.
6. Abaev, G.N., *Zh. Prikl. Khim.*, 1965, vol. 38, no. 10, pp. 2242–2252.
7. Agaev, A.A., Eminov, G.O., and Pashaev, Z.M., *Izv. Vyssh. Uchebn. Zaved., Khim. Khim. Tekhnol.*, 1989, no. 2, pp. 118–120.

Russian Journal of Applied Chemistry, Vol. 78, No. 4, 2005, pp. 685–687. Translated from Zhurnal Prikladnoi Khimii, Vol. 78, No. 4, 2005, pp. 692–694.
Original Russian Text Copyright © 2005 by V. Maslosh, Kotova, O. Maslosh.

BRIEF COMMUNICATIONS

Decreasing the Content of Free Formaldehyde in Urea–Formaldehyde Resins

V. Z. Maslosh, V. V. Kotova, and O. V. Maslosh

Institute of Applied Chemistry, Ministry of Science and Education of the Ukraine, Rubezhnoe, Lugansk oblast, Ukraine

Received June 14, 2004

Abstract—The possibility of decreasing the content of free formaldehyde in urea–formaldehyde resins by varying the pH and urea–formaldehyde ratio in various synthesis steps was examined. Urea–formaldehyde resins containing no free formaldehyde were prepared.

Urea–formaldehyde resins (UFRs) are widely used binders. Their significant drawback is the toxicity caused by the presence of free formaldehyde (FA); its content depends on the preparation conditions [1].

The influence of process parameters on the properties and structure of UFRs was examined in numerous studies [2–4], but the problem is far from being solved because of the complexity of the reactions involved in UFR formation. Polycondensation in the urea–FA system is accompanied by many side reactions (hydrolysis, cyclization, addition, etc.), affecting the functional composition of the product. The kinetic features and mechanisms of these reactions are different [5]. An additional factor complicating the mechanism of UFR formation is the polyfunctional nature of urea and FA.

In this study, we examined how the process parameters affect the content of free FA in UFRs prepared at varied pH values and urea : FA ratios in particular reaction steps.

EXPERIMENTAL

UFRs were prepared at 82 ± 3°C and varied pH in three steps. The urea : FA molar ratio in these steps was 1 : 4, 1 : 1.45, and 1 : 1.33. In the course of the synthesis, we monitored the content of free FA and methylol groups (MGs) [6]. The experimental results are shown in Fig. 1. In run nos. 1 and 2, step I was performed in an acidic solution (pH 4.5–5.0), and steps II and III, in an alkaline solution (pH 9.5–10.0). In run nos. 3 and 4, step I was performed in an alkaline solution (pH 9.5–10.0); step II, in an acidic solution (pH 4.5–5.0); and step III, again in an alkaline solution (pH 9.5–10.0). In run nos. 5 and 6, steps I and III were performed similarly to run nos. 3 and 4, and step II, at pH 2.0–2.5. In run nos. 7 and 8, all the three steps were performed in an alkaline solution (pH 9.5–10.0). In run nos. 1, 3, 5, and 7, urea was loaded in a single portion in each step; in run nos. 2, 4, 6, and 8, the same amounts of urea were loaded uniformly in equal portions during the course of the process step. A detailed protocol of UFR preparation and the UFR structure were reported in [7, 8].

Experimental data show that the properties and toxicity of UFRs are appreciably influenced by such process factors as the mode of loading urea, pH of the medium, and reaction time, and also by the concentrations of urea and FA. In the UFR synthesis in an alkaline solution, when urea is loaded in a single portion, the content of free FA is 0.13–0.14, and that of MGs, 18.6–19.8 wt % (Fig. 1d, curves *1* and *1*'); when urea is loaded uniformly, the content of free FA is 0.05–0.09, and that of MGs, 18.5–19.7 wt % (Fig. 1, curves *2* and *2*'). A longer reaction in alkaline solution does not result in an appreciable decrease in the free FA content.

In the synthesis of UFR in an alkaline solution, a steady decrease in the free FA content is accompanied by a smooth increase in the MG content, which reaches 23.0–23.5 wt % (Fig. 1, curves *1*' and *2*'). It has been shown previously [7] that the UFR formed under such conditions is of mostly linear structure, with a high content of methylene ether bonds. The ready hydrolysis of the methylene ether bonds and the equilibrium character of MG formation account for the reproducibly high content of free FA in UFR samples prepared in alkaline solution.

1070-4272/05/7804-0685 © 2005 Pleiades Publishing, Inc.

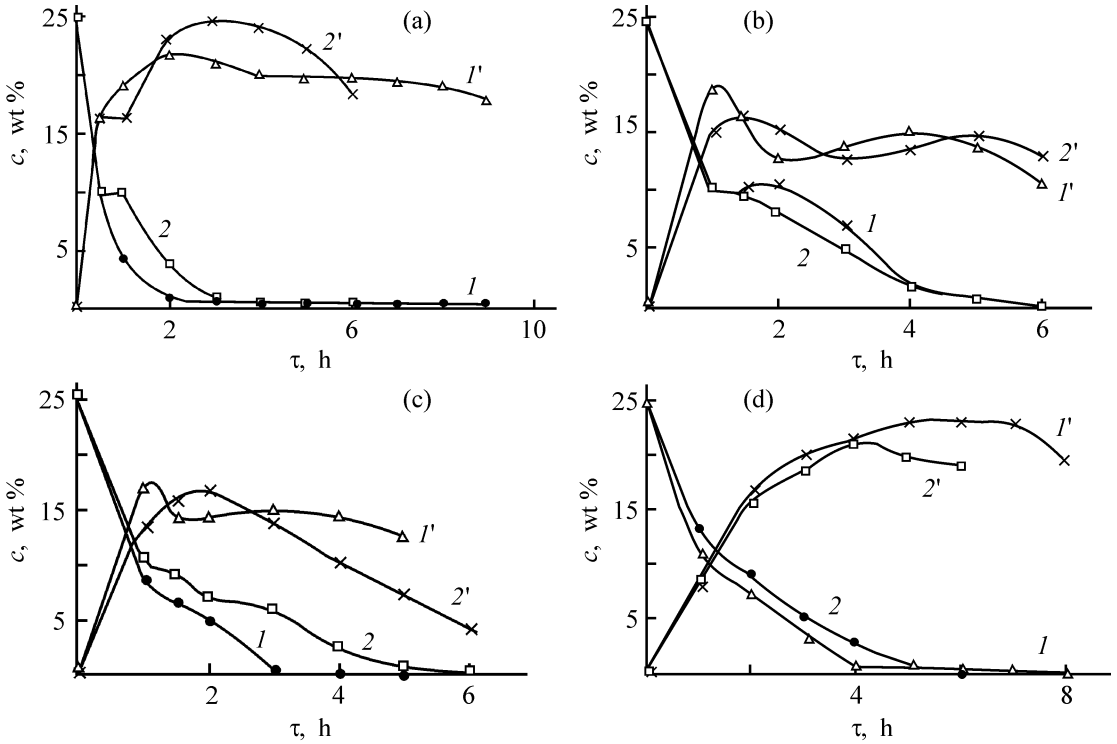


Fig. 1. Concentrations *c* of (*1*, *2*) free FA and (*1*', *2*') MGs vs. time τ in synthesis of UFR at varied pH. (a) Step I, pH 4.5; steps II and III, pH 9.5–10.0; urea loaded in a single portion in each step; (b) steps I and III, pH 9.5–10.0; step II, pH 4.0–4.5; (c) steps I and III, pH 9.5–10.0; step II, pH 2.0; and (d) whole synthesis in aklaline solution. MA loading mode: (*1*, *1*') in a single portion in each step and (*2*, *2*') uniformly in equal portions.

In the UFR prepared in acidic solution in step I and alkaline solution in steps II and III, the free FA content is high, 0.23–0.39 wt % (Fig. 1, curves *1* and *2*). A longer reaction does not result in a noticeable decrease in the free FA content. The MG content is considerably lower than in the preceding case, 18.0–18.5 wt % (Fig. 1, curves *1*' and *2*'). The UFR prepared under these conditions is characterized by the linear structure with small branchings and by the presence of MGs and methylene ether bonds [7], which are potential sources of free FA. Apparently, the main source of free FA in this case is unchanged FA.

The free FA content in UFRs was the lowest (0.03 wt %) when the resins were prepared in alkaline solution in step I, in acidic solution in step II, and again in alkaline solution in step III (Figs. 1b and 1c, curves *1* and *2*). When urea is added in a single portion in each step, the trends in variation of the FA concentration at pH 2.0–4.5 in step II are different (Figs. 1b and 1c, curves *1*). As pH 2.0–4.5 is established and a new portion of urea is added, the free FA content ceases to decrease until the pH is changed and a new portion of urea is added, after which the free FA content appreciably decreases again. When UFR is prepared under similar conditions but with uniform addition of urea, the free FA content decreases without interruptions (Figs. 1b and 1c, curves *2*). According to spectroscopic data, uronic rings are formed in step I in alkaline solution when urea is loaded in a single portion; upon completion of step II, these rings are cleaved with the release of free FA and its subsequent addition to amino and imino groups of urea derivatives. In the synthesis with uniform addition of urea, uronic rings are also formed in step I, but they are preserved in all the subsequent steps and in the final product. The alkaline–acidic–alkaline sequence provides conditions for formation of branched products, which are mainly formed in step II. The subsequent condensation in alkaline solution favors lengthening of the molecular chain of the reaction products formed in the preceding steps. Such a sequence of the pH variation at the chosen molar ratio of urea and FA results in formation of products with stronger bonds (including cyclic products). The residual release of free FA in these resins may be due to equilibrium reactions involving MGs and FA, and in the resins prepared by uniform addition of urea, also to reactions involving amino groups of urea which is present in the free state according to the spectroscopic data [7]. A longer reaction can yield under these conditions resins containing

no free FA. In storage of such resins, the equilibrium processes can cause fluctuations in the free FA content within the range 0.00 – 0.02 wt %.

CONCLUSION

The influence of process factors on the free formaldehyde content in urea–formaldehyde resins was revealed. The lowest content of free formaldehyde is attained when the first and third steps of the synthesis are performed in an alkaline solution, and the second step, in an acidic solution. Uniform addition of urea results in a larger extent of polycondensation, both in acidic and in alkaline solutions.

REFERENCES

1. Balakin, V.M., Toritsin, A.V., and Timoshenko, N.L., *Derevoobr. Prom–st.*, 1998, no. 4, pp. 21–23.
2. Slonim, I.Ya., Alekseeva, S.G., Urman, Ya.G., *et al.*, *Vysokomol. Soedin., Ser. A*, 1977, vol. 19, no. 4, pp. 776–784.
3. Slonim, I.Ya., Arshava, B.M., Aksel'rod, B.Ya., Smirnova, L.N., *et al.*, *Vysokomol. Soedin., Ser. A*, 1977, vol. 19, no. 4, pp. 793–806.
4. Slonim, I.Ya., Alekseeva, S.G., Urman, Ya.G., *et al.*, *Vysokomol. Soedin., Ser. A*, 1978, vol. 20, no. 7, pp. 1477–1485.
5. Wirpsza, Z. and Brzezinski, J., *Aminoplasty*, Warsaw: Naukowo-Techniczne, 1970.
6. Livshits, M.L., *Tekhnicheskii analiz i kontrol' proizvodstva lakov i krasok* (Technical Analysis and Monitoring of Paint-and-Varnish Production), Moscow: Vysshaya Shkola, 1980.
7. Maslosh, V.Z., Kotova, V.V., and Maslosh, O.V., *Zh. Prikl. Khim.*, 2003, vol. 76, no. 3, pp. 498–501.
8. Ukrainian Patent 21503A.

Russian Journal of Applied Chemistry, Vol. 78, No. 4, 2005, pp. 688–689. Translated from Zhurnal Prikladnoi Khimii, Vol. 78, No. 4, 2005, pp. 695–696.
Original Russian Text Copyright © 2005 by Morachevskii.

Professor Nikolai Nikolaevich Lyubavin (To 160th Anniversary of His Birthday)

Nikolai Nikolaevich Lyubavin, a graduate from St. Petersburg University and a pupil of N.N. Sokolov (1826–1877) and D.I. Mendeleev (1834–1907), is primarily known as the author of the book *Fizicheskaya khimiya* (Physical Chemistry) (first issue 1876, second issue 1877) and of a seven-volume textbook of technical chemistry.

Lyubavin was born on April 10 (22), 1845, into a wealthy merchant's family in St. Petersburg. He received his secondary education at St. Petersburg College of commerce. In 1867, he graduated from the natural department of the physicomathematical faculty of St. Petersburg University with a Ph. D. Beginning in early 1868, Lyubavin worked on his own initiative at a number of German chemical laboratories of the following scientists: H. Kolbe (1818–1884) in Leipzig, A. Baeyer (1835–1917, Nobel Prize in 1905) in Berlin, R. Bunsen (1811–1899) A. Ladenburg (1842–1911) in Heidelberg, and I. Hoppe-Seyler (1825–1895) in Tubingen. He also worked for a short time at M. Berthelot's (1827–1907) laboratory in Paris. During his stay in Germany, Lyubavin published results of his studies in the field of organic chemistry in four papers in German journals [1, 2].

In August 1870, the young scientist returned to St. Petersburg and at the beginning of 1871, occupied, by invitation of professor N.A. Menshutkin (1842–1907), a position of a laboratory assistant at the analytical department of his laboratory. Till the summer of 1886, Lyubavin supervised practical training in quantitative analysis. In 1874, he received his master's degree on passing appropriate examinations and defending a dissertation "Ammonia Compounds of Valeric Aldehyde." As a privatdocent, Lyubavin delivered a special course of lectures "Glycines and Amides of Carbonic Acid" in 1880–1882 and a general course of technical chemistry in 1885–1886. During his work at St. Petersburg University, Lyubavin continued experimental investigations in the field of organic chemistry. Among objects of his studies were valeric and other aldehydes, glyoxal, glyoxamine, cinchonine, glycines and amines of carbonic acid, and many other compounds. During the period



from 1871 to 1886, he published about 20 papers in *Zhurnal Russkogo fiziko-khimicheskogo obshchestva* (Journal of Russian Physicochemical Society). In the early 1880s, the scientist performed a number of investigations in the field of technical chemistry and studied iron-manganese ores and phosphorites. The first issue of Lyubavin's monograph *Fizicheskaya khimiya* (Physical Chemistry) was published in 1876, and the second issue, in 1977 (both issues combined include 20 chapters with a total volume of 806 pages). Lyubavin wrote the book on the assumption that theoretical chemistry, concerned with various chemical phenomena, can be divided into three sections: physical chemistry, descriptive chemistry, and analytical chemistry. In terms of this approach, physical chemistry is understood as a part of theoretical chemistry, which is concerned with fundamental aspects of chemical phenomena and chemical processes, irrespective of the nature of substances involved in these processes. The material is presented on the basis of a large number of diverse experimental investigations, with references given to original studies. The whole presentation is of nearly exclusively descriptive nature. Detailed descriptions of processes and phenomena, permanent references to experimental studies by various authors, the manner of presen-

1070-4272/05/7804-0688 © 2005 Pleiades Publishing, Inc.

tation, and the volume of the book give no way of referring this Lyubavin's work to merely the category of textbooks.

In 1886, having accepted an offer by professor V.V. Markovnikov (1837–1904), Lyubavin became a staff member at Moscow University and started to deliver the basic course of lectures in technical chemistry. The lectures were delivered during two semesters twice a week. The basic curse included the following topics: chemistry of combustibles; technical chemistry of heavy metals; silicates and cements; salts, alkalis, and acids; nutrients (including studies of fermentation); fats; oils and tars; and fibrous substances [3]. The chair of technical chemistry included two laboratories, of technical and agricultural chemistry. According to the Statute of Imperial Russian Universities, approved in 1863, chairs of technical chemistry were established at physicomathematical faculties. Even having no knowledge of certain engineering disciplines, students specialized in technical chemistry could well work in chemical industry. This was largely due to Lyubavin's efforts.

On having defended his doctoral dissertation "Pyridine Compounds, Lyubavin was appointed an extraordinary professor at the chair of technology and technical chemistry. In 1897 was published the first volume of the scientist's fundamental work *Tekhnicheskaya khimiya* (Technical Chemistry). In all, he wrote and published six volumes before 1914. The seventh volume remained unfinished and was published in parts in 1922–1926, under the editorship of a Lyubavin's pupil, professor A.M. Nastyukov (1868–1941). The first four volumes presented technical chemistry of inorganic substances, and the last three, that of organic substances.

In 1901, Lyubavin completed his 30-years term as a State employee and, in conformity with the regulations of that time, lost his position as a professor on the staff, but "retained his professor's status and right to teach at the University." He continued to deliver lectures and supervised practical training. In 1907, Lyubavin retired, terminated his teaching activities and concentrated his attention on writing next volumes of Technical Chemistry. During 20 years of his work at Moscow University, from 1886 to 1906, Lyubavin always delivered the basic course of technical chemistry himself. Privatdocents invited by him delivered separate special courses of lectures in varius sections of chemical technology. The position of the head of the chair of chemical technology at Moscow University was inherited by Nastyukov, who defended his doctoral dissertation in 1906 and was appointed professor in 1908.

Lyubavin did much for the improvement of the quality of teaching of technical chemistry at Moscow University and played an important role in training of specialists for industry. The construction of a new building for the laboratories of technical chemistry and agricultural chemistry was commenced in 1903 and completed in 1905 under Lyubavin. For Lyubavin, teaching at Moscow University was the main kind of activity; he did not occupy any positions not associated with his work at the University. The teaching of technical chemistry at Moscow University in 1855–1905 was described in detail by the scientist himself [3]. The organization of teaching and Lyubavin's contribution were discussed in [4–6]. Lyubavin's many-volume book Technical Chemistry was highly appreciated in P.M. Luk'yanov's monograph [7].

Lyubavin died on December 17, 1918.

REFERENCES

1. Blokh, M.A., *Biograficheskii spravochnik* (Biographical Reference Book) Leningrad: Nauch. Khim.-Tekh. Izd., 1929, vol. 1.
2. Blokh, M.A., *Zhurn. Russk. Fiz.-Khim. O–va, Chast' Khim.*, 1928, vol. 60, no. 5, pp. 8–148.
3. Lyubavin, N.N., *Russk. Arkhiv*, 1906, no. 8, pp. 563–594.
4. Shalfeev, V.M., *Uchen. Zp. Mos. Gos. Univ., Khim.*, 1940, no. 53, pp. 53–70.
5. Vol'fkovich, S.I. and Yur'eva, L.P., *Uchen. Zap. Mos. Gos. Univ., Neorg. Khim. Fiz. Khim.*, 1955, no. 174, pp. 177–206.
6. Figurovskii, N.A., Bykov, G.V., and Komarova, T.A., *Khimiya v Moskovskom universitete za 200 let, 1755–1955: Kratkii istoricheskii ocherk* (Chemistry at Moscow University during 200 Years, 1755–1955, A Brief Historical Essay), Moscow: Mos. Gos. Univ., 1955.
7. Luk'yanov, P.M., *Istoriya khimicheskikh promyslov i khimicheskoi promyshlennosti Rossii do kontsa XIX veka* (History of Chemical Works and Chemical Industry in Russia till the End of the XIX Century), Vol'fkovich, S.I., Ed., Moscow: Akad. Nauk SSSR, 1948, vol. 1.

A. G. Morachevskii

Russian Journal of Applied Chemistry, Vol. 78, No. 5, 2005, pp. 691–697. Translated from Zhurnal Prikladnoi Khimii, Vol. 78, No. 5, 2005, pp. 705–711.
Original Russian Text Copyright © 2005 by Vydysh, Naftal', Petrov, Batsunova.

INORGANIC SYNTHESIS AND INDUSTRIAL INORGANIC CHEMISTRY

Specific Features of Chemical Interactions in Atmospheric Purification of a Nickel–Cobalt Solution To Remove Copper

A. V. Vydysh, M. N. Naftal', A. F. Petrov, and I. V. Batsunova

Converter-Matte Plant, Norilsk Nickel Mining-and-Smelting Combine, Open Joint-Stock Company, Norilsk, Russia

Received February 24, 2005

Abstract—Atmospheric purification of a nickel–cobalt solution to remove copper with a high-copper converter matte was studied. The structural and textural characteristics and the phase and chemical composition of the high-copper converter matte and of the solid residue remaining after atmospheric copper removal were examined. The mechanism of copper precipitation and leaching-out of elements belonging to the iron triad was determined, and the extents of the main chemical reactions were calculated.

The technology of manufacture and hydrometallurgical processing of a granulated high-copper converter matte, developed for polymetallic raw materials with a high content of platinum-group metals from Norilsk,[1] has been rather thoroughly worked over in laboratory and, as regards certain procedures, on enlarged-laboratory and semicommercial scales.

It has been experimentally established that the key influence on parameters of the autoclave procedures of the technology is exerted by the mode of the leading procedure, copper removal. This fact, opening up an opportunity to control in rather simple ways the autoclave operations, has attracted the researchers' attention and has become a powerful stimulus to a comprehensive study of the fundamental aspects and specific features of chemical interactions occurring in purification of a nickel–cobalt solution to remove copper ions. Another factor requiring an in-depth analysis of copper removal processes is the need to calculate the distribution of metals and sulfur in the initial stages of converter matte hydrometallurgy, which are associated with development of process schedules and choice of apparatus.

The first stage of hydrometallurgical processing of the converter matte, selective purification of a nickel–cobalt solution to remove copper, is performed under atmospheric conditions with vigorous agitation of the slurry and aeration with air. The solution delivered from the stage of autoclave refining is purified with the initial crushed converter matte. In this case, the mode parameters of the process ensure that a final nickel–cobalt solution with a prescribed residual copper concentration (0.001 g dm^{-3}) is obtained. The main goal of this procedure consists in the maximum possible recovery of copper from solution into a solid precipitate directed into the stage of autoclave oxidative leaching (AOL). Another goal is to leach-out readily removable components of the converter matte, metallic alloy and, in part, heazlewoodite (Ni_3S_2). The leaching occurs in this procedure in the same chemical event as copper precipitation. Therefore, both these tasks are inseparably linked with each other.

It is known [1–4] that the most chemically active component of the converter mattes is the metallic phase. Leaching-out of its components mainly occurs by the reaction

$$M + H_2SO_4 + 0.5O_2 \rightarrow MSO_4 + H_2O, \qquad (1)$$

where M stands for Ni, Fe, Co, or Cu.

Because the recirculated solution delivered to the copper removal stage contains a considerable amount of free sulfuric acid, the acid leaching of heazlewoodite is possible [5–7]:

$$Ni_3S_2 + H_2SO_4 + 0.5O_2 \rightarrow NiSO_4 + 2NiS + H_2O. \qquad (2)$$

Despite that the atmospheric copper removal has been used for several decades in many schemes of atmospheric hydrometallurgy of converter matte, the mechanism of copper precipitation has not been conclusively elucidated. Published data on the mech-

[1] Developed by specialists from the Converter-Matte Plant of Norilsk Nickel Mining-and-Smelting Combine, Open Joint-Stock Company.

1070-4272/05/7805-0691 © 2005 Pleiades Publishing, Inc.

anism of this process are rather contradictory. This suggests the existence of several possible mechanisms of copper removal, with one or another dominating, depending on the composition of the converter matte and on operation conditions. In particular, the atmospheric purification of Ni–Fe–Co solutions to remove copper with a high-nickel converter matte (Ni : Cu ≈ 13 : 1), implemented at Harjavalta plant (Finland), occurs at pH values exceeding 4.5. In [4], the mechanism of this process, in which hydrolytic purification of the solution to remove iron occurs simultaneously with copper removal, is described by the following reactions:

$$CuSO_4 + (Ni \cdot Cu) + 0.5O_2 \rightarrow Cu_2O + NiSO_4, \quad (3)$$

$$2CuSO_4 + 2Ni_3S_2 + 0.5O_2 \rightarrow Cu_2O + 2NiSO_4 + 4NiS, \quad (4)$$

$$3CuSO_4 + 2Ni_3S_2 + O_2 + 2H_2O \rightarrow Cu_3SO_4(OH)_4 + 2NiSO_4 + 4NiS, \quad (5)$$

$$2CuSO_4 + (Ni \cdot Cu) + O_2 + 2H_2O \rightarrow Cu_3SO_4(OH)_4 + NiSO_4. \quad (6)$$

Iron present in the initial solution as Fe^{2+} is oxidized and precipitated mainly as FeOOH, in accordance with the equation

$$FeSO_4 + Ni_3S_2 + 0.75O_2 + 0.5H_2O \rightarrow FeOOH + NiSO_4 + 2NiS. \quad (7)$$

It can be seen from Eqs. (3)–(7) that, in the conditions under consideration (pH > 4.5), copper precipitates from solution in the form of cuprite (Cu_2O) and basic copper sulfate, whose composition corresponds to the formula of antlerite, $Cu_3SO_4(OH)_4$.

A study of the phase composition of solid residues formed in copper removal with a high-copper converter matte (Cu : Ni ≈ 2 : 1) at final pH values ~4.2–4.8 revealed noticeable amounts of basic copper sulfate described by the formula $Cu_5(SO_4)_2(OH)_6$[2]; among other newly formed phases of copper, produced in its precipitation from solution, secondary djurleite and covellite were found. X-ray diffraction studies of the residues revealed the absence of magnetite and bornite. Transfer of sulfide iron into solution in the course of copper removal may proceed by the following reaction to give elementary sulfur:

$$FeS + H_2SO_4 + 0.5O_2 \rightarrow FeSO_4 + S + H_2O. \quad (8)$$

[2] Carried out by specialists from Gipronikel' Institute, Open Joint-Stock Company.

Data on the process kinetics suggest the possibility of direct reaction between the freshly formed millerite and oxygen:

$$NiS + 2O_2 \rightarrow NiSO_4, \quad (9)$$

which also continues in the final stages of copper removal in the absence of copper and acid in solution.

The schedule of the copper removal process, developed for autoclave hydrometallurgy of high-copper converter matte, involves separate purification of nickel–cobalt solution to remove copper and iron. For this purpose, the copper precipitation is carried out at pH values not exceeding 3, which precludes formation of oxides and hydroxy compounds of copper (cuprite, basic sulfates) and coprecipitation of iron oxides. This specific feature of the copper removal mode leads to a fundamentally different course of the process, compared with that described above. The ability of copper–nickel converter mattes to precipitate copper ions has been used in hydrometallurgical practice for a comparatively long time. This effect has been attributed to a specific metallic property of a nickel atom in the heazlewoodite lattice, whence the term "cementation" has appeared. According to this concept, heazlewoodite is a complex in which nickel atoms are in different oxidation states, $Ni \cdot (2Ni_2 + S)$. Reznik *et al*. [8] assume that the copper precipitation with heazlewoodite can be represented as an exchange reaction

$$Ni_3S_2 + CuSO_4 \rightarrow Ni_2CuS_2\downarrow + NiSO_4, \quad (10)$$

according to which two of the three atoms of nickel contained in heazlewoodite remain in the precipitate in a complex intermediate phase. In accordance with the suggested mechanism, copper is in the atomic state in the complex intermediate phase. If the solution contains free acid and an oxidizing agent (oxygen) is present, reverse transfer of the active copper atom into solution is inevitable:

$$2NiS \cdot Cu + H_2SO_4 + 0.5O_2 \rightarrow 2NiS + CuSO_4 + 2H_2O. \quad (11)$$

The occurrence of reaction (11) leads to a paradoxical conclusion that precipitation of copper, which acts in the given process as a "mediator" that carries electrons from atomic nickel to oxygen molecules, is impossible.

The mechanism of copper precipitation by cementation with a converter matte from sulfate solutions was considered in [1, 2, 4, 5, 9]. According to the

results of these studies, the heazlewoodite leaching with simultaneous copper precipitation mainly occurs by the reaction

$$Ni_3S_2 + 2CuSO_4 \rightarrow NiS + 2NiSO_4 + Cu_2S. \quad (12)$$

The cementation reaction (12) is, undoubtedly, an overall reaction, because it is impossible to imagine congruent dissolution of a nickel metal atom from the heazlewoodite lattice and nickel ions chemically bound with sulfur. In addition, the mechanism of direct sulfidization of the copper(2+) atom remains unclear.

Rademan *et al.* [1] explained the interaction as occurring via the stage of formation of hydrogen sulfide:

$$Ni_3S_2 + 2H^+ \rightarrow H_2S + NiS + 2Ni^{2+} + 2e, \quad (12a)$$

$$2Cu^{2+} + H_2S + 2e \rightarrow Cu_2S + 2H^+, \quad (12b)$$

$$Ni_3S_2 + 2Cu^{2+} \rightarrow Cu_2S + NiS + 2Ni^{2+}. \quad (12)$$

There exists a concept that this reaction can proceed by the redox mechanism, without intermediate formation of hydrogen sulfide:

$$2NiS \cdot Ni \rightarrow 2NiS + Ni^{2+} + 2e, \quad (13a)$$

$$2Cu^{2+} + 2e \rightarrow 2Cu^+, \quad (13b)$$

$$Ni_3S_2 + 2CuSO_4 \rightarrow NiSO_4 + Cu_2SO_4 + 2NiS. \quad (13)$$

The active copper(1+) sulfate reacts with millerite to give copper(1+) sulfide:

$$NiS + Cu_2SO_4 \longrightarrow NiSO_4 + Cu_2S \quad (14)$$

In this case, the resultant reaction described by a sum of Eqs. (13) and (14) has the form corresponding to Eq. (12).

If this mechanism is operative, it follows from Eq. (12) that the stoichiometric recovery of copper into solution is 66%. At the same time, extensive studies of the process of copper removal, carried by us on real products, demonstrated that the actual level of copper recovery into solution does not exceed 25–30%.

EXPERIMENTAL

To determine the maximum recovery of nickel into solution in copper removal, laboratory studies of how the procedure duration and l/s ratio affect the parameters of the copper removal process were carried out.

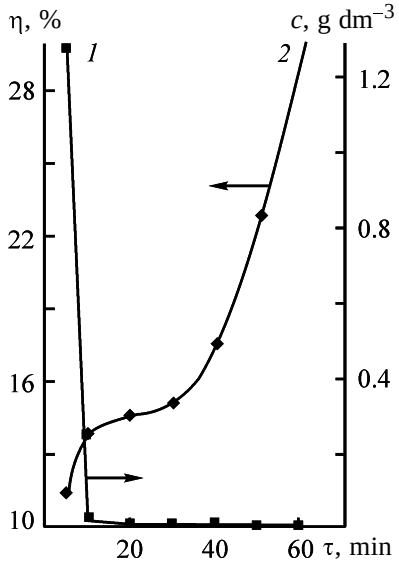


Fig. 1. (*1*) Residual content *c* of copper in solution and (*2*) nickel recovery η into solution vs. the duration of the copper removal process, τ.

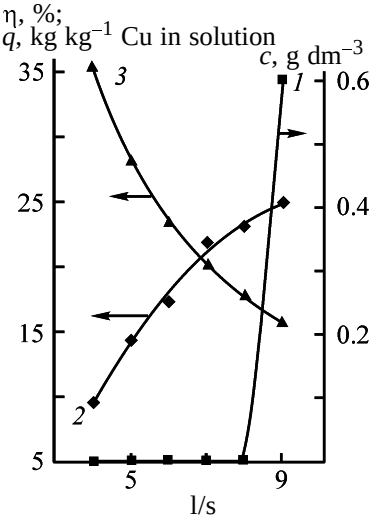


Fig. 2. (*1*) Residual content *c* of copper in solution, (*2*) nickel recovery η into solution, and (*3*) specific expenditure *q* of the converter matte vs. the l/s ratio in the initial sludge.

As starting ingredients were used a model solution of the composition simulating that of the recirculation solution from autoclave refining and sample no. 1 of a granulated high-copper converter matte of composition (%): Ni 26.20, Cu 46.6, Co 0.61, Fe 3.21, and S 21.4, crushed in a laboratory ball mill to a 90% content of particles of the –45-μm fraction. The copper removal was performed in a 1.0 dm^3 titanium reactor with mechanical agitation and electric heating. Air was supplied through a dispersant under a sludge bed, with its flow rate controlled with a calibrated rotameter. The results of these experiments are shown in Figs. 1, and 2.

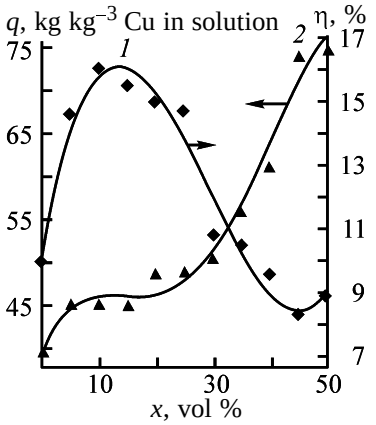


Fig. 3. (*1*) Nickel recovery η into solution and (*2*) specific expenditure *q* of the converter matte vs. the amount *x* of anolyte added.

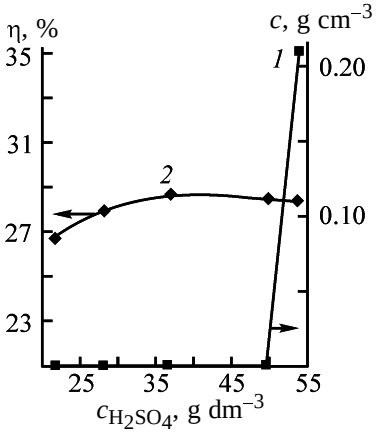


Fig. 4. (*1*) Residual content *c* of copper in the final solution and (*2*) nickel recovery η into solution vs. the content $c_{H_2SO_4}$ of the acid in the initial solution.

Figure 1 shows that sufficiently deep precipitation of copper occurs already in 20 min, with its residual concentration in solution equal to 1 mg dm^{-3}. The maximum recovery of nickel into solution was 30.19% at 60 min of copper removal.

Figure 2 shows how the recovery of nickel into solution depends on the l/s atio, i.e., on the amount of copper and sulfuric acid delivered to the process of copper removal with the recirculated solution.[3] The amount of copper and acid involved in the process grows simultaneously with an increase in the l/s ratio. Therefore, it is impossible to make an unambiguous conclusion about what mechanism, cementation (12) or acid dissolution (1) and(or) (2), predominantly affects the extent of nickel recovery into solution.

A possible way to raise the nickel recovery into solution was to deliver an additional amount of the acid into the copper removal process. In laboratory experiments, the acid was introduced into the process as a component of a nickel anoyte at a fixed l/s ratio. The laboratory experiments were performed with sample no. 2 of a granulated high-copper converter matte of composition (%): Ni 25.42, Cu 48.9, Co 0.72, Fe 2.27, and S 22.3, crushed in a laboratory ball mill to a 90% content of particles of the –45-μm fraction. The specific expenditure of the converter matte was raised, compared to that in preceding experiments, in order to diminish the influence exerted by copper arriving with the solution on the extent of nickel recovery from the converter matte. The experiment duration was the maximum possible, 60 min. In all the experiments, the required residual copper concentration in solution ($c \le 1$ mg dm^{-3}) was reached. The results obtained in copper removal are shown in Fig. 3.

Figure 3 shows that the dependence of the extent of nickel recovery on an anolyte addition shows an extremum. At small volumes of the anolyte, the nickel recovery into solution grows to reach a maximum at an anolyte expenditure of 10 vol %. However, further increase in the fraction of the anolyte in the liquid phase of the initial sludge leads to a decrease in the extent of nickel recovery into solution. The observed decline in the recovery may be due to a decrease in the amount of copper delivered into the process and to the resulting increase in the specific expenditure of the converter matte.

In the next stage of the study, it was necessary to determine how the nickel recovery into solution depends on the initial concentration of the acid in the recirculated solution. The duration of copper removal was 60 min. The initial solution with a fixed content of copper was acidified with concentrated sulfuric acid. The specific expenditure of the converter matte was 20.68 kg kg^{-1} copper in solution in all the experiments. The results obtained are shown in Fig. 4. It can be seen that, all other conditions being the same, introduction of an additional amount of the acid does not exert any decisive influence on the nickel recovery into solution, because the value of this parameter is about the same within experimental error.

The results of the study are summarized in Fig. 5. The data obtained indicate that the key influence is exerted on the extent of nickel recovery into solution by the ratio between the mass of the converter matte and amount of dissolved copper, delivered to the process of copper removal. In addition, the nickel recovery into solution is strongly affected by the degree of metallization of the converter matte, which, in turn,

[3] The duration of copper removal in experiments with varied l/s ratio was 40 min.

Table 1. Results of semicommercial tests of the atmospheric copper removal process (T = 85–90°C, air space velocity 2.2 $nm^3\ m^{-3}$ solution min^{-1}, τ = 60 min)

Phase	Content in precipitate, %, and in solution, g dm^{-3}					Recovered into solution, %			Degree of copper precipitation, %
	Ni	Cu	Co	Fe	S_{tot}	Ni	Co	Fe	
Solid residue	21.20	48.1	1.71	0.26	21.4	–	–	–	–
Solution	115.16	<0.001	0.89	5.78	86.0	18.18	59.54	43.55	99.99

depends on the content of sulfur in it. At a lowered content of sulfur in the converter matte, the amount of metallic nickel in the matte increases, reaction (1) of dissolution of the metallic component develops, and the dependence of nickel recovery into solution on the specific expenditure of the converter matte is less pronounced.

The minimum specific expenditure of the converter matte, which ensures that a prescribed residual concentration of copper in solution (0.001 g dm^{-3}) is reached, was 17.78 kg kg^{-1} Cu (Fig. 2); the maximum extent of nickel recovery into solution, achieved in the experiments, was 30.2% (Fig. 1). To determine the composition and structure of products formed in copper precipitation in atmospheric copper removal, samples of the initial and final solid products formed in this procedure were subjected to a mineralogical analysis.[4] In particular, the initial granulated high-copper converter matte (Ni 26.8, Cu 46.8, Co 0.67, Fe 3.1, and S 22.2%) and a solid residue formed in semicommercial purification to remove copper (Table 1) were analyzed. Composition of the initial solution (g dm^{-3}): Ni 114.1, Cu 7.19, Fe_{tot} 3.0, Co 0.01, and H_2SO_4 13.5.

A study of a sample of granulated high-copper converter matte demonstrated that the material contains three phase components: copper sulfide, nickel sulfide, and a metallic phase. Among the phases identified were djurleite, a tetragonal modification of $Cu_{1.96}S$, and heazlewoodite, Ni_3S_2, which are the main constituents of the converter matte. Also, a primary low-temperature chalcosine, an orthorhombic modification of Cu_2S, and a minor amount of low-temperature bornite (Cu_5FeS_4) were revealed. No independent mineral forms of iron and cobalt were established. Because of its extremely small dimensions, the composition of the metallic phase was determined semiquantitatively (wt %): Ni 75–80, Fe 10, Cu 10, and Co 2–3. The content of the metallic phase in a sample of the high-copper converter matte was approximately 3–5 wt %.

Coarse particles of the solid residue formed in purification to remove copper were close in their mineralogical composition to grains of the initial crushed converter matte. The finely dispersed component of the residue was mainly composed of copper sulfide (of predominantly secondary origin). A sample of the solid residue was composed both of particles containing all the three components and of those in which there was already no metallic phase. These latter had voids of a characteristic shape reproducing that of the initial metallic component, and these voids indicated that leaching of chemically free metals is selective. An unexpected and difficultly understandable fact was that the metallic phase simultaneously disappeared throughout the particle volume without any noticeable indications of their decryptation or formation of open pores. The main phase component of the sample formed in copper removal was relict djurleite ($Cu_{1.96}S$), containing virtually no iron. The composition of the metallic phase remained unchanged, but

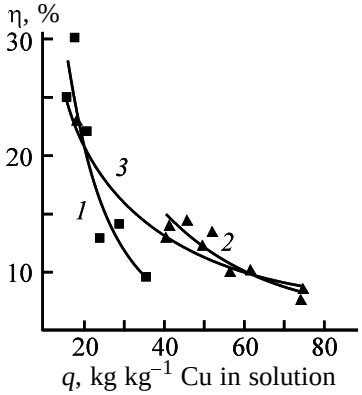


Fig. 5. Influence of the specific consumption q of the converter matte on the nickel recovery η into solution in atmospheric copper removal. Sulfur content (%) in the converter matte: (*1*) 21.4 and (*2*) 22.3; (*3*) generalized curve.

[4] Carried out by L.N. Ertseva using the conventional diagnostic techniques: X-ray diffraction and optical analyses and a set of modern methods for studying the composition of substances, including scanning electron microscopy and X-ray fluorescence microanalysis (Converter-Matte Plant, Norilsk Nickel Mining-and-Smelting Combine, Open Joint-Stock Company and Gipronikel' Institute, Open Joint-Stock Company).

Table 2. Calculated extents of the main chemical reactions in copper removal

Reaction	Metal being recovered	Extent of reaction with respect to metal being recovered into solution, %	Recovery of metal from converter matte, %	Fraction in total recovery of component, %
$Ni + H_2SO_4 + 0.5O_2 \rightarrow NiSO_4 + H_2O$	Ni	80.00	10.83	59.64
$Ni_3S_2 + 2CuSO_4 \rightarrow NiS + 2NiSO_4 + Cu_2S$	Ni	11.60	6.68	36.78
$Ni_3S_2 + H_2SO_4 + 0.5O_2 \rightarrow NiSO_4 + 2NiS + H_2O$	Ni	2.25	0.65	3.58
$Fe + H_2SO_4 + 0.5O_2 \rightarrow FeSO_4 + H_2O$	Fe	80.00	12.49	28.78
$Fe_2S_3 + 2CuSO_4 + Cu_2S \rightarrow 2FeSO_4 + 4CuS$	Fe	66.00	30.91	71.22
$Co + H_2SO_4 + 0.5O_2 \rightarrow CoSO_4 + H_2O$	Co	80.00	13.98	23.44
$Co_3S_2 + 2CuSO_4 \rightarrow CoS + 2CoSO_4 + Cu_2S$	Co	83.00	45.66	76.56
$Cu + H_2SO_4 + 0.5O_2 \rightarrow CuSO_4 + H_2O$	Cu	80.00	0.80	–

dissolution of its major part resulted in a decrease in the total content of iron and cobalt in the solid residue, compared with the initial converter matte. The decrease in the content of iron in the solid phase in the course of purification to remove copper is also due to its leaching-out from the bornite component, which probably yielded secondary copper sulfide. The phase component of nickel sulfide contained considerable amounts of copper impurity and, for the most part, had a formula close to $Ni_{50}Cu_{10}S_{40}$, which stoichiometrically corresponded to a mixture of $Cu_{2-x}S$ and Ni_3S_2. A minor amount of nickel sulfide was present in the form of millerite.

The possibility of copper precipitation in the course of copper removal by mechanism (12) is in good agreement with the results obtained when studying the phase composition of the product formed in the process, but this mechanism cannot be used to explain the effect of limited copper precipitation from solution. At the minimum specific expenditure of the converter matte equal to 17.78 kg kg^{-1} Cu in the recirculated solution, the calculated recovery of nickel from the solid phase by reaction (12) is 21.7%, in good agreement with the experimental results. However, it is unclear why the degree of solution purification decreases dramatically at a specific expenditure of the converter matte of less than 17.78 kg kg^{-1} Cu, despite that a considerable amount of heazlewoodite is still contained in the solid residue and there are no apparent reasons why reaction (12) cannot proceed further. It may be assumed that these reasons are of kinetic, rather than thermodynamic, origin.

The probable reasons for the hindrance to reaction (12) are as follows: diffusion hindrance associated with copper deposition onto the surface of converter matte particles in the form of dense films that preclude penetration of leaching agents into the reaction zone; kinetic hindrance of electrochemical nature, associated with the primarily occurring leaching-out of the metallic phase from the whole volume of a converter matte particle.

Elucidating the mechanism of hindrance and developing methods for its inhibition are a matter of current interest because, if the extent of reaction (12) is raised, the nickel recovery into solution in the atmospheric stage will substantially increase. A solution to this problem will markedly diminish the amount of expensive equipment required in the other stages of autoclave leaching.

The formation of a secondary copper sulfide with a composition close to Cu_2S suggests that the copper removal occurs under domination of the cementation mechanism by reaction (12). The extent of this reaction is determined from the amount of nickel recovered into solution, which is found in direct experiments with account of the dissolution of the metallized phase by reaction (1).

It may be assumed that the behavior of cobalt, which is isomorphically incorporated into the composition of heazlewoodite, in the reaction with copper sulfate is similar to that of nickel. This reaction yields higher cobalt monosulfide and chalcosine:

$$Co_3S_2 + 2CuSO_4 \rightarrow CoS + 2CoSO_4 + Cu_2S. \quad (15)$$

The acid fed into the process as a component of the initial solution is spent for dissolution of the metallic phase and oxidative leaching of heazlewoodite by reaction (2).

According to the results of mineralogical studies, the solid residue formed in copper removal contains virtually no bornite. This may be due to decomposition of iron and copper sulfides contained in it ($Cu_4^{1+}Cu_{0.5}^{2+}Fe^{3+}S_4 \rightleftarrows 2Cu_2S + 0.5CuS + 0.5Fe_2S_3$) to give iron sulfate and covelline:

$$Fe_2S_3 + 3CuSO_4 = Fe_2(SO_4)_3 + 3CuS, \quad (16)$$

$$Fe_2(SO_4)_3 + Cu_2S = 2FeSO_4 + CuS + CuSO_4, \quad (17)$$

$$Fe_2S_3 + 2CuSO_4 + Cu_2S = 2FeSO_4 + 4CuS. \quad (18)$$

The extent of this reaction was determined from the iron recovery into solution with account of the amount of iron dissolved by reaction (1). The main chemical reactions occurring in the course of copper removal and their extents are listed in Table 2.

The procedure for calculating the extent of the chemical reactions was based on the best possible fitting of the theoretical quantitative characteristics of the copper removal process to the parameters obtained in direct experiments (Table 1). The calculations were performed with account of the data obtained in an instrumental analysis of the structure and composition of the products under study.

CONCLUSIONS

(1) It was established experimentally and confirmed by calculation that the cementation precipitation of copper is incomplete despite the presence in the system of considerable amounts of the starting ingredients.

(2) The cementation mechanism of precipitation from solution is characteristic of copper; iron is leached-out both from the metallic phase of the converter matte and from the complex copper sulfide with a composition of bornite with predominance of the second mechanism; the recovery of nickel into solution is primarily due to leaching-out of the metallic phase and copper precipitation by the cementation mechanism, with the acid dissolution of heazlewoodite proceeding to only a minor extent.

(3) The results obtained in calculating the extent of the main chemical reactions were used for preliminary design and feasibility study of hydrometallurgical processing of a high-copper converter matte.

REFERENCES

1. Rademan, J.A.M., Lorenzen, L., van Deventer, J.S.J., *Hydrometallurgy*, 1999, vol. 52, pp. 231–252.
2. Hofirek, Z. and Kerfoot, D.G.E., *Hydrometallurgy*, 1992, vol. 29, pp. 357–381.
3. Maslenitskii, I.N., Dolivo-Dobrovol'skii, V.V., Dobrokhotov, G.N., *et al.*, *Avtoklavnye protsessy v tsvetnoi metallurgii* (Autoclave Processes in Autoclave Metallurgy), Moscow: Metallurgiya, 1969.
4. Knuutila, K., Hultholm, S.-E., Saxen, B., and Rosenback, L., in *ALTA 1997: Nickel–Cobalt Pressure Leaching and Hydrometallurgy Forum*, Hyatt Hotel, Perth (Western Australia), May 19–20, 1997.
5. Canadian Patent 1 173 655.
6. Fugleberg, S., Hultholm, S.-E., Rosenback, L., and Hololhan, T., *Hydrometallurgy*, 1995, vol. 39, pp. 1–10.
7. US Patent 6 206 951.
8. Reznik, I.D., Sobol', S.I., and Khudyakov, V.M., *Kobal't* (Cobalt), vol. 2: *Gidrometalurgiya* (Hydrometallurgy), Moscow: Mashinostroenie, 1995.
9. Llanos, Z.R., Queneau, P.B., and Rickard, R.S., *CIM Bull.*, 1974, vol. 67, pp. 74–81.

Russian Journal of Applied Chemistry, Vol. 78, No. 5, 2005, pp. 698–701. Translated from Zhurnal Prikladnoi Khimii, Vol. 78, No. 5, 2005, pp. 712–715.
Original Russian Text Copyright © 2005 by Kuznetsova, Shatov, Dryamina, Badertdinov.

INORGANIC SYNTHESIS AND INDUSTRIAL INORGANIC CHEMISTRY

Use of Wastes from Soda Production To Produce Nonshrinking Oil-Well Cement

T. V. Kuznetsova, A. A. Shatov, M. A. Dryamina, and R. N. Badertdinov

Soda Open Joint-Stock Company, Sterlitamak, Bashkortostan, Russia

Received September 20, 2004

Abstract—The possibility of using soda wastes to obtain sulfated clinkers was analyzed. The phase composition of the clinkers synthesized was determined. Processes of hydration of the cements obtained were examined. Semicommercial tests of formulations of nonshrinking oil-well cements were performed.

Disintegration of a cement ring in the annular space is largely due to its shrinkage stresses [1]. Therefore, the problem of development of an oil-well material with a compensated shrinkage in the course of hardening is still a matter of current interest.

As objects of study we chose raw materials used at the Podol'sk experimental cement plant: limestone, clay, cinders, gypsum, and materials of industrial origin, produced at the Soda Open Joint-Stock Company: carbonized and noncarbonized slurries [2]. The chemical compositions of the chosen components are listed in Table 1.

X-ray diffraction and petrographic analyses revealed that the limestone is mainly represented by calcite (>50%) and the clayey component mostly contains montmorillonite and a certain amount of hydromicas.

The slurries have close compositions. According to the results of an X-ray diffraction analysis, the material also contains calcium sulfate, calcium and aluminum oxychlorides, and a minor amount of magnesium hydroxychloride.

To examine the possibility of using carbonized and noncarbonized slurries, the compositions of raw mixes used to obtain sulfoferrite clinkers were calculated. The data obtained show that the chosen materials of industrial origin, wastes from the Soda Open Joint-Stock Company, can be used as a carbonate component. The presence of calcium sulfate in the wastes leads to a significant decrease in the amount of gypsum necessary for preparing the mixture (from 9.8% for mixtures prepared from the conventional components to 4.5% for a mixture prepared from a carbonized slurry) [3].

EXPERIMENTAL

To study processes of mineral formation, mixtures intended for production of low- and high-basic sulfoferrite clinkers and a clinker of intermediate composition were prepared. A control clinker was synthesized

Table 1. Chemical composition of raw components

Material	Content of oxides, wt %						
	SiO_2	Al_2O_3	Fe_2O_3	CaO	MgO	SO_3	calcination loss
Limestone	6.56	1.58	0.86	50.02	1.18	–	39.80
Clay	51.93	15.17	6.86	7.29	1.75	2.92	11.27
Cinders	13.05	3.80	75.32	1.38	1.47	3.77	1.21
Gypsum	4.59	1.18	0.55	34.08	3.13	38.20	18.15
Slurry:							
noncarbonized	4.10	0.35	0.15	63.50	3.50	4.10	21.50
carbonized	1.80	0.30	0.10	46.20	4.00	4.20	28.00

1070-4272/05/7805-0698 © 2005 Pleiades Publishing, Inc.

from raw materials used at the Podol'sk cement plant. The raw mixes were prepared by wet grinding in a laboratory porcelain mill for 6 h. Then the slurries obtained were dried in a drying box at 60±5°C to a residual moisture content of 1–2%.

The prepared raw mixes were used to form on a hydraulic press at a pressure P = 400 kg cm^{-2} cylindrical samples 5 cm in diameter and 3 cm high. The samples were calcined in a high-temperature furnace with lanthanum chromite heaters at 1100, 1150, 1180, and 1200°C, with isothermal heating for 5, 10, 15, 20, 30, and 60 min.

We found that the temperature of complete assimilation of CaO in heating of raw mixes depends on the basicity of a clinker. In a low-basic clinker, the degree of binding equal to 0.98–1.0 is reached at 1180°C. The degree of CaO assimilation is 0.73–0.78 upon an isothermal keeping for 5 min (T = 1180°C) and becomes as high as 0.98–1.0 when the time of heating is raised to 30 min.

Binding of calcium oxide in raw mixes for high-basic clinkers requires heating to a higher temperature of 1250°C, with a degree of limestone assimilation equal to 0.98–0.99 reached upon heating for 30 min. In clinkers of intermediate composition, the degree of CaO assimilation equal to 0.98–1.0 is reached at 1200°C (τ = 30 min). Data on the degree of assimilation of calcium oxide are listed in Table 2.

Comparison of the kinetics of CaO assimilation in mixtures based on solid residues formed in soda production and in control mixtures based on the conventional components shows that synthesis of minerals contained in the sulfoferrite clinker is considerably faster in the formulations developed, compared with control mixtures. The acceleration of the reactions of mineral formation is apparently due to the presence in slurries of chloride compounds, which act as mineralizers in calcination of a clinker [4, 5].

These results were used to calculate the rate constants of the reactions of CaO assimilation in formation of sulfated clinkers. An analysis of the data obtained demonstrated that the rate of CaO binding is limited by diffusion processes and is described by the Jander equation.

X-ray diffraction and petrographic analyses were used to determine the phase composition of the clinkers synthesized. It was established that the phase composition of a clinker produced by calcination of low-basic sulfoferrite raw mixes based on materials of industrial origin at a temperature of complete assimilation of CaO (T_c ≈ 1180–1200°C) significantly differs from that calculated. This is due to the appearance of a large amount of a melt and to the preferential formation of high-basic phases via the liquid phase. The content of phases in clinkers prepared from high-basic mixtures and those of intermediate composition was close to to that obtained by calculation (Table 3).

A study of hydration of the resulting clinkers by the petrographic method in micropreparations confirmed the conclusion that the hydration activity of products based on materials of industrial origin is higher [2]. Already in the first hours of hydration, ferruginous ettringite is formed in the samples studied;

Table 2. Degree of calcium oxide binding, α, in raw mixes

Mix	τ,* min	α at indicated temperature, °C		
		1100	1180	1250
Sulfoferrite clinker:				
low-basic (LSFC)	5	0.78	0.97	–
	10	0.83	0.98	–
	20	0.89	0.99	–
	30	0.92	0.99	–
	60	0.95	1.0	–
high-basic (HSFC)	5	0.75	0.87	0.99
	10	0.79	0.90	0.99
	20	0.83	0.96	1.0
	30	0.88	0.99	1.0
	60	0.88	1.0	1.0
of intermediate	5	0.73	0.85	0.98
composition (ISFC)	10	0.79	0.92	0.99
	20	0.81	0.98	0.99
	30	0.85	0.99	1.0
	60	0.85	1.0	1.0
Control clinker	5	0.72	0.85	0.97
	10	0.78	0.88	0.99
	20	0.83	0.92	0.99
	30	0.86	0.96	1.0
	60	0.88	0.97	1.0

* Time of isothermal heating.

Table 3. Phase composition of sulfoferrite clinkers

Run no.	Clinker	Content of indicated phase, %			
		C_2S	C_3S	$3CF\cdot CS$	$C_2F\cdot CS$
1	LSFC	32	10	32	18
2	HSFC	16	32	7	40
3	ISFC	24	25	17	28

Table 4. Material composition of cements

Run no.	Content of components, %				
	PCC	LSFC	HSFC	ISFC	gypsum
1	90	5	–	–	5
2	83	10	–	–	7
3	75	15	–	–	10
4	90	–	5	–	5
5	83	–	10	–	7
6	75	–	15	–	10
7	90	–	–	5	5
8	83	–	–	10	7
9	75	–	–	15	10

it remains stable for up to 14 days. This makes it possible to preserve the expansion effect in a system being hardened during a rapid buildup of strength and to eliminate the shrinkage deformations. In further hydration, the recrystallization of the ferruginous ettringite into a monosulfate form and the formation of a gel of iron hydroxide lead to reinforcement of the cement stone through mudding of the pore space.

The results obtained served as a basis for development of optimal compositions of zero-shrinkage oil-well cements.

Cements of various compositions (Table 4) were prepared on the basis of sulfoferrite clinkers (Table 3) and portland cement clinker (PCC) in an MBL laboratory mill.

The cements obtained were tested in conformity with the requirements imposed on oil-well materials at the following characteristics: w/c 0.45 and flowability within 205–230 mm. The results of physicomechanical tests are listed in Table 5.

Thus, the linear expansion of the samples increases from 0.03 to 0.24% as the amount of sulfoferrite clinker introduced into the cement is raised from 5 to 15 wt %. The strength of the cement stone remains virtually unchanged at small SFC doses (5–10%). As the amount of the sulfoferrite clinker in the cement is raised to 15 wt %, the strength characteristics deteriorate. This is due to formation of a greater amount of calcium hydrosulfoferrite of trisulfate form in hydration of the sulfoferrite clinker, with the expansion of the hardening system reaching such a level that destruction processes impair the strength characteristics.

Electron-microscopic examination of the cement stone demonstrated that, in the course of hydration of sulfoferrite phases, mainly ferruginous ettringite, calcium monohydrosulfoferrites and hydroferrites, and a gel of iron hydroxide are formed. In joint hydration of the minerals contained in portland cement and sulfoferrite clinkers, these phases are responsible for the expansion of the hardening system and densification of the cement stone.

Estimates of the rates of cement hydration make it possible to arrange the sulfoferrite-containing cements in the following order: low-basic SFC, that of intermediate composition, and high-basic SFC. This enables a considerable decrease in the amount of the sulfoferrite additive introduced, at the same linear expansions of the system.

These results served as a basis for tests at the Pilot Cement Plant of NIItsement (Research Institute of Cement).

Table 5. Strength of cement stone

Cement no.	Strength, MPa, at indicated age, days				Expansion, %, at indicated age, days	
	bending		compression		2	28
	2	28	2	28		
1	2.3	4.9	5.8	11.3	0.03	0.08
2	2.2	4.5	5.2	10.7	0.05	0.10
3	1.7	3.4	4.0	8.7	0.11	0.18
4	2.7	5.6	6.6	13.4	0.07	0.12
5	2.4	5.3	6.2	13.0	0.10	0.15
6	1.8	3.2	4.1	8.8	0.14	0.24
7	2.5	5.1	6.0	12.1	0.05	0.09
8	2.3	5.0	6.1	11.6	0.08	0.11
9	2.2	4.7	5.2	10.4	0.10	0.18

The tests were performed with the developed compositions of nonshrinking oil-well cements based on sulfated clinkers. The sulfoferrite clinker was obtained by calcination of a raw mix composed of limestone, pyrite cinders, and gypsum from the Podol'sk experimental cement plant and carbonized slurry from the Soda Open Joint-Stock Company in a forge at 1180°C.

A physicochemical analysis of the clinker obtained revealed that it is close in composition to high-basic sulfoferrite clinkers. The content of sulfated dicalcium ferrite is 38 wt %.

The oil-well cement was prepared by grinding in a batch mill of a stock composed of 80 wt % portland cement clinker, 10 wt % sulfoferrite clinker, and 10 wt % gypsum. The fineness of grinding of the cement was characterized by a 13% residue on sieve no. 008 at a specific surface area of about 3300 $cm^2\ g^{-1}$.

The physicomechanical properties of the cement obtained, determined in accordance with GOST (State Standard) 1581–78, are as follows: flowability at w/c = 0.44 equal to 195 mm; time of setting: onset 8 h 15 min, end 9 h 30 min; mortar density 1940 $kg\ m^{-3}$; ultimate strength of a 2-days-old cement stone: bending 3.0 MPa, compression 11.2 MPa; linear expansion of the cement stone 0.06%.

Thus, the cement tested can be classed with nonshrinking oil-well cements.

CONCLUSIONS

(1) The chemical and mineralogical composition of materials of industrial origin (carbonized and noncarbonized slurry), produced by the Soda Open Joint-Stock Company, enable their use as a raw mix component for obtaining sulfoferrite clinkers.

(2) A physicochemical analysis established the optimal compositions of the sulfoferrite clinker used as an expanding additive in production of nonshrinking cements. The clinker containing high-basic sulfated minerals is the most effective as regards the degree of hydration and physicomechanical properties of the resulting cements.

(3) The physicomechanical properties of sulfoferrite-containing cements demonstrated the possibility of development of a high-quality nonshrinking oil-well cement. The optimal cement formulations should not contain the sulfoferrite clinker in amounts exceeding 10 wt %.

(4) The pilot industrial tests performed at the Pilot Cement Plant of NIItsement confirmed the results of the laboratory studies.

REFERENCES

1. Karimov, N.Kh., Development of Formulations and Technology of Application of Expanding Oil-Well Materials for Cementation of Deep Wells under Difficult Geological Conditions, *Doctoral Dissertation*, Ufa, 1986.
2. Ponin, V.I., Babkov, V.V., Merkulov, Yu.M., *et al*., *Na Stroikakh Rossii*, 1984, no. 5.
3. Shatov, A.A., Salt and Oil-Well Formulations for Construction and Exploitation of Wells with the Use of Secondary Material Resources of Soda Production, *Doctoral Dissertation*, Ufa, 1995.
4. Maksin, V.I., Standritchuk, O.Z., and Petrenya, L.M., *Zh. Prikl. Khim*., 1988, vol. 51, no. 11, pp. 2424–2429.
5. Furman, A.A., *Neorganicheskie khloridy* (Inorganic Chlorides), Moscow: Khimiya, 1980.

Russian Journal of Applied Chemistry, Vol. 78, No. 5, 2005, pp. 702–706. Translated from Zhurnal Prikladnoi Khimii, Vol. 78, No. 5, 2005, pp. 716–720.
Original Russian Text Copyright © 2005 by Chizhova, Klyndyuk, Bashkirov, Petrov, Yanushkevich.

INORGANIC SYNTHESIS AND INDUSTRIAL INORGANIC CHEMISTRY

Structure and Properties of Solid Solutions in the System $YBaCuFeO_5$–$YBaCuCoO_5$

E. A. Chizhova, A. I. Klyndyuk, L. A. Bashkirov, G. S. Petrov, and K. I. Yanushkevich

Belarussian State Technological University, Minsk, Belarus
Institute of Solid State Physics and Semiconductors, Belarussian National Academy of Sciences, Minsk, Belarus

Received June 3, 2004; in final form, March 2005

Abstract—The crystal structure parameters of solid solutions $YBaCuFe_{1-x}Co_xO_5$ ($0 \le x \le 1$) were determined, and their thermal stability, thermal expansion, conductance, thermoelectromotive force, dielectric properties, and magnetic sensibility were studied.

At present, layered perovskite-like oxides $A'A''B_2O_{5.5\pm\delta}$ (A' is Y or rare-earth element; A'' is alkaline-earth element; B is 3*d* metal) attract appreciable interest. One of such compounds is yttrium barium ferrocuprate $YBaCuFeO_{5+\delta}$, which was described for the first time in [1].

The compound $YBaCuFeO_5$ has a tetragonal unit cell with the parameters $a = 0.3867$ and $c = 0.7656$ nm (space group $P4mm$, $z = 1$) [2], though, according to [3], this compound belongs to space group $P4/mmm$. At room temperature, $YBaCuFeO_5$ is antiferromagnetic (Neel temperature T_N is 440–475 K); its magnetic structure changes at 190–240 K [3–5] (a commensurate $\leftrightarrows$ incommensurate phase transition). The compound $YBaCuFeO_5$ is a *p*-type semiconductor [6] and shows anomalies of dielectric properties near 460 and 560 K [7]. The effect of iron replacement by nickel on the structure and properties of $YBaCuFe_{1-x}Ni_xO_5$ solid solutions was examined in [6]. Solid solutions $YBaCu_{1-x}Co_xFeO_{5+\delta}$, $YBaCu_{1-x}Fe_xFeO_{5+\delta}$, and $YBaCuFe_{1-x}Co_xFeO_{5+\delta}$ were obtained in [8], and their thermal stability in various gaseous media was examined in [9].

Here we report data on the crystal structure, thermal expansion, and electrophysical and magnetic properties of solid solutions $YBaCuFe_{1-x}Co_xO_5$.

EXPERIMENTAL

Samples of $YBaCuFe_{1-x}Co_xO_5$ ($0 \le x \le 1$) were prepared by a ceramic technique [6, 7] from Y_2O_3 (ItO-LYuM7), Fe_2O_3 (ultrapure 2-4 grade), CuO (ultrapure 9-2 grade), Co_3O_4 (analytically pure grade), and $BaCO_3$ (pure grade). The mixture was heated in air at 1173 K for 40 h. To study the thermal expansion, conductance, and thermoelectromotive force, the powders obtained were pressed in pellets 10 mm in diameter and 3–5 mm thick and bars of size $5 \times 5 \times 30$ mm, which were then sintered in air for 2–8 h at 1273 K. The density of the samples after sintering was no less than 80% of the X-ray density. The X-ray phase analysis (XRPA) of the resulting samples was carried out on a DRON-3 diffractometer (CuK_α radiation) at room temperature. The IR absorption spectra of the synthesized compounds in KBr (chemically pure grade) pellets in the frequency range 200–1500 cm^{-1} were recorded on Specord M-80 and Nexus (Thenno Nicolet) instruments. The thermal stability, thermal expansion, conductance, thermoelectromotive force, inductivity, and dielectric loss of the samples were studied in air according to the procedures described in [6, 7]. Before measuring the electrophysical properties, electrodes were applied onto end faces of the samples by burning-in a silver paste at 1073 K for 15 min. The temperature dependence of the magnetic susceptibility of $YBaCuFe_{0.8}Co_{0.2}O_5$ and $YBaCuFe_{0.7}Co_{0.3}O_5$ samples was studied by a ponderomotive method in a magnetic field H = 8.6 kOe in the temperatures range 77–1200 K, and that of $YBaCuFeO_5$ and $YBaCuFe_{0.9}Co_{0.1}O_5$ samples, by the Faraday method in a magnetic field of 4.5 kOe in the range 77–700 K.

The crystal structure of $YBaCuFe_{1-x}Co_xO_5$ solid solutions corresponded to the structure of $YBaCuFeO_5$. Figure 1 shows that the replacement of

1070-4272/05/7805-0702 © 2005 Pleiades Publishing, Inc.

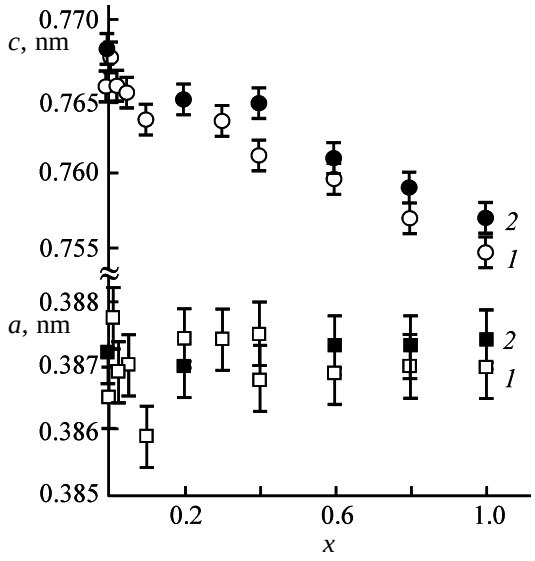


Fig. 1. Unit cell parameters a and c of $YBaCuFe_{1-x}Co_xO_5$ solid solutions as functions of the cobalt content x in $YBaCuFe_{1-x}Co_xO_5$ samples. Data: (*1*) this work and (*2*) [5].

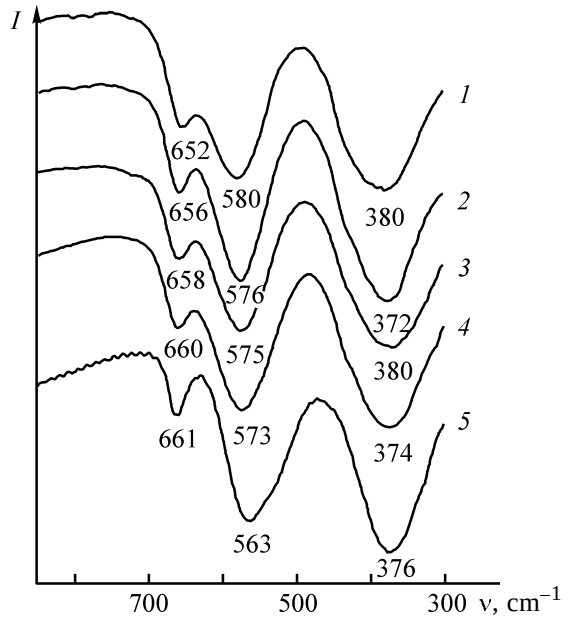


Fig. 2. IR absorption spectra of $YBaCuFe_{1-x}Co_xO_5$ solid solutions. (T) Transmittance and (ν) wave number. x: (*1*) 0, (*2*) 0.1, (*3*) 0.2, (*4*) 0.3, and (*5*) 1.0.

iron by cobalt results in an appreciable decrease in the unit cell parameter c, whereas the parameter a of $YBaCuFe_{1-x}Co_xO_5$ solid solutions remains practically constant up to $x = 1.0$. The data obtained agree well within the error limits with the results of [8]. Anomalies in the concentration dependences $a = f(x)$ and $c = f(x)$ at small ($x \le 0.1$) degrees of replacement are attributable to the fact that, in this case, cobalt in the lattice of $YBaCuFe_{1-x}Co_xO_5$ is in the form of Co^{3+} both in the high-spin (HS) and low-spin (LS) states, and at $x = 0.01$, partly or completely in the form of Co^{2+} ($r_{Fe^{3+}(HS)} = 0.0645$, $r_{Co^{3+}(HS)} = 0.0630$, $r_{Co^{3+}(LS)} = 0.0545$, $r_{Co^{2+}(HS)} = 0.0720$ nm for coordination number 6 [10]).

The IR absorption spectra of $YBaCuFe_{1-x}Co_xO_5$ solid solutions (Fig. 2) contain three absorption bands with maxima at 370–380 (ν_1), 560–580 (ν_2), and 650–660 cm^{-1} (ν_3), corresponding [11] to stretching (ν_2) and bending (ν_1) Cu(Fe)–O–Cu(Fe) vibrations of bonds in basal planes $[Cu(Fe)_2]_\infty$ and also to stretching vibrations of apical oxygen atoms of Cu–O–Fe bonds (ν_3). The replacement of iron by cobalt results in the shift of ν_1 and ν_2 bands to lower frequencies and of ν_3, to higher frequencies (Fig. 2). Thus, the increase in x in $YBaCuFe_{1-x}Co_xO_5$ results in a gradual decrease in the energy of metal–oxygen bonds in basal planes of $-[Cu(Fe)O_2]_\infty-$ layers. The energy of metal–oxygen bonds in the Cu–O–Fe-chains of the $YBaCuFe_{1-x}Co_xO_5$ crystal structure increases, which agrees with a decrease in the unit cell parameter c of $YBaCuFe_{1-x}Co_xO_5$ solid solutions as the degree of iron replacement by cobalt increases.

Samples of the compositions $YBaCuFeO_5$ and $YBaCuFe_{0.9}Co_{0.1}O_5$ were thermally stable in air in the range 293–1273 K, which agrees with the data of [9]. No anomalies were found in the temperature dependences of specific elongation for $YBaCuFe_{1-x}Co_xO_5$ solid solutions (Fig. 3a) within the entire temperature range under study, which points to the absence of structural transitions in these phases in air in this temperature range. A small hysteresis observed in the heating–cooling curves of certain solid solutions (Fig. 3a) is probably due to a low rate of reaching a thermal equilibrium in the samples under conditions of dynamic heating or cooling at a rate of 4–5 deg min^{-1}. The linear thermal expansion coefficient (LTEC) α of $YBaCuFe_{1-x}Co_xO_5$ solid solutions remains unchanged within the error limits when iron is replaced by cobalt (Table 1).

The conductance of $YBaCuFe_{1-x}Co_xO_5$ solid solutions is of the semiconductor nature ($d\sigma/dT > 0$) and tends to increase on replacing iron by cobalt (Fig. 4a). Anomalies in the $\sigma = f(x)$ dependences for $YBaCuFe_{1-x}Co_xO_5$ compounds (Fig. 4b), which are most strongly pronounced at near-room temperatures, can be caused by differences in the charge and spin states of cobalt ions in the composition of $YBaCuFe_{1-x}Co_xO_5$ solid solutions and also by different degrees of order-

Table 1. Coefficients of linear thermal expansion α, temperatures of bends T_{α_1} and T_{α_2}, and activation energies E_σ, E_s, E_p, E_m of charge-transfer processes in $YBaCuFe_{1-x}Co_xO_5$ solid solutions, calculated from the data on conductance and thermoelectromotive force

x	$\alpha \times 10^6$, K^{-1}	E_σ, eV			T_{σ_1}	T_{σ_2}	$E_s = E_p$	E_m
		$T < T_{\sigma_1}$	$T_{\sigma_1} - T_{\sigma_2}$	$T_{\sigma_2} < T$	K		eV	
0.000	14.3 ± 0.7	0.24	0.24	0.24	–	–	0.12	0.12
0.025	–	0.24	0.45	0.45	510	–	–	–
0.050	14.3 ± 0.7	0.10	0.41	0.41	410	–	–	–
0.100	14.1 ± 0.7	0.39	0.39	0.39	–	–	0.10	0.29
0.200	13.9 ± 0.7	0.18	0.30	0.30	390	–	–	–
0.300	–	0.12	0.31	0.31	430	–	0.17	0.14
0.400	13.9 ± 0.7	0.19	0.35	0.35	375	–	–	–
0.600	14.3 ± 0.7	0.12	0.33	0.18	380	880	–	–
0.800	14.9 ± 0.7	0.14	0.45	0.45	380	–	–	–
1.000	14.7 ± 0.7	0.14	0.39	0.25	390	795	–	–

ing of 3*d*-metal ions in the structure of these compounds. The activation energies of conductance E_σ calculated from the linear portions of the $\ln(\delta T) = f(1/T)$ dependences, and also the temperatures of bends T_{σ_1} and T_{σ_2} in these dependences are given in Table 1. The E_σ of $YBaCuFe_{1-x}Co_xO_5$ solid solutions at $T < T_{\sigma_1}$ decreases (except for the composition with $x = 0.1$), and at $T > T_{\sigma_1}$, increases as compared to E_σ of $YBaCuFeO_5$.

The thermoelectromotive force coefficient S of $YBaCuFe_{1-x}Co_xO_5$ phases in the entire temperature range under study was positive (Fig. 5). This indicates that "holes" are the main charge carriers in $YBaCuFe_{1-x}Co_xO_5$ and $YBaCuFeO_5$, i.e., these solid solutions are also *p*-type conductors (Fig. 4). A maximum near 480 K in the $S = f(T)$ dependence for $YBaCuFe_{1-x}Co_xO_5$ solid solutions can be caused by a change in the charge ($Co^{2+} \rightarrow Co^{3+}$) or spin [$Co^{3+}$(LS) $\rightarrow$ Co^{3+}(HS)] states of cobalt ions, though additional studies are necessary to elucidate unambiguously the causes of this anomaly. The thermoelectromotive force activation energies E_s calculated from the $S = f(1/T)$ dependences are presented in Table 1.

By applying the model of small-radius polarons (SRPs) [12] to the description of electrotransport properties of $YBaCuFe_{1-x}Co_xO_5$ solid solutions and comparing their measured conductance with the thermoelectromotive force, we can determine the activation (excitation) energy of charge-carrying SRPs (E_p, $E_p = E_s$) and also the activation energy of SRP

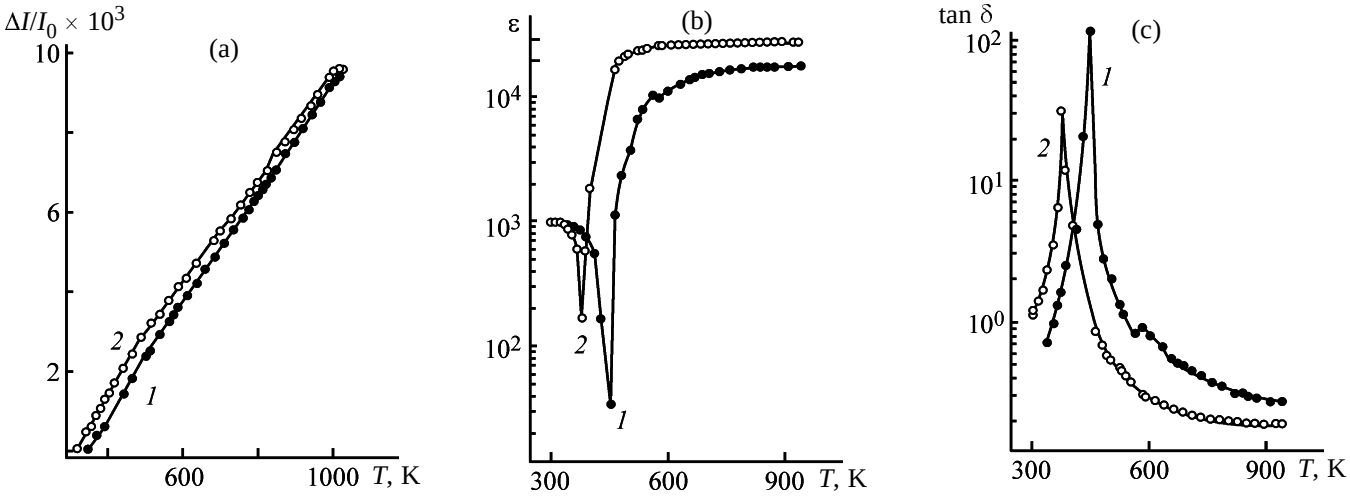


Fig. 3. Temperature dependences of the (a) relative elongation $\Delta l/l_0$ of $YBaCuFe_{0.9}Co_{0.1}O_5$ solid solution, (b) permittivity ε, and (c) tangent of the dielectric loss angle tanδ of the (*1*) $YBaCuFeO_5$ phase and (*2*) $YBaCuFe_{0.9}Co_{0.1}O_5$ solid solution. (a) (*1*) heating and (*2*) cooling.

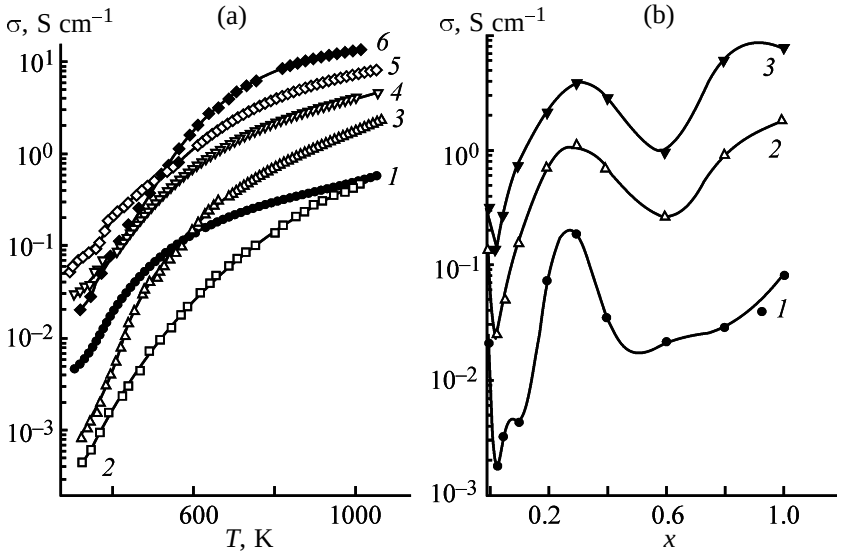


Fig. 4. Conductance σ of $YBaCuFe_{1-x}Co_xO_5$ solid solutions as a funcion of (a) temperature T and (b) cobalt content x. (a) x: (*1*) 0, (*2*) 0.025, (*3*) 0.1, (*4*) 0.2, (*5*) 0.3, and (*6*) 1.0. (b) T (K): (*1*) 400, (*2*) 600, and (*3*) 800.

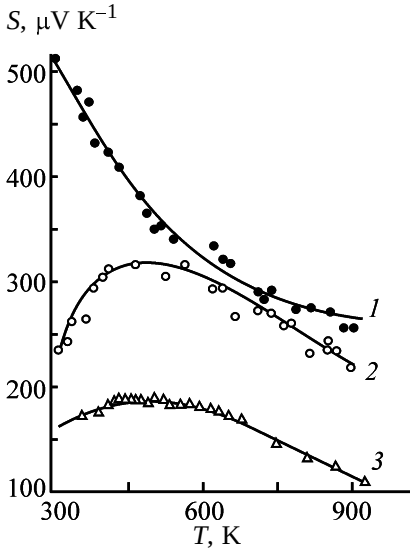


Fig. 5. Temperature dependence of the thermoelectromotive force S of $YBaCuFe_{1-x}Co_xO_5$ solid solutions. x: (*1*) 0, (*2*) 0.1, and (*3*) 0.3.

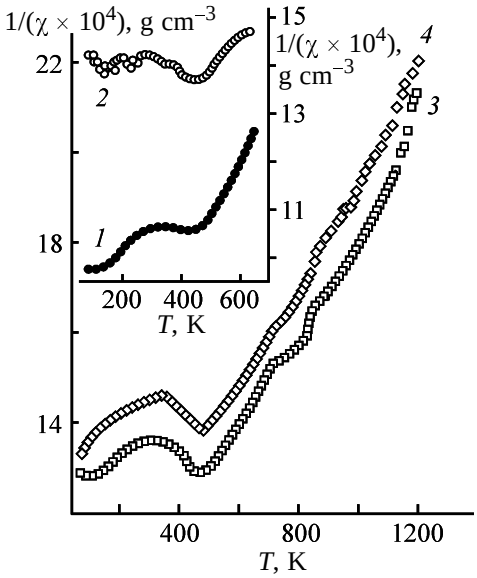


Fig. 6. Temperature dependence of reciprocal magnetic susceptibility 1/χ of $YBaCuFe_{1-x}Co_xO_5$ solid solutions. x: (*1*) 0, (*2*) 0.1, (*3*) 0.2, and (*4*) 0.3.

mobility (E_m, $E_m = E_\sigma - E_p$). Table 1 shows that the replacement of iron by cobalt slightly affects the excitation energy of the main charge carriers, "holes" (E_p); however, it result in hampering of their migration (E_m increases).

Partial replacement of iron by cobalt results in a shift of the permittivity anomalies (Fig. 3b) and of the tangent of the dielectric losse angle (Fig. 3c) toward lower temperatures (455 K for $YBaCuFeO_5$ and 380 K for $YBaCuFe_{0.9}Co_{0.1}O_5$).

The replacement of iron by cobalt noticeably reduces the magnetic susceptibility χ of $YBaCuFe_{1-x}Co_xO_5$ solid solutions (Fig. 6) compared to the compound $YBaCuFeO_5$ and does not appreciably affect their Neel temperature (Table 2). The χ is virtually independent of the degree of iron replacement by cobalt. In the paramagnetic region, the temperature dependence of the magnetic susceptibility for $YBaCuFe_{1-x}Co_xO_5$ solid solutions is described by the Curie–Weiss law $\chi = C/(T + \Theta)$, with C and Θ constants given in Table 2.

Table 2. Constants C and Θ and Neel temperature T_N of $YBaCuFe_{1-x}Co_xO_5$ solid solutions

x	$C \times 10^3$, $cm^3\ K\ g^{-1}$	Θ	T_N
		K	
0.0	8.90	–460	480
0.1	13.3	–1345	480
0.2	10.1	–808	460
0.3	9.27	–775	480

A preliminary test of the catalytic properties of $YBaCuFe_{1-x}Co_xO_5$ solid solutions has shown that they can be used as catalysts of the oxidation of hydrocarbons with atmospheric oxygen [13]. The fact that hydrocarbons are completely converted to CO_2 and H_2O on $YBaCuFe_{0.9}Co_{0.1}O_5$ makes this material promising as an afterburning catalyst (for example, in internal-combustion engines).

CONCLUSION

The effect of replacement of iron ions by cobalt ions on the crystal structure parameters and physical and chemical properties of solid solutions $YBaCuFe_{1-x}Co_xO_5$ ($0.0 \le x \le 1.0$) was studied. The parameters of electrotransport processes and constants of Curie–Weiss equations for the compounds studied were determined. The replacement of iron by cobalt leads to an increase in the conductivity and to a decrease in the thermoelectromotive force and magnetic susceptibility of samples and does not appreciably affect the coefficient of linear thermal expansion and temperatures of antiferromagnetic–paramagnetic transition of $YBaCuFe_{1-x}Co_xO_5$ solid solutions.

REFERENCES

1. Er-Rakho, L., Michel, C., LaCorre, Ph., and Raveau, B., *J. Solid State Chem.*, 1988, vol. 73, no. 2, pp. 531–535.
2. Meyer, C., Hartmann-Boutron, F., Gros, Y., and Strobel, P., *Solid State Commun.*, 1990, vol. 76, no. 2, pp. 163–168.
3. Ruiz-Aragon, M.J., Moran, E., Amador, U., *et al.*, *Phys. Rev. B*, 1998-II, vol. 58, no. 10, pp. 6291–6297.
4. Nagase, M., Linden, J., Miettinen, J., *et al.*, *Phys. Rev., B*, 1998-II, vol. 58, no. 6, pp. 3371–3376.
5. Mombru, A.W., Prassides, K., Christides, C., *et al.*, *J. Phys. Condens. Matter*, 1998, vol. 10, pp. 1247–1258.
6. Chizhova, E.A., Bashkirov, L.A., Klyndyuk, A.I., and Petrov, G.S., *Tr. Bel. Gos. Tekh. Univ., Ser. 3: Khim. Tekhnol. Neorg. Veshch.*, 2001, issue 9, pp. 3–7.
7. Klyndyuk, A.I., Petrov, G.S., and Bashkirov, L.A., *Izv. Ross. Akad. Nauk, Neorg. Mater.*, 1999, vol. 35, no. 9, pp. 1122–1124.
8. Rentschler, T., *J. Alloys Comp.*, 1996, vol. 232, pp. 43–52.
9. Rentschler, T., *Thermochim. Acta*, 1996, vol. 284, pp. 367–378.
10. Shannon, R.D. and Prewitt, C.T., *Acta Crystallogr., Sect. B*, 1969, vol. 25, no. 5, pp. 946–960.
11. Atanassova, Y.K., Popov, V.N., Bogachev, G.G., *et al.*, *Phys. Rev. B*, 1993, vol. 47, no. 22, pp. 15 201–15 207.
12. Mott, N.F. and Davis, E.A., *Electron Processes in Non-Crystalline Materials*, Oxford: Clarendon, 1979, 2nd ed.
13. Tchizhova, E.A., Klyndyuk, A.I., Petrov, G.S., *et al.*, in *Materialy Mezhdunarodnoi nauchno-tekhnicheskoi konferentsii "Noveishie dostizheniya v oblasti importozameshcheniya v khimicheskoi promyshlennosti i proizvodstve stroitel'nykh materialov"* (Proc. Int. Scientific and Technical Conf. "Recent Achievements in the Field of Import Replacement in Chemical Industry and Production of Building Materials"), Minsk, 2003, pp. 317–319.

Russian Journal of Applied Chemistry, Vol. 78, No. 5, 2005, pp. 707–710. Translated from Zhurnal Prikladnoi Khimii, Vol. 78, No. 5, 2005, pp. 721–724.
Original Russian Text Copyright © 2005 by Demidov, Markelov.

PHYSICOCHEMICAL STUDIES OF SYSTEMS AND PROCESSES

Thermodynamics of Reaction of Carbon with Oxygen

A. I. Demidov and I. A. Markelov

St. Petersburg State Polythechnic University, St. Petersburg, Russia

Received April 7, 2005

Abstract—The standard Gibbs energies of reactions proceeding in the C–O system are calculated per mole of carbon dioxide, per mole of the reaction product, and per mole of atoms of the initial substances. A comparative analysis of the calculation results is made.

The reactions of carbon with oxygen can be described by the following equations [1–5]:

$$2C + O_2 = 2CO, \quad (1)$$

$$C + O_2 = CO_2, \quad (2)$$

$$C + CO_2 = 2CO, \quad (3)$$

$$2CO + O_2 = 2CO_2. \quad (4)$$

These reactions are of practical significance for metallurgical, chemical, and fuel industry. The input data for calculating the standard Gibbs energy of the reactions were taken from a reference book [1]. The thermodynamic calculation of the Gibbs energy of reactions (1)–(4) per mole of oxygen [reactions (1), (2), (4)] or per mole of carbon dioxide [reaction (3)], as it was done in [2–6], yields the results given in Table 1 and Fig. 1.

In the range 298–2500 K, reactions (1), (2), and (4) are characterized by the negative standard Gibbs energy, and, consequently, by the high yield of the reaction products. The more negative the ΔG^0 values, the higher the yield of the reaction products [7]. The standard Gibbs energy of reaction (3) (straight line *3*) is negative above 1000 K. At the same time, the positive ΔG^0 values do not show that the reaction is improbable; they only show that the yield of the reaction products is very low [7].

Straight lines *1*, *2*, and *4* (Fig. 1) intersect at a temperature of about 1000 K. To the right from the interception point, straight line *1* passes below two others. This means that, above 1000 K, the chemical affinity of carbon for oxygen under conditions of CO formation is maximal. To the left from the interception point, i.e., below 1000 K, the most negative is the standard Gibbs energy of reaction (4). At temperatures of about 2100 K, straight lines *3* and *4* intersect. Above 2100 K, CO rather than CO_2 becomes the thermodynamically stable oxide.

The reactions in the C–O system can also be related to 1 mol of the reaction product [8, 9]:

$$C + 1/2O_2 = CO, \quad (1')$$

$$C + O_2 = CO_2, \quad (2')$$

$$1/2C + 1/2CO_2 = CO, \quad (3')$$

$$CO + 1/2O_2 = CO_2. \quad (4')$$

The results of the thermodynamic calculation of the standard Gibbs energy of reactions (1')–(4') are given in Table 1 and Fig. 2. As seen from Fig. 2, reaction (2') (straight line *2*') is characterized by the lowest standard Gibbs energy in the range 298–2500 K. This means that, in the reaction of carbon with oxygen over the entire temperature range studied,

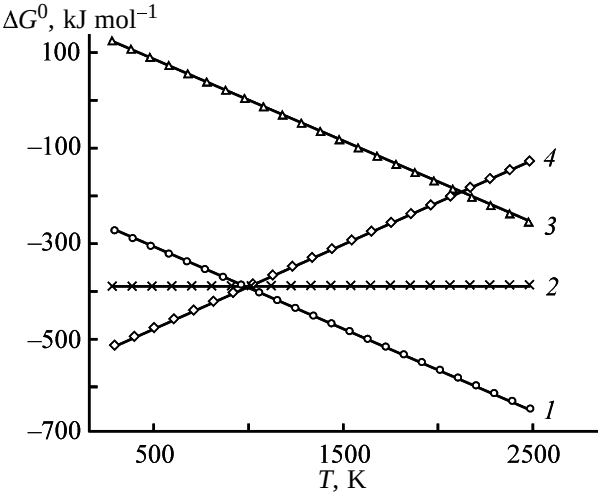


Fig. 1. Standard Gibbs energies ΔG^0 of reactions (1)–(4) vs. temperature *T*.

1070-4272/05/7805-0707 © 2005 Pleiades Publishing, Inc.

Table 1. Standard Gibbs energies of reactions (1)–(4) and (1')–(4') within 298–2500 K

T, K	ΔG^0, kJ mol^{-1}, for indicated reaction							
	(1)	(2)	(3)	(4)	(1')	(2')	(3')	(4')
298	–274.5	–394.6	120.1	–514.8	–137.3	–394.6	60.1	–257.4
300	–274.8	–394.6	119.8	–514.4	–137.4	–394.6	59.9	–257.2
400	–292.9	–394.9	102.1	–497.0	–146.4	–394.9	51.0	–248.5
500	–311.0	–395.2	84.2	–479.4	–155.5	–395.2	42.1	–239.7
600	–329.2	–395.5	66.3	–461.8	–164.6	–395.5	33.1	–230.9
700	–347.3	–395.7	48.4	–444.2	–173.6	–395.7	24.2	–222.1
800	–365.3	–395.9	30.6	–426.6	–182.6	–395.9	15.3	–213.3
900	–383.2	–396.1	12.9	–409.0	–191.6	–396.1	6.5	–204.5
1000	–400.9	–396.2	–4.7	–391.5	–200.4	–396.2	–2.3	–195.8
1100	–418.5	–396.3	–22.2	–374.1	–209.3	–396.3	–11.1	–187.1
1200	–436.0	–396.4	–39.6	–356.8	–218.0	–396,4	–19.8	–178.4
1300	–453.4	–396.4	–57.0	–339.5	–226.7	–396.4	–28.5	–169.7
1400	–470.7	–396.5	–74.3	–322.2	–235.4	–396.5	–37.1	–161.1
1500	–487.9	–396.5	–91.4	–305.0	–243.9	–396.5	–45.7	–152.5
1600	–505.0	–396.4	–108.6	–287.9	–252.5	–396.4	–54.3	–143.9
1700	–522.0	–396.4	–125.6	–270.9	–261.0	–396.4	–62.8	–135.4
1800	–538.9	–396.4	–142.5	–253.9	–269.4	–396.4	–71.3	–126.9
1900	–555.7	–396.3	–159.4	–236.9	–277.9	–396.3	–79.7	–118.5
2000	–572.5	–396.3	–176.2	–220.1	–286.2	–396.3	–88.1	–110.0
2100	–589.2	–396.2	–193.0	–203.3	–294.6	–396.2	–96.5	–101.6
2200	–605.8	–396.2	–209.6	–186.5	–302.9	–396.2	–104.8	–93.3
2300	–622.3	–396.1	–226.3	–169.8	–311.2	–396.1	–113.1	–84.9
2400	–638.8	–396.0	–242.8	–153.2	–319.4	–396.0	–121.4	–76.6
2500	–655.3	–396.0	–259.3	–136.7	–327.6	–396.0	–129.7	–68.3

the most thermodynamically stable oxide is CO_2. Straight lines *1'*, *2'*, and *4'*, characterizing the standard Gibbs energies of reactions (1'), (2'), and (4'), do not intersect in the temperature range studied. The difference in the results of a comparative thermodynamic analysis of reactions (1)–(4) and (1')–(4') is due to the fact that the Gibbs energy is an extensive quantity and depends on the amounts of substances participating in the reaction. When the reactions are related to 1 mol of oxygen, the number of moles of the reaction products is different from the case when they are related to 1 mol of carbon dioxide. When a reaction is related to 1 mol of the reaction product, the number of moles of the initial substances is different. Therefore, the equations of the chemical reactions related to 1 mol of oxygen [reactions (1), (2), (4)], 1 mol of carbon dioxide [reaction (3)], or 1 mol of the reaction product [reactions (1')–(4')] yield different results. In thermodynamic analysis of heterogeneous condensed systems, the thermodynamic characteristics are commonly calculated per mole of the alloy or the solution, or per gram-atom of a substance incorporated in the compound [10, 11]. Therefore, the standard Gibbs energies of the reactions between carbon and oxygen were calculated per mole of atoms of the initial substances:

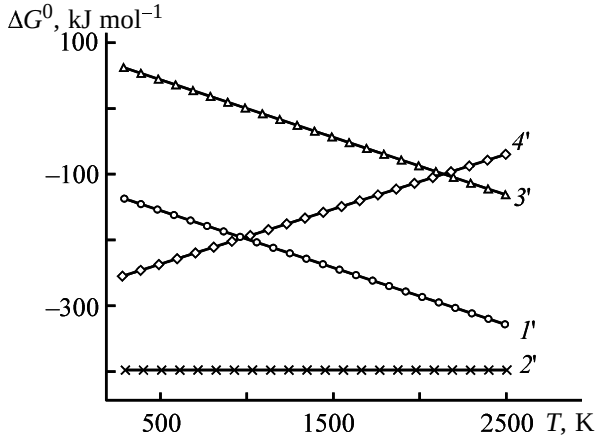


Fig. 2. Standard Gibbs energies ΔG^0 of reactions (1)–(4) (*1'–4'*, respectively) vs. temperature *T*.

$$1/2C + 1/4O_2 = C_{0.5}O_{0.5}, \quad (1'')$$

$$1/3C + 1/3O_2 = C_{0.333}O_{0.667}, \quad (2'')$$

Table 2. Standard Gibbs energies of reactions (1")–(4") within 298–2500 K

T, K	ΔG^0, kJ mol^{-1}, for indicated reaction			
	(1")	(2")	(3")	(4")
298	–68.6	–131.5	30.0	–85.8
300	–68.7	–131.5	30.0	–85.7
400	–73.2	–131.6	25.5	–82.8
500	–77.8	–131.7	21.0	–79.9
600	–82.3	–131.8	16.6	–77.0
700	–86.8	–131.9	12.1	–74.0
800	–91.3	–132.0	7.7	–71.1
900	–95.8	–132.0	3.2	–68.2
1000	–100.2	–132.1	–1.2	–65.3
1100	–104.6	–132.1	–5.5	–62.4
1200	–109.0	–132.1	–9.9	–59.5
1300	–113.4	–132.1	–14.2	–56.6
1400	–117.7	–132.2	–18.6	–53.7
1500	–122.0	–132.2	–22.9	–50.8
1600	–126.2	–132.1	–27.1	–48.0
1700	–130.5	–132.1	–31.4	–45.1
1800	–134.7	–132.1	–35.6	–42.3
1900	–138.9	–132.1	–39.8	–39.5
2000	–143.1	–132.1	–44.1	–36.7
2100	–147.3	–132.1	–48.2	–33,9
2200	–151.4	–132.1	–52.4	–31.1
2300	–155.6	–132.0	–56.6	–28.3
2400	–159.7	–132.0	–60.7	–25.5
2500	–163.8	–132.0	–64.8	–22.8

$$1/4C + 1/4CO_2 = C_{0.5}O_{0.5}, \quad (3")$$

$$1/3CO + 1/3O_2 = C_{0.333}O_{0.667}. \quad (4")$$

The results of the calculation are given in Table 2 and Fig. 3.

As seen from Fig. 3, the dependences depicting the standard Gibbs energy of reactions (1")–(4") markedly differ from those considered above. Straight line *1*" [reaction (1")] intersects with line *2*" [reaction (2")] at 1750 K. To the right from the interception point, straight line *1*" lies below line *2*". This shows that, in the range of high temperatures (above 1750 K), the chemical affinity of carbon for oxygen under the conditions of CO formation is maximal. At about 500 K, straight line *1*" intersects with straight line *4*" [reaction (4")]. Consequently, CO_2 is the most thermodynamically stable oxide below 500 K. As the temperature increases, the equilibrium of reaction (3") shifts further toward the formation of carbon monoxide, and the equilibrium of reaction (4"), toward the formation of carbon monoxide and oxygen. Above

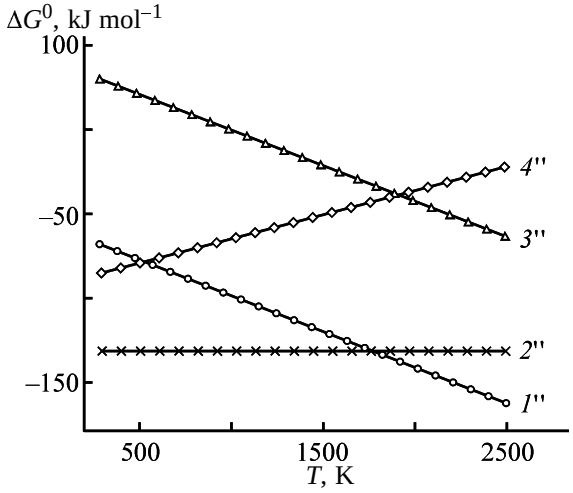


Fig. 3. Standard Gibbs energies ΔG^0 of reactions (1")–(4") (*1*"–*4*", respectively) vs. temperature T.

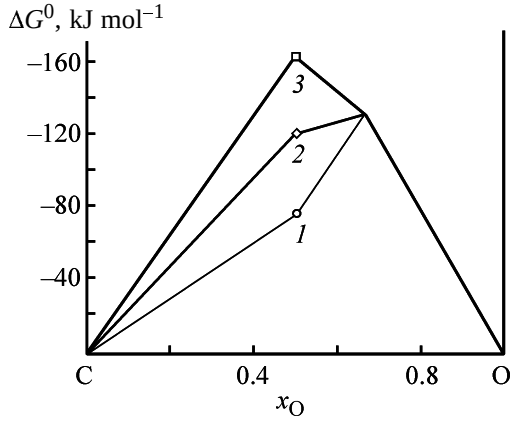


Fig. 4. Standard Gibbs energies ΔG^0 of reactions (1") and (2") vs. mole fraction of oxygen x_O at (*1*) 500, (*2*) 1500, and (*3*) 2500 K.

1900 K, the most thermodynamically stable oxide is CO. The dependences describing the Gibbs energy in the C–O system on the composition (x_O is the mole fraction of atomic oxygen) at 500, 1500, and 2500 K (Fig. 4) demonstrate how temperature affects the stability of carbon(II) and carbon(IV) oxides. At 2500 K, the most stable compound is carbon monoxide.

CONCLUSIONS

A comparative analysis of the Gibbs energies of the reactions occurring in the C–O system, calculated per mole of oxygen or carbon dioxide, per mole of the reaction product, and per mole of atoms of the initial substances shows that the results of the thermodynamic calculation and the conclusions about preferential formaiton of one or another product depend on the form of the equations of chemical reactions. To perform a comparative analysis, it is suggested to

relate the equations of chemical reactions to 1 mol of atoms of the initial substances.

REFERENCES

1. Barin, I., Knacke, O., and Kubaschewski, O., *Thermochemical Properties of Inorganic Substances*, New York: Springer, 1973.
2. Partington, J.R., *Introduction to General Thermodynamics and Its Applications to Chemistry and Physics*, London: Constable, 1950.
3. Kapustinskii, A.F., *Termodinamika khimicheskikh reaktsii i ee primenenie v metallurgii i neorganicheskoi tekhnologii* (Thermodynamics of Chemical Reactions and Its Application to Metallurgy and Inorganic Technology), Britske, E.V., Ed., Leningrad: Tsvetmetizdat, 1933.
4. Vvedenskii, A.A., *Termodinamicheskie raschety protsessov toplivnoi promyshlennosti* (Thermodynamic Calculation of Processes in Fuel Industry), Leningrad: Gostoptekhizdat, 1949.
5. Rostovtsev, S.T., *Teoriya metallurgicheskikh protsessov* (A Theory of Metallurgical Processes), Moscow: Metallurgizdat, 1956.
6. Ryzhonkov, D.I., Arsent'ev, P.P., Yakovlev, V.V., *et al*., *Teoriya metallurgicheskikh protsessov: Uchebnik dlya vysshikh uchebnykh zavedenii* (A Theory of Metallurgical Processes: A Textbook for Higher Schools), Moscow: Metallurgiya, 1989.
7. Gerasimov, Ya.I., Dreving, V.P., Eremin, E.N., *et al*., *Kurs fizicheskoi khimii* (A Course of Physical Chemistry), Gerasimov, Ya.I., Ed., Moscow: Khimiya, 1969, vol. 1.
8. Esin, O.A., and Gel'd, P.V., *Fizicheskaya khimiya pyrometallurgicheskikh protsessov* (Physical Chemistry of Pyrometallurgical Processes), part 1: *Reaktsii mezhdu gazoobraznymi i tverdymi fazami* (Reactions between Gaseous and Solid Phases), Sverdlovsk: Metallurgizdat, 1950.
9. Filippov, I.S., *Teoriya metallurgicheskikh protsessov* (Theory of Metallurgical Processes), Moscow: Metallurgiya, 1967.
10. Sirota, N.N., *Fiziko-khimicheskaya priroda faz peremennogo sostava* (Physicochemical Nature of Phases of Variable Composition), Minsk: Nauka i Tekhnika, 1970.
11. Morachevskii, A.G., *Termodinamika rasplavlennykh metallicheskikh i solevykh sistem* (Thermodynamics of Molten and Salt Systems), Moscow: Metallurgiya, 1987.

Russian Journal of Applied Chemistry, Vol. 78, No. 5, 2005, pp. 711–714. Translated from Zhurnal Prikladnoi Khimii, Vol. 78, No. 5, 2005, pp. 725–728.
Original Russian Text Copyright © 2005 by O. Sytnik, Krasnoperova, Lebedinets, K. Sytnik.

PHYSICOCHEMICAL STUDIES OF SYSTEMS AND PROCESSES

Polythermal Study of Solubility of *N*-[4-(Difluoromethylthio)phenyl]-2-Aminobenzoic Acid in the System Water–1,2-Propanediol

O. Yu. Sytnik, A. P. Krasnoperova, V. A. Lebedinets, and K. M. Sytnik

Chemical Research Institute, Karazin National University, Kharkov, Ukraine
Ukrainian National Pharmaceutical University, Kharkov, Ukraine

Received August 18, 2003; in final form, January 2005

Abstract—The solubility of *N*-[4-(difluoromethylthio)phenyl]-2-aminobenzoic acid in the system water–1,2-propanediol was studied over the entire range of the concentrations of the mixed solvent at 288.15–328.15 K.

Anthranilic acid derivatives are commonly used in modern pharmacology. *N*-[4-(Difluoromethylthio)-pheny]l-2-aminobenzoic acid (Difluorant, hereinafter DF), a nonsteroid antiphlogistic with antipsoriasis activity, is among them.

Difluorant is a hydrophobic organic compound, sparingly soluble in water, which makes it difficult to create on its basis water-containing medicines in the form of ointments, foams, and emulsions. Therefore, a study of the DF solubility in nonaqueous solvents, which can homogenize hydrophobic and hydrophilic compounds and their mixtures with water, is one of the main stages of development of highly effective and inexpensive drugs. The most commonly used solvent in soft medicines is 1,2-propanediol (1,2-PD) [1].

This study is concerned with the DF solubility in the water–1,2-PD system over the entire range of the concentrations of the mixed solvent at 288.15–328.15 K.

EXPERIMENTAL

The water–1,2-PD system was prepared gravimetrically. 1,2-Propanediol was preliminarily treated by double vacuum distillation [2]. The quality of 1,2-PD was checked by the density (ρ_4^{25} = 1032.8 kg m^{-3}) and dielectric permittivity (ε = 29.0 at 25°C). As second component was used double-distilled water. Prior to use, DF was dried for 2 h at 353 K under a pressure of 2.7 kPa. The quality of the preparation was checked by the melting point (T_m = 397 K).

The DF solubility was studied by the isothermal method, and the concentration of the saturated solution was determined by the electronic spectroscopy. To do this, excess amount of the substance under study was placed in flasks with ground-glass stoppers, the solvent of the required composition was added, and the mixture was kept at a constant temperature controlled to within $\pm$0.1 K with continuous agitation until the thermodynamic equilibrium was attained. The attainment of the equilibrium was monitored by taking the solution samples and measuring their optical density. The equilibrium was assumed to be attained when the optical density A of a series of successively taken solution samples became constant. Then, the solutions were allowed to settle for 3–4 h at the given temperature, after which they were sampled for the analysis. The saturation time was from 10 to 100 h, depending on the concentration of the nonaqueous component.

The optical density A was measured on a Specord M-40 spectrophotometer at λ = 310 nm. To do this, 2 ml of the transparent saturated solution was diluted with ethanol so that A of the solutions obtained was within 0.3–0.7. Each value of the solubility is the average of 3–4 measurements. The maximum average error in determining the solubility was 2–3% at a confidence probability of 0.95. The results obtained are presented in the table.

Our results show that the DF solubility varies within a wide range depending on the solvent composition and temperature and is not a linear dependence of the solvent composition.

Amino acids in strongly polar solvents are in the form of zwitterions [3, 4]. Since the zwitterions have

1070-4272/05/7805-0711 © 2005 Pleiades Publishing, Inc.

DF solubility L in the water–1,2-PD system

1,2-PD content		L, M at indicated temperature, K				
wt fraction	mole fraction	288.15	298.15	308.15	318.15	328.15
0.000	0.000	9.01×10^{-5}	1.10×10^{-4}	1.29×10^{-4}	1.84×10^{-4}	2.25×10^{-4}
0.111	0.029	8.89×10^{-5}	1.23×10^{-4}	1.71×10^{-4}	2.49×10^{-4}	3.08×10^{-4}
0.206	0.058	9.81×10^{-5}	1.46×10^{-4}	2.40×10^{-4}	3.66×10^{-4}	6.02×10^{-4}
0.313	0.097	1.70×10^{-4}	3.24×10^{-4}	4.83×10^{-4}	8.49×10^{-4}	1.56×10^{-3}
0.515	0.201	6.12×10^{-4}	1.30×10^{-3}	2.55×10^{-3}	4.60×10^{-3}	7.94×10^{-3}
0.612	0.272	2.32×10^{-3}	4.72×10^{-3}	7.47×10^{-3}	1.34×10^{-2}	2.46×10^{-2}
0.707	0.363	8.95×10^{-3}	1.58×10^{-2}	2.18×10^{-2}	3.54×10^{-2}	6.46×10^{-2}
0.800	0.485	3.38×10^{-2}	5.26×10^{-2}	7.41×10^{-2}	1.00×10^{-1}	1.58×10^{-1}
0.889	0.655	1.04×10^{-1}	1.58×10^{-1}	2.34×10^{-1}	3.39×10^{-1}	4.06×10^{-1}
0.960	0.851	3.72×10^{-1}	5.51×10^{-1}	8.31×10^{-1}	1.15	1.60
1.000	1.000	0.50	0.70	1.01	1.37	1.90

high dipole moments [5], the electrostatic interactions should largely contribute to the dissolution of bipolar compounds. It appeared, however, that the DF solubility in water is lower by four orders of magnitude than in 1,2-PD, despite the fact that the dielectric permittivity of water is considerably higher than that of 1,2-PD (ε = 80.1 against 30.8 at 20°C). In addition, the logarithm of the solubility $\log L$ in solvents of the same chemical nature is a linear function of reciprocal dielectric permittivity ε^{-1} [6], which is not the case in the system studied (Fig. 1). Hence, the solubility of the substance studied is primarily govened by interactions other than electrostatic.

The results obtained show that the specific interactions in the solute–solvent system and the specificity of the interparticle interactions in a binary solvent play the decisive role in DF dissolution. The fact that the DF solubility in water is lower than in 1,2-PD and in its aqueous mixtures is typical of a compound with large hydrophobic ions, which tend to structurization

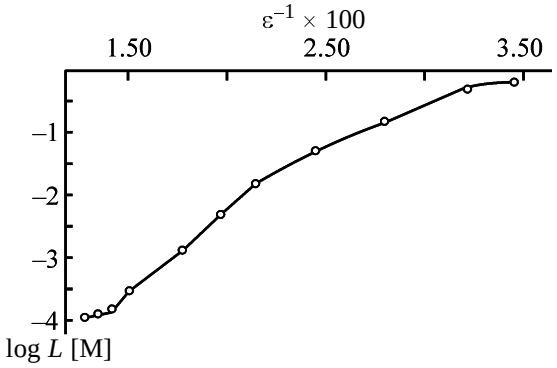


Fig. 1. Logarithm of the DF solubility $\log L$ vs. reciprocal dielectric permittivity ε^{-1} of the mixed solvent water–1,2-PD at 298.15 K.

in aqueous solvent owing to the enhancement of hydrogen bonding between the surrounding water molecules.

The deviations of the logarithm of the solubility from the additive values in the solvent studied were calculated from the data on the DF solubility [7]:

$$(\ln L)^E = \ln L - \sum_{i=1}^{2} \varphi_i \ln L_i, \qquad (1)$$

where L is the solubility of a substance in a mixed solvent (M); L_i, solubility of a substance in individual solvent i; $(\ln L)^E$, deviation of the logarithm of the solubility from the additive value; and φ_i, calculated volume fraction of individual solvent i in a mixed solvent in the water–1,2-PD system [8].

The logarithm of the DF solubility shows negative deviations from the additivity at all the studied temperatures and compositions of the mixed solvent (Fig. 2). Increasing temperature decreases the absolute values of $(\ln L)^E$. The $(\ln L)^E$ value is more than 10%, which shows that the features of the interparticle interaction in the binary mixed solvent considerably affect the DF solubility.

The heats of mixing of water and 1,2-PD in the water–1,2-PD system containing about 20 mol % 1,2-PD are maximal [9]. This fact suggests formation of relatively stable water–1,2-PD associates in which the water–dihydric alcohol bond is stronger than the water–water and diol–diol bonds, which is also confirmed elsewhere [8, 10–12].

The formation of mixed associates even more impedes dissolution of the third component. Apparently,

this fact explains why $(\ln L)^E$ at about 20 mol % 1,2-PD passes through a deep minimum.

A more detailed information about the processes affecting formation of saturated solution can be obtained from the thermodynamic characteristics of DF solution.

The solubility of substances is determined by two competing factors: changes in the Gibbs energy upon solvation and upon destruction of the crystal lattice [13]:

$$\Delta G_s^0 = \Delta G_{lat}^0 + \Delta G_{solv}^0, \quad (2)$$

where ΔG_s^0 is the Gibbs energy of solution (kJ mol^{-1}); ΔG_{lat}^0, Gibbs energy of crystal lattice destruction (kJ mol^{-1}); and ΔG_{solv}^0, Gibbs energy of solute solvation (kJ mol^{-1}).

Since the Gibbs energy ΔG_{lat}^0 of DF is the constant in Eq. (2), the decisive effect on the solubility in solvents with varied 1,2-PD concentration is exerted by ΔG_{solv}^0.

The lack of data on the thermodynamic characteristics of the crystal lattice formation prevents estimation of the thermodynamic characteristics of DF solvation from the solubility data. Therefore, the thermodynamic characteristics were calculated for the DF transfer from water into the water–1,2-PD mixed solvent [14].

The isotherms of the Gibbs energy of transfer ΔG_t^0 are nonlinear. The ΔG_t^0 is negative in the whole range of compositions of the mixed solvent (Fig. 3). Therefore, the DF solubility in 1,2-PD and in the binary solvent is higher than in water.

At the same time, when the concentration of the nonaqueous solvent in water is low, ΔG_t^0 depends only slightly on the solvent composition, and this is typical of low temperatures. Such a dependence of ΔG_t^0 on the composition of the mixed solvent is determined by a number of factors.

According to the physicochemical analysis [8], at low concentrations of 1,2-PD in water (5 mol %) the structure of water is stabilized with methyl radicals of 1,2-PD. The DF molecules in this region may undergo solvophobic solvation, which results in enhanced hydrogen bonding between the solvent molecules and their minimal contact with DF molecules. The solvophobic solvation of DF is typical of water, which explains the low solubility of DF in water. For a mixed solvent water–1,2-PD it is also typical in the regions of low 1,2-PD concentrations, where a small

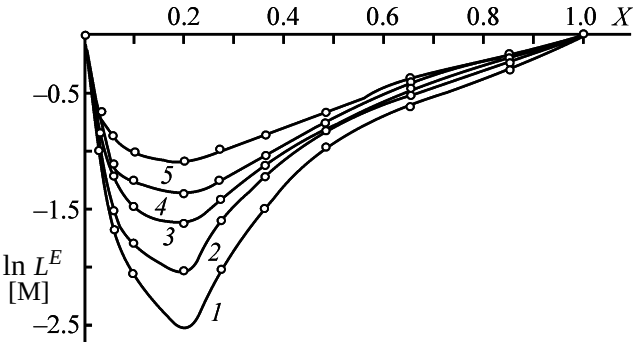


Fig. 2. Deviations of the logarithm of the DF solubility from the additive values $(\ln L)^E$ vs. the composition of the mixed solvent in the range 288.15–328.15 K. (*X*) Mole fraction of 1,2-PD in the mixed solvent. Temperature (K): (*1*) 288.15, (*2*) 298.15, (*3*) 308.15, (*4*) 318.15, and (*5*) 328.15; the same for Fig. 3.

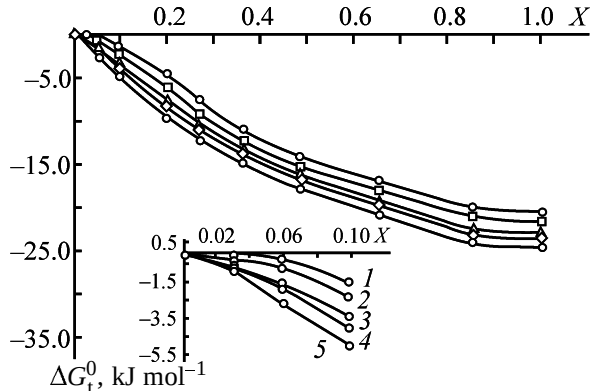


Fig. 3. Gibbs energy of DF transfer ΔG_t^0 from water into a mixed solvent water–1,2-PD vs. the mole fraction *X* of 1,2-PD in the mixed solvent.

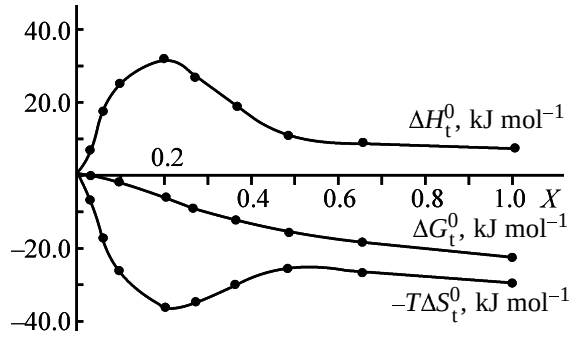


Fig. 4. Thermodynamic characteristics of DF transfer from water into a mixed solvent water–1,2-PD as functions of the mole fraction *X* of 1,2-PD at 298.15 K.

plateau disappearing at higher temperatures is observed in the isotherm of ΔG_t^0 of DF.

The ΔG_t^0 decreases with a further increase in the 1,2-PD concentration in the binary solvent. The large negative values of ΔG_t^0 in the 1,2-PD-rich binary solvent show that the solvates formed in the binary

solvent and in individual 1,2-PD are more stable than in water. The solvate stability in this region is of entropy origin, and the large negative values of $-T\Delta S_t^0$ confirm this conclusion.

The ΔH_t^0 and ΔS_t^0 isotherms have extrema; to the endothermic peak at about 20 mol % 1,2-PD in water corresponds the ΔS_t^0 maximum. Apparently, the extrema in the ΔH_t^0 and ΔS_t^0 curves in this region are due to the formation of water : 1,2-PD mixed associates of the composition 4 : 1.

CONCLUSION

The dependences of the Difluorant solubility in the water–1,2-PD system, dielectric permittivity, deviation of the logarithm of the solubility from additive values, and thermodynamic characteristics of Difluorant transfer from water into the mixed solvent on the composition of the mixed solvent, studied over the entire range of concentrations of the mixed solvent at 288.15–328.15 K, show that the specific interactions in the binary solvent and the Difluorant solvophobic solvation are the major factors affecting the Difluorant solubility.

REFERENCES

1. Jouyban-Gharamaleki, A., *Chem. Pharm. Bull*., 1998, vol. 46, no. 6, pp. 1058–1061.
2. Weissberger, A., Proskauer, E.S., Riddick, J.A., and Toops, E.E., *Organic Solvents*, New York: Interscience, 1955.
3. Mousa, M.A., and Hamed, M.M.A., *Thermochim. Acta*, 1988, vol. 136, pp. 23–31.
4. Majumder, K., Majumder, K., and Lahiri, S.C., *Z. Phys. Chem*., 2000, vol. 214, no. 3, pp. 285–299.
5. Jakubke, H.D. and Jeschkeit, H., *Aminosäuren, Peptide, Proteine. Eine Enführung*, Berlin: Akademie, 1969.
6. Izmailov, N.A., *Elektrokhimiya rastvorov* (Electrochemistry of Solutions), Moscow: Khimiya, 1966.
7. Nitta, T. and Katayama, T., *J. Chem. Eng. Jpn*., 1975, vol. 8, no. 3, pp. 175–180.
8. Chistyakov, Yu.V., and Egorova, I.V., in *Termodinamika i stroenie rastvorov: Mezhvuzovskii sbornik* (Thermodynamics and Structure of Solutions: Intercollegiate Coll.), Ivanovo, 1979, pp. 51–56.
9. Belousov, V.P., Morachevskii, A.G., and Panov, M.Yu., *Teplovye svoistva rastvorov neelektrolitov* (Thermal Properties of Nonelectrolyte Solutions), Leningrad: Khimiya, 1981.
10. Chistyakov, Yu.V., Egorova, I.E., and Krestov, G.A., *Zh. Strukt. Khim*., 1980, vol. 21, no. 5, pp. 83–85.
11. Chistyakov, Yu.V., Egorova, I.E., Krestov, G.A., and Karaseva, E.A., *Zh. Strukt. Khim*., 1980, vol. 21, no. 5, pp. 87–90.
12. Dyment, O.N., Kazanskii, K.S., and Miroshnikov, A.M., *Glikoli i drugie proizvodnye okisei etilena i propilena* (Glycols and Other Derivatives of Ethylene and Propylene Oxides), Moscow: Khimiya, 1976.
13. Berezina, G.R., Vorob'ev, Yu.G., and Smirnov, R.P., *Zh. Fiz. Khim*., 1996, vol. 70, no. 1, pp. 94–96.
14. Hefter, G., Marcus, Y., and Waghorne, W. E., *Chem. Rev*., 2002, vol. 102, pp. 2773–2836.

Russian Journal of Applied Chemistry, Vol. 78, No. 5, 2005, pp. 715–721. Translated from Zhurnal Prikladnoi Khimii, Vol. 78, No. 5, 2005, pp. 729–735.
Original Russian Text Copyright © 2005 by Simanova, Kuznetsova, Konovalov, Shchukarev.

SORPTION AND ION-EXCHANGE PROCESSES

Chemisorption of Platinum(II) and Platinum(IV) Chloride Complexes on Fibrous Sorbents Derived from Polyacrylonitrile Modified with Aminoguanidine

S. A. Simanova, T. V. Kuznetsova, L. V. Konovalov, and A. V. Shchukarev

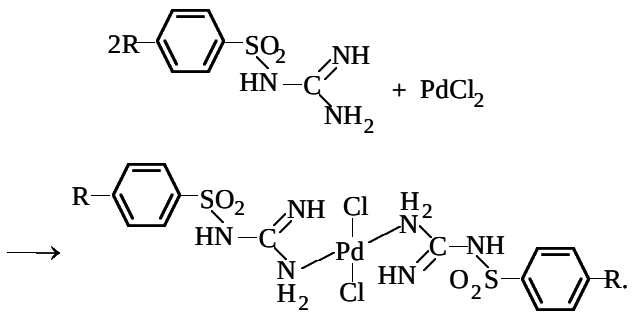
St. Petersburg State Technological Institute, St. Petersburg, Russia

Received February 28, 2004

Abstract—Sorption of platinum(II) and platinum(IV) chloride complexes on nitrogen-containing fibrous sorbents derived from polyacrylonitrile with aminoguanidine groups (GLIPAN-3) was studied as influenced by the temperature, platinum concentration in the solution, and pH of the solution. The kinetic sorption parameters and the sorption capacities of the sorbents in hydrochloric acid and chloride solutions were determined. The sorption mechanism and the composition of platinum compounds formed in the sorbent phase were suggested.

Complexing polyfunctional sorbents with various nitrogen-containing groups (aliphatic and aromatic amines, pyridine, pyrazole, and other nitrogen-containing heterocycles) are widely used to concentrate platinum metals in solutions and to recover them from solutions [1–4]. High sorption capacity of these sorbents for platinum metals in acidic solutions is due to, on one hand, protonation of the nitrogen-containing functional groups which facilitates their interaction with anionic complexes of platinum metals [1–3], and on the other hand, formation of strong platinum complexes with nitrogen-containing ligands [1, 2, 4].

As shown previously [5], polystyrene resin with sulfoguanidine groups sorbs quantitatively K_2PdCl_4 and does not sorb K_2PtCl_4 from perchloric acid solutions with different pH under the static conditions and under the dynamic conditions at constant stirring. Palladium(II) was desorbed with 3–4 M HCl [5]. The results of elemental analysis and IR spectroscopic study showed that the sorption could be described by the following equation:



Our previous study on sorption of palladium(II) chloride complexes on GLIPAN-3 fiber showed [6] that the apparent equilibrium in the palladium distribution between 1 M HCl and the fiber was attained within 40–60 min and the sorption half-time in this solution was 6 min. Onium palladium(II) complexes like $[RNHNHC(NH_2)NH_2]_2[PdCl_4]$ are formed in the fiber. Sorption of other metals including platinum on GLIPAN-3 fiber was not studied.

In this study we examined sorption of platinum(II) and platinum(IV) chloride complexes on nitrogen-containing GLIPAN-3 sorbent, composition and structure of platinum complexes formed in the fiber, and possibility of recovering platinum(II) from solutions containing Al(III), Fe(III), Ni(II), Co(II), and Cu(II) in a 1000-fold excess.

EXPERIMENTAL

Complexing fibrous sorbent GLIPAN-3 was prepared by Yu.E. Kazakevich (St. Petersburg State University of Technology and Design) by treatment of PAN fiber with aminoguanidine in ethylene glycol solution containing sodium hydroxide [6]. The fiber is yellow and contains aminoguanidine [NH_2–NH–C(=NH)–NH–] and carboxy (–COOH) groups. The static exchange capacity (SEC) for HCl and NaOH is 2.96 and 2.48 mmol g^{-1}, respectively. The sorbent is stable in 2 M H_2SO_4, 6 M HCl, and 0.5 NaOH for 24 h: the weight loss is 2–3 wt %. The aminoguani-

1070-4272/05/7805-0715 © 2005 Pleiades Publishing, Inc.

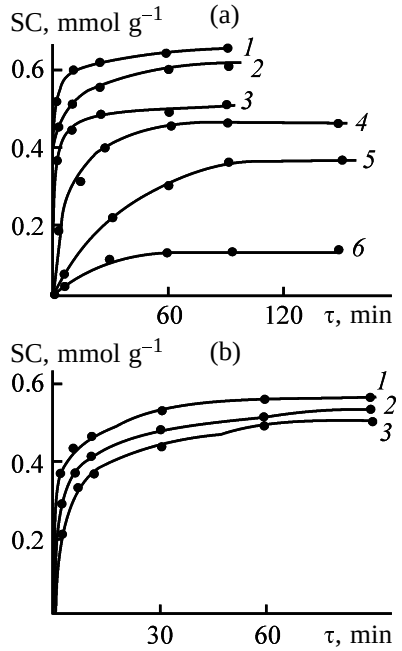
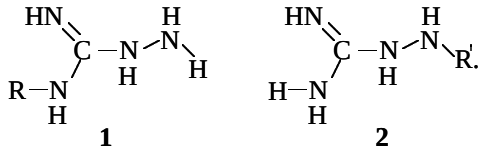


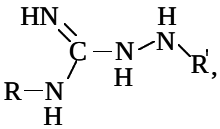
Fig. 1. Kinetic curves of (a) K_2PtCl_4 and (b) K_2PtCl_6 sorption from (*1–3*) 0.5 M HCl and (*4–6*) 0.5 M NaCl on GLIPAN-3 at (*1*, *4*) 90, (*2*, *5*) 50, (*3*, *6*) 18°C. (SC) sorption capacity and (τ) time. Platinum content (mM): (a) (*1–3*) 3.1 and (*4–6*) 3.3; (b) 2.9.

dine functional groups of the fiber have two structures:



1 **2**

Theoretically, guanidine can be bound to the matrix via both amino groups, but the content of these structures should be significantly smaller since the probability of reaction of two amino groups of an aminoguanidine molecule with the nitrile groups of the sorbent matrix is lower. Thus, the general structural formula of the fiber can be described as follows:



where R and R', in a particular case, can be hydrogen atoms.

We studied sorption of Pt(II) and Pt(IV) chloride complexes on GLIPAN-3 fiber under static conditions at continuous stirring (250 rocking min^{-1}, a T-22 rocker) at 18, 50, 76, and 90°C. The initial complexes $K_2[PtCl_4]$ and $K_2[PtCl_6]$ were prepared by the procedure in [7]. Sorption experiments were performed in freshly prepared 1–20 mM solutions of $K_2[PtCl_4]$ and $K_2[PtCl_6]$ in 0.1–4 M HCl and 0.5 M NaCl. In all cases, the solution volume was 20 ml and the sorbent weight was 0.1 g. The platinum content in the solutions before and after sorption was determined spectrophotometrically with a hydrochloric acid solution of tin(II) chloride [8]. The platinum sorption was determined as a difference between the platinum content in the solution before and after sorption. The IR spectra of fibers in the 400–4000 cm^{-1} range were recorded on an IKS-29 spectrophotometer and in the 140–400 cm^{-1} range (far IR region), on an FIS-3 spectrophotometer (Hitachi).

The procedure of sample preparation is described in our previous work [9]. Thermal analysis curves were recorded on an MOM derivatograph (Hungary) in the range 20–800°C at a heating rate of 10 deg min^{-1}. Isothermal hating of the sorbents was performed on a special installation equipped with a unit for qualitative analysis of gaseous thermolysis products. Thermal transformations of the samples (onset decomposition temperature, etc.) was visually observed with the aid of a Koefler stage [10]. The X-ray photoelectron spectra (XPS) of the platinum-containing samples were measured on a Kratos Axis Ultra electron spectrometer using AlK_α X-ray radiation with a power of 180 W. The sample was bombarded with slow electrons to compensate the surface charging. The measurements were performed at a residual pressure of 3×10^{-7} Pa. The quantitative analysis of the spectra and resolution of the spectra into separate lines were performed by conventional programs. The spectra were normalized to the C1*s* energy taken as 285.0 eV. The atomic concentrations were calculated from the corresponding peak areas.

The kinetic curves of K_2PtCl_4 and K_2PtCl_6 sorption from 0.5 M solutions of HCl and NaCl are shown in Figs. 1a and 1b. The equilibrium distribution of platinum(II) between the sorbent and hydrochloric acid and chloride solutions of K_2PtCl_4 at 50°C is attained in 60 and 120 min, respectively. The sorption half-time $\tau_{1/2}$ is 1 and 7 min, respectively. The degree of platinum(II) recovery from 0.5 M HCl (Fig. 1a, curve *2*) and 0.5 M NaCl (Fig. 1a, curve *5*) at 50°C is 95 and 54%, respectively.

In the case of K_2PtCl_6 (Fig. 1b), the sorption is somewhat slower and the degree of platinum recovery is lower than in the case of K_2PtCl_4. In acidic solutions at 50°C, τ_{app} is 80 min (Fig. 1b, curve *2*) and $\tau_{1/2}$ is 1.5 min. The degree of platinum(IV) recovery in 80 min is about 87%. The sorption from NaCl solutions is so slow that the apparent equilibrium between

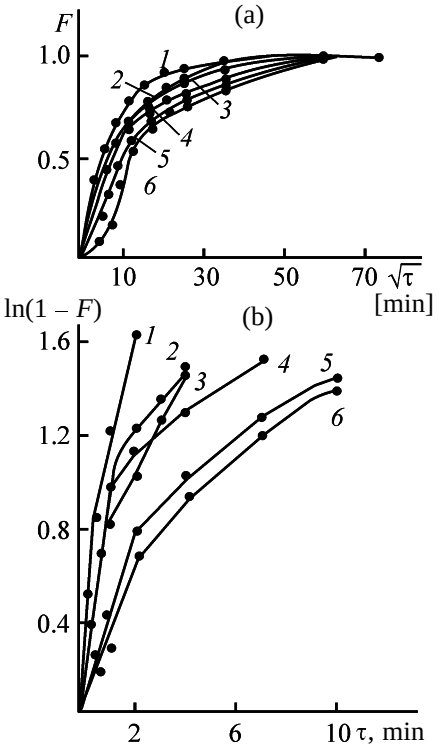


Fig. 2. (a) Degree of exchange F as a function of the square root of the sorption time τ and (b) $-\ln(1 - F)$ as a function of time τ of sorption of (*1–3*) K_2PtCl_4 and (*4–6*) K_2PtCl_6 on GLIPAN-3 from 0.5 M HCl at (*1*, *4*) 90, (*2*, *5*) 50, and (*3*, *6*) 18°C. $F = Q_\tau/Q_\infty$; (Q_τ) sorption of ions from solution in time τ and (Q_∞) equilibrium sorption. Platinum content (mM): (*1–3*) 3.1 and (*4–6*) 2.9.

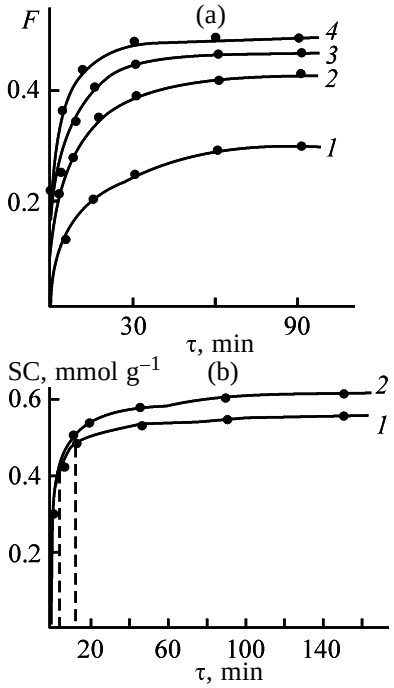


Fig. 3. Kinetic curves of K_2PtCl_6 sorption on GLIPAN-3 fiber from 0.5 M HCl at room temperature (a) with stirring of the solution at rate of (*1*) 0, (*2*) 29, (*3*) 69, and (*4*) 112–250 rocking min^{-1} and (b) (*1*) without interruption and (*2*) with 40-min interruption. (SC) sorption capacity and (τ) time. Platinum content (mM): (a) 2.9 and (b) 3.7.

the fiber and the solutions is not attained within 180 min and the degree of platinum recovery even on heating does not exceed 28%.

Generally, the rate-determining steps of the heterogeneous reaction can be (1) diffusion of reagents to the solid surface, (2) chemical reaction proper, and (3) diffusion of the reaction products from the solid phase into the solution. Since the sorption rate in hydrochloric acid solution is high and is almost independent of temperature, we suggest that the sorption of K_2PtCl_4 and K_2PtCl_6 occurs mainly by the anion-exchange mechanism to form onium complexes containing protonated amino groups [1, 2]. According to a large body of experimental data [1–4], slow sorption from chloride solutions suggests formation of intraspherical platinum complexes with aminoguanidine groups of GLIPAN-3 fiber.

Usually the type of diffusion kinetics is determined as follows: the dependence of the diffusion rate on the stirring rate (external diffusion) is studied; diffusion experiment is interrupted to determine the internal diffusion mechanism [1]]; and the F vs. $\tau^{0.5}$ and $-\ln(1 - F)$ vs. sortion time τ (where F is the degree of exchange, $F = Q_\tau/Q_\infty$, where Q_τ is the sorption of ions from solution in time τ and Q_∞ is the equilibrium sorption) are constructed. In the case of external diffusion kinetics, the $-\ln(1 - F)$ vs. τ curve is linear in the range from 0 to $\tau_{1/2}$. When the diffusion kinetics is external, the F vs. $\tau^{0.5}$ dependence is linear up to $F = 0.5$ [11]. The complex shape of the F vs. $\tau^{0.5}$ and $-\ln(1 - F)$ vs. τ dependence (Figs. 2a, 2b) and the presence of a linear section in them suggest [12] a mixed diffusion kinetics of sorption of platinum(II) and platinum(IV) chloride complexes from acidic solutions on GLIPAN-3. The apparent activation energies calculated by the Arrhenius equation [13] (7.1 and 7.5 kJ mol^{-1} for K_2PtCl_4 and K_2PtCl_6, respectively) confirm that the rate-determining step of the sorption is diffusion [12].

The kinetic curves of K_2PtCl_6 sorption from 0.5 M HCl at different stirring rates are shown in Fig. 3a. As seen from Fig. 3a, the sorption rate depends on the

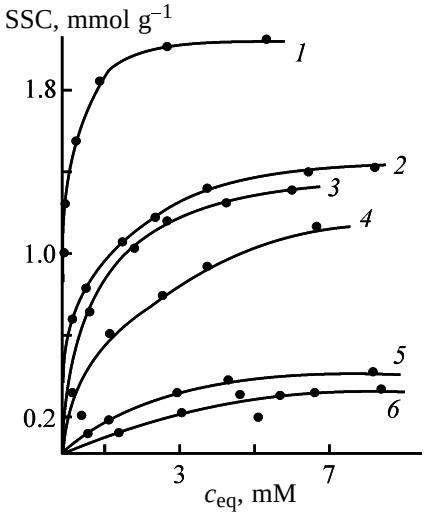


Fig. 4. Sorption isotherms of (*1, 2, 5, 6*) K_2PtCl_4 and (*3, 4*) K_2PtCl_6 at (*2, 4, 6*) 18°C and (*1, 3, 5*) 76°C from (*1–4*) 0.5 M HCl and (*5, 6*) 0.5 M NaCl. (SSC) Static sorption capacity and (c_{eq}) equilibrium Pt(II, IV) concentration.

stirring rate, which suggests diffusion control of the process. The sorption accelerates only insignificantly when the stirring rate increases in the range 112–250 rocking min^{-1}. The kinetic curves of K_2PtCl_6 sorption from 0.5 M HCl without interruption (curve *1*) and with a 40-min interruption (curve *2*) are shown in Fig. 3a. The fact that the SC measured in the experiment with interrupted sorption increases by 7% (Fig. 3b) suggests that not only external but also internal diffusion contribute to the sorption [12, 14]. Thus, these results also confirm mixed-diffusion mechanism of K_2PtCl_6 sorption on GLIPAN-3 from hydrochloric acid solutions.

The sorption isotherms of K_2PtCl_4 and K_2PtCl_6 from 0.5 M HCl and 0.5 M NaCl are shown in Fig. 4 (the initial platinum concentrations in the solutions are 1–20 mM). The shape of the sorption isotherm measured in hydrochloric acid solutions shows that GLIPAN-3 fiber can be used for platinum recovery from both dilute and concentrated solutions. The static sorption capacities (SSC) for K_2PtCl_4 and K_2PtCl_6 in 0.5 M HCl and 0.5 M NaCl are presented in the table. It should be noted that SSC for K_2PtCl_6 is almost independent of temperature, whereas SSC for K_2PtCl_4 increases by a factor of 1.5 on heating from 18 to 76°C, reaching 2.02 mmol g^{-1} at 76°C.

Table 1. Parameters of sorption of platinum(II) and platinum(IV) chloride complexes on GLIPAN-3

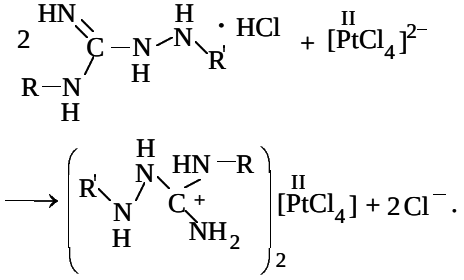
T, °C	Solution, 0.5 mM	Adsorbate	SSC, mmol g^{-1}
18	HCl	K_2PtCl_6	0.98
76			1.04
18	HCl	K_2PtCl_4	1.34
76			2.02
18	NaCl	K_2PtCl_4	0.33
76			0.38

Sorption of K_2PtCl_4 and K_2PtCl_6 substantially decreases with increasing HCl concentration. In the case of K_2PtCl_4, almost 100% of platinum(II) (SC = 0.94 mmol g^{-1}) is sorbed from 0.2 M HCl, whereas only 57% of Pt(II) (SC = 0.55 mmol g^{-1}) is sorbed at elevated temperature and 30% at room temperature (SC = 0.29 mmol g^{-1}) from 4 M HCl. Thus, sorption of platinum(II) and platinum(IV) chloride complexes from 0.2–0.5 M HCl is optimal.

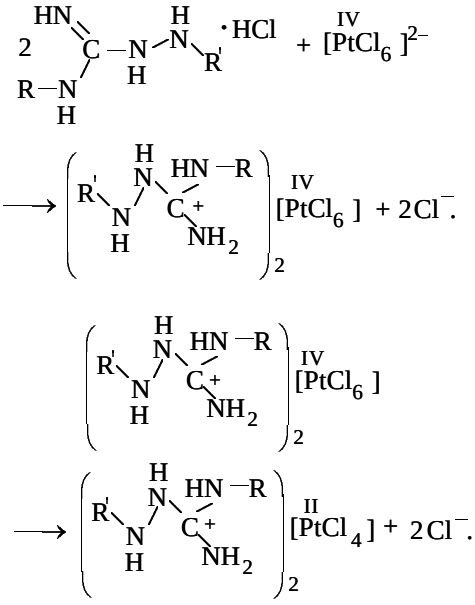
Comparison of the kinetic parameters of sorption of K_2PtCl_4 and K_2PtCl_6 on GLIPAN-3 and the capacity of this fiber for these complexes shows that the sorption of square planar tetrachloroplatinate on GLIPAN-3 is faster that that of hexachloroplatinate and the sorption capacity of the fiber for K_2PtCl_4 is higher than that for K_2PtCl_6. This is probably due to the fact that platinum(IV) complexes with $5d^5$ configuration of the central metal are more kinetically inert and the steric hindrance in sorption of larger $[PtCl_6]^{2-}$ anion with greater delocalization of the negative charge is stronger.

About 20% of platinum(II) and 25% of platinum(IV) can be desorbed from GLIPAN-3 fiber with 5 M HCl. Desorption of K_2PtCl_4 and K_2PtCl_6 with 0.5 M HCl does not exceed 5 and 10%, respectively. It should be noted that in all cases hexachloroplatinate is more readily desorbed than tetrachloroplatinate.

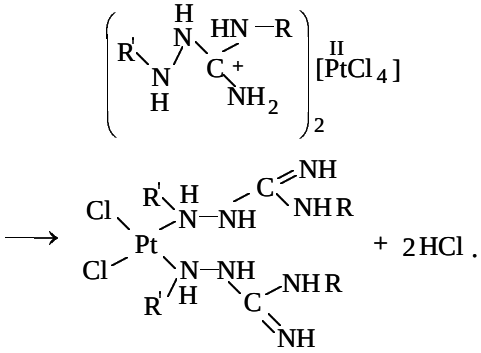
Analysis of the sorption kinetics of K_2PtCl_4 and K_2PtCl_6 on GLIPAN-3 and the capacity of this fiber for these complexes in acidic solution suggests that the complexes are sorbed mainly by the ion-exchange mechanism. Indeed, the FIR spectra of the fiber after sorption of K_2PtCl_4 from 0.5 M HCl (Fig. 5, curves *5*, *6*) suggest formation of onium platinum(II) complexes $[R'NHNHC(NH_2)NHR]_2[PtCl_4]$ (ν_{Pt-Cl} = 326 cm^{-1}) by the reaction



As determined by XPS, hexachloroplatinate is partially reduced to tetrachloroplatinate in the course of its sorption on GLIPAN-3 fiber [Pt4$f_{7/2}$ BE 72.9 and 75.0 eV agree well with the known BE for K_2PtCl_4 (73.1 eV) and K_2PtCl_6 (75.7 eV)] [15]. The Pt : Cl ratio on the fiber surface is 1 : 4.6 and the Pt(IV) : Pt(II) ratio is approximately 1 : 3. Formation of both onium platinum(II) chloride complexes and onium platinum(IV) chloride complexes, $[R'NHNHC(NH_2)\cdot NHR]_2[PtCl_6]$ is confirmed by the presence of a ν_{Pt-Cl} band at 330–334 cm^{-1} in the FIR spectra of the firber after sorption of K_2PtCl_6 from 0.5 M HCl. Platinum(IV) compounds can be reduced to platinum(II) compounds with hydrazine groups of aminoguanidine. Thus, sorption of K_2PtCl_6 can be described by the following scheme:



Formation of onium complexes of Pt(II) and Pt(IV) was also confirmed in special experiments. Intense liberation of hydrogen chloride was observed on isothermal heating of the sorbent that was washed with water to remove chloride ions and then was air-dried. The onium complex is converted to diamino chloride complex like $\{Pt[R'NHNHC(=NH)–NHR]_2Cl_2\}$ [10]:



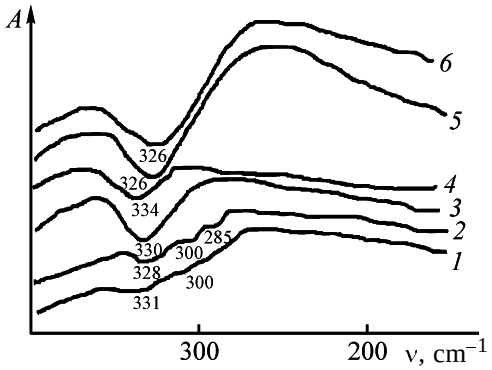


Fig. 5. Far IR spectra of GLIPAN-3 fiber after sorption of K_2PtCl_4 and K_2PtCl_6 for 3 h from (*1*, *2*) 0.5 M NaCl and (*3*–*6*) 0.5 HCl. C_{Pt} = 10 mM. (*A*) Absorption and (ν) frequency; the same for Fig. 3.

The temperature of this rearrangement cannot be accurately determined by thermal analysis, since it occurs simultaneously with water elimination and fiber degradation. The decomposition is complete at about 700°C with the formation of Pt metal.

Sorption of K_2PtCl_4 and K_2PtCl_6 from NaCl solutions is essentially different. Low sorption rate of these complexes and strong temperature dependence of the sorption rate and sorption capacity suggest formation of $\{Pt[R'NH–NH–C(=NH)–NHR]_2Cl_2\}$ complexes. Formation of these complexes is also confirmed by more complex shape of the FIR spectra of the fiber after sorption of K_2PtCl_4 from 0.5 M NaCl (Fig. 5, curves *1*, *2*) [16].

To confirm formation of these complexes by reaction of the platinum chloride complexes with aminoguanidine groups of the fiber, we prepared model Pt(II) complexes with aminoguanidine hydrochloride and guanidine hydrochloride. Solutions of K_2PtCl_4 and guanidine hydrochloride or aminoguanidine hydrochloride in a 1 : 2 ratio in 6 and 0.5 M HCl and water were heated on a boiling water bath for 5 h. Evaporation of the hydrochloric acid solutions gave red crystals of onium salts $[NH_2–NH–C(NH_2)–NH_2]_2\cdot[PtCl_4]$ or $[NH_2–C(NH_2)–NH_2]_2[PtCl_4]$. The FIR spectra of these complexes are similar to those of the fiber after sorption of K_2PtCl_4 from 0.5 M HCl and contain Pt–Cl bands at 323 and 326 cm^{-1} (Fig. 6) [17].

Prolonged heating of K_2PtCl_4 with aminoguanidine hydrochloride in an aqueous solution yields a dark finely crystalline product poorly soluble in water and ethanol. Elemental analysis of the product agrees with the formula $\{Pt[NH_2NHC(=NH)NH_2]_2Cl_2\}$: calculated M_w = 414.15, C 5.80, H 2.92, N 27.06; found: C 6.23, H 3.22, N 26.94. The FIR spectrum of this

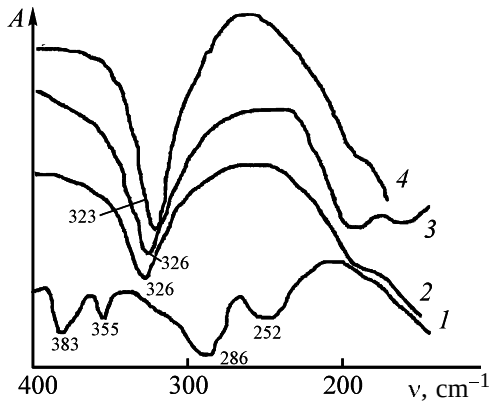
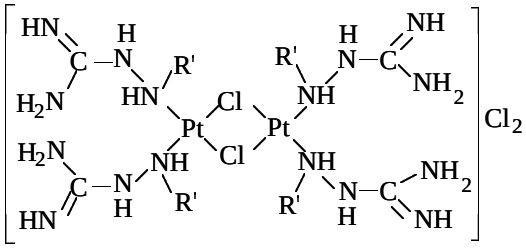


Fig. 6. FIR spectra of platinum(II) complexes with (*2*) guanidine and (*1*, *3*, *4*) aminoguanidine prepared from (*1*, *2*) 6 M HCl, (*3*) 0.5 M HCl, and (*4*) water.

compound is similar to the spectrum measured in [16]; the Pt–Cl stretching bands at 286 and 252 cm^{-1} are due to bridging chloride ions. The bands of terminal chloride ions are absent (Fig. 6, curve *1*). The structure of this complex can be described by the formula



Comparison of these data with the FIR spectra of the fiber after sorption of K_2PtCl_4 from neutral chloride solutions (Fig. 5, curves *1*, *2*) suggests that complexes containing bridging chloride ions (ν_{Pt-Cl} = 285 cm^{-1}), which are similar to the model compounds formed in aqueous solutions, are present in the polymeric matrix along with the amino chloride complexes.

We studied the possibility of using GLIPAN-3 fiber for separation of platinum metals from nonferrous metals and iron. Sorption was performed from 0.5 M HCl at 18 and 76°C for 3 h. The content of nonferrous metals and iron in the solution before and after sorption was determined by atomic emission spectroscopy (analysis was performed by S.N. Zimina, Mekhanobr Joint-Stock Company). The platinum content was determined by atomic absorption spectroscopy after precipitation on tellurium (L.A. Ushinskaya, Mekhanobr Joint-Stock Company). The main components of platinum-containing process solutions are nickel(II), copper(II), cobalt(II), and iron(III) chlorides. We studied sorption of tetrachloroplatinate(II) from model solutions of 1 M $NiCl_2$, $CuCl_2$, $CoCl_2$, and $FeCl_3$ in 0.5 M HCl (c_{Pt} = 1 mM) and sorption of K_2PtCl_4 against the background of a 1000-fold excess of $AlCl_3$ (solutions simulating process solutions formed in recovery of platinum metals from catalysts of gasoline afterburning). The solutions contained 1 M $AlCl_3$, 1 mM K_2PtCl_4, and 0.5 M HCl.

We found that about 25% of platinum was sorbed at 18 and 76°C. The main portion of nonferrous metals remained in the solution; their total recovery was no higher than 6–7%. At room temperature, about 83% of platinum and 13% of aluminum were sorbed, which allowed effective platinum concentration. Thus, GLIPAN-3 fiber can be used for platinum recovery at room temperature from solutions formed in processing of gasoline afterburning catalysts containing $AlCl_3$.

CONCLUSIONS

(1) Sorption of tetrachloroplatinate and hexachloroplatinate from hydrochloric acid solutions at the platinum concentration of 1–10 mM on GLIPAN-3 fibrous sorbent prepared by modification of polyacrylonitrile with aminoguanidines is fast and quantitative. In neutral solutions, the sorption is slow and is not quantitative [20–40% recovery of platinum(II)].

(2) Platinum chloride complexes are sorbed on GLIPAN-3 fiber from hydrochloric acid solutions by the anion-exchange mechanism to form $[R'NHNH \cdot C(NH_2)NHR]_2[PtCl_4]$ and $[R'NHNHC(NH_2)NHR]_2 \cdot [PtCl_6]$. Sorption from chloride solutions involves complexation with functional groups of the fiber.

(3) GLIPAN-3 fiber can be used to recover tetrachloroplatinate(II) from solutions containing 1000-fold excess of aluminum chloride and from solutions formed in processing of gasoline afterburning catalysts.

ACKNOWLEDGMENTS

The study was financially supported by the foundation supporting research work of postgraduate students of the Russian Ministry of Education (grant no. A03-2.11-224).

REFERENCES

1. Simanova, S.A. and Kukushkin, Yu.N., *Izv. Vyssh. Uchebn. Zaved., Khim. Khim. Tekhnol.*, 1985, vol. 28, no. 8, pp. 3–15.
2. Simanova, S.A. and Kukushkin, Yu.N., *Izv. Vyssh. Uchebn. Zaved., Khim. Khim. Tekhnol*., 1986, vol. 29, no. 8, pp. 3–14.

3. Myasoedov, G.V. and Komozin, P.N., *Zh. Neorg. Khim.*, 1994, vol. 39, no. 2, pp. 280–288.
4. Simanova, S.A. and Kukushkin, Yu.N., *Probl. Sovrem. Khim. Koord. Soedin.*, 1992, issue 10, pp. 125–141.
5. Gulko, A., Feigenbaum, H., and Schmukler, G., *Anal. Chim. Acta*, 1972, vol. 59, no. 3, pp. 397–402.
6. Simanova, S.A., Burmistrova, N.M., Kazakevich, Yu.E., *et al.*, *Zh. Prikl. Khim.*, 1996, vol. 69, no. 5, pp. 772–777.
7. *Sintez kompleksnykh soedinenii metallov platinovoi gruppy* (Synthesis of Platinum Metal Complexes), Chernyaev, I.I., Ed., Moscow: Nauka, 1964.
8. Ginzburg, S.I., Ezerskaya, N.A., Prokof'eva, I.V., *et al.*, *Analiticheskaya khimiya elementov: Platinovye metally* (Analytical Chemistry of Elements: Platinum Metals): Moscow: Nauka, 1972.
9. Simanova, S.A., Kuznetsova, T.V., Belyaev, A.N., *et al.*, *Zh. Prikl. Khim.*, 1999, vol. 72, no. 8, pp. 1276–1281.
10. Kukushkin, Yu.N., Budanova, V.F., and Sedova, G.N., *Termicheskie prevrashcheniya koordinatsionnykh soedinenii v tverdoi faze* (Thermal Transformations of Coordination Compounds in the Solid Phase), Leningrad: Leningr. Gos. Univ., 1981.
11. Kokotov, Yu.A. and Pasechnik, V.A., *Ravnovesie i kinetika ionnogo obmena* (Equilibrium and Kinetics of Ion Exchange) Leningrad: Khimiya, 1970.
12. Saldadze, K.M. and Kopylova-Valova, V.D., *Kompleksoobrazuyushchie ionity (kompleksity)* (Complexing Ion Exchanger (Complexites)), Moscow: Khimiya, 1980.
13. Emanuel', N.M. and Knorre, D.P., *Kurs khimicheskoi kinetiki* (Course of Chemical Kinetics), Moscow: Vysshaya Shkola, 1969.
14. Simanova, S.A. and Boichinova, E.S., in *Ionnyi obmen i ionometriya* (Ion Exchange and Ionometry), Leningrad: Leningr. Gos. Univ., 1998, no. 6, pp. 3–17.
15. Nefedov, V.I., *Rentgenoelektronnaya spektroskopiya khimicheskikh soedinenii. Spravochnik* (X-ray Photoelectron Spectroscopy of Chemical Compounds. Handbook), Moscow: Khimiya, 1984.
16. Finch, A., Gates, K., and Radcliffe, K., *Chemical Applications of Far Infrared Spectroscopy*, London: Academic, 1970.
17. Konovalov, L.V., *Koord. Khim.*, 1984, vol. 10, no. 10, pp. 1041–1047.

Russian Journal of Applied Chemistry, Vol. 78, No. 5, 2005, pp. 722–726. Translated from Zhurnal Prikladnoi Khimii, Vol. 78, No. 5, 2005, pp. 736–740.
Original Russian Text Copyright © 2005 by Kolomiets, Troshkina, Sheremet'ev, Konopleva.

SORPTION AND ION-EXCHANGE PROCESSES

Sorption of Uranium from Sulfuric Acid Leaching Solutions by Strongly Basic Anion Exchangers

D. N. Kolomiets, I. D. Troshkina, M. F. Sheremet'ev, and L. V. Konopleva

Mendeleev Russian Chemical Engineering University, Moscow, Russia
Russian Research Institute of Chemical Technology, Moscow, Russia

Received October 28, 2004; in the final form, February 2005

Abstract—The equilibrium and kinetic characteristics of uranium sorption from simulated sulfuric acid leaching solutions by AMP, Lewatit K 6367, Purolite A 500, Purolite A 600, and AM-p gel-like and porous strongly basic anion exchangers were studied.

Underground leaching is widely used in uranium mining. In leaching uranium with aqueous sulfuric acid, the leaching solutions containing neutral $[UO_2SO_4]^0$ and anionic $[UO_2(SO_4)_2]^{2-}$ and $[UO_2 \cdot (SO_4)_3]^{4-}$ complexes are formed. The yield of these complexes depends on the content of sulfuric acid and sulfate anions in the leaching solution [1].

The sorption recovery of uranium from sulfuric acid leaching solutions by strongly basic anion exchangers can be described by reactions of complexation and ion exchange [2]:

$$(R_4N^+)_2SO_4 + [UO_2SO_4]^0 \rightleftarrows (R_4N^+)_2[UO_2(SO_4)_2]^0,$$

$$2(R_4N^+)_2SO_4 + [UO_2(SO_4)_2]^{2-} \rightleftarrows (R_4N^+)_4[UO_2(SO_4)_3] + SO_4^{2-},$$

$$2(R_4N^+)_2SO_4 + [UO_2(SO_4)_3]^{4-} \rightleftarrows (R_4N^+)_4[UO_2(SO_4)_3] + 2SO_4^{2-}.$$

In this study we examined the equilibrium and kinetic characteristics of uranium sorption by anion exchangers from sulfuric acid solutions simulating the leaching solutions for underground uranium mining. Along with common AMP and AM-p anion exchangers, we tested new Lewatit K 6367, Purolite A 500, and Purolite A 600 strongly basic anion exchangers.

EXPERIMENTAL

In our experiments we studied sorption of uranium from simulated leaching solutions by commercial strongly basic anion exchangers in the SO_4^{2-} form. Anion exchangers of various brands were tested: AMP, AM-p (Smoly State Company, Ukraine); Purolite A 500, Purolite A 600 (Purolite International Limited, the United Kingdom); Lewatit K 6367 (Bayer AG, Germany). The main physicochemical characteristics of these resins, listed in Table 1, were published [3], taken from certificates (Lewatit K 6376, Purolite A 500, and Purolite 600), or determined in accordance with OST (Branch Standard) recommendations.

The factors for recalculating the mass sorption capacity (mg g^{-1}) of resins to their volume sorption capacity (mg cm^{-3}) were determined by the method reported in [4]. For the anion exchangers under consideration, these factors are as follows:

Anion exchanger	Recalculation factor, $cm^3\ g^{-1}$
AMP	1.9
Lewatit K 6367	1.8
Purolite A 500	2.7
Purolite A 600	2.5
AM-p	2.6

The sorption of uranium from simulated leaching solutions was studied at room temperature (20°C). The composition of these solutions was as follows (g dm^{-3}): uranium(VI) 0.058–0.063, sulfuric acid 4.8–5.0, iron (total) 1.50–1.65, aluminum(III) 1.30–1.35, calcium 0.50–0.57, magnesium 0.40–0.45, chloride anion 0.50–0.58, and sulfate anion (total) 19.5–20.5. The solid and liquid phases were stirred with a mechanical stirrer at a rate of 340 rpm.

The isotherms of uranium sorption were obtained at the uranium concentration in the solution ranging from 5 to 204 mg dm^{-3}. For solutions containing

1070-4272/05/7805-0722 © 2005 Pleiades Publishing, Inc.

Table 1. Main physicochemical characteristics of the tested anion exchangers in the Cl^- form

Characteristic	AMP (4% DVB)	Lewatit K 6367	Purolite A 500	Purolite A 600	AM-p (8.5% DVB)
Functional group	Benzylpyridine	Benzyltrimethyl-ammonium	Benzyltrimeth-ylammonium	Benzyltrimeth-ylammonium	Benzyltrimethyl-ammonium
Structure	Gel-like	Gel-like	Macroporous	Gel-like	Macroporous
Total exchange capacity, mg-equiv g^{-1},	3.10	4.41	3.98	4.17	3.30
Exchange capacity of weakly basic groups, mg-equiv g^{-1}	–	0.73	0.38	0.10	0.30
Specific swelling in distilled water, $cm^3\ g^{-1}$	2.70	2.85	3.15	2.5	3.85
Swelling coefficient in distilled water, $cm^3\ cm^{-3}$	1.43	1.65	1.33	1.48	2.55
Density, g cm^{-3} (for porous resins, the apparent and true densities are given)	1.14	1.08	1.09	Not determined	0.98; 1.15
Bulk weight, g cm^{-3}	700	640	668	685	680
Specific surface area, $m^2\ g^{-1}$	1.6	Not determined	31	Not determined	34
Average moisture content, %	52	55	46	56	55
Mechanical strength, %	99.0	100	99.0	99.5	99.5

5–30, 60–80, and 150–204 (mg U) dm^{-3}, the solution to sorbent ratio $V_l : V_s$ was 5000, 3000 and 1000, respectively. The time of contacting the sorbent and liquid phase was 24 h.

The isotherms of uranium sorption were treated with the Langmuir equation [5].

The kinetics of uranium sorption was studied at room temperature under static limited-volume conditions. The integral sorption kinetic curves were obtained at the contacting time of 1–24 h and the solution to sorbent ratio $V_l : V_s = 3000$.

The external uranium diffusion was estimated using a simplified approach [7] based on an assumption that, in the initial period of contact of the sorbent and solution, the solute content on the sorbent surface is zero and its diffusion into sorbent can be neglected:

$$\ln\frac{c(\tau)}{c_0} = -k\frac{A}{V}\tau, \qquad (1)$$

where $c(\tau)$ is the solute concentration (mg dm^{-3}) at time τ; c_0, initial solute concentration (mg dm^{-3}); A, exchanging surface area of the sorbent (m^2); and V, solution volume (dm^3).

The initial external mass transfer factor k (m s^{-1}) was determined from the plot of $\ln c(\tau)/c_0$ vs. the phase contact time.

The A/V ratio was calculated by the equation

$$A/V = 6m/d\rho_a, \qquad (2)$$

where m is the sorbent to solution ratio (g dm^{-3}); d, diameter of the sorbent granule (m); and ρ_a, apparent sorbent density (g dm^{-3}).

The average diameter of anion exchanger granules, as determined by dry sieving, was as follows (mm): AMP, 0.9; Lewatit K 6367, 0.7; Purolite A 500, 0.8; Purolite A 600, 0.7; and AM-p, 0.9. The apparent density of these sorbents was 1.15, 1.11, 1.12, 1.11, and 1.08 g cm^{-3}, respectively. In our kinetics sorption experiments, the A/V ratio, on the average, was 0.75, 0.72, 0.87, 1.00 and 0.74 m^{-1} for AMP, Lewatit K 6367, Purolite A 500, Purolite A 600, and AM-p anion exchangers, respectively.

The uranium diffusion within gel-like resins was analyzed by the equation deduced by Boyd, Adamson, and Myers [8]:

$$F = a_\tau/a_\infty = 1 - \frac{6}{\pi^2}\sum_{n=1}^{\infty}\frac{1}{n^2}\exp(\bar{D}\pi^2 n^2\tau/r_0^2), \qquad (3)$$

where $\bar{D}$ is the coefficient of internal diffusion ($m^2\ s^{-1}$); r_0, average radius of sorbent granule (m); a_τ and a_∞, sorption capacity of the resin for uranium

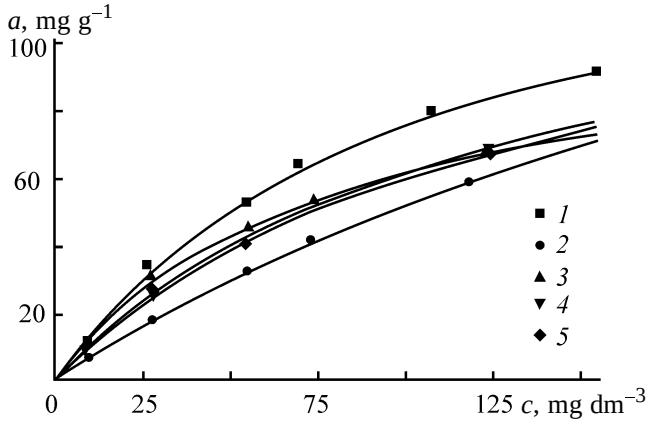


Fig. 1. Isotherms of uranium sorption by (*1*) AMP, (*2*) Lewatit K 6367, (*4*) Purolite A 600, and (*5*) AM-p anion exchangers and (*3*) apparent isotherm of uranium sorption by Purolite A 500 from simulated sulfuric acid leaching solutions. (*a*) Mass sorption capacity of anion exchanger for uranium and (*c*) uranium concentration in solution.

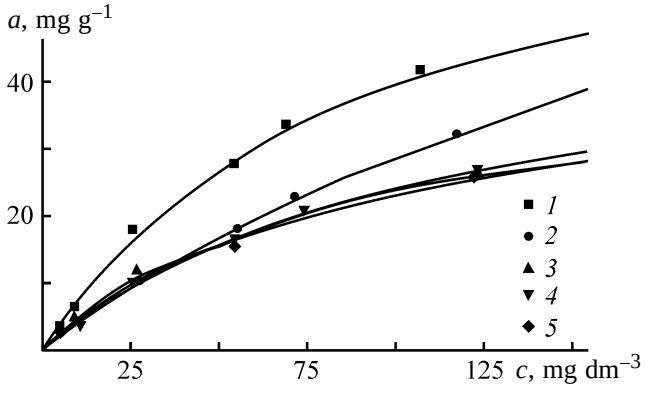


Fig. 2. Isotherms of uranium sorption by (*1*) AMP, (*2*) Lewatit K 6367, (*4*) Purolite A 600, and (*5*) AM-p anion exchangers and (*3*) apparent isotherm of uranium sorption by Purolite A 500 from simulated leaching solutions. (*a*) Volume sorption capacity of anion exchangers for uranium and (*c*) uranium concentration in solution.

Table 2. Parameters of isotherms of uranium sorption by AMP, Lewatit K 6367, Purolite A 500, Purolite A 600, and AM-p anion exchangers, calculated by the Langmuir equation

Anion exchanger	K, $dm^3\ g^{-1}$	A_∞, $g\ dm^{-3}$	R^2	$S \times 10^4$
AMP	8.5	86.4	0.962	1.4
Lewatit K 6367	3.1	123	0.977	0.8
Purolite A 500	10	45.8	0.988	1.7
Purolite A 600	6.5	61.3	0.949	2.6
AM-p	9.1	48.8	0.974	2.3

at the moment τ and at equilibrium ($mg\ g^{-1}$); and F, degree of the resin saturation depending only on the dimensionless parameter $B = \bar{D}\pi^2/r_0^2$.

At the degree of resin saturation $F > 0.7$, the terms of higher orders in Eq. (3) become small, and this equation is simplified:

$$F = 1 - \frac{6}{\pi^2}\exp(-B\tau). \quad (4)$$

After taking the logarithm, Eq. (4) is converted to a linear semilogarithmic equation $\ln(1 - F) = \ln(6/\pi^2) - B\tau$. This equation can be presented as the plot of $\log(1-F)$ vs. τ, whose slope is the B factor. After substitution of this factor into Eq. (3), the diffusion coefficient D was calculated.

The simplest and the most reliable procedure for determining the limiting stage of sorption is based on interruption of sorption [9]. According to this technique, after contact for 1 h, a resin is separated from the solution by vacuum filtration through a Schott filter, and both the sorbent and solution are kept separately. After the lapse of 3 h, the solution and sorbent are brought in contact again.

In sorption of uranium(VI) from model leaching solutions containing from 5 to 150 $(mg\ U)\ dm^{-3}$, the mass sorption capacity of anion exchangers for uranium decreases in the order AMP > AM-p, Purolite A 600, Purolite A 500 > Lewatit K 6367 (Fig. 1). Under the same conditions, the volume sorption capacity of these resins decreases in the order AMP > Lewatit K 6367 > AM-p, Purolite A 600, and Purolite A 500 (Fig. 2).

The residual uranium content in the leaching solution after the sorption is determined by the residual sorption capacity of regenerated resins for uranium. With the sorbents under consideration, the residual uranium concentration of 2 $mg\ dm^{-3}$ is attained at the following residual sorption capacities, $mg\ cm^{-3}$: AMP, 1.1–1.3; Lewatit K 6367, 0.6–0.8; Purolite A 500, 0.7–0.9; Purolite A 600, 0.6–0.8; and AM-p, 0.7–0.9.

Our sorption isotherms are well described by the Langmuir equation. The k and A_∞ parameters of the Langmuir equation for anion exchangers under consideration and also the approximation reliability factors R^2 and the residual variances S are listed in Table 2.

The rate of uranium sorption from simulated leaching solutions by the anion exchangers under consideration decreases in the order Lewatit K 6367 >

Table 3. Mass-transfer coefficient k and diffusion coefficient D of uranium(VI) in its sorption by AMP, Lewatit K 6367, Purolite A 500, Purolite A 600, and AM-p anion exchangers

Anion exchanger	$k \times 10^5$, m s^{-1}	R^2	S	$\bar{D} \times 10^{12}$, m^2 s^{-1}	R^2	S
AMP	2.10	0.957	0.0061	1.69	0.983	0.3247
Lewatit K 6367	2.00	0.990	0.0025	1.12	0.995	0.1189
Purolite A 500	0.54	0.954	0.0017	0.66	0.983	0.2062
Purolite A 600	0.83	0.983	0.0018	0.89	0.997	0.1136
AM-p	1.05	0.980	0.0018	0.98	0.981	0.1994

AMP > Purolite A 600, AM-p > Purolite A 500. The complete saturation of sorbents with uranium in sorption from its dilute sulfuric acid solutions was attained within the following time (h): Lewatit K 6367 6–10; AMP, Purolite A 600, 14–16; and AM-p, 20–24. In sorption of uranium by Purolite A 500, the sorption equilibrium was not attained within 25 h. Therefore, in this case the apparent isotherms of uranium sorption were obtained (Figs. 1, 2). Under the identical experimental conditions, the mass sorption capacity of AMP anion exchanger for uranium exceeds that of the other resins under consideration by 10–40%, and the volume sorption capacity, by 5–7%.

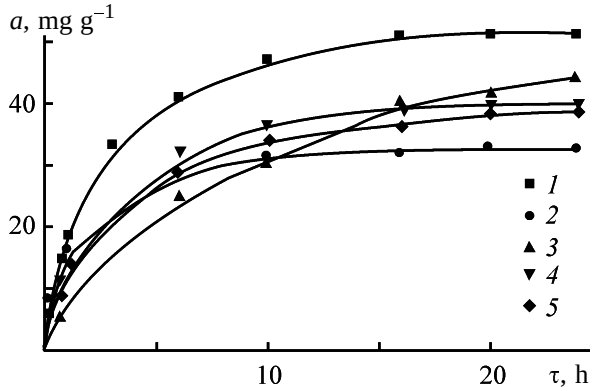


Fig. 3. Integral kinetic curves of uranium sorption by (*1*) AMP, (*2*) Lewatit K 6367, (*3*) Purolite A 500, (*4*) Purolite A 600, and (*5*) AM-p from simulated leaching solutions. (*a*) Mass sorption capacity for uranium and (τ) phase contact time; the same for Fig. 4.

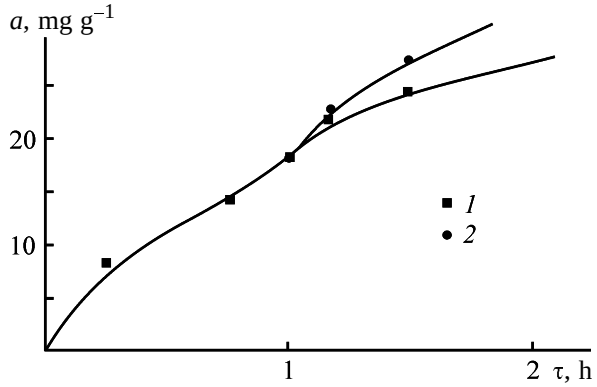


Fig. 4. Kinetic curves of uranium sorption from simulated leaching solutions: (*1*) without interruption and (*2*) with interruption.

Experiments on interruption of sorption showed that, in sorption of uranium with AMP, the intragranular (gel-like) diffusion starts to contribute to the total rate of uranium sorption at $\tau > 1$ h.

Under these conditions, after repeated phase contact, the rate of uranium sorption increases as compared to the rate of sorption before interruption. This effect is caused by the fact that, after interrupting the phase contact, uranium gets evenly distributed within the granule and, as a result, in the moment of repeated contact, the gradient of uranium concentration between the solution and the sorbent surface increases (Fig. 4). Whereas at a contact time $\tau < 1$ h uranium mainly diffuses by the film mechanism, at $\tau > 6$ h the intragranular gel-like diffusion of uranium predominates. At a contact time of 1–6 h, uranium is sorbed by the mixed mechanism.

The mass-transfer coefficients of uranium at a contact time $\tau < 1$ h and the uranium diffusion coefficients at the degree of sorbent saturation $F > 0.7$, calculated by Eqs. (1) and (4), are listed in Table 3.

The best kinetic characteristics of uranium sorption from simulated leaching solutions were exhibited by AMP and Lewatit K 6367 anion exchangers. The mass-transfer coefficients and the diffusion coefficients decrease in the order AMP > Lewatit K 6367 > AM-p > Purolite A 600 > Purolite A 500.

CONCLUSIONS

(1) Among anion exchangers used for uranium sorption from simulated leaching solutions for underground uranium mining (Lewatit K 6367, Purolite A 600, Purolite A 500, AMP, and AM-p), the highest sorption capacity for uranium is exhibited by standard

AMP anion exchanger. The isotherms of uranium sorption are well described by the Langmuir equation.

(2) AMP and Lewatit K 6367 anion exchangers show the best kinetics of uranium sorption from simulated leaching solutions. The experiments on interruption of uranium sorption showed that, whereas at a contact time $\tau < 1$ h uranium mainly diffuses by the film mechanism, at $\tau > 6$ h the intragranular gel-like diffusion predominates. At a contact time within 1–6 h, uranium diffuses by the mixed mechanism.

REFERENCES

1. Zefirov, A.P., Nevskii, B.V., Bakhurov, V.G., *et al*., in *Proc. IV Int. Conf. on the Peaceful Use of Atomic Energy*, Geneva: UN IAEA, 1972, vol. 8, no. 49, p. 45.
2. Beletskii, I.V., Bogatkov, L.K., Volkov, N.I., *et al*., *Spravochnik po geotekhnologii urana* (Handbook on Uranium Geotechnology), Skorovarov, D.I., Ed., Moscow: Energoatomizdat, 1997.
3. *Ionoobmenye materialy dlya protsessov gidrometallurgii, ochistki stochnykh vod i vodopodgotovki* (Ion-Exchange Materials for Hydrometallurgical Processes, Wastewater Decontamination, and Water Treatment), Moscow: Vses. Nauchno-Issled. Inst. Khim. Tekhnol., Gos. Komitet SSSR po Ispol'z. At. Energii, 1983.
4. Zhukova, N.G., Savina, L.A., Polyakova, O.P., *et al*., in *Sbornik metodik analiticheskogo kontrolya ionoobmennykh materialov dlya protsessov gidrometallurgii, ochistki stochnykh vod i vodopodgotovki* (Collection of Procedures for Analytical Monitoring of Ion-Exchange Materials for Hydrometallurgical Processes, Wastewater Decontamination, and Water Treatment), Moscow: Vses. Nauchno-Issled. Inst. Khim. Tekhnol., Gos. Komitet SSSR po Ispol'z. At. Energii, 1984.
5. Frolov, Yu.G., *Kurs kolloidnoi khimii: Poverkhnostnye yavleniya i dispersnye sistemy* (Course of Colloid Chemistry: Surface Phenomena and Disperse Systems), Moscow: Khimiya, 1988.
6. Znamenskii, Yu.P. and Bychkov, N.V., *Kinetika ionoobmennykh protsessov* (Kinetics of Ion-Exchange Processes), Obninsk: Piter, 2000.
7. Findon, A., McCay, G., and Blair, H.S., *J. Environ. Sci. Health*, 1993. part A28, pp. 173–185.
8. Boyd, G.E., Adamson, A.W., and Myers, L.S., *J. Am. Chem. Soc*., 1947, vol. 69, no. 11, pp. 2837–2848.
9. Zelikman, A.N., Vol'dman, G.N., and Belyaevskaya, L.V., *Teoriya gidrometallurgicheskikh protsessov* (Theory of Hydrometallurgical Processes), Moscow: Metallurgiya, 1983.

Russian Journal of Applied Chemistry, Vol. 78, No. 5, 2005, pp. 727–732. Translated from Zhurnal Prikladnoi Khimii, Vol. 78, No. 5, 2005, pp. 741–746.
Original Russian Text Copyright © 2005 by Dmitrieva, Tikhomolova, Chukhno.

SORPTION AND ION-EXCHANGE PROCESSES

Specific Features of 1,3-Diazole Adsorption on the Surface of NiO and Fe_2O_3

I. B. Dmitrieva, K. P. Tikhomolova, and A. S. Chukhno

St. Petersburg Academy of Pharmaceutical Chemistry, St. Petersburg, Russia
Research Institute of Chemistry, St. Petersburg State University, St. Petersburg, Russia

Received October 20, 2004; in final form, March 2005

Abstract—Variation of the electrokinetic potential of the surface of the oxides and of the amount of adsorbed diazole and its concentration in solution in systems constituted by aqueous solutions of 1,3-diazole and NiO and Fe_2O_3 adsorbents was studied in the course of a long time after bringing the phases in contact.

In this study, we proceed with analysis of the fundamental aspects of adsorption of nitrogen-containing five-membered heterocyclic organic compounds, azoles, from their aqueous solutions onto the surface of transition metal oxides [1–5]. Azoles are fragments of biologically important objects responsible for binding of metals in living bodies and show considerable promise for use in pharmacology and medicine. It is noteworthy that azole-containing fragments are incorporated in blood cells; numerous medical preparations (Analgin, antipyrine, pyramidone, etc.) and vitamins (B_1) are derivatives of azoles [6–8]. A study of adsorption of azoles on the surface of transition metal oxides will make it possible to understand and explain the mechanism of specific adsorption, which governs such biological processes as introduction of vitally important metals and removal of those with toxic properties from living bodies.

We chose as basic objects of study 1,3-diazole (imidazole) and Ni(II) and Fe(III) oxides. It is known that iron is the "metal of life" and nickel is a highly toxic metal.

The presence of nitrogen(III) in the imidazole molecule in position 1 (pyrrole-type nitrogen) determines its acid–base properties and the possibility of its existence in the anionic form, and nitrogen in position 3 (pyridine-type nitrogen) enables positive charging of the diazole molecule in its protonation. Imidazole can exist in aqueous solutions in three forms: neutral, cationic, and anionic. Consequently, the imidazole molecule can form, depending on conditions, an electrostatic bond with the charged surface of the oxide as a cation (at negatively charged surface) or anion (at a positive charge). It should, however, be noted that imidazole dissociates in water mainly by the basic type; the anionic form appears in noticeable amounts (>3%) at pH > 12 (pK_a 14, pK_{BH^+} – 6.99 [5]).

The imidazole cation is rather stable and can form, under the optimal conditions, large aggregates in the form of long chains with 20 and more molecules linked by hydrogen bonds $N_1 \cdots H \cdots N_3$. The neutral form of the molecules can also produce chains, which are, however, considerably shorter; the anionic form typically shows no aggregation [9].

At the same time, nitrogen atoms can be involved in bonding by the donor–acceptor mechanism with the metal ion belonging to an active center on the oxide surface. It is noteworthy that the property of aromaticity, generally characteristic of heterocycles, is rather poorly pronounced in imidazole.

The iron(III) and nickel(II) ions we chose for the study belong to metal ions exhibiting a variable acceptor power [10]. Depending on the pH value, the surface of their oxide may be charged both positively (at low pH) and negatively (at higher pH values), which is determined by its adsorption capacity for $[H^+]$ and $[OH^-]$ ions. The pH value at the isoelectric point (pH_{IEP}), found from electrokinetic measurements, depends on the acid–base properties of the active center on the oxide surface. For the oxides used in the study, these values were 7.6 for NiO and 6.1 for Fe_2O_3.

The interaction of azoles with an oxide surface can be judged from the manner in which the electrokinetic potential ζ, position of pH_{IEP}, and amount Γ of adsorbed nitrogen (found from its loss from solution) vary with the pH value of the system, intial nitrogen

1070-4272/05/7805-0727 © 2005 Pleiades Publishing, Inc.

concentration c_N^0, and time t_c of contact between the phases.

The powder of iron(III) oxide, used in the study, was composed of crystalline particles of three modifications, γ-Fe_2O_3, δ-Fe_2O_3, and α-Fe_2O_3; powdered nickel oxide was composed of particles of a single modification. To remove surface impurities, we repeatedly washed the metal oxides with distilled water to a constant electrical conductivity and pH value of washing water and dried in an oven at 105°C.

We studied the adsorption properties of the oxides, as regards the parameter Γ (henceforth, "adsorption properties" without specifying the characteristic parameter), on powders with a particle size of 0.5–10.0 μm, fractionated by sedimentation in water. The specific surface areas S_{sp} of this fraction, determined by BET, were ($m^2\ g^{-1}$) 3.3 for NiO and 2.8 for Fe_2O_3. To study the adsorption properties as regards the parameter ζ (henceforth "electrokinetic properties"), a powder fraction with a particle size of 0.5–10.0 μm was separated by sedimentation.

The concentrations of imidazole solutions were, before the solutions were brought in contact with the oxides, 1×10^{-3} and 1×10^{-4} M. We used solutions with various pH values: that corresponding to an imidazole solution of a given concentration without any additives during the entire experiment; pH 3; and, in the case of electrokinetic experiments, also pH 4. The initial pH of the aqueous imidazole solutions was 7.6 (solution no. 1). Solutions with pH 3 and 4 (solution nos. 2 and 3, respectively) were obtained by adding a certain amount of 1×10^{-1} M HCl, and these values were maintained constant during the entire experiment by adding an acid or an alkali. With solution no. 1, the pH values varied in the course of an experiment, but only slightly, by 0.3–0.4 pH units; they decreased during the first hour and then increased in the course of 120 h. In the latter case, they reached pH 8.0 when working with NiO, and 7.7, with Fe_2O_3.

All the solutions were prepared using distilled water with an electrical conductivity of $(1–2) \times 10^{-6}$; the 1×10^{-1} M HCl solution was prepared from a reference sample; all the chemicals used were of analytically pure grade. According to the speciation diagram calculated from K_a and K_{BN^+} [2, 3], at pH 7.6 about 30% of imidazole molecules carry a positive charge and about 70% are neutral; at pH 7.3 about 35–40% are in the cationic form; at pH 8.0 only 10% are charged positively and about 90% are neutral. In all the cases considered, only trace amounts of the anionic form are found.

The electrokinetic potential was determined by the microelectrophoretic method [11, 12]. The dispersion contained 0.5 g of a metal oxide and 200 ml of a solution. The electrophoretic mobility of dispersion particles was measured in a plane-parallel cell (cross-sectional area of the channel 17.8 mm^2). The ζ potential was calculated by the procedure corresponding to that repeatedly described in the literature [2, 3, 12].

To determine the adsorption of imidazole, weighed portions of NiO (Fe_2O_3) were poured over with 0.15 l of its solution ($c = 1 \times 10^{-3}$ M).[1] After 15, 30, and 45 min, and 1, 1.25, 1.5, 2, 3, and 24 h the solution was separated from the solid phase by filtration. The adsorption Γ was calculated from the difference of the imidazole concentrations (initial c_a^0 and that in a sample being measured, c_a) by the formula

$$\Gamma = \frac{(c_a^0 - c_a)V}{mS_{sp}},$$

where Γ is the adsorption (mol m^{-2}); c_a^0, concentration of the initial solution (M); c_a, running concentration of the solution in the course of adsorption (M); V, solution volume (l); m, mass of the adsorbent (g); and S_{sp}, specific surface area of NiO (Fe_2O_3) ($m^2\ g^{-1}$).

The concentration of imidazole in the solution bulk in adsorption on iron(III) oxide was determined spectrophotometrically with an SF-24 spectrophotometer at λ = 220 nm using 10-mm-thick quartz cells. Prior to measurements, the dispersion was exposed to a strong magnetic field to achieve a more complete separation of iron(III) oxide particles. In studying the adsorption on nickel oxide, the imidazole concentration was determined using the Kjeldahl method [13].

Let us first discuss the results obtained with solutions with $c_a^0 = 1 \times 10^{-3}$ M. Figures 1a and 1b show the $\zeta = f(t_c)$ dependences for Ni(II) and Fe(III) oxides at all of the above-mentioned pH values. For comparison, curves describing similar dependences for imidazole-free systems are presented. The corresponding solutions having the same pH values as solution nos. 1–3 (henceforth, solution nos. *1*'–*3*') are termed "background" solutions.

Here and hereinafter, the scale of the time variable (abscissa axis) in all the figures describing the kinetics of the processes under study as regards the ζ potential gives no way of plotting the potentials (ordinate axis) for $t_c < 0.25$ h. Therefore, two points are plotted on

[1] It is noteworthy that the relative amounts of the adsorbent and solution, as well as the above-mentioned particle sizes, are different in experiments in which Γ and ζ are measured.

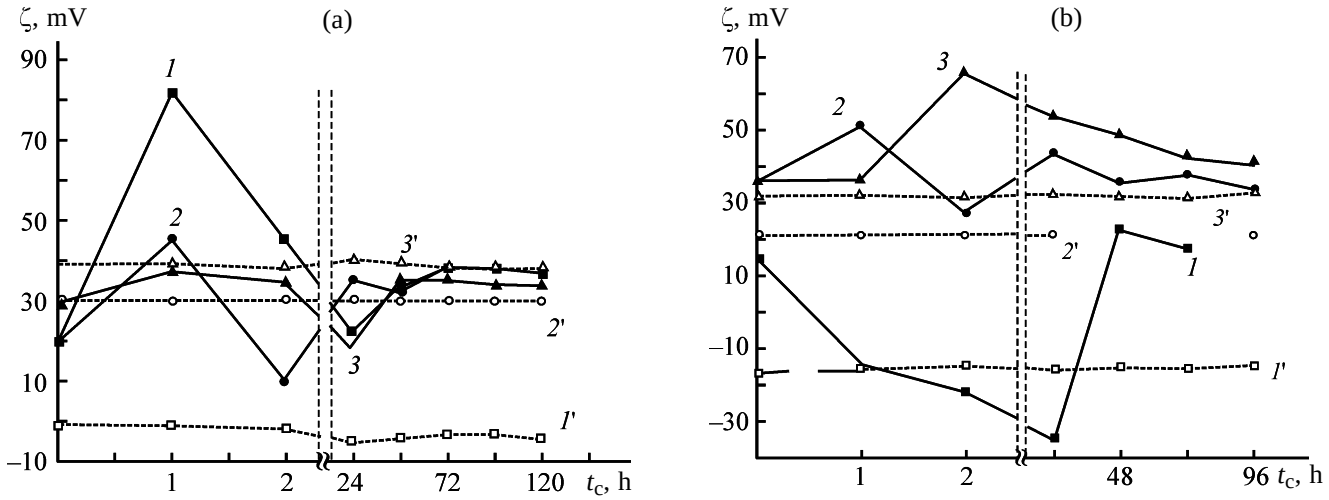


Fig. 1. The ζ potential of (a) NiO and (b) Fe_2O_3 particles vs. the time t_c of their contact with aqueous imidazole solutions with $c_a = 1 \times 10^{-3}$ M (solid lines) and with background solutions (HCl and KCl) (dashed lines) at different pH values. pH: (*1*, *1*') 7.6 (solution nos. *1*, *1*'), (*2*, *2*') 4 (solution nos. *2*, *2*'), and (*3*, *3*') 3 (solution nos. *3*, *3*').

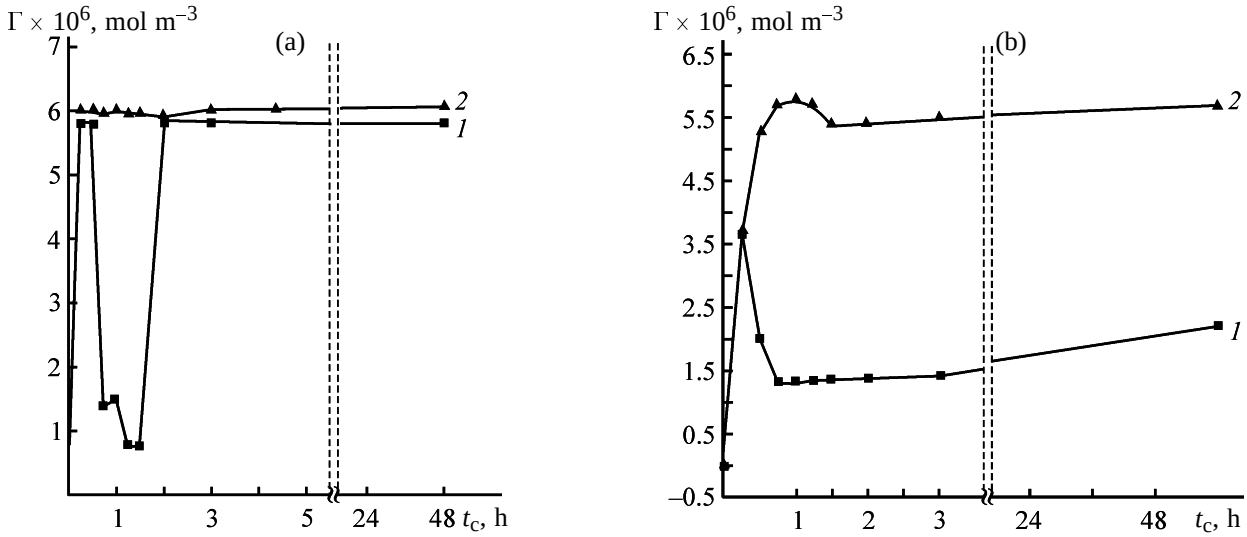


Fig. 2. Γ vs. time t_c of phase contact in systems constituted by aqueous imidazole solutions with $c_a = 1 \times 10^{-3}$ M and (a) NiO and (b) Fe_2O_3. pH: (*1*) 7.6 (solution no. 1) and (*2*) 3 (solution no. 3).

the ordinate axis at $t_c = 0$ in each run: that for a background solution and that with imidazole. The noncoincidence of these points suggests the occurrence of the adsorption governed by electrostatic forces.

It can be seen that the ζ potentials in simple electrolytes rapidly reach their steady-state values and further remain virtually unchanged in the course of time. In imidazole solutions, the ζ potential vs. time plots show extrema at all pH values. Qualitatively, the $\zeta = f(t_c)$ dependences are similar. In all cases, the potential substantially grows during the first hour of contact (in the system constituted by Fe_2O_3 and solution no. 1, already in the first few minutes) and then equally substantially decreases during several hours and after that either flattens out or slowly increases. However, the extrema are the more pronounced, the higher the pH, and at a given pH they are somewhat more pronounced in the case of NiO, compared to Fe_2O_3.

The experimental dependences of Γ on t_c are shown in Fig. 2a (NiO dispersion) and 2b (Fe_2O_3 dispersion). It can be seen that the $\Gamma = f(t_c)$ dependences obtained in solution no. 1 show a behavior differing from that of the corresponding $\zeta = f(t_c)$ dependences, which, however, also show pronounced maxima. In the case under consideration, Γ substantially grows

during a certain initial interval of time and then steeply decreases, after which it again starts to grow [relatively steeply in the case of nickel(II) oxide and rather gradually for iron(III) oxide], and the curve flattens out. It is noteworthy that the differences between the $\zeta = f(t_c)$ and $\Gamma = f(t_c)$ dependences at those t_c values for which the direction of the run of the corresponding curve shows the most pronounced changes can be, in principle, attributed to the above-mentioned difference of the grain-size distribution of the objects in electrokinetic and adsorption experiments. In the case of systems with low pH (pH 3), the run of the curves is rather smooth, with Γ substantially changing only in the first several minutes.

Let us now discuss the experimental results concerning the $\zeta = f(t_c)$ dependence. We are primarily interested in the noncoincidence of points on the ordinate axis that correspond to systems with imidazole ("zero points") and without it (background curves) at the same pH value. The increase in the positive potential upon appearance of imidazole in the system indicates that the imidazolium cation is adsorbed. Figure 1b shows that, in the case of a system constituted by Fe_2O_3 and imidazole solution no. 1, the sign of the ζ potential changes from negative to positive. This fact can be qualitatively understood as resulting from adsorption of the imidazolium cation onto the originally negatively charged surface of the adsorbent under the action of Coulomb forces; this process comes to saturation very rapidly (within fractions of second or several seconds). However, the noncoincidence of zero points in all other cases cannot be attributed to a simple electrostatic interaction. The adsorption of the cation on a positive (or neutral) surface indicates that specific adsorption forces are important already in the first minutes of contact.

The more or less prolonged rise in the ζ potential, observed during the first hours of the phase contact (Figs. 1a, 1b; 1 h for systems with NiO and 1–2 h in the case of Fe_2O_3), indicates that the specific adsorption of imidazolium cations continues. We believe that the absence of a portion of this kind in curve *1* in Fig. 1b is due to the active involvement of Coulomb forces (the only case of an originally negatively charged surface of the oxide), and the corresponding rise in the positive potential occurs in full measure within a few minutes.

We call attention to two facts characteristic of the interval of time from zero to 1 h when working with a NiO dispersion. The first is that the $\Delta\zeta$ corresponding to this time of the experiment is rather large in the case of solution no. 1. The second is that $\Delta\zeta$ decreases as the pH value becomes lower, but remains significant in more acidic solutions. A substantial rise in the ζ potential in solution no. 1 has been observed previously [3]. In our opinion, the increase in positive values of the ζ potentials in the initial period of time is due to adsorption of the already mentioned long chains formed in solution from protonated forms of imidazole molecules. These chains can be adsorbed on the oxide surface via formation of donor–acceptor bonds between a metal ion in the oxide and a molecular unit at the end of a chain. The appearance of such "polycations" in the surface layer introduces into it a large positive charge fixed on the oxide surface.

In addition to the specific adsorption of positively charged chains, the anionic form of imidazole can also be adsorbed. The adsorption of the anionic form must, in principle, lead to an increase in magnitude of the negative ζ potential; however, the contribution of this form is negligible under the experimental conditions. In addition to charged forms, the neutral form can also be adsorbed, which somewhat increases the magnitude of the ζ potential because of the steric effect on the distribution of counterions in the electrical double layer [14]. However, their role is incomparable with that of positive chains. A positive chain formed by protonated forms of imidazole molecules can have one its end attached to the oxide surface and the other (tail) directed into the solution, or both of its ends attached to the surface, with its shape resembling in this case a loop or a bridge. It should be added that a large number of counterions (inorganic anions in the given case) are situated between the tails and within the loops formed by the positive chains, and these counterions contribute to the electrokinetic flow.

The calculated values of the ζ potential are a consequence of the overall effect of all the forms.

The fact that $\Delta\zeta$ becomes lower with increasing solution acidity apparently reflects a decrease in aggregation between imidazole molecules at a higher concentration of H^+ ions. The aggregation of imidazole occurs via formation of hydrogen bonds between nitrogen atoms in one imidazole molecule and hydrogen atoms in the other. In the presence of a large number of hydrogen cations in solution, there occurs competition between free hydrogen cations and hydrogen atoms in a diazole molecule.

The results obtained for the interval of time from 0 to 2 h when working with iron(III) oxide dispersions can, on the whole, be explained from the same standpoint, although the influence of pH is manifested in an increase in the time interval after the maximum is observed, rather than in its magnitude.

We now pass to that portion of the curve in which the ζ potential falls. As before, we primarily choose for more clarity systems with solution no. 1. We attribute the behavior in this case to prevalence of the effect of chain disintegration over adsorption of long aggregates. This process is due to the relay-race mechanism of rupture of hydrogen bonds, i.e., formation of strong donor–acceptor bonds at chain ends leads to subsequent disintegration of the whole chain. As a result, a large number of imidazolium cations not bound with the surface can be found in its vicinity. This means that the equivalent amount of counterions previously contributing to the electrokinetic flow cease to be electrokinetically active [14]. As a result, the ζ potential decreases.

The rather fast, with account of the occurrence of the components in the bulk of the aqueous phase, rise in the ζ potential in the first period of interaction between the active centers of the surface and the solution components and its decrease in the second period are in full qualitative agreement with the experimental results obtained in determining the adsorbed amount, which reflect the fast increase in Γ in the first 15–20 min and an equally rapid decrease in Γ in the subsequent 30 min. The fact that the duration of these periods of fast growth and decrease in the amount of adsorbed diazole does not coincide with that estimated from the ζ potential is in all probability due to the above-emphasized difference in the relative amounts of phases in the dispersions used in ζ and Γ measurements.

It should be noted that the result of the interaction between the metal ions of a surface center and imidazole in the stages of rise and decrease of ζ and Γ is determined by the dynamic nature of attainment of their final values and the prevalent state of imidazole in solution.[2]

The abscissas of the minimum values indicate that, by the given time, the processes of chain adsorption and disintegration are complete and all the possible (in accordance with the Langmuir theory) active centers of the surface are bound with separate imidazole molecules or small associates only.

[2] The chains, being adsorbed, disintegrate; separate molecules from the surface layer find their way into solution bulk to form there new chains, which come to free surface centers to be again disintegrated, etc. The stage of rise in ζ and Γ means that, during this period, there still is a large number of long chains in solution, whereas the stage of a decreasing height of the peak in the ζ–t_c curve and a dip in the Γ–t_c curve corresponds to disintegration of long chains, whose number becomes small by that time.

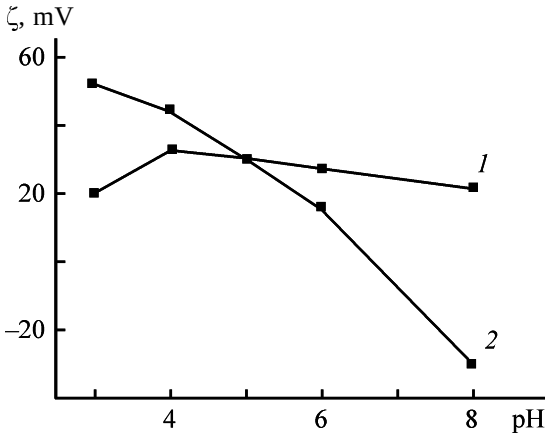


Fig. 3. The ζ potential of (*1*) NiO and (*2*) Fe_2O_3 particles vs. pH of aqueous imidazole solutions with $c_a = 1 \times 10^{-3}$ M.

The last stage of rise in the ζ potential in the absence of changes in Γ apparently indicates that there occur surface chemical reactions with the already formed surface compound [15]. In this context, it should be noted that, in the case of Fe(III) oxide, the pH values of solution no. 1 correspond to the region of strong hydrolysis, whereas in the case of Ni(II), the hydrolysis is considerably weaker [16].

To conclude, we note that the increments in the absolute values of the parameters in the stage of their rise and decrease are less pronounced in the case of Fe_2O_3, compared to NiO. These facts are in agreement with the repeatedly published concept that the energy of interaction between the ligand and Fe(III) is lower than that with Ni(II) [17]. The above concept suggesting the key role of specific interaction between nickel(II) or iron(III) ions of an active surface center and imidazole molecules is confirmed by the shift of pH_{IEP} values in imidazole solutions, compared to those in solutions containing no organic ligands (with HCl or KOH). According to the data obtained (Fig. 3), the pH_{IEP} value in systems with imidazole is shifted, for both NiO and Fe_2O_3, into the alkaline region, compared to systems with HCl, suggesting specific adsorption of the imidazolium cation. The shift in the system with Ni(II) oxide is so strong that pH_{IEP} lies far in the alkaline region (ΔpH_{IEP} markedly exceeds 2–3 pH units). In the system with Fe(III) oxide, the shift is considerably smaller (ΔpH_{IEP} = 0.5–0.6 units). The strong shift of pH_{IEP} in the case of Ni(II) oxide and the weak shift for Fe(III) oxide suggest that imidazole is a ligand with a rather low electrostatic component of the ligand field.

The main specific features of the dependences described, $\zeta = f(t_c)$ and $\Gamma = f(t_c)$, and their influence

on pH were qualitatively manifested also at a lower imidazole concentration of 1×10^{-4} M. As for the quantitative aspect, changes in the parameters were markedly smaller in this case. Such an influence of the imidazole concentration on $\Delta\zeta$ and $\Delta\Gamma$ is apparent and requires no special discussion.

CONCLUSIONS

(1) It was found that, in NiO and Fe_2O_3 dispersions in aqueous solutions of 1,3-diazole, the dependences of the electrokinetic potential and amount of adsorbed substance on the time of contact between the phases pass through a clearly pronounced maximum and a minimum following immediately after, and then show a prolonged ascent and flatten out.

(2) The height of the corresponding peak and depth of the dip in the curves depend on pH (higher and deeper, respectively, at pH 6.7–7.6, and less so at lower pH), initial imidazole concentration (stronger effect at higher concentrations), and kind of a metal oxide (considerably better pronounced in a dispersion with NiO, compared to Fe_2O_3).

(3) In the dispersions under study, pH_{IEP} is shifted, for both NiO and Fe_2O_3, into the alkaline region, compared to the pH_{IEP} of these oxides in HCl and NaOH solutions. The shift of pH_{IEP} exceeds 3 pH units for NiO, but is considerably smaller in the case of Fe_2O_3 (0.5–0.6 pH units).

ACKNOWLEDGMENTS

The study was supported by the grant of the President of the Russian Federation for Support of Leading Scientific Schools (no. NSh-789.2003.3) and by the Russian Foundation for Basic Research (project no. 03-03-32418).

REFERENCES

1. Tikhomolova, K.P., Dmitrieva, I.B., and Ivanova, M.V., Abstracts of Papers, *1-ya Mezhdunarodnaya konferentsiya "Khimiya vysokoorganizovannykh veshchestv i nauchnye osnovy nanotekhnologii"* (1st Int. Conf. "Chemistry of Highly Organized Substances and Scientific Foundations of Nanotechnology"), Sankt-Peterb. Gos. Univ., 1996, part 2, pp. 318–321.
2. Dmitrieva, I.B., Tikhomolova, K.P., Ivanova, M.V., and Antonova, I.G., *Kolloidn. Zh.*, 1997, vol. 59, no. 6, pp. 747–750.
3. Tikhomolova, K.P., Dmitrieva, I.B., and Ivanova, M.V., *Zh. Prikl. Khim.*, 1998, vol. 71, no. 4, pp. 536–543.
4. Tikhomolova, K.P., Dmitrieva, I.B., Ivanova, M.V., and Koldobskii, G.I., *Zh. Prikl. Khim.*, 2000, vol. 73, no. 3, pp. 391–396.
5. Tikhomolova, K.P., Dmitrieva, I.B., Ivanova, M.V., and Koldobskii, G.I., *Zh. Prikl. Khim.*, 2000, vol. 73, no. 7, pp. 1094–1098.
6. Mashkovskii, M.D., *Lekarstvennye sredstva* (Medicinals), Moscow: Medgiz, 1958.
7. Berezin, T.T., *Biologicheskaya khimiya* (Biochemistry), Moscow: Univ. Druzhby Narodov, 1970.
8. Granik, V.G., *Osnovy meditsinskoi khimii* (Fundamentals of Medical Chemistry), Moscow: Vuzovskaya kniga, 2001.
9. Paquette, L.A., *Principles of Modern Heterocyclic Chemistry*, New York: Benjamin, 1968.
10. Tikhomolova, K.P. and Urakova, I.N., *Zh. Prikl. Khim.*, 2002, vol. 75, no. 6, pp. 913–919.
11. Grigorov, O.N., Karpova, I.B., Koz'mina, Z.P., *et al.*, *Rukovodstvo k prakticheskim rabotam po kolloidnoi khimii* (Manual of Colloid Chemistry), Leningrad: Khimiya, 1964.
12. Grigorov, O.N., *Elektrokineticheskie yavleniya* (Electrokinetic Phenomena), Leningrad: Leningr. Gos. Univ., 1973.
13. *Gosudarstvennaya farmakopeya SSSR: Obshchie metody analiza* (State Pharmacopoeia of the USSR: General Methods of Analysis), Babayan, E.A., Mashkovskii, M.D., and Oboimakov, A.N., Eds., Moscow: Meditsina, 1987, 11th ed., issue 1, pp. 180–183.
14. Tikhomolova, K.P., *Elektroosmos* (Electroosmosis), Leningrad: Khimiya, 1989.
15. Tikhomolova, K.P. and Demin, S.A., *Fiz.-Khim. Mekh. Liofil'n. Dispersn. Sist.*, 1991, no. 22, pp. 77–86.
16. Baes, C.F. and Mesmer, R.E., *The Hydrolysis of Cations*, New York: Wiley–Interscience, 1976.
17. Suvorov, A.V. and Nikol'skii, A.B., *Obshchaya khimiya* (General Chemistry), St. Petersburg: Khimiya, 1994.

Russian Journal of Applied Chemistry, Vol. 78, No. 5, 2005, pp. 733–736. Translated from Zhurnal Prikladnoi Khimii, Vol. 78, No. 5, 2005, pp. 747–750.
Original Russian Text Copyright © 2005 by Malov.

SORPTION AND ION-EXCHANGE PROCESSES

Adsorption of Aliphatic Acids from Aqueous Solutions at the Interface with the Gas Phase

V. A. Malov

St. Petersburg State Technological Institute, St. Petersburg, Russia

Received October 15, 2004; in final form, March 2005

Abstract—The type of the dependence of the Gibbs relative adsorption on the concentration of an ideal solution of a surfactant was studied. The applicability of the hypothesis of monomolecular adsorption at the interface between an aqueous solution of aliphatic acids and the gas phase was assessed.

An important role in studying the adsorption from solutions at the interface with the gas phase is played by the dependence of the surface tension σ on the solution concentration x. Among a number of $\sigma = f(x)$ equations that have been suggested (for reviews, see [1, 2]), the best known and the most frequently cited is the equation empirically obtained by Shishkovskii [3]:

$$\Delta\sigma = B\ln(1 + xA), \quad (1)$$

where $\Delta\sigma = \sigma_0 - \sigma$; σ_0 and σ, surface tensions of the solvent and solution, respectively; and A and B, constants.

Equation (1) was theoretically substantiated in [4, 5] as the $\sigma = f(x)$ dependence for an ideal solution.

The interest in Eq. (1) is largely due to the fact that its application in the Gibbs adsorption equation yields the equation of the Langmuir isotherm for monomolecular adsorption. Therefore, the adequacy of Eq. (1) to experimental data gives reason to believe that the adsorption is monomolecular and to identify the Gibbs surface excess with the surface concentration. The applicability of Eq. (1) is most frequently judged from the presence of a linear portion in the surface tension isotherm plotted on the semilog scale. In this portion, the specific adsorption and the solution concentration in the surface layer reach their limiting values.

In a number of studies [6, 7], the experimental $\sigma = f(x)$ dependence was processed graphically or by numerical differentiation without using Eq. (1) and adsorption isotherms with a peak, untypical of monomolecular adsorption, were obtained. Adsorption isotherms with such a specific feature can be obtained from an approximate form of Eq. (1), which was not analyzed in [4].

Equation (1) can be written as

$$\Delta\sigma = -B\ln[1 - Ax/(1 + Ax)] = -B\ln(1 - \theta). \quad (2)$$

If the quantity $Ax/(1 + Ax) = \theta$, which characterizes the filling of the surface with the adsorbate in the case of monomolecular adsorption, is considerably less than unity ($\theta \ll 1$), then it is possible to keep in the power series expansion of the logarithmic function only the first term and to take that

$$\Delta\sigma = BAx/(1 + Ax). \quad (3)$$

Published data show that an equation of a fractionally linear function (3) was semiempirically obtained and experimentally verified in four studies [8–11]. In these cases, the $\sigma = f(x)$ dependences were represented in a form different from that of Eq. (3), but can be readily reduced to it. It was shown in [12] that introduction into Eq. (2) of an additional term $a\theta^2$, which accounts for the attractive interaction of adsorbed molecules, improves the agreement between the experimental and calculated data. Noteworthy is the fact that, upon this transformation of Eq. (1), the $\sigma = f(x)$ dependence becomes closer to the fractionally linear function (3).

In [9], Eq. (3) was derived on the assumption that the surface tension of a solution linearly depends on the solute concentration y in the surface layer:

$$\sigma = \sigma_0(1 - y) + \sigma_1 y, \quad (4)$$

where σ_0 and σ_1 are the surface tensions of the solv-

1070-4272/05/7805-0733© 2005 Pleiades Publishing, Inc.

Table 1. Constants *A* and *B* and correction for nonideality of aqueous solutions of organic acids

Acid	$d\ln\gamma/dx$	*A*	*B*
Acetic	–1.7	33.94 ± 0.7	0.03354 ± 0.002
Propionic	–5.0	104.90 ± 10.5	0.04033 ± 0.0056
Butyric	–8.2	290.77 ± 5.9	0.04291 ± 0.0012
Valeric	–11.4	1095.2 ± 10.8	0.04125 ± 0.0024
Caproic	–14.6	2459.8 ± 13.0	0.05205 ± 0.0021

ent and solute, respectively; *y* is the mole fraction of the solute in the surface layer.

To Eq. (3) leads substitution into formula (4) of the following known equation relating the solution compositions in the surface layer and in the bulk [4, 9]:

$$y = \frac{kx}{1 + (k - 1)x}, \quad (5)$$

where *y* and *x* are the mole fractions of the solute in the surface layer and in the solution bulk, respectively; $k = A + 1$ is the constant of equilibrium between the surface layer and the bulk of the solution.

The adsorption isotherm equation derived from the Gibbs adsorption equation and Eq. (3) has the form

$$\Gamma = \frac{B}{RT}\frac{Ax}{(1 + Ax)^2}. \quad (6)$$

Analysis of Eq. (6) for an extremum shows that, graphically, this adsorption isotherm is a curve with a peak of height $\Gamma_{max} = [B/(4RT)]$, lying at $x_0 = 1/A$. As follows from Eq. (5), the mole fraction of the solute in the surface layer is given by $y = (A + 1)/(2A)$ at $x = 1/A$ and equals 0.5 at $A \gg 1$. In the case of monomolecular adsorption, the mole fraction $y = 0.5$ corresponds to half-filling of the surface layer if the area occupied by a solute molecule is equal to the molecular area of the solvent. Therefore, the capacity of a saturated monolayer must be $\Gamma_\infty = 2\Gamma_{max} = B/(2RT)$ for a solution of this kind.

As known, the shape of an adsorption isotherm depends on various types of intermolecular interactions responsible for nonideality of solutions. The influence exerted by the nonideality of solutions on the adsorption can be analyzed using the Gibbs equation written as

$$\Gamma = -\frac{x}{RT}\frac{d\sigma}{dx}\left(1 + x\frac{d\ln\gamma}{dx}\right)^{-1}, \quad (7)$$

where Γ is the relative adsorption, and γ is the activity coefficient of the solute.

In [6], adsorption isotherms with a peak were obtained in a study of adsorption from aqueous solutions of aliphatic acids. In these systems, the influence exerted by nonideality of solutions was weak, which can be judged from the $\ln\gamma/dx$ values taken from this paper (Table 1). Therefore, it was of interest to compare the results obtained in processing of the experimental dependence $\sigma = f(x)$ by Eq. (3) with the results of [6].

A verification of the applicability of Eq. (3) demonstrated that the experimental dependences $\sigma = f(x)$ plotted in the coordinates of the linear form of Eq. (3), i.e., $x/\Delta\sigma = f(x)$, are straight lines with a satisfactory accuracy. The intercepts and slopes of these straight lines were used to calculate constants *A* and *B* listed in Table 1. It can be seen from Table 1 that constant *A*, which characterizes the slope of the adsorption isotherm at low concentrations, increases by, on average, a factor of 3 on passing from one homolog to another (in accordance with the Traube rule). As follows from Eq. (6), at $x > x_0$ the adsorption decreases as constant *A* becomes larger. Such a behavior was experimentally revealed in [7] in a study of adsorption of alcohols from aqueous solutions.

To illustrate the capabilities of Eq. (3), Table 2 lists the experimental [6] and calculated (from constants *A* and *B*) values of the surface tension of aqueous solutions of aliphatic acids. The specific adsorption Γ_c, calculated by Eq. (6) with a correction for the nonideality of the solutions, is given in Table 3.

As seen from Tables 3 and 4, the agreement between the results of [6] and data calculated by Eq. (6) is satisfactory at $x \le x_0$, i.e., in that concentration range in which the accuracy of numerical differentiation, used in [6] to calculate the specific adsorption Γ, is sufficiently high.

An assumption was made in [6, 13, 14] that the adsorption of butyric, valeric, and caproic acids cannot be understood in terms of the concept of monomolecular adsorption. As a criterion for monomolecular nature of the adsorption layer can serve the area S_0 occupied by a molecule in a saturated monolayer with molecules oriented perpendicularly to the surface:

$$S_0 = 1/(\Gamma_\infty N_A). \quad (8)$$

S_0 can also be calculated using the formula relating the relative adsorption Γ and the mole fraction *y* of the adsorbate in the surface layer. It was shown in [15]

Table 2. Experimental [6] and calculated [by Eq. (3)] values of the surface tension σ of aqueous solutions of aliphatic acids

Acid	x	σ, N m^{-1}	σ_c, N m^{-1}	Δ, %
Acetic	0	0.07196		
	0.0039	0.0679	0.06804	–0.206
	0.0069	0.0659	0.06560	0.460
	0.0147	0.0606	0.06080	–0.326
	0.0321	0.0545	0.05447	0.0489
	0.0748	0.0479	0.04790	0.00117
Propionic	0.0004	0.0695	0.07034	–1.203
	0.0011	0.0677	0.06779	–0.130
	0.0043	0.0591	0.05942	–0.548
	0.0107	0.0515	0.05063	1.684
	0.0257	0.0423	0.04254	–0.576
Valeric	0.00008	0.0674	0.06864	–1.836
	0.00016	0.0648	0.06581	–1.559
	0.00024	0.0625	0.06338	–1.400
	0.0004	0.0592	0.05940	–0.3296
	0.0006	0.0556	0.055604	–0.0071
	0.0008	0.0528	0.05270	0.1932
	0.001	0.0506	0.05040	0.3959
	0.0012	0.0486	0.04854	0.1309
	0.0016	0.0457	0.04570	0.0010
	0.002	0.0435	0.04364	–0.3259
	0.0024	0.0421	0.04208	0.04543
Butyric	0.0005	0.0661	0.06651	–0.626
	0.001	0.0624	0.06229	0.169
	0.002	0.0565	0.05618	0.561
	0.003	0.052	0.05197	0.0583
	0.004	0.0493	0.04889	0.833
	0.005	0.0468	0.04654	0.558
	0.006	0.0446	0.04469	–0.193
	0.007	0.0433	0.04319	0.257
	0.008	0.042	0.04195	0.112
	0.009	0.0408	0.04092	–0.284
	0.01	0.0398	0.04003	–0.586
Caproic	0.00005	0.0662	0.06626	–0.0893
	0.00008	0.0636	0.06340	0.313
	0.00016	0.0565	0.05726	–1.344
	0.00024	0.0528	0.05263	0.308
	0.00031	0.0494	0.049440	–0.08033
	0.00039	0.0468	0.04647	0.698
	0.00047	0.0445	0.04405	1.014
	0.00054	0.0424	0.04226	0.322
	0.00062	0.0408	0.04052	0.684
	0.00069	0.0389	0.03921	–0.784
	0.00078	0.0374	0.03774	–0.912

Table 3. Specific adsorption of aliphatic acids, Γ, reported in [6] and calculated by Eq. (6) with account of a correction for the nonideality of solutions

x	$\Gamma \times 10^6$	$\Gamma_c \times 10^6$	x	$\Gamma \times 10^6$	$\Gamma_c \times 10^6$
	mol m^{-2}			mol m^{-2}	
Acetic acid, $1/A$ = 0.02947					
0.001	0.37	0.4305	0.030	3.18	3.5659
0.002	0.71	0.8085	0.050	3.52	3.4518
0.004	1.39	1.4343	0.075	3.64	3.1420
0.007	2.37	2.1250	0.10	3.79	2.8673
0.010	2.79	2.6052	0.15	4.87	2.4936
0.015	3.04	3.1052	0.20	5.13	2.2957
0.020	3.38	3.3751			
Butyric acid, $1/A$ = 0.003439					
0.00005	0.31	0.2447	0.004	4.5	4.4509
0.00010	0.54	0.4759	0.005	4.41	4.3602
0.00015	0.7	0.6944	0.006	4.32	4.2184
0.00050	1.8	1.9271	0.007	4.19	4.0588
0.001	2.8	3.0474	0.008	4.0	3.8970
0.002	4.1	4.0936	0.009	3.91	3.7404
0.003	4.59	4.4181			
Caproic acid, $1/A$ = 0.0004065					
0.000004	0.26	0.2027	0.00032	5.05	5.2023
0.000016	0.83	0.7656	0.00040	5.43	5.2830
0.000030	1.33	1.3452	0.00046	5.6	5.2679
0.000046	1.85	1,1998	0.00054	5.76	5.1890
0.000100	3.48	3.3338	0.00062	5.67	5.0713
0.000164	3.81	4.3136	0.00070	4.99	4.9335
0.00024	4.46	4.9213			
Propionic acid, $1/A$ = 0.009533					
0.00016	0.28	0.2645	0.0072	3.61	4.1392
0.00032	0.54	0.5123	0.0096	3.86	4.2744
0.00048	0.77	0.7447	0.016	4.84	4.1394
0.00064	0.97	0.9627	0.020	5.01	3.9535
0.00096	1.4	1.3595	0.024	4.84	3.7635
0.0020	2.4	2.3568	0.030	5.12	3.5042
0.0040	3.29	3.4583			
Valeric acid, $1/A$ = 0.0009131					
0.000012	0.32	0.2132	0.000600	4.05	4.0113
0.000036	0.77	0.6078	0.000798	4.4	4.1812
0.000078	1.39	1.2082	0.000996	4.33	4.2019
0.000162	1.8	2.1346	0.001200	4.15	4.1419
0.000240	2.3	2.7514	0.001596	2.88	3.9251
0.000402	3.18	3.5500	0.001998	2.9	3.6674

Table 4. Areas S_0 calculated by formulas (8) and (9)

Acid	y	x	$\Gamma_{max} \times 10^6$, mol m^{-2}	$S_0 \times 10^{20}$, m^2	
				(8)	(9)
Acetic	0.5147	0.0321	3.570	24.5	23.2
Propionic	0.5048	0.0107	4.285	20.4	19.4
Butyric	0.5017	0.0035	4.457	19.2	18.6
Valeric	0.5004	0.0009	4.201	19.9	19.7
Caproic	0.5002	0.0004	5.280	15.8	15.7

that, if the molar surface areas of the solvent and solute are equal, the following expression is valid for the ideal solution:

$$y = S_0 N_A \Gamma + (1 - S_0 N_A \Gamma)x, \quad (9)$$

where N_A is the Avogadro number.

The results of calculation of S_0 by formulas (8) and (9) at x and y corresponding to the maximum adsorption Γ_{max}, listed in Table 4, give reason to assume that the adsorption of aliphatic acids, with the exception of caproic acid, has a monomolecular nature because, according to [16], $S_0 = 20.5 \times 10^{-20}$ m^2 for aliphatic acids.

CONCLUSIONS

(1) An isotherm equation for the relative adsorption at the liquid–gas interface for ideal solutions was derived. A distinctive feature of this equation is that it gives an adsorption isotherm with a peak. It was shown that the suggested adsorption isotherm satisfactorily describes, with account taken of the nonideality of solutions, the adsorption of aliphatic acids from aqueous solutions.

(2) The areas occupied by molecules of a number of aliphatic acids in the surface layer were calculated. For all the acids, except caproic acid, the molecular areas suggest monomolecular adsorption.

REFERENCES

1. Semenchenko, V.K., *Poverkhnostnye yavleniya v metallakh i splavakh* (Surface Phenomena in Metals and Alloys), Moscow: Gos. Izd. Tekhniko-Teoreticheskoi Literatury, 1957.
2. Adamson, A.W., *Physical Chemistry of Surfaces*, New York: Wiley, 1976.
3. Shishkovskii, B., *Z. Phys. Chem.*, 1908, vol. 64, pp. 385–410.
4. Zhukhovitskii, A.A., *Zh. Fiz. Khim.*, 1944, vol. 18, no. 2, pp. 214–221.
5. Guggenheim, E.A., *Trans. Faraday Soc.*, 1945, vol. 41, p. 150.
6. Litvinov, V.F., Levichev, S.A., and Rusanov, A.I., *Kolloidn. Zh.*, 1974, vol. 36, no. 5, pp. 872–878.
7. Butler, J.A.V., Wightman, A., and Maclennan, W.H., *J. Chem. Soc.*, 1934, no. 2, pp. 528–532.
8. Reshetnikov, M.A., *Izv. Sekt. Fiz.-Khim. Anal.*, 1949, vol. 19, p. 165.
9. Eberhart, J.G., *J. Phys. Chem.*, 1966., vol. 70, no. 4, pp. 1183–1186.
10. Stachorsky, K.M., *Z. Elektrochem.*, 1928, vol. 34, pp. 111–112.
11. Pavlov, P.N., *Tr. Odess. Gos. Univ.*, 1949, vol. 5(58), p. 5.
12. Frumkin, A.N., *Z. Phys. Chem.*, 1925, vol. 116, p. 466.
13. Ying Fu and Bartell, F.E., *J. Phys. Chem.*, 1950, vol. 54, pp. 537–546.
14. Ekserova, D., Sheludko, A., and Zakharieva, M., *God. Sofiisk. Univ.*, 1966/1967, vol. 61, p. 383.
15. Rusanov, A.I., *Fazovye ravnovesiya i poverkhnostnye yavleniya* (Phase Equilibria and Surface Phenomena), Leningrad: Khimiya, 1967.
16. Zhukov, I.I., *Kolloidnaya khimiya* (Colloid Chemistry), Leningrad: Leningr. Gos. Univ., 1949.

Russian Journal of Applied Chemistry, Vol. 78, No. 5, 2005, pp. 737–740. Translated from Zhurnal Prikladnoi Khimii, Vol. 78, No. 5, 2005, pp. 751–754.
Original Russian Text Copyright © 2005 by Kolosnitsyn, Minnikhanova, Karaseva, Dmitriev, Muratov.

APPLIED ELECTROCHEMISTRY AND CORROSION PROTECTION OF METALS

Effect of Ca^{2+}, Mg^{2+}, Fe^{3+}, and Al^{3+} Ions on the Deposition of Electrolytic Manganese Dioxide from Chloride Solutions

V. S. Kolosnitsyn, E. A. Minnikhanova, E. V. Karaseva, Yu. K. Dmitriev, and M. M. Muratov

Institute of Organic Chemistry, Ufa Scientific Center, Russian Academy of Sciences, Ufa, Bashkortostan, Russia
Kaustik Private Company, Sterlitamak, Bashkortostan, Russia

Received September 1, 2004; in final form, February 2005

Abstract—The effect of Ca^{2+}, Mg^{2+}, Fe^{3+}, and Al^{3+} ions on the deposition of electrolytic manganese dioxide from chloride solutions was studied.

In the world practice, the raw materials for production of electrolytic manganese dioxide (EMD) and electrolytic manganese metal (EMM) are rich manganese ores, which are virtually lacking in Russia. Therefore, it is of specific interest to use lean manganese ores, e.g., manganese limestones, for the production of manganese compounds. The largest deposit of manganese limestone ores is the Ulu-Telyak deposit (Bashkortostan). Manganese limestones have the following average chemical composition (wt %): Mn 9–15, SiO_2 5–10, Al_2O_3 3–5, Fe 1.2–1.5, CaO 30–40, S 0.04–0.06, P 0.02–0.04, MgO 3–5, and H_2O 1.0–1.5.

In hydrometallurgical reprocessing of lean manganese ores, as leaching agents are used mineral acids, H_2SO_4, HCl, and HNO_3. The choice of the acid is mainly determined by its cost and accessibility rather than by leaching power. For example, a large volume of a 20–25% hydrochloric acid is formed at chlorine production plants as waste, which can be utilized for ore leaching.

It should also be noted that leaching of manganese ores with hydrochloric acid has a number of advantages. For example, in leaching of manganese from limestone ores with hydrochloric acid, in contrast to sulfuric acid leaching, no sparingly soluble compounds adversely affecting the process equipment are formed. Moreover, in reprocessing of ores containing manganese in higher oxidation states, chlorine can be obtained, which is a valuable chemical raw material.

At the same time, in hydroelectrometallurgical reprocessing of manganese ores, there is also a number of problems, first of all, the problem of purification of leaching solutions to remove undesirable impurities. As a rule, the processing solutions of hydrochloric acid leaching contain, apart from $MnCl_2$, also $CaCl_2$, $MgCl_2$, $FeCl_3$, and $AlCl_3$ as main impurities. Prior to use for the electrolysis, they should be treated to remove the impurities that adversely affect the electrolysis and the composition and properties of the products. A common treatment method is the hydrolytic purification [1], which allows the content of readily hydrolyzable compounds, Fe^{3+} and Al^{3+} chlorides, to be decreased to the acceptable value. However, presumably, these compounds would not adversely affect the electrodeposition of MnO_2 and its properties.

Therefore, it was of practical significance to study the effect exerted by calcium, magnesium, aluminum, and iron ions on the composition of electrolytic manganese dioxide and the electrolysis parameters.

EXPERIMENTAL

The electrolysis was performed in an electrolyzer with parallel-plate Plexiglas electrodes. A VT-1-00 titanium was anode and NKh18N10T stainless steel, a cathode. The electrodes were polarized with a stabilized B5-47 current source. The electrode potentials were measured relative to a silver chloride reference electrode.

The change in the acidity of the electrolyte solutions before and after the electrolysis was determined with a portable microprocessor HI-9025 pH/mV/°C meter (Portugal).

The experiments were performed at 75°C and a current density of 5 mA cm^{-2}.

1070-4272/05/7805-0737 © 2005 Pleiades Publishing, Inc.

Current efficiency and degree of recovery of manganese(IV) oxide at various electrolyte compositions (current density 5 mA cm^{-2}, temperature 75°C, $MnCl_2$ 1 M, and HCl 0.05 M)

Impurity, M	pH		CE, %	Degree of Mn electrodeposition, %	U, V	E_a, V	Apparent density of MnO_2, g cm^{-3}
	before electrolysis	after electrolysis					
$CaCl_2$:							
0.05	0.65	0.30	92	15.5	2.58	1.62	1.55
0.25	0.45	0.27	93	16.5	2.83	1.88	1.43
1.0	0.08	0.04	89	14.2	3.23	2.14	1.58
$MgCl_2$:							
0.05	0.68	0.53	92	15.8	2.40	1.47	1.62
0.25	0.58	0.37	95	17.0	2.45	1.57	1.49
1.0	0.31	0.12	90	15.3	2.85	1.69	1.55
$AlCl_3$:							
0.05	0.52	0.33	80	13.0	2.34	1.48	1.55
0.25	0.42	0.22	75	11.0	2.43	1.52	1.56
1.0	0.10	0.08	Solution after electrolysis is turbid. Breakdown of anode surface. Voltage across the electrolyzer increased from 2.43 to 6 V				
$FeCl_3$:							
0.05	0.35	0.13	64	8.0	2.82	1.84	1.33
0.25	0.08	0.02	Solution after electrolysis is turbid. Breakdown of anode surface. Voltage across the electrolyzer increased from 2.43 to 6 V.				

The time of all the experiments was 60 min. Under the given conditions, the current efficiency was 95–97% and the degree of manganese electrodeposition, 18–20%. To retain the relatively constant composition of the components in the electrolytes, the process was not performed to greater extents of manganese electrodeposition. The electrolytes were prepared from chemically pure and analytically pure grade chemicals.

The product obtained was analyzed for the content of MnO_2 and of calcium, magnesium, iron, and aluminum impurity ions. The manganese content was determined by Volhard's method [2]. The microimpurities of calcium, magnesium, aluminum, and iron ions were determined by emission spectroscopy on an ISP-30 spectrometer. The apparent density was determined by the volumetric-gravimetric method [3].

In Ca^{2+}-containing electrolytes, the current efficiency (CE) is 75–93%, and it decreases with growing Ca^{2+} concentration (see table). As the concentration of the calcium ions in the electrolyte increases, the voltage across the electrolyzer and the anode potentials increase. For example, in the electrolyte containing 0.05 M Ca^{2+}, the voltage across the electrolyzer is 2.6 V, whereas in that containing 1 M Ca^{2+} it is 3.2 V.

In the course of the electrolysis, the anode potential first decreases and then increases, whereas the cathode potential always decreases (Fig. 1a).

Irrespective of the Ca^{2+} concentration in the electrolyte, MnO_2 is deposited onto the anode in the form of a black lustrous flaky film easily exfoliating from the electrode. The weight fraction of MnO_2 in the product obtained was 99.7% and the calcium concentration, less than 0.01%.

In magnesium-containing electrolytes, the current efficiency was 90–95% (see table). The behavior of the anode and the cathode potentials and of the voltage across the electrolyzer was similar to that in calcium-containing electrolytes (Fig. 1b), with the anode potential and voltage across the electrolyzer being somewhat lower. For example, the voltage across the electrolyzer was 2.4 and 2.85 V at 0.05 and 1 M Mg.

At any concentration of Mg^{2+} in the electrolyte, MnO_2 was deposited onto the anode in the form of a black flaky film easily exfoliating from the surface. The deposited film contained 99.7% MnO_2 and no more than 0.01% magnesium.

When the electrolysis was performed in the presence of aluminum ions, the current efficiency was 75–80%, and it decreased as the Al^{3+} concentration was increased (see table). For example, at an Al^{3+} concentration of 0.05 M, the current efficiency was 80% and at 0.25 M, 75%. In an electrolyte containing 1 M Al^{3+}, the anode was damaged and the electrolyte became turbid.

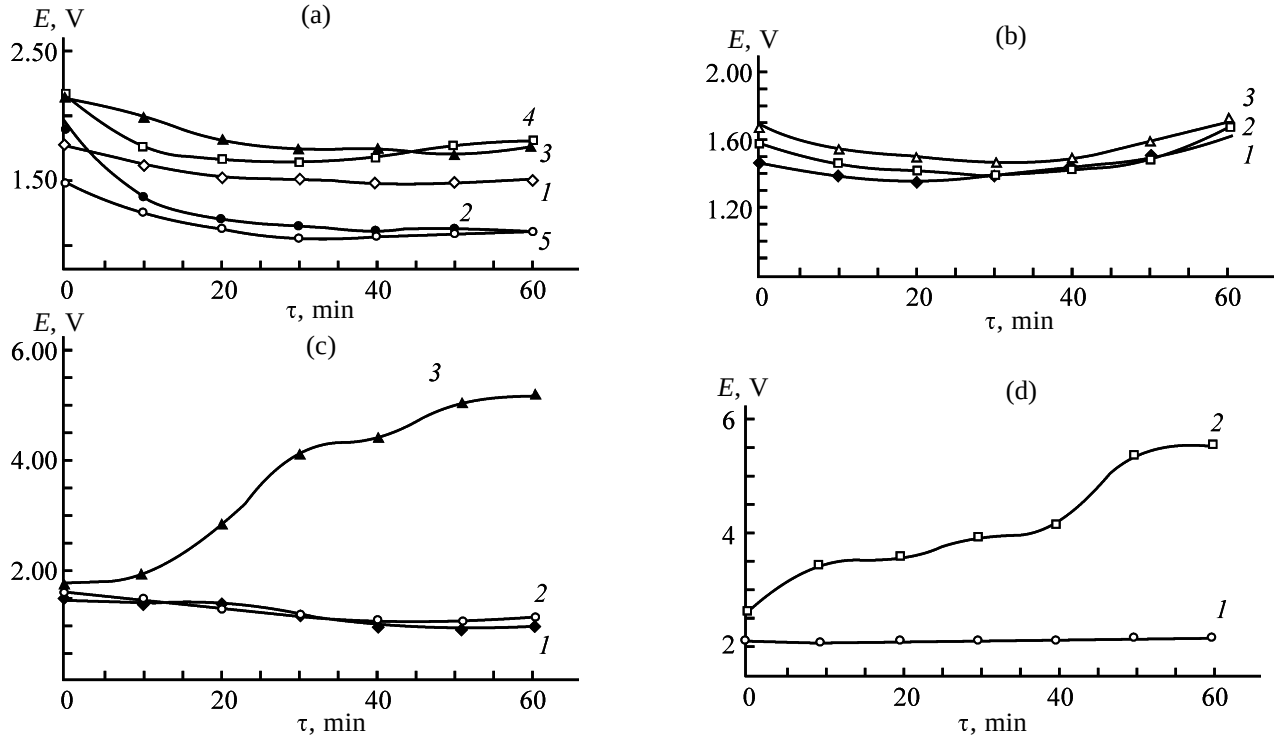


Fig. 1. Influence of the concentrations of (a) Ca^{2+}, (b) Mg^{2+}, (c) Al^{3+}, and (d) Fe^{3+} ions on variations of the anode potential E with time τ. Electrolyte (M): 1.0 $MnCl_2$ and 0.05 HCl. (a) $CaCl_2$ concentration (M): (*1*) 0.05, (*2*) 0.25, (*3*) 1.0, (*4*) 2.0, and (*5*) 0.0. (b) $MgCl_2$ concentration (M): (*1*) 0.05, (*2*) 0.25, and (*3*) 1.0. (c) $AlCl_3$ concentration (M): (*1*) 0.05, (*2*) 0.25, and (*3*) 1.0. (d) $FeCl_3$ concentration (M): (*1*) 0.05 and (*2*) 0.25.

In electrolytes with a low concentration of Al^{3+} ions (0.05 M), variations of the anode potential and voltage across the electrolyzer in the course of the electrolysis were similar to those in the Ca^{2+}- and Mg^{2+}-containing electrolytes. With the Al^{3+} concentration increased from 0.25 to 1 M, the anode potential (Fig. 1c) and voltage across the electrolyzer increased.

The manganese dioxide film deposited onto the anode was dense and difficult-to-detach from the surface. The film contained 99.5 wt % MnO_2 and no more than 0.03 wt % aluminum.

In the electrolytes containing Fe^{3+}, the current efficiency by MnO_2 was only 64% even at small iron concentrations (0.05 M Fe^{3+}) (see table). With increasing iron concentration, the voltage across the electrolyzer and the anode potential sharply increased (Fig. 1d).

The electrolyte containing 0.25 M $FeCl_3$ became turbid after the electrolysis. In the course of the electrolysis, the damage of the anode was observed, with its small areas coated with a fine MnO_2 deposit.

Manganese dioxide was deposited onto the anode as a dense dull black film difficult-to-detach from the surface. The deposited film contained 99 wt % MnO_2 and no more than 0.03–0.1 wt % iron.

The electrolysis of chloride solutions yields manganese tetrachloride, which hydrolyzes to form manganese dioxide [4, 5]:

$$MnCl_4 + 2H_2O \rightarrow MnO_2\downarrow + 4HCl. \quad (1)$$

The study showed that the effects exerted by calcium, magnesium, iron, and aluminum salts on the electrolysis of manganese chloride solutions differ essentially. The Ca^{2+} and Mg^{2+} ions do not noticeably affect the voltage across the electrolyzer, current efficiency, and chemical composition of MnO_2. On the contrary, the Fe^{3+} and Al^{3+} ions exert a very strong effect on both the electrolysis parameters and the chemical composition of the forming products. Probably, this is due to their different acid–base properties.

The Al^{3+} and Fe^{3+} ions are strong Lewis acids. In acid solutions, they form metallic acids:

$$FeCl_3 + HCl \rightarrow HFeCl_4, \quad (2)$$

$$AlCl_3 + HCl \rightarrow HAlCl_4. \quad (3)$$

Therefore, in electrolyte solutions they compete with Mn^{4+} ions for chloride ions. The binding of chloride ions with Al^{3+} and Fe^{3+} ions can accelerate the $MnCl_4$ hydrolysis. Therefore, MnO_2 is formed both in the bulk of the solution and on the anode surface, forming strong films with a poorly developed crystal structure.

The fact that CE considerably decreases in the presence of Fe^{3+} ions can be accounted for as follows. The iron ions in electrolytes are reduced on the cathode and oxidized on the anode in the course of electrolysis [6]. This results, on the one hand, in a decrease in the current efficiency of the MnO_2 electrodeposition owing to Fe^{2+} oxidation on the anode and, on the other hand, in a decrease in the Mn^{4+} concentration owing to the redox reactions

$$Fe^{2+} + Mn^{4+} \rightarrow Mn^{3+} + Fe^{3+}, \quad (4)$$

$$2Fe^{2+} + Mn^{4+} \rightarrow Mn^{2+} + 2Fe^{3+}. \quad (5)$$

A fast increase in the anode potential and, consequently, in the voltage across the electrolyzer may be due to formation on the anode of a dense passivation film with a low electrical conductivity. On the damaged areas of this film, the current densities increase, which results in the damage of the anodes by electroerosion.

Continuous electrolysis of electrolytes containing calcium and magnesium compounds will result in the formation of spent electrolytes with relatively high concentrations of Ca^{2+} and Mg^{2+} ions and hydrochloric acid. The results of this study showed that spent electrolytes can be used for leaching manganese compounds. In the process, a part of Ca^{2+} and Mg^{2+} ions passes into the leaching sludge by an ion-exchange reaction. The leaching of manganese compounds from ores with calcium chloride solutions has been described in [7, 8]. Moreover, the concentration of calcium ions in the spent electrolyte can be decreased to a required value by adding sulfuric acid. Calcium sulfate formed in the process can be used in building industry.

Thus, our results show that electrolytic MnO_2 with a low concentration of impurities can be prepared directly from processing solutions of hydrochloric acid leaching of manganese ores without their exhaustive purification.

CONCLUSION

Calcium and magnesium ions do not affect adversely the electrolysis of manganese chloride electrolytes and the quality of manganese dioxide being formed. The presence of iron and aluminum ions in the electrolyte solutions markedly deteriorates electrolysis process and the quality of the MnO_2 deposit.

REFERENCES

1. USSR Inventor's Certificate no. 1 497 252.
2. Charlot, G., *Quantitative Inorganic Analysis*, London: Wiley, 1957.
3. Pisarenko, V.V., and Zakharov, L.S., *Tekhnicheskii analiz* (Technical Analysis), Moscow: Vysshaya Shkola, 1972.
4. Lisov, V.N., in *Gidroelektrometallurgiya khloridov* (Hydroelectrometallurgy of Chlorides), Kiev: Naukova Dumka, 1964, pp. 76–98.
5. Stender, V.V., and Lisov, V.N., *Zh. Prikl. Khim.*, 1967, vol. 40, no. 3, pp. 570–576.
6. Antropov, L.I., *Teoreticheskaya elektrokhimiya* (Theoretical Electrochemistry), Moscow: Vysshaya Shkola, 1975, vol. 1.
7. Pozin, M.S., *Tekhnologiya mineral'nykh solei* (Technology of Mineral Salts), Moscow: Khimiya, 1975, vol. 1.
8. Lavrukhina, A.K., and Yukina, L.V., *Analiticheskaya khimiya margantsa* (Analytical Chemistry of Manganese), Moscow: Nauka, 1974.

Russian Journal of Applied Chemistry, Vol. 78, No. 5, 2005, pp. 741–746. Translated from Zhurnal Prikladnoi Khimii, Vol. 78, No. 5, 2005, pp. 755–760.
Original Russian Text Copyright © 2005 by Sokolov, Tarlakov, Ustinov, Pronkin.

APPLIED ELECTROCHEMISTRY AND CORROSION PROTECTION OF METALS

Structure and Electric Properties of Lithium Phosphate Glasses

I. A. Sokolov, Yu. P. Tarlakov, N. Yu. Ustinov, and A. A. Pronkin

St. Petersburg State Technological Institute, St. Petersburg, Russia

Received April 6, 2005

Abstract—The temperature–concentration dependence of the conductivity in glasses of the system Li_2O–P_2O_5 was studied. The content of extrinsic hydrogen in the structure of glasses was estimated by IR transmission spectra. The effect of hydrogen on the electrical properties and structure of the glasses studied was considered.

A large interest in the development of chemical power sources (CPSs) with a high specific energy is accompanied by active search for substances with a high conductivity. This is apparently responsible for researchers' interest in interrelations between physicochemical (especially electrical) properties and structures of model glasses such as M_2O–P_2O_5 (M = Li, Na,). Particular attention is given to glasses of the system Li_2O–P_2O_5 [1–10], allowing development of CPSs with a solid electrolyte (SEL), exhibiting unipolar conductance caused by migration of lithium ions. Furthermore, lithium glasses are promising materials for studying the effect of the ratio Li_2O/P_2O_5 = *R* on their structure and physicochemical properties [9]. Metaphosphate structural units (SUs) are formed in the glass at *R* = 1. These units consist of oxygen tetrahedra $[PO_4]$ connected in chains by bridging oxygen atoms. In this case, the following SUs can be distinquished [9]:

(1) "single" $[PO_4]^{3-}$ group sharing three oxygen atoms with adjacent $[PO_4]$ groups, thus forming "branching points" (B);

(2) "middle" $[PO_4]^{-}$ group sharing two oxygen atoms with adjacent $[PO_4]$ groups (M);

(3) "terminal" $[PO_4]^{2-}$ group sharing one oxygen atom with an adjacent $[PO_4]$ group, with two negative charges localized on two oxygen atoms (T).

Reactions of the following type proceed in phosphate melts [9]:

$$2MPO_3(M) \leftrightarrows PO_{2.5}(B) + MPO_{3.5}(T).$$

These reactions were studied later for seven binary mixtures, and it was shown that the equilibrium constant is virtually independent of the rate of cooling the melt when synthesizing the glasses [11]. These data suggest that the structure of the anionic matrix of the glasses being prepared is maximally close to the structure of the equilibrium melt at a preset temperature of the synthesis and depends only on the $[M_2O]/[P_2O_5]$ ratio. Compared to glasses of the systems M_2O–P_2O_5 (M = Na, K), in the lithium system the number of branchings is larger, and their concentration is less dependent on *R*.

At *R* > 1, the number of terminal oxygen atoms grows. The length of phosphate chains decreases, which results in increasing SU mobility. The number of pyro- and orthophosphate groups in the structure of glasses increases. An attempt to estimate quantitatively how the degree of polymerization of phosphate SUs forming the glass anionic matrix depends on *R* was undertaken in [12]. The results obtained confirm the assumed gradual depolymerization of the glass anionic matrix and formation of shorter-chain SUs [6].

To obtain high specific characteristics of a chemical power source, the electrolyte should have a minimal resistance. One way to increase SEL conductivity is to increase the concentration of lithium ions, which are current carriers in glasses of the Li_2O–P_2O_5 system. Another way for increasing the conductivity can be modification of the glass anionic matrix with the aim of decreasing the tightness of fixation of current-carrying ions in the structure. It will increase the degree of dissociation of polar structural chemical units (SCUs). According to [13], a three-dimensional network of a binary glass, e.g., Li_2O–P_2O_5, can be presented as a combination of polar $Li^+O^-PO_{3/2}$ $\begin{bmatrix} O_{3/2}P–O^-Li^+ \\ H^+O^–PO_{3/2} \end{bmatrix}$, $[O_{3/2}P–O^-Li^+]$, $[O_{2/2}P–O^-H^+]$ and nonpolar ($PO_{4/2}$) SCUs. At $[Li^+] < 8 \times 10^{-3}$ mol cm^{-3} ($R \cong 0.15$), polar SCUs are separated from each other by a nonpolar medium. When polar

1070-4272/05/7805-0741 © 2005 Pleiades Publishing, Inc.

SCUs dissociate, lithium ions should come out into the nonpolar medium and migrate in it. An increase in the concentration of lithium ions ($R > 1$) results in decreasing length of phosphate chains, as it was mentioned above, whereas polar SCUs form tie chains threading the entire glass volume. In this case ($[Li^+] < 8 \times 10$ mol cm^{-3}), polar SCUs dissociate much more easily, and dissociated lithium ions migrate in the medium of polar SCUs [6, 13]. The conductivity itself sharply increases owing to a decrease in the activation energy of conductivity [4].

In view of the aforesaid, it seemed appropriate to study glasses of the system Li_2O–P_2O_5 with the aim to obtain more specific information on the nature of current carriers and on the effect of anionic matrix on the electric current transport.

EXPERIMENTAL

Glasses were synthesized in crucibles made from SU-2000 carbon glass under dry argon. We used chemically pure grade Li_2CO_3 and H_3PO_4 as starting reagents. To study the effect of synthesis conditions on the physicochemical properties, the charge was prepared by two techniques. In the first case, the mixture of the components was heated in steps up to the temperature of glass founding. The charge was prepared by the sol–gel method. Lithium carbonate was mixed with orthophosphoric acid, and the resulting solution was evaporated to form a highly homogeneous charge.

In the second case, the charge was prepared from lithium oxide and metaphosphate preliminarily calcined to constant weight under dry argon.

In both cases, the glass melt was kept at 800–850°C for approximately 30 min. This time ensured good reproducibility and was sufficient for complete fusion of the glass. Samples of glasses were obtained by casting the melt on a steel plate, which was followed by annealing for 1 h in a muffle oven at temperatures lower than T_g by 10–15°C and cooling with the oven. Annealed samples were ground and polished to a thickness of 1.50 ± 0.01 mm and stored in a desiccator.

In view of the data of [10, 11], the structure of the anionic component of the resulting glasses can be considered as maximally approaching that of the equilibrium melt at the synthesis temperature.

The density of the glasses was determined by hydrostatic weighing in toluene. The reproducibility of the data obtained was no worse than ± 0.01 g cm^{-3}. The IR absorption spectra were recorded on a Perkin–Elmer 156 instrument. A weighed glass sample (~10 mg) was preliminarily crushed in an agate mortar to a dispersity of about 0.1 mm, and then it was transferred into a vibration mill and treated for 3 min. A weighed portion (~3 mg) of the resulting powder with a grain size of 5–40 μm was mixed with a weighed portion of KBr (~700 mg) in a vibration mill for 3 min, after which the mixture was pressed in pellets. The water content in the glasses were monitored by comparing their transmission spectra (1600–4000 cm^{-1}) with the spectra of samples prepared by as Nujol mulls.

The estimation of the electronic conduction component (Liang–Wagner polarization procedure [14]) showed that the contribution of the electronic component to the overall conductivity does not exceed 10^{-2}% (sensitivity of the procedure). The stationary conductivity was studied on direct current using active electrodes [4, 6]. The voltage applied to the samples ensured implementation of Ohm's law (electric field strength less than 10 kV cm^{-1}), which is a particular case of the general dependence between the current strength and voltage. The measurement was carried out in the temperature range from room temperature to temperatures lower than T_g by 15–20°C, using an ED-05M electrodynamic dc amplifier. The voltage was taken from a B5-49 stabilized dc source or a PI-50-1.1 potentiostat. To eliminate the surface conduction arising from the interaction of samples with the environment, the measurements were carried out using protective electrodes according to GOST (State Standard) 6433.2–71. The relative measurement error was 5–7%. Within the entire temperature range, a linear dependence $\log\sigma = f(1/T)$ was observed. The measurement of the conductivity in the heating and cooling modes showed the absence of hysteresis. The activation energy of conductivity E_σ was calculated by the equation

$$\sigma = \sigma_0 \exp[-E_\sigma/(2kT)].$$

The results of studying the temperature–concentration dependence of the conductivity are given in Table 1. The concentration dependence of the conductivity and the activation energy of conductivity of glasses of the system Li_2O–P_2O_5, obtained in this study, are compared with the published data [1, 4, 7] in Fig. 1. It is seen that an increase in the volume concentration of lithium ions from 2.12×10^{-2} to 3.08×10^{-2} mol cm^{-3} (from 30 to 58 mol % Li_2O) is accompanied by the growth of the conductivity by approximately four orders of magnitude (at 25°C). In

Table 1. Electrical properties of glasses of the system Li_2O–P_2O_5

Content, mol %		$[Li^+] \times 10^2$, mol cm^{-3}	E_σ, eV	$\log \sigma_0$ (σ, Ω^{-1} cm^{-1})	–log σ (σ, Ω^{-1} cm^{-1}) at indicated T, °C		
Li_2O	P_2O_5				25	100	200
40.0	60.0	2.38	1.64	3.1	10.75	7.95	5.65
40.0*	60.0	2.39	1.62	3.15	10.55	7.8	5.5
45.0	55.0	2.54	1.48	2.7	9.8	7.3	5.1
45.0*	55.0	2.55	1.47	2.9	9.55	7.05	4.95
50.0	50.0	2.73	1.38	3.25	8.4	6.1	4.1
50.0*	50.0	2.74	1.36	3.05	8.45	6.15	4.2
55.0	45.0	2.93	1.23	2.7	7.7	5.6	3.85
55.0*	45.0	2.94	1.21	2.75	7.5	5.45	3.7
58.0	42.0	3.09	1.15	2.6	7.1	5.15	3.5
58.0*	42.0	3.08	1.12	2.6	6.85	4.95	3.4
60.0	40.0	3.11	1.14	2.65	7.0	5.05	3.45

* Data of [4].

this case, the activation energy of the conductivity decreases from 1.65 to 1.12 eV, the density of the glasses under study increases, and their molar volume decreases (Table 2). The results obtained agree well with the data of [4, 7] on the conductivity of glasses of the system Li_2O–P_2O_5 for the molar ratio $[Li_2O]/[P_2O_5]$ from 0.7 to 1.22.

It was shown that an increase in the content of lithium oxide is accompanied by a linear increase in the conductivity. The fulfillment of Faraday's laws in glasses of this system was studied by Pronkin *et al*. [4]. They found that 99.1% of lithium was precipitated on the cathode in the electrolysis of the glass $0.425Li_2O$–$0.45P_2O_5$. Plyshevskii *et al*. [15] studied the removal of water from bulk phosphate glasses by a thermal method and showed that it was impossible to remove water completely from the glass by this technique. The content of hydrogen ("water") in lithium metaphosphate was qualitatively estimated in [16] (Table 3). It is evident from these data that, although the content of residual water is reduced as the temperature and the duration of the synthesis increase, it remains quite measurable, which should essentially affect the physicochemical and especially electrical properties of glasses. On this basis, Pronkin *et al*. [4] assumed that protons take part in the current transport in glasses of the system Li_2O–P_2O_5 along with lithium ions, with the contribution of protons to current transport decreasing as the Li_2O content increases. The participation of OH^- groups and hydrated protons (H_3O^+) in the current transport is improbable.

It is seen from the above data that a noticeable difference in the electrical properties of glasses is ob-

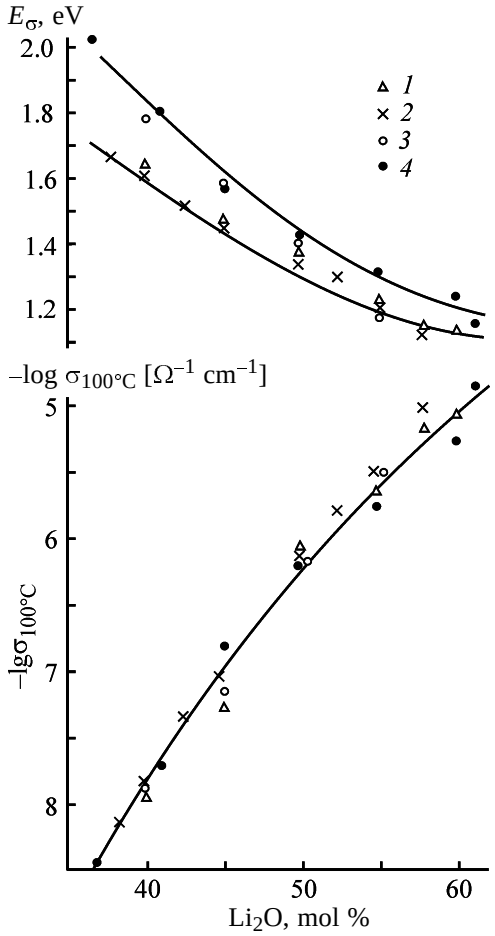


Fig. 1. Concentration dependence of the conductivity $\sigma_{100°C}$ and activation energy of conductivity of glasses of the system Li_2O–P_2O_5. Data: (*1*) this work, (*2*) [1], (*3*) [7], and (*4*) [4].

Table 2. Density d and molar volume V_{mol} of glasses of the system $Li_2O–P_2O_5$

Li_2O content, mol %	d, g cm^{-3}	V_{mol}, cm^3 mol^{-1}
40.0	2.31	42.08
45.0	2.33	39.31
50.0	2.35	36.60
55.0	2.35	34.21
58.0	2.37	32.51
60.0	2.37	31.56

Table 3. Content of residual water in lithium metaphosphate as a function of synthesis conditions (data of [16])

T, °C	τ, min	D_2O content, wt %
800	15	5.42
900	10	5.20
900	15	4.62
920	20	2.83
950	30	2.21
980*	120	0.63

* Bubbling of dry oxygen through the melt.

served at the concentrations of lithium oxide less than 50 mol % ($R < 1$), whereas at $R \geq 1$ they are rather constant. This fact seems to be caused by the presence of appreciable amounts of extrinsic hydrogen in the structure of the glasses under study, the content of which depends on their composition and synthesis conditions.

According to Van Wazer [9], the structure of phosphoric anhydride is formed by $[PO_{4/2}]$ tetrahedra linked to each other in infinite chains by bridging oxygen ions. The introduction of lithium oxide into P_2O_5 is accompanied by depolymerization of polyphosphate chains. Thus, according to the ^{31}P NMR data, as the content of lithium in glasses of the $Li_2O–P_2O_5$ system increases, the mean length of polyphosphate ions decreases from 22 (for the glass $0.5Li_2O–0.5P_2O_5$) to 7 units (for the glass $0.55Li_2O–0.45P_2O_5$) [17]. Thus, the introduction of lithium oxide in P_2O_5 is accompanied by cleavage of bridging P–O–P bonds according to the scheme

$$O_{3/2}P–O–PO_{3/2} + Li_2O \rightarrow 2[Li^+O^- – PO_{3/2}].$$

As mentioned above, Plyshevskii *et al*. [15] believe that it is impossible to remove hydrogen completely from the glass structure by thermal methods. This seems to be due to different positions of hydrogen in the structure of glasses. Water can be removed virtually completely from the glass only by chemical methods [4]. Therefore, the fact that the hydrogen content in the structure of glasses of the system $Li_2O–P_2O_5$ decreases as the concentration of lithium oxide increases is attributable to the substitution of lithium ions for hydrogen in the glass structure according to the scheme

$$2[O_{3/2}P–O^-H^+] + Li_2O \rightarrow [O_{3/2}P–O^-Li^+] + H_2O\uparrow.$$

Thus, according to [13], the structure of glasses of the system $Li_2O–P_2O_5$ can be presented as a combination of polar $\begin{bmatrix} O_{3/2}P–O^-Li^+ \\ H^+O^–PO_{3/2} \end{bmatrix}$, $[O_{3/2}P–O^-Li^+]$, $[O_{2/2}P–O^-H^+]$ and nonpolar $[PO_{4/2}]$ SCUs.

The dissociation energy of lithium SCGUs $O_{3/2}P–O^-Li^+$ is lower than that of mixed quadrupoles; $Li^+O^–PO_4$ therefore, the amount of current-carrying lithium ions and the conductivity of the glasses increase. At $R < 1$, the structure of the glasses is mainly determined by a combination of $[O_{3/2}P–O^-Li^+]$, $\begin{bmatrix} O_{3/2}P–O^-Li^+ \\ H^+O^–PO_{3/2} \end{bmatrix}$, and $[PO_{4/2}]$ SCUs. The structure of lithium metaphosphate ($R = 1$) consists mainly of polar SCUs $[O_{3/2}P–O^-Li^+]$ and of a small amount of $\begin{bmatrix} O_{3/2}P–O^-Li^+ \\ Li^+O^–PO_{3/2} \end{bmatrix}$ and $\begin{bmatrix} O_{3/2}P–O^-Li^+ \\ H^+O^–PO_{3/2} \end{bmatrix}$ SCUs. In this case, the concentration of quadrupoles $\begin{bmatrix} O_{3/2}P–O^-Li^+ \\ H^+O^–PO_{3/2} \end{bmatrix}$ decreases as the Li_2O content increases. At $R > 1$, only polar SCUs are formed in the structure of glasses, and the concentration of lithium quadrupoles increases as the concentration of lithium oxide increases.

Changes occurring in the structure of the glasses are proved by IR spectra, which correlate with the results of an IR study of glasses of the system $Li_2O–P_2O_5$ [7, 10, 12]. Broad bands with maxima near 3300 and 2600 cm^{-1} are observed in the IR transmission spectra in the region of vibrations of hydroxy groups. Their intensity increases as the content of lithium oxide decreases in glasses of both series examined in this study. However, in samples prepared by the first procedure, the relative content of water was somewhat less than in samples prepared by the second procedure. The IR absorption spectra of the samples prepared by the first procedure are given in Fig. 2. It is seen that the absorption in the range 910–1160 cm^{-1} changes essentially as the Li_2O content increases. The intensity of bands in the range 1050–1160 cm^{-1} in-

Table 4. Electric properties of lithium metaphosphate

$-\log\sigma$ (σ, Ω^{-1} cm^{-1}) at indicated T, °C			$\log\sigma_0$ (σ, Ω^{-1} cm^{-1})	E_σ, eV	T, °C	References
25	100	200				
8.0	5.55	3.5	4.15	1.44*	70–200	[18]
8.45	6.15	4.2	3.05	1.36	20–290	[4, 6]
8.3	5.95	3.95	3.45	1.39	20–290	
7.3	5.2	3.5	2.95	1.21	20–290**	
8.7	6.3	4.3	3.15	1.40	25–T_g	[3]
8.55	6.15	4.15	3.3	1.40*	20–260	[7]
8.95	6.55	4.45	3.25	1.45*	40–140	Watanabe M. [19]
8.6	6.25	4.15	3.45	1.43	25–230	[1]
8.4	6.1	4.1	3.25	1.38	25–275	This work

* The activation energy was recalculated by the equation $\sigma = \sigma_0 \exp[-E_0/(2kT)]$.

** Synthesis in an induction oven: heating to 900°C within approximately 5 min followed by exposure for 15 min; starting reagent: polycrystalline $LiPO_3$ of chemically pure grade.

creases, which seems to be due to the appearance of pyrophosphate groups [$\nu_{as}(PO_3)$]. At the same time, the intensity of the band at 1270 cm^{-1} [$\nu_{as}(PO_2)$] slightly decreases, and also the intensity of the band of bending vibrations (~500 cm^{-1}) decreases. Thus, as the content of Li_2O increases from 40 to 50 mol %, the position and shape of a number of bands change slightly, suggesting the preservation of the main metaphosphate motif of the glass. A sharp decrease in the intensity of the $\nu_{as}(PO_2)$ band and an increase in the intensity of $\nu_{as}(PO_3)$ are observed in the glass with 55 mol % Li_2O, which is due to increasing content of pyro- and orthophosphate groups and agrees well with the NMR data for the glasses of this system [17].

These conclusions are supported by the data on the density of the glasses: as the content of Li_2O increases, the density of the glasses increases (Table 2), which is attributable to more compact packing of the newly formed short-chain SCUs. Simultaneously the molar volume decreases (Table 2).

The effect of synthesis conditions on the electrical properties of glasses is illustrated by Table 4, in which the data of several authors on the conductance of lithium metaphosphate are compared. The observed discrepancy seems to be due to different techniques of the charge preparation and different thermal conditions of glass founding, as these factors determine the content of residual water in the glass structure, which noticeably affects the electrical properties of the glasses.

CONCLUSION

The temperature–concentration dependence of the conductivity in glasses of the system Li_2O–P_2O_5 was interpreted in terms of the structure-chemical microheterogeneity of the glass structure: in the region of low Li_2O concentrations, extrinsic hydrogen forms mixed quadrupoles $\begin{bmatrix} O_{3/2}P–O^-Li^+ \\ H^+O^–PO_{3/2} \end{bmatrix}$, retaining lithium ions more strongly than do homogeneous quadrupoles $\begin{bmatrix} O_{3/2}P–O^-Li^+ \\ Li^+O^–PO_{3/2} \end{bmatrix}$, and thus eliminating these ions from the electricity transfer. As the con-

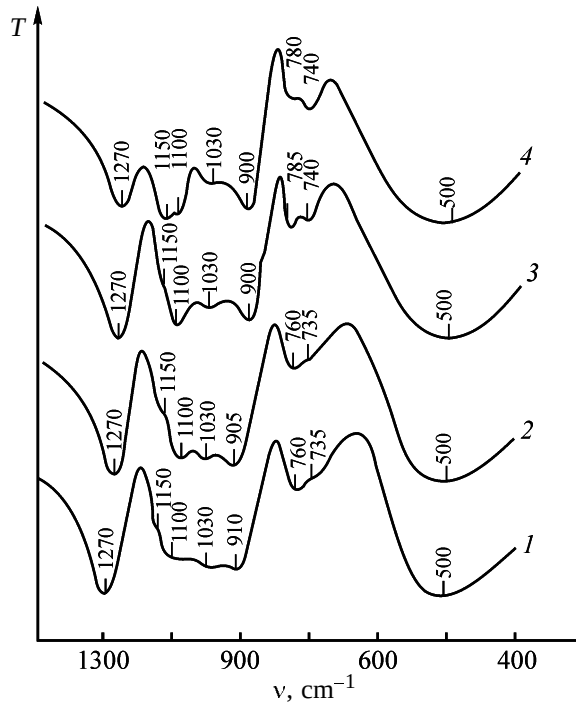


Fig. 2. IR spectra of glasses of the system xLi_2O–$(1 - x)P_2O_5$. x: (*1*) 0.4, (*2*) 0.45, (*3*) 0.50, and (*4*) 0.55. (T) Transmition and (ν) wave number.

centration of lithium oxide increases, the amount of extrinsic hydrogen decreases, which is accompanied by an increase in the conductance due to an increase in the concentration of current carriers and to a change of the mechanism of their migration.

REFERENCES

1. Martin, S.W. and Angell, C.A., *J. Non-Cryst. Solids*, 1986, vol. 83, no. 11, pp. 185–207.
2. Martin, S.W., *J. Am. Ceram. Soc*., 1991, vol. 74, no. 8, pp. 1767–1784.
3. Ravaine, D., *J. Non-Cryst. Solids*, 1980, vols. 38–39, pp. 185–207.
4. Pronkin, A.A., Murin, I.V., Sokolov, I.A., *et al*., *Fiz. Khim. Stekla*, 1997, vol. 23, no. 5, pp. 547–554.
5. Martin, S.W., *Eur. J. Solid. State Inorg. Chem.*, 1991, vol. 28, no. 1, pp. 163–205.
6. Pronkin, A.A., A Study in the Field of Physical Chemistry of Halogen-Containing Glasses, *Doctoral Dissertation*, Leningrad, 1979.
7. Osipov, A.B., Physicochemical Properties and Structure of Alkaline Phosphate and Halophosphate Glasses, *Cand. Sci. Dissertation*, Leningrad, 1983.
8. Kozlova, M.O., Structure and Properties of Alkaline Halophosphate and Potassium Silicate Glasses, *Cand. Sci. Dissertation*, Leningrad, 1989.
9. Van Wazer, I.R., *Phosphorus and Its Compounds*, New York: Interscience, 1958.
10. Pakhomov, G.B. and Neverov, S.L., *Fiz. Khim. Stekla*, 1997, vol. 23, no. 2, pp. 199–211.
11. Neverov, S.L., Effect of Rearrangement in Melts on the Anionic Structure of Glassy Phosphates of Alkali Metals, *Cand. Sci. Dissertation*, Yekaterinburg, 1994.
12. Cherches, G.S., Pechkovskii, V.V., Kuz'menkov, M.I., and Barashnikov, T.I., *Fiz. Khim. Stekla*, 1978, vol. 4, no. 2, pp. 233–237.
13. Myuller, R.L., *Elektroprovodnost' stekloobraznykh veshchestv* (Conductance of Glassy Substances), Leningrad: Leningr. Gos. Univ., 1968.
14. Liang, C., *Trans. Faraday Soc*., 1969, vol. 65, pp. 3369–3374.
15. Plyshevskii, S.V., Makatun, V.N., and Kuzmenkov, M.N., *Fiz. Khim. Stekla*, 1975, vol. 1, no. 3, pp. 279–285.
16. Ass, H.M.I. van and Stevels, I.M., *J. Non-Cryst. Solids*, 1974, vol. 16, no. 2, pp. 161–170.
17. Yumashev, N.I., Pronkin, A.A., and Yumasheva, L.V., *Fiz. Khim. Stekla*, 1995, vol. 21, no. 3, pp. 279–283.
18. Al-Rihabi, H.A. and Souquet, I.L., *C. R. Acad. Sci. Paris*, 1979, vol. 288, no. 23, pp. 549–552.
19. Mazurin, O.V., Strel'tsina, M.V., and Shvaiko-Shaikovskaya, T.P., *Svoistva stekol i stekloobraznykh rasplavov: Spravochnik* (Properties of Glasses and Glassy Melts: Handbook), Leningrad: Nauka, 1987, vol. 5.

Russian Journal of Applied Chemistry, Vol. 78, No. 5, 2005, pp. 741–746. Translated from Zhurnal Prikladnoi Khimii, Vol. 78, No. 5, 2005, pp. 755–760.
Original Russian Text Copyright © 2005 by Sokolov, Tarlakov, Ustinov, Pronkin.

APPLIED ELECTROCHEMISTRY AND CORROSION PROTECTION OF METALS

Structure and Electric Properties of Lithium Phosphate Glasses

I. A. Sokolov, Yu. P. Tarlakov, N. Yu. Ustinov, and A. A. Pronkin

St. Petersburg State Technological Institute, St. Petersburg, Russia

Received April 6, 2005

Abstract—The temperature–concentration dependence of the conductivity in glasses of the system Li_2O–P_2O_5 was studied. The content of extrinsic hydrogen in the structure of glasses was estimated by IR transmission spectra. The effect of hydrogen on the electrical properties and structure of the glasses studied was considered.

A large interest in the development of chemical power sources (CPSs) with a high specific energy is accompanied by active search for substances with a high conductivity. This is apparently responsible for researchers' interest in interrelations between physicochemical (especially electrical) properties and structures of model glasses such as M_2O–P_2O_5 (M = Li, Na,). Particular attention is given to glasses of the system Li_2O–P_2O_5 [1–10], allowing development of CPSs with a solid electrolyte (SEL), exhibiting unipolar conductance caused by migration of lithium ions. Furthermore, lithium glasses are promising materials for studying the effect of the ratio Li_2O/P_2O_5 = *R* on their structure and physicochemical properties [9]. Metaphosphate structural units (SUs) are formed in the glass at *R* = 1. These units consist of oxygen tetrahedra $[PO_4]$ connected in chains by bridging oxygen atoms. In this case, the following SUs can be distinquished [9]:

(1) "single" $[PO_4]^{3-}$ group sharing three oxygen atoms with adjacent $[PO_4]$ groups, thus forming "branching points" (B);

(2) "middle" $[PO_4]^{-}$ group sharing two oxygen atoms with adjacent $[PO_4]$ groups (M);

(3) "terminal" $[PO_4]^{2-}$ group sharing one oxygen atom with an adjacent $[PO_4]$ group, with two negative charges localized on two oxygen atoms (T).

Reactions of the following type proceed in phosphate melts [9]:

$$2MPO_3(M) \leftrightarrows PO_{2.5}(B) + MPO_{3.5}(T).$$

These reactions were studied later for seven binary mixtures, and it was shown that the equilibrium constant is virtually independent of the rate of cooling the melt when synthesizing the glasses [11]. These data suggest that the structure of the anionic matrix of the glasses being prepared is maximally close to the structure of the equilibrium melt at a preset temperature of the synthesis and depends only on the $[M_2O]/[P_2O_5]$ ratio. Compared to glasses of the systems M_2O–P_2O_5 (M = Na, K), in the lithium system the number of branchings is larger, and their concentration is less dependent on *R*.

At *R* > 1, the number of terminal oxygen atoms grows. The length of phosphate chains decreases, which results in increasing SU mobility. The number of pyro- and orthophosphate groups in the structure of glasses increases. An attempt to estimate quantitatively how the degree of polymerization of phosphate SUs forming the glass anionic matrix depends on *R* was undertaken in [12]. The results obtained confirm the assumed gradual depolymerization of the glass anionic matrix and formation of shorter-chain SUs [6].

To obtain high specific characteristics of a chemical power source, the electrolyte should have a minimal resistance. One way to increase SEL conductivity is to increase the concentration of lithium ions, which are current carriers in glasses of the Li_2O–P_2O_5 system. Another way for increasing the conductivity can be modification of the glass anionic matrix with the aim of decreasing the tightness of fixation of current-carrying ions in the structure. It will increase the degree of dissociation of polar structural chemical units (SCUs). According to [13], a three-dimensional network of a binary glass, e.g., Li_2O–P_2O_5, can be presented as a combination of polar $Li^+O^-PO_{3/2}$ $\begin{bmatrix} O_{3/2}P–O^-Li^+ \\ H^+O^–PO_{3/2} \end{bmatrix}$, $[O_{3/2}P–O^-Li^+]$, $[O_{2/2}P–O^-H^+]$ and nonpolar ($PO_{4/2}$) SCUs. At $[Li^+] < 8 \times 10^{-3}$ mol cm^{-3} ($R \cong 0.15$), polar SCUs are separated from each other by a nonpolar medium. When polar

1070-4272/05/7805-0741 © 2005 Pleiades Publishing, Inc.

SCUs dissociate, lithium ions should come out into the nonpolar medium and migrate in it. An increase in the concentration of lithium ions ($R > 1$) results in decreasing length of phosphate chains, as it was mentioned above, whereas polar SCUs form tie chains threading the entire glass volume. In this case ($[Li^+] < 8 \times 10$ mol cm^{-3}), polar SCUs dissociate much more easily, and dissociated lithium ions migrate in the medium of polar SCUs [6, 13]. The conductivity itself sharply increases owing to a decrease in the activation energy of conductivity [4].

In view of the aforesaid, it seemed appropriate to study glasses of the system Li_2O–P_2O_5 with the aim to obtain more specific information on the nature of current carriers and on the effect of anionic matrix on the electric current transport.

EXPERIMENTAL

Glasses were synthesized in crucibles made from SU-2000 carbon glass under dry argon. We used chemically pure grade Li_2CO_3 and H_3PO_4 as starting reagents. To study the effect of synthesis conditions on the physicochemical properties, the charge was prepared by two techniques. In the first case, the mixture of the components was heated in steps up to the temperature of glass founding. The charge was prepared by the sol–gel method. Lithium carbonate was mixed with orthophosphoric acid, and the resulting solution was evaporated to form a highly homogeneous charge.

In the second case, the charge was prepared from lithium oxide and metaphosphate preliminarily calcined to constant weight under dry argon.

In both cases, the glass melt was kept at 800–850°C for approximately 30 min. This time ensured good reproducibility and was sufficient for complete fusion of the glass. Samples of glasses were obtained by casting the melt on a steel plate, which was followed by annealing for 1 h in a muffle oven at temperatures lower than T_g by 10–15°C and cooling with the oven. Annealed samples were ground and polished to a thickness of 1.50 ± 0.01 mm and stored in a desiccator.

In view of the data of [10, 11], the structure of the anionic component of the resulting glasses can be considered as maximally approaching that of the equilibrium melt at the synthesis temperature.

The density of the glasses was determined by hydrostatic weighing in toluene. The reproducibility of the data obtained was no worse than ± 0.01 g cm^{-3}. The IR absorption spectra were recorded on a Perkin–Elmer 156 instrument. A weighed glass sample (~10 mg) was preliminarily crushed in an agate mortar to a dispersity of about 0.1 mm, and then it was transferred into a vibration mill and treated for 3 min. A weighed portion (~3 mg) of the resulting powder with a grain size of 5–40 μm was mixed with a weighed portion of KBr (~700 mg) in a vibration mill for 3 min, after which the mixture was pressed in pellets. The water content in the glasses were monitored by comparing their transmission spectra (1600–4000 cm^{-1}) with the spectra of samples prepared by as Nujol mulls.

The estimation of the electronic conduction component (Liang–Wagner polarization procedure [14]) showed that the contribution of the electronic component to the overall conductivity does not exceed 10^{-2}% (sensitivity of the procedure). The stationary conductivity was studied on direct current using active electrodes [4, 6]. The voltage applied to the samples ensured implementation of Ohm's law (electric field strength less than 10 kV cm^{-1}), which is a particular case of the general dependence between the current strength and voltage. The measurement was carried out in the temperature range from room temperature to temperatures lower than T_g by 15–20°C, using an ED-05M electrodynamic dc amplifier. The voltage was taken from a B5-49 stabilized dc source or a PI-50-1.1 potentiostat. To eliminate the surface conduction arising from the interaction of samples with the environment, the measurements were carried out using protective electrodes according to GOST (State Standard) 6433.2–71. The relative measurement error was 5–7%. Within the entire temperature range, a linear dependence $\log\sigma = f(1/T)$ was observed. The measurement of the conductivity in the heating and cooling modes showed the absence of hysteresis. The activation energy of conductivity E_σ was calculated by the equation

$$\sigma = \sigma_0 \exp[-E_\sigma/(2kT)].$$

The results of studying the temperature–concentration dependence of the conductivity are given in Table 1. The concentration dependence of the conductivity and the activation energy of conductivity of glasses of the system Li_2O–P_2O_5, obtained in this study, are compared with the published data [1, 4, 7] in Fig. 1. It is seen that an increase in the volume concentration of lithium ions from 2.12×10^{-2} to 3.08×10^{-2} mol cm^{-3} (from 30 to 58 mol % Li_2O) is accompanied by the growth of the conductivity by approximately four orders of magnitude (at 25°C). In

Table 1. Electrical properties of glasses of the system Li_2O–P_2O_5

Content, mol %		$[Li^+] \times 10^2$, mol cm^{-3}	E_σ, eV	$\log \sigma_0$ (σ, Ω^{-1} cm^{-1})	–log σ (σ, Ω^{-1} cm^{-1}) at indicated T, °C		
Li_2O	P_2O_5				25	100	200
40.0	60.0	2.38	1.64	3.1	10.75	7.95	5.65
40.0*	60.0	2.39	1.62	3.15	10.55	7.8	5.5
45.0	55.0	2.54	1.48	2.7	9.8	7.3	5.1
45.0*	55.0	2.55	1.47	2.9	9.55	7.05	4.95
50.0	50.0	2.73	1.38	3.25	8.4	6.1	4.1
50.0*	50.0	2.74	1.36	3.05	8.45	6.15	4.2
55.0	45.0	2.93	1.23	2.7	7.7	5.6	3.85
55.0*	45.0	2.94	1.21	2.75	7.5	5.45	3.7
58.0	42.0	3.09	1.15	2.6	7.1	5.15	3.5
58.0*	42.0	3.08	1.12	2.6	6.85	4.95	3.4
60.0	40.0	3.11	1.14	2.65	7.0	5.05	3.45

* Data of [4].

this case, the activation energy of the conductivity decreases from 1.65 to 1.12 eV, the density of the glasses under study increases, and their molar volume decreases (Table 2). The results obtained agree well with the data of [4, 7] on the conductivity of glasses of the system Li_2O–P_2O_5 for the molar ratio $[Li_2O]/[P_2O_5]$ from 0.7 to 1.22.

It was shown that an increase in the content of lithium oxide is accompanied by a linear increase in the conductivity. The fulfillment of Faraday's laws in glasses of this system was studied by Pronkin *et al*. [4]. They found that 99.1% of lithium was precipitated on the cathode in the electrolysis of the glass $0.425Li_2O$–$0.45P_2O_5$. Plyshevskii *et al*. [15] studied the removal of water from bulk phosphate glasses by a thermal method and showed that it was impossible to remove water completely from the glass by this technique. The content of hydrogen ("water") in lithium metaphosphate was qualitatively estimated in [16] (Table 3). It is evident from these data that, although the content of residual water is reduced as the temperature and the duration of the synthesis increase, it remains quite measurable, which should essentially affect the physicochemical and especially electrical properties of glasses. On this basis, Pronkin *et al*. [4] assumed that protons take part in the current transport in glasses of the system Li_2O–P_2O_5 along with lithium ions, with the contribution of protons to current transport decreasing as the Li_2O content increases. The participation of OH^- groups and hydrated protons (H_3O^+) in the current transport is improbable.

It is seen from the above data that a noticeable difference in the electrical properties of glasses is ob-

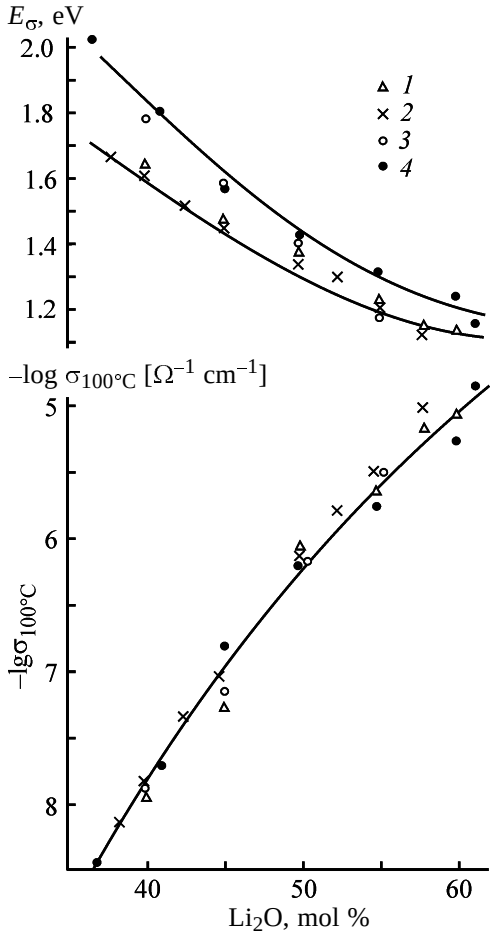


Fig. 1. Concentration dependence of the conductivity $\sigma_{100°C}$ and activation energy of conductivity of glasses of the system Li_2O–P_2O_5. Data: (*1*) this work, (*2*) [1], (*3*) [7], and (*4*) [4].

Table 2. Density d and molar volume V_{mol} of glasses of the system $Li_2O–P_2O_5$

Li_2O content, mol %	d, g cm^{-3}	V_{mol}, cm^3 mol^{-1}
40.0	2.31	42.08
45.0	2.33	39.31
50.0	2.35	36.60
55.0	2.35	34.21
58.0	2.37	32.51
60.0	2.37	31.56

Table 3. Content of residual water in lithium metaphosphate as a function of synthesis conditions (data of [16])

T, °C	τ, min	D_2O content, wt %
800	15	5.42
900	10	5.20
900	15	4.62
920	20	2.83
950	30	2.21
980*	120	0.63

* Bubbling of dry oxygen through the melt.

served at the concentrations of lithium oxide less than 50 mol % ($R < 1$), whereas at $R \geq 1$ they are rather constant. This fact seems to be caused by the presence of appreciable amounts of extrinsic hydrogen in the structure of the glasses under study, the content of which depends on their composition and synthesis conditions.

According to Van Wazer [9], the structure of phosphoric anhydride is formed by $[PO_{4/2}]$ tetrahedra linked to each other in infinite chains by bridging oxygen ions. The introduction of lithium oxide into P_2O_5 is accompanied by depolymerization of polyphosphate chains. Thus, according to the ^{31}P NMR data, as the content of lithium in glasses of the $Li_2O–P_2O_5$ system increases, the mean length of polyphosphate ions decreases from 22 (for the glass $0.5Li_2O–0.5P_2O_5$) to 7 units (for the glass $0.55Li_2O–0.45P_2O_5$) [17]. Thus, the introduction of lithium oxide in P_2O_5 is accompanied by cleavage of bridging P–O–P bonds according to the scheme

$$O_{3/2}P–O–PO_{3/2} + Li_2O \rightarrow 2[Li^+O^- – PO_{3/2}].$$

As mentioned above, Plyshevskii *et al*. [15] believe that it is impossible to remove hydrogen completely from the glass structure by thermal methods. This seems to be due to different positions of hydrogen in the structure of glasses. Water can be removed virtually completely from the glass only by chemical methods [4]. Therefore, the fact that the hydrogen content in the structure of glasses of the system $Li_2O–P_2O_5$ decreases as the concentration of lithium oxide increases is attributable to the substitution of lithium ions for hydrogen in the glass structure according to the scheme

$$2[O_{3/2}P–O^-H^+] + Li_2O \rightarrow [O_{3/2}P–O^-Li^+] + H_2O\uparrow.$$

Thus, according to [13], the structure of glasses of the system $Li_2O–P_2O_5$ can be presented as a combination of polar $\begin{bmatrix} O_{3/2}P–O^-Li^+ \\ H^+O^–PO_{3/2} \end{bmatrix}$, $[O_{3/2}P–O^-Li^+]$, $[O_{2/2}P–O^-H^+]$ and nonpolar $[PO_{4/2}]$ SCUs.

The dissociation energy of lithium SCGUs $O_{3/2}P–O^-Li^+$ is lower than that of mixed quadrupoles; $Li^+O^–PO_4$ therefore, the amount of current-carrying lithium ions and the conductivity of the glasses increase. At $R < 1$, the structure of the glasses is mainly determined by a combination of $[O_{3/2}P–O^-Li^+]$, $\begin{bmatrix} O_{3/2}P–O^-Li^+ \\ H^+O^–PO_{3/2} \end{bmatrix}$, and $[PO_{4/2}]$ SCUs. The structure of lithium metaphosphate ($R = 1$) consists mainly of polar SCUs $[O_{3/2}P–O^-Li^+]$ and of a small amount of $\begin{bmatrix} O_{3/2}P–O^-Li^+ \\ Li^+O^–PO_{3/2} \end{bmatrix}$ and $\begin{bmatrix} O_{3/2}P–O^-Li^+ \\ H^+O^–PO_{3/2} \end{bmatrix}$ SCUs. In this case, the concentration of quadrupoles $\begin{bmatrix} O_{3/2}P–O^-Li^+ \\ H^+O^–PO_{3/2} \end{bmatrix}$ decreases as the Li_2O content increases. At $R > 1$, only polar SCUs are formed in the structure of glasses, and the concentration of lithium quadrupoles increases as the concentration of lithium oxide increases.

Changes occurring in the structure of the glasses are proved by IR spectra, which correlate with the results of an IR study of glasses of the system $Li_2O–P_2O_5$ [7, 10, 12]. Broad bands with maxima near 3300 and 2600 cm^{-1} are observed in the IR transmission spectra in the region of vibrations of hydroxy groups. Their intensity increases as the content of lithium oxide decreases in glasses of both series examined in this study. However, in samples prepared by the first procedure, the relative content of water was somewhat less than in samples prepared by the second procedure. The IR absorption spectra of the samples prepared by the first procedure are given in Fig. 2. It is seen that the absorption in the range 910–1160 cm^{-1} changes essentially as the Li_2O content increases. The intensity of bands in the range 1050–1160 cm^{-1} in-

Table 4. Electric properties of lithium metaphosphate

$-\log\sigma$ (σ, Ω^{-1} cm^{-1}) at indicated T, °C			$\log\sigma_0$ (σ, Ω^{-1} cm^{-1})	E_σ, eV	T, °C	References
25	100	200				
8.0	5.55	3.5	4.15	1.44*	70–200	[18]
8.45	6.15	4.2	3.05	1.36	20–290	[4, 6]
8.3	5.95	3.95	3.45	1.39	20–290	
7.3	5.2	3.5	2.95	1.21	20–290**	
8.7	6.3	4.3	3.15	1.40	25–T_g	[3]
8.55	6.15	4.15	3.3	1.40*	20–260	[7]
8.95	6.55	4.45	3.25	1.45*	40–140	Watanabe M. [19]
8.6	6.25	4.15	3.45	1.43	25–230	[1]
8.4	6.1	4.1	3.25	1.38	25–275	This work

* The activation energy was recalculated by the equation $\sigma = \sigma_0 \exp[-E_0/(2kT)]$.

** Synthesis in an induction oven: heating to 900°C within approximately 5 min followed by exposure for 15 min; starting reagent: polycrystalline $LiPO_3$ of chemically pure grade.

creases, which seems to be due to the appearance of pyrophosphate groups [$\nu_{as}(PO_3)$]. At the same time, the intensity of the band at 1270 cm^{-1} [$\nu_{as}(PO_2)$] slightly decreases, and also the intensity of the band of bending vibrations (~500 cm^{-1}) decreases. Thus, as the content of Li_2O increases from 40 to 50 mol %, the position and shape of a number of bands change slightly, suggesting the preservation of the main metaphosphate motif of the glass. A sharp decrease in the intensity of the $\nu_{as}(PO_2)$ band and an increase in the intensity of $\nu_{as}(PO_3)$ are observed in the glass with 55 mol % Li_2O, which is due to increasing content of pyro- and orthophosphate groups and agrees well with the NMR data for the glasses of this system [17].

These conclusions are supported by the data on the density of the glasses: as the content of Li_2O increases, the density of the glasses increases (Table 2), which is attributable to more compact packing of the newly formed short-chain SCUs. Simultaneously the molar volume decreases (Table 2).

The effect of synthesis conditions on the electrical properties of glasses is illustrated by Table 4, in which the data of several authors on the conductance of lithium metaphosphate are compared. The observed discrepancy seems to be due to different techniques of the charge preparation and different thermal conditions of glass founding, as these factors determine the content of residual water in the glass structure, which noticeably affects the electrical properties of the glasses.

CONCLUSION

The temperature–concentration dependence of the conductivity in glasses of the system Li_2O–P_2O_5 was interpreted in terms of the structure-chemical microheterogeneity of the glass structure: in the region of low Li_2O concentrations, extrinsic hydrogen forms mixed quadrupoles $\begin{bmatrix} O_{3/2}P–O^-Li^+ \\ H^+O^–PO_{3/2} \end{bmatrix}$, retaining lithium ions more strongly than do homogeneous quadrupoles $\begin{bmatrix} O_{3/2}P–O^-Li^+ \\ Li^+O^–PO_{3/2} \end{bmatrix}$, and thus eliminating these ions from the electricity transfer. As the con-

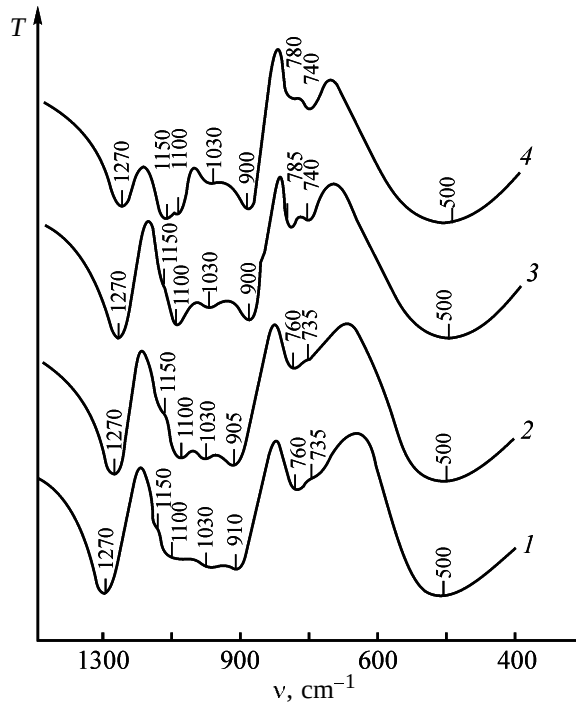


Fig. 2. IR spectra of glasses of the system xLi_2O–$(1 - x)P_2O_5$. x: (*1*) 0.4, (*2*) 0.45, (*3*) 0.50, and (*4*) 0.55. (T) Transmition and (ν) wave number.

centration of lithium oxide increases, the amount of extrinsic hydrogen decreases, which is accompanied by an increase in the conductance due to an increase in the concentration of current carriers and to a change of the mechanism of their migration.

REFERENCES

1. Martin, S.W. and Angell, C.A., *J. Non-Cryst. Solids*, 1986, vol. 83, no. 11, pp. 185–207.
2. Martin, S.W., *J. Am. Ceram. Soc*., 1991, vol. 74, no. 8, pp. 1767–1784.
3. Ravaine, D., *J. Non-Cryst. Solids*, 1980, vols. 38–39, pp. 185–207.
4. Pronkin, A.A., Murin, I.V., Sokolov, I.A., *et al*., *Fiz. Khim. Stekla*, 1997, vol. 23, no. 5, pp. 547–554.
5. Martin, S.W., *Eur. J. Solid. State Inorg. Chem.*, 1991, vol. 28, no. 1, pp. 163–205.
6. Pronkin, A.A., A Study in the Field of Physical Chemistry of Halogen-Containing Glasses, *Doctoral Dissertation*, Leningrad, 1979.
7. Osipov, A.B., Physicochemical Properties and Structure of Alkaline Phosphate and Halophosphate Glasses, *Cand. Sci. Dissertation*, Leningrad, 1983.
8. Kozlova, M.O., Structure and Properties of Alkaline Halophosphate and Potassium Silicate Glasses, *Cand. Sci. Dissertation*, Leningrad, 1989.
9. Van Wazer, I.R., *Phosphorus and Its Compounds*, New York: Interscience, 1958.
10. Pakhomov, G.B. and Neverov, S.L., *Fiz. Khim. Stekla*, 1997, vol. 23, no. 2, pp. 199–211.
11. Neverov, S.L., Effect of Rearrangement in Melts on the Anionic Structure of Glassy Phosphates of Alkali Metals, *Cand. Sci. Dissertation*, Yekaterinburg, 1994.
12. Cherches, G.S., Pechkovskii, V.V., Kuz'menkov, M.I., and Barashnikov, T.I., *Fiz. Khim. Stekla*, 1978, vol. 4, no. 2, pp. 233–237.
13. Myuller, R.L., *Elektroprovodnost' stekloobraznykh veshchestv* (Conductance of Glassy Substances), Leningrad: Leningr. Gos. Univ., 1968.
14. Liang, C., *Trans. Faraday Soc*., 1969, vol. 65, pp. 3369–3374.
15. Plyshevskii, S.V., Makatun, V.N., and Kuzmenkov, M.N., *Fiz. Khim. Stekla*, 1975, vol. 1, no. 3, pp. 279–285.
16. Ass, H.M.I. van and Stevels, I.M., *J. Non-Cryst. Solids*, 1974, vol. 16, no. 2, pp. 161–170.
17. Yumashev, N.I., Pronkin, A.A., and Yumasheva, L.V., *Fiz. Khim. Stekla*, 1995, vol. 21, no. 3, pp. 279–283.
18. Al-Rihabi, H.A. and Souquet, I.L., *C. R. Acad. Sci. Paris*, 1979, vol. 288, no. 23, pp. 549–552.
19. Mazurin, O.V., Strel'tsina, M.V., and Shvaiko-Shaikovskaya, T.P., *Svoistva stekol i stekloobraznykh rasplavov: Spravochnik* (Properties of Glasses and Glassy Melts: Handbook), Leningrad: Nauka, 1987, vol. 5.

Russian Journal of Applied Chemistry, Vol. 78, No. 5, 2005, pp. 753–757. Translated from Zhurnal Prikladnoi Khimii, Vol. 78, No. 5, 2005, pp. 767–771.
Original Russian Text Copyright © 2005 by Skorokhodova, Kobotaeva, Sirotkina.

CATALYSIS

Reactivity of Copper Nanopowders in a Model Reaction of Isopropylbenzene Oxidation

T. S. Skorokhodova, N. S. Kobotaeva, and E. E. Sirotkina

Institute of Petrochemistry, Siberian Division, Russian Academy of Sciences, Tomsk, Russia

Received July 27, 2004; in final form, December 2004

Abstract—The reactivity of copper nanopowders produced by an electric explosion of a conductor or mechanochemically was studied. Oxidation of isopropylbenzene was used as a model reaction. The dependence of the oxygen uptake rate on the specific surface area of a copper nanopowder and on the method used for its production is discussed. A possible mechanism of isopropylbenzene oxidation in the presence of copper nanopowders is suggested.

The intermediate position occupied by nanoparticles in passing from a bulk metal to a separate atom predetermines the deviation of their physicochemical properties from those of bulk metals, on the one hand, and from the properties of isolated atoms, on the other. This deviation is manifested in electronic, magnetic, optical, and other properties of nanoparticles with a characteristic size of several tens of nanometers to several nanometers [1]. Numerous summarizing papers concerning methods for preparation and stabilization of nanoparticles and their optical and other properties have already appeared, whereas studies of chemical transformations involving nanoparticles are only in their initial stage [2].

It is known [3] that nanosize powders (NPs) of metals show an increased reactivity, compared to compact metals. For example, reactions that do not occur in the presence of some metals or require severe conditions readily proceed in the presence of metal nanopowders. In particular, synthesis of complex compounds (phthalocyanines and tetraphenylporphyrins) with the use of copper and indium NP [4, 5] is performed under milder conditions (room temperature and atmospheric pressure) than the conventional synthesis with metal salts. Use of metal NPs as catalysts for oxidation of organic compounds is known. It was shown in [6] that the uptake of oxygen in oxidation of isopropylbenzene (IPB) in the presence of NPs of copper and cobalt proceeds at a sufficiently high rate even at 30°C without any initiator.

In this study we examined the reactivity of copper NP, obtained by an electric explosion of a conductor (EEC) or mechanochemically, in a model reaction of IPB oxidation.

EXPERIMENTAL

As objects of study served copper NP obtained by an electric explosion of a conductor in the atmosphere of nitrogen, argon, and xenon, as well as copper NP produced mechanochemically on an AGO-2 installation in the presence of organic and inorganic additives.[1] The additives were used to raise the specific surface area of the mechanochemically produced NP [7]. Copper nanopowders were produced by mechanical treatment (MT) in AGO-2 planetary-centrifugal high-energy-intensity mills in the presence of an organic surfactant (2,2,3,3,4,4,5,5-octafluorovaleramide) in an amount of 10% for 10 (Cu I), 20 (Cu II), and 30 min (Cu III). Copper powders were also prepared by mechanical treatment in the presence of 15 wt % $CuCl_2$ ($CuCl_2$ was washed out with ethanol after MT) on an AGO-2 installation for 10 (Cu 1), 20 (Cu 2), and 30 min (Cu 3). The physicochemical parameters and the preparation conditions of copper NPs used in this study are listed in Table 1.

IPB was oxidized on a gasometric installation [8]. A 0.7-M portion of IPB and 0.12 wt % copper NP were placed in the reactor. The reaction was performed at 30 and 60°C without initiator (azodiisobutyronitrile, AIBN). The reaction was stopped at the minimum rate of oxygen uptake (10–15 μl min^{-1}), which is determined by the scale factor of the buret in the gasometric installation. In some cases, repeated oxidation was performed 24 h after the end of the first

[1] Electric-explosion Cu NPs were obtained at the Institute of High-Current Electronics, Siberian Division, Russian Academy of Sciences, Tomsk; mechanochemical Cu NPs, at the Institute of Solid-State Chemistry and Mechanochemistry, Siberian Division, Russian Academy of Sciences, Novosibirsk.

1070-4272/05/7805-0753© 2005 Pleiades Publishing, Inc.

Table 1. Physicochemical parameters and preparation conditions of copper nanopowders

Powder	Preparation technique	E/E_s*	S_{sp}, $m^2\ g^{-1}$	Medium	Additive	Time of MT, min	W_{max},** $\mu l\ min^{-1}$	Induction period, min
Cu 8	EEC	1.0	8.7	Nitrogen	–	–	335	–
Cu 11	EEC	1.2	6.0	Xenon	–	–	300	–
Cu 13	EEC	0.8	2.2	Argon	–	–	100	–
Cu 18	EEC	2.0	2.1	Nitrogen	–	–	100	–
Cu 18(2)	EEC	2.0	9.7	Nitrogen	–	–	365	–
Cu 19	EEC	1.0	5.6	Nitrogen	–	–	280	–
Cu I	MT	–	3.2	Air	$H(CF_2CF_2)_2CONH_2$	10	–	19
Cu II	MT	–	3.9	Air	$H(CF_2CF_2)_2CONH_2$	20	–	17
Cu III	MT	–	5.2	Air	$H(CF_2CF_2)_2CONH_2$	30	–	6
Cu 1	MT	–	4.3	Air	$CuCl_2$	10	–	–
Cu 2	MT	–	6.2	Air	$CuCl_2$	20	–	–
Cu 3	MT	–	6.9	Air	$CuCl_2$	30	–	–

* E, supplied energy; E_s, energy of metal sublimation.
** W_{max}, maximum rate of oxygen uptake.

oxidation. Liquid reaction products (acetophenone, AP, and dimethylphenylcarbinol, DMPC), were analyzed by gas–liquid chromatography on a Perkin–Elmer Sigma 2B chromatograph with a flame-ionization detector on an SE-52 column (column length 33 m) in the programmed-temperature mode: initial thermostat temperature 80°C, temperature raised at a rate of 3 deg min^{-1} to 150°C. Carrier gas helium. Quantitative analyses were performed with an internal reference (*n*-hexane). IPB hydroperoxide (IPB HP) was determined iodometrically by the standard procedure [9].

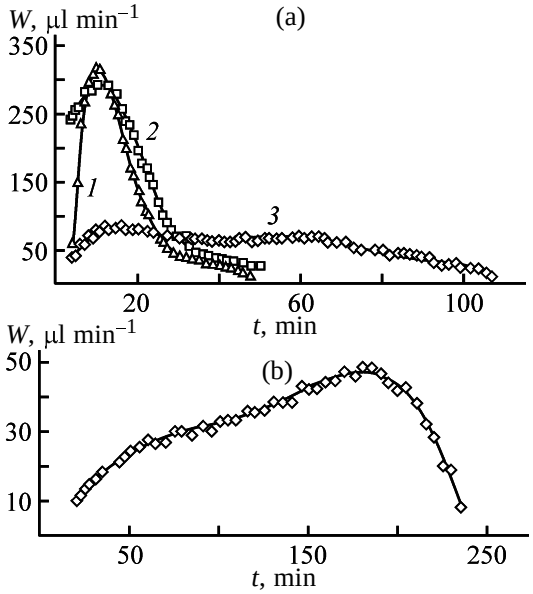


Fig. 1. Rate W of oxygen uptake vs. time t in oxidation of IPB in the presence of nanopowders. Nanopowder: (a) (*1*) Cu 8, (*2*) Cu 11, and (*3*) Cu 13; (b) Cu II. Temperature 60°C; the same for Fig. 2.

X-ray diffraction analysis was made on a DRON-1 instrument with a cobalt radiation source.[2] The X-ray diffraction patterns were recorded by point-by-point scanning with a step of 0.05°, with recording into a file for further computer processing.

The efficiency of copper NPs as catalysts for IPB oxidation was judged from the rate of oxygen uptake by a system constituted by IPB and Cu NP. Figure 1a shows the most typical kinetic curves of oxygen uptake in oxidation of IPB in the presence of 0.12 wt % Cu NP produced by EEC in various inert gases. Curves *1* and *2* are characteristic of Cu NP possessing a sufficiently large specific surface area [Cu 18(2), Cu 8, Cu 19, and Cu 11]. The run of the kinetic curves is about the same irrespective of the medium in which a powder was obtained: an exceedingly high rate at the beginning of the reaction and an abrupt fall in 10–15 min (Fig. 1). In the system constituted by IBP and Cu 13 NP with a small specific surface area (S_{sp} = 2.2 $m^2\ g^{-1}$), oxygen is taken up at a low rate during the entire reaction course (Fig. 1, curve *3*). For Cu NP produced by EEC, the following tendency can be noted: the larger the specific surface area of Cu NP, the higher the rate of oxygen uptake by the system constituted by IBP and Cu NP (Table 1).

A somewhat different behavior is exhibited in IBP oxidation by Cu NP produced mechanochemically. Irrespective of an additive, the rate of oxygen uptake gradually increases with time (Fig. 1b), with this type of curves characteristic of all mechanochemical Cu

[2] X-ray studies were carried out at the Institute of Strength Physics and Materials Science, Siberian Division, Russian Academy of Sciences, Tomsk.

Table 2. Composition of products formed in isopropylbenzene oxidation in the presence of a copper nanopowder

Powder	Yield, %			Conversion, %	Concentration of copper powder, %	Oxidation temperature, °C
	IPB HP	AP	DMPC			
Cu 8	0.53	0.30	0,35	1.18	0.12	60
Cu 11	0.6	0.32	0.44	1.36	0.13	60
Cu I	0.59	0.77	1.00	2.36	0.12	60
Cu II	0.8	0.88	1.25	2.93	0.12	60
Cu III	0.69	0.5	0.64	1.83	0.14	60
Cu 0	–	–	–	–	–	60
Cu 0	Trace amounts	–	–	–	–	80
Initiator	1.75	–	–	–	0.12	60

NPs. The powders are as if "shaken up" in the course of time. The oxygen uptake in IPB oxidation in the presence of mechanochemical Cu NP begins only after a certain induction period (Table 1).

The time in which the minimum rate of oxygen uptake (10–15 μl min^{-1}) is reached depends on the method by which Cu NPs are obtained: for NP produced by EEC, the minimum oxidation rate is reached rather rapidly (in 30–40 min), and this occurs the faster, the larger the specific surface area of the powder. For mechanochemical Cu NP, the time in which the minimum rate of oxygen uptake is reached is long and independent of the specific surface area of the powder. After the minimum rate of oxygen uptake is reached, the reaction may continue during an infinitely long time until the whole amount of IPB enters into the reaction or the reaction terminates because of recombination processes.

IPB oxidation in the presence of a Cu powder with a particle size of 40 μm and a specific surface area of 0.016 $m^2 g^{-1}$ (Cu 0) deserves separate consideration. Copper with such a specific surface area does not catalyze the IPB oxidation at 60°C. At 80°C, the reaction starts in 15 min, and then oxygen is adsorbed at a very low, nearly constant rate.

A chromatographic analysis of the reaction products formed in IPB oxidation in the presence of Cu NP demonstrated the presence of not only IPB HP, but also AP and DMPC (Table 2), irrespective of the preparation method, specific surface area, preparation medium, and other physicochemical properties of NP (Table 1). When used in the form of shavings, metallic copper decomposes hydroperoxides [10]; probably, the same behavior is characteristic of Cu NPs because it was impossible to selectively obtain only IPB HP in the presence of Cu NP. For electric-explosion Cu NPs, which have a large specific surface area and exhibit a high rate of oxygen uptake at the beginning of the reaction, the amount of reaction products is insignificant, in contrast to those characteristic of mechanochemical Cu NPs, at the same oxygen uptake. For example, the conversion is 1.36% (0.60 IPB HP, 0.32 AP, 0.44 DMPC) for electric-explosion copper Cu 11 with a specific surface area of 6 $m^2 g^{-1}$ and 2.9% (0.80 IPB HP, 0.88 AP, 1.25 DMPC) for mechanically treated Cu II NP. An increase in the mass of Cu NP by a factor of nearly 10 does not lead to any significant rise in the yield of the reaction products.

It is known [11] that IPB oxidation in the presence of a copper catalyst occurs by the radical-chain mechanism, with the primary radicals appearing on the surface of copper. This makes it possible to suggest a heterogeneous-homogeneous mechanism of the reaction by the scheme

$$\begin{aligned} (M) + O_2 &\rightarrow (M^+)\cdots(O\text{–}O)^-, \\ (M^+)\cdots(O\text{–}O)^- + RH &\rightarrow (M^+) + (OOH)^- + R^\bullet, \\ (M^+) + (OOH)^- &\rightarrow (M) + HO_2^\bullet, \\ HO_2^\bullet + RH &\rightarrow H_2O_2 + R^\bullet. \end{aligned} \quad (1)$$

The performance of a catalyst depends on the rate at which the active centers on the catalyst surface can adsorb reactants, retain them during the chemical transformation, and then release the reaction products to be free to perform a new catalytic cycle [1].

Probably, fast sorption of oxygen at the first instant of time is natural for Cu NPs with a sufficiently large specific surface area. After the surface of copper is saturated with oxygen, the rate of uptake decreases significantly because three processes start to compete: oxygen uptake, formation of reaction products on the surface, and desorption of the reaction products into solution. Chromatographic analysis for the reaction products, made immediately after the reaction ter-

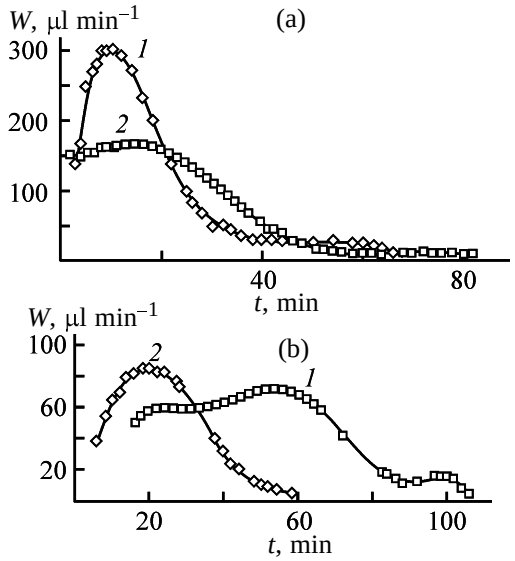


Fig. 2. Rate *W* of oxygen uptake vs. time *t* in oxidation of IPB in the presence of (a) Cu 8 and (b) Cu I nanopowders. Oxidation: (*1*) first and (*2*) repeated in 24 h.

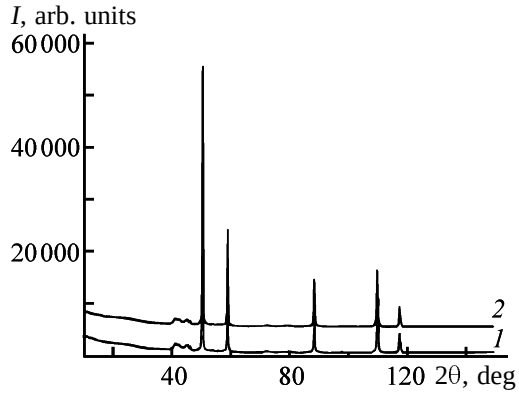


Fig. 3. X-ray diffraction patterns of Cu 11 powder (*1*) before and (*2*) after the oxidation. (*I*) Intensity and (2θ) Bragg angle.

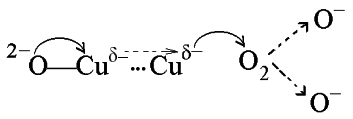
minated, reveals trace amounts of AP and DMPC. This means that the oxygen sorption is faster than formation of the reaction products and their desorption from the surface into the bulk. Nevertheless, after a certain time, when all the products would have diffused from the surface into the bulk, the conversion in the oxidation in the presence of electric-explosion Cu NPs with a large specific surface area is considerably lower than that with mechanochemical NPs. Probably, part of oxygen involved in oxidation is irreversibly sorbed on these NPs. Repeated oxidation of the system constituted by IPB and Cu NPs was performed in 24 h. The rate of oxygen uptake in the repeated oxidation of the system constituted by IPB and Cu NP prepared by the EEC method is always lower than that in the first oxidation of the same system, irrespective of the specific surface area of the NP (Fig. 2a). This means that the surface is not "freed" of oxygen even in the course of time. The curve of oxygen uptake in the repeated oxidation in the presence of mechanochemical Cu NP runs somewhat higher than that of the first oxidation (Fig. 2b). It was assumed that oxygen is consumed for oxidation of copper, and an X-ray diffraction analysis was carried out. However, an X-ray diffraction analysis did not reveal any additional formation of copper oxides after the reaction. Oxygen sorbed on the surface does not oxidize copper, but, probably, can be rather firmly retained on the surface of powder particles, without being involved in IPB oxidation to give reaction products; for example, it may form charge-transfer complexes with copper.

Figure 3 shows X-ray diffraction patterns of Cu 11 NP before and after the oxidation. The patterns reveal no difference between the structures of the initial NP and that isolated after the reaction. For example, the lattice constants (fcc unit cell) differ by less than 0.01% and the size of crystallites, determined from the angular broadening of the lines, was 60 and 62 nm in the initial and treated states, respectively. The only difference that could be revealed in the X-ray diffraction patterns is that the intensity of weak lines at 40°–48°, which, according to a phase analysis made on the basis of the ASTM file, belong to CuO (tenorite structure, 41-254 card), changes: after treatment of the powder, their intensity increases.

It was of interest to reveal the nature of the active center in Cu NPs, which can activate oxygen by scheme (1) and give rise to radical-chain transformations. A study was carried out[3] in order to elucidate the reasons for the increase in the reactivity of a mechanochemically treated copper powder, compared to the same powder in the initial state. It was demonstrated by X-ray photoelectron spectroscopy (XPS) that the intensity of oxygen peaks with a binding energy of 530.9–531.1 eV, which is not characteristic of adsorbed oxygen or copper oxides, increases in mechanochemically treated copper NPs [12]. The authors of this study believe that this peak may belong to the lattice, or suboxide, oxygen bound with defective sites in copper powder particles. In view of the fact that the bonding energy of the lattice oxygen exceeds that in the oxides CuO and Cu_2O, it may be stated that the bonding of copper atoms with the lattice oxygen is largely covalent, i.e., the suboxide oxygen donates its excess electron density to a copper atom bonded with it. The authors assume that the role of active centers in a copper sample activated by

[3] At the Institute of Solid-State Chemistry and Mechanochemistry, Siberian Division, Russian Academy of Sciences.

mechanical treatment or other methods leading to saturation with the lattice oxygen is played by oxygen atoms covalently bonded to copper atoms. Therefore, they suggest the following model of interaction of such an active center with molecular oxygen:



The lattice oxygen donates its excess electron density to the neighboring Cu atom, whose charge rapidly reaches the surface atom. The presence of an excess electron density on surface atoms leads to activation of molecular oxygen, which can then initiate radical-chain transformations in the catalytic oxidation of IPB.

The data of [12] can be used to explain the results obtained in this study. The copper NPs mechanically treated in ball mills in air probably contain a larger amount of suboxide oxygen capable of formation of active centers giving rise to radical chain reactions, because a 2 times greater amount of reaction products is formed. In addition, it is possible that the mechanochemical Cu NP treated in the presence of organic additives has on its surface a smaller number of free active sites at which oxygen not involved in the oxidation could be adsorbed. This is so because these sites, represented by various dislocations and structural surface defects, are already occupied in part by surfactants (e.g., by an organic surfactant, 2,2,3,3, 4,4,5,5-octafluorovaleramide), which can themselves form complexes with copper.

For copper NP produced by EEC in an inert atmosphere, presence of a large amount of suboxide oxygen is unlikely, and, therefore, it may be assumed that most part of absorbed oxygen is not activated and is not involved in the oxidation, being irreversibly sorbed at defective sites on the surface.

CONCLUSIONS

(1) In oxidation of isopropylbenzene in the presence of electric-explosion copper nanopowders obtained in an inert atmosphere, the maximum rate of oxygen uptake depends on the specific surface area of the nanopowders. The rate of oxygen uptake in the first oxidation run exceeds that in the case of a repeated oxidation run.

(2) With mechanochemically produced copper nanoparticles, the rate of oxygen uptake in the repeated oxidation runs exceeds that in the first oxidation of isopropylbenzene, which may be due to the high degree of caking of these powders and their "shake-up" in the course of time.

(3) The final products are isopropylbenzene hydroperoxide, acetophenone, and dimethylphenylcarbinol. The relative amounts of the reaction products depend on the method used to produce the nanopowders.

(4) A possible mechanism of isopropylbenzene oxidation in the presence of Cu nanopowders was suggested. This mechanism is associated with the presence of suboxide oxygen, which is involved in the oxidation and activates molecular oxygen.

REFERENCES

1. Bukhtiyarov, V.I. and Slin'ko, M.G., *Usp. Khim.*, 2001, vol. 70, no. 2, pp. 167–181.
2. Sergeev, G.B., *Usp. Khim.*, 2001, vol. 70, no. 10, pp. 915–933.
3. Gusev, A.I., *Nanokristallicheskie materialy: metody polucheniya i svoistva* (Nanocrystalline Materials: Preparation Methods and Properties), Yekaterinburg: Ural'sk. Otd. Ross. Akad. Nauk, 1998.
4. RF Patent 2103995.
5. RF Patent 2157373.
6. Sirotkina, E.E., Kobotaeva, N.S., Svarovskaya, N.V., *et al.*, in *32nd Int. Annual Conf. of ICI*, Karlsruhe (Germany), July 3–6, 2001, pp. 97–105.
7. Polyboyarov, V.A., Lapin, A.E., Korotayeva, Z.A., *et al.*, Abstracts of Papers, *Int. Conf. "Fundamental Bases of Mechanochemical Technologies,"* Novosibirsk (Russia), August 16–18, 2001, pp. 67–69.
8. Emanuel', N.M., Gladyshev, G.P., Denisov, E.T., *et al.*, *Poryadok testirovaniya khimicheskikh soedinenii kak katalizatorov polimernykh materialov* (Procedure for Testing of Chemical Compounds as Catalysts for Polymeric Materials), Chernogolovka: Otd. Inst. Khim. Fiz. Akad. Nauk SSSR, 1976.
9. Houben-Weyl, *Methoden der organischen Chemie*, vol. 2: *Analytische Methoden*, Stuttgart: Georg Thieme, 1953.
10. Lebedev, N.N., *Khimiya i tekhnologiya osnovnogo organicheskogo i neftekhimicheskogo sinteza* (Chemistry and Technology of Basic Organic and Petrochemical Synthesis), Moscow: Khimiya, 1981.
11. Shalya, V.V., Kolotusha, B.I., Yampol'skaya, F.A., and Gorokhovatskii, Ya.B., *Kinet. Katal.*, 1972, vol. 13, no. 2, pp. 404–408.
12. Polyboyarov, V.A., Lapin, A.E., Korotayeva, Z.A., *et al.*, Abstracts of Papers, *Int. Conf. "Mechanochemical Synthesis and Sintering,"* Novosibirsk (Russia), June 14–18, 2004, pp. 122–123.

Russian Journal of Applied Chemistry, Vol. 78, No. 5, 2005, pp. 758–764. Translated from Zhurnal Prikladnoi Khimii, Vol. 78, No. 5, 2005, pp. 772–778.
Original Russian Text Copyright © 2005 by Zhizhina, Simonova, Russkikh, Matveev.

CATALYSIS

New Catalytic Reactions in the Presence of Mo–V-Phosphoric Heteropoly Acid Solutions

E. G. Zhizhina, M. V. Simonova, V. V. Russkikh, and K. I. Matveev

Boreskov Institute of Catalysis, Siberian Division, Russian Academy of Sciences, Novosibirsk, Russia
Vorozhtsov Institute of Organic Chemistry, Siberian Division, Russian Academy of Sciences, Novosibirsk, Russia

Received September 30, 2004; in final form, February 2005

Abstract—The possibility of performing new catalytic reactions in the presence of solutions of $H_{x+3}PMo_{12-x}V_xO_{40}$ Mo–V-phosphoric heteropoly acids was examined.

Solutions of Mo–V-phosphoric heteropoly acids (HPAs) of the Keggin structure and the composition $H_{x+3}PMo_{12-x}V_xO_{40}$ (HPA-*x*, *x* = 2–6) find expanding application as effective catalysts of oxidation of organic compounds with oxygen [1–3]. In the presence of HPAs, these reactions often proceed in two steps performed in different reactors. In step (1), substrate H_2Su is oxidized with HPA to form the reaction product SuO and reduced HPA H_mHPA. In step (2), HPA is regenerated with oxygen. Catalytic reaction (3) is a sum of these reactions; it proceeds in the mode of non-steady-state catalysis. In these reactions, HPA acts as reversible oxidant.

$$m/4H_2Su + m/4H_2O + HPA \rightarrow m/4SuO + H_mHPA, \quad (1)$$

$$H_mHPA + m/4O_2 \rightarrow HPA + m/2H_2O, \quad (2)$$

$$H_2Su + O_2 \xrightarrow{HPA} SuO + H_2O. \quad (3)$$

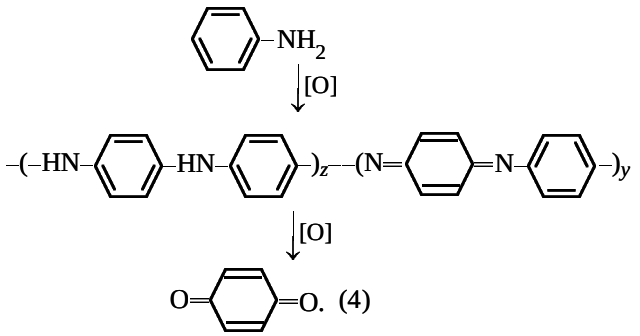
In HPA solutions, only vanadium ions undergo reversible redox transformations: V(V) → V(IV). Separate performance of reactions (1) and (2) provides high selectivity of reaction (1).

In this work we studied the oxidation of new substrates [aniline (An), *o*-toluidine (TD), hydroquinone (HQ), and partially hydrogenated quinones of naphthalene and anthracene series] in the presence of 0.2–0.25 M aqueous solutions of HPAs-*x* (*x* = 3–6, where *x* is the number of vanadium atoms in the molecule). Also, synthesis of 9,10-anthraquinone (AQ) was performed by combining the diene synthesis and oxidation of the adducts.

EXPERIMENTAL

In all the processes, HPA solutions were regenerated at 150–160°C and oxygen pressure of 6–9 atm [4, 5]. Almost complete regeneration of the activity of HPA solutions allowed their multiple reuse.

Oxidation of aniline and *o*-toluidine. Aniline and other aromatic amines are often oxidized with strong oxidants such as $NaClO_3$, $K_2Cr_2O_7$, etc. Depending on the oxidant and conditions, the reaction can yield 1,4-benzoquinone (BQ) or polyaniline (PAn), a product of oxidative polymerization {scheme (4) [6–8]}. Polyaniline can be quantitatively oxidized to BQ [8]:



(4)

Being a conducting polymer, PAn is widely used in chemical current sources [9, 10] and as stable black dye [11]. Development of environmentally safe procedures for catalytic oxidation of aniline to form PAn is an urgent problem.

We attempted to solve this problem using solutions of HPAs-*x* (*x* = 3, 4). Here we report the data on oxidation of AN and TD in HPA solutions; depending on the reaction conditions, either PAn or BQ can be obtained.

1070-4272/05/7805-0758© 2005 Pleiades Publishing, Inc.

Aromatic amines were oxidized in a 100-ml flask at stirring with a magnetic stirrer. Aniline (5.5 mmol) was added to a 0.2 M aqueous solution of HPA-3 (3.66 mmol), and a black precipitate (0.4858 g) that formed upon stirring of the reaction mixture for 30 min at 22°C was filtered off. The properties of this black compound correspond to those of PAn prepared by noncatalytic oxidation of aniline [7, 12]. This product is insoluble in organic solvents, organic acids (e.g., acetic, oxalic, and tartaric acids), and concentrated HCl, and is poorly soluble in concentrated KOH and NaOH. It is soluble only in concentrated H_2SO_4 and, with oxidation, in concentrated HNO_3. Except the 1000–800 cm^{-1} range, the IR spectrum of this compound essentially coincided with the IR spectrum of PAn [poly(*p*-phenylenaminimine)] [12].

The composition of this product is as follows, %: C 59.36, H 4.39, and N 11.98. Calculated composition of PAn {$z = y$ in scheme (1) [7]}, %: C 79.56, H 4.97, and N 15.47. The C/N ratio in our compound and in those prepared in [7] is 4.95 and 5.14, respectively. This difference is probably due the fact that x and z in the formula of the PAn obtained in our work differ from those in the formula $C_6H_{4.5}N$ {$z = y$, scheme (1) [7]}.

o-Toluidine was oxidized under the similar conditions (22°C, 30 min). For this purpose, the substrate (5.5 mmol) was added to a 0.2 M aqueous solution of HPA-3 (3.66 mmol). As a result, we obtained methylated PAn (0.5620 g) of the following composition, %: C 60.62, H 6.30, and N 6.59 [calculated, %: C 82.76, H 3.45, and N 13.79]. Higher content of H and C in the product is due to the additional methyl group in the monomer.

The GLC and ^1H NMR data show that, at 90–100°C, PAn prepared by low-temperature oxidation of An dissolves in excess HPA-3 or HPA-4 to form BQ at the molar ratio HPA-x : aniline = 3, recalculated to the initial An concentration. This result agrees with published data [8] and additionally confirms formation of PAn. If An is oxidized directly in excess HPA-x (x = 3, 4) at temperature higher than 70°C, BQ is formed in a quantitative yield.

As seen from Table 1, the yield of PAn depends on the HPA-3 : An molar ratio. The yield of PAn is low at HPA-3 deficiency due to incomplete An conversion, whereas at HPA-3 excess it decreases owing to partial oxidation of An to BQ. In HPA-4 solutions the highest yield of PAn is observed at the molar ratio HPA-4 : An = 0.5, which is due to larger number of vanadium(V) atoms than in HPA-3, i.e., to greater oxidative power.

Table 1. Yield of PAn in oxidation with HPA-3 solution at 22°C for 30 min; An content 0.5115 g (5.5 mmol)

Amount of An, mmol	HPA-3 : AN molar ratio	Amount of PAN, g	PAn : An weight ratio
4.58	0.83	0.3802	0.74
3.66	0.67	0.4858	0.95
1.83	0.33	0.0912	0.18

* PAn was separated from HPA-3 solution by filtration, washed, and dried over $CaCl_2$.

Our data show that, depending on the experimental conditions, An and TD are oxidized in HPA-x solutions yielding either the corresponding PAn or the corresponding 1,4-quinone. Regeneration of HPA-x with oxygen by reaction (2) [4, 5] closes the catalytic cycle and thus allows development of a catalytic process for synthesis of PAn in the presence of HPA solutions.

Preparation of 1,4-benzoquinone, 1,4-naphthoquinone, and 9,10-anthraquinone by oxidative dehydrogenation. *p*-Quinones are usually obtained by oxidation of appropriate substrates with strong oxidants. For example, BQ is prepared by oxidation of hydroquinone with salts of copper(II) [13], iron(III) [14], chromium(VI) [15], and sodium nitrosodisulfonate (Fremy salt) [16]. 1,4-Naphthoquinone (NQ) is prepared by oxidation of naphthalene with salts of chromium(VI) and cerium(IV) [17]. Anthraquinone is most often prepared from anthracene by oxidation with air at 360–380°C in the presence of V_2O_5 catalyst [18] or with such strong oxidants as $ZnCr_2O_7 \cdot 3H_2O$ or AcO_2H [17]. These processes are economically inefficient because of high cost of the oxidant; moreover, they are environmentally hazardous because of significant amount of wastes requiring utilization. Therefore, development of environmentally safe catalytic processes to prepare *p*-quinones is urgent. Owing to high oxidative power and reversible redox cycle [1, 19], the use of HPA-x solutions as oxidation catalysts seems promising.

It was found [20–22] that alkyl-substituted phenols of the benzene and naphthalene series can be oxidized in the presence of HPA solutions to form the corresponding *p*-quinones with high selectivity (85–99%). These reactions are usually carried out in two-phase systems (e.g., HPA aqueous solution + solution of substrate and reaction products in organic solvent). In this study, we also used HPA solutions for catalytic oxidation with air (oxidative dehydrogenation) of partially hydrogenated phenols of benzene, naphthalene, and anthracene series to prepare the corresponding *p*-quinones [23].

Table 2. Oxidative dehydrogenation of partially hydrogenated quinones in a 0.25 M solution of HPA-4 ($H_7PMo_8V_4O_{40}$, 5.62 mmol)

Substrate, mmol	HPA : substrate molar ratio	Solvent, ml	*T*, °C	τ, h	Yield, %		Substrate conversion, %
					quinone	dihydroquinone	
DDN:		1-Octanol:			NQ:		
1	5.62	10	65	2.5	67	–	100
2	2.81	4	68	2.5	62	–	100
4	1.40	4	68	1	68	–	100
						DHN:	
4	1.40	Chloroform, 5	50	1	30	59	97
4	1.40	–	70	1	82	6	100
4	1.40	Hexane, 5	60	1	71	11	92
THN, 4	1.40	–	70	1	96	–	100
THA:					AQ:	DHA:	
4	1.40	–	80	1	5	67	72
4	1.40	Octanol, 4	90	3	49	37	100
4*	1.56	–	60	3	33	67	100
HQ:		Chloroform:			BQ:		
4	1.40	7	45	0.5	82	–	100
8	0.70	5	24	0.5	97	–	100

* Experiment was performed with 0.25 M solution of HPA-6 ($H_9PMo_6V_6O_{40}$, 25 ml, 5.62 mmol).

Oxidative dehydrogenation was carried out with stirring in a 100-ml temperature-controlled conical flask equipped with a reflux condenser. In the case of two-phase systems, the reaction products are separated from the catalyst by phase separation. If the reaction was performed in the absence of organic solvent, the solid products were filtered off from the HPA solution. For more complete isolation of the reaction products, they were extracted with an organic solvent (chloroform, benzene); the extracts were dried over $CaCl_2$ and evaporated to dryness. The components of the residue were separated chromatographically (SiO_2, hexane, benzene, and chloroform eluents). The yields of the products were determined from the ^1H NMR spectra. The data on the oxidative dehydrogenation of several compounds studied are listed in Table 2.

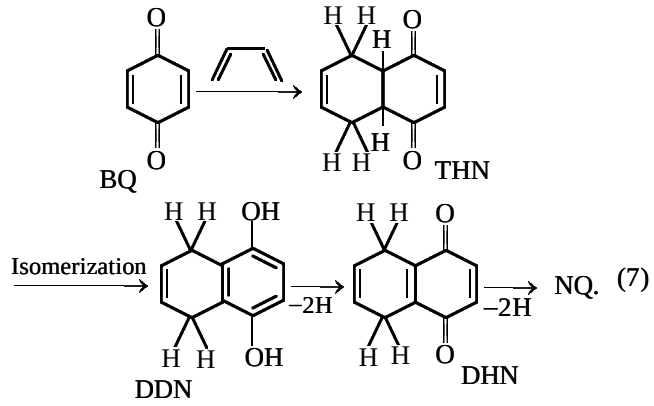
The oxidative dehydrogenation of 1,4-dihydroxy-5,8-dihydronaphthalene (DDN) in 0.25 M solution of HPA-4 at 50–70°C gives NQ in a yield from 30 to 82% and 5,8-dihydronaphthalene-1,4-dione (DHN) in a yield of up to 59% [scheme (5)]. With increasing temperature, the yield of NQ increases:

$$\mathrm{DDN} \xrightarrow[50\text{–}70^\circ\mathrm{C},\ 1\text{–}2.5\ \mathrm{h}]{\text{HPA-4}} \underset{\leq 59\%}{\mathrm{DHN}} + \underset{30\text{–}82\%}{\mathrm{NQ}}. \qquad (5)$$

This reaction can be performed without organic solvent. A solid substrate is added into an HPA solution heated to a required temperature before switching on stirring. As the initial substrate we can use 4a,5,5,8a-tetrahydronaphthalenedione (THN), and not the product of its isomerization (DDN). In this case, the yield of NQ reached 96%. No DHN was found in the reaction mixture (Table 2):

$$\mathrm{THN} \xrightarrow[70^\circ\mathrm{C},\ 1\ \mathrm{h}]{\text{HPA-4}} \underset{\leq 96\%}{\mathrm{NQ}}. \qquad (6)$$

These data suggest that the known procedure [24, 25] for preparing NQ [scheme (7)], which requires preliminary isomerization of THN in DDN and subsequent two-stage oxidation first into DHN and then into NQ using two different oxidants, can be significantly simplified and performed in one stage in the presence of HPA solutions:



(7)

The oxidative dehydrogenation of 1,4,4a,9a-tetrahydro-9,10-anthraquinone (THA) to 1,4-dihydro-9,10-anthraquinone (DHA) (Table 2) in the presence of HPA-4 solutions proceeds under more severe conditions than hydrogenation of THN and DDN:

$$\underset{}{\text{THA}} \xrightarrow[60\text{–}90^\circ\text{C},\ 1\text{–}3\ \text{h}]{\text{HPA-4}} \underset{37\text{–}67\%}{\text{DHA}} + \underset{5\text{–}49\%}{\text{AQ}}. \qquad (8)$$

On the contrary, hydroquinone is readily oxidized into BQ even at room temperature with a high yield (up to 98%), and with increasing temperature the yield of BQ decreases:

$$\underset{}{\text{HQ}} \xrightarrow[24\text{–}25^\circ\text{C},\ 0.5\ \text{h}]{\text{HPA-4}} \underset{82\text{–}98\%}{\text{BQ}}. \qquad (9)$$

The above data show that *p*-quinones of the benzene, naphthalene, and anthracene series can be prepared by oxidation of their partially hydrogenated derivatives in HPA solutions. Since DDN and THA are rather expensive, commercial synthesis of NQ and AQ should be based on more available substrates. However, the successful oxidative dehydrogenation of various substrates (Table 2) shows that the HPA solutions can be used as bifunctional catalysts for preparing 1,4-naphthoquinone and 9,10-anthraquinone.

Diene synthesis of 9,10-anthraquinone. Anthraquinone and its derivatives are intermediate products in synthesis of dyes, analytical reagents, and drugs [26]. 9,10-Anthraquinone is used as a catalyst of redox reactions, in particular, in production of hydrogen peroxide [27]. Moreover, AQ and its derivatives catalyze wood delignification and increase the yield of cellulose, degree of its bleaching, and its strength properties [28]. For this purpose, "soluble AQ," i.e., sodium salt of THA (intermediate product in the diene synthesis of 9,10-anthraquinone), is widely used [29].

Known procedures for preparing AQ can be subdivided in two groups. The first group includes oxidation of anthracene into AQ with atmospheric oxygen and other oxidants at 350–400°C [17, 26], and the second group is based on the cyclization reactions involving inter- and intramolecular acylation and Diels–Alder diene synthesis [26]. In the case of acylation, benzene and phthalic anhydride are the initial reagents and synthesis is carried out in several steps. The first stage yields 2-benzoylbenzoic acid, which is then dehydrated in the presence of various heterogeneous catalysts to form AQ [30].

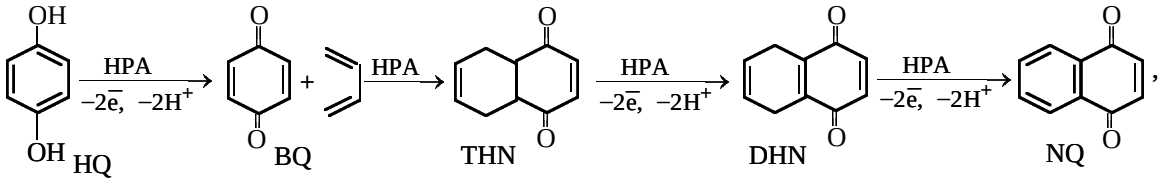
Diene synthesis is one of the commercial procedures for preparing THA, DHA, and AQ. It is based on the catalytic gas-phase oxidation of naphthalene into NQ and its subsequent reaction with 1,3-butadiene [26]. The primary addition products (adducts) are obtained in organic solvents either at elevated pressure of 1,3-butadiene of 0.3–2.0 MPA or in the presence of organic acids to decrease the pressure. In the presence of oxygen or alkalis, THA (adduct of diene synthesis) isomerizes to form 1,4-dihydro-9,10-dihydroxyanthracene, and this product is then oxidized in DHA and AQ with strong oxidants in acidic solutions or with atmospheric oxygen in an alkaline medium.

All modern procedures for preparing AQ and its derivatives are multistage and environmentally hazardous; each step produces significant amount of wastes including strong acids, spent acid catalysts, and oxidants, e.g., toxic compounds of chromium(VI) and (III), which require recycling.

Growing demand for AQ and its derivatives cannot be complied using outmoded and environmentally hazardous processes. Russia has no large-scale commercial production of AQ, and only foreign companies supply the required reagent. Hence, development of the domestic environmentally safe production of AQ and its derivatives is a very urgent problem.

Catalysts based on HPA show promise for this purpose. For example, condensation of NQ with 2,3-dimethyl-1,3-butadiene (Diels–Alder reaction) in the presence of tungsten HPA ($H_3PW_{12}O_{40}$ and $Ce_{0.87}H_{0.4}PW_{12}O_{40}$) yields substituted THA (70–80%) [31]. No oxidation of this product was observed because these HPAs exhibit no oxidative power [1, 31].

In the diene synthesis, we used solutions of HPA-*x* (*x* = 4–6) [23], which are both strong acids catalyzing Diels–Alder reaction and strong reversible oxidants. In contrast to Meuzelaar *et al*. [31], we succeeded in combining the diene synthesis with oxidation of the adducts in the presence of HPA solutions [23]. 9,10-Anthraquinone and its derivatives were prepared by one-pot synthesis:

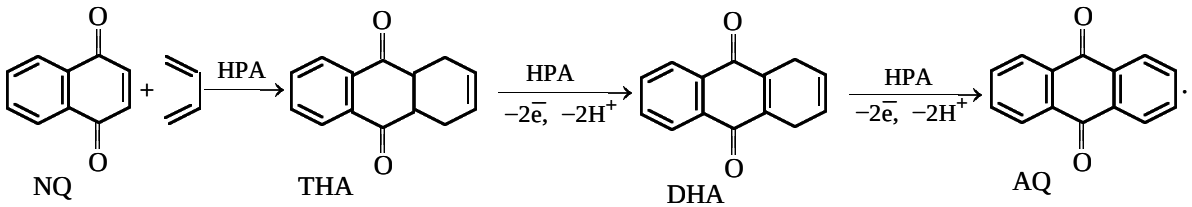


(10)

Table 3. Preparation of a mixture of THA, DHA, and AQ from HQ in 0.25 M solution of HPA-6 ($H_9PMo_6V_6O_{40}$) by the Diels–Alder reaction. 1,3-Butadiene medium, initial content of HQ 5 mmol, reaction time 10 h, conversion of HQ 100%; content of the reaction products in the reaction mixture was determined chromatographically

HPA-6, mmol	HPA-6 : HQ molar ratio	Solvent, ml	*T*, °C	Reaction products, %			
				AQ	DHA	THA	NQ
6.25	1.25	Chloroform, 5	23	–	1	23	71
6.25	1.25	Trichloroethylene, 5	23	–	2	46	47
6.25	1.25	–	23	9	3	67	15
6.25	1.25*	–	23	10	4	65	17
12.5	2.5	–	23	19	9	45	21
12.5	2.5	–	40	19	4	49	22

* 0.25 M solution of HPA-6 acidic salt $NaH_8PMo_6V_6O_{40}$ was used in the experiment.



(11)

Hydroquinone was used as the initial substrate [schemes (10), (11)]. It was oxidized to BQ and then condensed with 1,3-butadiene. The adducts of the diene synthesis were oxidized to NQ in the same HPA-*x* solution. In the second step of the process [scheme (11)], NQ was condensed with 1,3-butadiene to form THA, which was then oxidized to DHA and AQ. All the above reactions were performed as one-pot process owing to bifunctional properties of HPA acting as both acid and oxidation catalyst. In the course of this process, HPA was reduced to H_mHPA, where *m* is the number of electrons accepted by the HPA molecule. After the reaction completion, poorly soluble products (AQ, DHA, THA) were filtered off from the aqueous solution of H_mHPA. The solution of HPA-*x* was regenerated at 150–160°C under oxygen pressure, as in the case of oxidation of aniline, which allows multiple reuse of the HPA solutions.

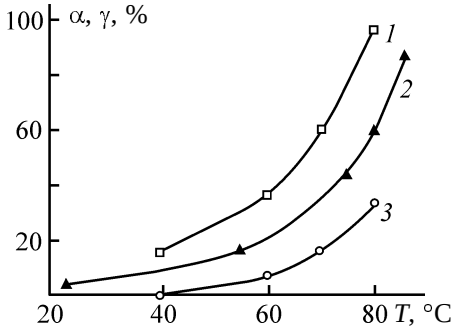


Fig. 1. (*1, 2*) Conversion of NQ γ and (*3*) yield of AQ α as functions of temperature *T*. 1,3-Butadiene medium, 0.2 M HPA-4 (25 ml), NQ 0.79 g. Conversion of NQ: (*1*) after 7 h (^{1}H NMR data) and (*2*) after 5 h (GLC data); (*3*) yield of AQ in 7 h (^{1}H NMR data).

First we studied preparation of AQ and its hydrogenated derivatives THA and DHA from HQ in HPA solutions by reaction schemes (10) and (11). The experimental results are listed in Table 3. As seen, with increasing temperature and HPA-6 : HQ molar ratio, the content of AQ in the reaction mixture increases, whereas addition of a solvent decreases the AQ yield.

For better understanding of processes (10) and (11), we studied separately step (11), i.e., preparation of a mixture of AQ, THA, and DHA from NQ. These data are also of independent importance. For example, if NQ as initial substrate will be acceptable by a cheap method (e.g., by oxidation of naphthalene), then the one-pot process for preparing AQ from NQ will be competitive, because at present HQ is a cheaper substrate as compared to NQ.

We found that the rate of reaction (11) strongly depends on temperature. At 40°C, the rate of the diene synthesis is low, but with increasing temperature to 80°C the conversion of NQ and the yield of AQ rapidly increase (Fig. 1). Simultaneously the solubility of NQ in HPA-*x* solution also increases, which promotes

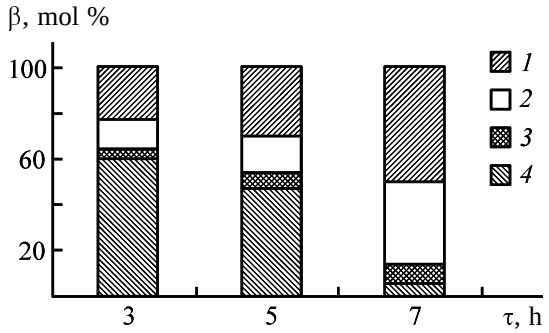


Fig. 2. Changes in the composition of the reaction products β with reaction time τ. 1,3-Butadiene medium, 80°C, 0.2 M HPA-4 (25 ml), NQ 0.79 g. (*1*) AQ, (*2*) DHA, (*3*) THA, and (*4*) NQ.

the reaction. The NQ conversion and AQ yield increase with time. The dependence of the precipitate composition on the reaction time (based on the ^{1}H NMR data) is shown in Fig. 2. As seen, the fraction of DHA in the reaction mixture is greater than that of THA. This suggests that the oxidation of DHA in AQ is slower than the oxidation of THA to DHA.

We also studied the condensation of HPA-4 with 1,3-butadiene as influenced by some organic solvents. We found that such solvents as toluene, benzene, and chloroform do not noticeably affect the NQ conversion and AQ yield. These results agree with the data on the diene synthesis of NQ with 1,3-butadiene in HPA-6 solution (Table 2).

We also studied how the HPA-4 : NQ molar ratio affects the composition of the reaction products of the diene synthesis of NQ with 1,3-butadiene and subsequent oxidation of the adducts [scheme (11)]. The HPA-4 : NQ molar ratio was varied by changing the content of NQ at constant content of HPA-4; the results are listed in Table 4.

As seen, with increasing HPA-4 : NQ molar ratio the yield of AQ increases. At high molar ratios (HPA-4 : NQ > 2), the catalysts retains high oxidative potential for a longer period, which provides higher conversion in reaction (11).

Table 4. AQ yield in the diene synthesis as influenced by HPA-4 : NQ molar ratio. 1,3-Butadiene medium, 0.2 M HPA-4 (25 ml), time 5 h, temperature 80°C

Weighed portion of NQ, g	HPA-4 : NQ molar ratio	AQ yield, %
1.58	0.5	7.2
0.79	1	12.9
0.40	2	38.2
0.20	4	40.3

CONCLUSIONS

(1) Aniline and *o*-toluidine in solutions of Mo–V-phosphoric heteropoly acids are oxidized to 1,4-benzoquinone or undergo oxidative polymerization to form polyanilines.

(2) The adducts of the Diels–Alder reaction are oxidized with heteropoly acid solutions to the corresponding *p*-quinones.

(3) Solutions of heteropoly acids can be used as bifunctional catalysts, i.e., acid catalysts in the Diels–Alder reaction and oxidation catalysts. In the presence of HPA-*x* (x = 4–6) solutions, a mixture of the products is obtained with a high content of 9,10-anthraquinone and 1,4,4a,9a-tetrahydro-9,10-anthraquinone at nearly quantitative conversion of the initial substrate (hydroquinone, 1,4-benzoquinone, or 1,4-naphthoquinone). The one-pot process combines reactions of diene synthesis and oxidation of its products.

REFERENCES

1. Kozhevnikov, I.V., *Catalysis by Polyoxometalates*, Chichester: Wiley, 2002.
2. Grate, J.H., *J. Mol. Catal., Ser. A*, 1996, vol. 114, nos. 1–3, pp. 93–101.
3. Neumann, R., *J. Org. Chem*., 1989, vol. 54, no. 19, pp. 4607–4610.
4. Zhizhina, E.G., Odyakov, V.F., Simonova, M.V., and Matveev, K.I., *React. Kinet. Catal. Lett*., 2003, vol. 78, no. 2, pp. 373–379.
5. Zhizhina, E.G., Simonova, M.V., Odyakov, V.F., and Matveev, K.I., *Khim. Inter. Ustoich. Razv*., 2004, vol. 12, no. 6, pp. 683–688.
6. Geniès, E.M., Lapkowski, M., and Tsintavis, C., *New J. Chem*., 1988, vol. 12, no. 4, pp. 181–196.
7. Tarasevich, M.R., Orlov, S.B., and Shkol'nikov, E.I., *Elektrokhimiya polimerov* (Electrochemistry of Polymers), Moscow: Nauka, 1990.
8. Willstatter, R. and Dorogi, S., *Chem. Ber*., 1909, vol. 42, no. 12, pp. 4118–4121.
9. Serville, R., Jozefowicz, M., and Yu, L.T., *Electrochim. Acta*, 1968, vol. 13, no. 2, p. 1451.
10. JPN Patent 2002371219.
11. Novak, P., Müller, K., Santhanam, K.S.V., and Haas, O., *Chem. Rev*., 1997, vol. 97, no. 1, pp. 207–281.
12. Wudl, F., Angus, R.O., Lu, F.L. *et al*., *J. Am. Chem. Soc*., 1987, vol. 109, pp. 3677–3684.

13. Sakamoto, T., Yonehara, H., and Pac, C., *J. Org. Chem.*, 1997, vol. 62, no. 10, pp. 3194–3199.
14. Scheib, S., Cava, M.P., Baldwin, J.W., and Metzger, R.M., *J. Org. Chem.*, 1998, vol. 63, no. 4, pp. 1198–1202.
15. Owton, W.M., *J. Chem. Soc. Perkin Trans.*, 1999, no. 17, pp. 2409–2420.
16. Zimmer, H., Lankin, D.C., and Horgan, S.W., *Chem. Rev.*, 1971, vol. 71, no. 2, pp. 229–236.
17. Hudlicky, M., *Oxidation in Organic Chemistry*, Washington, DC, 1990.
18. Pielichowski, J., Gurtat, P., and Polaczek, J., *Przem. Chem.*, 1997, vol. 76, no. 2, pp. 49–52.
19. Zhizhina, E.G., Simonova, M.V., Odyakov, V.F., and Matveev, K.I., *React. Kinet. Catal. Lett.*, 2003, no. 4, pp. 171–179.
20. Matveev, K.I., Zhizhina, E.G., and Odyakov, V.F., *Khim. Prom–st.*, 1996, no. 3, pp. 173–179.
21. Matveev, K.I., Odyakov, V.F., and Zhizhina, E.G., *J. Mol. Catal., Ser. A*, 1996, vol. 114, nos. 1–3, pp. 151–160.
22. Kolesnik, I.G., Zhizhina, E.G., and Matveev, K.I., *React. Kinet. Catal. Lett.*, 1999, no. 2, pp. 339–346.
23. Zhizhina, E.G., Matveev, K.I., and Russkikh, V.V., *Khim. Inter. Ustoich. Razv.*, 2004, vol. 12, no. 1, pp. 47–51.
24. Fieser, L.F., *J. Am. Chem. Soc.*, 1948, vol. 70, no. 10, pp. 3165–3166.
25. Fieser L.F. and Fieser M., *Reagents for Organic Synthesis*, New York: Wiley, 1968.
26. Gorelik, M.V., *Khimiya antrakhinonov i ikh proizvodnykh* (Chemistry of Anthraquinones and Their Derivatives), Moscow: Khimiya, 1983.
27. Efimov, N.K., Zhitkov, I.V., and Trubkin, V.E., *Khim. Prom–st.*, 1995, no. 12, pp. 751–753.
28. Burasko, L.V., Men'shikov, S.Yu., Ageev, A.Ya., *et al.*, *Lesn. Zh.*, 1994, no. 3, pp. 94–99.
29. Russkikh, V.V., *Khim. Inter. Ustoich. Razv.*, 1999, vol. 7, no. 1, pp. 85–88.
30. Tesser, R., Di Serio, M., and Ambrosio, M., *Chem. Eng. J.*, 2002, vol. 90, nos. 1–2, pp. 195–201.
31. Meuzelaar, G.J., Maat, L., Sheldon, R.A., and Kozhevnikov, I.V., *Catal. Lett.*, 1997, vol. 45, nos. 3–4, pp. 249–251.
32. Zhizhina, E.G., Odyakov, V.F., and Matveev, K.I., *Zh. Prikl. Khim.*, 2000, vol. 73, no. 5, pp. 777–780.

Russian Journal of Applied Chemistry, Vol. 78, No. 5, 2005, pp. 765–768. Translated from Zhurnal Prikladnoi Khimii, Vol. 78, No. 5, 2005, pp. 779–782.
Original Russian Text Copyright © 2005 by Zakharov, Berlin, Monakov.

CATALYSIS

Decrease in Content of Insoluble Fraction in *cis*-1,4-Polyisoprene in Formation of Titanium Catalyst in Turbulent Flow

V. P. Zakharov, Al. Al. Berlin, and Yu. B. Monakov

Bashkir State University, Ufa, Bashkortostan, Russia
Semenov Institute of Chemical Physics, Russian Academy of Sciences, Moscow, Russia
Institute of Organic Chemistry, Ufa Scientific Center, Russian Academy of Sciences, Ufa, Bashkortostan, Russia

Received October 14, 2004

Abstract—The effect caused by using a tubular prereactor of the diffuser–confuser design operating in the turbulent flow mode on the content of the insoluble gel fraction in *cis*-1,4-polyisoprene obtained on a Ti/Al catalyst is studied.

SKI-3 large-scale synthetic isoprene rubber is synthesized on Ti/Al Ziegler–Natta catalysts on the basis of the *cis* isomer and is used primarily in production of tires, conveyer belts, and other industrial and medical goods. Performance of goods manufactured from *cis*-1,4-polyisoprene and their application areas are controlled to a considerable extent by the molecular characteristics of the macrochains, particularly, by the content of the insoluble fraction (gel fraction) in the polymer, which may be as large as 20–30% [1]. Rubber stocks based on *cis*-1,4-polyisoprene with decreased insoluble fraction can be processed by molding, and SKI-3-based rubber stocks with low gel fraction content demonstrate better adhesiveness and lower shrinkage [1].

Muzhai *et al*. [2] suggested that formation of the gel fraction in stereoregular polymerization of dienes on Ziegler–Natta catalysts is initiated by secondary cationic reactions involving the macrochain at the solid surface of the heterogeneous catalyst. Most likely, these reactions are intra- and intermolecular interactions between the double bonds of the ready polymer chain and also chain propagation. At the same time, we have demonstrated previously that, in polymerization of isoprene on $TiCl_4$–$Al(i\text{-}C_4H_9)_3$, the use of a tubular turbulent prereactor installed before the bulk polymerizer with longer residence time affects the catalyst particle size distribution, particularly, reduces the particle size in the catalytically active precipitate. Evidently, this alters the insoluble fraction content in *cis*-1,4-polyisoprene, allowing development of a procedure aimed at decreasing the gel fraction content in isoprene rubber and improving performance characteristics of the products.

Therefore, in this study we examined the effect of the stereoregular polymerization procedure, namely, of the formation of the $TiCl_4$–$Al(i\text{-}C_4H_9)_3$ catalyst in a turbulent flow provided by the use of a tubular turbulent prereactor of the diffuser–confuser design on the content of the insoluble fraction in *cis*-1,4-polyisoprene.

The experimental setup for isoprene polymerization was described elsewhere [3]. The starting reactants were purified by standard methods accepted in stereoregular polymerization on Ziegler–Natta catalysts. In the experiments we varied the process procedure, the polymerization conditions remaining unchanged.

Method no. 1 simulated the traditional industrial polymerization process. Separately prepared solutions of the catalytic system [binary $TiCl_4$–$Al(i\text{-}C_4H_9)_3$ or ternary (modified) $TiCl_4$–$Al(i\text{-}C_4H_9)_3$–piperylene (piperylene as a modifier was introduced in the catalytic complex solution at the stage of its preliminary keeping)] kept for 30 min at 273 K and of the monomer were directly introduced into the apparatus (flask) with gentle stirring.

Method no. 2. The preliminarily kept catalytic system and the solvent were mixed in a tubular apparatus operating in the turbulent flow mode. Then the catalyst solution was fed to a stirred vessel. The monomer was added with gentle stirring.

Method no. 3. Separately prepared solutions of $TiCl_4$ and $Al(i\text{-}C_4H_9)_3$ were mixed in the tubular apparatus. The fast formation of the catalytically active precipitate proceeded in a turbulent flow, followed by keeping for 30 min with gentle stirring in the vessel at 273 K. Finally, the monomer was added.

1070-4272/05/7805-0765© 2005 Pleiades Publishing, Inc.

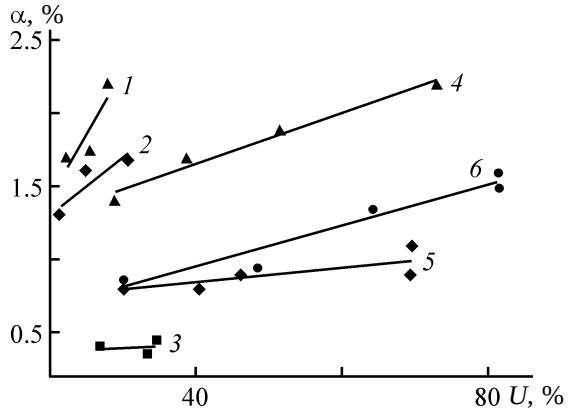


Fig. 1. Content of the gel fraction α as a function of the yield of *cis*-1,4-polyisoprene *U* on (*1*–*3*) $TiCl_4$–Al(*i*-C_4H_9)$_3$ and (*4*–*6*) $TiCl_4$–Al(*i*-C_4H_9)$_3$–piperylene catalysts. Ti : Al : piperylene molar ratio 1 : 1.25 : 2; solvent toluene; c_{Ti} = 6 mM; c_M = 1.5 M; 298 K. Polymerization conditions: (*1*, *4*) method no. 1 (conventional), (*2*, *5*) method no. 2 (exposure of the catalyst particles to turbulent flow), (*3*) method no. 3 (formation of the catalytic system in turbulent flow), and (*6*) method no. 4 (formation of the reaction mixture in turbulent flow).

Method no. 4. Separately prepared solutions of the preliminarily kept ternary catalytic system and monomer were mixed in the tubular apparatus and then fed into the bulk reactor. In this case, the catalyst particles were exposed to the turbulent flow. The procedure ensured fast initiation (addition of the first monomer molecule to the active center) and uniform distribution of the growth centers on the surface of the heterogeneous catalyst throughout the bulk of the reaction mixture.

In method nos. 2–4, the residence time of the reaction mixture in the tubular turbulent prereactor of the diffuser–confuser design was about 2–3 s.

The insoluble fraction in *cis*-1,4-polyisoprene was determined by extraction with hot toluene for 150 h [4]. For extraction, a 0.2-g sample was placed in cambric bag. The content of the insoluble fraction was determined gravimetrically.

Grechanovskii and Poddubnyi [5] have demonstrated that the insoluble fraction in polyisoprene consists of conglomerates of particular molecules, representing a physical gel rather than a cross-linked polymer. In this case, the conglomerates pass into solution upon stirring. The catalyst deactivation procedure used in this study involved vigorous mechanical action on both the polymer solution and polymer at the stage of precipitation with methanol. In this case, the physical gel is broken down, and the analysis for the insoluble fraction content in *cis*-1,4-polyisoprene reflects the content of the gel fraction formed by cross-linked macromolecules (chemical gel). As a result, the content of the insoluble fraction in *cis*-1,4-polyisoprene appears to be small, being below 3% (Fig. 1).

The content of the insoluble fraction increases with increasing polymer yield. Exposure of the catalyst system to turbulent flow (Fig. 1, curve *2*) slightly decreases the gel fraction content in the polymer as compared to the conventional method (Fig. 1, curve *1*). The minimal content of the gel fraction in *cis*-1,4-polyisoprene was observed when the fast reaction of the starting $TiCl_4$ and Al(*i*-C_4H_9)$_3$ solutions was conducted in a tubular turbulent prereactor with formation of a finely dispersed catalyst (Fig. 1, curve *3*). Modification of the $TiCl_4$–Al(*i*-C_4H_9)$_3$ catalyst by addition of piperylene decreases the gel fraction content under the same polymerization conditions (Fig. 1, curves *1* and *4*, and *2* and *5*). Furthermore, in the case of the modified catalyst, the effect of the turbulent flow on the gel fraction content is more pronounced.

It was demonstrated in our previous paper [6] that the polymerization procedure, particularly, the use of a tubular turbulent prereactor influences the molecular weight distribution of *cis*-1,4-polyisoprene, growth center concentration, and polymerization rate. An integral characteristic of the process is the amount of macrochains per active center. Therefore, it appeared advisable to examine the interrelation between the insoluble fraction content in the polymer and this integral parameter.

The amount of polymer chains in the reaction mixture *N* is written as

$$N = c_M U/P_n, \quad (1)$$

where c_M is the initial monomer concentration; *U*, polymer yield; and P_n, number-average degree of polymerization.

In turn, the amount of polymer chains *n* per active center is written as

$$n = c_M U/P_n c_a, \quad (2)$$

where c_a is the concentration of active centers.

In accordance with Eq. (1), with increasing polymer yield, the amount of macrochains in the reaction mixture increases as well as the probability of secondary processes, particularly, cross-linking, in the polymer chains. All this results in formation of a polymer with a high gel fraction content, as demonstrated experimentally (Fig. 1). At the same time, analysis

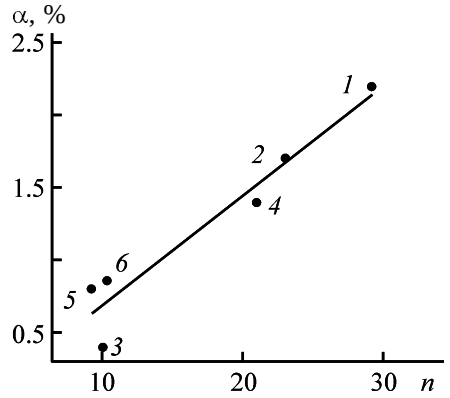


Fig. 2. Content of the gel fraction in *cis*-1,4-polyisoprene α as a function of the amount of macromolecules *n* per active center in polymerization on (*1–3*) $TiCl_4$–$Al(i\text{-}C_4H_9)_3$ and (*4–6*) $TiCl_4$–$Al(i\text{-}C_4H_9)_3$–piperylene catalysts. Polymerization conditions: (*1, 4*) conventional method, (*2, 5*) exposure of the catalyst particles to turbulent flow, (*3*) formation of the catalytic system in turbulent flow, and (*6*) formation of the reaction mixture in turbulent flow (polymer yield 30%).

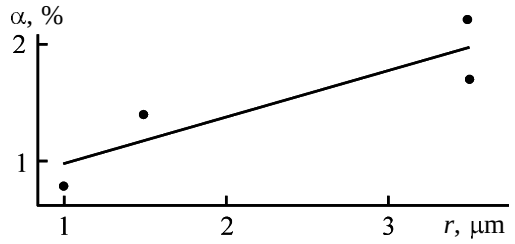


Fig. 3. Content of the gel fraction α as a function of the radius of the particles of the Ti/Al catalyst *r*.

of data on the insoluble fraction in *cis*-1,4-polyisoprene synthesized on $TiCl_4$–$Al(i\text{-}C_4H_9)_3$ and $TiCl_4$–$Al(i\text{-}C_4H_9)_3$–piperylene catalytic systems under various polymerization conditions revealed a general trend in this parameter as a function of the amount of macrochains per active center (Fig. 2).

It is known that active centers of stereoregular polymerization of isoprene on $TiCl_4$–$Al(i\text{-}C_4H_9)_3$ catalyst are located on the defects of the β-$TiCl_3$ crystal lattice [7]. In accordance with Eq. (2), this implies the interrelation between the insoluble fraction content in the polymer and the particle size of the heterogeneous catalyst as obtained by the sedimentation analysis [3] (Fig. 3). Decreasing radius of the catalyst particles results in a decrease in the insoluble fraction in *cis*-1,4-polyisoprene. In turn, the catalyst particle size and, as follows from Fig. 3, the insoluble fraction content can be affected by addition of a diene to the catalytic system and also by modification of the procedure of formation of the $TiCl_4$–$Al(i\text{-}C_4H_9)_3$ catalyst using the effect of a turbulent flow [3, 6]. Indeed, the minimal amount of macrochains per active center as well as the minimal gel fraction content are observed in formation of the catalytic system in a turbulent flow, when a fast chemical reaction proceeds with formation of a finely dispersed catalytically active precipitate (Fig. 2). It is clear that further decrease in the catalyst particle size should result in a decrease in the insoluble fraction in the polymer (Fig. 3). This is confirmed by the lack of the gel fraction in the polymers obtained on pseudohomogeneous lanthanide-based catalysts [8].

Evidently, the trend observed in this study (Fig. 3) is caused by the fact that, with decreasing particle size of the catalyst, the polymeric shell on its surface, consisting of growing macromolecules, becomes close to a monomolecular adsorption layer. In this case, the probability of cross-linking through collision of internal double bonds near the active center on the catalyst surface decreases, as evidenced by the results obtained in [7, 9] that the smaller the catalyst particle size, the thicker the polymeric shell (in a monomolecular layer the thickness of the adsorption layer approaches the length of the macromolecule), and the macromolecules growing in these shells are one-end connected to the catalyst surface. It is obvious that the indicated trends in evolution of the gel fraction formed by chemically cross-linked macromolecules (chemical gel) are valid also for the insoluble fraction formed by physically bound macrochains (physical gel).

CONCLUSIONS

(1) A correlation is found between characteristics of the $TiCl_4/Al(i\text{-}C_4H_9)_3$ heterogeneous catalyst and the particle size and content of the insoluble fraction in *cis*-1,4-polyisoprene. Modification of the catalytic system with a diene and hydrodynamic effects in a tubular prereactor of the diffuser–confuser design operating in the turbulent flow mode decrease the catalyst particle size as well as the content of the insoluble gel fraction in the polymer.

(2) The minimal content of the gel fraction in *cis*-1,4-polyisoprene was observed when the fast reaction of the starting $TiCl_4$ and $Al(i\text{-}C_4H_9)_3$ solutions was conducted in a tubular turbulent prereactor with formation of a finely dispersed catalyst.

ACKNOWLEDGMENTS

The work was financially supported by the Russian Foundation for Basic Research (project no. 02-01-97913) and Division of Chemistry and Materials

Sciences, Russian Academy of Sciences (project 10 002-251/OKhNM-08/131-141).

REFERENCES

1. Bashkatov, T.V. and Zhitalin, Ya.L., *Tekhnologiya sinteticheskikh kauchukov* (Technology of Synthetic Rubbers), Leningrad: Khimiya, 1987.
2. Muzhain, A., Bresler, L.S., Grechanovskii, V.A., and Poddubnyi, I.Ya., *Dokl. Akad. Nauk SSSR*, 1968, vol. 180, no. 4, pp. 920–922.
3. Zakharov, V.P., Sadykov, I.V., Minsker, K.S., *et al.*, *Zh. Prikl. Khim.*, 2004, vol. 77, no. 2, pp. 302–305.
4. Allen, P.W., *Techniques of Polymer Characterization*, London: Butterworths, 1959.
5. Grechanovskii, V.A. and Poddubnyi, I.Ya., *Dokl. Akad. Nauk SSSR*, 1971, vol. 197, no. 3, pp. 643–645.
6. Zakharov, V.P., Sadykov, I.V., Minsker, K.S., *et al.*, *Vysokomol. Soedin., Ser. A*, 2004, vol. 46, no. 10, pp. 1765–1769.
7. Grechanovskii, V.A., Andrianova, L.G., Agibalova, L.V., *et al.*, *Vysokomol. Soedin., Ser. A*, 1980, vol. 22, no. 9, pp. 2112–2120.
8. Monakov, Yu.B. and Tolstikov, G.A., *Kataliticheskaya polimerizatsiya 1,3-dienov* (Catalytic Polymerization of 1,3-Dienes), Moscow: Nauka, 1990.
9. Grechanovskii, V.A. and Poddubnyi, I.Ya., *Vysokomol. Soedin., Ser. B*, 1974, vol. 16, no. 12, pp. 875–878.

Russian Journal of Applied Chemistry, Vol. 78, No. 5, 2005, pp. 769–772. Translated from Zhurnal Prikladnoi Khimii, Vol. 78, No. 5, 2005, pp. 783–786.
Original Russian Text Copyright © 2005 by Koval', Bolotov, Zhukova, Safronova, Tregubkin.

CATALYSIS

Modification with *d* Metals of Zeolite Catalysts for Conjugated Conversion of Methanol and Lower Alkanes

L. M. Koval', V. V. Bolotov, N. V. Zhukova, S. S. Safronova, and R. A. Tregubkin

Tomsk State University, Tomsk, Russia

Received July 6, 2004; in final form, April 2005

Abstract—Joint conversion of methanol and lower alkanes on modified zeolites of the ZSM-5 type was studied.

A promising method for processing of hydrocarbon raw materials is conjugated conversion of alkanes C_3–C_4 and methanol. The most efficient catalysts in this process are zeolite catalysts of the Pentasil family, modified with various elements. The modifying elements strongly affect the selectivity and catalytic activity of zeolites, depending on their nature and method of introduction into the initial zeolite. A combination of unique structural and acid properties of Pentasils with the dehydrogenating capacity of modifiers makes it possible to develop the most selective catalysts for obtaining the desired conversion products.

The aim of this study was to examine the conjugated conversion of methanol and lower alkanes on high-silica zeolites (HSZs) modified by various methods with Group IV *d* metals and to determine how their acid and catalytic properties are related.

EXPERIMENTAL

High-silica zeolites of the ZSM-5 type with a mass ratio $SiO_2 : Al_2O_3 = 50$ (NVLTs-50) were prepared by the procedure developed in [1].

Modified HSZs (MHSZs) were produced by ion exchange (IE) and mechanical mixing (MM). In introducing a modifying element by the IE technique, a calculated amount of a soluble salt of a metal was added to an HSZ under vigorous agitation. The volume of the salt solution added was chosen so that the degree of proton exchange for metal cations was 95–100%. The modification by the MM method was performed by adding the oxide of an appropriate metal to HSZ, with subsequent mechanochemical activation in a ball mill at 293 K for 24 h. Thus, Zr-HSZ and Hf-HSZ were obtained by the IE method, and 5% TiO_2–HSZ, 5% ZrO_2–HSZ, and 5 wt % HfO_2–HSZ, by that of mechanical mixing; Ti-HSZ was produced by impregnation to saturate the moisture capacity.

As a raw material for joint conversion we used a gas mixture consisting (wt %) of methane (0.5), propane (80), and butane (19.5) and methanol. The catalytic conversion of lower alkanes and methanol was performed under atmospheric pressure, with the reaction temperature varied from 723 to 873 K. Methanol and the alkanes were fed at space velocities of 1.4 and 240 h^{-1}, respectively.

The catalytic properties of the modified zeolites are presented in Table 1.

The modification technique strongly affects the distribution of the products of joint conversion and the conversion of the raw material. As seen in Table 1, raising the reaction temperature from 773 to 873 K favorably affects the conversion of the starting alkanes for samples modified both by IE and by MM. For MHSZ produced by the IE technique, raising the temperature in the above range leads to an increase in the conversion γ from 34 to 63%. Similarly to the conversion of the starting substances, the selectivity α with respect to alkenes increases with temperature from 3.7 to 28.9 wt %; accordingly, the value of α for aromatic hydrocarbons, on the whole, falls from 13.6 to 4.5 wt %.

The maximum values of γ and α for alkenes are observed for MHSZ modified by IE in the case of Zr-HSZ: 63 and 28.9%, respectively.

For samples modified by MM (Table 1), raising the temperature from 773 to 873 K favors a more pronounced rise in γ of the starting alkanes, from 40 to 73%, compared both with the initial HSZ and with zeolites modified by IE. The selectivity of these catalysts with respect to alkenes increases with temperature to a considerably greater extent, from 12.1 to 36.2 wt %. The selectivity with respect to alkenes is the highest at 873 K for catalysts modified by the MM method (wt %): 33.4 for 5% TiO_2–HSZ, 36.2 for 5%

1070-4272/05/7805-0769© 2005 Pleiades Publishing, Inc.

Table 1. Composition of products formed in joint conversion of methanol and alkanes on MHSZ

Catalyst	γ, %	Composition of hydrocarbons, wt %													
		H_2	CH_4	C_2H_6	C_3H_8	C_2H_4	propene	isobutene	C_6H_6	toluene	xylenes	arenes C_{9+}	alkanes C_1–C_4	alkenes C_1–C_4	arenes C_6–C_{10}
Ion exchange															
T = 773 K															
Ti-HSZ	36	4.5	14.4	2.2	25.8	10.5	8.9	1.2	1.3	4.2	4.5	3.6	43.6	19.4	13.6
Zr-HSZ	37	8.8	14.2	10.3	19.9	4.9	4.2	5.7	1.3	5.1	4.3	1.3	50.1	9.1	12.0
Hf-HSZ	34	5.5	11.2	6.7	24.2	2.5	1.2	7.9	0.7	4.3	4.4	1.4	50.0	3.7	10.8
T = 823 K															
Ti-HSZ	52	3.6	13.4	2.1	26.2	9.8	11.0	0.9	1.1	3.2	5.7	3.5	42.6	20.8	13.5
Zr-HSZ	56	13.4	13.8	10.6	18.1	11.8	11.9	3.9	0.5	2.3	2.7	0.9	46.4	23.7	6.4
Hf-HSZ	38	15.0	10.6	5.5	26.7	5.0	3.7	5.8	0.5	3.0	2.9	1.1	48.6	8.7	7.5
T = 873 K															
Ti-HSZ	57	3.5	16.2	1.6	30.6	10.1	13.1	0.9	1.0	1.8	3.6	1.5	49.4	23.6	7.9
Zr-HSZ	63	16.8	12.6	10.8	18.4	16.4	12.5	1.2	0.4	1.6	1.9	0.6	42.8	28.9	4.5
Hf-HSZ	46	15.2	10.8	6.0	24.3	7.9	7.4	4.7	0.7	3.2	3.8	1.1	45.8	15.3	8.8
Mechanical mixing															
T = 773 K															
5% TiO_2–HSZ	48	16.8	11.0	6.8	25.8	11.3	7.1	2.7	0.9	3.0	2.8	1.4	46.3	18.4	8.1
5% ZrO_2–HSZ	45	9.2	9.9	3.6	37.4	14.0	9.9	4.0	0.7	3.3	6.1	1.9	54.9	23.9	12.0
5% HfO_2–HSZ	40	12.3	12.3	10.5	18.7	4.4	7.7	4.9	0.8	4.2	4.9	1.6	46.4	12.1	11.5
T = 823 K															
5% TiO_2–HSZ	60	16.2	11.0	7.3	17.6	15.4	10.2	3.2	0.6	2.0	2.4	1.0	38.1	25.6	6.0
5% ZrO_2–HSZ	64	11.8	11.9	5.5	27.3	22.0	10.6	1.9	0.4	2.1	3.4	1.1	46.6	32.6	7.0
5% HfO_2–	43	19.5	11.5	12.0	27.5	9.8	10.1	3.4	0.5	2.5	2.5	0.7	54.4	19.9	6.2
T = 873 K															
5% TiO_2–HSZ	66	15.5	11.2	9.3	14.2	17.7	15.7	0.9	0.4	1.6	1.9	0.8	35.6	33.4	4.7
5% ZrO_2–HSZ	73	16.0	12.4	6.8	28.1	22.2	14.0	1.2	0.4	2.2	1.5	0.7	48.5	36.2	4.8
5% HfO_2–HSZ	54	16.5	11.4	8.4	19.8	12.8	10.5	1.2	0.4	1.5	2.0	0.5	40.8	23.3	4.4

ZrO_2–HSZ, and 23.3 for 5% HfO_2–HSZ, which markedly exceeds the selectivity of the initial zeolite and samples modified by IE. A specific feature of the joint conversion of methanol and lower alkanes C_3–C_4 on MHSZ is the low content of benzene in the products (0.5–1.5 wt %), compared to alkylbenzenes, i.e., the role of methanol as an alkylating additive is apparent.

The difference in the catalytic activity between MHSZs obtained in different ways is due to the fact that acid centers differing both in concentration and strength and in nature are formed on the catalyst surface, depending on the modification technique. The acid parameters of the surface of the samples studied were evaluated by temperature-programmed desorption (TPD) of ammonia. The TPD spectra of all

Table 2. Acid parameters of modified HSZ

Catalyst	T_{max}, °C		Amount of acid centers, μmol g^{-1}		E_a of desorption, kJ mol^{-1}		Σ*
	I	II	I	II	I	II	
HSZ-50	290	475	433	313	72.5	155	746
Zr-HSZ (IE)	260	450	487	199	43	128.5	786
Hf-HSZ (IE)	260	450	450	180	50.3	119.7	630
5% TiO_2–HSZ (MM)	275	475	437	298	66	149	735
5% ZrO_2–HSZ (MM)	275	470	466	304	56	146	790
5% HfO_2–HSZ (MM)	280	475	428	210	70.6	124.7	638

* Total amount of type I and type II acid centers.

the samples show two types (I, II) of acid centers, with the low-temperature form identified [2–4] as weak type I acid centers with predominance of Lewis centers (LCs) and the high-temperature peak corresponding to strong type II acid centers mostly represented by Brønsted centers (BCs).

The amount of ammonia desorbed in the temperature ranges mentioned above, which can serve as a measure of the number of both types of centers, and the positions of peaks in the TPD spectra of ammonia, which indirectly characterize the strength of the acid centers present on the surface of MHSZ, are listed in Table 2.

Introduction of modifying elements into the initial zeolite changes to a certain extent the acid properties of its surface, depending on the modification technique. As seen in Table 2, introduction of Zr and Hf into the initial zeolite by IE leads to a decrease in the temperatures of peak I and II by 30 and 15°C, respectively. Also, the concentration of type II centers, to which BCs are predominantly attributed, decreases. The decrease in the temperatures of the peaks for the samples produced by IE indicates that the strengths of acid centers of both types decrease, which is also confirmed by the lower activation energy of desorption, E_a, as compared to the initial HSZ-50. For the samples modified by MM method, a significant increase in the concentration of type II acid centers is observed, by a factor of approximately 1.5 as compared to the catalysts produced by IE; the increase in E_a of desorption also indicates that the strength of these acid centers becomes higher. The concentration of type I centers (LCs) remains virtually the same as that for the initial zeolite, but the strength of these centers is somewhat higher than that for the samples modified by IE.

It is known [5] that a polyvalent modifier introduced by IE is incorporated in the cationic positions of the initial HSZ in the form of $MO(OH)^+$ species. Isolated $MO(OH)^+$ species have a coordination sphere of a larger radius and create steric hindrance, with the result that the acid centers become less accessible.

In explaining the enhanced surface acidity and high catalytic activity exhibited in alkene formation by samples modified by MM, it was suggested that isomorphic substitution of aluminum by a modifying element occurs in the mechanochemical activation in the solid phase. As a consequence, the concentration of LCs remains virtually the same as that in the initial zeolite, but their strength somewhat decreases. It may be suggested, based on the hypothesis that dehydrogenation of alkanes involves strong LCs incorporating ions of the modifying metals [6, 7] and on the experimental data obtained, that, for catalysts modified by MM, the strength of LCs is the optimal strength for formation of alkenes without their further aromatization.

CONCLUSIONS

(1) With modified high-silica zeolites used in joint conversion of methanol and lower alkanes (C_3–C_4), the chemical nature of the modifying agent and the method of modification strongly affect the distribution of conversion products.

(2) The active centers present on the surface of zeolites modified by ion exchange and mechanical mixing differ in chemical nature.

(3) The maximum selectivity with respect to alkenes is observed for a zirconium-containing zeolite catalyst modified by mechanical mixing. The resulting concentration and strength of various acid centers are optimal for formation of olefins.

ACKNOWLEDGMENTS

The study was financially supported by the Ministry of Education of the Russian Federation (grant A 03-2.11-699).

REFERENCES

1. RF Patent 1527154.
2. Koval', L.M. and Gaivoronskaya, Yu.I., *Izv. Vyssh. Uchebn. Zaved., Khim. Khim. Tekhnol.*, 1999, vol. 42, no. 6, pp. 121–126.
3. Yushchenko, V.V., Zakharov, A.N., and Romanovskii, B.N., *Kinet. Katal.*, 1986, vol. 27, no. 2, pp. 474–478.
4. Erofeev, V.I., Trofimova, A.S., Koval', L.M., and Ryabov, Yu.V., *Zh. Prikl. Khim.*, 2000, vol. 73, no. 12, pp. 1967–1974.
5. Kucherov, A.V. and Slinkin, A.A., *Kinet. Katal.*, 1986, vol. 27, no. 3, pp. 678–684.
6. Minachev, Kh.M. and Dergachev, A.A., *Itogi Nauki Tekh., Kinet. Katal.*, 1990, vol. 23, no. 3, pp. 46–55.
7. Lapidus, A.L., Dergachev, A.A., Kostina, V.A., and Mishin, I.V., *Izv. Ross. Akad. Nauk, Ser. Khim.*, 2003, no. 5, pp. 1035–1040.

Russian Journal of Applied Chemistry, Vol. 78, No. 5, 2005, pp. 773–775. Translated from Zhurnal Prikladnoi Khimii, Vol. 78, No. 5, 2005, pp. 787–789.
Original Russian Text Copyright © 2005 by Baranov, Tsypin, Malin, Laskin.

ORGANIC SYNTHESIS AND INDUSTRIAL ORGANIC CHEMISTRY

Synthesis of 2-Chloromethyl-5-aryl-, 2-Chloromethyl-5-(5-methyl-2-furyl)-, and 2-Chloromethyl-5-(1,5-dimethyl-2-pyrrolyl)-1,3,4-oxadiazoles from Tetrazole Derivatives

A. B. Baranov, V. G. Tsypin, A. S. Malin, and B. M. Laskin

Prikladnaya Khimiya Russian Scientific Center, St. Petersburg, Russia

Received October 26, 2004

Abstract—Acetylation of 5-aryltetrazoles, 5-(5-methyl-2-furyl)tetrazole, and 5-(1,5-dimethyl-2-pyrrolyl)tetrazole with chloroacetyl chloride was studied.

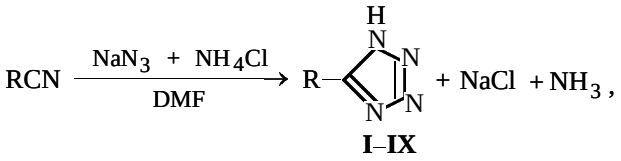
1,3,4-Oxadiazoles are key fragments of various drugs, from antiviral agents to antidepressants; they are used as organic scintillators and are components of specialty polymerizing formulations, etc. [1].

The goal of this study is the development of a one-pot procedure for preparing 5-aryl-2-chloromethyl-1,3,4-oxadiazoles and previously unknown 2-chloromethyl-5-(5-methyl-2-furyl)- and 2-chloromethyl-5-(1,5-dimethyl-2-pyrrolyl)-1,3,4-oxadiazoles from appropriate tetrazole derivatives. These 1,3,4-oxadiazoles are of interest as biologically active substances and reagents for further fine organic synthesis. Similarly to other 1,3,4-oxadiazoles [2], they can be involved in the peptide synthesis by the subsequent reactions with amino acids.

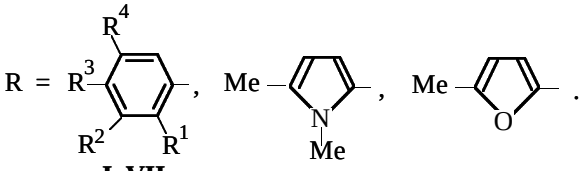
2,5-Disubstituted 1,3,4-oxadiazoles of various structures can be prepared by several procedures. The starting compounds can be carboxylic acids and hydrazine; they are converted into diacylhydrazides via several intermediates. The cyclodehydration of diacylhydrazides under the action of $POCl_3$ yields 1,3,4-oxadiazoles; these compounds can also be prepared by cyclodehydration of diaroylhydrazines and diacylhydrazines under the action of various dehydrating agents (organic acid anhydrides, PCl_5, H_2SO_4 [2–5]).

A procedure developed in [6] for preparing 2,5-diaryl-1,3,4-diazoles by the reactions of tetrazoles with benzoyl chlorides in *o*-xylene or toluene on heating was applied here to the synthesis of 2-chloromethyl-5-aryl-, 2-chloromethyl-5-(5-methyl-2-furyl)-, and 2-chloromethyl-5-(1,5-dimethyl-2-pyrrolyl)-1,3,4-oxadiazoles from tetrazoles and chloroacetyl chloride.

Tetrazoles are prepared starting from aromatic and heterocyclic nitriles [7]. Their azidation with NaN_3 is performed in the presence of NH_4Cl in DMF at 110–120°C. Following the procedures from [8–10], we prepared 5-phenyltetrazole **I**, 5-(2-chlorophenyl)tetrazole **II**, 5-(2-nitrophenyl)tetrazole **III**, 5-(2-ethoxyphenyl)tetrazole **IV**, 5-(3-methylphenyl)tetrazole **V**, 5-(2,4-dimethoxyphenyl)tetrazole **VI**, 5-(3,4,5-trimethoxyphenyl)tetrazole **VII**, and also previously unknown 5-(1,5-dimethyl-2-pyrrolyl)tetrazole **VIII** and 5-(5-methyl-2-furyl)tetrazole **IX**. The reaction conditions, yields, melting points, and analytical data for **VIII**, **IX**, and products of their further transformations (**X**–**XVIII**) are given in Table 1, and the ^1H NMR data, in Table 2.



I–**IX**



I–**VII** **VIII** **IX**

$R^1 = R^2 = R^3 = R^4 = H$ (**I**); $R^1 = Cl$, $R^2 = R^3 = R^4 = H$ (**II**); $R^1 = NO_2$, $R^2 = R^3 = R^4 = H$ (**III**); $R^1 = OEt$, $R^2 = R^3 = R^4 = H$ (**IV**); $R^2 = Me$, $R^1 = R^3 = R^4 = H$ (**V**); $R^1 = R^3 = OMe$, $R^2 = R^4 = H$ (**VI**); $R^2 = R^3 = R^4 = OMe$ (**VII**).

From tetrazoles **I**–**IX**, we prepared 2-chloromethyl-5-phenyl-1,3,4-oxadiazole **X**, 2-chloromethyl-5-(2-chlorophenyl)-1,3,4-oxadiazole **XI**, 2-chloromethyl-5-(2-nitrophenyl)-1,3,4-oxadiazole **XII**, 2-chloromethyl-5-(2-ethoxyphenyl)-1,3,4-oxadiazole **XIII**, 2-chloromethyl-5-(3-methylphenyl)-1,3,4-oxadiazole **XIV**, 2-chloromethyl-5-(2,4-dimethoxyphenyl)-1,3,4-oxadi-

1070-4272/05/7805-0773© 2005 Pleiades Publishing, Inc.

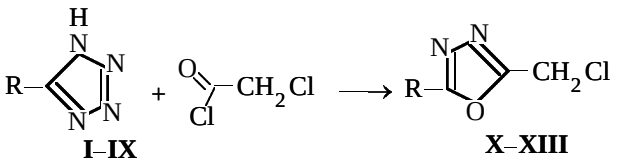
Table 1. Reaction conditions, melting points, elemental analyses, and yields of **VIII**–**XVIII**

Compound	Reaction conditions		mp, °C	Found, %			Formula	Calculated, %			Yield, %
	T, °C	τ, h		C	H	N		C	H	N	
VIII	115–120	14	188–187	51.50	5.51	42.91	$C_7H_9N_5$	51.53	5.52	42.95	81
IX	110–115	5	174–175	48.04	4.02	37.30	$C_6H_6N_4O$	48.00	4.00	37.33	85
X	115–120	5	119–120, (129–131 [2])	55.48	3.55	14.42	$C_9H_7ClNO_2$	55.53	3.60	14.40	86
XI	120–125	4	120–122, (93–94 [3])	47.12	2.60	12.20	$C_9H_6Cl_2N_2O$	47.16	2.62	12.22	87
XII	105–110	4	71–72, (65–68 [3])	45.10	2.50	17.52	$C_9H_6ClN_3O_3$	45.09	2.51	17.54	83
XIII	115–120	3	75–76	55.30	4.60	11.73	$C_{11}H_{11}ClN_2O_2$	55.34	4.61	11.74	84
XIV	110–115	5	61–62	57.52	4.31	13.41	$C_{10}H_9ClN_2O$	57.55	4.32	13.43	86
XV	120–125	4	143–145	51.85	4.31	11.00	$C_{11}H_{11}ClN_2O_3$	51.87	4.32	11.0	93
XV	120–125	8	120–122, (215 [3])	50.60	4.56	9.86	$C_{12}H_{13}ClN_2O_4$	50.62	4.57	9.84	89
XVII	110–115	10	76–78	51.03	4.72	19.85	$C_9H_{10}ClN_3O$	51.06	4.73	19.86	80
XVIII	110–115	5	88–89	48.35	3.52	14.10	$C_8H_7ClN_2O_2$	48.36	3.53	14.11	92

Table 2. ^{1}H NMR spectra pf **V**–**XVI** in DMSO-d_6

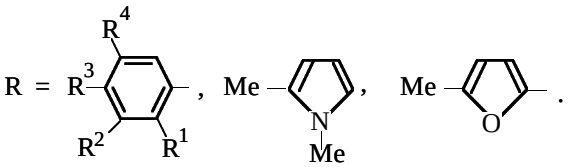
Compound	^{1}H NMR spectrum, δ, ppm	
	CH_2Cl	other signals
VIII		2.28 s (3H, CH_3), 3.93 s (3H, NCH_3), 5.91 d (1H, pyrrole), 6.69 d (1H, pyrrole), 16.06 s (1H, NH-tetrazole)
IX		2.42 s (3H, CH_3), 6.26 d (1H, furan), 7.06 d (1H, furan), 16.40 s (1H, NH-tetrazole)
X	4.90 s (2H)	7.33–7.94 m (5H, phenyl)
XI	4.97 s (2H)	7.31–7.93 m (4H, phenyl)
XII	5.01 s (2H)	7.87–8.18 m (4H, phenyl)
XIII	5.11 s (2H)	4.18 q (2H, OCH_2), 1.37 t (3H, CH_3), 7.10–7.84 m (4H, phenyl)
XIV	5.12 s (2H)	2.42 s (3H, CH_3), 7.45–7.85 m (4H, phenyl)
XV	4.73 s (2H)	3.91 s (3H, OCH_3), 3.92 s (3H, OCH_3), 6.91–7.59 m (3H, phenyl)
XVI	4.98 s (2H)	3.90 s (6H, OCH_3), 3.78 s (3H, OCH3), 7.22 s ((2H), phenyl)
XVII	4.71 s (2H)	6.02 d (1H, pyrrole), 6.80 d (1H, pyrrole), 3.93 s (3H, NCH_3), 2.29 s (3H, CH_3)
XVIII	4.99 s (2H)	6.35 d (1H, furan), 7.17 d (1H, furan), 2.44 s (3H, CH_3)

azole **XV**, 2-chloromethyl-5-(3,4,5-trimethoxyphenyl)-1,3,4-oxadiazole **XVI**, and also previously unknown 2-chloromethyl-5-(1,5-dimethyl-2-pyrrolyl)-1,3,4-oxadiazole **XVII** and 2-chloromethyl-5-(5-methylfuryl)-1,3,4-oxadiazole **XVIII**. These compounds are potentially bioactive and are of considerable interest as drug precursors.



I–**IX** **X**–**XIII**

+ HCl,



X–**XVI** **XVII** **XVIII**

$R^1 = R^2 = R^3 = R^4 = H$ (**X**); R^1 = Cl, $R^2 = R^3 = R^4 =$ H (**XI**); $R^1 = NO_2$, $R^2 = R^3 = R^4 =$ H (**XII**); $R^1 =$ OEt, $R^2 = R^3 = R^4 =$ H (**XIII**); R^2 = Me, $R^1 = R^3 = R^4 =$ H (**XIV**); $R^1 = R^3 =$ OMe, $R^2 = R^4 =$ H (**XV**); $R^2 = R^3 = R^4 =$ OMe (**XVI**).

1,3,4-Oxadiazoles **X**–**XVIII** were prepared in 80–93% by a one-pot procedure involving the reaction of **I**–**IX** with chloroacetyl chloride in *o*-xylene at 110–120°C for 3–10 h. The structures of **VIII**–**XVIII** were confirmed by elemental analysis and ^{1}H NMR spectroscopy. The melting points given in the literature for **X**–**XII** and **XVI** are different and depend on the synthesis procedure. We determined the melting points of **VIII**–**XVIII** (Table 1) on a PTP device at a heating rate of 1 deg min^{-1}.

EXPERIMENTAL

The ^{1}H NMR spectra were recorded on a DPX-300 spectrometer (300 MHz), solvent DMSO-d_6, internal reference TMS. The elemental analysis was performed on a Hewlett–Packard automatic C, H, N analyzer. The melting points were determined on a PTP device. The TLC analyses were performed on Silufol UV-254 plates (eluent $CHCl_3$–methanol, 90/10 by volume); development by UV light or with iodine vapor.

5-(1,5-Dimethyl-2-pyrrolyl)tetrazole VIII and 5-(5-methyl-2-furyl)tetrazole IX. To a solution of 3.6 g of NaN_3 in 25 ml of DMF, we added 5 g of 1,5-dimethyl-2-cyanopyrrole or 2-cyano-5-methylfuran and 3 g of NH_4Cl. The mixture was cooled, and excess DMF was distilled off at 20 mm Hg. The remaining solution was slowly poured into water with cooling and stirring and then was acidified with 10% HCl. The precipitate thus formed was filtered off, dried in air, and recrystallized from ethanol.

5-Aryl-2-chloromethyl-1,3,4-oxadiazoles X–XVI, 2-chloromethyl-5-(1,5-dimethyl-2-pyrrolyl)-1,3,4-oxadiazole XVII, and 2-chloromethyl-5-(5-methyl-2-furyl)-1,3,4-oxadiazole XVIII. A 5-g portion of **I**–**IX** was dissolved in 30 ml of *o*-xylene. The solution was heated with stirring to 30–40°C, and 3.6 g of chloroacetyl chloride in 10 ml of *o*-xylene was added. The mixture was cooled, and excess *o*-xylene was distilled off at 20 mm Hg. The remaining solution was slowly poured with cooling into 10% NaOH. The precipitate thus formed was filtered off, dried in air, and recrystallized from ethanol.

CONCLUSION

5-Aryl- and 5-heteryltetrazoles react with chloroacetyl chloride in *o*-xylene to form 5-aryl-2-chloromethyl-1,3,4-oxadiazoles, 2-chloromethyl-5-(1,5-dimethyl-2-pyrrolyl)-1,3,4-oxadiazole, and 2-chloromethyl-5-(5-methyl-2-furyl)-1,3,4-oxadiazole in 80–93% yields.

REFERENCES

1. *Comprehensive Heterocyclic Chemistry*, Katritzky, A.R. and Ress, C.W., Eds., Oxford: Pergamon, 1984, vol. 6, pp. 427–446.
2. Vakula, T.R. and Srinivasan, V.R., *Ind. J. Chem.*, 1973, vol. 11, no. 8, pp. 732–734.
3. Cojocariu, I., Cojocaru, Z., and Nistor, C., *Rev. Chim.*, 1977, vol. 28, no. 1, pp. 15–18.
4. Levin, Ya.A. and Skorobochatova, M.S., *Khim. Geterotsikl. Soedin.*, 1967, no. 6, pp. 1114–1126.
5. Weidinger, H. and Kranz, J., *Chem. Ber.*, 1963, no. 3, pp. 1049–1058.
6. Huisgen, R., Sauer, J., Sturm, H.J., and Markgraf, J.H., *Chem. Ber.*, 1960, no. 9, pp. 2106–2124.
7. Zil'berman, E.N., *Reaktsii nitrilov* (Reactions of Nitriles), Moscow: Khimiya, 1972.
8. Kondrat'eva, G.Ya. and Neng, Kh.Ch., *Zh. Obshch. Khim.*, 1962, vol. 32, pp. 2348–2353.
9. *Heterocyclic Compounds*, Elderfield, R.C., Ed., New York: Wiley, 1967, vol. 8. Translated under the title *Geterotsiklicheskie soedineniya*, Moscow: Mir, 1969, vol. 8, pp. 7–87.
10. Koldobskii, G.I. and Ostrovskii, V.A., *Usp. Khim.*, 1994, vol. 63, no. 10, pp. 847–865.

Russian Journal of Applied Chemistry, Vol. 78, No. 5, 2005, pp. 776–780. Translated from Zhurnal Prikladnoi Khimii, Vol. 78, No. 5, 2005, pp. 790–795.
Original Russian Text Copyright © 2005 by Chernyshev, Gaidukova, Zemlyakov, Taranushich.

ORGANIC SYNTHESIS AND INDUSTRIAL ORGANIC CHEMISTRY

Synthesis of 1-Acyl- and 1-Arylsulfonyl Derivatives of 3,5-Diamino-1,2,4-triazole

V. M. Chernyshev, G. V. Gaidukova, N. D. Zemlyakov, and V. A. Taranushich

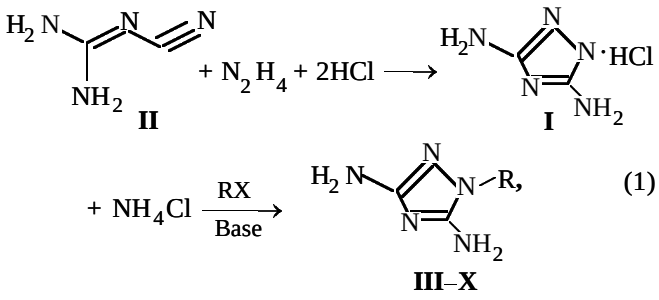
South Russian State Technical University, Novocherkassk, Rostov oblast, Russia

Received August 20, 2004; in final form, February 2005

Abstract—Acylation of 3,5-diamino-1,2,4-triazole with anhydrides and chlorides of alkane- and arenecarboxylic acids and arenesulfonyl chlorides in aqueous solutions and under phase-transfer catalysis was studied.

Acyl, aroyl, and arenesulfonyl derivatives of 3,5-diamino-1,2,4-triazoles are used as intermediates for preparing nitro and azido derivatives of 1,2,4-triazoles [1–3], and also drugs and herbicides [4–7]. The most general route to acyl derivatives of 3,5-diamino-1,2,4-triazole is acylation of 3,5-diamino-1,2,4-triazole **I**, which can yield mono-, di-, and triacetyl derivatives depending on the reaction conditions [1, 4, 8–10]. However, triazole **I** is expensive, despite the fact that it is prepared from available substances: dicyanodiamide **II** and hydrazine [11]. The high cost of **I** is due to its difficult isolation from reaction mixtures. Our previous studies [12, 13] showed that some derivatives of **I** can be prepared from dicyanodiamide and hydrazine without isolation of **I**.

In this study we developed a procedure for preparing 1-acyl-, 1-aroyl-, and 1-arenesulfonyl-3,5-diamino-1,2,4-triazoles by acylation of products of the reaction of nitrile **II** with hydrazine without isolation of **I**:



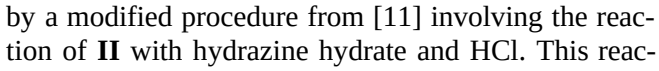
where R = Ac (**III**), EtCO (**IV**), PrCO (**V**), BuCO (**VI**), PhCO (**VII**), $PhSO_2$ (**VIII**), *p*-$MeC_6H_4SO_2$ (**IX**), *p*-$ClC_6H_4SO_2$ (**X**).

The reaction mixtures for acylation were prepared by a modified procedure from [11] involving the reaction of **II** with hydrazine hydrate and HCl. This reaction gave hydrochloride of **I** in 92–97% yield (determined according to [14]), with NH_4Cl as by-product.

Initially we studied acylation of the reaction mixtures with acetic anhydride, since 1-acetyl-3,5-diamino-1,2,4-triazole **III** is widely used as a reagent for preparing various 1,2,4-triazole derivatives, and, among the existing routes to **III**, the most convenient is acylation of **I** with acetic anhydride in aqueous solution [1].

Since triazole **I** occurs in the reaction mixture in the protonated form (pH 2–3), which does not react with acylating agents, the mixture should be preliminarily alkalized to convert the salt of **I** into the free base. However, for the acylation to be selective, ammonia should remain in the salt form. According to published data, for the equilibrium $\mathbf{I}\cdot H^+ \rightleftarrows \mathbf{I} + H^+$ $pK_a = 4.43$ [15], and for $NH_4^+ \rightleftarrows NH_3 + H^+$, $pK_a = 9.27$ [16]. Hence, pH 6.4–7.3 is an optimum at which the salt $\mathbf{I}\cdot H^+$ is virtually fully deprotonated but ammonia remains in the salt form. As bases in acylation with acetic anhydride, we used NaOH, Na_2CO_3, $NaHCO_3$, and sodium acetate.

At the equimolar ratio of **I** and base (pH 4.6–8.4), the major product of the reaction with acetic anhydride is **III**; its yield is virtually independent of particular base. Other acyl derivatives of **I** were not detected in the reaction mixtures. With sodium carbonate, hydrocarbonate, or acetate taken in excess, the reaction selectivity and yield of **III** remain unchanged. With excess NaOH (pH > 10), the yield of **III** decreases to 10–15%, because of the hydrolysis of ammonium chloride and competing reaction of the more nucleophilic ammonia with acetic anhydride:



1070-4272/05/7805-0776 © 2005 Pleiades Publishing, Inc.

Free ammonia can also cause ammonolysis of the target product:

$$\mathbf{III} + NH_3 \longrightarrow \mathbf{I} + AcNH_2. \quad (3)$$

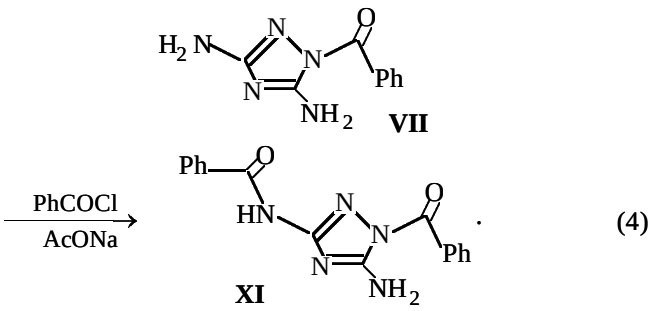
As the molar ratio $\mathbf{I} : Ac_2O$ is changed from 1 : 1 to 1 : (1.25–1.5), the yield of **III** increases from 62–71 to 78–80% (Table 1); larger excess of Ac_2O does not cause a further increase in the yield of **III**.

It is noteworthy that heating does not appreciably affect the selectivity of acylation with acetic anhydride and the yield of the target product (Table 2). In contrast to the majority of *N*-acyl azole derivatives, compound **III** shows enhanced resistance to hydrolysis, which may be due to the electron-donor effect of the 3,5-amino groups.

Thus, it is advisable to perform acylation with acetic anhydride at the molar ratio $\mathbf{I} : \text{base} : Ac_2O$ = 1 : (1–1.2) : 1.25. As in the range 0–50°C the acylation selectivity varies insignificantly, all the steps can be performed at the same temperature as one-pot synthesis. The use of NaOH is not appropriate, because excess NaOH can cause hydrolysis of NH_4Cl and decrease the reaction selectivity because of competing ammonolysis of the acylating agent.

Compounds **IV**–**VII** were prepared under similar conditions using appropriate anhydrides (Table 3). Compound **VII** is isolated from the reaction mixture together with benzoic acid. Benzoic acid can be readily removed by recrystallization from ethanol; yield of purified compound **VII** 35–40%.

With carboxylic acid chlorides and arenesulfonyl chlorides as acylating agents, it is necessary to introduce an additional amount of a base to bind the released HCl. Acylation with aliphatic acyl chlorides resulted only in their hydrolysis. Acylation with benzoyl chloride, which is more resistant to hydrolysis, at 20°C in the presence of sodium acetate gave a mixture of products consisting, according to liquid chromatography, of 14% **VII**, 42% 5-amino-3-benzamido-1-benzoyl-1,2,4-triazole **XI**, and 44% benzoic acid. Compound **XI** is apparently formed by acylation of **VII**:



(4)

Table 1. Yield of **III** at 20°C and pH 4.6–8.4

Molar ratio $\mathbf{I} : Ac_2O$	Yield, %	Molar ratio $\mathbf{I} : Ac_2O$	Yield, %
1 : 1.0	62	1 : 1.5	80
1 : 1.1	71	1 : 1.75	80
1 : 1.25	78	1 : 2.0	75

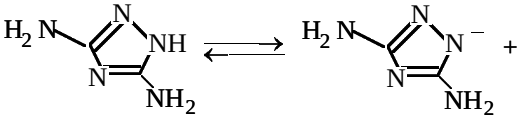
Table 2. Yield of **III** at the molar ratio $\mathbf{I} : Na_2CO_3 : Ac_2O$ = 1 : 1 : 1.25

T, °C	Yield, %	*T*, °C	Yield, %
0	79	50	77
30	78	70	72
40	77	90	68

Apparently, the rate of formation of **VII** is comparable with the rate of its subsequent acylation with benzoyl chloride into **XI**. We failed to prepare **VII** selectively even at a twofold excess of **I** relative to benzoyl chloride. This may be due to the fact that benzoyl chloride and compound **I** occur in different phases. Benzoyl chloride is poorly soluble in water, whereas triazole **I** is very well soluble; therefore, compound **VII** is mainly formed at the phase boundary. After being formed, compound **VII** dissolves in benzoyl chloride and undergoes further acylation.

The reaction with benzenesulfonyl chloride under the same conditions yielded compound **VIII** but was very slow; the yield of the target product did not exceed 35% in 72 h. Crystalline *p*-toluenesulfonyl chloride and *p*-chlorobenzenesulfonyl chloride under the same conditions gave **IX** and **X**; their yield in 3 days did not exceed 10%, and the major isolated compounds were unchanged arenesulfonyl chlorides.

We suggested that the selectivity of acylation with carboxylic acid chlorides and arenesulfonyl chlorides could be increased by converting triazole **I** into the anion and performing the reaction with phase-transfer catalysis. The anion should be considerably more nucleophilic and reactive as compared to the neutral molecule. For equilibrium (5), pK_a = 12.12 in water at 20°C [17]. Hence, at pH > 14.12, compound **I** in water occurs in the anionic form:



(5)

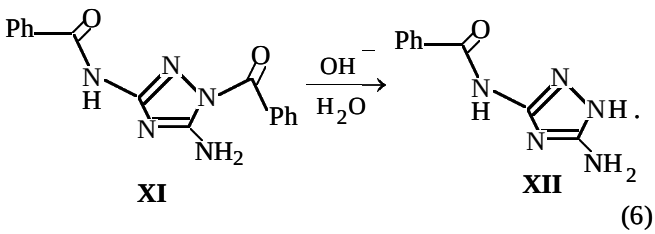
To provide the required basicity, no less than 3 mol of NaOH per mole of **II** should be added to the reac-

Table 3. Synthesis conditions, yields, and properties of acylation products **III**–**XII** (molar ratio **I** : acylating agent = 1 : 1)

Compound	Acylating agent	Base	Molar ratio **I** : base	*T*, °C	τ, h	Yield, % (synthesis procedure)	mp,[1] °C	Found, % / Calculated, %			Formula
								C	H	N	
III	AcCl	NaOH	1 : 1.2[2]	5	0.5	28 (*b*)	228 (dec.)[3]	34.00 / 34.04	5.07 / 5.00	49.59 / 49.62	$C_4H_7N_5O$
IV	$(EtCO)_2O$	NaOAc	1 : 1.25	20	1.0	75 (*a*)	166–167	38.75 / 38.65	5.83 / 5.85	45.18 / 45.34	$C_5H_9N_5O$
V	$(PrCO)_2O$	NaOAc	1 : 1.25	20	1.0	70 (*a*)	112–113	42.80 / 42.60	6.52 / 6.55	41.41 / 41.39	$C_6H_{11}N_5O$
	PrCOCl	NaOH	1 : 1.2[2]	5	0.5	29 (*b*)					
VI	$(BuCO)_2O$	NaOAc	1 : 1.25	20	1.0	75 (*a*)	123–124	45.93 / 45.89	7.20 / 7.15	38.25 / 38.22	$C_7H_{13}N_5O$
VII	$(PhCO)_2O$	NaOAc	1 : 1.25	45	1.0	47 (*a*)[4]	154–156	53.26 / 53.32	4.39 / 4.46	34.50 / 34.40	$C_9H_9N_5O$
	PhCOCl	NaOAc	1 : 2.25	20	2.0	8 (*a*)[4]					
	PhCOCl	NaOH	1 : 1.0[2]	5	0.5	58 (*b*)					
	PhCOCl	NaOH	1 : 1.2[2]	5	0.5	52 (*b*)					
VIII	$PhSO_2Cl$	NaOAc	1 : 2.25	20	72	35 (*a*)	222–224[5]	40.84 / 40.16	3.80 / 3.79	29.20 / 29.27	$C_8H_9N_5O_2S$
	$PhSO_2Cl$	NaOH	1 : 1.2[2]	5	0.5	70 (*b*)					
IX	*p*-$MeC_6H_4SO_2Cl$	NaOAc	1 : 2.25	20	72	10 (*a*)	216–217	43.00 / 42.68	4.38 / 4.38	27.20 / 27.65	$C_9H_{11}N_5O_2S$
	p-$MeC_6H_4SO_2Cl$	NaOH	1 : 1.2[2]	5	0.5	60 (*b*)					
X	*p*-$ClC_6H_4SO_2Cl$	NaOAc	1 : 2.25	20	72	9 (*a*)	213–215	35.21 / 35.11	2.89 / 2.95	25.66 / 25.59	$C_8H_8ClN_5O_2S$
	p-$ClC_6H_4SO_2Cl$	NaOH	1 : 1.2[2]	5	0.5	50 (*b*)					
XI	PhCOCl	NaOAc	1 : 2.25	20	72	41 (*a*)[4]	198 (dec.)	65.66 / 62.53	4.18 / 4.26	23.00 / 22.79	$C_{16}H_{13}IN_5O_2$
	PhCOCl	NaOH	1 : 1.0[2]	5	0.5	15 (*b*)[4]					
XII	PhCOCl	NaOH	1 : 1.2[2]	5	0.5	12 (*b*)	310–312	46.00 / 45.89	7.24 / 7.15	37.60 / 38.22	$C_9H_9N_5O$

[1] Compounds **III**–**VII** and **XI** were crystallized from ethanol; **VIII**–**X** and **XII**, from ethanol–DMF. [2] Additional 2 mol of NaOH was introduced per mole of **II**. [3] mp 228–230°C [9]. [4] According to liquid chromatography. [5] mp 225°C [18].

tion mixture [see scheme (1)]. Since NH_4Cl is fully hydrolyzed under these conditions, the released ammonia was removed by boiling the reaction mixture. The subsequent acylation with acetyl and butyryl chlorides in a CH_2Cl_2–water mixture in the presence of benzyltriethylammonium chloride yielded only 1-acyl derivatives **III** and **V**, and the reaction with benzoyl chloride, along with the major product **VII**, yielded also **XI** or 5-amino-3-benzamido-1,2,4-triazole **XII** depending on the molar ratio **I** : NaOH (Table 3, method *b*). Compound **XII** is apparently formed by hydrolysis of **XI**:



XI **XII** (6)

In particular, at an equimolar ratio of triazole **I** to NaOH, compound **XI** was isolated in 15% yield

(Table 3), and compound **XII** was not detected. At a 20% excess of alkali, compound **XI** was absent in the reaction products, and compound **XII** was isolated from the aqueous phase in 12% yield. Hence, compound **VII** formed under the conditions of phase-transfer catalysis is subsequently "slowly" acylated to dibenzoyl derivative **XI**, which is hydrolyzed to product **XII** with excess alkali. Probably, the hydrolysis of **XI** is promoted by an acidic proton of the benzoylamino group, responsible for the dissociation of **XI** in an alkali solution with the dissolution of **XI** in the aqueous phase and its subsequent hydrolysis.

The low yields of the acetyl (**III**) and butyryl (**V**) derivatives and the lack of acylamino derivatives in the reaction products may be due to the high rate of hydrolysis of aliphatic acyl chlorides.

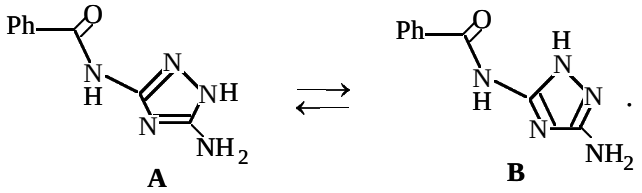
Acylation of **I** under the phase-transfer conditions is also an efficient route to 1-arenesulfonyl-3,5-diamino-1,2,4-triazoles. Under these conditions, from appropriate arenesulfonyl chlorides, we prepared compounds **VIII**–**X** in 50–70% yields (Table 3). The main substance content in the crude products was no less than 90% according to the ^{1}H NMR data.

The composition and structure of the compounds synthesized were confirmed by elemental analysis (Table 3) and by IR, UV, and ^{1}H NMR spectroscopy.

In the IR spectra of acyl derivatives **III**–**VII** and **XI**, the stretching vibration bands of the carbonyl group bonded to the nitrogen atom of the triazole ring are manifested at 1680–1710 cm^{-1}, whereas the vibration frequencies of the "amide" carbonyl group in **XI** and **XII** are lower: 1650–1660 cm^{-1}. The spectra of arenesulfonyl chlorides **VIII**–**X** contain a strong absorption band at 1150–1160 cm^{-1}, which was assigned to the symmetric vibrations of the SO_2 group.

The UV spectra of **III**–**VII** are similar to the spectra of 5-amino-1-acyl-1,2,4-triazoles reported in [9] and exhibit two maxima at 217–230 and 273–290 nm. The spectra of 1-arenesulfonyl-3,5-diamino-1,2,4-triazoles **VIII**–**X** are also characterized by two maxima in the ranges 220–234 and 261–269 mn. The UV spectrum of 5-amino-3-benzamido-1,2,4-triazole **XII** differs from that of isomeric 1-benzoyl-3,5-diamino-1,2,4-triazole **VII** by the absence of the long-wave maximum at about 290 nm and the presence of a shoulder at about 253 nm; this is consistent with the data for 3-R-5-acylamino-1,2,4-triazoles [9].

The NMR spectra of 1-acyl- and 1-arenesulfonyl-3,5-diamino-1,2,4-triazoles **III**–**X** contain two singlets from protons of amino groups. The 3-NH_2 protons give a signal at 5.36–5.65 ppm, and the 5-NH_2 protons, a signal at 7.32–7.55 ppm for acyl derivatives **III**–**VII** and at 6.90–6.97 ppm for arenesulfonyl derivatives **VIII**–**X**. The spectrum of **XI** does not contain the 3-NH_2 signal but contains a singlet of the amide proton at 10.67 ppm; the 5-NH_2 signal is shifted downfield relative to **VII** owing to the electron-withdrawing effect of the additional benzoyl group. According to the NMR spectrum, compound **XII** in DMSO occurs in the form of tautomers **A** (major) and **B**:



A **B**

EXPERIMENTAL

The ^{1}H NMR spectra were recorded on a Varian Unity-300 spectrometer (300 MHz) in DMSO-d_6, internal reference TMS. The IR spectra were recorded on a Specord IR-75 spectrometer from mulls in mineral oil. The UV spectra (aqueous solutions) were taken on an SF-26 spectrophotometer. High-performance liquid chromatography was performed on a Milikhrom chromatograph equipped with a UV detector and a 60 × 3-mm column (sorbent Silasorb C_{18}, 5 μm, mobile phase methanol, elution rate 5 μl min^{-1}, detection at 230 nm).

1-Acyl- and 1-arenesulfonyl-3,5-diamino-1,2,4-triazoles III–X and 5-amino-3-benzamido-1-benzoyl-1,2,4-triazole XI. (*a*) To 0.0333 mol of hydrazine hydrate (55% solution), we added dropwise with stirring at a temperature not exceeding 50°C 0.0666 mol of HCl (30% solution) and 0.0333 mol of **II** over a period of 10–15 min; the mixture was heated for 1 h at 50°C. Then the required amount of a base was added, and the acylating agent was added dropwise with stirring at the required temperature (Tables 1–3). The mixture was stirred for a period indicated in Table 3; the precipitate was filtered off, washed with water, dried, and analyzed by ^{1}H NMR and HPLC. The precipitates of **III**–**VI**, according to ^{1}H NMR, contained no less than 90% main substance, and compound **VII**, according to HPLC, contained ~50% benzoic acid. Compounds **III**–**VII** were purified by recrystallization from ethanol. To separate mixtures from acylation with benzoyl chloride, the precipitate was dissolved in 60 ml of boiling ethanol, and the solution was cooled. The precipitate of **XI** was filtered off, recrystallized, and analyzed. The mother liquor after the separation of **XI** was evaporated to a volume

of 15 ml and cooled; the precipitate of **VII** was recrystallized and analyzed. Compounds **VIII**–**X** were washed with chloroform to separate unchanged arenesulfonyl chloride, recrystallized, and analyzed.

(*b*) To the solution from the reaction of hydrazine hydrate, HCl, and compound **II** by method *a*, we added the required amount of NaOH (Table 3) and boiled until the evolution of NH_3 was complete (30–40 min); water was added to compensate for the evaporation. The mixture was diluted with distilled water to a volume of 12.5 ml and cooled; 0.003 mol of benzyltriethylammonium chloride and a solution of the acylating agent in 6 ml of CH_2Cl_2 were added. The mixture was stirred for 20 min; the precipitate of the target product was filtered off, washed successively with water and methylene chloride, dried, and analyzed. Compounds **III**–**XI** were purified similarly to method *a*.

5-Amino-3-benzamido-1,2,4-triazole XII. (*a*) The reaction mixture after the separation of compound **VII** prepared by method *b* at the molar ratio **I** : NaOH = 1 : 1.2 was neutralized with 10% HCl to pH 7–8. The precipiptate thus formed was filtered off, washed with 5 ml of boiling ethanol to separate benzoic acid, and crystallized from DMF–ethanol.

Compound **XII** was also prepared in 86% yield by independent synthesis: hydrolysis of 0.001 ml of **XI** in 10 ml of 1 M NaOH at 5°C for 2 h.

CONCLUSIONS

(1) One-pot procedures were developed for acylation and arenesulfonylation of 3,5-diamino-1,2,4-triazole in reaction mixtures from the reaction of dicyanodiamide with hydrazine.

(2) It is advisable to prepare 1-acyl-3,5-diamino-1,2,4-triazoles by acylation of 3,5-diamino-1,2,4-triazole with carboxylic acid anhydrides in aqueous solution (70–80% yields), and 1-arenesulfonyl-3,5-diamino-1,2,4-triazoles, by acylation of 3,5-diamino-1,2,4-triazole with arenesulfonyl chlorides under conditions of phase-transfer catalysis (50–70% yields).

REFERENCES

1. Pevzner, M.S., Gladkova, N.V., and Kravchenko, T.A., *Zh. Org. Khim.*, 1996, vol. 32, no. 8, pp. 1230–1233.
2. USSR Inventor's Certificate no. 979342.
3. Kofman, T.P. and Namestnikov, V.I., *Zh. Org. Khim.*, 2003, vol. 39, no. 4, pp. 615–620.
4. Selassie, C.D., Lien, E.J., and Khwaja, T.A., *J. Pharm. Sci.*, 1981, vol. 70, no. 11, pp. 1281–1283.
5. Kleschik, W.A., Dunbar, J.E., Snider, S.W., and Vinogradoff, A.P., *J. Org. Chem.*, 1988, vol. 53, no. 13, pp. 3120–3122.
6. Maybhate, S.P., Rajamohanan, P.P., and Rajappa, S., *Synthesis*, 1991, no. 3, pp. 220–222.
7. Chibale, K., Dauvergne, J., and Wyatt, P.G., *Synthesis*, 2002, no. 2, pp. 185–190.
8. Bos, B.G. van den, *Recl. Trav. Chim. Pays-Bas*, 1960, vol. 79, no. 8, pp. 836–842.
9. Reiter, J., Pongo, L., and Dvortsak, P., *J. Heterocyclic Chem.*, 1987, vol. 24, no. 1, pp. 127–142.
10. Stolle, R. and Ditrich, W., *J. Prakt. Chem.*, 1934, vol. 139, no. 2, pp. 193–210.
11. US Patent 2648671.
12. Chernyshev, V.M., Zemlyakov, N.D., Taranushich, V.A., and Rakitov, E.A., *Zh. Prikl. Khim.*, 1999, vol. 72, no. 10, pp. 1688–1691.
13. Chernyshev, V.M., Zemlyakov, N.D., Il'in, V.B., and Taranushich, V.A., *Zh. Prikl. Khim.*, 2000, vol. 73, no. 5, pp. 791–793.
14. Chernyshev, V.M., Zemlyakov, N.D., and Taranushich, V.A., *Zh. Prikl. Khim.*, 2000, vol. 73, no. 5, pp. 857–858.
15. Voronkov, M.G., Kashik, T.V., Makarskii, V.V., *et al.*, *Izv. Akad. Nauk SSSR*, 1976, vol. 227, no. 5, pp. 1116–1119.
16. Albert, A. and Serjeant, E., *Ionization Constants of Acids and Bases. A Laboratory Manual*, New York: Wiley, 1962.
17. Kröger, C.F. and Freiberg, W., *Z. Chem.*, 1969, vol. 5, no. 10, pp. 381–382.
18. Schulze, W., Letsch, G., and Fritzsche, H., *J. Prakt. Chem.*, 1965, vol. 30, no. 5, pp. 302–313.

Russian Journal of Applied Chemistry, Vol. 78, No. 5, 2005, pp. 781–786. Translated from Zhurnal Prikladnoi Khimii, Vol. 78, No. 5, 2005, pp. 796–801.
Original Russian Text Copyright © 2005 by Dyubchenko, Nikulina, Terakh, Prosenko, Grigor'ev.

ORGANIC SYNTHESIS AND INDUSTRIAL ORGANIC CHEMISTRY

Synthesis and Antioxidative Activity of *N*,*N*-Dialkyl-ω-[4-hydroxy(methoxy)aryl]alkylamines and Their *N*-Oxides

O. I. Dyubchenko, V. V. Nikulina, E. I. Terakh, A. E. Prosenko, and I. A. Grigor'ev

Research Institute of Chemistry of Antioxidants, Novosibirsk State Pedagogical University, Novosibirsk, Russia
Vorozhtsov Novosibirsk Institute of Organic Chemistry, Siberian Division, Russian Academy of Sciences, Novosibirsk, Russia

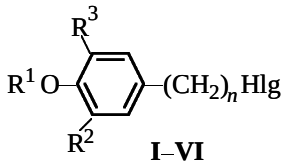
Received September 1, 2004; in final form, January 2005

Abstract—Aminoalkylphenols of various structures were prepared by reactions of ω-[4-hydroxy(methoxy)-aryl]haloalkanes with dialkylamines. The corresponding *N*-oxides were prepared by oxidation of aminoalkylphenols with hydrogen peroxide and cumene hydroperoxide. The inhibiting activities of these compounds in a model reaction of thermal autooxidation of lard were compared.

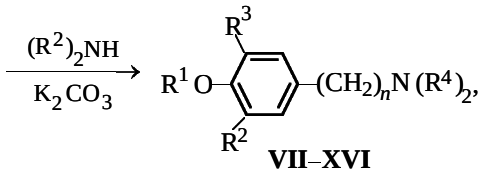
Aminoalkylphenols containing a phenolic fragment and an alkylamino group are highly effective inhibitors of free-radical oxidation of various organic substrates. According to patent data [1–3], they can be used as stabilizers of polymeric materials, rubbers, lubricating oils, and diesel and jet fuels. Furthermore, aminoalkylphenols show a wide spectrum of biological activity; in particular, they exhibit antiphlogistic, antirheumatic, antiallergic, antidiabetic, and other properties [4–10]. The mechanism of the antioxidative effect of aminoalkylphenols responsible for their high performance is not yet fully elucidated; for its better understanding, it is necessary to study the structure–inhibiting activity relationship for aminoalkylphenols and to examine their oxidation products in which one of the groups responsible for the antioxidative power is inactivated.

Therefore, in this study we prepared aminoalkylphenols differing in the extent of steric shielding of the phenolic OH group, structure of the *N*-substituents, and distance between the amino group and aromatic core; also we prepared the corresponding *N*-oxides and compared the inhibiting powers of the compounds synthesized in the model reaction of thermal autooxidation of lard.

By the reaction of ω-[4-hydroxy(methoxy)aryl]-haloalkanes **I**–**VI** with dialkylamines, we prepared the corresponding alkylphenols **VII**–**XVI**:



I–**VI**



VII–**XVI**

where R^1 = H, R^2 = R^3 = *t*-Bu: *n* = 2, Hlg = Cl (**I**); *n* = 2, R^4 = Me (**VII**), Et (**VIII**); *n* = 3, Hlg = Cl (**II**); *n* = 3, R^4 = Me (**IX**), Et (**X**), Pr (**XI**); *n* = 4, Hlg = Cl (**III**); *n* = 4, R^4 = Me (**XII**), Et (**XIII**); R^1 = R^2 = H, R^3 = *t*-Bu, *n* = 3: Hlg = Cl (**IV**), R^4 = Me (**XIV**); R^1 = R^2 = R^3 = H, *n* = 3: Hlg = Br (**V**), R^4 = Me (**XV**); R^1 = Me, R^2 = R^3 = H, *n* = 3: Hlg = Br (**VI**), R^4 = Me (**XVI**).

The syntheses were performed in ampules in ethanol in the presence of K_2CO_3 at 120°C for 7 h; the molar ratio of the starting haloalkane, dialkylamine, and K_2CO_3 was 1 : 2 : 2. Yields of **VII**–**XVI** 60–93%.

It is known [11–14] that tertiary aliphatic amines react with peroxy compounds to form *N*-oxides. We performed the oxidation of aminoalkylphenols **IX**–**XI** with hydrogen peroxide and cumene hydroperoxide in 2-propanol at 60°C for 3 h and obtained the corre-

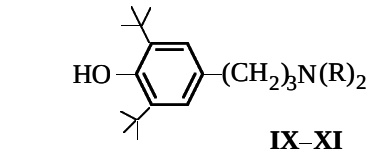
1070-4272/05/7805-0781 © 2005 Pleiades Publishing, Inc.

Induction period τ of lard oxidation, inhibited by phenolic antioxidants (1.5 μmol g^{-1}, 130°C)

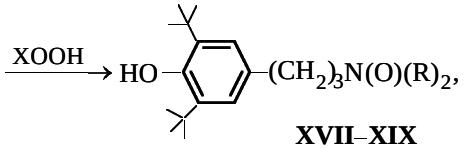
Antioxidant*	τ, min
$R(CH_2)_2N(Me)_2$ (**VII**)	288 ± 10
$R(CH_2)_2N(Et)_2$ (**VIII**)	298 ± 7
$R(CH_2)_3N(Me)_2$ (**IX**)	334 ± 5
$R(CH_2)_3N(Et)_2$ (**X**)	307 ± 5
$R(CH_2)_3N(Pr)_2$ (**XI**)	277 ± 7
$R(CH_2)_4N(Me)_2$ (**XII**)	435 ± 5
$R(CH_2)_4N(Et)_2$ (**XIII**)	335 ± 5
$R'(CH_2)_3N(Me)_2$ (**XIV**)	143 ± 5
$R''(CH_2)_3N(Me)_2$ (**XV**)	51 ± 5
$R(CH_2)_3N(O)(Me)_2$ (**XVII**)	170 ± 5
$R(CH_2)_3N(O)(Et)_2$ (**XVIII**)	150 ± 5
$R(CH_2)_3N(O)(Pr)_2$ (**XIX**)	110 ± 5
$RCH_2N(Me)_2$ (**XX**)	110 ± 5
RCH_3 (Ionol)	165 ± 5
$C_{12}H_{25}N(Me)_2$ (DMDA)	20 ± 3
RCH_3 + DMDA (synergistic mixture)	198 ± 5
Control	20 ± 3

* R = 3,5-di-*tert*-butyl-4-hydroxyphenyl, R' = 3-*tert*-butyl-4-hydroxyphenyl, and R'' = 4-hydroxyphenyl.

sponding *N*-oxides **XVII**–**XIX** in 43–90% yields:



IX–**XI**



XVII–**XIX**

where X = H, $PhC(Me)_2$; R = Me (**XVII**), Et (**XVIII**), Pr (**XIX**).

The compositions and structures of aminoalkylphenols **VII**–**XVI** and their *N*-oxides **XVII**–**XIX** were confirmed by elemental analysis and spectroscopy. In the ^1H NMR spectra of *N*-oxides **XVII**–**XIX**, compared to the corresponding aminoalkylphenols **IX**–**XI**, the signals of the methylene protons of the *p*-alkyl substituent are shifted downfield, which suggests an increase in the polarizing power of the N-containing fragment, i.e., its oxidation. The IR spectra of **XVII**–**XIX** contain absorption bands at 950–970 cm^{-1}, characteristic of the N–O stretching vibrations. These bands are absent in the spectra of the corresponding aminoalkylphenols **IX**–**XI**.

A search in the STN International database showed that compounds **VIII**, **XI**–**XIV**, and **XVII**–**XIX** were unknown previously. Aminoalkylphenol **VII** is mentioned in [6] without spectral characteristics, and amines **XV** and **XVI** are reported in [8] only as hydrochlorides.

The antioxidative activity (AOA) of aminoalkylphenols **VII**–**XV** and their *N*-oxides **XVII**–**XIX** was evaluated from their inhibiting effect on thermal autooxidation of lard. As references we used commercial inhibitors 2,6-di-*tert*-butyl-4-methylphenol (Ionol) and *N*,*N*-dimethyl(3,5-di-*tert*-butyl-4-hydroxybenzyl)amine **XX**, and also a 1 : 1 synergistic mixture of Ionol and *N*,*N*-dimethyldodecylamine (DMDA).

We found that di-*tert*-butyl-substituted aminoalkylphenols **VII**–**XIII** are effective inhibitors of lard oxidation (see table); in their antioxidative power they appreciably surpass the commercial antioxidants and the Ionol–DMDA mixture.

A previous study of the antiradical activity of 2,6-di-*tert*-butyl-substituted aminoalkylphenols **VII**, **IX**, and **XX** in a model reaction of initiated oxidation of methyl oleate in chlorobenzene at 60°C showed that these compounds are highly reactive toward peroxy radicals [15]. The rate constants k_7 of their reaction with peroxy radicals

$$PhOH + ROO^{\bullet} \longrightarrow PhO^{\bullet} + ROOH \qquad (1)$$

were similar to those characteristic of Ionol. This fact suggests that the higher inhibiting power of aminoalkylphenols **VII**–**XIII**, compared to Ionol, in autooxidation of lard is due to the bifunctional mechanism of theit antioxidative effect, namely, to a combination of the antiradical activity of the phenolic group and antioxidative activity of the alkylamino group. The significance of the contribution of the alkylamino group to AOA of aminoalkylphenols is also confirmed by the fact that the corresponding *N*-oxides **XVII**–**XIX** are comparable with, or even inferior to Ionol as inhibitors of lard oxidation. The low AOA of benzylamino derivative **XX** compared to aminoalkylphenols **VII**–**XIII** in oxidation of lard at 130°C is apparently caused by the thermal instability of **XX** [16].

It is known [17, 18] that aliphatic amines in mixtures with phenolic antioxidants can act as synergistic agents. The synergistic effect is usually evaluated by the induction period and characterized by $\Delta\tau_{syn}$ [19]:

$$\Delta\tau_{syn} = \tau_{1,2} - (\tau_1 + \tau_2),$$

where $\tau_{1,2}$ is the induction period in the presence of two inhibitors; τ_1 and τ_2, induction periods in the presence of individual inhibitors.

In the experiments on lard oxidation, the nonadditive effect of coinhibitors was revealed for the system Ionol–DMDA; the synergistic effect, calculated by the formula

$$\Delta\tau_{syn} = (\tau_{PhOH+DMDA} - \tau_0) - (\tau_{DMDA} + \tau_{PhOH} - 2\tau_0),$$

where τ_0 is the induction period of the noninhibited oxidation of lard; τ_{DMDA} and τ_{PhOH}, induction periods in the presence of DMDA and Ionol, respectively; and $\tau_{PhOH+DMDA}$, induction period in the presence of the Ionol–DMDA mixture, amounted to 33 min. For 2,6-di-*tert*-butyl-substituted aminoalkylphenols **VII**–**XIII**, the synergistic effect was more pronounced, and $\Delta\tau_{syn}$, calculated as

$$\Delta\tau_{syn} = (\tau_{AAP} - \tau_0) - (\tau_{DMDA} + \tau_{PhOH} - 2\tau_0),$$

where τ_{AAP} is the induction period of lard oxidation in the presence of aminoalkylphenols, ranged from 112 to 270 min. Thus, we can state that the high antioxidative acitivity of aminoalkylphenols in lard oxidation is associated not only with the bifunctional mechanism of their antioxidative effect but also with the pronounced synergistic effect which, most likely, is of intramolecular origin and is due to structural features of these molecules.

The occurrence of intramolecular synergism in bifunctional inhibitors, in particular, in sulfur-containing derivatives of sterically hindered phenols, was repeatedly discussed in [20–22]; however, its origin was not elucidated. The intramolecular synergism may be due to favorable steric arrangement of the phenolic and sulfur-containing fragments, allowing the hydroperoxide formed by reaction (1) to be deactivated with the sulfur-containing fragment without escaping into the bulk of the substrate [22]. A similar pattern can be expected for aminoalkylphenols.

Since the extent of the intramolecular synergism can depend on the distance between the alkylamino group and aromatic core, the difference in the AOA of aminoalkylphenols **VII**–**X**, **XII**, **XIII**, and **XX** containing different number of carbon atoms in the *p*-alkyl chain becomes quite understandable. In the series of *N,N*-dimethyl- and diethyl-substituted aminoalkylphenols, in the most effective inhibitors of lard oxidation the alkylamino group was separated from the aromatic core by four carbon atoms. Apparently, in this case the mutual arrangement of the phenolic and alkylamino groups is the most favorable for the intramolecular synergism.

The antioxidative activity of aminoalkylphenols also strongly depended on the structure of *N*-substituents and extent of steric shielding of the phenolic OH group. In going from *N,N*-dimethyl-substituted amine **IX** to its diethyl (**X**) and dipropyl (**XI**) analogs, the inhibiting activity decreased.

Aminoalkylphenols differing in the extent of steric shielding of the phenolic OH group can be ranked in the following order with respect to the capability to inhibit lard oxidation: **IX** > **XIV** > **XV**. A decrease in AOA of aminoalkylphenols in this series corresponds to an increase in the reactivity of the corresponding phenoxy radicals in the reaction

$$PhO^{\bullet} + RH \longrightarrow PhOH + R^{\bullet}. \qquad (2)$$

In particular, according to the existing estimates, *o*-unsubstituted phenoxyls are 10^3–10^4 times (at 60°C) more active than 2,6-di-*tert*-butyl-substituted phenoxy radicals [23]. Compound **XV** at the *o*-positions contains no bulky *tert*-butyl substituents sterically hindering reaction (2), which accounts for the lowest AOA of this compound in the examined series.

EXPERIMENTAL

The ^{1}H NMR spectra were recorded on a Bruker spectrometer (500 MHz), solvents $CDCl_3$ and CD_3OD, internal reference TMS; the IR spectra were taken on a Specord M80 spectrometer in $CHCl_3$. The melting points were determined on a PTP device. The starting ω-[4-hydroxy(methoxy)aryl]haloalkanes **I**–**VI** were prepared as described previously [24], and *N,N*-dimethyl(3,5-di-*tert*-butyl-4-hydroxybenzyl)amine **XX**, by the procedure described in [3].

***N,N*-Dimethyl-2-(3,5-di-*tert*-butyl-4-hydroxyphenyl)ethylamine VII.** A 50-ml ampule was charged with 5.0 g (18.6 mmol) of chloride **I**, 5.1 g of dimethylamine solution (37.2 mmol), 5.1 g (37.2 mmol) of K_2CO_3, and 10 ml of ethanol. The ampule was sealed, placed in a thermostat equipped with a shaker, and heated for 7 h at 120°C. After cooling, the ampule was opened, and the reaction mixture was treated with alkali and extracted with toluene. The extract was washed with water and dried over Na_2SO_4; the solvent was distilled off, and the residue was distilled in a vacuum. Yield of amine **VII** 4.0 g (78%), bp 140–142°C (1 mm Hg), mp 84–85°C. ^{1}H NMR spectrum, δ, ppm: 1.44 s (18H, *t*-Bu), 2.32 s [6H, $N(CH_3)_2$], 2.55 m (2H, CH_2N), 2.69 m (2H, $ArCH_2$), 4.91 s (1H, OH), 6.99 s (2H, H_{arom}). IR spectrum, ν, cm^{-1}: 3640 (OH).

Found, %: C 78.08, H 11.47, N 5.39.
$C_{18}H_{31}ON$.
Calculated, %: C 77.92, H 11.26, N 5.05.

***N*,*N*-Diethyl-2-(3,5-di-*tert*-butyl-4-hydroxyphenyl)ethylamine VIII** was prepared similarly from 5.2 g (19.3 mmol) of chloride **I**, 2.8 g (38.7 mmol) of diethylamine, and 5.4 g (38.7 mmol) of K_2CO_3. Yield 5.4 g (91%), bp 122–124°C (1 mm Hg). ^{1}H NMR spectrum, δ, ppm: 1.08 t [6H, $N(CH_2CH_3)_2$], 1.45 s (18H, *t*-Bu), 2.63 q [4H, $N(CH_2CH_3)_2$], 2.69 s (4H, $ArCH_2CH_2$), 5.07 s (1H, OH), 7.01 s (2H, H_{arom}). IR spectrum, ν, cm^{-1}: 3640 (OH).

Found, %: C 78.48, H 11.47, N 4.24.
$C_{20}H_{35}ON$.
Calculated, %: C 78.63, H 11.55, N 4.58.

***N*,*N*-Dimethyl-3-(3,5-di-*tert*-butyl-4-hydroxyphenyl)propylamine IX** was prepared similarly from 5.0 g (17.7 mmol) of chloride **II**, 4.8 g of dimethylamine solution (35.4 mmol), and 4.9 g (35.4 mmol) of K_2CO_3. Yield 4.6 g (90%), bp 130°C (1 mm Hg), mp 44–45°C (published data: 31–33°C) [5]. ^{1}H NMR spectrum, δ, ppm: 1.49 s (18H, *t*-Bu), 1.82 m (2H, $ArCH_2CH_2$), 2.30 s [6H, $N(CH_3)_2$], 2.38 t (2H, CH_2N), 2.60 t (2H, $ArCH_2$), 5.11 s (1H, OH), 7.06 s (2H, H_{arom}). IR spectrum, ν, cm^{-1}: 3640 (OH).

Found, %: C 78.11, H 11.58, N 4.81.
$C_{19}H_{33}ON$.
Calculated, %: C 78.29, H 11.41, N 4.85.

***N*,*N*-Diethyl-3-(3,5-di-*tert*-butyl-4-hydroxyphenyl)propylamine X** was prepared similarly from 4.7 g (16.7 mmol) of chloride **II**, 2.4 g (33.4 mmol) of diethylamine, and 4.6 g (33.4 mmol) of K_2CO_3. Yield 4.9 g (93%), bp 150–153°C (1 mm Hg). ^{1}H NMR spectrum, δ, ppm: 1.04 t [6H, $N(CH_2CH_3)_2$], 1.46 s (18H, *t*-Bu), 1.79 m (2H, $ArCH_2CH_2$), 2.50–2.58 m [8H, $ArCH_2$, CH_2N, $N(CH_2CH_3)_2$], 5.05 s (1H, OH), 7.02 s (2H, H_{arom}). IR spectrum, ν, cm^{-1}: 3640 (OH).

Found, %: C 78.82, H 11.75, N 4.22.
$C_{21}H_{37}ON$.
Calculated, %: C 78.94, H 11.67, N 4.38.

***N*,*N*-Dipropyl-3-(3,5-di-*tert*-butyl-4-hydroxyphenyl)propylamine XI** was prepared similarly from 5.0 g (17.5 mmol) of chloride **II**, 3.8 g (35.1 mmol) of dipropylamine, and 4.8 g (35.1 mmol) of K_2CO_3. Yield 5.1 g (84%), bp 161–164°C (2 mm Hg). ^{1}H NMR spectrum, δ, ppm: 0.96 t [6H, $N(CH_2CH_2 \cdot CH_3)_2$], 1.51 s (18H, *t*-Bu), 1.51 m [4H, $N(CH_2 \cdot CH_2CH_3)_2$], 1.77 m (2H, $ArCH_2CH_2$), 2.43 t [4H, $N(CH_2CH_2CH_3)_2$], 2.48 t (2H, CH_2N), 2.58 t (2H, $ArCH_2$), 4.96 s (1H, OH), 6.97 s (2H, H_{arom}). IR spectrum, ν, cm^{-1}: 3640 (OH).

Found, %: C 79.89, H 11.95, N 4.05.
$C_{23}H_{41}ON$.
Calculated, %: C 79.49, H 11.89, N 4.03.

***N*,*N*-Dimethyl-4-(3,5-di-*tert*-butyl-4-hydroxyphenyl)butylamine XII** was prepared similarly from 5.0 g (16.8 mmol) of **III**, 4.6 g of dimethylamine solution (33.7 mmol), and 4.7 g (33.7 mmol) of K_2CO_3. Yield 4.4 g (85%), bp 148–150°C (1 mm Hg), mp 90–91°C. ^{1}H NMR spectrum, δ, ppm: 1.47 s (18H, *t*-Bu), 1.57 m (2H, $ArCH_2CH_2CH_2$), 1.63 m (2H, $ArCH_2CH_2$), 2.26 s [6H, $N(CH_3)_2$], 2.32 t (2H, CH_2N), 2.58 t (2H, $ArCH_2$), 5.07 s (1H, OH), 7.01 s (2H, H_{arom}). IR spectrum, ν, cm^{-1}: 3640 (OH).

Found, %: C 78.97, H 11.81, N 4.65.
$C_{20}H_{35}ON$.
Calculated, %: C 78.63, H 11.55, N 4.58.

***N*,*N*-Diethyl-4-(3,5-di-*tert*-butyl-4-hydroxyphenyl)butylamine XIII** was prepared similarly from 5.2 g (17.5 mmol) of **III**, 2.6 g (35.0 mmol) of diethylamine, and 4.8 g (35.0 mmol) of K_2CO_3. Yield 5.3 g (91%), bp 145–147°C (1 mm Hg). ^{1}H NMR spectrum, δ, ppm: 1.06 t [6H, $N(CH_2CH_3)_2$], 1.48 s (18H, *t*-Bu), 1.60 m (4H, $ArCH_2CH_2CH_2$), 2.49–2.58 m [8H, $N(CH_2CH_3)_2$, CH_2N, $ArCH_2$], 5.05 s (1H, OH), 7.02 s (2H, H_{arom}). IR spectrum, ν, cm^{-1}: 3640 (OH).

Found, %: C 79.65, H 11.81, N 4.05.
$C_{22}H_{39}ON$.
Calculated, %: C 79.92, H 11.78, N 4.20.

***N*,*N*-Dimethyl-3-(3-*tert*-butyl-4-hydroxyphenyl)propylamine XIV** was prepared similarly from 5.0 g (22.1 mmol) of chloride **IV**, 6.0 g of dimethylamine solution (44.1 mmol), and 6.1 g (44.1 mmol) of K_2CO_3. Yield 4.4 g (85%), mp 90–91°C. ^{1}H NMR spectrum, δ, ppm: 1.39 s (9H, *t*-Bu), 1.80 m (2H, $ArCH_2CH_2$), 2.27 s [6H, $N(CH_3)_2$], 2.36 t (2H, CH_2N), 2.51 t (2H, $ArCH_2$), 6.48 d (1H, H_{arom}), 6.78 d.d (1H, H_{arom}), 7.01 d (1H, H_{arom}), 8.0 br.s (1H, OH). IR spectrum, ν, cm^{-1}: 3608 (OH).

Found, %: C 76.28, H 10.25, N 5.30.
$C_{15}H_{25}ON$.
Calculated, %: C 76.55, H 10.70, N 5.52.

***N,N*-Dimethyl-3-(4-hydroxyphenyl)propylamine XV** was prepared similarly from 5.0 g (23.3 mmol) of bromide **V**, 6.4 g of dimethylamine solution (46.5 mmol), and 6.4 g (46.5 mmol) of K_2CO_3. The contents of the ampule were transferred into a round-bottomed flask, and the solvent was distilled off on a rotary evaporator. The dry residue was dissolved in ethanol on heating, and the undissolved substance was filtered off. The solvent from the filtrate was distilled off, and the target product was recrystallized from benzene. Yield 2.5 g (61%), mp 114–116°C. ^{1}H NMR spectrum, δ, ppm: 1.77 m (2H, $ArCH_2CH_2$), 2.24 s [6H, $N(CH_3)_2$], 2.32 t (2H, CH_2N), 2.54 t (2H, $ArCH_2$), 5.05 s (1H, OH), 6.73 d (2H, H_{arom}), 7.03 d (2H, H_{arom}). IR spectrum, ν, cm^{-1}: 3612 (OH).

Found, %: C 73.58, H 9.44, N 7.93.
$C_{11}H_{17}ON$.
Calculated, %: C 73.70, H 9.56, N 7.81.

***N,N*-Dimethyl-3-(4-methoxyphenyl)propylamine XVI** was prepared similarly from 5.7 g (24.4 mmol) of bromide **VI**, 6.7 g of dimethylamine solution (48.8 mmol), and 6.7 g (48.8 mmol) of K_2CO_3. Yield 4.0 g (85%), bp 108–110°C (1 mm Hg). ^{1}H NMR spectrum, δ, ppm: 1.78 m (2H, $ArCH_2CH_2$), 2.22 s [6H, $N(CH_3)_2$], 2.32 t (2H, CH_2N), 2.57 t (2H, $ArCH_2$), 3.70 s (3H, OCH_3), 6.85 d (2H, H_{arom}), 7.12 d (2H, H_{arom}).

Found, %: C 74.28, H 10.03, N 7.55.
$C_{12}H_{19}ON$.
Calculated, %: C 74.57, H 9.91, N 7.24.

***N,N*-Dimethyl-3-(3,5-di-*tert*-butyl-4-hydroxyphenyl)propylamine *N*-oxide XVII.** To a solution of 2.0 g (6.9 mmol) of amine **IX** in 15 ml of 2-propanol, we added 0.84 ml (10.3 mmol) of 30% H_2O_2. The mixture was stirred at 60°C for 3 h, the solvent was distilled off, and the residue was recrystallized from toluene. Yield 1.9 g (90%), mp 165°C. ^{1}H NMR spectrum, δ, ppm: 1.43 s (18H, *t*-Bu), 2.21 m (2H, $ArCH_2CH_2$), 2.60 t (2H, $ArCH_2$), 3.19 s [6H, $N(CH_3)_2$], 3.30 t (2H, CH_2N), 5.26 s (1H, OH), 6.99 s (2H, H_{arom}). IR spectrum, ν, cm^{-1}: 3640 (OH), 954 (NO).

Found, %: C 74.46, H 10.95, N 4.24.
$C_{19}H_{33}NO_2$.
Calculated, %: C 74.21, H 10.81, N 4.56.

***N,N*-Dimethyl-3-(3,5-di-*tert*-butyl-4-hydroxyphenyl)propylamine *N*-oxide XVII** was also prepared by oxidation of 2.0 g (6.9 mmol) of amine **IX** with 1.5 ml (10.3 mmol) of an 80% solution of cumene hydroperoxide. The procedure was similar to that described above. Yield 0.9 g (43%).

***N,N*-Diethyl-3-(3,5-di-*tert*-butyl-4-hydroxyphenyl)propylamine *N*-oxide XVIII** was prepared similarly by oxidation of 2.0 g (6.3 mmol) of **X** with 0.76 ml of hydrogen peroxide solution (9.4 mmol). Yield 1.7 g (82%), mp 167°C. ^{1}H NMR spectrum ($CDCl_3$), δ, ppm: 1.21 s [6H, $N(CH_2CH_3)_2$], 1.37 s (18H, *t*-Bu), 1.98 m (2H, $ArCH_2CH_2$), 2.50 t (2H, $ArCH_2$), 3.00 t (2H, CH_2N), 3.10 q [4H, $N(CH_2CH_3)_2$], 5.17 s (1H, OH), 6.84 s (2H, H_{arom}). IR spectrum, ν, cm^{-1}: 3640 (OH), 948 (NO).

Found, %: C 75.48, H 11.70, N 4.30.
$C_{21}H_{37}NO_2$.
Calculated, %: C 75.17, H 11.11, N 4.18.

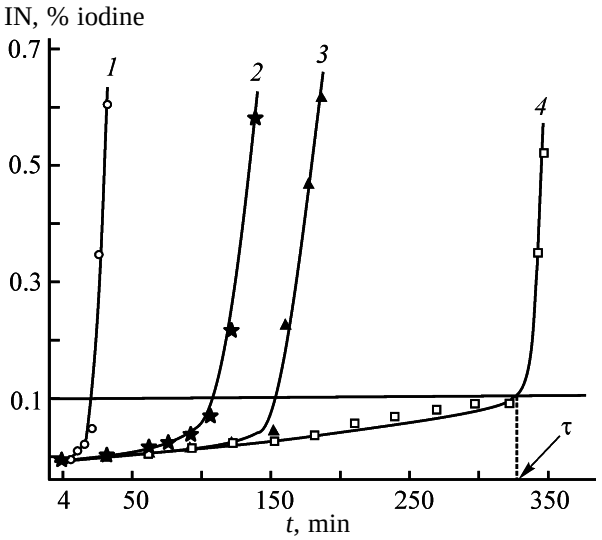
***N,N*-Dipropyl-3-(3,5-di-*tert*-butyl-4-hydroxyphenyl)propylamine *N*-oxide XIX was prepared similarly by oxidation of 1.0 g (2.9 mmol) of amine XI** with 0.35 ml of hydrogen peroxide solution (4.3 mmol). Yield 0.8 g (80%), mp 105°C. ^{1}H NMR spectrum ($CDCl_3$), δ, ppm: 0.92 t [6H, $N(CH_2CH_2CH_3)_2$], 1.40 s (18H, *t*-Bu), 1.70 m [4H, $N(CH_2CH_2CH_3)_2$], 2.02 m (2H, $ArCH_2CH_2$), 2.52 t (2H, $ArCH_2$), 3.10 t [4H, $N(CH_2CH_2CH_3)_2$], 3.15 m (2H, $ArCH_2CH_2CH_2$), 5.00 s (1H, OH), 6.87 s (2H, H_{arom}). IR spectrum, $CHCl_3$, ν, cm^{-1}: 3640 (OH), 966 (NO).

Found, %: C 76.03, H 11.54, N 3.93.
$C_{23}H_{41}NO_2$.
Calculated, %: C 75.98, H 11.37, N 3.85.

We also examined the inhibiting activity of 2,6-di-*tert*-butyl-4-methylphenol (Ionol) and *N,N*-dimethyldodecylamine (Acros Organics). Oxidation of lard (Novosibirsk Meat-Canning Plant) was performed under the conditions of oxygen bubbling at 130°C in an oxidation cell similar to that described in [19]. The weight of the lard sample was 50 g, and AO concentration, 1.5 μmol per gram of lard. In the course of the oxidation, 1-g samples of the lard were taken, and the concentration of peroxy compounds was determined by iodometric titration [25]. The kinetic curves were plotted (see figure), and the induction period (time in which the lard was oxidized to a peroxide number of 0.1) was determined graphically. All the measurements were repeated 3–4 times; the mean results with the rms errors are listed in the table.

CONCLUSIONS

(1) *N,N*-Dialkyl-ω-[4-hydroxy(methoxy)aryl]alkylamines of various structures, forming structurally related series, and their *N*-oxides were prepared.



Kinetic curves of oxidation of lard. Inhibitor: (*1*) none, (*2*) amine **XX**, (*3*) Ionol, and (*4*) amine **IX**. (PN) Peroxide number and (*t*) time.

(2) The aminoalkylphenols synthesized, owing to the bifunctional mechanism of the antioxidative effect and the occurrence of intramolecular synergism, surpass in the inhibiting activity commercial antioxidants and show promise as inhibitors preventing oxidation of fat-containing products.

(3) The inhibiting activity of the aminoalkylphenols synthesized increases with an increase in the distance between the nitrogen atom and aromatic core, decrease in the length of *N*-alkyl substituents, and increase in the extent of steric shielding of the phenolic OH group; in going from aminoalkylphenols to the corresponding *N*-oxides, the antioxidative activity decreases.

ACKNOWLEDGMENTS

The authors are grateful to the Russian Foundation for Basic Research for the access to the STN International database (project no. 00-03-32721) through the Novosibirsk STN Center, Novosibirsk Institute of Organic Chemistry, Siberian Division, Russian Academy of Sciences.

REFERENCES

1. US Patent 5814695.
2. US Patent 5340369.
3. US Patent 3305483.
4. EP Patent 500336.
5. US Patent 3202711.
6. EP Patent 474403.
7. US Patent 5281623.
8. Klein, C.D.P., Klingmuller, M., Schellinski, C., *et al.*, *J. Med. Chem.*, 1999, no. 42, pp. 3874–3888.
9. Kandalintseva, N.V., Dyubchenko, O.I., Prosenko, A.E., *et al.*, *Khim.-Farm. Zh.*, 2001, vol. 35, no. 3, pp. 22–25.
10. Kandalintseva, N.V., Dyubchenko, O.I., Terakh, E.I., *et al.*, *Khim.-Farm. Zh.*, 2002, vol. 36, no. 4, pp. 13–15.
11. *Comprehensive Organic Chemistry. The Synthesis and Reactions of Organic Compounds*, Barton, D. and Ollis, W.D., Eds., vol. 2: *Nitrogen Compounds*, Oxford: Pergamon, 1979.
12. Prilezhaeva, E.N., *Reaktsiya Prilezhaeva: Elektrofil'noe okislenie* (Prilezhaev Reaction: Electrophilic Oxidation), Moscow: Nauka, 1974.
13. USSR Inventor's Certificate no. 362825.
14. US Patent 4247480.
15. Dyubchenko, O.I., Prosenko, A.E., Terakh, E.I., *et al.*, *Nauch. Vestn. Tyumensk. Med. Akad.*, 2003, no. 1, pp. 23–26.
16. Gershanov, F.B., Gurvich, Ya.A., Dolidze, V.O., *et al.*, *Prom–st. Sint. Kauchuka*, 1973, no. 12, pp. 7–9.
17. Voigt, J., *Die Stabilisierung der Kunststoffe gegen Licht und Wärme*, Berlin: Springer, 1966.
18. *Ingibirovanie protsessov okisleniya polimerov smesyami stabilizatora* (Inhibition of Polymer Oxidation with Mixtures of Stabilizers), Moscow: NIITEKhIM, 1970.
19. Emanuel', N.M. and Lyaskovskaya, Yu.N., *Tormozhenie protsessov okisleniya zhirov* (Inhibition of Fat Oxidation), Moscow: Pishchepromizdat, 1961.
20. Farsaliev, V.M., Fernando, W.S., and Skott, G., *Eur. Polym. J.*, 1978, vol. 14, no. 10, pp. 785–788.
21. Skott, G. and Tusoff, M., *Eur. Polym. J.*, 1980, vol. 16, no. 6, pp. 497–501.
22. Terakh, E.I., Prosenko, A.E., Nikulina, V.V., and Zaitseva, O.V., *Zh. Prikl. Khim.*, 2003, vol. 76, no. 2, pp. 261–265.
23. Roginskii, V.A., *Fenol'nye antioksidanty: Reaktsionnaya sposobnost' i effektivnost'* (Phenolic Antioxidants: Reactivity and Performance), Moscow: Nauka, 1988.
24. USSR Patent 1376511.
25. Zinov'ev, A.A., *Khimiya zhirov* (Chemistry of Fats), Moscow: Pishchepromizdat, 1952.

Russian Journal of Applied Chemistry, Vol. 78, No. 5, 2005, pp. 787–790. Translated from Zhurnal Prikladnoi Khimii, Vol. 78, No. 5, 2005, pp. 802–806.
Original Russian Text Copyright © 2005 by Yutilov, Svertilova, Minkina, Kirillova, Smolyar.

ORGANIC SYNTHESIS AND INDUSTRIAL ORGANIC CHEMISTRY

Improvement of the Synthesis of 6-Bromo-5-methylimidazo[4,5-*b*]pyridine, a Stabilizer for Color Photography

Yu. M. Yutilov, I. A. Svertilova, L. V. Minkina, K. M. Kirillova, and N. N. Smolyar

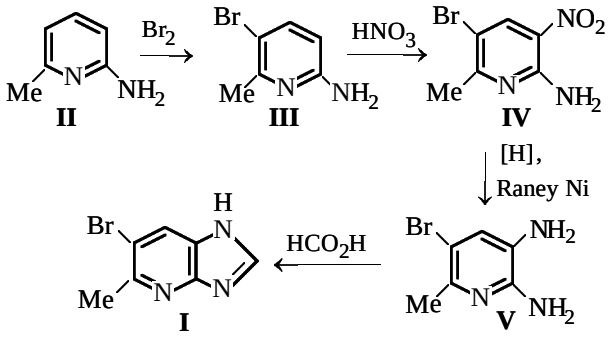
Litvinenko Institute of Physical Organic and Coal Chemistry, National Academy of Sciences of Ukraine, Donetsk, Ukraine

Received October 14, 2004; in final form, February 2005

Abstract—Procedures were suggested for preparing 6-bromo-5-methylimidazo[4,5-*b*]pyridine, a stabilizer for TsMF-2 color photographic moment, a component of developing pastes of the photographic kit.

Imidazo[4,5-*b*]pyridine derivatives exhibit unique antifogging properties among color photographic materials [1–8]. A particular mention should be made of 6-bromo-5-methylimidazo[4,5-*b*]pyridine **I**, which is simultaneously a stabilizer of a photographic layer and a component of developing pastes of the Polaroid color photographic kit; it provides high quality of a photographic image.

Data on the synthesis of **I** are available from two patent [1, 2]. The suggested four-step procedure involves bromination of 2-amino-6-methylpyridine **II**, nitration of the resulting 2-amino-5-bromo-6-methylpyridine **III**, reduction of 2-amino-3-nitro-6-methylpyridine **IV** to diamine **V**, and its subsequent cyclization into **I**. According to [1, 9], bromo derivative **III** is prepared by bromination of **II** with bromine in 20% sulfuric acid. An experimental check of the procedures from [1, 9] shows that the yield of **III** after purification is as low as 50–55%. It is known that amino and hydroxy derivatives of nitrogen heterocycles are smoothly halogenated in aqueous solutions or in glacial acetic acid [10, 11]:



Attempted bromination of **II** with an equivalent amount or small excess of bromine in aqueous solution at 20–70°C results in low yields of the reaction product. Bromination of **II** in glacial acetic acid at room temperature gives the product in almost quantitative yield. To bind HBr that is released in the reaction and may prevent the bromination of **II**, an equivalent amount of sodium acetate was added to the reaction mixture. The melting point of the resulting bromopyridine **III**, 73–74°C, somewhat differs from the value reported in the literature (70–71°C [1]).

A GLC analysis of this product revealed the presence of two impurities (10 wt %) along with the main substance **III**. The first impurity was unchanged substrate **II**, and the second, 2-amino-3,5-dibromo-6-methylpyridine **VI**, identified by comparison with an authentic smaple specially prepared by bromination of **II** under the conditions described in [9]. When the bromination of **II** was performed at 10–15°C, the content of unchanged **II** decreased to a minimum, but the content of dibromo derivative **VI** remained virtually the same, 7–8 wt %. By-product **VI** could be eliminated neither by decreasing the amount of bromine taken for the reaction, nor by repeated recrystallization of bromination product **III** from various organic solvents. We found that the concentration of **VI** in the reaction product depends on the rate of adding bromine: The lower the bromine concentration in the reaction mixture, the lower the probability of dehydrobromination. However, we failed to ensure formation of **III** as the only product. To separate **VI**, we took advantage of the fact that monobromo derivative **III** forms with acetic acid a salt readily soluble in water (30 g in 100 g of water at 23°C), whereas 3,5-dibromo derivative **VI** does not form such a salt and is virtual-

1070-4272/05/7805-0787 © 2005 Pleiades Publishing, Inc.

ly insoluble in water. After the bromination completion, the acetic acid was distilled off almost to dryness, and water was added to the residue. By-product **VI** remained in the insoluble residue, and it was filtered off. By alkalization of the filtrate, we isolated virtually pure **III**, without impurity of **VI**.

The nitration of amine **III** under the conditions described in [1, 2] often yielded, instead of the expected nitro compound **IV**, a black precipitate from which we failed to isolate the desired product by recrystallization from solvents in the presence of activated carbon or alumina, or by reprecipitation with alkalis from weakly acidic solutions. In nitration of 2-amino-5-bromopyridine **VII** under the same conditions, a significant amount of 3-nitro-5-bromo-2-pyridone **VIII** is formed along with the desired 3-nitro derivative of **VII** [13].

Nitration of **III** under the similar conditions is also accompanied by deamination. From dark tarry products, we isolated a compound identified as 3-nitro-5-bromo-6-methyl-2-pyridone **IX**.

To avoid formation of **IX** in nitration of **III**, we changed the order of mixing the reactants. Fuming nitric acid was added to a solution of **III** in sulfuric acid not at 55–60 but at 0–5°C, after which the temperature was gradually raised to 55–60°C. By so doing, we considerably reduced the yield of tars. However, after recrystallization of the products from methyl ethyl ketone, we detected **IX** in an amount comparable with that of the target product. By-product **IX** is insoluble in methyl ethyl ketone, alcohol, water, and the majority of aprotic solvents. At decreased nitration temperatures, the amount of **IX** decreased considerably (to 5–10 wt % relative to **IV**).

We examined the influence exerted by the conditions of nitration of **III** on the composition of the reaction products. It is advisable to perform nitration at 0–5°C in concentrated sulfuric acid with 60–63% nitric acid. In isolation of the desired nitro compound **IV**, to avoid formation of tarry impurities, the mixture should be neutralized to pH 2–3 with sodium acetate; in this case, the yield of **IV** is 80–85%. However, even with all these conditions observed, a certain amount of tar is formed; it decreases the melting point of **IV** by 10–20°C. Even a slight excess of nitric acid in nitration of amine **III** causes strong darkening of **IV**. For accurate dosage of nitric acid in nitration, we used instead of amine **IV** its nitrate **X** and added this salt with vigorous stirring at 15°C to concentrated sulfuric acid. Salt **X** is readily formed by mixing a melt of **III** with 60–63% nitric acid in water. Salt **X** can be obtained from crude **III** without its drying. To obtain pure nitro compound **IV** after the transformation of **X** in concentrated sulfuric acid, the acid solution after the nitration was neutralized with sodium acetate. After adding a half of the amount of sodium acetate required for complete neutralization of the reaction mixture, a bright yellow precipirtate of **IV** containing no by-products is formed. Neutralization of the filtrate after the isolation of **IV** to pH 6–7 allows isolation of the precipitate of dibromo derivative **VI**. If salt **X** taken for the nitration is free of amine **VI**, almost quantitative yield of **IV** can be attained, and its purity considerably increases. After recrystallization of **IV** from DMF, its melting point increases by 2–3°C (mp 213°C).

When in nitration of **III** HNO_3 is replaced by a less aggressive and more convenient in handling agent, e.g., KNO_3 in concentrated H_2SO_4, the reaction at 0–10°C yields no nitro compound **IV**, and heating to 40–50°C causes formation of pyridone **IX**. The nitration of **III** in glacial acetic acid also gives negative results.

According to [1, 2], nitro compound **IV** is reduced to diamine **V** with hydrogen in the presence of Raney nickel. Despite a fairly high yield of **V**, ~70%, this procedure is not quite feasible for industrial application, because the catalyst is pyrophoric and hydrogen is dangerously explosive. In the reduction of **IV** with $SnCl_2$ in concentrated HCl according to [12], the yield of **V** does not exceed 60%, and diamine **V** is contaminated with by-products and requires additional purification. Taking into account the fact that structurally related 2-amino-3-nitro-5-chloro(bromo)-6-methylpyridine is smoothly reduced with sodium sulfide in aqueous solution [10], we examined the applicability of this procedure to the reduction of **IV** at 60–100°C. At 60°C, no reduction occurs, and at 100°C the reaction is accompanied by extensive tarring. At 75–80°C, the yield of **V** does not exceed 40%. Experiments on reduction of **IV** with iron in aqueous solution containing a small amount of HCl showed that, when iron dust is added in small portions to a solution of **IV** at 80–90°C, the reduction occurred readily without self-heating and could be controlled. The yield of **V** reached 80% and did not decrease when the reaction time and amount of iron were decreased by half.

The most efficient is the reduction of **IV** with hydrazine hydrate. Refluxing of **IV** with a 15-fold excess of hydrazine hydrate for 5–6 h results in the formation of **V** in 68–70% yield. When the process is performed in a solvent, the consumption of hydrazine hydrate can be decreased by a factor of more than 3. 1-Butanol appeared to be the best solvent for this

purpose, because of high solubility of **IV** and **V** in it and sufficiently high boiling point providing the required reaction temperature. However, the reaction in 1-butanol requires longer time. To accelerate the reduction, we tested the following metals as catalysts: Raney nickel, iron of various brands, powdered aluminum, and zinc dust. The best results were obtained with zinc dust.

By varying the amounts of hydrazine hydrate, 1-butanol, and zinc dust, and also the temperature, we obtained highly pure diamine **V** in 87–90% yield.

When optimizing the synthesis of **I**, we started from the procedure [1, 12] involving heating of diamine **V** in 98–100% formic acid. Our experiments showed that the yield of **I** did not change at the consumption of formic acid decreased by a factor of 3 and the reaction time, by a factor of 2. The by-product was the *N*-formyl derivative of **V**. It seemed appropriate to use as a cyclizing agent pentyl formate suggested previously for the synthesis of a series of imidazo[4,5-*b*]- and -[4,5-*c*]pyridine derivatives [14]. This agent has significant advantages over formic acid: it is less toxic and does not cause scalds and damage mucous membranes of lungs and eyes. Furthermore, the consumption of pentyl formate for preparation of 1 kg of **I** is 5 l, whereas the required amount of formic acid is two times greater. The yield of **I** in refluxing of **V** in pentyl formate is 90–91%.

EXPERIMENTAL

The purity of volatile products was checked in an LKhM-72 analytical chromatograph (2000 × 4-mm column, stationary phase 15% Apiezon on Chromaton N-AW-DMC, carrier gas He, column temperature 220°C). Nonvolatile compounds were analyzed by TLC on Silufol UV-254 plates (eluent ethanol).

2-Amino-5-bromo-6-methylpyridine III. Amine **II** (16.1 g) and anhydrous sodium acetate (12.3 g) were dissolved in 126 ml of glacial acetic acid with stirring at 20–22°C. Then the mixture was cooled to 10–15°C, and a solution of 7.7 ml of bromine in 21 ml of glacial acetic acid was added dropwise at this temperature. After adding the whole amount of bromine, the mixture was stirred at 15°C for 1 h. The solvent was distilled off almost to dryness (~150 ml), and the residue was filtered off, washed with 10 ml of glacial acetic acid, and mixed at 20–25°C with 100 ml of water. The insoluble residue ot **VI** was filtered off, washed with 5 ml of water, and dried in air. Yield of by-product **VI** 2.1 g, mp 142–143°C [5]. The aqueous filtrate was alkalized with 6 ml of 30% NaOH to pH 8, and the colorless precipitate of bromo derivative **III** was filtered off. The product was washed with 5 ml of water, recrystallized from 20% acetic acid, and dried. Yield 25 g (90%), mp 80–82°C. According to [21], mp 71–72°C.

2-Amino-5-bromo-6-methylpyridinium nitrate X. To 16 ml of water heated to 80–85°C we added with stirring 7.6 g of molten 2-aminopyridine **III**. To the resulting emulsion, we added over a period of 5–10 min 3.4 ml of 60% HNO_3. In so doing, base **III** dissolved, and nitrate **X** started to precipitate on cooling the reaction mixture to 60–55°C. After cooling to 10–15°C, the precipitate was filtered off. Yield of **X** 9.7 g (95.5%), mp 170–172°C.

Found, %: C 28.59, H 3.16, N 16.61.
$C_6H_7BrN_2 \cdot HNO_3$.
Calculated, %: C 28.82, H 3.22, N 16.80.

2-Amino-3-nitro-5-bromo-6-methylpyridine IV. Nitrate **X** (21 g) was added in small portions to 45 ml of concentrated sulfuric acid cooled to 10–15°C. The mixture was stirred for 1 h and poured onto 160 g of ice, and 110 g of sodium acetate ($CH_3COONa \cdot 3H_2O$) was added. The light yellow precipitate was filtered off, washed with 10 ml of water and 5 ml of acetone, and dried; 19.5 g (~100%) of nitro compound **IV** was obtained, mp 211–213°C (from DMF); according to [12], mp 210–213°C.

2,3-Diamino-5-bromo-6-methylpyridine V. (*a*) To a mixture of 24 ml of 2-propanol, 6 ml of water, 5.6 g of aminonitropyridine **IV**, and 0.8 ml of concentrated HCl, we added with stirring at 70–75°C 5.6 g of iron carbonyl in portions over a period of 2 h, so that the mixture mildly boiled. Then the mixture was refluxed for 2 h and filtered while hot. The black precipitate on the filter was washed with hot 2-propanol, and the wash solution was combined with the filtrate. The resulting solution was alkalized with 25% aqueous ammonia to pH 8 and refluxed for 0.5 h. The precipitated iron oxides were filtered off, and 2-propanol and then water were distilled off in a water-jet-pump vacuum to ~1/4 of the initial volume. The residue was cooled to 15–20°C, and the precipitate of diamine **V** was filtered off. Yield 4.04 g (80%), mp 135–137°C (from H_2O). According to [12], mp 136–137°C.

(*b*) To a mixture of 5.8 g of **IV**, 50 ml of 1-butanol, and 7 ml of hydrazine hydrate, we added with stirring at 100°C 1.0 g of zinc dust in portions over a period of 2 h. The mixture was refluxed for 3–4 h until the gas evolution ceased. Then the mixture was cooled to 60–70°C and filtered. The gray precipitate

on the filter was washed with 20 ml of hot 1-butanol, and the wash solution was combined with the filtrate. Then 55–60 ml of 1-butanol was distilled off in a water-jet-pump vacuum. The residue was cooled to 15–20°C, and the precipitate of **V** was filtered off. Yield 4.55 g (90%), mp 135–137°C (H_2O).

6-Bromo-5-methylimidazo[4,5-*b*]pyridine I. A mixture of 5 g of **V** and 7 ml of pentyl formate was heated at 170–175°C for 2 h until 0.4–0.5 ml of water was released and then at 170–180°C for 2 h more. Pentyl formate and 1-pentanol were distilled off in a water-jet-pump vacuum (40–50°C, 25–30 mm Hg) to dryness, and the residue was crystallized from ethyl acetate or water–2-propanol (5 : 1). Yield 4.75 g (90.5%), mp 206–207°C. According to [12], mp 204–205°C.

CONCLUSION

Procedures were suggested for preparing 2-amino-5-bromo-6-methylpyridine by bromination of 2-amino-6-methylpyridine in glacial acetic acid in the presence of anhydrous sodium acetate in 90% yield, nitration of the resulting compound in the form of nitrate in concentrated sulfuric acid at 10–15°C (~100% yield), reduction of the product in an acidified alcohol with iron carbonyl (~80% yield) or with hydrazine hydrate and zinc (~87–90% yield), and cyclization of 2,3-diamino-6-methylpyridine in refluxing pentyl formate to 6-bromo-5-methylimidazo[4,5-*b*]pyridine (~90.5% yield), an antifogging compound for color photographic materials.

ACKNOWLEDGMENTS

The authors are grateful to L.I. Shcherbina for the assistance in the manuscript preparation.

REFERENCES

1. US Patent 3473924.
2. US Patent 3629272.
3. US Patent 3687660.
4. French Patent 2134750.
5. Australian Patent 461229.
6. US Patent 4071366.
7. US Patent 4102685.
8. US Patent 4134768.
9. Adams, R. and Schrecker, A.W., *J. Am. Chem. Soc.*, 1949, vol. 71, no. 4, pp. 1186–1195.
10. Israel, M. and Day, A.R., *J. Org. Chem.*, 1959, vol. 24, no. 10, pp. 1455–1460.
11. Weygand–Hilgetag, *Organisch-chemische Experimentierkunst*, Leipzig: Johann Ambrosius Barth, 1964, 3rd ed.
12. Graboues, H. and Day, A.R., *J. Am. Chem. Soc.*, 1957, vol. 79, no. 24, pp. 6421–6426.
13. Abramovich, A.B., *Pyridine and Its Derivatives*, New York, 1974, vol. 14, part 3.
14. USSR Inventor's Certificate no. 717055.

Russian Journal of Applied Chemistry, Vol. 78, No. 5, 2005, pp. 791–793. Translated from Zhurnal Prikladnoi Khimii, Vol. 78, No. 5, 2005, pp. 807–809.
Original Russian Text Copyright © 2005 by Gizatulina, Chebotok, Novikov, Konovalova.

ORGANIC SYNTHESIS AND INDUSTRIAL ORGANIC CHEMISTRY

Kinetics of Acid Hydrolysis of Acetylglucosamine

G. A. Gizatulina, E. N. Chebotok, V. Yu. Novikov, and I. N. Konovalova

Murmansk State Technical University, Murmansk, Russia
Knipovich Arctic Research Institute of Marine Fishery and Oceanography, Murmansk, Russia

Received January 26, 2005

Abstract—The kinetics of acid hydrolysis of *N*-acetylglucosamine at different temperatures and reagent concentrations was studied. A mathematical model of the hydrolysis was proposed. The rate constant and activation energy of deacetylation were calculated.

Utilization of large volumes of chitin-containing waste of crustaceans involves usually chemical hydrolysis of chitin and chitosan. Under these conditions, chitin is hydrolyzed to its monomers: glucosamine (GA) and acetylglucosamine (AGA). Complete depolymerization of chitin and chitosan is usually performed in an acidic solution at elevated temperatures [1]. Under these conditions, the glucoside bonds in the polysaccharide are ruptured to form the monomers. Deacetylation occurs in parallel with depolymerization. The deacetylated monomer is usually isolated in the form of its salt of the acid used for hydrolysis. The study of the mechanisms of acid hydrolysis of chitin and chitosan as influenced by the degree of deacetylation and molecular weight of the initial polysaccharide and hydrolysis conditions (temperature and acid concentration) is of both practical and theoretical interest.

Acid hydrolysis of chitin and chitosan was extensively studied [1–5]. However, the kinetics of this process was not understood and the rate constants of its elementary steps were not determined. Previously we suggested a mathematical model of acid deacetylation of chitin [6, 7]. We found that the chitin deacetylation is described by the first-order kinetic equation and the dependence of the reaction rate passes through a maximum at the hydrochloric acid concentration w_{HCl} = 29.8%.

The aim of this study was to estimate the rate constant and activation energy of AGA deacetylation and to determine the hydrolysis rate of the acetamide bond as influenced by the degree of polymerization of the polysaccharide.

EXPERIMENTAL

We used *N*-acetylglucosamine (AGA) prepared by acetylation of *D*-glucosamine with acetic anhydride by the reaction [8]

$$C_6H_{11}NO_5 + (CH_3CO)_2O \rightarrow C_8H_{15}NO_6 + CH_3COOH. \quad (1)$$

Acetylation was performed as follows. A 900-ml portion of AV-17-8 anion exchanger converted into the CO_3 form by treatment with 10% aqueous solution of sodium carbonate was placed into a flask equipped with a stirrer. A 900-ml portion of 0.38 M aqueous solution of *D*-glucosamine hydrochloride [75 g (0.46 mol) GA·HCl] and 90 ml of ethanol (w = 96%) were added at 0–5°C. Acetic anhydride (45 ml, 0.64 mol, w = 99%) was added in small portions at 0–5°C. The reaction mixture was stirred for 3 h at 0–5°C. The resin was filtered off, washed with 500 ml of distilled water, and regenerated.

The filtrate and wash waters were evaporated under reduced pressure (10–20 mm Hg) at 50–60°C to a viscous syrup containing crystals. Ethanol (75 ml, w = 96%) was added, and the resulting mixture was left to crystallize at 0–5°C for 12–15 h.

The crystals were filtered off, washed with 300 ml of acetone (chemically pure grade) to remove water, and dried in a vacuum. The *N*-acetylglucosamine yield was 73.5% of the theoretical yield corresponding to Eq. (1).

N-Acetylglucosamine was hydrolyzed in hydrochloric acid with a concentration from 10 to 37.2% at 40, 60, and 80°C. The hydrolyzate was neutralized first with 2.7 M NaOH and then with 0.1 M NaOH to pH 7.0, filtered through a Schott filter (pore diameter no larger than 10 μm, POR 10), and analyzed for AGA and GA content (M).

The AGA content was determined by the procedure described in [9]; the total AGA + GA content, by the procedure from [10]. The GA amount was calculated

1070-4272/05/7805-0791 © 2005 Pleiades Publishing, Inc.

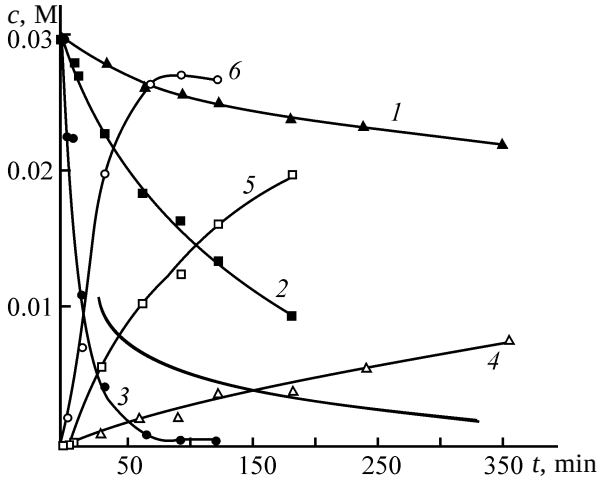


Fig. 1. Kinetic curves of AGA hydrolysis at (*1*) 313, (*2*) 333, and (*3*) 353 K and kinetic curves of GA formation at (*4*) 313, (*5*) 333, and (*6*) 353 K. c_{HCl} = 6.02 M (w_{HCl} = 20%). (*c*) concentration of AGA and GA and (*t*) hydrolysis time.

as the difference between the total AGA + GA amount and the AGA amount. The kinetic curves of AGA consumption and GA accumulation in 20% HCl at different temperatures are shown in Fig. 1. Hydrolysis of AGA is accelerated with increasing temperature. The major product of AGA hydrolysis is glucosamine:

$$C_8H_{15}NO_6 + H_2O \rightarrow C_6H_{11}NO_5 + CH_3COOH. \quad (2)$$

Analysis of the kinetic curves of AGA hydrolysis shows that the reaction can be described by a first-order kinetic equation. The rate constants of AGA deacetylation and GA formation at different temperatures were calculated by the first-order kinetic equation [11]

$$k = 1/t \ln(c_0/c), \quad (3)$$

where t is the reaction time (s^{-1}); c, current concentration of the reactant at time t (M); and c_0, initial concentration of the reactant (M).

The results of these calculations are presented in Table 1.

Table 1. Rate constants of AGA hydrolysis and GA formation. c_{HCl} = 6.02 M (w_{HCl} = 20%)

T, K	AGA		GA	
	k, s^{-1}	$\ln k$	k, s^{-1}	$\ln k$
313	0.00129	–6.653	0.00079	–7.143
333	0.00804	–4.824	0.00638	–5.055
353	0.0544	–2.912	0.0369	–3.301

Table 2. Rate constants of deacetylation of chitin and AGA at T = 353 K

Compound	w_{HCl}, %	c_{HCl}, M	k, s^{-1}
Chitin	35.8	11.57	0.0523
	29.8	9.38	0.0558
AGA	20	6.02	0.0544
	37.2	12.08	0.0428

The rate constants of AGA deacetylation were compared with the rate constant of acid deacetylation of chitin, determined in our previous study [6]. The rate constants of chitin deacetylation at 353 K, calculated by Eq. 3, are presented in Table 2.

As seen from Table 2, the rate constants of deacetylation of AGA and chitin at 353 K are of the same order. These results suggest that the rate constant of deacetylation of chitin and oligomeric and monomeric products of its acid hydrolysis is independent of the molecular weight.

The activation energy of hydrolysis of the acetamide bond was calculated from the temperature dependence of the rate constant by the Arrhenius equation [11]:

$$k = Ae^{-E_a/RT}. \quad (4)$$

The activation energy is 85.7 kJ mol^{-1}.

The calculations were performed on the assumption that the AGA deacetylation is described by the first-order kinetic equation and the true (second) reaction order is reduced owing to large excess of hydrochloric acid [11]. Since the rate of chitin deacetylation depends on the hydrochloric acid concentration [6], we studied the similar dependence for AGA.

The dependence of the rate constant of AGA deacetylation at T = 353 K on the hydrochloric acid concentration is shown in Fig. 3.

The dependence of the rate constant of chitin deacetylation on the hydrochloric acid concentration is similar [6]: it passes through a maximum at the hydrochloric acid concentration of 9 M (w = 29%) and then decreases with a further increase in c_{HCl}.

Since the acid is involved in the catalytic reaction, its concentration should enter into the pseudo-first-order rate constant $k = k'c_{HCl}$. However, the sharp ac-

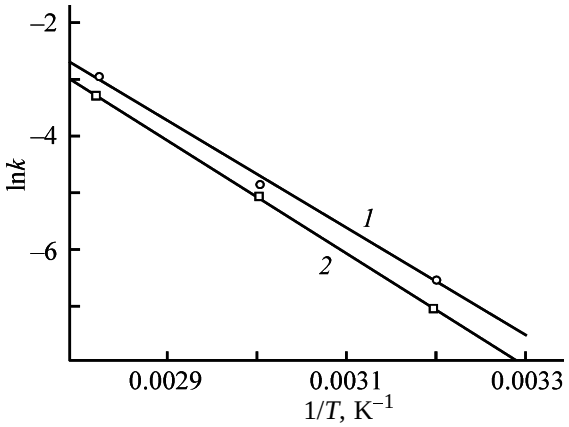


Fig. 2. Logarithms of rate constants ln*k* of (*1*) AGA hydrolysis and (*2*) GA formation as functions of 1/*T*.

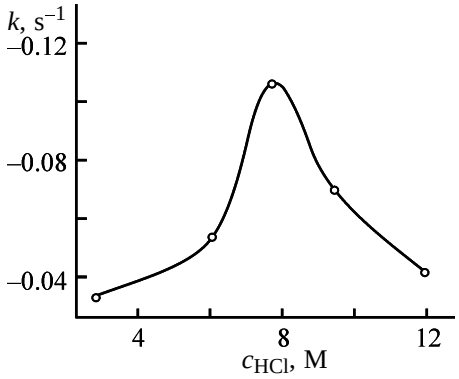


Fig. 3. Rate constant *k* of AGA deacetylation at 353 K as a function of the hydrochloric acid concentration c_{HCl}.

celeration of the reaction in 9 M HCl (Fig. 3) is difficult to explain.

The fact that the dependence for acid hydrolysis of chitin is similar additionally confirms that the mechanism of acid deacetylation of the monomeric and polymeric species is the same.

CONCLUSIONS

(1) The rate constant of acid hydrolysis of acetamide bonds in chitin is similar to that in its oligomers and *N*-acetylglucosamine.

(2) The dependence of the rate of *N*-acetylglucosamine deacetylation on the hydrochloric acid concentration passes through a maximum at $c_{HCl} \sim 8$ M ($w_{HCl} = 26\%$).

REFERENCES

1. Horowitz, S.T., Roseman, S., and Blumental, H.J., *J. Am. Chem. Soc*., 1957, vol. 79, no. 18, pp. 5046–5049.
2. Capon, B. and Foster, R.L., *J. Chem. Soc. Sec. C*, 1970, no. 12, pp. 1654–1655.
3. *Chitin Handbook*, Muzzarelli, R.A.A. and Peter, M.G., Eds., Grottamare, 1977, pp. 195–198.
4. Chang, K.L.B., Lee, J., and Fu, W.-R., *J. Food Drug Anal*., 2000, vol. 8, no. 2, pp. 75–83.
5. Varum, K.M., Ottoy, M.H., and Smidsrod, O., *Carbohydr. Polym*., 2001, vol. 46, no. 1, pp. 89–98.
6. Novikov, V.Yu., *Zh. Prikl., Khim*., 1999, vol. 72, no. 1, pp. 147–152.
7. Novikov, V.Yu., *Zh. Prikl. Khim.*, 2004, vol. 77, no. 3, pp. 490–493.
8. Roseman, S. and Ludowieg, J., *J. Am. Chem. Soc*., 1954, vol. 76, no. 1, pp. 301–302.
9. Reissig, J.L., Strominger, J.L., and Leloir, L.F., *J. Biol. Chem*., 1955, vol. 217, no. 2, pp. 959–966.
10. Imoto, T. and Yagishita, K., *Agr. Biol. Chem*., 1971, vol. 35, no. 7, pp. 1154–1156.
11. Semiokhin, I.A., Strakhov, B.V., and Osipov, A.I., *Kinetika gomogennykh khimicheskikh reaktsii* (Kinetics of Homogeneous Chemical Reactions), Moscow: Mosk. Univ., 1986.

Russian Journal of Applied Chemistry, Vol. 78, No. 5, 2005, pp. 794–797. Translated from Zhurnal Prikladnoi Khimii, Vol. 78, No. 5, 2005, pp. 810–813.
Original Russian Text Copyright © 2005 by Sazanov, Novoselova, Amsharov, Ugolkov, Andreeva, Gribanov.

MACROMOLECULAR CHEMISTRY AND POLYMERIC MATERIALS

Prospects for Using Polyacrylonitrile for Preparing Carbonized Polymeric Composites

Yu. N. Sazanov, A. V. Novoselova, K. Yu. Amsharov, V. L. Ugolkov, O. A. Andreeva, and A. V. Gribanov

Institute of Macromolecular Compounds, Russian Academy of Sciences, St. Petersburg, Russia
Institute of Silicate Chemistry, Russian Academy of Sciences, St. Petersburg, Russia

Received January 27, 2005

Abstract—The thermochemical cyclization of different polyacrylonitrile samples prepared by radical and anionic polymerization was studied by thermal analysis, spectroscopy, and AM1 semiempirical calculations. The possibility of using polyacrylonitrile as a cocarbonizate for preparing mixed carbon composites with nitrogen-containing polysaccharides was examined.

Our previous studies were aimed to enhance the heat resistance of polymers by their compounding with polyimides [1–4]. Some of the carbonized residues showed fairly high coke numbers (CNs) and exhibited properties deserving a special study. Another heat-resistant polymer is polyacrylonitrile (PAN), with which, as with polyimides, mixed composites with enhanced heat resistance and strength were prepared [5].

In the context of development of various carbon materials based on polymers, it is interesting to examine the effect of PAN on the thermochemical carbonization of other polymers and hence on the properties of the resulting products. From the viewpoint of the PAN reactivity, the most promising is the step of thermal cyclization occurring in the range 200–300°C. Despite numerous papers concerning this process, its mechanism is not yet elucidated unambiguously. The scheme of formation of "ladder" polymers as infinite chains of cyclic sequences, postulated in early studies [6–9], was not confirmed and gave way to the concept [10–16] according to which cyclization of PAN yields chains with the number of cyclic sequences not exceeding 8–10. Attempts to consider the mechanism of PAN cyclization taking into account the conformation of macromolecules [17, 18] were not properly developed, as major attention was given to solution of materials-science and processing problems. A number of tentative schemes reflecting attempts to take into account the features of production of real items, mainly fibers, were suggested [19].

Our goal was to develop procedures for preparing cocarbonizates from PAN and cellulose derivatives. The first step was to find the most probable routes that could ensure incorporation of the PAN structure into other polymers by their thermochemical reaction. To this end, we modeled cyclization of PAN in the absence of chemical additives (catalysts, oxidants, accelerators). Solution of this problem is complicated by the difficulties associated with preparation of PAN samples free of oxygen-containing functional groups remaining in the polymer after its isolation and purification. Such polymers cannot be prepared by radical polymerization (r-PAN). Polymerization of acrylonitrile by the anionic mechanism under definite conditions yields samples whose thermal cyclization in an inert atmosphere [20, 21] gives products containing no impurities and volatile low-molecular-weight cyclization products. For such samples of anionic PAN (a-PAN), the exothermic effect appreciably shifted toward higher temperatures. Thus, the conditions of PAN activation can correspond to the conditions of thermochemical reactions with other polymers. The most suitable for this purpose are cellulose derivatives; their thermal degradation occurs most actively in the same temperature range (200–300°C) as the cyclization of PAN [22, 23].

EXPERIMENTAL

Returning to the modeling of suitable PAN structures, we chose samples prepared by the radical and anionic polymerization mechanism, with different ratio of the atactic, isotactic, and syndiotactic structures [15, 24].

1070-4272/05/7805-0794© 2005 Pleiades Publishing, Inc.

Structural and calorimetric characteristics of PAN samples*

Sample	$M \times 10^{-5}$	MWD	s, %	a, %	i, %	CB	T_{max}, °C	ΔT, °C	ΔH, kJ mol^{-1}	Δm_1, %	Δm_2, %
r-PAN	6	–	24	47	29	1.0	318 302	210 87	182.44 26.04	2.53 0.83	7.42 18.1
a-PAN-i	3	1,8	27	43	30	1.5	276 276	205 73	86.20 21.00	0.2 1.0	6.41 3.3
a-PAN-s	6	1,5	34	41	25	1.3	317 310	95 88	50.82 23.10	0.3 0.8	8.2 15.6

* Thermal analysis was performed by DSC in air (numerator) and nitrogen (denominator). PAN structure: (s) syndiotactic, (a) atactic, and (i) isotactic; (CB) coefficient of stereoblock structure of the polymers [19]; (T_{max}) temperature of the exothermic maximum of PAN cyclization; (ΔT) temperature interval of the exothermic peak; (ΔH) heat of cyclization up to T_{max}; (Δm_1) PAN weight loss up to T_{max}; and (Δm_2) PAN weight loss in the whole interval of temperatures of the exo effect.

The table shows that the structure of r-PAN is less regular than that of a-PAN. To simplify the subsequent presentation, we denote the samples in accordance with the structures whose content in the given sample is maximal: r-PAN, atactic; a-PAN prepared in toluene, isotactic (a-PAN-i); and a-PAN prepared in DMF, syndiotactic (a-PAN-s). The temperature and energy characteristics of the cyclization show certain correlation with the features of the steric structure of each sample. However, actually each sample contains all the three types of structure, with a high content of atactic structures; therefore, for some of the parameters the structure–property correlation is not unambiguous.

It is interesting to compare the DSC (differential scanning calorimetry) data for PAN samples in air and nitrogen (see table). Both in nitrogen and in air, the a-PAN-i samples are characterized by the noticeably lower temperatures of the exothermic effects associated with PAN cyclization and by lower weight loss in the cyclization. The pyrolysis of a-PAN-s in air is characterized by high T_{max} and the narrowest temperature interval of the exothermic effect of cyclization, with the minimal weight loss. The r-PAN sample is characterized by the highest levels of heat release and weight loss and by a broad temperature interval of the exothermic effect. In an inert atmosphere, the thermal cyclization of all the samples occurs in a narrower interval with a considerably weaker exothermic effects and weight losses. When interpreting the results, we should take into account the qualitative composition of the polymers and procedures for their preparation and purification. In particular, the IR spectra of a-PAN contain absorption bands of carbonyl groups. These groups appear in the polymer in the course of its synthesis in a nonpolar medium owing to the reaction of organometallic initiators with cyano groups [12]. Weak "foreign" bands in the IR spectra of a-PAN-s suggest the presence of traces of the solvent (DMF) in which the synthesis was performed. A band at 775 cm^{-1}, sometimes termed the PAN ordering band, is noticeable in all the samples studied, and it grows in intensity in going from r-PAN to a-PAN-i and a-PAN-s.

To examine the influence exerted by the structural organization of PAN macromolecules on the energy characteristics of thermal cyclization, we performed AM1 semiempirical calculations. For a polymeric chain of nine monomeric units with various steric arrangements, we calculated the heats of formation of rings in the iso- and syndiotactic polymers. We found that the initial step of cyclization (formation of primary naphthyridine units) is accompanied by the release of 766.92 kJ mol^{-1} at the isotactic arrangement of the cyano groups and 756.41 kJ mol^{-1} at the syndiotactic arrangement. An increase in the length of the cyclic sequences in the course of further cyclization is accompanied by the invesion of this ratio. In particular, the cyclization energy in the step of formation of an eight-ring chain is 884.31 kJ mol^{-1} for a-PAN-i and 906.15 kJ mol^{-1} for a-PAN-s. Hence, to obtain longer cyclic macromolecules, it is energetically preferable to use a-PAN-s. In this case, the cyclized syndiotactic isomer acquires the shape of a double helix, which is more favorable for the subsequent formation of oriented carbonizates. As the length of the cyclic chain in a-PAN-i increases, the steric hindrance associated with the growing internal strain in the forming ladder structure becomes more pronounced [25]. Figures 1 and 2 illustrate the steric rearrangement of iso- and syndiotactic PAN in the course of stepwise cycli-

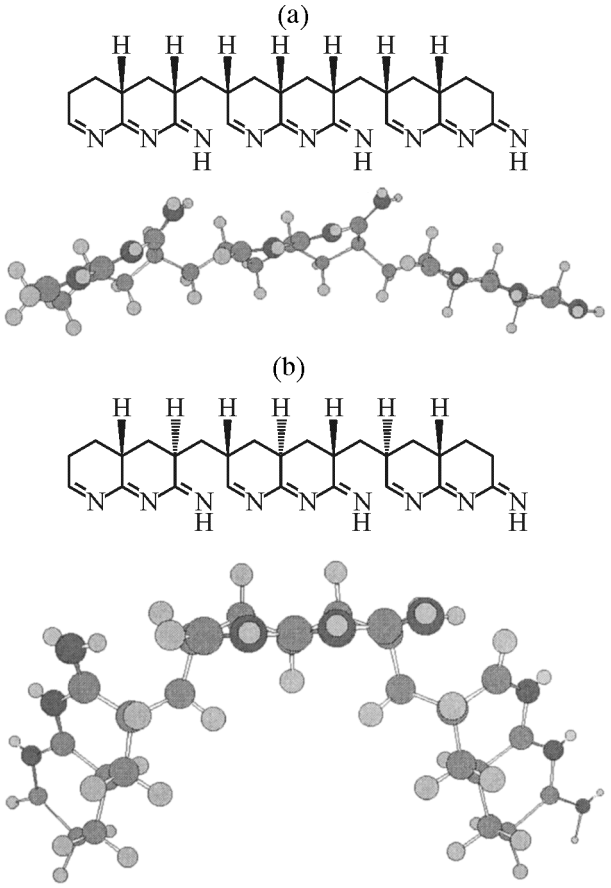


Fig. 1. Schematic and calculated structures of (a) isotactic and (b) syndiotactic PAN in the step of formation of naphthyridine rings.

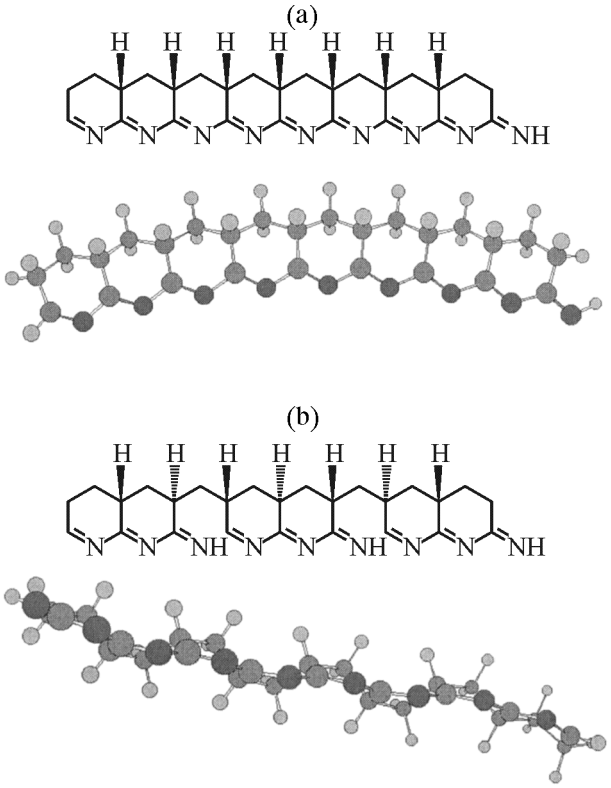


Fig. 2. Schematic and calculated structures of (a) isotactic and (b) syndiotactic PAN in the step of formation of a chain of eight cyclic units.

zation, from the closure of naphthyridine rings (Fig. 1) to formation of a chain of eight cyclic units (Fig. 2).

Our calculations reflect a trend that should be taken into account when choosing a procedure for preparing PAN so as to obtain structures with the required properties. Thus, the steric orientation of PAN macromolecules may be of decisive importance when the conditions of synthesis and isolation of the polymers and of their transformation into cyclic products are strictly observed. Our experiments showed that thermal cyclization of r-PAN in air is accompanied by degradation, which is confirmed by high thermal effects and significant weight loss. The heat release in the interval 250–350°C is a superposition of at least two exothermic processes: cyclization and oxidation with the release of low-molecular-weight products. Furthermore, r-PAN samples are characterized by high polydispersity and chain branchings. Therefore, the packing density of r-PAN macromolecules in precipitation from a solution is low, and powdered samples are subject to more intense thermal oxidation. In contrast to r-PAN, a-PAN polymers have narrow molecular-weight-distribution (MWD) and contain no low-molecular-weight fractions and branchings. These factors, along with the stereoblock structure (see table), are responsible for the high density of a-PAN [13]. In addition, the PAN packing density is appreciably affected by the presence of intermolecular bonds whose content depends on the steric ordering of macromolecules. In solution, a-PAN macromolecules have, to a certain extent, the double helix shape due to the interaction between the cyano groups and α-H atoms, between two cyano groups of adjacent PAN chains [26, 27], and, in some cases, between the adjacent cyclic structures [18]. These factors cause an appreciable shift of the exothermic cyclization toward higher temperatures and a decrease in the content of volatiles in the initial step of cyclization [21]. These structural features of a-PAN result in the prevalence of the cyclization over thermal degradation. As for the related reactions with r-PAN samples, the prevalence of heterostructures, presence of low-molecular-weight

fractions, broad MWD, significant branching, and presence of various functional (mainly oxygen-containing) groups make possible a wide spectrum of low-energy reactions yielding diverse reactive by-products. These factors, along with the fact that the temperature ranges of the highest reactivity of both components coincide (200–300°C), are necessary conditions for efficient cocarbonization with cellulose derivatives (ethers, esters, chitin, chitosan) releasing a number of reactive compounds in thermal degradation [22, 23]. It was also shown in [22, 23] that cyano derivatives of these carbohydrates are characterized by a high yield of the coke residue.

CONCLUSIONS

(1) The energetic, temperature, and gravimetric parameters of thermal cyclization of polyacrylonitrile prepared by radical and anionic polymerization were determined.

(2) The most suitable for cocarbonization with cellulose ethers and esters, chitin, and chitosan are samples of atactic polyacrylonitrile with a broad molecular-weight distribution, the presence of branchings, and a high content of low-molecular-weight fractions and thermoreactive groups.

REFERENCES

1. Sazanov, Yu.N., Szekely, T., Antonova, T.A., *et al.*, *Thermochim. Acta*, 1986, vol. 102, pp. 223–238.
2. Sazanov, Yu.N., Simanovich, I.E., Fedorova, G.N., *et al.*, *J. Thermal Anal.*, 1988, vol. 34, no. 2, pp. 289–295.
3. Sazanov, Yu.N., *J. Thermal Anal.*, 1990, vol. 36, no. 2, pp. 361–376.
4. Sazanov, Yu.N., Spirina, T.N., Shibaev, L.A., *et al.*, *J. Thermal Anal.*, 1990, vol. 36, no. 12, pp. 2329–2338.
5. Sazanov, Yu.N., Silinskaya, I.G., Spirina, T.N., *et al.*, *Vysokomol. Soedin., Ser. A*, 1991, vol. 33, no. 8, pp. 1617–1624.
6. Madorsky, S.L., *Thermal Degradation of Organic Polymers*, New York: Interscience, 1964.
7. Watt, W., *Nature*, 1969, vol. 222, no. 5190, pp. 265–266.
8. Grassie, N., McNeill, I., and Hay, G.N., *J. Polym. Sci.*, 1958, vol. 31, no. 1, pp. 205–210.
9. Konkin, A.A., *Uglerodnye i drugie zharostoikie volokonistye materialy* (Carbon and Other Heat-Resistant Fibrous Materials), Moscow: Khimiya, 1974.
10. Erusalimskii, B.L., *Ionnaya polimerizatsiya polyarnykh monomerov* (Ionic Polymerization of Polar Monomers), Leningrad: Nauka, 1970.
11. Erussalimsky, B.l. and Novoselova, A.V., *Faserforsch. Text. Tech.*, 1975, vol. 26, pp. 292–299.
12. Novoselova, A.V., Nefedov, P.P., Frenkel', S.Ya., *et al.*, *Vysokomol. Soedin., Ser. B*, 1974, vol. 16, no. 10, pp. 751–756.
13. Kipper, A.I., Novoselova, A.V., Zgonnik, V.N., and Klenin, S.I., *Vysokomol. Soedin., Ser. A*, 1992, vol. 34, no. 3, pp. 85–90.
14. Klimenko, I.B., Platonova, N.V., Novoselova, A.V., *et al.*, *Vysokomol. Soedin., Ser. A*, 1995, vol. 37, no. 6, pp. 969–973.
15. Khachaturov, A.S., Abramenko, E.A., Novoselova, A.V., *et al.*, *Vysokomol. Soedin., Ser. B*, 1988, vol. 30, no. 6, pp. 891–896.
16. Kanovich, M.M. and Rudenko, A.P., *Khim. Volokna*, 1982, no. 3, pp. 19–21.
17. Fialkov, A.S., *Uglerod, mezhsloevye soedineniya i kompozity na ego osnove* (Carbon and Intercalation Compounds and Composites Based on It), Moscow: Aspekt, 1997.
18. Rumynskaya, I.G., Agranova, S.Ya., Novoselova, A.V., *et al.*, *Vysokomol. Soedin., Ser. A*, 1999, vol. 41, no. 6, pp. 1–5.
19. Varshavskii, V.Ya., *Obzornaya informatsiya, ser.: Promyshlennost' khimicheskikh volokon* (Review, ser.: Chemical Fiber Industry), Moscow: NIITEKhIM, 1989.
20. Spirina, T.N., Sazanov, Yu.N., Shibaev, L.A., *et al.*, *J. Thermal Anal.*, 1990, vol. 36, pp. 2329–2338.
21. Novoselova, A.V., Zgonnik, V.N., Sazanov, Yu.N., *et al.*, *Vysokomol. Soedin., Ser. A*, 1992, vol. 34, no. 3, pp. 59–63.
22. Sazanov, Yu.N., Nud'ga, L.A., Novoselova, A.V., *et al.*, *Zh. Prikl. Khim.*, 2004, vol. 77, no. 4, pp. 643–648.
23. Sazanov, Yu.N., Nud'ga, L.A., Petrova, V.A., *et al.*, *Zh. Prikl. Khim.*, 2004, vol. 77, no. 8, pp. 1366–1369.
24. Sazanov, Yu.N., Shirokov, N.A., and Gjltsin, B.E., *Thermochim. Acta*, 1978, vol. 24, pp. 81–88.
25. Gribanov, A.V. and Sazanov, Yu.N., *Zh. Prikl. Khim.*, 2000, vol. 73, no. 6, pp. 987–991.
26. Henrici-Olive, G. and Olive, S., *Adv. Polym. Sci.*, 1979, vol. 32, pp. 125–152.
27. Beevers, R.B., *Macromol. Rev.*, 1968, vol. 3, pp. 113–254.

Russian Journal of Applied Chemistry, Vol. 78, No. 5, 2005, pp. 798–801. Translated from Zhurnal Prikladnoi Khimii, Vol. 78, No. 5, 2005, pp. 814–817.
Original Russian Text Copyright © 2005 by Kiryukhin, Kichigina, Zubakova, Moskvina.

MACROMOLECULAR CHEMISTRY AND POLYMERIC MATERIALS

Radiation-Initiated Copolymerization of *N*-Vinylpyrrolidone with Triethylene Glycol Dimethacrylate

D. P. Kiryukhin, G. A. Kichigina, L. B. Zubakova, and I. Yu. Moskvina

Institute of Problems of Chemical Physics, Russian Academy of Sciences, Chernogolovka, Moscow oblast, Russia

Received June 16, 2004; in final form, March 2005

Abstract—The kinetics of radiation-initiated copolymerization of *N*-vinylpyrrolidone with triethylene glycol dimethacrylate was studied. The variation of the composition of the 3D cross-linked copolymer and of the amount of *N*-vinylpyrrolidone homopolymer in the course of the process at various initial monomer ratios was monitored.

Polyvinylpyrrolidone and its copolymers are used in various branches of chemistry, medicine, and food and perfumery industries [1]. The use of triethylene glycol dimethacrylate (TGM-3) as a long-chain cross-linking agent in copolymerization with *N*-vinylpyrrolidone (*N*-VP) allows preparation of sorbents that efficiently recover polyphenols from food and perfumery liquids and are used for stabilization and clarification of juices, wine materials, and strong drinks [2–4]. The sorbent performance is largely determined by the composition and structure of the copolymer. The sorption properties of the sorbent are due to the presence of carbonyl oxygen atoms in *N*-VP units. However, as TGM-3 is more reactive than *N*-VP, it is difficult to prepare the product of the required structure in a high yield.

The goal of this study was to examine the kinetic relationships of radiation-initiated (^{60}Co γ-radiation) copolymerization of *N*-VP with TGM-3 and find the optimal conditions for preparing the sorbent. The reaction was monitored calorimetrically. A combination of the calorimetry with radiation initiation is very convenient for studying the block polymerization of a cross-linking system, as it allows the reaction rate to be measured directly during the process and the degree of conversion of double bonds in the monomers to be estimated up to high conversions.

EXPERIMENTAL

N-Vinylpyrrolidone was purified by double distillation in a vacuum, and TGM-3, by threefold filtration through a column packed with activated alumina. To perform the reaction, a monomer mixture of a definite composition was placed in glass calorimetric cells, deoxygenated, and sealed.

The radiation copolymerization was monitored calorimetrically [5]. A calorimeter with the reaction cell was placed in the chamber of a Gammatok-100 γ-ray installation, theromstated at the required temperature, and irradiated at a dose rate of 1.5 Gy s^{-1}. In the course of the experiment, we monitored how the rate of the heat release due to the polymerization varies in time. The degree of conversion and reaction rate were calculated using the following heats of polymerization (kJ mol^{-1}): 58.6 for *N*-VP [6] and 114.0 for TGM-3 [7].

After the reaction completion, the product was precipitated with diethyl ether and dried to constant weight in a vacuum, after which the total polymer yield was determined gravimetrically. To remove the soluble linear homopolymer of *N*-VP (PVP), the product was washed with distilled water, and the insoluble cross-linked copolymer was dried. The yield of PVP was calculated from the difference between the total yield of the polymer and the yield of the insoluble cross-linked copolymer.

The composition of the 3D copolymers were determined by elemental analysis for nitrogen.

To study the copolymerization of *N*-VP with TGM-3, we took samples of *N*-VP, TGM-3, and their mixtures with various initial molar ratios of the monomers. The calorimetric curves of the polymerization of *N*-VP and TGM-3 and of their copolymerization in the course of γ-irradiation at 295 K are shown in Fig. 1a, and the time dependences of the consumption of the

1070-4272/05/7805-0798© 2005 Pleiades Publishing, Inc.

double bonds during irradiation, calculated from these calorimetric curves, in Fig. 1b.

The calorimetric curves of *N*-VP polymerization show that, after the start of γ-irradiation, the reaction rate reaches a constant value and then sharply increases (gel effect, Fig. 1a, curve *1*). Then the rate of the *N*-VP polymerization decreases because of the consumption of the monomer. The autoacceleration of the process, observed in this case at approximately 40% conversion, is usually attributed to a decrease in the termination rate constant with an increase in the viscosity of the system, caused by accumulation of the polymer. The PVP yield reaches 100% at an irradiation dose of 10.8 kGy (Fig. 1b, curve *1*).

The polymerization of TGM-3 in a γ-ray field is considerably more efficient than that of *N*-VP (Fig. 1a, curve *2*). It is known that the 3D polymerization of TGM-3, a typical oligoether acrylate with two C=C bonds, occurs by the pronounced microheterogeneous mechanism [8–10]. After starting the irradiation, the reaction first develops autocatalytically, the reaction rate increases, and then it reaches a maximum followed by the reaction deceleration. The content of unchanged C=C bonds in the cured block of the TGM-3 polymer (gel fraction) is relatively high (~10–15% at a dose of 8.1 kGy; Fig. 1b, curve *2*).

A study of the copolymerization of the monomers shows that, on adding TGM-3 to *N*-VP, the initial polymerization rate increases relative to the *N*-VP homopolymerization to the greater extent, the higher the TGM-3 content in the initial system (Fig. 1a, curves *3*–*5*). The shape of the calorimetric curves changes also. It is interesting that, for the samples with the initial *N*-VP content exceeding 85 mol %, the reaction rate passes through two maxima (Fig. 1a, curves *3*, *4*). Comparison of these calorimetric curves with that of the *N*-VP homopolymerization (Fig. 1a, curve *1*) suggests that the second peak is due to the *N*-VP homopolymerization. Indeed, the corresponding products contain, along with the cross-linked *N*-VP–TGM-3 copolymer, also a water-soluble polymer. According to elemental analysis, this water-soluble product is the *N*-VP homopolymer. The yield of the *N*-VP homopolymer in the samples with the initial *N*-VP content of 86 and 95 mol % after the reaction completion (irradiation dose 10.8 kGy) is 3 and 35%, respectively. In the samples with the initial *N*-VP content less than 85 mol %, no *N*-VP homopolymer was detected after the reaction completion.

Thus, at least two processes can occur in the *N*-VP–TGM-3 system upon radiation initiation: copolymerization of the monomers to form a cross-

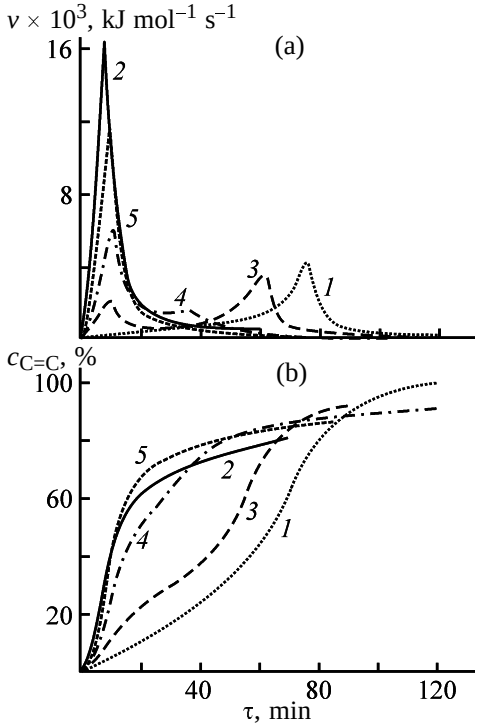


Fig. 1. (a) Rate of heat release *v* and (b) conversion of the double bonds $c_{C=C}$ as functions of the irradiation time τ in (*1*, *2*) homopolymerization of *N*-VP and TGM-3, respectively, and (*3*–*5*) their copolymerization at the initial *N*-VP : TGM-2 molar ratio of (*3*) 95 : 5, (*4*) 86 : 14, and (*5*) 57 : 43 at 295 K.

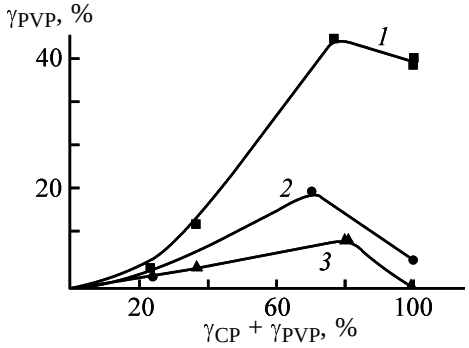


Fig. 2. Yield of the forming homopolymer PVP γ_{PVP} as a function of the total polymer yield $\gamma_{CP} + \gamma_{PVP}$. Initial monomer ratio in the *N*-VP : TGM-3 mixture, mol %: (*1*) 95 : 5, (*2*) 86 : 14, and (*3*) 72 : 28; the same for Fig. 3.

linked product and polymerization of *N*-VP to form a soluble homopolymer.

In this connection, it is interesting to examine the behavior of the system in the course of the process at various conversions. Figures 2 and 3 show how the amount of the forming *N*-VP homopolymer (Fig. 2) and the content of *N*-VP units in the cross-linked copolymer (Fig. 3) vary in the course of the process at three different initial ratios of *N*-VP and TGM-3.

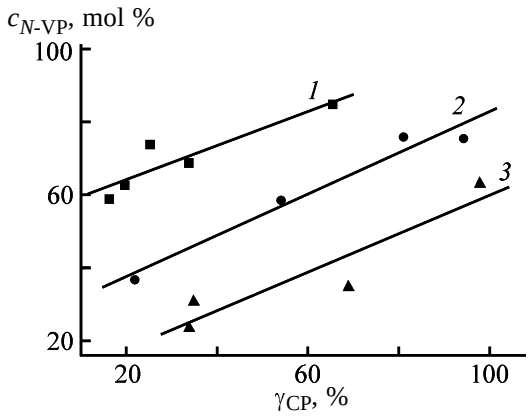


Fig. 3. Content of *N*-VP units $c_{N\text{-VP}}$ in the copolymer as a function of the yield of the cross-linked copolymer γ_{CP}.

These data show that the *N*-VP homopolymer is formed even at the beginning of the process (Fig. 2). The amount of the *N*-VP homopolymer increases in the course of the process, reaching a maximum at 70–80% conversions. Specifically these conversions correspond to the second maximum of the reaction rate for the samples containing 86 and 95 mol % *N*-VP. After passing through a maximum, the content of the homopolymer decreases. In the samples with the initial *N*-VP content of 95 mol %, the content of the homopolymer in the course of the process is considerably higher than in the samples with 86 mol % *N*-VP (Fig. 2, curves *1*, *2*).

The *N*-VP homopolymer is formed in the course of the process also at the initial *N*-VP content less than 85 mol % (Fig. 2, curve *3*). However, the final product in this case contains no homopolymer. A decrease in the amount of the homopolymer in the final steps of the process and its virtual disappearanece in the samples containing less than 85 mol % *N*-VP suggest that the PVP radicals generated by γ-radiation react with the unchanged C=C bonds of TGM-3, i.e., PVP is grafted to the copolymer.

It is known that the limiting conversion of the double bonds in radiation-initiated polymerization of TGM-3 is less than 100%. In particular, it follows from [11] that the content of the C=C bonds in the insoluble polymer (gel fraction) is not constant during the process and varies from 30% at the beginning of the process to 10% at its end. This fact indicates that, under γ-irradiation, the insoluble polymer phase undergoes further cross-linking involving the pendant C=C bonds.

Thus, in our case, along with the copolymerization of *N*-VP with TGM-3, grafting of PVP molecules to the three-dimensional framework is possible owing to the reactions between the PVP radicals generated by γ-irradiation and unchanged pendant double bonds. Note that the conversion of the double bonds increases with an increase in the *N*-VP content in the starting system (Fig. 1b, curves *1–5*).

The composition of the forming copolymer changes with the progress of the polymerization (Fig. 3). Irrespective of the initial comonomer ratio, the content of the *N*-VP units in the copolymer increases with an increase in the copolymer yield. The content of the *N*-VP units grows with an increase in the *N*-VP content in the initial mixture. In particular, the final copolymers prepared from mixtures containing 72, 86, and 95 mol % *N*-VP are characterized by the *N*-VP : TGM-3 molar ratio of ~65 : 35, 75 : 25, and 85 : 15, respectively.

The optimal monomer ratio for preparing the sorbent should be chosen so as to minimize the content of the *N*-VP homopolymer in the product (because the homopolymer should be separated) and, on the other hand, to provide the highest content of bound *N*-VP units in the copolymer (because these units are responsible for the sorption properties). Our results show that the initial *N*-VP : TGM-3 molar ratio of 86 : 14 is close to the optimum. Indeed, although the content of the *N*-VP units in the copolymer prepared at the initial *N*-VP : TGM-3 molar ratio of 95 : 5 is as high as ~85 mol %, the yield of the *N*-VP homopolymer is also relatively high (~35%). At the initial *N*-VP : TGM-3 molar ratio of 86 : 14, the content of the *N*-VP units in the copolymer is only slightly lower (~80 mol %), but the content of the *N*-VP homopolymer decreases considerably (to less than 3%). As the initial *N*-VP : TGM-3 molar ratio is decreased further, the content of the *N*-VP units in the copolymer becomes too low.

CONCLUSIONS

(1) Radiation-initiated copolymerization of triethylene glycol dimethacrylate with *N*-pyrrolidone yields the cross-linked 3D copolymer (major product) and the soluble *N*-vinylpyrrolidone homopolymer (by-product).

(2) With an increase in the *N*-vinylpyrrolidone concentration in the initial mixture, the content of the *N*-vinylpyrrolidone units in the copolymer increases, and a higher conversion of the double bonds in triethylene glycol dimethacrylate is attained.

(3) The optimal initial molar ratio of the comonomers for preparing the copolymers to be used as sorbents is 86 : 14.

ACKNOWLEDGMENTS

The authors are grateful to L.S. Kiryukhina for performing the elemental analysis.

The study was financially supported by the Russian Foundation for Basic Research and Ministry of Industry and Science of Moscow oblast (project no. 04-03-97237 r2004 for cities of science).

REFERENCES

1. Sidel'kovskaya, F.P., *Khimiya N-vinilpirrolidona i ego polimerov* (Chemistry of *N*-Vinylpyrrolidone and Its Polymers), Moscow: Nauka, 1970.
2. Zubakova, L.B., Osokina, M.P., Nikiforova, L.Ya., *et al.*, *Plast. Massy*, 1983, no. 2, pp. 19–21.
3. USSR Inventor's Certificate no. 1634671.
4. Pilina, I.Yu., Akhnazarova, S.L., Zubakova, L.B., and Ileneva, E.V., *Izv. Vyssh. Uchebn. Zaved., Khim. Khim. Tekhnol.*, 1998, vol. 41, no. 3, pp. 90–93.
5. Barkalov, I.M. and Kiryukhin, D.P., *Int. Rev. Phys. Chim.*, 1994, vol. 13, no. 2, pp. 337–357.
6. Ushakova, V.N., Panarin, E.F., Kiryukhin, D.P., *et al.*, *Vysokomol. Soedin., Ser. A*, 1991, vol. 33, no. 10, pp. 2151–2158.
7. Munikhes, V.M., Berezin, M.P., Kiryukhin, D.P., *et al.*, *Vysokomol. Soedin., Ser. A*, 1986, vol. 28, no. 2, pp. 358–363.
8. Berlin, A.A., Kefeli, T.Ya., and Korolev, G.V., *Poliefirakrilaty* (Polyether Acrylates), Moscow: Nauka, 1967.
9. Berlin, A.A., Korolev, G.V., Kefeli, T.Ya., and Sivergin, Yu.M., *Akrilovye oligomery i materialy na ikh osnove* (Acrylic Oligomers and Materials Based on Them), Moscow: Nauka, 1983.
10. Korolev, G.V., *Usp. Khim.*, 2003, vol. 72, no. 3, pp. 222–244.
11. Bol'bit, N.M., Duflot, V.R., Faizi, N.Kh., and Chikin, Yu.A., *Radiatsionnaya khimiya i tekhnologiya oligomernykh sistem* (Radiation Chemistry and Technology of Oligomeric Systems), Moscow: NIITEKhIM, 1985, pp. 9–11.

Russian Journal of Applied Chemistry, Vol. 78, No. 5, 2005, pp. 802–805. Translated from Zhurnal Prikladnoi Khimii, Vol. 78, No. 5, 2005, pp. 818–821.
Original Russian Text Copyright © 2005 by Man'ko, Mel'nichenko, Bovkunenko, Shendrik, Fedoseeva, Goncharov.

MACROMOLECULAR CHEMISTRY AND POLYMERIC MATERIALS

Radical Copolymerization of Fluoroalkyl Methacrylates with Methyl Methacrylate

K. I. Man'ko, V. I. Mel'nichenko, O. P. Bovkunenko, A. N. Shendrik, A. A. Fedoseeva, and E. N. Goncharov

Donetsk National University, Donetsk, Ukraine

Received January, 26, 2005

Abstract—Lauryl peroxide initiated radical copolymerization of 1,1,3-trihydroperfluoropropyl methacrylate and 1,1,5-trihydroperfluoroamyl methacrylate with methyl methacrylate was studied. The kinetic parameters of copolymerization for these systems were determined at low degrees of conversion. Optically transparent copolymers with glass transition points within 50–80°C were synthesized.

Polymers based on fluorine-containing acrylates and methacrylates find application in various fields of industry owing to an advantageous combination of properties: transparency and weather, thermal, and chemical resistance, as well as other parameters. They are used for impregnation of leather, paper, and textiles for imparting water-, oil-, and mud-repelling properties to these materials [1]. Because of high oxygen permeability, polyfluoroalkyl (meth)acrylates were patented as gas-separation membranes [2]. Optical properties (low refractive indices, high light transmittance) make these materials suitable for optical and optoelectronic applications [3]. In this context, polymerization of fluoroalkyl (meth)acrylates has recently received much attention [4, 5].

It should also be noted that some properties of homopolymers (water repellency, cold fluidity, low glass transition points), as well as high costs of the initial monomers, limit their application. These drawbacks can be eliminated to a certain extent by copolymerization of fluorinated monomers with vinyl monomers, for example, alkyl methacrylates, styrene, and methacrylic and acrylic acids. For such systems, it is urgent to carry out regular kinetic studies and also to establish the structure–property relationships.

In this work, we studied radical copolymerization of 1,1,3-trihydroperfluoropropyl methacrylate (F_1) and 1,1,5-trihydroperfluoamyl methacrylate (F_2) with methyl methacrylate (MMA) and the physicochemical properties of the copolymers synthesized.

EXPERIMENTAL

Copolymerization of F_1 and F_2 with MMA was carried out at 65°C. The monomers were purified by vacuum distillation in a nitrogen atmosphere. Lauryl peroxide which served as initiator was purified by reprecipitation from chloroform into methanol. The concentration of the initiator was 5×10^{-4} mol mol^{-1} of the monomer mixture. The content of the fluorinated components in the monomer mixture was varied from 9.09 to 83.3 mol%. The kinetics of copolymerization to high conversions were studied gravimetrically. The copolymers were isolated by reprecipitation from acetone into methanol. The composition of the copolymers was determined by IR spectroscopy. As analytical band served that corresponding to vibrations of the $–CF_2–$ groups at 800 cm^{-1} [6]. The IR spectra of the copolymers were recorded on a Specord 75-IR spectrometer in an acetonitrile solution in KBr cells with a layer thickness of 0.4 cm. The viscosity of the monomer mixtures was measured in an Ubbelohde viscometer. The thermomechanical properties of the polymers were studied by the method described in [7]. The water wettability of the polymers at 20°C was determined by measuring the contact angle [8]. The time dependences of the conversion of the monomer (Fig. 1) show that, in the initial stages of copolymeri-

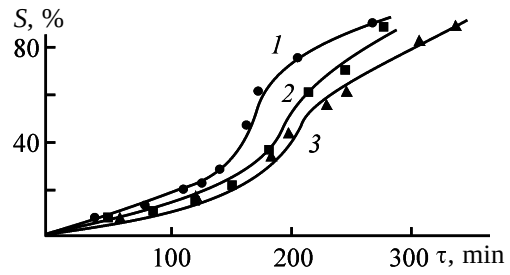


Fig. 1. Variation of the conversion of the monomer *S* with the time τ at *T* = 65°C. Mixture composition: (*1*) MMA, (*2*) F_1–MMA, and (*3*) F_2–MMA.

1070-4272/05/7805-0802 © 2005 Pleiades Publishing, Inc.

zation, the plots for these systems contain a linear portion, which is followed by autoacceleration at 25–30% conversions. The copolymerization rate in all the stages of synthesis is smaller than that of homopolymerization of MMA and tends to decrease with lengthening of the fluoroalkyl substituent, the gel effect being smoothened out. The length of the fluoroalkyl substituent affected the homopolymerization kinetics in studies of a number of fluoroalkyl acrylates as well [4].

It was found earlier [9] that the rate of homopolymerization of fluoroalkyl monomers in the initial stages (up to 10% conversion of the monomer) is 35–45% lower than the MMA homopolymerization rate. We estimated the ratio of the rate constants of addition of the "own" or "foreign" monomer to the propagating macroradical during copolymerization of the monomers by studying the composition of the copolymer formed in the initial stages of the reaction. From the IR data, we elucidated the compositions of the copolymers obtained by copolymerization of F_1 with MMA and F_2 with MMA, as well as their dependences on the composition of the initial monomer mixture (Fig. 2).

It is seen that the copolymers synthesized are enriched in fluorinated components. Table 1 presents the copolymerization constants r_1 and r_2 calculated by the Fineman–Ross method. For comparison, Table 1 also presents the copolymerization constants for these systems, calculated by the Alfrey–Price method using the published data on the Q–e parameters. The experimental and calculated copolymerization constants are close and suggest that the resulting macroradicals containing one of the monomers (fluoroalkyl methacrylate or MMA) as a terminal unit preferably add molecules of fluorinated monomers. Such a character of the chain propagation can be due to the known ability of fluoroalkyl methacrylates to form associates by hydrogen bonding between protons and $–CF_2–$ groups [10]. To estimate the degree of association of the mixtures of the monomers, we determined their viscosity at temperatures within 25–65°C and carried out calculations by the formula

$$g = \frac{2Nh}{\eta}\frac{\rho}{M}\exp\{1 + m[bT^m/(a + bT^m)]\}, \qquad (1)$$

where g is the degree of association; N, Avogadro number; h, Planck constant; a and b, constants from the equation $1/\eta = a + bT^m$; and m, varied parameter.

Figure 3 presents the dependence of the degree of association on the composition of the initial monomer

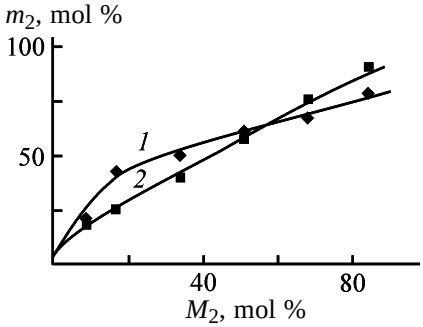


Fig. 2. Variation of the content of the F_1, F_2 units in copolymers (m_2) with the content of F_1, F_2 in the initial monomer mixture (M_2) for MMA copolymerization with (*1*) F_1 and (*2*) F_2.

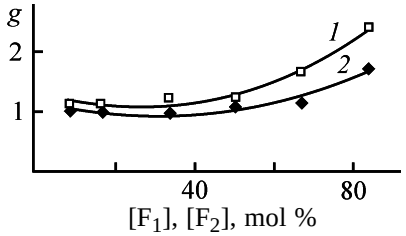


Fig. 3. Degree of association g of the MMA mixtures with (*1*) F_1 and (*2*) F_2 as a function of the content of fluoroalkyl methacrylates [F_1] and [F_2].

mixture. It is seen that the degree of association tends to increase with increasing proportion of the fluorinated component and length of the fluoroalkyl substituent. For example, for the F_2–MMA system, the degree of association is higher than for F_1–MMA. From the $\ln\eta$ vs. $1/T$ plot we determined the viscous flow activation energy E_a characterizing the energy of bonding between the molecules of the monomers (Table 2). It is seen that E_a tends to increase with increasing amount of the fluorinated component in the system. These data correlate with the degrees of association, calculated by formula (1).

It is known [11] that the structure of the associates in the liquid phase affects the polymerization kinetics, supramolecular structure of polymers, and their physical properties. This makes our data essential for interpreting the kinetic relationships in copolymerization in the systems of interest. For example, the relation-

Table 1. Constants of copolymerization of MMA (M_1) with fluoroalkyl methacrylates (M_2)

M_2	r_1	r_2	r_1*	r_2*
F_1	0.6 ± 0.4	3.1 ± 0.2	0.58	2.72
F_2	0.2 ± 0.1	1.7 ± 0.7	0.57	1.16

* Calculated by the Alfrey–Price method.

Table 2. Viscous flow activation energy E_a of the mixtures of F_1 and F_2 with MMA*

Monomer mixture	E_a, kJ mol^{-1}, at the indicated component molar ratio in the mixture					
	1:10	1:5	1:2	1:1	2:1	5:1
F_1 : MMA	8.3	8.3	9.4	10.7	13.0	13.7
F_2 : MMA	9.6	9.3	11.8	12.9	14.9	18.9

* Determined accurately to within 0.5–0.6 kJ mol^{-1}.

Table 3. Densities and refractive indices of the copolymers based on fluoroalkyl methacrylates (FMA) and MMA

FMA content in monomer mixture, mol %	d	d*	n_D^{20}
	g cm^{-3}		
F_1:			
9.1	1.2296	1.2153	1.475
16.6	1.2461	1.2366	1.472
33.3	1.3291	1.2833	1.467
50.0	1.3402	1.3301	1.462
66.7	1.3776	1.3767	1.447
83.3	1.4276	1.4236	1.205
F_2:			
9.1	1.2852	1.2365	1.474
16.6	1.3213	1.2756	1.469
33.3	1.4212	1.3608	1.463
50.0	1.5053	1.4471	1.457
66.7	1.5824	1.5314	1.449
83.3	1.6214	1.6181	1.443

* Calculated data.

ships for the rate of copolymerization of fluoroalkyl methacrylates with methyl methacrylate vs. the degree of association in the initial stages, which were established earlier [9] (Fig. 4), suggest that it affects the kinetics of the process: The higher the degree of association, the lower the rate. It is known that fluoroalkyl methacrylates form dimerized structures via cooperative interaction of the fluoroalkyl substituents of the neighboring molecules, and the energy of this interaction increases from 16.5 to 25.7 kJ mol^{-1} with increasing number of the $-CF_2-$ groups from 2 to 4 [12]. In this case, the most probable structure of the dimer being formed contains oxygen atoms and, correspondingly, the double bonds are at the maximal distance from one another. Probably, interaction of the propagating macroradical with such dimer does not result in its degradation. In this case, further propagation of the polymer chain is sterically hindered, which is responsible for deceleration of the process.

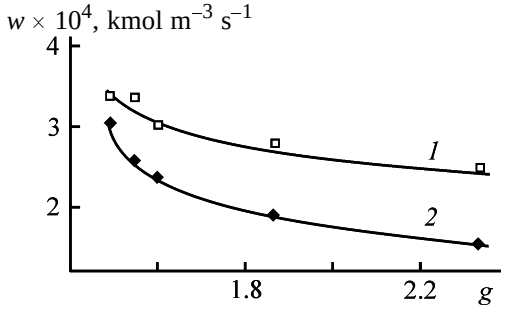


Fig. 4. Copolymerization rate w of MMA with (*1*) F_1 and (*2*) F_2 as a function of the degree of association g.

The copolymerization constants r_1 and r_2 that we determined show that, in the initial stages of copolymerization, the fluorinated monomer is consumed preferentially. With increasing extent of the reaction, the monomer mixture gets enriched in MMA, which favors formation of macromolecules with different compositions, though thermodynamically compatible, as suggested by the transparency of the copolymer throughout the composition range studied. For a number of the copolymers obtained, we determined the glass transition points, densities, and wettability with water. Thermomechanical measurements for the copolymers based on F_2–MMA showed that, with increasing proportion of the fluorinated component from 10 to 60 mol %, the glass transition point decreases from 80 to 50°C. The wetting contact angle varies from 65° to 80°, depending on the content of the fluoroalkyl methacrylate units in the copolymer.

We used the semiempirical method of group contributions proposed by Davies and Gottlieb [13], based on the principle of additivity, for establishing a relationship between the chemical composition and physical properties of the copolymers; Table 3 presents the calculated densities and refractive indices. These data suggest that the refractive index tends to markedly decrease with increasing amount of the fluoroalkyl methacrylate in the copolymer. Table 3 also presents the experimental densities of the copolymers based on fluoroalkyl acrylates and MMA, which slightly exceed the calculated data. Budovskaya *et al.* [14] showed that associates are formed not only between the fluoroalkyl acrylate molecules but also between the monomeric units of the homopolymer thereof, which is responsible for ordering of the structure and increase in the density of the copolymers. The discrepancy between the experimental densities and those calculated using the principle of additivity also suggests the possibility of formation of similar associative structures in these copolymers based on F_1 and MMA or F_2 and MMA.

CONCLUSIONS

(1) In the course of radical copolymerization of 1,1,3-trihydroperfluoropropyl methacrylate and 1,1,5-trihydroperfluoroamyl methacrylate with methyl methacrylate, the reaction rate decreases with increasing amount of the fluorinated monomer in the initial mixture. The compositions of the copolymers for these systems were determined, and the copolymerization constants were calculated.

(2) Transparent copolymers were synthesized from binary systems comprised of 1,1,3-trihydroperfluoropropyl methacrylate or 1,1,5-trihydroperfluoroamyl methacrylate and methyl methacrylate. These copolymers have glass transition points within 50–80°C and contact angles of wetting with water of 65°–80°, depending on the composition of the copolymer.

REFERENCES

1. US Patent 4 609 715.
2. JPN Appl. 62-127 306.
3. JPN Appl. 59-155 502.
4. Lachinov, M.B., Guliashvili, T.T., Chkheidze, N.R., and Lekishvili, N.G., *Vysokomol. Soedin., Ser. A*, 1998, vol. 40, no. 2, pp. 215–220.
5. Il'in, A.A, Smirnov, B.R., Golikov, I.V., and Mogilevich, M.M., *Izv. Vyssch. Uchebn. Zaved., Khim. Khim. Tekhnol.*, 1992, vol. 35, no. 8, pp. 105–106.
6. Pakhomov, P.M., Yakovleva, O.E., Perepelitsa, N.M., and Khizhnyak, S.D., *Vysokomol. Soedin., Ser. A.*, 1995, vol. 37, no. 2, pp. 223–229.
7. Toroptseva, A.M., Belogorodskaya, K.B., and Bondarenko, V.M., *Laboratornyi praktikum po khimii i tekhnologii vysokomolekulyarnykh soedinenii* (Laboratory Practical Guide on Chemistry and Technology of Macromolecular Compounds), Leningrad: Khimiya, 1972.
8. *Laboratornye raboty i zadachi po kolloidnoi khimii* (Laboratory Works and Problems on Colloid Chemistry), Frolov, Yu.G. and Grodskii, A.S., Eds., Moscow: Khimiya, 1986.
9. Mel'nichenko, V.I., Man'ko, K.I., and Bovkunenko, O.P., *Vestn. Donetsk. Univ., Ser. A*, 2003, no. 1, pp. 264–266.
10. Budovskaya, L.D., Ivanova, V.N., Oskar, L.N., *et al.*, *Zh. Fiz. Khim.*, 1989, vol. 63, no. 5, pp. 1231–1238.
11. Duflot, V.R., Faizi, N.Kh., and Chikin, Yu.A., *Vysokomol. Soedin., Ser. A*, 1982, vol. 24, no. 11, pp. 2363–2366.
12. Kuznetsova, N.P., Kanitskaya, L.V., Fedorov, S.V., and Ermakova, T.G., *Vysokomol. Soedin., Ser. B*, 2001, vol. 43, no. 9. pp. 1565–1569.
13. Van Krevelen, D.W., *Properties of Polymers. Correlations with Chemical Structure*, Amsterdam: Elsevier, 1972.
14. Budovskaya, L.D., Boyarchuk, Yu.M., and Denisov, V.M., *Vysokomol. Soedin., Ser. A*, 1992, vol. 34, no. 7, pp. 98–103.

Russian Journal of Applied Chemistry, Vol. 78, No. 5, 2005, pp. 806–810. Translated from Zhurnal Prikladnoi Khimii, Vol. 78, No. 5, 2005, pp. 822–826.
Original Russian Text Copyright © 2005 by Kuskov, Shtil'man, Tsatsakis, Torchilin, Yamskov.

MACROMOLECULAR CHEMISTRY AND POLYMERIC MATERIALS

Synthesis of Amphiphilic *N*-Vinylpyrrolidone and Acrylamide Polymers of Various Structures

A. N. Kuskov, M. I. Shtil'man, A. M. Tsatsakis, V. P. Torchilin, and I. A. Yamskov

Mendeleev Russian University of Chemical Engineering, Moscow, Russia
Nesmeyanov Institute of Organoelement Compounds, Russian Academy of Sciences, Moscow, Russia
Crete University, Iraklio, Greece
North-Eastern University, Boston, the United States

Received November 29, 2004

Abstract—Amphiphilic polymers of *N*-vinylpyrrolidone (M_n = 1100–11 000) and acrylamide (M_n = 2000–8000) with the terminal *n*-octadecyl group were prepared.

Nanosized carriers for biologically active substances and drugs (liposomes, nanoaggregates) attract much researchers' attention. They not only ensure controllable (prolonged) release of an active substance with a decreased probability of its side effects, but also make poorly soluble compounds lyophilic, allowing their administration in the form of disperse aqueous systems, e.g., by injection.

An efficient way to enhance the performance of nanosized carriers involves the use of water-soluble amphiphilic (diphilic) polymers for forming nanoaggregates and modifying liposomal membranes, thus increasing their stability. The most frequently used amphiphilic polymers are polyethylene oxides containing a terminal hydrophobic group [1–5].

Recently we suggested to use as such polymers amphiphilic derivatives of water-soluble carbon-chain polymers, primarily poly-*N*-vinylpyrrolidone (PVP), a component of many drug systems [6–10]. Modification of liposomes with amphiphilic *N*-vinylpyrrolidone polymers prolongs their circulation in the blood of laboratory animals and decreases their uptake by liver cells [6]. The interaction of aggregates of these polymers with proteins, including blood proteins, was considered [9, 10].

Here we consider the features of synthesis of amphiphilic *N*-vinylpyrrolidone and acrylamide polymers of various molecular weights with a single hydrophobic group of various structures.

EXPERIMENTAL

N-Vinylpyrrolidone was distilled in a vacuum at 363 K/14 mm Hg. Acrylamide was purified by recrystallization from benzene, mp 357–358 K. Azobis(isobutyronitrile) (AIBN) was purified by twofold recrystallization from ethanol, mp 378–379 K. Mercaptoacetic acid, 1,3-dicyclohexylcarbodiimide (DCC), and amines (*n*-octylamine, *n*-dodecylamine, *n*-hexadecylamine, *n*-octadecylamine, di-*n*-hexylamine, di-*n*-octylamine, di-*n*-octadecylamine) were used without additional purification. All the chemicals were purchased from Sigma.

Mercaptoethylamine was used as a solution in isopropyl alcohol; it was recovered from the hydrochloride (Sigma) by treatment with triethylamine. The reaction was performed in a round-bottomed flask equipped with a stirrer. The flask was charged with 11.35 g (0.1 mol) of mercaptoethylamine hydrochloride dissolved in 30 ml of dry isopropyl alcohol, and 10.1 g (0.1 mol) of triethylamine in 20 ml of dry isopropyl alcohol was added with cooling. The precipitate of triethylammonium chloride was filtered off, and the filtrate was stored at 275–278 K. The salt precipitate on the filter was washed with ether and dried to constant weight. Thus, a solution of 0.1 mol of mercaptoethylamine in 50 ml of isopropyl alcohol was obtained.

Stearoyl chloride was prepared by treatment of the acid with thionyl chloride. A flask for vacuum distillation, equipped with a tube for removal of HCl, was charged with 20 g (0.1 mol) of stearic acid. Thionyl chloride (29.28 g, 0.4 mol) was slowly added dropwise from a dropping funnel. A catalytic amount (0.8 ml) of dimethylformamide was added. The mixture was allowed to stand for 10 h, after which excess thionyl chloride was distilled off. The chloride was isolated by vacuum distillation (479 K/2 mm Hg). The

1070-4272/05/7805-0806© 2005 Pleiades Publishing, Inc.

N-Vinylpyrrolidone and acrylamide polymers with terminal functional groups

Polymer structure	Polymer	Amount of mercaptan, mol mol^{-1} monomer	Polymer yield, %	M_n*	M_n**	Number of unit in chain *N*
PVP–S–CH_2–COOH	1CPVP	0.16	86	1500	1450	12–14
	2CPVP	0.06	86	2000	1980	17–19
	3CPVP	0.012	90	2600	2640	22–24
	4CPVP	0.01	92	3300	3270	29–30
	5CPVP	0.008	92	4000	4050	35–37
	6CPVP	0.005	94	5500	5520	49–50
PAA–S–CH_2–COOH	1CPAA	0.24	75	1800	1870	24–26
	2CPAA	0.19	76	2100	2060	29–30
	3CPAA	0.01	81	3400	3350	47–49
	4CPAA	0.005	84	5000	5060	70–71
	5CPAA	0.0004	88	8000	7970	112–114
PVP–S–CH_2–CH_2–NH_2	1APVP	0.04	70	1100	1120	9–11
	2APVP	0.02	76	1400	1450	12–13
	3APVP	0.014	80	2100	2090	18–20
	4APVP	0.01	84	4200	4170	37–39
	5APVP	0.006	87	11 000	11 040	98–100

* Number-average molecular weight determined from the content of terminal groups.
** Number-average molecular weight determined by vapor osmometry.

product was stored in a refrigerator in sealed ampules filled with argon.

Solvents (dioxane, dimethylformamide, acetone, isopropyl alcohol, ethanol, chloroform, toluene, diethyl ether) were purified by common procedures.

N-Vinylpyrrolidone and acrylamide polymers containing a terminal amino or carboxy group were prepared as follows: 5.55 g (0.05 mol) of *N*-vinylpyrrolidone or 3.55 g (0.05 mol) of acrylamide and 0.05 g of AIBN initiator were dissolved in 10 ml of dioxane (35% or 25% solution of the monomer, respectively), and various amounts of mercaptoacetic acid or mercaptoethylamine were added. Ampules with the resulting solutions were purged with an inert gas, sealed, and kept at 343 K for 1 h. The polymers were isolated by precipitation into diethyl ether, purified by extraction with diethyl ether, and dried to constant weight in a vacuum. The yields of the polymers and amounts of the mercaptan added are given in the table. The content of terminal groups was determined by potentiometric titration.

N-Vinylpyrrolidone and acrylamide polymers containing terminal alkyl groups were prepared from the polymers with terminal carboxy or amino groups.

(1) A calculated amount of PVP or polyacrylamide (PAA) containing a terminal carboxy group (1CPVP–6CPVP; 1CPAA–5CPAA) was dissolved in dry isopropyl alcohol, and a solution of excess DCC (2.0 mol per mole of carboxy groups) in the same solvent was added with stirring. The mixture was stirred at 273 K for 1 h, after which a solution of appropriate aliphatic amine (*n*-octylamine, *n*-dodecylamine, *n*-hexadecylamine, *n*-octadecylamine, di-*n*-hexylamine, di-*n*-octylamine, di-*n*-octadecylamine; 1.5 mol per mole of carboxy groups) in dry isopropyl alcohol was added, and the mixture was heated for 2 h at 333 K. The precipitate that formed after cooling was filtered off, and the filtrate was evaporated to a volume of ~10 ml. The resulting polymer was precipitated into diethyl ether, extracted with diethyl ether, and dried in a vacuum to constant weight. The yield of the polymers was 75–80% in all the cases.

(2) A portion of PVP containing a terminal amino group (1APVP–5APVP) was dissolved in dry dioxane. To the resulting solution, the calculated amount of triethylamine in dioxane and then stearoyl chloride in dioxane were added with stirring at 273 K; the mixture was allowed to stand at room temperature for 2 h. The precipitate of triethylammonium chloride was filtered off, and the polymer was precipitated into diethyl ether, extracted with diethyl ether, and dried in a vacuum to constant weight.

The determinations of the number-average molecular weight by vapor osmometry were performed with a Knauer osmometer (Germany).

Amphiphilic derivatives of PVP and PAA containing terminal hydrophobic groups were prepared in two steps. The first step involved radical polymerization of the corresponding monomers in the presence of initiators generating primary radicals and radical-transfer agents which generate, under the action of primary radicals, new radicals initiating the chain propagation.

As such transfer agents we used mercaptans containing, along with the SH group, an additional functional group. The high reactivity of mercaptans in radical processes is well known [11–13]. With polystyrene and poly(methyl methacrylate) as examples, we demonstrated the feasibility of introducing terminal functional groups using mercaptans as chain-transfer agents [12].

Mercaproacetic acid and 2-mercaptoethylamine, used in this study, allowed introduction of a single terminal carboxy or amino group into the polymer.

The main reactions occurring in the system at a sufficient amount of a mercaptan can be described by the following scheme:

Generation of initiating radical

$$I \rightarrow [2R_1^{\bullet}],\ [2R_1^{\bullet}] \rightarrow R_1^{\bullet} + R_1^{\bullet}, \quad (1)$$

$$[2R_1^{\bullet}] \rightarrow R_1\text{–}R_1, \quad (2)$$

$$R_1^{\bullet} + H\text{–}S \rightarrow R_1\text{–}H + S^{\bullet}; \quad (3)$$

Initiation

$$S^{\bullet} + M \rightarrow S\text{–}M^{\bullet}, \quad (4)$$

$$R_1^{\bullet} + M \rightarrow R_1\text{–}M^{\bullet}; \quad (5)$$

Chain propagation

$$R_1^{\bullet}\text{–}M + M_n \rightarrow R_1\text{–}M_{n+1}^{\bullet}, \quad (6)$$

$$S\text{–}M^{\bullet} + M_n \rightarrow S\text{–}M_{n+1}^{\bullet}; \quad (7)$$

Chain termination

$$S\text{–}M_{n+1}^{\bullet} + H\text{–}S \rightarrow S\text{–}M_{n+1}\text{–}H + S^{\bullet}, \quad (8)$$

$$S\text{–}M_{n+1}^{\bullet} + {}^{\bullet}M_{n+1}\text{–}S \rightarrow S\text{–}M_{n+1}\text{–}M_{n+1}\text{–}S, \quad (9)$$

$$S\text{–}M_{n+1}^{\bullet} + S^{\bullet} \rightarrow S\text{–}M_{n+1}\text{–}S, \quad (10)$$

$$S\text{–}M_{n+1}^{\bullet} + R_1^{\bullet} \rightarrow S\text{–}M_{n+1}\text{–}R_1. \quad (11)$$

where I is the initiator; M, monomer; $R_1^{\bullet}$, primary radical formed by decomposition of the initiator; $S^{\bullet}$, radical formed from the mercaptan; $S\text{–}M^{\bullet}$, $R_1\text{–}M^{\bullet}$, $R_1\text{–}M_{n+1}^{\bullet}$, and $S\text{–}M_{n+1}^{\bullet}$, propagating polymeric radicals; $S\text{–}M_{n+1}\text{–}H$, $S\text{–}M_{n+1}\text{–}M_{n+1}\text{–}S$, $S\text{–}M_{n+1}\text{–}S$, and $S\text{–}M_{n+1}\text{–}R_1$, inert molecules; and H–S, molecule of the chain-transfer agent.

At a sufficient amount of a mercaptan, the chain propagation can be effected not by the primary radical formed by decomposition of the initiator but by the radical $S^{\bullet}$ formed by proton abstraction from the mercaptan, i.e., reaction (4) can prevail over reaction (5).

It is known that the rate of reaction of primary radicals with mercaptans exceeds the initiation rate by several orders of magnitude [14]. Therefore, presumably, the primary radical $R_1^{\bullet}$ is mainly consumed in reaction (3) rather than (5). Thus, under these conditions, the chain propagation is mainly initiated by the $S_1^{\bullet}$ radical, and the chain starts specifically from this group, which is confirmed by determinations of the number-average molecular weight of the polymers.

When studying polymerization of vinylpyrrolidone and acrylamide in the presence of a radical polymerization initiator (AIBN) and functional chain-transfer agents (mercaptoacetic acid, mercaptoethylamine), we examined how the amount of the mercaptan added affects the yield and molecular weight of the polymers formed.

In our case, the simplified reaction scheme is as follows:

$$AIBN \rightarrow 2CH_3\text{—}\overset{\displaystyle CH_3}{\overset{|}{\underset{|}{C^{\bullet}}}}\underset{\displaystyle CH_3}{} + N_2,$$

$$R_1^{\bullet} + HS\text{–}R' \rightarrow R_1\text{–}H + {}^{\bullet}S\text{–}R',$$

$$R_2^{\bullet} + nM \rightarrow R_2\text{–}(M)_{n-}^{\bullet}, \quad (R_3^{\bullet})$$

$$R_3^{\bullet} + HS\text{–}R \rightarrow R_3\text{–}H + R_2^{\bullet},$$

where M is a monomer molecule or monomeric unit; R' = $-CH_2COOH$ or $-CH_2CH_2NH_2$.

As seen from Figs. 1 and 2, the yield and molecular weight of the polymer decreased with an increase in the amount of the mercaptan added, which is apparently due to accelerated chain termination.

The polymers prepared contained a single terminal functional group, as confirmed by agreement of the molecular weights determined from the content of terminal groups and by vapor osmometry (see table).

Thus, this step yielded semitelechelic polymers with the molecular weights in the range suitable for

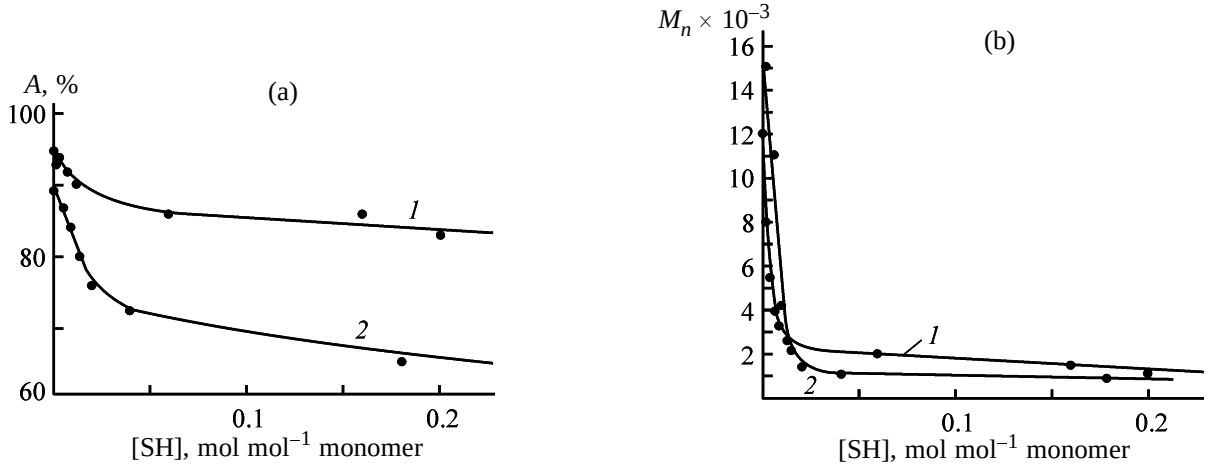


Fig. 1. Influence of mercaptan additions on the (a) yield *A* and (b) M_n of poly-*N*-vinylpyrrolidone. *N*-Vinylpyrrolidone and AIBN concentrations 35 and 1.5 wt %, respectively; 343 K; solvent dioxane. SH: (*1*) mercaptoacetic acid and (*2*) Mercaptoethylamine.

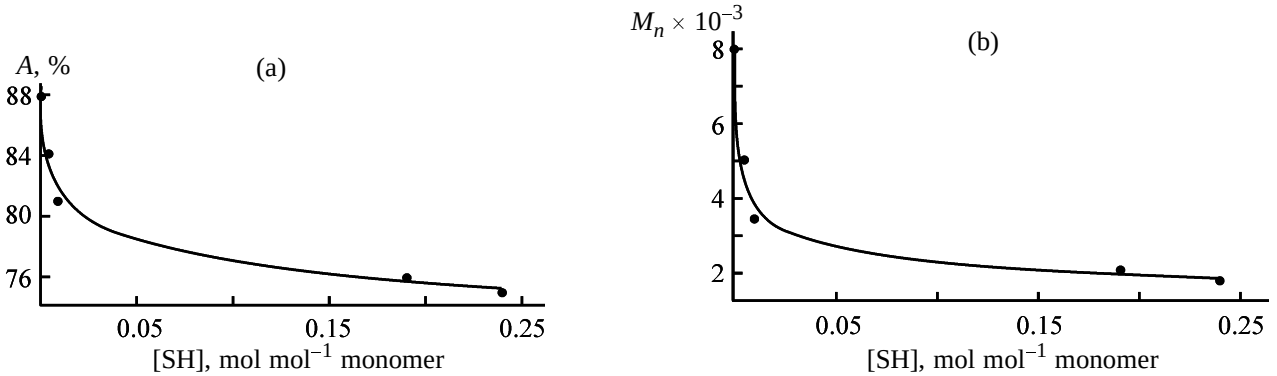


Fig. 2. Influence of mercaptoacetic acid additions on the (a) yield *A* and (b) M_n of polyacrylamide. Acrylamide and AIBN concentrations 25 and 1 wt %, respectively; 343 K; solvent dioxane.

preparing drug carriers. By varying the amount of the mercaptan added, it is possible to control the molecular weight of the products. We obtained in fairly high yield two series of polymers containing terminal amino and carboxy groups and having different molecular weights.

In the second step, into the semitelechelic polymers containing a terminal reactive group we introduced a long-chain alkyl group by the reaction with aliphatic amines containing various alkyl radicals (in the case of carboxy terminal group) or with an aliphatic acyl chloride (in the case of amino terminal group).

The modification of the carboxyl-containing polymer involved activation of the carboxy group with DCC followed by treatment with appropriate amine (*n*-octylamine, *n*-dodecylamine, *n*-hexadecylamine, *n*-octadecylamine, di-*n*-hexylamine, di-*n*-octylamine, di-*n*-octadecylamine), with *N*,*N*'-dicyclohexylurea (DCU) formed as by-product, and the modification of the amino-containing polymers, by treatment with stearoyl chloride, with the release of HCl.

This procedure allowed preparation of water-soluble amphiphilic polymers with the same hydrophobic terminal groups and different molecular weights of the polymeric fragment and with different hydrophobic terminal groups and the same molecular weight of the polymeric fragment. In the latter case, modification was performed with a PVP sample with M_n = 4000 and a terminal carboxy group.

Formation of amphiphilic polymers can be described by the following scheme:

$$\mathrm{H{-}[{-}M{-}]_n{-}SCH_2CH_2NH_2 + ClCO{-}C_{17}H_{35}}$$

$$\xrightarrow[-\mathrm{HCl}]{\mathrm{N(C_2H_5)_3}} \mathrm{H{-}[{-}M{-}]_n{-}SCH_2CH_2NHCO{-}C_{17}H_{35}},$$

$$\mathrm{H{-}[{-}M{-}]_n{-}SCH_2COOH + H_xNR_y}$$

$$\xrightarrow[-\mathrm{DCU}]{\mathrm{DCC}} \mathrm{H{-}[{-}M{-}]_n{-}SCH_2CONH_{x-1}R_y},$$

where M is a monomeric unit of *N*-vinylpyrrolidone

or acrylamide; H_xNR_y = $CH_3(CH_2)_{17}NH_2$, $[CH_3 \cdot (CH_2)_{17}]_2NH$, $CH_3(CH_2)_{15}NH_2$, $[CH_3(CH_2)_7]_2NH$, $CH_3(CH_2)_{11}NH_2$, $[CH_3(CH_2)_5]_2NH$, $CH_3(CH_2)_7NH_2$.

The degree of substitution of the reacting terminal groups was determined by potentiometric titration under the same conditions as in determination of these groups for evaluating the molecular weight. No residual terminal groups were detected, which suggests their virtually complete substitution. The elemental analysis is unsuitable for this purpose, because the difference in the C, H, N content due to substitution was insignificant in samples of higher molecular weights and did not exceed 1.5–2.5% in samples of lower molecular weights.

The IR spectra of the polymers (KBr pellets) in the range of carbonyl absorption exhibited, along with the major band corresponding to the fully substituted amide group in the pyrrolidone ring (~1650 cm^{-1}) and unsubstituted amide group in polyacrylamide (~1690 cm^{-1}), an additional band corresponding to a monosubstituted amine in the terminal group (~1680 and 1640 cm^{-1}). The relative intensity of this band increased with a decrease in the molecular weight of the polymer. Furthermore, the intensity of absorption of the methylene groups in the IR spectra of these polymers increased owing to introduction of long-chain terminal alkyl groups (633, 2850 cm^{-1}).

CONCLUSIONS

(1) Amphiphilic polymers containing a single terminal hydrophobic group were prepared.

(2) Reaction conditions were found for preparing amphiphilic *N*-vinylpyrrolidone and acrylamide polymers with the required molecular weight in the range M_n = 1500–11000; these polymers can be used for the development of new drug carriers.

REFERENCES

1. Torchilin, V.P., *J. Microencapsulation*, 1988, vol. 15, p. 1–19.
2. Gref, R., Minamitake, Y., Peracchia, M.T., *et al.*, *Science*, 1994, vol. 263, pp. 1600–1603.
3. Liaw, J., Aoyagi, T., Kataoka, K., *et al.*, *Pharm. Res.*, 1998, vol. 15, pp. 1721–1726.
4. Yasugi, K., Nakamura, T., Nagasaki, Y., *et al.*, *J. Macromol.*, 1999, vol. 32, pp. 8024–8032.
5. Jeong, Y.-I., Nah, J.-W., Lee, Y.-K., *et al.*, *J. Controll. Rel.*, 1999, vol. 188, pp. 49–58.
6. Torchilin, V.P., Shtilman, M.I., Trubetskoy, V.S., *et al.*, *Biochim. Biophys. Acta*, 1994, no. 1195, pp. 181–184.
7. Shtil'man, M.I., Tverdokhlebova, I.I., Yarmysh, M.Yu., *et al.*, *Vysokomol. Soedin.*, 1999, vol. 41, no. 5, pp. 906–909.
8. Torchilin, V.P., Levchenko, T.S., Whiteman, K.R., *et al.*, *Biomaterials*, 2001, vol. 22, no. 15, pp. 3035–3044.
9. Villemson, A.L., Malykh, E.V., Shtil'man, M.I., and Larionova, N.I., *Biokhimiya*, 2003, vol. 68, no. 8, pp. 1063–1069.
10. Villemson, A.L., Kuskov, A.N., Shtil'man, M.I., *et al.*, *Biokhimiya*, 2004, vol. 69, no. 6, pp. 621–629.
11. Sidel'kovskaya, F.P., *Khimiya N-vinilpirrolidona i ego polimerov* (Chemistry of *N*-Vinylpyrrolidone and Its Polymers), Moscow: Nauka. 1970.
12. Drobnik, J., Kaval, J., Dabrowska, L., *et al.*, *J. Polym. Sci., Polym. Symp.*, 1979, vol. 66, pp. 75–81.
13. Vlasak, J., Rypacek, F., Drobnik, J., and Saudek, V., *J. Polym. Sci., Polym. Symp.*, 1979, vol. 66, pp. 59–64.
14. Drobnik, J. and Rypacek, F., *IUPAC Macro Mainz, 26th Int. Symp. on Macromolecules*, Basel, 1979, vol. 3, pp. 1521–1528.

Russian Journal of Applied Chemistry, Vol. 78, No. 5, 2005, pp. 811–814. Translated from Zhurnal Prikladnoi Khimii, Vol. 78, No. 5, 2005, pp. 827–830.
Original Russian Text Copyright © 2005 by Bondar', Hong Je Kim, Yong Jin Lim.

MACROMOLECULAR CHEMISTRY AND POLYMERIC MATERIALS

Radiation-Induced Graft Polymerization of Glycidyl Methacrylate onto Nonwoven Polypropylene

Yu. V. Bondar', Hong Je Kim, and Yong Jin Lim

Institute of Environmental Geochemistry, Kiev, Ukraine

Received September 27, 2004; in final form, March 2005

Abstract—The influence of the major grafting parameters (irradiation dose, reaction time, and inhibitor concentration) on graft polymerization of glycidyl methacrylate from its 10% solution in methanol onto nonwoven polypropylene upon irradiation with an electron accelerator in air was studied.

Graft polymerization is an efficient method of modification of polymeric substrates. Economically efficient and environmentally clean radiation technologies, e.g., radiation-induced graft polymerizations, offer a number of undoubted advantages [1]. In particular, this method allows controlled introduction into an inert polymeric matrix of polymeric chains with functional groups and preparation of polymeric adsorbents (chemisorption fibers, fabrics, films) of the desired form and with varied concentration of ion-exchange groups. Functional groups can be introduced both by one-step radiation-induced graft polymerization of the appropriate monomers and by grafting of precursor monomers, followed by polymer-analogous reactions. In view of a limited number of accessible vinyl monomers with functional groups, the second option, in particular, grafting of glycidyl methacrylate (GMA), a vinyl monomer containing epoxy groups, showed much promise.

Radiation-induced (co)polymerization of GMA, as well as of other vinyl monomers, follows the chain radical mechanism, involving the double bonds, while epoxy rings remain fairly inert and contribute only slightly to formation of cross-links [2]. At the same time, the well-known [3] high reactivity of the epoxy rings of GMA in nucleophilic substitution reactions makes GMA a promising precursor monomer.

Radiation-induced graft polymerization and the subsequent modification of epoxy rings in GMA, aimed at preparation of adsorbents thereof, were actively studied by Saito, Kim, *et al.* [4–10]. Their technique included irradiation of the polymeric substrate with an electron accelerator in a nitrogen atmosphere up to a dose of 200 kGy, grafting of GMA chains in a 10% solution of GMA in methanol at 313 K, preparation of samples with the degree of grafting of 200% , and subsequent polymer-analogous reactions involving the epoxy rings.

More extensive information about the features of grafting GMA chains onto various polymeric substrates can be found in papers by Choi *et al.* [11–13]. They studied how the experimental parameters, namely, irradiation dose, monomer concentration (GMA–1,4-dioxane solution), temperature, and time of reaction affect the degree of graft polymerization of GMA upon irradiation of a polymeric substrate (^{60}Co source) in air. However, both research teams examined the influence of the experimental parameters only on the degree of graft polymerization of GMA chains (increase, in per cent, of the weight of the sample upon grafting). Therefore, we can only indirectly judge the efficiency of both grafting and conversion of the epoxy groups in GMA into functional groups during the subsequent polymer-analogous reactions.

In this study we examined how the major parameters of graft polymerization of GMA onto nonwoven polypropylene (PP) upon irradiation with an electron accelerator in air affect graft polymerization and represented the results as the plots of the density of grafted GMA chains vs. the degree of grafting.

EXPERIMENTAL

As a polymeric base for grafting GMA chains served nonwoven material from PP fibers, available from Saehan Filter Co Ltd, with an average thickness of 2 mm and density of 4.6×10^{-3} g cm^{-2}. Graft polymerization was performed by the pre-irradiation method [1]. Irradiation was carried out in an ELV-04 conveyor accelerator by a 1-MeV electron beam. After irradiation, the fabric was kept in a desiccator at room temperature, and polymerization was carried out with-

1070-4272/05/7805-0811 © 2005 Pleiades Publishing, Inc.

in 1–5 days after electron beam irradiation. In experiments we used GMA available from Aldrich. The irradiated sample was placed into a flask with an alcoholic solution of GMA; the resulting solution was purged with nitrogen, and the flask was closed tight and kept at the desired temperature, whereupon graft polymerization was carried out under continuous stirring and water cooling. The material was washed with tetrahydrofuran and then with methanol for 24 h to remove the homopolymer and unchanged monomer. The sample was dried to constant weight at 70°C.

The degree Q_{gr}, %, of grafting glycidyl methacrylate was estimated gravimetrically:

$$Q_{gr} = \frac{m_0 - m_1}{m_0} \times 100,$$

where m_0 and m_1 are the weights of the sample before and after grafting, respectively.

The density of the grafted GMA chains S_{GMA} (mmol g^{-1}) was calculated by the formula

$$S_{GMA} = \frac{(m_1 - m_0) \times 1000}{m_1 M_{GMA}},$$

where M_{GMA} is the molecular weight of GMA (142).

The presence of functional groups was judged from the IR spectra recorded on a Perkin–Elmer Golden Gate Single Reflection ATR System IR spectrophotometer.

The specific factor for graft polymerization by the pre-irradiation method is the absorbed irradiation dose, which governs the concentration of the active centers of grafting. However, by varying such parameters as temperature and time of reaction, the reaction medium, and the concentration of the sensitizing additives, it is possible to control the polymerization and prepare the product with the desired degree of grafting.

The specific features of radiation-induced graft polymerization of GMA onto various polymeric substrates (polyethylene, polypropylene, and polysulfone films, membranes, fibers) under irradiation with both γ-rays and accelerated electrons were considered in [4–13]. It was shown that efficient GMA grafting can be achieved in methanol, 1,4-dioxane, and water–methanol (1 : 1 by weight) system. Choi *et al.* [12, 13] noted a higher efficiency of grafting in the GMA–1,4-dioxane system, but their results did not differ essentially from those for the GMA–methanol system. In this study, we grafted the GMA chains onto nonwoven fabric made of polypropylene fibers in the GMA–methanol system, since methanol is relatively inexpensive and readily available.

As known, exposure of various polymers to radiation in the presence of atmospheric oxygen (pre-irradiation method) yields hydroperoxides as the main stable products [14], which are thermally stable at common temperatures and degrade upon heating above 60°C into macroradicals PPO$^{\bullet}$ and hydroxy radicals OH$^{\bullet}$. The macroradical provides the site for grafting, and the hydroxy radical can initiate homopolymerization of the monomers M. The scheme of this mechanism was discussed in numerous papers (e.g., in [15]) and can be represented as follows:

$$\text{PP–H} \xrightarrow{O_2} \text{PP–OOH} \xrightarrow{\Delta} \text{PPO}^{\bullet} + \text{OH}^{\bullet},$$

$$\text{PPO}^{\bullet} + n\text{M} \longrightarrow \text{PPO}^{\bullet}\text{–M}_n,$$

$$\text{M} + \text{OH}^{\bullet} \longrightarrow \text{M}^{\bullet}\text{–OH} \xrightarrow{n\text{M}} \text{M}^{\bullet}\text{–(M)}_n\text{–H},$$

$$\text{PPO}^{\bullet} + \text{M}^{\bullet}\text{–(M)}_n\text{–OH} \longrightarrow \text{PPO–M–(M)}_n\text{–OH}.$$

Homopolymerization of the monomers can be suppressed by addition of transition metal salts [16, 17], which increases the degree of grafting:

$$\text{OH}^{\bullet} + \text{Fe}^{2+} \longrightarrow \text{OH}^{-} + \text{Fe}^{3+}.$$

Transition metal salts favor efficient degradation of hydroperoxides at temperatures below 60°C:

$$\text{PP–OOH} + \text{Fe}^{2+} \longrightarrow \text{PPO}^{\bullet} + \text{OH}^{-} + \text{Fe}^{3+}.$$

Under excess of transition metal salts, active centers can be deactivated:

$$\text{PPO}^{\bullet} + \text{Fe}^{2+} \longrightarrow \text{PPO}^{-} + \text{Fe}^{3+}.$$

In [4–13], the influence of transition metal salts on the degree of graft polymerization of GMA was not discussed.

We studied how the absorbed dose affects graft polymerization of GMA from its 10% solution in methanol (Fig. 1). The reaction was run at 70°C, which favors degradation of hydroperoxides. However, for the samples irradiated at a dose under 40.2 kGy, grafting was not achieved even within 2 h of the reaction, and the degree of grafting of the samples irradiated at a dose of 70.5 kGy proved to be insignificant. This pattern may be due both to a low concentration of the macroradicals yielded by degradation of hydroperoxides and to the influence of

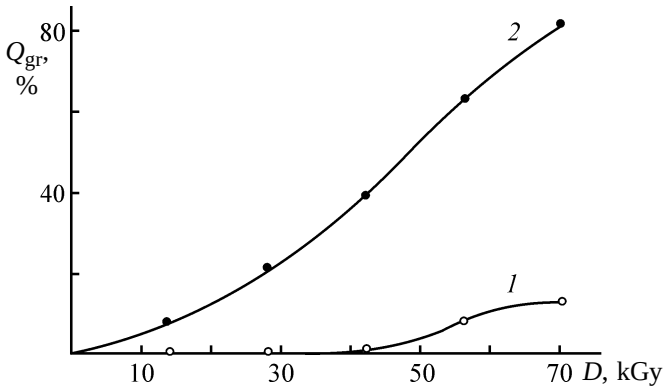


Fig. 1. Degree Q_{gr} of graft polymerization of GMA as a function of the absorbed dose D at the Mohr's salt content of (*1*) 10^{-2} and (*2*) 0 wt % (70°C, 2 h).

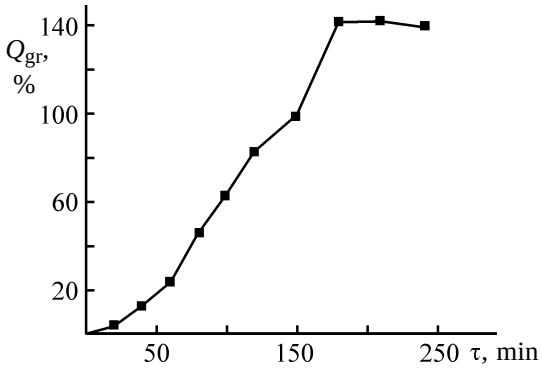


Fig. 3. Degree Q_{gr} of graft polymerization as a function of the reaction time τ. Irradiation dose 70.5 kGy, 70°C; Mohr's salt content 10^{-2} wt %.

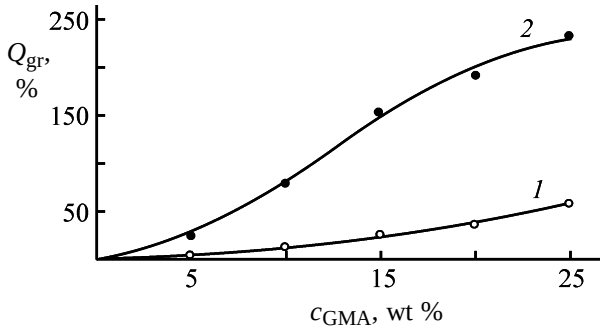


Fig. 2. Degree Q_{gr} of graft polymerization as a function of the monomer concentration c_{GMA} (*1*) upon addition of 10^{-2} wt % of Mohr's salt and (*2*) without Mohr's salt. Irradiation dose 70.5 kGy, 70°C, 2 h.

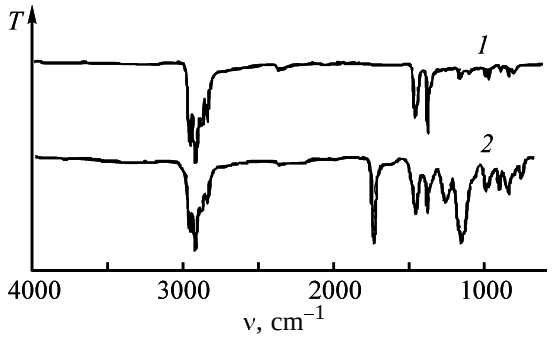


Fig. 4. IR spectra of polypropylene (*1*) before and (*2*) after GMA grafting. (*T*) Transmission and (ν) wave number.

homopolymerization. Grafting was intensified by addition of Mohr's salt (10^{-2} wt %) (Fig. 1, curve *1*). The degree of grafting GMA in this case increased with increasing absorbed dose from 14.1 to 70.5 kGy.

Also, we studied the sensitizing effect of the Mohr's salt on the degree of GMA grafting onto an nonwoven PP substrate from its 10% solution in methanol (irradiation dose 70.5 kGy, 70°C, 2 h). With increasing Mohr's salt concentration in solution from 0 to 0.03 wt % (0.5×10^{-5}, 10^{-4}, 5×10^{-3}, 10^{-2}, 2×10^{-2}, 3×10^{-2} wt %), the degree of grafting changed from 13.6 to 81.5% (13.6, 17.1, 51.0, 78.6, 81.5, 75.1, 74.8%, respectively). The maximal degree of grafting, 81.5%, was achieved upon addition of 10^{-2} wt % of Mohr's salt.

The dependence of the degree of GMA grafting on the monomer concentration was studied over the concentration range 0–25 wt % with and without Mohr's salt (Fig. 2). The degree of grafting of the GMA chains increases with increasing monomer concentration in both cases. However, addition of Mohr's salt (10^{-2} wt %) causes the degree of graft polymerization of GMA to increase 6–7-fold throughout the concentration range studied (Fig. 2, curve *1*). For example, the degree of grafting GMA from its 10% solution without Mohr's salt is 13.6%, and with Mohr's salt, 81.5%.

Also, we studied the kinetics of graft polymerizations of GMA onto a nonwoven PP substrate from its 10% solution in methanol. It is seen from Fig. 3 that the reaction goes fairly rapidly in the first 3 h, whereupon it is decelerated and attains saturation.

The presence of functional groups in the samples under study was judged from the IR spectra. Figure 4 shows the IR spectra of PP before and after GMA grafting. The IR spectrum of PP with grafted GMA chains contains absorption bands at 1730, 1300–1100 cm^{-1}, assigned to C=O and C–O–C vibrations, and also bands at 1260, 950–815, and 760 cm^{-1}, corresponding to vibrations of the epoxy groups.

Thus, by varying the experimental parameters [irradiation dose, time of reaction, inhibitor concentration in the course of graft polymerization at 70°C

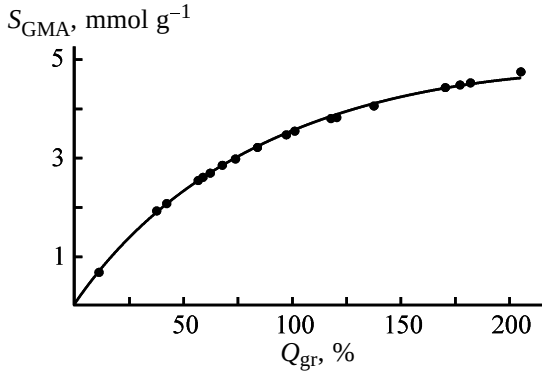


Fig. 5. Density of grafted GMA chains S_{GMA} as a function of the degree Q_{gr} of graft polymerization of GMA.

from 10% solutions of GMA in methanol (higher temperatures cause intensive evaporation of methanol under water cooling of the reactor)], we obtained samples with widely varying densities of epoxy groups, as seen in Fig. 5.

CONCLUSIONS

(1) Radiation-induced graft polymerization of glycidyl methacrylate chains onto nonwoven polypropylene fabric was studied. The influence of grafting parameters, namely, absorbed dose, concentration of the sensitizing additives (Mohr's salt), and time of reaction, on graft polymerization of glycidyl methacrylate from its 10% solution in methanol at 70°C was examined.

(2) Using pre-irradiation method, glycidyl methacrylate at 70°C can be grafted most effectively upon adding 10^{-2} wt % of Mohr's salt.

(3) The degree of grafting glycidyl methacrylate was studied as dependent on the density of its grafted chains on a nonwoven polypropylene substrate. This allows quantitative estimation of the efficiency of both grafting and conversion of the epoxy rings to functional groups in the subsequent polymer-analogous reactions.

REFERENCES

1. Ivanov, V.S., *Radiatsionnaya khimiya polimerov* (Radiation Chemistry of Polymers), Leningrad: Khimiya, 1988.
2. Fomina, N.V., Khoromskaya, V.A., and Shiryaeva, G.V., *Khim. Vys. Energ.*, 1987, vol. 21, no. 5, pp. 401–403.
3. Kalal, J., Svee, F., and Marousek, V., *J. Polym. Sci.*, 1974, vol. 47, no. 1, pp. 155–166.
4. Tsuneda, S., Saito, K., Furusaki, S., *et al.*, *J. Membrane Sci.*, 1991, vol. 58, no. 2, pp. 221–234.
5. Tsuneda, S., Saito, K., Furusaki, S. *et al.*, *J. Membrane Sci.*, 1992, vol. 71, nos. 1–2, pp. 1–12.
6. Kobayashi, K., Tsuneda, S., Saito, K. *et al.*, *J. Membrane Sci.*, 1993, vol. 76, nos. 2–3, pp. 209–218.
7. Kubota, N., Kounosu, M., Saito, K. *et al.*, *J. Chromatogr. A*, 1995, vol. 718, no. 1, pp. 27–34.
8. Kim, M., Kiyohara, S., Konishi, S., *et al.*, *J. Membrane Sci.*, 1996, vol. 117, nos. 1–2, pp. 33–38.
9. Sasagawa, N., Saito, K., Sugita, K., Kunori, S., and Sugo, T., *J. Chromatogr. A*, 1999, vol. 848, nos. 1–2, pp. 161–168.
10. Kim, M. and Saito, K., *React. Funct. Polym.*, 1999, vol. 40, no 3, pp. 275–279.
11. Yang, H.S., Choi, J.K., and Nho, Y.C., *J. Korean Ind. Eng. Chem.*, 1999, vol. 10, no. 3, pp. 477–485.
12. Choi, S.H., Lee, K.P., and Lee, J.G., *Microchem. J.*, 2001, vol. 68, nos. 2–3, pp. 205–213.
13. Choi, S.H., Jeong, Y.H., Ryoo, J.J., and Lee, K.P., *Radiat. Phys. Chem.*, 2001, vol. 60, nos. 4–5, pp. 503–511.
14. Sevost'yanov, V.S., Kritskaya, D.A., and Ponomarev, A.N., *Khim. Vys. Energ.*, 1986, vol. 20, no. 2, pp. 153–158.
15. Kaur, I., Kumar, S., Misra, B.N., and Chauhan, G.S., *Mater. Sci. Eng.*, 1999, vol. A270, no. 2, pp. 137–144.
16. Viengkhou, V., Ng, Loo-Teck, and Garnett, G.L., *Radiat. Phys. Chem.*, 1997, vol. 49, no. 5, pp. 595–602.
17. Chen, J., Nho, Y.C., and Park, J.S., *Radiat. Phys. Chem.*, 1998, vol. 52, nos. 1–6, pp. 201–206.

Russian Journal of Applied Chemistry, Vol. 78, No. 5, 2005, pp. 815–819. Translated from Zhurnal Prikladnoi Khimii, Vol. 78, No. 5, 2005, pp. 831–835.
Original Russian Text Copyright © 2005 by Grishin, Lazarev, Semenycheva, Nikolaev.

MACROMOLECULAR CHEMISTRY AND POLYMERIC MATERIALS

Emulsion Polymerization of Styrene in the Presence of *C*-Phenyl-*N*-*tert*-Butylnitrone

D. F. Grishin, M. A. Lazarev, L. L. Semenycheva, and E. Yu. Nikolaev

Lobachevsky Research Institute of Chemistry, Nizhni Novgorod State University, Nizhni Novgorod, Russia
Kargin Research Institute of Chemistry and Technology of Polymers with Pilot Plant, Dzerzhinsk, Nizhni Novgorod oblast, Russia

Received November 17, 2004; in final form, February 2005

Abstract—The radical polymerization of styrene in an emulsion stabilized with an ionic surfactant, with *C*-phenyl-*N*-*tert*-butylnitrone as chain-terminating agent and ammonium persulfate as initiator, was studied.

Pseudo-living radical polymerization is an actively developing field of synthetic chemistry of polymers [1–4]. Among chain-terminating agents used in these processes, stable nitroxyl radicals have been studied most comprehensively. With these radicals, the polymerization can be performed without gel effect, the molecular weight of macromolecular compounds can be linearly increased with conversion, and homo- and copolymers with relatively low polydispersity coefficients can be prepared. Furthermore, the polymers prepared in the presence of nitroxyls are macroinitiators themselves, which opens wide prospects for block copolymerization and design of macromolecules as a whole.

The most frequently used controlling agent in pseudo-living radical polymerization, both in the bulk [2–4] and in heterogeneous aqueous dispersions, including emulsions, suspensions, and miniemulsions [5–8], is 2,2,6,6-tetramethylpiperidine-1-oxyl (TEMPO). An essential disadvantage of this compoumnd as a chain-terminating agent is that, with this compound, the controlled polymerization takes place only at relatively high temperatures (120–140°C) and only with styrene and its derivatives. However, even under these conditions the polymerization rate is extremely low (e.g., for styrene at 120°C the reduced rate w/[styrene] does not exceed $\sim 2 \times 10^{-5}$ s^{-1} [9]).

A search for new effective chain life regulators led to development of a procedure for *in situ* preparation of nitroxyl radicals. The sources of stable radicals in [10–16] were spin traps, nitroso compounds and nitrones, which react with propagating radicals to form sterically hindered macromolecular nitroxyls. These radicals effect bulk polymerization in the pseudo-living/controlled mode of not only styrene, but also methyl methacrylate, butyl methacrylate, vinyl chloride, and acrylonitrile; furthermore, the process occurs at lower temperatures (50–100°C). Data on the use of *in situ* formed nitroxyls with a macromolecular "tail" for controlling the propagation of a polymeric chain under the conditions of emulsion radical polymerization are virtually lacking.

In this study we examined the emulsion polymerization of styrene in the presence of *C*-phenyl-*N*-*tert*-butylnitrone (PBN) as a potential source of stable nitroxyl radicals.

EXPERIMENTAL

Styrene and organic solvents (chloroform, isopropyl alcohol) were purified by standard procedures [17, 18]. *C*-Phenyl-*N*-*tert*-butylnitrone was prepared according to [19]. The initiator [ammonium persulfate (AP), Ekros Joint-Stock Company, chemically pure grade] and emulsifier [S-10, TU (Technical Specifications) 2492-366-00208947–2002, general formula n-C_8H_{17}–C_6H_4–$(CH_2$–$CH_2O)_n$–$CH_2CH_2OSO_3NH_4$ (n = 10–12, 62 wt % dry residue) was used without additional purification. Water was double-distilled.

The kinetics of emulsion polymerization of styrene was studied gravimetrically [20]. A four-necked flask equipped with a reflux condenser with a gas seal, a bubbler, and a sampler was charged with 10 g of styrene containing the dissolved chain-terminating agent (PBN concentration 0.1, 0.2, 0.3 mol %), and 0.75 g of the emulsifier dissolved in 30 ml of water was added. The mixture was emulsified for 30 min at a constant stirring rate of 500 ± 1 rpm. The inert atmosphere was provided by argon bubbling. The synthesis temperature was kept constant (70, 80, 90°C, respectively). Then a solution of 0.25 g of AP in 9 ml of double-distilled water was added through the reflux condenser.

1070-4272/05/7805-0815© 2005 Pleiades Publishing, Inc.

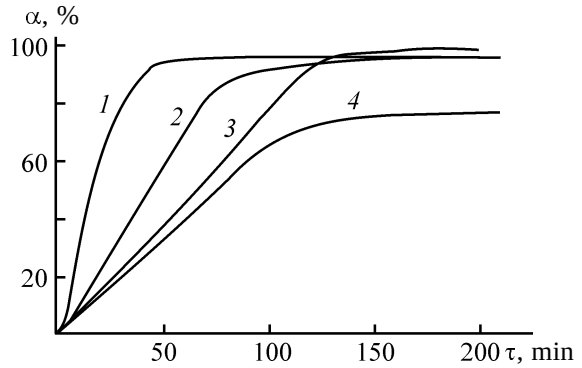


Fig. 1. Kinetic dependences of the emulsion polymerization of styrene at 70°C in the presence of 0.5 wt % PA and PBN. (α) Conversion and (τ) time. [PBN], mol %: (*1*) 0, (*2*) 0.1, (*3*) 0.2, and (*4*) 0.3.

Emulsion samples were taken at regular intervals, weighed on an analytical balance, dried to constant weight in a vacuum, and weighed again. The conversion α (%) was calculaed by the formula

$$\alpha = \frac{(m_3 - m_1) - a(m_2 - m_1)}{b(m_2 - m_1)} \times 100,$$

where m_1, m_2, and m_3 are the weights of the empty beaker, beaker with the latex, and beaker with the polymer, respectively; *a* is the correction for the emulsifier (0.015×0.62, i.e., the weight fraction of the emulsifier in the latex, multiplied by the dry residue of the emulsifier); and *b*, content of the monomeric fraction in the latex (20 wt %).

The molecular-weight characteristics of polymers were determined with a Knauer liquid chromatograph [21] equipped with a Phenomenex Phenogel 10u Linear (2) column (300×7.8 mm, 10 μm); the eluent was chloroform (flow rate 1 ml min^{-1}). The device was calibrated by polystyrene references with the molecular weight ranging from 900 to 1 049 000.

Polymer samples were ground in an agate mortar, washed with distilled water to remove water-soluble impurities (emulsifier and AP) and with isopropyl alcohol to remove impurities soluble in organic solvents (monomer, additives, etc.), and vacuum-dried to constant weight. Then the polymer samples were dissolved in chloroform, filtered through a glass frit (pore diameter 0.1 μm) to remove mechanical impurities, and analyzed by gel permeation chromatography.

The polymer isolated and purified to remove the initiator, monomer, and emulsifier (see above) was placed in an ampule (100 ± 0.2-mg portion, M_n = 7000 g mol^{-1}) and dissolved in 1 ml of styrene (macroinitiator concentration 1.57×10^{-2} M); then the solution was degassed by three freeze–pump–thaw cycles using liquid nitrogen. After that the ampule was sealed and placed in a thermostat to perform the postpolymerization at 90°C. The resulting polymer was analyzed as described above.

As already noted, PBN was successfully used previously in bulk polymerization of styrene [16]. Here we used this additive for the first time in polymerization of the same monomer in an emulsion stabilized with an ionic surfactant. As polymerization initiator we used AP, which is traditionally applied in industrial emulsion polymerization of vinyl monomers.

We found that PBN additions somewhat decelerate the emulsion polymerization of styrene (Fig. 1). However, even with excess nitrone the conversion in the first 30 min is as high as 60%. The decreased polymerization rate is undoubtedly due to the participation of the spin trap in the elementary steps of the process. In particular, the reaction of PBN with the propagating radicals (*in situ*) yields sterically hindered stable nitroxyl spin adducts [11]:

$$\sim P_n^{\bullet} + \underset{\underset{H}{|}}{\underset{\downarrow}{\underset{O}{|}}}{Ph–C=N–Bu^t} \rightarrow \sim P_n–\underset{Ph}{\underset{|}{CH}}–\underset{O^{\bullet}}{\underset{|}{N}}–Bu^t, \qquad (1)$$

where $\sim P_n$ is a macroradical containing *n* monomeric units.

Then the nitroxyl spin adducts react with the propagating radicals by the reversible inhibition scheme:

$$>N–O^{\bullet} + \sim P_n^{\bullet} \underset{k_d}{\overset{k_a}{\rightleftharpoons}} >N–O–P_n\sim, \qquad (2)$$

$$\sim P_n^{\bullet} \xrightarrow{+M,\ k_p} \sim P_n^{\bullet}$$

where $>N–O^{\bullet}$ is the nitroxyl radical; $\sim P_n^{\bullet}$, propagating radical; M, monomer, $>N–O–P_n$, alkoxyamine; and k_p, k_d, and k_a, rate constants of the propagation, dissociation, and accepting, respectively.

The molecular-weight characteristics of polystyrene are affected by the spin trap to a still greater extent. In particular, the molecular-weight distribution (MWD) curves of the samples synthesized in the presence of PBN (Figs. 2b, 2c) are shifted toward lower molecular weight compared to the polymers prepared without additions (Fig. 2a). With increasing concentration of nitrone, the general shape of the MWD curves changes. In particular, the samples prepared in the presence of 0.1 wt % PBN are essentially bimodal (Fig. 2b), which may be due to the realization of two mechanisms of chain propagation: common radical polymerization (high-molecular-weight shoulder) and polymerization in the reversible inhibition mode (2). As the PBN concentration is increased further, the

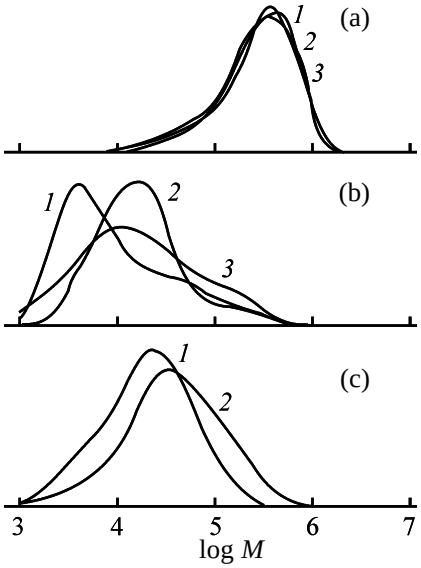


Fig. 2. MWD curves of polystyrene samples prepared at 70°C in the presence of AP (0.5 wt %) and PBN. (*M*) Molecular weight; the same for Figs. 3 and 5. [PBN], mol %: (a) 0, (b) 0.1, and (c) 0.2. Conversion, %: (a) (*1*) 27, (*2*) 55, and (*3*) 96; (b) (*1*) 8, (*2*) 58, and (*3*) 95; (c) (*1*) 53 and (*2*) 99.

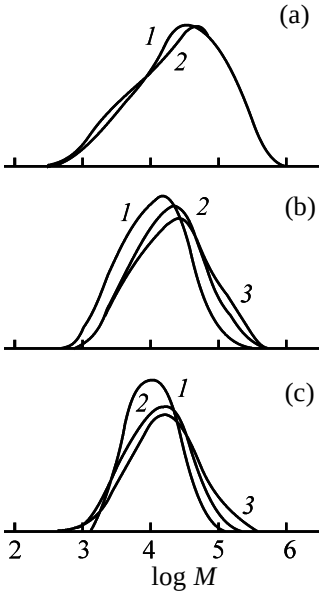


Fig. 3. MWD curves of polystyrene samples prepared in the presence of 0.5 wt % AP and 0.3 mol % PBN. Temperature, °C: (a) 70, (b) 80, and (c) 90. Conversion, %: (a) (*1*) 58 and (*2*) 79; (b) (*1*) 22, (*2*) 68, and (*3*) 92; (c) (*1*) 22, (*2*) 56, and (*3*) 98.

MWD curves become unimodal again, but are strongly broadened (Fig. 2c).

Thus, the experimental data show that the emulsion polymerization of styrene in the presence of PBN occurs by two mechanisms simultaneously: common radical and pseudo-living. It is known [22] that the equilibrium of reaction (2) shifts toward formation of radical products with increasing temperature. Hence, presumably, the contribution of the pseudo-living mechanism will also increase with temperature. Therefore, we studied the emulsion polymerization of styrene in the presence of 0.3 mol % PBN at 70, 80, and 90°C.

The MWD curves show that the polystyrene samples prepared at higher temperatures are less polydisperse (they have lower M_w/M_n, where M_w is the weight-average, and M_n, number-average molecular weight). This is manifested in narrowing of the MWD curves (Fig. 3). At higher synthesis temperatures, the MWD curves tend to shift toward higher molecular weights with increasing conversion. For the samples prepared at 90°C, *M* varies linearly with the conversion (Fig. 4). In contrast to the polymers prepared in the presence of low-molecular-weight nitroxyl radicals like TEMPO, for which the straight line reflecting this correlation passes through the origin [2–4], in our case $\lim_{\alpha\to 0} M_n \neq 0$.

According to the concept of classical pseudo-living radical processes [2], the radical initiating the polymerization directly adds to the stable nitroxyl radical to form alkoxyamine [similarly to scheme (2)]. After that, its length increases stepwise (in the controlled mode). Thus, the molecular weight of a polymer chain M_P will be $M_P = M_i + nM_M + M_N$, where M_i, M_M, and M_N are the molecular weights of the initiating radical, monomer, and nitroxyl radical, respectively; *n* is the number of elementary events of chain propagation. When the polymerization is performed in the presence of TEMPO, M_N is much lower than the molecular weight of the polymer (*nM*), and its contri-

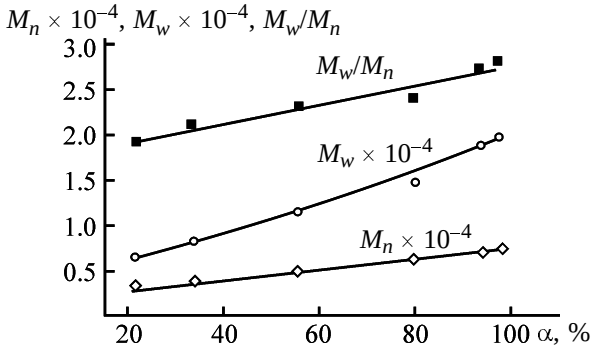


Fig. 4. Molecular-weight characteristics of polystyrene prepared at 90°C in the presence of 0.5 wt % AP and 0.3 mol % PBN as functions of conversion α: (M_n) Number-average and (M_w) weight-average molecular weights; (M_w/M_n) coefficient of polydispersity.

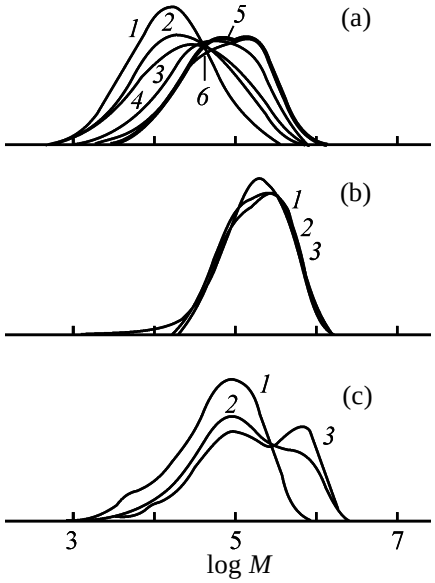


Fig. 5. MWD curves of polystyrene: (a) postpolymer, sample A; (b) thermal polymer, sample C; and (c) sample B. Conversion, %: (a) (*1*) initial polymer, (*2*) 8, (*3*) 14, (*4*) 24, (*5*) 26, and (*6*) 29; (b) (*1*) 7, (*2*) 20, and (*3*) 39; (c) (*1*) initial polymer, (*2*) 14, and (*3*) 23.

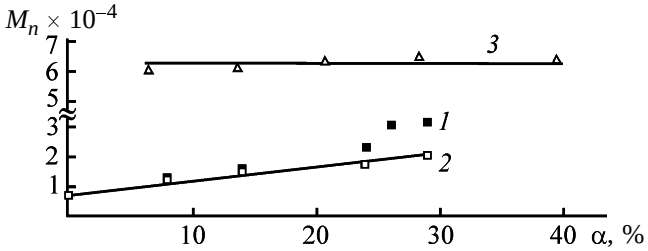


Fig. 6. Number-average molecular weight of polystyrene M_n as a function of conversion α: (*1*) postpolymer, (*2*) postpolymer without taking into account thermal polymer, and (*3*) thermal polymer.

bution to the total molecular weight of the macromolecules can be neglected; therefore, the linear dependence of *M* on the conversion passes virtually through the origin. In our case, on the contrary, the nitroxyl radical controlling the polymer chain propagation is formed *in situ* by the reaction of the spin trap with a polymeric radical [scheme (1)], and the contribution of *M* of such an adduct to the total molecular weight of the polymer is significant. It can be readily shown that in our system, on the average, M_N = 1800 g mol^{-1}. Thus, the polymeric radical bonded to PBN consists of 10–14 units. Therefore, in polymerization of styrene in the presence of PBN, the dependence of the molecular weight on conversion, though being linear, does not pass through the origin (Fig. 4).

One of the evidences of the living chain mechanism in radical processes is the postpolymerization in which the living polymeric chains, after removal of the initiator, residual monomer, and controlling additives can themselves act as initiators owing to the decomposition of active terminal groups [scheme (2)].

We found that the polystyrene isolated from the latex that was prepared in the presence of 0.3 mol % PBN at 90°C (sample A), after removal of residual initiator, monomer, and emulsifier, is indeed capable to initate the postpolymerization of a new portion of styrene. In particular, we prepared three series of samples under comparable conditions: sample A dissolved in styrene; solution of the polymer prepared under the same conditions as sample A but without PBN (sample B); and sample for thermal polymerization of styrene, containing the pure monomer only (sample C). The MVD curves for sample A (Fig. 5a) show that the curve maximum shifts toward higher molecular weights with increasing conversion. Correspondingly, in the region of $M \sim 1.5 \times 10^6$ ($\log M$ = 6.2), a shoulder appears, which is especially clearly seen in curve *5* (Fig. 5a). This high-molecular-weight shoulder is due to the occurrence of the polymerization by two mechanisms simultaneously: reversible inhibition and common radical mechanisms. In other words, both postpolymerization and common radical polymerization (due to thermal initiation) are observed in the system. It can be readily seen that the MWD maximum for the polymer (sample C) prepared by common (thermal) polymerization (Fig. 5b) coincides in the position with the high-molecular-weight shoulder in sample A (Fig. 5a). Sample B prepared without PBN shows no shift of the MWD curves toward higher molecular weights with the conversion (Fig. 5c). Thus, in this case no postpolymerization is observed. The polymer prepared by common radical polymerization (sample B), when added to the system, is inactive and remains dissolved as "dead ballast" in the monomer which, in turn, gradually polymerizes by the thermal mechanism. In this case, as in the case of the postpolymerization, a shoulder appears in the high-molecular-weight range, and its relative intensity grows with the conversion. The higher *M* of the thermal polymer is due to the initially higher viscosity of the monomer solution containing sample B.

The M_n of the postpolymer grows linearly with the conversion up to approximately 20% conversion (Fig. 6, curve *1*). The points corresponding to the samples with >20% conversion are shifted toward higher *M*. This is due to parallel formation in the system of the thermal polymer whose relative content increases in the course of the polymerization, introducing errors in the determination of M_n of the postpolymer.

To eliminate the disturbing effect of the thermal polymerization in the determination of *M* of the post-

polymer, we performed a mathematical treatment of the MWD curves. In so doing, we proceeded from the fact that the polymers formed in the system by thermal polymerization and pseudo-living mechanism have independent MWDs: for example, MWD of the thermal polymer is shown in Fig. 5b, and that of sample A, in Fig. 5a, curve *1*. Each of these distributions can be roughly approximated by a Gaussian curve. The superposition of the curves, taking into account the weight fraction of both kinds of the polymer, gives a bimodal curve, in particular, similar to that shown in Fig. 5a, curves *2–6*. Proceeding from these reasonings, we treated the experimental bimodal MWD curve as follows: first we took the logarithm $[\ln f(x)$, where $x = \log M]$ and then found its first derivative $\{\partial[\ln f(x)]/\partial x\}$.

By this sequence of operations, we brought the Gaussian function to the linear form: $\partial[\ln f(x)]/\partial x = y = x/\sigma^2 - m/\sigma$, where σ^2 is the variance and m is the mean value.

After the similar treatment of the experimental bimodal function, followed by singling out of linear portions, we decomposed this bimodal function into two unimodal functions. Taking into account the fractions of the postpolymer and thermal polymer in the mixture, we plotted the corresponding dependences of the number-average molecular weights of the samples on the conversion (Fig. 6). Thus, determination of the number-average molecular weight of the postpolymer proper (Fig. 6, curve *2*) showed that M of the postpolymer linearly increases with the conversion in the entire examined range of α.

CONCLUSION

Synthesis of polystyrene under the conditions of emulsion radical polymerization at 90°C in the presence of *C*-phenyl-*N*-*tert*-butylnitrone is characterized by the main features of the pseudo-living process: linear growth of the molecular weight of the polymer with the conversion, shift of the molecular-weight distribution toward higher molecular weights, and the possibility of block copolymerization.

ACKNOWLEDGMENTS

The study was supported by the Universities of Russia scientific and technical program of the RF Ministry of Education and Science.

REFERENCES

1. Matyjaszewski, K., *Controlled/Living Radical Polymerization*, Oxford: Univ. Press, 2000.
2. Korolev, G.V. and Marchenko, A.P., *Usp. Khim.*, 2000, vol. 69, no. 5, pp. 447–475.
3. Grishin, D.F. and Semenycheva, L.L., *Usp. Khim.*, 2001, vol. 70, no. 5, pp. 486–510.
4. Zaremskii, M.Yu. and Golubev, V.B., *Vysokomol. Soedin., Ser. C*, 2001, vol. 43, no. 9, pp. 1689–1728.
5. Qiu, J., Cheraleux, B., and Matyjaszewski, K., *Prog. Polym. Sci.*, 2001, vol. 26, no. 20, pp. 2083–2134.
6. Cunningham, M.F., *C. R. Cimie*, 2003, vol. 6, pp. 1351–1374.
7. Ma, J.W., Smith, J.A., McAuley, K.B., *et al.*, *Chem. Eng. Sci.*, 2003, vol. 58, pp. 1163–1176.
8. Pan, G., Sudol, E.D., Dimonie, V.L., and El-Aasser, M.S., *Macromolecules*, 2001, vol. 34, no. 3, pp. 481–488.
9. Fukuda, T., Terauchi, N., Goto, A., *et al.*, *Macromolecules*, 1996, vol. 29, no. 20, pp. 6393–6411.
10. Grishin, D.F., Semyonycheva, L.L., and Kolyakina, E.V., *Mendeleev Commun.*, 1999, no. 6, pp. 250–252.
11. Grishin, D.F., Semenycheva, L.L., and Kolyakina, E.V., *Zh. Prikl. Khim.*, 2001, vol. 74, no. 3, pp. 483–486.
12. Grishin, D.F., Semenycheva, L.L., Sokolov, K.V., and Pavlovskaya, M.V., *Zh. Prikl. Khim.*, 2001, vol. 74, no. 9, pp. 1546–1550.
13. Catala, J.M., Jousset, S., and Lamps, J.P., *Macromolecules*, 2001, vol. 34, no. 25, pp. 8654–8656.
14. Kolyakina, E.V., Semenycheva, L.L., and Grishin, D.F., *Vysokomol. Soedin., Ser. A*, 2001, vol. 43, no. 12, pp. 2092–2096.
15. Detrembler, C., Scianneamia, V., Koulic, C., *et al.*, *Macromolecules*, 2002, vol. 35, no. 19, pp. 7214–7223.
16. Grishin, D.F., Semenycheva, L.L., Bulgakova, S.A., *et al.*, *Vysokomol. Soedin., Ser. A*, 2003, vol. 45, no. 4, pp. 533–539.
17. *Analytical Chemistry of Polymers*, part 1: *Analysis of Monomers and Polymeric Materials*, Kline, G.M., Ed., New York: Interscience, 1959.
18. *Entsiklopediya polimerov* (Polymer Encyclopedia), Moscow: Sov. Entsiklopediya, 1976, vol. 1.
19. Terabe, S. and Konaka, S., *J. Chem. Soc., Perkin Trans. 2*, 1972, no. 14, pp. 2163–2172.
20. *Praktikum po khimii i fizike polimerov* (Practical Course of Polymer Chemistry and Physics), Kurenkov, V.F., Ed., Moscow: Khimiya, 1990.
21. Belen'kii, B.G. and Vilenchik, L.Z., *Khromatografiya polimerov* (Chromatography of Polymers), Moscow: Khimiya, 1978.
22. Zubarev, V.E., *Metod spinovykh lovushek* (Method of Spin Traps), Moscow: Mosk. Gos. Univ., 1984.

Russian Journal of Applied Chemistry, Vol. 78, No. 5, 2005, pp. 820–823. Translated from Zhurnal Prikladnoi Khimii, Vol. 78, No. 5, 2005, pp. 836–839.
Original Russian Text Copyright © 2005 by Galikhanov, Borisova, Deberdeev.

MACROMOLECULAR CHEMISTRY AND POLYMERIC MATERIALS

Changes in Electret Characteristics of Polymeric Formulations in Their Processing into Articles

M. F. Galikhanov, A. N. Borisova, and R. Ya. Deberdeev

Kazan State Technological University, Kazan, Tatarstan, Russia

Received September 21, 2004

Abstract—The process of fabrication of an article with electret properties from a sheet composite corona-electret based on low-density polyethylene and titanium dioxide by vacuum forming was studied. The influence exerted by temperature and deformation on the preservation of electret properties of their formulations in their processing into articles was revealed.

Filling of polymers makes it possible to obtain material with novel working properties. Fillers can exert various kinds of influence on properties of polymers, including electret properties [1]. Fillers of varied nature with various characteristics can both improve and deteriorate the electret properties of polymers [1–8]. However, the lack of a rigorous theoretical substantiation of manifestations of the electret effect in polymeric composites and the insufficient amount of experimental data on processes of formation and relaxation of charges in these materials strongly hinder technical application of composite electrets.

It has been shown previously that prolonged keeping of composite electrets at elevated temperatures does not lead to complete charge relaxation, in contrast to unfilled polymers. This allowed a conclusion that articles can be fabricated from electret films and plates by the conventional techniques for processing of plastics [7, 8]. However, processing of formulations also leads to deformation of the polymer matrix, which, undoubtedly, must affect the charge retention by electrets. Unfortunately, data of this kind are virtually lacking. Therefore, the aim of this study was to find out how the electret properties of polymeric formulations depend on deformation at elevated temperatures.

EXPERIMENTAL

As objects of study we chose low-density polyethylene of 11503-070 brand [GOST (State Standard) 16337–77] and titanium dioxide of the R-01 brand (GOST 9808–65) with a particle size of 0.3 μm and a specific surface area of 15 $m^2 g^{-1}$.

The polymers were mixed with fillers and Irgonox 1010 stabilizer (0.2 wt %) on a laboratory micro roll mill at 135 ± 5°C and a mixing time of 3 min. Plates 0.6 mm thick were produced by compaction in accordance with GOST 12019–66 at 170 ± 5°C and a time of keeping under pressure equal to 5 min. The polymeric plates were polarized in the field of a corona discharge with an electrode comprising 196 pointed needles uniformly distributed over an area of 49 cm^2 in the form of a square. The distance between the plates and the electrode was 20 mm, and the voltage and time of polarization were 35 kV and 90 s. Prior to polarization, the plates were kept in a heating box at 100°C for 10 min.

The electret characteristics were measured once a day with an IPEP-1 instrument, whose operation principle is based on periodic shielding of the receiving electrode situated at a certain distance from the electret surface. The error in measuring the surface potential U_e, electric field strength E, and surface density σ_{eff} of electric charges did not exceed 3%.

Spectra of thermally stimulated currents were measured under linear heating of samples in a special measuring cell with blocking aluminum electrodes and a Teflon spacer [1].

The electret plates were processed into articles by the method of vacuum forming in an installation with one-side IR heater and a mold in the form of a vessel of irregular shape. The time of heating of the plates was 90 s. The degree n (%) of extension in forming was found using the formula

$$n = (\sigma_{in}/\sigma_{fin})^{1/2} \times 100,$$

where σ_{in} is the initial thickness of the sheet blank

1070-4272/05/7805-0820© 2005 Pleiades Publishing, Inc.

(mm), and σ_{fin}, thickness of an article upon forming (mm).

The wide availability of polyethylene makes it a very promising material for production of electrets. Having a low electrical conductivity, such a nonpolar polymer is well polarized in the field of a corona discharge, when charge carriers penetrate into the material to be captured there by traps. The role of traps can be played by impurities, phase boundaries, free volume of a polymer, etc. [9].

The advantages of polymer polarization in the field of a corona discharge, high rate and simple equipment, are manifested in charging of sheet- and film-type materials on a production line. At the same time, many areas of practical application of electrets, electronics, machine building, and medicine, require electret articles of various shapes and configurations [1], whose polarization presents some technological difficulties. Therefore, forming of articles from electret sheets (by punching or pneumatic and vacuum forming) may be markedly simpler and less expensive than the existing techniques for their manufacture. The problem of loss of the electret properties upon heating of polymers is solved by introducing powder-like fillers [7, 8].

Formulations composed of low-density polyethylene and 4 vol % titanium dioxide, considered in [7], exhibit high and stable electret characteristics: the surface potential U_e exceeds 1 kV after 3 years of storage. Keeping such electrets at 150°C for 30 min leads to a decrease in U_e to 0.6 kV.

A study of spectra of thermally stimulated depolarization (TSD) of the electrets based on polyethylene and filled formulations (Fig. 1) demonstrated that a TSD spectrum contains, in addition to the peaks characteristic of polyethylene (at 75–80 and 105–115°C), two new peaks at 165–170 and 195–205°C. The peaks of TSD currents appear in disintegration of some group of traps containing a trapped injected charge. The peak at 75–80°C corresponds to the Vicat softening point, at which the mobility of macromolecules in polyethylene increases dramatically. The peak at 105–115°C lies near the melting point of low-density polyethylene, at which ordered supramolecular formations constituting the crystalline phase of the polymer undergo thermal disintegration. The intensive motion of terminal groups, double bonds, and oxidized fragments of macromolecules releases charges from traps situated at the interface between the amorphous and crystalline phases of polyethylene (Fig. 1). The slight difference between the melting point of polyethylene and disintegration temperature of these

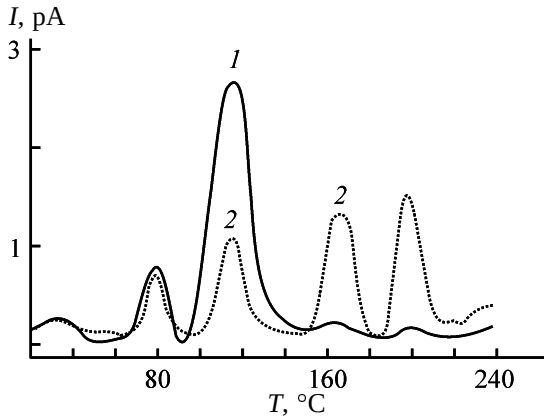


Fig. 1. Currents of thermally stimulated depolarization, *I–T*, of corona-electrets based on (*1*) low-density polyethylene and (*2*) polyethylene formulations with 4 vol % titanium dioxide.

category of traps is probably due to a too high rate of temperature variation in measuring the thermally stimulated currents, which is incomparable with the rate of relaxation of macromolecules of the polymer. The appearance of the peaks at 165–170 and 195–205°C (Fig. 1) is due to the Maxwell–Wagner polarization and to appearance of a new type of traps at the polymer–filler interface [7, 8]. Owing to the fact that these traps do not disintegrate at temperatures exceeding 150°C, the electret characteristics of the polyethylene formulations are not deteriorated down to zero at this temperature.

It is of interest that filling also changes the intensity and position of the TSD peaks characteristic of pure polyethylene. Presumably, this is due to the presence of a low-mobility adsorption layer of the polymer near the filler surface, which leads to a decrease in the mobility of various kinetic units of the polymer and to a broader range of relaxation times of its macromolecules.

In vacuum forming of a vessel of irregular shape from an electret composite plate, the material in different walls of the vessel is subjected to different extents of extension. This makes it possible to trace the effect of deformation at elevated temperatures on the retention of the electret effect in a polyethylene formulation. The data obtained revealed a rather interesting pattern. In deformation of composite plates, their electret characteristics (surface potential U_e, electric field strength E, and surface charge density σ_{eff}) decrease to a greater extent than do the parameters of undeformed plates, and this effect is less pronounced in the case of a 50% extension and more so at 25 and 75% extension (Fig. 2).

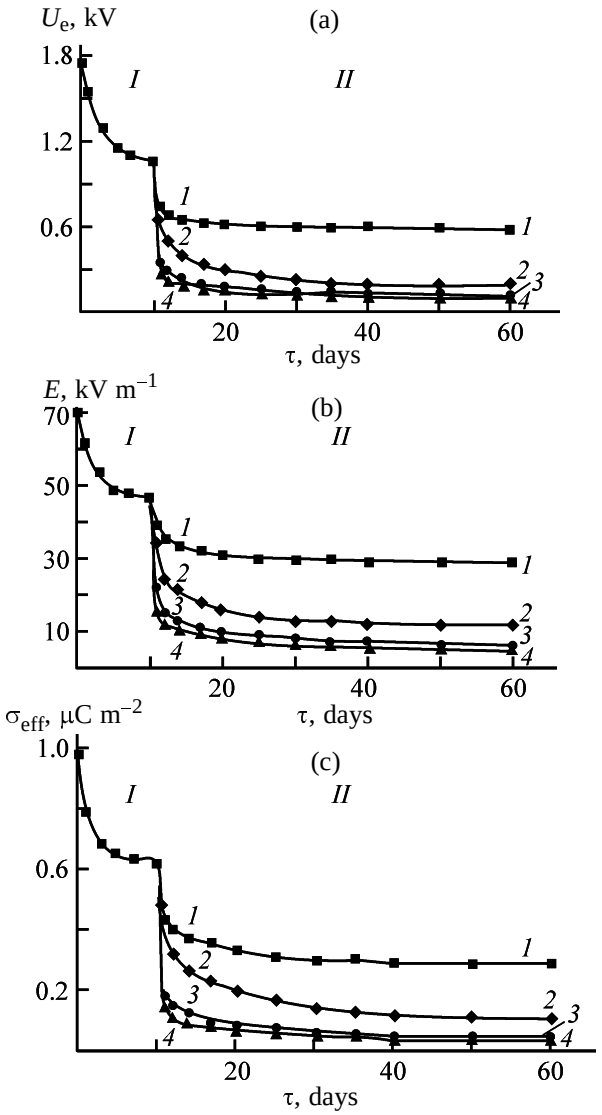


Fig. 2. (a) Surface potential U_e, (b) electric field strength E, and (c) surface charge density σ_{eff} of composite corona-electrets vs. storage time τ before (region *I*) and after (region *II*) vacuum forming. Degree of extension, %: (*1*) 0, (*2*) 50, (*3*) 25, and (*4*) 75.

The decrease in the electret characteristics of formulations under the action of temperatures exceeding the melting point of polyethylene (Fig. 2, curve *1*) is quite understandable. The depolarization resulting from disintegration of traps for injected carriers, which are characteristic of pure polyethylene, leads to partial relaxation of the charge. If account is taken of the fact that the area under the curve for the current is proportional to the charge of the electret [10], then disintegration of the first two trap levels in a polyethylene composite corona-electret (Fig. 1, curve *2*) must lead to a virtually 40% loss of electret properties, and this is the case in practice.

The deterioration of the electret characteristics of polyethylene corona-electrets in extension also would be expected. Borisova *et al.* [11] observed a similar phenomenon and identified two reasons why it occurred. First, a decrease in the film thickness and increase in the surface area at a fixed charge necessarily lead to a lower electret difference of potentials of the polyethylene films. Second, deformation of a polyethylene sample leads to disintegration of a part of structural traps because of the displacement of macromolecules of fragments of these, which releases injected charge carriers captured by these traps. Both these factors may also be responsible for the observed deterioration of the electret characteristics of polyethylene formulations in vacuum forming (Fig. 2, curves *2*–*4*).

At the same time, there is evidence that oriented polyethylene films considerably exceed unoriented films in their electret properties [12]. However, this is only observed in the cases of polarization of the already deformed polyethylene films.

In the context of the above considerations, it seems unreasonable that raising the degree of extension of an electret plate made of a polyethylene formulation containing 25 to 50% titanium dioxide leads to a slight improvement of electret characteristics (Fig. 2, curves *2*, *3*). Raising the degree of deformation of corona-electrets to 75% results in a decrease in U_e, E, and σ_{eff}, which would be expected (Fig. 2, curve *4*). However, such a dependence of the effective surface charge density in extension was observed in [13] in studying thermoelectrets based on polyethylene and its mixtures with silicon dioxide and powdered copper: under deformation, the charge first decreases, then starts to increase, and then again abruptly decreases. The rise in the charge at higher relative elongations in extension of unfilled and filled polyethylene films was attributed to formation and growth of microcracks, accompanied by charge formation on the surface of a film through emission of charge carriers and their capture by structural traps.

Indeed, the processes of carrier recapture in storage of electrets are markedly accelerated by elevated temperatures. Deformation of polymers leads to the following changes in their structure: the existing structural traps for charge carriers disintegrate and new traps, microcracks and radicals with a different trapping energy, are formed. It may be assumed that the recapture of carriers released from disintegrating traps into those newly formed at a 50% degree of extension occurs in a more optimal way than that at 25 and 75%. This may be also due to the possible partial recrys-

tallization of polyethylene, which occurs at >25% degrees of deformation and leads to changes in the area of the interface between the amorphous and crystalline phases.

Our results suggest that deformation of polymeric composite corona-electrets at elevated temperatures markedly impairs their electret characteristics, but does not lead to their fall to zero values in contrast to the case of unfilled polymeric electrets. This enables forming of articles with electret properties from sheet blanks, which markedly facilitates the technology of their manufacture, improves the productivity, and, consequently, makes lower the production cost. Undoubtedly, the charge distribution over the surface of a thus obtained article is nonuniform and depends on the degree of deformation of the material. However, this is not important in many cases of practical application of electrets.

CONCLUSIONS

(1) The electret characteristics of polyethylene formulations with titanium dioxide do not decrease in processing to zero values because of the presence in these formulations of high-energy levels of traps capturing charge carriers at the polymer–filler interface, which disintegrate at temperatures exceeding the flow point of polymers.

(2) Deformation of a sheet polyethylene composite corona-electret at elevated temperatures leads to a significant decrease in the surface potential, electric field strength, and surface density of electric charge. However, the residual level of the electret characteristics of the formulations makes it possible to produce articles with electret properties from sheet blanks. This can markedly facilitate the technology of their fabrication, raise the productivity, and, consequently, make lower the production cost.

(3) Raising the degree of extension of an electret plate made of a formulation composed of polyethylene and titanium dioxide from 25 to 50% leads to a slight improvement of their electret characteristics. This is accounted for by the more efficient recapture of carriers from disintegrating traps into those newly formed.

REFERENCES

1. Pinchuk, L.S. and Gol'dade, V.A., *Elektretnye materialy v mashinostroenii* (Electret Materials in Machine Building), Gomel: Infotribo, 1998.
2. Vertyachikh, I.M., Pinchuk, L.S., and Tsvetkova, E.A., *Vysokomol. Soedin., Ser. B*, 1987, vol. 29, no. 6, pp. 460–463.
3. Zhang, H., Yang, Q., Wang, W., *et al.*, in *Proc. 9th Int. Symp. on Electrets*, Shanghai (China), 1996, pp. 323–326.
4. Kravtsov, A.G., *Plast. Massy*, 1999, no. 9, pp. 39–42.
5. Goldade, V.A., Kravtsov, A.G., Pinchuk, L.S., *et al.*, in *Proc. Int. Conf. on Advances in Processing: Testing and Application of Dielectric Materials*, 2001, pp. 76–79.
6. Galikhanov, M.F., Eremeev, D.A., and Deberdeev, R.Ya., *Plast. Massy*, 2002, no. 10, pp. 26–28.
7. Galikhanov, M.F., Eremeev, D.A., and Deberdeev, R.Ya., *Vestn. Kazan. Tekhnol. Univ.*, 2003, no. 1, pp. 299–305.
8. Galikhanov, M.F., Eremeev, D.A., and Deberdeev, R.Ya., *Zh. Prikl. Khim.*, 2003, vol. 76, no. 10, pp. 1696–1700.
9. *Electrets*, Sessler, G.M., Ed., Berlin: Springer, 1980.
10. Gubkin, A.N., *Elektrety* (Electrets), Moscow: Nauka, 1978.
11. Borisova, M.E., Zakrevskii, V.A., Koikov, S.N., *et al.*, *Vysokomol. Soedin., Ser. B*, 1983, vol. 25, no. 8, pp. 571–574.
12. Zakrevskii, V.A., Pakhotin, V.A., and Fomin, V.A., *Vysokomol. Soedin., Ser. B*, 1976, vol. 18, no. 9, pp. 710–712.
13. Gol'dade, V.A., Voronezhtsev, Yu.I., Pinchuk, L.S., *et al.*, *Vysokomol. Soedin., Ser. B*, 1988, vol. 30, no. 7, pp. 511–514.

Russian Journal of Applied Chemistry, Vol. 78, No. 5, 2005, pp. 824–829. Translated from Zhurnal Prikladnoi Khimii, Vol. 78, No. 5, 2005, pp. 840–845.
Original Russian Text Copyright © 2005 by Galimzyanova, Bakirova, Valuev, Zenitova.

MACROMOLECULAR CHEMISTRY AND POLYMERIC MATERIALS

Mechanism and Relationships of Chemical Degradation of Rigid Polyurethane Foam

A. R. Galimzyanova, I. N. Bakirova, V. I. Valuev, and L. A. Zenitova

Kazan State Technological University, Kazan, Republic Tatarstan, Russia
Lebedev Research Institute of Synthetic Rubber, Federal State Unitary Enterprise, St. Petersburg, Russia

Received July 9, 2004; in final for, February 2005

Abstract—The regular trends in chemical degradation of rigid polyurethane foam under the action of oxypropylated hydroxy compounds were studied. The molecular-weight characteristics, functionality with respect to 4,4'-diphenylmethane diisocyanate and OH groups, viscosity, and the content of terminal OH groups of alcoholysis products at temperatures from 150 to 220°C were determined. A mechanism of degradation of the network structure of rigid polyurethane foam was suggested.

Owing to a unique combination of low thermal conductivity, low density, and high manufacturability rigid polyurethane foams (PUFs) are widely used in various branches of industry. An increase in their production volume estimated in 2003 at 2 000 000 tons results in accumulation of large amounts of wastes which are environmental pollutants. At the same time, a decrease in the natural resources and, as a result, rise of their price dictates the need of using secondary raw materials. The most promising solution of the above environmental and economic problem is chemical degradation of wastes from PUF production by alcoholysis.

The aim of this study was to reveal regular trends in the alcoholysis of rigid PUFs and to establish the mechanism of their chemical degradation.

EXPERIMENTAL

Experiments were performed with wastes from production of rigid PUF assigned for thermal insulation of refrigerating equipment. Foam plastic was prepared by the reaction of a hydroxy component with polyisocyanate (PIC) derived from 4,4'-diphenylmethane diisocyanate (MDI).

As a degradation agent (DA) we used oxypropylated hydroxy compound Laprol-564[1] (L-564), a polyether based on propylene oxide with a molecular weight M of approximately 500 and f_{OH} = 4. The weight ratio PUF : DA was 40 : 60 and was chosen experimentally based on evaluation of the maximum amount of wastes and minimum amount of DA.

Alcoholysis was carried out in the range 150–220°C. The instant of addition of PUF crumb was considered as the onset of degradation. Preliminary milled PUF was continuously added into DA at a stirring rate of 300 rpm. With increasing degradation temperature T_d, the monitored time interval decreased from 30 to 7 h. The alcoholysis products were analyzed starting from the instant of system homogenization.

The molecular-weight parameters were determined by gel permeation chromatography (GPC) with a chromatographic modular high-performance system designed from units produced by Waters-244. Chromatographing was carried out with Styrogel columns with the pore size of 10^4, 500, and 100 Å; the solvent was freshly distilled tetrahydrofuran (THF) prepurified to remove peroxy compounds; the concentration of sample solutions at the inlet of the chromatograph was 0.1–0.3 wt %. Detection was carried out with a refractometer and a photometer in parallel, which allowed determination of the polymer concentration at the outlet (refractometer) and the concentration of aromatic rings (photometer). The operating UV wavelength of the photometer was 255 nm.

The content of hydroxy groups c_{OH} in the alcoholysis products was determined by the acetylation method according to GOST (State Standard) 25 261-82.

The dynamic viscosity of the alcoholysis products η_{dyn} (Pa s) was determined on a Hoeppler rheovis-

[1] Produced by the Nizhnekamskneftekhim Joint-Stock Co.

1070-4272/05/7805-0824 © 2005 Pleiades Publishing, Inc.

cometer at 80±0.1°C [1]. The chemical structure of DA and alcoholysis products was studied by IR spectroscopy with a Specord 75-IR spectrophotometer. The samples for recording the spectra were prepared in the form of a drop pressed between NaCl plates.

A study of the parameters of molecular-weight distribution (MWD) of the alcoholysis products depending on the degradation conditions showed that, in the first hours of the process, the average M values decrease and then become constant (Table 1). For example, the weight-average molecular weight M_w, as the most sensitive to degradation processes, decreases from 8640 to 1370, and the number-average weight M_n, from 1100 to 660; the polydispersity coefficient M_w/M_n decreases from 7.85 to 2.09.

The decrease in the average M values is caused by development of the degradation processes, and their subsequent stabilization, by the attainment of the equilibrium state of the system. In this case, the higher is T_d, the lower is the equilibrium average M.

The progress of degradation can be judged from the differential MWD curves of alcoholysis products withdrawn in the course of degradation (Fig. 1). The content of fractions with high M decreases in the course of heating.

Data on distribution of alcoholysis products with respect to content of MDI fragments (Table 2) furnish more information on the mechanism of the polymer degradation. In the course of the process, the fraction of molecules containing six and more MDI fragments significantly decreases (functionality with respect to MDI fragments $f_{MDI} > 20$, from 15 to 0 wt %; $f_{MDI} > 10$, from 6 to 2 wt %; $f_{MDI} > 6$, from 16 to 2 wt %) with a simultaneous increase in the fraction of the compounds containing three aromatic fragments and less ($f_{MDI} = 3$, from 10 to 23 wt %; $f_{MDI} = 2$, from 3 to 17 wt %; $f_{MDI} = 1$, from 15 to 42 wt %).

In the course of alcoholysis, with increasing T_d f_{nMDI} decreases from 1.03 to 0.62, which confirms once again a decrease in the content of polymer molecules polyfunctional with respect to MDI fragments.

The most important parameter of alcoholysis products, allowing their use as polyol component in synthesis of polyurethane, is the nature and concentration of terminal functional groups, namely hydroxyls. As seen from Fig. 2, irrespective of the temperature and time of degradation, the concentration of OH groups remains constant and is equal to approximately 9.6 wt %, which corresponds to the amount of OH groups initially supplied by DA. The estimated number-average functionality with respect to OH groups f_{nOH} decreased from 6.1 to 4.72, which, as should be expected, exceeds the functionality of DA ($f_{nOH} = 4$).

Table 1. MWD parameters of alcoholysis products

T_d, °C	τ_d, h	M_w	M_n	M_w/M_n
150	7.5	8640	1100	7.85
	11.5	4470	1040	4.30
	15.5	4100	1020	4.08
	19.5	3820	950	4.02
	23.5	3850	960	4.01
	27.5	4040	1000	4.04
165	7.5	6986	1000	6.99
	12	3562	850	4.19
	18	3670	953	3.85
	24	3933	1030	3.82
	30	3735	885	4.22
180	8	3672	870	4.22
	12	3660	900	4.07
	18	3656	953	3.84
200	4	5100	945	5.40
	10	3150	850	3.71
	15	2350	802	2.93
220	2	3910	910	4.30
	3.5	3540	826	3.09
	7	1365	658	2.09

The kinetics of high-temperature alcoholysis with

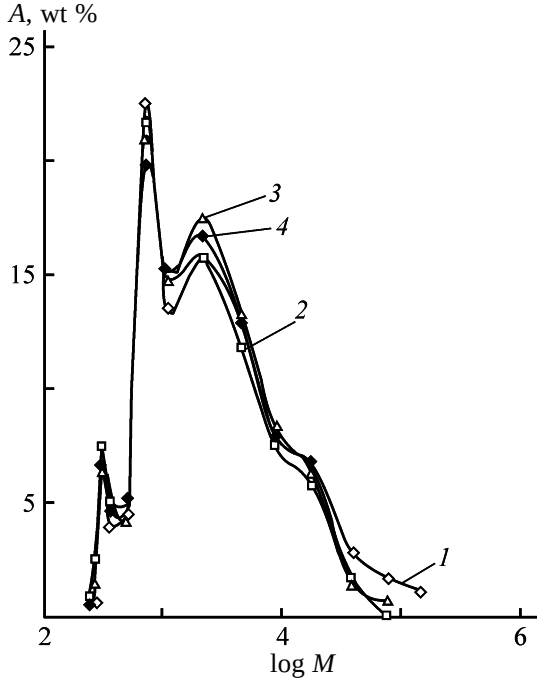


Fig. 1. Differential MWD curves of alcoholysis products at 165°C. (*A*) Content of fraction; (*M*) molecular weight. Heating time, h: (*1*) 7.5, (*2*) 12, (*3*) 18, and (*4*) 30.

Table 2. Distribution *D* of alcoholysis products with respect to the content of MDI fragments

T_d, °C	τ_d, h	$f_{n\text{MDI}}$		Weight content of fraction, %, with indicated *f*						
		GPC	D	>20	>10	>6	3	2	1	0
150	7.5	1.03	1.01	15	6	16	10	3	15	35
	11.5	0.97	0.96	13	7	15	12	4	16	33
	15.5	0.95	0.93	12	8	15	12	4	16	33
	19.5	0.89	0.86	10	8	12	12	8	19	31
	23.5	0.90	0.89	9	8	12	13	8	20	30
	27.5	0.93	0.91	10	7	13	13	8	19	30
165	7.5	0.93	0.91	10	8	13	10	12	21	26
	12	0.79	0.75	9	8	12	10	10	25	26
	18	0.89	0.85	8	8	8	10	15	26	25
	24	0.96	0.76	2	15	2	15	17	29	20
	30	0.83	0.77	2	14	13	5	14	25	27
180	8	0.81	0.74	7	8	12	10	12	24	27
	12	0.84	0.77	5	12	11	11	12	25	24
	18	0.89	0.80	2	15	10	10	13	26	24
200	4	0.88	0.80	4	7	10	20	7	31	21
	10	0.79	0.78	2	4	7	23	8	33	23
	15	0.75	0.73	–	3	6	21	9	35	26
220	2	0.85	0.81	2	5	10	22	7	32	22
	3.5	0.77	0.77	–	3	8	23	8	32	26
	7	0.62	0.67	–	2	4	11	9	42	32

respect to viscosity is shown in Fig. 3. In the course of degradation, the viscosity of alcoholysis products varies in agreement with the molecular weights. Initially the viscosity monotonically decreases owing to development of degradation processes and decrease in M_w of the alcoholysis products, which reach constant values at T_d 150, 165, and 180°C within 15, 12, and 8 h, respectively.

Qualitative analysis of the alcoholysis products was performed by IR spectroscopy. In the spectra of alcoholysis products (Fig. 4a) we found absorption bands characteristic of L-564 (Fig. 4b): strong bands of stretching vibrations of the ether group C–O–C at approximately 1080 cm^{-1}, stretching vibrations of associated OH group at approximately 3380 cm^{-1}, and in-plane bending vibrations of OH group at about 1400 cm^{-1}. In addition, new bands appeared: 1710 (C=O stretching vibrations of urethane group), 1600 (stretching vibrations of C=C bond in benzene ring), 1510 (N–H bending and C–N stretching vibrations of

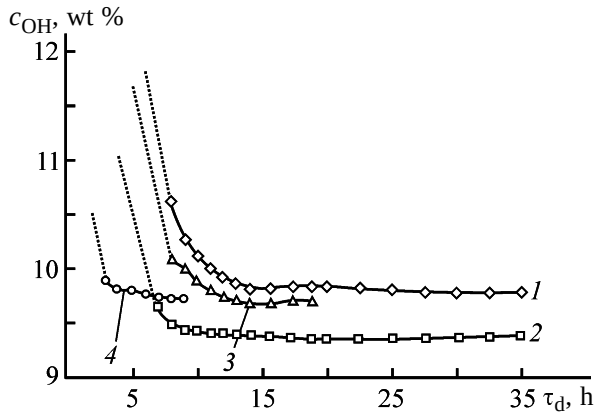


Fig. 2. Concentration of OH groups c_{OH} in alcoholysis products as a function of degradation duration τ_d. Process temperature, °C: (*1*) 150, (*2*) 165, (*3*) 180, and (*4*) 200.

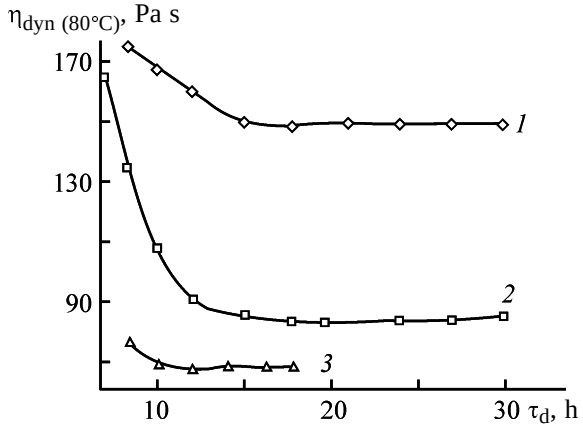


Fig. 3. Dynamic viscosity of alcoholysis products η_{dyn} as a function of process duration τ_d. Process temperature, °C: (*1*) 150, (*2*) 165, and (*3*) 180.

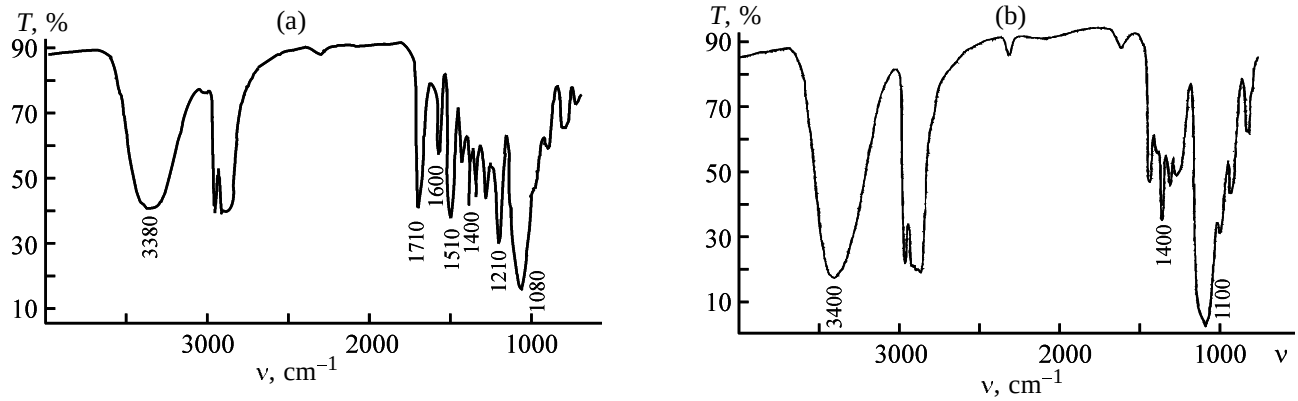


Fig. 4. IR spectra of alcoholysis products of (a) rigid PUF at T_d = 180°C and τ_d = 10 h and (b) L-564. (*T*) Transmission and (ν) wave number.

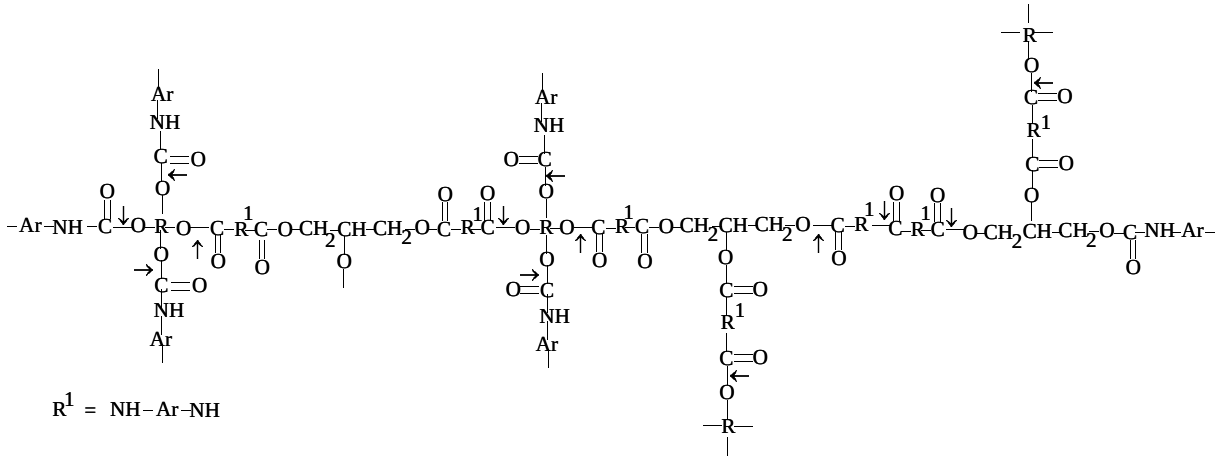
urethane group), and 1210 cm^{-1} (stretching vibrations of the C–N–H bond of the urethane group) [2–4]. Identification of the urea group is difficult since its characteristic absorption bands, such as N–H stretching vibrations at approximately 3300 cm^{-1} and C=O stretching vibrations in the range 1575–1660 cm^{-1}, overlap with stronger bands of hydroxy group and benzene ring.

The IR data show that alcoholysis products are compounds containing ether, urethane, urea, aromatic, and hydroxy groups.

Thus, the study of alcoholysis products showed that, in the course of degradation, the physicochemical characteristics (M_n, M_w, M_w/M_n, $f_{n\mathrm{MDI}}$, $f_{n\mathrm{OH}}$, and viscosity) decrease with their subsequent stabilization. The higher T_d, the lower the values of these parameters. Irrespective of the degradation conditions, c_{OH} remains constant.

Based on the IR data and the revealed regular trends in variation of the physicochemical parameters, taking into account the structure of the rigid polymer to be destroyed, we suggested a mechanism of chemical degradation of the polymer.

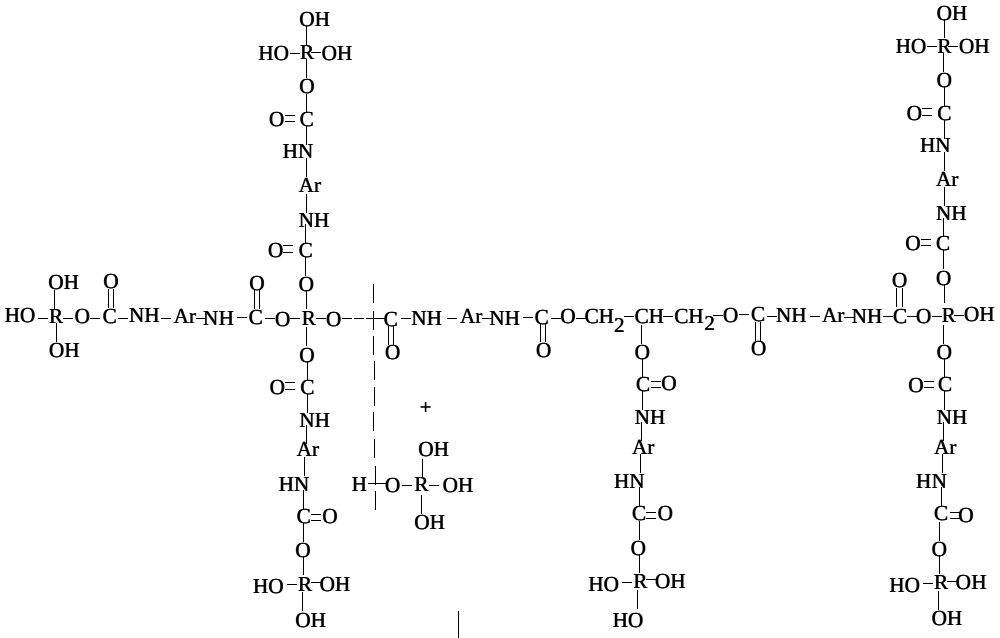
Polyurethane foam is a polymer with alternating laprolic, glycerol, and urea fragments linked through urethane bonds:



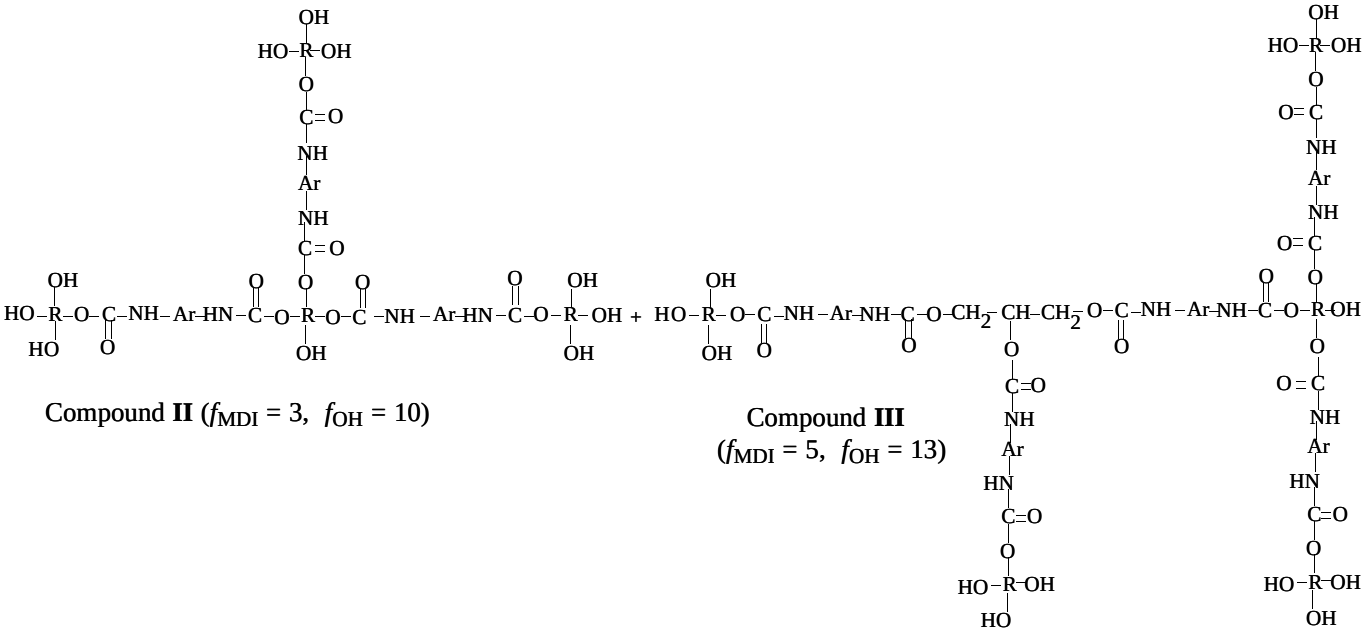
The mechanism of degradation of rigid PUF across urethane and urea bonds suggests their alcoholysis under the action of OH groups of L-584 by the ester interchange reaction. It is well known that alcoholysis of urethane groups is faster than that of urea groups; the most accessible are urethane bonds formed by OH groups of L-584 due to weaker steric hindrance.

In the initial period of degradation, large fragments of macromolecules are eliminated from the polymer matrix as a result of alcoholysis of less stable urethane bonds. Bulky branched molecules of compounds of type **I** with high functionality with respect to OH groups and aromatic fragments are formed. In these molecules, sterically hindered urethane and urea

groups as more resistant to hydrolysis are retained. This is confirmed by gel permeation chromatography. In particular, chromatograms of the samples withdrawn in the first hours after the start of degradation showed the presence of fractions with *M* of approximately 74000 and $f_{MDI} > 30$. Then, these macromolecular compounds undergo further alcoholysis to form smaller fragments. A longer polymer chain is subjected to degradation to a greater extent [5]:



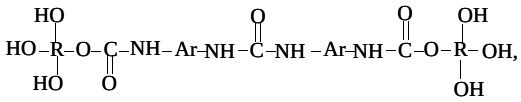
Compound **I** ($f_{MDI} = 8$, $f_{OH} = 19$)



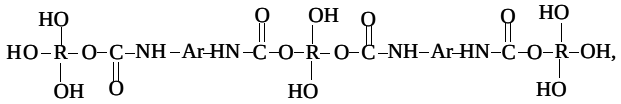
Compound **II** ($f_{MDI} = 3$, $f_{OH} = 10$)

Compound **III** ($f_{MDI} = 5$, $f_{OH} = 13$)

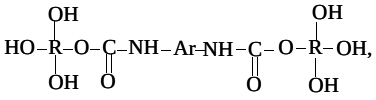
As the degradation develops further, compounds **II** and **III** degrade across the remaining urethane bonds to form compounds **IV**–**VII** containing 1–2 MDI fragments with $f_{OH} = 8–5$:



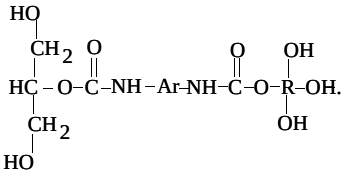
Compound **IV** (f_{MDI} = 2, f_{OH} = 6)



Compound **V** (f_{MDI} = 2, f_{OH} = 8)



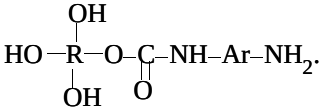
Compound **VI** (f_{MDI} = 1, f_{OH} = 6)



Compound **VII** (f_{MDI} = 1, f_{OH} = 5)

The resulting low-molecular-weight compounds, in turn, can serve as degradative agents with respect to polyfunctional macromolecules and to PUF.

Under prolonged action of heating (above 180°C), urea group can be subject to alcoholysis to form amino polyol:



Compound **VIII** (f_{MDI} = 1, f_{OH} = 3)

However, we detected compounds of type **VIII** neither by IR spectroscopy nor by chemical analysis. It is evident that formation of products with amino groups is insignificant due to low concentration of urea groups in the system (there is only one urea group per 14 urethane groups in a PUF unit). Hence, the terminal functional groups of the degradation products are mainly hydroxy groups.

Thus, the mechanism of alcoholysis of rigid PUF involves degradation of the network polymer matrix across urethane bonds to form primarily large macromolecules with a high content of aromatic fragments and their subsequent degradation to smaller fragments. In this case, the alcoholysis products are hydroxyl-containing compounds such as polyols, urethane–polyols, and urethane–urea–polyols with various *M* and functionality with respect to aromatic and terminal OH groups.

CONCLUSIONS

(1) The following features of chemical degradation of rigid polyurethane foams were established: with an increase in the process duration and the average molecular weights, the coefficient of polydispersity and the functionality with respect to fragments of 4,4'-diphenylmethane diisocyanate and OH groups of alcoholysis products decrease and subsequently attain constant values; with an increase in the alcoholysis temperature, the time of attainment of the equilibrium state and the corresponding parameter levels decrease; the concentration of terminal functional groups in the alcoholysis products is constant and is independent of the degradation conditions.

(2) The mechanism of chemical degradation of rigid polyurethane foam was suggested. This mechanism is based on alcoholysis of urethane and urea groups with formation of long multinuclear macromolecules, followed by cleavage with formation of smaller fragments such as polyols, urethane–polyols, urethane–urea–polyols, and amino polyols.

REFERENCES

1. *Analiz produktov proizvodstva sinteticheskikh kauchukov* (Analysis of the Products Formed in Production of Synthetic Rubbers), Garmonov, I.V., Ed., Moscow: Khimiya, 1984.
2. Smith, A.L., *Applied Infrared Spectroscopy: Fundamentals, Techniques, and Analytical Problem-Solving*, New York: Wiley, 1979.
3. Kazitsyna, L.A. and Kupletskaya, N.B., *Primenenie UF, IK i YaMR spektroskopii v organicheskoi khimii* (The Use of UV, IR, and NMR Spectroscopy in Organic Chemistry), Moscow: Vysshaya Shkola, 1971.
4. Nakanishi, K., *Infrared Absorption Spectroscopy*, Tokyo: Nankido, 1962.
5. Korshak, V.V. and Vinogradova, S.V., *Ravnovesnaya polikondensatsiya* (Equilibrium Polycondensation), Moscow: Nauka, 1968.

Russian Journal of Applied Chemistry, Vol. 78, No. 5, 2005, pp. 830–833. Translated from Zhurnal Prikladnoi Khimii, Vol. 78, No. 5, 2005, pp. 846–850.
Original Russian Text Copyright © 2005 by Uspenskaya, Sirotinkin, Yatsenko, Masik.

MACROMOLECULAR CHEMISTRY AND POLYMERIC MATERIALS

Formulations Based on Hollow Glass Spheres and Polyurethane Foams

M. V. Uspenskaya, N. V. Sirotinkin, S. V. Yatsenko, and I. V. Masik

St. Petersburg State University of Information Technology, Mechanics, and Optics, St. Petersburg, Russia
St. Petersburg State Technological Institute, St. Petersburg, Russia

Received September 14, 2004; in final form, March 2005

Abstract—Formulations based on hollow glass spheres and polyurethane foams were obtained and studied. The positive influence exerted by an inorganic filler, which improves the strength and heat resistance of the formulations and makes lower the probability of process defects in their application in heat networks and in building, was examined.

At present, polyurethane foams (PUFs) are rather well studied materials, which are widely used in various areas of science and engineering for more than 50 years. Depending on a particular application field, PUFs successfully compete with metals, plastics, rubbers, or other materials [1–3].

Rigid PUFs are widely used in world's building industry owing to their good characteristics and convenience in manufacture and application. The main requirements to PUF as a construction material are its heat heat resistance, high softening point, minimum density combined with high compression and bending strength, light fastness, and convenience of deposition by pouring or spraying.

The last achievement in this field is a polyurethane heat insulation combined with a surface waterproofing layer [4], which has such advantages as low thermal conductivity and density and high reliability during a prolonged service life.

At the same time, PUFs have a number of disadvantages, such as combustibility, necessity for additional surface protection, poor adhesion to shell materials, comparatively low compression strength, etc., which cannot be eliminated within the existing technology.

At present, intensive studies are being carried out in order to improve the physicomechanical and working properties of PUF-based materials. The main ways to control the properties of both rigid and elastic PUFs are chemical modification of the raw material used to obtain PUF and production of various composites [5].

The strength properties of formulations are largely determined by the type of filler. The cellular structure of PUF enables its combination with powdered solid materials, which improves the physicomechanical characteristics, diminishes the production cost, and creates a predictable inhomogeneity in the bulk of an article.

On the whole, the filler is a powerful tool for controlling the service characteristics, which is frequently used in those cases when the construction resources of the polymeric matrix are already exhausted. For example, to impart enhanced strength properties to a PUF, inorganic fillers with a high strength, such as sand, concrete, and glass, are introduced into the material (mostly into a rigid heat-insulating PUF) [6]. This also improves the fire safety of the material. The physicomechanical properties of polyurethanes can be improved by their filling with a dispersed quartz filler, with the strongest effect achieved in use of quartz with organosilicon glaze deposited on its surface [7].

Table 1 lists data characterizing the basic parameters of PUFs and a number of other, most widely used materials, e.g., those insulating steel heat-transfer pipes.

All rigid PUFs used as heat-insulating materials have low thermal conductivity, the best among other materials serving for similar purposes [8]. Along with the advantages of use of filled PUF for heat insulation, there also exist disadvantages: highly filled systems have a PUF density higher by an order of magnitude, which leads to an increase in the mass of heat insulation and to a higher thermal conductivity.

This study is devoted to production and study of formulations based on polyurethanes and hollow

1070-4272/05/7805-0830© 2005 Pleiades Publishing, Inc.

Table 1. Comparative properties of heat-insulating materials

Parameter	Foam stone concrete	Reinforced foam concrete	Bituminous perlite	Phenol plastic foam	Polyurethane foam
Density, kg m^{-3}	400–500	350–450	450–550	100	80
Strength, MPa:					
compression	2.5	0.8	0.5	0.56	0.2
bending	2.5–5.0	0.2–0.3	0.2	0.51	–
Adhesion to a steel pipe, MPa	0.4–0.6	0.007–0.1	–	0.046	0.3–0.5
Thermal conductivity, W m^{-1} K^{-1}	≤0.08	0.09–0.116	0.116–0.14	0.047	0.02–0.04
Maximum water absorption capacity at 20°C:					
wt %	≤15–23	95	81–102	80–140	55
in 30 days, vol %	5–10	52–55	30–38	60	–
True heat loss (compared with rated values), %	Lower by 20–30	Higher by 20–40	Higher by 20–40	Higher by 16	No data
Heat resistance, °C	150	≤500	≤130	≤150	≤190
Service life, years	30	15	8	15	30
Anticorrosion coating on a pipe to be heat insulated	None	Required	Required	Required	None

spheres used as fillers in order to eliminate some of the disadvantages mentioned above.

EXPERIMENTAL

Hollow glass spheres (GSs)[1] contain air and have a density of 140 kg m^{-3} and diameter of 140–160 μm, and, therefore, they must not lead to a significant increase in density.

The glass spheres were introduced into rigid PUF in amounts of 7, 11, 13, 15, and 28 wt %, relative to the block mass. Polyurethane foams were obtained using the spraying technique [1], with a binary Izolan 101 system used. Component A is A 1-17 N-1 manufactured by Izolan Open Joint-Stock Company (Vladimir), and component B is polyisocyanate of B brand. The components used in preparing the polyurethane foam system were taken in a 1 : 1 ratio.

In the case of concentrations in the range 0–15 wt %, GSs were introduced into component A, with the resulting mass thoroughly mixed so that the system remained stable for 4 h. The limiting content of GSs in component A corresponds to 15 wt % in the block, and, therefore, to raise their total content, GSs were introduced into both components: 15 and 13 wt % in components A and B, respectively.

[1] Supplied by NTS Ltd., St. Petersburg.

The kinetic parameters of foaming (times of onset, gelation, and foam rise) were monitored with a stopwatch. The samples were kept from the instant of fabrication to tests for no less than 24 h at 20°C.

The failure compression stress was determined in conformity with GOST (State Standard) 46 451–82 on a ZWICK-1445 tensile machine. In view of the construction features of the device, the test sample dimensions were 20 × 20 × 20 mm. The compression rate was 100 mm min^{-1}. The measurement error was ±0.03 MPa.

The apparent density was determined by the procedure prescribed by GOST 409–77. The error in determining the apparent density was ±0.5 kg m^{-3}.

The thermal conductivity λ (W m^{-1} K^{-1}) was determined by measuring the density of a stationary heat flux in a monotonic heating mode on an ITP-MG4 device in accordance with the operation manual. The measurement range was 0.04–0.8 W m^{-1} K^{-1}. The dimensions of the samples used were 100 × 100 × 20 mm. The thermal conductivity was found using the built-in calculating unit of the device with an error of ±0.002 W m^{-1} K^{-1}.

Table 2 illustrates the influence exerted by GSs on process parameters in spraying. It can be seen that, in mixing of filled components A and B in the presence of GSs, the onset and gelation times remain constant,

Table 2. Influence exerted by glass spheres on process parameters in spraying. Onset time 4–5 s, gelation time 15–20 s

GS content, wt %	Viscosity, mPa s, of indicated component		Curing time, min	PUF density, kg m^{-3}
	A	B		
0	440	600	25	51
7	4000	600	25	51.5
10.5	6000	600	25	52
13	8000	600	20	55
15	12 000	600	10	65
28	12 000	12 000	10	75

i.e., glass spheres act as an inert additive with respect to the macrokinetic parameters of foaming.

Viscosity measurements at different contents of GSs demonstrated that the rising curve follows the Chong–Christiansen dependence (Fig. 1), in which a characteristic point for monodisperse fillers is the filler content of 62 vol %. At a higher volume fraction, an asymptotic rise in viscosity is expected and motion in the system requires an extreme shear force.

As the content of hollow spheres becomes two times higher, the curing time of the system decreases

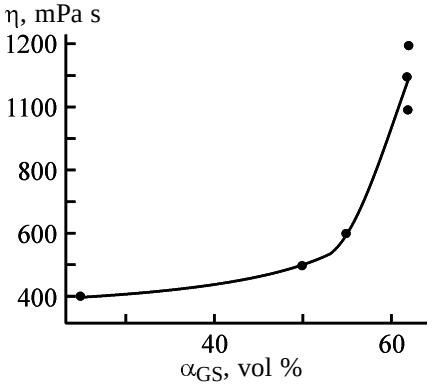


Fig. 1. Viscosity η of the formulation vs. the volume fraction α_{GS} of glass spheres.

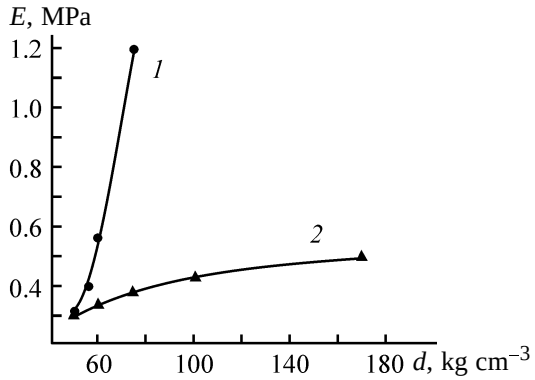


Fig. 2. Strength *E* vs. density *d* of PUF. PUF: (*1*) filled with glass spheres and (*2*) unfilled.

by a factor of 2.5, which indicates that the polymer cross-linking processes are accelerated.

Presumably, an increase in the area of contact with the material of glass spheres is important in the stage of formation of the final structure of polyurethane. It may be assumed in this case that the polyurethane structure in the surface adhesion–solvation layer differs from that in the bulk. The surface of glass spheres exerts an orienting influence on the structure of macromolecules:

$$V = V_{FVPU} + V_{ASLPU} + V_g,$$

where V is the total volume of the polymer binder; V_{FVPU}, free volume of polyurethane; V_{ASLPU}, volume of polyurethane in the adhesion–solvation layer; and V_g, gas volume.

As the content of glass spheres increases, the fraction of the polymer filler adsorbed on the surface grows.

It is known that use of fillers in foamed polymers yields articles that are nonuniform in density: the properties of the surface, crust layer differ from those in the bulk. The composite material based on PUF and hollow glass spheres, obtained in this study, is virtually isomorphic. It was found in determining the density of the casting sample with 12 wt % GS that samples taken at 10, 25, and 40 mm from the mold bottom have the same density of 60 kg m^{-3}.

The influence exerted by the density of unfilled and filled PUF on their strength varies (Fig. 2). As the density of a GS-filled PUF increases, the strength grows considerably faster and reaches markedly higher values. This fact can also be accounted for in terms of the theory of an adsorption–solvation interaction. Depending on the content of glass spheres, the structure of the formulations can be represented as follows (Fig. 3).

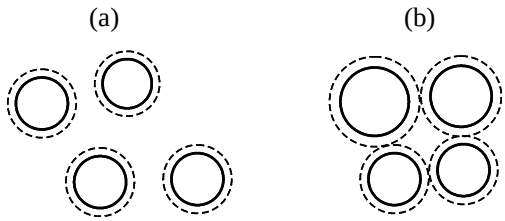


Fig. 3. Structure of a formulation based on PUF with glass spheres. Content of glass spheres (wt %): (a) <10 and (b) 10–30.

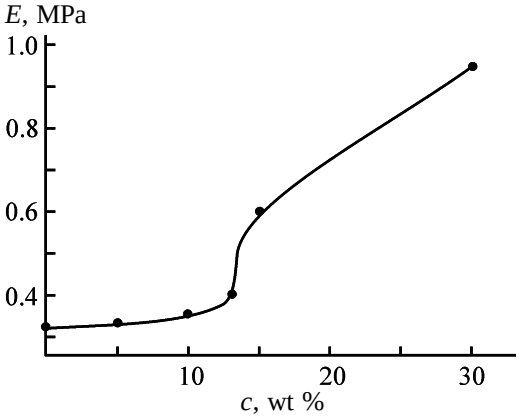


Fig. 4. Compression strength E of the formulation vs. filler content c.

Figure 4 shows how the compression strength of the polymers depends on the filler content. It can be seen that filling of PUF with hollows glass spheres leads to a significant increase in the compression strength of the polymer, especially at high contents. As the content of GS is raised from 5 to 13 wt %, the strength of the formulation under study steadily increases to 0.4 MPa; in the range 13–15 wt % filler, the strength steeply increases to 0.6 MPa; and in the range 15–20 wt % GS, the strength steadily grows to 0.95 MPa.

At a GS content lower than 5 wt %, the formulation properties are not modified to a sufficient extent, whereas in the case of GS present in amounts exceeding 30 wt %, spraying becomes impossible and the kinetics of casting significantly changes because of the high viscosity of the system.

It was shown that the thermal conductivity of an PUF-based composite material with 13 wt % GS is 0.06 W m^{-1} deg^{-1} at 20°C, and its bending strength, 2.5 MPa.

Thus, development of filled formulations based on PUF with an inorganic filler makes it possible to raise the strength and thermal resistance, diminish the probability and number of technological defects, ensure operation of heat-transfer networks at a temperature of the heat-carrying agent of up to 150°C, and make lower the moisture absorption, with the corrosion-protection properties of the coatings simultaneously improved.

CONCLUSIONS

(1) Hollow glass spheres are an inert additive with respect to the macrokinetic parameters of foaming of polyurethane foam, because the onset and gelation times remain unchanged.

(2) Raising the content of glass spheres in a polyurethane foam formulation accelerates formation of a network polymer.

(3) The composite based on polyurethane foam and glass spheres is virtually isomorphic and has a density of 60 kg m^{-3}, which expands the areas of its possible application.

(4) Filing of polyurethane foams with glass spheres leads to a considerable increase in the compression strength of the polymer from 0.32 to 0.95 MPa, and the bending strength is 2.5 MPa, which means that polyurethane foam materials with improved physicomechanical properties can be obtained.

REFERENCES

1. Reinhard, C., *Kunststoffe*, 1999, vol. 89, no. 10, pp. 162–168.
2. Gafiyatullin, R.V. and Zabelin, L.V., Abstracts of Papers, *Pervaya Ural'skaya konferentsiya "Poliuretany i tekhnologii ikh pererabotki"* (First Ural Conf. "Polyurethanes and Techniques for Their Processing"), Perm, 1995, p. 4.
3. Schluppkotten, J., Paßmann, K.-W., Kath, H., and Maier, M., *Kunststoffe*, 1998, vol. 88, no. 2, pp. 2176–2178.
4. Renders, J., *Urethanes Technol*., 1999, vol. 16, no. 3, p. 45.
5. Reilly, C.B. and Orchin, M., *Ind. Eng. Chem. Res*., 1956, vol. 48, pp. 59–60.
6. RF Patent 2123013.
7. Shandruk, M.I. and Kostyuk, L.I., *Ukr. Khim. Zh*., 2000, vol. 66, nos. 1–2, pp. 62–64.
8. *Khimicheskaya entsiklopediya* (Chemical Encyclopedia), Knunyants, I.L., Ed., Moscow: Sovetskaya Entsiklopediya) 1988, vol. 4.
9. US Patent 4246146.

Russian Journal of Applied Chemistry, Vol. 78, No. 5, 2005, pp. 834–838. Translated from Zhurnal Prikladnoi Khimii, Vol. 78, No. 5, 2005, pp. 851–855.
Original Russian Text Copyright © 2005 by Syroezhko, Pankova, Korchemkin, Otchayannyi, Proskuryakov.

MACROMOLECULAR CHEMISTRY AND POLYMERIC MATERIALS

Softeners for Rubber Based on Shale Thermal Dissolution Products

A. M. Syroezhko, Ya. I. Pankova, S. N. Korchemkin, N. N. Otchayannyi, and V. A. Proskuryakov

St. Petersburg State Technological Institute, St. Petersburg, Russia

Received January 19, 2005

Abstract—The source of raw materials for manufacturing softeners for rubber is extended through applying a nonwaste process of thermal dissolution of ordinary or enriched shale in crude producer-gas tar. The resulting products are less expensive than the conventional high-melting oil asphalts and oils.

Progress in the rubber industry is determined to a considerable extent by extension of the source of raw materials, i.e., by broadening of the spectrum of the products used. In production of elastomers, the weak point is a limited spectrum of softeners. Among the commonly used products of this type are asphaltic tar softeners, specialty bitumens, etc. Their introduction into rubber stocks allows control of the most important performance characteristics of rubber stocks and finished articles such as rubber-to-cord adhesion, ozone resistance, and abradability. These products serve also as dispersants for rubber stock components and as reinforcing agents.

Virtually the only source of softeners of this type is deep processing of oil. The rubber and tire industries are large-scale consumers of high-molecular-weight petroleum products such as PN-5 oil, black oils, tars, Rubraxes, and other asphaltic tar products. These softeners (plasticizers) demonstrate wide action spectrum: they reduce the shrinkage in calendering and extrusion molding of rubber stocks, improve the strength and heat resistance of rubber, and impart moisture resistance and solidity to finished articles [1, 2]. It was suggested that such products could be obtained from sapropelic coals, among them shales, whose reserves are huge.

In this study we examined the possibility of preparation of shale-oil bitumens by thermal dissolution of ordinary or enriched shales in shale-oil producer-gas tar and also of their use as softeners for rubber. Since bituminous softeners are used to improve performance characteristics of heavily extended elastomers and rubber stocks with a polymer body from rubber reclaim and SKD butadiene rubber, an associated task was to improve performance of the composites by introducing the indicated softeners, thus extending their application range.

Low branching of the macrochains and only slight temperature dependence of the viscosity of SKD cause its high cold flow in storage and transportation [3]. The processibility of SKD is characterized by its millability, estimated from the critical roll opening (mm). The millability of SKD ranges from 0.5 to 2 mm, depending on the molecular-weight distribution and polydispersity.

EXPERIMENTAL

Crude producer-gas tar and ordinary Baltic shale or enriched shale (Kerogen-70) (all the products from the Slantsy Works, Joint-Stock Company) were charged in 1 : 1 or 2 : 1 weight ratio into a three-necked flask equipped with a stirrer, electric heater, and outlet system for removal of liquid thermal dissolution products. The mixture was heated with continuous stirring for a fixed time (Table 1).

The effect of shale-oil bitumens A, B, and C (plasticizers) on properties of rubber stocks was studied in comparison with commercial plasticizers [bitumen BN-IV and bitumen G (Ukhta refinery)]. The characteristics of the plasticizers studied are summarized in Table 2.

The viscosity and tendency to scorching of the rubber stocks were determined with a Mooney viscometer according to GOST (State Standard) 10722–76. The tensile strength f_z, relative elongation (ε_z), and elongation set (θ) were determined on a tensile-testing machine (GOST 270–75).

1070-4272/05/7805-0834© 2005 Pleiades Publishing, Inc.

Table 1. Conditions of preparation of shale-oil bitumens

Shale-oil bitumens	Tar to shale weight ratio	T, °C	τ, h	Yield of shale-oil bitumen, wt %
A	1 : 1 (ordinary)	370	0.3	68.5
B	2 : 1 (ordinary)	360	0.67	56.6
C	1 : 1 (Kerogen-70)	400	0.17	52.6

Table 2. Characteristics of plasticizers

Characteristic	Bitumen G	BN-IV	A	B	C
Softening point, °C	132	>75	59	51.8	138
Penetration at 25°, 0.1 mm	2	32	30	109.8	1.5
Ash content, %	<0.2	Not determined	14.3	15.1	29.1

Table 3. Softener effect on the viscosity and initial vulcanization of rubber stocks at 140°C*

Characteristic	Ch-0 (no plasticizer)	Ch-G	Ch-BN	Ch-A	Ch-B	Ch-C
Mooney viscosity, arb. units	45	43	40	42	42	42
t, min	19	46	34	27	29	26
t_c, min	23	50	37	30	33.5	29

* The rubber stock designations reflect the filler (Ch = chalk) and plasticizer.

The Shore hardness of the rubbers *A* was determined according to GOST 263–75. The thermal aging tests were performed according to GOST 9.024–74 and swelling tests, according to GOST 9.030–74. The softening points of the softeners were determined according to GOST 11506–73; penetration (needle penetration depth), according to GOST 11501–78; and ash content, according to GOST 11512–65.

SKD rubber is characterized by high elasticity, frost resistance, and durability. It is widely used in various rubber stocks, including those for tire production. However, its processing characteristics are extremely unsatisfactory, so that, to improve them, bitumen plasticizers are always added into composites.

Rubber stock preparation procedure using a laboratory roll mills included two steps. First, mother stock, containing rubber and all other ingredients except for a softener and a filler (chalk), was prepared. The mother stock content was as follows (wt %): SKD 100, sulfur 2, sulfenamide C 0.7, zinc oxide 5, and stearin 2. Secondly, chalk (50 wt % relative to SKD) and a softener (5 wt %) were introduced into the mother stock.

In preparing the rubber stocks, all the tested softeners demonstrated a positive effect on the performance characteristics of the SKD-based rubber stocks.

It was demonstrated in rolling the rubber stocks that the critical roll opening increased from 0.5 to 2 mm. Bitumen G only slightly affected the millability of the rubber stocks because of its nonuniform distribution. Bitumen BN-IV improved the millability, but to a lesser extent as compared to shale-oil softeners. Shale-oil bitumens A and B have relatively low softening points, and they soil the rollers. The preparation time of rubber stocks with the indicated softeners increases as compared to that with the use of the most manufacturable high-melting shale-oil bitumen C (it does not soil the rollers and decreases the process duration by 30–40% in the absence of a plasticizer).

All the bitumens under examination demonstrated high plasticizing effect, decreasing the minimal viscosity of the resulting rubber stock (Table 3). The highest effect was observed with BN-IV. The plasticizing effect of all the softeners tested was approximately the same. The examined plasticizers exert a decelerating effect in the initial vulcanization stage, i.e., on the inductive period t and the period of the initial process rate t_c. Evidently, the differences in t and t_c can be attributed to different content of functional polar groups in oxidized oil asphalts and less oxidized shale-oil bitumens.

The plasticizer effect on the tensile strength f_z,

Table 4. Characteristics of vulcanizates

Rubber	f_z, MPa	ε_z, %	θ, %	Shore hardness, *A*, arb. units
Ch-0 (no plasticizer)	1.3	220	6	54
Ch-G	1.4	170	3	52
Ch-BN	1.4	200	3	52
Ch-A	1.3	190	4	48
Ch-B	1.3	250	3	52
Ch-C	1.4	270	4	49

Table 5. Effect of the content of bitumen C on the viscosity and initial vulcanization of rubber stocks at 140°C

Characteristic	Ch-0	Ch-5	Ch-10	Ch-15	Ch-30
Plasticizer content, wt %	–	5	10	15	30
Mooney viscosity, arb. units	95	89	84	85	54
t, min	19	26.5	34	42	52
t_c, min	26	32	42.5	50.5	67.5

relative elongation (ε_z), and elongation set (θ) of vulcanized rubbers is shown in Table 4. The best results were obtained with shale-oil bitumen C, which provided the highest relative elongation of the vulcanizate, the tensile strength being well comparable with other softeners. The use of bitumen softeners is often aimed at reducing the water absorption in vulcanizates. All the softeners studied reduced the swellability of the vulcanizate in water. In the rubbers prepared without plasticizers, after keeping in water, the weight increased by 2%, and in the rubbers with the indicated softeners, it decreased by up to 1% in 20 days. However, the weight of the rubber with plasticizer C remained practically unchanged even after long-time contact with water (weight loss 0.01–0.02%). Thus, plasticizer C imparts good performance characteristics to rubber stocks.

Addition of this plasticizer to the standard SKD-based rubber stock containing 50 wt % P-324 carbon black improved the performance characteristics of the product. After adding 5 wt % of the plasticizer, the critical roll opening was 2 mm, allowing ready manufacture of the rubber stock. Increase in the plasticizer content to 15 wt % did not deteriorate the performance of the rubber stock. At a 30 wt % content, we observed sticking of the rubber stock, which increased the time of its preparation. The effects of the content of bitumen C on the viscosity and initial vulcanization of rubber stocks were determined at 140°C by the standard method using a Mooney viscometer (Table 5).

As in the case of chalk-filled rubber stocks, introduction of bitumen C reduces the minimal viscosity of the product and decelerates the initial vulcanization step. With increasing plasticizer content, the induction period *t* regularly increases, the initial vulcanization rate decreases, and t_c grows. The observed abrupt decrease in the minimal viscosity of the rubber stock at a plasticizer content of 30 wt % is due to the fact that, at 140°C, the plasticizer is in the fluid state, and its amount is in excess relative to that sufficient to impregnate the solid components (note that the safety of rubber stock processing increases in parallel to the plasticizer content). However, these trends could result in a longer time required for vulcanization and attainment of the optimal mechanical characteristics of the vulcanizate by virtue of deceleration of the process in the major stage. Since the maximal decelerating effect was observed at a plasticizer content of 15 wt %, we prepared rubber stocks filled with carbon black without or with the indicated content of the plasticizer. Evolution of the mechanical characteristics of the rubber in the course of vulcanization of the indicated rubber stocks is shown in Fig. 1.

Introduction of the plasticizer only slightly affects the vulcanization rate. However, the softener effect on the performance of vulcanized rubbers is significant. Thus, the strength increases remarkably, regardless of the vulcanization mode, as well as the relative elongation and elongation set, as compared to unplasticized rubbers. The hardness index of plasticized rubbers depends on the vulcanization time, but it only slightly changes after reaching the optimal value (20 min). The plasticizer content influences the strength and hardness of rubber (Fig. 2, curves *1*, *2*) and relative elongation and elongation set (curves *3*, *4*). With increasing the plasticizer content to 30%, the strength and elasticity of vulcanizates increased. However, this is accompanied by an increase in the residual deformation, which is especially pronounced at high plasticizer content. The dependence of the hardness on the plasticizer content is represented by a curve with a maximum. The water absorption in plasticized products does not exceed that in the initial rubber stock.

Therefore, the recommended content of plasticizer C in vulcanizate is 10–15 wt %. The drawback of SKD-based rubbers is low vulcanization rate. Shale-oil bitumen C accelerates vulcanization, the effect being more clearly pronounced with the use of a

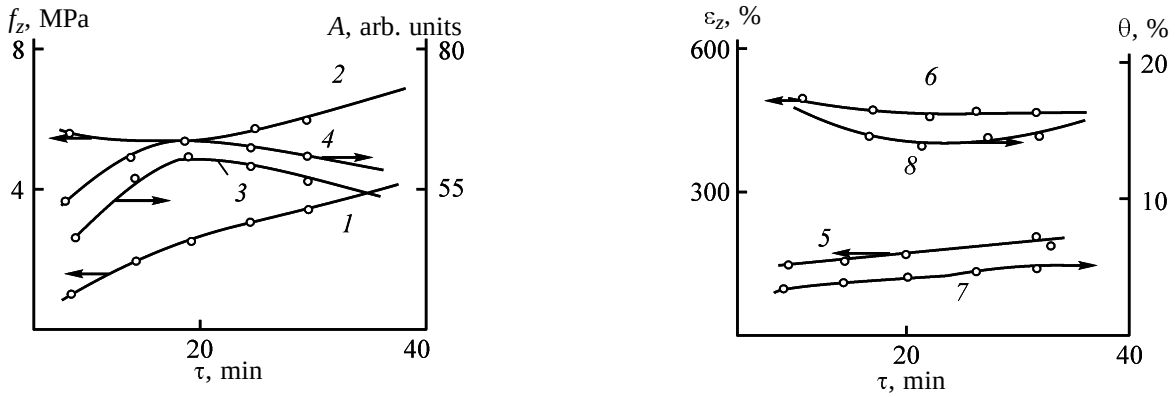


Fig. 1. (*1*, *2*) Tensile strength f_z, (*3*, *4*) Shore hardness A (arb. units), (*5*, *6*) relative elongation ε_z, and (*7*, *8*) elongation set θ of vulcanized rubber as functions of the vulcanization time. (*1*, *4*, *5*, *7*) C-0 and (*2*, *3*, *6*, *8*) C-15.

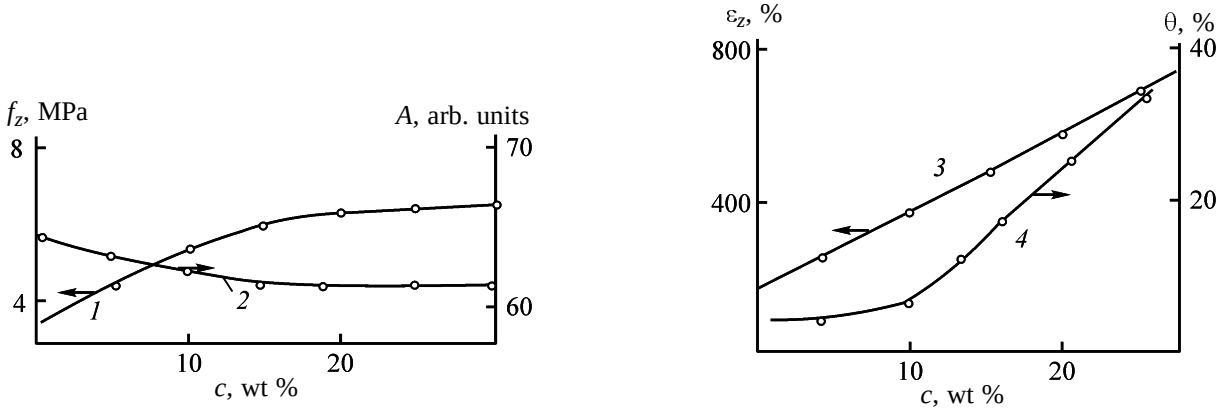


Fig. 2. (*1*) Tensile strength f_z, (*2*) Shore hardness *A*, (*3*) relative elongation ε_z, and (*4*) elongation set θ of vulcanized rubber as functions of the shale-oil bitumen content *c*.

modified plasticizer. To the rubber stock containing 10 wt % shale-oil bitumen C, we introduced tetramethylthiuram disulfide (TMTD) as a rubber accelerator in amount of 0.5–1.3 wt %. The characteristics of the resulting products are given in Table 6.

Increase in the activity of a rubber accelerator reduces the elasticity and elongation set of vulcanizates and increases the hardness. The tensile strength increases at small accelerator contents, and decreases at high contents, which is probably due to too high density of the resulting 3D structure and decrease in the capability of the macrochains for spatial orientation, as demonstrated by the decrease in the relative elongation in the rubber.

CONCLUSIONS

(1) High-melting shale-oil bitumen obtained by thermal dissolution of enriched shale in crude producer-gas tar is an efficient softener for rubber stocks based on SKD rubber filled with chalk, improving their millability and uniformity of distribution. The elasticity of rubbers with such a softener is higher than that with standard softeners, petroleum bitumens G and BN-IV.

(2) At optimal content of shale-oil bitumen (10–15 wt %), SKD-based carbon-filled rubber stocks with the desired critical roll opening can be produced without technological problems. In this case, the strength of the products increases by 25–100%; the relative

Table 6. Mechanical properties of vulcanized rubbers obtained using the rubber accelerator

TMTD content, wt %	Vulcanization time, min	f_z, MPa	ε_z, %	θ, %	Shore hardness *A*, arb. units
0.5	20	7.2	180	2	70
1.3	10	4.8	110	1	64
1.3	20	4.9	115	1	69
1.3	30	5.0	130	1	71

elongation, by a factor of 2–3; and the elongation set remains practically unchanged.

(3) Low-ductile high-melting shale-oil bitumen obtained by thermal dissolution of Kerogen-70 in crude producer-gas tar could be recommended for industrial application.

REFERENCES

1. Koshelev, F.F., Kornev, A.E., and Bukanov, A.M., *Obshchaya tekhnologiya resiny* (General Technology of Rubber), Moscow: Khimiya, 1978.
2. Sobolev, V.M. and Borodina, I.V., *Promyshlennye sinteticheskie kauchuki* (Commercial Synthetic Rubbers), Moscow: Khimiya, 1977.
3. Litvinova, T.V., *Plastifikatory dlya resinovogo proizvodstva* (Softeners for Rubber Production), Moscow: TsNIITEneftekhim, 1981.
4. Bodan, A.N. and Kostyk, B.L., *Asfal'teno-smolistye veshchestva – ingredienty rezinovykh smesei* (Asphaltic Tar Compounds as Ingredients of Rubber Stocks), Moscow: TsNIITEneftekhim, 1987.

Russian Journal of Applied Chemistry, Vol. 78, No. 5, 2005, pp. 839–842. Translated from Zhurnal Prikladnoi Khimii, Vol. 78, No. 5, 2005, pp. 856–859.
Original Russian Text Copyright © 2005 by Krul', Ivanova, Yakimtsova, Grinyuk.

MACROMOLECULAR CHEMISTRY AND POLYMERIC MATERIALS

Water-Soluble Polymers of Acrylamide as Labeling Adhesives

L. P. Krul', T. A. Ivanova, L. B. Yakimtsova, and E. V. Grinyuk

Belarussian State University, Minsk, Belarus

Received January 19, 2005

Abstract—The adhesive and rheological properties of high- and low-molecular-weight polyacrylamides and the products of their partial hydrolysis were studied. The suitability of the hydrolyzates of high-molecular-weight polyacrylamide as labeling adhesives in the glass–paper system was elucidated.

A major proportion of the labeling adhesives used for gluing paper labels to glass containers is accounted for by aqueous polymeric adhesives [1]. An important place among them is occupied by water-soluble copolymers of acrylamide (AA) with sodium acrylate, prepared by base hydrolysis of waste from polyacrylonitrile fiber production [2, 3]. However, the molar ratio of the acrylamide to acrylate units in the macromolecule of such copolymers, capable of modifying their adhesive properties, can be varied within very narrow range only (from 0.25 : 0.75 to 0 : 1) [4–6]. The reason is that a solid fiber can pass into solution only at high concentrations of the hydrolyzing agent. At the same time, hydrolysis of water-soluble polyacrylamide (PAA) allows preparation of a copolymer with the desired ratio of the acrylamide to acrylate units [7]. This makes possible preparation of labeling adhesives on the basis of partially hydrolyzed PAA (HPAA) with easily controllable adhesive properties. Water-soluble polymers of AA, including HPAA along with PAA proper, are capable of gluing together polar substrates, in particular, paper and glass [7]. However, the properties making these polymers suitable as labeling adhesives were studied to a lesser extent than the properties of hydrolyzates of polyacrylonitrile fibers [8–10].

In this study, we examined the adhesive properties of PAA and HPAA with various molecular weights, hydrolyzed to various degrees, in the glass–paper system.

EXPERIMENTAL

For synthesis of PAA we used AA available from REANAL (Hungary) with 98.7% main substance. The synthesis was run in 7% aqueous solutions of the monomer using the ammonium peroxodisulfate–sodium sulfite redox initiating system. The molecular weight (MW) of PAA was controlled by varying the total concentration of the components of the redox system and the component ratio in it. Base hydrolysis of PAA was conducted in 7% aqueous solutions of the polymer at their boiling point for 3 h at various ratios of the amounts of the polymer and NaOH. For procedures of the PAA synthesis and base hydrolysis of the polymer synthesized, see [11].

The viscosity-average MW was determined viscometrically. The specific viscosity was measured in a suspended-level Ubbelohde capillary viscometer with a capillary diameter of 0.86 mm at 25°C.

The adhesive properties of the solutions in the glass–adhesive–paper system were determined by the known procedure [12, 13] on an RMU-0.05-1 tensile-testing machine. After the paper was glued to glass, the sample was maintained at room temperature, whereupon the shear strength of the glue joint was determined. The time of keeping of the sample after gluing was 1, 2, 3, 5, 10, and 20 min. Simultaneously with the strength of the glue joint we determined the character of its failure.

The dynamic viscosity of the solutions was determined at 20 ± 0.1 °C on a Rheotest 2 rotary viscometer with the cylinder–cylinder working unit.

The quality of polymeric adhesives for the glass–paper system is determined, above all, by the character of failure of the glue joint. It is known that conventional labeling adhesives finding wide commercial application should provide a paper–glass joint so strong that, at attempted break of the glue joint after drying of the adhesive, the failure occurs across the paper texture [7]. Also, it is necessary that, before drying of the adhesive, the label will not come off from the glass surface, which is achieved through

1070-4272/05/7805-0839© 2005 Pleiades Publishing, Inc.

Kind of failure of the paper–glass glue joint as dependent on the nature of the AA polymer and time of keeping of the sample after gluing*

Polymer	PAA : NaOH, mol : mol	$-CONH_2$: –COONa	Solution concentration, %	Time after gluing, min					
				1	2	3	5	10	20
PAA HMW	–	1 : 0	7	A	A	A	A	A	A
HPAA HMW	1 : 0.2	0.70 : 0.30	7	B	A	A	A	A	A
	1 : 0.5	0.46 : 0.54	7	B	A	A	A	A	A
	1 : 0.7	0.31 : 0.69	7	B	B	B	A	A	A
	1 : 0.7	0.31 : 0.69	16	B	B	A	A	A	A
PAA LMW	–	1 : 0	7	C	C	C	C	C	C
HPAA LMW	1 : 0.2	0.75 : 0.25	7	C	C	C	C	C	C

* Failure: (A) cohesion, across the paper texture; (B) cohesion, across liquid adhesive; and (C) adhesion, at the glass–adhesive on paper interface.

the use of high-viscosity adhesives exhibiting non-Newtonian flow. It was noted earlier [7] for adhesives based on copolymers of AA with sodium acrylate, prepared by base hydrolysis of polyacrylonitrile fibers, that, at brief times of keeping after gluing (up to 5 min), the glue joint fails by the cohesion mechanism across the liquid adhesive, and at longer time periods, across the paper texture, which makes these adhesives suitable for labeling.

The tabulated data suggest the cohesion mechanism of failure of the glue joint across the paper texture even 1 min after gluing, when a high-molecular-weight PAA (PAA HMW) is used as adhesive. When adhesives from PAA HMW hydrolyzates are used, the glue joint can fail across both the liquid adhesive and the paper, depending on the time of keeping of the sample since gluing till testing. The time of keeping of the glue joint, required for changing from the failure across the liquid adhesive to that across the paper, is much smaller (1–3 min) in the case of PAA HMW hydrolyzates compared to adhesives from hydrolyzates of polyacrylonitrile fibers [7].

Whatever the time of keeping of the glued sample, for low-molecular-weight PAA (PAA LMW) and hydrolyzates of PAA LMW (HPAA LMW) failure of the glue joint follows the adhesion mechanism at the glass–adhesive interface. Without the stage of failure of the glue joint across the liquid adhesive, the use of PAA LMW and HPAA LMW as labeling adhesives is problematic, as labels easily come off from glass containers, especially when high-speed automatic devices are used.

With HPAA HMW as labeling adhesives, the ratio of the acrylamide to acrylate units in the macromolecule affects, above all, the period from formation of the glue joint till application of the shear load, in which the mechanism of its failure changes. For unhydrolyzed PAA HMW, this period is less than 1 min (approximately 15 s), for HPAA HMW with the $CONH_2$: COONa ratio of 0.70 : 0.30 and 0.46 : 0.54, 1–2 min, and for HPAA HMW with the $-CONH_2$: –COONa– ratio of 0.31 : 0.69, 2–3 min. Thus, the time of setting of the adhesive increases with increasing degree of hydrolysis.

The strength of the paper–glass glue joint in all cases is enhanced with increasing period between formation of the glue joint and the shear tests and reaches a limiting value within 10–20 min, corresponding in the case of PAA HMW and HPAA HMW to the dry paper strength (Figs. 1a, 1b). For PAA LMW and HPAA LMW, the limiting strength is half that for the high-molecular-weight analogs. However, the strengths of different adhesives correspond to different kinds of failure mechanisms. In the case of the initial, unhydrolyzed PAA HMW, paper fails at shear even within 1 min after gluing. Low strengths are due to a high content of water in paper. With increasing period between applying paper to glass and beginning the tests, the water from the glue joint evaporates through the capillary-porous system of paper, and the strength of paper, responsible for the strength of the glue joint, increases. For PAA HMW hydrolyzates, the observed shear strengths correspond to the strength of the adhesive for the periods when the glue joint fails across the liquid adhesive by the cohesion mechanism. With increasing period from gluing paper to glass till beginning the tests, it is paper, first wet and then dry, that fails.

Of much interest are the shear strengths of adhesives failing across the liquid adhesive. As regards

the adhesives tested in this study, this holds for HPAA HMW only. The shear strengths of the glue joints for HPAA HMWs, differing in the ratio of the acrylamide to acrylate groups in the macromolecules, were estimated at 6.2, 5.6, and 2.9 kPa at the $CONH_2 : COONa$ molar ratios of 0.70 : 0.30, 0.46 : 0.54, and 0.31 : 0.69, respectively, 1 min after formation of the glue joint, when the failure occurs across the liquid adhesive. Therefore, the adhesive properties of HPAA HMWs tend to deteriorate with increasing degree of hydrolysis.

Deteriorated gluing performance of HPAA HMWs with increasing degree of hydrolysis is due to a decrease in the viscosity of the solution. Figure 2 shows how the dynamic viscosity of HPAA HMWs varies with the shear rate. It is seen that, at small shear rates comparable with those in shear tests of the glue joints, the dynamic viscosity tends to sharply decrease with increasing degree of hydrolysis. With increasing degree of hydrolysis, the content of the carboxylate groups in the macromolecules tends to increase, thereby enhancing their mutual repulsion and decreasing the effective concentration of the sites of the fluctuation network of intermolecular contacts. As a result, intermolecular interaction in the liquid adhesive weakens, and the strength of the glue joint failing across liquid adhesive decreases.

The adhesive properties of HPAA HMW with a high content of acrylate groups can be improved by increasing the concentration of the polymer solution. For example, for HPAA with $CONH_2 : COONa$ = 0.31 : 0.69 mol : mol, an increase in the solution concentration from 7 to 16% substantially increases the solution viscosity and enhances intermolecular interaction, thereby significantly increasing the strength of the glue joint in the initial stage of its formation from 2.9 to 6.3 kPa.

CONCLUSIONS

(1) The kind of failure of the glue joint in the glass–paper system with water-soluble polymers of acrylamide as adhesives is governed by the molecular weight of the polymer and the degree of hydrolysis. For low-molecular-weight polyacrylamide and its hydrolyzates, the failure of the glue joint follows the adhesion mechanism at the glass–adhesive interface even in the initial stages of formation of the glue joint. At the same time, for high-molecular-weight polyacrylamide and its hydrolyzates, the failure of the glue joint follows the cohesion mechanism and occurs across the paper texture or liquid adhesive.

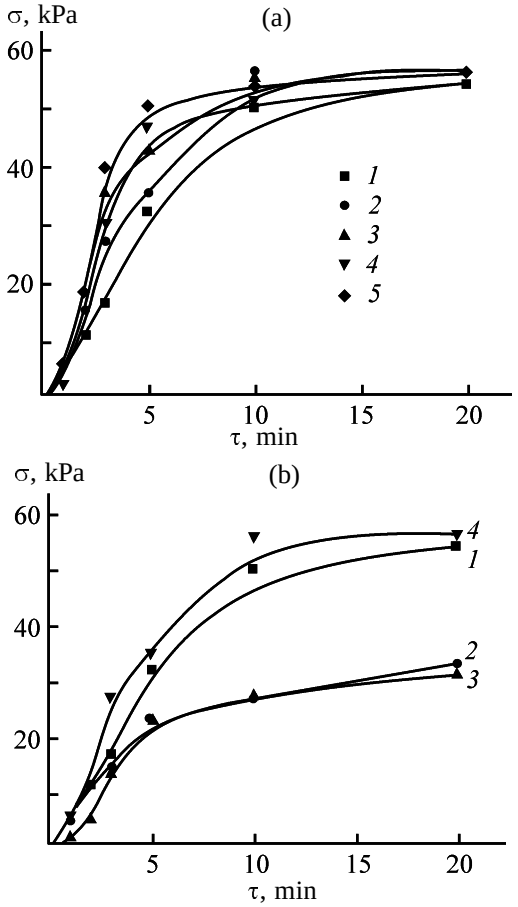


Fig. 1. Shear strength of the glue joint σ as a function of the time of keeping τ. (a) Polymer: (*1*) PAA HMW and (*2–5*) HPAA HMW. $–CONH_2 : –COONa$ molar ratio: (*2*) 0.70 : 0.30, (*3*) 0.46 : 0.54, and (*4, 5*) 0.31 : 0.69. Solution concentration, %: (*1–4*) 7 and (*5*) 16. (b) Polymer: (*1*) PAA HMW, (*2*) PAA LMW, (*3*) HPAA LMW, and (*4*) HPAA HMW. $–CONH_2 : –COONa$ molar ratio: (*3, 4*) 0.46 : 0.54. Solution concentration, %: (*1–4*) 7 and (*5*) 16.

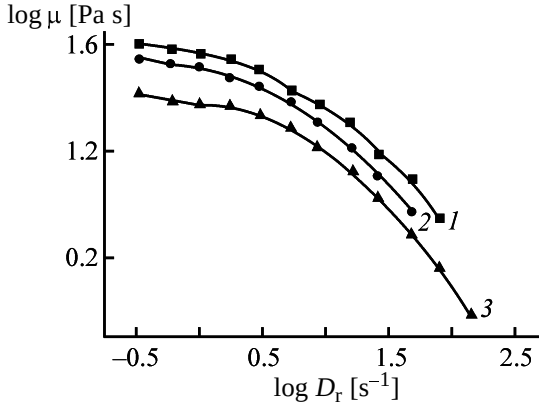


Fig. 2. Viscosity μ of 7% aqueous solutions of HPAA HMW as a function of the shear rate D_r. $–CONH_2 : –COONa$ molar ratio: (*1*) 0.70 : 0.30, (*2*) 0.46 : 0.54, and (*3*) 0.31 : 0.69.

(2) With increasing degree of hydrolysis of high-molecular-weight polyacrylamide, the period between formation of the glue joint and application of a shear load, within which the character of the glue joint failure changes from cohesion across the paper texture to cohesion across the liquid adhesive, increases. By contrast, the strength of the glue joint in the initial stage of its formation decreases, which correlates with a decrease in the dynamic viscosity of the adhesive.

(3) The adhesive properties of the high-molecular-weight polyacrylamide hydrolyzates are improved with increasing solution concentration.

REFERENCES

1. Freidin, A.S., *Polimernye vodnye klei* (Polymeric Aqueous Adhesives), Moscow: Khimiya, 1985.
2. Krul', L.P., *Tekhnol. Pererab. Upak.*, 2000, no. 1, pp. 15–17.
3. Krul', L.P., Brazhnikov, M.M., Brazhnikova, L.Yu., and Grinyuk, E.V., *Tekhnol. Pererab. Upak.*, 2002, no. 2, pp. 17–19.
4. Krul', L.P., Yakimtsova, L.B., Matusevich, Yu.I., and Krakodeev, D.V., *Izv. Nats. Akad. Nauk Bel., Ser. Khim. Nauk*, 2000, no. 1, pp. 103–105.
5. Krentsel, L.B., Kudryavtsev, Y.V., Rebrov, A.I., *et al.*, *J. Macromol. Sci*. A, 2001, vol. 34, no. 16, pp. 5607–5610.
6. Martinovich, V.I., Elinson, I.S., and Soldatov, V.S., *Izv. Nats. Akad. Nauk Bel., Ser. Khim. Nauk*, 2001, no. 4, pp. 39–43.
7. *Poliakrilamid* (Polyacrylamide), Kurenkov, V.F., Ed., Moscow: Khimiya, 1992.
8. Krul', L.P., Yakimtsova, L.B., Matusevich, Yu.I., *et al.*, *Mater. Tekhnol. Instr.*, 2000, vol. 5, no. 4, pp. 33–38.
9. Yakimtsova, L.B., Brazhnikov, M.M., and Krul', L.P., *Materialy 4-i mezhdunarodnoi nauchno-tekhnicheskoi konferentsii "Resursosberegayushchie ekotekhnologii: vozobnovlenie i ekonomiya energii, syr'ya i materialov"* (Proc. 4th Int. Scientific and Technical Conf. "Resource-Saving Ecotechnologies: Renewal and Saving of Energy, Resources, and Materials"), Sviridenko, A.I. and Mikhalevich, A.A, Eds., Grodno: Grodn. Gos. Univ., 2001, part 2, pp. 11–19.
10. Yakimtsova, L.B., Ivanova, T.A., Brazhnikov, M.M., and Krul', L.P., *Polimernye kompozity – 2000: Sbornik trudov mezhdunarodnoi nauchno-tekhnicheskoi konferentsii* (Polymeric Composites 2000: Coll. of Works of Scientific and Technical Conference), Gomel, 2000, pp. 197–201.
11. Krul', L.P., Ivanova, T.A., Yakimtsova, L.B., and Polikarpov, A.P., *Khimicheskie problemy sozdaniya novykh materialov i tekhnologii: Sbornik statei* (Chemical Problems of Development of New Materials and Technologies: Coll. of Papers), Ivashkevich, O.A., Ed., Minsk: Bel. Gos. Univ., 2003, issue 2, pp. 312–322.
12. Brazhnikov, M.M., Grinyuk, E.V., Brazhnikova, L.Yu., *et al.*, *Mater. Tekhnol. Instr.*, 2001, vol. 6, no. 3, pp. 37–39.
13. Brazhnikov, M.M., Grinyuk, E.V., Brazhnikova, L.Yu., and Krul', L.P., *Vestsi Nats. Akad. Navuk Bel., Ser. Khim. Navuk*, 2002, no. 2, pp. 91–93.

Russian Journal of Applied Chemistry, Vol. 78, No. 5, 2005, pp. 843–847. Translated from Zhurnal Prikladnoi Khimii, Vol. 78, No. 5, 2005, pp. 860–864.
Original Russian Text Copyright © 2005 by Nikolaev, Nikolaeva.

MACROMOLECULAR CHEMISTRY AND POLYMERIC MATERIALS

Synthesis of Phosphate Epoxy Hardener–Flame Retardant and Rheokinetics of Curing of Epoxy Composites with Its Use

P. V. Nikolaev and E. P. Nikolaeva

Ivanovo State University of Chemical Engineering, Ivanovo, Russia

Received May 25, 2004; in final form, February 2005

Abstract—The effect of phosphate hardener obtained from phosphoric acid and acetic anhydride on the rheokinetics of extended epoxy composite is studied.

In reactions of epoxy oligomers (EOs) with phosphoric acid (PA), water contained in the acid contributes significantly to the formation and hydrolysis of di- and triesters [1, 2], responsible for the formation of linear and network structures in the system low-molecular-weight EO–PA in curing.

Data on reactions between phenyl glycidyl ether, as a model for a low-molecular-weight EO, with PA in solution [1], combined with those on the oligomeric block system [2], confirmed the adequacy of the suggested mechanism of curing and revealed specific features of the oligomeric system, associated with incompatibility and limited viability of the cured composite. It was demonstrated that the curing can proceed through both increase in the linear dimension of the molecules (formation of diesters) and branching (formation of triesters by the reaction with epoxide). In the latter case, a 3D polymeric network structure is formed, since the initial PA has a tetrahedral structure [3]. It is known that, for epoxy materials (EMs) cured without heating, the time of establishment of the critical viscosity (viability) is one of the most significant processing characteristics, since the polymer starts to form immediately after introduction of a hardener. Therefore, in developing novel phosphate hardeners (PHs), in addition to determination of the degree of curing of epoxy materials, we studied the kinetics of increase in the viscosity after their introduction into the composite as well as the effects of various factors on the rheokinetic properties of the systems.

EXPERIMENTAL

In this study we examined commercial alkylresorcinol epoxy oligomer AREM 2-20 [TU (Technical Specifications) 38.39.101–87] with an epoxy group content of 19.5 wt %; crushed quartz sand KP-3 [GOST (State Standard) 9077–82] as a filler; and polyethylenepolyamine (PEPA) A (TU 6-02-594–85) as a reference epoxy hardener. The reference composite contained EO and filler in 1 : 1 weight ratio and 14 wt % PEPA (relative to the oligomer). PA was introduced into the EO–filler system in the same amount.

The viability of the composites was determined by two methods. In the first method we determined the temperature of the maximum of the exothermic peak observed after introduction of the hardener into EO. This method was demonstrated to be more suitable in the case of the reference composite containing PEPA as a hardener. With addition of powdered quartz sand as a filler, the temperature of the exothermic peak as well as the time of establishment of this maximum decreased.

In the second method, the reaction rates in the system EO–hardener were characterized using the rheokinetic method based on measuring the viscosity of the composite in time starting from the instant of introduction of the hardener. The viscosity was determined with a V3-7 cone funnel which is commonly used in studying viscous extended thermosetting materials. The funnel was filled with 50 g of the compound (EO : filler = 1 : 1; 14 wt % hardener). The filler and EO were introduced first and thoroughly mixed to obtain a homogeneous composition. The estimated amount of PH was added to the resulting suspension with vigorous stirring, and the viscosity was measured. The first measurement was made 2 min after addition of the hardener and thorough mixing of the components. The compound was thorough mixed for 1–1.5 min before each measurement. The exhaust time was determined as the time corresponding to a break

1070-4272/05/7805-0843 © 2005 Pleiades Publishing, Inc.

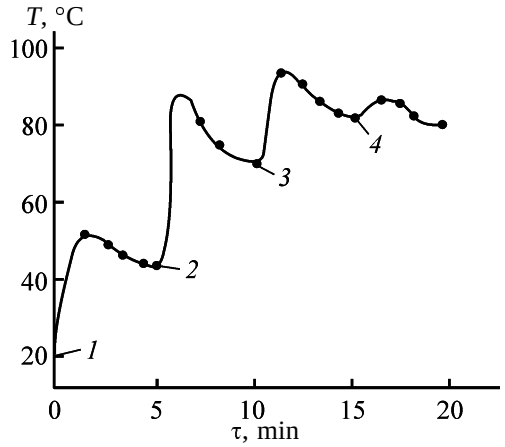


Fig. 1. Temperature T vs. time τ dependence for synthesis of the hardener based on aqueous PA and AcA. PA concentration 75.5 wt %. Total AcA content is equivalent to the water concentration in the acid. (*1–4*) Numbers of equal portions of the acid added to AcA.

of the flow of the compound at a distance of 40 mm from the funnel discharge. Simultaneously, the temperature of the composite was measured to characterize the exothermicity of the process. Each run involved 7–8 measurements of the viscosity. The experimental rheokinetic curve was compared with that obtained for the reference compound. For highly viscous systems we also used a semiquantitative method commonly applied in production of adhesives and compounds [4].

Our results showed that, thanks to high reactivity of the system, EO is cured with PA without heating even at large excess (up to twofold) of the epoxy groups relative to the hydroxy groups. However, the degree of cross-linking, being in direct proportion to the concentration and amount of the acid used, is low (maximal content of the gel fraction is 70 wt %). The presence of water in amounts up to tenfold molar excess relative to PA makes the components of the system incompatible, decreases the degree of curing, but increases the viability of the composite. These trends are caused by increasing volume of the aqueous phase and also by interaction of water with PA with formation of stable associates. We also observed the inhibiting effect of water in the reaction of α-oxo compounds with acids when studying the reaction kinetics in the model system containing phenyl glycidyl ether and *p*-dodecylbenzenesulfonic acid [5].

Keeping in mind the negative effect of water on curing and also the necessity in considerable improvement of the viability of composites based on low-molecular-weight EOs and PA, in developing PHs we used as modifiers such compounds that reacted with water contained in the acid with formation of nucleophilic compounds capable of reducing the activity of the acid in its reactions with epoxy groups of the oligomer. The use of carboxylic acid anhydrides appeared to be the simplest way to bind water. Comparison of acetic anhydride (AcA) with dicarboxylic acid anhydrides, phthalic and maleic, in reactions with aqueous phosphoric acid revealed considerable advantage of the former modifier [6]. The reactions of phthalic and maleic anhydrides with water produce the corresponding acids with high melting points (about 70°C above the melting points of the anhydrides). As a result of modification with these anhydrides, heterogeneous hardeners are formed, which are suitable only for organosoluble epoxy materials. Phosphate hardeners were prepared by stepwise addition of PA into AcA. Phosphate hardeners based on PA, AcA, and hexamethylenetetramine (HMTA) were prepared similarly. A part of water contained in the initial PA was bound with the equimolar amount of HMTA, estimated in accordance with the reaction

$$(CH_2)_6N_4 + 6H_2O \rightarrow 4NH_3 + 6CH_2O,$$

and the residual part, with the equimolar (relative to water) amount of AcA.

The synthesis of PHs based on aqueous PA and AA is spontaneous and autocatalytic, since acetic acid (HAc) formed by the reaction catalyzes the reaction of AcA with water [7]. The temperature–time relationship for the synthesis of PH based on aqueous PA (75.5 wt %) and AcA is shown in Fig. 1. As seen, the process is considerably exothermic, spontaneous, and autocatalytic. With excess of AcA relative to PA, it reacts with the acid with formation of acetic phosphoric anhydride (AcPA). Preparation of AcPA from anhydrous PA and AcA was described in [8]. AcPA demonstrates high activity in acetylation, suggesting high reactivity of the resulting PH with respect to both the initial secondary hydroxy groups of EO and hydroxy groups formed by opening of the epoxy ring of EO by the hardener.

The study of the rheokinetic characteristics of the system EO–filler–PH showed that the maximal viability of the composite is realized at the equimolar ratio of water contained in PA and AcA (Fig. 2). The viability of the composite depends also on the PH preparation procedure, increasing with increasing degree of completeness of the reactions occurring due to additional thermal cocondensation of the hardener components (Fig. 3). The use of EO to decrease the hardener activity, i.e., to convert it into an adduct,

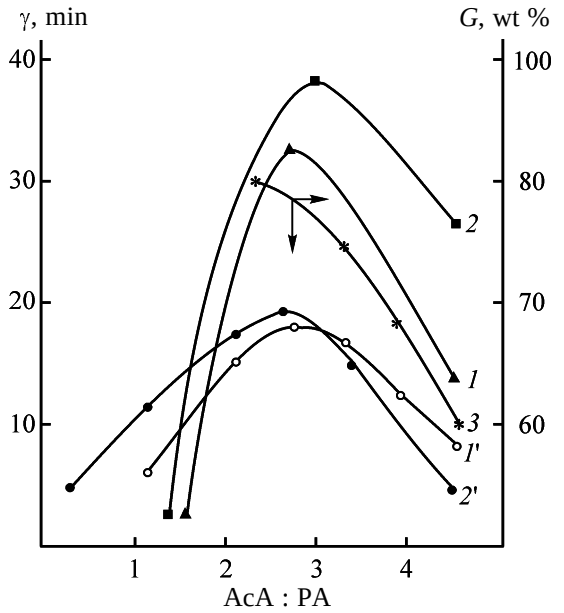


Fig. 2. (*1*, *1*', *2*, *2*') Viability and (*3*) gel fraction content in cured composite as functions of the PA concentration, AcA : PA weight ratio, and hardener preparation procedure. (γ) Viability and (*G*) gel fraction content. PA concentration, wt %: (*1*, *2*) 50 and (*1*', *2*') 75. Hardener preparation procedure: (*1*, *1*') without cocondensation, (*2*, *2*') with cocondensation, and (*3*) samples with PA-based hardener (75.5 wt %).

improves the viability of the composite. However, in this case, the viscosity of the curable systems considerably increases, thus deteriorating their processing characteristics (Fig. 3). This phenomenon is caused by considerable branching of the resulting acid adduct, and also by the fact that monophosphates formed by the reaction of PA with oxiranes are more reactive toward epoxy groups as compared to the initial PA [1].

Introduction of HMTA into the hardener also improves the viability of the system, but only at a fixed HMTA content in PH (Fig. 4) (viability of the composite may decrease as a result of interactions between HMTA decomposition products and EO).

Finally, our results obtained in studying the oligomeric systems confirmed the results of the kinetic studies in which we elucidated (with model systems) the mechanism of reaction of EO with acids, contribution of water to the formation of mono-, di- and triphenoxyhydroxypropyl phosphates and their derivatives [1]. These data were also used as a basis in developing novel phosphate hardeners and predicting their properties. In particular, higher reactivity of the monoesters formed by PA and EO causes abrupt

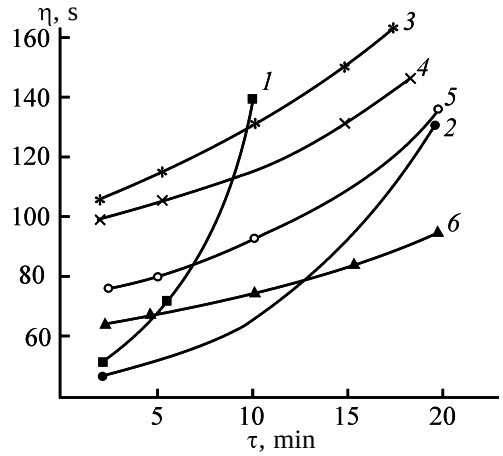


Fig. 3. Effect of the preparation procedure of PA–AcA hardener and EO in its composition on the rheokinetics in the system EO–filler–PH. PH content 15% (relative to the EO weight). (η) Viscosity and (τ) time; the same for Fig. 4. Hardener preparation procedure: (*1*, *3*, *5*) without cocondensation and (*2*, *4*, *6*) with cocondensation. EO content in PH (wt %): (*1*, *2*) 0, (*3*, *4*) 20, and (*5*, *6*) 10.

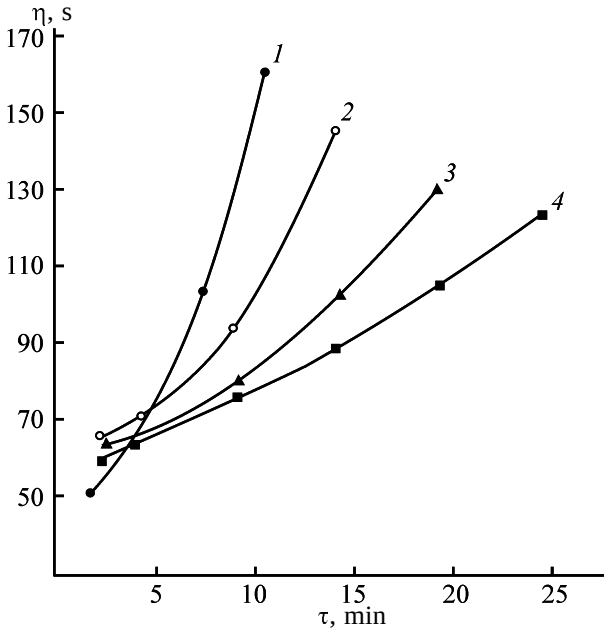


Fig. 4. Effect of the HMTA content in PH on the rheokinetics in the system EO–filler–PH: (*1*) no HMTA; proportions of water (initially present in OPA) bound by HMTA and AcA: (*2*) 50 : 50, (*3*) 75 : 25, and (*4*) 90 : 10%.

increase in the iniial viscosity of the composites cured with EO and PH adducts.

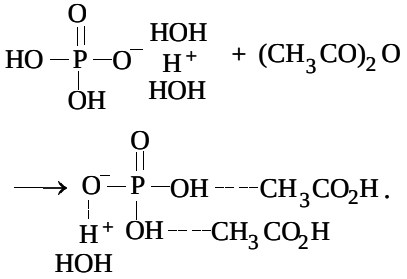
Evidently, acetic acid HAc, the product of the reaction of water contained in PA with AcA, like water, inhibits the reaction of the epoxy groups of PA with the acid hydroxy groups of PH. In this case, HAc acting as a nucleophile with respect to PA serves as

a solvating agent for the PA protons, reducing the reactivity of the EO–PH system. The interaction of PA with HAc involves protonation of the carbonyl oxygen of HAc. The hydroxy carbocation, an intermediate product of epoxy ring opening, also could be solvated by this mechanism [5]. It is not improbable that addition products of the mineral and organic acids are formed [3]. Here it should be taken into account that, in the reaction of 1 mol of water with 1 mol of AcA, 2 mol of HAc is formed, causing high degree of solvation of PA in PH.

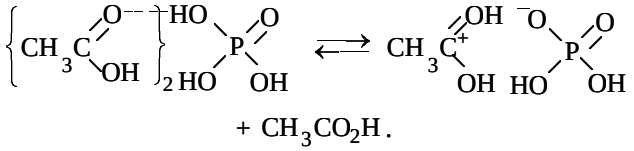
Taking into account the solvation effects, synthesis of PH and its reaction with EO can be described by the following scheme. Hydrous PA reacts with AcA with formation of solvated PA or of a mixture of hydrates and solvates, depending on the anhydride to water ratio:

$$H_3PO_4(H_2O)_n + (CH_3CO)_2O \rightarrow H_3PO_4(CH_3CO_2H)_{2n}.$$

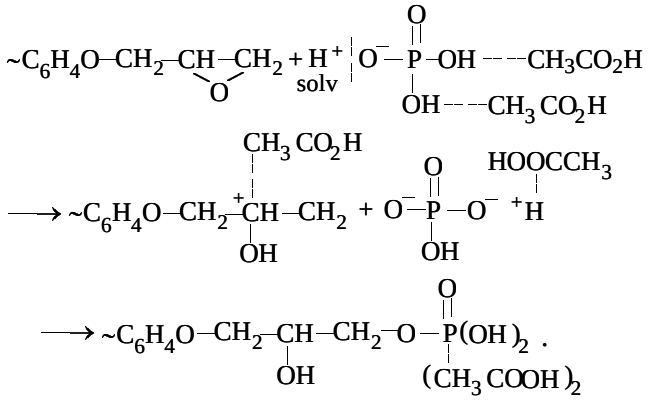
For example, at $n = 2$, since water is dimeric and the PA proton fluctuates between two water molecules [9], the interaction in the system aqueous PA–AcA produces PA solvatohydrate in which one proton is bound to the water molecule, and two other protons, to acetic acid molecules formed by the reaction of AcA with water:



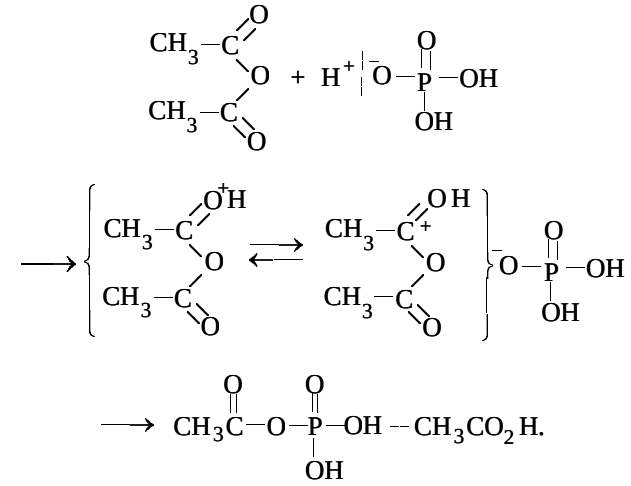
It is known that HAc occurs as fairly stable dimers both in liquid and vapor phases. Phosphoric acid, as a stronger acid, can replace a weak acid from the associate, which is also taken into account in the suggested solvation–hydration mechanism. As a result of this interaction, low-activity adducts (associates) are formed. Acetic acid, forming homoassociates, in the adducts acts as a nucleophile with respect to PA, so that a 1 : 1 individual addition product can be formed:



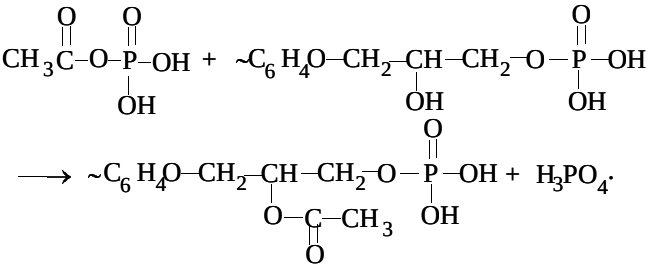
The formation of not only adduct, but also addition products of PA and AcA was reported earlier [3]. In the reaction of PH with the epoxy groups of EO, intermediate hydroxy carbocation is formed, which then reacts with the solvated anion of PA:



It should be pointed out that, in synthesis of PH with excess AcA as a reagent with respect to water and PA, solvated acetyl phosphate (AcPA) can be formed:



In the resulting AcPA, the positive charge δ^+ on the carbon atom (reactive center) increases by virtue of the intramolecular hydrogen bond between the carbonyl oxygen and the proton, making it possible for AcPA to react with not only the epoxy groups of EO (see scheme above), but also with the hydroxy groups of phenoxyhydroxypropyl phosphates (epoxy ring opening products), and also with the initial hydroxy groups of EO:



It is well known that AcPA is a convenient acetylating agent, which provides better results than the Fritz–Schenk reagent [8].

The indicated reaction, producing free PA, causes the decrease in the viability of the composites. The modification of EO in the course of curing proceeds through acetylation of the secondary hydroxy groups.

Sufficiently high degree of curing in the systems studies suggests that the side reactions involving the epoxy groups of EO and PH components, particularly HAc as a chain-terminating agent, only slightly contribute to the process. Furthermore, the presence of PA and HAc in the hardener reduces the inflammability of the resulting epoxy polymers without adding special flame retardants [6].

CONCLUSION

The presence of acetic acid in the phosphate hardener reduces the curing rate, i.e., increases the viability of epoxy composites. The rate of the epoxy ring opening with the mineral acid is controlled by its solvation with the organic acid. The duration of the induction period of gelation in curing of epoxy oligomers is determined by interactions between phosphoric and acetic acids.

REFERENCES

1. Sorokin, M.F., Kochnova, Z.A., Nikolaev, P.V., *et al*., *Lakokras. Mater. Ikh Primen*., 1989, no. 6, pp. 10–12.
2. Nikolaev, P.V., Lebedeva, L.N., and Poltavets, T.A., in *Okhrana okruzhayushchei sredy i resursosberezhenie: Mezhvuzovskii sbornik* (Environmental Protection and Resource Saving: Intercollegiate Collection), St. Petersburg: Sankt-Peterburg. Gos. Tekstil. Akad., 1995, pp. 93–98.
3. Corbridge, D.E., *Phosphorus. An Outline of Its Chemistry, Biochemistry and Technology*, Amsterdam: Elsevier, 1980.
4. *Klei i germetiki* (Adhesives and Sealants), Kardashov, D.A., Ed., Moscow: Khimiya, 1978.
5. Nikolaev, P.V. and Dmitrieva, M.A., *Zh. Obshch. Khim*., 1995, vol. 65, no. 1, pp. 116–120.
6. USSR Inventor's Certificate no. 1819889.
7. Moelwyn-Hughes, E.A., *The Chemical Statics and Kinetics of Solutions*, London: Academic, 1971.
8. Fieser, L.F. and Fieser, M., *Reagents for Organic Synthesis*, New York: Wiley, 1968. Translated under the title *Reagenty dlya organicheskogo sinteza*, Moscow: Mir, 1971, vol. 4, p. 95; vol. 5, p. 482.
9. Librovich, N.B., Maiorov, V.D., and Savel'ev, V.A., *Dokl. Akad. Nauk SSSR*, 1975, vol. 225, no. 6, pp. 1338–1361.

Russian Journal of Applied Chemistry, Vol. 78, No. 5, 2005, pp. 848–849. Translated from Zhurnal Prikladnoi Khimii, Vol. 78, No. 5, 2005, pp. 865–866.
Original Russian Text Copyright © 2005 by Studzinskii, Borisova, Ponomareva.

BRIEF COMMUNICATIONS

Haloalkane Derivatives as Light Stabilizers for Anthraquinone Dyes

O. P. Studzinskii, L. M. Borisova, and R. P. Ponomareva

St. Petersburg State Institute of Trade and Economy, St. Petersburg, Russia
Mechnikov St. Petersburg State Medical Academy, St. Petersburg, Russia

Received March 28, 2005

Abstract—The possibility of photostabilization of anthraquinone dyes with haloalkanols and haloalkanesulfonic acids was examined with model aminoanthraquinones.

Procedures for suppressing the photochemical degradation of optical brighteners and anthraquinone dyes with halide anions, complexones, arenes, arenesulfonic acids, haloarenes, and haloarenesulfonic acids [1–6] have certain drawbacks. In particular, bromide and iodide ions in a brightened or colored material are gradually oxidized with atmospheric oxygen to form free bromine and iodine, and arenes and their derivatives partially reabsorb the actinic light.

It is necessary to look for new ways of photostabilization, in particular, quenching the reactive excited states of the substrate with photochemically inactive additives that do not act on the substrate and material being brightened, do not reabsorb the excitation light, and are resistant to moisture and heat.

In this study we examined how haloalkanols (HAs) and sodium haloalkanesulfonates (HASs) affect the lightfastness of anthraquinone dyes (AQDs) using model anthraquinones (AQs) of a wide color range.

EXPERIMENTAL

Experiments with AQ + HA or AQ + HAS systems were performed in polyvinyl alcohol (PVAl) simulating the monomeric unit of cellulose and suitable for introduction of all the components (AQs, HAs, HASs) and for measuring the visible electronic absorption spectra (EASs) of AQs (analytical method; SF-46 spectrophotometer). The analytical wavelengths λ_a are listed in Table 1. They were chosen so that the optical density was less than 1 and could be reliably measured. The fluorescence of AQs was measured with a Neva-3 spectrofluorimeter.

The anthraquinones chosen (Central Laboratory, Rubezhnoe Chemical Combine, Ukraine) and their spectroscopic characteristics in PVAl are listed in Table 1. The compounds were purified by recrystallization from appropriate solvents followed by column chromatography on alumina or SiO_2. HAs and HASs were prepared as described in [6]; we chose 3-bromo-1-propanol **A**, 3-iodo-1-propanol **B**, sodium 3-bromo-1-propanesulfonate **C**, and sodium 3-iodo-1-propanesulfonate **D**, which appeared to be the most active with respect to optical brighteners [6]. Chemically pure grade PVAl was used without additional purification.

Films of pure PVAl (as reference samples in EAS measurements) and PVAl with additions of AQ, AQ + HA, and AQ + HAs were prepared by casting at a water : PVAl weight ratio of 1 : 1, so that the optical density at the excitation wavelength (366 nm) exceeded 2 (total absorption). The content of the additive (HA, HAS) was 20 wt % relative to AQ in all the cases. The film samples (5 cm in diameter) were ir-

Table 1. Anthraquinones, positions of absorption maxima in EASs (λ_{max}, nm), and analytical wavelengths (λ_a, nm)

Anthraquinone	λ_{max}	λ_a
Aminoanthraquinone **I**	484	504
2-Aminoanthraquinone **II**	455	490
1,8-Diaminoanthraquinone **III**	506	562
1-Amino-4-hydroxyanthraquinone **IV**	565	602
1,4-Diaminoanthraquinone **V**	592	623
1,5-Diaminoanthraquinone **VI**	490	528
1,2-Diaminoanthraquinone **VII**	531	585
2,6-Diaminoanthraquinone **VIII**	426	470
1,4,5,8-Tetraaminoanthraquinone **IX**	605	655
1,4-Diamino-2-methoxyanthraquinone **X**	542	586

1070-4272/05/7805-0848 © 2005 Pleiades Publishing, Inc.

Table 2. Photodecolorization of AQ in PVAl in the absence and in the presence of HAs and HASs

AQ	Additive	*Q*, %	AQ	Additive	*Q*, %
I	–	19.0	**VI**	–	19.8
I	**A**	15.7	**VI**	**A**	17.7
I	**B**	14.6	**VI**	**B**	16.5
I	**C**	10.7	**VI**	**C**	10.3
I	**D**	9.8	**VI**	**D**	9.1
II	–	20.0	**VII**	–	19.4
II	**A**	14.3	**VII**	**A**	13.8
II	**B**	13.7	**VII**	**B**	13.1
II	**C**	8.6	**VII**	**C**	7.1
II	**D**	8.5	**VII**	**D**	6.8
III	–	19.9	**VIII**	–	19.9
III	**A**	15.2	**VIII**	**A**	16.1
III	**B**	14.9	**VIII**	**B**	15.3
III	**C**	8.3	**VIII**	**C**	6.9
III	**D**	7.8	**VIII**	**D**	6.5
IV	–	18.9	**IX**	–	19.1
IV	**A**	14.7	**IX**	**A**	14.3
IV	**B**	14.5	**IX**	**B**	14.1
IV	**C**	8.4	**IX**	**C**	7.1
IV	**D**	7.7	**IX**	**D**	6.8
V	–	20.0	**X**	–	20.1
V	**A**	15.3	**X**	**A**	17.3
V	**B**	13.5	**X**	**B**	16.2
V	**C**	9.0	**X**	**C**	8.4
V	**D**	7.8	**X**	**D**	7.9

radiated on a UIS-1 installation in air under temperature control (25°C); the wavelength of 366 nm was cut with a system of glass color filteres. The irradiation time (constant for each dye) was chosen so that the optical density at the analytical wavelength (*A*) did not exceed 20%. The degree of photochemical degradation *Q* of AQs was measured in the course of photolysis from a decrease in *A*: $Q = [(A_0 - A)/A] \times 100\%$, where A_0 and *A* are the optical densities of the nonirradiated sample and sample irradiated for a definite time, constant for each AQ, respectively (Table 2).

The electronic absorption and fluoresence spectra show that HAs and HASs do not form with AQs any associates or charge-transfer complexes in the ground state and excimers in the electronically excited state, as follows from the lack of the effect of HAs and HASs on the electronic absorption and luminescence spectra of AQs.

In the presence of HAs **A** and **B**, the rate of photochemical degradation of **I**–**X** decreases by a factor of 1.3–1.5 and 2.5–3.2, respectively. The effect of HASs **C** and **D** is still stronger: The deceleration factor is 1.8–1.9 and 3.2–3.4, respectively. Apparently, the lower inhibiting activity of HAs compared to HASs may be due to association of HA molecules by hydrogen bonding, with a decrease in the content of active species inhibiting the AQ degradation.

An increase in the HA and HAs performance in going from the bromides to the iodides confirms the acceleration of conversion of photochemically excited AQs to the ground state without transfer of the excitation energy from AQ to HA or HAS. Both mechanisms of AQ photochemical degradation (reductive, under the action of labile hydrogen atom at the carbinol carbon atom, and oxidative, under the action of singlet oxygen generated by AQ) are suppressed simultaneously [7].

We have not revealed any trends in the effect of substituents on the rate of photodecolorization of AQ and performance of AQ light stabilizers (HAs, HASs).

CONCLUSION

In the presence of haloalkanes and sodium haloalkanesulfonates (Hlg = Br, I; light stabilizer content 20 wt % relative to the dye), the lightfastness of model anthraquinone dyes in cellulose-like materials increases by a factor of 1.2–3. The performance of the iodine-containing stabilizers is 1.3–1.5 times higher than that of their bromine analogs.

REFERENCES

1. Studzinskii, O.P., Grebenkina, V.M., and Ponomareva, R.P., *Izv. Vyssh. Uchebn. Zaved., Khim. Khim. Tekhnol.*, 1984, vol. 27, no. 7, pp. 799–801.
2. Ponomareva, R.P. and Studzinskii, O.P., *Zh. Obshch. Khim.*, 2001, vol. 71, no. 10, pp. 1704–1707.
3. Studzinskii, O.P., Ponomareva, R.P., and Borisova, L.M., *Zh. Obshch. Khim.*, 2003, vol. 73, no. 10, pp. 1674–1677.
4. Studzinskii, O.P., Borisova, L.M., and Ponomareva, R.P., *Zh. Obshch. Khim.*, 2003, vol. 73, no. 11, pp. 1904–1906.
5. Ponomareva, R.P., Studzinskii, O.P., and Borisova, L.M., *Zh. Obshch. Khim.*, 2002, vol. 72, no. 7, pp. 1180–1183.
6. Studzinskii, O.P., Borisova, L.M., and Ponomareva, R.P., *Zh. Obshch. Khim.*, 2005, vol. 75, no. 1, pp. 166–167.
7. Ponomareva, R.P. and Studzinskii, O.P., *Zh. Obshch. Khim.*, 2001, vol. 71, no. 5, pp. 809–813.

Russian Journal of Applied Chemistry, Vol. 78, No. 5, 2005, pp. 850–852. Translated from Zhurnal Prikladnoi Khimii, Vol. 78, No. 5, 2005, pp. 867–869.
Original Russian Text Copyright © 2005 by Ayurova, Maksanova, Starichenko, Shundrin, Bodoev, Mognonov.

BRIEF COMMUNICATIONS

A New Agent for Modification of the Teflon Surface

O. Zh. Ayurova, L. A. Maksanova, V. F. Starichenko, L. A. Shundrin, N. V. Bodoev, and D. M. Mognonov

East Siberian State Technological University, Ulan-Ude, Buryatia, Russia
Baikal Institute of Nature Management, Siberian Division, Russian Academy of Sciences, Ulan-Ude, Buryatia, Russia
Novosibirsk Institute of Organic Chemistry, Siberian Division, Russian Academy of Sciences, Novosibirsk, Russia

Received January 29, 2004; in final form, January 2005

Abstract—The possibility of preparing modification solutions from sodium naphthalenide wastes and their effect on Teflon adhesion were studied.

Organometallic complexes of alkali metals (Li, Na, K) and aromatic hydrocarbons (diphenyl, naphthalene, anthracene, etc.) are widely used to enhance adhesion of inert polymers, including Teflon [1, 2]. Wastes remaining after modifying the Teflon surface with Na-naphthalene complex comprise more than 70% of the initial active solution. The spent inactive solution containing various toxic compounds after neutralization is discharged into industrial sewage and pollutes the environment.

Arene complexes of metals are unstable; they are prepared under the anaerobic conditions [1, 3]. Previously [4], we attempted to prepare arene complexes of metals at room temperature in air using ethers [tetrahydrofuran (THF), dimethyl ethylene glycol, dimethyl diethylene glycol, diethyl diethylene glycol] and obtained dark solutions whose color was determined by the kind of metal and aromatic hydrocarbon.

In this study we examined by ESR solutions of sodium and naphthalene in THF, prepared at room temperature. We also examined the possibility of reusing the spent inactive solution of sodium naphthalenide to enhance the Teflon adhesion.

EXPERIMENTAL

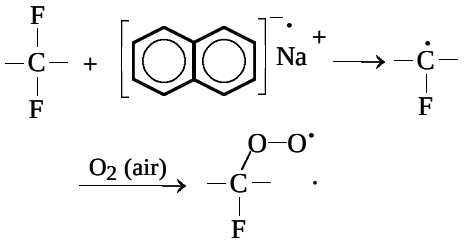
The ESR spectra were recorded on a Bruker ESR-300 spectrometer at T = 298 K. The g-factor in the ESR spectra of the solution in question agrees with that of the naphthalene radical anion [5].

We attempted to reuse the spent inactive solution. On adding sodium and naphthalene into the spent solution, its color changed from yellowish to dark brown; according to ESR data, this solution is diamagnetic.

The content of active sodium naphthalenide in the initial and regenerated solutions, determined on an LKhM-8MD chromatograph, was 12–13 and 18–20%, respectively.

The adhesion of Teflon films treated with solutions that had been prepared from the wastes is higher as compared to the films treated with solutions of the pure complexes. Probably, the Teflon surface is activated upon interaction with naphthalene radical anions and/or dianions, which can be formed under the experimental conditions studied [6].

As seen from the ESR spectra of the treated Teflon films, they contain paramagnetic centers probably belonging to the peroxy and carbon-centered radicals [7, 8]:

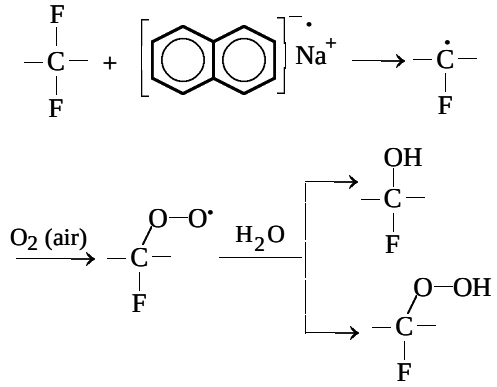


The IR spectra of the Teflon films treated with modifying solutions and washed with water exhibit bands in the 3600–3000 cm^{-1} range, belonging to hydroxy groups [9]:

1070-4272/05/7805-0850 © 2005 Pleiades Publishing, Inc.

Table 1. Breaking shear stress of the glued samples

Sample	Treatment with modifying complex in solution	Breaking shear stress, kN m^{-2}, at indicated temperature, °C								
		20			200	–12		–60		
		24 h	0.5 year	2 years	120 h	0.5 year	2 years	0.5 year	2 years	3 years
		BF-4 adhesive								
D-16T–Teflon	THF	176.4	210.1	196.3	–	–	–	215.2	187.2	205.8
	Ethylene glycol diether	157.8	194.2	180.5	–	–	–	215.6	210.2	206.9
	THF with wastes	209.3	221.4	217.3	–	–	–	235.1	229.1	228.7
Teflon–Teflon	THF	147.0	162.3	154.7	–	–	–	182.4	166.6	159.7
	Ethylene glycol diether	140.1	164.7	181.7	–	–	–	189.2	195.0	189.1
	THF with wastes	202.4	219.5	214.9	–	–	–	227.6	221.7	219.9
		K-300 adhesive								
D-16T–Teflon	THF	206.8	204.7	211.3	82.3	201.1	190.1	228.8	228.3	219.1
	Ethylene glycol diether	205.8	207.3	203.4	97.02	223.4	216.2	223.7	223.2	219.3
	THF with wastes	216.7	217.3	221.7	111.3	227.1	217.4	233.1	235.6	229.8
Teflon–Teflon	THF	157.8	174.5	173.1	75.5	191.4	214.2	228.8	215.6	217.7
	Ethylene glycol diether	175.4	184.4	181.3	81.3	207	200.9	229.1	225.2	219.5
	THF with wastes	207.6	221.7	217.7	101.5	224.1	211.3	231.7	229.1	229.5



Washing with water of untreated Teflon films does not result in appearance of such bands in the IR spectra.

Since the materials based on Teflon operate under various conditions, we studied the physicomechanical properties of activated glued Teflon films (Tables 1, 2).

The Teflon films were glued with metal support or with each other using adhesives BF-4 [GOST (State Standard) 12172–74] and K-300 (containing L-20 and SEDM-6 resins) at loads and drying modes corresponding to the GOST and TU (Technical Specifications) for the given adhesives. A plate (70 × 19.5 mm) of aluminum alloy (D 16T brand, GOST 21631–76) was used as a support. The mechanical strength of the resulting composites was evaluated from the breaking shear stress of the lapped glued samples (GOST 11262–80). The tests were performed on a ZM-40 tearing machine at a clamp velocity of 100 mm min^{-1}. The Teflon film thickness was 100 μm. The glued samples were tested in special temperature-controlled chambers at –12, –60, 20–22,

Table 2. Wetting angle of the treated Teflon films (wetting angle of untreated film 97°)

Storage temperature	Storage time, year	Wetting angle, deg
Treatment with sodium naphthalenide in THF		
20–22	1	57
	2	59
	3	62
12–14	1	56
	2	57
	3	60
Treatment with the complex from wastes in THF		
20–22	1	55
	2	55
	3	57
12–14	1	54
	2	55
	3	58

and 200°C. The strength parameters were recorded after storage for 1 day and 0.5, 1, 2, and 3 years (Table 1). Nine samples were used in each test. The results were treated using the procedures of mathematical statistics with 98% confidence probability. As seen from Table 1, the breaking shear stress for most of the glued samples changes insignificantly. However, certain trends in the strength properties can be revealed. The strength of the samples tested 1 day after gluing is lower than that of the samples stored for 0.5 year, and it slightly decreases (by 2–6%) upon storage for 2 and 3 years. At high temperature, changes in the sample strength are more pronounced. It is smaller by a factor of 1.5–2.0 than that of the samples stored at room and lower temperatures. Nevertheless, at 200°C the adhesion strength is fairly high, about 100 kN m^{-2}. With K-300 adhesive, the adhesion joint strength of the Teflon films is higher, and it only slightly changes in the temperature range studied. In the case of K-300 adhesive, the glue joint between the Teflon film and metal is stronger than that between two Teflon films, whereas with BF-4 adhesive the trend is opposite. The increase in the adhesion of the Teflon surface is confirmed by a decrease in the wetting angle of the samples treated with examined solutions (Table 2).

CONCLUSIONS

(1) According to the ESR data, sodium naphthalenide can be prepared in air in tetrahydrofuran (THF).

(2) The spent solution regenerated from the wastes by adding sodium and naphthalene increases the adhesion of the Teflon surface.

(3) Glued films of modified Teflon retain strength properties for a prolonged time in a wide temperature range.

REFERENCES

1. Talalaeva, T.V. and Kocheshkov, K.A., *Metody elementoorganicheskoi khimii: Litii, natrii, kalii, rubidii, tsezii* (Methods of Organometallic Chemistry: Lithium, Sodium, Potassium, Rubidium, and Cesium), Moscow: Nauka, 1971, book 1.
2. Panshin, Yu.A., Malkevich, S.G., and Dunaevskaya, Ts.S., *Ftoroplasty* (Fluoroplastics), Leningrad: Khimiya, 1978.
3. Fieser L.F. and Fieser M., *Reagents for Organic Synthesis*, New York: Wiley, 1968.
4. Maksanova, L.A. and Ayurova, O.Zh., *Vestn. Vost.-Sib. Gos. Tekhnol. Univ.*, 1999, no. 2, pp. 92–99.
5. Kuznetsov, A.N., *Metod spinovogo zonda* (Method of Spin Probe), Moscow: Nauka, 1976.
6. Rao, S.N.R., Kalianaraman, V., and George, M.V., *Usp. Khim.*, 1972, vol. 41, no. 5, pp. 940–976.
7. Smith, A.L., *Applied Infrared Spectroscopy: Fundamentals, Techniques, and Analytical Problem-Solving*, New York: Wiley, 1979.
8. Miroshnichenko, E.A., Mel'nikov, V.P., Vorob'eva, V.P., *et al.*, *Zh. Fiz. Khim.*, 1985, vol. 59, no. 12, pp. 2418–2430.
9. Bong Jin Jeong, Jin No Lee, and Hai Bang Lee, *J. Colloid Interface Sci.*, 1996, vol. 178, pp. 757–763.

Russian Journal of Applied Chemistry, Vol. 78, No. 5, 2005, pp. 853–855. Translated from Zhurnal Prikladnoi Khimii, Vol. 78, No. 5, 2005, pp. 870–872.
Original Russian Text Copyright © 2005 by Lebedeva, Yarkova, Platonov, Proskuryakov, Chernysheva.

BRIEF COMMUNICATIONS

Enhancement of Biological Activity of Humic Acids by Hydrobromination

G. F. Lebedeva, T. A. Yarkova, V. V. Platonov, V. A. Proskuryakov, and N. I. Chernysheva

Novomoskovsk Institute, Mendeleev Russian University of Chemical Engineering, Novomoskovsk, Tula oblast, Russia
Leo Tolstoy Teacher's Training University, Tula, Russia
St. Petersburg State Technological Institute, St. Petersburg, Russia

Received December 15, 2004; in final form, March 2005

Abstract—A procedure for preparing hydrobrominated peat humic acids with enhanced biological activity was developed.

Bromine is one of indispensible microelements of various human and animal tissues, ensuring normal development and activity of living bodies. In this connection, attempts were undertaken to prepare brominated humic acids (HA). Humic acids with a high bromine content (up to 18.6 wt %) were obtained by bromination of humic acids with bromine. It was found that bromination of humic acids is accompanied by their oxidation. Brominated humic acids are enriched in oxygen-containing functional groups, and their molecular weight decreases by a factor of 1.5–2.0 [1–4].

To prevent oxidative degradation of humic acids in the course of their bromination, we attempted to introduce bromine atoms into humic acid by hydrobromination.

EXPERIMENTAL

Table 1 shows how the time of hydrobromination of humic acids with 40% aqueous HBr at 20°C influences both their chemical characteristics (bromine and functional group content) and biological activity. It seen that, with increasing hydrobromination time from 0.5 to 2 h, the Br content in HA increases from 0.54 to 2.63 wt % and the content of the phenolic hydroxy groups increases from 3.86 to 5.95 mg-equiv g^{-1}. At the same time, under these conditions the content of the quinoid groups (QG) decreases from 2.34 to 0.61 mg-equiv g^{-1}, apparently due to formation of 5-bromohydroquinone groups. HBr can also add to alkene groups of HA and destroy the oxygen-containing heterocycles. As a result, after hydrobromination, the iodine number of HA and the oxygen content in heterocycles O_c decreases respectively, from 0.26 and 0.44 mg-equiv g^{-1} to zero.

In order to elucidate how atmospheric oxygen influences the hydrobromination of humic acids, this process was carried out both in air and under argon. Our experiments showed (Table 1) that, after hydrobromination for 2 h in air, the molecular weight of humic acids decreases by a factor of approximately 1.5. At the same time, after hydrobromination under argon, the decrease in the molecular weight was less pronounced (from 1400 to 1130). In going from air to argon, the effect exerted by hydrobromination on the content of functional groups noticeably changes. We suggest that, in hydrobromination in air, humic acid is partly oxidized with atmospheric oxygen. The hydrobromination of HA can be intensified by its treatment with concentrated aqueous HBr for 0.5–1.0 h. The biological activity of the initial and hydrobrominated humic acids was determined by a standard yeast technique with distilled water as a reference with zero biological activity. Our results showed that hydrobromination of humic acids, especially in the presence of air, enhances their biological activity.

Table 2 shows how treatment of HA with HBr of various concentrations for 0.5 h at 20°C influences the chemical characteristics (bromine and functional group content) and biological activity of humic acids. It seen that, in the presence of atmospheric oxygen, with increasing HBr concentration from 20 to 30 wt %, the bromine content in modified HA changed insig-

1070-4272/05/7805-0853 © 2005 Pleiades Publishing, Inc.

Table 1. Influence of hydrobromination time on chemical characteristics (bromine and functional group content) and biological activity of humic acids (c_{HBr} = 40%, T = 20°C)

τ, h	Yield of modified HA, %	c_{Br}, wt %	M	PhG	QG	IN	O_c	BA
				mg-equiv g^{-1}				
Initial HA		0.00	1400	3.86	2.34	0.26	0.44	1.06
0.5	94* (94)	0.54 (0.80)	1360 (1400)	4.91 (5.30)	1.40 (1.25)	0.24 (0.18)	0.26 (0.30)	1.18 (1.16)
1.0	91 (91)	0.65 (0.98)	1130 (1250)	5.30 (5.74)	1.21 (1.22)	0.20 (0.16)	0.20 (0.24)	1.39 (1.33)
1.5	86 (90)	1.75 (2.00)	1070 (1130)	5.38 (5.90)	0.95 (1.00)	0.15 (0.10)	0.18 (0.20)	1.27 (1.13)
2.0	76 (79)	1.88 (2.63)	1080 (1130)	5.79 (5.95)	0.74 (0.61)	0.12 (0.00)	0.00 (0.12)	1.47 (1.04)

* The quantities in parentheses and without them refer to hydrobromination under argon and in air, respectively. The same for Tables 2 and 3.

Table 2. Influence of hydrogen bromide concentration on the chemical characteristics (bromine and functional group content) and biological activity of humic acids (τ = 0.5 h, T = 20°C)

c_{HBr}, wt %	Yield of modified HA, %	c_{Br}, wt %	M	PhG	QG	IN	O_c	BA
				mg-equiv g^{-1}				
Initial HA		0.00	1400	3.86	2.34	0.26	0.44	1.06
20	92 (98)	0.30 (0.32)	1400 (1450)	4.20 (4.35)	2.14 (1.73)	0.20 (0.23)	0.42 (0.44)	1.10 (1.12)
30	96 (98)	0.38 (0.56)	1400 (1430)	4.63 (4.67)	2.00 (1.50)	0.22 (0.20)	0.33 (0.37)	1.12 (1.13)
40	94 (94)	0.54 (0.80)	1360 (1400)	4.91 (5.30)	1.40 (1.25)	0.24 (0.18)	0.26 (0.30)	1.18 (1.25)

nificantly (from 0.30 to 0.38 wt %), and the iodine number remained approximately constant (0.20–0.22 mg-equiv g^{-1}). With increasing HBr concentration from 20 to 40 wt %, the amount of oxygen atoms contained in heterocycles O_c decreased from 0.42 to 0.26 mg-equiv g^{-1}. The initial humic acid contained 0.44 mg-equiv g^{-1} O_c. The hydrobromination of HA in air either did not influence or somewhat decreased its molecular weight. At the same time, in several cases the hydrobromination under argon slightly increased the molecular weight of HA.

After hydrobromination under argon, the iodine number of humic acids decreased to a larger extent than after hydrobromination in air. These results suggest that, in going from air to argon, the addition of HBr to alkene groups becomes more efficient. For example, after HA treatment with 40% HBr for 2 h under argon, its iodine number decreased to zero. Under these conditions, the content of the quinoid groups in humic acids decreased by a factor of more than three. It was found also that hydrobromination increased the content of the phenolic groups in humic acids, and this effect was more pronounced under argon than in air. We believe that this difference is caused by oxidizing effect of atmospheric oxygen.

The hydrobromination of HA was studied in relation to temperature at an HBr concentration of 40 wt % under argon and in the presence of air. In these experiments, the hydrobromination time was 0.5, and 2 h and the temperature, –5, +10, and +20°C (Table 3). Table 3 shows that hydrobromination for 0.5 h under argon and in air weakly affected the HA characteristics. Its molecular weight remained practically constant, i.e., under these conditions humic acids did not degrade. We found no significant cleavage of the heterocyclic fragments. For example, after hydrobromination at 10°C in air, the O_c content decreased from 0.44 mg-equiv g^{-1} in the initial HA to 0.38 mg-equiv g^{-1}. At 20°C, O_c decreased to 0.26 mg-equiv g^{-1}. In going to argon, the degradative effect of hydrobromination slightly decreased. The bromine incorporation into HA did not exceed 0.8%. At the same time, the QG content decreased by a factor of approximately two and PG content increased from 3.86 to 5.30 mg-equiv g^{-1}. With increasing hydrobromination time from 0.5 to 2 h, the influence of temperature on the content of bromine and functional groups in humic acids sharply increased. After 2-h hydrobromination at 20°C, the characteristics of humic acids changed as follows: bromine content increased to 2.63 wt % (under argon), alkene groups were

Table 3. Influence of hydrobromination temperature on chemical characteristics (bromine and functional group content) and biological activity of humic acids (c_{HBr} = 40 wt %)

T, °C	τ, h	Yield of modified HA, %	c_{Br}, wt %	*M*	PhG	QG	IN	O_c	BA
					mg-equiv g^{-1}				
Initial HA			0.00	1400	3.86	2.34	0.26	0.44	1.06
–5	0.5	97	0.23	1400	4.00	2.16	0.20	0.44	1.07
		(97)	(0.60)	(1400)	(4.05)	(2.11)	(0.22)	(0.44)	(1.10)
10		95	0.40	1380	4.43	1.75	0.20	0.38	1.11
		(97)	(0.62)	(1400)	(4.72)	(1.48)	(0.20)	(0.40)	(1.18)
20		93	0.54	1360	4.91	1.40	0.24	0.26	1.18
		(94)	(0.80)	(1400)	(5.30)	(1.25)	(0.18)	(0.30)	(1.16)
–5	2.0	94	0.72	1360	4.16	2.10	0.25	0.35	1.15
		(93)	(0.80)	(1380)	(4.52)	(1.79)	(0.20)	(0.40)	(1.22)
10		89	1.30	1250	4.83	1.32	0.16	0.18	1.20
		(91)	(1.15)	(1300)	(5.40)	(1.08)	(0.12)	(0.27)	(1.30)
20		76	1.88	1080	5.79	0.74	0.12	0.00	1.47
		(79)	(2.63)	(1130)	(5.95)	(0.61)	(0.00)	(0.12)	(1.04)

completely saturated with HBr, molecular weight decreased by 35%, oxygen-containing heterocycles were completely cleaved, the QG content decreased by a factor of four (from 2.34 to 0.61 mg-equiv g^{-1}), PG content considerably increased (from 3.86 to 5.95 mg-equiv g^{-1}), and the biological activity increased by a factor of 1.5.

CONCLUSION

Treatment of humic acids with aqueous HBr (40 wt %) under argon for 1 h at 20°C ensures the optimal conditions for their bromination and enrichment with phenolic hydroxy groups, largely responsible for the biological activity.

REFERENCES

1. Platonov, V.V., Lebedeva, G.F., Khusam Al'-Din Taufik Mokhammed, *et al.*, Abstracts of Papers, *I Mezhdunarodnaya nauchnaya konferentsiya "Sovremennye problemy organicheskoi khimii, ekologii i biotekhnologii"* (First Int. Scientific Conf. "Modern Problems of Organic Chemistry, Ecology, and Biotechnology"), Luga, Krest'yanskii Univ im. Kirilla i Mefodiya, June 2001, p. 49.
2. Platonov, V.V., Lebedeva, G.F., Khusam Al'-Din Taufik Mokhammed, *et al.*, Abstracts of Papers, *I Mezhdunarodnaya nauchnaya konferentsiya "Sovremennye problemy organicheskoi khimii, ekologii i biotekhnologii"* (First Int. Scientific Conf. "Modern Problems of Organic Chemistry, Ecology, and Biotechnology"), Luga, Krest'yanskii Univ. im Kirilla i Mefodiya, June 2001, p. 48.
3. Platonov, V.V., Lebedeva, G.F., Chernysheva, N.I., *et al.*, in *Trudy XVI Mezhdunarodnoi konferentsiii molodykh uchenykh "Uspekhi v khimii i khimicheskoi tekhnologii"* (Proc. XVI Int. Conf. of Young Scientists "Progress in Chemistry and Chemical Technology"), Moscow: Ross. Khim.-Tekhnol. Univ., December 2002, pp. 53–56.
4. Khusam Al'-Din Taufik Mokhammed, Lebedeva, G.F., Platonov, V.V., *et al.*, Abstracts of Papers, *III Naucnotekhnicheskaya konferentsiya molodykh uchenykh i aspirantov Novomoskovskogo Inst. RKhTU* (III Scientific and Technical Conf. of Young Scientists and Post-Graduate Students of the Novomoskovsk Inst., Mendeleev Russian Univ. of Chemical Engineering,), Novomoskovsk, May 2001, pp. 252–253.

Russian Journal of Applied Chemistry, Vol. 78, No. 5, 2005, pp. 856–858. Translated from Zhurnal Prikladnoi Khimii, Vol. 78, No. 5, 2005, pp. 873–875.
Original Russian Text Copyright © 2005 by Morachevskii.

HISTORY OF CHEMISTRY AND CHEMICAL TECHNOLOGY

François Marie Raoult (To 175th Anniversary of His Birthday)

A French physicist and chemist F. Raoult made an outstanding contribution to the investigation into the nature of solutions, established a relationship between the reduction of the saturated vapor pressure over a solution and the mole fraction of a solute (Raoult law), suggested methods for determining the molecular weight of a solute from a depression of the freezing point of the solvent (cryoscopy) and from an elevation of the boiling point of a solution (ebullioscopy), and carried out a number of other studies. Raoult's works largely favored the appearance of investigations in the field of solutions, performed by founders of the present-day physical chemistry: J. van't Hoff (1852–1911, 1901 Nobel Prize in Chemistry), W. Ostwald (1852–1932, 1909 Nobel Prize in Chemistry), S. Arrhenius (1859–1927, 1903 Nobel Prize in Chemistry), and W. Nernst (1864–1941, 1920 Nobel Prize in Chemistry). In the lecture devoted to Raoult's memory, van't Hoff named him one of the most outstanding scientists of his century [1, 2].

François Marie Raoult was born on May 10, 1830, in Fournes in northern France into the family of a tax official with a moderate income. Raoult started his working activities as an official at a patent bureau in his native town, but soon moved to Paris to continue his education. The young student had to earn his living and tuition payments himself. Unfortunately, evidence concerning this period of Raoult's life is insufficient and contradictory. After publishing the results of his first electrochemical study in *C. R. Acad. Sci. Paris*, 1853, vol. 36, p. 826, Raoult became, presumably without having finished the university, a lecturer at a lyceum in Rheims. Beginning in 1855, he taught physics at College St. Dié. In 1856, Raoult became an adjunct professor at the same college and later headed the course of physics. In 1862, Raoult moved to a small provincial town of Sens, where he was a teacher at the local lyceum and prepared, in difficult conditions, his dissertation in electrochemistry for the degree of a doctor of physics. In 1863, he successfully defended it at the university in Paris and the degree of a docteur és sciences physiques was conferred on him. In 1867, the already known scientist was invited to teach chemistry at the University of



Grenoble, and all his further pedagogical and scientific activities were associated, till the end of his life, with the University of Grenoble. In 1870, he became a professor, and for a number of years was dean of the faculty of sciences. In Grenoble, world fame came to Raoult.

The scientific works of François Marie Raoult were to a certain extent ahead of his time, but all his conclusions were based on a thorough analysis of a vast body of experimental data. Three periods can be distinguished in his scientific activities. The earliest includes electrochemical studies: measurements of the electromotive forces of voltaic cells and evaluation of the heat effects of chemical reactions occurring in these cells. Continuing the investigations of P. Favre (1813–1880), also a French chemist, Raoult measured the heats of the chemical reactions and the electric work for various voltaic cells of a design similar to that of the Daniel cell. In contrast to the conclusions made by Favre and to the commonly accepted opinion of that time, Raoult established that, in the general case, these quantities do not coincide. In the second part of his investigations in this area, Raoult evaluated, using an instrument specially designed by him, the heat effects accompanying the decomposition

1070-4272/05/7805-0856© 2005 Pleiades Publishing, Inc.

of aqueous solutions of salts under the action of electric current. Describing this series of works, Raoult wrote: "I was the first to give a method for measuring the heat released or absorbed in chemical transformations under the action of electric current" [2]. Raoult repeatedly reverted to the problem of distinction between the "electric heat" and "chemical heat" in his subsequent investigations. As noted by W. Ostwald [2], Raoult convincingly demonstrated that the chemical and electric kinds of energy are not simply converted into one another, but a certain role is played here by heat. The Daniel cell is almost the only one in which the work is equal to the heat effect of the current-forming reaction. For the overwhelming majority of voltaic cells, the heat effect exceeds the electric work obtained. Being highly important, Raoult's electrochemical studies still did not bring scientific recognition to the author.

Beginning in 1870, Raoult makes the scope of his research work wider and pays increasing attention to various purely chemical studies, even though attempting to consider physical aspects of each chemical problem. Raoult studied the composition of natural gas from a deposit near Grenoble, examined the sorption of ammonia by ammonium nitrate, established the effects of light on the rate of inversion of cane-sugar, and considered how the content of CO_2 in the atmosphere affect breathing. During the period from 1870 till 1882, Raoult published 14 papers devoted to chemical issues in the *C. R. Acad. Sci. Paris*. All of these were carefully performed, but less interesting than those belonging to the preceding series of studies in the field of thermochemistry of electrochemical processes [4, 5].

In the late 1870s, Raoult found a new area of research and developed it for many years to come. In 1878 appeared the first Raoult's publication reporting the results obtained in determining the freezing point of the solvent in a solution (*C. R. Acad. Sci. Paris, Ser. 2*, 1878, vol. 87, p. 167). Already at the very beginning of his studies, Raoult established proportionality between the depression of the freezing point, reduction of the vapor pressure, and elevation of the boiling point. Aqueous solutions of both organic and inorganic compounds served as objects of study. In a separate set of experiments, water was replaced with benzene and other organic solvents.

In 1886, Raoult commenced measurements of vapor pressure in nonaqueous solutions, because salts and saltlike substances exhibited an anomalous behavior in aqueous solutions. Numerous experiments allowed Raoult to establish the independence of the molecular reduction of the vapor pressure from the nature of a solute, with only the ratio of the number of solvent molecules to that of solute molecules being important.

Summarizing the aforesaid, it may be stated that the main Raoult's contribution to investigation of solutions consisted in that he established, based on a vast experimental material accumulated by his predecessors, a simple and direct relationship between the solution composition, on the one hand, and reduction of the vapor pressure over a solution, depression of the melting point, and elevation of the boiling point, on the other. As already mentioned, Raoult's works in the field of solutions favored the development of a number of areas of research in the incipient physical chemistry. It became possible to determine from the depression of the freezing point the molecular weights of numerous liquids and solids that do not vaporize without decomposition, especially among organic compounds. Cryoscopic measurements affected the development of the method for analysis of substances, named thermal analysis by G. Tammann (1861–1938). An important conclusion from Raoult's studies was made by S. Arrhenius. In 1887, a quantitative explanation of violations of Raoult's law in aqueous solutions of salts, acids, and alkalis served as evidence in proof of the theory of electrolytic dissociation.

Raoult's studies of properties of solutions became widely known, they are described in courses of physical chemistry of any level. In historical regard, these investigations were analyzed in detail in monographs by P.I. Walden [6], Yu.I. Solov'ev [7], and J. Partington [8]. The results of basic Raoult's results were presented in the already mentioned lecture by van't Hoff [1], included in the collection of his selected works [2]. Raoult's cryoscopic investigations are considered in [9], where a certain biographic evidence is also presented. Raoult's contribution to the development of chemistry was noted by B.N. Menshutkin [10], a known historian of chemistry. Raoult's law and all its violations are discussed in detail in terms of the present-day concepts in a monograph by T.N. Sumarokova [11] and in numerous publications by M.I. Usanovich [12].

By 1888, Raoult became one of the best known French chemists, his investigations are highly appreciated. In 1889, he was awarded an International prize in chemistry. The British Royal Society awarded to Raoult the Davy medal; in 1895, he became a recipient of the Award of the French Academy of Sciences; in 1900, Raoult was decorated with the highest State

Award of France, he became chevalier of the Legion d'Honneur.

In 1890, the scientist was elected a corresponding member of the French Academy of Sciences and an honorary (foreign) member of the Rotterdam Scientific Society. In 1892, Raoult was elected an honorary member of the Manchester Literary and Philosophical Society; in 1898, he became a member of the London Chemical Society; in 1899, he was elected a foreign corresponding member of the St. Petersburg Academy of Sciences.

In April 1900, Raoult reached the retirement age, but, by decision of the council of the University of Grenoble, he was left in his position (in supernumerary status). By that time this was the proof of the high appreciation of his activities. In 1900 and 1901, Raoult published two extensive papers in which he presented his modern views on measurements of the vapor pressure (*La tonométrie*, Paris, 1900) and on cryoscopy (*La cryoscopie*, Paris, 1901). The known bibliographic reference book by Poggendorf lists more than 100 Raoult's papers (1898, vol. III, p. 1089; 1904, vol. IV, p. 1212). A large number of references to the most important Raoult's studies can be found in [1, 2, 6, 7].

Van't Hoff was not personally acquainted with Raoult and only rarely exchanged letter with him. Nevertheless, when assessing Raoult's personal qualities, van't Hoff wrote: "Raoult's personality is seen from his works: activity, patience, immense persistence and purposefulness, fine keenness of observation, especially in minutest details, and total independence in opinions and conclusions. At the same time, his self-criticism and acceptance of others' opinions together with those of his own, calm analysis of these opinions with a solid confidence that the final word belongs to the experiment. These features of his personality can be found on any page of his works and this should be known by the entire chemical community" [2]. He continued, with reference to a letter from Mrs. Raoult: "All of those who knew him in his private life always highly appreciated his good nature, elegancy, intellectuality, exclusive kindness, and modesty in any circumstances."

The sudden death of François Marie Raoult on April 1, 1901, was a tremendous loss not only to his relatives and friends, but also to the entire university, whole Grenoble, and the French science in general. The most prominent scientific journals published obituaries devoted to Raoult and noted that he had been an outstanding physical chemist of world level [13, 14].

REFERENCES

1. Van't Hoff, J.H., *J. Chem. Soc. Trans*. (London), 1902, vol. 81, pp. 969–981.
2. Van't Hoff, J.H., *Izbrannye trudy po khimii* (Selected Works in Chemistry), Moscow: Nauka, 1984.
3. Ostwald, W., *Elektrochemie, ihre Geschichte und Lehre*, Leipzig: Veit, 1896.
4. *Istoriya ucheniya o khimicheskom protsesse: Vseobshchaya istoriya khimii* (A History of the Theory of the Chemical Process: General History of Chemistry), Solov'ev, Yu.I., Ed., Moscow: Nauka, 1981.
5. Kuslan, L.I., *Dictionary of Scientific Bibliography*, New York: Charles Scribner's Sons, 1981, vol. 11, pp. 297–300.
6. Walden, P.I., *Teorii rastvorov v ikh istoricheskoi posledovatel'nosti* (Theories of Solutions in Their Historical Sequence), Petrograd: Nauch. Khim.-Tekh., 1921.
7. Solov'ev, Yu.I., *Istoriya ucheniya o rastvorakh* (A History of the Theory of Solutions), Moscow: Akad. Nauk SSSR, 1959.
8. Partington, J.R., *A History of Chemistry*, London, 1964, vol. 4.
9. Getman, F.H., *J. Chem. Educ*., 1936, vol. 13, no. 3, pp. 153–155.
10. Menshutkin, B.N., *Khimiya i puti ee razvitiya* (Chemistry and Ways of Its Development), Moscow: Akad. Nauk SSSR, 1937.
11. Sumarokova, T.N., *Kriometriya* (Cryometry), Alma-Ata: Nauka, 1970.
12. Usanovich, M.I., *Issledovaniya v oblasti teorii rastvorov i teorii kislot i osnovanii: Izbrannye trudy* (Investigations in the Theory of Solutions and Theory of Acids: Selected Works), Alma-Ata: Nauka, 1970.
13. Jones, H.C., *Science*, 1901, vol. 13, no. 336, pp. 881–883.
14. Ramsay, W., *Nature*, 1901, vol. 54, no. 1644, pp. 17–18.

A. G. Morachevskii

Russian Journal of Applied Chemistry, Vol. 78, No. 6, 2005, pp. 859–864. Translated from Zhurnal Prikladnoi Khimii, Vol. 78, No. 6, 2005, pp. 881–886.
Original Russian Text Copyright © 2005 by Malkov, Sosnov, Malygin.

INORGANIC SYNTHESIS AND INDUSTRIAL INORGANIC CHEMISTRY

Thermal Transformations of Titanium Oxochloride Nanostructures on Silica Surface

A. A. Malkov, E. A. Sosnov, and A. A. Malygin

St. Petersburg State Technological Institute (Technical University), St. Petersburg, Russia

Received March 2, 2005

Abstract—The nature of thermal transformations of titanium oxochloride surface groups on dispersed silica in the temperature range 25–600°C, both in the course of $TiCl_4$ chemisorption and in subsequent thermal treatments, is considered.

The problem of titanium(IV) chemisorption on silica has been studied extensively [1–10]. The available body of data indicates that the $TiCl_4$ chemisorption on silica in a wide temperature range mainly occurs by the reaction of electrophilic substitution of a proton in silanol groups to give titanium oxochloride groups $(\equiv Si–O–)_nTiCl_{4-n}$, where n = 1–3. The parameter n is used to evaluate the functionality of a surface group, i.e., the number of bonds between this group and the initial silica matrix. The functionality of titanium oxochloride surface structures formed in $TiCl_4$ chemisorption largely depends on the initial concentration of silanol groups, which is determined by the temperature T_0 of preliminary annealing of silica [2]. A review of the available experimental data on the influence exerted by T_0 on the nature of $TiCl_4$ chemisorption makes it possible to reveal the general pattern consisting in that the Cl/Ti ratio in surface groups increases from 1 to 3 as the concentration of ≡Si–OH decreases (with increasing T_0) [2, 6]. However, comparison of the results of syntheses performed at the same T_0 by different authors shows that the values of n widely vary. In the case of silicas thermally treated at moderate temperatures (180–300°C), the Cl/Ti ratio in the products synthesized varied between different studies from 0.5 to 2.6 [6]. Such strong discrepancies may occur for several reasons.

First, the concentration and topography of the reactive OH groups of silicas thermally treated at the same temperature, but obtained using different methods may widely differ [11].

Second, the accessibility of the OH groups to $TiCl_4$ molecules is determined both by the size of SiO_2 particles themselves and by the pore size [12]. In the case of nonporous pyrogenic silicas (aerosils), the nature of the interaction is affected by the curvature of the surface. For example, $TiCl_4$ chemisorption on an aerosil with $S_{sp} \geq 300$ $m^2 g^{-1}$ (particle diameter ≤8.5 nm) mainly yields $–OTiCl_3$ groups [9], each, in the authors' opinion, shielding two OH groups, which do not enter into the reaction because of the structural inaccessibility. The decrease in the radius of curvature of SiO_2 particles in aerosils with a smaller S_{sp} results in that chemisorption on these aerosils chemisorption occurs to give, in addition to $–OTiCl_3$ groups, also $(–O–)_2TiCl_2$ groups [9]. Presence of a porous structure in dispersed silicas (silica gels, silochromes), which have a negative radius of curvature of the pore surface, provides in $TiCl_4$ chemisorption not only a higher degree of hydroxylation of the pore surface as compared with pyrogenic forms of SiO_2, but also a firmer binding of titanium(IV) chloride molecules to give three bonds between titanium oxochloride structures and the surface, $(–O–)_3TiCl$ [1].

Third, the structure of titanium oxochloride groups is also affected by the experimental conditions (pressure, gaseous or liquid reaction medium, static or dynamic treatment modes, etc.). In $TiCl_4$ chemisorption from a solution of *n*-heptane or in a vacuum under static conditions, mostly $–OTiCl_3$ groups are formed on the surface of dehydrated silica [6]. Carrying out chemisorption under the same temperature conditions in a flow-through system with simultaneous removal of gaseous reaction products (HCl) makes it possible to shift the equilibrium toward a more complete course of the reaction [1]. In this case, the multiplicity of bonding between a titani-

1070-4272/05/7806-0859 © 2005 Pleiades Publishing, Inc.

Table 1. Influence of temperature of $TiCl_4$ chemisorption on the chemical composition of titanium oxochloride groups on ShSKG silica gel (T_0 = 600°C, content of OH groups [OH_{in}] = 1.66 mmol g_0)

T_{CS}, °C	g SiO_2/g	Content, mmol g_0		Cl/Ti	Relative content of indicated groups, %			OH_{spent}, %	Δm_{CS}, mg g_0^{-1}	
		Ti	$OH_{consumed}$		$-TiCl_3$	$=TiCl_2$	$\equiv TiCl$		chemical analysis	TG
25	0.925	0.67	0.69	2.97	97	3	–	41	101.2	103.8
100	0.925	0.75	1.16	2.44	44	56	–	70	99.3	–
200	0.928	0.73	1.29	2.23	23	77	–	78	91.8	88.5
300	0.942	0.58	1.20	1.93	–	93	7	73	66.3	–
400	0.950	0.49	1.08	1.80	–	80	20	65	53.6	–
500	0.950	0.50	1.12	1.75	–	75	25	68	53.7	–
600	0.951	0.49	1.16	1.65	–	65	35	70	51.4	51.9

um oxochloride group and the surface increases. Presence of trace amounts of moisture in the reaction medium (χ_{H_2O} > 16 mg m^{-3}) may distort the true value of the Cl/Ti ratio in surface groups on silica [13]. An additional important factor that affects the nature of chemisorption and the structure of the forming surface groups is the temperature at which the stage of $TiCl_4$ chemisorption is carried out (T_{CS}) or the products obtained are calcined (T_T) [14–16]. It may be assumed, on the basis of the results of [14, 15], that transformations caused by thermal instability of the titanium oxochloride groups synthesized may occur in the forming surface monolayer in the course of synthesis at temperatures higher than 200°C.

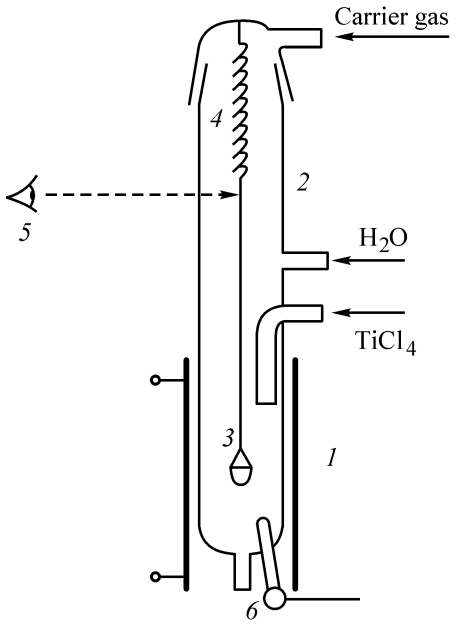


Fig. 1. Reactor with a quartz McBain balance. (*1*) Furnace for indirect heating, (*2*) flow-through quartz reactor, (*3*) vessel for silica, (*4*) quartz spring, (*5*) cathetometer, and (*6*) thermocouple.

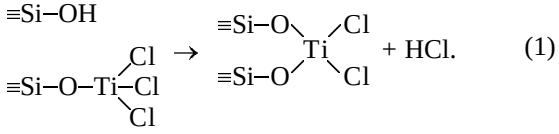
The aim of this study was to examine $TiCl_4$ chemisorption on silica and the subsequent thermal transformations of the reaction products in the temperature range 25–600°C.

The experiments were carried out with broad-porous silica of ShSKG brand (0.2–0.4-mm fraction), which was purified to remove iron ions by the procedure described in [17] and had a specific surface area (S_{sp}) of 235 $m^2 g^{-1}$, measured by the BET technique from low-temperature adsorption of air [18]. All silica samples were subjected to a preliminary thermal treatment at 600°C in air and then in a flow of dried argon for 6 h. After that the samples were treated with a $TiCl_4$ vapor at a fixed temperature T_{CS} in the range 25–600°C. The experiments were performed in flow-through conditions, which ensured continuous removal of gaseous reaction products from the reaction zone [13]. The thermal transformations of titanium oxochloride groups were studied in a flow-through reactor with a quartz-spring McBain balance (spring rate 3.3 mg mm^{-1}) (Fig. 1) on the basis of variation of the sample mass. In addition, the chemical composition of the initial samples and final solid and gaseous products of thermal transformations was monitored using the known techniques [19]. IR spectroscopic studies of products with surface titanium oxochloride groups were performed in the course of formation and subsequent thermal transformations on an IKS-29 instrument. The spectra were measured *in situ* in a flow-through reactor combined with a quartz cuvette with KBr windows [10]. The synthesis products were analyzed for the content of titanium(IV) [2, 20] and chloride ions [21]. To obtain the true stoichiometric ratios, the content of titanium(IV), chloride ions, and OH groups was recalculated to 1 g of anhydrous silica (to 1 g_0) [2].

Table 1 lists the chemical composition of products formed in interaction at various T_{CS} between $TiCl_4$ vapor and silica subjected to a preliminary thermal

treatment at 600°C. It can be seen that chemisorption of titanium(IV) chloride at 25°C yields mostly $-OTiCl_3$ surface groups (Cl/Ti ratio ~3.0). Raising T_{CS} to 100°C leads to a decrease in the Cl/Ti ratio in the synthesis products to 2.44, which indicates that polyfunctional titanium oxochloride structures are formed on the surface in this case. Together with the increase noted as T_{CS} is raised to 100–200°C, an increase in the content of titanium(IV) in the chemisorption products to 1.88–1.85 titanium atoms per 1 nm^2 is observed, compared with 1.68 titanium atoms per 1 nm^2 in samples obtained at 25°C (Fig. 2, curve *1*). Also significantly increases the consumption of OH groups in the reaction (from 41% at 25°C to 70–78% at 100–200°C, respectively). If T_{CS} is elevated further, the number of bonds between chemisorbed molecules and the surface increases, the total content of titanium(IV) and chloride ions decreases, and the number of OH groups involved in the reaction remains virtually unchanged.

To reveal the reasons for the above transformations, the possible ways in which temperature affects the system synthesized are now considered. It may be assumed that raising the chemisorption temperature from 25 to 100°C must lead to intensification of deformation vibrations of surface OH groups of the silica matrix and chemisorbed groups. Also possible is appearance at elevated temperatures of rotational degrees of freedom of surface OH groups about the bond between the oxygen atom of the OH group and silicon [22]. The whole set of the reasons mentioned above, as well as the known ability of surface silicon–oxygen tetrahedra in silicas to change without activation the Si–O–Si valence angle in the range 120–180°C [23], may lead to the following interactions of chemisorbed $-OTiCl_3$ groups with the unconsumed silanols by the scheme



(1)

The formation of titanium oxochloride groups bifunctionally bound to the silica surface, which occupy a significantly smaller surface area as compared with monofunctional groups ($S_{TiCl_3} \approx 0.37$ nm^2, $S_{TiCl_2} \approx 0.21$ nm^2)[1] leads to an increase in the consumption of the initial OH groups (Table 1). A calculation of the amount of OH groups consumed in chemisorption at T_{CS} = 100–600°C yields 1.17 ± 0.07 mmol g_0^{-1}, compared with 0.72 ± 0.03 mmol g_0^{-1}, the value characteristic of the samples obtained at T_{CS} = 25°C. Syntheses at $T_{CS} \geq 200$°C are accompanied by a decrease in the content of titanium(IV) and chloride ions in the surface groups synthesized, which is apparently due to their thermal instability [14, 15].

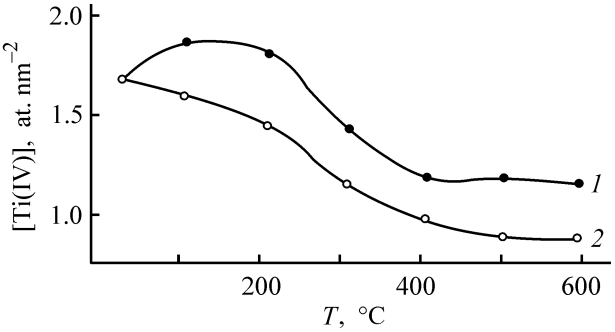


Fig. 2. (*1*) Concentration of Ti(IV) per unit surface area of Ti vs. the temperature T of $TiCl_4$ chemisorption and (*2*) variation of the same concentration in the course of thermal transformations of the product of chemisorption at T_{CS} = 25°C.

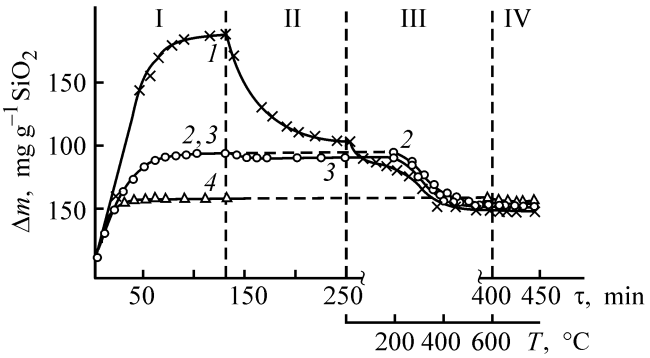


Fig. 3. Change in the sample mass, Δm, vs. time τ and temperature T of treatment of ShSKG silica gel with a $TiCl_4$ vapor and subsequent thermal treatment. T_0 = 600°C. T_{CS} (°C): (*1*) 25, (*2*, *3*) 200, and (*4*) 600. Stage: (I) $TiCl_4$ chemisorption, (II) $TiCl_4$ desorption in a flow of a carrier-gas at (*1*) 25 and (*3*) 200°C, (III) $TiCl_4$ desorption in thermal treatment of samples in a flow of the carrier-gas on raising T_T to 600°C, and (IV) $TiCl_4$ desorption in a flow of the carrier-gas at 600°C.

To verify the assumption made, the influence exerted by thermal treatment on the composition and structure of titanium oxochloride groups synthesized at 25°C was studied (Table 2; Fig. 3, curve *1*). For this purpose, a sample after chemisorption at T_{CS} = 25°C was subjected to a stepwise thermal annealing in a flow of an inert gas in the range 100–600°C, with the sample kept at each fixed temperature until

[1] The calculation was performed using the covalent radii of titanium, chlorine, and oxygen atoms, with account of the percentage of the ionic nature of bonding.

Table 2. Chemical composition of titanium oxochloride groups upon $TiCl_4$ chemisorption at 25°C by ShSKG silica gel and subsequent thermal treatment in the temperature range 100–600°C (T_0 = 600°C, content of OH groups 1.66 mmol g_0^{-1})

T_T, °C	g SiO_2/g	Content, mmol g_0^{-1}		Cl/Ti	Relative amount of indicated groups, %			Evolution, mmol g_0^{-1}		$\Delta Cl/\Delta Ti$
		Ti	$OH_{consumed}$		$-TiCl_3$	$=TiCl_2$	$\equiv TiCl$	ΔTi	ΔCl	
25	0.925	0.67	0.69	2.97	97	3	–	0.00	0.00	–
100	0.929	0.64	0.73	2.85	85	15	–	0.03	0.12	4.03
200	0.934	0.58	0.72	2.77	77	23	–	0.08	0.34	4.21
400	0.954	0.40	0.76	2.11	11	89	–	0.26	1.04	3.97
600	0.957	0.37	0.75	1.98	–	98	2	0.29	1.18	4.01

the evolution of chlorine-containing gaseous products ceased and a constant mass was reached. It can be seen from the data in Table 2 and curve *2* in Fig. 2 that calcination of a sample with titanium oxochloride groups obtained at 25°C leads to a decrease in the content of titanium(IV) and chloride ions, Cl/Ti ratio, and total mass. At the same time, calculation of the amount of OH groups involved in the formation of titanium oxochloride groups from the stoichiometric Cl/Ti ratio yields a virtually invariable value (0.72 ± 0.03 mmol g_0^{-1}) in the entire temperature range under consideration.

Analysis of the gaseous products at the reactor outlet in the course of stepwise heating demonstrates that titanium(IV) and chloride are present ions in a molar ratio close to 4 (4.06 ± 0.09). The results obtained indicate that the empirical formula of volatile compounds evolved in annealing is $TiCl_4$.

With account of the experimental data obtained, the possible course of interfunctional interactions of titanium oxochloride groups on the silica surface under thermal treatment can be represented as

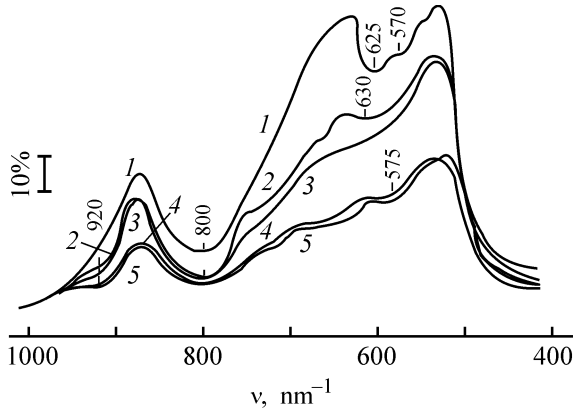
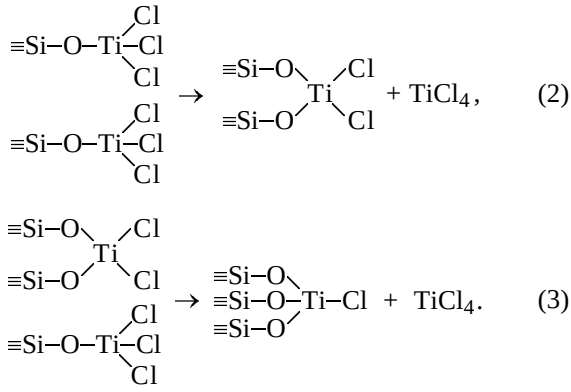


Fig. 4. IR transmission spectra of (*1*) initial silica gel with T_0 = 600°C, (*2*) that after $TiCl_4$ chemisorption at 25°C, and that after the subsequent thermal treatment at (*3*) 200, (*4*) 400, and (*5*) 600°C. (ν) Wave number.



The interfunctional interactions between $-OTiCl_3$ groups are the most pronounced in the T_T range 100–400°C, which points to a thermally activated nature of the rearrangement process. Its activation energy ΔE_a can be evaluated as

$$\Delta E_a = kN_A(T_T - T_{CS}), \quad (4)$$

where N_A is the Avogadro number and k is the Boltzmann constant. In the initial stage of the process (T_T = 25–100°C), the activation energy does not exceed 1 kJ mol^{-1}. At T_T > 400°C, the Cl/Ti ratio in the surface groups becomes less than 2.11, i.e., the remaining amount of closely spaced monofunctional titanium oxochloride groups is nearly zero, and, as a consequence, further decrease in the Cl/Ti ratio suggests that interfunctional transformations between $(-O-)_2TiCl_2$ and $-OTiCl_3$ groups in accordance with scheme (3) are possible. It should be noted here that, despite the removal of a part of titanium(IV) atoms from the surface in the form of $TiCl_4$, the amount of Si–O–Ti bonds between the silica substrate and surface titanium oxochloride groups remains virtually constant according to the results of a chemical analysis (Table 2). This is confirmed by IR spectroscopic studies of the products of thermal transformations (Fig. 4): the intensity of the ab-

sorption band at 920 cm^{-1}, which is associated with Si–O–Ti bonds, remains unchanged [7, 10]. The experimentally established pattern of structural-chemical transformations on the silica surface is in a good agreement with the results of a quantum-chemical simulation of structural transformations on the silica surface [24]. It was demonstrated in [24], based on the values obtained for the change in the Gibbs energy, that structural transformations of monofunctional, as well as mono- and bifunctional, titanium oxochloride groups with evolution of $TiCl_4$ into the gas phase proceed without any thermodynamic hindrance. The authors noted that an interaction between two structures bound to the surface by a single bond is more favorable than the reaction between the mono- and bifunctional groups.

The results obtained are in a good agreement with the previously made assumption that, depending on T_{CS}, interfunctional interactions may occur on the surface already directly in the course of synthesis, which results in that mostly $(–O–)_2TiCl_2$ and $(–O–)_3TiCl$ groups are formed at elevated temperatures [15]. Now, the experimentally determined content of chloride ions $[Cl_{exp}]$ in the products formed in interaction of $TiCl_4$ with silica at temperatures of 200–800°C [15] and the calculated Cl_{calc} in the samples obtained are compared on the assumption that mostly $TiCl_4$ is removed from the surface of silica containing titanium oxochloride groups on elevating the temperature from 200°C to T_{CS} at constant T_0:

$$(Cl_{calc})T_{CS} = (Cl_{exp})_{200} - 4[(Ti)_{200} - (Ti)_{T_{CS}}]. \quad (5)$$

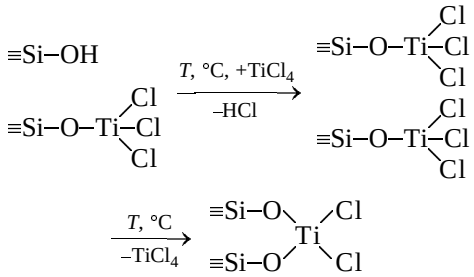
The good agreement between the experimentally determined and calculated content of chloride ions in titanium oxochloride groups (Table 3) convincingly confirms that interfunctional rearrangements of surface groups can occur directly in synthesis by the suggested schemes (2) and (3). It should be noted that the excess of $TiCl_4$ in the gas phase can strongly affect the process of interfunctional rearrangements. As can be seen from schemes (2) and (3), the occurrence of interfunctional interactions does not change the amount of OH groups consumed in chemisorption. However, a rearrangement in an inert medium (Table 2) results in that a significantly smaller amount of OH groups is consumed in the reaction even at T_T = 400–600°C, compared with the case of chemisorption under the same temperature conditions (Table 1). In all probability, presence of an excess amount of $TiCl_4$ ensures, under the conditions of a thermal treatment, an additional interaction of

Table 3. Comparison of the amount of chloride ions in titanium oxochloride groups, determined experimentally [15] and calculated by formula (5)

T_{CS}, °C	T_0, °C					
	300	400	500	600	700	800
300	1.88* 1.89	1.62 1.69	1.56 1.55	1.08 1.11	0.94 0.95	0.74 0.74
400		1.37 1.35	1.11 1.18	0.72 0.87	0.73 0.72	0.68 0.67
500			0.91 1.05	0.76 0.86	0.71 0.73	0.66 0.66
600				0.72 0.80	0.75 0.73	0.65 0.67
700					0.70 0.73	0.66 0.69
800						0.66 0.65

* Cl_{calc}, mmol g_0^{-1}/Cl_{exp}, mmol g_0^{-1}.

the $–OTiCl_3$ group with silanols, which can be represented as



(6)

Thus, the nature of thermal transformations of titanium oxochloride groups on the silica surface at 25–600°C depends on whether the initial reagent $TiCl_4$ is present or absent in the reaction space. In the presence of $TiCl_4$, the consumption of the initial OH groups grows from 40 to 70% as temperature increases from room temperature to 100°C and more, which is due to thermal activation of the chemisorption process. The dependence of the content of Ti(IV) is more complex: the Ti(IV) addition density per unit surface area grows as the chemisorption temperature increases from room temperature to 100–200°C and then decreases, approaching a constant value at T_{CS} of 400–600°C. The steady decrease in the Cl/Ti ratio in synthesis products from 3.0 to 1.65, observed in the entire temperature range under consideration, indicates that the amount of bonds between the groups synthesized and the silica surface increases.

In the absence of the initial reagent in thermal treatment in a flow of an inert gas, there occur structural-chemical transformations of monofunctionally bound titanium oxochloride groups, accompanied by evolution of $TiCl_4$ into the gas phase and formation of groups predominantly bifunctionally bound to the surface.

ACKNOWLEDGMENTS

The study was supported by the Program "Leading Scientific Schools of Russia" (project NSh 2236.2003.3 "Chemistry of Highly Organized Substances"), Russian Foundation for Basic Research (grant no. 04-03-32048), and programs of the Ministry of Science and Education of the Russian Federation.

REFERENCES

1. Kol'tsov, S.I., *Zh. Prikl. Khim.*, 1967, vol. 40, no. 4, p. 907.
2. Kol'tsov, S.I. and Aleskovskii, V.B., *Zh. Fiz. Khim.*, 1968, vol. 42, no. 5, pp. 1210–1214.
3. Kohlschutter, H.W. and Bogel, U., *Fortschr. Kolloide Polym.*, 1971, vol. 55, no. 1, pp. 29–33.
4. Velikova, M., Damyanov, D., and Mehandjiev, D., *BAS Commun. Depart. Chem.*, 1979, vol. 12, no. 4, pp. 647–651.
5. Chuiko, A.A., Tertykh, V.A., Kazakov, K.P., *et al.*, *Adsorbts. Adsorbenty*, 1980, no. 8, pp. 34–42.
6. Damyanov, D., Velikova, M., Ivanov, Iv., and Vlaev, L., *J. Non-Cryst. Solids*, 1988, vol. 105, no. 1, pp. 107–113.
7. Morrow, B.A. and McFarlan, A.J., *J. Non-Cryst. Solids*, 1990, vol. 120, no. 1, pp. 61–71.
8. Kytökivi, A. and Haukka, S., *J. Phys. Chem.*, 1997, vol. 101B, pp. 10365–10372.
9. Koval'kov, V.I., Malygin, A.A., Kol'tsov, S.I., and Aleskovskii, V.B., Available from VINITI, 1976, Leningrad, no. 1747–76Dep.
10. Khabibova, S.V., Tolstoi, V.P., Malkov, A.A., and Malygin, A.A., *Zh. Prikl. Khim.*, 1989, vol. 62, no. 2, pp. 341–344.
11. Lygin, V.I., *Zh. Fiz. Khim.*, 1997, vol. 71, no. 10, pp. 1735–1742.
12. Ellestad, O.H. and Blindheim, U., *J. Molec. Catal.*, 1985, vol. 33, no. 3, pp. 275–287.
13. Sosnov, E.A., Malkov, A.A., and Malygin, A.A., *Zh. Prikl. Khim.*, 2000, vol. 73, no. 7, pp. 1074–1080.
14. Riis, T., Dahl, J.M., and Ellestad, O.H., *J. Molec. Catal.*, 1983, vol. 18, no. 2, pp. 203–214.
15. Sosnov, E.A., Malkov, A.A., and Malygin, A.A., *Zh. Prikl. Khim.*, 1988, vol. 61, no. 1, pp. 29–34.
16. Haukka, S., Lakomaa, E.-L., and Root, A., *J. Phys. Chem.*, 1993, vol. 97, no. 19, pp. 5085–5094.
17. Kol'tsov, S.I. and Aleskovskii, V.B., *Silikagel', ego stroenie i khimicheskie svoistva* (Silica Gel: Structure and Properties), Leningrad: Goskhimizdat, 1963.
18. Klyachko-Gurvich, L.A., *Izv. Akad. Nauk SSSR, Otd. Khim. Nauk*, 1968, vol. 26, no. 10, pp. 1884–1891.
19. Malkov, A.A., Sosnov, E.A., and Malygin, A.A., *Zh. Prikl. Khim.*, 2004, vol. 77, no. 8, pp. 1245–1248.
20. Bulatov, M.I. and Kalinkin, I.P., *Prakticheskoe rukovodstvo po fotometricheskim metodam analiza* (Manual of Photometric Analytical Techniques), Leningrad: Khimiya, 1986.
21. Frumina, N.S., Lisenko, N.F., and Chernova, M.A., *Khlor* (Chlorine), Moscow: Nauka, 1983.
22. Ogenko, V.M., Rozenbaum, V.M., and Chuiko, A.A., *Teoriya kolebanii i pereorientatsii poverkhnostnykh grupp atomov* (Theory of Vibrations and Reorientations pf Surface Groups of Atoms), Kiev: Naukova Dumka, 1991.
23. Gibbs, G.V., *Amer. Minner.*, 1982, vol. 67, no. 1, pp. 421–428.
24. Kulakov, N.V. and Dubrovenskii, S.D., Abstracts of Papers, *Nauchno-prakticheskaya konferentsiya "Khimicheskie nanotekhnologii i funktsional'nye materialy" IV Mezhdunarodnogo kongressa khimicheskikh tekhnologii, 28–31 oktyabrya 2003 g. Sankt Peterburg* (Sci.-Pract. Conf. "Chemical Nanotechnologies and Functional Materials" at IV Int. Congr. For Chemical Technologies, October 28–31, 2003, St. Petersburg), St. Petersburg: RESTEK, 2003, pp. 36–37.

Russian Journal of Applied Chemistry, Vol. 78, No. 6, 2005, pp. 865–869. Translated from Zhurnal Prikladnoi Khimii, Vol. 78, No. 6, 2005, pp. 887–890.
Original Russian Text Copyright © 2005 by Charykov, Alekseev, Arapov, Alekhin, Gerasimov, Nekrasov, Polekhovskii, Semenov.

INORGANIC SYNTHESIS AND INDUSTRIAL INORGANIC CHEMISTRY

Modification of Natural Shungites To Obtain a Mixed Nanocarbon Material (MNS)

N. A. Charykov, N. I. Alekseev, O. V. Arapov, O. S. Alekhin, V. I. Gerasimov, K. V. Nekrasov, Yu. S. Polekhovskii, and K. N. Semenov

Innovatsii Leningradskikh institutov i predpriyatii (Innovations by Leningrad Institutes and Enterprises) Private Company, St. Petersburg, Russia

Ioffe Physicotechnical Institute, Russian Academy of Sciences, St. Petersburg, Russia

St. Petersburg State University, St. Petersburg, Russia

Received February 8, 2005

Abstract—An original technology for processing of a natural material, shungite-3 from the Zazhogino deposit (Karelia), was developed in order to obtain a new product, mixed nanocarbon material (MNS).

It is suggested to obtain a nanocarbon material (MNS) by using the available natural raw material, shungite rock widely occurring in the geologic profile of the world's largest Onega basin (Republic of Karelia) of Precambrian black-shale sedimentation. To the shungite rock is commonly related a large group of compositionally different carbon-containing Precambrian geologic formations. Commonly, rocks with 5–10% shungite substance are named shungitious, and those with 0.5–5%, shungite-containing. To high-carbon shungite rocks belong those in which the content of free shungite carbon exceeds 20%.

The total estimated resources of the shungite rock of the Onega basin according to Mikhailov [1] exceed one billion tons (1041 million), and the prospected resources (of classes B + C1 + C2) of the largest Zazhogino deposit (in Medvezh'egorskii district) are 148.8 million tons (reserves 321.8 million tons), with the average content of the shungite carbon, e.g., in the Maksovskaya bed, is about 31%.

Shungite (shungite rock) of the Zazhogino deposit is, on the average, composed of 30% carbon and 70% silicates [2]. It is by the content of carbon that it is referred [2] to the third variety of shungite rocks (shungite-3), or, according to the geological-genetic classification by Filippov, to maxovites, which are saprobitumolite rocks having the form of a fine homogeneous mixture of a shungite substance and a cryptocrystalline mineral substance. The conditions of the regional metamorphism of shungite rocks correspond to the chlorite and biotite zones of the greenshale facies. The microelements found in these rocks are Fe, Ti, V, Ni, Cu, and Zn, mainly in the sulfide (pyrite, pyrrhotine, sphalerite, etc.) and oxide (rutile etc.) mineral forms.

The conditions in which shungites are formed, as well as their chemical and phase composition, suggest that fullerenes and(or) fulleroid components of carbon fractions are present in natural shungites. Here and hereinafter by fullerenes are meant light fullerenes C_{60} and C_{70} and heavy fullerenes C_{76}, C_{78}, C_{84}, and C_{90}, as well as their mixtures; and by fulleroid materials are understood single- and multi-walled nabnotubes, nanobarrels, nano-onions, nanocones, and mixtures of these [4, 5].

The authors developed an original technique for mechanical and chemical processing of shungite-3 to obtain a heterogeneous catalyst. The technique includes the following processing stages: (a) decomposition of the rock in an alkaline (NaOH) melt at a temperature of 500–520°C to remove aluminosilicate and silicate components; (b) washing of carbon phases with water to remove trace amounts of the alkali, with the subsequent grinding and sieving to obtain a powder with a grain size of 80–100 μm; (c) acid treatment of carbon phases (HNO_3 65 wt %) at 60–65°C for 3–5 h to remove mixtures of metals, their oxides, and sparingly soluble salts and also to dissolve inactive amorphous carbon and graphite, which is present in carbon phases; (d) washing of carbon

1070-4272/05/7806-0865 © 2005 Pleiades Publishing, Inc.

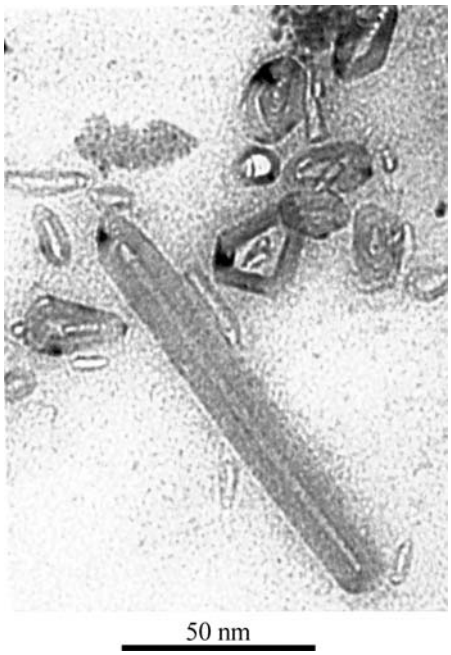


Fig. 1. Electron micrograph of modified shungite-3.

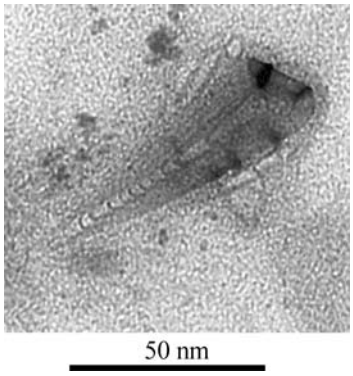


Fig. 2. Electron micrograph of a hollow nanocone in modified shungite-3.

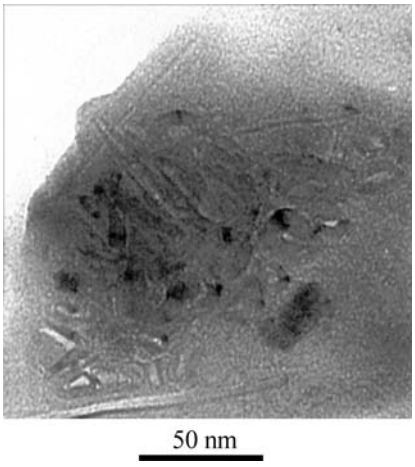


Fig. 3. Electron micrograph of a fragment of unmodified shungite-3.

phases with water to remove trace amounts of the acid and the forming salts and to oxidize the material with atmospheric oxygen at 650–700°C in the course of 10–15 h. Naturally, even if fullerenes or their derivatives were present in initial shungite samples, they would have irreversibly decomposed already in the first stage of treatment, in an alkali melt.

A natural, comparatively low-cost carbon nanomaterial was obtained for the first time by subjecting shungite-3 to a treatment of this kind. This material contained, depending on the extent of etching and quality of the starting shungite, 20 to 70 wt % fulleroid (mostly hollow) nanoparticles: multi- and single-walled nanotubes, nanobarrels, nano-onions, and nanocones. A typical electron micrograph (×500 000 magnification) of an as-modified shungite material (MNS) is shown in Fig. 1. A hollow, closed at both ends, multi-walled nanotube with a channel diameter of ~3 nm, outer diameter of ~20 nm, and length of ~0.2 μm is well seen, together with a set of fragments of singlewalled nanotubes, hollow nanobarrels, and nonhollow nano-onions. Also, rather exotic carbon nanoparticles and, in particular, hollow nanocones were found in shungite-3 (Fig. 2). Figure 3 shows for comparison a fragment image of an unmodified shungite material in which numerous fulleroid particles are embedded in silicate and aluminosilicate phases (naturally, the contrast in such an image is markedly lower than that in other images, and the fragment itself is rather untypical: fulleroid materials are rather nonuniformly distributed throughout the volume of shungite-3).

The authors estimate the total content of fulleroid particles in shungites-3 at 1 to 4 wt %, and the content of various nanotubes among other fulleroid particles may constitute 20 to 40 rel. % by mass. The total content of fulleroid particles in shungites with a high content of carbon phases may be a factor of 2 to 3 higher.

Up to 100 kg of the natural carbon nanomaterial MNS can be obtained from 1 ton of shungite-3 by the technique developed.

As the resources of oil are being exhausted all over the world, development of industrial technologies for synthesis of liquid hydrocarbons from other types of carbon-containing fossil fuels: coal, natural gas, peat, biomass of various types, etc., clearly becomes a matter of current interest.

It is suggested to use the new modified carbon material MNS, considered here, as a high-efficiency heterogeneous catalyst for processing of natural gas in a liquid, under normal conditions, mixture of hydro-

carbons (C_5-C_8). It was established in preliminary laboratory tests that MNS exhibits a rather well-pronounced sorption capacity for vapor of hydrocarbons (primarily methane) and oxygen- and nitrogen-containing compounds, hydrogen, and carbon(II) oxide, as well as for transition and heavy metals in sorption from solutions in a wide range of temperatures and pressures.

This made it possible to assume that MNS must have a high efficiency when used as a heterogeneous catalyst for processing of natural gas. Preliminary laboratory tests of MNS as a heterogeneous catalyst at temperatures of 200–450°C and pressures of up to 30 atm revealed that methane is effectively dehydrogenated to give a mixture of branched and normal saturated hydrocarbons (C_5-C_8) with a minor admixture of alkenes and aromatic compounds (up to several weight percent) at a sufficiently high completeness of methane conversion into the gasoline-ligroin fraction, of up to 30 wt %. The catalytic effect is strongly enhanced upon introduction of some elements (Ti, Zr, Al, Ru) in the form of metals and oxides into MNS in amounts not exceeding 1–2 wt %.

As analogous artificial carbon nanomaterials can be mentioned mixtures of single- or multi-walled carbon nanotubes open at both ends (SWNT and MWNT, respectively) [4] and mixtures of various fulleroid materials of unstable composition [5], the so-called astralenes (ASTR), fullerene black, or the so-called "washed" fullerene black (FB) [6]. The first two products (SWNT and MWNT) do exhibit a high heterogeneous-catalytic activity in processing of natural gas, which is comparable with that of the natural material, MNS. However, their manufacture is rather labor- and power-consuming. This is due to the use of the catalytic arc method for synthesis of SWNT, whose output capacity does not exceed 50 per 24 h per reactor, and to the necessity for subsequent multistage fine chemical purification. Similarly, the amount of SWNT and MWNT produced by CVD (chemical decomposition of carbon supports on a catalytically treated substrate) does not exceed several grams in 24 h [8], although the process of chemical purification is somewhat simpler in this case. These factors predetermine the very high cost of MWNT and SWNT. The prices for these materials are absolutely unacceptable for the chemical industry (they exceed the price of the developed material, MNS, by a factor of several hundreds). Two other types of materials are markedly less expensive; however, they have a smaller specific surface area and lower sorption capacity because the content of fulleroid carbon phases in these materials is significantly lower (up to 20–30 wt % in ASTR and not more than 1–2 wt % in FB). As a result, their heterogeneous-catalytic activity in reactions of chemicalization of natural gas is poorer than that of MNS.

The first report that fullerenes are contained in shungites appeared in 1992 [9]. Later, this issue was extensively studied, but the data obtained were contradictory. Some researchers found that the total content of fullerenes in natural shungites is about 1–3% relative to the mass of the shungite carbon [10–12], whereas others estimated it at 1–10 ppm [13]. First, we formulate what will be understood by the generalizing notion "fullerenes in shungites." These are light (C_{60} and C_{70}) and heavy (C_{76}, C_{78}, C_{84}, C_{90}, ...) fullerenes themselves, their oligomers [dimers, e.g., $(C_{60})_2$], and, possibly, some derivatives of fullerenes and their oligomers with undistorted or weakly distorted fullerene-type electronic structure: outer- and inner-sphere metal complexes; compounds with hydrogen, oxygen, sulfur, nitrogen, halogens, and hydroxy, carbonyl, and carboxyl groups with a moderate total number of substituents (≤6, best of all 1–2). We note several specific features of the analysis.

(1) When making an analysis, it is desirable to preliminarily remove from shungites silicate and, if possible, metal-containing phases, because fullerenes may be more or less strongly bound to components of these phases and, in any case, substantially blocked by these phases. This, undoubtedly, hinders their transfer into the liquid (e.g., in extraction) or vapor phase (e.g., in a mass-spectrometric determination).

(2) These phases should not be removed by strong oxidizing agents, e.g., molten alkalis, concentrated nitric or hydrochloric acid, because fullerenes are unstable in media of this kind and completely lose their fullerene structure upon oxidation.

(3) Direct determination of fullerenes in shungites (e.g., by mass-spectrometry in sublimation-ionization in a high vacuum) may lead to noticeable errors because of the possible direct synthesis of fullerenes from the carbon plasma generated directly in the course of a mass-spectrometric experiment.

In the experiments, the samples for analysis were prepared as follows:

(a) shungite-3 was ground in a ball mill;

(b) the fraction with a grain size of less than 40 μm was separated by sieving;

(c) the rock was decomposed in an acid (conc. HF) solution at 50–55°C in the course of 12–16 h to remove the aluminosilicate and silicate phases (as is known, fullerenes are quite stable against the action

of these hydrohalic acids in the comparatively mild conditions specified);

(d) a repeated acid treatment (HCl 36 wt %) at 50–55°C for 12–16 was performed to remove the mixture of metals, their oxides, and sparingly soluble salts;

(e) the carbon phases were washed with water to remove trace amounts of the acid and the forming salts;

(f) the material was dried in a vacuum oven at 100–110°C and a residual pressure of less than 0.1 mm Hg for 2 h (with carbon fractions that contain virtually zero amounts of other elements and can be used for direct chemical analysis obtained in an amount of up to 40 rel.% relative to the initial mass of the shungites);

(g) the carbon phases obtained were placed in a counterflow extractor of the type of a Soxhlet apparatus, and extraction with chemically pure *o*-dichlorobenzene, which is the most effective solvent for unmodified fullerenes [14], was carried out at 175–185°C under atmospheric pressure in the course of 240 h; (in the course of the extraction, the solvent acquired an increasingly intense yellow-brown coloration, which is rather characteristic of solutions of fullerene mixtures);

(h) the resulting solution was evaporated virtually to dryness in the vacuum oven at a pressure of 60–70 mm Hg;

(i) the residue was completely dried in the vacuum oven at 100–110°C and a residual pressure of less than 0.1 mm Hg for 8 h.

This procedure yielded a finely dispersed brown powder in an amount of 0.2–0.4 rel.% relative to the initial mass of shungites, and the sample preparation was complete.

Further, a sample was completely dissolved in chemically pure *o*-xylene and the absorption spectrum of the resulting solution was measured in the visible and near-UV spectral ranges in KU quartz cuvettes on an SF-46 instrument. The topological features of the spectrum obtained did not match the spectra of fullerenes and(or) their mixtures, dissolved in aromatic solvents [15]. For example, the band at 472 nm, characteristic of the C_{70} fullerene and heavier fullerenes is virtually absent; the UV part of the spectrum shows absorption steadily increasing as the wavelength becomes shorter; however, an exceedingly weakly pronounced, but reproducible shoulder is, nevertheless, observed at around 335.7 nm in the region characteristic of the absorption spectra of both light fullerenes. This shoulder can, in principle, be attributed to presence in the mixture of a certain, very small amount of fullerenes. A calculation performed using the absorption coefficients of light fullerenes at this wavelength [15] makes it possible to evaluate the possible content of fullerenes in shungites-3 at several hundredth of a weight percent (≤0.05 wt %). The concentrations of fullerenes were also measured by high-efficiency liquid chromatography with a UV detector (at 325 nm) upon a direct introduction of dilute samples dissolved in a mixture of *n*-hexane with toluene into the chromatographic column by the method described in [16]. As reference served solutions of individual light and heavy fullerenes and their mixtures of known composition.[1] Calculation by this method leads to virtually the same conclusion: the content of fullerenes in shungite-3 does not exceed 0.02 wt %.

CONCLUSION

The following fullerene materials were found in shungites in amounts of several weight percent: multi- and single-walled nanotubes, nanobarrels, nano-onions, nanocones (mostly hollow). Fullerenes themselves and their derivatives were virtually not detected at all by the measurement techniques employed.

REFERENCES

1. Mikhailov, V.P., *Uglerodsoderzhashchie formatsii v geologicheskoi istorii* (Carbon-containing Formation in the Geological History), Petrozavodsk: Karel'sk. Filial Akad. Nauk SSSR, 1998.
2. Sokolov, V.A., Kalinin, Yu.K., and Dyukkiev, E.F., *Shungity – novoe uglerodistoe syr'e* (Shungites, New Carboniferous Raw Materials), Petrozavodsk: Karel'sk. Filial Akad. Nauk SSSR, 1984.
3. Filippov, M.M., *Mineral'noe syr'e Karelii: Shungitovye porody Onezhskoi struktury* (Minera Raw Materials of Karelia: Shungite Rocks of the Onega Basin), Petrozavodsk: Petrozavodsk. Gos. Univ., 2002.
4. Iijima, S., *Nature*, 1991, vol. 354, pp. 56–65.
5. Harris, P.J., *Carbon Nanotubes and Related Structures*, Cambridge: Cambridge Univ., 2003.
6. Ponomarev, A.N., Barchenko, V.T., Charykov, N.A., *et al.*, *4th Bien. Int. Workshop "Fullerens and Atomic Clusters,"* St. Petersburg, 1999, p. 237.
7. Kajiura, H., Tsutsui, S., Huang, H., and Murakami, Y., *Chem. Phys. Lett.*, 2002, vol. 364, pp. 586–592.
8. Cumar, M. and Ando, J., *Chem. Phys. Lett.*, 2003, vol. 374, pp. 521–526.

[1] Manufacture by ILIP Private Company, St. Petersburg.

9. Buseck, P.R., Tsipursky, S.J., and Hettich, R., *Science*, 1992, vol. 257, pp. 215–221.
10. Polekhovskii, Yu.S. and Reznikov, V.A., *Obrazovanie i lokalizatsiya rud v zemnoi kore* (Formation and Localization of Ores in the Earth's Crust), St. Petersburg: SPb. Gos. Univ., 1999.
11. Reznikov, V.A. and Polekhovskii, Yu.S., *Zh. Prikl. Khim.*, 1999, vol. 72, no. 11, pp. 1746–1751.
12. Reznikov, V.A. and Polekhovskii, Yu.S., *Pis'ma Zh. Tekh. Fiz.*, 2000, vol. 26, no. 2, pp. 105–108.
13. Ozawa, E., *Fullerene Sci. Technol.*, 1999, vol. 7, pp. 637–658.
14. Semenov, K.N., Seregin, V.I., Arapov, O.V., and Charykov, N.A., *Russian J. Appl. Chem.*, 2004, vol. 77, no. 10, pp. 1627–1631.
15. Ponomarev, N., Yudovich, M.E., Charykov, N.A., *et al.*, *Opt. Spectr.*, 2000, vol. 88, no. 2, pp. 195–197.
16. *GOST* (State Standard) *8.563–96, Certification of MVI.*

Russian Journal of Applied Chemistry, Vol. 78, No. 6, 2005, pp. 870–879. Translated from Zhurnal Prikladnoi Khimii, Vol. 78, No. 6, 2005, pp. 891–900.
Original Russian Text Copyright © 2005 by Rubtsov, Kazakov, Kirpichev, Lempert, Manelis.

PHYSICOCHEMICAL STUDIES OF SYSTEMS AND PROCESSES

Kinetics and Mechanism of Thermal Decomposition of a Mixture of Ammonium Nitrate and Pyroxylin

Yu. I. Rubtsov, A. I. Kazakov, E. P. Kirpichev, D. B. Lempert, and G. B. Manelis

Institute for Problems of Chemical Physics, Russian Academy of Sciences, Chernogolovka, Moscow oblast, Russia

Received October 4, 2004

Abstract—The kinetics of heat release in thermal decomposition of a mixture of ammonium nitrate and pyroxylin was studied. To elucidate the mechanism of this process, the kinetics of heat release in oxidation of ammonium nitrate with nitrogen dioxide and of cellulose with a nitric acid solution was examined. The kinetic equations of the processes and the temperature dependence of the constants in these equations were established. The influence exerted by addition of diphenylamine on the rate of heat release in the system constituted by ammonium nitrate and pyroxylin was analyzed.

Pyroxylin, which is incomplete cellulose nitrate with a nitrogen content of 12–13.5%, has a negative oxygen balance; introduction of oxidizing agents into pyroxylin improves its energetic characteristics. A possible way in this direction is to use NH_4NO_3, whose mixtures with TNT (ammatols) have long been employed as explosives for various purposes [1]. An essential obstacle to application of NH_4NO_3-based formulations as composite fuels and gas-generating compositions is that phase transitions occur in NH_4NO_3, which disrupts the continuity of a sample when the temperature of the mixture passes across the phase transition temperatures. However, ways to strongly decelerate or even rule out such transitions have been under development recently. To make an objective assessment of the possibility of practical application of NH_4NO_3 mixed with pyroxylin at elevated temperatures it is necessary to study the fundamental kinetic aspects of thermal decomposition of these mixtures. Taken separately, pyroxylin and NH_4NO_3 have a thermal stability sufficiently high for many practical purposes and they are industrially manufactured in considerable amounts. However, these components can interact in a mixture, which may hinder practical application of these mixtures.

Various aspects of the reaction of thermal decomposition of pyroxylin have already been studied for about 100 years; the basic features of this process have been established and described in numerous publications [2]. The initial rate of pyroxylin decomposition has been extensively studied and the results obtained are in a satisfactory agreement [3], the rate in question being determined by the rate of NO_2 detachment from the nitrocellulose link. The fundamental aspects of how the reaction is accelerated depend on the possibility of accumulation of the reaction products and their removal into the gas phase; here, only qualitative results are available for the most part, and quantitative data, in separate cases. The influence exerted on the rate of pyroxylin decomposition by the main decomposition products, primarily by nitrogen oxides, nitric acid, and water, which all accelerate the decomposition, with the main part played by the reaction of acid hydrolysis of the nitroester bond, has been studied. However, the kinetics of heat release in pyroxylin decomposition has been the subject of only a single study [4]. Under the experimental conditions used in this study (open system in air or continuous removal of products by pumping), the autocatalysis is relatively weak and, therefore, the process was studied at a temperature of 140–165°C exceeding that used in the present study, and the decomposition kinetics was described by a first-order autocatalysis equation.

Pure NH_4NO_3 is markedly more stable and decomposes at a noticeable rate only at temperatures higher than its melting point (169°C) [2]. At the temperatures considered in this study, its own thermal transformations are insignificant. Reverse equilibrium dissociation of NH_4NO_3 into NH_3 and HNO_3 always occurs in NH_4NO_3. Although the degree of this dissociation is low, just the presence of these products in

1070-4272/05/7806-0870 © 2005 Pleiades Publishing, Inc.

the salt predetermines many of its properties. In particular, the rate of thermal decomposition of NH_4NO_3 is determined by presence of molecules of nitric acid in this compound. As HNO_3 makes higher the rate of pyroxylin decomposition, it would be expected that introduction of NH_4NO_3 into pyroxylin should also raise this rate, but the heterogeneity of the mixture may strongly hinder this influence. No direct kinetic analysis of thermal transformations in this mixture has been made, and, therefore, the aim of this study was to analyze quantitatively the kinetics of heat release in a mixture of NH_4NO_3 and pyroxylin under conditions as close as possible to those of the probable practical application of these mixtures.

EXPERIMENTAL

Industrial pyroxylin releasing 208.9 ml of NO per 1 g of the product in a standard analysis for the degree of nitration, which corresponds to a nitrogen content of about 13.1%, was used in the study. Ammonium nitrate was taken from three different sources: sample no. 1, fresh reagent of analytically pure grade, conforming to GOST (State Standard) 22867–77; sample no. 2, granulated NH_4NO_3 manufactured as a fertilizer at Kirovo-Chepetsk chemical combine; and sample no. 3, granulated NH_4NO_3 manufactured in France (Toulouse). All the NH_4NO_3 samples were preliminarily ground in an agate mortar, in order to make larger the surface area of contact between the components, and manually mixed with pyroxylin. The kinetic aspects of the thermal transformations were studied by analyzing the rate of heat release, using a DAK-1-1 differential automated calorimeter [5].

The equilibrium vapor pressures of NH_3 and HNO_3 over NH_4NO_3 strongly differ: a larger amount of NH_3 passes into the gas phase at elevated temperatures, which leads to the corresponding increase in the HNO_3 content in solid or liquid NH_4NO_3. This circumstance predetermines the dependence of the decomposition rate of NH_4NO_3 and the rate of its interaction with the other components on the gas volume of the system, V_g^0, because the rates of these processes are determined by the content of HNO_3 in the solid or liquid phase. For this reason, the experiments should be performed at as small V_g^0 as possible, in which case the deviation from stoichiometry of the initial salt and, accordingly, the decomposition rate will be lower. It is desirable to have no free gas volume at all; in this case, however, the evolving gaseous products will rapidly destroy the working ampule because of the buildup of an internal pressure exceeding its limiting strength. The experiments were performed in sealed glass ampules with an internal volume of about 2 cm^3, placed fully within the working cell of the microcalorimeter. Such experimental conditions simulate rather well the storage conditions of gas-generating compositions. It was possible to carry out the decomposition virtually to completion without disintegration of the ampule when a 0.02–0.03-g portion of pyroxylin was used. When it was necessary to use larger masses, the experiments were terminated at earlier stages of the reaction. In thermal decomposition of pyroxylin, the dependence of its rate on the gas volume is also strong: as the volume decreases, the degree of self-acceleration increases.

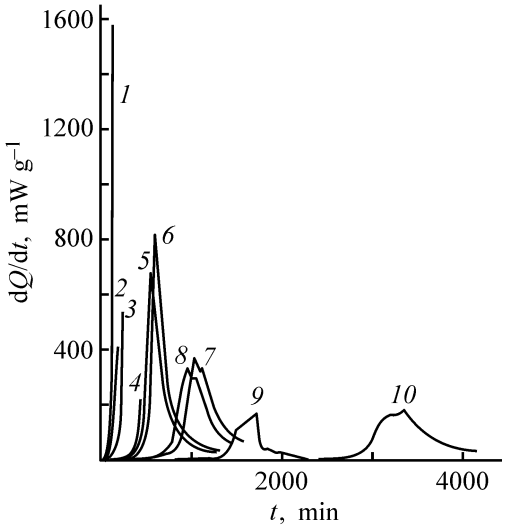


Fig. 1. Rate of heat release, dQ/dt vs. time t in thermal decomposition of a mixture of NH_4NO_3 with pyroxylin. Decomposition temperature (°C): (*1*) 121.6, (*2*) 117.1, (*3*) 112.8, (*4*) 106.3, (*5*) 104.3, (*6*) 104.3, (*7*) 99.0, (*8*) 98.9, (*9*) 96.8, and (*10*) 92.5.

First, the kinetics of heat release in thermal decomposition of the starting pyroxylin at a free gas volume V_g^0 = 65 cm^3 per 1 g of pyroxylin was studied in the temperature range 96.4–171.7°C, and that of a mixture of this pyroxylin with NH_4NO_3, under the same conditions at 92.5–121.6°C. The curves obtained for the mixture are shown in Fig. 1. The mixture contained about 30 wt % pyroxylin, which virtually corresponds to the oxygen balance, with the excess of oxygen equal to only 0.19 wt %. For all the three NH_4NO_3 samples studied, close results were obtained; sample no. 1 was used in further study. In all the experiments, the rate of heat release was calculated per 1 g of pyroxylin, which is convenient for analyzing the influence exerted by NH_4NO_3 on the heat and rate of the process; V_g^0 was also calculated per 1 g of pyroxylin.

The rate of intrinsic thermal decomposition of NH_4NO_3 at the temperatures studied is negligible, but

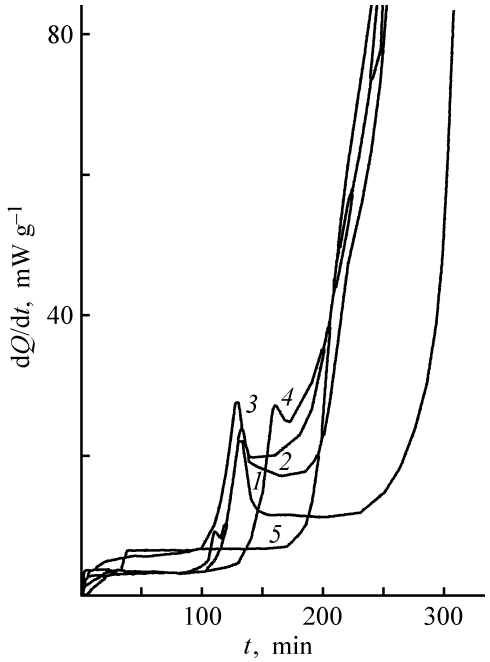


Fig. 2. Rate of heat release, d*Q*/d*t*, vs. time *t* in thermal decomposition of a mixture of NH_4NO_3 with pyroxylin at 113.3°C. NH_4NO_3 content in the mixture (wt %): (*1*) 25.05, (*2*) 39.20, (*3*) 57.46, (*4*) 77.12, and (*5*) 92.93.

it is involved in reactions with pyroxylin and products of its decomposition, which makes substantially higher the heat of the process in a mixture, compared with that in pure pyroxylin. The decomposition heat is about 3.1 kJ g^{-1} for pyroxylin and about 10.5 kJ g^{-1} for the mixtures with NH_4NO_3 under study. This points to a high extent of NH_4NO_3 involvement into the overall redox process, mainly in the reaction of NH_4NO_3 with the products formed in pyroxylin decomposition. The maximum possible heat of the process in this mixture can be calculated, provided that only liquid water and gaseous CO_2, N_2, and O_2 is formed, to be about 4.7 kJ per 1 g of the mixture or 15.8 kJ per 1 g of pyroxylin in the mixture. Comparison of the last value with that obtained in the experiment (10.5) shows that a larger part of the maximum possible heat of the process is released in thermal decomposition of the mixture.

Specific initial decomposition rates of pyroxylin and its mixture with NH_4NO_3

Pyroxylin		Pyroxylin–NH_4NO_3	
T, °C	$(d\eta/dt)_{t=0} \times 10^6$, s^{-1}	*T*, °C	$(d\eta/dt)_{t=0} \times 10^6$, s^{-1}
97	0.1	92.5	0.034
106.3	0.17	96.8	0.11
113.2	0.24	98.9	0.055
114	0.36	99	0.046
121.7	0.77	104.3	0.096
130.3	1.8	104.3	0.10
138.5	3.8	106.3	0.12
143.4	4.1	112.8	0.15
171.7	90	–	–

The initial rates of heat release in mixtures of pyroxylin with NH_4NO_3 are, on the average, 3.5 times those for pure pyroxylin, which virtually coincides with the increase in the total heat of the process. The initial specific rates for pyroxylin and mixtures $(d\eta/dt)_{t=0}$ (s^{-1}) nearly coincide and show the following temperature dependence:

$$(d\eta/dt)_{t=0} = 1.4 \times 10^{12} \exp(-138 \times 10^3/RT).$$

The rates are listed in the table.

The initial rates of heat release can be obtained from these values via multiplication by the corresponding heat of the process. Thus, introduction of NH_4NO_3 into pyroxylin has virtually no effect on the initial decomposition rate and only raises the total heat, which is apparently determined by the reaction of the products formed in pyroxylin decomposition with NH_4NO_3. The rate of this reaction must exceed the decomposition rate of pyroxylin. At the beginning of the process, HNO_3 and NH_4NO_3 have virtually no effect on the rate of pyroxylin decomposition, probably because of the heterogeneity of the mixture, and HNO_3 is in the NH_4NO_3 phase.

The values obtained for the initial rates of heat release from pyroxylin and its mixtures with NH_4NO_3 are close in magnitude to the values that can be calculated from the generalized temperature dependence of the initial decomposition rate of pyroxylin, obtained on the basis of a large number of experimental studies by different authors [3].

The influence exerted by the relative amount of the components in a mixture of NH_4NO_3 with pyroxylin on the kinetics of heat release in decomposition of the mixture was studied at 113.3°C (Fig. 2). In all the experiments, the mass of pyroxylin was the same, whereas the amount of NH_4NO_3 added was varied widely. It was found that, at the widely varying relative content of the components (40–90 wt % NH_4NO_3), the apparent rate of heat release is independent of the NH_4NO_3 content and starts to decrease only when it becomes lower than 40 wt %. The mixture under study is heterogeneous, the salt NH_4NO_3 and a macromolecular polymer pyroxylin can hardly dissolve in each other in noticeable amounts, and their interaction

is probably governed by reactions with gaseous products. The reasons for such a dependence of the rate on the mixture composition are discussed below.

Also, the influence exerted by V_g^0 on the kinetics of heat release in decomposition of a mixture of NH_4NO_3 with pyroxylin at 113.3°C was examined. The ampule volume is constant, and V_g^0 depends on the extent to which the mass of pyroxylin changes at the NH_4NO_3 content maintained within the limits ensuring a weak dependence of the kinetics on the NH_4NO_3 content. In accordance with published data on the effect of V_g^0 on the rate of pyroxylin decomposition, the extent to which the decomposition is accelerated decreases as V_g^0 becomes smaller, whereas the initial rate changes only slightly and in the opposite direction [2]. In a mixture of pyroxylin and NH_4NO_3, V_g^0 has a similar effect: as V_g^0 decreases, the initial rate of heat release becomes slightly slower, the maximum rate of heat release grows, and the time in which it is attained becomes shorter. In the range V_g^0 28.2–421 $cm^3\ g^{-1}$, the time in which the rate maximum is attained varies from 250 to 1170 min.

It was established by direct measurements of the rate of heat release that, both in pure pyroxylin and in its mixtures with NH_4NO_3, the rate of heat release grows slowly at the initial stage of decomposition, its value passes through a relatively weak maximum, and then the rate decreases equally slowly (Fig. 3). After the decomposition in a mixture of pyroxylin with NH_4NO_3 at temperatures lower than 115°C passes through the first maximum and about 80 $J\ g^{-1}$ of heat is released, the process rapidly accelerates following a second-order autocatalysis law until approximately 1000 $J\ g^{-1}$ is released. Then the parabolic dependence of the rate of heat release on the heat of the process changes for a weaker dependence and the rate continues to grow and reaches values exceeding those at the first maximum by a factor of several tens. After that, the rate slowly decreases because of the consumption of the components of the mixture (Fig. 1). The quadratic dependence of the rate on the degree of conversion has been repeatedly noted previously in studies of the thermal decomposition of various nitroesters [6, 7]. Because of such a nonlinear rise in the rate of heat release, critical jumps of the decomposition rate have been observed in mixtures of ammonium perchlorate and some nitroesters [8].

The rate constants of the catalytic stage, obtained from the dependence of the specific decomposition rate $(d\eta/dt)/(1 - \eta)$ on η^2 at running heats of the process in the range 80–1000 $J\ g^{-1}$ and V_g^0 = 65 cm^3 per 1 g of pyroxylin are listed below:

T, °C	92.5	96.8	98.9	99
$k_1 \times 10^3$, s^{-1}	0.86	1.9	2.1	1.4
T, °C	104.3	104.3	106.3	112.8
$k_1 \times 10^3$, s^{-1}	1.8	3.4	7.3	10

The temperature dependence of the rate constant k_1 (s^{-1}) has the form:

$$k_1 = 1.0 \times 10^{17} \exp(-154 \times 10^3/RT).$$

Within the measurement error, the temperature dependences of the rates of the decomposition reaction at the first $(d\eta/dt)_I$ (s^{-1}) and second $(d\eta/dt)_{II}$ (s^{-1}) maxima have the same activation energies and different pre-exponential factors:

$$(d\eta/dt)_I = 5.0 \times 10^{13} \exp(-154 \times 10^3/RT) \text{ and}$$

$$(d\eta/dt)_{II} = 2.0 \times 10^{15} \exp(-154 \times 10^3/RT).$$

In pure pyroxylin, the kinetic curve is qualitatively similar, the first maximum is also present, but shifted to higher conversions, and approaches the second maximum as temperature increases. The heat (and, accordingly, the extent) of the processes grows, on reaching the first maximum, from 20 to 110 $J\ g^{-1}$ as temperature increases in the range 96–130°C. At higher temperatures, this maximum merges with the second, stronger maximum. The first maximum has not been observed in previous studies concerned with

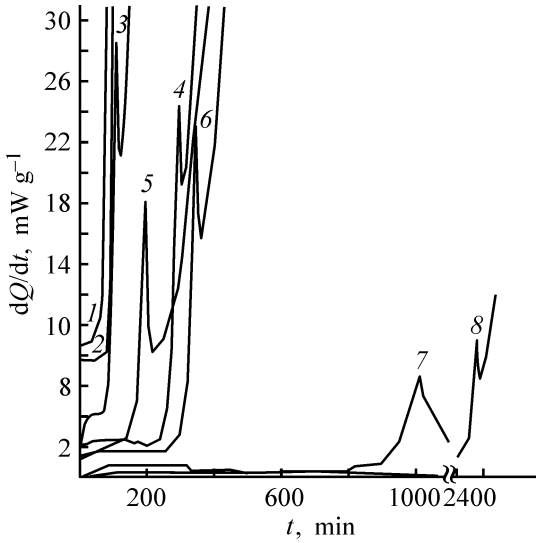


Fig. 3. Rate of heat release, dQ/dt vs. time t in thermal decomposition of a mixture of NH_4NO_3 with pyroxylin in the initial period of time. Decomposition temperature (°C): (*1*) 121.6, (*2*) 117.1, (*3*) 112.8, (*4*) 106.3, (*5*) 104.3, (*6*) 104.3, (*7*) 96.8, and (*8*) 92.5.

decomposition of nitroesters. Commonly, an initial period of slow growth is observed, which is probably due to difficulties encountered in revealing a weak maximum of the rate in the integral curve of accumulation of gaseous products. The rate of the process is measured directly on the dynamic calorimeter, and the measurement accuracy is sufficient for a reliable determination of this maximum. A similar maximum was observed in studying another batch of pyroxylin; it is probably due to a slow variation, in the course of decomposition, of the structure and molecular weight of pyroxylin, whose influence on the decomposition rate has been observed previously. It should be noted that, under the experimental conditions, the first maximum is observed at temperatures lower than 130°C in pure pyroxylin, and lower than 115°C in a mixture with NH_4NO_3; most of other published studies have been carried out at higher temperatures.

The curve for thermal decomposition of pyroxylin is described, in the range from the first maximum of the rate (on average, 2% degree of decomposition) to approximately 90% degree of decomposition, by the equation of a first-order autocatalytic reaction

$$d\eta/dt = (d\eta/dt)_{t=0}(1 - \eta) + k_2\eta(1 - \eta).$$

The rate constants of the noncatalytic stage are small and close in magnitude to the experimental initial specific rates of pyroxylin decomposition $(d\eta/dt)_{t=0}$. To a first approximation, the initial specific rate can be used in rate calculations instead of the constant of the noncatalytic stage. Below are given the resulting values of the rate constant of the catalytic stage, k_2

T, °C	96.4	106.3	114	121.7
$k_2 \times 10^4$, s^{-1}	1.6	5.0	5.1	6.1
T, °C	130.3	138.5	143.4	171.7
$k_2 \times 10^4$, s^{-1}	5.9	7.6	6.9	11

The temperature dependence of k_2 (s^{-1}) has the form

$$k_2 = 3\exp(-28 \times 10^3/RT)$$

The self-acceleration of the reaction of pyroxylin decomposition, which depends on temperature only very slightly, is considerably weaker than that in the system with NH_4NO_3 and begins later. Therefore, the temperatures studied for pure pyroxylin are, accordingly, higher. The lower activation energy of the rate constant in the catalytic stage of pyroxylin decomposition, compared with a similar value for decomposition of the mixed system, can probably be attributed to a more pronounced transfer of the catalytic agent into the gas phase at higher temperatures in the former case. In the mixed system, a considerable amount of NO_2 can be retained in the aqueous solution of NH_4NO_3, formed in the course of decomposition.

At temperatures exceeding 115°C, fundamental differences between the kinetic curves of heat release for thermal decomposition of a mixture of pyroxylin and NH_4NO_3 (Fig. 1) and pure pyroxylin are observed. In the mixed system at 117.1°C, the rate of heat release abruptly increases to values exceeding the measurement capabilities of the calorimeter already at the very beginning of decomposition, when approaching the first, relatively weak maximum of the heat release rate. This rate increases at 117.1°C very steeply, by about 0.2–0.35 W g^{-1} per minute. The true increase in the rate is probably even faster, because the dynamic characteristics of the calorimeter can markedly distort the kinetic curve at so fast changes in the rate of heat release. In an experiment of this kind, an explosive disintegration of the ampule was observed. At temperatures of 113.3°C and lower, only a monotonic, considerably slower variation of the rate of heat release was revealed in this part of the curve. In the stage of a developed self-acceleration of the process (at the second maximum), the rate of heat release considerably exceeds the level from which starts the steep increase in the rate at 117.1°C. Such a comparison demonstrates the nonthermal nature of the fast self-acceleration observed in the initial stage of the reaction, although a considerable warming-up of the mixture under study is observed in later stages of this process because high rates of heat release are reached. At a temperature of 115.3°C, which is a value intermediate between those considered above, a small plateau is observed at the first rate maximum; however, after that the rate starts, to grow rapidly to very high values instead of decreasing. The rise in this rate is somewhat slower than that at 117.1°C; a transition to a process with a fast acceleration is observed between 113.3 and 115.3°C. At a higher temperature of 121.6°C, the steep rise in the rate is even more pronounced and starts before the first maximum of the rate is reached. At still higher temperatures, the acceleration is even stronger, begins earlier, and has an explosive nature. However, no detailed studies of the rates of heat release were carried out in this range.

Here, a classical critical kinetic phenomenon is observed: a steplike change in the rate of the chemical process upon a small change in an external parameter, which is temperature in the case in question. Such a phenomenon may appear when equilibrium between formation and consumption of the intermediate reaction product, which is an active participant or a cata-

lyst of the process under study, is disturbed. In the given system, this is, most probably, NO_2. The main reactions leading to formation and consumption of NO_2 are presented below:

$$RONO_2 \rightarrow RO + NO_2, \quad (1)$$

$$RO + HNO_3(NO_2) \rightarrow \text{oxidation products}, \quad (2)$$

$$2NH_4NO_3 + 3NO_2 \rightarrow 2HNO_3 + 3NO + N_2 + 3H_2O, \quad (3)$$

$$4NH_4NO_3 + 3NO_2 \rightarrow 4HNO_3 + 3.5N_2 + 6H_2O, \quad (4)$$

$$RCH_2ONO_2 + H_2O(HNO_3) \rightarrow RCH_2OH + 2HNO_3, \quad (5)$$

$$RCH_2OH + 2HNO_3 \rightarrow RCHO + 2NO_2 + 2H_2O, \quad (6)$$

$$NO + 2HNO_3 \rightleftarrows H_2O + 3NO_2. \quad (7)$$

It is well known that the NO_2 molecule oxidizes most of organic substances at a considerably higher rate than does the HNO_3 molecule; the acceleration of the process in oxidation with nitric acid is commonly determined by accumulation of NO_2. However, water and HNO_3 can rather rapidly hydrolyze nitroesters. Nitrogen dioxide is incapable of reactions of this kind. At the same time, NO_2 is the primary product of monomolecular decomposition of pyroxylin and other nitroesters (1) and is partly consumed in the course of the process in various secondary oxidation reactions (2). In the presence of NH_4NO_3, nitrogen dioxide can be consumed at a high rate for oxidation of the ammonium into NH_4NO_3, with regeneration of nitric acid molecules by reactions (3) and (4). Reaction (4) has a higher heat, but leads to an irreversible consumption of nitrogen oxides. Water and HNO_3 formed in the process hydrolyze pyroxylin (5) with the subsequent oxidation of the alcohol and generation of NO_2 (6). Oxidation of NH_4NO_3 and organic compounds by the NO_2 molecule commonly yields NO, which can form in interaction with the accumulating HNO_3 three NO_2 molecules in accordance with equilibrium (7). This equilibrium is attained rather rapidly. Just this equilibrium leads to an increase in the content of NO_2 and to a strong self-acceleration of the reaction in which organic compounds are oxidized by nitric acid [9]. Possibly, just the turn-on of reaction (7), which occurs as nitric acid is accumulated, is the main reason for the critical jump of the rate.

To confirm the possibility of a fast reaction between NH_4NO_3 and NO_2, the kinetics of heat release in their mixture was measured. The required amount of gaseous NO_2 was refrozen into an ampule with a weighed portion of NH_4NO_3. Then the ampule was sealed and placed in a calorimeter, and the kinetics of heat release was studied in the temperature range 25–40.1°C. The rate of the reaction between NO_2 and NH_4NO_3 is high, and the process is rather fast even at room temperature. The heat effect of the oxidation reaction is about 3.3 kJ per 1 g of NO_2. The reaction occurs with a considerable self-acceleration, which is probably determined by accumulation of an HNO_3 solution in the ampule. Dissolution of NO_2 and NH_4NO_3 in this solution raises the rate of the reaction between these components, compared with that between gaseous NO_2 and solid NH_4NO_3. The resulting curves of heat release are described up to a 25% degree of decomposition by the kinetic equation of autocatalysis without burning-out

$$d\eta/dt = k_3 + k_4\eta.$$

The observed first order of the reaction with respect to the degree of conversion is determined by the proportional increase in the volume of the liquid phase. The subsequent decrease in the rate at higher degrees of conversion is due to consumption of NO_2. Below are given the resulting rate constants of the reaction in which NH_4NO_3 is oxidized by nitrogen dioxide:

T, °C	25	27.8	31.5	35.6	40.1
$k_3 \times 10^5$, s^{-1}	1.3	1.8	2.4	3.6	5.6
$k_4 \times 10^3$, s^{-1}	0.33	0.6	1.1	1.4	2.8

The temperature dependence of the rate constants k_3 and k_4 (s^{-1}) has the form

$$k_3 = 6.7 \times 10^7 \exp(-72\,000/RT),$$

$$k_4 = 3.2 \times 10^{14} \exp(-102\,000/RT).$$

The increase in the activation energy of the rate constant for the catalytic stage, k_4, as compared with that of k_3 may be due to a rise in the solubility of NH_4NO_3 in the forming aqueous solution with temperature. Also, the dependence of the rate of this reaction on the pressure of gaseous NO_2 in the ampule was studied and found to be directly proportional to this pressure. Calculation based on the kinetic data obtained shows that a 25% degree of NH_4NO_3 oxidation is achieved at 115°C already in 1 s, and this rate considerably exceeds the rate of pyroxylin decomposition.

Because of the high rate of the reaction between NH_4NO_3 and NO_2 in the case of the normal, smooth

course of the process, there is a competition between the formation and consumption of NO_2, and the quasi-stationary concentration of NO_2 in the system is low. Upon a critical increase in the rate, large amounts of NO_2 are formed. This means that a rise in the rate and an increase in the content of NO_2 are clearly related. The extent to which the overall reaction is accelerated is mostly determined by the slowest stage, reaction of NO_2 detachment from pyroxylin, and by other reactions of NO_2 formation. For this reason, the acceleration weakly depends on the content of NH_4NO_3, which is confirmed by the observed dependence of the process rate on the composition of the mixture (Fig. 2).

About 2 kJ per 1 g of NH_4NO_3 is released in reaction (3), which considerably exceeds the heat of its thermal decomposition, and about 3.5 kJ, in reaction (4). However, the latter reaction leads to chain termination, with NO_2 removed from the process. Together with reaction (6), these are the main processes leading to heat release. Reaction (7) is of equilibrium type and the equilibrium is attained rather rapidly; upon accumulation of HNO_3 in the system, this reaction may become the main reason for a rapid increase in the content of NO_2. Furthermore, an additional number of equilibria involving nitrogen oxides exist in the system; these equilibria have common products:

$$2NO_2 \rightleftarrows N_2O_4 \rightleftarrows NO^+ + NO_3^-,$$

$$2NO_2 + H_2O \rightleftarrows HNO_2 + HNO_3,$$

$$HNO_3(HNO_2) + H_2O \rightleftarrows H_3O^+ + NO_3^-(NO_2^-).$$

Owing to these equilibria, the concentrations of all the nitrogen-containing components in the system are interrelated, and, if the content of one of these is changed, the content of the others changes accordingly. NO_2 molecules formed in reaction (7) can again enter into the oxidation reaction to give NO; this process can be formally regarded as a chain reaction with continuous branching. In this case, the rate may grow very rapidly with a high oxidation rate constant; in the case in question, this is primarily the rate constant of the reaction between NO_2 and NH_4NO_3. Together with branching, chain termination reactions also occur in the system; the role of these reactions can be played both by reactions of oxidation by NO_2 molecules, with these molecules reduced to NO or N_2O, and by any reactions of NO reduction, yielding the same products. As in the case of an ordinary chain reaction, two modes of the process can be observed in the given case. In the first of these, quasi-stationary concentrations of NO and NO_2 are rapidly attained at virtually equal rates of their formation and consumption. This concentration gradually varies with time because of changes in the concentrations of the other components in the course of the reaction. All these changes determine the run of the corresponding kinetic curve with a comparatively slowly changing reaction rate. In the second mode, the content of NO_2 starts to grow rapidly if changes in the composition of the system or in the constants of formation and consumption of nitrogen oxides result in that the equilibrium between their formation and consumption is disturbed in favor of formation. Accordingly, the rate of the process increases virtually stepwise, and just this change is the critical phenomenon.

The excess of formation over consumption occurs because of the difference between the dependences of the corresponding rates on process parameters, primarily on temperature and component concentrations. For a critical phenomenon to occur, the dependences of the rates of formation and consumption of the leading component of the reaction on the other components must have different orders, and those on temperature, different activation energies, and the formation rate of the components whose accumulation gives rise to a critical phenomenon must grow faster. The most probable way to satisfy such a condition is a quadratic dependence of the rate of nitroester decomposition on the accumulation of decomposition products, with NO_2 formed and the rate of NO_2 consumption virtually always determined by a first-order reaction. A detailed study and analysis of dependences of this kind are beyond the scope of the present study. However, the key issue of the above consideration, which is the occurrence of a sufficiently fast reaction between NO_2 and NH_4NO_3 to give HNO_3, was tested and confirmed experimentally.

In a closed volume, pure pyroxylin always decomposes with a significant acceleration, which is predetermined by accumulation of nitrogen oxides and nitric acid. In view of this circumstance, stabilizers that can bind these products and thereby strongly diminish and, in the limit, eliminate the self-acceleration of the process are introduced into pyroxylin powders at the end of their shelf life. The historically first and the most frequently used stabilizer of pyroxylin is diphenylamine (DPA). It was appropriate to test the action of DPA also in the pyroxylin–NH_4NO_3 mixture, because the mechanism suggested for describing the acceleration of decomposition in this mixture is rather close to that for pure pyroxylin; anyway, binding of nitrogen oxides must diminish the acceleration of decomposition of the mixture.

A number of other experiments aimed to measure the rate of heat release in the ternary mixture pyroxylin–NH_4NO_3–DPA were performed. Some of the curves obtained are shown in Fig. 4. Introduction of DPA into the mixture changes the initial rate of heat release in the decomposition of the mixture only slightly, and even somewhat raises it, as it occurs in pure pyroxylin. Probably, this rise is determined by an increase in the total heat of the process through a turn-on of the reaction between nitrogen oxides and DPA.

Introduction of DPA into a mixture of pyroxylin and DPA strongly diminishes the main self-acceleration of the process and postpones its onset. However, the self-acceleration is not eliminated at all and the kinetic curve becomes more complex. For example, the first maximum is observed at 113.3°C in a mixture without DPA after 108 min and its magnitude is 0.03 W g^{-1}; the main acceleration reaches its maximum extent in 285 min, and the magnitude of this maximum is 2.2 W g^{-1}. Upon introduction of 4.2 wt % DPA, the first maximum is reached in 140 min and its magnitude decreases to 0.01 W g^{-1}. Then the second maximum with a magnitude of 0.033 W g^{-1} appears in 850 min, and after 4190 min comes the main acceleration with the maximum rate of 1.5 W g^{-1}. Upon introduction of 11 wt % DPA, the first maximum with 0.014 W g^{-1} occurs after 350 min, the second with 0.06 W g^{-1} appears in 990 min, and the development of the main acceleration is even slower, with the third rate maximum (0.5 W g^{-1}) reached in 6870 min. Upon introduction of 12.4 wt % DPA, the first maximum with a decreased magnitude of 0.011 W g^{-1} occurs in 350 min, and the second maximum (~0.06 W g^{-1}), in 1200 min; the maximum acceleration was not reached in this experiment. On the whole, raising the DPA content results in that the first maximum decreases in magnitude and occurs later and considerably later appears the second, also comparatively weak maximum, whose magnitude increases as the DPA content becomes higher; this is probably due to formation of products of DPA oxidation, which are oxidized easily or with a higher heat. The strongest stabilizing effect is observed in the development of the main acceleration process: introduction of 11.0 wt % DPA raises the time in which the maximum rate is reached by a factor of 27 and the rate itself decreases by a factor of 4.2. However, even addition of 11.0 wt % DPA does not fully eliminate the main acceleration of the process: after DPA is consumed in reactions with nitric acid and nitrogen oxides the acceleration develops as in a DPA-free mixture. The lower maximum rate of

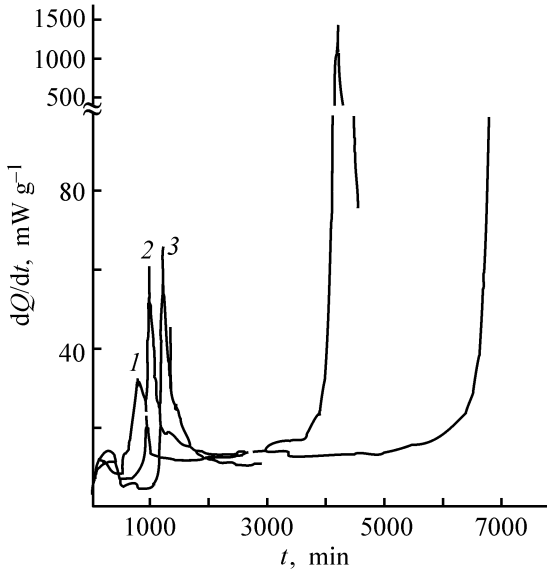


Fig. 4. Rate of heat release, dQ/dt vs. time t in thermal decomposition of a mixture of NH_4NO_3 with pyroxylin at 113.3°C. DPA content in the mixture (wt %): (*1*) 4.2, (*2*) 11.0, and (*3*) 12.4.

the process in this case is determined by the consumption of a considerable part of the components during the time before the beginning of a fast rise in the rate: at 11.0 wt % DPA, the degree of conversion during this time is 50–55%.

At temperatures exceeding the temperature of the critical rise in the decomposition rate, the influence of DPA is also important: the onset time of this acceleration strongly increases, but the acceleration itself still occurs. For example, at 121.3°C introduction of 8.9 wt % DPA results in that the time before the onset of an abrupt acceleration increases by a factor of 23, from 122 to 2850 min. The onset of acceleration is apparently determined by consumption of DPA in the course of decomposition: only after DPA is completely consumed, considerable amounts of nitrogen oxides can be accumulated.

To assess separately the contribution of nitrogen oxides to the acceleration of decomposition of the mixture, the following experiment was carried out. Carbamide was introduced into the reaction ampule with a mixture of NH_4NO_3 and pyroxylin in amount of 50% relative to the mass of the mixture in a separate glass vessel situated within the ampule over the mixture, so that carbamide could only interact with gaseous products. Carbamide rather rapidly reacts with nitrogen oxides and is used for preparative purposes to remove these oxides from HNO_3. If a mixture of pyroxylin with NH_4NO_3 is decomposed under these conditions at 116.2°C, the initial rate changes only

slightly, two weak peaks with a magnitude of about 0.03 W g^{-1} are observed in the kinetic curve after 450 and 1060 min, and no strong acceleration is obtained. This experiment shows that nitrogen oxides are a necessary factor in the development of a fast acceleration of the reaction in a mixture of pyroxylin and NH_4NO_3, and only an exceedingly small amount of HNO_3 passes into the gas phase at the temperature of the experiment. A similar curve is obtained under these conditions for pure pyroxylin, too: two weak peaks of the rate of heat release are observed and there is no strong acceleration at least during 4000 min; without introduction of carbamide into the upper position, the maximum rate of 0.4 W g^{-1} is reached already in 580 min. The heat released in the ampule under these conditions is close to 8.4 kJ g^{-1} and markedly exceeds the decomposition heat of pure pyroxylin (3.1 kJ g^{-1}), which results from oxidation of carbamide by nitrogen oxides in the upper vessel within the ampule.

At the same time, if decomposition of both the starting pyroxylin and its mixture with NH_4NO_3 is carried out at 113.2°C without additives, but in an open ampule, the initial rate of heat release is somewhat lower and the acceleration of decomposition is nearly completely eliminated. Under these conditions, all impurities in the starting components of the mixture and reaction products that have a noticeable vapor pressure at the temperature of the experiment, including water and nitrogen oxides, leave the reaction zone and are removed into the external atmosphere. In a hermetically sealed ampule, most part of water is in the liquid state, whereas in an open ampule, it passes into the gaseous state and is removed from the reaction zone, which strongly diminishes the role of hydrolytic reactions and the total heat of the process because of the consumption of the evaporation heat. At higher temperatures, the decomposition products probably have enough time, under these conditions, to partly enter into secondary reactions before passing into the gas phase and, as a result, a certain, but weaker acceleration of the process is observed [4].

In contrast to the case of full nitrates, an additional reaction is possible in a mixture of pyroxylin with NH_4NO_3: oxidation of free OH groups in nitrocellulose by HNO_3 molecules and nitrogen oxides. Such a reaction can lead to an increase in the reactivity of the neighboring nitrate groups of nitrocellulose and to formation of an additional amount of NO_2, which raises the rate of the overall interaction between the components of the system. This reaction was disregarded in the case of decomposition of pure pyroxylin, but the total content of HNO_3 is higher in the presence of NH_4NO_3, and, accordingly, the contribution of reactions involving the acid may become more important.

To assess the possible contribution from the reaction of oxidation of OH groups by molecules of nitric acid to the overall process, and primarily to the initial rate, the kinetics of heat release in a reaction between cellulose RB and a 45.1 wt % aqueous solution of HNO_3 was studied in the temperature range 65.1–133°C. Aqueous HNO_3 was used instead of NH_4NO_3 because it is difficult to bring cellulose RB in good contact with the NH_4NO_3 salt, and HNO_3 well impregnates cellulose. The concentration of HNO_3 molecules in the aqueous solution and in NH_4NO_3 can be evaluated by published data [10, 11]. The rate of the reaction is at a maximum at the beginning of the process and decreases as OH groups of cellulose are consumed. This rate for the most part obeys the kinetic law of a first-order reaction. The heat effect of the oxidation reaction is about 8.3 kJ per 1 g of cellulose. As HNO_3 is taken in a large excess, 120–210 mol per 1 mol of cellulose, its concentration remains virtually unchanged in the course of the process. Below are given the resulting values of the rate constant of the oxidation reaction:

T, °C	65.1	70.0	75.1	79.5	85.5	90.5
$k_5 \times 10^5$, s^{-1}	0.30	0.54	0.85	1.5	2.1	3.1

T, °C	96.5	116.8	121.0	126.8	133
$k_5 \times 10^5$, s^{-1}	4.5	17	25	41	61

The temperature dependence of the rate constant k_5 has the form

$$k_5 = 6.6 \times 10^7 \exp(-85.8 \times 10^3/RT).$$

The oxidation rate is rather high. An analysis of the rates obtained, which was made taking into account the difference in the content of HNO_3 molecules in an aqueous solution of HNO_3 and in NH_4NO_3 and the relatively low content of free OH groups in pyroxylin, demonstrated the following. In thermal decomposition of a mixture of NH_4NO_3 and pyroxylin, the possible contribution from the reaction of oxidation of OH groups of cellulose by nitric acid from NH_4NO_3 is rather important and accounts for up to 20–30% of the whole initial rate of heat release. It would be hardly expected for a mixture of two solid components that HNO_3 from an NH_4NO_3 crystal will be evenly distributed among NH_4NO_3 and pyroxylin. Therefore, the real contribution from oxidation of OH groups by nitric acid in pyroxylin will probably be considerably lower. It is quite possible that there is enough time for a certain amount of NO_2 to be formed

while the mixture is heated in the calorimeter. Then the contribution from the reaction with HNO_3 will be even smaller, and the rate of oxidation by nitrogen dioxide, lower than that with nitric acid [9]. The small contribution from the oxidation reaction to the initial rate of heat release in the mixture is also confirmed by the fact that the initial rates of heat release, related to the total heat of the process, virtually coincide. However, if the contact between NH_4NO_3 and pyroxylin is substantially improved, e.g., by compaction of their mixture, the initial rate of heat release may somewhat increase. In the case of a developed process, when a sufficiently large amount of HNO_3 is accumulated in the system through oxidation of NH_4NO_3, the contribution from the reaction of oxidation of OH groups will probably become important owing to, among other things, formation of a large amount of these groups in acid hydrolysis of pyroxylin.

CONCLUSIONS

(1) The specific initial rates of heat release in decomposition of pure pyroxylin and its mixture with NH_4NO_3 show the same temperature dependence. The observed difference between the initial rates of hear release in a mixture of NH_4NO_3 and pyroxylin and in a pure pyroxylin is due to the difference between the total heats of the processes.

(2) The degree of self-acceleration of the decomposition of a mixture exceeds that in decomposition of pure pyroxylin. Nitrogen dioxide is the active agent in the stage of acceleration of decomposition which produces in a fast reaction with NH_4NO_3 an equimolar amount of HNO_3. The acid, in turn, accelerates the decomposition of pyroxylin. In the temperature range 113.3–115.3°C, the degree of acceleration significantly changes upon a minor variation of temperature because of the different dependences of the rates of NO_2 formation and consumption on temperature and degree of conversion.

(3) Introduction of diphenylamine into a mixture of pyroxylin and ammonium nitrate diminishes the degree of acceleration in proportion to the added mass of NH_4NO_3 in all stages of the process, this effect being the most pronounced when the main acceleration process develops.

ACKNOWLEDGMENTS

The study was supported by the International Scientific Center (project MNTTs no. 1882–2001).

REFERENCES

1. Gorst, A.G., *Porokha i vzryvchatye veshchestva* (Powders and Explosives), Moscow: Mashinostroenie, 1972.
2. Manelis, G.B, Nazin, G.M., Rubtsov, Yu.I., *et al.*, *Thermal Decomposition and Combustion of Explosives and Propellants*, London: Taylor a. Francis Group, 2003.
3. Lur'e, B.A. and Svetlov, B.S., Abstracts of Papers, *Vsesoyuznaya konferentsiya "Khimiya i reaktsionnaya sposobnost' tsellyulozy i ee proizvodnykh"* (All-Union Conf. "Chemistry and Reactivity of Cellulose and Its Derivatives") Cholpon-Ata, 1991, pp. 184–188.
4. Manelis, G.B., Rubtsov, Yu.I., Smirnov, L.P., *et al.*, *Kinet. Kataliz*, 1962, vol. 3, no. 1, pp. 42–49.
5. Galyuk, O.S., Rubtsov, Yu.I., Malinovskaya, G.F., *et al.*, *Zh. Fiz. Khim.*, 1965, vol. 39, no. 9, pp. 2319–2322.
6. Svetlov, B.S., *Kinet. Kataliz*, 1961, vol. 2, no. 3, pp. 179–183.
7. Afanas'ev, A.G., Lur'e, B.A., and Svetlov, B.S., *Trudy Mos. Khim. Tekhnol. Inst. im. Mendeleeva*, 1967, no. 53, pp. 63–73.
8. Rubtsov, Yu.I. and Manelis, G.B., *Zh. Fiz. Khim.*, 1964, vol. 37, no. 10, pp. 2392–2396.
9. Rubtsov, Yu.I., Kazakov, A.I., Rubtsova, E.Yu., *et al.*, *Izv. Ross. Akad. Nauk, Ser. Khim.*, 1996, no. 8, pp. 1986–1991.
10. Chedin, J., *J. Chim. Phys.*, 1952, vol. 49, pp. 109–125.
11. Rubtsov, Yu.I., Kazakov, A.I., Lempert, D.B., *et al.*, *Zh. Prikl. Khim.*, 2004, vol. 77, no. 7, pp. 1098–1106.

Russian Journal of Applied Chemistry, Vol. 78, No. 6, 2005, pp. 880–883. Translated from Zhurnal Prikladnoi Khimii, Vol. 78, No. 6, 2005, pp. 901–904.
Original Russian Text Copyright © 2005 by Panasyugin, Kitikova, Bondareva, Sivak.

SORPTION AND ION-EXCHANGE PROCESSES

Sorption Characteristics of Pillared Ferruginous Montmorillonite Modified with Cetylpyridinium Bromide

A. S. Panasyugin, N. V. Kitikova, G. V. Bondareva, and Yu. B. Sivak

Branch Research Laboratory for Treatment of Airborne Effluents, Belarussian National Technical University, Minsk, Belarus

Institute of General and Inorganic Chemistry, Belarussian National Academy of Sciences, Minsk, Belarus

Received August 4, 2004; in final form, March 2005

Abstract—The sorption capacity of pillared ferruginous montmorillonite modified with cetylpyridinium bromide for iodine, methylene blue, and phenol was studied. Procedures for preparing a modified sorbent with the optimal sorption power for phenol were developed.

Industrial processes yield large volumes of wastewater. Among pollutants contained in wastewater, organic compounds are the most hazardous since they are poorly removed by common techniques of water treatment. Wastewater can be purified to remove organic pollutants by deep oxidation, membrane filtration, adsorption, and also by treatment with aerobic and anaerobic microflora [1–3].

As a rule, wastewater is purified to remove volatile organic pollutants, pesticides, surfactants and chlorine by its treatment with granulated activated carbon [4]. However, the sorption capacity of activated carbon and its service life noticeably decrease in decontamination of natural water containing humic acids [5]. Along with activated carbon, contaminated water can be purified to remove pollutants by its treatment with modified clay materials having high exchange capacity. The fixation of toxic chemicals and patogenic microflora by clay minerals has been extensively studied [6–8].

To improve the sorption selectivity of clays for organic pollutants, their surface should be made hydrophobic. One of methods for hydrophobization of the hydrophilic surface of clay minerals is based on substitution of its exchangeable inorganic cations by organic cations containing hydrophobic long-chain alkyl groups. Upon such a treatment, the clay surface is covered with hydrophobic groups. After hydrophobization by this procedure, clays become efficient sorbents for aromatic hydrocarbons, chlorophenols, and toxic metals [9, 10]. Another approach to modification of clay minerals to improve their sorption characteristics involves formation of metal oxide columns between structural layers of a lamellar clay mineral and filling of the interlayer space with bulky hydrophobic organic cations. The thus modified clay is calcined to obtain a pillared ferruginous clay material which can be repeatedly saturated with appropriate organic modifying agent to obtain an improved sorbent [10].

Phenol is one of organic pollutants which is hazardous for human health and environment even in the minor amounts. Ingress of phenol and its derivatives into air, water and soil, can lead to gene mutation in living bodies and, at high phenol concentrations, to deterioration of the range of species. The aim of this study was to prepare a pillared ferruginous montmorillonite modified with cetylpyridinium bromide and test its sorption power for iodine, methylene blue, and phenol.

EXPERIMENTAL

In our experiments, we used montmorillonite taken from the Askan deposit, Georgia. Its composition was as follows, wt %: SiO_2 53.5, Al_2O_3 18.1, Fe_2O_3 0.84, MgO 4.9, CaO 1.65, Na_2O 1.1, K_2O 0.32, and H_2O 7.98 [11]. Iron(III) polyhydroxo complex (PHC) and ferruginous montmorillonite (Fe-FM) were prepared by the procedures described in [12]. In our sorption experiments, we used Fe-FM prepared by treatment of 3% aqueous clay suspension with Fe(III) PHC (10 mg-equiv Fe^{3+} per gram of clay) at the molar ratio OH^-/Fe^{3+} = 2.0. The specific surface area of

1070-4272/05/7806-0880 © 2005 Pleiades Publishing, Inc.

Main characteristics of initial Fe-Fm and Fe-Fm containing varied amounts of cetylpyridinium bromide

Sample no.	Content of cetylpyridinium bromide, mmol per gram of clay	S_{sp}, $m^2\ g^{-1}$	Sorption capacity, mg g^{-1}		TG and DTA data endothermic effect			
			for iodine	for MB	I		II	
					T, °C	Δ*m*, %	*T*, °C	Δ*m*, %
1	Initial Fe-Fm	124	44	66	137	16.0	–	–
2	1	90	135	34	125	11.5	425	5.8
3	3	48	162	36	110	6.5	425	8.6
4	5	40	174	40	105	2.6	425	9.6
5	8	30	170	47	100	2.4	430	10.0
6	10	26	180	52	100	2.2	425	10.4

the initial Fe-Fm sample S_{sp} was 124 $m^2\ g^{-1}$. The initial Fe-Fm was washed with water and then, without drying, was treated with aqueous cetylpyridinium bromide (1, 3, 5, 8, and 10 mmol per gram of clay). The resulting suspension of organomodified clay (R · Fe-Fm) was settled for 1 day, separated from the liquid phase, washed with water, and dried first in air for 2 days and then at 120°C for 3 h.

A thermogravimetric analysis of R · Fe-Fm samples (500 mg) was carried out in air within the temperature range 20–800°C at a heating rate of 10 deg min^{-1}.

The specific surface area S_{sp} of R · Fe-Fm samples was determined by the BET technique based on measuring the low-temperature sorption of nitrogen with a Micromeritics 2200 express analyzer. The crystallographic parameter d_{001} was determined on a Siemens 500 diffractometer. The sorption capacity of R · Fe-Fm for methylene blue (MB) and iodine was measured under static conditions. In these experiments, 20 ml of aqueous MB (0.15 g l^{-1}) or 20 ml of aqueous iodine (10 g l^{-1}) was added to 100 mg of modified clay. The resulting suspension was kept with intermittent shaking at 20°C for 6 h. According to the data reported in [13], this time of phase contact is sufficient for the sorption equilibrium to be attained.

The sorption of phenol was studied under identical conditions from aqueous solutions containing from 5 to 400 mg l^{-1} of phenol. The equilibrium liquid phase was centrifuged and the phenol content in the resulting transparent centrifuged solution was determined by photometry of the colored complex of phenol with diazotized *p*-nitroaniline [14]. The MB and iodine content was determined photometrically and titrimetrically, respectively [15].

The table shows that, as the content of cetylpyridinium bromide in the modifying solution increases from 1 to 5 mmol per gram of Fe-Fm, the content of cetylpyridinium bromide in modified R · Fe-Fm grows from 5.8 to 10.4%. A further increase in cetylpyridinium bromide content in the modifying solution to 8 and 10 mmol per gram of Fe-FeM does not noticeably change the content of cetylpyridinium bromide in the modified material.

The DTA curves of R · Fe-Fm (Fig. 1) show a strong low-temperature endothermic peak accompanied by a weight loss assigned to the removal of adsorbed water [16]. As the content of cetylpyridinium bromide in R · Fe-Fm is raised to its maximum amount, the endothermic peak shifts toward lower temperatures and the weight loss decreases from 16.0 to 2.2%. We believe that this effect is caused by the fact that

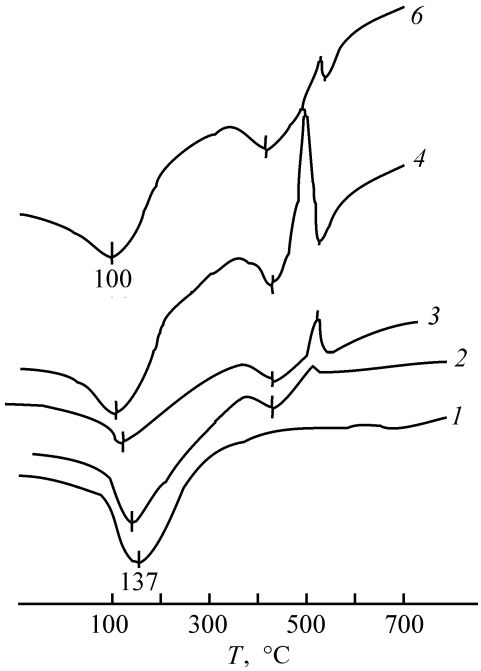


Fig. 1. DTA curves of the initial and modified Fe-FM. (*T*) Temperature. *Curve nos.* are sample nos. in the table; the same for Fig. 2.

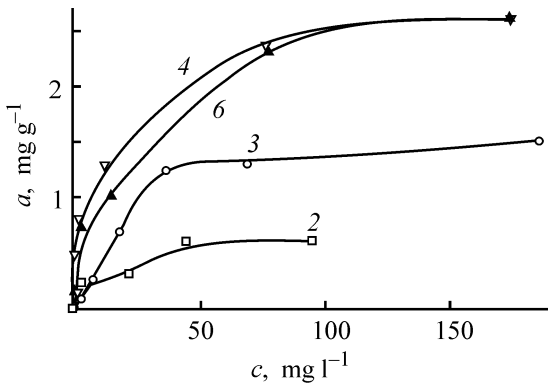


Fig. 2. Sorption isotherms of phenol on Fe-FM modified with cetylpyridinium bromide: (*a*) amount of sorbed phenol and (*c*) equilibrium phenol concentration in the aqueous phase.

the modification makes lower the hydrophilicity of R · Fe-Fm, and, as a result, facilitates the desorption of water at low temperature.

The DTA curves of R · Fe-Fm show one more weaker endothermic peak in the range 420–430 °C, associated with desorption of cetylpyridinium bromide, and an exothermic peak at 500°C, caused by oxidation of the modifying agent. The table shows that the content of the modifier in R · Fe-M does not affect the position of the endothermic peak, whereas the weight loss increases with the modifier content. It should be noted that the intensity of the endothermic peak for samples with an equal content of the modifier may noticeably differ (Fig. 1, curves *4*, *6*).

The table shows that the content of modifier in R · Fe-Fm correlates with its sorption capacity for iodine. In going from sample no. 1 to sample no. 4, the sorption capacity for iodine increases from 44 to 174 mg g^{-1} and does not appreciably change further, in going to samples nos. 5 and 6.

The sorption of MB is commonly used for evaluating the sorption power of sorbents. The table shows that the sorption capacity of the initial (nonmodified) Fe-M for MB exceeds that of the modified sorbent. After modification of Fe-M with a minimum addition of cetylpyridinium bromide, the sorption capacity for MB decreases by approximately a factor of two. However, a further increase in modifier content makes higher the sorption capacity of R · Fe-M for MB in spite of a decrease in S_{sp}. We believe that this phenomenon is caused by the fact that the sorption of alkylammonium cations on clay, as a rule, exceeds its cation-exchange capacity owing to association of alkylammonium cations with neutral amines and their salts [17]. The charged hydrophilic heads of these excess alkylamonium cations are oriended toward the aqueous phase. As a result, cationic groups sorbing MB appear in a certain amount on the hydrophobic surface of the modified clay. The content of these groups increases with the modifier content.

We found that phenol is not sorbed noticeably on the initial Fe-M. After modification of Fe-M with cetylpyridinium bromide, the sorption of phenol increases. The limiting sorption capacity of R · Fe-M for phenol is 2.5 mg g^{-1}. Similarly to iodine, the sorption of phenol does not change in going from sample no. 4 to sample nos. 5 and 6. We suggest that measurement of the sorption of iodine on R · Fe-Fm can be used for fast evaluation of the sorption capacity of this sorbent for phenol.

The sorption isotherms of phenol from aqueous solutions have a nonlinear shape (Fig. 2) typical of systems with prevalence of the physical sorption. At the content of phenol in the aqueous phase below 1 mg l^{-1}, the degree of phenol recovery is 80–95%.

CONCLUSION

Pillared ferruginous montmorillonite modified with cetylpyridinium bromide exhibits the best sorption properties for phenol at 5 mmol of cetylpyridinium bromide per gram of montmorillonite.

REFERENCES

1. Weber, W.J. and Le Boeuf, E.J., *Water Sci. Technol.*, 1999, vol. 40, nos. 4–5, pp. 11–19.
2. Teodosiu, C., Kennedy, M., van Straten, H.A., and Schippers, J.C., *Water Res.*, 1999, vol. 33, no. 9, pp. 2172–2180.
3. Castillo, R.L.A., Sillet, A., Roussy, J., *et al.*, *Water Sci. Technol.*, 2000, vol. 42, nos. 5–6, pp. 115–118.
4. Paune, F., Caixach, J., Espadaler, J., *et al.*, *Water Res.*, 1998, vol. 32, no. 11, pp. 3313–3324.
5. Hopman, R., Maarkerk, M.A., Wiegers, W.G., and Kruithof, J.C., *Water Supply*, 1994, vol. 12, no. 2, pp. 197–207.
6. Ake, C.L., Wiles, M.C., Hyebner, H.J., *et al.*, *Chemoshere*, 2003, vol. 51, no. 5, pp. 835–844.
7. Mortland, M.M., Shaobai, S., and Boyd, S.A., *Clays Clay Miner.*, 1986, vol. 34, no. 5, pp. 581–585.
8. Boyd, S.A., Shaobai, S., Lee, J.F., and Mortland, M.M., *Clays Clay Miner.*, 1988, vol. 36 no. 2, pp. 125–130.
9. Smith, J.A. and Jaffe, P.R., *J. Environ. Eng.*, 1994, vol. 120, no. 8, pp. 1559–1577.
10. Nolan, T., Srinivasan, K.R., and Fogler, H.S., *Clays*

Clay Miner., 1989, vol. 37, no. 5, pp. 487–492.

11. Tarasevich, Yu.I., *Prirodnye sorbenty v protsesse ochistki vody* (Natural Sorbents in Water Treatment), Kiev: Naukova Dumka, 1981.
12. Komarov, V.S., Panasyugin, A.S., Trofimenko, N.E., *et al.*, *Kolloidn. Zh.*, 1995, vol. 57, no. 1, pp. 51–54.
13. Shu Huai-Te, Danyun, Li, Scala, A.A., and Ma Yi Hua, *Sep. Purif. Technol.*, 1997, vol. 11, pp. 27–36.
14. *Sbornik metodik vypolneniya izmerenii, dopushchennykh k primeneniyu v deyatel'nosti laboratorii ekologicheskogo kontrolya predpriyatii i organizatsii Belarus Respublic* (Collection of Methods for Performing Measurements Accepted for Application in Functioning of a Laboratory for Environmental Monitoring of Enterprises and Organizations of Belarus Republic). Minsk, 1997, part 1,
15. Kreshkov, A.I., *Analiticheskaya khimiya* (Analytical Chemistry), Moscow: Khimiya, 1978, vol. 2.
16. Ivanova, V.P., Kasatov, B.P., Krasavina, T.N., and Rozinova, E.L., *Termicheskii analiz mineralov i gornykh porod* (Thermal Analysis of Minerals and Rocks), Moscow: Nedra, 1974.
17. Tarasevich Yu.I., *Adsorb. Adsorb.*, 1977, no. 5, pp. 58–62.

Russian Journal of Applied Chemistry, Vol. 78, No. 6, 2005, pp. 884–890. Translated from Zhurnal Prikladnoi Khimii, Vol. 78, No. 6, 2005, pp. 905–911.
Original Russian Text Copyright © 2005 by Mamchenko, Savchenko.

SORPTION AND ION-EXCHANGE PROCESSES

Determination of the Working Exchange Capacity of Weakly Basic Polyacrylic Anionites

A. V. Mamchenko and O. A. Savchenko

Institute of Colloid Chemistry and Chemistry of Water, National Academy of Sciences of the Ukraine, Kiev, Ukraine

Received June 3, 2004; in final form, January 2005

Abstract—The nonequilibrium dynamics of sorption of hydrochloric acid by weakly basic polyacrylic anionites was studied. An equation for calculating the working capacity of ion-exchange filters as a function of variable parameters (filtration rate, concentration of the starting solution, and height of the ionite bed in a filter) was derived using the theory of nonequilibrium dynamics of sorption.

In technological schemes intended for production of deeply desalinated water with exceedingly low electrical conductivity, weakly basic ionites are used in OH filters of the first stage to remove anions of strong acids from H-cationized water.

Matrices of weakly basic anionites can be obtained by copolymerization of styrene, esters of acrylic and metacrylic acids, and acrylonitrile with divinylbenzene, which is used as cross-linking agent. Polyacrylic anionites have a number of advantages over anionites synthesized on the basis of copolymers of styrene and divinylbenzene. Their matrix provides a reversible sorption of organic substances in a cycle of water treatment and ionite regeneration. They ensure a low specific consumption of an alkali per removal of a mole of anions of strong acids and specific expenditure of water for washing of the sorbent in the first-stage filter.

Under working conditions, the effectiveness and cost-efficiency of an ion-exchange resin is determined by its working capacity. It may constitute a larger or smaller fraction of the total exchange capacity, depending on a number of variable factors: concentration of ions to be sorbed, rate of water filtration, height of the resin bed, chemical composition, and concentration and amount of the regenerating solution.

Weakly basic polyacrylic anionites provide a complete regeneration at a nearly stoichiometric alkali expenditure. Therefore, the working capacity of ionites of this kind is determined by the stage of water desalination.

In industrial practice, all technological processes that employ ionites are carried out in the dynamic mode, because, in this case, the exchange capacity of the material is used the most completely [1]. In a dynamic system, equilibrium is not attained and the results obtained with ion-exchangers are affected by kinetic factors [2]. In view of this circumstance, the present study was concerned with the dynamics of sorption of hydrochloric acid by weakly basic polyacrylic anionites.

EXPERIMENTAL

As objects of study were chosen weakly basic polyacrylic anionites Amberlite IRA 67, Lewatit VP.OC.1072, Purolite A 845, Relite MG 1 , and MG 1/P. The first and second ionites contain only tertiary amino groups [3, 4]. Anionite Purolite A 845 contains, in addition to tertiary amino groups, a certain amount of strongly basic quaternary groups. This assumption can be made on the basis of an indirect information that this anionite can be used in cycles with regeneration with sodium hydroxide only at temperatures of 40°C and lower, because quaternary amino groups are decomposed at higher temperatures. Anionites Relite MG 1 and Relite MG 1/P both contain polyamines as exchange centers, but differ in matrix structure: the former is synthesized on a gel matrix,

1070-4272/05/7806-0884 © 2005 Pleiades Publishing, Inc.

Table 1. Main parameters of the weakly basic polyacrylic anionites under study

Ionite	Matrix structure	Type of functional groups	Total exchange capacity, M
Amberlite IRA 67	Gel-like	Tertiary	1.6 [3]
Lewatit VP.OC.1072	"	"	1.5 [4]
Purolite A 845	"	Tertiary and strongly basic	1.5 [5]
Relite MG 1	"	Polyamines	3.4 [6]
Relite MG 1/P	Porous	"	3.1 [6]

and the latter, on a porous matrix [6]. The main parameters of the ionites under study are listed in Table 1.

As a sorbate was chosen hydrochloric acid, because in water-treatment practice, first-stage OH filters are commonly cut-off, for regeneration to eliminate the breakthrough of chlorides [7, 8]. This is due to the following circumstances. First-stage OH filters in water desalination installations, which are charged with weakly basic anionites, are intended for absorption of sulfates and chlorides from solutions of the corresponding acids, formed in the stage of H-ionization of water [7–9]. In the case when a dissolved mixture of acids is passed through the anionites, anions of all strong acids are absorbed in the initial period of a filtering cycle. Then there occurs a breakthrough (in the form of acid) of the anion for which the sorption selectivity is the lowest, with the absorption of the other anions continued. As the initial solution is passed through the filter, the concentration of the anion for which the sorption selectivity is lower than that of other anions present in solution (chlorides in the case of first-stage OH filters) gradually increases and reaches a value equal to the total concentration (expressed in moles of equivalents of the substances) of all the anions in the initial solution. Passing the initial solution till the breakthrough of the sulfate ion into the filtrate is accompanied by a virtually complete displacement of previously absorbed chloride ions [9]. This circumstance makes it possible to simulate the operation of first-stage OH filters in water desalination installations by studying the sorption of only hydrochloric acid from its individual solution.

Experimental procedure. A sample of a commercial anionite, alternately treated with solutions of 1 M hydrochloric acid and sodium hydroxide and subjected to an intermediate washing with distilled water after measuring the sample volume in a graduated flask, was placed in a glass column in such a way that the bed height was approximately 1 m. A model solution of hydrochloric acid was pumped by a peristaltic pump across a bed of the anionite preliminarily regenerated with sodium hydroxide. The filtrate was collected in portions, the volume of the portions and the time during which each portion was collected were measured, and the acidity (alkalinity) of a solution of a portion was determined by titration with Methyl Red. The data obtained were used to calculate the linear velocity and volumetric rate of filtration of the liquid, as well as the amount of sorbed hydrochloric acid and the extent of acid breakthrough into the filtrate.

In a working cycle, weakly basic anionites in OH filters are in a dense bed. In this case, the theory of nonequilibrium dynamics of sorption is commonly used to describe the process.

Models constructed in terms of the theory of nonequilibrium dynamics of sorption can, in principle, describe the operation of ionite filters in any mode (of inner, outer, or mixed diffusion) [10–15]. However, it is necessary, in such a general case, to solve numerically systems of differential equations, which hinders application of the models to practical calculations. For particular cases, in which the sorption kinetics is limited only by outer or inner diffusion, the mass-transfer coefficient remains constant, and a parallel transfer of the sorption front occurs in the ionite bed, analytical solutions to a system of equations have been obtained, which makes it possible to prognosticate the working parameters of ionite filters [11, 14–20].

If the sorption kinetics is limited by outer mass transfer, then the following relation is valid [14, 15, 18]

$$t = a_0 h (v c_0)^{-1} - a_0 (c_0 \beta)^{-1} \times \{(B c_0)^{-1} \ln[(c_0/c) - 1] + \ln(c_0/c) - 1\}, \quad (1)$$

whereas in the case when the process is limited by inner-diffusion mass transfer, another equation is valid [14, 15, 19, 20]:

$$t = a_0 h (v c_0)^{-1} - \beta^{*-1} \times \{(B c_0)^{-1} \ln[(c_0/c) - 1] + \ln(1 - c/c_0) + 1\}. \quad (2)$$

Here, t is the time reckoned from the onset of the process; a_0, specific sorption of hydrochloric acid, calculated per unit volume of the bed under conditions of equilibrium between the ionite and the initial solu-

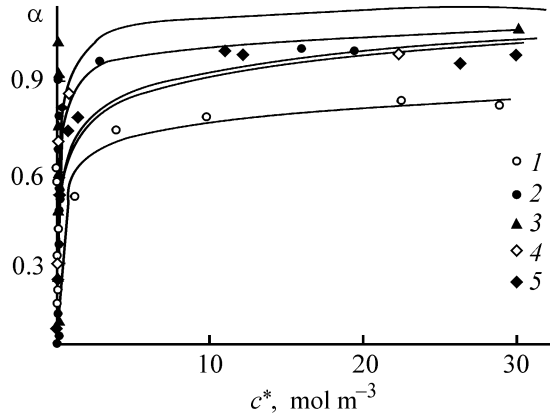


Fig. 1. Isotherms of equilibrium sorption of hydrochloric acid by weakly basic polyacrylic anionites. (α) Degree of neutralization of the anionite and (c^*) concentration of hydrochloric acid in the equilibrium solution; the same for Fig. 2. Anionite: (*1*) Amberlite IRA, (*2*) Lewatite VP.OC.1072, (*3*) Purolite A 845, (*4*) Relite MG, and (*5*) Relite MG 1/P; the same for Fig. 2.

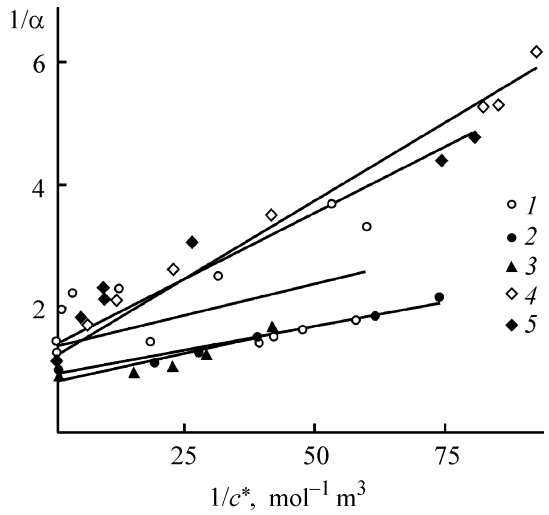


Fig. 2. Isotherms of equilibrium sorption of hydrochloric acid in the coordinates of the linear form of Eq. (4).

tion; h, height of the adsorbent bed; v, linear flow velocity of the liquid, calculated per total cross-section of the sorption column; c_0, concentration of the substance being sorbed in the initial solution; β and β^*, kinetic coefficients of inner and outer mass transfer, respectively; c, concentration of the substance being absorbed in the filtrate at instant of time t; and B, empirical coefficient of the sorption isotherm of the type of a Langmuir isotherm

$$a = f(c^*) = Ac^*/(1 + Bc^*). \quad (3)$$

Here, A is an empirical coefficient, and c^* is the concentration of the substance being sorbed (hydrochloric acid), which is in equilibrium with a.

Figure 1 shows isotherms of equilibrium sorption of hydrochloric acid by the anionites under study. It can be seen that these isotherms are strongly convex and can be identified as rectangular isotherms, for which formation of a stationary sorption front and its parallel transfer are characteristic [10, 11, 13, 21]. Equations (1) and (2) have been derived just for conditions of this kind [14, 15, 18–20].

To determine the coefficient B, Eq. (3) was brought to a linear form

$$1/\alpha = B/A^* + 1/(A^*c^*), \quad (4)$$

where α is the extent to which the anionite is converted to the salt form; $A^* = A/E_0$; and E_0, total exchange capacity of the anionite.

The average values of the total exchange capacity, obtained in a study of the equilibrium sorption, are listed in Table 2.

It follows from Fig. 2 that the dependence of $1/\alpha$ on $1/c^*$, plotted in the coordinates of the linear form of Eq. (4), satisfactorily describes the isotherm of sorption of hydrochloric acid by polyacrylic anionites. The values of parameter B, calculated by the least-squares method, are listed in Table 3.

Table 2. Total exchange capacity of weakly basic polyacrylic anionites with account of the specific volume, determined under static conditions

Ionite	$E_{0\,stat}$, mol kg^{-1}	V_{sp}, l kg^{-1}	$E_{0\,stat}V_{sp}^{-1}$, M
Amberlite IRA 67	2.87	1.65	1.73
Lewatit VP.OC.1072	2.71	1.99	1.36
Purolite A 845	2.52	1.75	1.44
Relite MG 1	5.30	1.56	3.39
Relite MG 1/P	4.57	1.60	2.85

Table 3. Values of parameter B, calculated by Eq. (4)

Ionite	B	$S(B)$
	m^3 mol^{-1}	
Amberlite IRA 67	81	39
Lewatit VP.OC.1072	77	14.5
Purolite A 845	90	30.7
Relite MG 1	37	1.8
Relite MG 1/P	37	3.5

Equations (1) and (2) make it possible to determine the limiting stage of the sorbate diffusion by processing of experimental data. The kinetic coefficient β^* in Eq. (2) is, by definition, independent of the hydrodynamic conditions of the process even if it depends on the composition of the resinates. By contrast, if the process is limited by outer diffusion, the kinetic coefficient β in Eq. (1) markedly increases with the linear velocity of filtration of the liquid phase [12–16, 18].

To analyze experimental data, it is appropriate to transform Eqs. (1) and (2) into expressions containing quantities directly determined from the experiment. Accordingly, Eqs. (1) and (2) take the form

$$Qc_0/W_0 = a_0 - [va_0/(\beta h)][(Bc_0)^{-1}\ln(c_0/c - 1) + \ln(c_0/c) - 1] = a_0 - (a_0/\beta)z. \quad (5)$$

Here, $z = v[(Bc_0)^{-1}\ln[(c_0/c) - 1] + \ln(c_0/c) - 1]/h$; Q, volume of filtrate passed across the ionite bed till breakthrough of the acid with concentration c; W_0, volume of the ionite charge in the filter; and

$$Qc_0/W_0 = a_0 - [vc_0/(h\beta^*)][(Bc_0)^{-1}\ln(c_0/c - 1) + \ln(1 - c/c_0) + 1] = a_0 - Z/\beta^*, \quad (6)$$

where

$$Z = (vc_0/h)\{(Bc_0)^{-1}\ln[(c_0/c) - 1] + \ln(1 - c/c_0) + 1\}.$$

According to Eq. (5), a linear dependence of Qc_0/W_0 on z must be observed in the case of the outer-diffusion sorption kinetics and any linear filtration velocity of the liquid phase. The plot must remain linear at different linear filtration velocities of water. However, the dependence of β on the hydrodynamic situation around ionite grains must lead to a decrease in the slope of the straight lines with increasing filtration velocity, because β grows owing to the decrease in the thickness of the immobile liquid film around an ionite grain.

When the process is controlled by inner-diffusion mass transfer, the dependences of Qc_0/W_0 on z must coincide in a wide range of linear filtration velocities of the liquid phase, although they may be nonlinear, because the theoretical model (5) is certainly inadequate to the real process.

Figure 3a shows, in the coordinates of the linear form of Eq. (5), the experimental data obtained in a study of the dynamics of sorption of hydrochloric acid by weakly basic polyacrylic anionites in a wide range of linear filtration velocities of the liquid.

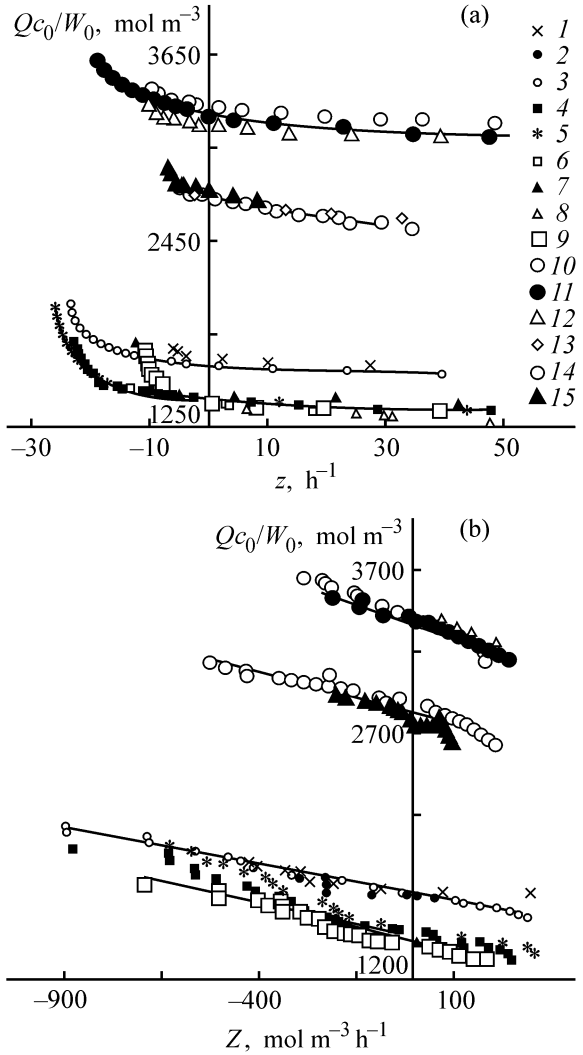


Fig. 3. Output sorption curves for hydrochloric acid, plotted in the coordinates of the linear form of equations (a) (*5*) and (b) (*6*) at various filtration velocities of the liquid through weakly basic polyacrylic anionites (*1–3*) Amberlite IRA 67, (*4–6*) Lewatit VP.OC.1072, (*7–9*) Purolite A 845, (*10–12*) Relite MG 1, and (*13–15*) Relite MG 1/P. (Qc_0/W_0) Total amount of counterions absorbed by the ionite bed. Filtration velocity v (m h^{-1}): (*1*) 8.4, (*2*) 17.3, (*3*) 23.2, (*4*) 4.5, (*5*) 20.2, (*6*) 22.9, (*7*) 7.3, (*8*) 11.8, (*9*) 13.0, (*10*) 15.0, (*11*) 20.0, (*12*) 22.0, (*13*) 8.0, (*14*) 14.0, and (*15*) 20.0.

As follows from Fig. 3, the experimental data are not described by the theoretical expression derived for the conditions in which the sorption kinetics is governed by outer diffusion. First, the experimental points fall on a clearly curved line, rather than on a straight line (is it would have been if Eq. (5) were adequate to the experimental data). Second, no dependence of the curves on the linear filtration velocity of the liquid phase is observed: irrespective of the flow rate of

Table 4. Experimental conditions and results of processing of experimental data on the dynamics of sorption of hydrochloric acid by weakly basic polyacrylic anionites, using Eq. (6)

Ionite	v, m h^{-1}	a_0	$S(a_0)$	$\Delta(a_0)$	β^*	$S(\beta^*)$	$\Delta(\beta^*)$
		M			h^{-1}		
Amberlite IRA 67	8.4	1.67	0.27	0.14	2.3	0.2	0.1
	16.3	1.68	0.43	0.35	2.0	0.3	0.2
	23.2	1.71	0.07	0.02	2.1	0.04	0.01
Average		1.69	0.26	0.17	2.2	0.2	0.2
Lewatit VP.OC.1072	20.2	1.50	0.15	0.55	1.95	0.10	0.04
	22.9	1.50	0.13	0.54	2.22	0.09	0.04
	14.5	1.49	0.27	0.87	2.04	0.18	0.06
Average		1.50	0.18	0.65	2.04	0.14	0.15
Purolite A 845	13.0	1.41	0.20	0.13	2.11	0.15	0.10
	7.3	1.41	0.29	0.24	2.00	0.21	0.17
	11.8	1.40	0.20	0.11	2.02	0.14	0.08
Average		1.41	0.23	0.15	2.05	0.17	0.12
Relite MG 1	15.0	3.38	0.29	0.11	0.99	0.04	0.02
	20.0	3.34	0.21	0.59	1.00	0.03	0.01
	22.0	3.42	0.64	0.27	1.01	0.10	0.04
Average		3.38	0.38	0.32	1.00	0.01	0.02
Relite MG 1/P	14.0	2.80	0.14	0.47	1.18	0.03	0.01
	20.0	2.84	0.57	0.27	1.16	0.12	0.05
	8.0	2.81	0.49	0.26	1.13	0.10	0.05
Average		2.82	0.40	0.33	1.16	0.02	0.03

water. This unambiguously shows that, at the flow rate in the range under study, the sorption kinetics of hydrochloric acid by weakly basic polyacrylic anionites is determined only by mass transfer within ionite grains. Consequently, relation (6) should be used for processing of experimental data.

Figure 3b shows dependences of Qc_0/W_0 on Z. It can be seen that, for all of the ionites studied, these dependences are linear and have the same slope rate. This corresponds to Eq. (6) and indicates that the kinetic coefficient of inner mass transfer of hydrochloric acid, β^*, is independent of the hydrodynamic conditions of the process. Consequently, the sorption of hydrochloric acid occurs in the inner-diffusion mode. Moreover, the chosen experimental conditions guarantee that a stationary sorption front is formed and the mechanism of its parallel transfer across the ionite bed is operative. Thereby, necessary and sufficient conditions are created for application of the theoretical model of the inner-diffusion sorption dynamics for an adequate description of the technological process.

Table 4 lists quantitative parameters characterizing the inner-diffusion kinetics of sorption of hydrochloric acid by weakly basic polyacrylic anionites at various linear filtration velocities of the initial solution. It can be seen that the values of the kinetic coefficient β^* coincide for all the ionites within the determination error [characterized by standard deviation $S(\beta^*)$ and confidence interval $\Delta(\beta^*)$ at a confidence probability of 0.95]. The values of parameter a_0, found by measuring the characteristics of the sorption dynamics, coincide for all the anionites. They are also in an agreement with the values of the total exchange capacity found in the case of sorption of hydrochloric acid by anionites under static conditions (with account of the specific volume) (Table 2) and those furnished

by the manufacturers (Table 1). Hence follows that parameter a_0 is the total exchange capacity of the anionites.

As can be seen from Table 4, the average values of the kinetic coefficients of inner mass transfer, β^*, coincide for anionites with the same amino groups. For example, $\beta^* \approx 2h^{-1}$ for ionites with tertiary amino groups: Amberlite IRA 67, Lewatit VP.OC.1072, and Parolite A 845.

For Relite MG 1 and Relite MG 1/P anionites, the value of the kinetic coefficient β^* is virtually independent of the presence or absence of porosity in grains of the ion-exchangers and is two times smaller (~1 h^{-1}) than that in the case of anionites with tertiary amino groups. This may be due to two factors: presence in the exchange centers of these anionites of groups with basic properties weaker than those in tertiary groups and smaller free volume in the gel phase of the anionites because of the presence of bulky polyamine chains.

As indicated by the data in Table 4, Relite MG 1 and Relite MG 1/P anionites show poorer kinetic characteristics than the anionites with tertiary amino groups, but have a considerably higher total exchange capacity.

However, the parameters found are insufficient for making a unique choice of an anionite for a technological process, because the operation cost of a filter is determined by the working capacity of the ionite used. The physical meaning of the working capacity of an ion-exchanger is the amount of acid anions that can be absorbed by unit volume of the bed until the concentration of the acid in the filtrate reaches the breakthrough value. The working capacity can be represented by the equation

$$E_w = \int_0^{Q_{br}} (c_0 - c)\, dQ/W_0, \qquad (7)$$

where Q_{br} is the volume of the initial solution that can be passed across the resin bed until the breakthrough concentration c of the acid is reached in the filtrate.

It is known from the experience of water treatment that the concentration of anions of strong acid in H-cationized water delivered to first-stage OH filters is 2–10 g-equiv m^{-3}. The breakthrough concentration of the acid, at which the filters are put out of operation and then are regenerated, is in the range 0.02–0.14 g-equiv m^{-3}. Because the breakthrough concentration is considerably lower than the concentration of the initial solution ($c << c_0$), it can be stated that, to a good approximation,

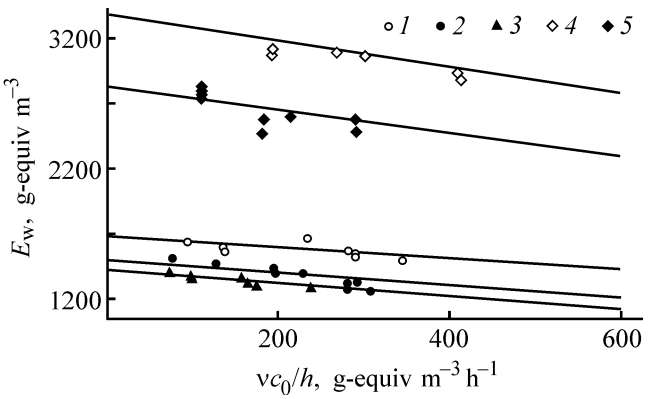


Fig. 4. Theoretical (*straight lines*) and experimental (*points*) dependences of the working capacity E_w on hydrodynamic conditions in the coordinates of the linear form of Eq. (9). (vc_0/h) Amount of counterions absorbed by the ionite bed in unit time.

$$E_w = Qc_0/W_0. \qquad (8)$$

Substitution of the value of Qc_0/W_0 from Eq. (6) into (8) yields the following equation for determining the working capacity of an ion-exchange filter:

$$E_w = E_0 - (vc_0/h)\beta^{*-1}\{(Bc_0)^{-1}\ln[(c_0/c) - 1] + \ln(1 - c/c_0) + 1\}. \qquad (9)$$

Equation (9) expresses the dependence of the working capacity E_w of an ionite on variable parameters of the process, such as linear filtration velocity v of the liquid phase, concentration c_0 of anions of strong acids in the initial water, and height h of the ionite bed in the filter. The parameters β^* and B are constant for each ionite. The c/c_0 ratio at the instant when the filter is put out of operation to be regenerated is also constant for a particular water composition. For the experimental conditions used (initial concentration of the model solution 10 ± 2 g-equiv m^{-3} and breakthrough concentration taken to be 0.1 g-equiv m^{-3}), the ratio is equal to 0.01.

Thus, it follows from Eq. (9) that the working capacity E_w of an ionite is a function of the linear filtration velocity of water, concentration of the initial solution, and height of the ionite bed in the filter.

Theoretical dependences of E_w on vc_0/h were calculated for weakly basic polyacrylic anionites with various types of amino groups in a wide range of linear filtration velocities of the liquid at certain values of the parameters β^*, B, h, and c_0 (Fig. 4). Figure 4

also shows the dependences of the working capacity on variable conditions, experimentally obtained in a study of the nonequilibrium dynamics of sorption of hydrochloric acid by these anionites. As can be seen in Fig. 4, the experimental values of the working capacity of the anionites fall on the theoretical curves with a satisfactory accuracy.

CONCLUSIONS

(1) It was established that the kinetics of sorption of hydrochloric acid by weakly basic polyacrylic anionites with amino groups of varied basicity is limited in water filtration modes characteristic of operation of first-stage OH filters in installations for desalination of water by diffusion within ionite grains.

(2) It was found that, irrespective of the porosity of anionites, the kinetic coefficient remains constant for ionites with identical groups and is determined by the chemical nature of ionogenic groups.

(3) An equation derived in terms of the theoretical model of inner-diffusion sorption dynamics was suggested for an *a priori* calculation of the working exchange capacity of ionite filters at any variable conditions of the process (linear filtration velocity of the initial solution, concentration of anions of strong acids in this solution, and bed height in the filter).

REFERENCES

1. Gel'ferikh F. *Ionity*, Moscow: IL, 1962. 490 s.
2. Kishnevskii, V.A., *Sovremennye metody obrabotki vody v energetike* (Modern Methods for Water Treatment in Power Engineering), Odessa: Odess. Gos. Polytekhn. Univ., 1999.
3. TU (Technical Specification) U 02071045-002–98, *Ion-exchange resins: Anionites: Requirements to the quality of anionites manufactured by Rohm and Haas Co.*
4. *Information Materials of Bayer Co.*, Leverkusen, Germany.
5. TU U 95.1.04.09.001–97, *Ion-exchange resins: Anionites: Requirements to the quality of anionites manufactured by Purolite Co.*
6. TU U 24.1-02071045.003–2003, *Ion-exchange resins: Anionites manufactured by Resindion S.R.L. Co., Mitsubishi Chemical Corporation.*
7. Feiziev, G.K., *Vysokoeffektivnye metody umyagcheniya, opresneniya i obessolivaniya vody* (High-Efficiency Methods for Softening, Desalination, and Deionization of Water). Moscow: Energoatomizdat, 1988.
8. Lifshits, O.I., *Spravochnik po vodopodgotovke kotel'nykh ustanovok* (Handbook of Water Treatment for Boiler Plants), 2-e izd. Moscow: Energiya, 1976.
9. Shkrob, M.S. and Prokhorov, F.G., *Vodopodgotovka i vodnyi rezhim paroturbinnykh elektrostantsii* (Water Treatment and Water Consumption Mode of Steam Power Plants), Moscow: Gosenergoizdat, 1961.
10. Zhukhovitskii, A.A., Zabezhinskii, Ya.L., and Tikhonov, A.N., *Zh. Fiz. Khim.*, 1945, vol. 19, no. 6, pp. 253–261.
11. Rosen, J.B., *J. Chem. Phys.*, 1952, vol. 20, no. 3, pp. 387–394.
12. Senyavin, M.M., Rubinshtein, R.N., Venitsianov, E.V., *et al.*, *Osnovy rascheta i optimizatsii ionoobmennykh protsessov* (Fundamentals of Calculation and Optimization of Ion-Exchange Processes), Moscow: Nauka, 1972.
13. *Ionity v khimicheskoi tekhnologii* (Ionites in Chemical Technology), Nikol'skii, B.P. and Romankov, P.G., Eds., Leningrad: Khimiya, 1982.
14. Koganovskii, A.M., Klimenko, N.A., Levchenko, T.M., *et al.*, *Ochistka i ispol'zovanie stochnykh vod v promyshlennom vodosnabzhenii* (Purification and Utilization of Wastewater in Industrial Water Supply), Moscow: Khimiya, 1983.
15. Koganovskii, A.M., *Adsorbtsiya i ionnyi obmen v protsessakh vodopodgotovki i ochistki stochnykh vod* (Adsorption and Ion Exchange in Water Treatment and Purification of Wastewater), Kiev: Naukova Dumka, 1983.
16. Serpionova, E.N., *Promyshlennaya adsorbtsiya gazov i parov* (Industrial Adsorption of Gases and Vapors), Moscow: Vysshaya Shkola, 1969.
17. Tikhonov, A.N. and Samarskii, A.A., *Uravneniya matematicheskoi fiziki* (Equations of Mathematical Physics), Moscow: Nauka, 1977.
18. Marutovskii, R.M., Koganovskii, A.M., and Roda, I.G., *Zh. Fiz. Khim.*, 1976, vol. 50, no. 2, pp. 443–448.
19. Roda, I.G., Koganovskii, A.M., and Marutovskii, R.M., *Zh. Fiz. Khim.*, 1976, vol. 50, no. 4, pp. 954–956.
20. Roda, I.G. and Zhuk, P.F., *Khim. Tekhnol. Vody*, 1985, vol. 8, no. 2, pp. 7–10.
21. Senyavin, M.M., *Ionnyi obmen v tekhnologii i analize neorganicheskikh veshchestv* (Ion Exchange in Technology and Analysis of Inorganic Substances), Moscow: Khimiya, 1980.

Russian Journal of Applied Chemistry, Vol. 78, No. 6, 2005, pp. 891–896. Translated from Zhurnal Prikladnoi Khimii, Vol. 78, No. 6, 2005, pp. 912–917.
Original Russian Text Copyright © 2005 by Kolosnitsyn, Minnikhanova, Karaseva, Dmitriev, Muratov.

APPLIED ELECTROCHEMISTRY AND CORROSION PROTECTION OF METALS

Possibility of Depositing Electrolytic Manganese Dioxide onto Titanium Anodes from Manganese Chloride Solutions

V. S. Kolosnitsyn, E. A. Minnikhanova, E. V. Karaseva, Yu. K. Dmitriev, and M. M. Muratov

Institute of Organic Chemistry, Ural Scientific Center, Russian Academy of Sciences, Ufa, Bashkortostan, Russia

Kaustik Private Company, Sterlitamak, Bashkortostan, Russia

Received September 1, 2004; in final form, February 2005

Abstract—Fundamental aspects of the deposition of electrolytic manganese dioxide from chloride electrolytes were studied. The optimal parameters of the electrolysis on titanium anodes were determined.

In production of organochlorine compounds, a large amount of hydrochloric acid is formed as a waste gas (HCl_{wg}). Therefore, it is necessary to develop processes that would make it possible to utilize HCl_{wg} to give a new commercial product. One of the main ways to utilize HCl is its use for leaching-out of manganese ions from oxidized manganese ores (substandard manganese ores, floatation tails, and other manganese-containing wastes).

When oxidized manganese ores are decomposed with hydrochloric acid, chlorine and manganese chloride solutions are formed by the reaction:

$$MnO_2 + 4HCl_{conc} \rightleftarrows MnCl_2 + Cl_2\uparrow + 2H_2O. \quad (1)$$

Chlorine can be used in manufacture of organochlorine compounds and $MnCl_2$ solutions, electrolytic manganese dioxide (EMD), and electrolytic manganese metal (EMM).

Thus, two problems can be solved in the same technological process: utilization of HCl_{wg} and processing of substandard manganese ores and other manganese-containing wastes. The use of HCl_{wg} and manganese-containing wastes as raw materials will make it possible to develop a competitive process for manufacture of EMD and EMM [1].

It should also be noted that MnO_2 obtained from chloride electrolytes is a more electrochemically active and pure material [2].

In developing a process for obtaining electrolytic MnO_2, a considerable attention is paid to the choice of the anode material. As the anode material for electrolysis of $MnCl_2$ solutions were used iridium [3], platinum [4], lead coated with lead dioxide [4], graphite [5], ORTA, and titanium electrodes coated with titanium carbide or manganese dioxide [6–8]. Because platinum and iridium are very expensive metals, it is unreasonable to use them in industrial electrolysis. Lead anodes contaminate MnO_2 with lead dioxide through their dissolution in the course of electrolysis. Graphite anodes gradually burn away because of the partial evolution of hydrogen and should be replaced at regular intervals.

We suggested that less expensive metal anodes, widely used in electrolysis with evolution of chlorine, can be used to obtain EDM, because a manganese dioxide film formed on titanium at the beginning of electrolysis will increase its corrosion resistance.

In this study, we examined the possibility of application of titanium anodes for deposition of EMD from $MnCl_2$ solutions.

EXPERIMENTAL

Manganese(IV) oxide was synthesized in a Plexiglas electrolyzer with plane-parallel electrodes. VT-1-00 titanium plates ($150 \times 70 \times 2$ mm) were used as the anode, and Kh18N10T stainless steel, as the cathode. The separation between the opposite electrodes was 5 mm.

Prior to the electrolysis, the surface of the electrodes was trimmed with an M-40 emery paper, washed

1070-4272/05/7806-0891 © 2005 Pleiades Publishing, Inc.

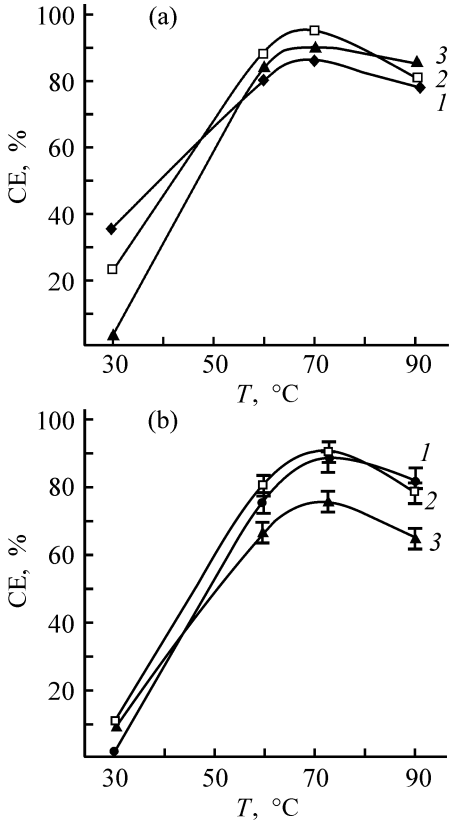


Fig. 1. Current efficiency CE by MnO_2 vs. temperature *T*. $MnCl_2$ concentration 1.0 M; the same for Figs. 2, 3. Current density (mA cm^{-2}): (a) 5.0 and (b) 10.0; the same for Fig. 2. HCl concentration (M): (*1*) 0, (*2*) 0.05, and (*3*) 0.25.

with distilled water and acetone, and dried in air for 1–2 min. The thus prepared electrodes were kept in a desiccator before the experiment.

The electrolyzer temperature was maintained constant with a U-8 water thermostat (Hungary). The anode and cathode potentials were measured relative to a silver chloride reference electrode.

The electrolyzer was polarized with a stabilized B5-47 dc power source. The voltage across the electrolyzer was measured with a V7-38 digital voltmeter. The electrode potentials and pH of the electrolytes were determined with an HI-9025 C portable microprocessor-controlled pH/mV/°C-meter (Portugal).

As electrolytes were used 1 M $MnCl_2$ solutions containing a varied amount of hydrochloric acid. The solutions were prepared from analytically pure $MnCl_2 \cdot 4H_2O$ and chemically pure HCl.

The manganese(II) content in the electrolytes was determined by back titration [9].

The experiments were performed as follows. First, the electrolyzer with the electrode system prepared was placed in the bath of the thermostat and kept there at a prescribed temperature for 1 h. The electrolysis time ensured deposition of 20–30% manganese from the electrolyte. The current efficiency (CE) was calculated from the loss of Mn(II) by the electrolyte solution after the electrolysis. The corrosion rate of the polarized and unpolarized (initial) titanium anodes was determined gravimetrically [10]. After the electrolysis, the electrodes were dried in air, and MnO_2 was carefully removed from their surface with a brush. Then, the electrodes were washed with 5% hydroxylamine hydrochloride and distilled water, and dried in air to constant mass. The accuracy in determining the corrosion rate was 7%.

The EDM deposited during the electrolysis was washed with distilled water to negative reaction for chloride ions. The MnO_2 deposit was dried to constant mass under an IR lamp at 105°C.

The temperature dependences of the current efficiency by MnO_2 at a current density of 5 and 10 mA cm^{-2} and different HCl concentrations are presented in Figs. 1a, 1b. It can be seen that the CE-vs.-temperature dependences are bell-shaped and pass through a maximum at 65–75°C. At a low temperature (30°C) and a current density of 5 mA cm^{-2} the current efficiency decreases with increasing HCl concentration (Fig. 1a). Raising the current density to 10 mA cm^{-2} makes the current efficiency significantly lower and changes the character of the dependence of CE on the HCl concentration (Fig. 1b). The lowest current efficiency is observed in the absence of the acid, and the highest, with 0.05 M of HCl.

As temperature increases, the current efficiency sharply grows. At temperatures close to the temperature of the maximum, the highest current efficiency is reached at an acid concentration of 0.05 M, irrespective of the current density (5 or 10 mA cm^{-2}). At 90°C, the current efficiency grows at j_a = 5 mA cm^{-2} as the HCl concentration becomes higher, and, reaches a the minimum at j_a = 10 mA cm^{-2}.

It should also be noted that titanium anodes rapidly disintegrate at low temperatures (30–40°C). The rate of this process increases as the density of polarizing current and the acid concentration become higher. In these conditions, the electrolyzer voltage reaches its maximum value of 10–12 V.

The dependences of the electrolyzer voltage on temperature and anode and cathode potentials at differ-

ent HCl concentrations are shown in Figs. 2a, 2b. It can be seen that the anode potential and the electrolyzer voltage decrease as the temperature becomes higher. The cathode potential is virtually temperature-independent. The electrolyzer voltage decreases with increasing HCl concentration in the electrolyte at a current density of 5 mA cm^{-2} and exhibits a complex dependence at 10 mA cm^{-2}. These results show that the electrolyzer voltage is mainly determined by the anode potential.

In the course of the electrolysis, a film consisting of the reaction products was formed on the anode. In the absence of the acid, the film was matte, uniform, black, and strongly adherent to the electrode surface. In the course of the electrolysis, the thickness of the product layer increased, but no flaking from the anode surface was observed. Addition of hydrochloric acid to the electrolyte changed the properties of the film. It acquired a metallic luster and became flaky, with flakes exfoliating from the electrode surface and going down to the bottom of the electrolyzer as their size increased. In the process, the initial film of the reaction products was retained on the anode surface. The surface film possessed a reasonably high corrosion resistance. According to a visual inspection and a gravimetric analysis, the film on the anode remained unchanged during several hundred hours after the current was switched off.

The variation of the electrolyzer voltage in the course of electrolysis is shown in Fig. 3. It can be seen that at 30°C the electrolyzer voltage first increases and then decreases. At temperatures of 60 to 90°C, the electrolyzer voltage somewhat decreases and then reaches a constant value or slightly increases.

The electrolytic deposition of EMD and EMM from $MnCl_2$ solutions was studied in [3, 5, 11]. In the course of electrolysis from manganese(II) chloride solutions, several electrochemical and chemical reactions proceed simultaneously at the anode and in the solution bulk, including the electrochemical oxidation of Mn^{2+} ions to the highest degrees of oxidation and the oxidation of chloride ions and water, which can be described by the following reaction equations:

$$Mn^{2+} + 2H_2O - 2e \rightarrow MnO_2\downarrow + 4H^+, \; E = +1.228 \text{ V}, \quad (2)$$

$$\text{pH} \sim 4\text{–}3,$$

$$Mn^{2+} - e \rightarrow Mn^{3+}, \; E = +1.510 \text{ V}, \quad (3)$$

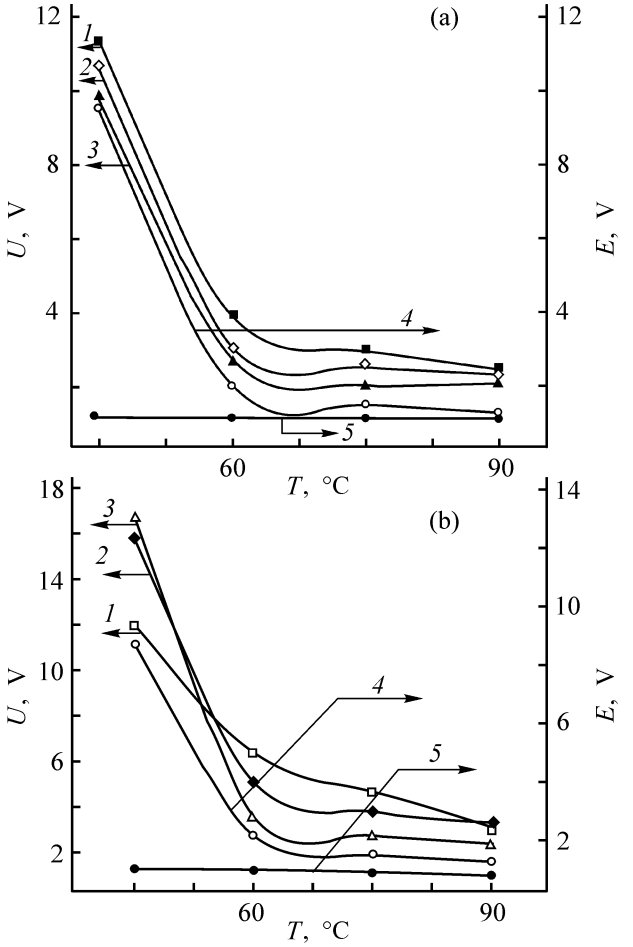


Fig. 2. Electrolyzer voltage U and the potential E of the (*4*) anode and (*5*) cathode vs. temperature T. HCl concentration (M): (*1*) 0, (*2*) 0.05, (*3*) 0.25, and (*4, 5*) 0.05.

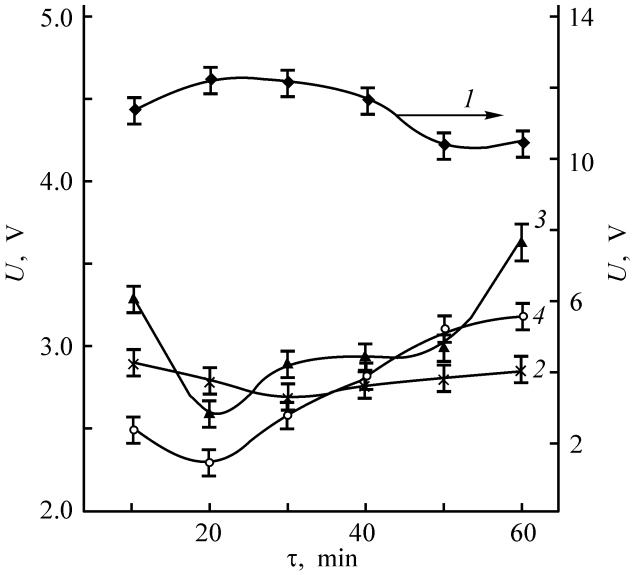


Fig. 3. Electrolyzer voltage U vs. time τ. Current density 5 mA cm^{-2}. Temperature (°C): (*1*) 30, (*2*) 60, (*3*) 75, and (*4*) 90.

$$Mn^{2+} - 2e \rightarrow Mn^{4+},\ E = +1.840\ V, \quad (4)$$

$$Mn^{2+} + 4H_2O - 5e \rightarrow MnO_4^- + 8H^+,\ E = +1.507\ V,\ pH \sim 2, \quad (5)$$

$$2Cl^- \rightarrow Cl_2 + 2e,\ E = +1.36\ V, \quad (6)$$

$$Cl_2 + H_2O \rightleftarrows HClO + HCl, \quad (7)$$

$$2HClO + ClO^- \rightleftarrows ClO_3^- + 2H^+ + 2Cl^-, \quad (8)$$

$$Mn^{2+} + x/2Cl_2 \rightleftarrows Mn^{(2+x)+} + xCl^-. \quad (9)$$

The resulting chlorine partly dissolves in the electrolyte to form hypochlorous and hydrochloric acids [reaction (7)], which results in a pronounced acidification of the electrolyte near the anode surface. In addition, the forming Cl_2 can oxidize Mn^{2+} to Mn^{4+} [reaction (9)]. The relative rates of the individual anodic reactions depend on the electrolysis conditions and are determined by the electrode potential and the temperature and acidity of the solution.

The rate of reaction (9) in the solution bulk is many times less than that of reactions (2) and (4) [3], which means that reactions (2) and (4) are the main source of manganese(IV).

In the course of the electrochemical oxidation of Mn^{2+}, the anode potential is the key parameter. Raising the anode potential favors successive oxidation of Mn^{2+} to Mn^{3+} and then to Mn^{4+}. At a potentials of approximately up to 1.5 V, Mn^{2+} is oxidized in solution to Mn^{3+} [equation (3)]. Another electrode reaction [equation (4)] takes place when the potential increases to 1.8 V.

Manganese(IV) can be also obtained by disproportionation of Mn^{3+} by the reaction

$$2Mn^{3+} \rightarrow Mn^{4+} + Mn^{2+}. \quad (10)$$

Manganese dioxide deposited from chloride solutions can be regarded as a product of hydrolysis [reaction (11)] of manganese(IV), which is formed by reactions (2), (4), (9), and (10):

$$MnCl_4 + 2H_2O \rightarrow MnO_2\downarrow + 4HCl. \quad (11)$$

Manganese tetrachloride may also decompose to yield $MnCl_2$ and Cl_2 via the inner-sphere redox reaction

$$MnCl_4 \rightarrow MnCl_2 + Cl_2\uparrow. \quad (12)$$

Apparently, the strong temperature dependence of CE is due to several factors: instability of higher manganese chlorides formed by electrolysis at high temperatures and by intense anodic dissolution of titanium at low temperatures, with both these factors being interrelated.

At low temperatures the hydrolysis rate of the Mn(IV) formed is low. Therefore, the reaction mainly proceeds in the bulk of the electrolyte rather than on the anode surface or in the near-anode space. Therefore, no MnO_2 film possessing high protective properties is formed on titanium. As a result, Ti undergoes at low temperatures a strong electrochemical dissolution to give a dense passivation film of titanium oxide. This is manifested in a fast increase in the anode potential, and, consequently, in the electrolyzer voltage. Owing to the intense passivation of titanium, the current is concentrated at those places where the passivation film is damaged, which results in a fast electroerosion disintegration of the anode.

Raising the temperature leads to an increase in the rate of $MnCl_4$ hydrolysis. Therefore, MnO_2 is formed on the surface of the titanium anode, rather than in the bulk of the electrolyte, to give a dense protective layer. This layer does not hinder reactions (2), (4), and (6) owing to its high electrical conductivity, but prevents the anodic dissolution of titanium.

It is known that the $MnCl_4$ dissociation at room temperature to form chlorine [reaction (12)] is extremely slow. The rate of this reaction sharply increases as temperature is raised [5]. As a result, the current efficiency starts to decrease above 60–70°C owing to the lowering of the Mn(IV) concentration.

As chloride ions compete with manganese(II) ions for the oxidation on the electrode, it may be suggested that an increase in the acidity would make lower the current efficiency by MnO_2. However, it can be seen from Figs. 1a, 1b that the dependence of CE on the concentration of hydrochloric acid is complex.

The decrease in CE upon an increase in the HCl concentration at low temperatures is probably due to a rise in the rate of anodic dissolution of titanium with increasing electrolyte acidity. The increase in CE from 80 to 95% as the HCl concentration is raised from 0 to 0.05 M may be due to a rise in the $MnCl_4$ concentration as a result of reaction (9).

The data obtained in studying the corrosion rate of unpolarized and polarized titanium anodes are listed

in Tables 1, 2 in relation to temperature and HCl concentration.

The results of the study show that titanium does not corrode in neutral $MnCl_2$ solutions. In the presence of HCl, titanium corrodes, but the corrosion rate is low. As the temperature and HCl concentration increase, the rate of titanium corrosion slightly grows. The results obtained are in a good agreement with reference data. For example, the corrosion rate of a titanium plate was zero after 200 h of electrolysis at 20°C in the presence of 5% HCl, 0.05 g m^{-2} h^{-1} after the same time of electrolysis at 60°C, and 4.23 g m^{-2} h^{-1} after as short a time as 25 h of electrolysis at 90°C [12].

Application of an anodic polarization makes the rate of titanium corrosion somewhat higher. As the temperature increases, the corrosion rate first grows, reaches a maximum at 75°C, and then falls, irrespective of the HCl concentration in the electrolyte. Raising the HCl concentration somewhat decreases the corrosion rate.

A visual inspection of the electrodes demonstrated that the MnO_2 deposit formed in electrolysis at 60°C is strongly adherent to the anode surface. Magnesium dioxide deposited at higher temperatures (75–90°C) has a weak adherence and exfoliates in the form of black flakes in the course of electrolysis, with the dense protective MnO_2 film retained on the surface of the titanium anode.

Several concurrent reactions, oxidation of titanium, evolution of Cl_2 and O_2, and formation of MnO_2, occur in the case of anodic polarization of the titanium electrode in HCl solutions [13]. A thin passivating TiO_2 film formed on the anode via oxidation at the beginning of the electrolysis hinders further ionization of titanium. As a result, the anode potential increases and reaches the potential of MnO_2 deposition. The thickness of the oxide film formed on the titanium electrode and, accordingly, its potential, depend on the current density, temperature, and electrolyte pH.

First, a primary passivating TiO_2 film exhibiting high protective properties is formed on the titanium surface at low current densities and relatively high temperatures. Then, the secondary passivating film, mostly composed of freshly deposited γ-MnO_2 is formed and reliably protects the titanium surface from disintegration. The protective properties of the MnO_2 film increase with temperature.

At low temperatures and high current densities, a titanium oxide layer with a high electrical resistance rapidly grows on the titanium surface. As a result, the anode potential increases to reach the potential of Cl_2 evolution. The distribution of the polarizing current along the anode surface is nonuniform. It is predominantly concentrated in the damaged areas of the passivating film, thus causing electroeroison of the anode.

Table 1. Chemical corrosion rate v_{ch} of VT-01-00 titanium at various temperatures and electrolyte compositions

c_{MnCl_2}, M	c_{HCl}, M	T, °C	τ, h	v_{ch}, g m^{-2} h^{-1}
1.0	–	60	6	0
1.0	–	75	15	0
1.0	–	90	15	0
1.0	0.05	60	6	0
1.0	0.05	75	10	2.4×10^{-4}
1.0	0.05	90	10	3.7×10^{-4}
1.0	0.25	60	6	1.1×10^{-4}
1.0	0.25	75	10	2.4×10^{-4}
1.0	0.25	90	10	6.7×10^{-4}
–	0.05	60	6	1.1×10^{-4}
–	0.05	75	10	2.6×10^{-4}
–	0.05	90	10	4.0×10^{-4}
–	0.25	60	6	8.0×10^{-4}
–	0.25	75	10	7.5×10^{-4}
–	0.25	90	10	9.3×10^{-4}

Table 2. Electrochemical corrosion rate v_{ech} of VT-01-00 titanium at various temperatures and HCl concentrations (Current density 5 mA cm^{-2}, $MnCl_2$ concentration 1 M)

c_{HCl}, M	T, °C	τ, h	U_{ini}, V	U_{fin}, V	v_{ech}, g m^{-2} h^{-1}
–	60	6	3.9	10.0	0
–	75	15	3.5	5.1	9.4×10^{-3}
–	90	15	2.6	5.1	7.2×10^{-3}
0.25	60	6	2.7	5.2	0
0.25	75	10	2.3	3.5	6.8×10^{-3}
0.25	90	10	2.9	3.2	2.8×10^{-3}

Calculations demonstrated that the rate at which the thickness of the titanium anodes decreases because of the chemical and electrochemical corrosion in the course of the electrolysis in manganese chloride electrolytes does not exceed 0.03 mm/year.

CONCLUSIONS

(1) VT-01-00 titanium can be used as anode in deposition of electrolytic manganese dioxide from chloride electrolytes.

(2) The optimal conditions for deposition of MnO_2 with a high current efficiency are as follows: temperature 70–75°C, current density 5 mA cm^{-2}, and HCl concentration 0.05 M. Under these conditions, the MnO_2 deposit has the form of coarsely crystalline aggregates that can be easily detached from the anode surface.

REFERENCES

1. Spotniz, R.M., Spilman, R.W., and Lundquist, J.T., *J. Electrochem. Soc.*, 2000, vol. 134, no. 10, pp. 2435–2441.
2. Roinishvili, L.I., Abstracts of Papers, *I Gruzinskaya Konferentsiya po elektrokhimii* (I Georgian Conf. on Electrochemistry), Tbilisi: Metsniereba, 1977, p. 99.
3. Stender, V.V. and Lisov, V.N., *Zh. Prikl. Khim.*, 1967, vol. 40, no. 3, pp. 570–576.
4. Kozin, L.F., Drozd, N.A., and Manilevich, F.D., *Zh. Prikl. Khim.*, 1996, vol. 69, no. 2, pp. 251–255.
5. Lisov, V.N., *Gidroelektrometallurgiya khloridov* (Hydroelectrometallurgy of Chlorides), Kiev: Naukova Dumka, 1964, pp. 76–98.
6. JPN Patent 2423.
7. USSR Inventor's Certificate, no. 220254.
8. USSR Inventor's Certificate, no. 1661247.
9. Charlot, G., *Quantitative Inorganic Analysis*, London: Wiley, 1957.
10. *TU* (Technical Specification) *2122-205-00203312–2000. Inhibited Hydrochloric Acid*.
11. Patrova, G.I., Yur'ev, B.P., and Shkol'nikov, S.N., *Zh. Prikl. Khim.*, 1979, vol. 52, no. 1, pp. 84–90.
12. Dyatlova, V.N., *Korrozionnaya stoikost' metallov i splavov* (Corrosion Resistance of Metals and Alloys) Moscow: Mashinostroenie, 1964.
13. Kalinovskii, E.A., Rossinskii, Yu.K., and Kebadze, Zh.M., *Zh. Prikl. Khim.*, 1988, vol. 61, no. 2, pp. 293–298.

Russian Journal of Applied Chemistry, Vol. 78, No. 6, 2005, pp. 897–902. Translated from Zhurnal Prikladnoi Khimii, Vol. 78, No. 6, 2005, pp. 918–923.
Original Russian Text Copyright © 2005 by Frolov, Bolotin, Panyshkin.

APPLIED ELECTROCHEMISTRY AND CORROSION PROTECTION OF METALS

Electrochemical Synthesis of Complex Compounds of Transition Elements with Carboxyl- and Carbonyl-containing Ligands

V. Yu. Frolov, S. N. Bolotin, and V. T. Panyshkin

Kuban State University, Krasnodar, Russia

Received February 25, 2004

Abstract—Complex compounds of *d*- and *f*-elements with carboxyl- and carbonyl-containing ligands were synthesized by the electrochemical method. The influence exerted by a number of factors on the process course was studied. The dependence of the electrosynthesis parameters on the composition of the forming compounds was established. The composition of these compounds was determined. A new method for anodic synthesis of these compounds was developed.

The electrochemical method simplifies synthesis of known compounds [1–5] and makes it possible to synthesize compounds that cannot be obtained otherwise [6]. Moreover, the advantage of the anodic synthesis is in that the process can be controlled and performed in mild conditions with a high yield and purity of the final products [7].

Despite that the electrosynthesis is one of the oldest methods for synthesis of coordination compounds [8], the analysis of the anodic synthesis methods in [1–7, 9–13] shows that many problems concerning the theory and practical application of the method have not been studied.

Transition-metal carboxylates of composition $M(O_2CR)_n$ (M = Cr; R = C_2H_5 or C_6H_5; n = 3; M = Mn, Fe, or Ni; R = CH_3, C_2H_5, C_6H_5, or n-C_7H_{15}; n = 2) have been prepared [14] by electrochemical oxidation of the corresponding metals in solutions of carboxylic acids RCOOH in acetonitrile. In [15–17], monocarboxylic acids containing one to four atoms in the carbon chain were successfully used to synthesize $M(O_2CR)_2$ salts. Oxalate complexes of iron and copper were synthesized by the electrochemical method in [18]. On the whole, publications devoted to carboxylate complexes are scarce and analyze a rather small number of the ligands.

The goal of this study was to develop new original methods that would enable application of the electrochemical synthesis in a wider range and to a larger number of objects and make it possible to perform directed syntheses in which the composition of the forming products is controlled by varying the process conditions (ligand concentration, temperature, solvent, and electrode potential), and also to compare the properties of compounds synthesized by electrochemical methods with those produced by chemical methods. Acetylacetonates of rare-earth elements (REE) were synthesized to confirm the suggestion that substances exhibiting a tendency toward sublimation, which could not be synthesized previously by other methods [19, 20], can be obtained by electrochemical synthesis.

EXPERIMENTAL

The installation for anodic synthesis (Fig. 1) comprised a three-electrode cell, PI-50-1 potentiostat,

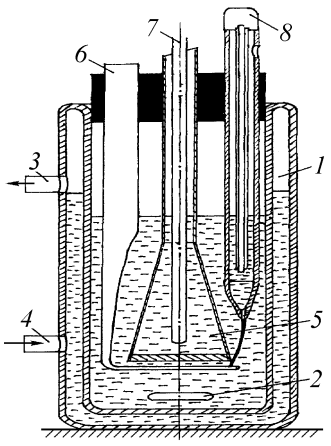


Fig. 1. Schematic of a three-electrode cell for electrochemical anodic synthesis (*1*) Thermostating jacket, (*2*) stirrer, (*3*) outlet, (*4*) inlet, (*5*) separator, (*6*) working electrode, (*7*) auxiliary electrode, and (*8*) reference electrode.

1070-4272/05/7806-0897 © 2005 Pleiades Publishing, Inc.

Complex compounds obtained by electrochemical synthesis

Compound	Formula	Ligand concentration, $c \times 10^2$, M	Supporting electrolyte and solvent	Anode	Cathode	Anode potential, V	Current density, A dm^{-2}		T, °C	Current efficiency, %
							anode	cathode		
I	$CuSuc \cdot 5H_2O$	10	H_2O	Cu	Cu	0.5	5	5	25	85.3
II	$CuSuc \cdot 5H_2O$	10	H_2O	Cu	Cu	0.5	5	5	60	80.6
III	$CuSuc \cdot 5H_2O$	10	H_2O–alcohol	Cu	Cu	0.05	5	5	25	53.2
IV	$ZnSuc \cdot 2H_2O$	10	H_2O	Zn	Zn	0.8	5	5	25	98.6
V	$ZnSuc \cdot 2H_2O$	10	H_2O	Zn	Zn	0.8	5	5	60	99
VI	$Cu(ButOH)_2 \cdot 2H_2O$	0.5	H_2O	Cu	Cu	0.5	5–10	5–10	25	78.7
VII	$Cu(ButOH)_2 \cdot 2H_2O$	0.5	H_2O	Cu	Cu	0.5	5–10	5–10	60	81.5
VIII	$Ni(ButOH)_2 \cdot 2H_2O$	5	H_2O	Ni	Ni	0.5	5–10	5–10	60	83.2
IX	$CuLac_2 \cdot 5H_2O$	5–10	H_2O	Cu	Cu	0.5–1	10–50	10–30	25	98.5
X	$CuLac_2$		LiCl, HLac	Cu	Cu	1–1.5	0.1–0.2	0.1–0.2	25–80	64.2
XI	$ZnLac_2 \cdot 2H_2O$	0.5	H_2O	Zn	Zn	0.8	5–10	5–10	60	87.8
XII	$CuMal \cdot 5H_2O$	1	H_2O	Cu	Cu	0.3	10–20	10–20	25	97.6
XIII	CuMal		LiCl, H_2Mal	Cu	Cu	1–1.5	0.1–0.2	0.1–0.2	135	45.9
XIV	$ZnMal \cdot 2H_2O$	1	H_2O	Zn	Zn	0.8	5–8	10–15	25	80.3
XV	$CuHCit \cdot 5H_2O$	0.5–1	H_2O	Cu	Cu	0.3–0.5	10–15	10–20	25	96.4
XVI	CuHCit	LiCl,	H_3Cit	Cu	Cu	1–1.5	0.1–0.2	0.1–0.2	165	35.6
XVII	$ZnHCit \cdot 2H_2O$	1	H_2O	Zn	Zn	0.8	3–10	10–15	25	87.8
XVIII	$CuArg_2 \cdot 5H_2O$	5–10	H_2O	Cu	Cu	0.15–0.3	10–15	10–20	25	89.6
XIX	$ZnArg_2 \cdot 2H_2O$	0.5–1	H_2O	Zn	Zn	0.5	5–8	10–20	25	81.5
XX	$NiArg_2 \cdot 3H_2O$	0.5	H_2O	Ni	Ni	0.5	1–5	5	25	78.9
XXI	$CuVal_2 \cdot 5H_2O$	5	H_2O	Cu	Cu	0.25	10–15	10–20	25	95.3
XXII	$ZnVal_2 \cdot 2H_2O$	1	H_2O	Zn	Zn	0.25	10–15	15–20	25	76.8
XXIII	$NiVal_2 \cdot 3H_2O$	0.5	H_2O	Ni	Ni	0.5	3–5	5–15	25	56.8
XXIV	$CuMet_2 \cdot 5H_2O$	10	H_2O	Cu	Cu	0.3	5–15	10–25	25	92.7
XXV	$ZnMet_2 \cdot 2H_2O$	1	H_2O	Zn	Zn	0.25	5–10	5–15	25	85.2
XXVI	$NiMet_2 \cdot 3H_2O$	50	H_2O	Ni	Ni	0.8	1–3	1–5	25	65.4
XXVII	$NdLac_3 \cdot 6DMF$	50	LiCl, DMF	Nd	Pt	0.5	1–3	1–5	25	
XXVIII	$TbLac_3 \cdot 8DMF$	50	LiCl, DMF	Tb	Pt	0.3–0.5	1–3	1–5	25	
XXIX	$GdLac_3 \cdot 8MDF$	50	LiCl, DMF	Gd	Pt	0.3–0.5	1–5	1–5	25	
XXX	$Nd_2Mal_3 \cdot 6MDF$	50	LiCl, DMF	Nd	Pt	0.5	1–5	1–5	25	
XXXI	$Tb_2Mal_3 \cdot 8DMF$	50	LiCl, DMF	Tb	Pt	0.5	1–3	1–5	25	
XXXII	$Er_2Mal_3 \cdot 10MDF$	50	LiCl, DMF	Er	Pt	0.5	1–5	1–5	25	
XXXIII	$NdLac_3$	50	LiCl, Acn	Nd	Pt	0.5	1–3	1–5	25	
XXXIV	$TbLac_3$	50	LiCl, Acn	Tb	Pt	0.3–0.5	1–3	1–5	25	
XXXV	$GdLac_3$	50	LiCl, Acn	Gd	Pt	0.3–0.5	1–5	1–5	25	
XXXVI	Nd_2Mal_3	50	LiCl, Acn	Nd	Pt	0.5	1–5	1–5	25	
XXXVII	Tb_2Mal_3	50	LiCl, Acn	Tb	Pt	0.5	1–3	1–5	25	
XXXVIII	Er_2Mal_3	50	LiCl, Acn	Er	Pt	0.5	1–5	1–5	25	
XXXIX	$NdAcac_3$	50	LiCl, Acn	Nd	Pt	0.5	10–15	10–15	25	
XL	$TbAcac_3$	50	LiCl, Acn	Tb	Pt	0.5	10–15	10–15	25	

PR-8 programmer, copper coulometer, instruments for external monitoring of the current and voltage (potential), magnetic or mechanic stirrer, and thermostat.

The working electrode was made of the metal subjected to anodic dissolution. Auxiliary electrodes were made of inert materials or of the same materials as working electrodes, depending on the objective. A standard silver chloride electrode served as a reference. In nonaqueous solvents, an electrolytic bridge was also used to prevent contamination of the solvent with water.

The cell includes a thermostated jacket for performing syntheses at elevated temperatures. In addition, the cathodic and the anodic compartments of the cell are separated with a porous glass separator. The electrochemical measurements can be performed

using a magnetic stirrer. The PR-8 programmer makes it possible to apply to the potentiostat a potential that can be varied by an arbitrary program, including linear or stepwise parts. The circuit includes a copper coulometer for determining the current efficiency.

The table lists the conditions in which complex compounds of zinc, copper, nickel, and a number of REEs (Nd, Tb, Pr, Gd, Er) with lactic (HLac), malic (H_2Mal), citric (H_3Cit), succinic (H_2Suc), and γ-oxybutyric (HButOH) acids, arginine (HArg), valine (HVal), methionine (HMet), and acetylacetone (HAcac) were synthesized. The presence of the compounds as individual phase was confirmed by elemental and thermogravimetric (TG) analyses and by IR spectroscopy.

The content of metals was determined by complexometric titration [21] and that of carbon, hydrogen, and nitrogen, by elemental gas-volumetric analysis.

The IR spectra were measured on a Perkin–Elmer 180 spectrophotometer in the range 4000 – 400 cm^{-1} in a Vaseline oil suspension. The IR spectra of the carboxylic acid compounds synthesized were mainly analyzed for the position of the absorption bands associated with the carboxylic group and carboxylate ion, which is consistent for the compounds studied with published data [20, 22–25] for compounds with similar structure and composition.

The thermogravimetric curves were measured at 20–1000°C on an MOM derivatograph (Hungary). We used platinum crucibles, a platinum–platinum-rhodium thermocouple, and aluminum oxide as reference. The weighed portions were 50 mg, and the heating rate, 10 deg min^{-1}. As objects of analysis of the thermogravimetric data served DTA, DTG, and TG curves. In those cases when the composition of the final phase formed by the thermolysis can be predicted rather reliably (e.g., formation of CuO as the final product for complex copper compounds), we performed a quantitative analysis for the content of the ligand. The results of such an analysis were always in an agreement with the data obtained by chemical analysis.

The synthesis was performed in water and in nonaqueous solvents: acetonitrile (Acn) and dimethylformamide (DMF). In aqueous solutions, the synthesis was carried out without a supporting electrolyte, with the electric conduction provided by ions formed upon the dissociation of the ligands (H^+, L^{n-}). The decrease in the electrical conductivity, which is due to the fact that these substances are weak electrolytes, is compensated for by the absence of foreign ions in the solution, and, consequently, by the formation of simpler complex compounds. The ions formed upon dissociation migrate toward the electrodes and enter into the electrode reactions [4, 12].

$$\text{C: } 2H^+ + 2e \rightarrow H_2 \quad (H_nL + ne \rightarrow L^{n-} + n/2H_2),$$

$$\text{A: } mL^{n-} + nM - (nm)e \rightarrow M_nL_m.$$

In the electrochemical systems Cu/HLac, Cu/H_2Mal, and Cu/H_3Cit, the synthesis was performed using a liquid (molten) ligand as a solvent. The working temperature of the synthesis (see table) was higher than the melting point of the ligand and lower than its decomposition point. Inorganic chlorides were added to the molten ligand, and the supporting electrolyte was formed directly by the reaction

$$n\text{LiCl} + H_nL \rightleftarrows Li_nL + n\text{HCl}\uparrow.$$

The synthesis in a liquid ligand was performed with a preliminary dehydration of the ligands to a water content of 1–10 mmol l^{-1}. The compounds obtained contained a large amount of water, but their degree of hydration was considerably lower than that for compounds obtained from solution and subjected to dehydration. Therefore, the synthesis in a melt can be recommended for obtaining substances with the minimum content of water or compounds hardly hydrated by the conventional methods. However, the process rate is low in this case.

To choose the optimal range of ligand concentrations for the anodic synthesis, we studied how the potential of the metal electrodes varies with the ligand concentration in the solution at a constant ionic strength (1 M LiCl).

The dependences of the electrode potentials on the ligand concentration in solution are shown in Fig. 2 for three typical systems. For the system constituted by copper and amino acid (curves *1*), extrema are observed in the ligand concentration range studied (0.005 M). In those cases when a complex compound has a low stability constant, the equilibrium potential of the electrode is mainly determined by the concentration of the metal aqua complexes. If the complex compound forms a sparingly soluble phase on the electrode surface and(or) a very stable complex compound is formed, then the electrode potential is also dependent on the concentration of the anionic form of the ligand in solution. This predetermines the complicated character of the dependences presented.

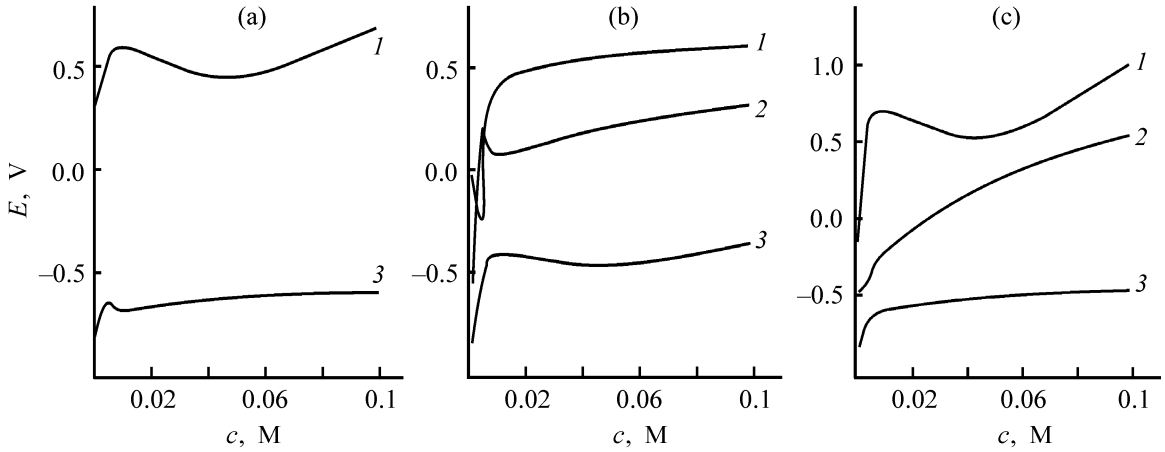


Fig. 2. Potential *E* of (*1*) copper, (*2*) nickel, and (*3*) zinc vs. the concentration *c* of (a) malic acid, (b) valine, and (c) arginine.

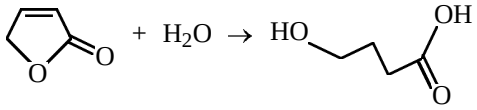
At low concentrations of the ligand (0.005 M and less), the electrode is frequently passivated. In the absence of a supporting electrolyte, such concentrations also lead to a low electrical conductivity of the solution. In these cases, it is suggested to perform electrolysis at high ligand concentrations by gradually raising the content of a ligand to the maximum possible value at a given temperature. For the amino acid systems, this means that the concentration can be raised from 0.005 M to the point of saturation (Fig. 2). It was found that such a procedure frequently makes it possible to avoid passivation of copper and zinc electrodes.

Copper easily dissolves in all the systems studied, with a high current efficiency at small shifts of the potential from the equilibrium value and high dissolution current densities.

Zinc dissolves well in the system with a stronger polarization, at higher anode potentials and lower current densities. Hydrogen is evolved at the cathode at the beginning of the process. Then, as metal ions are accumulated in the electrolyte, a parallel process of zinc separation commences, which decreases the current efficiency of the anodic process. The metal ions are discharged at the cathode to form dendrites, which are accumulated on the cell bottom because of the poor adherence to the electrode, thus creating additional difficulties in isolation of the final product. This difficulty is eliminated if a cell with separated electrode compartments is used. In all probability, the high current efficiencies by the zinc compounds are due to the simultaneous spontaneous dissolution of the zinc electrodes:

$$Zn + 2HL \rightarrow ZnL_2 + H_2\uparrow.$$

The electrosynthesis of the complex nickel compounds with hydroxy acids (except γ-hydroxy butyric acid) poses certain difficulties. When the electrode potentials are low (1–2 V), the electrode in the system chosen is passivated, the electrolysis proceeds very slowly, and the anodic products cannot be identified by analysis as individual compounds. At high anode potentials (up to 3 V), oxygen evolution from water proceeds at the anode, which makes the nickel electrode completely inert. The successful synthesis of the nickel(II) complex with γ-hydroxy butyric acid is probably favored by the fact that it is synthesized from the preligand (2-butenolide), the true concentration of the ligand near the anode surface is very low, and its loss is continuously compensated for by hydrolysis of 2-butenolide directly at the anode surface:



It was established for copper in an analogous system that copper compounds with different states degrees oxidation are formed by electrochemical synthesis at different temperatures: a pale green copper(II) complex insoluble in water (compound **VI**) is formed at 25°C, and a copper(I) complex insoluble in water (compound **VII**), at 65°C.

Comparison of the IR spectra of the compounds obtained in the REE(Nd, Tb)/HAcac system, which have, according to the results of an analysis, the composition $LnAcac_3$, with the spectrum of the pure ligand (shift of the carbonyl vibrational band at around 1650 cm^{-1} by 50–60 cm^{-1}) shows that a chemical carbonyl bond is formed [22]. The thermogravimetric

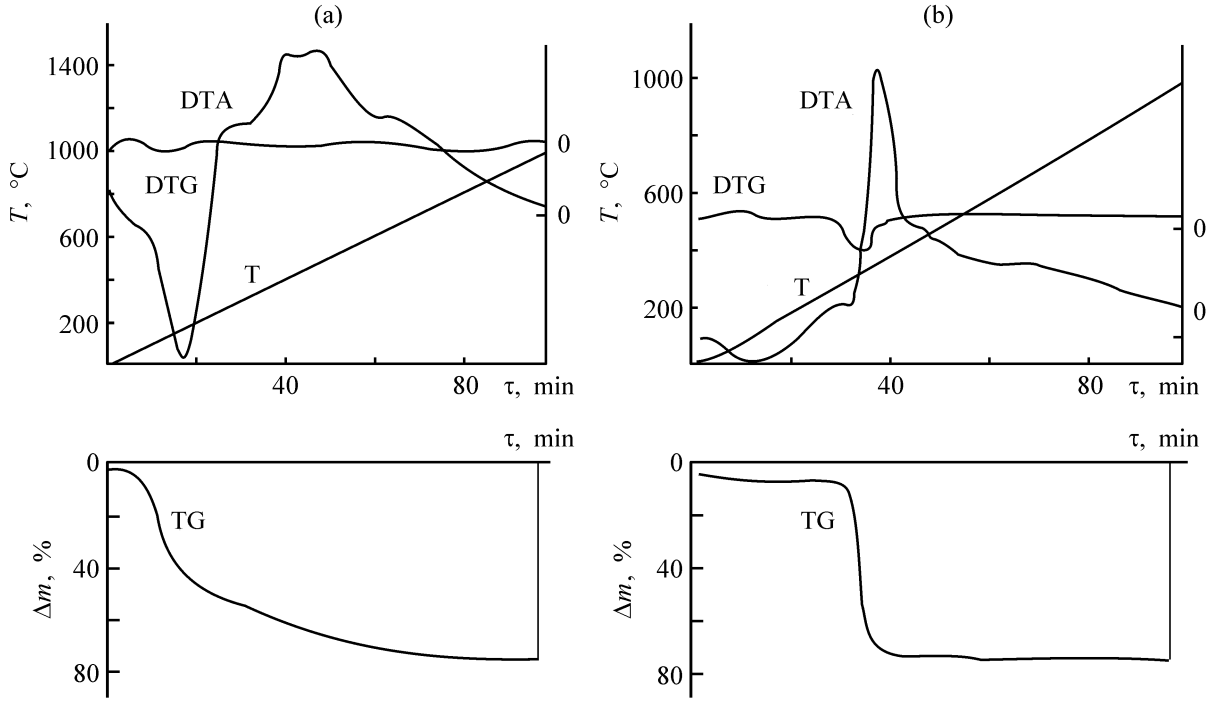


Fig. 3. Thermograms of (a) neodymium and (b) terbium trisacetylacetonates. (T) Temperature, (Δm) relative loss of mass, and (τ) time.

data in Fig. 3 suggest that the substances synthesized are volatile: a drastic mass loss (96%) observed at T = 310°C for compound (**XXXIX**) corresponds to a strong exothermic effect, which may be due to sublimation of a sample and its simultaneous combustion in the vapor state; for compound (**XL**), a 75%-loss of mass, accompanied by a pronounced endothermic effect, is observed at T = 220°C. Thus, the electrochemical synthesis of acetylacetonates of rare-earth elements is a simpler and less expensive method, and, which is the most important, it gives anhydrous compounds with a molecular crystal lattice [26].

In the course of synthesis in a system containing copper electrodes and an aqueous solution of lactic acid at high anode potentials (2–3 V), a finely dispersed colorless water-insoluble solid substance is formed at the anode alongside with a compound $CuLac_2 \cdot 5H_2O$, which is obtained in a very low yield (5–10%). An analysis of the compound obtained revealed neutral anhydrous copper carbonate $CuCO_3$. Therefore, it was suggested that the electrochemical anodic reaction of decarboxylation of lactic acid (Kolbe reaction) occurs in such a synthesis as a side process unknown previously for α-substituted hydroxy carboxylic acids and their salts. The process can be used to introduce into the anodic Kolbe synthesis new classes of organic substances, which is important for practice.

Various nonaqueous solvents also differently affect the composition of the products obtained and the process efficiency. Use of aqueous-alcoholic media in synthesis of *d*-element succinates was ineffective. It was found for aprotic solvents that there is a relationship between the solvent chosen and formation of solvated complexes. The formation of solvates (solvation) depends on the relative donor strength of the solvent and the ligand used and on the temperature mode of electrolysis. For example, solvated complexes are always formed in dimethylformamide, whereas in acetonitrile, this occurred only in several cases. It may be concluded that acetonitrile is the most suitable solvent for synthesis of unsolvated compounds.

The electrochemical synthesis has a high efficiency: the yield of substance and the current efficiency (>50%) are considerably higher than those in the conventional chemical syntheses. In addition, the electrochemical synthesis is a single-stage process, which also makes higher the yield of the product. In the general case, the yield of substance and the current efficiency may be different or may coincide.

The effect of the process temperature on the composition of the products obtained was especially strong in interaction of copper with 2-butenolide, when at a comparatively small temperature difference, two products of different compositions were formed, with

copper in different oxidation states. In other cases, differently solvated compounds were formed.

CONCLUSIONS

(1) The optimal concentration ranges of the ligand for electrochemical synthesis of complex compounds, temperature, solvent, and gaseous medium of synthesis were determined on the basis of potenstiostatic data.

(2) Anodes made of rare-earth metals were used in electrochemical synthesis for the first time. Thermogravimetric data demonstrated that the physical properties (high volatility) and structure of acetylacetonates of rare-earth elements synthesized by this method in anhydrous acetonitrile differ from the properties of the previously synthesized analogues.

(3) It was shown that the anodic dissolution of the metal facilitates decarboxylation of hydroxy acid.

REFERENCES

1. Habeeb, J.J., Tuck, D.G., and Walters, F.H., *Coord. Chem.*, 1978, vol. 8, no. 1, p. 27–33.
2. Habeeb, J.J., Nielson, L., and Tuck, D.G., *Inorg. Chem.*, 1978, vol. 17, no. 3, p. 306–310.
3. Habeeb, J.J., and Tuck, D.G., *J. Chem. Soc. Chem. Commun.*, 1975, vol. 5, no. 7, p. 808–809.
4. Konev, V.A., Kukushkin, V.Yu., and Kukushkin, Yu.N., *Zh. Neorg. Khim.*, 1986, vol. 31, no.7, p. 838–843.
5. Laube, B.L. and Schmulbach, C.D., *Prog. Inorg. Chem.*, 1971, vol. 14, no. 1, p. 65–181.
6. Chakravorti, M.C. and Subrahmanyam, G.V.B., *Coord. Chem. Rev.*, 1994, vol. 135, no. 1, pp. 65–92.
7. Garnovskii, A.D., Kharisov, A.I., Gokhon-Zorilla, G., and Garnovskii, D.A., *Usp. Khim.*, 1995, vol. 64, no. 3, p. 251–236.
8. Zamyatkina, V.M., Kukushkin, Yu.N., and Makarenya, L.A., *Lev Aleksandrovich Chugaev*, Moscow: Nauka, 1973.
9. Tuck, D.G., *Pure Appl. Chem.*, 1979, vol. 51, no. 2, p. 2005.
10. Bogdashev, N.N., Garnovskii, A.D., Osipov, O.A., *et al.*, *Zh. Obshch. Khim.*, 1976, vol. 46, no. 3, p. 675–680.
11. Garnovskii, A.D., Ryabukhin, Yu.I., and Kuzharov, A.S., *Koord. Khim.*, 1984, vol. 10, no. 8, p. 1011–1033.
12. Kukushkin, V.Yu. and Kukushkin, Yu.N., *Teoriya i praktika sinteza koordinatsionnykh soedinenii* (Theory and Practice of Synthesis of Coordination Compounds), Leningrad: Nauka, 1990.
13. Tomilov, A.P., Chernykh, I.N., and Kargin, Yu.N., *Elektrokhimiya elementoorganicheskikh soedinenii: Elementy I, II i III grupp periodicheskoi sistemy i perekhodnye elementy* (Electrochemistry of Hetero-Organic Compounds: Elements of Groups I, II, and III of the Periodic System and Transition Elements), Moscow: Nauka, 1985.
14. Kumar, N., Tuck, D.G., and Watson, K.D., *Canad. J. Chem.*, 1987, vol. 65, no. 6, p. 740.
15. Banait, J.S., and Pahil, P.K., *Polyhedron*, 1985, vol. 4, no. 6, p. 1031.
16. Banait, J.S., and Pahil, P.K., *Bull. Electrochem.*, 1989, vol. 5, no. 2, p. 264.
17. Bott, R., Healy, P.C., and Sagatys, D.S., *Chem. Commun.*, 1998, no. 21, p. 2403.
18. Kumar, N, and Tuck, D.G., *Canad. J. Chem.*, 1984, vol. 62, no. 14, p. 1701.
19. Przystal, J.K., Bos, W.G., and Liss, I.B., *J. Inorg. Nucl. Chem.*, 1971, vol. 33, no. 5, p. 679.
20. Panyushkin, V.T., *Spektroskopiya koordinatsionnykh soedinenii redkozemel'nykh elementov* (Spectroscopy of Coordination Compounds of Rare-Earth Elements), Rostov-on-Don: Rostov. Univ., 1984.
21. Schwarzenbach, G. and Flaschka, H., *Complexometric Titrations*, London: Methuen, 1969, 2nd ed.
22. Nakamoto, K., *Infrared and Raman Spectra of Inorganic and Coordination Compounds*, New York: Wiley, 1978, 3rd ed.
23. Ablov, A.V., Proskina, N.I., and Gapurina, P.F., Kolebatel'nye spektry v organicheskoi khimii (Vibrational Spectra in Organic Chemistry), Moscow: Nauka, 1971.
24. Bol'shakov, G.F., Glebovskaya, E.A., and Kaplan, Z.G., *Infrakrasnye spektry i rentgenogrammy geteroorganicheskikh soedinenii* (Infrared Spectra and X-Ray Diffraction Patterns of Hetero-organic Compounds), Leningrad: Khimiya, 1967.
25. Bellamy, L.J., *The Infrared Spectra of Complex Molecules*, New York: Wiley, 1975.
26. RF Patent 2 191 190.

Russian Journal of Applied Chemistry, Vol. 78, No. 6, 2005, pp. 903–906. Translated from Zhurnal Prikladnoi Khimii, Vol. 78, No. 6, 2005, pp. 924–927.
Original Russian Text Copyright © 2005 by Zaichenko.

APPLIED ELECTROCHEMISTRY AND CORROSION PROTECTION OF METALS

Magnetoelectrolytic Dispersion of Ferromagnetic Metals

V. N. Zaichenko

Institute of General and Inorganic Chemistry, Ukrainian National Academy of Sciences, Kiev, Ukraine

Received October 14, 2005; in final form, March 2005

Abstract—Processes of electrolytic dispersion of ferromagnetic metals (nickel and cobalt) to give oxides or metal powders were studied. The influence of an external magnetic field and current reversal on the processes of anodic dissolution was analyzed.

The known method for production of nickel(II) hydroxide (green) by electrochemical dissolution of rough nickel [1] cannot process lump or granulated metals. This problem was partly solved by the technique [2] that makes it possible to treat subquality powders. The electrochemical technology is the most suitable for this purpose, as it requires no chemicals and does not pollute the environment.

Also known is the intensification of certain diffusion-limited electrode processes by an external magnetic field [3]. This effect is due to a decrease in the thickness of near-electrode diffusion layers, which results from strong electrolyte flows tangential to the electrode surface, initiated by a one-dimensional magnetic field [4] and by that of a three-dimensional topography [5]. The anodic dissolution of nickel and cobalt in neutral solutions proceeds to give solid hydroxides, which are deposited onto the electrodes to form layers partially screening the electrode surface. Probably, this process can be prevented both by the action of an external magnetic field and by current reversal.

The known filled electrodes for anodic dissolution of nickel and cobalt, placed in perforated pockets made of a chemically resistant material (e.g., titanium), have the following drawbacks. First, the pockets screen no less than 50% of the surface area of a metal to be dissolved and, second, they are cluttered in the course of the electrolysis with hydroxides hardly removable through the perforation.

The aim of this study was to examine the effect of an external magnetic field and current reversal on the electrochemical dispersion of nickel and cobalt without screening of their surface and to assess the possibility of using ammonium chloride as an electrolyte, instead of sodium chloride.

To study the anodic dissolution of the metals, we used a 120-mm-high electrolyzer with a 160×280-mm cross-section and a standard electrochemical cell for recording of polarization curves. Solutions (2 M) of analytically pure sodium or ammonium chloride were used as electrolytes. A twofold decrease in the concentration of sodium chloride diminishes the conductivity of the solution by 80%, and an increase in this concentration results in an undesirable crystallization of salt on the electrolyzer walls above the electrolyte mirror.

To make a qualitative observation of the process, we first used a simplified electric circuit that allowed us to measure the current strength at a stepwise variation of the voltage across the electrolyzer. After that, the polarization of nickel and cobalt electrodes under potentiostatic conditions was studied with a PI-50-1.1 potentiostat. The efficiency of the anodic dissolution was estimated by the current efficiency, and the cost efficiency, by the expenditure of electricity per unit amount of the product.

The qualitative experiments were carried out in a 0.2-dm^3 cell. As the cathode served platinum, as the anode were used, in succession, nickel, cobalt, and titanium, as well as the nickel–titanium and cobalt–titanium combinations, with a working surface area of 4.0 ± 0.2 cm^2. Titanium was chosen as a metal for the current lead to lumpy nickel and cobalt owing to its chemical inertness. It was important to check its electrochemical stability in electrolysis in highly concentrated chloride solutions.

The experimental current-voltage dependences indicate that nickel and cobalt are anodically dissolved in a sodium chloride solution without any limitations (Fig. 1, curves *1* and *2*). Being a valve metal, titanium is anodically blocked: the current in the cell does not

1070-4272/05/7806-0903 © 2005 Pleiades Publishing, Inc.

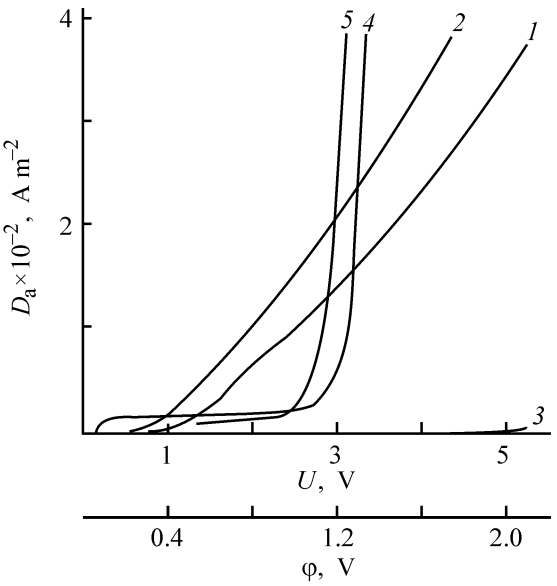


Fig. 1. Current density D_a vs. voltage U across a bath with (*1*) nickel, (*2*) cobalt, and (*3*) titanium anodes and a platinum cathode and vs. the anode potential φ for (*4*) nickel and (*5*) cobalt in a NaCl solution with a concentration of 120 g l^{-1}. Temperature 20 ± 1°C, pH 6.2.

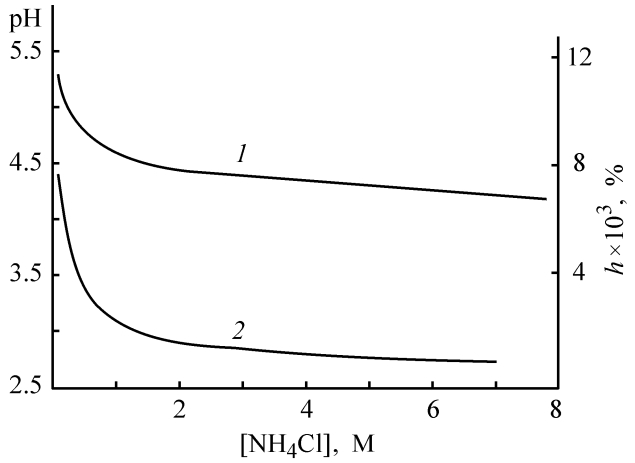


Fig. 2. (*1*) Solution pH and (*2*) degree h of hydrolysis vs. the concentration of NH_4Cl.

exceed 0.12 mA up to a voltage of 6 V; in the voltage range 6–15 V, the current increases to 0.4 mA due to a rise in the oxide film thickness; and only beginning at 16 V, a breakdown occurs in the film and the current increases to 1.5 A. In this case, white flakes, products of titanium(IV) hydrolysis, are formed in the solution. Under real conditions, the electrolyzer voltage does not exceed 10 V and, therefore, titanium is electrochemically inert.

To obtain more complete information on the anodic dissolution of Ni and Co in NaCl solutions, we recorded potentiostatic curves (Fig. 1, curves *4* and *5*) which also indicate that the dissolution proceeds without any hidrance.

As the sodium ion is an undesirable admixture in the final product, we checked up the possibility of carrying out the electrolysis in a NH_4Cl solution. It would be expected *a priori* that it is hardly possible to obtain precipitates of hydroxides under these conditions owing to the formation of soluble nickel complexes with ammonia. In this case, the anodic dissolution of nickel involves the following reactions:

$$Ni - 2e \rightarrow Ni^{2+}, \quad (1)$$

$$H_2O + 2e \rightarrow 2OH^- + H_2, \quad (2)$$

$$Ni^{2+} + 2OH^- \rightarrow Ni(OH)_2, \quad (3)$$

$$Ni(OH)_2 + 2NH_4^+ \rightarrow Ni^{2+} + 2NH_4OH, \quad (4)$$

$$Ni(OH)_2 + nNH_4OH \rightarrow [Ni(NH_3)_n]^{2+} + nH_2O + 2OH^-. \quad (5)$$

It was appropriate to find out whether there are ranges of pH values and NH_4Cl concentrations in which nickel(II) hydroxide can be precipitated in the presence of ammonium salts.

Compared with nickel, cobalt forms with ammonia stronger complexes and its precipitation as $Co(OH)_2$ in the presence of ammonium ions is virtually impossible.

According to the distribution diagrams of polyamine complexes with nickel(II) and cobalt(II) in 2 N solutions of their salts in the presence of ammonia, uncoordinated ions can exist only at p[(NH_3)] exceeding 4.4 and 3.5 or at concentrations less than 4.0×10^{-5} and 3.2×10^{-4} M, respectively, which corresponds to pH values less than 9.42 and 9.87.

The dependence of the solution pH on the salt concentration is calculated by the formula:

$$[H^+] = cK_w/K_b. \quad (6)$$

Here c is the concentration of NH_4Cl (M); K_w, ionic product of water; and K_b, constant of NH_4OH dissociation.

The calculated data are presented in Fig. 2, which shows that the pH of formation of nickel hydroxides in the presence of NH_4Cl can be reached only at concentrations of this salt less than 0.5 M. It is known [6] that, at an NH_4Cl concentration of 0.16 M (8.56 g l^{-1}), nickel(II) hydroxide is formed even at pH 3.3.

We carried out an experiment on anodic dissolution of nickel in such a solution at a current density of 125 A m^{-2} and a temperature of $20 \pm 1°C$, and found out that nickel(II) hydroxide is formed. However, the electrolyzer voltage increased to 8 V because of the low electrical conductivity of the solution. Therefore, dispersion of nickel under these conditions will involve an increase in the electricity consumption. It is also known that addition of boric acid makes lower the pH of hydroxide formation, but its application would lead to an increase in the consumption of deionized water for washing of precipitates.

In view of the aforesaid, a solution of kitchen salt is the most suitable electrolyte.

To make an electric contact with fragments of ferromagnetic metals, we used a magnetic block (Fig. 3) with an *m*-metal plate on the back side, which served as a magnetic core and diminished the magnetic leakage.

The magnetic block was assembled from flat permanent magnets with alternating poles. The magnetic induction of a single element was 0.04–0.50 T. The block provides an electric contact, via the titanium plate, with all fragments of a metal to be dissolved. Furthermore, this block creates in the near-electrode region a three-dimensional magnetic field whose component orthogonal to the electric field vector generates tangential electrolyte flows, which enhances the mass exchange. Moreover, nickel(II) and cobalt(II) hydroxides precipitated in a magnetic field have a better filterability.

Nickel and cobalt hydroxides $M(OH)_2$ formed in anodic dissolution partially adhere to the surface to screen it. Current reversal with a period of 5–30 min makes it possible to avoid this phenomenon almost completely due to hydrogen bubbling during the cathodic period.

The effect of a magnetic field and current reversal on the technological process is reflected in the table. These data were obtained on the above-mentioned laboratory electrolyzer in a NaCl solution with a concentration of 120 g l^{-1}. The amount of $Ni(OH)_2$ obtained in 20.8 h at an electricity consumption of 93.7 A h was 165.3 g. This intermediate product was further thermally reduced in a hydrogen medium to give 104.7 g of a nickel powder. The bath voltage was 2.6 V. The quantity of electricity consumed in magnetoelectrolytic dispersion was 2.33 kW h per 1 kg of the nickel powder.

In the course of the electrolysis, the electrolyte is somewhat alkalified. In our experiment, pH increased from 6.20 to 9.55 pH units in 20.8 h owing to the formation of a new phase from poorly soluble nickel(II) hydroxide, whose solubility product in the freshly precipitated state is 2.0×10^{-15}. Based on this value, we estimate the concentration of OH^- ions at 10^{-5} M (with the presence of a concentrated sodium chloride solution disregarded), which corresponds to pH 9. This satisfactorily accounts for the increase in the electrolyte pH.

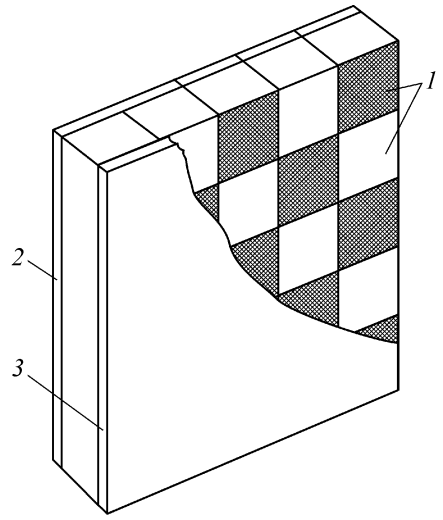


Fig. 3. Schematic of a magnetic block: (*1*) permanent magnets, (*2*) magnetic core, and (*3*) contact plate.

Effect of current density, external magnetic field, and current reversal on the magnetoelectrolytic dispersion of Ni and Co*

M	$D_a \times 10^{-2}$, A m^{-2}	B, T	τ_r, min	v_{md}, kg m^{-2} h^{-1}	Q, kW h kg^{-1}	Φ, l h^{-1}
Dispersion of nickel						
Ni	2.0	0.04	No	0.18	2.63	0.12
	2.0	0.25	5.0	0.21	2.47	0.23
	3.0	0.25	5.0	0.32	2.48	0.25
	3.0	0.50	5.0	0.34	2.33	0.41
	3.0	0.50	15.0	0.31	2.38	0.41
	3.0	0.50	30.0	0.31	2.40	0.41
Dispersion of cobalt						
Co	2.0	0.04	No	0.13	2.78	0.15
	2.0	0.25	5.0	0.15	2.51	0.26
	3.0	0.50	5.0	0.22	2.54	0.26

* *B* is the induction of a unit magnet; τ_r, reversal period, min; v_{md}, metal dissolution rate; *Q*, specific electricity consumption; and Φ, filterability.

Raising the electrolyte pH to 10 units has virtually no effect on the technological process and the product quality. Further increase in pH can be avoided by adjusting the electrolyte with hydrochloric acid.

An analysis of the reduced nickel powder for sodium demonstrated that its content does not exceed 0.03 wt %, which satisfies the requirements of GOST (All-Union Standard) 9722–97.

Similar experiments were carried out with an anode made of waste metallic cobalt. The technological process is similar to that of nickel dispersion.

In conclusion, it is necessary to note that dispersion of nickel at higher current densities yields black Ni(III) hydroxide, the same being true for cobalt.

COCNCLISIONS

(1) An external magnetic field intensifies the anodic dissolution of Ni and Co in NaCl solutions.

(2) Periodic current reversal prevents formation of hydroxide layers on the anode and intensifies the process, too.

(3) The calculated and experimental data obtained in this study demonstrate the possibility of precipitation of nickel(II) hydroxide by the electrochemical technique from NH_4Cl solutions with concentrations of 0.16 M and less.

REFERENCES

1. Kheifets, V.L. and Gran', T.V., *Elektroliz nikelya* (Electrolysis of Nickel), Moscow: Metallurgiya, 1975.
2. Ukrainian Patent 44430.
3. Zaichenko, V.N., *Vestn. Lviv. Univ., Ser. Khim.*, 2002, issue 42, part 1, pp. 102–104.
4. Fedot'ev, N.P. and Evstyukhin, A.I., *Trudy. Len. Khim.-Tekhnol. Inst. im. Lensoveta*, 1939, issue 7, pp. 32–41.
5. French Patent 2584621
6. Rotinyan, A.L. and Zel'des, V.Ya., *Zh. Prikl. Khim.*, 1951, vol. 24, no. 6, pp. 604–609.

Russian Journal of Applied Chemistry, Vol. 78, No. 6, 2005, pp. 907–911. Translated from Zhurnal Prikladnoi Khimii, Vol. 78, No. 6, 2005, pp. 928–932.
Original Russian Text Copyright © 2005 by Sedneva.

APPLIED ELECTROCHEMISTRY AND CORROSION PROTECTION OF METALS

Cerium(III) Electrooxidation in Nitric Acid Solutions of Rare-earth Elements

T. A. Sedneva

Tananaev Institute of Chemistry and Technology of Rare Elements and Mineral Resources, Kola Scientific Center, Russian Academy of Sciences, Apatity, Murmansk oblast, Russia

Received July 14, 2004; in final form, March 2005

Abstract—The electrochemical behavior of cerium(III) in nitric acid solutions of rare-earth elements was studied. The activation energy and reaction order of cerium(III) oxidation were determined for various levels of anodic polarization.

Published data [1–6] on cerium(III) recovery from a mixture of rare-earth elements (REEs) and preparation of its pure compounds show that the method of preliminary electrochemical oxidation of Ce(III) to Ce(IV), followed by separation by precipitation or extraction, is the most promising. The comparative simplicity of separation is based on the substantial difference in the chemical properties of REE(III) and Ce(IV). The advantages of the electrochemical oxidation are the absence of chemical oxidants, possibility of preparation of stable Ce(IV) solutions, feasibility of a continuous process, higher equipment productivity, and smaller working area. However, this method has been insufficiently developed for industrial application [7]. The high yield of Ce(III) oxidation is achieved at a low current efficiency.

In this study, we examined how the electrochemical oxidation of Ce(III) in nitric acid solutions depends on the current density i, Ce(III) concentration, and electrolyte stirring intensity (characterized by the Reynolds number Re). The conditions ensuring complete Ce(III) oxidation with a current efficiency exceeding 92% were determined.

EXPERIMENTAL

Nitric acid solutions of REEs containing approximately 200 g l^{-1} Ce(III) (recalculated to CeO_2)[1], which amounts to 54% of the sum of REE, were electrolyzed.

In an electrolyzer with unseparated electrode spaces, a cylindrical platinum grid with a 0.1-dm^2 surface area was the anode, and a coaxial titanium rod with varied surface area, the cathode. The electrolyte volume was 0.1 dm^3. The solution was stirred with a blade stirrer (blade diameter 30 mm) at varied rate.

Polarization measurements were performed on a PI-50-11 potentiostat equipped with an electrochemical cell containing a platinum working electrode with a 0.25-cm^2 surface area. The Ce(IV) concentration (g l^{-1}) in the solution was determined by titration with Mohr's salt in the presence of a Na DAS indicator. From the data of the analysis, the degree of Ce(III) oxidation C (%), current efficiency η (%), and rate of Ce(IV) accumulation in the electrolyte per unit anode surface area Q (kg m^{-2} h^{-1}) were calculated by the common methods.

To examine the influence of the electrode current density on the efficiency of electrochemical oxidation of Ce(III), the ratio of the anode and cathode surface areas, $S_a : S_c$, was varied from 1 : 2 to 6 : 1. Under these conditions, the cathode current density varied from 5 to 60 A dm^{-2}.

The following reactions can proceed in a nitric acid electrolyte under the action of direct current: at the anode

$$H_2O - 2e \rightarrow 1/2O_2 + 2H^+, \quad (1)$$

$$Ce(III) - e \rightarrow Ce(IV); \quad (2)$$

[1] In papers devoted to technology and analytical chemistry of REEs, their concentrations are usually expressed in terms of oxides. Hereinafter, the cerium concentration for both cerium oxidation states was recalculated to the CeO_2 content.

1070-4272/05/7806-0907 © 2005 Pleiades Publishing, Inc.

Table 1. Parameters of electrochemical oxidation of Ce(III) at various ratios of the electrode surface areas [$Ce(III)_{in}$ = 98 g l^{-1}, V_{el} = 0.1 l, S_a = 0.1 dm^2, τ = 10 min, and I = 1 A]

$S_a : S_c$	i, A dm^{-2}		Ce(IV), g l^{-1}	C, %	η, %
	anode	cathode			
1 : 2	10	5	0.09	0.09	0.8
1 : 1	10	10	0.54	0.55	4.9
2 : 1	10	20	2.00	2.04	18.3
3 : 1	10	30	4.42	4.52	40.4
4 : 1	10	40	6.85	6.99	62.5
5 : 1	10	50	7.65	7.80	69.8
6 : 1	10	60	8.02	8.18	73.2

Table 2. Parameters of Ce(III) oxidation at various anode current densities ($Ce(III)_{in}$ = 98 g l^{-1}, V_{el} = 0.1 l, S_a = 0.1 dm^2, τ = 10 min)

i, A dm^{-2}	Ce(IV), g l^{-1}	C, %	η, %	Q, kg m^{-2} h^{-1}
Re = 0				
1	0.84	0.85	76.4	0.51
5	3.91	3.97	71.2	2.35
10	7.70	7.81	70.1	4.62
30	15.8	16.0	47.9	9.48
50	5.61	5.69	10.2	3.37
Re = 54000				
1	1.1	1.12	100.1	0.66
5	5.40	5.48	98.3	3.24
10	10.9	11.1	99.2	6.54
30	31.8	32.3	96.5	19.1
40	38.9	39.5	88.5	23.3
50	26.5	26.9	48.3	15.9

at the cathode

$$H^+ + e \rightarrow 1/2H_2, \quad (3)$$

$$Ce(IV) + e \rightarrow Ce(III). \quad (4)$$

Reactions (2) and (3) are major reactions.

In the case of hydrogen ion deficiency (low acidity of the electrolyte), crystals of basic cerium nitrate of variable composition may precipitate:

$$Ce(IV) + xNO_3^- + yOH^- \rightarrow Ce(OH)_y(NO_3)_x\downarrow. \quad (5)$$

To avoid Ce(IV) redistribution between the liquid and solid phases, nitric acid should be introduced into the electrolyte in the amounts required for formation of $Ce(NO_3)_4$.

A study of the ratio of electrode surface areas during electrolysis showed that the Ce(IV) accumulation in the electrolyte is the most efficient when the cathode surface area is a factor of 5 and more smaller than the anode surface area, i.e., at cathode current densities higher than 50 A dm^{-2} (Table 1). For instance, as $S_a : S_c$ increases from 1 : 2 to 6 : 1, i.e., the cathode current density increases from 5 to 60 A dm^{-2}, the Ce(IV) current efficiency grows from 0.8 to 73.2%. In this case, the degree of Ce(III) oxidation increases from 0.09 to 8.18%, i.e., by more than a factor of 90. The effect observed can be attributed to the fact that the fraction of the current expended for hydrogen liberation substantially increases with the cathode polarization, and the Ce(IV) reduction is suppressed [reactions (3), (4)].

In studying the influence of the anode current density on the Ce(III) electrochemical oxidation, the current density was varied from 1 to 50 A dm^{-2} at the ratio of the electrode surface areas $S_a : S_c$ = 5 : 1.

Experiments without stirring (Re = 0) and with vigorous stirring (Re = 54000) of the electrolyte (Table 2) showed that the dependence of the rate of Ce(IV) accumulation, Q, on the anode current density shows a maximum, whereas the current efficiency η gradually decreases. The decrease in η can be caused by an increase in the overvoltage of Ce(III) discharge and a larger contribution of water electrolysis under these conditions [reaction (1)].

The above dependences show that Ce(III) oxidation is diffusion-controlled: stirring of the electrolyte favors delivery of cations to the anode surface and, under equal other conditions, makes higher the Ce(III) oxidation rate. Therefore, an increase in Re shifts the maximum efficiency to higher current densities. For instance, it is ~9.5 kg m^{-2} h^{-1} at the anode current density of 30 A dm^{-2} without stirring, and 23.3 kg m^{-2} h^{-1} at 40 dm^{-2} under conditions of a turbulent flow. It should be noted that stirring of the electrolyte substantially increases the process efficiency also at relatively low current densities, 1–30 A dm^{-2}. In this case, the current efficiency reaches 100–96.5%, being 76.4–47.9% without stirring.

The influence of the intensity of electrolyte agitation on the rate of Ce(III) oxidation was studied in detail in an electrochemical cell with a platinum elec-

Table 3. Activation energy at various electrolyte flows and polarizations, calculated by Arrhenius equation (ΔT = 30°C)

Re	ΔE, V	$\Delta \log i$	E, kJ mol^{-1}	Re	ΔE, V	$\Delta \log i$	E, kJ mol^{-1}
Laminar flows				Turbulent flows			
1516	0.1	0.45	29.3	29296	0.025	0.47	30.1
	0.2	0.22	13.8		0.05	0.23	14.6
	0.3	0.14	9.2		0.1	0.18	11.7
	0.5	0.13	8.8		0.3	0.15	9.6
3515	0.1	0.45	28.9		0.4	0.14	9.2
	0.2	0.22	14.2	71000	0.025	0.50	32.2
	0.3	0.16	10.5		0.05	0.25	15.9
	0.5	0.14	9.2		0.1	0.19	12.1
					0.4	0.14	9.2

trode with a surface area of 0.25 cm^2 at 20, 30, 40, and 50°C. The velocity of the electrolyte flow relative to anode surface was varied from 0 to 10 m s^{-1}, which corresponds to Re variation from 0 to 71000.

The typical polarization curves at 50°C are shown in Fig. 1. There are no well-defined limiting currents in all the polarization curves of Ce(III) oxidation. A smooth transition from the major reaction to the reaction occuring jointly with evolution of O_2 is observed. The electrolyte flow velocity strongly affects the current density at all polarizations. The effect increases with polarization. Comparison of the current densities at Re = 0 and Re = 71000 (developed turbulence) shows that, at a polarization of 0.025 V, the current density increases by a factor of 4, and at 0.4 V, by a factor of 12.8. Under the conditions of diffusion kinetics of Ce(III) oxidation on smooth electrodes, the rate of the process should increase by several orders of magnitude as the velocity is raised from 0 to 10 m s^{-1} (Re = 71000). The weaker effect of the flow velocity on the current density shows that electrolysis proceeds in the transition region (region of mixed kinetics) even at high polarizations.

To reveal the role of the chemical stage on the basis of the experimental polarization curves at 20–50°C and by analyzing the dependence $\log i = f(1/\tau)$ in term of the Arrhenius equation [from the shape of curves in Fig. 2 (Table 3)], we determined the equitransport activation energy of Ce(III) oxidation

$$\ln i = \ln A - E/RT, \qquad (6)$$

where i is the current density (A dm^{-2}); A, rate constant (A dm^{-2}); E, activation energy; R, gas constant; and T, temperature (K).

We found that the activation energy of Ce(III) oxidation under the conditions of both laminar and turbulent flows is virtually independent of the mass exchange intensity. Its deviation from the mean value

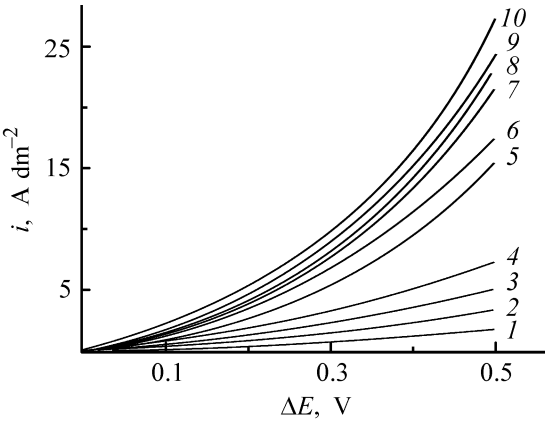


Fig. 1. Polarization curves of cerium oxidation at various electrolyte flow velocities. (i) Current density and (ΔE) polarization. Intensity of electrolyte stirring, Re: (*1*) 0, (*2*) 303, (*3*) 1516, (*4*) 3515, (*5*) 14406, (*6*) 16163, (*7*) 29296, (*8*) 39429, (*9*) 53422, and (*10*) 71000.

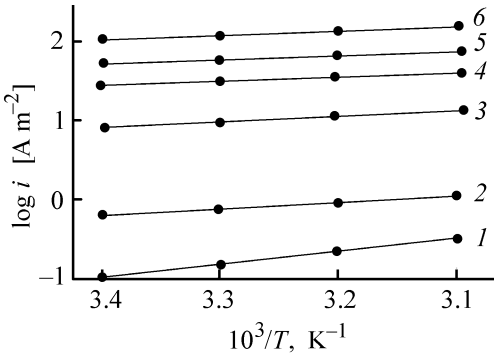


Fig. 2. Semilog plot of the current density i vs. the electrolyte temperature T at various polarizations. Polarization (V): (*1*) 0.025, (*2*) 0.05, (*3*) 0.1, (*4*) 0.2, (*5*) 0.3, and (*6*) 0.4.

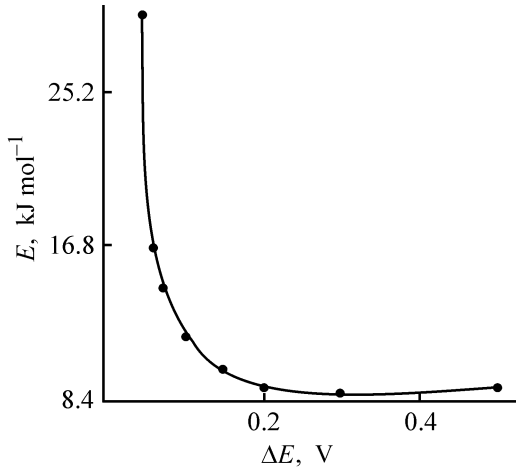


Fig. 3. Activation energy E of cerium(III) oxidation vs. the polarization ΔE.

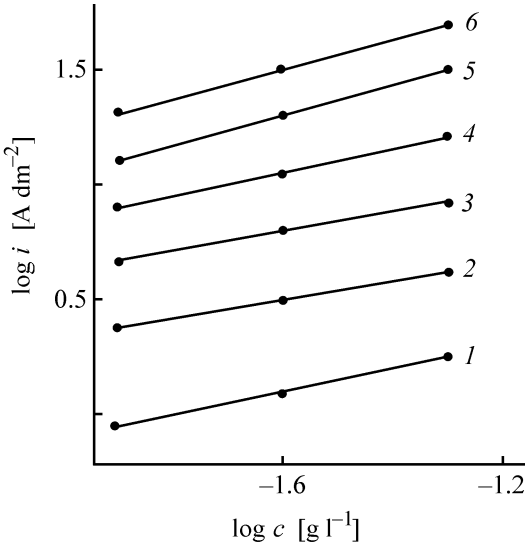


Fig. 4. Current density i vs. the cerium(III) concentration c. Polarization (V): (*1*) 0.025, (*2*) 0.05, (*3*) 0.1, (*4*) 0.2, (*5*) 0.4, and (*6*) 0.5.

at a constant polarization, as a rule, does not exceed the maximum error in determining the activation energy by this method, which is 1.7 kJ mol^{-1}. The dependence of the mean activation energy on polarization is shown in Fig. 3. It is 29.3 kJ mol^{-1} at a polarization of 0.025 V, smoothly decreases to 10.0 kJ mol^{-1} at 0.15 V, and then remains virtually constant up to 0.5 V. The decrease in the activation energy with increasing polarization shows that the role of the chemical stage in the process decreases as the polarization becomes stronger, but does not completely unimportant, because the activation energy would become zero other wise.

We also studied the effect of Ce(III) concentration on the rate of Ce(IV) accumulation under the conditions of a constant Ce(IV) : Ce(III) ratio (1 : 10), concentration of free nitric acid (30 g l^{-1}), and solution temperature (50°C). The dependence of the current density on the Ce(III) concentration at stirring with Re = 71 000 is shown in Fig. 4. From the slope of straight lines obtained, we found that, within the polarization range from 0.025 to 0.5 V, the formal reaction order with respect to Ce(III) changes from 0.6 to 0.94, whereas a first order with respect to the reacting substance is typical of the exclusively concentration control.

At high polarizations (0.4–0.5 V), when n = 0.94, we can speak of the diffusion control of the Ce(III) oxidation.

The instant of transition from the predominant Ce(III) oxidation to combined Ce(III) oxidation and oxygen evolution at the electrode cannot be derived from the shape of the polarization curves. Therefore, we performed special experiments at various current densities, with the Ce(IV) current efficiency determined (Table 4).

A $Ce(NO_3)_3$ solution with a Ce(III) concentration of 98 g l^{-1} was electrolyzed at 40°C and a flow velocity of 7.8 m s^{-1} (Re = 54 000). The data obtained show that the Ce(III) current efficiency remains close to 100% up to a current density of 35 A dm^{-2}. The electrolyte stirring allows the process to be performed efficiently at higher current densities and hence at a higher rate. When the above-indicated current density is exceeded, the current efficiency sharply decreases, suggesting a concurrent evolution of oxygen at the electrode. The dependence of the main elec-

Table 4. Current efficiency of Ce(III) oxidation at various anode current densities; oxidation to 4.7–5.3% [$Ce(III)_{in}$ = 98 g l^{-1}, V = 100 ml, Re = 71 000]

i, A dm^{-2}	τ, h	Ce(IV), g l^{-1}	η, %	i, A dm^{-2}	τ, h	Ce(IV), g l^{-1}	η, %
5	8.00	5.20	99.3	30	1.33	4.98	95.0
10	4.00	5.21	99.2	40	1.00	4.62	88.0
20	2.00	5.18	98.5	45	1.25	5.17	70.0

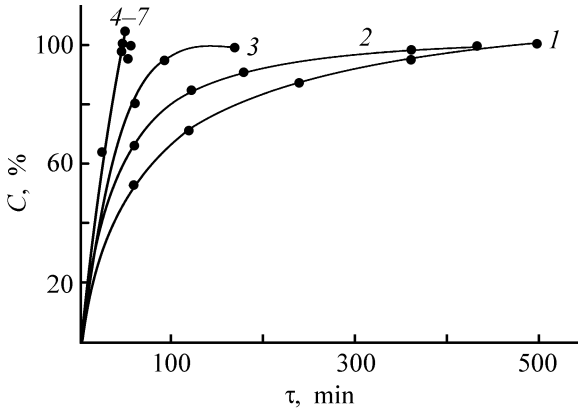


Fig. 5. Kinetic curves of cerium(III) oxidation at various intensities of electrolyte stirring Re. Initial cerium(III) concentration 98 g l^{-1}. (*C*) degree of oxidation, and (τ) time. Intensity of stirring, Re: (*1*) 286, (*2*) 428, (*3*) 2920, (*4*) 5840, (*5*) 11680 (*6*) 29400, and (*7*) 58400.

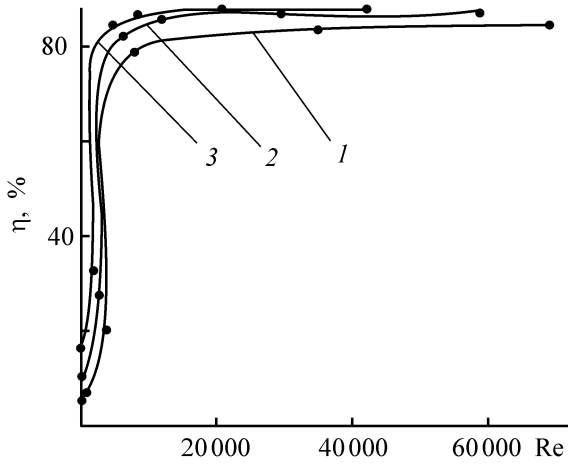


Fig. 6. Ce(IV) current efficiency η vs. the intensity of electrolyte stirring at various initial Ce(III) concentrations. Initial cerium(III) concentration (g l^{-1}): (*1*) 54, (*2*) 98, and (*3*) 210.

trolysis parameters *C* and η on the intensity of the electrolyte stirring is shown in Figs. 5 and 6. Transition from a laminar to a turbulent flow sharply increases the efficiency of Ce(III) oxidation.

Thus, an increase in the relative anode surface area (to $S_a : S_c \geq 5 : 1$), anode current density (to 30–40 A dm^{-2}), and turbulence of electrolyte flow (Re ≥ 10000) makes higher the efficiency of the Ce(III) electrochemical oxidation. The last two conditions are interconnected. The better the conditions of the mass exchange, the higher the current density at which the electrolysis can be performed.

CONCLUSIONS

(1) The activation energy of electrochemical oxidation of Ce(III) in a nitric acid solution of REEs is not higher than 32.2 kJ mol^{-1}; it decreases to 8.8 kJ mol^{-1} with increasing polarization, suggesting the transition to the diffusion control.

(2) The experimentally determined order of Ce(III) oxidation increases with polarization to $n = 0.94$, which also suggests the diffusion control of the Ce(III) oxidation.

(3) An increase in the anode polarization activates the side reaction of oxygen evolution, which decreases the current efficiency of Ce(III) oxidation.

(4) High parameters of Ce(III) electrochemical oxidation can be achieved at a relatively high cathode polarization ($i_c : i_a \geq 5 : 1$) and turbulent electrolyte flow (Re ≥ 10000).

REFERENCES

1. French Patent Application 8803021.
2. French Patent Application 2580273.
3. US patent 4417965.
4. Hamrah, H. and Kuhn, A.T., *J. Appl. Electrochem.*, 1980, vol. 10, pp. 635–647.
5. Kiekens, P., Steen, L., Donche, H., and Temmerman, E., *Electrochim. Acta*, 1981, vol. 26, pp. 841–845.
6. Songina, O.A. and Niyazbekova, A.S., *Radiokhimiya*, 1978, vol. 20, p. 807.
7. Mikhailichenko, A.I., Mikhlin, E.B., and Patrikeev, Yu.B., *Redkozemel'nye metally* (Rare-Earth Metals), Moscow: Metallurgiya, 1987.

Russian Journal of Applied Chemistry, Vol. 78, No. 6, 2005, pp. 912–916. Translated from Zhurnal Prikladnoi Khimii, Vol. 78, No. 6, 2005, pp. 933–937.
Original Russian Text Copyright © 2005 by Dobrovinskaya, Dobkina, Kuznetsova.

CATALYSIS

Study of the Stability of Catalysts for Decomposition of Spent Sulfuric Acid

N. A. Dobrovinskaya, E. I. Dobkina, and S. M. Kuznetsova

St. Petersburg State Technological Institute, St. Petersburg, Russia

Received November 15, 2004

Abstract—The influence of various factors on the stability of operation of heterogeneous catalysts for decomposition of spent sulfuric acid is analyzed.

The stability of operation of a catalyst [1] in decomposition of spent sulfuric acid (SSA) containing organic admixtures is strongly affected by several factors, including the mechanical action associated with the mode of the boiling bed and a long exposure to a high temperature. The first factor can promote destruction of the support and removal of active components. The second can diminish the catalytic activity through a transformation of the porous structure that leads to a decrease in the specific surface area. This study is devoted to examination and analysis of the effect of these factors on the catalyst.

EXPERIMENTAL

We used as real sulfuric acid waste to be subjected to decomposition the SSA formed in alkylation and in manufacture of methyl ethyl ketone. These two kinds of waste are representatives of concentrated and diluted SSA containing small amounts of organic admixtures (Table 1). The admixtures have a complex chemical composition including components of initial raw materials and products of target and side reactions. In view of the difficulties in determining such a composition, we estimated the amount of organic admixtures in SSA by a conventional method [2], by their sum in terms of carbon.

The abrasion resistance was estimated directly under conditions of SSA decomposition on an installation with a boiling-bed reactor (Fig. 1). The catalyst bed was poured on a porous quartz partition situated in the middle of a heated reactor *1* and brought into a fluidized state with air whose flow rate was measured with a rheometer *2*. Spent sulfuric acid was delivered by a mechanical batcher *3* into the catalyst bed through a side capillary built into a condenser *4* to prevent the catalyst coking. The loss of substance from the bed was judged from the increase in the mass of a trap *5* filled with fiberglass. To prevent condensation of sulfuric acid, the trap was placed in a furnace *6* which maintained its temperature at 300°C. To make a control measurement of the substance removal, the entire bed was additionally weighed every 10 h during the test.

The catalyst activity was estimated by the degree of SSA decomposition, β. It was studied on the same installation as the mechanical strength after dismantling the trap *5* and furnace *6*. A cooled gas mixture from the reactor *1* was analyzed by chromatography after removing SO_3 and water vapor.

The degree of SSA decomposition is the ratio between the amount of sulfur dioxide contained in the gas phase after the reactor and the total amount of sulfur dioxide in the SSA fed into the reactor.

The completeness of burning-out of organic admixtures was determined from the content of carbon oxide in gaseous decomposition products.

The wear resistance of the samples was studied *in situ* in the natural mode of the thermocatalytic decomposition of SSA. The samples were tested for 100 h

Table 1. Composition of industrial SSA

SSA	*c*, wt %	
	monohydrate	organic compounds in terms of carbon
Alkylation	85.0	3.0
Manufacture of methyl ethyl ketone	73.0	1.5

1070-4272/05/7806-0912 © 2005 Pleiades Publishing, Inc.

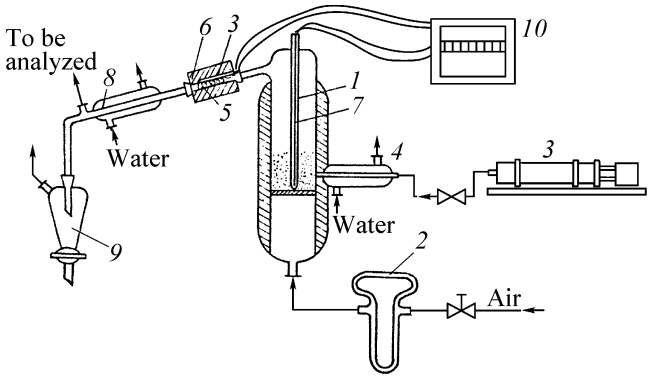


Fig. 1. Schematic of the installation for decomposition of spent sulfuric acid in a boling bed. (*1*) Reactor, (*2*) rheometer, (*3*) mechanical batcher, (*4*) capillary, (*5*) trap, (*6*) furnace, (*7*) thermocouple, (*8*) condenser, (*9*) condensate collector, (*10*) potentiometer.

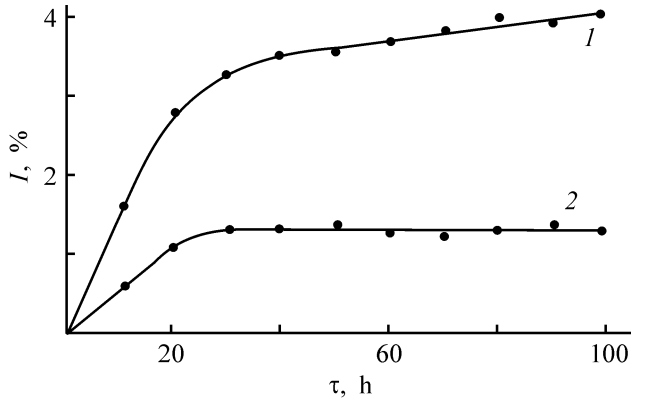


Fig. 2. Abradability I of supports vs. the working time τ in thermolysis of sulfuric acid. γ-Al_2O_3 support: (*1*) pure and (*2*) silicated.

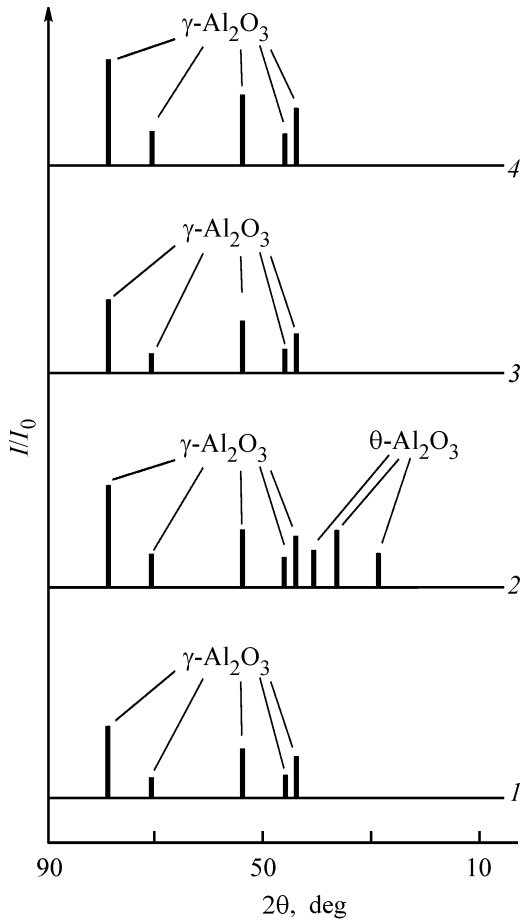


Fig. 3. X-ray diffraction patterns of supports. (I/I_0) Relative intensity and (2θ) Bragg angle. γ-Al_2O_3 support: (*1*) pure before test, (*2*) after test; (*3*) silicated before test, and (*4*) after test.

under conditions chosen on the basis of the experience gained in determining the optimal parameters of thermocatalytic decomposition of SSA in a boiling bed. Thee conditions were highly severe: T 850°C, load in terms of H_2SO_4 900 kg h^{-1} m^{-3}, and fluidization number 4. The results obtained in testing the supports are shown in Fig. 2. Comparison of curves *1* and *2*, corresponding to pure and silicated aluminum oxide [1], demonstrates not only the quantitative aspect of differences in abradability between these two supports, but also the fact that these dependences differ in their nature. For example, curve *2* of the time dependence of abradability of a silicated sample levels off after first 30 h of its operation, whereas the loss of pure γ-Al_2O_3 remains appreciable within the entire period of tests, although it becomes slower in the course of time. This can be explained as follows. In the course of the tests, unmodified γ-Al_2O_3 is subjected not only to a purely mechanical treatment, but also to a chemical action of the reaction medium, and undergoes polymorphic transformations under long-term influence of high temperatures. Probably, the action of the last two factors on silicated aluminum oxide is diminished due to a screening effect of the modifier. The abradability of such a support was about 0.2% per month.

An X-ray study of both samples (Fig. 3) demonstrated that they crystallize in 100 h of the tests (the intensity of discrete lines increases by 10–15%). The phase composition of silicated γ-Al_2O_3 remains virtually unchanged during the tests, whereas the initial Al_2O_3 is partially converted into the theta-form. Thus, the silication raises the stability of the phase composition and, accordingly, improves the performance of the support and, hence, of the catalyst itself.

Testing the wear resistance of finished iron-copper oxide catalysts based on the supports described above

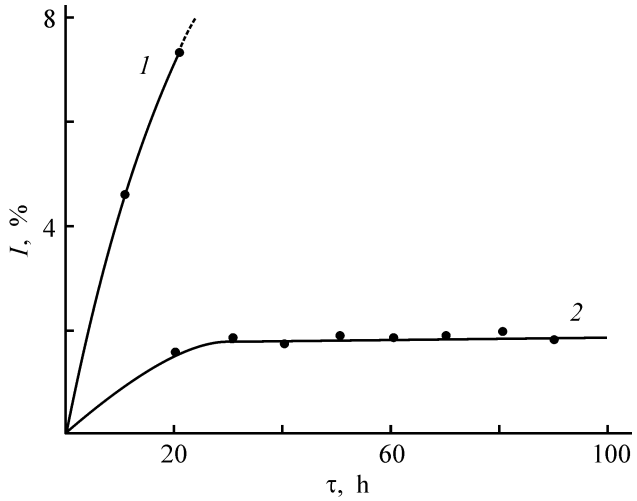


Fig. 4. Abradability I of iron-copper oxide catalysts vs. the working time τ in sulfuric acid thermolysis. Catalyst: (*1*) based on pure γ-Al_2O_3 and (*2*) based on silicated γ-Al_2O_3.

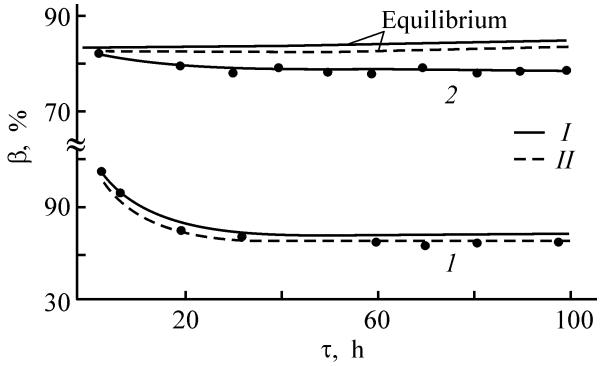


Fig. 5. Degree of decomposition of spent sulfuric acid, β, vs. the working time τ of a catalyst. Load by the acid (kg h^{-1} m^{-3}): (*1*) 900, (*2*) 500. SSA formed in (*I*) alkylation and (*II*) production of methyl ethyl ketone.

[1] is of special interest. Experiments demonstrated that use of an unmodified support for preparing a catalyst for SSA decomposition is unacceptable at all. As can be seen in Fig. 4 (curve *1*), the abradability of such a sample within the first 20 h of operation was 7.5%. Then the destruction process presumably passed from the surface into the bulk of grains. As a result, it was necessary to stop the test ahead of schedule because of the catalyst transformation into a shapeless mass. As to a sample prepared on a silicated support (Fig. 4, curve *2*), the loss of substance from it within the running-in period somewhat increased in comparison with that from the support (Fig. 2, curve *2*), probably through loss of a certain amount of active components. However, the abradability determined after this period remained unchanged and constituted 0.2% per month.

One of the main factors impairing the activity of the catalysts operating in high-temperature processes is their caking. It can lead to a decrease in the total surface area of a support and(or) in the dispersity of deposited components.

The most important function of the support is to minimize the rate of growth or migration of crystallites of the active components. Nevertheless, these processes are inevitable if a catalyst is used at high temperatures, because the caking of the support gradually diminishes its role as a dispersant, which adversely affects the activity of the catalyst.

To study the thermal stability of the iron-copper oxide catalysts synthesized, we tested them in decomposition of real sulfuric-acid wastes from the alkylation process for 100 h under conditions considerably more severe than the optimum, which long-run tests more objective.

We determined the following optimal parameters of the process, which provide a nearly equilibrium degree of SSA decomposition to sulfur dioxide at a complete oxidation of organic admixtures: temperature 850°C, fluidization number 3, specific load by SSA 500 kg h^{-1} m^{-3}, and contact duration 1.4 s.

A test of the chosen catalyst under conditions of decomposition of SSA formed in alkylation demonstrated (Fig. 5) that the catalyst activity steeply falls within the first 15–20 h of operation. Apparently, the decrease in the activity of this sample is determined by recrystallization processes occurring in it.

Three stages are commonly distinguished in the mechanism of caking of oxide supports with a developed surface [3]. The area of contact between fine particles increases in the first of these, and new closed pores appear as a result of overlapping of the newly formed contacts in the second. Both these stages are accompanied by an essential decrease in the surface area accessible to reagents. In the third stage, closed pores disappear completely. In this stage, which is most prolonged, the specific surface area changes less considerably. The experimental data on changes in the S_{sp} of the sample under study in thermocatalytic decomposition of SSA after alkylation are given below:

S_{sp} (mg^2 g^{-1}) after operation for τ (h)		
Initial	20	100
98.0	32.2	25.6

To gain a better insight into the processes occurring in the samples under study during the tests, we studied them by means of X-ray photoelectron spectroscopy.

It follows from these data (Table 2) that silicon, iron, and copper are at the surface of the support in the initial samples, as can be seen from a comparison of their relative concentrations at the surface (in a 2–5-nm-thick layer), determined from the intensities of XPS lines, and in the bulk, from the data of quantitative elemental analysis. The relative concentrations of these elements in the surface layer under study in spent samples decrease. This may occur for two reasons. First is a "transfer" of a certain amount of active components from the surface of a support into its bulk, which can take place upon formation of closed pores in caking. The second is formation of enlarged "islands" of the active components, i.e. a decrease in their dispersity.

It is evident that both these factors contribute to in the decrease in the activity of the sample under study. The first of these is inevitable, because the catalyst is indeed transformed, and the occurrence of the second is confirmed by an electron-microscopic study of the catalyst. Electron micrographs of the initial and spent samples prepared for analysis by a microdispersion technique are shown in Fig. 6. The magnification of 200 000 allowed us to examine the growth of crystallites of the active components of the catalyst in the course of its operation. The largest crystallites in the initial sample have projection dimensions of about 5×25, whereas the corresponding average values for the spent sample are 10×75 nm (Fig. 6). Thus, according to the electron-microscopic data, the dispersity of phases of the active components in the catalyst decreases by approximately a factor of 2–3 upon 100 h of operation under conditions of SSA decomposition.

Table 2. Relative amounts of elements in a supported iron-copper oxide catalyst

Sample	Relative atomic concentrations of elements					
	surface, as given by XPS			bulk, as given by elemental analysis		
	Cu/Al	Fe/Al	Si/Al	Cu/Al	Fe/Al	Si/Al
Initial	1.19	0.258	0.397	0.21	0.08	0.18
Spent	0.94	0.197	0.321	0.20	0.08	0.18

At the same time, according to the X-ray data, these phases in the spent sample remain, on the whole, rather highly dispersed, which is seen from the small increase in the intensities of the discrete lines associated with the active components (Fig. 7).

In this context, it is probable that the contribution of the decrease in the surface area to the fall of the catalyst activity is more important than that of caking of the active components themselves. It is also seen from Fig. 7 that higher iron and copper oxides, as well as copper ferrite $CuFe_2O_4$, are present in the initial catalyst. All these compounds were detected in trace amounts, which is, in all probability, a consequence of their high dispersity. The absence of peaks corresponding to CuO and α-Fe_2O_3 with $2\theta = 58°$ and 64° in the X-ray diffraction pattern of the sample after the test and the decrease in the intensity of the peak of α-Fe_2O_3 with $2\theta = 38.9°$ suggest that these phases

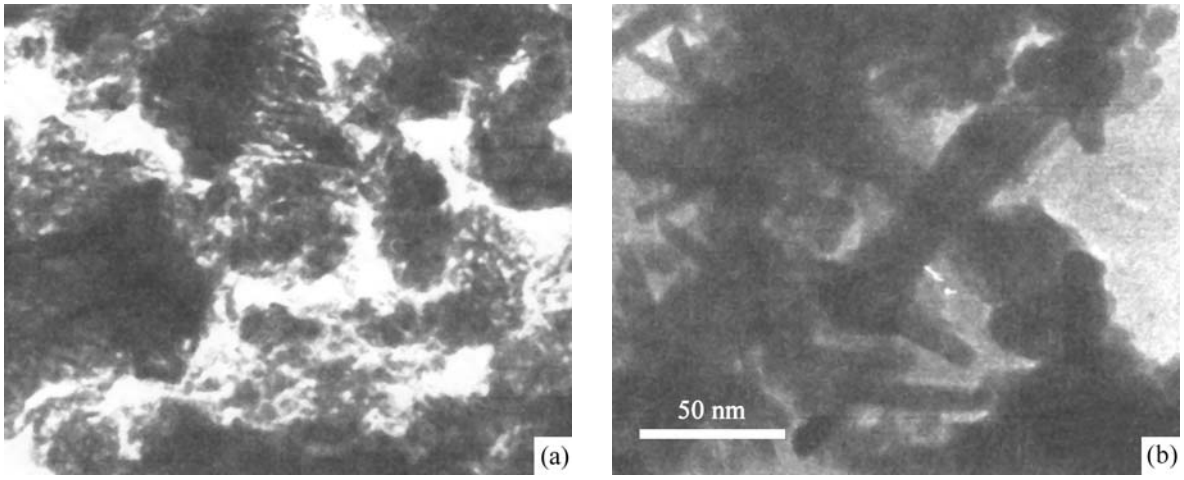


Fig. 6. Crystallization of active components under working conditions. Sample: (a) initial and (b) that after 100 h of operation.

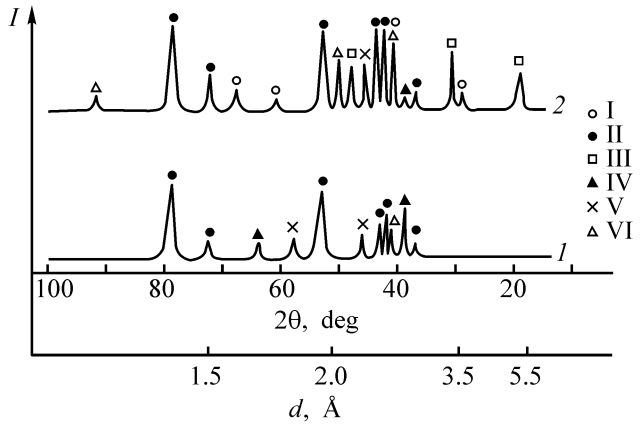


Fig. 7. X-ray diffraction patterns of (*1*) fresh and (*2*) spent catalysts. (*I*) Intensity, (2θ) Bragg angle, and (*d*) interplanar spacing. (I) α-Al_2O_3, (II) γ-Al_2O_3, (III) I-Al_2O_3, (IV) Fe_2O_3, (V) CuO, and (VI) $CuFe_2O_4$.

are consumed in catalyst operation. The increase in the intensity of $CuFe_2O_4$ (2θ = 41°), which is already present in the initial sample, and also the appearance of new peaks related to copper ferrite (2θ 50.6° and 92.4°) [4] suggest that iron and copper oxides react to give a ferrite. It is probable that the heat treatment of the catalyst during synthesis results in that only a part of iron and copper oxides enters into the reaction. The extent of ferrite formation increases further directly in the course of the sample operation during SSA decomposition. The formation of a more active phase of copper ferrite compensates for the decrease in the activity of the catalysts caused by a decrease in their specific surface area.

As to the support, it is represented in the initial sample by low-crystalline γ-Al_2O_3 (Fig. 7, curve *1*). During the test, it weakly crystallizes and undergoes insignificant polymorphic transformations. For example, a high-temperature phase *i*-Al_2O_3 and trace amounts of α-Al_2O_3 are observed in the spent catalyst (Fig. 7, curve *2*). The metastable phase of θ-Al_2O_3, formed in operation of non-silicated γ-Al_2O_3 (Fig. 3), is absent in this case.

CONCLUSIONS

(1) Comparative tests of the wear resistance of "pure" and silicated γ-Al_2O_3 and of catalysts prepared on their basis were carried out directly in decomposition of sulfuric acid.

(2) It was shown that silicating protects a support from the chemical action of the reaction medium, which prevents its destruction, and hinders the reaction of the support with the active components, thereby considerably improving the thermal stability of the catalyst.

(3) The abradability of iron-copper oxide catalysts was determined to be 0.2% per month.

(4) It was established that the decomposition of spent sulfuric acid is accompanied by caking, which results in a decrease in the surface area. Furthermore, active components are redistributed within catalyst grains.

(5) It was found that the highest stability of operation is exhibited by samples in which the CuO/Fe_2O_3 ratio is the closest to that in stoichiometric copper ferrite $CuFe_2O_4$.

REFERENCES

1. Dobrovinskaya, N.A., Dobkina, E.I., and Kuznetsova, S.M., *Zh. Prikl. Khim.*, 2004, vol. 77, no. 1, pp. 36–42.
2. Syunyaev, Z.I., *Neftyanoi uglerod* (Oil Carbon), Moscow: Khimiya, 1980.
3. Hughes, R., *Deactivation of Catalysts*, London: Academic, 1984. Translated under the title *Deactivation of catalysts*, Moscow: Khimiya, 1989.
4. Mirkin, L.I., *Rentgenostrukturnyi kontrol' mashinostroitel'nykh materialov: Spravochnik* (X-ray Control of Engineering Materials: Handbook), Moscow: Mashinostroenie, 1979.

Russian Journal of Applied Chemistry, Vol. 78, No. 6, 2005, pp. 917–923. Translated from Zhurnal Prikladnoi Khimii, Vol. 78, No. 6, 2005, pp. 938–944.
Original Russian Text Copyright © 2005 by Melezhik, Sementsov, Yanchenko.

CATALYSIS

Synthesis of Fine Carbon Nanotubes on Coprecipitated Metal Oxide Catalysts

A. V. Melezhik, Yu. I. Sementsov, and V. V. Yanchenko

TMSpetsmash Ltd., Kiev, Ukraine

Institute of Surface Chemistry, National Academy of Sciences of the Ukraine, Kiev, Ukraine

Received September 28, 2004; in final form, February 2005

Abstract—Catalysts for vapor-phase deposition of multi-walled carbon nanotubes are considered. A method for synthesis of iron-containing catalyst by coprecipitation of aluminum, magnesium, and iron(II) hydroxides is suggested.

Carbon nanotubes (CNT), which were only available in milligram amounts several years ago, are gradually becoming a product of large-tonnage synthesis. Simultaneously with the increase in the production scale, new application fields of CNT are being revealed. For example, Hyperion Catalysis International Co. (USA) manufactures CNT 10–15 nm in diameter and CNT-containing polymeric formulations. Introduction of 2–5% CNT into polymeric materials makes them electrically conducting and thereby hinders accumulation of static electricity [1]. Mechanical properties of CNT-filled polymeric materials have been studied [2–4]. CNT and CNT-based composites are under intensive scientific and technological development in China [5–10].

According to the results of [9], the most valuable are fine CNT less than 20 nm in diameter. In the best variants reported in numerous publications devoted to synthesis of multi-walled CNT by the chemical vapor deposition technique, the CNT diameter is 10–20 nm. The authors of the present study are not aware of any method for obtaining multi-walled CNT with an average diameter of less than 10 nm.

It is commonly believed, even though this issue remains insufficiently studied, that the diameter of a growing nanotube is determined by the size of the cluster of a catalytically active metal, e.g., iron, cobalt, or nickel. Presumably, the most efficient way to obtain and stabilize nanosize clusters of catalytically active metals is their immobilization on some highly dispersed or porous support, e.g., aluminum oxide, silicon, magnesium, or carbon. For this purpose, a dispersed support is impregnated with solutions of metal compounds (nitrates, acetylacetonates, salts of organic acids, etc.) On being introduced into a hot reactor, these compounds decompose to give, commonly, metal oxides, from which catalytically active metal clusters are formed in a reducing atmosphere (as a rule, a mixture of hydrogen and hydrocarbons). Such a procedure for fabrication of catalysts for synthesis of multi-walled CNT was described, e.g., in the patent [11]. Aluminum oxide with a particle size of about 10 nm was used as a highly dispersed support, and nitrates and acetylacetonates of iron, molybdenum, manganese, and chromium, and mixtures of these, as compounds of catalytically active metals. Ethylene mixed with hydrogen served as a source of carbon. The mass of the multi-walled CNT obtained was tens of times that of the catalytically active metals, and the diameter of the resulting CNT was in the range from 3.5 to 70 nm. The method described has the following disadvantage. As a result of impregnation and drying, particles of the material undergo aggregation and the size of metal oxide clusters formed in pyrolysis may markedly exceed the particle size of the highly dispersed support. Thus, the nanotubes obtained are nonuniform in diameter.

In another method, hydroxides of metals, e.g., of iron, cobalt, magnesium, or molybdenum, are coprecipitated, or mixed metal oxides are obtained by thermal decomposition of a mixture of appropriate compounds. Because oxides of catalytically active metals are uniformly distributed in the matrix of an inert oxide (of aluminum or magnesium), such an approach makes it possible to obtain more monodisperse catalytically active clusters and, consequently, finer carbon nanotubes that are more uniform in diameter.

For example, effective catalysts (or, more precisely, precursors of catalysts) for growth of multi-walled

1070-4272/05/7806-0917 © 2005 Pleiades Publishing, Inc.

CNT from acetylene, mixed oxides of magnesium and cobalt, were synthesized in [12, 13]. These catalysts were fabricated by drying an aqueous solution containing metal salts (nitrates, acetates) and citric acid, with the subsequent thermal treatment of the resulting xerogel at 700°C. A thermal treatment in the atmosphere of argon yielded a solid solution of oxides (homogeneous phase) of composition Co_xMg_{1-x} [12], whereas in thermal treatment in air, cobalt was partly oxidized to a trivalent metal to give a microheterogeneous mixture of phases Co_3O_4/MgO [13]. The average diameter of CNT fabricated using these catalysts could be varied within the range 16–70 nm by changing the composition of the gas mixture.

In the system under consideration, a homogeneous mixed oxide of magnesium and cobalt can be obtained owing to the fact that the ionic radii of bivalent cobalt and magnesium are nearly equal. One of the most effective catalytic systems for growth of multi-walled CNT from ethylene and propylene is a mixed oxide of iron, molybdenum, and aluminum. However, the ionic radii of these metals are different, and, therefore, special contrivances are necessary for obtaining a homogeneous mixed oxide or a nanosize microheterogeneous mixture. If these mixtures are obtained by coprecipitation of hydroxides from an aqueous solution of metal salts, the differences in pH values and rates of precipitation of different metals should also be taken into account. For example, the pH of the onset of precipitation of hydroxides from 1 M aqueous solutions of iron and aluminum salts is 1.5 for $Fe(OH)_3$ and 3.3 for $Al(OH)_3$ [14]. In addition, formation of soluble basic salts in the form of metastable solutions and gels is typical of aluminum, this being uncharacteristic of iron. Thus, precipitation of a considerable part of iron hydroxide in the form of a separate coarsely dispersed phase is probable upon addition of a precipitant to a mixture of aluminum and iron salts.

In [15], it was suggested to perform coprecipitation of iron, molybdenum, aluminum, and magnesium hydroxides in the presence of anions of carboxylic acids. Because it is known that carboxylic acids form rather stable complexes with Fe^{3+} ions, the role of these additives probably consists in that the precipitation rates of aluminum and iron hydroxides are equalized and(or) coagulation of iron hydroxide into a coarsely dispersed phase via adsorption of nanosize clusters of iron hydroxide is prevented.

Another approach to synthesis of homogeneous mixed metal oxides is also possible. It is known that, under certain conditions, hydroxides of bi- and trivalent metals form layered structures: anionic clays of composition $A_{1-x}B_x(OH)_2X_z \cdot mH_2O$, where A is a cation of a bivalent metal (e.g., Mg, Ni, Cu, Ca, Fe, Co, Sn, Mn, Cr, Cd, V, Zn); B, cation of a trivalent metal (e.g., Al, Fe, Ga, Co, Mn, Sc, Cr); and X, anion of an organic or inorganic acid [16]. Among the metal cations listed above are those exhibiting a catalytic activity in synthesis of carbon nanotubes. Thus, the given class of substances is of interest as regards the possibility of synthesis of oxide structures in which cations of catalytically active metals are uniformly distributed in an oxide matrix. In [17, 18], methods for synthesis of iron-containing hydrotalcites were suggested. In these syntheses, iron was introduced in the form of salts of bivalent iron. However, the catalytic activity of these substances in CNT growth has not been studied yet.

In [5], a nickel-containing hydrotalcite of composition $Ni_6Al_2(OH)_{16}Co_3 \cdot 4H_2O$ was deposited onto the surface of oxidized multi-walled CNT from a propylene–hydrogen gas mixture. Interestingly, the same nickel-hydrotalcite deposited in a pure form onto a substrate other than CNT yielded carbon nanofibers, instead of nanotubes. Thus, the nature of a substrate strongly affects the properties of the resulting catalyst.

The aim of this study was to examine the catalytic properties of hydrotalcite-like iron-containing substances in synthesis of carbon nanotubes.

EXPERIMENTAL

Iron-containing mixed metal hydroxides were synthesized by the conventional method of coprecipitation from aqueous solutions of metal (iron, aluminum, magnesium, ammonium molybdate) salts and a stoichiometric amount of aqueous ammonia. Iron was introduced into the reaction mixture in the form of a chloride of bivalent iron. The coprecipitated metal hydroxides were washed with water until the chlorine anion disappeared in the washing water, dried at 200°C, and ground in a vibration mill for 30–40 min. It should be noted that the bulk density of ground catalysts was rather high, 490–560 g dm^{-3}. With catalysts in this form, agglomeration of the forming carbon nanotubes into a loose solid mass was frequently observed, which is undesirable, especially in those cases when CNT are to be used in composites. The authors found that this adverse effect can be eliminated by mixing a ground catalyst with a highly dispersed pyrogenic silica (A-300 aerosil) in a mixer in the course of 5 min. In the process, the bulk density of the catalyst decreased by more than an order of

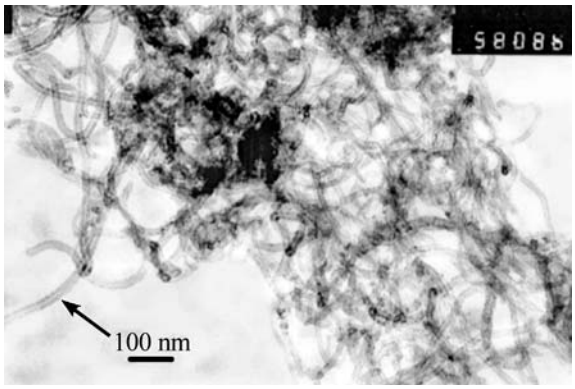


Fig. 1. Electron micrograph of carbon nanotubes grown on a $FeAlMo_{0.07}$ catalyst (synthesized by the method described in [15]; run no. 1).

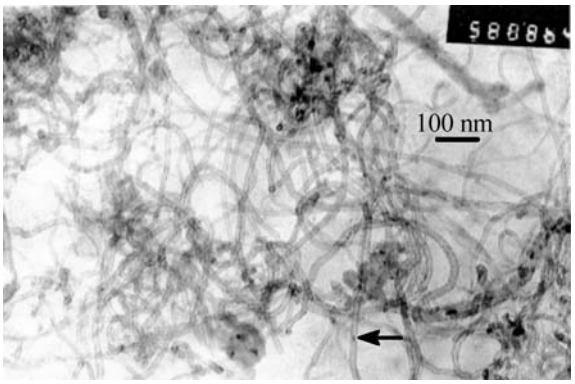


Fig. 2. Electron micrograph of carbon nanotubes grown on a $FeAlMo_{0.07}$ catalyst (synthesized by the method described in [15]) with addition of aerosil (run no. 3).

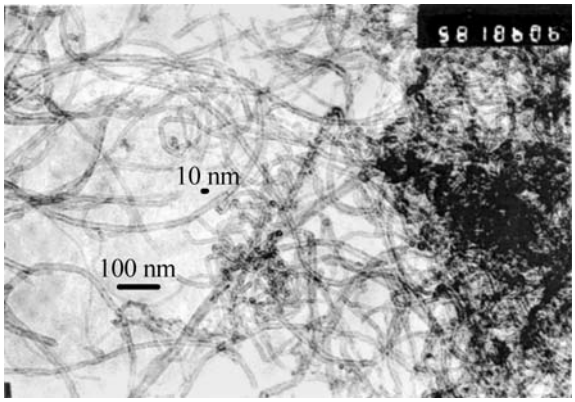


Fig. 3. Electron micrograph of carbon nanotubes grown on a $FeAlMgMo_{0.105}$ catalyst with addition of aerosil (run no. 8).

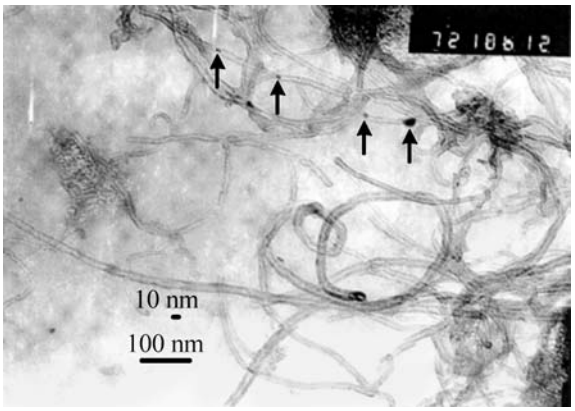


Fig. 4. Electron micrograph of carbon nanotubes grown on a $FeAl_2Mo_{0.2}$ catalyst with addition of aerosil (run no. 10).

magnitude. In one of the experiments, preliminarily synthesized nanotubes were used as a loosener instead of aerosil.

Carbon nanotubes were synthesized in a 2.1-dm^3 cylindrical quartz reactor with a catalyst bed agitated by rotating the reactor by means of an electric drive at a rate of 60–90 rpm. The rotation axis of the reactor was inclined at an angle of 8° to the horizon. The gas mixture was fed into the reactor through an immobile quartz extension connected to the reactor neck by a ground joint lubricated with a mineral oil. The reactor was placed in an electric furnace with controllable temperature.

Prior to the beginning of an experiment, a catalyst was introduced into the reactor and the temperature was raised to 680°C in a flow of argon. After this working temperature was reached, a gas mixture was fed into the reactor. The mixture was composed of ethylene (400 $cm^3\ min^{-1}$) and hydrogen (200 $cm^3\ min^{-1}$; the volumetric flow rate of the gases was measured at room temperature. After that, the flow of argon was turned off and the gases discharged from the reactor through a quartz tube were burnt. The flame coloration could be used to judge qualitatively the degree of ethylene conversion into carbon and to determine in this way how the catalyst activity varies with time. At a low conversion of ethylene, a bright yellow flare was observed, the flame at a high conversion being small and virtually colorless or pale yellow.

To remove mineral impurities, the products were treated with an alkali solution (to dissolve aerosil) and then with hydrochloric acid to dissolve metal oxides. It should be noted that, even upon a thorough purification (many-hour heating in conc. hydrochloric acid), the samples were noticeably attracted by a magnet, which points to incorporation of a certain fraction of iron into the nanotubes. Indeed, electron micrographs (Figs. 1–4) show inclusions at some places in the inner channel of nanotubes (indicated by arrows). Figure 4 shows a chain of four inclusions in the same

Composition of catalysts, synthesis modes, and properties of carbon nanotubes*

Run. no	Composition, catalyst fabrication procedure, mass in the reactor	Outward appearance, bulk density of the catalyst	Process duration, min; yield of carbon	Outward appearance of the product, mass, volume, bulk density, specific surface area
1	$FeAlMo_{0.07}$, in accordance with [15], ground in a mortar; 1.89 g charged into the reactor	Ocher-colored powder, 600 g dm^{-3}	90 min, C = 29.0 g (77%), C/Fe = 41	Nonpurified: black powder + loose lumps, 30.9 g, 0.4 dm^3, 77 g dm^{-3} Purified: black pieces; upon fluffing-up in a mixer, black powder, 72 g dm^{-3}, 220 m^2 g^{-1}, electron micrograph in Fig. 1
2	$FeAlMo_{0.07}$, in accordance with [15], grinding, 1 part of ground product + 1 part of fluffed-up A-300 5.2 g of the mixture into the reactor	Ocher-colored powder, without aerosil, 590 g dm^{-3}, with aerosil, 24 g dm^{-3}	180 min, C = 68.4 g (97%), C/Fe = 82	Nonpurified: black powder, 73.1 g, 1.7 dm^3, 43 g dm^{-3}
3	$FeAlMo_{0.07}$, in accordance with [15] (1 part) + A-300 (2 parts, grinding) + 4.35 parts of A-300, fluffing up; 11.6 g of the mixture in the reactor	Ocher-colored powder, 30 g dm^{-3}	100 min, C = 37.6 g (90%), C/Fe = 48	Nonpurified: black powder, 49.2 g, 1.5 dm^3, 33 g dm^{-3} Purified: black pieces, 255 m^2 g^{-1}, electron micrograph in Fig. 2
4	Run no. 2, in another grinding mode: $FeAlMo_{0.07}$, in accordance with [15] (2 parts) + A-300 (1 part, grinding) + A-300 (6 parts), fluffing up; 12 g of the mixture in the reactor	Ocher-colored powder, 24 g dm^{-3}	120 min, C = 43.6 g (87%), C/Fe = 51	Nonpurified: black powder, 55.1 g, 1.8 dm^3, 31 g dm^{-3}, 220 m^2 g^{-1}
5	$FeAlMo_{0.105}$, grinding; 3.0 g in the reactor	Ocher-colored powder, 550 g dm^{-3}	120 min, C = 35.1 g (70%), C/Fe = 34	Nonpurified: black powder + lumps, 37.8 g, 0.7 dm^3, 54 g dm^{-3}, 200 m^2 g^{-1}
6	$FeAlMo_{0.105}$, grinding; 1 part of ground product + A-300 (1 part), fluffing-up; 6.5 g of the mixture in the reactor	Ocher-colored powder, 26 g dm^{-3}	120 min, C = 46.0 g (92%), C/Fe = 41	Nonpurified: black powder + exceedingly loose lumps, 51.8 g, 1.65 dm^3, 31 g dm^{-3}, 210 m^2 g^{-1}
7	$FeAlMo_{0.105}$, grinding; 1 part of ground product + A-300 (2 parts), fluffing-up; 8.5 g of the mixture in the reactor	Ocher-colored powder, 19 g dm^{-3}	120 min, C = 49.5 g (92%), C/Fe = 42	Nonpurified: black powder, 54.2 g, 1.95 dm^3, 28 g dm^{-3}, 190 m^2 g^{-1}
8	$FeAlMo_{0.105}$, grinding; 1 part of ground product + 1 part of A-300, fluffing-up; 5.6 g of the mixture in the reactor	Ocher-colored powder, 32 g dm^{-3}	120 min, C = 40.0 g (87%), C/Fe = 55	Nonpurified: black powder, 45.3 g, 1.9 dm^3, 24 g dm^{-3}, 235 m^2 g^{-1} Purified: electron micrograph in Fig. 3
9	$FeAlMo_{0.105}$, grinding; 1 part of ground product + 1.67 parts of preliminarily synthesized CNT, fluffing up; 6 g of the mixture in the reactor	Brown-black powder 33 g dm^{-3}	85 min, C = 27.6 g (78%), C/Fe = 48	Nonpurified: black powder, 33.6 g, 1.3 dm^3, 26 g dm^{-3}, 220 m^2 g^{-1}

* Grinding: a catalyst was ground (with or without addition of aerosil) in a vibration mill; fluffing up: a catalyst was mixed (fluffed-up with aerosil in a mixer; carbon yield is given in grams, in percent relative to the theoretical value (in terms of ethylene passed through the reactor), and as a mass ratio of deposited carbon to elementary iron in the catalyst.

Table (Contd.)

Run. no	Composition, catalyst fabrication procedure, mass in the reactor	Outward appearance, bulk density of the catalyst	Process duration, min; yield of carbon	Outward appearance of the product, mass, volume, bulk density, specific surface area
10	$FeAlMo_{0.2}$, grinding; 1 part of ground product + 1 part of A-300, fluffing-up; 6.4 g of the mixture in the reactor	Ocher-colored powder, 26 g dm^{-3}	120 min, C = 43.4 g (86%), C/Fe = 54	Nonpurified: black powder, 49.6 g, 1.4 dm^3, 35 g dm^{-3}, 297 m^2 g^{-1} Purified: electron micrograph in Fig. 4
11	$FeAlMo_{0.2}$, grinding; 1 part of ground product + 1 part of A-300, fluffing-up; 9.9 g of the mixture in the reactor	Ocher-colored powder, 22 g dm^{-3}	120 min, C = 37.4 g (78%), C/Fe = 40	Nonpurified: black powder, 46.6 g, 1.4 dm^3, 33 g dm^{-3}, Purified: black lumps, 394 m^2 g^{-1}, electron micrograph in Fig. 5

nanotube, with the nanotube markedly dilated around the two right-hand inclusions.

The electron micrographs were obtained on a JEM-100 CXII transmission electron microscope.

The table lists the compositions of the catalysts (the atomic ratios of metals are given with oxygen and hydroxy groups disregarded) and modes of their preparation, synthesis modes, and properties of the carbon nanotubes obtained. If there is no reference to [15] in the table, the catalysts are synthesized by coprecipitation, with iron introduced in the form of iron(II) chloride. In several runs, catalysts fabricated by a method similar to that described in [15], with a solution of iron(III) formate-acetate, were used for comparison purposes.

In an analysis of the data in the table, the following should be noted. A catalyst of composition $FeAlMo_{0.07}$, synthesized by coprecipitation of iron(III) in the presence of anions of carboxylic acids by a procedure similar to that described in [15], is moderately active (carbon yield 77%) when used as a powder ground in a mortar (run no. 1). In this case, the CNT being formed tend to agglomerate into lumps and the carbon product has a comparatively high bulk density (77 g dm^{-3}). On grinding this catalyst in a vibration mill, with the subsequent fluffing-up of the ground product in a mixture with aerosil in a mixer (run nos. 2–4), the bulk density of the catalyst itself falls dramatically, the carbon yield increases to 87–97%, and the bulk density of the carbon product decreases to 31–43 g dm^{-3}. In this case, the product (CNT) is obtained in the form of a powder, rather than as lumps. Raising the amount of aerosil introduced (run nos. 3, 4) leads to a decrease in the bulk density of the carbon product. Probably, aerosil hinders aggregation of particles of both the catalyst and CNT, acting as a kind of a pseudoliquid solvent.

Judging from the electron micrographs (Figs. 1, 2) and the values of the specific surface area (see table), the diameter of the forming carbon nanotubes is little dependent on the mode of catalyst preparation and amount of aerosil introduced, being about 10–20 nm for the given catalyst, with a minor inclusion of thicker nanotubes. The diameter of the inner channel is, on the average, approximately half of the outer diameter.

Further, the results obtained with coprecipitated catalysts upon introduction of iron in the form of iron(II) chloride, without addition of carboxylic acids or their salts, are considered.

A catalyst of composition $FeAlMo_{0.07}$ without addition of aerosil (run no. 5) behaves similarly to the catalyst of the same composition, synthesized by the method described in [15] (run no. 1). Addition of aerosil makes it possible to markedly raise the yield of carbon and to eliminate the agglomeration of product particles (run nos. 6, 7).

Run no. 8 was carried out with a hydrotalcite-like catalyst of composition $FeAlMgMo_{0.105}$. The yield of catalyst was high, 87%. According to electron micrographs, the carbon nanotubes synthesized in run no. 8 (Fig. 3) do not differ significantly from the CNT obtained on the $FeAlMo_{0.07}$ catalyst [15] (Fig. 2, run no. 3). Thus, these catalysts are similar in activity and diameter of the forming nanotubes. However, the bulk density of the carbon product in run no. 8 is lower than that of the catalyst fabricated by the method described in [15]. This may be important for application of the CNT obtained in composites.

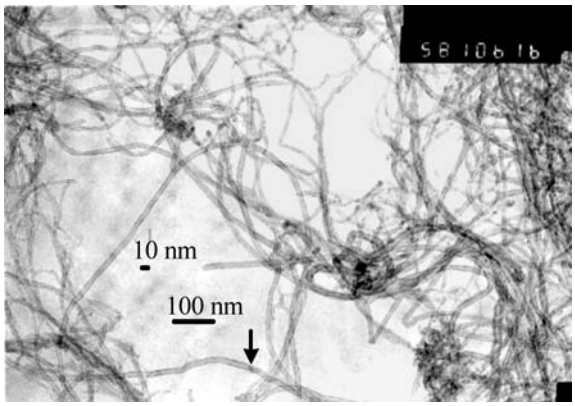


Fig. 5. Electron micrograph of carbon nanotubes grown on a $FeAl_3Mo_{0.2}$ catalyst with addition of aerosil (run no. 11).

In [5, 15], carbon nanotubes were studied as substrates for deposition of metal oxide catalysts, instead of mineral supports. Doing so makes it possible to diminish the content of mineral impurities in the final product and, in some applications, to skip the stage of its purification. However, treatment of carbon nanotubes in a solution is technologically inconvenient because CNT occupy a very large apparent volume (both in the dry state and as a suspension), and drying causes agglomeration, which gives rather dense lumps. The authors made an attempt to distribute a ground metal oxide catalyst of composition $FeAlMgMo_{0.105}$ on a CNT substrate by simple treatment of a dry mixture in a mixer and obtained good results for the carbon yield, bulk density, and specific surface area of the product (run no. 9).

As already noted, it is assumed that the diameter of the growing multi-walled CNT is determined by the size of clusters of the catalytically active metal. It would be expected that a decrease in the concentration of the oxide of a catalytically active metal in the oxide matrix of the type of hydrotalcite should yield finer CNT. For this purpose, catalysts with an increased content of magnesium, $FeAlMgMo_{0.105}$, were synthesized. It was found that doubling the content of magnesium in the catalyst leads to a decrease in the carbon yield to 34–42% and in the specific surface area of the carbon product to 160 $m^2 g^{-1}$, instead of the expected increase in the latter parameter.

However, dilution of iron oxide by raising the amount of aluminum oxide was successful (Figs. 4, 5; run nos. 10, 11). Although a minor decrease in the carbon yield was observed on raising the concentration of aluminum oxide, the specific surface area of the product increased substantially, from 200 to 297–394 $m^2 g^{-1}$. On certain assumptions, the specific surface area of multi-walled CNT can be regarded as being related to their diameter and number of carbon layers in a wall [19]. Consequently, the specific surface area and the average outer diameter of nanotubes can be used to roughly evaluate the number of carbon layers in the wall. For the product formed in run no. 10 ($FeAl_2Mo_{0.2}$ catalyst), the specific surface area is 297 $m^2 g^{-1}$, compared with 200–250 $m^2 g^{-1}$ in the preceding experiments. No differences can be revealed visually between the nanotubes in Fig. 4 and those in Figs. 2, 3. However, the nanotubes obtained in run no. 11 (Fig. 5, $FeAl_3Mo_{0.2}$ catalyst) were considerably thinner-walled than those in the preceding experiments. The average diameter of the nanotubes in Fig. 5 can be roughly estimated at 10–12 nm. Then, according to the data of [19], the number of carbon layers is 3–4.

Thus, dilution of iron oxide with aluminum oxide makes it possible to obtain thin-walled CNT with a small diameter and large specific surface area, which are promising as materials for electrochemical devices, adsorbents, and catalyst supports.

The output capacity of the above-described laboratory installation is (at the specified catalyst charges and ethylene flow rates) about 20–23 g of CNT per hour. On doubling the length and diameter of the reactor at the optimal catalyst charge, it is possible to raise the output capacity of the installation to 150–200 g of CNT per hour. It is unclear how the scaling factor will be manifested on making the reactor even larger. In [8], a reactor for continuous synthesis of CNT, in which the catalyst is supported in the suspended state by a gas flowing from below, was described. It is difficult to decide which design is more efficient. However, a supposedly higher degree of conversion of the gas serving as a source of carbon can be achieved in the rotating reactor. Because the gas medium within the reactor is mainly composed of hydrogen at a high degree of conversion, there is no need to add hydrogen to ethylene fed into the reactor, and this was experimentally confirmed in this study. For example, run no. 2 was repeated with hydrogen supply turned off 15 min after the beginning of the process (after the catalyst activation was complete), and it was found that the yield and properties of the resulting product remained virtually unchanged.

Mention should also be made of the different modes of CNT growth in a reactor with a fixed catalyst bed and in a rotating reactor, which affects the properties of the forming carbon products. For example, in the case of CNT grown from acetylene on the surface of thermally expanded graphite (TEG) promoted

with iron compounds in a horizontal tubular reactor with a fixed Fe/TEG bed, the specific surface area of the resulting (nonpurified) CNT/TEG composite was 110 $m^2 g^{-1}$ at a content of CNT equal to 35 wt % and decreased to 42 $m^2 g^{-1}$ at a CNT content of 85 wt % [20]. Carrying out the same process in a rotating reactor yielded carbon composites containing 20% TEG and 80% CNT, with a specific surface area of 304–387 $m^2 g^{-1}$, depending on the reactor charge. It may be assumed that CNT synthesis includes stages in which there occur addition of a molecule of an unsaturated hydrocarbon (acetylene, ethylene) to a catalytically active metal center and, further, several elementary events in which a hydrogen molecule is split off and the carbon nanostructure of a nanotube (nanofiber) is formed. If the tubular structure is formed more slowly than the preceding stages, carbon with an amorphous or imperfect structure may be obtained. If the substrate (catalyst) bed is agitated, a particle of the material is, at different instants of time, either in contact with the gas serving as a source of carbon or deep within the bed, where the gas diffusion is hindered. Thus, there is enough time for structuring of carbon clusters.

This mode reminds a "pulsed" supply of the gas serving as a source of carbon into the reactor, which was suggested in [21] and resulted in a higher yield of nanotubes and led to changes in their morphology.

CONCLUSIONS

(1) Iron-containing hydrotalcites are efficient catalysts for synthesis of carbon nanotubes by chemical vapor deposition.

(2) Dilution of the oxide of the catalytically active element (iron) in the hydrotalcite matrix with aluminum oxide leads to a decrease in the average diameter of the carbon nanotubes synthesized.

(3) Introduction of aerosil into a catalyst makes it possible to diminish the aggregation of the resulting carbon nanotubes and to prevent caking of the product.

(4) A rotating reactor is an efficient device for synthesis of carbon nanotubes by chemical vapor deposition.

REFERENCES

1. Pötschke, P., Bhattacharyya, A.R., and Janke, A., *Carbon*, 2004, vol. 42, pp. 965–969.
2. Breton, Y., Desarmot, G., Salvetat, J.P., *et al.*, *Carbon*, 2004, vol. 42, pp. 1027–1030.
3. Tang, W., Santare, M.H., and Advani, S.G., *Carbon*, 2003, vol. 41, pp. 2779–2785.
4. Bai, J., *Carbon*, 2003, vol. 41, pp. 1325–1328.
5. Li, C.-H., Zhao, Y., Yao, K.-F., and Liang, J., *Carbon*, 2003, vol. 41, pp. 2443–2446.
6. Qian, W., Liu, T., Wang, Z., *et al.*, *Carbon*, 2003, vol. 41, pp. 2487–2493.
7. Zhou, Z., Ci, L., Song, L., *et al.*, *Carbon*, 2003, vol. 41, pp. 2607–2611.
8. Hao, Y., Qunfeng, Z., Fei, W., *et al.*, *Carbon*, 2003, vol. 41, pp. 2855–2863.
9. Zou, Y., Feng, Y., Wang, L., and Liu, X., *Carbon*, 2004, vol. 42, pp. 271–277.
10. Lau, K.-T., Gu, C., Gao, G.-H., *et al.*, *Carbon*, 2004, vol. 42, pp. 426–428.
11. US Patent 5 500 200.
12. Soneda, Y., Szostak, K., Delpeux, S., *et al.*, *Carbon-2001, Int. Conf.*, July 14–19, Lexington, Kentucky, USA, Session 26.1.
13. Soneda, Y., Duclaux, L., and Beguin, F., *Carbon*, 2002, vol. 40, pp. 965–969.
14. Lur'e,Yu.Yu., *Spravochnik po analiticheskoi khimii* (Handbook of Analytical Chemistry), Moscow: Khimiya, 1965.
15. US Patent Application 20 010 014 307.
16. US Patent 5 728 364.
17. US Patent 4 415 555.
18. US Patent 4 629 626.
19. Peigney, A., Laurent, Ch., Flahaut, E., *et al.*, *Carbon*, 2001, vol. 39, pp. 507–514.
20. Ukrainian Patent 61 826.
21. Li, Q., Yan, H., Zhang, J., and Liu, Z., *Carbon*, 2003, vol. 41, pp. 2876–2878.

Russian Journal of Applied Chemistry, Vol. 78, No. 6, 2005, pp. 924–930. Translated from Zhurnal Prikladnoi Khimii, Vol. 78, No. 6, 2005, pp. 945–951.
Original Russian Text Copyright © 2005 by Melezhik, Sementsov, Yanchenko.

CATALYSIS

Synthesis of Porous Carbon Nanofibers on Catalysts Fabricated by the Mechanochemical Method

A. V. Melezhik, Yu. I. Sementsov, and V. V. Yanchenko

TMSpetsmash Ltd., Kiev, Ukraine

Institute of Surface Chemistry, National Academy of Sciences of the Ukraine, Kiev, Ukraine

Received September 28, 2004; in final form, February 2005

Abstract—A mechanochemical method for fabrication of catalysts for vapor-phase deposition of porous carbon nanofibers from acetylene is suggested.

Carbon nanotubes (CNT) and nanofibers (CNF) are the most promising materials for energy-storage devices: chemical power cells, supercapacitors, fuel cells, and hydrogen adsorbers [1–8]. The energy storage capacity is determined by the structure of the carbon materials. For example, the highest capacity for carbon has been observed for nanofibers in which the carbon layers are perpendicular to the fiber axis or have a "fir-tree" orientation. A reproducible capacity for hydrogen of about 15 wt % has been achieved [8].

Porous CNF with a developed surface have been synthesized. For example, chemical activation of CNT and CNF with molten potassium hydroxide makes it possible to raise manyfold the specific surface area through burning-out of a part of graphene layers and their unfolding [9, 10]. In [11], carbon nanofibers with porous walls in the form of honeycomb were obtained by chemical vapor deposition.

The main factors determining the structure of CNT and CNF in vapor-phase deposition are the composition and structure of the catalyst used. The conventional methods for fabrication of catalysts for the process in question (aerosol techniques are disregarded) are as follows: impregnation of porous or highly dispersed mineral substrates with solutions of compounds of catalytically active metals (most frequently, iron, cobalt, and nickel) [12], coprecipitation of a mixture of metal hydroxides [13], and thermal decomposition of a mixture of metal salts and organic acids [14]. The forming homogeneous or microheterogeneous mixtures of metal oxides give rise, under the conditions of vapor-phase deposition (temperature, reductive atmosphere), to clusters of catalytically active metals, on which CNT or CNF of certain structure grow. In the process, the structure is determined not only by the nature and size of clusters of the catalytically active metals, but also by the nature of a substrate. For example, it was shown in [15] that a mixed nickel-aluminum oxide deposited onto oxidized carbon nanotubes catalyzes growth of carbon nanotubes, and nanofibers grow on this mixed oxide without a carbon substrate. It was demonstrated in [16] that a thin layer of iron, deposited in a vacuum on a substrate made of a mixed indium-tin oxide, catalyzes growth of carbon nanocoils. At the same time, comparatively straight CNT or CNF are formed on other iron-containing catalysts.

A disadvantage of the impregnation or deposition from solution is that particles of the substrate or catalyst undergo aggregation upon drying. For example, highly dispersed pyrogenic oxides of aluminum and silicon, used as supports, lose fluffiness and turn into dense lumps of a xerogel upon impregnation with aqueous or methanol solutions and drying. In growth of CNT or CNF on catalysts of this kind, there appears a tendency toward agglomeration of the carbon product into more or less dense concretions, which is unfavorable for its use in composites.

The aim of this study was to analyze the possibility of obtaining catalysts for vapor-phase deposition of CNF by the mechanochemical method and to examine the properties of CNF formed on these catalysts.

EXPERIMENTAL

Technical-grade acetylene additionally purified by a procedure described in [17] was used in the study. Gas flow rates were measured with calibrated rheometers.

1070-4272/05/7806-0924 © 2005 Pleiades Publishing, Inc.

As highly dispersed materials-supports for the catalysts served aerosils manufactured by Kalusha pilot plant: A-300 aerosil (specific surface area 300 $m^2 g^{-1}$), GOST (State Standard) 14922–77; aluminoaerosil with a weight content of aluminum oxide equal to 3% and a specific surface area of 200 $m^2 g^{-1}$ (AA-200); and aluminoaerosil with a weight content of aluminum oxide equal to 4% and a specific surface area of 90 $m^2 g^{-1}$ (AA-90), TU (Technical Specification) U 88 251-02–84.

As precursors of the catalytically active metals were used metal stearates of composition $Fe_2^{III}(OH)_2St_4$, $CoSt_2$, and $Fe^{II}Sn^{IV}(OH)_2St_4$, synthesized by precipitation from an aqueous solution. The synthesis procedures were described in detail in [18].

X-ray diffraction patterns were recorded with a DRON-3 diffractometer; thermogravigrams, on a Q-1500D derivatograph; and electron micrographs, on JEM-100 CXII transmission electron microscope.

A vibration mill with steel balls was used for mechanochemical distribution of organic compounds of metals on aerosils. It was established in control experiments that, under the experimental conditions, the transfer of iron from the balls to a substance being treated is insignificant and has no effect on the catalytic activity.

After a mechanochemical distribution of metal stearates on aerosils, a thermal treatment was performed to remove organic groups. Upon a thermal treatment in air at 600°C, organic substances and the remainder of carbon completely burned out. However, it was found in a number of experiments that the catalytic activity in CNF formation markedly increases if the catalysts contain an admixture of carbon produced in carbonization of organic groups. For this purpose, the mixture subjected to a mechanochemical treatment in a vibration mill (MCT), was thermally treated at 250°C for several hours with a restricted access of air, and then a finishing thermal treatment at the working temperature of CNF synthesis (620°C) was carried out in a flow of argon. The thus treated catalysts had a black-brown coloration because of the formation of carbon. In the process, the oxidation catalyzed by iron or cobalt contained in the samples led to a partial burning-out of organic substances with a loss of mass equal to 30–70% relative to the mass of organic groups in the starting material.

The catalysts produced by the procedures described above had a bulk density of 120–200 g dm^{-3}. To obtain less dense catalysts, aerosil was added and the mixture was treated for several minutes in a mixer with a rotation frequency of the cross-shaped blade of 10000–15000 rpm. In this case, the bulk density decreased to 50–60 g dm^{-3}. The thus loosened catalysts provided fabrication of CNF in the form of a lightweight powder without agglomeration into lumps.

CNF were synthesized in a 2.1-dm^3 cylindrical quartz reactor in which the catalyst bed was agitated via rotation of the reactor at a rate of 60–90 rpm. The reactor design was described in detail in [18]. A gas mixture (hydrogen + argon + acetylene) was fed into the reactor. The working temperature was 620°C. The conversion of acetylene into carbon was qualitatively monitored by the coloration of the flame of burning waste gases. If the catalyst was sufficiently active, the flame was small and virtually colorless, because nearly pure hydrogen came out of the reactor. If, however, the conversion of acetylene was incomplete, the flame was large, bright yellow, and smoking. In this way, the activities of different catalysts could be qualitatively compared and the variation of their activity with time could be monitored. In most cases, the catalyst activity increased during the first 5–10 min of operation (probably, metal oxides were reduced by hydrogen) and then remained high (virtually 100% conversion of acetylene) for at least 3 h for good catalysts. In some cases, oligomerization of acetylene to give smoke at the reactor outlet was observed for low-activity catalysts.

The carbon products obtained were purified by their treatment with solutions of an alkali (to remove the aerosil) and hydrochloric acid (to dissolve metals and metal oxides). The purification procedure was described in detail in [18]. The weight content of ash in the purified samples did not exceed 1–2%.

Table 1 presents the composition, preparation procedure, and catalyst properties.

As can be seen from Table 1, the catalysts fabricated by the mechanochemical method are very lightweight powders with a bulk density of 120–200 g dm^{-3} without addition of a loosener, and 50–60 g dm^{-3} with a loosener. Thus, they have a large free volume for CNF growth. One more advantage of the mechanochemical method is that no organic solvents are used and a considerably wider variety of organic compounds of metals can be employed, including those nonvolatile and insoluble in water and organic solvents.

Table 2 illustrates the synthesis modes and properties of CNF obtained using the catalysts described above. The process was carried out at 620°C. If there is no indication of a loss of activity by a catalyst by

Table 1. Composition, preparation techniques, and properties of catalysts*

Run no.	Composition and preparation procedure	Outward appearance, bulk density, and content of catalytically active metal**
1	45 g AA-90 + 5 g $Fe_2(OH)_2St_4$; MCT 1 h; ACO, 4 h at 250°C; burning-out, 2 h at 600°C in air	Yellow powder, 180 g dm^{-3}, Fe = 0.96%
2	45 g AA-90 + 5 g $Fe_2(OH)_2St_4$; MCT 1 h; ACO, 4 h at 250°C; heating to 620°C in a flow of argon	Dark powder, 180 g dm^{-3}, Fe = 0.96%
3	17.5 g AA-90 + 5 g $CoSt_2$; MCT 1 h; + 5 g A-300 (loosener); ACO, 28 h at 250°C; heating to 620°C in a flow of argon	Dark gray powder, 60 g dm^{-3}, Co = 2.62%
4	17.5 g AA-90 + 5 g $CoSt_2$; MCT 1 h; + 5 g A-300 (loosener); ACO, 28 h at 250°C; burning-out 2 h 600°C in air	Pale blue powder, 60 g dm^{-3}, Co = 2.62%
5	30 g AA-200 + 5 g $Fe_2(OH)_2St_4$; MCT 1 h; ACO, 3 h at 250°C; heating to 620°C in a flow of argon	Dark powder powder, 120 g dm^{-3}, Fe = 1.44%
6	30 g A-300 + 5 g $Fe_2(OH)_2St_4$; MCT 1 h; ACO, 5 h at 250°C; + 15 g A-300 (loosener); heating to 620°C in a flow of argon	Dark gray powder, 50 g dm^{-3}, Fe = 1.44%
7	30 g AA-200 + 10 g $FeSn(OH)_2St_4$; MCT 1 h; ACO, 3 h at 250°C + 1 h at 300°C; heating to 620°C in a flow of argon	Dark powder powder, 140 g dm^{-3}, Fe = 1.37%
8	30 g AA-200 + 10 g $FeSn(OH)_2St_4$; MCT 1 h; ACO, 5 h at 250°C in a rotating reactor; heating to 620°C in a flow of argon	Dark powder powder, 140 g dm^{-3}, Fe = 1.37%
9	15 g previously synthesized purified CNF + 5 g $Fe_2(OH)_2St_4$; MCT 1 h; ACO, 5 h at 250°C; heating to 620°C in a flow of argon	Black powder, 200 g dm^{-3}, Fe = 2.83%
10	15 g previously synthesized purified CNF + 5 g $Fe_2(OH)_2St_4$; MCT 1 h; ACO, 5 h at 250°C; + 20 g A-300 (loosener); heating to 620°C in a flow of argon	Dark gray powder, 60 g dm^{-3}, Fe = 2.83%

* ACO, autocatalytic oxidation at 250°C.

** Mass content of catalytically active metals is given with the mass of loosener disregarded.

the end of the process, its activity did not decrease during the chosen reaction time. If there is no indication of smoke formation, no smoke was observed at the reactor outlet.

A comparison of the results obtained in tests of catalyst nos. 1 and 2 (Table 2) shows that the catalytic activity markedly increases (with virtually 100% conversion of acetylene into carbon during the entire process) if autocatalytic oxidation (ACO) is followed by further thermal treatment in the mode of carbonization of organic substances (catalyst no. 2). Moreover, the specific surface area of the resulting carbon material markedly increases, from 116 $m^2 g^{-1}$ (catalyst no. 1) to 210 $m^2 g^{-1}$ (catalyst no. 2).

Catalyst nos. 3 and 4 are similar to catalyst nos. 1 and 2, but contain cobalt, instead of iron, as a catalytically active metal. In this case, too, thermal treatment after ACO in the mode of carbonization of organic substances (catalyst no. 3) leads to a certain increase in the yield of the carbon product and to a considerable rise in the specific surface area, compared with catalyst no. 4, in which organic substances were completely burned-out in air at 600°C.

It may be assumed that carbon clusters formed in carbonization of organic substances hinder coarsening of clusters of catalytically active metals and their oxides and thereby favor growth of finer CNF with a high specific surface area. Possibly, nuclei of carbon nanostructures are formed already in the course of thermal treatment of a catalyst in an oxygen-free medium.

Also, experiments devoted to comparison of the activities of the same catalysts in reactions of formation of CNF from acetylene and CNT from ethylene were carried out. The conditions in which CNT are obtained from ethylene have been described previously [19]. It was found that an admixture of carbon in the catalyst, which raises the catalytic activity and specific surface area of CNF in the system with acetylene, completely suppresses the catalytic activity in the reaction of CNT deposition from ethylene. Further, iron- and tin-containing catalysts were found to be virtually inactive in the system with ethylene. These data indicate that the mechanisms of these processes are markedly different.

Iron-containing catalyst nos. 5 and 6 were obtained in about the same thermal treatment modes, but with

Table 2. Tests of catalysts in the reactor for synthesis of CNF

Catalyst no. in Table 1	Flow rate of gases fed into the reactor, $cm^3\ min^{-1}$, at 20°C; duration and stages of the process; degree of acetylene conversion (qualitatively, by flame coloration)	Outward appearance of raw product; parameters* *Y*, *S*, and *R*
1	Argon 1500, hydrogen 170, acetylene 420; first 10 min, smoke at the reactor outlet, flame large yellow; after 10 min, the smoke and flame coloration disappear; the following 1 h 10 min, flame colorless; further, during 15 min, gradual intensification of yellow flame coloration; run terminated	Loose lumps; Y = 34.3 g (78%), S = 116 $m^2\ h^{-1}$, R = 0.10 Ω cm
2	Argon 1500, hydrogen 170, acetylene 420; flame colorless from the very beginning for 3 h	Loose lumps; Y = 75.5 g (100%), S = 210 $m^2\ h^{-1}$, R = 0.09 Ω cm
3	Argon 700, hydrogen 170, acetylene 200; first 10 min, smoke from the reactor, flame yellow; during the following 1 h 30 min, flame colorless, no smoke; further, yellow flame appears and its intensity rapidly increases; run terminated	Loose lumps; Y = 19.6 g (98%), S = 274 $m^2\ h^{-1}$, R = 0.13 Ω cm
4	Argon 700, hydrogen 170, acetylene 200; during first 30 min, smoke from the reactor, flame small yellow; during the following 10 min, smoke and yellow flame disappear; further, during 2 h 10 min, no smoke, flame colorless; next 10 min, gradual enhancement of the flame; run terminated	Powder; Y = 34.5 g (96%), S = 213 $m^2\ h^{-1}$, R = 0.13 Ω cm
5	Argon 1500, hydrogen 170, acetylene 420; during first 5 min, small yellow flame; during the following 2 h 55 min, flame colorless	Powder; Y = 75.5 g (100%), S = 335 $m^2\ h^{-1}$, R = 0.12 Ω cm
6	Argon 1500, hydrogen 170, acetylene 420; during the first 10 min, flame colorless; during the following 10 min, thin smoke at the reactor outlet and small yellow flame; during the next 2 h 20 min, flame colorless, after which a yellow flame appears again and its intensity increases during the next 20 min; at this point, run terminated	Powder; Y = 67 g (89%), S = 125 $m^2\ h^{-1}$, R = 0.10 Ω cm
7	Argon 1500, hydrogen 170, acetylene 420; small yellow flame during the entire process (3 h)	Powder + elastic loose mass; Y = 71.7 g (95%), S = 340 $m^2\ h^{-1}$, R = 0.4 Ω cm
8	Argon 1500, hydrogen 170, acetylene 420; flame nearly colorless during the entire process; run terminated after 2 h 10 min because of the reactor overfilling with an exceedingly bulky product	Powder; Y = 51.8 g (95%), S = 475 $m^2\ h^{-1}$, R = 0.6 Ω cm
9	Argon 1500, hydrogen 170, acetylene 420; flame colorless from the very beginning during 4 h	Comparatively solid lumps Y = 101 g (100%), S = 300 $m^2\ h^{-1}$, R = 0.09 Ω cm
10	Argon 1500, hydrogen 170, acetylene 420; flame colorless from the very beginning during 3 h	Powder; Y = 75.5 g (100%), S = 338 $m^2\ h^{-1}$, R = 0.14 Ω cm

* *Y*, gain in carbon relative to the theoretical value for the amount of acetylene passed; *S*, specific surface area of purified CNF; and *R*, resistivity of a compacted (15 MPa) powder of purified CNF.

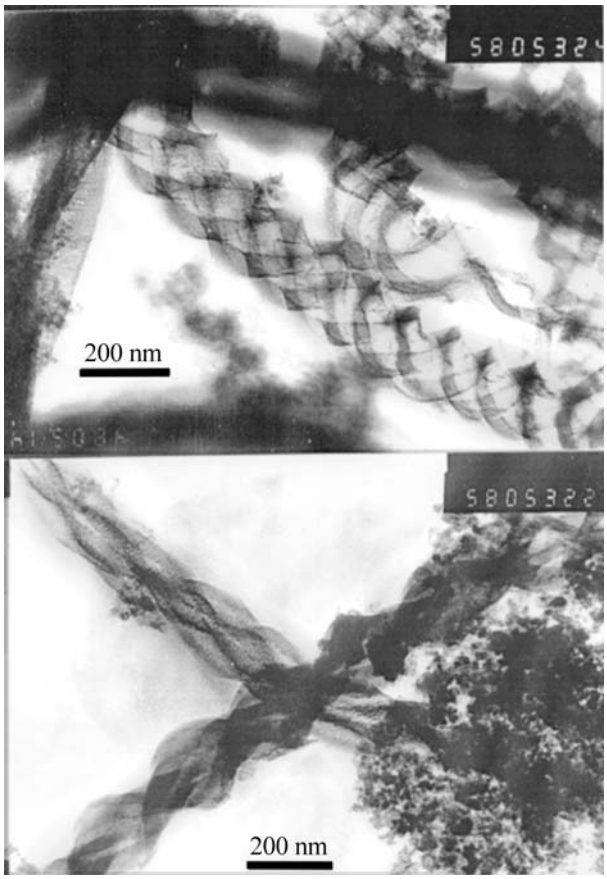


Fig. 1. Electron micrographs of a raw carbon material obtained on a tin-and-iron-containing catalyst no. 7.

different dispersed metal oxides as supports: aluminoaerosil AA-200 (catalyst no. 5) and aerosil A-300 (catalyst no. 6). Comparison of the results obtained in tests of these catalysts (Table 2) shows that use of aerosil A-300 as a support (catalyst no. 6) leads to a lower activity of the catalyst and incomplete conversion of acetylene, with the specific surface area of the carbon product decreasing. A comparison can also be made with catalyst no. 2, prepared using aluminoaerosil AA-90 at a somewhat lower content of iron.

To explain this phenomenon, it should be noted that aluminoaerosil contains on the surface of its particles rather strong acid centers, which are absent in the unmodified aerosil. These acid centers may be of both Brönsted (proton donors) and Lewis (acceptors of an electron pair) types. It is also known that Brönsted acid centers on the surface of mixed metal oxides eliminate water at high temperature to become Lewis centers. It can be assumed that presence of acid centers on the surface of support particles results in that clusters of a catalytically active metal (iron in the given case) interact with these centers with a partial transfer of the electron density to acceptor centers of the substrate. This stabilizes metal clusters and prevents their coarsening (and the ensuing decrease in their catalytic activity) through migration of metal atoms. It can also be assumed that, owing to the presence of Brönsted acid centers in the initial aluminoaerosil, organic compounds of iron interact with these centers in the course of MCT by the mechanism of ion exchange of a proton for a metal cation. This favors fixation of stearate clusters and, then, of the oxide of a catalytically active metal on the surface of aluminoaerosil particles.

Catalyst nos. 7 and 8, which contain tin and iron, differ in the mode of the ACO procedure. Comparison of the test results shows that ACO in a rotating reactor (catalyst no. 8, air passed through the reactor at a flow rate of 200 $cm^3\ min^{-1}$) yields a carbon product with a larger specific surface area (475 $m^2\ g^{-1}$) than that obtained upon ACO in a fixed bed (catalyst no. 7, 340 $m^2\ g^{-1}$). This is possibly due to the higher homogeneity of the product obtained with agitation of the catalyst in the course of ACO and to weaker aggregation of particles. In these systems, tin, which is not active by itself in the reaction of vapor-phase deposition of CNF, affects the structure of the forming CNF. Addition of tin makes it possible to obtain a carbon product with a large specific surface area and coil-like shape of fibers, as it is shown below in discussion of electron micrographs.

In fabrication of catalyst nos. 9 and 10, previously synthesized carbon fibers were used as a dispersed inorganic support. The catalytic activity of such a catalyst is very high, as can be seen from the results of tests. In this case, no mineral components are introduced into the system, with the exception of a minor amount of a catalytically active metal (iron), which markedly simplifies the purification of the carbon product or even makes it possible to do without purification if there are no stringent requirements to the content of mineral impurities. Introduction of a loosener (aerosil A-300, catalyst no. 10) prevents aggregation of particles of the carbon product in the course of synthesis and makes larger the specific surface area of the material.

Figure 1 shows TEM micrographs of a raw carbon material obtained using a tin-and-iron-containing catalyst no. 7. It can be seen that the material is mostly composed of nanofibers 50–200 nm in diameter, with a characteristic interweaving of the fibers into coils. It can be assumed that mobilization of nanofibers because of the agitation of the catalyst bed cor-

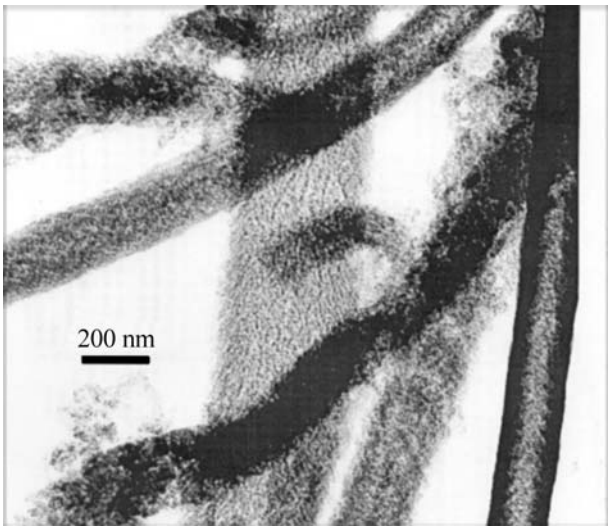


Fig. 2. Electron micrograph of a purified carbon material obtained on a tin-and-iron-containing catalyst no. 8.

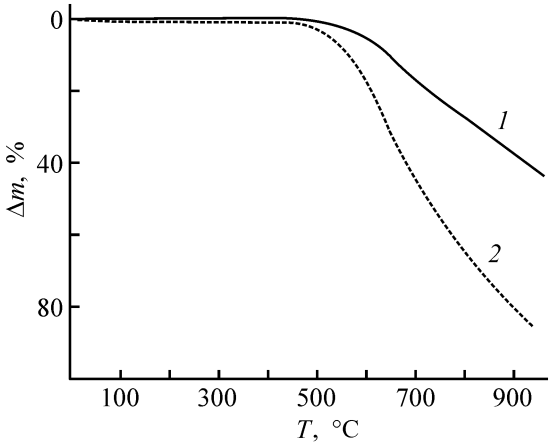


Fig. 4. Thermogravigrams of purified carbon nanofibers obtained on catalyst nos. (*1*) 5 and (*2*) 8. Rate of heating in air 10 deg min^{-1}. (Δm) Loss of mass and (T) temperature.

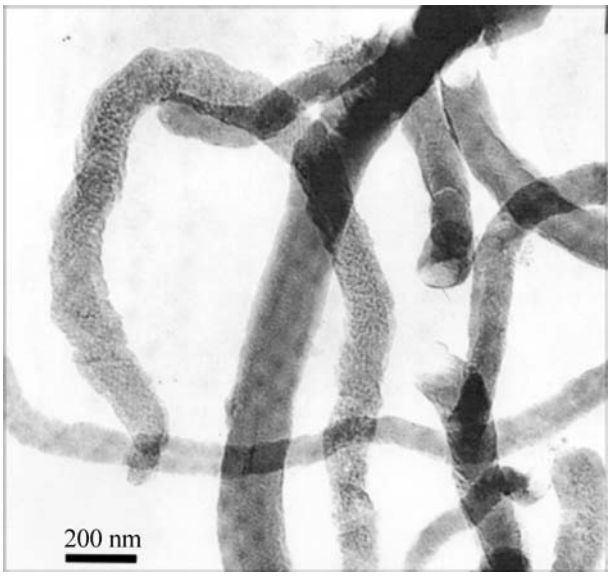


Fig. 3. Electron micrograph of a purified carbon material obtained on an iron-containing catalyst no. 5.

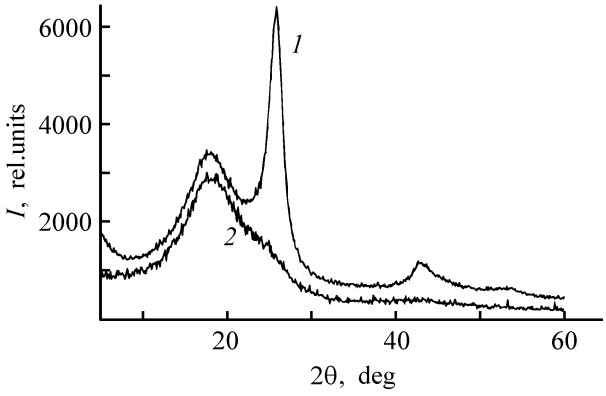


Fig. 5. X-ray diffraction patterns of purified nanofibers obtained on catalyst nos. (*1*) 5 and (*2*) 8. Cu_{K_α} radiation. (I) Intensity and (θ) Bragg angle.

responds to such an interweaving. The agitation results in that separate nanofibers collide in the course of growth and adhere to form a bundle under the action of intermolecular forces.

Figure 2 shows an electron micrograph of purified CNF obtained on catalyst no. 8 (with composition identical to that of catalyst no. 7, but a somewhat different ACO mode). It can be seen that nanofibers are composed of finer structural elements, which are poorly resolved by the available instrument. Possibly, these are bundles of thinner primary nanofibers or aggregates of bent graphene layers with pores in between.

The same fine structure is observed for nanofibers grown on the iron-containing catalyst no. 5 (Fig. 3).

Figure 4 shows thermogravigrams of purified carbon nanofibers obtained using catalyst nos. 5 and 8. It can be seen that these materials start to be oxidized in air at a noticeable rate at temperatures exceeding 500°C. As would be expected, the material with a larger specific surface area (catalyst no. 8) burns faster than catalyst no. 5. At the same time, it is known that amorphous carbon is rather rapidly oxidized in air even at 350–400°C. These data indicate that the admixture of amorphous carbon in the carbon materials obtained is insignificant. At the same time, the bends in the thermogravigrams indicate that carbon modifications with different types of structure are present in the samples.

Figure 5 shows X-ray diffraction patterns of purified carbon nanofibers obtained using catalyst nos. 5

and 8. It can be seen that the curve for sample no. 5 has two peaks at 2θ 17.9° and 25.9°, the second of which corresponds to an interplanar spacing of 3.44 Å in packets of turbostrate-disordered graphene layers. This peak is also characteristic of multi-walled carbon nanotubes. The structure of the phase corresponding to the first, broad peak (interplanar spacing of about 5.0 Å) is unclear. According to the X-ray pattern, sample no. 8 is entirely composed of this phase.

Thus, carbon fibers with different types of structure are obtained, depending on the catalyst composition, by chemical vapor deposition with the use of acetylene. The CNF obtained are promising for use in energy-storage devices. An activation of a carbon nanofiber synthesized from acetylene on a $Fe/C/SiO_2$ catalyst with molten potassium hydroxide yielded a carbon material with a specific surface area of 1700 $m^2 g^{-1}$ and a high electrical conductivity, which is promising for use in chemical power cells [20].

CONCLUSIONS

(1) The mechanochemical method makes it possible to obtain efficient catalysts for vapor-phase deposition of carbon nanofibers from acetylene.

(2) Thermal treatment a precursor of a catalyst in the mode of carbonization of organic groups markedly raises the catalytic activity and specific surface area of the forming carbon nanofibers.

(3) Introduction of tin into an iron-containing catalyst makes it possible to raise the specific surface area of carbon nanofibers to 475 $m^2 g^{-1}$. In this case, the peak at 3.44 Å, which corresponds to packets of graphene layers, disappears from the X-ray diffraction pattern of fibers.

REFERENCES

1. Yoon, S.-H., Park, C.-W., Yang, H., *et al.*, *Carbon*, 2004, vol. 42, pp. 21–32.
2. Li, W., Liang, C., Zhou, W., *et al.*, *Carbon*, 2004, vol. 42, pp. 436–439.
3. Liu, T., Sreekumar, T.V., Kumar, S., *et al.*, *Carbon*, 2003, vol. 41, pp. 2440–2442.
4. Hou, P.-X., Xu, S.-T., Ying, Z., *et al.*, *Carbon*, 2003, vol. 41, pp. 2471–2476.
5. Yang, H.F. and Yang, R.T., *Carbon*, 2002, vol. 40, pp. 437–444.
6. Fan, Y.-Y., Liao, B., Liu, M., *et al.*, *Carbon*, 1999, vol. 37, pp. 1649–1652.
7. Frackowiak, E. and Beguin, F., *Carbon*, 2002, vol. 40, pp. 1775–1787.
8. Gupta, B.K. and Srivastava, O.N., *Hydrogen Materials Science and Chemistry of Carbon Nanomaterials: VIII Int. Conf., Sudak, Crimea, Ukraine, September 14–20*, 2003, pp. 794–795.
9. Yoon, S.–H., Lim, S., Song, Y., *et al.*, *Carbon*, 2004, vol. 42, pp. 1723–1729.
10. Raymundo-Pinero, E., Cazorla-Amoros, D., Linares-Solano, A., *et al.*, *Carbon*, 2002, vol. 40, pp. 1614–1617.
11. Yan, G., Li, H., Hao, Z., and Han, H., *Carbon*, 2002, vol. 40, pp. 794–797.
12. US Patent 5 500 200.
13. US Patent Application 20 010 014 307.
14. Soneda, Y., Duclaux, L., and Beguin, F., *Carbon*, 2002, vol. 40, pp. 965–969.
15. Li, C.-H., Zhao, Y., Yao, K.–F., and Liang, J., *Carbon*, 2003, vol. 41, pp. 2443–2446.
16. US Patent Application 20 030 012 721.
17. Miller, S.A., *Atsetilen, ego svoistva, poluchenie i primenenie* (Acetylene: Properties, Production, and Use), Leningrad: Khimiya, 1969.
18. Ukrainian Patent 69 291.
19. Melezhik, A.V., Sementsov, Yu.I., and Yanchenko, V.V., *Zh. Prikl. Khim.*, 2005, vol. 78, no. 6 pp. 938–944.
20. Danilov, M.O. and Melezhik, A.V., *Zh. Prikl. Khim.*, 2004, vol. 77, no. 12, pp. 1980–1984.

Russian Journal of Applied Chemistry, Vol. 78, No. 6, 2005, pp. 931–935. Translated from Zhurnal Prikladnoi Khimii, Vol. 78, No. 6, 2005, pp. 952–956.
Original Russian Text Copyright © 2005 by V. Nekhoroshev, Ushakova, A. Nekhorosheva, Ruban.

CATALYSIS

Effect of Synthesis Conditions on Composition and Properties of Microspherical Catalyst for Polymerization of Propylene

V. P. Nekhoroshev, N. S. Ushakova, A. V. Nekhorosheva, and S. V. Ruban

Tomsk State University, Tomsk, Russia

Received January 31, 2005

Abstract—Experimental data on the influence exerted by the synthesis conditions on the composition and properties of a microspherical catalyst for polymerization of propylene are presented. The possibility of using this catalyst for synthesis of noncrystalline propylene polymers is demonstrated.

The problem of cost-efficiency and competitiveness of the product are commonly solved in manufacture of polypropylene in two ways, by using more efficient catalytic systems based on titanium-magnesium catalysts and by setting-up production of noncrystalline propylene polymers, which are in high demand on the market [1]. The first way requires a gross investment for reconstruction of a shop for synthesis of the catalyst and for licensing [2], and the second involves laboratory investigations. Despite that a single-stage synthesis of a microspherical catalyst (MSK-1) for propylene polymerization has been developed and brought to a commercial level [3], no scientific papers devoted to the influence exerted by the synthesis conditions on the composition and properties of MSK-1 have been published [4]. This is due to the fact that leading scientists and specialists in synthesis of catalysts for propylene polymerization have long believed that a single-stage synthesis of the catalyst is impossible, because low-temperature reduction of $TiCl_4$ with diethylaluminum chloride (DEAC) to $TiCl_3$, performed in three stages (MSK-3), is a more promising process for technological applications [5–7]. The idea of mixing all the reagents in the same reactor in a single stage in the course of 8–9 h was considered absurd and contradictory to the scientific concept of a prolonged multistage synthesis of MSK-3, controllable in many parameters [7]. As a scientific substantiation of the synthesis of MSK-3 can serve the general tendency toward a decrease in the reactivity of $TiCl_4$ and the reducing agent [DEAC or triethylaluminum (TEA)] via their preliminary binding into a donor–acceptor complex with an electron-donor compound (EDC). This idea proved to be fruitful and was confirmed virtually in the very first syntheses with dibutyl sulfide (DBS), dibutyl ether (DBE), diisoamyl ether (DIAE), and toluene as EDC. This made it possible to rule out use of low temperatures (down to –15°C), considerably shorten the time of synthesis, and simplify the technology of the process [8].

Synthesis of MSK-1, performed in a single stage in a hydrocarbon solvent, includes several steps. These are reduction of $TiCl_4$ with a DEAC complex in the presence of EDC, thermal treatment of the reduction products at an elevated temperature, settling with the subsequent decantation of the liquid phase and washing of the catalyst with a solvent, and discharging of the catalyst suspension with its simultaneous packaging.

In the course of synthesis, the most important parameters of the catalyst: activity, stereospecificity, and granulometric composition of its particles, are controlled. The reaction of $TiCl_4$ reduction in the presence of an aliphatic ether R_2O occurs by the scheme

$$TiCl_4 \cdot 0.2R_2O + 0.32(C_2H_5)_2AlCl \cdot 0.46R_2O$$

$$\rightarrow TiCl_3 \cdot 0.02AlCl_3 \cdot 0.05TiCl_4 \cdot 0.19R_2O \cdot Q,$$

where Q is the unidentified organic part of the catalyst, which constitutes 8.0–14.0 wt %; possibly, the main substance are oligomers of ethylene, formed in the course of the reaction.

The composition and properties of MSK-1 are affected by the synthesis conditions: relative content of the reagents, temperature mode of reduction and thermal treatment, and composition of the catalytic system

1070-4272/05/7806-0931 © 2005 Pleiades Publishing, Inc.

used in propylene polymerization. The primary role in synthesis of MSK-1 is played by processes of DIAE complexation with electron-acceptor compounds present in the reaction mixture, because the coloration of the reaction mass continuously changes in the course of synthesis: brown → green → brown → dark cherry. A characteristic feature of the synthesis is that the excess of the forming $AlCl_3$ passes in the form of ternary donor-acceptor complexes with an ether, of composition $TiCl_4 \cdot AlCl_3 \cdot 2(i\text{-}C_5H_{11})_2O$, into the solvent (heptane) and is removed together with the liquid phase in decantations and washing of the catalyst with the solvent. Commonly, such stable complexes have a large dipole moment and are strongly polar and insoluble in hydrocarbon media [8].

The goal of the present study was to examine the influence exerted by the synthesis conditions on the composition and properties of MSK-1 in order to determine the possibility of its use to obtain noncrystalline propylene polymers.

EXPERIMENTAL

MSK-1 was synthesized from $TiCl_4$ of special-purity grade, DIAE with the content of the main substance and isomers of no less than 99.9%, and DEAC with a content of butyl groups of no less than 2.0%. Compounds of DEAC and TEA were used in the form of 15% solutions in heptane; the chlorine-to-aluminum ratio was varied by adding a calculated amount of TEA to DEAC. As solvents in synthesis of the catalyst were used reference heptane, regenerated heptane, and cyclohexane, all dried over calcined zeolite of NaA and NaX brands. An inert atmosphere was created using dried argon with a purity of no less than 99.9%. The laboratory installation used to synthesize the catalyst comprises a four-necked flask with a stirrer and a thermostat filled with Vaseline oil. The flask is equipped with a pocket for a thermocouple, dropper for batching of the reducing agent, and connection pipes for input and discharge of the inert gas. After the batching of DEAC is complete, the dropper is replaced with a movable siphon through which the mother liquor and washing solution are discharged. The temperature is recorded with a KSP-4 instrument. Prior to the beginning of the synthesis, the reactor is purged with the inert gas for 30 min. The finished catalyst is discharged into ampules in the form of a suspension in a solvent, and the ampules are hermetically sealed. The catalyst has a dark violet color and contains spherical $TiCl_3$ particles 10–40 μm in size.

The general procedure for synthesis of MSK-1 consists in the following [9, 10]. A glass reactor is charged with 80 ml of a solvent, 64 ml of $TiCl_4$, and 22.5 ml of EDC. Another glass vessel is charged with 120 ml of the solvent, 20 ml of DEAC (in terms of the 100% concentration), and 58 ml of EDC. The $TiCl_4$ solution is heated in the reactor under stirring (240 rpm) to 25–50°C and a complex of DEAC with EDC is gradually added dropwise in the course of 4 h. The reaction mixture in the reactor is agitated for 1 h at 35°Cand then heated to 85–100°C in the course of 1.5 h and kept at this temperature for 2 h. The stirrer is switched off and, after 10 min of settling, the mother liquor is decanted from the reactor at 90°C with a retractable siphon. The catalyst obtained is thrice washed with the solvent (a 200-ml portion each time) at 65°C. To improve the granulometric composition of the catalyst, a employed batching of the DEAC : EDC complex is performed as follows. First, 20 ml of the complex is poured-in (about 10.0 vol %) in the course of 5 min, the reaction mixture is allowed to stand for 20 min for crystallization nuclei to be formed, and then the remaining part of the complex is measured out at a rate of 0.65 ml min^{-1}.

Propylene was polymerized in a 0.7-l stainless steel reactor with a stirrer and a heating jacket at 70°C and a pressure of 0.4 MPa, with the polymerization time equal to 5 h. The polymerization procedure was described in detail in [11]. The granulometric composition of the catalyst was determined by the known procedure [12] and that of the polypropylene powder, by sieving. The content of DIAE in MSK-1 was found by decomposition of the catalyst suspension with water, with the subsequent extraction of the ether released with heptane; the content of the ether in the extract was determined by gas–liquid chromatography. The stereoisomer composition of polypropylene was determined by extraction with, first, cold (25°C, 12 h) and then boiling heptane (98°C, 8 h). IR spectra of the polymers were measured on an Impact 410 Nicolet IR Fourier spectrometer, using the method of multiple frustrated total internal reflection on a zinc selenide crystal. The conditions under which the IR spectra were recorded were as follows: number of scans 36, resolution 4 cm^{-1}, amplification 4, scanning frequency 0.6329, aperture 35, detector DTGS KBr, scanning range 4000–650 cm^{-1}. The IR spectra were processed using the Omnic software. Polymer samples were identified using the computer database of IR spectra, with a special software employed to calculate the degree of coincidence of two spectra. The softening point of the polymers was determined by the ring-and-ball method, the dynamic viscosity was measured with a Brookfield programmable viscometer, and the penetration was found in accordance with TU

(Technical specification) 2211-056-05796653–98. The noncrystalline propylene polymers used to manufacture bituminous-polymeric binders at the Izofleks plant (Kirishi) were supplied by ALPHAMIN Co. (Belgium) (Table 1).

Polymer sample no. 1 (Table 1) is a mechanical mixture of isotactic and atactic polypropylene in approximately equal amounts. The degree of coincidence of the IR spectrum of this polymer with the spectra of isotactic and atactic polypropylene from the database is 88.4 and 87.3%, respectively (see Fig. 1a). A specific feature of the spectrum of sample no. 1 is the presence of a broad low-intensity band peaked at 1649 cm^{-1}, associated with stretching vibrations of olefin double bonds. This indicates that the polymer was preliminarily subjected to a prolonged thermal destruction at 300°C [13]. The polymer is supplied as 6-mm-thick plates. The whole set of the above data indicates that the noncrystalline propylene polymer of S-10 brand is manufactured at a plant employing the first-generation technology with a low-stereospecific catalytic system.

Polymer sample nos. 2 and 3 have an anomalously high melt viscosity and rather high softening points and penetrations, which is characteristic of noncrystalline copolymers of propylene and ethylene. They are exceedingly well mixed with molten bitumen at 180°C. The polymer of RSC brand corresponds to a block-copolymer of propylene and ethylene (degree of coincidence of the spectra 89.5%), and that of AAC brand, to a noncrystalline propylene copolymer containing 54 mol % ethylene units in the chain (degree of coincidence of the spectra 90.4%). The IR spectra of these polymers (see Figs. 1b, 1c) show an increase in the relative intensity of the bands peaked at 721 and 723 cm^{-1} [pendulum vibrations of the C-H bond in the methylene groups $(CH_2)_{n \geq 3}$]. This fact, combined with the increase in the relative intensity of the absorption band at 1376 cm^{-1} (deformation vibrations of methyl groups), indicates that methylene side chains C_4–C_8 are present in the form of alkyl branchings [14] formed in the course of polymerization in the presence of a third comonomer, α-olefin C_4–C_8. The branching of the ternary copolymer accounts for the anomalous properties of sample nos. 2, 3 (Table 1), i.e., the exceedingly high viscosity of the melts at an increased penetration, which imparts caoutchouc-like highly elastic properties to the copolymers.

The effect of the reagent ratio on the composition and properties of MSK-1 is illustrated in Table 2. The composition of MSK-1, having the general formula $TiCl_3 \cdot n_1AlCl_3 \cdot n_2TiCl_4 \cdot n_3R_2O \cdot Q$, varies

Table 1. Properties of noncrystalline propylene polymers

Sample no.	Polymer brand	Viscosity coefficient, 180°C, Pa s^{-1}	Softening point by the ring-and-ball method, °C	Penetration at 25°C, dmm
1	S-10	1.5	153	9.0
2	RSC	150.0	159	40.0
3	AAC	1600.0	165	50.0

within the following range: n_1 = 0.02–0.06, n_2 = 0.03–0.08, n_3 = 0.13–0.2; R = C_4H_9 or i-C_5H_{11}. It was established that, using DIAE in MSK-1 synthesis as an EDC provides a high stereospecificity of the catalytic system and a narrower granulometric distribu-

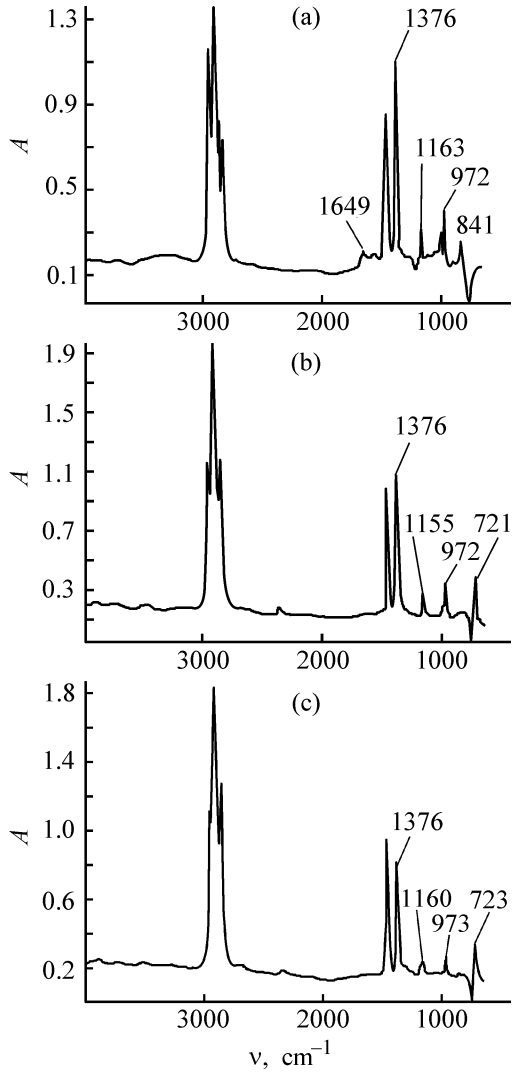


Fig. 1. IR spectra of (a) noncrystalline propylene polymers of S-10 brand and copolymers of propylene and ethylene of (b) RSC and (c) AAC brands. (*A*) Optical density and (ν) frequency.

Table 2. Effect of the relative amounts of reagents on the composition and properties of MSK-1

Sample no.	Molar ratio		Yield of atactic polypropylene, wt %	Activity, g of polypropylene/g of $TiCl_3$ h MPa
	$TiCl_4$: DEAC	ether : $TiCl_4$		
1	3.1 : 1.0	0.2 : 1.0	1.5	1750
2	3.4 : 1.0	0.1 : 1.0	1.0	1810
3	3.65 : 1.0	0.27 : 1.0	1.0	1900
4	4.0 : 1.0	0.2 : 1.0	0.5	2000

Table 3. Effect of the temperature mode of synthesis on the properties of MSK-1

Sample no.	Temperature		Yield of catalyst, g	Activity, g of polypropylene/g of $TiCl_3$ h MPa	Yield of atactic polypropylene, %
	reduction	thermal treatment			
5	25	85	75.2	1750	1.5
6	35	90	79.5	2000	0.5
7	50	100	71.4	1620	1.0
8	35	35	82.0	1690	8.3

tion of the catalyst (compared with DBE). Probably, the key role is played by the 3*D* branching and length of the aliphatic chains in the ether, which creates an additional steric hindrance in orientation of the monomer on a catalytic center. An increased yield of the atactic polypropylene is observed at a small $TiCl_4$: DEAC ratio (Table 2, run no. 1). The overall molar ratio of the reagents is maintained within $TiCl_4$: DEAC : ether = (3.4–3.7) : 1.0 : (2.1–2.5). $TiCl_4$ is reduced with DEAC containing up to 11.0 mol % ethylaluminum dichloride (EADC) or up to 20.0 mol % TEA.

An specific feature of the MSK-1 formulation consists in the increased content of the organic part (the content of the ether and ethylene oligomers combined is as high as 30.0 wt %) and of an admixture of cocrystallized $TiCl_4$. This provides its increased (by a factor of 6–7) poison resistance to impurities in the solvents used in the stages of synthesis and polymerization of propylene (alcohols, water, aromatic hydrocarbons, unsaturated and sulfurous compounds. The MSK-1 catalyst has a virtually uniform granulometric composition (96% of catalyst particles are 10–40 μm in size), which makes it possible to obtain an isotactic polypropylene powder with a high bulk density (420–500 g dm^{-3}) and a narrow granulometric distribution (92–100% of catalyst particles 250–710 nm in size). The technology of synthesis is simpler because there is no need to use low temperatures, the process is single-stage, and the regenerated heptane fraction of oil, which is widely used in polymerization of propylene, serves as a solvent in synthesizing the catalyst. If DEAC containing an admixture of TEA (up to 20 mol %) is used as a reducing agent, the yield of MSK-1 increases by 40%, which lowers its production cost by 25% [10]. In addition, MSK-1 has a 1.5 times higher thermal stability (compared with MSK-3), which allows propylene polymerization at higher temperatures, up to 90°C [15].

The temperature mode of reduction and thermal treatment strongly affects the streospecificity of MSK-1, and this can be used in synthesis of noncrystalline propylene polymers (Table 3).

Raising the reduction temperature from 25 to 50°C and that of thermal treatment to 100°C makes lower the yield of the catalyst in synthesis and diminishes its activity in polymerization of propylene (run no. 7). The catalyst synthesized without thermal treatment at an elevated temperature (run no. 8) has a low stereosopecificity and a sufficiently high activity in polymerization. The increased yield of the catalyst in this synthesis is due to the presence of a considerable amount of $AlCl_3$ in its composition.

The composition of the catalytic system used in propylene polymerization strongly affects its stereospecificity [16]. At a mass ratio DEAC : MSK-1 = 3 : 1 and less in the polymerization reactor, the yield of atactic polypropylene increases to 9 wt %.

Thus, the catalytic system for propylene polymerization and for synthesis of noncrystalline copolymers of propylene with ethylene and α-olefins, based on MSK-1 and having a low stereospecificity, should prepared with a mass ratio DEAC : MSK-1 = 2.5 : 1. The low-stereospecific MSK-1 is synthesized under the following conditions: molar ratio $TiCl_4$: DEAC : DIAE = 3.1 : 1.0 : 2.1, reduction temperature 25–35°C, no thermal treatment in synthesis. A propylene homopolymer obtained on MSK-1 under the conditions specified is subjected to initiated thermal destruction at 250°C in the presence of 0.1 wt % dicumyl peroxide for 4 h by the procedure described in [13]. The polymer obtained contains 32 wt % atactic fraction soluble in cold heptane, 55% fraction soluble in boiling heptane, and 45% isotactic fraction. The IR spectra and properties of the resulting noncrystalline propylene homopolymer correspond to those of S-10 brand (Table 1), which confirms the possibility of industrial synthesis of noncrystalline propylene polymers. With account of the high cost of noncrystalline propylene polymers ($1000 per ton) and posssibilty of their export in large amounts, the technique suggested for their synthesis on MSK-1 is economically sound.

CONCLUSIONS

(1) The influence exerted by the synthesis conditions on the composition and properties of the MSK-1 catalyst for propylene polymerization was experimentally studied. It was shown that a catalyst for propylene polymerization, having a low stereospecificity, can be obtained on the basis of MSK-1.

(2) Noncrystalline propylene homopolymer, having the necessary set of service characteristics, was synthesized.

ACKNOWLEDGMENTS

The study was supported by a grant from the administration of Tomsk oblast under contract no. 157 with Ataktika Ltd.

REFERENCES

1. Nekhoroshev, V.P., *Plast. Massy*, 1995, no. 5, pp. 42–46.
2. Vlasov, A.V., Dudchenko, V.K., and Maier, E.A., *Plast. Massy*, 2004, no. 5, pp. 7–9.
3. Khandorin, G.P., Polle, E.G., Labzovskii, S.Ya., and Maier, E.A., *Plast. Massy*, 1989, no. 2, pp. 3–5.
4. Bukatov, G.D., Sergeev, S.A., Zakharov, V.A., *et al.*, *Plast. Massy*, 2004, no. 5, pp. 9–10.
5. Bukatov, G.D., Zaikovskii, V.I., Zakharov, V.A. *et al.*, *Vysokomol. Soedin., Ser. A*, 1982, vol. 24, no. 3, pp. 542–548.
6. Denilov, R.Kh., Zhovoronkov, M.N., Shestak, N.P., *et al.*, *Plast. Massy*, 1986, no. 6, pp. 55–56.
7. Vermel', E.E., Zakharov, V.A., Fenelonov, V.B., *et al.*, *Kinet. Kataliz*, 1981, vol. 22, no. 2, pp. 480–487.
8. Nekhoroshev, V.P., Burmistrova, T.I., Ivanchev, S.S., *et al.*, *Kataliticheskie i initsiiruyushchie sistemy dlya sinteza i modifikatsii polimerov: Sbornik nauchnykgh trudov* (Catalytic and Initiating Systems for Synthesis and Modification of Polymers: Coll. of Sci. Works), Pavlyuchenko, V.N., Ed., Leningrad: ONPO Plastpolimer, 1984.
9. USSR Inventor's Certificate, no. 1436318.
10. USSR Inventor's Certificate, no. 1534821.
11. Maier, E.A., Shevchenko, S.A., Nekhoroshev, V.P., *et al.*, *Plast. Massy*, 1985, no. 6, pp. 12–13.
12. Antsiburov, K.A., Korsun, A.E., Chernikov, V.B., *et al.*, *Plast. Massy*, 1986, no. 4, pp. 48–49.
13. Volkov, A.M. and Nekhoroshev, V.P., *Zh. Prikl. Khim.*, 1985, vol. 58, no. 6, pp. 1416–1418.
14. Crompton, T., *Analiz plastikov* (Analysis of Plastics), Moscow: Mir, 1988.
15. Burmistrova, T.I., Shepel', V.M., Balakhonov, E.G., and Nekhoroshev, V.P., *Katalizatory i initsiatory dlya polucheniya polimerizatsionnykh plastmass: Sb. nauch. tr.* (Catalysts and Initiators for Synthesis of Polymerization Plastics: Coll. of Sci. works), Baulin, A.A., Ed., Leningrad: ONPO Plastpolimer, 1987.
16. Antsiburov, K.A., Balakhonov, E.G., Burmistrova, T.I., *et al.*, *Plast. Massy*, 1988, no. 7, pp. 63–64.

Russian Journal of Applied Chemistry, Vol. 78, No. 6, 2005, pp. 936–939. Translated from Zhurnal Prikladnoi Khimii, Vol. 78, No. 6, 2005, pp. 957–961.
Original Russian Text Copyright © 2005 by Gorbatenko, Pervova, Lipunova, Maslakova, Lipunov, Sigeikin.

CATALYSIS

Synthesis and Catalytic Properties of Copper(II) 1-Aryl-5-Benzothiazolylformazanates

Yu. A. Gorbatenko, I. G. Pervova, G. N. Lipunova, T. I. Maslakova, I. N. Lipunov, and G. I. Sigeikin

Ural State Forestry Engineering University, Yekaterinburg, Russia

Ural State Technical University, Yekaterinburg, Russia

Interdepartmental Center for Analytical Investigations in Physics, Chemistry, and Biology, Presidium of the Russian Academy of Sciences, Moscow, Russia

Received April 2, 2004; in final form, December 2004

Abstract—New copper(II) benzothiazolylformazane complexes were synthesized and immobilized on AN-18 anion exchanger. The influence of the composition of the coordination core of copper(II) benzthiazolylformazanates and temperature on their catalytic properties in decomposition of H_2O_2 and oxidation of Na_2S in aqueous solution was studied.

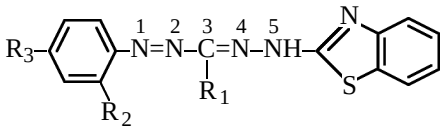
Development of heterogenized catalysts with a high concentration of active centers of known composition is an efficient way to obtain stable catalysts with a good reproducibility and high activity. The composition of active centers of such catalysts is similar to that of active centers of homogeneous catalysts; however, the active centers themselves are chemically bound with one or more ligands fixed on an insoluble support. Such complex catalysts combine properties of both homogeneous complexes (possibility of varying the type of the central atom and its ligand environment) and heterogeneous systems (formation of coordination-saturated structures on the support surface [1]). Ion exchangers of various types are widely used as solid supports. Their modification with functional complexing groups allows synthesis of new catalysts [2].

Anion exchangers with hetarylformazane groups have been prepared previously [3, 4], and it was shown that the formazan structure and the synthesis procedure substantially affect the catalytic activity of metal–formazan complexes in decomposition of H_2O_2 in aqueous solutions and liquid-phase oxidation of Na_2S.

In this study, we prepared certain copper(II) benzothiazolylformazanates and examined their composition and catalytic properties at various temperatures in the same reactions.

EXPERIMENTAL

To synthesize copper(II) complexes to be immobilized on the polymeric support, we used 1-aryl-3-alkyl-5-benzothiazolylformazans **I**–**III**:



where R_1, R_2, R_3 are CH_3, H, 4-SO_3H (**I**); CH_2Br, H, H (**II**); and CH_2Br, OH, 4-NO_2 (**III**), respectively.

It is known [5] that hetarylformazans are rather labile polydentate ligands and can form metal complexes of various compositions and structures depending on the substituent in 1-, 3-, and 5-positions.

First, the complexation of compounds **I**–**III** with copper(II) acetate in solution was studied by spectrophotometric titration. This method allows direct monitoring of the complexation process and calculation of the stoichiometry of the complexes formed [6, 7].

The clearest spectral pattern is observed with formazan **I**. In the course of titration of the ethanolic solution of this compound ($c_{\mathbf{I}} = 3 \times 10^{-5}$ M) with a copper(II) acetate aqueous solution ($c_{CuAc_2} = 10^{-3}$ M), the intensity of the absorption band of the initial formazan (λ_{max} = 430 nm) gradually decreases, and

1070-4272/05/7806-0936 © 2005 Pleiades Publishing, Inc.

that of the band at λ_{max} = 640 nm grows (Fig. 1). The spectral curves intersect at two isobestic points of titration, which indicates formation of two complexes. The complex with L : M = 2 : 1, showing a broadened band at 470–500 nm, and 1 : 1 complex with λ_{max} = 640 nm are formed when the copper(II) salt is in deficiency and excess, respectively.

Titration of formazan **II** with copper(II) acetate solution is also accompanied by a decrease in the intensity of the band of the initial compound (λ_{max} = 370 nm) and by appearance of a weak band at 610 nm. Only one isobestic point is observed in the titration curves, which corresponds to formation of the CuL complex. In the case of formazan **III**, the spectral pattern for titration with the copper(II) salt is more complex and cannot be interpreted unambiguously.

Based on the spectrophotometric titration data, we synthesized crystalline complexes of copper(II) with formazan **I** at L : M ratio of 1 : 1 and 2 : 1 complexes **IV** and **V**, with formazan **II**, at L : M = 1 : 1 complex **VI**, and with formazan **III**, at L : M = 1 : 1 and 2 : 1 complexes **VII** and **VIII** (Table 1).

Copper(II) formazanates **IV**–**VIII** were prepared by the following general procedure. To a solution of 0.15 mmol (or 0.30 mmol) of formazan in a minimal amount of ethanol (or aqueous ethanol for formazane **I**), a solution of 0.15 mmol of copper(II) sulfate in the minimal amount of water was added at 40°C with stirring, and the mixture was left for 1 h. The precipitate thus formed was filtered off, washed with water, and dried.

It follows from the elemental analysis that complexes **IV**, **VI**, and **VII** have the composition CuL, and **V** and **VIII**, CuL_2 (Table 1). All the compounds are crystal solvates with ethanol. The electronic absorption spectra of complexes **IV**–**VIII** in ethanol are similar to the spectra of Cu(II) formazanates obtained in titration of formazans **I**–**III**.

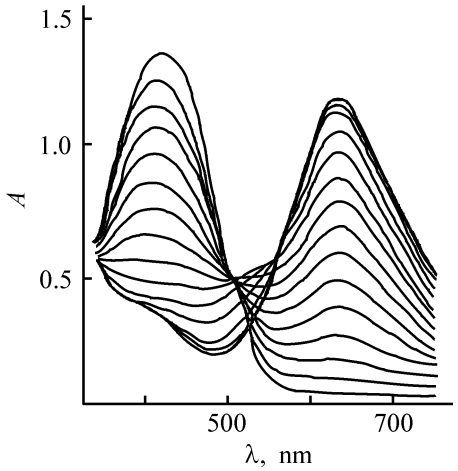
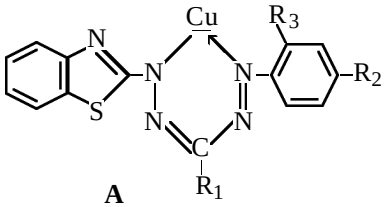


Fig. 1. Electronic absorption spectra of formazan **I** in ethanol in titration with aqueous solution of copper(II) acetate. $c_{\mathbf{I}} = 3 \times 10^{-5}$ M, $c_{CuAc_2} = 10^{-3}$ M, (λ) Wavelength; (*A*) transmittance.

The ESR spectra of copper(II) formazanates in toluene [8] suggest formation of a $Cu|4N|$ distorted tetrahedron for **V**, $Cu|4N|$ square-planar structure for **VIII**, and mixed nitrogen–oxygen $Cu|3N,O|$ structure for **VII**.

Our and published (for similar ligands [5]) data suggest structure **A** for copper(II) formazanates **V** and **VIII**:



A

Table 1. Characteristics of copper(II) formazanates **IV**–**VIII**

Compound	Ligand	L : Cu	mp, °C	λ_{max}, nm	Found, %				Empirical formula	Calculated, %			
					C	H	N (S)	Cu		C	H	N (S)	Cu
IV	**I**	1 : 1	>250	640 430	40.0	4.0	13.8 (12.5)	11.5	$C_{15}H_{12}N_5S_2O_3Cu \cdot 2C_2H_5OH$	40.0	4.5	13.2 (12.1)	12.0
V	**I**	2 : 1	235	640	44.8	3.8	15.9 (14.4)	7.6	$C_{30}H_{24}N_{10}S_4O_6Cu \cdot 2C_2H_5OH$	45.2	4.0	15.6 (14.2)	7.0
VI	**II**	1 : 1	>250	610	41.3	2.9	(6.9)	13.8	$C_{15}H_{11}N_5SBrCu$	41.2	2.5	(7.3)	14.6
VII	**III**	1 : 1	>250	470 640	37.3	3.1	15.3 (6.0)	11.7	$C_{15}H_9N_6SBrO_3Cu \cdot C_2H_5OH$	37.6	2.8	15.5 (5.8)	11.7
VIII	**III**	2 : 1	240	470 640	40.0	3.0	16.0 (5.9)	5.4	$C_{30}H_{20}N_{12}S_2Br_2O_6Cu \cdot 3C_2H_5OH$	40.4	3.5	15.7 (6.0)	5.9

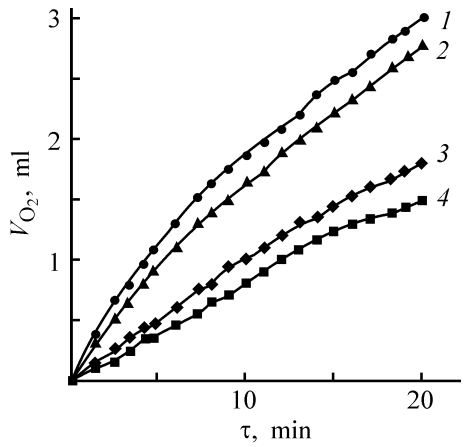


Fig. 2. Kinetic curves of decomposition of 1% H_2O_2 aqueous solution in the presence of copper(II) formazanates. T = 20°C, V_Σ = 27 ml, and c_{Cu} = 0.01 M. (V_{O_2}) oxygen volume and (τ) reaction time. Compound: (*1*) **VIII**, (*2*) **VII**, (*3*) **VIIIp**, and (*4*) **VIIp**; the same for Fig. 3.

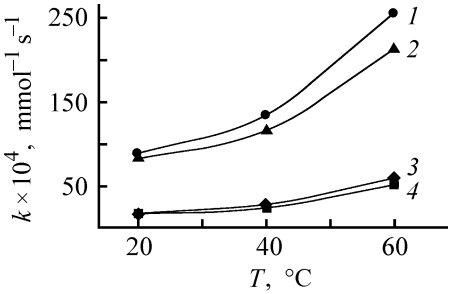
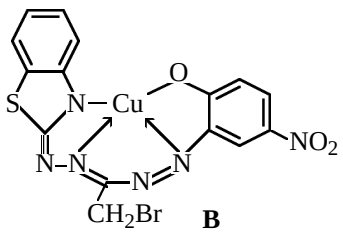


Fig. 3. Temperature (T) dependence of the rate constant of H_2O_2 decomposition (1% aqueous solution) in the presence of copper(II) formazanates.

The structure of complexes **IV** and **VI**, corresponding to the composition L : M = 1 : 1, is probably formed by additional coordination of $CuSO_4$ to nitrogen atoms of the benzothiazole fragment.

For complex **VII**, the structure **B** is the most probable:



B

To obtain metal complexes suitable for heterogeneous catalysis, we immobilized formazanates **IV**–**VIII** on AN-18 styrene-divinybenzene anion exchanger. The presence in its structure of primary and secondary amino groups allowed immobilization of formazanates **IV** and **V** containing sulfonate group in the ligand by ion exchange and of complexes **VI**–**VIII** containing labile bromine by covalent bonding.

Immobilization of Cu(II) formazanates was performed as follows. To a solution of **IV** in ethanol, a sample of AN-18 anion exchanger was added so that the copper ion concentration in the polymer was 0.01 mmol g^{-1}, and the mixture was stirred to complete decolorization of the solution. The modified anion exchanger was filtered off, washed with ethanol, and dried in air. In such a way, formazanate **IVp** was prepared. Similarly, formazanates **V**–**VIII** were immobilized to obtain catalysts **Vp**–**VIIIp**, which exhibit a high activity and can be easily separated from the reaction products.

The ESR data show the square-planar structure of the coordination core Cu|4N| for formazanate **VIIIp** and Cu|3N, O| for **VIIp**, similarly to the initial complexes **VIII** and **VII** [8, 9]. Presumably, immobilization of formazanates **IV**–**VI** on the polymeric support does not change the structure of the coordination core.

The catalytic properties of copper(II) formazanates **IV**–**VIII** and **IVp**–**VIIIp** were studied in the model reaction of H_2O_2 decomposition (1% aqueous solution). It is known [4] that complexes containing no more than 0.01 mmol of Cu(II) per gram of the polymeric matrix have the highest catalytic activity. Therefore, we studied the catalytic activity of **IV**–**VIII** and **IVp**–**VIIIp** under the similar conditions as follows. A sample of copper(II) formazanate [([0.1 g for **IVp**–**VIIIp** and 0.0028–0.0061 g for **IV**–**VIII**) was added to 27 ml of 1% H_2O_2 aqueous solution. The reaction curse was monitored by the volume of liberated oxygen at 20, 40, and 60°C.

The kinetic curves of H_2O_2 decomposition at 20°C for **VII**, **VIIp**, **VIII**, and **VIIIp** are shown in Fig. 2. Formazanates **VII** and **VIII** exhibit a high catalytic activity in H_2O_2 decomposition, which is probably caused by the square-planar structure of the metal chelate core. Copper(II) formazanates immobilized on the anion exchanger (**VIIp** and **VIIIp**) behave similarly. It should be noted that the related metal complex systems studied in [3, 4] show lower rate constants of H_2O_2 decomposition under the same conditions (0.12–11.78 × 10^{-4} mmol^{-1} s^{-1}).

Proceeding with the previous studies [3, 4], we examined the H_2O_2 decomposition in the presence of copper(II) formazanates at 40 and 60°C. The kinetic data obtained were used to calculate the rate constants of H_2O_2 decomposition [10] (Table 2).

The temperature dependences of the rate constants of H_2O_2 decomposition for complexes **VII**, **VIIp**, **VIII**, and **VIIIp**, as examples, are shown in Fig. 3.

Table 2. Catalytic activity of copper(II) formazanates in decomposition of 1% H_2O_2 aqueous solution and liquid-phase oxidation of 0.03% Na_2S solution at various temperatures

Compound no.	$k \times 10^4$, $mmol^{-1}\ s^{-1}$ at indicated temperature, °C			Degree of conversion S^{2-}, % at indicated temperature, °C		
	20	40	60	20	40	60
IV	46.8	89.9	203.6	–	–	–
IVp	0.7	2.6	11.2	31.2	64.0	71.3
V	57.5	95.1	219.0	–	–	–
Vp	1.2	5.6	17.3	34.1	64.9	74.1
VI	42.4	71.3	162.4	–	–	–
VIp	2.9	8.3	20.4	59.9	62.8	67.1
VII	82.3	114.8	212.0	–	–	–
VIIp	16.1	23.7	51.3	32.7	54.3	74.7
VIII	86.5	133.6	254.6	–	–	–
VIIIp	17.8	27.1	58.5	38.3	58.3	73.5

As can be seen from Fig. 3 and Table 2, the decomposition rate increases with temperature. For copper(II) formazanates **IVp**–**VIIIp**, the rate constants are lower than those for **IV**–**VIII**. Probably, this is caused by partial solubility of the "free" complexes, which increases with the temperature of the reaction mixture, thereby making the reaction conditions similar those in homogeneous catalysis.

In spite of the relatively low catalytic activity of **IVp**–**VIIIp** as compared to their crystalline analogues **IV**–**VIII**, they can be successfully used in heterogeneous catalysis, since their composition and the structure of the coordination core, and hence the catalytic properties, do not change in repeated use [11].

The liquid-phase Na_2S oxidation with molecular oxygen and calculation of the degree of catalytic conversion $S^{2-} \rightarrow SO_4^{2-}$ were performed by the method described in [11]. The use of **IV**–**VIII** as oxidation catalysts was unsuccessful because of their solubility in the reaction mixture. The catalytic activity of formazanates **IVp**–**VIIIp** in liquid-phase Na_2S oxidation is virtually independent of the composition and structure of the complexes (this is characteristic of the previously studied benzothiazolylformazanates [3, 4]) and slightly changes with the reaction temperature (Table 2).

CONCLUSIONS

(1) Complexation of 1-aryl-5-benzothiazolylformazans with copper(II) was studied by spectrophotometric titration, and the stoichiometry of complexes formed was calculated.

(2) It was found that the coordination core has the $Cu|4N|$ or $Cu|3N,O|$ structure. The crystalline copper(II) complexes synthesized were immobilized on a AN-18 solid support.

(3) The catalytic activity of immobilized copper(II) formazanates was studied in comparison with the initial analogues. The complexes with the square-planar copper environment show the highest activity.

ACKNOWLEDGMENTS

The study was financially supported by the Russian Foundation for Basic Research (projects nos. 02-03-96424-r2002 Ural and 03-03-32044).

REFERENCES

1. Boreskov, G.K., *Geterogennyi kataliz* (Heterogeneous Catalysis), Moscow: Nauka, 1988.
2. Pomogailo, A.D., *Polimernye immobilizovannye metallokompleksnye katalizatory* (Polymeric Immobilized Metal Complex Catalysts), Moscow: Nauka, 1988.
3. Lipunov, I.N., Pervova, I.G., Lipunova, G.N., *et al.*, *Koord. Khim.*, 1997, vol. 23, no. 12, pp. 934–937.
4. Pervova, I.G., Lipunova, G.N., Yushkova, O.G., *et al.*, *Sorb. Khromatogr. Prots.*, 2002, vol. 2, nos. 5–6, pp. 609–615.
5. Buzykin, B.I., Lipunova, G.N., Sysoeva, L.P., and Rusinova, L.I., *Khimiya formazanov* (Chemistry of Formazans), Moscow: Nauka, 1992.
6. Shlefer, G.L., *Kompleksoobrazovanie v rastvorakh* (Complexation in Solutions) Leningrad: Khimiya, 1964.
7. Babko, A.K. and Pilipenko, A.T., *Fotometricheskii analiz* (Photometric Analysis), Leningrad: Khimiya, 1968.
8. Vishnevskaya, G.P., Frolova, E.N., Pervova, I.G., *et al.*, *Strukt. Dinam. Mol. Sist.*, 2003, no. 10, part 3, pp. 190–195.
9. Molochnikov, L.S., Gorbatenko, Yu.A., Vishnevskaya, G.P., *et al.*, Abstracts of Papers, *XVII Mendeleevskii s'ezd po obshchei i prikladnoi khimii* (XVII Mendeleev Conf. on General and Applied Chemistry), Kazan, 2003, vol. 4, p. 439.
10. Kopylova, V.D., Frumkina, E.L., Mochalova, L.D., *et al.*, *Kinet. Katal.*, 1978, vol. 19, no. 15, pp. 1356–1370.
11. Astanina, A.N., Fung, T.Sh., Kopylova, V.D., *et al.*, Available from VINITI, July 5, 1983, no. 3676. *Vestn. Mosk. Univ., Ser. Khim.*, 1984, vol. 25, pp. 85–88.

Russian Journal of Applied Chemistry, Vol. 78, No. 6, 2005, pp. 940–943. Translated from Zhurnal Prikladnoi Khimii, Vol. 78, No. 6, 2005, pp. 962–965.
Original Russian Text Copyright © 2005 by Sergeeva, Aref'ev, Domnina, Komarova.

ORGANIC SYNTHESIS AND INDUSTRIAL ORGANIC CHEMISTRY

Synthesis and Antioxidative Properties of Conjugates of Dextran with 4-(4-Hydroxy-3,5-di-*tert*-butylbenzylidene)-2-phenyl-4,5-dihydrooxazol-5-one

O. Yu. Sergeeva, D. V. Aref'ev, N. S. Domnina, and E. A. Komarova

St. Petersburg State University, St. Petersburg, Russia

Received January 20, 2005

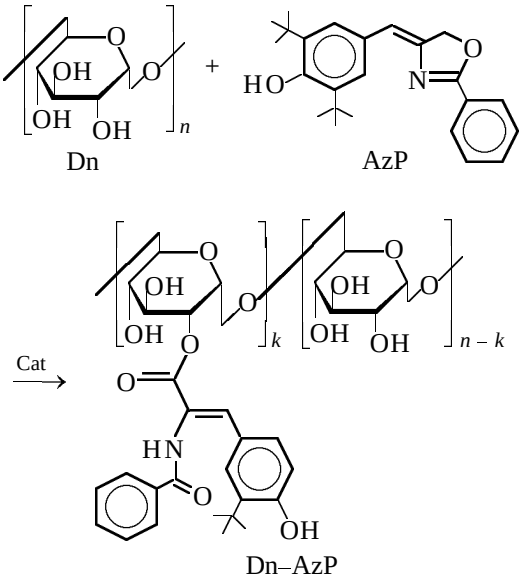
Abstract—The possibility of synthesis of conjugates differing in molecular weight, degree of substitution of the dextran glycoside units, and, accordingly, in the solubility in water from a hydrophilic polymer (dextran) and an azlactone derivative of a sterically hindered phenol, 4-(4-hydroxy-3,5-di-*tert*-butylbenzylidene)-2-phenyl-4,5-dihydrooxazol-5-one, was analyzed, and their antiradical and antioxidative activity was studied.

Search for, and study of biologically active substances with antioxidative properties become increasingly topical because of the important role of antioxidant-controlled free-radical processes in biological systems [1]. Among compounds exhibiting pronounced antioxidative properties and high biological activity, particular mention should be made of sterically hindered phenols (SHPs) [2]. Owing to their high antioxidative acvitivy (AOA) and nontoxicity of SHPs (Ionol, Probucol, Phenoxan, etc.), they are widely used in medicine and food industry [3, 4]. The recently developed polymeric SHP derivatives (conjugates) with hydrophilic polymers not only exhibit properties of the related macromolecular systems (prolonged effect, solubility in water, susceptibility to pH-dependent hydrolysis, etc.) [5, 6], but also show an enhanced antiradical activity (ARA), compared to the low-molecular-weight analogs. As shown in [7, 8], the high ARA of the conjugates is determined not only by the polymeric structure, but also by the structure of the spacer linking SHP to the polymer.

In this study, we suggested a procedure for preparing conjugates from dextran (Dn) and an azlactone derivative of SHP and examined the antioxidative properties of these compounds.

Dextran is a convenient polymeric carrier for immobilization of active substances, including antioxidants, owing to the presence of hydroxy groups and capacity for biodegradation in a living body.

The procedure for preparing Dn–SHP conjugates was based on acylation of alcohols with azlactones [9]. As azlactone we chose 4-(4-hydroxy-3,5-di-*tert*-butylbenzylidene)-2-phenyl-4,5-dihydrooxazol-5-one (AzP):



The most convenient solvent for modification of Dn with water-insoluble compounds is dimethyl sulfoxide

1070-4272/05/7806-0940 © 2005 Pleiades Publishing, Inc.

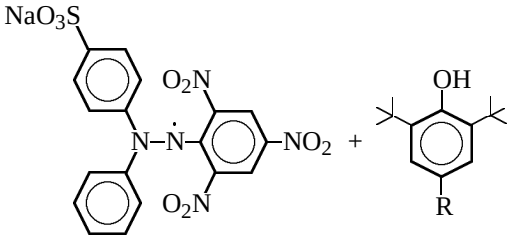
Table 1. Conditions of modification of dextran (MW 18000)

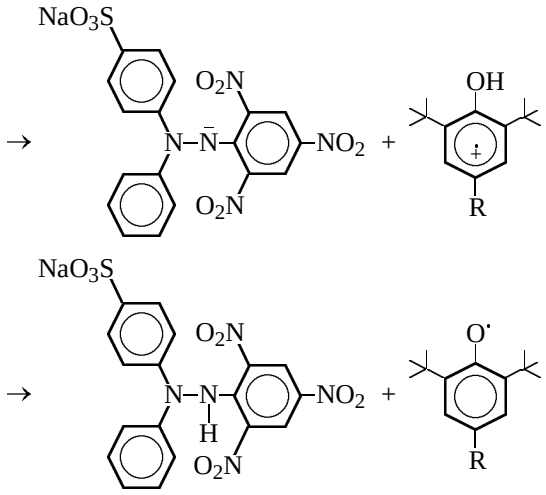
Molar ratio Dn : AzP : catalyst	Base	*T*, °C	τ, h	AzP content in conjugate	
				m, wt %	γ, mol %
2 : 1 : 0	–	20	24	0	0
2 : 1 : 0	–	40	72	0	0
2 : 1 : 0.5	Py	40	24	1.0	0.4
2 : 1 : 0.5	TEA	40	24	1.3	0.6
2 : 1 : 0.5	DMAP	40	24	5.0	2.3
2 : 1 : 0.5	DMAP	20	24	0	0
2 : 1 : 0.5	DMAP	50	24	11.0	5.3
2 : 1 : 0.5	DMAP	60	72	18.3	9.6

(DMSO) [10], and we used it to perform the reaction. As catalysts we chose tertiary amines: triethylamine (TEA), pyridine (Py), and *p*-dimethylaminopyridine (DMAP). Conjugates with different degree of substitution of the Dn glycoside units were prepared by varying the reactant ratio and the reaction temperature and time (Table 1). DMAP was found to be the best catalyst, and the optimal temperature was 60°C. The extent of modification of the glycoside units is virtually independent of the molecular weight (MW) of dextran (see figure). All the conjugates obtained are soluble in DMSO and in 1 : 1 (by volume) mixed solvents (water–dioxane, water–ethanol). The limiting degree of substitution of glycoside units in Dn, above which the conjugate becomes insoluble in water, is 6, 8, and 10 mol % at MW 200000, 40000, and 18000, respectively.

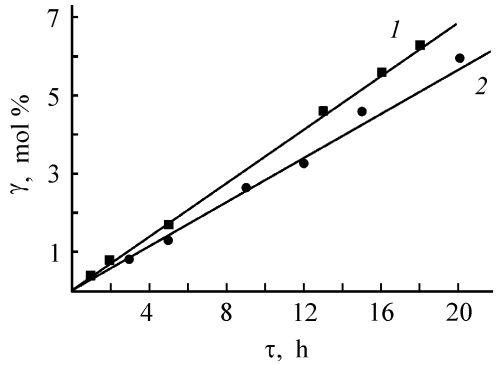
Thus, we found conditions in which conjugates differing in the content of SHP fragments and, accordingly, in the solubility in water can be prepared.

Sterically hindered phenols are highly reactive toward free oxygen-containing radicals, which determines their antiradical properties [2]. As shown in [11, 12], the reaction of SHPs and conjugates based on them with a water-soluble free radical, sodium salt of sulfonic acid derived from 2,2-diphenyl-1-picrylhydrazyl (DPPH–SO_3Na), can be a test for quantitative evaluation both antiradical and antioxidative properties of SHPs:





We found that the ARA in the reactions of our antioxidants with free radicals depends on the solvent polarity and, in the case of the conjugates, is also determined by the structure of the spacer between the polymer and SHP [11, 12]. As a solvent we chose aqueous dioxane (1 : 1 by volume) in which DPPH–SO_3Na,



Degree γ of substitution of glycoside units in dextran vs. reaction time τ (*T* = 60°C). Conjugates with MW (*1*) 40000 and (*2*) 200000.

Table 2. Rate constants of the reaction of DPPH–SO_3Na with conjugates and their low-molecular-weight models

Antioxidant*	k, l mol^{-1} s^{-1}	
	aqueous : dioxane (1 : 1 by volume)	water
Phenoxan	3.0 ± 0.2	35.7 ± 1.2
Dn–CP	3.5 ± 0.2	1100 ± 50
Model	1500 ± 100	–
Dn–AzP	7500 ± 500	Instantaneous reaction

*

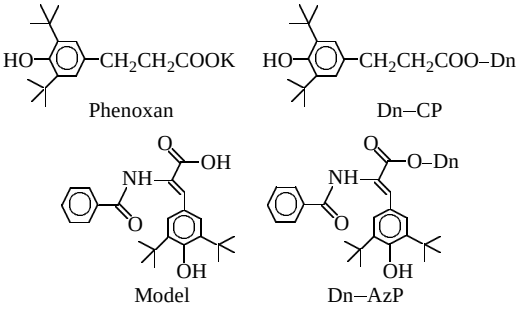


Table 3. Comparative characterization of the protective properties of low-molecular-weight antioxidants and Dn–AzP conjugate with respect to fibroblast culture in the presence of MMA

Antioxidant (AO)	$c_{AO} \times 10^4$, M	Enxyme activity, %, at indicated c_{MMA}, μg ml^{-1}	
		0.4	0.8
None	0	71	59
Phenoxan	4	100	71
α-Tocopherol	50	78	60
Conjugate (γ = 5.7 mol %, MW = 200 000)	4	100	100

the conjugates, and their low-molecular-weight analogs are soluble.

The rate constants obtained for the reaction with DPPH–SO_3Na indicate that the low-molecular-weight model (k = 1500 ± 100 l mol^{-1} s^{-1}) and, especially, the conjugates (k = 7500 ± 500 l mol^{-1} s^{-1}) exhibit high ARA. Under the same conditions, we determined the rate constans of the reaction of DPPH–SO_3Na with another conjugate, Dn–CP, containing an ester spacer (Table 2). Comparison of the constants obtained shows that just the spacer of a complex structure, with a system of conjugated bonds considerably enhances the ARA. On passing to a polar medium (water), the difference between the rate constants of the reactions of DPPH–SO_3Na with the conjugate containing an ester spacer and its low-molecular-weight analog dramatically increases. With our conjugates, we could not evaluate the ARA in water in the reaction with DPPH–SO_3Na, because this reaction occurred instantaneously when mixing the solutions.

We have shown previously that, in aqueous solutions of the conjugates, the SHP molecules covalently bound to dextran occur in the solvation shell of the polymer and react with a free radical within this shell [8]. Water forming the solvation shell of dextran exhibits a higher ionizing power [13], which, in our opinion, results in a stronger stabilization of the radical cation transition state in the conjugates, compared to the low-molecular-weight analogs. Apparently, this is the major factor responsible for the very high ARA of the conjugates.

The antioxidative activity of the conjugates was evaluated in simulating the toxic response of human cells in the presence of methyl methacrylate (MMA) toxicant [14] by the integral activity of mitochondrial respiratory enzymes. Since the activity of respiratory enzymes largely depends on the integrity of the internal mitochondrial membrane, the test results provide an indirect estimate of the extent of peroxide oxidation of lipids in cells.

Table 3 shows that MMA exerts a significant toxic effect on the total activity of the enzymes. α-Tocopherol, a well-known antioxidant, only slightly protects the enzymes from inactivation. In the presence of Phenoxan (synergistic water-soluble antioxidant), the enzymatic activity increases, and in the presence of the conjugate, it is fully preserved, which confirms the high antioxidative activity of the conjugates prepared and suggests their wider cytoprotective properties.

EXPERIMENTAL

We used dextran of linear structure (MW 18 000, 40 000, 200 000), purchased from Fluka. The sodium salt of sulfonic acid derived from 2,2-diphenyl-1-picrylhydrazyl was prepared as described in [15]. 4-(4-Hyroxy-3,5-di-*tert*-butylbenzylidene)-2-phenyl-4,5-dihydrooxazol-5-one was synthesized according to [16]. The conjugate with an ester spacer (Dn–CP) was prepared as described in [8]. Dioxane and DMSO were purified by standard procedures [17].

Dn–AzP conjugates were prepared in DMSO in the presence of a catalyst at 20, 40, 50, and 60°C. The mixture was precipitated into 2-propanol and then reprecipitated from aqueous DMSO into 2-propanol to remove low-molecular-weight impurities.

The amount of the added SHP fragments in the conjugate was determined with an SF-56 spectrophotometer (Leningrad Optical and Mechanical Association) in aqueous ethanol (1 : 1 by volume) at λ = 320 nm [18]. As a low-molecular-weight model of the conjugate, we used the related acid, β-(4-hydroxy-3,5-di-*tert*-butylphenyl)-2-benzoylaminoacrylic acid, prepared according to [16].

The ARA of the low-molecular-weight model and conjugates toward DPPH–SO_3Na was evaluated by comparing the rate constants of their reaction in aqueous dioxane (1 : 1 by volume) and in water at 20°C [19, 20]. The reaction was performed to 20% conversion of the radical at the initial antioxidant concentration of 2×10^{-5} M. The DPPH–SO_3Na concentration was determined spectrophotometrically at λ = 520 nm. The rate constants of the reactions of the conjugates and the model were calculated by the equation

$$k\tau = (y_0 - x_0)^{-1} \ln\left(\frac{x_0 y_\tau}{y_0 x_\tau}\right),$$

where k is the rate constant of the reaction of the antioxidant with the radical ($l\,mol^{-1}\,s^{-1}$); τ, reaction time (s); x_0, initial ($\tau = 0$) concentration of the antioxidant (M); y_0, initial ($\tau = 0$) concentration of the radical (M); x_τ, concentration of the antioxidant at time τ (M); and y_τ, concentration of the radical at time τ (M).

CONCLUSIONS

(1) Conjugates were prepared from 4-(4-hydroxy-3,5-di-*tert*-butylbenzylidene)-2-phenyl-4,5-dihydrooxazol-5-one and dextran of molecular weights 18000, 40000, and 200000.

(2) The conjugates show a high antioxidative and antiradical activity, compared to the known antioxidants, Phenoxan and α-tocopherol, and efficiently inhibit free-radical processes in model systems. The major role in the process is played by the spacer containing a conjugated bond chain.

ACKNOWLEDGMENTS

The authors are grateful to E.M. Eropkina (Vreden Institute of Traumatology and Orthopedics) for testing the conjugates in biological systems.

REFERENCES

1. Burlakova, E.B. and Khrapova, N.G., *Usp. Khim.*, 1985, vol. 54, no. 9, pp. 1540–1558.
2. Ershov, V.V., Nikiforov, G.A., and Volod'kin, A.A., *Prostranstvenno-zatrudnennye fenoly* (Sterically Hindered Phenols), Moscow: Khimiiya, 1972.
3. *Issledovanie sinteticheskikh i prirodnykh antioksidantov in vitro i in vivo: Sbornik nauchnykh statei* (In vitro and in vivo Studies of Synthetic and Natural Antioxidants), Burlakov, E.B., Kruglyakova, K.E., and Shishkina, L.N., Eds., Moscow: Nauka, 1992.
4. Emanuel', N.M., in *Materialy Vsesoyuznogo simpoziuma "Fenol'nye soedineniya i ikh biologicheskie funktsii"* (Proc. Int. Symp. "Phenolic Compounds and Their Biological Functions"), December 1966, Moscow: Nauka, 1968, pp. 274–280.
5. Nazarova, O.V., Domnina, N.S., Komarova, E.A., and Panarin, E.F., *Zh. Prikl. Khim.*, 1994, vol. 67, no. 5, pp. 843–847.
6. Karpova, S.V., Domnina, N.S., and Komarova, E.A., *Zh. Prikl. Khim.*, 1995, vol. 68, no. 3, pp. 494–498.
7. Domnina, N.S., Komarova, E.A., Aref'ev, D.V., *et al.*, *Vysokomol. Soedin., Ser. A*, 1997, vol. 39, no. 10, pp. 1573–1577.
8. Aref'ev, D.V., Domnina, N.S., Komarova, E.A., *et al.*, *Zh. Prikl. Khim.*, 1999, vol. 72, no. 4, pp. 670–673.
9. *Organic reactions*, Adams, R., Ed., New York: Wiley, 1947, vol. III.
10. Bamford, C.M., Middlton, J.P., and Al-Lame, K.G., *Polymer*, 1986, vol. 27, no. 12, pp. 1981–1985.
11. Gurvich, Ya.I., Arzamanova, I.G., and Zaikov, G.E., *Khim. Fiz.*, 1996, vol. 15, no. 1, pp. 54–72.
12. Burmistrov, S.O., Oparina, T.I., Prokopenko, V.M., and Arutyunyan, A.V., *Klin. Lab. Diagn.*, 1997, no. 11, pp. 14–17.
13. Sedlak, U. and Nordmeier, E., *Eur. Polym. J.*, 1996, vol. 32, pp. 1109–1112.
14. Kornilov, N.V., Eropkina, E.M., Eropkin, M.Yu., *et al.*, *Travmatol. Ortoped. Ross.*, 1999, no. 1, pp. 26–36.
15. Rozantsev, E.G. and Sholle, V.D., *Organicheskaya khimiya svobodnykh radikalov* (Organic Chemistry of Free Radicals), Moscow: Nauka, 1979.
16. Louis, A.C. and Willam, M.J., *J. Am. Chem. Soc.*, 1962, vol. 84, pp. 1629–1630.
17. Becker, H., Berger, W., Domschke, G., *et al.*, *Organikum. Organisch-chemisches Grundpraktikum*, Berlin: Wissenschaften, 1976.
18. Domnina, N.S. and Shagov, V.S., in *Rukovodstvo k prakticheskim rabotam po khimii polimerov* (Manual on Polymer Chemistry), Leningrad: Leningr. Gos. Univ., 1982, pp. 28–45.
19. Boguth, W. and Repges, R., *Int. Z. Vitaminforsch.*, 1969, vol. 39, no. 3, pp. 289–295.
20. Lebedev, A.V., Boguslavskaya, L.V., Levitskii, D.O., and Maksimov, V.A., *Biokhimiya*, 1988, vol. 53, no. 4, pp. 598–602.

Russian Journal of Applied Chemistry, Vol. 78, No. 6, 2005, pp. 944–949. Translated from Zhurnal Prikladnoi Khimii, Vol. 78, No. 6, 2005, pp. 966–971.
Original Russian Text Copyright © 2005 by Solodov, Varnavskaya, Khvatova, Fakhrutdinov, Lebedev, Diyarov.

ORGANIC SYNTHESIS AND INDUSTRIAL ORGANIC CHEMISTRY

Sorbitol-Based Demulsifying Agents and Their Surfactant Properties

V. A. Solodov, O. A. Varnavskaya, L. K. Khvatova, B. R. Fakhrutdinov, N. A. Lebedev, and I. N. Diyarov

Research Institute of Oilfield Chemistry (NIInefteprom khim), Joint-Stock Company, Kazan, Tatarstan, Russia

Kazan State Technological University, Kazan, Tatarstan, Russia

Received March 11, 2005

Abstract—Sorbitol-based block copolymers of ethylene and propylene oxides were synthesized and characterized as surfactants and demulsifiers.

The great diversity of oil production and treatment processes, as well as of the properties of produced oil, which vary not only on passing from one oil field to another, but also with time within the same oil field, make necessary a search for new high-performance demulsifiers.

An analysis of the available published data revealed that, at present time, the most efficient demulsifiers are nonionic surfactants, such as alkylene oxide block copolymers [1–3]. Nonionic surfactants are mostly synthesized from glycols, amines, synthetic fatty acids, and phenols.

Alkylene oxide block copolymers based on polyhydric alcohols have not been adequately explored as demulsifying surfactants [1–3].

Therefore, we prepared in this study sorbitol-based high-molecular-weight compounds and characterized their surfactant and demulsifying properties.

EXPERIMENTAL

In the syntheses, we used the conventional alkylene oxide addition route. First, we synthesized a prepolymer by adding 1 mol of propylene oxide (PO) per hydroxy group of the initial compound, and then PO and ethylene oxide (EO) were successively added.

Hydroxyalkylation was carried out at 120–160°C and 1.5–1.8 atm in the presence of a base catalyst.

As a result, we prepared a series of block copolymers with various hydrophobic to hydrophilic group ratios (Table 1).

Table 1. Characteristics of samples

Sample no.	Sample	OP : EO, wt %	MW	Cloud point, °C	Hydroxyl number, mg KOH g^{-1}		Mean demulsifying efficiency, %	
					experiment	theory	1*	2*
1	SPE80 : 20	80 : 20	11 313	–	32	29.7	57	47
2	SPE68 : 32	68 : 32	13 269	44	28	25.3	70	57
3	SPE66 : 34	66 : 34	13 665	55	28	24.6	70	57
4	SPE60 : 40	60 : 40	15 014	62	26	22.4	67	55
5	SPE50 : 50	50 : 50	17 980	70	23	18.7	63	43
6	SPE35 : 65	35 : 65	25 608	85	18	13.1	47	43

* Oil field: (1) Elabuga and (2) Kaliningrad.

1070-4272/05/7806-0944 © 2005 Pleiades Publishing, Inc.

The characteristic of the block copolymers that reflects the addition of ethylene oxide is the cloud point of their aqueous solutions.

When dissolved in water, nonionic substances form hydrates through hydrogen bonding between water molecules and ether oxygen atoms of the polyethylene glycol residue. With increasing temperature of the aqueous solution in which a nonionic substance is dissolved, these hydrogen bonds are broken, and the solution becomes turbid (the solute separates out as suspended droplets). After cooling, the solution becomes clear again. The cloud points of the samples obtained are listed in Table 1.

Table 1 shows that the cloud point increases with the number of the hydroxyethyl units, i.e., the number of hydrogen bonds between the EO units and water molecules.

Sample SPE80 : 20 is insoluble in water because of the high hydrophobicity, and, therefore, its cloud point has not been determined.

To determine the molecular weight, we measured the hydroxyl number by the procedure involving esterification of the hydroxy groups with acid chlorides or anhydrides. The theoretical and experimental hydroxyl numbers are also listed in Table 1.

As seen, the experimental hydroxyl numbers differ from the theoretical values, which can be attributed to formation of polyethylene glycols and also to the broad molecular-weight distribution in the resulting products. As the number of the hydroxyethyl groups added increases, the main reactions are accompanied by side reactions. On passing from step to step, both further hydroxyethylation of the polyethylene glycols present in the system and formation of new polyethylene glycols proceed. This makes more pronounced the difference between the experimental and theoretical data. However, this difference remains within the experimental error.

Among the significant characteristics of surfactants is their ability to reduce the surface tension at the interface between the solution and a gas or another liquid.

The surface tension of aqueous solution of nonionic surfactants at the interface with air, and the interfacial tension at the toluene/water interface, were measured by the ring detachment (Du Nouj) method using a LAUDA tensiometer. In this method, the force acting on an immersed body is measured electronically.

Figures 1a and 1b show the surface tension isotherms of aqueous solutions of the nonionic surfactants investigated at the air/water and toluene/water interfaces.

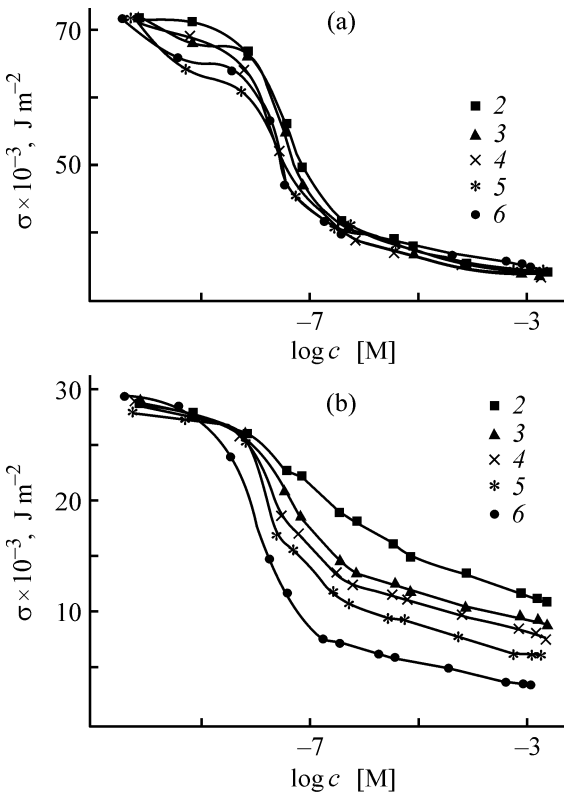


Fig. 1. Surface tension isotherms of the samples at (a) air/water and (b) toluene/water interfaces. (σ) Surface tension and (*c*) concentration. *The curve numbers* correspond to the sample numbers in Table 1.

The results show that the differences between the samples are more pronounced at the toluene/water interface, which is, most likely, due to a stronger influence exerted by toluene on the hydrophobic blocks, making less important the contribution of the steric factor.

We did obtain the isotherm for SPE80 : 20, since we failed to prepare its aqueous solution. However, we prepared a toluene solution of this sample and characterized its surfactant properties at the toluene/water interface.

There are two portions in the surface tension isotherms on passing from infinitesimal concentrations to the critical micelle concentrations (CMC). The samples demonstrate different variation ranges of the surface tension (Figs. 1a, 1b).

Petrov *et al.* [4] have shown that, in mixtures of ethers with different numbers of glycol residues, compounds with shorter polyglycol chains form micelles at a lower concentration, whereas longer-chain compounds have higher critical micelle concentrations [4]. Therefore, the surface tension isotherms level out

Table 2. Adsorption parameters of surfactants at the air/water interface

Sample no.	Sample	MW	CMC × 10^3, M	$\Gamma_m \times 10^6$, g-mol m^{-2}	$S_m \times 10^{17}$, m^2	W_a, kJ mol^{-1}	σ, J m^{-2}
1	SPE80 : 20	11313	–	–	–	–	–
2	SPE68 : 32	13269	0.301	0.435	0.382	49.940	34.0
3	SPE66 : 34	13665	0.320	0.333	0.499	52.786	33.9
4	SPE60 : 40	15014	0.400	0.193	0.859	53.999	34.3
5	SPE50 : 50	17980	0.560	0.187	0.890	53.492	34.5
6	SPE35 : 65	25608	1.120	0.203	0.818	48.548	35.1

Table 3. Adsorption parameters of surfactants at the toluene/water interface

Sample no.	Sample	MW	CMC × 10^3, M	$\Gamma_m \times 10^6$, g-mol m^{-2}	$S_m \times 10^{17}$, m^2	W_a, kJ mol^{-1}	σ, J m^{-2}
1	SPE80 : 20	11313	1.66	0.337	0.493	48.997	7.9
2	SPE68 : 32	13269	2.23	0.276	0.601	52.831	11.1
3	SPE66 : 34	13665	2.56	0.235	0.707	52.785	8.9
4	SPE60 : 40	15014	3.30	0.232	0.717	52.103	7.9
5	SPE50 : 50	17980	3.98	0.219	0.756	51.185	6.2
6	SPE35 : 65	25608	5.01	0.174	0.955	50.879	3.5

smoothly in our case, and the critical micelle concentration range is extended.

From the surface tension using the procedures described in [5–7] the following parameters: isotherms we estimated adsorption Γ; limiting adsorption Γ_m; work of adsorption, W_a; landing area of the molecule, S_m; and CMC.

The adsorption Γ (g-mol m^{-2}) was determined from the slope of the tangent to the initial portion of the isotherm. The slope $d\sigma/d\log c$ was then substituted in the Gibbs equation [6]:

$$\Gamma = -\frac{1}{2.3RT}\frac{d\sigma}{d\log c},$$

The limiting adsorption Γ_m (g-mol m^{-2}) was determined from the slope of the second portion of the isotherm, in which the limiting adsorption is attained. Again the slope $d\sigma/d\log c$ was substituted in the Gibbs equation [6]:

$$\Gamma_m = -\frac{1}{2.3RT}\frac{d\sigma}{d\log c}.$$

The landing area of the molecule, S_m (m^2), was estimated from the limiting adsorption [6]:

$$S_m = \frac{1}{\Gamma_m N}.$$

where N is the Avogadro number (6.02205 × 10^{23} mol^{-1}).

The work of adsorption, W_a (kJ mol^{-1}), is among the most significant characteristics of surfactants. It is the energy gain in transfer of a mole of the surfactant from the bulk to the interface [6]:

$$W_a = RT\ln\left(\frac{\Gamma}{\delta c}\right),$$

where δ is the adsorption layer thickness determined with account of the range of intermolecular forces at the interface and equal to 9×10^{-10} and 12×10^{-10} m for the air/water and toluene/water interfaces, respectively [5, 8].

The work of adsorption of the surfactants under study was estimated at the maximum dilution and extrapolated to zero concentration, i.e., for the case of ideal solution.

The CMC values were also determined from the surface tension isotherms (Tables 2, 3).

Using these data, we plotted vs. the degree of oxyethylation the limiting adsorption Γ_m; landing area of

the molecule, S_m; and work of adsorption, W_a. For the air/water and toluene/water interfaces, these plots are shown in Figs. 2, 3 and 4, 5, respectively. The resulting dependences are well consistent with the data from [5, 6, 9, 10].

As can be seen from Table 2, CMC grows, which is due to the increasing number of the oxyethyl chains in the samples (solubility increases, thus making higher the CMC).

The range of variation of the surface tension at the air/water interface with the experimental degree of oxyethylation is insignificant (Table 2), since the bulkier hydrophilic part of the molecule is retracted into the aqueous phase more strongly [5] and thereby adsorbed at the interface more weakely. We observed no decrease in the surface tension throughout the homologous series of the samples, and its insignificant increase is within the experimental error.

The dependence in Fig. 2 shows a gradual rise in the landing area of the molecule arranged in parallel to the interface. A further insignificant decrease can be attributed to stronger steric effects arising from twisting of the oxyethyl chains [9, 10]. At a low degree of oxyethylation, the hydrophilic chains are straightened in the aqueous phase, having the minimum landing area. With increasing number of the hydrophilic blocks, the oxyethyl units are twisted to form globular structures. In this case, a rise in the landing area is associated with an increase in the globule diameter. However, further growth of the oxyethyl part results in retraction of the globule into the aqueous phase, and the landing area of the molecule gradually decreases. The same factors are responsible for the changes in the limiting adsorption (Fig. 2).

The curve with a maximum, obtained for the work of adsorption (Fig. 3), may be interpreted in terms of self-association of the oxyethyl units with formation of globules [5, 10]. The resulting decreased hydration of the molecule makes lower the energy gain originating from the occurrence of the molecule in the aqueous phase, which leads to an increase in the contribution of the hydrophobic part and, accordingly, in the work of adsorption. With a further increase in the degree of oxyethylation, the solubility in water grows. The energy of globular oxyethyl chains prevails over the energy of the hydrophobic part. Evidently, this is responsible for the observed decrease in the work of adsorption.

In the case of the toluene/water interface, the indicated dependences are somewhat different.

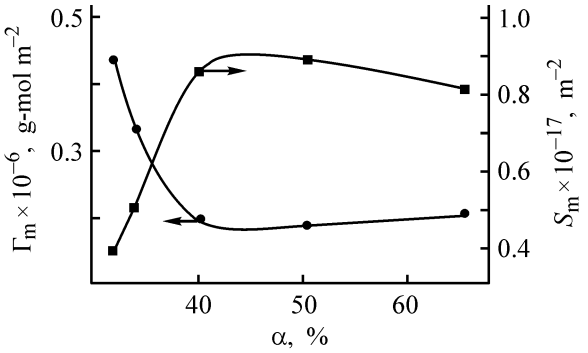


Fig. 2. Limiting adsorption Γ_m and landing area of the molecule, S_m, at the air/water interface vs. the degree of oxyethylation, α. (α) Percentage of EO in Table 1; the same for Figs. 3–5.

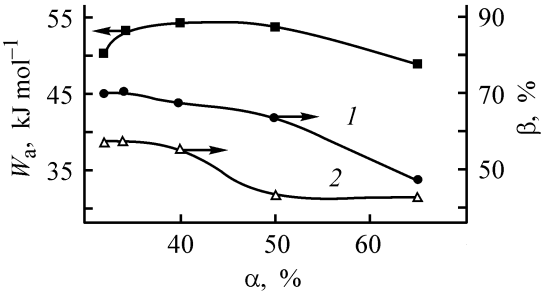


Fig. 3. Work of adsorption, W_a, and demulsifying efficiency β vs. the degree of oxyethylation, α (air/water interface). Oil field: (*1*) Elabuga and (*2*) Kaliningrad; the same for Fig. 5.

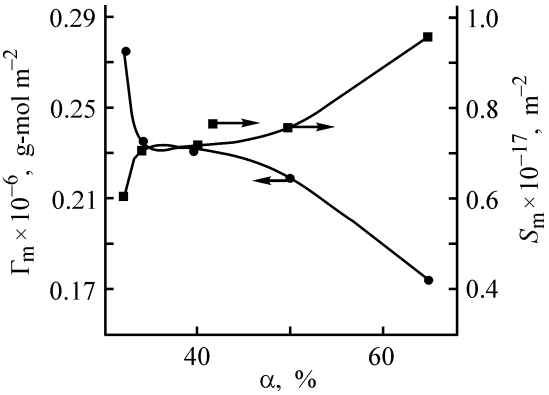


Fig. 4. Limiting adsorption Γ_m and landing area of the molecule, S_m, vs. the degree of oxyethylation α (toluene/water interface).

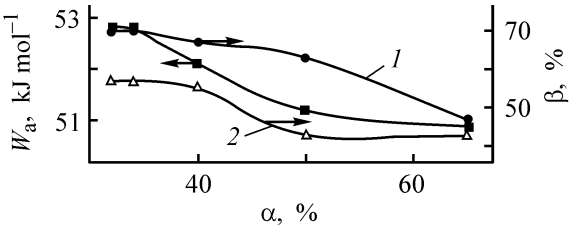


Fig. 5. Work of adsorption, W_a, and demulsifying efficiency β vs. the degree of oxyethylation, α (toluene/water interface).

Table 3 shows that, with increasing hydrophilicity of the molecule, the surface tension decreases throughout the homologous series, and CMC, by contrast, grows with the number of the oxyethyl groups added, which is associated with the enhanced hydrophilicity. The decrease in the surface tension at the toluene/water interface is more clearly pronounced, as a result of the effect of the organic solvent on both hydrophobic and hydrophilic blocks.

Figure 4 shows that the landing area of the molecule steadily increases with the amount of ethylene oxide added. This phenomenon is probably due to a different arrangement of the blocks in the molecule as compared to the case of the air/water interface. Here the hydrophobic parts of the molecules are regularly arranged at the interface, which is caused by intermolecular interaction of the surfactant molecules with water and toluene. The retraction into toluene of the hydrophilic part, in addition to the hydrophobic part, also straightens the molecular chains (in the case of the air/water interface, the chains take the shape of globules, which hinders their optimal arrangement at the interface).

The observed insignificant decrease in the work of adsorption (Fig. 5) is caused by the effect of the contacting phases on the hydrophilic and hydrophobic parts [6]. As the oxyethyl chain grows, occurrence of the molecule in the aqueous phase becomes more energetically favorable, and the fraction of the oxypropyl chains immersed in toluene decreases with respect to the total length of the molecule. As a result, the work done by the molecule on passing from the bulk to the interface decreases. The interaction of functional groups of the surfactant with the solvent hinders this transfer [11].

It was interesting to find a correlation between the demulsifying efficiency and the work of adsorption as the most relevant characteristic of the surface activity of a substance.

The demulsifying efficiency was studied using the conventional "bottle sampling" method with artificial emulsions. The emulsions (30% watering) were prepared from anhydrous coal-bearing oils from the Novo-Serebryanskoe oil field (Kaliningradneft' Joint-Stock Company) and from the Novo-Suksinskoe oil field (Tatneft' Joint-Stock Company, NGDU Prikamneft'), using a model stratal water.

The data obtained in testing the samples for the demulsifying efficiency are listed in Table 1. As seen, all the block copolymers investigated break the water/oil emulsions.

Comparison of the dependences of the demulsifying efficiency and work of adsorption on the degree of oxyethylation of the samples studied (Figs. 3, 5) shows that the most efficient are the samples with an oxyethyl group content of 32–40%. A decrease in the demulsifying efficiency correlates with the decreasing work of adsorption in the case of the toluene/water interface (Fig. 5).

In the case of the air/water interface (Fig. 3), no clear correlation is observed between the work of adsorption and the demulsifying efficiency, which is due to the lacking effect of the hydrophobic phase (toluene) on the nonionic surfactant molecules.

CONCLUSIONS

(1) Sorbitol-based block copolymers of ethylene and propylene oxides with various hydrophobic to hydrophilic part ratios demonstrate a surface activity and demulsifying action.

(2) The critical micelle concentration, surface tension, limiting adsorption, landing area of the molecule, work of adsorption, and demulsifying efficiency were determined as functions of the degree of oxyethylation of the samples. The highest demulsifying efficiency was shown by the compounds with a content of oxyethyl group equal to 32–40 wt %.

REFERENCES

1. Levchenko, D.N., Bergshtein, N.V., Khudyakova, A.D., and Nikolaeva, N.M., *Emul'sii nefti s vodoi i metody ikh razrusheniya* (Oil/Water Emulsions and Methods for Their Breaking), Moscow: Khimiya, 1981.
2. Tronov, V.P., *Promyslovaya podgotovka nefti* (Oil Treating), Kazan: Fen, 2000.
3. Volkov, Yu.M., Ranneva, E.A., Abdullina, L.L., and Bashukhina, I.N., in *Novoe v tekhnologii i primenenii PAV: Sbornik nauchnykh trudov* (Advances in Technology and Application of Surfactants: Collection of Scientific Works), Moscow: TsNIITEneftekhim, 1982, pp. 26–34.
4. Petrov, A.A., Pozdnyshev, G.N., and Smirnov, Yu.S., in *Sbor, transport, podgotovka nefti i avtomatizatsiya neftepromyslov: Sbornik nauchnykh trudov* (Oil Gathering, Transportation, and Treating, and Oil-Field Automation), Moscow: Gostoptekhizdat, 1963, issue 6, pp. 12–21.
5. Abramzon, A.A., *Poverkhnostno-aktivnye veshchestva: svoistva i primenenie* (Surfactants: Properties and Applications), Leningrad: Khimiya, 1981.

6. Abramzon, A.A., Zaichenko, L.P., Faingol'd, S.I., *et al., Poverkhnostno-aktivnye veshchestva. Sintez, analiz, svoistva, primenenie* (Surfactants: Synthesis, Analysis, Properties, and Applications), Leningrad: Khimiya, 1988.
7. Abramzon, A.A., Zaichenko, L.P., and Petukhova, L.A., *Metodicheskie ukazaniya k raschetnym zanyatiyam po svoistvam i primeneniyu PAV* (Guideline to Theoretical Studies in Properties and Applications of Surfactants), Leningrad: Khimiya, 1980.
8. Abramzon, A.A. and Pankratov, V.A., *Zh. Prikl. Khim.*, 1984, vol. 57, no. 2, pp. 293–297.
9. Pozdnyshev, G.N., *Stabilizatsiya i razrushenie neftyanykh emulsii* (Oil Emulsion Stabilization and Breaking), Moscow: Nedra, 1982.
10. Schönfeld, N., *Grenzflachenaktive Äthylenoxid-Addukte*, Stuttgart: Wissenschaftliche, 1976.
11. Abramzon, A.A., *Poverkhnostno-aktivnye veshchestva i moyushchie sredstva: Spravochnik* (Surfactants and Detergents: A Handbook), Moscow: Giperoks, 1993.

Russian Journal of Applied Chemistry, Vol. 78, No. 6, 2005, pp. 950–954. Translated from Zhurnal Prikladnoi Khimii, Vol. 78, No. 6, 2005, pp. 972–976.
Original Russian Text Copyright © 2005 by Glazko, Gur'yanova, Levanova, Kozlova, Neiman.

ORGANIC SYNTHESIS AND INDUSTRIAL ORGANIC CHEMISTRY

Synthesis of Esters of Dioxane Alcohols and Their Performance as Plasticizers for Polyvinyl Chloride Compounds

I. L. Glazko, O. P. Gur'yanova, S. V. Levanova, S. A. Kozlova, and N. S. Neiman

Samara State Technical University, Samara, Russia
Polimerstroimaterialy Combine, Joint-Stock Company, Samara, Russia

Received December 7, 2004; in final form, March 2005

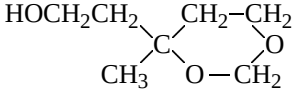
Abstract—A procedure was developed for preparing a plasticizer for polyvinyl chloride compounds from the fraction of dioxane alcohols. The main physicochemical properties of the new plasticizer were determined. Items prepared from formulations containing the new plasticizer were fabricated and tested in laboratory.

Since the discovery of the dioxane method for preparing isoprene, the utilization or reprocessing of dioxane alcohols has been topical problem.

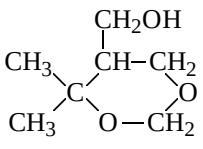
The world's annual production of isoprene reaches now 1000–1100 thousand tons, of which 250 thousand tons (23–25% of the total amount) is produced by the dioxane method. In Russia, the annual production of isoprene is 700–800 thousand tons, of which 190 thousand tons (24–27% of the total amount) is produced by the dioxane method. In this method, the amount of dioxane alcohols (by-products) reaches 100–110 kg per ton of isoprene. Thus, formation of large amounts of dioxane alcohols is inevitable [1].

The fraction of dioxane alcohols from the production of isoprene rubber is a colorless or light yellow mobile liquid containing 50–70 wt % dioxane alcohols; the boiling onset temperature is no less than 225°C, and the flash point, no less than 120°C. The fraction belongs to hazard class 3, recommended value of MPC (with respect to dioxane alcohol) 10 mg m^{-3}, LD_{50} for mice 2700 mg kg^{-1} [2].

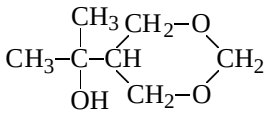
The fraction of dioxane alcohols contains three isomeric alcohols:



4-Methyl-4-hydroxyethyl-1,3-dioxane (**I**)



4,4-Dimethyl-5-hydroxymethyl-1,3-dioxane (**II**)



5-(1-Methyl-1-hydroxyethyl)-1,3-dioxane (**III**)

The major component (60–70% of the sum of the isomers) is 4-methyl-4-(2-hydroxyethyl)-1,3-dioxane **I**.

A number of possible applications of dioxane alcohols have been outlined in the literature: as an efficient solvent for nitrocellulose, nitrocellulose lacquers, rosin, lac, for bakelite, epoxy, and polyvinyl chloride resins, and for insulating lacquer; as a component of epoxy hardener [3–8]. One of promising ways of processing of the fraction of dioxane alcohols is preparation of plasticizers for polyvinyl chloride resins and rubbers [9–13].

However, proper utilization of this large-tonnage waste remains a matter of current interest.

We believe that the presence of hydroxy and acetal groups in molecules of dioxane alcohols, their low toxicity, absence of odor and color, and high boiling and flash points make these compounds interesting both as objects for theoretical studies (reactivity) and as potential raw materials for chemical industry.

Our goal was to examine the possibility of preparing esters from dioxane alcohols and carboxylic acids, as potential plasticizers.

1070-4272/05/7806-0950 © 2005 Pleiades Publishing, Inc.

EXPERIMENTAL

Esters of dioxane alcohols were prepared by two procedures.

(1) Carboxylic acids (acetic, adipic, phthalic, butyric, oxalic) were esterified with dioxane alcohols in the presence of acid catalysts (sulfuric, phosphoric, benzenesulfonic acids; KU-23 cation exchanger). The reactions were performed at 140–165°C for 4–6 h in an excess of dioxane alcohols (molar ratio 4 : 1). The acid conversion did not exceed 30%; the reaction mixture was dark.

(2) It was suggested to prepare esters of dioxane alcohols by ester interchange catalyzed by both acid and base catalysts, and also by transition metal salts [14].

The latter procedure involved two steps: esterification of adipic acid with butanol to obtain dibutyl adipate and ester interchange of dibutyl adipate with dioxane alcohols.

Esterification of adipic acid was performed with an excess butanol; concentrated sulfuric acid was used as a catalyst. The temperature was maintained within 90–117°C, which enabled distillation of the azeotrope. The concentration of adipic acid in the reaction mixture was monitored titrimetrically [15].

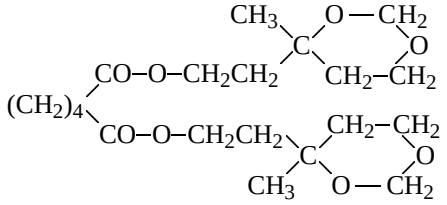
The reaction was stopped at a 98% conversion of adipic acid. Then the mixture was cooled and washed to neutral reaction. Water and excess alcohol were removed from the resulting crude ester by distillation at atmospheric pressure. The ester was distilled at 15 mm Hg; the fraction boiling at 210–213°C was collected. The dibutyl adipate obtained was analyzed for the acid number by the standard procedure [18]. The acid number of dibutyl adipate should not exceed 0.05 (mg KOH) g^{-1}. A higher acid number results in darkening of the reaction mixture in the step of ester interchange of dibutyl adipate with dioxane alcohols.

The ester interchange of dibutyl adipate was performed in an excess of dioxane alcohols in the temperature range 215–250°C, so as to ensure continuous distillation of the released butanol at a vapor temperature of 117–120°C. The released butanol can be returned to the step of esterification of adipic acid. As catalyst we used zinc stearate.

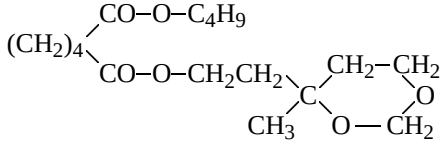
The completeness of the ester interchange was judged from the amount of the butanol released. The reaction was stopped at a 85–90% conversion of dibutyl adipate.

From the reaction mixture, we distilled off low-boiling components; the remaining target product (light yellow mass) was a mixture of esters of adipic acid and dioxane alcohols, with an admixture of dibutyl adipate and zinc stearate. The product yield was 97% of the theoretical value; the content of the mixture of the esters was no less than 98%.

The qualitative analysis of the product was performed by GC/MS on a Finnigan Trace DSQ device in the chemical ionization (isobutane) mode (in the electron impact mode, the molecular ions were not recorded). For the major components, we obtained *m*/*z* 331 and 403 ($[M + H]^+$), which corresponds to the molar weights of the following compounds:



M = 402 g mol^{-1}



M = 330 g mol^{-1}

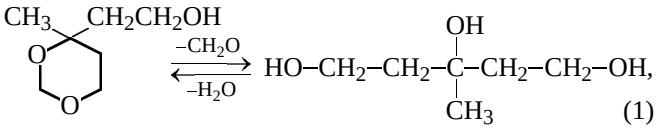
Thus, ester interchange of dibutyl adipate with dioxane alcohols yields a mixture of isomeric mono- and disubstituted esters.

To evaluate the plasticizing power of the product, we prepared samples of the middle PVC layer of calender-rolled linoleum. The samples had the following composition (%): PVC 51, chalk 21, dioctyl phthalate 13, test plasticizer 13, and calcium stearate 2.

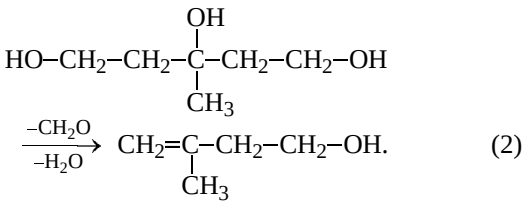
As the lower layer we used cotton underwarp (Netkol). A PVC film with a printed pattern is applied onto the upper layer; all the three layers are doubled on a Bersdorf continuous press.

The plastic compound was prepared from a suspension PVC, special stabilizers and pigments, and the test plasticizer (35–40 wt % of the total).

Our experiments showed that esters of dioxane alcohols could not be prepared in reasonable yields and with acceptable quality by esterification with carboxylic acid. Even weak acid catalysts, such as cation exchangers, caused dehydration of dioxane alcohols with ring opening and formation of triols and unsaturated compounds:



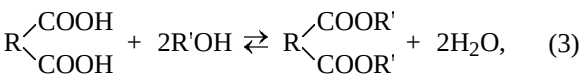
(1)



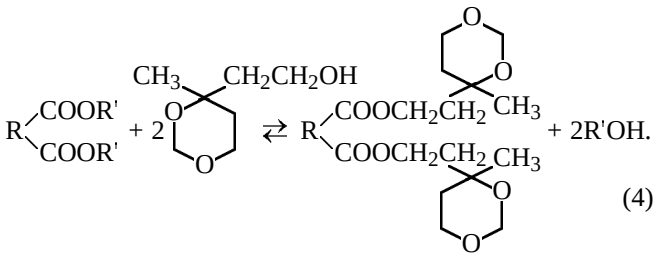
(2)

Analysis of the reaction mixture shows that dehydration occurs much faster than esterification. Water released in reaction (2) shifts the equilibrium of the target reaction (4), thereby decreasing the yield of the esters. The unsaturated compounds formed in the process undergo condensation, yielding tarry products which impair the quality of the esters.

The two-step procedure we suggested involves the following reactions:



(3)



(4)

In the first step (3), adipic acid is esterified with a primary aliphatic alcohol. The second step (4) is ester interchange of the adipic acid ester with dioxane alcohol. To esterify adipic acid, we used aliphatic alcohols that form heteroazeotropes, so as to continuously remove the released water and thus to reach a high conversion of adipic acid (98–99%).

For the product obtained, we determined the main physicochemical parameters [GOST (State Standard) 8728–77] and compared them with those of commercial analogs (Table 1).

Table 1 shows that the plasticizer prepared from dioxane alcohols is similar in physicochemical properties to high-quality commercial plasticizers, such as dioctyl adipate and dioctyl phthalate, and surpasses EDOS plasticizer, widely used today.

To confirm the plasticizing properties of the product we developed, we tested it in linoleum specimens (Table 2). The analysis showed that polyvinyl chloride (PVC-E, PVC-EP) swells in the suggested plasticizer to form fluid easy-to-apply pastes, thickening with time. We prepared specimens of linoleum and PVC RE-0.4 film (PVC-S : PVC-E = 5 : 1) and benzine-resistant plastic compound PB-BK, using the plasticizer developed.

As can be seen, replacement of EDOS plasticizer in the linoleum formulation with the new plasticizer enhances the strength of binding of the face layer and underwarp with the PVC layer. The ready linoleum exhibits higher tensile strength and higher elasticity.

With dioctyl phthalate replaced in the formulation of PB-BK benzine-resistant plastic compound with the new plasticizer, the compounding is quite feasible and the hardness and strength are enhanced relative to the commercial specimens; the benzine resistance remains high (see Table 3).

Table 1. Comparison of the physicochemical properties of the polyester plasticizer prepared in this study with those of commercially used plasticizers

Parameter	Dioctyl adipate	Dioctyl phthalate	EDOS, grade I	Plasticizer prepared
Flash point in open crucible, °C, no less than	190	205	150	216
Weight fraction of volatiles, wt %	0.07	0.1	0.25	0.2
Acid number, (mg KOH) g^{-1}	0.01	0.05	0.1	0.1–0.3
Density at 20°C, g cm^{-3}	0.92	0.98	1.08	1.1
Saponification number, (mg KOH) g^{-1}	298–307	284–290	–	350–364
Solidification point, °C	–	–55	–35	–50
Compatibility with PVC	Full	Full	Partial	Full

Table 2. Comparison of linoleum specimens prepared using the plasticizer developed in this study and EDOS

Parameter	Prescribed value	Specimen no. 1 (plasticizer developed)	Specimen no. 2 (EDOS)	Testing procedure
Strength of binding between face layer and PVC layer, kgf cm^{-1}, no less than	0.6	Longitudinal, 3.09 Transverse, 2.99	Longitudinal, 0.8 Transverse, 0.9	TU 5771-028-00282323–01 (PVC linoleum)
Strength of binding between the PVC layer and underwarp, kgf cm^{-1}, no less than	0.2	Longitudinal, 2.4 Transverse, 1.92	Longitudinal, 1.0 Transverse, 1.1	TU 5771-028-00282323–01 (PVC linoleum)
Absolute residual deformation, mm, no more than	1.0	0.55 0.35	0.47	TU 5771-028-00282323–01 (PVC linoleum)
Layer density, g cm^{-3}	–	1.25	1.39	GOST (State Standard) 11529
Breaking tensile stress, N cm^{-1}, no less than	215	416	–	TU 2245-016-00282323–98 (film material)
longitudinal transverse	196	458	–	
Changes in linear dimensions, %, no more than	1.0	Longitudinal, 0.4 Transverse, 0.3	Longitudinal, 0.11 Transverse, 0.08	TU 5771-028-00282323–01 (PVC linoleum)
Layer thickness, mm, no less than	1.3	1.69	1.96	TU 5771-028-00282323–01 (PVC linoleum)

* (TU) Technical specifications; the same for Table 3.

Table 3. Comparison of the properties of PB-BK plastic compound prepared with the plasticizer developed and with dioctyl phthalate

Parameter	Prescribed value	With plasticizer developed	With dioctyl phthalate	Testing procedure
Shore hardness, units	80 ± 0.5	80	79	TU 2246-022-00282323–01 (plastic compound for PVC tubes)
Benzine resistance, %, no more than	1.6	0.1	–	TU 2246-022-00282323–01 (plastic compound for PVC tubes)
Tensile strength, MPa, no less than	18.6	19.3	18.9	TU 2246-022-00282323–01 (plastic compound for PVC tubes)

CONCLUSIONS

(1) Previously unknown esters of adipic acid and dioxane alcohols were prepared.

(2) A catalyst for ester interchange of dibutyl adipate with the dioxane alcohol fraction was suggested, and the main process parameters were determined.

(3) The physicochemical properties of the mixture of dioxane alcohol adipates are comparable with those of commercial PVC plasticizers. The new plasticizer can be used for fabricating items with enhanced strength, elasticity, and benzine resistance.

REFERENCES

1. Sazykin, V.V., Abstracts of Papers, *Mezhdunarodnaya konferentsiya po kauchuku i rezine* (Int. Rubber Conf.), Moscow, June 1–4, 2004, pp. 157–158.
2. Ogorodnikov, S.K. and Idlis, G.S., *Proizvodstvo izoprena* (Production of Isoprene), Moscow: TsNIITE-Neftekhim, 1973.
3. Gur'yanova, O.P., Glazko, I.L., Levanova, S.V., *et al.*, *Ekol. Prom–st. Ross.*, 2004, June, pp. 28–30.
4. RF Patent 2 175 336.
5. RF Patent 2 172 767.
6. RF Patent 2 065 465.

7. RF Patent 2 121 487.
8. Sokolov, A.B., Glazko, I.L., Levanova, S.V., *et al.*, in *IX Mezhdunarodnaya konferentsiya "Okruzhayushchaya sreda dlya nas i budushchikh pokolenii"* (IX Int. Conf. "Environment for Us and Future Generations"), Samara, September 5–12, 2004, pp. 78–81.
9. RF Patent Appl. no. 2004 121 632/04 (023 235).
10. RF Patent 2 173 325.
11. RF Patent 2 199 617.
12. RF Patent 2 199 558.
13. RF Patent 2 100 356.
14. Gur'yanova, O.P., Glazko, I.L., Levanova, S.V., *et al.*, in *IX Mezhdunarodnaya konferentsiya "Okruzhayushchaya sreda dlya nas i budushchikh pokolenii"* (IX Int. Conf. "Environment for Us and Future Generations"), Samara, September 5–12, 2004, pp. 45–47.
15. RF Patent Appl. no. 2004 115 876.
16. Becker, H., Berge, W., Domschke, G. *et al.*, *Organicum. Organisch-chemisches Grundpractikum*, Berlin: Wissenschaften, 1976.
17. Dekhterman, A.Sh., *Laborant neftepererabatyvayushchego zavoda* (Laboratory Worker of Oil Refinery), Moscow: Khimiya, 1989.
18. Odabashyan, G.V., *Laboratornyi praktikum po tekhnologii osnovnogo organicheskogo sinteza* (Laboratory Manual on the Technology of Basic Organic Synthesis), Moscow: Khimiya, 1982.

Russian Journal of Applied Chemistry, Vol. 78, No. 6, 2005, pp. 955–961. Translated from Zhurnal Prikladnoi Khimii, Vol. 78, No. 6, 2005, pp. 977–983.
Original Russian Text Copyright © 2005 by Zhorin, Zelenetskii, Kiselev, Marevtsev, Shienok.

ORGANIC SYNTHESIS AND INDUSTRIAL ORGANIC CHEMISTRY

Coloration of Spirooxazine in Various Organic Matrices under Plastic Flow at High Pressure

V. A. Zhorin, A. N. Zelenetskii, M. P. Kiselev, V. S. Marevtsev, and A. I. Shienok

Semenov Institute of Chemical Physics, Russian Academy of Sciences, Moscow, Russia

Enikolopov Institute of Synthetic Polymer Materials, Russian Academy of Sciences, Moscow, Russia

Institute of Physical Chemistry, Russian Academy of Sciences, Moscow, Russia

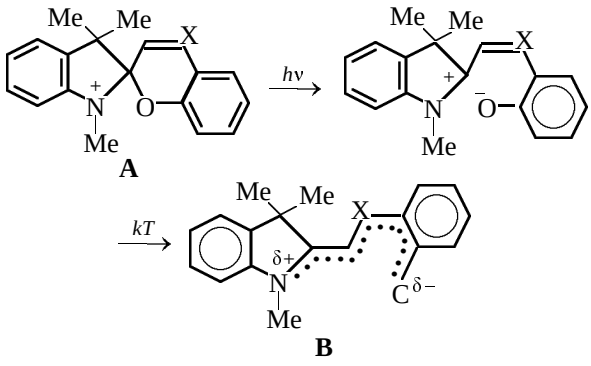
Received February 9, 2005

Abstract—The behavior of 1,3,3-trimethylspiro[indoline-2,3'-2*H*-naphtho[2,1-*b*][1,4]oxazine under plastic deformation was studied on high-pressure Bridgman anvil-type apparatus at 0.5–4 GPa and room temperature.

High pressures strongly modify various solids, e.g., cause an insulator–conductor transition, unusual chemical processes, changes in phase diagrams, etc. Substances subjected to high pressures are often exposed to shear stresses responsible for plastic deformations substantially affecting their behavior. A combined effect of high pressures and shear deformations on substances is strongly manifested in the case of high-pressure Bridgman anvil-type apparatus. In particular, various chemical reactions were revealed in the absence of initiators and catalysts for many classes of organic compounds. This suggests an electronic excitation of substances under such impacts. The rate of chemical processes under plastic deformations at high pressures is very weakly dependent on temperature, which supports the athermal mechanism of excitation of chemical transformations.

In the context of studying the excitation mechanisms of the electronic subsystem of solids under mechanical impacts, of much interest are organic reactions that can be photochemically initiated under ordinary conditions. For such systems, the positions of the ground and excited levels of the reacting molecules, the transition energies, and transformation pathways of the excited states are well understood. We have applied such an approach to a study of the behavior of linear annelated aromatic compounds [1]. It was shown that, under plastic deformation at high pressures, only 20% of the energy required for a chemical reaction to occur in the substances under study is due to high pressures, and the remainder comes from plastic deformation. In [2], we analyzed the baric dependences of a purely mechanical characteristic of solids (flow stress) for a wide variety of organic compounds and found that such dependences can be correlated with the processes occurring in the electronic subsystem of organic substances.

Another class of organic compounds whose photochemical transformations in solutions and polymer films are well understood are photochromes and, in particular, spiropyrans and spirooxazines [3–6]. Under photoirradiation in solution, they acquire a predominantly dark blue color (λ_{max} ~600 nm and over) owing to a transition of the molecule from a colorless initial state **A** with opening of the spiro bond into a colored merocyanine form **B**:



A **B**

where X = CH, N.

Under ordinary conditions, the equilibrium between the colored and colorless forms depends on the sol-

vent: the greater the solvent polarity, the stronger the shift of the equilibrium toward the colored form. Acid medium shifts the color of the spiro compound to the red spectral range, which has been attributed to formation of the protonated form [7].

The appearance of the red form of a spiro compound in an acid medium without UV irradiation has also been revealed by Kol'tsova *et al.* [8] who noted that this form is not decolorized, which was attributed to formation of a salt structure. Kozlovskaya *et al*. [9] studied transformations of selected spironaphthooxazines in various solvents in the presence of $LiClO_4$ when exposed to electric field with a strength of 5–100 V cm^{-1}. In this case, solutions turned red without UV irradiation, under electric field exposure only. It was suggested that the appearance of the red form is due to ionization of the molecules.

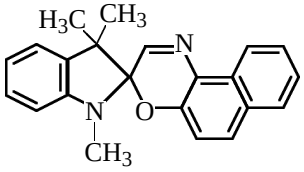
Certain spiro compounds exhibit photochromic properties in the solid phase as well. For example, Sychev *et al*. [10] showed that amorphous spirophenanthrooxazine films prepared by vacuum sputtering get colored under UV radiation and decolorize with time, which was attributed to crystallization.

Thus, the available experimental data suggest that transitions of spirooxazines to a colored form are extremely sensitive to the charge state of their surrounding molecules. This allows the changes induced in various solids by high pressure and shear deformation to be examined using molecules of photochromic spiro compounds as specific markers responding to changes in the environment.

Maksimychev *et al*. [11] and Zhorin *et al*. [12] found that, in the case of organic compounds having no conjugated bond system, compression to 4 GPa increases the average dielectric constant by a factor of 2–3.5. Under plastic deformation, this parameter can increase by 30% from the value achieved under pressure only. Also, under compression of organic compounds, a potential difference of several tens of volts appeared between the upper and lower surfaces of the samples placed between the metallic anvils. Thus, under plastic deformations at high pressures, organic molecules get polarized, which increases their reactivity. Also, Enikolopyan *et al*. [13–15] showed that high pressures intensify injection of electrons from the anvil metal into insulators being treated under pressure. Thus, the electrophysical state of organic substances subjected to plastic deformation at high pressures substantially differs from that under normal conditions.

EXPERIMENTAL

We examined 1',3'3'-trimethylspiro[indoline-2,2'-2*H*-naphtho[2,1-*b*][1,4]oxazine, mp 124–125°C, R_f = 0.93 (benzene : ether, 7 : 3, Silufol); λ_{max} 300 and 320 nm (dioxane, $\varepsilon = 9.75 \times 10^{-5}$ l mol^{-1} cm^{-1}); 1H NMR spectra ($C_6D_5CD_3$), δ, ppm; 1.08 and 1.2 (CMe_2), 2.45 (NMe), 7.58 (H^3). 8.93 (H^5), 7.43 (H^6), 7.20 (H^7), 7.48 (H^8), 7.29 (H^9), 6.73 (H^{10}), 6.90 ($H^{4'}$), 6.82 ($H^{5'}$). 7.00 ($H^{6'}$), and 6.30 ($H^{7'}$):



SPO

As matrices we used various chemically pure low-molecular-weight crystalline organic compounds (with physicochemical constants agreeing with reference data) and various commercial polymers, which were used without further purification.

Mixtures of 5 and 10% SPO with the substances chosen were prepared by mixing the initial powdered components in a mortar, which was followed by combined action of pressure in the range 0.5–4 GPa and shear deformations (the anvil rotation angles were varied from 10° to 400°). Pressures from 0.5 to 2 GPa were created on KhVG hardened steel anvils, and higher pressures, on VK6 hard alloy anvils. The changes in the color of the samples after plastic deformation at the chosen pressure were examined visually. Calorimetric studies were carried out on an MAS DSM-2M microcalorimeter at a heating rate of 8 deg min^{-1}; the sample weight was 20 mg. The deformation currents were measured with an M-95 indicator microammeter.

The results of the studies of the coloration of SPO under plastic deformation at 0.5–4 GPa suggest that, after treatment under pressure, the samples acquire a dark blue color whose intensity grows with increasing degree of deformation (anvil rotation angle). In this case, the most intensely colored samples lost their color at room temperature within ca. 1 h. All samples are completely dissolved in acetone, rapidly getting colorless in it, and such solutions, when exposed to UV radiation, acquire a dark blue color. Our data suggest that, during deformation, the initial SPO is not irreversibly changed, and all the arising colored states of the samples are metastable. The fact that

the times of decolorization of the dark blue samples treated within different pressure ranges are close suggests a similarity of the mechanisms and conditions of the relaxation processes.

An X-ray diffraction analysis showed that, after deformation at 1 and 4 GPa, the SPO samples are X-ray-amorphous; the time from termination of the treatment under pressure till the beginning of an X-ray diffraction analysis is sufficient for the samples to get completely colorless. Thus, the appearance of the dark blue form (DBF) in the SPO samples due to plastic deformation at different pressures is most likely not associated with degradation of the crystalline structure.

The DSC data in Fig. 1 suggest that, in the initial SPO, there are two crystalline phases with different melting points. The peak with mp 116°C is characterized by an enthalpy of 60 J g^{-1}, and that with mp 130°C, of 10 J g^{-1}. After treatment at 1 GPa, the low-temperature peak shifts to lower temperatures by 8°C, and its enthalpy decreases to 20 J g^{-1}; the position of the high-temperature peak on the temperature scale remains unchanged, and its enthalpy increases to 50 J g^{-1}. The thermograms of the samples treated at 4 GPa are identical to those of the samples treated at 1 GPa. It should be noted that, by the time of beginning of the calorimetric experiments, the samples treated under pressure were virtually colorless. Thus, the occurrence of endothermic peaks on thermograms of the colorless X-ray-amorphous samples of SPO suggests that, in the course of heating in the calorimeter, the substance undergoes recrystallization, yielding a structure different from that of the initial substance.

The effect of cathodochromism, consisting in coloration of various inorganic compounds under electron beam exposure, has been known since 1895 [16]. It could be assumed that a possible mechanism of coloration of SPO subjected to plastic deformation under pressure involves interaction of electrons injected from the anvil metal with SPO molecules. Measurements of thermostimulated currents in various polymers subjected to plastic deformations at high pressures showed that the injected electrons can penetrate the polymer samples to a depth of up to 40–50 μm. This situation with electron capture by the structural defects and their retention in the samples after removing the pressure can be compared to that arising after irradiation of the polymers with a 100-keV electron beam [17]. The electrons localized on the structural defects were liberated by heating the samples, when various kinds of molecular mobility of electrons in polymers existed. In this context, it can be

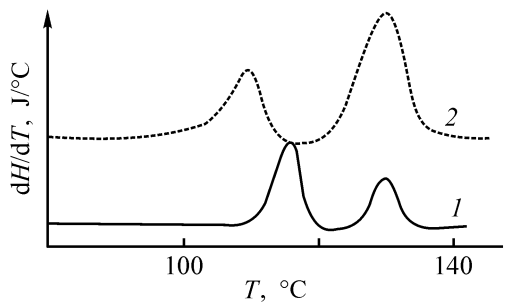


Fig. 1. Thermograms of SPO. Sample: (*1*) initial and (*2*) after treatment under 1 GPa. (*dH*/*dT*) Heat capacity change and (*T*) temperature.

assumed that decolorization of colored SPO is due to liberation of captured electrons from the structural traps.

We attempted to affect the liberation of electrons from the samples subjected to high pressure treatment and, thereby, to change the rate of their decolorization and the number of captured electrons in colored samples. In the case of the conventional experimental procedure, when, after removing the pressure, the anvils were taken out of the press and mounted on a dielectric support ("insulated"), the decolorization time was ca. 1 h. When the anvils remained in the press after removing the pressure (were "grounded"), the samples virtually lost their color within 10–15 min. To accelerate the charge leakage in the samples, we added 5–10 wt % powdered aluminum or copper to the initial SPO. After treatment under pressure, such samples were colorless. Thus, a facilitated charge leakage from the samples intensified their decolorization.

There are two processes occurring in samples treated under pressure: formation of structural defects at which charges can be localized and injection of electrons from the metal of an anvil into the material of the sample. As shown previously [18], the former process is virtually pressure-independent at pressures within 1–6 GPa and is determined by the magnitude of deformation (rotation angle of the anvils). The latter process is enhanced as the pressure at which the samples are subjected to deformation increases. It should be noted that, during plastic deformation, a part of the structural defects with captured electrons leaves the sample, but new defects are formed, which ensures dynamic equilibrium of the system.

The number of electrons remaining in the sample after removing the pressure can be controlled. To this end, the samples should be subjected first to a plastic deformation under pressure, when intense coloration is observed. Then, without terminating the de-

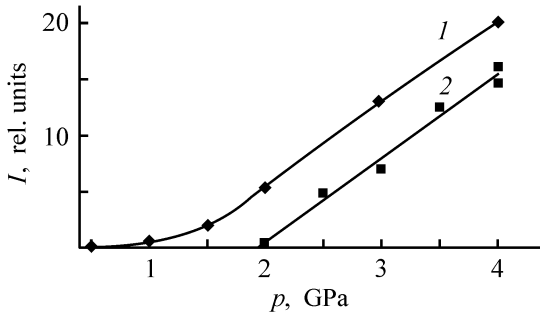


Fig. 2. Baric dependences of the deformation currents. (*I*) Current intensity and (*p*) treatment pressure. (*1*) SPO and (*2*) SPO in a mixture with succinic acid, 30 wt %.

formation, i.e., with the number of structural defects maintained constant, the pressure should be lowered. This will decrease the number of electrons injected and, consequently, captured by the structural defects. This procedure will remove from the sample the structural defects, together with the electrons localized on them. The number of charges retained in the samples will be much smaller than that in the case of a simple removal of the pressure after terminating the deformation.

Indeed, after treatment of the SPO samples preliminarily deformed at 2 GPa by the "deformation under pressure lowering" scheme, the samples are colorless. Our results suggest that the dark blue form of SPO, arising under plastic deformation at a high pressure, is at least partially due to the presence of injected electrons in the samples.

The presence of mobile charges in the SPO samples during treatment under pressure is evidenced by the deformation current. We reported in [19] that deformation currents flow through metal and metal-polymer composite samples subjected to plastic deformation under pressure. These currents are due to migration of charged structural defects. Figure 2 shows the baric dependence of the deformation current in SPO samples. At pressures under 1 GPa, the deformation current is manifested as individual pulses. During deformation at pressures of 2 GPa and over, the current monotonically increases with the degree of deformation to a limiting value achieved at the anvil rotation angles of 80°–100°. After terminating the rotation of the anvils, the current decreases to zero within several seconds. Under repeated deformation at the same pressure, the current exhibits identical dynamics.

Extensive experimental data suggest that, with increasing pressure, the substances under study begin to exhibit to ever growing degree the properties that evidence ionization and dissociation of molecules under plastic deformation. For example, deformation of maleic acid at 4 GPa yields a polyester, which suggests migration of the proton from the carboxy group to the double bond of the neighboring molecule [20]. Zhorin *et al*. [21] showed that, under plastic deformation of mixtures of organic acids with aromatic and aliphatic amines, a proton is transferred even in those acid–base pairs in which no salt is formed in liquid media. The proton transfer intensity increases with pressure; ion pairs were recorded by IR spectroscopy in samples subjected to treatment under pressure. Studies of the electrical conductivity of oxalic acid under pressure [22] showed that, at pressures above 2 GPa, a noticeable contribution to the conductivity comes from the ionic component. Formation of metal complexes of porphyrins from mixtures of metal-free porphyrins with metal salts and oxides under plastic deformation suggests dissociation of the metal salts and oxides under such conditions [23].

Thus, under plastic flow at high pressures, the electronic structure of bonds in organic molecules is substantially modified to the point of ionization and dissociation; the electronic excitation energy of ions of organic molecules is more than 2 times lower than that for molecules in the neutral state [24]. Also, a system of charged structural defects is formed in the material of the samples; local gradients of electric fields must exist in this system.

To further study the processes occurring in organic compounds under plastic deformation at high pressures and yielding, in the case of SPO, a colored form, we treated with pressure mixtures of SPO with various organic compounds, both low-molecular-weight and polymeric.

It turned out that all low-molecular-weight substances chosen as matrices can be divided into three groups: substances in which SPO turns blue; substances in which SPO turns red; and substances in which no coloration of SPO can be recorded.

Out of the totality of the organic matrices in which SPO is intensely colored, the amide and organic acid series can be singled out. The amide series includes acrylamide, methacrylamide, *N*,*N*'-methylenebisacrylamide, and propionamide. The first three members are unsaturated compounds arranged in order of decreasing tendency to polymerize under plastic flow at high pressure. In these matrices, SPO turns red. The intensity of SPO coloration varies in parallel with the activity of these unsaturated amides in polymerization. At the same time, a mixture of SPO with a saturated

analog of arcylamide, propionamide, acquires only a slightly blue color, rapidly disappearing under ambient conditions. We found that, when red samples of SPO mixed with unsaturated amides are dissolved, a part of the reaction mixture dissolves neither in acetone, nor in water; it dissolves only in dimethyl sulfoxide, yielding a red solution. Thus, red forms (RFs) appear only in mixtures with unsaturated amides. Evidently, coloration is due to chemical reactions of SPO with unsaturated amides.

With SPO–acrylamide mixtures as an example, we monitored the changes in the color of the samples with increasing degree of deformation (anvil rotation angle). We found that treatment at a pressure of 0.7 GPa and an anvil rotation angle of 50° yields a two-color sample, with a bright red peripheral zone and a dark blue center. Between these two extreme colors, there is a transition zone, in which both colors are present. The dark blue color disappears more rapidly, and the bright red color in the peripheral zone gets less intense in going to the center of the sample, and the center is virtually colorless. With increasing degree of deformation, the red zone tends to widen, and at the anvil rotation angles above 150° the whole sample is red. Thus, while the blue dark color in the samples treated under pressure is spread uniformly over the entire sample, the red color appears first in the peripheral zone of the sample; with increasing degree of deformation, the ring red zone tends to widen toward the center of the sample. Similar changes in the color of the samples have been observed previously, when substances subjected to plastic deformation at high pressures underwent chemical transformations into colored products (notably, the maximal deformation of the sample is observed in the peripheral ring zone).

The conclusion that formation of the red zone of SPO is due to the presence in the matrix molecules of active C=C bonds is confirmed by the results of treatment under pressure of the SPO mixtures with acenaphthylene and its saturated analogue, acenaphthene. We found that the SPO–acenaphthylene mixtures turn red, and the mixtures with acenaphthene are not colored.

As noted above, the color intensity of unsaturated amides depends on the reactivity of the double bond. It was of interest to study this effect for other compounds as well. To this end, we chose vinylcarbazole and tetraphenylethylene. In vinylcarbazole, the chemical activity of the double bonds is extremely low because of the strong steric hindrance. Therefore, for mixed samples based on vinylcarbazole we could record only a weak pink color in a narrow ring zone at the periphery of the samples. Even more hindered is the double bond in tetraphenylethylene, which is completely shielded by four phenyl rings. For this matrix, we could not record any coloration at all.

Thus, in mixtures with unsaturated amides, both the DBF and RF are manifested in SPO samples. Our results suggest that the DBF is formed in earlier stages of deformation, compared to the RF. The latter results in mixtures with amides from chemical reactions between the SPO molecules and unsaturated amide molecules.

To elucidate the influence exerted by organic acids on the coloration of SPO, we chose mono- and dibasic aromatic acids, as well as dibasic aliphatic acids; all these acids differed in strength.

In the case of mixtures of SPO with unsaturated dibasic acids, maleic and fumaric, we found that the RF was formed even under treatment at 1 GPa. To test the assumption concerning reactions between the SPO molecule and the double bonds of the matrix molecule, samples of the SPO–maleic acid mixtures were dissolved in various solvents after deformation under pressure. The samples are rapidly and completely soluble in acetone, the solution retaining a red color. About 50% of the substance is dissolved in water; the undissolved fraction has a dark brown, and the solution, a yellowish green color. Such a behavior of the samples in dissolution suggests chemical reactions between the mixture components during plastic deformation under pressure.

Mixtures of SPO with a saturated analogue of maleic and fimaric acids, succinic acid, were treated under pressures of 1–1.5 GPa. The samples with succinic acid have a dark blue-red color after treatment. Upon heating to 80–90°C, the dark blue color disappears, and the sample acquires an intense red color disappearing upon dissolution of the samples in acetone. The fact that the RF appears both in unsaturated acids and in their saturated analogue suggests that, in the acids, SPO can be colored not only due to reactions of the SPO molecules with the C=C bond, but also via protonation of the open form. Similarly to the case of SPO, deformation currents flow through the samples of the mixtures of SPO with succinic acid (the corresponding baric dependence is shown in Fig. 2).

Mixtures of SPO with a number of organic acids of different strengths were treated at 1–1.5 GPa. For comparison, we chose the series of acidity in water

Coloration of mixtures of SPO with organic acids after plastic deformation at 1.5 GPa, depending on the strength of the acid

Acid	pK_α	Color
Sebacic	4.55	Dark blue
Adipic	4.41	"
Glutaric	4.34	"
Succinic	4.21	Red
Benzoic	4.19	Dark blue
Cinnamic	3.89	"
Itaconic	3.85	"
Naphthylacetic	3.70	"
Isophthalic	3.62	"
o-Fluorobenzoic	3.27	"
Citric	3.13	Red
Fumaric	3.02	"
Phthalic	2.95	"
Malonic	2.86	"
Maleic	1.92	"
Pyromellitic	1.40	"
Oxalic	1.27	"

(see table). The tabulated data suggest that, within a certain pK_a range, organic acids favor appearance in the mixed samples of the red form of SPO, coexisting with the DBF. The monotonicity of the series established is violated by succinic acid: The dark blue and red forms are metastable, with the DBF being decolorized even during heating, and the RF, during dissolution in acetone. The most probable reason for the appearance of the RF is protonation of the SPO molecules with acids weak under ordinary conditions.

Protonation of SPO with weak organic acids formally means the enhancement of their acid properties. To estimate the possible magnitude of such an effect, we prepared solutions of trichloroacetic (pK_a = 0.66) and monochloroacetic (pK_a = 0.74) acids in acetone. Upon introduction of SPO into these solutions, they turn red. It should be noted that, when colored under pressure, the mixtures of SPO even with the strongest of the acids chosen, oxalic, are completely decolorized in acetone. Our data suggest that, for coloration of SPO in an acidic solution, the strength of the acid should be no lower than that of monochloroacetic acid; at the same time, coloration of SPO under pressure begins with citric acid. Thus, the degree of dissociation of citric acid under plastic flow at high pressures should formally increase by almost a factor of 300 to get equal to that of monochloroacetic acid.

The third group of the substances used to study the properties of SPO include propionamide, acenaphthene, anthracene, adamantane, pentaerythritol, pentaerythritol diformal, camphor, fluorene, carbazole, *N*-methylcarbazole, 9-propylcarbazole, 9-(2,3-dihydroxypropyl)carbazole, tetraphenylethylene, and triethylenediamine. For mixtures of SPO with these substances, we could not record after treatment at 2 GPa any color at all or it was very weak, bluish, and the mixture rapidly lost its color. This suggests that, in the substances discussed, SPO acquires a dark blue color, but in this case the decolorization rate is high. The substances in the third group are nonpolar and contain no functional groups that could stabilize the colored form of the SPO molecule, thereby decelerating decolorization.

Along with low-molecular-weight organic substances, we used the following polymers as matrices: high- and low-density polyethylene, polypropylene, polystyrene, cellulose, polyvinyl alcohol, polyvinyl chloride, and polycarbonate.

A characteristic feature of the mixtures of SPO with the polymers chosen is that, after treatment at 1–2 GPa, all the samples acquire either a dark blue-red or a pink-blue color. Within a period from 10 min to 1.5 h, the samples virtually lose the blue color and get pink-red or bordeaux. This color is retained for at least a month.

In samples of SPO mixtures with polymers (high-density polyethylene, polycarbonate, polyvinyl chloride), we recorded deformation currents. They belong to the same range as in the baric dependences shown in Fig. 2; after treatment under pressure, the samples were strongly electrified.

For the SPO mixtures with high-density polyethylene, we found that, under deformation at 2 GPa at small anvil rotation angles (50°), we can observe a blue color only. With increasing anvil rotation angle to 100°–150°, the samples acquire a pink tint. It intensifies with increasing degree of deformation, and the sample gets bright red at anvil rotation angles of 500°–700°.

The appearance of the red form of SPO in the polyethylene matrix is hardly attributable to chemical reactions or protonation, in contrast to the case of low-molecular-weight matrices. Here, it is appropriate to mention that coloration of SPO can be achieved by exposing the solution to an electric field.

Treatment under pressure of samples of SPO mixed with polyethylene yielded films easily detachable from the working surface of the anvils. This allowed measurement of the thermostimulated currents for such samples. The thermostimulated curent was

ca. 10^{-9} A in the polyethylene samples and 10^{-6} A in samples of the 30% SPO–polyethylene mixtures. Thus, the number of charges in the mixed samples is much greater than in individual polyethylene. Probably, this means that a large proportion of the SPO molecules occurs within the range of action of local electric fields.

CONCLUSIONS

(1) Under plastic deformation, spirooxazine can transform both to the dark blue and red forms. Early stages of deformation yield a dark blue form, and a more profound deformation, a red product.

(2) The dark blue form is an open merocyanine structure into which spiropyran is transformed. This process is strongly influenced by electrons injected from the anvil metal.

(3) The red form is the product of protonation of the open form, yielded by the reactions of the spirooxazine molecules with the matrix molecules. The appearance of the red form is favored by the action of electric fields arising in polymer matrices during treatment under pressure.

ACKNOWLEDGMENTS

This study was financially supported by the Russian Foundation for Basic Research (project no. 04-03-32 628).

REFERENCES

1. Zhorin, V.A. and Enikolopyan, N.S., *Dokl. Akad. Nauk SSSR*, 1985, vol. 285, no. 3, pp. 643–646.
2. Zhorin, V.A., *Zh. Fiz. Khim.*, 2001, vol. 75, no. 10, pp. 1825–1832.
3. *Photochromism and Systems*, Durr, H. and Bouas-Laurent, Eds., Amsterdam: Elsevier, 1990.
4. Marevtsev, V.S. and Zaichenko, N.L., *J. Photochem. Photobiol. A*, 1997, vol. 104, pp. 197–202.
5. Antipin, S.A., Petrukhin, A.N., Gostev, F.E., *et al.*, *Chem. Phys. Lett.*, 2000, vol. 331, no. 5, 6, pp. 378–381.
6. Bletz, M., Pfeifer-Fukumura, U., Kolb, U., and Baumann, W., *J. Phys. Chem. A*, 2002, vol. 106, pp. 2232–2239.
7. Arsenov, V.D., Marevtsev, V.S., Komlev, I.V., *et al.*, *Izv. Akad. Nauk SSSR, Ser. Khim.*, 1988, pp. 1019–1022.
8. Kol'tsova, L.S., Zaichenko, N.L., Shienok, A.I., and Marevtsev, V.S., *Izv. Ross. Akad. Nauk, Ser. Khim.*, 2001, no. 7, pp. 1157–1160.
9. Kozlovskaya, I.E., Sychev, I.Yu., Luchina, V.G., and Marevtsev, V.S., *Izv. Ross. Akad. Nauk, Ser. Khim.*, 1994, no. 5, pp. 836–840.
10. Sychev, I.Yu., Khamchukov, L.V., Marevtsev, V. S., *et al.*, *Zh. Nauch. Prikl. Fotogr.*, 2000, vol. 45, pp. 61–66.
11. Maksimychev, A.V., Zhorin, V.A., Ponomarenko, A.T., and Enikolopyan, N.S., *Dokl. Akad. Nauk SSSR*, 1979, vol. 244, no. 5, pp. 1153–1155.
12. Zhorin, V.A., Maksimychev, A.V., Ponomarenko, A.T., and Enikolopyan, N.S., *Izv. Akad. Nauk SSSR, Ser. Khim.*, 1979, no. 10, pp. 2256–2264.
13. Enikolopyan, N.S., Berlin, Yu.A., Beshenko, S.I., and Zhorin, V.A., *Pis'ma Zh. Eksp. Teor. Fiz.*, 1981, vol. 33, no. 10, pp. 508–509.
14. Enikolopyan, N.S., Berlin, Yu.A., Beshenko, S.I., and Zhorin, V.A., *Dokl. Akad. Nauk SSSR*, 1981, vol. 258, no. 6, pp. 1400–1403.
15. Berlin, Yu.A., Beshenko, S.I., Zhorin, V.A., and Enikolopyan, N.S., *Dokl. Akad. Nauk SSSR*, 1982, vol. 262, no. 2, pp. 364–366.
16. Barachevskii, V.A., Lashkov, G.I., and Tsekhomskii, V.A., *Fotokhromizm i ego primenenie* (Photochromism and Its Application), Moscow: Khimiya, 1977.
17. Zhorin, V.A., Lushcheikin, G.A., and Razumovskaya, I.V., *Vysokomol. Soedin, Ser. A*, 2001, vol. 43, no. 12, pp. 2163–2169.
18. Zhorin, V.A., Shashkin, D.P., and Enikolopyan, N.S., *Dokl. Akad. Nauk SSSR*, 1984, vol. 278, no. 1, pp. 1444–1446.
19. Zhorin, V.A., *Vysokomol. Soedin, Ser. A*, 1994, vol. 36 no. 4, pp. 559–579.
20. Solov'eva, A.B., Zhorin, V.A., and Enikolopyan, N.S., *Dokl. Akad. Nauk SSSR*, 1978, vol. 240, no. 1, pp. 125–127.
21. Zhorina, L.A., Vladimirov, L.V., Knunyants, M.I., *et al.*, *Dokl. Akad. Nauk SSSR*, 1991, vol. 320, no. 2, pp. 374–377.
22. Zhorin, V.A., Beshenko, S.I., Berlin, Yu.A., and Enikolopyan, N.S., *Zh. Fiz. Khim.*, 1984, vol. 58, no. 7, pp. 1799–1803.
23. Zhorin, V.A., Nikiforov, G.A., Khristyuk, A.L., and Enikolopyan, N.S., *Dokl. Akad. Nauk SSSR*, 1983, vol. 271, no. 3, pp. 650–652.
24. Terenin, A.N., *Fotonika molekul krasitelei i rodstvennykh organicheskikh soedinenii* (Photonics of the Molecules of Dyes and Related Organic Compounds), Leningrad: Nauka, 1967.

Russian Journal of Applied Chemistry, Vol. 78, No. 6, 2005, pp. 962–966. Translated from Zhurnal Prikladnoi Khimii, Vol. 78, No. 6, 2005, pp. 984–988.
Original Russian Text Copyright © 2005 by Andriyanova, Smirnova, Drozdov, Gracheva.

MACROMOLECULAR CHEMISTRY AND POLYMERIC MATERIALS

Structure and Characteristics of Graft Copolymers with Chitosan

N. A. Andriyanova, L. A. Smirnova, Yu. N. Drozdov, and T. A. Gracheva

Lobachevsky Nizhni Novgorod State University, Nizhni Novgorod, Russia
Institute of Physics of Microstructures, Russian Academy of Sciences, Nizhni Novgorod, Russia

Received December 16, 2004; in final form, February 2005

Abstract—Graft copolymers of acrylonitrile with chitosan were prepared by radical polymerization of acrylonitrile in aqueous acetic acid solution of chitosan.

The interest of applied chemists in natural polymers and, in particular, in polysaccharides, steadily grows. Among these polymers is chitosan, CTS [poly-β-(1,4)-2-amino-2-deoxy-*D*-glucosamine], the product of deacetylation of natural polymer chitin, which is a structural analogue of cellulose. The presence of an amino group in the monomeric unit of chitosan imparts to it solubility in dilute solutions of organic and some inorganic acids, and also a set of unique physicochemical and biological characteristics [1]. One of the promising applications of chitosan is preparation of membranes and fiber-forming materials based on it [2]. However, the widespread use of chitosan as a composite material is limited by its inadequate physicochemical parameters characteristic of all polysaccharides. Therefore, modification of chitosan and development of new materials based on chitosan with synthetic polymers are metters of current interest. It is of particular interest to use a fiber-forming synthetic polymer, polyacrylonitrile, for modification of chitosan. Combination of chitosan with this polymer can, on the one hand, improve the physicochemical characteristics of chitosan and, on the other hand, yield hygienic characteristics of polyacrylonitrile fiber dependent on the ratio of the components. In addition, the fairly high solubility of acrylonitrile (AN) in water (7.3 g per 100 ml H_2O at 20°C) is of significant importance, allowing modification of chitosan under homogeneous conditions.

The aim of this study was to examine the grafted polymerization of AN on chitosan and to analyze the properties of the products obtained.

EXPERIMENTAL

We used chitosan produced by Sonat Co. (Moscow) with molecular weight (MW) equal to 2.5×10^5 and degree of deacetylation of 82%. Before use, acrylonitrile was dried with NaOH for 4 h and distilled under atmospheric pressure on a setup equipped with a total-reflux head. The fraction with bp 78.5°C was collected. A 1.5% aqueous CH_3COOH served as a solvent; isopropanol of chemically pure grade was used as a precipitant.

Precipitation was performed in a three-necked flask equipped with a reflux condenser. The flask was charged with 100 g of a 3% solution of chitosan in 1.5% aqueous CH_3COOH, and then a weighed portion of monomer with dissolved initiator, azobis(isobutironitrile) (AIBN), was added. The process was carried out at 60°C.

The degree of conversion of AN in polymerization was monitored by three methods: chromatographic analysis, potentiometric titration of unchanged AN, and gravimetric analysis (by variation of the weight of the resulting product). For this purpose, samples of a certain weight were taken during the process, and the reaction product was precipitated, washed several times with isopropanol on a filter, and dried in a vacuum to constant weight. The filtrate was transferred into a measuring flask and analyzed for the AN content by chromatographic and potentiometric methods. The chromatographic analysis was performed on a Tsvet-500 chromatograph, 2000×4 mm column, sorbent SE, carrier gas argon, column temperature 75°C, detector temperature 103°C, and vaporizer temperature 130°C. The AN concentration in the samples was determined using n-butanol as internal reference. The unchanged AN was determined by potentiometric titration according to [3].

Films of the initial chitosan and products of its reaction with AN were prepared by casting from a solution in 1.5% aqueous CH_3COOH. One set of films

1070-4272/05/7806-0962 © 2005 Pleiades Publishing, Inc.

was dried in air for 40–48 h and then in a vacuum to constant weight. Another set was washed with 3% aqueous NaOH to remove CH_3COOH and then with distilled water to pH 7 and dried in a vacuum to constant weight. The tensile strength and relative elongation at break were determined on an RMI-5 tensile-testing machine at an extension rate of 50 mm min^{-1}.

IR Fourier spectra of the films were recorded on a Paragon 500 Perkin–Elmer Fourier spectrophotometer.

X-ray diffraction patterns were recorded on a DRON-4 diffractometer (Cu_{K_α} radiation, graphite monochromator, reflected beam).

The particle size of the graft product dispersion was determined by the turbidimetric method based on measurements of the intensity of scattered light passed through a disperse system, using a KFK-2-UKhL 4.2 device [4]. The electrokinetic potential of the dispersion particles was measured from the rate of electrophoresis by the method of a moving boundary [4].

The moisture absorption by films prepared from the graft copolymer of AN with chitosan was studied gravimetrically at 25°C. For this purpose, films of a certain weight were fixed on hooks and placed in a hermetically sealed beaker filled with distilled water. At certain intervals of time, the films were removed from the beaker, excess moisture was removed with a filter paper, and the films were weighed on an analytical balance. The percentage of swelling was evaluated by the formula

$$\omega = (m - m_0)/m_0 \times 100,$$

where m_0 and m are the weights of the initial and swollen films, respectively.

We studied how the polymerization conditions, such as initiator concentration, reactant ratio (chitosan : AN), and pH of the medium, affect the degree of AN conversion and the efficiency of grafting.

It should be noted that, in the course of polymerization, we used in all the runs an AN concentration lower than its limiting solubility in water (7.3 g per 100 ml H_2O at 20°C). At in the beginning of polymerization, the system was a homogeneous solution. The influence of chitosan concentration on the degree of AN conversion is illustrated by Fig. 1. It is seen that, at chitosan concentrations of 0.5 to 1.5 wt %, the maximum of AN conversion in the synthesis is as low as 25%, irrespective of the process duration. The AN conversion increases with the chitosan concentration and reaches 97.5% at a chitosan concentration of 3 wt %. Further increase in the chitosan concentration does not affect the limitingof AN conversion; therefore, all runs were performed at a chitosan concentration of 3 wt %. Since chitosan is a polyelectrolyte, we can suggest that the pH of the medium should noticeably affect the process. Actually, the limiting yield of AN is 93% at pH 3.9 and 97.5% at pH 5.5 (Fig. 2). In this case, the initial rate of the process increases by a factor of 1.3. The resulting product is an aggregatively stable dispersion with a particle size of 8.2×10^{-7} to 3×10^{-5} cm, remaining constant for no less than 8 months. This high aggregative stability of the dispersion of the graft copolymer in water is apparently caused by two factors: electrostatic

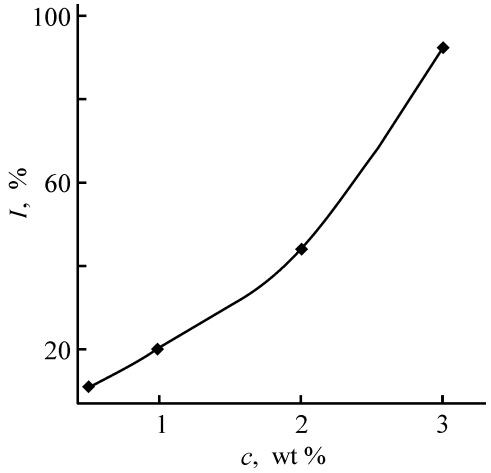


Fig. 1. Limiting degree of AN conversion, *I*, vs. chitosan concentration *c* in polymerization in a solution of chitosan. [AN] = 1.0 M, pH = 3.9, 60°C.

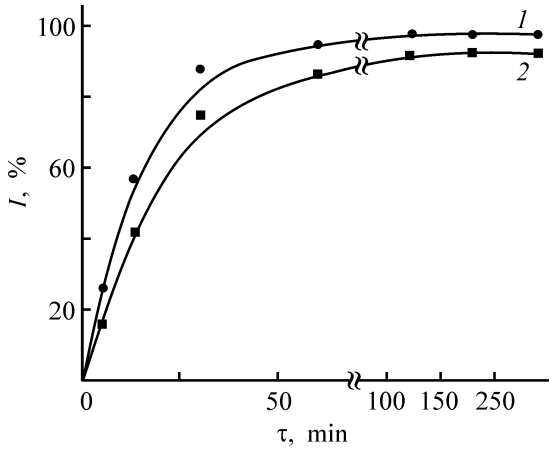


Fig. 2. Variation of the degree of AN conversion, *I*, with time τ in polymerization in a solution of chitosan at various pH of the reaction mixture. [AN] = 1.0 M, [CTS] = 0.187 M, $(\nu_{AN}/\nu_{CTS}) = 3.0$, ν_{AN} and ν_{CTS} are the number of AN moles and base-moles of chitosan, respectively, 60°C. pH: (*1*) 5.5 and (*2*) 3.9.

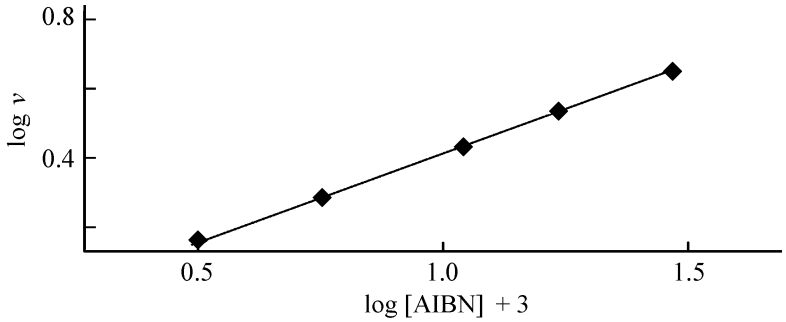


Fig. 3. A plot of log*v* vs. (log[AIBN] + 3). [AN] = 1.0 M, [CTS] = 0.187 M, 60°C, pH 3.9. (*v*) Initial polymerization rate.

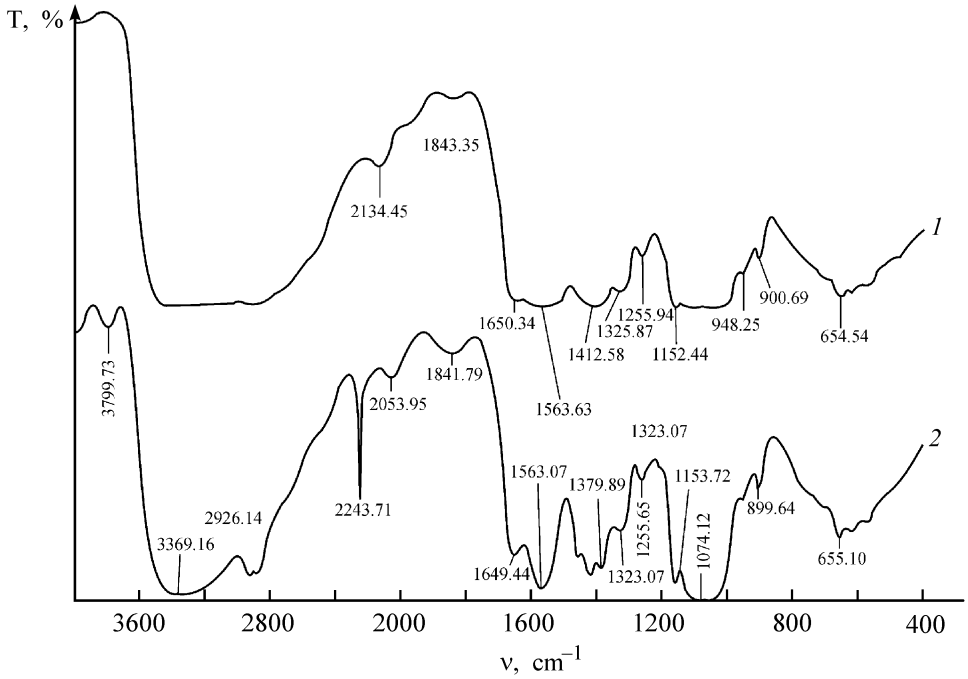


Fig. 4. IR Fourier spectra of samples of (*1*) the initial chitosan and (*2*) graft copolymer of chitosan with AN. (T) Transmission and (*v*) wave number.

repulsion of particles due to appearance of an electrical double layer at their surface caused by protonation of amino groups of chitosan (the electrokinetic potential of the dispersion particles determined by electrophoresis is approximately 56 mV; this significantly exceeds the critical value of 30 mV which, as a rule, corresponds to loss of stability by colloidal solutions) and structural mechanical factor [5].

As the concentration of the initiator increases from 2.8×10^{-3} to 2.8×10^{-2} M, the initial reaction rate grows by a factor of 1.5. The dependence of the initial reaction rate on the initiator concentration is linear. The reaction order with respect to the initiator was determined to be 0.65 (Fig. 3).

It is not improbable that the polymerization yields, in addition to the graft copolymer, also a PAN homopolymer. Therefore, to determine the degree and efficiency of grafting, the graft product and PAN were separated by extraction of the latter with dimethylformamide in a Soxhlet apparatus. Preliminary experiments on separation of a mixture of chitosan with PAN under the same conditions showed that the time required for complete removal of PAN from the mixture is approximately 40 h. It was found that the reaction product is mainly the graft copolymer. The content of the homopolymer does not exceed 3%. Formation of graft copolymers was proved by IR spectroscopy. After extraction in a Soxhlet apparatus, the sample of the copolymer was dissolved in 1.5% aqueous CH_3COOH and then films were prepared. The IR Fourier spectrum contains an absorption band at 2243.7 cm^{-1} corresponding to stretching vibrations of the –C≡N bond (Fig. 4).

For the optimum conditions of the process (pH 5.5, [AN] 1.0 M, [AIBN] 2.8×10^{-2} M), we calculated the degree of grafting (DG, weight of grafted AN/chitosan weight, %) and the efficiency of grafting (EG, weight of grafted AN/weight of polymerized AN, %). The degree and efficiency of grafting were 182 and 97%, respectively.

For the samples prepared under these conditions, the molecular weight of the grafted chains of PAN was determined. These chains were separated from chitosan chains by hydrolysis in the presence of a 3% NaOH solution for 30 min according to the procedure described in [6]; the precipitate was washed with water and methanol. Then, PAN was extracted with dimethylformamide and precipitated with methanol. The molecular weight of PAN (M_η) was calculated from viscometric data (DMF, 30°C) by the equation [7]

$$\log[\eta] = \log 2.3 \times 10^{-4} + 0.75 \log M_\eta,$$

where M_η of grafted chains was 2.2×10^4.

From the concentrations of chitosan and AN in synthesis, we calculated taking into account the efficiency of grafting, MW of chitosan (2.5×10^5), and MW of grafted PAN chains (2.2×10^4), the average number of grafted PAN chains per chitosan molecule. It was 20, i.e., one branching per 70 units of the chitosan chain.

The X-ray diffraction data (Fig. 5) for films of chitosan (curve *2*) and graft copolymer of chitosan with AN (curve *1*) indicate that their structures are strongly different. A high degree of structural ordering is characteristic of the initial sample of chitosan. The degree of crystallinity, evaluated by the procedure described in [8], was 41.8% for this sample. The positions of the main diffraction peaks correspond to the angles $2\theta_1 = 11.7°$, $2\theta_2 = 18.8°$, and $2\theta_3 = 21.6°$ (the respective interplanar spacings are $d_1 = 0.754$, $d_2 = 0.472$, and $d_3 = 0.411$ nm). Comparison of curves *1* and *2* shows that the diffraction respective characteristic of chitosan are absent in the X-ray diffraction pattern of the graft copolymer. Presumably, the grafted chains of PAN prevent ordered packing of chitosan chains, and its supramolecular structure becomes less ordered. At the same time, a sharp diffraction peak appears at $2\theta_4 = 17.2°$ against the background of the amorphous halo of chitosan; this peak corresponds to crystalline formations in the PAN structure [8]. In this case, the degree of crystallinity of the graft copolymer is as low as 16.1%. The improved physicomechanical characteristics of the graft copolymer in comparison with chitosan can be attributed to the decrease in the degree of crystallinity. The table shows that the ultimate tensile strength of graft copolymers of AN with chitosan increases to 600 MN m^{-2}, against the value of 290 MN m^{-2} for pure chitosan, and the degree of limiting deformation is approximately 30%, against 8% for pure chitosan. The moisture absorption of films prepared from the graft copolymer reaches 26%.

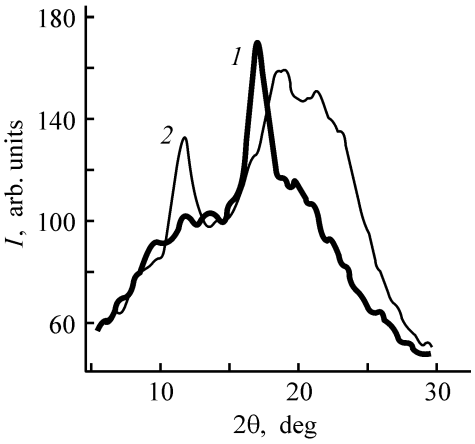


Fig. 5. X-ray diffraction patterns of the samples of (*1*) graft copolymer of chitosan with AN and (*2*) initial chitosan. (*I*) Intensity and (2θ) Bragg angle.

A comparison of the strength and relative elongation of the resulting graft copolymer with those of PAN fiber shows that these values are comparable: for PAN fiber, the tensile strength is 600 MN m^{-2} and the relative elongation is in the range 10–35% [9].

CONCLUSIONS

(1) Graft copolymer of acrylonitrile with chitosan with a high degree and efficiency of grafting was prepared in the form of a highly stable aqueous dispersion.

(2) Graft copolymers compare well with the polyacrylonitrile fiber in physicomechanical character-

Ultimate tensile strength σ and limiting strain ε of films prepared from graft copolymer chitosan–AN in relation to the AN content

[AN], M	σ, mN m^{-2}	ε, %
0	290	8
0.67	480	24
0.97	550	26
1.39	570	28
2.08	600	30

istics and have increased hygroscopicity and colorability.

REFERENCES

1. *Khitin i khitozan: Poluchenie, svoistva i primeneniya* (Chitin and Chitosan: Preparation, Characteristics, and Use), Skryabin, K.G., Vikhoreva, G.A., and Varlamov, V.P., Eds., Moscow: Nauka, 2002.
2. Marek, O. and Tomka, M., *Akrylove polymery*, Praha: SNTL, 1963. Translated under the title *Akrilovye polimery*, Moscow: Khimiya, 1966.
3. *Analiz polimerizatsionnykh plastmass* (Analysis of Polymerization Plastics), Bezuglyi, V.D., Ed., Moscow: Khimiya, 1965.
4. *Laboratornye raboty i zadachi po kolloidnoi khimii* (Practical Guide and Problems on Colloidal Chemistry), Frolov, Yu.G., Ed., Moscow: Khimiya, 1986.
5. Olieimeu, E.F. and Ebhoayl, J.E., *J. Appl. Polym. Sci.*, 1986, vol. 35, no. 31, pp. 1275–1279.
6. Martynov, M.A. and Vylegzhanina, K.N., *Rentgenografiya polimerov* (X-Ray Diffraction Analysis of Polymers), Moscow: Khimiya, 1972.
7. *Entsiklopediya polimerov* (Encyclopedia of Polymers), Kargin, V.A., Ed., Moscow: Sov. Entsiklopediya, 1972, vol. 1.
8. Frolov, Yu.G., *Kurs kolloidnoi khimii: Poverkhnostnye yavleniya i dispersnye sistemy* (Course of Colloidal Chemistry: Surface Phenomena and Disperse Systems), Moscow: Khimiya, 1989.
9. Shatenshtein, A.I., Vyrskii, Yu.P., Pravikova, N.A., *et al.*, *Opredelenie molekulyarnykh vesov polimerov* (Determination of Molecular Weights of Polymers), Moscow: Khimiya, 1964.

Russian Journal of Applied Chemistry, Vol. 78, No. 6, 2005, pp. 967–970. Translated from Zhurnal Prikladnoi Khimii, Vol. 78, No. 6, 2005, pp. 989–992.
Original Russian Text Copyright © 2005 by Suvorova, Tyukova, Smirnova, Tymchishina.

MACROMOLECULAR CHEMISTRY AND POLYMERIC MATERIALS

Rheological Properties of Blends of Ternary Copolyamide 6/66/610 with Chitosan

A. I. Suvorova, I. S. Tyukova, E. A. Smirnova, and N. M. Tymchishina

Gorky State University, Yekaterinburg, Russia

Received November 25, 2004; in final form, March 2005

Abstract—The viscosity of melts of a blend of a ternary copolyamide 6/66/610 and polysaccharide (chitosan) used as biodegradable additive was determined by capillary viscometry at 150–170°C.

Properties of blends of synthetic and natural polymers are studied to develop new environmentally clean materials temporarily used in homes, agriculture, and cosmetic and medical industry. The natural polymers contained in these blends promote degradation of the composite under the action of H^+ and OH^- ions, soil moisture, microorganisms, fungi, worms, and other biological and chemical agents causing degradation of polymers with subsequent decomposition of the disposed articles. Starch is most frequently used as a biodegradable component of polymer composites. Starch is a plant polysaccharide which readily degrades under the physiochemical and biological action of the environment [1, 2]. Another natural polysaccharide, chitin, produced by *Crustacea*, insects, and other living things, can also be used for this purpose. Chitin is a renewable natural polymer accumulated in large amounts. However, it is used to a lesser extent than starch [3, 4]. The acetamide group of chitin can be readily hydrolyzed to form chitosan, which is a copolymer of (2-amino-2-deoxy)- and (2-acetamido-2-deoxy)-β-1,4-*D*-glucans. Chitosan and chitin are biodegradable polymers [5]. The solubility of chitosan and its miscibility with other polymers are higher than those of chitin owing to formation of inermolecular hydrogen bonds between the components or of ion-polymer complexes with polyelectrolytes [6]. Therefore, blends of synthetic polymers with chitosan should be of practical interest.

Here we studied the rheological properties of chitosan blends with synthetic copolyamide (SPA) used in production of films and hot-melt adhesives. The miscibility of these polymers should be promoted by formation of hydrogen bonds between the amide groups –NH–CO– of the SPA macromolecule and chitosan. Previously, we have shown [7] that SPA forms homogeneous blends with starch in the presence of plasticizers (glycerol and water) providing the compatibility of the polymers (so-called compatibilizers). The similarity between the rheological properties of these blends and those of common synthetic polymers makes these mixtures promising for practical applications. A specific feature of the SPA–chitosan blend is that only relatively reactive compounds like acetic or formic acids are suitable as compatibilizers for these components. In this study, we used polymer blends free of these additives. The copolyamide served as a matrix, and chitosan, as a filler providing biodegradation of the composite. We used ternary copolyamide 6/66/610. Since the melting point of the copolyamide was lower by approximately 100°C than the temperature of thermal degradation of chitosan, the blends were prepared by direct addition of chitosan to an SPA melt.

Since the processing conditions of a polymer blend are determined by its rheological properties (viscosity), we studied the temperature dependence of the viscosity of chitosan–copolyamide melts as influenced by the chitosan content of the blend.

EXPERIMENTAL

We studied blends of ternary copolyamide 6/66/610 with chitosan. The copolyamide was prepared by cocondensation of caprolactam, and AG and SG salts taken in a 45/10/45 weight ratio. The molecular weigh and the degree of substitution of chitosan, determined by the procedure described in [8], were 1.2×10^5 and 89%, respectively. We used polymer powders with a particle size of about 7×10^{-5} m. Chitosan was X-ray-amorphous, and the degree of crystallinity of SPA

1070-4272/05/7806-0967 © 2005 Pleiades Publishing, Inc.

Properties of the polymers

Polymer	Density, kg m^{-3}	Intrinsic viscosity of solutions at 25°C, dl g^{-1}	mp, °C	Degree of crystallinity determined by XRD, %
SPA 6/66/610	1100	0.49*	135	10
Chitosan	1120	3.80**	–	0

* Solutions in formic acid.
** Solutions in acetate buffer [8].

6/66/610 was $n \approx 10\%$. The properties of these polymers are summarized in the table.

Prior to mixing, SPA was stabilized by addition of 1.0% Irganox antioxidant. Weighed portions of the powdered components were thoroughly mixed and pelletized. The pellets corresponded in the shape and size to the viscometer channel. The blends were pressed at 180°C under a pressure of 15 MPa.

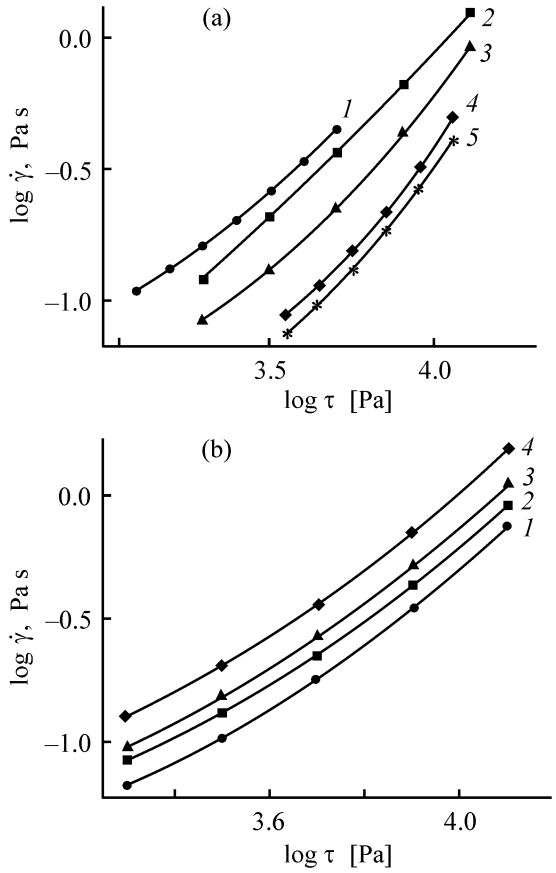


Fig. 1. Flow curves of SPA–chitosan blends. ($\dot{\gamma}$) Shear rate and (τ) shear stress. (a) 160°C; weight fraction of chitosan: (*1*) 0.0, (*2*) 0.05, (*3*) 0.1, (*4*) 0.12, (*5*) 0.15. (b) Weight fraction of chitosan 0.1; temperature (°C): (*1*) 150, (*2*) 155, (*3*) 160, and (*4*) 170.

The viscosity of SPA–chitosan melts η was measured at 150–170°C on an MV-2 microviscometer at a shear rate $\dot{\gamma} = 1 \times 10^{-2}$–$5 \times 10^{-1}$ s^{-1} and shear stress τ = 1.2–2.1 kPa. Since the ratio of the capillary length to its radius was 25, the viscosity was calculated without correction for the entrance effect [9]. The true flow curve (shear rate vs. shear stress) was constructed by the procedure described in [10] using the conventional Excel software.

The flow curves of SPA and its blends with chitosan at 160°C are shown in Fig. 1a. The shape of these curves is typical of pseudoplastic structured systems [11], in which the shear rate nonlinearly increases with the shear stress. As can be seen from Fig. 1a, deviation from linearity are more appreciable at increased chitosan content in the system. Similar rheological curves were obtained for all the examined systems at 150, 155, and 170°C.

The flow curves of a SPA–chitosan melt of one of the four compositions examined, measured at four temperatures, are shown in Fig. 1b. The viscosities of the melt are typical of melts of common synthetic polymers. As can be seen from Fig. 1, the shear rate, i.e., the flowability of the melt increases with temperature at a given shear stress. This trend is typical of polymer melts. Similar dependences were obtained for all the compositions examined.

The dependences of the viscosity of SPA–chitosan melts on the polysaccharide concentration are shown in Fig. 2. At all the temperatures examined, the viscosities of the melts increase with the chitosan content.

The activation enthalpy of viscous flow of SPA–chitosan melts was estimated by the Frenkel–Eyring equation [12]

$$\eta = A\exp[\Delta H/(RT)]. \quad (1)$$

The results are shown in Fig. 3 in the form of a dependence of ΔH on the polysaccharide concentration c in the melt at a constant shear stress. The activa-

tion enthalpy increases with the chitosan content. In the examined range of mole fractions of chitosan, the dependence can be approximated by a linear equation

$$\Delta H = 43.1 + 157.5c. \quad (2)$$

The rise in η and ΔH with increasing chitosan concentration is due to the introduction of a rigid-chain polymer with a higher molecular weight. This polymer can form $NH_2\ldots O{=}C<$ intermolecular bonds with the copolyamide. This assumption is confirmed by the IR spectra of films of chitosan blends with polycaprolactam and polyamide 66, whose units are similar in chemical stricture to those of SPA [13]. The concentration dependences of the viscosity and activation energy are similar and show a decrease in the viscosity of an SPA–chitosan melt (Figs. 2, 3) with increasing polysaccharide concentration.

The concentration dependence of the viscosity of a SPA–chitosan melt cannot be described by the Einstein equation for dispersions [14] since the components form intermolecular hydrogen bonds. To describe the rheological properties of the melts, we used the invariance principle applicable to different polymers and their blends [15, 16]. The maximum Newtonian viscosity of the melt η_0 was determined by extrapolation of the viscosity (Fig. 1a and 1b) to zero shear stress ($\tau \to 0$). These values were used to construct the dependence of the rheological properties of the system in the "invariance" coordinates: reduced viscosity η/η_0 vs. specific shear rate $\dot{\gamma}\eta_0$. The results are shown in Fig. 4. The points fall into a narrow band, which is typical of polymers [16]. A similar dependence was observed for various polymers and their blends, including a blend of synthetic ethylene–vinyl acetate copolymer (SEVA-15) with starch. In this case, the natural polymer was also used as the biodegradable filler [17]. The viscosity of SPA–chitosan blends can be calculated within the band shown in Fig. 4 at known shear rate and η_0.

Thus, we measured the viscosity of SPA–chitosan blends, determined the temperature dependence of the viscosity, and found that these systems follow the principle of invariance of rheological properties. Based on these results, the rheological properties of environmentally clean SPA–chitosan blend, required for their processing, can be predicted.

CONCLUSIONS

(1) Introduction of chitosan into synthetic copolyamide 6/66/610 leads to an increase in the viscosity

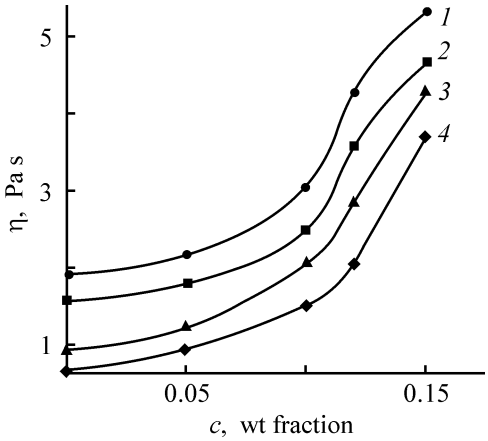


Fig. 2. Viscosity η of SPA–chitosan melts vs. the weight fraction of chitosan, *c*. Shear stress 5 kPa ($\log \tau = 3.7$); the same for Fig. 3. Temperature (°C): (*1*) 150, (*2*) 155, (*3*) 160, and (*4*) 170.

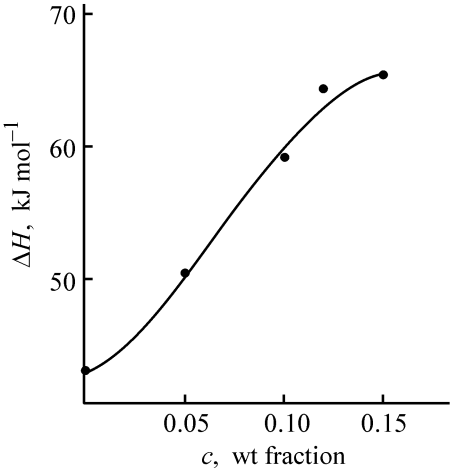


Fig. 3. Activation enthalpy of ΔH of viscous flow of SPA–chitosan melts vs. the weight fraction of chitosan, *c*.

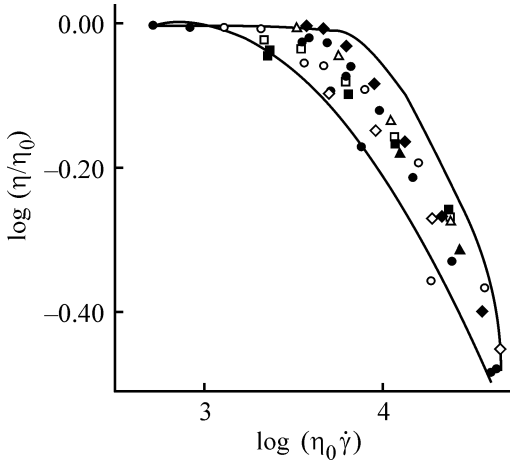


Fig. 4. Temperature-invariant characteristic of the viscosity of SPA–chitosan melts. (η/η_0) Reduced viscosity and ($\eta_0\dot{\gamma}$) specific shear rate. Filled and hollow symbols refer to 150 and 170°C, respectively.

of its melt and in the activation enthalpy of viscous flow of the blends.

(2) The dependences of the viscosity of SPA–chitosan blend on temperature and composition follow the principle of invariance of rheological properties, known for polymer systems, which can be used to predict the rheological properties of these blends in development of new biodegradable polymer materials.

ACKNOWLEDGMENTS

This study was financially supported by the Russian Foundation for Basic Research (project no. 04-03-96087) and by CRDF (grant NEK-005-XI).

REFERENCES

1. Suvorova, A.I., Tyukova, I.S., and Trufanova, E.I., *Usp. Khim.*, 2000, vol. 69, no. 5, pp. 494–503.
2. Fomin, V.A. and Guzeev, V.V., *Plast. Massy*, 2001, no. 2, pp. 42–46.
3. Chernekii, V.N. and Nifant'ev, N.E., *Zh. Ross. Khim. O–va im. D.I. Mendeleeva*, 1997, vol. 41, no. 1, pp. 80–83.
4. Hirano, S., *Applications of Chitin and Chitosan*, Goosen, M.F.A., Ed., Lancaster: Technomic, 1997, pp. 31–54.
5. Gooday, G.W., *Biodegradation*, 1990, vol. 1, pp. 177–190.
6. Peniche, C. and Argüelles-Monat, W., *Macromol. Symp.*, 2001, vol. 168, pp. 103–116.
7. Suvorova, A.I., Tyukova, I.S., and Sannikova, L.N., *Vysokomol. Soedin., Ser. A*, 2003, vol. 45, no. 5, pp. 797–803.
8. Vikhoreva, G.A., Rogovina, S.Z., Akopova, T.A., *et al.*, *Vysokomol. Soedin., Ser. B*, 1996, vol. 38, no. 10, pp. 1781–1785.
9. Gupta, R.K., *Polymer and Composite Rheology*, New York: Dekker, 2000, 2nd Ed.
10. Malkin, A.Ya. and Chalykh, A.E., *Diffuziya i vyazkost' polimerov: Metody izmereniya* (Diffusion and Viscosity of Polymers: Measurement Procedures), Moscow: Khimiya, 1979.
11. Gul', V.E. and Kuleznev, V.E., *Struktura i mekhanicheskie svoistva polimerov* (Structure and Mechanical Properties of Polymers), Moscow: Labirint, 1994.
12. Tager, A.A., *Fizikokhimiya polimerov* (Physical Chemistry of Polymers), Moscow: Khimiya, 1978.
13. Guerrero, C., Gonzalez, V., and Ortitz, U., *J. Polym. Eng.*, 1997, vol. 17, no. 2, pp. 109–133.
14. Shchukin, E.A., Pertsov, A.V., and Amelina, E.A., *Kolloidnaya khimiya* (Colloidal Chemistry), Moscow: Vysshaya Shkola, 2004,
15. Vinogradov, G.V., Malkin, A.Ya., and Prozorovskaya, N.V., *Dokl. Akad. Nauk SSSR*, 1964, vol. 154, no. 4, pp. 890–893.
16. Torner, R.V., *Teoreticheskie osnovy pererabotki polimerov (mekhanika protsessov)* (Theoretical Foundations of Polymer Processing (Mechanics of Processes)), Moscow: Khimiya, 1977.
17. Suvorova, A.I., Tyukova, I.S., and Smirnova, E.A., *Zh. Prikl. Khim.*, 2003, vol. 76, no. 12, pp. 2038–2042.

Russian Journal of Applied Chemistry, Vol. 78, No. 6, 2005, pp. 971–974. Translated from Zhurnal Prikladnoi Khimii, Vol. 78, No. 6, 2005, pp. 993–996.
Original Russian Text Copyright © 2005 by Alekseeva, Rozhkova, Eliseeva, Prusov.

MACROMOLECULAR CHEMISTRY AND POLYMERIC MATERIALS

Structural and Hydrodynamic Characteristics of Dextrans in Liquid-Phase Media

O. V. Alekseeva, O. V. Rozhkova, O. V. Eliseeva, and A. N. Prusov

Institute of Chemistry of Solutions, Russian Academy of Sciences, Ivanovo, Russia

Received February 9, 2005

Abstract—Viscous and volume properties of solutions of dextran with various molecular weights in water and dimethyl sulfoxide were studied.

In recent years, the researchers' attention has been attracted by natural polymer systems based on polysaccharides, which are not only biologically active compounds, but also an adequate model of amorphous regions of cellulose for studying solvation interactions in solution. Of particular interest are bacterial polymers, dextrans. Owing to their unique physicochemical properties, they are widely used in medicine and pharmacology. The practical use of these polysaccharides as effective blood substitutes makes a study of their behavior in dilute solutions a matter of current interest. Unfortunately, publications devoted to this issue are scarce [1].

In the present study, viscous and volume properties of solutions in water and dimethyl sulfoxide (DMSO) of dextrans with various molecular weights were subjected to a systematic analysis.

EXPERIMENTAL

Dextrans of Fluka AG Buchs brand, with molecular weights of 70×10^3–500×10^3, served as objects of study. The dextrans were dried in a vacuum at 330 K for 24 h. Water (twice distilled) and DMSO purified and dehydrated by the procedure described in [2] were used as solvents. The content of water in the solvent was determined by amperometric titration by the Fisher method to be ±0.002%. Polymer solutions were prepared gravimetrically using a VLR-200 balance with an accuracy of $\pm 5 \times 10^{-5}$ g. The viscosity of polymer solutions with concentrations of 3–16 kg^{-3} was measured with a capillary Ubbelohde viscometer at 293–303 K. The root-mean-square error in viscosity measurements was ±0.5%.

The dependences of the reduced viscosity of dilute solutions of dextrans, η_{sp}/c, on the polymer concentration c were linear for all the systems studied ($r = 0.98$). The viscometric Huggins constant was found using the equation from [3]:

$$\eta_{sp}/c = [\eta] + K_H c[\eta]^2, \quad (1)$$

where K_H is the Huggins constant, which describes the interaction of segment of polymer macromolecules with the solvent, and $[\eta]$ is the characteristic viscosity.

The solvent was characterized by K_H, $[\eta]$, and average statistical dimensions of macromolecular coils. The volume V_m of a polymer macromolecule and the root-mean-square distance $(\bar{h}^2)^{1/2}$ between the chain ends of polymer macromolecules were calculated by the formulas [4, 5]:

$$[\eta] = \Phi(\bar{h}^2)^{1/2}/M, \quad (2)$$

$$[\eta] = 2.5 N_A V_m/M, \quad (3)$$

were Φ is the Flory coefficient, which accounts for the deviation of the actual volume of the macromolecules from the spherical volume and for the partial permeability of the coil to the solvent; M, molecular weight of dextran; 2,5, form factor of a spherical particle; N_A, Avogadro number.

The density of dextran solutions was studied with a vibrational densitometer. The design of the densitometer and the experimental procedure were described in [6]. The error in density measurements was $\pm 2 \times 10^{-6}$ g cm^{-3}, which made it possible to calculate the volume characteristics of dextran with a sufficient reliability. The volume parameters were evaluated by an efficient procedure based on the experimentally measured solution density as the input value.

1070-4272/05/7806-0971 © 2005 Pleiades Publishing, Inc.

Table 1. Hydrodynamic parameters of dextran macromolecules in water and DMSO

M dextran	T, K	[η], $m^3\ kg^{-1}$	K_H	$(\bar{h}^2)^{1/2}$, nm	$V_m \times 10^{20}$, m^3
		Dextran–water			
70×10^3	293	0.019	1.068	17.95	0.088
	298	0.018	1.208	17.63	0.084
	303	0.016	1.766	16.95	0.074
	308	0.013	2.685	15.82	0.060
110×10^3	293	0.025	1.009	22.87	0.183
	298	0.022	1.115	21.91	0.161
	303	0.017	1.679	20.11	0.124
	308	0.014	1.802	18.85	0.102
500×10^3	293	0.040	0.773	44.30	1.329
	298	0.039	0.790	43.93	1.296
	303	0.035	1.046	42.37	1.163
	308	0.030	1.468	40.25	0.997
		Dextran–DMSO			
70×10^3	293	0.030	1.031	19.93	0.121
	298	0.028	1.198	19.13	0.107
	303	0.022	1.404	18.85	0.102
	308	0.020	1.532	18.26	0.093
110×10^3	293	0.043	0.623	27.40	0.314
	298	0.040	0.659	26.74	0.292
	303	0.038	0.707	26.29	0.278
	308	0.037	0.813	26.06	0.270
500×10^3	293	0.052	0.453	48.35	1.728
	298	0.050	0.484	47.72	1.661
	303	0.049	0.495	47.40	1.628
	308	0.048	0.501	47.08	1.595

To diminish the calculation error, partial molar volumes were calculated directly from experimental data on density by the equation [7]

$$V_2 = M_2/\rho - \frac{(1000 + mM_2)}{\rho^2}\frac{\partial\rho}{\partial m}, \quad (4)$$

where V_2 is the partial molar volume of the solute; M_2, molecular weight of the solute; ρ, solution density; and m, molal concentration of the solution (mol kg^{-1}).

The apparent molar volume V_Φ of the solute was calculated using the equation [8]:

$$V_\Phi = 1000(\rho_0 - \rho)/m\rho\rho_0 + M_2/\rho, \quad (5)$$

where ρ_0 is the density of the pure solvent.

The data in Table 1 demonstrate that solutions of dextrans with different molecular weights in water and DMSO have comparatively viscosities. The highest values of [η], V_m, and $(\bar{h}^2)^{1/2}$ are observed in DMSO, and the lowest, in water. At the same time, K_H has the minimum value in DMSO. Such a behavior of K_H is due to different mechanisms of solvation of polymer macrochains by molecules of water and DMSO. Water has a tetrahedral structure owing to the formation of strong hydrogen bonds between its molecules. Dimethyl sulfoxide is an associated liquid composed of clusters [9]. Having an unshared electron pair, the DMSO molecule can interact with both polar (ionic compounds) and nonpolar molecules and, therefore, dextran molecules are easily incorporated into the DMSO structure (because of the lower energy expenditure as compared with water) to form stable compounds with DMSO clusters. In this case, the macromolecular coil increases in size and a developed three-dimensional (3D) system of intermolecular bonds is formed. The strong intermolecular interaction between polysaccharide molecules and DMSO is confirmed by the negative enthalpy of dextran transfer from water into DMSO [1]. The increase in [η] and in average statistical dimensions of dextran macromolecules may be due in the given case both to a decrease in the thermodynamic lability of the molecular coil and to conformational changes (transition to a more unfolded state) through formation of new intermolecular complexes polymer–DMSO. In this case, the conformational lability of dextran is, as follows from NMR data, higher in water, compared with DMSO [10], which is in a good agreement with experimental data on viscosity.

Lowering the molecular weight of the polymer from 500×10^3 to 70×10^3 in the liquid-phase systems studied leads to an increase in K_H and decrease in [η] and in hydrodynamic dimensions of dextran macromolecules and is accompanied by their transition to a more folded conformation.

As temperature is raised from 293 to 313 K, the characteristic viscosity, dimensions of the macromolecular coil, and the intensity of intermolecular polymer–solvent interactions for dextrans with different molecular weights in water and DMSO decrease (Table 1). Presumably, this is due to structuring processes occurring in solutions because of the weakening of intermolecular interactions upon enhancement of the thermal motion.

To determine the structural changes in the systems under study, the enthalpies of activation of the viscous flow of polymers in solutions in the temperature

range 293–313 K were calculated. The enthalpies of activation of the viscous flow for samples of dextrans with molecular weights of 70×10^3–110×10^3 in water (9.2–10.3 kJ mol^{-1}) and DMSO (8.1–7.0 kJ mol^{-1}) differ only slightly. Another pattern is observed for samples of a dextran with a molecular weight of 500×10^3 in the solvents studied. As noted above, aqueous solutions of a dextran with $M = 500 \times 10^3$ have a lower viscosity than solutions in DMSO. However, the enthalpy of dextran activation in DMSO (3.7 kJ mol^{-1}) is lower than that in water (14.7 kJ mol^{-1}). The lower enthalpies of activation of the viscous flow of the polymer in DMSO are due to the following: a developed 3D system of intermolecular bonds is formed in DMSO, but it is not as stable as that in water, because dextran macromolecules are bound together by DMSO clusters. In this case, differences between the entropies of the viscous flow of solutions in water and DMSO must be observed. Indeed, the manner in which the entropy of activation changes in the systems under study indicates that orientation effects are predominant in a flow of dextran solutions in DMSO ($T\Delta S$ = –6.5 kJ mol^{-1}), compared with aqueous solutions ($T\Delta S$ = 5.6 kJ mol^{-1}), in which destruction of order dominates.

To confirm the previously advanced hypotheses, the volume properties of the polymers were studied. The figure and Table 2 show the concentration dependences of the density and the apparent and partial molar volumes of dextrans with different molecular weights in the solvents studied. It can be seen that the densities and volumes in equally concentrated solutions grow as the molecular weight of the polymer increases (Table 2). The types of behavior of the partial and apparent molar volumes of dextrans in water and DMSO with the polymer concentration were found to be different. As the polymer concentration in aqueous solutions is raised, the partial and apparent molar volumes grow and pass through a maximum, with the maximum becoming stronger at higher molecular weights of the polymer. In DMSO, a similar dependence passes through a minimum, and this minimum becomes more pronounced for dextrans with a molecular weight of 500×10^3. These differences may be due to different mechanisms of solvation of the polymer by molecules of water and DMSO.

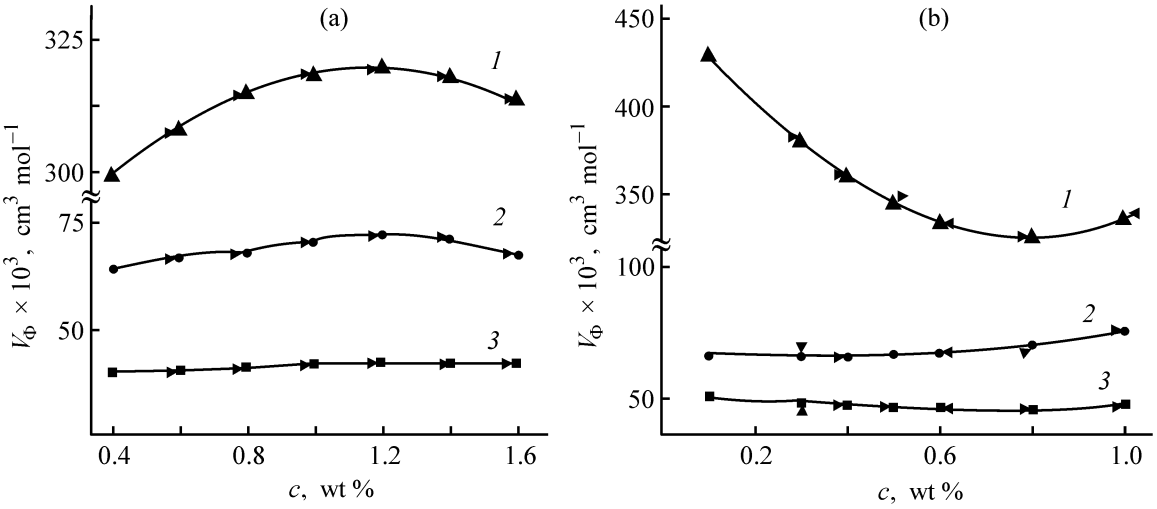
Thus, the results obtained in a study of the volume properties of dextran solutions are in a good agreement with their viscous characteristics. The data obtained are of interest for a deeper insight into the dextran structuring in liquid-phase media.

Table 2. Density ρ and partial molar volumes V_2 of dextrans in water and DMSO at 298 K

c, wt %	ρ, g cm^{-3}		V_2, cm^3 mol^{-1}	
	H_2O	DMSO	H_2O	DMSO
	$M = 70 \times 10^3$			
0	0.997075	1.089362	44260.54	51959.54
0.1	–	1.089600	–	48577.50
0.3	–	1.090216	–	44253.06
0.4	0.998512	1.090570	45529.72	43318.96
0.5	–	1.090933	–	43240.39
0.6	0.999208	1.091286	45929.95	44010.33
0.8	0.999898	1.091924	46172.76	48170.95
1.0	1.000583	1.092356	46254.42	55891.86
1.2	1.001269	–	46172.84	–
1.4	1.00196	–	45925.90	–
1.6	1.002664	–	45509.79	–
	$M = 110 \times 10^3$			
0	0.996982	1.089449	54688.79	67213.66
0.1	–	1.089824	–	65344.41
0.3	–	1.090613	–	64903.24
0.4	0.99855	1.090998	58881.22	66360.57
0.5	–	1.091365	–	68972.63
0.6	0.999288	1.091699	60046.7	72778.44
0.8	1.000017	1.092206	60588.36	83918.22
1.0	1.00074	1.092411	60489.06	99601.23
1.2	1.001473	–	59742.08	–
1.4	1.002228	–	58336.03	–
1.6	1.003014	–	56272.51	–
	$M = 500 \times 10^3$			
0	0.997060	1.089420	274067.42	460592.55
0.1	–	1.089491	–	399850.99
0.3	–	1.089990	–	315236.38
0.4	0.998660	1.090360	320252.52	291465.93
0.5	–	1.090793	–	279847.38
0.6	–	1.091216	334874.32	281502.08
0.8	1.000011	1.091991	330308.98	323744.82
1.0	1.000672	1.092437	317799.42	421363.45
1.2	1.001365	–	297331.00	–
1.4	1.002121	–	268899.31	–
1.6	1.002973	–	268899.31	–

CONCLUSION

The characteristic viscosities, Huggins constants, hydrodynamic dimensions of macromolecules, and partial and apparent molar volumes of dextran solu-



Apparent molar volumes V_Φ vs. the concentration c of dextrans in (a) water and (b) DMSO at 298 K. Molecular weight ($M \times 10^{-3}$): (*1*) 500, (*2*) 110, and (*3*) 70.

tions in water and dimethyl sulfoxide were calculated. The differences revealed in the behavior of dextrans were attributed to different mechanisms of solvation of polymer macrochains by solvent molecules.

REFERENCES

1. Myasoedova, V.V., Pokrovskii, S.A., Zav'yalov, N.A., *et al.*, *Usp. Khim.*, 1991, vol. 60, no. 9, pp. 1875–1897.
2. Gordon, A.J. and Ford, R.A., *The Chemist's Companion. A Handbook of Practical Data, Techniques and References*, New York: Wiley-Interscience, 1972.
3. Rabek, J.F., *Experimental Methods in Polymer Chemistry. Physical Principles and Applications*, Chichester: Wiley, 1980.
4. *Cellulose and Cellulose Derivatives*, part IV, Bikales, N.M. and Segal, L., Eds., New York: Wiley-Interscience, 1971.
5. Pavlova, S.A., *Metody issledovaniya tsellyulozy* (Methods for Study of Cellulose), Karlivan, V.P., Ed., Riga: Zinatne, 1981, pp. 179–191.
6. Korolev, V.V., *Zh. Fiz. Khim.*, 1989, vol. 64, no. 7, pp. 1701–1705.
7. Kolker, A.M. and Safonova, L.P., *Ionnaya sol'vatatsiya* (Ionic Solvation), Moscow: Nauka, 1987, pp. 199–226.
8. Eliseeva, O.V., Golubev, V.V., and Abakshin, V.A., Available from VINITI, 1997, Moscow, no. 2969-V97.
9. Yoshikata Koga, Yasutoshi Kaasahara, Kasumi Yoshino, and Keiko Nishikawa, *J. Solut. Chem.*, 2001, vol. 30, no. 10, pp. 885–893.
10. Daragan, V.A., Il'ina, E.E., and Myasoedova, V.V., Abstracts of Papers, *Vsesoyuznoe soveshchanie po kislotno-osnovnym vzaimodeistviyam i sol'vatatsii neelektrolitov* (All-Union Symp. on Acid-Basic Interactions and Solvation of Nonelectrolytes), Kharkov, 1987, p. 106.

Russian Journal of Applied Chemistry, Vol. 78, No. 6, 2005, pp. 975–980. Translated from Zhurnal Prikladnoi Khimii, Vol. 78, No. 6, 2005, pp. 997–1002.
Original Russian Text Copyright © 2005 by Bel'nikevich, Litvinova, Budtov.

MACROMOLECULAR CHEMISTRY AND POLYMERIC MATERIALS

Viscometric Behavior of Polystyrene in Binary Solutions Used as Eluents in Adsorption Chromatography

N. G. Bel'nikevich, L. S. Litvinova, and V. P. Budtov

Institute of Macromolecular Compounds, Russian Academy of Sciences, St. Petersburg, Russia

Received October 14, 2004; in final form, February 17, 2005

Abstract—Calculated and experimentally measured characteristic viscosities [η] of polystyrene in some binary solvents used as eluents in chromatographic experiments in a wide range of mixture compositions were compared. The values of [η] were measured in solvents of varied thermodynamic quality, including the theta solvent and mixtures of solvents of the following compositions: two good solvents; good solvent and theta solvent; good solvent and precipitant; poor solvent and theta solvent. An equation that relates the anomalies observed in the dependences of [η] on the composition of a solvent mixture to parameters of the Flory–Huggins thermodynamic interaction was suggested.

Ternary polymeric systems (a polymer in a binary solvent) have long attracted researchers' attention. Binary mixtures have been frequently used as theta solvents. Specific features in the behavior of these solutions, which cannot be understood in terms of the existing theories of polymer–solvent systems, have been revealed. Mixtures of solvents are widely used in practice of polymer processing. The recent interest in systems of this kind is due to their application in chromatography, and specifically in adsorption chromatography under critical conditions.

In the 1960–1970s, there appeared a large number of publications reporting on experimental and theoretical studies of polymer solutions in mixed solvents. In many systems, the dependences of the characteristic viscosity [η], second virial coefficient, sorption selectivity coefficient, and unperturbed size of macromolecular coils on the solvent composition were nonlinear [1]. This phenomenon has been mainly related by researchers to the balance of forces of intermolecular interactions in systems constituted by a polymer and solvent (1), polymer and solvent (2), solvent (1) and solvent (2), and two polymers. Numerous attempts have been made to introduce additional parameters, to take into account ternary interactions, into the equations used to calculate the size of macromolecular coils in binary solvents [1]. However, many of these parameters can be neither calculated nor measured [2]. Until now, the questions concerning the conformation of macromolecular chains, selective sorption of solvents, and effect of temperature in ternary systems constituted by a polymer in a binary solvent remain unanswered. It is known that the absolute viscosities of low-molecular nonelectrolyte liquids (binary and ternary) differ from the additive values by 10–18% [3], and the existence of dipole–dipole interactions in binary systems substantially enhances the deviations of their viscosity from linearity. In some cases, the dependences of the absolute viscosity on the mixture composition have an extremal nature [4].

It has been shown previously [5, 6] that the thermodynamic quality of the mobile phase is, under conditions of adsorption chromatography, a factor that affects the adsorption behavior of macromolecules and determines the degree of unfolding of the polymer chain in a single sorption–desorption event. To attain the same retaining factor of macromolecules, the polarity index of the mobile phase should be the higher, the better its thermodynamic quality. Therefore, the problem of the thermodynamic quality of a solvent used in chromatographic experiments is a matter of current interest.

Because the simplest way to compare the quality of solvents is to determine the characteristic viscosity [η], it seemed advisable to perform special-purpose experiments aimed to compare the calculated and measured values of [η] in some binary solvents used in chromatographic experiments, in a wide range of mixture compositions. In doing so, we made an at-

1070-4272/05/7806-0975 © 2005 Pleiades Publishing, Inc.

tempt to express the effects we observed in terms of the readily determinable parameter of the thermodynamic interaction, χ (Flory–Huggins parameter).

EXPERIMENTAL

It is known that the characteristic viscosity $[\eta]$ is proportional to the volume of macromolecules in solution and is related to the root-mean-square size of a thermodynamically unfolded coil by the following expressions:

$$[\eta]_\theta = \Phi_\theta (h_\theta^2)^{3/2}/M \text{ (in a theta solvent)}, \quad (1)$$

$$[\eta] = [\Phi_\theta (h_\theta^2)^{3/2}/M]\alpha^3 \text{ (in a good solvent)}, \quad (2)$$

where M is the molecular weight of the polymer; Φ_0, universal (under theta conditions) Flory constant; $(h_0^2)^{1/2}$, linear size of a chain molecule under theta conditions; and α, degree of swelling of the macromolecular coil [7, 8].

In good solvents, coils swell to a greater extent than in poor solvents, i.e., the better the thermodynamic quality of a solvent, the higher $[\eta]$:

$$[\eta] = [\eta]_\theta \alpha^3. \quad (3)$$

It is possible to determine $[\eta]$ for well-studied polymers, such as polystyrene and polymethyl methacrylate, in individual solvents by calculation, because the constants in the Mark–Kuhn–Houwink equation ($[\eta] = K_\eta M^a$) have been experimentally determined for most of solvents and can be found in the reference literature [9]. However, solvent mixtures are, as a rule, used as eluents in chromatographic experiments, and calculation of $[\eta]$ for these mixtures is, as shown above, a more complicated procedure. For example, a calculation of $[\eta]$ in a mixed solvent as a sum of products of $[\eta]$ in an individual solvent by the volume fraction of the solvent in the mixture, x_i, is only possible in the absence of specific polymer–solvent and(or) polymer–polymer intermolecular interactions [8]. In this case, the dependence of the additive viscosity $[\eta]_{ad}$ on the composition of the binary mixture is expressed by the equation

$$[\eta]_{ad} = [\eta]_1 x_1 + [\eta]_2 x_2, \quad (4)$$

where x_i is the volume fraction of a component, with $x_1 + x_2 = 1$.

The deviations $\Delta[\eta]$ of the experimental values of $[\eta]$ (or, accordingly, α^3) from their calculated additive values are occasionally related to the excess free energy of solvent mixing, ΔG. In particular, it follows from the equation suggested by Dondos and Patterson [10] that $\Delta[\eta]$ must be positive at $\Delta G > 0$ and negative at $\Delta G < 0$.

To relate the effects observed to the known constant χ_{ik} of the thermodynamic Flory–Huggins interaction, which characterizes intermolecular interactions in the system, we can use the following simple expression [8, 11]:

$$\varepsilon_i = 2\chi_{i3} - 1. \quad (5)$$

Here, the Flory–Huggins constant χ_{ik} is expressed in terms of the reduced excluded volume $-\varepsilon_i$, which also characterizes the interaction of the polymer with the mixture components:

$\varepsilon \approx -0.2\ldots0$ for good solvents, $\varepsilon \approx 0-0.1$ for bad solvents, and $\varepsilon > 0.3$ for precipitants.

Then we have for the mixture constituted by solvent (1), solvent (2), and polymer (3):

$$\varepsilon_m = x_1\varepsilon_1(1 - x_2\chi_{12}) + x_2\varepsilon_2(1 - x_1\chi_{12}) + x_1x_2[\Delta\chi^2 - \chi_{12}(2 - \chi_{12})], \quad (6)$$

where x_1 and x_2 are the volume fractions of the solvents ($x_1 + x_2 = 1$); χ_{12}, the solvent–solvent interaction parameter for easily mixed solvents, equal to 0.1–0.6; $\Delta\chi = \chi_{13} - \chi_{23}$; and χ_{13} and χ_{23}, interaction parameters for the polymer–solvent (1) and polymer–solvent (2) systems, respectively. Relation (6) can be represented as

$$\varepsilon_m = \varepsilon_{ad} + \Delta\varepsilon, \quad (7)$$

where

$$\varepsilon_{ad} = x_1\varepsilon_1 + x_2\varepsilon_2, \quad (8a)$$

$$\Delta\varepsilon = x_1x_2[\Delta\chi^2 - \chi_{12}(\chi_{12} - 2\chi_{13} - 2\chi_{23})]. \quad (8b)$$

It can be seen from relations (6), (7), (8a), and (8b) that a strong deviation from additivity is associated with the values of χ_{12} and $\Delta\chi^2$. An increase in $\Delta\chi^2$ always leads to a rise in $\Delta\varepsilon$, whereas the contribution from χ_{12} depends on the quality of a solvent used. It is known that, in some cases, the thermodynamic quality of a mixture of poor solvents is better than that of the initial components [1]. Simple calculations show that the strongest deviation from additivity must be observed at $x_1 = x_2 = 0.5$, i.e., at a 1 : 1 ratio of solvents in the mixture.

Flory–Huggins constants, second virial coefficients, reduced excluded volumes, C constants, and $\Delta[\eta]/x_1x_2$ [Eq. (14)] for polystyrene in individual solutions and mixtures of these

Solvent	χ	$A_2 \times 10^4$, mol cm^3 g^{-2}	ε_i	Mixed solvent	$-C$	$\Delta[\eta]/x_1x_2$
THF	0.4645	4.00	0.08	Toluene/CCl_4	20.0	–
Toluene	0.456	3.29	0.08	Toluene/Cyclohexane	17.6	0.88
CCl_4	0.463	2.60	0.07	THF/Cyclohexane	19.7	1.11
MEK	0.491	1.00	0.015	MEK/Cyclohexane	19.5	1.75
Cyclohexane (35°C)	0.5	0.93	0.0	–	–	–

It is known that the solvent quality also affects the Huggins constant K', which characterizes intermolecular and hydrodynamic interactions in a shear flow. Its values depend on the polymer–solvent interactions. For linear flexible-chain polymers, K' varies from 0.2 (good solvents) to 0.5 (bad solvents) [7, 8]. An expression describing K' in a wide range of α has been derived [8]:

$$K' = 0.25 + 0.3/\alpha^6. \quad (9)$$

The validity of expression (9) was confirmed for many polymer–solvent systems; however, this expression has not been extended to ternary polymeric systems until now. We found it appropriate to determine the dependence of K' on α [Eq. (9)] for polymers in binary solutions.

We chose for our experiments polystyrene with a weight-average molecular weight $M_w = 460 \times 10^3$ and a molecular-weight distribution $M_w/M_n < 1.1$. The values of $[\eta]$ were measured in good solvents: toluene, carbon tetrachloride CCl_4, and terahydrofuran (THF); in methyl ethyl ketone (MEK), a solvent with a poorer thermodynamic quality; in cyclohexane, a theta solvent; and solvent mixtures of the following compositions: two good solvents (1), good solvent and theta solvent (2), good solvent and precipitant (3), and poor solvent and theta solvent (4). The solvents were of analytically pure grade. All the solvents are indefinitely soluble in one another, with the exception of the MEK/cyclohexane pair, whose poor compatibility is indicated by the thermodynamic nature of the process of their mixing.

The thermodynamic quality of individual solutions with respect to polystyrene was well studied long ago. The relevant data are available in numerous publications and in the reference literature [9, 12]. This property of the solvents used was characterized by the second virial coefficient A_2 (see table).

The characteristic viscosities were measured in capillary viscometers of the Ubbelohde type with a suspended level. The time of solvent outflow was ~100 s, with the measurement error not exceeding 2%. The experiments were performed at 25°C, and those with cyclohexane-containing solutions, at 25 and 35°C.

We obtained an experimental dependence of $[\eta]$ of polystyrene on the composition of a binary solvent constituted by a pair of good solvents (toluene/CCl_4). As can be seen from Fig. 1 (curve *1*), the experimental values of $[\eta]$ coincide with the additive values [Eq. (4)]. The hydrodynamic volume of macromolecules is virtually independent of the solvent composition. The maximum deviation from the additive values of $[\eta]$, $\Delta[\eta]$, was 2.6%. The scatter of K' is also insignificant: 0.35–0.42.

The dependences of $[\eta]$ on the composition of mixtures constituted by a theta solvent and a good solvent, to which belong the mixtures cyclohexane/toluene (Fig. 1, curve *2*), cyclohexane/THF (Fig. 1, curve *3*), and cyclohexane/MEK (Fig. 2, curves *2* and *3*), exhibit deviations from linearity. As the fraction of cyclohexane increases from zero to 0.6 in a cyclohexane/THF mixture and to 0.4 in a cyclohexane/toluene mixture, the values of $[\eta]$ for polystyrene change only

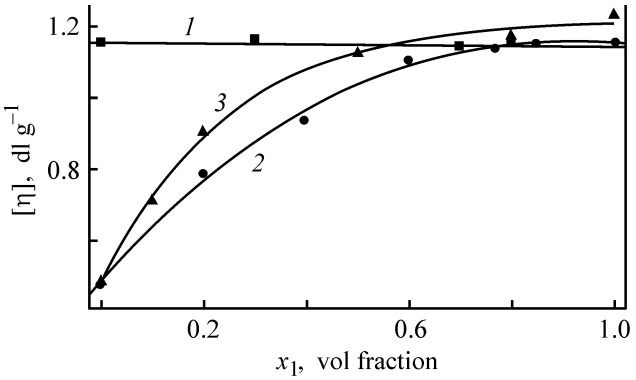


Fig. 1. Characteristic viscosity $[\eta]$ for polystyrene with $M_w = 460 \times 10^3$ in the mixtures (*1*) toluene/CCl_4, (*2*) toluene/cyclohexane, and (*3*) tetrahydrofuran/cyclohexane. (x_1) Volume fraction of toluene or tetrahydrofuran.

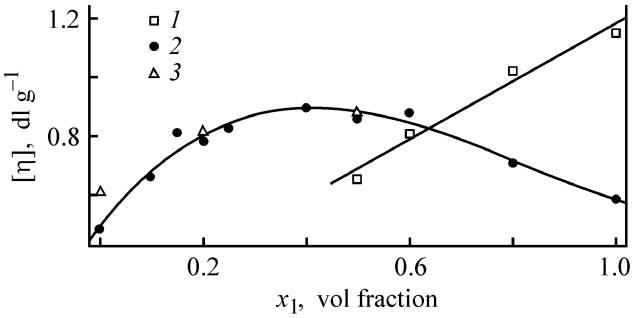


Fig. 2. Characteristic viscosity [η] of polystyrene with $M_w = 460 \times 10^3$ in the mixtures (*1*) toluene/hexane, (*2*) methyl ethyl ketone/cyclohexane at 25°C, and (*3*) the same mixture at 35°C. (x_1) Volume fraction of toluene or methyl ethyl ketone.

slightly: by 9 and 5%, respectively. Further addition of cyclohexane leads to their dramatic decrease, although the values of K' emain close to those for good solvents. This fact can be accounted for by selective sorption of the solvent by polystyrene molecules, which leads to an increase in the concentration of the good solvent in the solvation shell of a macromolecule, compared with its concentration in the surrounding solution. The degree of macromolecule swelling will be higher in this case.

An interesting pattern is observed for a mixture of two poor solvents: cyclohexane/MEK. Pure MEK is not a good solvent for polystyrene. This is also indicated by low [η] and K' close to 0.5. In addition, this is, as already noted, the only pair of solvents, of those used in the experiments, for which the mixing process is endothermic. A dependence of [η] on the solvent composition with a maximum was obtained for this mixture (Fig. 2). At the maximum, at a 1 : 1 component ratio, the value of [η] exceeds by 53% that for pure MEK, and by 87% that for pure cyclohexane.

The experiments were performed at two temperatures: 25 and (because the theta temperature for polystyrene in cyclohexane is 34°C) and 35°C. At all compositions of mixtures of these solvents, the values of [η] virtually coincide for these two temperatures. Differences are only observed in pure cyclohexane: [η] grows from 0.48 dl g^{-1} at 25°C to 0.607 dl g^{-1} at 35°C, in a good agreement with published data [13]. Similar nonlinear viscosity–composition dependences have been obtained previously for polystyrene in acetone/methyl cyclohexane and dioxan/chloroform mixtures [1].

As the values of [η] in MEK and cyclohexane are close, it may be considered that ε_1 and ε_2 are also close. Then, we have for the symmetric case ($\varepsilon_1 = \varepsilon_2$) from relation (6) that

$$\varepsilon_m = \varepsilon_1 - x_1 x_2 \chi_{12}(\varepsilon_1 + 2 - \chi_{12}). \qquad (10)$$

It can be seen that, for a mixture of solvents, the second term is always negative, i.e., the thermodynamic quality of the system is improved upon addition of the second component. The second term is at a maximum at $x_1 = x_2 = 0.5$, and just this is the case in the experiment.

In mixtures constituted by a solvent and a precipitant (toluene/hexane), the value of [η] steadily decreases as the fraction of the precipitant in the mixture increases till the onset of polymer precipitation (Fig. 2). At a 1 : 1 solvent/precipitant ratio, [η] decreases from 1.16 to 0.66 dl g^{-1} ($\Delta[\eta] = 43\%$), which means that the hydrodynamic volume of macromolecules considerably decreases. However, the values of [η] (and, accordingly, the volume of macromolecules) are somewhat higher than the additive values, which is also confirmed by chromatographic experiments. The run of these experimental curves is accounted for by the same selective polymer–solvent interactions as in the case of a system constituted by a good solvent as a theta solvent.

For the sake of convenience and simplicity of interpretation of the data obtained, let us revert to Eq. (3). According to Fixman's equation

$$\alpha^3 = 1 + 2z, \qquad (11)$$

where z is the known excluded volume parameter, which can be expressed in terms of the parameters ε_m, ε_{ad}, and $\Delta\varepsilon$, we introduced, as

$$\alpha^3 = 1 + C\varepsilon_m = 1 + C(\varepsilon_{ad} + \Delta\varepsilon), \qquad (12)$$

where C is a constant (negative, because ε_m is negative for good solvents), and ε_{ad} is the excluded-volume parameter calculated by the additive scheme [Eq. (8a)].

The values of ε_i, which can be readily found using relation (5) from the known Flory–Huggins parameters, are listed in the table. The same table presents values of C for the systems mentioned. The average value of C is –19.1.

Let us denote the deviations of $[\eta]_m$ from the additive value by

$$\Delta[\eta] = [\eta]_m - [\eta]_{ad}. \qquad (13)$$

Then, taking into account relations (3) and (12), we obtain

$$\Delta[\eta]/x_1x_2 = [\eta]_\theta |C| [\chi_{12}(2\chi_{23} + 2\chi_{13} - \chi_{12}) - \Delta\chi^2]. \quad (14)$$

It follows from Eq. (14) that an increase in the first term $\chi_{12}(2\chi_{23} + 2\chi_{13} - \chi_{12})$ virtually always leads to a rise in $\Delta[\eta]$, i.e., to a larger coil size. At the same time, an increase in the second term $\Delta\chi^2$ always leads to a decrease in $\Delta[\eta]$, i.e., to contraction of macromolecules.

Based on the experimental data, we obtained dependences of $\Delta[\eta]$ on the product x_1x_2 (Fig. 3). For all the systems constituted by a good solvent and a theta solvent, which we studied, these dependences are linear, in agreement with the theoretical predictions [Eq. (14)]. However, the slopes of these straight lines vary between different pairs of solvents and have the following values: 0.88 for toluene/cyclohexane, 1.11 for THF/cyclohexane, and 1.75 for MEK/cyclohexane. This means that the experimentally strongest effect is observed for a mixture constituted by a poor solvent and a theta solvent.

Figure 4 shows dependences of K' on α^3 for all the binary solution mixtures studied. It can be seen that all these dependences can be described by the same expression:

$$K' = 0.3 + 0.3/\alpha^6. \quad (15)$$

Thus, it was shown that the experimental dependences for ternary systems (a polymer in a binary solvent) are close to the dependences previously obtained for solutions of polymers in individual solvents, and Eq. (15) virtually coincides with relation (9), suggested in [8].

It is demonstrated that, in principle, values of $[\eta]$ in mixed solvents can be calculated. However, this calculation requires a knowledge of such thermodynamic characteristics as the interaction parameter for systems constituted by a polymer and solvent (1) or (2) or by solvent (1) and solvent (2) (χ_{12}, χ_{13}, and χ_{23}), which are not always available.

CONCLUSIONS

(1) It was shown that the values of $[\eta]$ measured for polystyrene in mixtures of two good solvents of various compositions are equal to the calculated additive values. The values of $[\eta]$, measured in solvent/precipitant mixtures, somewhat exceed the additive values. In mixtures constituted by a solvent and a theta solvent, nonlinear (and extremal for the MEK/cyclohexane mixture) dependences of $[\eta]$ of polystyrene on the solvent composition were obtained.

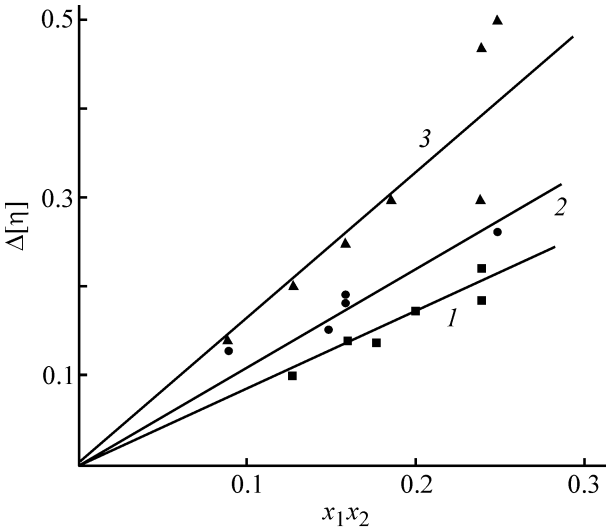


Fig. 3. Dependences of $\Delta[\eta]$ on x_1x_2 for different pairs of a solvent and a theta solvent. (*1*) toluene/cyclohexane, (*2*) THF/cyclohexane, and (*3*) MEK/cyclohexane.

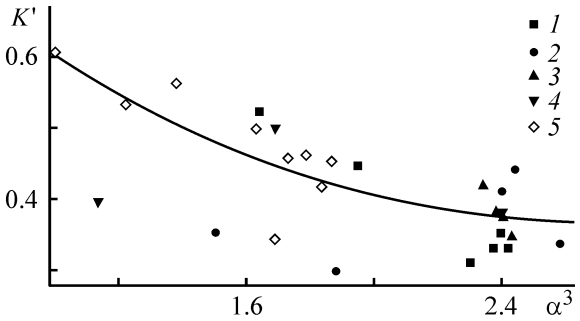


Fig. 4. Dependence of the Huggins constant K' on the degree of swelling, α^3, for polystyrene in mixtures (*1*) toluene/cyclohexane, (*2*) THF/cyclohexane, (*3*) toluene/CCl_4, (*4*) toluene/hexane, and (*5*) MEK/cyclohexane.

(2) The deviations of $[\eta]$ from the additive values, observed for polystyrene in mixed solvents, were attributed to selective solvation of macromolecules in ternary solutions, and this was confirmed by calculations of $\Delta[\eta]$ with account of the Flory–Huggins parameters of the thermodynamic interaction between the polymer and the solvent.

(3) It was shown that the experimental dependences of the Huggins constants on the degree of swelling of macromolecular coils for ternary systems (a polymer in a binary solvent) are close to the dependences previously obtained for solutions of polymers in individual solvents.

REFERENCES

1. Bekturov, E.A., *Troinye polimernye sistemy v rastvorakh* (Ternary Polymeric Systems in Solutions), Alma-Ata: Nauka Kazakhskoi SSR, 1975.
2. Quadrat, O., *Macromol. Chem. Rapid Commun.*, 1980, no. 1, pp. 651–654.
3. Pandey, J.D., Sushmita, M., Tripathi, S.B., *et al.*, *Indian J. Chem.*, 2001, vol. 40A, November, pp. 1214–1217.
4. Amalendu, P. and Rakesh, K.Bh., *Proc. Indian Acad. Sci. (Chem. Sci.)*, 2001, vol. 113, no. 3, pp. 215–225.
5. Litvinova, L.S. and Bel'nikevich, N.G., *3rd Int. Symp. "Molecular Order and Mobility in Polymer Systems,"* St. Petersburg, 7–10 June, 1999, P–096.
6. Litvinova, L., Bel'nikevich, N., and Tyihak, E.J., *Planar Chromatogr.*, 2000, vol. 13, no. 2, pp. 149–151.
7. Tsvetkov, V.N., Eskin, V.E., and Frenkel', S.Ya., *Struktura makromolekul v rastvorakh* (Structure of Macromolecules in Solutions), Moscow: Nauka, 1964.
8. Budtov, V.P., *Fizicheskaya khimiya rastvorov polimerov* (Physical Chemistry of Polymer Soutions), St. Petersburg: Khimiya, 1992.
9. Brandrup, J. and Immergut, E.H., *Polymer Handbook*, New York: Wiley Interscience, 1989.
10. Dondos, A. and Patterson, D., *J. Polymer Sci.*, 1969, vol. A2, no. 5, pp. 209–217.
11. Budtov, V.P., *Vysokomol. Soedin., Ser. A*, 1987, vol. 29, no. 9, pp. 1897–1901.
12. Kok, C.M. and Rudin, A.J., *Polym. Sci.*, 1982, vol. 27, no. 2, pp. 354–361.
13. Sun, S.F. and Fun Jingrung, *Polymer*, 1997, vol. 38, no. 3, pp. 563–570.
14. Litvinova, L. and Bel'nikevich, N., *J. Chromatogr.*, 2003, vol. 1005A, pp. 165–176.

Russian Journal of Applied Chemistry, Vol. 78, No. 6, 2005, pp. 981–984. Translated from Zhurnal Prikladnoi Khimii, Vol. 78, No. 6, 2005, pp. 1003–1005.
Original Russian Text Copyright © 2005 by Shkutina, Stoyanova, Selemenev.

MACROMOLECULAR CHEMISTRY AND POLYMERIC MATERIALS

Specific Features of Glucoamylase Immobilization by Adsorption on Fibrous Polyelectrolytes

I. V. Shkutina, O. F. Stoyanova, and V. F. Selemenev

Voronezh State University, Voronezh, Russia

Received March 2, 2005

Abstract—Some fundamental aspects of the immobilization of a hydrolytic enzyme glucoamylase via adsorption on aminocarboxylic ion-exchangers with fibrous structure were considered. The sorption capacity of amphoteric supports for the enzyme was studied in relation to the time of immobilization, concentration of hydrogen ions and the protein, and the ionic form of a polyelectrolyte. The catalytic properties of free and immobilized enzymes were compared.

Recently, the importance of reactions used to obtain products from renewable vegetable raw materials has been steadily increasing. A stage in production of glucose syrups widely used in food industry is saccharification of dextrinized starch, involving glucoamylase (α-1,4-glucanhydrolase, KF 3.2.1.3). The presently arising increased interest in immobilization of enzymes by supports of various kinds is due to the large potentialities in use of bound enzymes as specific and stable heterogeneous biocatalysts. A study of the immobilization of enzymes is primarily aimed to obtain data related to optimization of the process, which presumes an effective combination of the choice of a support with various conditions and parameters of the system and provides that the activity of the heterogeneous catalyst is preserved to the maximum possible extent.

Among the existing immobilization methods, the adsorption technique is distinguished by simplicity, requires no preliminary modification of a support, uses easily regenerated sorbents, and changes the structure of the enzyme to a lesser extent, compared with the case of covalent binding. In addition, of no less importance is the economic expediency and ecological safety of the method [2].

Despite that a large number of studies concerned with glucoamylase immobilization have been reported, the enzymatic process of hydrolytic amylolysis with a hereterogeneous catalyst has not been implemented [3, 4].

Previously, glucoamylase has been immobilized on a nonionogenic sorbent Stirosorb and granulated amphoteric ion-exchangers [5–7]. The present communication reports the results obtained in glucoamylase immobilization via adsorption on aminocarboxylic fibrous ion-exchangers of the Fiban type. The choice of sorbents as supports for enzyme immobilization is due to the similarity of the structural components of protein molecules and functional groups of polyelectrolytes. Use of fibers as supports is preferable in some cases to application of sorbents in other forms. Fiban fibers have a three-dimensional structure, highly developed surface, good mechanical strength, and chemical and osmotic resistance [8]. The physical form and properties of the biocatalyst obtained enable its use in continuous processes, e.g., in column reactors. The enzymes incorporated into its structure are protected from the inactivating influence of microorganisms.

EXPERIMENTAL

A hydrolytic enzyme glucoamylase from *Aspergillus awatori* was studied. As supports for glucoamylase immobilization served fibrous aminocarboxylic polyelectrolytes K-3, K-5, and AK-22-1, which contain $–NH_2$, =NH, ≡N, and –COOH as functional groups [9]. The ion-exchangers were prepared for immobilization by selecting a fraction with a required grain size, conditioning, and converting the ion-exchangers into the necessary ionic form [10].

1070-4272/05/7806-0981 © 2005 Pleiades Publishing, Inc.

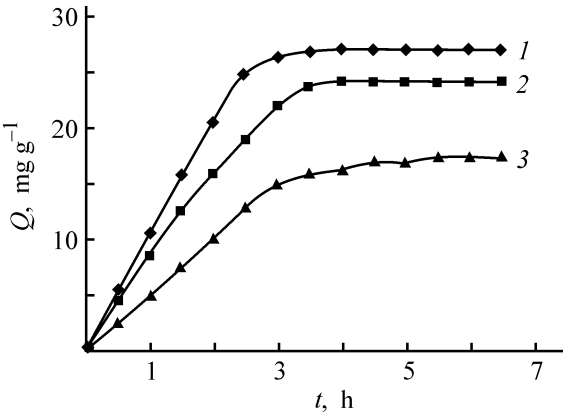


Fig. 1. Kinetic curves of glucoamylase sorption by fibrous ion-exchangers. (*Q*) Amount of sorbed glucoamylase and (*t*) process duration. (*1*) K-3, (*2*) K-5, (*3*) AK-22-1; the same for Figs. 2–4.

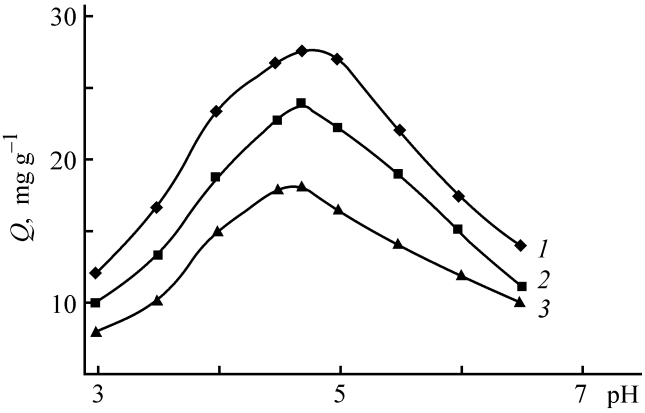


Fig. 2. Amount of sorbed glucoamylase, *Q*, vs. the pH value of the equilibrium solution.

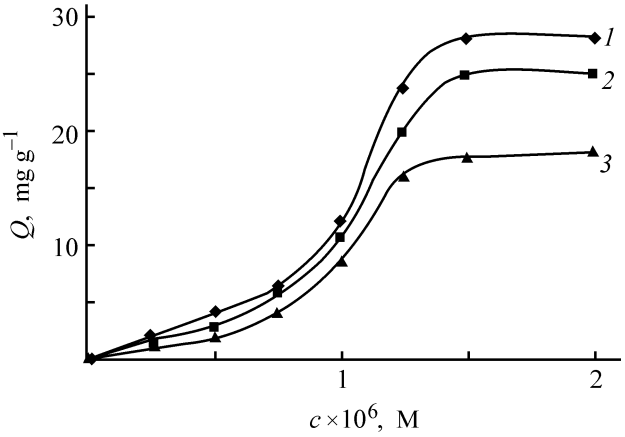


Fig. 3. Kinetic curves of glucoamylase sorption at pH 4.7. (*Q*) Amount of sorbed glucoamylase and (*c*) initial concentration of the protein in solution.

The immobilization was performed by the adsorption method under static conditions with periodic agitation at a temperature of 20°C. The desorption of the protein into buffer solutions did not exceed 5%. The total amount of the protein in native enzymatic preparations was determined by the Lowry method, and that in immobilized enzymes, by the modified Lowry method [11]. The catalytic activity of glucoamylase was measured by the glucose oxidase method [12]. As the activity unit of glucoamylase was taken such an amount of the enzyme, which catalyzes hydrolysis of starch at 25°C and pH 4.7 in 1 min to give 1 μmol of glucose. The mass of water in the sorbent was determined after phase separation by centrifugation at 3000 rpm for 5 min. The standard deviation of the results obtained did not exceed 0.05.

To determine the conditions in which glucoamylase can be immobilized the most effectively, the influence exerted by the time of immobilization and by the concentration of hydrogen ions on the amount of bound protein was studied. Figure 1 shows kinetic curves for immobilization of glucoamylase on fibrous supports. The shape of the curves obtained demonstrates that the sorption process occurs in about the same way on the ion-exchangers under study. Beginning at the very first minutes of phase interaction, the enzyme is sorbed at a rather high rate, so that the amount of adsorption in the first 2 h is 65–75% of the total amount of the bound protein. In all the cases under consideration, the amount of immobilized glucoamylase decreases in the final stages of the process and equilibrium is attained, on average, in 4 h.

The range of pH values in which an enzyme is selectively bound to supports depends on the electrochemical characteristics of the protein. The maximum sorption of glucoamylase is observed at pH 4.5–5.0, when most part of the enzyme is in the form of zwitter ions (Fig. 2).

The sorption curves shown in Fig. 3 point to a layer-by-layer nature of glucoamylase adsorption on fibrous supports. In an adsorption interaction of proteins with aminocarboxylic ion-exchangers, supramolecular complexes may be formed via interaction with, simultaneously, cationic, anionic, and neutral binding centers. Apparently, adsorption may occur via ion exchange at low enzyme concentrations in solution. Further, the interaction between sorbate molecules is more effective than the sorbent–sorbate interaction, and the subsequent distribution of the protein in the sorbent phase occurs mostly via non-ion-exchange binding.

The largest amount of glucoamylase is sorbed on a K-3 polyelectrolyte, in which acid groups predominate over basic groups. In this study, the acid-chloride form of ion-exchangers was used because it

Kinetic parameters of the reaction of starch hydrolysis by free and immobilized glucoamylase

Enzyme	$K_m \times 10^{-6}$, M	$V_{max} \times 10^{-4}$, mol min^{-1}	Enzyme	$K_m \times 10^{-6}$, M	$V_{max} \times 10^{-4}$, mol min^{-1}
Glucoamylase:			Glucoamylase:		
free	5.51	9.20	K-5	6.55	7.45
K-3	6.06	8.28	AK-22-1	6.72	7.18

was found in preliminary experiments that a 1.3–1.8 times greater amount of the protein is sorbed on the H–Cl form, compared with the H–OH and Na–OH forms of the same polyelectrolytes. It is known from the literature that, similarly to amino acids, polypeptides are better sorbed on hydrogen forms of ion-exchangers than on sodium forms [13]. This fact is probably due to recharging of ions in adsorption, with the result that the electrostatic repulsion between the sorbate and sorbent disappears.

An important role is played in immobilization by the effect of the medium as a result of interaction of solvent molecules with a support and the enzyme, as well as with one another. The adsorption of glucoamylase on fibers is accompanied by a considerable dehydration of the sorbents (Fig. 4), which indicates that the binding of the protein to the support surface becomes stronger.

In immobilization, the catalytic activity of the biocatalyst, which is dependent on the secondary and tertiary structure of the protein macromolecule, may decrease significantly. As a result of binding of the enzyme to the support, its structural-functional properties may change because the protein finds itself in a medium of a polymeric sorbent with other values of the local dielectric constant, electric potential, and concentration of hydrogen ions, compared with the solution. Immobilization may also lead to spatial hindrance to the action of factors controlling the rate of the enzymatic catalysis and to formation of a thermodynamically unfavorable conformation of the enzyme-substrate complex. As demonstrated by the experiments (see table), immobilization of glucoamylase on the ion-exchangers under consideration leads to an insignificant increase in K_m and a decrease in V_{max}, compared with the free enzyme, which indicates that the native structure of the protein is preserved.

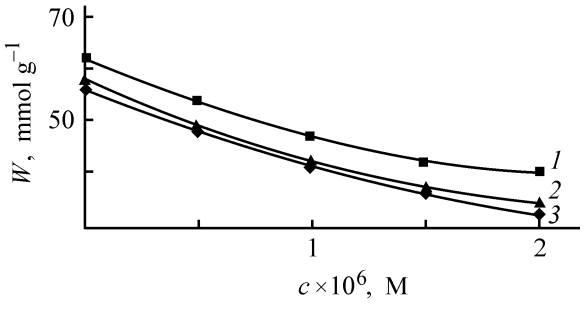


Fig. 4. Variation of the content of water in ion-exchangers in sorption of glucoamylase. (*W*) Amount of water in the sorbent and (*c*) initial concentration of the protein in solution.

Thus, the data obtained indicate that aminocarboxylic ion-exchangers are promising for immobilization of glucoamylase.

CONCLUSIONS

(1) The optimal conditions of adsorption immobilization of glucoamylase on aminocarboxylic polyelectrolytes with a fibrous structure were determined to be as follows: immobilization time 4 h, pH 4.5–4.7, sorbate concentration $(1.5–2.0) \times 10^{-6}$ M.

(2) It was established that the kinetic parameters of the reaction of starch hydrolysis for glucoamylase immobilized on K-3 ion-exchanger change to a lesser extent, compared with the native enzyme.

(3) It was shown that it is advisable to use the sorbents under consideration as supports for immobilization of glucoamylase.

REFERENCES

1. Zherebtsov, N.A., *Amilolitic heskie fermenty v pishchevoi promyshlennosti* (Amylolytic Enzymes in Food Industry), Moscow: Leg. Pishch. Prom–st., 1984.
2. Halgas, J., *Biocatalysts in Organic Synthesis*, Amsterdam: Elsevier, 1992.
3. Kovalenko, G.A., Komova, V.A., Simakov, A.V., *et al.*, *Biotekhnologiya*, 2002, no. 3, pp. 55–66.
4. *Microbial Enzymes and Biotechnology*, Fogarty, W.M., Ed., Elsevier Applied Scince, 1983. Translated under the title *Mikrobnye fermenty i biotekhnologiya*, Moscow: Agropromizdat, 1986.
5. RF Patent 2 181 770.

6. Shkutina, I.V., Stoyanova, O.F., and Selemenev, V.F., *Zh. Prikl. Khim.*, 2001, vol. 74, no. 5, pp. 869–871.
7. Shkutina, I.V., Stoyanova, O.F., Selemenev, V.F., and Grigor'eva, G.A., *Zh. Fiz. Khim.*, 2001, vol. 75, no. 11, pp. 2008–2010.
8. Soldatov, V.S., Martsinkevich, R.V., Pokrovskaya, A.I., and Shunkevich, A.A., *Zh. Prikl. Khim.*, 1994, vol. 67, no. 10, pp. 1640–1643.
9. Soldatov, V.S., Martsinkevich, R.V., Pokrovskaya, A.I., and Shunkevich, A.A., *Zh. Prikl. Khim.*, 1994, vol. 67, no. 10, pp. 1644–1647.
10. Selemenev, V.F., Slavinskaya, G.V., Khokhlov, V.Yu., *et al.*, *Praktikum po ionnomu obmenu* (Laboratory Manual of Ion Exchange), Voronezh: Voronezh. Gos. Univ., 2004.
11. Lowry, O.H., *J. Biol. Chem.*, 1951, vol. 193, pp. 265–275.
12. Chibata, I., *Pure Appl. Chem.*, 1978, vol. 50, no. 7, pp. 667–675.
13. Shataeva, L.K., Kuznetsova, N.N., and El'kin, G.E., *Karboksil'nye kationity v biotekhnologii* (Carboxylic Cationites in Biotechnology), Leningrad: Nauka, 1979.

Russian Journal of Applied Chemistry, Vol. 78, No. 6, 2005, pp. 985–988. Translated from Zhurnal Prikladnoi Khimii, Vol. 78, No. 6, 2005, pp. 1006–1009.
Original Russian Text Copyright © 2005 by Grebennikov, Smotrina, Anan'eva, Kuznetsov.

MACROMOLECULAR CHEMISTRY AND POLYMERIC MATERIALS

Porous Structure of Composites

S. F. Grebennikov, T. V. Smotrina, T. A. Anan'eva, and A. Yu. Kuznetsov

St. Petersburg State University of Technology and Design, St. Petersburg, Russia

Mari State Technical University, Yoshkar-Ola, Mari-El, Russia

Received January 12, 2005

Abstract—NMR and the sorption method were used to study the structure of composites based on ultrahigh-molecular-weight polyethylene and peat (filler).

Composite materials (CM) are widely used in various fields of technology (building and construction materials, supported catalysts, porous polymeric materials, sorption-active composites, etc.). The porous structure of composites plays a primary role in their application and determines their physicomechanical characteristics. In both cases, an important role is played by the interaction of components of the composite and the extent to which their surfaces overlap. In [1], the notions "host" and "guest" were introduced to characterize the interaction between the components of composites. The scheme of the host–guest interaction, suggested for catalysts [1], is to be extended for polymeric formulations, especially for those cases in which the guest is a fibrous ionexchange sorption-active or a fibrous material that is responsible for the large internal surface area of a composite and, simultaneously, is its physicomechanical skeleton. The possible schemes of the host–guest interaction are shown in Fig. 1. In position *a*, the guest is totally blocked by the polymeric matrix; in position *b*, part of the guest is in position *a*, and the other part may be in contact with the third phase or another part of the host. In position *c*, one side of the guest adheres t o the host surface. Scheme *d* is a superposition of states *a* and *b*. Most of polymers swell in some media. If a medium is inert for the host, but causes swelling of the guest, the polymeric matrix may be ruptured to give cracks (pores) (position *e*).

The structure of composites is analyzed by adsorption methods, and the state of the surface and the sorbate, by spectral techniques [1]. Here, the polymeric formulations also have specific features, because a noninert sorbate is absorbed by the bulk of the polymer and causes a sorption deformation of the polymer [2, 3], rather than remaining at the phase boundary. In the present study, composites based on a porous ultrahigh-molecular-weight polyethylene (UHMWP, molecular weight 1.5×10^6), which is the host, and a filler, guest, which is peat, were examined. Peat was introduced into the composite in amounts of 10 (CM-1 sample) and 30 wt % (CM-2 sample). A water vapor served as sorbate. The methods used to measure the amount of sorption and ^{1}H NMR spectra and to form the composites have been described previously [4, 5]. The most important characteristic of porous bodies is their specific surface area, which is commonly found [1] from the sorption capacity of a monolayer, a_m (mol g^{-1}), in the equation

$$\frac{h}{a(1-h)} = \frac{1}{a_m C} + \frac{C-1}{C a_m} h. \qquad (1)$$

Here a is the amount of sorption (mol g^{-1}); $h = p/p_0$, where p is the equilibrium pressure, and p_0, the saturated vapor pressure of the sorbate; and C is an energy constant.

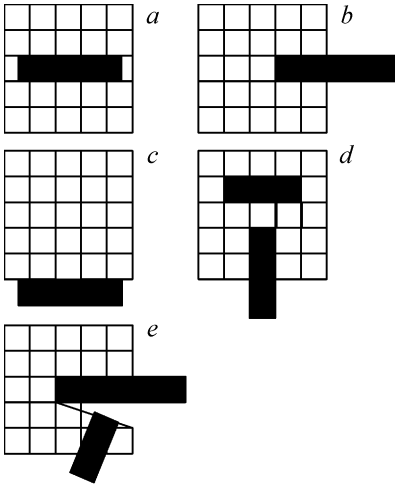


Fig. 1. Schemes of the host–guest interaction.

1070-4272/05/7806-0985 © 2005 Pleiades Publishing, Inc.

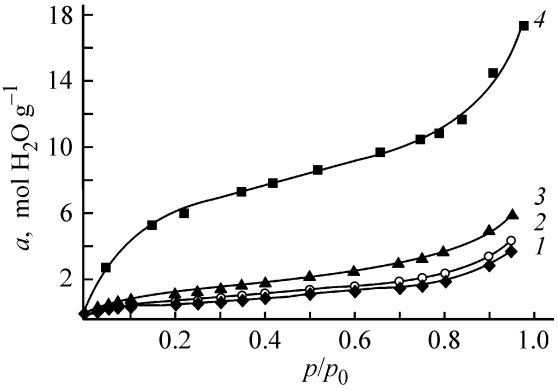


Fig. 2. Sorption isotherms (20°C) of water vapor. (*a*) Amount of sorption and (p/p_0) relative pressure of the sorbate. (*1*) UHMWP-1, (*2*) CM-1, (*3*) CM-2, and (*4*) peat; the same for Figs. 3, 4.

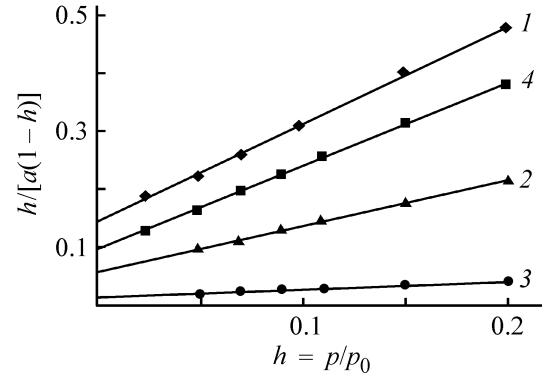


Fig. 3. Sorption isotherms of water vapor in the coordinates of Eq. (1).

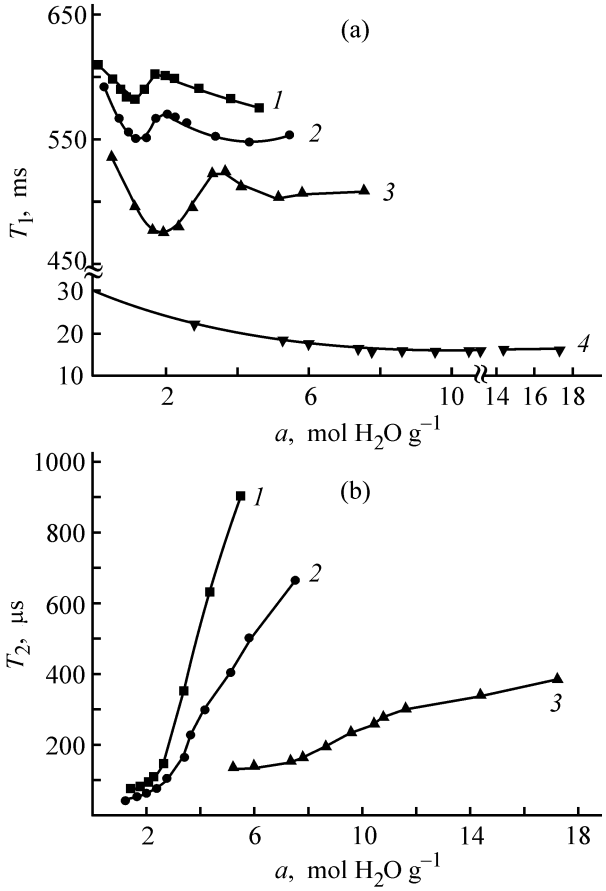


Fig. 4. Times of (a) spin–lattice (T_1) and (b) spin–spin (T_2) relaxation vs. the equilibrium water content *a*.

Figures 2 and 3 show sorption isotherms of water vapor in the ordinary coordinates and linear coordinates of Eq. (1). It can be seen from Fig. 3 that the initial portions of the isotherms satisfactorily obey Eq. (1). This made it possible to calculate the constants a_m (mmol g^{-1}): 0.53 (UHMWP), 0.66 (CM-1), 1.16 (CM-2), and 6.35 (peat); C: 13.4 (UHMWP), 15.2 (CM-1), 15.6 (CM-2), and 15.6 (peat).

For UHMWP, water is an inert sorbate and the data obtained make it possible to calculate the specific surface area by the equation

$$S_{sp} = a_m N_A \sigma, \quad (2)$$

where *A* is the Avogadro number; σ, the landing site area for a water molecule, which depends on the nature of the surface (with its common value of 0.105 nm^2, S_{sp} = 33.5 m^2).

The authors of [6] suggested a comparative method for determining the specific surface area of hydrophobic sorbents from water sorption isotherms. According to this method, 1.7, on average, adsorption layers are formed on hydrophobic surfaces at pressures close to the saturated vapor pressure. Then, $S_{sp} = 1.7a_m(26^{-1} \times 10^3)$ (a_m, mmol g^{-1}; $26^{-1} \times 10^3$, slope rate of the comparative plot); in the case in question, calculations yield S_{sp} = 34.6 m^2 g^{-1}), which is in a satisfactory agreement with the data obtained using Eq. (1). Interestingly, measurements in [7] demonstrated that, in the case of water adsorption on polyethylene films, approximately two monolayers are also formed at $h \to 1$. However, an analysis of this kind for the composite and peat is incorrect in the given case, because the constants obtained for Eq. (1) do not reflect the mechanism of water absorption by peat [8].

The state of UHMWP, composite, and water along the sorption isotherm was analyzed by ^{1}H NMR spectroscopy. Figure 4 shows how the time of spin–lattice relaxation, T_1 depends on the equilibrium water content.

A sample of pure UHMWP shows a longer time of spin–lattice relaxation along the entire sorption isotherm, compared with the composite. This is due to the chemically homogeneous regular structure of polyethylene (–CH_2–CH_2–), which contains no relaxation-active functional groups, on which the energy of the spin system is largely dissipated. Therefore, the process in which equilibrium is established between the spin system and the "lattice" at a slower rate. The minimum observed in the time of spin–lattice relaxation (Fig. 4a, curve *1*) indicates that the samples studied contain hydrophilic impurities and(or) a certain amount of oxidized groups acting as primary active sorption centers. The position of the minimum corresponds to a water content at which these centers are completely filled (the minimum is rather sharp, which points to a narrow distribution of the correlation times of different types of molecular motion, or, in other words, the sorption centers are rather uniform chemically and energetically).

Introduction of a filler into UHMWP leads to a pronounced shortening of the time of spin–lattice relaxation. Being a hydrophilic chemically inhomogeneous substance, peat contains a large number of polar groups of varied nature, which act as both sorption and relaxation centers (Fig. 4a, curve *4*). The irregular structure and the chemical inhomogeneity are the reason for very short times of spin–lattice relaxation of the filler in a wide range of water contents. Therefore, raising the content of the filler leads not only to a decrease in the time of spin–lattice relaxation, T_1, but also to an increase in the water content at its minimum and to broadening of this minimum. This indicates that the number of accessible sorption centers in the composites becomes larger and the chemical nonuniformity of these centers is enhanced. The general shape of the dependence of the time of spin–lattice relaxation on the water content for composite is, in the authors' opinion, a superposition of similar dependences for pure UHMWP and filler, because there is no exchange of protonic magnetization between them (Fig. 4a, curves *2*–*4*). Figure 4b also shows the dependences of the spin–spin relaxation of sorbed water (T_2) on the equilibrium water content of the samples, which can be used to judge the mobility of the sorbate. The highest sorption capacity and lowest mobility of sorbed water is observed for peat. This indicates a high hydrophilicity and amorphism of the filler.

Reverting to the method for analysis of composites, based on the balance between the surfaces of the guest, host, and composite [1], it should be noted that it is advisable, for complex systems constituted by an adsorbent and absorbent, to replace the balance of surfaces by the balance of amounts of sorption along the sorption isotherm. In the case of additivity of the contributions of the host and guest to the amount of sorption, a_{ad} (Figs. 1*b* and 1*c*), this quantity can be calculated by the equation

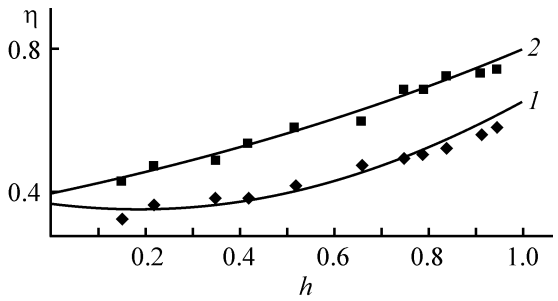


Fig. 5. Variation of the sorption activity coefficient η of the guest along the sorption isotherm, *h*.

$$a_{ad}(h) = a^0_{PE}(h)(1 - x) + a^0_P(h)x, \quad (3)$$

where a_{ad}, $a^0_{PE}(h)$, and $a^0_P(h)$ are the amounts of water sorption: additive and (by the initial UHMWP and peat) along the isotherm; x is the mass fraction of the guest.

On the assumption that the properties of the host are not changed in the presence of a guest, the amount of sorption along the isotherm, $a(h)$, is described by the expression

$$a(h) = a^0_{PE}(h)(1 - x) + a_P(h), \quad (4)$$

where $a_P(h)$ is the contribution of the guest to the total amount of sorption.

Then the dimensionless sorption activity of the guest, η, along the isotherm can be represented as (Fig. 5)

$$\eta = \frac{a_P(h)}{a^0_P x} = \frac{a(h) - a^0_{PE}(h)(1 - x)}{a^0_P x}. \quad (5)$$

Along most part of the isotherm, the sorption activity of the guest $\eta < 1$, i.e., a part of the filler is blocked by the host matrix in positions *a* and *d* (Fig. 1). At vapor pressures close to the saturated vapor pressure, swelling (increasing volume) of the guest may rupture the host (Fig. 1*e*), which is manifested in that $\eta \to 1$ at $h \to 1$. In approximately the same range of amounts of sorption, the curves of spin–lattice relaxation show a bend (Fig. 4). A similar, less pronounced, bend in the curve for UHMWP is possibly associated with capillary phenomena and with a disruption of the surface structure of polyethylene at $h \to 1$, suggested in [7].

CONCLUSIONS

(1) Adequate results were obtained in measuring the specific surface area in adsorption of water by porous polyethylene by the method of polymolecular adsorption and by the comparative method for analysis of water adsorption on hydrophobic surfaces.

(2) A scheme of interaction between the polymer and filler in a composite and a method for analysis of the state of the matrix of the composite in the case when the filler swels in a sorbate vapor were suggested.

REFERENCES

1. Fenelonov, V.B., *Vvedenie v fizicheskuyu khimiyu formirovaniya supramolekulyarnoi struktury adsorbentov i katalizatorov* (Introduction to the Physical Chemistry of Formation of a Supramolecular Structure in Adsorbents and Catalysts), Novosibirsk: Sib. Otd. Ross. Akad. Nauk, 2002.
2. Grebennikov, S.F. and Kynin, A.T., *Zh. Prikl. Khim.*, 1982, vol. 55, no. 10, pp. 2299–2303
3. Grebennikov, S.F., Kynin, A.T., and Grebennikova, O.D., *Zh. Prikl. Khim.*, 1984, vol. 57, no. 11, pp. 2459–2462.
4. Smotrina, T.V., Kynin, A.T., and Grebennikov, S.F., *Zh. Prikl. Khim.*, 2004, vol. 77, no. 3, pp. 487–489.
5. Nazarova, E.V., Anan'eva, T.A., Mikhailova, Yu.N., *et al.*, *Fizikokhimiya polimerov* (Physical Chemistry of Polymers), Tver: Tver. Gos. Univ., 2001, no. 7, pp. 192–197.
6. Vartapetyan, R.Sh. and Voloshchuk, A.M., *Usp. Khim.*, 1995, vol. 64, no. 11, pp. 1055–1072.
7. *Water in Polymers*, Rowland, S.P., Ed., Washington, D.C.: American Chemical Society, 1980. Translated under the title *Voda v polimerakh*, Moscow: Mir, 1984.
8. Klyuev, L.E. and Grebennikov, S.F., *Zh. Fiz. Khim.*, 1996, vol. 70, no. 11, pp. 2053–2058.

Russian Journal of Applied Chemistry, Vol. 78, No. 6, 2005, pp. 989–994. Translated from Zhurnal Prikladnoi Khimii, Vol. 78, No. 6, 2005, pp. 1010–1015.
Original Russian Text Copyright © 2005 by Druzhinina, Efremov, Struganova.

MACROMOLECULAR CHEMISTRY AND POLYMERIC MATERIALS

Mathematical Description of the Kinetics of the Heterophase Macromolecular Reaction of Hydrazidation of Grafted Polyglycidyl Methacrylate

T. V. Druzhinina, G. I. Efremov, and M. A. Struganova

Kosygin State University of Textile, Moscow, Russia

Received April 23, 2004; in final form, November 2004

Abstract—Hydrazidation of a grafted copolymer of polycaproamide and polyglycidyl methacrylate was mathematically modeled by solving the diffusion equation with a boundary condition in the form of a flow.

At present, an important role in the environment protection is played by sorption-active polymeric materials, including those in the fibrous form [1, 2]. However, only two kinds of chemisorption fibers are manufactured industrially (TsM-A2 and Mtilon-1) and the VION-KN fiber is produced at a pilot plant. Other types of fibrous chemisorbents are manufactured as one-time pilot batches. Of fundamental importance for the functioning of modern industrial processes used to manufacture chemisorption fibers is mathematical modeling, which makes it possible to create reliable systems for the control techniques being developed. In this context, the aim of this study was to construct a mathematical model of the heterophase macromolecular reaction in which a special class of branched polymers—grafted copolymers of polycaproamide (PCA) and polyglycidyl methacrylate (PGMA), undergoes hydrazidation, in order to solve the problem of optimization of the process for production of fibrous chemisorption materials with predictable sorption properties.

Among the known ways to obtain chemisorption fibers, the method based on the graft polymerization and chemical transformation in the polymer chains is the most promising [3]. This is because modification of a finished fiber is a simpler technological process, compared with that in which fibrous chemisorbents are obtained by synthesis of copolymers with functionally active groups and then fibers are formed. Owing to the distribution of sorption-active groups in the surface layers of the fiber, the sorbent has good mechanical properties and the highly developed specific surface area provides high rates of mass-exchange processes. The wide diversity of forms of fibrous sorption materials enables their efficient technological implementation in sorption processes [4].

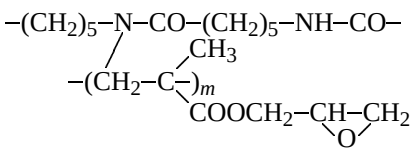
Previously, the modified quasi-stationary method (MQM) has been used for mathematical analysis of the occurring processes in studying the fundamental aspects of the kinetics of polymer-analogous transformations of grafted PGMA under the action of sulfur-containing compounds (thiourea and potassium thiocyanate) [5] and diamines (ethylenediamine and hexamethyldiamine) [6]. As this method is based on a simple summation of the kinetic and diffusion resistances, it can only be regarded as a simplified mathematical model, whose disagreement with the experiment may be as wide as 15% [7]. Therefore, a more precise mathematical kinetic model derived by analytical solution of the equation of isotropic diffusion [8] was adopted in the present study.

The interaction between the oxirane groups of a grafted PCA–PGMA copolymer and hydrazine hydrate underlies the method for production of the POLAN-OG chemisorption fiber having a high sorption capacity and good sorption kinetics [9]. The macrokinetics of this interaction was described by solving the equation of isotropic diffusion with a boundary condition in the form of a flow. Compared with the case of MQM, mathematical calculations of the kinetics of the macromolecular reaction by this method are somewhat more complicated, but provide a better precision of simulation. The method in which the diffusion equation is solved with a boundary condition in the form of a flow has been tested in analysis of some stages of the chemical technology of fibrous materials (dyeing, impregnation, washing, and drying) [7, 10].

As a polymeric matrix containing reactive oxirane groups providing a high rate of chemical transformations, with sorption-active groups introduced into the polymer, served grafted PCA–PGMA copolymer

1070-4272/05/7806-0989 © 2005 Pleiades Publishing, Inc.

with a fibrous structure, a 47 : 53 composition, and the following general structure:



Hydrazine hydrate was used as a modifying agent. To find the type of a solvent ensuring the greatest extent of polymer-analogous transformations, the process was performed in different media: water and aprotic bipolar solvents that cause swelling of the grafted polymer [11].

As applied to the polymer system under study, which is constituted by a grafted PCA–PGMA copolymer and a solution of hydrazine hydrate, the mathematical model of the kinetics of the reaction studied, based on solution of the diffusion equation with a boundary condition in the form of a flow, assumes that the first stage of hydrazidation of the grafted PGMA occurs at the initial instant of time ($\tau = 0$) on the surface of the fiber, with hydrazine hydrate distributed in the adjacent reaction solution. As shown by experimental data, the rate of the macromolecular reaction between polymeric oxirane and hydrazine depends on the concentration c_{HH} of the nucleophilic reagent at the phase boundary (fiber-reaction solution).

In this case, the equation of the isotropic molecular diffusion in the direction of the x axis has the form

$$\frac{\partial c}{\partial \tau} = D\frac{\partial^2 c}{\partial x^2}, \qquad (1)$$

and the boundary condition for the flow of the hydrazine hydrate solution at the phase boundary can be represented as

$$J = -D\frac{\partial c}{\partial x}\bigg|_{x=0} = k(c^* - c), \qquad (2)$$

where D is the diffusion coefficient; k, kinetic coefficient having the dimension of the reaction rate; c^* and c, content of the amine nitrogen in the reaction products upon completion of the reaction and its running concentration, respectively (%).

Using the Laplace operator method to solve the diffusion equation (1) with a boundary condition (2) yields, upon certain rearrangements, an equation for the process kinetics in the form of an error formula [8]:

$$\frac{c}{c^*}\operatorname{erfc}\left(\frac{x}{2\sqrt{D\tau}}\right) - e^{\frac{kx}{D}+\frac{k^2\tau}{D}}\operatorname{erfc}\left(k\sqrt{\frac{\tau}{D}} + \frac{x}{2\sqrt{D\tau}}\right), \qquad (3)$$

where $\operatorname{erfc}(a)$ is an error unction of argument a [7].

Expression (3) for the dimensionless concentration of the amine nitrogen, introduced into the grafted copolymer by the reaction of hydrazidation, at the fiber surface (at $x = 90$) is simplified:

$$\frac{c}{c^*} = 1 - e^{\frac{k^2\tau}{D}}\operatorname{erfc}\left(k\sqrt{\frac{\tau}{D}}\right), \qquad (4)$$

For simplicity of calculations, it is convenient to introduce into the algorithm for solving the diffusion equation with a boundary condition in the form of a flow a modified Fourier number:

$$\mathrm{Fo} = \frac{D}{k^2\tau}. \qquad (5)$$

Then Eq. (4) is transformed into the following expression:

$$\frac{c}{c^*} = 1 - e^{\frac{1}{\mathrm{Fo}}}\operatorname{erfc}\left(\frac{1}{\sqrt{\mathrm{Fo}}}\right), \qquad (6)$$

To account for the convective flows in the reaction medium, it is necessary to introduce an exponent n. In this case, Eq. (4) takes the form

$$\frac{c}{c^*} = 1 - e^{\frac{1}{\pi}\left(\frac{\tau}{\sigma}\right)^n}\operatorname{erfc}\left[\sqrt{\frac{1}{\pi}\left(\frac{\tau}{\sigma}\right)^n}\right], \qquad (7)$$

where σ is the characteristic time of the process (parameter with dimension of time),

$$\sigma = \frac{D}{\pi k^2}. \qquad (8)$$

A rearrangement of Eqs. (5) and (8) with account of the exponent n changes the expression for the modified Fourier criterion:

$$\mathrm{Fo} = \pi\left(\frac{\sigma}{\tau}\right)^n. \qquad (9)$$

A specific feature of Eq. (7) is that its solution has a discontinuity at $1/\mathrm{Fo} > 35$, and, therefore, it is inapplicable at large 1/Fo. To find a solution in this range, it is necessary to use in Eq. (7) an expansion of the error function $\operatorname{erfc}(a)$ into an asymptotic series [7]:

$$\operatorname{erfc}(a) \approx \frac{e^{-a^2}}{\pi}\left(\frac{1}{a} - \frac{1}{2a^3} + \frac{3}{4a^5} - \ldots\right). \qquad (10)$$

For two terms of the asymptotic series expansion of function, (7) leads to the expression

$$\frac{c}{c^*} = \left\{1 - \left[1 - \frac{\pi}{2}\left(\frac{\sigma}{\tau}\right)^n\right]\left[\sqrt{\left(\frac{\sigma}{\tau}\right)^n}\right]\right\}. \qquad (11)$$

An asymptotic solution of Eq. (11) for the interval $1/\mathrm{Fo} > 35$ with the use of expression (7) makes it possible to perform calculations in the entire range of variation of the modified Fourier criterion, with

the solutions overlapping at $13 < 1/Fo < 35$. As a consequence, it is recommended to use expression (11) for $1/Fo > 20$ and Eq. (7) for $1/Fo < 20$.

The above-described algorithm for solving the diffusion equation with a boundary condition in the form of a flow was used to process experimental data obtained in a study of the kinetic dependences $N_a = f(\tau)$ for polymer-analogous transformations of a grafted PCA–PMGA copolymer under the action of hydrazine. The macromolecular reaction of hydrazidation was performed at 80°C in various solvents: water, dimethyl sulfoxide (DMSO), dimethyl acetamide (DMAA), and dimethyl formamide (DMFA). The concentration of hydrazine hydrate in the reaction mixture was varied from 6.2 to 28.1 M. The experimental values of the content of the amine nitrogen in the reaction products and the corresponding parameters of the interaction involving the oxirane groups of grafted PGMA were mathematically processed using the Mathcad software. The exponents n were determined for all the experimental sets by the least-squares method. As a result, the following equations were obtained for the equilibrium content c^* of the amine nitrogen in the reaction products and the characteristic time σ as functions of the content of hydrazine hydrate in the reaction solution in various media:

Solvent of hydrazine hydrate	n	Expression for the parameters of Eqs. (7) and (11)	
DMSO	4.55	$c^* = 2.144 + 0.033c_{HH}$	(12)
		$\sigma = 5.331 - 0.108c_{HH}$	(13)
DMAA	5.97	$c^* = 1.816 + 0.046c_{HH}$	(14)
		$\sigma = 6.532 - 0.044c_{HH}$	(15)
DMFA	6.06	$c^* = 1.759 + 0.045c_{HH}$	(16)
		$\sigma = 8.006 - 0.147c_{HH}$	(17)
Water	5.13	$c^* = 1.431 + 0.028c_{HH}$	(18)
		$\sigma = 10.047 - 0.174c_{HH}$	(19)

A general analysis of Eqs. (12)–(19) points to an ambiguous influence exerted by the concentration of hydrazine hydrate and reaction duration on the rate and extent of hydrazidation of the oxirane groups of grafted PGMA: common terms and proportionality coefficients of the linear equations obtained are different. Their values well correlate with the dielectric constants ($\varepsilon_{DMSO} = 46.7$, $\varepsilon_{DMAA} = 37.8$, $\varepsilon_{DMFA} = 36.7$ [12]) and donor numbers ($DN_{DMSO} = 29.8$, $DN_{DMAA} = 27.8$, $DN_{DMFA} = 26.6$ [13]) of the solvents used, which lead to an increase in the nucleophilicity of hydrazine hydrate. The data obtained [Eqs. (12), (14), (16), (18)] indicate that, in accordance with the content of the amine nitrogen, the highest degree of conversion of polymeric oxirane is achieved when the reaction of hydrazidation is performed in DMSO, which will yield, in the end, a chemisorption fiber with better sorption characteristics.

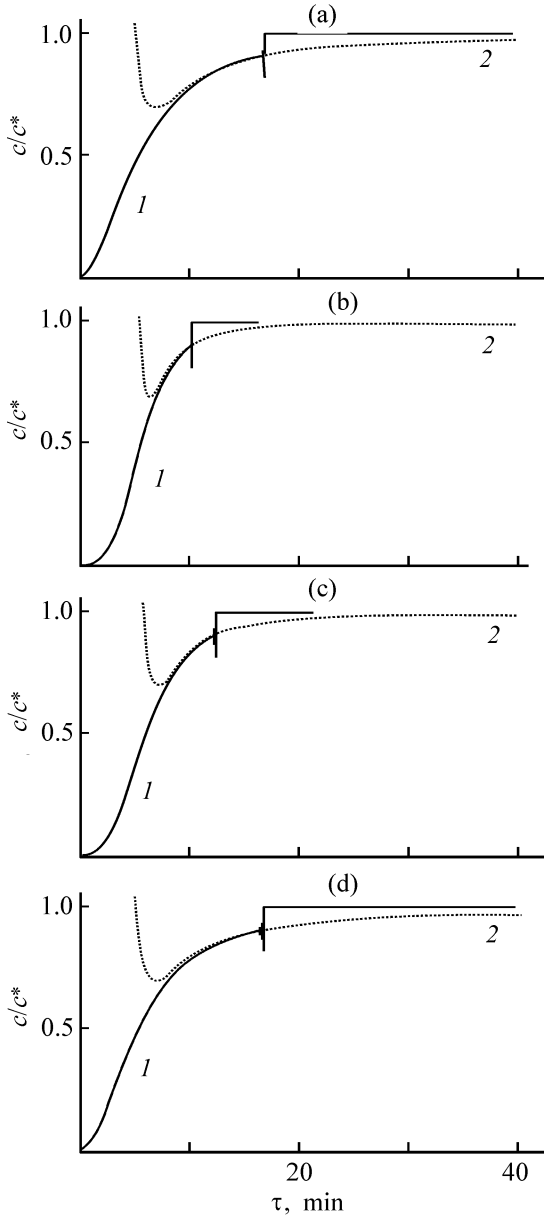


Fig. 1. Dimensionless content c/c^* of the amine nitrogen vs. the running time τ, according to Eqs. (7) and (11). $C_{HH} = 8.7$ M, temperature 80°C; solvent: (a) DMAA, (b) DMFA, (c) DMSO, and (d) water. (*1*) curve plotted with Eq. (7) and (*2*) that with Eq. (11).

Depending on the modification conditions (medium, concentration of hydrazine hydrate), the curves described by Eq. (7) (Fig. 1, curves *1*) have a discontinuity at different durations of the reaction of poly-

Table 1. Duration of the reaction of hydrazidation of grafted PCA–PMGA copolymer at various values of 1/Fo (Temperature 80°C, reaction duration 40 min, hydrazine hydrate concentration 18.7 M)

Solvent	$1/Fo_1 = 35$	$1/Fo_{cr} = 20$	$1/Fo_2 = 9$	Solvent	$1/Fo_1 = 35$	$1/Fo_{cr} = 20$	$1/Fo_2 = 9$
	τ, min				τ, min		
DMSO	12.3	11.1	9.6	DMFA	10.2	9.4	8.3
DMAA	13.7	12.4	10.8	Water	16.7	14.2	11.3

Table 2. $(\sigma/\tau)^n$ values at varied composition of the reaction solution

Solvent	n	τ, min	$(\sigma/\tau)^n$ at indicated concentration of hydrazine hydrate, M					
			6.2	12.5	15.6	18.7	25.0	28.1
DMSO	4.55	11.1	0.016	9.41×10^{-3}	6.31×10^{-3}	4.07×10^{-3}	1.43×10^{-3}	7.70×10^{-4}
DMAA	5.97	12.4	0.017	0.013	0.011	9.75×10^{-3}	7.24×10^{-3}	6.22×10^{-3}
DMFA	6.06	9.4	0.182	0.078	0.049	0.029	9.13×10^{-3}	4.65×10^{-3}
Water	5.13	14.2	0.095	0.048	0.034	0.023	9.23×10^{-3}	5.54×10^{-3}

mer-analogous transformations (Table 1) corresponding to $1/Fo_1 = 35$. The instability of the solution is also seen in the plot of Eq. (11) for processes in various media (Fig. 1, curves *2*) at τ in the range from 9.6 to 11.3 min (Table 1) and $1/Fo_2 = 9$. At the same time, both the curves plotted using the solutions to Eqs. (7) and (11) lie at the critical value $1/Fo_{cr}$ ($1/Fo_{cr} = 20$). Therefore, the τ values corresponding to $1/Fo_{cr} = 20$ should be used in further calculations.

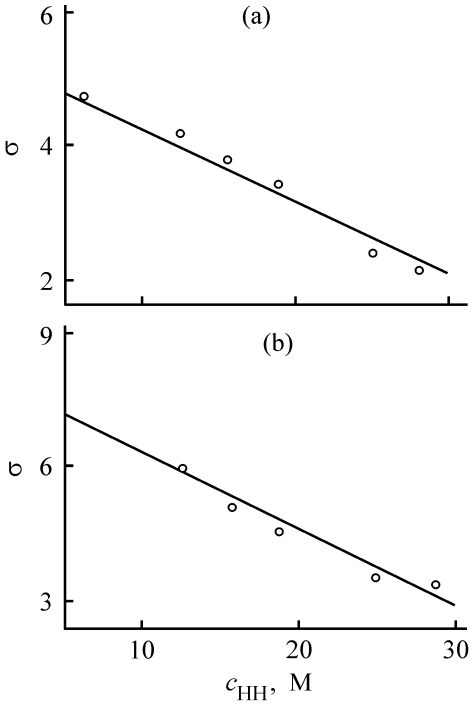


Fig. 2. Characteristic time σ of polymer-analogous transformations of grafted copolymers vs. the content c_{HH} of hydrazine hydrate in the reaction medium. Solvent: (a) DMSO and (b) DMFA.

To reveal the influence exerted by the duration of the process under study on the conversion of oxirane groups at various concentrations of hydrazine hydrate in the modifying solution and varied nature of the reaction medium, the values of the dimensionless time factor $(\sigma/\tau)^n$ were calculated using Eq. (11), which describes the dependence of c/c^* on the simplex $(\sigma/\tau)^n$ being varied. As can be seen from Table 2, the kinetic effect becomes less pronounced as the concentration of hydrazine hydrate in the reaction medium increases. Such a dependence is observed when polymer-analogous transformations are performed in any of the solvents used.

Analysis of the calculated values of $(\sigma/\tau)^n$ for different concentrations of the hydraziding reagent in order to compare the influence exerted by various media reveals the following efficiency series of hydrazine hydrate solvents in solutions of various concentrations: 6.2–18.7 M: DMSO < DMAA < water < DMFA; 25.0 M: DMSO < DMAA < DMFA < water; 28.1 M: DMSO < DMFA < water < DMAA.

As for the characteristic time, a linear dependence of the σ values on the concentrations of hydrazine hydrate in all of the solvents studied was obtained by the least-squares method (Fig. 2).

A mathematical simulation of the process of polymer-analogous transformations of the grafted PCA–PGMA copolymer under the action of hydrazine hydrate, by solving the diffusion equation with a boundary condition in the form of a flow, yielded two equa-

tions. One of these describes the interaction of polymeric oxirane with a hydraziding reagent up to τ values corresponding to $1/Fo_{cr} = 20$, and the other, the reaction at $1/Fo_{cr} > 20$.

Below are presented the corresponding equations derived for hydrazidation in various media with account of the empirical relationships found for dimethyl sulfoxide

$$\frac{c}{2.144 + 0.033c_{HH}} = 1 - e^{\frac{1}{\pi}\left(\frac{\tau}{5.331 - 0.108c_{HH}}\right)^{4.55}} \operatorname{erfc}\left[\sqrt{\frac{1}{\pi}\left(\frac{\tau}{5.33 - 0.108c_{HH}}\right)^{4.55}}\right], \quad (20)$$

$$\frac{c}{2.144 + 0.033c_{HH}} = \left\{1 - \left[1 - \frac{\pi}{2}\left(\frac{5.331 - 0.108c_{HH}}{\tau}\right)\right]^{4.55}\left[\sqrt{\left(\frac{5.331 - 0.108c_{HH}}{\tau}\right)^{4.55}}\right]\right\}; \quad (21)$$

for dimethyl acetamide

$$\frac{c}{1.816 + 0.046c_{HH}} = 1 - e^{\frac{1}{\pi}\left(\frac{\tau}{6.532 - 0.044c_{HH}}\right)^{5.97}} \operatorname{erfc}\left[\sqrt{\frac{1}{\pi}\left(\frac{\tau}{6.532 - 0.044c_{HH}}\right)^{5.97}}\right], \quad (22)$$

$$\frac{c}{1.816 + 0.046c_{HH}} = \left\{1 - \left[1 - \frac{\pi}{2}\left(\frac{6.532 - 0.044c_{HH}}{\tau}\right)\right]^{5.97}\left[\sqrt{\left(\frac{6.532 - 0.044c_{HH}}{\tau}\right)^{5.97}}\right]\right\}; \quad (23)$$

for dimethyl formamide

$$\frac{c}{1.759 + 0.046c_{HH}} = 1 - e^{\frac{1}{\pi}\left(\frac{\tau}{8.006 - 0.147c_{HH}}\right)^{6.06}} \operatorname{erfc}\left[\sqrt{\frac{1}{\pi}\left(\frac{\tau}{8.006 - 0.147c_{HH}}\right)^{6.06}}\right], \quad (24)$$

$$\frac{c}{1.759 + 0.045c_{HH}} = \left\{1 - \left[1 - \frac{\pi}{2}\left(\frac{8.006 - 0.147c_{HH}}{\tau}\right)\right]^{6.06}\left[\sqrt{\left(\frac{8.006 - 0.147c_{HH}}{\tau}\right)^{6.06}}\right]\right\}; \quad (25)$$

and for water

$$\frac{c}{1.431 + 0.028c_{HH}} = 1 - e^{\frac{1}{\pi}\left(\frac{\tau}{10.047 - 0.174c_{HH}}\right)^{5.13}} \operatorname{erfc}\left[\sqrt{\frac{1}{\pi}\left(\frac{\tau}{10.047 - 0.174c_{HH}}\right)^{5.13}}\right], \quad (26)$$

$$\frac{c}{1.431 + 0.028c_{HH}} = \left\{1 - \left[1 - \frac{\pi}{2}\left(\frac{10.047 - 0.174c_{HH}}{\tau}\right)\right]^{5.13}\left[\sqrt{\left(\frac{10.047 - 0.174c_{HH}}{\tau}\right)^{5.13}}\right]\right\}; \quad (27)$$

Equations (20), (22), (24), and (26) should be used to describe the interaction of the grafted PGMA with hydrazine hydrate in the initial stage of the process [by Eq. (7) in the algorithm of solution of the diffusion equation]. For further calculation of the hydrazidation reaction under study, it is necessary to use Eqs. (21), (23), (25), and (27), derived using the theoretical expression (11) and experimental kinetic coefficients.

The calculated values of the dimensionless content of the amine nitrogen in the reaction products are in a good agreement with the experimental data, which indicates that the given mathematical model is applicable to the polymeric system under study (Fig. 3). This mathematical model makes it possible to diminish the scatter of the experimental and calculated values of c/c^* to ±6%.

CONCLUSIONS

(1) The diffusion equation was solved with a boundary condition in the form of a flow for describing the kinetics of hydrazidation of a grafted copolymer of polycaproamide and polyglycidyl methacrylate with account of the influence exerted by the medium on the reaction course. This method was used to find the optimal parameters of the process under study

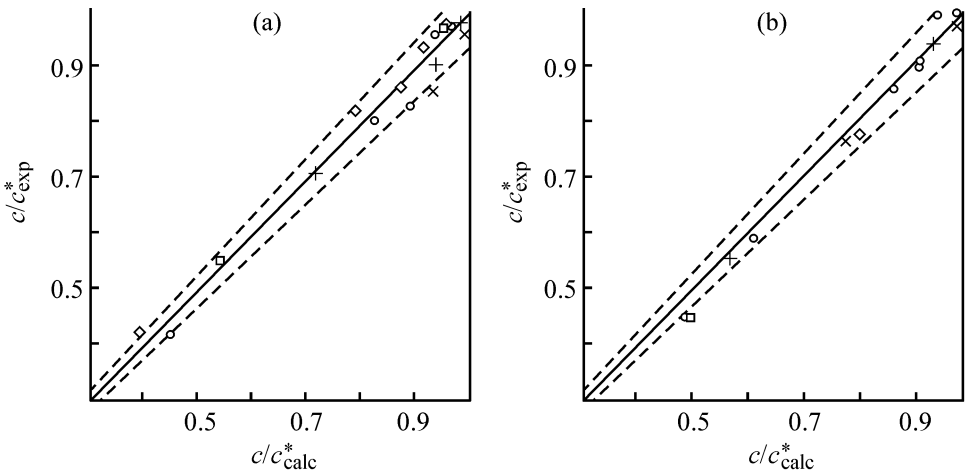


Fig. 3. Relationship between the experimental and calculated c/c^* in (a) DMSO and (b) DMFA.

(duration, reagent concentration), which ensured introduction of a prescribed amount of sorption-active groups into the polymer.

(2) The mathematical expressions derived in theoretical and experimental studies of the kinetics of a macromolecular interaction between grafted polyglycidyl methacrylate with hydrazine hydrate make it possible to control chemical transformations of polymeric oxiranes, which are used to produce chemisorption fibers and to obtain information about the extent of the reaction at a current instant of time.

REFERENCES

1. Abdulkhakova, Z.Z., Babich, I.I., Baskin, Z.L., *et al.*, *Ekol. Prom–st. Rossii*, 2000, April, pp. 12–13.
2. Zverev, M.P., Abdulkhakova, Z.Z., Polovikhina, L.A., *et al.*, *Ekol. Prom–st. Rossii*, 2002, April, pp. 16–18.
3. Druzhinina, T.V. and Nazar'ina, L.A., *Khim. Volokn.*, 1999, no. 4, pp. 8–16.
4. Zverev, M.P. and Abdulkhakova, Z.Z., *Voloknistye khemosorbenty* (Fibrous Chemisorbents), Moscow: Narodnyi Uchitel', 2001.
5. Druzhinina, T.V., Epifanova, N.Yu., and Efremov, G.I., *Zh. Prikl. Khim.*, 2000, vol. 73, no. 4, pp. 647–652.
6. Kardash, K.V., Druzhinina, T.V., and Efremov, G.I., *Khim. Volokn.*, 2002, no. 4, pp. 65–68.
7. Efremov, G.I., *Makrokinetika protsessov perenosa* (Macrokinetics of Transfer Processes), Moscow: Mos. Gos. Tekhn. Uch., 2001.
8. Frank-Kamenetskii, D.A., *Diffuziya i teploperedacha v khimicheskoi kinetike* (Diffusion and Heat Transfer in Chemical Kinetics), Moscow: Nauka, 1987.
9. Druzhinina, T.V., Smolenskaya, L.A., and Struganova, M.A., *Zh. Prikl. Khim.*, 2003, vol. 76, no. 12, pp. 1976–1980.
10. Efremov, G.I., Development of Generalized Methods for Calculation of Nonstationary Heterogeneous Processes in Chemical Technology and Finishing of Textile Materials, *Doctoral Dissertation*, Moscow, 1999.
11. Struganova, M.A. and Druzhinina, T.V., *Khim. Volokn.*, 2001, no. 6, pp. 6–10.
12. Rabinovich, V.A. and Khavin, Z.Ya., *Kratkii khimicheskii spravochnik* (Concise Chemical Reference Book), Leningrad: Khimiya, 1978.
13. Grekov, A.P. and Sukhorukova, S.A., *Polimery na osnove gidrazina* (Hydrazine-based Polymers), Kiev: Naukova Dumka, 1976.

Russian Journal of Applied Chemistry, Vol. 78, No. 6, 2005, pp. 995–999. Translated from Zhurnal Prikladnoi Khimii, Vol. 78, No. 6, 2005, pp. 1016–1020.
Original Russian Text Copyright © 2005 by V. Kurenkov, Trofimov, A. Kurenkov, Khartan, Lobanov.

MACROMOLECULAR CHEMISTRY AND POLYMERIC MATERIALS

Kinetics of Thermal Degradation of Copolymers of Acrylamide with Sodium Acrylate in Aqueous Solutions

V. F. Kurenkov, P. V. Trofimov, A. V. Kurenkov, Kh.-G. Khartan, and F. I. Lobanov

Kazan State Technological University, Kazan, Tatarstan, Russia

Stockhausen GMbH Company, Krefeld, Germany

Degussa Eurasia Joint-Stock Company, Moscow, Russia

Received September 13, 2004; in final form, March 2005

Abstract—The kinetics of thermal degradation of commercial samples of copolymers of acrylamide with sodium acrylate of various molecular characteristics in water and 1.5% NaCl aqueous solutions at 40–80°C was studied viscometrically.

Water-soluble polymers and, in particular, copolymers of acrylamide (AA) with sodium acrylate (Na-A) are used as accelerators in well-boring, thickening agents for water injected into oil strata to displace oil, structure-forming agents for preparing protective shields for an aquifer, agents lovering the water content in the extracted oil, etc. The efficiency of their use is determined by molecular properties of copolymers and their resistance to thermal degradation. The thermal degradation of polyacrylamide (PAA) in aqueous solutions at 75°C was studied in [1]. Previously, we have studied the degradation of partially hydrolyzed PAA in aqueous solutions at 40–70°C [2] and in aqueous salt solutions at 50°C in the presence of a degradation agent (potassium persulfate) [3] and some other additives [4]. An analysis of some features and of the mechanism of thermal degradation of AA copolymers with Na-A with a low content of ionic units (commercial Praestols) at 40–80°C showed that the polymer degrades under the effect of radicals formed by breakdown of the residual initiator in the commercial copolymers. As the temperature is elevated from 40 to 60°C, the molecular weight of the copolymers decreases owing to degradation, whereas on subsequent heating to 80°C, it increases due to possible intermolecular imidization of amide groups of the polymer. However, the possibility of imidization has not been confirmed experimentally.

In this study, we examined the thermal degradation of AA copolymers with Na-A of various compositions in water and 1.5% NaCl aqueous solution at 40–80°C and determined the content of imide units in the products of copolymer degradation.

EXPERIMENTAL

We studied samples of AA copolymers with Na-A (AA–Na-A), produced by Stockhausen GmbH (Krefeld, Germany); their properties are listed in the table. The experimental samples were prepared using distilled water and chemically pure grade chemicals.

The content of the ionic units, α, in AA–Na-A copolymers was determined by potentiometric titration [5]. The intrinsic viscosity $[\eta]$ of copolymer solutions was measured in a 0.5 M NaCl solution at 30°C on a VPZh-3 viscometer (d_c = 0.56 mm). The $[\eta]$ values were determined from the experimental linear depen-

Properties of AA–Na-A copolymers

Sample no.	Sample brand*	$[\eta]$, $cm^3\ g^{-1}$	$\bar{M}_\eta \times 10^{-6}$	Content of units, mol %	
				AA	Na-A
	Praestol:				
1	2500	990	3.9	97	3
2	2510	1080	3.3	92	8
3	2510 RDN	1450	4.1	87	13
4	2515 TR	1020	2.8	89	11
5	2530 TR	1780	4.2	80	20
6	2540 TR	890	1.6	72	28

* Unit structure in macromolecule:

sample no. 1: $-(CH_2-\underset{\underset{O=C-NH_2}{|}}{CH})_n-$

sample nos. 2–6: $[-(CH_2-\underset{\underset{O=C-NH_2}{|}}{CH})_n-(CH_2-\underset{\underset{O=C-ONa}{|}}{CH})_m-]_p$

1070-4272/05/7806-0995 © 2005 Pleiades Publishing, Inc.

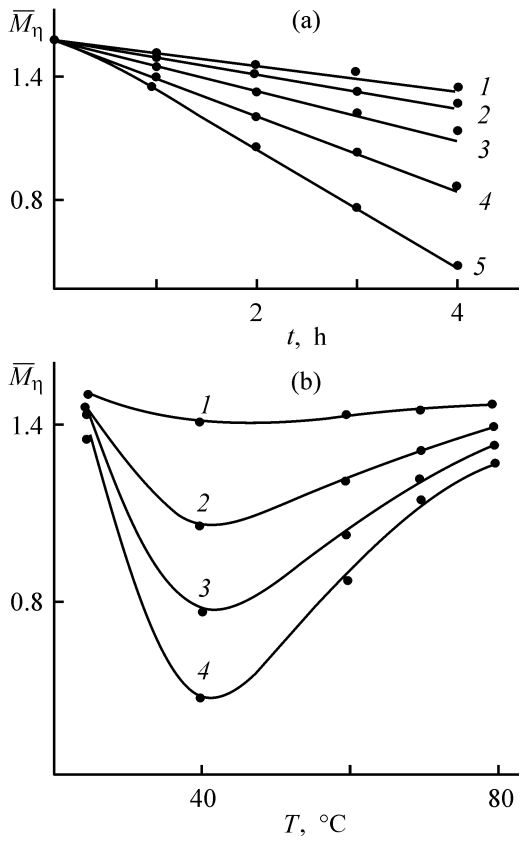


Fig. 1. $\bar{M}_\eta$ vs. (a) time *t* and (b) temperature *T* of degradation of an AA–Na-A copolymer (sample no. 5) in 1.5% NaCl solution. (a) Temperature, °C: (*1*) 26, (*2*) 80, (*3*) 70, (*4*) 60, and (*5*) 40. (b) Time, min; (*1*) 1, (*2*) 2, (*3*) 3, and (*4*) 4.

dence of the reduced viscosity $\eta_{sp}/c_p = f(c_p)$, where c_p is the copolymer concentration.

$$[\eta] = \lim(\eta_{sp}/c_p) \text{ at } c_p \to 0.$$

The viscosity-average molecular weight $\bar{M}_\eta$ of AA–Na-A copolymer was calculated using the Mark–Houwink equation

$$[\eta] = K\bar{M}_\eta^a,$$

where the factors *K* and *a* vary with the concentration of the ionic units in the copolymer; the numerical values of *K* and *a* were taken from [6].

The degradation was performed in 0.1% solutions of AA–Na-A copolymers at 60°C in the course of 4 h. The solvents were pure water and a 1.5% NaCl solution (model medium), because these copolymers are often used in aqueous salt systems.

The reactions were carried out in a glass vessel equipped with a thermostating jacket, magnetic stirrer (MM-5), outlet through which the samples were taken to determine [η], and VPZh-3 capillary viscometer (d_c = 0.56 mm) to monitor the viscosity of the reaction mixture in the course of degradation.

The degradation kinetics was monitored by viscometry [7]. For this purpose, we measured at certain intervals the times of outflow of the reaction mixture t_1 and calculated the reduced viscosities $\eta_{sp}/c_p = f(t)$, where $t = t_2 + t_1/2$ and t_2 is the period of time from the start of degradation to the start of viscosity measurements.

The total content of carboxy and imide groups in the degradation products of AA–Na-A copolymers was determined by the procedure described elsewhere [8]. In this case, a weighed sample of the copolymer was dissolved in 0.1 M NaOH and kept at room temperature for 20 h (during this time the imide groups are hydrolyzed [8], whereas the amide groups remain unchanged), and back titration was carried out according to the procedure reported in [5].

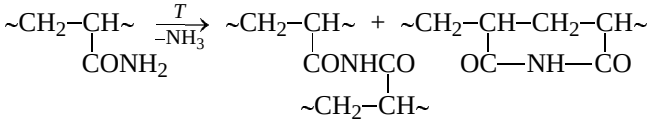
The solution acidity was measured with a pH-121 pH-millivoltmeter equipped with an ESL-63-07 working glass electrode and an EVL 1M-3 silver chloride reference electrode.

To evaluate the effect of temperature on the degradation of AA–Na-A copolymers (sample no. 6), the experiments were performed at 40–80°C, other experimental conditions being the same. The dependence of $\bar{M}_\eta$ on the reaction time is shown in Fig. 1a. As can be seen, $\bar{M}_\eta$ decreases in the course of degradation in the entire temperature range studied. This is due to rupture of the carbon–carbon bonds in the primary polymer chains under the effect of radicals R$^\bullet$ formed in thermal degradation of the residual initiator in the samples of the commercial copolymer.

The experimental data obtained at *t* = const show that $\bar{M}_\eta$ varies with temperature nonmonotonically (Fig. 1b). In the course of degradation, $\bar{M}_\eta$ first decreases as temperature increases from 26 to 40°C. This is obviously due to a rise in the rate of initiator decomposition, which makes higher the concentration of free radicals in the reaction mixture and, thus, promotes the copolymer degradation. In the second stage of degradation (40–80°C), $\bar{M}_\eta$ increases. These changes in $\bar{M}_\eta$ with temperature become more pronounced in the course of degradation (Fig. 1b, passing from curve *1* to curve *4*). For sample no. 2, temperature-related changes in $\bar{M}_\eta$ were similar.

The observed increase in $\bar{M}_\eta$ with temperature in the second step of degradation (Fig. 1b) is probably

due to acceleration of the cross-linking of macromolecules owing to intermolecular imidization of the amide groups of copolymer by the following reaction:



To confirm the possibility of imidization under the conditions of degradation of an AA–Na-A copolymer (sample no. 6), we experimentally determined the content of imide groups in the degradation products (Fig. 2). It can be seen that the content of these groups in the degradation products increases with temperature (in the range from 60 to 80°C) and time of degradation. Similar trends in variation of the content of imide groups in the course of degradation were found for sample no. 2. Thus, the intermolecular imidization during degradation of AA–Na-A copolymers at 60–80°C leads to an increase in $\bar{M}_\eta$, which exceeds the decrease in $\bar{M}_\eta$ caused by degradation of the copolymer backbones.

Let us compare the behavior of AA–Na-A copolymers of various compositions in the course of thermal degradation. The experiments were carried out in 1.5% NaCl solution at 60°C, other experimental conditions being the same. As can be seen from Fig. 3, $\bar{M}_\eta$ decreases in the course of degradation for all the samples studied. Moreover, despite the difference in the copolymer composition (see table), which can affect the process, the degradation rate increases with the initial $\bar{M}_\eta$ of copolymers. This trend agrees with the acceleration of PAA degradation in aqueous solutions as the initial $\bar{M}_\eta$ increases [9] and with data on degradation of some other copolymers [10]. Apparently, at equal number of breaks per macromolecule, a more pronounced decrease in $\bar{M}_\eta$ should be observed for heavier copolymers.

The data on degradation of an AA–Na-A copolymer (sample no. 6) in water and 1.5% NaCl are given for comparison in Fig. 4. As can be seen from the comparison of the experimental data at t = const, the reduced viscosities η_{sp}/c_p of the reaction mixtures and $\bar{M}_\eta$ both decrease on passing from water to a 1.5% NaCl aqueous solution (Figs. 4a and 4b, respectively). This is probably due to changes in the ionic strength of solution μ: with its increase, the electrostatic repulsion between similarly charged acrylate anions along the chain decreases. As a result, the effective size of copolymer aggregates and η_{cp}/c_p decrease. Therefore, the diffusion of the reagents (both degrading agent and macromolecules) becomes more intense with de-

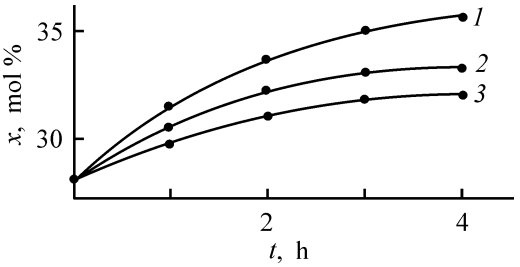


Fig. 2. Content x of imide groups in macromolecules vs. the time t of degradation of AA–Na-A copolymer (sample no. 5) in a 1.5% NaCl solution at various temperatures. Temperature, °C: (*1*) 60, (*2*) 70, and (*3*) 80.

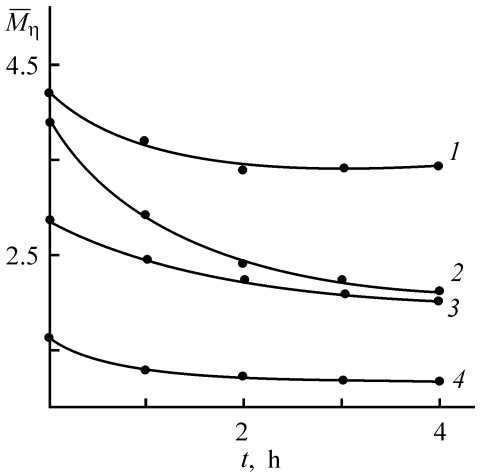


Fig. 3. $\bar{M}_\eta$ vs. the time t of degradation of AA–Na-A copolymers in a 1.5% NaCl aqueous solution. Sample no.: (*1*) 5, (*2*) 1, (*3*) 4, and (*4*) 6.

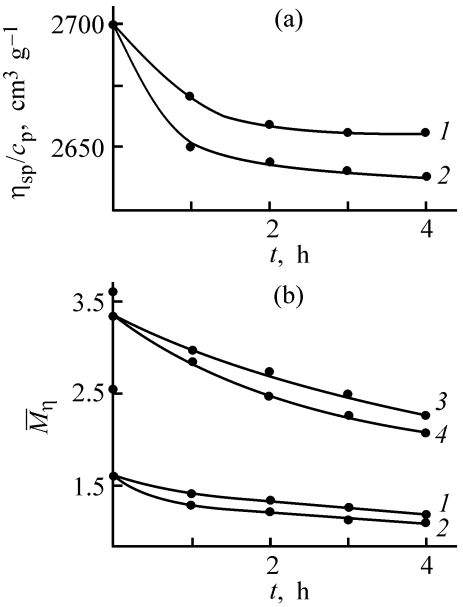


Fig. 4. (a) Reduced viscosity η_{sp}/c_p and (b) $\bar{M}_\eta$ vs. the time t of degradation of an AA–Na-A copolymer in (*1*, *3*) water and (*2*, *4*) 1.5% NaCl aqueous solution; c_p 0.001 g cm^{-3}, the same for Fig. 5. Sample no.: (*1*, *2*) 6 and (*3*, *4*) 2.

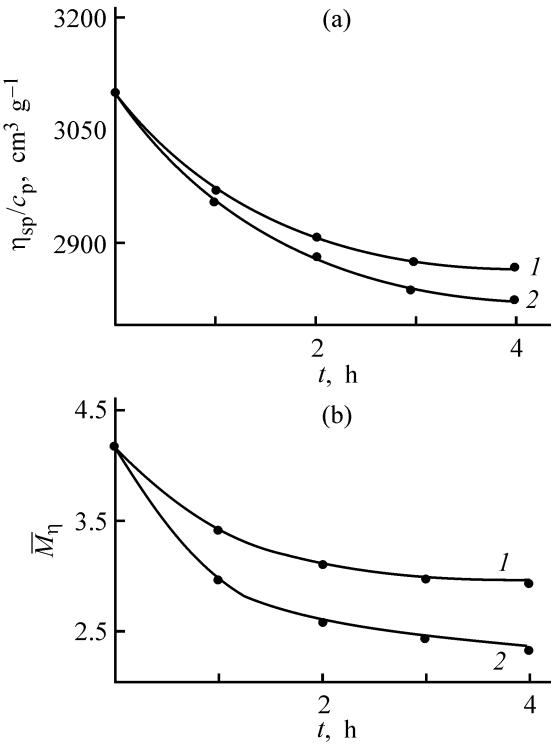


Fig. 5. (a) Reduced viscosity η_{sp}/c_p and (b) $\bar{M}_\eta$ vs. the time t of degradation of an AA–Na-A copolymer (sample no. 5) in a 1.5% NaCl aqueous solution at pH (*1*) 5.3 and (*2*) 9.

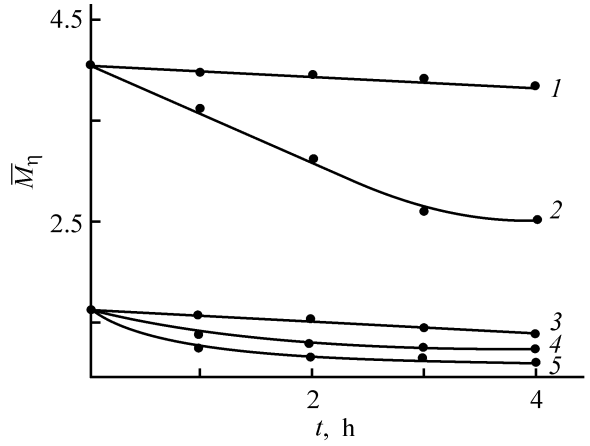


Fig. 6. $\bar{M}_\eta$ vs. time t of degradation of various AA–Na-A copolymers in a 1.5% NaCl solution (*2*–*5*) in the absence of additions and in the presence of (*1*) 0.1 KI, (*3*) 1.0 Na_2SO_3, and (*4*) 2.3% formaldehyde. Sample no.: (*1*, *2*) 3 and (*3*–*5*) 6.

creasing viscosity of the reaction mixtures, which enhances the copolymer degradation.

The dependences $\eta_{sp}/c_p = f(t)$ and $\bar{M}_\eta = f(t)$, recorded in the course of an AA–Na-A copolymer (sample no. 5) degradation in a 1.5% NaCl solution at pH 5.3 and 9, are shown in Fig. 5. It can be seen that with increasing pH, the reduced viscosities and $\bar{M}_\eta$ both decrease (t = const). These results are probably due to changes in μ, whose effect on the degradation was analyzed above.

To evaluate the possibility stabilization of 0.1%, solutions of an AA–Na-A copolymers in 1.5% NaCl aqueous solution at 60°C, we studied the effect of KI, Na_2SO_3, and formaldehyde on the degradation. As can be seen from Fig. 6, $\bar{M}_\eta$ of copolymer at t = const in the presence of KI (curve *1*), Na_2SO_3 (curve *3*), and formaldehyde (curve *4*) changes less strongly (especially in the presence of KI) than in the absence of the additives (curves *2*, *5*). This suggests that these additives deactivate the residual initiator in the commercial copolymer samples and thus suppress its promoting effect on the thermal degradation. Thus, these additives (KI, Na_2SO_3, and formaldehyde) can be used to suppress the thermal degradation of AA–Na-A copolymers.

CONCLUSIONS

(1) Data on the kinetics of thermal degradation of commercial samples of acrylamide copolymers with sodium acrylate of various compositions in 0.1% aqueous and 1.5% NaCl solutions at 40–80°C showed that $\bar{M}_\eta$ of the copolymers decreases as temperature increases from 26 to 40°C, pH grows from 5.3 to 9.0, time of degradation becomes longer, and water is chahged for a 1.5% NaCl solution; however, on heating from 40 to 80°C, it increases owing to intermolecular imidization of amide groups of the copolymer.

(2) Copolymer solutions can be stabilized using KI, Na_2SO_3, and formaldehyde additives.

REFERENCES

1. Klein, J. and Westerkamp, F., *J. Polym. Sci., Polym. Chem.*, Ed., 1981, vol. 19, pp. 707–714.
2. Kurenkov, V.F., Nagel', M.A., Kosterina, E.P., and Myagchenkov, V.A., in *Khimiya i tekhnologiya elementoorganicheskikh soedinenii i polimerov* (Chemistry and Technology of Organoelement Compounds and Polymers), Kazan, Kazan. Khem.-Tekhnol. Inst., 1984, pp. 34–38.
3. Kurenkov, V.F., Trifonova, M.P., Terent'eva, G.I., and Myagchenkov, V.A., in *Fiziko-khimicheskie osnovy sinteza i pererabotki polimerov* (Physicochemical Bases of Synthesis and Processing of Polymers), Gor'kii, Gor'k. Gos. Univ., 1987, pp. 74–78.
4. Nakonechnyi, I.I., Baiburdov, T.A., and Kuren-

kov, V.F., *Zh. Prikl. Khim.*, 1991, vol. 64, no. 5, pp. 1062–1065.

5. Kurenkov, V.F., Baiburdov, T.A., and Stupen'kova, L.L., in *Fiziko-khimicheskie osnovy sinteza i pererabotki polimerov* (Physicochemical Bases of Synthesis and Processing of Polymers), Gor'kii, Gor'k. Gos. Univ., 1985, pp. 79–86.
6. Klein, J. and Conrad, K.-D., *Makromol. Chem.*, 1978, vol. 179, pp. 1635–1638.
7. *Praktikum po khimii i fizike polimerov* (Laboratory Course on Chemistry and Physics of Polymers), Kurenkov, V.F., Ed., Moscow: Khimiya, 1995.
8. Zil'berman, E.N., Radina, I.A., and Spasskaya, R.I., *Vysokomol. Soedin., Ser. A*, 1978, vol. 20, no. 6, pp. 1240–1245.
9. Nagarajan, K. and Davies, G.S., *J. Inst. Eng. (India), Chem. Eng. Div.*, 1980, no. 2, pp. 41–44.
10. Kurenkov, V.F., Khartan, Kh.-G., and Lobanov, F.I., *Zh. Prikl. Khim.*, 2002, vol. 75, no. 7, pp. 1057–1068.

Russian Journal of Applied Chemistry, Vol. 78, No. 6, 2005, pp. 1000–1002. Translated from Zhurnal Prikladnoi Khimii, Vol. 78, No. 6, 2005, pp. 1021–1023.
Original Russian Text Copyright © 2005 by Khimich, Slabospitskaya, Korzhikov, Tennikova.

MACROMOLECULAR CHEMISTRY AND POLYMERIC MATERIALS

Synthesis of an Unsaturated β-Alanine Derivative

G. N. Khimich, M. Yu. Slabospitskaya, V. A. Korzhikov, and T. B. Tennikova

Institute of Macromolecular Compounds, Russian Academy of Sciences, St. Petersburg, Russia

Received July 26, 2004; in final form, January 2005

Abstract—A procedure was developed for preparing an acrylic derivative of β-alanine. A terpolymer of this compound with glycidyl methacrylate and ethylene glycol dimethacrylate was prepared.

Preparation of novel supports and sorbents for the analysis and isolation of biologically active substances is an actively developing field of polymer science.

The surface of supports used in affinity chromatography can be modified with ligands specific to target products [1]. An ideal case is direct synthesis of a peptide ligand on an appropriate matrix and its subsequent use for analytical or preparative separation [2, 3]. In so doing, the matrix should meet the requirements both to solid phases for peptide synthesis and to sorbents for chromatography.

Synthesis of acrylic derivatives of amino acids, capable of terpolymerization with glycidyl methacrylate (GMA) and ethylene glycol dimethacrylate (EDMA), is important in view of their use for preparation of monolithic porous sorbents [2] ready for analysis and use in solid-phase peptide synthesis. The capacity of the monolith, as determined by the amino group content, can be controlled by varying the monomer ratio.

Previously, we have demonstrated the possibility of preliminary covalent binding of a peptide with glycidyl methacrylate, followed by copolymerization of the resulting conjugate with GMA and EDMA [3]. A direct peptide synthesis was made on the GMA–EDMA monolithic sorbent modified with β-alanine, a stable and convenient anchor amino acid [4].

In this context, our goal was to prepare an acrylic derivative of β-alanine and to examine the possibility of preparing a terpolymer of this monomer with GMA and EDMA in the presence of a porogenic solvent.

EXPERIMENTAL

We used the following chemicals: glycidyl methacrylate (Fluka Chemie AG, Switzerland), 2,2-dimethyl-2-hydroxyacetophenone (Merck–Schuchard, Germany), ethylene glycol dimethacrylate, di-*tert*-butyl pyrocarbonate, β-alanine, cyclohexanol (all Sigma–Aldrich, Germany), 2,2'-azobis(isobutyronitrile) (Merck–Schuchard), dodecanol, ethylenediamine, 2-propanol, and acryloyl chloride (all Reakhim, Russia).

The ^{1}H NMR spectra were recorded on a Bruker AC 300 spectrometer (300 MHz) in acetone-d_6 or dimethylformamide-d_7.

The IR spectra were taken on a Bruker IFS 88 spectrophotometer.

UV irradiation was performed with a 125-W mercury lamp with a broad radiation spectrum and constant intensity.

Methyl 3-*tert*-butyloxycarbonylaminopropionate III. β-Alanine methyl ester hydrochloride (3.03 g, 21.6 mmol) was dissolved in 7 ml of MeOH. To the resulting solution, we added 60 ml of a 10% solution of triethylamine in methanol and then, in small portions, a 1.57 g (7.2 mmol) of di-*tert*-butyl pyrocarbonate. The mixture was heated to 50°C and kept at this temperature for 30 min. After that, it was left overnight at room temperature. Then the mixture was evaporated, diluted with 50 ml of ethyl acetate, and acidified with 2% $KHSO_4$. The resulting mixture was washed with water. The organic layer was dried over Na_2SO_4. The product was obtained as a colorless oil; yield 3.48 g (80%).

1070-4272/05/7806-1000 © 2005 Pleiades Publishing, Inc.

^{1}H NMR spectrum (300 MHz, acetone-d_6), δ, ppm: 1.41 s (9H, *t*-C_4H_9), 2.52 m (2H, C$\underline{H}_2$NH), 3.34 m (2H, COC$\underline{H}_2$), 3.6 s (3H, OCH_3).

Found, %: C 53.32, H 8.71, N 6.73.

$C_9H_{17}NO_4$.

Calculated, %: C 53.19, H 8.43, N 6.89.

Amine IV. Methyl 3-*tert*-butyloxycarbonylaminopropionate **III** (3.48 g, 17 mmol) was dissolved in 30 ml of methanol, and a solution of 30 ml of ethylenediamine in 60 ml of methanol was slowly added dropwise with stirring. The reaction was performed at room temperature in the dark for 5 days. Then the mixture was evaporated. The product was purified by column adsorption chromatography on silica gel (40–60 μm), with methylene chloride as eluent. The product was obtained as an oil; yield 2.94 g (75%).

^{1}H NMR spectrum (300 MHz, acetone-d_6), δ, ppm: 1.41 s (9H, *t*-C_4H_9), 2.31–2.46 m (2H), 3.24–3.33 m (4H), 3.34–3.45 m (2H).

Found, %: C 52.12, H 9.26, N 18.05.

$C_{10}H_{21}N_3O_3$.

Calculated, %: C 51.93, H 9.15, N 18.17.

Monomer V. To a solution of 1.43 g (6.2 mmol) of **IV** in 20 ml of methylene chloride, cooled with a mixture of ice and NaCl, we added with stirring 1.1 ml of triethylamine. Then we added dropwise a solution of 0.6 ml of acryloyl chloride in 5 ml of methylene chloride. The mixture was kept in a refrigerator for 7 days. After that, the mixture was diluted with 30 ml of methylene chloride and washed with water. The organic layer was dried over Na_2SO_4 and concentrated. The product was obtained as a white crystalline substance; yield 1.54 g (87%).

IR spectrum, ν, cm^{-1}: 3300, 3085, 1689, 1668 (C=O, amide I), 1540 (C=O, amide II). ^{1}H NMR spectrum (300 MHz, acetone-d_6), δ, ppm: 1.4 s (9H), 3.25–3.44 m (6H), 3.8 m (2H), 5.58 d.d (1H), 6.2 m (2H).

Found, %: C 54.87, H 8.21, N 14.83.

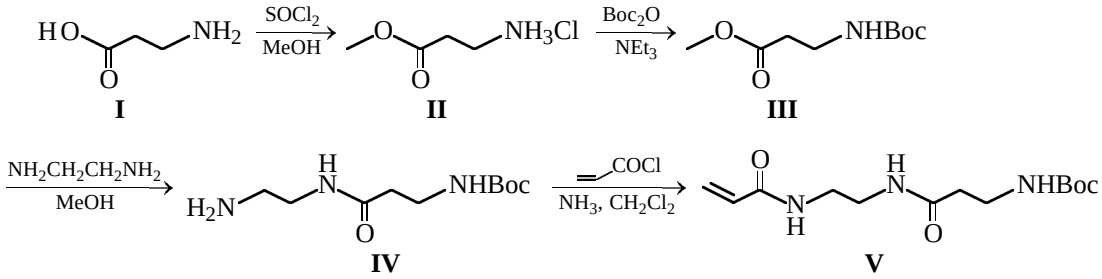
$C_{13}H_{23}N_3O_4$.

Calculated, %: C 54.72, H 8.12, N 14.73.

Free-radical copolymerization of GMA, EDMA, and the acrylic monomer (molar ratio 5.4 : 4 : 0.6) was performed under the photoinitiation conditions in cyclohexanol–dodecanol (7 : 3) in the presence of 2% Darocure 1173. The reaction time was 1 h. After the reaction was complete, the products were washed with ethanol and dried at 100°C.

Thermal copolymerization of GMA, EDMA, and the acrylic monomer (molar ratio 5.4 : 4 : 0.6) was performed in 2-propanol at 60°C, with 1% 2,2'-azobis(isobutyronitrile) as initiator, following the procedure described in [5]. The reaction time was 3 h. After the reaction was complete, the polymers were washed with ethanol and dried at 100°C.

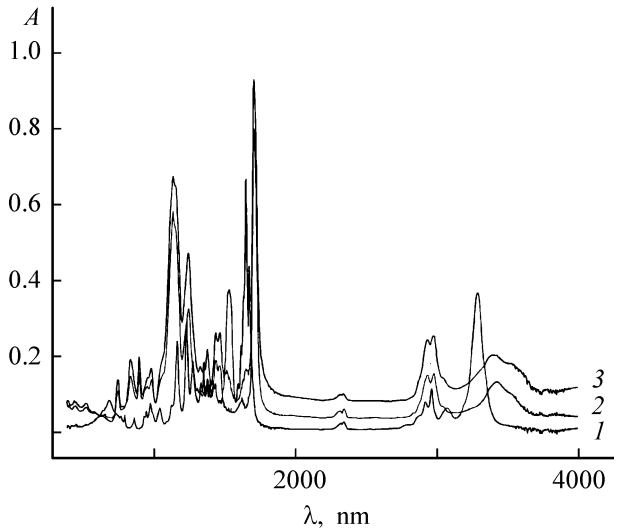
The synthesis of the acrylic derivative of β-alanine with a protected amino group involved several steps:



In the first step, the carboxy group of amino acid **I** was protected by conversion into methyl ester **II**. The reaction was performed in methanol in the presence of thionyl chloride [6].

The amino group of β-alanine methyl ester hydrochloride was protected with di-*tert*-butyl pyrocarbonate (Boc_2O). This reaction can be performed in aqueous–organic or organic media [6]. We found that the attempted protection in aqueous dioxane in the presence of NaOH is accompanied by saponification of the ester. Therefore, the Boc protection of the amino group in **II** was performed in the presence of a milder base, triethylamine [7]. The reaction was performed in methanol for 0.5 h at 50°C.

Boc-protected β-alanine ester **III** was converted to ethylenediamine derivative **IV** by the reaction with



IR spectra of (*1*) acrylic monomer, (*2*) GMA–EDMA copolymer, and (*3*) terpolymer of GMA, EDMA, and acrylic monomer. (*A*) Absorption and (λ) wavelength.

excess ethylenediamine. Acrylic monomer **V** was prepared by the reaction of the free amino group in **IV** with acryloyl chloride in dry methylene chloride at a low temperature (–5°C). A procedure was developed for isolation and purification of this monomer. The structures of the new compounds prepared in this study were confirmed by ^{1}H NMR spectroscopy and elemental analysis.

We examined the possibility of preparing a monolithic porous material by copolymerization of glycidyl methacrylate, ethylene glycol dimethacrylate, and monomer **V** containing an anchor amino acid, β-alanine. We found that, under the conditions of photoinitiated polymerization in the presence of 2,2-dimethyl-2-hydroxyacetophenone (Darocure 1173), with a 7 : 3 mixture of cyclohexanol and dodecanol as a porogenic solvent, monomer **V** is not involved in the copolymerization, as follows from the IR and analytical data. This may be due to the low solubility of **V** in the solvent chosen.

The terpolymer containing units with the anchor amino acid was successfully prepared by thermal copolymerization of GMA, EDMA, and monomer **V** in 2-propanol at 60°C for 3 h, with 2,2'-azobis(isobutyronitrile) as initiator.

The involvement of the acrylic monomer in the copolymerization was confirmed by elemental analysis and IR spectroscopy. The figure shows the IR spectra of monomer **V**, GMA–EDMA copolymer, and the terpolymer. The IR spectrum of the acrylic monomer contains the bands of stretching (3085 cm^{-1}) and bending (700 – 650 cm^{-1}) vibrations of the =C–H bond, the C=C stretching band (1620 cm^{-1}), and the amide C=O vibration bands (1689 and 1668 cm^{-1}, amide **I**; 1540 cm^{-1}, amide II), and also a strong N–H band (3300 cm^{-1}). The presence in the spectrum of the terpolymer of the amide bands (1678 cm^{-1}, amide **I**; 1546 cm^{-1}, amide II) confirms the involvement of acrylic monomer **V** in the copolymerization.

CONCLUSION

A monomer in which the acrylic residue is linked through a spacer with Boc-protected β-alanine was synthesized. A ternary copolymer was prepared by radical thermal copolymerization of glycidyl methacrylate, ethylene glycol dimethacrylate, and acrylic derivative of β-alanine.

REFERENCES

1. Merrifield, R.B., *J. Am. Chem. Soc.*, 1963, vol. 85, pp. 2149–2154.
2. Vlakh, E., Ostryanina, N., Jungbauer, A., and Tennikova, T., *J. Biotechnol.*, 2004, vol. 107, pp. 275–284.
3. Hahn, R., Podgornik, A., Merhar, M., *et al.*, *Anal. Chem.*, 2001, vol. 73, pp. 5126–5132.
4. Svec, F., Tennikova, T.B., and Deyl, Z., in *Monolithic Materials: Preparation, Properties and Applications*, Elsevier, 2003, vol. 67, p. 457.
5. US Patent 4 889 632.
6. Gershkovich, A.A. and Kireev, V.K., *Sintez peptidov: Reagenty i metody* (Peptide Synthesis: Reagents and Methods), Kiev: Naukova Dumka, 1987.
7. Ambade, A.V. and Kumar, A., *J. Polym. Sci., Part A: Polym. Chem.*, 2001, vol. 39, no. 9, pp. 1295–1304.

Russian Journal of Applied Chemistry, Vol. 78, No. 6, 2005, pp. 1003–1007. Translated from Zhurnal Prikladnoi Khimii, Vol. 78, No. 6, 2005, pp. 1024–1028.
Original Russian Text Copyright © 2005 by Khimich, Tennikova.

MACROMOLECULAR CHEMISTRY AND POLYMERIC MATERIALS

Synthesis of a Methacrylic Monomer Containing an *L*-Lysine-Based Dendron

G. N. Khimich and T. B. Tennikova

Institute of Macromolecular Compounds, Russian Academy of Sciences, St. Petersburg, Russia

Received July 26, 2004; in final form, January 2005

Abstract—Procedures were developed for preparing a polylysine dendron of second generation, containing terminal Boc-protected amino groups and a free focal amino group; from this substance, a previously unknown methacrylic monomer linked to the *L*-lysine-based dendron was prepared.

Much attention is given today to development of hybrid materials combining dendritic and linear structural fragments [1]. The use of dendritic monomers as building blocks along with linear monomers substantially extends the possibilities of macromolecular design; it has led to preparation of polymers of unusual architecture [2]. By using various structural elements forming a polymeric framework, it is possible not only to modify the physical properties of polymers, but also to impart additional functions to the polymer skeleton, such as complexing power, response to certain physical actions, and possibilities of further transformations. Introduction of dendrimers combining a high functionality with a compact molecular structure opens wide prospects for application of such materials in biology, medicine, and medical diagnostics [3–7].

Dendrimers prepared from natural amino acids by peptide synthesis [8–10] contain on the periphery a controllable amount of reactive functional groups.

The interest in polymers containing branched polylysine [11, 12] is due to the possibility of preparing new amphiphilic materials to be used in molecular biology. Dendrimers derived from *L*-lysine and block copolymers containing dendritic poly-*L*-lysine exhibit a high compacting power toward DNA [13, 14].

Two types of denritic-linear polymers containing poly-*L*-lysine fragments are known: dumbbell-like compounds prepared by reactions of bifunctional linear compounds (low-molecular-weight or polymeric) with dendritic fragments [12] and compounds in which one end of a polymer chain is linked to the focal point of a dendron [11, 12].

Published data on synthesis of dendritic polymers and copolymers containing monomeric units with dendritic poly-*L*-lysine fragments are lacking. There are three fundamentally different routes to such substances: (1) synthesis of a linear polymer, followed by addition of separately prepared dendrons to the chain (convergent route); (2) synthesis of a polymer with active substituents, followed by stepwise build-up of a dendron at the polymer chain (divergent route); and (3) synthesis of macromonomers, i.e., dendrons containing a polymerizable functional group at the focal point, followed by polymerization [1, 15]. Use of such macromonomers containing terminal functional groups capable of further chemical transformations under relatively mild conditions may be promising for preparation of new polymeric materials and macroporous polymeric sorbents [16].

The goal of this study was to develop a procedure for preparing a methacrylic monomer containing a fragment of a poly-*L*-lysine dendron of second generation.

EXPERIMENTAL

We used the following chemicals: *L*-lysine hydrochloride (Reanal, Hungary), di-*tert*-butyl pyrocarbonate, dicyclohexylcarbodiimide (DCC), *N*-hydroxybenzotriazole (HOBT) (all Sigma–Aldrich, Germany), methacryloyl chloride, and thionyl chloride (both Reakhim, Russia).

Methylene chloride, ethyl acetate, and chloroform were dried over P_2O_5 and then distilled (bp 40, 77, and 62°C, respectively). Tetrahydrofuran and diethyl ether were refluxed over alkali and then distilled (bp 65 and 35°C, respectively). Acetone was refluxed

1070-4272/05/7806-1003 © 2005 Pleiades Publishing, Inc.

over anhydrous K_2CO_3, distilled (bp 56°C), and stored over molecular sieves. Thionyl chloride was distilled (bp 79°C). Other solvents and solid chemicals were used without additional purification.

The ^1H and ^{13}C NMR spectra were recorded on Bruker AC 300 (300 MHz) and Bruker DRX 500 (500 MHz) spectrometers in DMSO-d_6 or acetone-d_6.

MALDI-TOF mass spectra were taken on a Bruker IV device. Samples were ionized with an N_2 laser from a matrix of 2,4-dihydroxybenzoic acid.

The IR spectra were recorded on a Bruker IFS 88 spectrophotometer.

***L*-Lysine methyl ester dihydrochloride I.** Thionyl chloride (8 ml) was added dropwise with stirring to 60 ml of methanol cooled to –5°C with an ice–salt mixture, after which *L*-lysine hydrochloride (9.13 g, 0.005 mol) was added in portions with cooling. The mixture was stirred for 40 min at room temperature and then refluxed for 80 min. After cooling, the mixture was left overnight. The precipitate was filtered off and washed with diethyl ether (1 : 1). The precipitate was dried in air and then in a desiccator over NaOH. Yield 10.17 g (87.2%); white crystals.

^1H NMR spectrum (DMSO-d_6), δ, ppm: 1.39 m (2H, CH_2), 1.59 m (2H, CH_2), 1.83 m (2H, CH_2), 2.74 m (2H, CH_2), 3.75 s (3H, OCH_3), 3.96 t (1H, CH), 8.16 br.s (NH_3^+), 8.72 (NH_3^+).

Di(*tert*-butoxycarbonylamino)-*L*-lysine II. To a solution of 3.2 g (0.08 mol) of NaOH in 30 ml of H_2O, we added with stirring *L*-lysine hydrochloride (7.306 g, 0.04 mol) and then sodium hydrocarbonate (1.68 g, 0.02 mol). A solution of 18.2 g (0.088 mol) of *tert*-butyl pyrocarbonate in 40 ml of ethanol was added dropwise with stirring to the solution of the amino acid, cooled with ice and water. The mixture was stirred for a day at room temperature, after which 50 ml of H_2O was added to dissolve the precipitate. Excess *tert*-butyl pyrocarbonate was extracted with petroleum ether. The aqueous phase was acidified with 1 M $NaHSO_4$. The product was extracted with ethyl acetate. The organic layer was washed with a saturated NaCl solution, dried over anhydrous Na_2SO_4, and evaporated; the residue was dried in a vacuum. Yield 10.98 g (85.4%); white crystals.

^1H NMR spectrum (DMSO-d_6), δ, ppm: 1.2–1.4 m (20H, *t*-C_4H_9, CH_2), 1.53 m (2H, CH_2), 1.61 m (2H, CH_2), 2.88 m (2H, CH_2NHBoc), 3.82 m (1H, OCCH), 6.72 t (1H, NH), 6.96 t (1H, NH), 12.35 s (1H, COOH).

Found, %: C 55.42, H 8.81, N 8.16.

$C_{16}H_{30}N_2O_6$.

Calculated, %: C 55.47, H 8.73, N 8.09.

CH_3OLys(LysBoc$_2$)$_2$ III. To a solution of 3.244 g (0.014 mol) of *L*-lysine methyl ester dihydrochloride in 20 ml of DMF, we added 4.6 ml (0.033 mol) of triethylamine to obtain mixture A. To a solution of 10.5 g (0.042 mol) of di(*tert*-butoxycarbonylamino)-*L*-lysine in 40 ml of DMF, we added 3.97 g (0.033 mol) of HOBT and 6.84 g (0.033 mol) of DCC. After standing for 40 min, the solution of the activated ester was filtered through a glass frit and added to mixture A. The mixture was stirred for a day, and the precipitate was separated. The filtrate was evaporated in a vacuum to 1/3 of the initial volume. The resulting solution was diluted with 100 ml of ethyl acetate and washed successively with saturated NaCl solution (40 ml), 2% $NaHSO_4$ solution (2 × 20 ml), 5% $NaHCO_3$ solution (2 × 20 ml), and H_2O (2 × 20 ml). The organic layer was dried over Na_2SO_4 and evaporated; the yellow oily residue was purified by preparative adsorption chromatography on a column packed with silica gel (40–60 μm). The major fraction was additionally purified by repeated chromatography on a similar column. A mixture of chloroform with methanol (ratio from 10 : 1 to 5 : 1) was used as eluent. A white crystalline substance was obtained; yield 9.84 g (86%).

^1H NMR spectrum (DMSO-d_6), δ, ppm: 1.10–1.75 m (54H; *t*-$C_4\underline{H}_9$, CH_2), 2.88 m (4H, $C\underline{H}_2$), 2.95–3.1 m (2H), 3.61 m (3H, $OC\underline{H}_3$), 3.80 m (1H, CH), 3.91 m (1H, CH), 4.20 m (1H, CH), 6.66 d (1H, NH), 6.71 m (3H, NH), 7.71 t (1H, NH), 8.05 t (1H, NH).

^{13}C NMR spectrum (DMSO-d_6), δ, ppm: 22.51, 22.72, 22.83, 24.48, 25.37, 28.22, 28.31, 28.61, 29.24, 29.26, 30.58, 31.64, 31.83, 33.38, 38.15, 39.72, 40.83, 47.55, 51.75, 54.03, 54.37, 77.34, 77.94, 155.28 (CO), 156.59 (CO), 171.95 (CO), 172.41 (CO), 172.53 (CO).

Found, %: C 57.41, H 8.95, N 10.40.

$C_{39}H_{72}N_6O_{12}$.

Calculated, %: C 57.33, H 8.88, N 10.29.

MALDI, *m*/*z*: 818.1 $[M + H]^+$, 840.1 $[M + Na]^+$, 856.1 $[M + K]^+$. IR spectrum, *ν*, cm^{-1}: 3150–3500 (NH), 2978 (*t*-C_4H_9), 1693 (C=O, amide **I**), 1525 (amide **II**), 1170 (CO).

$NH_2CH_2CH_2NH$Lys(LysBoc$_2$)$_2$ IV. A solution of 1.58 g (1.93 mmol) of dendron **III** in 15 ml of absolute methanol was added dropwise with stirring to 15 ml of ethylenediamine, cooled with ice. The mixture was purged with nitrogen and left in the dark at room temperature for 3 days. After that, the solvent and excess ethylenediamine were distilled off in a vacuum. The product was purified by preparative adsorption chromatography on a column packed with

silica gel (40–60 μm), with chloroform–methanol (5 : 1) as eluent. A white crystalline product was obtained; yield 1.38 g (83.8%).

^{1}H NMR spectrum (DMSO-d_6), δ, ppm: 1.10–1.75 m (56H), 2.54 m (2H, –CH_2–NH_2), 2.87 m (4H, CH_2), 2.95–3.08 m (4H, CH_2), 3.81 m (1H, CH), 3.85 m (1H, CH), 4.17 m (1H, CH), 6.66 d (1H, NH), 7.62 m (2H, NH), 6.86 d (1H, NH), 7.68 m (2H, NH), 7.79 t (1H, NH).

^{13}C NMR spectrum (DMSO-d_6), δ, ppm: 22.52, 22.83, 28.22, 28.32, 28.79, 29.24, 31.44, 31.89, 31.96, 38.41, 39.69, 41.25, 42.29, 52.38, 54.33, 54.54, 77.34, 77.93, 78.15, 155.29 (CO), 155.46 (CO), 155.61 (CO), 171.46 (CO), 171.90 (CO), 171.96 (CO).

Found, %: C 56.93, H 9.35, N 13.21.

$C_{40}H_{76}N_8O_{11}$.

Calculated, %: C 56.85, H 9.06, N 13.26.

MALDI, *m*/*z*: 846 $[M + H]^+$, 868 $[M + Na]^+$, 884 $[M + K]^+$. IR spectrum, ν, cm^{-1}: 3150–3500 (NH), 2978 (*t*-C_4H_9), 1695 (C=O, amide **I**), 1525 (amide **II**), 1169 (CO).

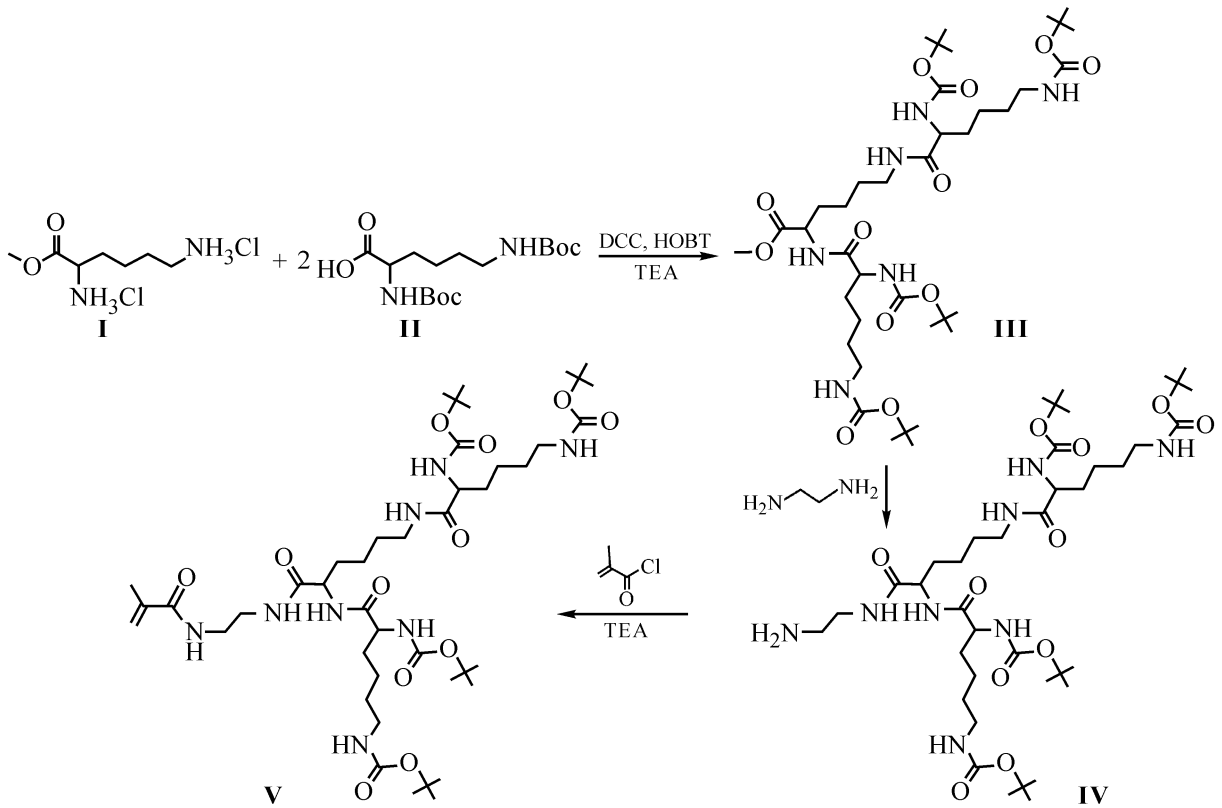
Methacrylic monomer V. To a solution of 0.97 g (1.45 mmol) of dendron **IV** in 12 ml of dry THF, cooled to –5°C, we added 0.223 ml (1.60 mmol) of triethylamine. Then we slowly added a solution of 1.167 g (1.6 mmol) of methacryloyl chloride in 2 ml of THF. The mixture was stirred for 3 h and left overnight. On the next day, the solvent was distilled off in a vacuum. The residue was dissolved in dichloromethane and washed with water, dilute Na_2CO_3, and again water. The organic layer was dried over Na_2SO_4 and concentrated. A white crystalline substance was obtained; yield 1.1 g (83.3%).

^{1}H NMR spectrum (DMSO-d_6), δ, ppm: 1.1–1.75 m (52H), 1.98 s (3H, C=CCH_3), 2.87 m (4H, CH_2NHCO), 3.03 m (2H), 3.15 m (4H), 3.82 m (2H), 4.18 m (1H, CH), 5.28 (1H), 5.62 (1H), 5.95–6.9 (a series of broad NH signals).

^{13}C NMR spectrum (DMSO-d_6), δ, ppm: 19.39, 21.55, 23.31, 23.66, 25.30, 25.97, 29.01, 29.10, 29.63, 30.06, 32.25, 32.71, 34.20, 39.81, 46.43, 48.37, 53.15, 55.15, 55.33, 55.70, 60.57, 67.86, 78.13, 78.72, 78.94, 119.93, 140.66, 156.09 (CO), 156.27 (CO), 156.40 (CO), 157.49 (CO), 168.37 (CO), 171.11 (CO), 172.62 (CO), 172.64 (CO).

MALDI-TOF, *m*/*z*: 935.7 $[M + Na]^+$, 951.7 $[M + K]^+$. IR spectrum, ν, cm^{-1}: 3150–3500 (NH), 3085 (=C–H), 2978 (*t*-C_4H_9), 1694 (C=O, amide **I**), 1642 (C=C), 1526 (amide **II**), 1169 (CO).

The poly-*L*-lysine dendritic macromonomer is prepared in several steps:



MALDI-TOF data

Dendron	Formula	Molar weight	MALDI-TOF data		
			$[M + H]^+$	$[M + Na]^+$	$[M + K]^+$
III	$C_{39}H_{72}N_6O_{12}$	817.02	818.02*	840.02	856.02
			818.1**	840.1	856.1
IV	$C_{41}H_{78}N_8O_{11}$	845.08	846.08	868.08	884.08
			846.1	868.1	884.1
V	$C_{44}H_80N_8O_{12}$	913.15	–	935.7	951.7
			–	935.7	951.7

* Found.

** Calculated.

First, we prepared by known procedures *L*-lysine methyl ester dihydrochloride and di-Boc-*L*-lysine. The carboxy group was protected by esterification with methanol in the presence of $SOCl_2$. The Boc protection of the amino groups of *L*-lysine was performed by a standard procedure with *tert*-butyl pyrocarbonate (Boc_2O) [17].

From *L*-lysine methyl ester hydrochloride **I** and di(*tert*-butyloxycarbonyl)-*L*-lysine **II**, we prepared a dendron of second generation, $CH_3OLys(LysBoc_2)_2$ **III**, containing four Boc-protected amino groups. For this reaction to be successful, the carboxy group should be activated. Various activating agents are used in the synthesis of dendritic poly-*L*-lysines. Choi *et al*. [12] used, when preparing a hybrid copolymer of poly(ethylene glycol) and polylysine dendron by a divergent procedure, *N*-α-*N*-ε-di-Fmoc-*L*-lysine (Fmoc = 9-fluorenylmethoxycarbonyl) and HOBT in the presence of diisopropylamine. Chapman et al. [11] used as reagent pentafluorophenyl ester of *N*-α-*N*-ε-di-Boc-*L*-lysine in the presence of diisopropylethylamine (DPEA).

In the synthesis of *L*-lysine dendron **III**, we activated the carboxy group with dicyclohexylcarbodiimide and *N*-hydroxybenzotriazole (DCC/HOBT). The reaction occurs within 3 days at room temperature. The product was purified by column chromatography on silica gel, with chloroform–methanol as eluent; yield 86%.

Compound **III** contains two types of protecting groups: Boc groups on the periphery and methyl group in the focal point. By saponification of the carboxy group, the dendron with the reactive carboxy group can be obtained; it can be used for preparing dendrons of further generations.

Schlüter *et al*. reported on preparation of dendron-containing monomers by a procedure involving addition of a spacer to an acrylic or methacrylic monomer, followed by its modification with a dendron containing an appropriate functional group [1, 18]. In this study, we modified dendron **III** with ethylenediamine to obtain $NH_2CH_2CH_2NHLys(LysBoc_2)_2$ **IV**. This compound contains a focal amino group. In the subsequent step, it is brought into condensation with methacryloyl chloride, i.e., the spacer is added directly to the dendritic fragment.

The structures of dendrons **III** and **IV** and of macromonomer **V** were confirmed by IR and ^1H and ^{13}C NMR spectroscopy, and also by MALDI-TOF spectrometry (see table).

CONCLUSIONS

(1) A poly-*L*-lysine dendron of second generation, containing a focal amino group and terminal Boc-protected amino groups, was prepared.

(2) A procedure was developed for preparing a methacrylic monomer linked to the poly-*L*-lysine dendron of second generation through a spacer.

REFERENCES

1. Zhang, A., Shu, L., Bo, Z., and Schlüter, A.D., *Macromol. Chem. Phys.*, 2003, vol. 204, no. 2, pp. 328–339.
2. Grinstaff, M.W., *Chem. Eur. J.*, 2002, vol. 8, no. 13, pp. 2839–2846.
3. Stiriba, S.-E., Frey, H., and Haag, R., *Angew. Chem.*, 2002, vol. 114, no. 8, pp. 1385–1390.
4. Ong, K.K., Jenkins, A.L., Cheng, R., *et al.*, *Anal. Chim. Acta*, 2001, vol. 444, no. 1, pp. 143–148.
5. Hudson, R.H.E. and Damha, M., *J. Am. Chem. Soc.*, 1993, vol. 115, no. 6, pp. 2119–2124.
6. Nilsen, T.W., Grayzel, J., and Prensky, W., *J. Theor. Biol.*, 1997, vol. 187, no. 2, pp. 273–284.

7. Stears, R.L., Getts, R.C., and Gullans, R.S., *Physiol. Genomics*, 2000, vol. 3, no. 1, pp. 93–99.
8. Kim, Y., Zeng, F., and Zimmerman, S.C., *Chem. Eur. J.*, 1999, vol. 5, no. 7, pp. 2133–2138.
9. Mong, T.K.-K., Niu, A., Chow, H.-F., *et al.*, *Chem. Eur. J.*, 2001, vol. 7, no. 3, pp. 686–699.
10. Tam, J.P., Lu Yi-An, and Yang Jin-Long, *Eur. J. Biochem.*, 2002, vol. 269, no. 3, pp. 923–932.
11. Chapman, T.M., Hillyer, G.L., Mahan, E.J., and Shaffer, K.A., *J. Am. Chem. Soc.*, 1994, vol. 116, no. 24, pp. 11 195–11 196.
12. Choi, J.S., Lee, E.J., Choi, Y.H., Jeong, Y.J., and Park, J.S., *Bioconj. Chem.*, 1999, vol. 10, no. 1, pp. 62–65.
13. Ohsaki, M., Okuda, T., Wada, A., *et al.*, *Bioconj. Chem.*, 2002, vol. 13, no. 3, pp. 510–517.
14. Okuda, T., Sugiyama, A., Niidome, T., and Aoyagi, H., *Biomaterials*, 2004, vol. 25, no. 3, pp. 537–544.
15. Schlüter, A.D. and Rabe, J.P., *Angew. Chem.*, 2000, vol. 112, no. 5, pp. 860–880.
16. US Patent 4 889 632.
17. Gershkovich, A.A. and Kireev, V.K., *Sintez peptidov: Reagenty i metody* (Peptide Synthesis: Reagents and Methods), Kiev: Naukova Dumka, 1987.
18. Wetter, S., Koch, S., and Schlüter, A.D., *J. Polym. Sci., Part A: Polym. Chem.*, 2001, vol. 39, no. 11, pp. 1940–1954.

Russian Journal of Applied Chemistry, Vol. 78, No. 6, 2005, pp. 1008–1012. Translated from Zhurnal Prikladnoi Khimii, Vol. 78, No. 6, 2005, pp. 1029–1033.
Original Russian Text Copyright © 2005 by Men'shikova, Evseeva, Shabsel's, Balanina, Sirotkin, Ivanchev.

MACROMOLECULAR CHEMISTRY AND POLYMERIC MATERIALS

Synthesis of Monodisperse Polystyrene Particles in the Presence of Sodium Dodecyl Sulfate and Carboxyl-containing Initiator

A. Yu. Men'shikova, T. G. Evseeva, B. M. Shabsel's, I. V. Balanina, A. K. Sirotkin, and S. S. Ivanchev

Institute of Macromolecular Compounds, Russian Academy of Sciences, St. Petersburg, Russia
Research Institute of Grippe, Russian Academy of Medical Sciences, St. Petersburg, Russia
St. Petersburg Branch, Boreskov Institute of Catalysis, Siberian Division, Russian Academy of Sciences, St. Petersburg, Russia

Received February 11, 2005

Abstract—Emulsion polymerization of styrene in the presence of an anionic surfactant, sodium dodecyl sulfate, in a concentration close to the critical micellization concentration, was studied, as influenced by the pH of the initial reaction mixture and the content of the carboxyl-containing azoinitiator.

Monodisperse polystyrene (PS) particles have long been used as calibration standard for electron microscopy. These particles are widely used for electron microscopic determination of the concentration of various components of natural water and, in particular, viruses, whose size is determined with the aid of an internal latex reference. To estimate quantitatively the virus population and the quality of drinking water, 50–150 nm latex monodispersions with similar polymeric structure are required. These references can also be used to estimate the retentivity of various antiviral filters and nutrient media and sera in production of vaccines and biologicals. Modification of the surface of latex particles with functional groups (e.g. carboxy groups) allows covalent binding of bioligands to the surface. The modified particles can be used to simulate virus particles not only in size but also in bioselective surface markers.

Submicrometer monodisperse microspheres of PS and poly(methyl methacrylate) (PMMA), containing surface carboxy groups, were prepared by emulsifier-free emulsion polymerization initiated by 4,4'-azobis(4-cyanoisovaleric acid) (CIVA) [1–3]. The stability of these particles against aggregation is provided by the surface charge produced in ionization of the terminal carboxy groups of the polymeric chains [4]. The degree of ionization of the initiator and polymerization products and, hence, the surface concentration of carboxy groups and the particle size depend on the pH of the reaction mixture. These particles can be used in biotechnology, since their carboxylated surface interacts with small biologically active compounds. The constancy of the polymeric structure of the particle surface makes it possible to provide the optimal conditions of immumochemical reactions with the surface change controlled by varying the pH of the reaction mixture.

To prepare 100-nm particles of this type, an emulsifier should be introduced into the reaction mixture to stabilize additionally the developed interface [5–7]. However, particles formed on the surface can migrate into the dispersion medium to promote there nucleation of new particles, thus broadening the particle size distribution of the latex.

To prepare 50–150-nm latex dispersions and to determine the factors affecting the dispersity of latex particles and the surface concentration of carboxy groups, we studied emulsion polymerization of styrene as influenced by the concentrations of emulsifier, sodium dodecyl sulfate (SDS), initiator (CIVA), and protons in the reaction mixture.

EXPERIMENTAL

Styrene was distilled under a reduced pressure. The procedures for treating CIVA are described in [4]. Sodium dodecyl sulfate (Serva) and standard solutions of HCl and NaOH were used as received. The polymerization was performed in double-distilled water. The procedure for preparing latexes has been described elsewhere [4]. The styrene to aqueous phase weight ra-

1070-4272/05/7806-1008 © 2005 Pleiades Publishing, Inc.

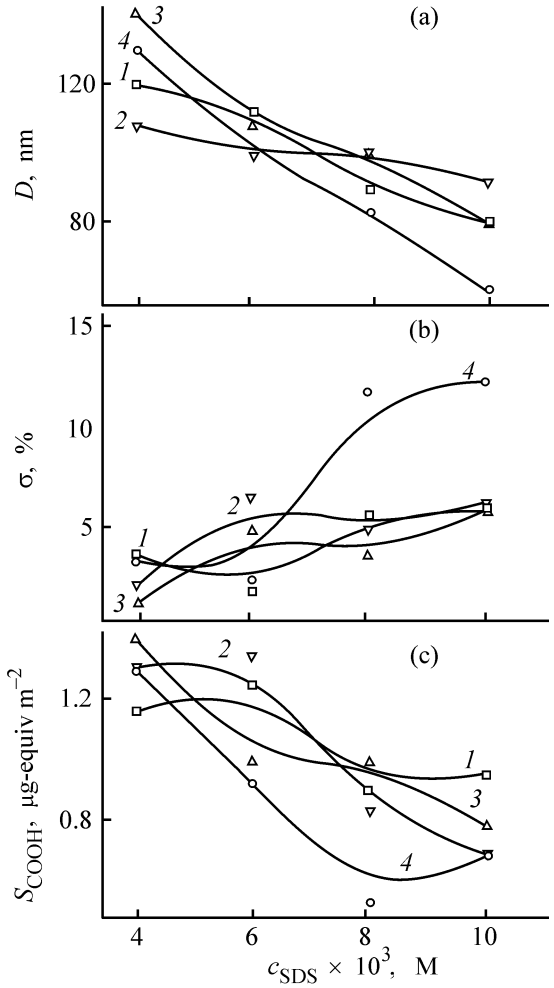


Fig. 1. (a) Diameter of PS particles (*D*), (b) root-mean-square variance of the diameter (σ), and (c) surface concentration of carboxy groups (S_{COOH}) vs. the SDS concentration c_{SDS}. CIVA content 3.57×10^{-3} M; the same for Fig. 2. Initial pH of the reaction mixture: (*1*) 8.7, (*2*) 9.5, (*3*) 10.7, and (*4*) 11.5.

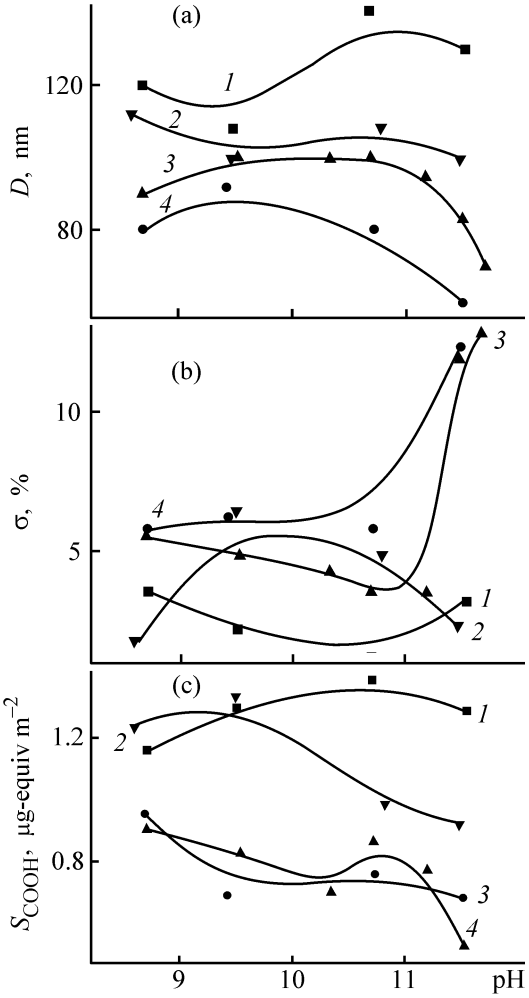


Fig. 2. (a) Diameter of PS particles *D*, (b) root-mean-square variance of the diameter σ and (c) surface concentration of carboxy groups S_{COOH} vs. the initial pH of the reaction mixture. SDS concentration in the reaction mixture (M): (*1*) 4×10^{-3}, (*2*) 6×10^{-3}, (*3*) 8×10^{-3}, and (*4*) 10^{-2}.

tio was 5%. The CIVA concentration in the aqueous phase was $(3.57–17.9) \times 10^{-3}$ M. Polymerization was performed at 363 K in the presence of $(4.08–10.20) \times 10^{-3}$ M SDS and pH of the initial emulsion 9.5–11.5.

The diameter of the latex particles was determined by electron microscopy (JEM 100 S microscope, JEOL, Japan). The root-mean-square variance σ and polydispersion coefficient *k* were calculated from diameters of more than 400 particles by the equation

$$k = D_m/D_n,$$

where D_m and D_n are the weight-average and number-average diameters, respectively.

Water-soluble impurities were removed from the latexes by dialysis for 7 days against double distilled water, which was replaced at regular intervals. The content of the surface carboxy groups was determined by conductometric titration [8].

To prepare monodisperse particles, their nucleation was performed under homogeneous conditions. For this purpose, SDS was introduced in an amount close to the critical micellization concentration (CMC) equal to 8.16×10^{-3} M at 25°C [10]. The maximal SDS concentration was 25% higher than the CMC.

The diameter of latex particles regularly decreased with increasing emulsifier concentration at all the examined initial pH values of the emulsion (Figs. 1a, 2a). This dependence was the most pronounced in strongly alkaline solutions. By contrast, the SDS concentration of 4.05×10^{-3} M is insufficient to decrease the par-

Influence of the initial concentration c_{CIVA} of the initiator, emulsifier concentration c_{SDS}, and initial pH (pH_0) on the properties of polystyrene latex particles

Sample no.	$c_{CIVA} \times 10^3$, M	pH_0	$c_{SDS} \times 10^3$, M	D_n, nm	k	σ, %	S^*_{COOH}, μg-equiv m^{-2}
1	3.57	9.5	4.08	108	1.0005	2.2	1.30
2	7.14	9.6	4.08	128	1.0007	2.7	1.37
3	8.93	9.6	4.08	145	1.0005	2.3	1.20
4	17.9	9.5	4.08	140	1.0052	7.2	1.54
5	3.57	10.4	8.16	100	1.0019	4.3	0.70
6	8.93	10.5	8.16	90	1.0061	7.8	0.93
7	17.9	10.5	8.16	78	1.0113	10.6	1.01

* S_{COOH} is the concentration of COOH groups on the surface of PS particles.

ticle size to 108 nm at pH 9.5, and a further increase in its concentration has virtually no effect on the particle size. These distinctions can be due to the fact that SDS and surfactant oligomers containing terminal COOH groups formed in the first polymerization steps are involved in the nucleation. Deprotonation of the carboxy groups with increasing pH affects the particle size in two ways. On the one hand, the ionization increases the surface charge of primary nuclei and gives rise to stable polymer-monomer particles (PMP) of smaller size. On the other hand, negatively charged carboxy groups of the oligomer and sulfo groups of the emulsifier compete for sorption on the particle surface, which is confirmed by a decrease in the surface concentration of carboxy groups with increasing SDS concentration (Fig. 1c) and pH (Fig. 2c, curves *2*–*4*). The degree of carboxylation of the particle surface is almost independent of pH (Fig. 2c, curve *1*) at the lowest concentration of SDS (4.08×10^{-3} M) in the reaction mixture, which indicates that the surface concentration of the emulsifier is low.

The latex particles growin size with as the initial concentration of the initiator increases at the SDS concentration of 4.08×10^{-3} M and pH 9.5–9.6 (see table, Fig. 3). The particle size distribution of the latex is substantially broadened at the maximal CIVA concentration (sample no. 4). A similar dependence has been observed for emulsifier-free polymerization of styrene initiated by potassium persulfate [6, 7].

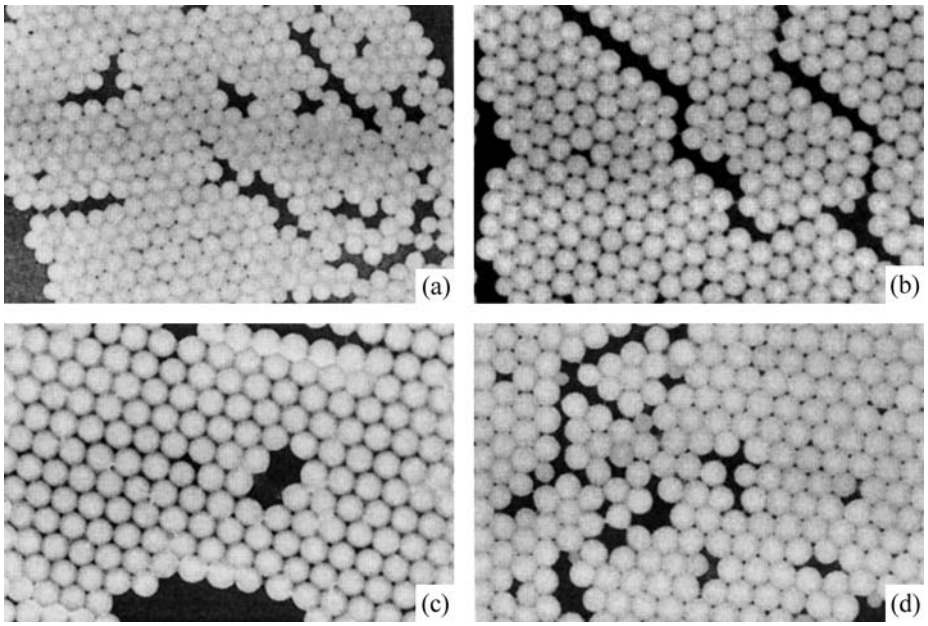


Fig. 3. Electron micrographs of latex nos. (a) 1, (b) 2, (c) 3, and (d) 4 (sample numbers are indicated in the table).

The negative concentration effect of high concentrations of water-soluble ionic initiators is due to an increase in the ionic strength of the reaction mixture and in the concentration of surfactant oligomers, which can form new PMPs in the course of polymerization, thereby making the latexes polydisperse. At pH 10.4–10.5 and the SDS concentration of 8.16×10^{-3} M, the dependence of the particle size on the CIVA concentration was inverse. The average particle diameter decreased and k and σ substantially increased owing to the above effects. The surface concentration of the terminal COOH groups also decreased. Therefore, most of the subsequent experiments were performed at the lowest CIVA concentration of (3.57×10^{-3} M).

The pH dependence of the particle diameter has a shallow minimum at pH 9.5 and SDS concentrations lower than CMC (Fig. 2a, curves *1*, *2*). This behavior is typical of an emulsifier-free polymerization of styrene, initiated by CIVA, and is caused by the fact that the degree of ionization of COOH groups on the surface of latex particles is at a maximum. In more alkaline solutions, $-COO^-Na^+$ ion pairs are formed owing to an increase in the ionic strength of the reaction mixture [1, 2]. By contrast, when the SDS concentration is equal to, or higher than CMC (Fig. 2a, curves *3*, *4*), this minimum is not observed and the diameter of particles formed in strongly alkaline solutions noticeably decreases. Clearly, both homogeneous and micellar nucleation mechanism are possible at SDS concentrations close to CMC. The average particle diameter decreases, the concentration of the surface COOH groups decreases, and the variance σ of the diameter of the latex particles substantially increases (Fig. 1b, curve *4*; Fig. 2b, curves *3*, *4*) as the SDS concentration decreases within the CMC range. However, monodisperse latexes with σ lower than 5–6% can be prepared in less alkaline solutions at this SDS concentration.

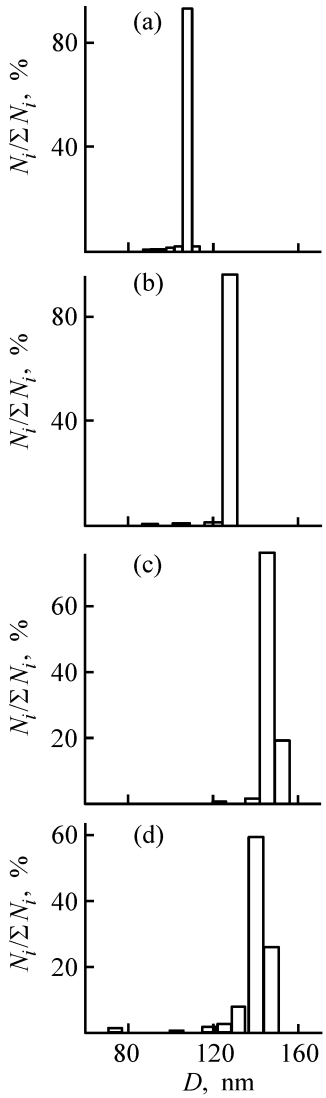


Fig. 4. Particle size distribution of latex nos. (a) 1, (b) 2, (c) 3, and (d) 4 (sample numbers are indicated in the table). ($N_i/\Sigma N_i$) Fraction of particles with a certain diameter and (D) particle diameter.

CONCLUSIONS

(1) Monodisperse 80–140-nm latex particles with a 0.50–1.35-μg-equiv m^{-2} surface concentration of carboxy groups were prepared by emulsion polymerization of styrene, induced by 4,4'-azobis(4-cyanoisovaleric acid) in the presence of sodium dodecyl sulfate in a concentration close to the critical micellization concentration.

(2) The particle diameter and the surface concentration of carboxy groups can be controlled in the indicated range by varying the pH of the initial reaction mixture and the azo initiator concentration in it. A dispersion characterized by a room-mean-square deviation from the average particle diameter lower than 5% can be prepared.

ACKNOWLEDGMENTS

This study was financially supported by the Russian Foundation for Basic Research (project no. 04-03-33080) and by research program of the Division of Chemistry and Material Science of the Russian Academy of Sciences "Preparation and Study of Macromolecules and Macromolecular Structures of New Generations."

REFERENCES

1. Lishanskii, I.S., Menshikova, A.Yu., Evseeva, T.G., *et al.*, *Vysokomol. Soerdin., Ser. B*, 1991, vol. 33, no. 6, pp. 413–416.
2. Men'shikova, A.Yu., Evseeva, T.G., Shabsel's, B.M., *et al.*, *Kolloidn. Zh.*, 1997, vol. 59, no. 5, pp. 671–675.
3. Men'shikova, A.Yu., Evseeva, T.G., Ivanchev, S.S., *et al.*, *Vysokomol. Soerdin., Ser. A*, 2001, vol. 43, no. 4, pp. 607–615.
4. Shubin, V.E., Isakova, I.V., Sidorova, M.P., *et al.*, *Kolloidn. Zh.*, 1990, vol. 52, no. 5, pp. 535–541.
5. Eliseeva, V.I., *Polimernye dispersii* (Polymer Dispersions), Moscow: Khimiya, 1980.
6. Kotera, A., Furasawa, K., and Takeda, Y., *Kolloid Z. Z. Polym.*, 1970, vol. 239, no. 2, pp. 677–681.
7. Kotera, A., Furasawa, K., and Kudo, K., *Kolloid Z. Z. Polym.*, 1970, vol. 240, nos. 1–2, pp. 837–842.
8. Labib, V.T. and Robertson, A.A., *J. Colloid Interface Sci.*, 1980, vol. 17, no. 1, pp. 151–161.
9. Abramson, A.A., *Poverkhnostno-aktivnye veshchestva: svoistva i primenenie* (Surfactants: Properties and Applications), Leningrad: Khimiya, 1981.

Russian Journal of Applied Chemistry, Vol. 78, No. 6, 2005, pp. 1013–1017. Translated from Zhurnal Prikladnoi Khimii, Vol. 78, No. 6, 2005, pp. 1034–1037.
Original Russian Text Copyright © 2005 by Zhokhova, Baskin, Palyulin, A. Zefirov, N. Zefirov.

MACROMOLECULAR CHEMISTRY AND POLYMERIC MATERIALS

A Study of the Affinity of Dyes for Cellulose Fiber within the Framework of a Fragment Approach in QSPR

N. I. Zhokhova, I. I. Baskin, V. A. Palyulin, A. N. Zefirov, and N. S. Zefirov

Lomonosov State University, Moscow, Russia

Received October 20, 2004; in final form, March 2005

Abstract—The affinity of azo and anthraquinone dyes for the cellulose fiber was first studied by the fragment approach in terms of the QSPR method. Linear-regression models that can prognosticate this parameter on the basis of descriptors taking into account the fragment composition of a molecule were suggested.

The interaction of various dyes with a cotton fiber is a complex physicochemical process governed by specific features of the structure of the textile polymer and by the nature of a dye molecule. This interaction is affected by various factors (electrostatic fields, Van der Waals forces, formation of hydrogen bonds, hydrophobicity, etc.), and the available experimental data are rather diverse. That is why theoretical methods for calculation of quantitative structure–property/activity relationships (QSPR/QSAR and 3D-QSAR) are widely used to study these interactions [1].

One of the main parameters characterizing the interaction of a dye with a fiber is the chemical affinity $-\Delta\mu^0$ (kJ mol^{-1}). It has been shown that, in the fixation of a dye molecule on a cellulose fiber, the key influence on the affinity of anionic and neutral azo [2, 3], heterocyclic monoazo [4], symmetric diazo [5], and anthraquinone [6] dyes for the cellulose fiber is exerted by electrostatic interactions. At the same time, it is commonly assumed thatthe binding of dye molecules may occur with specific binding centers involved, and the existence of these centers is due to the supramolecular structure of cellulose [7]. When studying dye–fiber intermolecular interactions, the authors of [8] concluded that steric factors are less important in this case than for the classical ligand–receptor interactions. As for the spatial structure of a dye molecule and presence of various kinds of substructures, they should be regarded as additional factors that affect the distribution of electrostatic potentials around a molecule, which are of primary importance for the dye–fiber interaction, too. In this context, it seems to be of interest to study how the affinity of dye molecules for cellulose depends on their fragment composition, which remains virtually unstudied. In the study, the affinity of a number of azo and anthraquinone dyes for cellulose was examined using the fragment approach the framework of the QSPR methodology.

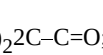
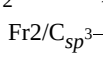
Previously, descriptors characterizing the fragment composition of a molecule have been successfully used for QSPR-prognostication of physicochemical properties of organic compounds of various classes, including the chromatographic retention indices [9], boiling point [9], flash point [10], sublimation enthalpy [11], polarizability [12], and magnetic susceptibility [13].

The study was performed using the NASAWIN QSAR/QSPR software package [14, 15] and the integrated FRAGMENT software. Databases were compiled using MEOW and BASTET software specially developed for creating and refining structural databases [12]. Three samples of compounds, containing 30 anionic sulfur-containing azo dyes [3] were studied (Database 1). The affinity of a dye for the fabric was chosen as the property to be modeled. It was calculated as the difference of the standard chemical potentials of a dye molecule fixed on the fabric surface and that in an aqueous solution. These thermodynamic data were experimentally obtained in aqueous solutions at three temperatures and were described in detail in [16]. Further, data for 49 anthraquinone dyes [8] were collected (Database 2). Finally, a combined sample was obtained, which contained both sets of structures (Database 3). Based on a preliminary verification of all the databases by the BASTED software, the following corrections were introduced, by agree-

1070-4272/05/7806-1013 © 2005 Pleiades Publishing, Inc.

Statistical parameters of QSPR models based on fragment descriptors for the affinity of azo and anthraquinone dyes for cellulose fiber

Model*	Database	R^2_{learn}	s	R^{2**}_{prog}	F	N***
1	Database 1 (azo dyes)	0.949	0.87	0.896	88.6	4/6
2		0.957	0.81	0.850	81.7	5/6
3		0.958	0.83	0.839	64.9	6/6
4		0.949	0.87	0.900	88.6	4/10
5		0.957	0.81	0.850	81.7	5/10
6		0.971	0.95	0.908	161.7	4/15
7	Database 2 (anthraquinone dyes)	0.918	0.56	0.860	51.1	7/15
8		0.924	0.55	0.866	47.5	8/15
9		0.931	0.53	0.866	44.9	9/15
10	Database 3 (azo and anthraquinone dyes)	0.940	1.66	0.765	94.3	9/15
11		0.942	1.65	0.772	86.6	10/15
12		0.945	1.63	0.785	80.7	11/15

* Model nos. 1–6: Fr1/=CR–C, Fr2/RC_{Ar}÷C_{Ar}–NH_2, Fr3/·=·–·÷·÷·÷· (· is an arbitrary atom), Fr4/  ; model nos. 2, 5: Fr5/C–$(C÷)_2$2C–C=O; model no. 3: Fr5/  , Fr6/  ; model no. 6: Fr4/C–C–$(C÷)_3$C–N=N–$(C÷)_5$C–N; model no. 7: Fr1/RC_{Ar}, Fr2/C_{sp^3}–NHR, Fr3/C_{Alk}–NR–C, Fr4/C_{Alk}–RC_{Ar}÷C_{Ar}, Fr5/C_{Alk}–C–NH–$(C_{Ar}÷)_2C_{Ar}$, Fr6/>N–$(C_{Ar}÷)_3C_{Ar}$–N<, Fr7/C_{sp^3}–O–$(C_{Ar}÷)_7C_{Ar}$–N<; model no. 8: Fr1–Fr4 as in model nos. 7, Fr5/$(C_{Ar}÷)_3C_{Ar}$–OH, Fr6, Fr7, Fr8 as Fr5, Fr6 and Fr7 model nos. 7, respectively; model no. 9: Fr1–Fr7 as in model nos. 8, Fr8/$(C_{Ar}÷)_5C_{Ar}$–Cl, Fr9 as Fr8 model nos. 8; model no. 10: Fr1/C=, Fr2/–OH, Fr3/C_{sp^3}–N_{sp^3}–C, Fr4/RC_{Ar}÷C_{Ar}÷C_{Ar}, Fr5/$(C÷)_3$C–N, Fr6/$(C_{Ar}÷)_3C_{Ar}$–C=O, Fr7/·–$(·÷)_4$·–·–·=· (· is an arbitrary atom), Fr8/=C–N_{sp^3}–$(C_{Ar}÷)_7C_{Ar}$–OH, Fr9/Cl–$C_{Ar}(÷C_{Ar}H)_2$; model no. 11: Fr1–Fr6 as in model nos. 10, Fr7/C–C–$(C_{Ar}÷)_3$C–N, Fr8, Fr9, Fr10 as Fr7, Fr8, Fr9 model nos. 10, respectively; model no. 12: Fr1–Fr4 as in model nos. 11, Fr5/N_{sp^3}–C_{Ar}÷C_{Ar}–N=, Fr6, Fr7, Fr8, Fr9, Fr10, Fr11 as Fr5, Fr6, Fr7, Fr8, Fr9, Fr10 model nos. 1 1.

** Control sample includes every fifth compound of a database.

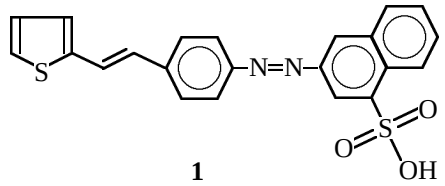
*** Number of fragment descriptors/Maximum number of atoms in a fragment.

ment with the authors of [8], into Database 2: substituent 1-$NHCOCH_3$ in structure no. 12 changed ws changed to 1-$NHCOCH_2Cl$, and the place of addition of the substituent –[4-$OCH_3C_6H_4CONH$–] in structure no. 41, from position 5 to position 4.

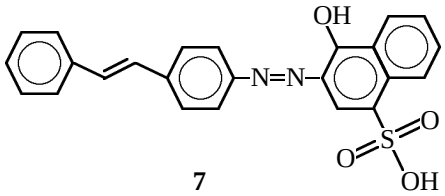
In the first stage of the study, linear-regression models based on descriptors characterizing fragments with the maximum chain lengths of 6, 10, and 15 atoms and an external control sample including every fifth compound of a database were constructed for the samples under study using the NASAWIN software package. These models (see table, model nos. 1–12) have good descriptive and prognosticating properties. The best prognosis quality was achieved with fragments having chains up to 15 atoms long included in the model.

The quality of fragment-based and published models obtained for the same samples by means of a comparative molecular field analysis and a multiple linear regression with the use of quantum-chemical descriptors (azo compounds) [3], and by the method of a comparative molecular surface analysis (CoMSA, azo and anthraquinone compounds) [8] was compared by constructing a number of models using a sliding control with exclusion of a single compound. The models obtained are comparable in their properties with those cited in the literature, and in some case, even surpass them. For example, the regression model constructed for Database 1 with four fragment descriptors (chain in a fragment up to 15 atoms long) has parameters (R^2_{learn} = 0.967; standard deviation s = 0.66; F = 181.6; squared correlation coefficient with a sliding control, Q^2 = 0.949; root-mean-square error RMS_{sl} = 0.74; standard deviation with a sliding control, s_{sl} = 0.80) exceeding those of the best regression model constructed for the same sample with the energies of the upper occupied and lower unoccupied molecular orbitals E_{HOMO}, E^2_{HOMO}, and E_{LUMO}, calculated by the AM1 method, used as descriptors (three descriptors, R^2_{learn} = 0.92, s = 1.02, F = 94.9, Q^2 = 0.89, standard deviation with a sliding control 1.19) [3]. For the PLS CoMFA [3] and CoMSA [8] models obtained for the given samples

the values of Q^2 fall within the ranges 0.63 – 0.75 and 0.829 – 0.970, respectively. The model constructed includes descriptors that describe the following fragments of azo compound molecules: =RC–C, RC_{Ar}÷C_{Ar}–NH_2, ·=·–·÷·÷·÷· (· is an arbitrary atom) and C–C–C÷(C÷)$_2$C–N=N–C÷ ÷(C÷)$_4$C–N. These fragment chains are more important for characterizing the affinity of the azo dyes. The largest difference between the calculated and experimental affinities is observed for structure **1** (1.3 kJ mol^{-1}) and **7** (1.2 kJ mol^{-1}):



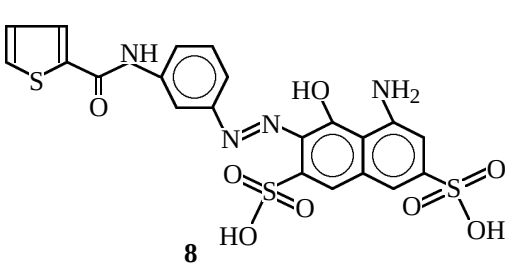
1



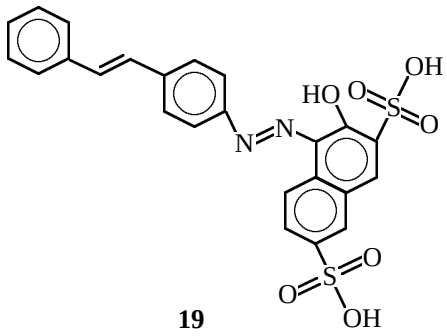
7

Combination of fragment descriptors with quantum-chemical descriptors of the energy of molecular orbitals, E_{HOMO} and E_{ILUMO} (data of [3] are used), fails to improve the quality of the models. Possibly, these descriptors are approximated by fragment descriptors.

The fragment models constructed for a sample of anthraquinone dyes (Database 2) also compare well in their prognosticating properties with published models [8]. Squared correlation coefficient with a sliding control for a model including eight descriptors (chains of 15 atoms; R^2_{learn} = 0.942, s = 0.46, F = 81.5, Q^2 = 0.915, RMS_{sl} = 0.50, s_{sl} = 0.55) exceeds the maximum value of Q^2 (0.88) for the Co MSA model [8]. The largest contribution to the model RC_{Ar}, and comes from the following components: C_{Ar}–N_{sp^3}–C, HC_{Ar}÷C_{Ar}–NHR, and C_{sp^3}–O–(C_{Ar}÷)$_7$ C_{Ar}–N_{sp^3}. The maximum deviation from the correlation is observed for structure **8** (0.98 kcal mol^{-1}) and **19** (0.94 kcal mol^{-1}):



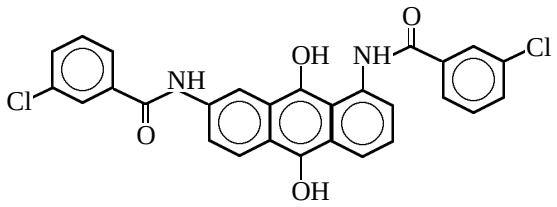
8



19

The most important fragments included in the models for azo and anthraquinone compounds are distinguished by the existence of long chains of conjugated systems, which reflects their importance for the characterization of the property being modeled.

An attempt was made to construct a more versatile model for describing the dye–cellulose affinity by merging narrow samples of azo and anthraquinone dyes (Database 3). The prognosticating ability of this model was assessed by using the sliding control method. To make Database 2 uniform, the affinities from this database (kcal mol^{-1}) were expressed in kJ mol^{-1}. The model obtained includes 10 fragment descriptors (chains of 15 atoms) and has the following parameters: R^2_{learn} = 0.933, s = 1.72, F = 94.7, Q^2 = 0.901, s_{sl} = 2.09, RMS_{sl} = 1.94. The largest deviation from the correlation is observed for compound no. 68 (5.5 kJ mol^{-1}):



Below, the model obtained with this structure excluded from the learning sample is presented:

$$-\Delta\mu^0 = -4.36 + 1.87Fr1 - 2.63Fr2 - 1.31Fr3 - 1.38Fr4 + 0.67Fr5 + 1.56Fr6 + 1.14Fr7 + 1.78Fr8 - 0.82Fr9 + 1.38Fr10, \quad (1)$$

where R^2_{learn} = 0.947, s = 1.47, F = 119.4, Q^2 = 0.909, s_m = 1.93, RMS_m = 1.79; Fr1/C=, Fr2/–OH, Fr3/C_{sp^3}–N_{sp^3}–C, Fr4/C_{Ar}–(C=)–C, Fr5/RC_{Ar}÷C_{Ar}÷C_{Ar}, Fr6/N–C÷C–N, Fr7/·–·–·–·=·–·; Fr8/C_{Ar}–(C=)–NR–(C_{Ar}÷)$_7$$C_{Ar}$–OH, Fr9/C–N–(C÷)7C–N–C=O, Fr10/Cl–C_{Ar}(÷C_{Ar}H)$_2$.

In contrast to the case of models constructed for narrow samples (Databases 1 and 2), the largest con-

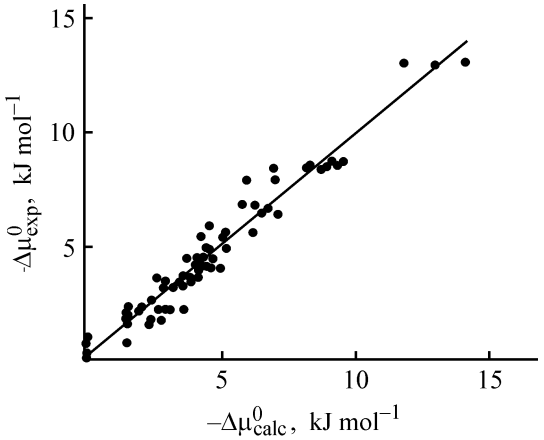


Diagram of scatter of the calculated and experimental values of the affinity of dyes for cellulose, $-\Delta\mu^0$, for a learning sample of Database 3, obtained in terms of the linear-regression model [Eq. (1)].

tribution to the combined model comes from descriptors of rather simple fragments: Fr1/C= and Fr2/–OH. The correlation plot for the calculated and experimental values of $-\Delta\mu^0$ for the combined model is shown in the figure.

Of interest is assessment of the prognosticating capacity of combined fragment models for the azo and anthraquinone dye samples under study. For this purpose, models were obtained using the combined Database 3 and the sliding control and were tested on two independent external samples including, respectively, every fifth compound from Databases 1 and 2. With these samples excluded from Database 3, the number of azo compounds and anthraquinones in the combined learning sample was 24 and 40, respectively. It was found that the prognosticating capacity of such a model (10 fragment descriptors, chains up to 15 atoms long) for an independent control sample of azo compounds considerably exceeds that for a sample of anthraquinones. For example, squared correlation coefficients between the experimental and predicted values, R^2_{prog}, for the appropriate control samples are 0.941 and 0.573, respectively. These data are in an agreement with the results of the study [8], in which the CoMSA models obtained for a sample of azo compounds surpass in prognosticating properties the models for a sample of anthraquinones. This confirms the efficiency of application of the fragment approach to modeling of the properties under study.

To improve the quality of the models, it seemed appropriate to include, in addition to the fragment descriptors, those characterizing the geometry (shape and size) of a molecule and making it possible to evaluate the degree of its compactness, i.e., topological indices. Descriptors of this kind were used to model the affinity of anthraquinone dyes for cellulose in [17]. More than 30 topological indices calculated using the EMMA software package [18, 19] were analyzed. However, the desired improvement of the quality of the models could not be achieved. This means that the set of fragment descriptors used in the present study enables a rather complete description of the relationship between the structural features of molecules of the dye groups studied and their affinity for cellulose.

CONCLUSION

Linear-regression QSPR models making it possible to prognosticate the affinity of azo and anthraquinone dyes for the cellulose fiber on the basis of descriptors that take into account the fragment composition of a dye molecule were suggested for the first time.

REFERENCES

1. Timofei, S., Schmidt, W., Kurunczi, L., and Simon, Z., *Dyes Pigm.*, 2000, vol. 47, nos. 1–2, pp. 5–16.
2. Funar-Timofei, S. and Schr uurmann, G., *J. Chem. Inf. Compt. Sci.*, 2002, vol. 42, no. 4, pp. 788–795.
3. Schr uurmann, G. and Funar-Timofei, S., *J. Chem. Inf. Compt. Sci.*, 2003, vol. 43, no. 5, pp. 1502–1512.
4. Timofei, S. and Fabian, W.M.F., *J. Chem. Inf. Compt. Sci.*, 1998, vol. 38, no. 6, pp. 1218–1222.
5. Fabian, W.M.F. and Timofei, S., *J. Mol. Struct., Theochem*, 1996, no. 362, pp. 155–162.
6. Fabian, W.M.F., Timofei, S., and Kurunczi, L., *J. Mol. Struct., Theochem*, 1995, no. 340, pp. 73–81.
7. French, A.D., Battisla, O.A., Cuculo, J.A., and Gray, D.G., *Kirk-Othmer Encyclopedia of Chemical Technology, 4th ed.*, New York: Wiley, 1993, vol. 5, p. 476.
8. Polanski, J., Gieleciak, R., and Wyszomirski, M., *J. Chem. Inf. Comp. Sci.*, 2003, vol. 43, no. 6, pp. 1754–1762.
9. Zefirov, N.S. and Palyulin, V.A., *J.Chem. Inf. Compt. Sci.*, 2001, vol. 41, no. 4, pp. 1022–1027.
10. Zhokhova, N.I., Palyulin, V.A., Baskin, I.I., *et al.*, *Izv. Akad. Nauk. Ser. Khim.*, 2003, no. 9, pp. 1787–1793.
11. Zhokhova, N.I., Palyulin, V.A., Baskin, I.I., *et al.*, *Zh. Prikl. Khim.*, 2003, vol. 76, no. 12, pp. 1914–1919.
12. Zhokhova, N.I., Palyulin, V.A., Baskin, I.I., *et al.*,

Izv. Akad. Nauk. Ser. Khim., 2003, no. 5, pp. 1005–1009.

13. Zhokhova, N.I., Palyulin, V.A., Baskin, I.I., *et al.*, *Zh. Strukt. Khim.*, 2004, vol. 45, no. 4, pp. 659–668.
14. Baskin, I.I., Palyulin, V.A., and Zefirov, N.S., *QSAR and Molecular Modelling: Concepts, Computational Tools and Biological Applications*, Sanz, F., Giraldo, J., and Manaut, F., Eds., Barcelona: Prous Sci. Publishers, 1995, p. 30.
15. Baskin, I.I., Palyulin, V.A., and Zefirov, N.S., *J. Chem. Inf. Comput. Sci.*, 1997, vol. 37, no. 4, pp. 715–721.
16. Alberti, G., Cerniani, A., de Giori, M.R., and Seu, G., *Tinctoria*, 1980, no. 5, pp. 141–143.
17. Timofei, S., Schmidt, W., Kurunczi, L., *et al.*, *Dyes Pigm.*, 1994, vol. 24, no. 4, pp. 267–279.
18. Petelin, D.E., Palyulin, V.A., and Zefirov, N.S., *Dokl. Akad. Nauk*, 1992, vol. 324, no. 5, pp. 1019–1022.
19. Zefirov, N.S. and Palyulin, V.A., *J. Chem. Inf. Compt. Sci.*, 2002, vol. 42, no. 5, pp. 1112–1122.

Russian Journal of Applied Chemistry, Vol. 78, No. 6, 2005, pp. 1018–1022. Translated from Zhurnal Prikladnoi Khimii, Vol. 78, No. 6, 2005, pp. 1038–1042.
Original Russian Text Copyright © 2005 by Troitskii, Khokhlova, Konev, Denisova, Novikova, Lopatin.

MACROMOLECULAR CHEMISTRY AND POLYMERIC MATERIALS

Influence of UV Pretreatment on Thermooxidative Degradation of Poly(Methyl Methacrylate) Films with Fullerene C_{60} or C_{70}

B. B. Troitskii, L. V. Khokhlova, A. N. Konev, V. N. Denisova, M. A. Novikova, and M. A. Lopatin

Razuvaev Institute of Organometallic Chemistry, Russian Academy of Sciences, Nizhni Novgorod, Russia

Received October 22, 2004; in final form, January 2005

Abstract—Wariation of the concentration of fullerenes C_{60} and C_{70} in poly(methyl methacrylate) films under UV exposure in atmospheric oxygen was studied. The mechanism of the influence exerted by addition of some photostabilizing polymers and xanthene dyes on the photooxidative degradation of fullerene in the polymer matrix was analyzed.

Poly(methyl methacrylate) (PMMA) and methyl methacrylate copolymers (MMACs) find practical application as organic glasses owing to their transparency, shock resistance, and stability against external factors.

Troitskii *et al.* [1, 3–6] and Shibaev *et al.* [2] have found recently that fullerenes C_{60} and C_{70}, thermally stable inorganic compounds, inhibit radical-chain reactions of thermal degradation of PMMA, MMACs, and branched chain reactions of thermooxidative degradation (TOD) of these polymers. An important feature of fullerenes as antioxidants is the deceleration of TOD of polymers at high temperatures of up to 340°C [7].

However, when exploited under natural conditions, organic glasses are subjected, above all, to solar radiation whose UV component exerts the strongest degrading action on the polymer and various additives introduced therein.

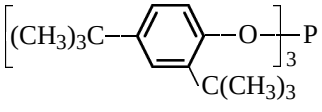
In this study, we examined (a) the influence of exposure to UV radiation in the presence of atmospheric oxygen on the concentrations of C_{60} and C_{70} dissolved in PMMA; (b) role of additives (selected photostabilizers and dyes) on this process; (c) mechanism of photooxidative degradation of fullerene in the polymer matrix; and (d) influence of a UV pretreatment on the TOD of PMMA with C_{60} and C_{70}.

EXPERIMENTAL

PMMA films of thickness 100 ± 20 μm, containing C_{60}, C_{70}, or a crude mixture of fullerenes, were prepared by the procedure described in [1].

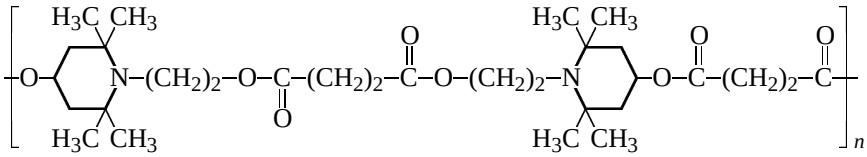
The films were irradiated in air with a 230-W DRT-230 (λ_{max} = 254 nm) low-pressure mercury lamp. The lamp was cooled with a quartz cooler through which distilled water was passed. The distance between the center of the lamp and the sample with an area of 2×4 cm^2 was 20 cm. The films were irradiated on both sides for the same time. The changes in the concentration of C_{60} and C_{70} in PMMA were monitored by the intensities of the absorption bands at 331 (C_{60}) and 331 and 375 nm (C_{70}). The spectra of the films in the UV and visible spectral ranges were recorded on a Perkin–Elmer Lambda 25 UV/VIS Spectrometer.

Polymer photostabilizers Irgafos 168, Tinuvin 622, Tinuvin 770, and Chimassorb 944 were available from Ciba Specialty Chemicals and used without further purification. Given below are the chemical formulas of the stabilizers: Irgafos 168, tri(2,4-di-*tert*-butylphenyl) phosphite

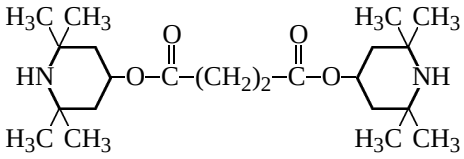


1070-4272/05/7806-1018 © 2005 Pleiades Publishing, Inc.

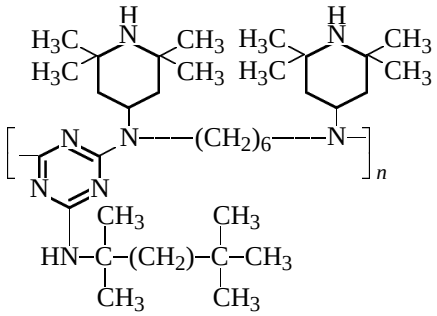
Tinuvin 622, oligomer, a sterically hindered amine



Tinuvin 770, a sterically hindered amine



Chimassorb 944, a sterically hindered amine, oligomeric product



As dyes served chemically pure rhodamine C and rhodamine G.

Thermooxidative degradation of the PMMA films with additives was studied by TGA at 277°C and an oxygen pressure of 200 mm Hg.

Figures 1a and 1b show that, as the time of UV irradiation of the PMMA films with fullerene additives increases, the fullerene concentration tends to regularly decrease, as can be seen from a decrease in the intensities of the absorption bands at 331 (Fig. 1a) and 375 (Fig. 1b) nm. Simultaneously, the absorption at 400–500 nm tends to increase.

It should be noted that the photophysical properties of thin films consisting of C_{60} and C_{70} molecules only are well understood [7, 8]. When exposed to UV radiation in a vacuum or in an inert gas atmosphere, fullerene molecules pass from the ground state S_0 to an excited S_1 singlet state. The $S_0 \rightarrow S_1$ transition energy E_S is 221.5 for C_{60} and 192.3 kJ mol^{-1} for C_{70}. From the S_1 state fullerene passes to an excited triplet state with a yield of nearly 100%. Arbogast *et al.* estimated the triplet state energy E_T for C_{60} as 156.8 ± 18.8 kJ mol^{-1} [7].

In the triplet state T_1, fullerene C_{60} reacts with the double bond of the neighboring unexcited molecule by the 2 + 2 cycloaddition mechanism, to give a dimer [8]. By analogous mechanism, dimers can be converted into trimers, etc., which are insoluble in solvents. This makes thin C_{60} films suitable for photolithographic application [8]. The activation energy of

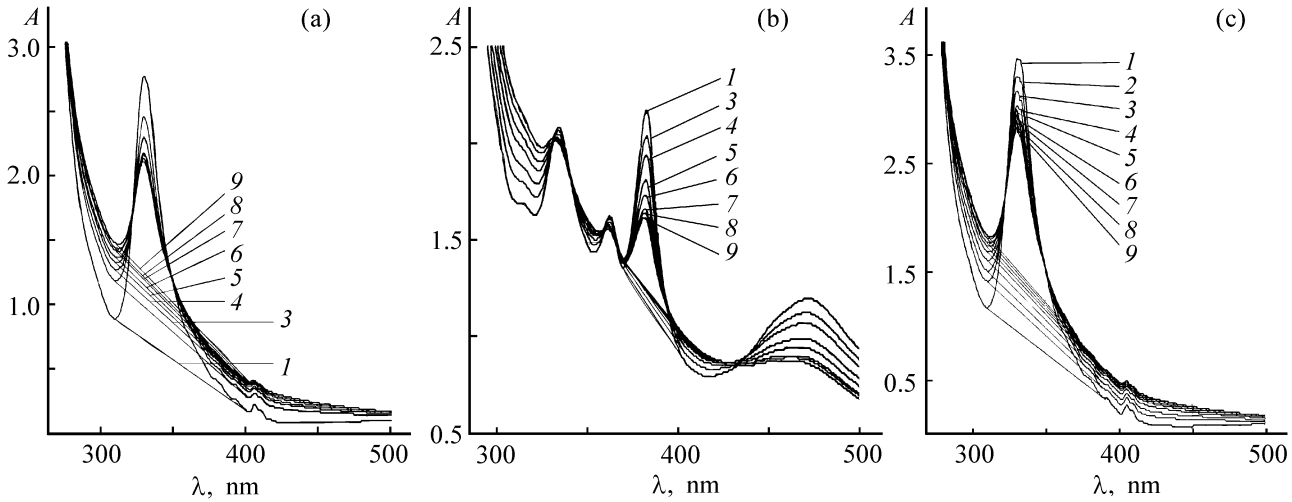
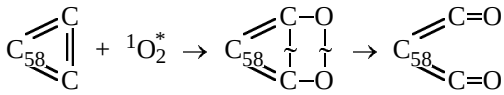


Fig. 1. Absorption spectra of UV-irradiated PMMA samples with various additives. (*A*) Absorption, and (λ) wavelength. Additive, mol kg^{-1}: (a) 3.3×10^{-3} C_{60}, (b) 4.1×10^{-3} C_{70}, and (c) 6×10^{-3} C_{60} + 0.3 wt % Tinuvin 622, (*1*) Nonirradiated sample; irradiation time, min: (*2*) 2×15, (*3*) 2×30, (*4*) 2×60, (*5*) 2×90, (*6*) 2×120, (*7*) 2×150, (*8*) 2×180, and (*9*) 2×210.

thermal degradation of the dimer was estimated as 120.4 kJ mol^{-1}. Above 100°C, the dimer degrades into the initial C_{60} [8]. Photodimerization and photopolymerization are much less pronounced in the case of C_{70}, compared to C_{60} [8].

When thin films of C_{60} or C_{70} are irradiated in the presence of oxygen, photodimerization and photopolymerization are completely suppressed, since oxygen quenches, with a huge rate constant $K_q(O_2) = 1.9 \times 10^9$ mol^{-1} s^{-1}, the triplet state of fullerene, passing to the excited singlet state [7, 8]. In the active singlet state, oxygen oxidizes fullerenes to give >C–O–, >C–O–C<, and >C=O [8].

The aforesaid suggests that UV irradiation of the PMMA films with fullerene additives involves photooxidation of fullerene by singlet oxygen by the scheme



(1)

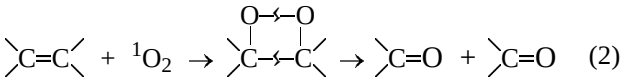
Formation of conjugated >C=C–C=O bonds is, evidently, responsible for the "broadening" of the absorption bands of fullerene and enhancement of absorption at 400–450 nm for C_{60} (Fig. 1a) and 430–500 nm for C_{70} (Fig. 1b).

Interestingly, reaction (1) results in degradation of the integral geometric structure of the fullerene (C_{60} is a sphere, and C_{70}, an ellipsoid) and formation of a "hole" at the site of rupture of the carbon–carbon double bond. Evidently, one molecule of fullerene C_{60} or C_{70} can add several molecules of singlet oxygen, with even more significant degradation of the geometric structure of the initial compound and formation of several holes on the surface of the sphere or ellipsoid.

In view of the fact that a fullerene molecule in the PMMA matrix is surrounded by fragments of macromolecules, it was reasonable to elucidate whether fullerene is a photosensitizer of photooxidation of the polymer. In other words, what is the probability of the reaction of the fullerene-activated singlet oxygen with fragments of macromolecules, rather than with fullerene, to yield active particles, with photooxidation of the polymer by the radical-chain mechanism.

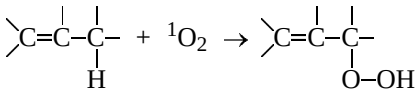
To this end, we carried out photooxidation of PMMA films with C_{60} and C_{70} in the presence of the known effective inhibitors of photooxidative degradation of polymers, Tinuvin 622, Tinuvin 770, and Chimassorb 944. Figure 1c shows how the intensity of the absorption band of fullerene C_{60} in the PMMA film with a Tinuvin 622 additive varies with the UV irradiation time. Similar spectra were obtained for other photooxidation inhibitors as well. Figure 1c shows that photooxidation of C_{60} and C_{70} fullerenes is unaffected by inhibitors of photooxidative degradation.

Evidently, photooxidation of films of PMMA with C_{60} and C_{70} leads, above all, to oxidation of the fullerene proper, without sensitizing the oxidation of the polymer. De Rosa and Crutchley [9] showed that singlet oxygen actively reacts with compounds containing carbon–carbon double bonds to give thermally unstable cyclic peroxide, degrading into carbonyl compounds:



(2)

Singlet oxygen, probably, reacts with the activated bond in the allyl position, to give hydroperoxide



(3)

Fullerene C_{60} contains 30 carbon–carbon double bonds, and fullerene C_{70}, 35 double bonds. At the same time PMMA macromolecules contain virtually no carbon–carbon double bonds and allyl groups (the concentration of the terminal double bonds in the macromolecules is very low, no more than 0.1 mol %). Therefore, oxidation of fullerene by singlet oxygen is more probable than oxidation of the surrounding fragments of macromolecules.

We studied how xanthene dyes affect the photooxidation in the PMMA–C_{60} system. Table shows that addition of rhodamine G and rhodamine C decelerates oxidation of C_{60}. Fullerene C_{60}, in turn, decelerates photooxidation of these dyes. Evidently, this is due to the shielding effect, since both the fullerene and dyes intensively absorb UV radiation.

The TGA studies of the thermooxidative degradation revealed that preirradiation of the PMMA films containing C_{60} (Fig. 2a), C_{70} (Fig. 2b), or a C_{60} (80%) + C_{70} (20%) mixture (Fig. 2c) deteriorates the antioxidative performance of the fullerenes in TOD of the polymer. The induction period of TOD of unirradiated polymer with addition of C_{60} is 40 min (Fig. 2a, curve *1*), decreases to 15 min after 60-min UV irradiation (curve *2*), and disappears after 120-min UV irradiation (curve *3*). Nevertheless, even after a 300-min UV irradiation, the initial rate of TOD for

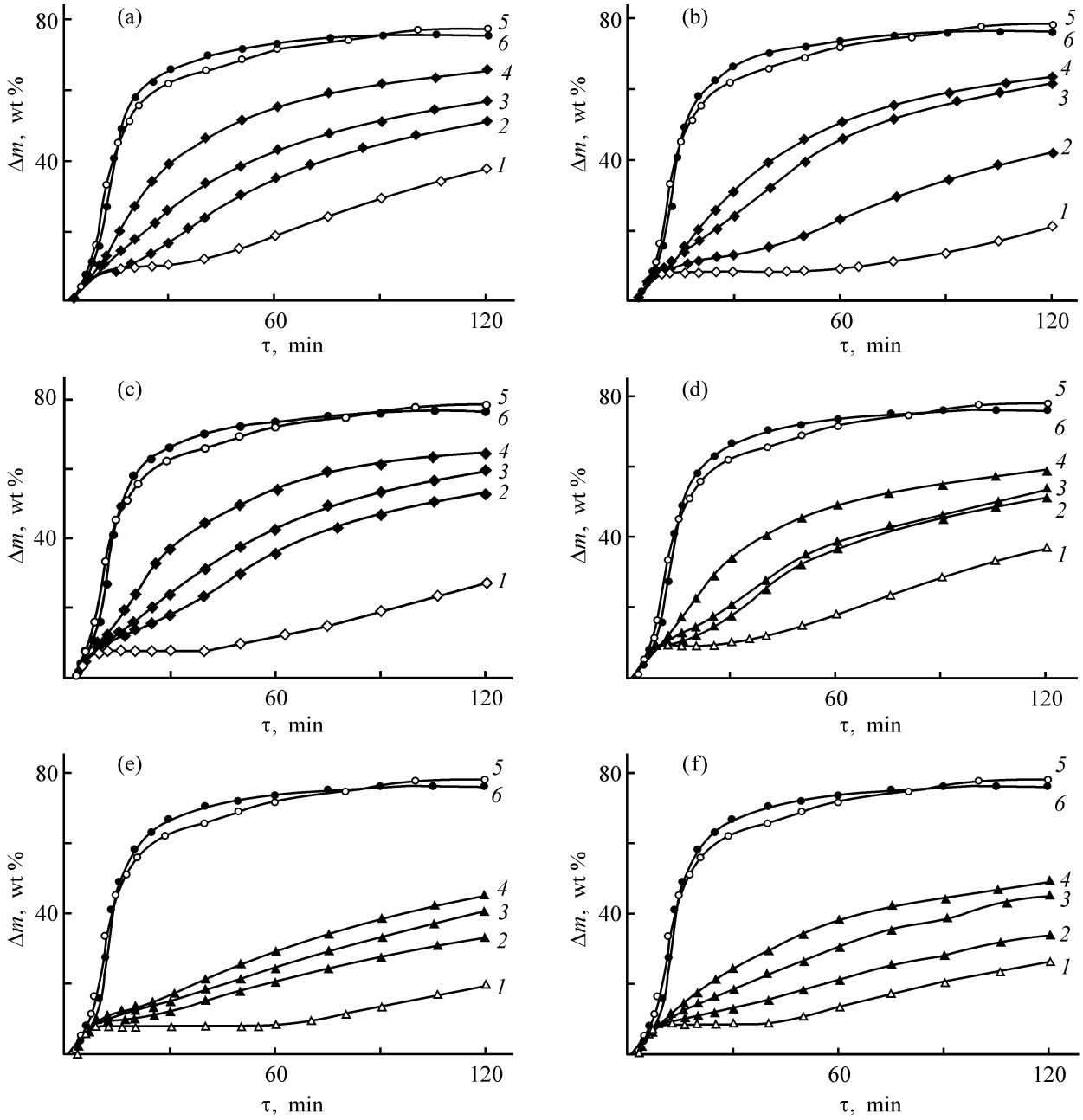


Fig. 2. TG (Δm) curves for thermooxidative degradation of PMMA (*1, 5*) before and (*2–4, 6*) after irradiation (*5, 6*) without and (*1–4*) with various additives. Irradiation time, min: (*2*) 60, (*3*) 120, (*6*) 180, and (*4*) 300. Addition, mol kg^{-1}: (a) 6×10^{-3} C_{60}, (b) 5.9×10^{-3} C_{70}, (c) 5.9×10^{-3} C_{60} + C_{70}, (d) 6×10^{-3} C_{60} + 0.29 wt % Irgafos 168, (e) 6×10^{-3} C_{60} + 0.294 wt % Chimassorb 944, and (f) 6×10^{-3} C_{60} + 0.3 wt % Tinuvin 622. T = 277°C; p_{O_2} = 200 mm Hg. (τ) Time.

PMAA with C_{60} is half that of PMMA without fullerene (Fig. 2a, curves *1* and *4*). After UV pretreatment, a fullerene mixture exhibits a stabilizing activity in TOD of PMMA (Fig. 2c), which is identical to that in the case of C_{60} (Fig. 2a). Fullerene C_{70} (Fig. 2b) is a more effective antioxidant than C_{60}, since the induction period in TOD of PMMA with C_{70} is 70 min, and that for PMMA with C_{60}, equals 40 min (Fig. 2a, curve *1*). However, the induction period disappears after a 120-min UV irradiation of PMMA with C_{70} (Fig. 2b, curve *3*). After 300-min irradiation of the PMMA film with C_{70} the initial rate of TOD of the polymer is three times lower (Fig. 2b, curve *4*), compared to PMMA without fullerene (Fig. 2b, curve *6*).

Decay of intensity *I* of the absorption band associated with the dye additive in PMMA during UV irradiation

Addition in PMMA	*I*, %, at indicated irradiation time, min					Addition in PMMA	*I*, %, at indicated irradiation time, min				
	0	60	120	240	360		0	60	120	240	360
	Band at 331 nm (C_{60})						Band at 535 nm (Rhodamine G)				
C_{60}	100	46	34	31	19	Rhodamine G	100	49	40	13	7
Rhodamine G + C_{60}	100	58	38	17	21	Rhodamine G + C_{60}	100	59	48	27	27
						Band at 556 nm (Rhodamine C)					
Rhodamine C + C_{60}	100	65	47	37	22	Rhodamine C	100	36	21	8	5
						Rhodamine C + C_{60}	100	49	30	17	7

The experimental data show that photochemical reactions of fullerene in PMMA films are responsible for the poorer performance of C_{60}, C_{70}, or a $C_{60} + C_{70}$ mixture as antioxidants in TOD of the polymer.

We found (Fig. 1c) that effective antioxidants of polymers Irgafos 168, Tinuvin 622, Tinuvin 770, and Chimassorb 944 virtually do not affect the decrease in the concentration of fullerenes C_{60}, C_{70}, or a $C_{60} + C_{70}$ mixture in PMMA films under UV irradiation at λ = 254 nm in the presence of atmospheric oxygen. Figure 2d shows that Irgafos does not affect TOD of PMMA with C_{60}. However, sterically hindered amines Tinuvin 622 and especially Chimassorb 944 (Fig. 2e, curve *3*, and Fig. 2f) significantly decelerate TOD of PMMA with C_{60}. This suggests that, at 277°C, these photostabilzers act as antioxidants in TOD of PMMA.

CONCLUSIONS

(1) UV irradiation of poly(methyl methacrylate) films containing fullerene C_{60} or C_{70} at 254 nm results in a regular decrease in the fullerene concentration with increasing irradiation time.

(2) Effective photostabilizers of polymers, Tinuvin 622, Tinuvin 770, and Chimassorb 944, do not affect the photooxidation of fullerenes. This suggests that oxidation follows the molecular, rather than the radical-chain, mechanism.

(3) Addition of Rhodamine G and Rhodamine C decelerates photooxidation of fullerenes C_{60} and C_{70} in the poly(methyl methacrylate) matrix, which is due to the shielding effect.

(4) Photochemical reactions of fullerenes in poly(methyl methacrylate) deteriorate the performance of fullerenes as antioxidants in thermooxidative degradation of the polymer.

(5) Sterically hindered amines Tinuvin 622, Tinuvin 770, and Chimassorb 944 at 277°C act as antioxidants in thermooxidative degradation of poly(methyl methacrylate) with addition of fullerenes and exhibit additional stabilizing effect in this process.

ACKNOWLEDGMENTS

The authors are deeply grateful to V.V. Arkhangel'skii for submitting the samples of the reagents.

REFERENCES

1. Troitskii, B.B., Troitskaya, L.S., Yakhnov, A.S., *et al.*, *Eur. Polym. J.*, 1997, vol. 33, nos. 10–12, pp. 1587–1590.
2. Shibaev, L.A., Antonova, T.A., Vinogradova, L.V., *et al.*, *Pis'ma Zh. Tekh. Fiz.*, 1997, vol. 23, no. 18, pp. 81–86.
3. Troitskii, B.B., Troitskaya, L.S., Yakhnov, A.S., *et al.*, *Dokl. Ross. Akad. Nauk*, 1998, vol. 363, no. 1, pp. 79–81.
4. Troitskii, B.B., Troitskaya, L.S., Dmitriev, A.A., and Yakhnov, A.S., *Eur. Polym. J.*, 2000, vol. 36, no. 7, pp. 1073–1084.
5. Troitskii, B.B., Domrachev, G.A., Khokhlova, L.V., and Anikina, L.I., *Vysokomol. Soedin., Ser. A*, 2001, vol. 43, no. 9, pp. 1540–1547.
6. Troitskii, B.B., Khokhlova, L.V., Konev. A.I., *et al.*, *Vysokomol. Soedin., Ser. A*, 2004, vol. 46, no. 9, pp. 1–8.
7. Arbogast, J.W., Darmanyan, A.P., Foote, C.S., *et al.*, *J. Phys. Chem.*, 1991, vol. 95, no. 1, pp. 11–12.
8. Eklund, P.C., Rao, A.M., Zhou, P., *et al.*, *Thin Solid Films*, 1995, vol. 257, pp. 185–203.
9. De Rosa, M.C. and Crutchley, R.J., *Coord. Chem. Rev.*, 2002, vols. 233–234, pp. 351–371.

Russian Journal of Applied Chemistry, Vol. 78, No. 6, 2005, pp. 1023–1026. Translated from Zhurnal Prikladnoi Khimii, Vol. 78, No. 6, 2005, pp. 1043–1046.
Original Russian Text Copyright © 2005 by Bublikov, Bespalova, Miroshnichenko, Sheveiko.

MACROMOLECULAR CHEMISTRY AND POLYMERIC MATERIALS

A Study of Thermal Properties of Fluoroplastic-based Polymeric Coatings

I. A. Bublikov, Zh. I. Bespalova, L. G. Miroshnichenko, and A. N. Sheveiko

South-Russia State Technical University (Novocherkassk Polytechnic Institute), Novocherkassk, Russia

Received August 4, 2004

Abstract—The possibility of using fluoroplastic with various fillers to obtain thin protective coatings on heat-exchange surfaces for systems of technical water supply was examined.

The operation of the heat-exchange equipment inevitably poses the problem of decreasing efficiency of the heat-exchange surface, caused by formation of various contaminations (scale). The low heat conductivity of these deposits (0.3–1.2 $W\,m^{-1}\,K^{-1}$) and the short time before the beginning of their strong influence on the heat exchange (200–300 h of operation) make it necessary to envisage a reserve heat-exchange surface area of 30–40% relative to the calculated value, thereby increasing the steel intensity of the apparatus.

The rate at which the deposits are formed and the energy of their binding to the heat-exchange surface are strongly affected by electric and electrostatic phenomena. To diminish the electrostatic forces and improve the corrosion resistance of the heat-exchange surface, it is coated with thin polymeric coatings (PC) [1]. Being insulators, they, on the one hand, make markedly slower the rate of deposit formation, and on the other, reduce the total heat-transfer coefficient of the apparatus. The contribution of PC to the decrease in the heat-transfer coefficient can be found from

$$\alpha = \frac{K_{ht} - K_c}{K_{ht}} = \frac{1}{1 + \lambda_c/(K_{ht}\delta_t)^{-1}}, \quad (1)$$

where K_{ht}, K_c is the running heat-transfer coefficient without and with PC; λ_c, heat conductivity with a coating; and σ_t, PC thickness.

The quantity K_{ht} is variable and decreases with time following the dependence established in [2]:

$$K_{ht} = \frac{K_0}{1 + D[1 - \exp(-3 \times 10^{-10} H_0)]},$$

where H_0 is the homochronicity factor and D is a parameter dependent on technological (specific heat flux, flow mode R_e), design (material of the heat-exchange surface and its position, vertical or horizontal), and chemical factors (total content and concentration of suspended particles and $CaCO_3$ in water).

The experience of work with heat-exchange apparatus with coated tubes [2] shows that, in the course of time, the heat-transfer coefficient remains unchanged or decreases only slightly (within 5%), i.e., there comes a time when K_{ht} becomes equal to K_c.

Polyethylene, epoxy mixtures, etc. are commonly used as protective PC in heat-exchange apparatus [3]. However, these PC fail to provide the necessary thermal and physical properties: heat conductivity, viscosity, and elasticity. At a heat conductivity on the same order of magnitude, fluoroplastic can be deposited onto a surface as a 10–20 times thinner controllable layer, which results in the accordingly lower thermal resistance of the PC layer.

The aim of this study was to examine the thermal properties of thin protective PC formed from a fluoroplastic-based composite and the possibility of their use for protecting a heat-exchange apparatus from scaling.

Polymeric coatings were deposited on the surface of 08KP steel samples with or without a phosphate layer by auto- and electrophoresis. The phosphating was performed using the standard procedure [4].

A bath for PC deposition was fabricated from polymethyl methacrylate. The deposition was performed at 18–25°C. Prior to deposition of PC, a sample was attached with a special device to a mechanical stirrer and submerged in a polymeric dispersion, with the rotation frequency of the stirrer equal to 60 rpm. Electrodeposition was carried out on an installation com-

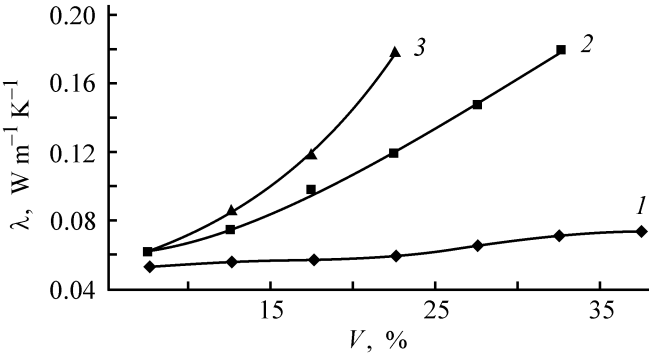


Fig. 1. Heat conductivity λ of filled fluoroplastic vs. volume content *V* of inclusions. (*1*) Model of series conductivity, (*2*) dependence by Bruggeman, and (*3*) dependence by Odolevskii.

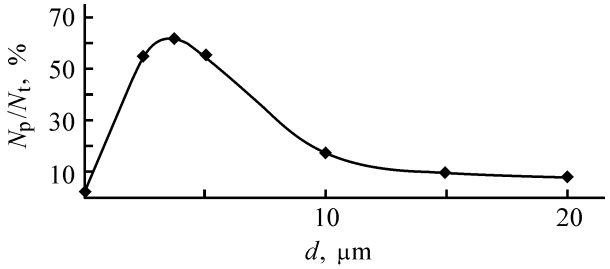


Fig. 2. Particle size distribution of inclusions. (N_p/N_t) Relative number of particles and (d) particle size.

prising a rectifier, voltmeter, ammeter, and an electrophoretic bath in the constant-voltage mode (25 V s^{-1}). The heat conductivity was determined by the method of a dynamic calorimeter on an IT-λ-400 installation.

The coating thickness and the volume content of inclusions were determined by measuring and weighing the samples with a micrometric ruler, VLA-200 analytical balance, and MBS-10 microscope. The thickness of the PC was determined at six points of a sample, with six or seven measurements at each point, after which the values obtained were averaged. Using the geometric and weight characteristics of the samples, the volume content *V* of the filler was determined by the formula

$$V = \frac{m_{PC}(V_{PC})^{-1} - \rho_{PC}}{\rho_{inc} - \rho_{fl}}, \quad (2)$$

where m_{PC} is the mass of PC; V_{PC}, volume of PC; and ρ_{inc} and ρ_{fl}, the densities of the dispersed phase and the fluoroplastic, respectively.

The particle size distribution of the polydisperse inclusions was determined by means of a sedimentation analysis [5].

The pH value of the formulation was measured with a pH-340 laboratory pH-meter.

A polymeric coating was obtained from a composite containing as its main component a fluoroplastic of 4D and 4MD brands, introduced into the formulation in the form of an aqueous suspension stabilized with a surfactant.

As fillers served highly heat-conducting copper, bronze, and colloid carbon black (or graphite). For a better compatibility and wettability by the polymeric phase, the fillers were dressed with modifying agents, including heterocyclic compounds from the vinylpyrrolidone group, and hydroxyethylated alkyl phenol.

The dry residue of the initial composition was 55%, viscosity 15 St (by VZ-246), pH 6.5. In the case of the autophoretic method of PC deposition, the pH value of the initial composition was adjusted to 3 with orthophosphoric acid ($\rho = 1.3 \times 10^3$ kg m^{-3}).

The study demonstrated that, in contrast to the previously published dependences obtained in tests of an epoxy compound [1], the heat conductivity coefficient of a fluoroplastic with finely dispersed inclusions varies with the volume content of these additives in accordance with the Bruggeman dependence, rather than by the Odolevskii model. The deviation of the experimental data does not exceed 30% (Fig. 1).

The size distribution of the polydisperse inclusions is shown in Fig. 2. It can be seen that the size of certain inclusions exceeds the PC thickness (which was 2.5 to 20 μm), i.e., there appears a local possibility of heat transfer in accordance with the combined parallel-consecutive model. In this case, it is difficult to describe theoretically the mechanism of heat conduction in the initial stage, and it can be empirically represented as an expression similar to the Bruggeman formula [1]:

$$\lambda_0 = \frac{\lambda_1}{(1 - V)^n}, \quad n = 3. \quad (3)$$

The necessary slope of the curve describing the experimental data can be reached by making larger the exponent *n*. It can be described as a function of the particle size d_p, volume content V_p of particles, and PC layer thickness δ_l:

$$n = \frac{a d_p}{\delta_l V_p}, \quad (4)$$

where *a* is a coefficient that accounts for the material of inclusions: $a = 1/35$ for dispersed copper particles and 1/50 for bronze particles.

Effect of the volume content of inclusions in a formulation on the heat conductivity of coatings obtained by the autophoresis method

Deposition time, min	Sample thickness, μm	Layer thickness, μm	PC mass, mg	*V*, %	$\lambda \times 10^2$, W m^{-1} K^{-1}
		Copper as filler			
2	616.0	8.0	34.35	30.3	3.2
2	625.9	16.1	0.05	6.03	7.2
2	618.8	9.8	7.95	15.9	5.6
5	607.2	7.2	3.8	20.5	4.5
5	581.6	6.5	9.4	48.1	2
5	680.7	9.1	20.4	9.7	4.8
10	605.4	1.9	31.5	13.9	6.9
10	582.1	11.8	36.25	18.2	6.5
10	620.6	12.9	33.2	13.1	4.3
		Bronze as filler			
2	582.8	5.6	34.5	49.6	3.2
2	584.0	2.5	11.3	33.4	0.8
2	554.0	8.8	13.95	3.4	3.2
5	539.3	4.8	10.15	8.8	2.5
5	581.4	2.8	13.95	37.9	1.2
5	527.3	4.8	14.65	18.5	2.5
10	586.0	4.0	12.6	19.3	1.6
10	587.3	10.15	17.75	5.0	3.5
10	78.0	3.35	29.2	76.0	1.6
15	554.0	13.0	34.0	13.9	4.1
15	610.2	8.7	16.0	5.9	4.1
15	596.0	10.9	25.2	10.7	6.4

The suggested exponent *n* in the Bruggeman formula makes it possible to extend its applicability limits, because it can take a value of 3 for finely dispersed inclusions of certain size. With the exponent used in experimental data processing, more reliable heat conductivity data could be obtained (Fig. 1).

The data calculated using formula (1) are in a good agreement with the experimental values if $\rho_{inc} > \rho_{fl}$. The results of experimental studies are presented in the table and Fig. 3.

It can be seen from Fig. 3 that the heat conductivity of fluoroplastic-based multicomponent formulations decreases as the volume content of inclusions increases. This can be attributed to the fibrous structure of interwoven macromolecules. Introduction of various inclusions into a structure of this kind disrupts the arrangement of fibers and leads to destructuring of the PC layer. A noticeable effect of the destructuring is already observed at a low content of inclusions. For example, this threshold is 10% for copper and 5% for bronze. The difference in the threshold values is due to the fact that copper inclusions have a smaller size of dispersed particles than bronze inclusions. Thus, the larger dispersed particles of the filler in the fluoroplastic, the more pronounced, all other conditions being the same, the destructuring and the stronger their influence on the heat conductivity. As the volume content of inclusions of the same size exceeds a certain value, the heat conductivity starts to grow. This value varies between 30 and 40% for copper and

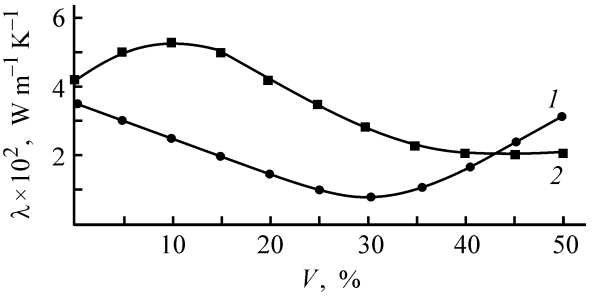


Fig. 3. Heat conductivity λ vs. volume content *V* of inclusions. Formulation: (*1*) with bronze and (*2*) with copper.

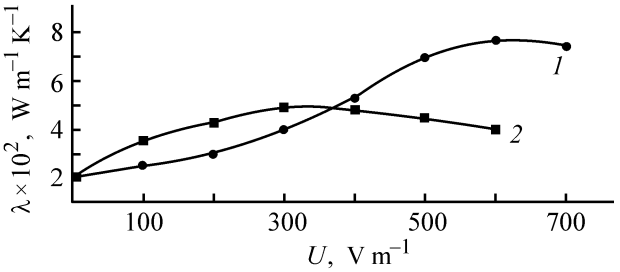


Fig. 4. Heat conductivity λ vs. the electric field strength *U* at a carbon black content of (*1*) 7 and (*2*) 3 wt %.

is 30% for bronze. In this case, copper and bronze inclusions cease to be dispersed and become a continuous phase diluted by the fluoroplastic.

Thus, filling of the fluoroplastic with high-heat-conductivity dispersed inclusions of copper or bronze fails to lead to the expected result and cannot make higher the heat conductivity of PC. In all probability, these inclusions loosen the polymer structure and do not favor formation of stronger polarized bonds between polymer molecules. In this connection, it was suggested to enhance the polarization of molecules in deposition by using electrophoresis and thereby to obtain denser structures having a higher heat conductivity.

The assumption is confirmed by an analysis of coatings deposited by electrophoresis at different electric field strengths. The heat conductivity of PC is 0.1 $W m^{-1} K^{-1}$ in this case.

Under similar conditions, a composite filled with a colloid carbon black (or graphite) was studied at a content of the colloid carbon black (or graphite) in the formulation equal to 3–7 wt %. If the density of inclusions is lower than that of the fluoroplastic (in the case of filling with a carbon black with ρ = 165 $kg m^{-3}$ and λ = 0.07–0.12 $W m^{-1} K^{-1}$), the heat conductivity grows to the value characteristic of the dispersed phase as the content of the filler increases to 7% (Fig. 4). Polymeric coatings deposited by electrophoresis at a varied voltage across the electrodes show a gradual rise in heat conductivity at a low content of inclusions. The curves show a bend at low voltages, which suggests that the voltage across the electrodes affects the amount of filler codeposited with the fluoroplastic. As the voltage decreases, the content of carbon black in the coatings becomes lower. This leads to formation of a looser structure with a low ?conductivity, which gives rise to peaks.

CONCLUSIONS

(1) Raising the electric field strength leads to a more significant increase in the heat conductivity of polymeric coatings than making higher the concentration of the filler, colloid carbon black (graphite).

(2) The heat conductivity increases only until the electric field strength reaches a certain value corresponding to a bath voltage of 70 V. As the field strength is raised further, the heat conductivity decreases to 0.1–0.15 $W m^{-1} K^{-1}$.

(3) The dependence of the coating density on the electric field strength exhibits a similar behavior, i.e., as the field strength increases to 2300 $V m^{-1}$, the density first grows to 80–90 and then decreases by 20%.

(4) The thermal resistance of the polymeric coatings is $(5–8) \times 10^{-4}$ $K m^2 W^{-1}$ and they can be rather effectively used at heat-transfer coefficients of 1200–200 $W m^{-2} K^{-1}$.

(5) Use of the fluoroplastic for obtaining thin protective coatings on heat-exchange surfaces for technical water supply systems can be regarded as promising in the case of deposition of coatings with a controllable thickness of 15–20 μm. As a filler of the fluoroplastic can be used, at the given thickness, finely dispersed particles of size not exceeding 1–2 μm: colloid carbon black or graphite.

REFERENCES

1. *Sovremennye tendentsii konstruktirovaniya, tekhnologii izgotovleniya i rascheta teploobmennogo oborudovaniya* (Modern Tendencies in the Design, Fabrication Technology, and Calculation of Heat-Exchange Apparatus), Pugaga, V.V., Ed., Moscow: Neftemash, 1987.
2. Vasil'ev, L.P. and Tanaeva, S.A., *Teplofizicheskie svoistva poristykh materialov* (Thermal Properties of Porous Materials), Minsk: Nauka i Tekhnika, 1971.
3. Miropol'skii, Z.L., Bublikov, I.A., and Novikov, B.E., *Teploenergetika*, 1992, no. 5, pp. 71–74.
4. Grilikhes, S.Ya. and Tikhonov, K.I., *Elektroliticheskie i khimicheskie pokrytiya* (Electrolytic and Chemical Coatings), Leningrad: Khimiya, 1990.
5. *Laboratornye raboty i zadachi po kolloidnoi khimii* (Laboratory Works and Tasks in Colloid Chemistry), Frolov, Yu.G. and Grodskii, A.S., Eds., Moscow: Khimiya, 1986.

Russian Journal of Applied Chemistry, Vol. 78, No. 6, 2005, pp. 1027–1030. Translated from Zhurnal Prikladnoi Khimii, Vol. 78, No. 6, 2005, pp. 1047–1049.
Original Russian Text Copyright © 2005 by Ginzburg, Tuichiev, Tabarov, Lavrent'ev, Melenevskaya, A. Pozdnyakov, O. Pozdnyakov, Shepelevskii, Shibaev.

MACROMOLECULAR CHEMISTRY AND POLYMERIC MATERIALS

Effect of Fullerene C_{60} on Structuring of Toluene

B. M. Ginzburg, Sh. Tuichiev, S. Kh. Tabarov, V. K. Lavrent'ev, E. Yu. Melenevskaya, A. O. Pozdnyakov, O. F. Pozdnyakov, A. A. Shepelevskii, and L. A. Shibaev

Institute of Problems of Mechanical Engineering, Russian Academy of Sciences, St. Petersburg, Russia

Tajik State National University, Dushanbe, Tajikistan

Institute of Macromolecular Compounds, St. Petersburg, Russia

Ioffe Physicotechnical Institute, Russian Academy of Sciences, St. Petersburg, Russia

Received June 9, 2004

Abstract—Toluene solutions of fullerene C_{60} with concentrations of 0.001, 0.01, and 0.2 wt % were studied by small-angle X-ray diffraction analysis. The radii of gyration of scattering elements were determined from the small-angle diffraction patterns plotted in the Guinier coordinates.

Toluene is a solvent widely used for recovering fullerenes from fullerene soot and for studying various fullerene-containing systems. Mass spectrometric data [1] showed that a certain fraction of toluene present in a fullerene C_{60} film is strongly retained when the film is heated in a vacuum to the point of its breakdown upon C_{60} sublimation. Such a behavior of toluene suggests that toluene strongly interacts with fullerene and thus fullerene dissolved in it can strongly change the structure of the solvent itself. In this paper, solutions of fullerene C_{60} in toluene were studied by small-angle X-ray scattering. Previously, similar studies have been performed with fullerenes C_{60} and C_{70} dissolved in *o*-xylene [2, 3]. In these studies, nonuniform areas were found in the entire concentration range examined. From the authors' viewpoint, the number of fullerene molecules in the associate is no more than four. No free single fullerene molecules were observed.

EXPERIMENTAL

The measurements were carried out on a KRM-1 device (Cu_{K_α}, Ni filter) with a slit collimation of the primary X-ray beam; the width of the intensity distribution in the primary beam was 5′ near the profile bottom of the corresponding curve. The scattering range was from 15′ to 2°. The error of the intensity measurements did not exceed ±2 pulse s^{-1} in the entire scattering range studied, i.e., it was as low as 2–4%.

Rectangular cells were prepared from a 7.5–10-μm polymeric film. Empty cells showed no noticeable scattering in the angle range studied. Then, the cells were filled with a sample to be analyzed, sealed, and placed in an evacuated chamber of the diffractometer.

The transmission measurements were carried out at 25–30°C. The cell with a solvent was placed at the center of a goniometer perpendicularly to the primary beam, and diffraction pattern 1 was recorded. Then, the sample was placed before the first slit and the contour of the primary beam after passing through the cell was recorded (diffraction pattern 2), and curve 2 was subtracted from diffraction pattern 1. These resulting difference patterns are given as the experimental curves $I(s)$, where $s = 4\pi\sin(\varphi/2)\lambda$, φ is the scattering angle, and λ is the wavelength of the X-ray radiation. Since the scattering angles are small, we consider that $s = 2\pi\varphi/\lambda$.

It should be noted that the scattering intensity in curves 2 at 15′ angle (scattering start) was similar within the measurement error for both solvent and C_{60} solutions in the entire concentration range; as a result, normalization of the curves to the same intensity of the primary beam was unnecessary. Fullerene C_{60} (99.7%) obtained by the Huffman-Kraetschmer method, was used to prepare solutions of fullerene C_{60} in toluene with the following concentrations: 0 (pure solvent), 0.001, 0.01, 0.1, and 0.2 wt %.

1070-4272/05/7806-1027 © 2005 Pleiades Publishing, Inc.

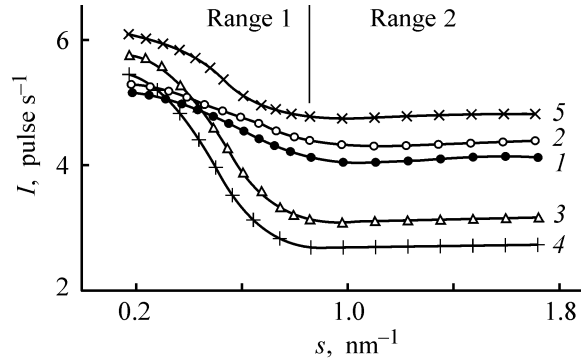


Fig. 1. Small-angle scattering patterns I–s of fullerene C_{60} solutions in toluene (Cu_{K_α} radiation). Fullerene C_{60} concentration, %: (*1*) 0 (pure toluene), (*2*) 0.001, (*3*) 0.01, (*4*) 0.1, and (*5*) 0.2; the same for Fig. 3.

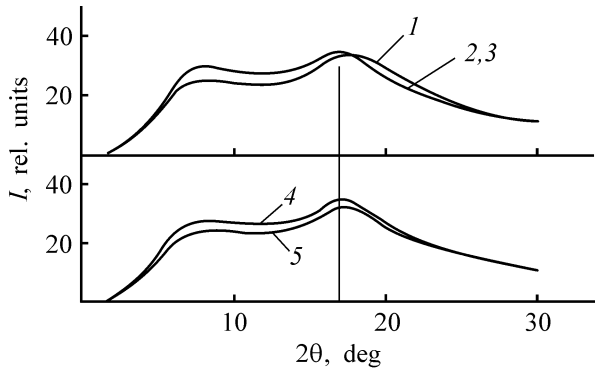


Fig. 2. Wide-angle scattering patterns I–2θ of fullerene C_{60} solutions in toluene (Cu_{K_α} radiation). Fullerene C_{60} concentration, %: (*1*) 0 (pure toluene), (*2*) 0.005, (*3*) 0.05, (*4*) 0.1, and (*5*) 0.2.

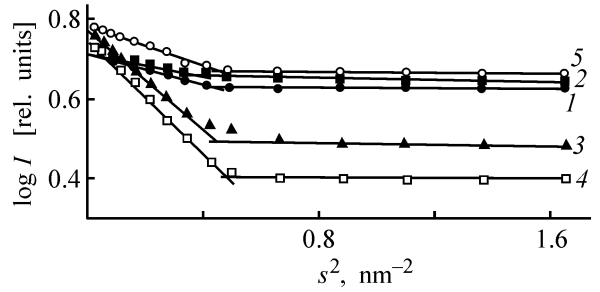


Fig. 3. Small-angle scattering patterns log I–s^2 of fullerene C_{60} solutions in toluene (Cu_{K_α} radiation) in the Guinier coordinates.

The resulting diffraction patterns are shown in Fig. 1. All the curves monotonically descend with increasing scattering angle (range 1) and then asymptotically reach constant I_c (range 2) at scattering angles of about 70′. Flattening-out of the curves is typical of homogeneous liquids and glasses [4], and, in this case, scattering can be accounted for by thermal fluctuations of the density. As temperature becomes lower, I_c decreases.

However, the dependence of I_c on the fullerene C_{60} concentration is rather unusual. At a 0.001% concentration, the shape of the scattering curve is close to that of the pure solvent, but with slightly higher intensities. This fact is probably due to an increase in the density of fluctuations involving fullerene molecules, because the electron density of fullerene molecules is higher than that of the solvent.

Sharp changes are observed at concentrations of 0.01 and 0.1% (Fig. 1, curves *3* and *4*); in this case, nearly the entire scattering curve runs below that of the solvent. These changes in I_c are probably due to the solvent structuring, when the thermal density fluctuations (with dimensions of about 35 Å and smaller, down to 6 Å, typical of short-range order) are suppressed by fullerene.

The wide-angle X-ray diffraction patterns of the solutions under study showed no changes in the amorphous halo (within the measurement error), i.e., the intermolecular spacing remains unchanged. However, the width of the halo slightly decreases, probably owing to an increase in the coherent scattering areas (Fig. 2), which agrees with the assumption that the solvent gets structured. The solvent structuring causes appearance of a negative entropy decrement in dissolution of fullerene in toluene (calorimetry data [5]).

Simultaneously with the decrease in I_c, the curve slope in range 1 increases on passing to small angles. At a concentration of 0.2%, I_c increases, whereas the curve slope at small angles decreases.

Figure 3 shows the same small-angle diffraction patterns plotted in the Guinier coordinates $\log I = f(s^2)$, which enables evaluation of the radius of gyration R_g of the scattering structural elements [6]. The values of I_c and R_g are listed in the table. As can be seen, the concentration dependences of I_c and R_g are opposite. To determine the number of molecules of structured solvent per fullerene molecule, we consider that the whole amount of the solvent is structured when I_c is at a minimum, i.e., at concentration of 0.1%. In this case, there are about 8000 toluene molecules per fullerene molecule.

Let us compare the radii of gyration with the size of C_{60} molecule. This molecule can be well approximated by a spherical shell with inner (R_i) and outer (R_e) radii of 200 and 357 nm, respectively [7]. The radius of gyration for a spherical shell with a uniform density distribution can be represented as

$$R_g = (3/5)^{1/2} R_e [(1 - C^5)/(1 - C^3)]^{1/2}, \qquad (1)$$

where $C = R_i/R_e$.

Thus, on the assumption of an equilibrium distribution of the electron density in a C_{60} molecule, its radius of gyration is 0.30 nm, which is smaller than our experimental results.

As can be seen from published data [8], the concentration dependence of the toluene solution density on the concentration of C_{60} passes through a maximum at a fullerene concentration of 0.05%. This fact indicates a compaction of the solution, probably due to its structuring. However, the electron density of fullerene exceeds that of liquid toluene by almost a factor of 2. As a result, the effect of ordered solvent on the fullerene molecules or aggregates can be neglected in our estimations of smallangle scattering.

Since the calculated and experimental radii of gyration are quite different, the model involving separate molecules C_{60} (even with a solvation shell) should be abandoned.

More adequate is a model based on fullerene aggregates. The size of the corresponding aggregates, calculated for a model sphere with uniform density from the experimental radii of gyration, and the number of C_{60} molecules accommodated in this sphere with hexagonal close packing are listed in the table. As can be seen, the number of fullerene molecules in this sphere is 80–90; in real aggregates, this value will be smaller, because the packing density should be lower than that in crystals.

The reasons for an increase in I_c and R_g at a fullerene concentration of 0.2% are still unknown. Probably, this is due to the approach to the solution saturation (2.15 mg ml^{-1} or 0.24% [9]). It is obvious that the model of supramolecular structure of solutions cannot be developed without additional independent data [2, 3]. We prefer the model of two-dimensional clusters, because the experimental data [9] suggest the fractal structures in fullerene solutions with a dimension close to 2. From our viewpoint, both the formation of fractal clusters and the long-range effect of fullerene on the solution structure probably suppress thermal density fluctuations.

Dimensions of nonuniform areas in the samples studied*

Sample	Range 1			Range 2
	R_g, nm	R_e, nm	$N_{C_{60}}$	$\log I_c$, arb. units
Toluene	–	–	–	0.63
Toluene + C_{60}, %:				
0.001	1.0	1.3	10	0.66
0.01	2.1	2.7	80	0.49
0.1	2.2	2.8	90	0.40
0.2	1.3	1.7	–	0.67

* R_c is the uniform sphere radius, and $N_{C_{60}}$ is the number of C_{60} molecules in this sphere.

** Range 1 corresponds to the small-angle section of the broken line in Fig. 3, and range 2, to the section parallel to the abscissa.

CONCLUSIONS

Solutions of fullerene C_{60} in toluene in the concentration range from 0.001 to 0.2% were studied by small- and wide-angle X-ray diffraction analysis. In all the small-angle diffraction patterns, the intensity decreases to some constant value I_c with increasing scattering angle. As the fullerene concentration becomes higher I_c first slightly increases, then sharply decreases, and finnaly increases again. The sharp decrease in I_c can be attributed to suppression of thermal fluctuations of the solution density. The radii of gyration were determined from the small-angle diffraction patterns plotted in the Guinier coordinates, which suggest that fullerene clusters consisting of 80–90 molecules are formed in the toluene solution.

ACKNOWLEDGMENNTS

This study was financially supported by the St. Petersburg Interdisciplinary Scientific Center (project "Structure and Properties of Fullerene Solutions in Organic Solvents"), International Science and Technology Center (ISTC project no. T-1145, "Study of Structure and Physical properties of Polymers at Complex External Action"), Program no. 13 of Basic Research of the Division of Power Engineering, Mechanical Engineering, Mechanics, and Management Processes of the Russian Academy of Sciences, and "Fullerenes and Atomic Clusters" Program of the Russian Foundation for Basic Research (project no. 03-03-32 633).

REFERENCES

1. Pozdnyakov, O.F., Redkov, B.P., Ginzburg, B.M., Pozdnyakov, A.O., *Pis'ma Zh. Tekh. Fiz.*, 1998, vol. 24, no. 23, pp. 29–34.
2. Golubkov, V.V., Shakhmatkin, B.A., Charykov, N. A., and Aksel'rod, B.M., *Zh. Fiz. Khim.*, 2001, vol. 75, no. 10, pp. 1821–1824.

3. Golubkov, V.V., Shakhmatkin, B.A., Charykov, N. A., and Aksel'rod, B.M., *Zh. Fiz. Khim.*, 2002, vol. 76, no. 3, pp. 562–564.
4. Svergun, D.I. and Feigin, L.A., *Rentgenovskoe i neitronnoe malouglovoe rasseyanie* (Small-Angle X-ray and Neutron Scattering), Moscow: Gos. Izd. Fiz.-Mat. Lit., 1986.
5. Herbst, M.H., Dias, G.H.M., Magalhaes, J.G., *et al.*, *J. Mol. Liq.*, 2005, vol. 118, nos. 1–3, pp. 9–13.
6. Guinier, A., *Theorie et Technique de la Radiocristallorgraphie*, Paris: Dunod, 1956. Translated under the title *Rentgenografiya kristallov*, Moscow: Gos. Izd. Fiz.-Mat. Lit., 1961.
7. Eletskii, A.V. and Smirnov, B.M., *Usp. Fiz. Nauk*, 1995, vol. 165, no. 9, pp. 977–1009.
8. Mekalova, N.V., *Fullereny v rastvorakh* (Fullerenes in Solutions), Ufa: Ufimsk. Gos. Neft. Tekh. Univ., 2001.
9. Bezmel'nitsyn, V.N., Eletskii, A.V., and Okun', M.V., *Usp. Fiz. Nauk.*, 1998, vol. 168, no. 11, pp. 1195–1220.

Russian Journal of Applied Chemistry, Vol. 78, No. 6, 2005, pp. 1031–1033. Translated from Zhurnal Prikladnoi Khimii, Vol. 78, No. 6, 2005, pp. 1050–1052.
Original Russian Text Copyright © 2005 by Smirnova, Vasil'eva, Persinen.

MACROMOLECULAR CHEMISTRY AND POLYMERIC MATERIALS

Electron-Beam-Cured Adhesives Based on Low-Molecular-Weight Carboxylated Butadiene-Nitrile Rubber

Yu. A. Smirnova, I. V. Vasil'eva, and A. A. Persinen

St. Petersburg State Technological Institute, St. Petersburg, Russia

Radiant Technology Center, Limited Liability Company, St. Petersburg, Russia

Abstract—Effects of a series of additives on the initial sticking and autohesion dynamics of electron-beam-cured adhesives for adhesive tapes, based on low-molecular-weight carboxylated butadiene-acrylonitrile rubber, were examined.

Modification of pressure-sensitive adhesives (PSAs) with telechelic butadiene-acrylonitrile rubbers was reported in [1]. It is also known that liquid butadiene-acrylonitrile rubber with terminal carboxy groups is rapidly cured by electron beam at room temperature in air to give a rubber-like material (oligomer MW 1700; carboxy group content 3%).

In this study, we examined the possibility of synthesis of electron beam-cured PSA based on domestic carboxylated low-molecular-weight butadiene-nitrile rubbers SKN-10-1 and SKN-10-KTR [mean MW 1500; functional groups (3%) are arranged in the backbone or as terminal groups; acrylonitrile units are arranged in microblocks, each consisting of several units; butadiene units are connected essentially at the 1,4-positions.

To optimize the formulations, we studied the effects of a series of organic and mineral components on the radiation stability of the investigated formulation, autohesion of electron beam-cured PSAs, and sticking dynamics.

EXPERIMENTAL

The formulations were prepared by mixing the components at room temperature. As a support material we used a tape made of carbon-black-extended PVC. The electron-beam curing of the composites applied onto the PVC tape surface was carried out in air, using an RTE-1V experimental setup [2] (electron energy 500 keV; beam current 1 mA). The target material was passed under the accelerator scan-horn at a speed of 1 m min^{-1}.

The criteria for determination of the absorbed dose optimal for polymer conversion were the lack of a contact pattern of the tested layer on glass and of traces of low-molecular-weight fractions. The absorbed dose was determined by film dosimetry, using standard polycarbonate detectors with a phenazine dye [PD(F)-150/500 dosimetric films]. The optical density of the irradiated detectors was measured on an SF-46 spectrophotometer at 512 nm.

The adhesiveness of the resulting samples was determined according to GOSTs (State Standards) [3, 4]. As a measure of the adhesiveness we used the time in which the sample was separated under a fixed stress. The quality of the materials tested was evaluated by comparison of their adhesiveness with that of similar domestic commercial products meeting the requirements of GOST [5], using the procedure employed in this study (the thus obtained adhesiveness of the commercial products was 8 s).

By electron-beam treatment in air of PVC-supported straight SKN-10-1 elastomer, we obtained a constant-adhesiveness pressure-sensitive adhesive (absorbed dose 400 kGy; autohesion 11 s). On the surface of PSA obtained by electron-beam curing of SKN-10-KTR, we observed, even at an absorbed dose of 600 kGy, a layer of the low-molecular-weight fraction, which can be attributed to exudation of stabilizers. Therefore, the subsequent experiments were performed with SKN-10-1 rubber.

Mineral additives were introduced into low-molecular-weight rubber for the following reasons. It is known that extenders are sensitizers for the overwhelming majority of rubbers. They reduce the mac-

1070-4272/05/7806-1031 © 2005 Pleiades Publishing, Inc.

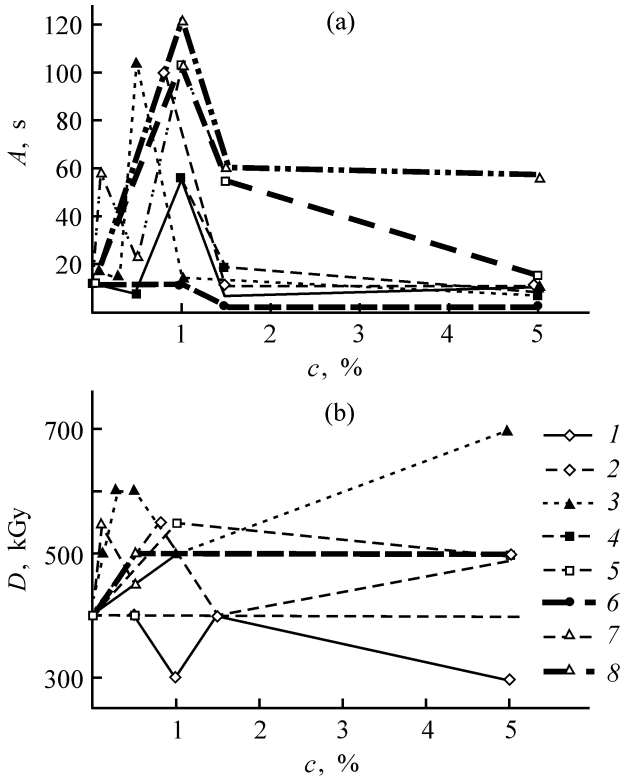


Fig. 1. (*1*) Initial adhesiveness of SKN-10-1-based PSA *A* and absorbed dose *D* vs. the additive concentrations. Additives: (*1*) TMPTA, (*2*) EHA, (*3*) MBT, (*4*) EAS-16, (*5*) EAS-20, (*6*) DEP-331, (*7*) Aerosil, and (*8*) alumina.

roscopic viscosity of the system, promote egress of the chain ends from the globules, and increase the probability of polymer branching [6]. Thus, the maximal initial adhesiveness of PSA was obtained by introducing inorganic additives in an amount of about 1 wt % (Fig. 1a), but, in this case, the absorbed dose increased (Fig. 1b).

Introduction into SKN-10-1 of monomers, such as trimethylolpropane triacrylate (TMPTA) and 2-ethylhexyl acrylate (EHA), was expected to decrease the macroscopic viscosity of the system, to promote egress of the chain ends from the globules, and to increase the probability of polymer branching. Indeed, over the experimental concentration range, the adhesiveness of PSA was at a maximum, and the absorbed dose changed noticeably as compared to that observed for the reference rubber (Fig. 1). The maximal adhesiveness of PSA was observed at a TMPTA concentration of 1 wt %. In this case, the dose required for preparation of a pressure-sensitive layer decreased as compared to the polymer without additive. For EHA, the absorbed dose increased at a concentration of 0.8 wt % corresponding to the maximal adhesiveness.

It is well known that sulfur-containing compounds, various acrylates, and polyfunctional oligoether acrylates demonstrate a high sensitizing power. For example, introduction of mercaptobenzothiazole (MBT) into rubber noticeably affects the parameters investigated (Fig. 1): the absorbed dose increases nonlinearly, and the maximal initial adhesiveness is observed at a concentration of 0.5 wt %. Introduction of epoxy-acrylate resins (EASs) has an effect on the homogeneity of the composite. Because of the low compatibility with the polymer, EAS can be regarded as an interstack plasticizer: the resin is primarily introduced between the coarsest supramolecular structures, breaking them and thus providing more favorable conditions for an adhesion contact. Therefore, we expected a considerable increase in the adhesion strength [9]. Introduction of epoxy-acrylate resins EAS-16 and EAS-20 did not decrease the absorbed dose, and the adhesion strength of PSA showed the maximum at an additive concentration of about 1 wt %. With epoxy-acrylate acrylated to 50% (DEP-331), we observed no noticeable change in the parameters investigated (Fig. 1).

Introduction into the elastomer of polypropylene glycol (PPE) or low-molecular-weight polysiloxanes (SKTN) increases the absorbed dose required for elastomer conversion, except for the formulation with 1 wt % SKTN. Polysiloxane strongly affects the initial adhesiveness of PSA. The optimal combination of performance characteristics was obtained with 1 wt % SKTN: initial adhesiveness 18 s at absorbed dose of 400 kGy. With 1 wt % PPG, the initial adhesiveness of 11 s was obtained at a dose of 500 kGy.

The ability of electron-donor and electron-acceptor additives to sensitize or inhibit the cross-linking suggests that charged species formed under the action of ionizing radiation are involved in the formation of the 3*D* network structure. For thermochemical PSAs, the curve of the adhesion strength passes through a maximum at an additive concentration of 0–2% [6]. Our results show that the radiation-chemical PSAs behave similarly.

The trends in the adhesion strength evolution with time are shown in Fig. 2. Two major features can be distinguished: exponentially decreasing initial maximum and fluctuating initial values. In the first case, the initial adhesiveness of PSA is an order of magnitude higher than that of the additive-free elastomer.

The observed differences in the adhesiveness dynamics can be attributed both to transient processes, such as after-effect upon completion of the formation of the adhesion layer and to conformational and re-

laxation processes prolonged by development of side and secondary reactions (for example, polymer-analogous transformations or cross-linking) and by aging in storage [7, 8].

CONCLUSIONS

(1) It was shown that organic and mineral additives affect the radiation sensitivity of low-molecular-weight carboxylated butadiene-acrylonitrile rubber and also the adhesiveness of pressure-sensitive adhesives prepared on its basis.

(2) The sensitizing effect was initiated by the addition of trimethylolpropane triacrylate (1 wt %).

(3) A high initial adhesiveness of pressure-sensitive adhesives was obtained by adding the additives investigated in an amount of about 1 wt %. However, the effect was short-term, and the initial adhesiveness decreased to below acceptable values in a month. Nevertheless, the results obtained demonstrate the possibility of preparing a pressure-sensitive adhesive on the basis of low-molecular-weight carboxylated butadiene-acrylonitrile rubber.

REFERENCES

1. *Adhesive Chemistry. Developments and Trends*, Lee, L.-H., Ed., New York: Plenum, 1984.
2. Svinin, M.P., Ivanov, A.S., Ovchinnikov, V.P., *et al.*, Abstracts of Papers, *Sixth Int. Conf. on Electron Beam Technologies*, Varna, 2000, p. 83.
3. *GOST* 28019–89, *Adhesive Insulation Tapes: Testing Methods*.
4. *GOST* 20477–86, *Polyethylene Adhesive Tape: Technical Specifications.*
5. *GOST* 16214–86, *PVC Adhesive Insulation Tape: Technical Specifications*.
6. Berlin, A.A. and Baskin, V.E., *Osnovy adgezii polimerov* (Principles of Polymer Adhesion), Moscow: Khimiya, 1974.
7. Ivanov, V.S., *Radiatsionnaya khimiya polimerov* (Radiation Chemistry of Polymers), Leningrad: Khimiya, 1988.
8. Shiryaeva, G.V. and Kozlov, Yu.D., *Tekhnologiya radiatsionnogo otverzhdeniya pokrytii* (Technology of Radiation Curing of Coatings), Moscow: Atomizdat, 1980.

Russian Journal of Applied Chemistry, Vol. 78, No. 7, 2005, pp. 1035–1037. Translated from Zhurnal Prikladnoi Khimii, Vol. 78, No. 7, 2005, pp. 1057–1059.
Original Russian Text Copyright © 2005 by Basiev, Batyrev, Voronov, Konyushkin, Kuznetsov, Osiko, Samartsev, Samoilova, Fedorov.

INORGANIC SYNTHESIS AND INDUSTRIAL INORGANIC CHEMISTRY

Hydration of Strontium Chloride and Rare-Earth Element Oxychlorides

T. T. Basiev, N. I. Batyrev, V. V. Voronov, V. A. Konyushkin, S. V. Kuznetsov, V. V. Osiko, A. M. Samartsev, E. B. Samoilova, and P. P. Fedorov

Scientific Center of Laser Materials and Technologies, Institute of General Physics, Russian Academy of Sciences, Moscow, Russia
Lomonosov Moscow State Academy of Fine Chemical Technology, Moscow, Russia

Received November 15, 2004

Abstract—Hydration and dehydration (on calcination) of $SrCl_2$, YOCl, and HoOCl powders were studied.

Single-crystal chloride materials are of interest for photonics owing to their transparence in the IR range and a "soft" photon spectrum. The main problem in both growing the crystals and working with them is their hydration. In particular, chlorides of rare-earth elements are very hygroscopic; hydrated rare-earth chlorides are readily hydrolyzed on heating [1–6]. This substantially complicates the use of such materials, though the spectroscopic characteristics, e.g., of $LaCl_3 : R^{3+}$ single crystals are highly promising [7]. Among matrices resistant to moisture are $PbCl_2$ and KPb_2Cl_5 [8–10].

In this study we examined the hydration of $SrCl_2$ powders and also of oxychlorides of rare-earth elements. Strontium chloride crystallizing in a cubic lattice of the fluorite type has a high isomorphous capacity with respect to chlorides of rare-earth elements [11]. Properties of $SrCl_2$ single crystals and of $Sr_{1-x}R_xCl_{2+x}$ solid solutions have been studied repeatedly [12–14]. Oxychlorides of rare-earth elements are more resistant to moisture than the chlorides [15]. Therefore they could be a convenient form for introducing dopants.

We used ultrapure 7–4 grade $SrCO_3$, chemically pure grade ammonium chloride NH_4Cl, and chemically pure grade hydrates of rare-earth elements $RCl_3 \cdot 6H_2O$ as starting substances. The initial chemicals were characterized by X-ray diffraction. The X-ray phase analysis was carried out on a DRON-2 diffractometer (CuK_α radiation, focusing monochromator from pyrolytic graphite). We recorded variations in sample weights on an Acculab V-200 electron balance. The humidity was measured with a psychrometer. The hydration was carried out at 19 ± 2°C and the relative humidity of 38 ± 5%.

We prepared strontium chloride by the reaction

$$SrCO_3 + 2NH_4Cl = SrCl_2 + H_2O\uparrow + CO_2\uparrow + 2NH_3\uparrow. \quad (1)$$

We used a fourfold excess of NH_4Cl. The reaction was carried out in an alundum crucible at 150–350°C for 6 h. The yield of $SrCl_2$ was 99%. The resulting $SrCl_2$ had a cubic fluorite-type lattice with a = 6.977 Å, which agrees with the published data (PDF card no. 38-0496). On exposure to air, the sample weight continuously increased; the process gradually decelerated with time (Fig. 1). The increase in the substance weight in the first hour was 7%. The increase in the sample weight was accompanied by changes in its X-ray pattern. Along with the $SrCl_2$ lines, an additional set of reflections appeared, and their intensities rapidly increased, whereas the lines of $SrCl_2$ weakened (Fig. 2). Analysis of the pattern using the PDF database revealed mixture of mono-, di-, and hexahydrates of $SrCl_2$. The final hydration product was $SrCl_2 \cdot 6H_2O$. On calcination of strontium chloride hexahydrate at 350°C for 2 h, the weight loss corresponded to complete dehydration. The subsequent

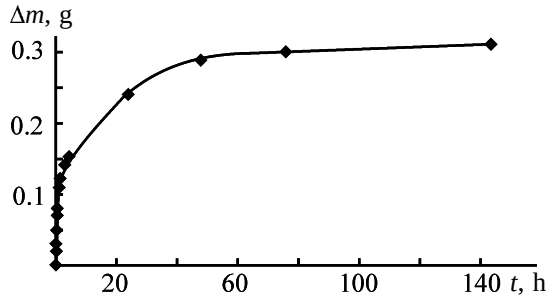


Fig. 1. Kinetics of $SrCl_2$ hydration. (Δm) Change in the weight of the sample and (t) time.

1070-4272/05/7807-1035 © 2005 Pleiades Publishing, Inc.

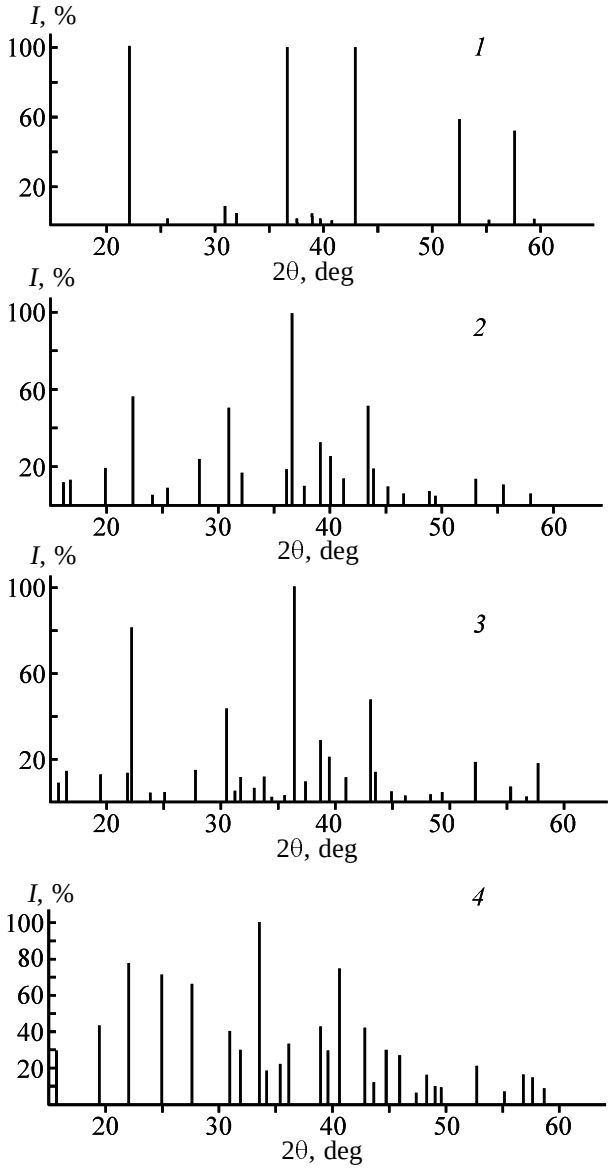


Fig. 2. X-ray patterns of $SrCl_2$ samples depending on the time of exposure to air. (*I*) Intensity and (2θ) Bragg's angle. Time, h: (*1*) 0.5, (*2*) 2, (*3*) 3, and (*4*) 24.

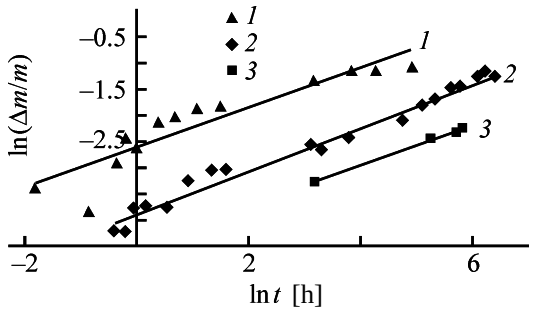


Fig. 3. Hydration of (*1*) $SrCl_2$, (*2*) HoOCl, and (*3*) YOCl samples. (Δ*m*/*m*) Relative weight gain of a sample and (*t*) time.

exposure to air resulted in repeated hydration. However, in this case only the lines of di- and hexahydrates of $SrCl_2$ were observed in the X-ray patterns.

We prepared yttrium and holmium oxychlorides by thermal decomposition of the crystal hydrates by the equation

$$RCl_3 \cdot 6H_2O \rightarrow ROCl + 5H_2O\uparrow + 2HCl\uparrow. \quad (2)$$

The reaction was performed in porcelain crucibles at 350°C for 2 h to obtain YOCl and for 5 h to obtain HoOCl. Tetragonal modifications of oxychlorides were obtained; their X-ray patterns corresponded to the published data (PDF nos. 85-0951 and 85-0897). On exposure of the oxychloride samples to air, their weight increased in a similar manner as with $SrCl_2$, but more slowly. An increase in the weight of YOCl was 0.2%. and that of HoOCl, 2.3% in the first hour of the exposure. No lines of any new phases were observed in the X-ray patterns, but only the intensities of the main peaks of oxychlorides decreased. On calcination, the starting weight of the samples and the X-ray pattern were restored. In the case of incomplete reaction (2), the hydration occurred more actively.

We found that the curves of the weight gain of the substances can be satisfactorily fitted in all cases by equations of the type

$$\Delta m/m = at^n,$$

where m and Δm are the weight of a sample and its gain, respectively (g); t is the time (h) (Fig. 3).

The exponent n in the equation is almost the same ($n = 0.380 \pm 0.015$) for the substances under study.

On the whole, moderate rates of hydration in air and the possibility of reversible removal of water by heating to 350°C indicate that the compounds under study may be promising for obtaining single crystals.

CONCLUSIONS

(1) The final product of hydration of $SrCl_2$ in air is the hexahydrate $SrCl_2 \cdot 6H_2O$. In the initial step of the process, mono- and dihydrates are formed as intermediates.

(2) The absorption of atmospheric moisture by Y(III) and Ho(III) oxychlorides is not accompanied by formation of new phases of hydrated compounds.

(3) Heating the products of $SrCl_2$, YOCl, and HoOCl hydration yields the starting anhydrous compounds.

ACKNOWLEDGMENTS

This study was financially supported in part by EOARD–ISTC (grant no. 2022TO).

The authors are grateful to A.G. Papashvili for submitting samples of hexahydrates of rare-earth elements.

REFERENCES

1. Johnson, K.E. and Mackenzie, J.R., *J. Inorg. Nucl. Chem.*, 1970, vol. 32, no. 1, pp. 43–48.
2. Fox, D.E. and Fong, F.K., *J. Crystal Growth*, 1973, vol. 20, pp. 233–237.
3. Laptev, D.M., Poshevneva, A., Astakhova, I.S., and Kulagin, N.M., *Zh. Neorg. Khim.*, 1976, vol. 21, no. 9, pp. 2317–2320.
4. Lyzlov, Yu.N. and Nisel'son, L.A., *Zh. Neorg. Khim.*, 1978, vol. 23, no. 3, pp. 857–859.
5. Garton, G. and Walker, P.J., *Mater. Res. Bull.*, 1982, vol. 17, no. 10, pp. 1227–1234.
6. Meyer, G. and Ax, P., *Mater. Res. Bull.*, 1982, vol. 17, no. 11, pp. 1447–1455.
7. Boody, F., 100-MV, 1.6 μm Pr^{3+} : $LaCl_3$ Up-Conversion Laser for Space Propulsion, *CLEO Europe EQLEC*, 2003, Advance Program, p. 84.
8. Nitsch, K., Dysek, M., Niki, M., *et al.*, *Progr. Crystal Growth Charact.*, 1995, vol. 30, pp. 1–22.
9. Tkachuk, A.M., Ivanova, S.E., Isaenko, L.I., and Eliseev, A.P., *Spektrosk. Tverd. Tela*, 2002, vol. 92, no. 1, pp. 89–101.
10. Basiev, T.T., Danilenko, Yu.K., Dmitruk, L.N., *et al.*, in *Proc. Fifth Int. Conf.: Single Crystal Growth and Heat and Mass Transfer*, Obninsk, 2003, vol. 1, pp. 331–335.
11. Blachnik, R., Alberts, G., and Enninga, E., *Z. Anorg. Allg. Chem.*, 1985, vol. 522, pp. 207–216.
12. Croatto, U. and Bruno, M., *Gazz. Chim. Ital.*, 1946, vol. 76, pp. 246–254.
13. Hutchings, V.T., Clausen, K., Dickens, M.H., *et al.*, *J. Phys. C: Solid State Phys.*, 1984, vol. 17, pp. 3903–3940.
14. Bendall, J.P., Catlow, C.R.A., and Fender, B.E.F., *J. Phys. C: Solid State Phys.*, 1984, vol. 17, pp. 797–814.
15. Drobot, D.V., Physicochemical Studies of Chlorine Derivatives of Rare-Earth Elements and Yttrium, *Cand. Sci. (Chem.) Dissertation*, Moscow, 1966.

Russian Journal of Applied Chemistry, Vol. 78, No. 7, 2005, pp. 1038–1042. Translated from Zhurnal Prikladnoi Khimii, Vol. 78, No. 7, 2005, pp. 1060–1064.
Original Russian Text Copyright © 2005 by Kopilevich, Voitenko, Zhilyak.

INORGANIC SYNTHESIS AND INDUSTRIAL INORGANIC CHEMISTRY

Hydrated Zinc Ammine Diphosphate Isolated from Water–Ammonia Solutions and Its Thermal Properties

V. A. Kopilevich, L. V. Voitenko, and I. D. Zhilyak

National Agricultural University, Kiev, Ukraine

Received November 29, 2004; in final form, April 2005

Abstract—A synthesis of amorphous hydrated zinc ammine diphosphate was described. Thermal properties of this compound were studied and schemes of thermal transformations were suggested.

Compounds of transition metal phosphates obtained from ammonia solutions and containing ammonia coordinated to a metal ion are of interest due to their possible catalytic activity [1, 2]. This especially concerns amorphous phosphate compounds exhibiting a high reactivity owing to their thermodynamic instability [3]. Published data on the synthesis and thermal behavior of zinc ammine diphosphate are extremely scarce [4].

The goal of this study was to prepare hydrated zinc ammine diphosphate and to examine its thermal properties.

EXPERIMENTAL

Hydrated zinc ammine diphosphate was prepared by its salting-out with an organic solvent from an ammonia solution [5]. The starting zinc diphosphate $Zn_2P_2O_7 \cdot 5H_2O$ (41.2% ZnO) synthesized according to [6] in an amount of 6 g was dissolved in 62 ml of a 23% ammonia solution. The resulting solution was poured into tetrahydrofuran (70 ml). The precipitate thus formed was separated from the mother solution and kept at 15–25°C up to complete hardening in air (to constant weight). For zinc ammine diphosphate of the composition $Zn_2P_2O_7 \cdot 3.0NH_3 \cdot 1.5H_2O$ (**I**):

Found, %: ZnO 42.40, P_2O_5 37.11, NH_3 13.20, H_2O 7.20.
Calculated, %: ZnO 42.51, P_2O_5 37.08, NH_3 13.34, H_2O 7.06.

The anionic composition of the compound synthesized was determined by quantitative paper chromatography [7]; relative to total P_2O_5, it is as follows (%): $P_2O_7^{4-}$ 92.40 and PO_4^{3-} 7.60. The starting zinc diphosphate contained 6.00 rel. % of P_2O_5 in the form of PO_4^{3-}.

The content of zinc(II) was determined by EDTA titration [8], that of phosphorus, by gravimetric analysis [9], that of ammonia, by its distillation on a Seren'ev apparatus [10], and the total content of water and ammonia, by the weight loss at 750°C in 2 h. The X-ray diffraction analysis was carried out on a DRON-UM1 diffractometer (CuK_α radiation). A graphite single crystal arranged in the diffracted beam was used as a monochromator. The diffraction patterns were taken by step scanning in the range of angles $2\theta = 4°–80°$. The scanning step was 0.05°, and the exposure time in a point, 3–9 s. The measured diffraction maxima were approximated by a pseudo-Voigt function with selecting the K_{α_1} component. The IR spectra were recorded on a Specord 75-IR spectrophotometer. Samples for the measurements were prepared as 0.2–0.3 wt % KBr pellets.

Transformations of $Zn_2P_2O_7 \cdot 3.0NH_3 \cdot 1.5H_2O$ on heating were studied by thermal analysis with a Q-1500D derivatograph. Samples were heated in air in the range 15–900°C up to termination of the weight loss. Dynamic experiments were carried out using capped cylindrical platinum crucibles; weighed samples of compound **I** were 0.400–0.500 g. Final and all intermediate decomposition products were obtained at a heating rate of 2.5 deg min^{-1}. In quasi-isothermal experiments, 0.500-g samples were placed in a platinum labyrinthine crucible and heated under controlled conditions.

Anionic compositions of the intermediate decomposition products were determined by paper chromatography [7].

An X-ray phase analysis showed that the starting $Zn_2P_2O_7 \cdot 5H_2O$ was crystalline. We found that the zinc ammine diphosphate synthesized on its basis was X-ray amorphous. A reflection maximum for com-

1070-4272/05/7807-1038 © 2005 Pleiades Publishing, Inc.

pound **I** is observed at 2θ = 28°, which can correspond to a proportional distance in the compounds at the subsequent formation of the crystal structure (Fig. 1). The thermolysis products are also X-ray amorphous except for the sample obtained at 900°C, which corresponds to anhydrous $Zn_2P_2O_7$ [11].

A strong broad band corresponding to stretching vibrations of NH and OH groups is observed in the range 3400–3000 cm^{-1} in the IR spectrum of **I**; the absorption bands corresponding to bending vibrations of water and asymmetric bending vibrations of ammonia in ammines are present in the range 1650–1545 cm^{-1}. The absorption in the range 1485–1420 cm^{-1} in the spectrum of **I** is indicative of hydrogen bonding between an ammonia molecule coordinated to a Zn(II) ion and a $P_2O_7^{4-}$ anion, which is accompanied by averaging of the electron density over the entire chain of atoms forming the hydrogen bond [12]. The absorption related to symmetric bending vibrations of coordinated ammonia molecules is observed at about 1260 cm^{-1} [13]. Antisymmetric and symmetric stretching vibrations of the $P_2O_7^{4-}$ group are observed in the range 1120–900 cm^{-1} as strong absorption bands. Weak absorption bands at 720–540 cm^{-1} correspond to vibrations of the P–O–P and O–P–O groups. The bands of stretching vibrations of the Zn–N and Zn–O bonds in **I** are observed in the range 510–465 cm^{-1} [14, 15].

Thus, the IR spectrum suggests that at least a part of coordinated ammonia molecules in **I** participates in the hydrogen bonding with oxygen atoms of water molecules and $P_2O_7^{4-}$ anions.

According to the thermal analysis (Fig. 2), the thermolysis of **I** occurs in a wide temperature range (approximately from 75 to 460°C) and, as follows from the DTA curve, is accompanied by three endothermic effects with minima at 125, 272, and 295°C. At 460°C, a exothermic peak is observed, which is superimposed by an endothermic effect, as demonstrated, in particular, by abrupt weight loss of the sample in the DTG and TG curves.

According to the TG curve, the sample undergoes weight loss in the range 75–460°C. Chemical analysis of the decomposition products of **I** (Fig. 2, curves *3*, *4*) shows that in the range 75–150°C $Zn_2P_2O_7 \cdot 3.0NH_3 \cdot 1.5H_2O$ loses 0.64 mol of H_2O and 0.30 mol of NH_3. According to the chromatographic data (Table 1), the sample taken at 150°C contains 29.5% of P_2O_5 in the form of PO_4^{3-} and 70.5%, in the form of $P_2O_7^{4-}$. The chemical analysis of the thermolysis

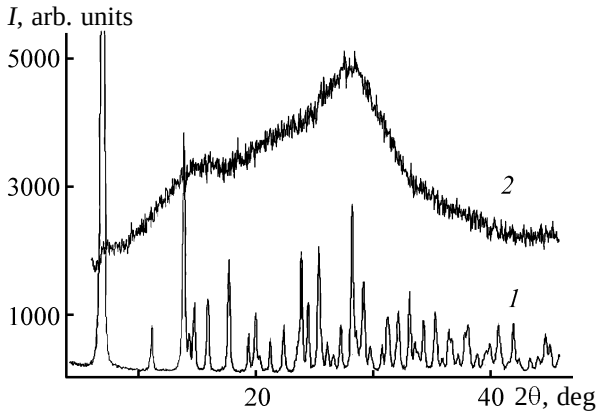


Fig. 1. Diffraction patterns of (*1*) $Zn_2P_2O_7 \cdot 5.0H_2O$ and (*2*) $Zn_2P_2O_7 \cdot 3.0NH_3 \cdot 1.5H_2O$. (*I*) intensity and (2θ) Bragg angle.

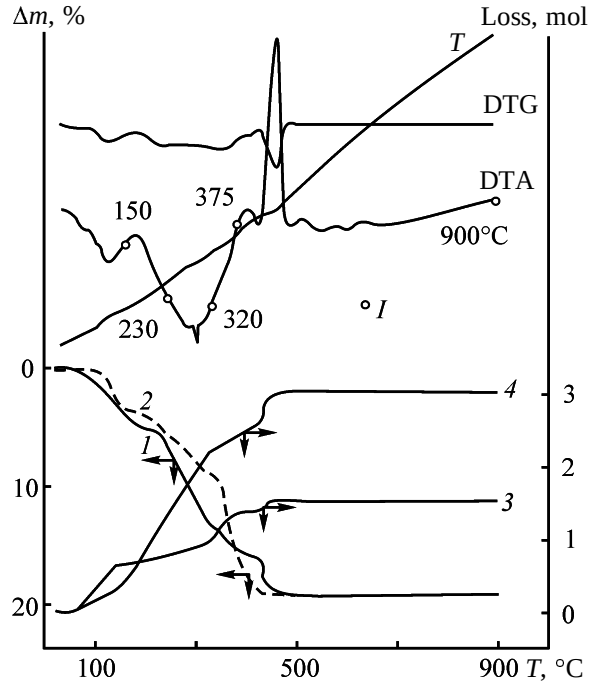


Fig. 2. TG curve of heating of $Zn_2P_2O_7 \cdot 3.0NH_3 \cdot 1.5H_2O$. (Δ*m*) Weight change and (*T*) temperature. Circles denote sampling points. (*1*) Dynamic heating at a rate of 2.5 deg min^{-1} and (*2*) quasi-isothermal mode; loss of (*3*) NH_3 and (*4*) H_2O from the substance on heating.

products shows that the first step involves mainly removal of water:

$$[Zn_4(NH_3)_6(H_2O)_2(P_2O_7)_2] \cdot H_2O$$

$$\xrightarrow{75\text{–}150^\circ C} 1.3H_2O + 0.6NH_3$$

$$+ Zn_4(NH_3)_{5.4}(H_2O)_{1.7}(P_2O_7)_2.$$

The quantitative chromatography (Table 1) shows that the thermolysis of **I** at temperatures of up to

Table 1. Changes in elemental and chemical compositions of zinc ammine diphosphate during thermolysis in the dynamic mode

T, °C	Composition according to chemical analysis	Distribution of P_2O_5, rel. %			Removed from starting compound, mol	
		PO_4^{3-}	$P_2O_7^{4-}$	$P_3O_{10}^{5-}$	NH_3	H_2O
Starting	$2.0ZnO \cdot P_2O_5 \cdot 3.0NH_3 \cdot 1.50H_2O$	7.6	92.3	–	0	0
150	$2.0ZnO \cdot P_2O_5 \cdot 2.7NH_3 \cdot 0.86H_2O$	29.5	70.5	–	0.30	0.64
230	$2.0ZnO \cdot P_2O_5 \cdot 1.8NH_3 \cdot 0.75H_2O$	44.7	55.3	Traces	1.16	0.75
320	$2.0ZnO \cdot P_2O_5 \cdot 0.9NH_3 \cdot 0.60H_2O$	39.0	56.0	5.0	2.10	0.90
375	$2.0ZnO \cdot P_2O_5 \cdot 0.7NH_3 \cdot 0.18H_2O$	22.8	66.7	10.5	2.34	1.32
900	$2.0ZnO \cdot P_2O_5$	Traces	100	–	3.00	1.50

230°C involves partial (approximately 50%) transformation of diphosphate anions according to the scheme

$$[Zn_4(NH_3)_6(H_2O)_2(P_2O_7)_2] \cdot H_2O$$

$$\xrightarrow{75–230°C} Zn_4(NH_3)_{3.6}(H_2O)_{1.5}(PO_4)_2(P_2O_7)_1.$$

A further increase in temperature in the range 230–375°C results in the condensation of monophosphate and diphosphate ions into tripolyphosphate ions, which is accompanied by the additional removal of 2.34 mol of ammonia and 1.32 mol of water. In this case, according to the chromatographic data, the product of thermolysis at 375°C contains 22.8% of P_2O_5 in the form of PO_4^{3-}, 66.7% in the form of $P_2O_7^{4-}$, and 10.5% in the form of $P_3O_{10}^{5-}$. Such a distribution of P_2O_5 over oligomeric species can be presented by the following scheme of this thermolysis step, taking into account the available data on thermal transformations of hydrated phosphates [16]:

$$Zn_4(NH_3)_{3.6}(H_2O)_{1.5}(PO_4)_2(P_2O_7)_1$$

$$\xrightarrow{230–375°C} 2.2NH_3 + 1.1H_2O$$

$$+ Zn_4(NH_3)_{1.4}(H_2O)_{0.4}(PO_4)_{0.44}(P_2O_7)_{1.28}(P_3O_{10})_{0.33}.$$

At 460°C, a new phase crystallizes from X-ray amorphous thermolysis products. Its structure remains unchanged on further heating up to 900°C. This process is accompanied by a powerful exothermic effect and by simplification of the anionic composition of samples due to a decrease in the content of tri- and monophosphate ions. The X-ray pattern of the final thermolysis product of **I** corresponds, as a whole, to the X-ray pattern of $Zn_2P_2O_7$ [11]. The scheme of this transformation step is as follows:

$$Zn_4(NH_3)_{1.4}(H_2O)_{0.4}(PO_4)_{0.44}(P_2O_7)_{1.28}(P_3O_{10})_{0.33}$$

$$\xrightarrow{460°C} 1.4NH_3 + 0.4H_2O + 2Zn_2P_2O_7.$$

Also, the dehydration of **I** was studied under near-equilibrium conditions, i.e., in the quasi-isothermal heating mode at a partial pressure of water vapor over the sample of about 0.8 atm. The thermolysis in this mode occurs in the temperature range 95–448°C (Fig. 2, curve *2*), and the sequence of the transformations on heating is similar to that in the schemes considered above.

The sequence of water and ammonia removal from the substance, with appreciable differences in temperature ranges of particular thermolysis steps, taking into account the specific features of variation of the composition of phosphate anions in the calcination products, is accounted for by different nature of binding of H_2O and NH_3 molecules in the structure and by their contribution to the formation of the averaged electron density within the chain [Zn–NH_3–H_2O–P_2O_7] [16, 17].

When the temperature is increased to 375°C, the maximum of the strong broad absorption band of ν(NH) vibrations in the IR spectra of the thermolysis products of **I** is shifted from 3450 to 3180 cm^{-1} (Table 2). The IR spectra of the starting compound **I** and its thermolysis products contain absorption bands characteristic of diphosphate ions (520–1195 cm^{-1}). The band ν_{as}(POP) [P_2O_7] (700–730 cm^{-1}) observed in the spectra of all the decomposition products suggests the presence of a nonlinear POP bridge in the diphosphate ion. The ν(OH) and ν(NH) vibrations of ammonia and water molecules are mainfested in the range 2800–3500 cm^{-1} as a very broad band, suggesting formation of strong hydrogen bonds. The spectrum of the product obtained at 900°C corresponds to anhydrous zinc diphosphate $Zn_2P_2O_7$ [11].

Table 2. IR spectra of $Zn_2P_2O_7 \cdot 3.0NH_3 \cdot 1.5H_2O$ (**I**) and products of its calcination*

Starting compound **I**	Products of calcination at indicated *T*, °C					Assignment of frequencies
	150	230	320	375	900	
3450 sh	3325 w	3300–150 s.br	3200 m	3250–3180 s.br		
3400–3100 s.br.	3200 w					
2800 sh	3050 sh	3050 sh	3050 sh	3050 sh		$\nu(H_2O)$, $\nu_{as}(NH_3)$
		2950 sh	2950 sh	2850 sh		
		2850 sh				
1650 sh	1650 sh	1640 w	1650 w			
1625 m	1600 m	1610 m		1610 sh		$\nu(H_2O)$, $\delta_{as}(NH_3)$
1545 sh	1500 sh		1500 sh			
1485 sh		1480 sh				
1445 m	1430 m	1430 m				$\delta_s(NH_3)$
1420 sh			1420 m	1420 m		
1260 w	1300 sh			1300 sh		$\delta_s(NH_3)$
	1265 w	1250 sh	1280 sh			
1125 sh	1150 w	1150 sh	1180 sh	1195–1070 s.br	1195 s	$\nu_{as}(PO_3)$ $[P_2O_7]$
1100 s	1110 s	1100–990 s.br	1120 sh		1150 w	
1085 sh	1090 s		1100 s	1010 w	1100 w	
1030 w	1020 sh		1010 sh	990 w	1070 w	
					1040 s	
900 s	900 s	910 s	920 s	920 s	935 s	$\nu_s(PO_3)$ (PO)
715 w		700 sh	720 w	730 m	710 m	$\nu_{as}(POP)$ $[P_2O_7]$
640 w	650 sh	670 w				$\delta_{as}(OPO)$
600 sh	560 sh	600 sh				
540 m	520 s	550 m	560 sh		540 sh	$\delta_s(OPO)$
510 m		510 sh	540 m	520 sh	520 m	} ν(Zn–N), ν(Zn–O)
470 sh	450 w	460 sh	510 sh	440 sh	420 sh	
			440 sh			

* (s) Strong, (m) medium, (w) weak, (br) broad, and (sh) shoulder.

CONCLUSION

Solid X-ray amorphous hydrated ammonia zinc diphosphate of the composition $Zn_2P_2O_7 \cdot 3.0NH_3 \cdot 1.5H_2O$ was isolated in the individual form from a water–ammonia solution. Its thermal behavior in the range 20–900°C was studied. It was found that the final thermolysis product is anhydrous crystalline zinc diphosphate and that the process occurs stepwise.

REFERENCES

1. Kopilevich, V.A., Kokhan, S.S., and Voitenko, L.V., in *Proc. 11th World Fertilizer Congr. of CIEC*, Ghent (Belgium), 1997, vol. 2, p. 296.
2. Voitenko, L.V., Hydrated Cobalt(II), Copper(II), and Zinc Ammine Phosphates, *Cand. Sci. Dissertation*, Kiev, 1994.
3. Voitenko, L.V., Zhilyak, I.D., and Kopilevich, V.A., *Zh. Prikl. Khim.*, 2004, vol. 77, no. 9, pp. 1421–1424.
4. Acharyya, H. and Roy, H., *Technology* (India), 1972, vol. 9, no. 4, pp. 273–277.
5. Ukrainian Patent 62 782.
6. Kokhanovskii, V.V., *Zh. Neorg. Khim.*, 1995, vol. 40, no. 1, pp. 173–176.
7. Shchegrov, L.N., *Fosfaty dvukhvalentnykh metallov* (Phosphates of Bivalent Metals), Kiev: Naukova Dumka, 1987.
8. Přibil, R., *Komplexometrie*, Prague: Chemapol, 1955.
9. *GOST* (State Standard) *20 851–75: Mineral Fertilizers: Methods of Analysis*, Moscow: Izd. Standartov, 1986.
10. Gorodnii, M.M., Kopilevich, V.A., Serdyuk, A.G., *et al.*, *Agrokhimichnyi analiz* (Agrochemical Analysis), Kiev: Vishcha Shkola, 1995.
11. Morozova, N.Yu., Selivanova, N.M., and Khozhainova, T.I., *Zh. Neorg. Khim.*, 1978, vol. 23, no. 2, pp. 331–340.

12. Voitenko, L.V., Kopilevich, V.A., and Shchegrov, L.N., *Zh. Neorg. Khim*., 1992, vol. 37, no. 9, pp. 2055–2060.
13. Shevchenko, Yu.N., Coordination Compounds of 3*d*-Transition Metals with Hydroborate Anions, *Doctoral Dissertation*, Moscow, 1991.
14. Nakamoto, K., *Infrared Spectra of Inorganic and Coordination Compounds*, New York: Wiley, 1963.
15. *Atlas IK spektrov fosfatov: Dvoinye mono- i difosfaty* (Atlas of IR Spectra of Phosphates: Double Mono- and Diphosphates), Pechkovskii, V.V., Ed., Moscow: Nauka, 1990.
16. Kopilevich, V.A., Synthesis and Thermal Transformations of Pure and Nitrogen-Containing Manganese(II), Cobalt(II), Copper(II), and Zinc Phosphates, *Doctoral Dissertation*, Kiev, 1994.
17. Shchegrov, L.N., Kopilevich, V.A., and Voitenko, L.V., *Zh. Neorg. Khim*., 1991, vol. 36, no. 8, pp. 2095–2156.

Russian Journal of Applied Chemistry, Vol. 78, No. 7, 2005, pp. 1043–1047. Translated from Zhurnal Prikladnoi Khimii, Vol. 78, No. 7, 2005, pp. 1065–1069.
Original Russian Text Copyright © 2005 by Eremina, Avvakumov, Zelinskii.

INORGANIC SYNTHESIS AND INDUSTRIAL INORGANIC CHEMISTRY

Properties of a Fireproofing Formulation Based on Liquid Glass and Mechanically Activated Aluminum Oxide

N. V. Eremina, E. G. Avvakumov, and V. Yu. Zelinskii

Institute of Solid-State Chemistry and Mechanochemistry, Siberian Division, Russian Academy of Sciences, Novosibirsk, Russia

Korund Ltd., Ust'-Kamenogorsk, Kazakhstan

Received November 17, 2004; in final form, April 2005

Abstract—Moistening of filler particles with binder, curing, and high-temperature synthesis were studied in a liquid-glass formulation based on aluminum oxide. Selected kinetic parameters of these processes were determined. The influence exerted by the phase composition and mechanical activation on the adhesion, yield of the synthesis product, and basic properties of the formulation were analyzed.

Liquid-glass formulations (LGFs)containig mineral fillers and some functional additives creating a combustion-inert atmosphere are used as fireproofing materials [1–3]. The most important properties of LGFs: long working life, good adhesion, and high fireproofing efficiency, are determined by processes that involve the binder and filler, including synthesis of phases in the high-temperature zone at the seat of fire. One of the main ways to affect the properties of an LGF is to change the chemical activity of fillers [4]. However, the expected result may vary between different properties. Raising the activity of a filler improves the fire-proofing efficiency, but, as a result of coagulation, impairs the adhesion and service life of an LGF. Mechanical activation (MA) is commonly used as an effective method for enhancing the reactivity of powdered media, but it virtually has not been studied at all as applied to LGF [5].

The aim of this study was to examine the adhesion properties of a liquid-glass formulation containing mechanically activated Al_2O_3 in stages of moistening and curing. The products formed in its thermal treatment in the range 200–1000°C were determined.

The choice of Al_2O_3 was governed by the strong variation of the chemical activity of this oxide with its phase composition. Alumina of G-00 brand [75 wt % γ-phase and α-phase, GOST (State Standard) 13078], was taken for MA. The powder was activated in a planetary-centrifugal mill with rubberized drums and corundum balls, at a material : balls ratio of 1 : 3 and a rotary acceleration of 18*g*. Alumina of GK brand, containing 100 wt % α-phase (GOST 30559), served as a chemically inert filler; and $Al(OH)_3$ (GOST 11841), as the most active filler passivated by annealing at 500, 700, 900, and 1000°C, which was accompanied by formation of transient Al_2O_3 phases of γ-, χ, æ-, and θ-types [6]. According to the results of an X-ray phase analysis, the phase composition of the annealing products varied as follows: 500°C, aluminum hydroxide and trace amounts of the γ-phase; 700°C, γ-phase and trace amounts of the χ-phase; 900°C, χ-phase and trace amounts of the æ- and θ-phases; and 1000°C, æ- and θ-phases. To eliminate any influence of the dispersity of a filler in LGF, the powder fraction obtained by sedimentation in water was used. According to the results of a granulometric analysis on a Sedigraf 5000 ET instrument, the fraction contained the following types of particles: 3–5 μm, up to 15 wt %; 5–10 μm, up to 73 wt %; and 10–15 μm, the rest.

A sodium liquid glass with a silica ratio of 2.8 and density of 1.34 g cm^{-3} was taken as a binder. The choice of the chemical composition of the binder was governed by the possibility of maximal accumulation of water in the hydration environment of the cation. It has been established that the fraction of crystallization-bound water for Na^+ considerably exceeds that for K^+ [5]. Intensive dehydration in the temperature range 150–450°C must markedly raise the porosity of LGF in the initial stages of a fire, which improves the fireproofing efficiency of a coating.

The formulation based on liquid glass contained 48 vol % binder and 52 vol % filler. The composition was chosen empirically, as providing the highest

1070-4272/05/7807-1043 © 2005 Pleiades Publishing, Inc.

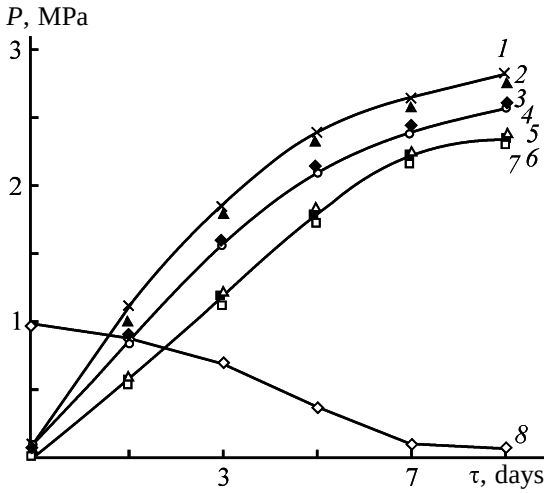


Fig. 1. Adhesion *P* of LGF in the stage of particle moistening at different preparation techniques and formulation compositions. (τ) Time of LGF keeping. Additive: (*1*) urea + G-00 (MA in air), (*2*) urea + G-00 (MA in water), (*3*) G-00 (MA in water), (*4*) G-00 (MA in air), (*5*) α-Al_2O_3, (*6*) nonactivated G-00, (*7*) $Al(OH)_3$ calcined at 700°C, and (*8*) uncalcined $Al(OH)_3$.

adhesion of the formulation to a wood substrate. The requirements to the substrate material were in conformity with GOST 16363 for tests of the fireproofing efficiency of coatings. LGF was modified with a urea additive in an amount of 3.5 wt % (GOST 6691). X-ray diffraction patterns were measured on a DRON 3M diffractometer with Cu*K* radiation, and IR spectra, on a Specord 75-IR instrument in KBr pellets. The adhesion was measured using the method of film detachment from a wood substrate [1].

After a filler is introduced into the LGF, its particles are moistened by the binder. The components come close to within the range of action of intermolecular forces, which markedly enhances the adhesion [7]. In an LGF with Al_2O_3 as a filler, the adhesion increases in the stage of moistening by a factor of 3–5 at a process duration of 6–7 days (Fig. 1). Mechanical activation of Al_2O_3 makes moistening faster and, consequently, enhances the adhesion. The disintegration of a film with $Al(OH)_3$ filler is accounted for by chemical interaction between the components, to give sparingly soluble alkaline aluminosilicates of the composition $Na_4Al_3Si_3O_{12}(OH)$ and $1.08Na_2O \cdot Al_2O_3 \cdot 1.68SiO_2 \cdot 1.8H_2O$ (Fig. 2a). After annealing of $Al(OH)_3$ at 700°C, neither synthesis of the abovemention compounds nor disintegration of the formulation were observed. Further increase in the annealing temperature impaired the adhesion.

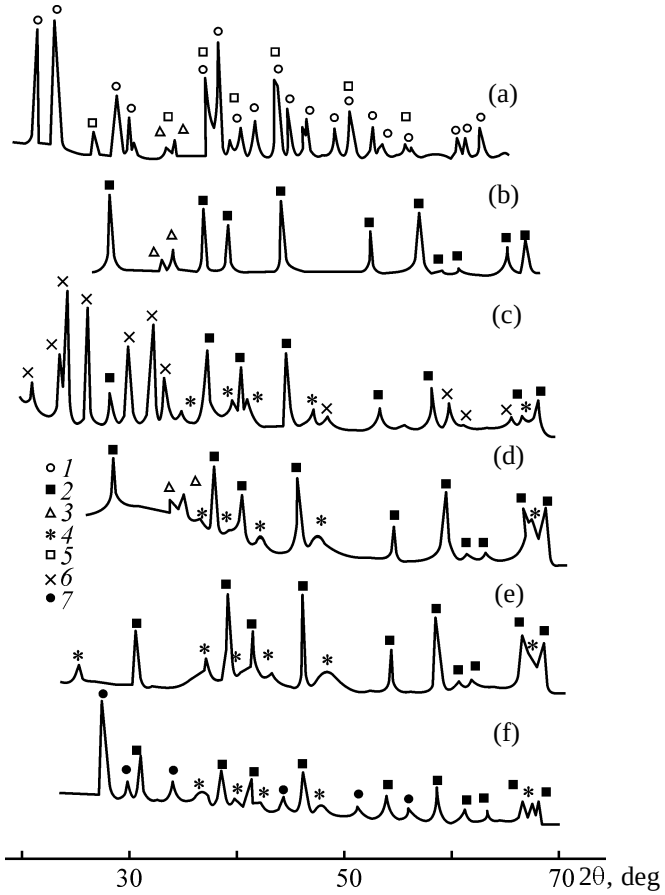


Fig. 2. X-ray diffraction patterns of samples of fireproofing formulations. (2θ) Bragg angle. Phase composition: (a) LGF + $Al(OH)_3$, (b) LGF + α-Al_2O_3, (c) LGF + G-00 (annealing at 1000°C), (d) LGF + G-00, (e) nonactivated G-00, and (f) LGF + G-00 (MA in air) + urea. (*1*) $Al(OH)_3$, (*2*) α-Al_2O_3, (*3*) $Na_2SiO_3 \cdot xH_2O$, (*4*) γ-Al_2O_3, (*5*) $Na_4Al_3 \cdot Si_3O_{12}(OH)$ or $1.08Na_2O \cdot Al_2O_3 \cdot 1.68SiO_2 \cdot 1.8H_2O$, (*6*) $Na_2O \cdot Al_2O_3 \cdot 2SiO_2$, and (*7*) $(NH_2)_2CO$.

In the X-ray diffraction patterns of LGF with G-00 alumina, the intensity of a γ-phase-related reflection from the plane with d = 0.456 nm and I_{rel} = 12% decreases to the background level (Fig. 2d). The same reflection is absent in powdered G-00 alumina mechanically activated in water or in air. For planes of the short-range order of the crystal structure, the decrease in the intensity of the diffraction profile is mostly due to appearance of static displacements [8]. These displacements arise under the action of external factors and are temperature-independent. The magnitude of the displacements was 0.03 nm under the given conditions of X-ray pattern recording, at a decrease in the profile intensity at the point of maximum by 5–7% to the background level.

The appearance of static displacements in a plane poorly populated by atoms with relatively weak intra-

crystalline bonds indicates that formation of chemisorption bonds is possible. In this case, the interatomic distance between the species involved must decrease, which is manifested experimentally in a decrease in the intensity of reflections in the X-ray diffraction pattern. With account of the occurrence of chemical reactions between the binder and Al^{3+} contained in $Al(OH)_3$, oxygen ions O^{2-} from siloxane links may form the chemisorption bond on the binder side, and Al^{3+} cations from γ-Al_2O_3, on the side of alumina particles. The phase composition of LGF with GK alumina corresponds to that of the starting components (Fig. 2b), which characterizes corundum as an inert filler interacting with the silicate binder by the mechanism of physical adsorption [7].

The observed increase in adhesion in the stage of moistening was used to study the process kinetics. The temperatures of isothermal keeping were 9, 22, and 40°C. Further lowering of the temperature terminated moistening because of a considerable increase in the viscosity of LGF, whereas heating to higher temperatures stopped the process because of the rapidly increasing loss of water. The maximum duration of keeping of the formulation corresponded to the actual length of the moistening period equal to 7 days, and that of coating curing in adhesion measurements, to 6 h. The apparent activation energy of the process was calculated using the Arrhenius equation. The rate constant was determined by differentiating the approximating equation with respect to time. The best fit was obtained for a power equation of the form $P = c\tau^n$, where P is the adhesion of a film; τ, moistening duration; and c and n, constants. The apparent activation energies E_m of moistening are listed in the table.

According to the data obtained, E_m decreases for an LGF containing a mechanically activated powder and reaches a minimum in the case of activation in air. As indicated above, a possible reason for the decrease in E_m is the static displacement of atoms in the plane with d = 0.456 nm of the γ-phase of Al_2O_3 in the course of MA. In the case of a nonactivated powder, such a displacement occurs in LGF after mixing of the powder with a binder. The lower E_m in formulations with a mechanically activated filler makes it possible to perform moistening at a lower temperature, which makes less stringent the requirements to the temperature conditions of LGF deposition onto a surface.

Urea has been conventionally used as a modifier of the properties of liquid glass [4]. Its introduction into a formulation in an amount of up to 3.5 wt % raised the adhesion by 18–20% and accelerated curing of LGF at a lowered temperature. The effectiveness of the additive increased in formulations based on a mechanically activated filler (Fig. 1). No effect of urea on the duration of the moistening process was observed. In the course of curing, urea crystallized into its own phase. X-ray diffraction patterns of LGF contained additive-related reflections from planes with d 0.4, 0.362, 0.305, 0.283, 0.253, 0.242, 0.223, 0.199, 0.187, and 0.167 nm. In formulations with mechanically activated fillers, the intensity of reflections increased to 30%, especially for a powder activated in air.

Apparent activation energies of moistening (E_m) and curing (E_c)

Composition	E_m, kJ mol^{-1}	E_c, kJ mol^{-1}, for indicated formulation	
		with urea	without urea
LGF with G-00 alumina:			
MA in water	35	32	63
MA in air	25	38	72
nonactivated	45	72	73
Liquid glass		67	65

The sorption of urea molecules on the surface of filler particles and the influence exerted on this process by mechanical activation of Al_2O_3 are confirmed by the IR data (Fig. 3). The most abundant in the spectrum are various kinds of vibrations of NH_2 and CN groups of urea [9]. The absorption by the oxide is observed at 1057 cm^{-1}. The absorption band of the carbonyl group CO is superimposed on NH_2 bending

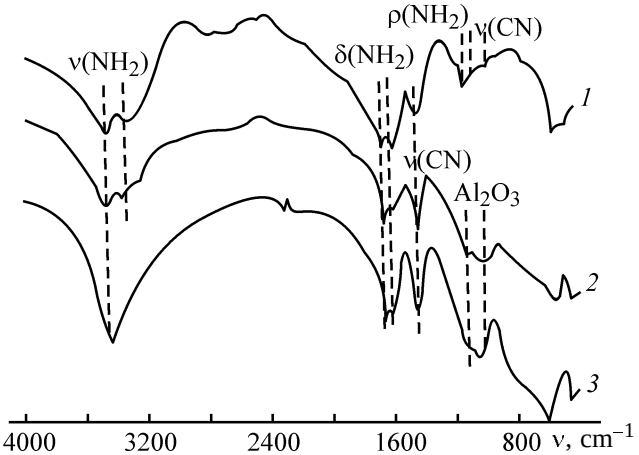


Fig. 3. IR spectra of fireproofing formulations. (ν) Wave number. (*1*) Urea, (*2*) LGF + G-00 (MA in water) + urea, and (*3*) LGF + G-00 (MA in air) + urea.

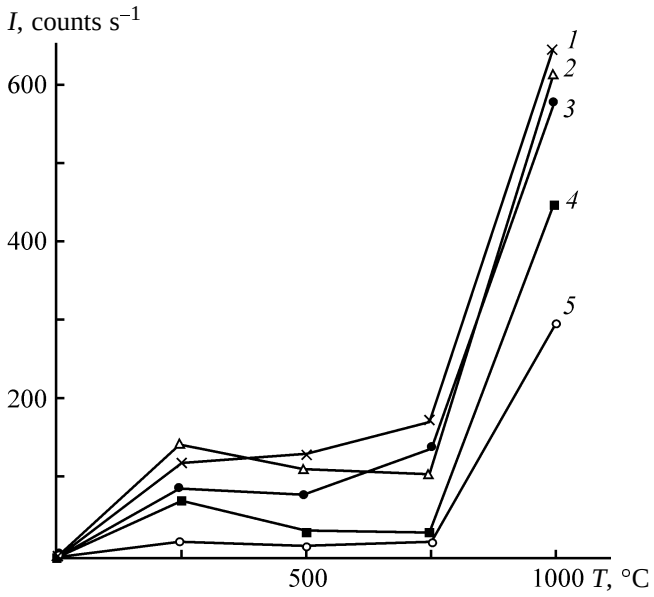
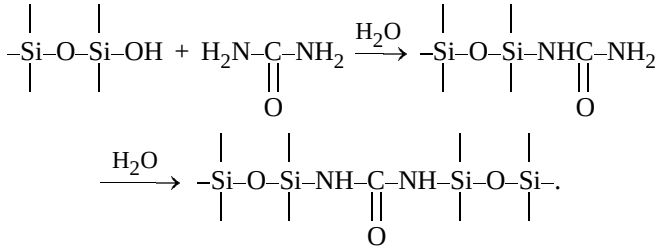


Fig. 4. Synthesis of nepheline from LGF. (*T*) Temperature and (*I*) absolute intensity. (*1*) G-00 (MA in air for 120 min, with subsequent disaggregation), (*2*) G-00 (MA in water for 30 min), (*3*) G-00 (MA in air for 30 min), (*4*) nonactivated G-00, and (*5*) G-00 (MA in air for 120 min).

(δ) vibrations. In contrast to that of pure urea, the spectrum of the formulation contains no stretching (ν) vibrations of the CN group or second overtones of NH_2 ν-vibrations. With a filler activated in air, the symmetric band of the NH_2 ν-vibrations becomes extinct. A similar behavior has been observed upon an increase in the coordination number of nitrogen atoms from 3 for the NH_3 molecule to 4 for the NH_4^+ cation [10]. An additional chemisorption bond between N^{3-} of the amide group and Al^{3+} cations of the γ-Al_2O_3 phase of alumina, disordered in the plane with d = 0.456 nm, may appear in an LGF with urea. The formation of this new bond can account for sorption of urea molecules at the interface between the solution and filler particles. This makes larger the fraction of the crystalline phase in curing and thereby leads to an increase in the experimentally observed intensity of reflections in the diffraction profile.

The kinetics of LGF curing after the moistening stage was studied in the isothermal mode. For this purpose, freshly prepared formulations were kept at 25°C for 7 days. The curing duration of the films was 0.5 to 6 h at 9, 22, and 40°C. The apparent activation energies E_c found for formulations without a urea additive are virtually the same and independent of the formulation composition and MA conditions (see table). E_c decreased by a factor of more than 2 upon introduction of urea into an LGF with an activated powder. The additive had no effect on E_c if other fillers were used.

In an LGF with an activated filler, the sorption activity of the amide group NH_2 of urea may increase via formation of a chemisorption bond. A local increase in the concentration of polymeric anions of the binder in the surface region may result in that the solubility limit will be exceeded and a precipitate will be formed. The weakening of the N–H bond in N^{3-} chemisorbed on the surface of Al_2O_3 particles makes probable the involvement of the urea additive in the reaction



Further, particles of this kind serve as growth centers of the solid phase.

Phase transformations that occur in high-temperature annealing of LGF are illustrated in Fig. 4. Heating to 200°C leads to appearance of the nepheline phase ($Na_2O \cdot Al_2O_3 \cdot 2SiO_2$). Reflections from the $Na_2SiO_3 \cdot xH_2O$ phase become extinct at the same temperature because of the transition to a readily fusible glassy state and dehydration. An increase in the rate of nepheline synthesis is observed at about 800°C. The yield of nepheline is primarily affected by the surface area of filler particles, which is characteristic of processes occurring at a phase boundary. The amount of the product synthesized decreases dramatically as the phase boundary area becomes smaller through aggregation of particles upon activation of the powder in air for 120 min. After disaggregation of the same powder (mechanical activation in an aqueous solution of liquid glass), the yield of $Na_2O \cdot Al_2O_3 \cdot 2SiO_2$ increases. The involvement of the γ- and α-phases of mechanically activated Al_2O_3 in synthesis is not the same. γ-Al_2O_3 is consumed from G-00 alumina to a greater extent. The consumption of the oxide phases in an LGF with a nonactivated filler is virtually the same.

Nepheline has a melting point of 1526°C. It forms with aluminum oxide, which is present in the formulations under study in a large excess, a eutectic that contains 7 wt % Al_2O_3 and melts at 1475 ± 10°C [11]. It would be expected that the material compares well in its fireproofing properties with the conventional refractories of mullite composition.

The formation of nepheline must lead to an increase in the heterodiffusion porosity of the coating. The volume of its unit cell exceeds that of γ-Al_2O_3 by a factor of 2. In the case of liquid-phase sintering of LGF at high temperatures, this hinders the rise in heat conductivity and provides a high fireproofing efficiency. Use of mechanically activated Al_2O_3 will improve the fireproofing efficiency of the coating, because it makes synthesis of nepheline faster.

CONCLUSIONS

(1) The processes occurring in liquid-glass formulations at the interface between the binder and filler are governed by the chemical activity of the filler. In a formulation with $Al(OH)_3$, there occurs a chemical interaction to give sparingly soluble alkaline silicates. The moistening of α-Al_2O_3 particles, which are chemically inert in liquid glass, occurs under the conditions of physical adsorption, whereas that of γ-Al_2O_3 particles yields a chemisorption bond that involves Al^{3+} and siloxane links.

(2) Mechanical activation of Al_2O_3 makes lower the apparent activation energy of particle moistening. Urea introduced into the composition is sorbed on the Al_2O_3 surface. In a formulation with a mechanically activated γ-Al_2O_3, a chemisorption bond is formed between Al^{3+} and N^{3-} of the amide group and the activation energy of curing decreases.

(3) The nepheline phase is synthesized at high temperatures. This phase forms, in a mixture with Al_2O_3, a high-temperature eutectic (mp 1475 ± 10°C). The synthesis occurs at the interface between the binder and filler. It becomes faster when mechanically activated Al_2O_3 is used.

(4) Use of mechanically activated Al_2O_3 makes it possible to perform a fireproofing treatment at lowered temperature and improves the adhesion and the fireproofing efficiency of a coating.

REFERENCES

1. Eremina, N.V., Zelinskii, V.Yu., and Avvakumov, E.G., *Khim. Inter. Ustoich. Razv.*, 2004, vol. 12, no. 3, pp. 331–337.
2. Eremina, N.V., Avvakumov, E.G., and Zelinsky, V.Yu., in *Proc. X APAM Topical Seminar and III Conf. "Materials of Siberia,"* Novosibirsk, June 2–6, 2003, p. 185.
3. RF Patent 2 223 244.
4. Korneev, V.I. and Danilov, V.V., *Rastvorimoe i zhidkoe steklo* (Soluble and Liquid Glass), St. Petersburg: Stroiizdat, 1996.
5. Avvakumov, E.G., *Mekhanicheskie metody aktivatsii khimicheskikh protsessov* (Mechanical Methods for Activation of Chemical Processes), Novosibirsk: Nauka, 1986, 2nd ed.
6. Vereshchagin, V.I., Zelinskii, V.Yu., Khabas, T.A., and Kolova, N.N., *Zh. Prikl. Khim.*, 1982, vol. 55, no. 9, pp. 1946–1951.
7. Kopeikin, V.A., Kliment'eva, V.S., and Krasnyi, B.L., *Ogneupornye rastvory na fosfatnykh svyazuyushchikh* (Fireproof Solutions Based on Phosphate Binders), Moscow: Metallurgiya, 1986.
8. Rusakov, A.A., *Rentgenografiya metallov* (X-ray Diffraction Analysis of Metals), Moscow: Atomizdat, 1980.
9. Gradolnik, J. and Marechal, Y., *J. Mol. Struct.*, 2002, vol. 615, pp. 177–189.
10. Boldyrev, A.I., *Infrakrasnye spektry mineralov* (IR Spectra of Minerals), Moscow: Nedra, 1976.
11. Toropov, N.A., Barzakovskii, V.P., Lapin, V.V., *et al.*, *Diagrammy sostoyaniya silikatnykh sistem: Spravochnik* (Phase Diagrams of Silicate Systems: Reference Book), issue 3: *Troinye silikatnye sistemy* (Ternary Silicate Systems), Leningrad: Nauka, 1972.

Russian Journal of Applied Chemistry, Vol. 78, No. 7, 2005, pp. 1048–1051. Translated from Zhurnal Prikladnoi Khimii, Vol. 78, No. 7, 2005, pp. 1070–1073.
Original Russian Text Copyright © 2005 by Zarubitskii, Dmitruk.

INORGANIC SYNTHESIS AND INDUSTRIAL INORGANIC CHEMISTRY

Reaction of Corundum with a Molten Mixture of Potassium and Sodium Tetrafluoroborates

O. G. Zarubitskii and B. F. Dmitruk

Vernadsky Institute of General and Inorganic Chemistry, National Academy of Sciences of the Ukraine, Kiev, Ukraine

Received December 22, 2004; in final form, April 2005

Abstract—Dissolution of synthetic corundum in KBF_4–$NaBF_4$ melts was studied as influenced by the composition of the salt mixture and temperature. The optimal parameters of the process for removal of synthetic corundum rods from internal channels of castings were determined.

A severe difficulty encountered in fabrication of gas-turbine engines is removal of ceramic rods composed of the chemically inert aluminum oxide from internal cavities in blades, which are important elements of these devices [1].

At present, industry uses for this purpose the method of dissolution of these rods in molten KHF_2 [2], which has a number of disadvantages: The process is performed at a temperature at which KHF_2 rapidly decomposes, the melt aggressively acts upon the alloy of castings, the quality of cleaning of channels in precision castings does not conform to the requirements imposed, and the expenditure of KHF_2 is too high (0.5–0.7 kg for removal of a rod with a mass of 12–15 g).

EXPERIMENTAL

Molten alkali metal tetrafluoroborates (MBF_4) were used in the process under consideration. It was found in experiments on removal of ceramic rods from internal cavities in turbine blades that the rod dissolution rate in this method is comparable with that in the existing technique [2]. Therefore, it was necessary to find an additive to KBF_4 that would raise the etching rate of the ceramic by a factor of no less than 2–3. In addition, the advantageous effect of the additive might consist in that it would raise the flowability of the molten mixture and make higher the limiting solubility of aluminum oxide, i.e., improve the reactivity of the fluoroborate melt or diminish the specific expenditure of salts for blade cleaning and simplify removal of the residue of the fluoroborate fusion cake by washing from the internal cavities in castings.

The experiments were performed using the procedure described in [3, 4]. The reactivity of the melts was studied on planar rectangular samples of a virtually pore-free synthetic corundum. After being treated in the melts, the samples were washed to remove reaction products by prolonged boiling in distilled water with a short-time intermediate treatment with a 10% HCl solution. The samples were dried to complete removal of moisture and then weighed. The change in the sample mass was used to calculate the specific reaction rate. The dissolution experiments were carried out using corundum rods taken from internal cavities in turbine blades quantity-produced at an aviation plant. The porosity of the rods was 15–18% at a grain size of 10–14 μm. KBF_4 and $NaBF_4$ of chemically pure grade were used. Thermogravimetric, X-ray phase, chemical, and microscopic analyses were made.

As possible additives for improving the removal of rods in a melt based on KHF_2 were tested KF and NaF, KCl, KNO_3, KHF_2, CaF_2 and BaF_2, and Na_2SiF_6 and NaB_4O_7. The experiments were performed at 600–700°C.

It was found that the most promising among the compositions studied, as regards their reactivity and other properties, are molten mixtures of KBF_4 and $NaBF_4$. For example, the dissolution time τ (h) of a synthetic corundum ceramics (rod) from a blade in KBF_4–$NaBF_4$ mixtures with a 1 : 1 mass ratio of the components is approximately three times that in pure molten KBF_4 (Table 1). It was found that the dissolution rate of synthetic corundum in KBF_4–$NaBF_4$ mixtures increases with the $NaBF_4$ content up to 65 wt %, and then falls abruptly (see figure). Other

1070-4272/05/7807-1048 © 2005 Pleiades Publishing, Inc.

advantages of the KBF_4–$NaBF_4$ melt were also revealed: It has an enhanced reactivity, i.e., provides dissolution of greater amounts of the ceramics, compared to the case when individual salts KBF_4 and $NaBF_4$ are used; after dissolution of a certain amount of Al_2O_3 (about 1%), the melt is covered with a crust which hinders volatility of the salts; and the viscosity of the mixtures is lower than those of individual KBF_4 and $NaBF_4$.

Attempts were made to find why the rate of reaction between aluminum oxide and molten KBF_4–$NaBF_4$ mixtures at a given temperature shows an abnormal dependence on the mixture composition (see figure). The peculiar shape of the dependence at $NaBF_4$ content below and above 65 wt % is due to the change of the reaction mechanism in the system. Below this $NaBF_4$ content, the process rate is limited by the chemical stage, with the main reaction product, potassium–sodium cryolite K_2NaAlF_6, being liquid at the temperature of the experiments. As the $NaBF_4$ content of the melt increases further, the process rate falls dramatically because of the formation on the Al_2O_3 surface of a layer (film) of a solid product, which is mostly a sparingly soluble glassy phase $MOBF_2$. It should be noted that reactions with Al_2O_3 in individual melts of KBF_4 and $NaBF_4$ proceed via different intermediates. Potassium tetrafluoroaluminate $KAlF_4$, which is in the liquid state at the temperature of the experiment (mp 574°C), is formed in a KBF_4–Al_2O_3 mixture, and a solid chiolite $Na_5Al_3F_{14}$ (mp 737°C), in a $NaBF_4$–Al_2O_3 mixture.

The following problems were solved in order to optimize the technology: the optimal process temperature was chosen; the duration of rod removal as a function of the amount of the ceramics introduced into the tetrafluoroborate melt and its limiting reactivity were determined; an efficient procedure was developed for washing of castings to remove the residue of the tetrafluoroborate fusion cake; the corrosion of the material of the castings was studied and its nature was determined; and the composition of the crust formed on the surface of the working melt was found by X-ray phase analysis.

The corrosion of samples of a heat-resistant alloy ZhS32 (material of castings) in the KBF_4–$NaBF_4$ melt of an equimass composition was determined at 600–750°C. It was found that the corrosion rate of the alloy, which is insignificant at 600–700°C, increases dramatically at 750°C. A microscopic study of the metal surface demonstrated that the corrosion is mostly uniform. Thickening of the melt with aluminum oxide leads to a considerable decrease in the corrosion rate. In particular, it decreases twofold at 700°C upon dissolution of 5 wt % Al_2O_3 in the KBF_4–$NaBF_4$ melt.

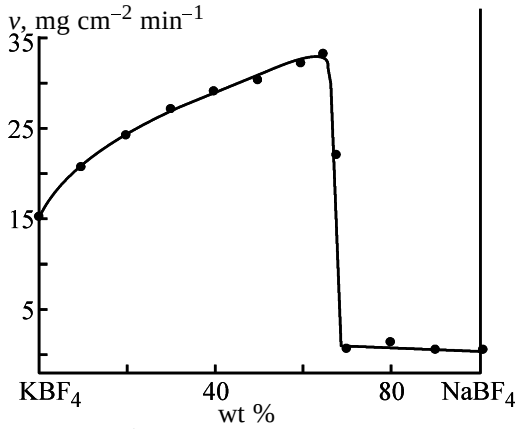
Table 1. Cleaning of castings of gas-turbine engines to remove the synthetic corundum ceramics in KBF_4 and KBF_4–$NaBF_4$ melts

Melt composition, wt %		*T*, °C	τ, h
KBF_4	$NaBF_4$		
100	–	600	4.0
100	–	650	3.0
100	–	680	2.4
50	50	600	1.4
80	20	650	1.5
35	65	650	0.8
50	50	650	1.0
50	50	680	0.8

The optimal temperature of rod removal in the KBF_4–$NaBF_4$ melt was chosen taking into account the corrosion behavior of the material of the castings and the intensity of rod dissolution. The rate of rod removal was determined on castings produced by oriented crystallization (rod length 86 mm). Below is given the duration of rod dissolution as influenced by temperature. In each experiment, 650 g of a freshly prepared molten KBF_4–$NaBF_4$ mixture was used; the rod mass was about 15 g. Thus, thickening of the melt with the ceramics was about 2% by the end of the experiment:

T, °C	600±5	630±5	655±5	695±5
τ, min	≥150	90±10	60±5	50±5

It follows from the data obtained that the temperature of 600–630°C cannot be recommended for use



Etching rate *v* of aluminum oxide in molten KBF_4–$NaBF_4$ mixtures at 650°C.

Table 2. Melting points and crystallization temperatures of KBF_4–$NaBF_4$ salt mixtures

Mixture composition, wt %		mp, °C	Crystallization onset temperature, °C
KBF_4	$NaBF_4$		
100	–	565	–
90	10	508	505
80	20	482	455
70	30	463	445
60	40	427	403
50	50	400	385
40	60	380	350
20	80	360	322
10	90	372	340
–	100	406	–

in the process because of the insufficient intensity of rod etching. In the course of casting treatment, the melt is continuously thickened by dissolution products and its reactivity decreases. Consequently, the working temperature should not be lower than 650°C. The upper limit to the working temperature was chosen taking into account the fact that, above 700°C, the volatility of the melt and its corrosivity toward the material of the castings substantially increase.

To choose the optimal composition and working mode of the fluoroborate melt, it is important to know the melting point and crystallization temperature of KBF_4–$NaBF_4$ mixtures. The parameters of the phase diagram of the KF–NaF–BF_3 system were reported in [5]. With account of the specific features of the behavior of fluoroborates (e.g., their decomposition can change the initial composition) and the conditions of the process being developed, the fusibility diagram of the system KBF_4–$NaBF_4$ was studied again by integrated thermal and X-ray phase analyses. The data obtained somewhat differ from those reported in [2]. Table 2 lists only the liquidus and solidus temperatures for a number of compositions. The temperature corresponding to the endothermic minimum in the DTA curve was taken as the melting point in heating the mixture, and that corresponding to the onset of the exothermic effect of crystallization, as the crystallization temperature in cooling the sample. It was found that the melting point of the KBF_4–$NaBF_4$ mixtures recommended as the optical composition is 400–410°C.

The reactivity of the KBF_4–$NaBF_4$ melt is largely determined by the composition of the interaction products and their solubility in a borofluoride mixture. It was found by X-ray phase analysis that mostly mixed cryolite is formed under the process conditions:

$$4KBF_4 + 2NaBF_4 + Al_2O_3 = 2K_2NaAlF_6 + 3BF_3 + (BOF)_3.$$

Simultaneously occur some other reactions to give potassium and sodium cryolites K_3AlF_6 and Na_3AlF_6, oxofluoroborates $NaBOF_2$ and $KBOF_2$, and sodium chiolite $Na_5Al_3F_{14}$. It is noteworthy that the solubility of cryolites in the KBF_4–$NaBF_4$ mixture markedly exceeds that in KBF_4, with the reactivity of the melt being, accordingly, higher, too.

The intensity of rod removal in the working melt depends on both the temperature and the thickening of the melt by interaction products. It was established that the rate of rod dissolution markedly decreases until approximately 3 wt % Al_2O_3 is accumulated in the melt at 650°C, and until 4–5 wt % Al_2O_3 is accumulated at 700°C. These values are apparently close to the solubility of Al_2O_3 in the form of the above-mentioned compounds. When these limits are reached, the rate of Al_2O_3 dissolution virtually stabilizes. The duration of rod removal strongly depends on the mass ratio between the molten KBF_4–$NaBF_4$ mixture and Al_2O_3, as well as on the amount of a ceramics introduced into the melt. Table 3 lists the results obtained in an experiment in which the minimum expenditure of the KBF_4–$NaBF_4$ melt is reached at a virtually

Table 3. Dissolution of a corundum rod in a KBF_4–$NaBF_4$ melt at 650°C

Casting mass, g		Mass of removed ceramics, g	Thickening of melt by ceramics, wt %	Rod removal
before experiment	after experiment			
253.7	240.4	13.3	1.9	Complete
254.5	241.2	13.3	3.8	Residue present
251.5	237.2	14.3	5.8	Complete
251.4	237.3	14.1	7.9	〃
257.5	242.5	15.0	10.0	〃

constant treatment duration of 1 h. Initial mass of the melt 700 g, treatment temperature 650°C.

In this experiment, the expenditure of the melt per blade was 140 g. Then, 15 more blades were processed and it was found that the minimum expenditure of the melt for cleaning of one casting (with a rod of mass 14 ± 1 g) is 115 g.

The most important among the secondary procedures of the process is their washing to remove the residue of the tetrafluoroborate melt. The difficulties encountered in washing are mostly due to the low solubility of KBF_4 and products formed in interaction between the ceramics and the melt (cryolites etc.). KBF_4 and $NaBF_4$ strongly differ in the solubility in water. For example, the solubilities of these salts in 100 g of water at different temperatures are as follows (g):

T, °C	20	25	30	40	100
KBF_4	0.45	0.55	0.98	1.4	6.3
$NaBF_4$	–	107.4	–	–	210.0

Consequently, the solubility of the KBF_4–$NaBF_4$ mixture in water is sufficiently high owing to the dissolution of $NaBF_4$. As shown by the experiments, the residue of the fusion cake of the fluoroborate mixture can be completely removed both from the surface and from the internal channels of the casting by washing with warm flowing water and by boiling in distilled water. If, however, the amount of the ceramics dissolved in the melt is considerable, cleaning to remove the fusion cake of KBF_4–$NaBF_4$ is hindered: in some cases, high-quality washing cannot be achieved even on repeating the procedures many times.

In view of the fact that the given procedure, which uses only water, is not efficient enough, other methods for removing the reaction products from internal cavities in a casting were sought for. As a dissolving medium were used acid and alkaline solutions (of sulfuric and oxalic acids) and low-melting substances (KOH–NaOH, KHF_2, NH_4KF_2, KOH, NaOH). It was found that complete removal of the residue of the fusion cake from the channels of castings is only guaranteed in melts of potassium hydroxide or hydrofluoride.

The reaction of tetrafluoroborate with an alkali is strongly exothermic, and, therefore, it is recommended to process castings at a temperature only slightly exceeding the melting point of KOH (400–450°C) in the course of 10–15 min. After the rods are removed in the KBF_4–$NaBF_4$ melt, the castings are cooled to the crystallization temperature of the tetrafluoroborate melt in order to preclude any interaction between the liquid melt of the salts and the alkali.

CONCLUSIONS

(1) The rate of the reaction between molten KBF_4–$NaBF_4$ mixtures and corundum at 600–700°C grows as the content of $NaBF_4$ in the melt increases to 65 wt %, and then strongly decreases at still higher concentrations of this salt.

(2) A method for removing synthetic corundum rods from internal channels of high-precision castings in melts was developed. The method includes treatment in a molten mixture of KBF_4 (50–55 wt %) and $NaBF_4$ (45–50 wt %) at 650–700°C for 1–2 h as the main process, as well as some additional procedures.

(3) The advantages of the new process are as follows: the intensity of rod removal increases by a factor of 2–3, the expenditure of the melt for removal of a rod is three times lower, the molten mixture of tetrafluoroborates is less corrosive toward the material of castings, and the contamination of the atmosphere and environment by noxious waste is diminished.

REFERENCES

1. Chumakov, V.A., Stepanov, V.M., Ivanov, B.G., *et al*., *Litein. Proizv.*, 1978, no. 1, pp. 23–24.
2. USSR Inventor's Certificate no. 1 401 071.
3. Dmitruk, B.F., Zarubitskii, O.G., and Orel, V.P., *Zh. Prikl. Khim.*, 1981, vol. 54, no. 12, pp. 2659–2662.
4. Dmitruk, B.F., Marchenko, V.A., Dotsenko, V.K., *et al*., *Zashch. Met.*, 1982, vol. 18, no. 3, pp. 376–380.
5. Barton, C.J., Gilpatcrick, L.O., Borman, I.A., *et al*., *J. Inorg. Nucl. Chem.*, 1971, vol. 33, pp. 345–350.

Russian Journal of Applied Chemistry, Vol. 78, No. 7, 2005, pp. 1052–1057. Translated from Zhurnal Prikladnoi Khimii, Vol. 78, No. 7, 2005, pp. 1074–1079.
Original Russian Text Copyright © 2005 by Morachevskii, Tsymbulov, Kolosova, Tsemekhman.

PHYSICOCHEMICAL STUDIES OF SYSTEMS AND PROCESSES

Thermodynamic Properties of Liquid Alloys of the System Iron–Copper–Cobalt

A. G. Morachevskii, L. B. Tsymbulov, E. Yu. Kolosova, and L. Sh. Tsemekhman

St. Petersburg State Polytechnic University, St. Petersburg, Russia
Gipronikel' Institute, Joint-Stock Company, St. Petersburg, Russia

Received May 12, 2005

Abstract—Integral molar excess Gibbs energy, enthalpy of mixing of liquid alloys of the ternary system iron–copper–cobalt, and component activities at 1600°C were calculated by various methods from data on boundary binary systems.

Previously, thermodynamic properties of liquid alloys in the ternary systems nickel–copper–iron, nickel–copper–cobalt, and iron–nickel–cobalt were calculated from the available data on boundary binary systems [1–4]. Various geometric models and analytical Redlich–Kister polynomials were used in calculation. The fact that the results of calculation by six to eight geometric models, differing in the description of the surface of a thermodynamic property, and those obtained in calculation by geometric models and polynomials are in good agreement shows that the calculation methods are suitable for describing rather reliably the dependence of thermodynamic functions on the composition in the above systems.

Unfortunately, experimental data on liquid ternary alloys formed by copper and iron-group metals are virtually lacking. For a large number of more fusible systems and for the extensively studied ternary metallic systems, a possibility of describing thermodynamic properties by a particular model was repeatedly demonstrated by comparison of experimental and calculated values.

The thermodynamic properties of liquid alloys in the system Fe–Cu were repeatedly studied by various methods. The results presented in [5–7] were used in the calculations. In the Fe–Cu system at 1600°C, the isotherms of the component activities exhibit considerable positive deviation from the ideal behavior; the integral excess molar Gibbs energy ΔG^{exc} and the enthalpy of mixing ΔH are positive over the entire composition range. The thermodynamic functions of liquid alloys in the Fe–Cu system are close [8–11].

The thermodynamic properties of liquid alloys in the Cu–Co system, unlike those in the Fe–Cu system, have been examined in a few studies. A more detailed study was performed by Taskinen [12] who used the emf method with a $ZrO_2 + MgO$ solid oxygen-conducting electrolyte in the temperature range 1097–1457°C for compositions within $0.03 \le x_{Co} \le 0.70$ (x_{Co} is the mole fraction of cobalt in the alloy). The liquidus line in the same region of the compositions was determined in [12]. Previously, Timberg *et al.* [13] used the mass-spectrometric method to study the thermodynamic properties of liquid alloys formed by copper and cobalt ($0.060 \le x_{Co} \le 0.949$, 1422–1597°C). The component activities were calculated from data on their ion currents at 1550°C. Also, liquid alloys in the Cu–Co system were studied by the

Table 1. Integral thermodynamic characteristics of the binary systems accepted for calculating thermodynamic properties of the ternary system Fe–Cu–Co at 1600°C*

x_2,** mole fraction	Fe–Cu		Cu–Co		Co–Fe	
	ΔG^{exc}	ΔH	ΔG^{exc}	ΔH	ΔG^{exc}	ΔH
	kJ mol^{-1}					
0.10	3.05	6.11	3.01	3.42	0.66	–0.59
0.20	4.98	9.37	5.04	5.76	1.06	–1.05
0.30	6.44	10.3	6.30	7.30	1.32	–1.38
0.40	7.28	9.75	6.95	8.22	1.42	–1.54
0.50	7.49	8.70	7.07	8.61	1.35	–1.53
0.60	7.11	7.49	6.68	8.48	1.09	–1.38
0.70	6.36	6.28	5.81	7.76	0.73	–1.10
0.80	5.17	4.98	4.41	6.29	0.40	–0.74
0.90	3.26	3.10	2.49	3.82	0.14	–0.35

* Standard state (pure liquid metals).
** x_2 is the mole fraction of the component indicated second.

1070-4272/05/7807-1052 © 2005 Pleiades Publishing, Inc.

calorimetric method [7, 14]. The system exhibits positive deviation from the ideal behavior. The results of the main studies of the system [12, 13] are in good agreement.

The thermodynamic properties of liquid alloys of the Co–Fe systems reported until 1980 are analyzed in [6]. Relatively complete set of the thermodynamic data devoted to this subject is presented in [15]. The isotherms of component activity in liquid alloys of the Co–Fe system show small deviation from the ideality, but the character of this deviation is controversial. Results of [16, 17] are the most reliable from the viewpoint of the research methods.

Table 1 presents the integral excess molar Gibbs energies and enthalpies of mixing of liquid binary systems used for calculating the corresponding integral characteristics of the ternary system Fe–Cu–Co. The calculation is based on the geometric models, which are described in detail in [18] and were used in our previous studies [1–4]. The four geometric models known as the Toop's (I), Kohler's (II), Muggiani's (III), and Colinet's (IV) models were used. The geometric schemes of the calculation are presented in Fig. 1 and the algorithms corresponding to them are reported in [1]. The ΔG^{exc} values in the ternary system calculated from the above models are in reasonable agreement (Table 2). This is largely due to the fact that the deviation from ideality in all the three boundary systems is similar, i.e., $\Delta G^{exc} > 0$. Because the ΔH values in the boundary binary system Co–Fe are negative, the surface of the enthalpy of mixing in the ternary system has the more complex shape. This is especially revealed in estimation of ΔH of the ternary system at low concentrations of copper (Table 3).

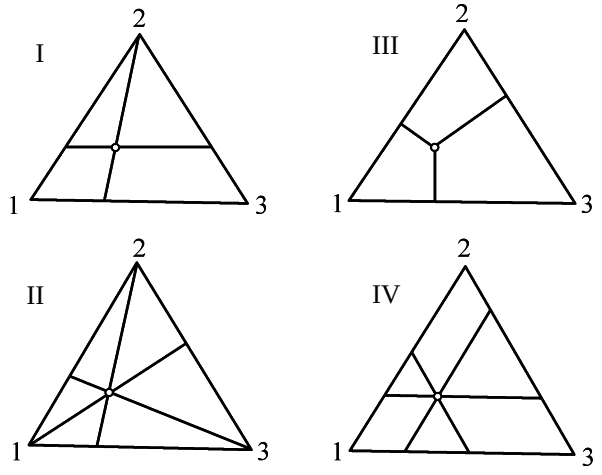


Fig. 1. Scheme for calculation of the integral molar properties of a ternary system from data on boundary binary systems. For explanations, see text.

Table 2. ΔG^{exc} of the Fe–Cu–Co ternary system at 1600°C, calculated by geometric models I–IV

x_{Cu}, mole fraction	ΔG^{exc}, kJ mol^{-1}, by indicated model				Average ΔG^{exc}
	I	II	III	IV	
Section $x_{Fe} : x_{Co} = 3 : 1$					
0.2	5.19	5.18	5.29	5.23	5.22
0.4	7.33	7.44	7.47	7.43	7.42
0.6	7.16	7.43	7.38	7.34	7.33
0.8	5.16	5.44	5.33	5.32	5.31
Section $x_{Fe} : x_{Co} = 1 : 1$					
0.2	5.67	5.53	5.53	5.55	5.57
0.4	7.47	7.50	7.55	7.49	7.50
0.6	7.25	7.63	7.53	7.45	7.47
0.8	5.16	5.56	5.38	5.37	5.37
Section $x_{Fe} : x_{Co} = 1 : 3$					
0.2	5.33	5.29	5.35	5.27	5.31
0.4	7.27	7.34	7.41	7.26	7.32
0.6	7.29	7.59	7.44	7.34	7.42
0.8	5.12	5.45	5.29	5.28	5.29

Table 3. ΔH of the Fe–Cu–Co ternary system at 1600°C, calculated using geometric models I–IV

x_{Cu}, mole fraction	ΔH, kJ mol^{-1}, by indicated model				Average ΔH
	I	II	III	IV	
Section $x_{Fe} : x_{Co} = 3 : 1$					
0.2	8.02	7.23	6.85	6.62	7.18
0.4	9.10	8.31	8.42	8.18	8.50
0.6	7.52	7.49	7.51	7.39	7.48
0.8	5.14	5.39	5.28	5.26	5.27
Section $x_{Fe} : x_{Co} = 3 : 1$					
0.2	6.85	5.59	5.56	5.10	5.78
0.4	8.56	7.40	7.91	7.49	7.84
0.6	7.61	7.62	7.73	7.52	7.62
0.8	5.31	5.68	5.53	5.50	5.51
Section $x_{Fe} : x_{Co} = 3 : 1$					
0.2	6.27	5.17	5.50	5.04	5.50
0.4	8.35	7.59	8.04	7.63	7.90
0.6	7.84	7.79	8.00	7.81	7.86
0.8	5.52	5.81	5.69	5.66	5.67

Table 4. Results obtained in calculation of ΔG^{exc} and ΔH in the Fe–Cu–Co ternary system at 1600°C using polynomial expressions

x_{Cu}, mole fraction	ΔG^{exc}	ΔH
	kJ mol^{-1}	
Section $x_{Fe} : x_{Co} = 3 : 1$		
0.20	5.23	6.54
0.40	7.37	8.19
0.60	7.45	7.44
0.80	5.28	5.22
Section $x_{Fe} : x_{Co} = 1 : 1$		
0.20	5.46	5.09
0.40	7.48	7.51
0.60	7.53	7.54
0.80	5.29	5.46
Section $x_{Fe} : x_{Co} = 1 : 3$		
0.20	5.25	5.05
0.40	7.29	7.64
0.60	7.39	7.82
0.80	5.21	5.64

As noted previously [1, 5, 18], ΔG^{exc} and ΔH of the ternary systems can be calculated from the Redlich–Kister polynomials. For binary systems, the dependences of ΔG^{exc} and ΔH on the composition can be expressed in the following polynomial form:

$$\Delta G^{exc} = x_1(1 - x_1)[b + c(2x_1 - 1) + d(2x_1 - 1)^2], \quad (1)$$

$$\Delta H = x_1(1 - x_1)[b' + c'(2x_1 - 1) + d'(2x_1 - 1)^2]. \quad (2)$$

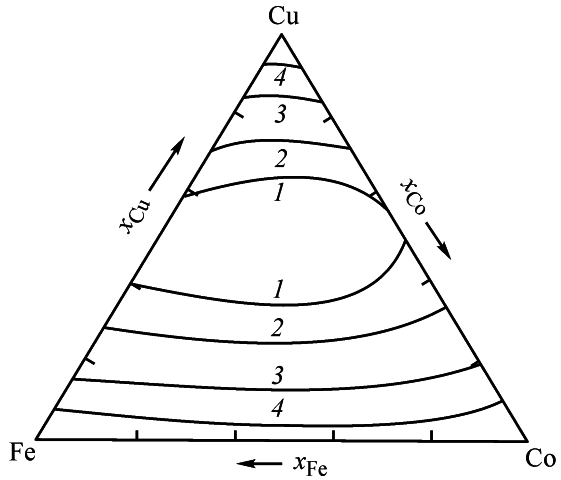


Fig. 2. Lines of equal integral molar excess Gibbs energies of liquid alloys of the Fe–Cu–Co system at 1600°C. (x_{Cu}, x_{Co}, x_{Fe}) Mole fractions of the component in the alloy; the same for Figs. 3 and 5. ΔG^{exc}, kJ mol^{-1}: (*1*) 7, (*2*) 6, (*3*) 4, and (*4*) 2.

To describe the concentration dependence of the integral thermodynamic functions in liquid binary metallic systems, it is not necessary to use polynomials of a higher degree [19].

For the binary systems considered, the following coefficients [ΔG^{exc} and ΔH (kJ mol^{-1})] were obtained:

Coefficient	Fe–Cu	Cu–Co	Co–Fe
b	29.6447	28.2676	5.2978
c	–0.3889	3.2043	3.4429
d	6.8478	3.5208	–1.9655
b'	34.9418	34.4250	–6.1419
c'	22.7298	–2.7500	–1.6528
d'	26.5721	9.0240	1.5121

For all the three binary systems, x_1 in Eqs. (1) and (2) corresponds to the components indicated first. The ΔG^{exc} can be calculated from the equation

$$\Delta G^{exc} = x_1x_2[b_{12} + c_{12}(x_1 - x_2) + d_{12}(x_1 - x_2)^2] + x_2x_3[b_{23} + c_{23}(x_2 - x_3) + d_{23}(x_2 - x_3)^2] + x_3x_1[b_{31} + c_{31}(x_3 - x_1) + d_{31}(x_3 - x_1)^2], \quad (3)$$

where x_1–x_3 characterize the composition of the ternary system and the subscripts in the polynomial coefficients denote the binary systems Fe–Cu (1–2), Cu–Co (2–3), and Co–Fe (3–1).

The similar equation with coefficients b', c', and d' can be written for the enthalpy of mixing in the ternary system.

Tables 2–4 show that ΔG^{exc} and ΔH calculated for the ternary system from different geometric models are in good agreement with those calculated using polynomials. The lines of the equal values of ΔG^{exc} and ΔH for liquid alloys in the Fe–Cu–Co system are plotted in Fig. 2.

As noted previously [3, 4], the partial molar thermodynamic characteristics of all the three components of the system can be estimated from the known relation connecting partial and integral molar quantities. For example, for component 2 at the composition along the secant with a constant ratio of two other components (x_2, x_1/x_3), we can write

$$\Delta G_2^{exc}(x_2, x_1/x_3) = \Delta G^{exc}(x_2, x_1/x_3) + (1 - x_2)(\partial \Delta G^{exc}/\partial x_2)_{x_1/x_3}. \quad (4)$$

Combining Eq. (4) and the Toop's expression for ΔG^{exc}, we obtain the following dependence [20, 21]:

$$\Delta G_2^{exc}(x_2, x_1/x_3) = [x_1 \Delta G_{2(1)}^{exc}/(1 - x_2) + x_{31} \Delta G_{2(3)}^{exc}/(1 - x_2)]_{x_2} - (1 - x_2)^2(\Delta G_{13}^{exc})_{x_1/x_3,\, x_2 = 0}. \quad (5)$$

In Eqs. (4) and (5). $\Delta G_2^{exc}(x_2, x_1/x_3)$ is the excess partial molar Gibbs energy of component 2 at the composition determined by the mole fraction of component 2 (x_2) and by the ratio of the mole fractions of the other two components (x_1/x_3); ΔG^{exc} is the integral molar Gibbs energy of the ternary system at the same composition; $\Delta G_{2(1)}^{exc}$ and $\Delta G_{2(3)}^{exc}$ are the partial molar Gibbs energies of component 2 in the boundary binary systems 1–2 and 2–3; ΔG_{13}^{exc} is the integral molar excess Gibbs energy of the boundary system 1–3 at the composition determined by the x_1/x_3 ratio.

The similar equations can be written for components 1 and 3. In total, the activity coefficients and component activities at 1600°C were calculated for 81 compositions of the ternary system. The data obtained were used to construct the lines of equal activity of the components (Fig. 3). The results of the calculation are also presented in Table 5 for a number of compositions.

Only positive deviation from the ideal behavior was observed for all the compositions of the ternary system. It was of interest to estimate the mutual consistency of the results obtained by the different calculation methods. To do this, the calculated values of the molar excess Gibbs energy of all the three components were used to calculate ΔG^{exc} by the equation

$$\Delta G^{exc} = x_1\Delta G_1^{exc} + x_2\Delta G_2^{exc} + x_3\Delta G_3^{exc} \qquad (6)$$

and the results obtained were compared with the ΔG^{exc} calculations based on geometric models (Table 2) and polynomials (Table 4). The agreement was quite satisfactory. The dependence of ΔG^{exc}, as calculated by different methods, on the composition along the secant with a constant ratio of the mole fractions of iron and cobalt equal to 3 : 1 is shown in Fig. 4.

A number of studies summarized in [18] has demonstrated the applicability of the Zdanovskii's rule to the description of liquid metallic systems. As known, this rule formulated nearly 70 years ago states that electrolyte solutions having similar water vapor pressures and not entering into chemical reactions with each other form a solution with the same pressure of water vapor (i.e., they form an isopiestic ideal solution). It is reasonable to represent the composition of a ternary system in the orthogonal coordinates (first Roozeboom's method [22]). The composition of the isopiestic ideal solutions in mixing changes along

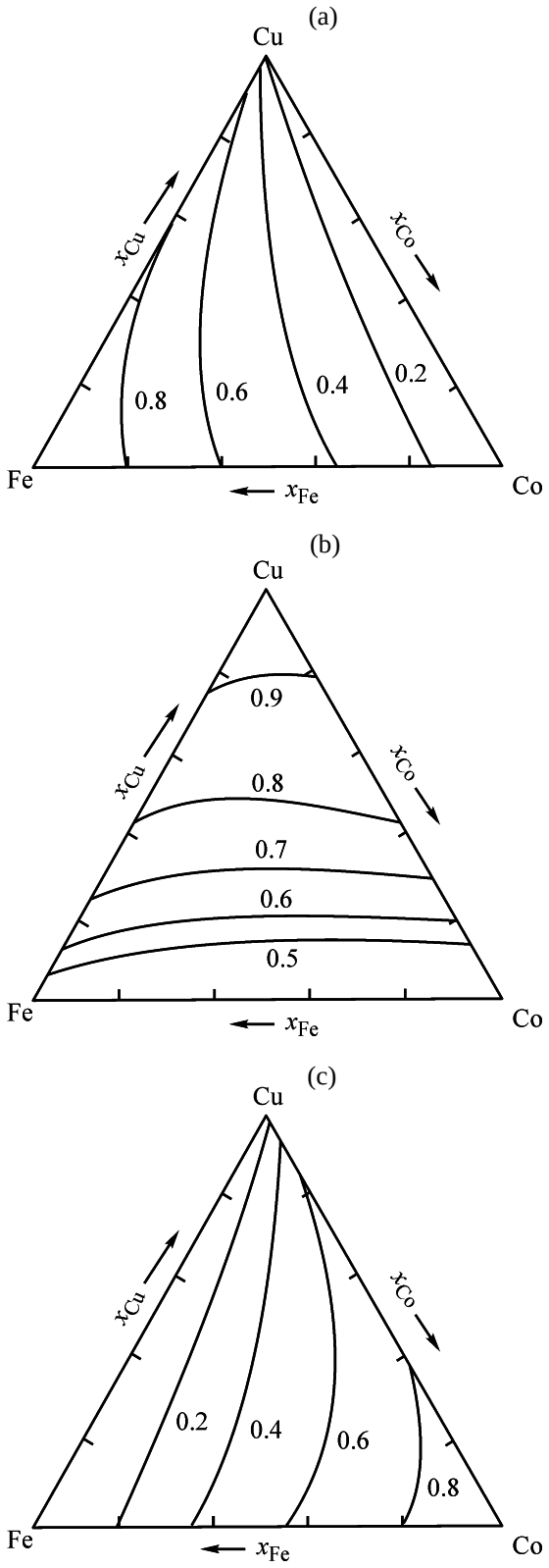


Fig. 3. Lines of equal activity of the components in liquid alloys of the Fe–Cu–Co ternary system at 1600°C. Activity: (a) iron, (b) copper, and (c) cobalt.

Table 5. Activity and activity coefficient of the components of liquid alloys of the Fe–Cu–Co ternary system at 1600°C

Alloy composition (mole fraction)			Component activity			Activity coefficient		
x_{Fe}	x_{Cu}	x_{Co}	a_{Fe}	a_{Cu}	a_{Co}	γ_{Fe}	γ_{Cu}	γ_{Co}
0.23	0.69	0.08	0.55	0.87	0.22	2.39	1.26	2.75
0.20	0.60	0.20	0.41	0.84	0.40	2.05	1.40	2.00
0.08	0.69	0.23	0.25	0.87	0.54	3.13	1.26	2.35
0.43	0.43	0.14	0.24	0.77	0.22	0.56	1.79	1.57
0.33	0.33	0.33	0.43	0.71	0.43	1.30	2.15	1.30
0.14	0.43	0.43	0.24	0.77	0.59	1.71	1.79	1.37
0.69	0.23	0.08	0.79	0.64	0.10	1.14	2.78	1.25
0.60	0.20	0.20	0.66	0.63	0.24	1.10	3.15	1.20
0.43	0.14	0.43	0.60	0.52	0.49	1.40	3.71	1.14
0.20	0.20	0.60	0.26	0.59	0.66	1.30	2.95	1.10
0.08	0.23	0.69	0.12	0.64	0.76	1.50	2.78	1.10
0.69	0.08	0.23	0.70	0.42	0.27	1.01	5.25	1.17
0.23	0.08	0.69	0.29	0.36	0.72	1.26	4.50	1.04

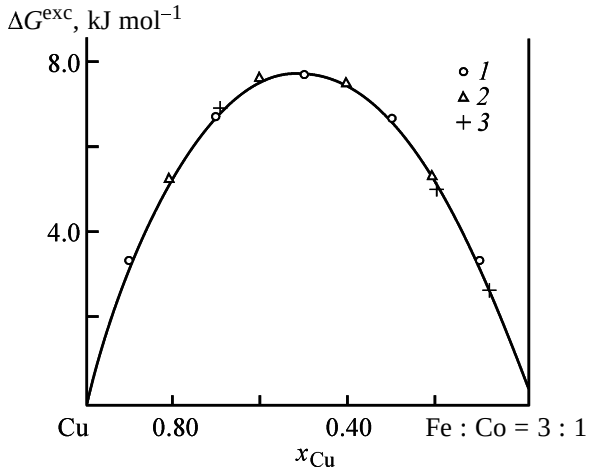


Fig. 4. Integral molar excess Gibbs energy ΔG^{exc} of the ternary Fe–Cu–Co system along the section $x_{Fe} : x_{Co} = 3 : 1$ at 1600°C. Calculation: (*1*) by geometric models, (*2*) by polynomial expressions, and (*3*) from coefficients of component activities.

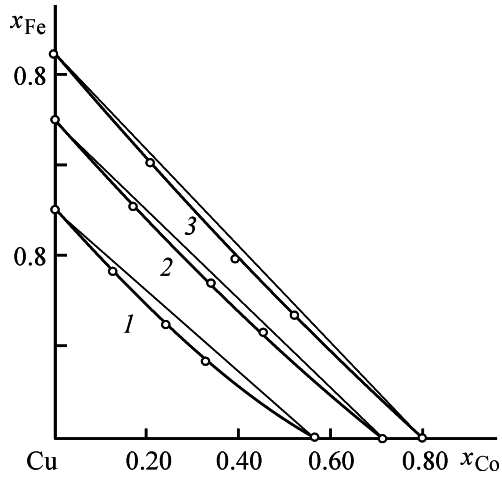


Fig. 5. Lines of equal activity of copper in liquid alloys of the Fe–Cu–Co system at 1600°C in the orthogonal coordinates. a_{Cu}: (*1*) 0.80, (*2*) 0.70, and (*3*) 0.60.

a straight line between the compositions of the binary mixtures. The analogous simple dependences were also observed for liquid metallic systems [18]. In the ternary Fe–Cu–Co system discussed here, lines of copper activity, if copper is solvent, only slightly differ from the straight lines (Fig. 5), which shows that deviation from the Zdanovskii's rule is minimal.

CONCLUSIONS

(1) The calculations of the integral thermodynamic characteristics of mixing of liquid alloys of the iron–copper–cobalt system based on geometric models (Toop, Kohler, Muggiani, and Colinet's models) and Redlich–Kister polynomials yield fairly consistent results. At 1600°C, the system exhibits positive deviation from the ideal behavior.

(2) The calculated activities of all the three components of the Fe–Cu–Co ternary system in the liquid state agree well with the integral thermodynamic characteristics of the system obtained by the independent methods.

(3) With copper as solvent, the Fe–Cu–Co system (at 1600°C) exhibits only minimal deviation from the Zdanovskii's rule.

REFERENCES

1. Morachevskii, A.G., Fedorova, N.A., Tsymbulov, L.B., and Tsemekhman, L.Sh., *Zh. Prikl. Khim.*, 2002, vol. 75, no. 11, pp. 1801–1805.
2. Morachevskii, A.G., Tsemekhman, L.Sh., Tsymbulov, L.B., and Fedorova, N.A., *Zh. Prikl. Khim.*, 2003, vol. 76, no. 11, pp. 1779–1784.
3. Morachevskii, A.G., Tsymbulov, L.B., and Kolosova, E.Yu., *Zh. Prikl. Khim.*, 2004, vol. 77, no. 9, pp. 1438–1441.
4. Morachevskii, A.G., Tsymbulov, L.B., Kolosova, E.Yu., and Tsemekhman, L.Sh., *Zh. Prikl. Khim.*, 2005, vol. 78, no. 1, pp. 59–65.
5. Batalin, G.I., and Sudavtsova, V.S., *Izv. Akad. Nauk SSSR, Metally*, 1980, no. 2, pp. 45–49.
6. Batalin, G.I., *Termodinamika zhidkikh splavov na osnove zheleza* (Thermodynamics of Liquid Iron Alloys), Kiev: Vishcha Shkola, 1982.
7. Belousov, A.A., Bakhvalov, S.G., Aleshina, S.N., *et al.*, *Fiziko-khimicheskie svoistva zhidkoi medi i ee splavov: Spravochnik* (Physicochemical Properties of Liquid Copper and Its Alloys: Handbook), Yekaterinburg: Inst. Metallurgii, Ross. Akad. Nauk, Ural. Otd., 1997.
8. Chuang, Y.-Y., Schmid, R., and Chang, Y.A., *Met. Trans.*, 1984, vol. 15A, October, pp. 1921–1930.
9. Turchanin, M.A., Porokhnya, S.V., and Kokhan, A.V., *Rasplavy*, 1995, no. 1, pp. 9–13.
10. Sorokin, M.L., Andryushechkin, N.A., and Nikolaev, A.G., *Izv. Vyssch. Uchebn. Zaved., Tsvetn. Metall.*, 1996, no. 6, pp. 10–14.
11. Turchanin, M.A., and Agraval, P.G., *Poroshk. Metall.*, 2001, nos. 7–8, pp. 34–53.
12. Taskinen, P., *Z. Metallkunde*, 1982, vol. 73, no. 7, pp. 445–450.
13. Timberg, L., Toguri, J.M., and Azakami, T., *Met. Trans. B.*, 1981, vol. 12B, June, pp. 275–279.
14. Turchanin, M.A., and Nikolaenko, I.V., *Rasplavy*, 1989, no. 5, pp. 80–82.
15. Nishizawa, T., and Ishida, K., *Bull. Alloy Phase Diagr.*, 1984, vol. 5, no. 3, pp. 250–259, 305–306.
16. Belton, G.R., and Fruehan, R.J., *J. Phys. Chem.*, 1967, vol. 71, no. 5, pp. 1403–1409.
17. Tomiska, J., and Neckel, A., *Z. Metallkunde*, 1986, vol. 77, no. 10, pp. 649–653.
18. Morachevskii, A.G., Voronin, G.F., Geiderikh, V.A., and Kutsenok, I.B., *Elektrokhimicheskie metody issledovaniya v termodinamike metallicheskikh sistem* (Electrochemical Methods in Studying the Electrodynamics of Metallic Systems), Moscow: Akademkniga, 2003.
19. Morachevskii, A.G., and Erofeev, K.B., *Zh. Prikl. Khim.*, 2000, vol. 73, no. 6, pp. 1032–1034.
20. Olson, N.J., and Toop, G.W., *Trans. Met. Soc. AIME*, 1966, vol. 256, April, pp. 590–592.
21. Jacob, K.T., and Fitzner, K., *Thermochim. Acta*, 1977, vol. 18, pp. 197–206.
22. Anosov, V.Ya., Ozerova, M.I., and Fialkov, Yu.Ya., *Osnovy fiziko-khimicheskogo analiza* (Principles of Physicochemical Analysis), Moscow: Nauka, 1978.

Russian Journal of Applied Chemistry, Vol. 78, No. 7, 2005, pp. 1058–1063. Translated from Zhurnal Prikladnoi Khimii, Vol. 78, No. 7, 2005, pp. 1080–1084.
Original Russian Text Copyright © 2005 by Lokshin, Tareeva, Ivlev, and Kashulina.

PHYSICOCHEMICAL STUDIES OF SYSTEMS AND PROCESSES

Solubility of Double Alkali Metal (Na, K) Rare-Earth (La, Ce) Sulfates in Sulfuric–Phosphoric Acid Solutions at 20°C

E. P. Lokshin, O. A. Tareeva, K. G. Ivlev, and T. G. Kashulina

Tananaev Institute of Chemistry and Technology of Rare Elements and Mineral Resources, Kola Scientific Center, Russian Academy of Sciences, Apatity, Murmansk oblast, Russia

Received January 26, 2005

Abstract—The dependence of the solubility of $NaLa(SO_4)_2 \cdot H_2O$, $NaCe(SO_4)_2 \cdot H_2O$, $KLa(SO_4)_2 \cdot H_2O$, and $KCe(SO_4)_2 \cdot H_2O$ on the concentration of acids in sulfuric, phosphoric, and sulfuric–phosphoric acid solutions containing up to 36 wt % H_2SO_4 and 33.12 g l^{-1} H_3PO_4 was studied at 20°C.

The most promising method of the recovery of lanthanides from phosphogypsum and phosphosemihydrate, which are formed in the manufacture of phosphoric acid by the processing of apatite concentrate with sulfuric acid, is the sulfuric acid leaching [1, 2]. Because these products contain sodium and potassium hexafluorosilicates, sparingly soluble double sulfates of lanthanides with sodium and (or) potassium can be formed in the leaching solutions. In addition, the sulfuric acid leaching solutions contain residual phosphoric acid from phosphogypsum. $NaLa(SO_4)_2 \cdot H_2O$ and $KLa(SO_4)_2 \cdot H_2O$ are poorly soluble in water [3, 4]. Data on the solubility of double sulfates $MLn(SO_4)_2 \cdot H_2O$ in sulfuric and sulfuric–phosphoric acid solutions are lacking. The concentration of lanthanum and cerium oxides in the sum of lanthanide oxides in the apatite concentrate exceeds 70 wt % [5]. Therefore, data on the solubility of lanthanum and cerium compounds are especially important for understanding processes that occur in sulfuric acid leaching of lanthanides. The goal of this study was to determine the solubility of double sulfates $M'M''(SO_4)_2 \cdot H_2O$ (M' = Na, K; M'' = La, Ce) in sulfuric and sulfuric–phosphoric acid solutions of low and medium concentrations.

EXPERIMENTAL

We used analytically pure grade chemicals. The double sulfates were synthesized by the standard procedure [4, 6], i.e., by evaporation of an aqueous solution containing lanthanide and alkali metal sulfates, with alkali metal sulfates taken in a 20% excess above stoichiometry. The precipitates were filtered off, the residual mother liquor was pressed out by filter centrifugation, excess alkali metal sulfates were removed from the mother liquor by washing with 3% H_2SO_4, the residue of the washing solution was pressed out by filter centrifugation, and the precipitate was dried at 125–150°C. The chemical analysis of the products synthesized (Table 1) was consistent (taking into account 3% error of the atomic absorption method used), and the X-ray phase analysis revealed no impurity phases. According to the thermogravimetric (TG) analysis, the products synthesized are monohydrates.

The sulfuric–phosphoric acid solutions were prepared by adding small amounts of 85 wt % H_3PO_4 into sulfuric acid solution of prescribed concentration $c_{H_2SO_4}$; the corresponding change in $c_{H_2SO_4}$ was neglected. The H_3PO_4 concentration $c_{H_3PO_4}$ in the solutions was in the range typical of process solutions obtained from leaching of phosphosemihydrate waste with sulfuric acid.

The content of lanthanides in the solutions was determined by oxalate gravimetric method [7] and by atomic-emission spectrometry with an inductively coupled plasma source on a Plasma 400 spectrophotometer (Perkin–Elmer). The low concentrations were analyzed spectrophotometrically with Arsenazo III [8]. The concentration of the sodium or potassium ions was determined by the atomic absorption method in acetylene–air flame on an AAS-30 spectrophotometer (Carl Zeiss, Jena) [9].

The solubility was studied by the isothermal method. Excess double sulfate was added to initial solutions of prescribed concentration. The mixtures were kept at agitation in hermetically sealed vessels at 20 ± 0.5°C until the equilibrium was attained (≥720 h).

1070-4272/05/7807-1058© 2005 Pleiades Publishing, Inc.

Table 1. Composition of the double sulfates synthesized

Double sulfate	Content, wt %					
	calculated			found		
	Na_2O	K_2O	Ln_2O_3	Na_2O	K_2O	Ln_2O_3
$NaLa(SO_4)_2 \cdot H_2O$	8.33		43.79	8.25		43.70
$NaCe(SO_4)_2 \cdot H_2O$	8.31		43.98	8.50		43.25
$KLa(SO_4)_2 \cdot H_2O$		12.14	41.98		12	41.94
$KCe(SO_4)_2 \cdot H_2O$		12.09	42.16		12.1	42.87

Table 2. Experimentally found concentrations of La_2O_3 and Na_2O in sulfuric and sulfuric–phosphoric acid solutions of $NaLa(SO_4)_2 \cdot H_2O$ at 20°C

$c_{H_2SO_4}$, wt %	Content of La_2O_3 (numerator) and Na_2O (denominator) at indicated $c_{H_3PO_4}$, g l^{-1}			
	0	6.90	16.56	27.6
0	2.35/0.44	0.03/0.38	0.044/0.54	0.060/0.59
4	2.69/0.53	2.80/0.54	2.82/0.54	2.92/0.57
8	2.76/0.56	2.74/0.54	2.81/0.53	2.82/0.53
12	2.55/0.48	2.48/0.47	2.64/0.49	2.49/0.49
16	2.20/0.41	2.20/0.41	2.15/0.40	2.19/0.42
20	1.76/0.34	1.90/0.36	2.00/0.38	1.74/0.33
24	1.31/0.26	1.29/0.25	1.24/0.24	1.27/0.24
28	0.95/0.19	0.90/0.17	0.86/0.16	0.84/0.15
32	0.46/0.088	0.51/0.093	0.42/0.080	0.41/0.075
36	0.32/0.060	0.33/0.063	0.33/0.062	0.35/0.067

Table 3. Experimentally found concentrations of Ce_2O_3 and Na_2O in sulfuric and sulfuric–phosphoric acid solutions of $NaCe(SO_4)_2 \cdot H_2O$ at 20°C

$c_{H_2SO_4}$, wt %	Content of Ce_2O_3 (numerator) and Na_2O (denominator) at indicated $c_{H_3PO_4}$, g l^{-1}			
	0	6.90	16.56	27.6
0	2.00/0.36	0.009/0.40	0.0042/0.29	0.009/0.30
4	2.29/0.40	2.26/0.40	2.27/0.42	2.28/0.41
8	1.90/0.33	1.88/0.34	1.90/0.35	1.90/0.33
12	1.76/0.32	1.72/0.30	1.73/0.31	1.73/0.32
16	1.50/0.26	1.68/0.31	1.60/0.28	1.61/0.27
20	1.39/0.25	1.38/0.24	1.32/0.23	1.26/0.22
24	0.85/0.15	0.86/0.15	0.86/0.15	0.83/0.15
28	0.57/0.10	0.64/0.12	0.57/0.10	0.58/0.10
32	0.47/0.083	0.40/0.07	0.39/0.069	0.38/0.068
36	0.34/0.063	0.30/0.053	0.25/0.043	0.24/0.046

The equilibrium was considered to be attained when the results of the analysis of the liquid-phase samples ceased to change. The experimental data are presented in Tables 2–5.

Tables 2–5 show that potassium and sodium were virtually the only ions that passed into dilute phosphoric acid solutions ($c_{H_2SO_4} = 0$), which may be due to secondary formation of hydrated lanthanum and cerium phosphates sparingly soluble under these conditions.

In sulfuric and sulfuric–phosphoric acid solutions of double sulfates, the molar ratio of lanthanide and

Table 4. Experimentally found concentrations of La_2O_3 and K_2O in sulfuric and sulfuric–phosphoric acid solutions of $KLa(SO_4)_2 \cdot H_2O$ at 20°C

$c_{H_2SO_4}$, wt %	Content of La_2O_3 (numerator) and K_2O (denominator) at indicated $c_{H_3PO_4}$, g l^{-1}			
	0	6.90	16.56	27.6
0	4.00/1.24	<0.001/1.00	<0.001/0.68	<0.001/0.59
3	5.14/1.71	–	–	5.43/1.28
6	5.68/1.84	5.10/1.51	5.37/1.50	5.60/1.45
9	5.85/1.99	5.29/1.33	5.40/1.43	5.74/1.49
12	6.19/1.99	6.68/1.86	6.78/1.71	6.04/1.78
16	5.56/1.77	6.29/1.80	5.64/1.59	5.35/1.62
20	4.43/1.57	4.98/1.46	4.77/1.22	4.81/1.28
24	4.30/1.33	4.40/1.34	4.27/1.31	3.77/1.71
28	3.15/0.98	3.16/0.98	3.14/0.98	3.12/0.96
32	2.57/0.78	2.53/0.74	2.56/0.75	2.59/0.75
36	1.88/0.58	1.82/0.56	1.78/0.54	1.74/0.53

Table 5. Experimentally found concentrations of Ce_2O_3 and K_2O in sulfuric and sulfuric–phosphoric acid solutions of $KCe(SO_4)_2 \cdot H_2O$ at 20°C

$c_{H_2SO_4}$, wt %	Content of Ce_2O_3 (numerator) and K_2O (denominator) at indicated $c_{H_3PO_4}$, g l^{-1}			
	0	6.90	16.56	27.6
0	4.30/1.19	0.048/0.82	0.041/0.53	0.015/0.51
4	6.29/1.65	5.60/1.56	5.24/1.43	4.95/1.41
8	6.38/1.72	6.10/1.60	6.30/1.67	6.00/1.64
12	5.81/1.62	6.28/1.69	6.10/1.60	5.90/1.62
16	5.52/1.52	5.70/1.58	5.61/1.56	5.61/1.57
20	4.67/1.33	4.76/1.31	4.86/1.35	5.14/1.33
24	3.80/1.06	3.90/1.11	3.80/1.05	3.90/1.06
28	2.95/0.80	2.95/0.81	2.95/0.85	2.86/0.82
32	2.20/0.63	2.29/0.64	2.38/0.64	2.48/0.68
36	1.90/0.52	1.90/0.52	1.90/0.53	2.00/0.54

alkali metal oxides commonly ranged from 0.91 to 1.09 (Table 6), i.e., was close to unity within the error of the analytical method (≤4.5 rel. % for single determination). At the same time, only double sulfates as individual phases were revealed by the X-ray and crystal-optical analyses of the solid phases separated after the reaction of the double sulfates with both sulfuric acid and sulfuric–phosphoric acid solutions. Consequently, the deviation of the molar ratio from unity is due to the fact that the mother liquor of alkali metal sulfates could not always be washed out completely in the synthesis of the double sulfates. The dissolution of alkali metal sulfates in sulfuric acid can result in the salting-out of sparingly soluble double sulfates. As a result, the solubilities could be underestimated. This effect will be especially pronounced at increased concentrations of sulfuric acid $c_{H_2SO_4}$, when the solubility of the double sulfates is considerably lower.

In estimating the true solubility of the double sulfates, we assumed that their dissolution in water and sulfuric acid proceeds by the scheme

$$M^IM^{III}(SO_4)_2 \cdot H_2O \rightleftarrows M^I + M^{III} + 2SO_4^{2-}. \quad (1)$$

Then, the solubility product

$$SP = [M^I][M^{III}](SO_4^{2-})^2. \quad (2)$$

In the case of the dissolution in water, $[M^I] = [M^{III}] = x$, and $[SO_4^{2-}] = 2x$. Then, $SP = 4x^4$.

Table 6. $M^{III}_2O_3/M^{I}_2O$ molar ratio in equilibrium sulfuric acid solutions of $M^{I}M^{III}(SO_4)_2 \cdot H_2O$

$c_{H_2SO_4}$, wt %	Ce_2O_3/Na_2O molar ratio at indicated $c_{H_3PO_4}$, g l^{-1}			
	$NaLa(SO_4)_2 \cdot H_2O$	$NaCe(SO_4)_2 \cdot H_2O$	$KLa(SO_4)_2 \cdot H_2O$	$KCe(SO_4)_2 \cdot H_2O$
0	1.02	1.05	0.93	1.04
3	–	–	0.87	–
4	0.96	1.08	–	1.09
6	–	–	0.89	–
8	0.94	1.09	–	1.06
9	–	–	0.85	–
12	1.01	1.05	0.90	1.03
16	1.02	1.09	0.91	1.04
20	0.98	1.06	0.82	1.01
24	0.96	1.07	0.93	1.03
28	0.95	1.08	0.93	1.06
32	0.99	1.08	0.95	1.00
36	1.01	1.02	0.94	1.05

In the presence of a small excess of an alkali metal sulfate, the following relationships are valid for the experimentally found concentrations of alkali metal $[M^{I}]_{exp}$ and lanthanide $[M^{III}]_{exp}$:

$$[M^{I}]_{exp} = x_{exp}, \quad [M^{III}]_{exp} = y_{exp},$$

$$[SO_4^{2-}]_{exp} = 0.5(x_{exp} + 3y_{exp}), \text{ and}$$

$$SP_{exp} = 0.25x_{exp}y_{exp}(x_{exp} + 3y_{exp})^2.$$

Since $SP = SP_{exp}$, then

$$x = 0.5[x_{exp}y_{exp}(x_{exp} + 3y_{exp})^2]^{1/4}. \quad (3)$$

In estimation of solubility in sulfuric acid, a slight change in $c_{H_2SO_4}$ due to the dissolution of the double sulfates was neglected. In the dissolution of a double sulfate, the concentrations of alkali metal and lanthanide cations in the equilibrium solution are equal, i.e., $[M^{I}] = [M^{III}]$. Then,

$$SP = [M^{III}]^2[SO_4^{2-}]^2 = [M^{I}]_{exp}[M^{III}]_{exp}[SO_4^{2-}]^2, \quad (4)$$

where $[M^{III}]_{exp}$ and $[M^{I}]_{exp}$ are the experimentally determined concentrations of lanthanide and alkali metal ions, respectively. Hence,

$$[M^{III}] = [M^{I}]^{0.5}_{exp}[M^{III}]^{0.5}_{exp}. \quad (5)$$

In concentrated sulfuric acid solutions ($c_{H_2SO_4} \geq 15$ g-equiv l^{-1}), lanthanides exist in the form of acid sulfate anionic complexes [3, 5]. Since at a constant concentration of H_2SO_4 in a solution slight changes in the concentration of alkali metal cations should not affect the composition of these complexes, Eq. (5) is also applicable to this case.

The solubility of the double sulfates studied, calculated by Eqs. (2) and (4), is presented in Table 7. As seen, the solubility of double cerium sulfates in water and sulfuric acid solutions of similar composition is lower than that of lanthanum sulfates, and that of double sodium sulfates is markedly lower than that of potassium sulfates. With increasing $c_{H_2SO_4}$, the solubility of the double sulfates, like that of lanthanide sulfates [10], first increases, reaches a maximum, and then decreases. The maximum concentration of the lanthanide ions in the solution is observed at $c_{H_2SO_4}$ equal to 0.418 g-equiv l^{-1} for $NaLa(SO_4)_2 \cdot H_2O$ and $NaCe(SO_4)_2 \cdot H_2O$. For $KLa(SO_4)_2 \cdot H_2O$, it is observed at $c_{H_2SO_4}$ equal to 1.32 g-equiv l^{-1}, and for $KCe(SO_4)_2 \cdot H_2O$, at 0.858–1.32 g-equiv l^{-1}.

An increase in the solubility with an increase in $c_{H_2SO_4}$ at relatively low concentrations is probably due to replacement of alkali metal cations by H^+ ions, which becomes more intense at higher $c_{H_2SO_4}$, and its subsequent decrease is due to the salting-out effect, which is also observed with lanthanide sulfates [6].

No salting-out effect was exerted by the SO_4^{2-} ion at low concentrations of sulfuric acid, which suggests that, in sulfuric acid solutions, the lanthanide anionic complexes are formed not only at $c_{H_2SO_4} \geq 15$ g-equiv l^{-1}, but also at lower concentrations.

The calculated solubility products in water at 20°C are 1.48×10^{-7}, 0.426×10^{-8}, 1.62×10^{-6}, and $1.05 \times$

Table 7. Solubility of double alkali metal (Na, K) rare-earth (La, Ce) sulfates in sulfuric acid solutions at 20°C

$c_{H_2SO_4}$		Solubility in terms of Ln_2O_3 (Ln = La, Ce), g l^{-1}			
wt %	g-equiv l^{-1}	$NaLa(SO_4)_2 \cdot H_2O$	$NaCe(SO_4)_2 \cdot H_2O$	$KLa(SO_4)_2 \cdot H_2O$	$KCe(SO_4)_2 \cdot H_2O$
0	0	2.34	1.88	4.11	4.20
3	0.312	–	–	5.59	–
4	0.418	2.73	2.20	–	–
6	0.635	–	–	6.19	6.18
8	0.858	2.85	1.82	–	–
9	0.971	–	–	6.43	–
12	1.320	2.54	1.73	6.62	5.73
16	1.810	2.18	1.44	5.91	5.41
20	2.325	1.77	1.36	4.97	4.65
24	2.864	1.34	0.82	4.51	3.75
28	3.432	0.97	0.55	3.31	2.87
32	4.029	0.46	0.45	2.67	2.20
36	4.656	0.32	0.34	1.97	1.86

10^{-6} for $NaLa(SO_4)_2 \cdot H_2O$, $NaCe(SO_4)_2 \cdot H_2O$, $KLa(SO_4)_2 \cdot H_2O$, and $KCe(SO_4)_2 \cdot H_2O$, respectively.

According to the data of [3, 4, 11], the solubility products of $NaLa(SO_4)_2 \cdot H_2O$, $KLa(SO_4)_2 \cdot H_2O$, and $KCe(SO_4)_2 \cdot H_2O$ at 25°C are 2.12×10^{-6}, $(1.45–8.01) \times 10^{-6}$, and 1.37×10^{-5}, respectively. This fact shows that the solubility of the double sulfates in water slightly increases with temperature.

Addition of H_3PO_4 in the examined concentration range to sulfuric acid solutions usually did not affect the solubility of all the double sulfates studied [the exception was $KCe(SO_4)_2 \cdot H_2O$, whose solubility in 4% H_2SO_4 decreased by 27 rel. % after 27.6 g l^{-1} of H_3PO_4 was added].

The data obtained suggest that the low solubility of the double sodium rare-earth (La, Ce) sulfates is one of the most important factors that restrict accumulation of lanthanides in the solutions in leaching of phosphogypsum and phosphosemihydrate with sulfuric acid.

CONCLUSIONS

(1) The solubilities of $NaLa(SO_4)_2 \cdot H_2O$, $NaCe(SO_4)_2 \cdot H_2O$, $KLa(SO_4)_2 \cdot H_2O$, and $KCe(SO_4)_2 \cdot H_2O$ at 20°C in water, sulfuric acid, and sulfuric–phosphoric acid solutions containing 0–36 wt % H_2SO_4 and 0–33.12 g l^{-1} H_3PO_4 was determined.

(2) The solubility of double cerium sulfates in water and sulfuric acid solutions of the same composition is lower than that of the related lanthanum compounds, and that of the double sodium sulfates is markedly lower than that of the potassium sulfates. As the H_2SO_4 concentration increases, the solubility of the double sulfates first increases, reaches a maximum, and then decreases. The maximum solubility is observed at the H_2SO_4 concentration of 0.418 g-equiv l^{-1} for $NaLa(SO_4)_2 \cdot H_2O$ and $NaCe(SO_4)_2 \cdot H_2O$, at 1.32 g-equiv l^{-1} for $KLa(SO_4)_2 \cdot H_2O$, and at 0.858–1.32 g-equiv l^{-1} for $KCe(SO_4)_2 \cdot H_2O$.

(3) Increasing the phosphoric acid concentration within the examined concentration range at a constant concentration of H_2SO_4 only slightly affects the solubility of $KLa(SO_4)_2 \cdot H_2O$ and $KCe(SO_4)_2 \cdot H_2O$. An exception is $KCe(SO_4)_2 \cdot H_2O$, whose solubility at $c_{H_2SO_4} \leq 4$ wt % markedly decreases as the H_3PO_4 concentration in the solution increases.

(4) In sulfuric acid solutions, the lanthanide anionic complexes are apparently formed not only at $c_{H_2SO_4} \geq 15$ g-equiv l^{-1}, but also at lower concentrations.

(5) The low solubility of the double sodium rare-earth (La, Ce) sulfates is one of the most important factors that restrict accumulation of lanthanides in sulfuric–phosphoric acid solutions in leaching of phosphogypsum and phosphosemihydrate with sulfuric acid.

ACKNOWLEDGMENTS

The study was financially supported by the Leading Research Schools grant (project no. NSh-1616–2003.03).

REFERENCES

1. Lokshin, E.P., Vershkov, A.V., and Vershkova, Yu.A., *Metally*, 2001, no. 1, pp. 42–50.
2. Malikov, V.A. and Krylova, O.K., *Tsvetn. Met.*, 2003, no. 4, pp. 63–64.
3. Tulinova, V.B., Plyushchev, E.V., Ternovskaya, I.V., *et al*., *Zh. Neorg. Khim.*, 1960, vol. 5, no. 3, pp. 695–700.
4. Iskhakova, L.D., and Plyushchev, V.E., *Zh. Neorg. Khim.*, 1970, vol. 15, no. 9, pp. 2526–2530.
5. Mineev, D.A., *Lantanoidy v rudakh* (Lanthanides in Ores), Moscow: Nauka, 1974.
6. Komissarova L.N., Pushkina, G.Ya., Shatskii, V.M., *et al*., *Soedineniya redkozemel'nykh elementov: Sul'faty, selenaty, telluraty, khromaty* (Rare-Earth Compounds: Sulfates, Selenates, Tellurates, and Chromates), Moscow: Nauka, 1986.
7. Laitinen, H.A. and Harris, W.E., *Chemical Analysis*, New York: McGraw-Hill, 1960.
8. Marczenko, Z., *Kolorymetryczne oznaczanie pierwiastkow*, Warszawa: Naukowa-Techniczne, 1968.
9. Fritz, J.S., and Schenk, G.H., *Quantitative Organic Analysis*, New York: Wiley, 1957.
10. Wirth, F., *Z. Anorg. Chem.*, 1912, vol. 76, pp. 174–180.
11. Schröder W., and Schackmann, H., *Z. Anorg. Allg. Chem.*, 1934, vol. 220, pp. 389–410.

Russian Journal of Applied Chemistry, Vol. 78, No. 7, 2005, pp. 1064–1066. Translated from Zhurnal Prikladnoi Khimii, Vol. 78, No. 7, 2005, pp. 1085–1087.
Original Russian Text Copyright © 2005 by Blinkova, Eliseev.

PHYSICOCHEMICAL STUDIES OF SYSTEMS AND PROCESSES

Dissolution of Calcium Carbonate in Aqueous Solutions of Acetic Acid

E. V. Blinkova and E. I. Eliseev

Ural State Technical University, Yekaterinburg, Russia

Received July 14, 2004; in final form, February 2005

Abstract—A kinetic equation for the calcium carbonate dissolution, fitting the experimental data to within 8.1%, was obtained. The additional diffusion hindrance caused by the CO_2 evolution in the course of the dissolution was considered.

To extract zinc from slimes obtained in blast furnace gas treatment, a process based on the acetate leaching with acetic acid solutions was suggested [1]. The blast furnace slime contains about 6% calcium, mainly in the form of carbonate [2], which is formed by the reaction of CaO and CO_2 in the gas-conduit channel of a blast furnace.

Since the slurry from the treatment of blast furnace gases to remove dust contains calcium oxide and dissolved carbon dioxide, calcium carbonate is also formed in the course of its transportation by the pipe system. Calcium carbonate in the form of thin crystals is deposited on the walls of the pipes and causes their overgrowing. Therefore, the pipelines, which are relatively long, get out of order from time to time. One of the methods for overcoming this negative phenomenon is the dissolution of salt crystals in a solution of acetic acid.

To choose proper conditions for this process, it is necessary to study the calcium carbonate dissolution in acetic acid solutions. This reaction was not comprehensively studied previously.

The acetate method of the calcium carbonate dissolution is described by the reaction

$$CaCO_3 + 2C_2H_4O_2 = Ca(CH_3CO_2)_2 + H_2O + CO_2\uparrow. \quad (1)$$

EXPERIMENTAL

We used a 1 : 3 aqueous solution of analytically pure acetic acid. The concentration of the CH_3COOH (HAc) solution was determined by potentiometric titration with NaOH.

The $CaCO_3$ dissolution was studied by the rotating disc method. The discs were made of white marble, which, according to the data of the potentiometric titration, contained 98.9% $CaCO_3$. Samples in the form of a cylinder (diameter 29 mm) were cut out from a bulk mineral with a tubular cutter. The discs were attached to an ebonite cartridge with a silicone acryl sealant. Prior to each experiment, the disc was trimmed with an emery paper (fineness 0.2) and flush-mounted to the cartridge.

The dissolution conditions were varied in the following ranges: temperature, from 283 to 343 K, CH_3COOH concentration in the initial solution, from 0.3 to 3.1 g dm^{-3}, and the disc rotation frequency, from 3.6 to 18.5 Hz. The process was performed in a beaker (inner diameter 14 cm).

The content of the dissolved substance was judged from the content of Ca(II) in the solution. The solutions were analyzed for the Ca(II) content by the volumetric (complexometric) titration with Acid Chrome Dark Blue indicator [3], using a plunger microburet. The analytical error in determining the Ca(II) concentration did not exceed 1.5%. The experimental time was 3 h.

During the experiment, the rate of the $CaCO_3$ dissolution remained virtually constant and increased with the CH_3COOH concentration. The reaction order with respect to HAc was 0.5.

The dissolution rate was a linear function of the square root of the rotation frequency n in the frequency range 3.6–18.5 Hz (Fig. 1), which is one of the essential evidences of a diffusion-controlled process.

One of the reasons why dissolution is diffusion-controlled is formation of new (gas) phase [4]. The diffusion limitations due to CO_2 evolution should be

1070-4272/05/7807-1064© 2005 Pleiades Publishing, Inc.

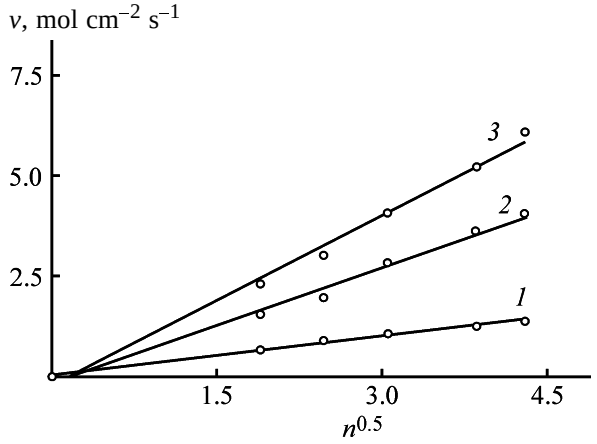


Fig. 1. Rate of $CaCO_3$ dissolution v vs. rotation frequency $n^{0.5}$. Temperature, K: (*1*) 283, (*2*) 323, and (*3*) 343.

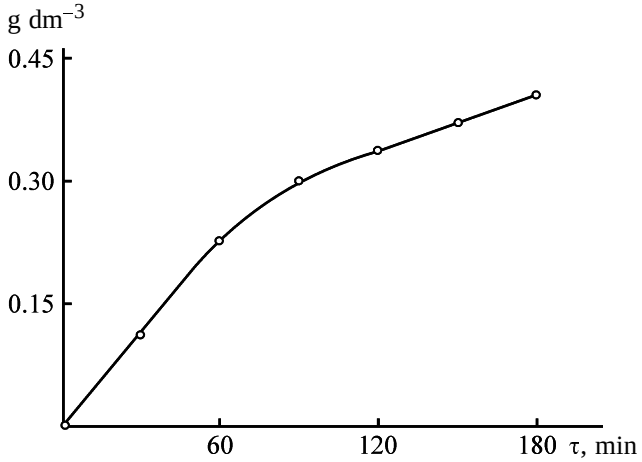


Fig. 2. Kinetic curve of $CaCO_3$ dissolution at 343 K and a disc rotation frequency of 14.9 Hz. (*c*) Calcium concentration and (τ) time; the same for Fig. 4.

less pronounced at low temperature, since the gas solubility in an aqueous solution is higher under these conditions [5]. At a higher temperature (343 K), additional factors affected the rate of the marble dissolution (especially at $n > 14.9$ Hz) after 60 min elapsed from the start of the experiment (Fig. 2). In this case, the initial linear portion of the kinetic curve was used for calculating the dissolution rate.

Increasing temperature within 283–343 K increases the dissolution rate over the entire range of the rotation frequences, i.e., the $CaCO_3$ dissolution is diffusion-controlled (Fig. 3). The temperature dependence of the dissolution rate of $CaCO_3$ was used to calculate the apparent activation energy of the process by the Arrhenius law.

The apparent activation energies calculated at different rotation frequencies were also typical of a diffusion-controlled process over the entire frequency range.

The discs subjected to the experiment at 343 K had a convex surface owing to evolution of CO_2 in the course of the dissolution. In the central part of the disc surface, where the centrifugal force developed in the rotation is minimal, the most stable CO_2 layer preventing dissolution was accumulated. The part of the blocked surface increased with the growth of this layer. Therefore, the dissolution mainly proceeded in the peripheral zone of the disc.

The effect exerted by the forming gas phase on the dissolution was eliminated in the presence of a surfactant. For this purpose we used a detergent, which, being a hydrophilizing agent, made the gaseous film less adhesive to the sample and facilitated its removal by the centrifugal force. Unlike the experiment performed without surfactant under the similar initial conditions, the plot of the Ca(II) concentration vs. dissolution time was linear (Fig. 4a). This was due to accessibility of the whole working surface area of the disc, which ensured the constant process rate. The rate of the $CaCO_3$ dissolution in the presence of surfactant was, however, lower, i.e., the surfactant concentrating at the interface created an additional diffusion hindrance.

The same result was obtained by lifting from time to time the disc over the solution to remove the accumulating CO_2. Under the conditions of vigorous evolution of CO_2 (at 343 K), the dissolution rate was constant only during the first 60 min and then markedly decreased. At this moment (90 min after the start of the experiment), the disc was removed from the solution for a short time. As a result, the gas phase was completely removed, and the initial dissolution rate was restored (Fig. 4b).

Thus, we obtained a kinetic equation of the $CaCO_3$ dissolution:

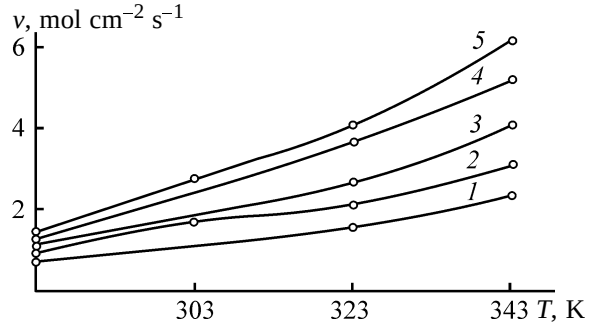


Fig. 3. Influence of temperature T on the rate of $CaCO_3$ dissolution v. Disc rotation frequency, Hz: (*1*) 3.6, (*2*) 6.2, (*3*) 9.4, (*4*) 14.9, and (*5*) 18.5.

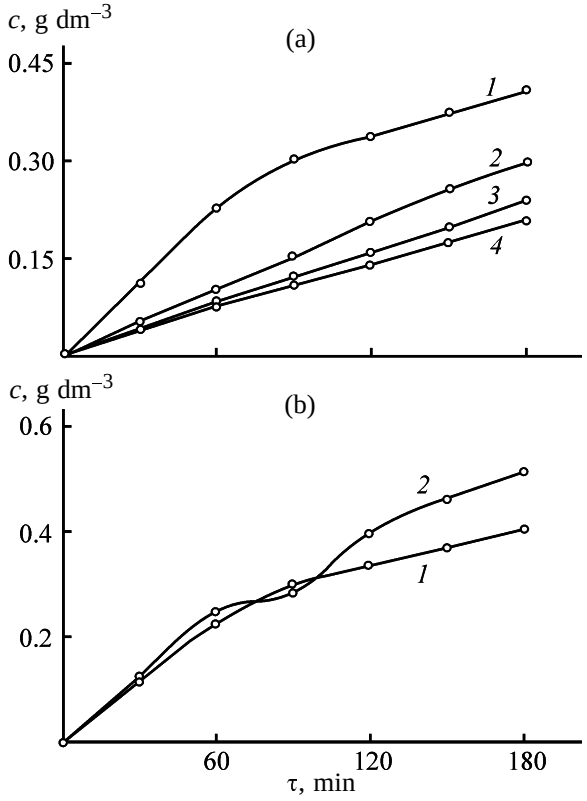


Fig. 4. Variation of the $CaCO_3$ dissolution rate due to blocking of the sample surface by gaseous film: (a) in the presence of surfactant and (b) with renewal of the surface. (a) Surfactant concentration, g dm^{-3}: (*1*) 0.00, (*2*) 0.025, (*3*) 0.050, and (*4*) 0.100; (b) (*1*) without and (*2*) with lifting the disc.

Experimental and calculated rates of $CaCO_3$ dissolution

T, K	*n*, Hz	c_{HAc}, g dm^{-3}	$v \times 10^8$, mol cm^{-2} s^{-1}		Relative error, %
			experimental	calculated	
283	3.6	3.1	6.96	6.78	–2.6
	6.2	3.1	9.23	8.90	–3.6
	9.4	3.1	10.98	10.96	–0.2
	18.5	3.1	14.22	15.37	8.1
283	3.6	0.6	3.11	2.86	–7.9
	3.6	3.1	6.96	6.78	–2.6
283	3.6	3.1	6.96	6.78	–2.6
343	3.6	3.1	23.32	24.36	4.5

$$v = k c_{HAc}^{m} n^{0.5} \exp(-E_a/RT),$$

where v is the specific dissolution rate (mol cm^{-2} s^{-1}); k, rate constant [(mol dm^{-3})$^{0.5}$ cm^{-2} $s^{-0.5}$]; m, reaction order with respect to HAc (0.5); c_{HAc}, HAc concentration (mol dm^{-3}); n, disc rotation rate (Hz); E_a, apparent activation energy (J mol^{-1}); R, universal gas constant (J mol^{-1} K^{-1}); and T, temperature (K).

From the results of 22 experiments performed under different conditions, we obtained $k = (2.46 \pm 0.08) \times 10^{-4}$ (mol dm^{-3})$^{0.5}$ cm^{-2} $s^{-0.5}$. The rates of the $CaCO_3$ dissolution calculated from this value were in satisfactory agreement with the experimental values (see table).

CONCLUSIONS

(1) At c_{HAc} = 3.1 g dm^{-3} and 283–343 K, the dissolution of $CaCO_3$ in acetic acid is a diffusion-controlled process with an apparent activation energy of 17.2 ± 2.6 kJ mol^{-1}.

(2) At 343 K and higher temperatures, the diffusion control of the process may be due to formation of a gaseous CO_2 film on the $CaCO_3$ surface. The order of the $CaCO_3$ dissolution reaction with respect to acetic acid is 0.5.

(3) The obtained kinetic equation of the $CaCO_3$ dissolution is adequate under the following conditions: temperature 283–343 K, HAc concentration 0.3–3.1 g dm^{-3}, and rotation rate 3.6–18.5 Hz.

REFERENCES

1. USSR Inventor's Certificate no. 1 092 195.
2. Shutikova, V.F., Vychaev, A.V., Larina, T.P, *et al*., *Kompleksn. Ispol'z. Miner. Syr'ya*, 1991, no. 2, pp. 69–72.
3. Zhivopistsev, V.P., and Selezneva, E.A., *Analiticheskaya khimiya elementov: Kal'tsii* (Analytical Chemistry of Elements: Calcium), Moscow: Nauka, 1975.
4. Aksel'rud, G.A., and Gumnitskii, Ya.M., *Zh. Prikl. Khim*., 1986, vol. 59, no. 10, pp. 2185–2189.
5. *Spravochnik khimika* (Chemist's Handbook), Nikol'skii, B.P., Ed., Leningrad: Khimiya, 1964, vol. 3.
6. Spitsyn, V.I., Pchelkin, V.A., and Goncharov, I.V., *Fiz. Khim*., 1961, vol. 137, no. 5, pp. 1158–1161.

Russian Journal of Applied Chemistry, Vol. 78, No. 7, 2005, pp. 1067–1072. Translated from Zhurnal Prikladnoi Khimii, Vol. 78, No. 7, 2005, pp. 1088–1093.
Original Russian Text Copyright © 2005 by G. Mikhailov, V. Mikhailov, Reva, Ryabchuk.

PHYSICOCHEMICAL STUDIES OF SYSTEMS AND PROCESSES

Precision Fitting of the Temperature Dependence of Density and Prediction of the Thermal Expansion Coefficient of Liqiuds

G. M. Mikhailov, V. G. Mikhailov, L. S. Reva, and G. V. Ryabchuk

Volgograd State Technical University, Volgograd, Russia

Received, July 9, 2004; in final form, May 2005

Abstract—An equation for precision fitting of the temperature dependence of density of any substance in the entire temperature range of its liquid state and an equation for the prediction of the coefficient of thermal expansion, derived from this dependence, was considered. Constants of the equation for 50 liquids were tabulated.

The main applied importance of an equation for precision fitting of the temperature dependence of the density or specific volume of liquids is connected with its use for the prediction of thermal expansion coefficients as functions of temperature, which are required for various process calculations.

The following equation is used today for precision fitting of the specific volume of liquids [1, 2]:

$$V = V_0(1 + at + bt^2 + ct^3), \quad (1)$$

where a, b, and c are experimental coefficients given in reference literature for various liquids with indication of the temperature range of the equation applicability; V_0 is the specific volume at $t = 0$°C; V, specific volume at a current temperature; and t, current temperature (°C).

Various methods for the prediction of thermal expansion coefficients using Eq. (1) are given in [3, 4]. It should be noted that these methods are too cumbersome, which does not count in favor of the prediction accuracy. By definition, the thermal expansion coefficient is

$$\beta = \frac{1}{V}\frac{dV}{dt}. \quad (2)$$

Hence, it follows from Eq. (1) with a mathematical exactitude that the thermal expansion coefficient is

$$\beta = \frac{a + 2bt + 3ct^2}{1 + at + 2bt^2 + ct^3}. \quad (3)$$

The basic disadvantage of Eqs. (1) and (3) is their applicability in rather narrow temperature ranges. For example, the following ranges of the applicability of Eq. (1) are suggested in [1, 2]: for water, $t = 0$–33; for sulfuric acid, 0–30; for isopentane, 0–27, and for methyl formate, 0–10°C. Furthermore, it is assumed that Eq. 1 is applicable in the vicinity of $t = 0$°C. Therefore, Eq. (1) basically is unsuitable for condensed gases, molten metals, and also organic and inorganic substances with high melting points.

Here we suggest Eq. (4) for precision fitting of the temperature dependence of density of any substances on the saturation line within the entire temperature range of their liquid state:

$$\rho = \rho_{cr} e^{[A\theta + B\theta^2 + (C\theta)^n]}, \quad (4)$$

where ρ_{cr} is the density under critical conditions (kg m^{-3}); $\theta = t_{cr} - t = T_{cr} - T$, temperature measured from the critical point (K); t and T, current temperature (°C and K); t_{cr} and T_{cr}, critical temperature (°C and K); and A, B, C, and n, constants depending on the kind of the liquid and determined by regression analysis of a series of experimental data.

Table 1 contains constants of Eq. (4) for various liquids, as determined by regression analysis of the experimental data [1, 5]. When the constants given in Table 1 are used, deviations of Eq. (4) from the experimental data in specific cases exceed 0.1% (Table 2). The experimental data on any liquids starting from hydrogen, including metal melts, up to the highest-molecular-weight organic liquids are equally well described by this equation. The only exception is the temperature range $t = 0$–200°C for water.

1070-4272/05/7807-1067 © 2005 Pleiades Publishing, Inc.

Table 1. Constants of Eq. (4)

Formula	Liquid	t, °C	ρ_{cr}, kg m^{-3}	A, K^{-1}	B, K^{-2}	C, K^{-1}	n
Ar	Argon	–122.3	535.6	-1.78713×10^{-3}	6.69296×10^{-6}	1.77087×10^{-2}	0.329
Cl_2	Chlorine	144	573	4.05161×10^{-4}	-3.91772×10^{-7}	4.53934×10^{-3}	0.2723
Cs	Cesium	1777	430	-1.20699×10^{-2}	2.85486×10^{-7}	1.62074×10^{-2}	0.92
H_2	Hydrogen	239.93	31.6	-4.81085×10^{-3}	-4.17178×10^{-5}	5.20431×10^{-2}	0.3163
He	Helium	–267.96	69.3	2.41728×10^{-3}	-4.83371×10^{-3}	1.30314×10^{-1}	0.254
Hg	Mercury	1490	5500	-1.26469×10^{-4}	3.98736×10^{-8}	6.82681×10^{-4}	0.275
K	Potassium	1977	160	3.75237×10^{-4}	-4.21767×10^{-8}	1.06199×10^{-3}	0.109
Kr	Krypton	–63.76	911	-2.50555×10^{-4}	3.41734×10^{-8}	1.10922×10^{-2}	0.3016
Li	Lithium	3527	100	2.23838×10^{-4}	-1.32227×10^{-8}	3.73420×10^{-4}	0.2
N_2	Nitrogen	–146.96	313	1.19685×10^{-3}	-6.15372×10^{-6}	1.41600×10^{-2}	0.273
Na	Sodium	2227	180	5.84806×10^{-5}	6.07382×10^{-9}	2.30299×10^{-3}	0.25
Ne	Neon	–228.76	483	-1.35808×10^{-3}	4.68067×10^{-6}	4.61334×10^{-2}	0.294
O_2	Oxygen	–118.39	405.8	-9.88542×10^{-4}	1.38740×10^{-6}	2.04821×10^{-2}	0.299
Rb	Rubidium	1827	350	4.62152×10^{-4}	-5.34634×10^{-8}	2.42377×10^{-2}	0.079
Xe	Xenon	16.54	1110	-1.61824×10^{-3}	4.24831×10^{-6}	1.10919×10^{-2}	0.332
CO	Carbon(II) oxide	–140	301	-3.66449×10^{-3}	1.76142×10^{-5}	2.60124×10^{-2}	0.342
CO_2	Carbon(IV) oxide	31	468	-3.45981×10^{-3}	2.13455×10^{-5}	1.49707×10^{-2}	0.34
H_2O	Water*	374.12	317.8	-3.77374×10^{-4}	-2.78180×10^{-7}	7.35050×10^{-3}	0.294
NH_3	Ammonia	132.4	235	-9.59559×10^{-4}	1.23699×10^{-6}	1.02061×10^{-2}	0.3304
SO_2	Sulfur(IV) oxide	157.5	525	-1.52357×10^{-3}	1.54593×10^{-6}	1.05995×10^{-2}	0.365
CCl_4	Carbon tetrachloride	283.2	588	-8.73256×10^{-4}	1.01339×10^{-6}	5.73583×10^{-3}	0.354
CF_3Cl	Trifluorochloromethane	29.13	571.43	-7.93146×10^{-4}	1.72836×10^{-6}	1.04507×10^{-2}	0.308
CH_4	Methane	–82.61	162.3	-1.15631×10^{-2}	2.91462×10^{-5}	3.72405×10^{-2}	0.487
CH_4O	Methanol	240	275	-1.73487×10^{-3}	1.99347×10^{-6}	1.11118×10^{-2}	0.339
$C_2F_3Cl_3$	Trifluorotrichloroethane	214.1	576.37	3.05394×10^{-4}	6.24242×10^{-8}	4.02836×10^{-3}	0.235
C_2H_2	Acetylene	35.5	230	4.25880×10^{-4}	-3.86365×10^{-7}	7.01284×10^{-3}	0.267
$C_2H_4O_2$	Acetic acid	321.6	351	-6.95833×10^{-4}	7.86327×10^{-7}	6.49919×10^{-3}	0.313
C_2H_6	Ethane	32.34	212.18	-1.98722×10^{-3}	4.14743×10^{-6}	1.17927×10^{-2}	0.331
$C_2H_8O_3$	Glycerol	432.84	361.16	2.62766×10^{-4}	-1.33817×10^{-6}	5.82579×10^{-3}	0.358
C_3H_8O	Propyl alcohol	263.7	273	-5.56445×10^{-4}	-1.36344×10^{-8}	7.84442×10^{-3}	0.302
C_4F_8	Octafluorocyclobutane	115	619.96	-2.29751×10^{-3}	4.74875×10^{-6}	1.28025×10^{-2}	0.348
$C_4H_{10}O$	Diethyl ether	193.8	265	-6.70394×10^{-3}	9.22197×10^{-7}	7.32230×10^{-3}	0.316
C_5H_{12}	Pentane	196.62	232	-3.4526×10^{-4}	5.58777×10^{-7}	6.40284×10^{-3}	0.2933
C_6H_5Cl	Chlorobenzene	359.2	365	-2.34096×10^{-4}	3.42803×10^{-7}	4.79524×10^{-3}	0.286
C_6H_6	Benzene	289.45	303.95	-1.24583×10^{-4}	2.52336×10^{-7}	4.95321×10^{-3}	0.29
C_6H_{12}	Cyclohexane	279.9	270	-2.46939×10^{-3}	1.66143×10^{-6}	1.05244×10^{-2}	0.46
C_6H_{14}	Hexane	234.7	234	-2.48121×10^{-4}	3.88235×10^{-7}	5.90923×10^{-3}	0.29
C_7H_8	Toluene	320.8	290	-1.96584×10^{-3}	1.34748×10^{-7}	9.45861×10^{-3}	0.428
C_7H_{16}	Heptane	267.01	235	-6.46796×10^{-4}	7.71002×10^{-7}	6.87633×10^{-3}	0.313
C_8H_{10}	Ethylbenzene	346.4	290	-3.42672×10^{-4}	4.62080×10^{-7}	5.00840×10^{-3}	0.298
C_9H_{20}	Nonane	322	236	8.47280×10^{-4}	-3.75733×10^{-7}	1.62557×10^{-3}	0.163
$C_{10}H_{22}$	Decane	346	236	9.07322×10^{-4}	-4.06751×10^{-7}	1.28166×10^{-3}	0.151
$C_{12}H_{26}$	Dodecane	386	237	2.49087×10^{-4}	4.66285×10^{-8}	3.38824×10^{-3}	0.24
$C_{13}H_{28}$	Tridecane	404	240	-2.75530×10^{-3}	1.48263×10^{-6}	1.02820×10^{-2}	0.5
$C_{15}H_{32}$	Pentadecane	437	240	-2.98450×10^{-3}	1.48837×10^{-6}	1.04188×10^{-2}	0.521
$C_{16}H_{34}$	Hexadecane	452	240	2.73394×10^{-4}	-6.20462×10^{-8}	2.92198×10^{-3}	0.263
$C_{17}H_{36}$	Heptadecane	462	240	-4.59136×10^{-4}	3.75839×10^{-7}	4.95668×10^{-3}	0.34
$C_{18}H_{38}$	Octadecane	477	240	-5.09698×10^{-4}	3.83613×10^{-7}	4.97525×10^{-3}	0.351
$C_{19}H_{40}$	Nonadecane	487	240	-8.79226×10^{-4}	5.36080×10^{-7}	5.83539×10^{-3}	0.391
$C_{20}H_{44}$	Eicosane	502	240	-4.30930×10^{-4}	3.12529×10^{-7}	4.60537×10^{-3}	0.353

* For water, the temperature range t = 0–200°C is not covered by Eqs. (4) and (6).

Table 2. Comparison of the results of calculations by Eqs. (4) and (5) with the experimental data [5]

Rubidium				Ammonia				Eicosane			
T, K	ρ	ρ_{calc}	δ, %	T, K	$V\times10^3$	$V_{calc}\times10^3$	δ, %	t, °C	ρ	ρ_{calc}	δ, %
	kg m^{-3}				m^3 kg^{-1}				kg m^{-3}		
312.7	1481	1470.8	–0.688	200	1.372	1.3712	–0.058	40	775.6	775.65	0.006
400	1432	1431.4	–0.841	210	1.394	1.3937	–0.025	60	762.4	762.37	–0.004
450	1408	1408.7	0.051	220	1.417	1.4172	0.011	80	749.1	749.06	–0.006
500	1385	1385.9	–0.004	230	1.441	1.4418	0.058	90	742.4	742.38	–0.003
550	1383	1363.1	0.007	240	1.467	1.4679	0.059	100	735.7	735.68	–0.003
600	1340	1340.2	0.014	250	1.495	1.4954	0.029	110	729.0	728.96	–0.005
650	1323	1317.2	–0.437	260	1.524	1.5248	0.051	120	722.2	722.22	0.002
700	1294	1294.2	0.017	270	1.556	1.5561	0.010	130	715.4	715.44	0.006
750	1271	1271.2	0.016	280	1.589	1.5899	0.058	140	708.7	708.63	–0.009
800	1248	1248.2	0.012	290	1.626	1.6265	0.030	150	701.8	701.79	–0.002
850	1225	1225.1	0.008	300	1.667	1.6664	–0.035	160	694.8	694.90	0.014
900	1202	1202.0	0.000	310	1.711	1.7104	–0.035	170	687.8	687.96	0.024
950	1179	1179.0	0.000	320	1.760	1.7593	–0.038	180	680.8	680.98	0.026
1000	1156	1156.0	0.000	330	1.815	1.8145	–0.028	190	673.8	673.93	0.019
1050	1133	1132.9	–0.006	340	1.878	1.8776	–0.020	200	666.8	666.82	0.003
1100	1110	1109.9	–0.005	350	1.952	1.9513	–0.035	210	659.7	659.64	–0.008
1150	1087	1087.0	0.000	360	2.039	2.0396	0.032	220	652.5	652.39	–0.017
1200	1064	1064.0	0.000	370	2.148	2.1495	0.069	230	645.2	645.05	–0.023
1250	1041	1041.1	0.013	380	2.292	2.2941	0.091	240	637.8	637.62	–0.028
1300	1015	1018.3	0.322	390	2.502	2.5049	0.117	250	630.2	630.10	–0.016
				400	2.903	2.9034	0.012	260	622.5	622.46	–0.006
				405.6	4.255	4.255	0.080	270	614.7	614.71	0.001
								280	606.8	606.82	0.004
								290	598.7	598.80	0.017
								300	590.3	590.62	0.054

Equation (4) can be presented as

$$V = V_{cr}e^{-[A\theta + B\theta^2 + (C\theta)^n]}, \quad (5)$$

where V is the specific volume under critical conditions (m^3 kg^{-1}).

Some examples showing how the results of calculations by Eqs. (4) and (5) agree with the experimental data are given in Table 2.

A high accuracy of the fitting allows us to use Eq. (5) for deriving an equation for predicting thermal expansion coefficients of liquids as functions of temperature. Substituting Eq. (5) in (2), we obtain

$$\beta = A + 2B\theta + n\theta^{-1}(C\theta)^n, \quad (6)$$

Some examples showing how the results of calculations by Eqs. (6) agree with the experimental data [4] are given in Table 3. The deviations, except a few cases, do not exceed ±5%. Such a fitting accuracy provided by Eq. (6) should be considered as acceptable, the more so as experimental data on the thermal expansion coefficients of liquids are not highly accurate.

It was noted above that Eqs. (4)–(6) do not cover the temperature range t = 0–200°C for water. Therefore, we offer special Eq. (7) applicable to this case:

$$\rho = 1000\exp\{a\eta^2 + b[1 - (1 + c\eta)e^{-c\eta}]\}, \quad (7)$$

where $a = -3.325848\times10^{-6}$ K^{-2}, $b = -1.925639\times10^{-2}$, $c = 2.165\times10^{-2}$ K^{-1}, $\eta = t - 4$, and t is temperature (°C).

Equations (4) and (7) are compared with the experimental data for water in Table 4, which shows that Eq. (7) fits the experimental data on the water density at t = 0–200°C with a very high accuracy. Therefore, Eq. (7) can be used to derive an equation for satisfactory fitting of the thermal expansion coefficient even in the vicinity of its zero value. Taking Eqs. (2) and (7) into account, we obtain Eq. (8):

Table 3. Comparison of the results of calculations by Eq. (6) with the experimental data [4]

Parameter	Temperature, °C							
	–20	0	20	40	60	80	100	120
Ammonia:								
$\beta \times 10^3$, K^{-1}	1.84	2.15	2.42	2.8	3.2	4.3	6.2	14.5
$\beta_{calc} \times 10^3$, K^{-1}	1.9261	2.1245	2.3944	2.7762	3.3490	4.2975	6.1953	12.530
δ, %	4.681	–1.188	–1.057	–0.851	4.655	–0.057	–0.076	–13.59
Benzene:								
$\beta \times 10^3$, K^{-1}	–	1.18	1.22	1.26	1.3	1.37	1.43	1.57
$\beta_{calc} \times 10^3$, K^{-1}	–	1.1337	1.1816	1.2374	1.3029	1.3805	1.4738	1.5876
δ, %	–	–3.921	–3.144	–1.792	0.222	0.769	3.063	1.120
Hexane:								
$\beta \times 10^3$, K^{-1}	1.16	1.22	1.37	1.48	1.57	1.7	1.8	1.97
$\beta_{calc} \times 10^3$, K^{-1}	1.2316	1.2927	1.3658	1.4543	1.5629	1.698	1.8711	2.0596
δ, %	6.16	5.957	–0.304	–1.733	–0.452	–0.092	1.164	0.579
Sulfur(IV) oxide:								
$\beta \times 10^3$, K^{-1}	1.64	1.75	1.92	2.23	2.61	3.15	3.9	4.4
$\beta_{calc} \times 10^3$, K^{-1}	1.6151	1.7575	1.9473	2.2052	2.5667	3.10	3.9525	5.54
δ, %	–1.5169	0.431	1.424	–1.112	–1.651	–1.603	1.345	23.973
Diethyl ether:								
$\beta \times 10^3$, K^{-1}	1.45	1.51	1.63	1.76	1.85	2.1608	2.6	3.1
$\beta_{calc} \times 10^3$, K^{-1}	1.4268	1.5083	1.6123	1.7465	1.9229	2.608	2.4948	2.55
δ, %	–1.597	–0.114	–1.088	–0.75	3.940	0.031	–4.062	–3.524
Methanol:								
$\beta \times 10^3$, K^{-1}	1.09	1.14	1.19	1.27	1.3	1.42	1.61	1.81
$\beta_{calc} \times 10^3$, K^{-1}	1.1031	1.1226	1.1569	1.2100	1.2874	1.3368	1.5505	1.7675
δ, %	1.198	–1.5303	–2.781	–4.723	–0.973	–1.631	–3.696	–2.249
Toluene:								
$\beta \times 10^3$, K^{-1}	1	1.04	1.07	1.11	1.17	1.24	1.33	1.44
$\beta_{calc} \times 10^3$, K^{-1}	1.0252	1.0448	1.0708	1.1062	1.1523	1.2112	1.2858	1.3802
δ, %	2.517	0.406	0.074	–0.338	–1.513	–2.324	–3.321	–4.152
Acetic acid:								
$\beta \times 10^3$, K^{-1}	–	1.05	1.07	1.11	1.14	1.18	1.23	1.3
$\beta_{calc} \times 10^3$, K^{-1}	–	1.0358	1.0596	1.0900	1.1283	1.1762	1.2360	1.3108
δ, %	–	–1.352	–0.969	–1.801	–1.028	–0.325	0.485	0.832
Chlorobenzene:								
$\beta \times 10^3$, K^{-1}	0.92	0.94	0.97	1.0	1.03	1.07	1.11	1.16
$\beta_{calc} \times 10^3$, K^{-1}	0.9208	0.9424	0.9675	0.9967	1.0309	1.0708	1.1178	1.1734
δ, %	0.083	0.251	–0.260	–0.326	0.085	0.078	0.704	1.134
Carbon tetrachloride:								
$\beta \times 10^3$, K^{-1}	1.14	1.18	1.22	1.26	1.32	1.37	1.5	1.62
$\beta_{calc} \times 10^3$, K^{-1}	1.1615	1.1849	1.2163	1.2573	1.3101	1.3778	1.4646	1.5765
δ, %	1.883	0.418	–0.303	–0.216	0.751	0.568	–2.363	–2.685

$$\beta = (t - 4)(6.6517 + 9.8424e^{-2.165 \times 10^{-2}t}) \times 10^{-6}. \quad (8)$$

The results of calculations by Eqs. (6) and (8) are compared with the experimental data in Table 5.

Thus, unlike Eq. (3), Eq. (6) allows us to predict the thermal expansion coefficient of any substances except water within the entire temperature range of their liquid state. In the temperature range from 200°C to t_{cr}, Eq. (6) is also applicable to water, whereas in the range 0–200°C Eq. (7) must be applied.

In view of low compressibility of liquids, Eqs. (4) and (6)–(8) are also applicable at pressures moderately exceeding the saturation pressure. For exam-

Table 4. Comparison of the results of calculations by Eqs. (4) and (7) with the experimental data for water [5]

t, °C	ρ, kg m^{-3}	Equation (4)		Equation (7)	
		ρ_{calc}, kg m^{-3}	δ, %	ρ_{calc}, kg m^{-3}	δ, %
0	999.9	–	–	999.87	–0.003
1	999.9	–	–	999.93	0.003
2	1000	–	–	999.97	–0.003
3	1000	–	–	999.99	–0.001
4	1000	–	–	1000	0.000
5	1000	–	–	999.99	–0.001
6	1000	–	–	999.97	–0.003
7	999.9	–	–	999.93	0.003
8	999.9	–	–	999.88	–0.002
9	999.8	–	–	999.81	0.001
10	999.7	–	–	999.73	0.003
15	999.1	–	–	999.13	0.003
20	998.2	–	–	998.23	0.003
30	995.7	–	–	995.65	–0.005
40	992.2	–	–	992.18	–0.002
50	988.1	–	–	987.98	–0.013
60	983.1	–	–	983.13	0.003
70	977.7	–	–	977.71	0.001
80	971.8	–	–	971.77	–0.003
90	965.3	–	–	965.32	0.002
100	958.4	–	–	958.40	0.000
120	943.1	–	–	943.16	0.006
140	926.1	–	–	926.10	0.000
160	907.4	–	–	907.27	–0.014
180	886.9	–	–	886.72	–0.020
200	864.7	864.66	–0.005	864.53	–0.020
220	840.3	840.37	0.009	–	–
240	813.6	813.66	0.007	–	–
260	784.0	784.00	0.000	–	–
280	750.7	750.64	–0.008	–	–
300	712.5	712.39	–0.016	–	–
320	667.1	667.10	0.000	–	–
340	610.2	610.25	0.009	–	–
360	528.0	527.62	–0.072	–	–
374.12	317.8	317.80	0.000	–	–

ple, the specific volume of liquid methane at 95 K on a saturation line (P_{sat} = 0.1969 bar) is V_{sat} = 0.002236 m^3 kg^{-1}, and at P = 3 bar V = 0.002235 m^3 kg^{-1}. The discrepancy of the specific volumes is less than 0.05%. The specific volume of liquid ammonia at 310 K on the saturation line (P_{sat} = 14.249 bar) is V_{sat} = 0.001711 m^3 kg^{-1}, and at P = 20 bar V = 0.001710 m^3 kg^{-1}. The discrepancy of the specific volumes is less than 0.06%.

Table 5. Comparison of the results of calculations by Eqs. (6) and (8) with the experimental data for water

t, °C	$\beta \times 10^4$, K^{-1}		Equation (6)		Equation (8)	
	[4]	[1]	$\beta_{calc} \times 10^4$, K^{-1}	δ, %	$\beta_{calc} \times 10^4$, K^{-1}	δ, %
0	–0.63	–	–	–	–0.6598	4.73
4	–	0	–	–	0	0.000
7	–	0.46	–	–	0.453	–1.46
10	–	0.88	–	–	0.875	–0.60
15	–	1.507	–	–	1.514	0.47
20	–	2.069	–	–	2.086	0.80
25	–	2.572	–	–	2.600	0.80
30	3.21	–	–	–	3.066	–4.48
40	3.87	–	–	–	3.885	0.39
50	4.49	–	–	–	4.593	2.30
60	5.11	–	–	–	5.229	2.32
70	5.7	–	–	–	5.817	2.06
80	6.32	–	–	–	6.38	0.93
90	6.95	–	–	–	6.93	–0.34
100	7.5	–	–	–	7.47	–0.40
110	8	–	–	–	8.01	0.19
120	8.6	–	–	–	8.57	–0.40
130	9.2	–	–	–	9.12	–0.82
140	9.7	–	–	–	9.69	–0.08
150	10.3	–	–	–	10.27	–0.29
160	10.8	–	–	–	10.86	0.53
170	11.5	–	–	–	11.45	–0.40
180	12.2	–	–	–	12.06	–1.16
190	–	13.04	–	–	12.67	–2.83
200	–	13.40	13.42	0.14	13.29	–0.81
210	–	14.50	14.23	–1.85	–	–
220	–	15.13	15.13	0.00	–	–
230	–	16.13	16.13	0.00	–	–
240	–	17.90	17.26	–3.59	–	–
250	–	18.78	18.53	–1.31	–	–

CONCLUSIONS

(1) A four-constant correlation equation for precision prediction of the density of any substances within the entire temperature range of their liquid state was suggested, and its constants were determined by regression analysis of reference experimental data for 50 elements, inorganic compounds, and organic compounds.

(2) An equation for predicting the thermal expansion coefficients of liquids was obtained on the basis of the suggested correlation equation for density.

REFERENCES

1. *Spravochnik khimika* (Chemist's Handbook), Nikol'skii, B.P., Ed., Leningrad: Khimiya, 1971, vol. 1, 3rd ed.
2. *Chemical Engineer's Handbook*, Perry, J.H., Ed., New York: McGraw-Hill, 1963.
3. Pavlov, K.F., *Primery i zadachi po kursu protsessov i apparatov khimicheskoi tekhnologii* (Examples and Problems on the Course of Processes and Apparatus of Chemical Engineering), Pavlov, K.F., Romankov, P.G., and Noskov, A.A., Eds., Leningrad: Khimiya, 1970, 7th ed.
4. Pavlov, K.F., *Primery i zadachi po kursu protsessov i apparatov khimicheskoi tekhnologii* (Examples and Problems on the Course of Processes and Apparatus of Chemical Engineering), Pavlov, K.F., Romankov, P.G., and Noskov, A.A., Eds., Leningrad: Khimiya, 1981, 9th ed.
5. Vargaftik, N.B., *Spravochnik po teplofizicheskim svoistvam gazov i zhidkostei* (Handbook on Thermal Properties of Gases and Liquids), Moscow, Nauka, 1972, 2nd ed.

Russian Journal of Applied Chemistry, Vol. 78, No. 7, 2005, pp. 1073–1076. Translated from Zhurnal Prikladnoi Khimii, Vol. 78, No. 7, 2005, pp. 1094–1098.
Original Russian Text Copyright © 2005 by Berezkin, Balushkin, Nepoklonov.

SORPTION AND ION-EXCHANGE PROCESSES

Electroosmotic Circular Thin-Layer Chromatography

V. G. Berezkin, A. O. Balushkin, and E. B. Nepoklonov

Topchiev Institute of Petrochemical Synthesis, Russian Academy of Sciences, Moscow, Russia

Received December 16, 2004; in final form, March 2005

Abstract—A new version of electroosmotic thin-layer chromatography, circular electroosmotic chromatography, was suggested and a prototype apparatus for its implementation was designed.

In the recent decade, liquid thin-layer chromatography (TLC) has been under intensive development. The cheapness and high selectivity of the technique, as well as its quite satisfactory performance and simplicity, led to a wide use of TLC in various fields of science and technology and in environmental monitoring [1–3].

One of the most efficient versions of TLC is circular TLC, which was first suggested by Izmailov and Shraiber [4] and is the first known kind of thin-layer chromatography. The theoretical foundations and experimental implementation of circular TLC, as well as the advantages and shortcomings of the method, were considered in detail in [1, 5, 6]. Compared with the linear version of TLC, widely used in chromatographic practice at present, the circular technique has the following important advantages [1, 5]: higher resolution, higher sensitivity of detection of chromatographic bands (as a result of their narrowing, i.e., concentration), and lower expenditure of the mobile phase. However, the version of circular TLC under discussion also shows a number of shortcomings [1, 5]: a decrease in the average flow velocity of the mobile phase, poorer resolution in analyses for compounds with high R_f (0.6), and impossibility of implementation of the two-dimensional version of TLC.

The basic specific feature of the chromatographic process in circular TLC (compared with the linear modification) consists in the existence of a velocity gradient in the flow of the mobile phase along the direction in which compounds being analyzed are eluted. This leads to an automatic narrowing of chromatographic bands in circular TLC, i.e., to a higher efficiency of chromatographic separation, because the velocity at the peak front is smaller than that at its backside.

It would be expected that application of the electroosmotic effect in circular TLC should make higher the motion velocity of the mobile phase, and effect of narrowing of chromatographic bands, characteristic of the conventional circular chromatography, must also be inherent in circular electroosmotic TLC (EO-TLC). Consequently, this version of EO-TLC must be more efficient as compared with linear electroosmotic thin-layer chromatography.

This study is devoted to development of a new chromatographic method and design of a new apparatus for implementation of circular EO-TLC and to analysis of its basic chromatographic characteristics.

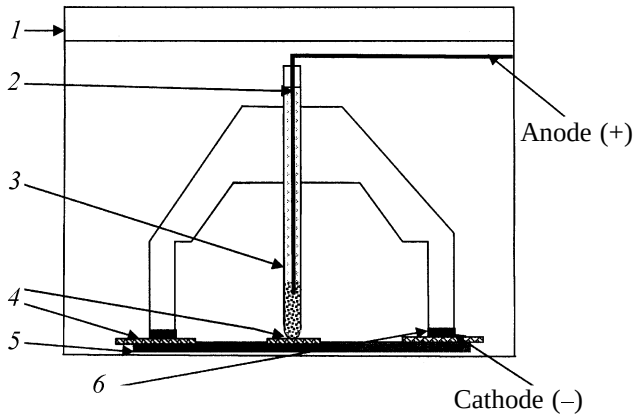
EXPERIMENTAL

The figure shows schematically the apparatus for the method under study.[1] The electroosmotic flow of a mobile liquid phase in circular EO-TLC was created using two electrodes: circular (positioned on the periphery; outer diameter ~9 cm, inner diameter ~8 cm; stainless steel) and central electrodes.

The central electrode was placed in a glass tube about 10 cm long, with an inner diameter of 7.5 cm. The end of the glass tube, brought in contact with the adsorption layer of a TLC plate, had a constriction (inner diameter 0.5 mm, outer diameter 3 mm). The glass tube was densely packed with a filter paper moistened with the mobile phase. A Nichrome-wire electrode (anode) was placed at the center of the tube. The mobile phase was delivered to the central part of the plate from the glass tube with the electrode at the center of a circular piece of filter paper (8 mm in diameter), placed in the central part of the TLC plate. As compounds subjected to chromatographic analysis served selected dyes or a mixture of these. The dye mixture to be separated was deposited with a micro-

[1] Designed at Institute of Petrochemical Synthesis, Russian Academy of Sciences.

1070-4272/05/7807-1073 © 2005 Pleiades Publishing, Inc.



Schematic of a chamber for electroosmotic circular chromatography: (*1*) poly(methyl methacrylate) chamber; (*2*) electrode (central); (*3*) glass tube with a constriction at end, packed with filter paper moistened with the mobile phase, with an electrode placed within the tube; (*4*) filter paper [(i) filter paper circle 8 mm in diameter, placed at the center, and (ii) filter paper square with a circular cut at the center (this filter paper is placed between the external electrode and the adsorption layer on the TLC plate)]; (*5*) TLC plate (adsorption layer on top); and (*6*) electrode (external).

syringe at a distance of 1 mm from the central filter paper circle. With silica gel as a fixed phase, the electroosmotic flow is directed from the anode to the cathode, with the silica gel surface charged negatively [7]. In accordance with the Joule–Lenz law, heat is released in EO-TLC, when electric current flows across the sorption layer. This leads to an intensive uncontrollable evaporation of volatile components of the mobile phase, with the result that the chromatographic experiment becomes poorly reproducible. Therefore, the plate used in separation in the circular EO-TLC mode was preliminarily moistened with a low-volatile mobile phase with a pulverizer, or a plate with a sorption layer protected from evaporation was used [8].

The study was carried out with Sorbfil plates,[2] with ethanol and dimethyl sulfoxide (DMSO) as mobile phases.

As basic characteristics of the new chromatographic method were chosen, first, the rapidity of the technique (motion velocity of the mobile phase or of the central part of the band corresponding to a dye under study) and, second, its performance, i.e., the effective number of theoretical plates, $N_{\text{eff}} = 16(l/w)^2$. Here l is the distance traveled by the central part of the band in a time t (from the point of sample deposition on the sorption layer), and w is the longitudinal width of the band. It is noteworthy that the experimentally determined number of theoretical plates in TLC and in the method in question should be regarded as an effective characteristic, because, strictly speaking, application of the quantity "theoretical plate" to characterization of the gradient chromatographic technique under study is not substantiated theoretically. However, the quantity used in this study (N_{eff}) undoubtedly enables a comparative evaluation of the real chromatographic processes of band smearing.

The experiments performed confirmed the improved (compared with the linear version) performance of circular EO-TLC.

To illustrate the high performance of circular EO-TLC, the following experimental data are presented. For example, HETP = 14 μm for circular EO-TLC with ethanol as a mobile phase (voltage 1.5 kV) at a displacement of the band of the dye (Rhodamine B) by 20 mm and HETP = 37 μm under conditions of the conventional circular TLC, i.e., the performance of EO-TLC is higher (by a factor of ~2.6). These experimental data were obtained on plates with an adsorption layer protected by a polyethylene film, which virtually terminates evaporation of the mobile phase and improves the reproducibility of the process. Thus, EO-TLC with a protected sorption layer exhibits a higher performance, compared with the conventional circular TLC.

Table 1 lists the experimental data obtained, which allow a comparative evaluation of the basic chromatographic characteristics of circular EO-TLC in which the adsorption layer is protected by a polyethylene film. It is seen that the velocity of motion of the dyes used as test compounds along the layer (rapidity of the method) increases by a factor of 3.5–5.6, and the performance becomes tens of times higher for some compounds. Thus, our experiments demonstrate that the basic chromatographic characteristics of the new method are markedly improved and, consequently, its use in analytical chromatography to solve various analytical problems is advisable.

As is known, a disadvantage of electroosmotic TLC consists in intensive evaporation of the mobile phase in the course of an experiment [9]. Therefore, an additional new version of circular EO-TLC was developed, in which low-volatile DMSO served as the mobile phase. The results obtained are listed in Table 2. It can be seen that the motion velocity of the bands of the compounds subjected to chromatographic analysis increases in the new version of

[2] Sorbpolimer Company (Krasnodar).

Table 1. Comparison of basic chromatographic characteristics of the conventional circular TLC and circular EO-TLC. Mobile phase ethanol, TLC plates with an adsorption layer protected by a polyethylene film

TLC version	Dye subjected to chromatographic analysis	Relative motion velocity of band	N_{eff}, TP	Relative increase in N_{eff}
Conventional circular, protected layer	Rhodamine C	1.0	80	1.0
	Brilliant Green	1.0	50	1.0
EO-TLC, protected layer, voltage 1.0 kV	Rhodamine C	3.5	4100	51
	Brilliant Green	4.6	2100	42

Table 2. Characteristics of the conventional circular TLC and circular EO-TLC in the case of a low-volatile mobile phase (DMSO)

TLC version	Sorbate	Displacement of sorbate band on plate, mm	Average motion velocity of band, mm min^{-1}	Relative average motion velocity of bands	N_{eff}, TP	Relative increase in N_{eff}
Conventional circular	Sudan (II)	13	1.3	1.0	2500	1.0
	Crystal Violet	2	0.18	1.0	50	1.0
	Rhodamine G	7	0.36	1.0	300	1.0
EO-TLC, voltage 1.5 kV	Sudan (II)	19	1.9	1.5	4300	1.8
	Crystal Violet	12	1.2	6.7	1700	34
	Rhodamine G	15	1.5	2.1	970	3.2

EO-TLC by a factor of 1.8–3.4, with a simultaneous pronounced (severalfold) rise in the performance. Thus, in the version of circular EO-TLC with low-volatile mobile phases, suggested in this study, such most important chromatographic characteristics as rapidity and performance are markedly improved, compared with the conventional version of circular TLC.

It is also noteworthy that circular EO-TLC can be used as a concentration technique. In chromatographic analyses of strongly diluted samples, the weight of a sample being analyzed and, consequently, its linear dimensions are raised in order to improve the sensitivity of impurity determination. Therefore, the positive effect can be achieved in this case only if a sample is made only moderately larger, because a further increase in the sample size already leads to a noticeable extension of the initial width of the band, which impairs the efficiency of the subsequent chromatographic separation [10].

The smearing of chromatographic bands in circular TLC automatically decreases because of the existence of a velocity gradient of the mobile phase. Therefore, it would be expected that the effect under discussion, i.e., the narrowing of the broad initial band of a sample, must also be observed in the case of EO-TLC. To confirm the occurrence of this effect under the conditions of circular EO-TLC, special experiments at a voltage of 1 kV were performed with DMSO as a mobile phase to study changes in chromatographic characteristics for Crystal Violet (compound subjected to chromatographic analysis). Under the conditions specified above, the broad initial band of the dye (width 10 mm) decreases to 8.5 mm (–15%) upon elution for 10 min and to 7.0 mm (–30%) upon elution for 20 min. This means that it is, in principle, possible to use in EO-TLC a broad initial band narrowing under the experimental conditions. This effect, combined with an increased sample volume, improves the efficiency of determination of impurity components.

Table 3 compares the basic characteristics of circular EO-TLC and circular conventional TLC. It can be seen that, according to its characteristics, circular EO-TLC is more promising than the classical linear version.

Finally, it should be noted that it is advisable to develop further the suggested version of circular EO-TLC in two ways: (1) to improve further the technique and the apparatus for its implementation and (2) to determine the optimal areas of its practical application.

Table 3. Comparison of circular EO-TLC with the conventional circular TLC

Characteristic of TLC	Conventional circular TLC	Circular EO-TLC
Phenomenon (principle) on which the motion of the mobile phase is based	Wetting of the sorption layer by the mobile phase	Electroosmosis: motion of the mobile phase relative to the adsorption layer under the conditions of formation of an electrical double layer (zeta potential) in an electric field gradient
Implementation conditions of the conventional TLC and EO-TLC	Mobile phase wets the adsorbent layer used	The mobile phase moves in an electric field relative to the solid sorbent (electroosmosis). Development of an electric field gradient and formation of an electrical double layer at the interface between the mobile phase and the sorbent are conditions for implementation of the method. To preclude evaporation of the conventional mobile phases in order to achieve stable operation of the technique, it is advisable to use a plate with a protected layer or a low-volatile mobile phase
Advantages of circular EO-TLC	Conventional circular TLC serves as a basis for comparison with EO-TLC	Positive specific features of circular EO-TLC (compared with conventional circular TLC): (1) higher rapidity and (2) higher performance

CONCLUSION

Compared with circular thin-layer chromatography, the circular electroosmotic thin-layer chromatography (both with a protected sorption layer and with low-volatility mobile phases) suggested in this study has the following advantages: (1) higher rapidity (by a factor of 1.5 –6.7), (2) 1.8–51 times higher performance, and (3) narrowing of the initial broad bands.

ACKNOWLEDGMENTS

The authors are deeply grateful to Acad. B.F. Myasoedov for a detailed discussion of the manuscript and valuable critical remarks.

REFERENCES

1. Geiss, F., *Fundamentals of Thin-Layer Chromatography*, Heidelberg: Alfred Hüthig, 1987.
2. Poole, C.F., *The Essence of Chromatography*, Amsterdam: Elsevier, 2003.
3. Sumina, E.G., Shtykov, S.N., and Tyurina, N.V., *Tonkosloinaya khromatografiya: Teoreticheskie osnovy i prakticheskoe primenenie* (Thin-Layer Chromatography: Theoretical Foundations and Practical Use), Saratov: Saratov. Univ., 2002.
4. Izmailov, N.A. and Shraiber, M.S., *Farmatsiya*, 1938, no. 3, pp. 1–6.
5. *Vysokoeffektivnaya tonkosloinaya khromatografiya* (High-Performance Thin-Layer Chromatography), Zlatkis, A. and Kaiser, R.E., Eds., Moscow: Mir, 1979.
6. Kaiser, R.E., *Einführung in die HPPLC (Hochdruck-Planar-Flüssigkeitschromatographie)*, Heidelberg: Hüthig, 1987.
7. Rozylo, J.K. and Malinowska, I., *Planar Chromatography: A Retrospective View for the Third Millennium*, Nyiredy, Sz., Ed., Budapest: Springer, 2001, pp. 200–219.
8. Berezkin, V.G. and Buzaev, V.V., *Dokl. Ross. Akad. Nauk*, 1996, vol. 347, no. 4, pp. 481–485.
9. Nurok, D., Frost, M.C., and Chenoweth, D.M., *J. Chromatogr. A*, 2000, vol. 903, pp. 211–218.
10. Berezkin, V.G. and Gorshunov, O.L., *Zh. Fiz. Khim.*, 1968, vol. 42, no. 10, pp. 2587–2590.

Russian Journal of Applied Chemistry, Vol. 78, No. 7, 2005, pp. 1077–1083. Translated from Zhurnal Prikladnoi Khimii, Vol. 78, No. 7, 2005, pp. 1099–1105.
Original Russian Text Copyright © 2005 by Zosin, Priimak, Koshkina, Masloboev.

SORPTION AND ION-EXCHANGE PROCESSES

Sorption-Active Materials Based on an Acid-Nonresistant Aluminosilicate Nepheline, Used for Defluorination of Industrial Sewage

A. P. Zosin, T. I. Priimak, L. B. Koshkina, and V. A. Masloboev

Institute for Problems of Industrial Ecology of the North, Kola Scientific Center, Russian Academy of Sciences, Apatity, Murmansk oblast, Russia

Received June 10, 2003; in final form, June 2005

Abstract—A method for obtaining sorption-active materials based on a solidifying mineral dispersion composed of nepheline, hydrochloric acid, and water was suggested. The hardening processes and conditions under which sorption-active compounds are formed were studied. The mechanism of sorption of F^- ions on the sorbents developed was determined.

A topical environmental problem of the Kola region is purification of mine water and underground water to remove fluoride ions. All the methods presently used for this purpose can be divided into two groups: (1) coprecipitation and coagulation on freshly synthesized aluminum and magnesium hydroxides and calcium phosphate and (2) ion exchange of fluorine-selective ion exchangers, e.g., activated aluminum oxide, which is a strongly basic anion exchanger. However, use of these expensive ways to defluorinate water is unacceptable in the case of large-tonnage wastes. Defluorination of sewage from mining plants require granulated sorbents, which can be used by creating check dams before discharging, e.g., mine water into natural water basins. To solve this problem, it is suggested to prepare sorption-active materials by the technology of self-hardening binder systems. By binders (self-hardening) are understood systems containing, in certain relative amounts, the solid and liquid phases that can interact to give new condensed phases and are capable of hardening [1, 2]. It is known that condensed reaction products formed in hardening of water-containing binder systems, with aluminosilicates used as a solid phase, are salts of complex composition. These salts contain oxyhydrates, hydrosilicates, and hydroaluminates, which exhibit sorption properties under certain conditions [5].

In development of sorbents for defluorination of wastewater, the mineral phase of the self-hardening binder system should be composed of acid-nonresistant aluminum-containing minerals that can interact with aqueous solutions of acids to give hydroxo compounds of aluminum, which are anion-active sorbents under certain conditions [4]. The search for starting raw materials was limited to the natural resources of the Kola Peninsula. Preference was given to nepheline-containing raw materials, whose advantage over other types of raw materials consists in larger resources, fast decomposition by acids, and high content of alumina (up to 30 wt % Al_2O_3). In view of the fact that aluminum hydroxides exhibiting the highest activity toward fluoride ions are formed in hydrolysis of its oxychlorides [4], a hydrochloric acid solution was chosen as the second component of the binder system for synthesis of a fluorine-selective sorbent.

The aim of this study was to find conditions under which granulated sorption-active materials to be used in treatment of mine wastewater can be formed by the binder technology in the system constituted by nepheline, hydrochloric acid, and water and to determine the optimal application conditions of the materials obtained.

We used a nepheleine concentrate produced by the Apatit Open Joint-Stock Company, ground to a specific surface area of 2600 $cm^2\ g^{-1}$. The concentrate contained up to 80–81 wt % nepheline and had the following chemical composition (wt %): SiO_2 42.60, Al_2O_3 29.30, Na_2O 13.96, and K_2O 7.13. The concentration of hydrochloric acid was varied from 5 to 35%. The degree of nepheline decomposition was controlled by changing the amount of HCl contained in the starting binder system and calculated in accor-

1070-4272/05/7807-1077 © 2005 Pleiades Publishing, Inc.

Table 1. Synthesis conditions and strength characteristics of sorbents

Sample no.	α, %	c_{HCl}, %	s : l	c_{F^-}, mg g^{-1}	R_{comp}, MPa
1	6–7	17	3 : 1	20.7	2.5–3.5
2	25	17	1 : 1.5	33.0	1.0
3	50	17	1 : 3	64.5	0.4
4	75	17	1 : 4	65.0	0.2
5	100	39	1 : 4	52.0	0.2
6	100	17	1 : 5.5	22.0	Less than 0.2
7	100	17	1 : 15	24.0	″ ″
8	75	9.5	1 : 8	33.0	″ ″
9	50	3.5	1 : 15	32.0	″ ″

dance with the reaction of complete (stoichiometric) decomposition of nepheline:

$$(Na_3K)O_2 \cdot 2Al_2O_3 \cdot 4SiO_2 + 16HCl \rightarrow 3NaCl + KCl + 4AlCl_3 + 4SiO_2 + 8H_2O.$$

It was assumed that 100% decomposition of nepheline occurs in those reaction mixtures in which the amount of hydrochloric acid corresponded to that required by the stoichiometry. In what follows, the degree of decomposition α is given in percent relative to total decomposition.

The concentration of fluoride ions, c_{F^-}, was measured potentiometrically with an EF-VI fluorine-selective electrode in the presence of a citrate buffer solution. The citrate buffer solution was used to break down complexes formed by F^- ions with aluminum cations, which may be present in solution.

The products formed in the reaction of nepheline with hydrochloric acid were studied by X-ray diffraction analysis, IR spectroscopy, and mass spectrometry.

EXPERIMENTAL

The technique used to obtain materials was the same for all the compositions: finely ground nepheline concentrate was poured-over with an HCl solution, the mixture was agitated for 15 min, and the resulting mass was kept at 22°C for 24 h, and then thermolysis was performed at 105°C to constant weight.

To determine the strength characteristics (compression strength R_{comp}) of the materials synthesized, $2 \times 2 \times 2$-cm samples were fabricated. For this purpose, the mass formed was cast into molds, kept at 22°C for 24 h, and then heat-treated at 105–110°C for 1 h. The water resistance of the materials synthesized was evaluated by the loss of strength by the samples kept in water for 7 days.

The sorption and the kinetics of leaching-out of the sorbent components were determined under static conditions at a sorbent : sorbate ratio of 1 : 100, temperature of 22°C, and intermittent agitation, with the time of contact varied from 15 min to 72 h. The data obtained are listed in Table 1. The results of the study demonstrated that a granulated water-resistant material should be synthesized in a narrow range of compositions of the starting binder system: the amount of hydrochloric acid corresponds to α = 6–7%, and the concentration of water, to an s : l ratio of 2.8 : 1 to 3 : 1. As α increases, the strength and water resistance of grains decrease dramatically. The technique that can be used to obtain the sorbent includes the following operations: grinding of the nepheline concentrate to a specific surface area of 2500–3000 $cm^2\ g^{-1}$, mixing of the ground concentrate with a 7% HCl solution at a phase ratio of 3 : 1, granulation of the resulting mass, and thermolysis at 105°C.

The reaction products responsible for formation of a strong water-resistant stone and sorption-active phases were for the most part studied using physicochemical methods. This is due to difficulties in isolation of the newly formed phases from the whole mass of a solidified dispersion. To make simpler the identification of the reaction products, all the physicochemical studies were carried out with samples synthesized on nepheline crystals ground to a specific surface area of 2600 $cm^2\ g^{-1}$. This is justified by the fact that the main impurity minerals (feldspar, titanomagnetite) contained in the nepheline concentrate are considerably more resistant to solutions of acids, compared with nepheline, and have no effect on the hardening processes.

It is known that the key role in hardening of binder formulations and in sorption interactions in materials synthesized by the technology of binder systems is played by water molecules, which are in a firmly bound state in the reaction products [3–4]. The role played by water molecules in the sorbent synthesized from nepheline was revealed using mass-spectrometric analysis, which makes it possible to record not only the loss of mass by a sample, but also the molecular weight of the thermolysis products being removed and their qualitative composition. The results obtained demonstrated that three temperatures of water removal can be distinguished in the mass spectrum of the

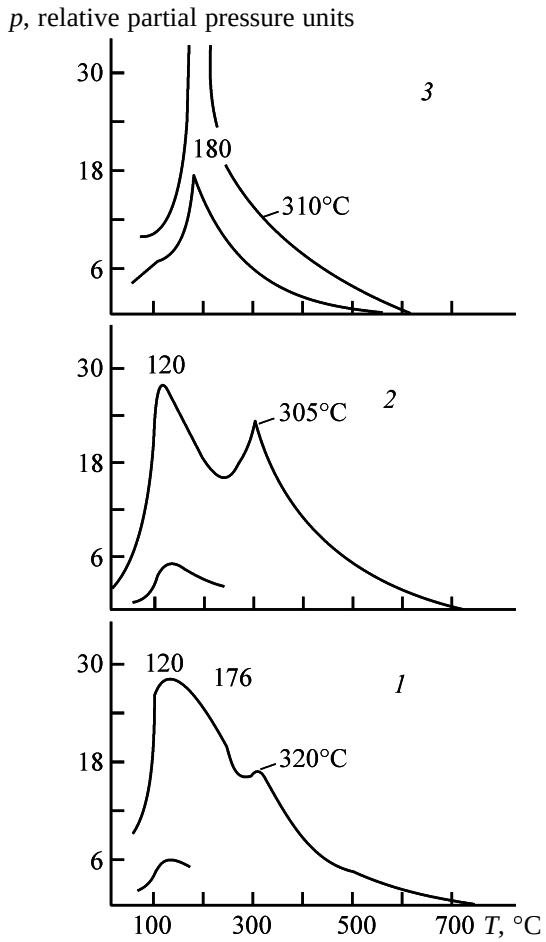


Fig. 1. Mass-spectrometric monitoring of thermal removal of water from the nepheline sorbent synthesized at various α and s : l ratios. (*p*) Relative pressure and (*T*) temperature. (*1*) α = 7% at s : l = 3 : 1, (*2*) α = 50% at s : l = 1 : 2.5, and (*3*) α = 50% at s : l = 1 : 5.

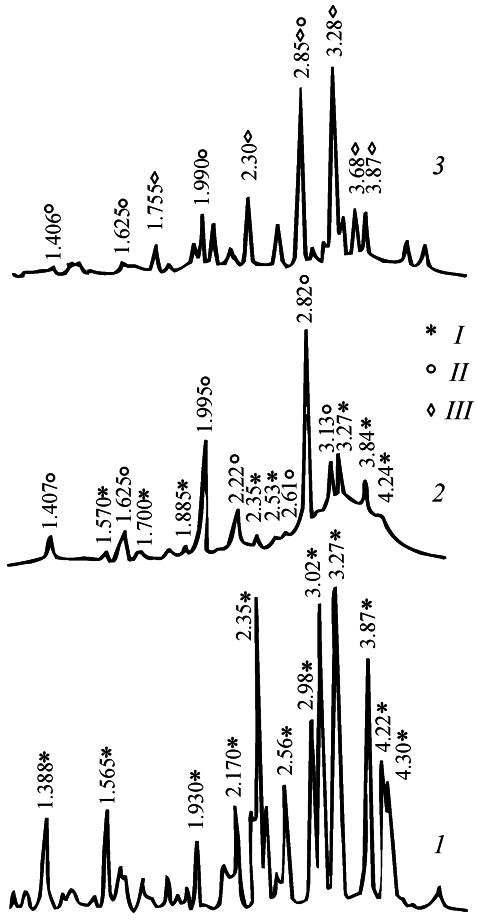


Fig. 2. X-ray diffraction patterns of nepheline and the nepheline sorbent synthesized at various s : l ratios. (*1*) Starting nepheline, (*2*) α = 50% at s : l = 1 : 2.5, and (*3*) α = 50% at s : l = 1 : 5. (*I*) Nepheline, (*II*) sodium chloride, and (*III*) hydrated aluminum chloride.

sample obtained at α = 7% (s : l = 3 : 1), with the following distribution of intensities: 120 > 175 > 320°C (Fig. 1). As α increases to 50%, an increase in the amount of OH_n groups removed at at T > 320°C and a decrease in that of OH_n groups removed at 175°C are observed at a water deficiency (s : l = 1 : 2.5). As the content of water in the starting dispersion increases (α = 50% at s : l = 1 : 5), the fraction of water removed at 175–180°C increases, and the content of firmly bound OH_n groups decreases.

The mass spectra of hydrogen chloride demonstrate that chlorides and hydroxochlorides decomposing at 320, 410, and 520°C are present in a weakly treated material (α = 7%).

Thus, the materials synthesized on the basis of binder systems with a low degree of nepheline decomposition contain, in contrast to materials with a high degree of decomposition, H_2O and HCl in a firmly bound state, which are removed at temperatures exceeding 350°C. This is in agreement with the variation of the strength characteristics of samples with their synthesis conditions (Table 1).

X-ray diffraction studies of the products formed in the reaction of nepheline with a hydrochloric acid solution demonstrated (Fig. 2) that the phase composition of the compounds formed is primarily determined by the amount of water contained in the starting dispersion, which presumably affects the diffusion of mobile elements in the nepheline structure. In the case of an excess of water, separate phases recorded in the X-ray diffraction pattern are formed. In the dispersions synthesized at s : l = 1 : 5, the reflections associated with nepheline disappear already at α = 50% and the phase of aluminum hydrochlorides (Fig. 2, X-ray diffraction pattern *3*) and that of amorphous hydrated silicon oxide are formed in the reaction prod-

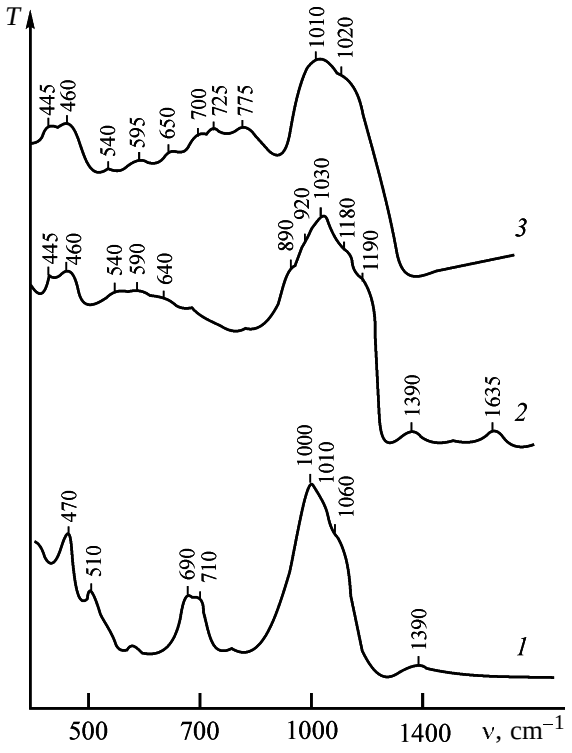


Fig. 3. IR spectra of nepheline and the nepheline sorbent synthesized at α = 50% and s : l = 1 : 2.5. (*T*) Transmission and (ν) wave number. (*1*) Nepheline, (*2*) nepheline sorbent, and (*3*) the sorbent heat-treated at 400°C.

ucts in addition to chlorides of alkali metals. In the case of deficiency of water (s : l = 1 : 2.5), formation of reaction products as separate phases is hindered and a broad band centered at about 3.7 Å is observed on the background of reflections associated with nepheline and alkali metal compounds. This band characterizes the amorphization of the aluminosilicate skeleton: reflections related to $AlCl_3 \cdot 6H_2O$ are absent (Fig. 2, pattern *2*).

The behavior revealed was also observed in a study of the reaction products formed at α = 100% at various s : l ratios: 17% HCl at s : l = 1 : 15 and 36% HCl at s : l = 1 : 3. The X-ray diffraction patterns of the samples obtained with excess water (s : l = 1 : 15) contain reflections associated with chlorides of alkali metals, hydrated aluminum chloride, and hydrated amorphous silicon oxide. With a deficiency of water, only NaCl, KCl, and amorphous aluminosilicates are manifested in the X-ray diffraction patterns. After washing of the reaction products with water, only a broad band associated with amorphous aluminosilicates is observed in both cases. The shift of its center from 3.7 to 3.3 Å in water-deficient systems indicates that this phase is enriched with aluminum oxides [5]. The $SiO_2 : Al_2O_3$ ratio in the reaction products is 1 : 0.04 in the system with an excess of water and 1 : 0.25 in that with a deficiency of water. This indicates that the extent to which aluminum oxides are removed from the aluminosilicate skeleton decreases as the concentration of H_2O in the starting dispersion becomes lower. The nepheline structure disintegrates incongruently: the egress of alkaline cations is ahead of the diffusion of Al^{3+} from the nepheline structure, which leads to formation of a sparingly soluble amorphous phase of aluminosilicates.

The results of X-ray diffraction studies are confirmed by the IR data (Fig. 3). A pronounced increase in the absorption at 960 cm^{-1} and in the range 540–640 cm^{-1} in nepheline treated with hydrochloric acid under conditions of water deficiency (s : l = 1 : 2.5) is due to hydroxylation of the surface and formation of Al–OH and Si–OH bonds [6]. The presence of hydrated aluminosilicates in the products formed in the reaction of nepheline with hydrochloric acid under conditions of water deficiency is indicated by the fact that the IR spectra contain a broad band at 2800–3740 cm^{-1}. The shoulders at 3560–3680 cm^{-1} correspond to stretching vibrations of silanol groups involved in hydrogen bonding and to isolated silanol groups. This interpretation is supported by the fact that the absorption in these spectral ranges decreases upon removal of water from the samples at 400°C. The partial cleavage of Si–O–Al bonds characterizing the ordered isomorphism in the aluminosilicate skeleton of nepheline and the appearance of purely Si–O and Al–O bonds is confirmed by broadening of the band of symmetric stretching vibrations ν_{as} of Si–O–Si and Si–O–Al bonds (920–1200 cm^{-1}) and by weakening of doublets of bending vibrations ν_s (690–710 cm^{-1}) and δ (470–510 cm^{-1}) of these bonds [6]. It should also be noted that all the samples under study exhibit absorption at 590–650 cm^{-1}, suggesting the presence of aluminum compounds with an octahedral coordination [6–9].

The results of physicochemical studies of the reaction products formed in the dispersions composed of nepheline, hydrochloric acid, and water indicate that the amorphous phase of oxyhydrate aluminum-containing compounds is formed on the sorbent surface. These compounds incorporate H_nO and HCl in a bound state, which are removed at temperatures higher than 350°C. These reaction products, formed in a narrow range of compositions, are responsible for the dispersion hardening and sorption processes.

To determine the optimal application conditions of

nepheline sorbents, the kinetics of leaching-out of the main components of the sorbent and its sorption characteristics were studied under varied conditions [4]. As is known, sorption of fluoride ions on oxyhydrate aluminum-containing sorbents occurs via formation of insoluble polymolecular fluoroaluminate complexes AlF_x^{3-x} (x = 1–6) through ion exchange or chemical interaction. The main exchange centers in amorphous aluminum oxyhydrates are molecules of coordination water and bridged and terminal OH groups [10]. Formation of various types of centers and occurrence of one or another sorption mechanism are affected by the solution pH, concentration of active Al^{3+} on the sorbent surface, and concentration of F^- in solution [10]. In the case of the nepheline concentrate, as active aluminum was regarded that contained in the reaction products, i.e., in the active phase. The amount of the active phase was evaluated by the degree of nepheline breakdown, α, i.e., by the amount of hydrochloric acid, with water contained in the dispersion disregarded. The study was carried out with a nepheline concentrate of the optimal composition. The kinetics of leaching-out of the main components was examined under static conditions. The concentration of fluoride ions in solutions, varied from 19 to 190 mg l^{-1}, was measured in the presence of a citrate buffer solution and without this solution. The difference between the concentrations of fluoride ions measured with and without the citrate buffer solution corresponded to the content of fluorine bound in fluoroaluminate complexes [8]. The solution pH was adjusted on the background of a constant concentration of NaCl (1 N solution) by adding NaOH and HCl.

Sorption of fluoride ions is primarily governed by the fundamental aspects of dissolution of aluminum from the active phase under the given conditions. The degree of dissolution of aluminum from the active phase of the sorbent was determined in percent relative to the total amount of aluminum in the active phase and was denoted by $\beta = Al^{3+}_{\text{in sol.}}/Al^{3+}_{\text{act}}$. A study of the kinetics of leaching-out of aluminum from the active phase of the sorbent into solution and of the hydrolytic equilibrium at various pH values and concentrations of the F^- ion revealed the following pattern (Figs. 4, 5; Table 2). It was established that, at $4 < pH_{in} < 10$, the fraction of Al^{3+} ions that passed into solution in the absence of fluoride ions is 20% of their total amount in the active phase (Fig. 4). The pH of the equilibrium solution in this range is 4.8–5.0 (Fig. 5), which indicates that compounds that can be hydrolyzed by the acid or base mechanism, depending on pH_{in}, are contained in the sorbent.

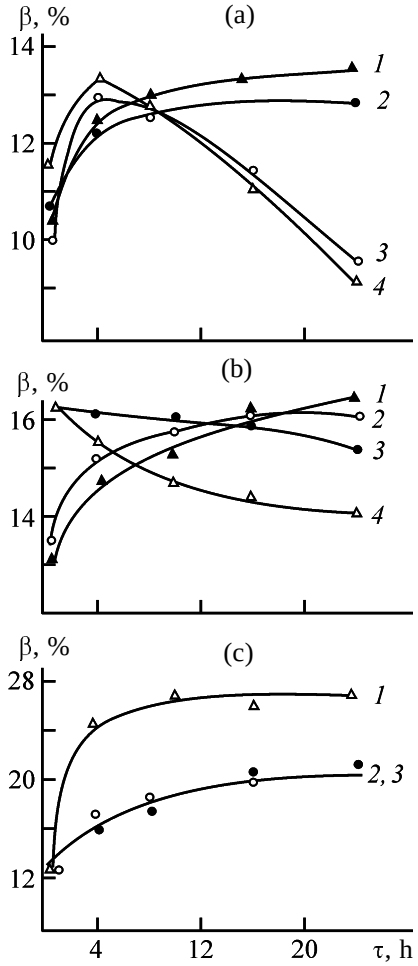


Fig. 4. Kinetic curves of redistribution β of active aluminum in relation to the solution pH and c_{F^-} in the contact solution. (τ) Time. c_{F^-}, mg g^{-1}: (a) 80, (b) 19, and (c) 0. pH: (a) (*1*) 3.08, (*2*) 11.18, (*3*) 4.35, and (*4*) 9.78; (b) (*1*) 3.01, (*2*) 10.81, (*3*) 3.88, and (*4*) 9.17; (c) (*1*) 3.02, (*2*) 5.93, and (*3*) 9.08.

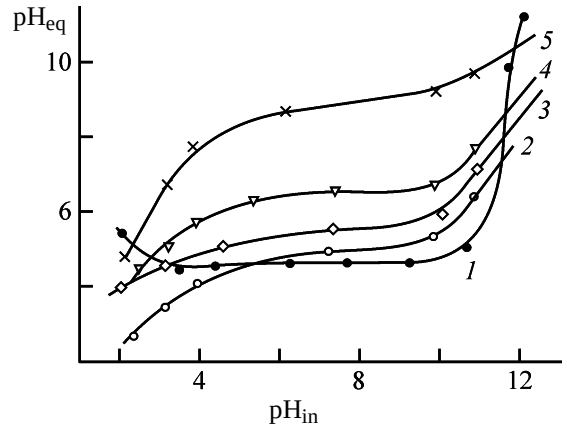


Fig. 5. Effect of pH and c_{F^-} in solution on the hydrolytic equilibrium in a system. (*1*–*4*) Nepheline sorbent and sodium fluoride solution and (*5*) activated aluminum oxide and sodium fluoride solution. c_{F^-}, mg g^{-1}: (*1*) 0, (*2*) 19, (*3*) 30, (*4*) 80, and (*5*) 19.

Table 2. Kinetics of sorption of fluoride ions by the nepheline sorbent in relation to the pH of the initial solution

Initial solution		Time of contact, h					
		1		4		24	
c_{F^-}, mg g^{-1}	pH	β, %	A, mg g^{-1}	β, %	A, mg g^{-1}	β, %	A, mg g^{-1}
80	2.0	36.0	0.0	38.0	0.10	45.0	0.17
	4.0–4.3	10.2	1.3	13.0	1.73	9.7	4.11
	7.0–7.2	11.7	1.3	13.2	2.25	9.2	4.11
	9.8–10.1	11.7	1.7	12.1	3.11	8.4	4.43
	10.8–11.2	10.7	1.3	12.2	1.73	12.9	3.57
19	2.0	43.0	0.0	47.0	0.10	49.0	0.15
	4.0–4.3	16.5	0.37	15.0	0.37	12.6	0.99
	7.0–7.2	16.3	0.4	16.5	0.98	15.0	0.97
	9.8–10.1	16.5	0.59	14.7	0.62	13.2	1.23
	10.8–11.2	12.6	0.0	15.2	0.27	16.3	0.27

Table 3. Change in the chemical composition of mine water after its treatment with the nepheline adsorbent

Characteristic of water	Content of indicated components, mg g^{-1}									pH
	Na^+	Al^{3+}	Ca^{2+}	Mg^{2+}	Cl^-	SO_4^{2-}	HCO_3^-	F^-	suspension	
Before treatment	600	1.8	0.7	1.0	5	10.5	20.1	60	465	10.15
After treatment to breakthrough	600	2.9	0.7	1.0	15.0	10.5	20.1	0.5	1.2	8.6

In the nepheline sorbent, these salts are, probably, hydrated aluminum oxychlorides. At pH < 3 and pH > 10, the active phase dissolves and the fraction of aluminum passing into solution increases dramatically. In the presence of fluoride ions in solution, the fundamental aspects of aluminum leaching-out from the sorbent vary over the entire range of pH values studied. At pH < 3 and pH > 10, the solubility of aluminum in the presence of fluoride ions somewhat decreases, although no sorption of the fluoride ion occurs. At $4 < pH_{in} < 10$, the solubility of aluminum from the active phase decreases substantially, and this decrease is the stronger, the higher the concentration of fluorine (Fig. 4, Table 2). In this pH range, sorption of fluoride ions is observed. The sorption capacity A (mg g^{-1}) is at a maximum at pH in the range from 9 to 10 (Table 2). The correlation between the sorption processes and the solubility of aluminum belonging to the active phase confirms the previously made assumption that aluminum-containing compounds are responsible for sorption processes involving fluoride ions.

The study performed made it possible to develop a technique for defluorination of mine and pit wastewater from plants for mining and dressing of phosphate and rare-metal raw materials at the Kola Peninsula. The mine wastewater from the Lovozero ore mining and processing combine contains up to 60 mg g^{-1} of fluoride ions at a high total salinity of the discharged water. The defluorination technique developed is based on synthesis and use of nepheline-containing sorbents in sorption filters with a fixed filtering bed, mounted as cartridges in gallery drains. The degree of purification of process wastewater to remove fluoride ions was 98.5–99.0% (Table 3). Spent sorbents are used to fill worked out mine spaces at mines of the Lovozero combine as a fluorine-containing additive to portland cement fill mixtures, which leads to an increase in the strength and water resistance of the fill [2].

CONCLUSIONS

(1) To prepare sorbents for defluorination of large-tonnage sewage formed in mining and processing of rare-metal and phosphate raw materials at the Kola peninsula, a procedure involving the use of a self-hardening dispersed system constituted by a nephe-

line-containing waste, hydrochloric acid, and water is suggested. The synthesis of a solid product exhibiting a sorption activity is governed by incongruent dissolution of nepheline at a high concentration of the solid phase in the initial dispersion (s : l = 3 : 1) and small value of α (7% anhydrous HCl relative to the amount required by stoichiometry for complete decomposition of nepheline). The adsorption-active phase formed under the given conditions is composed of the amorphous phase of aluminosilicates, which contains bound H_2O and HCl (removed at $T > 350°C$). Adsorption of fluoride ions presumably occurs via formation of sparingly soluble aluminosilicofluorides.

(2) The sorbent passed semicommercial tests at the Lovozero ore mining and processing combine. Implementation of the technique suggested in the study makes it possible to organize a closed cycle of processing of mined raw materials.

REFERENCES

1. Fedorov, N.F., *Vvedenie v khimiyu i tekhnologii spetsial'nykh vyazhushchikh* (Introduction to Chemistry and Technologies of Special Binders), Leningrad: Leningr. Tekhnol. Inst. im. Lensoveta, 1976, part 1, p. 26.
2. Sychev, M.M., *Trudy VI Mezhdunarodnogo kongressa po khimii tsementa* (Proc. VI Int. Congr. on Chemistry of Cement), Moscow: Stroiizdat, 1986, vol. 2, book 1, pp. 48–58.
3. Granovskii, I.G., *Strukturoobrazovanie v mineral'nykh vyazhushchikh sistemakh* (Structuring in Mineral Binder Systems), Kiev: Naukova Dumka, 1984.
4. Sukharev, Yu.I., *Sintez i primenenie spetsificheskikh oksigidratnykh sorbentov* (Synthesis and Use of Specific Oxyhydrate Sorbents), Moscow: Energoatomizdat, 1987.
5. Iler, R.K., *The Chemistry of Silica*, New York: Wiley–Interscience, 1979.
6. D'yakonov, S.S., Lychin, V.I., Shalumov, V.S., *et al.*, *Kolloidn. Zh.*, 1985, vol. 47, no. 1, pp. 146–149.
7. Farmer, V.C., *Infrared Spectra of Minerals*, London: Mineralogical Soc., 1974.
8. Mudgley, D. and Torrance, K., *Potentiometric Water Analysis*, Chichester: Wiley, 1978.
9. *Fizicheskaya khimiya* (Physical Chemistry), Nikol'skii, B.P., Ed., Leningrad: Khimiya, 1987.
10. Hao, O.J. and Huang, C.P., *J. Environ. Eng.*, 1986, vol. 112, no. 6, pp. 1054–1069.

Russian Journal of Applied Chemistry, Vol. 78, No. 7, 2005, pp. 1084–1087. Translated from Zhurnal Prikladnoi Khimii, Vol. 78, No. 7, 2005, pp. 1106–1109.
Original Russian Text Copyright © 2005 by Grishina, Udalova.

APPLIED ELECTROCHEMISTRY AND CORROSION PROTECTION OF METALS

Characterization of the Electrical Conductivity of Concentrated Suspensions of Silica in Aqueous Solutions of Sulfuric Acid

E. P. Grishina and A. M. Udalova

Institute of Chemistry of Solutions, Russian Academy of Sciences, Ivanovo, Russia

Received February 3, 2005

Abstract—The electrical conductivity of stable concentrated suspensions of SiO_2 in aqueous solutions of sulfuric acid was studied as influenced by the concentration and size of SiO_2 particles.

Electrolytes are an important constituent of any electrochemical system. A particular group of electrolytes is formed by dispersed systems composed of a solid dispersed phase and a liquid dispersion medium, in which the part of conducting elements can be played by solid particles (e.g., particles of carbon black) and by a dispersion medium (electrolyte solutions). An example of their practical use in applied electrochemistry are thickened electrolytes for chemical power cells and tantalum electrolytic capacitors and, in particular, gel-like electrolytes based on silica and H_2SO_4 [1–7]. Use of thickened electrolytes makes it possible to create hermetically sealed chemical power cells and to improve the performance of these devices [1].

Electrolyte systems constituted by an aqueous solution of H_2SO_4 and silica exhibit thixotropy, i.e., ability to be reversibly liquefied under mechanical stress [1]. It was shown in [8] that the magnitude of thixotropy grows with the H_2SO_4 concentration. The duration of the thixotropic period strongly depends on the particle size of the dispersed phase and decreases as SiO_2 grains become larger [9]. After the mechanical load is removed, the viscosity of the thickened electrolyte increases and its electrical conductivity becomes lower because of structuring processes that occur in the heterogeneous system.

The electrical conductivity and its temperature dependence are important parameters of an electrolyte system, which strongly affect the performance of electrotechnical devices. In impregnation of silica gel with an already formed system of pores and capillaries, the amount of absorbed acid grows with the silica gel pore volume and H_2SO_4 concentration [10]. For a 5 M H_2SO_4 solution, the electrical conductivity was at a maximum at 40–60°C and remained high at 100°C owing to physically adsorbed water retained in silica gel pores.

The aim of this study was to examine the electrical conductivity of stable highly concentrated SiO_2 suspensions in strong aqueous solutions of H_2SO_4 in relation to the concentration of components, size of SiO_2 particles, and temperature.

EXPERIMENTAL

Suspensions were prepared from SiO_2 powders with grain sizes of 45–55 and 100–110 μm (which correspond to peaks in the particle size distribution curves, sedimentation analysis was made with Analysette 22 Fritsch Particle Sizer). According to [11], their specific surface area was approximately 0.9×10^3 and 0.4×10^3 $cm^2\ g^{-1}$, respectively. Prior to being used, the SiO_2 powder was dried at 120°C to remove physically adsorbed water [12].

H_2SO_4 solutions were prepared from chemically pure grade H_2SO_4 with a density of 1.83 $g\ cm^{-3}$ and distilled water.

The electrical conductivity was measured for stable suspensions (without any indications of sedimentation of particles of the dispersed phase) with an R5021 ac bridge under a polarizing cell voltage of 10 mV [13]. In accordance with the recommendation of [13], the design of the conductometric cell included platinum electrodes without platinum black to preclude damage inflicted on the porous coatings by solid SiO_2 particles in cell filling. In this connection, the frequency dependence of the cell resistance was measured at ac frequencies in the range 0.3–30 kHz, the frequency-independent resistance of the electrolyte system was determined, and the electrical conductivity χ was cal-

1070-4272/05/7807-1084© 2005 Pleiades Publishing, Inc.

culated using these data. The cell constant was determined with a 1 M KCl solution [14]. The electrical conductivity was measured under isothermal conditions in the temperature range 15–70°C, with temperature maintained constant within ±0.1°C. Tests with aqueous sulfuric acid solutions demonstrated agreement with published data within ±4%.

The temperature coefficient of electrical conductivity, α, was calculated from values of the electrical conductivity of the electrolyte systems under study, using the equation [15]

$$\chi_2 = \chi_1[1 + \alpha(t_2 - t_1)],$$

where χ_1 and χ_2 are the electrical conductivities of the suspension at temperatures t_1 and t_2, respectively.

The structural resistance factor β, which characterizes changes in the conducting properties of heterogeneous systems with a liquid dispersion medium and solid dispersed phase, was calculated using the equation [12]

$$\beta = R_s/R_e,$$

where R_s is the suspension resistance and R_e is the electrolyte resistance in the absence of a nonconducting solid phase.

The calculations were carried out with the electrical conductivity of liquid and thickened electrolytes at the same percentage concentration of sulfuric acid.

A stable state of the suspensions prepared, without any indications of settling, is reached in those cases when the content of the dispersed phase is high (about 30%). These systems exhibit a pronounced thixotropy and, presumably, are pseudogels [16]. Figure 1 shows the experimental values of the electrical conductivity of the systems under study as compared with the concentration dependence of χ of aqueous H_2SO_4 solutions, constructed using the data of [17]. These dependences show a weakly pronounced maximum at H_2SO_4 concentrations of 33–35 wt %, with, on the whole, a more than twofold decrease in χ, which is more pronounced for suspensions with larger SiO_2 particles. For electrotechnical and electronic devices, not only the electrical conductivity, but also the total resistance Z of an electrolyte system used, is important [18]: $Z = [R^2 + (1/\omega C)^2]^{1/2}$. Here R and C are, respectively, the ac resistance and capacitance of the cell; and $\varphi = 2\pi f$ (f is the ac frequency) (Table 1). The values of Z, calculated for suspensions with different initial sulfuric acid concentrations, were found to differ less widely than χ (Table 1).

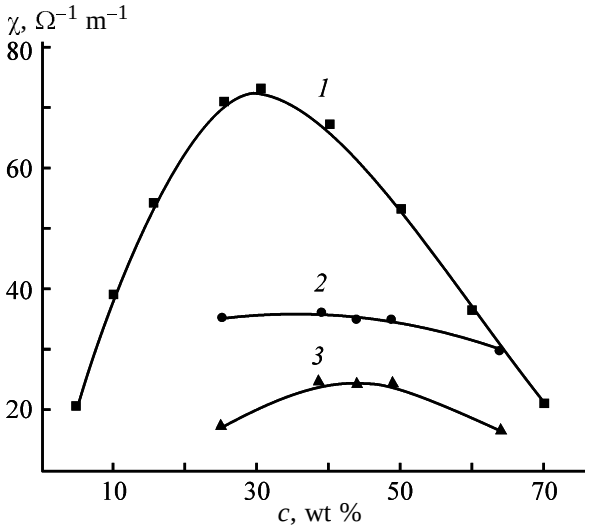


Fig. 1. Electrical conductivity χ of (*1*) H_2SO_4 [17] and (*2*, *3*) SiO_2 suspensions on its basis vs. H_2SO_4 concentration c (18°C). Suspension composition: 10 ml H_2SO_4 + 6.5 g SiO_2. SiO_2 particle size, μm: (*2*) 45–55 and (*3*) 100–110.

Introduction of SiO_2 into an H_2SO_4 solution leads to an increase in the dielectric loss tangent ($\tan\delta = \omega RC$ [18]), which is due to formation of a system of pores and capillaries in the thickened electrolyte (Table 2). Table 2 shows that the structural resistance factor grows with the particle size of the dispersed phase, with the thixotropic period becoming shorter,

Table 1. Values of Z in relation to the initial H_2SO_4 concentration and SiO_2 particle size. Suspension composition: 6.5 g SiO_2 + 10 ml H_2SO_4, 18°C, f = 10 kHz

SiO_2 particle size, μm	Z, Ω, at indicated H_2SO_4 concentration, wt %				
	25	39	44	49	64
45–55	10.2	9.7	9.3	9.0	8.9
100–110	13.7	10.5	9.3	9.7	9.8

Table 2. Effect of SiO_2 additives on the parameters χ and β of a thickened aqueous solution of H_2SO_4 and tanδ (f = 10 kHz) of the cell at 18°C

System, wt %	χ, Ω^{-1} m^{-1}	β	tanδ
H_2SO_4, 27.2	74.58	–	0.159
H_2SO_4, 27.2 + SiO_2 (45–55 μm), 31.5	34.8	2.14	0.173
H_2SO_4, 27.2 + SiO_2 (100–110 μm), 31.5	24.79	3.01	0.174

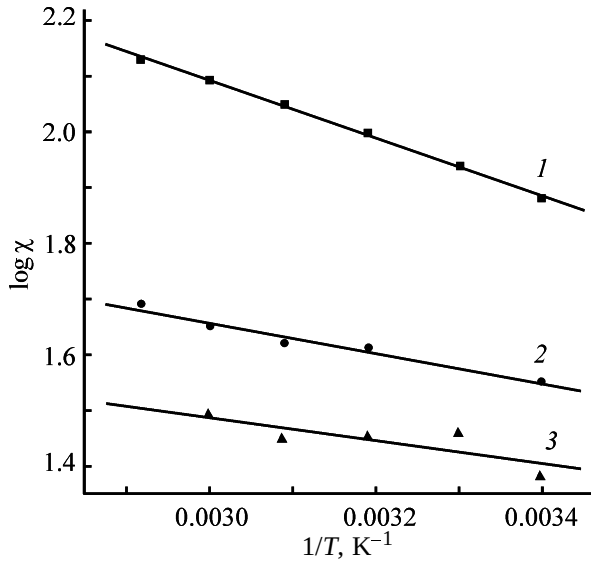


Fig. 2. log χ of the systems vs. 1/*T*. System, wt %: (*1*) 29.5H_2SO_4, (*2*) 29.5H_2SO_4 + 32.7SiO_2 (45–55 μm), and (*3*) 29.5H_2SO_4 + 32.7SiO_2 (100–110 μm).

as demonstrated in [9]. Presumably, large SiO_2 particles can form denser structures because the Coulomb repulsion forces between protonated surface groups of hydrated silica ($\equiv SiOH_2^+$) is overcome in this case more effectively [19].

The temperature dependence of the suspensions under study (Fig. 2), similarly to the case of aqueous H_2SO_4 solutions, is satisfactorily described by the Arrhenius equation [20]: $\chi = \alpha_\chi \exp(-E_{eff}/RT)$. Here, α_χ is the preexponential factor; E_{eff}, effective activation energy of electrical conductivity; R, universal gas constant; and T, temperature (K).

This made it possible to calculate E_{eff} for the systems under study, which were found to be comparable with E_{eff} for H_2SO_4 (Table 3).

Table 3. Values of α and E_{eff} of electrical conductivity of electrolytes based on H_2SO_4

System, wt %	α, Ω^{-1} m^{-1} deg^{-1}	E_{eff}, kJ mol^{-1}
H_2SO_4, 29.5%	0.0157 [21]	9.8 (calculated using the data of [22])
H_2SO_4, 29.5% + SiO_2 (45–55 μm), 32.7%	0.0076	5.1
H_2SO_4, 29.5% + SiO_2 (100–110 μm), 32.5%	0.0077	5.0

Table 3 shows that χ for the system constituted by a solid dispersed phase and a liquid dispersion medium is less sensitive to changes in temperature than an aqueous solution of H_2SO_4, and migration of charged particles and, primarily, H^+ is strongly hindered in the volume-porous structure formed by SiO_2 particles.

CONCLUSION

The electrical conductivity of thickened electrolytes is considerably lower than that of an aqueous solution of sulfuric acid. This is presumably due to appearance of siloxane and hydrogen bonds between SiO_2 particles in the systems studied and to formation of a system of pores and capillaries. The system of pores and capillaries formed by SiO_2 particles creates an additional resistance, and the structural resistance factor strongly depends on the particle size of the dispersed phase.

REFERENCES

1. Bagotskii, V.S. and Skundin, A.N., *Khimicheskie istochniki toka* (Chemical Power Cells), Moscow: Energoizdat, 1981.
2. JPN Patent Appl. 26933.
3. FRG Patent 1796066.
4. UK Patent 1364438.
5. USSR Inventor's Certificate no. 171460.
6. JPN Patent Appl. 15785.
7. US Patent 3202611.
8. Wu Ling, Jiang Xiong, Chen Hong-yu, *et al.*, *J. S. China, Norm. Univ. Natur. Sci.*, 2002, no. 3, pp. 54–58.
9. Grishina, E.P. and Filatova, A.E., *Izv. Vyssh. Uchebn. Zaved., Khim. Khim. Tekhnol.*, 2004, vol. 47, no. 9, pp. 158–161.
10. Matsuda Atsunori, Kanzaki Takao, Tadanaga Kiyoharu, *et al.*, *J. Electrochem. Soc.*, 2002, vol. 149, no. 8, pp. E292–E297.
11. Chelidze, T.D., *Elektropoverkhnostnye yavleniya v dispersnykh sistemakh* (Electrosurface Phenomena in Disperse Systems), Moscow: Nauka, 1972, pp. 40–45.
12. Fridrikhsberg, D.A., *Kurs kolloidnoi khimii* (A Course of Colloid Chemistry), Leningrad: Khimiya, 1984.
13. Lopatin, B.A., *Teoreticheskie osnovy elektrokhimicheskikh metodov analiza* (Theoretical Foundations of Electrochemical Analytical Methods), Moscow: Vysshaya Shkola, 1975.

14. Pratt, K.W., Koch, W.F., Wu, Y.C., and Berezansky, P.A., *Pure Appl. Chem.*, 2001, vol. 73, no. 11, pp. 1783–1793.
15. Damaskin, B.B., Petrii, O.A., and Tsirlina, G.A., *Elektrokhimiya* (Electrochemistry), Moscow: Khimiya, 2001.
16. Balezin, S.A., Erofeev, B.V., and Podobaev, N.I., *Osnovy fizicheskoi i kolloidnoi khimii* (Fundamentals of Physical and Colloid Chemistry), Moscow: Prosveshchenie, 1975.
17. *Spravochnik khimika* (Chemist's Handbook), Nikol'skii, B.P., Ed., Moscow: Khimiya, 1964, vol. 3.
18. Grafov, B.M. and Ukshe, E.A., *Elektrokhimicheskie tsepi peremennogo toka* (Electrochemical ac Circuits), Moscow: Nauka, 1973.
19. *Kapillyarnaya khimiya* (Capillary Chemistry), Slinkina, A.A., Ed., Moscow: Mir, 1983.
20. Fialkov, Yu.Ya. and Grishchenko, V.F., *Elektrovydelenie metallov iz nevodnykh rastvorov* (Electrodeposition of Metals from Nonaqueous Solutions), Kiev: Naukova Dumka, 1985.
21. Dobos, D., *Electrochemical Data*, Budapest: Akad. Kiado, 1978.
22. Maksimova, I.N., Pravdin, N.N., Razuvaev, V.E., *et al*., *Rastvory elektrolitov v vysoko- i nizkotemperaturnom rezhimakh: Fiziko-khimicheskoe issledovanie* (Electrolyte Solutions in High- and Low-Temperature Modes: A Physicochemical Syudy), Leningrad: Leningr. Gos. Univ., 1980, p. 104.

Russian Journal of Applied Chemistry, Vol. 78, No. 7, 2005, pp. 1088–1092. Translated from Zhurnal Prikladnoi Khimii, Vol. 78, No. 7, 2005, pp. 1110–1113.
Original Russian Text Copyright © 2005 by Kurta, Mykytyn, Khaber.

CATALYSIS

Influence of Regeneration Conditions on the Activity of the Catalyst for Oxidative Chlorination of Ethylene

S. A. Kurta, I. M. Mykytyn, and M. V. Khaber

Stefanik Precarpathian National University, Kalush, Ivano-Frankovsk oblast, Ukraine

Received October 13, 2004; in final form, March 2005

Abstract—The possibility of thermochemical regeneration of an industrial batch of a spent and partially deactivated catalyst to improve its activity and selectivity in oxidative chlorination of ethylene to give 1,2-dichloroethane was studied.

In the existing process for manufacture of vinyl chloride by a balanced scheme, 1,2-dichloroethane 1,2-$C_2H_4Cl_2$ is produced by direct and oxidative chlorination of ethylene. The oxidative chlorination process uses as a catalyst $CuCl_2$ supported by γ-Al_2O_3 [1]. The reaction requires a slight excess of C_2H_4 and occurs in accordance with the overall equation [2]

$$C_2H_4 + 2HCl + 0.5O_2 \rightarrow C_2H_4Cl_2 + H_2O + Q. \quad (1)$$

The main reaction is accompanied by side reactions: complete and incomplete combustion of C_2H_4 to give CO and CO_2 [3]:

$$C_2H_4 + 3O_2 \rightarrow 2CO_2 + 2H_2O, \quad (2)$$

$$C_2H_4 + 2O_2 \rightarrow 2CO + 2H_2O. \quad (3)$$

Other possible side reactions yield CCl_4, chloral, trichloroethane, trichloroethylene, etc. (a total of up to 2% relative to 1,2-$C_2H_4Cl_2$ obtained) [4].

In the course of the process, redox reactions may occur on the catalyst surface [5]:

$$C_2H_4 + 2CuCl_2 \rightarrow C_2H_4Cl_2 + 2CuCl, \quad (4)$$

$$2CuCl + 0.5O_2 + 2HCl \rightarrow 2CuCl_2 + H_2O. \quad (5)$$

The appearance of iron in the catalyst can be accounted for by the following reactions between the reactor walls and the catalyst:

$$Fe + CuCl_2 \rightarrow FeCl_2 + Cu, \quad (6)$$

$$4FeCl_2 + O_2 + 4HCl \rightarrow 4FeCl_3 + 2H_2O, \quad (7)$$

$$2FeCl_3 + 3H_2O \xrightarrow{\Delta} Fe_2O_3 + 6HCl. \quad (8)$$

EXPERIMENTAL

The study was performed on the newly created experimental laboratory installation that operates on real process gases (taken from the stage of ethylene oxychlorination at a shop of Lukor Private Company, Kalush) and adequately models the industrial process.

After two years of operation, the characteristics of the catalyst changed, which led to a decrease in its activity in oxychlorination. Therefore, our goal was to study the possibility of regenerating the oxychlorination catalyst and to analyze methods of such a regeneration under the conditions maximally similar to those used in the industry.

Experiments on catalyst regeneration were performed in two ways: by thermal treatment of the catalyst in a fluidized bed in oxygen-rich gas mixture or in air and by washing the catalyst in dichloroethane. In addition, the physicomechanical properties of catalyst samples before and after regeneration were studied.

The regeneration was performed in two modes: in air with heating to 180, 210, and 250°C and at increased oxygen content (20, 30, and 40 vol %) and nitrogen content of 80, 70, and 60 vol %, respectively. Simultaneously, analyses for the content of copper(I, II, total) chloride and iron(III) in the catalyst were made, with the bulk weight m_b, specific surface area S_{sp}, and pore volume V in the catalyst determined before and after regeneration. The data obtained are listed in the table.

In addition, the table lists data on washing of the catalyst to remove iron(III) chloride by extraction into dichloroethane and describes changes in the physicomechanical properties of the catalyst.

1070-4272/05/7807-1088 © 2005 Pleiades Publishing, Inc.

Physicomechanical properties of the catalyst for oxychlorination of ethylene before and after its regeneration in the air and oxygen-rich gas mixture. Regeneration duration 8 h

Catalyst	Cu(I, II) content, wt %	Fe(III) content, wt %	V, $cm^3\ g^{-1}$	S_{sp}, $m^2\ g^{-1}$	m_b, $g\ cm^{-3}$	Color
Fresh	4.2	0.12	0.36	140.0	1.02	Green
Without regeneration	4.15	0.30	0.26	74.5	1.31	Brown
After regeneration:						
180°C	4.10	0.30	0.26	78.5	1.29	Dark green
210°C	4.51	0.301	0.276	85.0	1.28	Green
250°C	4.585	0.30	0.286	99.0	1.27	Lettuce-green
Extraction in dichloroethane:						
80°C	4.75	0.254	0.276	101.2	1.12	Dark green
60°C (agitation)	4.58	0.255	0.269	100.0	1.12	Green
After regeneration with O_2/N_2, vol %:						
210°C 30/70	4.18	0.31	0.27	100.5	1.27	〃
210°C, 40/60	4.76	0.275	0.28	105.0	1.26	Light green
250°C, 40/60	4.77	0.26	0.32	108.0	1.25	Green

As the concentration of oxygen in the regenerating gas increases, the bulk weight of the catalyst decreases from 1.3 to 1.27–1.25 $g\ l^{-1}$, which is due to partial removal of by-products formed in the oxychlorination. This may be confirmed by a simultaneous increase in the pore volume in the catalyst, with this dependence being more pronounced at 250°C.

Gradually raising the temperature from 180 to 250°C in regeneration leads to a considerable increase in the pore volume from 0.25 to 0.3–0.33 $cm^3\ g^{-1}$, and this dependence is stronger at increased concentrations of oxygen, compared with the regeneration in air.

As seen from the table, the content of Fe(III) in the catalyst remains, on the whole, unchanged when the temperature is raised in air and decreases from 0.3 to 0.26 wt % in the case of regeneration in the oxygen-rich gas mixture. The best results, as regards the decrease in the amount of Fe(III), were obtained in extraction washing of the catalyst in boiling dichloroethane. In this case, the content of Fe(III) in the catalyst decreased to 0.25 wt %. Apparently, dichloroethane can dissolve $FeCl_3$ [1], which makes it possible to use this method to partly diminish the amount of Fe(III) formed on the oxychlorination catalyst and poisoning it.

After regeneration for 8 h at a prescribed temperature, the activity and selectivity of the regenerated catalyst in oxidative chlorination of C_2H_4 was studied in the standard operation mode: 225°C, $C_2H_4 : HCl : O_2 = 1.07 : 2 : 0.7$, flow rate of the circulation gas (60% CO_2) 72–80 $l\ h^{-1}$, temperature of the quenching column 87–100°C, pressure in the system 7–12 kPa, total flow rate of exhaust gases 76–86 $l\ h^{-1}$, and experiment duration 1 h. Additionally, the circulation gas was analyzed for the content of CO, CO_2, C_2H_4, and O_2 in the course of an experiment. After the experiment, the weight of the dichloroethane formed was determined, its purity and the content of microimpurities were analyzed chromatographically, and the content of unchanged HCl was measured. After that, the conversion in terms of hydrogen chloride and C_2H_4 and the yield of dichloroethane in percent relative to the theoretical value before and after regeneration in air and in oxygen-rich gas mixture were calculated.

Figure 1 (curves *1*, *2*) shows that the conversion of hydrogen chloride remains unchanged (~98.5%) upon regeneration of the catalyst in air and O_2. At the same time, the conversion of C_2H_4 upon regeneration (curves *3*, *4*) grows from 89 to 94–95% as the content of O_2 in the regenerating gas increases from 20 to 40%, with this trend being particularly pronounced at 250°C.

Figure 2 shows how the combustion of C_2H_4 on the catalyst subjected to regeneration depends on the content of O_2 in the regenerating gas at 210 and 250°C.

After regeneration of the catalyst, the combustion of C_2H_4 in synthesis of 1,2-dichloroethane (Fig. 2)

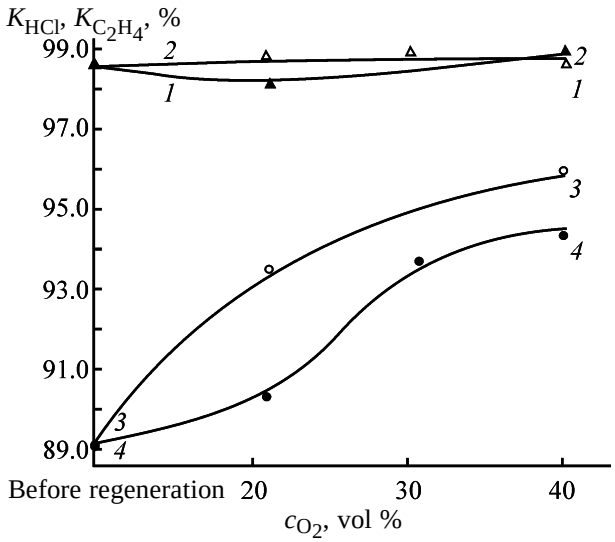


Fig. 1. Conversion of (*1*, *2*) HCl (K_{HCl}) and (*3*, *4*) C_2H_4 ($K_{C_2H_4}$) on a regenerated catalyst vs. the content of oxygen, c_{O_2}, in the regenerating gas. Temperature, °C: (*1*, *3*) 210 and (*2*, *4*) 250.

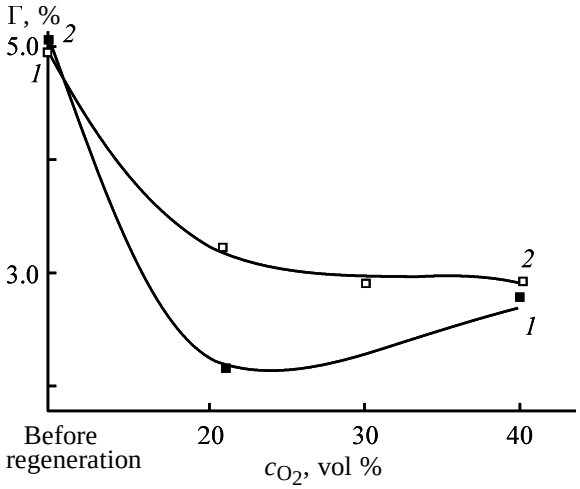


Fig. 2. Combustion Γ of C_2H_4 on a regenerated catalyst vs. the content of oxygen, c_{O_2}, in the regenerating gas. Temperature, °C: (*1*) 250 and (*2*) 210.

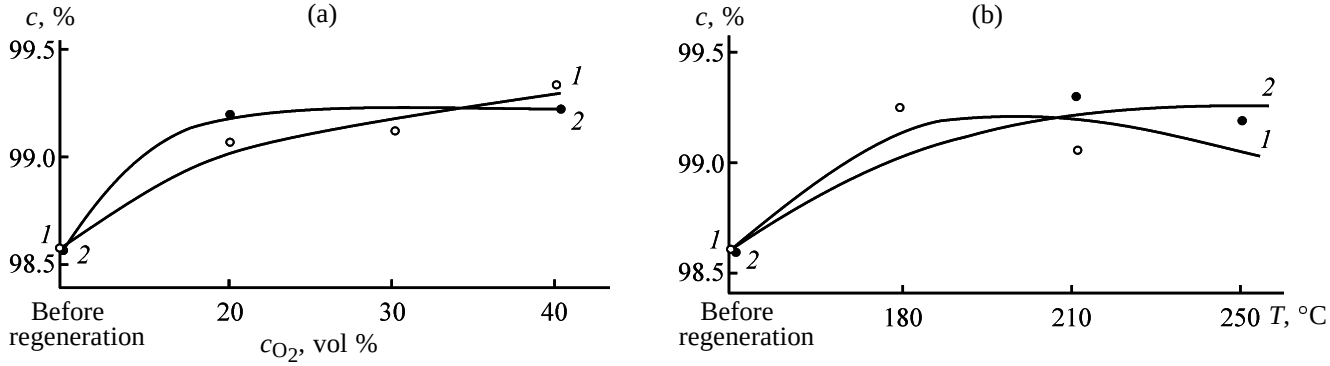


Fig. 3. Purity *c* of dichloroethane obtained on a regenerated catalyst vs. (a) content of oxygen, c_{O_2}, in the regenerating gas and (b) temperature *T* of the catalyst regeneration. (a) Temperature, °C: (*1*) 210 and (*2*) 250. (b) Medium: (*1*) air and (*2*) 40 vol % oxygen; the same for Fig. 4.

decreases from 5 to 2.5–3% in proportion to an increase in the content of O_2 in the regenerating gas. The same trend is observed on raising the regeneration temperature from 180 to 210 and 250°C.

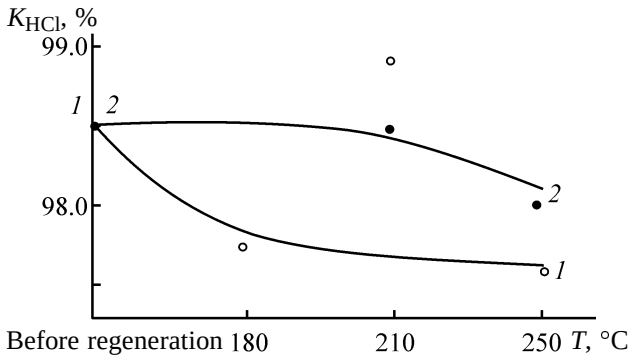


Fig. 4. Conversion of HCl, K_{HCl}, on a regenerated catalyst vs. the temperature *T* of catalyst regeneration.

Figures 3a and 3b show how the purity of dichloroethane in synthesis of 1,2-dichloroethane depends on the content of O_2 in the regenerating gas and on the temperature of catalyst regeneration. It can be seen that the purity of dichloroethane grows from 98.6% before regeneration to 99.5% after regeneration as the temperature is raised or the content of O_2 in the regenerating gas is made higher. In this case, the tendency toward an increase in the purity of dichloroethane is more pronounced when the regeneration is performed in an oxygen-rich gas mixture (Figs. 3a, 3b; curves *2*).

Figure 4 shows how the conversion of HCl in the catalytic synthesis of 1,2-dichloroethane depends on the temperature of the catalyst regeneration in air and in an oxygen-rich gas mixture (Fig. 4, curves *1*, *2*). It can be seen that the conversion of HCl decreases

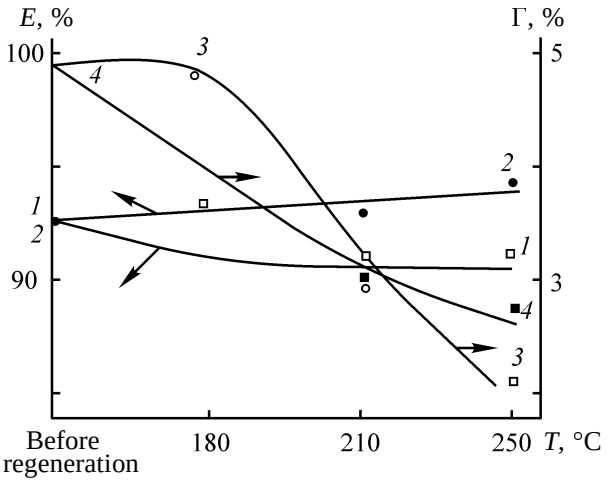


Fig. 5. (*1, 2*) Efficiency E of C_2H_4 conversion and (*3, 4*) C_2H_4 combustion Γ on a regenerated catalyst vs. the temperature T of catalyst regeneration. Medium: (*1, 3*) air and (*2, 4*) oxygen-rich gas mixture; the same for Fig. 6.

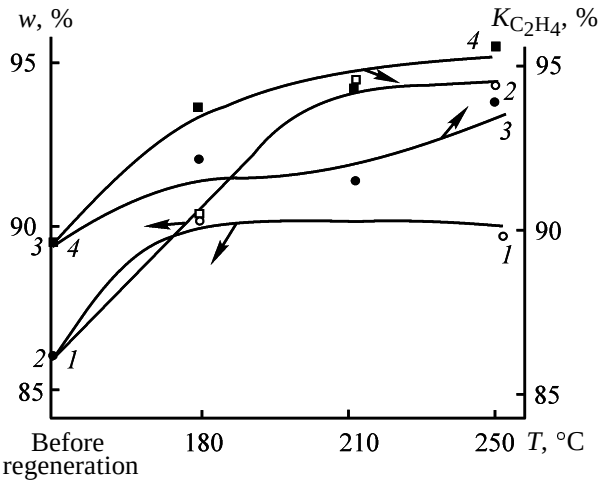


Fig. 6. (*1, 2*) Yield w of dichloroethane (relative to the theoretical value) and (*3, 4*) C_2H_4 conversion $K_{C_2H_4}$ on a regenerated catalyst vs. the temperature T of catalyst regeneration.

from 98.5 to 97.5–98%. This decrease is more pronounced in the case of regeneration in air, compared with that in the oxygen-rich gas mixture.

The increase in the conversion of C_2H_4 and decrease in its combustion after regeneration is understandable, because they are associated with partial restoration of the structure and activity of the catalyst after its thermochemical treatment in an O_2 atmosphere, which is due to oxidation of the catalyst surface and removal of tar and carbon black therefrom. This is, in turn, confirmed by the improvement of the physicomechanical properties of the catalyst, namely, by an increase in the specific surface area and pore volume and decrease in the bulk weight (see table).

Figure 5 shows how the efficiency of C_2H_4 conversion (curves *1, 2*) and C_2H_4 combustion (curves *3, 4*) in synthesis of 1,2-dichloroethane on a regenerated catalyst depend on the temperature of catalyst regeneration in air and an oxygen-rich gas mixture. It can be seen that the efficiency of C_2H_4 conversion into dichloroethane grows from 92.5 to 93–94% as the regeneration temperature increases from 180 to 250°C in the oxygen-rich has mixture (Fig. 5, curve *2*). Simultaneously, the combustion of C_2H_4 decreases from 5% before regeneration to 2–2.5% after regeneration as the temperature of catalyst regeneration is increased to 250°C.

Additionally, we calculated the yield of dichloroethane in synthesis of 1,2-dichloroethane (relative to the theoretical value) and its dependence on the temperature of catalyst regeneration (Fig. 6, curves *1, 2*). These data are compared with the dependence of the ethylene conversion in synthesis of 1,2-dichloroethane on the temperature of the catalyst regeneration (Fig. 5, curves *1, 2*) in the air and oxygen-rich gas mixtures. Figure 5 shows that the C_2H_4 conversion and yield of dichloroethane relative to the theoretical value tend to increase on a regenerated catalyst as the temperature of catalyst regeneration is raised. In this case, the C_2H_4 conversion increases by 5–7% upon regeneration, the yield of dichloroethane also grows by 5–7%. This confirms once more the fact that the catalyst activity in C_2H_4 conversion into dichloroethane increases after regeneration. The yield of by-products, trichloroethane, trichloroethylene, and others, does not increase in the case of a partly regenerated catalyst, and the combustion of C_2H_4 is suppressed.

CONCLUSIONS

(1) A partly deactivated catalyst for C_2H_4 oxychlorination can be regenerated. The regeneration in an oxygen-rich gas mixture (30–40 vol % O_2) is more effective than that in air (20 vol % O_2) under the same treatment conditions (180–210–250°C, 8 h).

(2) The regeneration improved the physicomechanical properties of the catalyst, namely, increased the pore volume and the specific surface area (by 10–20%) and decreased the bulk weight, and thus enhanced the activity and selectivity of a regenerated catalyst in oxychlorination of ethylene into 1,2-dichloroethane.

REFERENCES

1. Flid, M.R., Resource-Saving Chlorine-Balanced Processes for Synthesis of Vinyl Chloride from Ethane–

Ethylene Raw Materials, *Doctoral Dissertation*, Sintez Research Institute with a Design Office, Federal State Unitary Enterprise, 2002.

2. Flid, M.R., Kurlyandskaya, I.I., Solomonik, I.G., and Babotina, M.V., *Khim. Prom–st.*, 1996, no. 18, p. 38.
3. Kurta, S.A., Khaber, M.V., and Mikitin, I.M., *Khim. Prom–st. Ukr.*, 2003, no. 2 (55), pp. 9–14.
4. *Promyshlennye khlororganicheskie produkty: Spravochnik* (Industrial Organochlorine Products: Reference Book), Oshin, L.A., Ed., Moscow: Khimiya, 1978.
5. Kurta, S.A. and Mikitin, I.M., Abstracts of Papers, *Naukovo-tekhnichna konferentsiya "Postup v naftogazopererobnii ta naftokhimichnii promislovosti"* (Scientific and Technical Conf. "Advances in Oil-and-Gas-Processing and Petrochemical Industry"), Lviv, September 13–16, 2004.

Russian Journal of Applied Chemistry, Vol. 78, No. 7, 2005, pp. 1093–1095. Translated from Zhurnal Prikladnoi Khimii, Vol. 78, No. 7, 2005, pp. 1114–1116.
Original Russian Text Copyright © 2005 by Kagarlitskii, Krichevskii, Balpanov.

CATALYSIS

Synthesis of 2-Methylpyrazine on Ternary Oxide Catalysts

A. D. Kagarlitskii, L. A. Krichevskii, and D. S. Balpanov

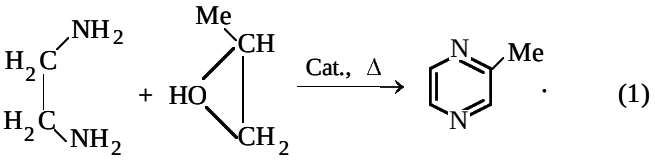
Institute of Phytochemistry, Ministry of Education and Science of the Kazakhstan Republic, Karaganda, Kazakhstan

Received July 20, 2004; in final form, April 2005

Abstract—Synthesis of 2-methylpyrazine by cyclocondensation of ethylenediamine with 1,2-propylene glycol in the presence of zinc–molybdenum–chromium catalysts was studied.

2-Methylpyrazine (MP) is used as an intermediate in synthesis of pyrazine-2-carboxamide (the basis of Pyrazinamide antituberculous drug [1]), but the existing procedures of its preparation are not perfect.

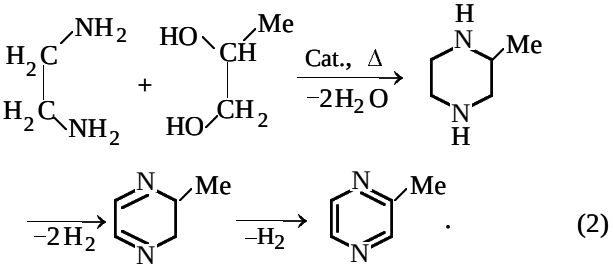
MP can be prepared by the reaction of propylene oxide with ethylenediamine (EDA) in methanol in the presence of zinc–molybdenum–chromium oxide catalyst (yield 63%) [2]:



(1)

The similar process was developed by the Prikladnaya Khimiya Russian Scientific Center [3]. An important draw-back of this process is the use of highly explosive initial products (propylene oxide and hydrogen) and of toxic methanol as a solvent.

From the viewpoint of industrial safety and availability of fairly cheap starting compounds, the catalytic dehydrocyclization of EDA with 1,2-propylene glycol (1,2-PG) is a more promising route to MP:



(2)

The attempts to use Al_2O_3 as a catalyst of this process failed due to its low selectivity [4]. However, the purity of alkylpyrazines was improved and the yield of MP was increased to 64% with zinc oxide catalysts [5–7].

In dehydrocyclization of EDA with 1,2-PG on the Pd/Zn–Cr–O catalyst (Zn : Cr = 1 : 3), the limiting stage of the process is the reaction of 1,2-PG adsorbed on the catalyst surface with EDA supplied with the gas phase to form MP (387°C) [8]. The system EDA–1,2-PG is more complicated than that described by the reaction equation, since synthesis of MP is accompanied by formation of by-products [9].

Initially this process was studied in the presence of granulated binary zinc–molybdenum oxide catalysts. The highest yield (75%) was obtained with the catalyst of the composition ZnO : MoO_3 = 1.0 : 0.3 (granule size 1.0–2.0 mm) [10].

EXPERIMENTAL

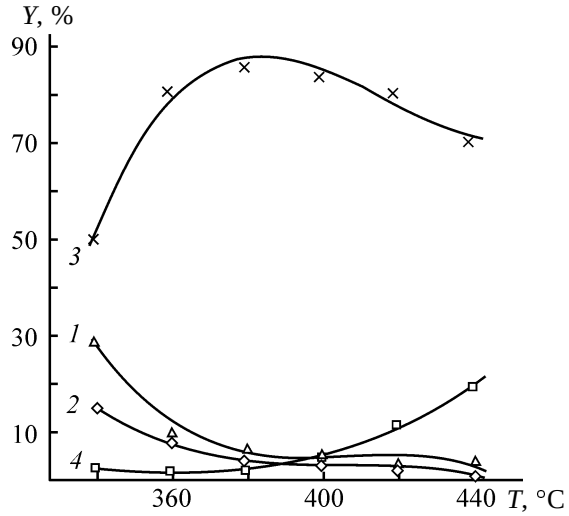
To increase the yield of the target product through decreasing the amount of polymeric deposits at the catalyst surface, it was suggested to add chromium(III) oxide to binary oxide systems, since Cr_2O_3 has high oxidation and dehydrogenation power. In addition, it was assumed that, owing to its characteristics, it will enhance the mechanical strength of the catalyst granules during thermal drying.

Table 1 shows how the ratio of components of

Table 1. Yield of MP at various catalyst compositions. Temperature 460°C, contact time 3.3 s

Molar ratio ZnO : MoO_3 : Cr_2O_3	Catalyst operation time, h	Yield of MP, %
1.00 : 0.30 : 0.05	7	67
1.00 : 0.30 : 0.10	9	78
1.00 : 0.30 : 0.15	10	69
1.00 : 0.40 : 0.10	23	73
1.00 : 0.40 : 0.15	27	82
1.00 : 0.40 : 0.20	21	76
1.00 : 0.50 : 0.15	17	71
1.00 : 0.50 : 0.20	22	76
1.00 : 0.50 : 0.25	24	64

1070-4272/05/7807-1093 © 2005 Pleiades Publishing, Inc.



Yield in synthesis of MP *Y* as a function of the process temperature *T* at a contact time of 4.2 s. (*1*) EDA, (*2*) 1,2-PG, (*3*) MP, and (*4*) PCPs.

mixed zinc–molybdenum–chromium oxide granulated catalyst affects the MP yield.

The yield of the target product on the catalysts tested was from 65 to 82%. When the content of zinc and molybdenum(III) oxides in these catalysts corresponded to the molar ratio of 1.0 : 0.3, they lost their activity and selectivity in 7–10 h, whereas at the molybdenum(III) oxide content of 0.4 and 0.5 mol per mole of zinc oxide they operated without regeneration for a period from 21 to 27 h depending on the amount of chromium(III) oxide added.

Table 2. Yield of MP at various contact times τ_c. Temperature 390°C

τ_c, s	Unchanged, wt %		Yield, %	
	EDA	1,2-PG	PCPs	MP
1	2	3	4	5
1.5	15	18	2	65
3.0	10	12	1	77
4.4	3	5	4	88
6.0	2	4	10	85
7.5	2	5	21	72
9.0	1	2	32	55

Table 3. Yield of MP at various time τ. Temperature 390°C, contact time 4.4 s

τ_c, s	Unchanged, wt %		Yield, %	
	EDA	1,2-PG	PCPs	MP
10	16	2	5	77
20	8	3	3	86
30	4	5	1	90
40	2	8	2	87
50	1	9	5	85
60	5	11	10	74

The best result were obtained with the catalyst of the composition $ZnO : MoO_3 : Cr_2O_3$ = 1.00 : 0.40 : 0.15.

The yield of MP exceeding 70% is reached on this catalyst in a wide temperature range, from 370 to 430°C, and the highest yield (80–90%), at 380–395°C, which is a relatively low temperature for these reactions (see figure).

As regards contact time, it can be varied in a wide range (from 1.5 to 7.5 s), and in this case the yield of MP can be no less than 65% due to decreasing content of polycondensation products (PCPs) in the catalyzate (Table 2). In the range 4.4–6.0 s, the yield of the target product reaches 80–88%.

Evaluation of the working time of the catalyst showed that the catalyst is able to operate for 55–57 h without noticeable variation of selectivity with respect to the target product, ensuring its yield as high as 85–90% (Table 3).

The $ZnO : MoO_3 : Cr_2O_3$ = 1.0 : 0.4 : 0.15 catalyst was prepared by mixing zinc, molybdenum(III), and chromium oxides to obtain a homogeneous mass. Granules were prepared from this mixture on a pan granulator with adding 5% NaOH and 10% aqueous polyvinyl alcohol for strengthening. The granules were sifted through a sieve, and a 1.0–2.0-mm fraction was collected. Then, the granules were dried for 3 h at 105°C. Dry granules were promoted with 3% aqueous $MnSO_4$ and 1% H_3PO_4. After promotion, the granules were subjected to air calcination for 5 h with a stepwise increase in temperature in the range 100–150, 150–250, 250–350, and 350–600°C. The final catalyst consists of greenish porous granules.

MP was synthesized on an installation equipped with a stainless steel flow-type tubular reactor (tube diameter 20 mm, length 80 cm), in which 150 cm^3 of the catalyst was placed. An equimolar mixture of EDA with 1,2-PG, diluted with water (20 vol %) and preliminarily passed through a vapor heater with a temperature of 280–300°C, was fed to the reactor. The experiments were carried out for 1 h. The reaction products were cooled in a trap system. In a typical synthesis, a mixture containing 67 ml of EDTA (1 mol), 73 ml of 1,2-PG (1 mol), and 28 ml of water

(1.56 mol) was fed into the reaction mixture with a dosing pump at a rate of 0.79 ml min^{-1}. MP was isolated from the reaction mixture by distillation on a column in the form of an azeotropic mixture with water (bp 97°C/737 mm Hg, MP content 45% [11]), from which the target product was extracted with chloroform or diethyl ether. After drying and removal of the solvent, MP was extracted by distillation on a column; a fraction with bp 133–135°C was collected. After the second distillation, MP had the following characteristics: bp 135°C, n_D^{20} 1.5050, d_4^{20} 1.030, which is in good agreement with published data [12].

The quantitative content of the unchanged starting components and the reaction product was determined by gas–liquid chromatography (Chrom-5, flame-ionization detector, glass column 3.5 m long with 0.3 cm inner diameter, packed with Chromaton NAW-HMDS and 5% SE-30 silicone elastomer); column temperature 150°C, vaporizer temperature 180°C, detector temperature 190°C; carrier gas argon, flow rate 20 ml min^{-1}.

Quantitative analysis was performed using benzonitrile as internal reference.

CONCLUSION

The catalyst Zn : MoO_3 : Cr_2O_3 = 1.00 : 0.40 : 0.15 was developed. The use of this catalyst in cyclocondensation of ethylenediamine with 1,2-propyleneglycol allows preparation of 2-methylpyrazine in 85–90% yield. The working life of the new catalyst before regeneration reaches 50–55 h, and the total working life of the catalyst is 400–450 h.

REFERECES

1. Mashkovskii, V.V., Shchekina, E.G., and Chernova, T.M., *Provizor*, 2002, no. 10, pp. 44–46.
2. JPN Patent Appl. no. 55-45610.
3. *TU* (Technical Specifications) *24-44-00480689–94: 2-methylpyrazine*, St. Petersburg: Prikladnaya Khimiya Russia Scientific Center, 1994.
4. Okada, D. and Nakano, K., *Yakugaku Zasshi*, 1971, vol. 91, no. 3, pp. 416–421.
5. US Patent no. 4097478.
6. JPN Patent Appl. no. 54-132588.
7. JPN Patent Appl. no. 53-37675.
8. Forni, L. and Polessel, P., *J. Catal.*, 1999, vol. 130, no. 2, pp. 403–410.
9. Forni, L., *Appl. Catal.*, 1988, vol. 11, no. 1, pp. 199–209.
10. Balpanov, D.S., Kagarlitskii, A.D., and Krichevskii, L.A., *Zh. Prikl. Khim.*, 2001, vol. 74, no. 12, pp. 2065–2067.
11. Ogorodnikov, S.K., Lesteva, T.M., and Kogan, V.B., *Azeotropnye smesi: Spravochnik* (Azeotropic Mixtures: A Handbook), Leningrad: Khimiya, 1971, pp. 1265–1266.
12. Bader, A., Harvey, D., and Nagarkatti, G., *Aldrich Handbook of Fine Chemicals*, Milwaukee, Wisconsin: Aldrich Chem., 1990, p. 1113.

Russian Journal of Applied Chemistry, Vol. 78, No. 7, 2005, pp. 1096–1100. Translated from Zhurnal Prikladnoi Khimii, Vol. 78, No. 7, 2005, pp. 1117–1121.
Original Russian Text Copyright © 2005 by Golovashin, Lazarev, Mamontov.

PROCESSES AND EQUIPMENT OF CHEMICAL INDUSTRY

Kinetic Characteristics of Reverse-Osmosis Separation of an Aqueous Solution of Aniline in a Flat-Frame Apparatus

V. L. Golovashin, S. I. Lazarev, and V. V. Mamontov

Tambov State Technical University, Tambov, Russia

Received April 5, 2005

Abstract—Reverse-osmosis separation of an aqueous solution of aniline on a flat-frame reverse-osmosis installation was studied for two types of industrial polymeric membranes in relation to the concentration and pressure of the solution in the intermembrane channel. The behavior of the main kinetic characteristics of separation was analyzed and explained for different physical conditions of the process.

The goal of this study was to examine membrane methods in separation of aqueous solutions of low-molecular-weight organic substances in manufacture of intermediates of organic synthesis and in treatment of wastewater from chemical and related plants. An aqueous solution of aniline, which is present in many kinds of industrial solutions and wastewater from production of dyes, served as a model.

Our studies were aimed to reveal the influence exerted by the concentration of a solute and the pressure on the specific flux of a solvent and on the retention factor of the membranes. The experiments were performed on an installation with a closed circulation of the solution in a two-chamber cell of the flat-frame type with industrial composite membranes of MGA-95K and OPM-K brands (manufactured by Vladipor Joint-Stock Company, Vladimir, Russia). The flow velocity of the solution in the intermembrane channel was 0.4 m s^{-1}, and the solution temperature, 22°C. The model solution was prepared using aniline of pure grade and distilled water. The experiments were performed using the procedure and apparatus described in [1].

The retention factor of membranes depends on a large number of factors (material of a membrane, nature of a solute and its concentration, working pressure, temperature, hydrodynamic situation over the membrane, etc.) [2–6] and is an integral quantity.

The dependences of the retention factor of the membranes on the concentration of the solution under study and on the working pressure are shown in Fig. 1. It can be seen that the aniline retention factors and the trends in their variation with the solution concentration strongly differ for the membranes studied (MGA-95K and OPM-K) and have negative and posi-

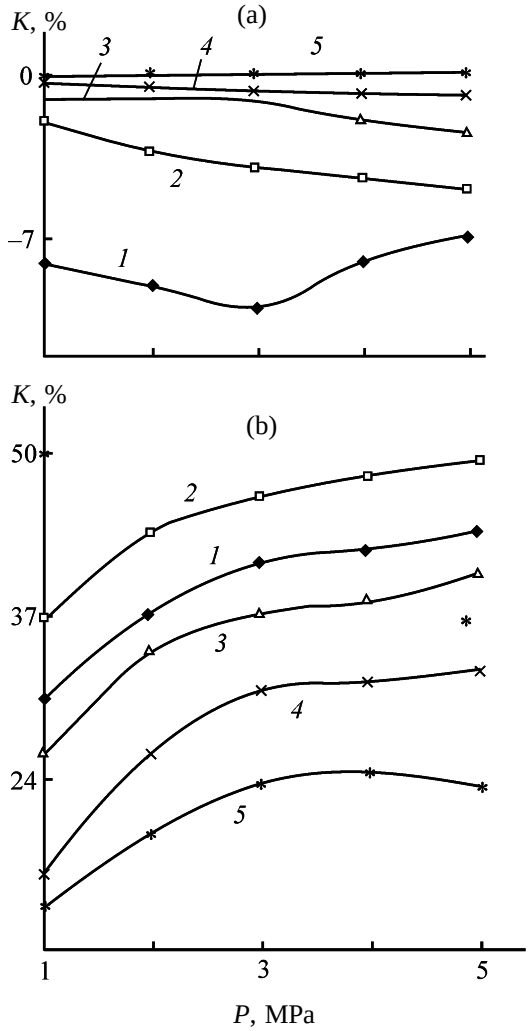


Fig. 1. Retention factor K of (a) MGA-95K and (b) OPM-K membranes for an aqueous solution of aniline vs. pressure P. Concentration of the starting aniline solution (kg m^{-3}): (*1*) 0.507, (*2*) 3.85, (*3*) 7.0, (*4*) 9.63, and (*5*) 14.18; the same for Fig. 2.

1070-4272/05/7807-1096 © 2005 Pleiades Publishing, Inc.

tive values. The manner in which the retention factor varies with the solution concentration and pressure applied can be explained using the hypothesis of a solution flow across the membrane as a flow through pores with the potential barrier overcome by the solute [6]. This hypothesis is an outgrowth of the sorption-sieve hypothesis [7, 8].

In the case of the MGA-95K membrane, the retention factor for an aqueous solution of aniline varies with concentration as follows: as the aniline concentration grows, the retention factor of the membrane passes from negative to zero values (Fig. 1). This effect can be understood on the basis of the following considerations: being a polar low-molecular-weight organic compound [9], aniline can form hydrogen bonds with the material of the MGA-95K membrane, and, therefore, a considerable amount of aniline is sorbed on its surface and within its pores (the content of aniline in the near-membrane layer becomes higher than that in the solution bulk, which is indicated by previous studies of sorption [10]). Aniline is mainly transferred across the membrane surface by a convective flow, with a negative retention factor observed in this case. A further increase in the concentration leads to filling of the membrane pores with aniline, with the "finest" pores blocked. The concentration of water decreases and the convective flow rate also becomes lower, with the result that the retention factor of the membrane becomes zero. It is known that, for low-molecular-weight organic substances, there exist narrow concentration ranges of aqueous solutions [11, 12] in which physicochemical parameters of these solutions (viscosity, density, surface tension) have an extremum. Probably, this range for the aqueous solution of aniline is 2–4 kg m^{-3}, and, therefore, the retention factor for the OPM-K membrane has a maximum within this range. As the concentration increases further, the retention factor decreases. At the same time, it should be taken into account that the properties of the solution within fine pores of the membrane may strongly differ from those in the free volume and be dependent on the sign and magnitude of the surface charge. As a result, the energy of interaction between the solute molecules and the surface of membrane pores changes (and, consequently, so does the distribution coefficient), which leads to a change in the retention factor of the membrane.

The above analysis is also valid for the OPM-K membrane. However, it is necessary to take into account a different pore radius distribution in the active layer of the membrane and its higher porosity, which probably leads to higher retention factors (which are all in the positive region), compared with the MGA-95K membrane. It should be noted that the substance is transferred across the membrane by two flows, convective and of the diffusion type. The data previously obtained in determining the diffusion permeability indicated that the diffusion transfer of the substance predominates, because the diffusion permeability coefficient has large values [13].

Table 1. Coefficients for calculation of the retention factor of membranes and the specific flux of the solvent

Membrane	Retention factor			Specific flux	
	k_1	k_2	k_3	k_1	n
MGA-95K	0.29	0.058	5	–0.5	0.6
OPM-K	0.02	1.1	0.1	1.9	–0.06

The retention factor of the membranes was calculated using formula (1) reported in [6]. In this formula, the diffusion coefficient in the membrane is replaced with the ratio of the diffusion permeability of the membrane to the distribution coefficient, and the thickness of the diffusion boundary layer, with the expression taken from [16]:

$$K = 1 - \{1 + [1/(k_d - k_1) - 1][1 - \exp(-J\delta k_d k_2/P_d)] \times \exp[J \times 0.0021 k_3/(D_0 w^{1/2})]\}^{-1}, \quad (1)$$

where J is the specific flux of the solvent across the membrane ($m^3\ m^{-2}\ s^{-1}$); w, solution flow velocity in the intermembrane space ($m\ s^{-1}$); P_d, diffusion permeability of the membrane ($m^2\ s^{-1}$); δ, membrane thickness (m); D_0, diffusion coefficient of aniline in solution ($m^2\ s^{-1}$); k_d, distribution coefficient; and k_1–k_3, numerical coefficients.

The coefficients for the solution and membranes studied are listed in Table 1. The disagreement between the results of calculation by formula (1) and the experimental data, listed in Table 2, does not exceed ±20%.

Let us then consider the influence exerted by the solute concentration on the specific flux of the solvent across the membrane. The dependences of the specific solvent flux across the MGA-95K and OPM-K membranes on the concentration of the solution under study and the working pressure are plotted in Fig. 2. It can be seen that the specific solvent flux across the membrane strongly depends on the concentration and

Table 2. Experimental and calculated data on reverse-osmosis separation of a model aqueous solution of aniline

P, MPa	c_{in}, kg m^{-3}	*K*, %		$J \times 10^6$, m^3 m^{-2} s^{-1}	
		expt.	calc.	expt.	calc.
		MGA-95K membrane			
1	0.507	–8	–8.8	1.3	1.2
2		–9	–11.5	2.6	2.5
3		–10	–11.2	3.8	3.7
4		–8	–9.6	5.1	4.9
5		–7	–7.86	6.4	6.1
1	3.85	–2	–6.2	0.75	0.73
2		–3.3	–9.7	1.28	1.46
3		–4	–11.3	2.03	2.19
4		–4.5	–11.6	2.99	2.9
5		–5	–11.2	3.42	3.7
1	7.0	–1	–0.78	0.46	0.45
2		–1.1	–1.36	0.83	0.9
3		–1.2	–1.76	1.28	1.35
4		–2	–2.02	1.8	1.8
5		–2.5	–2.2	2.08	2.25
1	9.63	–0.3	–0.32	0.32	0.3
2		–0.57	–0.57	0.64	0.6
3		–0.78	–0.78	0.96	0.9
4		–0.9	–0.94	1.18	1.2
5		–1	–1.06	1.6	1.5
1	14.18	–0.02	–0.013	0.142	0.149
2		–0.025	–0.025	0.34	0.298
3		–0.035	–0.035	0.48	0.447
4		–0.045	–0.045	0.71	0.596
5		–0.054	–0.054	0.86	0.744
		OPM-K membrane			
1	0.507	30.4	20.66	2.99	2.78
2		37.2	34.13	5.128	5.57
3		41.2	43.61	8.29	8.36
4		42.2	50.64	11.36	11.14
5		43.4	56.1	13.03	13.93
1	3.85	36.6	18.92	2.4	2.22
2		43.6	31.75	4.63	4.44
3		46.3	41.01	6.94	6.7
4		48	48.03	9.09	8.88
5		49.1	53.52	11.31	11.1
1.0	7.0	26	18.47	1.85	2.1
2.0		34	31.11	3.89	4.18
3.0		37.2	40.32	6.12	6.26
4.0		38	47.32	8	8.35
5.0		40	52.82	10.25	10.44
1.0	9.6	16.4	18.23	1.67	2.0
2.0		26	30.78	3.43	4.0
3.0		30.9	39.95	5.7	6.0
4.0		31.5	46.94	7.32	8.0
5.0		32.5	52.44	9.55	10.11
1.0	14.2	13.7	17.94	1.6	1.95
2.0		19.6	30.37	3.34	3.89
3.0		23.5	39.5	4.91	5.84
4.0		24.2	46.5	7.05	7.78
5.0		23.3	51.97	8.99	9.73

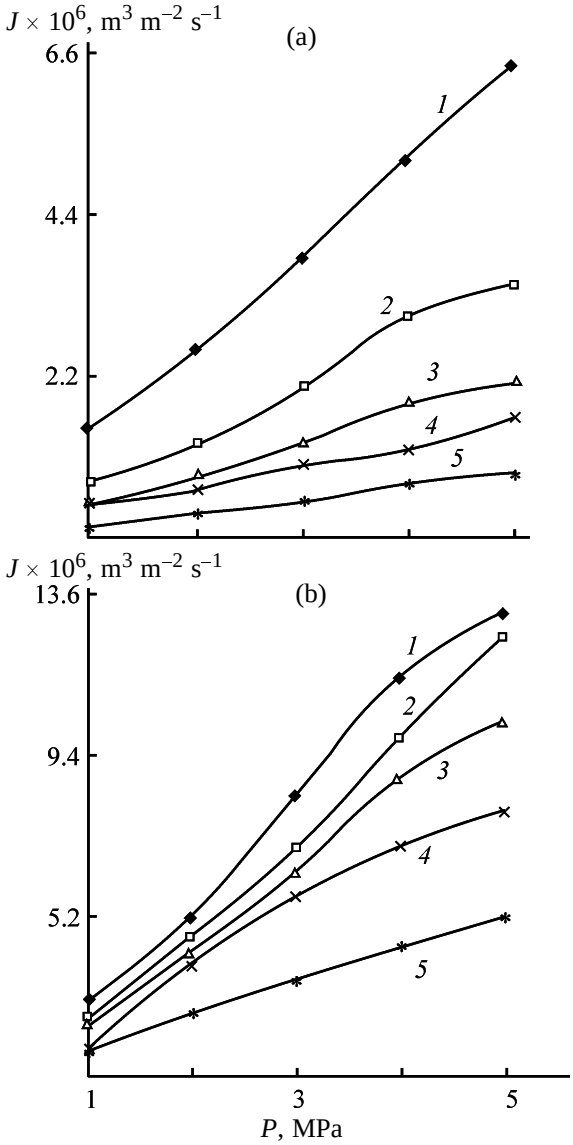


Fig. 2. Specific flux *J* of the solvent across (a) MGA-95K and (b) OPM-K membranes for an aqueous solution of aniline vs. pressure *P*.

working pressure. The specific flux of the solvent across a membrane depends on a number of factors: nature of membranes and solutions, solute concentration, solution temperature, working pressure, hydrodynamic situation over the membrane, etc. [1–5].

As the concentration of aniline in the working solution increases, the specific flux of the solvent across the membrane markedly decreases. Probably, the key factor for the solution studied is the interaction of the solute with the material constituting the active layer of the membrane. Being a strongly polar low-molecular-weight organic substance, aniline is sorbed by the surface of pores in the membrane, which makes

narrower the free cross section of the pores. As the concentration of the external solution grows, total "blocking" of the finest pores becomes possible, which leads to a substantial decrease in the specific flux of the solvent across the membrane. It should be noted that the specific flux of the solvent is affected not only by the decrease in the cross section, but also by an increase in the osmotic pressure of the solution and, as a consequence, by the osmotic flow of the solvent. For an aqueous solution of aniline, which has a low osmotic pressure, the influence of the osmotic flow is insignificant.

As the working pressure is raised from 1.0 to 5.0 MPa, the specific flux of the solvent across the membrane becomes higher. This can be explained as follows. Being the driving force of the reverse osmosis, the pressure is directly related to the specific flux of the solvent across membranes. Therefore, an increase in pressure in the course of reverse osmosis (in the absence of sedimentation or structural changes of the membrane) always leads to a rise in the specific flux of the solvent across the membrane.

The following formula, based on the known expressions from [2, 15, 16], was suggested for calculating the specific flux of the solvent across the membrane as a function of the solution concentration and pressure applied:

$$J = (k\Delta P - P_{osm}\Delta c/\delta)\exp(k_1 c^n), \quad (2)$$

where k is the water-permeability coefficient of the membrane ($m^3\ m^{-2}\ s^{-1}\ Pa^{-1}$); ΔP, pressure applied (Pa); P_{osm}, osmotic permeability of the membrane ($m^5\ kg^{-1}\ s^{-1}$); Δc, difference of the concentrations in the solution bulk and in the permeate ($kg\ m^{-3}$); δ, membrane thickness (m); c, concentration of aniline in the solution bulk ($kg\ m^{-3}$); and k_1 and n, numerical coefficients.

The values of the coefficients for the membranes and solutions studied are listed in Table 1.

The experimental values of the specific flux of the solvent across the membrane and those calculated by formula (2) are listed in Table 2. It can be seen that the experimental and calculated values of J are in rather good agreement (±20%).

CONCLUSIONS

(1) The influence exerted by the concentration of an aqueous solution of aniline and by the pressure applied on the retention factor of MGA-95K and OPM-K membranes was studied. It was established that, as the concentration of aniline in the solution is raised, the retention factor of the MGA-95K membrane increases and shows an inflection point. The retention factor of the OPM-K membrane grows with the concentration of aniline.

(2) The dependence of the specific flux of the solvent across the membrane on the pressure applied and on the solute concentration was studied. It was found that the specific flux of the solvent across the OPM-K membrane markedly exceeds that across the MGA-95K membrane (all other conditions being the same).

REFERENCES

1. Lazarev, S.I., Korobov, V.B., Kliot, M.B., and Pirogov, P.A., *Izv. Vyssh. Uchebn. Zaved., Khim. Khim. Tekhnol.*, 1993, vol. 46, no. 6, pp. 78–80.
2. Dytnerskii, Yu.I., *Baromembrannye protsessy: Teoriya i raschet* (Baromembrane Processes: Theory and Calculation), Moscow: Khimiya, 1986.
3. Hwang, S.-T. and Kammermeyer, K., *Membranes in Separations*, New York: Wiley, 1975.
4. Karelin, F.N., *Obessolivanie vody obratnym osmosom* (Water Desalination by Reverase Osmosis), Moscow: Stroiizdat, 1988.
5. Bryk, M.T. and Tsapyuk, E.A., *Ul'trafil'tratsiya* (Ultrafiltration), Kiev: Naukova Dumka, 1989.
6. Deryagin, B.V., Churaev, N.V., Martynov, G.A., *et al.*, *Khim. Tekhnol. Vody*, 1981, vol. 3, no. 2, pp. 99–104.
7. Sourirajan, S., *Pure Appl. Chem.*, 1978, vol. 50, pp. 593–615.
8. Tone, S., Shinohara, K., Igorashi, Y., and Otake, T., *J. Membrane Sci.*, 1984, vol. 19, pp. 195–208.
9. Reid, K.F., *Properties and Reactions of Bonds in Organic Molecules*, London: Longmans, 1968.
10. Sorption of Low-Molecular-Weight Organic Substances from an Aqueous Solution by an MGA-95K Reverse-Osmosis Membrane, *Trudy TGTU: Sbornik nauchnykh statei molodykh uchenykh i studentov* (Transactions of Tambov State Technical University: Coll. of Scientific Papers by Young Scientists and Students), Tambov: Tambov Gos. Tekh. Univ., 2001, issue 8, pp. 140–143.
11. Koganovskii, A.M., Levchenko, T.M., Kirichenko, V.A., *et al.*, *Adsorbtsiya rastvorennykh veshchestv* (Adsorption of Dissolved Substances), Kiev: Naukova Dumka, 1977.

12. Koganovskii, A.M., Klimenko, I.A., Levchenko, T.M., *et al*., *Adsorbtsiya organicheskikh veshchestv iz vody* (Adsorption of Orgabnic Substances from Water), Leningrad: Khimiya, 1990.
13. Golovashin, V.L. and Lazarev, S.I., *Izv. Vyssh. Uchebn. Zaved., Khim. Khim. Tekhnol*., 2000, vol. 43, no. 5, pp. 79–81.
14. Kul'skii, L.D., *Elektrokhimiya v protsessakh obrabotki vody* (Electrochemistry in Water Treatment), Kiev: Tekhnika, 1987.
15. Churaev, N.V., *Fizikokhimiya protsessov massoperenosa v kapillyarno-poristykh telakh* (Physical Chemistry of Mass Transfer in Capillary-Porous Bodies), Moscow: Khimiya, 1990.
16. Deryagin, B.V., Churaev, N.V., and Muller, M.V., *Poverkhnostnye sily* (Surface Forces), Moscow: Nauka, 1985.

Russian Journal of Applied Chemistry, Vol. 78, No. 7, 2005, pp. 1101–1105. Translated from Zhurnal Prikladnoi Khimii, Vol. 78, No. 7, 2005, pp. 1122–1126.
Original Russian Text Copyright © 2005 by Medyantseva, Varlamova, Bikkenina, Budnikov.

ENVIRONMENTAL PROBLEMS OF CHEMISTRY AND TECHNOLOGY

Preconcentration of Simazine from Aqueous Solutions with an Immunosorbent and Its Quantitative Determination

E. P. Medyantseva, R. M. Varlamova, D. R. Bikkenina, and G. K. Budnikov

Kazan State University, Kazan, Tatarstan, Russia

Received December 6, 2004; in final form, April 2005

Abstract—The optimal conditions were found for sorption preconcentration of Simazine (herbicide of *sym*-1,3,5-triazine group) from aqueous solution with immobilized antibodies. The main characteristics of immobilized antibodies as sorbents for Simazine were determined.

Virtually all the pesticides applied in agriculture are potential environmental pollutants. Among them Simazine (SM) belonging to the *sym*-1,3,5-triazine group (ST) of herbicides is widely used in agricultural practice. Its content in water, soils, and atmosphere must not exceed the permissible level established by the corresponding regulations [1, 2]. Simazine exhibits high mobility and chemical stability in soils irrespective of the climatic zone. Owing to the above-noted features and large-scale application, SM is the most frequently detectable pesticide in ground and surface water. Therefore, the development of sensitive and selective methods for determining herbicides of the triazine group in the environment and food is an urgent problem.

Microamounts of herbicides (including those of the triazine group) are commonly determined by various kinds of chromatography: thin-layer (TLC) [3], gas–liquid (GLC) [4], high-performance liquid (HPLC) [5], and micellar electrokinetic (MEC) [6]. Although chromatography ensures high sensitivity and selectivity of herbicide determination, this technique requires complicated and labor-consuming pretreatment of samples, highly skilled staff, and expensive equipment.

The demand for more efficient methods for analysis of soils and water for microamounts of *sym*-triazines stimulated development of immunochemical analytical technique based on specific complexation of the herbicide with an antibody (AB). This technique is characterized by very high sensitivity and selectivity, simplicity of sample pretreatment (in some cases, it is not required at all), promptness, and also low cost of equipment and easy automation. Various types of immunochemical technique are used today for determining microamounts of Simazine-group herbicides: polarization-fluorescent [7], chemiluminescence [8], and solid-phase enzyme-mediated immunoassay (EIA), ELISA [9].

A promising technique for analysis of pesticide microamounts is based on their preconcentration on solid sorbents followed by quantitative determination by chromatography [10], mass spectrometry [11], microwave absorption [12], and capillary electrophoresis [13]. These methods were used for determining pesticides of various kinds: phenylureas, triazines, organochlorine and organophosphorus compounds.

A combination of immunochemical analytical technique with solid-phase preconcentration allows development of more sensitive and selective techniques for determining various physiologically active compounds. In this relation, the sorption of herbicides on immobilized antibodies (IAB) shows much promise. These processes, however, are poorly understood today.

To develop an efficient immunosorption method for selective determination of herbicides, e.g. Simazine, in a multicomponent system, we must optimize conditions for their immunosorption recovery from aqueous solutions and determine the main physicochemical characteristics of IAB as immunosorbent.

Our version of immunochemical determination of SM is based on its selective sorption concentration from aqueous solution on immobilized antibodies followed by ammetric determination with a biosensor based on choline esterase. The determination of Simazine with this technique includes the following steps: formation of a sorption complex between immobilized antibody and Simazine on the immunosorb-

1070-4272/05/7807-1101 © 2005 Pleiades Publishing, Inc.

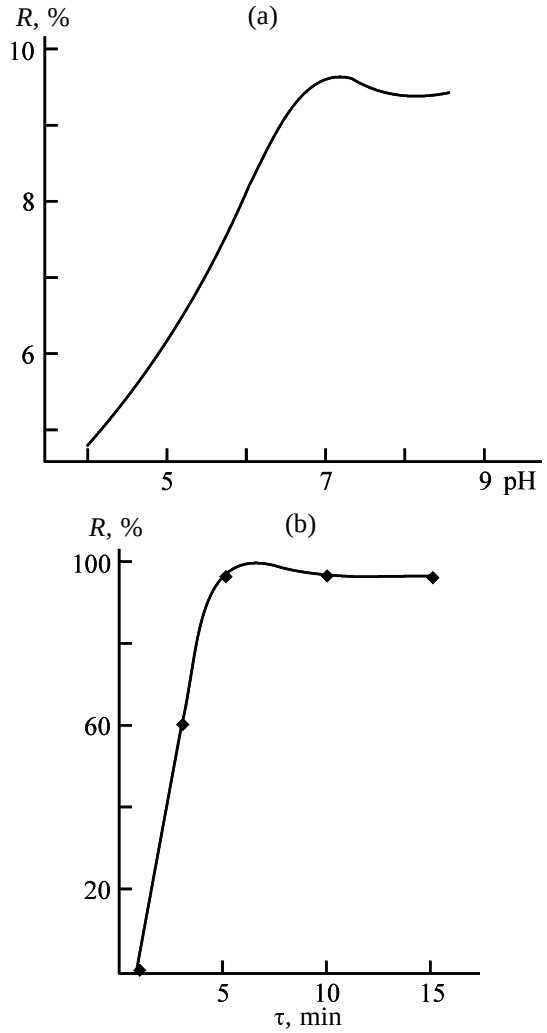


Fig. 1. Degree of Simazine sorption recovery *R* with IAB as a function of (a) pH and (b) contact time τ.

ent surface, breakdown of this complex with the release of Simazine, and ammetric determination of the released Simazine with a biosensor.

The Simazine content was determined ammetrically with a choline esterase (CE) biosensor (ACEBS) consisting of enzyme (choline esterase), appropriate substrate, and mercury electrode. The voltammetric measurements were carried out at cathodic polarization voltage of –0.55 V corresponding to the reversible reduction of Hg(I, II) mercaptide formed by the reaction of thiol with metallic mercury as electrode material [14].

There are different viewpoints on the problem of how herbicides of the triazine group affect the choline esterase catalytic activity. It was found [15] that these compounds inhibit CE with the inhibition factor of 27.7±5.3%. We found that, under identical conditions, Simazine microamounts (10^{-6}–10^{-9} M) also inhibit CE irrespective of its state (native or immobilized in nitrocellulose film). As a result, in the presence of SM the analytical signal of the biosensor (electrical current at polarization voltage $E = -0.55$ V produced by reduction of a redox-sensitive product of hydrolysis of sulfur-containing substrate) decreases.

Thus, Simazine is a relatively weak nonspecific inhibitor for CE. This inhibiting effect may be caused by interaction of SM with hydrophobic parts of the enzyme, making the active sites of choline esterase less accessible to substrate molecules.

We found that Simazine inhibits the enzymatic reaction in the enzyme–substrate system (butyrylthiocholine iodide–choline esterase immobilized in nitrocellulose film) by 27.6±0.6%. This inhibiting effect can be used for quantitative determination of Simazine with an ACEBS.

Mechanism of Simazine preconcentration by sorption on immobilized antibodies. The efficiency of sorption recovery and preconcentration of Simazine with an immunosorbent depends on its physicochemical properties. In our experiments we determined the main characteristics of recovery of Simazine from aqueous solutions with the biosorbent based on immobilized AB.

The degree of Simazine sorption recovery *R* (%) was determined from the residual Simazine content in the aqueous phase after its contact for a certain time (with stirring) with the antibody immobilized in a nitrocellulose film. The *R* value was calculated as the percent ratio of the Simazine amount sorbed on immobilized antibody to the Simazine amount in the initial solution.

To optimize conditions for the sorption preconcentration of Simazine and its quantitative determination, we examined the dependence of *R* (%) on pH (Fig. 1a). Figure 1a shows that in the pH range 7–8.6 Simazine is practically completely recovered from aqueous solution with IAB in single phase contact. In this pH range, choline esterase shows high enzymatic activity in the absence of the pesticide, and the pesticide is chemically stable. Under these conditions, IAB exhibits very high sorption power for Simazine, and, therefore, the repeated treatment of the solution with a fresh portion of the immunosorbent virtually does not affect the biosensor response.

In our experiments, the contact time was varied from 1 to 15 min. Figure 1b shows that, after 5-min contact of the immunosorbent with Simazine, the formation of the sorption complex SM–IAB is com-

plete. Longer contact does not noticeably affect the sorption of Simazine.

The sorption capacity of IAB for Simazine was determined from the Simazine distribution between the immunosorbent and aqueous phase at various Simazine contents.

Figure 2 shows the sorption isotherm of Simazine on immobilized antibodies [sorption capacity SC of Simazine was calculated per unit of the film surface area ($\mu g\ cm^{-2}$)]. It is seen that this isotherm is linear up to the point corresponding to complete exhaustion of the sorption power of IAB for Simazine. The projection of this point onto the abscissa axis is the maximal sorption capacity of the immunosorbent for Simazine. After saturation of the sorbent with Simazine, the sorption isotherm flattens out, i.e., sorption of Simazine stops.

We found that the maximal sorption capacity of IAB for Simazine is $50.3 \pm 0.9\ \mu g\ cm^{-2}$ at the initial concentration of immobilized antibodies in nitrocellulose equal to $0.076\ mg\ ml^{-1}$.

The efficiency of sorption of Simazine with the immunosorbent was characterized by its distribution factor determined as the ratio of the Simazine concentration on IAB to that in the equilibrium aqueous solution. Under our experimental conditions, the distribution factor of Simazine varied from 12 to 49, i.e., the degree of Simazine recovery was no less than $96 \pm 4\%$.

Owing to fairly high sorbability of Simazine on IAB, this immunosorbent can be used for preconcentrating Simazine from its dilute solutions (10^{-9}–10^{-10} M). We studied the recovery of Simazine from its 10^{-10} M aqueous solutions of the following volumes, ml: 25, 35, 100, 500, and 1000.

Desorption of Simazine from IAB samples used in these sorption experiments with water (5 ml) resulted in Simazine preconcentration by factors of 5, 7, 20, 100, and 200, respectively (Table 1).

Procedures for breaking down sorption complexes Simazine–immobilized antibody. The fact that Simazine is virtually completely recovered from its aqueous solutions with immobilized antibodies shows that Simazine forms fairly strong complexes with immobilized antibodies. The same conclusion was made in [16]. In order to determine the Simazine amount accumulated in the immunosorbent, the Simazine–antibody complexes should be broken down to release the Simazine molecules.

It is known that herbicides can be released from their complexes with an immubosorbent by their treatment with buffer solutions of appropriate pH, aqueous urea, sodium thiocyanate, etc. [17].

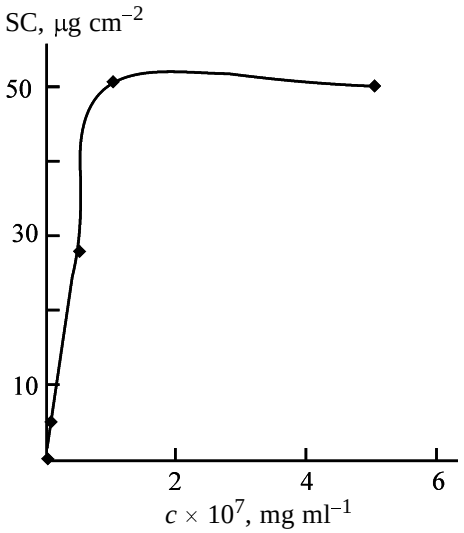


Fig. 2. Sorption capacity of immobilized antibodies SC for Simazine vs. Simazine concentration in the aqueous phase *c*.

In this study, the Simazine–antibody complexes were broken down with aqueous HCl containing 0.15 M NaCl (pH 4). It was found that, under these conditions, the sorption complexes are virtually completely broken down within 20 min.

Determination of Simazine microamounts in aqueous solution involves the following steps: (1) A nitrocellulose film containing immobilized antibodies is placed into a solution (pH 7) containing Simazine to be determined, and this system is stirred for 5 min at 20°C. Under these conditions, Simazine is completely

Table 1. Characteristics of sorption preconcentration of Simazine and accuracy of its determination.* Simazine content in the initial solution 1×10^{-10} M, $n = 3$, and $P = 0.95$

V, ml	c, M		S_r	γ
	calculated	found		
25	5×10^{-10}	$(4.8 \pm 0.7) \times 10^{-10}$	0.156	5
35	7×10^{-10}	$(7.3 \pm 0.9) \times 10^{-10}$	0.134	7
100	2×10^{-9}	$(2.5 \pm 0.3) \times 10^{-9}$	0.121	20
500	1×10^{-8}	$(1.2 \pm 0.2) \times 10^{-8}$	0.171	100
1000	2×10^{-8}	$(1.8 \pm 0.4) \times 10^{-8}$	0.212	200

* (V) initial solution volume, ml; (c) Simazine content after preconcentration; (S_r) determination error; and (γ) degree of Simazine preconcentration.

Table 2. Ammetric determination of Simazine with an ACEBS combined with sorption on immobilized antibodies. AB concentration 0.076 mg ml^{-1}, n = 5, P = 0.95

Introduced	Found	S_r
M		
5×10^{-8}	$(4.6\pm0.2)\times10^{-8}$	0.020
5×10^{-9}	$(4.8\pm0.2)\times10^{-9}$	0.022
5×10^{-10}	$(4.7\pm0.2)\times10^{-10}$	0.028

collected on the antibody sorbent. (2) The Simazine-containing nitrocellulose film is washed with distilled water and transferred into an aqueous solution (5 ml) containing 1 M NaCl + HCl (pH 4), and this mixture is kept for 20 min. Under these conditions, Simazine is completely released from the Simazine–antibody complex. (3) A solution formed after breakdown of the Simazine–anibody complex (0.5–2.5 ml) is placed into a 5-ml volumetric flask, and then 2×10^{-4} M BTCI (0.5 ml) and borate buffer (pH 9.05) (to a mark) are successively added. (4) The resulting mixture is placed into an electrochemical cell, atmospheric oxygen is removed from the solution by purging with hydrogen for 15 min, and then a cyclic voltammetric curve is recorded in the potential range from –0.1 to –0.9 V relative to a saturated calomel reference electrode. The potential sweep rate is V s^{-1}. The electric current at the polarization voltage of –0.55 is measured, and the Simazine concentration is determined using the calibration curve.

The sorption equilibrium in the system Simazine-IAB is characterized by a certain ratio between the antibodies bound with Simazine and occuring in the free state. Therefore, the Simazine concentration can be determined by the calibration plot built in the coordinates Simazine concentration in aqueous phase–electric current. Our experiments showed that the Simazine detection limit was 10^{-10} M.

In the systems under consideration, at the Simazine concentration ranging from 10^{-6} to 10^{-9} M, the relative electric current is a linear function of the logarithm of the Simazine concentration:

$$I_p/I_0 = (27\pm4) + (7.9\pm0.8)(-\log c),\ r = 0.9908.$$

This equation was used for determining the Simazine concentration. The accuracy of Simazine determination was evaluated as the difference between the Simazine amount introduced into a model solution and that determined in this model solution using our technique (Table 2). The determination of pesticides in various natural waters with our technique (n = 5, P = 0.95) revealed the presence of Simazine in some of them.

Water	Initial herbicide content, M	Herbicide content after sorption treatment with immunosorbent, M	S_r
Lake Chistoe	$(1.3\pm0.4)\times10^{-10}$	$(1.8\pm0.3)\times10^{-8}$	0.21
Well no. 20	–	$(2.1\pm0.4)\times10^{-9}$	0.20
Murzinka river	$(2.2\pm0.3)\times10^{-10}$	$(2.0\pm0.5)\times10^{-8}$	0.18

EXPERIMENTAL

The voltammetric measurements were carried out with a PI-50-1.1 potentiostat equipped with a computer. An electrochemical cell was temperature-controlled with a TC-50 thermostat. A saturated calomel electrode was used as the reference electrode. A biosensor based on choline esterase, ACEBS, was used as a working electrode; it was prepared as described in [14]. It consisted of a stationary mercury film electrode applied to a silver support and butyrylcholine esterase immobilized in a nitrocellulose membrane.

The immobilized antibodies were prepared as follows. An antibody-containing solution was applied to commercial nitrocellulose membranes (Sartorius) with the surface area of 2 cm^2 and pore diameter of 0.2 μm, and the membranes were kept over aqueous glutaraldehide (12.5%). Thereafter the membranes were kept for 12 h in a hermetically sealed vessel with humid air. After such pretreatment, the membranes were soaked in a solution of human serum albumin to bind the free reactive groups of glutaraldehyde. The final samples of immobilized antibodies were stored at +4°C. The Simazine-containing solutions to be analyzed were deoxygenated by bubbling electrolytic hydrogen. In the course of voltammetric measurements, hydrogen was passed over the solution.

The substrate based on butyrylthiocholine iodide was prepared by dissolving its accurately weighed sample in the working buffer solution. In the course of experiments, this solution was refreshed after each 3-h use. Butyrylcholine esterase of horse serum (EC 3.1.1.8) with activity of 110 AU mg^{-1} was produced by the Biomed Research and Production Association (Perm).

Choline esterase was immobilized with nitrocellulose of colloxylin type with the mean nitrogen content of 11.5–12.0 wt %, prepared in the form of films. Antibodies were immobilized on commercial nitrocel-

lulose membrane filters with the pore size of 0.2 μm, produced by Sartorius.

The following organic solvents were used in our experiments: butyl acetate, toluene, hexane (high purity), aqueous glutaraldehyde (25%) (ICN), and human serum albumin (Reanal, Hungary). Simazine solutions were prepared from its 0.1 M reference solution produced by the Ural Research Institute of Metrology.

In our experiments we used polyclonal antibodies prepared at the Chair of Chemical Enzymology, Moscow State University. The antibody content in working solution prepared by dissolving antibodies in double-distilled was water determined from its optical density at λ = 280 nm (25°C) by the equation

$$c_{AB} = A_{280} n/1.3,$$

where c_{AB} is the antibody concentration (mg ml^{-1}); A_{280}, optical density of solution; n, dilution factor; and 1.3, recalculation factor determined from the calibration curve. The AB content in the stock solution was 0.076 mg ml^{-1}.

In our experiments pH was adjusted with borate buffer (pH 9.05 ± 0.05). pH was measured on a pH-150 pH meter with a glass electrode calibrated against standard buffer solutions.

It should be noted that, in voltammetric analysis of systems under consideration, no catalytic electrochemical discharge of protons (hydrogen current) was observed. At the same time, this current appears, for example, in solutions of a chemically pure grade Co(II) salt (10^{-2} M) in ammonia buffer (pH 9–10). We believe that this difference in electrochemical behavior is caused by strong binding of immobilized antibodies with the nitrocellulose matrix.

CONCLUSIONS

(1) A technique for determining Simazine microamounts in aqueous solutions was developed. The procedure includes its sorption preconcentration on immobilized antibodies through formation of a strong Simazine–antibody complex, breakdown of this complex, and ammetric determination of the released Simazine with a biosensor.

(2) The Simazine–antibody immunocomplexes are broken down with an aqueous solution containing 0.1 M HCl and 0.15 M NaCl.

(3) The main characteristics of immobilized antibodies as sorbents for Simazine from aqueous solutions (degree of recovery, sorption capacity, distribution factor) were determined.

(4) Sorption of Simazine on immobilized antibodies ensures its preconcentration from dilute aqueous solutions (10^{-10} M) with a factor of 5–200.

REFERENCES

1. *European Communities, Council Directive of 15th July 1980 Relating to the Quality of Water Intended for Human Consumption [80/778/EEC], Drinking Water Directive no. L.229*.
2. Mel'nikov, N.N., Novozhilov, K.V., and Pylova, T.N., *Khimicheskie sredstva zashchity rastenii: Spravochnik* (Chemicals for Plant Protection: Handbook), Moscow: Khimiya, 1980.
3. Tuzimski, T. and Soczewinski, E., *J. Cromatogr. A*, 2002. vol. 961, no. 2, pp. 277–283.
4. Ranskii, A.P., Sandomirskii, A.V., and Gaididei, O.V., *Vopr. Khim. Khim. Tekhnol*., 2003, no. 4, pp. 50–53, 181, 187.
5. Baglio, D., Kotzias, D., and Larsen, B.R., *J. Chromatogr*., 1999, vol. 854, nos. 1–2, pp. 207–220.
6. Komarova, N.V. and Kartsova, L.A., *Zh. Anal. Khim*., 2003, vol. 58, no. 8, pp. 881–885.
7. Samsonova, Zh.V., Eremin, S.A., and Egorov, A.M., *Vopr. Med. Khim*., 1994, vol. 40, no. 4, pp. 53–56.
8. Samsonova, J.V., Rubtsova, M.Yu., Kiseleva, A.V., *et al*., *Biosens. Bioelectron*., 1999, vol. 14, pp. 273–281.
9. Yazynina, E.V., Zherdev, A.V., Dzantiev, V.V., *et al*., *Anal. Chim. Acta*, 1999, vol. 399, nos. 1–2, pp. 151–160.
10. Goncalves, C. and Alpendurada, M.F., *J. Chromatogr. A*, 2002, vol. 968, nos. 1–2, pp. 177–190.
11. Pepa Fernando, Cardenas Soledad, Gullego Mercedes, and Valcarcel Miguel, *Talanta*, 2002, vol. 56, vol. 4, pp. 727–737.
12. Lee, H.K. and Shen, G., *J. Chromatogr. A*, 2003, vol. 985, nos. 1–2, pp. 167–174.
13. Weidong Qin, Wei Hong Ping, and Li Sam Fong Yau, *J. Chromatogr. Sci*., 2002, vol. 40, no. 7, pp. 387–391.
14. Il'cheva, N.Yu., Beilinson, R.M., Medyantseva, E.P., *et al*., *Vestn. Mosk. Gos. Univ*., 2003, vol. 43, no. 6, pp. 408–411.
15. Ying Jin-Clarc, Michael J. Lydy, and Kun Yan Zhu, *Environ. Toxicol. Chem*., 2002, vol. 21, no. 2, pp. 598–603.
16. Il'cheva, N.Yu., Medyantseva, E.P., and Budnikov, G.K., *Anal. Kontr*., 2002, vol. 6, no. 5, pp. 538–544.
17. Ruoslahti, E., *Immunoadsorbents in Protein Purification*, Baltimore: Univ. Park, 1976.

Russian Journal of Applied Chemistry, Vol. 78, No. 7, 2005, pp. 1106–1109. Translated from Zhurnal Prikladnoi Khimii, Vol. 78, No. 7, 2005, pp. 1127–1129.
Original Russian Text Copyright © 2005 by Bubnov, Burova, Grinevich, Kuvykin.

ENVIRONMENTAL PROBLEMS OF CHEMISTRY AND TECHNOLOGY

Combined Plasma-Induced and Catalytic Decomposition of Phenols

A. G. Bubnov, E. Yu. Burova, V. I. Grinevich, and N. A. Kuvykin

Ivanovo State University of Chemical Engineering, Ivanovo, Russia

Received February 9, 2005

Abstract—Decomposition of phenol and its derivatives, resorcinol and pyrocatechol, was studied in barrier-discharge plasma in the presence of substances exhibiting catalytic properties.

Methods of high-energy chemistry find application in water treatment and purification. In particular, the use of barrier discharge plasma makes it possible to improve the water quality via decreasing the concentrations of organic pollutants by factors of several tens [1]. A new line in this area is application of combined plasma-induced and catalytic processes (CPICPs) accelerating decomposition of organic compounds, i.e., increasing the energy efficiency of the process. When introduced directly into the plasma zone, the catalyst and the solution being treated are exposed to all active species, including short-lived species that are formed in the gas and liquid phases. Active species in plasma can activate the catalyst at low temperatures, or active species capable of initiating and accelerating decomposition of organic compounds in water can be formed on the catalyst.

In this work we studied the kinetics of transformation of phenols when exposed to active species of barrier-discharge plasma (BDP) and in CPICP.

EXPERIMENTAL

The experiments were run on a setup described in [1]. Technical-grade oxygen (99.8 vol % pure, with nitrogen and argon as main impurities) served as plasma-forming gas. The flow rate of O_2 was constant in all the experiments (3.2 $cm^3\ s^{-1}$). Barrier discharge was excited from a high-voltage transformer (alternate current with a frequency of 50 Hz); the voltage applied to the electrodes was 16 kV. As model pollutants we chose phenol (PN) and its derivatives, resorcinol (RS) and pyrocatechol (PC), with different initial concentrations. During the studies we controlled the content of phenol in water before and after plasmochemical treatment.

Aqueous solutions of phenol were treated both in the presence and absence of compounds exhibiting catalytic properties. In the former case, prior to introducing the water being treated into the setup in the plasma burning zone, a catalyst (a nickel-containing compound) was preliminary applied to the hydrophilic inert material (fiber glass) coating the central noninsulated electrode.

The catalyst was applied to the fiber glass fabric by the following procedure. The fabric was leached with an HNO_3 solution (5.5 wt %) at 90°C for 10 min, whereupon it was dried at 110°C and calcined in air at 250°C [2]. Next, the fiber glass fabric was placed into an aqueous NaOH solution (pH 7–11), and a weighed portion of a salt, $Ni(NO_3)_2$, was added to yield 0.2 M solution. After 40 min, the fabric was repeatedly dried at 110°C and calcined at 250°C for 30–40 min [3].

The qualitative characteristics of the initial and treated waters were estimated by the procedures described in [4].

We found earlier [1, 5] that the efficiency α of plasma-induced decomposition of organic compounds dissolved in water depends on a multitude of parameters, including the time of contact of the gas and solution with the plasma zone τ, specific power W contributed to the discharge, and the initial concentration of the solute c_i. Our experiments showed (Fig. 1) that, with increasing initial concentration of the phenols in water, α tends to decrease, most profoundly in the case of PN and least profoundly, in the case of PC.

This is also evident from Fig. 2 demonstrating the efficiency of decomposition of the phenols in BDP. The decomposition rates for PN, RS, and PC (Fig. 2) are related as 1 : 1.2 : 1.4. Thus, PN proved to be the

1070-4272/05/7807-1106© 2005 Pleiades Publishing, Inc.

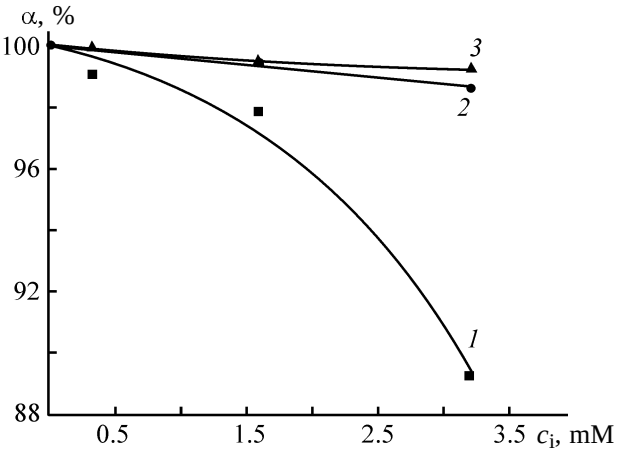


Fig. 1. Efficiency α of decomposition of phenols in BDP as a function of their initial concentration c_i as recalculated for the total content of carbon atoms in the molecules in solution. W = 28 mW cm^{-3}, τ_c = 50 s. (*1*) Phenol, (*2*) resorcinol, and (*3*) pyrocatechol; the same for Figs. 2–4.

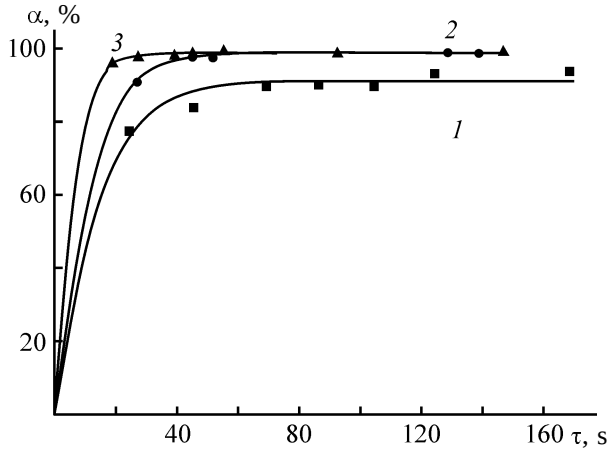


Fig. 2. Efficiency α of decomposition of phenols in BDP as a function of the time of the solution–plasma zone contact τ in BDP (c_i = 3.2 mM).

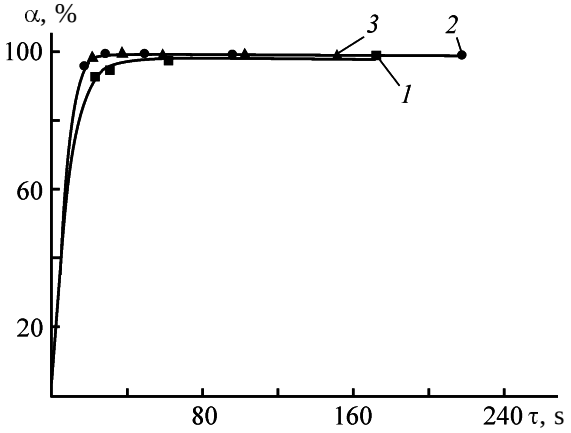


Fig. 3. Efficiency α of decomposition of phenols in CPICP as a function of the time of the liquid–plasma zone contact τ.

most stable and PC, the least stable, under plasma. It should be noted that the previous studies of oxidation of phenols with ozone [6] showed that the apparent rate constants of its reactions with RS and PC are close, with a 12.5% difference in favor of RS. In oxidation processes, PC is capable of forming quinoid structures, which is not characteristic of RS [6]. Evidently, specifically such structures are responsible for the effect observed.

Our measurements showed that the efficiency of decomposition of phenols in CPICP is much higher than in plasma-induced processes. For example, when the initial concentration of PN was increased from 2 to 200 mg l^{-1}, α decreased from 99.9 to 36% (by a factor of 2.8) [in the plasma-induced process], and from 99.9 to 86% (by a factor of 1.2), in the combined process. Similar results were obtained for PC and RS (Fig. 2). In CPICP, the decomposition rate increased by a factor of 1.3 for PN, by a factor of 1.2 for RS, and remained virtually unchanged in the case of PC.

Table 1 presents the calculated apparent rate constants k_{app} of decomposition of phenols in BDP and CPICP.

The apparent rate constants k_{app} of PN, RS, and PC in BDP are related as 1 : 5 : 19, and in CPICP, as 1 : 1.9 : 4.3.

Thus, CPICP proved to be the most efficient in decomposition of PN (k_{app} increases by a factor of nearly 11), and the least efficient in decomposition of PC (k_{app} increases by a factor of 2.5). It should be noted that k_{app} depends on c_i [6]. Comparison of the apparent rate constants for CPICP and ozonation of the phenols showed that combined plasma-induced catalytic decomposition of phenols dissolved in water offers significant advantages over ozonation, since

Table 1. Apparent rate constants of decomposition of the phenols in BDP and CPICP (c_i = 3.2 mM) and by ozonation [6]

Compound	k_{app}, l mol^{-1} s^{-1}		
	BDP	BDP + catalyst	ozonation [6]
PN	291 ± 51	3116 ± 460	1400 ± 500
RS	1501 ± 100	5956 ± 357	4000 ± 300
PC	5434 ± 907	13 546 ± 2050	3500 ± 400

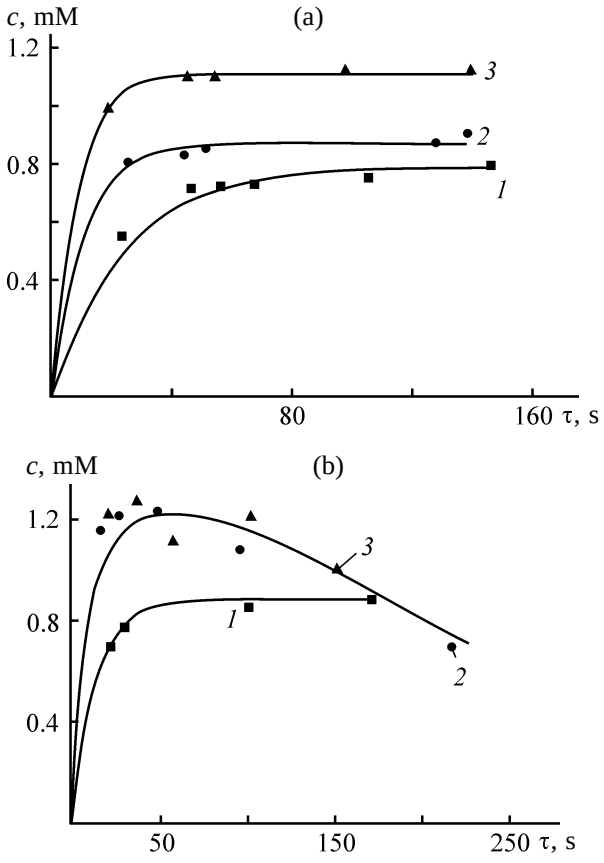


Fig. 4. Kinetic curves of formation of carboxylic acids for treatment of phenols in (a) BDP and (b) CPICP on a Ni catalyst. (*c*) Concentration of carboxylic acids in solution and (τ) solution–plasma zone contact time.

the apparent rate constants in the former case are larger by a factor of 1.5–3.9.

The main active species being formed in BDP is ozone [7]. Ozonation of aromatic hydrocarbons involves cleavage of the aromatic ring and formation of muconic acid derivatives which are further converted into moieties containing 2–4 carbon atoms. These species are oxidized to carbonyl and carboxy compounds containing 1–3 carbon atoms [6]. The main intermediate and final products of the phenol decomposition in the case of ozonation [1] and plasma treatment are carboxylic acids. Figure 4 presents the kinetics of accumulation of these acids (as recalculated for acetic acid). The yield of carboxylic acids is at a maximum when PC is exposed to active plasma species (by a factor of 1.7 larger than in the case of treatment of aqueous solutions of PN).

Table 2. Maximal yield of carboxylic acids (based on the initial content of carbon in solution) in decomposition of the phenols

Compound	Yield of acids (recalculated for acetic acid), %	
	BDP	BDP + Ni
PN	49	56
RS	50	68
PC	61	68

It should be noted that, in going from BDP to CPICP, the kinetics of formation of carboxylic acids remained virtually unchanged for PN. Whereas the kinetics of accumulation of carboxylic acids in BDP for RS and PC are described by an exponential dependence (like in the case of PN), those in CPICP are described by a typical curve with a maximum. This may be due to the fact that, for RS and PC, which are the least stable in plasma-induced processes, carboxylic acids are not the final oxidation products and only further decompose to CO_2 and HCO_3^-. Table 2 lists the maximal yields of carboxylic acids in oxidation of phenols. It is seen that, in CPICP, from 56 (PN) to 68% (RS, PC) of the initial carbon content in solution is converted into carboxylic acids, i.e., their yield is fairly high. In CPICP, the rate of formation of carboxylic acids increases by a factor of 1.4, 1.6, and 1.2 for PN, RS, and PC, respectively.

Thus, decomposition in CPICP is accelerated most efficiently for PN, and least efficiently, for PC.

CONCLUSIONS

(1) Barrier-discharge plasma affords high efficiency of decomposition of phenol and its derivatives (up to 99%), with phenol being the most resistant, and pyrocatechol, the least resistant to plasma.

(2) In combined plasma-induced and catalytic process, the apparent rate constant of decomposition increases relative to plasma-only treatment by a factor of 11, 4, and 2.5 for phenol, resorcinol, and pyrocatechol, respectively. From 56 (for phenol) to 68% (for resorcinol and pyrocatechol) of the initial carbon in solution is converted to carboxylic acids.

(3) Combined plasma-induced and catalytic processes are suitable for treating water to remove plasma-resistant compounds such as phenol or for treating water with high concentrations of phenols.

ACKNOWLEDGMENTS

This work was financially supported by the Russian Foundation for Basic Research (project no. 03-03-96441).

REFERENCES

1. Bubnov, A.G., Grinevich, V.I., Kuvykin, N.A., and Maslova, O.N., *Khim. Vys. Energ*., 2004, vol. 38, no. 1, pp. 44–49.
2. Simonova, L.G., Barelko, V.V., Lapina, O.B., *et al*., *Kinet. Katal*., 2001, vol. 42, no. 5, pp. 762–772.
3. Elizarova, G.L., Matvienko, L.G., Peskunova, O.P., *et al*., *Kinet. Katal*., 1998, vol. 39, no. 1, pp. 49–55.
4. Lur'e, Yu.Yu., *Analiticheskaya khimiya promyshlennykh stochnykh vod* (Analytical Chemistry of Industrial Wastewater), Moscow: Khimiya, 1984.
5. Bubnov, A.G., Grinevich, V.I., and Kuvykin, N.A., *Khim. Vys. Energ*., 2004, vol. 38, no. 5, pp. 380–386.
6. Razumovskii, S.D. and Zaikov, G.E., *Ozon i ego reaktsii s organicheskimi soedineniyami (kinetika i mekhanizm)* (Ozone and Its Reactions with Organic Compounds: Kinetics and Mechanism), Moscow: Nauka, 1974.
7. Lunin, V.V., Popovich, M.P., and Tkachenko, S.N., *Fizicheskaya khimiya ozona* (Physical Chemistry of Ozone), Moscow: Mosk. Gos. Univ., 1998.

Russian Journal of Applied Chemistry, Vol. 78, No. 7, 2005, pp. 1110–1114. Translated from Zhurnal Prikladnoi Khimii, Vol. 78, No. 7, 2005, pp. 1130–1134.
Original Russian Text Copyright © 2005 by Bashkatova, Miryasova, Cherezova, Bukharov.

ORGANIC SYNTHESIS AND INDUSTRIAL ORGANIC CHEMISTRY

Synthesis and Antioxidative Properties of Bis(3,5-di-*tert*-butyl-4-hydroxyphenyl) Polysulfides

T. V. Bashkatova, F. K. Miryasova, E. N. Cherezova, and S. V. Bukharov

Kazan State Technological University, Kazan, Tatarstan, Russia

Received March 4, 2005

Abstract—An efficient procedure was developed for preparing bis(3,5-di-*tert*-butyl-4-hydroxyphenyl) polysulfides in the presence of phenolic Mannich bases. The antioxidative activity of the resulting bis(polysulfides) in rubbers of various structures and in their vulcanizates was examined.

Sterically hindered phenols (SHPs) find growing use for antioxidative stabilization of polymeric materials, thanks to the strong protective effect of SHPs and their low toxicity. Today the researchers' attention is focused on molecular structures containing, along with an SHP moiety, also additional groups or atoms suppressing the radical-chain oxidation in various steps and by different mechanisms [1, 2]. Such stabilizers can exhibit intramolecular synergism and substantially surpass in the antioxidative performance classical mixed synergistic stabilizing systems [1]. Among polyfunctional SHP antioxidants are compounds containing simultaneously SHP fragments and sulfide groups [1, 3].

SHP sulfides were prepared previously by reactions of 2,6-dialkylphenols with S_2Cl_2 and SCl_2 [4]. However, this route has certain disadvantages: relatively low yield of the target product, formation of a large amount of the by-product, and release of hydrogen chloride contaminated with sulfur chlorides. SHP polysulfides can also be prepared using elemental sulfur. According to [5], the reactions of SHPs with sulfur are performed in the presence of an at least equimolar amount of alkali relative to 2,6-dialkylphenol and of a large excess of sulfur. This makes the process technologically unfeasible, because of the necessity of utilizing large amounts of acidic aqueous-organic wastes. However, the procedure for preparing SHP polysulfides using elemental sulfur is attractive in connection with the pressing problem of utilization of "gas" sulfur, a by-product of hydrorefining of crude oil and hydrocarbon raw materials.

The goals of this study were to develop a feasible procedure for preparing sterically hindered phenol sulfides by the reaction of 2,6-dialkylphenol with elemental sulfur and to examine their antioxidative (AO) performance in various rubbers and polymeric materials based on them.

EXPERIMENTAL

The following chemicals were used in the study.

2,6-Di-*tert*-butylphenol. White crystals, mp 36–37°C, MW 206. Readily soluble in benzene, acetone, and isopropanol.

Sulfur. mp 112.8°C, density 1960–2070 kg m^{-3}. A yellow crystalline solid, insoluble in water, sparingly soluble in alcohol and ether, and readily soluble in carbon disulfide. The molecular weight of sulfur at low temperatures corresponds to the formula S_8.

2-Dimethylaminomethylphenol. A light yellow liquid; it contained a 1.88% impurity of phenol.

2,6-Bis(dimethylaminomethyl)phenol. A light yellow liquid; it contained a 2.4% impurity of phenol.

4-Dimethylaminomethyl-2,6-di-*tert*-butylphenol. mp 93–95°C (from acetone). MW 263. White or slightly yellowish crystals soluble in the majority of organic solvents.

***N,N'*-Diphenyl-1,4-phenylenediamine (Diafen FF).** mp 152°C. MW 310. Dark gray crystalline powder; soluble in alcohols, acetone, benzene, chloroform, xylene, aniline, and chlorobenzene; insoluble in water.

Acetone anil P $(C_{12}H_{15}N)_n$. An oligomer of 2,2,4-trimethyl-1,2-dihydroquinoline. mp 65–75°C. MW 400–500. Soluble in chloroform, benzene, alcohols, and acetone; insoluble in water.

1070-4272/05/7807-1110 © 2005 Pleiades Publishing, Inc.

2,2'-Methylenebis(4-methyl-6-*tert*-butylphenol) (Agidol-2). mp 128–129°C. MW 340. White crystalline powder. Soluble in ethanol, ethyl acetate, and methylene chloride; virtually insoluble in water.

Procedure for preparing bis-SHP polysulfide. A four-necked flask equipped with a stirrer, a reflux condenser, a thermometer, and a tube for feeding a gas was charged with 14 g (0.0679 mol) of 2,6-di-*tert*-butylphenol, 25 g (0.0976 mol) sulfur, a catalyst, and 20 ml of DMF. The mixture was heated to 100–145°C, and the reaction was continued with stirring for 1.5–4 h, under bubbling with an inert gas (N_2, Ar) at a rate of 100 l h^{-1}. Then the mixture was cooled to room temperature and allowed to stand for a day until unchanged sulfur fully settled. The precipitate was filtered off, and the DMF was distilled off in a vacuum. The resulting product was a red-brown glassy resin without odor; softening point 75–80°C. ^{1}H NMR spectrum ($CDCl_3$), δ, ppm: 1.25–1.60 (36H, CMe_3), 6.55–6.80 (2H, OH), 7.25–7.65 (4H, ArH). Aryl proton signals are doublets with ^4J 2.4 Hz.

The ^{1}H NMR spectra were recorded on a Gemini-200 spectrometer operating at 200 MHz.

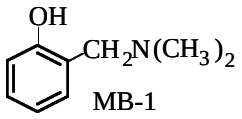
The IR spectra of SKI-3 rubber films were taken with a Perkin–Elmer 16PC-FT-IR spectrometer in the range 4000–400 cm^{-1}. Films 1.0–1.2 μm thick were prepared on a poly(ethylene terephthalate) support (0.04±0.01 mm thick) from a solution of SKI-3 in toluene.

The induction periods of oxidation of the polymer were estimated according to [6] at an oxygen pressure of 250 mm Hg.

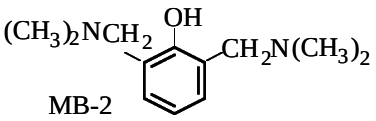
The composition of the rubber stock was as follows (wt parts): BNKS-18 butadiene–acrylonitrile rubber 100, zinc oxide 4, sulfenamide Ts 1, dithiodimorpholine 2, thiuram D 1, PM-50 carbon black 120, stearic acid 1, EDOS plasticizer 45, and stabilizer 3–4.

In the previous studies, we considered a procedure for preparing 2,6-di-*tert*-butylphenol (2,6-DTBP) sulfides by the reaction with elemental sulfur in polar aprotic solvents (DMF, DMSO, HMPA, *N*-methylpyrrolidone) [7]. With these solvents, a base catalyst appeared to be unnecessary. However, the reaction performed at 145–165°C with inert gas bubbling took no less than 6 h.

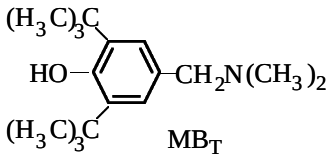
To examine the possibility of making the reaction of 2,6-DTBP with elemental sulfur more feasible (decrease the reaction time and temperature), we made experiments in a polar solvent in the presence of a series of commercially available Mannich bases (MBs): 2-dimethylaminomethylphenol (MB-1), 2,6-bis(dimethylaminomethyl)phenol (MB-2), and *N,N*-dimethyl-3,5-di-*tert*-butyl-4-hydroxybenzylamine (MB_T). We expected that the MBs would behave as base catalysts:



MB-1



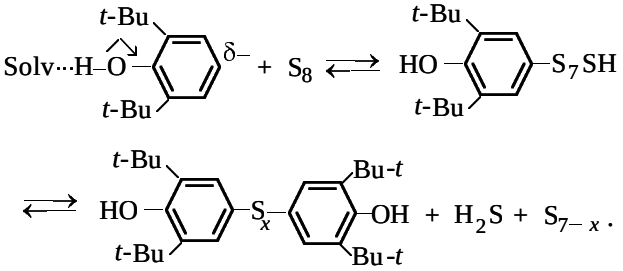
MB-2



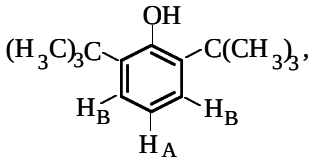
MB_T

These compounds are attractive in the synthesis of SHP polysulfide as they themselves are stabilizing additives to polymeric materials [8]; therefore, the removal of these catalysts in the commercial synthesis is unnecessary.

The reaction was performed at 100–145°C and was monitored by thin-layer chromatography:



The reaction was stopped when the 2,6-DTBP spot disappeared from the TLC plate. The reaction mixtures after removing the solvent were analyzed by ^{1}H NMR spectroscopy. The intensity of the H_A aryl proton (triplet at 6.90 ppm) of 2,6-DTBP was compared with those of the signals of the H_B aryl protons of bis-SHP polysulfide (singlets at 7.10–7.60 ppm):



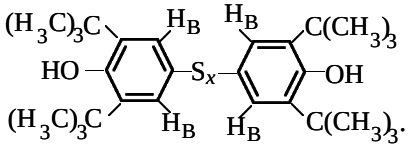


Table 1. Conversion of 2,6-DTBP in the reaction with sulfur in the presence of MB-2 as catalyst (140°C, 210 min, DMF, nitrogen flow)

MB-2 concentration, wt % relative to 2,6-DTBP	Conversion, %
10	96.9
5	96.7
3	96.6
1	96.4
0.5	60.8

Table 2. Conversion of 2,6-DTBP in the reaction with sulfur in the presence of 1 wt % catalyst (140°C, DMF, nitrogen flow)

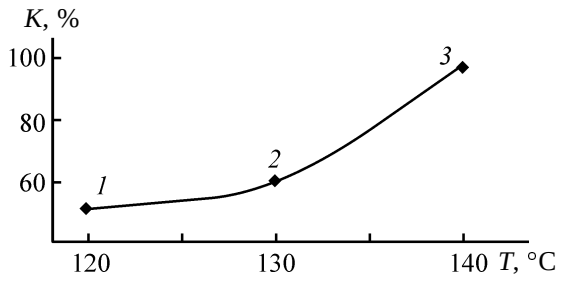
Catalyst	Reaction time, min	2,6-DTBP conversion, %
MB-2*	210	96.4
MB_T**	210	100
	180	98.3
	120	97.3
	90	96.8
MB-1	180	96.1

* When the reaction was performed in a melt, the 2,6-DTBP conversion was 14.3%.

** Without nitrogen bubbling, the 2,6-DTBP conversion was 80%.

First we optimized the amount of the catalyst taken. The MB concentration was varied from 10 to 0.5 wt %. As seen from Table 1, addition of ≥1 wt % MB-2 to the reaction mixture ensured virtually complete conversion of 2,6-DTBP in 3–3.5 h. At lower catalyst concentrations, the reaction rate drastically decreased.

A similar dependence of the 2,6-DTBP conversion on the catalyst concentration was observed with MB-1. With 1 wt % MB_T, the complete conversion of 2,6-DTBP was attained in 90 min.



Conversion *K* of 2,6-DTBP as a function of the reaction temperature *T*. DMF, 1 wt % MB_T, reaction time 120 min. Conversion, %: (*1*) 50.76, (*2*) 60, and (*3*) 96.8.

To ensure efficient conversion of 2,6-DTBP, it is important to remove H_2S (this is provided by inert gas bubbling), because of the reversibility of the reaction. In particular, when the reaction catalyzed with MB_T (1 wt %) was performed for 210 min at 140°C without nitrogen bubbling, the 2,6-DTBP conversion decreased to 80% (Table 2).

It should be particularly noted that the 2,6-DTBP conversion drastically decreases when the reaction is performed in the absence of a polar solvent (Table 2). This fact indicates that the polar solvent plays an important role of a dissociating medium enhancing the nucleophilicity of 2,6-DTBP.

With a decrease in temperature, the reaction rate decreased considerably (see figure).

The synthesized product was tested as antioxidant for various rubbers: both highly unsaturated (SKI-3, SKB) and containing a small amount of multiple bonds (BK, SKEPT). To evaluate the performance of the stabilizer, we used the manometric method for measuring the induction periods of oxidation of the polymers [6]. This method is based on studying the kinetics of thermal oxidation and involves monitoring of the oxygen uptake by the polymer in the course of heating under O_2 or in air. In the first (induction) period, the oxygen uptake is fully suppressed or strongly decelerated depending on the AO performance. The induction period ends at virtually complete consumption of the stabilizer, and its duration can be a measure of both the AO performance and rubber stability.

The performance of the bis-SHP polysulfide prepared was compared with that of commercial AOs used for stabilization of the same polymers. In particular, amine antioxidants Diafen FF (or Diafen FP) and acetone anil are used for stabilization of SKI-3 and SKB, respectively, and phenolic antioxidant Agidol-2, for stabilization of BK and SKEPT rubbers [6].

As seen from Table 3, the additive synthesized is an effective antioxidant for the majority of the polymers studied, increasing (compared to commercial stabilizers) the induction periods of oxidation of rubbers.

The stability of rubbers can also be judged from variation of the IR spectra of the polymer films in the course of thermal oxidation. The process is usually monitored by the >C=O stretching vibration band at 1720 cm^{-1} [9].

In this study, the polymer films were oxidized at 100°C in air. Experimental data showed that thermal

Table 3. Induction periods τ (min) of thermal oxidation of rubbers stabilized with bis-SHP polysulfide

Rubber	Oxidation temperature, °C	Reference stabilizer		τ, min, at indicated bis-SHP polysulfide concentration, wt %				
		name (*c*, wt %)	τ, min	0	0.1	0.2	0.3	0.4
SKI-33	130–135	Diafen FF (0.3)	80	10	45	50	55	–
SKB	130–135	Acetone anil P (0.3)	20	10	60–65	190–200	260	410
BK	170–175	Agidol 2 (0.2)	150	15	235	420	>520	>520
SKEPT	170–175	Agidol 2 (0.2)	220	40	110	130	260	280

Table 4. Effect of bis-SHP polysulfide on the time from the start of thermal oxidation of SKI-3 films (oven, air, 100°C) until the appearance of the carbonyl bands in the IR spectra

Concentration, wt %	Presence of peak at 1721 cm^{-1} [ν(C=O)] in the IR spectrum (+) after oxidation for indicated time, h						
	0	8	32	64	83	99	131
0	–	+	+	+	+	+	+
0.1	–	–	–	–	+(weak)	+	+
0.2	–	–	–	–	–	–	+(weak)
0.3	–	–	–	–	–	–	–

Table 5. Effect of stabilizers on the properties and stability of vulcanizates based on BNKS-18 (thermal aging: 100°C, 72 h; vulcanization: 143°C, 30 min)

Parameter	Rubber stocks		
	control	I	II
Nominal tensile strength, MPa	15.4	15.7	15.2
Relative elongation at break, %	240	230	250
Elongation set, %	6	4	6
Aging coefficient with respect to nominal tensile strength	1.08	0.96	1.06
Aging coefficient with respect to relative elongation at break	0.69	0.65	0.64
Stabilizer	Content, parts per 100 parts of rubber		
Diafen FP	1	–	–
Acetone anil	3	–	–
SHP polysulfide	–	4	3

oxidation for 8 h of SKI-3 containing no antioxidant caused the following changes in the IR spectra: bands appeared at 1721 [ν(C=O)] and 3475 cm^{-1} [ν(OH)], and the bands at 1666 (C=C) and at about 890 cm^{-1} (H–C=C) decreased in the intensity. On adding bis-SHP polysulfide to SKI-3, the heating time required for the ν(C=O) band (1721 cm^{-1}) to appear increased by a factor of several tens (Table 4).

We examined the possibility of using the synthesized bis-SHP polysulfide as antioxidant for the vulcanizate based on butadiene–acrylonitrile rubber. The formulation we used corresponds to the commercial rubber stock. As seen from Table 5, replacement of the commercial Diafen FP–acetone anil mixture by the synthesized bis-SHP polysulfide does not impair the initial properties and heat resistance of the vulcanizate.

CONCLUSIONS

(1) A feasible procedure was developed for preparing bis-SHP polysulfide by the reaction of 2,6-DTBP with elemental sulfur in a polar aprotic solvent, in

which the use of catalytic amounts of phenolic Mannich bases allowed the synthesis time to be reduced to 1.5–3 h.

(2) Bis-SHP polysulfide shows a high antioxidative activity in stabilization of various rubbers (SKI-3, SKB, SKEPT, BK, BNSK). This additive increases the induction period of the polymer oxidation and the time in which carbonyl groups started to form. The synthesized SHP polysulfide does not impair the initial properties and heat resistance of the vulcanizate based on BNSK-18.

REFERENCES

1. Emanuel', N.M. and Buchachenko, A.L., *Khimicheskaya fizika molekulyarnogo razrusheniya v stabilizatsii polimerov* (Chemical Physics of Molecular Degradation and Stabilization of Polymers), Moscow: Nauka, 1988.
2. US Patent 3310587.
3. Aslanov, A.D., Zolotova, N.V., Denisov, E.T., and Kuliev, F.A., *Neftekhimiya*, 1982, vol. 22, no. 3, pp. 394–399.
4. Shlyapintokh, V.Ya., *Fotokhimicheskie prevrashcheniya i stabilizatsiya polimerov* (Photochemical Transformations and Stabilization of Polymers), Moscow: Khimiya, 1979.
5. Voronkov, M.G. and Deryagina, E.N., *Zh. Obshch. Khim.*, 2001, vol. 71, no. 12, pp. 1941–1965.
6. Piotrovskii, K.B. and Tarasova, Z.N., *Starenie i stabilizatsiya sinteticheskikh kauchukov i vulkanizatorov* (Aging and Stabilization of Synthetic Rubbers and Vulcanizates), Moscow: Khimiya, 1980.
7. Bukharov, S.V., Konoshenko, L.V., Solov'eva, S.E., *et al.*, *Zh. Prikl. Khim.*, 1999, vol. 72, no. 4, pp. 641–644.
8. *Khimicheskie dobavki k polimeram: Spravochnik* (Chemical Additives to Polymers: Handbook), Moscow: Khimiya, 1972.
9. *Issledovanie i razrabotka tekhnologii proizvodstva monomerov i sinteticheskikh kauchukov* (Research and Development of a Process for Production of Monomers and Synthetic Rubbers), Moscow: TsNIITENeftekhim, 1983.

Russian Journal of Applied Chemistry, Vol. 78, No. 7, 2005, pp. 1115–1118. Translated from Zhurnal Prikladnoi Khimii, Vol. 78, No. 7, 2005, pp. 1135–1138.
Original Russian Text Copyright © 2005 by A. Samuilov, Zenitova, Solov'eva, Ya. Samuilov.

ORGANIC SYNTHESIS AND INDUSTRIAL ORGANIC CHEMISTRY

Composition of Laprol-373 and Products of Its Reaction with 2,4-Toluylene Diisocyanate

A. Ya. Samuilov, L. A. Zenitova, S. E. Solov'eva, and Ya. D. Samuilov

Kazan State Technological University, Kazan, Tatarstan, Russia
Arbuzov Institute of Organic and Physical Chemistry, Kazan Scientific Center, Russian Academy of Sciences, Kazan, Tatarstan, Russia

Received March 24, 2005

Abstract—The composition of oligoethers that are components of Laprol-373 and of products of their reaction with 2,4-toluylene diisocyanate were studied by matrix-assisted laser desorption ionization mass spectrometry (MALDI-TOF).

Oligoethers with terminal hydroxy groups prepared by copolymerization of ethylene and propylene oxides in the presence of polyol alcoholates as initiators are widely used in production of polyurethanes [1–3]. The parameters (hydroxy number, viscosity, IR and NMR data) used to characterize these oligoethers (Laprols) reflect their statistical mean properties. They are undoubtedly important for applications of Laprols, but for polymer chemistry it is important to know the structures of specific components of one or another Laprol.

The compositions of Laprol-373 and of products of its reaction with 2,4-toluylene diisocyanate (2,4-TDI) were studied by MALDI-TOF mass spectrometry. This method involves mild ionization of organic compounds, so that the degree of fragmentation of molecular ions is minimal compared to other mass-spectroscopic methods [4]. MALDI-TOF mass spectroscopy involves the following procedure. A substance to be studied is mixed with a matrix substance capable to absorb the laser radiation, and this mixture is applied onto a special metallic plate containing Na and K. The sample is irradiated with a laser beam. In so doing, the molecules of the test substance get ionized. The positive molecular ions formed pass into the gas phase and are recorded with time-of-flight mass-spectrometric detectors [5]. If the test substances are capable of complexing with sodium and potassium ions, they are detected as single-charged positive molecular ions of the complexes. Therefore, the same compound can give three signals in the mass spectrum, belonging to its radical cations and complexes of the neutral molecule with the sodium and potassium ions. This feature of MALDI-TOF mass spectroscopy makes the results obtained more reliable. The problems of ionization of compounds in this procedure were discussed in [6]. The intensity of signals in MALDI-TOF mass spectroscopy depends both on the amount of the test substance in the sample and on its electron-donor properties. Therefore, data obtained by this method furnish reliable information on the composition and structure of molecules but are less suitable for quantitative determinations. As shown by Meier *et al.* [7], the quantitative data obtained in analysis of molecular weights and molecular-weight distribution (MWD) of oligostyrenes by gel permeation chromatography and MALDI-TOF mass spectroscopy are mutually consistent. The possibility of using MALDI-TOF mass spectrometry for analysis of a series of oligoethers and oligoesters was demonstrated in [8].

EXPERIMENTAL

Laprol-373 [Nizhnekamskneftekhim Joint-Stock Company, TU (Technical Specifications) 2226-017-10 488 057–97) was vacuum-dried (133 Pa, 80°C) before use. 2,4-TDI was purchased from Bayer (Germany). The 2,4-TDI samples freshly distilled in a vacuum had the following characteristics: bp 120–121°C/1330 Pa (121°C/1330 Pa [9]), n_D^{20} 1.5680 (1.5678 [9]).

The reaction of Laprol-373 with 2,4-TDI was performed in the bulk under the conditions of a slight excess of isocyanate groups relative to hydroxy groups, without catalysts. Under these conditions, the oligomerization was insignificant, and modified Laprols with terminal isocyanate groups were obtained.

1070-4272/05/7807-1115 © 2005 Pleiades Publishing, Inc.

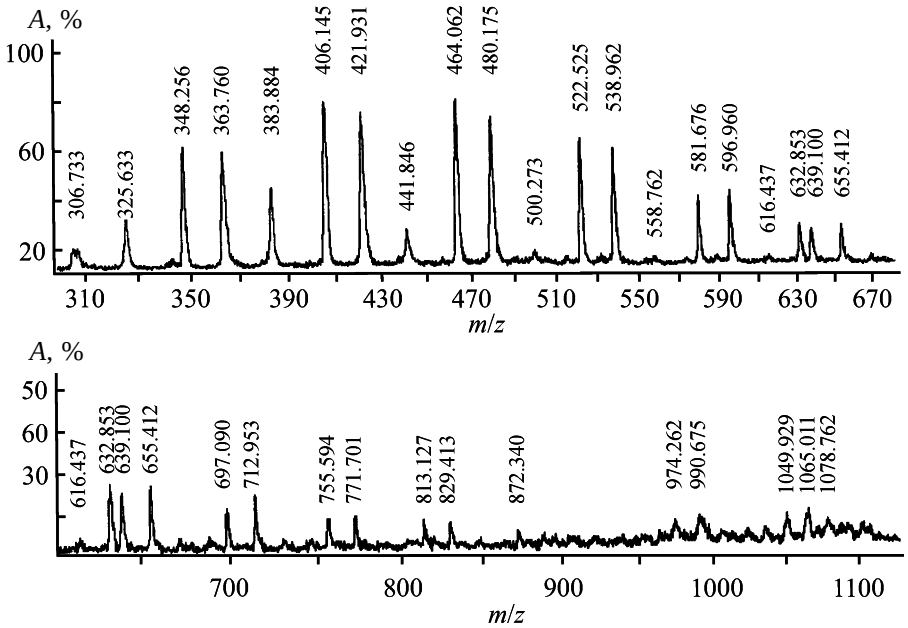


Fig. 1. MALDI-TOF mass spectrum of Laprol-373. (*A*) Intensity; the same for Fig. 2.

Laprol-373 (100 g) was kept for 30 min in a vacuum (residual pressure 18 620 Pa) at 80°C. After that, it was cooled, the pressure was brought to atmospheric pressure, and 130 g of 2,4-TDI was added (molar ratio of the HO and NCO groups 1 : 1.5). In so doing, the mixture spontaneously warmed up to 60°C. The reaction was performed for 30 min with stirring in a vacuum (residual pressure 18 629 Pa) at 60°C. The mass spectra were recorded on a Finnigan MALDI-TOF Dynamo device, using 1,8,9-trihydroxyanthracene as matrix. The weights were determined with an accuracy of ±(1–2) amu.

Table 1. Structure of oligomers **Ia**–**Im**, according to mass-spectroscopic data

Compound	*m*	*n*	*m*/*z*(**I**)	*m*/*z*(**I** + Na)*	*m*/*z*(**I** + K)*
Ia	4	0	(268)**	(291)	307
Ib	4	1	326	349	365
Ic	4	2	384	407	423
Id	4	3	442	465	481
Ie	4	4	500	523	539
If	4	5	558	581	597
Ig	4	6	616	639	655
Ih	4	7	(674)	697	713
Ii	4	8	(732)	755	771
Ij	4	9	(790)	813	829
Ik	4	10	(848)	871	(887)
Il	5	11	(950)	973	989
Im	7	11	(1038)	1061	1077

* The *m*/*z* ratio is given for complexes of **Ia**–**Im** with sodium and potassium ions.

** The weights of ions that were not detected are given in parentheses; the same for Figs. 2 and 3.

Laprol-373 is a product of copolymerization of ethylene and propylene oxides in the presence of potassium monoglycerate; its structure is described by the formula

$$C_3H_5O_3(CH_2CH_2O)_m(CH_2\text{–}\underset{\displaystyle CH_3}{\underset{|}{CH}}\text{–}O)_nCH_3$$

Ia–**Im**.

Figure 1 shows the mass spectrum of Laprol-373. It is seen that the substance has a broad molecular-weight distribution.

The ions detected (or expected) in the MALDI-TOF mass spectrum of Laprol-373 are given with assignments in Table 1.

Compounds **Ia**–**Im** are detected in the mass spectra not only in the form of molecular ions, but also as complexes with sodium and potassium ions; the intensity of their signals is higher than that of the free molecule. This fact indicates that oligoethers readily form complexes with alkali metal cations [10].

The principal structural unit of **Ia**–**Ik** is an oligoether formed by addition of four ethylene oxide mole-

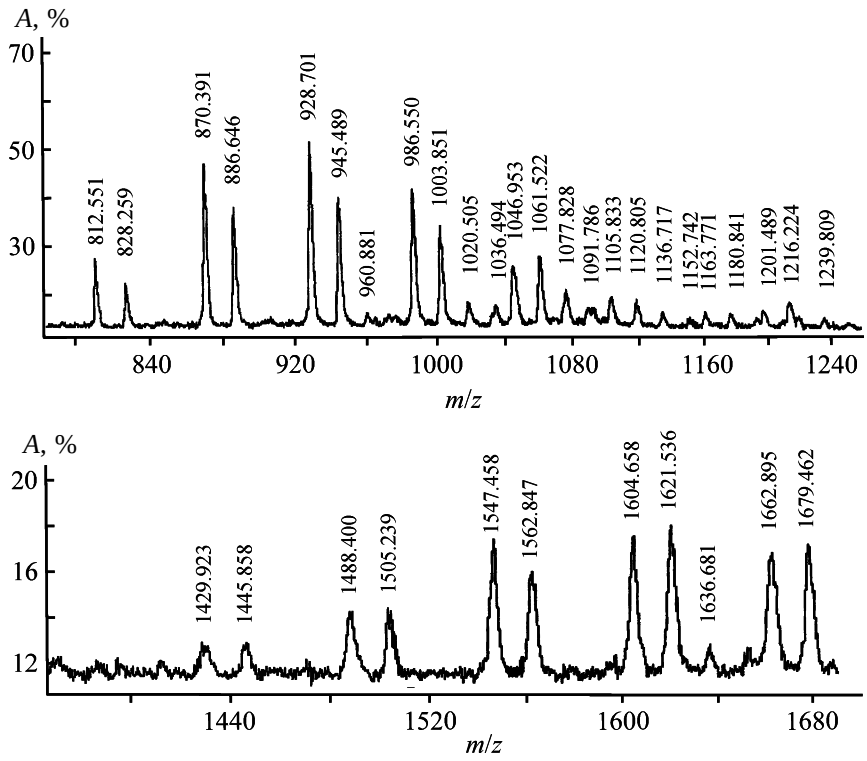


Fig. 2. Mass spectrum of compounds formed in the reaction of Laprol-373 with 2,4-TDI.

cules to a glycerol molecule (compound **Ia**). Further complication of the structure occurs through successive addition of propylene oxide molecules to **Ia**. Laprol-373 contains also compounds **Il** and **Im** of relatively high molecular weights, with more than four ethylene oxide fragments.

Figure 2 shows the mass spectrum of products formed in the reaction of a mixture of **Ia**–**Im** with 2,4-TDI:

$$\textbf{Ia–Im} + 3OCNC_6H_3NCO \rightarrow C_3H_5O_3(CH_2CH_2O)_m\cdot$$

$$(CH_2\text{–}\underset{\displaystyle CH_3}{\underset{|}{CH}}\text{–}O)_n[CONHC_6H_3(CH_3)NCO]_3.$$

Without catalysts, the 4-NCO group in 2,4-TDI is more reactive toward alcohols [11, 12]. The causes of such a selectivity are discussed in [13, 14].

The mass-spectrometric data for preisocyanates **IIa**–**IIh** are given in Table 2.

In the mass spectra, we detected no signals of preisocyanates **IIi**–**IIm**, expected products of addition of 2,4-TDI to oligoethers **Ii**–**Im**. This may be due to a low content of **Ii**–**Im** in Laprol-373.

In most cases, compounds **II** are manifested in the mass spectra only as complexes with sodium and potassium ions. This fact indicates that the addition of 2,4-TDI to oligoethers **Ia**–**Im** enhances their capability for complexation with alkali metal ions.

The products of the reaction of 2,4-TDI with oligoethers **I** contain, along with the above-mentioned compounds, also compounds formed by the reaction of two oligoether molecules with five 2,4-TDI molecules:

$$2(\textbf{I}) + 5(2,4\text{-TDI}) \rightarrow (\textbf{III}).$$

Table 2. Structures of compounds **IIa**–**IIh**, according to mass-spectrometric data (m = 4)

Compound	n	m/z(**II**)	m/z(**II** + Na)*	m/z(**II** + K)*
IIa	0	(790)	813	829
IIb	1	(848)	871	887
IIc	2	(906)	929	945
IId	3	(964)	987	1003
IIe	4	(1022)	1045	1061
IIf	5	(1080)	1103	1119
IIg	6	1138	1161	1177
IIh	7	(1169)	1219	1235

* The m/z ratio is given for complexes of **IIa**–**IIh** with sodium and potassium ions.

Table 3. Structures of compounds **III**, according to mass-spectrometric data

Compound	Fragments of oligoethers **I** in **III**		*m*/*z*(**III**)	*m*/*z*(**III** + Na)	*m*/*z*(**III** + K)
IIIa	**Ia**	**Ia**	(1406)	1429	1445
IIIb	**Ia**	**Ib**	(1464)	1487	1503
IIIc	**Ib**	**Ib**	(1522)	1545	1561
IIId	**Ib**	**Ic**	(1580)	1603	1619
IIIe	**Ic**	**Ic**	(1638)	1661	1677

In the process, two oligoether molecules are bound with two isocyanate groups of one 2,4-TDI molecule; the remaining hydroxy groups, in turn, react with four 2,4-TDI molecules. As a result, large molecules containing four terminal isocyanate groups are formed. Compounds **III** can be formed by coupling of different oligoethers **I** with 2,4-TDI. The detected compounds **III** are listed in Table 3.

Urethane diisocyanates **III**, like the compounds discussed above, are manifested in the mass spectra in the form of complexes with cations.

CONCLUSIONS

(1) The major fraction of oligomers that are components of Laprol-373 are formed by addition of propylene oxide molecules to the product of addition of four ethylene oxide molecules to a glycerol molecule.

(2) Oligoethers **I** in the reaction with 2,4-toluylene diisocyanate without catalysts, even with excess isocyanate, form not only trifunctional but also tetrafunctional urethane diisocyanates containing two fragments of oligoethers **I**.

(3) Both oligoethers **I** and products of their reaction with 2,4-toluylene diisocyanate are capable of complexation with sodium and potassium ions in the gas phase.

REFERENCES

1. Saunders, J.H. and Frish, K.C., *Polyurethanes. Chemistry and Technology*, part 1: *Chemistry*, New York: Interscience, 1962.
2. Kirpichnikov, P.A., Zenitova, L.A., and Bakirova, I.N., *Khim. Komp'yut. Model.: Butlerovsk. Soobshch.*, 1999, vol. 1, no. 1, pp. 57–60.
3. Zenitova, L.A., Bakirova, I.N., Mukmeneva, N.A., *et al.*, *Khim. Komp'yut. Model.: Butlerovsk. Soobshch.*, 2002, vol. 3, no. 11, pp. 45–47.
4. Schiller, J. and Arnold, K., *Encyclopedia of Analytical Chemistry*, Meyers, R.A., Ed., Chichester: Wiley, 2000, pp. 559–585.
5. Karas, M., Bachmann, D., and Hillenkamp, F., *Anal. Chem.*, 1985, vol. 57, no. 14, pp. 2935–2939.
6. Pshenichnyuk, S.A., Asfandiarov, N.L., Fal'ko, V.S., *et al.*, *VIII Vserossiiskaya konferentsiya "Struktura i dinamika molekulyarnykh sistem: Yal'chik-2001" (sbornik statei)* (VIII Russian Conf. "Structure and Dynamics of Molecular Systems: Yal'chik-2001" (Coll. of Papers)), Ioshkar-Ola, 2001, part 2, pp. 58–61.
7. Meier, M.A., Hoogenboom, R., Fijten, V.W., *et al.*, *J. Comb. Chem.*, 2003, no. 5, pp. 369–374.
8. Lawson, G., Bartram, S., Fitchner, S., and Woodland, E.D., *Analyst*, 2000, vol. 125, no. 1, pp. 115–118.
9. *Khimicheskaya entsiklopediya* (Chemical Encyclopedia), Knunyants, I.L., Ed., Moscow: Sov. Entsiklopediya, 1990, vol. 2, p. 402.
10. Kron, T.E. and Tsvetkov, E.N., *Usp. Khim.*, 1990, vol. 59, no. 3, pp. 483–508.
11. Boitsov, E.N. and Trub, E.P., *Kinet. Katal.*, 1984, vol. 25, no. 2, pp. 279–282.
12. Sumkina, V.G., Palyutkin, G.M., and Zharkov, V.V., *Kinet. Katal.*, 1985, vol. 26, no. 2, pp. 476–480.
13. Samuilov, A.Ya., Zenitova, L.A., and Samuilov, Ya.D., *Khim. Komp'yut. Model.: Butlerovsk. Soobshch.*, 2004, vol. 5, no. 2, pp. 51–53.
14. Samuilov, A.Ya., Zenitova, L.A., Palyutin, F.M., and Samuilov, Ya.D., *Khim. Komp'yut. Model.: Butlerovsk. Soobshch.*, 2004, vol. 5, no. 3, pp. 1–10.

Russian Journal of Applied Chemistry, Vol. 78, No. 7, 2005, pp. 1119–1121. Translated from Zhurnal Prikladnoi Khimii, Vol. 78, No. 7, 2005, pp. 1139–1141.
Original Russian Text Copyright © 2005 by Storozhakova, Khaled Khedar Nasser Akhmed, Rakhimov.

ORGANIC SYNTHESIS AND INDUSTRIAL ORGANIC CHEMISTRY

Catalytic Synthesis of Low-Molecular-Weight Oligomers of *N*-Adamantanoyl-ε-aminocaproic Acid

N. A. Storozhakova, Khaled Khedar Nasser Akhmed, and A. I. Rakhimov

Volgograd State Technical University, Volgograd, Russia
Institute of Chemical Problems of Ecology, Russian Academy of Natural Sciences, Volgograd, Russia

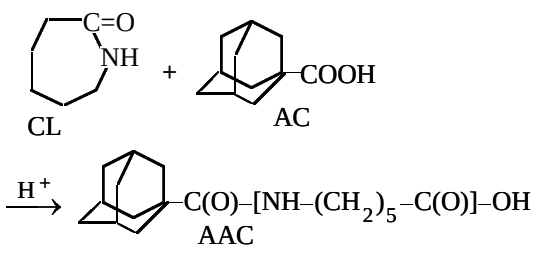
Received March 16, 2005

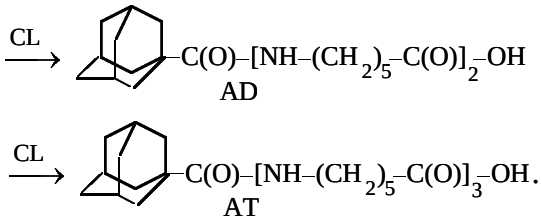
Abstract—The synthesis of the dimer and trimer of *N*-adamantanoyl-ε-aminocaproic acid by the reaction of adamantanecarboxylic acid with ε-caprolactam in the presence of a catalyst, *p*-toluenesulfonic acid, was studied.

ε-Aminocaproic acid and its *N*-acetyl derivative are used in medicine [1, 2]. One of the routes to *N*-acyl derivatives of ε-aminocaproic acid oligomers is the acid-catalyzed reaction of carboxylic acids with ε-caprolactam (CL).

The reactions of aliphatic carboxylic acids containing 8–26 carbon atoms with CL are performed in the presence of sulfuric, boric, toluenesulfonic, or methanesulfonic acid, or their mixtures [3, 4]. Water is added to the reaction mixture, which results in the formation of ε-aminocaproic acid; this acid is subsequently acylated at the NH_2 group, and the resulting *N*-acyl derivative reacts with a new CL molecule; the major products of the reaction are oligomers containing 5–10 monomeric units.

Synthesis of low-molecular-weight oligomers of *N*-1-adamantanoyl-ε-aminocaproic acid (AAC) was not studied previously. At the same time, according to the prediction made with the PASS C & T 1.41 program [5], AAC is expected to exhibit antiviral and nootropic activity. Therefore, our goal was to study the synthesis of the dimer (AD) and trimer (AT) of AAC by the reaction of 1-adamantanecarboxylic acid (AC) with CL in the absence of water and in the presence of a catalyst, *p*-toluenesulfonic acid.





EXPERIMENTAL

The IR spectra of liquid substances were recorded with a Specord M82 spectrophotometer from thin films, and those of solids, from mulls in mineral oil. The ^1H NMR spectra were taken on a Varian Mercury Plus spectrometer (300 MHz, CCl_4, internal reference TMS).

The rates of consumption of CL and AC and of formation of *N*-1-adamantanoyl dimer (AD) and trimer (AT) of ε-aminocaproic acid via intermediate monomer (AAC) were estimated by the ampule method.

Ampules containing CL, AC, and a catalyst (*p*-toluenesulfonic acid) in a 1 : 1 : 0.1 molar ratio were placed in a thermostat. At equal intervals (15 min), an ampule was withdrawn, and its contents were analyzed. To this end, the reaction mixture was treated with chloroform in which CL and AC are soluble, after which the precipitate was filtered off. The precipitate consisted of a mixture of AD and AT.

To separate AD and AT, their mixture in ethanol was heated to boil. The solution was filtered while hot and cooled, after which AT precipitated and was filtered off, whereas AD, which is readily soluble in ethanol, remained in the solution; it was isolated by evaporation of the mother liquor, followed by recrys-

1070-4272/05/7807-1119 © 2005 Pleiades Publishing, Inc.

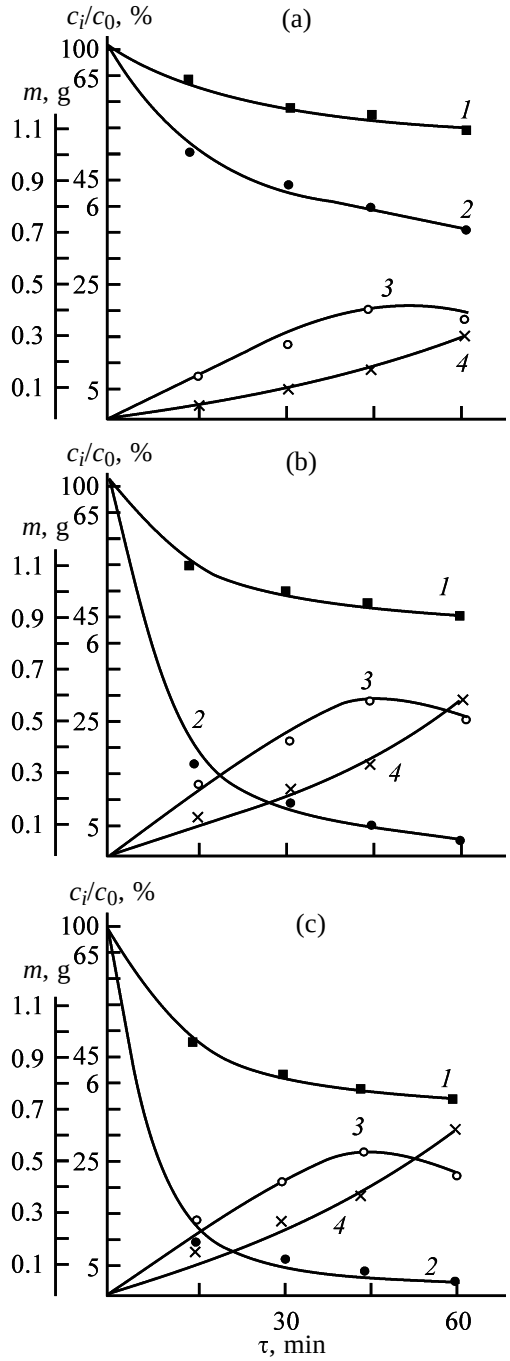


Fig. 1. Consumption of reactants and formation of oligomers in the reaction of CL with AC: (c_i/c_0) content of *i*th compound relative to its initial content (for reactants) or theoretical yield (for products), (*m*) AD and AT weight, and (τ) time. (*1*) AC, (*2*) CL, (*3*) AD, and (*4*) AT. Temperature, °C: (a) 180, (b) 195, and (c) 210.

tallization. The chloroform solution containing CL and AC was evaporated. Then a mixture of CL and AC was treated with hexane, and AC was recovered from the solution.

Nitrogen content in AD, %: found 6.88, calculated for $C_{23}H_{38}N_2O_4$ 6.89; mp 135–138°C. Nitrogen content in AT, %: found 8.23, calculated for $C_{29}H_{49}N_3O_5$ 8.10; mp 172–174°C. The structures of AD and AT were proved by IR and ^{1}H NMR spectroscopy.

The IR spectrum of AD contains amide I and amide II bands at 1680 and 1576 cm^{-1}, respectively, and also the NH stretching band at 3328 cm^{-1}. In the IR spectrum of AT, the amide I and amide II bands are observed at 1640 and 1540 cm^{-1}, respectively, and the NH stretching band, at 3296 cm^{-1}. ^{1}H NMR spectrum of AD (CCl_4), δ, ppm: 7.19 s (H, OH), 6.4 s (2H, NH), 3.1 t (4H, CHNH), 2.3 m [4H, $CH_2C(O)$], 0.8–1.9 m [27H, Ad, $(CH_2)_6$].

Figures 1a–1c show the kinetic curves of the reactant consumption (c_i/c_0, ratio of the current amount of reactant to its initial amount) and product (AD, AT) formation at different temperatures. The initial period is characterized by a high rate of CL consumption. The initial rate of reactant consumption, min^{-1}, is as follows: at 180°C, CL 0.05 and AC 0.03; at 195°C, CL 0.10 and AC 0.04; and at 210°C, CL 0.13 and AC 0.06.

The ratio of consumptions of the reactants in the first 15 min depends on the temperature. The consumptions (%) of CL and AC change as follows: 90 CL and 55 AC (210°C); 85 CL and 45 AC (195°C); and 50 CL and 35 AC (180°C). In this period, the content of AD is 55% of that in a maximum at 210°C (Fig. 1c), 50% at 195°C (FIg. 1b), and 35% at 180°C (Fig. 1a). At the same time, the amount of AT formed in 15 min, relative to that isolated after 60 min, is 30% at 210°C (Fig. 1c), 25% at 195°C (Fig. 1b), and 16% at 180°C (Fig. 1a).

Hence, in the initial period (first 15 min), the major reaction is that of CL with AC, yielding AAC, which subsequently reacts with CL to form AD.

The highest yield of AD is observed 45 min after the start of the reaction (at both 210 and 195°C). The AT content in the system increases monotonically, and in 60 min it starts to exceed the AD content, which tends to decrease after 45 min.

The optimal conditions for preparing AD are 195°C and 45 min; the AD yield is 54% based on CL.

The optimal conditions for preparing AT are 210°C and 45 min; the AT yield is 72% based on CL. Longer heating results in formation of higher oligomers.

The yields of AD and AT under these conditions are considerably higher than under the conditions described in [3, 4]. This is due to the fact that, in the

absence of water, CL reacts directly with AC, without formation of AAC. To prove this assumption, we performed the reaction of AAC with AC under the conditions similar to those described in the Experimental. The reaction of AC with AAC gave higher AAC oligomers containing 10.5–11.20% N, with mp 176–182°C; these products were virtually insoluble in water.

Under the conditions of the reaction of AC with CL, AAC is more reactive than AC. This fact allows preparation of AD (54% yield) and AT (72% yield) under the optimal conditions.

CONCLUSION

Monitoring of the consumption of the reactants (ε-caprolactam and 1-adamantanecarboxylic acid) in the course of the catalytic synthesis of the dimer and trimer of *N*-adamantanoyl-ε-aminocaproic acid revealed significantly larger consumption in the first 15 min of ε-caprolactam (85–90%) relative to 1-adamantanecarboxylic acid (45–55%), which indicates that the forming *N*-1-adamantanoyl-ε-aminocaproic acid is more reactive than 1-adamantanecarboxylic acid in the acid-catalyzed reaction with ε-caprolactam. This fact allows efficient synthesis of the dimer and trimer of *N*-1-adamantanoyl-ε-aminocaproic acid.

REFERENCES

1. Mashkovskii, M.D., *Lekarstvennye sredstva* (Drugs), Moscow: Meditsina, 1993.
2. Popova, V.V., Sernov, L.N., and Novikov, V.V., Abstracts of Papers, *4-i Rossiiskii natsional'nyi kongress* (4th Russian National Congr.), Moscow, April 12–18, 1997, p. 285.
3. US Patent 2956068.
4. US Patent 5414099.
5. *GU NII Biomeditsinskoi khimii im. V.N.Orekhovicha RAMN: programma PASS [Elektronnyi resurs]* (Orekhovich Research Inst. of Biomedical Chemistry, Russian Acad. of Medical Sci.: PASS Program [Electronic Resource]), 2003. Available from http://www.ibmh.msk.su/ibmh-rus.

Russian Journal of Applied Chemistry, Vol. 78, No. 7, 2005, pp. 1122–1125. Translated from Zhurnal Prikladnoi Khimii, Vol. 78, No. 7, 2005, pp. 1142–1145.
Original Russian Text Copyright © 2005 by Fomina, Chervyakova, Kurskii, Sineokov.

ORGANIC SYNTHESIS AND INDUSTRIAL ORGANIC CHEMISTRY

Reaction of Dimerized Fatty Acid with Aliphatic Diamines and Properties of Reaction Products

E. V. Fomina, G. N. Chervyakova, Yu. A. Kurskii, and A. P. Sineokov

Kargin Research Institute of Polymers, Federal State Unitary Enterprise, Dzerzhinsk, Nizhni Novgorod oblast, Russia

Received February 9, 2005

Abstract—The reactions of dicarboxylic acids with di- and triamines were studied, and the properties of the resulting polyamides were examined in relation to the structure and ratio of the starting reactants.

Among numerous polyamide derivatives [1, 2], a particular place is occupied by aliphatic polyimides prepared from dimerized fatty acid (DFA). The presense of a bulky alkylene segments between the carboxy groups of DFA makes the resulting polyamide considerably more elastic, decreases its softening point, and enhances its adhesion properties. This is important for preparing thermoplastic adhesive compounds [3–5].

The possibility of using polyamides derived from DFA for preparing hot-melt adhesives was reported in [6–8]. However, the purposeful development of adhesive formulations with the preset physicomechanical properties was prevented by the lack of data on how the properties of the polyamides depend on the structure of the starting components. Therefore, it seemed important to study the synthesis of polyamides from DFA and to reveal the main parameters affecting the reaction course and the properties of the final product.

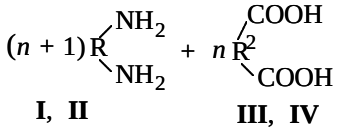
The goals of this study were to optimize the synthesis conditions (so as to attain the maximal conversion of the reactants), examine how the properties of the resulting polyamides depend on the structure and ratio of the reactants, and optimize the process as a whole.

EXPERIMENTAL

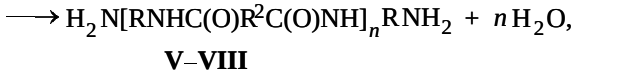
In our study we used DFA of PRIPOL 1017 DIMER ACID brand (the Netherlands, CAS registry no. 61788-89-4), sebacic acid [SA, TU (Technical Specifications) 6-02-1091–83], abietic acid [AbA, GOST (State Standard) 14201–83], acetic acid (AcA, GOST 61–75), hexamethylenediamine (HMDA, TU 6-09-36–73), and diethylenetriamine (DETA, EC no. 203-865-4, fraction distilled at 82–85°C/1.33 kPa).

Syntheses of polyamides were performed in a reactor equipped with a stirrer, a thermometer, a descending condenser, and a receiver. As DFA is viscous, after loading the reactants in the required ratio the reactor contents were heated to 120°C, and only after that the stirrer was switched on. The mixture was heated to 160°C with efficient stirring; the condensation with the water release started at this temperature. The temperature was gradually (over a period of 5–6 h) raised to 230°C. The synthesis was performed until the water release ceased.

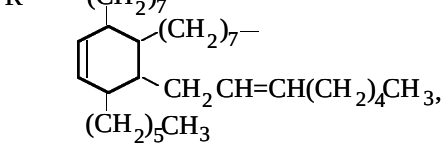
The general scheme of formation of polyimides in the reaction of DFA with amines can be represented as follows:



I, II **III, IV**



V–VIII



where R = $(CH_2)_6$ (**I**), $C_2H_4NHC_2H_4$ (**II**); R^2 = $C_{34}H_{62}$ (**III**), $(CH_2)_8$ (**IV**); R = $(CH_2)_6$, R^2 = $C_{34}H_{62}$ (**V**); R = $C_2H_4NHC_2H_4$, R^2 = $C_{34}H_{62}$ (**VI**); R = $(CH_2)_6$, R^2 = $C_{34}H_{62}$ and $(CH_2)_8$ (**VII**); R = $C_2H_4 \cdot NHC_2H_4$, R^2 = $C_{34}H_{62}$ and $(CH_2)_8$ (**VIII**); n = 3–30.

The IR spectra of the polyamides obtained were taken on a Specord M 80 spectrometer in the range 4000–700 cm^{-1}. A drop of a sample was pressed between NaCl plates. The NMR spectra were recorded

1070-4272/05/7807-1122 © 2005 Pleiades Publishing, Inc.

Table 1. Synthesis and properties of polyamides **V** and **VI**. Initial amount of DFA 0.25 molar equiv in all the experiments

Run no.	Initial amine amount, molar equiv	AmN	AcN	*M*	*T*, °C
		(mg KOH) (g polyamide)$^{-1}$			
	HMDA:				
1	0.30	6.5	2.0	13200	93
2	0.35	36.1	1.2	3010	85
3	0.40	48.3	0.8	2290	83
	DETA:				
4	0.30	8.4*	2.9	9930	45
5	0.35	39.0*	1.7	2760	40
6	0.40	50.4*	0.9	2190	39

* The amine number was determined for primary amino groups only [12].

on a Bruker DPX-200 spectrometer operating at 200 MHz for ^{1}H and 50 MHz for ^{13}C; solvent $CDCl_3$, internal reference TMS.

The amine and acid numbers and molecular weights *M* of polyamides were determined by procedures described in [9], and the softening points T_s, by the ring-and-ball method (GOST 11506–73).

The polycondensation progress was monitored by variation of the acid and amine numbers, and also by the amount of the released water. The starting components are mainly exhausted (Figs. 1, 2) in the first 2–3 h; however, as the reactant concentartions decrease and the viscosity of the reaction mixture grows, the reaction decelerates. To attain the maximal conversion of the reactants, the final step of the synthesis was performed in a vacuum at 1.33 kPa and 160–220°C for 1–1.5 h, which favored faster shift of the equilibrium toward formation of the desired polyamide, due to efficient removal of water from the reaction mixture (Fig. 1). It should be noted that the ratio of DFA and amine was chosen so as to obtain products with terminal primary amino groups.

As shown in Fig. 2, in the system DFA–HMDA (0.25 : 0.30 ratio), the amine and acid numbers vary in parallel, and a polyamide with a measurable softening point is formed. However, in the system DFA–DETA, in which the amine contains two primary and one secondary amino groups, at the same ratio of the components, the reaction performed to conversions exceeding 70% yields an insoluble and nonmelting product. This phenomenon is due to involvement of secondary amino groups in the reaction and formation of a network polymer. In view of the undesirable gelation, it is appropriate to use the molar equivalent of DETA equal to 2, taking into account the fact that primary amino groups are more nucleophilic than secondary amino groups and undergo amidation first [10].

Polyamides **V** and **VI** synthesized at various ratios of DFA and amines **I** and **II** are transparent golden yellow solids with a weak amine odor (Table 1).

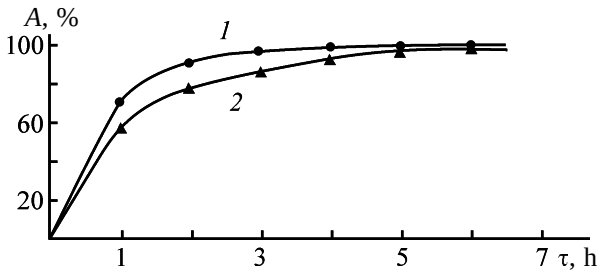


Fig. 1. Amount of the released water *A* in the synthesis of polyamides **V** and **VI** as a function of time τ. DFA : amine ratio 0.25 : 0.30. (*1*) DFA + HMDA and (*2*) DFA + DETA; the same for Fig. 2.

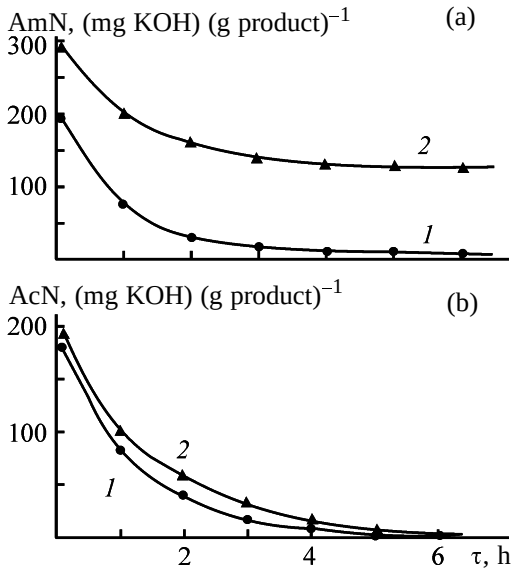


Fig. 2. Variation of the (a) amine number AmN (for the system with DETA, total amine number) and (b) acid number AcN with time τ in the course of the synthesis of polyamides **V** and **VI**. DFA : amine ratio 0.25 : 0.30.

Table 2. Synthesis and properties of copolyamides **VII** and **VIII**

Run no.	Starting reactants and their ratio		AmN	AcN	*M*	T_s, °C
	dicarboxylic acid	amine	(mg KOH) (g polyamide)$^{-1}$			
1	DFA, 0.10; SA, 0.15	HMDA, 0.30	4.0	1.0	22 450	104
2	DFA, 0.15; SA, 0.10	HMDA, 0.35	30.3	1.3	3550	102
3	DFA, 0.20; SA, 0.05	HMDA, 0.40	43.2	1.6	2505	97
4	DFA, 0.10; SA, 0.15	DETA, 0.30	5.6*	1.8	15 165	49
5	DFA, 0.15; SA, 0.10	DETA, 0.35	33.7*	1.5	3190	48
6	DFA, 0.20; SA, 0.05	DETA, 0.40	49.2*	2.0	2190	46

* The amine number was determined for primary amino groups only [12].

It should be noted that the polycondensation under N_2 yields less colored products than that performed in air.

With DETA taken instead of HMDA, the softening point of the resulting polyamide decreases from ~100 to ~50°C, which is due to the presence of a secondary amino group in DETA [11].

Along with the polyamides prepared from DFA, we also prepared copolyamides **VII** and **VIII** with sebacic acid additionally introduced into the reaction mixture (Table 2). The initial ratio of the sum of DFA and SA to diamines was the same as in Table 1.

As seen from Table 2, introduction of sebacic acid into the copolyamides increases their molecular weight and softening point compared to the products prepared from DFA only. The observed increase in the softening point by 10–15°C is apparently caused by the more ordered molecular structure of the polyamide, due to the presence of normal alkylene fragments of sebacic acid, in contrast to branched alkylenecycloaliphatic segments of DFA. The increased softening point of **VII** and **VIII** may also be associated with their somewhat higher molecular weight, compared to the polyamides prepared from DFA only. This fact is due to the presence of up to 3% monocarboxylic acids, terminating the propagating chain, in the starting DFA. When DFA is partially replaced by SA, the concentration of chain-terminating agents decreases.

The structure of the synthesized products was studied by IR and NMR (^{1}H, ^{13}C) spectroscopy. The IR spectra of **V**–**VIII** contain strong absorption bands in the ranges 1650–1680 cm^{-1} (C=O stretching vibrations, amide I band) and 1550–1640 cm^{-1} (mainly NH bending vibrations, amide II band). In contrast to the products derived from HMDA, the spectra of polyamides derived from DETA contain bands at 3200–3500 cm^{-1} with a maximum at about 3320 cm^{-1}, corresponding to vibrations of the secondary NH groups.

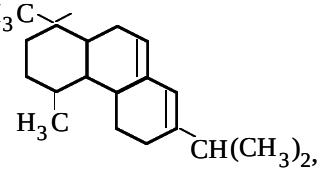
The ^{1}H NMR spectra of **V**–**VIII** contain signals of methylene protons adjacent to amide and carboxy groups [–CH_2C(O)NH–, –CH_2C(O)OH] at 2.2 ppm and to the nitrogen atom [–C(O)NHCH_2–] at 3.2 ppm. The ^{13}C NMR spectra contain strong signals at 173.2, 173.3, and 173.4 ppm, belonging to CONH groups.

As polyamides **V**–**VIII** contain terminal amino groups, their subsequent use as thermoplastics in hot-melt adhesive formulations may involve reactions altering the physicomechanical properties of the products owing to amide interchange [13]. To exclude these processes, the polyamide compounds prepared were stabilized with monocarboxylic acids (abietic or acetic). The required amount of the monocarboxylic acid was calculated from the amine number of the polymer. The monocarboxylic acid was added to the polyamide reaction mixture cooled to 120–150°C, the mixture was stirred for 15 min, and then it was gradually heated to 220–240°C until the water evolution ceased. The reaction with monocarboxylic acids follows the scheme

$$\mathbf{V}\text{–}\mathbf{VIII} + 2R^3COOH \quad (\mathbf{IX}, \mathbf{X})$$

$$\rightarrow R^3C(O)NH[RNHC(O)R^2C(O)NH]_nRNHC(O)R^3 + H_2O. \quad (\mathbf{XI}\text{–}\mathbf{XVIII})$$

where R^2 =



R^3 = $C_{19}H_{29}$ (**IX**), CH_3 (**X**); R = $(CH_2)_6$, R^2 = $C_{34}H_{62}$, R^3 = CH_3 (**XI**); R = $(CH_2)_6$, R^2 = $C_{34}H_{62}$, R^3 = $C_{19}H_{29}$ (**XII**); R = $C_2H_4NHC_2H_4$, R^2 = $C_{34}H_{62}$, R^3 = CH_3 (**XIII**); R = $C_2H_4NHC_2H_4$, R^2 = $C_{34}H_{62}$, R^3 = $C_{19}H_{29}$ (**XIV**); R = $(CH_2)_6$, R^2 = $C_{34}H_{62}$ and

$(CH_2)_8$, $R^3 = CH_3$ (**XV**); R = $(CH_2)_6$, $R^2 = C_{34}H_{62}$ and $(CH_2)_8$, $R^3 = C_{19}H_{29}$ (**XVI**); R = $C_2H_4NHC_2H_4$, $R^2 = C_{34}H_{62}$ and $(CH_2)_8$, $R^3 = CH_3$ (**XVII**); R = $C_2H_4NHC_2H_4$, $R^2 = C_{34}H_{62}$ and $(CH_2)_8$, $R^3 = C_{19}H_{29}$ (**XVIII**); n = 3–30.

Polyamides **XI**–**XVIII** have the following characteristics: amine number (for primary amino groups) 0.5–1.2 (mg KOH) (g polyamide)$^{-1}$; acid number 0.3–1.0 (mg KOH) (g polyamide)$^{-1}$; softening point 43–104°C. It should be noted that the softening point of stabilized compounds **XI**–**XVIII** does not change after heating at 250°C for 2 h, whereas that of **V**–**VIII** changes after heating at 250°C for 1 h. Introduction of the abietic acid residue enhanced the adhesion properties of the polyamides.

CONCLUSION

The conditions for preparing polyamides from dimerized fatty acid, sebacic acid, and aliphatic amines were optimized. The ratio of dicarboxylic acids and amines largely determines the softening point of the polyamides. Replacement of hexamethylenediamine in the reaction mixture by diethylenetetramine decreases the softening point from ~100 to ~50°C, which is associated with the structure of the amine.

REFERENCES

1. Korshak, V.V. and Frunze, T.M., *Sinteticheskie geterotsepnye poliamidy* (Synthetic Heterochain Polyamides), Moscow: Akad. Nauk SSSR, 1962.
2. Makarov, V.G. and Koptenarmusov, V.B., *Promyshlennye termoplasty: Spravochnik* (Commercial Thermoplastics: Handbook), Moscow: Khimiya, 2003.
3. World Appl. 9524439.
4. Huang Yue, Li Weihua, and Yan Deyue, *Polym. Bull.*, 2002, vol. 49, nos. 2–3, pp. 111–118.
5. Sorokin, M.F., Kochnova, Z.A., and Shode, L.G., *Khimiya i tekhnologiya plenkoobrazuyushchikh veshchestv* (Chemistry and Technology of Film-Forming Substances), Moscow: Khimiya, 1989.
6. Popova, T.A., Zhilina, N.V., Rodivilova, L.A., *et al.*, *Proizvodstvo oligoamidov za rubezhom: Obzornaya informatsiya* (Production of Oligoamides Abroad: Review), Ser.: *Plasticheskie massy i sinteticheskie smoly* (Plastics and Synthetic Resins), Moscow: NII-TEKhIM, 1979.
7. Fomina, E.V., Guzeev, V.V., and Fomin, V.A., Abstracts of Papers, *VIII Mezhdunarodnaya konferentsiya po khimii i fizikokhimii oligomerov "Oligomery-2002"* (VIII Int. Conf. on Chemistry and Physical Chemistry of Oligomers "Oligomers-2002"), Chernogolovka, September 9–14, 2002, p. 117.
8. Fomina, E.V., Nosova, Yu.E., and Kurskii, Yu.A., Abstracts of Papers, *Tret'ya Vserossiiskaya Karginskaya konferentsiya "Polimery-2004"* (Third Russian Kargin Conf. "Polymers-2004"), Moscow, January 27–February 1, 2004, vol. 1, p. 155.
9. Toroptseva, A.M., Belogorodskaya, K.V., and Bondarenko, V.M., *Laboratornyi praktikum po khimii i tekhnologii vysokomolekulyarnykh soedinenii* (Laboratory Manual on Chemistry and Technology of Macromolecular Compounds), Leningrad: Khimiya, 1972.
10. Zarinskii, V.A. and Kotov, A.V., *Izv. Akad. Nauk SSSR, Ser. Khim.*, 1968, no. 11, pp. 2639–2640.
11. Floyd, D.E., *Polyamide Resins*, New York: Reinhold, 1958.
12. Kreshkov, A.P., Bykova, L.N., and Kazaryan, N.A., *Kislotno-osnovnoe titrovanie v nevodnykh rastvorakh* (Acid–Base Titration in Nonaqueous Solutions), Moscow: Khimiya, 1967.
13. *Comprehensive Organic Chemistry. The Synthesis and Reactions of Organic Compounds*, Barton, D. and Ollis, W.D., Eds., vol. 2: *Carboxylic Acids, Phosphorus Compounds*, Oxford: Pergamon, 1979.

Russian Journal of Applied Chemistry, Vol. 78, No. 7, 2005, pp. 1126–1130. Translated from Zhurnal Prikladnoi Khimii, Vol. 78, No. 7, 2005, pp. 1146–1150.
Original Russian Text Copyright © 2005 by A. Radbil', Zhurinova, Starostina, B. Radbil'.

ORGANIC SYNTHESIS AND INDUSTRIAL ORGANIC CHEMISTRY

Preparation of High-Melting Polyterpene Resins from α-Pinene

A. B. Radbil', T. A. Zhurinova, E. B. Starostina, and B. A. Radbil'

Lesma Research and Promotion Limited Liability Company, Nizhni Novgorod, Russia

Received February 3, 2005

Abstract—The $AlCl_3$-catalyzed low-temperature polymerization of α-pinene in the presence of various activating additives was studied.

Polyterpene resins (PTRs) are prepared by acid-catalyzed polymerization in the course of deep processing of turpentine. These resins are widely used in industry, especially beyond Russia. Depending on the composition of the raw materials and preparation procedure, PTRs have different consistency: from viscous liquids to high-melting solids. The wide spectrum of physicochemical properties determines the applications of PTRs. Of most interest are solid high-melting PTRs with the ring-and-ball softening point T_s above 90°C (PTR_{90}). Specifically these products, produced mainly in the United States from turpentine enriched in β-pinene, are successfully used for more than 30 years as thermoplastic adhesive additives in production of hot-melt and pressure-sensitive adhesives, and also of paint-and-varnish, sealing, and insulating materials [1–4]. In oleoresin and sulfate turpentine produced in Russia, the content of β-pinene does not exceed 5%, and the major component is α-pinene, from which it is difficult to prepare PTR_{90} in a high yield [5–10]. This is primarily due to the specific features of the molecular structure of α-pinene, in which the double bond, in contrast to β-pinene, is sterically shielded, which hinders the polymeric chain propagation. Therefore, the development and choice of the best catalytic systems and conditions for α-pinene polymerization, providing high yield of PTR_{90}, is of considerable theoretical and applied interest.

The polymerization of α-pinene was studied in the temperature range from –28 to +10°C in the presence of a mixture of Friedel–Crafts catalysts ($AlCl_3$ and $SbCl_3$), and also of heteropoly acids (HPAs) $H_3PW_{12}O_{40}$ (PW_{12}) and $H_4SiMo_{12}O_{40}$ ($SiMo_{12}$). As a result, we obtained PTR_{90} samples in yields reaching 84%. These samples were solid glassy substances with the color from light yellow to light brown and T_s = 92–115°C (Table 1). The molecular weight (MW) of PTR_{90} is 580–800, and the intrinsic viscosity η at 20°C, 0.0124–0.0289 dl g^{-1}. The PTR_{90} is a mixture of oligomers of monoterpene hydrocarbons with the chain length from 3 to 6 $C_{10}H_{16}$ units (so-called polyterpenes, PTs) and of a small amount of dimers of α-pinene and/or other monoterpene hydrocarbons (diterpenes, DTs).

The DT fraction isolated from PTR_{90} is a transparent light yellow oily liquid with a kinematic viscosity at 20°C of 130–200 $mm^2 s^{-1}$ and a density of 936–942 g dm^{-3}. The boiling point of DT is 150–200°C at 0.5 kPa, refractive index n_D^{20} 1.5126–1.5157, and MW 270–290.

The polymerization of α-pinene is accompanied by its isomerization; along with PTR_{90}, the products contain camphene, dipentene, terpinolene, and *p*-cymene. As shown in [5–7], the same monoterpenoids are formed by polymerization of α-pinene at temperatures exceeding 100°C in the presence of acid catalysts of other types: aluminosilicates, natural zeolites, or titanium catalyst.

The influence of the composition of the catalytic system on T_s of PTRs prepared by polymerization of α-pinene at –(3±2)°C for 3 h is illustrated by Fig. 1. These data show that $SbCl_3$ is an effective cocatalytic additive to $AlCl_3$. On adding even 0.1 wt % $SbCl_3$ to 4 wt % $AlCl_3$, PTR_{90} samples with T_s = 92°C are obtained (Fig. 1, curve *1*). As the $SbCl_3$ content is increased to 0.3 wt %, T_s of PTR_{90} increases to 113°C and does not further change at higher concentrations of $SbCl_3$. The yield of PTR_{90} obtained in the presence of this catalytic system is 78–84%, and MW is in the range 584–790.

When the content of the main catalyst, $AlCl_3$, is decreased to 3 wt %, the noticeable cocatalytic effect of $SbCl_3$ is preserved (Fig. 1, curve *2*). However, in this case $SbCl_3$ should be added in a substantially larger amount (0.9 wt %) to obtain PTR_{90}. The re-

1070-4272/05/7807-1126 © 2005 Pleiades Publishing, Inc.

Table 1. Conditions for preparing PTR_{90} from α-pinene. Polymerization time 3 h

Catalytic system, wt % of α-pinene			T, °C	Yield of PTR_{90}, %	Composition of PTR_{90}, wt %		Properties of PTR_{90}		
$AlCl_3$	$SbCl_3$	PW_{12}			DT	PT	T_s, °C	MW	η, dl g^{-1}
4	0.1	–	–(3±2)	78	16	84	92	584	0.0175
4	0.2	–	–(3±2)	80	11	89	103	640	0.0190
4	0.3	–	–(3±2)	82	5	95	113	790	0.0289
4	0.5	–	–(3±2)	84	5.5	94.5	112	759	–
3	0.2	0.6	–(3±2)	83	13	87	98	598	–
3	0.2	1.0	–(3±2)	82	7	93	108	720	0.0242
3	0.2	1.0*	–(3±2)	81	6.5	93.5	109	726	–
3	0.4	0.6	–(3±2)	83	10	90	104	637	–
3	0.4	1.0	–(3±2)	83	6	94	110	746	0.0229
3	0.9	–	–(3±2)	78	14.5	85.5	94	592	0.0178
3	0.9	0.6	–(3±2)	81	4.5	95.5	114	784	–
3	0.9	0.6*	–(3±2)	79	4.5	95.5	115	798	0.0288
3	0.9	1.0	–(3±2)	83	5	95	112	756	–
3	1.5	–	–(3±2)	81	6	94	110	748	0.0252
3	1.5	–	–(25±3)	82	6	94	109	756	0.0240
3	1.5	–	–(15±3)	81	5.5	94.5	112	764	–
3	1.5	–	–(8±2)	82	6	94	109	750	–
3	1.5	–	3±2	80	12	88	101	619	0.0185
3	1.5	–	8±2	81	15	85	94	581	0.0169

* $SiMo_{12}$.

quired amount of $SbCl_3$ can be appreciably reduced by adding HPAs PW_{12} and $SiMo_{12}$ into the catalytic system. As seen from Fig. 1 (curves *3*, *4*), on adding 0.6–1.0 wt % PW_{12} to the binary catalytic system $AlCl_3$–$SbCl_3$, T_s of PTR sharply increases, especially at the $SbCl_3$ concentration in the range 0.2–0.5 wt %. At higher $SbCl_3$ concentrations, the effect of PW_{12} on T_s of PTR is less significant, and starting from 0.9 wt % $SbCl_3$ additions of HPAs to the catalytic system no longer affect the composition and physicochemical properties of the resins.

It should be noted that $SiMo_2$ behaves in the examined reactions of α-pinene polymerization similarly to PW_{12}. These HPAs have similar structure and similar acid-catalytic properties; therefore, the mechanism of their effect is presumably similar.

Table 1 and Fig. 2 show that the yield and composition of PTR_{90} prepared by polymerization of α-pinene for 3 h in the presence of a mixture of 3 wt % $AlCl_3$ and 1.5 wt % $SbCl_3$ are independent of the reaction temperature in the range from –28 to 0°C. The softening point of the PTR_{90} thus formed is 109–112°C, and MW, 750–764. When the temperature is increased to 3±2°C and then to 8±2°C, the PTR_{90} yield remains constant, and T_s decreases to 101 and 94°C, respectively. When the polymerization temperature is increased further to 15±2°C, T_s of the PTR drastically decreases (to 62°C).

From these data, we plotted the correlation of T_s of PTRs prepared by polymerization of α-pinene with their MW (Fig. 3). This correlation is important for preparing PTRs with preset physicochemical properties. Figure 3 shows that, with an increase in MW

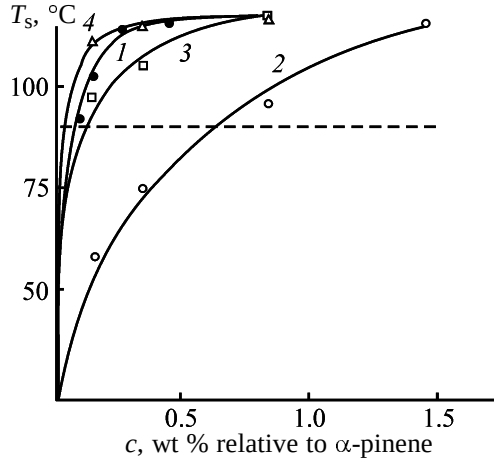


Fig. 1. Softening point T_s of PTR prepared in the presence of the $AlCl_3$–HPA catalytic system as a function of the $SbCl_3$ content c. $AlCl_3$: HPA (wt % relative to α-pinene): (*1*) 4 : 0, (*2*) 3 : 0, (*3*) 3 : 0.6, and (*4*) 3 : 1. α-Pinene polymerization at –(3±2)°C for 3 h.

Table 2. Kinetics of α-pinene polymerization. Catalyst (wt% relative to α-pinene): $AlCl_3 : SbCl_3 = 3 : 1.5$; –(3±2)°C

τ, h	Reaction mixture composition, wt %							Properties of PTR_{90}	
	α-pinene	polymerization product				content in PTR_{90}			
		camphene	dipentene	*p*-cymene	terpinolene	DT	PT	T_s, °C	MW
–	96.0	1.1	1.1	0.5	Traces	–	–	–	–
0.5	45.0	1.5	9.4	0.6	4.5	2.0	35.5	111	760
1	37.7	2.0	5.0	0.8	1.5	3.1	48.6	109	748
2	17.3	2.1	2.5	1.5	0.5	4.5	70.3	110	755
3	6.5	2.5	1.1	2.0	Traces	5.2	81.4	110	750
6	5.5	2.5	1.0	3.1	〃	5.1	81.5	111	764

from 450 to 580, T_s of PTR grows considerably, from 40 to 90°C, whereas with a further increase in MW to 800 T_s grows less significantly, from 90 to 115°C. It can be expected that PTR_{90} with MW > 800, if obtained, will have only slightly higher T_s. For comparison, according to [4, 11], T_s of PTR_{90} samples with MW 1500–2000 prepared from α-pinene is 125–130°C.

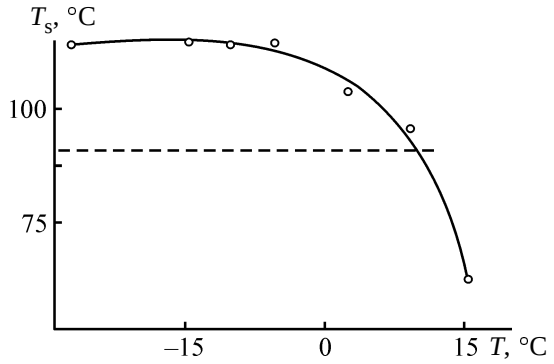


Fig. 2. T_s of PTR as a function of α-pinene polymerization temperature T. Catalyst (wt % of α-pinene) $AlCl_3 : SbCl_3 = 3 : 1.5$; polymerization time 3 h.

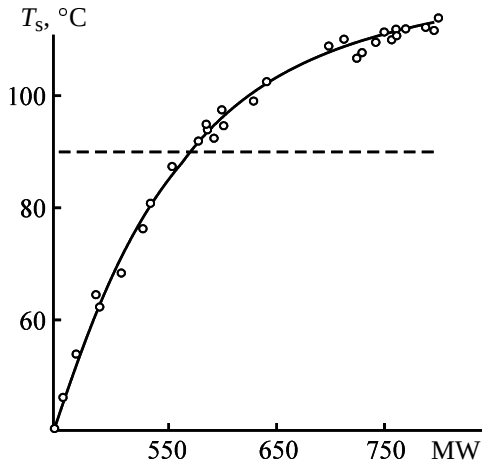


Fig. 3. Correlation of T_s of PTR with its MW.

In Fig. 4 and Table 2 we present the kinetic data on the polymerization of α-pinene in the presence of the catalytic system 3 wt % $AlCl_3$ + 1.5 wt % $SbCl_3$ at –(3±2)°C. It is seen that it is appropriate to perform the polymerization of α-pinene for 3 h, as the content of PT (81.4%) and hence the yield of PTR_{90} under these conditions reach a maximum. Longer reaction (6 h) does not further change the PT content. It should be noted that the physicochemical properties of PTR_{90} prepared from α-pinene under these conditions are independent of the reaction time (Table 2).

As seen from Fig. 4, the kinetic curves of accumulation of α-pinene isomerization products in the course of its polymerization are different. Dipentene and terpinolene (curves *5*, *7*) are rapidly accumulated in the initial period; their content reaches a maximum 0.5 h after the start of the reaction, after which they are virtually completely consumed, especially in the interval 0.5–2 h. Thus, these monoterpenoids undergo secondary transformations. The content of *p*-cymene (curve *6*) in the reaction mixture gradually increases throughout the process, and the weight fraction of camphene (curve *4*) slightly increases in the first hour of the reaction and then remains virtually constant.

The results of this study are well consistent with the well-known and generally accepted cationic mechanism of α-pinene polymerization in the presence of Lewis acids [3].

The cocatalytic effect of $SbCl_3$ and HPA additions to $AlCl_3$ and of HPA additions to an $AlCl_3$–$SbCl_3$ mixture is apparently associated with stabilization of the growing intermediate carbenium ion, i.e., with extension of its "life" during which it can attack the next α-pinene molecule. Simultaneously, the contribution of the reaction pathway leading to DT decreases. A similar hypothesis on the mechanism of the effect of activating additives on the α-pinene polymerization

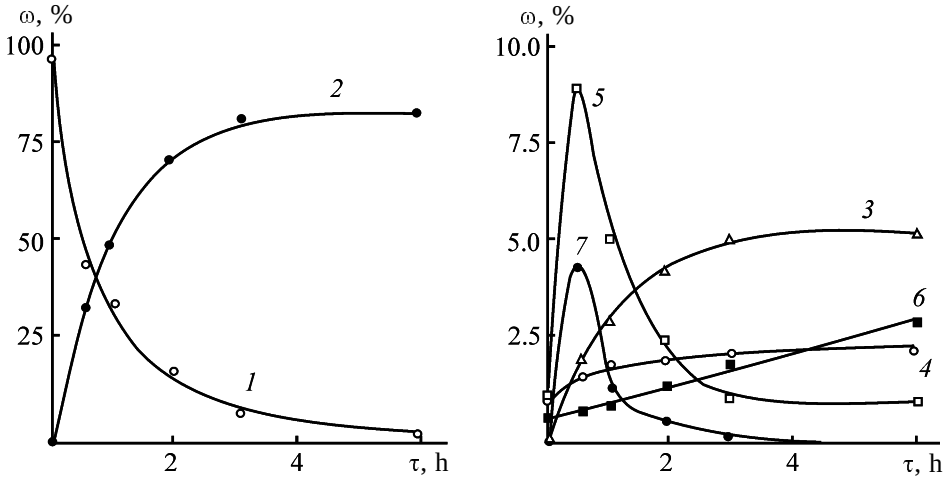


Fig. 4. Kinetic curves of polymerization of α-pinene: (ω) weight fraction of reaction products and (τ) polymerization time. (*1*) α-Pinene, (*2*) PT, (*3*) DT, (*4*) camphene, (*5*) dipentene, (*6*) *p*-cymene, and (*7*) terpinolene.

in the presence of $AlCl_3$ was formulated previously [3, 4, 11] as applied to Sb, Si, and Ge halides.

The stabilization of the growing carbenium ion and propagation of the polymer chain are also favored by the negative temperature of the α-pinene polymerization. The reaction is exothermic (thermal effect 1000–1200 kJ kg^{-1}), and when it is performed at temperatures in the range from –28 to 0°C, the temperature in the reaction zone can be readily controlled; under these conditions, the major pathway is PT formation.

It is well known and generally accepted that acid-catalyzed isomerization of monoterpenoids by the mechanism described in [12] occurs at elevated temperatures. Our results show that, with the examined catalytic systems, the same carbocationic mechanism is realized at low and even negative temperatures.

The kinetic studies show that dipentene and terpinolene formed by isomerization of α-pinene, apparently, polymerize subsequently through the intermediate tertiary carbenium ion to form DT and PT.

The results of this study serve as a basis for the development of a process for preparation of solid polyterpene resins from turpentine produced by Russian coniferous trees.

EXPERIMENTAL

α-Pinene [technical-grade purified sulfate pinene, TU (Technical Specifications) 13-00 281 074-268–96] contained 94–98 wt % main substance and 0.001–0.005 wt % moisture. The other chemicals were of chemically pure or analytically pure grade and were used without additional purification.

Polymerization of α-pinene was performed in a reactor equipped with a descending condenser and a blade stirrer. The temperature in the reactor was maintained constant (±2°C) with a cooling agent. The reactor was charged with the required amount of toluene (solvent), after which the required amounts of the catalyst and additives were added with stirring, and the contents were stirred to obtain a uniform mass. After the required temperature was attained, α-pinene was gradually added at a rate at which spontaneous self-heating could be avoided. The moment of completion of adding α-pinene was considered as the start of the reaction. After a definite time, the reaction was stopped by adding excess water, which caused deactivation of the catalyst. Then the contents were transferred into a separating funnel, and the upper layer (solution of reaction products in toluene) was separated after settling. This solution was treated with CaO, again washed with water, dried over Na_2SO_4, and subjected to fractional distillation at 0.5 kPa. The following fractions were collected: toluene <45°C and monoterpene hydrocarbons 45–110°C. After that, the distillation was stopped, the still was cooled, and the residue was analyzed to determine the weight fraction of DT in PTR_{90} (by GLC) and other physicomechanical parameters of PTR_{90}.

The chromatographic analysis of DT was performed with a Chrom 5 chromatorgaph equipped with a flame-ionization detector and a packed stainless steel column 5 m long, liquid phase SE-30, column temperature 180–200°C, vaporizer temperature 290°C, nitrogen flow rate 60 ml min^{-1}. The fraction of monoterpene hydrocarbons was analyzed with a packed stainless steel column 3 m long; liquid phase tricresyl

phosphate, column temperature 110–115°C, vaporizer temperature 250°C, nitrogen flow rate 60 ml min^{-1}.

The amounts of the reaction mixture components were determined with an internal reference. The components of the reaction mixture were identified using reference compounds or from the relative retention of terpenoids [12]. The relative error of a single analysis at a confidence level of 0.95 was within ±2%. The results of five replicate runs were averaged.

The softening point of PTR_{90} was determined according to GOST (State Standard) 23863–79 with changes 1 and 2 (ring-and-ball method), and the intrinsic viscosity (in toluene), by the procedure described in [13]. The molecular weights of PTR_{90} and DT were determined cryoscopically in benzene [13].

To isolate DT, PTR_{90} was distilled at 0.5 kPa, and the DT fraction boiling at 115–200°C was collected. The density, kinematic viscosity, and refractive index of DT were determined according to TU 2416-018-02067907–2001 "Liquid Polyterpenes."

CONCLUSIONS

(1) Polymerization of α-pinene gave a solid polyterpene resin with a softening point above 90°C in 81–84% yield.

(2) The low-temperature polymerization of α-pinene catalyzed by $AlCl_3$ in the presence of activating additives ($SbCl_3$, heteropoly acids) occurs presumably by the cationic mechanism. The cocatalytic effect of the additives is associated with the stabilization of the growing carbenium ion, which favors formation of polyterpenes and decreases the contribution of the dimerization of the monoterpene hydrocarbons.

(3) The low-temperature polymerization of α-pinene is accompanied by acid-catalyzed isomerization of monoterpenoids by the carbenium ion mechanism with the formation of *p*-cymene, camphene, dipentene, and terpinolene and subsequent polymerization of dipentene and terpinolene.

(4) The results obtained serve as a basis for the development of a commercial process for preparation of solid polyterpene resins from turpentine produced in Russia.

REFERENCES

1. Shavyrin, S.V. and Rubtsov, V.V., *Ispol'zovanie politerpenovykh smol: Ekspress-informatsiya: Zarubezhnyi opyt* (Applications of Polyterpene Resins: Express Information: Foreign Experience), Moscow: VNIPIEIlesprom, 1987, issue 1.
2. Starostina, E.B. and Chashchin, A.M., *Politerpeny: sintez, stroenie, primenenie: Obzornaya informatsiya* (Polyterpenes: Synthesis, Structure, and Applications: Review), Moscow: VNIPIEIlesprom, 1987, issue 3.
3. Ruckel, E.R. and Arit, H.G., Jr., *Naval Stories Rev.*, 1984, vol. 94, no. 1, pp. 1–6.
4. Lu, J., Liang, H., Zhang, R.J., *et al.*, *Acta Polym. Sinica*, 1998, vol. 26, no. 6, pp. 698–703.
5. Popov, A.A., Larionov, V.P., Starostina, E.B., *et al.*, *Gidrolizn. Lesokhim. Prom–st.*, 1987, no. 6, pp. 16–18.
6. Popov, A.A., Starostina, E.B., Larionov, V.P., *et al.*, *Sovershenstvovanie proizvodstva kanifol'no-skipidarnykh produktov: Sbornik trudov TsNILKhI* (Improvement of the Production of Rosin–Turpentine Products: Coll. of Papers of the Central Research Inst. of Forest Management), Gor'kii: Volgo-Vyatskoe Knizhnoe, 1986, pp. 64–73.
7. Soboleva, S.V., Preparation of Polyterpenes from Turpentine Using Sakhaptin Natural Zeolite, *Cand. Sci. Dissertation*, Krasnoyarsk, 2001.
8. Higashimura, T., Lu, J., Kamigaito, M., *et al.*, *Macromol. Chem.–Macromol. Chem. Phys.*, 1993, vol. 194, no. 12, pp. 3441–3453.
9. Higashimura, T., Lu, J., Kamigaito, M., *et al.*, *Macromol. Chem.–Macromol. Chem. Phys.*, 1993, vol. 194, no. 12, pp. 3455–3465.
10. Higashimura, T., Lu, J., Kamigaito, M., *et al.*, *Macromol. Chem.–Macromol. Chem. Phys.*, 1992, vol. 193, no. 9, pp. 2311–2321.
11. Lu, J., Liang, H., and Zhang, R.J., *Chem. J. Chinese Univ.*, 1996, vol. 17, no. 6, pp. 1314–1318.
12. Rudakov, G.A., *Khimiya i tekhnologiya kamfary* (Chemistry and Technology of Camphor), Moscow: Lesnaya Prom–st., 1976.
13. Toroptseva, A.M., Belogorodskaya, K.V., and Bondarenko, V.M., *Laboratornyi praktikum po khimii i tekhnologii vysokomolekulyarnykh soedinenii* (Laboratory Manual on Chemistry and Technology of Macromolecular Compounds), Leningrad: Khimiya, 1972.

Russian Journal of Applied Chemistry, Vol. 78, No. 7, 2005, pp. 1131–1136. Translated from Zhurnal Prikladnoi Khimii, Vol. 78, No. 7, 2005, pp. 1151–1156.
Original Russian Text Copyright © 2005 by Egorov, Matyukhova, Nikishova, Platonov, Proskuryakov.

ORGANIC SYNTHESIS AND INDUSTRIAL ORGANIC CHEMISTRY

Reaction of Benzyl Bromide with Mn(0) in Dimethylformamide

A. M. Egorov, S. A. Matyukhova, Yu. A. Nikishova, V. V. Platonov, and V. A. Proskuryakov

Tula State University, Tula, Russia
Moscow State University, Moscow, Russia
Leo Tolstoy Tula State Pedagogical University, Tula, Russia
St. Petersburg State Technological Institute, St. Petersburg, Russia

Received December 15, 2004; in final form, May 2005

Abstract—The reaction of Mn(0) with benzyl bromide in dimethylformamide was studied.

Coordination compounds of Mn in various oxidation states are used in industry as selective catalysts of various chemical processes [1]. With the aim to optimize the conditions for preparing complexes of manganese(II) bromide with organic ligands, we examined in detail the mechanism and kinetics of the reaction of Mn(0) with benzyl bromide in the presence of dimethylformamide (DMF).

The kinetics of oxidative dissolution of Mn(0) in the system benzyl bromide–DMF was studied resistometrically. This method allows kinetic studies of fast heterogeneous reactions; it ensures high accuracy and reproducibility of the results [2, 3].

To determine the kinetic characteristics of the process, the reaction was performed in an inert solvent (benzene, $DN_{SbCl_5} = 0.42$ kJ mol^{-1}) [3].

The kinetic curves are shown in the figure. The dependences of the reaction rate on the benzyl bromide concentration at the DMF concentration varied in the range from 0.2 to 2 M have a similar shape with a pronounced maximum, suggesting that the reaction follows the Langmuir–Hinshelwood scheme with the adsorption of the reagent and solvent on the same active centers of the metal surface [4]:

$$PhCH_2Br + S \overset{K_1}{\rightleftarrows} (PhCH_2Br)S, \quad (1)$$

$$DMF + S \overset{K_2}{\rightleftarrows} (DMF)S, \quad (2)$$

$$(PhCH_2Br)S + (DMF)S \xrightarrow{k_3} \text{reaction products}, \quad (3)$$

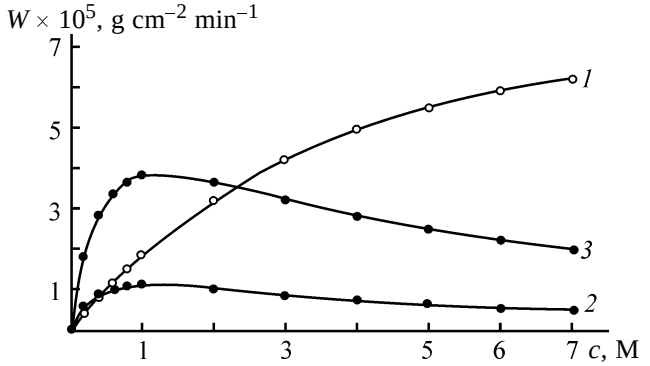
where K_1 and K_2 are the equilibrium constants of adsorption of benzyl bromide and DMF, respectively; k_3 is the rate constant of the chemical process; and S denotes active centers on which benzyl bromide and DMF are adsorbed.

The kinetic equation for this case includes the degree of the surface coverage, determined from the Langmuir isotherm for the adsorption of each component; the equation for the reaction rate W has the form

$$W = k\frac{K_1 K_2 [PhCH_2Br][DMF]}{(1 + K_1[PhCH_2Br] + K_2[DMF])^2}, \quad (4)$$

where $k = KN^2$, N is the number of active centers of the metal surface on which benzyl bromide and DMF are adsorbed.

Treatment of the experimental dependences (see figure) using Eqs. (1)–(3) allowed determination of the equilibrium constants of adsorption of benzyl bromide (K_1) and DMF (K_2) on the Mn surface and



Rate of oxidative dissolution of Mn(0) W in the benzyl bromide–DMF system as a function of the initial component concentrations c in benzene at 353 K: (*1*) $W = f(c_{DMF})$, $c_{PhCH_2Br} = 0.5$ M; (*2*) $W = f(c_{PhCH_2Br})$, $c_{DMF} = 0.5$ M; and (*3*) $W = f(c_{PhCH_2Br})$, $c_{DMF} = 2$ M.

1070-4272/05/7807-1131 © 2005 Pleiades Publishing, Inc.

Table 1. Kinetic and thermodynamic parameters of oxidative dissolution of Mn(0) in the system benzyl bromide–DMF, calculated in terms of the Langmuir–Hinshelwood scheme for adsorption of the reagent and solvent on the same active centers of the metal surface*

T, K	$k \times 10^5$	K_1	K_2
313	0.58 ± 0.03	1.80 ± 0.07	0.189 ± 0.009
323	2.40 ± 0.05	1.52 ± 0.06	0.167 ± 0.008
333	6.70 ± 0.07	1.32 ± 0.06	0.151 ± 0.008
338	14.00 ± 0.07	1.19 ± 0.06	0.142 ± 0.008
343	23.00 ± 0.07	1.12 ± 0.05	0.132 ± 0.007
353	70.00 ± 0.09	0.98 ± 0.05	0.120 ± 0.007
R	0.999	0.999	0.998
ΔE_a, kJ mol^{-1}	108.9 ± 5.4		
$\Delta H^0_{PhCH_2Br}$, kJ mol^{-1}		–14.0 ± 0.8	
ΔH^0_{DMF}, kJ mol^{-1}			–10.5 ± 0.7

* (R) Estimated correlation coefficient; (ΔE_a) activation energy of the process; ($\Delta H^0_{PhCH_2Br}$, ΔH^0_{DMF}) enthalpies of adsorption of benzyl bromide and DMF, respectively, on the metallic Mn surface.

Table 2. ESR parameters a of the benzyl radical in solid matrices

g-Factor	$a^H_{CH_2}$	a^H_o	a^H_m	a^H_p	References
	G				
2.002 ± 0.001	16.4 ± 0.5	5.5 ± 0.5	–	5.5 ± 0.5	This work
–	16.5	6	–	6	[5]
–	16.5 ± 1.0	5.5 ± 0.5	–	5.5 ± 0.5	[6]
2.0026	16.34	5.13	1.77	6.17	[7]

the reaction constant k. From the kinetic data obtained at different temperatures, we determined E_a of the chemical reactionm and the enthalpies of adsorption of the reactants ($\Delta H^0_{PhCH_2Br}$, ΔH^0_{DMF}) on the Mn surface. The results are listed in Table 1.

The Langmuir–Hinshelwood scheme for this process suggests that the limiting step is the reaction of the reactant molecules adsorbed on the metal surface, i.e., the chemical reaction on the surface.

In the absence of atmospheric oxygen (including oxygen adsorbed on the metal surface), the dehalogenation of benzyl bromide with Mn(0) in DMF yields Mn(II) coordination compounds, 1,2-diphenylethane, and traces of 4,4'-ditolyl (<0.1%):

$$2PhCH_2Br + Mn + 2DMF \rightarrow [MnBr_2 \cdot 2DMF] + PhCH_2CH_2Ph + \underset{<0.1\%}{p\text{-}MeC_6H_4C_6H_4Me\text{-}p}.$$

As proved by ion chromatography, only Mn(II) complexes are formed in the process. Cocondensation of atomic Mn generated by the metal evaporation in a low-voltage electric arc with benzyl bromide (Mn : benzyl bromide ratio 1 : 100) deposited in the molecular-beam mode on a surface cooled with liquid nitrogen gave white films stable at 77 K for no less than 24 h; these films became transparent at the melting point of the samples. The samples were treated with H_2O and D_2O. The melts contained a small amount of white solid inclusions. An analysis by ion chromatography revealed the presence of Mn^{2+} and Br^- in a ratio corresponding to the formula $MnBr_2$.

The formation of 1,2-diphenylethane and traces of 4,4'-ditolyl suggests that the oxidative dissolution of Mn(0) in the benzyl bromide–DMF system occurs by the radical mechanism.

The ESR spectrum of the cocondensate of atomic Mn with benzyl bromide at 77 K is a triplet of quartets with the full width of about 50 G and g-factor of approximately 2.002. Based on data from [5–7], this spectrum was assigned to the benzyl radical in a solid matrix (Table 2).

The fact that the ESR spectrum at 77 K contains no signals from Mn atoms, radical pairs, and tolyl radicals, and also formation of white films suggest that dehalogenation of benzyl bromide with atomic Mn generated by evaporation in a low-voltage electric arc occurs predominantly in the gas phase rather than in the benzyl bromide matrix, and the recombination and isomerization of benzyl radicals and formation of their radical pairs occur at temperatures above 77 K. Indeed, when the Mn–benzyl bromide cocondensates are warmed up to 130 K, the signals of the benzyl radicals decrease in the intensity; at 130–150 K, the resolution of the ESR spectra gets considerably worse because of the superposition of the signals from the benzyl and tolyl radicals and from the corresponding radical pairs.

The detection of small amounts of toluene and polybenzyls (compounds containing no halogen) after the defrosting and hydrolysis of the samples suggests the following reaction scheme:

$$2PhC\dot{H}_2 \longrightarrow PhCH_3 + PhC\ddot{H},$$

$$n PhC\ddot{H} + 2\,PhC\dot{H}_2 \longrightarrow CH_2(Ph)\text{–}\left(CH(Ph)\right)_n\text{–}CH_2(Ph),$$

where n = 1–5.

In the reaction of atomic Mn generated by the metal evaporation in a low-voltage electric arc with benzyl bromide, after defrosting and treatment of the samples with water, we detected molecular hydrogen (<0.02%). This may be due to the reaction of unchanged Mn with water or to hydrolysis of benzylpolymanganese bromide and benzylpolymanganese hydride formed by the scheme [8, 9]

$$PhCH_2Br + Mn_n \longrightarrow \overline{PhCH_2Br^{\bullet-}Mn_n^{\bullet+}} \longrightarrow PhCH(Br)Mn_nH,$$

$$PhCH_2Br + Mn_n \longrightarrow \overline{PhCH_2^{\bullet}\cdots Mn_nBr} \longrightarrow PhCH_2Mn_nBr,$$

where n > 1.

As the amount of hydrogen is small, the content of benzylpolymanganese bromide and/or hydride in the reaction mixture is low or zero. Hence, the reaction of atomic Mn generated by the metal evaporation in a low-voltage electric arc with benzyl bromide does not yield noticeable amounts of the $[Mn_nBr]^{\bullet}$ radical.

Formation of a white matrix in the cocondensation of atomic Mn generated by the metal evaporation in a low-voltage electric arc with benzyl bromide at 77 K suggests that charge-transfer complexes are not noticeably formed on the Mn surface either.

These facts suggest that the Mn atoms react with benzyl bromide already in the gas phase:

$$PhCH_2Br + Mn \longrightarrow PhC\dot{H}_2 + \dot{M}nBr.$$

After the cocondensation, the radicals occur in a cage of solid benzyl bromide (molar ratio $PhCH_2Br$: Mn = 100 : 1); therefore, the radical $\dot{M}nBr$ does not disproportionate at 77 K but reacts with $PhCH_2Br$, abstracting the halogen atom:

$$PhCH_2Br + \dot{M}nBr \longrightarrow PhC\dot{H}_2 + MnBr_2.$$

Toluene detected in the reaction mixtures after defrosting and hydrolysis of the samples may originate from decomposition of $PhCH_2MnBr$ with water or from the reaction

$$PhC\dot{H}_2 + PhCH_2Br \longrightarrow PhCH_3 + PhC\dot{H}Br.$$

However, recombination products of the Ph–$\dot{C}$HBr radical were not detected in the reaction mixtures, and the deuterolysis yielded $PhCH_2D$. Hence, the presence of toluene in the reaction mixture after defrosting and hydrolysis of the samples with water suggests that the reaction of benzyl halide with atomic Mn involves formation of organomanganese compounds:

$$PhCH_2Br + Mn \longrightarrow PhCH_2MnBr.$$

The radical species in solutions were detected and identified using spin traps.

When a stable radical, 2,2,6,6-tetramethylpiperidyl-1-oxyl (TEMPO), reacting with radical intermediates, was added to the reaction mixture, its ESR signals disappeared in the course of the reaction, suggesting the radical mechanism of the oxidative dissolution of Mn(0) in the benzyl bromide–DMF systems, since the ESR signals of TEMPO do not appear after oxidation of Mn(0) to Mn(II) and reduction of the mixtures with KI in acetate buffer solution [10, 11].

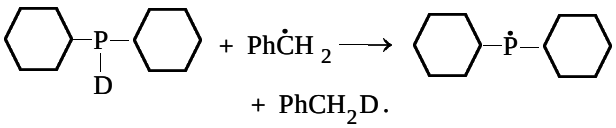
As a chemical radical trap we used dicyclohexyldeuterophosphine (DCPD), which is successfully used for this purpose and allows not only the detection of radical intermediates but also determination of their content in solution [9].

In the dehalogenation of benzyl bromide with Mn(0) in DMF in the presence of DCPD, the composition of the reaction products changes and shows a dependence on the Mn(0) : DCPD molar ratio. At a Mn(0) : DCPD molar ratio of 1 : 5, 1,2-diphenyl-

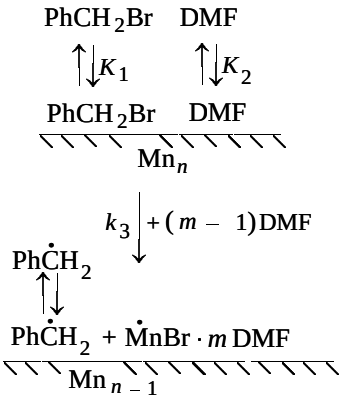
ethane was not detected, but an equivalent amount of α-deuterotoluene (97 ± 1%) was detected instead:

$$2PhCH_2Br + Mn + DMF \xrightarrow{DCPD} [MnBr_2 \cdot 2DMF] + 2PhCH_2D.$$

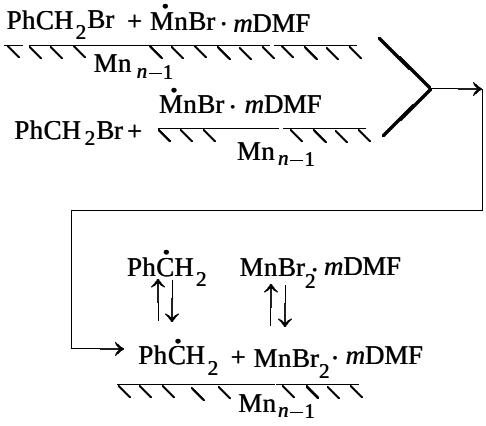
An analysis of the reaction products in the absence and in the presence of radical traps indicates that the reaction occurs by the radical mechanism via benzyl radical:



Thus, dehalogenation of benzyl bromide occurs on the Mn(0) surface by the radical mechanism via benzyl radicals; their recombination occurs in the solution. The adsorption of the reagent and solvent occurs by the Langmuir–Hinshelwood mechanism on the same active centers of the metal surface:



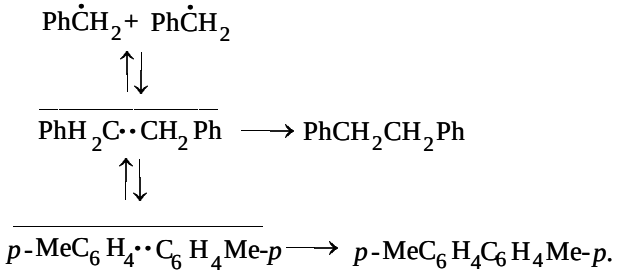
The $\dot{M}nBr \cdot m$DMF radical rapidly reacts with a new benzyl bromide molecule by the Lamgmuir–Hinshelwood or Ealy–Rideal mechanism:



$$MnBr_2 \cdot m\text{DMF} + (2 - m)\text{DMF} \rightarrow MnBr_2 \cdot 2\text{DMF},$$

where $m = 1, 2$; $n \geq 1$.

In the solution, the benzyl radicals either recombine via formation of a radical pair or again return to the Mn surface:



EXPERIMENTAL

The ESR spectra were recorded on a Radiopan spectrometer at 77 and 293 K by the procedures described in [10–12]. TEMPO was used as a spin trap at 298 K. The IR spectra were taken on an Impact 400d spectrophotometer (Nicolet).

To monitor the purity of the starting compounds and quantitatively analyze the organic products, we used gas–liquid chromatography (GLC); the conditions are described in [8].

White solid inclusions were analyzed by ion chromatography on a Tsvet 3006 chromatograph equipped with a conductometric detector. Anions were analyzed on a steel column (l = 200 mm, d = 4 mm), sorbent KhIKS-1 (Institute of Chemistry, Academy of Sciences of Estonia; particle size 15 μm), eluent 0.03 M Na_2CO_3 in water, elution rate 2 ml min^{-1}, sample volume 10 μl. Cations were analyzed on a Diakat-3 column (Elsiko, Moscow; l = 150 mm, d = 3 mm), mobile phase ethylenediamine : tartaric acid : citric acid = 1.5 : 3.5 : 3.5 (molar ratio), elution rate 1.5 ml min^{-1}.

A GC–MS analysis of the reaction products was performed on a Hewlett–Packard gas chromatograph–mass spectrometer (the United States; HP-5972 mass detector, HP-5890 chromatograph) equipped with a capillary column (l = 30 m, d = 0.25 mm), stationary phase poly[diphenylsiloxane (5%)–dimethylsiloxane]. The column was heated from 40 to 250°C at a rate of 30 deg min^{-1}. The carrier gas was helium (flow rate 1 ml min^{-1}). The vaporizer and detector temperatures were 250 and 280°C, respectively.

The ^1H NMR spectra (δ, ppm) were recorded on a Jeol LTD FX-90Q NMR Fourier spectrometer from 25–30% solutions of samples in CCl_4 or $CDCl_3$, internal reference HMDS. The chemical shifts were determined with an accuracy of ± 0.01 ppm. The reaction products were isolated by preparative liquid chro-

matography on a Tsvet-304 chromatograph equipped with a UV detector (λ = 254 nm) and a steel column (l = 25 cm, d = 4 mm), sorbent Silasorb 600 (Chemapol, Czechia; fraction 15–25 μm). A 5 : 1 (by volume) hexane–diethyl ether mixture was used as eluent.

Manganese powder [99.8% purity, Reakhim, Moscow; GOST (State Standard) 6008–90] was used without additional purification.

Samples of manganese wire used for kinetic studies were prepared by electroplating of a copper wire (0.05 mm in diameter) with Mn metal (coating thickness 0.075 mm). Just before an experiment, the sample was kept for 5–10 s in concentrated HCl and washed successively with water, acetone, and DMF. All the organic compounds were commercial chemicals. Dimethylformamide was purified by slow double vacuum distillation from a large amount of P_2O_5 [13]. Acetone, benzene, and other solvents were purified by standard procedures [14]. All the solvents were degassed by repeated freeze–pump–thaw cycles and stored in ampules without air access.

Manganese(II) complexes. To 1.1 g of Mn(0) powder we added 10 ml of DMF and 10 ml of benzyl bromide. The reaction was performed under pure dry Ar at 70°C for 8 h. After the dissolution of Mn, the reaction mixture was treated with 20 ml of absolute diethyl ether. The crystalline precipitate of [$MnBr_2 \cdot 2DMF$] was separated, washed with hexane, and vacuum-dried. Yield 5.92 g (82%), decomposition point 156°C (published data: decomposition point 156°C [15]). IR spectrum (KBr), ν, cm^{-1}: 1649 (CO), 1445 (CH_3), 1248 (CN), 1113 (CN), 678 (OCN).

Found, %: C 19.94, H 3.95, Br 44.30, Mn 15.21, N 7.74. $C_6H_{14}Br_2MnN_2O_2$.
Calculated, %: C 19.95, H 3.91, Br 44.28, Mn 15.22, N 7.76.

Treatment of the reaction mixture with moist diethyl ether gave [$MnBr_2 \cdot 2DMF \cdot 2H_2O$], yield 6.59 g (87%), mp 85°C (published data: mp 85°C [15]). IR spectrum (KBr), ν, cm^{-1}: 3470 (OH), 1660 (CO), 1620 (HOH), 1450 (CH_3), 1255 (CN), 1120 (CN), 682 (OCN).

Found, %: C 18.11, H 4.58, Br 40.07, Mn 13.82, N 7.09. $C_6H_{18}Br_2MnN_2O_4$.
Calculated, %: C 18.15, H 4.57, Br 40.05, Mn 13.84, N 7.06.

In the ether solution, we detected unchanged benzyl bromide and DMF, and also 1,2-diphenylethane and traces of 4,4'-ditolyl. 1,2-Diphenylethane, yield 3.54 g (97%), mp 51–52°C (published data: mp 51–52°C [16]). ^{1}H NMR spectrum ($CDCl_3$), δ, ppm: 2.82 s (4H, CH_2), 7.02 m (10H, Ph). Mass spectrum (70 eV), m/z [I_{rel} (%)]: 182 $[M]^+$ (23), 91 $[M/2]^+$ (100). 4,4'-Ditolyl. Mass spectrum (70 eV), m/z [I_{rel} (%)]: 182 $[M]^+$ (100), 167 $[M - CH_3]^+$ (56), 152 $[M - 2CH_3]^+$ (15).

The ESR spectra were taken directly from the reaction mixtures at 298 K by the procedure described in [10, 11]. As a stable radical we used TEMPO [10, 11] at the molar ratio Mn : $PhCH_2Br$: DMF : TEMPO = 1 : 5 : 8 : 0.2. 2,2,6,6-Tetramethylpiperidyl-1-oxyl[1] had mp 39°C (published data: mp 39°C [17]). IR spectrum (KBr), ν, cm^{-1}: 1330, 1180, 1060, 975, 950. ESR spectrum: g = 2.0055, a_N = 17.2 ± 0.1 G, a_H = 0.2 ± 0.2 G, ΔH = 1.5 G. After the oxidation of Mn, the reaction mixtures were reduced with KI in an acetate buffer solution or with H_2O_2 in an alkaline solution directly in the ampule placed in the spectrometer cavity.

Experiments in the presence of the spin trap were performed similarly. As spin trap we used dicyclohexyldeuterophosphine (DCPD) [9]. The Mn(0) : DCPD ratio was 1 : 5.

In ether solutions, we detected unchanged benzyl bromide and DMF, and also α-deuterotoluene (yield 97%). ^{1}H NMR spectrum ($CDCl_3$), δ, ppm: 2.32 m (2H, CH_2), 7.15 m (5H, Ph). Mass spectrum (70 eV), m/z [I_{rel} (%)]: 93 $[M]^+$ (100), 92 $[M - H]^+$ (93), 91 $[M - D]^+$ (46), 66 $[M - C_2H_3]^+$ (9), 65 $[M - C_2H_2D]$ (11).

Reaction of atomic Mn with benzyl bromide was performed in a high-vacuum unit similar to that described in [18] and equipped with a device for metal evaporation in a low-voltage electric arc. The reagents were vaporized in an evacuated ($p = 10^{-4}$ torr) reactor (V = 10 l) and condensed on a surface cooled with liquid nitrogen. Atomic Mn was generated by evaporation of the purified metal in a low-voltage electric arc (15 V, 32 A) formed between two Mn electrodes. The vapors of compounds to be condensed together with the evaporated metal were sprayed in the vessel just below the arc. The rate of Mn evaporation was 0.2 mmol min^{-1}. Benzyl halide was evaporated at 273–308 K ($PhCH_2Br$: Mn ratio 100 : 1). The cocondensation was performed for 2–4 h. The cocondensation of atomic Mn generated by the metal evaporation in a low-voltage electric arc with benzyl halides deposited in the molecular beam mode on a surface

[1] Submitted by F. Kayumov.

cooled with liquid nitrogen gave white films stable at 77 K for no less than 24 h.

After the polycondensation completion, the evacuation was stopped, and the reactor was filled with pure dry Ar (p = 760 mm Hg). The samples were warmed up to 298 K. When the melting point was reached, the films became transparent. The resulting melts contained a small amount of white solid inclusions. The reaction mixtures were treated with H_2O and D_2O at 298 K under pure dry Ar. Products in the gas phase were analyzed by gas chromatography; white solid inclusions were filtered off and analyzed by ion chromatography; the liquid phase was analyzed by GLC; organic products were isolated by preparative liquid chromatography. We isolated 1,2-diphenylethane (yield 98%), 4,4'-ditolyl (yield 1%), and hydrogen (yield 0.02%).

The kinetics of the reaction of Mn with benzyl bromide in DMF was studied resistometrically [2] by the procedure described in [19] in an atmosphere of dry deoxygenated Ar, with benzene as inert solvent [3]. The independence of the Mn(0) dissolution rate in the examined media from the stirring rate indicates that the process is kinetically controlled.

CONCLUSION

Oxidative dissolution of Mn(0) in the system benzyl bromide–dimethylformamide in the absence of oxygen occurs on the metal surface by the mechanism of one-electron transfer with the generation of the benzyl radical whose recombination and isomerization occur in the solution.

ACKNOWLEDGMENTS

The study was financially supported by the Ministry of Education of the Russian Federation, scientific program "Basic Research of Higher School in the Field of Natural Sciences and Humanities. Russian Universities" (project no. UR.05.01.012).

REFERENCES

1. Cahier, G., Bernard, D., and Normant, F., *J. Organomet. Chem.*, 1976, vol. 113, nos. 1–2, pp. 107–111.
2. Nifontova, G.A., Echmaev, S.B., Sikorenko, Yu.B., and Lavrent'ev, I.P., *Zh. Fiz. Khim.*, 1998, vol. 72, no. 1, pp. 147–151.
3. Kondin, A.V., Tabachkova, T.V., Alyasov, V.N., and Maslennikov, V.P., *Metalloorg. Khim.*, 1992, vol. 5, no. 5, pp. 993–1000.
4. Kondin, A.V., Berezina, N.V., Cherkasov, V.K., and Maslennikov, V.P., *Zh. Obshch. Khim.*, 1993, vol. 63, no. 10, pp. 2210–2216.
5. Buben, N.Ya., Tolkachev, V.A., and Chkheidze, I.I., *Kinet. Katal.*, 1963, vol. 4, no. 5, pp. 683–687.
6. Tolkachev, V.A., Chkheidze, I.I., and Buben, N.Ya., *Dokl. Akad. Nauk SSSR*, 1962, vol. 147, no. 3, pp. 643–644.
7. Neta, P. and Shuler, R.H., *J. Phys. Chem.*, 1973, vol. 77, no. 11, pp. 1368–1370.
8. Egorov, A.M. and Anisimov, A.V., *Appl. Organomet. Chem.*, 1995, vol. 9, no. 2, pp. 285–289.
9. Ashby, E.C. and Oswald, J., *J. Org. Chem.*, 1988, vol. 53, no. 26, pp. 6068–6076.
10. Letuchii, Ya.A., Lavrentev, I.P., and Khidekel', M.L., *Koord. Khim.*, 1982, vol. 8, no. 11, pp. 1477–1484.
11. Golubev, V.A., Sen', V.D., and Rozantsev, E.G., *Izv. Akad. Nauk SSSR, Ser. Khim.*, 1979, no. 9, pp. 2091–2095.
12. Sergeev, G.B., Smirnov, V.V., and Zagorskii, V.V., *Vestn. Mosk. Gos. Univ.*, 1980, vol. 21, no. 3, pp. 257–261.
13. Artamkina, G.A., Beletskaya, I.P., and Reutov, O.A., *Zh. Org. Khim.*, 1973, vol. 9, no. 9, pp. 1769–1776.
14. Gordon, A.J. and Ford, R.A., *The Chemist's Companion. A Handbook of Practical Data, Techniques, and References*, New York: Wiley, 1972.
15. Imanakunov, B.I., Kim, T.P., and Baidinov, T., *Reaktsii formamida i dimetilformamida s neorganicheskimi solyami* (Reactions of Formamide and Dimethylformamide with Inorganic Salts), Frunze: Ilim, 1986.
16. Caubere, P. and Moreau, J., *Tetrahedron*, 1969, vol. 25, no. 12, pp. 2469–2486.
17. Biere, R., Lemaire, H., and Rassat, M., *Bull. Soc. Chim. Fr.*, 1965, no. 11, pp. 3273–3283.
18. *Cryochemistry*, Moskovits, M. and Ozin, G.A., Eds., New York: Wiley, 1976.
19. Sergeeva, V.P., Kondin, A.V., Alyasov, V.N., *et al.*, *Zh. Obshch. Khim.*, 1990, vol. 90, no. 10, pp. 2268–2272.

Russian Journal of Applied Chemistry, Vol. 78, No. 7, 2005, pp. 1137–1144. Translated from Zhurnal Prikladnoi Khimii, Vol. 78, No. 7, 2005, pp. 1157–1164.
Original Russian Text Copyright © 2005 by Kalnin'sh, Semenov.

MACROMOLECULAR CHEMISTRY AND POLYMERIC MATERIALS

Excited Biradicals in Thermal Dimerization and Polymerization of Bicyclobutanes

K. K. Kalnin'sh and S. G. Semenov

Institute of Macromolecular Compounds, Russian Academy of Sciences, St. Petersburg, Russia
St. Petersburg State University, St. Petersburg, Russia

Received April 21, 2005

Abstract—The structure and electronic parameters of 1-cyanobicyclobutane and 1-cyano-3-vinylbicyclobutane were determined by RHF, ROHF, and GVB (TCSCF)/6-31G* quantum-chemical calculations.

Theoretical study of the polymerization mechanism at the level of elementary steps gives an insight into the regioselectivity, chemical structure of the products, and reaction rates. Not only well-understood polymerization reactions (i.e., anionic polymerization of 1,3-butadiene or isoprene [1]) but also other little known reactions are of interest in this respect. 1-Cyanobicyclobutane (**I**) and 1-cyano-3-vinylbicyclobutane (**II**) have unusual steric structure and are highly reactive. These are colorless compounds stable at –80°C in the presence of a free-radical inhibitor [2, 3]. Compound **I** in the liquid state or in a solution dimerizes on heating to +80°C. At ~150°C, the trimer of this compound is formed [2]. Carbonitrile **I** polymerizes at room temperature or on mild heating in the presence of a radical initiator, with the polymer skeleton consisting mainly of four-membered carbon monocycles [2, 3]. Carbonitrile **I** can copolymerize with acrylonitrile, styrene, methyl methacrylate, vinyl chloride, isobutene, sulfur dioxide, and other monomers. The products are high-melting thermally stable polymers soluble in polar solvents [2].

This study is based on the theoretical concept on electronically excited biradicals or their complexes formed in thermal reactions occurring on molecular collisions [4]. Generally, neutral or charged excited radicals (biradicals) (thermoexciplexes or thermoexcimers) of various chemical structures should be considered. The main feature of these species is low energy (<1 eV) relative to that of free reagents. These states are populated at ordinary temperatures. The final reaction step is recombination of the radicals to form stable molecular products. Previously, with perfluorinated olefins as example, we showed [1] that electronically excited biradical quasi-degenerate states $(S{\cdot}T)_1$ are involved in thermal dimerization. The experimental heats of formation of the intermediates were correlated with the calculated excitation energies of the olefins.

The existence of these electronic states and the possibility of their thermal population are indicated by instability of bicyclobutanes in the absence of radical initiators at temperatures higher than –80°C. In this study, *ab initio* quantum-chemical calculations of the molecular geometries of **I** and **II** in the ground and lowest excited states were performed with the aim to determine the mechanism of dimerization and polymerization of these compounds.

Calculation procedures. Quantum-chemical calculation of the electronic and steric structure, vibrational spectra, and relative energies of the compounds in the ground (S_0) and triplet (T_1, T_2) electronic states were performed by restricted Hartree–Fock methods (RHF/6-31G* and ROHF/6-31G*) using GAMESS software [5] (version pcGAMESS 6.2 [6]). In the case of lowest excited singlet electronic states (S_1, S_2), we used the generalized two-configuration version of the valence bond procedure (TCSCF GVB/6-31G*). The geometric parameters of the triplet states were calculated by energy minimization at the ROHF level without symmetry restrictions. The geometry of the singlet excited states was assumed to be identical to that of T_1 and T_2 states and then was optimized at the GVB level by minimization of total energies at fixed populations of the active natural MO $n_1 = n_2 = 1$. It should be noted that the two-configuration method of generalized valence bonds, used to calculate the singlet excited state, corresponds to the ROHF calculation of the triplet state.

The valence V_A of each atom A in a molecule or free radical is a sum of the indices of the chemical

1070-4272/05/7807-1137 © 2005 Pleiades Publishing, Inc.

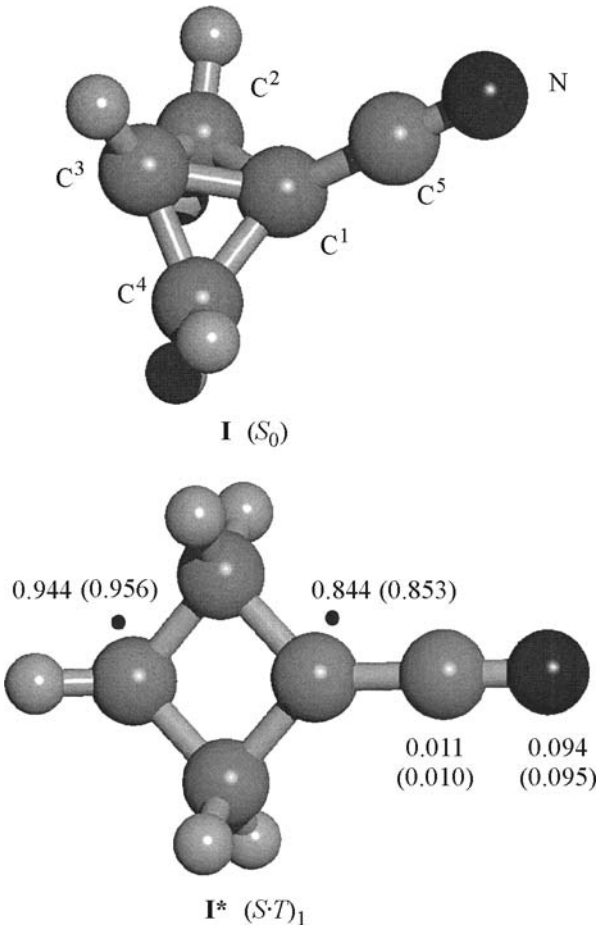


Fig. 1. Molecular structure of 1-cyanobicyclobutane **I** and free valances of the triplet and singlet (in parentheses) states.

bonds I_{AB} and free valence F_A [7], which can be calculated by the equation

$$F_A = V_A - \sum_{B(\neq A)} I_{AB}, \quad (1)$$

where

$$V_A = \sum_{a \in A} [2n_a^M - (n_a^M)^2] - \sum_{a \neq a'} (PS)_{aa'}(PS)_{a'a} \text{ [8]}, \quad (2)$$

$$I_{AB} = \sum_{a \in A} \sum_{A \in B} (PS)_{ab}(PS)_{ba} \text{ [9]}, \quad (3)$$

There are no free valences in the ground electronic state S_0 of a molecule: $F_A = 0$ and $V_{mol} = F_{mol} = 0$. In the excited states T_1 and S_1, the molecule becomes biradical: $V_{mol} = F_{mol} = 2$. Indices F_A characterize the distribution of the total valence of the biradical between its atoms [1]. The parameter F_A can be used to estimate the relative reactivity of atoms and to determine reaction sites in excited molecules, free radicals, and biradicals.

Structure of the monomers. The equilibrium nuclear configuration of **I** and **II** is characterized by nonplanar carbon skeleton and shortening of the interatomic distances typical for small rings. Substitution of hydrogen atoms of the tertiary carbon atom of the ring by a vinyl group has virtually no effect on the structural parameters of 1-cyanobicyclobutane (Table 1).

Quasi-degeneration of the energy levels of triplet T_1 and singlet S_1 states of **I** and **II** and the similarity in their structural parameters indicate that the lowest equilibrium excited states of the molecules are biradicals. The electronic excitation $S_0 \rightarrow (S{\cdot}T)_1$ results in rupture of the C^1–C^3 bond common for the two three-membered rings of bicyclobutanes. The bicyclic system is rearranged into a four-membered monocyclic biradical with a definite localization of free valences (Figs. 1, 2). In the lowest excited states, the C^1 and C^3 atoms of **I** and C^1 atom and terminal C^7 atom of the vinyl group of **II** have free valences. At the same time, the free valence of the biradical of **II** in the higher electronic state $(S{\cdot}T)_2$ is delocalized between vinyl carbon atoms (Fig. 2).

The four-membered rings of **I** and **II** in the lowest excited states $(S{\cdot}T)_1$ are flattened, the bond distances in the rind increase, and the exocyclic bonds with the cyano group are shortened. The bond between the ring and the vinyl group in **II** in the excited state $(S{\cdot}T)_1$ is shortened to the greatest extent and virtually becomes double, $C^3{=}C^6$. The bond angles ∠HCH in methylene groups of the ring appreciably decrease after excitation (Table 1).

Dimerization mechanism of 1-cyanobicyclobutane I. Since a molecule of 1-cyanobicyclobutane **I** contains the polar cyano group, it has a considerable dipole moment: 4.2 D in the ground state and 4.4 D in the excited biradical state $(S{\cdot}T)_1$. The charge distribution is presented in Table 2. The largest negative and positive charges are localized, respectively, on the nitrogen and adjacent carbon atoms of the cyano group. Electrostatic interactions suggest formation of =C–N= intermolecular bonds (with bicyclobutyl substituents at the carbon atoms). However, NMR, IR, and mass-spectroscopic studies showed that the only dimerization product is 1-cyano-3-(3-cyanocyclobut-1-yl)cyclobut-1-ene **VI** (Fig. 3).

Dimerization of 1-cyanobicyclobutane observed experimentally is inconsistent with the charge control of the reaction and becomes clear within the frame-

Table 1. Geometric parameters of 1-cyanobicyclobutane **I** and 1-cyano-3-vinylbicyclobitane **II** molecules in the equilibrium states S_0, S_n, and T_n, calculated by RHF, GVB, and ROHF/6-31G* methods

Molecule	Parameter	S_0 (RHF)	S_1 (GVB)	T_1 (ROHF)	S_2 (GVB)	T_2 (ROHF)
I	Bond length, Å:					
	C^1C^2	1.495	1.516	1.513	–	–
	C^2C^3	1.483	1.524	1.520	–	–
	C^1C^3	1.477	2.080	2.072	–	–
	C^1C^5	1.428	1.413	1.413	–	–
	C^5N	1.137	1.140	1.140	–	–
	C^3H	1.069	1.074	1.074	–	–
	C^2H; C^4H	1.08	1.09	1.09	–	–
	Angle, deg:					
	$\angle C^2C^1C^4$	98.3	93.9	94.1	–	–
	$\angle C^2C^3C^4$	99.3	93.2	93.5	–	–
	$\angle C^2C^1C^3$	59.9	–	–	–	–
	$\angle C^2C^3C^1$	60.7	–	–	–	–
	$\angle C^1C^2C^3$	59.5	86.3	86.2	–	–
	$\angle C^3C^1C^5$	130.7	174.9	173.9	–	–
	$\angle C^1C^3H$	128.8	155.8	155.5	–	–
	$\angle C^1C^5N$	180.0	180.0	180.0	–	–
	$\angle H'C^2H''$	114.5	108.5	108.1	–	–
	$\angle C^2C^1C^3C^4$	122.0	3.7	1.9	–	–
II	Bond length, Å:					
	C^1C^2	1.493	1.512	1.511	1.493	1.493
	C^1C^4	1.493	1.512	1.512	1.494	1.494
	C^2C^3	1.490	1.527	1.526	1.488	1.487
	C^3C^4	1.490	1.526	1.525	1.486	1.486
	C^1C^3	1.476	2.081	2.078	1.501	1.500
	C^1C^5	1.428	1.411	1.411	1.426	1.426
	C^5N	1.137	1.399	1.140	1.137	1.137
	C^3C^6	1.483	1.328	1.329	1.459	1.460
	C^6C^7	1.318	1.435	1.432	1.473	1.470
	C^2H; C^4H	1.08	1.09	1.09	1.08	1.08
	C^6H	1.078	1.078	1.078	1.076	1.077
	C^7H	1.076	1.073	1.073	1.076	1.076
	Angle, deg:					
	$\angle C^2C^1C^4$	96.2	94.2	94.2	98.0	98.0
	$\angle C^2C^3C^4$	98.5	93.0	93.1	98.6	98.6
	$\angle C^2C^1C^3$	60.2	–	–	59.6	59.6
	$\angle C^2C^3C^1$	60.5	–	–	59.9	60.0
	$\angle C^1C^2C^3$	59.3	86.4	86.4	60.5	60.4
	$\angle C^3C^1C^5$	130.3	179.7	180.0	130.0	130.0
	$\angle C^1C^3C^6$	131.3	179.8	179.8	132.2	132.3
	$\angle C^1C^5N$	180.0	180.0	180.0	180.0	180.0
	$\angle C^3C^6C^7$	123.2	124.7	124.7	122.2	122.1
	$\angle H'C^2H''$	114.6	108.5	108.4	114.4	114.4
	$\angle H'C^7H''$	116.8	117.9	117.9	117.5	117.1
	$\angle C^2C^1C^3C^4$	121.0	0.0	0.0	122.2	122.2

work of the concept of thermal excitation of **I** to the biradical states. The equilibrium excited state $(S{\cdot}T)_1$ (E = 20 kcal mol^{-1}) can be populated by thermal excitation. The calculated singlet–triplet splitting of the level is 2 kcal mol^{-1}. In biradical **I***, the carbon atom C^3 located at the maximal distance from the cyano group and bound with the hydrogen atom has the maximal index of free valence (Fig. 1). High reac-

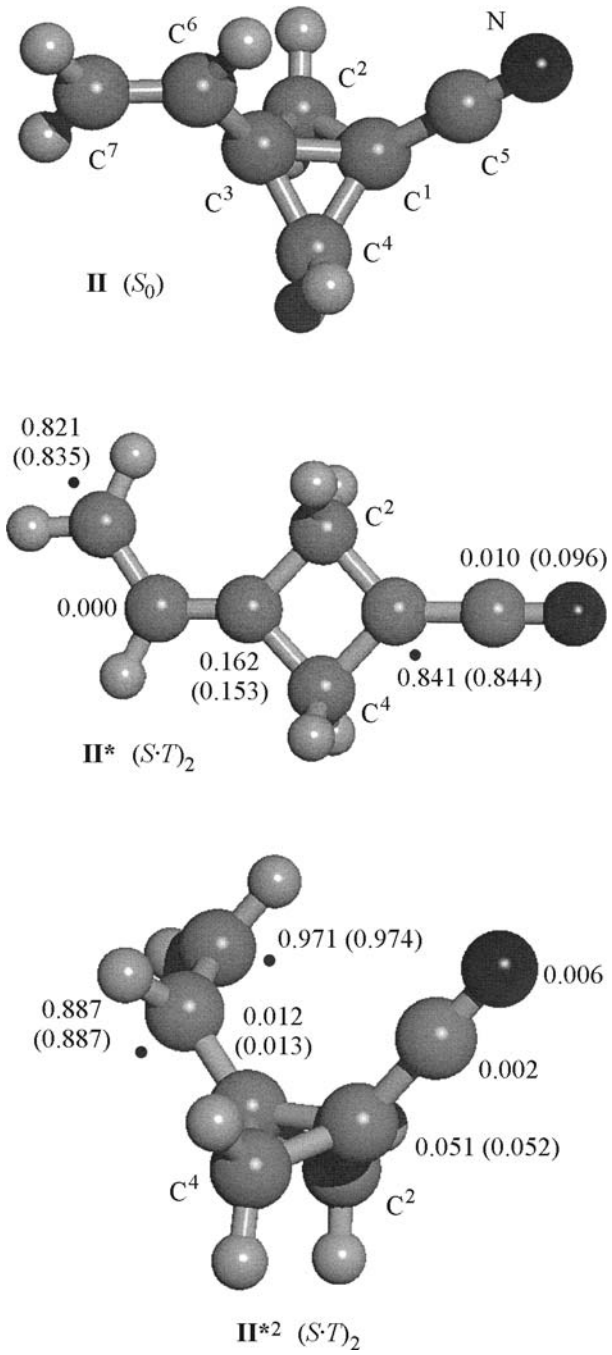


Fig. 2. Molecular structure of 1-cyano-3-vinylbicyclobutane **II** and free valances in its triplet and singlet (in parentheses) states.

tivity of this atom favors formation of a new carbon–carbon bond with the similar atom of another monomer. The radical centers recombine to form biradical **III***. Formation of biradicals **IV*** and **V*** by other coupling routes is energetically unfavorable (Fig. 4) and hence is improbable.

Table 2. Mulliken charge distribution (au) in molecules of **I** and **II** in the equilibrium states S_0, S_1, and T_1, calculated by RHF, GVB, and ROHF/6-31G* methods

Molecule	Atom	S_0 (RHF)	S_1 (GVB)	T_1 (ROHF)
I	C^1	–0.053	0.030	0.031
	C^2	–0.341	–0.348	–0.348
	C^3	–0.160	–0.156	–0.156
	C^4	–0.341	–0.348	–0.348
	C^5	0.321	0.287	0.286
	N	–0.462	–0.463	–0.462
II	C^1	–0.059	0.044	0.044
	C^2	–0.335	–0.349	–0.350
	C^3	0.003	0.057	0.057
	C^4	–0.335	–0.356	–0.356
	C^5	0.318	0.271	0.271
	C^6	–0.155	–0.223	–0.222
	C^7	–0.369	–0.385	–0.386
	N	–0.460	–0.462	–0.462

The final dimerization step is hydrogen atom transfer from the methylene group of one of the four-membered rings to the valence-active C^1 atom of the adjacent ring, i.e., reaction of two biradicals **III*** to form stable final reaction products: *trans*-**VI** and *cis*-**VI** (Fig. 3). The calculated energies of the stereoisomers of **VI** are similar. However, the dipole moment (5.0 D) and the energy of solvation of the *cis* isomer of dimer **VI** are higher than those of the *trans* isomer (1.4 D). The sterochemistry of dimerization of 1-cyanobicyclobutane was not considered in the experimental study [2].

The energy of hypothetical product **VII** is close to that of experimentally detected dimerization products **VI**. However, the energies of biradical intermediates **III*** and **IV*** differ substantially. Hence, the dimerization pathway **I** $\rightarrow$ **III*** $\rightarrow$ **VI** is more favorable than **I** $\rightarrow$ **IV*** $\rightarrow$ **VII**. Our calculation also showed that the preservation of the bicyclic structure of one of two components in dimer **IX** and the presence of adjacent cyano groups in dimer **VIII** are energetically unfavorable. The energy of hypothetical compound **X** formed by binding of valence-unsaturated carbon atoms of intermediate dimer **IV*** and containing the six-membered ring including two four-membered rings (Fig. 4) is the highest.

Dimerization mechanism of 1-cyano-3-vinylbicyclobutane II. The calculated dipole moments of **II** in the ground S_0 (4.4 D) and excited $(S{\cdot}T)_1$ (4.6 D) states are close to those of **I**. The atomic charges in these molecules are also close (Table 2). However,

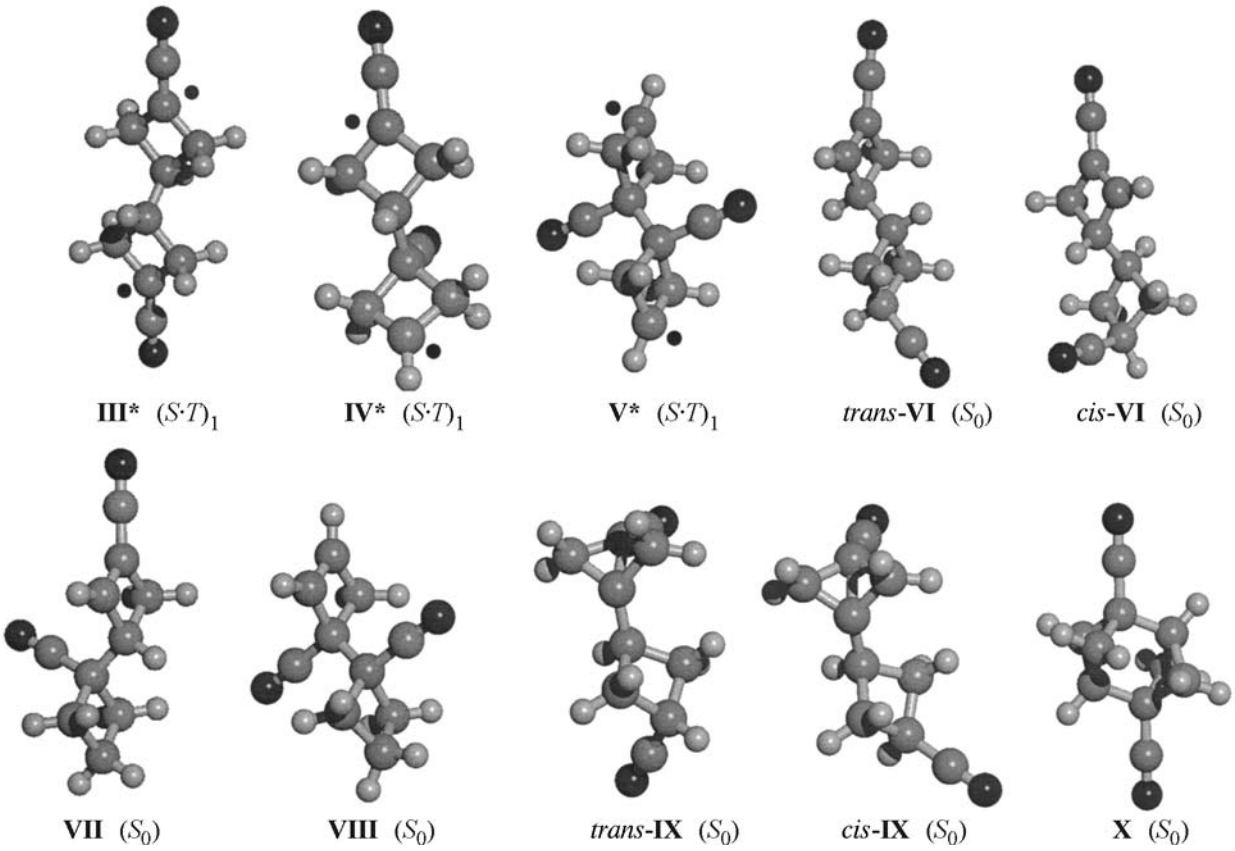


Fig. 3. Structure of biradical intermediates **III***–**V*** and hypothetical final products **VI**–**X** of dimerization of 1-cyanobicyclobutane **I**.

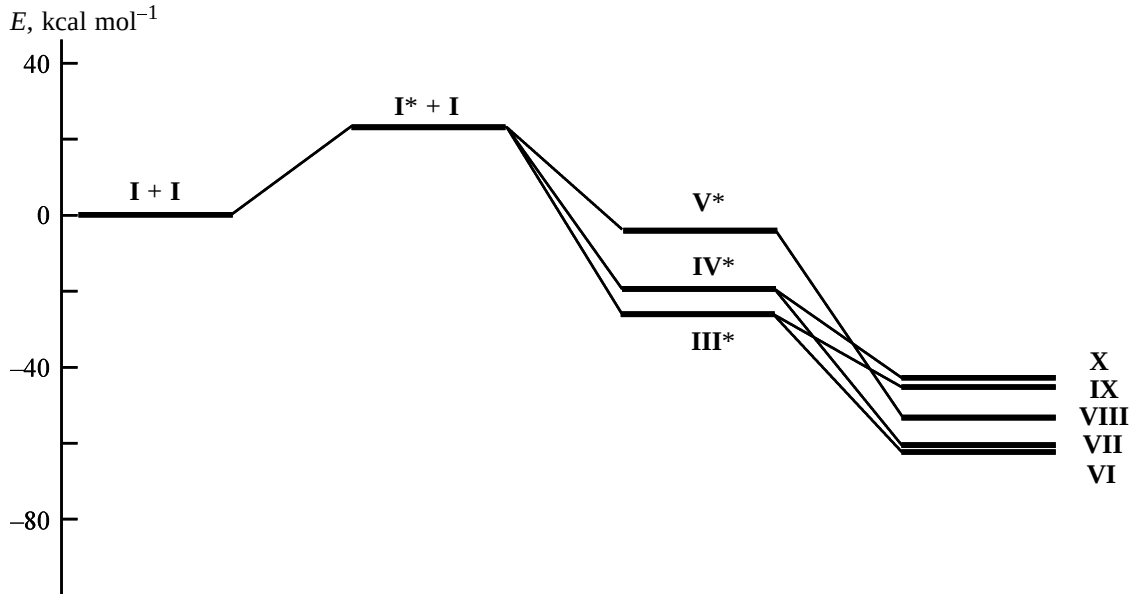


Fig. 4. Energy levels *E* of molecules of 1-cyanobicyclobutane **I**, biradical intermediates **III***–**V***, and hypothetical final dimerization products **VI**–**X**.

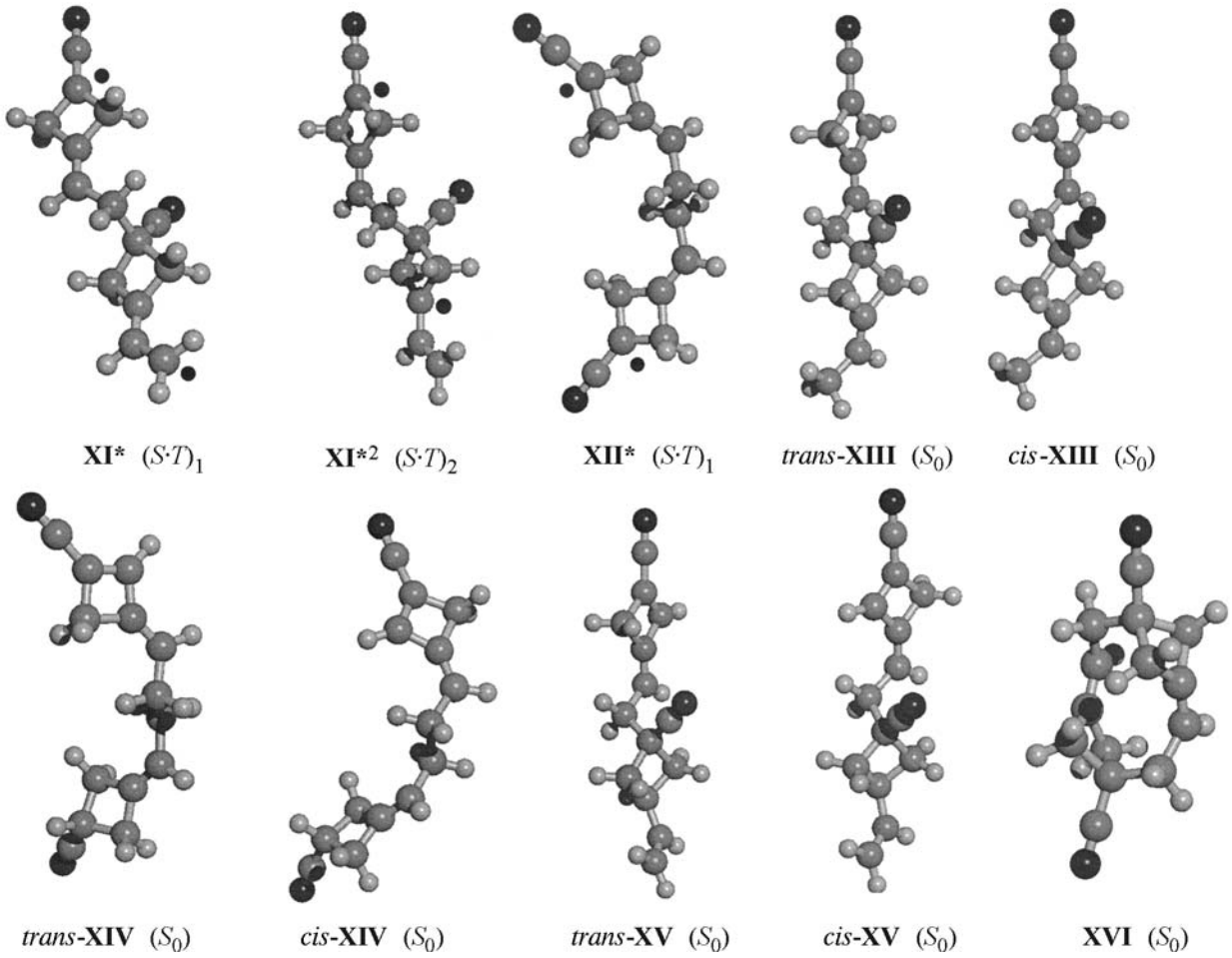


Fig. 5. Structure of biradical intermediates **XI*** and **XII*** and of hypothetical final dimerization products **XIII**–**XVI** of 1-cyano-3-vinylbicyclobutane.

the dimerization mechanism and the dimerization products are determined by free valence distribution and by the energy of the lowest equilibrium excited state, affecting the probability of its thermal population, rather than by the charge distribution (the charge control principle).

The calculated excitation energy of **II** in the biradical state $(S\cdot T)_1$ is as low as 12 kcal mol^{-1}, with the singlet–triplet splitting being negligibly small (0.5 kcal mol^{-1}). Clearly, extremely high reactivity of 1-cyano-3-vinylbicyclobutane, which is manifested in its instability at room temperature in the absence of initiators [3], is due to the low-lying excited state $(S\cdot T)_1$. The valence of biradical **II*** is delocalized almost equally between the C^1 atom of the ring and terminal C^7 atom of the vinyl group. Coupling of the carbonitriles via C^1 atoms is ruled out since, as shown above, formation of biradical **V*** containing two neighboring cyano groups is energetically unfavorable. Other binding types yield dimeric biradicals **XI***–**XII*** (Fig. 5).

Monomolecular binding of valence-unsaturated carbon atoms in intermediate dimer **XI*** does not involve hydrogen transfer and yields tricyclic dimer **XVI** consisting of ten-membered unsaturated ring and two four-membered rings (Fig. 6).

It should be noted that biradical **XI*** can exist in two quasi-degenerate equilibrium states differing in the bond lengths in the vinyl group. The free valence of **XI*** is localized on the terminal carbon atom (Fig. 5), and the free valence of **XI***^{2}, on the carbon atom of the ring bound with the vinyl group. Hence, hydrogen transfer in **XI*** can yield two stable dimerization products of 1-cyano-3-vinylbicyclobutate, namely, **XIII** and **XV**. Biradical **XII*** transforms into stable dimer **XIV**. Since each compound has its stereoisomer, the number of possible dimerization products is doubled (Fig. 6).

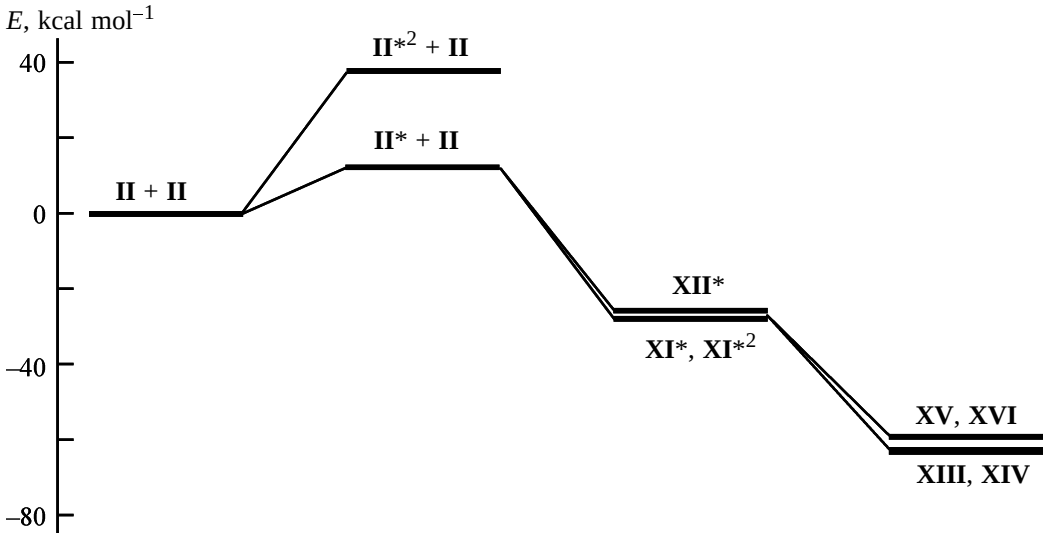


Fig. 6. Energy levels *E* of molecules of 1-cyano-3-vinylbicyclobutane **II**, biradical intermediates **XI***–**XXI***, and hypothetical dimerization products **XIII**–**XVI**.

Since the hydrocarbon chain of the intermediate isomers of 1-cyano-3-vinylbicyclobutane dimerization is flexible and the distance between valence-unsaturated carbon atoms in these compounds is sufficiently long, the energy levels of the intermediates are close. The splitting of the energy levels of all the examined stereoisomers is lower than 0.5 kcal mol^{-1}.

The energy of the biradical state $(S \cdot T)_2$ (39 kcal mol^{-1}, singlet–triplet splitting 1.4 kcal mol^{-1}) is too high for this state to be formed in thermal reactions at room temperature. Generation of this biradical is possible only in photochemical reactions of 1-cyano-3-vinylbicyclobutate.

Polymerization mechanism of 1-cyanobicyclobutanes. An excited monomer whose free valence is only weakly shielded by neighboring atoms can react with a radical initiator R*. Generation of a polymeric chain of 1-cyanobicyclobutane should involve formation of R–CH$(CH_2)_2$C$^{\bullet}$–C≡N radical.

This radical is added to the most reactive atom of thermally excited 1-cyanobicyclobutane to form a dimeric radical:

$$\text{R–CH}(\text{CH}_2)_2\text{C}^{\bullet}\text{–C}{\equiv}\text{N} + \text{H–C}(\text{CH}_2)_2\text{C}^{\bullet}\text{–C}{\equiv}\text{N}$$

$$\rightarrow \text{R–CH}(\text{CH}_2)_2\text{C(CN)–CH}(\text{CH}_2)_2\text{C}^{\bullet}\text{–C}{\equiv}\text{N}. \quad (4)$$

The resulting radical is bound with further monomer molecules in the similar way.

In the case of 1-cyano-3-vinylbicyclobutane, consecutive reactions (5) and (6) are possible. The skeleton of the resulting polymer contains atoms of exocyclic vinyl group

$$\text{R}^{\bullet} + \dot{\text{C}}\text{H}_2\text{–CH=C}(\text{CH}_2)_2\text{C}^{\bullet}\text{–C}{\equiv}\text{N}$$

$$\rightarrow \text{R–CH}_2\text{CH=C}(\text{CH}_2)_2\text{C}^{\bullet}\text{–C}{\equiv}\text{N}, \quad (5)$$

$$\text{R–CH}_2\text{CH=C}(\text{CH}_2)_2\text{C(CN)–CH}_2\text{CH=C}(\text{CH}_2)_2\text{C}^{\bullet}\text{–C}{\equiv}\text{N}$$

$$+ \text{H}_2\text{C}^{\bullet}\text{–CH=C}(\text{CH}_2)_2\text{C}^{\bullet}\text{–C}{\equiv}\text{N}$$

$$\rightarrow \text{R–CH}_2\text{CH=C}(\text{CH}_2)_2\text{C(CN)–CH}_2\text{CH=C}(\text{CH}_2)_2\text{C(CN)–}$$

$$\text{–CH}_2\text{CH=C}(\text{CH}_2)_2\text{C}^{\bullet}\text{–C}{\equiv}\text{N}. \quad (6)$$

These polymers can be cross-linked on exposure to UV radiation owing to the presence of double bonds in the polymeric chain.

CONCLUSIONS

(1) Steric and electionic structures of 1-cyanobicyclobutanes and 1-cyano-3-vinylbicyclobutane and radical intermediate and stable products of their dimerization and polymerization were determined by *ab initio* quantum-chemical calculations.

(2) Low calculated energies (<1 eV) of excitation of bicyclobutanes to $(S \cdot T)_1$ states suggest thermal population of these states under ordinary conditions. Mechanisms of dimerization and polymerization involving biradical states $(S \cdot T)_1$ were suggested, and the structures of the reaction products were determined.

REFERENCES

1. Kalnin'sh, K.K. and Semenov, S.G., *Zh. Prikl. Khim.*, 2003, vol. 76, no. 10, pp. 1585–1600.
2. Hall, H.K., Jr., Blanchard, E.P., Jr., Cherkofsky, S.C., *et al.*, *J. Am. Chem. Soc.*, 1971, vol. 93, no. 1, pp. 110–120.
3. Hall, H.K., Jr. and Yancy, R.E., III, *J. Org. Chem.*, 1974, vol. 39, no. 19, pp. 2862–2866.
4. Kalnin'sh, K.K., *Elektronnoe vozbuzhdenie v khimii* (Electronic Excitation in Chemistry), St. Petersburg: Sankt-Peterb. Gos. Univ. Tekhnol. i Dizaina, 1998.
5. Schmidt, M.W., Baldridge, K.K., Boatz, J.A., *et al.*, *J. Comput. Chem.*, 1993, vol. 14, pp. 1347–1363.
6. Granovsky, A.A., http://classic.chem.msu.su/gran/gamess/index.html.
7. Takatsuka, K., Fueno, T., and Yamaguchi, K., *Theor. Chim. Acta*, 1978, vol. 48, pp. 175–183.
8. Dmitriev, I.S. and Semenov, S.G., *Kvantovaya khimiya – ee proshloe i nastoyashchee: Razvitie elektronnykh predstavlenii o prirode khimicheskoi svyazi* (Quantum Chemistry—Its History and Modern State of the Art: Evolution of the Concept on Chemical Bond), Moscow: Atomizdat, 1980.
9. Giambiagi, M., Giambiagi, M., Grempel, D.R., and Heymann, C.D., *J. Chim. Phys.*, 1975, vol. 72, no. 1, pp. 15–22.

Russian Journal of Applied Chemistry, Vol. 78, No. 7, 2005, pp. 1145–1148. Translated from Zhurnal Prikladnoi Khimii, Vol. 78, No. 7, 2005, pp. 1165–1168.
Original Russian Text Copyright © 2005 by Mokeev, Gribanov, Sazanov, Goikhman, Fedorova.

MACROMOLECULAR CHEMISTRY AND POLYMERIC MATERIALS

Influence of Allotropic Forms of Carbon on Formation and Cross-Linking of Heat-Resistant Polymer Binders

M. V. Mokeev, A. V. Gribanov, Yu. N. Sazanov, M. Ya. Goikhman, and G. N. Fedorova

Institute of Macromolecular Compounds, Russian Academy of Sciences, St. Petersburg, Russia

Received February 8, 2005

Abstract—The thermochemical reactions of polyimide binder with various allotropic forms of carbon, fullerene C_{60} and ultradispersed artificial diamonds, were studied by thermal and spectral analyses.

Derivatives of polyimides, which are among the most heat-resistant commercially produced polymer materials, came recently onto use as binders for development of carbon–carbon composites (CCC). The prepolymer of polyimide, polyamido acid (PAA) prepared by the reaction of tetracarboxylic dianhydrides and diamines of various structures, was the first polyimide binder used for this purpose [1]. In the past decade, the variety of polyimide derivatives used as impregnating materials in production of CCC and more advantageous than PAA has extended. Among these derivatives are polyimides synthesized from aromatic tetracarboxylic acids or their anhydrides and tetraacetyl derivatives of various aromatic diamines [2, 3]. The thermochemical cross-linking of the polycondensation product of 3,3',4,4'-benzophenonetetracarboxylic dianhydride (BCDA) and bis(4-acetylaminophenyl) ether (TAA, ITA-31) was studied previously [4], and the mechanism of these reactions depending on process conditions was established. The possibility of formation of composite materials based on pitch using ITA-31 for impregnation of a heat-resistant band from Elur (product of polyacrylonitrile carbonization) was shown. Thus, the active role of ITA-31 in cross-linking of CCC gives grounds to consider the problem of production of CCC using some active additives, among which some allotropic forms of carbon such as fullerene and diamond began to play the leading role in recent years.

The aim of this work is to compare the features of the reactions of polyimide ITA-31 and two different allotropic forms of carbon, fullerene C_{60} (mixed sp^2/sp^3 hybridization of carbon atoms) and artificial diamonds (sp^3 hybridization).

EXPERIMENTAL

To prepare samples of composites of the ITA-31 binder, 40 wt % fullerene C_{60} (or ultradispersed artificial diamonds with the average particle size of 90 nm) was added to the melt of the monomer mixture, and the mixture was heated to 260°C for 12–15 min with vigorous stirring; after that, the thermal imidization of the polymer was carried out with stepwise heating from room temperature to 300°C. After cooling, the resulting composition was milled, sifted, and studied by thermal gravimetric analysis (TGA) and high-resolution solid-state (HR SS) ^{13}C NMR. To compare the thermal effects of cross-linking of filled ITA-31 with the data on formation of ITA-31 itself and to reveal the influence of fillers on this process, we performed TGA and DTA (differential thermal analysis) of a mixture of these compounds.

TGA was performed on an MOM derivatograph (Hungary) at a heating rate of 10 deg min^{-1} with 50-mg weighed portions in a self-generated medium.

The HR SS ^{13}C NMR spectra were recorded at room temperature on a Bruker CXP-100 spectrometer using magic angle spinning (MAS) and cross-polarization (CP). The MAS technique (without polarization transfer from protons) was used to obtain spectra of the samples containing fullerene and diamond, because of the absence of protons in their composition. The ^{13}C NMR spectra were recorded at 25.18 MHz, spinning rate 3–4 kHz. Chemical shifts (ppm) were referred to tetramethylsilane.

Data of thermal analysis (Figs. 1, 2) of a mixture of the starting compounds used for production of ITA-31 (BCDA + TAA) without fillers and also with C_{60} and

1070-4272/05/7807-1145 © 2005 Pleiades Publishing, Inc.

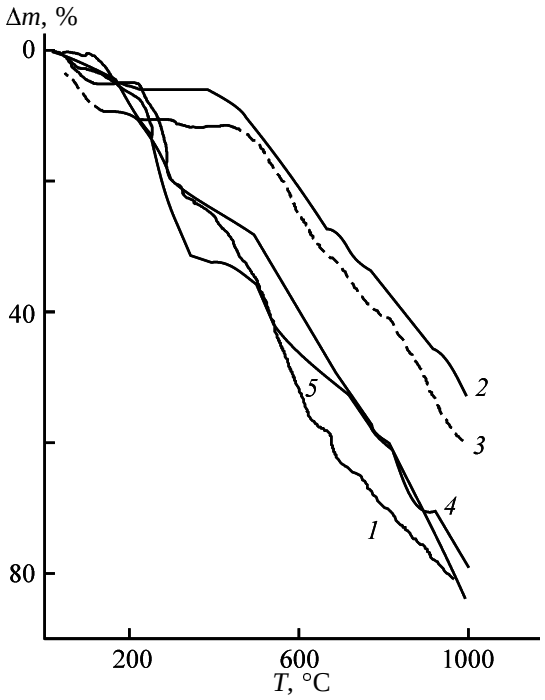


Fig. 1. TGA curves: (Δ*m*) weight loss and (*T*) temperature. (*1*) BCDA + TAA, (*2*) C_{60}, (*3*) diamond, (*4*) BCDA + TAA + C_{60}, and (*5*) BCA + TAA + diamond; the same for Fig. 2.

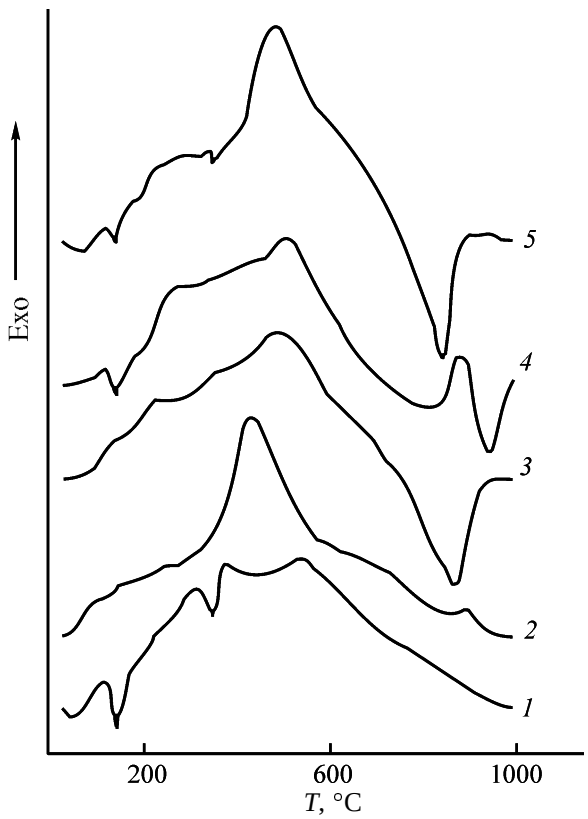


Fig. 2. DTA curves: (*T*) temperature.

diamond show noticeable distinctions in the character of their thermal degradation and cross-linking.

As found previously [4], the reaction of BCDA with TAA after their melting at 140–150°C is accompanied by the release of acetic anhydride and products of its degradation, which comes to the end at 350–360°C with complete removal of volatile substances and formation of cyclochain product having mp 354°C. From 360 to 500°C, there is a noticeable interval of thermal stability, with no weight loss. The resulting compound is cross-linked polymer. Above 500°C, a gradual weight loss accompanied by weak exothermic effects is observed. This pattern is typical for carbonization of polymers of this type [5].

Addition of fullerene to the initial mixture of monomers does not alter the thermal gravimetric characteristics of the resulting polymer, but substantially changes the structure of its intermediates and final products. The analysis of thermal effects proceeding in conversion of ITA-31 in the presence of C_{60} (Fig. 2, curves *1* and *4*) shows that the cross-linking of the reacting substances starts even at 240–250°C. This fact is further confirmed by the absence of the endothermic effect at 354°C. Contrary to the initial mixture, in the presence of fullerene at elevated temperature the exothermic effect of oxidation of the reaction product is enhanced. This phenomenon is apparently caused by superposition of fullerene oxidation (according to DTA, maximum at 410°C, Fig. 2) and polymer oxidation (maximum at 556°C). The most unexpected result is the appearance of a strong exothermic effect in the range 830–910°C. Understanding of this heat release requires additional studies, especially, identification of structural transformation of the carbonizate in this stage.

When finely dispersed diamond powder is added to the initial monomer mixture, in the low-temperature stage of thermal degradation a smooth weight loss is observed over the entire range of release of volatile products formed in the reaction of the monomers. The thermal stability interval is practically absent; the carbonization begins from 400°C and proceeds similarly to carbonization of the other samples considered. The thermal effect reflects the specific features of each component. A peak corresponding to melting of the resulting polymer is observed at 360°C, and after 450°C the effects corresponding to diamond oxidation with a maximum at 500°C and sublimation with an endothermic maximum at 900°C predominate (Fig. 2, curves *3* and *5*).

In the HR SS ^{13}C NMR spectra (Fig. 3a) of the composition with fullerene subjected to heating at

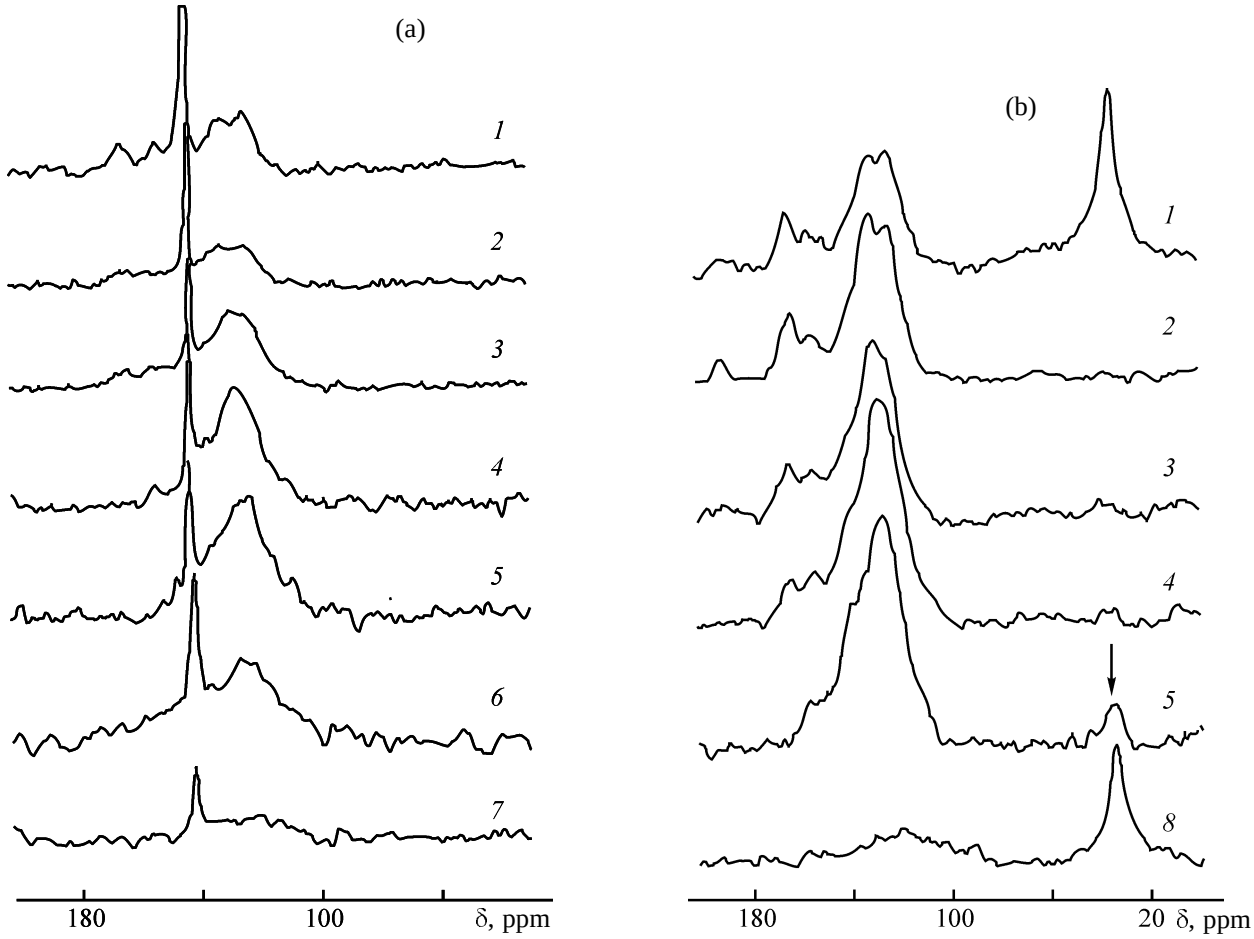


Fig. 3. HR SS ^{13}C NMR spectra of compositions (a) BCDA + TAA + C_{60} and (b) BCDA + TAA + diamond. (δ) Chemical shift. (*1*) Initial mixture; heat treatment of the mixture at temperature, °C: (*2*) 400, (*3*) 550, (*4*) 600, (*5*) 700, (*6*) 800, (*7*) 850, and (*8*) 900.

various temperatures in a vacuum, there is a stable signal at 143 ppm corresponding to C_{60} molecule [6]. This signal is observed in the spectra of the reaction products up to 900°C. The relative integral intensity of the ^{13}C NMR signal of fullerene in the sample obtained at 900°C is more than 30%. After the heat treatment of the composition at 600°C in air, the signal of fullerene disappears from the spectrum, which is apparently caused by oxidation and degradation of fullerene. Experiments on pyrolysis of the initial fullerene C_{60} in a vacuum show that above 600°C it starts to sublime, and by 900°C the weight loss is more than 90%.

Another important characteristic of the HR SS ^{13}C NMR spectra is the linewidth of the fullerene signal ($\Delta_{1/2}$). It should be noted that in the case of crystalline fullerene C_{60} $\Delta_{1/2}$ is extremely low (approximately 10 Hz), which is caused by high rotation mobility of this molecule in the solid state [7]. Therefore, we can judge on the degree of free rotation of C_{60} molecules in the composition. Up to 700°C $\Delta_{1/2}$ remains almost unchanged (approximately 35 Hz) and then abruptly increases by a factor of approximately 2, after which it varies only slightly up to 900°C. It should be noted that, although the increased $\Delta_{1/2}$ for fullerene (60–70 Hz) reflects certain decrease in the mobility of fullerene molecules in this temperature range, its value remains typical for extremely mobile molecular systems.

Thus, a part of fullerene molecules in the composition remains unbonded, i.e., they do not lose extremely high rotation mobility. However, with heating this high mobility somewhat decreases. It can be assumed that, as the carbonizate structure becomes more perfect with increasing temperature, the cavities in the carbonizate accommodating unbonded fullerene molecules decrease in size, which apparently restricts the mobility of these molecules.

In the case of the composition with diamond, the HR SS ^{13}C NMR spectra reflect the process of polymer carbonization, largely similar to carbonization of both unfilled ITA-31 and an ITA-31–fullerene mixture. However, there are some differences, namely, an increase in temperature of stepwise thermal degradation of the polymer in the presence of diamond, compared to the unfilled polymer and fullerene-containing composition.

It is seen from the spectra of the system ITA-31–diamond (Fig. 3b) that the signals of both carbonyl carbon atoms (164 ppm) and aromatic carbon atoms directly bonded to ether oxygen (155 ppm) do not noticeably vary in the intensity after the thermal treatment at temperatures of up to 600°C. The latter signal in the residual form remains up to 700°C, which is a unique fact itself. It should be noted that, in the spectra recorded using the CP MAS technique, a weak signal of diamond (34 ppm) appears at the same temperature (700°C). This means that a fairly large number of diamond atoms protonated with hydrogen atoms from carbonizate appeared in the system. Presumably above 700°C diamond begins to serve as a trap for nitrogen and oxygen heteroatoms living the carnonizate.

CONCLUSIONS

(1) In carbonization of ITA-31 polymer with added fullerene C_{60}, in the first stage (up to 550°C) a part of C_{60} molecules are apparently incorporated in the network structure, which results in a decrease in their mobility to the level of the average mobility of precarbonizate fragments. The other part of C_{60} molecules remains unbonded and does not lose high rotation mobility up to 900°C.

(2) Carbon atoms of finely dispersed diamond partially inhibit thermal degradation of ITA-31 due to retention of degradation products in the crystal lattice of diamond. In the stage of high-temperature carbonization of ITA-31, carbon atoms of diamond get protonated and scavenge a part of heteroatoms of ITA-31.

REFERENCES

1. Fitzer, E., *Carbon*, 1987, vol. 25, no. 1, pp. 163–168.
2. Burger, A., Fitzer, E., Heym, M., and Terwiesch, B., *Carbon*, 1975, vol. 13, no. 3, pp. 149–157.
3. Bessonov, M.I., Koton, M.M., Kudryavtsev, V.V., and Laius, L.A., *Poliimidy – klass termostoikikh polimerov* (Polyimides as a Class of Heat-Resistant Polymers), Leningrad, Nauka, 1983.
4. Goikhman, M.Ya., Koton, M.M., and Bolotnikova, L.S., *Zh. Prikl. Khim.*, 1991, vol. 64, no. 3, pp. 649–655.
5. Gribanov, A.V., Sazanov, Yu.N., Beloborodova, E.V., *et al.*, *Zh. Prikl. Khim.*, 1999, vol. 72, no. 3, pp. 518–520.
6. Tycko, R., Haddon, R.C., Dabbagh, G., *et al.*, *J. Phys. Chem.*, 1991, vol. 95, no. 2, pp. 518–520.
7. Johnson, F.D., Bethune, D.S., and Yannoni, C.S., *Acc. Chem. Res.*, 1992, vol. 25, no. 3, pp. 169–175.

Russian Journal of Applied Chemistry, Vol. 78, No. 7, 2005, pp. 1149–1153. Translated from Zhurnal Prikladnoi Khimii, Vol. 78, No. 7, 2005, pp. 1169–1173.
Original Russian Text Copyright © 2005 by Dryabina, Malysheva, Navrotskii, Mokharam, Novakov.

MACROMOLECULAR CHEMISTRY AND POLYMERIC MATERIALS

Flocculation and Precipitation in the Presence of Binary Polyelectrolytes

S. S. Dryabina, Zh. N. Malysheva, A. V. Navrotskii, R. Mokharam, and I. A. Novakov

Volgograd State Technical University, Volgograd, Russia

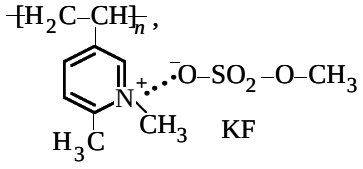
Received December 4, 2004; in final form, April 2005

Abstract—Flocculation of kaolin suspension with a binary mixture of cationic polyelectrolytes is studied by optical microscopy and turbidimetry. Interrelation between the thermodynamic compatibility of components in the solution and flocculation conditions is examined.

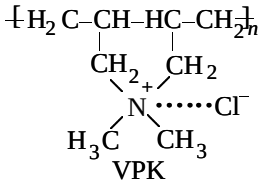
According to the modern concept of the flocculation, the flocculation efficiency can be increased by adding some mixed reagents. Recently, steadily growing interest was shown in the effect exerted on the flocculation by mixtures of cationic and anionic derivatives of polyacrylamide [1–8] and also of reagents based on nonionic polymers [4–7, 9, 10]. It was demonstrated previously [11] that adsorption of polymers from a mixture depends on the thermodynamic compatibility of components in the solution. It is also well known that it is the adsorption of macromolecules on particles of the dispersed phase that controls the flocculation efficiency and dispersion clarification rate [1–8]. It may be suggested that the conditions of adsorption as well as flocculation considerably change, depending on the thermodynamic compatibility of polymers. Therefore, in this work we studied the hydrodynamic behavior and flocculating capacity of a binary mixture of likely charged polymers.

EXPERIMENTAL

As cationic polyelectrolytes we used poly-1,2-dimethyl-5-vinylpyridinium methyl sulfate (KF) [12–14], poly-*N*,*N*-dimethyldiallylammonium chloride (VPK) [15–17], and their mixtures:



KF



VPK

Characteristics of the polyelectrolytes are given in Table 1.

The intrinsic viscosity of the polyelectrolytes [η] was measured to within 2% with an Ubbelohde glass viscometer (capillary diameter 0.34 mm) at 30°C in 2.0 M NaCl. The relative viscosity η_r was measured in double-distilled water at a polymer concentration of 0.01 wt %. The coefficient of swelling of the macromolecular globule α_η was estimated by Eq. (1):

$$\alpha_\eta = (\eta_r/[\eta])^{1/3}. \quad (1)$$

The flocculation in the presence of a mixture of the indicated polyelectrolytes was studied with an aqueous suspension of kaolin (KSD grade; mean particle size 18 μm) as a model, at a concentration of the dispersed phase of 0.8 wt %.

The flocculation kinetics was studied turbidimetrically. The optical density A was measured on a UNICO 1201 spectrophotometer (United Products&Instruments Inc., the United States). The flocculation rate was determined from the kinetic curves of the optical density as the slope of the initial linear portion $(-dA/d\tau)_{\tau \to 0}$.

The particle-size distribution characteristics of the dispersions [number-average (R_n), surface-average (R_s), and weight-average (R_m) particle radii], and also the polydispersity coefficient k_p and form factor ψ were determined by optical microscopy (OM) as in [13, 14].

The compaction kinetics of the precipitates was determined by the motion of the boundary between

Table 1. Characteristics of polyelectrolytes

Flocculant	N, mg-equiv g^{-1}	[η], dl g^{-1}	η_r, dl g^{-1} (c_p = 0.01 g dl^{-1})	α_η
KF	4.08	3.21	73.3	2.84
VPK	6.19	0.27	13.8	3.71

1070-4272/05/7807-1149 © 2005 Pleiades Publishing, Inc.

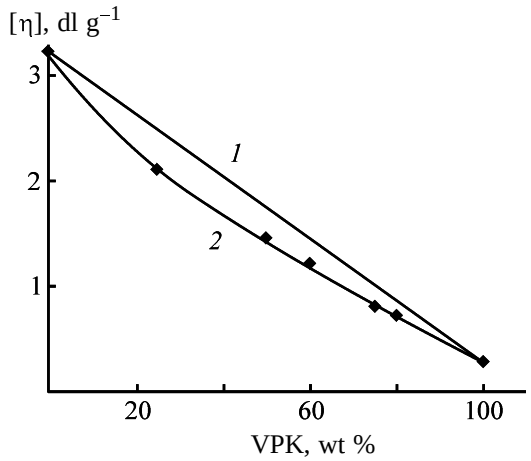


Fig. 1. Intrinsic viscosity [η] as a function of the composition of the binary mixture. (VPK) VPK concentration in the mixture (wt %); the same for Figs. 2–4 and 6. (*1*) Additivity curve obtained by Eq. (2) and (*2*) experimental curve.

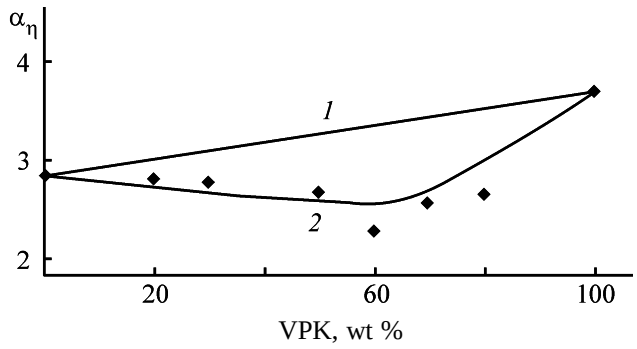


Fig. 2. Coefficient of swelling α_η as a function of the composition of the binary mixture. (*1*) Additivity curve obtained by Eq. (3) and (*2*) experimental curve.

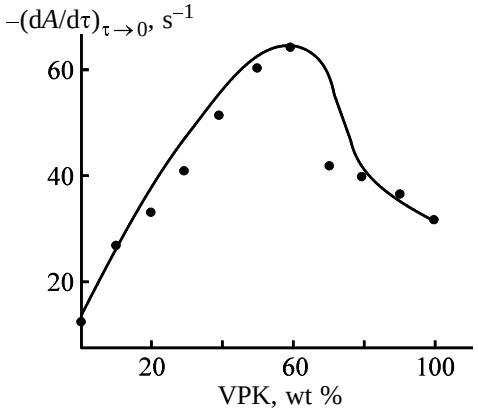


Fig. 3. Effect of the composition of the KF–VPK system on the flocculation rate in the kaolin suspension $(-dA/d\tau)_{\tau\to 0}$.

the clarified and unclarified layers of the suspension. The initial compaction rates V were estimated in the presence of both individual flocculants and their mixture.

The interaction between the components in mixed polymer solutions can be characterized using data on their hydrodynamic properties. The simplest and most adequate method is analysis of the viscosity curves in mixtures of various compositions [18]. The viscosity of polyelectrolytes can be determined under conditions of suppressed ionization and the compact conformation of the globule or in the case when the macromolecules are swollen and take the form of unfolded macroions.

Figures 1 and 2 show that the composition dependences of the intrinsic viscosity and coefficient of swelling run below the additivity lines, which, with no specific intermolecular interactions, are estimated by Eqs. (2) and (3):

$$[\eta]_{ad} = [\eta]_{KF} W_{KF} + [\eta]_{VPK} W_{VPK}, \quad (2)$$

$$\alpha_{\eta ad} = \alpha_{\eta KF} W_{KF} + \alpha_{\eta VPK} W_{VPK}, \quad (3)$$

where $[\eta]_{KF}$ and $[\eta]_{VPK}$ are the intrinsic viscosities of the polyelectrolytes KF and VPK, respectively; $\alpha_{\eta KF}$ and $\alpha_{\eta VPK}$, coefficients of swelling; and W_{KF} and W_{VPK}, the contents of the polyelectrolytes in the mixture.

The highest negative deviations are observed at a VPK content in the mixture of 50–70 wt %, suggesting deterioration of the thermodynamic quality of the mixed solvent as compared to the pure solvent. In this case, some compaction of the polyelectrolyte globules occurs, as demonstrated by the decreases in the intrinsic viscosity and coefficients of swelling in the mixed solutions.

Evidently, in the mixtures with 50–70% VPK, the conditions of adsorption of the macromolecules on the surface of the particles and also the flocculation conditions change to a larger extent in the presence of the polyelectrolyte mixture as compared to the individual reagents.

The concentration dependences of the flocculation in the kaolin suspension show that, with increasing concentration, the aggregating capacity of KF and VPK increases, remaining practically unchanged over the concentration ranges 0.3–1.0 and 0.5–1.0 mg l^{-1}, respectively. Therefore, we selected 1.0 mg l^{-1} as the optimal concentration of the binary mixture.

The effects of the individual polyelectrolytes and of their mixture are clearly seen from the optical density curve. In Fig. 3, the flocculation rate is presented as s function of the composition of KF–VPK system. The flocculation rate increases with increasing VPK concentration in the mixture, reaches a maximum, and

then decreases. However, at any KF : VPK ratio, the experimental values are above the additivity curve.

In this connection, it was necessary to analyze the behavior of other parameters characterizing the flocculation in binary polyelectrolyte mixtures. Figure 4 shows that the compaction rate of the kaolin precipitate in the KF–VPK system passes through a maximum. In the individual flocculant KF, the compaction rate is 95, which is about twice that in VPK. Seemingly, addition of straight VPK favors the formation of more compact floccules, which remains practically unchanged in settling, while in the case of KF, the precipitate is further compacted through closer packing of the floccules. Therefore, it was necessary to determine parameters of the floccules formed in the binary cationic polyelectrolyte.

To characterize the aggregating capacity of the polyelectrolyte, we examined the dependences of the degree of aggregation α_s as a function of the polyelectrolyte concentration and composition (Fig. 5). The degree of aggregation of the kaolin particles in the presence of KF amounts to 20–30 (curve *1*), while in the presence of VPK, only to 5–10 (curve *2*) over the experimental concentration range (up to 1 mg l^{-1}). With the binary flocculant KF + VPK (curve *3*), the floccules of an intermediate size are formed. From data on the particle-size distribution obtained by optical microscopy, we also estimated such parameters as the polydispersity of the kaolin suspension k_p and the form factor of the floccules ψ. The latter was used for estimating the Stokes density of the floccules (Fig. 6). As seen, the composition dependence of the density also passes through a maximum located in the same composition range as the clarification rate (Fig. 3). Similar increase in the density of the floccules at low degree of aggregation was observed for the flocculation with 1,2-dimethyl-5-vinylpyridinium methyl sulfate [14], but the absolute values of the density of the floccules formed in the KF–VPK mixtures are higher than those in the presence of individual FK or its copolymers with *N*-vinylpyrrolidone and acrylamide.

Comparison of data on the viscosity of the polyelectrolyte mixture with the parameters characterizing the flocculation suggests a significant effect of the thermodynamic quality of the mixed solvent. The floccules formed upon introduction of the polyelectrolytes are rather loose aggregates containing a large amount of the dispersion medium in addition to kaolin particles. The reason is the adsorption of the macromolecules on the particle surface. Considerable part of the units of these macromolecules can be unbound,

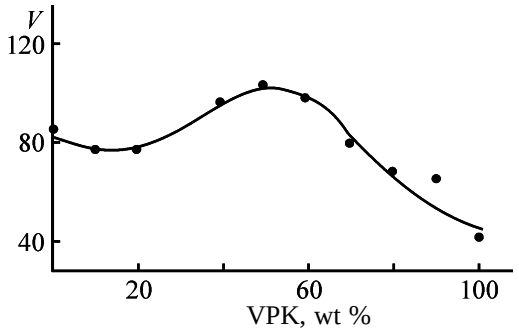


Fig. 4. Compaction rate V of the precipitate in the kaolin suspension in the presence of KF–VPK mixtures.

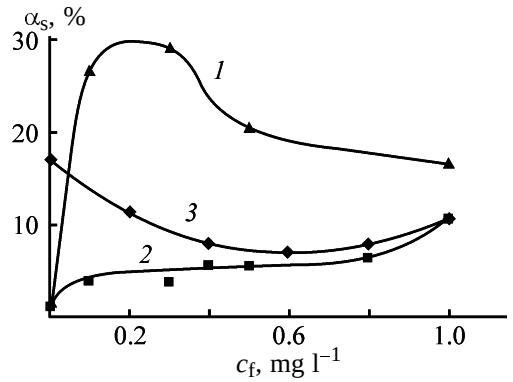


Fig. 5. Degree of aggregation of the kaolin particles α_s as a function of the individual polyelectrolyte concentration c_f and of the composition of the KF–VPK mixture. The concentration of the mixed reagent is expressed in the VPK fractions (KF + VPK = 1 mg l^{-1}). Flocculant: (*1*) KF, (*2*) VPK, and (*3*) KF + VPK.

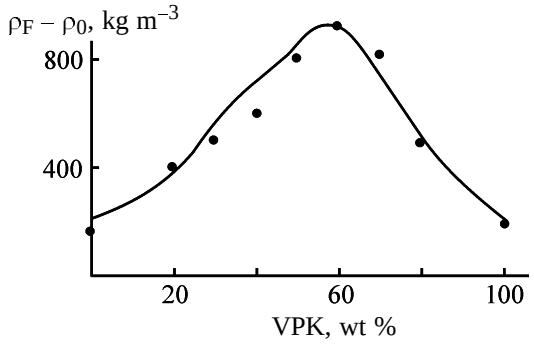


Fig. 6. Density of floccules $\rho_F - \rho_0$ in the kaolin suspension in the presence of KF–VPK mixture.

being arranged in the surface layer as coils and tails. In this connection, it may be suggested that it is conformation of these fragments that controls the structure of the floccules.

Polyelectrolyte chains are strongly swollen in polar solvents at low ionic strength, this effect being more clearly pronounced as compared to the swelling of

Table 2. Characteristics of floccules and precipitates in kaolin suspension in the presence of flocculants

System	$R_n \times 10^5$, m	$R_s \times 10^5$, m	$R_m \times 10^5$, m	α_s	k_p	ψ	$\rho_F - \rho_0$, kg m^{-3}
Aqueous kaolin dispersion, c_f = 0.8 wt %	1.2	1.7	2.4	1	0.49	2.1	
Kaolin (c_{dp} = 0.8 wt %) + flocculant:							
KF	5.2	28.4	34.7	16.7	0.15	1.8	165
VPK	4.3	18.4	24.3	10.8	0.17	1.8	185
KF : VPK*	2.1	12.0	15.6	7.0	0.14	1.7	927

* KF : VPK = 40 : 60; c_f = 1.0 mg l^{-1}.

uncharged macromolecules in a good solvent. As a result, in flocculation of dispersions with homopolymer polyelectrolytes, the density of the floccules formed is close to that of the dispersion medium. The structure of the floccules can change significantly in the presence of copolymer polyelectrolytes.

Introduction of nonionic groups incapable of dissociation results in remarkable increase in the density of the floccules [13]. However, our experiments show that the compaction of the structure of the floccules occurs also in the presence of a mixture of two homopolymer polyelectrolytes. In this case, the reasons for the compaction of the floccules could not be the same as in the presence of copolymer polyelectrolytes having the units capable of association. Most likely, the observed effects can be attributed to thermodynamic incompatibility of polymers of different nature. Adsorption and aggregation of the particles in the system provide concentration of the macromolecules in the bulk of the floccules. However, the coexistence of the coils of different nature in a microscopic volume is thermodynamically disadvantageous. Furthermore, since the macromolecules are bound to the surface via a cooperative system of chemical and physical bonds, they cannot be desorbed to leave the volume of the floccules. Evidently, in this case, the coils collapse so as to minimize the contacts with "foreign" units. As a result, compaction of the floccule as a whole occurs, increasing the clarification rate. It may be suggested that this trend is typical not only of this particular pair of polyelectrolytes, but of any mixture of thermodynamically incompatible polymers.

CONCLUSIONS

(1) It was demonstrated in studying the flocculation of kaolin suspension in the presence of the cationic polyelectrolytes poly-1,2-dimethyl-5-vinylpyridinium methyl sulfate and poly-*N*,*N*-dimethyldiallylammonium chloride that the flocculating capacity of their binary mixture is higher than that of the individual reagents, which is caused by the formation of more compact floccules. As a result, the clarification rate increases.

(2) The effects observed in flocculation in the presence of the likely charged polyelectrolytes are probably due to thermodynamic incompatibility of these polymers, which is reflected in significant deviations of hydrodynamic parameters of the system from the additivity at a 50–70 wt % content of poly-*N*,*N*-dimethyldiallylammonium chloride in the mixture.

REFERENCES

1. Zapol'skii, A.G. and Baran, A.A., *Koagulyanty i flokulyanty v protsessakh ochistki vody: Svoistva. Poluchenie. Primenenie* (Coagulants and Flocculants in Water Treatment Processes: Synthesis, Characterization, and Applications), Leningrad: Khimiya, 1987.
2. Kul'skii, F.M., *Osnovy khimii i tekhnologii vody* (Foundations of the Chemistry and Technology of Water), Kiev: Naukova Dumka, 1991.
3. Kurenkov, V.F., Snegirev, S.V., and Kogdanina, L.S., *Zh. Prikl. Khim.*, 2001, vol. 74, no. 1, pp. 83–87.
4. Myagchenkov, V.A. and Proskurina, V.E., *Zh. Prikl. Khim.*, 2000, vol. 73, no. 6, pp. 1007–1010.
5. Myagchenkov, V.A., Proskurina, V.E., and Malysheva, Zh.N., *Khim. Tekhnol. Vody*, 2000, vol. 22, no. 5, pp. 462–472.
6. Proskurina, V.E. and Myagchenkov, V.A., *Zh. Prikl. Khim.*, 2001, vol. 74, no. 3, pp. 499–504.
7. Myagchenkov, V.A. and Proskurina, V.E., *Zh. Prikl. Khim.*, 2000, vol. 73, no. 12, pp. 2030–2035.
8. Karelin, A.Ya., Popova, I.A., Evseeva, L.A., and Evseeva, O.Ya., *Ochistka stochnykh vod neftepererabatyvayushchikh zavodov* (Wastewater Treatment at Oil Refineries), Moscow: Stroiizdat, 1982, pp. 88–89.

9. Myagchenkov, V.A. and Proskurina, V.E., *Kolloidn. Zh.*, 2000, vol. 62, no. 5, pp. 654–659.
10. Myagchenkov, V.A., Proskurina, V.E., Bulidorova, G.V., *et al.*, *Khim. Tekhnol. Vody*, 2001, vol. 23, no. 35, pp. 285–296.
11. Lipatov, Yu.S., Todosiichuk, T.T., and Chornaya, V.N., *Usp. Khim.*, 1995, vol. 64, no. 5, pp. 497–504.
12. Novakov, I.A., Navrotskii, A.V., Navrotskii, V.A., *et al.*, *Nauka Proizvod.*, 2000, no. 1, pp. 40–43.
13. Navrotskii, A.V., Dryabina, S.S., Malysheva, Zh.N., and Novakov, I.A., *Zh. Prikl. Khim.*, 2000, vol. 73, no. 12, pp. 1940–1944.
14. Navrotskii, A.V., Dryabina, S.S., Malysheva, Zh.N., and Novakov, I.A., *Kolloidn. Zh.*, 2003, vol. 65, no. 3, pp. 368–373.
15. Gandurina, L.V., Zubakova, L.B., Myasnikov, I.N., and Butseva, L.N., *Plast. Massy*, 1976, no. 5, pp. 59–61.
16. Butseva, L.N. and Gandurina, L.V., in *Ochistka stochnykh vod neftepererabatyvayushchikh zavodov kationnymi flokulyantami: Sbornik nauchnykh trudov* (Wastewater Treatment at Oil Refineries with Cationic Flocculants: Collection of Scientific Works), Moscow: VODGEO, 1987, pp. 30–32.
17. Myasnikov, I.N., Butseva, L.N., Gandurina, L.V., and Potanina, V.A., in *Issledovanie protsessov smesheniya i khlop'eobrazovaniya pri ochistke stochnykh vod s primeneniem kationnykh flokulyantov: Sbornik nauchnykh trudov* (Mixing and Flocculation in Wastewater Treatment with Cationic Flocculants: Collection of Scientific Works), Moscow: VODGEO, 1981, pp. 48–56.
18. Bel'nikevich, N.G., Budtova, T.V., Nikolaeva, O.V., and Vesnebolotskaya, S.A., *Vysokomol. Soedin.*, 2002, vol. 44, no. 2, pp. 341–346.

Russian Journal of Applied Chemistry, Vol. 78, No. 7, 2005, pp. 1154–1157. Translated from Zhurnal Prikladnoi Khimii, Vol. 78, No. 7, 2005, pp. 1174–1177.
Original Russian Text Copyright © 2005 by Verezhnikov, Min'kova, Poyarkova.

MACROMOLECULAR CHEMISTRY AND POLYMERIC MATERIALS

Interaction of a Cationic Polymeric Flocculant with Anionic Stabilizers in Latex

V. N. Verezhnikov, T. V. Min'kova, and T. N. Poyarkova

Voronezh State University, Voronezh, Russia

Received October 26, 2004; in final form, April 2005

Abstract—Turbidimetric titration of aqueous solutions of sodium dodecyl sulfate and Leukanol and coagulation titration of polystyrene and polybutadiene latexes containing various amounts of these surfactants are performed.

In separating rubber from latex by flocculation with cationic polyelectrolytes, it is important to neutralize anions of the surfactants used as stabilizers through chemical binding with cationic groups of the flocculant macromolecules. As a result of such interaction, insoluble undissociated ionic complexes are formed, thus decreasing the surface charge and electrostatic repulsion energy of the particles. It is commonly accepted that the maximum of flocculating activity of a polymer corresponds to the full neutralization of all negative charges on the particle surface, and that adsorption of the macromolecules upon introduction of some excess of the polyelectrolyte (PE) results in the recharge and restabilization of the system reflected in the appearance of a maximum in the concentration dependences of the flocculating efficiency of PE.

The factors complicating such a simple flocculation mechanism are the contribution of bridging to the destabilization of the colloid system and the interaction of surfactant anions with the macromolecules, depending on the nature of latex stabilizers. In the case of commercial latex, the latter factor is significant because of the use of two different types of surfactants responsible for the aggregative stability of the latex. The first type is represented by low-molecular-weight emulsifiers, particularly, salts of fatty and resin carboxylic acids, and alkane- and alkylbenzenesulfonates. Also micelle nonforming oligomeric surfactant known as Leukanol (Lk) (sodium salts of the condensation product of β-naphthalenesulfonic acid and formaldehyde) is used. Leukanol serves as an additional stabilizer; its small additions (mostly 0.3 wt % calculated per monomer) considerably increase the stability of the emulsion in the course of polymerization, at the stage of latex degassing, etc. It is significant that, in contrast to paraffinates and rosin soaps, Lk preserves its stabilizing activity in acidic media also, complicating the rubber separation.

It is interesting how the optimal flocculation conditions relate to the completeness of binding of the anionic groups with the cationic groups of flocculant macromolecules for both types of surfactants. Here we report data characterizing the interaction of sodium dodecyl sulfate (SDS) and Lk with the cationic polyelectrolyte (CPE) in aqueous solutions and in latex flocculation.

EXPERIMENTAL

Sodium dodecyl sulfate was purified by fivefold recrystallization from ethanol [1]. The purity of the product was controlled by disappearance of the minimum in the concentration dependence of the surface tension. Leukanol [GOST (State Standard) 6848–73] was purified by gel filtration on Sephadex G-25.

As a flocculant we used poly(dimethylaminoethyl methacrylate) hydrochloride (PDM·HCl), which was obtained by random polymerization in an aqueous solution [2] and dewatered by freeze drying. The mean molecular weight $\overline{M}$ (2.04×10^5) was determined from the viscometric data ($[\eta] = 0.96$ dl g^{-1}, where $[\eta]$ is the intrinsic viscosity in 0.5 N aqueous KCl) using the Mark–Houwink equation ($[\eta] = K\overline{M}^{\alpha}$ [3] with $K = 6.15 \times 10^{-5}$ and $\alpha = 0.79$) [4]).

In synthesis of polystyrene latex (PSL) we used SDS (4.5 wt % calculated per monomer) as an emulsifier. Its content in the dialyzed latex was determined by coagulation titration with cetylpyridinium bromide (CPB) [6]. Recalculated to the polymer weight, it was

1070-4272/05/7807-1154© 2005 Pleiades Publishing, Inc.

1.5×10^{-4} mol g^{-1}. The polymer concentration in the latex was 9.6 g l^{-1}. The mean particle size was estimated by the Rayleigh equation [5] to be 36 nm.

Additionally we used a sample of polybutadiene latex (PBL) (emulsifier: a mixture of potassium resinate with potassium salts of maleinated α-olefins C_{12}–C_{14}).[1]

The interaction of the components in aqueous solutions and the flocculation of latexes were studied turbidimetrically. The turbidity τ was measured on an NFM visual turbidimeter.

Initially we titrated aqueous solutions of SDS and Lk with PDM·HCl. The dependence of τ on the CPE concentration is given in Fig. 1. In all cases, the curves pass through a maximum, as reported previously, for example, in [7, 8] for interaction of SDS with solutions of quaternized poly-4-vinylpyridine derivatives. The observed increase in the turbidity is caused by increasing amount of the insoluble polymer–colloid complex (PCC) formed as a result of electrostatic binding of the surfactant anions with the cationic centers of the macromolecules [9, 10] and then separated from the aqueous phase. The peak concentration c_m corresponds to saturation of all the cationic centers and maximal hydrophobization of the macromolecular globule. With further increasing CPE concentration (right branch in the τ–c_{CPE} curves), the turbidity decreases, which, according to the modern views [7, 8], is caused by increase in the solubility of PCC through hydrophobic interaction of the surfactant ions with the hydrocarbon fragments of the macromolecules resulting in the orientation of the polar group toward the aqueous phase. Such an "adsorption" of the ions causes hydrophilization of the macromolecules and also their recharging, which, acting in combination, result in progressive degradation of the PCC aggregates. This interpretation of the τ–c_{CPE} curves is supported by the experimental data on the electrophoretic mobility of the PCC aggregates and also on the solubilization of a dye [7].

Figure 2 presents c_m as a function of surfactant (SDS and Lk) concentration. The dotted line corresponds to the equivalent binding of the anionic and cationic groups of the components (z = 1, where z is the anionic to cationic group molar concentration ratio in the mixture). There is certain difference between the low-molecular-weight and oligomeric surfactants in the binding nature. In rough approximation, c_m for SDS corresponds to $z \approx 1$. Similar result was obtained in [8]: the maximum in the turbidimetric titration curves of poly-4-vinyl-*N*-butylpyridinium bromide with SDS approximately corresponds to the full binding of the surfactant (according to the potentiometric

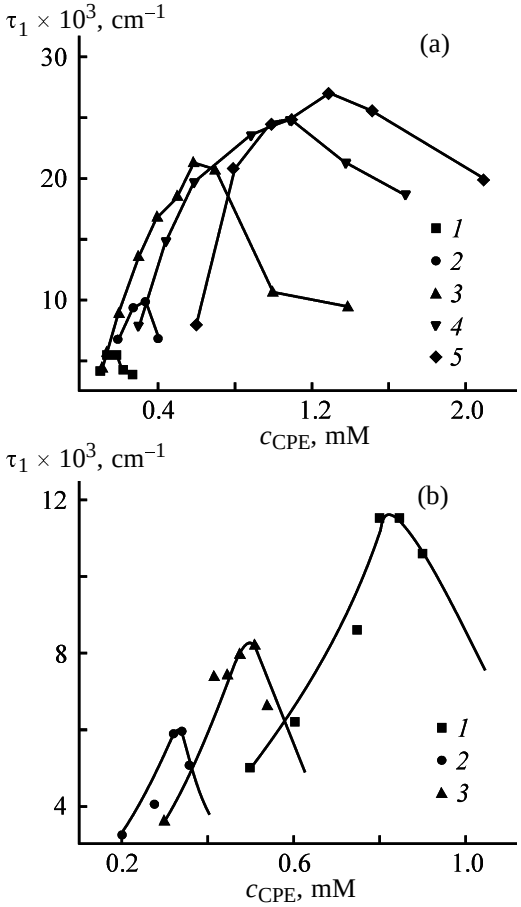


Fig. 1. Turbidimetric titration curves of aqueous solutions of (a) SDS and (b) Lk with PDM·HCl. (τ) Turbidity and (c_{CPE}) PDM·HCl concentration. Surfactant concentration (mM): (a) (*1*) 0.28, (*2*) 0.34, (*3*) 0.5, (*4*) 0.74, and (*5*) 1.0; (b) (*1*) 0.2, (*2*) 0.3, and (*3*) 0.5.

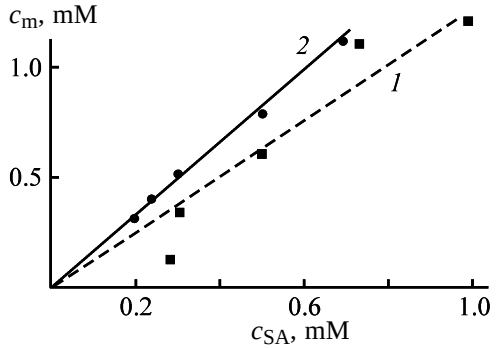


Fig. 2. PDM·HCl concentration c_m corresponding to the maximal flocculating effect as a function of the surfactant concentration c_{SA} in turbidimetric titration of aqueous solutions of (*1*) SDS and (*2*) Lk with PDM·HCl.

[1] Synthesized at the Voronezh Branch, Research Institute of Synthetic Rubber.

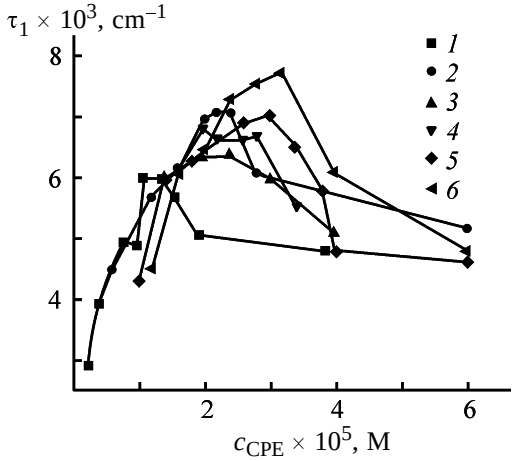


Fig. 3. Initial flocculation rate of polystyrene latex as a function of the PDM·HCl concentration c_{CPE}). (τ_1) Turbidity. SDS concentration in latex $c \times 10^5$ (M): (*1*) 0.96, (*2*) 2.6, (*3*) 4.0, (*4*) 5.4, (*5*) 8.0, and (*6*) 13.0.

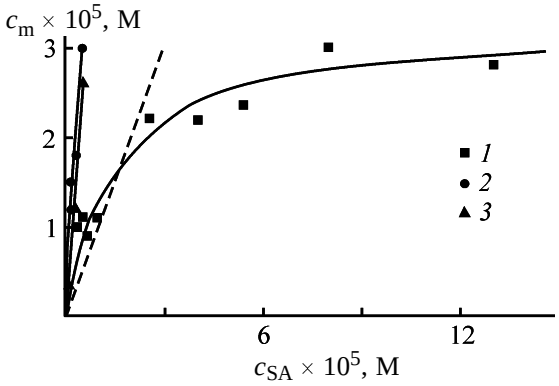


Fig. 4. PDM·HCl concentration c_m corresponding to the maximal flocculating effect as a function of the surfactant concentration c_{SA} in latex. (*1*) PSL + SDS, (*2*) PSL + Lk, (*3*) PBL + Lk [for dependences (*2*) and (*3*), the ordinate scale is increased by a factor of 4].

data obtained using a DS-reversible electrode). At the same time, for Lk, the dependence c_m–c_{Lk} is linear with a slope corresponding to $z = 0.6$. In this case, the maximal PCC concentration is attained at a considerable deficiency of the anionic groups of the oligomeric surfactant or with excess of the cationic groups (excess expenditure) of CPE.

To characterize quantitatively the interaction of the flocculant with the latex stabilizers in the course of flocculation, we studied the initial flocculation rate (IFR) as a function of the CPE concentration at various stabilizer concentrations. As a measure for IFR we used the turbudity τ_1 of a dilute ($1 : 10^4$) latex 1 min after the onset of flocculation (1-min turbidity method [5]). The experimental procedure was as follows. A fixed volume of 10^{-2} M CPE was introduced in a 25-ml volumetric flask and the volume was adjusted to the mark with distilled water. Then the estimated volume of 10^{-2} M surfactant or latex (diluted in proportion 1 : 100) was added. The turbidity τ_1 was measured after 1 min of stirring. Latex samples with various SDS and Lk contents were prepared by introducing incremental doses of the corresponding surfactant to the initial and dialyzed latexes. The concentration of SDS in polystyrene latex (PSL) was selected on the basis of the adsorption titration curve of the latex [5]. Leukanol was added in amounts not exceeding 5 wt % relative to rubber, since, according to our data, higher concentrations decrease the aggregative stability of latex [10]. The surfactant concentration in the initial latexes and final samples was determined by coagulation titration with CPB [6].

Figure 3 shows as an example the τ_1–c_{CPE} curves for PSL samples containing various SDS concentrations. Similar curves were also obtained for PSL and PBL containing various concentrations of Lk. In all cases, the curves pass through a maximum (optimum flocculation), which is typical of the flocculation of negatively charged sols with cationic polyelectrolytes [9]. Figure 4 shows the optimum flocculation as a function of the surfactant concentration in the latexes. It is noteworthy that the trend observed for the low-molecular-weight surfactant strongly differs from that for Lk. In the case of SDS, the optimum flocculation is mostly found considerably below c_{CPE} corresponding to the full binding of the surfactant with the flocculant macromolecules (dotted line). Thus, the maximal flocculation is observed when a considerable electric charge (and potential) induced by free dodecyl sulfate anions still remains on the particle surface. This conclusion is supported by the results of analysis of the dependences of the flocculation efficiency and electrokinetic potential of AgI [11], polystyrene latex [12], and kaolin [14] on the flocculant concentration. In such cases, the major factor controlling the flocculation is the formation of molecular bridges via the adsorbed macromolecules of the polymer rather than neutralization of charges on the particle surface [13]. It should be pointed out that, according to [13, 14], the neutralization mechanism of flocculation is observed for low-molecular-weight (~10^3) flocculants with high charge density on the macromolecular chain.

In the case of Lk, over the entire experimental concentration range, the optimum flocculation for both latexes (PSL and PBL) is observed with CPE taken in excess over the equivalent quantity. The dependence c_m–c_{Lk} is linear, z (0.57 and 0.63, respectively) being practically coincident with that found for interaction of the components in aqueous solutions, which can be

probably due to the oligomeric nature of Lk (it is a mixture of homologs containing from 1 to 10 naphthalene units per molecule [15]). The product after gel filtration should be enriched in heavier nuclei. It is natural to suggest that, in interaction of oppositely charged chain macroions, the formation of stoichiometric complexes requires a uniform or nearly uniform charge distribution along the macromolecular chain. However, this condition is not actually fulfilled. In the case of Lk, in accordance with its structure (methylene groups of the backbone are separated by the naphthalene rings), one could expect a longer distance between the charged sulfonate groups than that between the neighboring cationic centers of PDM · HCl, which should hinder approach of the oppositely charged groups to a distance sufficient for strong binding. As a result, the full neutralization of Lk becomes possible only with excess of the cationic groups of the flocculant, i.e., at its excess expenditure (by a factor of about 1.5 relative to the stoichiometry, as demonstrated by the slopes of curves *2* and *3* in Fig. 4).

CONCLUSION

Full binding of sodium dodecyl sulfate with poly(dimethylaminoethyl methacrylate) hydrochloride is attained at the equivalent proportion of the reagents, while in the case of Leukanol, a 1.5-fold excess of the cationic polyelectrolyte is required.

REFERENCES

1. Verezhnikov, V.N., *Praktikum po kolloidnoi khimii poverkhnostno-aktivnykh veshchestv* (Practical Course of Colloid Chemistry of Surfactants), Voronezh: Voronezh. Gos. Univ., 1984.
2. Verezhnikov, V.N., Min'kova, T.V., and Poyarkova, T.N., *Zh. Prikl. Khim.*, 2004, vol. 77, no. 5, pp. 835–839.
3. Semchikov, Yu.D., *Vysokomolekulyarnye soedineniya* (Macromolecular Compounds), Moscow: Akademiya, 2003.
4. Askarov, M.A., Mukhitdinova, N.A., and Nazarov, A., *Polimerizatsiya aminoalkilmetakrilatov* (Polymerization of Aminoalkyl Methacrylates), Tashkent: Fan, 1974.
5. *Kolloidnaya khimiya sinteticheskikh lateksov* (Colloid Chemistry of Synthetic Latexes), Neiman, R.E., Ed., Voronezh: Voronezh. Gos. Univ., 1984.
6. Verezhnikov, V.N., Poyarkova, T.N., Vostrikova, G.Yu., and Rassokhin, A.V., *Vestn. Voronezh. Gos. Univ.*, 2002, issue 1, pp. 12–14.
7. Tret'yakova, A.Ya., Novikova, I.R., and Barabanov, V.P., *Vysokomol. Soedin., Ser. B*, 1985, vol. 27, no. 9, pp. 665–668.
8. Bilalov, A.V., Manyurov, I.R., Tret'yakova, A.Ya., and Barabanov, V.P., *Vysokomol. Soedin., Ser. A*, 1996, vol. 38, no. 1, pp. 94–102.
9. Baran, A.A., *Polimersoderzhashchie dispersnye sistemy* (Polymer-Containing Disperse Systems), Kiev: Naukova Dumka, 1986.
10. Baran, A.A. and Solomentseva, I.M., *Khim. Tekhnol. Vody*, 1983, vol. 5, no. 2, pp. 120–127.
11. Baran, A.A., Tusupbaev, N.K., Solomentseva, I.M., *et al.*, *Kolloidn. Zh.*, 1980, vol. 42, no. 1, pp. 11–18.
12. Solomentseva, I.M., Tusupbaev, N.K., Baran, A.A., and Musabekov, K.B., *Ukr. Khim. Zh.*, 1980, vol. 46, no. 9, pp. 928–932.
13. Baran', Sh. and Gregory, D., *Kolloidn. Zh.*, 1996, vol. 58, no. 1, pp. 13–18.
14. Walles, W.E., *J. Colloid Interface Sci.*, 1968, vol. 27, no. 4, pp. 797–803.
15. Poyarkova, T.N., Volume and Surface Properties of Aqueous Solutions of Leukanol Latex Stabilizer, *Cand. Sci. Dissertation*, Moscow, 1984.

Russian Journal of Applied Chemistry, Vol. 78, No. 7, 2005, pp. 1158–1161. Translated from Zhurnal Prikladnoi Khimii, Vol. 78, No. 7, 2005, pp. 1178–1182.
Original Russian Text Copyright © 2005 by Petrova, Evtushenko, Chikhacheva, Zubov, Kubrakova.

MACROMOLECULAR CHEMISTRY AND POLYMERIC MATERIALS

Effect of Microwave Irradiation on the Cross-Linking of Polyvinyl Alcohol

N. V. Petrova, A. M. Evtushenko, I. P. Chikhacheva, V. P. Zubov, and I. V. Kubrakova

Lomonosov Moscow State Academy of Fine Chemical Technology, Moscow, Russia
Vernadsky Institute of Geochemistry and Analytical Chemistry, Russian Academy of Sciences, Moscow, Russia

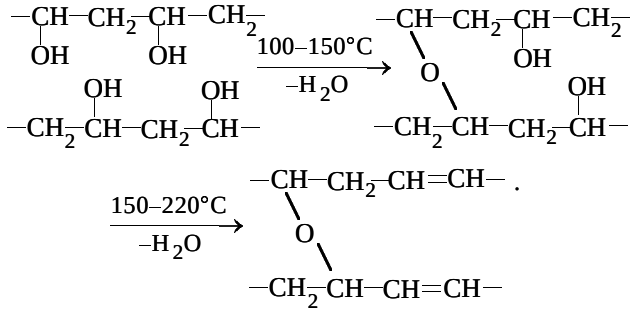
Received April 5, 2004; in final form, June 2005

Abstract—The possibility of dehydration (cross-linking) of polyvinyl alcohol upon microwave irradiation of thin polymer films was examined. The properties of polyvinyl alcohol samples treated by convection heating and irradiation were compared. Immobilization of polyvinyl alcohol on polymer matrices by microwave irradiation was studied.

The effect of microwave irradiation (MWI) on chemical reactions, especially on those involving low-molecular-weight substances, is a subject of a growing number of papers; MWI also shows promise in synthesis and modification of polymers [1–5].

Intensification of chemical reactions by MWI is due to the effect of an electromagnetic field on the solvent and reactants. Along with the thermal effect (sample heating), there may be specific effects caused by the excitation effect of the field; these effects in some cases alter the preexponential factor, reaction entropy, etc.

In this study we examined the effect of heating and MWI on reactions of polyvinyl alcohol (PVAl). When heated to 100–150°C, this substrate tends to dehydrate with cross-linking through ether bridges [6]. Heating to higher temperatures (150–220°C) causes formation of double bonds, and the arising conjugated structures impart a dark color to the polymer:



An additional goal of our study was optimization of a process for converting the water-soluble polymer into an insoluble form. Cross-linked PVAl shows promise for use in aqueous media as biosorbent, biological carrier, material for water filters, etc. [6].

EXPERIMENTAL

The electromagnetic field was generated with an MDS-2000 oven (CEM, the United States) operating at 2.45 GHz; the temperature was measured with an optical-fiber probe.

The substrates to be treated by MWI or heating were solid PVAl films 25 to 250 μm thick (molecular weight of the polymer M = 70 000–100 000), formed from an 8% aqueous solutions of the polymer. For the treated films, we determined the limiting swelling and the amount of insoluble (cross-linked) polymer after repeated extraction of the samples at room temperature; the films were analyzed by IR (EGUINOX-55) and UV (Specord M-40) spectroscopy. The double bond content was determined with an ADS-4M double bond analyzer from the amount of ozone taken up by 1 g of the substance (accuracy 2.5%).

The PVAl films were found to warm up under MWI. This fact indicates that the rotations and vibrations of polar groups are excited by the electromagnetic field. In contrast to the behavior of low-molecular-weight compounds in solutions, the motion of a PVAl molecule as a whole in the solid state is impossible; the warming-up of of the polymer film under MWI is more likely due to the mobility (vibration) of a macromolecule segment or its part. At the same time, the segmental mobility of a macromolecule determines its flexibility and the glass transition point of the polymer. An increase in the mobility of a polymer chain results in its more efficient interaction with the radiation, and, after reaching the glass transition point (85°C), as the polymer passes from the glassy to elastic state, the temperature rise accelerates (Fig. 1). A certain role in the change in the mobility of PVAl

Table 1. Effect of MWI on the PVAl properties. Irradiation power 350 W

h, μm	T,* °C	τ, min	$(P - P_0)/P \times 100$, %	Content of cross-linked polymer, %	Content of C=C bonds, rel. units**
90	Initial PVAl (before irradiation)		88–94	51	1.0
30	70	8	81–88	64	1.0
100	100	5	78–85	68	1.0
130	120	8	62–64	96	1.1
160	175	5	50–60	98	3.0
250	190	3	38–42	100	6.9
25	80	10	93	49	1.0
40	109	10	90	64	1.0
55	129	10	84	86	1.1
95	180	10	38	100	3.1

* Sample temperature after irradiation.
** Relative to the background uptake of ozone by the initial PVAl; the same for Table 3.

macromolecules is apparently played by cleavage of hydrogen bonds on heating the polymer to the softening point (50–60°C), which corresponds to appearance of the hyperelastic properties [6].

Compounds acting as plasticizers increase the mobility of the segment and, correspondingly, the warming-up rate (under equal other conditions). On the contrary, compounds with a high glass transition point decrease the microwave heating temperature. In this connection, polyacrylic acid (PAA) can act as PVAl "antiplasticizer." It is known [7] that the cohesion energies of the hydroxy and carboxy groups are 21.4 and 23.4 kJ mol^{-1}, respectively, and the glass transition point of PAA exceeds that of PVAl (106 and 85°C). The temperature of a film prepared from a PVAl–PAA blend decreases with an increase in the PAA content: at PVAl : PAA = 7.5 : 1, it is 172°C; at 5 : 1, 157°C; and at 3 : 1, 112°C. Also, a decrease in the temperature may be due to formation of an interpolymeric complex of PVAl with PAA, which also decreases the mobility of the macromolecules.

Table 1 shows that, with increasing film thickness, under equal other conditions, the temperature of the polymer increases upon MWI to a greater extent, and the limiting swelling $[(P - P_0)/P] \times 100\%$ (P is weight of the swollen film, and P_0, that of the dry film, g) decreases. Apparently, for a thin film, the contribution of the surface heat exchange and convection cooling of the external layers of the material, affecting the temperature profile of the samples and hence their properties, is more significant.

Introduction into PVAl of compounds that actively interact with the radiation increases the temperature of the system and hence the reaction rate, under equal other conditions. We performed MWI of films preliminarily swollen in water (to 40–45% swelling) and PVAl films containing 10–12 wt % glycerol. As seen from Table 2, both water and glycerol promote the cross-linking.

For comparison, we examined the behavior of PVAl films at thermal heating. Table 3 shows that, with an increase in the temperature and time of the treatment, the degree of cross-linking (amount of the polymer remaining after repeated washing with water) increases and the limiting swelling decreases.

Examination of the IR spectra of PVAl films after MWI and thermal treatment shows that, in both cases, the bands characteristic of OH (3440 cm^{-1}) and CH_2 (2940–2910, 1375, 920 cm^{-1}) groups slightly decrease in the intensity, the absorption of C–H bonds (2840–2850 cm^{-1}) increases, and the absorption in the region characteristic of C–O–C groups (1140 cm^{-1}) increases substantially. Changes in the spectra are proportional to the sample temperature. The IR spectra confirm the published data [6] on the composition of the main products formed by thermal dehydration of

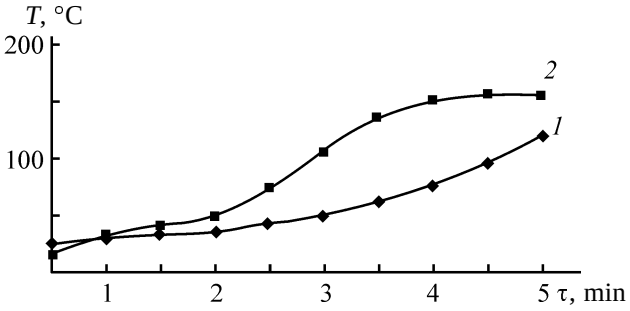


Fig. 1. Temperature T of PVAl films as a function of MWI time τ. Film thickness, μm: (*1*) 50 and (*2*) 100.

Table 2. Influence of water and glycerol on the properties of PVAl upon MWI for 2 min

Sample	T_{MWI}, °C	$(P - P_0)/P \times 100$, %	Content of cross-linked polymer, %
PVAl + water	95	64	96–100
PVAl + glycerol	130	60	100

PVAl. Strong absorption of alcoholic OH groups (3150–3500 cm^{-1}) and the bands of acetate groups and water (1570–1740 cm^{-1}) present in PVAl obscure the bands characteristic of multiple bonds [8–10]; in this case, more information is furnished by UV spectra. Thermal heating of PVAl (178°C) results in its brown coloration, suggesting formation of a conjugated structure [6]. The UV spectra (Fig. 2) show strong absorption in the range 250–400 nm; the growth of absorption at λ = 330 nm assignable to polyconjugated unsaturated structures [10, 11] is more pronounced than at λ = 280 nm. At the same time, when heated to almost the same temperature (170°C) but in the MWI mode, the films became yellow and not brown, and the absorption at λ = 280 nm increased to a greater extent.

The data obtained are in good agreement with the results of determination of the double bond content in the treated samples. The content of double bonds in MWI-treated samples is lower compared to the thermally treated samples. At both heating modes, the content of double bonds increases with temperature, but at thermal heating this trend is more pronounced. In particular, upon MWI, the content of double bonds increases from 1.9 (150°C) to 2.7 rel. units (170°C), and upon thermal heating, from 2.5 (150°C) to 5.4 rel. units (178°C). Furthermore, upon heating to moderate temperatures (70–100°C), C=C bonds formed only at the thermal heating mode (1.2–1.7 rel. units).

Thus, presumably, an electromagnetic field acting on polar groups of PVAl increases the probability of dehydration mainly via intermolecular reaction of hydroxy groups (although intramolecular cyclization also cannot be ruled out). In convection heating, both hydroxy and nonpolar methylene groups (see scheme) get involved in the dehydration, and the process involving methylene groups becomes particularly noticeable at T > 150°C, resulting in active formation of by-products and imparting a dark color to the polymer. At the same time, for MWI, a lower temperature (down to 120°C) is optimal, and addition of glycerol allows the cross-linking time to be decreased to 3–5 min.

Table 3. Effect of thermal heating on the properties of PVAl

h, μm	T_{heat}, °C	τ, min	Limiting swelling	Content of cross-linked polymer	Content of C=C bonds, rel. units
			%		
90	Initial film (without heating)		88–94	51	1.0
90	70	30	85–90	51	–
30	120	30	83–86	75	3.0
90	120	30	77–80	86	3.2
150	120	30	67–70	96	–
25	80	10	96	11	1.3
40	109	10	95	18	1.5
55	129	10	93	43	1.7
95	180	10	78	95	5.4
30	150	30	64–67	98	4.8
90	150	15	71–75	82	3.3
90	150	30	55–57	99	–
150	150	30	41–44	99	–
30	180	30	24–26	100	7.5
90	180	5	63–65	87	4.5
90	180	15	39–41	92	–
90	180	30	26–28	100	–
150	180	30	24–26	100	–
30	210	30	22–24	100	26.2
90	210	30	19–21	100	15.9
150	210	30	23–25	100	–

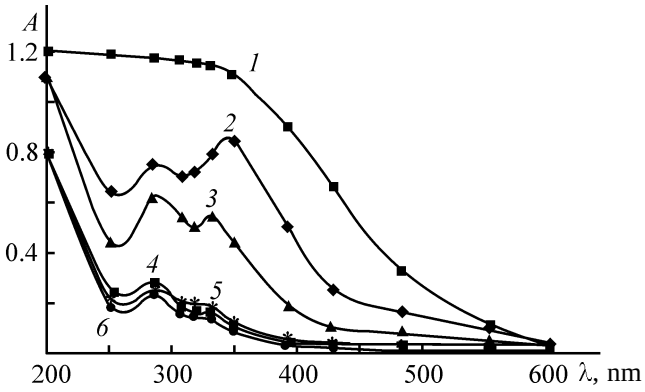


Fig. 2. UV spectra of PVAl films after thermal heating at (*1*, *2*) 178 and (*5*) 150°C, and after microwave heating to (*3*) 170 and (*4*) 150°C. (*A*) Optical density and (λ) wavelength. Film thickness, μm: (*1*, *3*) 150 and (*2*–*4*, *6*) 90; (*6*) Initial PVAl film.

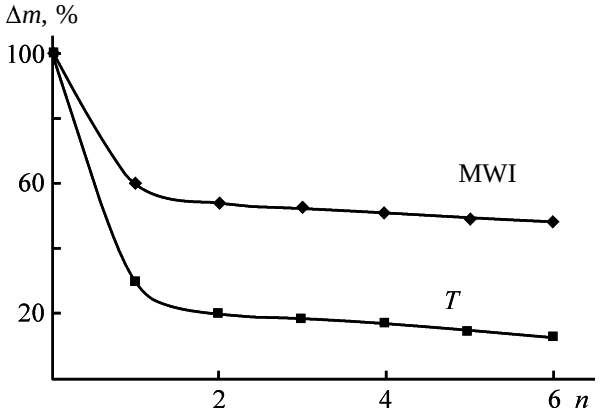


Fig. 3. Weight loss Δ*m* of PVAl samples applied onto polypropylene fiber upon their washing with water after MWI (100°C, 10 min) and thermal treatment (100°C, 10 min). (*n*) Number of washing runs.

A selective action of MFI on the polar groups allows cross-linking of PVAl applied onto polypropylene (PP) or polyethylene (PE) supports, i.e., onto matrices with a low heat resistance (the working temperature should not exceed 100–120°C). As seen from Fig. 3, MWI allows more efficient immobilization of PVAl on the PP fiber, compared to the thermal heating under equal other conditions.

Thus, MWI is a promising procedure for imparting water resistance to PVAl films. Further experimental studies are required to assess the prospects for using MWI in synthesis and modification of other macromolecular compounds.

CONCLUSIONS

(1) Microwave irradiation of polyvinyl alcohol films results in their heating; the temperature attained depends on the film thickness and determines the degree of the polymer cross-linking.

(2) Under equal other conditions, the degree of cross-linking of polyvinyl alcohol films subjected to microwave irradiation is higher compared to convection heating; the difference increases with a decrease in the treatment temperature.

(3) The amount of immobilized polyvinyl alcohol on a polypropylene support upon microwave irradiation is larger than upon thermal heating, other conditions being the same.

(4) The results obtained suggest that the contribution of intermolecular etherification reactions involving hydroxy groups and resulting in cross-linking of polyvinyl alcohol is greater upon microwave irradiation compared to thermal heating.

ACKNOWLEDGMENTS

The study was financially supported by the Ministry of Education of the Russian Federation (project no. E02-5.0-121).

REFERENCES

1. Kubrakova, I.V., *Usp. Khim.*, 2002, vol. 71, no. 4, pp. 327–340.
2. Dikusar, M.A., Kubrakova, I.V., Chinarev, A.A., and Bovin, N.V., *Bioorg. Khim.*, 2001, vol. 27, no. 6, pp. 457–461.
3. Perreux, L. and Loupy, A., *Tetrahedron*, 2001, vol. 57, pp. 9199–9223.
4. Lidstrom, P., Tierney, J., Wathey, B., and Westan, J., *Tetrahedron*, 2001, vol. 57, pp. 9225–9283.
5. Wittaker, A.G. and Mingos, D.M.P., *J. Microwave Power Electromagn. Energy*, 1994, vol. 29, no. 4, pp. 195–219.
6. Ushakov, S.N., *Polivinilovyi spirt i ego proizvodnye* (Polyvinyl Alcohol and Its Derivatives), Moscow: Akad. Nauk SSSR, 1960, vols. 1, 2.
7. *Entsiklopediya polimerov* (Polymer Encyclopedia), Kargin, V.A., Ed., Moscow: Sov. Entsiklopediya, 1972–1977, vols. 1–3.
8. *Fizika polimerov* (Polymer Physics), Vol'kenshtein, M.V., Ed., Moscow: Inostrannaya Literatura, 1960.
9. Dechant, J., Danz, R., Kimmer, W., *et al.*, *Ultrarotspektroskopische Untersuchungen an Polymeren*, Berlin: Akademie, 1972.
10. *Chemical Applications of Spectroscopy*, West, W., Ed., New York: Interscience, 1956.
11. Rao, C.N.R., *Ultra-Violet and Visible Spectroscopy: Chemical Applications*, London: Butterworth, 1961.

Russian Journal of Applied Chemistry, Vol. 78, No. 7, 2005, pp. 1162–1165. Translated from Zhurnal Prikladnoi Khimii, Vol. 78, No. 7, 2005, pp. 1183–1186.
Original Russian Text Copyright © 2005 by Nemilov, Orlova, Chulkova.

MACROMOLECULAR CHEMISTRY AND POLYMERIC MATERIALS

Kinetics of Polycondensation of Betulin with Adipic Acid

V. E. Nemilov, T. V. Orlova, and Yu. S. Chulkova

St. Petersburg State University of Technology and Design, St. Petersburg, Russia

Received November 23, 2004; in final form, April 2005

Abstract—The influence of various factors on the kinetics of polycondensation of betulin (a triterpene alcohol of the lupane series) with adipic acid was studied.

Extension of the range of polymeric binders for composite materials involves a search for nontraditional sources of monomers. One of such sources can be by-products from processing of vegetable raw materials and from wood-chemical and wood-processing industry. These by-products contain a large amount of various polyfunctional organic compounds.

Of certain interest in this respect is betulin, a triterpene alcohol of the lupane series containing primary and secondary hydroxy and isopropenyl groups, which creates prerequisites for preparing linear thermoplastic polymers [1]. Since the isopropenyl group does not tend to polymerize because of its structural features, the probability of formation of branching polymers in this case will be low. The most acceptable procedure for polycondensation of betulin with dibasic organic acids is polycondensation in the melt, since the agents involved are thermally stable above the melting points of the monomers.

EXPERIMENTAL

Betulin was isolated from birch crust; its characteristics were as follows: hydroxy number 253.1, iodine number 47.6, and acid number 0, which corresponds to 99.5% purity of the product. Adipic acid dried at 80°C met the requirements of GOST (State Standard) 10558–80.

When studying the kinetic features of the process, we used the method of separate samples; to reduce the thermal oxidative degradation, the synthesis was performed in a nitrogen flow. In analysis of the kinetic features of the polycondensation of these monomers, it is difficult to determine with sufficient accuracy the changes in the concentrations of primary and secondary hydroxy groups of betulin separately. Therefore, we determined the overall changes in the concentration of hydroxy groups by acylation with acetic anhydride in pyridine. The carboxy groups were determined by neutralization, and double bonds, by the iodine–bromine method. It should be noted that the concentration of double bonds remained constant in the course of the synthesis, which confirmed the low reactivity of the double bond in betulin. The ratio of the hydroxy and carboxy groups remained equimolar; therefore, the kinetic parameters determined for the hydroxy and carboxy groups coincided.

In this study we considered the kinetic features of polycondensation of betulin with adipic acid in a melt; the upper limit of the polycondensation temperature is determined by the thermal stability of betulin (265°C), and the lower limit (215°C), by the solubility of betulin in adipic acid at the equimolar reactant ratio.

The variation of the concentration of the hydroxy groups at various temperatures is shown in Fig. 1. As seen, the polycondensation shows no deviations; however, the plot of $\ln w$ vs. $\ln c$ (w is the reaction rate, and c, concentration) is not a straight line but consists

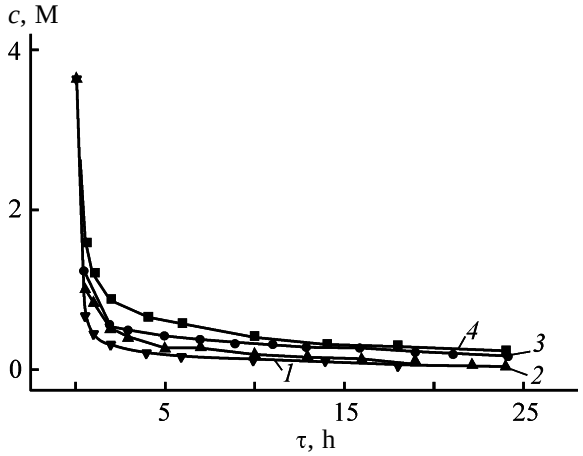


Fig. 1. Concentration of OH groups c as a function of reaction time τ. T, °C: (*1*) 265, (*2*) 250, (*3*) 230, and (*4*) 215.

1070-4272/05/7807-1162 © 2005 Pleiades Publishing, Inc.

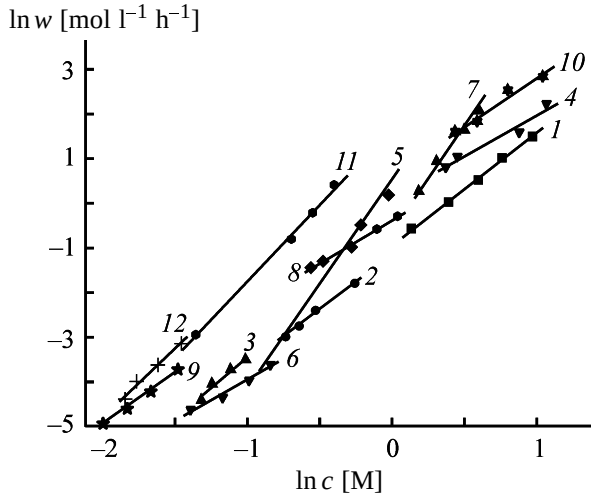


Fig. 2. Plot of ln*w* vs. ln*c* at various temperatures. *T*, °C: (*1*–*3*) 215, (*4*–*6*) 230, (*7*–*9*) 250, and (*10*–*12*) 265.

of three portions (Fig. 2). The plots are shown with breaks corresponding to the transition regions. It could be expected from the different reactivity of the hydroxy groups of betulin that the plot of ln*w* vs. ln*c* would consist of two portions, with the first portion corresponding to the simultaneous transformations of primary and secondary hydroxy groups and the second portion, to the state when the equilibrium has already been attained for the primary OH groups but has not yet been attained for the secondary OH groups. The observed dependence of ln*w* on ln*c* is attributable to a decrease in the molecular mobility in the course of the polycondensation (due to growing viscosity), or to possible manifestation of the thermotropic properties of the polymer (formation of mesomorphic structures in solution, as shown in [2]). Furthermore, when the ln*w*–ln*c* dependences are plotted for different reaction times, different rate constants are obtained (Fig. 2). The changes in the polycondensation kinetics are seen more clearly from the *w/c*–*c* plot (Fig. 3). Moreover, the dependence of *w/c* on *c* allows us to derive a polynomial equation describing the concentration dependence of the reaction rate:

$$d[c]/d\tau = a_1[c^2] + a_2[c],$$

where a_1 and a_2 are constants, *c* is concentration, and τ is time.

The form of this polynomial suggests the occurrence of parallel reactions of different orders with respect to *c*. Furthermore, this equation shows that both hydroxy groups participate in the reaction through out the process (24 h), and the equilibrium is not attained even with primary OH groups. It is also

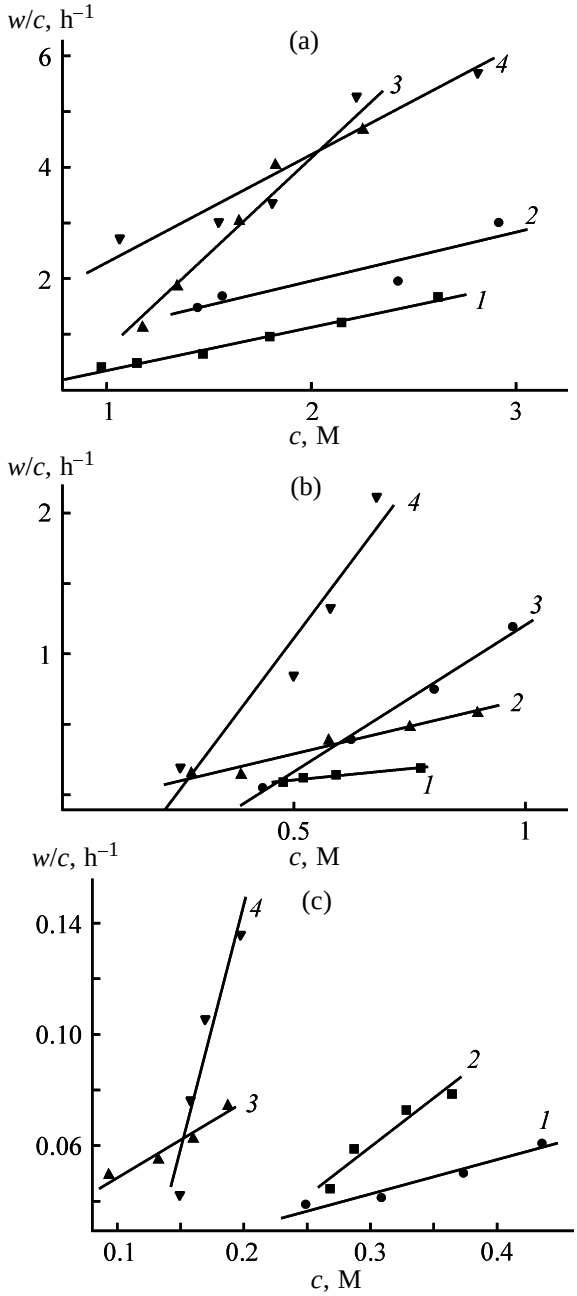


Fig. 3. Plot of *w/c* vs. *c*. Reaction step: (a) initial, (b) middle, and (c) final. *T*, °C: (*1*) 230, (*2*) 250, (*3*) 215, and (*4*) 265.

seen that the reactions are not catalyzed by components of the system.

The reaction rate constants and reaction orders in relation to the reaction time are given in Table 1.

Table 1 shows that, in portion I of the kinetic curve (low conversions), the reaction follows the commonly accepted mechanism and is not complicated by the influence of the forming polymer and by the growing viscosity of the melt [3]. In portion II, the polycon-

Table 1. Kinetic parameters of the reaction for different portions of the concentration–time dependences

T, °C	Portion	Apparent rate constant, l mol$^{-(n-1)}$ $c^{-(n-1)}$	Reaction order
215	I	0.381	2.52
	II	0.353	2.64
	III	0.523	2.81
230	I	1.110	1.83
	II	1.298	3.41
	III	0.120	1.84
250	I	0.740	3.84
	II	0.786	1.97
	III	0.191	1.59
265	I	2.338	1.85
	II	5.067	3.41
	III	1.241	3.02

densation rate constant increases (except for 215°C), which may be due to appearance of mesomorphic structures promoting the reaction; this effect is stronger than that exerted by the melt viscosity. At 215°C, the viscosity is so high that formation of ordered structures is hindered; correspondingly, the polycondensation rate decreases. In portion III, the melt viscosity increases to such an extent (owing to an increase in the molecular weight of the polymer) that the effect of mesomorphic structures is not manifested.

Thus, our data allow calculation of the rate constants of the process, but do not allow determination of the equilibrium constants for the whole process at various temperatures and for primary and secondary hydroxy groups. The equilibrium constant K in this case depends only on temperature, which allows determination of K at least for the initial portion, in which the process is controlled only by the rate of reaction of the functional groups. For this purpose, it is sufficient to ensure the pseudo-first-order reaction conditions. According to published data, the error in determining the reaction parameters at a fivefold excess of one of the agents is 5%, which is quite acceptable for kinetic measurements [4]. In this case, the equilibrium constant can be determined only with excess betulin; otherwise, the polycondensation may be catalyzed by the carboxy groups of adipic acid. Figure 4 shows the plot of $\ln c$ vs. τ, confirming the occurrence of parallel first-order reactions with the common product. From the dependence of w on c, we can determine the reaction rate constants for primary and secondary hydroxy groups. Knowing the rate constants, we can obtain the dependence of $\ln(c - c_{eq})$ on time τ. The equilibrium concentration c_{eq} is chosen so as to obtain a linear dependence. The slope of this dependence is equal to $-(k_+ + k_-)$. Knowing the equilibrium concentration of each type of hydroxy groups and the quantity $-(k_+ + k_-)$, we can find the rate constants of the forward and reverse reactions and the equilibrium constant of the polycondensation for primary and secondary hydroxy groups. The results are listed in Table 2.

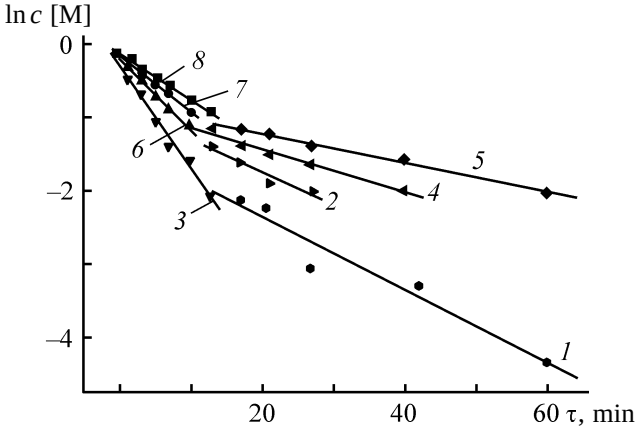


Fig. 4. Plot of $\ln c$ vs. time τ (pseudo-first order). T, °C: (*1*, *3*) 270, (*2*, *6*) 260, (*4*, *7*) 250, and (*5*, *8*) 240.

Table 2 shows that the equilibrium constant, as expected, increases with temperature; also, the rate constants determined allow estimation of the reactivity of the hydroxy groups. The primary hydroxy groups are 5.5 times more reactive than the secondary hydroxy groups, and this reactivity ratio is independent of temperature. The pseudo-first-order reaction parameters found for the 5 : 1 molar ratio allow calculation of the reaction parameters for the 1 : 1 molar ratio. The calculated parameters are listed in Table 3.

As already noted, the equilibrium constants obtained refer not to the whole process but only to the interval from the start of the process to the moment when the concentration of OH groups reaches 0.8 M. If these parameters referred to the whole process up to the maximum attainable conversion, their calculated values would be as follows: 215°C, 0.92; 230°C, 0.94; 250°C, 0.96; and 265°C, 0.97. However, actually the conversion in 24 h reaches 0.98. This is possible only if the equilibrium constant increases with the molecular weight [5].

It is interesting that, at 250°C, the rate constants of the forward and reverse reactions decrease, which may be due to formation of structures in which the reaction of the terminal groups is hindered. This decrease is also observed in other portions of the kinetic plots and is confirmed by Table 1.

Table 2. Equilibrium constants of polycondensation and rate constants of the forward and reverse reactions

T, °C	Primary OH groups			Secondary OH groups		
	K	k_+	k_-	K	k_+	k_-
		$\min^{-1}$			$\min^{-1}$	
240	41.3	0.113	0.0027	46.0	0.0196	0.000426
250	46.0	0.166	0.0036	51.9	0.0294	0.000567
260	51.9	0.219	0.0042	69.5	0.0414	0.000596
270	69.3	0.394	0.0057	83.6	0.0702	0.000839

Table 3. Parameters of the polycondensation at the 1 : 1 molar ratio in the concentration range from the initial concentration to 0.8 M

T, °C	Primary OH groups			Secondary OH groups		
	K	k_+	k_-	K	k_+	k_-
		$l\ mol^{-n}\ h^{-n}$			$l\ mol^{-n}\ h^{-n}$	
215	24.1	0.310	0.013	24.3	0.056	0.002
230	33.0	0.912	0.028	36.0	0.166	0.004
250	46.0	0.613	0.013	69.5	0.112	0.002
265	60.2	1.946	0.032	75.5	0.355	0.005

CONCLUSIONS

(1) The kinetics of the polycondensation of betulin with adipic acid depends on the molecular weight of the polymer. The kinetic plots consist of three portions, each characterized by specific reaction parameters.

(2) The equilibrium constants were found, and the possibility of using the pseudo-first-order conditions for their determination was demonstrated.

(3) The polycondensation of betulin with adipic acid shows an anomaly at 250°C.

REFERENCES

1. Nemilov, V.E., Nemilova, T.V, Nachinkin, O.I., and Tsarev, G.I., *Zh. Prikl. Khim.*, 1999, vol. 72, no. 9, pp. 1534–1537.
2. Nemilov, V.E. and Orlova, T.V., in *Fizikokhimiya polimerov: Sbornik trudov* (Physical Chemistry of Polymers: Coll. of Papers), Tver, 2001, issue 7, pp. 57–59.
3. Sokolov, L.B., *Osnovy sinteza polimerov metodom polikondensatsii* (Principles of Polymer Synthesis by Polycondensation), Moscow: Khimiya, 1979.
4. Schmid, R. and Sapunov, V.N., *Non-Formal Kinetics*, Weinheim: Chemie, 1982.
5. Zhubanov, B.A., *Vysokomol. Soedin., Ser. A*, 1978, vol. 20, no. 4, pp. 273–282.

Russian Journal of Applied Chemistry, Vol. 78, No. 7, 2005, pp. 1166–1169. Translated from Zhurnal Prikladnoi Khimii, Vol. 78, No. 7, 2005, pp. 1187–1190.
Original Russian Text Copyright © 2005 by Semchikov, Bulgakova, Mazanova.

MACROMOLECULAR CHEMISTRY AND POLYMERIC MATERIALS

Use of Organohydridodisilanes for Controlling the Molecular-Weight Distribution of High-Conversion Polymers

Yu. D. Semchikov, S. A. Bulgakova, and L. M. Mazanova

Research Institute of Chemistry, Lobachevsky Nizhni Novgorod State University, Nizhni Novgorod, Russia
Lobachevsky Nizhni Novgorod State University, Nizhni Novgorod, Russia

Received March 2, 2005

Abstract—The polymerization of methyl methacrylate to high conversion in the presence of a series of disilanes as chain-transfer agents was studied, and the chain-transfer constants at low and high conversions were determined. The molecular-weight characteristics of the polymers were estimated by gel permeation chromatography.

The molecular-weight distribution (MWD) of polymers mainly affects the rheological properties of their solutions and melts. This influence is the most pronounced in the case of a flow under a high shear stress [1]. Therefore, the development of methods for controlling MWD, suitable for industrial applications, is an urgent problem, since polymers are mainly processed in the form of melts.

Recently there has been a considerable progress in the controlled pseudo-living radical polymerization [2, 3] allowing preparation of virtually monodisperse polymers. However, this result is provided by reversible inhibition, which leads to low polymerization rates even at very high temperatures (100–120°C). Therefore, it is urgent to find the conditions of radical polymerization ensuring preparation of polymers with fairly narrow MWD without decreasing the polymerization rate at acceptable temperature. For this purpose, we studied the molecular-weight characteristics of polymers prepared in the presence of polyfunctional silicon hydrides, which are effective chain-terminating agents for polymers [4].

EXPERIMENTAL

The organosilicon hydrides (main substance content 98–99%) were prepared at the Institute of Organometallic Chemistry, Russian Academy of Sciences (Nizhni Novgorod) and were used without additional purification. The procedures for preparing the hydrides were described in [5–8]. Dodecyl mercaptan (DDM) was purified by vacuum distillation; methyl methacrylate (MMA), by vacuum recondensation; and azobis(isobutyronitrile) (AIBN, initiator), by recrystallization from ethanol. The polymerization was performed in sealed dilatometric ampules at 60°C, both to low (≤10%) and to high conversions, at which the reaction mixture lost fluidity. Prior to the experiments, the ampules were treated to remove atmospheric oxygen. The initial polymerization rate was monitored dilatometrically. The resulting polymers were purified by triple reprecipitation from acetone into petroleum ether and were dried to constant weight in a vacuum.

The relative chain-transfer constants C_s and the apparent chain-transfer constants at high conversions C_s^{app} were calculated from the Mayo graphical dependence

$$1/P_n = 1/P_0 + C_s[S]/[M],$$

where P_n and P_0 are the degrees of polymerization of the polymer obtained in the presence and in the absence of the chain-transfer agent, respectively; [S] and [M] are the molar concentrations of the chain-transfer agent and monomer, respectively.

The viscosity-average molecular weights (MWs) of the polymers were determined viscometrically. The measurements were performed with an Ubbelohde viscometer in methyl ethyl ketone (MEK) at 30°C; MW was calculated by the formula $[\eta] = 5.907 \times 10^{-4} M^{0.5716}$ [9]. The previously determined constants of the chain transfer through organosilicon hydrides [4] are given in Table 1. The molecular-weight characteristics of the polymers were determined by GPC

1070-4272/05/7807-1166 © 2005 Pleiades Publishing, Inc.

Table 1. Relative chain-transfer constants at initial (C_s) and high (C_s^{app}) conversions in polymerization of MMA in the presence of organosilicon chain-transfer agents and DDM

Compound	Structural formula	$C_s \times 10^3$	$C_s^{app} \times 10^3$
DS-2	$H_2(Me)Si–Si(Me)H_2$	234	184
DS-4	$Me_2(HMe_2SiO)Si–Si(OSiMe_2H)Me_2$	2.43	2.8
DS-8	$H(Me_2)Si–Si(Me)(i\text{-Pr})H$	139	199
DS-9	$Me_3Si–Si(Me_2)H$	56	110
DS-10	$H(n\text{-Bu})(Me)Si–Si(Me)(n\text{-Bu}_2)$	50	77
DS-11	$Me_2(HMe_2SiO)Si–Si(OSiMe_2H)_2Me$	3.93	3.48
DS-12	$H(i\text{-Bu})(Me)Si–Si(Me)(i\text{-Bu}_2)$	13	66
DS-13	$H(i\text{-Pr})(Me)Si–Si(Me)(i\text{-Pr})H$	72	138
DS-14	$H(Me_2)Si–Si(Me_2)H$	175	120
DS-15	$(Me_3Si)_3SiH$	8300	660
DDM	$C_{12}H_{25}SH$	207	220

Table 2. Molecular-weight characteristics of high-conversion PMMA samples prepared in the bulk at 60°C

Conditions of PMMA preparation	$M_n \times 10^3$	$M_w \times 10^3$	$M_z \times 10^3$	M_w/M_n
[AIBN] = 2×10^{-1} M	115	438	1230	3.81
[AIBN] = 5×10^{-3} M, $c_{DS\text{-}9}$ = 0.5 wt %	284	600	1100	2.12
[AIBN] = 5×10^{-3} M, c_{DDM} = 0.35 wt %	240	500	930	2.10

on a Waters chromatograph with a set of five Styrogel columns with the pore diameter of 10^5, 3×10^4, 10^4, 10^3, and 250 Å. The eluent was tetrahydrofuran. An RD-410 differential refractometer was used as detector.

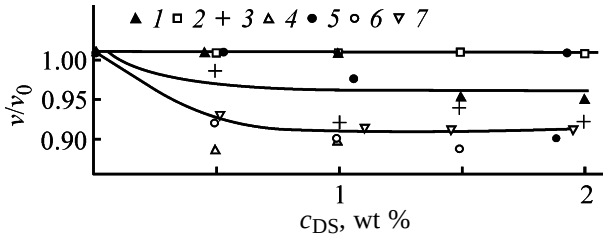
It is known that the necessary condition for processing polymers through the melt is MW of the order of 10^5. As polymerization to high conversions usually yields polymers with MW by an order of magnitude higher, the MW should be controlled. Table 2 presents the results of GPC analysis of PMMA samples prepared using two main methods for decreasing MW: increasing the initiator concentration and adding chain-transfer agents to the formulation. Table 2 shows that, in the polymerization to high conversions, both methods allow the molecular weight of PMMA to be decreased by an order of magnitude. However, polymers prepared in the presence of chain-transfer agents with active S–H and Si–H groups have a narrower MWD. It is important that the polydispersity parameter of such polymers virtually reaches the theoretical value, $M_w/M_n \cong 2$, corresponding to the Flory exponential distribution characteristic of radical polymerization with the chain termination through disproportionation of radicals and/or chain transfer.

The above-indicated limit can be overcome by using polyfunctional silicon hydrides as chain-transfer agents. Table 3 shows that, in polymerization of MMA to high conversions in the presence of trimethylisopropyldisilane (DS-8) containing two Si–H groups in the molecule, the polydispersity index M_w/M_n becomes as low as 1.51.

This value corresponds to the minimal polydispersity of a polymer attainable under the conditions of radical polymerization. It theoretically corresponds to the Schultz distribution characteristic of radical polymerization with recombination (coupling) of radicals and of polycondensation. It can be readily shown that specifically this distribution is characteristic, to one or another extent, of the polymerization performed in the presence of bifunctional disilanes as chain-transfer agents. Assume that both Si–H groups of the disilane

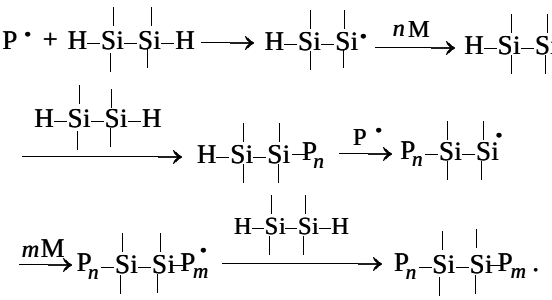
Table 3. Molecular-weight characteristics of high-conversion PMMA samples prepared in the presence of disilanes of various structures

Disilane, wt %	$M_n \times 10^3$	$M_w \times 10^3$	M_w/M_n
DS-2, 1.0	4.9	8.7	1.79
DS-4, 0.56	51	97	1.89
DS-8, 0.42	8.9	13.6	1.51
DS-11, 1.0	107	198	1.85
DS-15, 0.72	44.9	9.7	4.64



Initial relative polymerization rate v/v_0 of MMA in the bulk at 60°C in the presence of 5×10^{-3} M AIBN as a function of concentration c_{DS} of various disilanes: (*1*) DS-8, (*2*) DS-4, (*3*) DS-9, (*4*) DS-10, (*5*) DS-11, (*6*) DS-12, and (*7*) DS-2.

participate in the chain transfer:



Then it can be assumed that any macromolecule with the degree of polymerization p is formed from propagating radicals with the degrees of polymerization p' and $p - p'$. The probability of formation of such macromolecules is described by an expression similar to that for the chain termination through recombination of radicals:

$$q(p) = A\sum_{p'=1}^{p'=p-1}(1-\varepsilon)^{p'}\varepsilon(1-\varepsilon)^{p-p'}\varepsilon = A\sum_{p'=1}^{p'=p-1}(1-\varepsilon)^{p}\varepsilon^2, \quad (1)$$

where $\varepsilon = \Sigma v_0/(\Sigma v_0 + v_p)$ is the probability of chain termination; v_p, rate of chain propagation; v_0, total rate of chain termination reactions; and $A = 1$, quantity determined from the normalization conditions [10].

Therefore, expression (1) corresponds to the numerical distribution function of macromolecules with respect to the degree of polymerization. Passing to the continuous distribution, we obtain

$$q(p)\mathrm{d}p = p\varepsilon^2 e^{\varepsilon p}. \quad (2)$$

Expression (2) is the Schultz distribution characteristic of radical polymerization with the predominant chain termination through the recombination of radicals. In this case,

$$M_z/M_w/M_n = (k + 3)/(k + 2)/(k + 1), \quad (3)$$

where k is determined by the fraction of radicals participating in the chain termination through recombination; at $k = 1$, $M_w/M_n = 1.5$.

Thus, the existing theory of radical polymerization explains why the polydispersity of polymers prepared by radical polymerization in the presence of silicon dihydrides is lower, compared to the polymerization in the presence of monohydrides and mercaptans.

Data in Table 3, especially for DS-8, suggest that k is close to unity. This means that the Si–H group in the disilane bound to a macromolecule is more reactive than the same group in the initial chain-transfer agent. This conclusion is supported, in particular, by comparison of C_s for the initial polymerization step in the presence of mono- and disilanes (Table 1): $1/2C_s$(DS-8) > C_s (DS-9). This relationship may be due, among other things, to the fact that the terminal organosilicon group as a "foreign" unit is expelled to the border of the coordination sphere of the macromolecular coil, which increases the probability of its reaction with propagating macroradicals from the standpoint of the North's diffusion theory of chain termination [11].

As already noted, the existing methods for "cardinally" decreasing the polydispersity involve, as a rule, a decrease in the polymerization rate, which is unacceptable for the commercial process. Therefore, it is very important that the participation of the Si–H group in the chain transfer exerts virtually no effect on the polymerization rate. As seen from the figure, the polymerization rate does not noticeably change as the concentration of the majority of the tested silanes is increased up to 2 wt %, i.e., to the level exceeding the reasonable concentration of silanes in controlling the MW of the polymers under the conditions of bulk polymerization.

The abnormally high polydispersity of the PMMA sample prepared in the presence of DS-15 deserves certain discussion. This result is undoubtedly associated with the abnormally high chain-transfer constant, $C_s = 8.3$, due to the presence in the chain-transfer agent of a group of four silicon atoms located closely to the hydrogen atom. As shown in [4], polysilicon fragments in silanes activate the Si–H bond. At $C_s \gg 1$, the relative concentration of the chain-transfer agent [S]/[M] rapidly decreases in the course of the polymerization, which results in an appreciable decrease (by more than an order of magnitude in our case) in the apparent chain-transfer constant, in formation of a higher-molecular-weight polymer, and hence in the higher polydispersity of the final product. It should be

noted in conclusion that similar effects can be expected in the case of polystyrene, as judged from the constants of chain transfer through disilanes in polymerization of styrene [4].

CONCLUSIONS

(1) In radical polymerization of methyl methacrylate, addition of disilanes decreases the degree of polydispersity of the high-conversion polymers to M_w/M_n = 1.5–1.89; the performance of the chain-transfer agent depends on its functionality, i.e., on the number of the Si–H bonds. In the presence of silicon dihydrides, polymers with the molecular-weight distribution close to the Schultz distribution (M_w/M_n = 1.5) are formed.

(2) Decreasing the degree of polydispersity of the polymer by adding polyfunctional silicon hydrides to the reaction system does not require high temperatures and is not accompanied by a noticeable decrease in the rate of the radical polymerization.

REFERENCES

1. *Entsiklopediya polimerov* (Polymer Encyclopedia), Kargin, V.A., Ed., Moscow: Sov. Entsiklopediya, 1977, vol. 2, pp. 283–295.
2. Korolev, G.V. and Marchenko, A.P., *Usp. Khim.*, 2000, vol. 69, no. 5, pp. 447–475.
3. Zaremskii, M.Yu. and Golubev, V.B., *Vysokomol. Soedin., Ser. C*, 2001, vol. 43, no. 9, pp. 1689–1728.
4. Bulgakova, S.A., Mazanova, L.M., Semenov, V.V., and Semchikov, Yu.D., *Vysokomol. Soedin., Ser. A*, 2001, vol. 43, no. 8, pp. 1293–1298.
5. Kumada, M. and Tamao, K., *Adv. Organomet. Chem.*, 1968, vol. 6, pp. 19–117.
6. Hengge, E., *Top. Curr. Chem.*, 1974, vol. 51, pp. 1–127.
7. Semenov, V.V., Ladilina, E.Yu., Chesnokova, T.A., *et al.*, *Izv. Ross. Akad. Nauk, Ser. Khim.*, 1995, no. 5, pp. 954–957.
8. Semenov, V.V. and Chesnokova, T.A., *Zh. Obshch. Khim.*, 1990, vol. 60, no. 1, pp. 150–159.
9. Lipatov, Yu.S., Nesterov, A.E., Gritsenko, T.M., and Veselovskii, R.A., *Spravochnik po khimii polimerov* (Handbook of Polymer Chemistry), Kiev: Naukova Dumka, 1971.
10. Semchikov, Yu.D., *Vysokomolekulyarnye soedineniya* (Macromolecular Compounds), Moscow: Akademiya, 2003.
11. Benson, S.W. and North, A.M., *J. Am. Chem. Soc.*, 1962, vol. 84, no. 6, pp. 935–940.

Russian Journal of Applied Chemistry, Vol. 78, No. 7, 2005, pp. 1170–1175. Translated from Zhurnal Prikladnoi Khimii, Vol. 78, No. 7, 2005, pp. 1191–1196.
Original Russian Text Copyright © 2005 by Kurenkov, Zhelonkina, Nefedova, Lobanov.

MACROMOLECULAR CHEMISTRY AND POLYMERIC MATERIALS

Copolymerization of Sodium 2-Acrylamido-2-methylpropane-1-sulfonate with *N*-Vinylpyrrolidone in Aqueous Dimethylformamide Solutions

V. F. Kurenkov, T. A. Zhelonkina, M. A. Nefedova, and F. I. Lobanov

Kazan State Technological University, Kazan, Tatarstan, Russia
Degussa Eurasia Joint-Stock Company, Moscow, Russia

Received September 2, 2004; in final form, January 2005

Abstract—The kinetics of radical copolymerization of sodium 2-acrylamido-2-methylpropane-1-sulfonate with *N*-vinylpyrrolidone in water, water–dimethylformamide (1 : 1) solutions, and dimethylformamide at pH 9 and 60°C in the presence of initiators [azobis(isobutyronitrile) and ammonium persulfate] was studied by dilatometry.

The reaction medium strongly affects both the kinetic parameters of copolymerization of salts of 2-acrylamido-2-methylpropane-1-sulfonic acid (H-AMS) with *N*-vinylpyrrolidone (VP) and the properties of the resulting copolymers. This is due to the features in the behavior of ionic monomers [1, 2] and nonionic VP monomer [3, 4] in the processes of radical (co)polymerization. Previously we studied copolymerization of sodium 2-acrylamido-2-methylpropane-1-sulfonate (Na-AMS) with VP in aqueous [5–7] and dimethyl sulfoxide [8] solutions and examined how the ionic strength of the solution and kind of mono- [9, 10] and bivalent [10, 11] cations affect the copolymerization in aqueous solutions.

In this work we studied the dependences of radical copolymerization of Na-AMS and VP in water, water–dimethylformamide (1 : 1) solutions, and dimethylformamide (DMF). These data are not only of theoretical but also of practical importance because, owing to the valuable properties of copolymers of Na-AMS and VP, they show promise for various branches of industry and medicine.

EXPERIMENTAL

Sodium salt Na-AMS was prepared by neutralization of aqueous solutions of H-AMS [Lubrisol-2404 (Lubrisol Corp., the United Kingdom), mp 185°C, main substance 99%] with NaOH to pH 9. *N*-Vinylpyrrolidone (Merck, Germany) was double-distilled in the presence of 0.1% KOH solution at 63°C in a vacuum (3 mm Hg) [n_D^{20} 1.5117, 99% main substance (GLC data)]. Ammonium persulfate (AP) was twice recrystallized from aqueous solutions [98.7% main substance (redox titration data)]. Azobis(isobutyronitrile) (AIBN) was twice recrystallized from methanol (mp 103.5°C). Dimethylformamide was distilled with a mixture of benzene and water in a vacuum (n_D^{20} = 1.4269). All the solutions were prepared using distilled water; the other chemicals were of chemically pure grade.

Copolymerization of Na-AMS with VP was performed in 7 cm^3 glass dilatometers and in 50 cm^3 weighing bottles for 2 h. The procedures of copolymerization and dilatometric analysis of the reaction kinetics were similar to those described in [6]. The initial sections of the kinetic curves obtained dilatometrically were linear, which allowed calculation of the initial copolymerization rate v_0 at low conversion ($x < 3\%$).

After copolymerization, the resulting polymers were precipitated from aqueous solutions with acetone, filtered off, washed with acetone, and dried to constant weight in a vacuum at 50°C. The yield of the copolymers was determined gravimetrically. The molecular weights of the copolymers (M) were calculated from the intrinsic viscosities [η] of their solutions, which were measured in a 0.5 M NaCl solution at 30°C on a VPZh-3 capillary viscometer (d_c = 0.43 mm). The experimental dependence of the reduced viscosity η_{sp}/c_p on the copolymer concentration c_p was plotted. Then, using the linear dependence $\eta_{sp}/c_p = f(c_p)$, we determined $[\eta] = \lim(\eta_{sp}/c_p)$ at $c_p \to 0$. The content of ionic units in the copolymer

1070-4272/05/7807-1170 © 2005 Pleiades Publishing, Inc.

of Na-AMS and VP was determined from the content of sulfur [12].

The potentiometric titration was carried out with a pH-121 pH-millivoltmeter equipped with an ESL-65-07 working glass electrode and an EVL 1MZ silver chloride reference electrode.

Copolymerization of Na-AMS (M_1) with VP (M_2) was performed in 20% solutions in water, H_2O : DMF = 1 : 1 mixture, and DMF at 60°C and pH 9. In all the solutions, the reaction was initiated by thermal decomposition of ammonium persulfate ([AP] = 7.4×10^{-4} M), additionally AIBN was used in the case of DMF ([AIBN] = 3×10^{-2} M). Maintaining pH 9 during initiation with AP [13] is necessary for providing fairly high and constant initiation rates when the ionic strength of solutions varies (due to changes in the Na-AMS concentration in the initial monomer mixture in the course of copolymerization [14]), and also for preventing hydrolysis of VP [15].

Our experiments showed that Na-AMS and VP did not noticeably polymerize in the absence of initiators in all the systems studied. In the presence of the initiator, the copolymerization in water and water : DMF = 1 : 1 mixture proceeds under homogeneous conditions, whereas in the case of DMF the reaction is heterogeneous: an opalescence appeared in solutions, though a solid phase did not precipitate.

The dependences of v_0 (curves *1*–*3*) and [η] (curves *1*'–*3*') of copolymers on the concentration of Na-AMS [M_1] in the initial monomer mixture in various solutions are shown in Fig. 1. As seen, v_0 decreases in the series water > water : DMF = 1 : 1 > DMF; the same trend is observed for [η]. These changes in v_0 with increasing content of the protic solvents in the reaction mixture well agree with the data on changes in the reaction rate on passing from aprotic to protic solvents in homopolymerization of H-AMS [16] and VP [17, 18]. In accordance with published data on several water-soluble monomers [3] and, in particular, on VP [19], acceleration of copolymerization of Na-AMS and VP in a protic solvent is caused by solvation of the monomers due to formation of hydrogen bonds between the C=O group of the monomer and solvent. This increases the polarity of the vinyl group in the monomers and, thus, enhances their activity in copolymerization.

The dependences of the current concentration of the Na-AMS–VP copolymer at low conversions (x < 3%) on the composition of the initial monomer mixture in different solvents are shown in Fig. 2. The dependences $m_1 = f(M_1)$ for copolymerization in

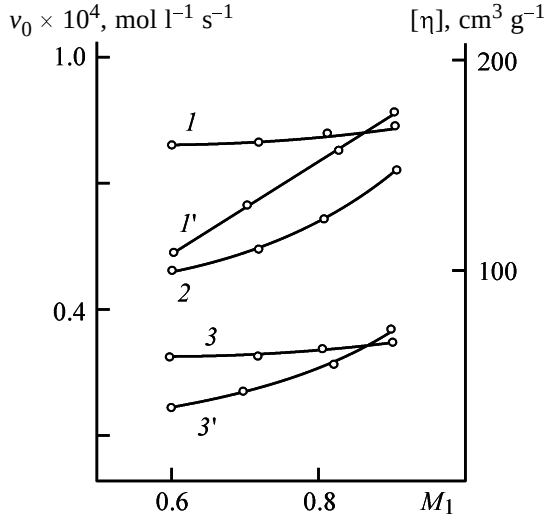


Fig. 1. (*1*–*3*) Initial copolymerization rate v_0 of Na-AMS and VP in the presence of AP and (*1*', *3*') intrinsic viscosity of copolymers [η] as functions of the Na-AMS mole fraction in the initial monomer mixture M_1. Solution: (*1*, *1*') H_2O, (*2*) H_2O : DMF = 1 : 1, and (*3*, *3*') DMF.

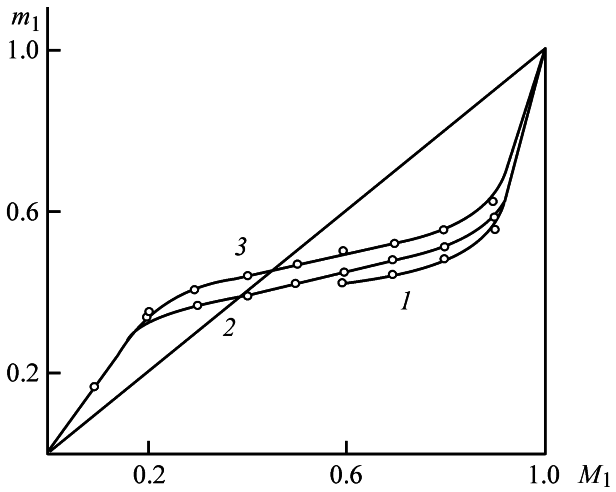


Fig. 2. Mole fraction of Na-AMS units in the copolymer m_1 at conversion x < 3% as a function of the Na-AMS mole fraction in the initial monomer mixture M_1 in copolymerization in (*1*) H_2O, (*2*) H_2O : DMF = 1 : 1, and (*3*) DMF in the presence of AP.

H_2O : DMF = 1 : 1 (Fig. 2, curve *2*) and DMF (Fig. 2, curve *3*) are S-shaped with the corresponding azeotropic points. From these data, using the Mayo–Lewis equation, we calculated the effective relative activities of the monomers in copolymerization $r_1 = k_{11}/k_{12}$ and $r_2 = k_{22}/k_{21}$ for Na-AMS and VP, respectively (see table). These data confirm that, in copolymerization in H_2O : DMF = 1 : 1 and pure DMF, both macroradicals react with the "foreign" monomer more readily than with their "own" monomer. The $r_1 r_2$ values confirm

Effective relative activities of the monomers r_1 and r_2 in copolymerization of Na-AMS and VP in solutions containing DMF at various initiator concentrations

Solution, initiator	r_1(Na-AMS)	r_2(VP)	$r_1 r_2$
AP–initiator			
Solution:			
H_2O : DMF = 1 : 1	0.02 ± 0.01	0.29 ± 0.08	0.06
DMF	0.09 ± 0.01	0.22 ± 0.04	0.02
DMF solution			
Initiator, M:			
AIBN, 3.0×10^{-2}	0.04 ± 0.01	0.70 ± 0.05	–
AP, 7.4×10^{-4}	0.09 ± 0.01	0.22 ± 0.04	–

the regular composition of the copolymers formed in the systems studied.

Comparison of the experimental data at M_1 = const shows that the content of Na-AMS units in the polymer chain increases in the following order: H_2O < H_2O : DMF = 1 : 1 < DMF, i.e., on passing from curve *1* to curve *3* (Fig. 2).

The above changes in the composition of Na-AMS–VP copolymer in the above solutions can be due to the effect of the solvent polarity on the ionization equilibrium of the ionic groups in Na-AMS and its units in the copolymer:

$$\underset{\text{I}}{A^-X^+} \overset{\leftarrow}{\rightarrow} \underset{\text{II}}{A^-} \parallel X^+ \overset{\leftarrow}{\rightarrow} \underset{\text{III}}{A^- + X^+}, \qquad (1)$$

where A^- is the anion of the monomer or macroradical; X^+ is the cation; and I, II, and III are the contact ion pairs, ion pairs separated with a solvent, and free ions, respectively.

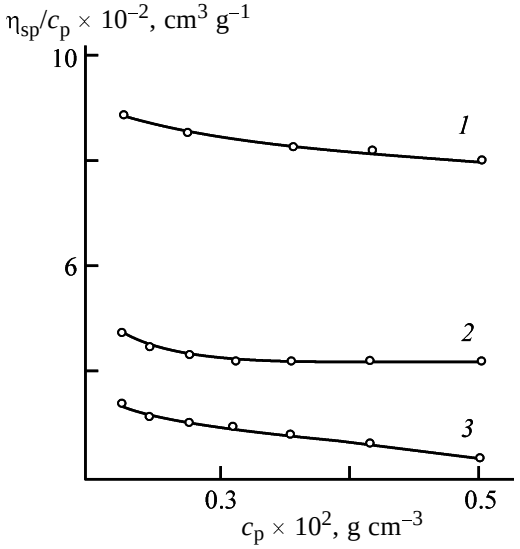


Fig. 3. Reduced viscosity η_{sp}/c_p of Na-AMS-VP copolymer ($[\eta]$ = 260 cm^3 g^{-1}, 33 mol % Na-AMS units) as a function of copolymer concentration c_p in (*1*) H_2O, (*2*) H_2O : DMF = 1 : 1, and (*3*) DMF at 30°C.

Changes in the solvent polarity affect the ionization of the ionic groups of Na-AMS and its units in macroradical. This shifts the ionization equilibrium (1) and changes the content in the reaction mixture of various ionic species and, thus, the intensity of intra- and intermolecular electrostatic interactions between them. As a result, the relative activities of ionic monomers in copolymerization r_1 and r_2 are variable, and the process cannot be described using the Mayo–Lewis equation with fixed r_1 and r_2.

With decreasing solvent polarity in the series H_2O > H_2O : DMF = 1 : 1 > DMF, the ionization equilibrium (1) is shifted to the left, which decreases the electrostatic repulsion between the similarly charged monomer Na-AMS and macroradical with terminal Na-AMS unit and thus increases the elementary constant of chain propagation k_{11} and promotes enrichment of the copolymer with Na-AMS units. On passing from water to DMF, the decrease in the electrostatic repulsion between similarly charged units along the chain decreases the effective size of macromolecular globules, which is indirectly confirmed by viscometry (Fig. 3). With decreasing charge of macromolecules in the series H_2O > H_2O : DMF = 1 : 1 > DMF, the local concentration of Na-AMS monomers in the vicinity of their "own" centers increases in the series H_2O < H_2O : DMF = 1 : 1 < DMF; as a result, the content of Na-AMS units in the copolymer grows. It should be noted that, since the copolymerization in DMF is a heterogeneous process, certain differences in the distribution and diffusion of comonomers in different phases and selective solvation of macroradicals with monomers can affect the kinetic parameters of copolymerization in the systems studied.

The effect of the initiator concentration on the composition of Na-AMS–VP copolymer was studied in the course of copolymerization in DMF in the presence of AP ([AP] = 7.4×10^{-4} M) and AIBN ([AIBN] = 3.0×10^{-2} M), other conditions being equal. For this experimental series, the dependence of the current composition of the copolymer on the composition of the initial monomer mixture is given in Fig. 4. As seen from a comparative analysis of these data at M_1 = const, in a wide range of compositions of the initial monomer mixture the content of Na-AMS units increases with decreasing content of the initiator (Fig. 4, passing from curve *1* to curve *2*), which is due to an increase in r_1 and decrease in r_2 in the system studied (see table). Changes in the copolymer

composition and in r_1 and r_2 values as influenced by AIBN content were also found by Begantseva *et al.* [20] who studied the copolymerization of styrene and acrylamide in DMSO. This suggests that a significant difference in the concentration of initiators (nearly two orders of magnitude) in the system studied provides formation of copolymers with different M, which, in accordance with [21, 22], affects the selective solvation of macroradicals with monomers and changes the composition of the resulting copolymers.

It is known that, in classical systems, the copolymer composition strongly depends on the conversion (except the case when $r_1 = r_2$); however, for some water-soluble polymers certain deviation from this trend in solutions is observed [23, 24], which was attributed to hydrophobic interactions in aqueous polymer solutions. To examine the effect of conversion on the molecular properties of the resulting Na-AMS–VP copolymers, we determined the copolymer composition and [η] in the course of copolymerization in the presence of AIBN in DMF at mole fractions M_1 0.3 and 0.5 (Fig. 5). As seen, in the course of copolymerization [η] increases (Fig. 5, curves *1*' and *2*'), which agrees with the data on the alternating copolymerization in other systems [25]. The copolymer composition at $M_1 = 0.5$ does not significantly change with increasing copolymerization time (Fig. 5, curve *1*), whereas at $M_1 = 0.3$, the changes are more pronounced (Fig. 5, curve *2*). The observed changes in the copolymer composition (Fig. 5) with increasing conversion are probably associated with different rates of consumption of the monomers owing to their different reactivity and with nonisoionic synthesis conditions, which affect the activity of the ionic monomer in copolymerization [2].

The kinetics of copolymerization of Na-AMS with VP in DMF in the presence of AIBN was studied at 60°C. The effect of the Na-AMS content in the initial monomer mixture M_1 on v_0 and [η] of Na-AMS–VP copolymer is illustrated by Fig. 6. As seen, the dependences $v_0 = f(M_1)$ and [η] = $f(M_1)$ show similar trends and pass through a maximum at $M_1 = 0.5$. These dependences well agree with the data on copolymerization of Na-AMS and VP in aqueous solutions [6] and suggest donor–acceptor interaction between Na-AMS and VP, which is confirmed by the IR data for nonaqueous solutions [26].

To determine the total rate of copolymerization of Na-AMS with VP in DMF, we carried out the experiments at different concentrations of the monomers and initiator, other conditions being equal. The dependences of v_0 on the initial concentrations of Na-AMS,

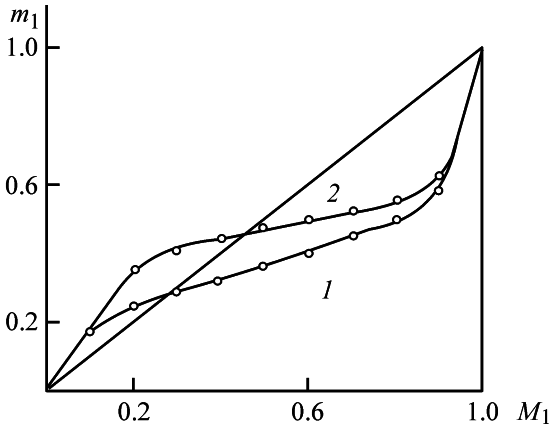


Fig. 4. Mole fraction of Na-AMS units in copolymer m_1 at low conversion ($x < 3\%$) as a function of the Na-AMS mole fraction in the initial monomer mixture M_1 in copolymerization of Na-AMS with VP in DMF in the presence of (*1*) AIBN ([AIBN] = 3.0×10^{-2} M) and (*2*) AP ([AP] = 7.4×10^{-4} M).

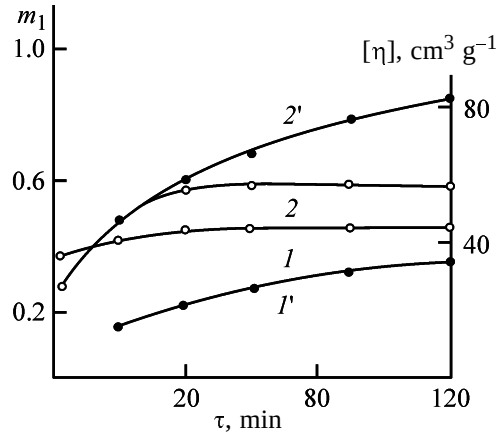


Fig. 5. (*1*, *2*) Mole fraction of Na-AMS units in copolymer m_1 and (*1*', *2*') intrinsic viscosity [η] in copolymerization of Na-AMS and VP as functions of time τ of copolymerization in DMF in the presence of AIBN. Mole fraction of Na-AMS in the initial monomer mixture M_1: (*1*, *1*') 0.5 and (*2*, *2*') 0.3.

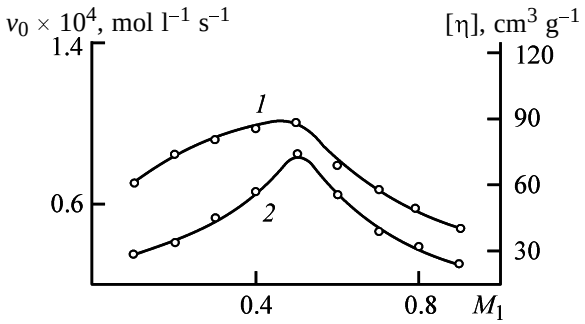


Fig. 6. (*1*) Initial copolymerization rate v_0 of Na-AMS and VP in DMF in the presence of AIBN and (*2*) intrinsic viscosity of copolymers [η] as functions of the Na-AMS mole fraction in the initial monomer mixture M_1.

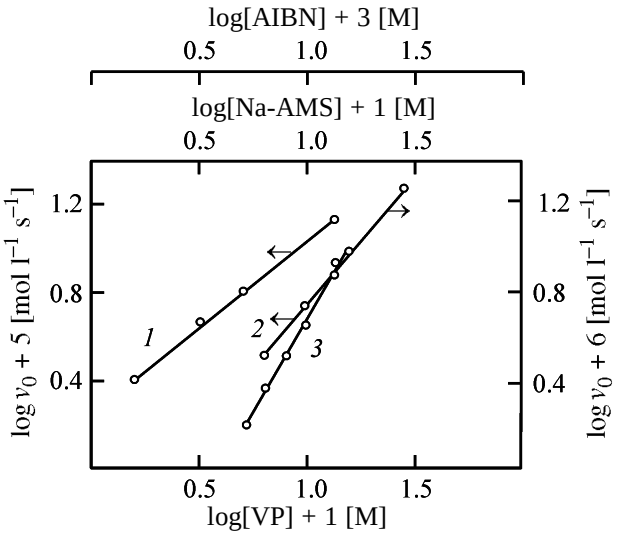


Fig. 7. Initial copolymerization rate v_0 of Na-AMS and VP in DMF as influenced by concentrations of (*1*) VP, (*2*) AIBN, and (*3*) Na-AMS (log–log plots). (*1*) [Na-AMS] = 0.587 and [AIBN] = 0.03 M; (*2*) [Na-AMS] = 0.587 and [AP] = 0.587 M; and (*3*) [VP] = 0.587 and [AIBN] = 0.03 M.

VP, and AIBN are shown in Fig. 7. As seen, v_0 increases with increasing concentrations of Na-AMS (from 0.362 to 0.724), VP (from 0.187 to 0.934), and AIBN (from 0.01 to 0.03 M) (Fig. 7, curves *3*, *1*, *2*). The reaction orders with respect to Na-AMS, VP, and AIBN were 1.5, 0.9, and 1.2, respectively. Using these experimental data, the equation of the total rate of copolymerization of Na-AMS and VP in DMF was evaluated:

$$v = k_c[\text{Na-AMS}]^{1.5}[\text{VP}]^{0.9}[\text{AIBN}]^{1.2}, \quad (2)$$

where k_c is the rate constant of copolymerization.

For the copolymerization of Na-AMS and VP in water, the following equation was given in [6]:

$$v = k_c[\text{Na-AMS}]^{0.9}[\text{VP}]^{0.7}[\text{AIBN}]^{0.5}. \quad (3)$$

Comparison of Eqs. (2) and (3) showed an increase in the reaction orders with respect to the comonomers and initiator on passing from water to DMF, which is probably due to the fact that, in the case of DMF, copolymerization proceeds as a heterogeneous process. The reaction order of 0.5 with respect to the initiator in Eq. (3) suggests bimolecular chain termination, which is typical for homogeneous polymerization. The reaction order of 1.2 with respect to the initiator in Eq. (2) suggests monomolecular chain termination owing to heterogeneous copolymerization of Na-AMS and VP in DMF.

CONCLUSIONS

(1) The copolymerization rate of sodium 2-acrylamido-2-methylpropanesulfonate with *N*-vinylpyrrolidone and molecular weight of the resulting copolymer increase, and the content of the ionic units in the copolymer decreases, on passing from water to dimethylformamide solvents.

(2) In copolymerization in dimethylformamide, the reaction rate increases with increasing concentrations of M_1, M_2, and azobis(isobutyronitrile) and passes through a maximum (similarly as molecular weight of the polymer) with changing $[M_1]/[M_2]$ in the initial monomer mixture (maximum at $[M_1]/[M_2] = 1:1$). The composition of the copolymer and relative activities of the monomers depend on the initiator concentration. With increasing conversion, the molecular weight of the copolymer and the content of the ionic units both increase.

REFERENCES

1. Kabanov, V.A. and Topchiev, D.A., *Polimerizatsiya ionizuyushchikhsya monomerov* (Polymerization of Ionizable Monomers), Moscow: Nauka, 1975.
2. Kurenkov, V.F. and Myagchenkov, V.A., *Zh. Prikl. Khim.*, 1999, vol. 72, no. 6, pp. 881–890.
3. Gromov, V.F., Bune, E.V., and Teleshov, E.N., *Usp. Khim.*, 1994, vol. 63, no. 6, pp. 530–541.
4. Sivtsov, E.V., Lavrov, N.A., and Nikolaev, A.F., *Plast. Massy*, 2001, no. 10, pp. 32–42.
5. Schultz, D.N., Kitano, K., Danik, J.F., and Kaladas, J.J., *Polym. Mater. Sci. Eng.*, 1987, vol. 57, pp. 149–153.
6. Kurenkov, V.F., Sirotkin, R.O., Beryachkova, E.A., and Khairullin, M.R., *Zh. Prikl. Khim.*, 1999, vol. 72, no. 8, pp. 1533–1537.
7. Kurenkov, V.F., Khabibullina, G.A., and Zaitseva, N.N., *Zh. Prikl. Khim.*, 2002, vol. 75, no. 11, pp. 1892–1895.
8. Kurenkov, V.F. and Zhelonkina, T.A., *Zh. Prikl. Khim.*, 2004, vol. 77, no. 2, pp. 310–314.
9. Kurenkov, V.F., Zaitseva, O.A., and Koryagina, S.V., *Vestn. Kazan. Tekhnol. Univ.*, 2000, nos. 1–2, pp. 121–126.
10. Kurenkov, V.F., Zaitseva, O.A., Khartan, Kh.G., and Lobanov, F.I., *Vestn. Kazan. Tekhnol. Univ.*, 2001, Suppl., pp. 1684–1687.
11. Kurenkov, V.F., Zaitseva, OA., and Isaeva, N.V., *Zh. Prikl. Khim.*, 2001, vol. 74, no. 10, pp. 1374–1378.
12. Charlot, G., *Les methods de la chimie analytique. Analyse quantitative minerale*, Paris: Masson, 1961, 4th ed.

13. Kholodnova, L.V., Pavlyuchenko, V.N., Alekseeva, Z.M., and Andreeva, A.I., in *Kataliticheskie i initsiiruyushchie sistemy dlya sinteza i modifikatsii polimerov* (Catalytic and Initiating Systems for Synthesis and Modification of Polymers), Leningrad: Plastpolimer, 1984, pp. 90–104.
14. Kolthoff, I.M. and Miller, I.K., *J. Am. Chem. Soc*., 1951, vol. 73, no. 7, pp. 3055–3059.
15. Sidel'kovskaya, F.P., *Khimiya N-vinilpirrolidona i ego polimerov* (Chemistry of *N*-Vinylpyrrolidone and Its Polymers), Moscow: Nauka, 1970.
16. Lisovtsev, V.V., Rostokin, G.A., Kulikova, A.E., and Khalistova, I.D., *Fiziko-khimicheskie osnovy sinteza i pererabotki polimerov* (Physicochemical Basis of Synthesis and Processing of Polymers), Gor'kii: Gor'k. Gos. Univ., 1984, pp. 8–11.
17. Senoglez, E. and Thomas, R., *J. Polym. Sci.: Polym. Symp. Ed*., 1975, vol. 49, pp. 203–209.
18. Karaputadze, T.M., Shumskii, V.I., and Kirsh, Yu.E., *Vysokomol. Soedin., Ser. A*, 1978, vol. 20, no. 8, pp. 1854–1859.
19. Kirsh, Yu.E., Kokorin, A.I., Karaputadze, T.M., and Kazarin, L.A., *Vysokomol. Soedin., Ser. B*, 1981, vol. 23, no. 6, pp. 444–448.
20. Begantseva, Yu.E., Malyshev, A.S., Zaitsev, A.S., and Semchikov, Yu.D., *Vysokomol. Soedin., Ser. A*, 2002, vol. 44, no. 4, pp. 560–566.
21. Harwood, H.J., *Macromol. Chem., Macromol. Symp*., 1987, vols. 10/11, pp. 331–338.
22. Semchikov, Yu.D., Smirnova, L.A., Knyazeva, T.Ye., *et al*., *Eur. Polym. J*., 1990, vol. 26, no. 8, pp. 883–890.
23. Barabanova, A.I., Gromov, V.F., Bune, E.V., *et al*., *Vysokomol. Soedin., Ser. A*, 1994, vol. 36, no. 6, pp. 901–907.
24. Gromov, V.F., Bune, E.V., Barabanova, A.I., *et al*., *Vysokomol. Soedin., Ser. A*, 1995, vol. 37, no. 11, pp. 1818–1822.
25. Kabanov, V.A., Zubov, V.P., and Semchikov, Yu.D., *Kompleksno-radikal'naya polimerizatsiya* (Coordination Radical Polymerization), Moscow: Khimiya, 1987.
26. Kurenkov, V.F., Zhelonkina, T.A., and Kovalenko, V.I., *Zh. Prikl. Khim*., 2005, vol. 78, no. 2, pp. 301–305.

Russian Journal of Applied Chemistry, Vol. 78, No. 7, 2005, pp. 1176–1181. Translated from Zhurnal Prikladnoi Khimii, Vol. 78, No. 7, 2005, pp. 1197–1202.
Original Russian Text Copyright © 2005 by Baklagina, Khripunov, Tkachenko, Kopeikin, Matveeva, Lavrent'ev, Nilova, Sukhanova, Smyslov, Zanaveskina, Klechkovskaya, Feigin.

MACROMOLECULAR CHEMISTRY AND POLYMERIC MATERIALS

Sorption Properties of Gel Films of Bacterial Cellulose

Yu. G. Baklagina, A. K. Khripunov, A. A. Tkachenko, V. V. Kopeikin, N. A. Matveeva, V. K. Lavrent'ev, V. K. Nilova, T. E. Sukhanova, R. Yu. Smyslov, I. S. Zanaveskina, V. V. Klechkovskaya, and L. A. Feigin

Institute of Macromolecular Compounds, Russian Academy of Sciences, St. Petersburg, Russia
St. Petersburg State University, St. Petersburg, Russia
Institute of Cytology, Russian Academy of Sciences, St. Petersburg, Russia
Institute of Crystallography, Russian Academy of Sciences, Moscow, Russia

Received February 2, 2005

Abstract—The structure and sorption properties of gel films of bacterial cellulose were studied in its interaction with polyvinylpyrrolidone and silver nanoparticles stabilized by this compound.

The influence exerted by the conditions of biosynthesis of *Acetobacter xylinum* cellulose (AXC) by the VKM V-880 strain on the structural properties of gel films of bacterial cellulose (GFBCs), formed in surface cultivation on low-cost nutrient media (industrial hydrolyzates of wood, peat, molasses, etc.) has been studied in the last decade [1, 2]. Particular attention has been given to structural changes of GFBCs at different conditions of their dehydration [3, 4].

Structural studies revealed that mainly highly crystalline cellulose of a polymorphic modification is formed in GFBC [1], and dried films show an axial-planar texture in which the $(\bar{1}10)$ crystallographic plane of the monoclinic cell is parallel to the sample plane. A conclusion was made that the texture of this kind, observed in macroscopic samples of AXC, is formed already in the stage of biosynthesis in microfibrillar bands, which have their primary hydroxy groups facing the surface of the nutrient medium on coming out of the terminal complex of a bacterium. According to electron diffraction data, such a microfibrillar band is a 50–100-nm-wide single-crystal formation with a length exceeding this diameter by a factor of 1000 and more [4, 5]. Motion of bacteria in the course of biosynthesis and growth of microfibrillar bands at the surface of the nutrient medium give rise to a GFBC structure with various types of packing, the densest of which are polycrystalline domains (Fig. 1). The specificity of growth of the crystalline domains of AXC is determined by interaction of microfibrils via primary hydroxy groups, which form a crystallographic plane at the phase boundary between the domain and the nutrient medium. This plane has an interplanar spacing d = 0.59–0.61 nm, which corresponds both to monoclinic I_β and triclinic I_α unit cells [6]. In the process, there arises a network of hydrogen bonds with water, which is preserved in purification and storage of gel films [3, 4].

Thus, microfibrillar bands lying in the film plane serve two functions: form hydrophilic layers that can retain a large amount of water and act as a reinforcing network, which, according to electron-microscopic data, occupies a considerable part of the volume of a gel film (Fig. 1) [3, 4]. Specifically this feature of the supramolecular organization of GFBCs enables their use as a matrix for medicines capable of a specific interaction, via hydrogen bonds, with the crystallographic plane filled with primary hydroxy groups. Such a matrix has a unique axial-planar texture, which favors preservation by GFBC of good sorption and strength characteristic in the course of its purification after biosynthesis to remove bacterial cells and in prolonged storage in distilled water at 5°C or after sterilization, and also after its saturation with various medical preparations [7].

One of the most promising areas of GFBC application in medicine is its use as high-efficiency bandaging materials, especially in curing of burns. This is because GFBCs are elastic, show low adhesion to the wound surface, and do not damage skin when a bandage is removed.

To impart antimicrobial properties to GFBC, a modern highly effective antibacterial agent, Poviargol,

1070-4272/05/7807-1176© 2005 Pleiades Publishing, Inc.

is introduced into its matrix. This agent is composed of nanoparticles of a zerovalent metallic silver, which are stabilized by polyvinylpyrrolidone (PVP–nano-Ag^0). This preparation shows, in addition to the antimicrobial action, also a preparative and immunopotentiating activity [8].

It is known that PVP and its copolymers are widely used in medical practice because they are low-toxic and form complexes with various biologically active substances [9]. Being dissolved in water, PVP acts as a structure-forming agent upon water molecules to form H-bound complexes of various stoichiometric compositions. It has also been shown that water clusters are formed on carbonyl groups of two neighboring pyrrolidone rings, with PVP hydrates being rather thermally stable, and an absolutely anhydrous polymer cannot be obtained even upon heating to 250°C [10]. In this context, it is assumed that PVP is involved in complexation with other substances via bound water molecules.

Therefore, of particular interest is an analysis of sorption and desorption interactions of PVP and Poviargol with the GFBC matrix, which is a network constituted by highly crystalline cellulose microfibrils surrounded by an enormous number of water molecules, and this is the subject of our study.

EXPERIMENTAL

Gel films of bacterial cellulose produced by the VKM V-880 strain of *Acetobacter xylinum* (AXC) were synthesized on a previously described nutrient medium [3]. After 80–90% of the initial amount of water was removed from GFBCs, samples were placed in aqueous solutions of PVP or Poviargol of a required concentration. The amount of substances sorbed in the GFBC matrix varied with their concentration (3–10 wt %) and exposure (1–20 h). The content of adsorbed substances in the composites obtained was monitored by X-ray diffraction analysis after drying the samples at room temperature.

Medicinal PVP of pharmacopoeia grade with a molecular weight MW 12 600 and Poviargol medicine with a silver content of 8%, manufactured by Tekhnolog Special Engineering and Design Office (St. Petersburg), were used in the studies. X-ray diffraction analyses were made on a DRON-2 installation with Ni-filtered copper radiation. For electron-microscopic studies, dry films of GFBC and GFBC–PVP–nano-Ag^0 were embedded in Araldite. Sections were made on an LKB-III ultramicrotome and examined with

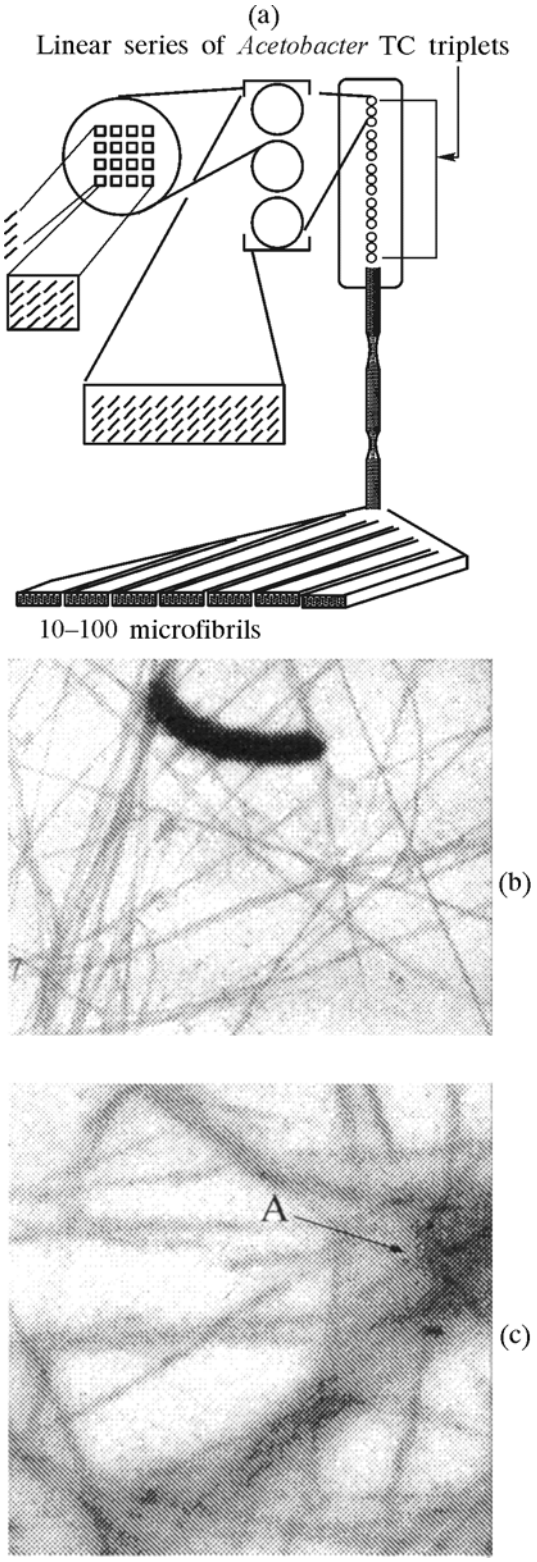


Fig. 1. (a) Scheme of AXC biosynthesis after Brown [5] and electron micrographs of *A. xylinum* bacteria on the background of microfibrillar networks created by this bacterium after (b) 3 and (c) 6 h of synthesis [3, 4]. (A) Crystalline domain and (TC) terminal complex.

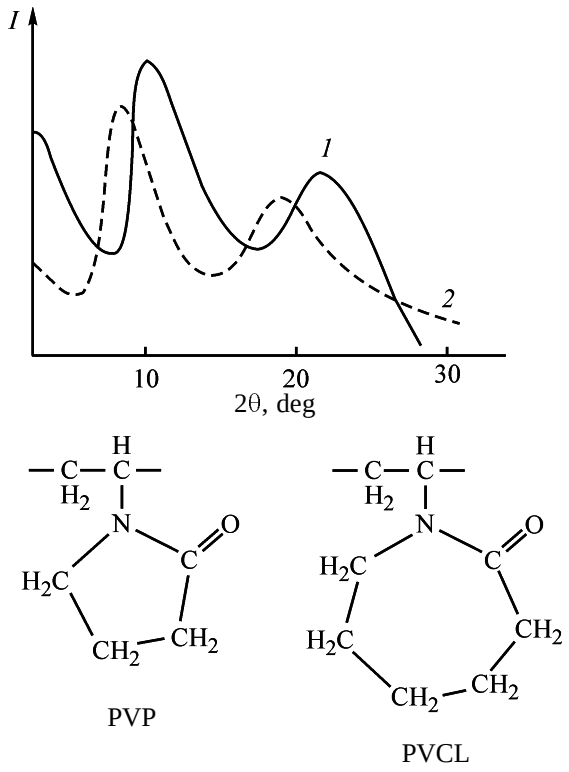


Fig. 2. X-ray diffraction patterns of (*1*) polyvinylpyrrolidone and (*2*) polyvinylcaprolactam. (*I*) Intensity and (2θ) Bragg angle; the same for Figs. 3–5.

a JEM-7A electron microscope at an accelerating voltage of 80 kV at magnifications of 1500 to 21000.

The X-ray diffraction pattern of compacted powders and films of PVP, obtained from various solvents (water, ethanol, acetone, etc.), exhibits two broadened reflections (Fig. 2, curve *1*) at reflection angles 2θ 11.3°–11.7° and 20°–21°. It is commonly believed that this polymer, widely used in medicine, has an amorphous structure. However, the authors of [9–13], who analyzed X-ray data for polymers exhibiting, similarly to PVP, two or three broadened reflections believe that these polymers contain a certain fraction of ordered structures in the amorphous phase. It should be emphasized that such an "amorphous-like" nature of X-ray diffraction patterns is attributed to the two-phase nature of the polymer if the halfwidth of the strongest first reflection, which, as a rule, corresponds to interchain distances, is $\varphi_{1/2}$ = 2°–4°.

The mesomorphic nature of the mutual packing of PVP chains is well confirmed by comparison of two diffraction curves in Fig. 2. Curve *2* was obtained for a film of polyvinylcaprolactam (PVCL), which differs from PVP in the presence of a seven-membered pendant ring [10]. It can be seen that the first reflection is shifted in the case of PVCL to smaller angles (2θ = 9°–9.5°), and the lower-intensity broad reflection is observed at 2θ = 18°–19°. It should be noted that the halfwidth of the first reflections of PVP and PVCL films deposited from different solvents onto different substrates (glass, metal, Teflon) remained virtually unchanged ($\varphi_{1/2}$ = 3°–4°).

As the PVP and PVCL chains have a cylindrical symmetry despite the difference in the content of *cis* and *trans* conformers [9], they can be involved in the formation of a pseudo-hexagonal structure even though the conformational disorder in the arrangement of monomer units along the polymer chains is preserved. This is confirmed by the existence of a high-intensity diffraction peak corresponding to an interchain period $L = 0.76 \pm 0.03$ nm for PVP and $L = 0.95 \pm 0.03$ nm for PVCL. According to experimental X-ray data and conformational calculations, these ordered parts of pseudohexagonal type in PVP and PVCL show a two-dimensional translation order in the plane perpendicular to chain axes and only orientational ordering in the third direction. Indeed, the patterns of X-ray scattering from PVP films stretched by a factor of 3–5 show no reflections associated with periodicity along the polymer chain. Similar results were obtained by Nishio *et al.* [13] in a study of the structure of strongly stretched films formed from a mixture of PVP and polyvinyl alcohol solutions with a mass ratio of 70 : 30.

The information about the PVP structure was used in a study of sorption properties of GFBCs. Figure 3 shows X-ray diffraction patterns of samples (dried at room temperature) of the starting GFBC (curve *1*), PVP films (curve *2*), and GFBC brought in contact with a 10% aqueous solution of PVP for 1 h (curve *3*). It can be seen that, in contrast to the diffraction pattern of the starting GFBC, curve *3* exhibits a broad reflection, similar to the first reflection from the PVP film (curve *2*), at reflection angles 2θ = 10°–12°. The same results were obtained with GFBC samples brought in contact with a 1–3% solution of PVP for 10–15 h. Hence follows that the structural parameters remain unchanged when AXC is introduced into its matrix. The position and intensity of the first reflection from PVP have no effect on the position and shape of the 110 crystal reflection (at 2θ = 17°) for the monoclinic modification of cellulose itself, but masks the 110 reflection (2θ = 15°), whose low intensity (curve *1*) indicates that an axial-planar structure exists in the starting GFBC [3, 4]. The second broad reflection from PVP has no effect, either, on the position of AXC reflections from the 102 and 012 (2θ = 21°) and 200 (2θ = 23°) planes of the monoclinic lattice,

but changes the background ratio in the diffraction curves *1* and *3* at reflection angles of 20°–30°. Indeed, the background intensity $I_b(20°)$ at $2\theta = 20°$ is equal to the background level at $2\theta = 30°$ for the starting GFBC [$I_b(30°)$], but $I_b(20°) \gg I_b(30°)$ for the GFBC–PVP composite (curve *3*). Such a change in the background intensity at 20°, compared with that at 30°, indicates that the second reflection from PVP makes a significant contribution to the total reflection from GFBC–PVP. The distinct reflection at $2\theta = 35°$ is associated with periodicity along the axis of the AXC chain in crystalline domains (004). This reflection is present in diffraction patterns of any modified sample of GFBC.

The sorption properties of GFBC with respect to PVP were studied in more detail by comparing the diffraction patterns obtained for GFBC–PVP samples (Fig. 3, curve *3*) with the patterns for the same sample after treatment with water for 2 (curve *4*) and 12 h (curve *5*). It can be seen that the first reflection, assigned to PVP, markedly decreases in intensity in curve *4* and totally disappears in curve *5*. The fact that the diffuse background level at $2\theta = 20°$ in curves *4* and *5* is substantially higher than that at $2\theta = 30°$ is possibly due to incomplete desorption of PVP from the GFBC matrix.

The most interesting results were obtained in a study of sorption and desorption of Poviargol (PVP–nano-Ag^0) on a GFBC matrix. The diffraction pattern of PVP–nano-Ag^0 (Fig. 4, curve *1*) contains reflections from two individually manifested structural phases: PVP at reflection angles of 5° to 30° and reflections that belong to the crystal structure of silver (2θ 38.4° and 44°) [14]. Figure 4 shows curves for GFBC–PVP–PVP–nano-Ag^0 composite samples obtained upon adsorption of a 3% solution of Poviargol for 1 (curve *2*), 2 (curve *3*), and 19 h (curve *4*) at room temperature with the subsequent drying on glass. Comparison of the diffraction patterns of these three samples shows that the strongest reflection from PVP is observed in curve *3*, i.e., upon exposure of a gel film of AXC in an aqueous solution of Poviargol for 2 h. After a 19-h exposure, the intensity of this reflection ($2\theta = 10°$–$12°$) noticeably decreased (Fig. 4, curve *4*), whereas the reflection associated with silver ($2\theta = 38.4°$) reached its maximum value. Apparently, a prolonged exposure of GFBC to a Poviargol solution leads to irreversible adsorption of silver on the surface and within the matrix of AXC, with PVP partly displaced into the aqueous phase.

To obtain a more detailed information about the phase composition, structure, and sorption properties

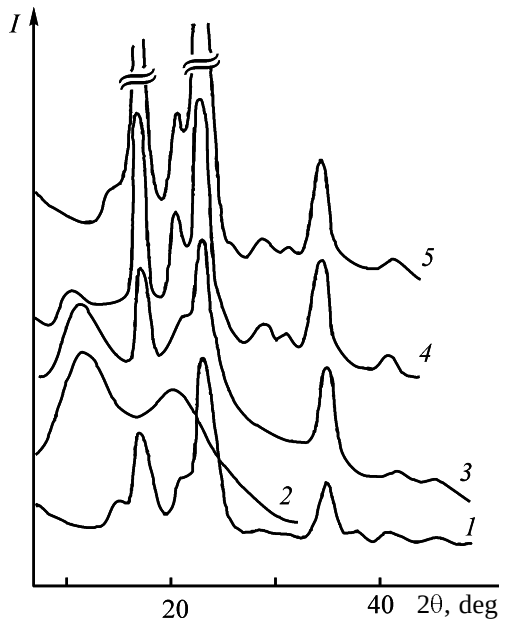


Fig. 3. X-ray diffraction patterns of dried samples of (*1*) GFBC, (*2*) PVP, and (*3*–*5*) GFBC–PVP composites (*3*) after bringing GFBC in contact with a 3% aqueous solution of PVP and subsequent washing of the films with distilled water for (*4*) 2 and (*5*) 12 h.

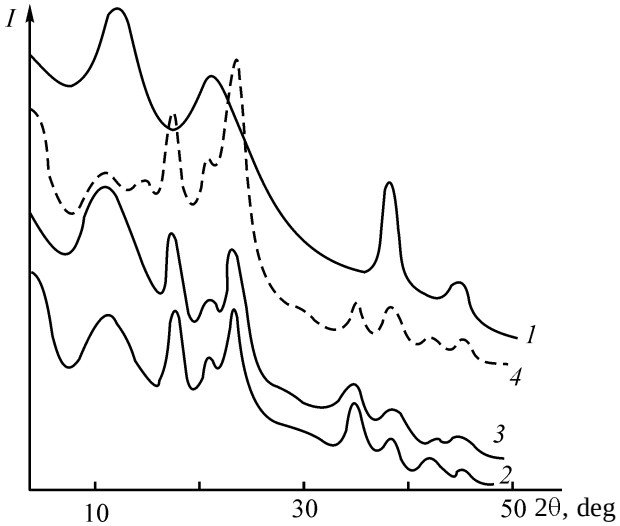


Fig. 4. X-ray diffraction patterns of (*1*) powdered Poviargol and dry films of GFBC–Poviargol composites obtained by bringing GFBC in contact with a 3% solution of Poviargol for (*2*) 1, (*3*) 2, and (*4*) 19 h.

of the GFBC matrix, the kinetics of desorption of PVP and nanoparticles of silver from gel films upon their being submerged in distilled water was studied. For this purpose, diffraction patterns of dry GFBC–PVP–PVP–nano-Ag^0 films were measured and the films were placed in water for 20 h. Then the samples were dried and another set of their diffraction patterns

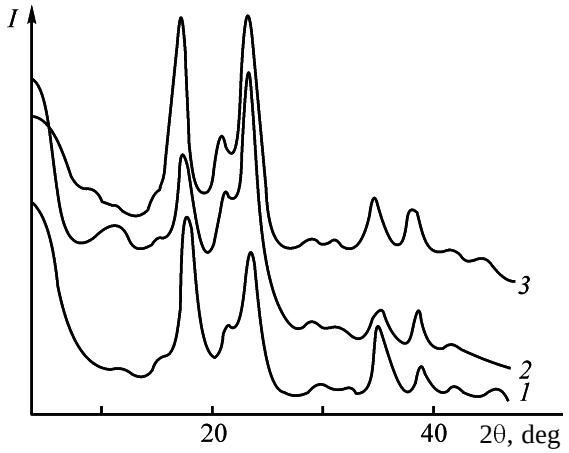


Fig. 5. X-ray diffraction patterns of dried GFBC–Poviargol samples after their preliminary multiple washing with distilled water in the course of 20 h. The initial composite samples were obtained by bringing GFBC in contact with a 3% solution of Poviargol for (*1*) 1, (*2*) 2, and (*3*) 19 h.

was obtained (Fig. 5). It can be seen in the scattering curves obtained after a 20-h treatment of all the samples that the position and sharpness of the reflections associated with crystalline domains of AXC and silver remain unchanged. The reflections associated with the presence of the PVP polymer in the GFBC matrix were observed after desorption only from GFBC–PVP–nano-Ag^0 samples obtained upon a 2-h exposure to Poviargol (Fig. 5, curve *2*).

Figure 6 shows cross-sectional electron micrographs of gel films modified with the PVP–nano-Ag^0 composite. An analysis of micrographs obtained at different magnifications (8000–21 000) revealed that the distribution of silver nanoparticles over the surface (Fig. 6a) and across the thickness (Fig. 6b) of a film is nonuniform. Characteristically, the silver clusters localized on the surface of gel films are larger than those in the film matrix. Presumably, the nonuniformity of the nanoparticle distribution is due to a distribution of water cavities with nonuniform dimensions in the microfibrillar network of GFBC. The difference in the number and size of clusters of adsorbed silver between the outer surface and the interior of the films is probably due to a specific texture of gel films formed in the course of biosynthesis and to its changes in squeezing of the films with removal of 80–90 wt % of water from GFBCs to enable adsorption of PVP–

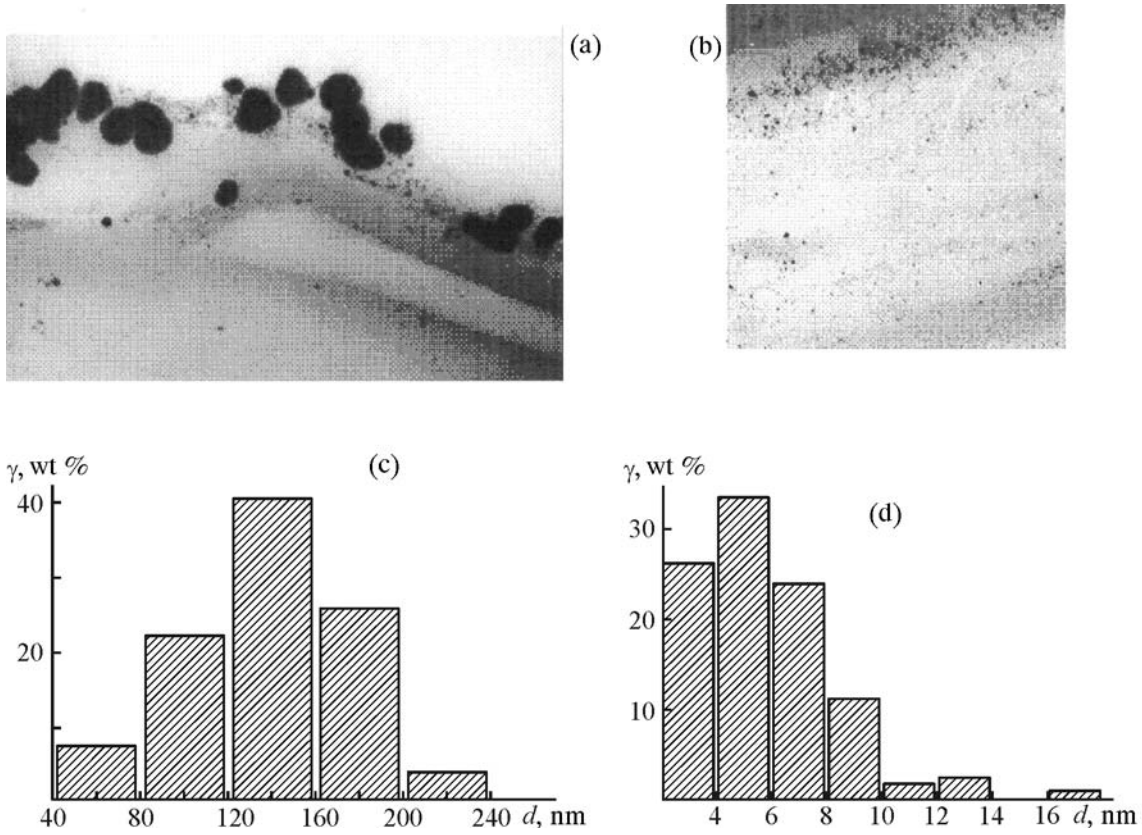


Fig. 6. Electron micrographs and histograms of dry samples of GFBC–Poviargol composites with silver distribution (a, c) over the surface and (b, d) across the film thickness. (γ) Content of grains and (*d*) grain diameter.

nano-Ag^0. The size distribution of silver nanoparticles deep in the cross section in regions with the highest content of silver in the cellulose matrix is shown in Figs. 6b and 6d. It was established that a major fraction of the particles (60%) is constituted by 2–6-nm particles, and 35% of the particles are 6–10 nm in size. The dimensions of the surface clusters of silver fall within the range 40–240 nm, with the maximum content (80%) of particles 100–180 nm in size. It is from these clusters that the diffraction patterns shown in Figs. 4 and 5 were obtained.

CONCLUSIONS

(1) X-ray diffraction analysis shows that the crystal structure of the cellulose under study remains unchanged when polyvinylpyrrolidone or its complex with silver nanoparticles is incorporated into its matrix.

(2) Electron microscopic examination shows that, in intercalation of gel films of bacterial cellulose with the polyvinylpyrrolidone–nano-Ag^0 complex, silver nanoparticles 2–10 nm in size penetrate deep into the matrix and larger clusters of silver are localized on its surface.

(3) Polyvinylpyrrolidone is readily removed from dried composite gel films of bacterial cellulose and polyvinylpyrrolidone or Poviargol by washing with distilled water without any changes in the cellulose structure and amount of adsorbed silver.

ACKNOWLEDGMENTS

R.Yu. Smyslov is grateful to the Foundation for Support of Domestic Science for financial support within the framework of a Grant for young candidates of science.

REFERENCES

1. RF Patent 2 141 530.
2. RF Patent 2 189 394.
3. Baklagina, Yu.G., Khripunov, A.K., Tkachenko, A.A., *et al.*, *Zh. Prikl. Khim.*, 2003, vol. 76, no. 6, pp. 1017–1024.
4. Klechkovskaya, V.V., Baklagina, Yu.G., Stepina, N.D., *et al.*, *Kristallografiya*, 2003, vol. 48, no. 5, pp. 813–820.
5. Brown, R.M., Jr., *J.M.S. Pure Appl. Chem.*, 1996, vol. A33, no. 10, pp. 1345–1373.
6. Sugiyama, J., Young, R., and Chanzy, H., *Macromolecules*, 1991, vol. 24, no. 14, pp. 4168–4175.
7. Khripunov, A.K., Tkachenko, A.A., Baklagina, Yu.G., *et al.*, *Materialy II Mezhdunarodnoi konferentsii "Sovremennye podkhody k razrabotke effektivnykh perevyazochnykh sredstv, shovnykh materialov i polimernykh implantantov"* (Proc. II Int. Conf. "Modern Approaches to Development of Effective Bandaging and Suture Materials and Polymeric Implants), Moscow, November 21–23, 1995, pp. 71–73.
8. Kopeikin, V.V. and Panarin, E.F., *Dokl. Ross. Akad. Nauk*, 2001, vol. 380, no. 4, pp. 497–550.
9. Kirsh, Yu.E., *Poli-N-vinilpirrolidon i drugie poli-N-vinilamidy* (Poly-*N*-vinylpyrroidone and Other Poly-*N*-vinylamides), Moscow: Nauka, 1998.
10. Lebedev, T.L., Fel'dshtein, M.M., Kuptsov, S.A., and Plate, N.A., *Vysokomol. Soedin., Ser. A*, 2000, vol. 42, no. 9, pp. 1504–1526.
11. Plate, N.A., Antipov, E.M., Teplyakov, V.V., *et al.*, *Vysokomol. Soedin., Ser. A*, 1990, vol. 32, no. 6, pp. 1123–1138.
12. Khotimskii, V.S., Matson, S.M., Litvinova, E.G., *et al.*, *Vysokomol. Soedin., Ser. A*, 2003, vol. 45, no. 8, pp. 1259–1267.
13. Nishio, Y., Haratani, T., and Takanashi, T., *J. Polym. Sci. B: Polym. Phys.*, 1990, vol. 28, pp. 355–376.
14. Kitaigorodskii, A.I., *Rentgenostrukturnyi analiz melkokristallicheskikh i amorfnykh tel* (X-ray Diffraction Analysis of Finely Crystalline and Amorphous Substances), Moscow: GITTL, 1952.

Russian Journal of Applied Chemistry, Vol. 78, No. 7, 2005, pp. 1182–1184. Translated from Zhurnal Prikladnoi Khimii, Vol. 78, No. 7, 2005, pp. 1203–1205.
Original Russian Text Copyright © 2005 by Osovskaya, Poltoratskii, Dmitrieva, Kamyshanskaya.

MACROMOLECULAR CHEMISTRY AND POLYMERIC MATERIALS

Hydrophilic Characteristics of Cellulose Treated with Saturated Water Vapor

I. I. Osovskaya, G. M. Poltoratskii, E. A. Dmitrieva, and Ya. V. Kamyshanskaya

St. Petersburg State Technological University of Plant Polymers, St. Petersburg, Russia

Received November 2, 2004; in final form, March 2005

Abstract—The reaction of water with cellulose treated with saturated water vapor at various temperatures for various times was studied. Trends in variation of its sorption and hydrophilic characteristics were examined.

The system of hydrogen bonds, macromolecular mobility, and regularity in arrangement of macromolecules in cellulose can be varied by physical or chemical actions [1–5]. One of the ways is treatment of cellulose with saturated water vapor. Sorption of water vapor with cellulose at various temperatures was considered previously [6, 7]. However, the influence of conditions of cellulose treatment with saturated water vapor on its physicochemical characteristics remains poorly understood, although such a treatment of dry cellulose material can be used in preparation of cellulose for chemical processing and paper production [8].

Formation of hydrogen bonds of water molecules with active groups of the polymer in this treatment and also partial breakdown of the system of intramolecular and intermolecular hydrogen bonds in the glassy component of cellulose affect subsequent sorption activity and reaction of the treated polymer with water.

Therefore, the goal of this study is a search for optimal conditions of cellulose treatment with saturated water vapor to restore its capillary-porous structure lost under drying in production of pulp.

We mainly used thermodynamic methods reflecting sorption and energy characteristics of cellulose fibers. Absorption of water with cellulose from liquid and gas phases was monitored from the enthalpy of wetting and desorption isotherms; variation of the internal surface area was characterized by sorption of a dye.

EXPERIMENTAL

Kraft whitened cellulose (SP-1650, degree of ordering 0.65, α-cellulose content 95.5%) was the subject of the study. The degree of polymerization was determined viscometrically at 298 K. Sodium ferric tartrate complex was used as a solvent. The degree of ordering was determined by X-ray diffraction analysis, and α-cellulose content, by dissolution of cellulose in 17.5% aqueous NaOH. The industrial samples of air-dry cellulose were treated under conditions of constant 100% relative humidity at temperatures T of 353, 373, and 438 K for the time τ from 3 to 15 min. Dehydration of the samples for calorimetric measurements and the study of dye sorption were performed by the inclusion method. Recording of desorption isotherms did not require additional treatment of the samples.

The thermal effects of the interaction of cellulose with water ΔH were obtained on a calorimeter equipped with an isothermal shell; the average relative error was ±1%. The desorption isotherms of water

Table 1. Heat of cellulose wetting

Sample no.	Conditions of treatment with water vapor		$-H$, J g^{-1}
	T, K	τ, min	
1*	–	–	49.0
2	438	3	70.6
3	438	5	84
4	438	7	70.2
5	438	10	60.2
6	373	5	60.2
7	373	10	70
8	373	15	54.4
9	353	5	53.8
10	353	10	64.2
11	353	15	68.8
12**	–	–	84.8

* Initial cellulose.
** Non-dried cellulose.

1070-4272/05/7807-1182 © 2005 Pleiades Publishing, Inc.

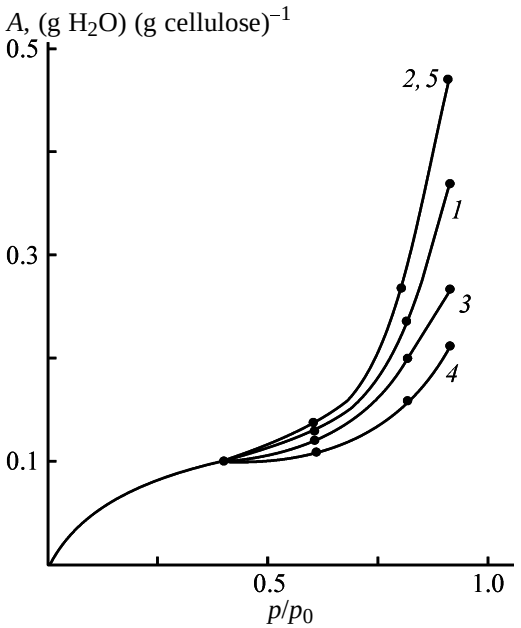


Fig. 1. Desorption (*A*) isotherms of water vapor after pretreatment of cellulose with water vapor at 438 K for (*1*) 3, (*2*) 5, and (*3*) 10 min. (p/p_0) Relative pressure; the same for Fig. 2. (*4*) Initial and (*5*) nondried cellulose.

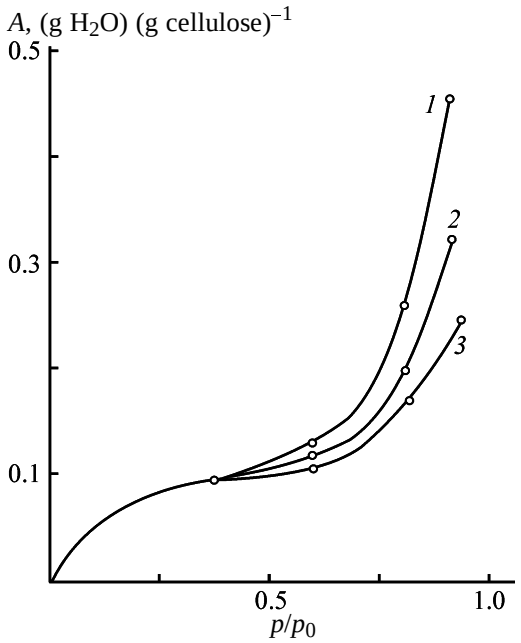


Fig. 2. Desorption (*A*) isotherms of water vapor after pretreatment of cellulose with saturated water vapor for 5 min at (*1*) 438, (*2*) 373, and (*3*) 353 K.

vapor were recorded at 298 K by the tensimetric method; the relative error was ±3%. The amount of a dye adsorbed with cellulose was determined with a ±3% error. As a dye we used Direct Green Triaza dye (trade mark).

Variations of ΔH depending on duration of pretreatment with saturated water vapor are presented in Table 1, and the isotherms of desorption of water vapor, in Figs. 1 and 2.

The results of calorimetric measurements showed clear dependence of ΔH on T and τ. As seen from Table 1, the dependence of ΔH on τ has an extremum, the most pronounced at 438 K.

As seen from Figs. 1 and 2, the desorption of water vapor *A* also depends on the temperature and time of the pretreatment. It should be noted that, at low relative pressure of water vapor ($p/p_0 < 0.6$), the *A* values of all the samples are small; in this case, water is sorbed by the mechanism of local sorption on polar centers of macromolecules accessible to the sorbate. However, at increased p/p_0, especially at $p/p_0 = 0.975$, when the water desorption with the capillary system of the monofiber becomes noticeable, the influence of the pretreatment conditions is more significant.

Figure 1 shows that desorption isotherms *2* and *5* practically coincide. This suggests complete reconstruction of the capillary-porous structure of cellulose upon treatment with saturated water vapor at 434 K for 5 min. An increase in the action duration to 5 min results in a decrease in the water retention *A*.

The extremum in the dependence of the heat of wetting and the water retention on the duration of pretreatment with saturated water vapor suggests the occurrence of two opposite processes, each affecting the sorption characteristics and hydrophilicity of cellulose. With increasing temperature and treatment duration, the energy of thermal motion of macromole-

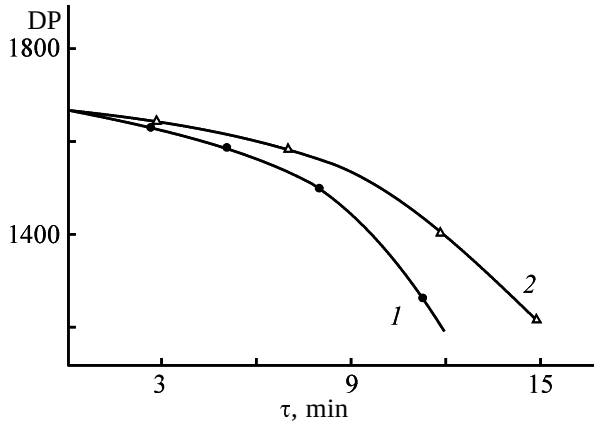


Fig. 3. Average degree of polymerization of cellulose DP as a function of duration of pretreatment with saturated water vapor τ at (*1*) 438 and (*2*) 373 K.

Table 2. Sorption of Direct Green Triazo dye with cellulose

Sample no.	Conditions of treatment with water vapor		Amount of dye sorbed with cellulose, mg g^{-1}
	T, K	τ, min	
1*	–	–	6.2
2	438	5	5.8
3	438	10	4.2
4	373	10	4.8
5	373	10	4.2
6**	–	–	4.0

* Non-dried cellulose.
** Initial cellulose.

cules increases and the system of hydrogen bonds is reorganized toward a decrease in their energy. The rupture of hydrogen bonds promotes swelling of the fiber and opening of pores and capillaries closed in drying. However, with increasing treatment duration the enthalpy of wetting and the water retention decrease due to recrystallization of the polymer and onset of degradation processes, also promoting formation of hydrogen bonds and decrease in the hydrophilicity of the polymer. The dependence of the average degree of polymerization of cellulose (DP) on τ is shown in Fig. 3.

The relationship between the treatment conditions and cellulose characteristics is suggested by variation of the dye sorption (Table 2). An increase in the amount of sorbed dye suggests maximum development of the capillary-porous structure of cellulose in treatment with saturated water vapor at 438 K for 5 min.

CONCLUSION

Studies of the physicochemical characteristics of cellulose treated with saturated water vapor at 353–438 K for 3–15 min by calorimetry, tensimetry, and dye sorption methods showed that the sorption and hydrophilic characteristics of cellulose are improved to the greatest extent by treatment at 438 K for 5 min.

REFERENCES

1. Azarov, V.I., Burov, A.V., and Obolenskaya, A.V., *Khimiya drevesiny i sinteticheskikh polimerov* (Chemistry of Wood and Synthetic Polymers), St. Petersburg: Lesotekhn. Akad., 1999.
2. Rogovin, Z.L., *Khimiya tsellyulozy* (Cellulose Chemistry), Moscow: Khimiya, 1972.
3. *Cellulose and Cellulose Derivatives*, Bikales, N. and Segal, L., Eds., New York: Wiley, 1991.
4. Osovskaya, I.I. and Poltoratskii, G.M., *Izv. Vyssh. Uchebn. Zaved., Lesn. Zh.*, 1999, no. 1, pp. 101–106.
5. Osovskaya, I.I. and Poltoratskii, G.M., *Zh. Prikl. Khim.*, 2001, vol. 74, no. 3, pp. 505–507.
6. *Water in Polymers*, Rowland, S.P., Ed., Washington: Am. Chem. Soc., 1980.
7. Frainberg, E.Z. and Papkov, S.P., *Vysokomol. Soedin.*, 1967, vol. 9, pp. 1483–1488.
8. RF Patent 1779081.

Russian Journal of Applied Chemistry, Vol. 78, No. 7, 2005, pp. 1185–1189. Translated from Zhurnal Prikladnoi Khimii, Vol. 78, No. 7, 2005, pp. 1206–1210.
Original Russian Text Copyright © 2005 by Shulevich, A. Navrotskii, Kovaleva, V. Navrotskii, Novakov.

MACROMOLECULAR CHEMISTRY AND POLYMERIC MATERIALS

Synthesis of Polymer–Colloid Complexes by Polymerization of Ionic Monomers in a Surfactant Solution

Yu. V. Shulevich, A. V. Navrotskii, O. Yu. Kovaleva, V. A. Navrotskii, and I. A. Novakov

Volgograd State Technical University, Volgograd, Russia

Received October 6, 2004; in final form, May 2005

Abstract—The possibility of synthesis of polymer–colloid complexes by polymerization of 1,2-dimethyl-5-vinylpyridinium methyl sulfate and *N*,*N*,*N*,*N*-trimethyl(methacryloyloxyethyl)ammonium methyl sulfate in a solution of sodium dodecyl sulfate was examined.

Interaction of linear polyelectrolytes (PEs) with oppositely charged surfactants produces polymer–colloid complexes (PCCs). Such complexes find a broad spectrum of applications, as being efficient emulsifiers, flocculants, foaming agents, and dispersion stabilizers [1].

Polymer–colloid complexes represent compounds stabilized by a system of cooperative ionic bonds and hydrophobic interactions [2]. The common method for their preparation is mixing of PE and surfactant solutions. At the same time, it is known that polymer complexes formed by electrostatically complementary polyelectrolytes can be prepared by template polymerization in the presence of macromolecular matrices [3]. In this case, the role of the matrix could be played by colloid particles [4]. It was suggested that PCCs could be synthesized by polymerization of ionic monomers in surfactant solutions.

It is known that polymeric quaternary salts of vinylpyridinium and *N*,*N*-dimethylaminoethyl methacrylate are effective polyelectrolyte reagents for separating disperse systems [5, 6]. It was demonstrated previously [7] that performing polymerization in the presence of organic peroxides allows preparation of high-molecular-weight polyelectrolytes with a viscosity-average molecular weight M_η of (1–12) × 10^6 in the theoretical yield in the form of concentrated aqueous solutions. The polymerization of the monomers in surfactant solutions can differ significantly from both the polymerization of ionic monomers in aqueous solutions and classical template polymerization.

The goal of this work was to synthesize PCCs by polymerization of monomers in a solution of an electrostatically complementary surfactant.

EXPERIMENTAL

As ionic monomers we used 1,2-dimethyl-5-vinylpyridinium methyl sulfate (M1) and *N*,*N*,*N*,*N*-trimethyl(methacryloyloxyethyl)ammonium methyl sulfate (M2); and as a surfactant, sodium dodecyl sulfate (SDS), whose behavior in complexation is well studied in a number of systems [8].

Monomers M1 and M2 and the surfactant were purified by recrystallization from methanol, acetone, and ethanol, respectively, and vacuum-dried. The critical micelle concentration (CMC) of SDS was found to be 0.008 M, which is well consistent with that reported in [9]. Interaction of the monomers with SDS was studied by the Rebinder method [10] and also by UV spectroscopy. The UV spectra were recorded on an SF-26 spectrophotometer over the range 190–220 nm in a 1-cm cell. In all the experiments we used water distilled under Ar. pH of the SDS and M2–SDS solutions was measured on a Delta 320 pH-meter (Mettler Toledo).

The polymerization was performed in Ar under isothermal conditions at 30 and 50°C for M1 and M2, respectively. As initiators we used *tert*-butylperoxy-2-propanol (TBPP) and potassium persulfate (PP) for M1 and M2, respectively. The polymerization kinetics was studied by microcalorimetry on a DAK-1-2M calorimeter in the mode of direct registration of the heat liberation rate. The limiting conversion was determined photometrically. The current conversion of the monomer and polymerization rate were estimated using the values of 79.4 and 56.8 kJ mol^{-1} for the polymerization enthalpies of M1 and M2, respectively. The experiments were carried out at an initial monomer concentration of 2 M and initiator concen-

1070-4272/05/7807-1185 © 2005 Pleiades Publishing, Inc.

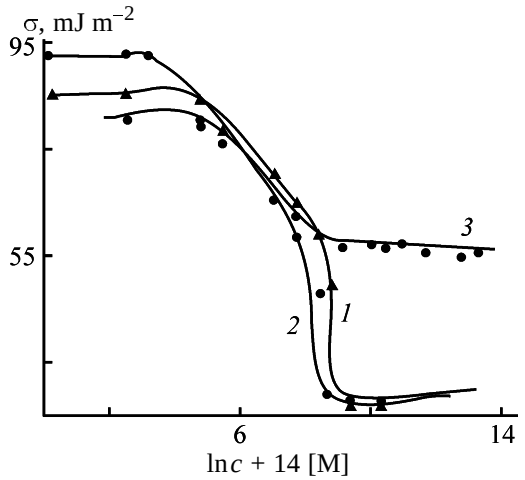


Fig. 1. Surface tension σ of the SDS solutions as a function of the logarithm of the SDS concentration *c*. M2 concentration (M): (*1*) 2, (*2*) 0.05, and (*3*) 0.25.

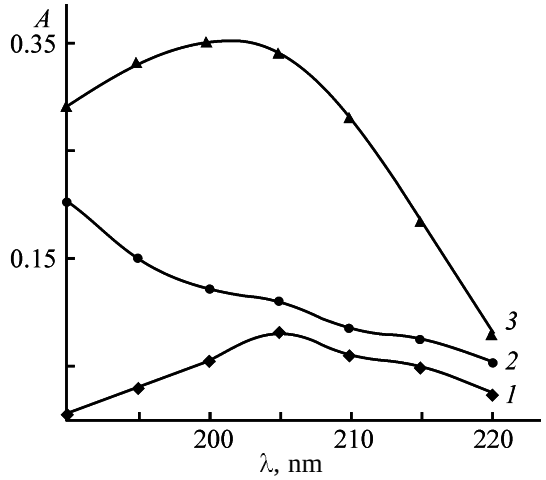


Fig. 2. Optical density *A* of the aqueous solutions of (*1*) M2, (*2*) SDS, and (*3*) SDS–M2 as a function of the wavelength λ. Solution concentration 5×10^{-5} M.

tration of 0.001 M; the SDS concentration was varied over the range 0–0.7 M. The composition of the resulting complexes was characterized by the parameter *W* defined as

$$W = [SA]/[M], \quad (1)$$

where [SA] and [M] are the surfactant and monomer concentrations (M).

The PCC solutions (PCC-m) were prepared by mixing the PE and surfactant stock solutions in a common solvent. The stock surfactant solution was added dropwise with vigorous stirring to the PE solution. The solutions were prepared using double-distilled water. In preparing PCC-m, we used PE with $M_\eta = 2.2 \times 10^6$. The insoluble fraction of PCC was separated by centrifugation (1000 rpm) for 30 min. The composition of the resulting solutions *Z* was characterized by the surfactant to PE concentration ratio in the system. The characteristics of the solutions were examined at least a day after preparation. The intrinsic viscosity of the polymer solutions [η] (dl g^{-1}) was determined with an Ubbelohde viscometer at 30°C in 0.005 M NaCl. The intrinsic viscosity was estimated using double extrapolation of the specific viscosity η_{sp} and of the logarithm of the ratio of the relative viscosity η_{rel} to the polymer concentration *c* (M) to the zero concentration of the polymer.

It is known that, under certain conditions, ionic surfactants form micelles, which, on the one hand, hold the counterions around themselves, and on the other hand, are capable of solubilizing hydrophobic compounds. It is also known that ionic monomers are compounds demonstrating surface activity [11]. Therefore, being dissolved in an SDS solution, they can interact with each other by two possible mechanisms. The first mechanism produces so-called mixed micelles through transformation of the initial micelles initiated by surface activity of both components [12]. The second mechanism is driven by the electrostatic complementarity of the components, i.e., by the ability of the monomer to be sorbed at the micellar surface with formation of the monomer–SDS associate.

To study the nature of the interaction, we examined the concentration dependence of the surface tension σ (mJ m^{-2}) of the SDS solution at various M2 contents (Fig. 1). The critical micelle concentration of SDS was found to be 0.007, 0.006, and 0.01 M at a monomer concentration of 2, 0.25, and 0.05 M, respectively. As seen, CMC of SDS remains unchanged within the experimental error, being equal to that in water. The UV spectrum of the M2 solution (Fig. 2, spectrum *1*) shows a maximum at 200–210 nm, which is typical of compounds with double bonds [13]. The spectrum of the SDS solution shows no maximum in the range studied (Fig. 2, spectrum *2*). The spectrum of the M2–SDS mixture demonstrates a maximum in the same region as that of the monomer. However, in this case, the molar extinction increases from 8000 (M2) to 35 000 l cm^{-1} mol^{-1} (M2–SDS). This increase is probably due to intermolecular interaction [13] resulting in most cases in formation of stable associates.

Comparison of the tensiometric and UV spectroscopic data suggests that addition of M2 to the SDS micellar solution initiates partial substitution of

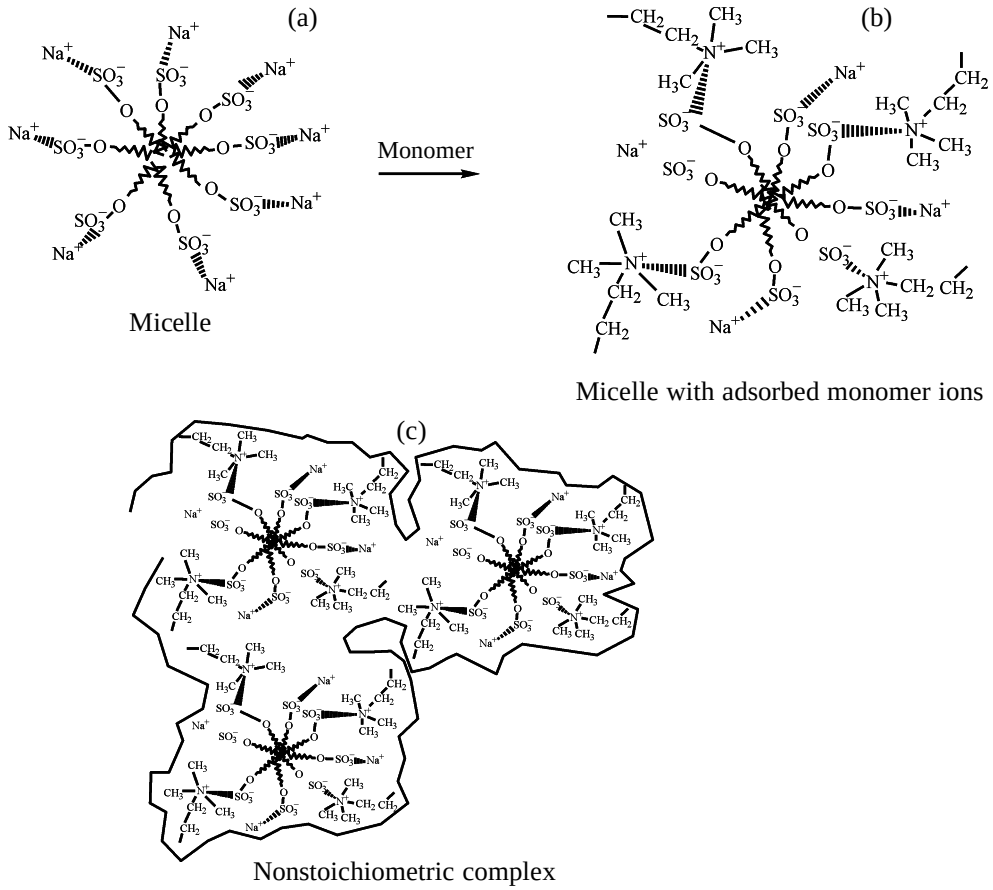


Fig. 3. Structural transformations in the micellar solution of SDS initiated by addition of the monomer and its subsequent polymerization.

the cations of the monomer for the Na^+ counterions of the micelle (Figs. 3a and 3b). Addition of the initiator to such a monomer–micellar system can initiate polymerization of both free and adsorbed monomer.

Keeping in mind the tendency of M2 to hydrolysis, we monitored pH in the M2–SDS system (Fig. 4). The 0.1–0.7 M SDS solutions are characterized by increased pH (7.18–9.48), promoting base hydrolysis of M2 with formation of a copolymer containing methacrylate units. However, addition of M2 to the SDS solutions, to obtain a concentration of 2 M, considerably decreases pH over the entire SDS concentration range, so that pH of the SDS–M2 solutions only slightly changes, remaining within the range 2.41–3.04. It is known [14] that acid hydrolysis of quaternary salts of *N*,*N*-dimethylaminoethyl methacrylate is also possible. However, the methyl sulfate of M2 is subject to hydrolysis to a lesser extent as compared to others. Its hydrolysis can proceed only under rigorous conditions (70°C, H_2SO_4 concentration 0.5 M).

Analysis of the concentration dependences of the initial polymerization rates of M1 and M2 in SDS solutions shows that the effect of SDS on the polymerization kinetics becomes clearly pronounced only at SDS concentrations exceeding CMC. The maximal

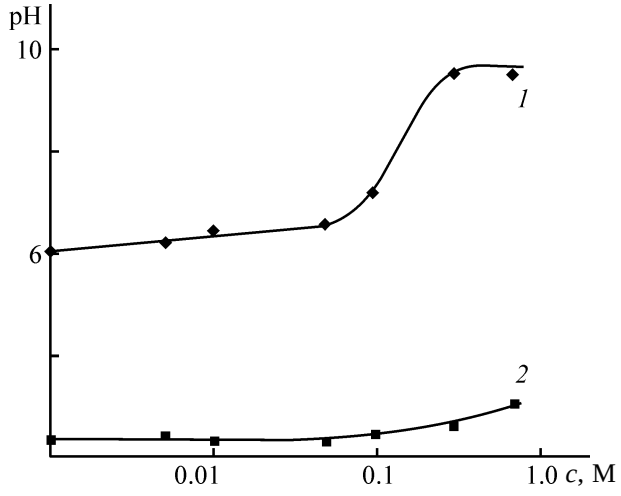


Fig. 4. pH of (*1*) SDS and (*2*) SDS–M2 solutions as a function of the SDS concentration *c*.

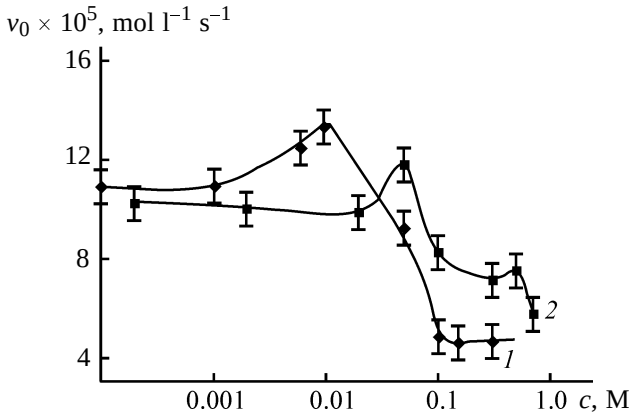


Fig. 5. Initial polymerization rate v_0 of (*1*) M1 and (*2*) M2 as a function of the SDS concentration *c*.

polymerization rate is observed at a surfactant concentration of 0.1 and 0.05 M for M1 and M2, respectively. Further increase in the SDS concentration considerably decreases the rate. Most likely, the observed influence of SDS on the polymerization rate is associated with the template effect and diffusion control.

In contrast to the classical template polymerization, no formation of a stoichiometric complex was observed in the systems in hand. The polymerizate remains homogeneous at any conversion of the monomer. The most probable reason is the detachment of the propagating radical from the SDS micelle in the course of polymerization. Further propagation of the chain proceeds by virtue of the polymerization of both free monomers and monomers adsorbed on other micelles, producing a nonstoichiometric complex (Fig. 3c).

It was demonstrated in [15] that, in formation of the complexes by mixing, PE macromolecules coexist with the nonstoichiometric complex, or stable dispersion of the nonstoichiometric and stoichiometric complexes exists, depending on the PE to surfactant ratio in the system. The M2-based polymeric complexes formed in the course of polymerization at $W \le 0.25$ form a true solution, but at $W \ge 0.25$, they become insoluble in water, being only capable of limited swelling. However, these complexes are soluble in aqueous electrolyte (NaCl) solutions. The solubility of PCCs is controlled by the possibility of migration of the surfactant ions along the PE chain. In the case of hindered migration, PCCs with random distribution of the surfactant ions are formed, making improbable the formation of long sequences of ionized PE units responsible for dissolution of the PCC particles. Being introduced in the reaction mixture, a low-molecular-weight electrolyte competes for the formation of ionic bonds with the reagents, making it possible for the surfactant ions to migrate, so that the PE chain takes the conformation representing a compromise between the maximal number of contacts of hydrophobic groups of the surfactant ions contained in the PCC particles and the minimal entropy stress in the PE chain [16].

Hydrodynamic characteristics of M1-based polymer–colloid complexes prepared by mixing and polymerization

Preparation method					
mixing (PCC-m)			polymerization (PCC-p)		
Z	$[\eta]$, dl g^{-1}*	$[\eta]/[\eta]_0$	*W*	$[\eta]$, dl g^{-1}*	$[\eta]/[\eta]_0$
0	3.54	1.00	0	3.54	1.00
0.010	3.77	1.06	0.005	3.76	1.06
0.030	3.95	1.12	0.025	4.86	1.37
0.050	3.18	0.90	0.050	4.70	1.33
0.150	2.77	0.78	0.075	2.73	0.77
			0.150	2.81	0.79

* 0.05 M NaCl, 30°C; ($[\eta]$, $[\eta]_0$) intrinsic viscosities of PCC and PE, respectively, dl g^{-1}.

The study of the hydrodynamic properties of the polymer complexes obtained by two different methods (polymerization and mixing of predissolved components) showed (see table) that the intrinsic viscosity of the complexes only slightly depends on the composition (some tendency to increase is observed in the range of low concentrations). The intrinsic viscosities of the PCC-p and PCC-m solutions differ insignificantly from each other. Evidently, the hydrodynamic dimensions of the complexes obtained by different methods are well comparable. Taking into account that $[\eta]$ of PCCs only slightly differ from that of straight PE, it may be suggested that high-molecular-weight complexes are formed in the course of polymerization in the SDS micellar solution, as in the case of preparation of PCCs by mixing.

CONCLUSIONS

(1) The initial polymerization rates of 1,2-dimethyl-5-vinylpyridinium methyl sulfate and *N*,*N*,*N*,*N*-trimethyl(methacryloyloxyethyl)ammonium methyl sulfate in sodium dodecylsulfate solution decreases at the surfactant concentrations in the solution above the critical micelle concentration.

(2) High-molecular-weight complexes are formed in the course of polymerization in the sodium dodecyl sulfate micellar solution, as in the case of preparation

of polymer–colloid complexes by mixing the predissolved components.

ACKNOWLEDGMENTS

The study was financially supported by the Competition Center for Basic Natural Science (project A04-2.11-185).

REFERENCES

1. Babak, V.G., *Kolloidnaya khimiya v tekhnologii mikrokapsulirovaniya* (Colloid Chemistry for Microencapsulation Processes), Sverdlovsk: Ural. Gos. Univ., 1991.
2. Kabanov, V.A. and Papisov, I.M., *Vysokomol. Soedin., Ser. A*, 1979, vol. 21, no. 2, pp. 243–281.
3. Papisov, I.M., *Vysokomol. Soedin., Ser. B*, 1997, vol. 39, no. 3, pp. 563–574.
4. Goddard, E.D. and Ananthapadmanabhan, K.P., *Interactions of Surfactants with Polymers and Proteins*, New York: CRC, 1993.
5. Novakov, I.A. and Navrotskii, A.V., *Vysokomol. Soedin., Ser. C*, 2002, vol. 44, no. 9, pp. 1660–1676.
6. Panarin, E.F., *Usp. Khim.*, 1991, vol. 60, no. 3, pp. 629–630.
7. Novakov, I.A., Navrotskii, A.V., Starovoitova, Ya.M., *et al., Zh. Prikl. Khim.*, 2003, vol. 76, no. 7, pp. 1200–1206.
8. Kasaikin, V.A., Litmanovich, E.A., Zezin, A.B., *et al.*, *Dokl. Ross. Akad. Nauk*, 1999, vol. 367, no. 3, pp. 359–362.
9. Abramzon, A.A., *Poverkhnostno-aktivnye veshchestva* (Surfactants), Leningrad: Khimiya, 1986.
10. Frolov, Yu.G. and Grodskii, A.S., *Laboratornye raboty i zadachi po kolloidnoi khimii* (Experimental Works and Exercises on Colloid Chemistry), Moscow: Khimiya, 1986.
11. Batrakova, E.V., Orlov, V.N., and Egorov, V.V., *Kolloidn. Zh.*, 1985, vol. 47, no. 1, pp. 131–134.
12. Egorov, V.V. and Ksenofontova, O.B., *Vysokomol. Soedin., Ser. A*, 1991, vol. 33, no. 8, pp. 1780–1785.
13. Sverdlova, O.V., *Elektronnye spektry v organicheskoi khimii* (Electronic Spectra in Organic Chemistry), Leningrad: Khimiya, 1973.
14. Kuznetsova, N.A., Kazantsev, O.A., Shirshin, K.V., *et al., Zh. Prikl. Khim.*, 2003, vol. 76, no. 7, pp. 1150–1153.
15. Zakharova, Yu.A., Otdel'nova, M.V., Aliev, I.I., *et al.*, *Kolloidn. Zh.*, 2002, vol. 64, no. 2, pp. 170–175.
16. Ibragimova, Z.Kh., Ivleva, E.M., Pavlova, N.V., *et al.*, *Vysokomol. Soedin., Ser. A*, 1992, vol. 34, no. 9, pp. 139–147.

Russian Journal of Applied Chemistry, Vol. 78, No. 7, 2005, pp. 1190–1193. Translated from Zhurnal Prikladnoi Khimii, Vol. 78, No. 7, 2005, pp. 1211–1214.
Original Russian Text Copyright © 2005 by Kovaleva, V. Navrotskii, Shulevich, A. Navrotskii, Novakov.

MACROMOLECULAR CHEMISTRY AND POLYMERIC MATERIALS

Synthesis and Hydrodynamic Behavior of Stoichiometric Complexes of Cationic Polyelectrolytes with Amphiphilic Anions

O. Yu. Kovaleva, V. A. Navrotskii, Yu. V. Shulevich, A. V. Navrotskii, and I. A. Novakov

Volgograd State Technical University, Volgograd, Russia

Received October 6, 2004; in final form, April 2005

Abstract—Complexation of poly(*N*,*N*-dimethyl-*N*-benzyl-*N*-methacryloyloxyethyl)ammonium chloride with oppositely charged amphiphilic compounds was studied. The solubility and hydrodynamic properties of the resulting complexes in chloroform, methanol, and chloroform–hexane and chloroform–toluene mixtures were determined.

Polyelectrolytes (PEs) interact with oppositely charged diphilic ions of micelle-forming surfactants to form polyelectrolyte complexes (PECs) with unique physicochemical properties [1]. Studies of such interactions are necessary for understanding the processes that occur in natural PECs of biopolymers and diphilic compounds [2–4] and the behavior of PECs at flocculation and stabilization of dispersions [5]. It is known [6–9] that stoichiometric PECs (SPECs) formed by anionic surfactants and polydimethyldiallylammonium chloride (PDMDAAC) or poly-*N*-ethyl-4-vinylpyridinium bromide (PEVPB) (M_w 10^4–10^5) are soluble in low-polar organic solvents. However, the features of hydrodynamic behavior of SPECs of macromolecular polyelectrolytes based on aminoalkyl acrylates are still poorly understood. Poly(*N*,*N*-dimethyl-*N*-benzyl-*N*-methacryloyloxyethyl)ammonium chloride (PE-1) shows promise for preparing hydrophobic complexes, as it has higher molecular weight as compared to poly-*N*,*N*-dimethyldiallylammonium chloride (PE-2) and exhibits pronounced hydrophobic properties imparted by the benzyl substituent [10].

In this work we studied the features of interaction between various amphiphilic anions and PE-1 and the hydrodynamic behavior of the resulting SPECs in chloroform, methanol, and mixed solvents.

EXPERIMENTAL

Polyelectrolyte PE-1 was prepared by radical polymerization of the monomer, which was synthesized by alkylation of dimethylaminoethyl methacrylate with benzyl chloride at 0–3°C in acetone and recrystallized from acetone–acetonitrile mixture. Radical polymerization was performed in an aqueous solution (2 M monomer concentration) at 25 ± 0.5°C up to 96–98% conversion. Then, the polymerizate was dissolved in methanol and precipitated with diethyl ether. *tert*-Butylperoxy-2-propanol used as initiator was prepared by the procedure given in [11]. The resulting polymer was additionally purified by recrystallization from methanol with diethyl ether and dried in a vacuum (1.5–2.0 mm Hg, 20 ± 0.5°C) to constant weight.

In our study we used commercial aqueous solutions of PE-2 (40 wt %). The solutions of PE-2 of various concentrations were prepared from the initial solution by successive dilution.

The intrinsic viscosities of PE-1 and PE-2 determined in 0.1 M NaCl at 30°C were 4.7 and 1.4 dl g^{-1}, respectively.

Anionic surfactants such as sodium dodecyl sulfate SDS (chemically pure grade, Merck) and Volgonat-emul'gator (VE) [mixture of sodium salts of alkylsulfonic acids RSO_3Na, R = C_{16}–C_{18}, Khimprom Joint-Stock Company, Volgograd, Russia; STP (Enterprise Standard) 2480-282-05 763 458–99] were used without additional purification.

The stoichiometric polyelectrolyte complexes of surfactants were prepared from the aqueous solutions of components with vigorous stirring. The concentrations of polyelectrolytes and surfactants were 0.01 and 0.1 M, respectively. The resulting precipitate of SPEC was separated, washed with water, and dried in a desiccator to constant weight.

The composition of the reaction mixture *Z* was determined as the ratio of the concentration of the surfactant ions to the concentration of PE units in the

1070-4272/05/7807-1190 © 2005 Pleiades Publishing, Inc.

Synthesis of insoluble complexes based on PE-1 and PE-2

PE–surfactant	*Z*	SPEC yield, wt %	S, wt %	N, wt %	S/N	φ, mol	η_r, dl g^{-1}*
PE-1–SDS	1.0	65	5.5	2.30	2.4	1.00	5.3
	1.5	68	3.1	1.70	1.8	0.80	4.6
	3.0	–	4.7	2.70	1.7	0.76	–
PE-1–VE	1.0	84	5.8	2.28	2.5	1.10	6.3
	1.5	86	4.9	2.56	1.9	0.84	5.2
	3.0	–	5.4	2.20	2.4	1.07	5.1
PE-2–SDS	1.0	59	6.9	2.70	2.5	1.09	–
	1.5	63	–	–	–	–	–
	3.0	–	–	–	–	–	–
PE-2–VE	1.0	38	7.4	3.40	2.2	0.95	–
	1.5	63	–	–	–	–	–
	3.0	–	–	–	–	–	–

* Reduced viscosity of the chloroform solution of the complex (0.2 g dl^{-1}).

system (*Z* = [surfactant]/[PE]). The composition of PEC φ was characterized by the ratio of the number of diphilic surfactant ions in PEC to the number of PE units in the polymeric complex (φ = $[surfactant]_{PEC}/[PE]_{PEC}$. The composition of the resulting PECs was determined by chemical analysis.

To determine the solubility and hydrodynamic properties of SPECs in organic solvents, the samples were placed in chemically pure grade methanol, chloroform, benzene, toluene, and butyl acetate.

The viscosities of the SPEC solutions in chloroform, methanol, and mixed solvents were measured with an Ubbelohde viscometer (0.34 mm capillary diameter).

A distinctive feature of the interaction of diphilic surfactant ions with oppositely charged macroion is that the phase state of the reaction system depends on the initial reagent ratio *Z*, and certain *Z* values characterize different phase states of PECs [12].

In the reaction of PE-1 with SDS and VE, the precipitate is formed only at the reagent ratio close to stoichiometric.

The table shows that quantitative yield of the insoluble complex is never obtained at the stoichiometric reagent ratio, and with increasing *Z* above the stoichiometric ratio the yield of all the SPECs studied increases. It should be noted that the yields of the complexes in the PE-2–SDS and PE-2–VE systems are lower than those in the corresponding systems with PE-1. The possibility of SPEC formation is determined by the size ratio of the polymer chain and internal surfactant micelles. Moreover, the composition of the precipitated complex can be determined by the polyanion chain length. For example, PEVPB with the degree of polymerization of 1000 yields SPEC with φ = 1.0 [13], whereas the same polymer with the higher degree of polymerization (2000) gives an insoluble SPEC with φ = 0.85. A similar trend is observed with the complexes PE-2–SDS and PE-1–VE (φ = 1.09 and 0.84, respectively). This suggests that certain decrease in φ is associated with the length of the polymeric ion, because the probability of formation of various defects (e.g., loops) increases with increasing length of the polymer chain. These defects are also typical for double-stranded chains of stoichiometric complexes of oppositely charged polymeric ions [14]. These defects are formed owing to conformational noncomplementarity of the polymer chain and surfactant micelles, because the structure of SPEC is a compromise between the conformation of polymeric ion and geometric characteristics of the surfactant aggregates. The mismatch of these parameters will be greater in the case of longer chains, which causes appearance of unlinked sections in the polymer chain. As a result, φ of the resulting complexes is smaller than unity.

It is known that the major factor determining whether the polymer will dissolve or swell is its specific interaction with the solvent. In this connection, we studied the behavior of SPECs in various organic solvents. It was found that these complexes dissolve in chloroform and methanol, whereas in aliphatic and aromatic hydrocarbons and ethyl and butyl acetates they occur in the swollen state. Taking into account the polarity and proton-donor power of methanol and chloroform, we suggest that the dissolution of SPECs in them proceeds owing to the solvation of the ion pairs and ester fragments. The other

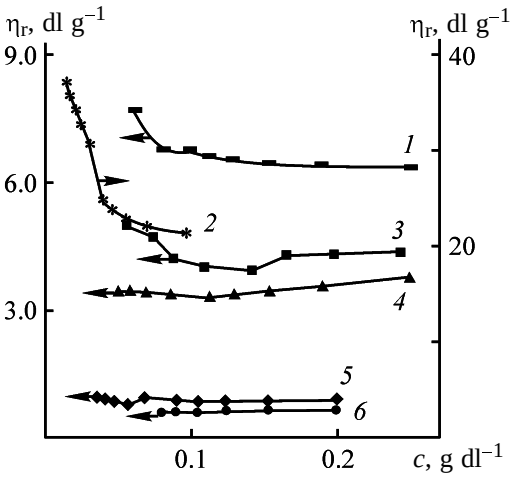


Fig. 1. Reduced viscosity η_r as a function of PEC concentration c in chloroform, methanol, and mixed solvents. (*1*) Chloroform, (*2*) methanol, (*3*) chloroform : hexane = 70 : 30, (*4*) chloroform : hexane = 50 : 50, (*5*) chloroform : toluene = 70 : 30, and (*6*) chloroform : toluene = 50 : 50 (volume ratio in all cases).

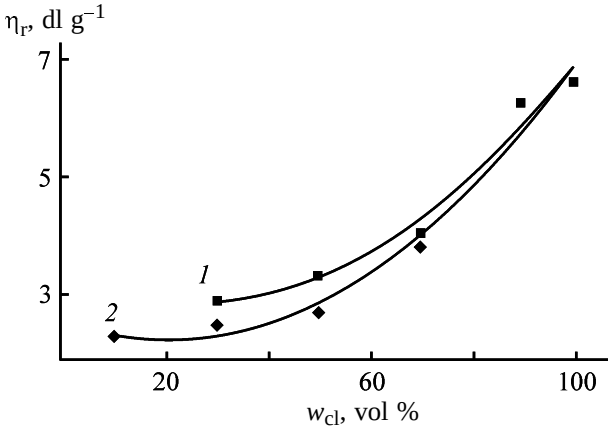


Fig. 2. Reduced viscosity η_r of PE-1–VE in the mixed solution as a function of chloroform concentration w_{cl}; PE-1–VE concentration 0.11 g dl^{-1}. Second component of the solvent: (*1*) hexane and (*2*) toluene.

solvents studied cannot dissolve SPECs, as they are incapable of specific interactions with SPECs.

The dependence of the reduced viscosity on the concentration of the complex in methanol is typical for dissociating polyelectrolytes (Fig. 1). The reduced viscosity of the complex η_r in methanol at a concentration c 0.015 g dl^{-1} is 37.1 dl g^{-1}, which is comparable with η_r for PE-1 (43.3 dl g^{-1}). Thus, in methanol the complex dissociates, and owing to the electrostatic repulsion the complex macromolecules occur in the form of a strongly swollen globule.

The solutions of PE-1–VE in chloroform also exhibit abnormal concentration dependences of η_r (Fig. 2), which strongly increases at concentrations lower that 0.1 g dl^{-1}. Similar effect was observed for complexes of sodium polystyrenesulfonate with alkyltrimethylammonium bromides in ethanol, DMF, and isopropanol [15]. This phenomenon was attributed to the effective charge on the polymer chains even in a low-polarity solvent, which enhances the electrostatic repulsion and increases the hydrodynamic size of the polymer globule. At the same time, in chloroform η_r of the complexes is significantly lower than that in methanol. The η_r values given in the table are comparable with [η] of PE-1 in an aqueous-salt solution (4.7 dl g^{-1}), which suggests that SPECs occur in chloroform as loose swollen globules.

The behavior of the complexes in question strongly differs from that of the complexes based on PDMDAAC or PEVPB for which [η] is 0.35–0.55 dl g^{-1} and their Huggins constants k' = 0.66 are typical for linear flexible-chain macromolecules in thermodynamically good solvents. The η_r values linearly decrease with dilution, which is typical for uncharged polymers.

Since no dissolution of SPECs in individual hydrocarbons was observed, their hydrodynamic behavior was studied using mixed systems with chloroform and toluene or hexane. The viscometric measurements performed in a wide range of solvent compositions showed no phase separation at a chloroform content from 10 to 90 vol %.

It was expected that addition of hydrocarbons exhibiting affinity for surfactant chains and benzyl groups into the mixed solvent would cause solvation of the above fragments and enhance swelling of the polymer globule. However, as seen from Figs. 1 and 2, in the mixed solvents η_r sharply decreases with increasing hydrocarbon content. This is probably due to the deterioration of the conditions of the ion pair solvation. The effect of this factor is more decisive than the increase of the affinity for the hydrocarbon polymer fragments. As a result, more compact polymer globules are formed in the mixed solvents. Thus, the solubility of the complexes and swelling of their globules are primarily promoted by weakening of the interionic interaction.

The revealed features in the hydrodynamic behavior of PE–surfactant complexes suggest the possibility of their use for modifying the rheological properties of organic liquids.

CONCLUSIONS

(1) Complexing of poly(*N*,*N*-dimethyl-*N*-benzyl-*N*-methacroyloxyethyl)ammonium chloride with ani-

onic surfactants gives hydrophobic complexes (yield 63–86%) with φ = 0.8–1.1 at the initial component ratio Z = 1–3.

(2) Solutions of the polymeric complexes in methanol and chloroform exhibit abnormal hydrodynamic behavior typical for polyelectrolytes. The solubility and high viscosity of solutions of the complexes are enhanced by solvation of the ion pair and polar fragments with proton-donor solvents.

REFERENCES

1. Goddard, E.D. and Ananthapadmanabhan, K.P., *Interactions of Surfactants with Polymers and Proteins*, New York: CRC, 1993.
2. Kabanov, V.A., *Vysokomol. Soedin., Ser. A*, 1994, vol. 36, no. 2, pp. 183–197.
3. Panarin, E.F. and Kopeikin, V.V., *Vysokomol. Soedin., Ser. C*, 2002, vol. 44, no. 12, pp. 2340–2351.
4. Izumrudov, V.A. and San Khyun Lin, *Vysokomol. Soedin., Ser. A*, 1998, vol. 40, no. 3, pp. 459–465.
5. Kabanov, V.A., Zezin, A.B., Kasaikin, V.A., *et al.*, *Usp. Khim.*, 1991, vol. 60, no. 3, pp. 595–601.
6. Bakeev, K.N., Yan Min Shu, Zezin, A.B., and Kabanov, V.A., *Dokl. Ross. Akad. Nauk*, 1993, vol. 332, no. 4, pp. 450–453.
7. Lezov, A.B., Mel'nikov, A.B., Kolomiets, I.P., *et al.*, *Vysokomol. Soedin., Ser. A*, 1995, vol. 37, no. 11, pp. 1904–1909.
8. Lezov, A.B., Kolomiets, I.P., Ryumtsev, E.I., *et al.*, *Vysokomol. Soedin., Ser. A*, 1995, vol. 37, no. 11, pp. 1910–1915.
9. Bobrov, A.B., Skorikova, E.E., Sul'yanov, S.N., *et al.*, *Vysokomol. Soedin., Ser. A*, 1997, vol. 39, no. 4, pp. 627–631.
10. Kotlyarevskaya, O.O., Navrotskii, A.V., Orlyanskii, M.V., *et al.*, *Zh. Prikl. Khim.*, 2004, vol. 77, no. 4, pp. 626–631.
11. Navrotskii, A.V., Novakov, I.A., Lotov, V.V., and Navrotskii, V.A., in *Khimiya i tekhnologiya elementoorganicheskikh monomerov i polimernykh materialov: Mezhvuzovskii sbornik nauchnykh trudov* (Chemistry and Technology of Organoelement Monomers and Polymeric Materials: Intercollegiate Collection of Works), Volgograd: Gos. Tekh. Univ., 1995, pp. 13–19.
12. Zakharova, Yu.A., Otdel'nova, M.V., Alieva, I.I., *et al.*, *Kolloidn. Zh.*, 2002, vol. 64, no. 2, pp. 170–175.
13. Otdel'nova, M.V., Zakhariova, Yu.A., Ivleva, E.M., *et al.*, *Vysokomol. Soedin., Ser. A*, 2003, vol. 45, no. 9, pp. 1524–1532.
14. Zezin, A.B. and Kabanov, V.A., *Usp. Khim.*, 1982, vol. 51, no. 9, pp. 1447–1483.
15. Antonietti, M., Förster, S., Zisenis, M., and Conrad, J., *Macromolecules*, 1995, vol. 28, no. 7, pp. 2270–2275.

Russian Journal of Applied Chemistry, Vol. 78, No. 7, 2005, pp. 1194–1196. Translated from Zhurnal Prikladnoi Khimii, Vol. 78, No. 7, 2005, pp. 1215–1217.
Original Russian Text Copyright © 2005 by Tagirzyanov, Yakubov, Morozov, Yakubova.

CHEMISTRY OF FOSSIL FUEL

Method of Unification of the Relative Measurement Units for the Concentrations of V(IV) and Free Radicals in Crude Oils and Asphaltenes

M. I. Tagirzyanov, M. R. Yakubov, V. I. Morozov, and S. G. Yakubova

Arbuzov Institute of Organic and Physical Chemistry, Kazan Scientific Center, Russian Academy of Sciences, Kazan, Tatarstan, Russia

Received October 20, 2004; in final form, April 2005

Abstract—The potential of the method for unification of the relative units for measuring the concentration of V(IV) and free radicals in crude oils and asphaltenes was examined.

Studies of the macromolecular components of crude oils, natural bitumens, and other oil-like systems are necessary for solving a complex of problems in extraction, preparation, transportation, and processing of oil raw materials. Macromolecular components of oil systems include, above all, asphaltenes and resins, whose structures concentrate most of the heteroatoms contained in crude oils [1]. Moreover, asphaltenes rank among concentrates of oil paramagnetics [2] because of a fairly high content (ca. 10^{19} spin) of stable free radicals. Some metal ions entering into the composition of the macromolecular components of oil exhibit paramagnetism (V^{4+}, Fe^{3+}, Mn^{2+}). The highest concentrations in crude oils are characteristic of vanadium [3], which mainly occurs as paramagnetic vanadyl ion VO^{2+}, entering into composition of complexes with various structures.

Studies of the structure, behavior, and distribution over oil components of free radicals (FRs) and vanadyl complexes (VCs) by ESR have some specific features. As known, one of the main problems in measuring the content of the paramagnetic centers in oil objects is the choice of the reference. It is suggested either to "permanently" place a standard ruby rod into an ESR spectrometer [2], or to calculate the mass of each oil sample in the part of the ampule occurring in the region where the data are taken. It is possible to reject determining the absolute concentrations of the paramagnetics and to base all conclusions on measuring the relative changes in the ESR spectra. This gives rise to another problem: The relative measurement units for the concentration of the paramagnetics in crude oils, resins, asphaltenes, and other oil components will have different "relativities." However, it is possible to use a simple technique for unification of the relative units for measuring the content of paramagnetics in crude oils and asphaltenes so as to avoid errors due to nonideal character of references and the infeasibility of permanently placing a reference sample in the spectrometer cavity.

EXPERIMENTAL

Asphaltenes were precipitated from crude oils with hexane at the crude oil : hexane volume ratio of 1 : 20 and washed in a Soxhlet apparatus until decolorization of the solvent. From the Soxhlet apparatus, asphaltenes were washed out with benzene, which was then distilled off. The resulting asphaltenes were vacuum-dried to constant weight.

The content of vanadium in the crude oils and asphaltenes was determined by direct flame atomic absorption spectrometry on an AAS-IN spectrophotometer. A weighed sample solution was sprayed in acetylene–nitrogen(II) oxide flame. As solvent served a mixture of *o*-xylene (80 vol %), acetone (10 vol %), and ethanol (10 vol %). The concentration of vanadium was determined from calibration curves, with V^{2+} dibutyldithiocarbamate in the above-mentioned solvent mixture as the reference [4].

All measurements of the content of paramagnetics in oil objects were run under identical conditions at 20°C on an SE/X-2544 ESR spectrometer. The content of paramagnetics in crude oils was measured in a quartz glass ampule with the internal diameter of 6 mm, which was filled with crude oil to a full volume within the zone of the ESR spectrometer

1070-4272/05/7807-1194© 2005 Pleiades Publishing, Inc.

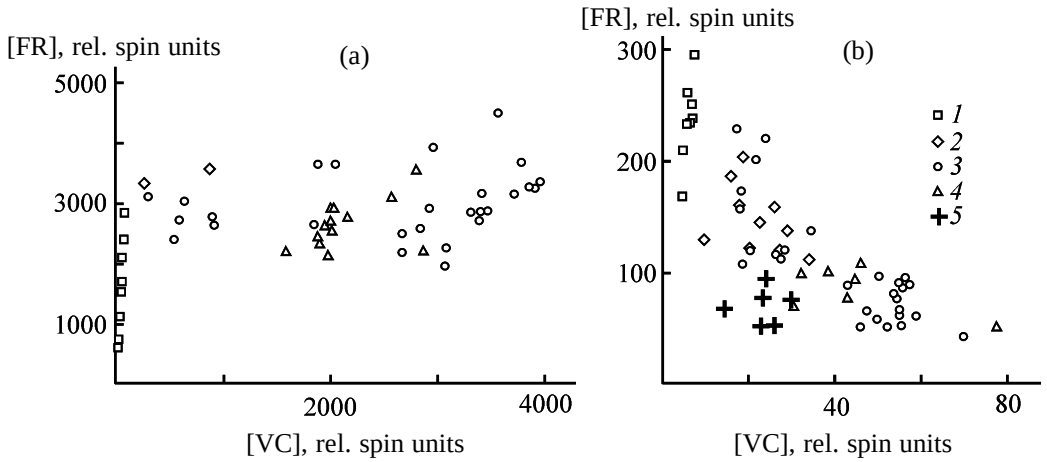


Fig. 1. Variation of the FR content with increasing concentration of the VCs in (a) crude oils from deposits of different ages and (b) asphaltenes. ([FR], [VC]) Contents of FRs and VCs, respectively; the same for Fig. 4. Geological age of the objects under study: (*1*) Middle Devon, (*2*) Upper Devon, (*3*) Lower Carbon, (*4*) Middle Carbon, and (*5*) Perm.

cavity. The line intensity of free radicals was determined from the amplitude of a separate line at the center of the ESR spectrum. To calculate the intensity of the lines belonging to vanadyl complexes, we measured the amplitude of the +1/2 line neighboring with that of a free radical in the region of a weaker magnetic field.

To determine the content of paramagnetics in crude oil asphaltenes, we used ampules with the internal diameter of 3 mm made of molybdenum glass which gave no noticeable signal in the ESR spectrum. The ampules were compactly packed with asphaltenes to a height of 13–14 mm; the sample was located in the region corresponding to the maximal sensitivity of the cavity. The signal intensities of free radicals and vanadyl complexes were calculated in relative spin units per gram of a substance (rel. spin units/g). The content of free radicals was additionally recalculated with different signal widths taken into account.

Figure 1 presents the measured contents of FRs and VCs in crude oils and oil asphaltenes. The relativity of the units for measuring the content of paramagnetics in crude oils differs from that for asphaltenes. This hinders comprehensive analysis of our results, and we have to restrict ourselves to the search for general trends in variation of the FR content with increasing VC concentration.

We suggest a method to unify the relative units for measuring the concentration of paramagnetics in crude oils and asphaltenes. To avoid technical problems mentioned in the introduction, we compared the content of vanadium in the oil objects, determined by direct flame atomic absorption spectrometry ("total vanadium"), with that of paramagnetic vanadium, determined by ESR.

Using the concentrations of the total vanadium in crude oils and asphaltenes and the V^{4+} content, we plotted the $\log[VC] = f(\log[V])$ dependence for crude oils and asphaltenes (Fig. 2).

It is seen that, for both crude oils and asphltenes, the plots of the content of the vanadyl complexes vs. the total vanadium content are straight lines with almost identical slopes.

Having solved a system of equations describing the dependences of the content of VCs on the total vana-

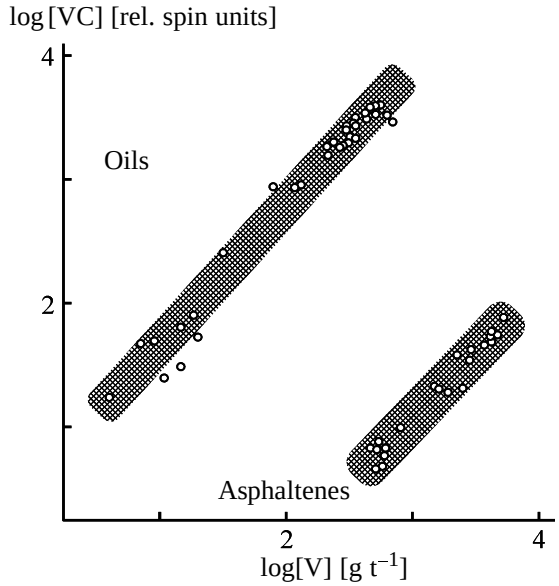


Fig. 2. Variation of the VC content in asphaltenes with the V content in crude oils and asphaltenes. ([VC], [V]) Contents of VCs and V, respectively.

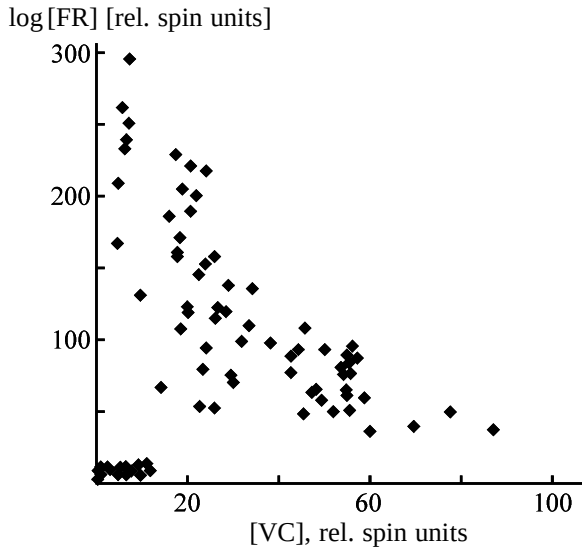


Fig. 3. Variation of the FR content with increasing VC concentration in crude oils and asphaltenes. ([FR], [VC]) Contents of FRs and VCs, respectively.

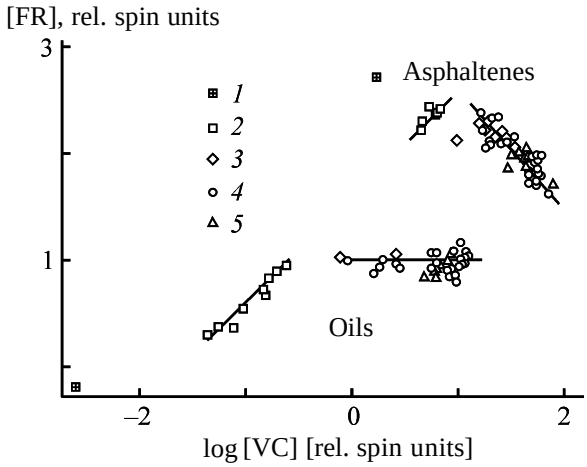


Fig. 4. log[FR] vs. log[VC] plots in crude oils and asphaltenes from deposits of different ages. Geological age of the objects under study: (*1*) Cambrian, (*2*) Middle Devon, (*3*) Upper Devon, (*4*) Lower Carbon, and (*5*) Middle Carbon.

dium content, we found a dimensionless coefficient, $10^{2.5}$, which brings the concentrations of paramagnetics in crude oils to an identity with that in asphaltenes.

Thus, the FR–VC scale for crude oils can be converted to that for asphaltenes using the following equations:

$$\log[VC_c] = \log[VC_i] - 2.5$$

$$\log[FR_c] = \log[FR_i] - 2.5$$

where c refers to the converted values, rel. spin units, and i, to the initial values, rel. spin units.

Recalculation of all the data for crude oils yielded an "integrated" plot of the FR content vs. the VC concentration for crude oils and asphaltenes (Fig. 3).

A huge (by a factor of $10^{2.5}$) difference in the concentrations of paramagnetics in crude oils and asphaltenes hinders visual perception and examination of the resulting dependences. Therefore, it is more convenient to characterize the VC and FR content with logarithms of their relative contents (log[VC] and log[FR], respectively) (Fig. 4).

In crude oils and asphaltenes with a low content of vanadium, the FR and VC concentrations vary in the same direction. In vanadium-rich crude oils, the FR content weakly changes with increasing VC content, and in asphaltenes it decreases.

CONCLUSIONS

(1) A methodical approach to analysis of paramagnetics in crude oils and asphaltenes was suggested. It consists in unification of the relative measurement units for the concentrations of vanadyl complexes and free radicals in crude oils and asphaltenes by comparing the content in oil objects of vanadium, determined by atomic absorption spectroscopy, with that of paramagnetic vanadium, determined by ESR.

(2) The resulting "integrated" pattern of distribution of crude oils and asphaltenes in the coordinates of the concentrations of free radicals and vanadium complexes simplifies studies of distribution of paramagnetics and throws light on a number of structural features of asphaltenes.

REFERENCES

1. Pokonova, Yu.V. and Speight, J.G., *Ispol'zovanie neftyanykh ostatkov* (Use of Oil Residues), St. Petersburg, IK SINTEZ, 1992.
2. Unger, F.G. and Andreeva, L.N., *Fundamental'nye aspekty khimii nefti: priroda smol i asfal'tenov* (Fundamental Aspects of Petroleum Chemistry: Nature of Resins and Asphaltenes), Novosibirsk: Nauka, 1995.
3. Tagirzyanov, M.I., Yakubov, M.R., Morozov, V.I., and Galimov, R.A., *Interval: Pered. Neftegaz. Tekhnol.*, 2003, no. 12(59), pp. 26–28.
4. RF Inventor's Certificate no. 1749793.

Russian Journal of Applied Chemistry, Vol. 78, No. 7, 2005, pp. 1197–1198. Translated from Zhurnal Prikladnoi Khimii, Vol. 78, No. 7, 2005, pp. 1218–1219.
Original Russian Text Copyright © 2005 by Kukharev, Stankevich, Klimenko, Lelyukh, Kukhareva, Timofeeva.

BRIEF COMMUNICATIONS

Polyvinyloxyalkylammonium Chlorides and Their Use in Pressure Flotation of Lignin Sludge

B. F. Kukharev, V. K. Stankevich, G. R. Klimenko, T. F. Lelyukh, V. A. Kukhareva, and S. S. Timofeeva

Favorskii Irkutsk Institute of Chemistry, Russian Academy of Sciences, Siberian Division, Irkutsk, Russia

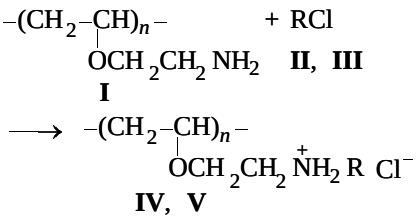
Received March 2, 2005

Abstract—Polyvinyloxyalkylammonium chlorides were synthesized in up to 82% yields by alkylation of monoethanolamine polyvinyl ether with higher alkyl chlorides. The suitability of the resulting polyvinyloxyalkylammonium chlorides for treatment of lignin-containing wastewater by pressure flotation was tested.

The suitability of water-soluble polymers for wastewater treatment is well known [1]. One of serious environmental problems in pulp and paper industry is more efficient exploitation of the acting complex facilities for wastewater treatment to remove such a large-capacity waste as lignin. Modern technology of wastewater treatment to remove lignin consists in flotation of lignin sludge with polyacrylamide (PAA) [2].

In this work we synthesized polyvinyloxyalkylammonium chlorides from monoethanolamine polyvinyl ether and tested them as flotation agents in pressure flotation of lignin sludge.

Monoethanolamine polyvinyl ether **I**, prepared by polymerization of monoethanolamine vinyl ether [3], was alkylated with equimolar amount of dodecyl chloride **II** or hexadecyl chloride **III**. The resulting polyvinyloxyalkylammonium chlorides **IV** and **V** were isolated by reprecipitation:



where n = 6–9; R = $C_{12}H_{25}$ (**II**, **IV**) or $C_{16}H_{33}$ (**III**, **V**).

The flotation properties of polyvinyloxyalkylammonium chlorides **IV** and **V** were studied with real lignin sludge currently treated at the Baikal Pulp and Paper Combine (BPPC).

The results of our experiments are presented in the table. It is seen that changing from polyacrylamide to polyvinyloxyalkylammonium chlorides, even in a concentration by a factor of 1.3 lower, allows the flotation rate to be increased by a factor of 1.8–2.5. Furthermore, the wastewater treatment efficiency is improved as regards both the color index (by 5.2–5.7%) and the content of suspended matter (by 3–6.5%). At identical concentrations of these reagents, the flotation rate increases by a factor of 2.37–2.75, and the wastewater treatment efficiency, by 6.5–6.8 and 6.5–11.3% for the color index and the content of suspended matter, respectively.

EXPERIMENTAL

Poly-*N*-(2-vinyloxyethyl)-*N*-dodecylamonium chloride IV. To a solution of 87 g (1 mol of monomeric units) of monoethanolamine polyvinyl ether **I** with a weight-average molecular weight of 720 in 500 ml of isopropyl alcohol, 204.8 g (1 mol) of dodecyl chloride was added, and the resulting mixture was refluxed for 16 h. The solution was cooled, and then petroleum ether was added until the polymer ceased to precipitate. The resulting polymer was isolated and vacuum-dried; 239.4 g (82%) of polymer **IV** was obtained as a viscous dark-brown resin.

Found, %: C 65.31, H 11.03, Cl 12.44, N 4.52. $C_{16}H_{34}ClNO$.
Calculated, %: C 65.84, H 11.74, Cl 12.15, N 4.80.

Poly-*N*-(2-vinyloxyethyl)-*N*-hexadecylamonium chloride V. Similar to **IV**, 87 g of monoethanolamine polyvinyl ether **I** and 260.9 g of hexadecyl chloride

1070-4272/05/7807-1197 © 2005 Pleiades Publishing, Inc.

Results of wastewater treatment to remove lignin sludge using polyvinyloxyalkylammonium chlorides **IV** and **V** and PAA as flotation agents

Reagent	Reagent dose, mg l^{-1}	Flotation time, min	Treatment efficiency, %		Average rate constant of flotation, min^{-1}
			in color index	in content of suspended matter	
IV	60	2	91.1	62.4	0.15
		5	93.4	66.6	
		10	94.2	73.1	
		15	95.2	74.4	
		20	95.7	81.3	
	80	2	92.5	64.8	0.19
		5	94.6	68.8	
		10	95.6	76.1	
		15	96.2	78.8	
		20	96.5	84.8	
V	60	2	90.0	60.0	0.20
		5	92.5	64.8	
		10	93.7	71.2	
		15	95.0	74.8	
		20	95.2	84.8	
	80	2	92.5	64.8	0.22
		5	95.1	68.8	
		10	95.6	76.1	
		15	96.8	80.8	
		20	96.8	89.6	
PAA	80	20	90.0	78.3	0.08

yielded 271.4 g (78%) of polymer **V**.

Found, %: C 69.48, H 12.52, Cl 10.31, N 3.78. $C_{20}H_{42}ClNO$.
Calculated, %: C 69.03, H 12.16, Cl 10.19, N 4.02.

To a 500-ml wastewater sample containing 4 g l^{-1} of lignin sludge (pH 5.3), 6.4 ml of 0.8% solution of ammonium sulfate and 3–4 ml of 1% aqueous solution of polyvinyloxyalkylammonium chloride **IV** or **V** was added. The resulting mixture was fed into a 1-l flotation column and saturated with air at a pressure of 0.2 MPa. Next, the pressure was released, and the rate of compaction of lignin sludge was monitored from migration of its boundary. For each time period, we calculated the first-order rate constant of flotation and then the average constant throughout the flotation period (20 min). The characteristics of the treated water were determined by known methods.

CONCLUSIONS

(1) The polyvinyloxyalkylammonium chlorides synthesized accelerate the pressure flotation by a factor of 2.3–2.75 compared to polyacrylamide.

(2) When polyvinyloxyalkylammonium chlorides are used in identical with polyacrylamide amounts, the efficiency of treatment of lignin-containing wastewaters is 89.6 and 96.8% in the content of suspended matter and color index, respectively. This is, respectively, 11.3 and 6.8% greater than the efficiencies achieved with polyacrylamide.

REFERENCES

1. Veitser, Yu.I., *Vysokomolekulyarnye flokulyanty v protsesse ochistki vody* (Macromolecular Flocculants in Water Treatment), Moscow: Stroiizdat, 1975.
2. Leonov, S.B., Rusetskyaya, G.D., and Mel'nikova, V.S., Abstracts of Papers, *III Vsesoyuznaya konferentsiya "Vodorastvorimye polimery i ikh primenenie"* (III All-Union Conf. "Water-Soluble Polymers and Their Application", Irkutsk: Vostochno-Sibirskaya Pravda, 1987, p. 222.
3. Chekulaeva, I.A., Lipovich, I.V., and Shostakovskii, M.F., *Izv. Akad. Nauk SSSR, Otd. Khim. Nauk*, 1963, no. 3, pp. 535–540.

Russian Journal of Applied Chemistry, Vol. 78, No. 7, 2005, pp. 1199–1201. Translated from Zhurnal Prikladnoi Khimii, Vol. 78, No. 7, 2005, pp. 1220–1222.
Original Russian Text Copyright © 2005 by Gaikalova, D'yakonov.

BRIEF COMMUNICATIONS

Influence of the Components of the Conserving Polymeric Composition on Preservation of a Photographic Image

E. S. Gaikalova and A. N. D'yakonov

St. Petersburg State University of Motion Pictures and Television, St. Petersburg, Russia

Received December 9, 2004; in final form, June 2005

Abstract—The possibility of improving a latex composition for conservation of archival and historically valuable photodocuments by introducing additives was substantiated. The inertness of these additives to the photographic materials during long-term storage was tested.

A vast amount of photographic materials is of historical and art value, and their careful preservation is an important task. Wide application in restoration practice is found by polymeric materials, of which aqueous polymeric dispersions are the most promising.

Along with film-forming substances, latexes contain various functional additives such as, e.g., conservants, making them resistant to mold formation and bacterial degradation, as well as foam quenchers and inhibitors preventing corrosion of the surface being protected.

To impart additional characteristics to latex compositions for conservation of photographic documents, it seems reasonable to introduce into them such additives as biocidal systems and light stabilizers.

A special place is occupied by coalescent additives intended for formation of a uniform polymer phase at lower and more technologically "convenient" temperatures, at which the "barrier" of the glassy state, characteristics of (co)polymers, is overcome. Generally, coalescence of globules consists in their mutual approach, followed by deformation and contacts with one another. When the protecting barrier is eliminated (by introducing coalescents), such mutual approach should have a fluctuation character. If the barrier is preserved, it is overcome owing to moisture evaporation, because the globules are forced to approach one another to distances shorter than the critical distance. The amount of water retained in the interglobular spaces is insufficient for hydration of the protecting layers, and the system gets destabilized [1].

Some latex brands do not require introducing coalescents, while formation of films from other brands requires introducing coalescents. Suitable as coalescents are nontoxic substances dissolving the polymer, which are usually selected taking into account the donor–acceptor mechanism of dissolution. Coalescents should act as solvents and plasticizing agents with respect to polymers and also be volatile, but they should evaporate not very fast and at a controllable rate.

In conservation of photodocuments, one of the most significant criteria governing the choice of coalescents is their absolute inertness to photographic materials during long-term storage. Hence, in this work we chose as conservants methylene chloride (MC), ethanol (E), and acetone (A), used in preparation of the base for film and photographic materials and satisfying the above-mentioned requirements.

Our experiments showed (Table 1) that the coalescent being introduced virtually does not affect the preservation of the image. Thus, the choice of coalescents should be dictated by their physicochemical properties. From the viewpoint of the uniform character of application of the coating and the time of its drying, as well as of the above-mentioned factors, methylene chloride seems the most acceptable coalescent, as confirmed by its solubility parameters ($J^{1/2}$ $cm^{-3/2}$):

PMMA	18.6
MC	19.8
A	20.5
E	26.0

These data show that the solubility parameters are the closest for solid poly(methyl methacrylate) (PMMA) and solvent, MC.

From the viewpoint of the solvency, the most advantageous is the solvent whose solubility param-

1070-4272/05/7807-1199 © 2005 Pleiades Publishing, Inc.

Table 1. Variation of the optical density of the monochrome photographic paper samples (%) relative to the initial optical density during long-term (450 h) forced aging

Copolymer coating*	Blue sample	Purple sample	Yellow sample	White sample	Black sample
S–BA + A	4.5	0.8	0.9	15.7	1.5
S–BA + MC	3.2	1.0	1.1	16.9	1.9
S–BA + E	3.2	0.8	1.6	9.0	0.9
BA–MMA + A	2.4	1.8	2.5	23.8	1.0
BA–MMA + MC	3.6	1.7	2.7	26.0	0.9
BA–MMA + E	3.0	1.6	2.1	18.4	1.6

* S–BA is copolymer of styrene (S) with butyl acrylate (BA), and BA–MMA, copolymer of BA with methyl methacrylate (MMA).

Table 2. Variation of the optical density of the monochrome photographic paper samples relative to the initial optical density during dark aging. Humidity 100%, temperature 60°C

Copolymer coating	Blue sample	Purple sample	Yellow sample	White sample	Black sample
S–BA	4.5/3.8*	3.2/2.8	1.1/1.5	38.3/28.3	5.4/3.4
	4.9/3.3	3.1/2.8	1.2/1.7	44.3/35.3	6.3/4.1
	3.9/3.8	2.9/2.1	1.1/1.6	40.7/35.7	5.5/3.3
B**–S	3.8/2.8	2.5/1.9	0.7/1.1	28.8/24.8	4.0/1.8
BA–MMA	3.6/3.0	1.8/1.5	0.5/0.5	21.6/23.6	3.2/1.0
Reference	6.3/5.6	3.3/3.3	1.6/2.6	54.8/46.8	8.4/7.2

* Samples coated with latexes with/without biocide introduced.
** B is butadiene.

eter is equal to that of the solid substance, which will accelerate coalescence as well.

Protection of archival documents against biodamage is extremely important for their long-term preservation. Microbiological studies in this area are carried out along the following lines: (1) studies of microorganisms; (2) development of methods; and (3) infection prevention.

For restoration and preservation–prevention purposes, film and photographic documents are treated with fungicidal preparations [2].

By imparting antiseptic properties to a latex-based conserving composition, it is possible to prevent not only bacterial damage to the polymer but also mold damage to the archival material intended for long-term storage, as well as repeated damage to the material after the restoration treatment.

There are two lines in protection of film and photographic documents against biodamage. The first line consists in selection of such ingredients for polymeric compositions that do not serve as nutrition sources for fungi and bacteria, and the second line, in introduction of biocides (chemical agents protecting against biodamage) into the polymeric formulation. The latter line is advantageous, since it allows preparation of biostable materials with the desired set of properties.

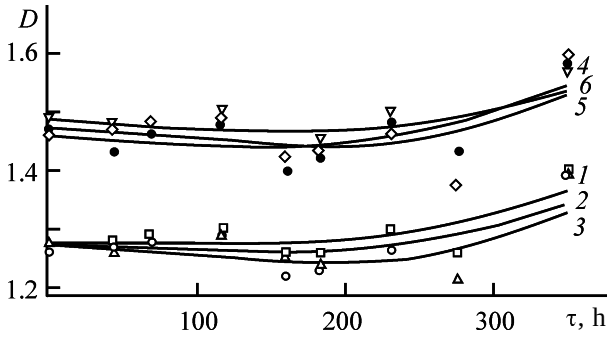
The biocidal system being introduced must not only prevent biological damage to the material but also be absolutely inert to the material during long-term storage.

In view of the fact that introduction of biocides is required for materials to be stored at elevated humidities, we carried out the experiments in a thermostat at 100% humidity and 60°C. For procedure of monitoring the constancy of the humidity, see [3].

Table 2 shows that the results of our experiments on aging of a coating with and without a biocidal additive at a constant temperature are fairly consistent with each other. This suggests that the biocide does not influence the conservation power of the latex and preservation of the photographic material.

Of no less importance is introduction into the formulation of the conserving composition of substances enhancing the light stability of the polymer.

Light exposure causes various transformations in the polymer, leading eventually to its degradation. Exposure to solar radiation with $\lambda > 290$ nm near the Earth surface leads to formation of radicals and is accompanied by polymer degradation [4].



Influence of the light stabilizer on variation of the optical density *D* of the image of a paper-based positive material under UV radiation exposure. λ = 254 nm. (τ) Time. Copolymer: (*1*, *4*) Styrene–butyl acrylate, (*2*, *5*) styrene–butadiene, and (*3*, *6*) butyl acrylate–methyl methacrylate. Material coated with copolymer: (*1*–*3*) without and (*4*–*6*) with stabilizer.

There are several methods to protect the polymer: (1) light reflection by filling agents reflecting UV or visible radiation; (2) introduction of UV light absorbers, namely, those from a class of substances that absorb light and whose reaction products then emit energy as a heat, whereupon the system returns to the initial state; (3) introduction of the so-called excited state quenchers, i.e., substances converting the polymer from an excited to the ground state; and (4) introduction of highly efficient stabilizers, whose photodegradation yields stable radicals reacting with the primary radicals generated by photolysis of the polymers, thus terminating the photodegradation chains.

Our data (see figure) show that introduction of light-stabilizing additives substantially depresses yellowing of the photographic paper, which is manifested most prominently in variation of the optical density of white samples.

CONCLUSION

The above-mentioned classes of substances are suitable for conservation of archival and historically valuable photodocuments, since they perform the main function of the additives introduced, namely, impart additional characteristics to the conserving polymeric composition and are inert to photographic materials during long-term storage.

REFERENCES

1. Erkova, L.N., *Lateksy* (Latexes), Leningrad: Khimiya, 1983.
2. *Obespechenie fiziko-khimicheskoi sokhrannosti kino-fotodokumentov i mikrofil'mov* (Ensuring Physicochemical Preservation of Film and Photographic Documents and Microfilms), Krestovskaya, K.V. and Mikhailov, O.L., Eds., Moscow: NIItsentr Tekhnicheskoi Dokumentatsii SSSR, 1981.
3. Benval'd, S.A., Kartuzhanskii, A.L., and Potapovich, S.I., *Tekh. Kino Televid.*, 1989, no. 1, pp. 14–15.
4. Ivanova, A.V., *Restavratsiya, issledovanie i khranenie muzeinykh khudozhestvennykh tsennostei* (Restoration, Investigation, and Storage of Items of Art Value in Museums), Moscow, 1983.

Russian Journal of Applied Chemistry, Vol. 78, No. 7, 2005, pp. 1202–1203. Translated from Zhurnal Prikladnoi Khimii, Vol. 78, No. 7, 2005, pp. 1223–1224.
Original Russian Text Copyright © 2005 by the Editorial Board.

OBITUARIES

Florentina Alekseevna Belinskaya

On June 2, 2005, our science suffered a severe loss. Florentina Alekseevna Belinskaya, doctor of chemical science, professor, leading researcher of the Chemical Faculty and the Research Institute for Chemistry of St. Petersburg State University, and, for a long time, active member of the Editorial Board of *Zhurnal Prikladnoi Khimii* (Russian Journal of Applied Chemistry), died at the age of 76.



In 1953, a young graduate from the Chair of Physical Chemistry, Florentina Alekseevna was left at the University as a post-graduate student and, since that time, worked at the Leningrad (St. Petersburg) University. Showing a goal-seeking behavior and persistence in overcoming the difficulties encountered in solving scientific problems, Florentina Alekseevna made a career from a student and post-graduate student, whose work was supervised by Academician B.P. Nikol'skii, to a professor, head of laboratory, and a leading specialist in theory and practice of ion exchange and chromatography.

Having defended her candidate dissertation devoted to electrode properties of membranes made of organic ion-exchange resins in 1959, Belinskaya took active part in the development of work on ionometry and then headed a new promising area of synthesis and physicochemical studies of inorganic ion-exchange materials. Just in this area of research, Florentina Alekseevna's work received ample recognition and support among her colleagues, "ion-exchange researchers," in the Soviet Union and abroad. In 1974, she became head of the Laboratory of Ion Exchange at the Chair of Physical Chemistry, in which whole classes of new inorganic sorbents were synthesized on the basis of oxygen compounds of antimony, titanium, silicon, tin, tellurium, and mixed oxyhydrates of these elements. A generalization of the diverse experimental data obtained enabled Belinskaya to suggest a truly pioneering approach to description of inorganic ion exchangers as polymeric complex compounds. In 1984, Florentina Alekseevna defended her doctoral dissertation "Fundamental Aspects of Ion Exchange on Inorganic Ion-Exchange Materials," in which she formulated for the first time the basic principles of directed synthesis of inorganic compounds with predictable properties and presented an original technique for thermodynamic description of the ion-exchange equilibrium, named the step-exchange method by her.

Florentina Alekseevna Belinskaya had never been an armchair scientist having no idea about what might be the practical importance of her work. Her distinctive feature was persistence in a search for the possible practical implementation of her scientific ideas. She received as a co-author about fifteen inventor's certificates and was awarded the "Inventor of the USSR" badge. The list of scientific-technological and humanitarian programs in which Florentina Alekseevna took direct part is rather extensive: "Sorbents for Radionuclides," "High Technology," "Environmental Safety of Russia," etc. Undoubtedly, the most prominent and interesting practical applications are radioprotective medicinal preparations Polisur'min, an antidote for radioactive strontium, and Ferrotsin, which removes radioactive cesium from human and animal bodies. In addition, Ferrotsin can serve as an antidote in poisoning with thallium salts and can also be used to adjust the electrolyte composition of blood. These preparations were created at the laboratory of ion exchange, in cooperation with medical researchers, on the basis of inorganic ion-exchange materials. After the Chernobyl accident, Florentina Alekseevna Belinskaya went to a special business trip to Perm oblast to rapidly set up a process for manufac-

1070-4272/05/7807-1202 © 2005 Pleiades Publishing, Inc.

ture of Ferrotsin. Later, the ample experience in this area enabled Belinskaya to take part in the humanitarian program "Children from Chernobyl" and to work at the nongovernmental institution "Chernobyl–Help." For her studies of inorganic ion-exchange materials and development of radioprotective medicinal preparations, Belinskaya was awarded II Prize of Mendeleev All-Union Chemical Society in 1988 and II University Prize in 1989.

One more point of practical application of Belinskaya's scientific interests was integrated processing of natural mineral raw materials and large-tonnage industrial wastes. Owing to Florentina Alekseevna's ideas, wastes from a number of industries can be successfully converted into effective sorbents.

For many years of her life, Florentina Alekseevna was engaged in pedagogical activities. In 1991, Belinskaya was given an academic status of a professor in physical chemistry. She delivered courses of lectures on theory of ion exchange and fundamentals of chromatography at the chemical faculty and that of biology and soil science of St. Petersburg State University. An extremely broad-minded person, not confined to her narrow specialization, Florentina Alekseevna always came to understanding with young people and her ideas were captivating for them. She brought up more than 40 specialists, including candidates of science.

During the decades of her scientific activities, Florentina Alekseevna Belinskaya published more than 150 works, was a co-author of the textbook *Fizicheskaya khimiya. Teoreticheskoe i prakticheskoe rukovodstvo* (Physical Chemistry. Theoretical Foundations and Manual), monograph *Ionity v khimicheskoi tekhnologii* (Ion Exchangers in Chemical Technology); she was a scientific editor of 10 issues of the intercollegiate collection of works *Ionnyi obmen i ionometriya* (Ion Exchange and Ionometry) and of the book devoted to the centennial anniversary of Nikol'skii's birthday, *Akademik B.P. Nikol'skii. Zhizn'. Trudy. Shkola* (Academician B.P. Nikol'skii. Life. Works. School) (St. Petersburg State University, 2000).

Belinskaya was an organizer and permanent supervisor of the seminar "Chemistry and Technology of Inorganic Sorbents," which was established in 1972 as an unpretentious meeting of like-minded persons and then became international. It is largely due to her efforts that the city seminar "Ion Exchange, Chromatography, and Alternative Methods," held under the aegis of the Russian Chemical Society and formerly co-chaired by her, still continues to exist. Florentina Alekseevna was an active member of the Editorial Board of *Zhurnal Prikladnoi Khimii* and *Vestnik Sankt-Peterburgskogo universiteta* (Gerald of St. Petersburg University) and a member of specialized dissertation councils at St. Petersburg State University and State Technological University of Plant Polymers.

Florentina Alekseevna was a surprisingly persistent optimist. She was born and grew up in the family of a professional serviceman, she was familiar with the hardship of the migratory mode of life, wartime childhood, and hunger in youth. Maybe, just for this reason she could appreciate all the good that fell to her lot, liked and understood the poetry, painting, and music. Florentina Alekseevna was a person with high moral criteria, who was faithful to her choice not only in the profession, but also in her private life. She was hand in hand with a loving husband for 51 years, brought up wonderful children, son and daughter, three excellent grandchildren, and was lucky to see her great-grandson. It is difficult to Florentina Alekseevna's relatives and colleagues to bear with her death.

Florentina Alekseevna left a firm trace in that area of physical chemistry to which she devoted her whole life. Her works will long serve her disciples and followers as a source of fruitful ideas.

St. Petersburg State University; Editorial Board and Editorial Staff of *Zhurnal Prikladnoi Khimii*

Russian Journal of Applied Chemistry, Vol. 78, No. 7, 2005, pp. 1204–1207. Translated from Zhurnal Prikladnoi Khimii, Vol. 78, No. 7, 2005, pp. 1225–1228.
Original Russian Text Copyright © 2005 by Morachevskii.

HISTORY OF CHEMISTRY AND CHEMICAL TECHNOLOGY

Professor Aleksandr Aleksandrovich Krakau (to 150th Anniversary of His Birthday)

A.A. Krakau, professor of chemistry at Emperor Alexander III Electrotechnical Institute in St. Petersburg, occupies an honorable place in the history of domestic chemistry owing not only to his studies in the field of organic chemistry, but also to the fact that he was the first who started to deliver a special course of electrochemistry and organized training of electrochemical engineers.

Aleksandr Aleksandrovich Krakau was born on July 30 (August 11), 1855, in St. Petersberg in a rather well-cultured family. His father Aleksandr Ivanovich Krakau was a known architect, and his mother, Anna Vasil'evna (nee Grigorovich) was of artistic origin [1]. Having finished Mai Gymnasium, one of the best in St. Petersburg [2], Krakau entered the natural department of the physicomathematical faculty of St. Petersburg State University in 1873. Already when being a student, he commenced experimental studies in the area suggested by A.M. Butlerov (1828–1886, academician since 1874). On May 4(16), 1887, at a meeting of the Russian Physicochemical Society, Krakau reported on his studies of styrene polymerization under the action of alkali metals [3]. This work was an important part in the investigations of polymerization of unsaturated compounds, carried out by Butlerov and his disciples. At the end of April 1879, Krakau graduated from the university with a degree of candidate and was left at the university for two years to be prepared for pedagogical activities.

In May 1881, Krakau became a laboratory assistant at the chemical laboratory of the Academy of Sciences, where his work was first (till August 1886) supervised by Butlerov and later (till January 1891) by N.N. Beketov (1827–1911, academician since 1886). Beginning in 1888, Krakau occupied the position of a senior laboratory assistant.

Simultaneously, in those same years, Krakau was engaged in pedagogical activities. In 1880–1883, he was Butlerov's lecturer's assistant at St. Petersburg women's (Bestuzhev) courses, and in 1883–1884, supervised laboratory exercises on analytical chemistry. The Bestuzhev courses, opened in 1878, were the first Russia's women's university, at which lectures were delivered and laboratory exercises were supervised by leading scientists of St. Petersburg [4].



Aleksandr Aleksandrovich Krakau

In June 1886, the first Russia's Technical School of the Postal-Telegraph Service was organized in St. Petersburg. In the last quarter of the XIX century, the leading position among all areas of electrical engineering was occupied by telegraphy, and training of specialists in this field undoubtedly satisfied the demand of the country. Krakau was invited to teach chemistry at this educational institution. In June 1891, the technical school was reorganized into Electrotechnical Institute, with the education term increased from three to four years. Finally, in June 1898, a five-year education term was established and the institute was given all the rights of a higher-school institution.

In 1891, Krakau completely turned to teaching of chemical disciplines at the Electrotechnical Institute and became a professor. In addition to the general course of chemistry, he taught, beginning in 1892, foundations of electrochemistry in the form of the course "Study of Voltaic Cells" [5]. Since 1895,

1070-4272/05/7807-1204© 2005 Pleiades Publishing, Inc.



Main building of the Electrotechnical Institute (1905).

Krakau was not only engaged in pedagogical activities, but also occupied the position of the head of studies at the Institute. Krakau made a major contribution to the reorganization of the Electrotechnical Institute into a higher-school institution with a five-tear education term, he took an active part in all meetings at which the corresponding decision was made. The curriculum developed in 1898 included electrochemistry as an independent discipline subdivided into theoretical foundations of electrochemistry and applied electrochemistry. The studies of the course were accompanied by laboratory exercises in the specially designed electrochemical laboratory. The new curriculum also included physical chemistry, taught by the already known, by that time, scientist N.S. Kurnakov (1860–1941, academician since 1913), professor of the Mining Institute. The studies of the course were accompanied by laboratory exercises, supervised by N.A. Pushin (1875–1947), a laboratory assistant of the chair. A graduate from St. Petersburg University, a well-educated specialist, and a closest associate of Kurnakov, Pushin made a major contribution to the development of the chair of chemistry at the Electrotechnical Institute. He became an extraordinary professor in 1909 and ordinary professor in 1913, and emigrated in 1920 [6, 7]. The curriculum also included studies of technical chemistry.

The gradual increase in the number and volume of chemical disciplines led to a fundamental change of the Institute's curriculum. By Krakau's initiative and with an active involvement of Pushin, two departments, electrotechnical and electrochemical, with separate admission of first-year students were organized at the Institute. The necessity for intensive development of the electrochemical industry in Russia required that engineers of the corresponding specialties should be trained in due time. In Krakau's opinion, an electrochemist should not only be well chemically educated, but also be a good physicist and possess a comprehensive knowledge in electrical engineering. Such a combination of chemical and electrotechnical disciplines was characteristic of the curriculum of the newly created electrochemical department. Thus, two higher school institutions in St. Petersburg, Emperor Alexander III Electrotechnical Institute and Emperor Peter the Great Polytechnic Institute, opened in 1902, started training of broad specialists in electrochemical engineering already at the very beginning of the XX century. The Polytechnic Institute had, since the time of its organization, an electrochemical subdepartment as a part of the metallurgical department.

In 1893, Krakau published the first edition of his textbook on electrochemistry (second edition, in 1898). This was the first textbook on electrochemistry written in Russia.

Being head of studies (inspector) at the Institute,

Krakau was, together with the director of the Institute, N.N. Kachalov (1852–1909) and other known scientists, a member of the Commission that supervised the construction of a new complex of buildings for the Institute, at the intersection of Aptekarskii avenue and Pesochnaya street (now Professor Popov street). The construction work was commenced in May 1900, and the Institute moved to its new buildings in 1903. The construction work was carried out under supervision of A.N. Vekshinskii, an academician of architecture. Krakau paid a considerable attention to equipment of chemical laboratories, went to business trips abroad, and visited laboratories at some of the best-known scientific centers. Four laboratories were organized in the new complex of buildings: those of inorganic chemistry, physical chemistry, analytical chemistry, and electrochemistry. In 1903, the Council of the Electrotechnical Institute conferred on Krakau the title of honorary electrical engineer.

Two periods can be distinguished in Krakau's scientific activities: the first, associated with investigations in the field of organic chemistry, and the second, with electrochemistry as new branch of physical chemistry by that time. As already mentioned, Krakau was the first to pay attention to the ability of alkali metals to initiate polymerization of unsaturated hydrocarbons. Unfortunately, the study was not published in full measure. This idea was further developed by M.G. Kucherov (1850–1911) and I.L. Kondakov (1857–1931). Krakau's work and its impact on the development of further studies in the field of polymerization with the use of alkali metals were analyzed in detail by K.B. Piotrovskii [8].

In 1885–1887, Krakau published in *Zhurnal Russkogo Fiziko-Khimicheskogo Obshchestva* (Journal of the Russian Physicochemical Society) and in French chemical journals quite a number of papers devoted to the action of caustic alkalis on cinchonine, quinine, and quinidine. Krakau also observed hindrance to polymerization of unsaturated compounds by iodine, sulfur, and bromine [8].

In 1892 was published first Krakau's electrochemical study. He examined the operation of various types of Meidinger cells, widely used at that time in communication systems [9]. Later appeared a number of Krakau's publications concerned with electrical conductivity and dissociation pressure of palladium compounds with hydrogen. In 1898, he published a paper devoted to the method suggested by Herz for electrochemical ac/dc conversion. At that year, Krakau took part in the congress of electrochemists in Munich and published a detailed report about this event [10].

In early January 1900, Krakau delivered at the first All-Russia electrotechnical congress a detailed report "On the Modern State of the Electrochemical Industry" [11]. The same topic was analyzed with account of new evidence in a large report "An Outline of the Development and Modern State of the Electrochemical Industry" at the First Mendeleev Congress on General and Applied Chemistry, held in St. Petersburg at the end of December 1907 [12]. The author analyzed in detail the processes of refining of copper, silver, gold, and other metals, considered the possibility of manufacture of aluminum, magnesium, sodium, and calcium, and discussed prospects for production of chlorine and alkalis and for electrolysis of water. Krakau's report also considered electrothermal processes (manufacture of calcium carbide, phosphorus, etc.).

Krakau's contemporaries highly appreciated his pedagogical and scientific activities. One of the oldest at that time Russian chemists, academician Beketov, wrote in connection with the election of Krakau a professor of the Electrotechnical Institute in 1891: "...I personally know A.A. Krakau as my former assistant at the Laboratory of the Imperial Academy of Sciences. I could make certain not only of his all-round knowledge in all areas of chemistry, but also of his skill to conduct chemical and physicochemical investigations..." [8]. Krakau's experimental investigations and pedagogical activities in the field of chemistry and electrochemistry were also highly appreciated by Professor D.P. Konovalov (1856–1929, academician of the Academy of Sciences of the USSR since 1923) [8]. The role of Krakau in that St. Petersburg Electrotechical Institute was one of the most prominent centers of electrochemical research in the first quarter of the XX century is difficult to overestimate. Among those who worked at the Institute were, together with Pushin, I.V. Grebenshchikov (1887–1953, academician of the Academy of Sciences of the USSR since 1932), P.F. Antipin (1890–1960, academician of the Academy of Sciences of the USSR since 1939), M.S. Maksimenko (1878–1942), a prominent specialist in technology of electrothermal industries, and their disciples and co-workers. Aluminum and magnesium were for the first time produced from fully domestic raw materials [7] and foundations of manufacture of magnesium and sodium in Russia were laid at the laboratory of the Electrotechnical Institute, headed by Pushin, in 1913–1915.

Aleksandr Aleksandrovich Krakau, an ordinary professor of chemistry and electrochemistry at the Electrotechnical Institute, honorary electrical engineer, and senior state councilor, untimely died on March 16(29), 1909, at the age of fifty-three.

REFERENCES

1. Krakau, T.K., *Izv. Sankt-Peterb. Gos. Elektrotekh. Univ. "LETI," Ser. Istor. Nauki, Obraz. Tekh.*, 2001, no. 1, pp. 23–25.
2. *Pyatidesyatiletie shkoly K.I. Maya. 1856–1906* (50th Foundation Anniversary of Mai School 1856–1906), St. Petersburg, 1907.
3. Krakau, A.A., *Zh. Ross. Fiz.-Khim. O–va.*, 1878, vol. 10, no. 6, pp. 237–238.
4. Fedosova, E.P., *Bestuzhevskie kursy – pervyi zhenskii universitet v Rossii* (1878–1918) (Bestuzhev Courses, the First Women's University in Russia (1878–1918)), Moscow: Pedagogika, 1980.
5. *Leningradskii elektrotekhnicheskii institut imeni V.I. Ul'yanova-Lenina (1886–1961)* (Ul'yanov-Lenin Electrotechnical Institute in Leningrad (1886–1961)), Leningrad: Leningr. Univ., 1963.
6. Morachevskii, A.G., *Izv. Sankt-Peterb. Gos. Elektrotekh. Univ. "LETI," Ser. Istor. Nauki, Obraz. Tekh.*, 2002, no. 1, pp. 28–30.
7. Morachevskii, A.G., *Ocherki ob uchenykh-khimikakh Sankt-Peterburga* (Essays about Chemists of St. Petersburg), St. Petersburg: Politekh. Univ., 2004.
8. Piotrovskii, K.B., *Usp. Khim.*, 1954, vol. 23, no. 1, pp. 123–128.
9. Krakau, A.A., *Zh. Ross. Fiz.-Khim. O–va.*, 1892, vol. 24, no. 5, pp. 325–330.
10. Krakau, A.A., *Elektrotekh. Vestn.*, 1898, vol. 5, no. 49, pp. 33–43.
11. Krakau, A.A., in *Trudy Pervogo Vserossiskogo elektrotekhnicheskogo s''ezda* (Proc. First All-Russia Electrotechnical Congr.), St. Petersburg, 1901, vol. 2, pp. 172–185.
12. Krakau, A.A., in *Trudy Pervogo Mendeleevskogo s''ezda po obshchei i prikladnoi khimii* (Proc. First Mendeleev Congr. on General and Applied Chemistry), St. Petersburg, 1909, pp. 350–356.

A. G. Morachevskii

Russian Journal of Applied Chemistry, Vol. 78, No. 7, 2005, p. 1208. Translated from Zhurnal Prikladnoi Khimii, Vol. 78, No. 7, 2005, pp. 1229.
Original Russian Text Copyright © 2005 by Morachevskii, Beloglazov.

BOOK REVIEWS

Borovichskii kombinat ogneuporov (Borovichi Combine of Refractories)

Mozhzharin, V.A., Ed., Moscow: Ruda i Metally, 2005, 136 pp.

The book, whose publication was timed with the approaching 150th foundation anniversary of the enterprise, briefly describes the historical events associated with the revival of the refractory trade in Russia, development of the refractory industry in Borovichi, Novgorod oblast, and present-day state of affairs at Borovichi Combine of Refractories.

The book comprises an introduction and three parts. The brief introduction (pp. 3–6) gives a general notion of various aspects of the activities of the Borovichi Combine of Refractories, Open Joint-Stock Company and on solution of production-related and social problems. The first park of the book (pp. 7–36) is devoted to the history of manufacture of refractories in Borovichi. The availability of high-quality refractory clays had long been known, but serious attention to this fact was given only in mid-XIX century. After the railway between Moscow and St. Petersburg, passing at a distance of 30 km from Borovichi, was put in operation in 1851, it became possible to ship raw materials to large plants in St. Petersburg. The manufacture of refractories directly in Borovichi, set in 1855, is associated with the activities in Russia of Emmanuel Nobel (1801–1872) and sons. The production volume was approximately up to 100 hundred thousand refractory bricks per year. In view of the comparatively moderate demand for refractories, the plant was cost-inefficient and existed for only several years.

In 1880, a plant for manufacture of refractory bricks and other articles was constructed near Borovichi by K.L. Vakhter, a St. Petersburg businessman. The joint-stock company organized by him later, in 1897, became monopolist in Russia's market of refractories. In 1919, all Borovichi plants and mines were nationalized.

The second part of the book (pp. 37–100) contains comprehensive evidence concerning the operation of Borovichi Combine of Refractories under the present-day conditions. Since 1992, it has been a joint-stock company. The main consumers of its production are the largest plants of domestic ferrous metallurgy, Cherepovets, Novolipetsk, and Magnitogorsk combines, and other metallurgical and metal-working plants and enterprises of nonferrous metallurgy.

The third part of the book (pp. 101–132) is a catalogue of the products manufactured by the combine: a wide variety of aluminosilicate refractories, from fireclay to high-alumina types. In each type of aluminosilicate refractories, manufacture of varied-purpose articles has been mastered. Quite a number of articles of other kinds are produced.

The book provides a comprehensive idea of the creation history and modern state of the first Russia's industrial plant for manufacture of refractories and about its functioning in the conditions of market economy. The book is very well published and it contains a large number of photographs. It may be of use for teachers and students of the corresponding specialties of higher-school and post-secondary educational institutions and to consumers of various kinds of refractories.

A. G. Morachevskii and I. N. Beloglazov

1070-4272/05/7807-1208© 2005 Pleiades Publishing, Inc.

Russian Journal of Applied Chemistry, Vol. 78, No. 8, 2005, pp. 1209–1212. Translated from Zhurnal Prikladnoi Khimii, Vol. 78, No. 8, 2005, pp. 1233–1236.
Original Russian Text Copyright © 2005 by Lembrikov, Volkova, Konyakhina, Korneva, Pokidova.

INORGANIC SYNTHESIS AND INDUSTRIAL INORGANIC CHEMISTRY

A Study of Viscosity in the Extraction System Constituted by Tributyl Phosphate and Phosphoric Acid

V. M. Lembrikov, V. V. Volkova, L. V. Konyakhina, Z. N. Korneva, and O. V. Pokidova

Voskresenskii NIUiF (Voskresensk Research Institute of Fertilizers and Phosphoric Acid) Open Joint-Stock Company, Voskresensk, Moscow oblast, Russia

Received May 13, 2005

Abstract—Data on the kinematic viscosity of phosphoric acid solutions in technical-grade tributyl phosphate and in an industrial extract from a technological purification system based on tributyl phosphate, which contain 0–18% phosphoric acid in terms of P_2O_5, at 10–70°C are presented.

One of methods used to obtain pure phosphoric acid is purification of extraction phosphoric acid (EPA) with organic solvents. In Russia, Voskresenskii NIUiF (Voskresensk Research Institute of Fertilizers and Phosphoric Acid) Open Joint-Stock Company employs on the industrial scale a purification technique in which tri-*n*-butyl phosphate (TBP) serves as an extracting agent [1].

When working with the installation used to purify EPA, it is necessary to improve the quality of the acid manufactured and to raise the output capacity of the installation. This is achieved by selecting and developing a perfect equipment. Doing so requires that the physicochemical parameters of the extraction system, including the viscosity of an extract from the industrial technological system at various contents of phosphoric acid in the extract, should be known.

This communication presents data on the kinematic viscosity of phosphoric acid solutions in technical-grade tributyl phosphate [2] and in an industrial extract from a technological purification system based on technical-grade TBP, which contain 0–18% phosphoric acid in terms of P_2O_5, at 10–70°C. The choice of these temperature and concentration ranges was governed by real conditions of the industrial process for purification of extraction phosphoric acid. The solutions were prepared by saturating technical-grade TBP and the extracting agent from the industrial system.

The kinematic viscosity ν of organic solutions was measured with a capillary glass viscometer of the VPZh type. The content of phosphoric acid was determined potentiometrically [3]. The temperature of the experiments was maintained by thermostating within ±0.5°C. The resulting values of the kinematic viscosity are listed in Table 1.

A graphical analysis and mathematical processing of the data obtained demonstrated that the dependence $\nu = f(c, t)$ is logarithmic. It can be represented as

$$\ln \nu = ac + b, \quad (1)$$

where ν is the kinematic viscosity ($mm^2\ s^{-1}$); *c*, content of P_2O_5 (wt %); and *a*, *b*, coefficients of the equation.

Table 2 lists values of the coefficients *a* and *b*, as well as the approximation reliability R^2 for each curve. The data of Table 2 were used to plot the temperature dependences of the coefficients *a* and *b* (see figure) for technical-grade TBP and for the extracting agent from the industrial system. It is noteworthy that the temperature dependences of the coefficients are similar for both types of solutions.

The temperature dependence of the coefficient *a* can be described by the equation

$$a = kT + m, \quad (2)$$

and that of the coefficient *b*, by

$$b = n\exp(pT), \quad (3)$$

where *T* is temperature (°C); *k*, *m*, coefficients in Eq. (2); and *n*, *p*, coefficients in Eq. (3).

1070-4272/05/7808-1209 © 2005 Pleiades Publishing, Inc.

Table 1. Kinematic viscosity ν of phosphoric acid solutions in technical-grade TBP and in an extracting agent from the technological system

P_2O_5, wt %	10°C				20°C				30°C				40°C			
	ν, $mm^2 s^{-1}$	ln ν		Δ, %	ν, $mm^2 s^{-1}$	ln ν		Δ, %	ν, $mm^2 s^{-1}$	ln ν		Δ, %	ν, $mm^2 s^{-1}$	ln ν		Δ, %
		experiment	calculation			experiment	calculation			experiment	calculation			experiment	calculation	
Technical-grade TBP																
0	5.30	1.67	1.69	–1.54	3.97	1.38	1.40	–1.57	3.16	1.15	1.18	–2.65	2.85	1.05	0.99	5.76
0.05	6.72	1.91	1.70	10.63	4.17	1.43	1.41	1.32	3.67	1.30	1.19	8.50	3.12	1.14	1.00	12.44
4	9.18	2.22	2.49	–12.24	7.15	1.97	2.13	–8.24	5.43	1.69	1.84	–8.76	4.33	1.47	1.58	–7.70
5.4	17.97	2.89	2.77	4.22	9.86	2.29	2.38	–4.13	8.30	2.12	2.07	2.15	5.19	1.65	1.79	–8.54
11.6	56.41	4.03	4.00	0.81	35.06	3.56	3.51	1.29	23.22	3.14	3.09	1.64	16.60	2.81	2.70	3.78
Extracting agent from the industrial system																
0.03	5.92	1.78	1.82	–2.46	5.09	1.63	1.55	4.96	3.77	1.33	1.34	–1.21	3.25	1.18	1.17	0.94
2	7.94	2.07	2.14	–3.05	6.22	1.83	1.84	–0.86	4.51	1.51	1.62	–7.57	3.54	1.26	1.43	–12.95
3.28	9.74	2.28	2.34	–2.76	8.60	2.15	2.04	5.40	6.65	1.89	1.80	4.92	5.66	1.73	1.60	7.86
3.95	14.01	2.64	2.45	7.36	8.71	2.16	2.14	1.30	6.76	1.91	1.90	0.82	6.17	1.82	1.69	7.36
6.23	15.04	2.71	2.81	–3.61	12.13	2.50	2.48	0.70	8.83	2.18	2.22	–1.83	6.96	1.94	1.99	–2.42
14	53.12	3.97	4.05	–1.84	39.58	3.68	3.65	0.90	26.85	3.29	3.32	–0.76	20.34	3.01	3.01	–0.05
15	60.67	4.11	4.20	–2.42	43.61	3.78	3.80	–0.53	30.38	3.41	3.46	–1.24	22.54	3.12	3.15	–0.99
16	74.31	4.31	4.36	–1.29	58.19	4.06	3.95	2.90	31.25	3.44	3.60	–4.52	26.01	3.26	3.28	–0.62
18.5	119.82	4.79	4.76	0.50	81.12	4.40	4.32	1.70	56.54	4.03	3.95	2.09	38.61	3.65	3.61	1.22
P_2O_5, wt %	50°C				60°C				70°C				40°C*			
	ν, $mm^2 s^{-1}$	ln ν		Δ, %	ν, $mm^2 s^{-1}$	ln ν		Δ, %	ν, $mm^2 s^{-1}$	ln ν		Δ, %	ν, $mm^2 s^{-1}$	ln ν		Δ, %
		experiment	calculation			experiment	calculation			experiment	calculation			experiment	calculation	
Technical-grade TBP																
0	2.24	0.81	0.81	–0.09	2.00	0.69	0.63	8.62	1.73	0.55	0.45	17.23	2.85	1.05	1.20	–14.52
0.05	2.44	0.89	0.81	8.88	2.05	0.72	0.64	10.99	1.73	0.55	0.46	16.29	3.12	1.14	1.21	–6.19
4	3.46	1.24	1.33	–7.37	2.63	0.97	1.09	–12.64	2.05	0.72	0.84	–17.05	4.33	1.47	1.73	–18.02
5.4	3.52	1.26	1.51	–20.47					2.93	1.07	0.98	9.04	5.19	1.65	1.92	–16.43
11.6	11.65	2.46	2.33	5.28	7.62	2.03	1.95	3.81	5.16	1.64	1.58	3.75	16.60	2.81	2.74	2.54
Extracting agent from the industrial system																
0.03	2.55	0.93	1.01	–7.67	2.18	0.78	0.85	–9.39	1.83	0.61	0.70	–15.60	3.25	1.18	1.20	1.48
2	2.74	1.01	1.25	–24.03									3.54	1.26	1.47	15.44
3.28	4.37	1.47	1.41	4.59	3.87	1.35	1.22	9.62	3.18	1.16	1.04	9.80	5.66	1.73	1.64	5.65
3.95	5.09	1.63	1.49	8.44	4.04	1.40	1.30	6.96	3.57	1.27	1.11	12.54	6.17	1.82	1.72	5.23
6.23	5.14	1.64	1.77	–8.08	4.13	1.42	1.56	–9.94	3.30	1.19	1.35	–13.33	6.96	1.94	2.03	–4.46
14	14.11	2.65	2.73	–3.04	10.72	2.37	2.45	–3.18	7.79	2.05	2.17	–5.73	20.34	3.01	3.06	–1.46
15	16.01	2.77	2.85	–2.78	11.65	2.46	2.56	–4.33	8.38	2.13	2.28	–7.05	22.54	3.12	3.19	–2.37
16	19.15	2.95	2.97	–0.73	12.92	2.56	2.68	–4.59	14.45	2.67	2.38	10.87	26.01	3.26	3.32	–1.95
18.5	26.89	3.29	3.28	0.31	18.29	2.91	2.96	–1.89	12.60	2.53	2.64	–4.33	38.61	3.65	3.65	0.03

* Values of ln ν were calculated using *a* simplified equation (6) for the coefficient *b*.

Table 2. Coefficients a and b in Eq. (1) and approximation reliabilities R^2

Coefficients in Eq. (1)	Temperature, °C						
	10	20	30	40	50	60	70
Technical-grade TBP							
a	0.1957	0.1849	0.1664	0.1457	0.1347	0.1144	0.095
b	1.7183	1.3458	1.1799	1.0079	0.7637	0.6532	0.5066
R^2	0.9642	0.9910	0.9846	0.9669	0.9470	0.9760	0.9569
Extracting agent from the industrial system							
a	0.1574	0.1507	0.1405	0.1318	0.1247	0.1074	0.1034
b	1.8016	1.5859	1.3222	1.1741	0.9434	0.8717	0.7064
R^2	0.9933	0.9976	0.9933	0.9901	0.9843	0.9863	0.9475

Table 3. Coefficients and approximation reliabilities R^2 for Eqs. (2), (3), and (4)

Organic phase	Coefficients of Eq. (2)		R^2	Coefficients of Eq. (3)		R^2	Coefficients of Eq. (6)		R^2
	k	m		n	p		d	q	
Technical-grade TBP	–0.0017	0.2159	0.9945	2.129	–0.0155	0.9936	–0.0194	1.8017	0.9746
Extracting agent from the industrial system	–0.0009	0.1686	0.9852	2.096	–0.0198	0.9926	–0.0182	1.9283	0.9816

Table 3 lists the values of the coefficients in Eqs. (2), (3) and of the approximation reliability R^2 for technical-grade TBP and for the extracting agent from the technological system.

Thus, the kinematic viscosity of phosphoric acid solutions in technical-grade TBP can be calculated by the equation

$$\ln \nu = (-0.0017T + 0.2159)c + 2.129\exp(-0.0155T), \quad (4)$$

and that of phosphoric acid solutions in the extracting agent from the industrial system, by the equation

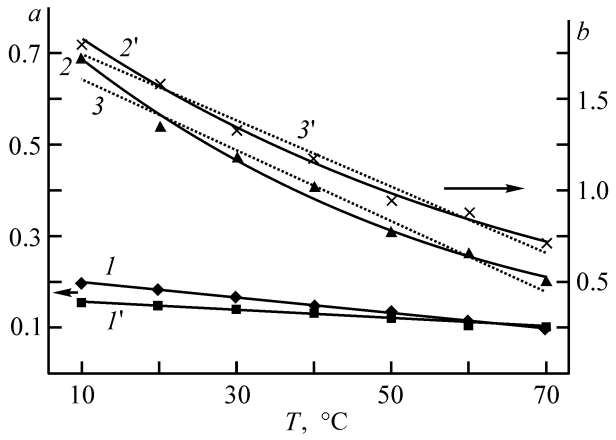
$$\ln \nu = (-0.0009T + 0.1686)c + 2.096\exp(-0.0198T). \quad (5)$$

For simplicity, the logarithmic dependence of the coefficient b in Eq. (1) can be replaced with a linear dependence (see figure, curves *3* and *3*'). Then, the temperature dependence of the coefficient b can be represented as

$$b = dT + q, \quad (6)$$

where T is temperature (°C), and d, q are the coefficients in Eq. (6).

The values of the coefficients in Eq. (6) and the approximation reliability R^2 are listed in Table 3 for both types of solutions. In the case of simplification, the kinematic viscosity is described by Eq. (7) for solutions based on technical-grade TBP and Eq. (8) for solutions based on the extracting agent:



Coefficients a and b in Eq. (1) vs. temperature T for (*1*–*3*) technical-grade TBP and (*1*'–*3*') extracting agent from the technological system.

$$\ln \nu = -0.0017cT + 0.2159c - 0.0194T + 1.8017, \quad (7)$$

$$\ln \nu = -0.0009cT + 0.1686c - 0.0182T + 1.9283. \quad (8)$$

Both pairs of equations, (4), (5) and (7), (8) can be used to calculate the viscosity, but it should be noted that application of Eqs. (4), (5) yields a smaller discrepancy $\left(\Delta = \frac{\ln \nu_{exp} - \ln \nu_{calc}}{\ln \nu_{exp}} \times 100\%\right)$ between the experimental and calculated values listed in Table 1. (For brevity, the comparison of both the calculation methods is limited to the values at 40°C).

An analysis of the viscosities of organic solutions of phosphoric acid revealed a certain difference between the kinematic viscosity of the extracting agent from the industrial system and the viscosity of technical-grade dibutyl phosphate. This is due to presence of organic impurities in the extracting agent [4, 5].

CONCLUSION

Analytical dependences of the viscosity of phosphoric acid solutions in tri-*n*-butyl phosphate on the temperature and composition of the organic solutions were obtained for the temperature range 10–70°C and P_2O_5 content of the organic phase of 0–18 wt %.

REFERENCES

1. Lembrikov, V.M., Konyakhina, L.V., Nikitin, V.G., and Volkova, V.V., *Khim. Technol.*, 2004, no. 8, pp. 4–8.
2. Skornyakova, R.A., Konyakhina,L.V., and Tokmakova, T.V., *Ekspress informatsiya: Otechestvennyi proizvodstvennyi opyt, Ser. Metody analiza i kontrolya proizvodstva* (Express Information: Domestic Industrial Experience, Series Methods for Analysis and Monitoring the Industrial Production), Moscow: NIITEKhIM, 1985, no. 6, pp. 20–22.
3. *TU* (Technical Specification) *2435-05-05763458–01, Technical-grade tributyl phosphate.*
4. Lembrikov, V.M., Konyakhina, L.V., Volkova, V.V., *et al.*, *Zh. Prikl. Khim.*, 2004, vol. 77, no. 9, pp. 1425–1429.
5. Lembrikov, V.M., Konyakhina, L.V., Volkova, V.V., *et al.*, *Khim. Tekhnol.*, 2004, no. 9, pp. 2–4.

Russian Journal of Applied Chemistry, Vol. 78, No. 8, 2005, pp. 1213–1217. Translated from Zhurnal Prikladnoi Khimii, Vol. 78, No. 8, 2005, pp. 1237–1241.
Original Russian Text Copyright © 2005 by Krut'ko, Dikhtievskaya, Markin, Shevchuk, Gorbachev, Varava, Kirienko.

INORGANIC SYNTHESIS AND INDUSTRIAL INORGANIC CHEMISTRY

Adsorption-induced Depression of the Strength of Potassium Chloride Grains under the Action of Fatty Amines and Water

N. P. Krut'ko, L. V. Dikhtievskaya, A. D. Markin, V. V. Shevchuk, A. S. Gorbachev, M. M. Varava, and V. M. Kirienko

Institute of General and Inorganic Chemistry, National Academy of Sciences of Belarus, Minsk, Belarus

Belarus'kalii Production Association, Republican Unitary Enterprise, Soligorsk, Minsk oblast, Belarus

Received November 4, 2004; in final form, April 2005

Abstract—The surface activity of higher aliphatic amines and their salts at the interface between their solutions and air, oil, and KCl grains and their influence on the strength characteristics, moisture absorption, and caking of the grains were studied.

The problem of improving the quality of granulated potassium fertilizers and their physicomechanical properties remains a matter of current interest. Modern conditioners for potassium fertilizers contain several components, which most frequently include surfactants and oil hydrocarbons [1–3].

The aim of the present study was to examine the influence exerted by surfactants (higher aliphatic amines and their salts) and moisture on the strength of potassium chloride grains and on their moisture absorption and caking. As objects of study served industrial grains of flotation KCl, manufactured by Belarus'kalii Production Association, Republican Unitary Enterprise. Individual aliphatic amines of Armeen-D brand, their acetic salts of Armac-D brand, and technical-grade amine of Flotigam brand were used as amines; dodecane, vacuum gas oil (VGO), and slop wax served as hydrocarbons.

The quality of grains was assessed by a comprehensive study of their basic physicochemical properties: destructibility, static strength, moisture absorption, degree of hydrophobization, and caking. The destructibility of grains was evaluated by the content of destroyed grains (–0.5-mm fraction) upon a vibrational and impact treatment on the –4…+2-mm fraction in a vibration mill for 30 min. The static strength of grains was found with an IPG-1 instrument intended for determining the strength necessary for grain crushing. The absorption of atmospheric moisture by grains, W (g H_2O/100 g KCl), was determined using the "desiccator" method under the following conditions: air humidity 80%, temperature 25°C, weighing accuracy 1×10^{-4} g, time of sample keeping in a desiccator equal to 1 to 7 days. The degree of hydrophobization, H (%), was calculated from the difference of masses of moisture absorbed by the initial (M_0) and modified (M) samples, using the formula

$$H = \frac{M_0 - M}{M_0} \times 100.$$

The caking was evaluated by the force necessary for crushing a briquette of the granulated material, preliminarily moistened with water to 3% moisture content and kept in molds under a pressure of 0.8 kg cm^{-2} at a temperature of 60°C for 24 h.

EXPERIMENTAL

Higher aliphatic amines and their salts are cationic surfactants. To study the surface activity of the amines, isotherms of surface tension σ at the interface between an aqueous solution of a surfactant and air and the interfacial tension at the interface between the aqueous solution of the surfactant and oil were measured by the Wilhelmi method (Fig. 1). The isotherms obtained were used to calculate the basic parameters of the adsorption layer at solution–air and solution–oil interfaces (Table 1): minimum surface or interfacial tension σ_{min}, surface activity G_m, saturation concentration c_n of the adsorption layer, critical micelle concentration c_{cr}, maximum adsorption Γ_m of a surfactant at the interface, area S_m occupied by the molecule of the sur-

1070-4272/05/7808-1213 © 2005 Pleiades Publishing, Inc.

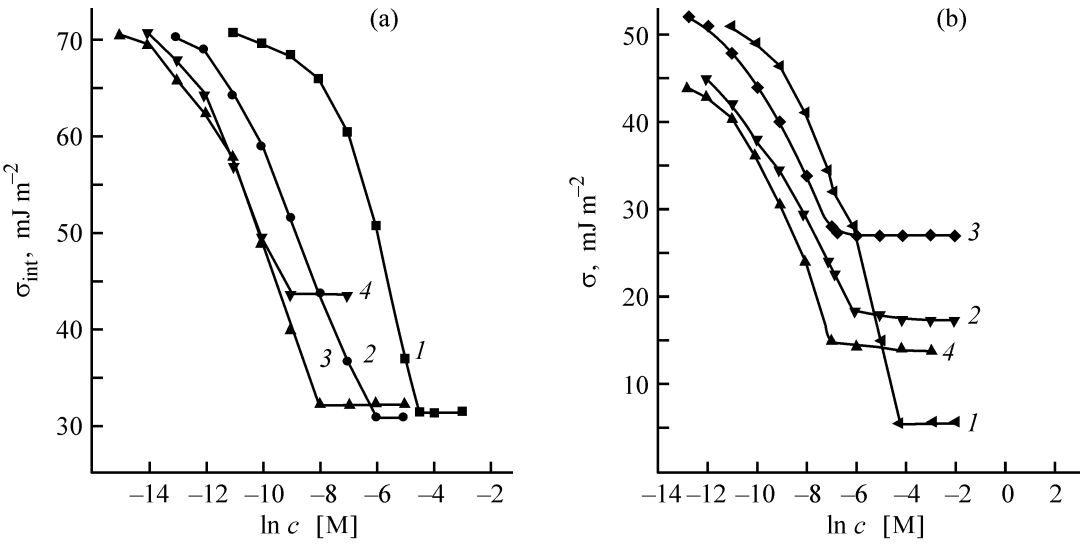


Fig. 1. Isotherms of surface tension of amine acetates at the interface between their aqueous solutions and (a) air or (b) dodecane. (σ, σ_{int}) Surface and interfacial tension, respectively; (c) amine concentration. Amine acetate: (*1*) $C_{12}H_{25}NH_2 \cdot CH_3COOH$, (*2*) $C_{14}H_{29}NH_2 \cdot CH_3COOH$, (*3*) $C_{16}H_{33}NH_2 \cdot CH_3COOH$, and (*4*) $C_{18}H_{37}NH_2 \cdot CH_3COOH$; the same for Fig. 2.

factant under study in the saturated adsorption layer, and the thickness δ of this layer.

It can be seen that the cation-active surfactants exhibit a high surface activity both at the interface with air and at that with oil. For example, the work of adsorption per a methylene group of the hydrocarbon chain of the amines is 0.78 kT at the solution–air interface and 0.66 kT at the solution–oil interface. It is noteworthy that the Traube rule is observed in the C_{12}–C_{16} amine series. However, the variation pattern of the surface activity is violated on passing to the C_{18} amine, which is possibly due to appearance of new conformational states in the longest-chain member of the homologous series under consideration or to presence of associates in its solutions even at low concentrations. Having such a high adsorption activity, amines can reduce the surface tension to 30–40 mJ m^{-2} at the solution–air interface, against 72 mJ m^{-2} for water, and to 5–26 mJ m^{-2} at the solution–oil interface, against 51 mJ m^{-2} for oil (Table 1). The adsorption layer is saturated at such mobile interfaces at amine concentrations an order of magnitude lower than the critical micelle concentration.

In the presence of inorganic electrolytes, such as KCl or NaCl, the surface activity and adsorption increase, and, consequently, so does the packing density of molecules in the surface layer. Also, the satura-

Table 1. Colloid-chemical characteristics of alkylamine acetates at the interface between their aqueous solutions and air or dodecane

Amine acetate	σ_{min}, mJ m^{-2}	G_m, J m kmol^{-1}	c_n, M	c_{cr}, M	$\Gamma_m \times 10^6$, mol m^{-2}	$S_m \times 10^{20}$, m^2	$\delta \times 10^{10}$, m
Air							
C_{12}	31	3	1.5×10^{-3}	1.3×10^{-2}	4.9	33.9	12.0
C_{14}	31	18	2.0×10^{-4}	2.2×10^{-3}	4.0	41.5	11.0
C_{16}	32	58	6.7×10^{-5}	6.8×10^{-4}	2.6	63.8	7.8
C_{18}	43	322	5.5×10^{-6}	8.5×10^{-5}	2.7	61.5	9.1
Dodecane							
C_{12}	5	3	4.1×10^{-31}	1.5×10^{-2}	3.9	42.9	9.5
C_{14}	17	13	5.0×10^{-4}	2.4×10^{-3}	2.5	66.4	7.6
C_{16}	26	21	2.0×10^{-4}	1.1×10^{-3}	2.5	66.4	7.6
C_{18}	15	38	5.5×10^{-6}	9.1×10^{-4}	3.0	53.6	10.2

Table 2. Effect of electrolyte on the colloid-chemical properties of tetradecylamine chloride

NaCl, M	G_m, J m kmol^{-1}	c_n, M	c_{cr}, M	$\Gamma_m \times 10^6$, mol m^{-2}	$S_m \times 10^{20}$, m^2
0	15	3.3×10^{-4}	3.1×10^{-3}	2.8	59.3
0.003	27.3	2.0×10^{-4}	3.1×10^{-3}	3.8	49.6
0.005	33.2	1.6×10^{-4}	1.4×10^{-3}	4.6	36.1
0.01	56.0	1.0×10^{-4}	8.3×10^{-4}	5.8	28.6
0.05	160.0	5.5×10^{-5}	2.9×10^{-4}	6.9	24.1
0.1	244.7	3.7×10^{-5}	1.9×10^{-4}	6.3	26.4

tion concentration of the adsorption layer and the critical micelle concentration decrease, i.e., addition of inorganic electrolytes is equivalent to an increase in the oil-receptivity of surfactant molecules (Table 2) [4]. The effects observed in the presence of inorganic electrolytes are due to the action of three main factors: (i) screening and neutralization of the charge of the polar groups of surfactant molecules by counter-ions (contraction of the electric double layer), (ii) decrease in the degree of hydration of surfactant molecules, and (iii) change in the structure of the solvent (water). As the hydrophobic radical in amine molecules becomes longer, smaller amounts of inorganic electrolytes are to be added to reach the same increase in the surface activity and decrease in c_n and c_{cr}. For example, the concentration of effective NaCl additives is as high as 1–2 M for a salt of dodecylamine C_{12}, and as low as 10^{-3}–10^{-4} M for hexadecylamine C_{16}.

It can be seen in Fig. 2 that salts of higher aliphatic amines also have a high adsorption activity on KCl crystals [5].

The results obtained in a study of the influence exerted by amines on the moisture absorption, degree of hydrophobization, static strength, destructibility, and caking of grains of flotation KCl are listed in Table 3. It can be seen that, being adsorbed on KCl crystals, the amines have an anticaking and water-repellent effect. The hydrophobization processes are based on oriented adsorption of modifier molecules on the solid surface of the crystals to form mono- or polymolecular layers. It is commonly believed that the maximum hydrophobicity of the product is only reached when a saturated layer of a water-repellent agent is formed. The amount of C_{12}–C_{18} amines sufficient for such a monomolecular film to be created on the surface of KCl grains of various fractions (from –4 to +0.25 mm) is 5–20 g per ton of the grained material [6]. In fact, a larger amount of the amine is necessary for creating the sufficient water-repellent and anticaking effect (Table 3).

However, the high activity of the amines adversely affects the strength of KCl grains (Tables 3, 4). The reason is as follows. Surfactant molecules present on the surface of a real solid penetrate close to the predisintegration zone (e.g., crack tip) owing to their high surface activity and surface mobility, diminish the surface tension, and thereby make smaller the work of formation of a new surface (Rebinder effect) [7]. An adsorption event must occur simultaneously with an event of bond rupture at the instant of formation of a new unit cell on the surface. Thus, an obligatory combination of the action of the medium and of mechanical stresses is characteristic of the adsorption-induced depression of the strength of a solid. As is known, the media that can impair the strength of ionic crystals are not only surfactants, but also water and aqueous electrolyte solutions.

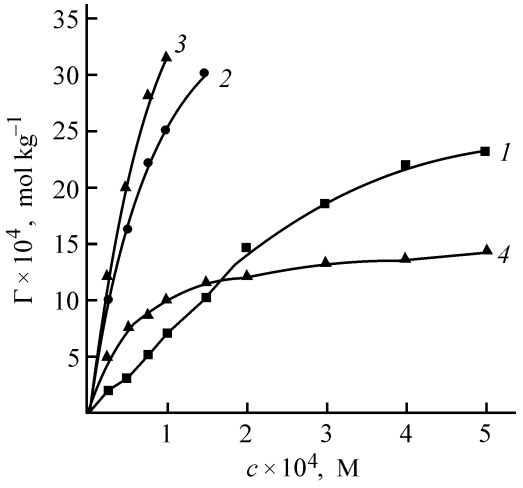


Fig. 2. Isotherms of adsorption Γ of amine acetates on KCl crystals at 20°C. (*c*) Amine concentration. The amines were introduced from starting solutions heated to 70°C.

Table 3. Effect of the expenditure of the amine of the Flotigam brand (taken individually and in combination with oil products) on the physicochemical properties of granulated flotation KCl

Mode of grain conditioning, additive g ton^{-1}	Time of sample keeping, days				Static strength of separate grains, kgf, at indicated moisture content of grains, %		Destructibility, %, of the –0.5-mm fraction at indicated moisture content of grains, %		Caking	
	1		7							
	W, g H_2O per 100 g KCl	H, %	W, g H_2O per 100 g KCl	H, %	0_{cond}	0.2	0_{cond}	0.2	kgf cm^{-2}	%
Initial	0.145	0	0.328	0	10.6	6.5	1.0	1.4	3.0	100
Amine:										
25	0.135	7	0.321	2	–	–	1.0	1.7	–	–
50	0.130	10	0.312	5	9.0	5.2	1.1	2.2	2.2	73
75	0.128	12	0.305	7	–	5.0	1.3	3.0	1.0	66
100	0.125	13	0.298	9	–	5.2	1.5	3.8	0.9	59
200	0.123	15	0.295	10	–	3.0	2.0	4.7	1.5	50
400	0.120	17	0.292	11	7.0	2.5	2.2	7.7	0.8	25
VG, 2500 + amine, 50	0.106	27	0.256	22	9.9	7.4	1.1	1.8	1.0	35
VG, 2500 + amine, 75	0.096	34	0.230	30	9.4	7.2	1.1	2.0	0.9	30
VG, 2500 + amine, 100	0.080	45	0.203	38	9.2	7.0	1.2	2.4	0.7	22
Slop wax, 2500 + amine, 100	0.080	45	0.200	39	9.2	7.0	1.2	2.4	0.7	22

Table 4. Effect of the moisture content and storage time of grains treated with a formulation composed of VG (2500 g ton^{-1}) and amine (50 g ton^{-1}) on their destructibility

Moisture content, %	Storage time, days	Destructibility of the –0.5-mm fraction, %	Moisture content, %	Storage time, days	Destructibility of the –0.5-mm fraction, %
0_{cond}	1	1.4	0.20	15	2.8
0.20	1	2.2	0.35	1	2.6
0.20	7	2.5	0.50	1	3.0

Tables 3, 4 clearly demonstrate a tendency toward disintegration of KCl grains under the action of amines and moisture. On dry grains, the disintegrating effect of the amines is insignificant. On humid grains, the destructibility of grains is rather strong and becomes more pronounced as the amine expenditure or amount of absorbed moisture grows. At amine expenditure of 50 g per ton of the granulated material, this effect is 2.2% at a fixed moisture content of 0.2%, against 1.4% for the initial, amine-untreated granulated material. As the content of the amine in the system increases, the amount of the –0.5-mm fraction after vibrational crushing grows to become 4.7% at a content of the amine equal to 200 g, and 7.7% at 400 g of the amine per ton of the granulated material. In the presence of moisture, the destructibility of grains under the action of amines and water grows in the course of time (Table 4).

If amine–hydrocarbon mixtures are used to treat KCl grains, the destruction power of amines decreases. Thus, the strength and elasticity of the hydrophobic coating increase in the presence of a surfactant. However, an inverse effect is also observed: apolar compounds favor adsorption of the amine on the KCl surface [8]. When amine–hydrocarbon formulations are used, the distribution of an amine over the grain surface is more uniform and the hydrocarbons and amines are more firmly fixed on the KCl surface, which leads, in the end, to a stronger hydrophobization of the surface.

CONCLUSION

It was established that surface-active modifiers, to which belong higher aliphatic amines and their salts, exert a water-repellent and anticaking action

on the granulated potassium material. However, the strength of KCl grains decreases and their destructibility increases in the presence of moisture. In view of this fact, it is necessary to minimize the expenditure of surfactants in treatment of granulated fertilizers under industrial conditions. This can be achieved by using amine–hydrocarbon mixtures with a low content of an amine (1–2%).

REFERENCES

1. Kuznetsov, F.M., Sokolov, I.D., Volkov, V.A., *et al., Khim. Tekhnol.*, 1982, no. 4, pp. 6–9.
2. Korshuk, E.F., Dikhtievskaya, L.V., Kirilenko, O.I., *et al., Zh. Prikl. Khim.*, 1999, vol. 72, no. 4, pp. 559–563.
3. Korshuk, E.F., Dikhtievskaya, L.V., Kirilenko, O.I., *et al., Zh. Prikl. Khim.*, 2000, vol. 73, no. 2, pp. 195–198.
4. Dikhtievskaya, L.V. and Mozheiko, F.F., *Dokl. Nats. Akad. Nauk Belarusi, Ser. Khim. Nauk*, 1999, vol. 43, no. 5, pp. 58–61.
5. Aleksandrovich, Kh.M., Mozheiko, F.F., Korshuk, E.F., and Markin, A.D., *Fizikokhimiya selektivnoi flotatsii kaliinykh solei* (Physical Chemistry of Selective Flotation of Potassium Salts), Minsk: Nauka i tekhnika, 1983.
6. Pol'kin, S.I., *Flotatsiya rud redkikh metallov i olova* (Flotation of Ores of Rare Metals and Tin), Moscow: Khimiya, 1960.
7. Rebinder, P.A., *Izbrannye trudy* (Selected Works), Moscow: Nauka, 1978, pp. 74–121.
8. Glembotskii, P.A., Dmitrieva, G.M., and Sorokin, M.M., *Apolyarnye reagenty i ikh deistvie pri flotatsii* (Apolar Reagents and Their Effect in Flotation), Moscow: Nauka, 1968.

Russian Journal of Applied Chemistry, Vol. 78, No. 8, 2005, pp. 1218–1222. Translated from Zhurnal Prikladnoi Khimii, Vol. 78, No. 8, 2005, pp. 1242–1246.
Original Russian Text Copyright © 2005 by Luneva, Petrovskaya, Lyudchik, Ezovitova.

INORGANIC SYNTHESIS AND INDUSTRIAL INORGANIC CHEMISTRY

Thermal Decomposition of the System $CO(NH_2)_2$–H_3PO_4 in the Presence of Nitrate Compounds

N. K. Luneva, L. I. Petrovskaya, I. A. Lyudchik, and T. I. Ezovitova

Institute of General and Inorganic Chemistry of the National Academy of Sciences of Belarus, State Research Institution, Minsk, Belarus

Received January 26, 2005

Abstract—Chemical, derivatographic, IR spectral, and X-ray diffraction analyses were used to study thermal transformations in the system $CO(NH_2)_2$–H_3PO_4 and in the same system with addition of KNO_3, $CsNO_3$, $LiNO_3 \cdot 3H_2O$, and NH_4NO_3 salts in the temperature range 20–600°C. The influence of the chosen nitrate compounds on the process of reorganization of the constituent ingredients, evolution of nitrogen into the gas phase, yield of the solid residue, and preservation of nitrogen and phosphorus was revealed.

Recently, nitrogen-phosphorus compounds have been widely used as cellulose modifiers and combustion inhibitors for various polymeric materials.

The efficiency of nitrogen-phosphorus fire-retardants depends on the chemical nature of the nitrogen-containing component, degree of condensation of the phosphates used, ratio of the main components (nitrogen to phosphorus), additives introduced, and some other factors [1–7].

It is known that the nature of the metal cation in inorganic additives present in nitrogen–phosphorus systems can strongly modify their fire-extinguishing properties and decomposition temperature [2, 3]. For example, amidophosphate formulations are effective fire-protecting means. However, studies of the thermal decomposition of phosphorus-nitrogen mixtures and of the influence exerted by addition of inorganic salts on the structural-chemical transformations in the course of their heating are virtually not reflected in the literature at all.

EXPERIMENTAL

Systems composed of a mixture of phosphoric acid and carbamide, $CO(NH_2)_2$–H_3PO_4 (NP), at a mass ratio N : P = 1 : 2, and the same formulations with addition of NH_4NO_3, KNO_3, $LiNO_3 \cdot 3H_2O$, and $CsNO_3$ (Table 1) were chosen for study.

The NP systems were prepared by successive introduction of carbamide and appropriate nitrate salts into phosphoric acid. The content of nitrogen and phosphorus after thermal treatment was determined using procedures described in [8, 9].

The X-ray diffraction patterns of the samples studied were recorded with a monochromatic Cu_{K_α} radiation on an IRS-50M installation, and the IR spectra, on a Perkin-Elmer instrument by the sandwich technique [10] in a polyethylene film in the frequency range 400–3900 cm^{-1}. The course of the thermal decomposition process was recorded with an MOM Q-1000 derivatograph (Hungary), with temperature raised at a rate of 10 deg min^{-1} in the interval 20–600°C. In view of the fact that vigorous gas evolution with ejection of the samples under study from crucibles occurred on heating the NP system with nitrate additives, thermograms were only recorded for the additives introduced into the system.

It is known that carbamide forms with phosphoric acid associates of acid carbamide phosphates [1, 11–13].

Table 1. Parameters of the nitrogen-phosphorus compounds studied

System no.	System	N_a^* : P
1	NP	
2	NP–NH_4NO_3	1 : 5.4
3	NP–NH_4NO_3	1 : 2.2
4	NP–$LiNO_3$	1 : 9.3
5	NP–$LiNO_3$	1 : 3.8
6	NP–$CsNO_3$	1 : 11.0
7	NP–KNO_3	1 : 5.8

* N_a is nitrogen contained in an additive.

1070-4272/05/7808-1218 © 2005 Pleiades Publishing, Inc.

Table 2. Results of a chemical analysis of the products formed in thermal decomposition of nitrogen–phosphorus systems

System no.*	*T*, °C	Yield a product, wt %	Found, wt %		System no.*	*T*, °C	Yield a product, wt %	Found, wt %	
			N	P				N	P
1	20	100.00	5.06	23.57	5	20	100.00	3.95	18.07
	180	91.13	5.40	23.39		180	86.07	4.53	19.76
	260	77.50	6.00	28.51		260	61.50	5.35	28.00
	460	69.70	6.10	32.00		460	53.10	5.72	30.60
	600	60.00	2.70	34.17		600	48.70	1.27	33.27
2	20	0	5.56	19.70	6	20	100.00	3.67	18.00
	180	86.26	6.35	21.60		180	91.36	3.30	20.10
	260	73.30	7.10	28.18		260	70.70	3.99	23.80
	460	63.90	7.62	31.60		460	61.62	3.36	27.80
	600	56.20	3.17	32.34		600	54.80	2.12	30.50
3	20	100.00	6.62	20.50	7	20	100.00	3.67	17.40
	180	91.55	7.10	19.70		180	85.80	3.82	20.90
	260	69.70	8.10	26.69		260	67.40	4.30	24.90
	460	58.60	7.39	32.70		460	53.50	2.50	32.70
	600	50.00	2.65	33.31		600	51.40	0.76	34.20
4	20	100.00	4.50	20.42					
	180	90.92	4.89	21.39					
	260	70.20	5.77	27.30					
	460	61.50	6.32	30.80					
	600	53.00	1.40	33.14					

* System numbers correspond to those of nitrogen–phosphorus systems in Table 1.

It has been shown previously [3, 14] that thermal decomposition of associates of this kind is a complex chemical process that simultaneously involves chemical decomposition of adducts, interaction of the forming gaseous compounds with solid products of decomposition of the systems, formation of new crystalline phases, and condensation of phosphates. The yield of a residue from such systems depends on the temperature to which a formulation is heated, N : P ratio, and nature of the additives introduced.

According to the results of a thermogravimetric analysis, the KNO_3 and $CsNO_3$ salts used as additives in the nitrogen–phosphorus system $CO(NH_2)_2$–H_3PO_4 (NP) are not decomposed in the temperature range under study. $LiNO_3 \cdot 3H_2O$ crystal hydrate loses virtually only the crystallization water; as for the NH_4NO_3 additive, its loss of mass is 44.6 wt %. Table 2 lists data characterizing the thermal decomposition of nitrogen–phosphorus systems. For a system with addition of nitrates, the yield of the solid product decreases, compared with that for the NP system without additives. For example, the yield of the residue (wt %) for the NP system containing no additives was 60.0 at 600°C; upon addition of equal amounts of $LINO_3$, KNO_3, or $CsNO_3$, it was 48.7, 51.4, and 54.8, respectively. At a higher content of $LINO_3$ or NH_4NO_3 in NP formulations, the yield of the solid product at 600°C decreases. For example, as the content of the $LiNO_3$ additive increased (N : P ratio 1 : 9.3 and 1 : 3.8), the yield at 600°C was 53.0 and 48.7 wt %, respectively. For the system containing NH_4NO_3, the yield of residues at 60°C was 58.0 wt % (N : P = 1 : 5.4) and 55.3 wt % (N : P = 1 : 2.2).

Figure 1 shows the content of nitrogen in products of thermal decomposition of nitrogen–phosphorus

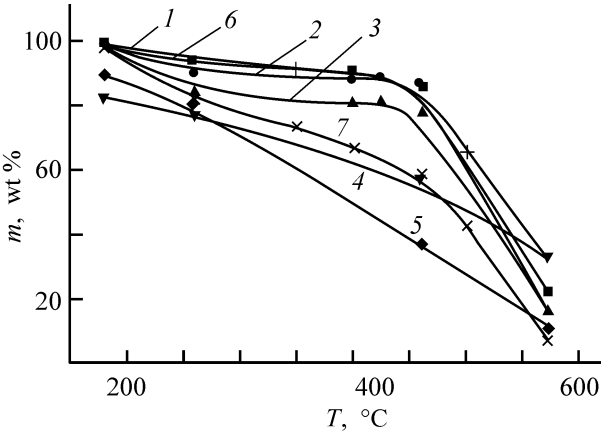


Fig. 1. Content of nitrogen in products of thermal decomposition of nitrogen–phosphorus systems. (*T*) Temperature and (*m*) amount of nitrogen. System: (*1*) no. 1, (*2*) no. 4, (*3*) no. 5, (*4*) no. 6, (*5*) no. 7, (*6*) no. 2, and (*7*) no. 3.

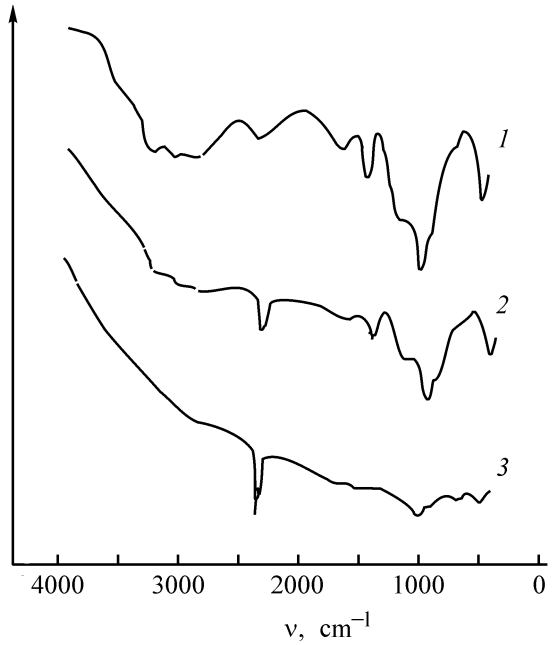


Fig. 2. IR spectra of samples obtained upon thermal decomposition of nitrogen–phosphorus systems. (ν) Wave number. Sample: (*1*) NP–NH_4NO_3 (N_a : P = 1 : 5.4), (*2*) NP, and (*3*) NP–$LiNO_3$ (N_a : P = 1 : 9.3).

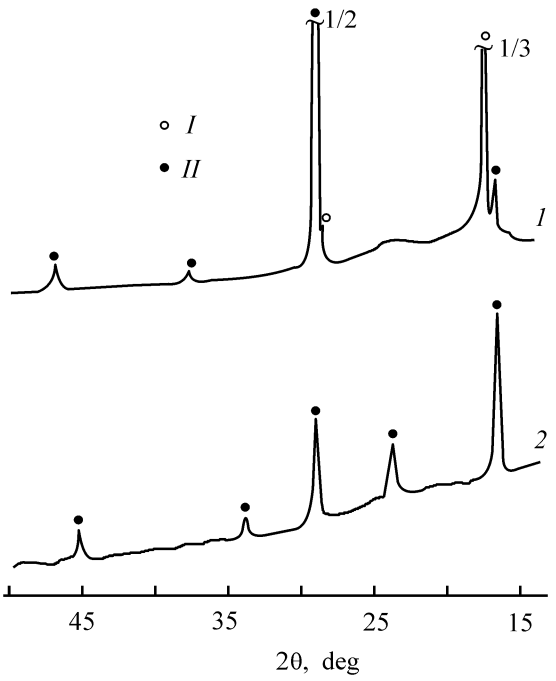


Fig. 3. X-ray diffraction patterns of samples obtained upon thermal decomposition of nitrogen–phosphorus systems. (2θ) Bragg angle. Sample: (*1*) NP, (*2*) NP–NH_4NO_3 (N_a : P = 1 : 2.2). Phase: (*I*) $(NH_4)_2HPO_4$ and (*II*) $NH_4H_2PO_4$.

systems in the temperature interval 20–600°C. All the nitrate additives introduced into the NP system in the interval 180–460°C favor a stronger evolution of nitrogen into the gas phase, compared with a system without additives. Raising the content of the $LiNO_3$ additive in the nitrogen–phosphorus system (N : P = 1 : 9.3 and 1 : 3.8) leads to a decrease in the preservation of nitrogen at 460°C from 86.1 to 77.0 wt %.

At virtually the same content of KNO_3, $LiNO_3$, and $CsNO_3$ additives in NP systems, the smallest amount of nitrogen (36.5 wt %) was observed in products obtained at 460°C with a KNO_3 additive, whereas for systems with $LiNO_3$ and $CsNO_3$ additives, the content of nitrogen was 77.0 and 56.4 wt %, respectively. The preservation of nitrogen in the initial NP system at the same temperature was 84.0 wt %. Here, the total amount of the ammonia and carbamide nitrogen was taken as 100%.

A chemical analysis demonstrated that nitrogen is present in samples of all the systems, thermally treated at 600°C, as NH_4^+ ions. This is also confirmed by the IR spectra of these samples (Fig. 2). For example, the following absorption bands were observed in the IR spectra (cm^{-1}): 1438 (ν_4NH_4), 1667 (ν_2NH), 2876 (ν_1NH), and 3040 (νNH_4). According to [15–19], these bands can be assigned to the NH_4^+ ion.

Thermal treatment of all the nitrogen–phosphorus systems at 180–460°C yields cakes, and that at 600°C, glassy products. Keeping in air samples of NP systems and those with addition of NH_4NO_3, thermally treated at 260°C, leads to crystallization of compounds that belong, according to X-ray phase analysis (Fig. 3), to the crystalline phases $NH_4H_2PO_4$ and $(NH_4)_2HPO_4$ [20]. The formation of these compounds indicates that H_3PO_4 reacts with NH_3 evolved upon heating of nitrogen–phosphorus systems. Further increase in the temperature of thermal treatment (T > 260°C) of nitrogen–phosphorus formulations leads to formation of polyphosphorus compounds, which is confirmed by the IR spectra of thermal decomposition products in Fig. 2, in which the following absorption bands are observed (cm^{-1}): 494 (δ_s PO_3), 725 (ν_s POP), 987 (ν_{as} POP), 997 (ν_s PO_3), 1146 (ν_{as} PO_3), and 1433, 3242 (ν_{as} PO_2), which are characteristic of vibrations of the phosphate groups of chain polyphosphates [17, 18, 21, 22]. The formation of polyphosphates upon heating of nitrogen–phosphorus systems is accompanied by a minor loss of phosphorus.

In the interval 180–600°C, the preservation of phosphorus in thermal decomposition products is

rather high and the minimum retention factor is 0.82 (Table 3). The content of phosphorus is the highest in the system with a KNO_3 additive (retention factor 0.99 at 600°C); in the systems with $CsNO_3$ and $LiNO_3$ it is 0.93 and 0.90, respectively.

Thus, it was established that, when subjected to a thermal treatment, all the systems studied undergo significant transformations, which are due to loss of phosphorus and nitrogen and to reorganization of the phosphate structures. The systems with $CsNO_3$ and KNO_3 show at 600°C a minor loss of mass and higher retention factors for phosphorus, and, therefore, they may be of interest as combustion inhibitors for polymeric materials.

The efficiency of the formulations studied in fireproofing (30 wt % in an aqueous solution) was evaluated by treating wood with these materials [tests in conformity with GOST (State Standard) 16363–98]. Table 4 lists data obtained in evaluating the fireproofing properties of treated wood (150 × 60×30-mm sticks).

It can be seen that the smallest loss of mass (15 wt %) in fire tests is observed for wood sticks (pine) treated with an NP system with addition of KNO_3. Thus, this system is a more efficient combustion inhibitor for cellulose-containing materials.

CONCLUSIONS

(1) It was shown in a study of thermal decomposition of the system $CO(NH_2)_2$–H_3PO_4 with and without addition of KNO_3, $CsNO_3$, $LiNO_3 \cdot 3H_2O$ salts by methods of physicochemical analysis that all the additives introduced affect the yield of the solid product. The mass fraction of the solid product depends on the nature of nitrate compounds and their quantitative content in nitrogen–phosphorus systems. The lowest yield of the product was observed for a nitrogen-phosphorus system with addition of $LiNO_3 \cdot 3H_2O$ or KNO_3.

(2) It was established that the thermal decomposition of nitrogen–phosphorus systems involves, together with evolution of gaseous products into the gas phase, reactions of their interaction with solid thermal decomposition products and reorganization of the latter to form polyphosphorus compounds.

(3) It was revealed that all the nitrate additives introduced intensify nitrogen evolution into the gas phase in the temperature range 180–460°C, with the strongest influence exerted by the KNO_3 additive.

Table 3. Preservation of phosphorus and nitrogen in the products of thermal decomposition of nitrogen–phosphorus systems

System no.*	T °C	Retention factor	
		P	N
1	20	1.00	1.00
	180	0.90	0.97
	260	0.94	0.92
	460	0.95	0.84
	600	0.87	0.21
2	20	1.00	1.00
	180	0.94	0.99
	260	1.05	0.94
	460	1.03	0.88
	600	0.92	0.32
3	20	1.00	1.00
	180	0.88	0.98
	260	0.91	0.85
	460	0.94	0.66
	600	0.82	0.20
4	20	1.00	1.00
	180	0.96	0.99
	260	0.94	0.90
	460	0.93	0.86
	600	0.86	0.16
5	20	1.00	1.00
	180	0.94	0.99
	260	0.95	0.83
	460	0.90	0.77
	600	0.90	0.16
6	20	1.00	1.00
	180	1.02	0.82
	260	0.93	0.77
	460	0.95	0.56
	600	0.93	0.32
7	20	1.00	1.00
	180	1.01	0.89
	260	0.94	0.80
	460	0.98	0.37
	600	0.99	0.12

* System numbers correspond to those nitrogen–phosphorus systems in Table 1.

Table 4. Efficiency of fireproofing properties of the nitrogen–phosphorus systems

Impregnating solution	Gain in solution weight, g mm^{-2}	Loss of mass, wt %
NP	250	20.1
NP–$CsNO_3$	250	18.1
NP–KNO_3	250	15.0

(4) Systems with KNO_3 and $CsNO_3$ additives possess improved fireproofing properties and can be used as combustion inhibitors for cellulose-containing materials.

REFERENCES

1. Leonovich, A.A. and Sheloumov, A.V., *Khim. Prom–st.*, 2003, vol. 80, no. 7, pp. 11–15.
2. Bazhenov, S.V., Duberov, N.G., Nozhinovskii, Yu.K., and Naumov, Yu.V., *Sbornik trudov II Mezhdunarodnoi konferentsii po polimernym materialam ponizhennoi goryuchesti* (Proc. II Int. Conf. on Polymeric Materials with Lowered Combustibility), Volgograd, 1992, pp. 56–59.
3. Luneva, N.K., Petrovskaya, L.I., and Rekashova, N.I., *Zh. Prikl. Khim.*, 2000, vol. 73, no. 10, pp. 1585–1590.
4. Luneva, N.K., Petushok, I.A., Vorob'ev, V.K., and Dmitrichenko, A.S., *Materialy II Mezhdunarodnoi nauchno-prakticheskoi konferentsii "Pozharnaya bezopasnost'": Informatsionnyi sbornik "Nauchnoe obespechenie pozharnoi bezopasnosti"* (Proc. II Int. Sci.-Pract. Conf. "Fire Safety": Inf. Coll. of Articles "Scientific Foundations of Fire Safety"), Minsk: Resp. Nauchn. Prikl. Tsentr Pozharn. Bezopasn., 1997, issue 4, pp. 116–117.
5. Leonovich, A.A., *Ognezashchita drevesiny i drevesnykh materialov* (Fire Protection of Wood and Wood Materials), St. Petersburg: SPb. Gos. Lesotekhn. Akad., 1994.
6. Luneva, N.K., Vorob'ev, V.K., Petushok, I.A., and Komarov, V.S., *Vestsi Akad. Nauk Belarusi*, 1994, no. 1, pp. 15–20.
7. Vorob'ev, V.K., Luneva, N.K., Petushok, I.A., and Komarov, V.S., *Problemy sozdaniya informatsionnykh tekhnologii: Sbornik nauchnykh trudov* (Problems of Development of Information Technologies: Coll. of Sci. Works), Minsk, 1996, pp. 80–83.
8. Losev, I.P. and Fedotova, O.P., *Praktikum po khimii VMS* (Laboratory Works in Chemistry of Macromolecular Compounds), Moscow: Khimiya, 1959.
9. Mikhailin, A.D., Postnikov, N.I., and Klenitskii, A.M., *Trudy NIUIF*, 1969, issue 211, pp. 36–42.
10. Gusev, S.S., Skorynina, I.S., Vorob'eva, N.K., and Ermolenko, I.N., *Obshchaya i prikladnaya khimiya: Sbornik trudov Belorusskogo tekhnologicheskogo institute* (General and Applied Chemistry: Coll. of Works of Belarussian Technological Institute), Minsk: Vysheisha Shkola, 1974, pp. 123–128.
11. Sarsembinova, B.T., Nikitina, I.I., and Titov, K.M., *Izv. Akad. Nauk KazSSR, Ser. Khim. Nauk*, 1991, no. 6, pp. 53–58.
12. Emsley, J. and Niazu, S., *J. Chem. Soc. Dalton Trans.*, 1982, no. 12, pp. 2527–2531.
13. McCullough, J.E., Sheridan, R.C., and Frederick, L.L., *J. Agric Food Chem.*, 1978, vol. 26, no. 3, pp. 670–675.
14. Luneva, N.K., Petrovskaya, L.I., and Lyudchik, I.A., *Zh. Prikl. Khim.*, 1999, vol. 72, no. 2, pp. 190–194.
15. Kiss, A.B., *Acta chim. Acad. Scient. hung.*, 1973, vol. 75, no. 7, pp. 351–368.
16. Nakamoto, K., *Infrared Spectra of Inorganic and Coordination Compounds*, New York: John Wiley & Sons, 1963.
17. Korzhuev, V.N., A Physicochemical Study of Ammonium Triphosphates, *Cand. Sci. Dissertation*, Minsk, 1984.
18. Bellamy, L.J., *The Infra-Red Spectra of Complex Molecules*, New York: John Wiley, 1957.
19. Kiss, A.B. and Chudik-Majer, Z.M., *Acta chim. Acad. Scient. hung.*, 1976, vol. 78, no. 3, pp. 237–251.
20. Luneva, N.K., Vorob'ev, V.K., and Petushok, I.A., *Zh. Prikl. Khim.*, 1997, vol. 70, no. 10, pp. 1729–1734.
21. Prodan, E.A., Prodan, L.I., and Ermolenko, N.F., *Tripolifosfaty i ikh primenenie* (Triphosphates and Their Use), Minsk: Nauka i Tekhnika, 1969.
22. Mel'nikova, R.Ya., Korzhuev, V.N., Prodan, E.A., and Malashonok, I.E., *Zh. Prikl. Spektrosk.*, 1984, vol. 41, no. 4, pp. 597–601.

Russian Journal of Applied Chemistry, Vol. 78, No. 8, 2005, pp. 1223–1228. Translated from Zhurnal Prikladnoi Khimii, Vol. 78, No. 8, 2005, pp. 1247–1251.
Original Russian Text Copyright © 2005 by Lekanova, Ryabkov, Sevbo, Filippov.

INORGANIC SYNTHESIS AND INDUSTRIAL INORGANIC CHEMISTRY

Interactions in the Al_2TiO_5–Ti_2O_3 System

T. L. Lekanova, Yu. I. Ryabkov, O. A. Sevbo, and V. N. Filippov

Institute of Chemistry, Komi Scientific Center, Ural Division, Russian Academy of Sciences, Syktyvkar, Komi Republic, Russia
Institute of Geology, Komi Scientific Center, Ural Division, Russian Academy of Sciences, Syktyvkar, Komi Republic, Russia

Received December 9, 2004; in final form, May 2005

Abstract—Interactions in the Al_2TiO_5–Ti_2O_3 system were studied and the regions of existence of $Al_{2-2x}Ti^{3+}_{2x}Ti^{4+}O_5$ solid solutions with a pseudobrookite structure were determined.

A distinguishing feature of ceramics based on aluminum titanate is their refractoriness and low overall coefficient of linear thermal expansion [1]. Owing to this property, it is expedient to use aluminum titanate, in processes that occur in nonstandard operation modes, as a material resistant to thermal shocks. Aluminum titanate is used as a heat insulator in propulsion engineering, material for crucibles in ferrous and nonferrous metallurgy, and support for catalysts [2, 3].

Aluminum titanate Al_2TiO_5 belongs to an isomorphous series of binary oxides A_2BO_5 with a pseudobrookite structure (also including Fe_2TiO_5, Ti_3O_5, and Ti_2MgO_5), in which A and B atoms may be isovalently substituted by various cations, with continuous series of solid solutions formed [4, 5]. Aluminum titanate has an orthorhombic lattice with a *Cmcm* space group, with the following lattice constants: $a = 0.3591$, $b = 0.9429$, and $c = 0.9636$ nm [4]. A characteristic feature of the representatives of the isomorphous A_2BO_5 series is the anomalously high anisotropy of thermal expansion, caused by distortion of $[MO_6]$ octahedra and different lengths of M–O bonds [6, 7].

Titanium pentoxide Ti_3O_5 has two, high- and low-temperature, modifications [8]. Crystals of anosovite (high-temperature modification of Ti_2O_5) [9, 10] belong to the rhombic crystal system, are characterized by the *Cmcm* space group, and have the following lattice constants: $a = 0.3747$, $b = 0.9465$, and $c = 0.9715$ nm. The crystal structure of the low-temperature modification of Ti_3O_5 belong to the monoclinic system, is characterized by the *C*2/*m* space group, and has the following lattice constants: $a = 0.3808$, $b = 0.9442$, $c = 0.9752$ nm, and $\beta = 91.55°$.

The high- and low-temperature modifications of Ti_3O_5 are rather easily transformed one into the other at a temperature of about 120°C. At slightly higher temperatures [8], the structure Ti_3O_5 is similar to that of orthorhombic anosovite, but is slightly distorted (monoclinic), with lattice constants $a = 0.378$, $b = 0.997$, $c = 0.982$ nm, and $\beta = 91.0°$. At higher temperatures, the monoclinic angle gradually approaches 90°, and the lattice constants, those of anosovite. The crystal structure of the high-temperature modification can also remain stable at low (room) temperatures in the presence of a certain amount (several weight percent) of iron, magnesium, or aluminum. In the absence of admixtures, titanium pentoxide has at room temperature the structure of its low-temperature modification. According to the refined data [11], the lattice constants of the low-temperature modification of Ti_3O_5 are $a = 0.3801$, $b = 0.9441$, $c = 0.9748$ nm, and $\beta = 91.53°$.

The sinterability of aluminum titanate ceramics is commonly improved, and its thermal stability, raised, by introducing mineralizers into the stock [12–14]. The stability of the structure of the high-temperature modification of Ti_3O_5 at room temperature in the presence of a minor amount of Al_2O_3 admixture was confirmed in [13]: solutions of composition $[(Ti_{1-x}Al_x)_2O_3TiO_2]$ with $0 \le x \le 0.4$ have the structure of low-temperature Ti_3O_5, and compounds with $x \ge 0.08$ are structurally similar to high-temperature Ti_3O_5. A transition from the monoclinic crystal system, to which the crystal structure of compounds with $0 \le x \le 0.2$ belongs, to the rhombic crystal system characteristic of compounds with $0.3 < x < 1$ was found [13].

To perform a directed synthesis of ceramic materials, it is necessary to study in detail the structural

1070-4272/05/7808-1223 © 2005 Pleiades Publishing, Inc.

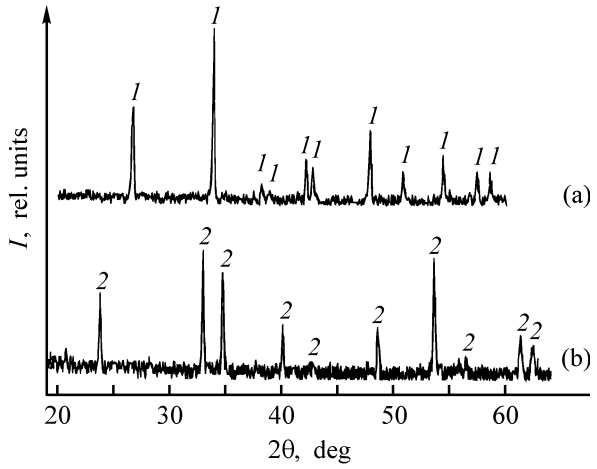


Fig. 1. X-ray diffraction patterns of the starting powders of (a) Al_2TiO_5 and (b) Ti_2O_3. (*1*) Al_2TiO_5 and (*2*) Ti_2O_3. (*I*) Intensity and (2θ) Bragg angle; the same for Fig. 3.

parameters of the forming samples and their correlation with the properties of the samples. A study of real structure of substances with all its defects makes it possible to search for new compounds with valuable properties and to improve processes of their synthesis by using various methods of control over their composition and the distortion of their structure. In this study, we examined the phase formation in the Al_2TiO_5–Ti_2O_3 system and the physicochemical properties of ceramic materials based on $Al_{2-2x}Ti^{3+}_{2x}Ti^{4+}O_5$ solid solutions with a pseudobrookite structure.

EXPERIMENTAL

To prepare the starting mixtures, we used Al_2O_3 of pure grade, TiO_2 of special-purity grade, and BAU-A activated carbon. Aluminum titanate was synthesized at 1400°C in the course of 9 h from an equimolar mixture of aluminum and titanium(IV) oxides (Fig. 1, diffraction pattern a). Ti_2O_3 was prepared by reducing TiO_2 with carbon in a vacuum (residual pressure 10^{-3}–10^{-1} Pa) at 1600°C with an isothermal exposure for 3 h [15]. The correspondence of the material synthesized to the stoichiometric formula Ti_2O_3 was monitored by the weight gain in the oxidation of the material to titanium dioxide by annealing in air at 1000°C for 2 h in accordance with the reaction

$$Ti_2O_{3+x} + \frac{1-x}{2}O_2 \rightarrow 2TiO_2. \quad (1)$$

The discrepancy revealed between the composition of the material synthesized and the stoichiometric formula is rather small (x = 0.011). The presence of an excess oxygen is a consequence of the insufficient amount of carbon in the reduction reaction; an exact calculation of the stock composition is complicated by the fact that the humidity of activated carbon, which is used as a source of carbon, varies from 8 to 10 wt %. The X-ray data (Fig. 1, diffraction pattern b) also confirm that the substance obtained is titanium(III) oxide.

To determine the ranges of existence of $Al_{2-2x}Ti^{3+}_{2x} \cdot Ti^{4+}O_5$ solid solutions, we prepared $Al_2TiO_5 + xTi_2O_3$ mixtures (x is the number of Ti_2O_3 moles, varied from zero to unity with a step of 0.1). Billets 20 mm in diameter and 5 mm high for high-temperature treatment were prepared by semidry compaction under a pressure of 150 MPa. The samples were thermally treated under atmospheric pressure in argon at 1400°C for 4 h.

The phase composition of the samples subjected to thermal treatment was studied by X-ray phase analysis on a DRON-3M installation (Cu_{K_α} radiation), using the JCPDS-ICDD database of powdered standards. We used the Powder Cell software [16] to evaluate the content of crystalline phases in the thermal treatment products (with an accuracy of ±5 vol %) and analyze the line intensities by the Rietveld method. The software makes it possible to construct and predict structural models of a solid solution based on aluminum titanate. The position parameters of the aluminum titanate lattice are listed in Table 1. The construction is based on substitution of a part of Al^{3+} ions

Table 1. Position parameters of the crystal structure of aluminum titanate (*Cmcm* space group) [17]

Atom	Ion	Position	*x*	*y*	*z*	Occupancy
Ti	Ti^{3+}	4*c*	0.0000	0.1863	0.2500	0.3330
	Al^{3+}					0.6670
Al	Al^{3+}	8*f*	0.0000	0.8649	0.4387	0.6670
	Ti^{4+}					0.3330
O	O^{2-}	4*c*	0.0000	0.7590	0.2500	1.0000
O	O^{2-}	8*f*	0.0000	0.9520	0.8820	1.0000
O	O^{2-}	8*f*	0.0000	0.6830	0.9250	1.0000

Table 2. Lattice constants (nm) of $Al_{2-2x}Ti^{3+}_{2x}Ti^{4+}O_5$ solid solutions and Ti_2O_3 content in the starting mixture and annealing products (composition of the starting mixture Al_2TiO_5–xTi_2O_3)

x	Phase composition of products, vol %			a	b	c	Ti_2O_3, mol %	
	$Al_{2-2x}Ti^{3+}_{2x}Ti^{4+}O_5$	α-Al_2O_3	Magneli phases				initial	products
0	~100	≤5	–	0.359	0.946	0.967	–	4.0
0.1	90	10	–	0.360	0.947	0.968	9.09	10.6
0.2	90	10	–	0.360	0.947	0.968	16.7	18.8
0.3	90	≤5	≤5	0.361	0.947	0.969	23.1	25.0
0.4	85	≤5	10	0.361	0.948	0.969	28.5	32.8
0.6	80	≤5	15	0.361	0.948	0.969	37.4	41.0
0.8	75	≤5	20	0.361	0.948	0.970	44.5	49.0
1.0	75	≤5	20	0.361	0.948	0.970	50.0	51.0

in 4*c* and 8*f* positions in the Al_2TiO_5 structure [17] with Ti^{3+}. The occupancy of the specified positions by Al^{3+} was varied in the range 0.6670 – 0.4670, that by Ti^{3+}, in the range 0 – 0.2000. The experimental and theoretical X-ray patterns were compared within the entire pattern profile, and the convergence factor was output as the result of the calculation. The variant with a lower *R*-factor represents the model configuration. The software also makes it possible to compare a description of the structure of a solid solution with experimental data and to carry out a quantitative phase analysis. The lattice constants of the solid solutions based on aluminum titanate (orthorhombic crystal system) were determined using the least-squares method for 12 highest-intensity peaks in the 2θ range from 10° to 80°.

The open porosity *P* and water absorption *W* of the samples were determined in conformity with GOST (State Standard) 18847–84 by hydrostatic weighing. The acid resistance A of the samples synthesized was evaluated, according to GOST 473.1–81, by the change in the mass of the ceramic material after its treatment with concentrated sulfuric acid.

The content of Ti_2O_3 in the calcination products was determined by the method of complete oxidation from the weight gain of samples exposed in air at 1000°C for 2 h. The atomic composition of the crystalline phases of the ceramics was found by electron microprobe analysis using a JSM-6400 electron scanning microscope equipped with a Link X-ray energy-dispersion spectrometer with ISIS-300 software. The volume of the substance analyzed was 1 μm^3. The constituent phases of the samples were analyzed for the content of Al, Ti, and O. To reliably determine the amounts of elements in a phase, we made up to 10 measurements on the sample surface. We used as standards certified Microspec reference samples. The measurement error was ±1%.

Our studies revealed that the phase composition of the samples and the lattice constants of the pseudobrookite phase change, depending on the parameter *x* of the starting Ti_2O_3, upon calcination of the Al_2TiO_5–xTi_2O_3 mixture. The weight loss upon heat treatment of compacts did not exceed 0.5% for the entire range of compositions, $0 \le x \le 1$. According to the results of an X-ray analysis (Table 2), up to 5 vol % α-Al_2O_3 is contained in the heat-treatment products at $x = 0$. All the reflections of the aluminum titanate phase in the X-ray diffraction pattern are shifted to smaller 2θ angles owing to the formation of the $Al_{2-2x}Ti^{3+}_{2x}Ti^{4+}O_5$ solid solution via dissociation of aluminum titanate in the atmosphere of argon:

$$Al_2TiO_5 = (1/1 + 2x)Al_{2-2x}Ti^{3+}_{2x}Ti^{4+}O_5 + (3x/1 + 2x)Al_2O_3 + (x/1 + 2x)O. \quad (2)$$

Analysis for the content of Ti_2O_3 confirms the presence of 1.6 mol % Ti^{3+} in the heat-treatment products. The lattice constants of the $Al_{2-2x}Ti^{3+}_{2x}Ti^{4+}O_5$ solid solution, $a = 0.359$, $b = 0.946$, and $c = 0.967$ nm, exceed those of stoichiometric Al_2TiO_5 [17]. An examination of the profile of the X-ray diffraction pattern demonstrated that the intensity of peaks changes when the occupancy by Al^{3+} of the positions 4*c* and 8*f* decreases through partial substitution by Ti^{3+}. The best result in describing the experimental X-ray pattern was achieved in the case when 5% of Al^{3+} positions in the Al_2TiO_5 structure were substituted with Ti^{3+}.

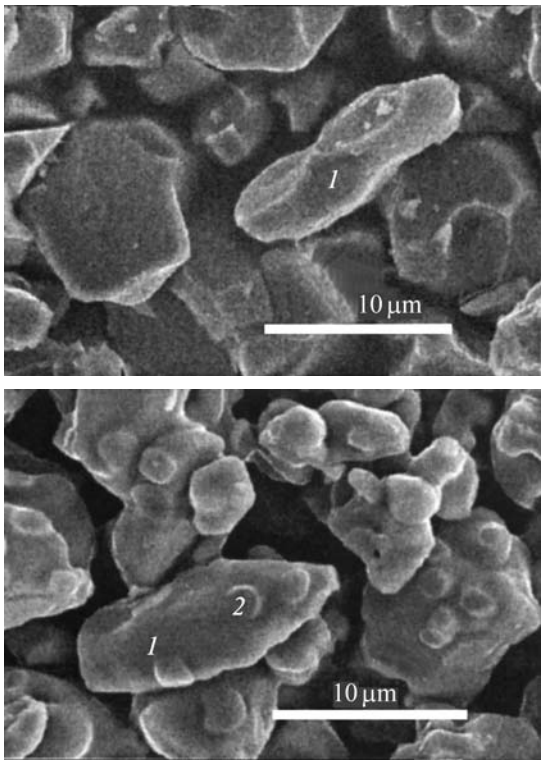


Fig. 2. Electron micrographs of the thermal treatment products (a) Al_2TiO_5 synthesized in air and (b) that calcined in argon. (*1*) Al_2TiO_5 and (*2*) $Al_{2-2x}Ti^{3+}_{2x}Ti^{4+}O_5$.

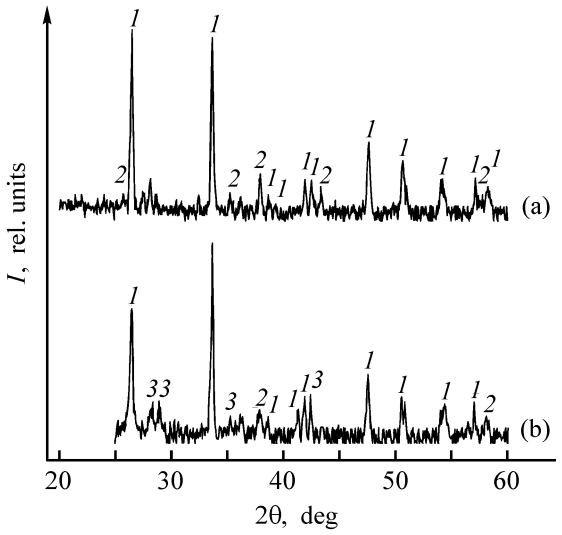


Fig. 3. X-ray diffraction patterns of thermal-treatment products: (a) $Al_2TiO_5 + 0.1\,Ti_2O_3$, (b) $Al_2TiO_5 + 1.0\,Ti_2O_3$. (*1*) $Al_{2-2x}Ti^{3+}_{2x}Ti^{4+}O_5$, (*2*) Al_2O_3, and (*3*) Magneli phases.

According to electron-microscopic data, aluminum titanate synthesized in air is composed of regularly shaped particles less than 10 μm in size, with the following atomic composition (mol %): Al 25.0, Ti 12.0, and O 63.0, which corresponds to that of stoichiometric Al_2TiO_5 (Fig. 2a). Areas with an increased content of titanium (13.0 mol %) are formed on the surface of aluminum titanate particles after annealing of the samples in argon (Fig. 2b). The averaged data of the electron microprobe analysis of the compound correspond to the chemical formula $Al_{1.9}Ti^{3+}_{0.1}Ti^{4+}O_5$.

An $Al_{2-2x}Ti^{3+}_{2x}Ti^{4+}O_5$ solid solution and α-Al_2O_3 (10 vol %) are formed in the thermal treatment products at $x = 0.1$ (Fig. 3, X-ray diffraction pattern a). The reaction of Al_2TiO_5 with Ti_2O_3 can be represented by the following equation:

$$Al_2TiO_5 + xTi_2O_3 = Al_{2-2x}Ti^{3+}_{2x}Ti^{4+}O_5 + xAl_2O_3. \quad (3)$$

Triple-charged titanium atoms isovalently substitute aluminum atoms in the Al_2TiO_5 crystal lattice to form the individual phase α-Al_2O_3. In this concentration range ($x = 0.1$), aluminum titanate partially dissociates in accordance with Eq. (1), because the Ti^{3+} content in calcination products (4.2 mol %) exceeds its amount in the starting stock (3.6 mol %). According to the averaged data of the electron microprobe analysis, the compound synthesized contains (mol %): Al 21.0, Ti 16.0, and O 63.0, which corresponds to the chemical formula $Al_{1.7}Ti^{3+}_{0.3}Ti^{4+}O_5$.

An increase in the Ti_2O_3 content to $x = 0.2$ is accompanied by formation of α-Al_2O_3 (up to 10 vol %) in the thermal-treatment products. As Ti^{3+} ions substitute Al^{3+} ions in aluminum titanate the lattice constants of $Al_{2-2x}Ti^{3+}_{2x}Ti^{4+}O_5$ increase further (Table 2). This is due to the larger ionic radius of titanium(III) in octahedral coordination as compared with aluminum [18]: $R(Ti^{3+}) = 0.67$ Å, $R(Al^{3+}) = 0.53$ Å. In modeling of the structure of the solid solution $Al_{2-2x}Ti^{3+}_{2x}Ti^{4+}O_5$ in the sample under consideration, the best result corresponds to the occupancies by Al^{3+} and Ti^{3+} of 0.557 and 0.110, respectively, in Ti^{3+} substitution for Al^{3+} in the aluminum titanate structure [17]. For the composition $x = 1.3$, the content of α-Al_2O_3 in the final products virtually does not increase. Thus, under the chosen thermal treatment conditions (1400°C), Ti^{3+} occupies no more than 20% of Al^{3+} positions in the Al_2TiO_5 structure, and the region of isovalent substitution is limited to the $Al_{1.6}Ti^{3+}_{0.4}Ti^{4+}O_5$ composition.

In the concentration range $0.3 \le x \le 1$, Magneli phases Ti_nO_{2n-1} ($4 < n < 9$) appear in the thermal-treatment products in addition to the phases of the $Al_{2-2x}Ti^{3+}_{2x}Ti^{4+}O_5$ solid solution and α-Al_2O_3

(Fig. 3, diffraction pattern b). Aluminum titanate reacts with Ti_2O_3 to form Ti_nO_{2n-1} in accordance with the equation

$$(n - 2)Al_2TiO_5 + Ti_2O_3 = Ti_nO_{2n-1} + (n - 2)Al_2O_3. \quad (4)$$

The sum of reactions (3) and (4) has the form

$$(n - 1)Al_2TiO_5 + (x + 1)Ti_2O_3 = Al_{2-2x}Ti^{3+}_{2x}Ti^{4+}O_5 + Ti_nO_{2n-1} + (n - 2 + x)Al_2O_3. \quad (5)$$

The results of an electron microprobe analysis of the products of calcination of the starting Al_2TiO_5–$1.0\,Ti_2O_3$ sample confirm the presence of the Magneli phase (Ti 34.5 mol % and O 65.5 mol %) and that of the $Al_{1.75}Ti^{3+}_{0.25}Ti^{4+}O_5$ solid solution. In the concentration range $0.2 < x < 1$, the lattice constants of the resulting $Al_{2-2x}Ti^{3+}_{2x}Ti^{4+}O_5$ solid solutions are close within the experimental error and independent of the Ti_2O_3 content in the starting stock (Table 2).

The dependences of the physical characteristics of samples on the content of titanium(III) oxide in $Al_2TiO_5 + xTi_2O_3$ starting mixtures, obtained in this study, show that the water absorption by the material decreases from 17.9 to 4.6%, and the open porosity, from 39.0 to 17.7%, as the Ti_2O_3 content in the stock increases, which points to activation of sintering processes (Fig. 4). The strongest effect of the compaction of aluminum titanate ceramics is achieved when 23 mol % Ti_2O_3 is introduced, and further increase in the content of Ti_2O_3 does not improve the physical characteristics. The resistance of the samples synthesized (Fig. 4) to concentrated H_2SO_4 increases as the content of the $Al_{2-2x}Ti^{3+}_{2x}Ti^{4+}O_5$ solid solution enriched with titanium, relative to that of aluminum titanate, in a sample increases. Such a dependence of the acid-resistance on the sample composition can be attributed to a lower mobility of titanium atoms, compared with aluminum atoms, resulting from the difference in their radii [$R(Ti^{3+}) > R(Al^{3+})$]. The improvement of the physical characteristics and the chemical resistance of a ceramic material by introducing Ti_2O_3 enables extension of the application area of materials based on Al_2TiO_5.

CONCLUSIONS

It was found that, under the chosen conditions of thermal treatment (1400°C), Ti^{3+} occupies no more than 20% of Al^{3+} positions in the Al_2TiO_5 structure and the range of isovalent substitution is limited to the $Al_{1.6}Ti^{3+}_{0.4}Ti^{4+}O_5$ composition.

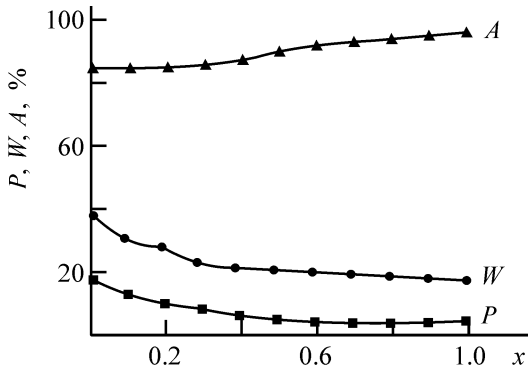


Fig. 4. Water absorption *W*, open porosity *P*, and acid-resistance *A* of the material obtained from the Al_2TiO_5 + xTi_2O_3 starting mixture vs. the parameter *x*.

The strongest effect of compaction of ceramics based on aluminum titanate is achieved by introducing up to 23 mol % Ti_2O_3, and further increase in the content of Ti_2O_3 does not result in any noticeable improvement of physical characteristics. The resistance of a ceramic material based on aluminum titanate to concentrated sulfuric acid increases with the content of titanium(III) in the samples studied.

REFERENCES

1. Bobkova, N.M. and Silich, L.M., *Zh. Vses. Khim. O–va im. D.I. Mendeleeva*, 1991, vol. 36, no. 5, pp. 564–569.
2. Dlitr, I.A., Podkovyrkin, M.I., and Kleshcheva, T.M., *Steklo Keram.*, 1990, no. 1, pp. 27–29.
3. Thomas, H.A. and Stevens, R., *Br. Ceram. Trans. J.*, 1989, vol. 88, no. 5, pp. 184–190.
4. Morison, B. and Lynch, R.W., *Acta. Cryst.*, 1972, vol. 28, pp. 1040–1046.
5. Austin, A.E. and Schwartz, C.M., *Acta. Cryst.*, 1953, vol. 6, pp. 812–813.
6. Ohya, Y., Nakagava, Z., and Hamano, K., *J. Am. Ceram. Soc.*, 1987, vol. 70, no. 8, pp. 184–186.
7. Goldberg, D., *Rev. Int. Hautes. Temp. Refract.*, 1968, vol. 5, pp. 181–194.
8. Asbrink, S. and Magneli, A., *Acta Cryst.*, 1959, vol. 12, pp. 575–581.
9. Rusakov, A.A. and Zhdanov, G.S., *Dokl. Akad. Nauk SSSR*, 1951, vol. 77, no. 3, pp. 411–414.
10. Zhdanov, G.S. and Rusakov, A.A., *Dokl. Akad. Nauk SSSR*, 1952, vol. 82, no. 6, pp. 901–904.
11. Onoda, M., *J. Solid State Chem.*, 1998, vol. 136, pp. 67–73.

12. Shveikin, G.P., Dudkin, B.N., Lekanova, T.L., and Sevbo, O.A., *Neorg. Mater.*, 1993, vol. 29, no. 6, pp. 859–861.
13. Goldin, B.A., Ryabkov, Yu.I., Istomin, P.V., and Grass, V.E., *Vysokotemperaturnaya vosstanovitel'naya pererabotka oksidnogo mineral'nogo syr'ya (malozhelezistye boksity i leikoksen)* (High-temperature Reductive Processing of Oxide Mineral Raw Materials (Low-Ferrous Bauxites and Leucoxene), Yekaterinburg: Ural. Otd. Ross. Akad. Nauk, 2001.
14. Giordano, L., Viviani, M., Bottino, C., *et al.*, *J. Eur. Ceram. Soc.*, 2002, vol. 22, pp. 1811–1822.
15. *Handbuch der Praparativen Anorganischen Chemie*, Bd. 2, von Baudler, M., Brauer, G., Feher, F., *et al.*, Stuttgart: Ferdinand Enke, 1978.
16. Kraus, W. and Nolze, G., *J. Appl. Crystallogr.*, 1996, vol. 29, p. 301.
17. *Data file JCPDS-ICDD*, 71–356.
18. Shannon, R.P. and Prewitt, C.T., *Acta Cryst.*, 1969, vol. 25, p. 725–949.

Russian Journal of Applied Chemistry, Vol. 78, No. 8, 2005, pp. 1229–1234. Translated from Zhurnal Prikladnoi Khimii, Vol. 78, No. 8, 2005, pp. 1252–1257.
Original Russian Text Copyright © 2005 by Kirsanov.

INORGANIC SYNTHESIS AND INDUSTRIAL INORGANIC CHEMISTRY

Comparative Study of the Combustion of Formulations Based on Sodium Chlorate and Polyethylene in the Form of Powder or Tubes

O. N. Kirsanov

Prikladnaya Khimiya Russian Scientific Center, Federal State Unitary Enterprise, St. Petersburg, Russia

Received March 20, 2003; in final form, June 2005

Abstract—A comparative study of the combustion rate under atmospheric conditions, of formulations with different compositions based on sodium chlorate and polyethylene in the form of powder or tubes (layered system) was carried out.

Previously, the combustion rate of formulations based on $NaClO_3$ and polyethylene (PE) and kerogen in the form of powders, which are typical disordered systems for gunpowder and explosives, have been studied [1]. This was done in a narrow range of compositions, evaluated by the oxidant excess coefficient of 0.37 to 1.5 for kerogen and 0.5 to 1.5 for polyethylene as combustibles. It became necessary to carry out studies in a wider range of compositions and with polyethylene in the form of tubes, a layered system. This is due to the necessity to determine the limits of stable combustion of the formulations considered and to examine in more detail the combustion process itself. Based on the data obtained, the present study assessed the possibility of transition of the combustion from deflagration to detonation.

In this stage, we studied the macrokinetics of combustion of formulations based on $NaClO_3$ and PE in the form of a powder, with an oxidant content increased to the point of combustion damping, and with PE in the form of tubes (layered system), also, when possible, as far as the stable-combustion boundaries, on a laboratory setup. The interest in a layered system is due to its presumably higher stability against transition from deflagration to detonation. The study was carried out in order to search for, and create, new materials necessary for mining industry for extraction of block stone and for building industry for safe destruction of natural and artificial objects.

EXPERIMENTAL

We studied the combustion of a formulation composed of $NaClO_3$ and polyethylene experimentally on a setup similar to that used previously [1]: the transit time of a combustion front between two reference points spaced by a distance l = 55 mm (determined when assembling the of contacts). The measuring system included two electric circuits with one dc power source (V = 25 V) connected to the electrically conducting case. Each circuit had an electric contact introduced via a ceramic nonconducting channel into the case. Ionization contacts were mounted at a distance of 10–15 mm from the upper and lower edges of the cylindrical case in order to preclude any influence of transients in ignition and termination of combustion. The instants at which the combustion surface passed the contacts (reference points) were recorded as successive closure of the contacts of two electric circuits connected to a P14M electric stopwatch. The tests were performed under atmospheric pressure at ambient temperature. The combustible formulation included $NaClO_3$ of a 25–150-μm fraction (60% 25–65-μm fraction) as oxidant and PE in the form of a powder of a 10–180-μm fraction (71% 15–65-μm fraction) or as tubes (d 5–7 mm, wall thickness 150–500 μm) as a combustible. The mass of $NaClO_3$ was varied in each experiment within the range 57–82 g. A preliminarily blended mixture of $NaClO_3$ and PE of a prescribed (as regards the oxidant excess coefficient) composition was charged to a height of 80 mm into an experimental steel vessel (d 30 mm, wall thickness 1 mm) made of Kh18N9T steel, and the mass of the experimental vessel and of the formulation charged was measured. The scatter in bulk density did not exceed ±7% for an oxidant excess coefficient equal to unity and ±4% for other compositions. When studying the layered system, we first charged tubes of required dimensions and amount (mass) prescribed by calcula-

1070-4272/05/7808-1229 © 2005 Pleiades Publishing, Inc.

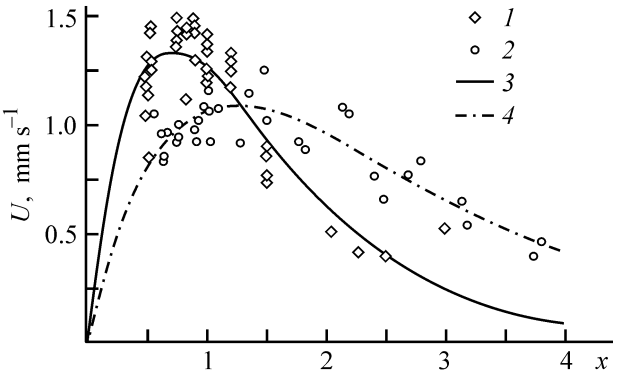


Fig. 1. Linear combustion velocity U of the formulations vs. the oxidant excess coefficient x. Experimental data for formulations: (*1*) $NaClO_3$ + PE (powder), (*2*) $NaClO_3$ + PE (tubes), (*3*) approximation for formulation *1*, and (*4*) approximation for formulation *2*.

tion into the gas-generator case, weighed the vessel on a VLK-500 balance, and charged $NaClO_3$ in several stages, with the vessel tapped from time to time (manual vibration compaction). The scatter in bulk density did not exceed ±7% in this case. The fuel formulation was ignited by lighting a 1-g portion of black powder with a Nichrome coil (V = 12 V, R = 1 Ω). To obtain more reliable results, we performed all the tests at least twice. The linear combustion velocity U (mm s^{-1}) of the formulation was determined by the equation

$$U = l t_c^{-1},$$

where l is the distance between the reference points (mm, absolute measurement error 1 mm), and t_c is the combustion time of the formulation between the reference points (s, absolute measurement error 0.01 s).

The total relative error in measuring the linear combustion velocity did not exceed 3%:

$$3\% \le \left(\frac{100}{55} + \frac{0.01}{50}\right) \times 100\%.$$

The main results of the experiments on the influence exerted by composition (evaluated by the oxidant excess coefficient x) on the linear combustion velocity of combustion of the formulations studied are presented in Fig. 1. The lines in the figure are plotted using regression equations obtained in a polynomial processing of the experimental data by the least-squares method. For a formulation composed of $NaClO_3$ and PE powder, the following regression equation was obtained with a correlation coefficient of 0.92:

$$U = 5.024x \exp(-1.387x).$$

According to the calculation, the maximum linear combustion velocity of the given formulation is 1.33 ± 0.04 mm s^{-1} at an oxidant excess coefficient x = 0.72. The fact that the regression equation of the process differs from that used previously [1] is largely due to the wider variation range of the formulation composition. It follows from these data that the interval of oxidant excess coefficients in which the combustion of the powder system is reliable and stable is $0.5 \le x \le 2.3$.

For the layered system, the regression equation (correlation coefficient 0.91) has the form

$$U = 2.211x \exp(-0.78x), \text{ mm } s^{-1}.$$

For this formulation, the maximum linear combustion velocity is 1.09 ± 0.04 mm s^{-1} at an oxidant excess coefficient x = 1.26. For the layered system, the interval of compositions with a reliable stable combustion is considerably wider than that for the powdered system: $0.5 \le x \le 3.7$, although a stable combustion was observed in a gas-generator 40 mm in diameter even at an oxidant excess coefficient of 5.7. It can be seen from the results presented that, first, the combustion velocity of the powdered formulation in the stoichiometric region exceeds that of the layered system and, second, the interval of stable combustion of the layered system is considerably wider than that for the powdered (disordered) system. This can be attributed to a difference in the rates of processes of purely physical nature: both to a higher rate of gasification of a PE powder and $NaClO_3$, compared with gasification of tubes (thickness 25–65 and 150–500 μm, respectively), and to a shorter time of gas mixing for the powdered system. This time can be evaluated using the Fourier diffusion criterion:

$$\text{Fo} = D_{i,j} \tau l^{-2},$$

where $D_{i,j}$ is the diffusion coefficient of the components (taken to be the same for all the components in the case in question, with only gases involved); τ, time of mixing of the gases; and l, mixing path proportional to the geometrical parameters of the systems (grain size or tube diameter).

Then the ratio of the mixing times will be on the order of

$$\frac{\tau_1}{\tau_2} \approx \frac{D_1}{D_2}\left(\frac{d_1}{d_2}\right)^2,$$

where subscript 1 refers to the layered system, and subscript 2, to the disordered (powdered) system.

Our calculation shows that the maximum mixing time for the layered system (tube diameter 5.0 mm) exceeds that for the powdered system (grain size 60 μm) by two to three orders of magnitude. This is one of the main reasons why the combustion velocity of the powdered system exceeds that for the layered system.

It is necessary to take into account the fact that PE gasification occurs with heat consumption. Therefore, the larger the mass of PE, the lower the overall rate of the process. Probably, the wider interval of stable combustion of the formulation composed of $NaClO_3$ and PE tubes, with an oxidant excess coefficient exceeding 1.5, and its lower combustion velocity in the stoichiometric region can be understood as follows. The combustion of the oxidant and combustible in a layered system undergoing gasification [2, 3] occurs in the mixing zone, similarly to the combustion of unmixed gases, with the same cross-sectional inhomogeneity of the concentration fields and the same composition dependence of the flame jet length (10 to 30 cm). The main source of heat is localized near the surface of PE tubes undergoing gasification. The gasification rate of the components depends on the heat flux. A part of the heat released in the combustion is consumed for gasification of an additional mass of $NaClO_3$. It is necessary to take into account that $NaClO_3$ heated to above 623 K decomposes with release of approximately 54.76 J mol^{-1} [4]. All these factors, combined, provide a wider interval of stable combustion of the layered system. In an ordinary disordered system (with powdered components), heat is released uniformly over the entire cross-section. The experimental data on the relative combustion velocities of the layered and disordered systems, presented here, differ from the results obtained with a model system [2]. Possibly, this can be attributed to the fact that the study [2] was performed on models having the form of separate Plexiglas tubes with oxidants ($KClO_4$, $KClO_3$) compacted within the tubes.

To confirm the hypothesis that the gasification rate affects the whole process, we performed a qualitative numerical experiment to evaluate, under certain assumptions, the time and rate of heating of PE and $NaClO_3$ powders (loose material) and of a PE film. As the diameter of the PE tubes exceeds by approximately an order of magnitude the wall thickness, the latter can be considered a planar thin film. Let us take the grain size of PE and $NaClO_3$ to be 60 μm, and the wall thickness of PE tubes, 300 μm (a size promising for practical implementation). The thermal properties of the material are believed to be constant [4, 5]. All the calculations of nonstationary heat exchange are simplified if the body has a low internal resistance (Bio criterion $Bi = \alpha l \lambda^{-1} < 0.1$ [6]). In this case, the temperatures of the surface and mid-part of a body being heated or cooled are nearly the same [6].

Let us determine the interval in which this criterion varies for a film at the following values of the parameters involved: $\lambda = 0.418–0.440$ W m^{-1} deg^{-1} and $\alpha = 2.5–250$ W m^{-2} deg^{-1}. Then we have for the film $0.002 < Bi < 0.18$. We calculate the interval of variation of the Bio criterion for a $NaClO_3$ powder for the following values of the parameters: $\lambda = 0.64–1.28$ W m^{-1} deg^{-1} and $\alpha = 2.5–250$ W m^{-2} deg^{-1}. The calculation yields $0.00004 < Bi < 0.008$. Thus, the absence of a temperature gradient over the cross-section of the materials under consideration makes it possible to calculate the time (and rate) of heating by the following formulas [6]:

$$\tau = \frac{l}{2}\frac{\rho C_p}{\alpha}\ln\frac{T - T_{in}}{T - T_{fin}},$$

for a PE film and

$$\tau = \frac{r}{3}\frac{\rho C_p}{\alpha}\ln\frac{T - T_{in}}{T - T_{fin}},$$

for $NaClO_3$ and PE grains. Here, ρ is the component density (kg m^{-3}); α, heat-transfer coefficient (W m^{-2} deg^{-1}); l, PE film thickness (m); r, $NaClO_3$ (PE) grain radius (m); C_p, specific heat of the component (J kg^{-1} deg^{-1}); T, flame temperature (K); T_{in}, initial temperature of the component (K); and T_{fin}, final temperature of the component (K).

We take the following values of the parameters: $C_p = 1880$ J kg^{-1} deg^{-1} for polyethylene and 1200 J kg^{-1} deg^{-1} for $NaClO_3$; ρ, 959 and 2490 kg m^{-3}, respectively; initial temperature of the components, 293 K; final temperature equal to the destruction temperature of 763 K for PE [5]; and decomposition temperature of technical-grade $NaClO_3$ equal to 643 K [4]. More reliable results, even for a qualitative numerical experiment, would be obtained by direct measurements on the surface of the components during combustion, as it was done by Zenin [7], or by using the Mikhel'son equation. Experimental data [7] on the temperature profile refer to a layer of a solid substance, gunpowder N, with the temperature gradient in the condensed phase reaching a value of approximately 2000 deg mm^{-1}. Such a temperature gradient is impossible for thin bodies [6]. When using the Mikhel'son equation, it is necessary to calculate the thermal diffusivity of a loose material composed of dissimilar substances (PE and $NaClO_3$). The pres-

Table 1. Time of heating of a polyethylene film in relation to flame temperature and heat-transfer coefficient

T, K	τ, s, at indicated α, W m^{-2} deg^{-1}					
	2.5	25	50	100	150	250
2345	28.482	2.848	1.424	0.712	0.475	0.285
2703	23.747	2.375	1.187	0.594	0.396	0.237
2981	21.034	2.103	1.052	0.526	0.351	0.21
3199	19.307	1.931	0.965	0.483	0.322	0.193
3342	18.32	1.832	0.916	0.458	0.305	0.183
3357	18.222	1.822	0.911	0.456	0.304	0.182
2930	21.484	2.148	1.074	0.537	0.358	0.215
2545	25.626	2.563	1.281	0.641	0.427	0.256
2030	34.558	3.456	1.728	0.864	0.576	0.346
1719	43.823	4.382	2.191	1.096	0.73	0.438
1516	53.185	5.319	2.659	1.33	0.866	0.532

Table 2. Heating velocity *W* of a polyethylene film in relation to flame temperature and heat-transfer coefficient

T, K	*W*, mm s^{-1}, at indicated α, W m^{-2} deg^{-1}					
	2.5	25	50	100	150	250
2345	0.011	0.105	0.211	0.421	0.632	1.053
2703	0.013	0.126	0.253	0.505	0.758	1.263
2981	0.014	0.143	0.285	0.57	0.856	1.426
3199	0.016	0.155	0.311	0.622	0.932	1.554
3342	0.016	0.164	0.328	0.655	0.983	1.638
3357	0.016	0.165	0.329	0.659	0.988	1.646
2930	0.014	0.14	0.279	0.559	0.838	1.396
2545	0.012	0.117	0.234	0.468	0.702	1.171
2030	0.009	0.087	0.174	0.347	0.521	0.868
1719	0.007	0.068	0.137	0.274	0.411	0.685
1516	0.006	0.056	0.113	0.226	0.338	0.564

ently existing methods for evaluation of this coefficient give a gross error [8]. Below are listed preliminary results of a thermodynamic calculation of the combustion temperature *T* in relation to the oxidant excess coefficient *x*:

x	*T*	*x*	*T*
0.5	2345	1.0	3357
0.6	2703	1.5	2930
0.7	2981	2.0	2545
0.8	3199	3.0	2030
0.9	3342	4.0	1719

It is necessary to take into account that the real combustion temperature is lower than the calculated value by the amount of loss of heat, which is proportional to that presented. Table 1 lists the calculated times of heating of a PE film to the destruction temperature (taken to be equal to the gasification temperature) in relation to the flame temperature and heat-transfer coefficient. The last row presents data for an oxidant excess coefficient $x = 5$ and flame temperature of 1516 K.

The velocity of heating *W* to a prescribed temperature (destruction temperature) can be obtained (Table 2) by dividing the film thickness by the time listed in Table 1.

For comparison, we present data on the time of heating of a $NaClO_3$ powder to the decomposition

Table 3. Time of heating of a $NaClO_3$ powder in relation to flame temperature and heat-transfer coefficient

T, K	τ, s, at indicated α, *W* m^{-2} deg^{-1}					
	2.5	25	50	100	150	250
2345	22.352	2.235	0.224	0.112	0.056	0.022
2703	18.755	1.876	0.188	0.094	0.047	0.019
2981	16.673	1.667	0.167	0.083	0.042	0.017
3199	15.338	1.534	0.153	0.077	0.038	0.015
3342	14.573	1.457	0.146	0.073	0.036	0.015
3357	14.497	1.45	0.145	0.072	0.036	0.014
2930	17.02	1.702	0.17	0.085	0.043	0.017
2545	20.188	2.019	0.202	0.101	0.05	0.02
2030	26.894	2.689	0.269	0.134	0.067	0.027
1719	33.66	3.366	0.337	0.168	0.084	0.034

temperature (Table 3) at the same heat-transfer coefficients and flame temperatures as those for the PE film.

As can be seen from Tables 1 and 3, the time of PE heating to the destruction temperature exceeds by more than an order of magnitude the time of $NaClO_3$ heating to the decomposition temperature. Consequently, the influence of heating of the $NaClO_3$ powder can be neglected. As the velocity of heating of the PE film must exceed the overall combustion velocity (about 1 mm s^{-1}), it is sufficient to consider only the last two columns in Table 2 in a comparison with the experimentally measured motion velocity of the combustion front. Figure 2 shows, as functions of the oxidant excess coefficient, experimental data on the combustion velocity (curve *1*) and PE film heating velocities for heat-transfer coefficients of 250 and 150 W m^{-2} deg^{-1} (curves *2* and *3*, respectively). It can be seen that the run of the curves describing the PE film heating velocity virtually coincides with the experimental data on the combustion velocity. Thus, there is reason to believe that the heating process noticeably affects the entire process, being, in fact, of the diffusion type. This is not the case for a formulation composed of $NaClO_3$ and powdered PE (typical disordered system). It follows from the calculations that the time of PE powder heating virtually coincides with that of $NaClO_3$ powder heating, being more than order of magnitude shorter than that for the PE film. Therefore, the powder heating process cannot exert the same influence (diffusion hindrance) on the overall process as the process of heating of the PE film.

As another evidence in favor of the influence exerted by the heating velocity (diffusion factor) on the overall process can serve the type of dependence of the reaction rate on the reciprocal temperature, which can be used to determine the region in which the process occurs and to evaluate the activation energy. We can calculate this parameter by the known formula [9], taking the combustion velocity as the reaction rate (which is possible because the velocity ratios are considered):

$$E = \frac{8.314 \ln (u_2/u_1)}{1/T_1 - 1/T_2},$$

where u_1, u_2 are the combustion velocities U (mm s^{-1}) at temperatures T_1 and T_2, respectively.

Let us substitute into the formula the combustion velocities from the regression equations and the corresponding temperatures from a thermodynamic calculation. As the combustion velocity passes through a maximum, parameters referring either to the ascending or to the descending portion of the curve for

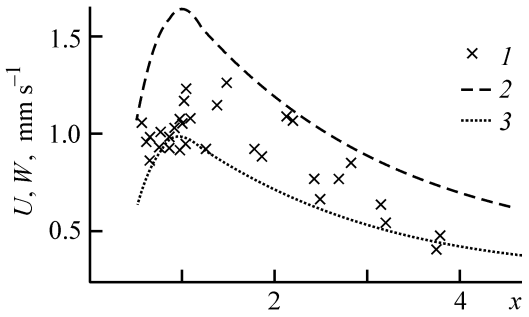


Fig. 2. Comparison of (*1*) combustion velocity *U* of a formulation composed of PE tubes and $NaClO_3$ with (*2*, *3*) heating velocity *W* of a PE film (tubes). (*x*) Oxidant excess coefficient. Heat-transfer coefficient (W m^{-2} deg^{-1}): (*2*) 250 and (*3*) 150.

the combustion velocity can be taken for the calculation. We assume that the activation energy remains constant during the process under study. For the layered system, the flame temperature T_1 = 2545 K and the combustion velocity found from the equation, u_1 = 0.93 mm s^{-1}, for an oxidant excess coefficient x = 2, and T_2 = 1719 K and u_2 = 0.391 mm s^{-1} for x = 4. Substituting these values into the equation, we obtain E = 38 kJ mol^{-1}. The results of the calculation indicate that the combustion of the layered system occurs in an intermediate region that is far from the kinetic zone and is closer to the purely diffusion region. Consequently, the process of combustion of such a system cannot pass from deflagration to detonation under the real application conditions (gas-generator diameter not exceeding 75 mm). For a formulation with powders, the pattern is entirely different: T = 2980 K, u = 1.33 mm s^{-1} for an oxidant excess coefficient x = 0.72, and T = 2545 K and u = 0.63 mm s^{-1} for x = 2.0. Calculation gives E = 141.7 kJ mol^{-1}. This means that the combustion of the powdered system occurs in the kinetic region, and, consequently, a transition of the ordinary deflagration combustion to the detonation mode is possible. The hypothesis suggested was confirmed by the UN test 1(a) (iii), paragraph 5. Two experiments were performed for each formulation, and one, for a neutral mixture (sand + salt). The tube rupture for the layered system was similar to that for the neutral mixture, which classes the layered system under study with nonexplosive materials. The formulation composed of $NaClO_3$ and diesel fuel (tested by the same procedure) belongs to explosives.

CONCLUSIONS

(1) An analysis of how the combustion velocity of formulations based on $NaClO_3$ and polyethylene in the form of a powder (disordered system) or tubes (layered system) depends on the relative content of the oxidant and combustible at an oxidant excess coefficient x varied from 0.5 to 3.7 demonstrated that the combustion velocity depends on the composition of the formulations under study and reaches a maximum in the region close to the stoichiometry.

(2) The maximum linear combustion velocities are 1.33 mm s^{-1} for the powdered system (oxidant excess coefficient 0.72) and 1.09 mm s^{-1} for the layered system (oxidant excess coefficient 1.26).

(3) The formulations exhibit reliable combustion at oxidant excess coefficients in the range 0.5–2.3 for the disordered system and 0.5–3.7 for the layered system, with this range being extendible in the latter case. Making larger the diameter of the experimental vessel extends the range of stable combustion to larger oxidant excess coefficients.

(4) The run of the curves describing the heating velocities of polyethylene films virtually coincides with that of the curves for the combustion velocities of the layered system.

(5) The combustion of the layered system occurs in the diffusion region, which follows from the results obtained in determining the activation energies and from the collinearity of the curves for the combustion and heating velocities. The combustion of systems of this kind occurs only in the deflagration (nondetonation) mode.

ACKNOWLEDGMENTS

The author wishes to thank V.B. Ulybin for help in the study and valuable comments taken into account in revising the manuscript.

REFERENCES

1. Kirsanov, O.N., Berezuev, Yu.A., Ostrovskii, V.I., and Tyminskii, V.N., *Zh. Prikl. Khim.*, 2003, vol. 76, no. 5, pp. 734–737.
2. Bakhman, N.N. and Belyaev, A.F., *Gorenie geterogennykh kondensirovannykh system* (Combustion of Heterogeneous Condensed Systems), Moscow: Nauka, 1967.
3. Librovich, V.B., *Prikl. Mat. Tekh. Fiz.*, 1962, no. 4, pp. 33–39.
4. Blinov, I.F., *Khloratnye i perkhloratnye vzryvchatye veshchestva* (Chlorate and Perchlorate Explosives), Moscow: Oborongiz, 1941.
5. Gordon, G.Ya., *Stabilizatsiya sinteticheskikh polimerov* (Stabilization of Synthetic Polymers), Moscow: Goskhimizdat, 1963.
6. Shorin, S.N., *Teploperedacha* (Heat Transfer), Moscow: Vysshaya Shkola, 1964.
7. Novozhilov, B.V., *Nestatsionarnoe gorenie tverdykh raketnykh topliv* (Nonstationary Combustion of Rocket Propellants), Moscow: Nauka, 1973.
8. Vasil'ev, L.L. and Tanaeva, S.A., *Teplofizicheskie svoistva poristykh materialov* (Thermal Properties of Porous Materials), Minsk: Nauka i Tekhnika, 1972.
9. Frank-Kamenetskii, D.A., *Diffuziya i teploperedacha v khimicheskoi kinetike* (Diffusion and Heat Transfer in Chemical Kinetics), Moscow: Nauka, 1987.

Russian Journal of Applied Chemistry, Vol. 78, No. 8, 2005, pp. 1235–1244. Translated from Zhurnal Prikladnoi Khimii, Vol. 78, No. 8, 2005, pp. 1258–1267.
Original Russian Text Copyright © 2005 by Prikhodko, Chudakov.

PHYSICOCHEMICAL STUDIES OF SYSTEMS AND PROCESSES

Application of the Hole Group Quasi-Chemical Model to Evaluation of Azeotropic Properties[1]

I. V. Prikhodko and A. M. Chudakov

St. Petersburg State University, St. Petersburg, Russia

Received May 12, 2005

Abstract—Azeotropic parameters (composition, boiling point, equilibrium pressure) were calculated in terms of the Viktorov–Smirnova lattice-hole quasi-chemical group model for binary and ternary systems in which there is no stratification of solutions formed by various components (hydrocarbons, alkanols, acetic acid, ethanoates, chloroform, acetone, pyridine, and water). Azeotropes of various kinds (positive, negative, saddle-type) were found using simple algorithms, including composition variation. Thirty binary, nine ternary, and one quaternary systems were considered. New group parameters were evaluated. The results of calculations of azeotropes were compared with published experimental data.

Information about existence of azeotropes and knowledge of their characteristics in binary and multicomponent systems are necessary for analysis of the phase behavior in designing technological schemes for separation processes and, in particular, azeotropic rectification. Because an azeotrope is an important feature of the phase diagram, calculation of parameters of the azeotropic state is an important aspect of the general problem of modeling of the phase equilibrium. Such a calculation is simultaneously an effective means of verification of a method used to model the vapor–liquid equilibrium.

Previously, Storonkin and co-workers carried out extensive studies of azeotropic properties. In particular, they formulated rigorous thermodynamic expressions for Vrevsky rules, found factors determining how the composition of azeotropes varies with temperature and pressure, and derived for systems with solution stratification expressions similar to Vrevsky rules for multicomponent systems. They found experimentally how the composition of azeotropes varies with external conditions for numerous binary and ternary systems. The main results of this set of investigations were summarized in the monograph [1]. No studies devoted to prognostication of azeotropic properties with model equations were carried out at that time because equations of local composition and others had not been known yet.

Since the 1970s, models of local composition (e.g., Wilson, NRTL, and UNIFAC equations) have been the most frequently used in practical calculations of phase equilibria at low pressures [2]. At elevated pressures, equations of the Van der Waals type (Peng–Robinson, Soave–Redlich–Qwong equations etc.) [3, 4] have been widely used. The above models we used to determine parameters of a wide variety of azeotropes [5–16].

In the present study, the azeotropic properties were evaluated using a group equation of state based on the lattice-hole model (HM) suggested by Smirnova and Viktorov [2, 17]. The HM was successfully tested on single-component, binary, and multicomponent systems in widely varying conditions [2, 17–26]. The model satisfactorily describes equilibria of fluid phases in various mixtures in a wide range of temperatures and pressures. However, the problem of determining the ability of HM to prognosticate azeotropic parameters has not been specially considered previously. In addition, the HM has not been tested at all on a number of systems. In particular, the necessary parameters of the model for chloroform, cyclohexane, and perfluorobenzene have not been determined. The aim of the present study was to describe the vapor–liquid equilibrium for a number of binary systems including the above-mentioned substances, evaluate new group

[1] Reported at the XVI International Congress on Chemical Technology, CHISA2004, Prague, Czechia, August 22–26, 2004.

1070-4272/05/7808-1235 © 2005 Pleiades Publishing, Inc.

Table 1. Group parameters* and the results of description of the thermodynamic properties of pure substances: liquid density ρ_l and equilibrium pressure P

Type of groups s and t	w_{st}	h_{st}	c_{st}
3Cl–CH (chloroform)	–2.6683	–3.0774	0.2282
CH–hole (chloroform)	–0.0311	0.0168	–0.1717
3Cl–hole (chloroform)	–0.0311	0.0168	–0.1717
CH_2–hole (cyclohexane)	0.2199	0.2342	–0.0304
CF–hole (perfluorobenzene)	0.2142	0.2437	–0.0400

Substance	T, K	$\delta\rho_l$,** %	δP,** %
Chloroform	216–431	0.2	1.4
Cyclohexane	279–491	2.3	0.2
Perfluorobenzene	293–473	2.0	1.3

* Chloroform: $r_{CH} = 0.6090$, $l_{CH} = 1.5$; $r_{3Cl} = 3.4104$, $l_{3Cl} = 0.5$. Cyclohexane: $r_{CH_2} = 1.1847$, $l_{CH_2} = 1.0$. Perfluorobenzene: $r_{CF} = 1.2579$, $l_{CF} = 1.0$.

** $\delta A = \frac{100}{N}\sum_{i=1}^{N}\left|\frac{A_i^{exp} - A_i^{calc}}{A_i^{exp}}\right|$, where A^{exp} is the experimental value of a property (density of the liquid phase or saturation pressure); A^{calc}, the corresponding calculated value; and $i = 1, ..., N$, number of points.

parameters, predict azeotropic properties of mixtures with different numbers of components with the help of HM, and compare the calculated results with experimental data. Homogeneous azeotropes of various kinds were found using simple, well-proven techniques based on successive changes in the molar fractions of the components [2, 6].

According to HM, pressure P is a sum of two contributions, repulsive (P_{rep}) and residual (P_{res}).

The repulsive pressure component, which takes into account differences in size and shape between molecules constituting a system, is evaluated by the Staverman formula. The residual contribution takes into account differences in interaction energy between neighboring pairs of different types and reflects orientation effects appearing because of the energy-nonuniformity of the molecular surface. This contribution is calculated in the quasi-chemical approximation:

$$P = P_{rep} + P_{res},$$

$$P_{rep} = -\frac{RT}{v^*} \times \left\{-\ln(1-\tilde{\rho}) + \tilde{\rho}\frac{\sum_{i=1}^{n} x_i l_i}{\sum_{i=1}^{n} x_i r_i} + \frac{z}{2}\ln\left[1 - \tilde{\rho}\left(1 - \frac{\sum_{i=1}^{n} x_i q_i}{\sum_{i=1}^{n} x_i r_i}\right)\right]\right\},$$

$$P_{res} = -\frac{RT}{v^*}\left\{z \ln X_0\right\}, \quad (1)$$

where v^* is the molar volume per lattice site (volume of a standard segment); x_i, mole fraction of ith component; $l_i = -z(q_i - r_i)/2 - (r_i - 1)$, molecule volume factor; z, coordination number of the lattice; r_i and q_i, geometric parameters of the model, which characterize the volume and surface area of ith molecule and are related to the corresponding quantities for groups constituting the molecule by $r_i = \sum_s \nu_s r_s$ and $q_i = \sum_s \nu_s q_s$, where ν_s is the of groups of sth kind in ith molecule; $\tilde{\rho} = v^* \sum_{i=1}^{n} \nu_i r_i / v$, reduced density ($v$, molar volume); and X_0, solution to a system of quasichemical equations

$$X_s \sum \alpha_t X_t \exp\left(-\frac{\Delta\varepsilon_{st}}{kT}\right) = 1.$$

Here, subscripts s and t designate regions of the molecular surface (group) whose interaction is described by interchange energies $\Delta\varepsilon_{st}$, with $s = 0$ for vacant lattice sites (holes); α_t is the fraction of the surface area occupied by groups of tth kind in the system.

The values of $\Delta\varepsilon_{st}$ are temperature-dependent:

$$\frac{\Delta\varepsilon_{st}}{kT} = w_{st} + h_{st}\frac{T_0 - T}{T} + c_{st}\left(\ln\frac{T_0}{T} - \frac{T_0 - T}{T}\right),$$

where w_{st}, h_{st}, and c_{st} are, respectively, the free energy, enthalpy, and specific heat of interchange (dimensionless energy parameters of the model); and T_0 is the chosen standard temperature.

To carry out calculations in terms of the lattice-hole model, it is necessary to have a set of geometric (r_s, q_s) and energy (w_{st}, h_{st}, c_{st}) parameters of the groups. The HM and the algorithm of calculations in terms of this model were described in most detail in [2, 17].

The geometric and energy parameters of the HM have been obtained previously for quite a number of chemical groups [2, 18–22, 24–26]. In particular, the model has been applied to description of systems containing various hydrocarbons, alkanols, esters (ethanoates), water, acetone, acetic acid, etc. In the group approach used in the HM, component molecules were divided into groups as follows: two

Table 2. Energy parameters of the hole model for mixtures (T_0 = 298.16 K, c_{st} = 0.0)

Type of groups *s* and *t*	w_{st}	h_{st}	Type of groups *s* and *t*	w_{st}	h_{st}
CH_2(alkanes)–CH($CHCl_3$)	–1.9110	–4.3685	CH_3CCH_3(acetone)–ACH (aromatic compounds)	0.0288	–0.0303
CH_2(alkanes)–3Cl($CHCl_3$)	–0.0775	0.2197			
CH_3(alkanes)–CH($CHCl_3$)	–1.9110	–4.3685	O(acetone)–ACH(aromatic compounds)	–0.1799	1.5390
CH_3(alkanes)–3Cl($CHCl_3$)	–0.0775	0.2197			
ACH(aromatic compounds)–CH($CHCl_3$)	–1.9807	–5.6882	CH_3CCH_3(acetone)–CH($CHCl_3$)	–0.1213	–0.1604
			CH_3CCH_3(acetone)–3Cl($CHCl_3$)	–0.1213	–0.1604
ACH(aromatic compounds)–3Cl($CHCl_3$)	–0.1078	0.3462	O(acetone)–CH($CHCl_3$)	–1.6609	1.9743
			O(acetone)–3Cl($CHCl_3$)	–1.6609	1.9743
CH_2(cyclohexane)–ACH (aromatic compounds)	0.0135	0.0327	MeO(MeOH)–CH($CHCl_3$)	–1.6298	2.2354
			MeO(MeOH)–3Cl($CHCl_3$)	–0.1569	–0.6408
CH_2(cyclohexane)–C_2H_5(EtOH)	–0.0264	–0.0264	H(MeOH)–CH($CHCl_3$)	–0.1569	–0.6408
CH_2(cyclohexane)–O(EtOH)	0.0896	0.0896	H(MeOH)–3Cl($CHCl_3$)	–1.6298	2.2354
CH_2(cyclohexane)–H(EtOH)	0.0896	0.0896	C_2H_5(EtOH)–CH($CHCl_3$)	0.0581	0.0838
CH_3(MeAc)–CH($CHCl_3$)	–2.0624	–8.3652	C_2H_5(EtOH)–3Cl($CHCl_3$)	0.0581	0.0838
CH_3(MeAc)–3Cl($CHCl_3$)	–0.1145	0.2286	O(EtOH)–CH($CHCl_3$)	–2.4172	–2.9135
Ac(MeAc)–CH($CHCl_3$)	–2.0624	–8.3652	O(EtOH)–3Cl($CHCl_3$)	–0.8470	–0.0447
Ac(MeAc)–3Cl($CHCl_3$)	–0.1145	0.2286	H(EtOH)–CH($CHCl_3$)	–2.4172	–2.9135
CH_3CCH_3(acetone)–Ac(MeAc)	0.0632	–0.2270	H(EtOH)–3Cl($CHCl_3$)	–0.8470	–0.0447
O(acetone)–Ac(MeAc)	–0.4773	–0.3174	CF(C_6F_6)–ACH(aromatic compounds)	–0.0009	–0.0136
CH_3CCH_3(acetone)–(CH_3MeAc)*	–0.0009	0.0100			
			CF(C_6F_6)–CCH_3(aromatic compounds)	–0.0132	–0.0425
O(acetone)–CH_3(MeAc)**	2.0704	11.1325			

* c_{st} = 0.4706. ** c_{st} = –58.8266.

types of groups, CH and 3Cl, were distinguished for chloroform $CHCl_3$, and six CH_2 and CF groups for cyclohexane and hexafluorobenzene, respectively. In the calculations in terms of HM, the molar volume of a standard segment was taken to be v^* = 14.244 $cm^3\ mol^{-1}$, and the coordination number of the lattice, z = 10. For groups of chloroform, the volume factors were evaluated using Bondi tables [27]. For the molecules C_6H_{12} and C_6F_6, which have a cyclic structure, the volume factor l = 1. The values of the group parameters, obtained in this study, and the results obtained in describing the saturated vapor pressure and the liquid phase density for these substances are listed in Table 1. It can be seen that the values of the properties, calculated using the HM, are in a good agreement with experimental data [28].

New energy parameters of group interaction (Table 2) for mixtures containing acetone, benzene, methyl acetate, chloroform, cyclohexane, and perfluorobenzene were evaluated using experimental data on the vapor–liquid equilibrium in binary systems (pressure–solution composition). The results of modeling are listed in Table 3, with the predicted values of the equilibrium pressure denoted by abbreviation "pred." The results obtained in calculating the liquid–vapor equilibria can be considered quite satisfactory. The list of the new parameters (Tables 1 and 2), combined with those obtained previously for other chemical groups, is sufficient for describing the liquid–vapor equilibrium and calculating azeotropes in binary and multicomponent mixtures containing a variety of organic components, including those mentioned above.

Now, the calculation of azeotropes will be described in more detail. The homogeneous azeotrope was found in accordance with the equation

$$x_i = y_i,\ i = 1, 2, ..., n, \qquad (2)$$

where x_i and y_i are the mole fractions of *i*th component in the liquid and vapor phases, respectively; $\sum_{i=1}^{n} x_i = 1$, $\sum_{i=1}^{n} y_i = 1$.

In a search for an azeotrope, it is convenient to introduce the distribution coefficient defined by

$$K_i = y_i/x_i,\ i = 1, 2, ..., n, \qquad (3)$$

and calculated in terms of the model at a given solution composition.

Table 3. Results of description of the vapor–liquid equilibrium for binary mixtures

System	T, K	P, mm Hg	δP, %	Δy,* %	Experimental data
Acetone + $CHCl_3$	238–330	760	pred. 0.9	1.3	[29]
	329–337	760	pred. 1.1	1.2	[29]
	298	162–224	1.6	2.5	[7]
	308	251–348	pred. 1.3	1.3	[29]
	328	547–731	pred. 0.7	0.9	[29]
C_6H_6 + $CHCl_3$	330–348	760	pred. 3.0	2.0	[30]
	298	106–186	0.7	0.9	[29]
	308	164–262	0.6	0.9	[29]
	318	247–422	1.6	2.1	[29]
C_6H_{14} + $CHCl_3$	333–342	760	pred. 1.9	0.5	[29]
	308	247–310	0.2	1.0	[29]
	318	365–453	1.2	1.0	[29]
	328	519–636	0.6	1.7	[29]
MeAc + $CHCl_3$	331–338	760	2.1	3.1	[29]
	323	500–571	1.2	1.4	[31]
MeOH + $CHCl_3$	326–336	760	pred. 1.5	0.6	[32]
	298	137–237	1.7	2.0	[7]
	313	301–454	1.2		[33]
	323	448–671	0.8		[33]
C_6H_6 + C_6H_{12}	350–370	760	pred. 1.4	0.8	[29]
	298	102–109	0.7	0.5	[34]
	313	192–206	1.6	0.6	[34]
	328	341–364	0.9	0.6	[34]
	343	562–596	1.3	0.9	[34]
EtOH + C_6H_{12}	323	272–428	0.2	0.9	[34]
Acetone + C_6H_6	353–329	760	pred. 1.2	4.5	[29]
	347–329	750	pred. 1.0	1.9	[34]
	298	98–227	0.1	0.2	[29]
	308	150–344	0.1	0.3	[29]
	323	271–614	0.2	0.4	[34]
Acetone + MeAc	328–329	760	pred. 0.4	0.5	[34]
	293	170–182	0.6	0.4	[35]
	303	270–283	0.5	0.5	[35]
	313	402–431	0.5	0.3	[35]
EtOH + $CHCl_3$	308	111–306	2.0	0.6	[29]
	318	181–456	pred. 1.8	0.4	[29]
	328	340–653	1.5	0.3	[29]
C_6H_6 + C_6F_6	303	106–119	1.8	1.6	[34]
	323	253–273	1.6	1.4	[34]
	343	535–557	1.4	1.1	[34]
C_7H_8 + C_6F_6	303	41–98	2.2	1.5	[29]
	323	104–235	1.8	1.4	[29]
	343	230–498	1.8	1.3	[29]

* $\Delta y = \frac{1}{N}\sum_{i=1}^{2}\sum_{j=1}^{N}\left|y_{i,j}^{\exp} - y_{i,j}^{\mathrm{calc}}\right|$, where $y^{\exp}$ is the experimental vapor composition, and y^{calc}, that obtained by calculation; i = 1, 2 (components); j = 1, ..., N (number of points).

The composition of an azeotrope can be found by minimizing the functional [2, 6]

$$F = \sum_{i=1}^{n} |K_i - 1|. \quad (4)$$

This functional is convenient for calculating azeotropes of various kinds under both isothermal and isobaric conditions and is sensitive to minor changes in the concentration of the mixture. The deviation of F from zero can be used to characterize the precision of solution to system (3).

In the present study, the minimum of the function F was sought using the method of coordinate-wise dichotomy. The search for an azeotrope was continued until the condition $F < 10^{-4}$, which corresponds to the experimental error in determining the azeotropic composition, was satisfied. If the required accuracy could not be achieved by means of this algorithm, the search was continued with other starting composition approximations. Under isobaric conditions, the temperature was calculated by iterations, until the calculated and prescribed values of the total pressure coincided to within $\left|\left(P_i^{\exp} - P_i^{\text{calc}}\right)/P_i^{\exp}\right| \le 10^{-5}$. In a search for the minimum of the target function (4), the equilibrium properties of the vapor–liquid mixture [vapor composition y_i, distribution coefficients K_i, boiling point (P = const) or saturation pressure (T = const)] were calculated at each running value of the solution composition. The clearly pronounced positive azeotropes (with a minimum boiling point and maximum vapor pressure) were also found using another method. Such an n-component azeotrope can be calculated as a final point to which tends the line of conjugated liquid–vapor nodes [2]. In this case, a value of the equilibrium vapor composition, calculated in a preceding step, is assigned to the mole fraction of the solution in any succeeding step of the search. The calculation is continued until the value of F, given by expression (4), becomes smaller than 10^{-4}.

Now the results of the calculation will be discussed. First, several general remarks should be made. It is noteworthy that azeotropic data were not used to determine or refine the HM parameters. The method of coordinate-wise dichotomy proved to be rather effective for finding an azeotrope in the binary, ternary, and quaternary systems under consideration (Tables 4–6) under isobaric and isothermal condi-

Table 4. Results for binary azeotropic systems

System* (1) + (2)	P, mm Hg	Properties of azeotropes			
		composition, mole fraction		$T^{\exp}$	T^{calc}
		$x_{\exp}$	x_{calc}	K	
C_6H_6 + MeOH	760	0.390	0.375	331.31	331.81
C_6H_6 + EtOH	760	0.569	0.535	337.96	341.07
C_7H_8 + MeOH	412	0.130	0.143	321.16	321.76
	512	0.125	0.140	326.66	326.89
	613	0.122	0.137	331.16	331.29
	760	0.118	0.133	336.66	336.71
C_7H_8 + EtOH	412	0.222	0.211	334.66	334.99
	510	0.209	0.195	339.66	339.99
	610	0.198	0.182	344.16	344.31
	760	0.182	0.165	350.16	349.80
C_7H_8 + PrOH	413	0.452	0.399	348.66	347.38
	513	0.429	0.373	355.16	352.86
	612	0.412	0.350	359.16	357.45
	760	0.384	0.321	365.66	363.28
C_7H_8 + BuOH	409	0.734	0.655	359.16	357.73
	510	0.718	0.630	365.66	364.01
	610	0.699	0.607	371.16	369.28
	759	0.674	0.578	378.66	375.95

* Experimental data on azeotropic properties taken from [7, 32, 33, 36–38].

Table 4. (Contd.)

System (1) + (2)	P, mm Hg	Properties of azeotropes			
		composition, mole fraction		T^{exp}	T^{calc}
		x_{exp}	x_{calc}	K	
MeAc + MeOH	100	0.772	0.825	281.66	281.28
	200	0.737	0.802	294.66	295.56
	300	0.720	0.784	303.56	304.76
	400	0.700	0.767	310.36	311.66
	600	0.678	0.739	320.41	322.07
	760	0.680	0.719	327.16	328.46
EtAc + MeOH	760	0.285	0.297	335.36	335.76
EtAc + C_6H_{14}	760	0.344	0.396	338.31	338.83
PrAc + PrOH	200	0.562	0.605	333.12	333.88
	400	0.477	0.500	350.22	351.03
	600	0.420	0.423	361.20	361.91
	760	0.381	0.372	367.96	368.56
BuAc + BuOH	760	0.222	0.177	389.64	390.16
Acetone + MeOH	760	0.785	0.747	328.36	328.49
Acetone + $CHCl_3$	760	0.360	0.408	337.66	336.70
Acetone + C_6H_{14}	760	0.625	0.598	322.76	319.10
MeOH + $CHCl_3$	760	0.347	0.331	326.51	326.64
EtOH + $CHCl_3$	200	0.081	0.094	297.75	297.47
	600	0.151	0.140	326.05	325.10
	760	0.159	0.151	332.45	331.92
C_6H_{14} + $CHCl_3$	760	0.218	0.104	333.00	333.70
MeAc + Acetone	400	0.429	0.391	311.16	311.57
	500	0.457	0.399	317.06	317.28
	600	0.470	0.403	321.96	322.12
	700	0.483	0.406	325.66	326.36
	760	0.390	0.407	329.25	328.67
MeAc + $CHCl_3$	760	0.322	0.346	337.96	339.50
MeAc + C_6H_{14}	400	0.618	0.667	307.26	306.97
	500	0.633	0.673	312.46	313.00
	600	0.644	0.679	318.06	318.12
	700	0.653	0.684	322.46	322.59
	760	0.669	0.686	324.96	325.03
EtOH + C_6H_{12}	296	0.384	0.394	314.36	317.30
	420	0.407	0.433	322.46	325.81
	643	0.436	0.440	333.96	335.02
C_6H_6 + C_6H_{12}	760	0.520	0.517	350.76	350.12
EtOH + C_6H_{14}	760	0.332	0.357	331.85	333.57
H_2O + EtOH	276	0.085	0.042	327.97	327.83
	380	0.103	0.111	336.66	334.74
	760	0.105	0.207	351.25	350.87
CH_3COOH + C_6H_{14}	760	0.111	0.098	341.50	340.55
CH_3COOH + C_7H_{16}	760	0.255	0.258	368.15	364.63
CH_3COOH + C_8H_{18}	760	0.687	0.517	378.85	381.90
CH_3COOH + C_9H_{20}	760	0.826	0.923	385.95	390.69

Table 4. (Contd.)

System (1) + (2)	T, K	Properties of azeotropes			
		composition, mole fraction		P^{exp}	P^{calc}
		x_{exp}	x_{calc}	mm Hg	
H_2O + C_5H_5N	323.15	0.740	0.683	115.0	116.5
	353.15	0.750	0.715	444.0	442.3
Acetone + MeOH	298.15	0.912	0.890	231.2	230.7
	323.15	0.799	0.773	628.5	626.5
Acetone + $CHCl_3$	298.15	0.405	0.413	161.4	160.3
	313.15	0.382	0.404	308.0	305.5
	323.15	0.376	0.393	454.5	448.9
Acetone + C_6H_{14}	308.16	0.634	0.612	447	421
	328.16	0.646	0.630	906	884
MeOH + $CHCl_3$	298.15	0.262	0.240	237.4	240.8
	313.15	0.309	0.294	454.0	459.8
	323.15	0.340	0.322	670.4	672.0
C_6H_{14} + $CHCl_3$	308.16	0.232	0.213	311	310
	328.16	0.227	0.142	637.5	635
C_6H_6 + C_6H_{12}	323.55	0.512	0.506	307	310.8
	373.15	0.555	0.552	1440	1437
EtOH + C_7H_{16}	303.16	0.553	0.554	121.23	120.21

tions. As shown in [2, 6], this method successfully works for homogeneous azeotropes of various kinds (positive, negative, and saddle-type) and is suitable for mixtures with a tangential azeotropy. It was found that the method of conjugated nodes is insensitive to the choice of a starting compositional approximation (except at $x_i = 0$) and is quite reliable in determining clearly pronounced positive binary and ternary homoazeotropes. The coordinates of a positive azeotrope, found using the method of conjugated nodes and by successive variation of mole fractions virtually coincide.

The results of a calculation of azeotropic parameters of binary systems are listed in Table 4. The hole lattice model adequately reflects the shift of the azeotrope on changing the pressure (temperature). Also correctly reproduced is the tendency toward variation of the parameters of azeotropes in homologous series of mixtures (e.g., toluene + alkanols, acetic acid + alkanes). The model well reproduces the coordinates of azeotropes at temperatures of 400–500 K. For the mixtures tested, the absolute deviation of a calculated azeotropic composition from the experimental value is within 0.001–0.1 mol fraction. The boiling point and the pressure of the azeotrope, predicted using the HM, are close to the corresponding experimental values.

An interesting system in which an unusual phase behavior was observed (double azeotropy) is a mixture of benzene and perfluorobenzene. However, the HM erroneously predicts the phase diagram of this system: only a single positive azeotrope can be found, with its composition and pressure at a given temperature markedly deviating from the values observed in the experiment.

Table 5 demonstrates the results obtained in prognostication of azeotropic properties for ternary mixtures. As examples were chosen systems with both positive and saddle-type azeotropes; systems with a low content of one of the components in an azeotropic mixture. As in the case of binary systems, the calculated boiling points (equilibrium pressures) are rather close to the experimental values. However, the compositions of the tangential and saddle-type azeotropes, predicted by the HM for a number of mixtures, markedly differ from the experimental values (Table 5, system nos. 5 and 7).

Table 5. Results for ternary azeotropic systems

System no.	System (1) + (2) + (3), type of azeotrope	P, mm Hg	Properties of azeotropes					
			composition, mole fraction				T^{exp}	T^{calc}
			x_1^{exp}	x_2^{exp}	x_1^{calc}	x_2^{calc}	K	
1	Acetone + $CHCl_3$ + MeOH, saddle-type [36, 38]	760	0.318	0.241	0.362	0.244	330.83	330.97
2	MeAc + MeOH + C_6H_{14}, positive [37]	400	0.352	0.290	0.384	0.260	307.25	304.36
		500	0.336	0.305	0.358	0.286	313.05	310.06
		600	0.328	0.322	0.334	0.309	318.05	314.86
		700	0.316	0.335	0.312	0.330	322.45	318.96
		800	0.306	0.346	0.291	0.349	326.65	322.56
3	Acetone + MeOH + C_6H_{14}, positive [37]	400	0.393	0.206	0.468	0.158	303.86	305.11
		500	0.376	0.227	0.397	0.231	309.56	310.92
		600	0.360	0.248	0.337	0.288	314.26	315.77
		700	0.341	0.268	0.283	0.337	318.36	319.93
		800	0.333	0.277	0.232	0.380	321.86	323.58
4	Acetone + MeAc + C_6H_{14}, positive (tangential) [37]	400	0.582	0.039	0.615	0.009	304.66	305.40
		500	0.583	0.039	0.615	0.020	310.46	311.59
		600	0.590	0.041	0.615	0.029	315.56	316.82
		700	0.597	0.041	0.615	0.048	319.96	321.35
		800	0.600	0.045	0.605	0.054	324.16	325.38
5	Acetone + MeAc + MeOH, positive (tangential) [37]	400	0.028	0.694	0.403	0.403	310.06	310.69
		500	0.033	0.671	0.397	0.397	315.66	316.33
		600	0.038	0.652	0.391	0.391	320.36	321.12
		700	0.044	0.635	0.386	0.386	324.46	325.29
		800	0.048	0.620	0.380	0.381	328.26	328.99
6	MeAc + $CHCl_3$ + MeOH, saddle-type [36]	760	0.250	0.292	0.212	0.327	329.57	330.02
7	$CHCl_3$ + Acetone + C_6H_{14}, saddle-type [36]	600	0.601	0.076	0.397	0.161	326.15	328.22
		760	0.697	0.080	0.415	0.157	333.95	335.25
8	C_6H_6 + EtOH + C_7H_{16}, positive (tangential) [36]	180	0.646	0.331	0.671	0.328	305.55	305.40
9	C_6H_{12} + EtOH + C_6H_6, positive (tangential) [36]	760	0.460	0.430	0.504	0.428	337.85	339.80

System no.	System (1) + (2) + (3), type of azeotrope	T, K	Properties of azeotropes					
			composition, mole fraction				P^{exp}	P^{calc}
			x_1^{exp}	x_2^{exp}	x_1^{calc}	x_2^{calc}	mm Hg	
1	Acetone + $CHCl_3$ + MeOH, saddle-type [7, 33]	298.15	0.402	0.401	0.278	0.368	188.4	210.2
		313.15	0.314	0.281	0.346	0.289	376.8	398.6
		323.15	0.313	0.254	0.367	0.258	566.8	579.9

Table 6. Comparison of the results of prediction of a quaternary azeotrope in the system acetone (1) + chloroform (2) + methanol (3) + benzene (4) at P = 760 mm Hg

Composition, mole fraction				$\Delta\bar{x}^*$	T, K	Reference
x_1	x_2	x_3	x_4			
0.182	0.120	0.500	0.198		331.05	Experimental data of [38]
0.197	0.237	0.442	0.124	0.066	330.60	HM
0.295	0.148	0.463	0.094	0.071	330.30	Wilson 1 [9]**
0.313	0.222	0.440	0.025	0.117	330.35	NRTL 1 [9]**
0.251	0.154	0.477	0.118	0.052	330.63	Wilson 2 [10]**
0.357	0.166	0.427	0.050	0.111	330.20	NRTL 2 [10]**

* $\Delta\bar{x} = \frac{1}{4}\sum_{i=1}^{4}\left|x_i^{\text{az.exp}} - x_i^{\text{az.calc}}\right|$, where $x^{\text{az.exp}}$ and $x^{\text{az.calc}}$ are the experimental and calculated values of the azeotrope composition; i = 1–4 (components).

** Designations Wilson 1 and NRTL 1 mean that the corresponding models of local composition and the method of branches and boundaries are used; Wilson 2 and NRTL 2 correspond to use of the above models in combination with the method of interval analysis.

Table 6 compares the results of calculations for a quaternary azeotrope, obtained using different models, with the experimental data for the system acetone + chloroform + methanol + benzene. Among the binary subsystems of this four-component mixture, two are nonazeotropic (benzene + acetone and chloroform + benzene); these subsystems were used to evaluate new energy parameters of the HM (Table 2). As can be seen in Table 6, all the models used describe, for the above mixture, rather reasonably describe the composition and the boiling point of the azeotrope. The results obtained with different models and methods of search for an azeotrope suggest that the HM and the Wilson equation have an advantage. The results obtained in modeling the liquid–vapor equilibrium for the binary mixtures considered, both containing and not containing an azeotrope (Table 3), suggest that the HM is a suitable method for prognostication of a multicomponent azeotrope.

The discrepancy between the calculated and experimental azeotropic properties is due to an inaccuracy of both the model used and algorithm chosen for a search for an azeotrope, which is confirmed by the results of [9–12]. As demonstrated by tests, simple methods of search for azeotropes can be of use in engineering calculations. In particular, the method of conjugated nodes proved to be rather effective for finding a pronounced positive n-azeotrope in an n-component system. However, this method cannot be used for finding saddle-type (and tangential) azeotropes. It should be noted that the method of coordinate-wise dichotomy is devoid of this disadvantage and allows calculation of azeotropes of these types.

CONCLUSIONS

(1) The database of group parameters of the hole model was expanded. It was supplemented with parameters necessary for calculation of phase equilibria in systems containing hydrocarbons (saturated cyclic, aromatic), methyl acetate, chloroform, acetone, alkanols (methanol, ethanol), and perfluorobenzene.

(2) Tests of the Viktorov–Smirnova lattice-hole group model demonstrated that it predicts azeotropic properties for most of binary mixtures with accuracy satisfactory for technological applications.

(3) For ternary systems with a clearly pronounced positive azeotrope, the hole model predicts azeotropic parameters with an acceptable accuracy. For mixtures with tangential or saddle-type azeotropes, the model gives a good agreement between the experimental and calculated boiling points and pressure; however, the composition may show strong deviations.

(4) Simple calculation algorithms of search for homogeneous azeotropes proved to be quite effective for the systems considered.

ACKNOWLEDGMENTS

The authors thank Aleksei Gerogievich Morachevskii and Aleksei Ismailovich Viktorov for reading the manuscript and making valuable remarks.

The study was supported by the Russian Foundation for Basic Research (project nos. 02-03-32709, 05-03-33267) and by the Presidential Grant of

the Russian Federation "Leading Scientific Schools" (project no. HSh-676.2003.03).

REFERENCES

1. Storonkin, A.V., *Termodinamika geterogennykh sistem* (Thermodynamics of Heterogeneous Systems), Leningrad: Khimiya, 1967, parts 1, 2.
2. Morachevskii, A.G., Smirnova, N.A., Piotrovskaya, E.M., *et al.*, *Termodinamika ravnovesiya zhidkost'–par* (Thermodynamics of the Liquid–Vapor Equilibrium), Leningrad, 1989.
3. Viktorov, A.I., Kuranov, G.L., Morachevskii, A.G., and Smirnova, N.A., *Zh. Prikl. Khim.*, 1991, vol. 64, no. 5, pp. 961–978.
4. IUPAC, vol. V: *Equations of State for Fluids and Fluid Mixtures*, Sengers, J.V., Kayser, R.F., Peters, C.J., and White, H.J., Eds., Amsterdam: Elsevier, 2000, parts 1, 2.
5. Aristovich, V.Yu. and Stepanova, E.I., *Zh. Prikl. Khim.*, 1970, vol. 43, no. 10, pp. 2192–2200.
6. Moracevski, A.G. and Pukinskij, I.B., *Modellierung von Phasengleichgewichten als Grundlage von Stoffrennprozessen (in German)*, Berlin: Akademie, 1981, pp. 295–328.
7. Tamir, A., Apelblat, A., and Wagner, M.,. *Fluid Phase Equilib.*, 1981, vol. 6, pp. 113–139.
8. Demirel, Y., *Fluid Phase Equilib.*, 1993, vol. 86, pp. 1–13.
9. Harding, S.T., Maranas, C.D., McDonald, C.M., and Floudas, C.A., *Ind. Eng. Chem. Res.*, 1997, vol. 36, pp. 160–178.
10. Maier, R.W., Brennecke, J.F., and Stadtherr, M.A., *Am. Iust. Chem. Eng. J.*, 1998, vol. 44, pp. 1745–1755.
11. Hua, J.Z., Maier, R.W., Tessier, S.R., *et al. Fluid Phase Equilib.*, 1999, vol. 158–160, pp. 607–615.
12. Maier, R.W., Brennecke, J.F., and Stadtherr, M.A., *Comput. Chem. Eng.*, 2000, vol. 24, pp. 1851–1861.
13. Wang, S.-H. and Whiting, W.B., *Ind. Eng. Chem. Proc. Des. Dev.*, 1986, vol. 25, pp. 547–551.
14. Chen, S.-F., Chen, Y.-P., and Tang, M., *J. Chem. Eng. Japan*, 1994, vol. 27, pp. 512–516.
15. Segura, H., Wisniak, J., Toledo, P.G., and Mejia, A., *Fluid Phase Equilib.*, 1999, vol. 166, pp. 141–162.
16. Aslam, N. and Sunol, A.K., *Chem. Eng. Sci.*, 2004, vol. 59, pp. 599–609.
17. Smirnova, N.A. and Victorov, A.I., IUPAC, vol. V: *Equations of State for Fluids and Fluid Mixtures*, Amsterdam: Elsevier, 2000, pp. 255–288.
18. Smirnova, N.A. and Victorov, A.I., *Fluid Phase Equilib.*, 1987, vol. 34, pp. 235–263.
19. Prikhodko, I.V., Shmel'tser, Yu., Viktorov, A.I., and Smirnova, N.A., *Zh. Prikl. Khim.*, 1989, vol. 62, no. 12, pp. 2738–2744.
20. Victorov, A.I. and Fredenslund, A., *Fluid Phase Equilib.*, 1991, vol. 66, pp. 77–101.
21. Deak, A., Victorov, A.I., and de Loos, Th.W., *Fluid Phase Equilib.*, 1995, vol. 107, pp. 277–301.
22. Prikhodko, I.V., Victorov, A.I., Smirnova, N.A., and de Loos, Th.W., *Fluid Phase Equilib.*, 1995, vol. 110, pp. 17–30.
23. Viktorov, A.I., Morachevskii, A.G., Prikhodko, I.V., and Smirnova, N.A., *Vestn. SPb. Gos. Univ., Ser. 4*, 1995, no. 3, pp. 24–32.
24. Prikhodko, I.V., Letcher, T.M., and de Loos, Th.W., *Ind. Eng. Chem. Res.*, 1997, vol. 36, pp. 4391–4396.
25. Prikhodko, I.V. and Vinogradova, I.V., *Zh. Prikl. Khim.*, 2002, vol. 75, no. 11, pp. 1810–1815.
26. Chudakov, A.M., Vinogradova, I.V., and Prikhod'ko, I.V., *Vestnik SPb. Gos. Univ., Ser. 4*, 2004, issue 1, no. 4, pp. 53–69.
27. Bondi, A., *Physical Properties of Molecular Crystals, Liquids and Glasses*, New York: Willey, 1968.
28. Smith, B.D. and Srivastava, R., *Thermodynamic Data for Pure Compounds: Physical Sciences Data*, parts A, B, Amsterdam: Elsevier, 1986.
29. Kogan, V.B., Fridman, V.M., and Kafarov, V.V., *Ravnovesie mezhdu zhidkost'yu i parom* (Liquid–Vapor Equilibrium), Moscow: Nauka, 1966, vols. 1, 2.
30. Kurihara, K., Hori, H., and Kojima, K., *J. Chem. Eng. Data*, 1998, vol. 43, pp. 264–268.
31. Nagata, I. and Hayashida, H., *J. Chem. Eng. Japan*, 1970, vol. 3, pp. 161–166.
32. Hiaki, T., Kurihara, K., and Kojima, K., *J. Chem. Eng. Data*, 1994, vol. 39, pp. 714–719.
33. Goral, M., Kolasińska, G., and Oracz, P., *Fluid Phase Equilib.*, 1985, vol. 23, pp. 89–116.
34. Lyudmirskaya, G.S., Barsukova, T.A., and Bogomol'nyi, A.M., *Ravnovesie zhidkost'–par: Spravochnik* (Liquid–Vapor Equilibrium: Reference Book), Leningrad, 1987.
35. Bekárek, V., *Collect. Czech. Chem. Commun.*, 1968, vol. 33, pp. 2608–2619.
36. Ogorodnikov, S.K., Lesteva, T.M., and Kogan, V.B., *Azeotropnye smesi: Spravochnik* (Azeotropic Mixtures: Reference Book), Leningrad: Khimiya, 1971.
37. Pivovarov, A.M., Marinichev, A.N., and Susarev, M.P., *Vestn. Len. Gos. Univ., Fiz. Khim.*, 1976, issue 1, pp. 100–105.
38. Gmehling, J., Menke, J., Krafczyk, J., and Fischer, K., *Azeotropic Data*, Weinheim: VCH, Germany, 1994, parts I, II.

Russian Journal of Applied Chemistry, Vol. 78, No. 8, 2005, pp. 1245–1248. Translated from Zhurnal Prikladnoi Khimii, Vol. 78, No. 8, 2005, pp. 1268–1271.
Original Russian Text Copyright © 2005 by Sladkov, Pobedonostseva.

PHYSICOCHEMICAL STUDIES OF SYSTEMS AND PROCESSES

Calculation of the Critical Parameters of Inorganic Compounds by the Additive Method

I. B. Sladkov and E. V. Pobedonostseva

St. Petersburg State Polytechnic University, St. Petersburg, Russia

Received April 7, 2005

Abstract—A set of 100 substances was studied to obtain data that would allow application of the additive method to calculation of critical parameters of inorganic compounds. An additive scheme that makes it possible to improve the accuracy of calculation of the critical pressure of inorganic compounds was suggested.

At present, methods of the thermodynamic similarity theory are widely used to prognosticate physicochemical properties of substances [1, 2]. In this case, the critical parameters of substances serve as input data for a calculation. Published data on critical parameters are rather scarce. Experimental determination of critical parameters involves severe difficulties. Of particular practical importance in this context is determining the critical parameters by calculation.

A possible way to calculate the critical parameters is to sum up the corresponding increments for the elements constituting the molecule of a compound. This method is attractive in that it is based on the minimum amount of information about the substance under study, which frequently does not include any data except the stoichiometric formula.

The additive method for calculation of critical parameters is widely used for prognosticating the critical parameters of organic substances [1, 3]. The potentialities of this technique, as applied to determination of the critical parameters of molecular inorganic compounds, are unknown. This is because the increments are available in the literature for less than 10 elements. These are nonmetals (C, H, O, S, N, F, Cl, Br, I), which constitute molecules of organic substances. However, data on the increments for metals contained in molecules of inorganic and organometallic substances are lacking completely.

The goals of this study were as follows: (a) to obtain missing information about the increments of metals from experimental data on critical parameters and (b) to determine, using the data obtained, the accuracy of calculation of the critical parameters by the additive method for inorganic and organometallic compounds.

The most widely used in the literature is the additive scheme suggested by Leadersen [1]. In this technique, atomic constituents (increments) of the reduced temperature at the boiling point are summed up for determining the critical temperature:

$$\theta = T_{boil}/T_{cr}, \quad (1)$$

where T_{boil} and T_{cr} are, respectively, the temperatures at the normal-boiling and critical points.

The calculational formula for determining θ for a binary compound of the AB_n type has the form

$$\theta = 0.576 + \Sigma\Delta_T - (\Sigma\Delta_T)^2, \quad (2)$$

$$\Sigma\Delta_T = \Delta_T(A) + n\Delta_T(B), \quad (3)$$

where $\Delta_T(A)$ and $\Delta_T(B)$ are the increments of the reduced boiling point θ for elements A and B, respectively; and n is the number of B atoms in compound AB_n.

The critical volume is found in the Leadersen method by the formula

$$V_{cr} = 40 + \Sigma\Delta_V. \quad (4)$$

The critical pressure (MPa) is given by

$$P_{cr} = 0.101325M/(\Sigma\Delta_P + 0.34)^2, \quad (5)$$

where M is the molecular weight of the compound.

In Eqs. (4) and (5), the sum of increments Δ_V and Δ_P is calculated in accordance with Eq. (3).

1070-4272/05/7808-1245 © 2005 Pleiades Publishing, Inc.

Table 1. Increments of the critical temperature (K), critical volume, and Van der Waals constant ($cm^3\ mol^{-1}$)

Element	Δ_T	Δ_V	Δ_P	Element	Δ_T	Δ_V	Δ_P
H^{1-}	0	5	5.8	$S^{2+,\ 4+}$	0.006	47*	30
H^{1+}	–0.005	2	8.6	S^{6+}	–0.023	47*	22.8
F	0.018*	18*	11	Se^{2-}	0.032	65	35
Cl	0.017*	49*	26.4**	Se^{4+}	–0.006	55	30
Br	0.010*	70*	34	Se^{6+}	–0.028	66	31
I	0.012*	95*	45	Te^{2-}	0.016	99	43
Hg^{2+}	–0.002	33	26	Te^{4+}	0.028	74	21
B^{3+}	0.032	30	13.4	Te^{6+}	–0.006	92	41
C^{4+}	0.022	37	19.3	Cr^{6+}	0.004	80	33
Si^{4+}	0.035	81	36.5	$Mo^{5+,\ 6+}$	–0.020	83	33.6
Ge^{4+}	0.033	84	42.5	$W^{5+,\ 6+}$	–0.008	89	34.6
Sn^{4+}	0.034	110	53	Tc^{6+}	–0.036	78	34
Pb^{4+}	0.017	110	52	Re^{6+}	–0.028	82	37
Ti^{4+}	0.019	86	45	$Os^{5+,\ 6+}$	–0.040	84	37.5
V^{4+}	–0.005	92	35	Os^{8+}	–0.048	94	28
$N^{1+,\ 2+,\ 3+}$	0.008	28	19	$Ir^{5+,\ 6+}$	–0.028	92	36
P^{3+}	0.006	56	36	Pt^{6+}	–0.033	82	37
P^{5+}	0.025	80	37	$Ru^{5+,\ 6+}$	–0.037	70	33
As^{3+}	–0.012	60	36	Ru^{8+}	–0.026	90	25
Sb^{3+}	0.011	61	39	U^{6+}	–0.025	107	48
Sb^{5+}	–0.005	110	43	Np^{6+}	–0.026	102	45
Bi^{3+}	–0.012	63	31	CH_3***	0.022	68	33
O	0.020*	11*	13.4**	C_2H_5***	0.028	126	56

* Calculation by Leadersen [1].

** Calculation by Heukelom [6].

*** Increments for the CH_3 and C_2H_5 radicals were determined for organometallic compounds.

Table 2. Increments of the critical parameters of silicon, obtained for various silicon compounds

Compound	Δ_T	Δ_V	Δ_P	Compound	Δ_T	Δ_V	Δ_P
$SiCl_4$	0.026	90.0	0.529	$SiCl_2F_2$	0.025	68.0	0.564
$SiBr_4$	0.042	62.0	0.628	$SiCl_3F$	0.024	75.0	0.560
$SiHCl_3$	0.025	81.0	0.394	$SiBrCl_3$	0.036	89.0	0.610
$SiHBr_3$	0.054	75.1	0.539	$SiBr_2Cl_2$	0.032	86.0	0.643
$SiClF_3$	0.034	60.0	0.547	$SiBr_3Cl$	0.043	85.0	0.665

In the first stage, it was necessary to find the increments Δ_T, Δ_V, and Δ_P for elements-metals. For this purpose, substances with known critical parameters were chosen and Δ(A) (increment for the element-metal A) was found by an inverse calculation by Eqs. (1)–(5) from the known Δ(B) (increment for element B in compound AB_n).

The values of the critical parameters were taken from the reference book [4], with only experimental data used. The data array under study included experimental values of the boiling point and critical parameters for 100 molecular inorganic compounds, 90% of which were compounds of the AB_n type. The resulting values of the increments are listed in Table 1. For most of elements, the increments were determined for several compounds.

As an example of the scatter of increments obtained for different compounds of the same element, Table 2 lists increments of critical parameters for silicon. Use of averaged values of the increments for silicon

Table 3. Average error in calculation of the critical parameters

Data array	Average calculation error, %				Data array	Average calculation error, %			
	T_{cr}	V_{cr}	P_{cr}			T_{cr}	V_{cr}	P_{cr}	
			by Leadersen	this study				by Leadersen	this study
10*	0.9	3.5	6.9	2.1	100**	1.5	3.6	11.8	3.0

* Silicon compounds listed in Table 2.

** All the inorganic compounds considered in this study.

Table 4. Calculation of the critical parameters* of compounds with a complex stoichiometry and organometallic compounds

Compound	Reference	T_{cr}, K		V_{cr}, $cm^3\ mol^{-1}$		P_{cr}, MPa	
		found	error, %	found	error, %	found	error, %
$SiHCl_3$	[7]	479.0	–1.3	268.0	0.2	4.17	1.1
Si_2Cl_6O	[7]	578.0	–2.3	560.0	9.7	2.35	2.1
PCl_2OF	[4]	510.0	–0.1	247.0	0.1	4.79	–0.2
$Si(CH_3)_3Cl$	[8]	497.8	–0.3	365.6	2.3	3.21	–0.7
$Si(CH_3)_2Cl_2$	[8]	520.4	–1.1	349.9	1.5	3.48	–1.0
$SiCH_3Cl_3$	[9]	517.8	–1.4	339.8	–1.1	3.51	1.7
$Si(C_2H_5)_3Cl$	[10]	600.0	1.5	520.0	5.4	2.84	–3.5
$Si(C_2H_5)_2Cl_2$	[10]	595.8	0.2	455.0	3.5	3.06	0.7
$SiC_2H_5Cl_3$	[10]	560.8	–0.8	402.7	–2.2	3.33	1.1

* T_{cr}, critical temperature; V_{cr}, critical volume; and P_{cr}, critical pressure.

(Table 1) leads to calculation errors of the critical parameters of silicon compounds, listed in Table 3.

Table 3 also presents the error of the Leadersen method for a set of 100 molecular inorganic compounds. It should be noted for comparison that the accuracy of the Leadersen method (average error) for organic substances is less than 2% for the critical temperature [1], 3.2% for the critical volume [5], and 3.8% for the critical pressure [1]. Thus, the data on the critical temperature and critical volume, obtained for inorganic substances, are in a good agreement with those for organic substances.

It can be seen from Table 3 that, as applied to inorganic compounds, the Leadersen method provides a high accuracy of prognostication of the critical temperature and a satisfactory accuracy of prognostication of the critical volume.

At the same time, the calculation error is unacceptable in the case of the critical pressure. An additive scheme that allows reliable prognostication of the critical pressure of inorganic compounds was developed in this study. The essence of the additive scheme suggested is in the following.

The critical pressure was calculated from the Van der Waals constant b:

$$P_{cr} = RT_{cr}/8b. \quad (6)$$

The critical temperature in Eq. (6) was calculated by the Leadersen equations (1)–(3), and the Van der Waals constant was found using the conventional additivity rule:

$$b = \Sigma\Delta_b = \Delta_b(a) + n\Delta_b(B).$$

The increments of the Van der Waals constant, determined in the study, are listed in Table 1.

As can be seen in Table 3, the method suggested provides a significantly improved accuracy of prognostication of the critical pressure.

The increments obtained in this study make it possible to reliably prognosticate the critical parameters of molecular inorganic compounds with any stoichiometry, as well as those of organometallic compounds (Table 4).

CONCLUSIONS

(1) Data were obtained, which allow application of the additive method to calculation of the critical parameters of inorganic compounds.

(2) The accuracy of prognostication of the critical parameters was established for a set of 100 compounds.

(3) It was shown that the accuracy of data on the critical temperature and critical volume exactly coincides with that of published data for organic compounds.

(4) It was found that the additive scheme suggested makes it possible to improve the accuracy of calculation of the critical pressure for inorganic compounds.

REFERENCES

1. Reid, R.G. and Sherwood, T.K., *The Properties of Gases and Liquids*, New York: McGraw-Hill Book, 1966.
2. Filippov, L.P., *Podobie svoistv veshchestv* (Similarity of Substance Properties), Moscow: Mos. Gos. Univ., 1978.
3. Viktorov, M.M., *Metody vychisleniya fiziko-khimicheskikh velichin i prikladnye raschety* (Methods for Calculation of Physicochemical Quantities and Applied Calculations), Leningrad: Khimiya, 1977.
4. Morachevskii, A.G. and Sladkov, I.B., *Fiziko-khimicheskie svoistva molekulyarnykh neorganicheskikh soedinenii* (Physicochemical Properties of Molecular Inorganic Compounds), Leningrad: Khimiya, 1996.
5. Fedors, R.F., *Am. Inst. Chem. Eng. J.*, 1979, vol. 25, no. 1, pp. 202–206.
6. Heukelom, W., *Rec. Trav. Chim.*, 1949, vol. 68, no. 9/10, pp. 661–680.
7. Lapidus, I.I. and Nisel'son, L.A., *Tetrakhlorsilan i trikhlorsilan* (Tetrachlorosilane and Trichlorosilane), Moscow: Khimiya, 1978.
8. Stepanov, N.G. and Nozdrev, V.F., *Zh. Fiz. Khim.*, 1968, vol. 42, no. 10, pp. 2456–2461.
9. Stepanov, N.G., *Zh. Fiz. Khim.*, 1972, vol. 46, no. 3, pp. 801–802.
10. Myers, K.H. and Danner, R.P., *J. Chem. Eng. Data*, 1993, vol. 38, no. 2, pp. 175–200.

Russian Journal of Applied Chemistry, Vol. 78, No. 8, 2005, pp. 1249–1252. Translated from Zhurnal Prikladnoi Khimii, Vol. 78, No. 8, 2005, pp. 1272–1275.
Original Russian Text Copyright © 2005 by Egiazarov, Shachenkova, Radkevich, Lysenko, Cherches.

SORPTION AND ION-EXCHANGE PROCESSES

Synthesis, Structure, and Thermal Stability of a Sulfonic Cation Exchanger Grafted to Carbonized Fiber

Yu. G. Egiazarov, L. N. Shachenkova, V. Z. Radkevich, G. N. Lysenko, and B. Kh. Cherches

Institute of Physical Organical Chemistry, Belarussian National Academy of Sciences, Minsk, Belarus

Received January 14, 2004; in final form, February 2005

Abstract—A new kind of sulfonic cation exchanger based on carbonized fiber modified with poly(styrene–divinylbenzene) was prepared by radiation grafting. The structural features and thermal stability of the cation exchangers prepared were studied.

The reduction of toxicity of the automobile exhaust is a topical environmental problem. The solution of this problem includes the exclusion of tetraethyllead as an antiknock additive to gasoline. With this aim, benzine from catalytic craking and reforming is modified by adding high-octane oxygen-containing compounds: methyl *tret*-butyl ether (MTBE) and methyl *tret*-amyl ether (MTAE). In industrial production of these additives, granulated sulfonic cation exchangers Amberlyst 15, Dowex msm 31, KU-23, etc. are used as catalysts [1–3].

It has been reported [4, 5] that FIBAN K-1 gel-like sulfonic cation exchanger based on polypropylene fiber [6] more effectively catalyzes MTBE and MTAE formation than KU-2 × 8 granulated gel-like and Dowex msm 31 macroporous sulfonic cation exchangers.

In this context, it was of interest to develop a catalyst for preparing MTBE and MTAE based on carbonized fiber. Owing to several features (high porosity, small thickness, non swelling in polar solvents), carbonized fibers are more favorable for preparing grafted cation exchangers. In addition, these fibers exhibit a high electrical conductivity. Therefore, we can expect that sulfonic cation exchangers grafted to carbonized fiber will exhibit electrical conductivity irrespective of the moisture content. No data have been reported on sulfonic cation exchangers grafted to carbonized fibers.

EXPERIMENTAL

In our experiments, a nonwoven carbonized fabric Carbopon prepared by carbonization of viscose fiber was used as a fibrous base for a sulfonic cation exchanger.

The main characteristics of Carbopon were as follows: fiber diameter 5–10 μm, capillary moisture capacity 0.64 ml g^{-1}, average pore diameter d_{av} 23 Å, average surface area determined from low-temperature sorption of nitrogen 780 $m^2 g^{-1}$.

In preparing sulfonic cation exchanger grafted to Carbopon, the following procedures were used. A weighed sample of air-dried Carbopon (5 g) was placed on the bottom of a 50-ml test tube and kept under vacuum (1 mm Hg) for 2 h at 90°C. Two identical Carbopon samples were used in parallel experiments. The test tubes containing Carbopon were cooled to room temperature, and a mixture of monomeric styrene and divinylbenzene (10 ml) in methanol (25 ml) was added. The styrene to divinylbenzene molar ratios in the reaction mixtures were 98 : 2 and 75 : 25, which corresponded to their relative content in gel-like (sample no. I) and maroporous (sample no. II) cation exchangers, respectively. The test tubes containing Carbopon and monomer mixture were closed, kept for 4h at 20°C and then placed in a channel of a RKhM-gamma-20 cobalt (Co^{60}) unit for radiation grafting of styrene and divinylbenzene to Carbopon and their simultaneous copolymerization. In these experiments, the exposure time was 15 h, and the irradiation dose up to 4.5 Mrad. After the radiation treatment was complete, the test tubes were removed from the unit, the liquid phase was decanted, and the resulting matrix [poly(styrene–divinylbenzene) grafted to Carbopon] was washed with methanol and then dried at 90 °C.

The content X (weight fraction) of grafted poly(styrene-divinylbenzene) is commonly determined gravimetrically. However, because the resin samples obtained in our experiments are small and their loss is inevitable, the gravimetric measurements are unsuitable. Therefore, we developed a new technique ensur-

1070-4272/05/7808-1249 © 2005 Pleiades Publishing, Inc.

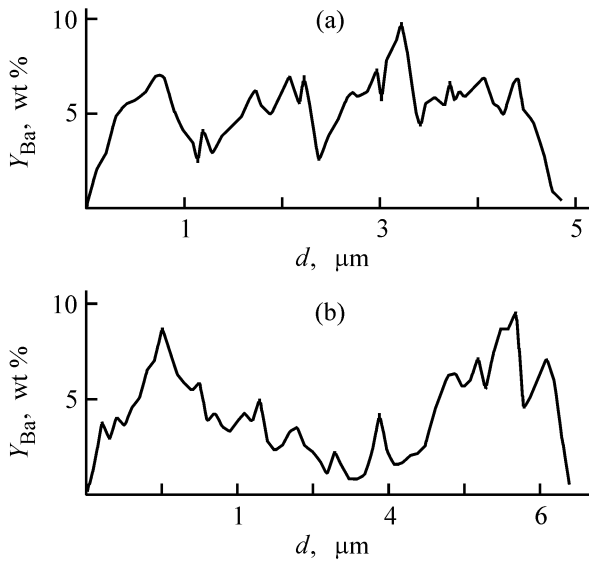


Fig. 1. Distribution of Ba (ion-exchange groups) across the fiber of sulfonic cation exchanger grafted to Carbopon. (Y_{Ba}) Barium content and (*d*) fiber diameter. Sample no.: (a) I and (b) II.

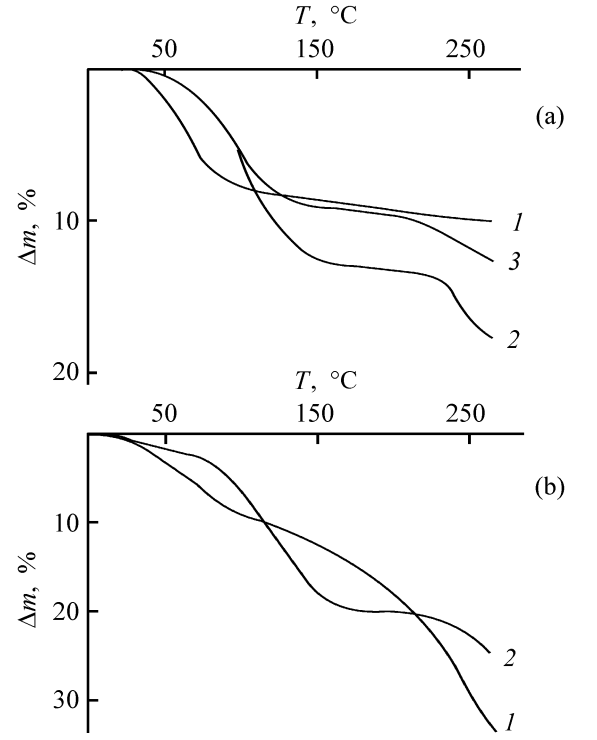


Fig. 2. Weight loss of Carbopon and cation exchangers, Δ*m*, vs. temperature *T*. (a) (*1*) Carbopon, (*2*) sample no. I, and (*3*) sample no. II. (b) (*1*) FIBAN K-1 and (*2*) DOWEX msm 31.

ing correct determination of *X* under our experimental conditions. According to this method, the C/H ratios in both the thoroughly dried initial Carbopon [$(C/H)_{Carb}$] and the matrix based on poly(styrene–divinylbenzene) grafted to Carbopon fiber [$(C/H)_{matr}$] were determined. Taking into account that the C/H ratio in poly(styrene–divinylbenzene) is 12, *X* was determined from the equation

$$12X + C/H_{Carb}(1 - X) = C/H_{matr}.$$

We found that $(C/H)_{Carb}$ is 36.7, and $(C/H)_{matr}$, 27.2 and 27.9, for sample nos. I and II, respectively. The calculated *X* values were 0.38 and 0.35 for samples nos. I and II, respectively. The degree of grafting (the weight ratio of the grafted copolymer to the initial Carbopon) was 61 and 54 for sample nos. I and II, respectively.

A matrix based on poly(styrene–divinylbenzene) grafted to Carbopon was sulfonated with concentrated sulfuric acid (d = 1.84 g cm^3) in a glass reactor for 4 h at 90–95°C. The resulting sulfonated matrix was washed with water to neutral reaction to remove H_2SO_4 and dried at room temperature.

The sorption exchange capacity of sample nos. I and II, determined by procedure reported in [7], was 1.7 and 1.3 mg-equiv g^{-1}, respectively.

The distribution of cation-exchange groups across the fibers of the sulfonic cation exchangers was determined as follows. An excess of 1 N aqueous $BaCl_2$ was passed though a column packed with a weighed sample of the cation exchanger tested until the pH of both the eluent and eluate became equal [8]. Under these conditions, the initial sulfonic cation exchanger is converted to the Ba^{2+} form. This resin was washed with water to complete absence of chloride anions in the wash water and then was air-dried at room temperature. The distribution of Ba across the fiber was determined X-ray fluorescence microanalysis on a Cam Scan electron microscope equipped with an AN-10 000 energy-dispersive spectrometer (Link Analytical, UK).

The X-ray fluorescence microanalysis showed that the gel-like cation exchanger (sample no. I) has uniform distribution of cation-exchange sites across the fiber (Fig. 1a). At the same time, the macroporous cation exchanger is characterized by increased functional group concentration on the fiber periphery (Fig. 1b).

A thermogravimetric analysis of cation exchangers was carried out in air within the temperture range 20–250 °C at a heating rate of 5 deg min^{-1}. The heating of initial Carbopon from room temperature to 90–100 °C is accompanied by large weight loss due to vaporization of water from pores. In going to a grafted sulfonic cation exchanger, the temperature range corresponding to intensive weight loss is shifted to higher temperatures (130–150°C) (Fig. 2a). The weight loss

by sample no. I is larger than that by sample no. II. In the temperature range 150–220 °C, the weight loss is small. Taking into account that the cation exchangers are anhydrous within this temperature range, a certain decrease in their weight may be due to weak thermal degradation of the resin. Further heating is accompanied by a sharp weight loss caused by intensive thermal degradation of resins.

Comparison of the temperature dependences of the weight loss by FIBAN K-1 and Dowex msm 31 shows that FIBAN-1 is less heat-resistant (Fig. 2b). The sulfonic cation exchangers grafted to Carbopon show a higher heat resistance at elevated temperatures. The weight of resin sample nos. I and II decreases at 250°C by 12 and 18%, respectively. Under identical conditions, the weight of Dowex msm 31 and FIBAN K-1 decreases by 23 and 32%, respectively.

Our results show that the sulfonic cation exchanger starts to degrade before the resin dehydration is complete. Therefore, we cannot correctly determine the onset temperature of the degradation of functional groups. In order to overcome this difficulty, we developed a method sensitive to the onset of degradation of functional groups.

This method is based on the following procedures. An air-dry weighed sample of tested resin (approximately 0.5 g) is placed in a U-shaped reactor immersed in an oil thermostat, and nitrogen is passed through the reactor at a rate of 30 ml min^{-1}. The nitrogen is preliminarily dried and purified to remove atmospheric oxygen by passing through a column packed with calcined $CaCl_2$ and reduced Ni catalyst. After passing through the reactor, the nitrogen flow is directed into a Drechsel bottle (20 mm in diameter and 80 mm high) filled with 0.003 N aqueous acidified (pH 1) $KMnO_4$ (10 ml). Thereafter the reactor temperature is raised to 120 °C with a temperature-control unit. At this temperature the cation exchanger is kept in a nitrogen flow for 1 h. If the $KMnO_4$ solution is not decolorized, the temperature is raised by 10°C, and the procedure is repeated. These stepwise heating runs are repeated until aqueous $KMnO_4$ becomes colorless. Taking into account that $KMnO_4$ decolorization is caused by its reaction with gaseous reductants formed by thermal degradation of the sulfonic cation exchanger (sulfur dioxide, hydrocarbon fragments), the temperature at which the released gases causes decolorization of the $KMnO_4$ solution can be accepted as the onset temperature of resin degradation.

To refine the onset temperature of resin degradation found in the first experiment, this factor was determined repeatedly. In doing so the reactor containing the cation exchanger being tested was heated to a temperature 10°C lower than the onset temperature of resin degradation, determined in the first experiment. Thereafter, the reactor temperature was raised by 5°C, and the resin sample was kept at this temperature for 1 h in a nitrogen flow. If aqueous $KMnO_4$ retained its color under these conditions, the reactor temperature was raised again by 5°C. This procedure was repeated until aqueous $KMnO_4$ became colorless. This technique allows determination of the temperature of the resin degradation with an accuracy of about ±5°C.

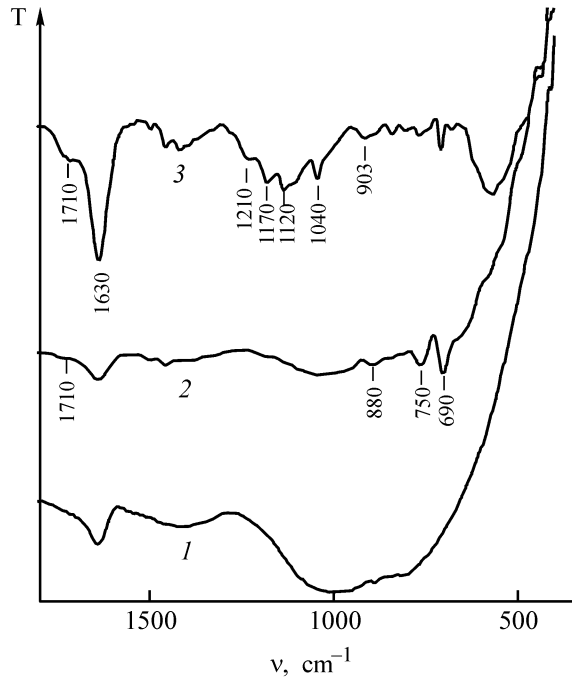


Fig. 3. IR spectra of Carbopon, carbonized fibers modified with poly(styrene–divinylbenzene), and sulfonic cation exchangers grafted to Carbopon. (T) Transmission and (ν) wave number. (*1*) Carbopon, (*2*) carbonized fiber modified with poly(styrene–divinylbenzene), and (*3*) sulfonic cation exchanger (sample no. I).

The thermogravimetric studies showed that Carbopon was heat resistant within the temperature range 120–250°C. The grafted gel-like and macroporous sulfonic resins start to degrade at 135 and 145°C, respectively, which virtually coincides with the related characteristics of the structurally similar resins FIBAN K-1 (130 °C) and Dowex msm 31 (145°C).

The IR spectra of the initial Carbopon and poly(styrene–divinylbenzene)–Carbopon matrix (sample no. I, styrene to divinylbenzene ratio 98 : 2) before and after sulfonation were studied. The samples were ground,

mixed with KBr powder dehydrated by heating at 150°C for 2 h, and compacted into thin pellets by the standard technique. The sample content in the KBr pellet was 0.4 wt %. The IR spectra were recorded on a Protege 460 IR Fourier spectrometer (Nicolet, USA). The scan number was 128, and the spectral resolution, 4 cm^{-1}. The IR spectra were processed using OMNIC software.

The IR spectrum of the initial Carbopon (Fig. 3, spectrum *1*) contains a broad unresolved absorption band of glycoside bond vibrations (1200–700 cm^{-1}), the band of bending vibrations of the CH groups (1500–1300 cm^{-1}), and the absorption band of the H_2O bending vibrations (1630 cm^{-1}).

The IR spectrum of the matrix based on Carbopon modified with poly(styrene–divinylbenzene) contains several narrow absorption bands of different intensities, belonging to the out-of-plane CH vibrations of the benzene ring [9] (690, 750, 880 cm^{-1}) (Fig. 3, spectrum *2*) against the broad background of the skeleton vibrations. The CO stretching vibrations νCO are manifested as a weakly pronounced shoulder (1710 cm^{-1}) on the high-frequency wing of the absorption band of the H_2O bending vibrations at 1630 cm^{-1}.

The IR spectra of sulfonated matrix contain an intensive absorption band of the H_2O bending (Fig. 3, spectrum *3*) vibrations and a series of well-resolved absorption bands belonging to vibrations of deprotonated sulfonic groups with iequivalent SO bonds (1210, 1170 and 1040 cm^{-1}) [10], [11]. The planar skeleton vibrations of the benzene ring with the SO_3H substituent are manifested as the absorption band at 1120 cm^{-1}. The absorption band at 903 cm^{-1} can be assigned to the S–OH vibrations. The presence of this band shows that some sulfonic groups are present in the protonated state. The absorption band at 560 cm^{-1} is caused by the C–S vibrations. Generally, the IR spectra of sulfonic cation exchangers grafted to Carbopon are similar to those of known fibrous and granulated sulfonic cationexchange resins.

CONCLUSIONS

(1) A new kind of sulfonic cation exchangers was prepared by radiation grafting of poly(styrene–divinylbenzene) to nonwoven carbonized fabric Carbopon, followed by sulfonation of the resulting matrix.

(2) The degree of grafting and exchange capacity of gel-like grafted sulfonic cation exchangers exceed those of macroporous grafted resins. The cation-exchange groups of grafted gel-like resins are uniformly distributed across the fiber, whereas those of grafted macroporous resin are mostly concentrated on the fiber periphery.

(3) The IR spectra of grafted sulfonic cation exchangers are similar to those of the known fibrous and granulated sulfonic resins.

ACKNOWLEDGMENT

The study was financially supported by INTAS (project no. 00-291).

REFERENCES

1. Crause, A.D. and Hammarstrom, L.G., *Appl. Catal.*, 1987, vol. 30, no. 2, pp. 313–318.
2. Stryakhileva, M.N., Krylova, G.N., Chaplits, D.N., *et al.*, *Proizvodstvo metil-tret-alkilovykh efirov-vysokooktanovykh komponentov benzina* (Production of Methyl *tert*-Alkyl Ethers as Components of High-Octane Gasoline), Moscow: NIITEneftekhim, 1988.
3. Pavlov, S.Yu., Gorshkov, V.A., and Churkin, V.N., *Khim. Prom–st.*, 1995, no. 5, pp. 9–11.
4. Cherches, B. Kh., Shunkevich, A.A., Belotserkovskaya, T.N., and Egiazarov, Yu.G., *Zh. Prikl. Khim.*, 1999, vol. 72, no. 4, pp. 623–627.
5. Cherches, B.Kh., Kovalenko, M.A., Shunkevich, A.A., *et al.*, *Neftekhimiya*, 2002, vol. 42, no. 1, pp. 28–31.
6. Soldatov, V.S., Pokrovskaya, A.I., and Martsinkevich, R.V., *Zh. Prikl. Khim.*, 1984, vol. 57, no. 9, pp. 2030–2034.
7. Polyanskii, N.G., Gorbunov, G.V., and Polyanskaya, N.A., *Metody issledovaniya ionitov* (Methods for Studying Ion Exchangers), Moscow: Khimiya, 1976.
8. Radkevich, V.Z., Kistanova, I.E., Soldatov, V.S., and Egiazarov, Yu. G., *Zh. Prikl. Khim.*, 2001, vol. 74, no. 9, pp. 1407–1409.
9. Bellamy, L.J., *The Infra-Red Spectra of Complex Molecules*, London: Methuen, 1957.
10. Cherches, B.Kh., Lysenko, G.N., and Egiazarov, Yu.G., *Zh. Prikl. Spektrosk.*, 2000, vol. 67, no. 5, pp. 587–590.
11. Zundel, G., *Hydration and Intermolecular Interaction. Infrared Investigations with Polyelectrolyte Membranes*, New York: Academic, 1969. Translated under the title *Gidratatsiya i mezhmolekulyarnye vzaimodeistviya*, Moscow: Mir, 1972.

Russian Journal of Applied Chemistry, Vol. 78, No. 8, 2005, pp. 1253–1257. Translated from Zhurnal Prikladnoi Khimii, Vol. 78, No. 8, 2005, pp. 1276–1279.
Original Russian Text Copyright © 2005 by Stavitskaya, Goba, Tomashevskaya, Kartel'.

SORPTION AND ION-EXCHANGE PROCESSES

Manufacture of Carbon Materials of Aerogel Type from Carbon Blacks of Various Origins

S. S. Stavitskaya, V. E. Goba, A. N. Tomashevskaya, and N. T. Kartel'

Institute of Sorption and Endoecology Problems, National Academy of Sciences of the Ukraine, Kiev, Ukraine

Received April 20, 2004; in final form, March 2005

Abstract—The influence exerted by the structure and origin of samples of technical grade carbon, conditions of their thermal treatment (temperature, nature of a gas medium) and preliminary impregnation with activating additives, and other factors on the final characteristics of carbon aerogels: density, specific surface area, and sorption capacity, was studied.

Of particular interest among new carbon materials, which may have, depending on the starting raw material and treatment methods, widely diverse forms and physicomechanical and chemical properties, are low-density carbon materials of the aerogel type.

Low-density carbon materials, carbon aerogels, were first synthesized in 1989 [1] by pyrolysis of a resorcinol–phenol-formaldehyde resin, with subsequent high-temperature activation of the resulting carbonizate in an inert atmosphere. Later, carbon aerogels were obtained from various organic polymers [2–8], including those of the expanded type, by using various treatments, organic additives, fillers [NaCl, Na_2CO_3, $Ca(OH)_2$], and cross-linking agents (e.g., melamine) Primary attention was given to properties of the starting oligomers, their thermal stability, and relative content of their components; also, the effect of solvents and catalysts used in synthesis of the starting organic aerogels on the final properties of the carbon aerogels obtained and, for the most part, on their porous structure and electrical conductivity was studied [2–4, 9].

In recent years, the interest in this class of compounds has increased because of the widely diverse possibilities of their use (owing to the uniquely high porosity, chemical stability, and electrical properties) as effective sorbents-fillers in chromatographic columns and materials for absorption and accumulation of small gas molecules, e.g., of hydrogen, which may be rather promising for obtaining a fuel of a new generation. Carbon aerogels are used in electrical engineering for fabrication of new electrodes in high-capacity power cells, molded articles with prescribed electrical properties, as well as heat insulators, various filters, catalyst supports, and catalysts themselves [2–9].

However, it should be noted that the literature on carbon aerogels has virtually no reports devoted the possibility of changing or controlling their porous structure or, the more so, the chemical nature of the surface of the carbon aerogels by its direct modification with special treatments, impregnations, etc.

A search for new ways to create carbon aerogels with unique properties by using unconventional sources of raw materials and new forms of low-density carbon materials of the aerogel type is of permanent current interest.

In this study, samples of finely dispersed carbon blacks (technical-grade carbon) were used as a starting substance to obtain carbon aerogels. The blacks were prepared by thermal decomposition of natural gas (C-1) or by thermal-oxidative decomposition of liquid hydrocarbons, as it has become usual in recent years (henceforth C-2). These samples differed in the initial apparent density (d = 470 and 240 mg cm^{-3}, respectively) and in the degree of graphitization, which was substantially higher for C-2, compared with C-1.

The specific features of the structure of technical-grade carbon as a most finely dispersed material give reason to believe that its thermal oxidative-destructive treatment as a starting substance can yield carbon aerogels. Indeed, carbon blacks have a strongly developed chain structure; it is known that any carbon

1070-4272/05/7808-1253 © 2005 Pleiades Publishing, Inc.

Table 1. Effect of gamma irradiation and ultrasound on technical-grade carbon samples of varied nature

Treatment conditions	C-1 carbon bla1ck		C-2 carbon black	
	d, mg cm^{-3}	W_s, cm^3 g^{-1}	d, mg cm^{-3}	W_s, cm^3 g^{-1}
Initial sample	470	0.026	240	0.047
Gamma irradiation* at indicated dose, rad:				
50	750	0.015	220	0.050
300	510	0.018	240	0.032
500	750	0.017	230	0.044
Ultrasound:				
τ = 30 min	750	0.013	240	0.045
τ = 60 min	440	0.020	230	0.050

* Irradiation in evacuated ampules (with 0.5 g of sorbent in an ampule); τ, treatment duration.

black particle contains a large number of pseudographite carbon crystallites and amorphous ("unorganized") carbon. Separate elementary particles have an approximately spherical shape. Rigid chains of particles, which determine the degree of cross-linking of carbon black, are composed of particles with about the same diameter in the range from 100 to 2500 Å.

In an oxidative atmosphere, the inner part of the particles must burn out under the action of a high temperature considerably faster, to give voids. The reactivity and properties of technical-grade carbon blacks are largely determined by the size of primary carbon black aggregates. It was assumed that the density of these substances can be changed (lowered) via formation of voids in burning-out of the inner part of carbon black particles, which is commonly represented by the so-called unorganized carbon, whereas the outer part is, as a rule, composed of more ordered, thermally stable carbon crystallites [10]. Such a process, occurring in an oxidative atmosphere at high temperatures, can be affected by the temperature mode, treatment duration, type of a gas atmosphere, etc.

EXPERIMENTAL

The aim of this study was to examine the preparation conditions of carbon materials of the aerogel type and to reveal the influence exerted by the type of the starting carbon material, gas atmosphere, temperature mode, treatment duration and other factors on the final properties of the carbon aerogels synthesized (apparent density, burnout, sorption capacity for a benzene vapor), determined by the standard methods [11]. In addition, the stability of these samples of technical-grade carbon against the action of ultrasound and gamma irradiation and the possibility of a "chemical" activation of carbon-black particles were analyzed. In the latter case, the samples were preliminarily treated with substances that could decompose, in the course of the subsequent thermal treatment, into gaseous products directly within the carbon black particles, which also had to promote their loosening and to impair their strength. For this purpose, samples of technical-grade carbon were impregnated with solutions of ammonium acetate or hydrocarbonate or subjected to a two-stage impregnation with sulfuric acid and ammonium hydrocarbonate. The thermal treatment was done in air or in the atmosphere of CO_2, water vapor, hydrogen, or argon.

To raise the dispersity, carbon blacks of varied origin were subjected to the action of ultrasound or to gamma irradiation. In doing so, the effect of the treatment time and irradiation dose on the dispersity of blacks and on their properties was studied (Table 1).

It was found that the action of ultrasound (30 min) on C-1 carbon black is similar to that of vibration milling, in which the chain structure disintegrates into separate fragments and a decrease in porosity is observed [10]. The higher dispersity of the system is also indicated by an increase in the apparent density d (i.e., the packing density) and decrease in the porosity (sorption capacity) for benzene, W_s [11].

High-energy gamma irradiation (50–500 rad) also leads to an increase in dispersity. The change in the degree of cross-linking of C-1 carbon black samples subjected to irradiation treatment was also confirmed by the results of X-ray diffraction analysis. For the carbon black of C-2 brand, the above-mentioned parameters remain virtually unchanged under similar conditions (Table 1).

A strong difference between the final parameters of the materials obtained was also observed upon thermal treatment of C-1 and C-2 samples at 600–900°C in the presence of water vapor, CO_2, or air. Such an oxidative-destructive treatment, high-temperature activation, was used to raise the density of finely dispersed blacks in order to obtain aerogels on their base. In the process, the optimal preparation conditions of carbon aerogels were studied, the main activation parameters were determined, and the effect of various factors (temperature mode, time of contact

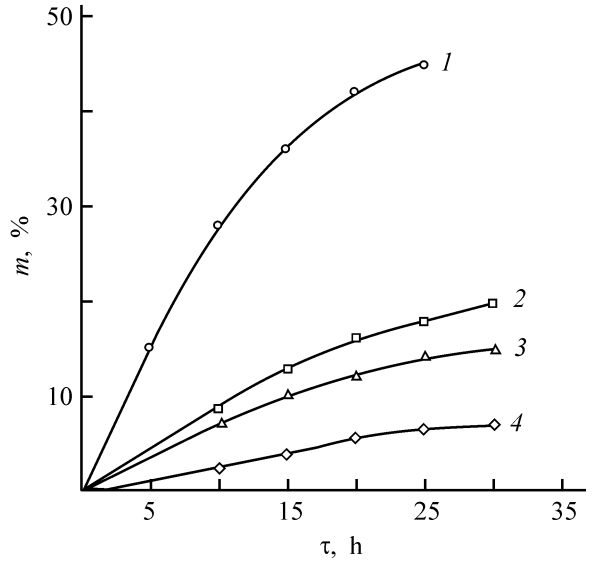


Fig. 1. Burnout m of (*1*, *3*) C-1 and (*2*, *4*) C-2 carbon blacks in the atmosphere of argon vs. the time τ of an experiment on thermal treatment. Temperature (°C): (*1*, *2*) 800 and (*3*, *4*) 600.

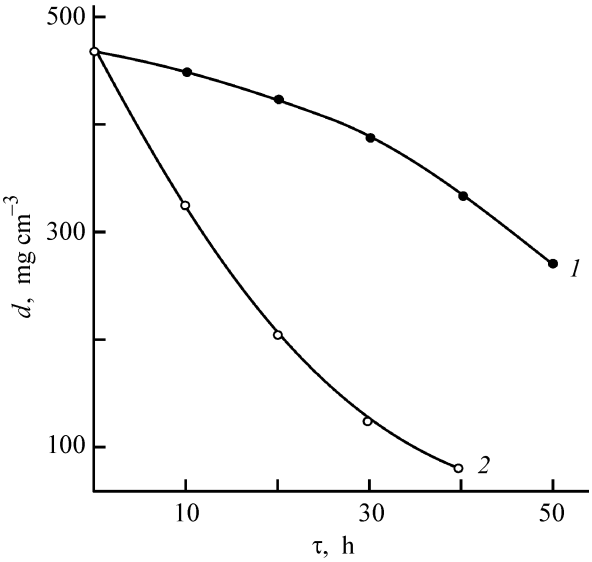


Fig. 2. Variation of the apparent density d in thermal activation of C-1 carbon black in a flow of CO_2 at temperatures of (*1*) 800 and (*2*) 900°C with time τ.

between a sample and the activating agent, and nature of the starting material and the oxidant used) on the final properties of carbon were revealed. The quality of the samples obtained was monitored by their density d, burnout m, and sorption capacity for C_6H_6, W_s. The data obtained are listed in Table 2 and shown in Figs. 1 and 2.

The porous structure (not to be confused with the degree of cross-linking, i.e., extent to which carbon black particles are connected [10]), by which the internal structure of particles is understood, is manifested in carbon blacks only upon their prolonged, deep oxidation with atmospheric oxygen at 450°C for 50 h [10]. In the present study, such conditions were used only in exceptional cases (Table 2). For this reason, the porous structure parameters (volume of pores of a certain size, pore radius distribution, geometric surface area of pores, etc.) are not given in this communication. The specific surface areas [11] of the initial samples and of the most promising materials of the aerogel types were obtained to be 25 and 21 $m^2 g^{-1}$ for C-1 and C-2, respectively, and 106 and 191 $m^2 g^{-1}$ for low-density samples with d = 80–90 mg cm^{-3}.

It can be seen from Table 2 and Figs. 1 and 2, which show typical curves of variation of the burnout and apparent density of samples in their thermal treatment, that the less graphitized samples C-1 exhibit, together with the burnout caused by formation of phase oxides of carbon, a significant increase in the sorption capacity for benzene and a decrease in the apparent density. The processes are strongly affected by the treatment temperature (Table 2, Fig. 2). Under certain conditions (900°C, treatment with water vapor or CO_2), samples with an apparent density of 160–80 mg cm^{-3}, i.e., carbon aerogels, can be obtained. A strong difference was revealed between the final parameters of samples thermally treated in the presence of water vapor and CO_2 (Table 2): the low density, characteristic of aerogels, was reached fast, but at very high burnout (up to 90%). Thus, use of water vapor for activation of technical-grade carbon to obtain aerogels was found to be inexpedient because of the resulting low yield of the product.

A considerably smaller burnout and lower density of final samples were observed in the case of thermal

Table 2. Parameters of C-1 carbon black samples after thermal treatment (initial density d = 470 mg cm^{-3}, benzene sorption with W_s = 0.026 $cm^3 g^{-1}$)

Gas medium	T, °C	τ, h	m, %	d, mg cm^{-3}	W_s, $cm^3 g^{-1}$
H_2O	600	30	45	460	0.126
	700	20	69	320	0.170
	900	30	90	160	1.100
CO_2	800	50	30	270	0.440
	900	40	54	80	0.730
Air + CO_2	900	20	50	90	0.700

Table 3. Parameters of carbon black samples after preliminary impregnation and thermal treatment (thermal treatment duration 1 h, calcination temperature 900–950°C)

Impregnating agent	Gas medium in thermal treatment	d, mg cm^{-3}	W_s, cm^3 g^{-1}
	C-1 carbon black		
NH_4HCO_3 + H_2SO_4	Air	360	0.04
H_2SO_4 + NH_4HCO_3	"	320	0.07
	C-2 carbon black		
H_2SO_4 + NH_4HCO_3	Argon	180	0.02
CH_3COONH_4	"	240	0.04
NH_4HCO_3	"	350	0.07
CH_3COONH_4	Hydrogen	310	0.05
NH_4HCO_3	"	340	0.07

treatment in the atmosphere of CO_2. A thermal treatment of C-2 samples failed to yield similar results. It can be seen from Fig. 1, that, all the conditions being the same, a considerably smaller burnout of C-2 carbon black was observed as compared with that for C-1. In this case, the apparent density changed only slightly, from 240 to 225 mg cm^{-3} at a 50% burnout; no aerogels were formed.

It was found preferable to obtain carbon aerogels from C-1 carbon black by a combined treatment: with atmospheric oxygen at 450°C to destroy the ordered outer shell of carbon black particles and the subsequent treatment in the atmosphere of CO_2 at 900°C to remove unorganized carbon from the inner part. Samples with density conforming to the term aerogel (80–90 mg cm^{-3}) were obtained in a considerably shorter time (Table 2). It is also noteworthy that the carbon aero-gels obtained exhibited a considerably higher sorption capacity for benzene vapor, compared with the initial samples (Table 2).

Further, it was found in special-purpose experiments that an additional high-temperature (~1000°C) treatment with hydrogen of a gas black preliminarily subjected to an oxidative activation yields sorbents with a very high sorption capacity W_s for benzene, 0.8 to 1.1 cm^3 g^{-1}, which considerably exceeds the same parameter for ordinary activated carbon [11]. However, this leads to a significant decrease in the dispersity of the samples obtained, presumably, because of aggregation of their particles, caused by formation under these conditions of rather active surface radicals [10].

Substances of the aerogel type were also synthesized from technical-grade carbon by the method of chemical activation. Samples saturated with ammonium acetate and hydrocarbonate solutions or those impregnated in two stages with sulfuric acid and ammonium hydrocarbonate were first thermally treated in an inert atmosphere (Ar, H_2) and then subjected to the action of an oxidizing agent.

The studies demonstrated (Table 3) that the sorption capacity of samples obtained by thermal treatment of carbon blacks preliminarily impregnated with various substances (chemical activation) increased. However, the decrease in the apparent density of the more reactive C-1 was comparatively small, whereas for C-2, this parameter even somewhat increased, probably because of an incomplete removal of impregnating impurities. The results obtained with the chemical activation demonstrated that the most efficient technique is that involving a two-stage saturation (H_2SO_4 + NH_4HCO_3) combined with thermal treatment, which yielded a sample with a density d = 180 mg cm^{-3}.

CONCLUSIONS

(1) The possibility of obtaining carbon materials of the aerogel type from separate samples of finely dispersed carbon blacks with a lower degree of graphitization in their thermal-oxidative treatment was demonstrated.

(2) It was found preferable to obtain carbon aerogels (with a density of 80–90 mg cm^{-3}) by combined treatment with atmospheric oxygen at 450°C and then in the atmosphere of CO_2 at 900°C.

(3) It was established that the more ordered (graphitized) C-2 samples, which are stable against physical (ultrasonic and gamma irradiation) and chemical ac-

tions, show no tendency toward a change in the density of the material obtained (no aerogel formation).

REFERENCES

1. Pekala, R.W., *J. Mater Sci.*, 1989, vol. 24, no. 9, pp. 3221–3231.
2. Petricevic, M., Glora, M., and Fricke, J., *Carbon*, 2001, vol. 39, no. 6, pp. 857–867.
3. Yamashita, J., Ojima, T., Hatori, H., and Yamada, Y., *Carbon*, 2003, vol. 41, no. 2, pp. 285–295.
4. Guotong Qin and Shucai Guo, *Carbon*, 2001, vol. 39, no. 12, pp. 1935–1937.
5. Thorikawa, T., Ogawa, K., Mizuno, K., *et al.*, *Carbon*, 2003, vol. 41, no. 3, pp. 465–472.
6. Petricevic, R., Reichenauer, G., and Fricke, J., *J. Non-Cryst. Solids*, 1998, vol. 225, no. 1, pp. 41–51.
7. Noriko Yoshizawa, Yasushi Soneda, Hiroaki Hatori, and Yohko Hanzawa, *Proc. Int. Conf. on Carbon, 6–10 July, 2003, Oviedo*, Spain, CD–ROM JSBN 0–9674971–2–49674972.
8. Li, W.C., Lu, A.H., and Guo, S.C., *Carbon*, 2001, vol. 39, no. 12, pp. 1989–1994.
9. Pekala, R.W., Farmer, J.C., Alviso, C.T., and Tran, T.D., *J. Non-Cryst. Solids*, 1998, vol. 225, no. 1, pp. 74–80.
10. Samoilov, V.S., Senin, N.D., and Smirnov, V.N., *Proizvodstvo i svoistva uglerodnykh sazh* (Manufacture and Properties of Carbon Blacks), Omsk, 1980.
11. Kel'tsev, N.V., *Osnovy adsorbtsionnoi tekhniki* (Fundamentals of the Adsorption Technology). Moscow: Khimiya, 1984.

Russian Journal of Applied Chemistry, Vol. 78, No. 8, 2005, pp. 1258–1265. Translated from Zhurnal Prikladnoi Khimii, Vol. 78, No. 8, 2005, pp. 1280–1287.
Original Russian Text Copyright © 2005 by Stavitskaya, Goba, Tomashevskaya, Tsyba.

SORPTION AND ION-EXCHANGE PROCESSES

New Carbon Aerogels Fabricated from Polymeric Materials and Their Properties

S. S. Stavitskaya, V. E. Goba, A. N. Tomashevskaya, and N. N. Tsyba

Institute of Sorption and Endoecology Problems, National Academy of Sciences of the Ukraine, Kiev, Ukraine

Received June 16, 2004; in final form, April 2005

Abstract—Electron microscopy and adsorption-structural, X-ray phase, and thermal analyses were used to determine the density, porosity, microstructure, electrical conductivity, and reactivity of new carbon aerogels based on phenol-formaldehyde polymers.

Low-density carbon materials, carbon aerogels (CA), were first produced by pyrolysis of organic aerogels [1–3]. All the subsequent studies were devoted to synthesis and analysis of the structural parameters and adsorption and electrical properties of carbon aerogels [4–8]. Carbon aerogels were obtained by the classical scheme in three steps: sol-gel polymerization of organic oligomers (synthesis of organic aerogels), high-efficiency drying in a flow of CO_2, and high-temperature carbonization of the resulting organic aerogels (synthesis of carbon aerogels).

In the first stage, the influence exerted by the relative content of starting components [4], thermal stability of chosen resins [5] and solvents (mostly alcohols) [6], and presence in the course of polymerization of catalysts [$Ca(OH)_2$, Na_2CO_3] [7] and cross-linking agents (e.g., melamine) [8] on the final properties of the carbon aerogels obtained was studied in detail. Commonly, resorcinol–formaldehyde, phenol–furfural, melamine–formaldehyde, polyurethane, and, less frequently polyvinyl chloride systems are used as starting components [9].

The interest in materials of the aerogel type is due to the wide opportunities for their use in chemical technology and electrical engineering, provided by their uniquely high porosity, electrical conductivity, corrosion and acid resistance, and biological stability [3, 4, 7, 8, 10–14].

Published studies have been mainly concerned with methods for synthesis of carbon aerogels and properties of these materials, with little attention given to the possibility of controlled variation of the porous structure and chemical nature of the surface of the resulting carbon aerogels, e.g., by special treatment and directional modification. Therefore, a search for new ways of synthesis and new forms of carbon aerogels is a matter of current interest.

EXPERIMENTAL

This study is concerned with properties of new carbon aerogels prepared from phenol-formaldehyde oligomers (PFO) and with changes in the structural parameters, porosity, nature of the surface, and electrical properties upon their thermal treatment (activation) in the atmosphere of CO_2 and oxidation with nitric acid.

Carbonized products differing in degree of branching, porosity, and other structural parameters and texture can be obtained by using in synthesis the phenol-formaldehyde resin, which can form 3*D* hexagonal carbon networks in carbonization, and various relative amounts of the same components and additives.

PFO was carbonized in a flow of N_2, with the treatment time of the starting polymer varied within 2–4 h and the carbonization temperature gradually elevated from 400 to 600°C. The activation was done in the atmosphere of CO_2 at 850°C during a varied time and the oxidation was performed with concentrated HNO_3 [15]. The porous structure was characterized by electron microscopy and adsorption-structural analysis by sorption of benzene vapor and H_2O, and low-temperature (77 K) sorption of N_2. The gas-chromatographic method of thermal desorption of argon was used to measure the specific surface area S_{sp} of the samples studied. The nature and amount of oxygen-containing functional surface groups was determined by chemical

1070-4272/05/7808-1258 © 2005 Pleiades Publishing, Inc.

Table 1. Sorption parameters of carbon aerogels prepared from phenol-formaldehyde oligomers and selected activated carbons*

Sample	d, mg cm^{-3}	W_s	U_Σ	Sample	d, mg cm^{-3}	W_s	U_Σ
		cm^3 g^{-1}				cm^3 g^{-1}	
CA-1	20	0.20	1.1	CA_2-A	115	0.33	8.4
CA-2	90	0.17	2.6	Raw PF	920	0.12	1.4
CA-3	145	0.20	3.4	PF-A	690	0.50	1.8
CA_1-A	125	0.34	41.9	BAC	250	0.34	1.8

* CA_1-A and CA_2-A, aerogels activated in a flow of CO_2 for 2 and 4 h, respectively; PF-A, carbon activated from phenol-formaldehyde resin; BAC, birch activated carbon.

Table 2. Physicochemical parameters of the initial (raw PF) and activated phenol-formaldehyde (PF-A) carbons and carbon aerogels synthesized on their basis*

Sample	d, mg cm^{-3}	W_s	V_{micro}	V_{meso}	V_{macro}	S_{sp}, m^2 g^{-1}	E_o, kJ mol^{-1}	$B \times 10^6$	W_o, cm^3 g^{-1}
		cm^3 g^{-1}							
Raw PF	920	0.12	0.02	0.01	–	150	–	–	–
PF-A	690	0.34	0.09	0.14	–	170	–	–	–
CA-1	30	0.17	0.100	0.036	0.875	228	16.6	1.18	0.15
CA-2	45	0.20	0.178	0.047	–	235	17.0	1.50	0.19
CA-3	60	0.22	0.176	0.079	0.662	265	23.6	0.66	0.14
CA-4	70	0.25	0.246	0.064	–	300	24.2	0.66	0.14
CA-5	85	0.22	0.178	0.093	0.660	370	31.2	0.82	0.22
CA-6	140	0.20	0.141	0.035	0.590	418	23.6	0.66	0.11
CA_1-A	140	0.34	0.204	0.006	0.550	358	27.4	1.30	0.09
CA_2-A	150	0.35	0.186	0.032	0.590	407	10.6	1.80	0.10
CA-O	73	0.33	0.196	0.064	0.599	300	–	–	–

* CA-1–CA-6, carbon aerogels, carbonizates of phenol-formaldehyde resins of different compositions and densities; CA_1-A and CA_2-A, carbon aerogels additionally activated in a flow of CO_2 for 2 and 4 h, respectively' CA-O carbon aerogel oxidized in the liquid phase with nitric acid.

titration [15]. The structure and reactivity of carbon aerogels was also subjected to X-ray phase and thermographic analyses [16, 17].

Phenol-formaldehyde resins with prescribed texture and varied ratio of the components were used as starting materials to obtain, after carbonization in the atmosphere of N_2, carbon aerogels with a widely variable apparent density d, which was in the range 20–150 mg cm^{-3} for different samples. It should be noted that the density of the carbon aerogel samples obtained is considerably lower than that of an untreated, additionally expanded graphite (d = 350 mg cm^{-3}) and aerosils (150–180 mg cm^{-3}).

Compared with the conventional activated carbons, synthetic low-density carbon aerogels exhibit rather high sorption parameters (Table 1) (specific volume of sorption pores, W_s, found by the desiccator method from the of sorption of a benzene vapor is 0.35 cm^3 g^{-1}) and a high total porosity U_Σ [16], which, in some cases, exceeds that of BAC and activated phenol-formaldehyde carbons by an order of magnitude (Table 1) [15, 18].

Electron-microscopic studies demonstrated that carbon aerogels have a strongly inhomogeneous microcellular structure. The surface of the aerogels is pierced by coarse macropores (2×10^3–1×10^4 nm and more, up to several tens of micrometers, depending on the sample density). It is the presence of a large number of macropores that is responsible for the high total porosity and 90–95 : 100 ratio of the apparent and true densities. The electron-microscopic data obtained were used to calculate the wall thickness of carbon aerogels, which varied widely, from 10 to 600 nm.

As indicated by the sorption data (for benzene and water vapor, Table 2), carbonizates of carbon aerogels

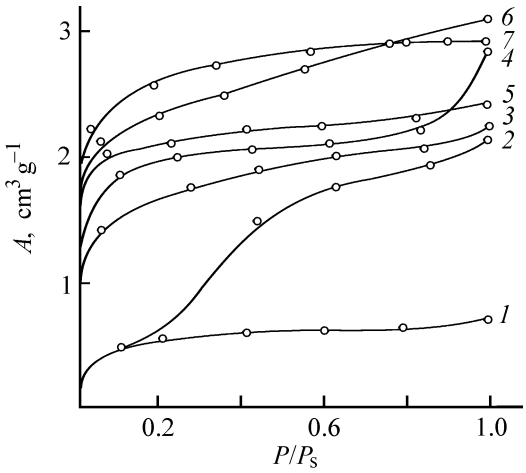


Fig. 1. Isotherms of benzene vapor sorption by carbon aerogels with different densities and varied chemical nature of the surface and by activated carbon prepared from a phenol-formaldehyde resin, obtained on an adsorption-gravimetric setup (McBain balance). (*A*) Adsorption and (P/P_s) relative pressure. CA sample, density (mg cm^{-3}): (*1*) oxidized CA-O, 30; (*2*) CA, 30); (*3*) CA, 45; (*4*) CA, 85; (*5*) CA, 140; (*6*) CA_1-A (activated) 140; and (*7*) activated carbon prepared from a phenol-formaldehyde resin.

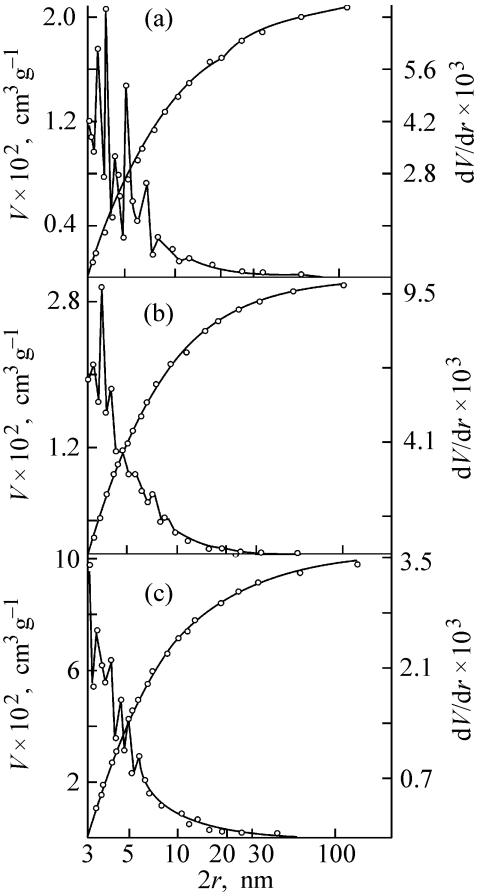


Fig. 2. Differential (d*V*/d*r*) and integral (*V*) distributions of pores over radii *r* in (a) initial aerogel, (b) activated CA, and (c) oxidized CA-O.

of the same nature have, in contrast to low-porosity raw carbon based on phenol-formaldehyde resins, a rather developed system of micropores, which is formed already in the carbonization stage. In activated carbons prepared from phenol-formaldehyde resins, micropores appear only in the course of activation.

The benzene sorption isotherms obtained (Fig. 1) and the structural parameters calculated from these isotherms (Table 2) indicate that all the carbon aerogel samples contain micro- (V_{micro}), meso- (V_{meso}), and macropores (V_{macro}), whose volume *V* strongly depends on the sample density. An increase in the density of carbon aerogels makes larger the volume of the sorption space (amount *A* of adsorbed benzene vapor, Fig. 1), that of mesopores (V_{meso}), and specific surface area S_{sp}.

An additional activation of carbon aerogels also makes higher their sorption capacity via development of micropores, with, however, strongly decreasing mesoporosity.

The presence of micropores in carbon aerogels is confirmed by the values of the main parameters of the microporous structure [19], structural constants *B* and W_o in the equation of the theory of volume filling of micropores and the characteristic adsorption energy E_o, which are found from data on water sorption at $P/P_s = 1$ (Table 2). Constant W_o is the limiting volume of the adsorption space, and constant *B* characterizes the size of micropores [19]. An increase in constant *B* indicates that micropores become larger; at small *B*, W_o is close to the volume of micropores.

As the density of carbon aerogels increases, the surface area of the samples becomes larger. In some cases, it reaches values typical of activated carbons. An increase in the characteristic energy E_o, with a simultaneous decrease in the structural constant *B*, indicates that small micropores and even ultramicropores are predominant in the structure of aerogels with a sufficiently high density ($d \approx 100$ mg cm^{-3}) [15, 18].

The presence of a microporous structure in the carbon aerogels synthesized is also confirmed by the results of a study of their structural-sorption parameters for N_2, obtained on a Quantachrome NOVA 2200E high-speed gas sorption analyzer. Figures 2a–2c show pore radius distributions for, respectively, the starting sample (carbonizate), activated CA–A, and oxidized CA–O, which were calculated using the Barrett–Joyrnal–Halenda (BJH) method [20]. The initial nonacti-

Table 3. Structural-sorption parameters of some of the samples studied, found from the low-temperature adsorption of nitrogen (BJH method)*

Sample	A, $cm^3\ g^{-1}$, at $P/P_s = 1$	Average pore width, nm	V_{micro}, $cm^3\ g^{-1}$	S_{micro}	S	E, kJ mol^{-1}
				$m^2\ g^{-1}$		
Raw PF	12.0	8.2	0.0	6.5	6.2	3.2
CA-A	21.0	6.6	0.2	8.9	630	3.9
CA-O	280.0	2.4	0.4	10.1	969	11.0

* A, nitrogen adsorption at 77 K; V_{micro}, volume of micropores, calculated by the BJH method; S_{micro}, surface area of micropores; S, total surface area; and E, adsorption energy.

vated aerogel contains micropores of various sizes, whereas in the activated and oxidized sample, only 3–5-nm micropores were observed, i.e., the carbon aerogels synthesized are nanosize and uniformly microporous, which is a rater valuable property as regards their practical application. Table 3 lists the structural-sorption parameters of some of the samples under study, found from the low-temperature adsorption of N_2, using the BJH method.

In order to study the possibility of controlling the structure and chemical nature of the surface of carbon aerogels and imparting new properties to these materials, the reactivity and thermal stability of carbon aerogels were examined in various oxidizing media (CO_2, O_2) at different temperatures.

To develop the microporosity and raise the sorption capacity, samples of varied density were subjected to a high-temperature (850°C) activation with carbon dioxide. In doing so, the main activation parameters were determined and data on how the density of carbon aerogels varies in the process (Fig. 3) were obtained.

High-temperature treatment of finished samples of carbon aerogels in the atmosphere of CO_2 makes higher the total porosity, number of micropores, absorption capacity for benzene and water, and S_{sp}, but diminishes the number of meso- and macropores (Table 2). As the BJH method yields clear-cut data on the content of micro- and mesopores [20], the volume of macropores in the carbon materials studied was determined [20] as the difference between the total volume of pores, found from the moisture absorption capacity of the carbons, and the maximum volume of sorbed benzene, W_s. The following specific features of the process of thermal treatment of the carbon aerogels prepared are noteworthy. It was found, in particular, that d is virtually the same for samples with a low initial density, subjected to activation for different periods of time (Fig. 3). At the same time, the density of samples with an initial density $d > 50$ mg cm^{-3} decreases during thermal treatment till a certain instant of time, presumably via burning-out of the most reactive amorphous part of carbon and further development of porosity, whereas at longer treatment, a structural transformation of the skeleton occurs and the density increases to nearly its initial value. This may be due to changes in the texture of carbon aerogels in prolonged thermal treatment.

Thus, the optimal activation conditions and, in particular, the time of activation for aerogels of varied density, at which the quality of the aerogels is markedly improved, were revealed.

The reactivity of carbon aerogels toward oxygen was determined from the results of a thermogravimet-

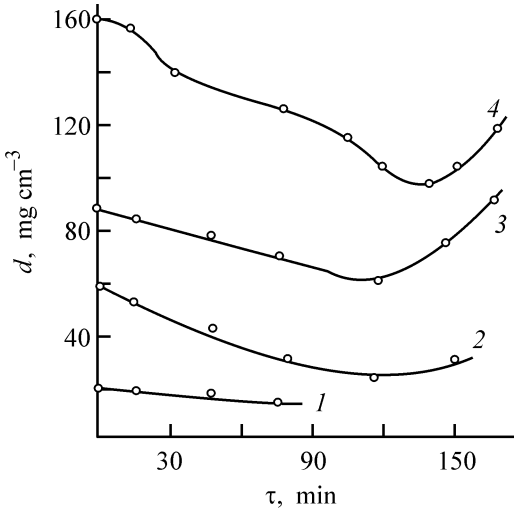


Fig. 3. Kinetics of variation of the apparent density d of carbon aerogels. (τ) Activation time. Carbon aerogel: (*1*) CA-1, (*2*) CA-3, (*3*) CA-5, and (*4*) CA_2-A.

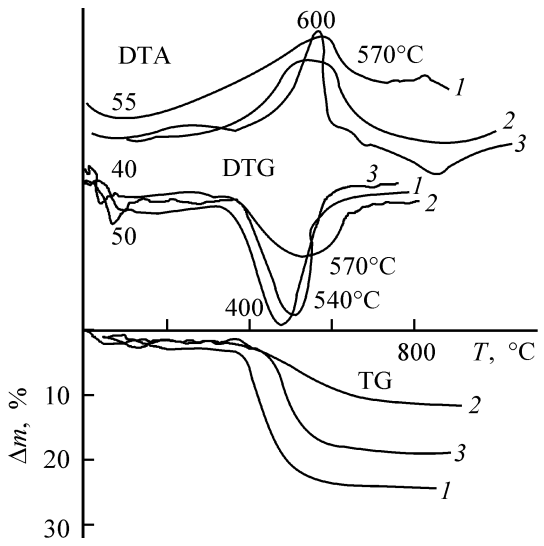


Fig. 4. Thermograms of carbon aerogels, obtained in air. (T) Temperature and (Δm) loss of mass. Sample, d (mg cm^{-3}): (*1*) starting carbonizates of CA-1, 30; (*2*) CA-6, 140; and (*3*) activated CA_2-A, 140.

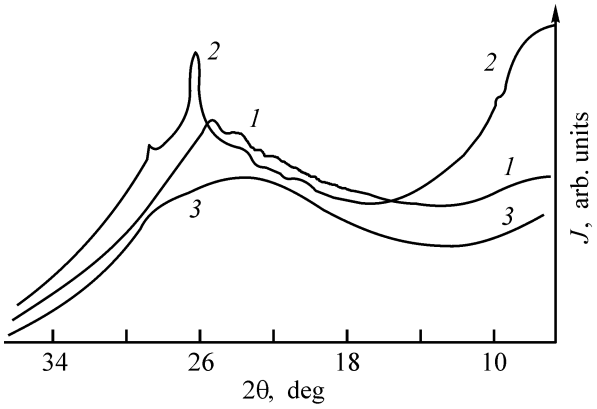


Fig. 5. X-ray diffraction patterns of carbon aerogels and raw phenol-formaldehyde carbon. (J) Signal intensity and (2θ) Bragg angle; the same for Fig. 6. CA sample, d (mg cm^{-3}): (*1*) CA-3, 60; (*2*) CA-6, 140; and (*3*) raw PF.

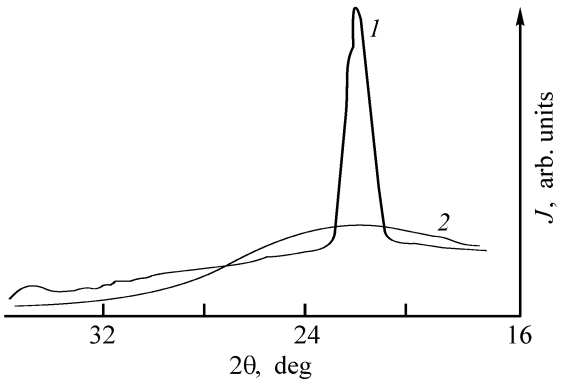


Fig. 6. X-ray diffraction patterns of (*1*) activated aerogel CA_1-A and (*2*) activated phenol-formaldehyde carbon PF-A.

ric analysis (Fig. 4), performed both in air and in an inert atmosphere (Ar) [21] on an MOM derivatograph (Hungary). The weighed portions were 100 mg, the temperature was raised at a rate of 5 deg min^{-1}. Heating of carbon aerogels first leads to a minor endothermic effect at 40–55°C. This effect should be attributed to removal of sorbed water. As the temperature is raised to 540–600°C, the carbon mass of all of the samples studied burns out, which is accompanied by an exothermic effect. The rates of carbon destruction at different times of contact with the oxidant are not the same, which is indicated by the TG curves showing the loss of the carbon mass. The higher the density of carbon aerogel samples, the better their thermal stability: a low-density sample (curve *1*) burns out faster than do aerogels with d = 140 mg cm^{-3} (curves *2*, *3*). In the inert medium, the thermal stability of carbon aerogels is considerably higher.

The reactivity of carbon materials depends not only on their porous structure, but also on the forms in which carbon exists in their structure and on its valence state.

According to the results of an X-ray phase analysis on a DRON-2 instrument, the carbon skeleton of low-density aerogels (d = 30–50 mg cm^{-3}) is mostly composed of disordered amorphous carbon.

In this case, however, the intensity of the diffuse halo increases with the sample density and diffraction peaks appear on its background, which points to a crystalline ordering of carbon, compared with the very diffuse halo from activated carbon of the same nature (Fig. 5). In the X-ray scattering curves of carbonizates of aerogels with a comparatively high density (d > 100 mg cm^{-3}), the intensity of the diffraction peaks grows, which points to predominance of the crystalline form size and larger of carbon crystallites.

Particularly strongly different are the X-ray spectra of activated samples of carbon aerogels and phenol-formaldehyde carbon (Fig. 6). The X-ray diffraction patterns of an activated aerogel show a clearly pronounced diffraction peak of the 002 band, which indicates a considerable increase in the content of crystalline carbon in the microstructure upon activation, untypical of the ordinary activated carbon.

The position of the 002 band in the X-ray diffraction patterns of aerogel samples and its halfwidth were used to calculate by the Warren equation [22] the average size of carbon crystallites in the micro-

structure of the aerogels: L_a, height of packets of atomic networks; L_d, diameter of these packets (Table 4).

As can be seen in Table 4, the parameters of the microstructure of carbon aerogels significantly differ from the same parameters of the known carbon materials (e.g., in the larger interplanar spacing L = 4.1 Å. This fact can account for the discrepancy between the true densities of activated phenol-formaldehyde carbon (1.65 g cm^{-3}) and of the carbon skeleton of carbon aerogels (0.9–1.25 g cm^{-3}).

Growth of crystallites and their ordering are favored by an additional high-temperature activation, which is indicated by an increase in the height of atomic-network packets to 60 Å and in their diameter to 115 Å at a constant interplanar spacing.

The considerable fraction of crystalline carbon in the carbon aerogels synthesized leads to their higher (compared with the corresponding samples of PF-A activated carbon) electrical conductivity (Table 5).

As is known [15], the conduction in carbons as graphite bodies is mainly effected by π-electrons moving along planes of hexagonal networks (via the system of conjugated bonds). The electrical resistance of powdered carbon materials is determined, as in other crystalline bodies, by their internal microstructure and contacts (barriers) between particles. The electrical resistance of the barriers depends both on the state of the particle surface (presence of functional groups, adsorbed substances, impurities on the surface) and on the particle size and pressure applied to the powder [21, 23]. To exclude the influence of the last factors, which are not related to the nature of a material under study, the electrical resistance was measured under identical conditions (grain size, pressure, etc.).

To determine the electrical resistance, carbon aerogels and carbons were taken in the form of a ground (D = 0.25 mm) freely poured powder. A weighed portion of a powder was placed in a 1-cm-long porcelain tube with an inner diameter of 6 mm and the tube was clamped between two metallic cylinders. The measurements were carried out under constant pressure at 20°C in the ac mode. The electrical resistance was determined by the voltmeter-ammeter method [23]. A G3-43 generator working in the frequency range 0.15–30 MHz served as a voltage source. The voltage drop across a sample was measured with a V3-4 valve voltmeter.

As demonstrated by the data obtained, the highest electrical conductivity χ (lowest electrical resistivity ρ) was observed for low-density carbon aerogels. As the density of the aerogels becomes higher, their electrical resistance increases, possibly because of the higher content ratio of amorphous and crystalline carbon in the microstructure of the aerogels. In this case, however, ρ of carbon aerogels is an order of magnitude lower than that of activated carbon. Additional activation of carbon aerogels (Table 5, samples CA_1–A and CA_2–A) diminishes their electrical resistance.

Table 4. Comparative characteristics of microstructures of various carbon materials

Carbon material	L	L_c	L_a
	Å		
Graphite	3.34–3.35	200	6.69
Carbon blacks, fossil coals, sugar coke	3.44	26–28	9–12
PF-A	3.5–3.6	58–83	22–24
CA	4–4.1	22–46	11–21
CA_1-A	–	15	28
CA_2-A	–	115	57

Table 5. Electrical properties of carbon materials

Sample	d, mg cm^{-3}	ρ, Ω cm	χ, Ω^{-1} cm^{-1}
Aerogel	30	20.5	4.9×10^{-2}
	45	22.1	4.4×10^{-2}
	70	41.7	2.4×10^{-2}
	85	58.7	1.7×10^{-2}
	120	99.5	1.1×10^{-2}
CA_1-A	140	32.5	3.1×10^{-2}
CA_1-A (H_2)*	140	68.2	1.4×10^{-2}
Raw PF	–	247	4.1×10^{-3}
PF-A**	–	132	7.6×10^{-3}

* Activated CA additionally treated in a flow of H_2 at 850°C to remove possible surface oxides.

** Activated in a flow of CO_2.

It should be noted that the possibility of obtaining carbon aerogels with a sufficiently high electrical conductivity is rather important for technology, especially for fabrication of molded articles of prescribed configuration on the basis of carbon aerogels.

It is known [15] that presence of acidic surface functional groups on the carbon surface strongly changes not only the sorption and catalytic properties of carbon materials, but also the electrical parameters and performance of articles containing various modifications of free carbon.

In this context, the possibility of changing the chemical nature of the surface of carbon aerogels and

obtaining their oxidized forms by treatment of activated carbon aerogels with concentrated HNO_3 solutions was also analyzed [15]. In the process, samples with a high cation-exchange capacity of up to 4 mmol g^{-1} and different compositions of surface functional groups with varied acidity were prepared. It should be noted that preparation of oxidized carbons with SEC exceeding 2 mmol g^{-1} is commonly accompanied by destruction of the carbon substance to give fulvic acids and coloring humic acids [15], which is untypical of oxidized aerogels.

The relative contents of surface functional groups in carbon aerogels, obtained here, approximately correspond to the known distributions of such groups, observed on ordinary oxidized carbons [15]. The change of the chemical nature of the surface in oxidized carbon aerogels, compared with activated carbons of the same density, is also confirmed by the results of a thermogravimetric analysis. These data indicate that the onset of the reaction between oxygen and the carbon mass is observed in oxidized carbon aerogels at a higher temperature (540–560°C) than that in activated carbons (440–470°C). Presumably, this results from the shielding effect of oxygen-containing surface functional groups. It should be noted that there is no evidence concerning the synthesis and analysis of properties of their oxidized forms in the literature devoted to carbon aerogels.

CONCLUSIONS

(1) New low-density carbon materials, aerogels with a widely controllable apparent density (20–150 mg cm^{-3}), were synthesized from phenol-formaldehyde polymers by carbonization.

(2) It was shown that the carbon aerogels synthesized show high sorption capacity (for benzene, water, and nitrogen) and total porosity. In addition to a large number of macropores, the materials under study possess a rather well-developed microporous structure. In contrast to that of ordinary carbons based on phenol-formaldehyde oligomers, this microporous structure is formed already in the carbonization stage and leads to a high sorption capacity and large specific surface area comparing well with that in industrial carbons.

(3) An X-ray phase analysis demonstrated an increased content of crystalline carbon in the microstructure of carbon aerogels after their activation, which is untypical of the ordinary activated carbon. The samples synthesized also differ from those of ordinary activated carbon in the parameters of microstructure, considerably larger interplanar spacings (up to 4.1 Å), which leads to their lower true density, compared with that of ordinary carbons based on the phenol-formaldehyde resin.

(4) It was found that the aerogel samples studied exhibit a high electrical conductivity typical of carbon materials of this kind. The electrical conductivity exceeds that of phenol-formaldehyde carbons by a factor of 2–5.

(5) Cation-exchange (oxidized) forms of carbon aerogels with a high sorption capacity (SEC of up to 4 mm g^{-1}) and various compositions of acidic surface functional groups were obtained. It was established that, when such an exchange capacity is reached, no destruction of the carbon substance occurs and no coloring humic and fulvic acids are formed. This points to a high chemical stability of the carbon skeleton obtained.

(6) The study of the properties of the carbon aerogels synthesized made it possible to suggest that materials of this kind can find use as effective adsorbents, various filter media, fillers of chromatographic columns, etc.

REFERENCES

1. Pekala, R.W., *J. Mater Sci.*, 1989, vol. 24, no. 9, pp. 3221–3231.
2. US Patent 476778.
3. Pekala, R.W., Farmer, J.C., Alviso, C.T., and Tran, T.D., *J. Non-Cryst. Solids*, 1998, vol. 225, no. 1, pp. 74–80.
4. Petricevic, M., Glora, M., and Fricke, J., *Carbon*, 2001, vol. 39, no. 6, pp. 857–867.
5. Yamashita, J., Ojima, T., Hatori, H., and Yamada, Y., *Carbon*, 2003, vol. 41, no. 2, pp. 285–295.
6. Guotong Qin and Shucai Guo, *Carbon*, 2001, vol. 39, no. 12, pp. 1935–1937.
7. Thery, A., Clinard, C., Beguin, F., *et al.*, *Proc. Int. Conf. on Carbon, 2002, Bejihg, China*, CD-ROM SBN 7-900362-03-7/G03.
8. Rui Zang, Zhihong Li, Yiao Xu, *et al.*, *Proc. Int. Conf. on Carbon, September 15–20, 2002, Bejing, China*, CD-ROM SBN 7-900362-03-7/G03.
9. Thorikawa, T., Ogawa, K., Mizuno, K., *et al.*, *Carbon*, 2003, vol. 41, no. 3, pp. 465–472.
10. Petricevic, R., Reichenauer, G., and Fricke, J., *J. Non-Cryst. Solids*, 1998, vol. 225, no. 1, pp. 41–51.
11. Gilow, K.M. and Shapovalova, L.N., *Polym. Degrad. Stab.*, 1992, vol. 38, no. 1, pp. 27–34.
12. Mitrofanov, V.D., Manakov, A.I., and Shveikin, G.P., *Karbidy i materialy na ikh osnove* (Carbides and

Materials on Their Basis), Kiev: Inst. Probl. Materialoved., Akad. Nauk SSSR, 1991.

13. Noriko Yoshizawa, Yasushi Soneda, Hiroaki Hatori, and Yohko Hanzawa, *Proc. Int. Conf. on Carbon, July 6–10, 2003, Oviedo, Spain,* CD-ROM JSBN 0-9 674 971-249 674 972.
14. Li, W.C., Lu, A.H., and Guo, S.C., *Carbon*, 2001, vol. 39, no. 12, pp. 1989–1994.
15. Tarkovskaya, I.A., *Okislennyi ugol'* (Oxidized Carbon), Kiev: Naukova Dumka, 1981.
16. Nefedov, V.I., *Rentgenoelektronnaya spektroskopiya khimicheskikh soedinenii* (X-ray Photoelectron Spectroscopy of Chemical Compounds), Moscow: Khimiya, 1984.
17. Larina, A.A., Tarkovskaya, I.A., Zakolodyazhnaya, O.V., *et al.*, *Teor. Eksperim. Khim.*, 1984, no. 4, pp. 496–501.
18. Dubinin, M.M., *Poristaya struktura i adsorbtsionnye svoistva aktivnykh uglei* (Porous Structure and Adsorption Properties of Activated Carbons), Moscow: Voen. Akad. Khim. Zashchity, 1965.
19. Kolyshkin, D.A. and Mikhailova, K.K., *Aktivnye ugli: Spravochnik* (Activated Carbons: Reference Book), Leningrad: Khimiya, 1993.
20. Gregg, S.J. and Sing, K.S., *Adsorption, Surface Area and Porosity*, London: Acad., 1982.
21. Stavitskaya, S.S., Larina, A.A., Tarkovskaya, I.A., and Zakolodyazhnaya, O.V., *Khim. Tverd. Tela*, 1990, no. 5, pp. 111–113.
22. Spiridonov, E.P., Barykin, B.M., Drozdov, R.Ya., *et al.*, *Strukturnaya khimiya ugleroda i uglei* (Structural Chemistry of Carbon and Coals), Kasatochkin, V.I., ED., Moscow: Nauka, 1969.
23. Tarkovskaya, I.A., Kozub, G.M., Goba, V.E., and Stavitskaya, S.S., *Ukr. Khim. Zh.*, 1978, vol. 44, no. 5, pp. 489–493.

Russian Journal of Applied Chemistry, Vol. 78, No. 8, 2005, pp. 1266–1269. Translated from Zhurnal Prikladnoi Khimii, Vol. 78, No. 8, 2005, pp. 1288–1291.
Original Russian Text Copyright © 2005 by Bondarenko, Boichinova.

SORPTION AND ION-EXCHANGE PROCESSES

Sorption of Some Metal Ions on Inorganic Electron and Ion Exchangers Based on Zirconium(IV)

T. S. Bondarenko and E. S. Boichinova

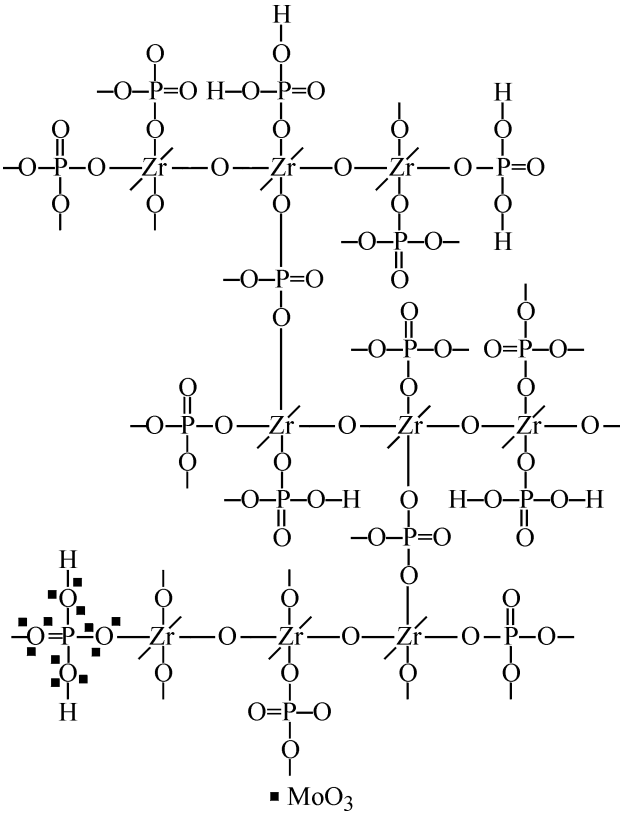
St. Petersburg State Technological Institute, St. Petersburg, Russia

Received July 19, 2004; in final form, July 2005

Abstract—Conditions of sorption of nonferrous metal ions on inorganic electron and ion exchangers based on zirconium(IV) were analyzed. The sorption capacity was evaluated as influenced by pH, concentration, and temperature of the contacting solutions and nature and chemical composition of the ion exchanger.

Sorbents operating under severe conditions are required in many branches of science and industry. In contrast to organic sorption materials, inorganic sorbents show high chemical resistance to aggressive solutions and high stability at elevated temperatures and pressures or under irradiation. Therefore, a study of the properties of these materials as influenced by various operation factors is rather urgent. Synthesis of inorganic sorbents based on zirconium–oxygen matrix involves formation of polymers with Zr–O–Zr units on adding polybasic acids or their salts in aqueous solutions of zirconium(IV). The residues of polybasic acids link with zirconium–oxygen chains to form simple or complex functional groups exhibiting ion-exchange, redox, and some other properties.

In this study, we examined the effect of some factors on the ion-exchange properties of inorganic electron and ion exchangers (EIEs) based on zirconium(IV), with functional groups containing phosphorus(V) and molybdenum(VI) (zirconium phosphomolybdate, ZPM[1]), tungsten(VI) and vanadium(V) (zirconium tungstovanadate, ZTV [2], and silicon(IV) and molybdenum(VI) (zirconium silicomolybdate, ZSM [3]). The ion-exchange properties of these sorbents are due to the residues of polybasic acids of molybdenum(VI), phosphorus(V), tungsten(VI), and silicon(IV) and hydroxy groups, and the redox properties are associated with the formation of the corresponding heteropoly acid residues in the course of synthesis. In this study, we analyzed only the ion-exchange power of EIEs in comparison with hydrated zirconium dioxide (HZD) [4]. The structure of EIE based on zirconium(IV), molybdenum(VI), and phosphorus(V) is given below.



It is known that the sorption properties depend not only on the nature and composition of a sorbent, but also on the sorption conditions, such as the solution pH, ionic composition of the solution (nature of anions, impurity electrolytes), contact time (sorption kinetics), temperature, etc.

All the sorbents were prepared from zirconium oxynitrate by the procedures given elsewhere [1–4].

1070-4272/05/7808-1266 © 2005 Pleiades Publishing, Inc.

The sorption capacity Q was determined under the static conditions and calculated as the difference of the concentrations of the adsorbed ion in the contacting solution before sorption and after attainment of a quasi-equilibrium (chelatometry [5]).

The solid to liquid ratio was 1 : 100; the working fractions of the sorbent were 0.25–0.50 and 0.50–0.80 μm and sorption time τ = 24 h (unless otherwise indicated). The required pH of the initial contact solution was adjusted with an appropriate acid. The half-time of exchange was determined from the kinetic curves. The temperature was maintained with a Universal Termostat U-8 unit with an accuracy of ±0.02°C. In our experiments, we used the sorbents in the H form.

The time in which the equilibrium is attained (sorption kinetics) is of practical importance. As can be seen from Table 1, the half-time of exchange of various sorbents changes with their composition. The time of attainment of the quasi-equilibrium in the distribution of a given ion between the sorbent and solution depends on the nature of the adsorbed ion. A comparison of the data on several three-component inorganic EIEs based on zirconium(IV) [1–3] showed that ZSM sorbents exhibit the best kinetic parameters in sorption of nonferrous metals.

In the case of ZSM, the half-times of exchange of copper(II) and nickel(II) ions are shorter than those with ZPM and ZPM (Table 1). The sorption capacity of the sorbents in question changes in the following order: ZSM, $Ag^+ > Co^{2+} > Cu^{2+} > Ni^{2+}$; ZTM, $Cu^{2+} > Co^{2+} > Ni^{2+}$; and ZPM–$Ag^+ > Cu^{2+} > Co^{2+} > Ni^{2+}$.

Only in the case of ZSM the degree of exchange changes in accordance with the increasing ionic radius of metals, whereas for ZPM and ZTV this trend is broken: $Co^{2+} > Cu^{2+} > Ni^{2+}$ [7].

It is known that the sorption capacity of weakly basic and weakly acidic exchangers depends on the pH of the contacting solution. With increasing pH, the sorption capacity of ZTV and ZSM grows (Table 2), which is due to stronger dissociation of the functional groups of the exchanger. Thus, our experimental data confirm that sorbents of this type are cation exchangers [1–3].

In contrast to ZTV, the sorption capacity of ZSM depends on the electrolyte composition (Table 3). It has been found that the salt anion in the solution from which sorption is carried out strongly affects the sorption capacity [8]. For example, ions of cobalt(II), nickel(II) and copper(II) are readily recovered by alumina from sulfate solutions, whereas

Table 1. Sorption-kinetic characteristics of electron and ion exchangers based on zirconium(IV) (initial metal concentration c 5×10^{-2} M)

Sorbent	Adsorbed ion,	Q, mmol g^{-1}	$\tau_{1/2}$, h	$D^* \times 10^{10}$, cm s^{-1}	τ, h
ZSM [3]	Cu^{2+}	0.70 ± 0.02	3.0	39.00	24
	Co^{2+}	1.00 ± 0.03	8.4	14.00	48
	Ni^{2+}	0.40 ± 0.01	1.4	67.00	24
	Ag^+	1.3 ± 0.03	2.6	10.00	24
ZTV [2]	Cu^{2+}	0.40 ± 7.02	10.5	–	24
	Co^{2+}	0.28 ± 0.03	–	–	24
	Ni^{2+}	0.27 ± 0.01	–	–	24
ZPM [1]	Cu^{2+}	0.67	6.0	0.27	24
	Co^{2+}	0.46	–	–	24
	Ni^{2+}	0.33	6.2	0.59	84
	Ag^+	0.83	0.5	9.10	24

* The diffusion coefficients D were calculated using the Boyd equation at the degree of exchange F = 0.5 for pore-diffusion kinetics, whose mechanism was determined by special experiments using the Helfferich criteria [6].

Table 2. Sorption properties* of ZTV and ZSM sorbents as influenced by the concentration and pH

Sorbent	Sorbed ion	pH		c, M	K_d, ml g^{-1}
		initial solution	after sorption		
ZSM [3]	Cs^+	5.90	3.67	1×10^{-1}	9.52
		5.50	3.57	1×10^{-2}	186.70
	Co^{2+}	5.58	4.79	5×10^{-2}	4.25
		5.58	4.70	2×10^{-2}	6.43
		1.68**	1.68	5×10^{-2}	1.43
	Cu^{2+}	4.26	3.10	5×10^{-2}	4.79
		2.10***	2.00	5×10^{-2}	1.56
ZTV [2]	Zn^{2+}	–	1.90***	5×10^{-2}	3.00
		–	6.10	5×10^{-2}	10.40

* c is the concentration of the adsorbed ion and K_d is the distribution coefficient.

** Acidified with hydrochloric acid.

*** Acidified with sulfuric acid.

no sorption is observed from nitrate solutions. In the case of HZD, the sorption capacity with respect to transition metals is also determined by the kind of the anion. The same phenomenon was found for ZSM: The distribution coefficients of Co(II) and Cu(II) in sorption from sulfate solutions differ from those in sorption from chloride solutions. This difference in sorption on exchangers with the zirconium-oxygen matrix is probably due to the nature of the elements forming its functional groups and to the ion-dipole interaction of the sorbed ions with polar matrix.

Table 3. Sorption capacity of ZTV and ZSM sorbents as influenced by the electrolyte anion (electrolyte concentration 5×10^{-2} M)

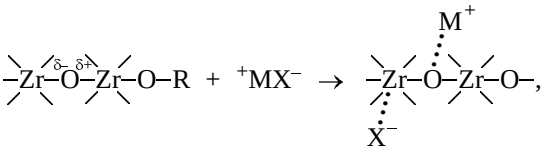
Sorbent	Electrolyte	pH		K_d, ml g^{-1}	Sorbent	Electrolyte	pH		K_d, ml g^{-1}
		initial solution	after sorption				initial solution	after sorption	
ZSM [3]	$CoSO_4$	3.78	3.20	9.7	ZTV* [2]	$CuSO_4$	4.15	3.66	21.8
	$CoCl_2$	5.58	4.70	6.4		$CuCl_2$	4.17	3.50	22.2
	$CuSO_4$	4.41	3.30	8.8		$CoSO_4$	4.88	3.37	16.4
	$CuCl_2$	4.26	3.10	4.8		$CoCl_2$	5.04	3.15	18.4

* ZTV was prepared from zirconium(IV) sulfate.

Table 4. Sorption capacity of ZSM and HZD sorbents as influenced by temperature (electrolyte concentration 5×10^{-2} M)

Sorbent	Sorbed ion	τ, h	Q, mmol g^{-1}, at indicated temperature, °C				
			20	40	50	65	80
HZD [4]	Cu^{2+}	6	0.92 ± 0.10	1.10 ± 0.1	–	–	1.48 ± 0.11
		12	1.03 ± 0.11	1.26 ± 0.12	–	–	1.79 ± 0.13
	Ni^{2+}	12	0.58 ± 0.06	0.48 ± 0.05	–	–	0.53 ± 0.05
	Pb^{2+}	6	0.13 ± 0.06	0.53 ± 0.05	–	–	No sorption
ZSM [3]	Cu^{2+}	5	0.50 ± 0.01	–	1.70 ± 0.01	2.80 ± 0.01	–

The contribution of the ion-dipole interaction is probably rather high, because the activity coefficients of sulfate solutions are smaller than those of nitrate and chloride solutions. As a result, although the sorption from nitrate and chloride solutions should seemingly be higher, the sorption capacity of the sorbent is actually higher in sulfate solutions owing to significant contribution of the ion-dipole interaction to the total sorption. The high polarity of the zirconium–oxygen matrix increases the dispersion interaction and promotes penetration of the electrolyte into the sorbent phase, i.e., the so-called molecular sorption proceeds and electrolyte interacts with the matrix dipoles by the ion-dipole mechanism. In this case, the sorption capacity is determined not only by the strength of binding between a cation and the negative end of the dipole of the matrix, but also by that between an anion and the positive end of the dipole. The complexing power of chloride and nitrate ions with respect to zirconium(IV) are similar, and their contribution to the molecular sorption are also similar. Complexes of zirconium(IV) with sulfate anions are significantly stronger. Since secondary sorption can proceed on the HSO_4^- groups, the stronger the complexes formed by sulfate anions with the sorbed cation, the stronger the sorption of cations from sulfate solutions. At the same time, the sorption capacity of ZTV sorbent is independent of the electrolyte anion (Table 3). Probably, formation of functional groups with a weaker electron-acceptor power diminishes the effective charge on zirconium(IV); as a result, interaction of the anion with Zr(IV) becomes weaker. The higher the electron-acceptor power of the functional group, the stronger the ion-dipole interaction. As compared to ZTV, the ion-dipole interaction of the ZSM matrix with the electrolyte ions is somewhat stronger, probably due to the functional groups containing Mo(VI) and Si(IV), which make the matrix somewhat more polar. The sorption by the ion-dipole mechanism can be represented as:



where R are the residues of molybdic, tungstic, phosphoric acids, and heteropoly acids.

Temperature is an important factor affecting the sorption properties of ion exchangers. A systematic study of the ion-exchange equilibrium as influenced by temperature was performed in [9]. The qualitative data on the effect of temperature on sorption of copper(II) ions on ZSM showed that, with the sorption temperature increasing from 20 to 65°C, the static capacity for copper(II) grows by nearly a factor of 5.6 [10]. An increase in the sorption capacity of HZD for copper with temperature was found in [4].

At the same time, at the temperature increases to above 40°C, the sorption of lead(II) sharply decreases. As for sorption of nickel(II) on HZD, no significant changes in the sorption capacity were observed in the entire temperature range studied (Table 4). It is difficult to explain the effect of temperature on the sorption capacity, because it is determined by the relative contribution of different sorption mechanisms, influenced by solvation (hydration), dissociation of the functional groups, etc. In our experiments, copper(II) was sorbed on HZD and ZSM from sulfate solutions, and nickel(II) and lead(II) on HZD, from nitrate solutions. Apparently, with increasing temperature, the ion-dipole interaction is enhanced, strengthening the bond between zirconium(IV) and sulfate ions; as a result, sorption of sulfate and, thus, copper(II) ions increases. Moreover, owing to close radii of Zr(IV) and Cu(II), copper ion can penetrate into the sorbent matrix, increasing the total content of copper in the exchanger phase.

Natural aging of ion exchangers based on zirconium(IV) depends on a particular sorbent. This is especially the case for the redox sorbents exhibiting both ion-exchange and redox properties. The ion-exchange properties of inorganic three-component redox sorbents based on zirconium(IV) are rather stable. For example, the sorption capacity for copper(II) of the ZSM sorbent remained unchanged even after storage for 3 years.

Our experimental data show that the sorption activity of EIEs based on zirconium(IV) is close to that of HZD type sorbents. These sorbents can be recommended as ion exchangers for sorption of single- and multicharged metal ions from solutions of various compositions.

CONCLUSIONS

(1) The sorption capacity of Zr(IV)-based sorbents with respect to Cu(II), Co(II), and Ni(II) depends on the concentration, pH, and temperature of the contacting solution.

(2) The decrease in pH in the course of sorption of Cu(II), Co(II) and Ni(II) ions on the electron and ion exchangers confirms the cation-exchange mechanism of sorption.

(3) The effect of the anion in the contacting solution depends on the chemical composition of the ion exchanger.

REFERENCES

1. Vinter, I.K., Synthesis and Study of an Inorganic Electron and Ion Exchanger Based on Zirconium(IV), Molybdenum(VI) and Phosphorus(V), *Cand. Sci. Dissertation*, Leningrad, 1970.
2. Kryuchkova, N.Ya., Synthesis and Study of Electron and Ion Exchangers Based on Zirconium(IV), Tungsten(VI), and Vanadium(V), *Cand. Sci. Dissertation*, Leningrad, 1980.
3. Bondarenko, T.S. and Boichinova, E.S., *Ionn. Obmen Ionom.*, 1996, no. 9, pp. 32–36.
4. Chernykh, O.A., Ion-Exchange Properties of Hydrated Zirconium Dioxide, *Cand. Sci. Dissertation*, Leningrad, 1972.
5. Pribil, R., *Komplexony v chemicke analyse*, Praha: Nakl. Ceskoslovenske akad., 1957.
6. Helfferich, F., *Ionenaustauscher*, Bd. 1, Weinheim: Chemie, 1959.
7. Kurilenko, O.D., *Kratkii spravochnik po khimii* (Brief Handbook on Chemistry), Kiev: Naukova Dumka, 1965.
8. Bondarenko, T.S., Boichinova, E.S., and Abovskaya, N.V., *Zh. Obshch. Khim.*, 1994, vol. 64, no. 5, pp. 708–713.
9. Soldatov, V.S. and Starobinets, G.L., *Issledovanie svoistv ionoobmennykh materialov* (Study of the Properties of Ion Exchangers), Chmutov, K.V., Ed., Moscow: Nauka, 1964.
10. Bondarenko, T.S. and Boichinova, E.S., *Sorbts. Khromatogr. Protsessy*, 2001, vol. 1, no. 3, pp, 478–480.

Russian Journal of Applied Chemistry, Vol. 78, No. 8, 2005, pp. 1270–1272. Translated from Zhurnal Prikladnoi Khimii, Vol. 78, No. 8, 2005, pp. 1292–1295.
Original Russian Text Copyright © 2005 by Sedelkin, Surkova, Denisova, Ramazaeva.

SORPTION AND ION-EXCHANGE PROCESSES

Adsorption of Amino Acids on Cellulose Diacetate Membranes

V. M. Sedelkin, A. N. Surkova, G. P. Denisova, and L. F. Ramazaeva

Engels Technological Institute, Saratov State Technical University, Engels, Saratov oblast, Russia

Received October 5, 2004; in final form, May 2005

Abstract—Adsorption of a series of amino acids on cellulose diacetate membranes was studied. Adsorption isotherms were constructed and thermodynamic characteristics of adsorption (chemical potential of the adsorbent and Gibbs energy) were determined.

In separating curdy whey albumin, a cellulose diacetate (CA) membrane retains soluble and other dispersed particles for several reasons, including the adsorption on the membrane surface. The contribution of this process is not clearly understood yet.

Flory and Huggins were first who derived, using statistical thermodynamics, theoretical relationships that take into account these effects, with certain assumptions made, for highly elastic polymers in athermic or quasiathermic processes. At the same time, glassy polymers characterized by S-shaped sorption isotherms cannot be described in the framework of this theory. Until now, a considerable success has been achieved in the development of the physicochemical theory of adsorption through application of thermodynamic, semiempirical, and empirical approaches to description of the formal statics of sorption. The most rigorous approaches are based on the osmotic and stoichiometric theories of adsorption. The consequences of these theories for swellable polymers with nearly zero porosity are presented in [1]. The adsorption on swellable porous sorbents, e.g., in baromembrane processes has been studied to a lesser extent [1, 2]. In particular, this is true for cellulose acetate membranes, which are widely used in processing of dairy products [3]. In this study, we examined the adsorption properties of cellulose diacetate membranes with respect to a series of amino acids.

EXPERIMENTAL

To improve the efficiency of utilization of curdy whey, we experimentally studied the adsorption from model systems containing amino acids (isoleucine, threonine, phenylalanine, methionine, lysine, and valine) on CA membranes. The membranes were produced from a 10% solution of cellulose diacetate in aqueous–acetone mixtures (95 : 5 by volume) using dry-wet formation procedure. The solution was placed in a specially designed cylindrical mold with a face ground-in to a glass plate. Acetone was evaporated for 12 h at 20 ± 2°C in a draft, using a draft hood for acetone recovery. In this way, we prepared isotropic membranes with a 0.05–0.8-μm filtering layer (commercial CA ultrafiltration membranes, e.g., UAM-500, have a filtering layer of 0.01–0.05 μm) and a through-pore diameter of 0.01–0.1 μm (0.03 μm in the case of UAM-500). The membrane thickness and pore size were varied by adjusting the concentration and volume of the initial CA solution. The resulting UAM-SF membranes (dry-wet formation ultrafiltration cellulose diacetate membranes) were tested in separating curdy whey albumin. The ultrafiltration was carried out on a laboratory unit at a pressure of 0.15 MPa and 20°C. The permeability of the membranes to distilled water was 2.6–2.8 $l\,m^{-2}\,min^{-1}$, and to curdy whey, 0.72–1.0 $l\,m^{-2}\,min^{-1}$; the selectivity with respect to curdy whey albumin was 70–72%.

In practice, the separation processes are performed in aqueous solutions. Therefore, we subjected the membranes to swelling in distilled water for 10 h prior to the experiments. Then the membranes were immersed in solutions of amino acids.

The adsorption was determined interferometrically. The error of determination of the refractive index was 1×10^{-4} [1, 2]. In the static experiments, the specific adsorption (amount of adsorbed substance per gram of adsorbent) was estimated by Eq. (1):

$$n = \frac{c_0 - c_1}{m} V, \qquad (1)$$

1070-4272/05/7808-1270 © 2005 Pleiades Publishing, Inc.

Table 1. Amino acid concentrations in the initial solutions

Initial solution c, mg l^{-1}	c_0, mole fraction					
	isoleucine	threonine	phenylalanine	methionine	lysine	valine
0.48	0.0037	0.0040	0.0030	0.0032	0.0033	0.0041
0.8	0.0061	0.0067	0.0048	0.0054	0.0055	0.0068
1.12	0.0085	0.0094	0.0068	0.0075	0.0077	0.0096
1.6	0.0122	0.0134	0.0097	0.0107	0.0109	0.0137
4.0	–	–	–	0.0120	–	–

Table 2. Adsorption of amino acids on AC membranes

Initial solution c, mg l^{-1}	c_1, mg l^{-1}					
	isoleucine	threonine	phenylalanine	methionine	lysine	valine
0.48	0.34	0.31	0.29	0.37	0.32	0.31
0.8	0.72	0.63	0.62	0.73	0.67	0.67
1.12	0.98	0.92	0.91	0.97	0.93	0.93
1.6	1.43	1.39	1.38	1.45	1.41	1.41
4.0	–	–	–	0.0120	–	–

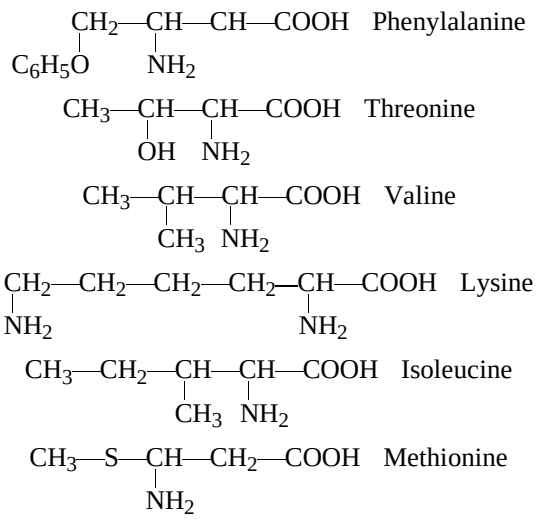
where c_0 and c_1 are the initial and equilibrium solution concentrations (M); m, weight of the adsorbent sample (g); and V, solution volume (l).

The initial concentrations of amino acids, c_0, were selected taking into account their solubility (Table 1).

It was demonstrated that 24 h is a sufficient time for the adsorption equilibrium to be attained in the cases of isoleucine and methionine (Fig. 1a). Similar results were obtained for the other amino acids.

In the adsorption experiments, the equilibrium concentrations of amino acids were estimated from the experimental optical densities of the solutions (Table 2).

The adsorption of amino acids decreases in the order



The presence of two amino groups as well as of sulfur in the backbone decreases the adsorption on CA membranes.

Figure 1b shows the adsorption isotherms at 20°C for three amino acids (isoleucine, threonine, and phenylalanine). All of them are S-shaped. Similar isotherms were obtained for the other amino acids

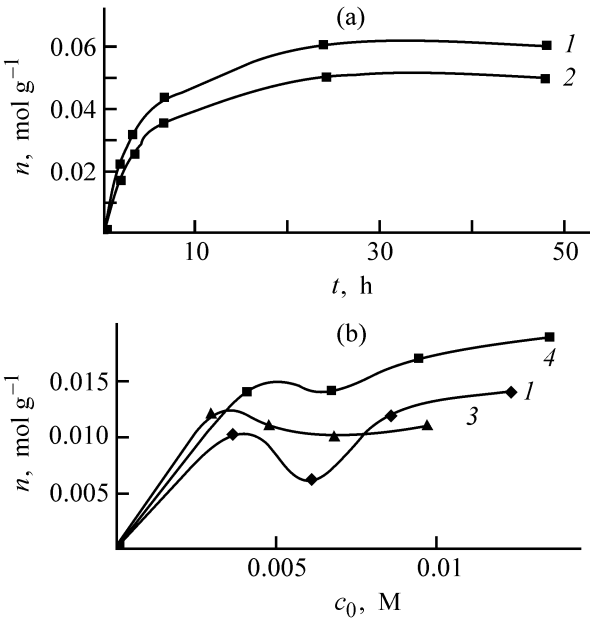


Fig. 1. Adsorption n vs. (a) adsorption time τ and (b) solution concentration c_0: (*1*) isoleucine, (*2*) methionine, (*3*) phenylalanine, and (*4*) threonine.

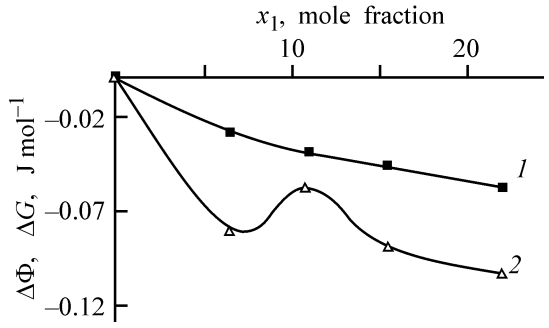


Fig. 2. (*1*) Chemical potential of the sorbent $\Delta\Phi$ and (*2*) Gibbs energy ΔG vs. the solution concentration x_1 in the system threonine–CA membrane.

studied. Arbitrarily, the isotherms could be divided into three groups. In the initial stage of adsorption, the amino acids form monolayers on the membrane surface. The decrease in the adsorption with increasing concentration of the amino acid can be attributed to its reorientation in the adsorption layer, which is particularly clearly pronounced for threonine containing a hydroxy group. With the concentration increasing further, the adsorption noticeably grows, which is probably due to formation of the second and next layers. For isoleucine, as a less adsorbable amino acid, this stage is not pronounced. We found no correlation between the adsorption and molecular weight of the amino acids.

We analyzed the experimental data using excess Gibbs functions [4]. Adsorption is accompanied by a decrease in the free energy of the system. We estimated the free Gibbs energy ΔG and the chemical potential of the sorbent $\Delta\Phi$ in the systems in hand. The change in the chemical potential of the sorbent can be written as

$$\Delta\Phi = \Phi_{x_1} - \Phi_{x_2} = RT\int_0^x \frac{n}{x(1-x)}\,dx_1,$$

where $R = 8.314$ J mol^{-1} K^{-1}; T, temperature (K); n, adsorption (mol g^{-1}); and x_1, mole fraction of the component (initial concentration).

The change in the free energy can be found as the difference between the free energies of the system before and after brinding the adsorbent in contact with the solution:

$$\Delta G = -(\Phi_x - \Phi_X) + n_0 RT\sum_{n=1}\left(x_i \ln\frac{X}{x}\right),$$

where $X_i = 0.1n_1 + x_i$, $n_0 = 10$.

Using the calculated data, we constructed the concentration dependences of the chemical potential of the sorbent $\Delta\Phi$ and of the free Gibbs energy ΔG for the system constituted by threonine and the CA membrane at 293 K over the entire experimental concentration range (Fig. 2). The calculations were also done for the other investigated systems amino acid and the CA membrane. Our results show that the chemical potential of the sorbent and the free Gibbs energy of the systems decrease with increasing amino acid content in the solution.

Finally, in separating curdy whey albumin on CA membranes, adsorption of the protein containing the amino acids investigated on the membrane surface can contribute to the process efficiency.

CONCLUSIONS

(1) Adsorption of a series of amino acids (isoleucine, threonine, phenylalanine, methionine, lysine, and valine) on the surface of cellulose diacetate membranes was studied. The adsorption isotherms were constructed and the thermodynamic characteristics of adsorption (chemical potential of the adsorbent and Gibbs free energy) were determined.

(2) The adsorption of amino acids on cellulose diacetate membranes depends on the structure of an amino acid. Two amino groups and sulfur in the backbone decrease the adsorption.

REFERENCES

1. Tolmachev, A.M., *Zh. Fiz. Khim.*, 1978, vol. 52, no. 3, p. 105.
2. Kiselev, A.V. and Shikalova, I.V., *Zh. Anal. Khim.*, 1956, vol. 30, no. 1, pp. 94–108.
3. Fetisov, E.A. and Chagorovskii, A.P., *Membrannye molekulyarnositovye metody pererabotki moloka* (Membrane Molecular-Sieve Methods for Milk Processing), Moscow: Agropromizdat, 1991.
4. Gibbs, J.W., *The Collected Works of J. Willard Gibbs*, New Haven: Yale Univ., 1948.

Russian Journal of Applied Chemistry, Vol. 78, No. 8, 2005, pp. 1273–1275. Translated from Zhurnal Prikladnoi Khimii, Vol. 78, No. 8, 2005, pp. 1296–1298.
Original Russian Text Copyright © 2005 by Shaglaeva, Amosova, Shaulina, Golentovskaya, Sultangareev, Pinigina.

SORPTION AND ION-EXCHANGE PROCESSES

Divinyl Sulfide–4-Vinylpyridine Copolymer as an Effective Sorbent for Mercury

N. S. Shaglaeva, S. V. Amosova, L. P. Shaulina, I. P. Golentovskaya, R. G. Sultangareev, and O. P. Pinigina

Favorskii Institute of Chemistry, Siberian Division, Russian Academy of Sciences, Irkutsk, Russia

Irkutsk State University, Irkutsk, Russia

Received May 19, 2005

Abstract—The sorption power of divinyl sulfide–4-vinylpyridine copolymer toward Hg(II) ions was studied. The influence of the kind and concentration of an acid on the sorption characteristics is examined. Mechanisms of the interaction of the active sorption centers of the copolymer with Hg(II) ions are discussed.

Polymeric complexing sorbents are successfully used for determining low concentrations of toxic heavy metals in multicomponent samples. With such sorbents, the effect of the sample matrix is substantially weaker, and the detection limit of the target components is lower [1]. The use of divinyl sulfide as a cross-linking agent allows preparation of porous polymers resistant to acids, and the sulfur atom exhibiting donor properties affects the sorption characteristics [2, 3].

In this study, we examined the properties of a new sorbent, a divinyl sulfide–4-vinylpyridine copolymer, toward Hg(II) ions.

Divinyl sulfide (DVS) was prepared according to [4] and was distilled just before use. Commercial 4-vinylpyridine (VP) was purified by repeated vacuum distillation. The purity of the monomers was monitored chromatographically.

Radical copolymerization was performed in ampules in the presence of AIBN at 60°C. Insoluble DVS–VP copolymers were washed with solvents (benzene, acetone, water) and dried to constant weight in a vacuum. The compositions of the copolymers were found by elemental analysis. The degree of swelling of DVS–VP copolymers was determined gravimetrically. The IR spectra were measured for KBr pellets or mulls in mineral oil on an IFS-25 spectrometer.

The sorption of Hg(II) ions from aqueous solutions was studied in a static mode at room temperature. Mercury(II) was taken as a nitric acid solution with the initial Hg(II) concentration of 2.79 mg ml^{-1}. The solid phase was separated by filtration, and the residual Hg(II) concentration in solution was determined by an extraction-photometric procedure [5].

The DVS–VP copolymers were obtained as yellow powders stable in prolonged storage and insoluble in organic solvents and solutions of acids and alkalis. The copolymerization results are listed in Table 1.

Table 1. Copolymerization of DVS with VP (AIBN concentration 0.5 wt %, 60°C, 6 h)

Copolymer no.	Initial mixture composition, mol %		Content, wt %		Copolymer composition, mol %		Yield, %
	VP	DVS	N	S	VP	DVS	
1	20.00	80.00	5.01	23.42	32.11	67.89	65
2	40.10	59.90	7.90	16.83	54.36	45.64	75
3	50.00	50.00	8.78	12.67	61.23	38.77	92
4	80.00	20.00	12.11	3.45	88.75	11.25	80

1070-4272/05/7808-1273 © 2005 Pleiades Publishing, Inc.

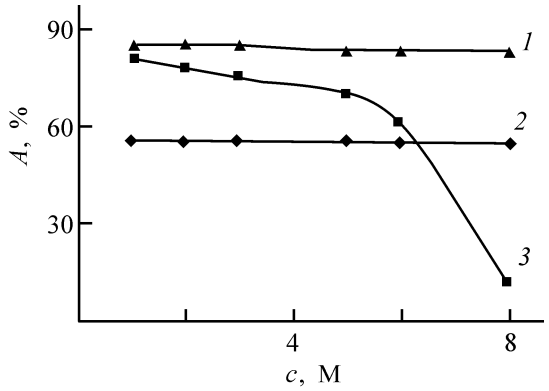


Fig. 1. Influence of the kind and concentration c of acid on the recovery of Hg(II) ions, A, from solutions. m_{sorb} = 10 mg, $m_{Hg^{2+}}$ = 5.6 mg, sorption time 2 h. Acid: (*1*) H_2SO_4, (*2*) HNO_3, and (*3*) HCl; the same for Fig. 2.

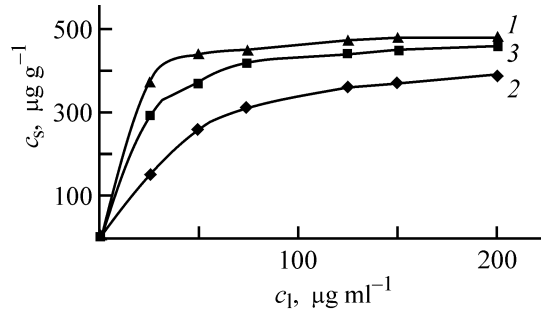
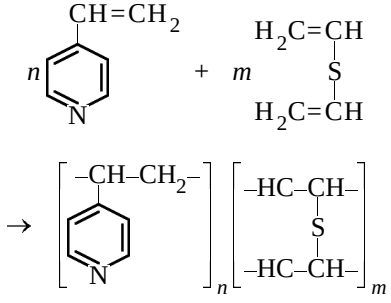


Fig. 2. Curves of equilibrium distribution of Hg(II) at its different concentrations in 1 M acids. m_{sorb} = 10 mg, sorption time 2 h. Hg(II) concentration: (c_l) in solution and (c_s) in the solid phase.

The IR spectra of the copolymers contain no bands characteristic of the VP vinyl group (1640 cm^{-1}), but the pyridine absorption bands (1600, 1555, 1490, 1068 cm^{-1}) remain unchanged. The band at 660 cm^{-1} is assignable to the C–S stretching vibrations.

Calculation of the copolymer compositions from the N and S contents gave reasonably consistent results.

The formation of the insoluble product, as well as the IR spectra and analytical data, suggest that the copolymerization of DVS with VP involves cleavage of two double bonds in DVS, yielding a network copolymer:

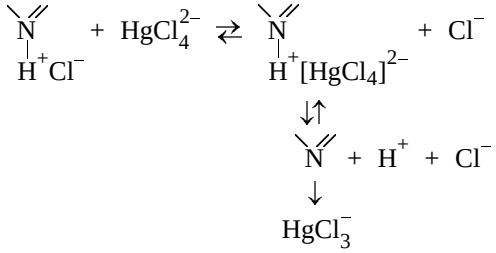


The resulting copolymers swell in organic solvents (to 500% in acetone and 300% in hexane).

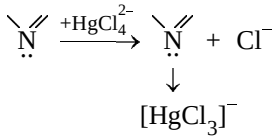
Copolymer no. 3 (Table 1) in the preliminary tests showed the highest activity in the sorption of Hg(II) ions from aqueous solutions. Therefore, this copolymer (38.77 mol % divinyl sulfide units) was chosen for a more detailed study of the sorption characteristics. The sorption equilibrium in solution was attained in 2 h, with the sorption half-time being 10–15 min.

To find the optimal sorption conditions, we studied the sorption of Hg(II) from HNO_3, H_2SO_4, and HCl solutions in relation to the acid concentration (Fig. 1). We found that the recovery of Hg(II) was virtually independent of the concentrations of HNO_3 and H_2SO_4 (Fig. 1, curves *1*, *2*). At the same time, with increasing concentration of HCl, the sorption activity drastically decreased (Fig. 1, curve *3*). These trends are associated with the sorption mechanism. From HNO_3 and H_2SO_4 solutions, the sorption occurs through donor–acceptor interaction of Hg(II) with both S and N atoms. At the same time an ion-exchange sorption mechanism becomes operative in HCl solutions, in which anionic chloride complexes are formed, and at high HCl concentrations the sorption is suppressed because of the competing effect of chloride ions. However, the coordination interaction is also possible along with the ion-exchange interaction.

To confirm the sorption mechanism, we recorded the IR spectra of the initial sorbents, sorbents treated with acids, and the concentrates. We found that the band at 1600 cm^{-1} in the spectrum of the initial copolymer shifted to 1630 cm^{-1} in going to the concentrate and acid-treated sorbent. This shift points to protonation of the N atom with the formation of the pyridinium ion, or to a coordination interaction of this atom with a metal ion. As shown in [6], sorption of metals that occur in solutions in the form of anionic complexes involves first anion exchange and then coordination. Thus, the ionic interaction is followed by the displacement of the chloride ion from the first coordination sphere of the metal:



The sorption on the nonprotonated form occurs exclusively as replacement of chloride ions with the ligand groups of the copolymer:



To estimate the sorption capacity, we studied the equilibrium distribution of mercury between the solid phase and solutions of Hg(II) in 1 M acids (Fig. 2). From the sorption isotherms, we determined the sorption capacities of the polymer and distribution coefficients of Hg(II) (Table 2).

The sorption capacities show that the copolymer is highly active toward Hg(II) ions. It effectively takes up Hg(II) from sulfuric and hydrochloric acid solutions (SC 480 and 460 mg g^{-1}, respectively). The relatively high distribution coefficients, especially in HCl solution, show that the sorbent can recover trace amounts of Hg(II) from solution.

Iron(II), cobalt(II), nickel(II), and zinc(II) ions are not sorbed under the conditions of Hg(II) recovery, but copper(II) ions are sorbed.

The applicability of a sorbent is largely determined by the possibility of the metal desorption from the concentrate, allowing regeneration of the sorbent.

As can be seen from Fig. 1, the recovery of Hg(II) decreases with increasing concentration of HCl, to become as low as 12% in 8 M HCl. Therefore, we examined the possibility of mercury desorption with various volumes of 9 M HCl at various treatment times. We found that 5 ml of 9 M HCl desorbs 65% of Hg(II) from the concentrate, and 10 ml of 9 M HCl desorbs Hg(II) quantitatively within 30 min.

We also examined the possibility of recycling the sorbent. After a sorption cycle, the sorbent was regenerated by treatment with 9 M HCl, washed with distilled water, dried, and reused for the sorption of Hg(II) ions under the optimal conditions. In four cycles, the recovery of Hg(II) was 56–49% at the initial Hg(II) concentration of 2.5 mg in 20 ml.

The stable high performance of the sorbent after the desorption may be due to the elasticity of the cross-linking fragment (DVS). When a mercury(II) atom is coordinated, a sort an energy cell is formed in the vicinity of the S atom; the parameters of this cell match the characteristics of Hg(II) ions only [7], and, apparently, the introduction and removal of Hg(II) ions can occur repeatedly.

Table 2. Sorption capacities of the copolymer and distribution coefficients of Hg(II) in sorption from 1 M acids

Acid	Sorption capacity (SC), mg g^{-1}	Distribution coefficient *D*, cm^3 g^{-1}
HNO_3	380	4.5×10^3
H_2SO_4	480	6.0×10^3
HCl	460	1.6×10^4

CONCLUSIONS

(1) A divinyl sulfide–4-vinylpyridine copolymer containing 38.77 mol % divinyl sulfide units was prepared by radical copolymerization of the monomers.

(2) It was found that the copolymer has a high sorption capacity for Hg(II) ions and can recover trace amounts of Hg(II) from solutions.

(3) It was shown that the sorption activity of the copolymer is fully restored after its regeneration with 9 M HCl.

REFERENCES

1. Myasoedova, G.V. and Savvin, S.B., *Khelatoobrazuyushchie sorbenty* (Chelating Sorbents), Moscow: Nauka, 1984.
2. Golentovskaya, I.P., Kirillov, I.I., *et al.*, *Izv. Vyssh. Uchebn. Zaved., Khim. Khim. Tekhnol.*, 1982, vol. 25, no. 10, pp. 37–38.
3. Golentovskaya, I.P., Shaulina, L.P., *et al.*, *Izv. Vyssh. Uchebn. Zaved., Khim. Khim. Tekhnol.*, 1985, vol. 28, no. 2, pp. 56–59.
4. Trofimov, B.A. and Amosova, S.V., *Divinilsul'fid i ego proizvodnye* (Divinyl Sulfide and Its Derivatives), Novosibirsk: Nauka, 1983.
5. Marczenko, Z., *Kolorymetryczne oznaczanie pierwiastkow*, Warsaw: Naukowa-Techniczne, 1968.
6. Saldadze, K.M. and Kopylova-Valova, V.F., *Kompleksoobrazuyushchie ionity* (Complexing Ion Exchangers), Moscow: Khimiya, 1980.
7. Krakhmalets, I.A., Synthesis and Properties of Ion Exchangers and Sorbents Based on Copolymers of Monovinyl Monomers and Divinyl Sulfide, *Cand. Sci. Dissertation*, Kemerovo, 1980.

Russian Journal of Applied Chemistry, Vol. 78, No. 8, 2005, pp. 1276–1279. Translated from Zhurnal Prikladnoi Khimii, Vol. 78, No. 8, 2005, pp. 1299–1302.
Original Russian Text Copyright © 2005 by Lebedev, Brusakov, Shkuryakov.

APPLIED ELECTROCHEMISTRY AND CORROSION PROTECTION OF METALS

Express Monitoring of $MgCl_2$ Concentration in the Electrolyte of Magnesium Electrolyzers

O. A. Lebedev, I. Yu. Brusakov, and N. P. Shkuryakov,

St. Petersburg State Electrotechnical University, St. Petersburg, Russia

Received May 12, 2005

Abstract—A method and apparatus were developed for express monitoring of the $MgCl_2$ concentration in a molten electrolyte and of the temperature conditions in electrolytic manufacture of magnesium.

In electrolytic production of magnesium from chloride melts, the most significant influence on the technological parameters of the process is exerted by the electrolyte temperature and the concentration of magnesium chloride in a melt [1, 2]. Therefore, the technological schedule of the electrolysis process includes a systematic monitoring of the above parameters in order to control the processing conditions. The working temperature of the electrolyte is measured three or four times a day with a displaceable Chromel–Alumel thermocouple and a millivoltmeter,[1] and the electrolyte samples are taken and then analyzed by a chemical laboratory for the content of magnesium chloride and, if necessary, other components of the electrolyte.

The main drawback of the existing monitoring system is the long lag (several hours) between the time of sampling of the electrolyte and that when the results of analysis are obtained, which makes virtually impossible any online control over the processing conditions.

The difficulties encountered in maintaining the optimal processing conditions (with a simultaneous on-line monitoring of the efficiency of separate electrolyzers) are strongly aggravated if magnesium is manufactured by electrolysis in the flow-line mode. In this case, the current efficiency is taken into account as a batch-average, because doing so for each electrolyzer is impossible. The temperature conditions in separate electrolyzers are largely equalized owing to circulation of the electrolyte between electrolyzers via overflow channels.

[1] Fixed Chromel–Alumel thermocouples can also be installed in the electrolyzers, with their signals displayed at the central control panel.

A method and the corresponding apparatus were developed for determining the magnesium chloride concentration in the electrolyte 3–4 min after electrolyte sampling.

The method developed consists in the following. A melt sample taken with a special sampler is allowed to cool in air, which makes it possible to measure the cooling curve of the electrolyte and to determine the liquidus temperature. The working temperature is accurately recorded immediately after extracting a sample.

The concentration of magnesium chloride is determined using the formula:

$$c = c_0 - (T_l - T_{l.r})/K, \quad (1)$$

where c is the magnesium chloride concentration (wt %) in the electrolyte sample; c_0, magnesium chloride concentration (wt %) at the liquidus temperature of the electrolyte, taken as the reference point; T_l, liquidus temperature of the working electrolyte (°C); $T_{l.r}$, liquidus temperature of the electrolyte, taken as the reference point (°C); and K, coefficient that is found from the ternary fusibility diagram of the KCl–NaCl–$MgCl_2$ system as a function of the KCl : NaCl ratio in the working electrolyte and characterizes the extent to which the liquidus temperature depends on the magnesium chloride concentration (°C / %).

It should be emphasized that K is mostly affected by such components of the electrolyte as NaCl and KCl, whereas the effect produced by $CaCl_2$ and CaF_2 additives is insignificant. A study of the regions with 15–5 wt % $MgCl_2$ in the KCl–NaCl–$MgCl_2$ ternary diagram [3, 4] at various KCl : NaCl ratios

1070-4272/05/7808-1276 © 2005 Pleiades Publishing, Inc.

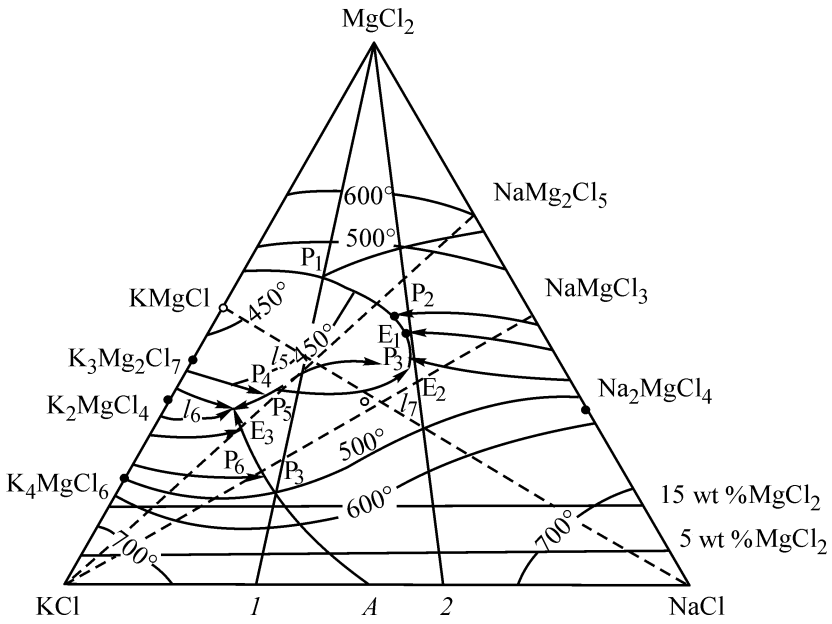


Fig. 1. Fusibility diagram of the system KCl–NaCl–$MgCl_2$. Electrolyte: (*1*) potassium and (*2*) sodium–potassium.

in the working electrolytes led to a conclusion that the dependence of the liquidus temperature on the $MgCl_2$ concentration is nearly linear, which predetermined the type of Eq. (1).

Figure 1 shows the fusibility diagram for the KCl–NaCl–$MgCl_2$ system [4]. The $MgCl_2$–*1* line corresponds to variation of the $MgCl_2$ concentration during electrolysis of the so-called potassium electrolyte with a KCl : NaCl ratio of ~3 (by mass). The $MgCl_2$–*2* line corresponds to electrolysis of a sodium–potassium electrolyte with a KCl : NaCl ratio of ~0.8–1.0 (by mass). The lines corresponding to variation of the $MgCl_2$ concentration from 15 to 5 wt % are also plotted in Fig. 1.

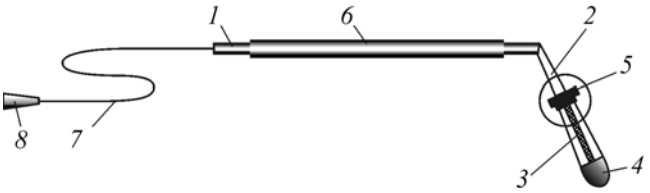


Fig. 2. Measuring probe. (*7*) Connection cable and (*8*) connector; [for explanation of (*1*–*6*, see text].

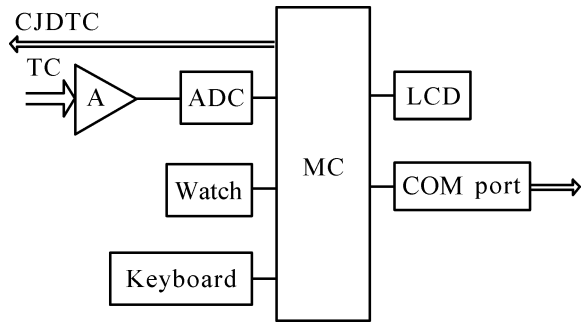


Fig. 3. Block diagram of the electronic unit. (CJDTC) cold junction of a differential thermocouple, (TC) thermocouple, (A) amplifier, (ADC) analog-to-digital converter, (MC) microcontroller, (LCD) liquid-crystal display, (COM port) connection to a computer.

A system for express determination of the magnesium chloride concentration in the electrolyte of a magnesium electrolyzer [5] comprises two main subsystems: (1) a probe with a sensor and sampler (Fig. 2) and (2) an electronic unit (Fig. 3).

The major element of the probe is pipe *1*, to which pipe *2* is jointed, with a cable thermocouple *3* passed through the pipes. The cold junction of the thermocouple is fixed within the unit serving for compensation of the cold junction temperature (not shown in Fig. 2), which is situated at the left-hand (in figure) end of pipe *1*. The working junction of the thermocouple is placed within sampler *4* and secured against a shift in the mounting unit *5*.

Operator's handle *6* serves as a probe extender and an insulator to improve the safety of the operator. It can be freely moved along pipe *1* and fixed in a desired position with a tightening nut.

The absolute error in determining the liquidus temperature does not exceed ±2°C, and the resolution in measuring the points of the cooling curve is 0.1°C.

c_{MgCl_2} is determined with an error not exceeding 0.5% at a resolution of 0.1%.

The apparatus is $110 \times 100 \times 40$ mm in size and has a weight of 0.7 kg.

In sampling the melt, the electronic unit records the working temperature of the electrolyte, determined by the thermocouple, and then the temperature measured at prescribed intervals of time, and the values obtained are loaded into the memory of a computer. Simultaneously, the electronic unit analyzes the resulting temperature curve to find the inflection point, which is recorded as the liquidus temperature of electrolyte, and, based on the prescribed values of K, c_0, and $T_{l.r}$, indicates the magnesium chloride concentration on an LCD.

The apparatus design developed was first tested in laboratory conditions on synthetic electrolytes of the $MgCl_2$–KCl–NaCl system for a long time. In the concentration range 5–10%, the difference in the $MgCl_2$ concentrations measured by the apparatus and determined by chemical analysis of the electrolyte did not exceed 0.3–0.5% (see table).

The apparatus was successfully tested in industrial electrolyzers at the Solikamsk Magnesium Plant (SMP) and Berezniki Titanium-Magnesium Plant.

In Solikamsk, the apparatus was tested on four diaphragmless electrolyzers with carnallite feeding. It was established that at high concentrations of $MgCl_2$ in the electrolyte (~14–15%), which occurred after the main filling, the discrepancy between the values measured by the apparatus and those furnished by chemical analysis of electrolyte samples at the central laboratory of the plant is about 2%. As the $MgCl_2$ concentration in the electrolyte is lowered to 9–10% and 6–7% %, the discrepancy becomes 0.6–0.8 and 0.2–0.3%, respectively.

The wider discrepancy at 14–15% $MgCl_2$ can be accounted for by a deviation of the dependence of the liquidus temperature on the $MgCl_2$ concentration from linearity in these regions of the fusibility diagram. A certain role was played by the fact that the apparatus was calibrated for the KCl : NaCl ratio, which was somewhat different from that in the SMP electrolytes. The time necessary for an analysis with the apparatus is 2–3 min.

An appropriate adjustment of the apparatus software to measurements at concentrations of 15–10% $MgCl_2$ showed that the values measured deviate from the data of chemical analysis by no more than 0.2% over the entire concentration range (5–15%)

Results of the study

Run no.	$MgCl_2$ concentration, wt %	
	results of analysis	measured by apparatus
Potassium electrolyte, KCl : NaCl = 3		
1	5.2	5.1
2	6.8	7.0
3	7.6	8.0
4	10.3	10.8
Sodium–potassium electrolyte, KCl : NaCl = 0.8–1.0		
5	4.8	4.7
6	6.8	7.0
7	8.3	8.6
8	9.85	10.3

Measurements were also made on diaphragmless electrolyzers with magnesium chloride feeding, for which the KCl : NaCl ratio differed for an even greater extent from the calibration ratio as compared with the potassium electrolytes used at SMP. Nevertheless, the apparatus demonstrated a clearly pronounced tendency toward variation of the $MgCl_2$ concentration with time on separate electrolyzers, with a certain systematic difference between the data furnished by the device and the results of a chemical analysis.

The tests showed that, with a certain modification, the apparatus can successfully operate in electrolyzers with magnesium chloride feeding.

The main advantage of the apparatus developed is that the loss of $MgCl_2$ with spent electrolyte can be substantially reduced when working with carnallite. According to the technological schedule, the concentration of $MgCl_2$ in a spent electrolyte discharged from electrolyzer baths should not exceed 5%. However, this value is frequently as high as 6–7% in actual practice.

The express determination of the $MgCl_2$ concentration will make it possible to strictly satisfy the technological requirements and to diminish the loss of $MgCl_2$ with spent electrolyte.

The apparatus will be rather useful for analysis of electrolyzers in the start-up period (in the case of separate feeding with raw materials) and for a comparative analysis, based on loss of $MgCl_2$, of the influence exerted by various parameters (electrolyte temperature, draw-off flow from the cathode, $MgCl_2$ concentration in the working electrolyte, and concentration of F^- ions) on the technical and economical efficiency of the electrolysis process.

Use of the apparatus in a flow-line mode will allow an on-line control of the current efficiency and fast determination of the working efficiency both for any separate electrolyzer and for the entire production line [6]. For this purpose, it is necessary to measure the temperature and concentration of magnesium chloride with samplers (equipped with thermocouples connected to an electronic unit) installed at the inlet of each electrolyzer of the production line and at the outlet of the last electrolyzer.

The samplers are mechanically extracted with a pneumatic system (or in some other way) on a prescribed schedule. Then, the cooling rate of the electrolyte is analyzed by the electronic unit, and the current efficiency in each electrolyzer is determined by the formula:

$$\eta = a\eta_\Sigma / b, \quad (2)$$

where η is the current efficiency of a given electrolyzer (%); a, difference between the magnesium chloride concentrations at the inlet and outlet of the given electrolyzer (%); η_Σ, current efficiency averaged over all the electrolyzers of the production line (%); b, difference between the magnesium chloride concentrations at the inlet of the head electrolyzer and at the outlet of the last electrolyzer, divided by the number of electrolyzers in the line (%).

Mounting mechanically extractable samplers with thermocouples on all electrolyzers of a production line will make it possible to feed the signals of the thermocouples into the electronic unit at the central control panel, which is successively connected to the samplers of different electrolyzers on a prescribed schedule.

REFERENCES

1. Lebedev, O.A., *Proizvodstvo magniya elektrolizom* (Manufacture of Magnesium by Electrolysis), Moscow: Metallurgiya, 1988.
2. Shchegolev, V.I. and Lebedev, O.A., *Elektroliticheskoe poluchenie magniya* (Eletrolytic Production of Magnesium), Moscow: Ruda i Metally, 2002.
3. Orekhova, A.I., Physicochemical Foundations of a Technique for Dehydration of Magnesium Chloride Raw Materials, *Doctoral Dissertation*, Leningrad: 1984.
4. Podlesnyak, N.P., Orekhova, A.I., and Dieva, E.N., *Izv. Vyssh. Uchebn. Zaved. Tsvet. Metall.*, 1987, no. 4, pp. 105–106.
5. RF Patent no. 2204630.
6. RF Patent no. 2238350.

Russian Journal of Applied Chemistry, Vol. 78, No. 8, 2005, pp. 1280–1282. Translated from Zhurnal Prikladnoi Khimii, Vol. 78, No. 8, 2005, pp. 1303–1305.
Original Russian Text Copyright © 2005 by Demidov, Kokhatskaya,Sun Lyu Bin.

APPLIED ELECTROCHEMISTRY AND CORROSION PROTECTION OF METALS

Determination of Residual Alkalinity in Positive and Negative Electrodes of a Worked-out Nickel–Iron Battery

A. I. Demidov, M. S. Kokhatskaya, and Sun Lyu Bin

St. Petersburg State Polytechnic University, St.Petersburg, Russia

Received May 12, 2005

Abstract—The content of sodium carbonate and sodium hydrocarbonate in the active paste of the positive and negative electrodes of a worked-out nickel–iron battery after their prolonged storage in air was determined by means of a conductometric analysis.

Nickel–iron battery suggested by Edison at the beginning of the last century belongs to alkaline lamellar cells, in which potassium and sodium hydroxide solutions with a reasonably high electrical conductivity in a wide temperature range are commonly used as electrolytes [1]. The use of the sodium electrolyte is due to its favorable influence on the nickel oxide electrode at elevated temperatures. The potassium electrolyte is preferable at low temperatures owing to its higher electrical conductivity and lower freezing point [2]. The drawback of alkaline electrolytes is their susceptibility to carbonization, which mainly occurs via absorption of atmospheric carbon dioxide and results in accumulation of a carbonate in the electrolyte in the course of operation of a battery [1].

Prolonged storage of positive and negative electrodes of worked-out nickel–iron batteries in air leads to further carbonization of the electrolyte remaining in pores of the active paste. As a result, sodium hydroxide is converted into carbonate and then hydrocarbonate by the reaction:

$$2NaOH + CO_2 \rightarrow Na_2CO_3 + H_2O,$$
$$Na_2CO_3 + H_2O + CO_2 \rightarrow 2NaHCO_3.$$

In hydrometallurgical processing of worked-out electrodes of nickel–iron batteries, it is necessary to know the residual content of carbonate and bicarbonate in the active paste, because their amount affects the expenditure of sulfuric acid for recovery of positive electrodes containing nickel hydroxide and the quality of the active paste of the negative electrode, obtained in processing.

In this study, the content of sodium carbonate and bicarbonate in the active paste of the positive and negative electrodes of a worked-out nickel–iron battery was determined by conductometric titration.

Titration, which underlies the classical titrimetric analysis, is a virtually versatile technique widely applied in physicochemical analytical techniques. In these methods, the electrical parameters of the systems being analyzed, which change as a result of chemical reactions, are measured and recorded [3]. To these techniques belongs conductometric titration, in which the equivalence point is found by measuring the change in the electrical conductivity of a solution during the reaction of the titrant with the substance to be determined. The equivalence point is determined from the sharp break in a titration curve, which reflects the change in the electrical conductivity of the solution being analyzed upon addition of a titrant in the course of titration [4].

We used in the study the active paste extracted from lamellas of a worked-out nickel–iron battery of the TNZh-250-U2 type and chemically pure sulfuric acid. The content of carbonate and hydrocarbonate in the active paste of the worked-out electrodes kept in contact with air for a long time was determined by conductometric titration of the filtrate obtained upon treatment of the active paste with distilled water. In the course of the experiment, the solution was vigorously agitated with a magnetic stirrer and its resistance was measured using an E7-15 immittance meter with the use of graphite electrodes. No less than 5–7 experiments were carried out in parallel.

During the titration of a filtrate containing sodium carbonate and hydrocarbonate with a standard solution of sulfuric acid, first, sodium carbonate reacts with the strong acid to yield sodium hydrocarbonate and sulfate. Then, sodium bicarbonate contained in the ini-

1070-4272/05/7808-1280 © 2005 Pleiades Publishing, Inc.

tial solution and sodium carbonate obtained in titration are neutralized to give sodium sulfate.

To construct the theoretical dependence of the electrical resistivity of the solution on the number of titrant equivalents, we suggested in this study that the electrical conductivity of the initial solution is a sum of the electrical conductivities of the corresponding salts, i.e., $\chi_\Sigma = \chi_{Na_2CO_3} + \chi_{NaHCO_3}$, where χ_Σ is the total electrical conductivity of the initial solution, and $\chi_{Na_2CO_3}$ and χ_{NaHCO_3} are the electrical conductivities of sodium carbonate and sodium hydrocarbonate solutions, respectively. The calculation was performed for solutions containing equivalent amounts of sodium carbonate and hydrocarbonate (0.01, 0.02, 0.05, and 0.1 N) [5].

During titration, the electrical conductivity of the solution varies as follows: Before the first equivalence point, at $0 < y < 1$,

$$\chi_\Sigma = \chi_{Na_2CO_3}(1 - y) + \chi_{NaHCO_3}(1 + y) + \chi_{Na_2SO_4}y,$$

where $\chi_{Na_2SO_4}$ is the electrical conductivity of the sodium sulfate solution, and y, the number of titrant equivalents.

At the first equivalence point, at $y = 1$,

$$\chi_\Sigma = 2\chi_{NaHCO_3} + \chi_{Na_2SO_4}.$$

In titration to the second equivalence point, at $1 < y < 3$,

$$\chi_\Sigma = \chi_{NaHCO_3}(3 - y) + \chi_{Na_2SO_4}y.$$

At the second equivalence point, at $y = 3$,

$$\chi_\Sigma = 3\chi_{Na_2SO_4}.$$

In titration after the second equivalence point, at $3 < y < 5$,

$$\chi_\Sigma = 3\chi_{Na_2SO_4} + \chi_{H_2SO_4}(y - 3),$$

where $\chi_{H_2SO_4}$ is the electrical conductivity of sulfuric acid.

The resulting values of the total electrical conductivity were used to construct the theoretical dependences of the electrical conductivity of the solutions on the number of titrant equivalents (Fig. 1). As can be seen, the titration curves for dilute solutions of sodium carbonate and sodium hydrocarbonate (0.01 and 0.02 N) show two clearly pronounced inflections at the first and the second equivalence points, respectively.

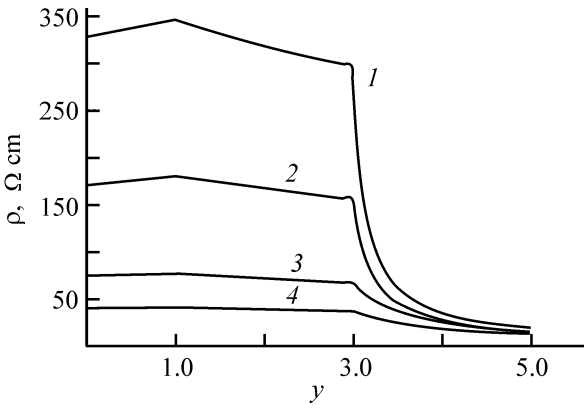


Fig. 1. Theoretical dependence of the electrical resistivity ρ of the solution on the number of titrant equivalents, *y*, taken during titration of a solution containing sodium carbonate and sodium hydrocarbonate at a ratio of 1 : 1 with 0.1 NH_2SO_4 at 25°C. Concentration (g-equiv l^{-1}): (*1*) 0.01, (*2*) 0.02, (*3*) 0.05, and (*4*) 0.1.

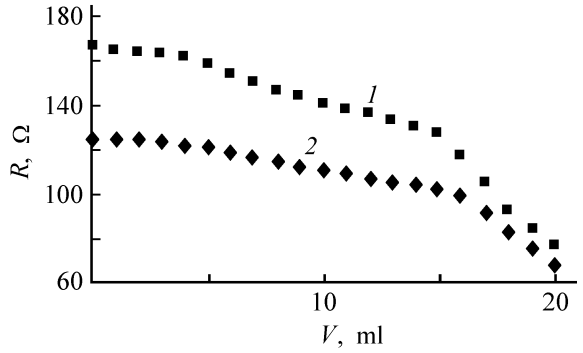


Fig. 2. Conductometric titration curves of the filtrate obtained by treating the active paste of the positive electrode with distilled water. (*R*) Resistance; (*V*) titrant volume. Experiments: (*1*) initial and (*2*) after half a year.

In the experiments, a 2-g portion of the active paste was placed in distilled water, the solution was filtered, and the titration was performed with a standard solution of 0.1 N sulfuric acid. In each titration, the readings of the immitance meter were recorded and the values obtained were used to plot the titration curves and to calculate the residual alkalinity of the solution. The dependences obtained in conductometric titration are shown in Fig. 2. As can be seen, the curves have two inflections at the two equivalence points.

Comparison of the calculated titration curves with the experimental curves shows their identical character. As can be seen from Fig. 2, the amount of carbonate in the solution decreases in the course of time, whereas the amount of bicarbonate increases.

The amount of sulfuric acid spent for titration was calculated from the curves of conductometric titration,

and the amount of sodium carbonate and bicarbonate in a weighed portion of the active paste was calculated from the equivalence law. The content of sodium carbonate and hydrocarbonate was $(6.1 \pm 1.0)\%$ and $(7.3 \pm 1.0)\%$ in the positive electrode and (0.8 ± 0.2) and $(2.2 \pm 0.2)\%$, respectively, in the negative electrode.

It was established for the example of the active paste of the positive electrode that sodium carbonate is converted into bicarbonate in electrodes of worked-out nickel–iron batteries stored in air for a long time. As a result, the content of sodium carbonate in the active paste decreases, and that of sodium hydrocarbonate, increases. A repeated analysis of the active paste of a worked-out positive electrode, made in half a year, demonstrated that the content of sodium carbonate and hydrocarbonate in the active paste changed to $(5.7 \pm 0.6)\%$ and $(9.0 \pm 0.6)\%$, respectively.

CONCLUSIONS

(1) The content of sodium carbonate and sodium hydrocarbonate in the active paste of positive and negative electrodes of a worked-out nickel–iron battery was determined by conductometric titration.

(2) It was established for the example of the active paste of a positive electrode that the content of sodium carbonate in the active paste in electrodes of worked-out nickel–iron batteries stored in air for a long time decreases, and that of sodium bicarbonate increases.

REFERENCES

1. Vyrypaev, V.N., *et al., Khimicheskie istochniki toka: Uchebnoe posobie dlya khimiko-tekhnologicheskikh spetsial™nostei vysshikh uchebnykh zavedenii* (Chemical Power Cells: Textbook for Students Specialized in Chemical Engineering), Moscow: Vysshaya Shkola, 1990.
2. *Khimicheskie istochniki toka: Spravochnik* (Chemical Power Cells: Reference Book), Korovin, N.V. and Skundin, A.M., Eds., Moscow: Mosk. Energ. Inst., 2003.
3. Kreshkov, A.P., *Osnovy analiticheskoi khimii: Fizicheskie i fiziko-khimicheskie (instrumental'nye) metody analiza* (Principles of Analytical Chemistry: Physical and Physicochemical (Instrumental) Methods of Analysis), Moscow: Khimiya, 1977, vol. 3.
4. Khudykova, T.A., and Kreshkov, A.P., *Konduktometricheskii metod analiza: Uchebnoe posobie dlya vysshikh uchebnykh zavedenii* (Conductometric Analysis: Textbook for Higher School Students) Moscow: Vysshaya Schkola, 1975.
5. *Spravochnik fizicheskikh, khimicheskikh i tekhnologicheskikh velichin* (Reference Book of Physical, Chemical, and Technological Values), Martens, L.K., Ed., Moscow: Sov. Entsiklopediya 1930, vol. 4.

Russian Journal of Applied Chemistry, Vol. 78, No. 8, 2005, pp. 1283–1287. Translated from Zhurnal Prikladnoi Khimii, Vol. 78, No. 8, 2005, pp. 1306–1310.
Original Russian Text Copyright © 2005 by Nizhnikova, Podterob.

APPLIED ELECTROCHEMISTRY AND CORROSION PROTECTION OF METALS

Determination of Antiseptic Dyes with Ion-Selective Electrodes

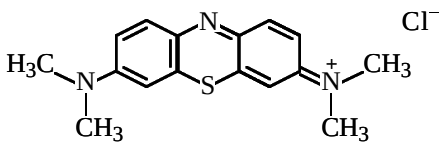
E. V. Nizhnikova and A. P. Podterob

Belarussian State University, Minsk, Belarus

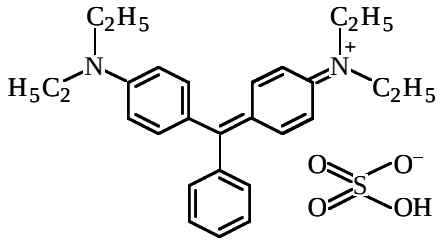
Received October 5, 2004; in final form, April 2005

Abstract—The possibility of determining Methylene Blue and Brilliant Green antiseptic dyes in solutions with the use of ion-selective electrodes based on trioctyl oxybenzosulfonic acid was examined. Data on application of the electrodes fabricated to analysis of powdered dyes are presented. A gravimetric method for analysis for Brilliant Green was suggested and used as a comparative technique.

Methylene Blue (MB, *N*,*N*,*N*',*N*'-tetramethyl thionine chloride) and Brilliant Green [BG, bis(*para*-diethylamino)-triphenyl anhydrocarbinol oxalate) are used as antiseptics:



MB



BG

Methylene Blue is effective as an antidote in poisoning with hydrocyanic acid and its salts and as an agent for neutralization of hemiglobin-forming poisons (nitrites, aniline, and their derivatives) [1, 2]. Together with other dyes of the thiazine series, MB is contained in reagents for hematological analyses and, in particular, in the Eosin-methylene Blue solution by Mey-Grunwald. It is also used to determine the content of carboxy groups in oxidized celluloses [3]. Brilliant Green finds wide use in various fields of science: analytical [4–6], physical [7], and radiation chemistry [8], microbiology [9, 10], neurophysiology [11], veterinary science [12], and medicine [1, 13, 14].

MB is commonly determined by spectrophotometry [15], redox colorimetric titration [16, 17], nonaqueous acid–base titration and gravimetry [18], polarography [19–21], potentiometric titration [17, 18, 22–25], and direct potentiometry [26]. Methods for determining MB with electrodes are indirect [17, 18, 22–25] (in most cases, this is back titration), which undoubtedly impairs the accuracy of determination. An ion-selective electrode (ISE), selective with respect to MB, was first suggested in [26]. This electrode, containing an ionic complex of MB with phosphoric-tungstic acid as an electrode-active substance, can be used in direct potentiometric determination of MB. However, it is known that the determination error strongly depends in this case on the accuracy with which the potential is measured. The 10th edition of the State Pharmacopoeia recommends performing quantitative analyses for MB by its precipitation with potassium dichromate and subsequent iodometric determination of the excess amount of potassium dichromate [16, 27]. The method includes several stages and requires visual indication of the equivalence point. Similar disadvantages are also characteristic of the method of iodometric determination of MB [28]. Direct photometry is not used to determine MB mainly because the shape of the absorption spectrum and the molar absorption coefficient are concentration dependent [28, 29]. As BG is a quaternary ammonium salt and belongs to dyes of the triphenylmethane series, information about methods for its quantitative analysis can be found in the literature [16, 30, 31]. These reports present the general procedures used in analysis for medical preparations belonging to the group of quaternary ammonium salts [31], de-

1070-4272/05/7808-1283 © 2005 Pleiades Publishing, Inc.

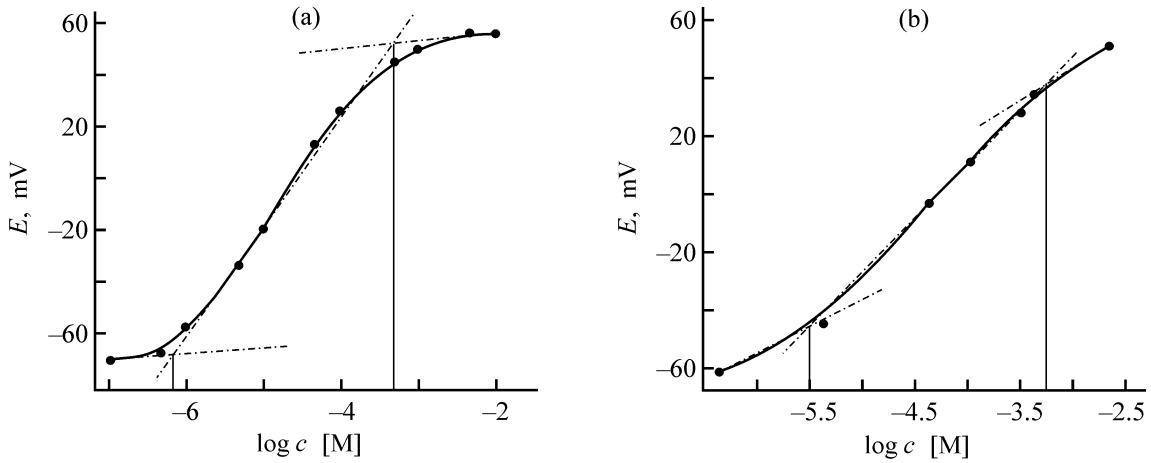


Fig. 1. Calibration plot for ISEs selective toward (a) MB and (b) BG. (*E*) Potential and (*c*) dye concentration.

scribe methods for quantitative determination of quinoid dyes by reduction of the quinoid ring with titanium(III) [16], and give a direct description of a method for quantitative iodochlorometric determination of BG [30].

Analysis of published data suggests that most of the known methods for determination of MB and BG are either labor-consuming or insufficiently accurate. Therefore, development of new techniques is a matter of current interest.

This study analyzes the possibility of employing ISEs for determining the antiseptic dyes MB and BG, widely used in medical practice. Data are presented on their application in a variant of potentiometric titration, which improves its accuracy. In the case of MB, results of potentiometric titration are compared with those furnished by the pharmacopoeic method; a gravimetric comparative method is suggested for BG.

EXPERIMENTAL

All the substances used in the study were of no less than analytically pure grade. The solutions used were prepared with distilled water.

Polyvinyl chloride membranes plasticized with dibutyl phthalate were prepared using the standard procedure [32]. Trioctyl oxybenzosulfonic acid was used as a cation exchanger, with its concentration in the membrane equal to 1×10^{-2} M in terms of dibutyl phthalate. Prior to being used, ISEs were soaked in a saturated solution of an appropriate antiseptic dye.

The characteristics of the ISEs were studied in aqueous solutions of the dyes. The calibration plots are shown in Figs. 1a and 1b. A standard silver chloride electrode filled with a saturated solution of NaCl (EVL-1 M3.1) served as an external reference. All the measurements were carried out at 20 ± 2°C. The resistances of galvanic cells were 1–2 MΩ, which is characteristic of film electrodes plasticized with dibutyl phthalate. The stability of operation of the electrodes was monitored during a month, with all the parameters being well reproducible (Table 1). The response time was less than 1 min at concentrations of 10^{-2}–10^{-4} M and 1–2 min at 10^{-5}–10^{-6} M. In going from concentrated to dilute solutions, it is necessary to wash the electrodes with distilled water for 5–10 min. The washing quality can be monitored visually.

The influence exerted by the pH value on the potential of film electrodes selective toward antiseptic

Table 1. Parameters of ISEs selective toward MB and BG

Parameter	MB	BG
Slope of the electrode function, mV/log *c*	53.3 ± 0.5	39.0 ± 0.7
Const	250.7 ± 5.9	166.6 ± 9.8
Region of linearity of the electrode function, M	1×10^{-6}–1×10^{-4}	5×10^{-6}–5×10^{-4}
Lower detection limit, M	$(6.17 \pm 0.80) \times 10^{-7}$	$(3.24 \pm 0.75) \times 10^{-6}$

dyes was studied at pH 1–12 by adding minor amounts of HClconc and NaOH to a solution of the corresponding ye. A study of the effect of the medium on the electrode potentials demonstrated that, as the concentration of an aseptic dye decreases, the range of pH values at which the ISE potential is constant becomes narrower. For example, the ISE potential remains constant at a BG concentration of 1×10^{-2} M in the range pH 3–12, whereas at a BG concentration lowered to 1×10^{-4} M, this range becomes narrower: pH 4–8. For MB, passing from a concentration of 1×10^{-3} to 1×10^{-5} M results in that the range of constant ISE potential narrows down from pH 4–11 to pH 7–8. The decrease in the ISE potential in an acid medium (at pH $\leq$ 3–4) is possibly due to protonation of the tertiary nitrogen atom in the molecule of an antiseptic dye to give a double-charged cation, toward which the selectivity of ISE is lower. The decrease in the ISE potential in an alkaline medium is due to formation of a sparingly soluble base of MB or BG [28, 29].

The selectivity coefficients of the ISEs toward cations of alkali and alkaline-earth metals were determined by the method of mixed solutions at a fixed concentration of an interfering ion in the range 0.01–0.1 M (Table 2). The method used was described in [33].

The MB and BG solutions prepared by dissolving weighed (with an accuracy as good as 0.0001 g) portions of a powder in distilled water were analyzed by precipitation potentiometric titration with sodium tetraphenylboron (STPB) (the titration curves are shown in Fig. 2), using the electrodes fabricated, and, additionally, by the pharmacopoeic method in the case of MB and by gravimetry in the case of BG (Table 3) [34].

In measurement by the method of precipitation potentiometric titration, a weighed portion of a powder, with a mass m (g), was dissolved in a volumetric flask of volume V (mm), with m and V chosen in such a way that the solution prepared contained about 10^{-3} M of MB and 10^{-4} M of GB. An aliquot for titration, of volume V_{al} (ml), was taken from the solution prepared. The variation of the potential was recorded with an EV-74 ion meter. The precise concentration of the STPB solution was determined by precipitation potentiometric titration with a K-valinomycin electrode as an indicator. The results obtained in the titration were used to calculate the content of a dye in the powder, ω (wt %):

$$\omega = \frac{c_{TPBS} V_{TPBS} M_{BG^+HSO_4^-} V}{V_{al} \times 1000 m} \times 100,$$

Table 2. Selectivity coefficients K_s of electrodes selective toward antiseptic dyes, with respect to inorganic cations

Dye	K_s for indicated interfering ion			
	K^+	Na^+	Mg^{2+}	Ca^{2+}
MB	2.1×10^{-5}	2.0×10^{-5}	1.9×10^{-5}	5.1×10^{-6}
BG	1.2×10^{-5}	1.2×10^{-5}	1.1×10^{-5}	5.5×10^{-5}

where c_{STPB} is the concentration of the tetraphenylborate titrant (M); V_{STPB}, volume of the titrant consumed for titration (ml); $M_{BG^+HSO_4^-}$, molar mass of BG hydrosulfate (g mol^{-1}); V_{al}, volume (ml) of the aliquot of a dye solution prepared by dissolving a dye powder of mass m (g) in a volumetric flask of volume V (ml), taken for titration; and 1000 is the scaling factor for recalculation of the mass into grams.

The gravimetric method for determining BG consists in that it is precipitated with iodine in the presence of CH_3COONa and the forming tetraiodine derivative is weighed after purification and calcination at 110°C. The content of BG in the powder, ω (wt %), was calculated by the formula

$$\omega = \frac{m_{precipitate} M_{BG^+HSO_4^-} V}{m_{weighed.portion} M_{C_{27}H_{29}N_2I_4^+I^-}} \times 100,$$

where $m_{weighed.portion}$ is the mass of the weighed portion of the dye powder (g); $m_{precipitate}$, mass of the precipitate of BG hydrosulfate formed; $M_{BG^+HSO_4^-}$, molar mass of BG hydrosulfate (g mol^{-1}); and $M_{C_{27}H_{29}N_2I_4^+I^-}$,

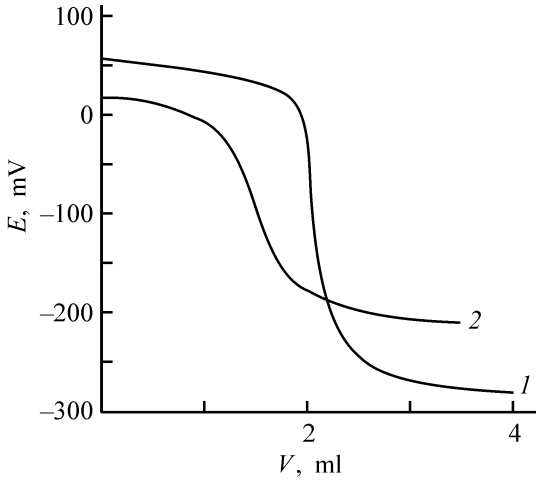


Fig. 2. Curves of titration of antiseptic dyes with an STPB solution. (E) Potential and (V) volume of tetraphenylboron sodium. Solution (M): (*1*) MB (~10^{-3}) and (*2*) BG (~10^{-4}). STPB (M): (*1*) 9.52×10^{-3} and (*2*) 9.52×10^{-4}.

Table 3. Results of determination of powdered antiseptic dyes*

Found, %			
MB		BG	
1	2	1	3
96.99	101.15	80.9	87.7
95.66	98.20	80.9	91.4
97.43	99.28	76.7	82.6
99.23	98.74	87.3	78.6
98.25	93.16	84.4	78.1
98.61	94.57	78.1	76.6
99.45		93.4	77.9
95.69		92.5	80.1
96.97			
98.85			
99.03			
x = 97.83, s = 1.40	x = 97.52, s = 3.03	x = 84.3, s = 6.31	x = 81.6, s = 5.30
$F(P = 0.99, f_1 = 5, f_2 = 10)$ = 5.64 F = 4.68 $F < F(P = 0.99, f_1 = 5, f_2 = 10)$ t (P = 0.99, f = 15) = 2.95 t = 0.29 $t < t$ (P = 0.99, f = 15)		$F(P = 0.95, f_1 = f_2 = 7)$ = 3.80 F = 1.42 $F < F(P = 0.95, f_1 = f_2 = 7)$ t (P = 0.95, f = 14) = 2.14 t = 0.93 $t < t$ (P = 0.95, f = 14)	

* (1) Potentiometric titration, (2) pharmacopoeic method, and (3) gravimetric method.

molar mass of a tetraiodine derivative of BG ($g\,mol^{-1}$).

The results obtained in the analysis are listed in Table 3.

CONCLUSIONS

(1) Ion-selective electrodes with a film membrane containing polyvinyl chloride, dibutyl phthalate, and a salt formed by the cation of an antiseptic dye and anion of trioctyl oxybenzosulfonic acid (1×10^{-2} M in terms of dibutyl phthalate) have the following parameters: sensitivity for Methylene Blue and Brilliant Green dyes of 53.3 and 39.0 mV/log c, respectively; detection limit, 6.17×10^{-7} and 3.24×10^{-7} M; and linearity range of the calibration plot, 1×10^{-6}–1×10^{-4} and 5×10^{-6}–5×10^{-4} M. The lower sensitivity of the electrodes fabricated with respect to the theoretical value is, in all probability, due to partial extraction of the dye by the membrane in the form of an ionic associate, rather than by the exchange mechanism.

(2) The potential of an ion-selective electrode exhibiting selectivity toward antiseptic dyes depends on the pH value of the medium, with this dependence becoming more pronounced as the solution is diluted. Consequently, a strict control over the pH value is necessary in the case of a direct potentiometric determination of the dyes. Inorganic cations (sodium, potassium, magnesium, calcium) virtually do not interfere with determination of antiseptic dyes.

(3) Determination of antiseptic dyes in solution by titration with sodium tetraphenylboron with a potentiometric indication of the equivalence point has high accuracy, reproducibility, rapidity, and simplicity. To assess the significance of differences between the results obtained in determining the dyes by different methods, their standard deviations and average values were compared by statistical criteria. The difference between the results obtained by the two methods in the case of both the antiseptic dyes studied is nonsignificant.

REFERENCES

1. Mashkovskii, M.D., *Lekarstvennye sredstva* (Medicinal Agents), Moscow: Novaya Volna, 2000, vol. 2.
2. *Spravochnik Vidal' – 2003: Lekarstvennye preparaty v Rossii* (Vidal Reference Book of 2003: Medicinal Preparations in Russia), Moscow: AstraFarmServis, 2003.
3. Ermolenko, I.N., *Spektroskopiya v khimii okislennykh tsellyuloz* (Spectroscopy in Chemistry of Oxidized Celluloses), Minsk: Akad. Nauk BelSSR, 1959.
4. Patel, R. and Patel, K.S., *Analyst*, 1998, vol. 123, pp. 1691–1695.
5. Pyka, A., Gurak, D., and Bober, K., *J. Liq. Chrom. Rel. Technol.*, 2002, vol. 25, pp. 1483–1495.
6. Shaopu, L., Zhongfang, L., Ming, L., *et al., Fresenius J. Anal. Chem.*, 2000, vol. 368, pp. 848–852.
7. Bhattacharyya, K.G. and Sarma, A., *Dyes Pigments*, 2003, vol. 57, pp. 211–223.
8. Khan, H.M., Anwer, M., and Chaudhary, Z.S., *Radiation Phys. Chem.*, 2002, vol. 63, pp. 713–718.
9. Bolton, D.I., Pearce, R., Sheridan, J.J., *et al. J. Appl. Microbiol.*, 2003, vol. 94, no. 6, pp. 1036–1042.
10. Menon, T. and Ponnuvel, K.M., *Mycoses*, 2000, vol. 43, no. 5, pp. 165–168.
11. Bufler, J., Cordes, A., Heineke, W., *et al., Neurosci Lett.*, 2001, vol. 312, no. 2, pp. 91–95.
12. Ogawa, E., Ota, C., Fujise, H., and Kobayashi, K.,

The Japan. J. Veterinary Sci., 1988, vol. 50, no. 2, pp. 577–586.

13. Bakker, P., Van Doome, H., Gooskens, V., and Wieringa, N., *Int. J. Dermatol.*, 1992, vol. 31, no. 3, pp. 210–213.
14. Wachenheim, D.E., Blythe, L.L., and Craig, A.M., *Appl. Environ. Microbiol.*, 1992, vol. 58, no. 8, pp. 2559–2564.
15. Muralikrishna, U., Ramanadham, G.V., and Someswara, R.N., *Fresenius' Zeitschrift für Analytische Chemie*, 1976, vol. 279, no. 3, p. 208.
16. Lastovskii, R.P. and Vainshtein, Yu.I., *Tekhnicheskii analiz v proizvodstve promezhutochnykh produktov i krasitelei* (Technical Analysis in Manufacture of Intermediates and Dyes), Moscow: Goskhimizdat, 1958.
17. Rukmini, N., Kavitha, V.S.N.P., and Pulla, R.Y., *Talanta*, 1979, vol. 26, no. 5, pp. 409–410.
18. Burgess, C., Fogg, A.G., and Burns, D.T., *Laboratory Practice*, 1973, vol. 22, no. 7, pp. 472–474.
19. Senkevich, V.V., Sister, Yu.D., and Lyalikov, Yu.S., *Zh. Anal. Khim.*, 1972, vol. 27, no. 2, p. 380.
20. Stuzka, V. and Ruzicka, O., *Acta Universitatis Palackianae Olomucensis, Facultas rerum naturalium*, 1979/80, vol. 61/65, pp. 161–168.
21. Stuzka, V. and Ruzicka, O., *Acta Universitatis Palackianae Olomucensis, Facultas rerum naturalium*, 1983, vol. 76, pp. 61–71.
22. Vytras, K., *Ion-Selective Electrode Rev.*, 1985, vol. 7, no. 1, pp. 77–107.
23. Dessouky, Y.M., Toth, K., and Pungor, E., *The Analyst*, 1970, vol. 95, no. 1137, pp. 977–1048.
24. Vytras, K., *Collection Czechoslov. Chem. Commun.*, 1977, vol. 42, pp. 3168–3174.
25. Fogg, A.G., Al-Sibaai, A.A., and Yoo, K.S., *Analytical Lett.*, 1977, vol. 10, no. 3, pp. 173–182.
26. Wen, M.L., Zhao, Y.B., Chen, X., and Chang, Y.W., *Croatica Chemica Acta*, 1998, vol. 71, no. 3, pp. 757–764.
27. *Gosudarstvennaya farmakopeya* (State Pharmacopoeia), Moscow: Meditsina, 1968, 10th ed.
28. Khaletskii, A.M., *Farmatsevticheskaya khimiya* (Pharmaceutical Chemistry), Leningrad: Meditsina, 1966.
29. Dawson, R.M.C., Elliot, D.C., Elliot, W.H., and Jones, K.M., *Data for Biochemical Research*, Oxford: Clarendon, 1986. Translated under the title *Spravochnik biokhimika*, Moscow: Mir, 1991.
30. Lastaeva, S.M., *Farmatsiya*, 1972, vol. 21, no. 3, pp. 80–81.
31. Pohloudek-Fabini, R. and Beyrich, Th., *Organische Analyse*, Leipzig: Academische Verlagsgesellschaft Geest and Portig K.-G., 1975. Translated under the title *Organicheskii analiz*, Leningrad: Khimiya, 1981.
32. Repin, V.A., Egorov, V.V., and Starobinets, G.L., *Zh. Anal. Khim.*, 1988, vol. 43, no. 7, pp. 1318–1320.
33. Nikol'skii, B.P. and Materova, E.A., *Ionoselektivnye elektrody* (ion-Selective Electrodes), Leningrad: Khimiya, 1980.
34. Doerfel, K., *Statistic in der analytischen Chemie*, Leipzig: Leuna-Merseburg, 1966. Translated under the title *Statistika v analiticheskoi khimii* Moscow: Mir, 1994.

Russian Journal of Applied Chemistry, Vol. 78, No. 8, 2005, pp. 1288–1293. Translated from Zhurnal Prikladnoi Khimii, Vol. 78, No. 8, 2005, pp. 1311–1316.
Original Russian Text Copyright © 2005 by Pisarska, Dylevski.

APPLIED ELECTROCHEMISTRY AND CORROSION PROTECTION OF METALS

Analysis of Preparation Conditions of H_2SO_4 and NaOH from Sodium Sulfate Solutions by Electrodialysis

B. Pisarska and R. Dylevski

Institute of Inorganic Chemistry, Gliwice, Poland
Silesian Technical University, Gliwice, Poland

Received February 7, 2002

Abstract—Preparation of sulfuric acid and sodium hydroxide from solutions containing sodium sulfate was studied by the electrodialysis method in a three-chamber (?three-compartment) electrodialyzer equipped with two membranes, an anion-exchange membrane AESD-2a and a cation-exchange membrane Nafion 427.

Manufacture of some fatty acids [1, 2], synthetic fibers, and inorganic and organic compounds [3] and integrated processing of worked-out lead batteries [4] yield spent solutions containing sodium sulfate, which are considered nontoxic and are discharged as wastewater. In most cases, sodium sulfate is formed in spent solutions when sulfuric acid and sodium hydroxide are used as technological solutions. Hence follows that it would be possible to solve the ecological problems associated with the formation and discharge of spent solutions containing sodium sulfate if there existed an effective and cost-efficient method for their processing to obtain sulfuric acid and sodium hydroxide. This would enable development of integrated (conjugated) closed cycles. H_2SO_4 and NaOH of purity and concentration sufficient for recycling can be obtained at a plant using sulfuric acid and sodium hydroxide, with sodium sulfate solutions formed along with the target product [5, 6].

The possible technologies based on this principle of processing of spent solutions containing sodium sulfate were described in [4]. It was suggested to use for this purpose electrodialysis in a three-chamber apparatus (electrodialyzer) with two, anion-exchange and cation-exchange, membranes.

The aim of this study was to determine how the current density in the range 2.5–10.0 A dm^{-3}, initial concentration of sodium sulfate (50 and 100 g dm^{-2}), and dialyzate composition affect the current efficiency by sulfuric acid and sodium hydroxide and the direction of transfer and amount of water transferred across the membranes in the course of electrodialysis.

EXPERIMENTAL

The electrodialyzer is shown schematically in Fig. 1. It comprises clamping plates *1, 9*, anode chamber *2*, anode *3* made of perforated lead sheet, anion-exchange membrane *4*, central chamber *5*, cation-exchange membrane *6*, cathode *7* made of perforated nickel sheet, and cathode chamber *8*. The separate elements are connected via 2-mm-thick rubber sealing gaskets. The whole set is assembled into a rigid stack by means of steel coupling bolts. The working size of each membrane and electrode is 5×20 cm.

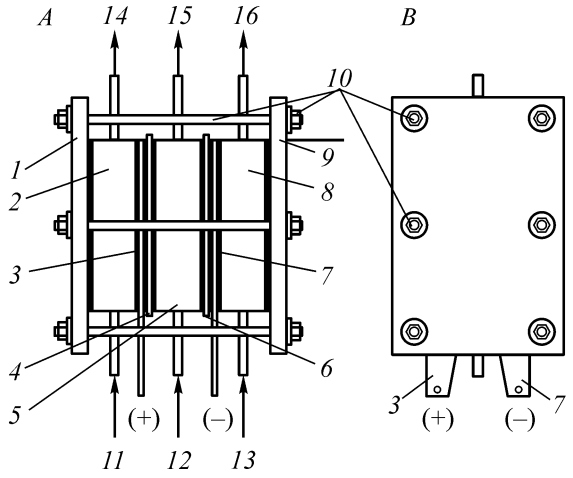


Fig. 1. Schematic of the electrodialyzer unit. (*A*) Front view and (*B*) side view. (*10*) Coupling bolts, (*11*) inlet for water (dilute H_2SO_4), (*12*) inlet for Na_2SO_4 solution, (*13*) inlet for water (dilute NaOH), (*14*) outlet for H_2SO_4 solution and oxygen, (*15*) outlet for dialyzate, and (*16*) outlet for NaOH solution and hydrogen. The rubber separators are colored black.

1070-4272/05/7808-1288 © 2005 Pleiades Publishing, Inc.

The AESD-2a membrane manufactured by GALENA pharmaceutical plant (Wroclaw) is a single-layer anion-exchange membrane used without a reinforcing grid at temperatures of up to 45°C [7]. The membrane is fabricated from polyethylene modified with a copolymer of styrene and divinylbenzene, functionalized with $–NH(CH_3)$ groups, and has thickness of 170 μm. The formal selectivity of the membrane is 0.93, and the swelling capacity, 22–24%.

The Nafion 427 membrane manufactured by E.I. Du Pont de Nemours & Co (USA) is a single-layer cation-exchange membrane composed of a perforated mass with $–SO_3H$ functional groups. The membrane has a thickness of 127 μm, mass equivalent ME = 1200, and a reinforcing Teflon fabric of T-12 brand. Nafion 427 membranes are intended for regeneration of technological media, including acids and alkalis [8].

The installation is shown schematically in Fig. 2. It comprises three reservoirs preliminarily filled with an anolyte, a Na_2SO_4-containing solution, and a catholyte. The anolyte (H_2SO_4 solution of initial concentration 16 g dm^{-3}) is delivered from a reservoir *1* by a dosing pump *2* and passes through an anode chamber *3* into a sulfuric acid collector *4*. The catholyte (NaOH solution of initial concentration 12 g dm^{-3}) from a reservoir *5* is delivered by a dosing pump *6* and passes through a cathode chamber *7* into a collector *8*. The sodium sulfate solution from a reservoir *9* is delivered by a dosing pump *10* into a central chamber *11* and then into a dialyzate collector *12*. Gaseous products of electrodialysis (oxygen and hydrogen) are released into the atmosphere.

The volume of the solutions obtained (anolyte, catholyte, and dialyzate) was measured at certain intervals of time. The concentration of sulfuric acid was measured in the anolyte, and that of sodium hydroxide, in the catholyte. A selective determination of SO_4^{2-} ions in the catholyte gave a negative result. SO_4^{2-} ions and an excess amount of free acid or hydroxide were found in the dialyzate. These data were used to calculate the concentrations of Na_2SO_4 and H_2SO_4. The results obtained were used, together with the data furnished by direct determination of the products concentration and dialyzate composition, to calculate the current efficiency by sulfuric acid and sodium hydroxide, as well as the amount of water transferred across both the ion-exchange membranes.

The results obtained were mathematically processed using the procedure suggested by Kafarov [9]. For this purpose, equations describing the dependences of the current efficiency on the process parameters

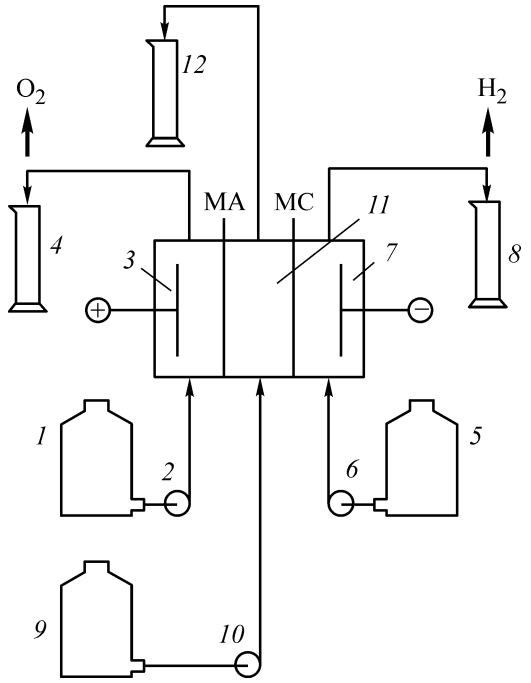


Fig. 2. Schematic of the installation for electrodialysis. Membrane: MA, of anion-exchange, and MC, of cation-exchange types.

were set up in the form of second-degree polynomials including all combinations of the process parameters (as independent variables). Statgraph software was used to calculate the numerical coefficients of individual terms and to analyze their significance. Using terms with a significance level higher than 0.05, we derived functions with only significant terms, which makes it possible to determine the influence exerted by separate parameters on the current efficiency. As two products (sulfuric acid and sodium hydroxide) are formed in the course of electrodialysis, the equations for sulfuric acid for sodium hydroxide were set up and processed independently

$$CE_{H_2SO_4} = f(K_1,\ j_m,\ c_{H_2SO_4}), \quad (1)$$

$$CE_{NaOH} = f(K_2,\ j_m,\ c_{NaOH}), \quad (2)$$

where $CE_{H_2SO_4}$ and CE_{NaOH} are the current efficiencies by sulfuric acid and sodium hydroxide, respectively (%); K_1 and K_2, constants (free terms reflecting the influence of the membrane characteristics); j_m, current density recalculated to the geometric area of the membrane (A dm^{-2}); and $c_{H_2SO_4}$ and c_{NaOH}, concentrations of H_2SO_4 and NaOH in the solutions flowing out of the respective chamber of the electrodialyzer (g dm^{-3}).

Table 1. Parameters and efficiency of electrodialysis (initial solution contains 50 g dm^{-3} Na_2SO_4)

j_m, A dm^{-2}	Dialyzate,* g dm^{-3}	Catholyte			Anolyte		
		c_{NaOH}, g dm^{-3}	CE,** %	Water transport, mole H_2O/mole NaOH	$c_{H_2SO_4}$, g dm^{-3}	CE,*** %	Water transport, mole H_2O/mole H_2SO_4
2.5		14.95	78.43		19.22	71.26	
2.5		17.81	78.56		22.72	71.24	
2.5		20.64	78.80		26.28	71.31	
2.5		23.45	78.94		29.98	71.60	
2.5	21.56	26.22	79.12		33.64	71.52	
2.5	1.15	28.98	79.01	+4.39	37.43	71.41	–12.31
5.0		18.15	80.94		22.82	71.96	
5.0		24.06	81.12		30.20	72.09	
5.0		29.85	81.28		38.03	72.16	
5.0		34.53	81.28		46.35	72.16	
5.0	5.92	41.41	81.28		56.13	72.16	
5.0	5.29	46.57	81.28	+4.22	66.40	72.02	–15.42
7.5		21.28	82.48		25.94	71.96	
7.5		28.77	82.36		37.34	72.16	
7.5		36.17	82.30		49.89	72.30	
7.5		43.63	82.24		63.74	72.11	
7.5	6.93	51.27	81.98		79.12	72.02	
7.5	4.43	59.25	81.90	+3.83	96.32	71.92	–19.56
10.0		23.73	80.10		31.93	70.86	
10.0		35.41	79.96		47.66	70.78	
10.0		47.02	79.58		63.36	70.64	
10.0		58.55	79.32		80.00	70.64	
10.0	6.86	70.07	79.06		97.58	70.49	
10.0	4.02	81.56	78.91	+4.15	117.14	70.40	–17.68

* Numerator, Na_2SO_4 concentration; denominator, H_2SO_4 concentration.

** $CE_{NaOH} = 72.81 + 2.57j_m + 0.42c_{NaOH} - 0.17j_m^2 - 0.0067j_m c_{NaOH}$, $R^2 = 95.09\%$. (3)

*** $CE_{H_2SO_4} = 69.29 + 0.94j_m + 0.011c_{H_2SO_4} - 0.08j_m^2 - 0.00011c_{H_2SO_4}^2$, $R^2 = 95.32\%$. (4)

The data obtained for the initial Na_2SO_4 concentrations c_0 of 50 and 100 g dm^{-3} are listed in Tables 1 and 2. The sign (+) stands for water transfer from the central chamber into the electrode chamber, and the sign (–), for water transfer from the electrode chamber into the central chamber.

It follows from the data in Table 2 that the current efficiency by sodium hydroxide increases from 78 to 85% as the current density is raised from 2.5 to 10.0 A dm^{-2}. Simultaneously, the current efficiency by sulfuric acid increases from approximately 72.3 to 74%. The increase in the current efficiency can be explained as follows. The product yield is determined by competition of two processes. These are, first, an increase in the amount of the product as a result of electrodialysis and transfer of Na^+ and SO_4^{2-} ions under the action of electric current, and, second, loss of the product via exchange with the membrane, which results from the fact that the true selectivity of the membrane is always lower than inity (frequently, even lower than the formal selectivity given in the data sheet). The ion transfer in an electric field, e.g., across a membrane, is associated with the transport of an electric current and depends on its density. At the same time, the effects of exchange of solution components via diffusion and osmosis mainly depend on the solution composition and time of exchange. Hence follows that the higher the current density, the faster the accumulation of the product obtained and, thereby, the smaller the amount of loss.

With some simplification, the current density can be considered a factor determining the processing rate of the substrate (Na^+ and SO_4^{2-} ions) fed into the central chamber. The throughput of this processing depends on the content of the substrate in the dialyzate.

Comparison of the data in Tables 1 and 2 shows that the current efficiencies by both the products are

Table 2. Parameters and efficiency of electrodialysis (initial solution contains 100 g dm^{-3} Na_2SO_4)

j_m, A dm^{-2}	Dialyzate,* g dm^{-3}	Catholyte			Anolyte		
		c_{NaOH}, g dm^{-3}	CE,** %	Water transport, mole H_2O/mole NaOH	$c_{H_2SO_4}$, g dm^{-3}	CE,*** %	Water transport, mole H_2O/mole H_2SO_4
2.5		16.83	78.02		21.64	72.28	
2.5		21.28	77.96		27.67	72.32	
2.5		25.56	78.02		33.92	72.32	
2.5		29.70	77.96		40.39	72.30	
2.5	81.02	33.71	78.04		47.12	72.32	
2.5	2.28	37.64	78.04	+5.72	54.14	72.36	–13.76
5.0		22.28	82.59		27.28	73.12	
5.0		32.40	83.10		40.42	73.07	
5.0		42.29	83.23		55.05	73.07	
5.0		52.02	83.20		71.33	73.07	
5.0	87.44	61.62	83.15		89.69	72.81	
5.0	1.56	71.14	83.05	+3.75	110.49	72.98	–19.28
7.5		27.83	84.24		32.83	73.35	
7.5		43.30	84.16		53.22	73.35	
7.5		58.52	84.06		76.93	73.82	
7.5		73.26	84.10		104.85	73.66	
7.5	54.20	87.94	84.06		138.10	73.24	
7.5	3.68	101.90	84.06	+3.54	179.72	73.18	–21.28
10.0		32.62	85.18		38.49	74.18	
10.0		53.11	85.10		64.85	74.06	
10.0		73.56	85.10		95.23	73.92	
10.0		94.01	85.04		127.56	73.82	
10.0	46.12	114.45	84.96		164.58	73.66	
10.0	3.89	134.92	84.96	+3.92	206.34	73.66	–22.94

* Numerator, Na_2SO_4 concentration; denominator, H_2SO_4 concentration.

** $CE_{NaOH} = 71.88 + 2.95j_m + 0.00086c_{NaOH} - 0.16j_m^2$, $R^2 = 96.88\%$. (5)

*** $CE_{H_2SO_4} = 71.53 + 0.35j_m + 0.000012c_{H_2SO_4} - 0.0096j_m^2$, $R^2 = 95.40\%$. (6)

lower at a lower initial concentration of Na_2SO_4 and a lower concentration of the dialyzate. The difference is the larger, the higher the current density. The current efficiency by H_2SO_4 and NaOH at the initial Na_2SO_4 concentration of 50 g dm^{-3} is determined by the transfer of Na^+ and SO_4^{2-} ions. This is indicated by the fact that the current efficiency decreases as the current density increases from 7.5 to 10.0 A dm^{-2} (Table 1). This behavior is observed at c_0 = 100 g dm^{-3} Na_2SO_4 (Table 2).

The concentrations of sodium sulfate in the solution fed into the central chamber of the dialyzer, which are used in the study, are comparable with the concentrations in spent solutions and have comparatively low values: the Na_2SO_4 concentration of 100 g dm^{-3} corresponds to a concentration of about 0.7 mol dm^{-3}, and 50 g dm^{-3}, to 0.35 mol dm^{-3}. In the central chamber, the concentration decreases to the value found for the dialyzate. As the rate of the solution flow through the central chamber was 1–2 cm min^{-1}, it may be suggested that a concentration gradient is formed: the highest concentration of the solution is observed in the bottom part and the lowest, in the top part (on the feed side).

The current efficiencies by sodium hydroxide and sulfuric acid are different, with that by sodium hydroxide higher in all cases. Accordingly, the dialyzate outflowing from the central chamber contains, in addition to sodium sulfate, also sulfuric acid, whose concentration depends on the transport number and on the solution flow rate. Generalization of this fact shows that, if the current efficiencies by the products

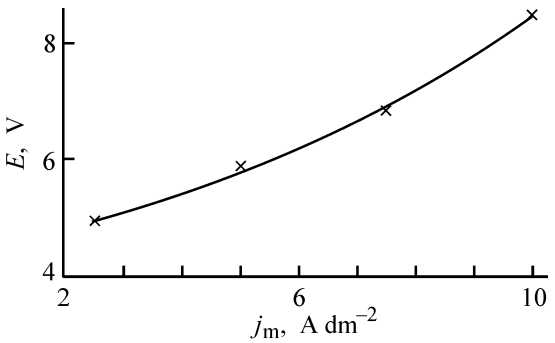


Fig. 3. Electrodialyzer voltage E vs. the current density on the membrane j_m. Initial solution contains 50 g dm^{-3} Na_2SO_4.

obtained in the electrode chambers of the electrodialyzer are different (which is primarily determined by the characteristics of the membranes used), then the product with a lower current efficiency will be also present in the dialyzate.

The presence of sulfuric acid in the central chamber, which results from the lower selectivity of the anion-exchange membrane, may be responsible for the decrease in the current efficiency by sodium hydroxide obtained in the cathode chamber. This is because the solution contains, in addition to Na^+ cations, also hydroxonium ions H_3O^+ involved in the transfer across the cation-exchange membrane. The transfer of H_3O^+ ions from the central chamber to the catholyte does not yield sodium hydroxide and only promotes transport of water, thereby diluting the catholyte. Each hydroxonium ion that passes into the catholyte across the membrane interacts with a hydroxy ion to form water:

$$H_3O^+ + OH^- = 2H_2O.$$

Analysis of Eqs. (3)–(6) confirms the above observations. In these dependences, the influence of the membranes on the CE is reflected by the free term, with this effect being predominant. It may be considered that use of membranes with certain characteristics predetermines the limiting current efficiency, whereas changing the electrodialysis parameters produces a considerably weaker effect.

The numerical coefficients in the terms containing the current density j_m are positive, which confirms the character of their influence on the current efficiency. The presence of j_m terms (with considerably smaller numerical coefficients) shows that this influence is not linear. However, use of very high current densities in the process under discussion is unfeasible for economic reasons and the optimal current density is considerably lower than its highest admissible value indicated by membrane manufacturers. Thus, the solution in the central chamber (dialyzate) should change its concentration in the course of the electrodialysis to an as low value as possible and its electrical conductivity should be low. Under the conditions described in Table 1, the process performed at a current density j_m = 2.5 A dm^{-2} occurred at a voltage E = 4.9 V, and that carried out at j_m = 7.5 A dm^{-2}, at 6.8 V. Hence follows that the rise in the current efficiency by a value not exceeding 4 % was determined by an increase in the voltage by more than 1.9 V, i.e., by approximately 39 % (Fig. 3). Although the dependence of the voltage E on the current density is determined by the electrodialyzer design and can be improved, it would be expected that the optimal current densities in an industrial process should be the same as those in a typical electrodialysis process, i.e., in the range from one to several amperes per square decimeter.

Varying the concentration of sulfuric acid in the anolyte and that of sodium hydroxide in the catholyte at a constant current density within the range studied has no significant effect on the current efficiency.

The purpose of application of electrodialysis is to process sodium sulfate solutions to obtain reusable sulfuric acid and sodium hydroxide. However, a dialyzate containing sodium sulfate and a minor amount of sulfuric acid or sodium hydroxide is also formed, in addition to these products. The desire to obtain in electrodialysis a dialyzate of purity conforming to, at least, the requirements to wastewater commonly leads to gross energy expenditure because of the low current efficiency and the low electrolytic conductivity of the solution in the middle chamber. This adverse effect can be diminished by making the middle chamber very narrow (about 2 mm). The problems encountered when using the dialyzate can be solved in many cases in integrated systems. Commonly, at least one of these products can contain sodium sulfate in an industrial process using sulfuric acid and sodium hydroxide. If this is, i.e., sulfuric acid (as it occurs when obtaining pure silica), then the dialyzate can be used to feed the anode chamber. In this case, all the dialyzate components remain in the closed cycle of the solutions. If, however, the resulting sulfuric acid is of high purity (as is the case in integrated processing of scrap lead batteries [3]) and a sodium hydroxide solution used for desulfation of the sulfate–oxide fraction contains sodium sulfate, then the dialyzate is fed into the cathode chamber. In systems of this kind, the electrolytic conductivity of the dialyzate may be reasonably high at a low energy

expenditure (depending on the admissible Na_2SO_4 concentration), and sodium sulfate does not penetrate into wastewater at all.

CONCLUSIONS

(1) Electrodialysis is the process that makes it possible to obtain sulfuric acid, sodium hydroxide, and a dialyzate from a spent solution containing sodium sulfate, and is especially suitable for closed integrated systems. The current efficiency by the products primarily depends on the parameters of ion-exchange membranes and, to a considerably lesser extent, on the process parameters.

(2) If the membranes used in electrodialysis have different selectivities, the dialyzate contains, in addition to the residual sodium sulfate, also the product (acid or hydroxide) obtained in an electrode chamber with a lower current efficiency.

(3) In the case when one of the electrodialysis products contains sodium sulfate, the dialyzate can be used to feed that electrode chamber in which this product is formed. This makes it possible to diminish the energy expenditure, facilitates enables closed circulation of the solutions, and prevents penetration of sodium sulfate into wastewater.

REFERENCES

1. Drozdetskaya, E.P., Skripchenko, V.I., and Il™in, K.G., *Khim. Prom–st.*, 1985, no. 11, pp. 677–678.
2. Baidin, I.I., Bogdanov, Yu.S., and Korobova, E.S., *Khim. Prom–st.*, 1975, no. 6, pp. 422–424.
3. Delewski, R., *Chemik*, 2001, vol. 54, no. 1, pp. 8–12.
4. Morachevskii, A.G., *Zh. Prikl. Khim.*, vol. 70, no. 1, pp. 3–15.
5. Veličkovic', D.P., Jokic', A.M., and Jakšic', M.M., *Hem. Ind. (Yug).*, 1989, vol. 43, no. 2, pp. 45–60.
6. *Membrany i membranowe techniki rozdzialu* (Membranes and Membrane Separation Techniques), Narebskiej, A., Ed., Torun: Uniwersytetu M. Kopernika, 1997, pp. 261–332.
7. Wisniewska, G. and Wiśniewski, J., *Environment. Protection Eng.*, 1989, vol. 15, no. 3–4, pp. 155–162.
8. Mazanko, A.F., Kamar'yan, G.M., and Romashin, O.P., *Promyshlennyi membrannyi elektroliz* (Industrial Membrane Electrolysis), Moscow: Khimiya, 1989.
9. Kafarow, W.W., *Metody cybernetyki w chemii i technologii chemicznej* (Cybernetic Methods in Chemistry and Chemical Engineering), Warsaw: WNT, 1979.

Russian Journal of Applied Chemistry, Vol. 78, No. 8, 2005, pp. 1294–1300. Translated from Zhurnal Prikladnoi Khimii, Vol. 78, No. 8, 2005, pp. 1317–1323.
Original Russian Text Copyright © 2005 by Yablonskii.

PROCESSES AND EQUIPMENT OF CHEMICAL INDUSTRY

Effect of Rheological Properties of the Dispersion Medium on Separation of Suspensions in Hydrocyclones with Various Working Space Configurations

V. O. Yablonskii

Volgograd State Technical University, Volgograd, Russia

Received March 16, 2005

Abstract—The model of separation of suspensions with a non-Newtonian dispersion medium in a cylindroconical hydrocyclone, which takes into account the effect of the Coriolis force on solid particles, was constructed and applied to analysis of the rheological properties of the dispersion medium on separation of suspensions in hydrocyclones with various working space configurations.

Hydrocyclones are one of multi-purpose types of apparatus for separation of heterogeneous systems in chemical, microbiological, food, and other industries. Use of hydrocyclones yields a pronounced economic effect through intensification of technological processes. The economic feasibility and efficiency of separation processes are determined by the degree of thickening of the dispersed phase and by its loss. In this context, optimizing the design parameters of hydrocyclones and determining the optimal modes of their operation are important problems, which can lead, when solved, to intensification and accelerated development of numerous branches of industry.

Until now, there has been no rigorous theory of motion of two-phase systems in a swirling vortex flow. The overwhelming majority of modern studies [1–6] are based on the equation of a unidimensional motion of a small spherical particle suspended in a viscous incompressible turbulent flow.

In [1], methods for calculation of predictable separation parameters and other important performance characteristics of cylindroconical hydrocyclones were developed in the framework of a unified stochastic approach. As noted by the authors, an exact analytical description of particle motion in a centrifugal field, based on Navier–Stokes and flow continuity equations, requires that a number of not quite correct assumptions should be made, because of the complexity of the hydrodynamic situation in hydrocyclones, which impairs the adequacy of the suggested analytical descriptions of the real hydrodynamic pattern.

In [2, 3], fundamental aspects of a calculation of turbulent particle transport in a hydrocyclone, based on the continuity equation for the solid phase flow, were considered. Such an approach makes it possible to calculate both the amount of the solid phase recovered in a hydrocyclone and its parameters (concentration, granulometric composition) at any point of the apparatus. In [4], a numerical study of the flow structure and separation processes in a hydrocyclone was carried out using the Navier–Stokes equations. The momentum transfer by the dispersed phase was described in terms of the theory of multispeed continuum. By now, the equation of radial motion of particles in hydrocyclones of various designs has been solved with account of the action of inertia and Coriolis forces on a particle [5–7]. This made it possible to calculate the size distribution of particles of the dispersed phase and to determine their content in target separation products.

The difficulty encountered in solving equations that characterize sedimentation of solid particles in a hydrocyclone consists in that, in order to satisfy the requirement that the system of equations should be closed, it is necessary to use those solutions to equations of hydrocyclone hydrodynamics, which rigorously relate the circumferential, radial, and axial components of the fluid velocity over the entire working space of the apparatus. In addition, suspensions separated in chemical industry are, in most cases, non-Newtonian media whose effective viscosity decreases as the intensity of deformation rates becomes higher, which affects the hydrodynamics of apparatus.

1070-4272/05/7808-1294 © 2005 Pleiades Publishing, Inc.

It was concluded in [8, 9] that the rheological equation of state of a non-Newtonian liquid, which is commonly written in the form of the Ostwald–de Weyl power law, is applicable to multiphase heterogeneous systems.

A numerical study of the flow of a film of a non-Newtonian fluid in a cylindroconical hydrocyclone, based on solution of complete equations of rheodynamics, was carried out in [10]. Description of separation processes in a hydrocyclone with a freely forming surface of a non-Newtonian fluid phase by solving complete equations of rheodynamics has not been provided until now, but it is of considerable theoretical and practical interest.

The hydrocyclone comprises a cylindrical chamber, into which a suspension to be separated is fed tangentially through the inlet pipe mounted in its upper part, and a conical section. The height of the cylindrical chamber of the hydrocyclone is equal to its diameter. The suspension delivered into the hydrocyclone flows down, swirling, along its walls, having a radial (V_r), circumferential (V_φ), and axial (V_z) velocity components. Solid particles are thrown by the centrifugal force to apparatus walls and are then removed via an unloading device at the bottom discharge. The clarified suspension is also removed via the bottom discharge.

The efficiency of suspension separation in a hydrocyclone is determined by hydrodynamic parameters of a preliminarily swirled suspension film flowing down along the case walls under the action of the gravity force and pressure created by centrifugal forces.

The problem was mathematically formulated under the following assumptions: particles of the substance being recovered are uniformly distributed in the inlet pipe of the hydrocyclone; their concentration at the hydrocyclone inlet is c_0; for a film-type flow of a suspension with a non-Newtonian dispersion medium with a high effective viscosity, the flow mode is laminar and the sedimentation mode of solid particles is laminar [11].

The mathematical modeling of the concentration field in a flow of a suspension with a non-Newtonian dispersion medium in a cylindroconical hydrocyclone is performed by using the differential equation of convective diffusion in cylindrical coordinates, which can be written at a molecular diffusion coefficient equal to zero as follows [12]:

$$\mathrm{div}(\mathbf{V}_\mathrm{h} c) = 0, \tag{1}$$

where $\mathbf{V}_\mathrm{h}$ is the vector of velocity of solid particles, and c is the concentration of these particles (kg m^{-3}).

Equation (1) can be brought to the form

$$\mathbf{V}_\mathrm{h}\,\mathrm{grad}\,c + c\,\mathrm{div}\,\mathbf{V}_\mathrm{h} = 0. \tag{2}$$

As the velocity of solid particles differs from the velocity of a continuous flow of the dispersion medium, $\mathrm{div}\,\mathbf{V}_\mathrm{h} = \dfrac{1}{r}\dfrac{\partial[r(V_{r\mathrm{h}} - V_{r\mathrm{l}})]}{\partial r}$ and Eq. (2) takes the following form:

$$V_{r\mathrm{h}}\frac{\partial c}{\partial r} + V_{z\mathrm{h}}\frac{\partial c}{\partial z} = -c\left\{\frac{1}{r}\frac{\partial[r(V_{r\mathrm{h}} - V_{z\mathrm{h}})]}{\partial r}\right\}, \tag{3}$$

where $V_{r\mathrm{h}}(r, z)$ and $V_{z\mathrm{h}}(r, z)$ are the radial and axial velocity components of solid particles (m s^{-1}); $V_{r\mathrm{l}}(r, z)$, radial velocity component of the dispersion medium (m s^{-1}); r, z, radial and axial coordinates (m); h, solid particle; and l, dispersion medium.

This equation is solved together with the equation of motion of a solid particle.

It is assumed that the solid phase of a suspension being separated is monodisperse, which makes it possible to achieve a required degree of thickening of solid particles in modeling the separation process for the finest fraction. The inertia force acting on a solid particles in the axial direction, gravity force, and Archimedes buoyancy force are neglected by assuming that the axial component of the velocity of a solid particle, $V_{z\mathrm{h}}(r, z)$ is equal to the axial component of the velocity of the dispersion medium, $V_{z\mathrm{l}}(r, z)$. This assumption is well justified in practice because separation in hydrocyclones with a non-Newtonian dispersion medium having high effective viscosity occurs at larger Froude numbers Fr (separation factors).

Taking into account that suspensions with a non-Newtonian dispersion medium are separated in hydrocyclones under the conditions in which the Reynolds number, which characterizes the sedimentation mode of a solid particle, is not large, the Magnus force can be neglected. If a centrifugal Archimedes force, resistance force, and a Coriolis force act upon a solid particle, the equation of motion of a solid particle can be written, in projections onto the r and φ axes, as

$$\left.\begin{aligned} V_{r\mathrm{h}}\frac{\mathrm{d}V_{r\mathrm{h}}}{\mathrm{d}r} + V_{z\mathrm{h}}\frac{\mathrm{d}V_{r\mathrm{h}}}{\mathrm{d}z} &= \frac{V_{\varphi\mathrm{h}}^2}{r}\left(1 - \frac{\rho_\mathrm{l}}{\rho_\mathrm{h}}\right) - \frac{3}{4}\frac{K_{fr}\rho_\mathrm{l}(V_{r\mathrm{h}} - V_{r\mathrm{l}})|V_{r\mathrm{h}} - V_{r\mathrm{l}}|}{\rho_\mathrm{h} d_\mathrm{h}\Phi(B)}, \\ V_{r\mathrm{h}}\frac{\mathrm{d}V_{\varphi\mathrm{h}}}{\mathrm{d}r} + V_{z\mathrm{h}}\frac{\mathrm{d}V_{\varphi\mathrm{h}}}{\mathrm{d}z} &= \frac{V_{\varphi\mathrm{h}}V_{r\mathrm{h}}}{r} - \frac{3}{4}\frac{K_{f\varphi}\rho_\mathrm{l}(V_{\varphi\mathrm{h}} - V_{\varphi\mathrm{l}})|V_{\varphi\mathrm{h}} - V_{\varphi\mathrm{l}}|}{\rho_\mathrm{h} d_\mathrm{h}\Phi(B)}, \end{aligned}\right\} \tag{4}$$

where K_{fr}, $K_{f\varphi}$ are the coefficients of resistance to particle motion in the radial and circumferential directions; $V_{\varphi h}(r, z)$, circumferential velocity component of solid particles (m s^{-1}); d_h, diameter of solid particles (m); ρ_h, ρ_l, densities of solid particles and dispersion medium, respectively (kg m^{-3}); and φ, circumferential coordinate (deg).

The resistance coefficients for radial motion of a particle in a non-Newtonian fluid, K_{fr}, can be calculated using the empirical formula [13]

$$K_{fr} = \frac{24f_1(n)}{\mathrm{Re}_{nr}} + \frac{f_2(n)}{(\mathrm{Re}_{nr})^{f_3(n)}}, \quad (5)$$

where

$$f_1(n) = 3^{1.5(n-1)}\frac{2 + 29n - 22n^2}{n(n+2)(2n+1)},$$

$$f_2(n) = 10.5n - 3.5, \quad f_3(n) = 0.32n + 0.13.$$

$\mathrm{Re}_{nr} = [\rho_l(d_h)^n(V_{rh} - V_{rl})^{2-n}]/k$, local Reynolds number characterizing the sedimentation mode of solid particles; k, consistency index (Pa s^{n-1}); and n, nonlinearly index of the flow curve.

The resistance coefficient for circumferential motion of a particle, $K_{f\varphi}$, is calculated using similar dependences, but with the corresponding difference of particle and fluid velocities in the circumferential direction taken as a characteristic velocity difference.

The coefficient $\Phi(B)$, which accounts for the hindered conditions of particle sedimentation, is calculated using the formula suggested by Sokolov [14]:

$$\Phi(B) = 10^{-1.82(1-B)}, \quad (6)$$

where $B = 1 - c_0/\rho_h$, is a part of a unit volume of the suspension that is occupied by the dispersion medium, and c_0 is the concentration of solid particles in the inlet pipe of the hydrocyclone (kg m^{-3}).

The initial fraction of the suspension volume occupied by solid particles, equal to $1 - B$, was taken to be 0.05.

In accordance with the method of characteristics [15], the system of differential equations in partial derivatives, (3) and (4), is reduced to an equivalent system of ordinary differential equations, which can be represented in dimensionless form as

$$\frac{dR}{dZ} = \frac{G_h}{H_h},$$

$$\frac{dC}{dZ} = -\frac{C}{H_h}\left[\frac{d(G_h - G_l)}{dR} + \frac{G_h - G_l}{R}\right],$$

$$\left.\begin{aligned}\frac{dG_h}{dZ} &= -\frac{\Theta_h^2}{H_h R}(1-P) - \frac{3}{4}\frac{K_{fr}P(G_h - G_l)|G_h - G_l|}{D_h\Phi(B)},\\ \frac{d\Theta_h}{dZ} &= \frac{\Theta_h G_h}{H_h R} - \frac{3}{4}\frac{K_{fr}P(\Theta_h - \Theta_l)|\Theta_h - \Theta_l|}{D_h\Phi(B)},\end{aligned}\right\} \quad (7)$$

where $G_h(R, Z) = [V_{rh}(r, z)]/U_0$, $H_h(R, Z) = [V_{zh}(r, z)]/U_0$, $\Theta_h(R, Z) = [V_{\varphi h}(r, z)]/U_0$, are the dimensionless radial, axial, and circumferential velocity components of particles of the solid phase; $\Theta_l(R, Z) = [V_{\varphi l}(r, z)]/U_0$, $G_l(R, Z) = [V_{rl}(r, z)]/U_0$, dimensionless circumferential and radial velocity components of the dispersion medium; $C = c/c_0$, dimensionless concentration of solid particles; $P = \rho_l/\rho_h$, density parameter; $D_h = d_h/r_k$, dimensionless diameter of solid particles; $R = r/r_k$, $Z = z/r_k$, dimensionless radial and axial coordinates; U_0 average suspension velocity in the inlet pipe of the hydrocyclone (m s^{-1}); and r_k, radius of the cylindrical chamber of the hydrocyclone (m).

The boundary conditions for the system of ordinary differential equations (7) has the form

$$Z = 0, \quad 1 - F \le R \le 1, \quad C_0 = 1, \quad (8)$$

where C_0 is the dimensionless concentration of solid particles in the inlet pipe of the hydrocyclone; $F = f/r_k$, dimensionless width of the inlet pipe of the hydrocyclone; and f, width of the initial pipe of the hydrocyclone (m).

The approximating dependences for the radial $[H_l(r, z)]$ and axial $[\Theta_l(r, z)]$ velocity components of the dispersion medium can be represented as

$$\left.\begin{aligned}H_l(R, Z) &= H_{ls}(Z)\left[1 - \left(1 - \frac{1-R}{\Delta(Z)}\right)^{M(Z)}\right],\\ \Theta_l(R, Z) &= \Theta_{ls}(Z)\left[1 - \left(1 - \frac{1-R}{\Delta(Z)}\right)^{M(Z)}\right],\end{aligned}\right\} \quad (9)$$

where $H_l(R, Z) = V_{zl}(r, z)/U_0$ is the dimensionless axial velocity component of the dispersion medium; $H_{ls}(Z)$, $\Theta_{ls}(Z)$, dimensionless axial and circumferential velocity components of the dispersion medium at the film surface; $\Delta(Z) = \delta(z)/r_k$, dimensionless thickness of the suspension film; $L(Z)$, $M(Z)$, completeness coefficients of the radial distributions of the circumferential and axial velocity components; $\delta(z)$ suspension film thickness (m).

The values of $H_{ls}(Z)$, $\Theta_{ls}(Z)$, $M(Z)$, $L(Z)$, and $\Delta(Z)$ were approximated with fourth-order polynomials.

The first equation of the system (7) determines the motion trajectory of a solid particle, which de-

pends on the place of particle entry into the apparatus, i.e., sets the direction of the characteristic. The second equation yields the value of the function, i.e., the dimensionless concentration of solid particles, which indicates the degree of concentration of solid particles, on the characteristic. The remaining equations make it possible to find the radial (G_h) and circumferential (Θ_h) velocity components of the particle.

The system of differential equations (7) was solved by the fourth-order Runge–Kutta method with a fixed step. The rate of variation of the axial coordinate for a trajectory approaching the wall is many times that of the radial coordinate in the case of a small Re_{nr} number. Therefore, the given system of equations is a stiff set [16] and its solution requires a very large number of steps. the integration interval from the lower boundary of the inlet pipe of the hydrocyclone to the outlet orifice of the conical part of the case was divided into $M = 3 \times 10^5$ steps along the Z axis and the system of differential equations (7) was integrated using a software composed in Compaq Visual Fortran language. The error in solving the system, evaluated by doubling the number of steps, did not exceed 1×10^{-5}.

The separation of suspensions with a non-Newtonian dispersion medium in a hydrocyclone was simulated by modeling the velocity and pressure component fields in a flow of a non-Newtonian fluid in a cylindroconical hydrocyclone [10] and then approximating the results obtained. This was done by solving the system of differential equations (7) at a boundary condition (8) for widely varied defining similarity numbers and rheological constants of the dispersion medium. The flow of a non-Newtonian fluid in the hydrocyclone is characterized by a centrifugal Froude number Fr (separation factor), modified Reynolds number Re_n, dimensionless flow rate parameter Q, and nonlinearity index n of the flow curve. Sedimentation of solid particles in the field of centrifugal forces in a non-Newtonian dispersion medium is characterized by a local Reynolds number Re_{nr}, which varies along the trajectory of a particle.

The defining similarity numbers [10] were calculated as follows:

$$\mathrm{Fr} = \frac{U_0^2}{gr_k}, \quad \mathrm{Re}_n = \frac{\rho_l U_0^{2-n} r_k^n}{k}, \quad Q = \frac{q}{\pi r_k^2 U_0} = \frac{ef}{\pi r_k^2}, \quad (10)$$

where q is the suspension flow rate ($m^3\ s^{-1}$); e, height of the inlet pipe of the hydrocyclone (m); and g, acceleration of gravity ($m\ s^{-2}$).

The width F of the inlet pipe of the hydrocyclone was divided in the radial direction into 20 equal intervals and, for each point at boundaries between the intervals, a calculation of the corresponding trajectory and concentrations of solid particles along this trajectory was commenced. This was done so because the trajectory of a particle at prescribed hydrodynamic parameters of a suspension film is uniquely determined by the place of its entry into the apparatus. The arrival of a solid particle to the wall was determined from the condition $1 - R \le D_h$ with account of the accumulation of a deposit layer on the wall. As a solid particle arrived to the wall, the calculation for the given trajectory was terminated and a calculation of the next trajectory was commenced. The results obtained in the numerical simulation are shown in Figs. 1, 2.

Fig. 1a (*I*) shows the trajectories of solid particles, and Fig. 1b (*I*), the distributions of the concentrations of solid particles along the respective trajectories at Fr = 85, $Re_n = 4 \times 10^3$, $Q = 3.98 \times 10^{-2}$, $n = 0.6$, and $\alpha = 5°$. Analysis of Fig. 1a (*I*) demonstrates that the most intense sedimentation of solid particles in a centrifugal field occurs in the cylindrical chamber of the hydrocyclone, in which solid particles are in the zone of high values of the circumferential velocity component of the dispersion medium, Θ_l, near the surface of the suspension film. In the bottom zone of the conical part of the case, the film becomes considerably thicker and the radial velocity component of the dispersion medium, G_l, directed toward the apparatus axis, grows, with the result that particles move away from the case wall.

The concentrations of solid particles grow along the trajectories because of the thickening of the solid phase, and this increase is the most pronounced in regions close to the boundary between the thickened and clarified suspension.

Fig. 1 (*II*, *III*) shows the trajectories and concentration distributions for Fr, Re_n, Q, and n corresponding to Fig. 1 (*I*) at $\alpha = 10$ and 15°, respectively. Analysis of Fig. 1 (*I–III*) demonstrates that the maximum dimensionless concentration of solid particles, characterizing the degree of its thickening, is observed for $n = 0.6$ at $\alpha = 5°$. This is due to the low rate of decay of the circumferential velocity component of the dispersion medium, Θ_l, in the direction of the Z axis and to the high value of the completeness coefficient L of the radial distribution of Θ_l at a more pronounced anomaly of the non-Newtonian

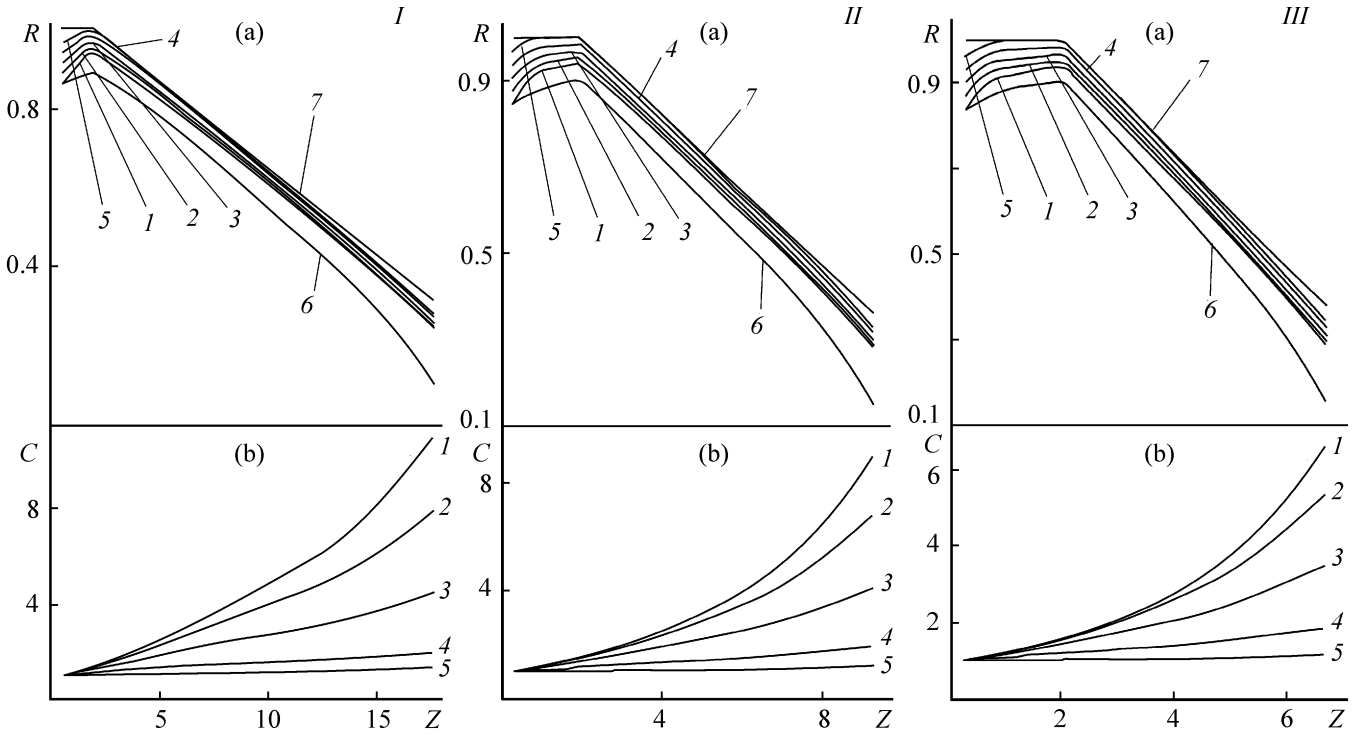


Fig. 1. (a) Trajectories of solid particles and (b) distribution of the concentrations C along the trajectories at Fr = 85, $\mathrm{Re}_n = 4 \times 10^3$, $Q = 3.98 \times 10^{-2}$, $n = 0.6$, $D_\mathrm{h} = 1.75 \times 10^{-3}$, and $P = 0.5$. (R) Dimensionless radial coordinate and (Z) dimensionless axial coordinate; the same for Fig. 2. α (deg): (*I*) 5, (*II*) 10, and (*III*) 15; the same for Fig. 2. (*1*) Trajectory corresponding to the boundary between the zones of clarified and thickened suspension, (*2*–*5*) trajectories of solid particles, (*6*) boundary of the suspension film, (*7*) wall of the hydrocyclone case; the same for Fig. 2.

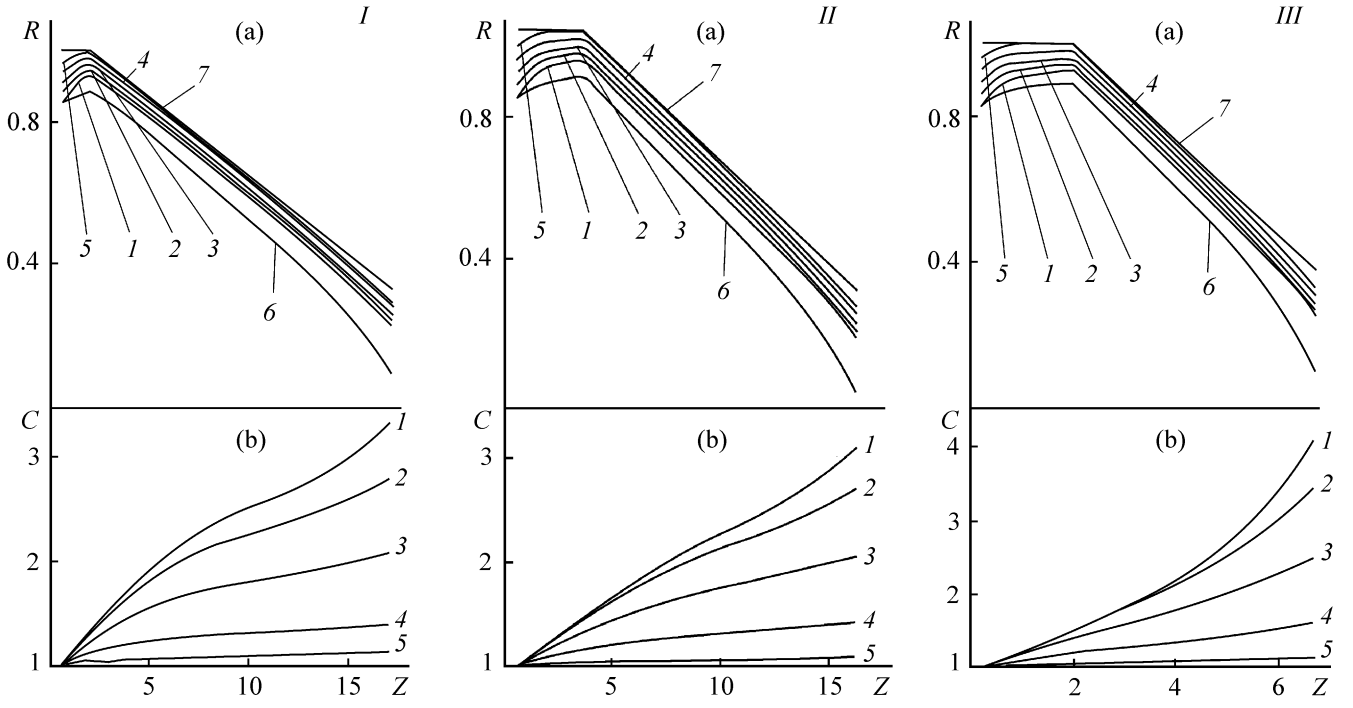


Fig. 2. (a) Trajectories of solid particles and (b) distribution of the concentrations C along the trajectories at Fr = 85, $\mathrm{Re}_n = 4 \times 10^3$, $Q = 3.98 \times 10^{-2}$, $n = 0.8$, $D_\mathrm{h} = 1.75 \times 10^{-3}$, and $P = 0.5$.

properties of the dispersion medium (n = 0.6). This yields a high degree of thickening of solid particles, because the length of the conical part of the hydrocyclone case is larger in the direction of the Z axis at $\alpha = 5°$, which makes longer the residence time of the suspension in the separation zone.

Fig. 2 (*I–III*) shows the trajectories and concentration distributions for Fr, Re_n, and Q corresponding to Fig. 1 (*I–III*) at n = 0.8 and $\alpha = 5°$, 10°, and 15°, respectively. Comparison of the concentration distributions at n = 0.8 [Fig. 2 (*I–III*)] and n = 0.6 [Fig. 1 (*I–III*)] shows that the degree of thickening of solid particles is lower at n = 0.8, which can be attributed to a faster decay of the circumferential velocity component Θ_1 in the direction of the Z axis and to a lower completeness coefficient L of the radial distribution of Θ_1 at a less pronounced anomaly of the non-Newtonian properties of the dispersion medium. Comparison of the data in Fig. 2 (*I–III*) suggests that the highest degree of thickening of solid particles at n = 0.8 is observed at $\alpha = 15°$, because this angle of conicity provides the minimum decay of the circumferential velocity component Θ_1 in the direction of the Z axis. At $\alpha = 5°$, the degree of thickening of solid particles exceeds that at $\alpha = 10°$, because the strong decay of the Θ_1 component along the Z axis at 5° is compensated for by the large length of the conical part of the hydrocyclone case in the direction of the apparatus axis.

As follows from the analysis of the calculated data for Fr, Re_n, and Q corresponding to Fig. 1 (*I–III*), even lower degrees of thickening of solid particles are obtained at n = 1.0 (Newtonian fluid), compared with the case of n = 0.8, because the rate of decay of the circumferential velocity component Θ_1 in the direction of the Z axis increases as the anomaly of the non-Newtonian properties of the dispersion medium becomes less pronounced. The lowest degree of thickening of solid particles is observed at $\alpha = 5°$ because of the strong decay of the Θ_1 component along the Z axis. At α = 10 and 15°, the degrees of thickening of solid particles are approximately the same because of the opposite kinds of influence exerted on the degree of thickening by such factors as the rate of decay of the circumferential velocity component Θ_1 of the dispersion medium along the Z axis and the length of the conical part of the hydrocyclone case in the direction of the apparatus axis.

CONCLUSIONS

(1) The degree of thickening of solid particles of the suspension in a cylindroconical hydrocyclone grows as the anomaly of the non-Newtonian properties of the dispersion medium becomes more pronounced because of the decrease in the rate of decay of the circumferential velocity component of the dispersion medium along the hydrocyclone axis and increase in the completeness coefficient of its radial distribution.

(2) The influence exerted by the angle of conicity of the hydrocyclone case on the degree of thickening of solid particles depends on the rheological properties of the dispersion medium, which determine the rate of decay of the circumferential velocity component of the dispersion medium along the hydrocyclone axis, because the rate of decay decreases and, simultaneously, so does the length of the conical part of the case along the apparatus axis, which makes shorter the residence time of the suspension in the separation zone.

(3) The mathematical model of separation of suspensions with a non-Newtonian dispersion medium in a cylindroconical hydrocyclone, constructed in the study, makes it possible to calculate the degree of thickening of solid particles as a function of the defining similarity numbers and rheological properties of the dispersion medium and can be used as a basis for developing a procedure for engineering calculations of hydrocyclones for separation of rheologically complex media.

REFERENCES

1. Ternovskii, I.G. and Kutepov, A.M., *Gidrotsiklonirovanie* (Hydrocyclonation), Moscow: Nauka, 1994.
2. Kudryavtsev, I.A. and Mikhotov, V.V., *Teor. Osn. Khim. Tekhnol.*, 1989, vol. 23, no. 1, pp. 120–121.
3. Kosoi, G.M. and Sapeshko, V.V., *Teor. Osn. Khim. Tekhnol.*, 1983, vol. 17, no. 5, pp. 637–641.
4. Dik, I.G., Matvienko, O.V., and Neesse, T., *Teor. Osn. Khim. Tekhnol.*, 2000, vol. 34, no. 5, pp. 478–488.
5. Baranov, D.A., Kutepov, A.M., and Lagutkin, M.G., *Teor. Osn. Khim. Tekhnol.*, 1996, vol. 30, no. 2, pp. 117–122.
6. Lagutkin, M.G., Baranov, D.A., Bulychev, S.Yu., and Baranova, E.Yu., *Khim. Neftegaz. Mashinostr.*, 2004, no. 5, pp. 3–6.
7. Lagutkin, M.G. and Baranov, D.A., *Teor. Osn. Khim. Tekhnol.*, 2004, vol. 38, no. 1, pp. 9–13.
8. Romankov, P.G., *Teor. Osn. Khim. Tekhnol.*, 1972, vol. 6, no. 6, pp. 855–871.

9. Vainshtein, I.A., *Inzh.–Fiz. Zh.*, 1983, vol. 45, no. 4, pp. 602–608.
10. Yablonskii, V.O., *Zh. Prikl. Khim.*, 2004, vol. 77, no. 6, pp. 971–977.
11. Dyakowski, T., Hornung, G., and Williams, R.A., *Chem. Eng. Res. Des. A.*, 1994, vol. 72, no. 4, pp. 513–520.
12. Bird, R.B., Stewart, V.E., and Lightfoot, E.N., *Transfer Phenomena*, New York: John Wiley and Sons, 1965. Translated under the title *Yavleniya perenosa*, Zhavoronkov, N.M. and Malyusov, V.A., Eds., Moscow: Khimiya, 1974.
13. Acharya, A., Mashelkar, R.A., and Ulbrecht, J., *Rheol. Acta*, 1976, vol. 15, no. 9, pp. 454–463.
14. Sokolov, V.I., *Tsentrifugirovanie* (Centrifugation), Moscow: Khimiya, 1976.
15. Matveev, N.M., *Differentsial'nye uravneniya* (Differential Equations), Minsk: Vysheisha Shkola, 1976.
16. Cahaner, D., Mowler, C., and Nash, S., *Chislennye metody i programmnoe obespechenie* (Numerical Methods and Software), Moscow: Mir, 2001.

Russian Journal of Applied Chemistry, Vol. 78, No. 8, 2005, pp. 1301–1305. Translated from Zhurnal Prikladnoi Khimii, Vol. 78, No. 8, 2005, pp. 1324–1328.
Original Russian Text Copyright © 2005 by A.Magerramov, M.Magerramov, Makhmudova, Alizade.

ORGANIC SYNTHESIS AND INDUSTRIAL ORGANIC CHEMISTRY

Synthesis of *N*-Substituted Oxazolidines and Morpholines

A. M. Magerramov, M. N. Magerramov, Kh. A. Makhmudova, and G. I. Alizade

Baku State University, Baku, Azerbaijan

Received July 28, 2004; in final form, April 2005

Abstract—A series of *N*-substituted oxazolidines and morpholines were prepared and characterized.

Among synthetic antioxidants, amine and diamine derivatives are the most similar to natural antioxidants in the antiradical activity [1]. Therefore, it was of interest to prepare new oxazolidine and morpholine derivatives and to study their antioxidant properties.

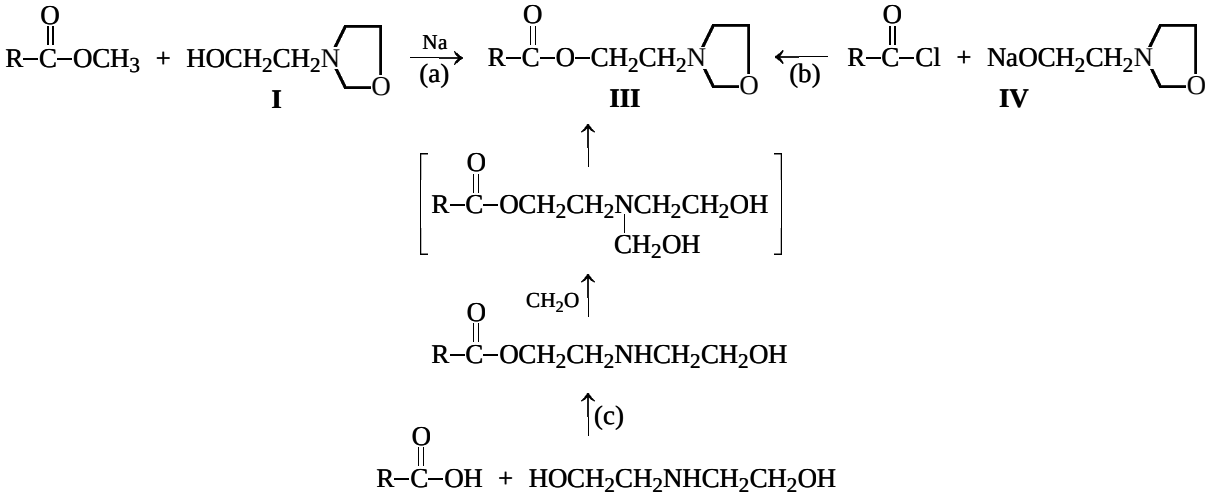
Condensation of *N*-methylethanolamine with aldehydes yielded *N*-methyloxazolidines [2]. Among *N*-substituted morpholine derivatives, 4-(2-hydroxyethyl)-, 2-methyl-4-(2-hydroxyethyl)-, and 2,2-dimethyl-4-(2-hydroxyethyl)morpholines and 4-benzyl-4-(2-benzyloxyethyl)morpholinium chloride are known [3].

In this study, we prepared new nitrogen-containing compounds, *N*-(2-alkanoyloxyethyl), *N*-(halobenzyl), and *N*-(halobenzyloxyethyl) derivatives of 1,3-oxazolidine and morpholine by reacting carboxylic acids and halobenzyl chlorides with ethanolamine, diethanolamine, ethylene chlorohydrin, morpholine, *N*-(2-hydroxyethyl)-1,3-oxazolidine, and *N*-(2-hydroxyethyl)-1,3-morpholine.

As a route to *N*-(2-alkanoyloxyethyl) derivatives of 1,3-oxazolidine and morpholine, we first examined the thermal esterification of carboxylic acids with *N*-(2-hydroxyethyl)oxazolidine **I** and *N*-(2-hydroxyethyl)morpholine **II**. Oxazolidine **I** was prepared by condensation of diethanolamine with formaldehyde [4], and morpholine **II**, by the reaction of morpholine with ethylene chlorohydrin.

The esterification was performed by the procedure described in [5]. We found that, in the reactions of carboxylic acids with oxazolidine **I**, the oxazolidine ring is cleaved first, yielding a complex mixture of products; in esterification of propionic acid, we isolated a product identified by ^{1}H NMR spectroscopy as $(CH_3CH_2COOCH_2CH_2)_2NCH_3$.

We succeeded in preparation of *N*-(2-alkanoyloxyetyhyl)-1,3-oxazolidines **III** by three routes: ester interchange of carboxylic acid methyl esters with *N*-(2-hydroxyethyl)-1,3-oxazolidine **I** (route a), reaction of carboxylic acid chlorides with *N*-(2-hydroxyethyl)-1,3-oxazolidine sodium derivative **IV** (route b), and esterification of carboxylic acids with diethanolamine, followed by condensation of the resulting ester with formaldehyde (route c):

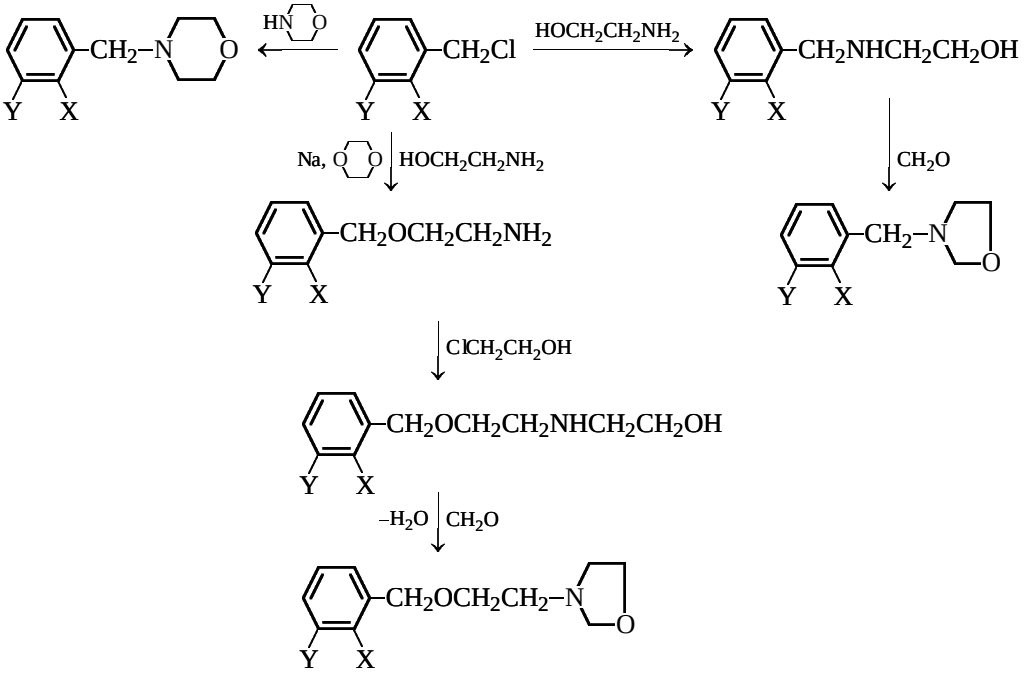


1070-4272/05/7808-1301 © 2005 Pleiades Publishing, Inc.

Synthesis of esters **III** by the reaction of carboxylic acids with diethanolamine is complicated by formation of a minor amount of *N*-acyldiethanolamine, which is difficult to separate.

In contrast to oxazolidine **I**, thermal esterification of carboxylic acids with morpholine **II** occurs without complications and yields *N*-(2-alkanoyloxyethyl)morpholines **V** in high yield (80–90%).

Then we prepared new *N*-substituted 1,3-oxazolidine and morpholine derivative by the reactions of halobenzene chlorides with ethanolamine or morpholine:



where Y = H, X = F: Y = Cl, X = H.

Among the compounds synthesized, *N*-(2-ethanoyloxyethyl)-1,3-oxazolidine was tested as antioxidant in studying the photosynthetic activity of *Synechococcus sp*. PCC 7942 (*Cyanophyceae*) cells as influenced by various doses of UV-C radication and the effect of various chronic doses of UV-C radiation on the duplication cycles of the population density of these cells. We found that the antioxidant deactivates the radicals generated in the cell throughout the experiment and thus increases the relative contribution from stimulation of cell fission by small doses of UV-C radiation; upon a single introduction into the cultural medium, the antioxidant restores the suppression of the fission rate of the irradiated cells by chronically high UV-C radiation doses to the level of the control population.

EXPERIMENTAL

The ^{1}H NMR spectra were recorded on a Bruker-300 spectrometer.

***N*-(2-Hydroxyethyl)-1,3-oxazolidine I**. a. A 55-g portion of diethanolamine was added dropwise over a period of 20 min to a stirred mixture of 15 g of paraform and 50 ml of benzene, heated to 80°C. After that, the stirring was continued for an additional 1.5 h. After the reaction completion, the solvent was distilled off; by distillation of the residue in a nitrogen flow under reduced pressure, we isolated 53 g (87%) of *N*-(2-hydroxyethyl)oxazolidine **I**, bp 79–80°C (4 mm Hg), d_4^{20} 1.1236, n_D^{20} 1.4764. ^{1}H NMR spectrum, δ, ppm: 2.68 (2H, NCH_2), 2.98 (2H, NCH_2), 3.61 t (2H, OCH_2), 3.75 t (2H, OCH_2), 4.25 s (2H, NCH_2O), 4.7 s (H, OH). ^{13}C NMR spectrum, δ_C, ppm: 52.5, 57.0, 62.0, 66.0, 87.0.

Di(2-propanoyloxyethyl)methylamine. b. A mixture of 11.7 g of oxazolidine **I** and 22.2 g of propionic acid was stirred at 130°C for 6 h. After the reaction completion, the mixture was neutralized with KOH and filtered to remove the potassium propionate precipitate. By distillation in a nitrogen flow under re-

duced pressure, we isolated 4 g (25%) of di(2-propanoyloxyethyl)methylamine, bp 102–103°C (2 mm Hg), d_4^{20} 1.0202, n_D^{20} 1.4400. ^{1}H NMR spectrum, δ, ppm: 1.18 t (6H, $2CH_3$), 2.32 q (4H, $2CH_2$), 2.4 s (3H, CH_3), 2.71 t [4H, $N(CH_2)_2$], 4.15 t (4H, $2OCH_2$). ^{13}C NMR spectrum, δ_C, ppm: 9.9, 27.0, 43.0, 56.0, 62.0, 172.5.

***N*-(2-Alkanoyloxyethyl)oxazolidines**. c. A solution of 0.09 ml of **I** in *m*-xylene was added dropwise to 0.005 mol of finely divided Na in 20 ml of *m*-xylene. After the completion of the initially vigorous reaction, the mixture was heated to 60°C, and the stirring was continued at this temperature until the sodium fully dissolved. Then 0.08 mol of appropriate carboxylic acid methyl ester was added dropwise at 120°C to the alcoholate, and the released methanol was distilled off. After cooling, the organic matter was separated, the residue was washed with benzene, and, after common work-up, the target products were isolated by distillation in a nitrogen flow under reduced pressure.

N-(2-Butanoyloxyethyl)-, *N*-(2-pentanoyloxyethyl)-, *N*-(2-hexanoyloxyethyl)-, and *N*-(2-octanoyloxyethyl)-1,3-oxazolidines were prepared (see table).

Yields, constants, and NMR spectra of the compounds synthesized

Compound	Yield, %	bp, °C (*P*, mm Hg)	n_D^{20}	d_4^{20}	NMR spectrum, δ, ppm
N-(2-Butanoyloxyethyl)oxazolidine	50	90–92 (2)	1.4540	1.0560	^{1}H NMR: 1.02 (3H, CH_3), 1.69 m, (2H, CH_2), 2.31 t, (2H, CH_2), 2.78 t, (2H, OCH_2), 3.72 t, (2H, OCH_2), 4.16 t, (2H, OCH_2), 4.22 s, (2H, NCH_2O). ^{13}C NMR: 12, 18, 37, 52, 62, 88, 172
N-(2-Pentanoyloxyethyl)oxazolidine	53	97–98 (2)	1.4534	1.0372	^{1}H NMR: 0.99 (3H, CH_3), 1.41 m, (2H, CH_2), 1.62 m, (2H, CH_2), 2.3 m, (2H, CH_2), 2.7 t, (2H, NCH_2), 3.0 t, (2H, OCH_2), 3.72 t, (2H, NCH_2), 4.15 t, (2H, OCH_2), 4.25 s, (2H, NCH_2O). ^{13}C NMR: 14, 22, 24, 33.5, 53.5, 54, 62.8, 63.2, 86.75, 173
N-(2-Hexanoyloxyethyl)oxazolidine	55	108–109 (2)	1.4490	1.0023	–
N-(2-Octanoyloxyethyl)oxazolidine	54	125 (2)	1.4520	0.9841	–
N-(2-Ethanoyloxyethyl)morpholine	70	69–70 (3)	1.4560	1.0723	–
N-(2-Propanoyloxyethyl)morpholine	75	80–81 (2)	1.4553	1.0439	–
N-(2-Butanoyloxyethyl)morpholine	90	108–109 (4)	1.4540	1.0231	^{1}H NMR: 1.08 t, (3H, CH_3), 1.75 m, (2H, CH_2), 2.37 t, (2H, CH_2), 2.58 t, (4H, $N(CH_2)_2$), 2.68 t, (2H, NCH_2), 3.71 t, (4H, $O(CH_2)_2$), 4.28 t, (2H, OCH_2). ^{13}C NMR: 14, 18, 37, 54, 58, 62, 67, 172
N-(2-Pentanoyloxyethyl)morpholine	80	115–116 (3)	1.4540	1.0072	–
N-(2-Hexanoyloxyethyl)morpholine	66	122–123 (3)	1.4555	0.9922	–
N-(2-Octanoyloxyethyl)morpholine	78	128–129 (2.5)	1.4560	0.9786	–
N-(*o*-Fluorobenzyl)morpholine	67	98–99 (5)	1.5140	1.1213	^{1}H NMR: 2.32 t, (4H, $N(CH_2)_2$), 3.45 s, (2H, $C_6H_4CH_2$), 3.54 t, (4H, $O(CH_2)_2$), 6.86–7.34 m, (4H, C_6H_4). ^{13}C NMR: 53, 57, 67, 115, 123, 129, 132, 159.9, 163
N-(*m*-Chlorobenzyl)morpholine	64	134 (3)	1.5180	1.1477	–
N-(*o*-Fluorobenzyl)-ethanolamine	60	120–122 (3)	1.5140	1.1449	–

Table (Contd.)

Compound	Yield, %	bp, °C (*P*, mm Hg)	n_D^{20}	d_4^{20}	NMR spectrum, δ, ppm
N-(*m*-Chlorobenzyl)-ethanolamine	60	138–140 (3)	1.5310	1.1709	–
N-(*o*-Fluorobenzyl)-oxazolidine	77	87–88 (2)	1.5240	1.1680	–
N-(*m*-Chlorobenzyl)-oxazolidine	87	108–110 (3)	1.5470	1.2010	^{1}H NMR: 2.8 t, (2H, NCH_2), 3.55 s, (2H, $C_6H_4CH_2$), 3.64 t, (2H, OCH_2), 4.1 s, (2H, NCH_2O), 7.08–7.3 m, (4H, C_6H_4). ^{13}C NMR: 52, 57.5, 86, 126.5, 127.5, 128.5, 129.5, 134, 141.5
N-(*o*-Fluorobenzyl)-ethylamine	50	86–87 (2)	1.5000	1.1012	–
N-(*m*-Chlorobenzyl)-ethylamine	50	110–112 (2)	1.5330	1.1489	–
N-(*o*-Fluorobenzyl-oxyethyl)ethanol-amine	30	150–151 (2)	1.5110	1.1418	–
N-(*m*-Chlorobenzyl-oxyethyl)ethanol-amine	30	170–172 (2)	1.5340	1.1683	^{1}H NMR: 1.72 s, (2H, NH_2), 2.7 t, (2H, NCH_2), 3.35 t, (2H, OCH_2), 4.35 s, (2H, $C_6H_4CH_2$), 7.0–7.25 m, (4H, C_6H_4), ^{13}C NMR: 42, 72, 73, 125, 127, 129, 134, 142
N-(*o*-Fluorobenzyl-oxyethyl)oxazolidine	76	134–135 (2)	1.5070	1.1349	–
N-(*m*-Chlorobenzyl-oxyethyl)oxazolidine	72	148–149 (2)	1.5370	1.1786	^{1}H NMR: 2.66 t, (2H, NCH_2), 2.86 t, (2H, NCH_2), 3.49 t, (2H, OCH_2), 3.61 t, (2H, OCH_2), 4.15 s, (2H, NCH_2O), 4.4 s, (2H, $C_6H_4CH_2$), 7.0–7.3 m, (4H, C_6H_4). ^{13}C NMR: 53, 54, 62, 71, 73, 87, 125, 129, 134, 141

***N*-(2-Ethanoyloxyethyl)-1,3-oxazolidine**. A solution of 5.7 g of **I** in benzene was added dropwise to 1.124 g of finely crushed Na in 20 ml of benzene. After the completion of the initially vigorous reaction, the mixture was heated to 60°C, and the stirring was continued at this temperature until the sodium fully dissolved. Then 3.82 g of acetyl chloride was added dropwise to the alcoholate at 20–22°C over a period of 2 h, after which the mixture was stirred for an additional 4 h. After the reaction completion, the organic phase was filtered to remove NaCl, the solvent was distilled off, and the residue was distilled in a nitrogen flow under reduced pressure to obtain 4 g (40%) of *N*-(2-ethanoyloxyethyl)-1,3-oxazolidine, bp 90°C (2 mm Hg), d_4^{20} 1.0998, n_D^{20} 1.4520. ^{1}H NMR spectrum, δ, ppm: 2.1 t (3H, CH_3), 2.75 t (2H, NCH_2), 3.0 t (2H, NCH_2), 3.72 t (2H, OCH_2), 4.15 t (2H, OCH_2), 4.21 s (2H, NCH_2O). ^{13}C NMR spectrum, δ_C, ppm: 20.0, 54.0, 62.5, 87.0, 170.0.

***N*-(2-Pentanoyloxyethyl)-1,3-oxazolidine**. A mixture of 10.5 g of diethanolamine, 10.2 g of valeric acid, and 30 ml of toluene was refluxed until the release of water was complete, after which the mixture was neutralized with KOH and filtered to remove KCl; the solvent was distilled off, and distillation of the residue in a nitrogen flow under reduced pressure gave 5 g (26%) of 2-(2-hydroxyethyl)aminoethyl valerate, bp 135–137°C (2 mm Hg), d_4^{20} 1.0816, n_D^{20} 1.4730.

The condensation of 2-(2-hydroxyethyl)aminoethyl valerate was performed by procedure a. The yield and physicochemical constants of *N*-(2-pentanoyloxyethyl)-1,3-oxazolidine coincided with those of the same product obtained by method c.

***N*-(2-Hydroxyethyl)morpholine**. To a mixture of 34.8 g of morpholine and 32.2 g of ethylene chlorohydrin, we added dropwise at 40–45°C over a period of 1.5 h 32 g of a 50% NaOH solution. After the reaction completion, the organic layer was separated and dried over sodium sulfate; by distillation in a nitrogen flow under reduced pressure, we isolated 35 g (67%)

of *N*-(2-hydroxyethyl)morpholine, bp 104°C (10 mm Hg), d_4^{20} 1.0742, n_D^{20} 1.4766. ^{1}H NMR spectrum, δ, ppm: 2.52 t (2H, NCH_2), 2.53 t [4H, $N(CH_2)_2$], 3.66 t [4H, $O(CH_2)_2$], 4.23 s (H, OH). ^{13}C NMR spectrum, δ, ppm: 54.0; 58.0, 61.0, 66.5.

***N*-(2-Alkanoyloxyethyl)morpholines** were prepared by esterification of carboxylic acids with morpholine **II**. The reactions were performed similarly to the preparation of *N*-(2-pentanoyloxyethyl)-1,3-oxazolidine. *N*-(2-Ethanoyloxyethyl)-, *N*-(2-propanoyloxyethyl)-, *N*-(2-butanoyloxyethyl)-, *N*-(2-pentanoyloxyethyl)-, *N*-(2-hexanoyloxyethyl)-, and *N*-(2-octanoyloxyethyl)morpholines were prepared (see table).

***N*-(Halobenzyl)morpholines**. To a stirred solution of 0.125 mol of morpholine in 60 ml of benzene, heated to 80°C, we added dropwise over a period of 1 h 0.125 mol of halobenzyl chloride, after which the mixture was stirred for an additional 3 h. After the reaction completion, the mixture was neutralized with a 5% $NaHCO_3$ solution, washed with water to neutral reaction, and dried over sodium sulfate. After distilling off the solvent, the desired compounds were isolated by distillation in a nitrogen flow under reduced pressure.

***N*-(*o*-Fluorobenzyl)- and *N*-(*m*-chlorobenzyl)morpholines** were prepared (see table). Data on *N*-(halobenzyl)-1,3-oxazolidines are listed in the table.

***N*-(*m*-Chlorobenzyl)- and *N*-(*o*-fluorobenzyl)ethanolamines**. Halobenzyl chloride (0.12 mol) was added dropwise to a stirred mixture of 1 mol of ethanolamine and 30 ml of benzene, after which the mixture was refluxed with stirring for 4 h, neutralized after cooling with KOH, and filtered to remove KCl. The benzene was distilled off, and the target products were isolated by distillation in a nitrogen flow under reduced pressure.

***N*-(*m*-Chlorobenzyl)- and *N*-(*o*-fluorobenzyl)oxazolidines** were prepared similarly to *N*-(2-hydroxyethyl)-1,3-oxazolidine. Data on *N*-(halobenzyloxyethyl)-1,3-oxazolidines are listed in the table.

β-(*m*-Chlorobenzyloxy)- and β-(*o*-fluorobenzyloxy)ethylamines. Ethanolamine (0.1 mol) was added dropwise to 0.25 mol of finely divided Na in 25 ml of dioxane. After the completion of the initially vigorous reaction, the mixture was heated to reflux and stirred at this temperature until the sodium fully dissolved. Then, while cooling below 15°C, 0.19 mol of halobenzyl chloride was added dropwise, and the resulting mixture was stirred for 5 h. After the reaction completion, the mixture was filtered to remove NaCl, the dioxane was distilled off, and the desired products were isolated by distillation in a nitrogen flow under reduced pressure.

***N*(*m*-Chlorobenzyloxyethyl)- and *N*-(*o*-fluorobenzyloxyethyl)ethanolamines** were prepared similarly to *N*-(*m*-chlorobenzyl)- and *N*-(*o*-fluorobenzyl)-1,3-oxazolidines.

***N*-(*m*-Chlorobenzyloxyethyl)- and *N*-(*o*-fluorobenzyloxyethyl)oxazolidines** were prepared similarly to *N*-(2-hydroxyethyl)-1,3-oxazolidine.

CONCLUSION

Thermal esterification of carboxylic acids with *N*-(2-hydroxyethyl)morpholine gives *N*-(2-alkanoyloxyethyl)morpholines in high yield (80–90%). With *N*-(2-hydroxyethyl)-1,3-oxazolidine, a complex mixture of products is formed; the desired products were obtained in 50–80% yield by indirect procedures.

REFERENCES

1. Berkman, B.E., *Promyshlennyi sintez aromaticheskikh nitrosoedinenii i aminov* (Industrial Synthesis of Aromatic Nitro Compounds and Amines), Moscow: Khimiya, 1964, pp. 30–50.
2. Knorr, L. and Mattes, H., *Ber.*, 1901, vol. 34, no. 5, pp. 3484–3486.
3. Azizov, A.M., Reactions of 1,2-Amino Alcohols and Their Quaternary Salts with Organohalogen Compounds and Bases, *Doctoral Dissertation*, Baku, 1991.
4. Gadzhiev, G.Yu. and Veiisov, K.V., *Khim. Geterotsikl. Soedin.*, 1976, no. 4, pp. 447–449.
5. Magerramov, M.N., Makhmudova, Kh.A., Magerramov, G.Kh., and Lyutfaliev, A.N., *Izv. Bak. Univ., Ser. Estestv. Nauk*, 2001, no. 1, pp. 99–100.

Russian Journal of Applied Chemistry, Vol. 78, No. 8, 2005, pp. 1306–1308. Translated from Zhurnal Prikladnoi Khimii, Vol. 78, No. 8, 2005, pp. 1329–1332.
Original Russian Text Copyright © 2005 by Efanov, Dudkin, Galochkin.

ORGANIC SYNTHESIS AND INDUSTRIAL ORGANIC CHEMISTRY

Mechanochemical Synthesis of Nitrogen-containing Derivatives of Flax Boon

M. V. Efanov, D. V. Dudkin, and A. I. Galochkin

Altai State University, Barnaul, Russia

Received March 10, 2005; in final form, May 14, 2005

Abstract—The influence exerted by the conditions of the mechanochemical synthesis [time (100–100 min), air pressure (1–9 atm), temperature (30–90°C), amount of ammonia (0.5–3.0 g g^{-1} raw material)] on the content of nitrogen and functional groups in the products of oxidative ammonolysis of flax boon was studied. The resulting products were tested as nitrogen-containing ion exchangers in sorption of heavy metals.

In processing of plant raw materials, the modern trends are toward integrated chemical processing of the whole biomass to obtain polymeric compounds with prescribed properties. One of the ways of utilizing plant wastes is their use as raw materials for preparing fertilizers and sorbents [1, 2].

To obtain a nitrogen-containing fertilizer from wood bark, Deineko et al. suggested a process involving chemical treatment of the plant raw material with oxygen in aqueous ammonia (oxidative ammonolysis) [3]. The main disadvantages of this process are high temperature (75–200°C), high oxygen pressure (up to 8 MPa), and relatively low nitrogen content in the resulting fertilizer (1.0–3.5%).

Oxidation of lignocarbohydrate materials with ammonium persulfate in ammonia under mild conditions yielded valuable nitrogen-containing derivatives suitable as nitrogen-containing organic fertilizers and ion exchangers [4]. However, commercial use of this process is restricted by the high cost of ammonium persulfate and its large consumption. We have developed a new mechanochemical procedure for preparing nitrogen-containing derivatives of lignocarbohydrate materials by oxidation with atmospheric oxygen in aqueous ammonia [5].

Flax boon is a fairly valuable plant raw material; it is available in large amounts as a waste from flax processing in Altai krai and finds no proper use today. The possibility of using flax boon oxidation products as nitrogen-containing organic fertilizers was shown in [6].

In this study, we examined how the conditions of flax boon oxidation with atmospheric oxygen in aqueous ammonia affect the composition and properties of the resulting nitrogen-containing derivatives.

EXPERIMENTAL

As the raw material we used finely cut flax boon from the Biisk Flax Joint-Stock Company as air-dry particles ~0.5 mm in size.

According to chemical analysis [7], the raw material contained 37.2% cellulose, 25.6% hemicellulose, and 35.8% lignin.

The oxidative ammonolysis was performed as follows. A 5.0-g sample of air-dry flax boon was placed in a 300 cm^3 cylindrical reactor of a vibration mill (IV-98B vibrator, frequency 2800 cm^{-1}) with 15 steel rods (10 × 100 mm).

The temperature-controlled reactor was charged with 25% aqueous ammonia in an amount of 0.5–3.0 g of NH_3 per gram of the raw material, air was pumped in with a compressor to the final pressure of 1–9 atm, and the mixture was vigorously milled for 10–100 min. The temperature in the reaction chamber was 30–90°C. After the process completion, the products were unloaded, separated from the rods, washed with water to neutral reaction, and dried in a desiccator to constant weight.

The products were analyzed for the content of fixed nitrogen by the Kjeldahl method [8], for the content of carboxy groups by conductometric back-titration, and for the content of phenolic hydroxy groups by a chemisorption method as described in [9]. The sorption power of the nitrogen-containing flax boon derivatives

1070-4272/05/7808-1306 © 2005 Pleiades Publishing, Inc.

toward Cu(II) and Cd(II) ions was determined under the equilibrium conditions as described in [2].

Figure 1a shows how the duration of the mechanochemical synthesis affects the functional composition of the products of oxidative ammonolysis of flax boon. It is seen that the mechanochemical treatment for a time exceeding 60 min does not lead to further changes in the content of fixed organic nitrogen and functional groups.

In the first 30 min of the process, the content of phenolic hydroxy groups steadily decreases, and carboxy groups are accumulated. The nitrogen content grows insignificantly. However, the content of carboxy groups increases to a greater extent than decreases the content of phenolic groups. Apparently, carboxy groups in the macromolecular components of the boon are formed not only by oxidation of phenolic groups but also by demethoxylation. This was shown in our previous study [10].

In the interval from 40 to 60 min, fixed organic nitrogen is accumulated, and the content of carboxy groups decreases. This is apparently due to the reaction of ammonia with carboxy groups to form amide groups.

Figure 1b shows that the dependence of the content of fixed nitrogen on the air pressure flattens out. An increase in the oxygen pressure above 6 atm does not result in a significant increase in the content of fixed nitrogen. The content of carboxy groups varies insignificantly, which is apparently due to possible decarboxylation and formation of amide groups at 70°C under the conditions of mechanochemical synthesis.

Table 1 shows how the amount of ammonia affects the functional composition of the products of the

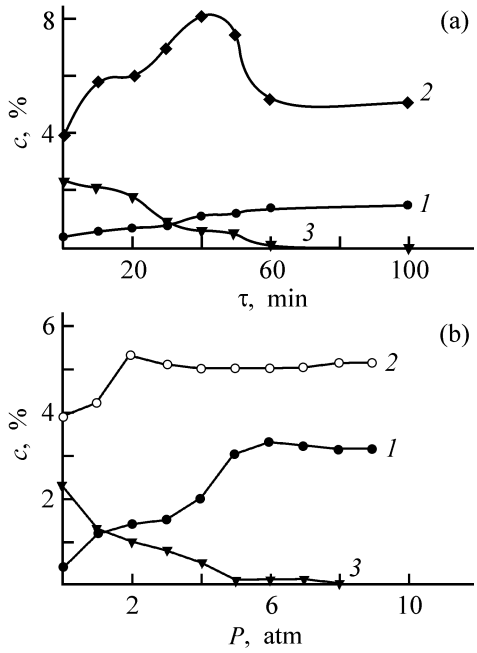


Fig. 1. Content *c* of (*1*) nitrogen, (*2*) COOH groups, and (*3*) phenolic OH groups in the products of oxidative ammonolysis of flax boon vs. the (a) duration *t* of mechanochemical treatment and (b) air pressure *P*.

oxidative ammonolysis. With an increase in the ammonia amount from 0.5 to 1.5 g g^{-1} raw material, the content of fixed nitrogen increases from 1.6 to 5.6%. A decrease in the content of carboxy groups is apparently due to decarboxylation or formation of amide groups. A further increase in the ammonia content to 3.0 g g^{-1} does not lead to significant changes in the content of fixed nitrogen and carboxy groups.

We examined the influence of temperature on the functional composition of the products of oxidative ammonolysis of flax boon (Table 2) and revealed no definite trends.

Table 1. Influence of the ammonia amount on the content of fixed nitrogen and carboxy groups in products of oxidative ammonolysis of flax boon (reaction time 60 min, air pressure 6 atm, temperature in the reactor 70°C)

NH_3, g g^{-1} raw material	Content, %	
	N	COOH
0.5	1.6	5.7
1.0	3.5	5.1
1.5	5.5	4.1
2.0	5.5	3.8
2.5	5.5	3.5
3.0	5.6	3.4

Table 2. Influence of temperature on the content of fixed nitrogen and carboxy groups in products of oxidative ammonolysis of flax boon (reaction time 60 min, air pressure 6 atm, 1.5 g of ammonia per gram of the raw material)

T, °C	Content, %	
	N	COOH
30	3.0	4.1
40	3.8	4.4
50	4.2	3.9
60	4.4	4.0
70	5.5	4.0
80	4.1	4.4
90	3.8	3.9

Table 3. Content of cellulose and lignin in the product of oxidative ammonolysis of flax boon. (treatment time 60 min, air pressure 6 atm, amount of ammonia 1.5 g per gram of the raw material)

Component	Content, wt %	
	initial flax boon	oxidative ammonolysis product (5.5% N)
Cellulose	37.2	34.2
Lignin	35.8	35.3

Table 4. Sorption power of nitrogen-containing flax boon derivatives toward transition metal ions (MSO_4 concentration 0.05 g-equiv l^{-1})

Sample	Pressure, atm	Content, %		SEC, mg-equiv g^{-1}	
		N	COOH	Cu^{2+}	Cd^{2+}
Initial boon	–	0.5	3.9	0.8	0.6
1	1	1.2	4.2	2.2	2.8
2	6	3.5	5.1	3.4	3.9

The content of fixed nitrogen is maximal (5.5%) upon treatment at 70°C. Thus, the following conditions of oxidative ammonolysis should be considered as optimal: treatment time 60 min, temperature 70°C, and air pressure 6 atm.

Formation of various forms of fixed nitrogen was confirmed by IR spectra. The spectra of the products contain absorption bands characteristic of carboxy groups (1720 cm^{-1}), amide groups (1650 cm^{-1}), and heterocyclic structures of the indole type (1585 and 1550 cm^{-1}).

In the product of oxidative ammonolysis of flax boon, containing 5.5% nitrogen, we determined the cellulose content by the Kürschner method and the lignin content by the Komarov method [7] (Table 3). The content of lignin in the initial flax boon and in the product of its oxidative ammonolysis is the same, i.e., no delignification occurs in the solid phase. The cellulose content changes insignificantly (by 3%).

Data on the sorption power of nitrogen-containing flax boon derivatives toward Cu(II) and Cd(II) cations are given in Table 4. As seen, the static exchange capacity (SEC) of the products of oxidative ammonolysis of flax boon for Cu(II) and Cd(II) cations increases with the content of nitrogen and COOH groups.[1]

CONCLUSIONS

(1) A procedure was developed for preparing nitrogen-containing derivatives of flax boon by its oxidative ammonolysis with atmospheric oxygen in aqueous ammonia by a mechanochemical procedure. Products containing up to 5.5% fixed organic nitrogen and up to 8.0% carboxy groups were obtained.

(2) The products exhibit high sorption power toward Cu(II) and Cd(II) ions and can be used as ion exchangers and nitrogen-containing fertilizers of prolonged action, increasing the yield of food grains by 19–24%.

REFERENCES

1. USSR Inventor's Certificate, no. 545627.
2. Efanov, M.V., Dudkin, D.V., and Galochkin, A.I., *Zh. Prikl. Khim.*, 2002, vol. 75, no. 10, pp. 1745–1746.
3. Deineko, I.P., Deineko, I.V., and Kornilova, L.I., *Zh. Prikl. Khim.*, 2002, vol. 75, no. 3, pp. 502–505.
4. RF Patent 2185394.
5. RF Patent 2215755.
6. Efanov, M.V., Panchenko, O.A., and Zabelina, A.V., *Khim. Rast. Syr'ya*, 2004, no. 3, pp. 95–97.
7. Obolenskaya, A.V., Shchegolev, V.P., Akim, G.L., *et al.*, *Prakticheskie raboty po khimii drevesiny i tsellyulozy* (Practical Works on Chemistry of Wood and Cellulose), Moscow: Lesnaya Prom–st., 1965.
8. Klimova, V.A., *Osnovnye mikrometody analiza organicheskikh soedinenii* (Main Methods of Organic Microanalysis), Moscow: Khimiya, 1975.
9. Zakis, G.F., *Funktsional'nyi analiz ligninov i ikh proizvodnykh* (Functional Analysis of Lignins and Their Derivatives), Riga: Zinatne, 1987.
10. Efanov, M.V. and Dudkin, D.V., *Khim. Prirodn. Soedin.*, 2004, no. 3, pp. 235–236.

[1] The product containing 5.5% fixed nitrogen was tested as a nitrogen-containing organic fertilizer for spring wheat of the Altaiskii Prostor strain (1.5 t ha^{-1}). According to the results of the field tests, the effect of the fertilizer based on the product of oxidative ammonolysis of flax boon is comparable with the effect of ammonium sulfate. The products obtained are nitrogen-containing organic fertilizers of prolonged action, increasing the yield of spring wheat by 19–24% during a period of 2–3 years.

Russian Journal of Applied Chemistry, Vol. 78, No. 8, 2005, pp. 1309–1311. Translated from Zhurnal Prikladnoi Khimii, Vol. 78, No. 8, 2005, pp. 1333–1335.
Original Russian Text Copyright © 2005 by Talzi, Doronina, Belyi.

ORGANIC SYNTHESIS AND INDUSTRIAL ORGANIC CHEMISTRY

Quick Determination of the Total Content of Aromatic Hydrocarbons in Reformer Naphthas by ^{1}H NMR Spectroscopy

V. P. Talzi, S. S. Doronina, and A. S. Belyi

Institute of Problems of Hydrocarbon Processing, Siberian Division, Russian Academy of Sciences, Omsk, Russia

Received April 20, 2005

Abstract—A procedure for fast determination of the total content of arenes in reformer naphthas by ^{1}H NMR spectroscopy was developed and tested. Their content is determined from the ratio of the integral intensities of the signals of aromatic protons and alkane methyl protons, using a calibration plot constructed on the basis of GLC data.

The procedure suggested for fast (<10 min) and relatively accurate determination of the total content of aromatic hydrocarbons in reformer naphthas by ^{1}H NMR spectroscopy may be of use not only for research but also plant laboratories, since the GLC analysis is relatively complex and time-consuming. As a rule, laboratories of oil refineries are not equipped with NMR spectrometers. This is caused by insufficient demand, rather than by the high cost of these devices: The analytical problems that could be efficiently solved by NMR and could justify the use of this method under industrial conditions are yet few. Fast and accurate determination of the total content of aromatics in reformer naphthas could be one of such problems. Also, we have recently developed a procedure [1] based on ^{1}H and ^{13}C NMR for monitoring the composition (and thus the service characteristics) of aqueous monoethanolamine solutions used at the majority of oil refineries for treating process gases.

Quantitative analysis of mixtures of organic substances by ^{1}H NMR spectroscopy, from the integral intensities of nonoverlapping signals of components, is a routine procedure that has been used for many decades [2]; it is not inferior to GLC in the accuracy.

Figures 1a and 1b show the ^{1}H NMR spectra of a reformer naphtha sample obtained on a laboratory rig. All the aromatic protons of its components, from mesitylene (upfield border of the range) to naphthalene (downfield border), give signals in the range from 6.6 to 7.7 ppm; no other protons give signals in this range. Thus, the integral intensity of signals in this range of the ^{1}H NMR spectra can be an adequate measure of the total content of aromatic hydrocarbons in the sample. As the absolute intensities of signals, as a rule, do not bear analytical information, it is necessary to choose an appropriate reference signal in the

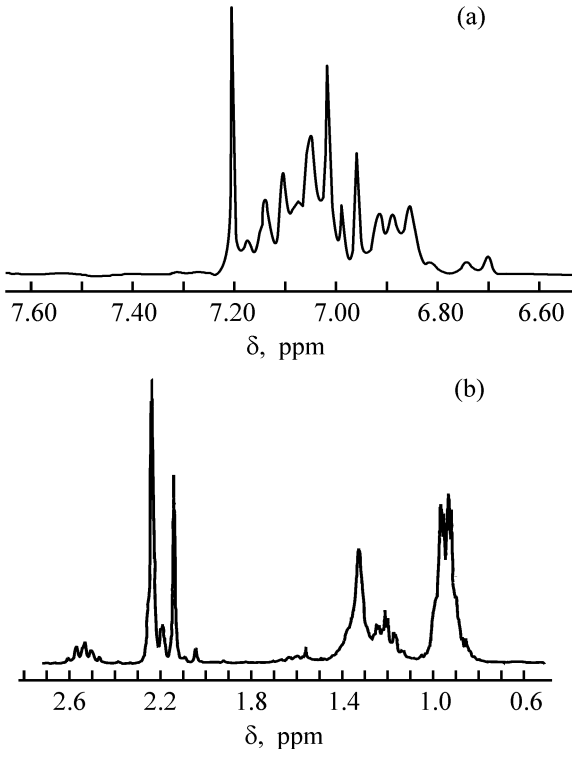


Fig. 1. (a) Low-field (aromatic protons) and (b) high-field parts of the ^{1}H NMR spectrum of a reformer naphtha sample. In the range 3.0–6.6 ppm, there are no signals. (δ) Chemical shift.

1070-4272/05/7808-1309 © 2005 Pleiades Publishing, Inc.

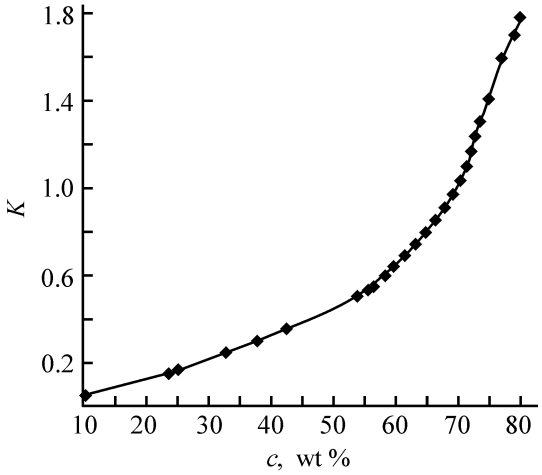


Fig. 2. Calibration curve plotted to determine total content of arenes in reformer naphthas, according to ^{1}H NMR spectrum. (*K*) Ratio of the integral intensities of the signals from the aromatic and aliphatic protons at 6.7–7.7 and 0.8–1.0 ppm and (*c*) total content of arenes in the samples produced by GLC.

^{1}H NMR spectrum, so that the ratio of the intensities of the signals from aromatic protons and the reference signal should be the measure of the content of arenes. As such a reference signal we chose a broad signal at 0.7–1.0 ppm belonging to methyl groups of the aliphatic components. Among aromatic compounds, only methyl groups of *n*-propylbenzene, butylbenzenes, and higher alkylbenzenes contribute to the absorption in this range. Since the content *n*-propylbenzene, the most abundant among these compounds, does not exceed 1%, this contribution can be neglected, i.e., the ratio of the integral intensities of the signals at 6.6–7.7 and 0.7–1.0 ppm can be considered as adequately reflecting the ratio of aromatic and aliphatic hydrocarbons in a sample and can be used, after appropriate calibration, as the measure of the total content of arenes in reformer naphthas.

Total content of arenes in reformer naphthas, according to GLC and NMR data

Run no.	Content, %	
	NMR	GLC
1	59.2	62.5
	66.0	66.0
	71.5	69.7
	75.1	75.3
2	63.2	62.4
	69.4	68.9
	71.3	71.1
	77.6	77.2
3	65.2	63.1
	70.5	70.2
	72.6	72.8
	77.5	80.6
4	58.3	59.9
	62.3	62.5
	63.8	64.9
	69.9	69.9
5	59.0	59.3
	61.3	62.3
	65.9	67.4
	68.0	69.2

According to reference data [3], the narrow singlet at 7.20 ppm belongs to benzene (Fig. 1a); the singlet at 7.02 ppm, to *p*-xylene; the next singlet at 6.95 ppm, to *p*-ethyltoluene; and the fourth singlet at 6.99 ppm, presumably to *p*-diethylbenzene or *p*-*n*-propyltoluene. The weak signals at 7.30 and 7.65 ppm belong to naphthalene, and the high-field signals at 6.70 and 6.75 ppm, to mesitylene and durene, respectively.

The weak signals at about 2.8 ppm belong to aliphatic protons of indan (Fig. 1b); the signals at 2.6–2.4 ppm, to α-CH_2 groups of alkylbenzenes (ethylbenzene, ethyltoluenes, *n*-propylbenzene, etc.); the signals at 2.0–2.34 ppm, to CH_3 groups of methylbenzenes; the signal at 1.25–1.40 ppm, mainly to CH_3 groups of alkanes; the triplet at 1.1–1.2 ppm, to CH_3 groups of ethylarenes; and the signal at 0.8–1.0 ppm, to CH_3 groups of alkanes and some alkylbenzenes [3].

Figure 2 shows a calibration curve plotted as the intensity ratio of the above-indicated signals of aromatic and methyl protons in the ^{1}H NMR spectra (along the ordinate) vs. the total content of aromatic hydrocarbons in the reformer naphthas according to GLC data (along the abscissa).

The curve in Fig. 2, though having numerous inflection points, is steadily ascending. The steep slope of the curve in the range of arene content typical of reformer naphthas (60–80%) means that the intensity ratio of the analytical signals appreciably changes even upon minor changes in the total content of arenes, which makes the suggested method highly accurate.

Representative data on the total content of arenes in various reformer naphtha samples, determined by NMR with the calibration curve shown in Fig. 2 and by GLC, are listed in the table. The agreement is quite reasonable, the more so as we deal with the concentrations determined by two different methods, rather than with "introduced–found" data. If similar raw materials are fed and the same catalyst is used in the reforming, the analysis accuracy is determined by

the accuracy of construction of the calibration curve. In the case of a correct calibration, the concentrations determined by NMR may be even more correct and reproducible than those determined by GLC, because recording of an NMR spectrum is not accompanied by decomposition of the sample and does not alter the results of the subsequent determinations, and the relative intensity of the signals does not appreciably depend on the quality and working status of the spectrometer and, in particular, on the uniformity of the magnetic field. Furthermore, only two groups of signals are integrated in the NMR procedure, whereas a GLC analysis involves integration of several tens of peaks, sometimes ill-resolved.

When the feed source and catalyst are replaced in a laboratory or industrial reforming installation, it is not necessary to construct a new calibration curve (Fig. 2) provided that the fractional composition of the feed with respect to major components remains similar and the new catalyst does not alter significantly the ratio of different arenes in the reformer naphtha. The data listed in the table were obtained with similar feed from several oil refineries and with several batches of commercial and experimental catalysts. At the same time, when a considerably lower-boiling benzine fraction (C_6) is used as a feed, the content of arenes in the reformer naphtha obtained by GLC (e.g., 20%) appears to be appreciably lower than that determined by NMR using the calibration curve in Fig. 2 (31%). Thus, a new calibration curve should be constructed in this case.

The approach suggested can also be used for fast estimation of the benzene content in reformer naphthas. Because the benzene signal in the ^{1}H NMR spectrum (Fig. 1a) only slightly overlaps with signals of other arenes, the ratio of the integral intensity of this signal to the total integral intensity of signals of aromatic protons can be correlated with the relative content of benzene in the sum of arenes, determined by GLC. By determining the total content of arenes (by the procedure suggested) and multiplying it by the ratio of the integral intensity of the benzene signal (7.2 ppm) to the total integral intensity of signals of aromatic protons in the ^{1}H NMR spectrum and then by the calibration factor (0.5–0.6, estimated by comparing the GLC and NMR data), it is possible to determine the benzene concentration with a relative accuracy of about 10%, at least for reformer naphthas containing 60–80% arenes.

EXPERIMENTAL

Reformer naphtha samples were obtained on an OL-120 pilot installation under typical conditions of catalytic reforming of a hydrorefined 85–120°C benzine fraction from Omsk Oil Refinery. Before measurements, naphtha samples were stabilized by the standard procedure.

The content of specific hydrocarbons and of the sum of arenes in naphtha samples was determined by gas–liquid chromatography on a Tsvet-800 analytical gas chromatograph equipped with an RTX-60 capillary column and a flame-ionizattion detector (for more detail, see [4, 5]).

The ^{1}H NMR spectra were recorded on a Bruker ACP-200P spectrometer.

CONCLUSION

Provided that similar feed and similar catalysts are used for reforming, the total content of arenes and the relative content of benzene in reformer naphthas can be determined rapidly and fairly accurately by ^{1}H NMR spectroscopy.

REFERENCES

1. Talzi, V.P., *Zh. Prikl. Khim.*, 2004, vol. 77, no. 3, pp. 437–441.
2. Emsley, J.W., Feeney, J., and Sutcliffe, L.H., *High Resolution Nuclear-Magnetic Resonance Spectroscopy*, Oxford: Pergamon, 1965.
3. Pouchert, Ch.J. and Campbell, J.R., in *The Aldrich Library of NMR Spectra*, 1974.
4. *Programma sbora i obrabotki khromatograficheskikh dannykh "Tsvet-Analitik dlya Windows"* (Tsvet-Analytic for Windows: Program for Collection and Processing of Chromatographic Data).
5. Rudenko, B.A., *Kapillyarnaya khromatografiya* (Capillary Chromatography), Moscow: Nauka, 1978.

Russian Journal of Applied Chemistry, Vol. 78, No. 8, 2005, pp. 1312–1315. Translated from Zhurnal Prikladnoi Khimii, Vol. 78, No. 8, 2005, pp. 1336–1339.
Original Russian Text Copyright © 2005 by Chursin.

ORGANIC SYNTHESIS AND INDUSTRIAL ORGANIC CHEMISTRY

Colloid-Chemical Properties of Organic–Aqueous Surfactants

V. I. Chursin

Research Institute of Tanning Industry, Federal State Unitary Enterprise, Moscow, Russia

Received March, 24, 2005

Abstract—The colloid-chemical properties of organic–aqueous formulations including a nonionic surfactant, an organic solvent, and polyethylenepolyamine were studied. The most efficient methods for preparation of a new degreasing material, Skianol, were determined.

Efficient degreasing of leather and fur raw material implies use of surfactants with high dispersing and washing properties, whose components promote dissolution of natural skin fats. We suggested the compositions for such formulations in [1]. However, development of a universal organic–aqueous composition affording the maximum extent of fat removal requires optimization of both the method of its preparation and its composition.

In this study, we examined how an organic solvent and an amine-containing additive affect the colloid-chemical properties of an organic–aqueous formulation and its preparation in the optimal, from the viewpoint of the technological use, consistency, namely, as a gel. We showed in [1] that introduction of an organic solvent into aqueous solutions of surfactants decreases the surface tension of the system formed. It can be assumed that other properties of these systems will change as well. Organic-aqueous systems are of both scientific and practical interest. It is known that the nature of the intermolecular interactions and morphological structures formed in such systems depends on the content of the organic solvent [2]. A study of the electrical conductivity of organic–aqueous formulations can facilitate the choice of the optimal composition.

We studied the properties of aqueous solutions of Neonol 9-10 and Neonol 9-12 in the presence of an organic solvent (turpentine) and an amine-containing compound (polyethylenepolyamine, PEPA). The concentration of the surfactant in the aqueous solutions was 50%, and that of PEPA, 2 %. The electrical conductivity of the solutions was measured on a Hanna conductometer.

Figure 1 shows the results of conductometric titration of an aqueous solution of the surfactant with an organic solvent in the presence of an auxiliary amine-containing additive. It is seen from Fig. 1 that, upon addition of the organic component to the aqueous solution of the surfactant, the electrical conductivity of the latter decreases. This is due to a decrease in the dielectric constant of the system. On the whole, the electrical conductivity of the solutions in the presence of the amine-containing compound is higher than that in the systems containing solely the surfactant. Introduction of the solvent into the system without a surfactant also causes the electrical conductivity to decrease; but this process is characterized by the lack of kinetic stability of the system owing to a nonuniform distribution of the organic component throughout of the system.

When a certain amount of the organic solvent was introduced into the system during conductometric titration of the surfactant solutions, the system turned

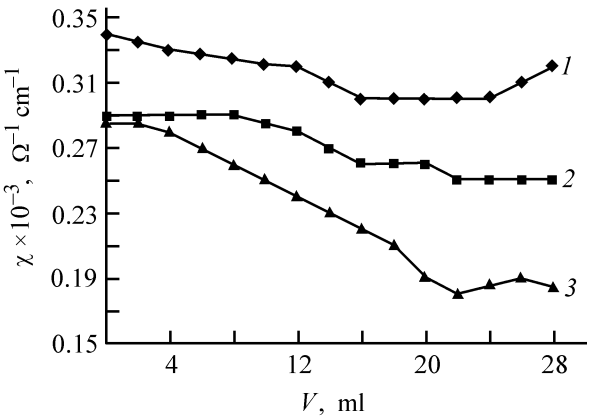


Fig. 1. Electrical conductivity χ of the surfactant solutions vs. the volume V of the solvent. (*1*) PEPA–Neonol 9-10, (*2*) PEPA–Neonol 9-12, and (*3*) Neonol 9-12.

1070-4272/05/7808-1312 © 2005 Pleiades Publishing, Inc.

turbid, and this was followed by gelation. The dip in the plot for the electrical conductivity may be due to presence in the system of large micelles and, according to published data, can be interpreted as the critical micelle concentration (CMC). In the case of Neonol 9-12, this dip in curve *3* (Fig. 1) corresponds to 22 ml of the organic solvent. Characteristically, the presence of the amine-containing auxiliary additive does not affect the amount of the organic solvent, required for gelation. However, the pattern of variation of the electrical conductivity near the CMC suggests that, in the system constituted by a surfactant, an amine-containing additive, and an organic solvent, the mechanism of intermolecular interactions has some distinctive features. This may be due to changes in the structure and shape of the mixed micelles.

The specific interactions of the surfactant with the organic component of the formulation can be judged from variation of the cloud point, a characteristic parameter of nonionic surfactants (CMC). The curves in Fig. 2 furnish information on the state of colloid solutions constituted by a surfactant, an organic component, and water. It is seen that, for the systems studied, the cloud point, corresponding to formation of a micellar solution, is below that for a binary solution of the surfactant in water. In this case, the turbidity is due to formation of a complex of the surfactant with the organic solvent. A decrease in the cloud point is most likely caused by distribution of the organic component between two other components and by an increase in the size of the micelles as a result of adsorption of surfactant molecules on nonpolar segments of terpene compounds or via formation of molecular associates. The resulting mixed micelles act as surfactants, thereby reducing the CMC in solutions [3].

The cloud point decreases the most steeply upon introduction of minor (4–8% relative to the weight of the surfactant) amounts of the organic solvent. Further addition of the organic solvent causes a proportional decrease in the cloud point of the system. The onset of gelation virtually coincides with the inflection point on the plot of the cloud point against the amount of the solvent.

In the presence of PEPA, the cloud point of the organic–aqueous systems tends to decrease, to the greatest extent with Neonol 9-12 as surfactant. This may be due to cleavage of the hydrogen bonds between water molecules and ether oxygen atoms in the surfactant molecule with a large number of oxyethyl units.

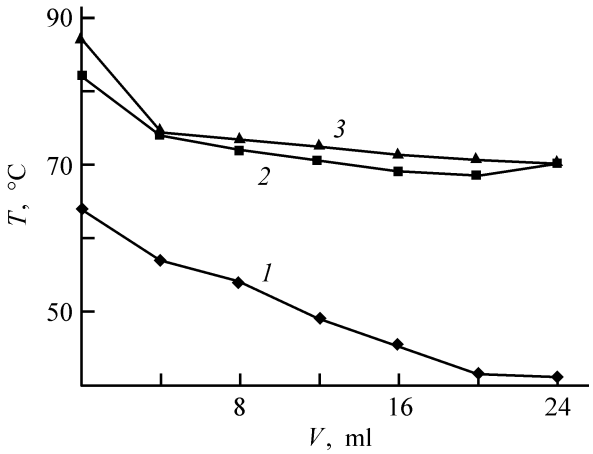


Fig. 2. Effect of the organic solvent volume *V* on the cloud point *T* of the surfactant solution. (*1*) PEPA–Neonol 9-10, (*2*) PEPA–Neonol 9-12, and (*3*) Neonol 9-10.

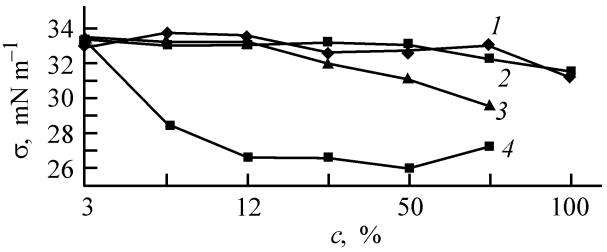


Fig. 3. Surface tension σ vs. the concentration *c* of the solutions of the surfactants in the presence of organic solvent. *V*, ml: (*1*) without solvent, (*2*) 2, (*3*) 21, and (*4*) 30.

Thus, from the physicochemical viewpoint, the gels formed in organic–aqueous systems can be regarded as dispersed systems consisting of a component forming a three-dimensional structure (surfactant) and a liquid component (organic solvent), immobilized in this matrix as a coherent medium. In terms of the basic classification, the gels formed can be attributed to ordered gel mesophases [4].

We studied how the concentration affects the surface tension of organic–aqueous surfactants containing different amounts of the organic solvent. We found that, on the whole, the surface tension of the organic–aqueous compositions is lower than that of an aqueous solution of the surfactant. This is consistent with published data on the influence of hydrophobic additives on the properties of surfactant solutions [5]. Figure 3 shows that, with increasing proportion of the organic solvent in the system, the surface tension of the solutions tends to decrease and reaches the minimum value upon introduction of 30 ml of the organic component. The CMC is shifted toward lower concentrations, namely from 23% without the solvent to 13%. Interestingly, at formulation concentrations

Table 1. Characteristics of the samples

Sample	Preparation procedure	Changes observed	Appearance
Skianol 1	The surfactant was mixed with the organic solvent, whereupon a special additive was introduced, and the resulting mixture was diluted with water	After addition of water into the composition, a gel was formed, which passed to a viscous solution in the course of time under stirring	Transparent liquid
Skianol 2	The surfactant was mixed with hot water, whereupon the additive was introduced, and, next, the organic solvent	The components formed a transparent solution. Upon addition of the organic solvent, the composition got turbid and later became transparent again	A liquid with white embedded particles and clots
Skianol 3	The surfactant was introduced into hot water, whereupon the additive and the organic solvent were introduced	Formation of a gel. Upon introduction of the organic solvent, the system got turbid	A stiff white paste
Skianol 4	The organic solvent and the auxiliary additive were introduced into hot water, whereupon the system was emulsified with the surfactant	First, the system got stratified; then a turbid gel was formed	A liquid with gray inclusions and clots
Skianol 5	The surfactant was emulsified in hot water, whereupon the additive was introduced, and the organic solvent was added	Upon introduction of the organic solvent, a milky-white viscous system was formed	A stiff white paste

Table 2. Colloid-chemical properties of the samples

Sample	Solution density d, g cm^{-3}	Surface tension coefficient σ, mN m^{-1}	Wetting coefficient $K \times 10^{-4}$, m s^{-1}
Skianol 1	1.015	31.78	2.33
Skianol 2	1.08	32.89	1.43
Skianol 3	1.010	32.22	1.6
Skianol 4	1.07	32.00	1.97
Skianol 5	1.010	31.33	1.77

above CMC, the surface tension continues to decrease, which suggests an increase in the content of the surfactant in the surface layer [6, 7].

Based on our experimental data, we developed a composition of the organic–aqueous degreasing formulation which was termed Skianol. Table 1 summarizes various methods of preparation and characteristics of the samples of the organic–aqueous formulations. These formulations differed in the physical state, and the surface tension was measured in 50% aqueous solutions. The experimental results are listed in Table 2.

Our data suggest that the lowest surface tension is characteristic of sample nos. 5 and 1. Thus, we showed that, despite the components of all the preparations are identical, their surface-active properties depend on the method of introduction of individual components during preparation of the end product. Based on the surface tension, the samples studied can be ranked as follows: $5 < 1 < 4 < 3 < 2$.

An important characteristic of the efficiency of the surfactants used or of their systems is the wetting power with respect to the material being processed. We estimated the influence of the method of preparation of organic–aqueous systems on the wetting power from the rate at which the front of the liquid ascends along a filtering paper. Table 2 confirms the existing relationship between the surface tension coefficient of the solution and the wetting power of the surfactant. Certain differences in these parameters for sample nos. 1, 5, and 4 are, probably, due to the differences in the physical condition of the initial preparations.

Probably, particles of the liquid preparation Skianol 1 more easily penetrate into the structure of the filtering paper, which affects the rate at which the front of the liquid ascends. For the gel form of the sample of Skianol 5, such penetration is sterically hindered.

Thus, our experiments suggest that, from the viewpoint of the preparation methods, the optimal preparations are sample nos. 1, 5, and 4. However, sample no. 4 does not satisfy the requirements concerning the outward appearance (Table 1). Considering the unstable consistency of sample no. 1 in storage and taking into account the colloid-chemical characteristics of Skianol 5, this formulation was chosen as the optimal composition. The comparative assessment of the degreasing power of this material with pork skins showed a high efficiency of Skianol 5, for which the degree of degreasing was over 65 %. This parameter is almost twice that achieved with Neonol.

CONCLUSIONS

(1) The organic solvent and amine-containing additive affect the colloid-chemical properties of nonionic surfactants.

(2) The formulation and method of preparation of a new organic–aqueous composition Skianol were developed. Skianol efficiently removes natural fat from the tanning raw material.

REFERENCES

1. Chursin, V.I., Abstracts of Papers, *XI konferentsiya "Poverkhnostno-aktivnye veshchestva: nauka i proizvodstvo"* (XI Conf. "Surfactants: Science and Production"), Belgorod, 2003, pp. 70–71.
2. Kudryavtsev, D.K., Ibragimov, A.R., and Valeeva, F.G., in *Fizikokhimiya polimerov: sintez, svoistva i primenenie: Sbornik nauchnykh trudov* (Physical Chemistry of Polymers: Synthesis, Properties, and Application: Coll. of Scientific Works), Tver, 2002, issue 8, pp. 44–49.
3. Cheshkova, A.V., Pankova, M.V., and Kozlov, V.A., *Izv. Vyssh. Uchebn. Zaved., Khim. Khim. Tekhnol.*, 2001, vol. 44, no. 5, pp. 157–160.
4. Daniels, R., *Syr'e Upak.*, 2004, no. 1, pp. 8–11.
5. Schonfeldt, N., *Grenzflachenaktive Athylenoxid-Addukte*, Stuttgart: Wissenschaftliche, 1976.
6. Abrosimov, V.K., Korolev, V.V., Afanas'ev, V.N., *et al., Eksperimental'nye metody khimii rastvorov: densimetriya, viskozimetriya, konduktometriya i drugie metody* (Experimental Methods of Chemistry of Solutions: Densimetry, Viscometry, Conductometry, and Other Methods), Moscow, Nauka, 1997.
7. Rusanov, A.I., *Mitselloobrazovanie v rastvorakh poverkhnostno-aktivnykh veshchestv* (Micellization in Surfactant Solutions), St. Petersburg: Khimiya, 1992.

Russian Journal of Applied Chemistry, Vol. 78, No. 8, 2005, pp. 1316–1319. Translated from Zhurnal Prikladnoi Khimii, Vol. 78, No. 8, 2005, pp. 1340–1343.
Original Russian Text Copyright © 2005 by Panarin, Ivanova.

MACROMOLECULAR CHEMISTRY AND POLYMERIC MATERIALS

Synthesis of Copolymers of Vinylformamide with *N*-Methacryloylglucosamine

E. F. Panarin and N. P. Ivanova

Institute of Macromolecular Compounds, Russian Academy of Sciences, St. Petersburg, Russia

Received July 12, 2005

Abstract—Copolymers of vinylformamide with *N*-methacryloylglucosamine were prepared. Acid hydrolysis of these copolymers yielded terpolymers of vinylformamide, vinylamine, and *N*-methacryloylglucosamine. A ^{1}H NMR study showed that the hydrolysis of the vinylformamide homopolymer under the same conditions is virtually complete.

Poly-*N*-vinylamides derived from cyclic *N*-vinylamides are widely used in medicine, biotechnology, and engineering [1], whereas poly-*N*-vinylamides derived from fatty carboxylic acids are poorly studied. Some of them are water-soluble and can be used as synthetic precursors of functional polymers owing to the presence of an acyl-protected amino group. Of particular interest is polyvinylformamide, in which the formyl group can be removed fairly readily. Copolymerization of vinylformamide (VFA) with other vinyl monomers opens prospects for preparing reactive polymers containing a primary amino group, including new water-soluble polymers suitable as carriers of biologically active substances.

The possibility of preparing *N*-vinylpyrrolidone (VP)–vinylamine copolymers by copolymerization of VP with VFA, followed by acid deformylation, was demonstrated in [2].

The goal of this study was to prepare water-soluble copolymers of *N*-methacryloylglucosamine (MGA) with VFA and to examine the possibility of selective deformylation with the aim to obtain a polyvinyl saccharide containing primary amino groups.

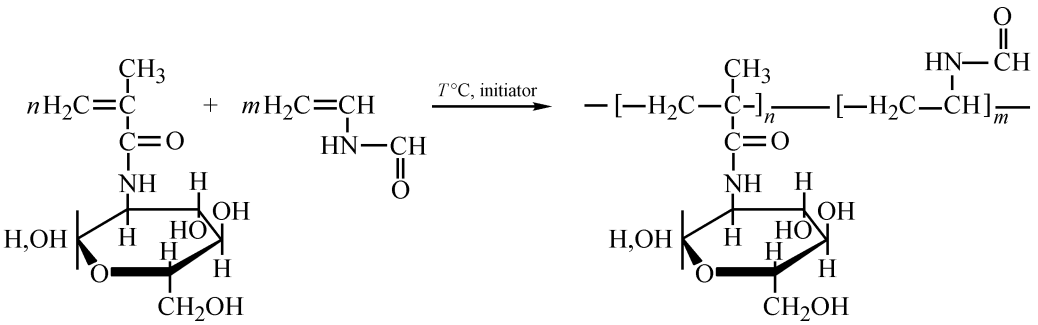
VFA and MGA are active comonomers and readily copolymerize. Copolymerization occurs with a high yield both in water and in organic solvents (see table). By varying the copolymerization conditions (primarily solvent and initiator), it is possible to prepare copolymers of different compositions with a widely varying molecular weight.

When choosing the conditions (reaction time, solvent, monomer concentrations) of copolymerization

Copolymerization conditions and characteristics of copolymers (1 wt % initiator relative to sum of monomers in all runs)

Initiator	Composition of monomer mixture, mol %		Solvent, wt %	Time, h	Yield, %	Copolymer composition, mol %		$[\eta]^{25}$, dl g^{-1}
	VFA	MGA				VFA	MGA	
AIBN	90	10	DMF, 15	24	72	88	12	0.39
AIBN	90	10	Ethanol, 10	4	66	86	14	1.30
AMPDDC	90	10	Water, 10	3	87	85	15	1.60
AIBN	90	10	Isopropanol : water, 9 : 1	22	75	80	20	0.46
AIBN	70	30	DMF, 15	21	70	75	25	0.10
AMPDDC	70	30	Water, 10	1.5	60	90	10	1.60
AIBN	50	50	DMF, 15	6	60	40	60	0.20
AMPDDC	50	50	Water, 10	5	98	45	55	1.25

1070-4272/05/7808-1316 © 2005 Pleiades Publishing, Inc.



Scheme of copolymerization of VFA with MGA.

of VFA with MGA (see scheme), we took into account published data on the synthesis of polyvinylacetamide [3] and on the hydrodynamic properties of poly-*N*-methacryloylglucosamine (PMGA) [4].

Experiments on copolymerization of VFA with MGA at various monomer ratios (90 : 10, 70 : 30, 50 : 50 mol %) in different solvents showed that both monomers are fairly active in copolymerization, which allowed preparation of copolymers of different compositions with a widely varying molecular weight. The strongest effect on the molecular weight is exerted by the solvent used for the reaction. The copolymers prepared in DMF have the lowest intrinsic viscosity.

The structures of the copolymers were confirmed by ^{1}H NMR spectroscopy (Fig. 1). The spectra contained signals assignable to the carbohydrate and amide units. The copolymer compositions were determined from the intensity ratio of the formyl proton signal at δ 8 ppm (VFA fragment) and

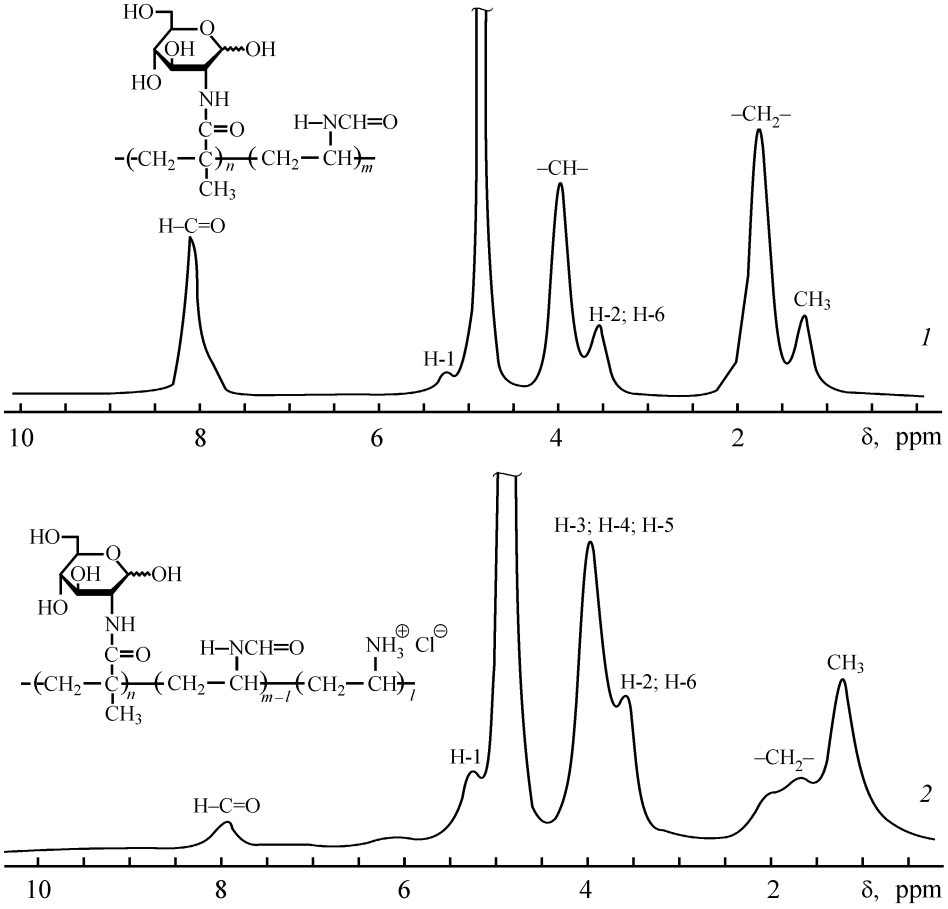
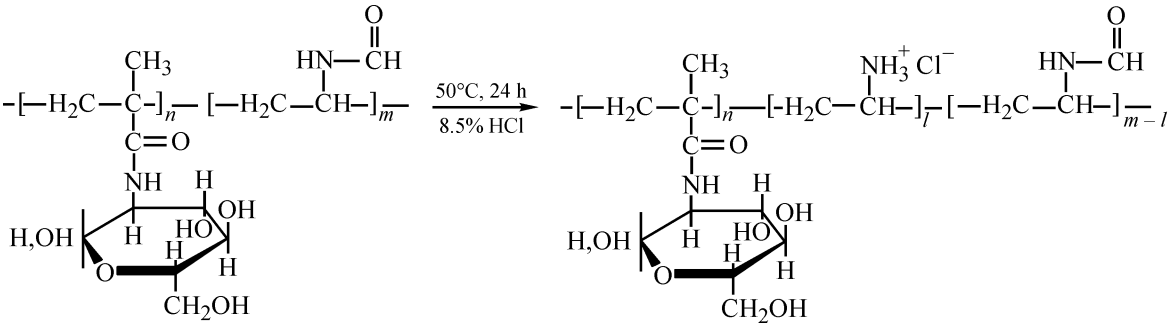


Fig. 1. ^{1}H NMR spectra of VFA–MGA copolymer (90 : 10 mol %) in D_2O: (*1*) before and (*2*) after hydrolysis.

the CH signals of the carbohydrate fragments at δ 1.3 ppm.

VFA–MGA copolymers were subjected to acid hydrolysis with HCl to obtain products containing reactive NH_2 groups. The hydrolysis conditions were chosen so as to avoid the hydrolysis of MGA units. First we studied the hydrolysis of PVFA and PMGA. Poly-*N*-methacryloylglucosamine was dissolved in 8.5 wt % HCl and heated at 50°C for 24 h. The occurrence of hydrolysis was judged from the appearance of glucosamine in the reaction products. To detect glucosamine, samples of the reaction mixture were analyzed by TLC on silica gel plates. The resistance of PMGA to hydrolysis under these conditions was also confirmed by the absence of the proton signal of the carboxy group in the ^{1}H NMR spectrum in D_2O, which should appear after removal of the glucosamine moiety.

The PVFA hydrolysis kinetics was monitored by taking hydrolyzate samples and analyzing them by ^{1}H NMR spectroscopy after dialysis and freeze drying (from the loss of the intensity of the formyl proton signal at δ 8.0 ppm) and by conductometric titration with silver nitrate. The kinetic curve is shown in Fig. 2. Heating of a PVFA solution in 8.5% HCl at 50°C for 3 days results in virtually complete deformylation, with the degree of hydrolysis as high as 90–95%. In VFA–MGA copolymers, irrespective of the composition, the hydrolysis of VFA units under the same conditions occurs to 50% only, probably because of steric effects of bulky carbohydrate fragments. Partial hydrolysis of VFA units in VFA–MGA copolymer yields terpolymers containing, along with VFA and MGA, also vinylamine (VA) units:



EXPERIMENTAL

N-Vinylformamide (Aldrich) was vacuum-distilled; bp 80°C (10 mm Hg), n_D^{20} 1.4940.

Azobis(isobutyronitrile) initiator (AIBN) was twice recrystallized from ethanol–chloroform (3 : 1), mp 103°C; 2,2'-azobis(2-methylpropanediamine) dihydrochloride (AMPDDC) was prepared according to [4].

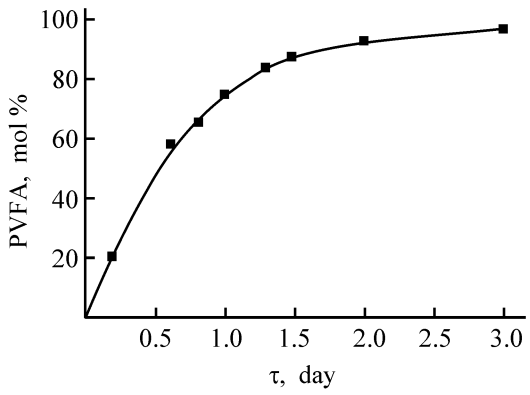


Fig. 2. Degree of PVFA hydrolysis vs. time τ.

N-Methacryloylglucosamine was prepared by treatment of glucosamine hydrochloride with methacryloyl chloride in methanol in the presence of triethylamine [5].

Dimethylformamide was purified according to [6].

Polymerization was performed in sealed ampules at 60°C. The polymers were isolated by precipitation from DMF into diethyl ether and from aqueous solutions into acetone and were purified by reprecipitation from water into methanol. Hydrolyzed VFA–MGA copolymers were purified by dialysis.

Thin-layer chromatography was performed with ATSKh-st. plates (Lenkhrom), eluent ethyl acetate–isopropyl alcohol–water (5.0 : 3.2 : 1.6), development with aniline–diphenylamine mixture [7].

The intrinsic viscosity was measured in 0.1 M CH_3COONa with an Ubbelohde viscometer.

The ^{1}H NMR spectra were recorded on a Bruker AC 200 spectrometer (Germany) at a working frequency of 200 MHz in D_2O.

CONCLUSIONS

(1) *N*-Vinylformamide–*N*-methacryloylglucosamine copolymers of various compositions and molecular weights were prepared.

(2) It was found that acid hydrolysis of *N*-vinylformamide–*N*-methacryloylglucosamine copolymers allows preparation of *N*-vinylformamide–vinylamine–*N*-methacryloylglucosamine terpolymers.

ACKNOWLEDGMENTS

The study was financially supported within the framework of the Biomolecular and Medical Chemistry Program of the Division of Chemistry and Materials Science, Russian Academy of Sciences.

The authors are grateful to A.Yu. Ershov for the interpretation of the ^{1}H NMR spectra.

REFERENCES

1. Kirsh Yu.E. *Poli-N-vinilpirrolidon i drugie N-vinilamidy* (Poly-*N*-vinylpyrrolidone and Other *N*-Vinylamides), Moscow: Nauka, 1998.
2. Ershov, A.Yu., Gavrilova, I.I., and Panarin, E.F., *Zh. Prikl. Khim.*, 1995, vol. 68, no. 9, pp. 1522–1526.
3. Pavlov, G.M., Korneeva, E.V., Mikhailova, N.A., *et al.*, *Vysokomol. Soedin., Ser. A*, 1993, vol. 35, no. 10, pp. 1647–1651.
4. Harada, S. and Hasegawa, S., *Makromol. Chem., Rapid Commun.*, 1984, vol. 5, no. 1, pp. 27–31.
5. Mataklyama, T., *Chem. Abstr.*, 1983, vol. 98, abstr. no. 180070.
6. *Laboratorni technika organicke chemie*, Keil, B., Ed., Prague, 1963.
7. Pohloudek-Fabini, R. and Beyrich, Th., *Organische Analyse*, Leipzig: Geest und Portig, 1975.

Russian Journal of Applied Chemistry, Vol. 78, No. 8, 2005, pp. 1320–1324. Translated from Zhurnal Prikladnoi Khimii, Vol. 78, No. 8, 2005, pp. 1344–1348.
Original Russian Text Copyright © 2005 by Sazanov, Novoselova, Nud'ga, Ugolkov, Fedorova, Kulikova, Kostycheva, Gribanov.

MACROMOLECULAR CHEMISTRY AND POLYMERIC MATERIALS

Cocarbinization of Blends of Polyacrylonitrile with Chitin and Chitosan

Yu. N. Sazanov, A. V. Novoselova, L. A. Nud'ga, V. L. Ugolkov, G. N. Fedorova, E. M. Kulikova, D. M. Kostycheva, and A. V. Gribanov

Institute of Macromolecular Compounds, Russian Academy of Sciences, St. Petersburg, Russia
Institute of Silicate Chemistry, Russian Academy of Sciences, St. Petersburg, Russia

Received April 20, 2005

Abstract—The possibility of thermochemical cocarbonization of polyacrylonitrile with chitin and chitosan by combined heat treatment of their blends was examined. It was concluded that the components form complexes in dimethylformamide and dimethylacetamide at the temperature of polyacrylonitrile cyclization (230–300°C). The main thermal characteristics and the coke numbers of the cocarbonization products were determined.

Preparation of carbon composites with valuable properties is a topical problem of applied organic chemistry. One of important lines in this field is the use of polymers commercially produced on a large scale, such as polyacrylonitrile (PAN) and cellulose derivatives, for which the raw materials are readily available. In [1], we substantiated theoretically and experimentally the thermochemical reactions of PAN with chitin (CT) and chitosan (CTS), nitrogen-containing cellulose derivatives. As shown in [2, 3], cellulose derivatives containing nitrile groups and graft copolymers of PAN with cellulose ethers or esters are promising as raw materials for preparing cocarbonizates with a high coke number (CN). However, preparation of cyano derivatives of cellulose involves certain problems, and alternative routes should be sought for.

In this study, we examined the cocarbonization of CT and CTS with PAN by heat treatment of a blend of these polymers in the solid phase and in solution. Based on the previous data [1], we chose for the reaction the temperature range 200–350°C. At these temperatures, the thermal degradation and cross-linking of PAN and polysaccharides are the most intense. In this temperature range, PAN undergoes cyclization (initial step) with release of such volatile products as HCN, ammonia, acrylonitrile, acetonitrile; CT and CTS undergo degradation with release of large amounts of water, methanol, acetamide, pyridine, levoglucosan, and other compounds. Such a set of reactive substances released from the polymer blend in the above temperature interval may initiate formation of new structures serving as carbonization nuclei in the subsequent high-temperature process. It is known that, as carbonization of polymer blends is usually diffusion-controlled, it is necessary to ensure the maximally efficient contact of the components in an isolated volume to attain a high CN of the products.

EXPERIMENTAL

PAN was prepared by radical polymerization [4], $[\eta] = 6$ (in DMF). Chitin and chitosan were prepared by processing of crab shells (CT: mean molecular weight 282 kDa, ash residue 0.1%: CTS: mean molecular weight 245 kDa, degree of deacetylation 0.79).

To study the thermochemical reactions of PAN with CT and CTS, the initial polymers were taken as blends of powders (1 : 1 by weight, total weight 5 to 100 mg), pressed pellets, or films or blocks prepared from DMF solutions of the polymer blends. Samples were arranged in special holders of thermoanalytical devices and tested under the conditions described previously [2, 3], with the gravimetric and thermal characteristics of the intermediate and final cocarbonization products recorded.

Experiments with blended powders, performed in open crucibles, revealed no changes in the gas evolution kinetics and in the rate and value of the weight

1070-4272/05/7808-1320 © 2005 Pleiades Publishing, Inc.

Weight loss of samples of PAN, CT, CTS, and their mechanical blends (50 : 50) upon isothermal heating in a vacuum at 200, 250, and 300°C for 2 h, followed by heating to 900°C in the dynamic mode (3 deg min^{-1})

Sample	Weight loss Δm, %			Total weight loss, %, of samples heated to 900°C		
	200°C	250°C	300°C	200°C	250°C	300°C
PAN	15.1	45.2	59.4	83.2	77.5	76.2
CT	16.6	59.0	85.0	91.6	96.4	93.2
CTS	32.6	57.1	65.3	68.0	66.7	72.8
PAN + CT	13.7	49.3	67.6	81.3	83.1	81.9
	15.8*	52.3*	72.2*	87.4*	87.0*	84.7*
	+2.1**	+2.8**	+4.6**	+6.1**	+3.9**	+2.8**
PAN + CTS	26.1	50.4	55.0	76.8	74.8	74.3
	23.8*	51.1*	62.4*	75.6*	72.2*	74.5*
	–2.3**	+0.7**	+7.6**	–1.2**	–2.6**	+0.2**

* $\Delta m_{tot} = 0.5(\Delta m_{PAN} + \Delta m_{CT\,or\,CTS})$.

** SE = $\Delta m_{tot} - \Delta m_{bl}$, stabilizing effect.

loss throughout the experiment, compared to the polymers taken separately. Certain changes in the character of thermal degradation in the self-generated atmosphere at a constant heating rate were observed with large samples of the polymer blend, exceeding the standard samples in weight by a factor of 2–3. However, these changes are attributable to the scale effect, rather than to fundamental changes in the mechanism of the reaction between the starting polymers.

Experiments on heat treatment of powdered blends of PAN with CT and CTS in a vacuum in the isothermal mode at 200, 250, and 300°C (see table) revealed the effect of PAN on the thermal characteristics of the blends. Comparison of the total weight loss of the individual polymers at fixed temperatures, Δm_{tot}, with the weight loss of the blend, Δm_{bl}, allows evaluation of the stabilizing effect of PAN (positive quantities) in the blend. It can be readily seen that the strongest stabilizing effect of PAN is observed at 300°C, i.e., at a temperature corresponding to the onset of PAN cyclization. In particular, the weight loss of CT and CTS at 300°C decreases by 15–20% in the presence of PAN, compared to the polymers taken separately. Apparently, certain reactions of thermal degradation of CT and CTS at this temperature are inhibited; formation of intermediate bonds between the PAN and CT (or CTS) macromolecules at the instant of their thermal degradation is also possible. The strongest effect is observed with the PAN–CTS blend, for which the CN at 900°C is comparable with that of PAN. This fact is due to the increased reactivity of the amino group of CTS, compared to the *N*-acetyl group of CT, at the temperatures of thermal degradation of these polymers.

Then we studied the influence exerted by compaction of the polymer blends, intended to facilitate the mutual diffusion of the components in the course of the thermal degradation. We compacted pellets from 1 : 1 (by weight) blends of PAN and CT (or CTS) powders. A thermal analysis showed that the compaction of the components facilitates their reaction. Processing of the TG and DTA curves reveals changes in the gravimetric and energetic parameters of the exothermic step of the process, indicating that the degradation–cross-linking balance of macromolecules is shifted toward cross-linking. In particular, the weight loss of the blend in the interval 230–300°C is 21.6%, whereas the additive value is 26.8%. The heat release from the blend sample under the same conditions is almost equal to that from pure PAN, and the exothermic peak is shifted by 8°C to lower temperatures. It should also be noted that an increase in CN for the blend does not correspond to the additive value: CN is 24.8% for the blend, 45.6% for PAN, and 10.6% for CTS.

Comprehensive thermal analysis of blends prepared as films from mixed solutions of PAN and CT in DMF reveals a difference in the thermochemical reactions of the blends and individual compounds (Fig. 1). The mixed solutions show a tendency to react at lower temperatures on their keeping for a long time (curves *1*, *3*, *4*).

To sum up, the predominant reaction in the temperature range examined is cyclization of PAN, accompanied by a strong exothermic effect. It is known [4, 6, 7] that the magnitude of this effect is propor-

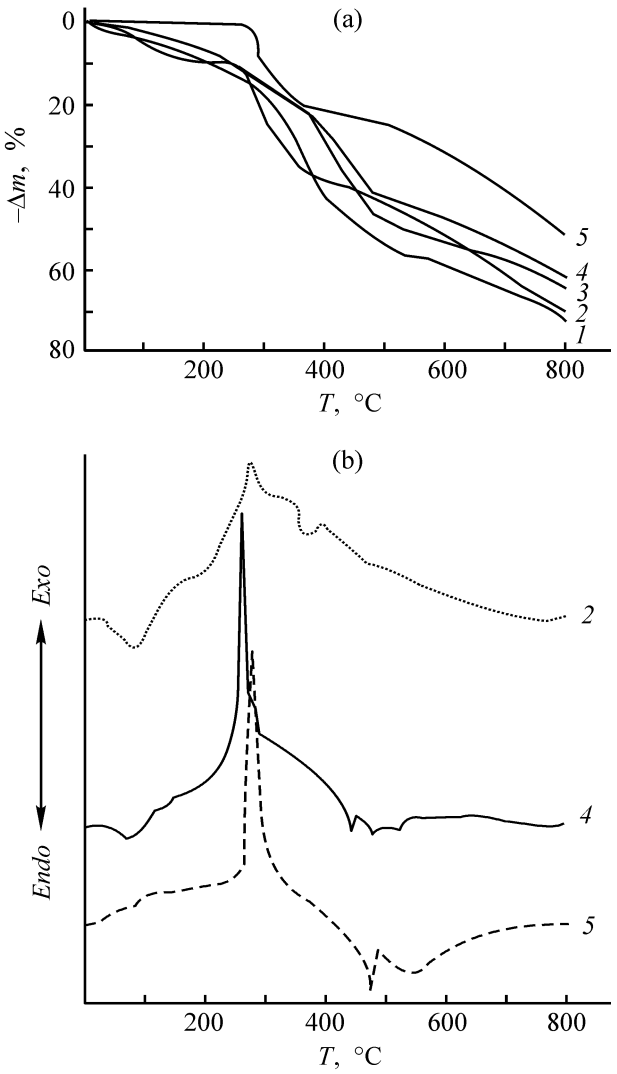


Fig. 1. (a) TG and (b) DTA curves of samples of PAN, CT, and their blends, recorded in air. Heating rate 10 deg min^{-1}, sample weight 50 mg. (T) Temperature and (Δm) weight loss; the same for Figs. 2 and 3. (*1*) PAN + CT film (1 : 1 by weight) cast immediately after mixing solutions in DMF; (*2*) CT powder; (*3*) PAN + CT film cast after keeping the solutions in DMF for 72 h; (*4*) CT powder in a solution of PAN in DMF; and (*5*) PAN powder.

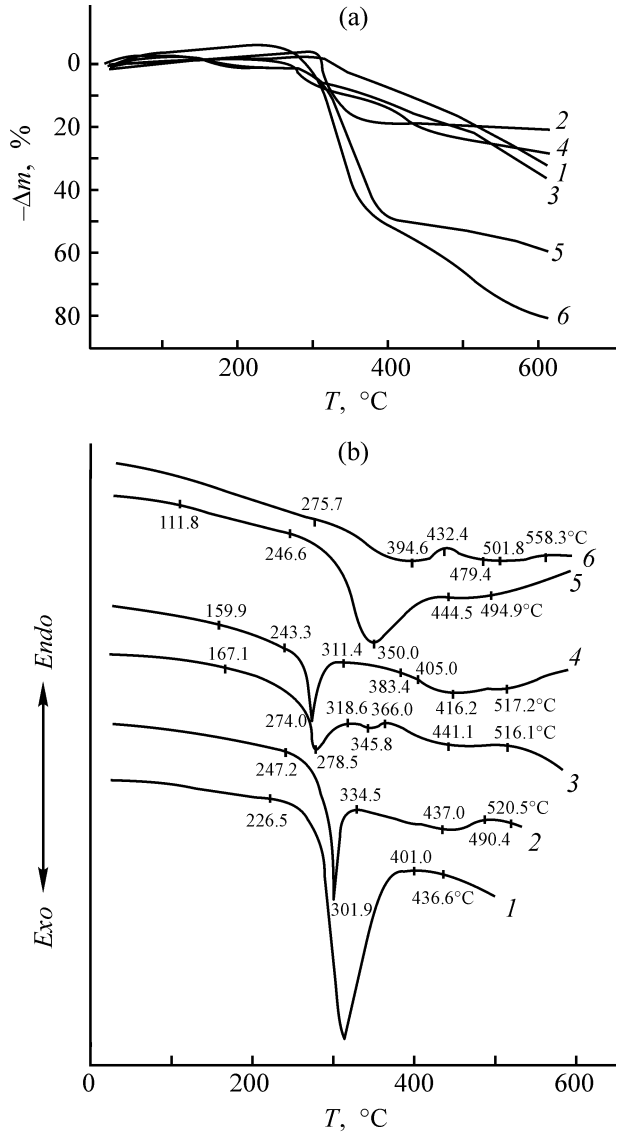


Fig. 2. (a) TG and (b) DSC curves of samples of PAN, CT, and PAN + CT film (prepared from DMF solution). Heating rate 10 deg min^{-1}, sample weight 5 mg; the same for Fig. 3. (*1*, *2*) PAN powder, (*3*, *4*) film of PAN + CT blend, and (*5*, *6*) CT powder. (*1*, *3*, *5*) In air and (*2*, *4*, *6*) in a nitrogen flow.

tional to the amount of oxygen coming to the reaction system from air, and also to the amount of oxygen-containing compounds formed during synthesis and isolation of PAN. Apparently, oxygen prevents, to a certain extent, the reaction of PAN with CT and CTS, shifting the reaction balance toward formation of volatile products of thermal oxidative degradation. To reveal the effect of atmospheric oxygen, we made a series of experiments on the thermochemical reaction of the components in a nitrogen atmosphere.

Figure 2 shows the TG and DSC curves obtained with PAN, CT, and PAN + CT blend film in the course of heating in air and in a nitrogen flow. The most interesting fact is the enhanced heat resistance and increased CN of the film prepared from mixed solutions of PAN and CT in DMF and subjected to prolonged drying and keeping at an elevated temperature. Comparison of the TG curves shows that the composite film (curves *3*, *4*) noticeably differs from the samples of the individual polymers in the thermal and

gravimetric characteristics. The behavior of the weight loss in the range 20–600°C suggests the occurrence of a thermochemical reaction of PAN with CT. The initial step, Δm = 5–6%, is observed in the interval 130–270°C. It can be assigned to removal of residual DMF, which is known [8, 9] to participate in the formation of interpolymeric complexes upon heat treatment of polymers. Above 270°C, the weight loss accelerates owing to the development of thermal degradation. A distinctive feature of the degradation of the composite films in this step is that Δm is appreciably smaller, compared to powdered PAN and CT samples. In particular, in the range 270–315°C, Δm is 2.5–4% for the composite film, 1–7.5% for PAN, anmd 11–6% for CT. Thus, in the region of the maximum intensity of thermal reactions (250–320°C) involving the individual polymers, the thermal degradation reactions characteristic of CT are almost fully inhibited, and the balance of volatile products of PAN degradation is altered.

One more feature of this process is a weak effect of thermal oxidation reactions on the degradation of the composite film, compared to the thermal oxidation of CT (the above-given quantities refer to TGA in air and in a nitrogen flow, respectively). Heating to higher temperatures (315–400°C) induces the carbonization of PAN and the film composite, characterized by a decrease in the weight loss rate and in the amount of the released volatile products. Chitin undergoes, in the same temperature interval, further degradation slightly decelerating at temperatures above 400°C. In the step of formation of the coke residue (above 600°C), the CN of the film composite is 58 and 71% (heating in air and in a nitrogen flow, respectively) and is comparable with CN of PAN (66 and 80%, respectively). At 1000°C, the CN of the film composite in nitrogen is 43%. These facts suggest that complex thermochemical reactions involve the reaction of CT with PAN to form a cross-linked structure differing from the structure of the starting polymers.

Similar conclusions follow from analysis of the effects that accompany the thermochemical reactions of the samples in hand. The DSC curves (Fig. 2b) demonstrate significant differences in the temperature and energy characteristics of the individual polymers and the composite film. When choosing components for cocarbonization, it is essential that the temperature intervals of the most intense thermal transformations of both polymers should coincide. In our case, this rule is observed: The exothermic maxima in the DSC curves of PAN and CT (curves *1*, *5*) are observed at 317.9 and 350.0°C, respectively; the ranges of these peaks are 232–400°C for PAN and 246–405°C for CT. The overall activation energy of these processes is 344.15 and 198.66 kJ mol^{-1}, respectively. In the case of PAN, this energy is the sum of the contributions from cyclization and partial oxidation, and in the case of CT, a superposition of oxidation, thermal degradation, and evaporation of volatile degradation products. In a nitrogen atmosphere, the values are appreciably lower: 70.52 kJ mol^{-1} for PAN and 67.28 kJ mol^{-1} for CT, which is due to the absence of oxidation reactions. The pattern of the heat release in the case of the film composites essentially differs from that observed with the individual polymers. For the composites, the temperatures of the peak maxima are lower by 40–60°C, and the boundaries of the range of the thermal effect, by 70–120°C; the activation energies are lower by 40 kJ mol^{-1} on the average, irrespective of the gas medium.

Thus, the best procedure for thermochemical cocarbonization of PAN with CT consists in combining their solutions in DMF and keeping the resulting blend to obtain stable complexes with the solvents. Prolonged low-temperature heat treatment (120–200°C) results in a gradual decomposition of the complexes, apparently with the formation of an intermediate compound of CT with PAN, in which CT (namely, its *N*-acetyl or free hydroxy groups) acts as an initiator of PAN cyclization. The possibility of formation of intermediate PAN compounds was discussed in detail in [10]; the existence of ionized structures involving solvent (DMF) molecules was confirmed. Similar structures may also initiate the reaction of PAN with CT, which occurs at lower temperatures than the PAN cyclization.

To reveal the role of the *N*-acetyl group in CT, we performed experiments on combined heat treatment of PAN and CTS solutions. For this purpose, we prepared a mixture of concentrated (~10 wt %) solutions of PAN and CTS in DMF; this mixture was subjected to prolonged drying in the stepwise heating mode at temperatures of 140 to 400°C for 45 h. In the first step of the heat treatment (24 h), an interpolymeric complex of the starting component with DMF molecules was formed, and this was accompanied by evaporation of the excess solvent. As a result, a viscous inhomogeneous product containing 12–14% solvent in a complex with the polymer blend was obtained. The subsequent heating at 160°C for 7 h did not result in destabilization of the complex, and its noticeable degradation occurred only upon heating at 200°C. In the interval 250–300°C, thermochemical reactions of PAN with CTS occurred with the release of ~26–28% volatile products apparently formed by the cyclization of PAN, degradation of

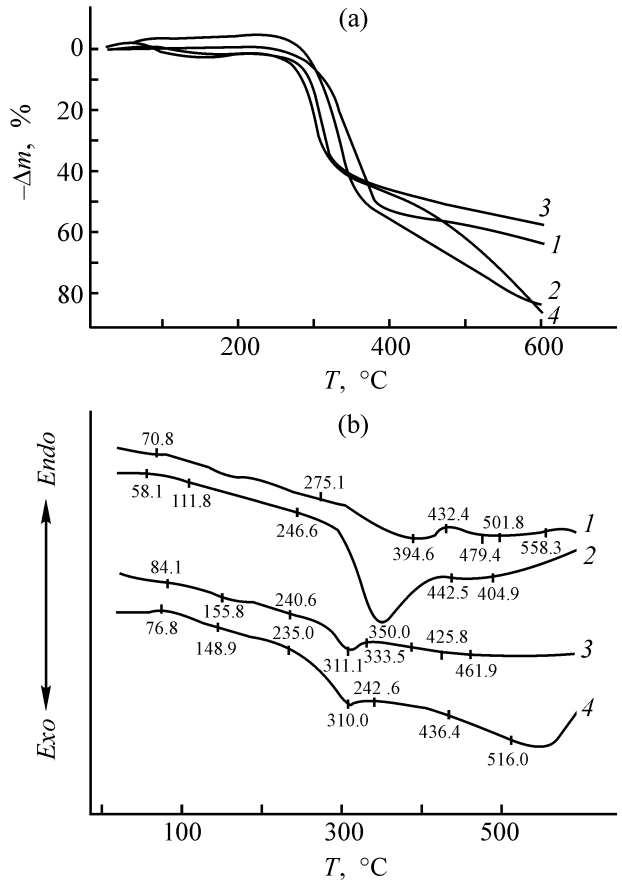


Fig. 3. (a) TG and (b) DSC curves (*1*, *2*) CT and (*3*, *4*) CTS powders (*1*, *3*) under nitrogen and (*2*, *4*) in air.

CTS, and probably reaction of PAN with CTS. As shown previously [11], replacement of the acetylamino group in CT with the amino group favors rapid cross-linking of CTS at elevated temperatures. Furthermore, the reaction of the amino groups with the nitrile groups of PAN becomes possible, by analogy with the results of our previous study [12] in which PAN was modified with ethanolamine at temperatures above 100°C; the process started with a nucleophilic addition of the amino group to the cyano group and formation of *N*-hydroxyethylamidine units. The same conclusion followed from a comparison of the results of a thermal analysis of CT and CTS under the conditions of the dynamic heating in air and in a nitrogen flow (Fig. 3). According to TGA, the thermal degradation of CTS starts in an inert atmosphere at a temperature 20°C higher, compared to CT, and is complete at 315°C, with a total weight loss of 32%, whereas the weight loss of CT is about 50%. The CNs at 600°C are 50 and 60%, respectively. In air, the differences are noticeable only in the step of thermal degradation, in which the weight loss of CT and CTS is appreciably larger than that in nitrogen, and the degradation is accompanied by an exothermic effect with a maximum at 350°C, especially strong for CT.

CONCLUSIONS

(1) A laboratory procedure was developed for cocarbonization of polyacrylonitrile with chitin and chitosan, based on thermochemical transformations of the starting polymers in the step of an interpolymeric complex with an aprotic polar solvent in the temperature range of polyacrylonitrile cyclization (230–300°C).

(2) The cocarbonization of the polymer blend differs in the thermal characteristics from the carbonization of the individual polymers, and the coke numbers at 800°C are close to that of polyacrylonitrile (70–80%).

REFERENCES

1. Sazanov, Yu.N., Novoselova, A.V., Amsharov, K.Yu., *et al.*, *Zh. Prikl. Khim.*, 2005, vol. 78, no. 5, pp. 810–813.
2. Sazanov, Yu.N., Nud'ga, L.A., Novoselova, A.V., *et al.*, *Zh. Prikl. Khim.*, 2004, vol. 77, no. 4, pp. 643–648.
3. Sazanov, Yu.N., Nud'ga, L.A., Petrova, V.A., *et al.*, *Zh. Prikl. Khim.*, 2004, vol. 77, no. 8, pp. 1366–1369.
4. Gryaznov, N.S., O*snovy teorii koksovaniya* (Principles of the Coking Theory), Moscow: Metallurgiya, 1976.
5. Sazanov, Yu.N., Shirokov, N.A., and Goltsin, B.E., *Thermochim. Acta*, 1978, vol. 24, pp. 81–88.
6. Fialkov, A.S., *Uglerod, mezhsloevye soedineniya i kompozity na ikh osnove* (Carbon, Intercalation Compounds, and Composites Based on Them), Moscow: Aspekt, 1997.
7. Panova, L.G., Artemenko, S.E., and Besshaposhnikova, V.I., *Khim. Volokna*, 2003, no. 6, pp. 56–58.
8. Sazanov, Yu.N., Spirina, T.N., Shibaev, L.A., *et al.*, *J. Therm. Anal.*, 1990, vol. 36, no. 12, pp. 2329–2338.
9. Sazanov, Yu.N., Silinskaya, I.G., Spirina, T.N., *et al.*, *Vysokomol. Soedin., Ser. A*, 1992??, vol. 33??, no. 8, pp. 1617–1624.
10. Platonova, N.V., Klimenko, I.B., and Maiburov, S.P., *Vysokomol. Soedin., Ser. B*, 1991??, vol. 32??, no. 9, pp. 698–707.
11. Sazanov, Yu.N., Fedorova, G.N., Plisko, E.A., and Nud'ga, L.A., *Zh. Prikl. Khim.*, 1980, vol. 53, no. 9, pp. 2143–2146.
12. Josseland, J.F., Forestiere, A., Petratiu, A., and Dima, M., *J. Polym. Sci.*, 1981, vol. 19, no. 12, pp. 2869–2878.

Russian Journal of Applied Chemistry, Vol. 78, No. 8, 2005, pp. 1325–1328. Translated from Zhurnal Prikladnoi Khimii, Vol. 78, No. 8, 2005, pp. 1349–1352.
Original Russian Text Copyright © 2005 by Grishin, Valetova, Semenycheva, Il'ichev.

MACROMOLECULAR CHEMISTRY AND POLYMERIC MATERIALS

(Allylbenzene)tricarbonylchromium in Radical Polymerization of Methyl Methacrylate and Styrene

D. F. Grishin, N. B. Valetova, L. L. Semenycheva, and I. S. Il'ichev

Research Institute of Chemistry, Lobachevsky Nizhni Novgorod State University, Nizhni Novgorod, Russia

Received December 9, 2004; in final form, April 2005

Abstract—The effect of (allylbenzene)tricarbonylchromium on the kinetic parameters of radical polymerization of methyl methacrylate and styrene and on the molecular-weight characteristics of the resulting polymers was studied.

Control over the kinetic parameters of radical polymerization of vinyl monomers and over the molecular-weight characteristics of the resulting polymers under the conditions maximally similar to those of their commercial synthesis is an urgent line of macromolecular chemistry [1, 2].

Nitroxyl radicals and their sources [3, 4] and organometallic compounds [2, 4], including metal-containing monomers [5, 6], are actively used today to control the chain propagation in radical polymerization processes. In particular, (α-methylstyrene)tricarbonylchromium affects the propagation step in polymerization of methyl methacrylate (MMA), styrene (ST), and butyl acrylate [6]. The controlling effect of organochromium additives is due to their reaction with initiator radicals and propagating macroradicals to form relatively stable carbon-centered organometallic radicals directly affecting the polymerization rate and molecular weight of the polymers [5, 6].

In this study, we examined the polymerization kinetics of MMA and ST and the molecular-weight characteristics of the resulting polymers, as influenced by addition of (allylbenzene)tricarbonylchromium (ABC). It is known [7] that the polymerization of allyl monomers has certain specific features associated with the formation of stabilized allyl radicals in the course of chain propagation. Therefore, it is of indubitable interest to examine the effect exerted on elementary steps of polymerization by compounds containing simultaneously an allyl fragment and a stabilizing tricarbonylchromium group.

EXPERIMENTAL

(Allylbenzene)tricarbonylchromium was prepared by the procedure described in [8]; its physicochemical constants were consistent with published data. The monomers were purified by standard procedures [9]. Commercial azobis(isobutyronitrile) (AIBN) used as initiator was recrystallized from methanol. Nitrosodurene used as spin trap was prepared according to [10].

The polymerization of MMA and ST was performed in evacuated temperature-controlled ampules. The polymerization kinetics was monitored derivatographically and thermographically [11]. The polymers formed were purified to remove residual monomers by reprecipitation with hexane from a solution in ethyl acetate under argon. The ABC content in double-reprecipitated samples was determined from the chromium content evaluated spectrophotometrically [12]. The molecular weight (MW) and molecular-weight distribution (MWD) of poly(methyl methacrylate) (PMMA) and polystyrene (PS) were estimated by gel permeation chromatography (GPC) [13] using, respectively, a single Phenogel column (Linear-2 Phenomenex) and a set of five Styrogel columns (Waters). As detectors we used R-2301 (Knauer) and R-403 (Waters) differential refractometers. The eluents were THF for PS and chloroform for PMMA.

The ESR specrta were taken on an AE-4700 commercial radiospectrometer in special ampules. As reference for magnetic field calibration we used Mn^{2+} ions incorporated in the MgO lattice.

1070-4272/05/7806-1325 © 2005 Pleiades Publishing, Inc.

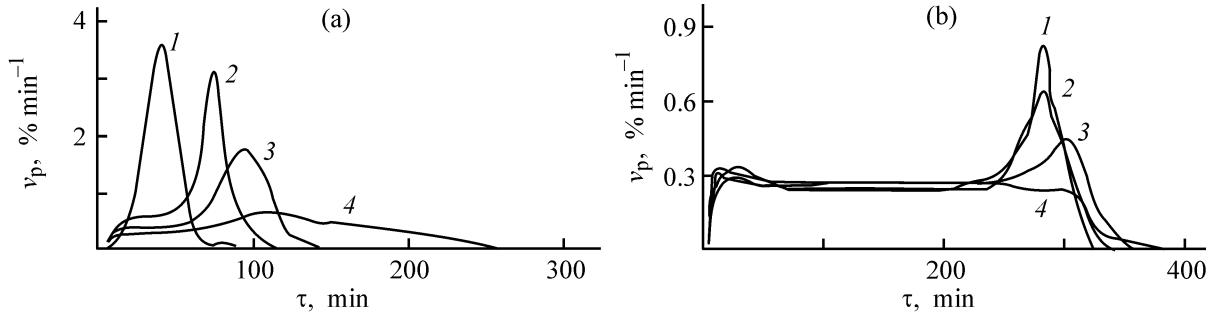
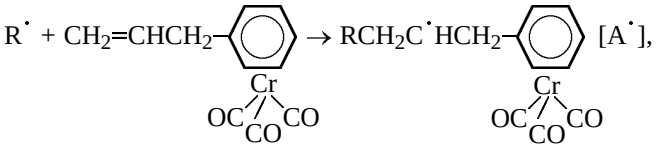
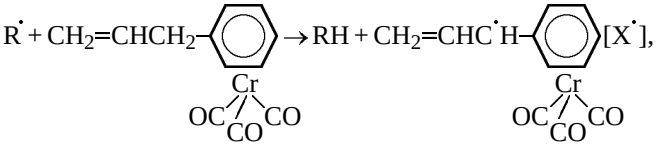


Fig. 1. Differential kinetic curves of the polymerization of (a) MMA and (b) ST in the presence of ABC at 70°C: (v_p) polymerization rate and (τ) time. Initiator AIBN; concentration, mol %: (a) 0.1 and (b) 0.8. ABC concentration, mol %: (a) (*1*) 0, (*2*) 0.5, (*3*) 0.8, and (*4*) 1.0; (b) (*1*) 0, (*2*) 0.5, (*3*) 2.0, and (*4*) 5.0.

A kinetic study of the radical polymerization of MMA and ST in the presence of AIBN (initiator) and ABC showed that ABC appreciably decelerates the polymerization and exerts a significant effect on the polymer chain propagation, decreasing the polymerization rate and simultaneously eliminating the gel effect at moderate temperatures (70°C) (Figs. 1a, 1b). However, to suppress the autoacceleration virtually fully, relatively high concentrations of ABC are required: 1.0 mol % in the synthesis of PMMA and 5.0 mol % in the polymerization of ST.

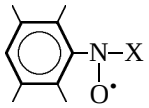
The strong effect of ABC on the kinetic parameters of the polymerization is apparently associated with the direct involvement of the organochromium compound in the chain propagation step. It is known [7, 14] that the reactivity of allyl monomers is appreciably lower than that of vinyl monomers, which is due, on the one hand, to isolated position of the π bond and lack of conjugation between the π bond and the functional group and, on the other, to formation of a relatively stable allyl radical in reactions of allyl compounds with the propagating radical or radical generated from the initiator. Apparently, these reactions are also possible in the polymerization of MMA and ST in the presence of ABC:





where R$^{\cdot}$ is the propagating radical or radical generated from the initiator.

Using ESR with nitrosodurene added as spin trap, we detected in the reaction system a spin adduct of radical X$^{\cdot}$ [scheme (2)], giving a triplet of doublets (a_N = 13.8 Oe, a_H = 0.5 Oe), which allows this adduct to be identified as radical B$^{\cdot}$. This fact unambiguously confirms that ABC is involved in the polymerization and gives a sterically hindered carbon-centered radical stabilized, on the one hand, by a conjugated π bond (π–e conjugation) and, on the other, by an arenetricarbonylchromium moiety:



[B$^{\cdot}$]

The propagating radical of (allylbenzene)tricarbonylchromium [radical A$^{\cdot}$, scheme (1)] was not detected by the spin trap technique.

Experiments on MMA polymerization in the presence of various concentrations of ABC showed that this chromium-containing monomer does not noticeably copolymerize with MMA. In particular, when 5 to 25 mol % (allylbenzene)tricarbonylchromium was added to a solution of 0.1 mol % AIBN in MMA, the polymer obtained at ≤10 wt % conversion contained only traces of chromium, irrespective of the initial amount of the chromium-containing monomer in the reaction mixture. This fact indicates that the copolymer of MMA with ABC is not formed in this case.

The failure of attempts to prepare (allylbenzene)tricarbonylchromium copolymers is well consistent with the ESR data. Furthermore, comparison with the published data on the reactivity of the organic analogue of ABC, allylbenzene, which copolymerizes with acrylic and methacrylic monomers under the conditions of radical initiation [15], indicates that introduction of

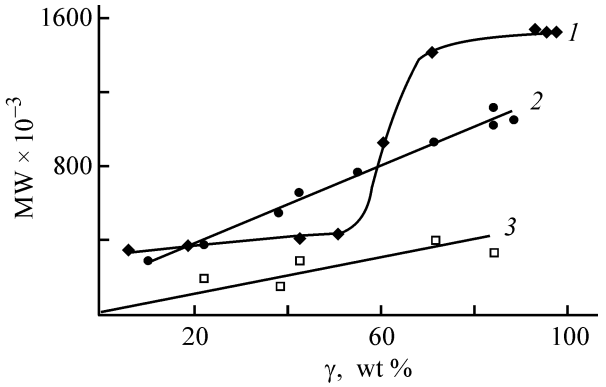


Fig. 2. (*1*, *2*) Viscosity-average and (*3*) number-average MW of PMMA formed in the presence of ABC vs. conversion γ. [AIBN] = 0.1 mol %, T = 70°C. ABC concentration, mol %: (*1*) 0 and (*2*, *3*) 1.0.

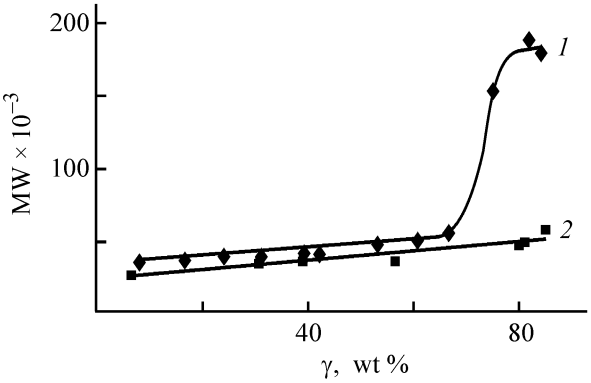


Fig. 3. (*1*) Viscosity-average and (*2*) number-average MW of PS formed in the presence of ABC vs. conversion γ. [AIBN] = 0.8 mol %, T = 70°C. ABC concentration, mol %: (*1*) 0 and (*2*) 5.0.

a bulky arenetricarbonylchromium group decreases the polymerization activity of the allyl fragment.

As noted above, addition of ABC to the reaction mixture appreciably affects the polymerization kinetics of ST and MMA, which is apparently due to the reaction of propagating radicals with the chromium-containing monomer to form a sterically hindered carbon-centered radical stabilized by the arenetricarbonylchromium group [scheme (2)]. It is reasonable to expect that stabilized radicals of this type can efficiently control the molecular-weight characteristics of polymers.

We found that the ST and MMA polymers formed in the presence of ABC have an appreciably decreased molecular weight (see table). As shown by the example of PMMA, this effect is determined by the ABC concentration. In particular, as the ABC concentration is raised from 5 to 25 mol %, the number-average MW M_n of the polymer regularly decreases from 11.1×10^4 to 4.7×10^4. The M_n of PMMA prepared under the similar conditions, but without adding ABC, is 20.6×10^4.

Furthermore, the table and Figs. 2 and 3 show that, when ABC is added in amounts comparable with the initiator concentration, M_n linearly increases with the monomer conversion. The dependences of M_n of PMMA and PS on the conversion in the absence of ABC, with AIBN as initiator, are shown in Figs. 2 and 3 for comparison. As seen from these data, in the absence of ABC M_n shows a spontaneous uncontrollable growth in the course of the polymerization.

It is known [2–4] that specifically the linear dependence of the molecular weight of a polymer on the conversion is one of the major evidences of polymerization in the "living" chain mode. This means that, starting from low conversions, the molecular weight of the polymer continuously increases in the course of the synthesis owing to the fragmentary chain propagation, and specifically M_n linearly increases with the conversion. Hence, the synthesis of PMMA and PS in the presence of ABC follows the chain propagation scheme (3) characteristic of controlled radical polymerization:

$$\sim P_n^{\bullet} + {}^{\bullet}X \rightleftarrows \sim P_n\text{---}X,$$

$$\wedge\!\wedge P_n\text{—}X \underset{k_c}{\overset{k_d}{\rightleftarrows}} \wedge\!\wedge P_n^{\bullet} + {}^{\bullet}X,$$

where $\sim P_n^{\bullet}$ is the propagating radical and ${}^{\bullet}X$ is the carbon-centered chromium-containing radical.

Molecular-weight characteristics of PMMA and PS synthesized in the presence of ABC at 70°C (AIBN initiator, 0.1 and 0.8 mol %, respectively)

Starting monomer	ABC added, mol %	Monomer conversion, wt %	$M_n \times 10^{-3}$	$M_w^* \times 10^{-3}$	M_w/M_n
MMA	0	90.3	661	1604	2.4
	1	9.5	123	227	1.8
		22.1	199	417	2.1
		42.3	319	715	2.2
		84.6	360	856	2.4
ST	0	84.0	77	246	3.2
	5	6.4	26	39	1.5
		30.8	35	51	1.5
		39.3	37	54	1.5
		79.6	44	86	1.9
		80.6	47	95	2.0
		84.9	58	128	2.2

* (M_w) Weight-average MW.

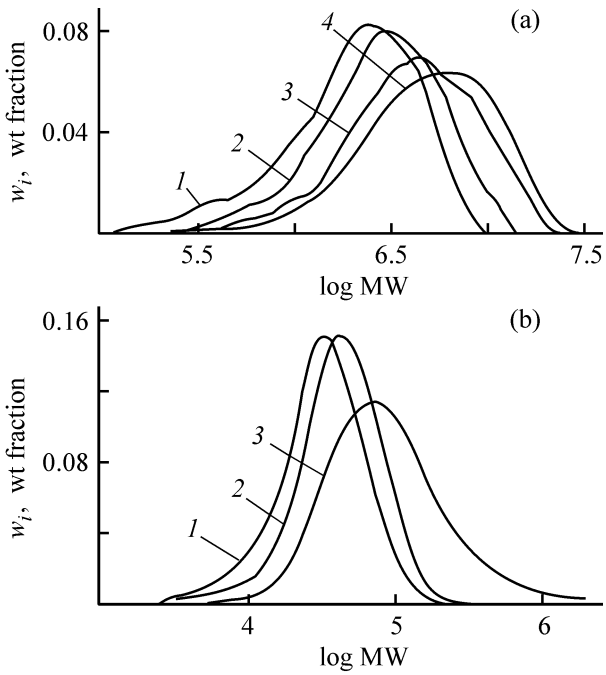


Fig. 4. MWD curves for (a) PMMA and (b) PS samples synthesized to various conversions at 70°C in the presence of (a) 0.1 and (b) 0.8 mol % AIBN and of (a) 1.0 and (b) 5.0 mol % ABC. (w_i) Weight fraction of molecules of the given MW. γ, wt %: (a) (*1*) 9.5, (*2*) 22.1, (*3*) 42.3, and (*4*) 84.6; (b) (*1*) 6.4, (*2*) 30.8, and (*3*) 84.9.

Figures 4a and 4b show the MWD curves of PMMA and PS samples prepared in the presence of ABC. A trend characteristic of "pseudoliving" polymerization is observed: The MWD curves shift toward higher MW as the conversion increases, which also counts in favor of the occurrence of a controlled chain propagation in the polymerization of MMA and ST in the presence of ABC [scheme (4)].

It should be noted that, at high conversions, the MWD curves get broadened (Figs. 4a, 4b), and the polydispersity coefficients increase (see table). This trend is untypical of classical polymerization in the living chain mode and is apparently due to formation of a "dead" polymer in the system as a result of bimolecular termination of the propagating chains. This process can occur in parallel with the pseudoliving polymerization and is observed, e.g., in controlled radical polymerization in the presence of triphenylmethyl and some other sterically hindered carbon-centered radicals [16].

CONCLUSION

A sterically hindered organochromium allyl monomer, (allylbenzene)tricarbonylchromium, is a novel agent for controlling the chain propagation in radical polymerization of vinyl monomers at temperatures optimal for the commercial synthesis of macromolecular compounds.

ACKNOWLEDGMENTS

The authors are grateful to A.N. Artemov and E.V. Sazonova for the assistance in the experiments.

The study was supported by the Ministry of Education and Science of the Russian Federation and by the Russian Foundation for Basic Research.

REFERENCES

1. *Controlled Radical Polymerization*, Matyjaszewski, Kr., Ed., Oxford: Oxford Univ., 1998.
2. Hawker, C.J., Bosman, A.W., and Harth, E., *Chem. Rev.*, 2001, vol. 101, no. 12, pp. 3611–3688.
3. Grishin, D.F. and Semenycheva, L.L., *Usp. Khim.*, 2001, vol. 70, no. 5, pp. 486–510.
4. Zaremskii, M.Yu. and Golubev, V.G., *Vysokomol. Soedin., Ser. C*, 2001, vol. 43, no. 9, pp. 1689–1728.
5. Grishin, D.F., Semyonycheva, L.L., Artemov, A.N., *et al.*, *Appl. Organomet. Chem.*, 2003, vol. 17, no. 2, pp. 717–722.
6. Grishin, D.F., Semenycheva, L.L., Telegina, E.V., and Cherkasov, V.K., *Vysokomol. Soedin., Ser. A*, 2003, vol. 45, no. 2, pp. 211–216.
7. Vorob'eva, A.I., Prochukhan, Yu.A., and Monakov, Yu.B., *Vysokomol. Soedin., Ser. C*, 2003, vol. 45, no. 12, pp. 2118–2136.
8. Trahanovsky, W.S. and Hall, R.A., *J. Am. Chem. Soc.*, 1975, vol. 96, no. 1, pp. 71–82.
9. *Analiticheskaya khimiya polimerov* (Analytical Chemistry of Polymers), Klain, T., Ed., Moscow: Mir, 1966.
10. *Organic Syntheses*, Blatt, A.H., Ed., New York: Wiley, 1944, vol. 2.
11. Arulin, V.I. and Efimov, L.I., *Tr. Khim. Khim. Tekhnol.* (Gor'kii), 1970, issue 2, pp. 74–77.
12. Borisova, L.N. and Guseva, T.V., *Khim. Elementoorg. Soedin.* (Gor'kii), 1978, issue 6, pp. 78–80.
13. Belen'kii, B.G. and Vilenchik, L.Z., *Khromatografiya polimerov* (Chromatography of Polymers), Moscow: Khimiya, 1978.
14. *Allilovye monomery: sintez i primenenie* (Allyl Monomers: Synthesis and Applications), Moscow: NIITEKhIM, 1989.
15. Tadatoshi, O., Seizo, M., and Chiyoko, A., *Kobunshi Kagaku*, 1973, vol. 30, no. 336, pp. 223–238.
16. Korolev, G.V. and Marchenko, A.P., *Usp. Khim.*, 2000, vol. 69, no. 5, pp. 447–475.

Russian Journal of Applied Chemistry, Vol. 78, No. 8, 2005, pp. 1329–1332. Translated from Zhurnal Prikladnoi Khimii, Vol. 78, No. 8, 2005, pp. 1353–1356.
Original Russian Text Copyright © 2005 by Sultanova, Rakhmatullina, Akhmed'yanova, Liakumovich.

MACROMOLECULAR CHEMISTRY AND POLYMERIC MATERIALS

Emulsion Polymerization of Styrene in the Presence of a Mixture of Potassium Stearate and Oleate

G. I. Sultanova, A. P. Rakhmatullina, R. A. Akhmed'yanova, and A. G. Liakumovich

Kazan State Technological University, Kazan, Tatarstan, Russia

Received April 21, 2005

Abstract—The features of emulsion polymerization of styrene in the presence of a mixture of potassium stearate and oleate was studied. The effect of these salts on the polymerization rate and the yield and molecular weight of polystyrene was examined.

Making the existing processes for latex production more feasible and efficient remains a topical problem. This goal can be accomplished, in particular, by choosing effective emulsifiers that could provide a high conversion of the monomers and aggregative stability of the latexes.

It is known that effective emulsifying systems for synthesis of diene–styrene and styrene–acrylate dispersions contain mixtures of different types of surfactants [1]. At the same time, impurities of potassium myristate, palmitate, stearate, or linoleate in the commercially used emulsifier, potassium oleate, decrease the polymerization rate and mechanical stability of butadiene–styrene latex [2].

We found previously that a 40 : 60 (by weight) mixture of stearic and oleic acids exhibits synergism in its effect on some properties of rubber stocks and vulcanizates [3–5]. This fact suggests that these surfactants may affect nonadditively the preparation and properties of other polymers.

As a model for examining the effect of a mixture of stearic and oleic acids in the form of potassium salts on the emulsion polymerization, we chose polymerization of styrene.

EXPERIMENTAL

The emulsion polymerization was performed at 80°C for 90 min. The composition (wt parts) of the reaction mixture was as follows: styrene 100, fatty acid 1.2, KOH 0.18, $K_2S_2O_8$ 0.5, and water 160. The reaction progress was monitored gravimetrically. Samples were taken at definite intervals and analyzed to determine the polymer yield (%) by the formula [6]

$$N = P_p \times 100/P_m,$$

where P_p is the polymer weight in the sample (g), and P_m is the monomer weight in the sample (g), calculated from the initial monomer concentration.

The viscosity-average molecular weight of the isolated polystyrene was determined by the procedure described previously [7].

The surface tension of aqueous solutions of potassium soaps of fatty acids was determined by the Du Nouy method [8]. The limiting adsorption Γ_∞ was determined graphically from the adsorption isotherms of the surfactants [9, 10]. The negative logarithm of the surfactant concentration at which σ decreases by 20 mN m^{-1} (pC_{20}) was determined by a procedure described in [11], and the critical micellization concentration (CMC), according to [12, 13].

Figures 1a–1c show that the polymerization kinetics depends on the emulsifier composition, namely, on the ratio of stearic (St) and oleic (Ol) acids in the potassium salts [K(St : Ol)]. The styrene conversion as a function of the emulsifier composition passes through a maximum at the K(St : Ol) ratio ranging from 40 : 60 to 60 : 40 wt %, with the polystyrene yield (Fig. 2, curve *1*) equal to 99.9%.

The viscosity-average molecular weight ($\bar{M}_\eta$) of polystyrene as a function of the K(St : Ol) ratio also passes through a maximum, 460 000, observed at K(St : Ol) = 40 : 60 wt % (Fig. 2, curve *2*).

The dependences of the mean reaction rate (W_m) on the styrene conversion (Fig. 3) are, on the whole, similar at different emulsifier compositions, with the highest W_m attained at 60% conversion. However,

1070-4272/05/7808-1329 © 2005 Pleiades Publishing, Inc.

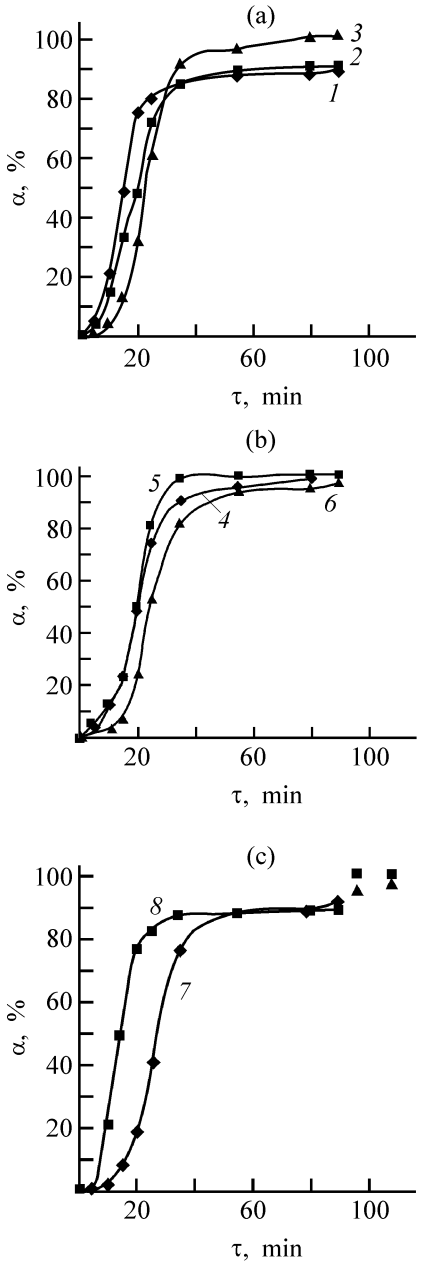


Fig. 1. Styrene conversion α vs. time τ at various ratios of stearic and oleic acids in the emulsifier. St : Ol, wt %: (*1*) 100 : 0, (*2*) 0 : 100, (*3*) 40 : 60, (*4*) 70 : 30, (*5*) 60 : 40, (*6*) 30 : 70, (*7*) 10 : 90, and (*8*) 90 : 10.

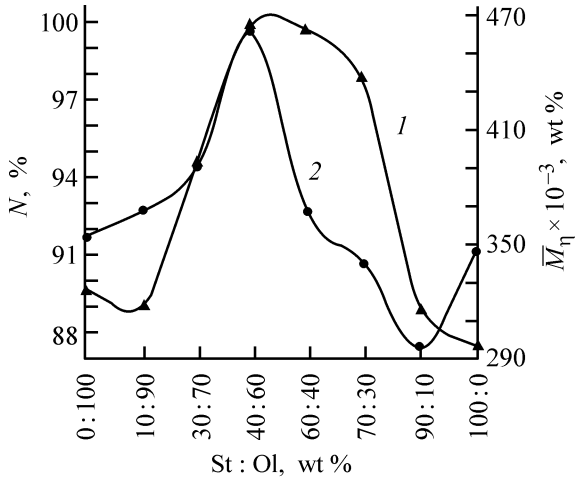


Fig. 2. (*1*) Yield *N* and (*2*) viscosity-average molecular weight $\bar{M}_\eta$ of polystyrene vs. the ratio of stearic and oleic acids in the emulsifier.

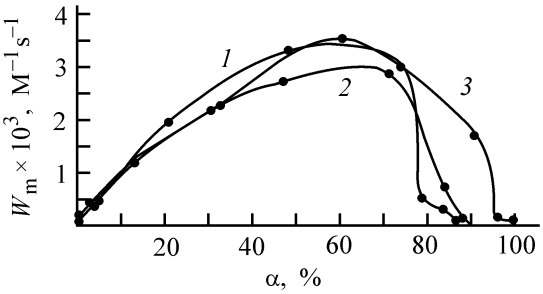


Fig. 3. Variation of the mean rate of styrene polymerization W_m with the conversion α. Emulsifier: (*1*) potassium stearate, (*2*) potassium oleate, and (*3*) potassium salts of a mixture of stearic (40 wt %) and oleic (60 wt %) acids; the same for Figs. 4 and 5.

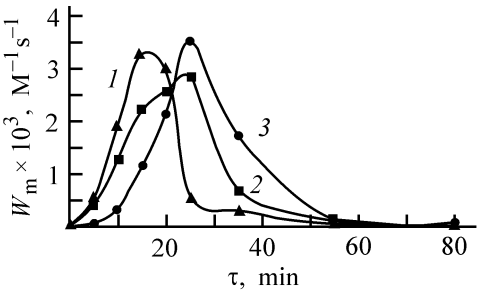


Fig. 4. Mean rate of styrene polymerization W_m vs. polymerization time τ.

the curve shape depends on the emulsifier composition. This effect is especially pronounced at high monomer conversions when the mean polymerization rate in the presence of the mixed emulsifier (Fig. 3, curve *3*) is higher than that observed with the individual surfactants. With the mixed emulsifier, virtually 100% conversion of styrene is attained in 1.5 h.

The plots of W_m vs. polymerization time (Fig. 4) show that the K(St : Ol) = 40 : 60 wt % mixture has a nonadditive effect on the reaction kinetics.

It should be noted that, although the mean polymerization rates observed in the presence of the individual emulsifiers are different, the monomer conversions and viscosity-average molecular weights of

Colloid-chemical properties of aqueous solutions of potassium salts of fatty acids

Surfactant	σ, mN m^{-1}	C_{20}, g dm^{-3}	$\Gamma_\infty \times 10^6$, mol m^{-2}	CMC, g dm^{-3}
Potassium stearate	43.0	0.041	3.3	0.48
Potassium oleate	33.5	0.007	4.6	0.75
Mixture of potassium salts of St (40 wt %) and Ol (60 wt %)	33.0	0.003	5.0	0.50

the polymer samples prepared in the presence of both emulsifiers are virtually equal.

The nonadditive effect is most probably associated with the colloid-chemical characteristics of the surfactants used. Stearic and oleic acids do not differ in the length of the hydrocarbon substituent, but differ in its nature: In oleic acid, the hydrocarbon substituent contains a double bond.

It has been found previously that the surface tension of a mixture of stearic and oleic acids is lower than the additive value and has a minimum in the composition range St : Ol (33–40) : (67–60) wt % at temperatures of 60 to 80°C [14]. Similar effects would be expected with aqueous solutions of the potassium salts of St and Ol and of their mixture (40 : 60 wt %). In this connection, we constructred the isotherms of surface tension at the aqueous solution|air phase boundary (Fig. 5).

The lowest σ (11.5% lower than the additive value) was observed with the K(St : Ol) = 40 : 60 wt % mixture (see table). With pure potassium stearate, the surface tension was the highest.

The C_{20} value for potassium stearate is higher by factors of 6 and 11 than that for potassium oleate and K(St : Ol) = 40 : 60 wt % mixture, respectively (see table). Hence, this mixture exhibits synergism with respect not only to an absolute quantity (surface tension) but also to a relative parameter (concentration providing a given decrease in σ).

The dispersing and stabilizing effect of a surfactant is due to its adsorption at the phase boundary. The limiting adsorption can be considered a criterion of the surfactant performance. As can be seen from the table, potassium stearate shows the lowest adsorption, and the K(St : Ol) = 40 : 60 wt % mixture, the highest, and hence it is a more effective dispersant and stabilizer for emulsions, compared to the individual potassium carboxylates.

The critical micelle concentration (CMC) is one of the most important physicochemical characteristics of surfactants. Among the surfactants studied, potassium oleate has the highest CMC, and potassium stearate, the lowest (see table). The CMC of the K(St : Ol) = 40 : 60 wt % mixture is lower than the additive value and approximately equal to that of potassium stearate. The lower CMC of potassium stearate, compared to oleate, is most probably due to lower degree of dissociation of this soap.

Since the emulsion polymerization of styrene was studied in the range of emulsifier concentrations exceeding CMC of all the emulsifiers examined, the observed effects should be attributed to differences in the amount and size of the micelles, as it is known [15] that the rate of emulsion polymerization depends, under equal other conditions, on the solubilizing power of aqueous solutions of emulsifiers.

CONCLUSIONS

(1) The yield of polystyrene in emulsion polymerization reaches a maximum (99.9%) when a mixture of potassium stearate and oleate (ratio from 40 : 60 to 60 : 40 wt %) is used as emulsifier.

(2) In emulsion polymerization of styrene in the presence of potassium stearate and oleate taken in a ratio of 40 : 60 wt %, the high mean polymerization rate is preserved at high conversions of the monomer, in contrast to the process performed in the presence of each of these salts taken separately.

(3) Polystyrene prepared using a mixture of potassium stearate and oleate in a ratio of 40 : 60 wt % has

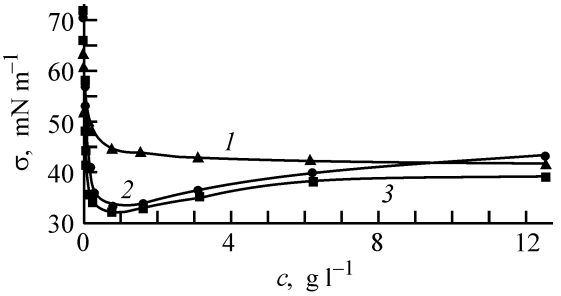


Fig. 5. Surface tension isotherms. (σ) Surface tension and (*c*) emlusifier concentration.

the highest viscosity-average molecular weight ($\overline{M}_\eta$ = 460 000), whereas $\overline{M}_\eta$ of polystyrene prepared in the presence of potassium stearate or oleate taken separately is about 350 000.

REFERENCES

1. Petukhova, A.V., Synthesis of Diene–Styrene Latexes in the Presence of Surfactant Mixtures, *Cand. Sci. Dissertation*, Moscow, 2003.
2. Lebedeva, T.A. and Mironova, N.M., Abstracts of Papers, *2-ya Mezhrespublikanskaya nauchnaya konferentsiya studentov vuzov SSSR "Sintez, issledovanie svoistv, modifikatsiya i pererabotka vysokomolekulyarnykh soedinenii"* (2nd Interrepublican Scientific Conf. of Higher School Students of the Soviet Union "Synthesis, Properties, Modification, and Processing of Macromolecular Compounds"), Kazan, 1981, p. 17.
3. Rakhmatullina, A.P., Zavarikhina, L.A., Akhmed'yanova, R.A., and Liakumovich, A.G., *Kauchuk Rezina*, 2001, no. 6, pp. 44–45.
4. Rakhmatullina, A.P., Zavarikhina, L.A., Mokhnatkina, O.G., *et al.*, *Vopr. Khim. Khim. Tekhnol.*, 2002, pp. 124–126.
5. Mokhnatkina, O.G., Features of Behavior of Mixtures of Stearic and Oleic Acids in Tire Protector Rubbers Based on Butadiene–Methylstyrene Rubber, *Cand. Sci. Dissertation*, Kazan, 2003.
6. Toroptseva, A.M., Belogorodskaya, K.V., and Bondarenko, V.M., *Laboratornyi praktikum po khimii i tekhnologii VMS* (Laboratory Manual on Chemistry and Technology of Macromolecular Compounds), Leningrad: Khimiya, 1972.
7. Averko-Antonovich, Yu.O., *Metodicheskie ukazaniya k laboratornomu praktikumu po khimii i fizike VMS* (Methodical Instructions to the Laboratory Course of Chemistry and Physics of Macromolecular Compounds), Kazan: Kazan. Gos. Tekhnol. Univ., 2001.
8. Abramzon, A.A., Zaichenko, L.P., and Faingol'd, S.I., *Poverkhnostno-aktivnye veshchestva* (Surfactants), Leningrad: Khimiya, 1988.
9. Aivazov, V.V., *Praktikum po khimii poverkhnostnykh yavlenii i adsorbtsii* (Practical Course of Chemistry of Surface Phenomena and Adsorption), Moscow: Vysshaya Shkola, 1973.
10. Averko-Antonovich, I.Yu. and Averko-Antonovich, Yu.O., *Metodicheskie ukazaniya po kursu "Tekhnologiya sinteticheskogo kauchuka"* (Methodical Instructions to the Course "Technology of Synthetic Rubber"), Kazan: Kazan. Khimiko-Tekhnol. Inst., 1991.
11. Rosen, M.J., *Surfactants and Interfacial Phenomena*, New York: Wiley, 1978.
12. *Praktikum po kolloidnoi khimii* (Practical Course of Colloid Chemistry), Neiman, R.E., Ed., Moscow: Vysshaya Shkola, 1972.
13. Vyaseleva, G.Ya., Kurmaeva, A.I., and Tret'yakova, A.Ya., *Praktikum po kolloidnoi khimii* (Practical Course of Colloid Chemistry), Kazan: Kazan. Khimiko-Tekhnol. Inst., 1979.
14. Rakhmatullina, A.P., Zavarikhina, L.A., Mokhnatkina, O.G., *et al.*, *Zh. Prikl. Khim.*, 2003, vol. 76, no. 4, pp. 680–684.
15. Eliseeva, V.I., Ivanchev, S.S., Kuchanov, S.I., and Lebedev, A.V., *Emul'sionnaya polimerizatsiya i ee primenenie v promyshlennosti* (Emulsion Polymerization and Its Industrial Applications), Moscow: Khimiya, 1976.

Russian Journal of Applied Chemistry, Vol. 78, No. 8, 2005, pp. 1333–1336. Translated from Zhurnal Prikladnoi Khimii, Vol. 78, No. 8, 2005, pp. 1357–1360.
Original Russian Text Copyright © 2005 by Udoratina, Demin.

MACROMOLECULAR CHEMISTRY AND POLYMERIC MATERIALS

Degradation of Hardwood Sulfate Pulp in Aqueous Dioxane

E. V. Udoratina and V. A. Demin

Institute of Chemistry, Komi Scientific Center, Ural Division, Russian Academy of Sciences, Syktyvkar, Komi Republic, Russia

Received March 2, 2005

Abstract—Degradation of unbleached hardwood sulfate pulp in aqueous dioxane in the presence of catalytic amounts of HCl was studied. The kinetic constants and the apparent activation energy of pulp degradation in the range 343–363 K were calculated.

Treatment of cellulose with organic solvents containing a mineral acid in the presence or in the absence of water results in cleavage of glycoside bonds between its monomeric units, which leads to a decrease in the degree of polymerization, i.e., to degradation [1]. In production of fibrous semifinished products for paper, the pulp degradation is undesirable. By contrast, preparation of powdered cellulose products, including microcrystalline cellulose, is based on the pulp degradation.

The objectives of this study are determined by the growing researchers' interest in the development of nonaqueous processes for pulp production, based on organic liquids, with complete regeneration and recycling of the solvents [2, 3]. These processes show much promise, as they decrease the consumption of natural water and energy for the process. Although delignification of wood with organic solvents has been the subject of numerous studies, the effect of organic solvents on sulfate pulp and the possibilities of using these processes for pulp bleaching are insufficiently understood. In this study, we examined the degradation of unbleached sulfate pulp in aqueous dioxane. This treatment was used in [4] for recovering residual lignin with the aim to study its properties. In [5], we showed that, depending on treatment conditions, 29–80% of residual lignin dissolves on treatment of sulfate pulp with aqueous dioxane in the course of its bleaching.

EXPERIMENTAL

Experiments were performed with unbleached hardwood sulfate pulp with a Bjorkman hardness of 77 permanganate units and a degree of polymerization of 1031. The pulp was treated in a 9 : 1 dioxane–water mixture in the presence of an acid catalyst (0.0–0.2 M HCl) at a slurry concentration of 5 wt % absolutely dry pulp. Treatments were performed at 343–363 K for 1–5 h. The treated pulp was washed with warm distilled water and dried. The pulp degradation was evaluated by a decrease in its degree of polymerization, determined viscometrically in Cadoxen [6]. The resulting pulp samples were also analyzed photometrically for lignin [7].

We examined how the degradation of sulfate pulp is influenced by the acid catalyst (HCl) concentration (first series of experiments) and temperature (second series). The first series was performed in the course of 1 h at 343 K, and the acid catalyst concentration was varied from 0.00 to 0.20 M. Preliminary studies of sulfate pulp delignification in this medium showed that, at lower temperatures, the degree of removal of residual lignin is unsatisfactory. Data on the intrinsic viscosity in Cadoxen and degree of polymerization of the pulp are listed in Table 1.

Table 1. Intrinsic viscosities in Cadoxen [η] and degrees of polymerization $[DP]_\eta$ of hardwood sulfate pulp after its treatment in aqueous dioxane at various HCl concentrations

Run no.	HCl concentration, M	[η]	DP_η^*	Relative lignin content
1	Initial pulp	4.95	1031	1.00
2	0.000	4.30	910	0.90
3	0.005	4.23	890	0.74
4	0.010	3.68	770	0.69
5	0.020	3.12	650	0.63
6	0.050	2.92	600	0.60
7	0.200	2.01	400	0.45

* The degree of polymerization was estimated from the equation $[\eta] = DP^{0.04} \times 7.1 \times 10^{-3}$ [5].

1070-4272/05/7808-1333 © 2005 Pleiades Publishing, Inc.

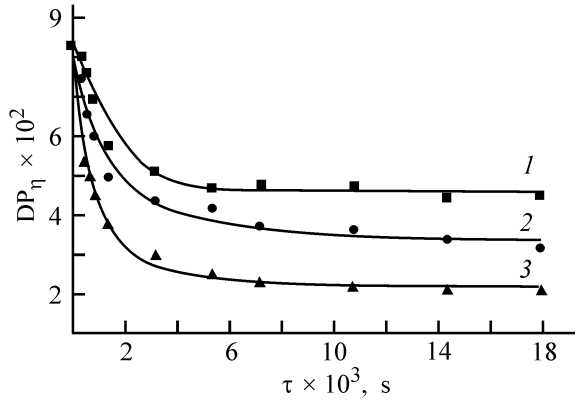


Fig. 1. Degree of polymerization DP_η of pulp vs. the treatment time τ at various temperatures. Temperature, K: (*1*) 343, (*2*) 353, and (*3*) 363; the same for Figs. 2 and 4.

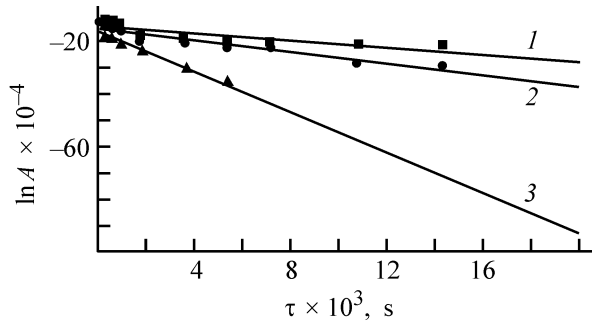


Fig. 2. Semilog kinetic plots of pulp degradation at 343–363 K. $A = (DP^n - 1)/DP^n$; (τ) treatment time.

In the absence of an acid and at its small amounts in the system (run nos. 2, 3), the degree of polymerization of the pulp after an 1-h treatment decreased, on the average, by 12% relative to the initial values, and at HCl concentrations of 0.01–0.05 M, by 25–42% (to 770–600, respectively). At the HCl concentration increased to 0.20 M, the degree of polymerization decreased drastically, to 400, i.e., by almost a factor of 3, compared to the initial sample.

Table 2. Calculated kinetic parameters of delignification of hardwood sulfate pulp in aqueous dioxane

Treatment temperature, K	Calculated kinetic parameters		
	$k_{app} \times 10^8$, s^{-1}	$-\ln k_{app}$	E_{app}, kJ mol^{-1}
343	6.9	16.5	
353	11.4	16.0	88.6 ± 11.8
363	38.4	14.8	

Data on the relative content of lignin in the pulp treated with aqueous dioxane solutions are also listed in Table 1. As the acid catalyst concentration is increased from 0.00 to 0.05 M, the residual lignin content decreases from 0.90 to 0.60 relative to the initial level. At the highest tested concentration of HCl, the residual lignin is removed by half. Taking into account published data [8], we can suggest that, in the solvent system examined, residual lignin of sulfate pulp undergoes degradation with partial dissolution.

The dependence of the DP of pulp on the treatment temperature was examined in the range 343–363 K at an acid catalyst concentration of 0.02 M. At this acid content (which is ten times lower than that in classical acidolysis of wood), lignin undergoes relatively deep degradation (Table 1, run no. 5), but the DP of pulp remains sufficient for the use in paper production. The upper limit of the temperature range examined corresponds to the boiling point of the solvent mixture.

The kinetic curves of pulp degradation are shown in Fig. 1.

The kinetic curves indicate that a major decrease in the degree of polymerization of pulp occurs in the initial period of the treatment. Within 5 h, the DP of the pulp decreases to 541 at 343 K, to 328 at 353 K, and to 219 at 363 K; in the last case, the pulp loses the fibrous structure.

To determine the kinetic parameters of degradation of sulfate pulp, we used a first-order equation characterizing the concentration of bonds in the cellulose macromolecule, which has the following form in the logarithmic coordinates [9]:

$$-\ln[(DP^n - 1)/(DP^n)] = -\ln[(DP_0^n - 1)/(DP_0^n)] + k\tau,$$

where DP^n is the number-average degree of polymerization, determined using the formula for the mean polydispersity coefficient: $n = DP_\eta/DP^n$.

According to [10], $n = 1.25$.

The rate constants of pulp degradation were calculated from the equations for the kinetic curves linearized in the semilog coordinates (Fig. 2). When plotting these straight lines, we used the initial DP of the pulp.

The apparent rate constants k_{app} of pulp degradation in aqueous dioxane increase from 6.9×10^{-8} to 38.4×10^{-8} s^{-1} in going from 343 to 363 K (Table 2).

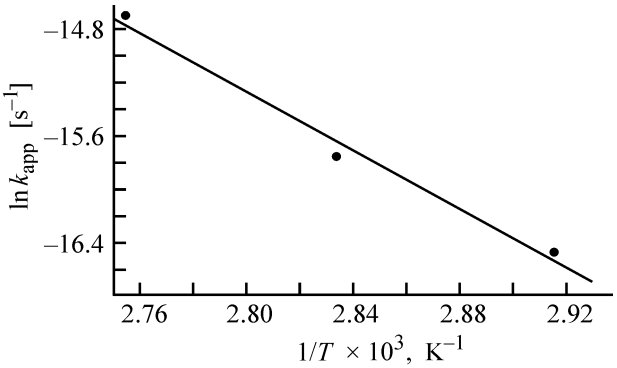


Fig. 3. Arrhenius plot for degradation of sulfate pulp in the range 343–363 K. Fitting equation: $\ln k_{app} = (14.50 \pm 4.04) - (10.66 \pm 1.42) \times 10^3/T$, $R = 0.99$; (T) temperature.

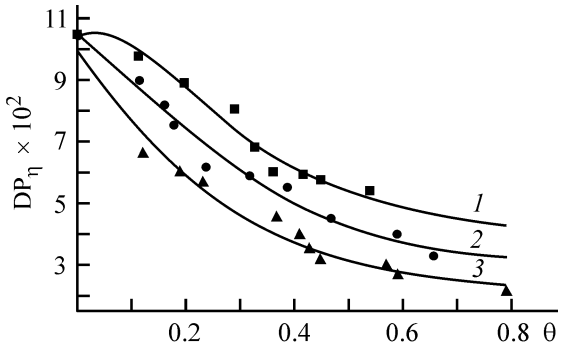


Fig. 4. Selectivity of treatment of hardwood sulfate pulp in aqueous dioxane containing 0.02 M HCl at various temperatures. (DP_η) Degree of polymerization and (θ) degree of delignification of pulp.

The temperature coefficient $\alpha(T^{10})$, i.e., the factor by which k_{app} increases as the temperature is elevated by 10 K, is 1.7–3.4.

From the slope B of the Arrhenius dependence $\ln k_{app}$–$1/T$ (Fig. 3),

$$B = \ln(k_1/k_2)/(1/T_2 - 1/T_1)$$

we calculated the apparent activation energy E_{app} by the equation

$$E = BR,$$

where R is the universal gas constant. We obtained $E_{app} = 88.6 \pm 11.8$ kJ mol^{-1}, which is comparable with E_{app} of oxidative hydrolysis and acid hydrolysis reactions [11], ~95–100 kJ mol^{-1}.

We assessed the feasibility of aqueous-dioxane treatment of sulfate pulp in the course of bleaching, in particular, in the first steps of delignification. The major parameter of the bleaching process is the delignification selectivity. It can be characterized by the dependence of DP_η on θ, where θ is the degree of pulp delignification (Fig. 4).

The curves obtained show that both lignin and cellulose undergo simultaneous and substantial degradation even under mild treatment conditions (343 K). Raising the temperature to 353–363 K favors degradation of cellulose to a greater extent, compared with residual lignin.

Thus, treatment of sulfate pulp in aqueous dioxane occurs with a low selectivity and may be of limited use in pulp treatment for paper production. However, treatment under mild conditions can be used for delignification in production of fibrous cellulose, and treatment under more severe conditions, in production of powdered cellulose materials for chemical processing, e.g., of microcrystalline cellulose.

CONCLUSIONS

(1) Treatment of unbleached hardwood sulfate pulp in a dioxane–water–HCl solution results in degradation and partial delignification of the pulp.

(2) With an increase in the temperature by 10 K, the rate of degradation of hardwood sulfate pulp grows by a factor of 2–3. The apparent activation energy of the process is 88.6 ± 11.8 kJ mol^{-1}.

REFERENCES

1. Blažej, A. and Košik, M., *Cellulose and Its Derivatives: Chemistry, Biochemistry and Applications*, Kennedy, J.F. *et al.*, Eds., 1985, pp. 97–117.
2. Petrova, S.N., Zakharov, A.G., Matveeva, I.Yu., and Ivanova, O.N., in *5-ya Mezhdunarodnaya nauchnaya konferentsiya "Teoreticheskie i eksperimental'nye osnovy sozdaniya novykh vysokoeffektivnykh khimiko-tekhnologicheskikh protsessov i oborudovaniya": Sbornik trudov* (Proc. 5th Int. Scientific Conf. "Theoretical and Experimental Principles of Development of New High-Performance Chemical Processes and Equipment"), Ivanovo, 2001, p. 441.
3. Aziz, S. and Sarkanen, K., *TAPPI J.*, 1989, vol. 72, no. 3, pp. 169–175.
4. Bogomolov, V.D., Demin, V.A., Davydov, V.D., and Popova, G.I., *Izv. Vyssh. Uchebn. Zaved., Lesn. Zh.*, 1977, no. 1, pp. 96–99.
5. Udoratina, E.V. and Demin, V.A., in *Khimiya vysokomolekulyarnykh soedinenii, lesokhimiya i organi-*

cheskii sintez: Sbornik statei Komi nauchnogo tsentra (Chemistry of Macromolecular Compounds, Forest Chemistry, and Organic Synthesis: Coll. of Papers of Komi Scientific Center), Syktyvkar, 2002, no. 167, p. 19.

6. Bolotnikova, L.S., Danilov, S.N., and Samsonova, T.I., *Zh. Prikl. Khim.*, 1966, vol. 39, no. 1, pp. 176–180.
7. Vlasova, T.E. and Nekhaichuk, A.D., *Tsellyuloza, Bumaga, Karton*, 1974, issue 9, p. 9.
8. Grushnikov, O.P. and Elkin, V.V., *Dostizheniya i problemy khimii lignina* (Advances and Problems of Lignin Chemistry), Moscow: Nauka, 1973.
9. Emanuel', N.M. and Knorre, D.G., *Kurs khimicheskoi kinetiki* (A Course of Chemical Kinetics), Moscow: Vysshaya Shkola, 1974.
10. Sokolov, O.M., Demin, V.A., Karmanov, A.P., and Korobova, E.N., *Lesn. Zh.*, 1990, no. 4, pp. 78–83.
11. Khol'kin, Yu.I., *Teoriya gidroliza rastitel'nogo syr'ya* (Theory of Hydrolysis of Plant Raw Materials), Leningrad: Lesotekh. Akad., 1987.

Russian Journal of Applied Chemistry, Vol. 78, No. 8, 2005, pp. 1337–1342. Translated from Zhurnal Prikladnoi Khimii, Vol. 78, No. 8, 2005, pp. 1361–1366.
Original Russian Text Copyright © 2005 by Luchkina, Askadskii, Bychko.

MACROMOLECULAR CHEMISTRY AND POLYMERIC MATERIALS

Composite Polymeric Materials Based on Polyisocyanurates and Polyurethanes

L. V. Luchkina, A. A. Askadskii, and K. A. Bychko

Nesmeyanov Institute of Organoelement Compounds, Russian Academy of Sciences, Moscow, Russia

Received October 14, 2004

Abstract—Network poly(urethane–isocyanurate) systems were synthesized from polyurethanes and polyisocyanurates, and the process for preparing composite materials based on them was examined.

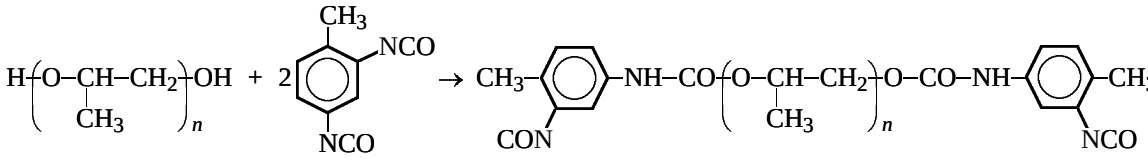
Polyurethane materials find growing applications, primarily thanks to a unique combination of high hardness and elasticity, and also to the exceedingly high tear and wear resistance. Composite polymeric materials (CPMs) have been prepared from polyisocyanurate and polyurethane compounds. These materials preserve elasticity at any elastic modulus and contain a voluminous highly porous support exerting no effect on the elastic properties of the CPMs. Previously CPMs have been prepared from polyisocyanurates, but these materials show poor wear resistance, and the low-modulus samples based on them exhibit an accelerated weather aging. Therefore, it seemed appropriate to prepare materials containing a polyurethane component [1, 2].

In this study, we examined the process for preparing composite polymeric materials from polyisocyanurate and polyurethane compounds.

EXPERIMENTAL

As polymeric binders we used compounds of varied composition, based on 2,4-toluylene diisocyanate (TDI), a diamine [di(3-chloro-4-aminophenuyl)methane], and an oligomeric rubber with terminal hydroxy groups, polypropylene glycol (PPG) [Bayer, MW 2200, hydroxyl number 56.7 (mg KOH) g^{-1}, n_D^{30} = 1.4500, moisture content ≤0.03%]. The prepolymer, oligoether diisocyanate (OEC), was prepared as described in [3]. The reaction progress was monitored by IR spectroscopy from the intensity of the band at 2280 cm^{-1} and from the bands of hydroxy groups at 3500–3600 cm^{-1} [4]. The content of isocyanate groups (%) was estimated from their reaction with dibutylamine; excess amine was titrated with an acid [5]. According to the potentiometric titration data, in the course of the OEC synthesis (T = 70°C, 5 h) the content of isocyanate groups decreases by approximately a factor of 2 (from 10.1 to 4.7%, Fig. 1).

The IR spectrum of the reaction product contained characteristic bands of urethane groups at 3300–3400 cm^{-1} [6]. OEC was obtained as a viscous colorless liquid (at room temperature); n_D^{30} 1.4711, ρ 1.057 g cm^{-3}. The prepolymer is formed by the following reaction:

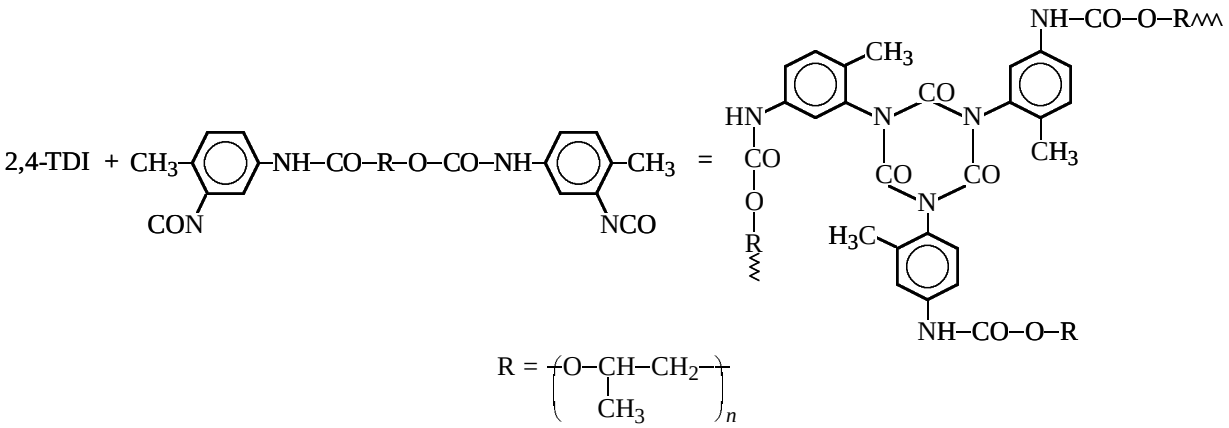


(1)

where n = 38.

In the second step, the prepolymer was mixed with a varied amount of TDI and di(3-chloro-4-aminophenyl)methane. A calculated amount of carbon black (P 803 brand) was added to obtain black articles. The reaction occurred in the presence of a complex catalyst prepared by mixing dimethylbenzylamine (DMBA) with ED-22 epoxy oligomer in a 1 : 20 molar ratio [3]:

1070-4272/05/7808-1337 © 2005 Pleiades Publishing, Inc.



(2)

In turn, the reaction of the macrodiisocyanate with the diamine initially yielded linear polyurethane–ureas, as confirmed by a spectroscopic analysis (intensity of the band at 1550 cm^{-1}) [6]:

$$\text{OCN}\sim\text{NCO} + \text{H}_2\text{N–R–NH}_2 + \text{OCN}\sim\text{NCO} + \text{H}_2\text{N–R–NH}_2$$
$$\rightarrow \text{–OC–NH}\sim\text{NH–CO–NH–R–NH–CO–NH}\sim\text{NH–CO–NH–R–NH–}, \quad (3)$$

where ∼ is a macrodiisocyanate molecule.

An excess unchanged macrodiisocyanate caused cross-linking of the chain. At temperatures above 100°C, the macrodiisocyanate added to the preliminarily formed urea bonds, which are sufficiently reactive toward diisocyanate groups. As a result, a new kind of fragments, biuret groups, appeared in the cross-linked rubbers:

$$\text{–OC–NH}\sim\text{NH–CO–NH–R–NH–CO–NH}\sim\text{NH–CO–NH–R–NH–} + \text{OCN}\sim\text{NCO}$$
$$+ \text{ –OC–NH}\sim\text{NH–CO–NH–R–NH–CO–NH}\sim\text{NH–CO–NH–R–NH–}$$
$$\rightarrow \text{ –OC–NH}\sim\sim\text{NH–CO–N(C=O–NH≋NH–C=O)–R–NH–CO–NH}\sim\sim\text{NH–CO–NH–R–NH–} \quad (4)$$
$$\text{–OC–NH}\sim\sim\text{NH–CO–N(C=O–NH≋NH–C=O)–R–NH–CO–NH}\sim\sim\text{NH–CO–NH–R–NH–}$$

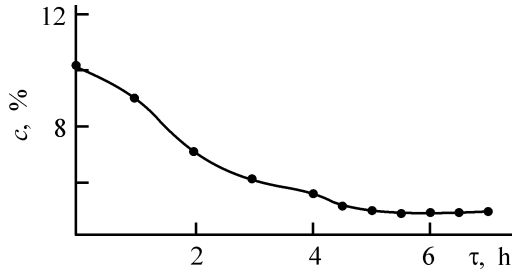


Fig. 1. Variation of the concentration of isocyanate groups *c* in the course of OEC synthesis. (τ) Time.

The IR spectra of the resulting polymers contained bands at 1310 cm^{-1}, characteristic of allophanate structures [6] and suggesting that the reaction between the urethane and isocyanate groups in the course of the synthesis of the poly(urethane–isocyanurate) materials is quite probable at temperatures increased to 120–140°C.

The reactions of urea and urethane group with isocyanate are very important in the synthesis of poly(urethane–isocyanurate) gradient materials, as they give rise to branched and cross-linked structures in

polyurethanes; this is, apparently, one of the factors providing the high strength and wear resistance of these materials. The above reactions are slow (they take 5–6 h), but occur at temperatures commonly used in syntheses of polyisocyanurates, including the commercial synthesis.

Materials with different elastic moduli were obtained by varying the ratio of the prepolymer, TDI, and diamine.

The dynamic and "conventional" viscosities (η^{30}) of polymer solutions were determined by standard procedures using VPZh-2 capillary viscometers (inner capillary diameters 3.00 and 1.31 mm) and a VZ-246 viscometer (orifice diameter 2, 4, and 6 mm). The density of the solutions was determined pycnometrically [7].

The success in preparation of CPMs based on polyisocyanurate and polyurethane compounds and the quality of these materials are governed by a proper choice of highly porous supports and of conditions for their impregnation with prepolymeric binders. The course of impregnation, in turn, depends on the support structure and process conditions, namely, on the pressure, temperature, and time of impregnation, and also on the viscosity of the polymeric binder and conditions of its penetration into support pores. In this context, taking into account data from [1], we chose the following supports for the polymeric compounds: a highly porous nonwoven fibrous framework material continuous in two directions (synthetic felt, Synthepon, PET fiber) and a gas-filled foamed material with an open-cell structure [elastic polyurethane foam of PPU-EM-1 brand, Porolone (PUF)]. Additional experiments on the choice of supports for the polymeric compounds suggested that Hollowfan and Shersticron are also suitable (Table 1). Shersticron is a nonwoven fabric, a thermally bound material consisting of 60% natural wool and 40% polyester fibers. Hollowfan is a nonwoven fabric produced from hollow highly tortuous polyester fibers bound by a two-component fiber. These supports do not noticeably affect the elastic modulus of poly(urethane–isocyanurate) materials, because their own elastic modulus is low and the content in the composite material does not exceed 3–4% because of the high porosity (96–98%).

The porosity of the supports and press materials was determined pycnometrically. The content of open pores in supports of polymeric compounds was determined from the acetone absorption, according to [1].

The supports were impregnated with the compounds at room temperature and atmospheric pressure. The samples were pressed by the procedure from [3].

Table 1. Characteristics of supports for precursors of reactive poly(urethane–isocyanurate) compounds

Support	Support thickness *h*, mm	Support density ρ, g cm^{-3}		Porosity, %
		true	apparent	
Porolone	50	1.27	0.0193	98.5
	20	1.28	0.0147	98.85
	10	1.22	0.0185	98.5
Shersticron	50	1.35	0.0351	98.2
Hollowfan	50	1.41	0.0191	98.6

We examined the conditions for preparation of composite materials based on polyisocyanurates and polyurethanes, using a "solution" method of combining the binder with the support, and also for the subsequent processing of the materials into articles with prescribed properties by hot pressing (a process yielding an article of the required shape in one pressing cycle).

The process for preparing such materials consists of the following steps: (1) compounding of the ingredients for the impregnation; (2) impregnation of the support; (3) prepolymerization (gelation); (4) polycyclotrimerization and chain elongation reactions at 100–140°C; and (5) pressing.

To determine the optimal parameters of the impregnation, drying, and pressing, we obtained unimodular samples at various ratios of OEC, TDI, and diamine.

We considered the influence exerted on the degree of filling of the supports by the following factors: viscosity of the starting compounds, impregnation time, and porosity (initial and residual) of the supports.

In the synthesis of CPMs based on polyisocyanurates and polyurethanes, OEC has the highest viscosity (η^{30} = 2.7 Pa s), and with addition of TDI (η^{30} = 2.5×10^{-3} Pa s) the viscosity of the polyisocyanurate compound correspondingly decreased, which allowed the use of this compound for impregnating the supports without preliminary dilution with acetone. However, when the catalyst was added to the polyisocyanurate compound and the resulting formulation was mixed with the polyurethane compound, the viscosity of the impregnation solutions increased owing to the occurrence of the polycyclotrimerization even at room temperature, and rapid cross-linking of the compound hindered the impregnation. Therefore, we controlled the viscosity of the compounds by adding a diluent (acetone) [1], which had to be removed from the material just before pressing.

Table 2. Density of poly(urethane–isocyanurate) solutions at various TDI contents in formulations

100% solution		90% solution	
TDI content, wt %	density, g cm^{-3}	TDI content, wt %	density, g cm^{-3}
60	1.126	54	1.063
48	1.115	43	1.045
36	1.108	32	1.023
30	1.105	27	1.015
24	1.085	22	1.005
12	1.050	11	0.995
0	0.995	0	0.985

Our experiments showed that the decisive factor governing the degree of support impregnation was the viscosity of the impregnating solutions. However, a too high content of the diluent was undesirable, as it led to a decrease in the amount of the polymer in the CPM, and evaporation of a large amount of the diluent caused formation of pores unfilled with

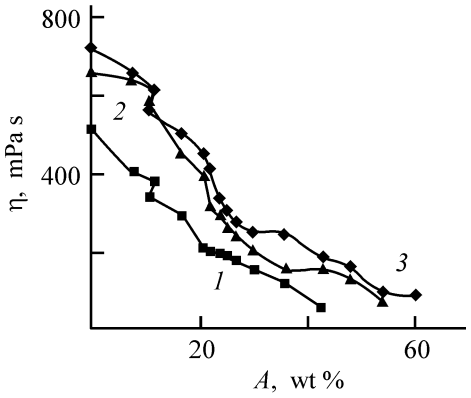


Fig. 2. Viscosity of precursors η vs. the TDI content in solution *A*. Concentration of solutions in acetone, %: (*1*) 70, (*2*) 90, and (*3*) 100.

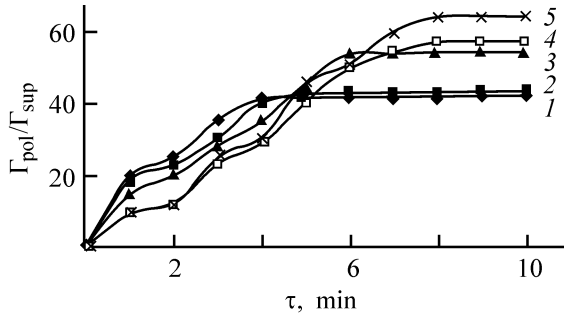


Fig. 3. Precursor uptake $\Gamma_{pol}/\Gamma_{sup}$ by the support (PUF, h = 20 mm) vs. the impregnation time τ. Solution concentration, %: (*1*) 60, (*2*) 70, (*3*) 80, (*4*) 100, and (*5*) 90.

with the polymer. By varying the concentration of the impregnating solutions (60, 70, 80, 90, and 100%), we found that the amount of the polymer introduced is at a maximum, and the residual porosity at a minimum, with 90% solutions. The concentration dependence of the degree of impregnation passes through a maximum. At low concentrations (and, hence, low viscosity), the impregnation is faster, but the polymer flows out from the support pores. As a result, most of the polymer remains on the support surface and retains air inside the prepregs, which adversely affects the uniformity of the pressed composite materials.

It is known [8, 9] that the elastic modulus of polymeric materials depends on the TDI content in reaction formulations. As the TDI content in the compounds increases, the viscosity of the polymer solutions decreases (Fig. 2). The densities of the polymer solutions show the same trend (Table 2). We used for the impregnation 60–100% solutions (10% step) containing 0.5 wt % catalyst relative to TDI. The impregnating solutions (except 100% solutions) were kept at room temperature before the impregnation to ensure the prepolymerization in solution. The experimental data show that the prepolymerization in solution in this step does not noticeably affect the elastic modulus of the resulting samples. However, this step is required to reduce the gelation time of the poly(urethane–isocyanurate) polymeric materials. The reaction is faster in more concentrated (90–100%) solutions and in formulations containing more TDI. In 90% solutions, an increase in the viscosity with increasing TDI content is more pronounced than in the less concentrated solutions.

We determined the optimal time of impregnation of the highly porous supports (5–7 min), in which the constant degree of filling was attained at all the concentrations and compositions of the solution. The support is impregnated most rapidly with a 60% solution (Fig. 3). This solution is the least viscous, and the impregnation time increases with the solution concentration. Thus, the amount of the polymer (so-called degree of filling, DF) introduced in one impregnation cycle increases with the polymer content in the solution. Despite the longer impregnation time, it is preferable to use 90% solutions, which ensures high degree of filling (63 g of polymer per gram of support) and high impregnation quality. As for 100% polyisocyanurate compounds, the apparently larger size of the oligomeric molecules, high viscosity, and fast cross-linking of the compound hinder its penetration into the finely porous structure of the support; as a result, the polymer content is lower: 50–56 g g^{-1} support.

Table 3. Characteristics of poly(urethane–isocyanurate) polymeric materials prepared by hot pressing*

Sample no.	Content, wt %		Carbon black P 803, wt %	Precursor support density, kg m^{-3}	Elastic modulus E, MPa	Sample density, kg m^{-3}
	PU in PUIC	TDI in PIC				
1	0	50	2	1.28	472	1.193
2	20	40	2	1.28	385	1.185
3	40	30	2	1.28	179	1.170
4	50	25	2	1.28	97.5	1.165
5	60	20	2	1.28	54.4	1.141
6	80	10	2	1.28	26.5	1.132
7	100	0	2	1.28	3.6	1.065
8	0	60	2	1.28	1250	1.215
9	20	48	2	1.28	517	1.198
10	40	36	2	1.28	293	1.175
11	50	30	2	1.28	127	1.169
12	60	24	2	1.28	21.7	1.148
13	80	12	2	1.28	14.4	1.114
14	0	50	2	1.42	423	1.189
15	0	50	3**	1.35	318	1.171

* Compound: (PU) polyurethane, (PIC) polyisocyanurate, and (PUIC) poly(urethane–isocyanurate).

** The sample contains 3 wt % phthalocyanine blue pigment.

At all the solution concentrations, more porous supports take up more polymer; hence, such supports will exert a weaker effect on the properties of the composite materials. In preparation of composite materials, it is also necessary to take into account the residual porosity of the prepregs after the impregnation. It should be as low as possible. When comparing the quality of impregnation of Porolone and Synthepon with compounds based on PPG under the same conditions, we noted that the residual porosity of Porolone was 10%, and the degree of filling, 40–60 g of the polymer per gram of support. For Synthepon (including Shersticron and Hollowfan), the residual porosity was 8–12%, and the degree of filling, 30–35 g of the polymer per gram of support.

The polycyclotrimerization continued in the materials in the step of acetone removal, and the compounds transformed from the liquid viscous-flow state into a gel-like state. The materials lost stickiness and became suitable for the subsequent hot pressing. However, the polycyclotrimerization rate depended not only on temperature, but also on the compound composition. The support impregnated with a TDI-rich compound lost stickiness after keeping for 1 h at 60–65°C; with a decrease in the TDI content and an increase in the content of the polyurethane component, the gel time increased, and the stickiness did not disappear. Therefore, taking into account the conditions of polyurethane synthesis [10], we heated the impregnated samples at 120°C for 4.5–5 h prior to pressing; this step did not impair the molding properties of the materials.

The formation of the network structure and the molding of articles are completed in the step of hot pressing. By varying the temperature, pressure, and time, taking into account the process features of the polyurethane synthesis, we found the following pressing conditions to be the best: T = 120–140°C and specific pressure of 25 kg cm^{-2}. The pressing time was determined as 1 min of pressing per 1 mm of sample thickness. The characteristics of some poly(urethane–isocyanurate) polymeric materials prepared by hot pressing are listed in Table 3.

CONCLUSIONS

(1) Conditions were found and optimal parameters determined for preparing prepregs (pressure, temperature, impregnation time, viscosity of polymeric binder, conditions of its penetration into support pores) based on polyisocyanurate and polyurethane compounds.

(2) Polymeric materials of desired shape, with an elastic modulus of 3.6 to 1250 MPa, were prepared by hot pressing at varied ratio of the prepolymer, TDI, and diamine.

(3) Synthepon, Porolone, Hollowfan, and Shersticron were chosen as highly porous supports exerting no effect on the properties of the resulting materials.

REFERENCES

1. Askadskii, A.A., Goleneva, L.M., Simonov-Emel'yanov, I.D., *et al.*, *Plast. Massy*, 2001, no. 7, pp. 21–26.
2. Goleneva, L.M., Almaeva, E.S., Simonov–Emel'yanov, I.D., *et al.*, *Vysokomol. Soedin., Ser. A*, 2002, vol. 44, no. 2, pp. 268–274.
3. Askadskii, A.A., Luchkina, L.V., Goleneva, L.M., *et al.*, *Elektron. Zh. Issled. Ross.*, 2004, vol. 69, pp. 751–769; http://zhurnal.ape.relarn.ru/articles/2004/069.pdf.
4. Bellamy, L.J., *The Infra-Red Spectra of Complex Molecules*, New York: Wiley, 1957.
5. *Entsiklopediya polimerov* (Polymer Encyclopedia), Moscow: Sov. Entsiklopediya, 1972, vol. 1 (A–K).
6. Rait, P. and Kamming, A., *Poliuretanovye pokrytiya* (Polyurethanic Coatings), Leningrad: Khimiya, 1973.
7. *Analytical Chemistry of Polymers*, Kline, G.M., Ed., New York: Interscience, 1959. Translated under the title *Analiticheskaya khimiya polimerov*, Moscow: Mir, 1966.
8. Askadskii, A.A., Luchkina, L.V., Konstantinov, K.V., *et al.*, *Vysokomol. Soedin., Ser. A*, 2004, vol. 46, no. 4, pp. 567–571.
9. Askadskii, A.A., Luchkina, L.V., Konstantinov, K.B., *et al.*, *Russ. Polym. News*, 2003, vol. 8, no. 4, pp. 66–76.
10. Saunders, J.H. and Frish, K.C., *Polyurethanes. Chemistry and Technology*, part 1: *Chemistry*, New York: Interscience, 1962.

Russian Journal of Applied Chemistry, Vol. 78, No. 8, 2005, pp. 1343–1350. Translated from Zhurnal Prikladnoi Khimii, Vol. 78, No. 8, 2005, pp. 1367–1374.
Original Russian Text Copyright © 2005 by Kocheva, Borisenkov, Karmanov, Mishurov, Spirikhin, Monakov.

MACROMOLECULAR CHEMISTRY AND POLYMERIC MATERIALS

Structure and Antioxidant Characteristics of Wheat and Oat Lignins

L. S. Kocheva, M. F. Borisenkov, A. P. Karmanov, V. P. Mishurov, L. V. Spirikhin, and Yu. B. Monakov

Institute of Chemistry, Komi Scientific Center, Russian Academy of Sciences, Syktyvkar, Komi Republic, Russia

Institute of Physiology, Komi Scientific Center, Russian Academy of Sciences, Syktyvkar, Komi Republic, Russia

Syktyvkar Forestry Institute, Syktyvkar, Komi Republic, Russia

Institute of Biology, Komi Scientific Center, Russian Academy of Sciences, Syktyvkar, Komi Republic, Russia

Institute of Organic Chemistry, Ufa Scientific Center, Russian Academy of Sciences, Ufa, Bashkorkostan, Russia

Received November 1, 2004; in final form, June 2005

Abstract—The chemical structure of dioxane lignins recovered from Gramineal plants, wheat and oats, was studied by IR, ESR, and ^{13}C spectroscopies, and elemental and chemical analyses. The antioxidant characteristics of lignins were estimated.

Lignins are natural heterochain copolymers composed of structural units of the guaiacyl, syringyl, and *p*-coumaric types. The specific feature of lignin is a variety of chemical and topological structures, which are mainly governed by the taxonomic origin and poorly investigated processes of dynamic self-organization, which occur in biosynthesis of this polymer by plants functioning under conditions of a variable exogenous situation. In this connection, many aspects of structural organization of lignins remain unstudied. The influence of lignins on the human health has not been established either. As is known, a significant amount of lignins of various botanic origins are supplied to the human body with vegetable food. According to published data [1], some types of lignins can suppress the free-radical oxidation of biopolymers, acting as natural antioxidants. Considering modern views on the nature of malignant tumors and other aging pathologies [2, 3] establishment of a relationship between the structure and physicochemical, among them antioxidant, characteristics of lignin polymers is a topical problem.

The goal of this study was to estimate antioxidant characteristics and chemical structure of lignins recovered from Gramineal plants.

EXPERIMENTAL

As the initial plant material served mature stalks of oats *Avena sativa L.* and wheat *Triticum sp.* The raw materials were prepared at a pilot plantation of the Sysola strain-testing plant of the Komi Republic at the end of the vegetation period. The composition of oat stalks was as follows (%): lignin 22.5, cellulose 48.7, readily hydrolyzable polysaccharides 20.9, ash 5.0, and nitrogen 0.7. The composition of wheat stalks was as follows: lignin 22.0, cellulose 48.7, readily hydrolyzable polysaccharides 20.5, ash 3.1, and nitrogen 0.8.

The samples of oat lignins (DL-O) and wheat lignins (DL-W) were recovered by the dioxane procedure [4]. The samples were purified by twofold precipitation from dioxane into diethyl ether. The amount of carbohydrate impurities in DL-O was 2.0%, and in DL-W, 2.4%. The samples were freeze-dried. The yield of DL-O was 20% and that of DL-W, 25% relative to the content of Komarov lignin in the initial raw material. An elemental analysis of the recovered samples was performed on a Hewlett–Packard analyzer (USA). The standard methods of wood chemistry were used for quantitative estimation of functional

1070-4272/05/7808-1343 © 2005 Pleiades Publishing, Inc.

Table 1. Antioxidant activity of lignins and other samples ($n = 5$, $p = 0.95$)

Plant raw materials	Sample	AOA, kC per 100 g	
		$(X \pm S)^*$	S_r^*
Oats	DL-O	69.4 ± 2.8	0.04
Wheat	DL-W	61.3 ± 2.1	0.03
Fescue meadow (Festuca pratensis)	DL-FM	41.5 ± 2.8	0.07
Fungus Betulinus	Aqueous extract	4.9 ± 0.2	0.03
Hydrolyzed industrial lignin	Polyphen	1.7 ± 0.1	0.04
–	Mitofen	87.6 ± 6.6	0.07

* X is the arithmetic mean of five determinations of AOA ($n = 5$); S, standard deviation; and S_r, relative standard deviation (confidence level $p = 0.95$).

groups. The content of methoxy groups was determined by the Viebock-Schwappach method, and that of phenolic and carboxy groups, by the barium chloride method [5].

The ^{13}C NMR spectra were recorded in a pulsed mode on a Bruker AM-300 spectrometer operating at 75.5 MHz. The spectrum width was 18 kHz, pulse length, 2 μs, and pulse separation, 6 s. DMSO-d_6 containing 0.02 M chromium triacetylacetonate (relaxing agent) served as a solvent. The solution concentration was 30%. The acquisition number was 20000. The ^{13}C NMR were quantitatively interpreted according to the procedures described in [6]. The results of calculations are presented as a number of carbon atoms of certain type per aromatic ring (AR) n_x:

$$n_x = (p_x/f_a) \times 6,$$

where $p_x = I_x/I_{tot}$ is the relative content of carbon atoms of the given type; I_x, integral intensity of the signal from the given type of atoms; I_{tot}, total intensity of the spectrum; f_a, aromaticity of lignin, evaluated as the ratio of the integral intensities of signals from aromatic carbon atoms I_a (at 103–160 ppm) to the total intensity of the spectrum, $f_a = I_a/I_{tot}$; and 6, number of carbon atoms in an aromatic ring.

The ESR spectra of the compounds were recorded on an SE/X-2547 spectrometer (RadioPAN, Poland) in the X-frequency range with 100-kHz HF modulation at room temperature; the UHF field power was 2.2 mW. An RX102 rectangular cavity with the TE102 mode was used. The concentration of free radicals was estimated using reference samples of diphenylpicrylhydrazyl with spin concentrations of $(7.0 \pm 0.7) \times 10^{16}$ and $(2.7 \pm 0.3) \times 10^{18}$ spin g^{-1}. The error in determining the concentration of paramagnetic centers (PMCs) was 15%.

The IR spectra were recorded from KBr pellets on a Specord M80 spectrometer and MIR8000 Fourier IR spectrometer equipped with a DTGS detector. The IR spectra were processed by the well-known procedure [7] using the baseline method and normalization with respect to the strongest absorption line.

The antioxidation activity (AOA) was estimated by coulometric titration [8]. The quantity of electricity expressed in coulombs, consumed per 100 g of the product, was calculated by the formula

$$Q = 100It/V_{al},$$

where I is the current strength; t, time in which the final point of titration is reached; and V_{al}, aliquot volume.

Lignins, along with cellulose and hemicelluloses, are components of plant food fibers. Lignins are polyphenolic compounds containing phenolic groups of various types with different acidities, and also stable radicals. This creates prerequisites for manifestation of antioxidant characteristics.

For quantitative estimation of AOA, we used a coulometric procedure allowing estimation of the total content of antioxidants in various substrates. This procedure is based on coulometric titration of substances with electrolytically generated bromine species (Br_3^-, Br_2, and $Br^\bullet$), which are able to enter into various reactions: radical, redox, electrophilic substitution, and addition to multiple bonds [8]. It should be noted that comparative studies of AOA of a series of samples by coulometric titration and chemiluminescence, one of the classical ways to determine AOA, revealed a high degree of correlation of the results furnished by these two methods ($r = +0.94$).

Table 1 shows the results of measurements of AOA of the lignin samples from wheat and oats and also of a number of other samples of plant and synthetic origin. As the studies showed, the AOA value of the DL-W sample was 61.3 ± 2.1 kC per 100 g. The higher value of AOA, 69.4 ± 2.8 kC per 100 g, was found for the DL-O sample. For all other samples, including medical lignin Polyphen, the antioxidant activity was noticeably lower. The exception is Mitofen [sodium poly(*p*-dihydroxy-*p*-phenylene)-thiosulfonate], which is not surprising since this medication belongs to a number of the most effective and acknowledged antioxidants and is widely used in medical practice. Among drawbacks of Mitofen is,

apparently, its synthetic origin. The results obtained suggest that lignins prepared from grassy cereals may be of interest for development of pharmaceutical medications with tumor- and gerontoprotective effects. It is evident that high andioxidant characteristics of DL-W and DL-O lignins are caused by the features of molecular structure of these biopolymers. In this context, one of the topical problems of the development of highly effective natural antioxidants is elucidation of various aspects of the lignin structure and, primarily, of the chemical structure of the macromolecules.

The lignin content in plant substances depends on the vegetation period and exogenous natural factors. For a ripe plant, the lignin amount in grass xylem is usually 17–23%. In this case, plant raw materials, oak and wheat stalks, contain 22.5 and 22.0% lignin, respectively. The DL-O and DL-W lignin samples recovered by freeze-drying are light cream-colored porous powders readily soluble in dilute alkalis and polar solvents with a Hildebrand parameter 9–13 $(\text{cal cm}^{-3})^{0.5}$.

A study of lignins by the molecular hydrodynamics methods showed that the DL-O and DL-W samples are typical macromolecular compounds. The macromolecular characteristics of the samples are listed in Table 2.

The molecular weights of lignins, $M_{D\eta}$, determined by the sedimentation-diffusion analysis of fractionated DL-O and DL-W samples are 12.4×10^3 and 14.4×10^3, respectively. A large body of data on characteristics of dioxane lignins of various botanic origins shows that the molecular weight of the lignins studied does not noticeably differ from that of lignins of coniferous wood.

As is known [6, 9], lignins are characterized by diversity of the chemical structure of macromolecules, which is caused by a variety of monomeric precursors and the absence of genetic control over biosynthesis in the stage of growth of macromolecules. Macromolecules of lignins consist of phenylpropane units; the monomeric precursors of these polymers are derivatives of hydroxycinnamic alcohols: *p*-coumarol, coniferol, and sinapol

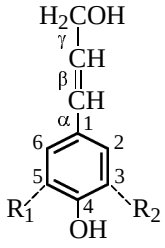


Table 2. Hydrodynamic characteristics of DL-O and DL-W lignins*

Polymer	$[\eta]$, $\text{cm}^{-3}\,\text{g}^{-1}$	$D \times 10^7$, $\text{cm}^2\,\text{s}^{-1}$	$(1 - \bar{\nu}p_0)$	$M_{D\eta} \times 10^{-3}$
DL-O	5.9	13.5	0.334	12.4
DL-W	6.2	12.5	0.338	14.4

* $[\eta]$ is the intrinsic viscosity; D, coefficient of translation diffusion; $(1 - \bar{\nu}p_0)$, factor of Archimedean floatability, where $\bar{\nu}$ is the specific partial volume of polymer, $\text{cm}^3\,\text{g}^{-1}$; p_0, solvent density, g cm^{-3}; and $M_{D\eta}$, molecular weight.

Table 3. Elemental composition and content of functional groups with account of the presence of carbohydrate impurities in DL-O and DL-W samples

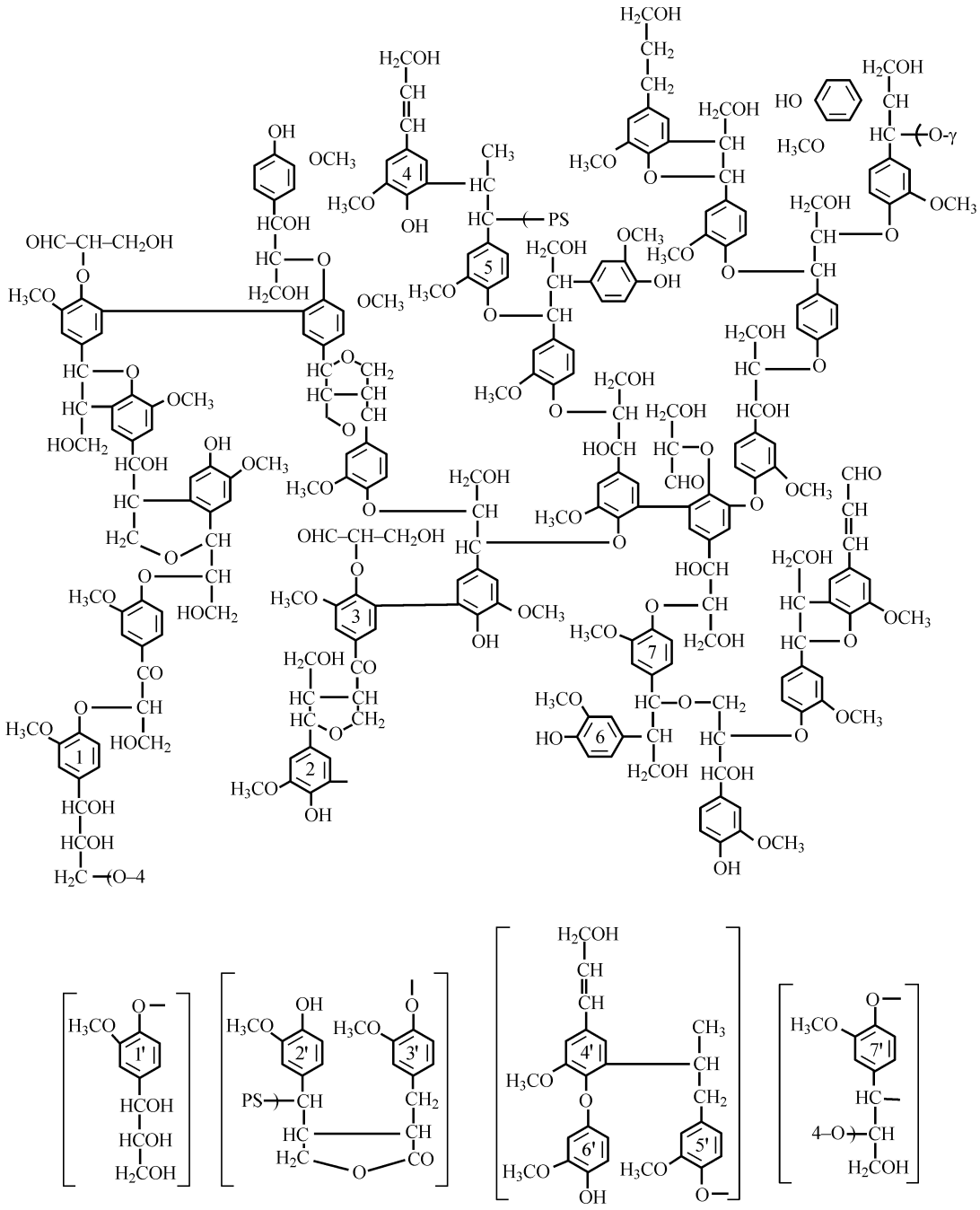
Sample	Content, %				
	OCH_3	COOH	OH_{phen}	C	H
DL-O	16.3	4.3	2.7	59.2	5.26
DL-W	15.4	4.2	2.6	60.3	5.66

where $R_1 = R_2 = H$ (*p*-coumarol); $R_1 = H$, $R_2 = OCH_3$ (coniferol); and $R_1 = R_2 = OCH_3$ (sinapol).

At present, all natural lignins are subdivided according to their botanic attribution into three groups: coniferous, deciduous, and grassy lignins. Coniferous lignins are mainly composed of guaiacylpropane structural units (monolignol coniferol); macromolecules of deciduous and grassy lignins contain units of all three types, with their ratio varies depending on the taxonomic origin. The structural units of various types are bonded by numerous bonds of various types [9]. The diversity of structural units, fragments, and functional groups of macromolecules hampers interpretation of the chemical structure of natural lignins. One of the numerous hypothetical and theoretically possible models describing the molecular structure of lignin of the guaiacylsyringyl type, suggested in [10], is presented below.

It should be noted that structural schemes have not yet been developed for grassy lignins.

A topical problem of the lignin chemistry today is elucidation of the structural features of lignins within the framework of individual taxonomic group of botanic classification. In this context, it is of interest to compare the chemical compositions and structural features of DL-O and DL-W macromolecules. The elemental compositions and contents of functional groups of these lignins are listed in Table 3.



(1)

(2)

Model of the structure of spruce lignin [10]: (1) general structure and (2) possible additional alternative structural fragments.

An elemental analysis of the samples showed that, in the carbon content, DL-O and DL-W correspond to guaiacylsyringyl lignins, for which the established carbon content is 57–61%. However, in the degree of methoxylation these lignins should be classed with guaiacyl lignins, i.e. coniferous lignins, since the number of OCH_3 groups per phenylpropane unit does not exceed 1.1. This follows from the evaluation of the average empirical formulas of the monomeric unit, $C_9H_{10.0}O_{3.9}(OH_3)_{1.1}$ (DL-O) and $C_9H_{10.2}O_{3.3}(OH_3)_{1.0}$ (DL-W).

Nevertheless, there are no contradictions between these data, since, as the studies show, the monomeric units of the guaiacyl type predominate in grassy lignin macromolecules at a noticeable amount of *p*-coumaric units. At the same time, these lignins have

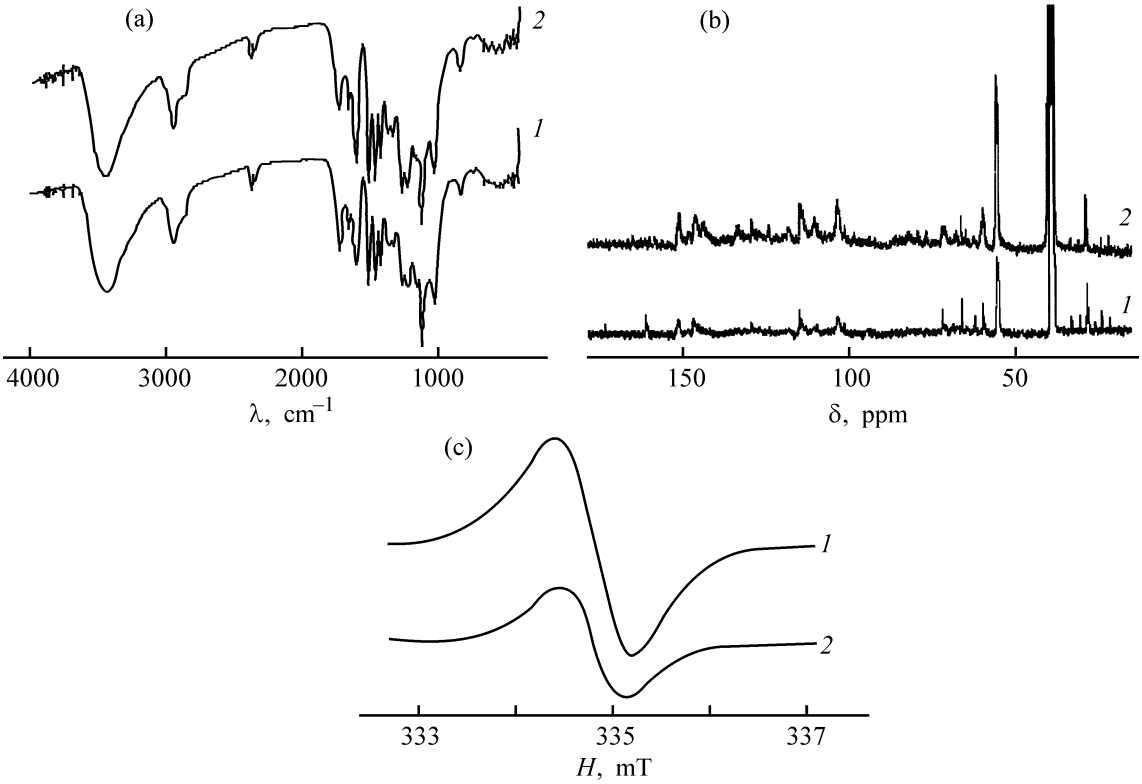


Fig. 1. (a) Fourier IR, (b) ^{13}C NMR, and (c) ESR spectra of (*1*) DL-O and (*2*) DL-W samples. (λ) Wave number, (δ) chemical shift, and (*H*) magnetic induction.

an increased content of such oxygen-containing functional groups as carboxy and phenolic (Table 3). Of special interest is that phenolic groups of several types differing in acidity (p*K* value) have been found in lignin macromolecules [11].

The IR spectra of the lignins studied (Fig. 1a, Table 4) contain a series of characteristic bands (cm^{-1}): 3440, 1725, 1600, 1520, 1470, 1430, 1330, 1270, 1140, 1035, and 840. Analysis of the spectra allows estimation of the amount of some func-

Table 4. IR characteristics of the samples of DL-O and DL-W lignins*

Range, cm^{-1}	Assignment	DL-O		DL-W	
		λ, cm^{-1}	*A*, %	λ, cm^{-1}	*A*, %
1720–1730	StM of unconjugated C=O bonds	1725	35	1720	36
1660–1675	StM of conjugated C=O bonds	1660	27	1660	26
1600–1610	ScM of aromatic ring	1605	78	1610	79
1505–1520	ScM of aromatic ring	1520	88	1515	74
1460–1470	BM of C–H bond in CH_3 and CH_2 groups (asymmetrical)	1470	73	1470	65
1420–1430	ScM of aromatic ring	1430	64	1430	56
1365–1370	BM of C–H bond in CH_3 and CH_2 groups (symmetrical)	1365	51	1365	49
1325–1335	ScM of S ring	1335	44	1330	47
1265–1270	ScM of G ring	1270	83	1270	82
1220–1230	ScM of G and S rings	1225	81	1230	76
1125–1140	BM of C–H bond of benzene ring (planar)	1130	100	1130	100
1030–1040	BM of C–H bond of benzene ring and BM of C–O in primary alcohols	1035	58	1040	57
835–860	BM of C–H in G and S ring	840	15	840	11

* (ScM) Skeleton modes, (BM) bending modes, (StM) stretching modes, (S) syringyl unit, (G) guaiacyl unit, and (*A*) absorption intensity in percent relative to that of the strongest absorption band.

Table 5. ^{13}C Chemical shifts δ of DL-O and DL-W lignins

δ, ppm		Assignment
DL-O	DL-W	
13.9, 22.1, 24.5, 26.8, 28.5, 29.0, 31.3, 33.6	13.8, 22.2, 24.5, 26.7, 28.5, 29.0, 31.4, 33.5	CH_3, CH_2 aliphatic
53.5, 53.8	53.5, 53.8	C_β in β-5 and (β-β)
55.7, 55.9	55.7, 55.9	Ar–OCH_3 G and S
60.3	60.1	C_γ in (β-O-4) G and S
62.6	62.9	C_γ in (β-5) and (β-O-4) G
71.5	71.6	C_γ in (β-β) G
72.3	72.3	C_α in (β-O-4) G and S
102.1, 103.7, 104.9	102, 103.9, 104.2	C-2 and C-6 S and S'
110.4	110.4	C-2 G
115.2, 115.8	115.5, 115.8	C-5 G and G'
119.1	119.1	C-6 G and G'
124.9	125.0	C-1 H
130.3	130.4	C_α and C_β in coniferyl-aldehyde structures and (or) C-2 and C-6
131.4	131.5	C-2 and C-6 H, H'
134.4, 134.9	134.4, 135.0	C-4 S and S'
145.4	145.4	C-4 G'
147.6	147.5	C-3 G
149.5	149.6	C-3 G'
152.1	152.1	C-3 and C-5 S'
160.1	160.1	C-4 H
166.7	166.5	C_β ethers of *p*-coumaric units

Table 6. Number of carbon atoms of various types per aromatic ring n_x, evaluated from the ^{13}C NMR spectra of DL-O and DL-W lignins

Type of C atom	δ, ppm	n_x	
		DL-O	DL-W
C_{Ar}–C, C_{Ar}–O	156–128	3.0	3.1
$C_{Ar\,tert}$	128–103	3.0	2.9
C-2, C-6 S	108–103	1.1	0.9
$C_{\alpha\beta}$ (β-O-4) (α-O-4) G and S	90–57.5	2.5	2.0
C in Ar–OCH_3	57.5–54	1.5	1.2
C_{aliph} (β-5) and (β-β)	54.5–53	0.1	0.1

tional groups and structural fragments. As follows from Table 4, DL-O and DL-W lignins have approximately the same content of aliphatic carboxyls (1720–1730 cm^{-1}), which is confirmed by chemical analysis (Table 3). The samples do not differ in the content of conjugated C=O groups in the coniferyl aldehyde groups (1660 cm^{-1}). The ratio of intensities of the bands at 1470 and 1430 cm^{-1} can be used for chemotaxonomic identification of lignins. In this case, the relationship is typical of guaiacyl (i.e. coniferous) rather than guaiacylsyringyl lignins: $A_{1500} > A_{1470} > A_{1430}$ cm^{-1}. In addition, as can be seen from Table 4, $A_{1270} > A_{1230}$, for DL-O and DL-W lignins although an inverse ratio of the intensities of these bands would be expected according to the Kawamura–Higuchi (K–H) chemotaxonomic classification [12]. Without any sophisticated analysis of all the spectral criteria, it should be noted that oat and wheat lignins are difficult to class with the well-known types of lignins N_s, L_s, and L_m within the framework of the K–H concept.

The ^{13}C NMR spectra of the DL-O and DL-W samples are shown in Fig. 1b. The chemical shifts and assignments of the signals are listed in Table 5. The signals of aliphatic carbon atoms in the CH, CH_2, and CH_3 groups not bonded to oxygen atoms are found in the range 5–45 ppm. In this range, there are numerous signals, suggesting the diversity of chemical structures of side aliphatic chains; however, the number and positions of these signals in the spectra of both samples coincide. Nevertheless, the lengths of side chains in two lignins are not equal: $n_{\Sigma\,10-35}$ = 2.0, for DL-O and less than 1.0 atom/AR for DL-W. In the spectra of the lignins studied there are signals at 53.5 and 53.8 ppm, assignable to the C_β atoms of the coumaran and pinoresinol structures. Table 6 shows that, according to the $n_{\Sigma\,54.5-53}$ values, the total amount of these structures in the DL-O and DL-W samples is the same. Carbon atoms in aromatic methoxyls give rise characteristic signals at 55.7 and 55.9 ppm. Integration of these signals (Table 6) shows that the number of C atoms in Ar–OCH_3 in the DL-O sample is higher than that in DL-W. This result agrees qualitatively with the estimation of the number of C-2 and C-6 atoms in the syringyl units S and S' from the integral intensity in the range of 108–103 ppm. Their amount is 1.1 in DL-O and 0.9 atom/AR in DL-W. In dioxane lignin of wheat stalks, $n_{\Sigma\,102-108}$ = 0.675 atom/AR [13].

A unique feature of lignin as a natural polymer is its paramagnetism caused by the presence of stable free radicals in the macromolecule. The ESR spectra can be characterized by the signal intensity, *g*-factor, and the shape and width ΔH of the resonance line (Fig. 1c). As the studies showed, the ESR signals of DL-O and DL-W lignins are virtually iso-

tropic singlets with a *g*-factor equal to 2.0042–2.0045 (Table 7).

The nature of lignin paramagnetism remains the matter of discussion. In studying the influence of various procedures of chemical treatment on lignin, Lin and Dence [14] concluded that radicals contained in lignins can be classed with semiquinone macroradicals. Semiquinone radical ions of benzoide structure were detected in samples of lignin treated with alkali [15]. The certain role of phenolic hydroxyls and, correspondingly, phenoxy radicals in lignin paramagnetism is suggested by published data [16], which show that, after methylation of pine lignin samples with diazomethane, the concentration of free radicals decreases by approximately a factor of 10. However, it should be noted that a decrease in the concentration of paramagnetic centers from the initial value of approximately 1.5×10^{17} to 1.4×10^{16} spin g^{-1} is scarcely significant. Based on studies of dioxane lignins, Chudakov and co-worker [17] cast doubt on the fact that paramagnetic characteristics of lignins are caused by the radicals of the phenoxyl or semiquinone type. They believe that the ESR spectra of lignins result from intermolecular and intramolecular interactions caused by the presence of conjugated double bonds. As shown previously on the basis of ozonolysis data [15], the number of double bonds in hydrolyzed lignin reaches 3×10^8 mol g^{-1}. Having analyzed published data and the ESR spectra of lignins measured by them in the 2-mm and 3-cm wavelength ranges, Kuzina and co-workers [15] concluded that singlet signals in the ESR spectra of lignins in the range of a *g*-factor of approximately 2.0 belong to radicals having a system of conjugated C–C bonds.

It should be noted that virtually all studies of paramagnetic properties have been performed with samples of lignins recovered from wood of guaiacyl type. In this context, the ESR spectra of lignins recovered from grassy plants with Gramineal plants as an example, are of considerable interest. As is known, the singlet linewidth is governed by the degree of delocalization of the spin density; therefore, the ΔH values characterize the difference of lignins in the size of the conjugated C–C bond system in lignin macromolecules. For DL-O lignins, the linewidth measured between the extremal points ΔH is 0.78 mT, which mainly coincides with the ΔH value for the samples of other grassy lignins. In particular, ΔH = 0.81, for lignin recovered from rye and ΔH = 0.63 mT for lignin from Fescue meadow. As a rule, the width of the ESR signal of lignins from wood is in the range 0.5–0.65 mT. The concentration of PMCs strongly depends not only on the origin of a lignin, but also on the procedures of its recovery. For example, spruce lignin has the following concentrations of radicals (spin g^{-1}): Browns lignin, 0.5×10^{17}; milled wood lignin, $(0.23–1.0) \times 10^{17}$; and dioxane lignin, 0.83×10^{17}. It should be noted that the concentration of PMCs in the samples studied is noticeably higher than that in wood lignins. However, for adequate comparison of lignins of various origins with respect to this characteristic, it is necessary to determine the concentration of PMCs in parallel in different samples under absolutely identical conditions. As the results obtained show (Table 1), the samples of grassy lignins are rated in the order of increasing AOA as follows: AOA(DL-FM) < AOA(DL-W) < AOA(DL-O). The concentration of PMCs increases in the same order (Table 7).

Table 7. Parameters of ESR spectra and PMC concentrations in various lignin samples

Sample	*g*-factor	ΔH, mT	$c \times 10^{-17}$, spin g^{-1}
DL-O	2.0044	0.78	2.2
DL-W	2.0042	0.81	1.2
DL-FM	2.0042	0.63	0.9

CONCLUSIONS

(1) The structure of natural lignins recovered from stalks of oats *Avena sativa L.* and wheat *Triticum sp.* was studied. The results of the IR, ESR, and ^{13}C NMR spectroscopic studies of lignins and also of chemical analysis suggest a similarity in the structural organization of lignins.

(2) Antioxidant characteristics of lignins and a series of other preparations of plant and synthetic origins were estimated. The results show that the development of new natural antioxidants based on lignins is promising.

ACKNOWLEDGMENTS

This study was financially supported by the Russian Foundation for Basic Research (project nos. 04-04-96022 and 04-03-96029) and by the Program of the Presidium of Russian Academy of Sciences "Basic Sciences for Medicine."

REFERENCES

1. Lapin, A.A., Karmanov, A.P., Borisenkov, M.F., and Kocheva, L.S., in *Problemy gerontologii i geriatrii-2004: Meterialy 2-i nauchno-prakticheskoi konferentsii s mezhdunarodnym uchastiem* (Problems of Gerontology and Geriatrics-2004: Proc. 2nd Scientific and Practical Conf. with Foreign Participants), Syktyvkar, 2004, pp. 73–75.
2. Anasimov, V.N., *Molekulyarnye i fiziologicheskie mekhanizmy stareniya* (Molecular and Physiological Mechanisms of Aging), St. Petersburg: Nauka, 2003.
3. Khavinson, V.Kh., Barinov, V.A., Arutyunyan, A.V., and Malinin, V.V. *Svobodnoradikal'noe okislenie i starenie* (Free-Radical Oxidation and Aging), St. Petersburg: Nauka, 2003.
4. Pepper, J.M., Baylis, P.E., and Adler, E., *Can. J. Chem.*, 1959, vol. 37, no. 8, pp. 1241–1245.
5. Zakis, G.F., Mozheiko, L.N., and Telysheva, G.M., *Metody opredeleniya funktsional'nykh grupp lignina* (Methods for Determination of Functional Groups of Lignin), Riga: Zinatne, 1975.
6. Kalabin, G.A., Kanitskaya, L.V., and Kushnarev, D.F., *Kolichestvennaya spektroskopiya YaMR prirodnogo organicheskogo syr'ya i produktov ikh pererabotki* (Qvantitative NMR Spectroscopy of Natural Organic Raw Materials and Products of Their Processing), Moscow: Khimiya, 2000.
7. Karklin', V.B. and Erin'sh, P.P., *Khim. Drev.*, 1971, no. 7, pp. 83–93.
8. Pogorel'tsev, V.I., Ziyatdinova, G.K., and Budnikov, G.K., *Primenenie metoda gal'vanostaticheskoi kulonometrii v klinicheskoi diagnostike antioksidantnogo statusa organizma cheloveka* (Application of Galvanostatic Coulometry in Clinical Diagnostics of Antioxidant Status of the Human Body), Kazan: Kazan Gos. Med. Univ., 2004.
9. Karmanov, A.P., *Samoorganizatsiya i strukturnaya organizatsiya lignina* (Self-Organization and Structural Organization of Lignin), Yekaterinburg: Ural. Otd. Ross. Akad. Nauk, 2004.
10. Sakakibara, M.A., in *Wood and Cellulose Chemistry*, New York: Marcel Dekker, 1991, pp. 111–168.
11. Karmanov, A.N., Davydov, V.D., and Bogomolov, B.D., *Khim. Drev.*, 1980, no. 3, pp. 78–83.
12. Kawamura, I. and Higushi, T., in *Khimiya i biokhimiya lignina, tsellyulozy i gemitsellyuloz: Materialy Mezdunarodnogo simpoziuma* (Chemistry and Biochemistry of Lignin, Cellulose, and Hemicelluloses: Proc. Int. Symp.), Grenoble, July 1964, Moscow: Lesn. Prom–st., 1969, pp. 196–212.
13. Kanitskaya, L.V., Rokhin, A.V., Kushnarev, D.F., and Kalabin, G.A., *Vysokomol. Soedin., Ser. A*, 1998, vol. 40, no. 5, pp. 800–805.
14. Lin, S.Y. and Dence, C.W., *Methods in Lignin Chemistry*, Berlin: Springer, 1992.
15. Kuzina, S.I., Demidov, S.V., Shilova, I.A., *et al.*, *Vysokomol. Soedin., Ser. A*, 2002, vol. 44, no. 8, pp. 1286–1294.
16. *Lignins: Occurrence, Formation, Structure, and Reactions*, Sarkanen, K.V. and Ludwig, C.H., Eds., New York: Wiley, 1971.
17. Raskin, M.N., Mal'tsev, V.I., and Chudakov, M.I., *Gidroliz. Lesokhim. Prom–st.*, 1968, no. 6, pp. 8–10.

Russian Journal of Applied Chemistry, Vol. 78, No. 8, 2005, pp. 1351–1354. Translated from Zhurnal Prikladnoi Khimii, Vol. 78, No. 8, 2005, pp. 1375–1378.
Original Russian Text Copyright © 2005 by Nikulin, Akatova, Sedykh.

MACROMOLECULAR CHEMISTRY AND POLYMERIC MATERIALS

Coagulation of Latex in the Presence of Viscose Fiber and Properties of the Resulting Rubbers, Rubber Stocks, and Vulcanizates

S. S. Nikulin, I. N. Akatova, and V. A. Sedykh

Voronezh State Academy of Forestry Engineering, Voronezh, Russia

Voronezh State Technological Academy, Voronezh, Russia

Received November 10, 2004; in final form, March 2005

Abstract—The effect of addition of viscose fiber on the recovery of butadiene–styrene rubber from a latex and on the properties of the commercial rubber and vulcanizates based on it was examined.

Preservation of the environment is one of the major problems of the mankind. This is connected with the increase in the extraction and processing of natural resources. The rise in the industrial potential is accompanied by the formation and accumulation of large amounts of wastes. Only 1/3 of the raw materials consumed goes for production of target products, with 2/3 giving wastes and by-products. The enhancement of the industrial impact on the nature gave rise to environmental problems [1, 2].

In Russia, the annual volume of wastes containing chemical fibers and threads in the 1980–1990s was, on the average, 9–10 thousand tons. Use of these wastes in industrial rubber and latex items and in various formulations not only would give a considerable profit due to production of additional items but also could solve environmental problems.

A certain part of textile wastes is used in various branches of industry. However, the major fraction of these wastes is not properly used as a secondary raw material and is dumped. Therefore, utilization of textile wastes is a topical problem [3].

It is suggested to use fibers of various origins in tire and rubber industry [4, 5]. In particular, textile materials can be reinforcing elements in many industrial rubber items for which the strength, durability, low weight, and wide range of operation temperatures are essential parameters [4].

In the above-mentioned studies, fibrous fillers were introduced on rollers in the course of compounding of rubber stocks. However, this procedure does not ensure uniform distribution of the fibrous filler in the bulk of the rubber stock, which, in turn, adversely affects the physicomechanical characteristics of the vulcanizates.

In this study, we examined the effect of viscose fiber introduced into SKS-30 ARK butadiene–styrene rubber (BSR) latex on the latex coagulation, rheoligocal and vulcanization properties of the rubber and rubber stock, and physicomechanical characteristics of the vulcanizates.

EXPERIMENTAL

The apparatus for studying the recovery of the rubber from the latex was a vessel equipped with a stirrer and placed in a thermostat to maintain the required temperature. The coagulator was charged with the butadiene–styrene latex (dry residue about 18 wt %) and thermostated at the required temperature for 15–20 min. The fibrous filler was introduced with an acidifying agent in the final step of rubber recovery from the latex [6–8]. The coagulation was performed with a 24 wt % NaCl solution; the constant pH of the coagulation (~2.0) was adjusted by adding 1–2 wt % H_2SO_4 solution.

Our experimental study consisted of two stages. In the first stage, we examined the effect of viscose fiber added with the acidifying agent (sulfuric acid) on the rubber recovery from the latex. The viscose fiber length was 2, 5, and 10 mm, and the fiber content, 0, 0.1, 0.3, 0.5, 0.7, and 1.0 wt % based on the rubber. The results are listed in Tables 1–3.

1070-4272/05/7808-1351 © 2005 Pleiades Publishing, Inc.

Table 1. Effect of viscose fiber additions on the degree of coagulation of SKS-30 ARK latex

NaCl consumption, kg t^{-1} rubber	Coagulation, %, at indicated fiber addition, wt % based on rubber																	
	2 mm*						5 mm						10 mm					
	0	0.1	0.3	0.5	0.7	1.0	0	0.1	0.3	0.5	0.7	1.0	0	0.1	0.3	0.5	0.7	1.0
25	8.9	12.6	12.6	10.6	9.4	11.7	8.9	11.0	9.9	10.0	10.3	11.6	8.9	9.3	7.7	8.1	9.8	10.7
50	21.4	23.1	22.5	21.8	21.5	20.3	21.4	22.8	20.9	21.0	23.3	22.3	21.4	20.4	20.7	19.9	20.9	17.8
75	32.8	31.6	39.8	31.5	33.7	29.1	32.8	28.3	30.9	31.6	30.2	28.8	32.8	32.1	28.7	30.4	34.2	26.9
100	62.7	44.3	46.7	46.6	45.3	44.4	62.7	43.7	46.1	39.7	46.9	41.3	62.7	42.4	39.5	37.9	42.3	37.7
125	80.6	83.6	92.6	79.6	86.3	70.1	80.6	85.0	92.7	84.8	85.7	75.4	80.6	89.2	81.6	83.9	83.0	88.6
150	93.4	97.7	95.4	96.8	94.8	94.3	93.4	98.7	99.0	96.7	96.9	94.5	93.4	96.5	96.1	95.1	94.8	94.1

* Fiber length

Table 2. Properties of rubbers, rubber stocks, and vulcanizates based on SKS-30 ARK. Vulcanization temperature 143°C, optimal vulcanization time 60 min

Parameter	Reference sample (no additives)	Fiber additive, wt % based on rubber				
		2 mm		5 mm		10 mm
		0.3	0.7	0.3	0.7	0.3
Mooney viscosity, MB 1 + 4 (100°C):						
of rubber	55	53	53	53	52	51
of rubber stock	57	55	56	55	56	55
Karrer plasticity of rubber stock, arb. units	0.34	0.38	0.31	0.32	0.35	0.36
Recovery, mm	1.4	1.4	1.7	1.8	1.5	1.4
Nominal stress at 300% elongation, MPa	9.4	3.9	4.9	6.3	5.8	6.0
Nominal tensile strength, MPa	26.3	24.3	20.0	23.0	22.0	23.0
Relative elongation at break, %	618	698	690	680	675	688
Relative residual strain, %	12	18	18	16	14	14
Rebound elasticity, %:						
20°C	40	43	43	46	44	44
100°C	53	49	50	53	50	51
Shore hardness A, arb. units	57	55	56	55	59	57
Resistance to repeated 100% extension, thousands of cycles	70	70	72	76	96	85
Tear resistance, kN m^{-1}	53	71	75	81	96	95
Aging coefficient (100°C, 72 h):						
for strength	0.44	0.63	0.77	0.53	0.56	0.60
for relative elongation	0.33	0.45	0.43	0.33	0.33	0.41

Table 3. Rheogram of vulcanization of rubber socks based on SKS-30 ARK rubber filled with viscose fiber

Parameter	Reference sample (no additives)	Fiber additive, wt % based on rubber				
		2 mm		5 mm		10 mm
		0.3	0.7	0.3	0.7	0.3
Torque, N m:						
minimal	4.8	6.3	6.0	5.5	5.5	6.5
maximal	36.5	30	32	34	33	36
Vulcanization onset time, min	3.5	5	4	4	5	4
Optimal vulcanization time, min	27.5	30	29	28	29	29

Table 4. Influence of the kind of solvent and size and content of viscose fiber added on the degree α_{max} and rate k of swelling of BSR-based vulcanizates

Fiber		*n*-Octane		Toluene		Chloroform	
size, mm	content, wt % based on rubber	α_{max}	k	α_{max}	k	α_{max}	k
2	0.3	168	–0.93	360	–1.43	675	–1.07
5	0.3	162	–0.93	316	–1.43	600	–1.07
10	0.3	145	–0.93	294	–1.43	582	–1.43
2	0.7	150	–1.19	302	–1.33	590	–1.33
5	0.7	154	–1.19	312	–1.33	614	–1.43

The experimental data show that the coagulum yield increased in all the cases. This is most probably due to a decrease in the rubber loss with the finely dispersed coagulum and wash waters and to the capture of the fibrous filler by the forming coagulum.

It should be noted that the size and content of the fibrous filler, varied in the ranges examined, have no effect on the degree of rubber recovery from the latex. However, with large amounts of the fibrous filler (more than 1.0 wt % based on the rubber), the slurry of the fiber in a sulfuric acid solution became too thick, which made its use unfeasible because of problems with transportation along pipelines and with dispersion in the latex in the final step of the rubber recovery from the latex.

Then we examined the influence exerted by the viscose fiber on the properties of rubber stocks and vulcanizates.

The rubbers were tested according to the requirements of GOST (State Standard) 15 627–79 to SKS-30 ARK rubber, in comparison with the reference sample.

Table 2 shows that, upon addition of the viscose fiber, the viscosity of the rubber and rubber stock slightly decreases (from 55 ro 51–53 and from 57 to 53–56 units, respectively), and the minimal torque increases from 4.8 (reference sample) to 5.5–6.5 N m (Table 3). The lack of orientation of poorly wettable viscose fibers in the rubber stock matrix in the direction perpendicular to the load direction (calender effect) accounts for the increase in the recovery of the samples from 1.4 to 1.8 mm (Table 2) and the corresponding decrease in the creep of rubber stocks. The fiber additions increase the scatter of the plasticity of the rubber stock within the limits 0.31–0.38 units.

The adsorption of a part of components of the vulcanizing group on the fiber surface (2-mm viscose fibers) causes an increase in the optimal vulcanization time from 27.5 (reference sample) to 29–30 min. The vulcanizates filled with 2–10-mm fibers show a decrease in the strength and stress at 300% elongation, compared to the samples without fiber, because of the lower degree of cross-linking.

A substantial increase in the tear resistance (from 53 to 71–96 kN m^{-1}) and in the resistance to multiple cyclic deformations from 70 to 96 thousand cycles is proportional to the content and length of the fibers and is due to their reinforcing effect, revealed previously for vulcanizates filled with fibers in the step of rubber compounding [9].

An increase in the resistance to aging (100°C, 72 h) may be due to the completion of the vulcanization as a result of desorption of the vulcanizing group components from the fiber surface.

Thus, we revealed an effect of small additions of a fiber on the viscosity and vulcanization characteristics of the rubber and rubber stock and on the service properties of the vulcanizates. An important parameter for evaluating the properties of the resulting composites is the occurrence or absence of the interphase interaction of the rubber matrix with the surface of viscose fiber introduced in the step of rubber recovery from the latex.

To evaluate the interphase interactions of small fiber additions with the rubber matrix, we examined, in the second stage of our study, the kinetics of swelling of BSR-based vulcanizates in solvents of various polarities.

The interphase interactions were evaluated by the equilibrium degree of swelling α_{max} and the rate constant of swelling k (h^{-1}) of vulcanizates containing the viscose filler in such solvents as *n*-octane, toluene, and chloroform (Table 4).

Irrespective of a particular solvent, the influence of the fiber content (varied in the range 0.3–0.7 wt %) on α_{max} was insignificant. With an increase in the sol-

vent polarity (octane, solubility parameter ρ_{oct} 15.4 $MJ^{0.5}\,m^{-1.5}$; toluene, ρ_{tol} 18.2 $MJ^{0.5}\,m^{-1.5}$; chloroform, ρ_{chl} 18.8 $MJ^{0.5}\,m^{-1.5}$ [10]), α_{max} grows from 154–168 to 312–369 and 614–675 wt %, irrespective of the fiber content. The highest α_{max} of BSR vulcanizate with the fibrous filler in chloroform indicates that the vulcanizate polarity increases and its solubility parameter approaches that of chloroform, ρ_{chl} 18.8 $MJ^{0.5}\,m^{-1.5}$, against 17.4 $MJ^{0.5}\,m^{-1.5}$ for the starting BSR, due to the presence of the fiber and appearance of the vulcanization network.

The apparent driving force equal to α_{max} did not affect the swelling rate. The difference in the thermodynamic compatibility of the solvents and BSR vulcanizate with the fiber determined the swelling rate. For the BSR vulcanizate–octane system, for which the compatibility parameter $\beta = (\rho_p - \rho_s)^2$ [10, 11] (4–12 $MJ\,m^{-3}$) is larger, the swelling rate is lower (k = 0.93–1.19 h), and for the BSR vulcanizate–toluene (or chloroform) system with lower β (0.4–2.0 $MJ\,m^{-3}$), k is higher (1.07–1.43 h^{-1}).

For viscose fibers, we revealed no significant effect of their content and size on the swelling rate, apparently because of the weak interphase interaction of the boundary layers as a result of large difference in ρ_{BSR} and ρ_f = 31.9 $MJ^{0.5}\,m^{-1.5}$ [$\beta = (\rho_{BSR} - \rho_f)^2 \approx$ 170–210].

CONCLUSIONS

(1) The optimal length of the viscose fiber is 2–5 mm, and its optimal content in the rubber, 0.3–0.7 wt %.

(2) Addition of viscose fiber in the step of the latex coagulation ensures uniform distribution of the fiber in the rubber bulk, which positively affects such properties of the resulting vulcanizates as tear resistance, resistance to repeated strains, and resistance to thermal aging.

(3) Addition of viscose fiber affects the rheological and vulcanization properties of rubbers and rubber stocks and the physicomechanical parameters of the vulcanizates.

(4) The fiber length (varied in the range 2–10 mm) and content (varied in the range 0.3–0.7 wt %) do not noticeably affect the viscosity of the rubber and rubber stock.

REFERENCES

1. Novikov, Yu.V., *Ekologiya, okruzhayushchaya sreda i chelovek* (Ecology, Environment, and Human), Moscow: Fair, 1999.
2. Chelnokov, A.A. and Yushchenko, L.F., *Osnovy promekologii: Uchebnoe posobie dlya uchashchikhsya spetsial'nykh uchebnykh zavedenii khimiko-tekhnologicheskikh spetsial'nostei* (Principles of Industrial Ecology: Textbook for Students of Colleges of Chemical Engineering Specialties), Moscow: Vysshaya Shkola, 2001.
3. Ozerova, N.V., in *Sbornik materialov V Mezhdunarodnoi nauchno-prakticheskoi konferentsii "Ekonomika prirodopol'zovaniya i prirodookhrany"* (Coll. of Papers of V Int. Scientific and Practical Conf. "Economy of Nature Management and Nature Protection"), Penza, 2002, p. 210.
4. Yagnyatinskaya, E.A., Gol'dberg, B.B., Leonov, V.V., *et al.*, *Tekhnologiya izgotovleniya, svoistva i osobennosti primeneniya rezin s voloknistymi napolnitelyami v RTI* (Production Process, Properties, and Specific Features of Application of Rubbers with Fibrous Fillers in Industrial Rubber Items), Moscow: TsNIITEneftekhim, 1979.
5. Guzina, R.V., Dostoyan, M.S., and Ionova, T.V., *Tekhnologiya obrabotki korda iz khimicheskikh volokon v rezinovoi promyshlennosti* (Technology for Treatment of Cord from Chemical Fibers in Rubber Industry), Moscow: Khimiya, 1973.
6. Akatova, I.N., Nikulin, S.S., Kondrat'eva, N.A., *et al.*, Abstracts of Papers, *X Yubileinaya nauchno-prakticheskaya konferentsiya "Rezinovaya promyshlennost': Syr'e, materialy, tekhnologiya"* (X Jubilee Scientific and Practical Conf. "Rubber Industry: Initial Substances, Materials, and Technology"), Moscow: Nauchno-Issled. Inst. Shinnoi Prom–sti., 2003, pp. 297–299.
7. Akatova, I.N., Nikulin, S.S., and Korystin, S.I., *Proizv. Ispol'z. Elastom.*, 2003, no. 1, pp. 7–11.
8. Akatova, I.N. and Nikulin, S.S., *Usp. Sovrem. Estestvozn.*, 2003, no. 4, p. 83.
9. Reznichenko, S.V., *Kauchuk Rezina*, 2002, no. 2, pp. 38–43.
10. Drinberg, S.A. and Itsko, E.F., *Rastvoriteli dlya lakokrasochnykh materialov* (Solvents for Paint-and-Varnish Materials), Leningrad: Khimiya, 1986.
11. Koshelev, F.F., Kornev, A.F., and Bukanov, A.M., *Obshchaya tekhnologiya reziny* (General Technology of Rubber), Moscow: Khimiya, 1978.

Russian Journal of Applied Chemistry, Vol. 78, No. 8, 2005, pp. 1355–1359. Translated from Zhurnal Prikladnoi Khimii, Vol. 78, No. 8, 2005, pp. 1379–1383.
Original Russian Text Copyright © 2005 by Kurbanova.

MACROMOLECULAR CHEMISTRY AND POLYMERIC MATERIALS

Influence of Modification on the Elastic-Relaxation Properties of Rubbers Based on Binary Blends of Diene Rubbers

N. I. Kurbanova

Institute of Polymeric Materials, Azerbaijan National Academy of Sciences, Sumgaiyt, Azerbaijan

Received April 21, 2005

Abstract—The elastic-relaxation properties of rubbers based on binary blends of diene rubbers were studied as influenced by the modifier, trichloroacetic acid.

The current trends in the development of chemistry and technology of composite materials are largely determined by the search for ways to develop materials with an improved set of properties. An efficient way to prepare new materials with desired properties consists in mixing of two or more polymers [1–3]. The conditions of preparation and processing of blends and introduction of various modifying additives strongly affect their structure and properties [4–6]. Polymer blends offer a number of advantages over conventional polymeric materials and often stimulate rapid scientific and technological progress in their application fields.

We have demonstrated earlier [7] how fillers affect the elastic-relaxation and strength properties of rubbers based on binary blends of diene rubbers [7]. In this study, we elucidated how the modifier affects the properties of binary blends of divinyl (SKD) and butadiene-styrene (SKS) rubbers with polyisoprene (SKI).

We used Cariflex IR309 polyisoprene available from Shell, cis-132 (96% cis) SKD, SBR-1500 SKS (styrene 23%) available from BSL Olefinverbund GmbH, Schkopau, and carbon black no. 330. Trichloroacetic acid (TCAA) (mp 58°C, bp 196.5°C) served as modifier.

The component ratio, mass fractions, in the formulations was as follows: SKD (SKS) : SKI : carbon black : TCAA = 50 : 50 : 50 : 5. Vulcanizing system, mass fractions: sulfur 2.0, stearic acid 2.0, ZnO 3.0, thiuram 0.65, Altax 1.0, Captax 1.25 for SKD/SKI blend, and sulfur 2.0, stearic acid 2.0, ZnO 2.0, and Altax 2.75 for SKS/SKI blend.

The rubbers were mixed under laboratory conditions in a 60-cm^3 Brabender Plasticorder mixer (initial temperature 50°C, degree of filling 0.75) for 6 min in the case of systems without the filler and for 7, 10, and 15 min in the case of formulations with the filler. The time, s, of introduction of the components into the mixer was as follows: SKD (SKS) 0, TCAA 60, SKI 120, carbon black 180 (in three portions), sulfur + stearic acid + ZnO + accelerators 240.

The blends were pressed in 1-mm-thick molds at 145°C.

The tensile tests were carried out on a tensile-testing machine at room temperature and a strain rate of 200 mm min^{-1}.

A dynamic mechanical analysis was carried out on a Gabo Qualimeter Eplexor 500 N (T from –120 to 120°C, frequency 1 Hz) at a heating rate of 1 deg min^{-1}.

We studied the physicomechanical properties of the initial filled and unfilled, as well as modified, vulcanizates of the resulting formulations under quasi-static and dynamic loads. The compositions and properties of the binary blend formulations (average of five measurements) are listed in the table.

As is known [8], of greatest interest in the case of elastomeric formulations is introduction of minor additives of highly polar compounds. They spread over the surface of the structural elements of the macromolecules, increase their mobility, and accelerate relaxation processes, thereby improving the properties of the polymeric materials.

With a modifier containing chlorine atoms and a carboxy group, it is possible to introduce into the elastomers functional groups creating new reactive centers that enhance their interaction with isoprene rubber and other components of the rubber stock.

1070-4272/05/7808-1355 © 2005 Pleiades Publishing, Inc.

Formulations and properties of formulations based on binary rubber blends*

Formulation	σ_t, MPa	ε, %	M_{100}	M_{200}	M_{300}	τ_v^{143}, min
			MPa			
SKD/SKI	0.9	980.6	0.2	0.3	0.3	11.7
SKD/SKI/TCAA	3.5	389	1.2	2.0	2.9	22.6
	10.1	128	7.8	0	0	11
SKD/SKI/carbon black (7, 10, 15 min)	10.7	173	7.3	0	0	7.9
	11.5	158	6.2	0	0	7.1
	10.2	202	4.8	10.1	0	18
SKD/SKI/TCAA/carbon black (7, 10, 15 min)	12.1	253	4.1	8.6	9.2	15
	13.5	318	3.3	7.1	11.6	13.5
SKS/SKI	4.7	995	0.5	0.7	1.0	22.5
SKS/SKI/TCAA	5.8	560.5	0.9	1.6	2.3	56.3
	21.9	432	4.0	8.9	14.5	14.1
SKS/SKI/carbon black (7, 10, 15 min)	21.1	512	3.3	7.1	11.7	15.7
	20.3	640	2.0	4.3	7.6	28
	22.4	506	4.8	10.1	18.2	16
SKS/SKI/TCAA/carbon black (7, 10, 15 min)	20.1	417	4.1	8.6	16.2	18
	16.2	273	3.3	7.1	11.7	25

* σ_t is tensile strength; ε, relative elongation at break; M_{100}, M_{200}, and M_{300}, stresses at 100, 200, and 300% elongation, respectively; and τ_v^{143}, vulcanization time at 143°C.

We showed in [7] that the optimal time of mixing of filled formulations based on binary rubber blends is 10 min. Introduction of a modifying agent allows preparation of vulcanizates with improved properties, when formulations are mixed for 7 min in the case of SKS/SKI and 10 min in the case of SKD/SKI system.

Table shows that, upon introduction of TCAA into an unfilled SKD/SKI (SKS/SKI) blend, the strength σ_t increases by a factor of 3.8 (1.25), but relative elongation at break ε decreases by a factor of 2.5 (1.77), and the stress at 300% elongation M_{300} increases from 0.3 to 2.9 MPa (from 0.1 to 2.3 MPa).

Combined use of the modifier and filler improves the properties of the formulations. Evidently, polar groups of the modifier enhance the general intermolecular interaction by making stronger the interaction with the filler through formation of chemical bonds and absorption binding, which increases the deformation stress and also accelerates crystallization.

It is known [6, 9] that the major factor in the modification, essential for improving the physicomechanical properties of rubbers, is the formation of chemical and intermolecular bonds in the filled elastomeric matrix when the rubber interacts with the filler or substrate, or the involvement in formation of additional vulcanization bonds. In this context, many researchers direct their efforts toward increasing the number of bonds being formed in rubbers, enhancing their strength, and creating cross-linked structures with different chains. In the context of increasing the resistance of rubbers to fatigue failure, of much importance is the capability of the broken bonds to recover after removal of the load. Consequently, rubbers with a set of strong and labile transverse bonds exhibit a high resistance to multiple deformations.

As is known [3, 6, 8], the structure of the vulcanizate results from various chemical and physicochemical interactions of the rubber stock components, governing eventually the properties of the rubbers. Polar functional groups (carboxy, chloride) introduced into the polymer chains should affect the nature of such an interaction.

The nature of the interaction of the polymeric chains of the elastomer with carbon black (filler) is very important in rubber reinforcement. This interaction is due to the formation of both physical and chemical bonds whose number and ratio may vary with the properties of the interacting components. Modification of polymers affects their interaction with carbon black.

Presumably, interaction of the functional groups of the polymer with active centers on the surface of the filler particles improves their wetting with the polymer and facilitates penetration of the polymer chain segments into the space between aggregates of carbon black. All this accelerates the disintegration of such aggregates during mixing and improves the dispersion of the primary particles of carbon black within the polymer matrix [9]. Evidently, with this type of dispersion of carbon black, new active centers appear on its particles, capable of further interaction with

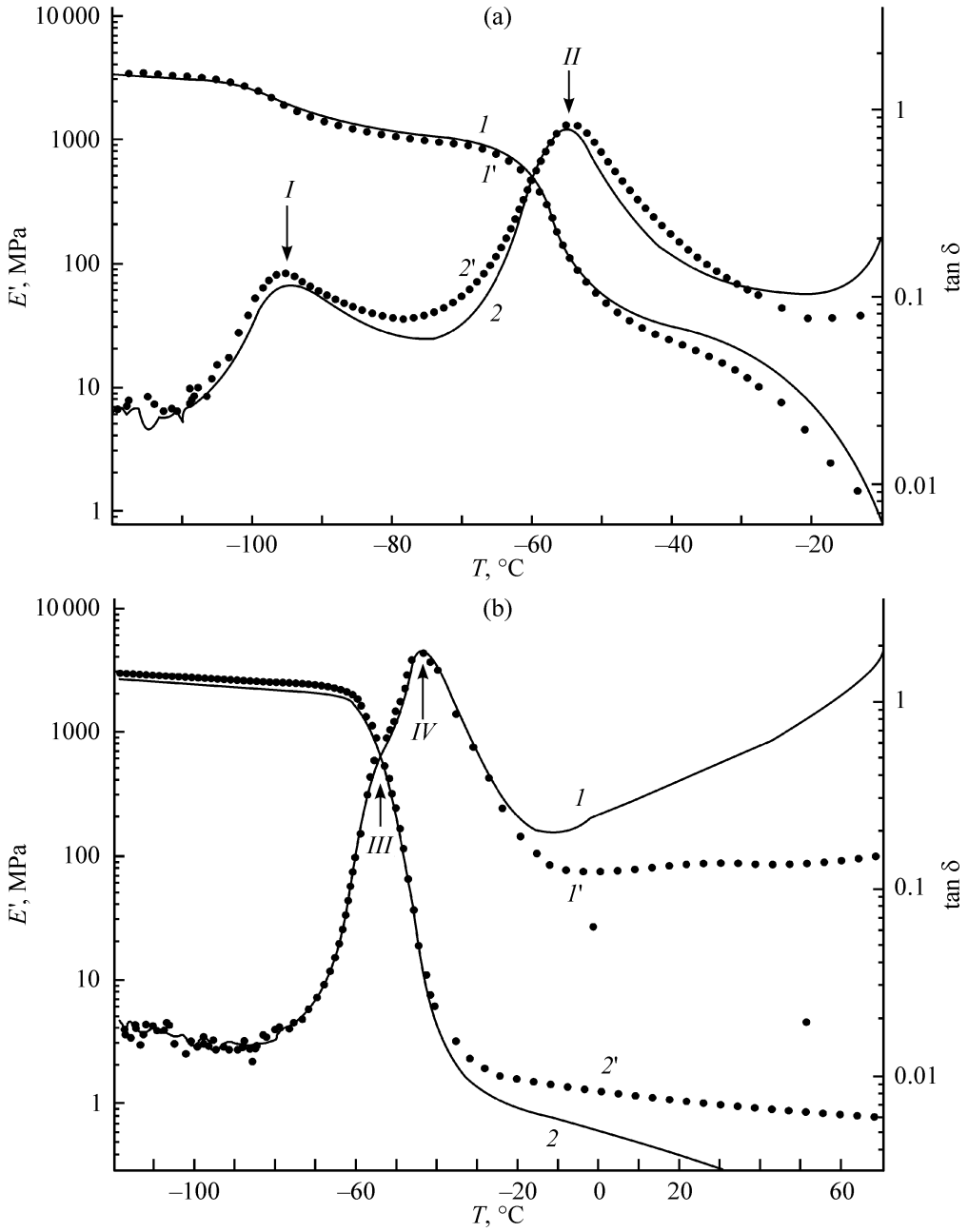


Fig. 1. Temperature dependences of the dynamic modulus of elasticity, E', and the mechanical loss tangent $\tan\delta$ of (a) SKD/SKI and (b) SKS/SKI unfilled formulations and (c) SKD/SKI and (d) SKS/SKI formulations filled with carbon black no. 330. ν = 1 Hz. Formulation: (*1*, *2*) unfilled and (*1*', *2*') modified with TCAA. Glass transition point, °C: (*1*) –94, SKD; (*II*, *III*) –54, SKI: and (*IV*) –44, SKS.

the polymer chains. All this favors a more uniform distribution of carbon black within the polymer matrix, as evidenced by an optical microscopic analysis. The enhancement of the interphase interaction in the systems based on modified rubbers plays the key role in improvement of such important characteristics as elastic properties of rubber stocks and elastic-relaxation properties of vulcanizates.

The results of the dynamic studies of the formulations obtained are presented in Fig. 1.

The dynamic studies of the vulcanizates of the binary blends of rubbers at temperatures of –120 to 70°C revealed two glass transition points T_g [T_g(SKD) = –94 and T_g(SKI) = –54°C for SKD/SKI system; T_g(SKS) = –44 and T_g(SKI) = –54°C for SKS/SKI

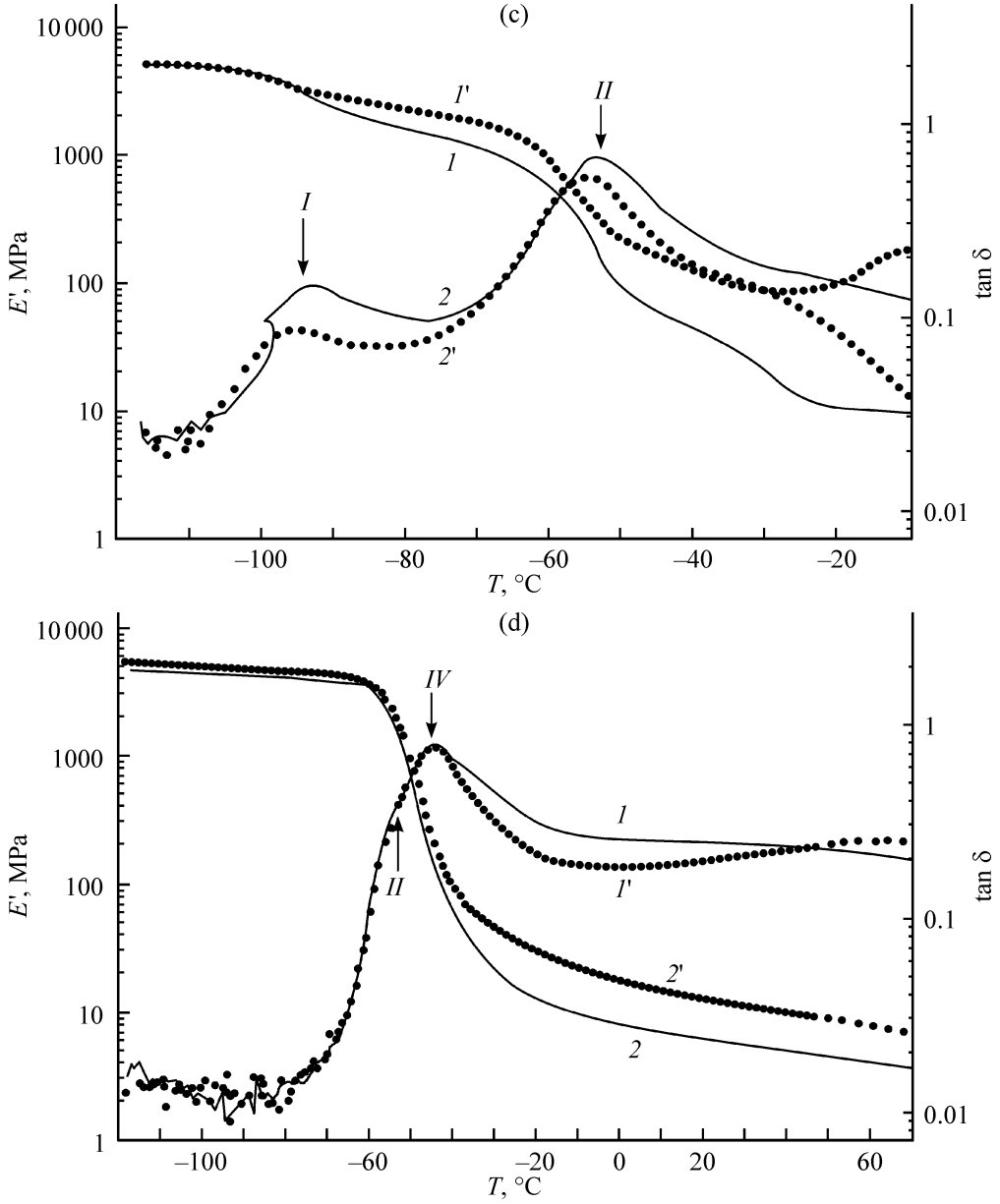


Fig. 1. (Contd.)

system] corresponding to each specific polymer; this means that these are two-phase systems. The temperature dependence of the modulus of elasticity, E', of the formulations exhibited a two-step pattern, and the curve describing the variation of the mechanical loss tangent tan δ had two peaks. For the SKS/SKI system, the glass transition points are close for both polymers, which is responsible for overlapping and broadening of the mechanical loss curve near the peak.

We have shown earlier [7] that the introduction of the filler, carbon black no. 330, does not affect the glass transition point of the polymers under study. Hence, the mobility of the chain segments is independent of the presence of filler particles; otherwise, T_g whould shift owing to changes in the macromolecular mobility. This suggests that the forces responsible for improvement of the mechanical properties of rubbers containing an active filler are of predominantly physical nature, and, evidently, chemical bonds are of minor significance.

Figures 1a and 1b show the temperature dependences of E' and tan δ for SKD/SKI and SKD/SKI/TCAA (SKS/SKI, SKS/SKI/TCAA) systems.

Figure 1a shows that introduction of TCAA into an unfilled SKD/SKI formulation only weakly affects

the modulus of elasticity, E' (1 MPa), but causes tan δ to decrease from 0.2 to 0.08 at $T = -10°C$. Figure 1b shows that, upon introduction of TCAA into the unfilled SKS/SKI formulation, E' increases from 0 to 1 MPa, and tan δ decreases by an order of magnitude, from 1.8 to 0.15 at $T = 30°C$. Figures 1a and 1b show that introduction of TCAA increases the modulus of elasticity of the system and decreases the mechanical loss tangent. The parameters E' and tan δ preserve improved values over a wide temperature range from –10 to 70°C, which extends the temperature range of applicability of the formulations.

Figures 1c and 1d show the temperature dependences of E' and tan δ for SKD/SKI/carbon black, SKD/SKI/carbon black/TCAA, SKS/SKI/carbon black, and SKS/SKI/carbon black/TCAA formulations. They suggest that combined introduction of TCAA and filler into the formulations based on binary rubber blends increases to the greatest extent the characteristics of the systems: E' increases from 1 and 4 to 10 MPa for SKS formulations and from 1 and 11 to 16 MPa for SKD formulations.

It is seen that the introduction of the modifier results in a shift of the glass transition point of the polymers by 2–3°C. This suggests that, in the structure of the vulcanization network, there are not only physical (owing to the filler) but also chemical [owing to the functional groups (carboxy, chloride) of the modifier] bonds.

We showed that combined introduction of the filler and modifier into formulations based on binary blends of rubbers significantly increases the modulus of elasticity and decreases by an order of magnitude the mechanical loss tangent. This is, evidently, due to an enhanced degree of crystallinity or a higher degree of cross-linking of the resulting vulcanizates.

The influence of the functional groups on the structure of vulcanizates can be analyzed from the viewpoint of the change in the degree of cross-linking and the type of the bonds being formed. In this context, of special interest is the possibility of formation of specific labile bonds via interaction of the functional groups of the elastomer with the vulcanizing agents. As is known [9], carboxy groups reacting with metal oxides or hydroxides form a network of labile, the so-called salt bonds. These are associates of charged particles, characterized by a relatively low energy, compared to disulfide bonds. The ability of these bonds to undergo rearrangement makes possible dissipation of overstresses arising in such systems, both during formation of the vulcanization network and during deformation of the final vulcanizates. The dissipation of overstresses is responsible for the increased resistance of rubbers to aging, tear, and multiple deformations.

CONSLUSIONS

(1) Introduction of carboxy groups and chlorine atoms into elastomers favors directed complex improvement of the properties of rubbers by changing the structure of the vulcanization networks, i.e., via creation of a combination of strong valence and labile bonds.

(2) Preparation of formulations with an improved set of properties extends the applicability field of the resulting materials in various branches of industry such as tire, cable, and industrial rubber articles.

ACKNOWLEDGMENT

The author is grateful to H.-J. Radusch (Institute of Materials Science, Martin-Luther University, Halle-Wittenberg, Germany) for assistance in preparation of formulations from binary blends of diene rubbers and in investigation of their properties.

REFERENCES

1. Pomogailo, A.D., *Usp. Khim.*, 2002, vol. 71, no. 1, p. 5.
2. Manson, J.A. and Sperling, L.H., *Polymer Blends and Composites*, New York: Plenum, 1976.
3. Kuleznev, V. I., *Smesi polimerov* (Polymer Blends), Moscow: Khimiya, 1980.
4. Evstratov, V.A., Lykin, A.S., Shvarts, A.G., and Kavun, S.M., *Vysokomol. Soedin., Ser. A.*, 1979, vol. 21, no. 11, pp. 2415–2416.
5. Bespalov, Yu.A. and Konovalenko, N.G., *Mnogokomponentnye sistemy na osnove polimerov* (Polymer-Based Multicomponent Systems), Leningrad: Khimiya, 1981.
6. Shvarts, A.G., *Khimicheskaya modifikatsiya rezin* (Chemical Modification of Rubbers), Moscow: TsNIITEneftekhim, 1980.
7. Kurbanova, N.I., *Zh. Prikl. Khim.*, 2004, vol. 77, no. 6, pp. 1041–1043.
8. Kargin, V.A., *Struktura i mekhanicheskie svoistva polimerov: izbrannye trudy* (Structure and Mechanical Properties of Polymers: Selected Works), Moscow: Nauka, 1979.
9. Poluektova, L.E., Mosagutova, L.V., Sapronov, V.A., and Lykin, L.S., *Kauchuk Rezina*, 1985, no. 1, pp. 16–18.

Russian Journal of Applied Chemistry, Vol. 78, No. 8, 2005, pp. 1360–1363. Translated from Zhurnal Prikladnoi Khimii, Vol. 78, No. 8, 2005, pp. 1384–1387.
Original Russian Text Copyright © 2005 by Lebedeva, Yarkova, Platonov, Proskuryakov.

CHEMISTRY OF FOSSIL FUEL

Chemical Modification of Peat Humic Acids To Increase Their Bioactivity

G. F. Lebedeva, T. Ya. Yarkova, V. V. Platonov, and V. A. Proskuryakov

Novomoskovsk Institute of Mendeleev Russian University of Chemical Engineering, Novomoskovsk, Tula oblast, Russia

Leo Tolstoy State Pedagogical University, Tula, Russia

St. Petersburg State Technological University, St. Petersburg, Russia

Received March 2, 2005

Abstract—The possibility of chemical modification of peat humic acids in order to increase their bioactivity by reduction with tin(II) chloride and sodium borohydride and also by carboxylation using the Kolbe method was analyzed.

It was demonstrated in [1–3] and our previous studies [4–6] that the bioactivity of humic acids (HA) is due to the presence of phenolic (PG) and carboxy (CG) groups, whereas the keto (KG) and quinoid (QG) groups have virtually no effect on this property of HA.

Therefore, it was of interest to modify the HA structure by converting some functional groups into groups responsible for bioactivity (BA). In this case, it is undesirable to use such destructive methods as oxidation with nitric acid or peroxide, etc., since oxidative degradation leads to a considerable decrease in the molecular weight of HA.

EXPERIMENTAL

In the study, we used humic acids extracted from peat obtained from Tver oblast (Russia). These humic acids are high-molecular-weight polyfunctional compounds (aromaticity 0.69, naphthenic index 0.10, and degree of alkylation 0.21). Their elemental composition (wt % daf) was as follows: C 59.11, H 5.09, N 3.01, O + S 32.79.

Reduction of HA with tin(II) chloride was carried out in alkaline solutions in air or in a CO_2 atmosphere, to reduce HA more deeply (Tables 1–3).

Table 1. Contents of functional groups *c* and bioactivity of humic preparations (HPs) at various τ times of HA reduction with $SnCl_2$ and $NaBH_4$* ($SnCl_2$: 20°C, HA : $SnCl_2$ weight ratio 2 : 1; $NaBH_4$: 25°C, HA : $NaBH_4$ 10 : 1)

Parameter	Initial HA	Reductant $SnCl_2$			Reductant $NaBH_4$		
		2 h	4 h	6 h	1 h	2 h	3 h
M	1400	1230 (1410)	1210 (1350)	1210	1350	1340	1300
c, mg-equiv g^{-1}:							
PG	3.86	4.76 (5.31)	4.90 (5.52)	5.12	4.70	4.86	4.88
QG	2.34	1.79 (1.10)	1.62 (1.06)	1.48	1.41	1.34	1.30
CG	2.73	2.70 (3.35)	2.70 (3.42)	2.70	2.73	2.72	2.70
KG	0.28	0.16 (0.11)	0.14 (0.08)	0.07	0.07	0.04	0.00
IN, mg-equiv g^{-1}	0.27	0.26 (0.22)	0.24 (0.20)	0.20	0.19	0.14	0.16
BA	1.06	1.18 (1.20)	1.20 (1.23)	1.21	1.14	1.16	1.12
HP yield, %	–	89 (95)	88 (96)	82	96	96	98

* Data for reduction in air and CO_2 are given without parentheses and in parentheses, respectively; (*M*) Molecular weight; BA was measured in 1×10^{-3} wt % HP; the same for Tables 2, 3.

1070-4272/05/7808-1360 © 2005 Pleiades Publishing, Inc.

Table 2. Contents of functional groups *c* and bioactivity of humic preparations at various temperatures *T* of HA reduction with $SnCl_2$ (HA : $SnCl_2$ weight ratio 2 : 1; 2 h)

Parameter	Initial HA	20°C	40°C	60°C
M	1400	1230 (1410)	1170 (1230)	1090 (1140)
c, mg-equiv g^{-1}:				
PG	3.86	4.76 (5.31)	5.03 (5.63)	5.29(5.65)
QG	2.34	1.79 (1.10)	1.31 (0.83)	0.95 (0.71)
CG	2.73	2.70 (3.35)	2.70 (3.44)	2.79 (3.83)
KG	0.28	0.16 (0.11)	0.06 (0.03)	0.04 (0.00)
IN, mg-equiv g^{-1}	0.27	0.26 (0.22)	0.26 (0.20)	0.24 (0.21)
BA	1.06	1.18 (1.20)	1.21 (1.22)	1.25 (1.25)
HP yield, %	–	89 (95)	82 (90)	76 (80)

Table 3. Contents of functional groups *c* and bioactivity of humic preparations at various reductant concentrations ($SnCl_2$: 20°C, 2 h; $NaBH_4$: 25°C, 1 h)

Parameter	Initial HA	HA : reductant weight ratio							
		$SnCl_2$				$NaBH_4$			
		10 : 1	5 : 1	2 : 1	1 : 1	10 : 1	5 : 1	3 : 1	2 : 1
M	1400	1300	1300	1230	1270	1350 (1380)	1350 (1350)	1350 (1360)	1350 (1360)
c, mg-equiv g^{-1}:									
PG	3.86	4.22	4.70	4.76	4.83	4.70 (5.16)	5.42 (5.34)	5.69 (5.72)	5.72 (5.70)
QG	2.34	2.00	1.82	1.79	1.70	1.41 (1.02)	1.07 (0.88)	0.79 (0.77)	0.74 (0.70)
CG	2.73	2.73	2.73	2.70	2.73	2.73 (3.50)	2.73 (3.49)	2.70 (3.72)	2.70 (3.78)
KG	0.28	0.26	0.19	0.16	0.16	0.07 (0.04)	0.03 (0.02)	0.00 (0.00)	0.00 (0.00)
IN, mg-equiv g^{-1}	0.27	0.26	0.26	0.26	0.24	0.19 (0.17)	0.12 (0.13)	0.11 (0.12)	0.10 (0.06)
BA	1.06	1.06	1.17	1.18	1.18	1.14 (1.14)	1.22 (1.21)	1.22 (1.35)	1.31 (1.28)
HP yield, %	–	96	95	89	90	96 (92)	88 (90)	90 (93)	87 (92)

A study of the process at 20°C, HA : $SnCl_2$ = 2 : 1, and a reaction time of 2 to 6 h (Table 1) revealed that, in air, quinoid groups are reduced into phenolic groups, whose content increased from 3.86 to 5.12 mg-equiv g^{-1} in 6 h. Simultaneously, the QG content decreased from 2.34 to 1.48 mg-equiv g^{-1}. Under these conditions, the carboxy groups were virtually not reduced. The content of keto groups decreased significantly (from 0.28 to 0.07 mg-equiv g^{-1}). Apparently, these groups were converted into the alcoholic groups (AG). The iodine number (IN) changed from 0.27 to 0.20 mg-equiv g^{-1}. The molecular weight decreased in the course of reaction from 1400 to 1210, the decrease being virtually independent of the reaction time.

The bioactivity of humic preparations was determined by the standard fermentation test based on the capability of biostimulants to increase the fermenting capacity of yeast. The bioactivity is expressed in fraction units relative to the bioactivity of distilled water. The bioactivity tests with the initial humic acid and reduced humic preparations were positive: for humic preparations, BA increased by 14%.

As expected, performing the reduction under the same conditions, but in the CO_2 atmosphere, increased not only the efficiency of reduction of QG, but also increased the content of carboxy groups. For example, in 4 h, the PG content increased to 5.52 mg-equiv g^{-1} (against 4.90 mg-equiv g^{-1} in air). In turn, the QG content decreased to 1.06 (1.62 mg-equiv g^{-1} in air), and the CG content increased from 2.73 in the initial HA to 3.42 mg-equiv g^{-1} in the resulting humic preparation. Accordingly, the bioactivity factor also increased after reduction of HA under CO_2. The unexpected increase in the CG content under the reducing conditions can be attributed to a parallel occurrence of the Kolbe reaction involving the phenolic fragments of the HA molecule, since, as known, this reaction occurs more readily in alkaline solutions. It should also be noted that, under CO_2, two practically important reaction proceed in parallel: reduction and carboxylation with virtually no change in the molecular weight of HA. Evidently, atmospheric oxygen promotes oxidative degradation of HA.

The effect of temperature on the reduction of HA is shown in Table 2. The experiments were carried

Table 4. Contents of functional groups *c* and bioactivity of humic preparations in the course of carboxylation of humic acids

Parameter	Initial HA	HP	
		$HA + SnCl_2$ (20°C, 2 h, 2 : 1)	$HA + NaBH_4$ (25°C, 1 h, 10 : 1)
M	1400*/1470	1230/1410	1350/1390
c, mg-equiv g^{-1}:			
PG	3.86/3.76	4.76/4.76	4.70/4.86
QG	2.34/2.34	1.79/1.79	1.41/1.34
CG	2.73/3.70	2.70/3.85	2.73/4.12
KG	0.28/0.25	0.16/0.14	0.07/0.07
IN, mg-equiv g^{-1}	0.27/0.27	0.26/0.20	0.19/0.10
BA**	1.06/1.15	1.18/1.17	1.14/1.18
HP yield, %	–/96	89/86	96/93

* Data before and after carboxylation are given in the numerator and denominator, respectively.

** BA was measured in 1×10^{-3} wt % HP.

out under similar conditions at 20, 40, and 60°C in air and CO_2 atmosphere. The general trends in the reduction and carboxylation of HA remained unchanged. As expected, the reduction rate increased with temperature. At the same time, because of the low heat resistance of HA, its molecular weight decreased to 1090 and 1140 at 60°C in air and under CO_2, respectively. Therefore, it is advisable to perform the reduction at 20–40°C under CO_2. The effect of the HA : $SnCl_2$ ratio is shown in Table 3. It was varied over a wide range from 10 : 1 to 1 : 1. The increase in the reductant concentration only slightly affected the functional composition of HA. Therefore, the 10 : 1 ratio can be recommended for the process.

Reduction of HA with sodium borohydride ($NaBH_4$). The reaction was performed in an alkaline solution at 25°C to prevent decomposition of the reagent (Tables 1 and 3).

When studying the effect of the reaction time, the reduction was carried out at HA : $NaBH_4$ = 10 : 1 for 1, 2, and 3 h. Table 1 shows that, like $SnCl_2$, $NaBH_4$ reduces QG into PG, and KG into AG, the CG content remaining unchanged.

A comparison of the two reducing agents studied revealed a higher efficiency of $NaBH_4$ under similar conditions (Tables 1 and 3). For example, the PG content increased upon reduction with $SnCl_2$ and $NaBH_4$ from 3.86 to 4.22 and 4.86 mg-equiv g^{-1}, respectively, with the QG content coming to equal to 0.55 and 1.00 mg-equiv g^{-1}, and the KG content, to 0.08 and 0.24 mg-equiv g^{-1}. Note that, with $NaBH_4$, the reduction in air had a smaller effect on the molecular weight of HA. In this case, it decreased by 4.5% against 7% with $SnCl_2$, which is probably due to evolution of hydrogen in the borohydride reduction. Indeed, data on IN revealed a partial hydrogenation of the multiple bonds.

Data on the effect of the reaction time on the reduction efficiency (Table 1) suggest that 1 h is a time sufficient for obtaining a satisfactory result.

Further, we studied the effect of the HA : $NaBH_4$ weight ratio, varied from 10 : 1 to 2 : 1, on the reduction efficiency (Table 3). The PG content and the degree of QG and KG reduction were at a maximum at HA : $NaBH_4$ = 3 : 1. In this case, the keto groups were fully reduced. In parallel, we carried out experiments in a CO_2 atmosphere (Table 3). As expected, the CG content increased under these conditions in parallel to that of PG (by 28–37%). The 3 : 1 proportion also provided the maximum bioactivity, which increased by 27%.

Carboxylation of HA by the Kolbe reaction. Positive results obtained in the reduction under CO_2 stimulated further experiments on carboxylation as a method for chemical modification of HA aimed at improving their bioactivity. This process was applied to the initial HA and also to the humic preparations obtained by reduction with $NaBH_4$ and $SnCl_2$ (Table 4). As a result, the CG content increased from 2.73 mg-equiv g^{-1} in the initial HA to 3.70–4.12 mg-equiv g^{-1}, the best result being obtained after the borohydride reduction. Comparison of these results with those obtained by the reduction under CO_2 (Table 1) shows that the carboxylation is a more efficient process. For example, the reduction with $SnCl_2$ and $NaBH_4$ under CO_2 increased the CG content to 3.35 and 3.50 mg-equiv g^{-1}, and the carboxylation of the reduced humic preparations, to 3.85 and 4.12 mg-equiv g^{-1}, respectively. Note that the carboxylation had virtually no effect on the molecular weight of the products, which can be attributed to intensive decomposition of potassium hydrocarbonate in the course of the reaction and also to the anaerobic conditions.

CONCLUSIONS

(1) Nondestructive reduction of peat humic acids with $SnCl_2$ and $NaBH_4$ increases (by 26–33%) the content of phenolic groups, influencing the bioactivity, without degradation of humic acid molecules. The best results were obtained with $NaBH_4$.

(2) Treatment of humic acids with $SnCl_2$ and $NaBH_4$ in a CO_2 atmosphere allows two practically important processes to be performed simultaneously: reduction and carboxylation without significant change in the molecular weight of the initial humic acids. In this case, the carboxy group content increased by 40%.

(3) Bioactivity of humic preparations obtained by reduction of humic acids with $NaBH_4$ under CO_2 at a humic acid to $NaBH_4$ weight ratio of 3 : 1 (25°C; 1 h) increased by 27%.

REFERENCES

1. Strochai, L.P., *Tr. Dnepropetrovsk. Sel'skokhoz. Inst.*, 1983, vol. 8, no. 1, pp. 47–50.
2. Sumina, A.D. and Starostin, A.I., Abstracts of Papers, *Pervaya mezhvuzovskaya konferentsiya "Biokhimiya i plodorodie pochv"* (First Intercollegiate Conf. "Biochemistry and Fertility of Soils"), Moscow: Mosk. Gos. Univ., 1967, pp. 67–68.
3. Pivovarov, L.N., *O prirode fiziologicheskoi aktivnosti guminovykh kislot v svyazi s ikh stroeniem* (On the Nature of Physiological Activity of Humic Acids in Light of Their Structure), Kiev: Naukova Dumka, 1962.
4. Lebedeva, G.F., Chernysheva, N.I., Platonov, V.V., and Proskuryakov, V.A., Abstracts of Papers, *XIII Mezhdunarodnaya nauchno-tekhnicheskaya konferentsiya Reaktiv-2000* (XIII Int. Scientific and Technical Conf. "Chemical-2000"), Tula: Tul'skii Gos. Pedagog. Univ., 2000, pp. 216–217.
5. Platonov, V.V., Lebedeva, G.F., Chernysheva, N.I., *et al.*, Abstracts of Papers, *XVI mezhdunarodnaya konferentsiya molodykh uchenykh "Uspekhi v khimii i khimicheskoi tekhnologii* (XVI Int. Conf. of Young Scientists "Advances in Chemistry and Chemical Technology"), Moscow: Ross. Khim.-Tekhnol. Univ., 2002, vol. 16, no. 4, pp. 109–110.
6. Platonov, V.V., Lebedeva, G.F., Yarkova, T.A., *et al.*, Abstracts of Papers, *IV Nauchno-tekhnicheskaya konferentsiya molodykh uchenykh, aspirantov i studentov* (IV Scientific and Technical Conf. of Young Scientists, Postgraduates, and Students), Novomoskovsk: Novomoskovsk. Inst. Ross. Khim.-Tekhnol. Univ., 2002, p. 142.

Russian Journal of Applied Chemistry, Vol. 78, No. 8, 2005, pp. 1364–1369. Translated from Zhurnal Prikladnoi Khimii, Vol. 78, No. 8, 2005, pp. 1388–1394.
Original Russian Text Copyright © 2005 by Nikulicheva, Fadeeva, Piottukh-Peletskii, Pokrovskii, Bogdanova, Yudina.

CHEMISTRY OF FOSSIL FUEL

An IR and GC–MS Study of Substances Extracted from Peat

O. N. Nikulicheva, V. P. Fadeeva, V. N. Piottukh-Peletskii, L. M. Pokrovskii, T. F. Bogdanova, and N. V. Yudina

Vorozhtsov Institute of Organic Chemistry, Siberian Division, Russian Academy of Sciences, Novosibirsk, Russia

Institute of Petroleum Chemistry, Siberian Division, Russian Academy of Sciences, Tomsk, Russia

Received February 1, 2005

Abstract—The substances extracted from peats were studied by IR spectroscopy and gas chromatography–mass spectrometry.

Peat is the product of partial degradation of bog plants. The properties of peat formed in different regions of Russia are diverse because of different peat-forming plants and widely varying conditions of peat accumulation. Peat contains both relatively simple and macromolecular organic compounds typical of plants, and these compounds may be useful for the national economy [1].

Peat contains a large amount of biologically active substances [2, 3] of the humus origin and of other classes. It is of scientific and practical interest to study organic compounds extractable from peat with organic solvents. The chemical composition and properties of extracts depend on the kinds of the peat and extractant. Extraction of peats, especially of those from Belarus, with various solvents has been studied previously [4, 5]. An ethanol extract from peat wax resin, exhibiting high antiphlogistic and antiviral activity, is used in medicine and cosmetology. Torfenal antiallergic agent, which is a component of ointments, lotions, and detergents, is commercially produced from these extracts [3].

The composition of extracts from Siberian peats has been poorly studied. In this study, we examined the extracts from some peats of the Tomsk oblast.

EXPERIMENTAL

Peats chosen for the study had different bedding depths and different degrees of degradation *R*. We took lowland peat from the Taganskoe deposit ($R \sim 30\%$), raised-bog peat from the Temnoe deposit ($R \sim 0$–5%), raised-bog peat from the Svetloe deposit ($R \sim 0$–5%), and mechanically activated raised-bog peat from the Svetloe deposit. The mechanical activation was performed with a vibrocentifugal mill. This treatment induces changes in the porous supramolecular structure, physical state, and properties of peats and enhances the efficiency of extraction with organic solvents [6, 7].

The extraction of peats was performed in a Soxhlet apparatus heated on a water bath (about 15 h). The elemental composition of peats and extracted substances was determined on a Carlo Erba Model 1106 CHN analyzer; the ash residue was determined gravimetrically. For the extracts, we determined the acid, iodine, carbonyl, and saponification numbers [8–11] and the content of triterpenic acids [12, 13]. The IR spectra were recorded on a Bruker Vector-22 IR Fourier spectrometer from thin films or KBr pellets in the range >400 cm^{-1}.

IR spectroscopy alone does not allow exhaustive determination of the structure of a compound; furthermore, we analyzed mixtures rather than individual compounds. Therefore, we used the IR spectra to search for structural fragments that could be present in the samples and to identify some compounds whose spectra taken from the database closely matched the experimental spectra of the samples.

The search for structural fragments in the database was performed in two modes: with Euclidean metrics (point-by-point comparison of spectral curves) and with IR descriptors (comparison of the positions and intensities of absorption bands). An analysis using the IK Ekspert (IR Expert) system [14] allowed us to find structures of the most probable fragments. The fragments were chosen on the basis of statistical

1070-4272/05/7808-1364 © 2005 Pleiades Publishing, Inc.

Table 1. Yield of extracted substances from peat

Extractant (sequential extraction)	Yield, wt %, from indicated peat	
	lowland*	raised-bog**
Hexane	0.7	1.3
Chloroform	1.3	2.6
Ethyl acetate	0.3	0.3
Methanol	1.2	1.6
Total	3.5	5.8

* Taganskoe deposit. ** Temnoe deposit.

evaluation of the so-called noncontingency factors of appearance of a fragment in search response structures. When calculating the noncontingency factors, we took into account the incidence of fragments in the search response structures and in database structures [15].

A GC–MS analysis was performed with a Hewlett–Packard 5890/II gas chromatograph (the United States) interfaced with an HP MSD 5971 quadrupole mass spectrometer. A 30-m quartz column was coated with polyphenylmethylsiloxane (HP-5MS, 5% phenyl groups); the carrier gas was He, flow rate 1 ml min^{-1}. The column temperature was programmed as follows: 50°C, 2 min; heating to 280°C, 4 deg min^{-1}; 280°C, 15 min. The molecules were ionized by electron impact (70 eV).

The extracted substances were separated into neutral and acid fractions; the acid fraction was methylated by standard procedures [16]. To choose an extractant, we extracted raised-bog and lowland peat samples with solvents of various polarities. The results of sequential extraction of peats with solvents, from low-polarity hexane to strongly polar methanol, are listed in Table 1, together with the total yield of the extracted substances.

We also tested as extractant methyl *tert*-butyl ether (MTBE), which appeared to be more efficient and more readily available than certain nonpolar solvents (hexane, petroleum ether) and was not inferior to some polar solvents like chloroform (extract yield about 4 wt %). Therefore, further extraction experiments were performed with MTBE.

The elemental composition of the peats and the elemental composition and characteristics of the extracted substances (averaged over 3–5 measurements) are listed in Tables 2 and 3. Sulfur was detected neither in peats nor in their extracts.

Table 3 shows that the substances extracted from different peats are similar in the content of free acids

Table 2. Results of C, H, N analysis of peats and extracts

Peat	Content, %						
	in peat				in extract		
	C	H	N	ash	C	H	N
Lowland*	33.3	4.9	2.9	26.9	73.4	10.0	0.3
Raised-bog**	49.3	6.7	1.5	4.3	72.5	9.8	0
Raised-bog***	51.0	6.4	1.6	3.7	71.5	9.5	0
Raised-bog mechanically activated raised-bog***	49.6	6.1	1.55	2.8	73.5	10.0	0

* Taganskoe deposit. ** Temnoe deposit. *** Svetloe deposit.

Table 3. Characteristics of substances extracted from peats

Extract from peat:	Acid number	Saponification number	Iodine number, g I_2 per 100 g substance	Carbonyl number, mg g^{-1} substance	Triterpene acids, wt %
	mg KOH g^{-1} substance				
Lowland*	6.8	12.0	30.0	6.6	0.25
Raised-bog**	6.5	12.0	–	–	–
Raised-bog***	6.6	14.0	41.0	5.3	1.5
Raised-bog mechanically activated raised-bog***	7.5	16.0	44.0	6.6	2.0

* Taganskoe deposit. ** Temnoe deposit. *** Svetloe deposit.

and esters, but differ in the content of unsaturated compounds (iodine number from 30 to 44 g I_2 per 100 g substance). For the mechanically activated peat, all the parameters are somewhat higher.

The peat extracts were separated into the neutral and acid fractions. The yield of the neutral fraction of nonactivated peats was 45–50% of the total amount of the extracted substances. In the extract from the mechanically activated peat, the content of the neutral fraction was 35.1%, and that of the acid fraction, 64.8%. Apparently, the mechanical activation results in partial oxidation of the peat dust by atmospheric oxygen [7].

The IR spectra of the substances extracted from the peat samples examined show that extracts are similar in the chemical composition and structure of the components. The major components of virtually all the extracts (total, neutral fraction, and acid fraction) are aliphatic carboxylic acid esters R^1COOOR^2, where R^1 and R^2 are long aliphatic chains containing a double bond, and products of their hydrolysis, free carboxylic acids R–COOH.

It should be noted that the keto group R^1COR^2, and not carboxy group, is often detected as a non-occasional fragment, i.e., ketones with long aliphatic chains (possibly branched) may be present in the samples.

The structures of components of the neutral and acid fraction, including the methylated acid fraction, were determined by GC–MS. The major components of the extracts, according to the GC–MS data (the content was calculated from the peak areas without correction factors), are listed in Table 4.

Table 4. Components of neutral and acid fractions of peat extracts, identified by gas chromatography–mass spectrometry

Neutral fraction	Content, wt %	Acid fraction	Content, wt %
Lowland peat, Taganskoe deposit			
1,4-Dimethylbenzene	1.14	Azelaic acid	1.35
2,4,4-Trimethylheptane	0.97	Tetradecanoic acid	1.40
Nonane	1.25	Hexadecanoic acid	4.56
2,6-Dimethyloctane	0.61	Methyl oleate	0.88
Propylbenzene	0.93	Octadecanoic acid	1.77
Ethylmethylbenzene	1.77	Dimethylhexadecanoic acid	1.14
Trimethylbenzene	2.95	9-Eicosene	0.82
3-Methylnonane	0.56	Eicosanoic acid	4.60
Tetramethyl-4-methylenehexane	7.02	Tetramethylheptadecan-4-olide	1.26
Decane	4.47	Octadecadienoic acid	7.97
Pentamethyl-3-heptene	8.47	Heneicosanoic acid	0.95
4-Methyldecane	1.55	1-Docosanol	2.42
Butylcyclohexane	0.85	Docosanoic acid	10.90
Methylpropylbenzene	1.32	Tricosanoic acid	1.66
Butylbenzene	1.45	1-Octadecanol	1.19
2-Methyldecane	0.70	Tetradecanoic acid	12.30
3-Methyldecane	0.82	Tetracosanedioic acid	6.16
Undecane	5.61	Heptacosanone	1.10
Amylcyclohexane	0.74	Hexacosanoic acid	9.02
2-Methylundecane	1.31	Heptacosanoic acid	1.72
Dodecane	4.19	Octacosanoic acid	2.33
3,6-Dimethylundecane	1.31	Triacontanoic acid	0.94
Tridecane	3.01	Friedelan-3-one	0.36
Methylnaphthalene	0.80	–	–
Tetradecane	1.86	–	–
Pentadecane	1.23	–	–
Hexadecane	0.71	–	–
γ-Sitosterol	1.12	–	–
Raised-bog peat, Temnoe deposit			
1,4-Dimethylcyclohexane	1.20	Azelaic acid	0.89
2-Methylheptane	1.35	Tetradecanoic acid	0.77
Toluene	3.12	Hexadecanoic acid	5.20
3-Methylheptane	0.98	Palmityl acrylate	0.65

Table 4. (Contd.)

Neutral fraction	Content, wt %	Acid fraction	Content, wt %
1,3-Dimethylcyclohexane	2.26	6-Octadecynoic acid?	1.40
Octane	3.43	Methyl oleate	1.77
Ethylcyclohexane	1.86	Octadecanoic acid	2.11
2,4-Dimethylheptane	1.31	Tetradecanoic acid	2.33
1,3-Dimethylbenzene	2.11	Hexadecanoic acid?	0.81
2-Methoxy-2,4,4-trimethylpentane	3.18	Stearyl acrylate	1.28
Nonane	1.76	Eicosanoic acid	3.32
2,2,6,6-Tetramethylheptane	2.82	Dihydroabietic acid	1.26
2,2,4,6,6-Pentamethyl-3-heptene	3.08	Heneicosanoic acid	1.90
Undecane	1.27	9,12-Octadecadienoic acid	0.94
Dodecane	3.39	Docosanoic acid	8.95
2,6-Dimethylundecane	1.41	7-Oxodihydroabietic acid	0.63
6,6-Dimethylundecane	1.07	Tricosanoic acid	1.25
Tridecane	5.54	Eicosanedionoic acid?	3.32
4,6-Dimethyldodecane	1.86	Tetracosanoic acid	1.25
Tetradecane	5.20	Pentacosanoic acid	1.53
Pentadecane	4.45	Docosanedionoic acid?	4.73
Hexadecane	3.42	Hexacosanoic acid	7.88
6-Methylpentadecane	1.54	Not identified	3.36
Heptadecane	3.41	Octacosanoic acid	1.56
2,6,10,14-Tetramethylpentadecane	2.81	*D:A*-Friedoolean-6-ene	0.93
Octadecane	3.09	Friedelin	12.06
Nonadecane	2.14	–	–
Eicosane	1.54	–	–
Heneicosane	1.66	–	–
Docosane	0.98	–	–
Tricosane	1.13	–	–
Pentacosane	1.05	–	–
Phthalate?	0.60	–	–
Heptacosane	0.61	–	–
γ-Sitosterol	14.21	–	–
	Raised-bog peat, Svetloe deposit		
Heptadecane	1.94	Azelaic acid	1.35
6,10,14-Trimethyl-2-pentadecanone	1.17	Tetradecanoic acid	1.40
Tricosane	0.70	Hexadecanoic acid	4.56
Cyclohexane	0.75	Methyl oleate	0.88
2,6,10,14-Tetramethylheptadecane?	2.26	Octadecanoic acid	1.77
Pentacosane	0.83	Eicosanoic acid	4.60
Heptacosane	1.24	Hexadecanoic acid?	1.14
Squalene	0.71	9-Eicosene	0.82
Nonacosane	0.98	Tetramethylheptadecane	1.26
2-Heptacosane	1.10	Octadecanoic acid	1.28
Taraxerin	2.15	Heneicosanoic acid	7.97
γ-Tocopherol	1.79	Tetradecanoic acid	0.93
Not identified	1.17	1-Docosanol	2.42
Hentriacontane	1.79	Docosanoic acid	10.91
Vitamin E	1.51	Tricosanoic acid	1.66
Campesterol	4.44	Eicosanedicarboxylic acid	3.47
Stigmasterol	6.00	1-Octadecanol	1.19
5α-Ergostan-3-one	0.81	Tetracosanoic acid	12.30
Not identified	2.06	Pentadecanoate?	1.00
β-Sitosterol	24.07	Docosanoic acid?	6.16
Stigmastan-3-ol	1.62	Hexacosanoic acid	1.10
Not identified	1.51	Hexacosanoic acid	9.02

Table 4. (Contd.)

Neutral fraction	Content, wt %	Acid fraction	Content, wt %
5α-Stigmastan-3-one	5.06	Heptacosanoic acid	1.72
Not identified	2.42	Octacosanoic acid	2.33
Not identified	5.08	Triacontanoate?	0.94
γ-Sitosterol	7.18	Stigmast-4-en-3-one	1.06
Not identified	4.89	Friedelan-3-one	0.40
Octadecyl palmitate	1.02	–	–
Mechanically activated raised-bog peat, Svetloe deposit			
Pentane	0.82	2-Octenoic acid	15.01
Heptane	0.97	Tridecanol	11.85
3-Heptene	1.16	Citronellyl acetate?	1.30
Dodecane	0.33	Hexadecanoic acid	2.53
2-Octenoic acid	10.05	Heneicosane	1.13
Tridecane	0.24	Octadecanoic acid	2.14
1-Dodecanol	1.34	*n*-Triacontane	4.11
2-Pentadecanone	0.63	2-Nonadecanone	1.62
Heneicosane	0.16	4,8,12,16-Tetramethylheptadecan-4-olide	2.50
Phytol	0.67	Pentacosane	3.13
Tricosane	0.87	Octadecadienoic acid	1.81
Pentacosane	0.89	Not identified	1.22
Heptacosane	1.25	Not identified	1.42
Nonacosane	0.81	Heptacosane	3.36
2-Heptacosanone	0.76	CH_3–CO–$(CH_2)_n$–CH_3	1.43
Not identified	1.74	Tetracosanoic acid	1.17
γ-Tocopherol	2.09	Not identified	1.08
Hentriacontane	1.34	Nonacosane	1.69
2-Nonacosanone	0.44	CH_3–CO–$(CH_2)_m$–CH_3	4.26
Vitamin E	2.14	Hexacosanoic acid	1.66
Not identified	1.48	Docosanedioic acid?	3.04
Campesterol	5.85	Hentriacontane	1.68
Stigmasterol	8.79	CH_3–CO–$(CH_2)_k$–CH_3	1.75
Tritriacontane	0.63	Vitamin E	3.49
Not identified	4.55	Octacosanoic acid	3.19
β-Sitosterol	22.87	Not identified	5.48
Stigmastan-3-one	0.72	Stigmast-4-en-3-one	3.49
Stigmast-4-en-3-one	2.04	Friedelin	3.70
Not identified	3.86	Not identified	4.85

The percentages given in Table 4 for certain components are estimates; however, these estimates give a qualitative pattern of the extract composition. The identified complex polycyclic structures, e.g., vitamin E, friedelin, and other steroid compounds, may have isomers with simlar mass spectra; therefore, conclusions about the presence of specific compounds were made only if a closely similar mass spectrum was found in the database.

CONCLUSIONS

(1) An IR and GC–MS study of the substances extracted from peats showed that the extracts are closely similar in the qualitative and quantitative composition. The extracts contain a large set of alkanes, aromatic compounds, esters, polyhydric alcohols, aliphatic fatty acids (including keto acids), and steroid compounds (including γ- and β-sitosterols).

(2) In the extract from the mechanically activated peat, the content of the acid fraction is appreciably higher, compared to the extract from the nonactivated peat, apparently because of the partial oxidation of aldehydes and ketons in the course of peat milling.

(3) Friedelin, phytol, triterpene acids, steroid compounds (including γ- and β-sitosterols), and the compound identical to vitamin E, identified in peat ex-

tracts, may be of interest as raw materials for preparing biologically active substances.

ACKNOWLEDGMENTS

The study was supported by the Siberian Division of the Russian Academy of Sciences (integration project no. 35) and, in part, by the Russian Foundation for Basic Research (project no. 04-03-32374).

REFERENCES

1. *Torf v narodnom khozyaistve* (Peat in the National Economy), Sokolov, B.N., Ed., M.: Nedra, 1988.
2. *Torf v biotekhnologii* (Peat in Biotechnology), Naumov, G.V., Ed., Minsk: Nauka i Tekhnika, 1987.
3. Dolidovich, E.F., Sheremet, L.S., Gusintseva, A.V., and Zaitseva, T.L., *Rast. Resursy*, 1995, no. 2, pp. 37–43.
4. *Torfyanoi vosk i soputstvuyushchie produkty* (Peat Wax and Concomitant Products), Bel'kevich, P.I., Ed., Minsk: Nauka i Tekhnika, 1977, pp. 11–40.
5. Ivanova, L.A., Chistyakova, E.I., and Yurkevich, E.A., *Khim. Tverd. Topl.*, 1996, no. 3, pp. 60–65.
6. Khrenkova, T.M., Kirda, V.S., and Antonova, V.M., *Khim. Tverd. Topl.*, 1991, no. 5, pp. 1–20.
7. Kashinskaya, T.Ya., Gavril'chik, A.P., Kalilets, L.P., *et al.*, *Khim. Tverd. Topl.*, 1997, no. 6, pp. 14–24.
8. *GOST* (State Standard) *5476–80 (COMECON Standard 4715–84): Vegetable Oils: Methods for Determination of the Acid Number*.
9. *GOST* (State Standard) *5475–69: Vegetable Oils: Methods for Determination of the Iodine Number*.
10. *GOST* (State Standard) *14618.2–78: Determination of Ketones and Some Substituted Aldehydes*.
11. *GOST* (State Standard) *5478–90: Vegetable Oils and Natural Fatty Acids: Method for Determination of the Saponification Number*.
12. Lishtvan, I.I., Dolidovich, E.F., and Sheremet, L.S., *Khim. Tverd. Topl.*, 1994, nos. 4–5, pp. 5–8.
13. Oganesyan, E.T., *Khim. Prirodn. Soedin.*, 1980, no. 5, pp. 647–651.
14. Piottukh-Peletskii, V.N., Chmutina, K.S., and Korolevich, M.V., *Zh. Strukt. Khim.*, 2003, vol. 44, no. 5, pp. 835–842.
15. Piottukh-Peletskii, V.N., Derendyaev, B.G., and Bogdanova, T.F., *Zh. Strukt. Khim.*, 1997, vol. 38, no. 1, pp. 155–166.
16. Lazurevskii, G.V., Terent'eva, I.V., and Shamshurin, A.A., *Prakticheskie raboty po khimii prirodnykh soedinenii* (Manual on Chemistry of Natural Compounds), Moscow: Vysshaya Shkola, 1961.

Russian Journal of Applied Chemistry, Vol. 78, No. 8, 2005, pp. 1370–1372. Translated from Zhurnal Prikladnoi Khimii, Vol. 78, No. 8, 2005, pp. 1395–1397.
Original Russian Text Copyright © 2005 by Yurkinskii, Firsova, Petrova.

BRIEF COMMUNICATIONS

Complexation of Lead(II) Ions with Hydroxide Ions in Nitrate-Chloride Solutions

V. P. Yurkinskii, E. G. Firsova, and N. V. Petrova

St. Petersburg State Polytechnical University, St. Petersburg, Russia

Received April 19, 2005

Abstract—Complexation of lead(II) ions with hydroxide ions in nitrate-chloride solutions at 298 K was studied using potentiometric titration.

The search for the optimal composition of the alkaline electrolyte is an important technological task in processing of scrap lead accumulators with an active paste containing lead(II) oxide [1].

The high solubility of PbO in alkaline solutions is known to be due to formation of strong lead(II) hydroxide complexes [2, 3]. The presence of both organic and inorganic admixtures and, in particular, chlorides in alkaline solutions strongly affects the complexation of lead(II) ions [1–5]. For example, it was found in [4] that mixed lead(II) hydroxidechloride complexes are formed at low alkali concentrations (<0.4 M) in a solution containing a mixture of sodium chloride and hydroxide.

Proceeding with the studies [4, 5], we examined the complexation of Pb(II) in mixed nitrate-chloride solutions containing sodium hydroxide as an additive in order to analyze the effect of the concentration of chloride ions on the formation of lead hydroxide complexes and, if possible, to determine the composition of mixed chloride-hydroxide complexes.

EXPERIMENTAL

The complexation of lead(II) ions was studied by potentiometric titration at 298 K. The experimental technique and the electrochemical cell have been described earlier [4, 5].

We used as a supporting electrolyte aqueous solutions containing a mixture of sodium nitrate (0.3–1.0 M) and sodium chloride (0–0.7 M) with concentrations that allowed us to obtain a solution with an ionic strength equal to unity (in the limiting case, no sodium chloride was present, and the nitrate concentration was 1.0 M).

The potentiometric titration was carried out with a sodium hydroxide solution containing sodium chloride, the concentrations of NaOH and NaCl being equal to the concentrations of $NaNO_3$ and NaCl, respectively, in the supporting electrolyte. This allowed us to maintain a constant ionic strength in a solution under study during all the experiments.

The half-cell of the electrochemical cell under study can be represented as:

$$-\mathrm{Pb(Hg)}\,|\,\mathrm{Pb(NO_3)_2},\ \mathrm{NaNO_3},\ \mathrm{NaOH},\ \mathrm{NaCl}, \qquad (1)$$

where Pb(Hg) is a lead amalgam electrode.

A typical dependence of the potential of the amalgam electrode on the logarithm of the alkali concentration in solutions containing sodium chloride is shown in Fig. 1. It can be seen that the E–$\ln c_{OH^-}$

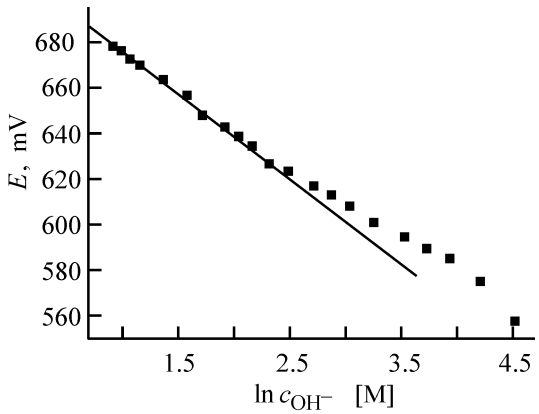


Fig. 1. Potential of the indicator electrode, E, vs. the logarithm of the total concentration of hydroxide ions $\ln c_{OH^-}$ in solution. Supporting electrolyte (M): 0.7 $NaNO_3$ + 0.3NaC1 + $1 \times 10^{-3}Pb(NO_3)_2$. ($c_{OH^-}$) Total concentration of hydroxide ions.

1070-4272/05/7808-1370 © 2005 Pleiades Publishing, Inc.

dependence deviates from linearity at low NaOH concentrations (0.05–0.25 M). The run of the curve is virtually independent of the sodium chloride content (0.1–0.7 M) in the solution. The range of NaOH concentrations at which the E–$\ln c_{OH^-}$ dependence is linear is shifted to higher concentrations of hydroxide ions as the concentration of chloride ions increases. In a solution containing only sodium chloride, a linear dependence is observed at NaOH concentrations $c \geq 0.4$ M [4].

It was found that such a run of the dependence under study can be accounted for by the low solubility of lead hydroxide in these solutions. At low sodium hydroxide concentrations, a $Pb(OH)_2$ precipitate appeared in solution. Its solubility in the aqueous solution is 1×10^{-4} wt % at 298 K [6] and, obviously, decreases when sodium chloride is added to the solution. The appearance of a lead hydroxide precipitate in the solution changes the concentration of potential-determining Pb(II) ions and leads to deviation of the E–$\ln c_{OH^-}$ curves from linearity. However, the solubility of $Pb(OH)_2$ increases with the concentration of NaOH and the E–$\ln c_{OH^-}$ dependence becomes linear.

It was noted in [3, 4] that mixed lead(II) chloride-hydroxide complexes can exist at low NaOH concentrations. Unfortunately, the presence of a $Pb(OH)_2$ precipitate in solution gave no way of determining their composition in the present study.

Lead(II) hydroxide complexes are formed at alkali concentrations for which the E–$\ln c_{OH^-}$ dependence is linear [4]. We determined the number n of ligands, OH^- ions, involved in Pb(II) complexation from the slope of the linear portion. The average number $\bar{n}$ is 2.96 ± 0.03. Therefore, lead(II) hydroxide complexes with coordination numbers 2 and 3 are present in a solution with a sodium hydroxide concentration $c >$ 0.05–0.4 M (depending on the concentration of sodium chloride), with the coordination number 3 predominating. Data for nitrate-chloride solutions, obtained in this study, are in a satisfactory agreement with the results of the earlier studies of individual nitrate and chloride solutions [4].

Thus, the joint presence of competitive ligands (hydroxide and chloride ions) in solution does not affect noticeably the composition of the forming lead(II) hydroxide complexes.

The stability constants of lead(II) hydroxide complexes, β_2 and β_3, were calculated using our experimental data (Fig. 1) and a standard software package by Eq. (2) [7, 8].

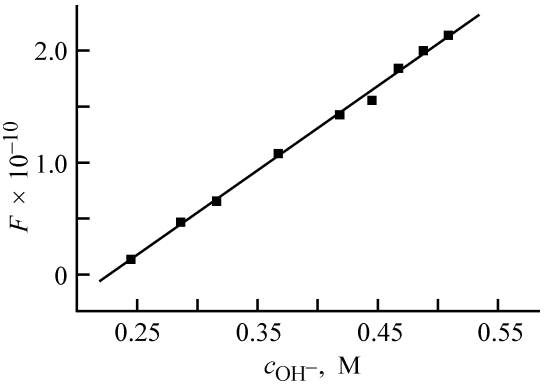


Fig. 2. Function $F = (\Phi - 1)/[OH^-]^2$ vs. the concentration of free hydroxide ions c_{OH^-}. Supporting electrolyte (M): $0.5NaNO_3 + 0.5NaCl + 1 \times 10^{-3}Pb(NO_3)_2$.

$$\Delta E = \frac{RT}{zF} \ln \frac{c^0_{Pb^{2+}}}{[Pb^{2+}]} = \frac{RT}{zF} \ln \Phi. \quad (2)$$

Here ΔE is the difference of the potentials of the amalgam electrode in the supporting electrolyte and in solutions with addition of a solution containing hydroxide ions; $c^0_{Pb^{2+}}$, total concentration of lead ions in solution (M); $[Pb^{2+}]$, concentration of free lead ions (M); Φ, function describing the degree of complexation of lead ions; and β_1, β_2, and β_3, stability constants of lead(II) hydroxide complexes containing one, two, or three hydroxide groups, respectively.

$$\Phi = 1 + \beta_1[OH^-] + \beta_2[OH^-]^2 + \beta_3[OH^-]^3. \quad (3)$$

We found that the constant β_1 in the system under consideration is virtually zero, in agreement with the data of [2–4].

Using the data of Fig. 1 and Eq. (2), we calculated values of the function Φ and analyzed the dependence of the type

$$(\Phi - 1)/[OH^-]^2 = f[OH^-]. \quad (4)$$

We determined constants β_2 and β_3 from this dependence (Fig. 2) with account of Eq. (3). The values of β_2 appeared to be one-and-a-half to two orders of magnitude lower than those of β_3. Introduction of sodium chloride into the solution leads to a noticeable decrease in the degree of complexation of lead(II) ions and, hence, in the values of the stability constants β_2 and β_3 of hydroxide complexes. The dependence of β_3 on the content of sodium chloride in solution

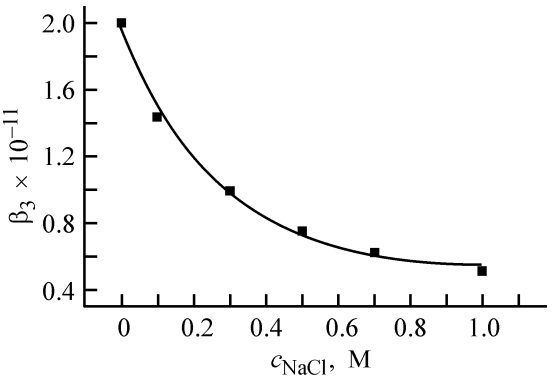


Fig. 3. Stability constant β_3 of a lead(II) hydroxide complex vs. the concentration c_{NaCl} of sodium chloride in solution.

is shown in Fig. 3. It can be seen that this constant noticeably decreases as the concentration of sodium chloride in solution grows. A similar dependence is also observed for the constant β_2. The results of the present study are in a reasonable agreement with the data [4] for individual sodium nitrate and chloride solutions.

CONCLUSIONS

(1) It was shown that a mixture of lead(II) hydroxide complexes, with a strong predominance of $Pb(OH)_3^-$ complexes, is formed in mixed nitrate-chloride solutions with addition of sodium hydroxide at NaOH concentration exceeding 0.05–0.4 M (depending on the content of sodium chloride in these solutions).

(2) It was found that the degree of complexation of lead(II) ions and, hence, the stability constants β_2 and β_3 steadily decrease as the concentration of sodium chloride in solution grows.

REFERENCES

1. Morachevskii, A.G., Vaisgant, Z.I., and Demidov, A.I., *Pererabotka vtorichnogo svintsovogo syr'ya* (Processing of Secondary Lead), St. Petersburg: Khimiya, 1993.
2. Carell, B. and Olin, A., *Acta Chem. Scand.*, 1960, vol. 14, no. 9, pp. 1999–2008.
3. Schorsch, G. and Ingri, N., *Acta Chem. Scand.*, 1967, vol. 21, no. 10, pp. 2727–2735.
4. Yurkinskii, V.P. and Sokolova, N.V., *Zh. Prikl. Khim.*, 1999, vol. 72, no. 10, pp. 1592–1595.
5. Yurkinskii, V.P. and Sokolova, N.V., *Zh. Prikl. Khim.*, 1999, vol. 72, no. 11, pp. 1917–1919.
6. Kirgintsev, A.N., Trushnikova, L.N., and Lavrent'eva, V.G., *Rastvorimost' neorganicheskikh veshchestv v vode* (Solubility of Inorganic Substances in Water), Leningrad: Khimiya, 1972.
7. Kravtsov, V.I., *Ravnovesie i kinetika elektrodnykh reaktsii kompleksov metallov* (Equilibrium and Kinetics of Electrode Reactions of Metal Complexes), Leningrad: Khimiya, 1985.
8. Vasil'ev, V.P., *Termodinamicheskie svoistva rastvorov elektrolitov* (Thermodynamic Properties of Electrolyte Solutions), Moscow: Vysshaya Shkola, 1982.

Russian Journal of Applied Chemistry, Vol. 78, No. 8, 2005, pp. 1373–1375. Translated from Zhurnal Prikladnoi Khimii, Vol. 78, No. 8, 2005, pp. 1398–1399.
Original Russian Text Copyright © 2005 by Titova, Nikol'skaya, Buyanov, Pudova.

BRIEF COMMUNICATIONS

Solubility and Stability of Peroxosolvates $Na_4P_2O_7 \cdot 3H_2O_2$ and $Na_2HPO_4 \cdot H_2O_2$ in Polyatomic Alcohols, Glycerol and Ethylene Glycol, and in Water–Alcohol Mixtures

K. B. Titova, V. P. Nikol'skaya, V. V. Buyanov, and O. B. Pudova

Institute for Problems of Chemical Physics, Russian Academy of Sciences, Chernogolovka, Moscow oblast, Russia

State Research Institute of Biological Instrument Making, Federal Russian Unitary Enterprise, Moscow, Russia

Received May 14, 2004

Abstract—Solubility and stability of peroxosolvates of sodium phosphates in polyatomic alcohols (glycerol and ethylene glycol) and in water–alcohol mixtures, as well as their applicability in development of disinfectants, were studied.

Salts of inorganic acids solvated by hydrogen peroxide show bactericidal activity. A series of disinfectants with a wide-range antimicrobial action have been created on the basis of potassium fluoride peroxosolvates $KF \cdot nH_2O_2$, n = 1, 1.5 [1, 2]. Use of viscous organic liquids, in addition to water, to produce such chemicals expands the opportunities for their application in disinfection. In a slow evaporation of the solvent, a viscous organic medium creates a reserve of hydrogen peroxide, from which it gradually diffuses to a surface being treated. This leads to a prolonged contact of the disinfectant with the object under treatment and improves the disinfection efficiency. It was found in [3] that KF peroxosolvates and disinfectants created on their basis are rather well soluble and stable in polyatomic alcohols (glycerol and ethylene glycol), and also in water–alcohol mixtures.

In this study, we examined the solubility and stability of peroxosolvates of sodium phosphates in the above-mentioned solvents. According to the data of [1], peroxosolvates of phosphates surpass peroxosolvates of potassium fluoride in bactericidal activity.

EXPERIMENTAL

Peroxosolvates of sodium diphosphate and hydrophosphate were synthesized by the reactions of their hydrates (of chemically pure grade) with hydrogen peroxide solutions of a concentration 47 wt %. Water and the excess of H_2O_2 were removed with a flow of air heated to 40–50°C over a solution placed in a polymeric pan. The content of H_2O_2 in the products obtained and in the saturated solutions prepared was determined by permanganatometric titration:

Found, %: H_2O_2 27.7.
$Na_4P_2O_7 \cdot 3H_2O_2$.
Calculated, %: H_2O_2 27.73.

Found, %: H_2O_2 32.3.
$Na_2HPO_4 \cdot 2H_2O_2$.
Calculated, %: H_2O_2 32.40.

Found, %: H_2O_2 19.0.
$Na_2HPO_4 \cdot H_2O_2$.
Calculated, %: H_2O_2 19.32.

It was found in the course of synthesis that sodium hydrophosphate yields, upon a prolonged drying, a stable monoperoxosolvate in addition to the previously obtained diperoxosolvate [4].

Solvents of chemically pure grade, glycerol and ethylene glycol, were used without additional purification and dehydration. Saturated solutions were pre-

1070-4272/05/7808-1373 © 2005 Pleiades Publishing, Inc.

Table 1. Solubility and stability of $Na_4P_2O_7 \cdot 3H_2O_2$ in polyatomic alcohols (glycerol and ethylene glycol) and in mixed alcohol–water solvents

Alcohol content, wt %	Solubility, wt % of H_2O_2	Storage time, days	Loss of H_2O_2, % day^{-1}	$k \times 10^4$, day^{-1}
Glycerol–water				
100	2.16	66	0.52 ± 0.23	2.5 ± 1.2
90	3.26	62	0.33 ± 0.13	1.4 ± 0.6
80	3.75	62	0.70 ± 0.03	3.4 ± 0.2
70	5.04	33	2.2 ± 0.8	10.9 ± 3.5
Ethylene glycol–water				
100	3.05	60	0.23 ± 0.04*	1.0 ± 0.4
90	4.22	66	0.10 ± 0.02*	0.4 ± 0.1
80	4.55	57	0.16 ± 0.06*	0.6 ± 0.4
70	5.97	51	0.49 ± 0.16*	2.4 ± 0.9

* Solutions do not lose H_2O_2 in the first 20–30 days; the figures above refer to subsequent storage.

Table 2. Solubility and stability of $Na_2HPO_4 \cdot H_2O_2$ in polyatomic alcohols (glycerol and ethylene glycol) and in mixed alcohol–water solvents

Alcohol content, wt %	Solubility, wt % of H_2O_2	Storage time, days	Loss of H_2O_2, % day^{-1}	$k \times 10^4$, day^{-1}
Glycerol–water				
100	2.02	20	3.69 ± 1.38	2.1 ± 0.6
90	2.13	24	1.30 ± 0.47	0.6 ± 0.1
80	3.28	24	2.54 ± 0.63	1.2 ± 0.2
70	4.77	26	3.09 ± 0.58	1.7 ± 0.1
Ethylene glycol–water				
100	1.19	24	2.33 ± 0.29	1.2 ± 0.2
90	1.72	48	1.10 ± 0.34	0.4 ± 0.2
80	3.17	48	2.24 ± 0.34	1.4 ± 0.1
70	4.64	48	1.09 ± 0.12	0.5 ± 0.0

pared as described in [3] at 20°C and kept in closed polymeric reservoirs. The solutions were analyzed at intervals of 3–5 days. The decomposition rate constants were calculated by the equation $c_0/c = k(\tau - \tau_0)$.

The solubility of peroxosolvates of the sodium phosphates under study in glycerol and water–glycerol mixtures, as well as in ethylene glycol and its mixtures with water, is much lower than that of KF peroxosolvates in the same media. A saturated solution of $KF \cdot H_2O_2$ in a solvent composed of 85 wt % glycerol and 15 wt % water contains 9.06 wt % H_2O_2, whereas the content of H_2O_2 in a saturated solution of $Na_4P_2O_7 \cdot 3H_2O_2$ in a solvent composed of 90 wt % glycerol and 10 wt % water is 3.26 wt % (Table 1). A saturated solution of $Na_2HPO_4 \cdot H_2O_2$ in the same solvent (Table 2) contains 2.13 wt % H_2O_2. As the content of water in a solvent increases, the solubility of peroxosolvates of phosphates grows, as it occurs in all the previously studied systems.

The solutions are sufficiently stable. In the system $Na_4P_2O_7 \cdot 3H_2O_2$, the average loss of H_2O_2 in 30–60 days is 0.5–2.1 % day^{-1} relative to its initial content (Table 1).

In the systems constituted by $Na_4P_2O_7 \cdot 3H_2O_2$, ethylene glycol, and water, no loss of H_2O_2 is observed within the first 20–30 days. Then, a slow H_2O_2 decomposition (0.1–0.5) begins. The stability of $Na_2HPO_4 \cdot H_2O_2$ in the systems constituted by an alcohol and water is noticeably lower, and the loss of H_2O_2 is 1.3–3.7 and 1.1–2.4 % day^{-1} for glycerol and ethylene glycol, respectively.

Diperoxosolvate $Na_2HPO_4 \cdot 2H_2O_2$ is unstable in glycerol and in water–glycerol mixtures. The content of H_2O_2 decreases to almost zero already during preparation of saturated solutions. Hydrogen peroxide completely decomposes within 2–3 days in dissolution of $Na_2HPO_4 \cdot H_2O_2$ in ethylene glycol–water mixtures initially containing 1–2 wt % H_2O_2.

Water–alcohol solutions of $Na_4P_2O_7 \cdot 3H_2O_2$ seem to be promising for application in disinfection. Solutions of this kind can be used both under normal conditions and at low temperatures.

CONCLUSION

The solubility of peroxosolvates of sodium phosphates in polyatomic alcohols (glycerol and ethylene glycol) at 20°C is 2.16 wt % H_2O_2 for $Na_4P_2O_7 \cdot 3H_2O_2$ and 3.05 wt % for $Na_2HPO_4 \cdot H_2O_2$. The solubility of the solvates in water–alcohol systems increases, to become a factor of 2–4 higher for solvents with a water content of 30 wt %. The solutions are stable. The average rate of decomposition of sodium peroxosolvate diphosphate in a water–glycerol mixture is 0.3–2.1 % day^{-1}, whereas solutions in water–ethylene glycol solvents are completely stable within 20–30 days, after which the decomposition rate is 0.1–0.5 % day^{-1}. For monoperoxosolvate of sodium hydrophosphate, these values are 1.3–3.4 and 1.0–2.4 % day^{-1}, respectively.

REFERENCES

1. Titova, K.V., Nikol'skaya, V.P., and Buyanov, V.V., *Koordinatsionnye soedineniya peroksida vodoroda: Sintez, stroenie, svoistva, sporotsidnaya aktivnost', tekhnologiya i proizvodstvo dezinfitsiruyushchikh preparatov* (Coordination Compounds of Hydrogen Peroxide: Synthesis, Structure, Properties, Antispore Activity, Technology, and Manufacture of Disinfectants), Chernogolovka: Inst. Probl. Khim. Fiz. Ross. Akad. Nauk, 2000.
2. Buyanov, V.V., Nikol'skaya, V.P., Pudova, O.B., *et al.*, *Peroksosol'vaty v dezinfectologii* (Peroxosolvates in Disinfection Technology), Chernogolovka: Inst. Probl. Khim. Fiz. Ross. Akad. Nauk, 2000.
3. Titova, K.V., Nikol'skaya, V.P., Buyanov, V.V., *et al.*, *Zh. Prikl. Khim.*, 2004, vol. 77, no. 3, pp. 409–413.
4. Titova, K.V., Kolmakova, E.I., and Gelyuk, I.P., *Zh. Neorg. Khim.*, 1994, vol. 39, no. 5, pp. 754–756.

Russian Journal of Applied Chemistry, Vol. 78, No. 8, 2005, pp. 1376–1378. Translated from Zhurnal Prikladnoi Khimii, Vol. 78, No. 8, 2005, pp. 1400–1402.
Original Russian Text Copyright © 2005 by Gaikalova, D'yakonov.

BRIEF COMMUNICATIONS

Use of Polymeric Coatings for Conservation of Archival and Historically Valuable Documentary Photographs

E. S. Gaikalova and A. N. D'yakonov

St. Petersburg State University of Cinematography and Television, St. Petersburg, Russia

Received December 9, 2004; in final form, June 2005

Abstract—The possibility of conservation of archival and historically valuable documentary photographs with polymeric coatings was substantiated. Coatings obtained from aqueous dispersions of polymers were considered. A dependence of the shelf life of the material on the coating thickness was established.

Conservation of documentary photographs is an important task of state archives. The main goal of a set of procedures for preservation of documents in storage is to slow down the process of aging and protect documents from the action of detrimental factors.

Of particular importance in preservation of the whole set of properties of a photographic system are a number of factors associated with the storage conditions and influence of atmospheric gases. In recent years, work has been conducted on development of digital technologies, which enabled restoration of many documents via their digitalization. This made it possible to significantly accelerate the restoration process, to lower its cost, and to solve the problem of transportation and storage of replicas. However, in the opinion of experts in restoration, digital technologies actually hinder true restoration of original documents, many of which are of historical and artistic value [1].

Chemical methods for restoration of documentary photographs may cause loss of image or impair the quality of the original image. For example, the method of autoradiography inevitably leads to a complete loss of the original [2]. Therefore, a copy is made before chemical treatment of a document, which makes it possible to retain the image, but not the document itself, which frequently is more valuable than the image.

The most important factor that affects the preservation of a photographic material is electromagnetic radiation in the ultraviolet and visible spectral ranges. Among other factors affecting the stability of photographs are temperature, humidity, and atmospheric contaminants. The presence of moisture catalyzes all undesirable chemical and biological processes. A relative humidity of more than 60% leads to fungal damage [3].

However, it was noticed as far back as 1888 [4] that the action of light is rarely the reason, by itself, for photochemical changes in materials of artistic and historical value. In most cases, decoloration occurs with active involvement of atmospheric oxygen and water vapor, which accelerate the process.

Analysis of the literature shows that the problem of preservation of documentary photographs can be solved in a simpler way by protection, rather than by restoration. The exceedingly high historical and artistic value of documentary photographs and motion pictures created during the years of development of photography and cinematography has been noted all over the world. However, the unsatisfactory storage conditions have been the reason for loss of, or damage to, numerous documents. Therefore, the more important is the work on preservation of the existing documentary photographs and motion pictures, of both color and white-and-black types.

The world's experience in storage of photographic materials is based on construction of depositories in which the materials are kept in the dark at the optimal temperatures under conditions of controlled humidity. Air is purified to the maximum possible extent to remove noxious impurities, and particularly valuable exhibits are stored in the atmosphere of an inert gas. However, invaluable historical-and-artistic articles are concentrated in museums, state institutions, architectural monuments, libraries, and private collections,

1070-4272/05/7808-1376 © 2005 Pleiades Publishing, Inc.

where the optimal storage conditions cannot be created in all cases. This huge wealth is also subject to aging, but, at present, there is no evidence concerning the preservation of documents stored outside specialized depositories.

Despite the large body of the accumulated factual material on use of polymers in the restoration practice [5], there is only limited evidence concerning the influence of polymers on the entire set of properties of a photographic material and on preservation of images. This makes studies of the conservation of documentary photographs by deposition of polymeric coatings a matter of current interest.

The most promising materials for this study are aqueous dispersions of polymers. As the liquid aggregative state of systems of this kind is provided by use of water as a dispersion medium, these systems have a number of advantages over solutions of synthetic resins.

Aqueous polymer dispersions with a high concentration (50%) have the minimum viscosity, whereas polymer solutions with such a concentration cannot be obtained at all [6]. Because of their low viscosity, they have a high penetrating power, dependent of the size of dispersion particles. The low surface tension of water, favors strong wetting of any surface by these dispersions [7].

Aqueous polymer dispersions are more technologically effective. Coatings of synthetic caoutchoucs have a number of advantages over other kinds of chemically stable coatings. They not only sustain prolonged action of various chemical media (solutions of acids, alkalis, salts), but also better withstand abrasive wear [8].

Taking into account the preservative nature of latexes and their availability, nontoxicity, convenience of use, transparency, and resistance to external action, latexes can be recommended for use in a study of the influence exerted by polymeric coatings on the efficiency of preservation, photographic properties, and aging of photographic materials. Polymer materials, of which aqueous polymer dispersions seem to be the most promising, are widely used in restoration practice.

Thus, the advantages of water-based polymeric films and coatings are determined by the technological effectiveness and ecological safety of their formation. The most promising are latex coatings deposited from high-concentration, low-viscosity systems at room temperature.

Variation of the optical density of a white sample of color photographic paper relative to the initial value under prolonged (450 h) UV irradiation with a wavelength λ = 254 nm

Dilution	Copolymer				
	S–BA			BA–MMA	S–B
5	0.88	1.00	0.88	0.80	0.63
10	1.55	1.55	1.55	1.55	1.55
15	1.77	1.66	1.77	1.88	1.77
20	2.11	2.37	2.57	2.22	2.22

For effective use of this class of compounds as preservative agents for photographic materials, it is necessary to reveal the influence of these substances on the physicochemical and service characteristics of the materials and to examine their influence on the process of image preservation.

Latex coatings are commonly prepared from dispersions of the following types: copolymers of acrylates, homo- and copolymers of vinyl acetate, and copolymers of styrene with butadiene. One of the main properties determining the choice of latexes as preservative agents for photographic materials is the nearly 100% transparency of latex coatings.

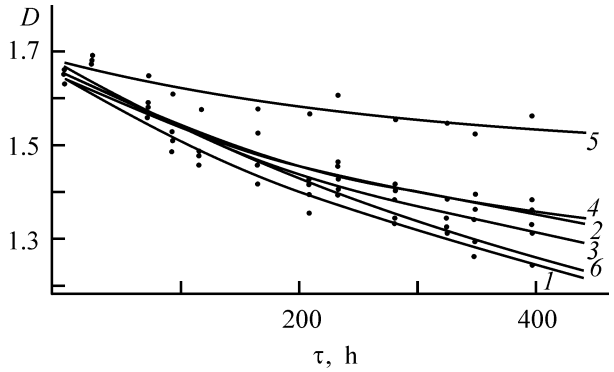
The following latex formulations were chosen for the study: copolymers of butyl acrylate (BA) and methyl methacrylate (MMA); styrene (S) and BA; and S and butadiene (B).

The formation conditions of a latex film coating may strongly affect the physicomechanical properties of a polymer: for example, it is important to select the optimal thickness of the coating obtained. The coating thickness can be controlled both by diluting the initial latex dispersion or by depositing several latex layers on a dried surface.

The table illustrates the influence exerted by the layer thickness on the variation of the optical density in prolonged storage of a white sample of color photographic paper.

The conclusion that raising the layer thickness makes the variation of the optical density in prolonged storage considerably narrower is confirmed by data obtained by coating a material with several layers of a 20-fold diluted latex.

The influence exerted by preservative polymeric coatings based on various latexes on the image stability was revealed by carrying out the experiment under severe conditions, with densitometric monitoring.



Effect of a preservative coating on the process of image aging in a paper-based positive material under UV irradiation at a wavelength λ = 254 nm. (*D*) Optical density and (τ) time. Copolymer: (*1*–*3*) styrene–butyl acrylate, (*4*) butyl acrylate–methyl methacrylate, (*5*) styrene–butadiene, and (*6*) control sample.

According to the data obtained (see figure), the smallest decrease in optical density *D* is observed for samples coated with a latex composed of copolymers of butadiene and styrene. This can be accounted for by the fact that the absorption spectra of both butadiene and styrene lie in the range 240–290 nm. For butadiene, this is due to the presence of various chromophore groups in the polymer chains [9]. For styrene, the absorption is due to a transition of the benzoic ring to the singlet state under the action of photons [10]. The mechanism of photooxidation of copolymers of butadiene and styrene is determined by a set of processes occurring in irradiation of polystyrene and butadiene. Thus, the copolymers readily absorb light with wavelengths of up to 350 nm, with the absorption rate proportional to the light intensity [11].

By contrast, polymethyl methacrylate exceedingly weakly absorbs light in the UV spectral range, and, consequently, incident light can penetrate deep into a polymer sample [12]. This makes polymethyl methacrylate highly resistant to the action of light, which indicates that the coatings themselves, rather that the surface protected by these coatings, is stable at a rather small coating thickness.

CONCLUSION

Use of polymeric coatings deposited from aqueous-dispersion systems can strongly affect the shelf life of a photographic material. With account of the ability of latexes to have low viscosity at high concentrations, the optimal coating thickness can be controlled by varying the initial concentration of latexes.

REFERENCES

1. Zone, R., *Am. Cinematographer*, 2001, vol. 82, no. 1, pp. 171–174.
2. Blyumberg, M.I., *Zh. Nauchn. Prikl. Fotogr. Kinematogr.*, 1993, vol. 38, no. 3, pp. 35–38.
3. *Obespechenie fiziko-khimicheskoi sokhrannosti kinofotodokumentov i mikrofil'mov* (Physicochemical Preservation of Documentary Photographs and Motion Pictures and Microfilms), Krestovskaya, K.V. and Mikhailov, O.L., Eds., Moscow: NIItsentr Tekhn. Dokumentats. SSSR, 1981.
4. Bril, T., *Svet: Vozdeistvie na proizvedeniya iskusstva* (Light: Effect on Works of Art), Moscow: Mir, 1983.
5. Ivanova, A.V., *Restavratsiya, issledovanie i khranenie muzeinykh khudozhestvennykh tsennostei* (Restoration, Study, and Storage of Museum Works of Art), Moscow: Bibl. Iskusstv, 1983.
6. Erkova, L.N., *Lateksy* (Latexes), Leningrad: Khimiya, 1983.
7. Eliseeva, V.I. and Sharkova, N.G., *Novye lateksnye plenkoobrazovateli* (New Latexs Film-forming Agents), Moscow: Mir, 1967, pp. 65–66.
8. Filipp, G.I., *Korroziya i zashchita ot korrozii v khimicheskoi promyshlennosti* (Corrosion and Corrosion Protection in Chemical Industry), Moscow: Nauka, 1983, pp. 42–48.
9. Morand, J.L., *Rubltr Chim. Technol.*, 1972, vol. 45, pp. 481–485.
10. Loux, G. and Weil, G.I., *Chim. Phys.*, 1964, vol. 61, pp. 484–487.
11. Ranby, B.J. and Rabek, J.F., *Photodegradation, Photooxidation, and Photostabilization of Polymers*, London: Wiley, 1975. Translated under the title *Fotodestruktsiya, fotookislenie, fotostabilizatsiya polimerov*, Moscow: Mir, 1978.
12. Gol'denberg, V.I. and Shlyapintokh, V.Ya., *Vysokomolek. Soedin.*, 1969, no. 11, pp. 13–19.

Russian Journal of Applied Chemistry, Vol. 78, No. 8, 2005, pp. 1379–1381. Translated from Zhurnal Prikladnoi Khimii, Vol. 78, No. 8, 2005, pp. 1403–1405.
Original Russian Text Copyright © 2005 by Morachevskii.

Ivan Ivanovich Andreev (To 125th Anniversary of His Birthday)

An engineer-technologist Ivan Ivanovich Andreev went down in the history of domestic chemistry and chemical technology owing to his vigorous activities in the organization of the nitrogen and other important industries during World War I (1914–1918), a hard time for Russia.

Andreev was born on July 20, 1880, in the town of Belozersk, an uezd center in Novgorod Province (now district center in Vologda oblast) into a wealthy landowners' family. He received his primary education at home and then studied at Novgorod gymnasium, which he finished with a gold medal. Having early lost his parents, Andreev was distinguished by self-dependence and sense of duty during his entire, unfortunately very short, life. In 1899, he entered the natural department of the physicomathematical faculty of St. Petersburg University, but, after seven semesters, left Russia for political reasons without completing his studies. He continued his education at the Polytechnic Institute (Higher Technical School) in Karlsruhe, Germany, wherefrom he graduated as an engineer-technologist-electrochemist. Having become a certified engineer, Andreev did not consider his education complete. According to the scarce available biographic evidence, he was engaged in 1906–1908 in research work at the laboratory of physical chemistry (St. Petersburg Polytechnic Institute), headed by professor V.A. Kistyakovskii (1865–1952, academician of the Academy of Sciences of the USSR since 1929) and at Leipzig University in Germany. For his study "Growth Rate and Dissolution of Crystals," published both in Germany (1907) and in Russia (1908), Andreev received from the Polytechnic Institute in Karlsruhe the degree of a doctor-engineer. To extend his knowledge in the field of mathematics and physics, Andreev passed a state graduation examination at the physicomathematical faculty of St. Petersburg University. In this way, the young scientist received a very good theoretical and engineering training.

In 1908, Andreev became a laboratory assistant at the chair of technology and merchandising at St. Petersburg Polytechnic Institute. During the time free from his basic duties, he commenced a set of investigations of the chemical action of ultraviolet light. The first results were published in *Izvestiya Sankt-Peterburgskogo politekhnicheskogo institute* (Transactions of St. Petersburg Polytechnic Institute) in 1911 and 1914. As noted by B.V. Byzov (1880–1934) in Andreev's obituary [1], the scientist was deeply interested in the influence exerted by ultraviolet light on chemical processes; the results of his studies in this field were published only in part and largely remained in the form of manuscripts.



In 1912, Andreev passed his master's examination at St. Petersburg University. In the same year, he took part in studies aimed to synthesize caoutchouc. The preliminary results obtained and the possible ways to solve this most important problem were analyzed by Andreev in the monograph *Sinteticheskii kauchuk* (Synthetic Caoutchouc, 1914).

In 1913, the scientist was sent to a business trip abroad to be prepared for professorship. He spent most time at the Polytechnic Institute in Zurich (Switzerland) and continued there his studies concerned with the chemical action of ultraviolet light

1070-4272/05/7808-1379 © 2005 Pleiades Publishing, Inc.

and with dissolution of gold and silver in potassium cyanide solutions. However, Andreev's dream to head a chemical chair at a higher school institution in Russia remained unfulfilled. In view of the beginning of World War I, the Central scientific and engineering laboratory was created by the Military ministry and Andreev headed its department of inorganic chemistry [2]. In 1914–1918, he took most active part in solution of extremely important defense-related problems, the central of which was the development of an industrial technology for manufacture of nitric acid [3–5].

In the early XIX century (1809), an exceedingly rich deposit of saltpeter $NaNO_3$ was discovered in Chile. In more than a hundred of years that followed, the Chilean saltpeter became the main source of fixed nitrogen all over the world. Ammonia was obtained in very small amounts as a by-product in coal coking. The manufacture of nitric acid in Russia was based solely on Chilean saltpeter, which was imported duty free. Saltpeter was also used as a nitrogen fertilizer. In 1900–1914, the import of saltpeter in Russia increased from 14.7 to 53.9 thousand tons. The war between Russia and Japan led to an increase in manufacture of nitric acid for production of explosives. The agrarian reforms carried out in Russia, beginning in 1906, also made higher the consumption of nitrogen fertilizers. It was necessary to have Russia's own sources of fixed nitrogen. It was also necessary to take into account that the whole amount of Chilean saltpeter was imported across the western boundary and via Baltic ports. It would be expected that, in case of military operations in this region, the import of saltpeter could be completely terminated, which would cut-off primarily the military industry from an exceedingly important source of raw materials.

Already in December 1905, a rather representative interdepartmental Commission for Manufacture of Nitric Acid by Oxidation of Atmospheric Nitrogen was created at the Main engineering directorate of the Military ministry [6, 7]. The organization of the Commission was initiated by professor A.I. Gorbov (1859–1939), a broadly educated chemist, A.M. Butlerov's pupil, and close friend of D.I. Mendeleev. Gorbov became the secretary of the Commission. Gorbov and professor V.F. Mitkevich (1872–1951, academician of the Academy of Sciences of the USSR since 1929), a specialist in electrical engineering, were charged with a task to consider the possibility of construction in Russia of a plant for oxidation of atmospheric oxygen in an electric-arc furnace. Such a plant existed in Norway, which possessed, already at that time, resources of low-cost hydroelectric power. Despite the successful work of the scientists, this project could not be rapidly carried out in Russia because of the exceedingly high consumption of electric power, which made necessary construction of a hydroelectric power plant [7].

Based on economical calculations, Andreev convincingly demonstrated that the method of ammonia oxidation to give nitric acid is considerably more cost-efficient than the arc method, even though being substantially less studied. Data necessary for designing Russia's first plant for manufacture of nitric acid by oxidation of ammonia were obtained at a laboratory of the Technological Institute in Petrograd and on a pilot installation in Makeevka (Donetsk basin). The plant was designed by engineer N.M. Kulepov, who also supervised its construction and put it in operation. Andreev, the creator of the technology, was actively involved in the designing work and in solution of problems associated with the construction of the plant and putting it in operation. In February 1917, less than a year after its construction was commenced, the plant yielded the first amounts of its product. Gaseous ammonia was delivered in a mixture with air into the catalytic apparatus, in which an alloy of platinum and rhodium served as a catalyst. A single apparatus hourly produced 16 kg of nitric acid (in terms of monohydrate). The daily output was up to 17 tons of nitric acid containing 33 wt % HNO_3. The yield of nitric acid was as high as 93% and more [3, 9, 10].

In addition to production of nitric acid, Andreev was engaged in those same years in studies and tests of gas masks. The main results he obtained were published in *Sbornik materialov po protivogazovym voprosam* (Coll. of Works on Gas Masks; first issue 1917; second issue, 1918). Andreev studied the dynamic activity of carbons toward various poison gases [11]. In particular, he revealed factors determining the dynamic activity of absorbents. The priority in the development of catalysts and universal absorbents based on activated carbons belongs to Andreev, together with N.D. Zelinski (1861–1953, academician of the Academy of Sciences of the USSR since 1929).

Andreev devoted a considerable attention to a search for sources of toluene necessary for manufacture of explosives. His considerations concerning this issue, which are both valuable and constructive, were summarized in the paper "Maikop Oil as a Source of Toluene." The country's demand for fuel forced Andreev to take active part in organization and work of the Sapropel Committee, aimed to study methods for utilization of the silt of our northern lakes. Andreev

constantly taking an active interest in domestic agriculture, its needs, and the possibility of its provision with various kinds of nitrogen fertilizers.

Andreev started his work on some of these problems at the Institute of Applied Chemistry, created in Petrograd in 1919. However, a long severe illness resulted in the scientist's death on December 16, 1919, at the age of only 39. Lieutenant-general V.N. Ipat'ev (1867–1952, academician since 1916), who, in fact, headed the whole military-chemical complex of Russia during World War I, highly appreciated Andreev and the results of his works [2, 12, 13]. During only several war years, Andreev showed himself as an erudite and talented scientist who could implement results of his studies in the industry. The premature death terminated his vigorous and efficient activities.

REFERENCES

1. Byzov, B.V., *Trudy Komissii po svyazannomu azotu VSNKh* (Proc. of the Commission for Fixed Nitrogen of the Supreme Council for National Economy), Petrograd, 1922, issue VII, pp. 7–10.
2. Ipat'ev, V.N., *Trudy Komissii po svyazannomu azotu VSNKh* (Proc. of the Commission for Fixed Nitrogen of the Supreme Council for National Economy), Petrograd, 1922, issue VII, pp. 5–7.
3. Luk'yanov, P.M., *Kratkaya istoriya khimicheskoi promyshlennosti SSSR* (A Brief History of the Chemical Industry of the USSR), Moscow: Akad. Nauk SSSR, 1959.
4. Luk'yanov, P.M., *Trudy Inst. Estestvozn. Tekhn.*, 1958, vol. 18, pp. 385–397.
5. Gamburg, D.Yu., *Usp. Khim.*, 1945, vol. 14, no. 3, pp. 239–252.
6. Sapozhnikov, A.V., *Azotnaya kislota iz vozdukha* (Manufacture of Nitric Acid from Air), St. Petersburg, 1911.
7. Morachevskii, A.G. and Bashenko, V.V., *Zh. Prikl. Khim.*, 2001, vol. 74, no. 1, pp. 169–171.
8. Andreev, I.I., *Trudy Komissii po svyazannomu azotu VSNKh* (Proc. of the Commission for Fixed Nitrogen of the Supreme Council for National Economy), Petrograd, 1922, issue VII, pp. 19–46.
9. Kolosov, A.K., *Kontaktnoe proizvodstvo azotnoi kisloty* (Catalytic Production of Nitric Acid), Petrograd: Nauch. Khim.-Tekhn. Izd., 1923.
10. Kolosov, A.K., in *Materialy po istorii otechestvennoi khimii* (Materials on the History of Domestic Chemistry), Moscow: Akad. Nauk SSSR, 1953, pp. 196–209.
11. Dubinin, M.M., in *Materialy po istorii otechestvennoi khimii* (Materials on the History of Domestic Chemistry), Moscow: Akad. Nauk SSSR, 1953, pp. 163–172.
12. Ipat'ev, V.N., *Rabota khimicheskoi promyshlennosti na oboronu vo vremya voiny* (Work of the Chemical Industry for Defense during the War), Petrograd, 1920.
13. Ipat'ev, V.N., *Khimicheskii komitet pri Glavnom artilleriiskom upravlenii i ego deyatel'nost' dlya razvitiya otechestvennoi khimicheskoi promyshlennosti* (Chemical Committee at the Main Artillery Directorate and Its Activities Aimed To Develop the Domestic Chemical Industry), Petrograd, 1921, part 1.

A. G. Morachevskii

Russian Journal of Applied Chemistry, Vol. 78, No. 8, 2005, p. 1382. Translated from Zhurnal Prikladnoi Khimii, Vol. 78, No. 8, 2005, p. 1406.
Original Russian Text Copyright © 2005 by Morachevskii, Beloglazov.

BOOK REVIEWS

Tsar'kov, V.A., *Opyt raboty zolotoizvlekatel'nykh predpriyatii mira* (Experience of Work of World's Gold-Recovery Plants), Moscow: Ruda I Metally Publ. House, 2004, 112 pp.

The small monograph analyzes the practice of 29 foreign and 14 domestic plants processing gold-bearing ledge ores. Rather valuable is the detailed information about resources of ore at various deposits, its quality, processing techniques, and production scale. The book comprises an introduction, three chapters, conclusion, and a combined list of references for all the chapters.

The brief introduction (pp. 5, 6) notes that the annual world's production of gold is about 3.5 thousand tons, of which more than 70% is recovered by processing of gold-bearing ledge ores. The world's leading countries in gold mining are South Africa, US, and Australia. The gradual depletion of the resources of rich ores and the increasing demand for gold force the gold mining companies all over the world to process lean ores having a complex mineralogical composition and containing noxious admixtures. The book considers modern technologies for recovery of gold from rich and lean ledge ores.

The first chapter (pp. 7–29) describes the general trends in the development of the technology for recovery of gold from ledge ores, discusses ore pretreatment, gravity concentration, flotation dressing, hydrometallurgical processing, cyanidation, and sorption technology. The recovery cost of a gram of gold at different plants depends on the content of gold in ores, conditions of ore occurrence, and technology of ore mining and processing and is commonly within the range 3.4–10 US dollars.

The second chapter (pp. 29–84) discusses the working practice of foreign gold-mining plants processing ledge ores. These plants are distributed among countries as follows: US 7, Canada 4, Indonesia 3, Uzbekistan 3, and Kazakhstan 2. Evidence is given concerning 10 more plants from other countries, but there is no information about such gross gold-mining countries as South Africa and Australia. No comments concerning this issue can be found in the text of the monograph.

For each of the gold-mining plants considered, a brief description of the deposit (type of ore, conditions of occurrence, proven resources, content of gold in the ore), basic technological procedures in processing of raw ore, and scale of gold mining are given. Mostly sorption-cyanide technology with activated carbon is used in ore recovery. For lean ores (with gold content less than 2.5 g per ton of ore) the heap leaching method is employed. Most of the 29 plants described in the second chapter were created at deposits discovered 10–15 years ago.

The third chapter (pp. 85–105) contains similar information about Russia's 14 gold-recovery plants, which are situated in the eastern part of the country, from South Urals to Chukotka.

The conclusion (pp. 106, 107) emphasizes that the basic process for gold recovery from easily dressed ledge ores is cyanidation with subsequent sorption from slurry onto activated carbon or ion-exchange resins. It is noted that 92% of gold is recovered from ores by this process. A steady tendency is revealed toward depletion of the resources of rich easily dressed ores and involvement of lean difficultly dressed ores of complex composition into processing, which makes necessary autoclave oxidation, calcination, or bacterial leaching. The author of the monograph notes that Russia is second in the world in gold resources. At the same time, only 165 tons of gold were produced in 2001 (sixth place in the world), which is largely accounted for by the uncoordinated work of our gold-mining plants. According to the data presented in the monograph, there were 639 gold-mining plants in Russia in 2001, 80% of which produced less than a ton of gold in a year. The recovery of gold at small-scale Russian plants is 75–80%, whereas at larger plants, such as Olimpiadinskaya (Krasnoyarsk krai) or Kubaka (Magadan oblast) the recovery is as high as 92–98%.

V.A. Tsar'kov's monograph gives a summary of data that are of indubitable interest for a wide audience of specialists in chemical metallurgy and for teachers from high-school institutions training specialists in chemical engineering and metallurgy.

A.G. Morachevskii and I.N. Beloglazov

1070-4272/05/7808-1382 © 2005 Pleiades Publishing, Inc.

Russian Journal of Applied Chemistry, Vol. 78, No. 9, 2005, pp. 1383–1385. Translated from Zhurnal Prikladnoi Khimii, Vol. 78, No. 9, 2005, pp. 1409–1411.
Original Russian Text Copyright © 2005 by Karapetyan, Senichenkov, Zenin, Ryabova.

INORGANIC SYNTHESIS AND INDUSTRIAL INORGANIC CHEMISTRY

Kinetics of Dissolution of Glassy Fertilizers

K. G. Karapetyan, V. A. Senichenkov, G. S. Zenin, and M. N. Ryabova

St. Petersburg State Polytechnic University, St. Petersburg, Russia
Northwest State Correspondence Technical University, St. Petersburg, Russia

Received March, 3, 2005

Abstract—Slowly soluble phosphate glasses are a promising material for new environmentally safe fertilizers. The kinetics of the dissolution of phosphate glasses used for the development of fertilizers was studied.

Modern nature management is impossible without application of mineral elements, because ions of potassium, magnesium, calcium, phosphorus, boron, and trace elements are irrevocably withdrawn from soil together with agricultural products. Existing mineral fertilizers have a number of principal drawbacks connected with their crystal structure and constant composition. These fertilizers are easily washed away and weathered from the soil, which gives rise to extreme workloads on soil microorganisms and root systems of plants. Annual world production and application of fertilizers reaching 400 million tons is not only prodigal, but also environmentally dangerous, as no less than 50% of fertilizers goes to subsoil waters and is weathered, causing environmental pollution.

The cardinal way of overcoming these drawbacks is to abandon traditional crystalline fertilizers and to develop essentially new highly effective fertilizers based on glassy amorphous materials. Glass is one of the most promising among these materials because of its favorable physical and chemical properties and feasibility of processing.

In the early 1980s, phosphate glasses were used to develop a new generation of fertilizers [1]. These fertilizers of the prolonged action are based on glassy potassium, magnesium, and calcium metaphosphates doped with microelements. Their preparation was based on long-term experience in the field of development of optical glasses and ion-exchange processes.

As a result of these studies [1, 2], a new type of glassy fertilizers (AVA) was developed; their high efficiency and environmental cleanliness are due to the high-temperature synthesis of phosphate systems, quenching of the structural state of the components in the form assimilable by plants, and their variable composition providing easy adaptation to regions of use, to types of soils, and to the kind of crops.

The rate of dissolution of such glasses depends on their chemical composition. Glass components, K, Ca, and P oxides, are nontoxic. Such glasses provide egress of the required compounds from the glass into the environment. The dissolution of a glass in water is accompanied by a chemical reaction between the glass and water, which results in cleavage of the >P–O–P< bonds and passing of phosphate ions into solution. Metal ions contained in the glass together with P_2O_5 pass simultaneously into the solution at a rate determined by the rate of the glass dissolution. The soluble phosphate glass can be used for delivering fertilizers with a specified intensity and substances for protection of plants.

According to published data [3, 4], the dissolution of phosphate glasses involves several steps: selective passing into a solution (leaching) of cations within the framework of internal diffusion and hydrolytic degradation of the anionic skeleton. However, the most important is the thermodynamically nonequilibrium structure of glasses, so that all the components remain in the cytosoluble state and are accessible to plants, and the glass dissolution is slow, with a constant thickness of the destroyed granule layer.

Various macro- and microelements are necessary for successful vital activity of plants. They are introduced in a balanced proportion and are not subject to selective leaching.

Owing to specific physicochemical properties, the rate of dissolution of a glassy fertilizer granule strongly depends on temperature. For example, at 50°C they are dissolved within 3 months and at 20°C, within 27 months (Fig. 1).

After introducing the fertilizers into a soil, they slowly (within several years) dissolve to release consecutively chemical components feeding plants.

1070-4272/05/7809-1383 © 2005 Pleiades Publishing, Inc.

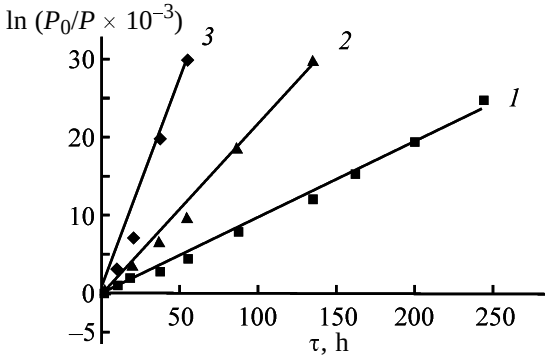


Fig. 1. Kinetics of dissolution of AVA fertilizer. (τ) Time. Temperature, °C: (*1*) 20, (*2*) 30, and (*3*) 50.

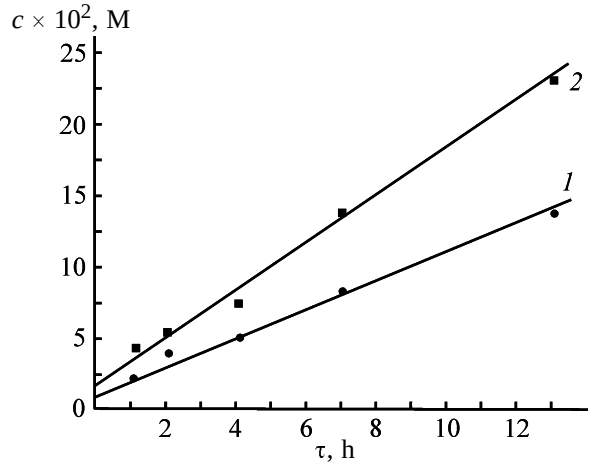


Fig. 2. Concentrations *c* of (*1*) K^+ and (*2*) PO_3^- ions in solution as functions of time τ at 60°C.

The time of dissolution at various temperatures is 90% dependent on the soil moisture content, heterogeneity of the structure of glasses, and the granule size distribution determining the specific surface area.

Successful application of glassy metaphosphate fertilizers has demanded a deeper study of the kinetics of passing of all fertilizer components into solutions. The monitoring of the kinetics of AVA dissolution by the weight loss of granules of various fractions suggested that two processes occur consecutively: the electrolytic dissociation connected with passing of metal cations into the solution and hydrolytic degradation of the polyanionic framework providing passing of phosphate ions and microelements into the solution.

The simulation of the dissolution kinetics for AVA is complicated by the long time of complete dissolution; therefore, our experiments involved dissolution of 2–3% of the initial weight, with the subsequent calculation of the dissolution parameters (rate and activation energy for each component).

EXPERIMENTAL

Samples of complex metaphosphate glassy systems under study had the following composition:

Compound	Content, wt %
P_2O_5	50
K_2O	20
CaO	10
MgO	6
SiO_2	2.5
Microelements: Na, Co, Zn, Mn	11.5

Granules of the samples (sample weight 0.5 g) were dissolved in water within 1–14 h at 60°C. The sampling (up to 5 ml) of solution for the capillary electrophoretic analysis [5] was carried out at 2-h intervals.

The principal possibility of determining chemically the structure of alkali metal phosphates was shown in [6]. Glassy $NaPO_3$ or a glass with the ratio Na : P ≥ 1.25 was dissolved in water under strictly controlled conditions. Polyphosphates were precipitated from aqueous solutions with acetone. The mobility of phosphate ions was determined by chromatography or electrophoresis [7].

In the case of glassy AVA fertilizers, K, Ca, and Mg cations and PO_3^- anions were separated in solution by capillary electrophoresis (CEP). This method is based on examination of the ion mobility in a thin capillary after the separation in a strong electric field; the detection was carried out at a wavelength of 254 nm [5]. The examination of the time dependences of the concentration of ions in solution (c_a–τ and c_c–τ) within the first hours of dissolution, as given by the CEP method, allows us to extrapolate the simulated dependence to the entire process of glass breakdown.

We studied the solubility of glassy KPO_3 under the same conditions to compare passing of metaphosphates into solution.

The time dependences of passing of potassium and phosphate ions into the solution within 14 h of granule dissolution are shown in Fig. 2. The kinetic curves for this period are approximated by a straight line, the fraction of the dissolved substance being approximately 1%. Two processes are observed: cation exchange and breakdown of the anionic framework of glassy metaphosphate, which is characteristic of dissolution of phosphate glasses [1, 2].

The slope of the kinetic curves of the dissolution (Fig. 3) for single-charged K^+ cations differs from that for double-charged Ca^{2+} and Mg^{2+} cations, showing

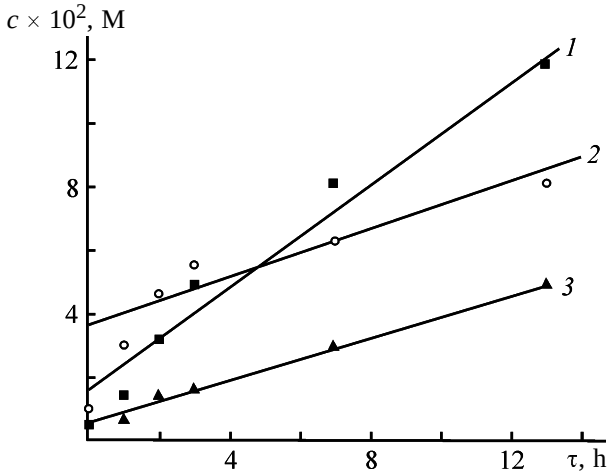


Fig. 3. Concentration c of cations in solution as a funciton of time τ at 60°C. (*1*) K, (*2*) Ca, and (*3*) Mg.

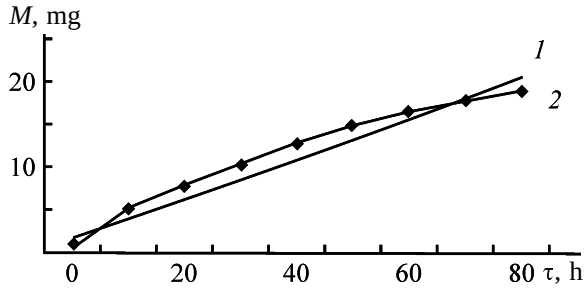


Fig. 4. Weight loss in the dissolution of glassy fertilizers: (*1*) calculation and (*2*) experiment. (*M*) Weight and (τ) time.

that single-charged cations (which have a higher weight fraction in the glass) preferentially pass into the solution compared to double-charged cations upon the dissociative rupture of ionic bonds with the anionic framework. Examination of the c–τ dependences for K^+ and PO_3^- for glassy KPO_3 and the data of [2] confirm the assumption that the corrosion stability of a phosphate glass increases with the concentration of oxides of double-charged metals.

We found that the dissolution of glassy fertilizers in water is described by a first-order kinetic equation, i.e., by the law $\ln(M_0/M) = k\tau$, where M_0 is the initial weight, and M, current weight of granules; k, rate constant of dissolution exponentially dependent on temperature; and τ, time.

When the reaction is of the first order, the total weight loss for a glass granule in time is described by the dependence

$$M_{sum}(\tau) = m_{01}F_1(1 - e^{-k_1}) + m_{02}F_2(1 - e^{-k_2}), \quad (1)$$

where m_{01} and m_{02} are weight fractions of components; $F_1(\tau)$ and $F_2(\tau)$ are functions describing the rate of egress of each component; k_1 and k_2 are rate constants [8].

Transformed equation (1) for the first-order reaction appears as

$$M(\tau) = m[1 - \exp(-km\tau/\rho d)], \quad (2)$$

where m is the initial weight of granules; ρ, their density; d, size of glass granules, and k, rate constant.

The initial conditions are as folllows: m = 0.5 g, d of a granule 0.2 cm, and ρ = 2.6 g cm^{-3}. The experimental constant ($k = 3 \times 10^{-1}$ h^{-1}) is used for calculating the weight loss of a fertilizer granule. The calculation by Eq. (2) gave the results consistent with the experiment (Fig. 4). The results obtained show that the approximations of the model are suitable for estimating the initial step of the dissolution of glassy fertilizers.

CONCLUSIONS

(1) The kinetics of the dissolution of glassy fertilizers AVA and of passing of K, Ca, and Mg cations into solution is described by a first-order equation.

(2) Equations (1) and (2) allow estimation of passing of ions into solution within the entire period of the dissolution of glass granules.

REFERENCES

1. Karapetyan, G.O., Petrovskii, G.T., Shashkin, V.S., and Yanush, O.V., Abstracts of Papers, *Perspective Technologies of Glass Used in Agriculture and Building: 4th European East-West Conf. and Exhibition on Materials and Processes*, St. Petersburg, October 16–19, 1993, report F 1–4, pp. 140–141.
2. Pakhomov, G.B. and Neverov, S.L., Abstracts of Papers, *Russian Conf. on the Chemistry of Solids*, Yekaterinburg, 1996, p. 89.
3. Pakhomov, G.B., Neverov, S.L., and Kochedykov, V.A., *Fiz. Khim. Stekla*, 1993, vol. 19, no. 6, pp. 864–870.
4. Vakhula, Ya.I., Semchuk, O.R., and Kozii, O.I., *Fiz. Khim. Stekla*, 2002, vol. 28, no. 4, pp. 364–368.
5. Anufrieva, R.M., Komarova, N.V., and Kamentsev, Ya.S., *Sistema kapillyarnogo elektroforeza* (System of Capillary Electrophoresis), St. Petersburg: Petropolis, 2001.
6. Van Wazer, I.R., *Phosphorus and Its Compounds*, New York: Wiley–Interscience, 1958.
7. Tianlin, W. and Li, S.F.Y., *Chromatography*, 1996, vol. 723A, no. 1, pp. 197–205.
8. Delmon, B., *Introduction á la Cinétique Hétérogene*, Paris: Technip, 1969. Translated under the title *Kinetika geterogennykh reaktsii*, Moscow: Mir, 1972, p. 556.

Russian Journal of Applied Chemistry, Vol. 78, No. 9, 2005, pp. 1386–1390. Translated from Zhurnal Prikladnoi Khimii, Vol. 78, No. 9, 2005, pp. 1412–1415.
Original Russian Text Copyright © 2005 by Isakova, Petrakovskaya, Glushchenko, Bulina, Churilov.

INORGANIC SYNTHESIS AND INDUSTRIAL INORGANIC CHEMISTRY

Platinized Fullerene Soots in the Synthesis of Fullerene-Containing Platinum Complexes

V. G. Isakova, E. A. Petrakovskaya, G. A. Glushchenko, N. V. Bulina, and G. N. Churilov

Kirenskii Institute of Physics, Siberian Division, Russian Academy of Sciences, Krasnoyarsk, Russia

Received April 15, 2005

Abstract—Thermal reaction of platinized fullerene soot and platinum(II) acetylacetonate occurs in the combustion mode. As shown by ESR, the combustion products contain compounds of platinum with fullerene. Water-soluble fullerene-containing platinum complexes with the parameters g_{eff} = 2 and ΔH = 84 mT were synthesized by the hydroxylation of combustion products with a nitric acid solution.

Carbon clusters, fullerenes and their compounds, have extremely wide spectrum of biological activity: antiviral, antimicrobial, and antitumor; they are active against HIV infection [1–4]. However, both fullerenes and overwhelming majority of their derivatives are insoluble in water, which makes them incompatible with physiological media and is one of the main obstacles in their use for biomedical purposes.

Polyhydroxylated fullerenes $C_{60}(OH)_x$ and $C_{70}(OH)_x$ (fullerenols) are water-soluble [4–7] and biologically active [8] compounds. As a rule, fullerenes are isolated with a large number of hydroxy groups as a mixture of isomers. The number of hydroxy groups in $C_{60}(OH)_x$ can reach 36. Recently the diols $C_{60}(OH)_2$ and $C_{70}(OH)_2$ were synthesized in the individual form [9]. Water-soluble metal-containing fullerenols were synthesized by the hydroxylation of endohedral fullerides C_{82} of *f* metals (Gd, Ho, Pr) [10, 11], but they are poorly accessible for wide-scale studies because of the lack of efficient procedures for the synthesis of higher fullerenes and their endohedral complexes. The formation of exohedrally bound compounds with metals is characteristic for more readily accessible fullerenes, C_{60} and C_{70}. They are described in numerous papers, but no water-soluble compounds of this type were reported. Anions C_{60}^{n-} were hydroxylated in lithium fullerides [12] to give fullerenol $C_{60}H_2(OH)_{24}$ readily soluble in water. It was interesting to carry out the hydroxylation of fullerides of *d* metals as a possible route to water-soluble fullerene-containing complexes of metals.

The aim of this work was to synthesize and study fullerene-containing platinum complexes.

EXPERIMENTAL

Platinized fullerene-containing soot (Pt/FS) [13] was the starting reagent. It was prepared in a plasmochemical reactor. Its operation is based on the vaporization of graphite under atmospheric pressure in an long plasma jet with a longitudinal (~1 m) temperature gradient from 5000 to 2000 K [14]. A metallic platinum powder was placed in the orifice of one of graphite electrodes between which the carbon plasma jet is formed. The reactor was cooled to room temperature. The resulting condensate (Pt/FS) contained approximately 8% of a mixture of fullerenes with the ratio C_{60}/C_{70} = 4/1 (the content of higher fullerenes in the fullerene mixture was less than 1%), approximately 5% of platinum in the form of finely dispersed metal particles, more than 80% of ultradispersed carbon not bound in fullerenes, and residual graphite [13].

Pt/FS with an addition (about 3–4%) of platinum acetylacetonate $Pt(acac)_2$[1] was heated to initiate the combustion of the reagents. On the reaction termination, the combustion products (Pt/FS_{comb}) were treated with a concentrated HNO_3 solution. The dissolved part of the products was separated by filtration. The solution was evaporated on a water bath to dryness, with full removal of acid vapor. The resulting amorphous brown-black powder **I** was readily soluble in water and insoluble in organic solvents. The yield was ~40% based on the weight of fullerenes in Pt/FS.

[1] Platinum acetylacetonate was prepared by G.I. Zharkova (Institute of Inorganic Chemistry, Siberian Division, Russian Academy of Sciences, Novosibirsk).

1070-4272/05/7809-1386 © 2005 Pleiades Publishing, Inc.

The electron spin resonance spectra (ESR) of the products isolated in the course of the synthesis were recorded on an SE/X-2544 ESR spectrometer at 77 and 293 K. The IR spectra were recorded on a Bruker spectrometer in KBr pellets. The electronic absorption spectra were taken on a Specord UV-VIS instrument from aqueous solutions. The X-ray phase analysis was carried out on a DRON-4 diffractometer using CuK_α radiation.

Previous studies showed that thermal reactions in solid-phase mixtures of fullerene C_{60} and metal acetylacetonates proceed in a catalytic combustion mode [15, 16]. The fullerene initiates the exothermic thermolysis of a metal complex. Reaction of the combustion products formed in the C_{60}/Fe(acac)$_3$ mixture with hydrochloric acid yielded iron fullerene complexes containing hydroxy groups [15]. The yield of the target product in the similar synthesis of platinum complexes was very low. Therefore, in this study, to prepare platinum fullerenol complexes, we used products of the thermal reaction of platinized fullerene soot and platinum acetylacetonate.

Heating a solid-phase mixture Pt/FS + Pt(acac)$_2$ results in combustion of the reagents [15] at ~200°C. In the absence of Pt(acac)$_2$, no combustion of Pt/FS was observed even above 400°C. Addition of platinum acetylacetonate to "empty" soot (fullerenes were extracted beforehand with toluene) does not give rise to combustion, i.e., the combustion of a Pt/FS + Pt(acac)$_2$ mixture is a consequence of the exothermic decomposition of platinum acetylacetonate initiated by fullerene. Ultradispersed carbon from Pt/FS is gasified in the course of the combustion. The total weight loss of the reagents is about 70%.

Phases of metallic platinum and residual graphite were detected in the X-ray diffraction patterns of the starting Pt/FS and combustion products of the Pt/FS + Pt(acac)$_2$ mixture. Fullerene reflections were observed in the Pt/FS pattern against the background of a halo from ultradispersed soot but were absent from the pattern of Pt/FS$_{comb}$. The ESR spectra suggest the presence of fullerenes both in Pt/FS and in Pt/FS$_{comb}$, as they both have an intensive absorption line characteristic of a radical of solid-phase fullerenes (fullerites) [17] (Fig. 1, line *3*). The line of the radical in the spectra of Pt/FS and Pt/FS$_{comb}$ is somewhat shifted and broadened as compared to the C_{60}/C_{70} sample, which is attributable to the presence of paramagnetic centers. Broad line *1* observed in the spectrum of the starting soot at 77 K refers to platinum compounds. In the spectrum of combustion products, this line becomes more intense (line *2*) and clearly observable

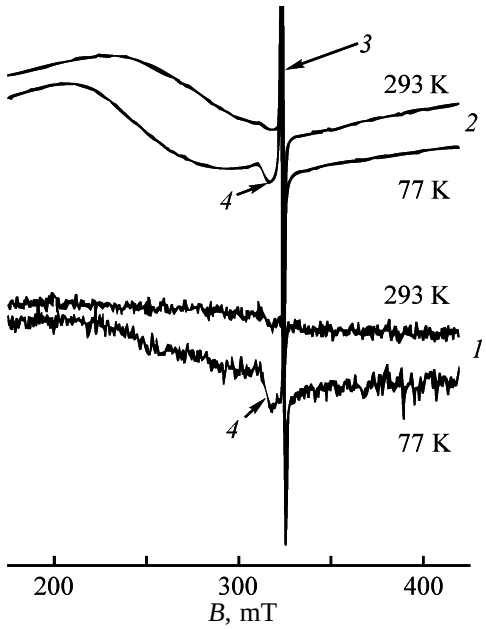


Fig. 1. ESR spectra: (*1*) Pt/FS, (*2*) Pt/FS$_{comb}$, (*3*) fullerite radical, and (*4*) platinum nanoparticles. (*B*) Magnetic field; the same for Fig. 3.

at room temperature. The parameters of the spectrum g_{eff} = 2.27, ΔH = 94 mT (293 K) and g_{eff} = 2.57, ΔH = 82 mT (77) correspond to Pt^{3+} [18]. Line skewness, which is more noticeable at 77 K, is due to a low-symmetry surrounding characteristic for Pt^{3+} ions; the increase in the ESR line symmetry at 293 K is caused by a high molecular mobility. As the temperature decreased, no increase in the line intensity, characteristic for paramagnetic centers, was observed. Presumably, there is an interaction between platinum ions, which is also proved by the downfield shift of the line at 77 K. The line narrowing at 77 K is attributable to an increase in the spin–lattice relaxation time. We believe that Pt/FS$_{comb}$ contains platinum fullerides Pt_nC_{60} and Pt_nC_{70} in an amorphous state typical of them [19].

Absorption lines (g_{eff} = 2.06, ΔH = 6 mT) in the spectra of starting soot and combustion products have an asymmetric shape characteristic of small metallic particles [20, 21], which allows them to be assigned to platinum nanoparticles of sizes no greater than 1 nm.

To hydroxylate fullerides in Pt/FS$_{comb}$, we used their reaction with concentrated HNO_3 [10]. When Pt/FS$_{comb}$ was treated with nitric acid, a part of the substance passed into solution, which became bright brown. The action of HNO_3 on Pt/FS yielded only a trace amount of a soluble product. This fact suggests that product **I** (in view of its rather high yield) is formed owing to the dissolution of the platinum-

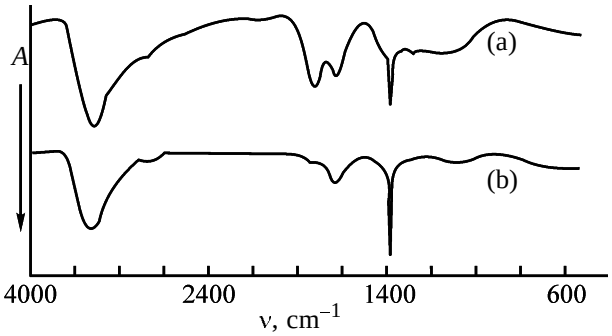


Fig. 2. IR spectra: (*A*) absorption and (ν) wave number. (a) Product **I** obtained by Pt/FS_{comb} hydroxylation and (b) product **II** obtained by the reaction of **I** with water.

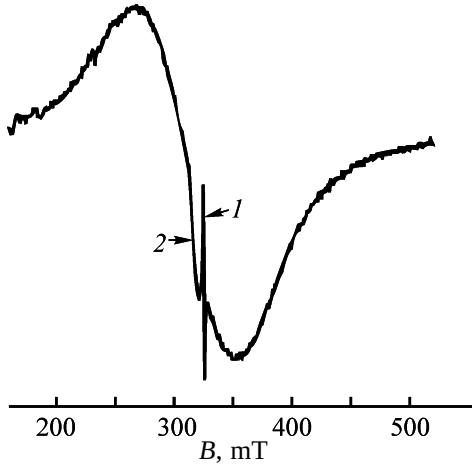


Fig. 3. ESR spectrum of product **I**: (*1*) line of a fullerenol radical and (*2*) line of platinum nanoparticles.

containing products of combustion of the Pt/FS + $Pt(acac)_2$ mixture in HNO_3.

The elemental analysis and thin-layer chromatography of product **I** (two major components are detected in a freshly prepared aqueous solution) allow us to conclude that **I** is a mixture of derivatives of (60)- and (70)-fullerenes with the composition $Pt_2(C_{60}/C_{70})\cdot N_{2.5}H_{42}O_{44}$ (C_{60}/C_{70} = 4/1).

Found, %: N 1.78, H 2.17, C 39.96, Pt 19.9.
Calculated, %: N 1.79, H 2.15, C 39.98, Pt 20.0.

We failed to isolate pure complexes by column chromatography of aqueous solutions (eluent: water–alcohol mixtures) because of smearing of the bands, their mixing, and increase in their number.

The IR spectra of products **I** and **II** are shown in Figs. 2a and 2b, respectively. Product **II** was prepared by the dissolution of **I** in water followed by evaporation of the solution. Both spectra resemble those of fullerenols [5, 6, 12] and the spectrum of the water-soluble endohedral complex $Pr_2C_{82}O_m(OH)_n$ ($m \sim 10$, $n \sim 10$) [10]. Strong bands at 3425 (broad) and 1384 cm^{-1} (narrow) correspond to stretching and bending vibrations of OH groups, respectively, and bands of medium intensity at 1634 (1629 cm^{-1} in the spectrum of **I**) and 1050 cm^{-1} correspond to C=C and C–O stretching vibrations. Very weak bands of C–H vibrations are also observed at 2852 and 2928 cm^{-1}. The absorption at 1580 cm^{-1} (shoulder), in the region of 1150–1290, and at 720 cm^{-1} (C=O vibrations), disappearing in the spectrum of **II**, is attributable to the substitution of water for nitrate groups bound to platinum [22] and by the hydrolysis of complexes **I**. As vibrations of any functional groups, except for OH, C–O, C=C, and C–H, are absent from the spectrum of **II**, it is most probable that product **I** is transformed into the corresponding aqua or aquahydroxofullerenol platinum complexes $Pt_2(H_2O)_n(C_{60}/C_{70})H_m(OH)_x$. The evaporation of the solution of **I** resulted in a partial loss of the solubility of the isolated product **II**, but at room temperature no precipitate was detected in a saturated solution of **I** even after storage for more than 10 days.

The ESR spectrum of **I** is shown in Fig. 3. The resonance from platinum ions is recorded at room temperature. The line is symmetric; ΔH = 84 mT and g = 2.1. A change in the g-factor as compared to Pt/FS_{comb} is due to a change in the local surrounding of ions and increasing splitting of platinum orbital levels, which results in a decrease in the contribution of orbital motion of electrons to g-factor of the observed Pt^{3+} spectral line and in approach of its value to 2. The position of the resonance line of the radical (g = 1.997, ΔH = 0.35 mT) corresponds to the radical anion of fullerene C_{60} [17], suggesting the formation of charge-transfer complexes. An absorption line referred to nanoparticles of metallic platinum (line *2*) is also present in the spectrum, which seems to be due to insignificant decomposition of the complexes to Pt(O) during their isolation from a nitric acid solution by evaporation.

The transformation of product **I** into **II** practically does not noticeably change the ESR spectrum. However, after a prolonged heating of solution **I** and its subsequent evaporation, the intensity of the resonance line of platinum ions in the spectrum of the isolated solid product decreases, which is attributable to the reduction of the complexes. The line of the radical of fullerenes becomes stronger.

Complexes **I** are reduced with ethanol at room temperature. When product **I** is treated with alcohol, it partially dissolves. Lines of Pt^{3+} ions are absent from the ESR spectra of the fractions insoluble (product **III**)

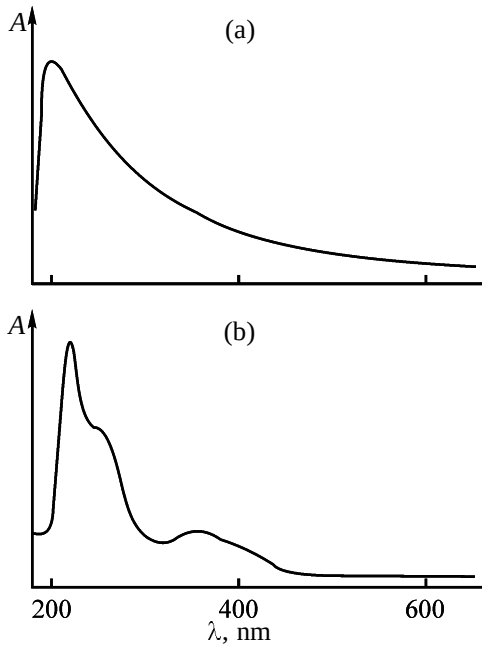


Fig. 4. UV and visible absorption spectra of aqueous solutions of products (a) **III** and (b) **IV**. (*A*) Absorption and (λ) wavelength.

and soluble in alcohol (product **IV**), which is a due to their reduction; the line of radicals increases in the intensity. The *g*-factor shifts relative to the radical of substance **I** (g = 2.0025, ΔH = 0.54 mT for **III** and g = 2.0027, ΔH = 0.34 mT for **IV**), which is probably due to a decrease in the charge of the radical anion.

It should be noted that products **III** and **IV** preserve the water solubility. The electronic absorption spectra of aqueous solutions of **III** (a) and **IV** (b) are shown in Fig. 4. These spectra are similar to the spectra of the fullerenols $C_{60}(OH)_2$ and $C_{70}(OH)_2$ [9], respectively, but the bands are shifted to the UV region owing to bonding of fullerenol groups with platinum. We believe that the difference in the solubility in alcohol makes it possible to separate the derivatives of (60)- and (70)-fullerenols in product **I**, but the separation is accompanied by reduction and probably by exchange processes.

CONCLUSIONS

(1) Products of the combustion of a mixture of platinized fullerene soot and platinum acetylacetonate contain platinum fullerides, which are hydroxylated when treated by nitric acid to form magnetic (60)- and (70)-fullerene-containing platinum complexes.

(2) The resonance from platinum ions is recorded in the ESR spectra of the starting fullerides and the hydroxylation products at room temperature. Parameters of the spectra are characteristic for Pt^{3+}. The position of the resonance line of the radical corresponds to the fullerene radical anion, suggesting the formation of charge-transfer complexes.

(3) The resulting complexes are readily soluble in water, preserve the solubility during transformations in aqueous solutions, and are fairly stable with respect to reduction. The separation of the complexes into C_{60} and C_{70} derivatives using a difference in their solubility in alcohol is accompanied by reduction, with the solubility in water of the reduced complexes being preserved. The synthesized water-soluble platinum fullerenol complexes are suitable for operation in physiological media. The suggested route of their synthesis excludes traditional steps of the extraction of fullerenes from fullerene soot by toxic organic solvents.

ACKNOWLEDGMENTS

This work was financially supported by the Program of the Siberian Division of Russian Academy of Sciences on the priority directions of science (project no. 9.2.1).

REFERENCES

1. Moussa Fathi, Chretien Pascale, Dubois Pierre, *et al*., *Fullerene Sci. Technol*., 1995, vol. 3, no. 3, pp. 333–342.
2. Jencen, A.W., Wilson, S.R., and Shuster, D.I., *Bioorg. Med. Chem. Lett*., 1996, no. 4, pp. 767–779.
3. Kiselev, O.I., Kozeletskaya, K.N., Melenevskaya, E.Yu., *et al*., *Dokl. Ross. Akad. Nauk*, 1998, vol. 361, no. 4, pp. 547–549.
4. Bagrii, E.I. and Karaulova, E.N., *Neftekhimiya*, 2001, vol. 41, no. 5, pp. 323–342.
5. Chiang, L.Y., Upasani, R.B., Swirczewski, J.W., and Soled, S., *J. Am. Chem. Soc*., 1993, vol. 11, no. 13, pp. 5453–5457.
6. Schneider, N.S., Darwish, A.D., Kroto, H.W., *et al*., *J. Chem. Soc., Chem. Commun*., 1994, no. 4, pp. 463–464.
7. Long, I.C., Fung-Jou, L., and Jow-Touwn, L., *Electrochem. Soc. Proc*., 1995, vol. 10, pp. 699–702.
8. Jin, H., Chen, W.Q., Tang, X.W., *et al*., *J. Neurosci. Res*., 2000, vol. 62, pp. 600–607.
9. Meier, M.S. and Kiegiel, J., *Org. Lett*., 2001, vol. 3, no. 11, pp. 1717–1719.
10. Sun Dayong, Huang Houjin, and Yang Shihe, *Chem. Mater*., 1999, vol. 11, no. 4, pp. 1003–1006.

11. Shuying Liu and Shuqing Sun, *J. Organomet. Chem.*, 2000, vol. 599, pp. 74–86.
12. Yu Chen, Rui-Fang Cai, Shiming Chen, and Zu-En Huang, *J. Phys. Chem. Solids*, 2001, vol. 62, pp. 999–1001.
13. Churilov, G.N., Isakova, V.G., Weisman, R.B., *et al.*, *Fiz. Tverd. Tela*, 2002, vol. 44, no. 4, pp. 579–580.
14. Churilov, G.N., Korets, A.Ya., and Titarenko, Ya.N., *Zh. Tekh. Fiz.*, 1996, vol. 66, no. 1, pp. 191–194.
15. Isakova, V.G., Petrakovskaya, E.A., Balaev, A.D., and Kolpakova, T.A., *Zh. Prikl. Khim.*, 2003, vol. 76, no. 4, pp. 597–601.
16. Isakova, V.G., Petrakovskaya, E.A., Isakov, V.P., *et al.*, Abstracts of Papers, *Euro-Asian Symp. "Trends in Magnetism,"* Krasnoyarsk, August 24–27, 2004, p. 354.
17. Zaritskii, I.M., Ishchenko, S.S., Konchits, A.A., *et al.*, *Fiz. Tverd. Tela*, 1996, vol. 38, no. 2, pp. 419–426.
18. Abragam, A. and Bleaney, B., *Electron Paramagnetic Resonance of Transition Ions*, Oxford: Clarendon, 1970.
19. Herbst, M.H., Pinhal, N.M., Demetrio, F.A.T., *et al.*, *J. Non-Cryst. Solids*, 2000, vol. 272, pp. 127–130.
20. Grobet, P.J. and Schoonheydt, R.A., *Surf. Sci.*, 1985, vol. 156, no. 4, pp. 893–898.
21. Tu, W., Takai, K., Fukui, K., *et al.*, *J. Phys. Chem.*, 2003, vol. 107, no. 37, pp. 10 134–10 140.
22. Kukushkin, Yu.N., *Khimiya koordinatsionnykh soedinenii* (Chemistry of Coordination Compounds), Moscow: Vysshaya Shkola, 1985.

Russian Journal of Applied Chemistry, Vol. 78, No. 9, 2005, pp. 1391–1397. Translated from Zhurnal Prikladnoi Khimii, Vol. 78, No. 9, 2005, pp. 1416–1422.
Original Russian Text Copyright © 2005 by Rodyagina, Chepurnaya, Vasil'eva, Timonov.

INORGANIC SYNTHESIS AND INDUSTRIAL INORGANIC CHEMISTRY

Synthesis and Properties of Polymeric Copper Complexes with Schiff Bases

T. Yu. Rodyagina, I. A. Chepurnaya, S. V. Vasil'eva, and A. M. Timonov

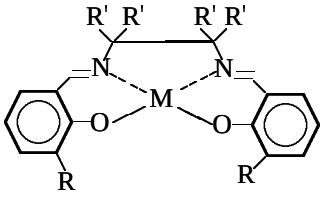
Herzen Russian State Pedagogical University, St. Petersburg, Russia

Received April 7, 2005

Abstract—The electrochemical synthesis and properties of polymeric copper complexes with tetradentate (N_2O_2) Schiff bases were studied. The effects of the metal center and ligand surrounding of the starting compounds on the mechanism and kinetics of the charge transport in the polymers are discussed.

Polymeric complexes of transition metals (M) with tetradentate (N_2O_2) Schiff bases {poly-[M(Schiff)]} have a number of unique properties, such as directed redox conductivity, electrochromism, and the capability of selective catalysis of important chemical processes involving organic compounds [1–3]. This set of properties of poly-[M(Schiff)] polymers makes them promising for development of new optoelectronic and sensory devices and energy-storing and catalytic systems.

Nickel(II) and copper(II) compounds are the most practically significant among poly-[M(Schiff)] polymers owing to a relatively low cost. Papers devoted to nickel-containing polymers are numerous, but only a few studies [4–6] concerned poly-[Cu(SalEn)] polymers



where M is Cu; R, R' = H, [Cu(SalEn)]; R = OCH_3, R' = H, [Cu(CH_3O–SalEn)]; R = H, R' = CH_3, [Cu(SaltmEn)]; R = OCH_3, R' = CH_3 [Cu(CH_3O–SaltmEn)].

Here we made a first systematic study of the formation and properties of [Cu(Schiff)] polymeric complexes. These results make it possible to carry out a purposeful synthesis of materials with preset properties for various applications.

EXPERIMENTAL

The complexes [Cu(CH_3O–SalEn)] and [Cu(SalEn)] were synthesized by the procedures from [5, 7], and [Cu(SaltmEn)] and [Cu(CH_3O–SaltmEn)], by the following procedure.

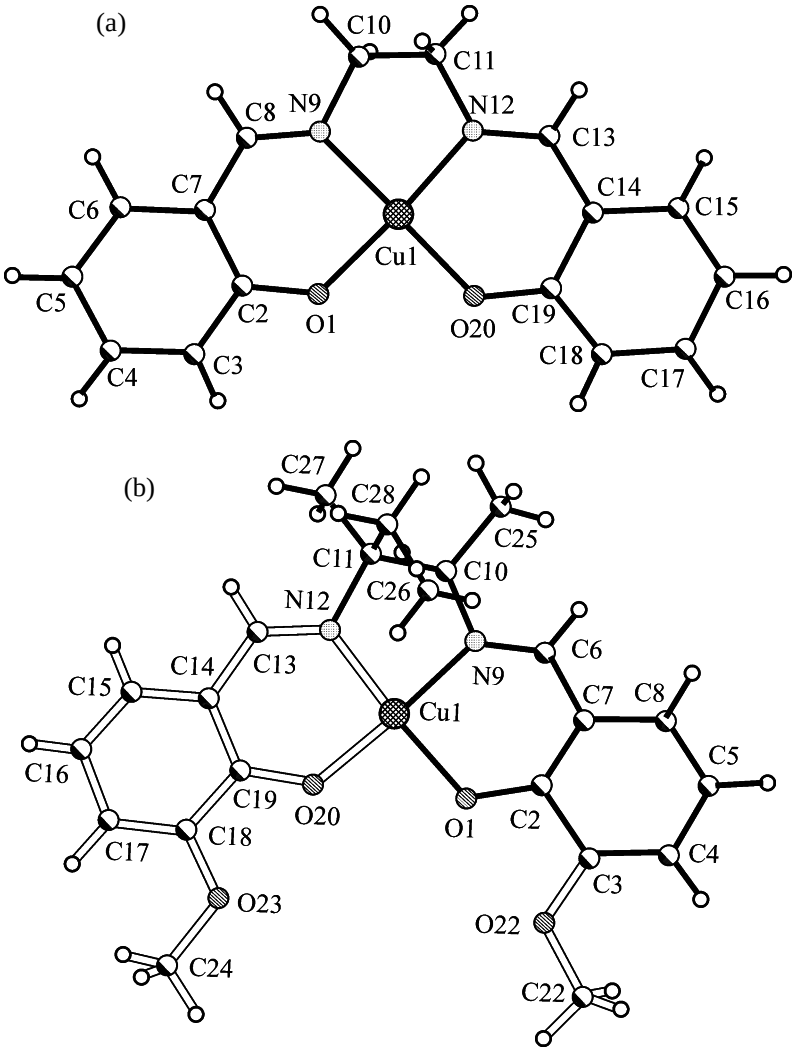
The ligands H_2SaltmEn and H_2CH_3O–SaltmEn were prepared by mixing hot saturated alcoholic solutions containing stoichiometric amounts of the corresponding aldehydes and diamino derivatives: salicylaldehyde (Aldrich) and 2,3-diamino-2,3-dimethylbutane (H_2SaltmEn) or *o*-vanillin (Aldrich, 97%) and 2,3-diamino-2,3-dimethylbutane (H_2CH_3O–SaltmEn). 2,3-Diamino-2,3-dimethylbutane was obtained by the reduction of 2,3-dimethyl-2,3-dinitrobutane (Aldrich) with hydrogen [8]. The resulting ligands were filtered under vacuum, washed with cold distilled water and ethanol, and dried in air.

To prepare the complexes, a saturated acetonitrile solution of appropriate ligand was added to a saturated aqueous solution of $Cu(CH_3COO)_2$ (Vekton, chemically pure grade); the solutions contained stoichiometric amounts of the reactants. Then the mixture of the reactants was refluxed for 20–30 min; the precipitates were washed with water and acetonitrile, filtered off, and recrystallized from acetonitrile. The yield of [Cu(CH_3O–SaltmEn)] and [Cu(SaltmEn)] was 44 and 49%, respectively.

All the complexes were identified by X-ray diffraction analysis using a Bruker D-5000 diffractometer. The composition and structure of the synthesized complexes [Cu(SaltmEn)] (a) and [Cu(CH_3O–SaltmEn)] (b) are shown below.

To prepare supporting electrolyte solutions, we used the following salts: tetraethylammonium tetrafluoroborate $(Et_4N)BF_4$, tetraethylammonium perchlorate $(Et_4N)ClO_4$, and tetraethylammonium hexafluorophosphate $(Et_4N)PF_6$ (all purchased from Merck, 97%). Before preparing the solutions, the salts

1070-4272/05/7809-1391 © 2005 Pleiades Publishing, Inc.



were dried at 125°C for 12 h in an inert atmosphere. Solvents were acetonitrile (AN, Kriokhrome, 0 grade) and dimethylformamide (DMF, Merck, 98%).

To determine the number of electrons participating in electrochemical processes, we used ferrocene $Fe(C_5H_5)_2$ (Merck, 98%) as a reference.

We used a computerized complex based on an Epsilon 2 (BAS) potentiostat for electrochemical experiments, which were carried out in a hermetically sealed three-electrode cell with separated electrode compartments. A working electrode was a BAS MF 2012 glassy graphite disk 3 mm in diameter (surface area 0.07 cm^2). The surface of the working electrode was polished prior to the experiments using diamond powders with particle sizes of 3 and 1 μm (BASi PK-4 polishing kit), washed with acetonitrile, and dried in air. The reference electrode was AgCl/Ag filled with a saturated NaCl solution (RE-5B BAS). All potentials are given relative to this reference electrode. An auxiliary electrode was a platinum grid (surface area about 5 cm^2). The voltammograms of the processes involving some of the complexes under study in acetonitrile solutions are given as an example in Fig. 1. The voltammograms were recorded by single scanning of the potential from 0 to the anode region up to 1.2–1.4 V and back. The anode part of the voltammograms is the most informative for studying electrolytic oxidation of the compounds under consideration, as the reverse potential scanning is accompanied by reduction of the forming polymeric complexes immobilized on the electrode surface, which is described by the relationships characteristic of thin-layer voltammetry. The voltammograms of all the complexes under study are characterized by the presence of two anode maxima; the overall shape of the anode branches of the voltammograms corresponds to the EEC [9] mechanism of the electrolytic oxidation

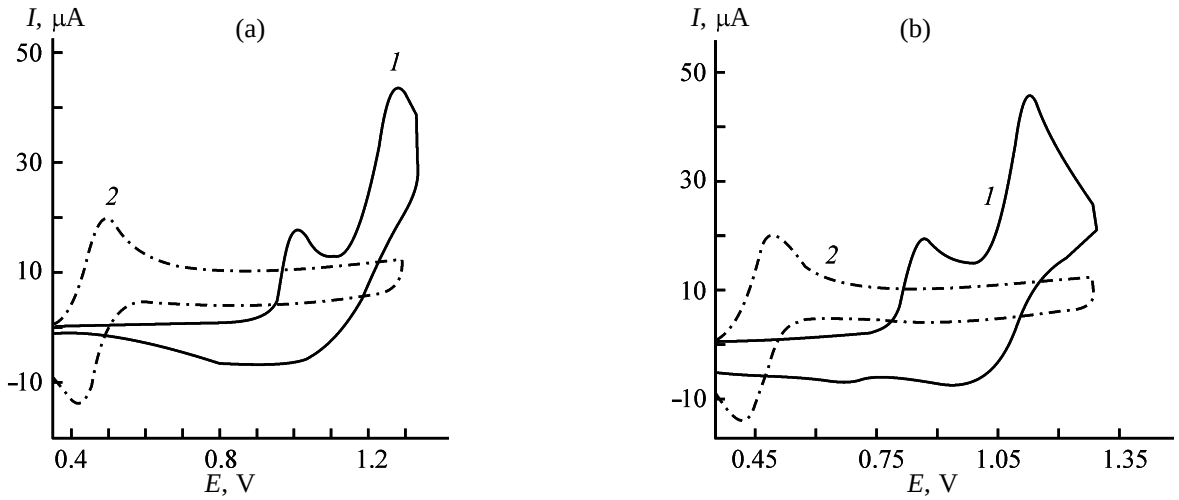


Fig. 1. Voltammograms of redox processes involving (*1*) complexes and (*2*) ferrocene, recorded with a glassy graphite electrode (S = 0.07 cm^2) in an AN solution. Potential scanning rate V_s = 0.05 V s^{-1}; the same for Fig. 2. Concentration (M): complexes and ferrocene 1×10^{-3}, $(Et_4N)BF_4$ 0.1. (*I*) current strength and (*E*) potential; the same for Fig. 2. (a) [Cu(SaltmEn)] and (b) [Cu(CH_3O–SaltmEn)]; the same for Fig. 2.

(E is an electrochemical stage, and C, a chemical reaction conjugated with it). Comparison of the oxidation voltammograms of the copper complexes and ferrocene used as a reference shows that both electrochemical steps are one-electron. The potentials of the anode maxima in the voltammograms of the complexes and individual ligands in AN and DMF solutions are given in Table 1.

An electrochemical study of the oxidation of [Cu(Schiff)] complexes revealed the following facts.

The formation of polymeric compounds on the electrode surface was observed only when the complexes were oxidized in a solvent with a low coordinating power (AN). As shown previously [10, 11] for the related nickel and palladium complexes, passing from AN to DMF having a higher donor number [10] favors stabilization of the electrochemical oxidation products in the form of inert octahedral complexes containing axially coordinated solvent molecules.

Using the reference compound, we found that the electrolytic oxidation of all the complexes under study is a two-electron process in both acetonitrile and DMF. When the complexes [Cu(SalEn)] and [Cu(SaltmEn)] are oxidized in DMF solutions, the potentials of the maxima of both oxidation waves are close to each other, and, as a result, only one anodic current maximum is observed in the voltammograms. At the same time, it was found by *in situ* microgravimetry [12] that the electrochemical oxidation of the copper complexes under consideration in acetonitrile solutions involves one electron per fragment of a [Cu(Schiff)] polymer. The whole set of these facts indicates that, when a polymer is formed, the two-electron oxidation of the starting complex is accompanied by a chemical reaction of the coordination of a [Cu(Schiff)] molecule to the product of the electrolytic oxidation.

The potentials E_{pa1} for [Cu(SalEn)] and [Cu(SaltmEn)] and E_{pa2} for [Cu(CH_3O–SalEn)] and [Cu(CH_3O–SaltmEn)] in the voltammograms of the complexes in acetonitrile solutions are close to each other (1.00–1.12 V), irrespective of the presence of electron-donor methoxy groups in the phenyl moiety. A similar fact is observed also in the voltammograms recorded in DMF (1.05–1.08 V).

Table 1. Potentials of anode maxima E_{pa1} and E_{pa2} of voltammograms of the complexes [Cu(Schiff)] and ligands H_2(Schiff). V_s = 0.05 V s^{-1}

Complex, ligand	AN		DMF	
	E_{pa1}	E_{pa2}	E_{pa1}	E_{pa2}
	V			
[Cu(SalEn)]	1.00	1.22	1.08	–
H_2(SalEn)	1.10*	1.24	1.34	–
[Cu(CH_3)O–SalEn)]	0.83	1.10	0.99	1.07
H_2(CH_3O–SalEn)	0.86	0.96	1.01	–
[Cu(SaltmEn)]	1.01	1.27	1.05	–
H_2(SaltmEn)	1.13	1.44	1.31	–
[Cu(CH_3O–SaltmEn)]	0.86	1.12	0.99	1.07
H_2(CH_3O–SaltmEn)	0.83	1.09	0.99	1.05

* Shoulder.

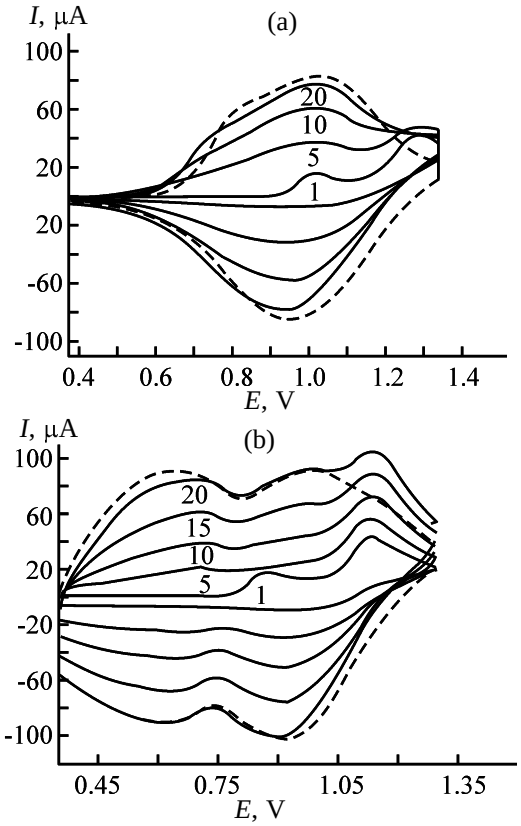


Fig. 2. Voltammograms of redox processes involving complexes, recorded with a glassy graphite electrode (S = 0.07 cm^2) in acetonitrile solutions. Concentration (M): complexes 1×10^{-3}, $(Et_4N)BF_4$ 0.1. (a) [Cu(SaltmEn)] and (b) [Cu(CH_3O–SaltmEn)]. Numbers at curves correspond to successive cycles. Dashed lines: voltammograms of polymers recorded after polymerization termination (20 cycles) and transfer of the modified electrode into a supporting electrolyte [0.1 M $(Et_4N)BF_4$, AN, V_s = 0.05 V s^{-1}].

Presumably, these oxidation waves correspond to the electron transfer from predominantly metal-centered orbitals of the complexes. Apparently, the second oxidation waves of the complexes [Cu(SalEn)] and [Cu(SaltmEn)] and the first oxidation waves of [Cu(CH_3O–SalEn)] and [Cu(CH_3O–SaltmEn)] are determined by the electron transfer from predominantly metal-centered orbitals. This is proved by the fact that the maxima of potentials of these waves are considerably shifted toward the negative region when electron-donor methoxy groups are introduced into the phenyl moieties.

The introduction of four methyl groups into the diamine bridge connecting the phenyl moieties does not result in a noticeable change in the electron density on the ligands, as methyl groups are weak donors. Therefore, the potentials of the current maxima in the oxidation voltammograms of the complexes [Cu(SalEn)] and [Cu(SaltmEn)] are close to each other. The same is also true for [Cu(CH_3O–SalEn)] and [Cu(CH_3O–SaltmEn)].

The limiting step of the polymerization of the complexes under study is the diffusion of the starting compounds to the electrode surface, which is confirmed by the fact that the currents of the anode maxima in the voltammograms increase linearly as the concentration of the starting substances in solution increases (in the range 1×10^{-4}–3×10^{-3} M).

On the whole, the experimental data for the complexes [Cu(Schiff)] agree with the general mechanism of the electrochemical oxidation of complexes [M(Schiff)] suggested previously [10, 11].

The formation of the polymeric complexes poly-[Cu(SaltmEn)] and poly-[Cu(CH_3O–SaltmEn)] on the surface of a glassy graphite electrode in the case of potential cycling is shown in Fig. 2. The voltammograms of the polymers recorded after the polymerization was complete and the modified electrode was transferred into the supporting electrolyte are also shown in Fig. 2 for comparison.

The regular increase in the currents of the anode and cathode maxima in the voltammograms correspond to the growth of polymeric compounds on the electrode. In the course of the formation of polymers, starting from the second cycle, a new broad anodic wave of the oxidation of polymers on the electrode surface is observed in the voltammograms at potentials more negative than E_{pa1}. At the same time, the anode wave corresponding to the transfer of the second electron, after which the formation of the polymer was observed according to [13], is absent from the voltammograms recorded in the supporting electrolyte solution with electrodes modified with the polymers (Fig. 2, dashed curves). The common trend for all the polymers studied is a shift of the region of redox processes to the side of less positive potentials when donor methoxy groups are introduced into the ligand. The introduction of methyl groups into the diamine bridges between phenyl moieties does not noticeably affect the shape and position of the voltammograms of the polymers. Thus, the voltammograms of the polymeric complexes poly-[Cu(SalEn)] and [Cu(SaltmEn)] only slightly differ from each other in the specified parameters.

Two pairs of anode and cathode waves are observed in the voltammograms of all the polymeric complexes studied. At the same time, it was found previously for nickel [14] and copper [12] polymeric complexes that the reduction–oxidation of polymers

in the range of potentials 0–1.3 V is characterized by the transfer of one electron per fragment. At present, the nature of processes giving rise to two pairs of waves in the voltammograms of the polymeric complexes under discussion is not determined unambiguously. A possible reason for the observed shape of the voltammograms can be the presence of two polymeric forms on the electrode surface, which are bound to the surface owing to the interaction between predominantly metal- or ligand-centered orbitals of the surface fragments of stacks and are correspondingly oxidized (or reduced) at different potentials. The other probable reason for the appearance of the broadened oxidation waves corresponding to the redox processes in the polymers can be the presence of polymeric stacks of different length on the surface, having different resistance to charge transfer.

Polymeric complexes can be formed also in a static mode when an electrode is polarized in a solution of the starting compound at a constant potential. In this case, the most important parameter is the polymer formation potential providing, on the one hand, a sufficient rate of the electrochemical process and, on the other hand, the absence of side reactions resulting in the degradation of the polymer or in the loss of its electrochemical activity. The criterion for choosing the optimal potential of the formation of polymers can be the charge diffusion coefficient D_{ct} reflecting the redox conductivity of the polymeric compounds.

To choose an optimal formation potential, we have prepared polymer films at various potentials in the range 0.9–1.2 V. The coefficients of charge diffusion in polymers were calculated by the Randles–Sevcik equation [15] on the basis of voltammograms recorded at potential scanning rates that provided the occurrence of redox processes in the polymer in the mode corresponding to the conditions of semiinfinite diffusion of current carriers. The calculation of the charge diffusion coefficients implies the exact knowledge of concentration of redox centers in the polymer, i.e., of the density of the polymeric film [16]. The density of the polymeric films based on the complexes with the ligand SalEn, about 1 g cm^{-3}, was determined previously by *in situ* ellipsometry [13]. Certainly, the density of the polymers depends on the presence of various substituents in the ligand surrounding, altering the geometry of the starting monomeric fragments. The exact values of the density of the polymers containing SaltmEn and CH_3O–SaltmEn ligands are unknown; therefore, the density of the polymers in these calculations was taken equal to 1 g cm^{-3}. This assumption does not allow us to compare the charge transfer rates in various polymers. Nevertheless, the resulting D_{ct} values can be used for comparison of charge transfer rates in the same polymer formed under different conditions.

The resulting D_{ct} values for all the complexes under study are close to each other and fall into the range $(1 \pm 0.5) \times 10^{-10}$ $cm^2\ s^{-1}$ for the range of the formation potential 1.00–1.10 V. This range of the polymer formation potentials is more positive than the potential of the first anodic maximum in the oxidation voltammograms of the starting complexes and, at the same time, overlaps with the range of potentials of the second oxidation process (Table 1). The formation of polymers at potentials lower than 0.95 V apparently results in the fact that the primary product of the electrolytic oxidation of the starting compound is partially stabilized owing to side processes involving a solvent, instead of the transfer of the second conduction electron. Monomeric and oligomeric fragments forming by the side processes can be captured by the growing polymeric film, which disturbs its structure and results in a decrease in the efficiency of the motion of charge carriers (in this case, the resulting D_{ct} values are close to 10^{-11} $cm^2\ s^{-1}$).

The formation of polymers at potentials higher than 1.2 V is accompanied by the irreversible oxidation of the ligand surrounding of the complexes and results in the loss of the polymer electrochemical activity.

The nature of the limiting step of charge transfer processes in the films of the polymers under study was determined by studying the effect of the size of charge-compensating ions (BF_4^-, ClO_4^-, and PF_6^-) [17] and concentration of supporting electrolytes (0.05–0.5 M) on D_{ct}. The experiments showed that the charge transfer rate in all the polymers studied is independent of the size of charge-compensating anions and of their concentration in solution. The results obtained show that the charge transfer in these films is limited not by the stage of diffusion of counterions in them, but by the rate of electron motion along polymeric stacks; therefore, the resulting D_{ct} values characterize the rate of specifically this process.

To compare characteristics of the charge transport in the polymeric complexes with various ligands and metallic centers, we can use the products of the concentrations of redox centers in a polymer c (mol cm^{-3}) by $D_{ct}^{1/2}$ values dependent on changes in the structure of polymers with variation of their composition and on the efficiency of the motion of charge carriers. The $cD_{ct}^{1/2}$ values for the poly-[Cu(Schiff)] polymers calculated by the Randles–Sevcik equation are given in Table 2; the related characteristics of nickel- and

Table 2. Values of $cD_{ct}^{1/2}$ for poly-[Cu(Schiff)] polymers

Complex	$cD_{ct}^{1/2} \times 10^8$, mol cm^{-2} s$^{-1/2}$	Complex	$cD_{ct}^{1/2} \times 10^8$, mol cm^{-2} s$^{-1/2}$
poly-[Ni(SalEn)]	4.0 ± 0.5	poly-[Ni(SaltmEn)]	12.0 ± 0.5
poly-[Pd(SalEn)]	2.5 ± 0.5	poly-[Pd(SaltmEn)]	5.6 ± 0.5
poly-[Cu(SalEn)]	1.5 ± 0.5	poly-[Cu(SaltmEn)]	2.0 ± 0.5
poly-[Ni(CH_3O–SalEn)]	5.0 ± 0.5	poly-[Ni(CH_3O–SaltmEn)]	5.5 ± 0.5
poly-[Pd(CH_3O–SalEn)]	3.0 ± 0.5	poly-[Pd(CH_3O–SaltmEn)]	4.6 ± 0.5
poly-[Cu(CH_3O–SalEn)]	1.5 ± 0.5	poly-[Cu(CH_3O–SaltmEn)]	2.0 ± 0.5

palladiuim-containing polymeric complexes obtained previously [18] are given for comparison.

Our results allow the following conclusions: (i) $cD_{ct}^{1/2}$ parameters for the copper complexes studied are lower than those for the polymeric nickel and palladium complexes; (ii) poly-[Cu(Schiff)] polymers are characterized by slow electron transport in stacks in contrast to nickel- and palladium-containing polymers, in which the limiting step of the charge transport is the motion of charge-compensating ions [18]; (iii) the effect of substituents in ligand surroundings on the behavior of compounds in polymeric complexes poly-[Cu(Schiff)] essentially differs from that in the nickel- and palladium-containing polymers owing to a change in the nature of the limiting step of the charge transport. In particular, for poly-[Ni,Pd(Schiff)] complexes, $cD_{ct}^{1/2}$ substantially increases on passing from the polymers with the SalEn ligand to those with the SaltmEn ligand. As shown in [19], the introduction of four methyl groups into the structure of the diamine bridge between the phenyl moieties results in a noticeable increase in the repulsive interactions between the polymer stacks and in the formation of a less compact polymeric film. For [Cu(Schiff)] polymers, such a change in the ligand surrounding results in increasing efficiency of the motion of charge-compensating ions, but does not noticeably affect the charge-transfer rate.

It is known that [Cu(Schiff)] complexes, unlike the related nickel and palladium compounds, form intermolecular associates in the solid phase, in which copper atoms are bound to each other through the oxygen atom of a Schiff base. In the associates, the length of the bond between the copper atom of one molecule and the oxygen atom of another molecule is 2.41 Å [20]. Presumably, in [Cu(Schiff)] the bonds between separate fragments in a stack are similar in nature [21]. At the same time, it was found that in the nickel and palladium polymeric complexes with Schiff bases, the bonds between separate fragments of stacks are formed by interaction of the metallic centers with the phenyl moieties of the ligands [22, 23]. The difference in the nature of bonds between fragments of stacks in the copper polymeric complexes compared to nickel- and palladium-containing polymers offers an explanation for the data obtained in this study, in particular, for a lower electronic conductivity of poly-[Cu(Schiff)] complexes.

CONCLUSIONS

(1) Previously unknown polymeric copper complexes with the ligands *N*,*N*'-2,3-dimethylbutane-2,3-diylbis(salicylidenimine) and *N*,*N*'-2,3-dimethylbutane-2,3-diylbis(3-methoxysalicylidenimine) were prepared. The conditions for the electrochemical synthesis of the polymers with the highest redox conductivity [optimal potentials of the formation of copper(II) polymeric complexes with Schiff bases, nature and concentration of the supporting electrolyte] were determined.

(2) The oxidation of the poly-[Cu(Schiff)] complexes occurs by the two-electron mechanism with the subsequent chemical step of the coordination of a starting complex molecule to the product of the electrochemical oxidation; the limiting step of the polymerization is the diffusion of the starting compounds to the electrode surface.

(3) A study of the mechanism and kinetics of charge transport showed that the electron transfer in a stack occurs through an oxygen atom. Therefore, these polymeric compounds are characterized by a slow electron transport along stacks, and the parameter $cD_{ct}^{1/2}$ for the copper(II) complexes studied is lower than for the related nickel and palladium polymeric complexes.

(4) Variation of the ligand surrounding does not affect the charge-transfer rate.

(5) The trends revealed in this study allow purposeful synthesis of electroactive polymeric materials with a preset range of potentials of the electrochemi-

cal activity and with the required rate of charge transport.

ACKNOWLEDGMENTS

This study was financially supported by the Russian Foundation for Basic Research (project no. 04-03-32979).

The authors are grateful to Dr. Dale Svensson (University of Iowa, the United States) for the assistance in X-ray diffraction analysis of the compounds.

REFERENCES

1. Popeko, I.E., Timonov, A.M., and Shagisultanova, G.A., *Zh. Prikl. Khim.*, 1990, vol. 63, no. 10, pp. 2207–2210.
2. Dahm, C.E. and Peters, D.G., *Anal. Chem.*, 1994, vol. 66, p. 3117.
3. Dahm, C.E. and Peters, D.G., *J. Electroanal. Chem.*, 1996, vol. 406, p. 119.
4. Hoferkamp, L.A. and Goldsby, K.A., *Chem. Mater.*, 1989, vol. 1, no. 3, pp. 348–352.
5. Audebert, P., Capdevielle, P., and Maumy, M., *New J. Chem.*, 1992, vol. 16, no. 6, pp. 697–703.
6. Orlova, I.A., Popeko, I.E., Timonov, A.M., *et al.*, *Zh. Prikl. Khim.*, 1993, vol. 66, no. 3, pp. 584–589.
7. Pfeiffer, P., Breith, E., Lubbe, E., and Tsumaki, T., *Justus Leibigs Ann. Chem.*, 1933, vol. 503, pp. 84–130.
8. Sayre, R., *J. Am. Chem. Soc.*, 1955, vol. 77, pp. 6689–6692.
9. Polcyn, D.S. and Shain, I., *Anal. Chem.*, 1966, vol. 38, pp. 370–385.
10. Vasil'eva, S.V., Balashev, K.P., and Timonov, A.M., *Elektrokhimiya*, 1998, vol. 34, no. 10, pp. 1090–1096.
11. Vasil'eva, S.V., Balashev, K.P., and Timonov, A.M., *Elektrokhimiya*, 2000, vol. 36, no. 1, pp. 85–89.
12. Rodyagina, T.J., Chepurnaya, I.A., Vasil'eva, S.V., and Timonov, A.M., in *Trudy XXII Mezhdunarodnoi Chugaevskoi konferentsii po koordinatsionnoi khimii* (Proc. XXII Int. Chugaev Conf. on Coordination Chemistry), Chisinau, 2005, p. 217.
13. Hamnett, A., Abel, J., Eameaim, J., *et al.*, *J. Phys. Chem. Chem. Phys.*, 1999, vol. 1, pp. 5147–5156.
14. Vilas-Boas, M., Freire, C., De Castro, B., and Hillman, R., *J. Phys. Chem. B.*, 1998, vol. 102, no. 43, pp. 8533–8540.
15. Galus, Zb., *Teoretyczue podstawy elektroanalisy chemicznej*, Warsaw: Naukowe, 1971.
16. Khannanov, N.K., Yatsun, T.F., Shafirovich, V.Ya., and Strelets, V.V., *Izv. Akad. Nauk SSSR, Ser. Khim.*, 1983, no. 6, pp. 1282–1290.
17. Hurrell, H.C. and Abruna, H.D., *Inorg. Chem.*, 1990, vol. 29, pp. 736–739.
18. Gaman'kov, P.V., Synthesis and Study of the Properties of Polymeric Ni and Pd Complexes with Schiff Bases, *Cand. Sci. (Chem.) Dissertation*, St. Petersburg, 2004.
19. Dmitrieva, E.A., Logvinov, S.A., Kurdakova, V.V., *et al.*, *Elektrokhimiya*, 2005, vol. 41, no. 4, pp. 433–441.
20. Hobday, M.D. and Smith, T.D., *Coord. Chem. Rev.*, 1972, vol. 3, pp. 311–316.
21. Shagisultanova, G.A. and Kuznetsova, N.N., *Koord. Khim.*, 2003, vol. 29, no. 10, pp. 760–765.
22. Popeko, I.E., Vasil'ev, V.V., Timonov, A.M., and Shagisultanova, G.A., *Zh. Neorg. Khim.*, 1990, vol. 35, no. 4, pp. 933–937.
23. Dahm, C.E., Peters, D.G., and Simonet, J., *J. Electroanal. Chem.*, 1996, vol. 410, pp. 163–171.

Russian Journal of Applied Chemistry, Vol. 78, No. 9, 2005, pp. 1398–1402. Translated from Zhurnal Prikladnoi Khimii, Vol. 78, No. 9, 2005, pp. 1423–1427.
Original Russian Text Copyright © 2005 by Mokhammad Arif, Samoilenko, Sergeev, Blinov.

PHYSICOCHEMICAL STUDIES OF SYSTEMS AND PROCESSES

Phase Diagram and Properties of Glasses of the System Sb_2S_3–AgI

Mokhammad Arif, G. V. Samoilenko, Yu. G. Sergeev, and L. N. Blinov

St. Petersburg State Polytechnic University, St. Petersburg, Russia

Received February 16, 2005

Abstract—The phase diagram of the system Sb_2S_3–AgI was constructed from data of the differential thermal and X-ray phase analyses. The physicochemical properties of glassy and crystalline alloys were studied.

The studies performed in Russia show that introduction of halides of heavy *p, d* elements into an Sb_2S_3 melt allows preparation of glassy alloys within a considerably extended region. The glasses show high stability and have high refractive index, which is necessary for manufacturing fiber optic elements for the IR range [1–4].

The system Sb_2S_3–AgI was also studied by Mentus *et al*. [5]. They measured the electrical conductivity of the glasses σ as a function of composition in the temperature range from room temperature to 280°C. By a number of parameters, a glass of the composition $(Sb_2S_3)_{0.4}(AgI)_{0.6}$ having a high ionic conductivity ($\sigma = 10^{-3}\ \Omega^{-1}\ cm^{-1}$) stands out. The impedance characteristics obtained in [5] showed that the electrical conductivity of this glass at 147°C changed jumpwise from 10^{-4} to $10^{-1}\ \Omega^{-1}\ cm^{-1}$. This behavior was attributed to the β-AgI–α-AgI phase transition.

The above system was also studied studied by Sun *et al*. [6]. In this system, the region of glass formation by hard quenching was 0.10–0.67 AgI (mole fraction scale), the remainder being Sb_2S_3. For certain compositions, the concentration dependence of the electrical conductivity was studied. An IR study suggested the occurrence of the exchange chemical reaction in the melts:

$$Sb_2S_3 + 2AgI \rightarrow Ag_2S + 2SbSI \qquad (1)$$

Formation of glassy alloys in the system Sb_2S_3–AgI was studied in the 1990s [7, 8]. This study was of practical significance for developing membranes of chemical sensors. A Mössbauer study with ^{129}I, ^{121}Sb, and ^{110}Ag isotopes ruled out the exchange reaction (1). It was established experimentally that silver is in the iodide rather than in the sulfide surrounding.

Thus, published data on the chemical interaction of components in the Sb_2S_3–AgI system are contradictory. In addition, the number of AgI modifications and their notations in different publications are inconsistent [9, 10, 15–20]. Therefore, we chose another approach. First we analyzed the possibility of occurrence of various chemical reactions by calculating the Gibbs energy ΔG^0 and then constructred the phase diagram and studied some optical properties (transparency in the IR region and refractive index).

To study the chemical interaction of components and assess the possibility of occurrence of exchange reactions in the Sb_2S_3–AgI system from ΔH_f^0 and ΔS_f^0 values [9, 10] (see table), we calculated the Gibbs energy ($\Delta G^0 \equiv \Delta H^0 - T\Delta S^0$) at T = 298 K for the reactions

$$Sb_2S_3 + 2AgI \rightleftarrows 2SbSI + Ag_2S, \qquad (2)$$

$$Sb_2S_3 + 6AgI \rightleftarrows 2SbI_3 + 3Ag_2S. \qquad (3)$$

The results obtained in calculating the isobaric–isothermal potential of the reaction ΔG^0 showed that reactions (2) and (3) cannot proceed, since $\Delta G^0 > 0$ [49.3 and 231.6 kJ mol^{-1} for reactions (2) and (3),

Thermodynamic characteristics of formation of the compounds

Compound	ΔH_f^0, kJ mol^{-1}	ΔS_f^0, J mol^{-1} K^{-1}	References
Sb_2S_3	–157.7	181.6	[9]
SbSI	–106.3	112.6	[10]
SbI_3	–100	216	[10]
Ag_2S	–32.8	144	[9]
AgI	–62	115.6	[9]

1070-4272/05/7809-1398 © 2005 Pleiades Publishing, Inc.

respectively]. Therefore, to solve properly the problem of chemical interaction of the system components, we constructed the phase diagram of the Sb_2S_3–AgI system. To do this, we performed the differential thermal (DTA) and X-ray phase (XPA) analyses.

EXPERIMENTAL

The glasses were synthesized in a horizontal electrical furnace at continuous agitation of the melt placed in preliminarily evacuated quartz ampules. The maximal temperature of the synthesis was 700°C and the synthesis time, 6 h. The ampules with the melt were cooled in air. The glasses were synthesized from antimony (SU-000 grade), sulfur (16-5 ultrapure grade), and AgI (chemically pure grade). Antimony trisulfide was synthesized in evacuated quartz ampules by the reaction $2Sb + 3S \rightarrow Sb_2S_3$ at $T_{max} = 700$°C. AgI was prepared by the reaction of $AgNO_3$ and KI solutions: $AgNO_3 + KI \longrightarrow AgI\downarrow + KNO_3$. All the reactants were of chemically pure grade. The yellow AgI precipitate was thoroughly washed many times with distilled water, filtered off, dried, and then heated in a vacuum ($P = 10^{-3}$ mm Hg) to 220°C for 3 h. After that, X-ray diffraction patterns (DRON-3 diffractometer, FeK_α radiation) were taken at room temperature. From these diagrams, Sb_2S_3 and AgI were identified and X-ray amorphous structure of the glassy compositions in the Sb_2S_3–AgI system was confirmed. The synthesis was performed no less than three times to obtain reproducible results.

The glass density ρ was determined by the method of hydrostatic weighing in toluene at room temperature. The density of toluene was checked by the density of a germanium single crystal. The refractive index n was determined on plane-parallel glass samples by a defocusing method with an MIK-1 microscope at $\lambda = 1.1$ μm. The IR transmission spectra were recorded on a UR-20 spectrophotometer.

The glass transition point T_g, the temperature of the glass–crystal transition (crystallization point) T_c, and the temperature of the end of the melting T_l were determined by the methods used in [12, 13]. To construct the phase diagram of the Sb_2S_3–AgI system, the alloys synthesized were annealed at a temperature below the crystallization point (200°C) for 100 h. The thermographic study of the samples was performed within 20–700°C on an installation described in [11]. The sample weight was 0.5 g.

The phase diagram of the Sb_2S_3–AgI system was constructed from the experimental data obtained by DTA and XPA of annealed crystalline samples

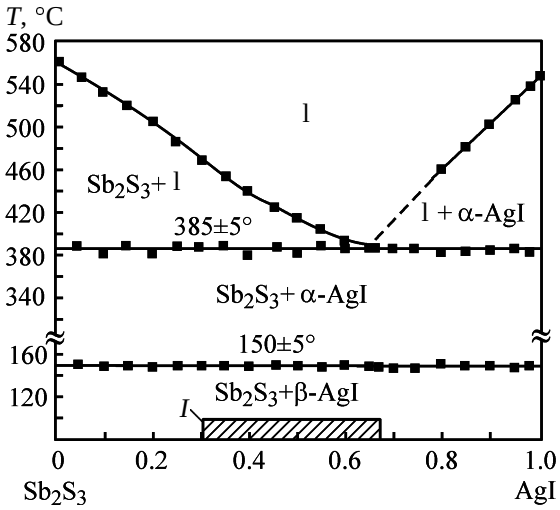


Fig. 1. Phase diagram of the system Sb_2S_3–AgI (mole fraction scale). (*T*) Temperature. (*I*) Glass formation range.

(Fig. 1). It was found that, upon spontaneous cooling of the melt in air, glassy alloys are formed in the composition range 0.30–0.67 AgI (mole fraction scale). Because the alloys tend to supercool, DTA curves were taken solely in the heating mode at a heating rate of 5 deg min^{-1}.

The glassy samples obtained were characterized by a shell-like fracture, X-ray amorphous structure, and existence of a glass transition point; they were transparent under an IR microscope. As illustration, we present X-ray diffraction patterns (Fig. 2) and thermograms (Fig. 3) of certain alloys in glassy and crystalline states.

The diffraction patterns of the glassy alloys exhibit no reflections (Fig. 2a), whereas the diffraction patterns of all the crystalline alloys contain reflections corresponding to Sb_2S_3 and AgI (Fig. 2b). This result agrees with the previous calculation of the Gibbs energy ΔG^0 of reactions of Sb_2S_3 and AgI and with the data of [7, 8].

The thermograms of the alloys studied exhibited peaks at T_g and T_c, along with the three thermal effects. The first effect corresponds to the temperature of the end of melting of the alloy T_l (liquidus line). The second is observed for all the alloys (except for the alloys of the initial components Sb_2S_3 and AgI) at 385 ± 5°C (solidus line T_s). Except for Sb_2S_3, the third thermal effect at 150 ± 5°C is observed in all the alloys and in AgI, with its value the lower, the smaller the AgI concentration (Fig. 3).

Our results suggest with confidence that (1) the constructed phase diagram of the Sb_2S_3–AgI system

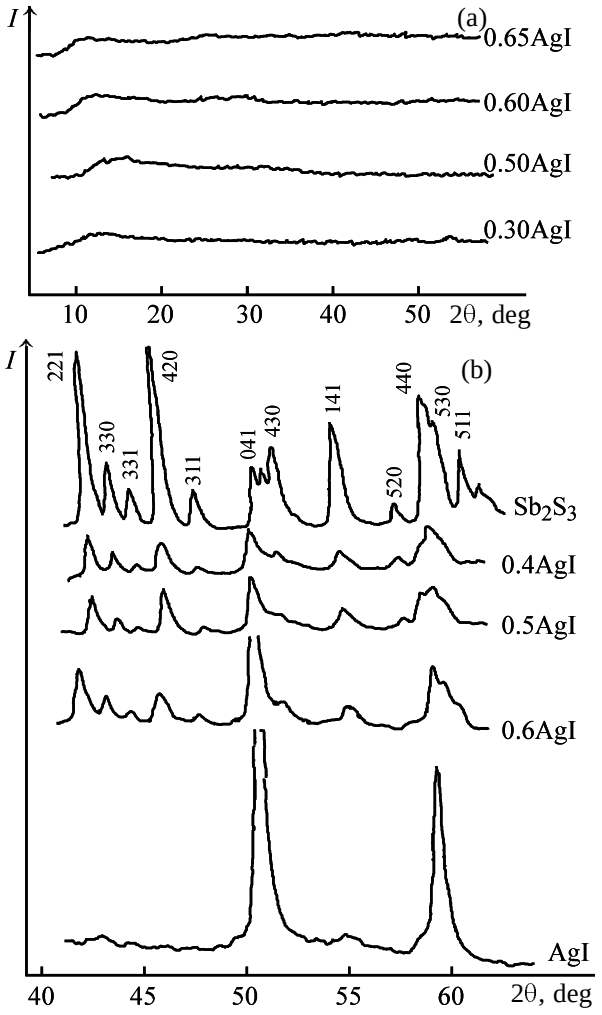


Fig. 2. X-ray diffraction patterns of (a) glassy and (b) crystalline alloys of the system Sb_2S_3–AgI (mole fraction scale). (*I*) Reflection intensity and (2θ) Bragg angle.

(Fig. 1) belongs to phase diagrams with nonvariant eutectic transformation ($l \rightleftarrows Sb_2S_3 + AgI$ at 385±5°C) and has an eutectic point at AgI mole fraction of 0.67; Sb_2S_3 crystallizes from the subeutectic alloys after a liquidus temperature T_l is attained, and AgI, from the supereutectic alloys; (2) at 145±5°C, β-AgI (hexagonal modification) undergoes a polymorphous transition into α-AgI (cubic modification), which is in line with the data of [15, 16]; below the line of the eutectic transformation (i.e., solidus line), there is a region in which two phases, Sb_2S_3 and AgI, are in equilibrium.

It should be noted that, in the range of AgI mole fractions of 0.7–0.8, the critical temperature T_l was not present in the thermograms. This is likely due to a small amount of heat released upon the crystallization of a small amount of the excess AgI phase, which

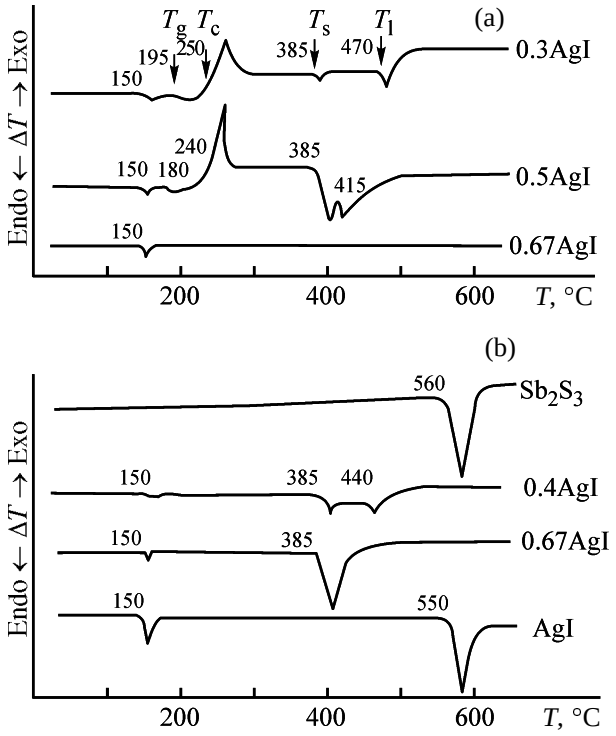


Fig. 3. DTA curves of (a) glassy and (b) crystalline samples in the Sb_2S_3–AgI system (mole fraction scale). (Δ*T*) Difference in temperatures between the sample and reference and (*T*) temperature.

is attributable to a regular decrease in the thermal effects with decreasing Sb_2S_3 concentration.

The dependences of T_g, T_c, and density ρ of the glassy samples on the composition are shown in Fig. 4a. With composition changing from 0.30 to 0.67 AgI (mole fraction scale), T_g and T_c decrease from 195 to 171°C and from 248 to 232°C, respectively, with the difference between them being about 50°C. In this case, the calculated criterion of the glass-forming ability, Hr, increases up to the AgI mole fraction of 0.67 and then decreases (Fig. 4b). As the AgI mole fraction is increased further above 0.67, the alloys are no longer amorphous. The density of the glasses regularly increases from 4.47 to 5.01 g cm^{-3} over the concentration range studied.

The Hruby criterion, Hr, is the ratio $Hr = (T_c - T_g)/(T_l - T_c)$. The larger $(T_c - T_g)$ and the smaller $(T_l - T_c)$, the larger the Hr value, and, consequently, the higher the glass-forming ability of the given melt. Published data show that, to compare the glass-forming abilities of different compositions, it is reasonable to calculate Hr. In this study, we made an attempt to find a correlation between Hr and an optical property, namely, the refractive index.

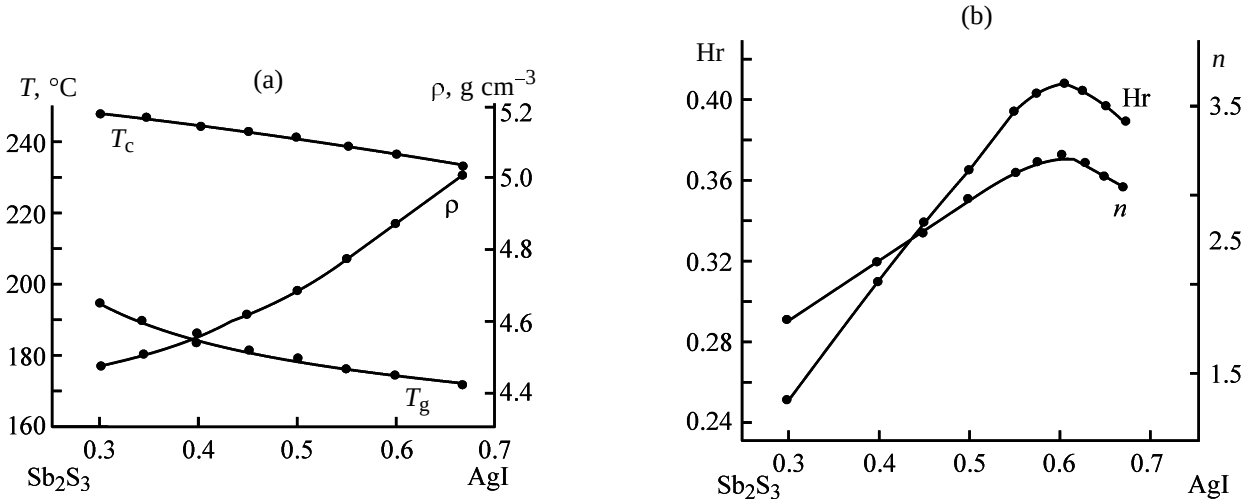


Fig. 4. (a) T_g, T_c, and ρ, and (b) refractive index n and Hr criterion vs. the composition of the Sb_2S_3–AgI glass (mole fraction scale).

The optical properties, refractive index n and transparency in the IR range, are important characteristics of iodine-containing chalcogenide glasses. Therefore, we studied how the composition affects these characteristics. The constructed dependence of the glass refractive index n on the AgI concentration in the alloy (Fig. 4b) shows that the refractive index from 1.90 to the maximum value n = 3.12 at AgI mole fraction of 0.60 and then decreases. The maximum n value is in the region of the eutectic composition. This is probably associated with higher homogeneity of the eutectic alloy in comparison with, e.g., subeutectic or supereutectic alloys.

The transmission spectra of two glassy compositions in the Sb_2S_3–AgI system are shown in Fig. 5.

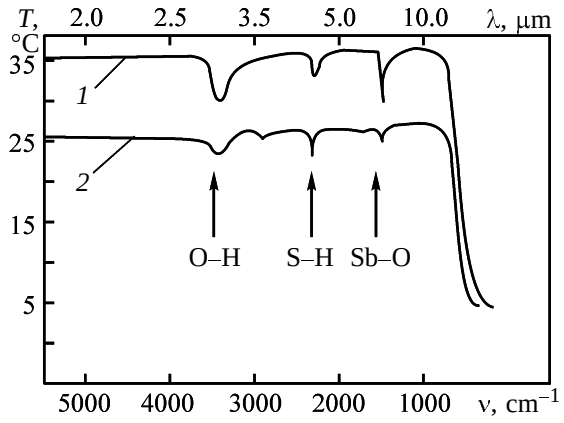


Fig. 5. IR transmission spectra of (*1*) $(AgI)_{0.4}(Sb_2S_3)_{0.6}$ and (*2*) $(AgI)_{0.6}(Sb_2S_3)_{0.4}$ glasses. Sample thickness 1.25 mm. (T_r) Transmission, (ν) wave number, and (λ) wavelength.

As seen, the glasses with the AgI mole fraction of 0.40 and 0.60 are transparent in the IR region up to a wavelength of 15 μm, and their optical transmission T (%) depends on the composition: the optical transmission of the glasses increases from 25 to 35% with increasing AgI content. At the same time, the intensity of the impurity absorption bands corresponding to O–H, S–H, and Sb–O in the transmission spectra increases. This fact shows that the initial AgI contains some water, which reacts with sulfur and antimony of the alloy. With changing composition, the absorption edge of the glasses studied does not noticeably shift to longer wavelengths.

CONCLUSIONS

(1) The phase diagram of the Sb_2S_3–AgI system with eutectic nonvariant transformation and polymorphous transition from the low-temperature β phase into the high-temperature α phase was constructed from data of differential thermal and X-ray phase analyses.

(2) The region of glass formation region in spontaneous cooling of the melts in air is within 0.30–0.67 AgI (mole fraction scale, remainder Sb_2S_3).

(3) In the region of the eutectic composition, the glasses studied have high, up to 3 and larger, refractive indices and are transparent in the IR range up to the wavelength λ = 15 μm.

(4) The glass with the AgI mole fraction of 0.60 can be used as a matrix for obtaining glasses with high ionic conductivity to produce on their basis

membranes for chemical sensors and a new class of biosensors to be used in medicine and biochemistry.

REFERENCES

1. Baidakov, L.A., and Arif, M., *Sovremennye materialy: tekhnologii i issledovaniya* (Advanced Materials: Technology and Study): *Tr. Sankt-Peterb. Gos. Tekh. Univ.*, 1996, no. 463, pp. 3–7.
2. Arif, M., and Baidakov, L.A., *Fiz. Khim. Stekla*, 1995, vol. 21, no. 6, pp. 627–629.
3. Arif, M., Tolochko, O.V., and Baidakov, L.A., *Fiz. Khim. Stekla*, 1996, vol. 22, no. 1, pp. 91–93.
4. Arif, M., Blinov, L.N., and Tolochko, O.V., *Fiz. Khim. Stekla*, 1998, vol. 24, no. 4, pp. 499–501.
5. Mentus, S.V., Susic, M.V., and Gajinov, S.P., *Solid State Ionics*, 1983, vol. 11, no. 2, pp. 143–149.
6. Sun, H.W., Tanguy, B., and Reau, J.-M., *J. Non-Cryst. Solids*, 1988, vol. 99, no. 2, pp. 222–232.
7. Vlasov, Yu.G., Bychkov, E.A., Legin, A.V., and Daved, M.M., *Elektrokhimiya*, 1991, vol. 27, no. 11, pp. 1432–1439.
8. Daved, M.M., Ionic Processes and Short-Range Order in Sulfide Glasses Activated with Silver Halides by Data of Radiochemical and Nuclear Spectroscopic Methods, *Cand. Sci. Dissertation*, St. Petersburg, 1992.
9. Rabinovich, V.A., and Khavin, Z.Ya., *Kratkii khimicheskii spravochnik* (Concise Chemical Handbook), St. Petersburg: Khimiya, 1978.
10. *Khimicheskaya entsiklopediya* (Chemical Encyclopedia), Zefirov, N.S., Ed., Moscow: Bol'shaya Rossiiskaya Entsiklopediya, 1995, vol. 4.
11. Brauer, G., *The Synthesis and Characterization of Inorganic Compounds. A Laboratory Manual*, Stuttgart: Enke, 1981.
12. Remy, H. von, *Lehrbuch der anorganischen Chemie*, Leipzig: Geest und Portig, 1961.
13. Karyakin, Yu.V., and Angelov, I.I., *Chistye khimicheskie veshchestva* (Pure Chemicals), Moscow: Khimiya, 1974.
14. Takahashi, T., Kuwabara, K., and Yamamoto, O., *J. Electrochem. Soc*., 1969, vol. 116, no. 3, pp. 357–360.
15. Takahashi, T., Ikeda, Sh., and Yamamoto, O., *J. Electrochem. Soc*., 1972, vol. 119, no. 4. pp. 477–482.
16. Takahashi, T., Ikeda, Sh., and Yamamoto, O., *J. Electrochem. Soc*., 1973, vol. 120, no. 5, pp. 647–651.
17. Hruby, A., *Czech. J. Phys*., 1972, vol. B22, no. 10, pp. 1187–1193.
18. Hruby, A., *Czech. J. Phys*., 1973, vol. B23, no. 11, pp. 1263–1272.
19. Samoilenko, G.V., Arif, M., Novikov, E.V., *et al*., *Fiz. Khim. Stekla*, 2004, vol. 30, no. 4, pp. 700–705.
20. Filippov, S.N., Arif, M., and Blinov, L.N., *XII Mezhdunarodnaya konferentsiya "Vysokie intellektual'nye tekhnologii obrazovaniya i nauki"* (XII Int. Conf. "High Intellectual Technologies of Science and Education"), St. Petersburg: Sankt-Peterb. Gos. Politekh. Univ., 2005, pp. 321–322.

Russian Journal of Applied Chemistry, Vol. 78, No. 9, 2005, pp. 1403–1407. Translated from Zhurnal Prikladnoi Khimii, Vol. 78, No. 9, 2005, pp. 1428–1432.
Original Russian Text Copyright © 2005 by Gaile, Kostenko, Semenov, Koldobskaya.

PHYSICOCHEMICAL STUDIES OF SYSTEMS AND PROCESSES

Extraction of 1-Methylnaphthalene, Benzothiophene, and Indole with *N*-Methylpyrrolidone from Their Mixtures with Alkanes

A. A. Gaile, A. V. Kostenko, L. V. Semenov, and L. L. Koldobskaya

St. Petersburg State Technological Institute, St. Petersburg, Russia
Kirishinefteorgsintez Production Association, Limited Liability Company, Kirishi, Leningrad oblast, Russia

Received September 1, 2004; in final form, July 2005

Abstract—Extraction of 1-methylnaphthalene, benzo[*b*]thiophene, and indole with *N*-methylpyrrolidone from their model mixtures with hexadecane in the absence and in the presence of lower-boiling *n*-alkanes (hexane, decane, dodecane) was studied.

The requirements to the environmental safety of motor and boiler fuels became considerably more stringent in the past 5–10 years. The permissible concentration of sulfur and aromatic hydrocarbons in automobile gasolines, diesel fuel, black oil for ships, and boiler fuel is restricted.

The content of nitrogen in fuels is not restricted. However, nitrogen compounds in fuels are catalytic poisons, and with an increase in their content the efficiency of hydrorefining decreases. Also decreases the yield of light petroleum products in catalytic cracking and hydrocracking of vacuum gas oils and black oils.

Exhaustive removal of sulfur and nitrogen compounds from fuels using traditional hydrogenation methods requires elevation of partial hydrogen pressures and upgrade of installations with inclusion of additional hydrorefining reactors because of low feed space velocities; this requires large investments and increases the power consumption. Hydrogenolysis of 4,6-dialkyl derivatives of dibenzothiophene is especially difficult because of steric hindrance [2].

In the alternative extraction procedure for fuel treatment, on the contrary, such heteroatomic aromatic or partially aromatic compounds should be readily removed, as suggested by higher, compared to arenes, stability constants of the complexes with polar solvents, low enthalpies of mixing, and low activity coefficients. In particular, the formation constants of complexes of *N*-methylpyrrolidone with benzo[*b*]thiophene and naphthalene at 20°C are 1.9 and 0.6 l mol^{-1}, respectively [3]. The activity coefficients of benzo[*b*]-thiophene and naphthalene at infinite dilution in diethylene glycol at 30°C are 6.6 and 11.2 [4]. The enthalpies of specific interaction of 1-methylnaphthalene, benzo[*b*]thiophene, and indole with *N*-methylpyrrolidone at 25°C are –33.5, –38.4, and –54.4 kJ mol^{-1}, respectively [5].

However, data on the extractive recovery of heteroatomic compounds and arenes are contradictory. For example, Podolyak *et al.* [6] report that benzothiophene is extracted better than naphthalene. At the same time, data obtained by Bikkulov *et al.* [7] indicate that naphthalene homologs are extracted from kerosene–gas oil fractions with *N*-methylpyrrolidone better than benzothiophene homologs.

Therefore, taking also into account problems with the determination of nitrogen compounds (whose content in petroleum fractions is by an order of magnitude lower than that of organosulfur compounds), it is urgent to examine the relative efficiency of extraction of arenes and aromatic sulfur and nitrogen compounds from model mixtures with saturated hydrocarbons.

The goals of this study were to compare the efficiency of the extraction of heterocyclic sulfur- and nitrogen-containing compounds and polycyclic arenes from model mixtures with *n*-alkanes and to elucidate the influence exerted by various nonpolar diluents on the efficiency of the extraction of heterocyclic compounds and arenes.

As a polar solvent for the extraction of heterocyclic compounds and arenes we chose *N*-methylpyrrolidone. This extractant is commercially used both for extraction of benzene, toluene, and xylene from reformer naphthas and for selective refining of oil fractions [8].

We found previously [9–11] that the separation factors of hydrocarbons substantially increase when the extraction of benzene and naphthalene homologs with polar extractants (acetonitrile, methyl Cellosolve,

1070-4272/05/7809-1403© 2005 Pleiades Publishing, Inc.

Table 1. Conditions of one-step extractions with aqueous *N*-methylpyrrolidone at 50°C

Run no.	Water content in *N*-methylpyrrolidone, wt %	Solvent : feed weight ratio	Nonpolar diluent	Nonpolar diluent : feed weight ratio
1	–	2 : 1	–	–
2	3	2 : 1	–	–
3	6	2 : 1	–	–
4	3	1.5 : 1	–	–
5	3	1 : 1	–	–
6	3	2 : 1	Hexane	0.5 : 1
7	3	2 : 1	Dodecane	0.5 : 1
8	3	2 : 1	Decane	0.5 : 1
9	3	2 : 1	″	1 : 1
10	3	2 : 1	″	1.5 : 1
11	–	2.06 : 1	–	–

dimethylformamide) from model mixtures with saturated hydrocarbons is performed in the presence of pentane or other low-boiling nonpolar diluents.

It seemed interesting to reveal how the molecular weight of *n*-alkanes affects the selectivity of the extractive recovery with *N*-methylpyrrolidone of not only arenes but also heterocyclic compounds. As nonpolar *n*-alkanes (diluents), we chose hexane, decane, and dodecane.

The model hydrocarbon system used as a feed contained (wt %) 49.67 hexadecane, 40.25 1-methylnaphthalene, 5.00 benzo[*b*]thiophene, and 5.08 indole. All the components of the model hydrocarbon system have relatively close boiling points (°C); the difference is, however, sufficient for separation on PFMS-4 nonpolar phase in GLC analysis: benzo[*b*]thiophene 221–222°C, 1-methylnaphthalene 245°C, indole 254°C, and hexadecane 286.5°C. Each of the heterocyclic and aromatic components contains two fused aromatic rings. With respect to the boiling point, these components belong to the diesel fraction.

It is known, however, that there are linear correlations between the selectivities of solvents to different arenes (e.g., to homologs of mono-, bi-, and tricyclic arenes), to indole and carbazole, or to benzo[*b*]thiophene and dibenzothiophene. This is due to a common mechanism of specific interactions of polar solvents with benzologs or homologs of arenes and heterocyclic compounds. Therefore, the relationships that will be revealed with the chosen model system will be applicable to higher-boiling components, e.g., to systems consisting of phenanthrene (or anthracene) homologs, dibenzothiophenes, and carbazole homologs (these compounds are present in vacuum gas oils and black oils).

EXPERIMENTAL

N-Methylpyrrolidone, benzo[*b*]thiophene, 1-methylnaphthalene, indole, *n*-hexadecane, *n*-dodecane, *n*-decane, and *n*-hexane were freshly distilled; the main substance content, according to GLC, was no less than 99.8 wt %. Experiments on one-step extraction were performed in a hermetically sealed vessel equipped with a magnetic stirrer. The raffinate and extract phases were sampled with a microsyringe after complete phase separation and were analyzed by GLC (column length 3 m, internal diameter 3 mm, stationary phase PFMS-4, solid support Chromaton N-AW-HMDS, carrier gas He, column temperature 160°C, vaporizer temperature 280°C, thermal conductivity detector, detector temperature 250°C). The compositions of the equilibrium phases were calculated using the calibration coefficients determined with reference mixtures: hexane 0.87, *N*-methylpyrrolidone 0.92, decane 0.94, benzo[*b*]thiophene 0.96, 1-methylnaphthalene 1.00, dodecane 1.10, hexadecane 1.16, and indole 1.22. With decane used as nonpolar diluent, an additional analysis on the Carbowax stationary phase was made.

We examined the influence exerted on the extraction efficiency by the following parameters (Table 1): water content in *N*-methylpyrrolidone (run nos. 1–3), extractant : feed ratio (run nos. 2, 4, 5), nonpolar diluent (decane) : feed ratio (run nos. 8–10), and molar weight of the nonpolar diluent, alkane (run nos. 6–8). Run no. 11 was performed with a different model mixture containing approximately equal amounts of the components to be extracted (wt %): benzo[*b*]thiophene 5.79, 1-methylnaphthalene 6.33, indole 4.74, and hexadecane 83.14. It is known that the distribution factors of components depend on their

Table 2. Material balance of run no. 6

Component	Content in feed		Content in indicated phase			
			raffinate		extract	
	g	wt %	g	wt %	g	wt %
N-Methylpyrrolidone	1.8047	55.37	0.0342	3.60	1.7705	76.67
Water	0.0558	1.71	–	–	0.0558	2.42
Benzo[*b*]thiophene	0.0466	1.43	0.0125	1.32	0.0341	1.48
1-Methylnaphthalene	0.3753	11.52	0.1081	11.39	0.2672	11.57
Indole	0.0474	1.45	0.0079	0.83	0.0395	1.71
Hexadecane	0.4631	14.21	0.4206	44.28	0.0425	1.84
Hexane	0.4663	14.31	0.3665	38.58	0.0998	4.32
Total	3.2592	100	0.9498	100	2.3094	100

Table 3. Distribution factors K_d and separation factors β in systems extractable component–hexadecane

Run no.	Distribution factor K_d				Separation factor β		
	1-methylnaphthalene	benzo[*b*]thiophene	indole	hexadecane	1-methylnaphthalene	benzo[*b*]thiophene	indole
1	0.84	1.07	2.52	0.086	9.77	12.44	29.30
2	0.77	0.88	1.93	0.061	12.62	14.43	31.64
3	0.65	0.77	1.42	0.038	17.11	20.26	37.37
4	0.92	1.07	1.83	0.05	18.40	21.40	36.60
5	1.12	1.28	1.70	0.04	28.00	32.00	42.50
6*	0.65	0.72	1.32	0.027	24.07	26.67	48.89
7*	0.72	0.86	1.84	0.029	24.83	29.66	63.45
8*	0.69	0.77	1.50	0.028	24.64	27.50	53.57
9*	0.58	0.66	1.17	0.017	34.12	38.82	68.82
10*	0.54	0.58	0.98	0.012	45.0	48.33	81.67
11	1.09	1.58	2.72	0.034	32.06	46.47	80.00

* The values of K_d and β were calculated from the compositions of phases, without taking into account the nonpolar diluent.

content in the feed; in run no. 11, this factor is virtually eliminated.

As example, we present the material balance for one of extraction runs, calculated using the yields of the raffinate and extract phases and their compositions determined by GLC (Table 2).

As seen from Tables 3 and 4, the efficiency of the extraction of the components (with respect to all the parameters) increases in the order 1-methylnaphthalene < benzo[*b*]thiophene < indole. The degree of recovery and the distribution and separation factors increase in the same order.

At similar concentrations of the extractable components in the feed (Table 3, run no. 11), the distribution factors of benzo[*b*]thiophene and indole are higher than those of 1-methylnaphthalene by factors of 1.5 and 2.5, respectively.

The increased distribution factors of benzo[*b*]thiophene and separation factors are due to the higher electron-donor power of this compound compared to 1-methylnaphthalene. Still higher distribution and separation factors for indole are due to an additional kind of specific interaction, hydrogen bonding between *N*-methylpyrrolidone and labile N–H proton of indole.

With moist *N*-methylpyrrolidone used instead of the anhydrous extractant, the separation factors and concentrations in the extract of 1-methylnaphthalene, benzo[*b*]thiophene, and indole increase, but the degree of recovery and the distribution factors decrease. This is caused by the high selectivity of water to arenes and aromatic heterocyclic compounds and by the low solvency of water.

With an increase in the extractant : feed ratio from

Table 4. Results of one-step extraction of 1-methylnaphthalene, benzo[*b*]thiophene, and indole from their mixture with hexadecane

Run no.	Raffinate yield, wt %	Concentration, wt %						Recovery α, wt %		
		in raffinate			in extract					
		1-methyl-naphthalene	benzo[*b*]-thiophene	indole	1-methyl-naphthalene	benzo[*b*]-thiophene	indole	1-methyl-naphthalene	benzo[*b*]-thiophene	indole
1	39.37	16.10	1.62	0.75	55.91	7.18	7.88	84.26	87.27	94.16
2	46.97	17.00	1.89	0.98	60.85	7.75	8.71	80.17	82.25	90.98
3	54.52	19.01	2.05	1.27	65.71	8.50	9.64	74.26	77.36	86.37
4	53.05	17.51	1.93	1.25	65.90	8.47	9.40	76.92	79.55	86.91
5	58.57	18.67	2.10	1.70	70.75	9.10	9.84	73.93	56.23	73.71
6	58.89	19.69	2.28	1.44	69.71	8.90	10.30	71.20	73.18	83.33
7	56.77	18.30	2.02	1.17	69.07	8.82	10.23	74.18	76.16	86.95
8	57.65	18.87	2.17	1.28	69.42	8.87	10.25	72.99	75.04	85.46
9	62.36	21.01	2.38	1.57	72.12	9.33	10.88	67.44	70.35	80.76
10	65.24	22.30	2.58	1.85	73.93	9.51	11.15	63.84	66.28	76.37
11	79.01	1.02	2.79	1.63	9.21	6.02	5.79	87.19	61.92	72.83

1 : 1 to 2 : 1 (run nos. 5 and 2), the degrees of recovery of the extractable components increase (for benzo[*b*]thiophene and indole to a greater extent than for 1-methylnaphthalene), but the concentrations of the extractable components in the extract and the separation factors decrease. These results are attributable to greater transfer of hexadecane to the extract phase with an increase in the extractant : feed ratio and to an increase in the distribution factor of hexadecane from 0.04 (run no. 5) to 0.061 (run no. 2).

It is interesting to compare the data on the extraction of *N*-methylpyrrolidone without nonpolar diluent and in the presence of various alkanes of lower molecular weight compared to hexadecane. With an increase in the number of carbon atoms in alkane molecules, their activity coefficients in *N*-methylpyrrolidone increase and the mutual solubility decreases, as indicated by the critical solution temperatures (CSTs). For example, the CSTs of hexane and hexadecane with *N*-methylpyrrolidone are 51.85 and 94.45°C, respectively [12].

Therefore, the distribution factor of hexane, calculated from data in Table 2 (K_d = 0.112), is considerably higher than that of hexadecane (K_d = 0.042) in the same run no. 6. Relatively low-boiling nonpolar solvent can be readily distilled off from the extract phase, to obtain increased concentrations of the extractable components in the extract. The separation factors for the systems hexadecane–arene and hexadecane–heterocyclic compounds also increase appreciably. This trend may be due to the fact that *N*-methylpyrrolidone concentrating in the extract phase is selective to aromatic compounds, whereas the nonpolar diluent concentrating in the raffinate phase is selective to hexadecane and favors its transfer to the raffinate phase.

A drawback of the exctraction using systems polar extractant–nonpolar diluent is decreased recovery of the extractable components. This is caused by the fact that these components are readily soluble not only in *N*-methylpyrrolidone but also in the nonpolar diluent. Both the separation factors and the degrees of recovery of arenes and heterocyclic compounds can be increased by taking a higher ratio of the polar solvent to the feed.

With a higher-boiling alkane, decane or dodecane, used as a nonpolar diluent instead of hexane, the separation factors of the components increase to a still greater extent. This result can be accounted for as follows. With a decrease in the difference between the molar volumes of the saturated hydrocarbons of the feed (hexadecane in our case) and nonpolar diluent, the entropy constituent of the activity coefficient of, e.g., hexadecane decreases in accordance with the Flory–Huggins equation, which results in the growth of the selectivity to hexadecane in the order hexane < decane < dodecane.

With an increase in the ratio of the nonpolar diluent (decane) to feed, the separation factors and concentrations of the extractable components in the extract increase to a still greater extent, but this is accompanied by a decrease in the degree of recovery.

Table 5. Changes in the extraction parameters in run no. 7 relative to run no. 3

Parameter	1-Methyl-naphthalene	Benzo[*b*]-thiophene	Indole
Concentration, rel %:			
in raffinate	–3.7	–1.5	–7.9
in extract	+5.1	+3.8	+6.1
Recovery, rel %	–0.1	–1.6	+0.7
Distribution factor, rel %	+10.8	+11.7	+29.6
Separation factor, rel %	+45.1	+46.4	+69.8

Thus, there are two ways to increase the separation selectivity at a fixed temperature: (1) using the moist extractant and (2) using the extraction system polar extractant–nonpolar diluent. The efficiencies of these two approaches are compared in Table 5 (extraction run nos. 3 and 7). In run no. 3, the extractant contained two times more water, and run no. 7 was performed in the presence of dodecane. Table 5 shows that the recovery of 1-methylnaphthalene, benzo[*b*]-thiophene, and indole in run nos. 3 and 7 is virtually equal, and with respect to all the other parameters the extraction in the presence of dodecane is more efficient: the distribution and separation factors and the concentrations of the extractable components in the extract are higher, and their residual concentrations in the raffinate are lower. The yield of the raffinate in run no. 7 is also higher (by 2.25 wt %) than in run no. 3.

The advantages of the extraction system extractant–nonpolar diluent, compared to the moist extractant, should become more pronounced in going from one-step to multistep extraction.

CONCLUSIONS

(1) The efficiency of extraction of aromatic compounds with *N*-methylpyrrolidone from mixtures with saturated hydrocarbons increases in the order alkylnaphthalenes < benzo[*b*]thiophene < indole. The separation factors in the systems with benzo[*b*]thiophene and indole are higher than in the systems with 1-methylnaphthalene by factors of approximately 1.5 and 2.5, respectively.

(2) Extraction of arenes and heterocyclic compounds with a polar extractant in the presence of a nonpolar diluent is a more efficient way to increase the separation selectivity, compared to the use of the moist extractant.

(3) The separation factors in the systems hexadecane–1-methylnaphthalene, benzo[*b*]thiophene, or indole in the extraction with *N*-methylpyrrolidone in the presence of a nonpolar diluent (alkane) increase in the order of diluents hexane < decane < dodecane.

REFERENCES

1. Kaminskii, E.F. and Khavkin, V.A., *Glubokaya pererabotka nefti: tekhnologicheskii i ekologicheskii aspekty* (Deep Oil Refining: Processing and Environmental Aspects), Moscow: Tekhnika, 2001.
2. Macaud, M., Milenkovic, A., Schulz, E., *et al.*, *J. Catal.*, 2000, vol. 193, no. 2, pp. 255–263.
3. Zaretskii, M.I., *Koks Khim.*, 2003, no. 10, pp. 29–32.
4. Zaretskii, M.I., Podolyak, V.G., Kononov, N.F., *et al.*, Abstracts of Papers, *XIII nauchnaya sessiya po khimii i tekhnologii organicheskikh soedinenii sery i sernistykh neftei* (XIII Scientific Session on Chemistry and Technology of Organic Sulfur Compounds and Sulfurous Crude Oils), Riga: Zinatne, 1974, pp. 333–334.
5. Krichman, E.S., Gaile, A.A., and Semenov, L.V., *Zh. Obshch. Khim.*, 1991, vol. 61, no. 3, pp. 694–697.
6. Podolyak, V.G., Zaretskii, M.I., and Taits, S.Z., *Neftekhimiya* (Petroleum Chemistry), Proskuryakov, V.A., Ed., Leningrad: Nauka, 1985, pp. 169–174.
7. Dushin, P.N., Sokov, Yu.F., Bikkulov, A.Z., *et al.*, *Neftepererab. Neftekhim.*, 1975, no. 9, pp. 27–28.
8. Bittrich, H.-J., Gaile, A.A., Lempe, D., *et al.*, *Razdelenie uglevodorodov s ispol'zovaniem selektivnykh rastvoritelei* (Separation of Hydrocarbons Using Selective Solvents), Leningrad: Khimiya, 1987.
9. Varshavskii, O.M., Gaile, A.A., Koldobskaya, L.L., *et al.*, *Ekstraktsiya i primenenie arenov srednedistillyatnykh neftyanykh fraktsii: Sbornik trudov OOO "KINEF"* (Extraction and Applications of Arenes from Middle Oil Distillates: Coll. of Papers of KINEF Limited Liability Company), Gaile, A.A. and Somov, V.E., St. Petersburg: Sintez, 1998, pp. 19–29.
10. Gaile, A.A., Kaifadzhyan, E.A., Semenov, L.V., *et al.*, *Zh. Prikl. Khim.*, 1998, vol. 71, no. 12, pp. 2003–2008.
11. Erzhenkov, A.S., Gaile, A.A., Somov, V.E., and Semenov, L.V., *Ekstraktsionnaya dearomatizatsiya neftyanykh fraktsii: Sbornik trudov OOO "KINEF"* (Extractive Dearomatization of Oil Fractions: Coll. of Papers of KINEF Limited Liability Company), Gaile, A.A. and Somov, V.E., Eds., St. Petersburg: Sankt-Peterb. Gos. Univ., 2002, pp. 94–101.
12. Hradetzky, G., Hammerl, Y., Kisan, W., *et al.*, *Data of Selective Solvents: DMFA–NMC–NMP*, Berlin: Wissenschaften, 1989.

Russian Journal of Applied Chemistry, Vol. 78, No. 9, 2005, pp. 1408–1410. Translated from Zhurnal Prikladnoi Khimii, Vol. 78, No. 9, 2005, pp. 1433–1435.
Original Russian Text Copyright © 2005 by M. Gavrilenko, N. Gavrilenko, Mokrousov.

PHYSICOCHEMICAL STUDIES OF SYSTEMS AND PROCESSES

Solid-Phase Extraction of Aliphatic Amines from the Aqueous Phase with a Methacrylate Polymer

M. A. Gavrilenko, N. A. Gavrilenko, and M. G. Mokrousov

Tomsk State University, Tomsk, Russia

Received December 30, 2004; in final form, April 2005

Abstract—Solid-phase extraction of aliphatic amines from aqueous solutions with a methacrylate polymer was studied. The possibility of simultaneous sorption of amines considerably differing in the boiling point was examined.

Aliphatic amines widely occur in the nature. They act as secondary pollutants forming by biodegradation of nitrogen-containing compounds, including proteins and amino acids [1]. The necessity of monitoring amines is caused not only by an unpleasant odor of some of them, but also by the possibility of their transformation under certain conditions into considerably more hazardous nitrosamines [2].

Toxic amines are particularly hazardous in aquatic objects [3]. Owing to high polarity, amines are readily soluble in water, and their recovery is difficult. Amines are usually determined by capillary gas and liquid chromatography [4, 5]. Despite high sensitivity of these methods, determination of amines requires preconcentration. This is usually done by liquid [6, 7] and solid-phase [8, 9] extraction. A relatively new approach is solid-phase preconcentration of amines on the microlevel [10] involving the use of a detector highly selective to nitrogen. Also, Baltussen *et al.* [11, 12] suggested a combined approach involving solid-phase extraction with polydimethylsiloxane or poly(butyl acrylate) followed by thermal desorption into the chromatograph injector. However, nonpolar sorbents poorly extract polar amines, and polar poly(butyl acrylate) in the step of thermal desorption gives noise and false peaks in the chromatograms.

The use of styrene–divinylbenzene polymers, XAD, and cyclodextrins for solid-phase extraction of amines was described in numerous papers [13–16], but no acceptable procedure has been developed. Thus, studies in the field of sorption of polar substances from aqueous media remain very urgent.

In this study we examined solid-phase extraction of dimethylamine (DMA), ethylamine (EA), diethylamine (DEA), triethylamine (TEA), propylamine (PA), dipropylamine (DPA), and tripropylamine (TPA) from aqueous solutions with a polar hydrophobic methacrylate polymer (PM), followed by determination of the amines by capillary gas chromatography.

EXPERIMENTAL

The study was performed with a Shimadzu GC-9A gas chromatograph (Japan); a 25000 × 0.25-mm capillary column was coated with SE-30 (30 μm). The temperature of the detector and injector was 200°C. The column temperature program was as follows: 70°C, 1 min; heating to 200°C, 5 deg min^{-1}; 200°C, 3 min. The sample was pumped through the sorbent with a Gilson Minipuls-2 micropump (the United States).

Stock solutions of amines (1 g l^{-1}) were prepared in MILLI-Q water (Millipore, the United States) and were stored at 6°C. Working solutions (20–50 μg l^{-1}) were prepared just before the experiments in double-distilled water. Acidic solutions (pH < 4) were prepared with hydrochloric acid. The buffer solution with pH 9 was prepared by mixing 0.1 M solutions of potassium dihydrogen phosphate and sodium hydroxide.

The polymethacrylate sorbent was prepared by radical block copolymerization of methacrylate monomers, with benzoyl peroxide as initiator [17]. A 10 × 5-mm steel precolumn was packed with the sorbent of particle size 0.1–0.15 mm. Aqueous solutions of DMA, EA, DEA, TEA, PA, DPA, and TPA (50 μg l^{-1} each) were passed through the PM sorbent at pH 9. To evaluate the extractive power, we took 10 ml of the solution that passed through the sorbent and the same aliquot of the initial solution. Both samples were extracted with 1 ml of diethyl ether. The extracts were dried over anhydrous sodium sulfate and evaporated to 100 μl prior to the analysis. Before extraction of

1070-4272/05/7809-1408© 2005 Pleiades Publishing, Inc.

amines from aqueous solution, the column was dried with a nitrogen flow for 5 min. The amines were desorbed with diethyl ether (flow rate 0.1 ml min^{-1}). The resulting extract was drier over anhydrous sodium sulfate for 6 h and concentrated to a volume of 100 μl on a rotary evaporator under nitrogen.

The recovery of amines with the polymethacrylate at pH 9 was close to 100%, as judged from the absence of chromatographic peaks of the amines in the sample treated with the sorbent. However, at pH 7 and 3 the recovery was lower, ranging for various amines from 22 to 58 and from 11 to 28%, respectively (see table).

To determine the optimal conditions of the extraction of the amines with the PM sorbent, we examined how the recovery depends on the volume of the amine solution (20–400 ml) at a constant amount of the sorbent (200 mg) (Fig. 1) and on the sorbent amount at a constant volume of the amine solution (100 ml) (Fig. 2). We also studied the desorption with various amounts of diethyl ether (0.5–10 ml) at constant volume of the amine solution (100 ml) and constant amount of the sorbent (400 mg).

The extraction of DMA (which is washed out most readily) with 200 mg of PM is complete up to passing 80–100 ml of the amine solution; this volume can be increased by taking larger amounts of the sorbent. Further experiments were performed with 100-ml portions of the amine solution. No significant differences were observed in the experiments performed with different amounts of the sorbent. Further experiments were performed with 400-mg portions of PM. The optimal volume of diethyl ether was 2 ml per 400 mg of the sorbent.

The efficiency of the solid-phase extraction of amines with PM depends on the flow rate of the amine solution through the sorbent (Fig. 3). The best results in the group preconcentration of amines were obtained at a flow rate of 2 ml min^{-1}. For individual amines, the optimal flow rate is 1–2 ml min^{-1} for highly volatile DMA and 2–4 ml min^{-1} in the other cases. The narrow interval of the optimal flow rate in the extraction of amines is associated with the specific features of two-step preconcentration of polar substances on hydrophobic polar sorbents [18]. In the first step, the preconcentration occurs on the hydrophobic PM surface, after which the polar substances can diffuse into the bulk of the sorbent. Therefore, in the determination of amines, the flow rate should not be lower than 2 ml min^{-1}. However, the same effect allows PM to be used for solid-phase extraction of volatile polar compounds at low flow rates in the sorption and desorption steps. The chromatogram of a model solution containing all the examined amines (50 μg l^{-1} each) is shown in Fig. 4a.

Extraction of amines from aqueous solution (100 ml) at various pH

Amine	Recovery, %, at indicated pH		
	3.0	7.0	9.0
DMA	28.2	55.8	98.9
EA	22.8	35.5	95.6
DEA	15.5	49.7	100.0
TEA	18.4	68.4	94.0
PA	10.6	24.5	88.2
DPA	25.1	52.1	94.3
TPA	16.3	22.6	98.9

The detection limit of the amines in the procedure involving extraction with PM sorbent and detection by capillary gas chromatography was evaluated as the minimal detectable concentration at a signal-to-noise

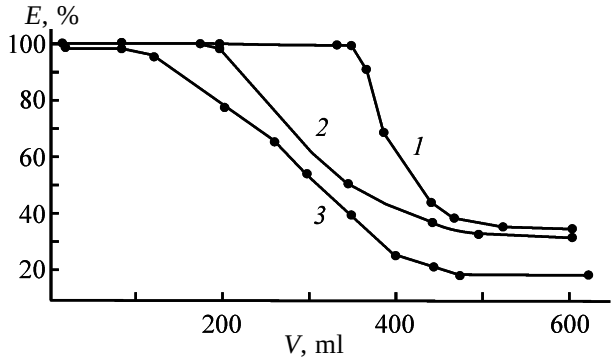


Fig. 1. Recovery *E* of amines from aqueous solution as a function of solution volume *V* at a constant amount of the sorbent (200 mg): (*1*) DPA, (*2*) DEA, and (*3*) DMA.

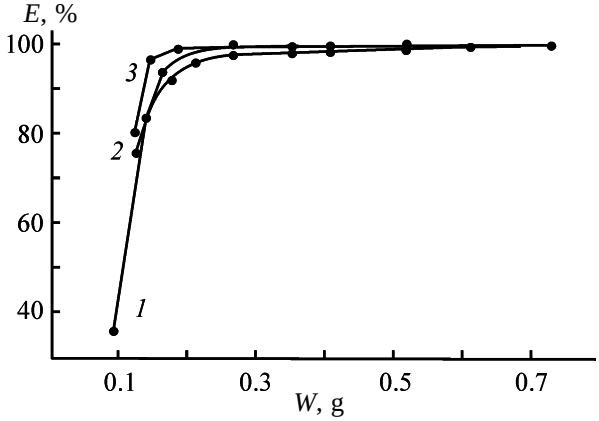


Fig. 2. Recovery *E* of (*1*) DMA, (*2*) DEA, and (*3*) DPA as a function of the sorbent weight *W* at a constant volume of the amine solution (100 ml).

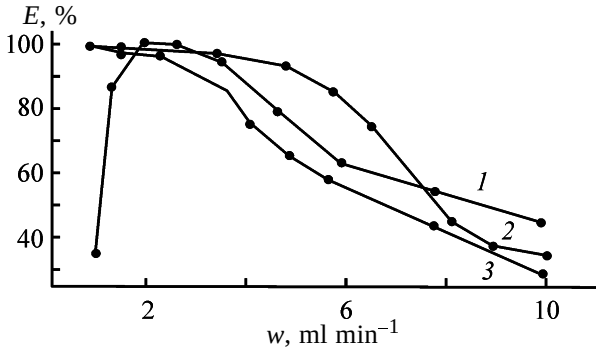


Fig. 3. Recovery *E* of (*1*) DEA, (*2*) DPA, and (*3*) DMA from aqueous solution as a function of the flow rate *w* of the amine solution through the sorbent.

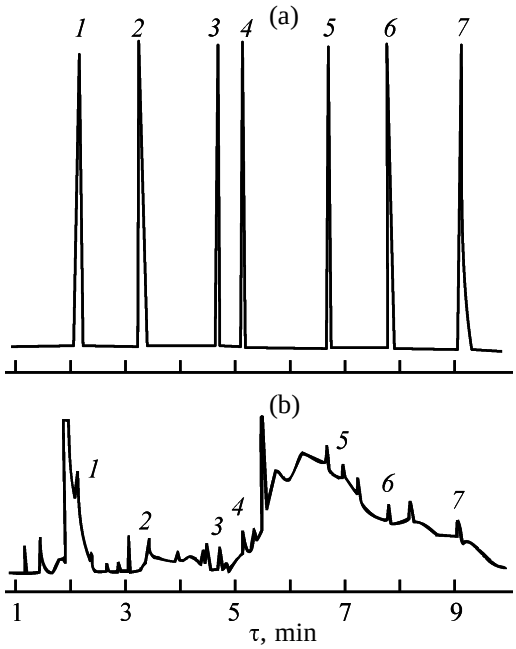


Fig. 4. Chromatograms: (a) reference solution of the amines (50 μg l^{-1} each) after solid-phase extraction with PM under optimal conditions and (b) river water sample (amine concentration 5 μg l^{-1}). (τ) Time. Amine: (*1*) DMA, (*2*) EA, (*3*) PA, (*4*) DEA, (*5*) TEA, (*6*) DPA, and (*7*) TPA.

ratio of 3 : 1. For the amines in question under the optimal conditions, the detection limit is 0.5–1.0 μg l^{-1}. At the sorbent weight increased to 600–800 mg and the sample volume, to 400 ml, the detection limit is 0.4–0.6 μg l^{-1} (Fig. 4b).

The suggested procedure of solid-phase extraction of amines was applied to analysis of river water samples. A 100-ml aliquot was filtered through a Nylon filter to remove solid particles and was adjusted to pH 9 with a buffer solution. No amines were detected by gas chromatography after preconcentration with the PM sorbent. Therefore, a solution of the amines used in our experiments was artificially added to the sample to obtain 5 μg l^{-1} concentration of each amine. The chromatogram of the resulting sample is shown in Fig. 4b.

CONCLUSION

Solid-phase extraction with a polymethacrylate sorbent allows efficient simultaneous preconcentration of amines with the boiling points varying in a wide range. Hydrophobic polar polymethacrylate sorbs polar amines and is chemically stable at various pH.

REFERENCES

1. Gao, C.-X., Krull, I.S., and Trainor, T., *J. Chromatogr. Sci.*, 1990, vol. 28, no. 3, pp. 102–108.
2. Tricker, A.R. and Preussmann, R., *Mutat. Res.*, 1991, vol. 259, nos. 3–4, pp. 277–289.
3. Riggin, R.M. and Howard, C.C., *Anal. Chem.*, 1979, vol. 51, pp. 210–214.
4. Terashi, A., Hanada, Y., Kido, A., *et al.*, *J. Chromatogr.*, 1990, vol. 503, pp. 369–376.
5. Pfundstein, B., Tricker, A.R., and Pressman, R., *J. Chromatogr.*, 1991, vol. 539, pp. 141–149.
6. Pietsch, J., Hampel, S., Schmidt, W., *et al.*, *Fresenius J. Anal. Chem.*, 1996, vol. 355, no. 2, pp. 164–173.
7. Sacher, F., Lenz, S., and Brauch, H.-J., *J. Chromatogr.*, 1997, vol. 764, pp. 85–93.
8. Djozan, D. and Farai-Zadah, M.A., *J. High Resol. Chromatogr.*, 1996, vol. 19, no. 11, pp. 633–638.
9. Matchett, W.H. and Brumley, W.C., *J. Liq. Chromatogr. Relat. Technol.*, 1997, vol. 20, no. 1, pp. 79–100.
10. Pan, L., Chong, J.M., and Pawliszyn, J., *J. Chromatogr.*, 1997, vol. 773, pp. 249–260.
11. Baltussen, E., Janssen, H.-G., and Sandra, P., *J. High Resol. Chromatogr.*, 1997, vol. 20, no. 6, pp. 395–399.
12. Baltussen, E., David, F., and Sandra, P., *J. High Resol. Chromatogr.*, 1998, vol. 21, no. 12, pp. 645–648.
13. Kawaguchi, Y., Tanaka, M., Nakae, M., *et al.*, *Anal. Chem.*, 1983, vol. 55, pp. 1852–1853.
14. Tanaka, M., Mizobuchi, Y., Kuroda, T., *et al.*, *J. Chromatogr.*, 1981, vol. 219, pp. 108–111.
15. Bhaskar, M., Aruna, P., and Jeevan, R.J.G., *Anal. Chim. Acta*, 2004, vol. 509, pp. 39–44.
16. Less, M., Schmidt, T.C., Low, E. von, *et al.*, *J. Chromatogr.*, 1998, vol. 810, pp. 173–182.
17. Gavrilenko, N.A., Mokrousov, G.M., and Dzhiganskaya, O.V., *Zh. Anal. Khim.*, 2004, vol. 59, no. 9, pp. 967–970.
18. Barnes, D.E., Marshall, G.D., and Staden, J.F. van, *Sep. Sci. Technol.*, 1995, vol. 30, pp. 751–762.

Russian Journal of Applied Chemistry, Vol. 78, No. 9, 2005, pp. 1411–1415. Translated from Zhurnal Prikladnoi Khimii, Vol. 78, No. 9, 2005, pp. 1436–1439.
Original Russian Text Copyright © 2005 by Blokhin, Amosov, Murashkin, Evdoshenko, Mikhailenko, Nikitin.

SORPTION AND ION-EXCHANGE PROCESSES

Sorption of Rhenium(VII) on Gel and Macroporous Anion Exchangers of Different Basicities from Solutions of Mineral Acids and Their Ammonium Salts

A. A. Blokhin, A. A. Amosov, Yu. V. Murashkin, S. A. Evdoshenko, M. A. Mikhailenko, and N. V. Nikitin

St. Petersburg State Technological Institute, St. Petersburg, Russia
Purolite Int. Ltd., Russian Representation, Moscow, Russia

Received June 9, 2005

Abstract—Equilibrium sorption of rhenium on strongly basic gel-like anion exchanger Purolite A600, on weakly acidic anion exchangers Purolite A170 and A172 with macroporous and gel structures and on composite anion exchanger Purolite SIM202, which is a synthetic sorbent based on super-cross-linked polystyrene impregnated with trialkylamine Alamine 336, was studied in a wide range of concentrations of sulfuric, hydrochloric, and nitric acids and of their ammonium salts.

Rhenium belongs to elements that are the least abundant in the earth's crust. No proper rhenium deposits are found in the nature. Rhenium is obtained as by-product of refinement of copper–molybdenum ores, which are a primary rhenium source. Also, it is extracted from spent catalysts of petrochemical industry, among which platinum–rhenium catalysts are a major secondary source of rhenium. Depending on the raw material type and method of its reprocessing, rhenium can be extracted primarily from sulfuric acid solutions (washing sulfuric acid used in wet dust collection systems of molybdenum production or in gas-treatment systems of copper production), and also from nitric acid solutions (obtained in breakdown of molybdenite concentrates with nitric acid), hydrochloric acid solutions (obtained by leaching of rhenium compounds from spent platinum–rhenium catalysts), and from solutions of the corresponding salts, mainly of ammonium salts, formed by neutralization of the acids.

The ion-exchange sorption, along with liquid extraction, is the most efficient method for extracting rhenium from multicomponent solutions. Available data on the effect exerted by the macrocomponent on the Re(VII) sorption on various ion exchangers are scarce [1–4]. No systematic studies were performed in this field.

This study is concerned with the Re(VII) sorption on gel and macroporous ion exchangers differing in the basicity and on composite ion exchanger based on granulated polystyrene impregnated with technical-grade trialkylamine. The sorption was performed from solutions of sulfuric, hydrochloric, and nitric acids and from acidified solutions of the corresponding ammonium salts (sulfate, chloride, and nitrate, respectively) of various concentrations.

EXPERIMENTAL

The objects of this study were ion exchangers differing in the basicity and pore structure, manufactured by Purolite Company in the form of commercial resins that showed good performance in recovery of rhenium from various objects and of pilot samples, including (1) gel-like highly basic anion exchanger A600 functionalized with quaternary ammonium groups $-N^+R_3$, (2) macroporous weakly basic anion exchanger A170 containing secondary amino groups –NHR, (3) gel-like weakly basic anion exchanger A172 functionalized with the same groups as A170 anion exchanger (pilot sample), and (4) a composite anion exchanger SIM202 based on super-cross-linked polystyrene with a developed porosity (Hypersol-Macronet sorbent) impregnated with trialkylamine Alamine 336 (extractant content 0.9 mmol l^{-1} of sorbent) and thus containing functional tertiary amino groups $-NR_2$ [5].

The experiments were performed under static conditions. The ratio of the weighed portion of the ion exchanger in terms of the absolute dry mass (g) to

1070-4272/05/7809-1411 © 2005 Pleiades Publishing, Inc.

the solution volume (ml) was 1 : 100, and the contact time was 5–7 days. After this period, the solutions were separated from the ion exchangers and analyzed for the content of rhenium(VII).

The concentration of Re(VII) in the solutions was determined by the thiocyanate method using a KFK-2MP photoelectrocolorimeter [6].

From the change in the Re(VII) concentration, we calculated the sorption capacity of the ion exchangers [mg Re(VII)/g of dry ion exchanger], taking into account the weighed portion of the ion exchanger and the solution volume. Then, the values obtained were recalculated to the volume capacity [mg Re(VII)/ml of swollen ion exchanger], taking into account the specific volume of the ion exchangers. The distribution coefficients of Re(VII) D were calculated as the ratios of the volume capacity of the ion exchanger to the Re(VII) concentration in the equilibrium solution.

First we studied how the concentration of mineral acids (sulfuric, hydrochloric, and nitric) and their ammonium salts (at a constant solution acidity of 0.1 M) affects the Re(VII) sorption on the chosen ion exchangers. The Re(VII) concentration in the initial solutions was constant and equal to 0.5 g l^{-1} (0.00269 M). The data obtained were plotted in the form of the dependences of the distribution coefficients of Re(VII) on the concentration of the corresponding acids and salts (Figs. 1A–1C). As seen, as the concentration of the acids and corresponding salts, i.e., of ions of macrocomponents competing with the perrhenate ion, increases, the distribution coefficients in sorption of Re(VII) on all the ion exchangers decrease, though to a different extent. The presence of H_2SO_4 and $(NH_4)_2SO_4$ in the solutions affects the Re(VII) sorption to the least extent, and the presence of HCl and NH_4Cl, to a greater extent. The strongest suppressing effect on the Re(VII) sorption is exerted by HNO_3 and NH_4NO_3. At the similar total concentration of the macroanions, the ammonium salts of the corresponding acids affect the Re(VII) sorption to a lesser extent than the acids themselves, i.e., a so-called acid effect is observed.

With respect to the negative effect exerted on the Re(VII) sorption, the acids can be ranked in the order $H_2SO_4 < HCl \ll HNO_3$, corresponding to the order of the affinity of their anions for the ion exchanger: $HSO_4^- < Cl < NO_3^-$. The same order is observed with the ammonium salts of the acids.

In general, the anion-exchange selectivity is most adequately explained in terms of the Diamond–Whitney's theory [7], according to which the selectivity of anion exchangers with respect to the anions is the higher, the larger the anion size, the smaller its charge, and thus, the weaker its hydration. Under the action of water structure, large anions having small charge, which are weakly hydrated, are more readily displaced into the phase of the anion exchanger, where water has less ordered structure, and form there ion pairs with large hydrophobic cations that are functional groups of anion exchangers. In the process, small anions, which are hydrated more strongly, are displaced into the solution phase. Indeed, the thermochemical radius is 0.282, 0.230, 0.181, and 0.189 nm for ReO_4^-, SO_4^{2-}, Cl^-, and NO_3^-, respectively, and the Gibbs energy of hydration is –921, –330, and –289 kJ mol^{-1} for SO_4^{2-}, Cl^-, and NO_3^-, respectively [8]. For perrhenate ion, we found no data in the literature on the Gibbs energy of hydration. At the same time, the value reported for the MnO_4^- ion (–231 kJ mol^{-1}) suggests that it should be considerably lower than that for sulfate, nitrate, and chloride ions. Hence, single-charged ion ReO_4^- having the largest size and thus the lowest capability for hydration should be sorbed on anion exchangers more selectivity than the other ions mentioned above. In addition, sulfate ion has the highest (in the absolute value) hydration energy. Therefore, it exerts a weak competing effect on the Re(VII) sorption. The hydration energy of the ions decreases in the order sulfate > chloride > nitrate ion. Therefore, their competition with the perrhenate ion in sorption on anion exchangers increases in the same order.

The acid effect can be accounted for as follows. The higher distribution coefficients in the Re(VII) sorption from $(NH_4)_2SO_4$ solutions compared to H_2SO_4 solutions are due to the fact that in solutions of sulfuric acid the sulfate ion is in the form of single-charged protonated hydrosulfate ion HSO_4^-, whereas in $(NH_4)_2SO_4$ solutions it is in the form of deprotonated sulfate ion SO_4^{2-}. Apparently, single-charged hydrosulfate ion is less hydrated than double-charged sulfate ion. Therefore, it is competitive with perrhenate ion to a greater extent. For hydrochloric acid and ammonium chloride, or nitric acid and ammonium nitrate, the nature of the acid effect is difficult to understand. Hydrochloric and nitric acids are strong acids, and their anions show no tendency to protonate. At the same time, it was suggested in [7] that, e.g., HCl_2^--like associates, whose selectivity relative to anion exchangers should be higher than that of chloride ion Cl^-, can be formed in concentrated HCl. The same may be true for nitric acid.

It is important that, contrary to the published data, in the capability to sorb Re(VII) from solutions of

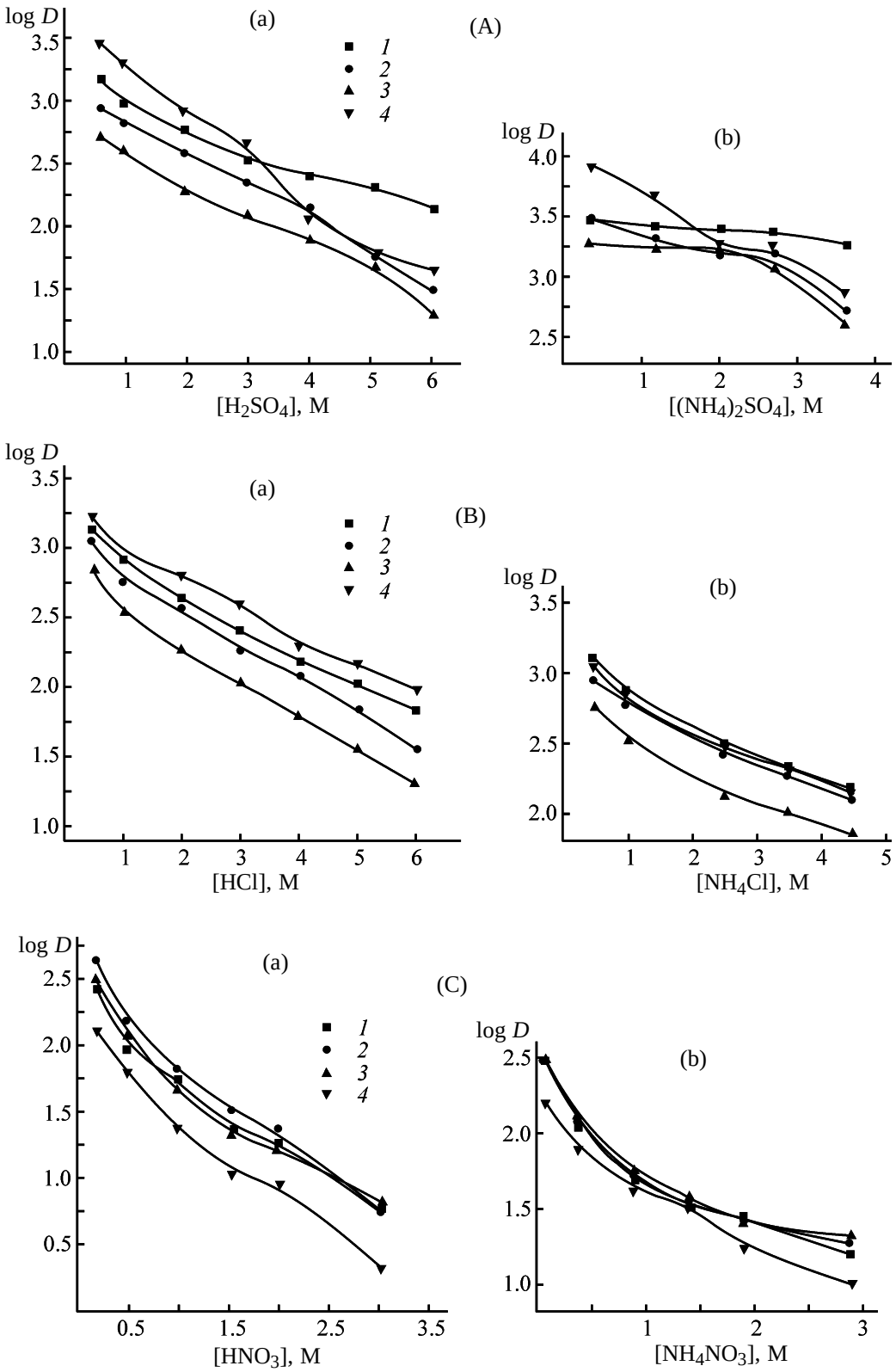


Fig. 1. Distribution coefficient of Re(VII) *D* vs. the concentration of (a) acid and (b) corresponding salt in sorption on Purolite anion exchangers. (A) H_2SO_4, $(NH_4)_2SO_4$; (B) HCl, NH_4Cl; and (C) HNO_3, NH_4NO_3. Ion exchanger: (*1*) A170, (*2*) A172, (*3*) A600, and (*4*) SIM202.

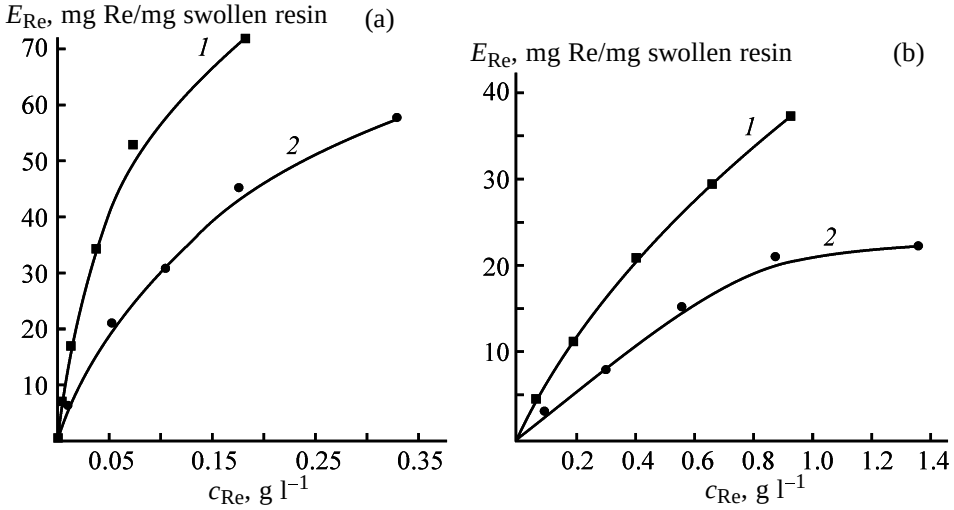


Fig. 2. Isotherms of Re(VII) sorption on A170 anion exchanger from (a) H_2SO_4 and (b) HNO_3 solutions. (E_{Re}) Sorption capacity of anion exchanger for Re(VII) and (C_{Re}) equilibrium rhenium concentration. Acid concentration, M: (a) (*1*) 1.0 and (*2*) 4.0; (b) (*1*) 1.0 and (*2*) 2.0.

different compositions with a high content of macrocomponents, the weakly basic anion exchangers tested here not only compete well with the strongly basic ion exchanger but also surpass it in sorption from solutions of sulfuric and hydrochloric acids and their ammonium salts. In HNO_3 and NH_4NO_3 solutions, the sorption on composite ion exchanger SIM202 is drastically deteriorated, whereas anion exchangers A170 and A172 show practically the same results as A600.

It seemed important to estimate the capacity characteristics of the ion exchangers for Re(VII) in a wide range of its concentrations at different concentrations of the macrocomponents in solutions. This was done by taking isotherms of Re(VII) sorption from H_2SO_4 solution, which suppresses the sorption to a minimal extent, and from HNO_3 solutions, whose negative effect on the Re(VII) sorption is especially strong, on A170 anion exchanger, which is a selective Re(VII) sorbent. The isotherms of Re(VII) sorption were taken from 1 and 4 M H_2SO_4 solutions and from 1 and 2 M HNO_3 solutions (Fig. 2).

The data obtained show that the Re(VII) sorption from sulfate solutions on anion exchangers is more efficient than from nitrate solutions over the entire range of its equilibrium concentrations. For example, the ion exchanger capacity relative to Re(VII) at its same equilibrium concentrations in sorption from 4 M H_2SO_4 is several times higher than in sorption from 1 M HNO_3. Thus, the selective weakly basic anion exchangers are suitable for efficient extraction of Re(VII) from concentrated H_2SO_4 solutions. At the same time, the ion-exchange method can hardly be recommended for Re(VII) extraction from nitrate solutions containing more than 1 M HNO_3.

CONCLUSIONS

(1) With respect to the negative effect exerted on the sorption of Re(VII) on strongly and weakly basic anion exchangers, mineral acids can be ranked in the order $H_2SO_4 < HCl \ll HNO_3$, in agreement with the order of the affinity of their anions for the anion exchangers ($HSO_4^- < Cl < NO_3^-$). The ammonium salts of the corresponding acids affect the Re(VII) sorption to a lesser extent.

(2) The weakly basic anion exchangers analyzed in this study surpass the highly basic anion exchanger in the capability to sorb Re(VII) from sulfate and chloride solutions.

(3) The sorption capacity of weakly basic anion exchanger A170 for Re(VII) from 4 M H_2SO_4 is several times higher than from 1 M HNO_3.

REFERENCES

1. *Ionity v tsvetnoi metallurgii* (Ion Exchangers in Nonferrous Metallurgy), Lebedev, K.B., Ed., Moscow: Metallurgiya, 1975.
2. Kholmogorov, A.G., Mokhosoev, M.V., and Zonkhoeva, E.L., *Modifitsirovannye ionity v tekhnologii molibdena i vol'frama* (Modified Ion Exchangers in

Molybdenum and Tungsten Technology), Novosibirsk: Nauka, 1985.

3. Kryukova, E.I., Zagorodnyaya, A.N., Lebedev, K.B., *et al.*, *Kompleksn. Ispol'z. Miner. Syr'ya*, 1986, no. 8, pp. 33–36.
4. Lebedev, K.B., Naimanov, S., and Tyurekhodzhaeva, T.I., in *Trudy Inst. Metallurgii i Obogashcheniya, Akad. Nauk Kaz. SSR* (Trans. Inst. of Metallurgy and Dressing, Acad. Sci. of Kazakh SSR), 1986, pp. 119–124.
5. Blokhin, A.A., Kopyrin, A.A., Mikhailenko, M.A., and Nikitin, N.V., *Tsvetn. Met.*, 2005, no. 2, pp. 59–62.
6. Borisova, L.V., and Ermakov, A.N., *Analiticheskaya khimiya reniya* (Analytical Chemistry of Rhenium), Moscow: Nauka, 1974.
7. Diamond, R.M., and Whitney, D.C., *Resin Selectivity in Dilute to Concentrated Aqueous Solutions, Ion Exchange, A Series of Advances*, chapter 8: *Ion Exchange*, Marinsky, J.A., Ed., New York: Dekker, 1966.
8. Krestov, G.A., *Termodinamika ionnykh protsessov v rastvorakh* (Thermodynamics of Ionic Processes in Solutions), Leningrad: Khimiya, 1987.

Russian Journal of Applied Chemistry, Vol. 78, No. 9, 2005, pp. 1416–1419. Translated from Zhurnal Prikladnoi Khimii, Vol. 78, No. 9, 2005, pp. 1440–1443.
Original Russian Text Copyright © 2005 by Tin'gaeva, Zil'berman.

SORPTION AND ION-EXCHANGE PROCESSES

Synthesis and Properties of Organomineral Sorbents

E. A. Tin'gaeva and M. V. Zil'berman

Perm State Technical University, Perm, Russia
Ekologiya Ural Research Institute, Perm, Russia

Received December 27, 2004; in final form, May 2005

Abstract—Composite sorbents including an active inorganic component and a polymeric binder were obtained. The effect of various factors on their sorption and strength properties was studied.

The high selectivity, heat resistance, and radiation stability of ion-exchange materials based on sparingly soluble inorganic compounds make such sorbents suitable for selective recovery of components from multicomponent solutions with the aim of utilization of these components or purification of process solutions and wastewater [1].

The possibility of effective use of inorganic ion-exchange materials is largely determined not only by their chemical properties, but also by the hydromechanical stability of granulates. As a rule, a sufficient hydromechanical stability of inorganic ion-exchange materials is achieved by creating composites [1], with inorganic materials commonly used as binders or supports.

Table 1 shows that a high mechanical stability of a material is, as a rule, provided by a significant decrease in the fraction of the active component in the sorption material.

An analysis of published evidence concerning the technology of polymeric materials and concepts of how stresses arise in granulated ion-exchange materials in their deformation [5] led to a conclusion that organic polymers can also be used as binders.

Here we describe fundamentals of a method for synthesis of organomineral sorbents, which yields granulates of inorganic sorbents with a content of the active component in a formulation exceeding 80 wt %, and report on certain properties of the ion-exchange materials obtained.

EXPERIMENTAL

The technique developed consists in the following. A suspension containing a polymer solution and a powdered inorganic sorbent is dispersed into a precipitant. The polymer is cured by washing-out the solvent from a drop of a suspension of the powdered inorganic component in a polymer solution, which is close to the known "wet" method for forming of synthetic and artificial fibers. The use of this method makes it possible to combine the processes of formulation curing and grain forming.

Some linear polymers, including perchlorovinyl (PCV), ABS plastics, and cellulose acetate, were tested as organic binders. These substances are well soluble in organic solvents, sufficiently wear-resistant, and nontoxic.

Water was used as a precipitant. This imposed certain requirements on the choice of a solvent for the polymer: this solvent should be fully miscible with water.

Acetone, dimethylformamide, and dimethylacetamide were tested as solvents meeting these requirements.

Hexacyanoferrates(II) and (III) of transition metals and hydrated titanium and aluminum oxides were used as active inorganic components.

The sorption properties of the organomineral

Table 1. Comparison of different techniques for production of granulates of inorganic ion-exchange materials

Technique	Fraction of the active component, %	Mechanical strength
Impregnation into finished supports	Up to 20	High [1]
Drying	100	Low [2]
Coprecipitation with silica gel	Uo to 50	High [3]
Sol–gel method	Up to 30	High [4]

1070-4272/05/7809-1416 © 2005 Pleiades Publishing, Inc.

sorbents were studied with respect to different ions, to assess the selectivity of the materials studied.

The sorption of chloride ions was studied on AAT-0P sorbent (with hydrated Al_2O_3 as support). The experiments were carried out under static conditions by the method of separate samples, using a 0.1 M NaCl solution with pH 3 (adjusted with an HCl solution); weighed portion of the sorbent 1 g, ratio between the solution volume and sorbent mass 100 : 1, time of contact 0.5 h.

The sorption of Cs^+ on samples of ferrocyanide sorbents was carried out from solutions containing 0.56 g dm^{-3} cesium ions; weighed portion of the sorbent 0.5 g, l : s = 160 : 1.

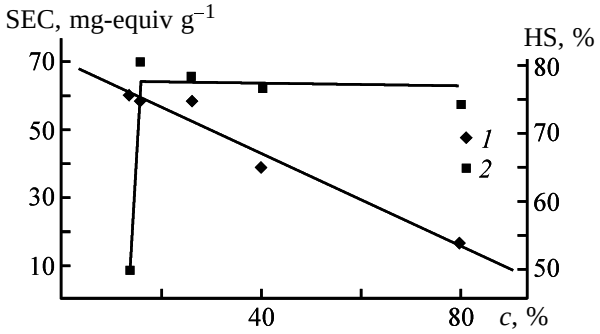
Dynamic experiments were performed by filtration of electrolyte solutions at a rate of 4–6 cm^3 h^{-1} across a 20-cm sorbent bed in a glass column 5 mm in diameter.

In these experiments, the sorption of Li^+ on ISTZh-1P sorbent with hydrated TiO_2 as the active component was carried out, similarly to [6], from a solution containing (g dm^{-3}): Li_2SO_4 5.5, NaCl 56.0, and NaOH 3.0. Cesium ions were sorbed from a 0.01 M CsCl solution.

The concentration of metal ions in model solutions, solutions after sorption, and eluates was determined by atomic-adsorption analysis, and that of Cl^- ions, by titration.

To evaluate the hydromechanical stability (HS), 30 cm^3 of a working solution was poured into a plastic vessel with 5 g of a sorbent. To enhance the mechanical impact upon the sorbent, a 20-g fluoroplastic disc was placed in the vessel. The contents of the vessel were shaken for 3 h at a frequency of 4 Hz with an amplitude of 20 mm. The amount of grains that remained undestroyed was taken as their HS (wt %).

Of particular importance in optimization of the synthesis conditions is the composition of the suspension delivered to dispersion and, in particular, the concentration of the polymer and the ratio between the polymer and the inorganic sorbent. As shown by experiments, the suspension is cured in washing-out of the organic solvent without any significant change in volume. Therefore, to raise the capacity of the granulate per unit volume, more concentrated suspensions should be used when possible. However, this leads to a rise in viscosity, mainly because of an increase in the concentration of the polymer solution. The apparatus employed (pneumatic nozzles and disc



(*1*) SEC for Cs^+ and (*2*) HS vs. the fraction *c* of the polymeric binder (cellulose acetate) in the formulation.

atomizers) enabled working with solutions containing up to 11 wt % polymer.

The figure shows how the sorption exchange capacity (SEC) and HS of organomineral sorbents depend on the polymer content in a formulation.

It can be seen that an increase in the polymer content in the formulation leads to a virtually linear decrease in capacity. The dependence of the hydromechanical stability of the sorbent is of a clearly pronounced steplike type. For example, HS is virtually constant at a polymer concentration exceeding 16 wt %. This indicates, in our opinion, that a continuous polymeric skeleton of a grain is formed just at this concentration.

Our results show that the optimal content of cellulose acetate is 16–30% for sorbents based on hexacyanoferrates(II) and (III) of transition metals. For sorbents based on hydrated titanium and aluminum oxides, the concentration optimum of the polymer is 11–20% [6, 7].

In this range of the polymer content, the organomineral sorbents retain a high ion-exchange capacity for the target ion, and a sufficiently strong, deformation-resistant packing is ensured.

The kinetic parameters of the organomineral sorbents are fairly high. The effective inner diffusion coefficients *D* in Cs^+ sorption on organomineral sorbents based on copper potassium hexacyanoferrate $KCu_{1.5}[Fe(CN)_6]$ (FOC Cu) and cellulose acetate are given in Table 2.

Table 2 shows that the kinetic parameters are only slightly dependent on the polymer content in a formulation. It should be noted that the effective inner diffusion coefficients markedly exceed the diffusion coefficients of ions in an aqueous solution.

This phenomenon can be attributed to concentration of cesium ions on the surface of the pore space

Table 2. Diffusion coefficients and exchange capacities of FOC Cu sorbent at different fractions of the polymer

Cellulose acetate, %	E, (mg-equiv Cs) g^{-1}		D, $mg^2\ s^{-1}$
	per gram of sorbent	per gram of inorganic substrate	
25	1.30	1.78	0.1946×10^{-8}
40	0.92	1.54	0.1738×10^{-8}
60	0.69	1.73	0.173×10^{-8}
80	0.37	1.87	0.173×10^{-8}

[8] and also to a nonuniform distribution of the active component in a grain.

As the fraction of the polymer in the sorbent increases, the exchange capacity of the polymer becomes smaller, but it remains virtually the same when recalculated per gram of the inorganic phase.

In the course of curing of a grain, the suspension components are spatially redistributed. In particular, the outer surface of the grain is enriched with the most hydrophilic component, the inorganic constituent of the composite sorbent. The deformations accompanying this redistribution give rise to undesirable mechanical stresses. It was suggested to perform a hydrothermal treatment in order to intensify the relaxation of internal stresses and to modify the structure of the pore space. This is commonly done in the polymer technology. For example, it was shown in [9] that heating of cellulose acetate to 70–90°C in an aqueous medium leads to relaxation of internal stresses. The best results in hydrothermal treatment of organomineral sorbents were obtained with aqueous-salt solutions. For example, a certain rise in the exchange capacity and diffusion coefficient was observed for a sorbent based on copper potassium hexacyanoferrate and cellulose acetate as the content of acetic acid increased from 4 to 8%, and the concentration of NaCl, from 10 to 80 g cm^{-3}.

A stronger effect is produced by boiling ISTZh-1P sorbent in 0.05 M LiOH for 1.5–2 h. As a result, the exchange capacity increases by 8–12%, and the HS, by 36–39%. Boiling of grains of AAT-0P sorbent in a 0.05 M solution of Na_2SO_4 also leads to an increase in the HS by 5–8%, and in the capacity by 17–52%.

According to the data obtained, hydrothermal treatment leads to redistribution of components within a grain toward coarsening of polymeric fragments, which improves their sorption and strength properties. In conclusion, a number of known sorption materials are compared with the organomineral sorbents (Table 3).

Table 3 shows that introduction of an organic binder into the materials raises their HS by a factor of 1.3–4.4. The hydromechanical stability of ferrocyanide organomineral sorbents containing 16% cellulose acetate and 17% PVC (with copper potassium hexacyanoferrate the rest) exceeds by 6–20% the wear resistance of ferrocyanide–silica gel formulations (fraction of the active component 62%).

The organomineral sorbents ISTZh-1P and AAT-0P, based on hydrated TiO_2 and Al_2O_3, retain a high DEC and SEC for lithium ions and chloride ions. Their capacities recalculated per gram of the inorganic substrate (Table 3, in parentheses) exceed the corresponding values for samples containing no polymeric binder.

CONCLUSIONS

(1) Organomineral sorbents containing an active inorganic constituent and a polymeric binder were

Table 3. Comparative parameters of inorganic sorbents and their organomineral formulations

Parameter	Sorbent						
	FS-10 [1]	FOC Cu + PCV	FOC Cu + cellulose acetate	ISTZh-1 [6]	ISTZh-1P	AAT-0 [7]	AAT-0P
HS, %	75.0	80.0	95.0	21.1	93.0	49.2	85.4
Dynamic exchange capacity, DEC, (mg-equiv M) g^{-1}	185 (Cs^+)	240	286	4.1 (Li^+)	3.9(5.0)	–	–
Static exchange capacity, SEC, mg-equiv g^{-1}	–	–	–	3.3	3.2(4.0)	2.4 (Cl^-)	2.7 (Cl^-)
Separation factor $P_{Li,Na}$	–	–	–	70–90	80–100	–	–
Capacity to 1% breakthrough, (mg Cs^+) g^{-1}	133	196	213	–	–	–	–

synthesized. The sorbents can be recommended for multicycle use in recovery of valuable components from multicomponent solutions or for purification of wastewater to remove heavy metal ions. It was established that the content of a polymer in a grain in synthesis of sorbents should be within 11–20% for perchlorovinyl and 16–30% for cellulose acetate.

(2) The conditions of a hydrothermal treatment of the granulate ensuring the high strength and good sorption-kinetic characteristics were found.

(3) The dependence of the rate of the ion exchange on the fraction of a polymer in the sorbent was determined; granulation with an organic binder does not diminish the accessibility of the active inorganic constituent.

REFERENCES

1. *Neorganicheskie sorbenty: Katalog-spravochnik* (Inorganic Sorbents: Catalog and Reference Book), Perm: Perm. Politekh. Inst., 1988, issue 1.
2. Kalinin, N.F., in *Khimiya i tekhnologiya neorganicheskikh sorbentov: Mezhvuzovskii sbornik* (Chemistry and Technology of Inorganic Sorbents: Intercollegiate Coll.), Perm: Perm. Politekh. Inst., 1979, pp. 111–114.
3. Vol'khin, V.V., Kalyuzhnyi, A.V., Zil'berman, M.V., *et al*., in *Khimiya i tekhnologiya neorganicheskikh sorbentov: Mezhvuzovskii sbornik* (Chemistry and Technology of Inorganic Sorbents: Intercollegiate Coll.), Perm: Perm. Politekh. Inst., 1980, p. 57.
4. Zil'berman, M.V., Kozlova, G.F., and Kor'eva, O.A., in *Khimiya i tekhnologiya neorganicheskikh sorbentov: Mezhvuzovskii sbornik* (Chemistry and Technology of Inorganic Sorbents: Intercollegiate Coll.), Perm: Perm. Politekh. Inst., 1985, pp. 26–27.
5. Sharygin, L.M., *Zh. Fiz. Khim.*, 1979, vol. 53, no. 3, pp. 706–710.
6. Onorin, S.A., Vol'khin, V.V., Khodyashev, M.V., *et al*., in *Khimiya i tekhnologiya neorganicheskikh sorbentov: Mezhvuzovskii sbornik* (Chemistry and Technology of Inorganic Sorbents: Intercollegiate Coll.), Perm: Perm. Politekh. Inst., 1989, pp. 124–129.
7. *TU* (Technical Specification) *6-09-40-1466–386: AAT-0 Ion Exchanger*, Perm, 1986.
8. Pan, L.S., Vol'khin, V.V., and Zil'berman, M.V., in *Khimicheskie problemy zashchity okruzhayushchei sredy: Mezhvuzovskii sbornik* (Chemical Problems of Environment Protection: Intercollegiate Coll.), Perm: Perm. Gos. Tekh. Univ., 1996, pp. 52–56.
9. Papkov, S.P., *Fiziko-khimicheskie osnovy pererabotki rastvorov polimerov* (Physicochemical Foundations of Processing of Polymer Solutions), Moscow: Khimiya, 1971.

Russian Journal of Applied Chemistry, Vol. 78, No. 9, 2005, pp. 1420–1426. Translated from Zhurnal Prikladnoi Khimii, Vol. 78, No. 9, 2005, pp. 1444–1450.
Original Russian Text Copyright © 2005 by Gelis, Chuveleva, Firsova, Kozlitin, Barabanov.

SORPTION AND ION-EXCHANGE PROCESSES

Optimization of Separation of Ytterbium and Lutetium by Displacement Complexing Chromatography

V. M. Gelis, E. A. Chuveleva, L. A. Firsova, E. A. Kozlitin, and I. R. Barabanov

Institute of Physical Chemistry, Russian Academy of Sciences, Moscow, Russia
Institute of Nuclear Research, Russian Academy of Sciences, Moscow, Russia

Received June 4, 2003; in final form, April 26, 2005

Abstract—Separation of large amounts (500 g) of ytterbium and lutetium by displacement complexing chromatography was studied. The optimal separation conditions were determined.

Detection of solar neutrinos is one of the most urgent problems of modern particle physics and astrophysics. Natural ytterbium can be used for preparing a solar neutrino detector. To detect ~100 events/year, the minimal weight of ytterbium contained in the detector should be 10–20 t. The lutetium concentration in ytterbium used for this purpose should not exceed 0.1 ppm (1×10^{-7} g lutetium per gram of ytterbium). To remove lutetium from ytterbium, we use displacement complexing chromatography [1]. Our preliminary experiments showed that the lutetium content can be decreased by a factor of 350 and ytterbium (1 g) with the lutetium concentration at a level of 0.05 ppm can be obtained by chromatographic separation of these elements on a series of columns packed with KU-2 × 8M cation exchanger (grain size 115 μm) at 70°C using 0.056 M solution of ethylenediaminetetraacetic acid (EDTA) as an eluent [2, 3]. The aim of this study was to develop a process for producing a large amount of pure ytterbium and to optimize the separation conditions of lutetium and ytterbium.

EXPERIMENTAL

Separation of ytterbium and lutetium was performed by displacement complexing chromatography (DCC) using a series of column one of which is a sorption column and the others are separating columns. Rare-earth elements (REEs) are sorbed as a uniform band on the sorption column and are separated on a series of columns packed with the resin in the form of retaining ion (Ni^{2+}, Cu^{2+}, H^+, etc.). The main role of the retaining ion is to decompose the REE complex during the whole separation time, which favors repeated sorption–desorption cycles. The complexes of the eluent with the retaining ion should be stronger than those with the ions being separated. The sorption of the retaining ion on the resin should be weaker than that of the ions being separated. To separate REEs, a complexing agent containing displacing ions, NH_4^+ or Na^+, is used. The sorption of this agent is stronger than that of REEs. When a column is washed with this agent, NH_4^+ cations substitute REE^{3+} cations. As a results, the resin is transformed into the NH_4^+ form and REE ions form complexes with the eluent (EDTA). These complexes are decomposed by reaction with the resin in the form of the retaining ion Ni^{2+}. The released REE ions are sorbed again and displace Ni^{2+}. Thus, separate REE bands are formed in the columns. The order of these bands corresponds to the strength of the REE complexes. As an eluent, we used 0.056 M aqueous solution of ethylenediaminetetraacetic acid (EDTA) neutralized to pH 7.0–7.5 with ammonia.

To remove small amounts of lutetium from a large amount of ytterbium (500 g), the optimal conditions of their chromatographic separation [number of chromatographic columns, their diameter (d) and height (h), height-to-diameter ratio, ratio of the cross sections of succeeding and preceding columns ($S_{n+1} : S_n$), order of attachment of the columns during the process] should be determined. In addition, the influence of the final step of the chromatographic process (complete elution with the complexing agent or partial elution followed by desorption of the residual ytterbium with the mineral acid to eliminate additional step of eluent separation in Yb_2O_3 recovery with the aim to accelerate the separation) on the ytterbium purity should also be studied. It was also necessary to check whether ytterbium was contaminated in the final separation steps. These preliminary estimations are required for preparation of ytterbium on a larger scale.

1070-4272/05/7809-1420 © 2005 Pleiades Publishing, Inc.

The ytterbium concentration was determined on an atomic absorption spectrometer (Perkin–Elmer 1100B) and an atomic emission spectrometer. The lutetium concentration was determined by γ-ray radiation of ^{176}Lu measured on a γ-ray spectrometer using 202 and 307 keV channels. The pH was measured on a pH211 pH-meter. An Ecoline VC-360 peristaltic pump was used to feed the solutions at the required rate. The elution rate was 4 ml min^{-1} cm^{-2}. Sulfonic acid cation exchangers in the hydrogen or nickel form were used as the sorbents.

To determine the optimal conditions of ytterbium recovery, we studied different factors affecting the chromatographic separation of ytterbium and lutetium on a series of columns. Among them are the ratio of the column height to its diameter ($h : d$) and the ratio of the cross sections of the succeeding and preceding columns ($S_{n+1} : S_n$).

Since under conditions of DCC the behavior of REEs is similar, the influence of these factors was studied with an example of separation of neodymium and europium labeled with ^{152}Eu, using 0.05 M ETDA as the element. The neodymium concentration was determined spectrophotometrically on an SF-16 spectrophotometer. The europium concentration was determined by the γ-activity of ^{152}Eu measured on an NRG-603 spectrometer (Czech Republic). The columns were packed with KU-2 sulfonic action exchanger in the H form. Nickel(II) (90 mg) was added to the solution along with europium and neodymium. Our preliminary experiments showed that in columns with $h : d < 10$ the elution front of the elements being separated is smeared. However, when the separation is performed on a series of columns attached in advance (i.e., the front of the REE band is at a distance of 5–7 cm from the end of the preceding column), with the elution rate set in accordance with the cross section of the attached column (4 ml min^{-1} cm^{-2}), the chromatographic separation becomes more efficient. If the cross sections of the adjacent columns differ by a factor of more than 4 (Fig. 2), the front of REEs gets distorted. As a result, the front and rear boundary of the europium band become smeared and the yield and purity of the element being separated are deteriorated. Hence, the ratio of the column cross sections should be no more than 2.

We compared two modes of the final step of ytterbium recovery: complete ytterbium elution with the complexing agent and partial ytterbium desorption from the terminal column with a mineral acid to eliminate the additional step of eluent removal in preparation of the final product, Yb_2O_3.

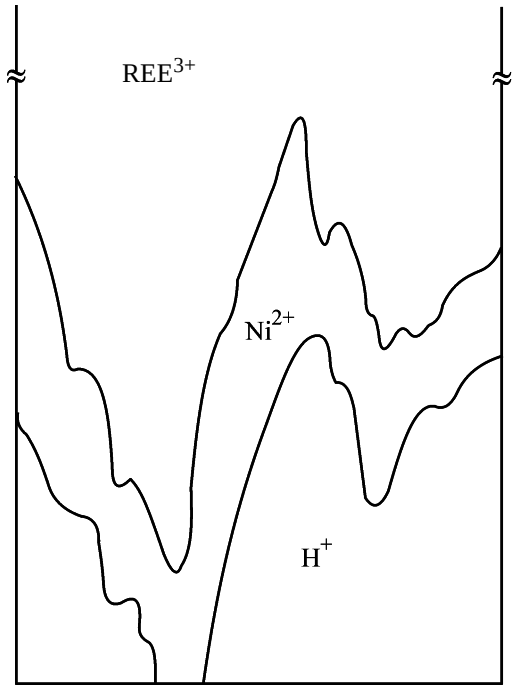


Fig. 1. Smearing of the front of the elements being separated on a column with a height-to-diameter ratio lower than 10.

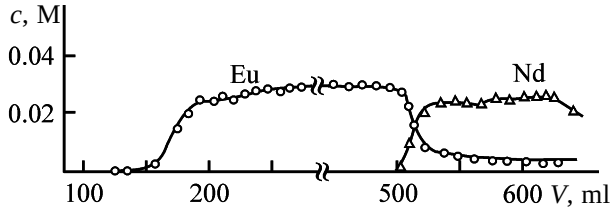


Fig. 2. Curves of elution of europium and neodymium with 0.05 M EDTA on columns with strongly different cross sections: (*c*) REE concentration and (*V*) eluent volume.

The results of these experiments are summarized in Tables 1 and 2. In each experiment we used 500 mg of lutetium and 374 mg of ytterbium.

Lutetium and ytterbium were separated on two columns with the following sizes: S_1 = 0.36 cm^2, h_1 = 80 cm and S_2 = 0.17 cm^2, h_2 = 80 cm. These elements were sorbed on the sorption column (S = 0.77 cm^2 and h = 11.3 cm). The columns were packed with KU-2 cation exchanger (industrial batch, 60–90 mesh) in the H form. Then the resin was converted into the Ni form. A 0.056 M EDTA solution neutralized with ammonia to pH 6.95 was used as the eluent. The elution rate was 4 ml min^{-1} cm^{-2}. The separation was performed at 70°C. The linear velocity of the REE band was 14 cm h^{-1}. Fractions (5–6 ml) were collected and analyzed for the lutetium content on

Table 1. Lutetium content in the samples (run no. 1)

Sample no.	Sample volume, ml	Lu concentration, mg ml^{-1}	Lu amount in the sample, mg	pH
8	5.7	8.5	48.5	2.25
10	5.5	6.5	35.8	2.30
12	5.3	6.2	32.9	2.25
14	4.4	6.0	26.4	2.25
16	5.6	1.53	8.6	2.25
18	6.0	0.424	2.5	2.25
20	8.2	<0.077	<1.5	2.25
21–25, 50% Yb	21.6	0.051	1.1	2.25–3.5

Table 2. Lutetium content in the samples (run no. 2)

Sample no.	Sample volume, ml	Lu concentration, mg ml^{-1}	Lu amount in the sample, mg	pH
6	5.7	7.89	45	2.25
8	5.6	7.46	41.8	2.25
10	4.4	7.08	31.2	2.25
12	5.7	5.92	33.7	2.25
14	3.8	6.77	25.7	2.28
16	7.5	1.27	9.5	2.25
17	3.9	0.43	1.7	2.25
18	3.3	<0.19	<0.62	2.25
19	4.6	<0.069	<0.31	2.25
H_2O	30	–	<0.15	
3 M HCl	44	–	<0.15	
3 M HCl	48	–	<0.15	

a Canberra γ-ray spectrometer with a 60 cm^3 germanium detector. The pH of the fractions was measured.

In the first experiment (Table 1), ytterbium was recovered by complete elution. As seen from Table 1, 50% of ytterbium eluted by the volume V = 21.6 ml (sample nos. 21–25) contains 1.1 mg of lutetium. Hence, the decontamination factor of ytterbium with respect to lutetium (the ratio of lutetium amount in the initial solution to that in the recovered ytterbium) is K_{dec} = 455.

In the second experiment (Table 2), lutetium and ytterbium were desorbed by the procedure of the first experiment. The elution was stopped when the distance from the rear of the ytterbium band and the lower part of the second separating column was 12 cm (50% elution). The column was washed with distilled water (V_1 = 30 ml) to remove EDTA and then with 0.5 M HCl to desorb ammonium ions (V_2 = 44 ml). After that ytterbium was desorbed with 3 M HCl (V_3 = 48 ml). The fractions were collected and analyzed for lutetium.

As seen from Tables 1 and 2, the last fractions before 50% elution of Yb in experiment nos. 1 and 2 contain similar lutetium amounts: $Lu_1 < 0.077$, $Lu_2 < 0.069$ mg ml^{-1}, respectively. In addition, 50% of Yb separated in the first and second experiments contains 1.1 and <0.15 mg of Lu, respectively. Thus, the purity of ytterbium recovered in the first experiment by elution with an EDTA solution is similar to that of ytterbium eluted with 3 M HCl after 50% separation of ytterbium with an EDTA solution. In the framework of LENS project, ultrapure ytterbium was recovered on a chromatographic unit with the productivity of 500 g of ytterbium in single sycle.[1]

The amount of the sorbent required for purification of 500 g of ytterbium was calculated from the number of separation bands by the equation

$$\nu = V/V_0 = [1 + (\alpha - 1)]/(\alpha - 1), \qquad (1)$$

where α is the separation coefficient of lutetium and ytterbium, equal to 2.09; N, fraction of the first component in the mixture (1.0); V_0, resin volume in the

[1] At Planck Institute of Nuclear Physics (Heidenberg, Germany).

Table 3. Parameters of ion-exchange columns

Column no.	Column diameter d, cm	Column cross section S, cm^2	Height of sorbent bed h, cm	Sorbent volume in column, l	$d : h$ ratio	Ratio of column cross sections	Height of Yb band, cm
1	8.0	50	100	5.0	1 : 12.5	1.0	100
2	8.0	50	100	5.0	1 : 12.5	1.7	100
3	6.0	29	100	2.9	1 : 16.7	1.8	172
4	4.5	16	100	1.6	1 : 22.7	5.3	312
5	2.0	3	100	0.3	1 : 50.0	–	1667

sorption column; and V, resin volume in the separation column.

Substitution of these values in Eq. (1) gives ν = 2.0. V_0 depends on the amount of the initial lutetium–ytterbium mixture (500 g) and the sorbent capacity (1.7 mg-equiv ml^{-1} of the resin). Therefore, the required resin volume in the sorption column is 5.0 l. The resin volume in separating columns V is determined by the number of separation bands $V = V_0 \nu$, i.e., $V = 2 \times 5 = 10$ l of the resin distributed between several columns in proportions corresponding to the optimal ratios $h : d$ and $S_{n+1} : S_n$. The required height of the ytterbium band in the last column and hence the column diameter is determined from the equation

$$\log(c_a/c_b) = l \log \alpha_b^a / \mathrm{HETP}, \quad (2)$$

where c_a and c_b are the ytterbium and lutetium concentrations in the solution, respectively; HETP is the height equivalent to the theoretical plate; α_b^a, separation coefficient of ytterbium and lutetium; and l, height of the mixing zone.

Substitution of $\log \alpha_{Yb}^{Lu} = 0.32$ and HETP = 1 cm in Eq. (2) gives for required height of the ytterbium band with the lutetium content of 1 ppm at a 50% ytterbium yield the value of 180 cm. If 70% yield is required, the height of the ytterbium band should be 300 cm. The diameter of the last column is determined from these data.

The chromatographic unit is shown in Fig. 3. The parameters of ion-exchange columns with heating jackets are presented in Table 3.

The columns were packed with Amberlite JR-120 (16–45 mesh) and Dowex-50 × 8 (50–100 mesh) sulfonic cation exchangers in the H form in the amounts given in Table 4.

We used ytterbium oxide Yb_2O_3 (YbO-1 trademark) containing Er_2O_3 <0.005, Tm_2O_3 <0.005, Lu_2O_3 0.018, Ca <0.005, Fe 0.003, and Cu <0.005 wt %.

Table 4. Amount of H form of the cation exchanger in the columns

Column no.	Cation exchanger (mesh)	Volume of cation exchanger in the column, l
1	IR-120 (16–45)	5.0
2	IR-120 (16–45)	5.0
3	IR-120 (16–45)	1.0 (top)
	Dowex-50 × 8 (50–100)	1.9 (bottom)
4	Dowex-50 × 8 (50–100)	1.6
5	Dowex-50 × 8 (50–100)	0.3

Ytterbium oxide (Yb_2O_3) was analyzed by spark mass spectrometry on a JMS01-BM2 double-focusing mass spectrometer (laboratory of mass spectrometry and chromatography, Moscow, Russia).

Ytterbium oxide was dissolved in portions on heating by addition of 65% HNO_3 in a 1.5-fold excess. The ytterbium concentration in the resulting solution (V = 38.2 l) was 14 g l^{-1}, i.e., the solution contained 534.8 g of Yb. Analysis of the solution performed in Germany showed the presence of 267 mg of lutetium,

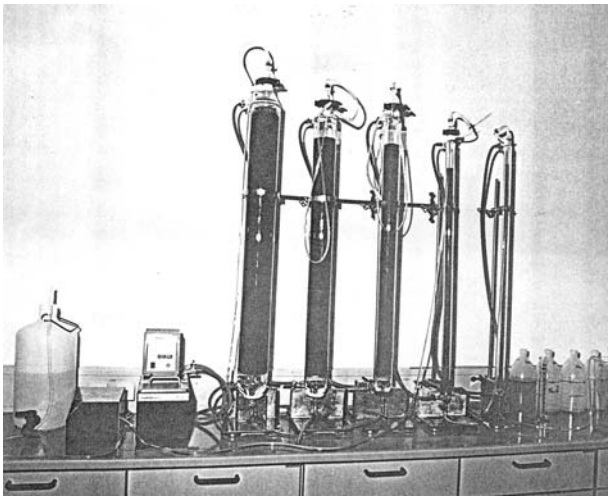


Fig. 3. Chromatographic unit.

Table 5. Parameters of ytterbium elution (experiment no. 1)

Solution no.	Ytterbium fraction	Fraction volume, l	Yb concentration, g l^{-1}	Yb amount, g	Lu amount, μg
1	Initial solution	38.2	14.0	534.8	499
2	Filtrate after Yb sorption and washing of the column with H_2O	15.5	5.04	78.1	–
3	Fraction 1 (Yb–EDTA)	1.5	6.22	9.3	1980
4	Fraction 2 (Yb–EDTA)	1.6	8.67	13.9	528
5	Fraction 3 (Yb–EDTA)	1.55	10.51	16.3	370
6	Fraction 4 (Yb–EDTA)	1.5	8.80	13.2	325
7	Fraction 5 (Yb–EDTA)	1.5	9.16	13.7	229
8	Fraction 6 (Yb–EDTA)	2.5	8.30	20.8	226
9	Fraction 7 (Yb–EDTA)	2.6	8.56	22.3	195
10	Fraction 8–9 (Yb–EDTA)	3.9	8.85	34.5	162
11	Fraction 10 (Yb–EDTA)	1.85	9.71	18.0	115
12	Washing of columns 3–5 with H_2O	7.9	3.40	26.9	–
13	Yb desorption with 3 M HCl (column 5)	2.9	11.40	33.1	43.2
14	Yb desorption with 3 M HCl (columns 3–4)	11.5	24.40	280.6	18.8

i.e., the lutetium content was 499 μg g^{-1} Yb. Ytterbium was sorbed at room temperature from the solution on the first column. The amount of the adsorbed ytterbium was 456.7 g, i.e., 1.58 mg-equiv ml^{-1} of the resin. The resin in columns 2–5 was converted into the nickel form by passing 0.5 M $NiCl_2 \cdot 6H_2O$. Separation of ytterbium and lutetium was performed at 70°C by elution with 0.056 M EDTA (pH 7.17–7.63). The number of separation bands was $\nu = 1.96$.

After sorption of the REEs, the first column was washed with distilled water, and then the first and the second columns were washed with 0.056 M EDTA at 70°C. The elution rate was 4 ml min^{-1} cm^{-2}. The velocity of the REE band ranged from 11 to 14 cm h^{-1}. Separation was performed by connection of the columns in series. When the distance between the lower point of the second column and the rear boundary of the nickel(II) band was 10 cm, the third column was attached and elution was performed through the first three columns. When the distance between the lower point of the third column and the rear boundary of the nickel(II) band was 10 cm, the fourth column was attached and elution was performed through a series of the first four columns. When the distance between the lower point of the fourth column and the rear boundary of the nickel band was 10 cm, the fifth column was attached and the first column was detached.

Ten ytterbium fractions were taken from the fifth column. The total volume of these fractions was 18.5 l. The total amount of the recovered ytterbium was 161.9 g (35% of the sorbed amount). After these manipulations, columns 3–5 were washed with distilled water and the residual ytterbium was desorbed with 3 M HCl. The results of these experiments are summarized in Table 5.

After desorption of REEs from the third and the fourth columns, the ytterbium and lutetium amounts in the solution were 280.6 g and 18.8 ppm, respectively. The decontamination factor K_{dec} was 25.7. From the fifth column, 33.1 g of ytterbium and 43.2 μg of lutetium (K_{dec} = 11.6) were desorbed. Thus, 313.7 g of ytterbium (68.7% of the sorbed amount) was recovered.

Since ytterbium recovered in the first cycle contained 18.8 μg g^{-1} of lutetium (i.e., 18.8 ppm), it was repeatedly treated to remove excess lutetium. For this purpose we used columns 2–5 packed, as in the first cycle, with Amberlite YR-120 and Dowex-50 × 8 cation exchangers.

Combined fractions 13 (Yb–HCl, 33.1 of ytterbium) and 14 (Yb–HCl, 280.6 g of ytterbium) were used as the initial solution, i.e., the total ammount of ytterbium recovered in the first cycle and used in repeated separation was 313.7 g. Ytterbium and lutetium were sorbed on the second column. Separation was performed by washing column 2–5 connected in series with 0.056 M EDTA at 70°C. The results are given in Table 6.

The Yb–EDTA fractions were taken first from the fourth column (fraction 1, 1.5 l, 5.6 g of ytterbium) and then from the fifth column (fractions 2–6 contain-

Table 6. Parameters of ytterbium elution (experiment no. 2)

Solution no.	Ytterbium fraction	Fraction volume, l	Yb concentration, g l^{-1}	Yb amount g
1	Fraction 13 (HCl) (run no. 1)	2.9	11.40	33.1
2	Fraction 14 (HCl) (run no. 1)	11.5	24.40	280.6
3	Combined fraction from run no. 1 (initial solution, run no. 2)	14.4	21.78	313.7
4	Fraction 1: from column 4 (Yb–EDTA)	1.5	3.74	5.6
5	Fraction 2: from column 5 (Yb–EDTA)	1.5	6.18	9.3
6	Fraction 3: from column 5 (Yb–EDTA)	1.5	7.76	11.6
7	Fraction 4: from column 5 (Yb–EDTA)	1.5	7.89	11.8
8	Fraction 5: from column 5 (Yb–EDTA)	1.5	7.92	11.9
9	Fraction 6: from column 5 (Yb–EDTA)	2.5	8.01	20.0
10	Fraction 7: from column 4 (Yb–EDTA)	1.35	7.75	10.5
11	Fraction 8: from columns 3–5 (Yb–EDTA) and washing with H_2O	2.9	2.73	7.9
12	Fraction 9: desorption from column 3 (Yb–HCl)	8.2	26.94	220.9
13	Fraction 10: desorption from column 4 (Yb–HCl)	1.4	23.26	32.6
14	Fraction 11: desorption from column 5 (Yb–HCl)	0.5	20.20	10.1

ing 64.6 g of ytterbium). After that the columns were washed with distilled water (fractions 7 and 8 containing 18.4 g of ytterbium).

Then ytterbium was desorbed with 3 M HCl from the third (fraction 9, 220.9 g of ytterbium), fourth (fraction 10, 32.6 g of ytterbium), and fifth (fraction 11, 10.1 g of ytterbium) columns. Fractions 9 and 10 were combined. The ytterbium amount in the combined fraction was 253.5 g (70% of the initial ytterbium amount). Then ytterbium oxalate $Yb_2(C_2O_4)_3$ was precipitated (so-called pure fraction). The lutetium content in this fraction was 0.833 ppm. The decontamination factor in the second cycle was K_{dec_2} = 23.3. The total K_{dec} was 499/0.83 = 599. Fractions 3–8 and 11 were also combined (72.2 g of ytterbium). Ytterbium oxalate (tail fraction) was precipitated from the resulting solution.

Previously we found that the decontamination factor of ytterbium with respect to lutetium in separation of small amounts of lutetium and ytterbium (up to 10 g) under the optimal conditions ($h : d > 10$ and $S_1 : S_2 = 2$, HETP = 1 cm) on KU-2 × 8M sulfonic cation exchanger (115 μm grain size) was 350–450. The lutetium content in the sample was lower than 0.05 ppm.

When larger ytterbium amounts (500 g) are treated, the use of the fourth and fifth columns with substantially different cross sections ($S_4 : S_5 = 5.3$) and of Amberlite-IR-120 (16–45 mesh) and Dowex-50 (50–100 mesh) cation exchangers decreases the decontamination factor owing to both smearing of the rear boundary of the lutetium band and of stronger overlap of the lutetium and ytterbium bands. However, in the case of two-step ytterbium recovery, the lutetium content can be decreased to 0.833 ppm and the decontamination factor can be as high as 599.

CONCLUSIONS

(1) Optimal conditions of separation of ytterbium and lutetium were determined. The yield and purity of the recovered ytterbium decrease when the separation is performed on columns with the height-to-diameter ratio lower than 10 ($h : d < 10$) and the cross-section ratio larger than 2–3.

(2) Two modes of ytterbium recovery were studied: (*1*) complete elution with the complexing agent and (*2*) partial desorption with a mineral acid in the final step. The ytterbium purity is independent of the recovery mode.

(3) Separation of ytterbium and lutetium was performed on a large-scale level (500 g). 252.5 g of ytterbium with the lutetium content of 0.833 ppm was recovered with the decontamination factor K_{dec} = 599.

ACKNOWLEDGMENTS

This study was financially supported by CRDF (project RP-23-MO-02).

REFERENCES

1. Tremillon, B., *les Separations par les resines exchangeuses d'Ions*, Paris: Gauthier Villars, 1965.
2. Firsova, L.A., Chuveleva. E.A., Gelis, V.M., *et al.*, *Zh. Fiz. Khim.*, 2001, vol. 75, no. 6, pp. 1068–1071.
3. Firsova, L.A., Chuveleva, E.A., Gelis, V.M., *et al.*, Purification of Ytterbium from Lutetium by Sorption Chromatography, *Preprint of the Inst. of Nuclear Research*, no. 1042/2000.
4. Sheptunov, V.N., Maslova, G.B., Nazarov, P.P., and Chmutov, K.V., *Zh. Fiz. Khim.*, 1972, vol. 46, no. 5, pp. 1174–1176.
5. Chmutov, K.V., Nazarov, P.P., Maslova, G.B., and Sheptunov, V.N., *J. Chromatogr.*, 1971, vol. 59, pp. 415–417.

Russian Journal of Applied Chemistry, Vol. 78, No. 9, 2005, pp. 1427–1429. Translated from Zhurnal Prikladnoi Khimii, Vol. 78, No. 9, 2005, pp. 1451–1454.
Original Russian Text Copyright © 2005 by Khasanov, Dychko, Kuryaeva, Ryzhova, Mal'tseva.

SORPTION AND ION-EXCHANGE PROCESSES

A New Procedure for Caffeine Determination

V. V. Khasanov, K. A. Dychko, T. T. Kuryaeva, G. L. Ryzhova, and E. V. Mal'tseva

Tomsk State University, Tomsk, Russia

Received August 24, 2004; in final form, February 2005

Abstract—The content of caffeine in multicomponent natural objects (tea leaves, coffee beans, and instant coffee) and caffeine-containing beverage foods was determined by ion-exchange chromatography.

Since caffeine is an inherent component of some plants and foodstuffs produced from them [1], availability of the reliable procedures of its determination is important for various-purpose analyses (such as technological, umpire, etc.). In accordance with GOST (State Standard) [2], the main method of caffeine analysis is a photometric determination based on hydrolytic oxidation of caffeine into tetramethylpurpuric acid followed by photometric registration of the absorption density at λ 540 nm. The main disadvantage of this procedure is underestimation of the caffeine content in the samples [1].

The most general procedure of caffeine determination used in laboratories beyond Russia is reversed-phase high-performance liquid chromatography (RP HPLC). Kusch and Knupp [3] compared the analytical data on the content of caffeine in beverage foods determined by high-performance thin-layer chromatography and RP HPLC. They found that, despite some restrictions, each procedure provides reliable results with small measurement errors. As for caffeine determination in vegetable extracts of tea and coffee, the problem is more complex. The content of caffeine in tea and coffee is so high that no additional procedures of its preconcentration (such as solid-phase extraction often used in the analysis of caffeine in biological liquids [4]) are required. With solid-phase extraction and RP HPLC, the detection limit of the caffeine in protein-containing samples was determined as 200 ng cm^{-3}. However, wide assortment of compounds extracted with water from tea and coffee hinders direct determination of caffeine by RP HPLC, which is probably due to the short retention times of the polar caffeine molecules, especially in sorbents with small and intermediate content of grafted hydrocarbon chains. As a result, the caffeine peaks overlap with peaks of concomitant compounds even in the case of gradient elution. Another technique recently tested for determination is capillary electrophoresis [5]. Though this method provides very high separation efficiency, it is not widely used yet.

Nishitani and Sagesaka [6] performed an HPLC analysis of green tea components (catechins, phenolic glycosides, acids, and caffeine) on a C18 Wakosil-II 5C18 HG (3 × 150 mm) reversed-phase column (Wako Pure Chemical Industries, Ltd., Japan) using complex gradient profile with changes in the flow rate. The analysis time was 40 min. Smaller amount of components (8) can be separated with this system in 20 min. The detection limit of the components varied from 1.4 to 3.5 ng and the concentration dependence was linear up to charges of 1500 ng; the introduced/found ratio was 96–103%.

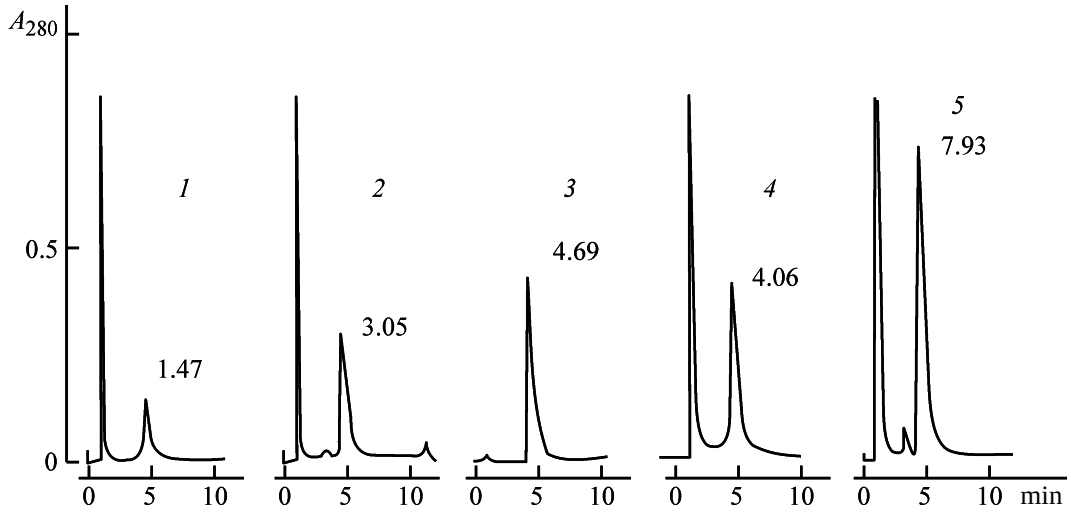
In this study we used a procedure more selective to caffeine, based on two separation mechanisms through ion-exchange and hydrophobic interactions.

EXPERIMENTAL

Analysis was performed on an FPLC liquid chromatograph (LKB Pharmacia, Sweden) equipped with a 50 × 5 mm column packed with Mono S sorbent (strong cation-exchanger with grafted sulfopropyl groups) produced by the same company. This sorbent is a hydrophilic polymer consisting of spherical particles (10 μm size) with a pore size of about 100 nm. A ready-to-use column was supplied by the company.

The elution was performed with a gradient in the organic modifier content. Two solutions were used: (A) 0.025 M sodium acetate (pH 6.8) and (B) 0.025 M sodium acetate (pH 6.8)–acetonitrile (70 : 30 volume ratio). The column was equilibrated for 4 min with a mixture A : B = 95 : 5; then the sample was injected, and after 4 min the gradient was switched on, up to the composition A : B = 15 : 85 in 10 min; the flow rate was 1 ml min^{-1} (300 cm h^{-1}).

1070-4272/05/7809-1427 © 2005 Pleiades Publishing, Inc.



Chromatographic patterns of the samples and caffeine reference; sample volume 100 μl, UV detector, λ 280 nm. (*1*) Georgian tea, (*2*) MK Gold tea, (*3*) reference, (*4*) Jacobs Meister coffee, and (*5*) Coca-Cola. Figures at peaks indicate the content of caffeine (in 100-μl sample volume).

The volume of the sample was varied from 100 to 500 μl (depending on the expected caffeine content); the process was monitored with a UV detector at λ 280 nm.

Before measurements, a weighed sample (100–200 mg) of tea or coffee was kept in solution A for 5–10 min at 90°C with stirring. Certain fraction of the extract was centrifuged for 5 min at 5000 rpm and filtered (0.45 μm).

The Coca-Cola and Pepsi caffeine-containing carbonated beverages were only filtered before analysis. Modern sorbents for ion-exchange HPLC exhibit pronounced hydrophobic properties of the hydrocarbon spacer retaining the ion-exchange group on the sorbent surface or even matrix material. The hydrophobic properties of the ion exchangers are weaker than those of reversed-phase sorbents. Thus, strongly ionized compounds will be retained on the ion exchangers predominantly by electrostatic interactions, and weakly ionized and nonionized compounds, by hydrophobic interactions. By varying the eluent pH, we can change the ratio of the ionized and nonionized caffeine molecules and, thus, control the contribution of one or another mechanism of retention in the column. At pH < 6, the electrostatic interactions of the caffeine molecules with a cation exchanger are so strong that they are poorly eluted from the column even by 1 M NaCl. Moreover, high concentrations of salt in the buffer solution enhance the hydrophobic interactions between caffeine and the sorbent. With changing pH from 6 to 7, the retention of caffeine decreases and it can be eluted with a gradient in the organic modifier concentration (as in the case of RP HPLC). The optimal pH value was determined experimentally. Under these conditions, polar and low-polar weakly ionized molecules of various compounds interfering with the caffeine determination on common reversed phases are not retained in the column and do not affect the analysis. After the gradient elution, the ion-exchange column is equilibrated with the initial eluent in less than 3 min and becomes ready for a new analysis. The chromatographic patterns of several samples are shown in the figure.

The main fraction of the concomitant compounds was eluted from the column immediately after the sample injection. The caffeine peak is easily separated from the peaks of concomitant compounds and thus is efficiently recorded. The absence of compounds simultaneously eluted with caffeine (peak purity) was tested using an RSD-2140 detector on diode matrices (Pharmacia-LKB, Sweden) by comparing the absorption spectra in the UV peak maxima of caffeine in the reference and samples studied.

The validation of the procedure suggested for the caffeine determination was performed in accordance with recommendation of the International Conference on Harmonisation (ICH Tripartite Guideline, CPMP/ICH/281/95), topic Q2B (Validation of Analytical Procedures: Methodology) [7]. The results are listed in Table 1. The accuracy of the procedure was evaluated at addition of the caffeine reference to the tea samples. For this purpose, the contents of caffeine added and determined from the experimental depen-

Table 1. Validation of the procedure suggested for caffeine determination*

Parameter	Caffeine reference	Test samples		
		tea	coffee	beverage
Linearity	0.9998	–	–	–
Detection limit, ng	15	–	–	–
Measurement limit, ng	100	–	–	–
Convergence, ng	4600.0 ± 14.6 (0.60%)	38.2 ± 0.02 (1.4%)	46.7 ± 0.02 (1.3%)	95.4 ± 0.50 (1.2%)
Accuracy, %	–	98.5	101.2	98.7

* Linearity of the procedure was studied in the ranges 100 ng–10 μg and 1–100 mg $^{-1}$ in the column and reference, respectively; detection and measurement limits, at signal : noise ratios of 3 : 1 and 10 : 1; and convergence, at three replicate measurements in three samples [for caffeine reference and samples, the results are given in ng and mg ml^{-1}, respectively, in the following order: average value ± standard deviation (relative error, %)].

dence were compared using three measurements and three replicate samples.

In the course of this study, the content of caffeine in some commercial brands of tea, coffee, and carbonated beverages was determined; the results of three replicate measurements are listed in Table 2.

Table 2. Content of caffeine in samples

Sample	Caffeine content	Relative error
Tea:		
Green Seal, India	2.95 ± 0.018	1.3
Crown of Russian Empire, Russia	3.83 ± 0.024	1.4
Spring Garden, China	3.15 ± 0.022	1.3
Dilmah, Sri Lanka	2.95 ± 0.017	1.4
Colombo Bay, Russia	3.55 ± 0.023	1.2
MK Gold, India	3.02 ± 0.020	1.2
Georgian, 1st grade		
Instant coffee:		
Nescafe Classic, Brazil	4.00 ± 0.024	1.2
Jacobs Merido, Germany	3.83 ± 0.019	1.2
Maxwell House, Brazil	4.00 ± 0.022	1.3
Jacobs Meister Rostung, Canada	4.67 ± 0.024	1.3
Beverage:		
Coca-Cola, Russia	80.1 ± 0.464	1.2
Pepsi, Russia	95.4 ± 0.474	1.2

* For tea and coffee, the content of caffeine is given in percents of the dry weight of the sample (moisture content of the packed product), and for carbonated beverages, in mg l^{-1}; average values ± standard deviation are given.

CONCLUSIONS

(1) Combination of the ion-exchange and hydrophobic mechanisms of retention in the liquid chromatography allows development of a new express and reliable procedure of caffeine determination.

(2) The relative error in the caffeine determination does not exceed 1.5%; quantitative analysis is performed by an absolute calibration procedure.

(3) The calibration dependence at caffeine concentration from 1 to 100 mg ml^{-1} is linear with the correlation coefficient $r > 0.999$.

(4) By this procedure, the content of caffeine can be determined on a standard HPLC unit.

REFERENCES

1. Solov'eva, S.I., Serazhutdinova, L.D., Malykh, M.A., *et al.*, *Partnery Konkurenty*, 2001, no. 5, pp. 13–17.
2. *GOST* (State Standard) *29148–97: Natural Instant Coffee: Technical Specifications*.
3. Kusch, P. and Knupp, G., *Chem. Educ.*, 2003, vol. 8, no. 3, pp. 201–205.
4. Abu-Qare, A.W. and Abou-Donia, M.B., *J. Pharm. Biomed. Anal.*, 2000, no. 6, pp. 939–947.
5. Boyce, M.C., *Electrophoresis*, 2001, vol. 22, no. 8, pp. 1447–1459.
6. Nishitani, E. and Sagesaka, Y.M., *J. Food Compos. Anal.*, 2004, vol. 17, no. 5, pp. 675–685.
7. *Q2B Validation of Analytical Procedure: Methodology. Int. Conf. on Harmonisation*, step 4: *Consensus Guideline*, November 6, 1996.

Russian Journal of Applied Chemistry, Vol. 78, No. 9, 2005, pp. 1430–1432. Translated from Zhurnal Prikladnoi Khimii, Vol. 78, No. 9, 2005, pp. 1455–1457.
Original Russian Text Copyright © 2005 by Arkhangel'skaya, Demidov, Loginova, Kas'yan, Apollonova.

APPLIED ELECTROCHEMISTRY AND CORROSION PROTECTION OF METALS

Effect of Lanthanide Additives to a Nickel Oxide Electrode of a Sealed Nickel–Zinc Battery on the Self-Discharge and Hydrogen Pressure

Z. P. Arkhangel'skaya, A. I. Demidov, M. M. Loginova, T. B. Kas'yan, and E. V. Apollonova

Rigel' Open Joint-Stock Battery Company, St. Petersburg, Russia
St. Petersburg State Polytechnic University, St. Petersburg, Russia

Received March 16, 2005

Abstract—The influence exerted by addition of a nickel-based alloy containing lanthanides (La, Ce, Nd, Pr) to the active paste of a nickel oxide electrode on the self-discharge and hydrogen pressure in a sealed nickel–zinc battery was studied.

Proceeding with studies of gas evolution and gas absorption in a sealed nickel–zinc (SNiZn) battery with a nickel oxide electrode (NOE) made of spherical nickel hydroxide [1], we examined the influence exerted by addition of a nickel-based alloy containing lanthanides (La, Ce, Nd, Pr) to the active paste of a nickel–oxide electrode on the self-discharge and hydrogen pressure in an SNiZn battery. Lanthanide oxides were introduced into the active paste of an NOE in order to raise the utilization coefficient of the active paste in the NOE and improve its preservation [2]. Erbium, thulium, ytterbium, and lutetium oxides were found to be the most effective additives at an elevated temperature (75°C).

Nickel-based lanthanide-containing alloys exhibit a high absorption capacity for hydrogen [3]. The replacement of a cadmium electrode with an electrode composed of a nickel alloy with lanthanides, which can absorb hydrogen and desorb it upon polarity reversal, gave rise to nickel–metal hydride batteries. As the interaction of nickel metahydroxide NiOOH with hydrogen is accompanied by reduction of the nickel ion Ni^{3+} and oxidation of hydrogen

$$2NiOOH + H_2 = 2Ni(OH)_2,$$

the influence of lanthanides on the self-discharge and hydrogen pressure in an SNiZn battery can be evaluated by a decrease in the NOE capacity and a change in the hydrogen pressure under cycling conditions.

EXPERIMENTAL

We introduced lanthanides into the active paste of an NOE in an amount of 1–2 wt % in the form of a nickel-based alloy containing La, Ce, Nd, and Pr. The study was performed on SNiZn batteries of the NTsG-25 type with an NOE composed of spherical nickel hydroxide [1]. The characteristics of the NOE studied in the batteries are listed in Table 1.

We determined the rated capacity of NOE by studying separate NOEs in prototype batteries. The electrodes were formed in two to three cycles, with a capacity equal to $1.1C_{th}$ of the positive electrode imparted in the first cycle, and $1.4C_{th}$, in the second and third cycles (C_{th} is the thermodynamic capacity). The zinc electrode contained 2 wt % CdO and 1 wt % PbO.

The open-circuit voltage U_{OC} of assembled batteries and the potential of NOE relative to a mercury

Table 1. Characteristics of NOE in NTsG-25 nickel–zinc batteries

Parameter	Content of alloy additive, wt %/g			
	0/0	0.5/1	1.0/2	2.0/4
Total amount of active paste, g	189	189	189	189
Ni + Co content, g	113	112	111	110
Capacity, A h:				
theoretical	51	51	51	50
rated	26	26	26	25

1070-4272/05/7809-1430 © 2005 Pleiades Publishing, Inc.

Table 2. U_{OC} of the batteries and the potential of NOE in the course of forming

Cycle	U_{OC} of battery, V				NOE potential, V			
	content of additive, wt %							
	0	0.5	1.0	2.0	0	0.5	1.0	2.0
Before forming	1.18	1.13	1.09	0.94		–0.19	–0.23	
First:								
after charging	1.85	1.85	1.85	1.85	0.51	0.50	0.50	0.50
after discharge	1.69	1.69	1.69	1.69	0.37	0.36	0.36	0.36
Second:								
after charging	1.84	1.84	1.84	1.84	0.45	0.50	0.50	0.45
after discharge		1.69	1.69					
Third, after discharge		1.79	1.80					

oxide electrode (Hg, HgO | OH^-) before the first forming charging depended on the content of the alloy in the active paste of the NOE (Table 2).

Table 2 shows that, before forming, the U_{OC} of the batteries decreases as the content of the additive in the active paste of NOE becomes higher. As the content of lanthanides increases, the potential of NOE shifts toward the negative direction and becomes more negative than the potential of the mercury oxide electrode. However, already after the first charging and during further discharge–charging cycles, the NOE potential becomes independent of the additive content and takes the characteristic value observed in the absence of an additive.

The open-circuit voltage and the charging-discharge characteristics of all the batteries under study become the same in the course of forming and cycling (Fig. 1).

The open-circuit voltage of batteries with NOE containing a lanthanide alloy (up to 2 wt %) and without additive varies in the course of storage in the same way (Fig. 2). However, the capacity in discharge after 29 days of storage of a battery containing 2 wt % alloy in the NOE is higher (Fig. 3). The loss of capacity in self-discharge is 30.6% for this battery and 36.0% for that containing no additive in its NOE. This result can be understood if we assume that the nickel-based lanthanide-containing alloy introduced into the active paste of the NOE is oxidized on its surface, but retains its ability to absorb hydrogen (Table 3).

Table 3 was compiled using data on self-discharge of ventilated nickel–zinc batteries, which is 10% in 30 days (2.5 A h) [4].

Calculation shows that the content of hydrogen in the alloy after 29-day storage of an SNiZn battery (0.32 A h) is close to the value characteristic of the alloy used as the active paste in the negative electrode of a nickel–metal hydride battery.

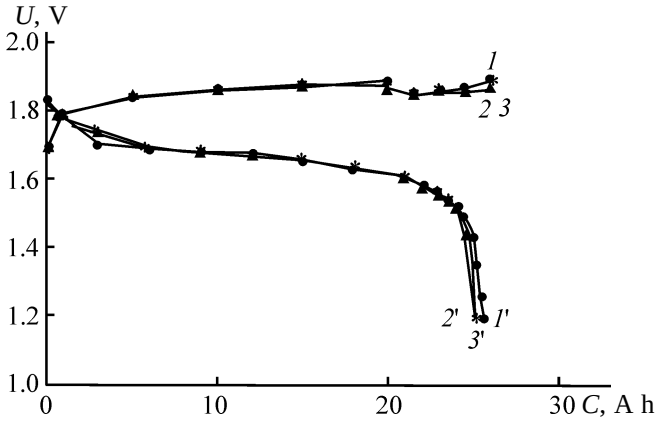


Fig. 1. Variation of the voltage U in (*1*–*3*) charging and (*1*'–*3*') discharge in the ninth cycle of an NTsG-25 battery with a lanthanide alloy added to the NOE. (*C*) Capacity: the same for Fig. 3. Additive content (wt %): (*1*, *1*') 0, (*2*, *2*') 1, and (*3*, *3*') 2.

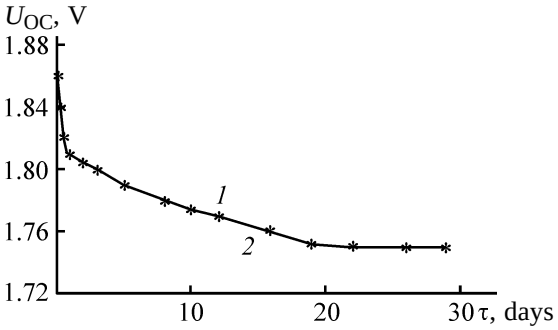


Fig. 2. Variation of U_{OC} in storage of charged NTsG-25 batteries (*1*) with addition of 2 wt % lanthanide alloy and (*2*) without additive. (τ) Time.

Table 3. Effect of the NOE composition on the self-discharge of NTsG-25

Battery	Capacity before (after) storage, A h	Decrease in capacity in storage, A h		Capacity of hydrogen absorbed by alloy, A h
		total	in oxidation by hydrogen	
NOE:				
without alloy additive	24.5 (15.7)	8.8	6.3	–
with alloy additive	24.5 (17.0)	7.5	5.0	1.3

In the course of cycling of an SNiZn battery, the pressure first increases and then reaches a constant value (Fig. 4). The maximum total pressure in the battery corresponds to the pressure of hydrogen and oxygen in charging, and the minimum pressure, to that of hydrogen in discharge. In the absence of an alloy additive in the NOE, the hydrogen pressure in the battery was $(2.0–2.2) \times 10^2$ kPa, and the total pressure of hydrogen and oxygen, 2.8×10^2 kPa. In the case of an NOE containing the additive in an amount of 2 wt %, the hydrogen pressure in the battery was $(1.6–1.8) \times 10^2$ kPa, and the total pressure of hydrogen and oxygen, 2.2×10^2 kPa. Thus, the introduction of a nickel-based lanthanide-containing alloy in the active paste of an NOE made it possible to diminish the total pressure in an NTsG-25 sealed battery by 60 kPa, and the hydrogen pressure, by 40 kPa.

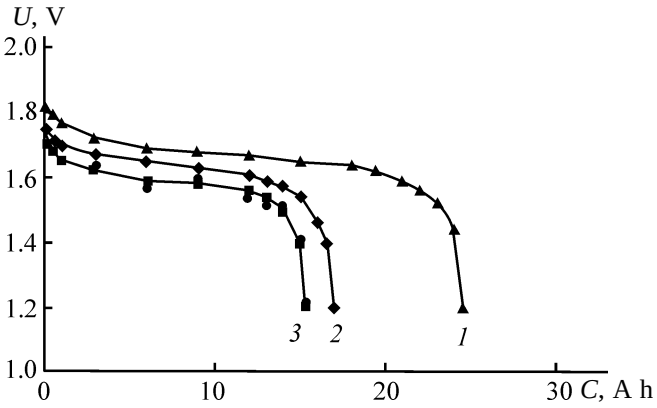


Fig. 3. Variation of the voltage *U* in discharge of NTsG-25 batteries (*1*, *2*) with addition of 2 wt % alloy of lanthanides to NOE and (*3*) without additive (*1*) before and (*2*, *3*) after storage for 29 days.

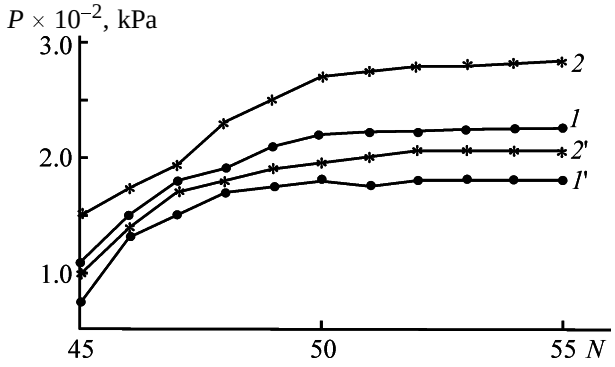


Fig. 4. Variation of (*1*, *2*) maximum and (*1*', *2*') minimum pressure *P* in an NTsG-25 battery (*1*, *1*') with addition of 2 wt % alloy of lanthanides and (*2*, *2*') without additive. (*N*) Number of cycles.

CONCLUSION

A nickel-based alloy containing lanthanides (La, Ce, Nd, Pr) introduced into a nickel oxide electrode retains its ability to absorb hydrogen. This leads to a decrease in the self-discharge of a sealed nickel–zinc battery in storage and makes lower the total pressure and hydrogen pressure in the battery in cycling.

REFERENCES

1. Arkhangel'skaya, Z.P., Loginova, M.M., Kas'yan, T.B., and Vinogradova, D.A., *Zh. Prikl. Khim.*, 2004, vol. 77, no. 1, pp. 70–74.
2. Masahiko, O., Masaharu, W., Kaori, S., and Mitsuhiro, K., *J. Electrochem. Soc.*, 2001, vol. 148, no. 1, pp. 67–73.
3. Tsenter, B.I. and Lyzlov, N.Yu., *Metall-vodorodnye elektrokhimicheskie sistemy: Teoriya i praktika* (Metal-Hydrogen Electrochemical Systems: Theory and Practice), Leningrad: Khimiya, 1989.
4. Loginova, M.M., Kas'yan, T.B., Arkhangel'skaya, Z.P., and Raikhel'son, L.B., *Zh. Prikl. Khim.*, 2003, vol. 76, no. 5, pp. 779–782.
5. *Khimicheskie istochniki toka: Spravochnik* (Chemical Power Cells: Reference Book), Korovin, N.V. and Skundin, A.M., Eds., Moscow: Mosk. Energ. Inst., 2003.

Russian Journal of Applied Chemistry, Vol. 78, No. 9, 2005, pp. 1433–1437. Translated from Zhurnal Prikladnoi Khimii, Vol. 78, No. 9, 2005, pp. 1458–1462.
Original Russian Text Copyright © 2005 by Arkhangel'skaya, Krasnobryzhii, Loginova, Kas'yan, Apollonova.

APPLIED ELECTROCHEMISTRY AND CORROSION PROTECTION OF METALS

Effect of the Electrolyte Concentration on the Reversibility of a Nickel Oxide Electrode in a Nickel–Zinc Battery

Z. P. Arkhangel'skaya, A. V. Krasnobryzhii, M. M. Loginova, T. B. Kas'yan, and E. V. Apollonova

Rigel' Open Joint-Stock Battery Company, St. Petersburg, Russia

Received March 16, 2005

Abstract—The degree of charging of a nickel oxide electrode composed of spherical nickel hydroxide in a nickel–zinc battery was studied in anodic oxidation of the electrode in KOH solutions of different concentrations, containing hydroxozincate ions.

The use of a nickel oxide electrode composed of spherical nickel hydroxide on a foamed nickel support (FNi NOE), instead of a metal–ceramic (MC) electrode, in nickel–cadmium (NiCd) and nickel–metal hydride (NiMH) batteries made it possible to markedly simplify the production process and raise by 30–50% their electrochemical parameters. At the same time, as applied to a nickel–zinc battery, NOE of the same type made longer the service life of the battery compared to similar batteries with metal–ceramic NOE (MC NOE) but gave no noticeable advantages in the energy storage capacity.

The achievable degree of oxidation of an NOE composed of spherical nickel hydroxide in its operation in NiCd and NiMH batteries is 0.85–1.0 in terms of the $Ni(OH)_2 \rightarrow NiOOH$ transition [1], whereas in forming of NiZn batteries with the same NOE, this parameter does not exceed 0.7–0.8 [2]. In the previously developed NiZn batteries with an MC NOE, the degree of its charging was virtually the same as that obtained in NiZn batteries (0.85–0.9). If an NOE composed of spherical nickel hydroxide is used instead of MC NOE, its low degree of oxidation leads to a necessity for raising the amount of the active paste per unit capacity and, consequently, to a decrease in the capacity ratio of the negative and positive electrodes. This, in the end, reduces the specific energy of an NiZn battery with FNi NOE to 60 W h kg^{-1}, i.e., to a level provided by a similar battery with an MC NOE [3].

The aim of this study was to reveal what processes limit the chargeability of an NOE composed of spherical nickel hydroxide on a foamed nickel support both in forming of an NiZn battery and in its subsequent cycling under the conditions of varying concentrations of KOH and hydroxozincate ions in the electrolyte.

A preliminary analysis of our previous publications [2, 3] demonstrated that the hindrance to egress of a proton (and an electron) in charging of an NOE under the forming conditions may be due to simultaneous intercalation of zinc(II) contained in the electrolyte into the $Ni(OH)_2$ structure. The intercalated zinc is not an active component involved in electrochemical processes in the subsequent operation of the electrode. However, it can affect the distribution and interaction of the other components (H_2O; OH^-, K^+, and CO_3^{2-} ions) in forming of the NOE structure. Its own position in the layered structure of nickel hydroxides may vary [4], which is reflected in the degree of ordering of the nickel hydroxide structure and in its formability [5].

Another reason may be the electrolyte composition and, primarily, the KOH concentration both during the forming cycles and in the subsequent reversible operation, because an electrolyte of lowered concentration is used in NiZn batteries in order to diminish the solubility of zinc. In the course of cycling, this concentration decreases to even greater, and considerably so, extent [3] because of the small volume of the electrolyte and use of materials containing an admixture of carbonates and oxidizable organic additives.

A number of studies have been concerned with the influence exerted by zinc as a stabilizing additive on processes that occur in NOE, including that directly devoted to the issue in question [4]. In this study, we examined the influence exerted by zinc on processes occurring in forming of the $Ni(OH)_2$ structure and its

1070-4272/05/7809-1433© 2005 Pleiades Publishing, Inc.

stabilization under conditions of NOE cycling in KOH solutions of different concentrations.

It was shown that the achievable degree of charging of an NOE containing incorporated zinc is lower than that of an electrode containing no zinc, but is distinguished by high stability of its capacity under cycling conditions. As the KOH concentration in the electrolyte was raised from 2 to 8 M, the degree of charging increased from 0.7 to 1.0. However, these results were obtained on electrodes with a constant content of zinc [6% Zn/(Zn + Ni)], and, therefore, they do not reflect specific features of the processes that occur in an NiZn battery, with the content of zinc in the NOE steadily increasing and the KOH concentration in the electrolyte simultaneously decreasing.

In nickel hydroxide with a structure of the β-phase, zinc can be incorporated in amounts of up to 15% Zn/Ni or 10–12% $Zn/Ni(OH)_2$ [4, 6]. When zinc is accumulated in NOE in such amounts, the β-phase starts to decompose with the subsequent gradual transformation into the α-phase, and the interplanar spacing between $Ni(OH)_2$ layers grows from 4.6 to 7 Å [5], with simultaneous increase in the structural disorder [5, 6]. By contrast, the structure of nickel(II, III) oxides is more stable at a $Zn/Ni(OH)_2$ ratio less than 10%, compared with that in the absence of zinc, and provides a virtually constant degree of proton (electron) egress.

EXPERIMENTAL

We performed the study on NiZn batteries and prototypes of varied capacity with a nickel oxide electrode composed of spherical nickel hydroxide on a foamed nickel support.

FNi NOE was fabricated from nickel hydroxide with particles 10–30 μm in diameter. The starting active paste contained 53–53.5% nickel and admixtures of cobalt (5.4%) and zinc (3.4%), introduced in synthesis of nickel hydroxide.

As shown in [2], the degree of NOE charging obtained in forming cycles depends on the imparted charging capacity. Among the modes tested, the highest capacity was provided by that in which a capacity of 100–110% relative to the theoretical value for the $Ni^{2+} \rightarrow Ni^{3+}$ transition was imparted in the first cycle, and 120–140%, in the second.

Charging with an excess imparted capacity is accompanied by a change in the electrolyte composition, because nickel hydroxide is oxidized with consumption of hydroxide ions and release of water:

$$Ni(OH)_2 + OH^- \rightarrow NiOOH + H_2O + e. \quad (1)$$

In the subsequent discharge, hydroxide ions are returned into the electrolyte and water is consumed, but not completely, because the charging capacity C_{ch} exceeds the discharge capacity C_d. As a result, the KOH concentration in the electrolyte may decrease to a varied extent, depending on the mode of battery forming.

The degree of NOE charging in the battery varied with the ratio of charging to theoretical capacity, C_{ch}/C_{th} (0.8–1.5), only slightly, from 0.65 to 0.75 [2]. Therefore, in order to obtain a noticeable effect in comparative analysis, forming was performed in this study at different C_{ch}/C_{th} ratios.

The degree of Ni charging obtained in the case when the charging is limited by the final voltage, $C_{ch} < C_{th}$, was determined as the C_d/C_{ch} ratio (current utilization coefficient), and that in charging with $C_{ch} > C_{th}$ imparted in the transition $Ni^{2+} \rightarrow Ni^{3+}$, as the C_{ch}/C_{th} ratio (nickel utilization coefficient).

Table 1 shows that the degree of FNi NOE charging in prototypes with a cadmium counterelectrode exceeds by 15–20% that in prototypes with a zinc electrode. This fact confirms that hydroxozincate ions are involved in the formation of the NOE structure and affect the achievable degree of NOE charging.

Table 2 shows that two cycles are sufficient for forming of an FNi NOE. In the third and subsequent cycles, the capacity changes only slightly. It should be noted that the values obtained on prototypes are smaller than those for batteries, which is due to different electrolyte volumes per unit NOE capacity. Therefore, the results obtained in tests with prototypes are regarded as tentative.

To obtain the most contrasting, as regards the degree of charging, results, we carried out forming of prototypes with electrolyte of varied concentration under the most severe conditions with a C_{ch}/C_{th} ratio increased to 1.5 (Table 2). However, as the initial KOH concentration was raised from 7.0 to 8.5 M and forming was performed with a zinc counterelectrode, i.e., in the presence of $Zn(OH)_4^{2-}$ ions, the degree of charging increased by only 10%, and by only the 10th training cycle.

The variation of the electrolyte concentration in forming of FNi NOE during the forming cycles was determined for batteries with a capacity of 50 A h (C_{th} = 100 A h) at an initial KOH concentration in

Table 1. Degree of charging of NOE composed of spherical nickel hydroxide on an FNi support in forming in prototype batteries with cadmium and zinc electrodes. C_{ch}/C_{th} = 0.88–0.95

C_{th} of NOE, A h	Concentration of the starting electrolyte, M		Current density, A dm^{-2}		Capacity in cycling A h		Degree of charging
	KOH	LiOH	charging	discharge	charging	discharge	
Nickel–cadmium system							
0.89	7.2	0.93	0.48 (first stage 0.24 (second stage)	0.125	1st, 0.82 2nd, 0.79 3rd, 0.85 4th, 0.80 5th, 0.79	0.43 0.55 0.61 0.56 0.58	0.48 0.62 0.68 0.63 0.65
Nickel–zinc system							
0.89	7.2	0.93	0.48 (first stage) 0.24 (second stage)	0.125	1st, 0.82 2nd, 0.79 3rd, 0.85 4th, 0.80 5th, 0.79	0.32 0.45 0.50 0.49 0.49	0.36 0.50 0.56 0.55 0.55

Table 2. Degree of charging of an NOE composed of spherical nickel hydroxide on a foamed nickel support in forming of prototype NiZn batteries with different initial concentrations of KOH in the electrolyte

Calculated capacity, A h	Cycle	Capacity, A h, at indicated initial KOH concentration, M		Degree of Ni charging at indicated initial KOH concentration, M	
		7	8.5	7	8.5
C_{th} = 3.5–3.6	Forming:				
	first	5.4/2.21*	5.4/2.18	0.62	0.62
	second	4.0/2.23	4.0/2.25	0.62	0.63
C_{in} = 2.0	Training:				
	first	2.4/2.06	2.4/2.08	0.56	0.58
	fifth	2.4/2.23	2.4/2.3	0.61	0.64
	tenth	2.8/2.21	2.8/2.34	0.63	0.68

* Charging/discharge capacity.

the electrolyte equal to 7 M and a C_{ch}/C_{th} ratio of 1.0 in the first and second cycles (Table 3). Even under these mild conditions, the electrolyte composition mainly changed during the forming cycles and varied only slightly in further cycling. In two forming cycles, the KOH concentration in the electrolyte decreased from 7 to 4 M in a charged battery, and to 5 M in a discharged one. In this case, the degree of NOE charging was 0.58–0.84. The high degree of charging obtained in these batteries is due to certain specific features of its operation.

The data in Tables 1–3 suggest that the impairment of the chargeability of FNi NOE in a NiZn battery is due to its forming directly in batteries and is associated with the influence exerted on the forming β-$Ni(OH)_2$ structure by zinc being intercalated from hydroxozincate ions at a decreasing KOH concentration in the electrolyte.

The data obtained in forming of FNi NOE were confirmed in determining the cyclic life of NiZn batteries with varied KOH concentration. The initial concentration of 7 M decreased in the forming cycles to 5 M and remained at a level of about 4 M in further cycling (Fig. 1). The degree of NOE charging was in this case in the range 0.65–0.60 and decreased to 0.45 after 200 cycles because of the accumulation of zinc in NOE in amounts leading to degradation of the active paste. The total cycling life of the batteries was 300–350 cycles.

Table 3. Variation of the KOH concentration in the electrolyte in the forming cycles and the achievable degree of NOE charging in a Ni/Zn battery. Rated capacity 50 A h, initial KOH concentration 7 M

Cycle	State	Capacity, A h	Current density, A dm^{-2}	C_{ch}/C_{th}	C_d/C_{th}	KOH concentration, M
Forming:						
first	Charged	100	0.23	1.0		4.4
	Discharged	58.5	0.27		0.585	5.0
second	Charged	100	0.23	1.0		4.0
	Discharged	84	1.8		0.84	
Training:						
fifth	Charged	84	0.32	0.9		3.8
	Discharged	80	1.8		0.80	4.0

At an initial value of 6 M, the KOH concentration was in the range 4.0–3.0 after the forming (Fig. 1). The degree of charging was in this case about 0.5 till 200th–250th cycle, but the total cycling life may start to decrease in earlier cycles because the zinc electrode may be passivated at the specified lower-limit KOH concentration.

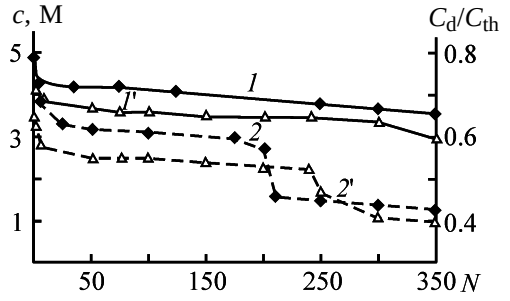


Fig. 1. Variation of (*1*, *1*') the KOH concentration in the electrolyte and (*2*, *2*') degree of charging of an NOE composed of spherical nickel hydroxide on an FNi support in the course of cycling of NTs-25 batteries. Initial KOH concentration, M: (*1*, *2*) 7 and (*1*', *2*') 6. (*N*) Number of cycles, (*c*) KOH concentration, and (C_d/C_{th}) degree of NOE charging; the same for Fig. 2.

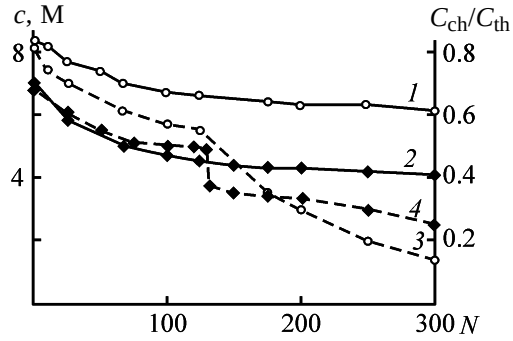


Fig. 2. Variation of (*1*, *1*') the KOH concentration in the electrolyte and (*2*, *2*') degree of charging of an MC NOE in the course of cycling of NTs-25 batteries. Initial KOH concentration, M: (*1*, *2*) 7 and (*1*', *2*') 6.

These results determine the lower limit to the KOH concentration in the electrolyte, at which the NOE retains its working efficiency.

To reveal specific features of the processes occurring in FNi NOE in electrolytes with different KOH concentrations, we compared the data considered above with the results obtained in testing under similar conditions batteries with MC positive electrodes (Fig. 2). It can be seen that the degree of charging of an MC NOE formed separately in an electrolyte containing no zincate ions in the initial cycles exceeds that of a compacted NOE composed of spherical nickel hydroxide on a foamed nickel support at any of the initial KOH concentrations used (8.5–7.0 M). However, it decreases in the course of cycling just as the KOH concentration does. This dependence reflects the extent to which the capacity of batteries with MC NOE is unstable with respect to service life.

The results obtained in cycling of batteries with MC NOE at a KOH concentration of 8.5 M indicate that it is inadvisable to use an electrolyte of this composition in batteries with FNi NOE, because its forming will occur at a high concentration of $Zn(OH)_4^{2-}$ ions, which will shorten the cycling life of the battery.

Thus, introduction of zinc into FNi NOE stabilizes its capacity by making weaker its dependence on the electrolyte concentration, but the achievable degree of charging decreases in this case. The actually achieved degree of charging of FNi NOE under the conditions of forming in a NiZn battery is lower than that possible for NiCd and NiMH batteries and in NiZn batteries with MC NOE. This is due to the presence in the electrolyte of zincate ions involved in the transformation of the active paste at a decreasing KOH concentration.

As shown in [4], the zinc-containing active paste is formed in an electrolyte with a low KOH concentra-

tion (6–4 M) in the solid phase with a direct transition β-$Ni(OH)_2 \rightarrow \beta$-NiOOH, for which the maximum degree of charging is 0.8. In this case, the specific capacity of FNi NOE is approximately equal to that of MC NOE because of the lower mass of the support of the former. A higher degree of charging is only achieved for a transition in forming via the γ-phase: $\beta_{(II)} \rightarrow \gamma \rightarrow \alpha \rightarrow \beta_{(III)} + \gamma$. For this phase to be formed in zinc-containing electrolytes, a higher KOH concentration is necessary, which is unacceptable for NiZn batteries.

CONCLUSIONS

(1) The degree of charging of a nickel oxide electrode on a foamed nickel support, obtained in forming in a nickel–zinc battery, does not exceed 0.7–0.85 of the calculated value corresponding to the transition $Ni^{2+} \rightarrow Ni^{3+}$, which is lower than the values obtained in nickel–cadmium and nickel–metal hydride batteries and in nickel–zinc batteries with a metal–ceramic nickel oxide electrode. This is due to the combined action of zinc introduced into the starting active paste of a nickel oxide electrode on a foamed nickel support and that contained in the electrolyte and to a decrease in the concentration of OH^- ions.

(2) The degree of charging of a nickel oxide electrode on a foamed nickel support obtained in subsequent cycling of nickel–zinc batteries is 0.6–0.5 and varies within this narrow range as the KOH concentration in the electrolyte decreases. In this case, the nickel oxide electrode on a foamed nickel support has about the same specific capacity as that of a metal–ceramic nickel oxide electrode because of the lighter support.

(3) Comparison of the degree of charging of the nickel oxide electrode on a foamed nickel support with that of the metal–ceramic nickel oxide electrode, obtained under similar conditions, shows that zinc intercalated into the electrode on a foamed nickel support stabilizes the capacity of the electrode and makes it less dependent on the varying electrolyte concentration, but simultaneously depresses the level at which this stabilization occurs.

REFERENCES

1. Hui, L., Yunchang, Y., Jiongliang, Y., and Zeyun, W., *J. Power Sources*, 1995, vol. 57, pp. 137–140.
2. Arkhangel'skaya, Z.P., Kas'yan, T.B., and Loginova, M.M., *Zh. Prikl. Khim.*, 2003, vol. 76, no. 12, pp. 1981–1986.
3. Arkhangel'skaya, Z.P., Kas'yan, T.B., and Loginova, M.M., *Elektrokhim. Energet.*, 2003, vol. 3, no. 4, pp. 192–199.
4. Tessier, C., Faure, C., Guerlou-Demourgues, L., *et al.*, *J. Electrochem. Soc.*, 2002, vol. 149, no. 9, pp. 1136–1145.
5. Sac-Epee, N., Falacin, L.R., Delahaye-Vidal, A., *et al.*, *J. Electrochem. Soc.*, 1998, vol. 145, no. 5, pp. 1434–1439.
6. Ezhov, B.B., Egorova, S.A., and Goryainova, T.I., *Zh. Prikl. Khim.*, 1992, vol. 65, no. 1, pp. 11–15.

Russian Journal of Applied Chemistry, Vol. 78, No. 9, 2005, pp. 1438–1443. Translated from Zhurnal Prikladnoi Khimii, Vol. 78, No. 9, 2005, pp. 1463–1468.
Original Russian Text Copyright © 2005 by Danilenko, Savel'ev, Yavorovskii, Yurmazova, Galanov, Balukhtin.

APPLIED ELECTROCHEMISTRY AND CORROSION PROTECTION OF METALS

Composition and Formation Kinetics of Erosion Products of the Metallic Charge in an Electric-Discharge Reactor

N. B. Danilenko, G. G. Savel'ev, N. A. Yavorovskii, T. A. Yurmazova, A. I. Galanov, and P. V. Balukhtin

Research Institute of High Voltages, Tomsk, Russia
Tomsk Polytechnic University, Tomsk, Russia

Received June 7, 2005

Abstract—The composition and formation kinetics of erosion products of the metallic charge (aluminum, iron) in an electric-discharge reactor operating at an open-circuit voltage of 500–1000 V, peak pulse current of 250 A, and pulse energy of 0.5–1 J were studied. Dispersion products of the charge were subjected to electron-microscopic and X-ray phase analyses. The energy yield of erosion products was determined by chemical analysis to be hundreds of times the calculated yields of electrolysis. The erosion kinetics was studied and the mechanism of erosion was considered.

Electric-discharge methods for purification of wastewater, based on electroerosion of electrodes [1, 2], find use because a wider variety of chemical processes can be provided by substances constituting the electrode. If, however, the discharge occurs in water, the erosion yield of the electrodes is low, and the energy expenditure is high. For example, it was found in [3, 4] that the energy expenditure for erosion of metals in this mode is 2.8×10^6 to 5.6×10^6 kJ mol^{-1} (~104 kW h kg^{-1}).

In electric-discharge erosion treatment, the energy expenditure is 1.2–12 kW h kg^{-1} [5–10]. In this case, a reactor with bulky electrodes is used, with metal in the form of grains or shavings more or less insulated from one another by oxide films or having point contacts charged in between. When an electric current is passed through the reactor, a breakdown occurs in the multitude of insulating gaps, with electric explosions at these gaps or at conducting microcontacts.

In the opinion of Fominskii [5] and Zubenko and Yushchishina [6], the electroerosion of metals in water occurred via breakdown of the oxide layer at the electrode surface and the subsequent melting and spraying of the metal. The efficiency of such a process was rather high, 3–4 kW h kg^{-1}. Similar results were obtained in [9, 10]. In [7], a system with an active charge in the form of metal shavings was tested. In this case, the curvature of the contacting surfaces is markedly higher and each current pulse gives rise to multiple discharges at randomly arranged contacts. In this case, electroerosion occurs via disintegration of contacts by the current, and purification of water is associated not only with discharges in water, but also with chemical reactions involving the charge. Preliminary experiments demonstrated that the energy efficiency of erosion may be in this case as high as 1.2 kW h kg^{-1} [7]. This indicates that the method in question is promising both for purification of potable water and wastewater and for synthesis of various materials.

This study is concerned with the energetics, chemical mechanism, and formation kinetics of erosion products of the metallic (aluminum, iron) charge of an electric-discharge reactor.

EXPERIMENTAL

The experimental setup comprised a vessel into which 200 g of metal shavings used as a chemically active charge was placed. Electrodes were lowered into the vessel and 950 ml of distilled water was poured in. The electrodes were connected to a two-circuit source of pulsed current with the following parameters: pulse width ε_p = 10 μs; pulse repetition rate 100 Hz; voltage U 500–1000V; and current in the first half-period of the pulse, I = 250–400 A.

The concentration of iron ions was determined colorimetrically [11]: Fe^{2+}, with 2,2'-bipyridine; ΣFe, with sulfosalicylic acid in an alkaline medium; and Fe^{3+}, as the difference $c(Fe^{3+}) = c(\Sigma Fe) - c(Fe^{2+})$.

1070-4272/05/7809-1438© 2005 Pleiades Publishing, Inc.

The specific surface area of the forming precipitate was measured by BET from thermal desorption of argon.

Electron-microscopic studies were carried out on a JEM-100 CXII electron microscope, and X-ray phase analysis, on a Shimadzu XRD 6000 diffractometer.

The energy expenditure for water purification was determined by obtaining current and voltage pulse oscillograms with an S8-17 oscilloscope. The pulse energy was calculated by integrating current and voltage oscillograms, to give values E 0.5–1.0 J pulse^{-1}. In addition, we measured the temperature of water in which an iron charge is subjected to the action of an electric discharge: at E = 0.5 J pulse^{-1} its rise was 0.53 deg min^{-1}.

When electric pulses act upon a charge poured-over with water, electric discharges are observed in the form of sparks all over the visible volume. After the iron charge is treated for several tens of seconds, a black suspension becomes noticeable, which partly turns brown in storage. In the case of an aluminum charge, a light gray suspension is formed, which becomes white in storage.

Spectral studies and X-ray phase analysis of products formed in dispersion of the charge demonstrated that the reaction of metal particles with water yields both hydroxides and oxides, which have a developed surface and fibrous structure for aluminum (Fig. 1a), and are of different shapes (plates, needles, and isometric crystals; Fig. 1b) for iron. The diameter of fibers of aluminum erosion products is 5–10 nm, and the diagonal dimensions of iron plates, about 100 nm. These structures have a large specific surface area (105 ± 5 m^2 g^{-1} for an iron charge dried at 110°C, and 293 ± 5 m^2 g^{-1} for an aluminum charge).

An X-ray phase analysis of products formed in erosion of the electrodes demonstrated that the products obtained mainly contain a crystalline substance with a structure close to that of Fe_3O_4 in the case of an iron charge, and boehmite AlOOH in the case of the aluminum charge.

To study the dynamics of accumulation of erosion products of an iron charge in various forms in water, both the forming suspension as a whole and, separately, the filtrate were analyzed after a certain time of treatment with electric discharges. The data on iron accumulation in various forms in solid erosion products are listed in the table.

The experimental data obtained were processed and dependences were plotted in the log–log coordinates (Figs. 2, 3). The total amount of iron (mg s^{-1}) removed from the electrodes (charge) is described as a function of the time of action of the discharge by the following empirical relations:

$$\log c_{Fe} = 0.72 \log t + 1.1331 \text{ or } c_{Fe} = 13.6 t^{0.72}. \quad \text{(I)}$$

The relative amount of Fe^{3+} in the suspension is

Data on accumulation of erosion products of the iron charge in various forms (Fe^0, Fe^{2+}, Fe^{3+}) in water

t, s	Fe^0,	Fe^{2+},	Fe^{3+}
	mg l^{-1}		
0	0	0	0
10	47	18	65
30	109	37	146
60	252	78	330
180	441	130	571
360	699	299	998
600	1086	445	1531
1800	1454	1221	2675

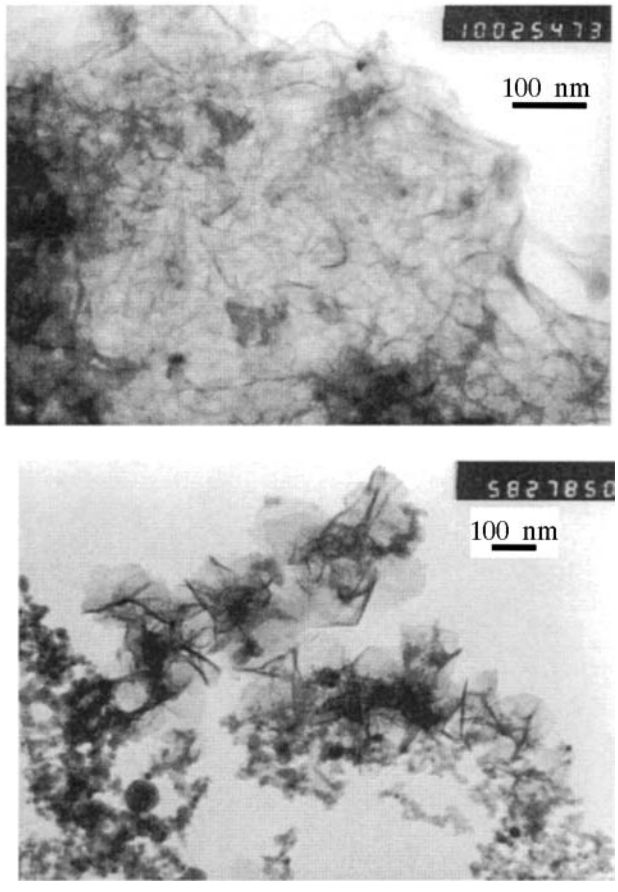


Fig. 1. Typical electron micrographs of solid products formed by electric discharges in water. Charge: (a) aluminum and (b) iron.

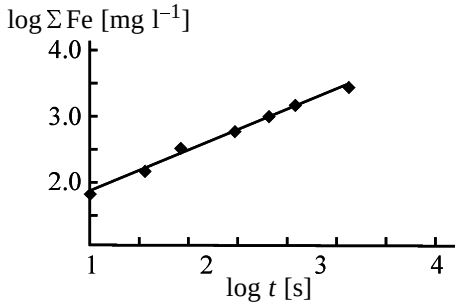


Fig. 2. Concentration Σ Fe of iron ions in erosion products (in suspension) vs. the treatment time *t*.

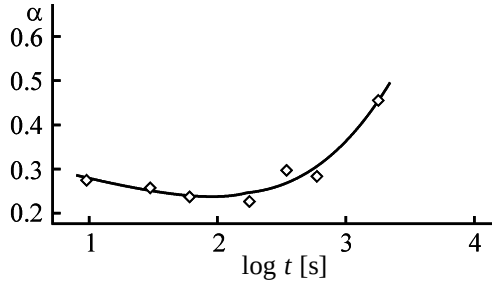


Fig. 3. Fraction of completely oxidized iron, $\alpha_{Fe^{3+}} = c_{Fe^{3+}}/c_{\Sigma Fe}$, vs. the erosion time *t*.

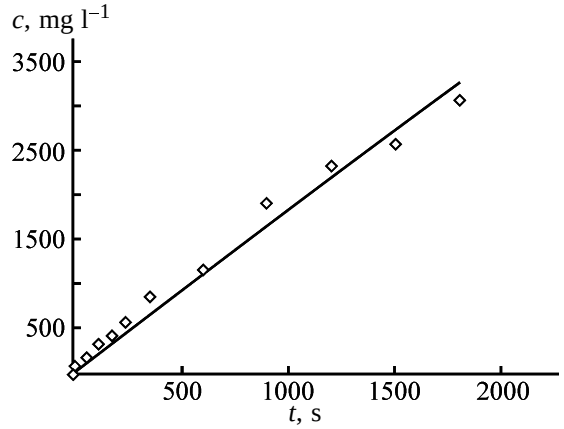


Fig. 4. Concentration c of aluminum ions in erosion products (in suspension) vs. the time *t* of action of an electric discharge.

shown in Fig. 3, whence follows that it passes through a minimum.

The variation of the concentration of Fe^{3+} and Fe^{2+} ions in the filtrate in electric-discharge treatment of water with an iron charge does not follow any regular pattern, and their concentration is approximately 1000 times less than that in the solid product, 0.187 to 2.347 mg l^{-1}.

The electroerosion kinetics of an aluminum charge was studied (Fig. 4). In contrast to the case of an iron charge, the dependence of the concentrations in the suspension and filtrate on the treatment time is linearized in the *c*–*t* coordinates [Al^{3+} concentration (mg l^{-1}) against the time of an electric-discharge treatment (s)].

The amount of aluminum removed from the electrodes (charge) is described as a function of the time of action of the discharge by the following empirical relation:

$$c_{Al^{3+}} = 1.82\,t. \qquad \text{(II)}$$

The installation used in the study shows a wide scatter of working characteristics, which is due to the structure and composition of the charge and to the dimensions and configuration of the reaction zone. Below, the results obtained in determining the energy expenditure in one of the runs are presented as an example.

In this run, the pulse repetition frequency was 100 Hz; energy released in a pulse, E = 0.5 J; mass of water, 950 g; mass of iron charge, 200 g; and mass of iron passing into suspension (in the form of oxide), 0.33 g min^{-1}. Hence, it can be calculated that the energy yield of iron was 7.0 mol (kW h)$^{-1}$, and the energy expenditure, 2.54 kW h kg^{-1} (0.142 kW h mol^{-1}) dispersed iron.

In this case, the balance of the electric and thermal energy has in this case the following form: with the loss of heat disregarded, a temperature rise by 0.714 deg min^{-1} corresponds to the experimentally determined uptake of electric energy equal to 3 kJ min^{-1}. In addition, chemical reaction may yield 16.5 kJ mol^{-1} in oxidation of iron with water, which may lead to a temperature rise by 0.01 deg min^{-1}, but more probable is oxidation of Fe with dissolved oxygen to give 376 kJ mol^{-1} (0.297 deg min^{-1}). The overall rise in temperature may constitute 1.0 deg min^{-1}. This value exceeds that found in the experiment (0.53 deg min^{-1}), which may be due both to thermal loss and to incomplete oxidation of iron to Fe^{3+}.

The energy expenditure obtained in this study markedly exceeds that reported previously (0.067 kW h mol^{-1} [7]), which is due to different geometric and other parameters of the experimental setup.

The energy expenditure in electroerosion of aluminum under comparable conditions was 0.046 kW h mol^{-1}. If the electroerosion mechanism consists in melting and spraying of the melt, the lower expenditure for heating to the melting point (30 and 9 kJ mol^{-1}) and for detachment of particles from the support (atomization heats 354 and 302 kJ mol^{-1})

may be responsible for the decrease in the energy expenditure.

It is of interest to compare the energy yield of the electroerosion product with the radiation-chemical and electrochemical yields of reactions in solutions and in an electric explosion of a wire [12–14].

For example, the energy yield of a product in nonchain radiation-chemical processes is commonly within 0.01–10 molecules per 100 eV. The above value of the yield for iron, 7.0 mol $(kW\ h)^{-1}$, corresponds to 19 molecules per 100 eV, and a value of 40 was obtained in [7].

In the case of a purely electrochemical oxidation of iron, the energy expenditure

$$W = znUF = 3 \times 1 \times 500 \times 97\,500 = 1.4 \times 10^8 \text{ J mol}^{-1} \text{ or}$$

$$714 \text{ kW h kh}^{-1}, \quad \text{(III)}$$

where z is the ion charge; n, number of metal equivalents; F, Faraday constant; and U, potential difference.

If 2.54 kW h is expended for oxidation of iron, only 3.6 g of the metal can be oxidized at a voltage of 500 V. As 1 kg is actually oxidized in this case, the amplification factor is more than 275, and even 550 according to [7].

A comparison with the process of metal dispersion by an electric explosion of a wire [12] can be made in the ratio of the supplied energy to the sublimation energy of the corresponding metal. In the given set of experiments, this value was 0.68 to 1.44 for electroerosion of iron, and 0.27 to 0.55 for aluminum. Commonly, metal powders are obtained by electric explosion of a wire at $E/E_c \approx 0.8$–2.5. If this procedure is carried out in the atmosphere of chemically active gases, the relative energy contribution may be ~0.6 and less.

Thus, the efficiency of electroerosion considerably exceeds that of processes in which each atom (molecule) of a reagent is subjected to an external action. This is evidence in favor of a collective or chain mechanism, in which energy is consumed for dispersion of the material via detachment of particles containing a large number of bound atoms, rather than by its evaporation. Alternatively, the process uses the energy of oxidation of the material with water or oxygen. The electroerosion resembles to the greatest extent the electric explosion of a metallic wire in an oxygen atmosphere [13, 14].

In the case when current pulses are passed through the metallic charge, the pulse energy probably mostly acts upon the metal, with the metal heated and small metal particles detached from the support. A particular detachment mechanism and the size of these particles will depend on the specific energy supplied and the rate of the energy supply. This may be evaporation of the metal, its melting and spraying, or mechanical detachment of nanoparticles. At the electric discharge parameters used in the study, the most probable in the primary process is formation of metal particles via spraying and detachment.

Apparently, the main stages of the process can be represented as the following scheme (M_c, compact metal; M_n, metal nanoparticles):

$$M_c \xrightarrow{\text{Electric-discharge erosion}} M_n, \quad (1)$$

reduction of water with the metal:

$$M_n + H_2O \longrightarrow M(OH)_n + H_2, \quad (2)$$

and oxidation of metallic particles with dissolved oxygen:

$$M_n + O_2 + H_2O \longrightarrow M(OH)_n. \quad (3)$$

The local temperature may be high because of the energy released by the electric discharge or by the exothermic oxidation [8]. Therefore, the resulting hydroxides may decompose partly (to oxohydroxides) or completely (to oxides). These are $Fe(OH)_2$, $Fe(OH)_3$, FeO, Fe_2O_3, Fe_3O_4, and FeO(OH) in the case of Fe, and $Al(OH)_3$, AlOOH, and Al_2O_3 for Al.

It is noteworthy that, in the mechanism described, the electric discharge acts upon the metallic electrode (charge), rather than upon water. In an alternative mechanism, the action of the electric discharge upon water is considered. This mechanism includes reactions in which O and OH radicals and H_2O_2 and O_3 molecules are formed in the electric discharge, with the subsequent oxidation of the compact material with these species. In this case, OH and O radicals presumably do not have enough time to react with M_n before their recombination to give H_2O_2, O_3, and O_2, and, therefore, the most probable pathway in this case is oxidation of the compact material with hydrogen peroxide and ozone, e.g., $Fe_c + H_2O_2 = Fe(OH)_2$.

The energy yield of reactions (1)–(3) under the action of an electric discharge on the metal should theoretically considerably exceed that for decomposition of water under the action of an electric discharge to give O_3 and H_2O_2 (without formation or involve-

ment of iron particles). This is due to the fact that, in the latter case, electric energy is expended for formation of each molecule of the product, whereas in the case of an electric discharge with electrode erosion, it is consumed for formation of a metal particle containing 107–108 atoms. At a particle size of 30–50 nm, only less than 1% of its bonds with the matrix are to be ruptured; further, nanoparticles react spontaneously to give the final product with energy release. The role of the electric discharge is reduced in this case to activation (depassivation) of the metal both via formation of nanoparticles and because of self-heating, with the amplification factor (per energy expended for detachment of a particle) exceeding 100. This estimate is made without regard for melting of the metal; taking this factor into account will make the amplification factor lower. The value calculated from the experimental data exceeds that expected on the basis of the above considerations by a factor of 2–3. This may be due to activation of the interaction between water and the metal matrix at the place of particle detachment or to a lower energy expenditure for dispersion of the metal by spraying.

The energy expenditure in electropulse erosion of iron, 0.067–0.142 kW h mol^{-1} (Fe), is markedly lower than that for electric-discharge synthesis of H_2O_2 molecules and OH radicals in water (0.12 molecule per 100 eV corresponds to 22.34 kW h mol^{-1} [15]), and, therefore, reactions of the type (1)–(3) are more probable; in the case of an iron charge, these reactions can be specified:

$$Fe_c \xrightarrow{\text{Electric-discharge erosion}} Fe_n, \quad (4)$$

$$Fe_n + H_2O \longrightarrow Fe(OH)_2 + H_2, \quad (5)$$

$$Fe(OH)_2 + O_2 + H_2O \longrightarrow Fe(OH)_3. \quad (6)$$

$$Fe_n + O_2 + H_2O \longrightarrow Fe(OH)_3 \text{ or } FeO(OH). \quad (7)$$

The fraction of completely oxidized iron passes through a minimum (Fig. 3), which may be due to consumption of dissolved oxygen by reactions (6) and (7), with the subsequent increase in this fraction through diffusion of oxygen to incompletely oxidized particles.

In the case of an aluminum charge, the occurring processes are simpler: aluminum particles formed in the electric discharge react with water and oxygen by reactions (2) and (3) to give a hydroxide, which can decompose to an oxohydroxide and oxide.

The main stages of the process for the aluminum charge can be represented as the following scheme:

$$Al_c \xrightarrow{\text{Electric-discharge erosion}} Al_n, \quad (8)$$

$$Al_n + H_2O \longrightarrow Al(OH)_3 + H_2, \text{ or } AlOOH + H_2, \quad (9)$$

$$Al_n + O_2 \longrightarrow Al_2O_3. \quad (10)$$

Complex ions, e.g., $[Al(H_2O)_5(OH)]^{2+}$ and $[Al(H_2O)_4(OH)_2]^{+}$, may be formed in solution.

Three mechanisms are possible for the erosion kinetics. The first consists in that erosion occurs via microscopic explosions of the material of the electrode (charge) at places of contacts, with the nature and number of these contacts remaining unchanged during erosion. This mechanism may become operative for a charge in the form of spheres or particles of other shapes, with surfaces of low curvature. This may be promoted by presence on the metal surface of thin dense films whose breakdown causes erosion, as well as by a low melting point of the metal and its low hardness. This is presumably the case for the aluminum charge, for which the erosion rate is constant (Fig. 4).

The second mechanism, which is characteristic of an iron charge, consists in that erosion occurs at irregularities with a high surface curvature (small radii of curvature). Electric discharge leads to a decrease in the height of projections and in the number of irregularities, and this decrease makes the resistance of breakdown gaps higher and the fraction of energy expended for spraying of the material lower.

The time dependence of the erosion rate can be represented in this case in the general form as

$$dc/dt = kc^{1/n}, \quad \text{(IV)}$$

where c is the concentration of the dispersed metal in the suspension, and n is the exponent dependent on the electrode configuration: $n = 3$ if the projections are eroded so that the volume of the metal being dispersed is proportional to the projection heights; $n = 2$ if the erosion products insulate or somehow diminish the active area of the electrodes; and $n = 1$ if the degree of erosion depends on the volume of the material removed in erosion (e.g., in the case of a decrease in the conductivity of the liquid, which is hardly probable).

Integration gives

$$c_{Fe} = \frac{n+1}{n} kt^{n/(n+1)} = k_n t^{\nu}. \quad \text{(V)}$$

Comparison of the experimentally obtained time dependences of the erosion yield [Fig. 2, formula (I)] shows that $\nu = 0.72$. This value corresponds to $1/n = 0.38$, which somewhat exceeds the theoretical value $1/n = 0.33$ for the case of erosion of projections.

The third mechanism consists in that, after primary erosion by, e.g., the second mechanism, a spontaneous topochemical reaction is initiated at damaged places. If this reaction is rapidly terminated (by fast formation of a protective film), the overall kinetics may correspond to formula (V). If, however, the specific rate of the reaction remains constant at the place of particle detachment, the kinetic equation becomes more complex:

$$dc/dt = k_1 c^{1/n} - k_2 c^m, \quad \text{(VI)}$$

where n is the configuration index for primary erosion; m, the index of the topochemical reaction, which is dependent on the configuration of the reaction zone; and k_1 and k_2, effective rate constants of the primary erosion and topochemical reaction, respectively.

Integration of this expression in the general form gives rather complex formulas inconvenient for analysis. However, rather simple expressions are obtained in certain particular cases, e.g., for $n = 3$ and $m = 1$:

$$t = 3(k_1 + k_2 c^{4/3})/4k_2. \quad \text{(VII)}$$

Such a mechanism is possible, e.g., in the presence of a catalyst.

CONCLUSIONS

(1) The action of pulsed electric discharges on a metallic charge causes its erosion with the subsequent oxidation of the forming micro- and nanoparticles. This gives precipitates with varied morphology: fibrous for Al and mixed (films, needles, nanocrystals) for Fe.

(2) The energy expenditure is 0.142 kW h mol^{-1} for Fe atoms, which is by a factor of 275 lower than that in electrolytic erosion. For the aluminum charge, the energy expenditure is approximately three times lower, which is due to the lower melting point of aluminum.

(3) A kinetic analysis demonstrated that, in electroerosion of a charge in the form of iron shavings, the erosion is hindered by dispersion of projections (points) and their resulting gradual smoothing. The electroerosion of aluminum occurs under similar conditions at a constant rate, at least during a time of about 30 min. This is probably due to higher plasticity and lower melting point of aluminum and to specific properties of the surface oxide film.

REFERENCES

1. USSR Inventor's Certificate no. 70 000.
2. Namitokov, K.K., in *Fizicheskie osnovy elektroiskrovoi obrabotki metallov* (Physical Foundations of Electric-Spark Treatment of Metals), Moscow: Nauka, 1966, pp. 86–108.
3. Goryachev, V.L., Korobochko, V.Yu., Kulishevich, A.I., *et al.*, *Izv. Ross. Akad. Nauk, Ser. Fiz.*, 1999, no. 11, pp. 2294–2297.
4. Goryachev, V.L., Ufimtsev, A.A., and Khodakovskii, A.M., *Pis'ma Zh. Tekh. Fiz.*, 1997, vol. 23, no. 10, pp. 25–29.
5. Fominskii, L.P., *Elektron. Obrab. Mater.*, 1980, no. 1, pp. 46–49.
6. Zubenko, A.A. and Yushchishina, A.N., *Elektron. Obrab. Mater.*, 2001, no. 6, pp. 60–65.
7. Shamanskii, V.V., Danilenko, N.B., and Gulak, N.V., in *Osnovnye vodokhozyaistvennye problemy i puti ikh resheniya. K 100-letiyu Tomskogo vodoprovoda: Materialy nauchno-prakticheskoi konferentsii* (Main Hydroeconomic Problems and Ways of Their Solution. To Centennial Anniversary of Tomsk Water-Supply System: Proc. Scientific and Practical Conf.), Tomsk: Tomskvodokanal, 2005, pp. 40–42.
8. Lyashko, A.P., Medvinskii, A.A., Savel'ev, G.G., *et al.*, *Kinet. Katal.*, 1990, vol. 31, no. 4, pp. 967–972.
9. Bairamov, R.K., *Zh. Prikl. Khim.*, 2003, vol. 76, no. 5, pp. 771–773.
10. Bairamov, R.K., *Zh. Prikl. Khim.*, 2003, vol. 76, no. 7, pp. 1067–1070.
11. *Unifitsirovannye metody analiza vod* (Unified Methods for Analysis of Water), Lur'e, Yu.Yu., Ed., Moscow: Khimiya, 1973.
12. Yavorovskii, N.A., *Izv. Vyssh. Uchebn. Zaved., Ser. Fiz.*, 1996, no. 4, pp. 114–136.
13. Kotov, Yu.A., in *Trudy Vserossiiskoi konferentsii "Fizikokhimiya ul'tradispersnykh sistem"* (Proc. Russian Conf. "Physical Chemistry of Ultradispersed Systems"), Moscow: Mosk. Inzh.-Fiz. Inst., 1999, pp. 60–66.
14. Savel'ev, G.G., Shamanskii, V.V., and Lerner, M.I., *Izv. Tomsk. Politekh. Univ.*, 2005, vol. 308, no. 1, pp. 97–102.
15. Piskarev, I.M., *Zh. Fiz. Khim.*, 2000, vol. 74, no. 3, pp. 546–551.

Russian Journal of Applied Chemistry, Vol. 78, No. 9, 2005, pp. 1444–1449. Translated from Zhurnal Prikladnoi Khimii, Vol. 78, No. 9, 2005, pp. 1469–1474.
Original Russian Text Copyright © 2005 by Turaev, Kruglikov, Parfenova.

APPLIED ELECTROCHEMISTRY AND CORROSION PROTECTION OF METALS

Regeneration by Membrane Electrolysis of an Etching Solution Based on Copper Chloride

D. Yu. Turaev, S. S. Kruglikov, and A. V. Parfenova

Mendeleev Russian University of Chemical Engineering, Moscow, Russia

Received March 24, 2005

Abstract—Regeneration of an acid solution for copper etching, based on copper(II) chloride, hydrochloric acid, and ammonium chloride, by membrane electrolysis was studied. The concentrations of copper(I, II) ions in the cathode and anode spaces, current efficiency, degree of copper recovery, and specific consumption of electric power at different quantities of electricity passed through the electrolyzer were measured. The influence exerted by the current density on the electric power expenditure for recovery of metallic copper was examined. The anode current efficiency by chlorine was determined with a spent etching solution and an H_2SO_4 solution used as anolyte.

One of the main procedures in manufacture of printed-circuit boards is copper etching, for which an acid solution based on Cu(II) chloride is frequently used. The working principle of this etching solution is based on the reaction

$$Cu^{2+} + Cu + 4Cl^- = 2[CuCl_2]^-, \quad (1)$$

whence follows that the etching solution should contain chloride ions in an amount sufficient for binding of the whole amount of copper(I) into a complex. The necessary excess of chloride ions is introduced into solution in the form of HCl, NH_4Cl, or NaCl. In the course of etching, the concentration of Cu(II) ions decreases through an increase in the concentration of Cu(I) ions, which makes slower the etching rate.

Under industrial conditions, such a spent etching solution can be regenerated [1] by oxidizing Cu(I) ions with atmospheric oxygen or hydrogen peroxide.

To maintain a constant, nearly optimal composition of the solution, all its components except Cu(II) ions should be added to it. As a result, each cycle of etching and chemical regeneration leads to a substantial increase in the volume of the etching solution and involves an additional expenditure of chemicals. Furthermore, the appearing excess amount of the solution requires an appropriate treatment, which consists at the majority of plants in the reagent method for production of metallic copper or of its sparingly soluble compounds (oxides, $CuO \cdot CuCl_2$).

Electrochemical regeneration of a spent etching solution in a two-chamber electrolyzer with cation-exchange membrane and circulation of the etching solution between the anode chamber and the etching machine was considered in [2]. It should be noted that the amount of ions of bivalent copper(II) formed at the anode in a process of this kind will always markedly exceed the amount of copper ions that passed across the membrane from the anode space into the cathode chamber. This mismatch leads to a decrease in the concentration of copper ions and increase in that of hydrogen ions in the catholyte. This, in turn, gives rise to a side reaction of hydrogen evolution at the cathode. Thus, circulation of the etching solution only between the anolyte and the etching machine leads to limitation of the rate of copper removal from the etching solution by the rate of its migration across the cation-exchange membrane from the anode space into the cathode space in the form of Cu^{2+} ions. In the steady state, the current efficiency by copper will be rather low, because it should be equal to the transport number of Cu^{2+} ions across the membrane. The additional supply of copper ions, which is necessary for maintaining their concentration in the catholyte at a prescribed level, can be provided by circulating the etching solution not only through the anode chamber, but also through the cathode chamber.

Copper is removed from the surface of printed-circuit boards in the etching machine by spraying of the etching solution over a printed-circuit board. Owing to the contact between the etching solution and atmospheric oxygen, copper(I) ions are partly oxidized to Cu(II) already in the etching machine. This reaction

1070-4272/05/7809-1444© 2005 Pleiades Publishing, Inc.

makes lower the concentration of copper(I) in the anolyte and thereby leads to a decrease in the quantity of electricity that should be passed through the anolyte before the onset of evolution of the toxic chlorine. This quantity of electricity is several times smaller than that necessary for removal of etched-off copper from the etching solution. Therefore, the scheme under consideration cannot balance the processes at the anode and cathode without formation of a chlorine–oxygen mixture at the anode.

Thus, a topical task is to modify the process of electrochemical regeneration to preclude formation of Cl_2 at the anode in considerable amounts. In this study, two possible ways to solve the problem are analyzed: (1) regeneration in two stages, with each portion of a spent etching solution electrochemically treated first in the cathode chamber and then in the anode chamber; and (2) electrochemical treatment of a spent etching solution only in the cathode chamber, with a sulfuric acid solution used as anolyte.

In the first version of the process, oxidation of $CuCl_2^-$ ions is the predominant anodic reaction, because nearly the whole amount of copper(II) contained in an etching solution during its residence in the cathode chamber will be converted either into the metal or into $CuCl_2^-$ ions.

In the second version, the rate of discharge of chloride ions at the anode will be limited by the rate of their transfer from the catholyte across the membrane, i.e., will be determined solely by the selectivity of the membrane.

EXPERIMENTAL

A two-chamber cell [3] with a Flemion cation-exchange membrane [4] was used in the study. The anode space was hermetically sealed in order to catch and absorb gases evolved at the anode. For a more effective removal of Joule heat, the cell was placed in a vessel with cold water. The current and voltage were monitored with a digital ammeter and an M-830B digital voltmeter. The cell was fed from a B5-48 dc power supply. A titanium plate with a working surface area of 0.25 dm^2 served as a cathode, and a platinum-plated niobium plate with the same working surface area, as an anode.

The electrolysis was carried out in accordance with the above-mentioned two schemes of the process. Scheme 1: an etching solution containing no Cu(I) ions in the 350-ml cathode chamber and a solution containing Cu(I) and Cu(II) ions in the 350-ml anode space; scheme 2: etching solution containing no Cu(I) ions in the cathode space and 1.0 N H_2SO_4 solution in the anode space.

Composition of the solutions used

Composition	Concentration, g l^{-1}		
	catholyte	anolyte	wash water
Cu^{2+}	39.3–41.2	24.1–34.6	2.54
NH_4Cl	150	150	9.46
HCl	50	50	3.15
Including Cu^+	0	23.8–33.5	0

Scheme 2 was also used in experiments simulating the recovery of copper ions from wash water in a trapping bath after etching. In these experiments, the catholyte simulated the wash water in the trapping bath and a 1 N H_2SO_4 solution served as the anolyte. The chlorine contained in the anode gas was absorbed with a 1 M solution of KI. The electrolysis was performed at current densities of 2 and 4 A dm^{-2}. The starting solution had the following composition (g l^{-1}): $CuCl_2 \cdot 2H_2O$ 106–111, NH_4Cl 150, and HCl 50. Metallic copper was dissolved to prepare the anolyte. The composition of the solutions poured into the cell before the experiments is listed in the table.

Cathodic and anodic polarization curves were obtained in the potentiodynamic mode at potential sweep rates of 0.5 and 1 mV s^{-1} with a PI-50-1.1 potentiostat. The content of Cu(I) and Cu(II) ions was determined in the starting solutions and in the anolyte in the course of electrolysis. In the experiments using an H_2SO_4 solution as the anolyte, the content of chloride ions was determined. The content of Cl_2 in the anode gas was found by titration of the iodine evolved in passing the anode gas through a KI solution.

Cathodic process. The scheme of processes occurring in the two-chamber electrolyzer in electrolysis of a chloride solution of copper is shown in Fig. 1.

The main cathodic reaction is reduction of Cu^{2+} ions, which occurs in two stages:

$$Cu^{2+} + 2Cl^- + e^- \rightarrow CuCl_2^-, \quad (2)$$

$$CuCl_2^- + e^- \rightarrow Cu + 2Cl^-. \quad (3)$$

In this case, it can be seen from curve *3* (Figs. 2a–2d) that, first, reaction (2) dominates, which is manifested in accumulation of Cu^+ ions in solution. Only after approximately 20 A h l^{-1} of electricity is passed, their concentration starts to decrease, i.e., the rate of further reduction becomes higher than the rate of their

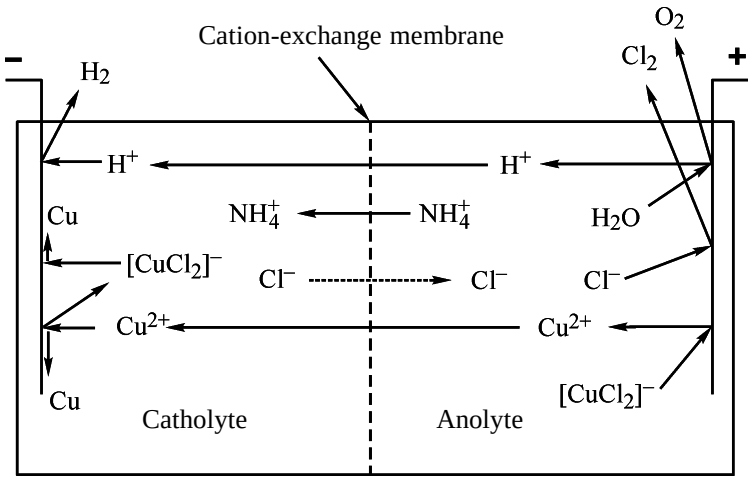


Fig. 1. Schematic of the processes occurring in a two-chamber cell.

formation. Presumably, the cathode potential is the main factor determining the predominance of a one- or two-electron process. This is indicated by the manner in which the current density affects the run of curve *3* (Figs. 2a–2d): at a current density of 2 A dm^{-2}, a higher concentration of Cu^+ ions is reached than that at a current density of 4 A dm^{-2}. This explanation is also supported by the faster decrease in the concentration of Cu^{2+} ions at a lower current density (Figs. 2a–2d, curves *2*). The cathode potential, naturally, depends on the current density and is steadily shifted in the course of electrolysis in the negative direction because of a change in the solution composition, which consists in that the total concentration of copper ions gradually decreases. At a lowered current density and, accordingly, at a more positive averaged cathode potential, it is possible to accumulate univalent copper in amounts exceeding the content of Cu^{2+} ions, which results in differential current efficiencies that exceed 100% (Figs. 3a–3d, curves *3*).

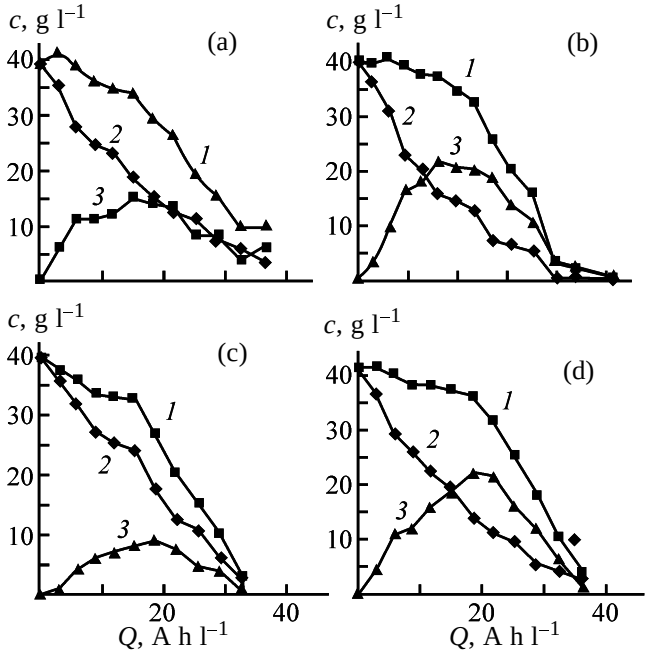


Fig. 2. Concentration *c* of copper ions in the catholyte vs. the amount *Q* of passed electricity. Anolyte: (a, b) Cu(I)-containing copper etching solution and (c, d) 1.0 N H_2SO_4 solution. Cathode current density, A dm^{-2}: (a, c) 4 and (b, d) 2. Concentration, g l^{-1}: (*1*) total, (*2*) Cu(II) ions, and (*3*) Cu(I) ions.

A considerable decrease in the concentration of Cu(I) and Cu(II) ions in the course of further electrolysis at an amount of passed electricity exceeding 30–40 A h l^{-1} will diminish the current efficiency by metallic copper and copper(I) to values that are markedly lower than 100%. With account of the fact that the concentrations of Cu(I) and Cu(II) are close, the decrease in the differential current efficiency can be only attributed to occurrence of a side process of hydrogen evolution. The results of polarization measurements confirm this conclusion (Fig. 4, curve *4*).

At a cathode current density of 4 A dm^{-2}, the average current efficiency by Cu^0 is, after the recovery of 62% of the whole amount of copper(I, II) present in the anolyte at the beginning of an experiment, 66%, and the average electric power consumption for recovery of Cu^0, 25.3 kW h kg^{-1}. At 2 A dm^{-2}, these values are strongly different: after the recovery of 77.1% of the whole amount of copper(I, II) contained in the catholyte at the beginning of an experiment, the average current efficiency by Cu^0 is 78.1%, and the average electric power expenditure for Cu^0 recovery,

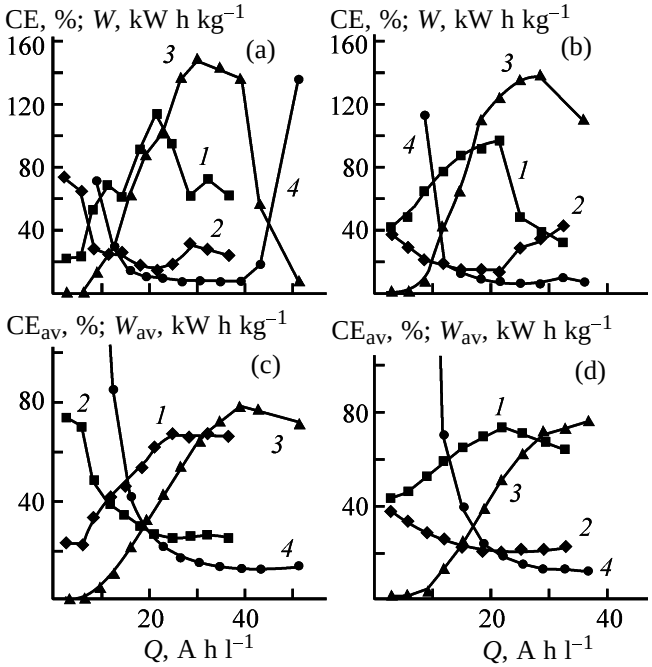


Fig. 3. Current efficiency CE by copper, specific electric power expenditure W, average current efficiency CE_{av}, and average specific electric power expenditure W_{av} vs. the amount Q of passed electricity at cathode current densities of (*1, 2*) 4 and (*3, 4*) 2 A dm^{-2}. Anolyte: (a, c) Cu(I)-containing copper etching solution and (b, d) 1.0 N H_2SO_4 solution. (a, b) (*1, 3*) CE and (*2, 4*) W; (c, d) (*1, 3*) CE_{av} and (*2, 4*) W_{av}.

11.7 kW h kg^{-1} (Fig. 3c). Use of a 1.0 N H_2SO_4 solution as anolyte at the same cathode current density does not lead to any significant changes in the dependence for the cathode space, compared with the anolyte in the form of a solution containing Cu(I, II) ions (Figs. 2, 3). Minor differences are, in all probability, due to transfer of Cu^{2+} ions from the anolyte into the catholyte, and also to different electrical conductivities of the anolytes compared.

Anodic processes. The total concentration of copper in the anode space decreases from 57.5 to 50.1 g l^{-1} (Figs. 5a, 5b; curves *1*) via migration of Cu(II) cations from the anode space into the cathode chamber. In the process, the concentration of copper(II) in the anode space increases (curve *2*), and that of Cu(I) decreases (curve *3*). To prevent evolution of the toxic Cl_2, the anode current density should not exceed the limiting current of diffusion of Cu(I) ions, which decreases with its concentration (Fig. 4, curves *1–3*). If a 1.0 N H_2SO_4 solution is used as anolyte, the anode current efficiency by chlorine (Figs. 5c, 5d; curves *4*) is limited by the concentration of chloride ions in the anolyte (Fig. 5, curves *5*), whose migration into the anolyte is governed by the

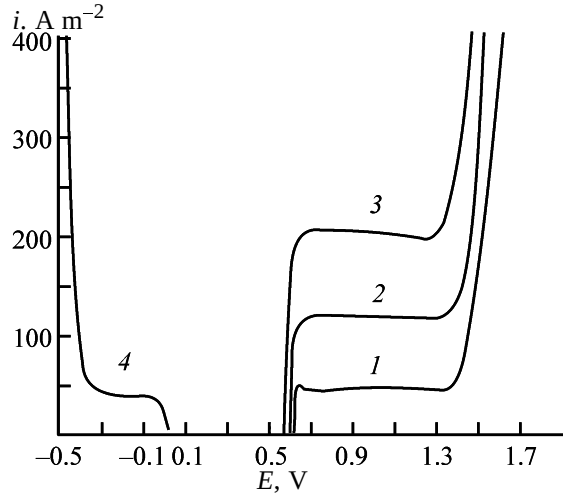


Fig. 4. (*1–3*) Anodic and (*4*) cathodic polarization curves. (*i*) Current density and (*E*) polarization. Curves *1–3* were measured with an anode made of platinum-plated niobium with a working surface area of 6.25 cm^2 (titanium as cathode) at a potential sweep rate of 0.5 mV s^{-1} in a solution of 50 g l^{-1} HCl and 150 g l^{-1} NH_4Cl. Content, g l^{-1}: (*1*) Cu^+ 7.62, Cu^{2+} 47.63; (*2*) Cu^+ 16.51, Cu^{2+} 43.18; and (*3*) Cu^+ 24.135, Cu^{2+} 40.00. Curve *4* was measured with a copper cathode with a working area of 5.72 mm^2 (platinum-plated niobium as anode) in a solution composed of 50 g l^{-1} HCl, 150 g l^{-1} NH_4Cl, and Cu_Σ 0.635 g l^{-1} at a potential sweep rate of 1 mV s^{-1}.

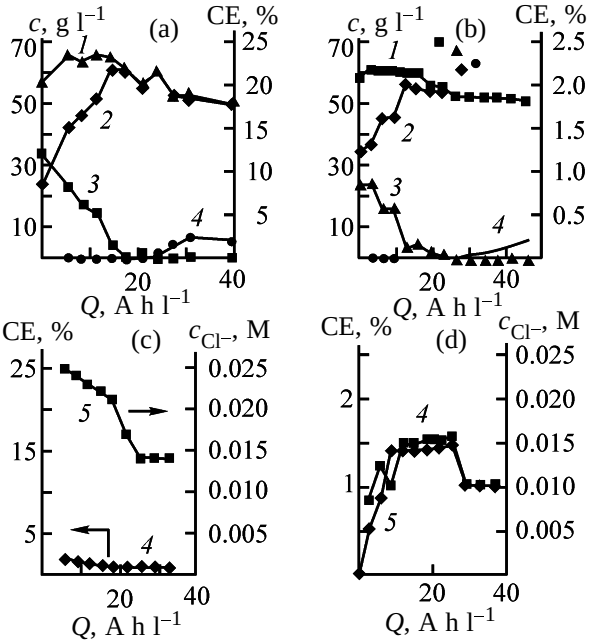


Fig. 5. Concentration of (a, b) copper ions c and (c, d) chloride ions c_{Cl^-} and (a–d) current efficiency CE by chlorine in the anolyte vs. the amount Q of electricity passed. Anolyte: (a, b) copper etching solution and (c, d) 1.0 N H_2SO_4 solution. Anode current density, A dm^{-2}: (a, c) 4 and (b, d) 2. Concentration, g l^{-1}: (*1*) total copper ions, (*2*) Cu(II) ions, and (*3*) Cu(I) ions; (*4*) current efficiency by chlorine; and (*5*) concentration of chloride ions.

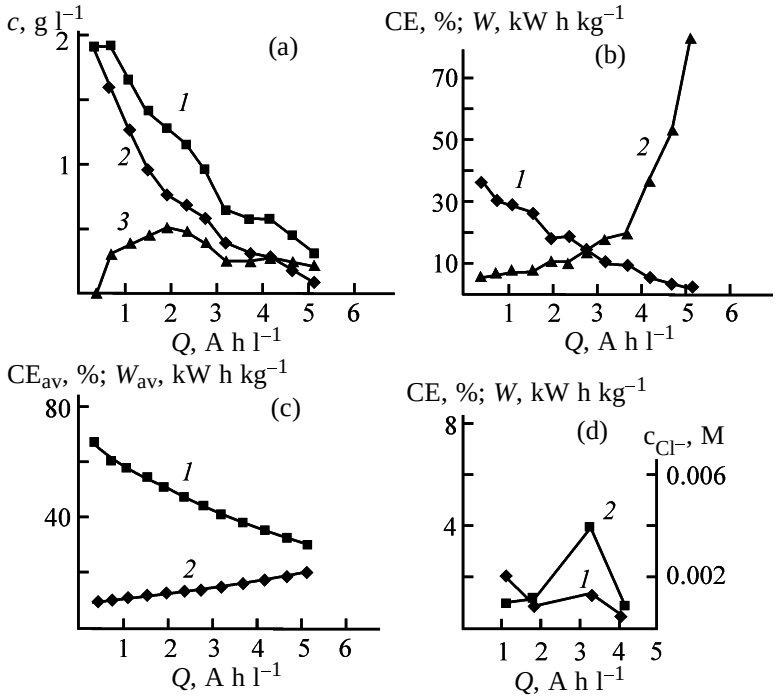


Fig. 6. Recovery of copper ions from the wash water from a trapping bath by membrane electrolysis. Two-chamber cell with a perfluorinated cation-exchange membrane; wash water from the trapping bath as catholyte and 1.0 N H_2SO_4 solution as anolyte; cathode and anode current density 1 A dm^{-2}. Dependence on the amount of passed electricity of (a) concentration *c* of copper ions in the catholyte: (*1*) total copper ions, (*2*) copper(II) ions, and (*3*) Cu(I) ions; (b) (*1*) current efficiency CE by copper and (*2*) electric power expenditure *W*; (c) (*1*) average current efficiency by copper and (*2*) average electric power expenditure; and (d) (*1*) concentration of chloride ions in the anolyte and (*2*) current efficiency by Cl.

selectivity of the cation-exchange membrane. It should be noted that, in the presence of chloride ions in the anolyte in a considerable concentration, the anode current efficiency does not exceed 2.5% at an anode current density of 4 A dm^{-2} and decreases with the current density (Figs. 5a, 5b; curves *4*). The regeneration by scheme (1) is particularly efficient if the concentration of Cu(I) ions in the solution being regenerated substantially exceeds that of Cu(II) ions. In this case, virtually complete oxidation of Cu(I) into Cu(II) is achieved at a simultaneous minor decrease in the total concentration of copper ions. If it is necessary to markedly diminish the total concentration of copper ions, Cl_2 inevitably evolves at the anode. The advantage of scheme (2) consists in the possibility of regeneration of copper etching solutions with any concentration ratio of Cu(I) and Cu(II) ions. Cl_2 evolved at the anode is completely absorbed via oxidation of Cu(I) into Cu(II). In both versions, it is advisable to use a low current density in order to make lower the electric power consumption.

The results obtained in a study of electrodeposition of Cu^0 from the wash water in the cathode space of the two-chamber electrolyzer with a hermetically sealed anode space are shown in Fig. 6. The curve describing the dependence of the concentration of copper ions in the catholyte on the amount of passed electricity show a run similar to that presented above. The current efficiency by Cu^0 decreases, which points to intense evolution of hydrogen during the entire experiment. This leads to an increase in the electric power consumption.

The electrochemical treatment of the wash water can decrease the concentration of copper ions in the trapping bath from 2.54 to 0.32 g l^{-1} on passing 5.1 A h l^{-1}, with the average current efficiency by copper equal to 30.5%, and the average electric power expenditure, to 20 kW h kg^{-1}.

CONCLUSIONS

(1) Separation of the cathode and anode spaces with a cation-exchange membrane makes it possible to prevent oxidation of copper(I) to Cu(II) at the anode, with its subsequent reduction to Cu(I) at the cathode, to raise the current efficiency by Cu^0, and to diminish the current efficiency by Cl_2.

(2) Use of low cathode and anode current densities

prevents or markedly diminishes the evolution of H_2 at the cathode and Cl_2 at the anode, and also reduces the electric power expenditure per kilogram of recovered Cu^0.

(3) Use of 1.0 N H_2SO_4 or a copper etching solution as anolyte enables regeneration of copper etching solutions with different Cu(I) and Cu(II) concentrations. However, this requires that the anode space should be hermetically sealed to trap the evolving chlorine and use it to oxidize Cu(I) ions.

(4) To decrease the loss of copper ions from the etching shop to wastewater, it is advisable to introduce a procedure of washing in the trapping bath, with a low concentration of copper ions maintained in the bath by means of membrane electrolysis.

REFERENCES

1. Kolesnikov, V.A., Kokarev, G.A., Kamynina, L.L., and Kapustin, Yu.I., *Ekologiya i resursosberezhenie v elektrokhimicheskikh proizvodstvakh* (Ecology and Resource Saving at Electrochemical Shops), Moscow: Ross. Khim.-Tekhnol. Univ. im. D.I. Mendeleeva, 1998, part II.
2. Il'in, V.A., *Khimicheskie i elektrokhimicheskie protsessy v proizvodstve pechatnykh plat* (Chemical and Electrochemical Processes in Manufacture of Printed-Circuit Bioards), issue 2, Supplement to *Gal'vanotekh. Obrab. Poverkhn*., Moscow, 1994.
3. Kruglikov, S.S., Turaev, D.Yu., and Gulina, V.V., *Gal'vanotekh. Obrab. Poverkhn*., 2003, no. 4.
4. Mazanko, L.F., Kamar'yan, G.M., and Romashin, O.P., *Promyshlennyi membrannyi elektroliz* (Industrial Membrane Electrolysis), Moscow: Khimiya, 1989.

Russian Journal of Applied Chemistry, Vol. 78, No. 9, 2005, pp. 1450–1453. Translated from Zhurnal Prikladnoi Khimii, Vol. 78, No. 9, 2005, pp. 1475–1478.
Original Russian Text Copyright © 2005 by Pisanenko, Pogrebova, Avilov, Yantsevich.

APPLIED ELECTROCHEMISTRY AND CORROSION PROTECTION OF METALS

Corrosion-Preventing Properties of Benzyl-Substituted *N*-Benzylpyridinium Chlorides

D. A. Pisanenko, I. S. Pogrebova, V. O. Avilov, and K. V. Yantsevich

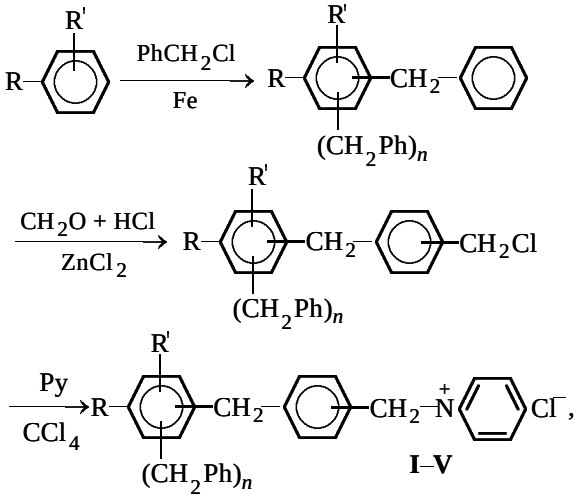
Kiev Polytechnic Institute, National Technical University of Ukraine, Kiev, Ukraine

Received May 4, 2005

Abstract—Benzyl-substituted *N*-benzylpyridinium chlorides were prepared by quaternization of pyridine with chloromethylated benzyl–substituted toluene, xylene, ethylbenzene, *o*-chlorotoluene, and phenetole. These compounds were studied as inhibitors of corrosion of 08 kp steel, 20 steel, and TsO zinc in solutions of sulfuric and hydrochloric acids at 20–80°C.

Quaternary ammonium salts are known [1] to be adsorption inhibitors of acid corrosion of metals. The inhibiting power of mixtures of these salts is frequently higher than that of the pure compounds [2]. Katapins used in industrial etching of ferrous and nonferrous metals with acids belong to this inhibitor type [3, 4]. The disadvantage of these inhibitors is irreproducibility of their protecting properties owing to the use in their synthesis of complex mixtures of alkylbenzens, nonaromatic hydrocarbons, and linear oligomer of benzyl chloride of uncontrolled composition. Therefore, preparation of inhibitors of this type from available compounds of known composition and study of their corrosion-preventing properties are urgent problems.

In this study we examined inhibition of acid corrosion of steels and zinc by benzyl-substituted *N*-benzylpyridinium chlorides prepared by the following scheme:



I–V

where n = 0–2; (**I**) R = Me, R'= H; (**II**) R = R' = Me; (**III**) R = Me, R' = 2–Cl; (**IV**) R = EtO, R'= H; (**V**) R = Et, R' = H.

To estimate the corrosion-protecting properties of salts **I**–**V** with respect to 08 kp steel, 20 steel, and TsO zinc, we measured the coefficient of corrosion deceleration γ, the degree of corrosion inhibition Z, and the shift of the corrosion potentials ΔE_c in the presence of these salts.

EXPERIMENTAL

The initial benzylarenes were prepared by the reaction of toluene, xylene, and ethylbenzene (technical grade) and of *o*-chlorobenzene and phenetole (reagent grade) with a threefold excess of benzyl chloride in the presence of iron chips [5] at 80–90°C for 5–6 h. The yield of benzylarenes was 61–89%. As determined by GLC, the ratio of mono-, di-, and trisubstituted benzylarenes in reactions with toluene, xylene, *o*-chlorobenzene, phenetole, and ethylbenzene was 62 : 26 : 12, 60 : 27 : 13, 65 : 25 : 10, 74 : 19 : 7, and 67 : 27 : 6, respectively. Benzylarenes of the known composition were chloromethylated in CCl_4 by the procedure described in [6]. Prior to the synthesis, a catalyst for this reaction was prepared. For this purpose, paraform and anhydrous $ZnCl_2$ were mixed in CCl_4 and dry HCl was bubbled through the mixture until complete dissolution of the components. To the freshly prepared catalyst, a solution of appropriate benzylarene in CCl_4 was added at simultaneous bubbling of dry HCl and stirring.

Monochloromethylation was performed for 4–6 h at the benzylarene : paraform : catalyst molar ratio

1070-4272/05/7809-1450 © 2005 Pleiades Publishing, Inc.

Table 1. Influence of salts **I**–**V** on corrosion of 08 kp steel and TsO zinc in solutions of sulfuric and hydrochloric acids. Salt concentration 3 g l^{-1}

Salt	20°C		40°C		60°C		80°C	
	γ	*Z*, %	γ	*Z*, %	γ	*Z*, %	γ	*Z*, %
08 kp steel, 3 M H_2SO_4								
I	20.06	95.01	39.75	97.48	55.42	98.19	128.62	99.22
II	14.50	93.10	22.82	95.61	37.38	97.32	130.07	99.23
III	12.49	91.99	31.78	96.85	49.64	97.98	140.36	99.28
IV	18.43	94.57	39.75	97.48	60.65	98.35	136.92	99.26
V	17.49	94.28	42.81	97.66	65.66	98.47	142.05	99.29
TsO zinc, 0.5 M H_2SO_4								
I	33.61	97.02	38.34	97.39	39.54	97.47	40.59	97.53
08 kp steel, 6 M HCl								
I	85.58	98.83	92.73	98.92	182.82	99.45	120.22	99.16
II	31.55	96.83	56.32	98.22	77.87	98.71	60.77	98.35
III	20.65	95.15	49.33	97.97	112.71	99.11	92.56	98.91
IV	76.53	98.69	118.69	99.15	133.63	99.25	100.12	99.00
V	66.27	98.49	23.69	95.77	33.77	97.03	26.24	96.18
TsO zinc, 6 M HCl								
I	12.54	92.02	39.62	97.47	90.01	98.88	96.86	98.96

of 1 : 2 : 0.3 and 70°C. After reaction completion, a solution of chloromethylated benzylarene in CCl_4 was decanted from the lower bed of the spent catalyst and purged with nitrogen. The number of CH_2Cl groups was determined by the intensity of the ^1H NMR signals of methylene protons [7]. The solutions of chloromethylated benzylarenes in CCl_4 were used in pyridine quaternization under conditions of Katapin preparation [3]. The products of pyridine quaternization were dried on a rotary evaporator under a reduced pressure of 30–40 mm Hg. The residual water content was determined by refluxing a weighed portion of the salts in toluene using a Dean–Stark trap. The yields of salts **I**–**V** based on the initial benzylarenes were 76, 72, 76, 62, and 75%, respectively.

Chromatographic analysis of benzylarenes was performed on a Biokhrom chromatograph (5% SE-30 elastomer on Chromosorb W, helium carrier gas). The ^1H NMR spectra were recorded on a Tesla BS-487 spectrometer (80 MHz) using HMDS as an internal reference.

The corrosion experiments were performed in 0.5 and 3 M H_2SO_4 and in 1 and 6 M HCl at 20°C for 24 h, at 40 and 60°C for 2 h, and at 80°C for 0.25 h. The corrosion was monitored gravimetrically. The polarization curves of a steel plate with the working surface area of 1×10^{-4} m^2 were recorded in the acid solutions in the absence and in the presence of the inhibitors. The electrode potentials were given vs. a hydrogen electrode.

Our experiments showed that all the examined compounds strongly inhibit corrosion of 08 kp steel and TsO zinc in concentrated sulfuric and hydrochloric acids at 20–80°C (Table 1). On heating from 20 to 80°C, the corrosion inhibition coefficients of 08 kp steel in 3 M H_2SO_4 steadily increase, whereas in 6 M HCl they reach a maximum at 60°C and then sharply decrease. The strengthening of the inhibiting effect is probably due to an increase in the specific adsorption of the salts by interaction of π electrons of benzene rings with the steel surface. The decrease in the corrosion inhibition coefficient in 6 M HCl at 80°C is caused by desorption of the salts from the metal surface owing to fast dissolution of the metal [1]. The fact that the inhibition power of all the examined salts at 20–60°C in hydrochloric acid solutions is higher than in sulfuric acid solutions is consistent with the well-known influence of chloride ions on the protecting effect of cationic inhibitors of metal corrosion [1]. Comparison of the inhibiting power of

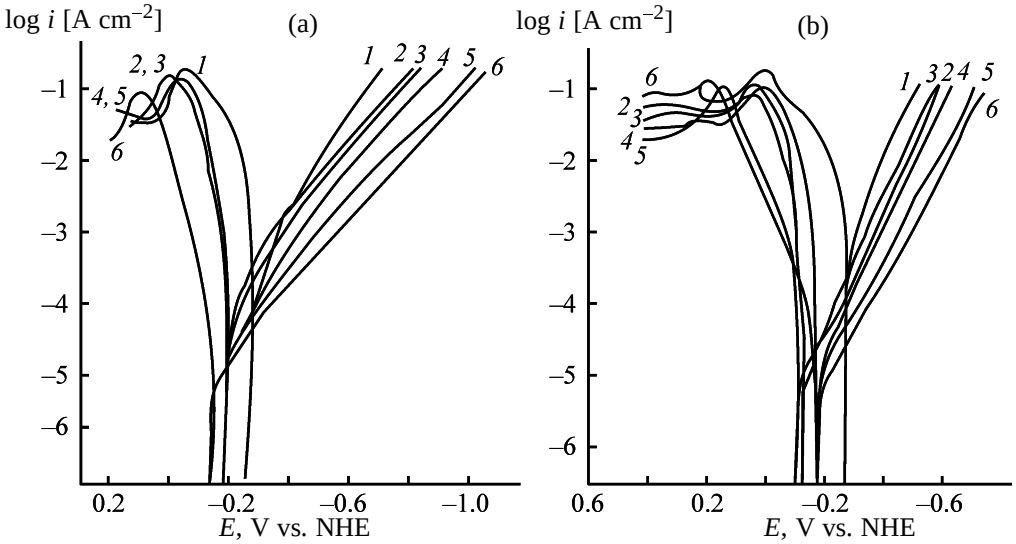


Fig. 1. Polarization curves of 20 steel in (a) 3 M H_2SO_4 and (b) 6 M HCl at 24°C in the presence of salts **I**–**V** (3 g l^{-1}). (*i*) Current density and (*E*) potential. (*1*) supporting electrolyte; (*2*) **II**, (*3*) **III**, (*4*) **IV**, (*5*) **V**, and (*6*) **I**.

salts **I**–**V** shows that both methyl (**II** and **III**) and bulky ethyl (**V**) substituents at the aryl fragment decrease the inhibiting power, probably due to steric hindrance in sorption of these compounds on the steel surface. The presence of the ethoxy groups in this fragment (compound **IV**) increases the protecting effect owing to specific interaction of the unshared electron pair of the oxygen atom of this group with the steel surface.

Adsorption on steel of salts **I**–**V** containing benzyl substituents directly bound to the aryl fragment is, on the whole, better than that of EPV, VPV and B-300 Katapins in which the sorption site, polybenzyl fragment, is remote from the pyridine ring [1, 8].

Table 2. Experimental (γ_{gm}) and calculated (γ_{pc}, $\gamma_{\Delta\psi1}$, and γ_θ) inhibition coefficient of 20 steel corrosion in 3 M H_2SO_4 and 6 M HCl at 24°C in the presence of salts **I**–**V**

Salt	ΔE_c, V	γ_{gm}	γ_{pc}	$\gamma_{\Delta\psi1}$	γ_θ	θ
			3 M H_2SO_4*			
I	0.080	26.22	26.31	75.85	–	–
II	0.030	13.51	10.11	7.32	1.84	0.46
III	0.030	14.41	10.22	5.85	2.46	0.60
IV	0.045	18.42	11.82	14.14	1.34	0.26
V	0.055	15.71	12.84	25.70	–	–
			6 M HCl**			
I	0.080	93.51	66.62	75.85	1.23	0.20
II	0.060	39.32	10.22	25.84	1.52	0.35
III	0.060	27.71	16.53	25.84	1.07	0.07
IV	0.060	60.32	12.32	28.84	2.09	0.53
V	0.070	56.64	31.62	44.67	1.26	0.21

* Calculated with b_c = –0.11 V, b_a = 0.029 V for **I** and **V** and b_a = 0.036 V for **II**–**IV**.

** Calculated with b_c = –0.11 V and b_a = 0.029 V.

The results of the voltammetric experiments in solutions of sulfuric and hydrochloric acids showed that compounds **I**–**V** inhibit both cathodic and anodic corrosion and shift the free corrosion potential E_c to the positive range. In most of experiments, the slopes of linear (Tafel) portions of the cathodic polarization curves b_c measured in the vicinity of steel potential E_c change slightly, and those of anodic polarization curves b_a change to a greater extent in the presence of these salts (Figs. 1a and 1b; Table 2). These changes, according to [1, 8], indicate that anions from the solution, sorbed on the metal surface and involved in its anodic dissolution, are displaced with the inhibitor. The anodic curved recorded in 6 M HCl in the presence of the most effective inhibitors **I**, **IV**, and **V** have two Tafel portions with different constants b_a. This is probably due to the fact that the adsorption of chloride ions increasing the efficiency of cationic inhibitors increases at anodic polarization [2]. The inhibition coefficients calculated from the polarization curves measured in hydrochloric acid solutions γ_{pc} differ from those calculated from the results of longer gravimetric monitoring γ_{gm} (Table 2). This difference can also be due to adsorption of chloride ions on the steel surface and decelerated formation of protecting inhibitor films containing organic cations and chloride anions.

To determine the inhibition mechanism, we studied the role of the energetic $\gamma_{\Delta\psi1}$ and blocking factors γ_0 in the course of steel corrosion inhibited by the exam-

ined salts. According to [9], the contribution of these factors into the inhibition coefficient γ_{gm} was estimated from the equation $\gamma_{gm} = \gamma_{\Delta\psi 1}\gamma_\theta = 10^{k\Delta\psi 1}(1 - \theta)^{-1}$. We assumed that $k = bk/b_0(b_a + b_c)$, $\Delta\psi_1 = \Delta E_c/[1 - b_a b_c/b_0(b_a + b_c)]$, where $\Delta\psi$ in the adsorption potential difference in the presence on an inhibitor; θ is the degree of coverage of the metal surface with the inhibitor; ΔE_c is the shift of the corrosion potential in the presence of the inhibitor; b_c and b_a are the Tafel slopes of the cathodic and anodic polarization curves; $b_0 = 2.3RT/F$.

The results of our calculations showed that most of the examined salts inhibit corrosion by the energy-blocking mechanism, with the energetic effect prevailing ($\gamma_{gm} > \gamma_{\Delta\psi 1} \gg \gamma_\theta$). The calculations for sulfuric acid solution containing salts **I** and **V** are complicated by the fact that $\gamma_{\Delta\psi 1}$ is higher than γ_{gm}. This difference is likely due to dependence of E_c on the following additional factors: coupled reduction of oxygen, adsorption of the inhibitors on the active sites of the metal surface, chemical reactions, etc. However, the linearity of $\log\gamma$–$\log c$ dependences (where c is the volume concentration of the inhibitor) for solutions of these compounds in sulfuric and hydrochloric acids suggests, in accordance with [1], that the energetic effect in the corrosion inhibition prevails.

CONCLUSIONS

(1) A procedure was developed for preparing benzyl-substituted *N*-benzylpyridinium chlorides by quaternization of pyridine with chloromethylated benzyl-substituted toluene, xylene, ethylbenzene, *o*-chlorotoluene, and phenetole (yield 62–76%).

(2) The benzyl-substituted *N*-benzylpyridinium chlorides are effective inhibitors of corrosion of carbon steels in solutions of sulfuric and hydrochloric acids.

REFERENCES

1. Reshetnikov, S.M., *Ingibitory kislotnoi korrozii metallov* (Inhibitors of Acid Corrosion of Metals), Leningrad: Khimiya, 1986.
2. Kuznetsov, Yu.I., *Usp. Khim.*, 2004, vol. 73, no. 1, pp. 79–93.
3. Gershenovich, A.I. and Stefanovich, V.V., *Khim. Prom.*, 1964, no. 6, pp. 416–418.
4. USSR Inventor's Certificate no. 280 162.
5. Olah, G.A., Kuhn, S.L., and Flood, S.H., *J. Am. Chem. Soc.*, 1962, vol. 84, no. 9, pp. 1688–1695.
6. Dashevskii, M.M. and Golivets, G.I., *Izv. Vyssh. Uchebn. Zaved., Khim. Khim. Tekhnol.*, 1967, vol. 10, no. 1, pp. 61–63.
7. Bible, R.H., *Interpretation of NMR Spectra. An Empirical Approach*, New York: Plenum, 1965.
8. Ivanov, E.S., *Ingibitory korrozii metallov v kislykh sredakh* (Inhibitors of Metal Corrosion in Acidic Solutions), Moscow: Metallurgiya, 1986.
9. Antropov, L.I. and Pogrebova, I.S., *Itogi Nauki Tekh., Ser: Korroz. Zashch. Korroz.*, 1973, vol. 2, pp. 27–112.

Russian Journal of Applied Chemistry, Vol. 78, No. 9, 2005, pp. 1454–1456. Translated from Zhurnal Prikladnoi Khimii, Vol. 78, No. 9, 2005, pp. 1479–1481.
Original Russian Text Copyright © 2005 by Korchagin, Sklyadnev.

ENVIRONMENTAL PROBLEMS OF CHEMISTRY AND TECHNOLOGY

Treatment of Highly Concentrated Wastewater with Spent Activated Carbon

V. I. Korchagin and E. V. Sklyadnev

Voronezh State Technological Academy, Voronezh, Russia

Received February 3, 2005; in final form, July 2005

Abstract—Sorption of the main polluting components of the wastewater from production of emulsion butadiene–styrene rubbers, soaps of synthetic and fatty acids and Leukanol, was studied on a preliminarily ground spent AG-3 activated carbon.

The world demand for adsorbents is expected to steadily grow in the future, since the amount of the water consumed tends to grow, and the quality of natural water is constantly deteriorated. Also, adsorbents are widely used in water and gas treatment. The use of adsorption processes suitable for exhaustive removal of organic compounds, in particular, surfactants, is hindered by complicated and expensive regeneration of adsorbents. For example, it is known [1] that regeneration of activated carbon costs approximately half as much as fresh carbon.

A peculiar way to solve the problem of sorption pretreatment of highly concentrated wastewater is the use of activated carbons from the main production. In particular, spent OU-A activated carbon from pharmaceutical production can remove 60–82% of organic pollutants from wastewater [2].

It is known [3] that sorption of technical surfactants involves no more than 1% of the surface area of SKT activated carbon, no more than 10–15% of that of KAD carbon, and no more than 20–25 of that of activated anthracite.

In sorption of surfactants, the surface of the sorbent macropores is of critical importance, as seen from characteristics of sorbents in [2]: SKT activated carbon has a macropore volume of 0.27, and KAD activated carbon, 0.52 $cm^3\ g^{-1}$. This can be confirmed by the data of Kisel'gof and Mikhailov [4] who reported that absorption of fairly hydrophilic Leukanol occurs on the sorbent surface.

It seems reasonable to use spent AG-3 activated carbon from the butadiene distillation stage of synthetic rubber production in treatment of highly concentrated wastewater from production of emulsion butadiene–styrene rubbers to remove surfactants, since AG-3 with a macropore volume of 0.41–0.52 $cm^3\ g^{-1}$ [2] belongs to macroporous sorbents, and the problem of its utilization still remains to be solved.

Specific pollutants in wastewater (serum) from the emulsion butadiene–styrene rubber coagulation stage are soaps of resin and synthetic fatty acids contained in the wastewater in amounts of ca. 500 mg dm^{-3}, as well as Leukanol, contained in amounts of 400 mg dm^{-3}. Leukanol belongs to "biologically hard" surfactants and occurs in water as individual molecules and associates, which complicates its sorption on granulated carbons.

The Leukanol concentration in solution was determined on an SF-46 spectrophotometer. In the UV region, the spectrum of Leukanol contains absorption bands with maxima near 227 and 235 nm. The Leukanol concentration was measured accurately to within 5.0 wt % [5].

Resin and synthetic fatty acid soaps were analyzed by direct titration with an alkali upon extraction from a model wastewater with an organic solvent, diethyl ether [6].

The total pollution indicator, chemical oxygen demand (COD), was determined titrimetrically [7]: Organic substances were oxidized with excess potassium dichromate in an H_2SO_4 solution under heating in the presence of a catalyst, silver sulfate. The residual potassium dichromate was determined by titration with a Mohr's salt solution, and the difference gave the amount of $K_2Cr_2O_7$ spent for oxidation of organic substances.

Testing preliminarily ground spent AG-3 activated carbon as sorbent in treatment of highly concentrated

1070-4272/05/7809-1454© 2005 Pleiades Publishing, Inc.

wastewaters to remove surfactants, in particular, Leukanol, showed that the sorption capacity of AG-3 varies with the degree of grinding. Figure 1 shows that the isotherms of Leukanol sorption on spent carbons substantially depend on the activated carbon particle size. For example, spent AG-3 carbon with the particle size of 5–20 μm has a higher sorption power than that with the particle size of 60–100 μm.

Low capacity of all granulated activated carbons with respect to surfactants is due to a small proportion in their structure of fairly large adsorption pores [3]. Therefore, we preliminarily ground the spent activated carbon in a disintegrator and a ball mill, which caused pore opening and restoration of the sorption surface. This yielded a finely dispersed activated carbon with a developed external surface, on which the adsorption virtually was not complicated by internal diffusion, in contrast to granulated carbons.

Figure 2 shows that, during the wastewater treatment, the total pollution indicator, COD, varies with the content of the spent AG-3 activated carbon and its particle size. Introduction of spent AG-3 carbon with the particle size of 5–20 μm in amounts of over 10 g dm^{-3} sharply decreases the COD to 80–120 mg O_2 dm^{-3}, which is due to adsorption of resin and synthetic fatty acid soaps, as well as of Leukanol. Removal of surfactants and Leukanol from the wastewater can be confirmed by plots of the surface tension vs. the content of the spent carbon, obtained in treatment of real wastewater, serum from SKS-30ARK production. The decrease in COD reflects reduction in the content of organic pollutants, and the growth of the surface tension is due to an increase in the surface energy at the interface owing to a decrease in the content of surfactants in solution because of sorption.

It should be noted that treatment of highly concentrated wastewaters from emulsion rubber production with spent activated carbon is efficient, as this is favored by real parameters of wastewater: pH 2.2–3.5, temperature 50–60°C, and content of sodium chloride up to 5.0 wt %.

The sorption capacity of AG-3 activated carbon depends on pH of the wastewater and, in absorption of anionic surfactants, is at a maximum in an acid medium (Fig. 3) due to conversion of the salts of surfactants to acid form.

It is known [2] that the sorption capacity with respect to surfactants is at a maximum at 35–60°C, and the sorption in treatment of highly concentrated wastewater significantly accelerates with temperature. The reason is rearrangement of the molecules in solu-

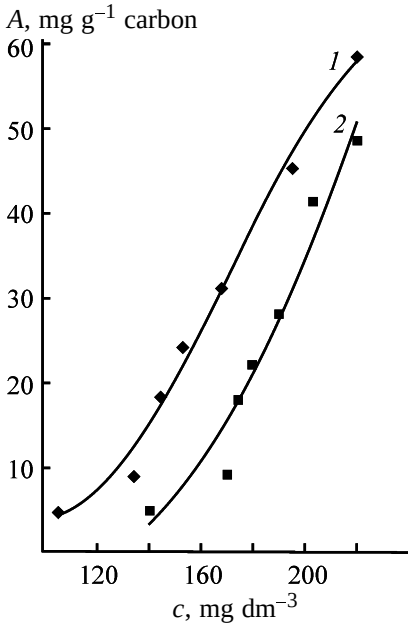


Fig. 1. Isotherms of Leukanol sorption on spent AG-3 carbon, depending on the AG-3 particle size. (*A*) Sorption capacity of carbon and (*c*) Leukanol concentration. Carbon fraction, μm: (*1*) 5–20 and (*2*) 60–100.

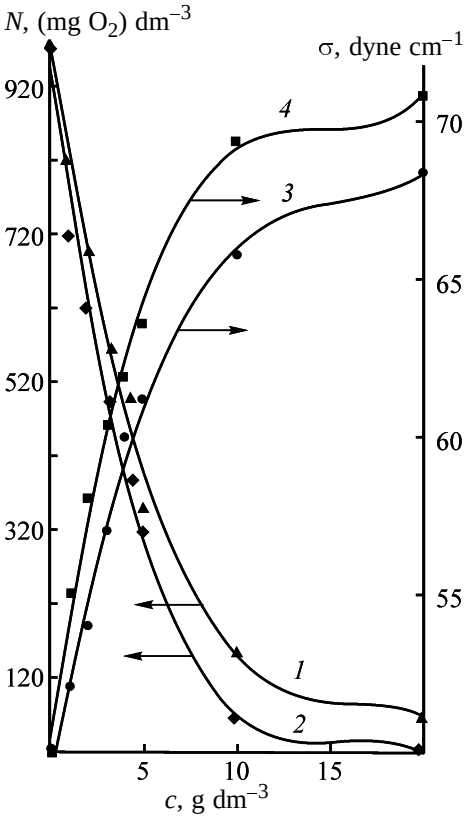


Fig. 2. Variation of COD *N* and surface tension σ with the content of spent AG-3 activated carbon *c*. COD upon introduction of fraction, μm: (*1*) 6–100 and (*2*) 5–20. Surface tension upon introduction of fraction, μm: (*3*) 60–100 and (*4*) 5–20.

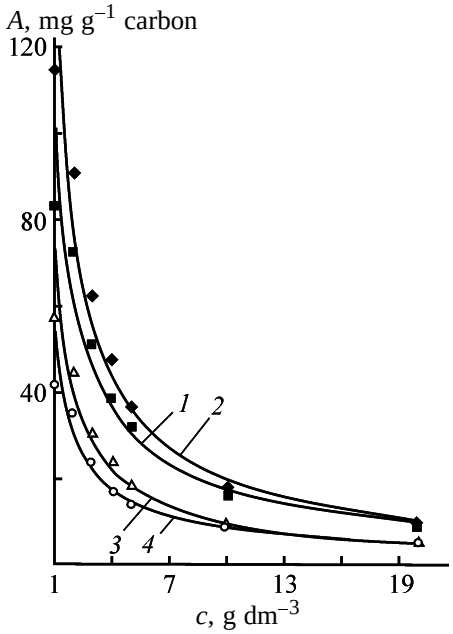


Fig. 3. Variation of the sorption capacity of carbon *A* with the content of spent AG-3 activated carbon at different pH and temperatures of the wastewater. pH: (*1*, *4*) 9 and (*2*, *3*) 2. Temperature, °C: (*1*, *2*) 60 and (*3*, *4*) 20.

tions, degradation of water–sorbate associates, and a decrease in the viscosity of the solution. At the same time, physical adsorption, like any exothermic process, becomes less efficient as a whole with temperature growth.

A similar influence is exerted by the temperature on adsorption of surfactants, in particular, Leukanol, on a ground spent AG-3 activated carbon (Fig. 3). The absorption power of the sorbent tends to increase upon washing with solutions of NaCl [3], which in our case is one of the wastewater components.

The above-mentioned factors in sorption from multicomponent systems, in particular, wastewater from synthetic rubber production, are manifested to a maximal extent at a certain temperature.

It is reasonable to concentrate the resulting aqueous dispersion of the spent activated carbon in order to make it suitable for subsequent utilization as a carbon-containing filler of polymeric systems in liquid-phase filling.

Upon treatment with preliminarily ground spent activated carbon to remove resin and synthetic fatty acid soaps, as well as a "biologically hard" NF dispersant, Leukanol, the wastewater from emulsion rubber production can be further supplied to the plant or municipal wastewater treatment facilities without preliminary dilution.

CONCLUSIONS

(1) Preliminarily ground spent activated carbon is suitable for local treatment of highly concentrated wastewater from emulsion rubber production.

(2) Soaps of resin and synthetic fatty acids, as well as Leukanol, are removed from the wastewater owing to pore opening and restoration of the sorption surface upon grinding of the spent activated carbon.

(3) Adsorption treatment of highly concentrated wastewater from emulsion rubber production is feasible, being the most efficient at the real values of the wastewater parameters: pH 2–3.5, T = 50–60°C, and salt content up to 5.0 wt %.

REFERENCES

1. *Ochistka i kontrol' stochnykh vod predpriyatii tsvetnoi metallurgii* (Treatment and Control of Wastewater from Nonferrous Metallurgy Enterprises), Lebedev, K.B., Ed., Moscow: Metallurgiya, 1983.
2. Smirnov, A.D., *Sorbtsionnaya ochistka vody* (Sorption Treatment of Water), Leningrad: Khimiya, 1982.
3. Koganovskii, A.M. and Klimenko, N.A., *Fiziko-khimicheskie osnovy izvlecheniya poverkhnostno-aktivnykh veshchestv iz vodnykh rastvorov i stochnykh vod* (Physicochemical Principles of Extraction of Surfactants from Aqueous Solutions and Wastewater), Kiev: Naukova Dumka, 1978.
4. Kisel'gof, G.V., Mikhailov, M.Yu., and Arkhangel'skii, L.K., *Zh. Prikl. Khim.*, 1994, vol. 67, no. 2, pp. 310–312.
5. Yakubenok, E.F., Poluektov, P.T., Svatikov, V.P., *et al.*, *Proizv. Izpol'z. Elastom.*, 1991, no. 9, pp. 3–4.
6. *Metodicheskie ukazaniya po analizu stochnykh vod promyshlennosti sinteticheskikh kauchukov* (Methodical Instructions on Analysis of Wastewater from the Synthetic Rubber Industry), Moscow: TsBNTI-leskhoza, 1977, pp. 61–62.
7. *PND* (Design and Normative Documentation) F 14.1: 2.100–97: *Quantitative Chemical Analysis of Waters: Technique for Titrimetric Measurement of the Chemical Oxygen Demand in Samples of Natural and Treated Wastewater*, Moscow: GUAK, 1997.

Russian Journal of Applied Chemistry, Vol. 78, No. 9, 2005, pp. 1457–1461. Translated from Zhurnal Prikladnoi Khimii, Vol. 78, No. 9, 2005, pp. 1482–1486.
Original Russian Text Copyright © 2005 by Lupeiko, Bayan, Gorbunova.

ENVIRONMENTAL PROBLEMS OF CHEMISTRY AND TECHNOLOGY

Use of a Carbonate-Containing Process Waste in Purification of Aqueous Solutions To Remove Zinc(II) Ions

T. G. Lupeiko, E. M. Bayan, and M. O. Gorbunova

Rostov State University, Rostov-on-Don, Russia

Received March 16, 2005

Abstract—A carbonate-containing waste from water-treatment installations of thermal power plants is tested as a sorbent for purifying aqueous solutions to remove zinc(II) ions. The effect of time, temperature, and other factors on sorption is evaluated.

The utilization of large-tonnage industrial wastes and, in particular, of the slurry formed in the flushing water of clarifying units at shops for chemical water treatment of thermal power plants is an important environmental problem. At present, most part of the forming waste is stockpiled on territories adjacent to power plants, occupies there an increasing space, and contaminates soil, as well as the surface and underground water. Therefore, development of methods for utilization of the water-treatment slurry, which will make it possible to convert this burdensome waste into "secondary resources," is a matter of current interest.

Previously, the composition and physicochemical properties of a waste formed in water treatment at Rostov Heat and Power Plant no. 2 has been studied [1], and it was shown that the slurry mainly contains calcium and magnesium carbonates, is homogeneous and finely dispersed, has a relatively constant composition, and is chemically and radiation safe. In [2, 3], we showed that the carbonate-containing waste (CCW) can be used for puryfing solutions to remove iron(III), copper(II), and chromium(III) ions.

Here we report the results obtained in studying the possibility of purification of aqueous solutions (real wastewater) to remove rather toxic zinc(II) ions with CCW.

According to the results of theoretical calculations, virtually complete recovery of zinc in the form of sparingly soluble $Zn(OH)_2$ requires that the precipitation should be performed at $8.0 \le pH \le 10.5$. In this case, it should be kept in mind that the precipitation of zinc(II) hydroxide onsets at pH 6.4, and at pH > 10.5 the precipitate starts to dissolve to form Zn(II) hydroxo ions, i.e., the recovery of zinc ceases to be complete [4]. The pH value of the CCW solution is ~9, which enables its use as a "mild" adaptive neutralizer precluding further dissolution of zinc(II) hydroxide. Also, in addition to the "hydrolysis" mechanism of the interaction of CCW with a zinc(II) solution, an exchange mechanism is possible, to give zinc carbonates in accordance with their solubility products: $SP_{MgCO_3} = 2.1 \times 10^{-5}$, $SP_{CaCO_3} = 3.8 \times 10^{-9}$, whereas $SP_{ZnCO_3} = 1.45 \times 10^{-11}$ [4].

In view of the aforesaid, removal of zinc(II) from solution can, theoretically, include the following processes.

(1) Partial dissolution of the carbonate components of a waste to form hydroxide anions, which leads to an increase in the solution pH:

$$CO_3^{2-} + H_2O \rightleftarrows HCO_3^- + OH^-,$$

$$HCO_3^- + H_2O \rightleftarrows OH^- + H_2CO_3,$$

$$H_2CO_3 \rightleftarrows H_2O + CO_2\uparrow.$$

(2) Shift of the equilibrium of zinc(II) hydrolysis toward formation of sparingly soluble hydroxo compounds and zinc hydroxide:

$$Zn^{2+} + HOH \rightleftarrows ZnOH^+ + H^+,$$

$$ZnOH^+ + HOH \rightleftarrows Zn(OH)_2\downarrow + H^+,$$

The addition of CCW to a solution of a zinc(II) salt will lead to mutual enhancement of the hydrolysis of the zinc salt and the carbonate component of the waste, leading in the end to precipitation of sparingly soluble hydroxo compounds or zinc hydroxide and to evolution of carbon dioxide.

1070-4272/05/7809-1457 © 2005 Pleiades Publishing, Inc.

Table 1. Degree of Zn^{2+} recovery in relation to the time of contact with the reagent for solutions of various concentrations

Run no.	τ, min	$pH_{filtrate}$	c_{res}^{Zn}, mg l^{-1}	α, %
c_{in} = 50 mg l^{-1}, pH_{in} = 5.70, CCW 40 g l^{-1}				
1	1	8.77	0.61	98.8
2	5	8.84	0.11	99.8
3	10	8.86	0.08	99.9
5	20	9.02	0.04	99.9
c_{in} = 200 mg l^{-1}, pH_{in} = 5.68, CCW 40 g l^{-1}				
1	1	7.73	56.40	71.8
2	5	8.01	10.32	94.8
3	10	8.08	7.47	96.3
4	15	8.12	2.53	98.7
5	30	8.18	0.49	99.8
6	60	8.31	0.11	99.9
c_{in} = 500 mg l^{-1}, pH_{in} = 5.62, CCW 40 g l^{-1}				
1	15	7.56	228.343	54.3
2	30	7.60	182.875	63.4
3	60	7.64	144.949	71.0
4	120	7.79	74.749	85.1
c_{in} = 50 mg l^{-1}, pH_{in} = 5.70, CCW 5 g l^{-1}				
1	5	7.73	14.702	70.6
2	10	7.81	9.366	81.3
3	15	7.86	6.039	87.9
4	20	7.89	4.382	91.2

(3) Formation of sparingly soluble carbonate, hydroxocarbonate, and other compounds of zinc at and on the surface of solid $CaCO_3$:

$$CaCO_3(s) + Zn^{2+} \rightleftarrows ZnCO_3(s) + Ca^{2+},$$

$$CaCO_3(s) + 2Zn^{2+} + 2OH^- \rightleftarrows (ZnOH)_2CO_3(s) + Ca^{2+}.$$

It is noteworthy that the last stage is less probable, because solid phases are formed during a long time and hydrolysis processes are fast. Thus, hydrolysis is preferable as regards kinetic characteristics.

EXPERIMENTAL

The precipitation of zinc(II) from solutions with CCW was studied on model solutions with initial concentrations of zinc(II), c_{in}^{Zn}, of 50, 100, 200, and 500 mg l^{-1}, prepared from $ZnSO_4 \cdot 6H_2O$ with account of the content of zinc(II) in wastewater from elecotroplating shops of plants [5]. Zinc(II) compounds were precipitated under static conditions: to 100 ml of a solution to be purified, with a prescribed concentration c_{in}^{Zn} (mg l^{-1}), was added a weighed portion of CCW with a particle size of 0.25–0.50 mm, and the mixture was agitated for a time τ (min). Further, the solutions were filtered. The pH value and the concentration of Zn^{2+} in solution were monitored before and after the contact with the reagent; the degree of metal recovery, α (%), was calculated from the difference of the initial (c_{in}^{Zn}) and residual (c_{res}^{Zn}) concentrations. The concentration of Zn^{2+} was determined spectrophotometrically by the standard procedure [6]. The optical density was measured with a KFK-3 photometer (error ±5%); the solution pH was monitored potentiometrically with an I-120M pH meter (accuracy ±0.05). For solutions with c_{in}^{Zn} of 50, 200, and 500 mg l^{-1}, the optimal purification time of aqueous solutions was determined (Table 1).

It was established that the recovery of zinc(II) is fast. For example, recovery from solutions with a concentration of zinc(II) lower than 200 mg l^{-1} (at CCW expenditure of 40 g l^{-1}) occurs during the first 5 min. At higher concentrations of zinc(II) ions in solution or at a smaller amount of the reagent, a longer contact is necessary. For example, at a concentration of zinc(II) ions equal to 500 mg l^{-1} and 40 g l^{-1} of the reagent, the duration of contact increases to 120 min, with the degree of metal recovery of 85%. In purification of a solution with c_{in}^{Zn} = 50 mg l^{-1} and 5 g l^{-1} CCW, α = 91% after 20 min; at the same time, on raising the amount of CCW to 40 g l^{-1}, the recovery occurs virtually instantaneously. It is also apparent that making the contact time longer and the weighed portion of the reagent larger leads to an increase in the pH value of the filtrate, which also supports the above-suggested mechanism of the process.

The effect of the CCW expenditure on the completeness of recovery at a varied time of contact between a solution being purified and CCW was studied in a solution with c_{in}^{Zn} of 50 mg l^{-1} at pH_{in} 5.70. As can be seen in Fig. 1, 20 g l^{-1} CCW is sufficient for detoxication of the solution under study to the maximum permissible concentration (MPC_{Zn} = 0.5 mg l^{-1} [6]). In this case, the degree of recovery exceeding 99.5% is reached in 10 min, i.e., c_{res}^{Zn} in the purified solutions is lower than the maximum permissible concentration. If 10 g l^{-1} CCW is added to this solution, MPC_{Zn} is reached in 30 min. Figure 1 also shows that the difference in time is only important at relatively small additions of CCW, the effect of time being insignificant at larger amounts of the reagent. Presumably, this is due to the dissolution rate of CCW,

which is rate-determining factor only at relatively small amounts of CCW.

For practical purposes, it was necessary to determine how the dispersity of CCW particles affects the efficiency of zinc(II) recovery from solutions. The main fractions of the slurry, with grain sizes of 0.1–0.25, 0.25–0.5, and 0.5–1.0 mm were used. A solution with c_{in}^{Zn} of 50 mg l^{-1} was used in the experiment, the time of contact between CCW and the solution was 10 min. As expected, the degree of recovery at the same time of contact with the solution is higher, and the expenditure of CCW, lower if the finely dispersed 0.1–0.25-mm fraction is used (Fig. 2). Apparently, this is due to an increase in the active surface area and in the dissolution rate of finer particles in an aqueous solution. The latter was experimentally confirmed in determining the pH of aqueous solutions of various CCW fractions (Table 2). However, the optimal, in the authors' opinion, is the 0.25–0.50-mm fraction. First, its content in the waste is the highest (nearly 50% [3]), and, second, the finer fraction more rapidly leads to clogging of filters, which hinders separation of the purified water from spent CCW.

Another important issue is the effect of the anionic component of solutions on the degree of zinc recovery, because the composition of wastewater from electroplating shops is rather diverse in this regard. Solutions with c_{in}^{Zn} of 50 mg l^{-1} were used in experiments aimed to elucidate this question, at a time of contact between CCW and a solution equal to 10 min. It was found that the anionic component has virtually no effect on the recovery of zinc(II) ions, provided that the pH values of the starting solutions are sufficiently close. However, the degree of recovery of Zn(II) ions decreases in a more acidic starting solution (as in the case of a chloride solution no. 2, Table 3), and the CCW expenditure increases, which is quite understandable.

It would also be expected that the precipitation of zinc(II) from solutions should be strongly affected by their temperature. Indeed, zinc ions are virtually completely removed at 40°C from a solution with c_{in}^{Zn} of 50 mg l^{-1} in the presence of 10 g l^{-1} slurry in 10 min, whereas reaching the same degree of recovery in the same time at 20°C requires a doubled amount of CCW (Fig. 3). Thus, in recovery of metal ions from hot solutions, the expenditure of CCW dramatically decreases, precipitation of zinc(II) ions becomes considerably faster, and a higher degree of purification is reached more easily. Presumably, this is due to an increased solubility of the slurry and to an enhanced hydrolysis of the carbonates it contains and the zinc

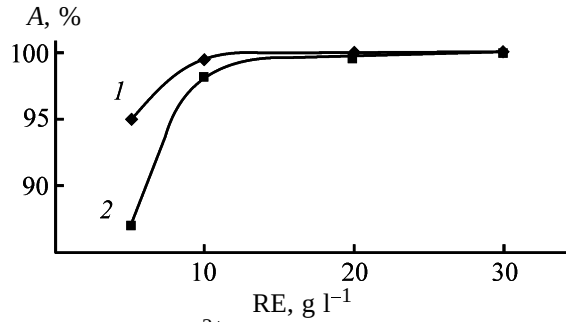


Fig. 1. Degree of Zn^{2+} recovery *A* vs. reagent expenditure RE. Sorption time, min: (*1*) 30 and (*2*) 10.

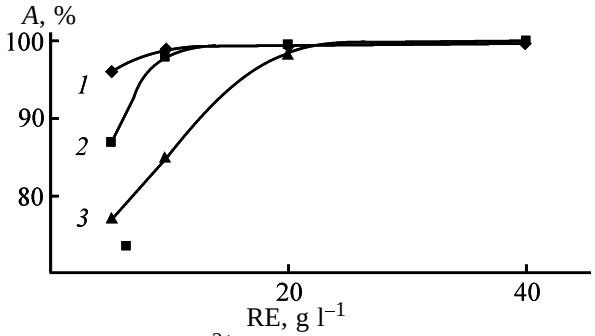


Fig. 2. Degree of Zn^{2+} recovery *A* vs. reagent expenditure RE. Particle diameter, mm: (*1*) 0.1–0.25, (*2*) 0.25–0.5, and (*3*) 0.5–1.0.

salt itself, which favors a more intense evolution of carbon dioxide, rise in the solution pH, and more complete precipitation of zinc in the form of sparingly soluble zinc hydroxo compounds.

One more issue of high practical importance is how iron(III) ions affect the degree of zinc(II) recovery from solution, because iron-containing articles are most frequently zinc-plated. A model solution containing a varied amount of iron(III) and 50 mg l^{-1} zinc(II) was used in experiments aimed to elucidate this question; the time of contact between the solution and CCW was 5 min. It was noted that the precipitation of zinc(II) in the presence of iron(III) (Fig. 4,

Table 2. Dependence of the solution pH on the CCW expenditure in dissolution of various fractions of the reagent

Amount of CCW, g l^{-1}	pH at indicated particle size, mm		
	0.1–0.25	0.25–0.5	>0.5
5	8.98	8.89	8.70
10	9.00	8.96	8.85
20	9.00	8.98	8.98
40	9.02	9.01	9.01

Table 3. Degree of Zn^{2+} recovery in relation to the CCW expenditure in sorption from sulfate, chloride, and nitrate solutions

Solution	pH	Reagent expenditure, g l^{-1}							
		5		10		20		40	
		pH	α, %	pH	α, %	pH	α, %	pH	α, %
Sulfate	5.53	8.06	86	8.44	98	8.76	99.7	8.99	99.9
Nitrate	5.61	7.80	85	7.82	98	8.08	99.5	8.75	99.9
Chloride no. 1	5.78	7.91	93	8.36	99	8.60	99.8	8.72	99.9
Chloride no. 2	2.63	7.62	66	7.78	96	7.89	98.3	8.18	99.1

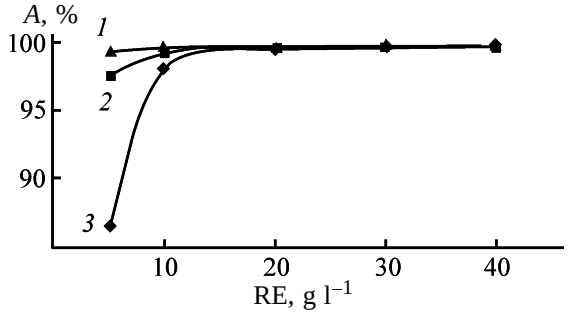


Fig. 3. Degree of Zn^{2+} recovery *A* vs. reagent expenditure RE. Temperature, °C: (*1*) 60, (*2*) 40, and (*3*) 20.

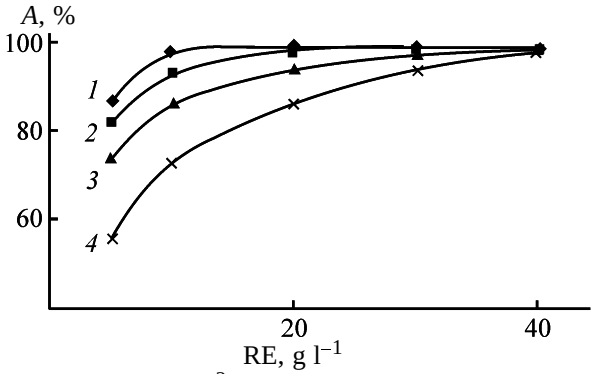


Fig. 4. Degree of Zn^{2+} recovery *A* vs. reagent expenditure RE. Iron concentration, mg l^{-1}: (*1*) 0, (*2*) 50, (*3*) 100, and (*4*) 150.

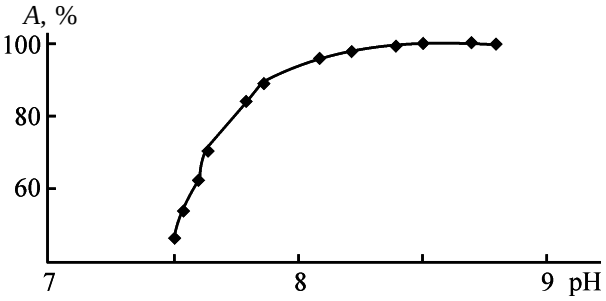


Fig. 5. Degree of Zn^{2+} recovery *A* vs. the pH of the medium.

curves *2–4*) is inferior to that from a pure solution (Fig. 4, curve *1*). Apparently, this is due to the fact that CCW is primarily consumed for precipitation of iron(III) ions. As shown previously [3], recovery of iron(III) is virtually instantaneous and the activity of CCW is in this case 200 mg Fe(III) per gram of the reagent. Therefore, only 0.75 g l^{-1} CCW is necessary for precipitation of iron(III) from the model solution being purified, with the rest of CCW consumed for recovery of zinc(II). In contrast to the case of iron(III), precipitation of zinc(II) requires a certain time and the expenditure of CCW for this process is considerably higher. Apparently, the reason is that precipitation of iron(III) is complete at a lower pH value (pH > 3) than that in removal of zinc(II). In addition, also different are the mechanisms of recovery of iron(III) and zinc(II). In the case of iron(III), the recovery mainly occurs via formation of a sparingly soluble hydroxide, whose solubility product is lower than those of the rest of phases. In removal of zinc(II), not only the hydroxide, but also hydroxo carbonate and carbonate can be formed by the exchange mechanism, and it is known that such a solid → solid conversion is slower than hydrolytic precipitation processes.

To determine how pH affects the recovery of zinc(II), we studied neutralization of a zinc solution with a slurry waste. Figure 5 shows that the degree of zinc(II) recovery exceeds 99%, which corresponds to the theoretically calculated value, on reaching pH 8.3. In addition, use of the CCW totally precludes dissolution of zinc(II) hydroxide caused by the overalkalization of the medium, because pH of a saturated slurry solution is 8.7. Thus, the slurry can serve as an effective and "mild" neutralizer of acid solutions, e.g., wastewater, because of the carbonate phases it contains.

The method suggested for purification of solutions to remove zinc(II) ions using CCW was successfully

tested on electroplating wastewater from the industrial plants of the city.

CONCLUSIONS

(1) Carbonate-containing waste formed in water treatment at electric power plants can be used for effective purification of acid aqueous solutions to remove zinc(II) ions to the MPC level. The expenditure of the carbonate-containing waste decreases, and the completeness of zinc(II) precipitation from a solution increases as the time of contact with the solution becomes longer, temperature increases, and the concentration of the solution being purified decreases.

(2) The 0.25–0.50-mm fraction of the carbonate-containing waste was chosen as the optimal for water purification.

(3) The anionic composition of the solution to be purified has virtually no effect on the interaction of zinc(II) ions with the carbonate-containing waste.

The results obtained in the study were confirmed by testing on wastewater from electroplating shops of various plants.

REFERENCES

1. Lupeiko, T.G., Bayan, E.M., Gorbunova, M.O., and Tsapkova, N.N., *Izv. Vyssh. Uchebn. Zaved., Sev.-Kavk. Region, Estestv. Nauki, Prilozh.*, 2003, no. 3, pp. 75–79.
2. Lupeiko, T.G., Ivleva, T.I., and Solov'ev, L.A., *Zh. Prikl. Khim.*, 2001, vol. 74, no. 4, pp. 567–570.
3. Lupeiko, T.G., Gorbunova, M.O., and Bayan, E.M., *Zh. Prikl. Khim.*, 2001, vol. 74, no. 10, pp. 1648–1650.
4. Lur'e, Yu.Yu., *Spravochnik po analiticheskoi khimii* (Handbook of Analytical Chemistry), Moscow: Khimiya, 1989.
5. Zhukov, A.I., Mongait, I.L., and Rodziller, I.D., *Kanalizatsiya promyshlennykh predpriyatii* (Sewage at Industrial Plants), Moscow: Gosstroiizdat, 1962.
6. *Rukovodstvo po khimicheskomu analizu poverkhnostnykh vod sushi* (Manual of Chemical Analysis of Land-Surface Water), Semenov, A.D., Ed., Leningrad: Gidrometeoizdat, 1977.

Russian Journal of Applied Chemistry, Vol. 78, No. 9, 2005, pp. 1462–1467. Translated from Zhurnal Prikladnoi Khimii, Vol. 78, No. 9, 2005, pp. 1487–1492.
Original Russian Text Copyright © 2005 by Ivanov, Babenko.

PROCESSES AND EQUIPMENT OF CHEMICAL INDUSTRY

Elementary Models of Extraction from Porous Particles under the Action of Pressure Pulses

E. V. Ivanov and Yu. I. Babenko

St. Petersburg Academy of Chemistry and Pharmacology, St. Petersburg, Russia
Prikladnaya Khimiya Russian Scientific Center, Federal State Unitary Enterprise, St. Petersburg, Russia

Received November 29, 2004; in final form, June 2005

Abstract—Extraction of target components from porous particles is analyzed for the case when a solution is displaced from coarse pores at the particle surface into the bulk of the extracting agent under the action of pressure pulses. Elementary mathematical models are suggested for the initial (hydraulic) and final (diffusion) stages of the extraction process.

In the overwhelming majority of studies concerned with the theory of extraction in a system constituted by a liquid and a solid porous body, the process is considered in terms of the diffusion extraction model [1, 2]. At the same time, the contribution of the convective component of the mass-transfer process in porous particles is rather important for apparatus with a fast rabble, those of pulsatory and vibration types, and apparatus with ultrasonic treatment, electric discharge, vacuum boiling, vacuum oscillation, "explosive" boiling-up, etc. [1, 3–7]. Filtration of the extracting agent occurs in coarse capillaries through squeezing of the raw material, collisions of particles with the working members of the apparatus, periodic changes in the pressure in the system, intense boiling-up of the extracting agent, collapse of cavitation bubbles near particles, etc.

Most of researchers consider the convective mass transfer in terms of diffusion models by introducing effective diffusion coefficients [8–10]. The exception are studies in which the diffusion of a substance to be recovered from deep inside a porous particle to coarse pores and the convective transfer through these pores to the surface of particles are considered simultaneously [11, 12].

The extraction in apparatus with an active hydrodynamic action upon porous particles occurs in three stages. In the initial stage, the extracting agent penetrates under the action of capillary forces into coarse pores and dissolves the target (being recovered) component contained in the pores and around them. The rate of the process is determined by that of the filtration displacement of the solution from pores into the extracting agent surrounding the particles. In what follows, this stage will be named hydraulic. In the second, diffusion-convective, stage the rate of diffusion of the target component into transport pores is comparable with that of solution removal from the pores. The fundamental aspects of such a process in a porous body with a bidisperse structure were studied in [11, 12]. In the third, diffusion, stage, the rate of the process is determined by that of molecular diffusion of the target component from deep inside a porous particle to transport pores.

It is noteworthy that the observed kinetic pattern of an extraction process that occurs in an exclusively diffusion mode is formally similar to that of a process occurring in an apparatus with a strong hydrodynamic action upon porous particles. However, the time in which the same degree of extraction is reached in extraction in the diffusion mode markedly exceeds that in the mode of a convective mass transfer in porous particles.

Here we suggest the simplest models of the hydraulic and diffusion stages, whose analysis is the most important for practical purposes.

Mathematical model of the hydraulic stage. Let us consider a single pore that pierces a particle and is filled with a solution containing the target component (Fig. 1a; presence of the target component is denoted by hatching). The pore mouths open at the particle surface and are in contact with the extracting agent containing no target component.

After the action of the first separate pressure pulse (e.g., as a result of collapse of a cavitation bubble near the pore mouth), the liquid is "pushed" through the

1070-4272/05/7809-1462 © 2005 Pleiades Publishing, Inc.

pore, with a volume ε of the extracting agent with the target component being removed from the pore (Fig. 1b; part of the pore free of the target component is not hatched).

Further, we assume that all the pressure pulses are identical, equal to the statistical-average pressure pulse, the probability of their occurrence at the left- and right-hand mouths of a pore are the same, and the pulses are distributed in time.

A second pressure pulse may arise both at the right-hand and at the left-hand opening of a pore. Therefore, two "states" of the pore are possible (Fig. 1c). In the first case, a volume ε of the extracting agent with the target component is extracted from the pore, whereas in the second, nothing is extracted, with a column of the extracting agent only moving within the pore. Thus, the average amount of substance extracted under the action of a single pressure pulse is ε/2.

After a next, third pulse appears, four states of the pore are possible. Two of these lead to extraction of the target component, with the two others being ineffective (Fig. 1d). Thus, a volume ε/2 of the liquid with the target component is, on the average, extracted per pressure pulse.

Analysis of the state of a capillary under the subsequent actions shows that the same amounts of the extracting agent with the target component is extracted in the *m*th and (*m* + 1)th stages (*m* ≥ 2). Therefore, it is appropriate, in deriving a general formula, to numerate the pairs (2, 3), (4, 5), (6, 7) ... by the values *n* = 1, 2, 3, ..., respectively. It was calculated that the average volume of the extracting agent with the target component, extracted per pressure pulse in a state *m*, equal to *V*(*m*), has the following values:

$$n = 1,\ V(2,\ 3)/\varepsilon = 1/2;\ n = 2,\ V(4,\ 5)/\varepsilon = 3/8;$$

$$n = 3,\ V(6,\ 7)/\varepsilon = 5/16;\ n = 4,\ V(8,\ 9)/\varepsilon = 35/128,\ \ldots$$

This sequence is generalized by the formula

$$V(m)/\varepsilon = V(m + 1)/\varepsilon = (-1)^n \binom{-1/2}{n}$$

$$= \pi^{-1/2}[\Gamma(n + 1/2)]/[\Gamma(n + 1)], \quad (1)$$

where Γ is the gamma function, and *n* is the number of a pair.

The volume of the extracting agent with the target component, extracted upon the action of the nth pair, is two times greater. Therefore, from (1) we obtain

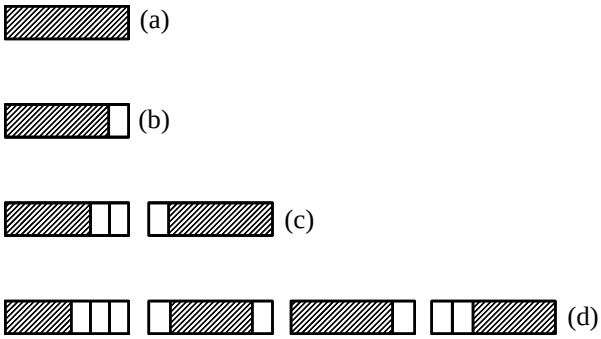


Fig. 1. Motion of the extracting agent within a pore under the action of pressure pulses. (a–d) For explanations, see text.

$$V(n)/\varepsilon = 2\pi^{-1/2}[\Gamma(n + 1/2)]/[\Gamma(n + 1)]. \quad (2)$$

The total volume of the extracting agent with the target component, *Q*(*N*), extracted upon the action of the first pulse and *N* following pairs of pressure pulses, is found by summation of expression (2):

$$Q(N)/\varepsilon = 1 + 2\pi^{-1/2}\sum_{n=1}^{N}[\Gamma(n + 1/2)]/[\Gamma(n + 1)]. \quad (3)$$

Formula (3) is remarkable in that the dependence on parameters of the system (pore size, pore tortuosity, viscosity of the extracting agent, etc.) and on those of the external action (pressure pulse intensity) are included in a single parameter ε, and the relative amount of the extracting agent with the target component is given by an algebraic expression.

This is an advantage of the model suggested, compared with the diffusion model, although the general type of the dependence is the same.

It should be mentioned, however, that the conclusion made implies that the pore has an infinite length. Therefore, formulas (1)–(3) are valid under real conditions only while the volume *Q* remains smaller than the capillary volume:

$$Q(N) < \pi d^2 l/4, \quad (4)$$

where *l* is the length of the capillary, and *d*, its diameter.

Let use convert expression (3) to a form convenient for practical use, keeping in mind the fact that *N* is rather large. In this case, the summation can be re-

Rate of removal of the extracting agent, $V(n)/\varepsilon$, and the total volume of removed extracting agent, $Q(N)/\varepsilon$

n, N	$V(n)/\varepsilon$	$Q(N)/\varepsilon$	n, N	$V(n)/\varepsilon$	$Q(N)/\varepsilon$	n, N	$V(n)/\varepsilon$	$Q(N)/\varepsilon$
1	0.500	1.500	13	0.155	4.184	45	0.084	7.632
2	0.375	1.875	14	0.149	4.334	50	0.080	8.039
3	0.313	2.188	15	0.144	4.478	60	0.073	8.795
4	0.273	2.461	16	0.140	4.618	70	0.067	9.491
5	0.246	2.707	17	0.136	4.754	80	0.063	10.139
6	0.226	2.933	18	0.132	4.886	90	0.059	10.749
7	0.209	3.142	19	0.129	5.015	100	0.056	11.326
8	0.196	3.338	20	0.125	5.140	120	0.051	12.399
9	0.185	3.524	25	0.112	5.726	140	0.048	13.387
10	0.176	3.699	30	0.103	6.257	160	0.045	14.306
11	0.168	3.868	35	0.095	6.747	180	0.042	15.170
12	0.161	4.03	40	0.089	7.203	200	0.040	15.988

placed with integration:

$$Q(N)/\varepsilon \approx 1 + 2\pi^{-1/2}\int_1^N \{[\Gamma(z + 1/2)]/[\Gamma(z + 1)]\}\mathrm{d}z, \quad N \gg 1. \tag{5}$$

Using an approximate expression for the gamma function [13]

$$\Gamma(z + 1) \approx (2\pi)^{1/2} z^{z+1/2}\exp[-z + \delta/(12z)],$$

$$z > 0,\ 0 < \delta < 1,\ z \to \infty$$

and neglecting the term $\delta/(12z)$, we rewrite (5) in the form

$$Q(N)/\varepsilon \approx 1 + 2(e/\pi)^{1/2}\int_1^N \{[(z + 1/2)^z]/z^{z+1/2}\}\mathrm{d}z \approx 1 + 2(e/\pi)^{1/2}$$

$$\times \int_1^N \{\exp z[\ln z + \ln(1 - 1/2z)]\}/\{\exp[(z + 1/2)\ln z]\}\mathrm{d}z.$$

Assuming, further, that $\ln[1 - 1/(2z)] \approx -1/2z$, we obtain

$$Q(N)/\varepsilon \approx 1 + 2\pi^{-1/2}\int_1^N z^{-1/2}\mathrm{d}z \approx 4\pi^{-1/2}(N^{1/2} - 1)$$

$$\approx 4\pi^{-1/2}N^{1/2}, \quad N \gg 1. \tag{6}$$

In practice, the number n of pressure pulse pairs is frequently small, with formula (6) inapplicable. The main error comes from the replacement of summation (3) with integration (5). The table lists the values of $V(n)$ and $Q(N)$, calculated by formulas (2) and (3) at $1 \le n \le 200$.

It was found that, at small n, dependence (2) is well approximated with a power function

$$V(n)/\varepsilon = An^{-\alpha}, \tag{7}$$

where $A = 0.505$ and $\alpha = 0.466$ at $1 \le n \le 10$; at $n \to 10\,000$, $\alpha \to 0.5$.

The rms deviation of the values of $V(n)/\varepsilon$, obtained using formula (7), from those given by formula (2) is $\sigma^2 = 1.21 \times 10^{-5}$.

Dependence (3) is rather well approximated by the expression

$$Q(N)/\varepsilon = 1 + \frac{A(n^{1-\alpha} - S^{1-\alpha})}{1 - \alpha} + \sum_{n=1}^{N} V(n)/\varepsilon. \tag{8}$$

For $N \le 100$, $S = 3$, $A = 0.505$, and $\alpha = 0.466$, the discrepancy between the values of $Q(N)/\varepsilon$, calculated by Eqs. (3) and (8), does not exceed 2%.

Use of power function of the type $Q(N)/\varepsilon = 1 + B_1N^{\beta}$ and $Q(N)/\varepsilon = B_2N^{\gamma}$ at $1 \le N \le 100$ gives an rms error $\sigma^2 = (0.5\text{–}7.3) \times 10^{-3}$, with the approximation error increasing with n; at $N \to 10\,000$, $\beta \to 0.5$ and $\gamma \to 0.5$.

The number of pairs of impacts, n, is a random function of time. In the stationary extraction mode, the average value of n (denoted by $\langle n\rangle$) is proportional to the process duration τ:

$$\langle n\rangle \sim \tau. \tag{9}$$

The dependence $V(n)/\varepsilon$ is, in fact, the rate of removal of the extracting agent from a pore at an instant of

time τ, corresponding to $\langle n \rangle$. It follows from the aforesaid that

$$V(\tau)/\varepsilon \sim 1/\tau^{1/2}. \quad (10)$$

It has been established in the diffusion theory of extraction [1] that the flux of the solute, q, from a single capillary and from a semiinfinite porous body can be calculated by dependences similar to (10):

$$q(\tau)/\varepsilon \sim 1/\tau^{1/2}. \quad (11)$$

However, the proportionality factor in expression (10) is determined by the hydrodynamic conditions of the process (via ε), and that in (11), by the molecular diffusion coefficient.

Equating the pore volume V_p to the volume of the extracting agent with the target component, removed from the pore [Eq. (6)], we can find the number of pairs of impacts, N^*, that provide complete replacement of the extracting agent in the pore with its "fresh" portion, coming from the bulk of the liquid:

$$N^* \approx \pi V_p^2/16\varepsilon^2. \quad (12)$$

In other words, the duration of extraction, $t \sim N^*$, to complete replacement of the extracting agent in pores is inversely proportional to the squared volume ε of the extracting agent, removed after the first pressure pulse:

$$t \sim 1/\varepsilon^2. \quad (13)$$

In the case of an intensive extraction ($\varepsilon/V_p \geq 0.01$, $N \leq 7840$), the dependence of the fraction φ of an unrenewed (not replaced with a "fresh" portion) extracting agent in a pore on the dimensionless time $\Theta = n/N^*$ can be conveniently approximated with the function

$$\omega = \Theta^k, \quad (14)$$

The exponent $k = 0.468–0.49$ for $\varepsilon/V_p = 0.01–0.25$, $k \to 0.5$, and $\varepsilon \to 0$.

Mathematical model of the diffusion stage. Let us assume that, after the diffusion-convective stage is complete, the content of the target component in transport pores is close to zero. In the third stage, there occurs a diffusion process not related to filtration motion of the extracting agent in pores. It is natural to choose the problem of diffusion in an infinite hollow circular cylinder as a model of this process. However, solution of a nonstationary problem for an annular region is exceedingly cumbersome [14]. Therefore, we replace the real medium with a model medium constituted by alternating planar layers of a solid body and planar pores. In Fig. 2, l is the average distance between the planar pores.

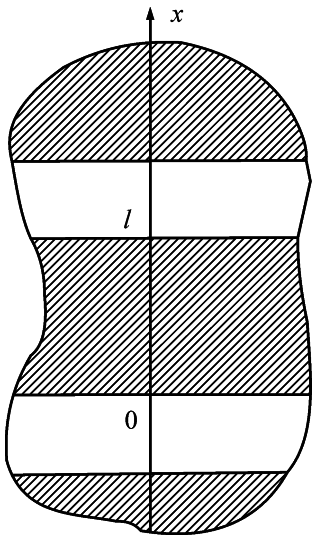


Fig. 2. Model of alternating planar layers of a solid body and planar pores.

In contrast to the cylindrical case, solution of the diffusion problem for a planar layer is rather simple [14]. Let us assume that at an instant of time $\tau = 0$ the concentration of the substance to be recovered in the layer is independent of the coordinate x and equal to c_0, and the concentration at the boundaries ($x = 0$, $x = l$) is zero. Then the local diffusion flux across the boundary $x = 0$ is given by

$$D\frac{\partial c}{\partial x}\Big|_{x=0} = \frac{4D}{l}c_0 \sum_{n=0}^{\infty} \exp\left[-\frac{4\pi^2 D}{l^2}(n + 1/2)^2\tau\right], \quad (15)$$

where D is the diffusion coefficient.

Qualitative analysis shows that the main amount of the substance being recovered leaves the layer at sufficiently large values of τ. Therefore, only the first term $n = 0$ can be kept in expression (15). Thus, we obtain the following approximate formula:

$$D\frac{\partial c}{\partial x}\Big|_{x=0} = \frac{4D}{l}c_0 \exp(-\pi^2 D\tau/l^2). \quad (16)$$

To find the full flux, it is necessary to multiply Eq. (16) by the surface area S of the pore, and to determine the total amount $Q(\tau)$ of the substance released by diffusion into the pore space, Eq. (16) should be integrated over the interval $[0, \tau]$:

$$Q = S\frac{4lc_0}{\pi^2}[1 - \exp(-\pi^2 D\tau/l^2)]. \quad (17)$$

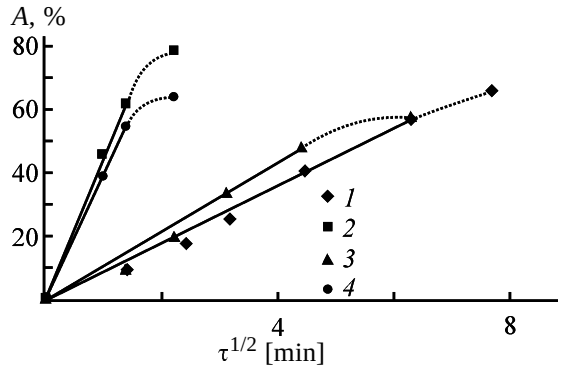


Fig. 3. Yield A of flavonoids from a vegetable raw material vs. $\tau^{1/2}$. (τ) Time. (*1*) Hawthorn, (*2*) licorice, (*3*) everlasting, and (*4*) galls; the same for Fig. 4.

Formula (17) overestimates the flux because the system of pores was replaced with a layer. Therefore, it is necessary to multiply expression (17) by a dimensionless factor $\chi < 1$, which characterizes the "filling" of the layer by pores:

$$Q = S\chi\frac{4lc_0}{\pi^2}[1 - \exp(-\pi^2 D\tau/l^2)]. \quad (18)$$

The factor before the square brackets in Eq. (18) is equal to the content of the target component in a particle before the beginning of the diffusion stage. The expression in the square brackets in formula (18) represents the time dependence of the fraction of the component recovered. Accordingly, the fraction of the unextracted component is given by

$$\bar{c}/c_0 = \exp(-\pi^2 D\tau/l^2), \quad (19)$$

where $\bar{c}$ is the average concentration of the target component in the solid after a time τ from the beginning of the diffusion stage.

The model of the hydraulic stage, suggested here, implies that the whole amount of the substance to be recovered is in the dissolved state and its content in the bulk of the extracting agent can be taken to be zero. In practice, the substance from the nearby lying layers of the porous material is permanently fed into pores via molecular diffusion and its content in the bulk of the extracting agent steadily increases. Therefore, the extraction yield may be proportional to a square root of τ only in the initial stage of the process, before the onset of the diffusion-convective stage. Nevertheless, a direct proportion to $\tau^{1/2}$ is observed during a long time in extraction from vegetable raw materials (Fig. 3).

Figure 3 shows experimental data on the kinetics of extraction of flavonoids (in terms of rutin) with an ethanol solution (40 vol %) from hawthorn fruits (70°C, s : l = 1 : 12) in the vacuum-oscillating mode (frequency of boiling-ups, 7.5 s^{-1}; amplitude of changes in the vapor space, 0.035 m), from licorice roots (25°C, s : l = 1 : 12) in a planetary apparatus (centrifugal acceleration at the drum circumference 28*g*, drum diameter 110 mm), and from everlasting flowers (70°C, s : l = 1 : 20) in the vacuum-boiling mode (temperature head 6.5°C). In addition, we used Balabudkin's data [15] on the kinetics of tannin extraction from galls in a rotary-pulsatory apparatus at a rotor rotation frequency of 2960 rpm. The rms deviation of the experimental data from the theoretical dependences (solid lines) in the initial stages of extraction of target components from licorice roots, everlasting flowers, and galls is 1.8%, and the maximum deviation, 2.9%. The rms deviation in extraction of flavonoids from hawthorn fruits is 2.9% at a maximum deviation of 5.3%.

Results similar to those presented in Fig. 3 were obtained in processing of experimental data on the kinetics of extraction of various kinds of vegetable raw materials in a pulsatory apparatus, apparatus with a fast rabble (3000 rpm), and in the case of an ultrasonic treatment of a suspension. The rms deviation of the experimental data from theoretical dependences was in the range 2.1–3.5% for various kinds of raw materials and extraction methods.

It is of interest to compare the model of the diffusion stage (15)–(19) with that of the final (the so-called regular) stage of a purely diffusion-type extraction [1, 2]. According to the latter, in the case of extraction of a target component from porous bodies of various shapes (sphere, infinite plate or cylinder), the dependence of the fraction of an unextracted component is described, beginning at a certain instant of time, by the formula [1, 2]

$$\bar{c}_D/c_{0D} = B_1\exp(-\mu_1^2 D\tau_D/R^2), \quad (20)$$

where $\bar{c}_0$ and c_{0D} are the average concentrations of the target component in a particle at, respectively the running and initial instants of time; B_1, coefficient dependent on the particle shape, Biot number, and root of the characteristic equation; R, radius of the sphere or cylinder or half plate thickness; and τ_D, total duration of the process.

Formulas (19) and (20) are formally similar, but the parameters appearing in these formulas are strongly different, with the exception of the diffusion coefficients D. Expression (19) contains the duration of the diffusion stage τ and the distance between pores l; the particle radius R (or half plate thickness) and total

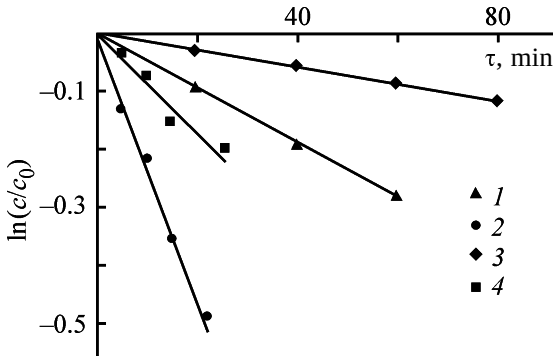


Fig. 4. $\ln(c/c_0)$ vs. the time τ of extraction in the diffusion stage.

duration of the process τ_D ($\tau_D \gg \tau$ and $R \gg 1$) appear in (20).

Experimental data on the extraction kinetics in the diffusion stage is well approximated (Fig. 4) with a dependence of the type (19). In extraction from hawthorn, the diffusion stage onsets approximately τ_{tot} = 60 min after the beginning of the process at a degree of extraction μ = 66%; for licorice, τ_{tot} = 10 min and μ = 69%; for everlasting, τ_{tot} = 80 min and μ = 64%; for galls, τ_{tot} = 10 min and μ = 72%. The rms deviation of the experimental data from the theoretical dependences is 1.2% at a maximum deviation of 3.3%.

Particles of the solid phase have rather diverse pore structures (pores may branch, have variable diameter, etc.), whereas the schemes considered are represented by the simplest models. Therefore, it should be emphasized that the adequacy of the accepted models was only established for those kinds of vegetable raw materials for which a comparison with experimental data was made. Formula (20) is frequently used to determine the effective diffusion coefficients, which presumably cannot be done with formula (19) because of the simplifying assumptions made in deriving Eqs. (18) and (19).

CONCLUSIONS

(1) The fundamental aspects of the extraction kinetics of target components from porous particles under the action of pressure pulses on their surface qualitatively coincide with those in diffusion extraction (Q–$\tau^{1/2}$). The extraction rate is only determined by the number of pulses in unit time and their power.

(2) The fundamental aspects of extraction in the final (diffusion) stage of the process can be described in terms of the simplest model in the form of a porous medium with alternation of planar layers of the solid and planar pores.

(3) Experimental data on the extraction kinetics of flavonoids from vegetable raw materials in apparatus with a strong hydrodynamic impact on porous particles are in good agreement with the theoretical models suggested.

REFERENCES

1. Aksel'rud, G.A. and Lysyanskii, V.M., *Ekstragirovanie (sistema tverdoe telo–zhidkost')* [Extraction (Solid–Liquid System)], Leningrad: Khimiya, 1974.
2. Aksel'rud, G.A. and Al'tshuler, M.A., *Vvedenie v kapillyarno-khimicheskuyu tekhnologiyu* (Introduction to Capillary-Chemical Technology), Moscow: Khimiya, 1983.
3. Dolinskii, A.A., *Inzh.-Fiz. Zh.*, 1996, vol. 69, no. 6, pp. 35–43.
4. Dolinskii, A.A. and Ivanitskii, G.K., *Prom. Teplotekh.*, 1997, vol. 19, nos. 4–5, pp. 13–25.
5. Sister, R.G. and Martynov, Yu.V., *Printsipy povysheniya effektivnosti teplomassoobmennykh protsessov* (Principles of Improvement of the Efficiency of Heat-and-Mass Transfer Processes), Kaluga: Izd. N. Bochkarevoi, 1998.
6. Khiterkheev, S.K. and Khiterkheeva, N.S., *Kavitatsionnye teplomassoobmennye apparaty* (Cavitation Heat-and-Mass Transfer Apparatus), Ulan-Ude: Vost.-Sib. Gos. Tekh. Univ., 1999.
7. Molchanov, G.I., *Intensivnaya obrabotka lekarstvennogo syr'ya* (Intensive Treatment of Medicinal Raw Materials), Moscow: Meditsina, 1981.
8. Lysyanskii, V.M. and Grebenyuk, S.M., *Ekstragirovanie v pishchevoi promyshlennosti* (Extraction in Food Industry), Moscow: Agropromizdat, 1987.
9. Lysyanskii, V.M., *Protsess ekstraktsii sakhara iz svekly: Teoriya i raschet* (Extraction of Sugar from Beet: Theory and Calculation), Moscow: Pishchevaya Prom–st., 1973.
10. Malyshev, R.M., Kutepov, A.M., Zolotnikov, A.N., *et al.*, *Dokl. Ross. Akad. Nauk*, 2001, vol. 381, no. 6, pp. 800–805.
11. Abiev, R.Sh. and Ostrovskii, G.M., *Teor. Osn. Khim. Tekhnol.*, 2001, vol. 35, no. 3, pp. 270–275.
12. Abiev, R.Sh., *Zh. Prikl. Khim.*, 2001, vol. 74, no. 5, pp. 754–761.
13. Abramovitz, M. and Stigan, I., *Spravochnik po spetsial'nym funktsiyam* (Reference Book of Special Functions), Moscow: Nauka, 1979.
14. Karslou, G. and Eger, D., *Teploprovodnost' tverdykh tel* (Heat Conductivity of Solids), Moscow: Nauka, 1964.
15. Balabudkin, M.A., *Rotorno-pul'satsionnye apparaty v khimiko-farmatsevticheskoi promyshlennosti* (Rotary-Pulsatory Apparatus in Chemical-Pharmaceutical Industry), Moscow: Meditsina, 1983.

Russian Journal of Applied Chemistry, Vol. 78, No. 9, 2005, pp. 1468–1473. Translated from Zhurnal Prikladnoi Khimii, Vol. 78, No. 9, 2005, pp. 1493–1498.
Original Russian Text Copyright © 2005 by Polotskaya, Gladchenko, Pen'kova, Kuznetsov, Toikka.

MACROMOLECULAR CHEMISTRY AND POLYMERIC MATERIALS

Synthesis of Fullerene–Polyphenylene Oxide Membranes for Separating Aqueous-Organic Mixtures

G. A. Polotskaya, S. V. Gladchenko, A. V. Pen'kova, V. M. Kuznetsov, and A. M. Toikka

Institute of Macromolecular Compounds, Russian Academy of Sciences, St. Petersburg, Russia
St. Petersburg State University, St. Petersburg, Russia

Received May 18, 2005

Abstract—Homogeneous fullerene–polyphenylene oxide membranes containing up to 2 wt % C_{60} are synthesized and characterized by the density, electrical resistivity, and contact angle with water and ethanol. The effect of fullerene additive on the transport characteristics of the membranes in pervaporation of water mixtures with ethanol and ethyl acetate is studied.

Membrane processes find steadily growing use for purification, concentration, and fractionation of liquid and vapor mixtures. Pervaporation (separation of binary and multicomponent mixtures by evaporation through a membrane) appears to be an efficient process in those cases when the use of conventional methods such as distillation and rectification is impractical or inadvisable (for example, separation of azeotropic mixtures and substances with close physicochemical properties). In pervaporation under reduced pressure, the driving force of transmembrane transport is the pressure gradient controlling the fluxes across the membrane. It is commonly accepted that the model "dissolution–diffusion" most adequately reproduces the mechanism of this process [1–4].

The selectivity and efficiency of pervaporation is controlled by such factors as the structure, chemical nature, and composition of the membrane material. The spectrum of commercial pervaporation membranes is rather limited. Therefore, searching for novel high-performance membranes is, without question, of significant scientific and practical interest. In this relation, membranes based on hybrid polymeric materials containing various ultradispersed and nano particles show promise for advanced membrane processes. It is obvious that of primary interest are polymeric composites containing highly physicochemically active substances. In this study we examined thin-film membrabes based on poly(2,6-dimethyl-1,4-phenylene oxide) (PPO) modified with fullerene C_{60}.

The modification yields PPO–C_{60} donor–acceptor complex. Rheological and hydrodynamic study of its solutions revealed that the donor–acceptor bond is strong enough to remain stable upon dilution, despite small decrease in the intrinsic viscosity and broken symmetry of the PPO molecule [5]. It was demonstrated by TGA–MS and differential calorimetry that modification with fullerene improves the heat resistance of PPO [6]. Biryulin *et al*. [7] studied photoluminescence spectra of C_{60}–PPO films. Molecular complexes were found in the films containing up to 2 wt % C_{60}, while in the 4% C_{60}–PPO films, the major part of fullerene molecules is free.

Only a few publications are devoted to properties of fullerene-containing membranes based on poly(trimethylsilylpropyne), polystyrene, and Martimide [8–10]. It was demonstrated in our previous studies that the presence of fullerene strongly affects the transport characteristics of polystyrene and PPO in gas separation to enrich air with oxygen, increasing the selectivity and decreasing the permeability [11, 12]. In this study we examined the effect of modification with C_{60} on physical and pervaporation characteristics of homogeneous PPO membranes. The transport properties of the membranes were studied in separating aqueous-organic systems with ethyl acetate and ethanol.

EXPERIMENTAL

In the study we used PPO with MW 178 000. Fullerene containing more than 98% of C_{60} (Ioffe Physicotechnical Institute, Russian Academy of Sciences) was dried by heating to 100°C in a vacuum. Composites C_{60}–PPO containing up to 2 wt % C_{60} were

1070-4272/05/7809-1468© 2005 Pleiades Publishing, Inc.

prepared by mixing toluene solutions of the components.

Membranes 50–80 μm thick were produced by removal of toluene at 40°C from the mixed solution poured onto cellophane. The density ρ of the membranes was determined at 25°C in the sucrose solution by the flotation method. The free volume v_f was estimated by Eq. (1):

$$v_f = v_{sp} - 1.3v_w, \quad (1)$$

where $v_{sp} = 1/\rho$ is the specific volume and v_w, van der Waals volume determined by the Bondi method. The contribution of C_{60} to the occupied volume and molecular weight of PPO monomeric unit was taken into account in estimating v_w of the C_{60}–PPO composites.

Dielectric measurements were carried out in a hermetically sealed glass cell using chrome-plated brass contact electrodes at 0.1 kHz in a vacuum. Contact angles of the membrane surface with water and ethanol were determined by the Wilhelmy method on a KRUSS contact angle measuring system with computer-controlled sample immersion rate and data processing.

The pervaporation experiments were conducted using a laboratory cell with an effective membrane area of 14.8 cm^2 with stirring of the feed mixture at 50°C over the membrane at a residual pressure under the membrane of 0.2 mbar. The compositions of the feed mixture and permeate were determined refractometrically or chromatographically. The partition factor α was estimated as

$$\alpha = (X_A/X_B)/(Y_A/Y_B), \quad (2)$$

where Y_A and Y_B are the weight fractions of A and B in the initial (feed) mixture and X_A and X_B, in the permeate. The transport characteristics were determined to within 5%.

The equilibrium swellability (sorption) was determined gravimetrically. The equilibrium sorption S was estimated by Eq. (3):

$$S = (m_s - m_0) \times 100/m_0 \quad (3)$$

where m_s and m_0 are the weights of the swollen and dry membrane, respectively.

The formation of C_{60}–PPO donor–acceptor complex imparts typical brown color to the modified PPO membranes; the color intensity depends on the percentage of C_{60}. We examined some physical characteristics of the C_{60}–PPO membranes, which are relevant to understanding the features of the transport of small molecules across homogeneous membranes. In particular, we have determined the distribution of C_{60} in PPO films (from the dielcometric measurements) and also the density of the films and contact angles.

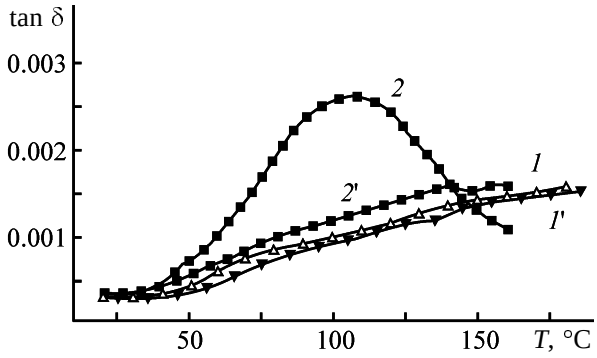


Fig. 1. Dielectric loss tangent tan δ as a function of the temperature *T*: (*1*, *1'*) PPO and (*2*, *2'*) 2% C_{60}–PPO. (*1*, *2*) Before heating and (*1'*, *2'*) after heating to 150°C without air access. Frequency 0.1 kHz.

Figure 1 shows the temperature dependences of the dielectric loss tangent tan δ of the initial PPO and 2% C_{60}–PPO membranes. At room temperature PPO occurs in the glassy state, demonstrating no dielectric relaxation range up to 180°C (Fig. 1, curve *1*). In the case of the C_{60}–PPO membranes we found a relaxation range at 80 to 120°C. Since $\tan\delta_{max}$ is observed only in the presence of C_{60}, it may be suggested that the occurrence of the relaxation range is associated with the mobility of the kinetic units of fullerene. Heat treatment of the C_{60}–PPO membrane suppresses the relaxation transition, and the temperature dependence of tan δ becomes similar to that of PPO.

It is known from the literature that fullerenes in solutions can form clusters [13]. It may be suggested that, as in the C_{60}–polystyrene system [12], the observed relaxation transition is associated with the mobility of the dipoles of fullerene clusters. However, in the C_{60}–PPO composite, the intensity of this transition is lower by an order of magnitude than that in the system with polystyrene, suggesting that only a small fraction of fullerene molecules in PPO films exist in the form of clusters. This is supported also by the lack of the $\tan\delta_{max}$ peak in the heat-treated sample (Fig. 1, curve *2'*). In preparing the composite films from solutions, the most of C_{60} molecules are more regularly distributed throughout the PPO film thanks to donor–acceptor interaction of C_{60} with the lone pair of the oxygen atom of PPO in addition to the interac-

Table 1. Selected physical characteristics of membranes

Polymer	$\log \rho_v^*$	Density, g cm^{-3}	Free volume, cm^3 g^{-1}	Contact angle, deg	
				water	ethanol
PPO	15.15	1.057	0.181	91.2	20.2
1% C_{60}–PPO	–	1.093	0.150	–	–
2% C_{60}–PPO	16.48	1.120	0.128	94.4	17.9

* (ρ_v) Electrical resistivity.

tion of the phenyl ring with the π system of C_{60}. The fullerene molecules associated with PPO are capable of strong intermolecular interactions resulting in physical cross-linking of the PPO chains via fullerene bridges, which is reflected in considerable increase in the dielectric permittivity of the C_{60}–PPO composites (Table 1) and also can increase the density.

Introduction of foreign particles into polymer systems may result in both compaction and loosening of the polymer structure. To elucidate the effect of C_{60}, we measured the density of PPO films with various C_{60} content and estimated their free volume. Table 1 shows that addition of C_{60} increases the density of PPO, i.e., the PPO globules becomes more compact, and the free volume of the fullerene-containing composites decreases, thus reflecting the intercomponent interactions.

The contact angle is a parameter most commonly used to characterize the surface tension of solids [14]. We determined the contact angles of PPO and C_{60}–PPO membranes with water and ethanol using the Wilhelmy technique (Table 1). The results show that PPO is a hydrophobic polymer (contact angle with water is above 90°). Addition of C_{60} increases the contact angle, i.e., the hydrophobicity. Inversely, the PPO surface is readily wetted with ethanol, and addition of C_{60} decreases the contact angle with ethanol. These results appeared to be significant for interpretation of the effect of C_{60} on the sorption and pervaporation characteristics of PPO membranes.

Table 2. Equilibrium sorption *S* and interaction parameters of membrane materials with components of liquid mixtures

Solvent	*S*, wt %		Interaction parameter χ	
	PPO	2% C_{60}–PPO	PPO	2% C_{60}–PPO
Ethyl acetate	23	26	1.22	1.13
Ethanol	13	15	1.45	1.34
Water	0	0	–	–

In pervaporation, polymeric membranes operate as molecular sieves, but having active sites capable of dipole–dipole, ion–dipole interactions or hydrogen bonding with components of a liquid mixture to be separated [15]. The mass transfer depends to a considerable extent on the affinity of the membrane material for components of the mixture [2, 4]. Quantitatively, this affinity is characterized by the Flory–Huggins interaction factor χ (as known, χ directly characterizes the solubility of a polymer in a given solvent [16]). In the case of equilibrium sorption and a one-component solvent, χ can be estimated by Eq. (4) [17]:

$$\chi = \frac{-\ln \varphi_i - \varphi_p}{\varphi_p^2}, \quad (4)$$

where φ_i and φ_p are the volume fractions of the solvent and polymer, respectively.

Therefore, the fraction of the solvent in the polymer phase increases with decreasing χ, i.e., the lower χ, the better sorption. Equation (4) can be used for estimating parameters of interaction in binary solvents also on the condition that these parameters are composition-independent [17]. To estimate the interaction parameter, we studied the sorption of ethyl acetate, ethanol, and water vapors on the homogeneous membranes. The results obtained after establishment of the equilibrium show (Table 2) that the affinity of the PPO and C_{60}–PPO membranes for the solvent decreases in the order ethyl acetate > ethanol >> water (water appears to be absolutely inert solvent with respect to the polymers studied). The C_{60}-modified membranes better sorb both ethyl acetate and ethanol.

Pervaporation of aqueous-alcoholic mixtures represents a classical task for this membrane separation technique [18–20]. We studied the effect of C_{60} on the pervaporation characteristics of PPO membranes

in pervaporation of the H_2O–EtOH mixture. Figure 2 shows the dependences of the EtOH concentration in the permeate and selectivity on the EtOH concentration in the feed mixture in pervaporation of the H_2O–EtOH mixture through PPO and C_{60}–PPO membranes. The trend of the concentration dependence for pervaporation differs significantly from the equilibrium liquid–vapor diagram in the system water–ethanol (Fig. 2a). In pervaporation, at any concentration of the feed mixture, a water-enriched permeate is formed, i.e., the membranes in hand are selective with respect to water. Addition of C_{60} decreases the alcohol concentration in the permeate, i.e., the selectivity increases (Fig. 2b). This fact can be attributed to decreasing free volume of PPO with addition of C_{60} (Table 1), which could cause a decrease in the size of the transport channels in the modified PPO membranes, and, therefore, an increase in the selectivity with respect to water.

Figure 3 shows the permeability Jl as a function of the ethanol concentration in the initial mixture in pervaporation of the water–ethanol mixture. Since the penetrant flux J is inversely proportional to the membrane thickness l, which varied from 50 to 80 μm for different samples, we used the product Jl, to compare transport characteristics of the homogeneous membranes (the use of this product was demonstrated to be more correct [21]. As seen from Fig. 3, addition of C_{60} increases the penetrant flux across the membrane. Furthermore, increasing concentration of less penetrating component, ethanol, in the initial mixture also increases the permeability of the membranes, which seems to be surprising. This fact can be attributed to the specific sorption features of the investigated membranes with respect to water and ethanol.

Figure 4 shows the dependence of the equilibrium sorption on the EtOH concentration in the water–ethanol mixture for PPO and 2% C_{60}–PPO membranes. As seen, all the membranes studied are inert with respect to water, but readily sorb ethanol. Therefore, even small amounts of ethanol in water initiate swelling of PPO. In this case, addition of C_{60} increases the sorption capacity, which is consistent with data of Table 2 demonstrating that, in ethanol, the interaction parameter and contact angle of fullerene-containing membranes decrease. This is responsible for the fact that, with increasing EtOH concentration in water, the sorption on C_{60}–PPO composite increases to a larger extent than for PPO.

To interpret the observed preferential transport of water in pervaporation of water–ethanol mixtures through hydrophobic PPO-based membranes, we sug-

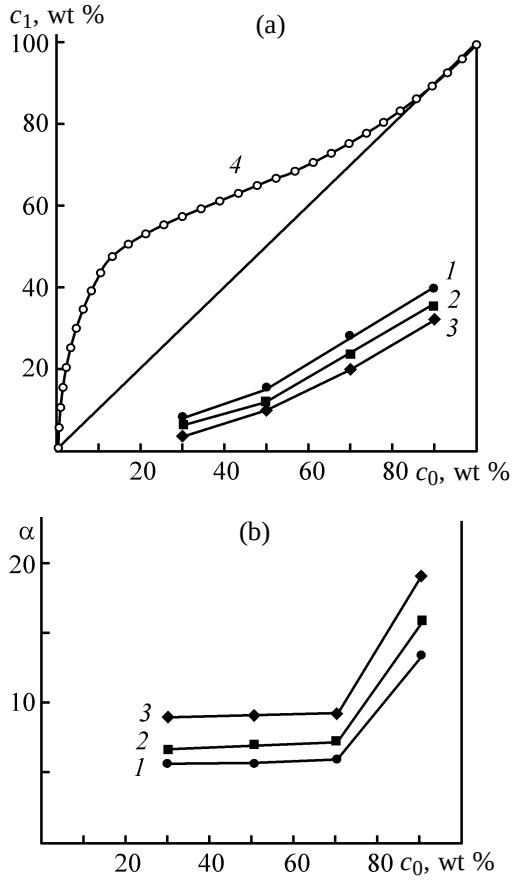


Fig. 2. (a) Ethanol concentration in the permeate c_1 and (b) partition factor α H_2O/EtOH as functions of the ethanol concentration in the initial mixture c_0 in pervaporation of the water–ethanol mixture: (*1*) PPO, (*2*) 1% C_{60}–PPO, (*3*) 2% C_{60}–PPO, and (*4*) liquid–vapor equilibrium curve at 50°C.

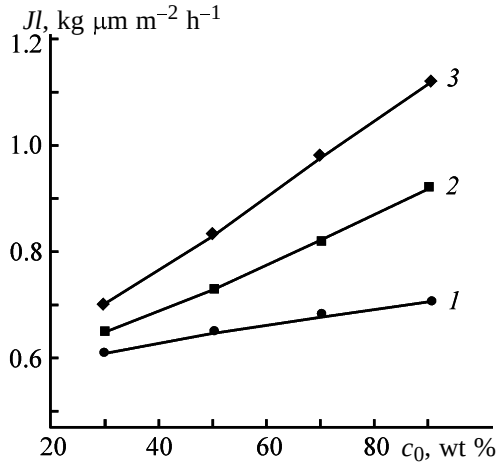


Fig. 3. Permeability Jl as a function of the ethanol concentration in the initial mixture c_0 in separating water–ethanol mixture by pervaporation on (*1*) PPO, (*2*) 1% C_{60}–PPO, and (*3*) 2% C_{60}–PPO membranes.

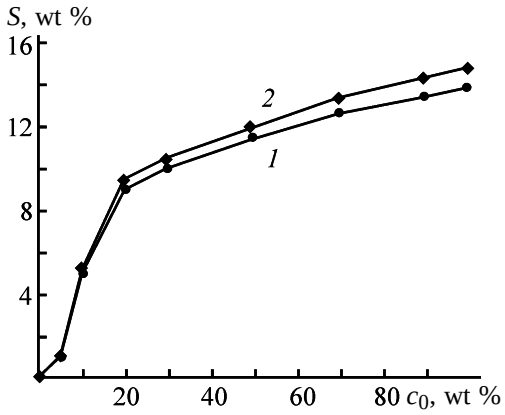


Fig. 4. Equilibrium sorption *S* as a function of the ethanol concentration in the water–ethanol mixture c_0 for (*1*) PPO and (*2*) 2% C_{60}–PPO membranes.

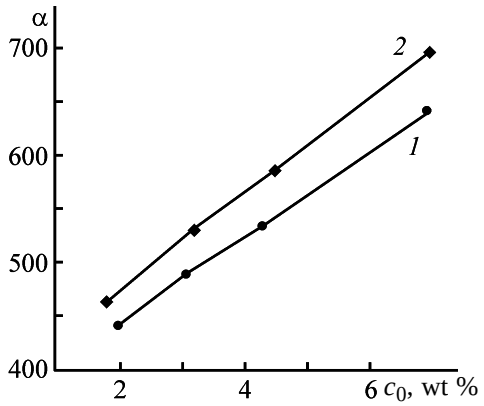


Fig. 5. Partition factor α for the pair ethyl acetate–water as a function of the ethyl acetate concentration in the initial mixture c_0 in pervaporation of the mixture water–ethyl acetate on (*1*) PPO and (*2*) 2% C_{60}–PPO membranes.

gested the following mechanism. Initially only ethanol molecules are involved in the sorption through interaction with the lone electron pair of the oxygen atom of the PPO backbone with formation of hydrogen bonds; in such a way ethanol molecules are retained in the membrane phase, creating transport channels. Thanks to a considerable affinity for ethanol, water penetrates these channels whose size is well comparable with the kinetic diameter of the water molecule, the penetrability of water being higher because of smaller size of its molecules as compared to ethanol. Increasing ethanol concentration as a swelling agent in the feed mixture weakens the intra- and intermolecular interactions in the PPO membrane, i.e., placticizes the membrane, favoring increase in the permeate flux across the membrane. The sorption data confirm the increase in the degree of plasticization of the PPO matrix as well as of the number of mass-transfer channels with increasing ethanol concentration in water. These transformations result in increasing penetrability of water and selectivity, the tendency being more clearly pronounced for C_{60}–PPO membranes.

In studying pervaporation in the system water–ethyl acetate, the primary attention was paid to separation of ethyl acetate from homogeneous water-rich mixtures (<7 wt % ethyl acetate). The reason is that the phase separation in this system occurs over a wide composition range, and the homogeneity ranges are found at an ethyl acetate concentration below 7 and above 97 wt %. We studied the transport characteristics of PPO and C_{60}–PPO membranes in pervaporation of dilute aqueous ethyl acetate solutions. For all the membranes studied we obtained high selectivity with respect to ethyl acetate (Fig. 5), which can be attributed to hydrophobic nature of PPO. After formation of the transport channels as a result of sorption and swelling of the membrane in ethyl acetate, penetration of water into these channels is hindered because of high activity coefficients of the components, which results in phase separation in the mixture at an ethyl acetate concentration above 7 wt %. Figure 5 shows that addition of C_{60} further increases the selectivity. At the same time, addition of C_{60} only slightly changes the flux across the membranes: from 0.48 to 0.52 kg m^{-2} h^{-1} on passing from PPO to 2% C_{60}–PPO in pervaporation of 7% aqueous ethyl acetate. This can be a resultant of two oppositely directed factors: decreasing free volume, on the one hand, and increasing swellability of fullerene-containing membranes in ethyl acetate, on the other hand. Note, as a conclusion, that data on pervaporation of aqueous ethyl acetate solutions in combination with those on the system water–ethanol are important for developing a process for synthesis of ethyl acetate using pervaporation.

CONCLUSIONS

(1) Homogeneous PPO membranes modified with up to 2 wt % C_{60} demonstrate higher electrical resistivity and density as compared to unmodified membranes. Also the modification strongly affects the contact angle with water and ethanol.

(2) In pervaporation of water–ethanol mixture through fullerene-modified membranes, both the selectivity with respect to water and permeability increase with increasing ethanol concentration in the initial mixture. Modification of PPO membranes with fullerene makes them more organophilic (swellability in ethanol increases with increasing fullerene content). Increasing fullerene concentration increases both the

sorption capacity of the modified membranes and their efficiency in pervaporation of water–ethanol mixtures.

(3) PPO-based membranes demonstrate high selectivity with respect to ethyl acetate in pervaporation of water-rich mixtures; the selectivity grows with increasing C_{60} content.

ACKNOWLEDGMENTS

The study was financially supported by the Russian Foundation for Basic Research (project no. 03-03-32379).

REFERENCES

1. Baker, R.W., *Membrane Technology and Applications*, New York: McGraw-Hill, 2000.
2. Mulder, M., *Basic Principles of Membrane Technology*, Dordrecht: Kluwer, 1991.
3. Staudt-Bickel, C. and Lichtenthaler R.N., *Vysokomol. Soedin.*, 1994, vol. 36, no. 11, pp. 1924–1945.
4. Feng, X. and Huang, R.Y.M., *Ind. Eng. Chem. Res.*, 1997, vol. 36, pp. 1048–1066.
5. Lavrenko, P.N., Evlamp'eva, N.P., Volokhova, D.M., *et al.*, *Vysokomol. Soedin., Ser. A.*, 2002, vol. 44, no. 2, pp. 289–296.
6. Shibaev, L.A., Egorov, I.M., Zgonnik, V.N., *et al.*, *Vysokomol. Soedin., Ser. A*, 2001, vol. 43, no. 1, pp. 211–216.
7. Biryulin, Yu.F., Melenevskaya, E.Yu., Mikov, S.N., *et al.*, *Fiz. Tekh. Poluprov.*, 2003, vol. 37, pp. 110–114.
8. Higuchi, A., Agatsuma, T., Uemiya, S., *et al.*, *J. Appl. Polym. Sci.*, 2000, vol. 77, pp. 529–538.
9. Higuchi, A., Yoshida, T., Imizu, T., *et al.*, *J. Polym. Sci., Polym. Phys.*, 2000, vol. 38, pp. 1794–1811.
10. Chung, T.-C., Chan, S.S., Wang, R., *et al.*, *J. Membrane Sci.*, 2003, vol. 211, pp. 91–103.
11. Polotskaya, G.A., Gladchenko, S.V., and Zgonnik, V.N., *J. Appl. Polym. Sci.*, 2002, vol. 85, pp. 2946–2951.
12. Polotskaya, G.A., Andreeva, D.V., and El'yashevich, G.K., *Pis'ma Zh. Tekh. Fiz.*, 1999, vol. 25, no. 14, pp. 14–19.
13. Bezmel'nitsyn, V.N., Eletskii, A.V., and Okun', M.V., *Usp. Fiz. Nauk*, 1998, vol. 168, no. 11, pp. 1195–1234.
14. *Physics to Technology*, Garbassi, F., Morra, M., and Occhielbo, E., Eds., New York: Wiley, 1994.
15. Semenova, S.I., Ohya, H., and Soontarapa, K., *Desalination*, 1997, vol. 110, pp. 251–268.
16. Prausnitz, J.M., Lichtenthaler, R.N., and Azevedo, E.G., *Molecular Thermodynamics of Fluid Phase Equilibria*, Upper Saddle River, NJ: Prentice-Hall, 1999, 3rd ed.
17. Khayet, M., Villaluenga, J.P.G., Godino, M.P., *et al.*, *J. Colloid Interface Sci.*, 2004, vol. 278, pp. 410–422.
18. Kirsh, Yu.E., Fedotov, Yu.A., Semenova, S.I., *et al.*, *J. Membrane Sci.*, 1995, vol. 103, pp. 95–103.
19. Kuznetsov, Yu.P., Kruchinina, E.V., Kononova, S.V., *et al.*, *Zh. Prikl. Khim.*, 1998, vol. 71, no. 9, pp. 1508–1512.
20. Buyanov, A.L., Revelskaya, L.G., Kuznetsov, Yu.P., *et al.*, *J. Appl. Polym. Sci.*, 1998, vol. 69, pp. 761–769.
21. Tanihara, N., Umeo, N., Kawabata, T., *et al.*, *J. Membrane Sci.*, 1995, vol. 104, pp. 181–198.

Russian Journal of Applied Chemistry, Vol. 78, No. 9, 2005, pp. 1474–1478. Translated from Zhurnal Prikladnoi Khimii, Vol. 78, No. 9, 2005, pp. 1499–1503.
Original Russian Text Copyright © 2005 by Goloudina, Luchinin, Pasyuta, Rozanov, Sklizkova, Kudryavtsev, Levin, Mayer, Paufler.

MACROMOLECULAR CHEMISTRY AND POLYMERIC MATERIALS

Specific Structural Features of Langmuir–Blodgett Films of a Rigid-Chain Polyimide

S. I. Goloudina, V. V. Luchinin, V. M. Pasyuta, V. V. Rozanov, V. P. Sklizkova, V. V. Kudryavtsev, A. A. Levin, D. C. Meyer, and P. Paufler

St. Petersburg State Electrotechnical University, St. Petersburg, Russia
Institute of Macromolecular Compounds, Russian Academy of Sciences, St. Petersburg, Russia
Institute of Analytical Instrument Making, Russian Academy of Sciences, St. Petersburg, Russia
Institut für Strukturphysik, Technische Universit ät Dresden, Dresden, Germany

Received April 27, 2005

Abstract—Atomic-force microscopy, reflectometry, and ellipsometry were applied to analysis of ultrathin films (3.3–13.6 nm) of a rigid-chain polyimide, formed on the surface of a silicon substrate by thermal imidization of Langmuir–Blodgett films of polyamido acid derived from 3,3',4,4'-diphenyltetracarboxylic acid and *ortho*-tolidine.

Formation of ultrathin films on the surface of solids and fabrication of nanolayer composites on their basis is an important part of modern micro- and nanotechnology. A particular place among polymeric dielectric materials used in microelectronics is occupied by polyimides (PI), because they possess a set of practically important properties, such as high thermal stability, mechanical and chemical stability, and radiation hardness [1]. The Langmuir–Blodgett method makes it possible to deposit onto the surface of solids PI films of thickness ranging from 0.5 to several hundreds of nanometers. The field of application of PI films produced by the Langmuir–Blodgett method is rapidly expanding. Introduction of functional groups into the polymer chain of polyimide makes it possible to obtain conducting films [2], as well as films possessing nonlinear optical [3], luminescent [4], and photoelectric properties [5]. These films can be used as antifriction [6] and water-proofing coatings [7] in microsystem devices. Deposition of Langmuir–Blodgett films (LBFs) of PI onto the surface of polymeric gas- and liquid-separating membranes markedly improves their selective properties [8, 9].

The most promising for practical use are LBFs of rigid-chain PI. For example, a rigid-chain PI obtained by imidization of a polyamido acid DP-*o*-TD synthesized from 3,3',4,4'-diphenyltetracarboxylic acid and *o*-tolidine has an exceedingly high thermal stability (the temperature of 5% weight loss is 560°C). In addition, this PI has a low thermal expansion coefficient (~0.5×10^{-5} K^{-1}) and exhibits a pronounced planarizing ability, high moisture resistance, and good adhesion to substrates used in the electronic industry.

PI LBFs are formed in two steps: first, monolayers of a diphilic prepolymer (ester or salt of a polyamido acid) are deposited by the Langmuir–Blodgett method on a solid substrate and then the film obtained is subjected to a chemical or thermal imidization. In the process, aliphatic radicals of the prepolymer molecule are removed, which leads to a significant decrease in the film thickness and to PI formation [10]. The homogeneity of the forming film and its surface roughness are largely determined by the structural organization of macromolecules in the PI film, which, in turn, depends on the structure of the prepolymer macromolecule, conditions in which LBFs are formed, and method of their imidization. Previous studies of PI films obtained by chemical and thermal imidization of the LBF prepolymer, alkylammonium salt of polyamido acid (PAA), DP-*o*-TD, with two multichains of tertiary amine, revealed the presence of a domain structure in the prepolymer LBF and in PI and showed that this structure depends on the pressure in the monolayer of a PAA salt and on the imidization method [11, 12].

The aim of this study was to examine PI films obtained through thermal imidization of an LBF of a PAA salt, with 7, 11, and 29 monolayers, by atomic-force microscopy, reflectometry, and ellipsometry.

1070-4272/05/7809-1474© 2005 Pleiades Publishing, Inc.

EXPERIMENTAL

The synthesis of the alkylammonium PAA salt DP-*o*-TD with multichains of a tertiary amine, the isotherm of compression of a monolayer of a PAA salt, and conditions of its transfer to a silicon substrate were reported in [12]. In this study, the surface pressure in a monolayer in its transfer to a solid substrate was 25 mN m^{-1}. Monolayers of a PAA salt were deposited onto a (100)Si-KDB1.0 substrate preliminarily etched in a dilute solution of hydrofluoric acid to make thinner the oxide layer. The first layer was deposited by lifting the substrate from water at a velocity of 0.2 cm min^{-1}, and the rest of the layers, at 0.5 cm min^{-1}. After each lift of the substrate from water, the film was dried in air for 15 min. PI films (7, 11, and 29 layers) were obtained by step heating to 400°C in a vacuum of PAA salt LBF containing 7, 11, and 29 monolayers.

Surface micrographs of PI LBF were obtained in air with an atomic-force microscope manufactured by NT-MDT, Russia. A semicontact (tapping) mode was used in scanning the surface. This mode ensures a milder action of the probe upon a sample and makes it possible to preclude any damage to its surface. A rectangular cantilever with a tip curvature radius of 10 nm was used. The resonance frequency of the cantilever was 230 kHz.

The PI films were characterized by reflectance ellipsometry on an LEF-101 ellipsometer. The ellipsometric angles were measured in air at 632.8 nm. The thickness of PI films was calculated in terms of a single-layer model by the Holmes method.

Small-angle X-ray reflection patterns were obtained at room temperature by the θ–2θ scanning method (θ, angle of incidence of X-rays onto the sample surface; 2θ, angle of reflection) on a Seifert FPM HZG4 X-ray diffractometer (Germany). A characteristic K_β radiation of an X-ray tube with a Cu anode and thin focus (focus width ~0.04 mm), monochromatized with a primary (111)Si monochromator, was used. The structural parameters of the film (thickness *t*, density ρ of the constituent layers, and roughness σ of interfaces) were determined by fitting calculated model small-angle X-ray reflection curves to those obtained in the experiment. The calculations and fitting were made with a REFSIM software (Siemens AG, 1994, Germany) based on the recursive approach of Parrat [13] to calculation of the intensity of reflected beams and the model of Sinha *et al.* [14], which takes into account the roughness of interfaces between the layers.

Previous studies of the morphology of PI films (29 layers) by atomic-force microscopy have shown that the profile and roughness of the surface are due to presence of a domain structure in a film [11]. The AFM images of PI films (7 and 29 layers), obtained in this study, also demonstrate the presence of domains (Fig. 1), and it can be seen that both separate domains and their aggregates are present on the surface of the films. The surface profile obtained on those parts of a film which are composed of separate domains gives a notion of their dimensions (Figs. 1a, 1b; right-hand diagrams). For the PI films with 7 layers, the domain diameter is 30–50 nm. As the number of layers in a film increases to 29, the domain diameter grows to approximately 100 nm, and, accordingly, the surface roughness of the films, defined as an arithmetic mean of the absolute values of deviations from the average profile height on an area of 3000×3000 nm, increases from 1.34(5) to 2.80(5) nm. It can be seen in the AFM image of the PI film with 7 layers that, in its certain parts, similarly oriented domains form rows of different lengths (up to 1 μm). The domains constituting the rows are elongated.

The results obtained in studying the PI films by reflectometry are presented in Fig. 2 and in the table. The experimental reflection patterns shown in Fig. 2 have a shape typical of homogeneous films with density not modulated periodically in the direction perpendicular to the surface and a rather pronounced surface roughness, which is indicated by the absence of Bragg reflections and clearly pronounced Kiessig oscillations in the reflection patterns. Indeed, as can be seen in the table and Fig. 2, there is good agreement between the experimental reflection patterns and those calculated on the assumption of a single-layer PI film on a Si substrate. The quality of fitting of the experimental and calculated curves was significantly improved on assuming that there exists a thin (~2 nm) additional oxide (SiO_2) layer covering the Si substrate.

The density of the PI films containing 7 and 11 layers, found by reflectometry, was 1.39(5) and 1.23(5) g cm^{-3}, respectively. This is close to the calculated density of DP-*o*-TD PI ($C_{30}H_{18}N_2O_4$), equal to 1.40 g cm^{-3} [15]. For a thicker PI film (29 layers), the density was lower, 1.00(5) g cm^{-3}. The thickest film also has the maximum roughness of 2.6(3) nm. The roughness of the films with 7 and 11 layers was 1.6(2) and 2.0(1) nm, respectively. The roughness determined by reflectometry well coincides with that obtained by analysis of the AFM images of PI films.

According to the results of X-ray reflectometry, the thickness of the PI films (7, 11, and 29 layers) was

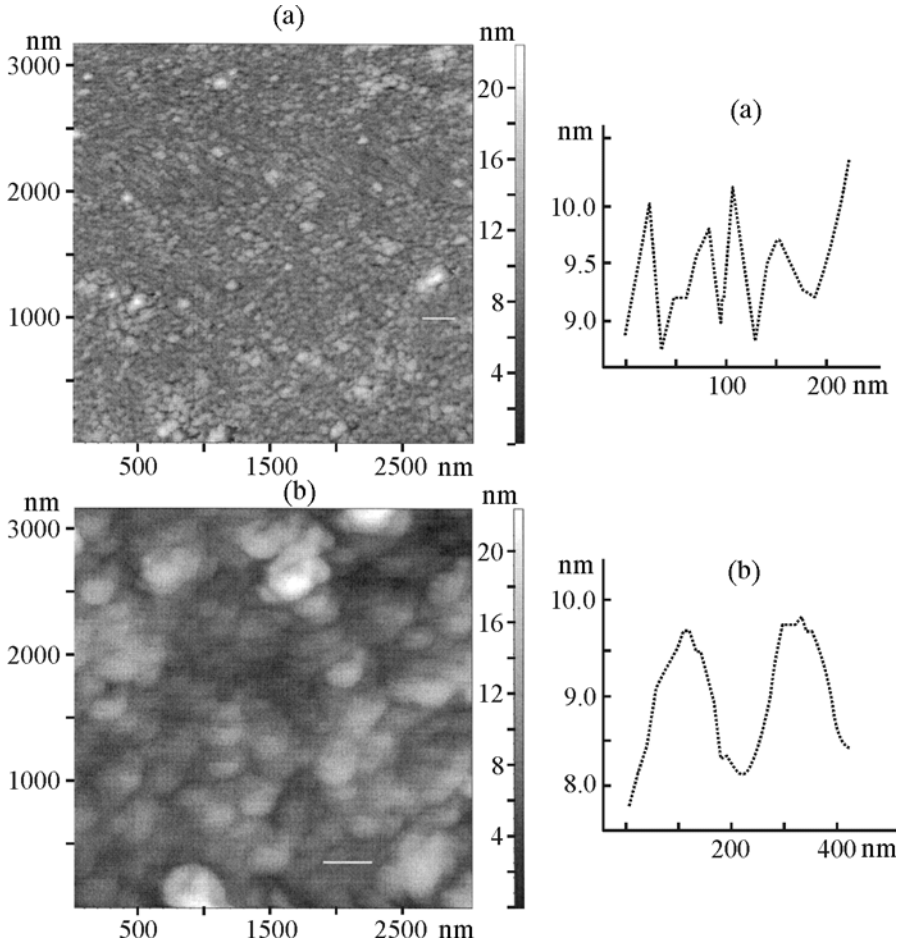


Fig. 1. AFM images of the surface of PI films and the profiles of regions (indicated by white lines) composed of separate domains. Number of layers: (a) 7 and (b) 29.

3.3(2), 5.3(3), and 13.6(5) nm, respectively (see table). The film thickness linearly depends on the number of monolayers in LBF of a PAA salt (Fig. 3). The calculated thickness of a PI layer is 0.474(7) nm (here the root-mean-square error characterizes the deviation of individual calculated thicknesses of a PI monolayer from the average value), which is in good agreement with model conformational calcula-

Parameters of the structural model of PI films

Number of PI layers	Layer	Thickness t, nm	Roughness σ, nm	Density, g cm^{-3}	
				ρ	ρ^{*}_{theor}
7	PI	3.3(2)**	1.6(2)	1.39(5)	1.40
	SiO_2	2.9(3)	1.1(1)	2.65(5)	2.65
	Si substrate	∞	0.3(2)	2.32(5)	2.32
11	PI	5.3(3)	2.0(1)	1.23(5)	1.40
	SiO_2	2.4(2)	0.7(1)	2.65(5)	2.65
	Si substrate	∞	0.3(3)	2.32(5)	2.32
29	PI	13.6(5)	2.6(3)	1.00(5)	1.40
	SiO_2	2.0(2)	0.9(1)	2.65(5)	2.65
	Si substrate	∞	0.5(4)	2.32(5)	2.32

* Calculated density. ** Standard errors for the parameters are given in parentheses.

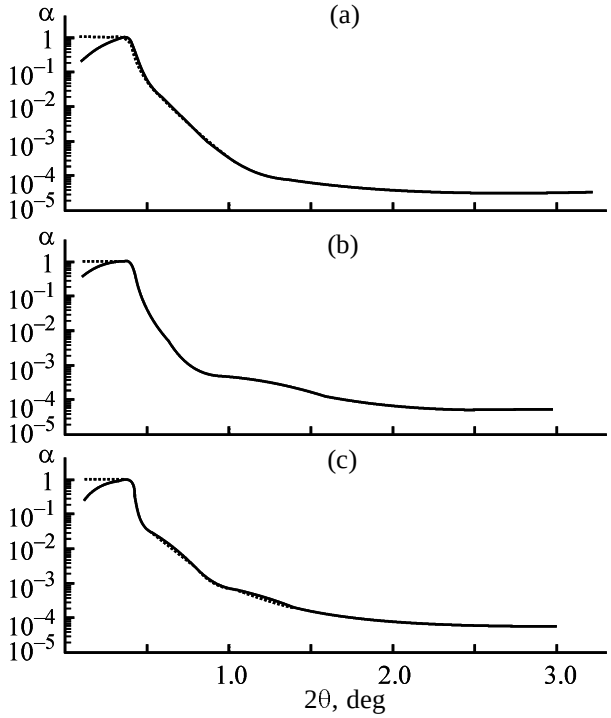


Fig. 2. Experimental (solid lines) and simulated (dashed lines) small-angle X-ray reflection patterns plotted against the diffraction angle 2θ for PI films produced by thermal imidization of LBF containing (a) 7, (b) 11, and (c) 29 monolayers of the PAA salt. (α) Reflectance. The structural parameters of model films are listed in the table.

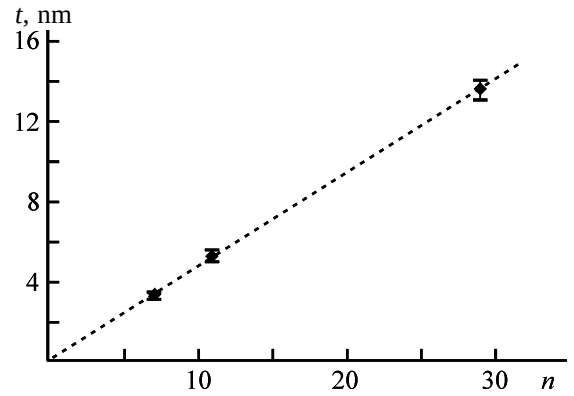


Fig. 3. Thickness *t* of a PI film vs. the number *n* of constituent layers.

tions of the structure of the PI macromolecule [11] and with published data on the thickness of a layer in PI LBF [16].

The ellipsometrically determined thickness of the film with 29 layers is 16.0(4) nm, which is close to that yielded by reflectometry. It was too difficult to determine by ellipsometry the thickness of thinner films.

Thus, as already noted, the reflection patterns obtained indicate that homogeneous PI films, without any pronounced layered structure, are formed on the surface of silicon. This fact is in agreement with the results previously obtained in a study of PI DP-*o*-TD LBF by electron diffraction analysis [11], which demonstrated that the packing of polymer chains in a film is mesomorphic. The presence of a mesomorphic and domain structure in a PI DP-*o*-TD film can be accounted for by specific structural features of the macromolecule of the prepolymer used, in which two molecules of tertiary amine are attached to a monomer unit of the polyamido acid, and each of these molecules contains three hydrocarbon chains with 17 methyl groups and one $-COO^-$ group. The interaction of the hydrocarbon chains within a molecule and that between neighboring molecules create a strong "contraction" effect, which favors aggregation of polymer chains both in the stage of formation of a monolayer and in its deposition onto a solid substrate. In addition, an ordered arrangement of polymer chains in a film is hindered by the presence of two methyl groups in the diamine moiety of the PAA macromolecule.

CONCLUSIONS

(1) Ultrathin Langmuir–Blodgett films of a DP-*o*-TD polymer, formed by thermal imidization of an alkylamine salt of polyamido acid with multichains of a tertiary amine, have a domain structure.

(2) The thickness of the polyimide film linearly depends on the number of layers in the Langmuir–Blodgett film of the prepolymer.

(3) As the film thickness increases from 3.3 to 13.6 nm, the domain size grows from 30–50 nm to approximately 100 nm, and the roughness, from 1.34 to 2.8 nm.

(4) The results obtained indicate that homogeneous films of the polyimide DP-*o*-TD, with a thickness of 3.3 to 16.0 nm, can be obtained on the surface of silicon, and the methods of X-ray reflectometry and atomic-force microscopy can be effectively used to evaluate their thickness, homogeneity, and roughness.

ACKNOWLEDGMENTS

The authors thank I.V. Gofman for carrying out the thermal imidization and to M.F. Panov for measuring the film thickness by ellipsometry. The study was in part supported by the Russian Foundation for Basic Research (project no. 05-03-33194) and by the grant NSh 1824.2003.3.

REFERENCES

1. Bessonov, M.I., Koton, M.M., Kudryavtsev, V.V., and Laius, A.A., *Poliimidy – klass termostoikikh polimerov* (Polyimides: a Class of Heat-Resistant Polymers), Leningrad: Nauka, 1983.
2. Akatsuka, T., Tanaka, H., Toyama, J., *et al*., *Chem. Lett*., 1990, pp. 975–978.
3. Kudryavtsev, V.V., Baklagina, Yu.G., Bitsenko, M.I., *et al*., *Inform. Byull. Ross. Fonda Fundam. Issl*., 1995, vol. 3, no. 3, p. 104.
4. Wu, A., Akagi, T., Jikei, M., *et al*., *Thin Solid Films*, 1996, vol. 273, pp. 214–217.
5. Kholmanskii, A.S., Rumyantsev, B.M., Gol'ding, I.R., *et al*., *Zh. Fiz. Khim*., 1990, vol. 64, no. 6, pp. 1630–1636.
6. Bliznyuk, V., Everson, M., and Tsukruk, V., *J. Tribol*., 1998, vol. 120, pp. 489–495.
7. Goloudina, S.I., Pasyuta, V.M., Luchinin, V.V., *et al*., *Peterb. Zh. Elektron*., 2001, no. 4, pp. 79–86.
8. Polotskaya, G.A., Sklizkova, V.P., Goloudina, S.I., *et al*,. Abstracts of Papers, *4th Int. Symp. "Molecular Order and Mobility in Polymer Systems,"* St. Petersburg, June 3–7, 2002, p. 125.
9. Marek, M., Brynda, E., Pientka, Z., *et al*., *Eur. Polym. J*., 1997, vol. 33, no. 10–12, pp. 1717–1721.
10. Suzuki, M., Kakimoto, M., Konishi, T., *et al*., *Chem. Lett*., 1986, pp. 395–398.
11. Goloudina, S.I., Sklizkova, V.P., Pasyuta, V.M., *et al*., *Poverkhn.: Rentgen. Sinkhrotr. Neitron. Issl*., 2003, no. 10, pp. 93–99.
12. Goloudina, S.I., Sklizkova, V.P., Pasyuta, V.M., *et al*., Abstracts of Papers, *XVI European Chemistry at Interfaces Conf*., Vladimir (Russia), May 14–18, 2003, p. 106.
13. Sinha, S.K., Sirota, E.B., Garoff, S., and Stanley, H.B., *Phys. Rev. B*, 1988, vol. 38, pp. 2297–2311.
14. Kaneda, T., Katsura, T., Nakagawa, K., *et al*., *J. Appl. Polym. Sci*., 1986, vol. 32, pp. 3151–3176.
15. Parrat, L.G., *Phys. Rev*., 1954, vol. 95, pp. 359–369.
16. Arslanov, A.A., *Usp. Khim*., 1994, vol. 63, no. 1, p. 3.

Russian Journal of Applied Chemistry, Vol. 78, No. 9, 2005, pp. 1479–1485. Translated from Zhurnal Prikladnoi Khimii, Vol. 78, No. 9, 2005, pp. 1504–1510.
Original Russian Text Copyright © 2005 by Mikhailov, Lebedeva.

MACROMOLECULAR CHEMISTRY AND POLYMERIC MATERIALS

Preparation and Modification of Chitin-Based Fibers

G. M. Mikhailov and M. F. Lebedeva

Institute of Macromolecular Compounds, Russian Academy of Sciences, St. Petersburg, Russia

Received April 21, 2003; in final form, July 2005

Abstract—Spinning solutions of chitin were modified with polyvinylpyrrolidone, methyl cellulose, and sulfite cellulose. The resulting systems were used for preparing fibers by the wet formation method. The deformation and strength characteristics of these fibers were determined, and their X-ray diffraction analysis was carried out. The influence of the modifying additives on the structure and characteristics of the systems prepared was explained.

Biological activity of a natural polysaccharide, chitin, makes it attractive for researchers in the context of preparation and use of materials thereof, in particular, fibers. Chitin accelerates 3–4 times healing of wounds, and chitin sutures give cosmetic seams [1–3]. Pilot sutures resolve in a patient's body within the period sufficient for complete healing of a wound. However, inadequate elasticity of chitin sutures precludes commercial production of resolving chitin-based surgical seam materials in world practice.

Sukhanova *et al*. [4] showed that brittle failure of chitin-based sutures is due to easy crystallizability of chitin. This property is exhibited by cellulose and a number of others polysaccharides. One of the ways to disturb the crystallinity of a chitin fiber is partial deacetylation of chitin, increasing the structural inhomogeneity of the suture.

An increase in the structural inhomogeneity of the system under partial heterogeneous deacetylation of chitin hinders crystallization of the polymer during preparation of the fiber and increases its elasticity [5]. At chitin deacetylation degree of ≤0.30, the fiber forms a knot and preserves 40% of its initial strength. Heterogeneous deacetylation involves a severe impact of a concentrated alkali (30–50%) at a high temperature on chitin and frequently yields products with difficultly reproducible characteristics. This makes unreasonable the use of such a step in the technology because of variable characteristics of the resulting copolymer (solubility, gel formation, possible formation of glucuronic acids, etc.), which not only complicates but frequently hinders preparation of spinning solutions and formation of a fiber.

Therefore, it is necessary to develop a method of structural modification suitable for hindering crystallization of the macromolecules of the polysaccharide, chitin, increasing the elasticity of fibers, and extending the application field of such a valuable polymer.

EXPERIMENTAL

We used the following chemicals: dimethylacetamide available from Vekton (it was dehydrated and vacuum-distilled, with collection of the fraction boiling at 42°C and a residual pressure of 7 mm Hg); lithium chloride crystal hydrate (dehydrated at 400°C); sulfite cellulose (Svetogorsk Paper and Pulp Combine), DP = 996; crab chitin (manufactured by Vostok-Bor Joint-Stock Company, Dal'negorsk), M = 170 kDa, without ash and proteins; chitin from the North Sea shrimp, M = 135 kDa, with ash and proteins removed; polyvinylpyrrolidone (PVP) (samples with different molecular weights were prepared by radiation-induced polymerization [6]); and methyl cellulose with DP = 980 and degree of substitution 0.94 (laboratory synthesis).

Spinning solutions were prepared by dissolving polymers in a dimethylacetamide + 5% LiCl mixture so that the total concentration of chitin and the modifying polymer was 3% [7, 8]. The desired systems were obtained by introducing into the chitin solution the required amount of the solution of the modifier, which was followed by thorough mixing and gas removal in a vacuum, whereupon the resulting mixture was used for formation of fibers.

Fibers were obtained on a PIFV-01 setup, using a dosing syringe and a 1/0.4 spinneret. For precipitation served an alcohol bath, and for plasticization, a water bath. The fibers were freed from LiCl by washing with hot water until complete absence of chloride ions

1070-4272/05/7809-1479 © 2005 Pleiades Publishing, Inc.

in the wash waters (test with $AgNO_3$). The fiber was dried at 105°C.

Mechanical tests were carried out on an Instron-110 universal tensile-testing machine. The stress–strain diagrams were obtained for a 50-mm sample at a loading speed of 5 mm min^{-1}. Before tests, the samples were kept for a day in a desiccator over a concentrated aqueous solution of magnesium acetate, i.e., at a relative humidity of 65%.

X-ray diffraction studies were carried out on a DRON-2 diffractometer and in an RKV-86 chamber using nickel-filtered CuK_α radiation.

To choose the main procedures for preparation and modification of chitin sutures, it is necessary to consider the physicochemical relationships in formation of fibers from polysaccharide solutions.

The mechanical properties of chemical fibers, in particular, synthetic fibers based on polysaccharides, chitin and cellulose, are governed by two major factors: (1) degree of orientation of the polymer macromolecules along the fiber axis and their stacking and (2) morphology of the fiber, character and presence of submicrodefects in its structure on the micro and macro levels.

Also, a specific feature of polysaccharides should be mentioned, namely, a strong crystal lattice due to high-energy hydrogen bonds and rigidity of the macromolecules due both to pyranose fragments of the polymer chain and intramolecular hydrogen bond between the hydroxy group at the C^3 atom in a pyranose fragment and the oxygen atom of the neighboring pyranose ring. This is specifically responsible for rigidity of the macromolecules of polysaccharides, chitin and cellulose, as well as for the specific features of their conversion into the dissolved state. Polysaccharides can be dissolved via preparation of labile low-substituted esters or ethers that are easily solvated or via dissolution of polymers in "straight" solvents, yielding addition compounds. The latter procedure seems preferable. Out of all systems able to dissolve cellulose and chitin, the most convenient is a complex solvent dimethylacetamide–lithium chloride [9–11] in which polysaccharides do not degrade. When protected from the impact of the environment, these solutions preserve their properties for years.

Dissolution of polysaccharides, e.g., cellulose, is commonly accelerated by treating successively with water and methanol, whereupon the latter is replaced by dimethylacetamide in order to make the reaction centers more accessible for solvation. Such a procedure, inclusion, allows transparent solutions of the polysaccharide with higher concentrations of the polymer in solution to be prepared in a shorter time. The time of preparation of the solution increases with an increase in the molecular weight of the polymer.

McCormick [11] prepared solutions of polysaccharides by heating the mixture to 150°C, followed by slow cooling under protection of the system with nitrogen against thermooxidative degradation, which yielded transparent solutions. In this study we took advantage of the given technique for preparing a solution of chitin to be used for forming fibers.

Fibers are formed by pouring the chitin solution into appropriate precipitating baths in which the addition compounds degrade with replacement of the solvent from the polymer solution jet with the precipitating agent. According to phase equilibrium laws, coagulation of the polymer occurs. The system separates into two phases, one of which is a concentrated solution of the polymer; a three-dimensional structure (gel) is formed. This phase has a high viscosity and imparts to the coagulated polymer the fiber-gel properties.

Subsequent processes occur simultaneously or in a certain sequence depending on the formation conditions chosen. Strengthening of the system is associated with orientation of the polymer macromolecules. It should be accomplished before the onset of crystallization, while the originally formed phase exhibits certain plasticity.

Thus, one of the prerequisites to preparation of high-strength polysaccharide fibers is prevention or deceleration of the polymer crystallization during formation of a suture. Above all, the water activity should be decreased. This can be done by using alcohols as precipitating agents for polysaccharides during fiber formation.

Also, crystallization during preparation of polysaccharide fibers can be decelerated by introducing into the system other polymeric substances capable of hindering crystallization of the polysaccharides by strong interchain interaction and yielding a highly oriented mesomorphic supramolecular organization and, as a result, a fine fibrillar structure making the fibers highly strong and elastic. These polymeric substances should be kinetically compatible with the polysaccharide, which will prevent phase segregation at high concentrations of the polymer in the spinning solution and ensure steric hindrance to premature crystallization of the polysaccharide macromolecules during formation of the fibers.

Table 1. Influence of the origin and concentration of chitin in solution on the deformation and strength characteristics of fibers

Sample no.	σ_t, MPa	ε_b, %	E, GPa	Origin	c, %	M, kDa
1	476	4.5	27.3	Crab	3.2	170
2	395	5.0	18.3	Shrimp	3.1	135
3	405	1.7	32.1	"	2.0	135

* σ_t is ultimate tensile strength of the fiber; ε_b, elongation at break; and E, initial modulus of elasticity (Young modulus).

Both the molecular weight of the polysaccharide and the concentration of the polymer in solution affect structure formation in the resulting sutures and, correspondingly, the deformation and strength characteristics of the fibers.

Table 1 presents the deformation and strength characteristics of the fibers obtained from crab chitin (sample no. 1) and chitin of the North Sea shrimp (sample nos. 2 and 3). At virtually identical concentrations of the polymers in the solutions (3.2 and 3.1%) and under identical conditions of formation, the fiber from crab chitin is characterized by higher strength and higher initial modulus of elasticity, while elongations at break are close. This can be due only to the difference in the molecular weight of the chitin samples (170 kDa for crab chitin and 135 kDa for shrimp chitin). At the same time, at different concentrations of the shrimp chitin in solutions (3.1 and 2.0%) but under identical formation conditions, the resulting fibers are close in the strength (395 and 405 MPa) but differ in the deformation properties: The elongation at break is 5 and 1.7%, respectively. Table 1 shows that, with decreasing concentration of the polymer in solution, the resulting sutures are more rigid (initial modulus of elasticity of sample nos. 3 and 2) and brittle (elongation at break is much lower, sample nos. 2 and 3).

Table 2 shows that, to achieve large elongations at break, formation should be carried out at negative spinneret extensions (when the solution is supplied from the spinneret at a velocity exceeding that of the fiber reception). The strength characteristics of the fibers are improved as well. This is presumably due to the conformational transformations of the glucopyranose rings of the polysaccharide macromolecules and, correspondingly, to the relaxation processes occurring during suture formation.

Table 3 presents the deformation and strength characteristics of the fibers obtained by modification of the chitin fibers with PVP. It is seen that the properties of the fibers are most strongly affected by minor (1–2.5%) PVP additions. PVP with molecular weight

Table 2. Influence of extension on the deformation and strength characteristics of the chitin fibers

Total degree of extension	σ_t, MPa	ε_b, %
1.17	155	3.6
0.80	158	6.4
0.68	168	6.0
0.45	171	7.4

Table 3. Deformation and strength characteristics of fibers obtained from a shrimp chitin–PVP blend

M_{PVP}, kDa	Blend, %		σ_t, MPa	ε_b, %	E, GPa
	chitin	PVP			
8.0	99.5	0.05	346	2.9	2.39
	99.0	1.0	384	3.7	2.47
	97.5	2.5	370	4.4	2.25
	95.0	5.0	366	3.8	2.22
	90.0	10.0	412	3.5	2.57
12.0	99.5	0.05	653	5.2	3.54
	99.0	1.0	773	4.0	4.28
	97.5	2.5	718	6.8	3.22
	95.0	5.0	577	6.1	3.04
	90.0	10.0	367	5.1	3.53
35.0	99.5	0.05	525	5.8	3.02
	99.0	1.0	573	5.5	3.01
	97.5	2.5	528	3.1	3.76
	95.0	5.0	484	5.1	2.58
	90.0	10.0	413	5.6	2.23
800.0	99.5	0.05	432	3.6	2.73
	99.0	1.0	416	2.5	3.04
	97.5	2.5	405	2.6	3.06
	95.0	5.0	391	3.4	2.50
	90.0	10.0	351	5.4	1.96
1500.0	99.5	0.05	403	4.8	2.22
	99.0	1.0	387	5.3	1.47
	97.5	2.5	461	5.2	2.38
	95.0	5.0	494	6.4	2.27
	90.0	10.0	410	4.3	1.96
Chitin without additives	100.0	0	300	1.9	2.49

Table 4. Influence of the content of methyl cellulose c_{MC} on the characteristics of the composite fibers

c_{MC}, %	σ_t, MPa	ε_b, %
0	305	2
0.5	767	3.7
1.0	834	4.5
2.5	752	4.2
5.0	696	3.9
10.0	596	3.9

M of 12 and 35 kDa proved to be the best modifier. Upon introduction of 2.5% PVP with *M* = 12 kDa into a spinning solution, the strength of the fiber increased to 718 MPa, and the elongation at break was 6.8%. With increasing PVP concentration in the spinning solution to above 2.5%, all the mechanical characteristics of the fiber, also strongly influenced by the molecular weight of PVP, tended to decrease. The optimal characteristics were obtained at the molecular weight of 12.0 kDa.

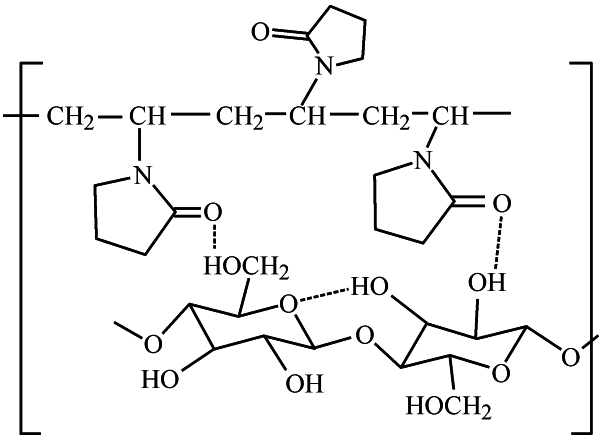
With a low- (*M* = 8.0 kDa) and a high-molecular-weight PVP (*M* > 800 kDa), the strength and elongation at break markedly decrease; the modulus of elasticity remains virtually unchanged, but with PVP having *M* = 800 and 1500 kDa it tends to sharply decrease. Such a dependence of the mechanical properties of the fiber on the molecular weight of PVP is, evidently, due to formation of microheterogeneous structures already in the spinning solution.

By using PVP with *M* = 12 kDa as modifier, the elongation at break of the fiber can be increased to 6.8%. Such a fiber preserves in the knot up to 40% of its initial strength.

X-ray diffraction studies [7] of the fiber obtained from chitin and composite fibers containing 1% PVP with the molecular weight of 12.0 and 35.0 kDa show that the fiber preserves a highly ordered structure typical for the unmodified chitin fibers. The X-ray diffraction patterns taken along the fiber axis (meridian) contain reflections at 2θ of 17° and 26°, corresponding to interplanar spacings of 5.02 and 3.36 Å, respectively. In the X-ray diffraction patterns of the fibers containing over 2.5% PVP, the reflection at 2θ = 9° it slightly blurred. The X-ray diffraction patterns taken across the fiber (equator) exhibit clear reflections at 2θ of 9° and 19°36′, also corresponding to interplanar spacings of 9.8 and 4.45 Å, typical for chitin fiber.

Thus, our X-ray diffraction studies show that, when introduced into a spinning solution in amounts up to 2.5% of those of chitin, PVP of varied molecular weights does not form a separate phase, and at a larger content of PVP the interplanar spacing in the system tends to increase.

Apparently, the macromolecules of the polysaccharide (chitin or cellulose) interact with PVP to form interchain hydrogen bonds:



This scheme shows that hydrogen bonding between the carbonyl oxygen from the pyrrolidone ring of PVP and hydroxy groups of the pyranose ring of the polysaccharide can involve the hydroxy group both at C^6 and at C^2 carbon atoms of the glucopyranose ring of the polysaccharide. The hydroxy group at C^3 forms an intramolecular hydrogen bond with the oxygen atom of the neighboring unit.

Also, the main chain of PVP is a hydrophobic element of the macromolecule and, when occurring in the interpolymer complex along with the modified system of hydrogen bonds of the polysaccharide, it decelerates crystallization of the polysaccharide macromolecules and modifies the supramolecular organization of the polysaccharide fibers. This improves the deformation characteristics of the fibers: They become more elastic, and their elongation at break increases. However, increases in the content of PVP and its molecular weight weaken the interchain interaction in polysaccharides and, consequently, deteriorate the deformation and strength characteristics of the fibers.

Introduction of up to 1.0% methyl cellulose into a solution of chitin [7] (Table 4) enhances the strength of a fiber to 834 MPa and increases its elongation at break to 4.5%. In the composition range studied (0.5–10.0%), the strength of the fiber shows a maximum at 1.0% content of methyl cellulose. Evidently, the methyl group of methyl cellulose hinders stacking of the macromolecules into crystal structures in the systems studied, decreases the density of the network of hydrogen bonds, as if plasticizing the system (as

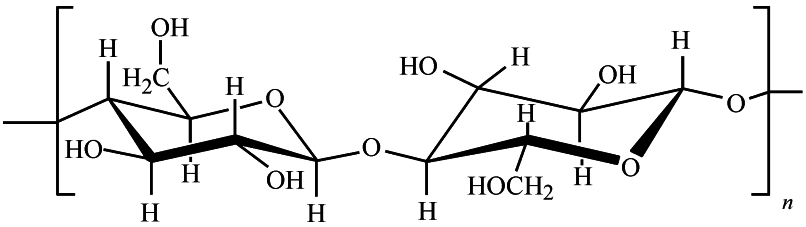
manifested in the changes in the strength and elongation at break of the fiber), and favors its orientation strengthening.

When chitin is modified with cellulose, or cellulose with chitin [8], at a low content of the modifier in the system, there is a sharp extremum of the ultimate tensile strength: a maximum at 0.5% cellulose in chitin and a minimum at 0.5% chitin in cellulose. Introduction of only 0.5% cellulose into chitin increases the strength of the fiber by 23% of the initial value, and at the modifier content of 2.5% the strength is 457 MPa, i.e., it deceases almost to the initial level (436 MPa). This local maximum of the strength is accompanied by a minimum of the elongation at break (2.2%). At a low (0.5%) content of chitin in cellulose, the fibers have a similarly homogeneous, though less clearly expressed, structure.

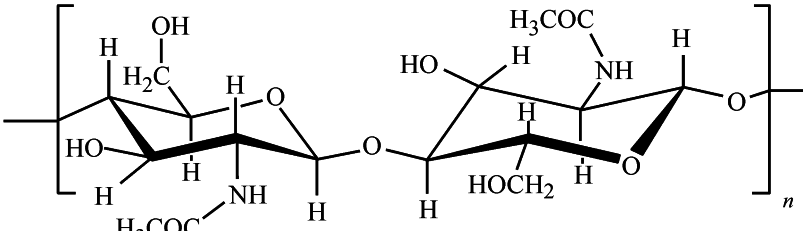
Bochek *et al*. [12] note that minor amounts of chitin and cellulose produce oppositely directed changes of the structure both in solutions and in a solid phase (films). Also, they reported that introduction of chitin into cellulose yields a more heterogeneous structure than introduction of cellulose into chitin.

The X-ray diffraction analysis of the systems with a low content of the modifier does not reveal the factors responsible for this phenomenon. However, studies of the structures of solutions of these polysaccharides [12], as well as of D_2O sorption by nonoriented films obtained from these systems [13], showed that the amount of the vapor sorbed tends to decrease upon introduction of 0.5% cellulose into chitin and to increase upon introduction of the identical amount of chitin into cellulose. Small-angle neutron scattering studies of these films showed that the scattering inhomogeneities are the smallest in the case of films with a low content of any component of the mixture. The size of the scattering inhomogeneities exhibits a local jumpwise decrease. The number of these inhomogeneities increases at 0.5% content of cellulose in chitin, and the structure of the film becomes more homogeneous.

Analysis of the chemical structures of chitin and cellulose will reveal the driving forces governing the morphology of the modified fibers:



A



B

The schematically presented fragments of the cellulose (**A**) and chitin (**B**) macromolecules show that the only difference between them consists in that, in the pyranose ring of chitin, one hydroxy group is replaced by acetamide group. The latter will hinder the stacking of the macromolecules during crystallization in the polysaccharide mixture and affect the character of the hydrogen bonds in the system.

When introduced into chitin in small amounts, cellulose can create a surface layer on the surpamolecular structural formations of chitin, whose "additional" hydroxy groups will strengthen the interstructural (interelement) interaction. This will be specifically responsible for enhanced rigidity of the system and the ensuing decrease in the elongation at break of the fibers. Thus, when added to chitin in minor amounts, cellulose acts as an antiplasticizer.

By contrast, introduction of chitin into cellulose should weaken the intermolecular interactions at the boundary separating the structural elements, since the

acetamide groups of chitin will sterically hinder the mutual stacking of the cellulose macromolecules. Hence, minor additives of chitin will act as plasticizers of the system. This can be responsible for an increase in the elongation at break of the cellulose fibers containing small amounts of chitin.

Thus, the influence of minor additives introduced into the polymer and substantially affecting its properties is exerted via changing the supramolecular ordering of highly organized polymeric systems. Presumably, these phenomena have the following mechanism. Spread of the modifier over the surface of the boundary separating the structural supramolecular formations of the polymer in some cases decreases the surface energy of interelement interaction, thereby increasing the mobility of the structural elements. In these cases, the modified system undergoes structural plasticization. In other cases, the energy of interaction of the interstructural elements increases, and the modifying additive acts as a structural antiplasticizer of the polymer. However, the phenomena of interest can be interpreted in such a way only when the structural elements of a polymer body are separated by a boundary, that is, this is a heterophase system. This is in line with the conclusions made by Papkov [14]. These effects are manifested only in heterophase systems with structural formations corresponding to the "macroscopic level" of the structure.

The modifier is localized on the boundary separating the macroscopic elements of the supramolecular structure of the polymer. This yields a heterophase system with the boundary at the location site of the modifier.

However, the term "heterophase nature" in its traditional sense is hardly applicable to so closely related polymers as chitin and cellulose, whose polymer chains are formed by glucopyranose rings. Instead, we should discuss a substantial change of the concentration of the hydrogen bonds on the surface of the micro- or macrofibrils. When cellulose is modified by microamounts of chitin, this concentration decreases, and when chitin is modified by cellulose, increases. In these cases, when chitin fibers are modified by minor additions of cellulose, the latter acts as a structural antiplasticizer, probably forming an epitaxial layer on the boundary separating the supramolecular formations and increasing the total energy of the interstructural interactions via increasing the density of the network of hydrogen bonds.

When cellulose is modified with chitin, minor additives of chitin act as structural plasticizers of the cellulose fibers. The plasticizing effect is due to a decrease in the density of the network of hydrogen bonds of the interstructural supramolecular formations.

In nature, similar role is played by cellulose satellites, hemicelluloses. Being natural structural modifiers, they affect the deformation and strength properties of plant materials. This makes of special importance the history of preparation of the sample of the polysaccharide and the ways of its isolation and preliminary processing, governing its purity, molecular weight, and polydispersity and affecting formation of the supramolecular structure and thus the characteristics of fibers thereof.

CONCLUSIONS

(1) Factors influencing the structure and the deformation and strength characteristic of polysaccharide fibers were established. High deformation and strength characteristics of fibers can be achieved with a polysaccharide having a maximal possible molecular weight and a maximal concentration of the polymer in solution, and sutures should be formed at negative spinneret extensions.

(2) The structure of polysaccharide fibers can be modified both by another polysaccharide or its derivative (partly substituted ethers or esters) and hydrophilic carbon-chain polymers.

(3) The deformation and strength characteristics are improved when a minor addition of a modifier acts as structural plasticizer decreasing the total energy of the network of hydrogen bonds at the boundary separating the supramolecular formations. When the modifier increases the total energy of the network of interstructural hydrogen bonds, it acts as a structural antiplasticizer, increasing the rigidity of the system and deteriorating the deformation characteristics of the fibers.

ACKNOWLEDGMENTS

The authors are grateful to V.S. Bozhko ("Vostok-Bor" Joint-Stock Company, Dal'negorsk) for the submitted crab chitin and for the interest and assistance in carrying out this study; to V.A. Petrov for the submitted solutions of chitin with polyvinylpyrrolidone; and to V.N. Ushakov for the submitted polyvinylpyrrolidone samples.

REFERENCES

1. Shigemasa, A. and Minami S., *Kobunshi Kako*, 1997, vol. 46, no. 2, pp. 27–33.

2. Oshihoma, Y., Nishino, K., Yonekura, Y., *et al*., *Eur. J. Plast. Surg*., 1987, vol. 10, pp. 66–69.
3. Tomihata, K. and Ikada, Y., *Biomaterials*, 1997, vol. 18, pp. 567–575.
4. Sukhanova, T.E., Sidorovich, A.V., Goryainov, G.I., *et al*., *Vysokomol. Soedin., Ser. B*, 1989, vol. 31, no. 5, pp. 381–384.
5. Nud'ga, L.A., Baklagina, Yu.G., Petropavlovskii, G.A., *et al*., *Vysokomol. Soedin., Ser. B*, 1991, vol. 33, no. 11, pp. 864–868.
6. Ushakova, V.N., Panarin, E.F., Kiryukhin, D.P., *et al*., *Vysokomol. Soedin., Ser. A*, 1991, vol. 33, no. 10, pp. 2151–2158.
7. Mikhailov, G.M., Lebedeva, M.F., Nud'ga, L.A., *et al*., *Zh. Prikl. Khim*., 2001, vol. 74, no. 7, pp. 1178–1181.
8. Mikhailov, G.M., Lebedeva, M.F., Nud'ga, L.A., *et al*., *Zh. Prikl. Khim*., 2001, vol. 74, no. 9, pp. 1526–1529.
9. McCormick, C.L. and Shen, T.S., *Macromolecular Solutions*, New York: Pergamon, 1982, pp. 101–107.
10. Dawsey, T.R. and McCormick, C.L., *J. Macromol. Sci.—Rev. Macromol. Chem. Phys*., 1990, vol. C30, nos. 3–4, pp. 405–440.
11. McCormick, C.L., Callais, P.A., and Hutchison, B.N., *Macromolecules*, 1985, vol. 18, no. 12, pp. 2394–2401.
12. Bochek, A.M., Nud'ga, L.A., Petrova, V.A., *et al*., *Zh. Prikl. Khim*., 1998, vol. 71, no. 12, pp. 2050–2055.
13. Nud'ga, L.A., Petrova, V.A., Bochek, A.M., *et al*., *Vysokomol. Soedin., Ser. A*, 1999, vol. 41, no. 11, pp. 1786–1792.
14. Papkov, S.P., *Fiziko-khimicheskie osnovy pererabotki rastvorov polimerov* (Physicochemical Principles of Polymer Solution Processing), Moscow: Khimiya, 1974.

Russian Journal of Applied Chemistry, Vol. 78, No. 9, 2005, pp. 1486–1488. Translated from Zhurnal Prikladnoi Khimii, Vol. 78, No. 9, 2005, pp. 1511–1513.
Original Russian Text Copyright © 2005 by Kulish, Kolesov.

MACROMOLECULAR CHEMISTRY AND POLYMERIC MATERIALS

A Study of Structure Formation in Chitosan–Polyvinyl Alcohol Blends by Turbidity Spectroscopy

E. I. Kulish and S. V. Kolesov

Bashkir State University, Ufa, Bashkortostan, Russia

Received March 21, 2005

Abstract—The structure formation of film samples of chitosan, polyvinyl alcohol, and their blends was studied by turbidity spectroscopy.

A blend of water-soluble polymers, polyvinyl alcohol (PVA) and aminopolysacharide, chitosan (CS), shows promise for preparing films and fibers combining high strength, biodegradability, and high hydrophilicity [1]. Introduction of PVA into CS, which is characterized by physiological activity, increases the flexibility of fairly brittle chitosan films [2]. Film materials based on PVA are widely used as membranes, artificial leather, and packing. Chitosan is used for reinforcing PVA films. Many properties of the polymeric composition are set in the stage of its formation and are determined by the phase and supramolecular structure of the polymer blend. The possibility of controlling the structure and properties of polymeric films, on the one hand, and unique properties of CS, on the other hand, give grounds to expect that polymeric films based on PVA and chitosan can serve as polymeric support for systems with controllable release of a drug.

In this study, we examined the structure of film samples of PVA and CS blends prepared from the combined solution and the principal possibility of release of a drug (gentamicin) from such films.

EXPERIMENTAL

PVA of 16/1 grade [GOST (State Standard) 10 779–78)] with M_η = 25 000, CS sample [TU (Technical Specification) 6-09-05-296–76] prepared by base deacetylation of crab chitin (degree of deacetylation 75%, M_η = 120 000), and gentamicin antibiotic were used without additional purification. Films of the individual polymers and their blends were prepared by casting the initial solutions onto the glass surface. The polymer concentration was varied from 0.2 to 5 g dl^{-1}. The solvent quality with respect to CS was controlled by varying the solution acidity [dissolution of CS in 5% aqueous ultrapure grade acetic acid (hereinafter these solutions are denoted as 5-AA) or 1% acetic acid (1-AA)]. To determine the average dimensions of supramolecular particles r and their number N in 1 cm^3 in the films, we used turbidity spectroscopy [3, 4]. The measurements were performed within λ = 340–590 nm at 20°C on a KFK-2MP photocolorimeter. The kinetics of gentamicin release from films placed in alkaline solution (pH 10) to prevent dissolution of CS was studied spectrophotometrically at λ = 240 nm (the absorption band of the pentosan ring of gentamicin) on a UV-VIS Specord M-40 spectrophotometer. The gentamicin content in the film was 2 wt %.

The study of PVA and CS films showed that the average turbidity of the films prepared from dilute solutions is substantially higher than that of the films prepared from more concentrated solutions (Fig. 1). Figure 2 shows that, with increasing concentration of the initial solution, the dimensions of supramolecular particles decrease and their number increases. This non-trivial result can be explained as follows. Forma-

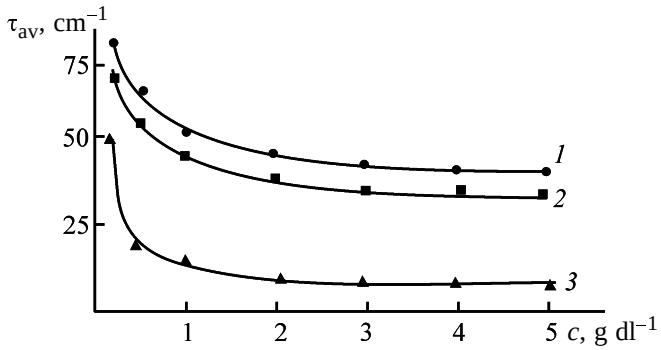


Fig. 1. Average turbidity τ_{av} of (*1, 2*) CS and (*3*) PVA films as a function of the polymer concentration c in the initial solution in (*1*) 5-AA and (*2, 3*) 1-AA.

1070-4272/05/7809-1486 © 2005 Pleiades Publishing, Inc.

tion of the film from dilute (0.2 g dl^{-1}) and concentrated (5.0 g dl^{-1}) solutions substantially differs in time. The initial 5% solution is viscous, and formation of the film proceeds very rapidly, within several hours. As a result, the film structure is similar to the structure of the initial solution. When the film is prepared from dilute solution, the solvent evaporation takes several days. The structure of the initial solution undergoes substantial transformation: supramolecular particles existing in the solution are consolidated, and, correspondingly, their number decreases.

It is of interest that the dimensions of supramolecular particles in CS films are substantially larger than in PVA films. This fact is consistent with the known tendency toward integration of CS crystallites in so-called clusters [5].

Apparently, films prepared from dilute and concentrated solutions should differ in their transport properties. It follows from Fig. 3 (curves *1*, *2*) that the release rate and degree of gentamicin release from the film prepared from the initially dilute solution are higher. This is apparently due to the fact that films prepared from the more concentrated solutions and hence having greater number of supramolecular particles with small dimensions will have denser packing and, correspondingly, reduced transport properties.

The films prepared from CS–PVA blends are microheterogeneous and contain crystalline areas of both CS and PVA [5]. At the same time, evident features of interpolymeric interaction appear in these blends. Figure 4 shows that, in the course of film formation from dilute solution, both more (5-AA) and less (1-AA) acidic, the trend in variation of the number and size of supramolecular particles with the CS to PVA ratio is the same. In both cases, the number of supramolecular particles in the blend is smaller and their size are larger than the corresponding additive values. Apparently, in this case we observe interpolymeric interaction, i.e., formation of CS–PVA heteroclusters, which, as known [6], are characterized by reduced packing density and larger size.

In the case of films prepared from concentrated solutions, the size of supramolecular particles in the region of small contents of CS in the mixture sharply increases (Fig. 5). It should be noted that just the blends with the prevalence of PVA (CS content 15–30 wt %) are characterized by elevated strength and the lowest crystallinity factor [7], which suggests the interpenetration of macromolecules.

This fact is indirectly confirmed by the data on the release of gentamicin from the films prepared from

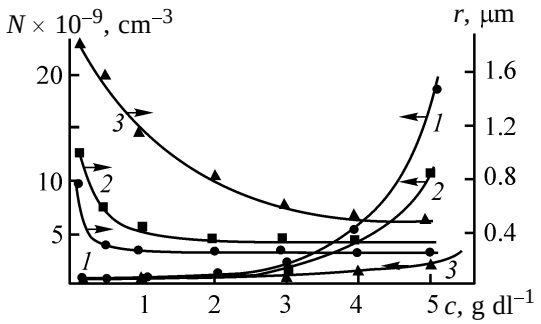


Fig. 2. Number *N* and size *r* of supramolecilar particles in (*1, 2*) CS and (*3*) PVA films as functions of the polymer concentration *c* in the initial solution in (*1*) 5-AA and (*2, 3*) 1-AA.

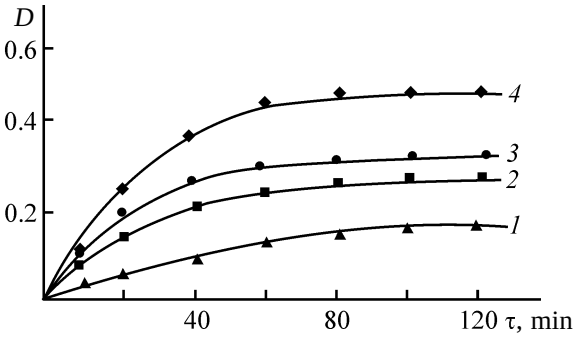


Fig. 3. Kinetics of gentamicin release from (*1, 2*) CS and CS-PVA films at weight ratio of CS to PVA of (*3*) 50 : 50 and (*4*) 20 : 80. (*D*) Optical density and (τ) time. Polymer concentration in 5-AA (g dl^{-1}): (*1*) 1 and (*2–4*) 0.2.

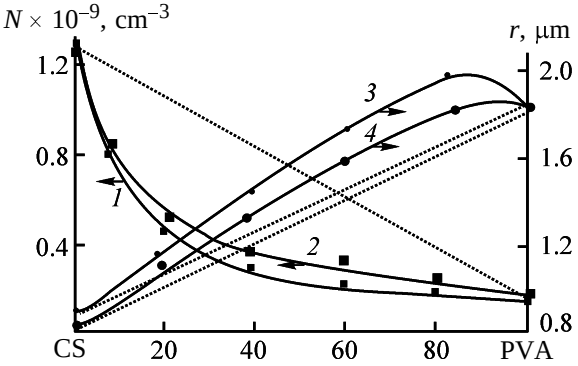


Fig. 4. (*1, 2*) Number *N* and (*3, 4*) size *r* of supramolecular particles in films prepared from 0.2% solution in (*1, 3*) 1-AA and (*2, 4*) 5-AA as functions of CS + PVA blend composition.

CS–PVA blend and pure CS. As seen from Fig. 3 (curves *3*, *4*), gentamicin is released from the CS–PVA film at a higher rate and to a greater degree than from the CS film (curve *2*). Apparently, films prepared from CS–PVA blends have less dense packing and, correspondingly, better transport properties, which is possible only in the case of formation of heteroclusters.

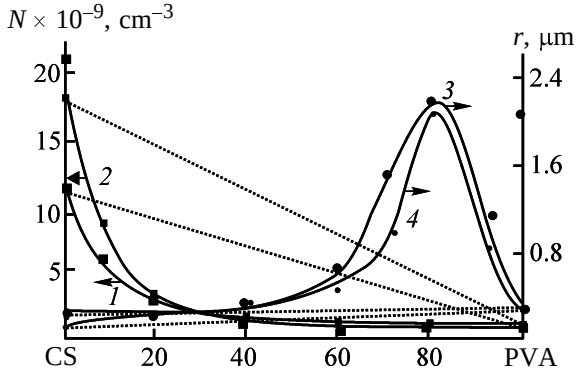


Fig. 5. (*1*, *2*) Number N and (*3*, *4*) size r of supramolecilar particles in films prepared from 5% solution in (*1*, *3*) 1-AA and (*2*, *4*) 5-AA as functions of CS + PVA blend composition.

CONCLUSIONS

(1) The conditions of formation of films from chitosan, polyvinyl alcohol, and their blends determine the number and size of supramolecular particles in the film. The number of supramolecular particles increases and their size, on the contrary, decreases with an increase in the concentration of the initial polymer solution. This fact is explained by consolidation of supramolecular particles at slow evaporation of the diluent in the course of film preparation from dilute solutions.

(2) A sharp increase in the size of supramolecular particles in films prepared from concentrated solutions with the prevalence of polyvinyl alcohol is attributed to formation of heteroclusters.

(3) The change in the structure of polymeric film due to change of the polymer concentration in the initial solution or introduction of the second polymer determines the film transport properties. The kinetics of gentamicin release from the films directly depends on the number and size of supramolecular particles formed in the film.

REFERENCES

1. Muzzarelli, R.A.A., *Chitin*, Oxford: Pergamon, 1977.
2. Nikolaev, A.F., Prokopov, A.A., Sul'gina, E.S., *et al.*, *Plast. Massy*, 1987, no. 7, pp. 40–41.
3. Klenin, V.I., *Termodinamika sistem s gibkotsepnymi polimerami* (Thermodynamics of Systems with Flexible-Chain Polymers), Saratov: Saratov. Univ., 1995.
4. Klenin, V.I., Shchegolev, S.Yu., and Lavrushin, V.I., *Kharakteristicheskie funktsii svetorasseyaniya dispersnykh system* (Characteristic Functions of Light Scattering of Disperse Systems), Saratov: Saratov. Univ., 1977.
5. Mukhina, V.R., Pastukhova, N.V., Semchukov, Yu.D., *et al.*, *Vysokomol. Soedin., Ser. A*, 2001, vol. 43, no. 10, pp. 1797–1804.
6. Kuleznev, V.N. and Krokhina, L.S., *Vysokomol. Soedin., Ser. A*, 1973, vol. 15, no. 4, pp. 906–915.
7. Prokopov, A.A. and Shul'gina, E.S., *Zh. Prikl. Khim.*, 1989, vol. 62, no. 6, pp. 1406–1407.

Russian Journal of Applied Chemistry, Vol. 78, No. 9, 2005, pp. 1489–1493. Translated from Zhurnal Prikladnoi Khimii, Vol. 78, No. 9, 2005, pp. 1514–1517.
Original Russian Text Copyright © 2005 by Kopeikin, Valueva, Kipper, Filippov, Borovikova, Suvorova, Nazarkina, Matveeva, Ostrovskaya.

MACROMOLECULAR CHEMISTRY AND POLYMERIC MATERIALS

Formation of Selenium Nanoparticles in the Selenite–Ascorbate Redox System in Aqueous Solutions of Polyelectrolyte Complexes of Various Compositions

V. V. Kopeikin, S. V. Valueva, A. I. Kipper, A. P. Filippov, L. N. Borovikova, E. I. Suvorova, Ya. I. Nazarkina, N. A. Matveeva, and L. D. Ostrovskaya

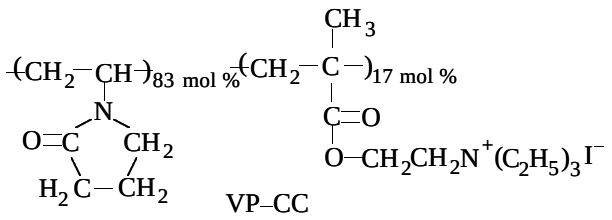
Institute of Macromolecular Compounds, Russian Academy of Sciences, St. Petersburg, Russia
Institute of Crystallography, Russian Academy of Sciences, Moscow, Russia

Received April 19, 2005

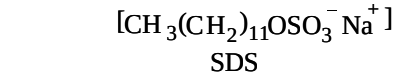
Abstract—Selenium nanoparticles were synthesized in aqueous solutions of polyelectrolyte complexes of sodium dodecyl sulfate, and the size and morphology of the forming nanostructures were determined.

Polyelecttrolyte complexes (PECs) of sodium dodecyl sulfate (SDS) with a cationic copolymer of *N*-vinylpyrrolidone and *N*,*N*,*N*,*N*-triethyl(methacryloyloxyethyl)ammonium iodide (VP–CC) are of particular interest as substances with a wide biological activity profile [1]:

PEC



VP–CC



SDS

Depending on the molar ratio γ of charged subunits in the complex (γ = SDS/CC), PECs exhibit a varied biological activity. The complex with γ = 0.5 is a strong competitive inhibitor of trypsin, whereas that with γ = 4.0 enhances the activity of this enzyme [2]. At γ = 0.5, PEC inhibits growth of animals, whereas at γ = 4.0 it possesses the highest growth-stimulating activity [1].

It has been established previously [3] that these complexes also differ in structural respect: at γ = 0.5, PEC has the form of micelles electrostatically bound to VP–CC; at γ = 4.0, a lamellar cluster of approximately 1000 SDS molecules is formed in a symmetric polymeric coil.

It is known that water-soluble polymers and anionic surfactants are effective stabilizers of silver [4] and palladium [5] particles. In an aqueous solution of SDS, palladium nanoparticles are stabilized via adsorption of SDS molecules on their surface and formation of a highly organized nanostructure of the 3D type "sphere around sphere" [5].

Of particular interest is the polymeric stabilization of nanoparticles of amorphous selenium, because, as established recently [6], nano-Se^0 stabilized with bovine serum albumin has a relatively low toxicity and retains a biological activity profile characteristic of ionic forms of selenium.

In view of the fact that the PECs mentioned above exhibit membranotropic properties and markedly raise the permeability of lipid bilayers [7], they can enhance the activity of selenium. Therefore, it seemed appropriate to synthesize nano-Se^0 in aqueous solutions of PECs and to determine the size and structural-morphological characteristics of the nanostructures formed in the process.

EXPERIMENTAL

We used a VP–CC copolymer with a molecular weight $M_w = 88 \times 10^3$, whose synthesis and purification have been described previously [3], and chemicals with a content of the main substance of no less than 99.9%. Polyelectrolyte complexes of various compositions were obtained by mixing aqueous solutions of VP–CC and SDS and then isolated in dry form by freeze drying. PEC with $M_w = 117 \times 10^3$ (γ = 0.5) and $M_w = 385 \times 10^4$ (γ = 4.0) were used. The reduction of ionic selenium was carried out at a 0.01% selenium

1070-4272/05/7809-1489© 2005 Pleiades Publishing, Inc.

concentration in the aqueous solution and a PEC : selenium mass ratio of 90 : 10, as in the case of the related selenium–polymer nanostructures [8]. The rate of Se(IV) reduction was evaluated in the thermostated mode (20°C) on a Specord M40 spectrophotometer by the rise with time in the optical density of a solution at a wavelength of 320 nm. The initial concentration of selenious acid was 1.0 mM (the pH of the reaction mass was 3.2 in both cases).

The molecular weights M_w and root-mean-square radii of inertia, R_g, of nanostructures were determined using the method of static light scattering [9], and their affinity for the solvent was found from the value of the second virial coefficient A_2. The ratio of the molecular weights of PECs and nanostructures formed by them was used to calculate the amount N of PECs adsorbed on the surface of nano-Se^0. The reduced intensity of scattering by solutions, R_θ, was measured with a Fica photogoniodiffusometer. The wavelength of the incident vertically polarized light was 546.1 nm. The measurements were performed at scattering angles in the range $\theta = 30°–150°$. The solutions and the solvent were purified by centrifugation at 15×10^3 rpm for 1–1.5 h. The increments of the refractive index, dn/dc, were determined by refractometric measurements on an IRF-23 instrument. For the system constituted by PEC, nano-Se^0, and water, $dn/dc = 0.244$ for $\gamma = 0.5$ and 0.198 for $\gamma = 4.0$.

The experimental data on light scattering by solutions of nanostructures were processed by the Zimm method by double extrapolation (to $c = 0$ and $\theta = 0$) of the plots of Kc/R_θ against $\sin^2(\theta/2) + kc$ (K, calibration constant; k, numerical constant).

The method of dynamic light scattering [10] was used to determine the average hydrodynamic dimensions of nanostructures, R_h. The ratio of the experimental values of R_g and R_h was used to find the value of the parameter ρ^* characterizing the structural-conformational state of the nanostructure [11–14]. The optical part of the installation for measuring the dynamic light scattering was equipped with an ALV-SP goniometer (Germany) (source of light: Spectra-Physics He–Ne laser, $\lambda = 632.8$ nm, power ~20 mW). The correlation function of the intensity of scattered light was determined using a Photo Cor-EC correlator with 288 channels (manufactured by Anteks Private Company, Russia). The correlation function was analyzed by Dynals software for processing of dynamic light scattering data (Gelios Company, Russia).

The data on M_w and root-mean-square radii of inertia were used to determine the average density of the nanostructures by the formula

$$\Phi^* = 3M_w/4\pi N_a R_{sph}^3, \quad (1)$$

where $R_{sph} = 1.29R_g$ [15].

The molecular dispersity of solutions of the nanostructures being formed was evaluated using the method of flow birefringence (FB) from the type of the gradient dependence of the magnitude of FB, Δn. In doing so, Δn was determined in relation to the gradient of the rate g of rotor rotation and to the PEC concentration c at a fixed concentration of selenium. We used a titanium dynamooptical caliper with an internal rotor of height 4 cm and a spacing of 0.03 cm between the rotor and stator. All the FB studies were performed with temperature-controlled solutions (21°C) in order to preclude changes in their viscosity and optical distortions caused by the temperature gradient. The installation was calibrated against phenylethyl alcohol, which exhibits a pronounced FB ($\Delta n/g = 17 \times 10^{-12}$), and the polystyrene–bromoform system. The error in determining the characteristic value of FB, $[n] = \lim_{g\to 0,\, c\to 0} (\Delta n/gc\eta_0)$ (η_0 is the solvent viscosity) did not exceed 10%. The measurements were performed at $g < g_k$, where g_k is the velocity gradient at which the flow becomes turbulent.

In the general case of $dn/dc \neq 0$, the experimental value of $[n]$ is constituted by three effects:

$$[n] = [n]_e + [n]_{fs} + [n]_f,$$

where $[n]_e$ is the intrinsic anisotropy; $[n]_{fs}$, microform effect; and $[n]_f$, macroform effect [16].

The quantity $[n]_f$ is related to the shape asymmetry of a particle, p, by the expression

$$[n]_f = [(n_s^2 + 2)/3]^2[M_w(dn/dc)^2 f(p)]/(30\pi RTn_s)$$

$$= \text{const}\, M_w(dn/dc)^2 f(p), \quad (2)$$

where n_s is the refractive index of the solvent; T, absolute temperature; R, universal gas constant; and $f(p)$, tabulated function of the ratio between the axes of a rigid (impermeable to the solvent) ellipsoid approximating a particle [16].

Electron micrographs of the forming nanostructures were obtained with a Philips CM300 FEG transmission electron microscope (accelerating voltage 300 kV). The samples had the form of thin films obtained upon drying of 100-fold diluted starting solutions on structureless carbon films of standard thickness. The dilution of the solutions was necessary to

Basic physical parameters of PECs of various compositions and of hybrid nanostructures formed by them with selenium nanoparticles in water

System	γ	$M_w \times 10^{-3}$	N	p	R_g, nm	R_h, nm	ρ^*	Φ^*, g cm^{-3}	$-\Delta G \times 10^5$, J m^{-2}	$A_2 \times 10^4$, cm^2 mol g^{-2}
PEC	0.5	117	–	–	22	–	–	–	–	0.8
	0.4	385	–		77	–	–	–	–	22
PEC–Se^0	0.5	10^4	85	1	40	40	1.0	0.07	0.059	0.5
	0.4	2×10^5	520	1	100	100	1.0	0.17	0.016	–1.8
SDS–Se^0	–	29×10^3	1611	1	40	40	1.0	0.08	0.042	0.2

prevent conglomeration of particles and formation of 3D agglomerates through drying.

In reduction of selenious acid in the presence of PEC, the rate constants of the process in which ascorbate is used as a reducing agent were 0.94×10^{-3} and 1.15×10^{-3} s^{-1} for γ = 0.5 and 4.0, respectively, i.e., the reaction rate was virtually independent of γ.

According to the data on static light scattering, M_w increased by a factor of 20 in going from γ = 0.5 ($M_w = 10^7$) to γ = 4.0 ($M_w = 20 \times 10^7$), i.e., 85 and 520 PEC particles, respectively, were adsorbed on the surface of nano-Se^0 (see table). In this case, the molecular-dispersed state of the solutions of nanostructures was preserved, which is indicated by the type of the $\Delta n = f(g)$ dependences: at $g < g_k$ they are well approximated by straight lines passing through the origin of coordinates for any c and γ [16].

The parameter p was estimated for the nanostructures under study in the approximation of $[n] \approx [n]_f$, using relation (2). It was found that a spherical nanostructure (p = 1) is formed at both values of γ. This is in full agreement with the data on the parameter ρ^* (see table): ρ^* = 1.0 (γ 0.5 and 4.0), which corresponds to a strictly spherical conformation of a particle.

However, experiments on static and dynamic light scattering revealed that nanostructures with different values of γ differ in R_g and R_h: $R_g = R_h$ = 40 nm (γ = 0.5) and $R_g = R_h$ = 100 nm (γ = 4.0) (see table), i.e., the nanostructure with a heavier molecular weight also has a large size (it is noteworthy that, in the absence of selenium in a solution, higher molecular weight and larger size are also observed for PEC with a higher content of SDS [3]).

A calculation of the average density Φ^* of a nanostructure by formula (1) demonstrated that a heavier particle (γ = 4.0) is also denser: Φ^* = 0.04 g cm^{-3} (Φ^* = 0.07 g cm^{-3} at γ = 0.5). This situation is different from that observed in [17], where a more compact nanostructure was denser. Apparently, these systems differ in the packing and distribution of organic molecules around selenium nuclei.

The second virial coefficient A_2 tends to zero for the nanostructure with γ = 0.5 ($A_2 = 0.5 \times 10^{-4}$ cm^2 mol g^{-2}), which characterizes the state of the solution as approaching the ideal. The value of A_2 for the nanostructure with γ = 4.0 is negative ($A_2 = -1.8 \times 10^{-4}$ cm^2 mol g^{-2}), which points to a poor thermodynamic quality of the solution. This results from orientation of hydrophobic alkyl chains of SDS toward the bulk phase of the solution. It should be emphasized that, at γ = 0.5, presence of selenium in a solution has virtually no effect on its thermodynamic state, whereas at γ = 4.0 transition from the PEC–water system to that constituted by PEC, nano-Se^0, and water is accompanied by a fundamental change in the thermodynamic state of the solution from good ($A_2 = 22 \times 10^{-4}$ cm^2 mol g^{-2}) to poor.

As is known [18], the Gibbs energy ΔG of the macromolecule–nanoparticle interaction, calculated per unit area of the particle surface, can be determined by the relation

$$\Delta G = kT \ln c / 4\pi R_{sph}^2, \quad (3)$$

where c is the initial concentration of the polymer (M).

It is noteworthy that relation (3) is valid for spherical nanostructures of arbitrary morphology in the range of formation of stable dispersions. Application of Eq. (3) to the nanostructures under study demonstrated that $\Delta G = -0.016 \times 10^{-5}$ J m^{-2} in the case of formation of a denser sphere (γ = 4.0). This value is considerably lower in magnitude than that in the case of a nanostructure with γ = 0.5, for which $\Delta G = -0.059 \times 10^{-5}$ J m^{-2}. The results we obtained are in qualitative agreement with the data on the parameter A_2 for the nanosystems studied.

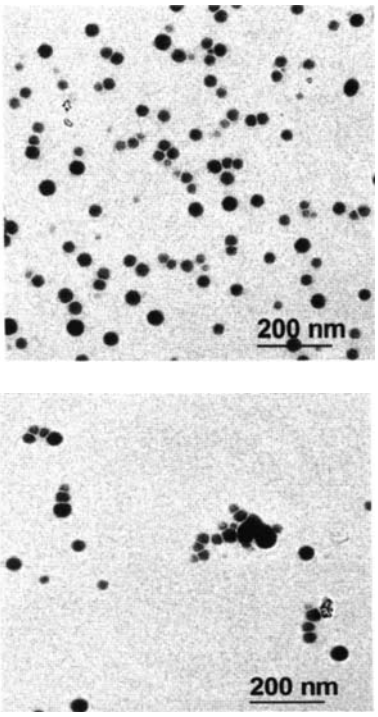


Fig. 1. Electron micrograph of a PEC–Se^0 film with γ = (a) 0.5 and (b) 4.0, formed by drying from an aqueous solution with a selenium concentration of 0.0001 wt %.

Thus, the energies and nature of interaction between nanoparticles and PEC in a complex multicomponent system constituted by PEC, nano-Se^0, and water strongly vary with γ (γ 0.5 and 4.0), which is reflected by the parameters ΔG and A_2. These nanostructures also strongly differ in the molecular weight, size, and density. Presumably, nanostructures with fundamentally different morphologies can be formed in the systems studied. Theoretically, their morphologies may be different for the polymer–nanoparticle systems [19].

This assumption is confirmed by the results obtained using high-resolution transmission electron microscopy for PEC films formed by drying from an aqueous solution with a selenium concentration of 0.0001 wt %. The nanosystem is mostly a mononuclear structure (Fig. 1a) for PEC with γ = 0.5, and mostly a polynuclear structure in the case of a PEC with γ = 4.0 (Fig. 1b).

In the physical parameters R_g, R_h, Φ^*, ΔG, and A_2 (see table), the PEC–Se^0 nanosystem with γ = 0.5 is close to the SDS–Se^0 nanosystem with the same selenium concentration and the same ratio of the components in solution [20]. This indicates that PEC mainly interacts with the selenium nucleus via SDS micelles.

CONCLUSIONS

(1) Hybrid selenium–polymer nanostructures fundamentally differing in their physical parameters and morphology were obtained for the first time by reduction of sodium selenite with ascorbate in aqueous solutions of polyelectrolyte complexes of a cationic copolymer and sodium dodecyl sulfate with various ratios of the charged subunits.

(2) The data obtained constitute a physicochemical basis for purposeful synthesis of potential selenium-based medicines with a lowered toxicity and high pharmacological activity.

ACKNOWLEDGMENTS

The authors thank Prof. Philippe A. Buffat (Centre for Electron Microscopy, Lausanne, Switzerland) for the opportunity to work at the Centre he heads.

The study was supported by the Russian Foundation for Basic Research (project no. 05-03-32842).

REFERENCES

1. Panarin, E.F. and Kopeikin, V.V., *Vysokomol. Soedin., Ser. C*, 2002, vol. 44, no. 12, pp. 2340–2351.
2. Kopeikin, V.V. and Afanakina, N.A., *Bioorg. Khim.*, 1988, vol. 14, no. 6, pp. 802–809.
3. Kopeikin, V.V. and Kipper, A.I., *Vysokomol. Soedin., Ser. B*, 2001, vol. 43, no. 7, pp. 1245–1250.
4. Kopeikin, V.V. and Panarin, E.F., *Dokl. Ross. Akad. Nauk*, 2001, vol. 243, no. 2, pp. 495–500.
5. Lee, C.-L., Wan, C.-C., and Wang, Y.-Y., *Adv. Funct. Mater.*, 2001, vol. 11, no. 5, pp. 344–347.
6. Zhang, J.S., Gao, X.Y., Zhang, L.D., and Bao, Y.P., *Biofactors*, 2001, vol. 15, no. 1, pp. 27–38.
7. Kopeikin, V.V., *Biol. Membr.*, 1988, vol. 5, no. 7, pp. 728–734.
8. Kopeikin, V.V., Valueva, S.V., Kipper, A.I., *et al.*, *Vysokomol. Soedin., Ser. A*, 2003, vol. 45, no. 4, pp. 615–622.
9. Eskin, V.E., *Rasseyanie sveta rastvorami polimerov i svoistva makromolekul* (Light Scattering by Polymer Solutions and Properties of Macromolecules), Leningrad: Nauka, 1986.
10. Brown, W., *Dynamic Light Scattering: the Method and Some Application*, Oxford: Clarendon, 1993.
11. Meewes, M., Ricka, J., De Silva, M., *et al.*, *Macromolecules*, 1991, vol. 24, no. 21, pp. 5811–5816.
12. Nishio, I., Shao Thang Sun, Swislow, G., and Tana-

ka, T., *Nature*, 1979, vol. 281, no. 5728, pp. 208–209.

13. Konishi, T., Yoshizaki, T., and Yamakawa, H., *Macromolecules*, 1991, vol. 24, no. 20, pp. 5614–5622.
14. *Laser Light Scattering in Biochemistry*, Harding, S.E., Satelle, D.B., and Bloomfield, V.A., Eds., Cambridge: Royal Soc. Chem., 1992, Inform. Services, pp. 3–21.
15. Pogodina, N.V. and Tsvetkov, N.V., *Macromolecules*, 1997, vol. 30, no. 17, pp. 4897–4904.
16. Tsvetkov, V.N., Eskin, V.E., and Frenkel, S.Ya., *Struktura makromolekul v rastvorakh* (Structure of Macromolecules in Solutions), Moscow: Nauka, 1964.
17. Valueva, S.V., Kopeikin, V.V., Kipper, A.I., *et al*., *Vysokomol. Soedin., Ser. B*, 2005, vol. 47, no. 5, pp. 857–860.
18. Litmanovich, O.E. and Papisov, I.M., *Vysokomol. Soedin., Ser. A*, 1999, vol. 41, no. 11, pp. 1824–1830.
19. Mayer, A.B.R., *Polym. Adv. Technol*., 2001, vol. 12, no. 1, pp. 96–106.
20. Kopeikin, V.V., Valueva, S.V., Kipper, A.I., *et al*., *Polym. Sci., Part A*, 2003, vol. 45, no. 6, pp. 963–969.

Russian Journal of Applied Chemistry, Vol. 78, No. 9, 2005, pp. 1494–1497. Translated from Zhurnal Prikladnoi Khimii, Vol. 78, No. 9, 2005, pp. 1518–1521.
Original Russian Text Copyright © 2005 by Legon'kova, Bokarev.

MACROMOLECULAR CHEMISTRY AND POLYMERIC MATERIALS

Physicomechanical and Rheological Characteristics of Composite Materials with Organic and Inorganic Fillers

O. A. Legon'kova and A. A. Bokarev

State Institution of Higher Vocational Education, Moscow, Russia
Moscow State University of Applied Biotechnology, Moscow, Russia

Received September 13, 2004; in final form, May 2005

Abstract—The strength and rheological characteristics of polymer composite materials based on synthetic copolymers and various fillers were studied. The influence of the filler on the characteristics of composites was revealed.

Polymer composite materials (PCMs) consisting of polymer materials and inorganic or organic substances of various chemical natures and structures find expanding applications in the form of mixtures or alloys [1].

As a rule, the characteristics of PCM are not a sum of characteristics of its components and are governed by a variety of chemical and physical processes involving the components and occurring at the phase boundary [2].

Polymer blends used today as biodegradable polymers [3–7] contain biodegradable components: cellulose and its ethers and esters, starch, etc., resulting in biodegradation of the composition as a whole. These materials are of interest for practice.

The physicomechanical and rheological characteristics of highly filled materials consisting of a polymer matrix and a mixture of fillers imparting the biodegradability to the composite as a whole were not adequately studied.

In this study we examined the physicomechanical and rheological characteristics of composites with organic (wastes from threshing of grains of the third category, particle size 63–240 μm, bulk density 350 kg m^{-3}, moisture content 4%) and inorganic filler {water-soluble complex mineral NPK fertilizer Rastvorin A [OST (Branch Standard) 10-193–96], containing N, P, K, Mg, Mn, Cu, Zn, B, and Mo in the form of salts, necessary for growth and development of plants}.

As a polymer component we used a copolymer of ethylene and vinyl acetate, Sevilen (SEVA) of the 11306–070 and 11506–070 brands, copolyamide (coPA) prepared by copolycondensation of adipic and sebacic acids with hexamethylenediamine of the N-005 brand [glass transition point T_g 115–120°C, melt flow index MFI 15 g $(10\ min)^{-1}$], and acrylate–styrene carboxylated latex Lenteks A4 [TU (Technical Specifications) 2241-001-47923137–01]. The criterion of choice of these polymers is the presence of functional groups in their compositions. The other important factor is fairly low temperature of treatment of these polymers (130–150°C), which is important for preservation of the characteristics of fillers added to the composite.

The physicomechanical characteristics of the samples were determined in a wide range of the component ratios according to recommendations of GOST (State Standard) 14236–82, and rheological characteristics of filled composites, by capillary viscometry from MFI depending on the filler concentration.

EXPERIMENTAL

In addition of fillers to SEVA, irrespective of its brand, it was found that with increasing content of both wastes and mineral fertilizer in the binary polymer–filler system, the strength and relative elongation decrease (Figs. 1a–1c). In the case of filling with organic fillers (wastes from grain production), the samples become harder, and in filling with inorganic filler (mineral fertilizer), even at its high concentration, the samples preserve fairly high plasticity. This behavior can be caused not only by decreasing concentration of the matrix in the composite, but also by the plasticizing effect of the inorganic filler.

As for ternary systems SEVA–wastes–fertilizer (Fig. 1d), it should be noted that an increase in the

1070-4272/05/7809-1494© 2005 Pleiades Publishing, Inc.

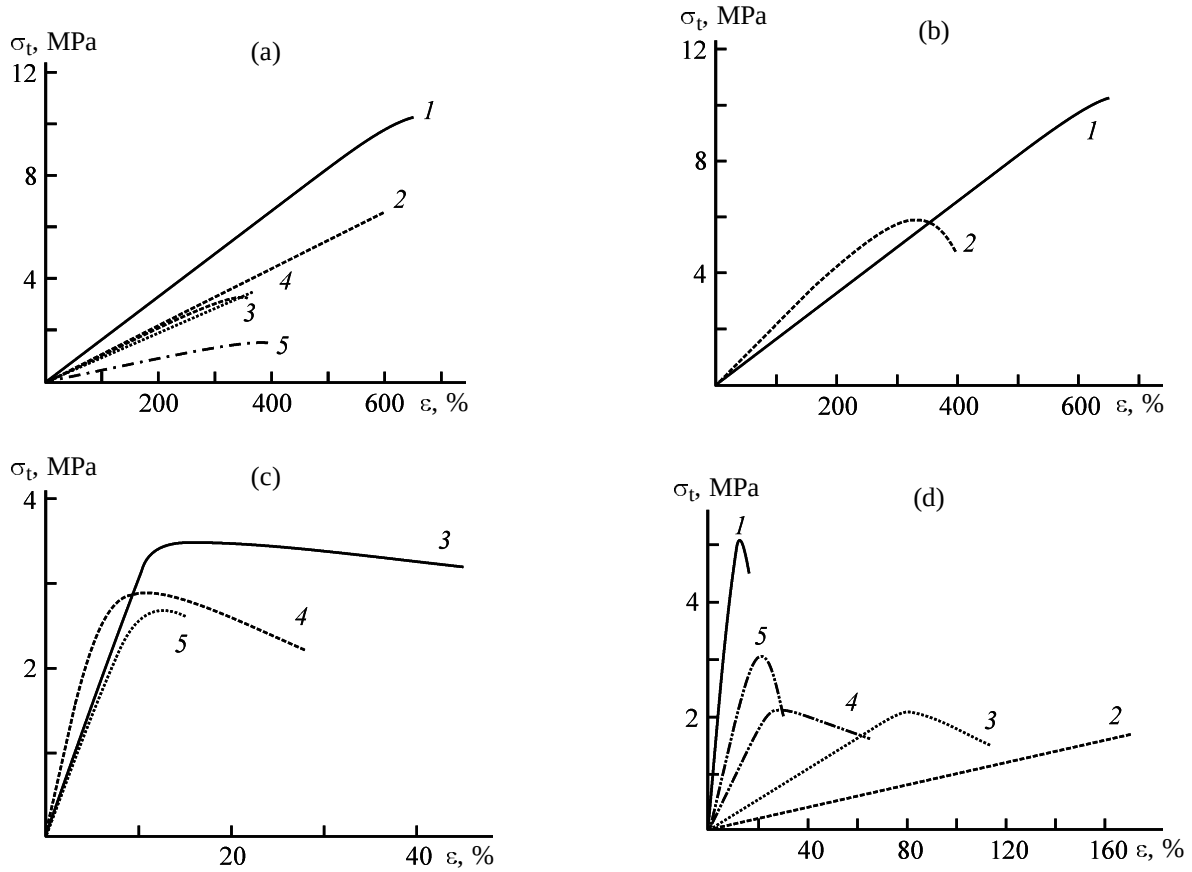


Fig. 1. Physicomechanical characteristics of (a) SEVA–fertilizer, (b, c) SEVA–wastes, and (d) SEVA–wastes–fertilizer system. (σ_t) Ultimate tensile strength and (ε) relative elongation; the same for Fig. 3. (a–c) SEVA/fertilizer, SEVA/wastes ratios, wt %: (*1*) 100/0, (*2*) 80/20, (*3*) 60/40, (*4*) 50/50, and (*5*) 40/60. (d) Ratio, wt %: (*1*) SEVA/wastes 50/50, (*2*) SEVA/fertilizer 50/50; (*3*) SEVA/wastes/fertilizer 50/13/37, (*4*) SEVA/wastes/fertilizer 50/25/25, and (*5*) SEVA/wastes/fertilizer 50/37/13.

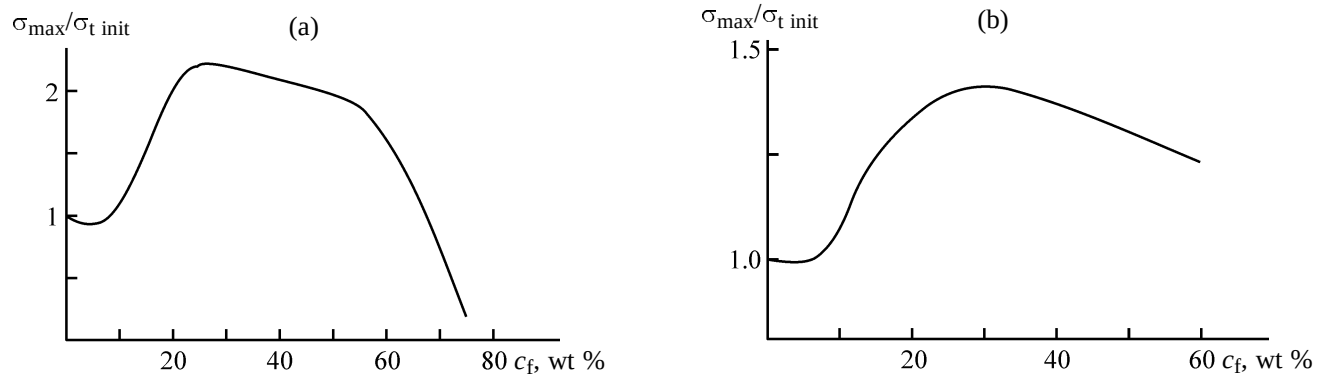


Fig. 2. Variation of the $\sigma_{max}/\sigma_{t\,init}$ ratio as a function of the concentration of (a) inorganic and (b) organic filler. (c_f) Filler concentration; the same for Fig. 4.

content of inorganic filler gives more plastic samples.

The variations of physicomechanical characteristics of the samples differing in the SEVA brand show similar trends.

Let us consider the behavior of the composite material based on coPA. The ratio of ultimate tensile strength of the filled sample to that of the initial nonfilled sample, $\sigma_{max}/\sigma_{t\,init}$, as a function of the concentration of the inorganic filler is shown in Fig. 2a. In addition of the fertilizer to the composite in the amount of up to 10% (Fig. 2a), the ultimate tensile

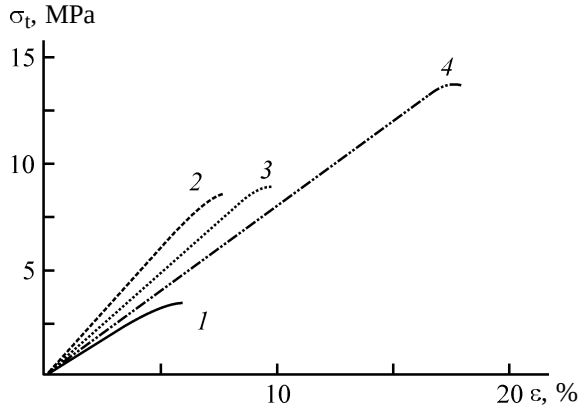


Fig. 3. Physicomechanical characteristics of coPA–wastes–fertilizer systems. coPA/wastes/fertilizer, wt %: (*1*) 50/10/40, (*2*) 50/20/30, (*3*) 50/25/25, and (*4*) 50/40/10.

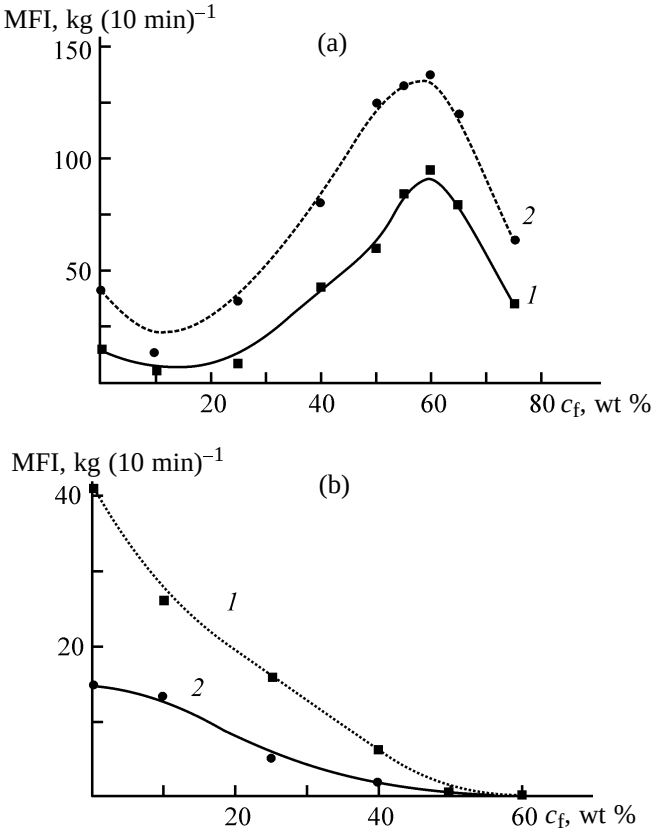


Fig. 4. Variation of MFI of filled coPA as a function of concentration of (a) inorganic and (b) organic fillers. Test temperature 130°C. (MFI) Melt flow index. Load, kgf: (*1*) 2.16 and (*2*) 5.0.

strength slightly decreases. This is apparently caused not only by decreasing content of the polymer per unit surface area, but also by the fact that at low degree of filling, even at a good adhesion between the polymer and filler, but in the absence of aggregation of powdered particles, the filler accumulates stresses and is a potential source of crack propagation [8]. With increasing concentration of the filler to 30%, the strength ratio $\sigma_{max}/\sigma_{t\,init}$ increases by a factor of more than 2. With increasing content of the filler, crack propagation becomes more hindered, and the amount of intermolecular interactions between components increases, which results in inhibition of the failure processes [9]. Further decrease in the strength is typical for highly filled polymers with a high content of inorganic filler and a low content of coPA. At a fertilizer concentration of approximately 75%, the sample becomes very brittle and has the strength by an order in magnitude lower than that of the initial sample. The relative elongation at break for all the samples decreases with increasing filling and finally becomes 2 times lower than that of the initial sample. With addition of wastes to coPA (Fig. 2b), the similar trend is observed, i.e., the system gets relatively strengthened; however, this effect is not so significant as in the two-component system with the inorganic filler.

The variations of the physicomechanical characteristics of the coPA–wastes–fertilizer system are shown in Fig. 3. The coPA content was constant, 50%. We varied the content of organic and inorganic fillers. At a high content of the filler, an increase in the content of wastes results in somewhat higher strength and rigidity of the composite. For the system with styrene acrylate–polymer matrix at 49% filling with inorganic filler, the ultimate tensile strength decreases by a factor of 0.9, and at filling with organic filler it increases by a factor of 2.7.

Addition of up to 10% inorganic filler to coPA results not only in insignificant decrease in the strength of the composite material but also in a decrease in MFI (Fig. 4a). With increasing content of inorganic filler to 60%, MFI increases significantly, which confirms the plasticizing effect of the fertilizer in the system. Then, MFI decreases, which is caused by saturation of the system with the filler, attainment of the filling limit, and decrease in the content of the thermoplastic component.

The revealed effect is governed by the total effect of components of the inorganic filler on the composite viscosity. Elucidation of this phenomenon is an important and sophisticated problem. Therefore, to understand the causes of extremal increase in the fluidity of systems filled with fertilizers, we filled the polymer with individual components of the complex mineral fertilizer. Filling was performed to a degree of 1–2%, taking into account that an increase in MFI was observed even at a fertilizer content of 25–30% (Fig. 4a) and the content of individual components in

MFI at various concentrations of salts

Sample	MFI, g (10 min)$^{-1}$, at indicated salt concentration, wt %	
	1	2
SEVA* + $MgCl_2$	7.5	7.1
SEVA + KCl	6.7	6.3
SEVA + P_2O_5	8.1	7.1
SEVA + KNO_3	2.9	Not determined because of
SEVA + NH_4NO_3	4.3	extremely high outflow rate

* MFI_{SEVA} = 7.8 g (10 min)$^{-1}$ (T_{test} 130°C).

complex fertilizer Rastvorin A was 5–15%. We added KCl, $MgCl_2$, P_2O_5, NH_4NO_3, and KNO_3 and found that specifically nitrogen-containing substances cause a significant decrease in MFI of the synthetic polymers (see table).

Addition of insignificant amounts of wastes from grain production increases the system viscosity, and on addition of 50 wt % of wastes the system practically loses the fluidity (Fig. 4b). The results obtained are typical for filled and highly filled systems in the absence of interaction between the filler and polymer matrix.

CONCLUSIONS

(1) Physicomechanical characteristics of polymer composites with inorganic filler depend on the kind of the polymer matrix: for SEVA, irrespective of its brand, and Lenteks A4, an increase in the fertilizer content results in a decrease in the ultimate tensile strength, and for the matrix based on coPA, in an increase in the strength by a factor of more than 2; for all polymer types, addition of the inorganic filler results in a decrease in the viscosity of the system.

(2) For all types of polymers, addition of the organic filler results in formation of a rigid system. In the case of using coPA and Lenteks A4 as a polymer matrix, the ultimate tensile strength increases.

(3) The order of addition of fillers into the system is of some importance for obtaining highly filled composites: first, highly filled two-component system polymer–fertilizer with the minimal viscosity should be prepared and then the organic filler should be added. In this case, the ternary system is homogeneous and compatible.

REFERENCES

1. *Napolniteli dlya polimernykh kompozitsionnykh materialov: Spravochnoe posobie* (Fillers for Polymeric Composite Materials: Handbook), Babaevskii, P.G., Ed., Moscow: Khimiya, 1981.
2. Lipatov, Yu.S., *Fiziko-khimicheskie osnovy napolneniya polimerov* (Physicochemical Principles of Polymer Filling), Moscow: Khimiya, 1981.
3. RF Patent 2 174 132.
4. RF Patent 2 126 427.
5. RF Patent 2 126 023.
6. RF Patent 2 123 014.
7. RF Patent 2 117 016.
8. Manson, J.A. and Sperling, L.H., *Polymer Blends and Composites*, New York: Plenum, 1976.
9. Lipatov, Yu.S., *Kolloidnaya khimiya polimerov* (Colloidal Chemistry of Polymers), Kiev: Naukova Dumka, 1984.

Russian Journal of Applied Chemistry, Vol. 78, No. 9, 2005, pp. 1498–1502. Translated from Zhurnal Prikladnoi Khimii, Vol. 78, No. 9, 2005, pp. 1522–1526.
Original Russian Text Copyright © 2005 by Konstantinova, Berezkin, Kurbatova, Finkel'shtein.

MACROMOLECULAR CHEMISTRY AND POLYMERIC MATERIALS

Relationship between Physicochemical Properties and Chromatographic Retention of Some Adamantane Derivatives

K. K. Konstantinova, V. G. Berezkin, S. V. Kurbatova, and E. E. Finkel'shtein

Samara State University, Samara, Russia
Institute of Petrochemical Synthesis, Russian Academy of Sciences, Moscow, Russia

Received February 3, 2005

Abstract—Correlations between physicochemical properties and chromatographic retention parameters of adamantane derivatives were studied. The Kovats indices and contributions of hydrocarbon radicals and functional groups to the chromatographic retention were calculated from the experimental data.

One of urgent problems of the modern chemistry is revealing quantitative relationships between the structures and physicochemical properties of compounds. This problem is solved within the framework of QSPR (Quantitative Structure–Property Relationships) studies [1]. One of promising lines in these studies is based on the use of chromatography as a powerful tool of organic chemistry used primarily for separating mixtures. Chromatography also finds increasing use as a method of structural analysis. The most widely used for this purpose is adsorption chromatography (chromatoscopy, according to A.V. Kiselev [2]), because it is commonly believed that, among macroscopic properties of molecular systems, adsorption on a uniform flat surface of an adsorbent at low fillings is the most strongly dependent on the geometric structure of molecules. Therefore, the QSRR (Quantitative Structure–Retention Relationships) approach is considered as a part of QSPR [1].

To reveal a correlation between the structure and chromatographic retention of organic molecules, it is necessary to understand what kinds of intermolecular interactions are characteristic of the given kind of molecules. It is assumed that the structure–property relationship for organic compounds is determined by the system of intermolecular interactions which, in turn, is governed by the energy of intermolecular bonds, internal rotation barriers of particular atomic groups, molecular symmetry, etc. [2]. At present, the problem of revealing correlations between the structure and chromatographic retention of organic compounds can be considered as solved for particular cases of homologous series [3]. The structure–retention relationships for wider taxonomic groups such as, e.g., structural analogs are studied to a lesser extent [4–6].

As investigation objects we chose structural analogs of adamantane, in view of the steadily growing interest in these derivatives. Data are available on the chromatographic behavior of alkyl, amino, hydroxy, and some other derivatives of adamantane [7–9]. Data on properties of adamantane-containing sorbents and stationary phases are virtually lacking. At the same time, it was shown that such sorbents can be efficient tools in studies of molecular structures of sorbates and intermolecular interactions [10, 11].

In construction of structure–chromatographic retention correlations for wide taxonomic groups, an effective approach is theoretical replacement of complex functional groups or structural fragments by simpler groups or vice versa. Therefore, the sample for revealing correlations includes either a large number of compounds with diverse structures or, on the contrary, a small number of structurally related compounds [9]. Previously [12, 13] we studied alkyl derivatives of adamantane and substances constituting a wide taxonomic group of cyclic compounds.

In this study we examined the chromatographic behavior of adamantane functional derivatives of various chemical nature on adamantylsilicone stationary phase.

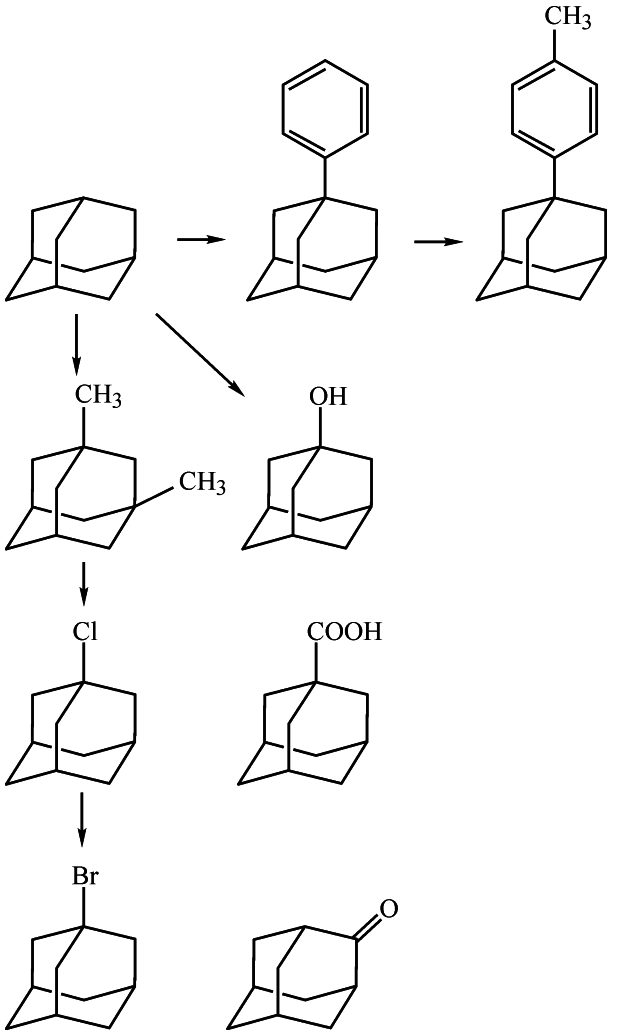
EXPERIMENTAL

We used capillary chromatography with flow splitting. The experiment was performed with a Tsvet-100 chromatograph equipped with a flame-ionization

1070-4272/05/7809-1498 © 2005 Pleiades Publishing, Inc.

detector. The column temperature was 160°C, and the vaporizer temperature, 200°C. The carrier gas was nitrogen; the flow splitting ratio at the column inlet was 1 : 60. A 22 m × 0.22 mm capillary column was coated with cross-linked adamantylsilicone (film thickness d_f = 0.2 μm). The chromatographic properties of the adamantylsilicone stationary phase were reported previously [11].

As investigation objects we chose the compounds shown below.[1] The purity of the compounds was confirmed by elemental analysis and by IR and NMR spectroscopy.



To determine the relationships in the chromatographic retention within wide taxonomic groups, we also used the previously obtained characteristics of the chromatographic retention of some carbo- and heterocycles [13].

The retention indices (RIs) were calculated by the Kovats formula [3]. The RIs were reproducible within the limits of 1–2 units.

The differential molar free energy of sorption ΔG was calculated by the formula $\Delta G = -RT\ln k\beta$, where k is the retention factor, and β, phase ratio [14].

The experimental indices I averaged over 7–10 values and the quantites ΔG are given in the table.

Quantum-chemical calculations were performed with HyperChem program package, version 6.0, by AM1 and PM3 semiempirical methods and MM+ molecular mechanics method. The calculated molar volumes V and polarizabilities α of the compounds are given in the table.

The main principle of using physicochemical methods for determining the molecular structure is proof of the presence (or absence) of certain fragments, i.e., group identification, with different levels of detailing the structural features of a compound. This approach is largely based on the concept that the properties of organic substances are additive and the CH_2 group gives a constant increment in estimation of a physicochemical property. In determination of the chromatographic parameters, the additive schemes and their elements are primarily represented in the so-called homomorphism factors and other related criteria [3]. The use of chromatographic retention parameters is quite justified in this case, because the decisive factor in determining the structure of a compound from the chromatographic data is that variations of the thermodynamic characteristic of the sorption should be adequate to structural changes in the sorbate molecules.

The chromatographic retention is governed by three major factors: nature of the chromatographic system (mobile and stationary phases between which the sorbate molecules are distributed), chromatographic conditions, and molecular structure of the sorbate [3]. The properties of the adamantylsilicone stationary phase used in this study were described previously [11]. It was shown that adamantylsilicone is fairly selective in separation of structural isomers.

For structural analogs of adamantane, we observed regular, on the whole, variation of the retention characteristics in going from cyclanes to aromatic compounds, from carbocycles to heterocycles, and from mono- to polycyclic analogs [13].

Since the adamantane molecule is highly symmetrical with an extremely small external surface area

[1] The adamantane derivatives were prepared at the Chair of Organic Chemistry, Samara State Technical University and submitted by Prof. Moiseev.

Chromatographic characteristics of compounds studied

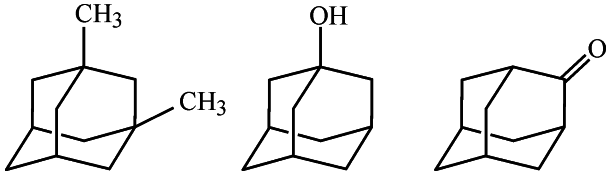
Compound	M	V, Å^3	α, Å^3	Ad–R					
				I_{ApL}	δI_{RApL}	I	$-\Delta G$, kJ mol^{-1}	δI_R	$\delta(\Delta G_R)$
Adamantane	136	482.79	16.80	1144	–	1123	16.246	–	–
1,3-Dimethyladamantane	164	570.88	20.47	1245	50.5	1171	17.071	48	0.825
1-Chloroadamantane	170	522.48	18.73	1350	206	1300	19.355	177	3.109
1-Bromoadamantane	215	539.80	19.43	1417	273	1386	20.201	263	3.935
Adamantan-1-ol	152	502.34	17.44	1333	189	1268	18.008	145	1.762
Adamantanone	150	490.19	16.89	–	–	1332	19.124	209	2.878
Adamantanecarboxylic acid	180	553.11	19.36	1498	354	1314	18.892	191	2.646
1-Acetyladamantane	194	611.77	21.19	–	–	1462	21.512	339	5.266
Phenyladamantane	212	679.44	26.46	–	–	1364	19.796	241	2.550
Tolyladamantane	226	732.01	28.30	–	–	1595	23.943	472	7.697

and weak intermolecular interactions in the crystal lattice, introduction of various substituents decreases the molecular symmetry and affects the physicochemical characteristics, including the chromatographic retention [7]. In this case, simple additive schemes assuming the constancy of increments for a given kind of atoms are unsuitable because of the mutual influence of the atoms (or bonds between them).

The contribution of substituents to the retention indices depends on their structure and position in the molecule. Substituents strongly affect the electron density distribution in the molecule. This effect is not uniform usually; it is transferred by several mechanisms depending on the properties of the substituent itself and on the type of the reaction center, molecular core, and even surrounding (temperature, pressure). The effect of a substituent can correspond to the sum of several effects. Therefore, in complex molecular systems, additive schemes used for determining the retention characteristics should take into account various intramolecular effects associated with the nature and position of the substituent. For example, it is known that substituents at the bridgehead carbon atoms in the adamantane molecule make a considerably lower contribution to the retention than the same substituents at the bridging carbon atoms, because of the so-called "cage effect" (overlap of the rear sides of the atomic orbitals of the tertiary carbon atoms in the adamantane framework).

The table shows that the order of elution of the examined adamantane derivatives on the nonpolar adamantanylsilicone phase corresponds to the order of increasing molecular size. It is known [3] that such an elution order is characteristic of systems in which the intermolecular interactions between the sorbate and stationary phase are determined by dispersion forces. These forces, in turn, are determined by the molecular polarizability, which increases with the molecular size. Comparison of the retention data for adamantane derivatives and other cyclic compounds shows that, in aromatic and cyclic hydrocarbons, the main fragment determining the chromatographic retention is the benzene (or other) ring. Therefore, as seen from Figs. 1 and 2, for adamantane analogs of different structures the retention characteristics vary in parallel with the molecular volume and polarizability.

At the same time, it is known that specific interactions make a certain contribution to interaction of silicone stationary phases with compounds containing elements with lone electron pairs [14]. This fact may be responsible for differences in the retention characteristics of some sorbates with similar molecular weight, despite the nonpolar character of adamantylsilicone:



$I_{Ad-R} = 1171$, $M = 164$ | $I_{Ad-R} = 1268$, $M = 152$ | $I_{Ad-R} = 1332$, $M = 150$

Therefore, points corresponding to compounds with similar electronic structure (e.g., compounds containing several aromatic or saturated rings) are arranged in separate areas of the plots (Figs. 1, 2), exhibiting additional relationships within the general trend.

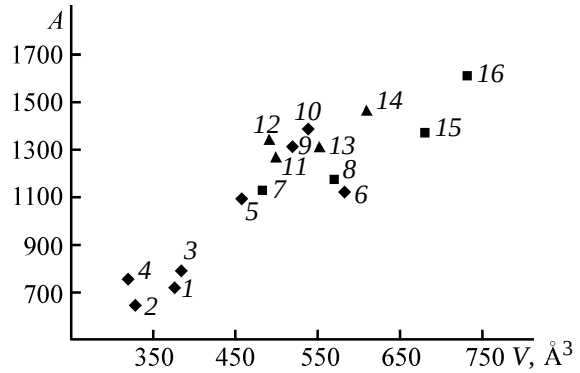


Fig. 1. Kovats indices *A* vs. molecular volumes *V*. (*1*) Cyclohexane, (*2*) benzene, (*3*) toluene, (*4*) pyridine, (*5*) naphthalene, (*6*) anthracene, (*7*) adamantane, (*8*) 1,3-dimethyladamantane, (*9*) 1-chloroadamantane, (*10*) 1-bromoadamantane, (*11*) adamantan-1-ol, (*12*) adamantanone, (*13*) adamantanecarboxylic acid, (*14*) acetyladamantane, (*15*) phenyladamantane, and (*16*) tolyladamantane; stationary phase adamantylsilicone; the same for Figs. 2 and 3.

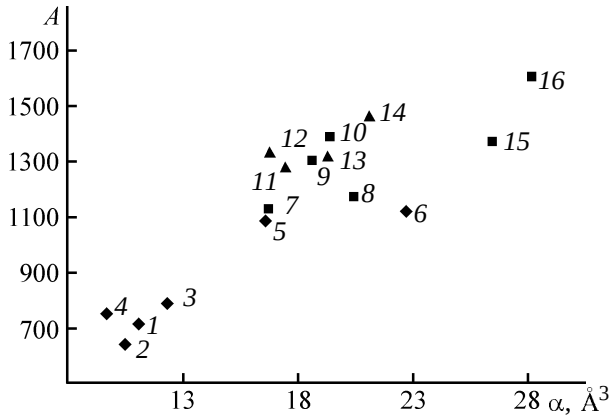


Fig. 2. Kovats indices *A* vs. molecular polarizabilities α.

On the whole, the retention characteristics of the examined compounds on adamantylsilicone are somewhat lower than on Apiezon L (ApL), which may be due to the steric effect of the adamantane core incorporated into the stationary phase.

Phenyl- and tolyladamantane having the largest molecular volume have also the largest retention indices. At the same time, the contribution of the phenyl (241) and tolyl (472) substituents to the retention of these compounds by adamantylsilicone in considerably lower than the retention indices of benzene (649) and toluene (796) molecules. This fact may be caused both by participation of the substituents in realization of the cage effect and by steric hindrance to interaction with the stationary phase.

The chromatographic retention of alkyladamantanes on stationary phases of various polarities was described in detail in [9]. It was showsn that the contribution of methyl radicals $\delta I(CH_3)$ in 1,3-dimethyladamantane is not additive because of their participation in realization of the cage effect and is as low as 31 units, whereas for *n*-alkanes this value is 100 units [3]. With the adamantylsilicone stationary phase, $\Delta I(CH_3)$ is 48 units. The suggested mechanism of the interaction of 1,3-dimethyladamantane with the stationary phase (with realization of the cage effect) is also confirmed by the fact that the retention index of this compound is considerably lower than it could be expected from its molecular volume.

It was determined previously [15] that, in going from adamantane to 1-fluoro-, 1-chloro-, and 1-bromoadamantane the retention index on nonpolar stationary phases increases by 100, 200, and 600 units, respectively [15]. This trend was attributed to an increase in the contribution of the induction interaction due to higher polarizability of the bromine atom compared to chlorine and fluorine. The contribution of the halogen to the retention is approximately the same as for haloalkanes on Apiezon L. On adamantylsilicone, the contribution of the Cl and Br atoms is 177 and 263 units, respectively. A significant decrease in the contribution of the Br atom on the adamantylsilicone stationary phase, compared to Apiezon L, is also attributable to steric hindrance caused by the presence of bulky adamantane fragments in both the sorbate and stationary phase.

It is known that ΔG is a quantitative characteristic of the structural and sorption properties of a substance being chromatographed and of the energy of its interaction with the stationary phase at a given temperature. The decisive factor in determining the structure of a compound from the chromatographic data is that variation of the thermodynamic characteristics of the sorption should be adequate to variation of the structure of the sorbate molecule. The differential molar free energy of sorption varies depending on the length of the alkyl chain and on the molecular structure as a whole. In many cases, the increment $\Delta G(CH_2)$ (with ΔH and ΔS, the pattern is similar) on certain sorbents is not constant within a homologous series. In such cases, ΔG does not always linearly correlate with the retention index. On the whole, if the dispersion component prevails in interactions between the sorbate and stationary phase, the free energy of sorption (and hence the retention characteristics) varies in parallel with the molecular weight [16]. Figure 3 shows that there is a good correlation between the retention indices of the examined compounds on adamantylsilicone and free energies of their sorption, indicating that ΔG in this series is an additive quantity.

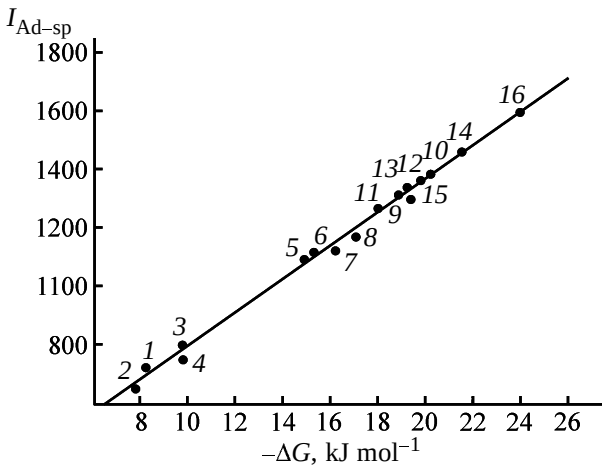


Fig. 3. Correlation between the Kovats indices I_{Ad-sp} and ΔG.

Thus, the chromatographic behavior of adamantane derivatives under the conditions of gas–liquid chromatography is determined by several factors. First, irrespective of the substituent at the adamantane core, the bulky adamantane fragment makes a major contribution to the retention on both polar and nonpolar stationary phases [9, 15]. Substituents cause redistribution of the electron density in the adamantane framework and correspondingly alter the retention characteristics. The contributions of substituents and functional groups to the retention on adamantylsilicone are somewhat smaller than on Apiezon L, which may be due to steric hindrance produced by the adamantane fragment of the stationary phase.

The relationships revealed can be used for predicting the retention and other physicochemical characteristics of adamantane derivatives and for developing identification procedures.

CONCLUSIONS

(1) Substituents cause redistribution of the electron density in the adamantane framework and the corresponding changes in the retention indices on the adamantylsilicone stationary phase.

(2) The steric hindrance produced by the adamantane core in the adamantylsilicone stationary phase causes a decrease, relative to Apiezon L, in the retention indices of adamantane derivatives.

REFERENCES

1. Raevskii, A.O. and Sapegin, A.M., *Usp. Khim.*, 1988, vol. 57, no. 9, pp. 1565–1586.
2. Kiselev, A.V., *Mezhmolekulyarnye vzaimodeistviya v adsorbtsii i khromatografii* (Intermolecular Interactions in Adsorption and Chromatography), Moscow: Vysshaya Shkola, 1986.
3. Vigdergauz, M.S., Semenchenko, L.V., Ezrets, V.A., and Bogoslovskii, Yu.N., *Kachestvennyi gazokhromatograficheskii analiz* (Qualitative Gas-Chromatographic Analysis), Moscow: Nauka, 1978.
4. Zenkevich, I.G., *Zh. Strukt. Khim.*, 1999, vol. 40, no. 1, pp. 121–130.
5. Zenkevich, I.G., *Zh. Strukt. Khim.*, 1996, vol. 37, no. 4, pp. 784–795.
6. Zenkevich, I.G., *Zh. Strukt. Khim.*, 1996, vol. 51, no. 11, pp. 1140–1148.
7. Bagrii, E.I., *Adamantany. Poluchenie, svoistva, primenenie* (Adamantanes: Preparation, Properties, Applications), Moscow: Nauka, 1989.
8. Suslov, I.A., Rudenko, B.A., and Arzamastsev, A.P., *Zh. Anal. Khim.*, 1988, vol. 43, no. 2, pp. 328–332.
9. Kurbatova, S.V., Moiseev, I.K., and Zemtsova, M.N., *Zh. Anal. Khim.*, 1998, no. 3, pp. 307–311.
10. Yang, S.S. and Gilpin, R.K., *J. Chromatogr.*, 1988, pp. 414–416.
11. Berezkin, V.G., Kurbatova, S.V., Finkel'shtein, E.E., *et al.*, *Zh. Prikl. Khim.*, 2004, vol. 77, no. 1, pp. 113–118.
12. Kurbatova, S.V., Finkel'shtein, E.E., Yashkin, S.N., and Kolosova, E.A., *Zh. Strukt. Khim.*, 2004, vol. 45, no. 1, pp. 144–149.
13. Kurbatova, S.V., Finkel'shtein, E.E., Kolosova, E.A., *et al.*, *Zh. Strukt. Khim.*, 2004, vol. 40, no. 1, pp. 150–157.
14. Grigor'eva, D.N., Vasil'ev, A.V., and Golovnya, R.V., *Zh. Anal. Khim.*, 1993, vol. 48, no. 7, pp. 1167–1173.
15. Kurbatova, S.V., Arutyunov, Yu.I., Moiseev, I.K., and Kudryashov, S.Yu., *Zh. Fiz. Khim.*, 1998, vol. 72, no. 8, pp. 1485–1489.
16. Anderson, A.A., *Gazovaya khromatografiya aminosoedinenii* (Gas Chromatography of Amino Compounds), Riga: Zinatne, 1982.

Russian Journal of Applied Chemistry, Vol. 78, No. 9, 2005, pp. 1503–1507. Translated from Zhurnal Prikladnoi Khimii, Vol. 78, No. 9, 2005, pp. 1527–1532.
Original Russian Text Copyright © 2005 by Lin, Vorob'eva, Marchenko.

MACROMOLECULAR CHEMISTRY AND POLYMERIC MATERIALS

Influence of Copper on Oxidation of Polyethylene Containing Antioxidants

D. G. Lin, E. V. Vorob'eva, and N. V. Marchenko

Skorina Gomel State University, Gomel, Belarus

Received May 3, 2005

Abstract—Thermal oxidation of polyethylene containing amine and phenolic antioxidants during contact with copper (metal support, powder) and the trends in variation of the antioxidant performance were studied.

Oxidation of noninhibited polyethylene (PE) in contact with catalytically active metals (including copper) is accompanied by dissolution of the metal support and transfer of the metal into the polymer bulk [1–3]. It was shown in [1–5] that noticeable metal transfer starts since the end of the induction period of polymer oxidation (IPO) (the IPO duration was estimated from the content of carbonyl groups in PE). Egorenkov [6] confirmed the carboxylate mechanism of the metal transfer suggested in [7–9]. The absorption bands characteristic of metal salts of fatty acids were found in the range 1500–1650 cm^{-1} in the IR spectra of PE films containing the transferred metal. Egorenkov [6] also confirmed the existence of two types of carboxylates (anhydrous and hydrated) in PE. It follows from [10] that, in the course of contact oxidation of PE on a copper support, the most probable scheme of metal transfer is diffusion in PE of low-molecular-weight metal carboxylates (which are products of contact reactions).

The transferred metal compounds affect the development of redox transformations in PE. For instance, the copper compounds taken in small concentrations catalyze PE oxidation, but at higher concentrations they, on the contrary, inhibit it. Similarly, copper(II) stearate affects oxidation of noninhibited PE [11]. Therefore, it was suggested to consider the catalysis of PE oxidation on copper supports as homogeneous, effected by the transferred copper-containing compounds, the more so as, in the course of contact oxidation of PE on a copper support, IPO practically coincides with the time after which the metal transfer into the PE film becomes noticeable.

An antioxidant (AO) introduced into PE increases the IPO. Data on the influence of catalytically active metals and their compounds on the oxidation of inhibited PE are fragmentary [12–14]. It was shown in [13] that IPO becomes shorter when PE containing a phenolic AO contacts with copper, i.e., the AO becomes less effective. In the case of PE inhibited with amine AO Neozon D, contact with copper, on the contrary, increases the IPO [14]. We suggested that, upon contact with copper, the amine AO transforms into a product with a higher inhibiting power. However, it remained unclear why the performance of the phenolic AO drastically decreases in the presence of copper [13]. It is of interest to determine how transformations of AO (phenolic or amine) are connected with the copper transfer into the polymer being oxidized. This was the subject of our study.

EXPERIMENTAL

We used unstabilized, high-density PE prepared at low pressure on complex organometallic catalysts [GOST (State Standard) 16338–85, base trade mark 20308-005]. Amine (Neozon D, *N*-phenyl-2-naphtylamine, GOST 39–79) and phenolic (Irganox 1010, pentaerythriol ester of 4-hydroxy-3,5-di-*tert*-butylphenylpropionic acid) AO were taken as inhibitors. To prepare compositions with PE, an AO powder was dissolved in acetone (GOST 2603–79), and the solution was stirred on a magnetic stirrer for 3 min. The AOs were introduced by wetting of a PE powder with an AO solution, followed by solvent evaporation at room temperature. For certain samples of inhibited PE, we used fillers: a copper powder (trade mark M1), which was introduced into the polymer by mechanical mixing, or copper(II) stearate [TU (Technical Specifications) 6-09-12-152–75] introduced similarly to AO through the solvent. From PE blends with AO and other modifiers, we prepared films (100 μm) by hot pressing (150°C, 30 s) and used them in the study.

1070-4272/05/7809-1503© 2005 Pleiades Publishing, Inc.

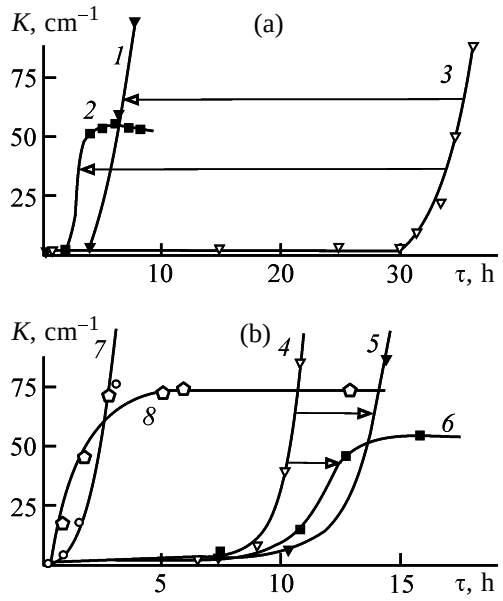


Fig. 1. Extinction index K of the absorption band at 1720 cm^{-1} in the IR spectra of PE films containing 0.1 wt % (a) Irganox 1010 and (b, curves *4–6*) Neozon D as a function of the time of their oxidation τ on (*1, 5, 8*) copper and (*2–4, 6, 7*) KBr supports. Oxidation temperature 150°C. (*2, 6*) Films contain 10 wt% copper powder.

The films were placed on a preliminarily purified copper (trade mark M1) foil. Simultaneously, these films were tested on inert supports (KBr plates).

The samples prepared were oxidized in air at 150°C in ovens. The degree of PE oxidation and the content of the transferred copper in PE were estimated.

The degree of PE oxidation was estimated from the IR spectra; the film was separated from the support when oxidation was performed on a copper foil and was not separated when the oxidation proceeded on a KBr plate transparent in the IR range. The IR spectra were recorded on an IR-75 double-beam spectrophotometer (Carl Zeiss, Jena) at 160 $cm^{-1}\,min^{-1}$ scanning speed. The extent of PE oxidation was evaluated by the extinction index (ratio of the optical density to the film thickness, cm) of the absorption band at 1720 cm^{-1} in the IR spectrum of the film. The band at 1460 cm^{-1} was used as an internal reference in determination of the optical density. The IPO duration we determined from the kinetic curves of carbonyl group accumulation; the IPO was considered to end when the extinction index reached 3–4 cm^{-1}.

The amount of the copper transferred into the PE film during the contact thermal treatment was determined by polarographic analysis [17]. To prepare working solutions for polarography, we used ash residue formed by two-step thermal treatment of the polymeric film [18] in an IR-20 muffle furnace [TU (Technical Specifications) 16-531.704–81]. The ash formed was dissolved in a supporting electrolyte (hydrochloric acid) prepared from reference solutions (TU 6-09-3780–74) using double-distilled water. The solutions were tested on a PU-1 device equipped with a mercury drop electrode; the metal content in the solution was determined with calibration graphs.

The data on oxidation of PE films inhibited with phenolic (Irganox 1010) and amine (Neozon D) AOs on the inert (KBr) and active (copper) supports are shown in Fig. 1. For comparison, the data on oxidation of noninhibited PE are also demonstrated. Noninhibited PE was oxidized on the inert support with a short (approximately 1 h) induction period, after which intense accumulation of oxygen-containing groups was observed (Fig. 1, curve *7*). The IPO decreased to several minutes when noninhibited PE was oxidized on the copper support (Fig. 1, curve *8*, initial portion). This is due to the catalytic effect of the metal compounds transferred. Then, after a time, the catalysis of PE oxidation on the copper support gives way to the inhibition due to accumulation of the critical amount of organometallic compounds, and the kinetic curve of the extinction index flattens out (Fig. 1, curve *8*, final portion).

Antioxidants (Neozon D, Irganox 1010) introduced into PE increase the stability of the polymer with respect to oxidation, and IPO increases (Fig. 1, curves *3*, *4*). At the same AO concentration (0.1 wt %), IPO increases to 8 (Neozon D) and 30 h (Irganox 1010). However, when the inhibited PO is oxidized on the copper support, the effects are opposite. Figure 1 shows that, for PE inhibited with Irganox 1010, IPO decreases from 30 to 4 h (curves *1, 3*), whereas for PE inhibited with Neozon D IPO increases from 8 to 11 h (curves *4, 5*). A similar pattern is observed for PE films filled with copper powder (10 wt %) (Fig. 1, curves *3, 2* and *4, 6*). In other words, the contact of inhibited PE with copper decreases the performance of phenolic AO, but increases the performance of the amine AO.

Let us consider the data on copper transfer into the inhibited PE heated on a copper support (Fig. 2, curves *2, 4*). Depending on AO type, the character of the kinetic curves of the metal accumulation in the film bulk differs in principle. With phenolic AO, the metal traces and metal transfer into the film are detected even during IPO (Fig. 2, curves *3, 4*). In the process, a well-defined absorption band at 1580–1620 cm^{-1} belonging to copper-containing com-

pounds appears in the IR spectrum of the polymer. By the end of IPO, the copper concentration in the polymer amounts to approximately 0.1 wt % according to polarography, which is fairly high metal concentration. In PE inhibited with Neozon D, there is no copper transfer during IPO. In this case, the metal and its complexes are detected in the PE film only when carbonyl-containing products of polymer oxidation appear. Therefore, we may conclude that, at the contact treatment of PE inhibited with amine AO, the IPO coincides with the induction period of the metal transfer.

The above features of copper transfer show that, at the contact oxidation of the inhibited PE, amine and phenolic AOs undergo different chemical transformations. As mentioned above, in the case of PE containing phenolic AO, the copper compounds are detected in the bulk of the polymer film before the appearance of the carbonyl-containing oxidation products. This fact means that, during the heat treatment, the redox transformations of the polymer with formation of organometallic compounds proceed in the copper-inhibited PE contact zone. These transformations cannot be monitored by transmission IR spectroscopy, since they proceed in a very fine boundary layer. The copper-containing compounds formed are transferred from the contact zone into the film bulk and catalyze there redox transformations. Since PE contains AO, the catalyzed process is terminated in the initial step, formation of the primary radicals. The phenolic AO is transferred into the zone containing the catalyst and deactivates the radicals formed. Such a mechanism of the AO consumption was described by Shlyapnikov *et al*. [19, 20]. They showed that, when oxidation zones are artificially organized in an inhibited polymer (e.g., by introducing oxidation catalysts), AO diffuses into these zones and is intensively consumed there. Similar process is observed in our case. As mentioned above, the copper-containing compounds diffuse into the film bulk from the contact zone and initiate formation of radical oxidation products. AO also migrates to this region from the whole film volume up to complete consumption. In this step of oxidation, the accumulation of copper-containing compounds and AO consumption proceed simultaneously. After AO consumption, IPO is ended, and the oxidation becomes autocatalytic. As a result, stable oxidation products (including carbonyl-containing compounds) are accumulated and may be monitored in the film.

Thus, the transfer of copper-containing compounds during IPO should accelerate the consumption of the phenolic AO in the whole film volume and, as a result, shorten IPO. To check this conclusion, we introduced into PE containing Irganox 1010 copper(II) stearate, which, as known [1, 11], is an analog of copper-containing compounds formed by the contact oxidation. In other words, we simulated accumulation of copper-containing compounds in the PE film in the step of IPO.

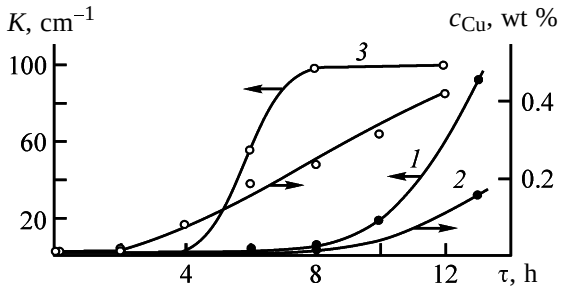


Fig. 2. (*1, 3*) Extinction index K of the absorption band at 1720 cm^{-1} in the IR spectra of PE films and (*2, 4*) concentration of the copper transferred into the film c_{Cu} as functions of the time of their oxidation τ at 150°C on the copper support. PE contains 0.1 wt % of (*1, 2*) Neozon G and (*3, 4*) Irganox 1010.

The concentration of copper introduced as copper(II) stearate was 0.05–0.4 wt %, i.e., this range covered the copper concentration accumulated in the film by the end of IPO (0.1 wt %).

The data on oxidation of PE inhibited with Irganox 1010 and containing various amounts of copper(II) stearate are shown in Fig. 3. As seen, copper(II) stearate catalyzes oxidation, since the IPO shortens, especially at 0.05 wt % copper (Fig. 3, curves *1, 2*). At higher copper concentrations, IPO increases, but remains shorter than IPO of the inhibited PE containing no copper(II) stearate (Fig. 3, curves *1, 5*). The data obtained undoubtedly indicate that the copper transfer into the PE bulk shortens IPO of the polymer. In turn, the IPO shortening is caused by accelerated consumption of AO during deactivation of the primary radicals whose formation is initiated by the copper compounds.

Oxidation of PE containing amine AO. It was mentioned above that, in oxidation of PE inhibited with amine AO, contact of the polymer with copper increases IPO. In the process, copper-containing compounds are not transferred into the polymer bulk during IPO (Fig. 2, curve *2*). Thus, in contrast to phenolic AO, amine AO suppresses the copper transfer into the film of the yet intact inhibited PE.

Presumably, in inhibition of PE oxidation with amine AO, the AO interaction with the copper support

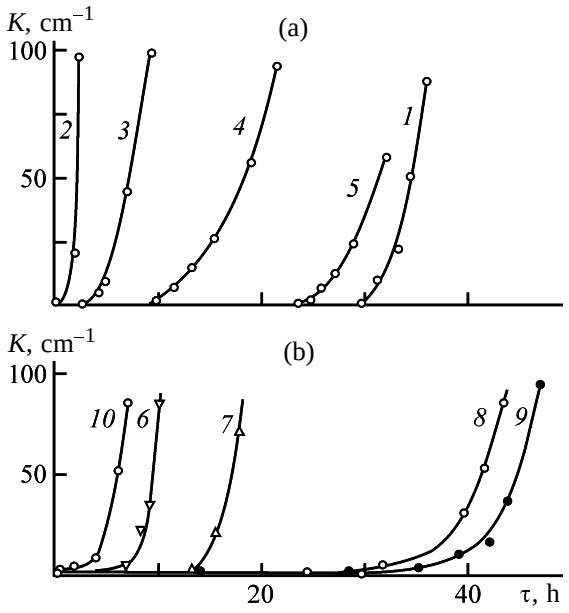


Fig. 3. Extinction index K of the absorption band at 1720 cm^{-1} in the IR spectra of PE films (a) containing 0.1 wt % Irganox 1010 and (*1*) 0, (*2*) 0.05, (*3*) 0.1, (*4*) 0.2, and (*5*) 0.4 wt % copper in form of copper(II) stearate as a function of the time of their oxidation τ at 150°C on KBr support, and (b) containing (*6*, *10*) initial Neozon D, (*7*) Neozon D thermally modified on copper support, (*10*) copper(II) stearate (0.111 wt %), and (*8*, *9*) thermally modified mixtures of copper(II) stearate and Neozon D as a function of the time of oxidation τ of the films at 150°C on (*6*) copper and (*7*–*10*) KBr supports. $(C_{17}H_{35}COO)_2Cu : C_{16}H_{12}NH$ (mol : mol): (*8*) 1 : 24 and (*9*) 1 : 246. (*2*) Heat treatment of blends and AO on the support for 10 h at 150°C; concentration of AO in the polymer 0.1 wt %.

or with copper-containing compounds is the main process, and it is localized in the contact zone. This reaction yields a new compound which is a more effective inhibitor as compared to the initial AO. This product of AO reaction with copper (or copper compounds) should be transferred back into the PE film and provide more efficient protection of the polymer against oxidation.

To check formation of this new compound, we performed the following experiment. A thin layer (approximately 1 mm) of Neozon D was placed on a copper support and heated at 150°C for 10 h in air. Then, the thus treated Neozon D (0.1 wt %) was introduced into the PE, and its inhibiting power was estimated from IPO (KBr support). We found that the thermal treatment substantially enhances the Neozon D inhibiting power: IPO increases by a factor of more than 2 (Fig. 3, curves *6*, *7*). The heat treatment of AO placed on the inert support (e.g., aluminum) does not change the AO properties: IPO of PE films containing such AO is approximately the same as IPO of films containing unmodified Neozon D.

A similar experiment was performed with two mixtures of AO with copper(II) stearate, in which the molar ratio of Neozon D to copper(II) stearate was 24 : 1 (blend A) and 242 : 1 (blend B), with the copper concentration of 1.0 and 0.1 wt %, respectively. In these mixtures, Neozon D was taken in a large excess relative to optimal ratio of 2 : 1 for formation of AO complexes with copper(II) stearate.

This statement requires comments. The enhancement of the inhibiting power of amine AO (Neozon D) in the presence of copper(II) stearate was observed previously with liquid hydrocarbons, in particular, *n*-decane [21–23]. Vetchinkina *et al*. [22] suggest two reactions converting AO into a more active product. In the first of them, *N*-phenyl-2-naphtylamine reacts with copper(II) stearate to form copper(I) complexes with the radical $C_{10}H_7N^{\bullet}C_6H_5$ and free stearic acid. In the second reaction, the stearic acid formed binds free AO and forms a salt that is incapable to react with copper(II) stearate. Vetchinkina *et al*. [22, 23] believe that just the copper(I) complexes are the effictive inhibitors that suppress PE oxidation after amine AO consumption. If we assume that in the system being oxidized AO is consumed only for the reaction with copper(II) stearate, in the mixture of Neozon D with copper(II) stearate the components should be taken in 2 : 1 molar ratio. Deviations from this ratio will result in preservation of either free AO or free copper(II) stearate.

After thermal treatment, the mixtures were introduced into PE in amounts corresponding to an AO concentration of 0.1 wt % in the polymer. It was found that the preliminary heat treatment of mixtures A and B substantially enhances the AO inhibiting pover: IPO increases by a factor 5 for A and 6 for B (Fig. 3, curves *8*, *9*). As seen, the inhibiting power of AO increases with a decrease in the copper content in the mixture. In the case of complex formation, we should expect an opposite trend, because increase in the copper concentration should increase the concentration of copper complexes and, as a result, increase IPO. However, this is not the case, i.e., another mechanism, differing from the mechanism acting in liquid low-molecular-weight hydrocarbons, is responsible for increasing inhibiting power of amine AO in the contact with copper and its compounds.

Hence, high performance in PE inhibition with Neozon D in contact with copper is caused by the catalytic influence of copper and its compounds on oxidation of Neozon-D molecules. As a result, stable

nitroxyl radicals are formed:

$$C_{10}H_7\text{–}NH\text{–}C_6H_5 \xrightarrow{Cu} C_{10}H_7\text{–}N^{\bullet}\text{–}C_6H_5$$

$$\xrightarrow{Cu} C_{10}H_7\text{–}NO^{\bullet}\text{–}C_6H_5.$$

These radicals (>NO$^{\bullet}$) repeatedly terminate chains in oxidative transformations of polymers [24]. This process ensures their high performance exceeding that of the initial AO.

CONCLUSION

When PE inhibited with phenolic AO is brought in contact with copper, the metal is actively transferred into the polymer bulk even during IPO. A decrease in the AO performance observed in this case is a result of accelerated consumption of AO for deactivation of free radicals formed in the local regions of the polymer under catalytic action of the transferred copper compounds. On the contrary, in contact with copper, Neozon D becomes more effective. In this case, the copper-containing compounds are actively transferred into the polymer inhibited with amine AO only after the end of IPO. An increase in the inhibiting power of Neozon D is caused by the catalytic effect of copper on AO oxidation.

REFERENCES

1. Lin, D.G., *J. Appl. Polym. Sci.*, 1994, vol. 54, pp. 1789–1793.
2. Lin, D.G. and Vorob'eva, E.V., *Zh. Prikl. Khim.*, 2002, vol. 75, no. 5, pp. 836–839.
3. Packham, D.E. and Evans, J.R.G., in *Industrial Division Annual Chemical Congr.*, Durham, 1980.
4. Chan, M.G. and Allara, D.L., *J. Colloid. Interface Sci.*, 1974, vol. 47, no. 697.
5. Allara, D.L., White, C.W., Meek, R.L., and Briggs, T.H., *J. Polym. Sci., Polym. Chem. Ed.*, 1976, vol. 14, p. 93.
6. Egorenkov, N.I., Trends in Variation of Adhesion, Friction, and Physicochemical Properties of Polymeric Films on Metal Supports under Thermal Treatment, *Doctoral Dissertation*, Kiev, 1986.
7. Belyi, V.A., Egorenkov, N.I., and Pleskachevskii, Yu.M., *Vysokomol. Soedin., Ser. B*, 1970, vol. 12, pp. 643–644.
8. Egorenkov, N.I., Lin, D.G., and Belyi, V.A., *Dokl. Akad. Nauk SSSR*, 1972, vol. 207, no. 2, pp. 397–400.
9. Egorenkov, N.I., Lin, D.G., and Belyi, V.A., *J. Polym. Sci., Polym. Chem. Ed.*, 1975, vol. 13, p. 1493–1498.
10. Lin, D.G. and Vorob'eva, E.V., *Zh. Prikl. Khim.*, 2001, vol. 74, no. 6, pp. 998–1002.
11. Vorob'eva, E.V. and Lin, D.G., *Materialy mezhdunarodnoi nauchno-prakticheskoi konferentsii "Kompozitsionnye materialy v promyshlennosti"* (Proc. Int. Scientific and Applied Conf. "Composite Materials in Industry"), Yalta, May 30–June 1, 2000, Kiev, 2000, pp. 43–44.
12. Kiryushkin, S.G., Kovalev, I.B., Panchenkov, G.M., *et al.*, *Plast. Massy*, 1982, no. 5, pp. 55–56.
13. Lin, D.G. and Vorobieva, E.V., *J. Adhes. Sci. Technol.*, 2003, vol. 17, no. 2, pp. 179–193.
14. Lin, D.G. and Vorob'eva, E.V., *Plast. Massy*, 2002, no. 1, pp. 9–11.
15. Lin, D.G. and Vorob'eva, E.V., *Zh. Prikl. Khim.*, 2003, vol. 76, no. 5, pp. 856–859.
16. Lin, D.G., Vorob'eva, E.V., and Marchenko, N.V., *Zh. Prikl. Khim.*, 2004, vol. 77, no. 9, pp. 1539–1542.
17. Sviridenko, V.G., Eliseeva, I.M., and Lin, D.G., *Vysokomol. Soedin.*, 1989, vol. 31, no. 4, pp. 885–887.
18. USSR Inventor's Certificate no. 1 226 119.
19. Shlyapnikov, Yu.A., Kiryushkin, S.G., and Mar'in, A.P., *Antiokislitel'naya stabilizatsiya polimerov* (Antioxidative Stabilization of Polymers), Moscow: Khimiya, 1986.
20. Shlyapnikov, Yu.A., *Eur. Polym. J.*, 1998, vol. 34, no. 8, pp. 1177–1184.
21. Maizus, Z.K., Skibida, I.P., and Emmanuel', N.M., *Zh. Fiz. Khim.*, 1966, vol. 40, no. 2, pp. 322–327.
22. Vetchinkina, V.N., Maizus, Z.K., Skibida, I.P., and Emanuel', N.M., *Dokl. Akad. Nauk SSSR*, 1967, vol. 177, no. 3, pp. 625–628.
23. Vetchinkina, V.N., Skibida, I.P., and Maizus, Z.K., *Izv. Akad. Nauk SSSR, Ser. Khim.*, 1977, no. 5, pp. 1008–1013.
24. Denisov, E.T., Sarkisov, O.M., and Likhtenshtein, G.I., *Khimicheskaya kinetika* (Chemical Kinetics), Moscow: Khimiya, 2000.

Russian Journal of Applied Chemistry, Vol. 78, No. 9, 2005, pp. 1508–1511. Translated from Zhurnal Prikladnoi Khimii, Vol. 78, No. 9, 2005, pp. 1533–1536.
Original Russian Text Copyright © 2005 by Beloshenko, Konstantinova, Borzenko, Glazunova.

MACROMOLECULAR CHEMISTRY AND POLYMERIC MATERIALS

Effect of Filler Aggregation on Properties of a Composite Based on Epoxy Polymer

V. A. Beloshenko, T. E. Konstantinova, A. P. Borzenko, and V. A. Glazunova

Galkin Physicotechnical Institute, Ukrainian National Academy of Sciences, Donetsk, Ukraine

Received December 22, 2004; in final form, May 2005

Abstract—The plasticity of a composite based on epoxy polymer was studied as influenced by the concentration of the filler, nanosized powders containing aggregates of strongly bound ZrO_2 particles.

Composites based on epoxy polymers (EPs) are widely used as building and functional materials. The operation properties of composites can be efficiently controlled either by changing epoxy oligomer–curing agent system or by adding appropriate filler. It is known [1–3] that the properties of these systems are determined by various factors, i.e., nature and concentration of the filler, its morphology, particle size, adhesion power, procedure of addition into the polymer matrix, etc.

Ultradispersed fillers (nanosized particles) allowing formation of composites with unique physicomechanical properties are actively studied today [4–7]. However, preparation of polymeric nanocomposites is a complex procedure, because nanoparticles strongly tend to aggregation. The effect of the resulting aggregates on the properties of epoxy polymers is poorly understood.

In this study we examined the effect of aggregation of zirconium dioxide nanoparticles on the deformation and strength properties of an epoxy composite used for preparing thermally shrinkable adapter fittings [8, 9]. These fittings are used to obtain strong and hermetically sealed adhesive joints of tubes and rods of various, even dissimilar, materials [9, 11].

EXPERIMENTAL

As polymeric matrices we used the epoxy compound containing diglycidyl ester (DGE) of hydrophthalic acid, block oligomer (BO) of aliphatic epoxy resin and acidic oligoester, epoxy–diphenylolpropane resin (ED) with molecular weight of 390–430, *iso*-methyltetrahydrophthalic anhydride (IMTHPA), and tris(dimethylaminomethyl)phenol (TDAP) [8] with the following component ratio, weight fraction: 77.5 DGE, 20 BO, 2.5 ED, 68 IMTHPA, and 0.7 TDAP.

The filler powders were prepared by precipitation from zirconium oxychloride solutions: no. 1, from chemical reagents in laboratory; no. 2, from industrial intermediate product (hydroxide) with subsequent treatment in laboratory; and no. 3 was commercial product. The filler concentration was varied from 0 to 30 wt % (with EP content taken as 100%).

The experimental samples were prepared by mixing of the epoxy composite components with ZrO_2 powder in a given ratio at 60–70°C on a mechanical stirrer with subsequent curing in appropriate molds at 120°C for 4 h. Curing was performed with rotation of the molds to prevent sedimentation. Depending on the filler, three types of polymeric composites were obtained.

Thermally shrinkable fittings (couplers) were prepared by rolling of tubular billets. The initial size of fittings was as follows: 20 mm internal diameter d_0, 35 mm height, and 3.5 mm thickness. Curing was carried out in the hyperelastic state with subsequent cooling of the deformed billet on a mandrel to the temperature lower than the glass transition point T_g of the polymer matrix. The degree of deformation was determined from the expression $\varepsilon = (d - d_0)/d$, where d is the mandrel diameter.

In accordance with GOST (State Standard) 11262–80, the tensile strength tests were carried out with 37×5 mm plates with thickness of 2 mm on a tensile-testing machine equipped with a thermal chamber; the rate of a mobile clamp was 10 mm min^{-1}.

The microhardness H_μ was measured using samples cut off from the fittings after thermal shrink-age. The load on the indenter was 5 N; the average H_μ was calculated from 10–15 marks.

Differential scanning calorimetry (DSC) and thermomechanical analysis (TMA) were performed on

1070-4272/05/7809-1508© 2005 Pleiades Publishing, Inc.

a Du Pont 9900 thermomechanical installation using the samples cut off from the fittings; the heating rates were 10 and 5 deg min^{-1} for DSC and TMA procedures, respectively.

The fractional composition and morphology of ZrO_2 powders were studied by transmission electron microscopy (TEM); the samples were prepared by an ultrasonic dispersion procedure developed at the Physicotechnical Institute (Ukrainian National Academy of Sciences, Donetsk, Ukraine). The average size of the coherent scattering areas (CSA) were calculated from the Selyanov–Scherrer equation from the half-width $B_{0.5}$ of the diffraction peaks from the (111) plane. The failure surfaces in the composites were studied on a JEM 200A unit (JEOL) using a two-step replica procedure.

The dependences of the ultimate strain at rolling (without failure of the billet) on the content of ZrO_2, shown in Fig. 1, refer to three types of composites with the filler prepared by three different procedures. In the case of composite no. 1, the dependence ε(c) passes through a maximum at the filler concentration *c* 15–20 wt %. In the case of composite no. 3, there is also a maximum, but the curve starts to ascend only at a filler content higher than 10 wt %, whereas at small concentrations ε is independent of *c*. The behavior of composite no. 2 is essentially different; with increasing ZrO_2 content its ultimate strain decreases.

In all the cases, the tubular billets were broken during their deformation in the hyperelastic state. For comparison, the failure strains of the standard EP samples and composites based on them were measured under similar conditions at 100°C. It was found that the failure strain values correlate with the dependences shown in Fig. 1; for EP it comprised 35%, whereas for composite nos. 1, 2, and 3 (15 wt % filling) it was 50, 30, and 40%, respectively.

As seen from Fig. 1, changes in H_μ largely agree with the results of mechanical tests and data on the ultimate strain of the fittings ε(*c*), though H_μ was measured using the glassy material. In the case of composite no. 2, H_μ slightly increases with increasing filler content, whereas for composite nos. 1 and 3 the dependences pass through a minimum at *c* 15 wt %. Since H_μ is proportional to the yield point σ_T [12], composite nos. 1 and 3 are weakened to the greatest extent at a filler content of 15 wt %, whereas for composite no. 2 σ_T is nearly constant.

The calorimetric data show that the fillers studied are not inert to the polymeric matrix. This is confirmed by differences in glass transition point T_g,

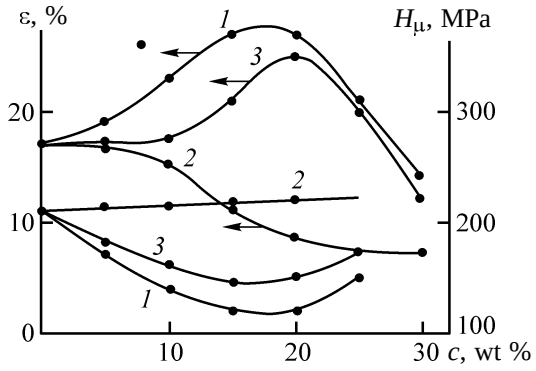


Fig. 1. Ultimate strain of the billet ε and microhardness H_μ as functions of the filler concentration *c*; curve nos. are composite nos.

glass transition width ΔT_g, and heat capacity change ΔC_p (Table 1). Higher values of T_g and ΔC_p for composites as compared to the polymeric matrix suggest a decrease in interstitial distances [13], which is due to the filling of the system with ZrO_2 particles acting as the points of the polymer network in the composite.

The DSC data well agree with TMA results, according to which the filler added to the polymer increases T_g and decreases the deformation changes at temperatures near T_g and the coefficient of thermal expansion in the hyperelastic state, i.e., it decreases the interstitial distances.

The XRD and electron microscopic data showed that ZrO_2 powders prepared under different conditions are characterized by CSA values typical for nanoparticles, but their morphology is different (Table 2).

Table 1. Thermal characteristics of composites based on EP

Composite formulation	T_g, °C	ΔT_g, °C	ΔC_p, J g^{-1} K^{-1}
EP	49	7	0.16
EP + 20% ZrO_2 no. 1	51	13	0.26
EP + 20% ZrO_2 no. 2	51	15	0.27
EP + 20% ZrO_2 no. 3	51	9	0.23

Table 2. Characteristics of the filler evaluated from XRD and TEM data

Filler	Size, nm			
	CSA	particles	aggregates	agglomerates
no. 1	37	40	200	500–1000
no. 2	35	20–40	300	300–2000
no. 3	24	20–100	300	2000–3000

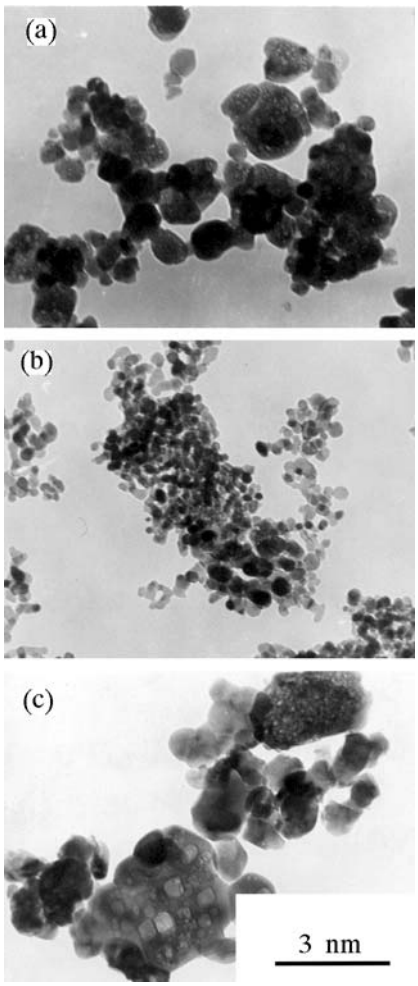


Fig. 2. Fractures of composite nos. (a) 1, (b) 2, and (c) 3 through the areas containing ZrO_2 particle aggregates.

Their features can be evaluated using TEM data on the size of the initial particles, aggregates (groups of initial particles), and agglomerates (groups of aggregates), and on the degree of particle binding in the aggregates. The degree of binding in the aggregates (i.e., aggregate density) can be evaluated from the dispersion of the particles in the electron-microscopic patterns taken after ultrasonic treatment (with power equal for all the samples) for breakdown of the aggregates and agglomerates.

As seen from Fig. 2, the particles in powder nos. 1 and 3 are characterized by strong bonds in the agglomerates and significant amount of pores, which suggests occurrence of the diffusion processes (sintering) in the powder system in the course of its annealing. Porous aggregate usually formed in the initial stages transforms into the polycrystalline particle at high-temperature treatment. In sample no. 2 (Fig. 2b), the interaction in the aggregates is rather weak.

As a rule, additives increase the strength and decrease the plasticity of polymer composites [14, 15]. In some cases, composites retain their plasticity at small charges of the filler [1, 16]. Thus, the increase in the composite plasticity with increasing filler content that we observed is unusual. The decrease in the plasticity of composite no. 2 and its increase in composite nos. 1 and 3 are still more surprising. The DSC, TEM, and XRD data do not provide unambiguous explanation of this difference in the mechanical properties of EPs and composites.

To reveal the other possible reasons of the unusual behavior of the composites under the load, we examined the fracture by electron microscopy. We found that the character of fractures in the samples is different. In composite nos. 1 and 2, the fracture passes through the aggregates (Figs. 2a, 2b). It should be noted that the density of particles in the aggregates of composite no. 1 is significantly greater than that in composite no. 2. In samples of composite no. 3, in which the particle density is comparable with that in composite no. 1, the crack passes through the boundary between the matrix and filler (Fig. 2c).

Analysis of the experimental and published data suggests that in our case the decisive role in the failure and, thus, in plasticity is played by the aggregates and degree of binding of the particles in them, rather than by the adhesion between the filler particles and matrix, as discussed in other papers. It should be noted that the phenomenon concerns nanoparticles. At present, our experimental data allow only qualitative explanation of the facts observed.

In the course of deformation, the structure of aggregates with strongly bound nanoparticles allows their turning and sliding [17], which consumes the energy of the growing crack and thus improves the material elasticity. The amount and distribution of the aggregates on the path of the growing crack are of particular importance. If their amount is small, the crack develops very rapidly, whereas when their amount is large, each aggregate acts as a barrier for the crack, exerting a certain strengthening affect. For example, with increasing content of ZrO_2 the plasticity of composite nos. 1 and 3 first increases and then decreases (Fig. 1). The shift of the maximum in the concentration dependence $\varepsilon(c)$ toward higher concentrations in the case of composite no. 3 is probably due to the fact that its aggregates are coarser, their amount is smaller, and porous ZrO_2 particles form polycrystalline aggregates. Turning and sliding of the particles in the above aggregates are hindered as

compared to composite no. 1; as a result, noticeable decrease in the plasticity is observed at higher concentrations of ZrO_2 as compared to composite no. 1. Owing to weak interaction of the particles in aggregates of composite no. 2, no turning and sliding between them is realized, causing the plasticity to decrease in the entire concentration range of the filler added; and the larger the number of particles in the aggregates, the greater the decrease in the plasticity.

It is known [18] that composites based on EPs may exhibit the plasticization effect, which is due to the selective sorption of components in the uncured polymer–filler system. Its appearance depends on various interrelated factors complicating specific interpretation of our experimental results. However, we can conclude that the complex effect of all the factors examined in this study causes an unusual change in the EP plasticity upon addition of ZrO_2 nanopowders.

CONCLUSIONS

(1) The morphology of aggregates and degree of binding of the filler particles (ZrO_2 nanopowder) strongly affect the deformation-strength characteristics of polymeric composites.

(2) The deformability of composites in the hyperelastic state increases by a factor of 1.5 on adding ZrO_2 nanopowders with significant porosity of aggregates formed by strongly bound primary particles.

(3) The plasticization of the polymeric composite was attributed to turning and sliding of the primary particles in the filler aggregates.

ACKNOWLEDGMENTS

The authors are grateful to G.Ya. Akimov and V.M. Timchenko for ZrO_2 powders and to M.K. Pakter for helpful discussion.

REFERENCES

1. Dubnikova, I.L., Topolkaraev, V.A., Paramzina, T.V., *et al.*, *Vysokomol. Soedin., Ser. A*, 1990, vol. 32, no. 4, pp. 841–847.
2. Lomonosova, N.V., Dobretsov, S.L., Matveev, V.K., *et al.*, *Plast. Massy*, 1995, no. 3, pp. 26–27.
3. Kaush, Kh.Kh., Begelin, F., and Fisher, M., *Mekh. Kompoz. Mater.*, 2000, vol. 36, no. 3, pp. 305–316.
4. Kang, S., Hong, S.I., Choe, C.R., *et al.*, *Polymer*, 2001, vol. 42, no. 3, pp. 879–887.
5. Urbonaite, V. and Simonov-Emel'yanov, I.D., *Plast. Massy*, 2002, no. 9, pp. 42–44.
6. Tjong, S.C., Meng, Y.Z., and Xu, Y., *J. Polym. Sci., Ser. B*, 2002, vol. 40, no. 24, pp. 2860–2870.
7. Xu, W., Bao, S., Shen, S., *et al.*, *J. Polym. Sci., Ser. B*, 2003, vol. 41, no. 4, pp. 378–386.
8. RF Patent no. 2 141 600.
9. Beloshenko, V.A., Beygelzimer, Ya.E., Stroganov, V.F., and Sheludchenko, V.I., *Eng. Mech.*, 2000, vol. 7, no. 3, pp. 231–237.
10. Ukrainian Patent 10 298.
11. RF Patent 2 216 679.
12. Balta Calleja, F.J., *Structure Development During Polymer Processing*, Dordrecht: Kluwer, 2000.
13. Bernshtein, V.A. and Egorov, V.M., *Differentsial'naya skaniruyushchaya kalorimetriya v fizikokhimii polimerov* (Differential Scanning Calorimetry in Physical Chemistry of Polymers), Leningrad: Khimiya, 1990.
14. Deev, I.S. and Kobets, L.P., *Vysokomol. Soedin., Ser. A*, 1996, vol. 38, no. 4, pp. 627–633.
15. Dubnikova, I.L., Petrosyan, A.I., Topolkaraev, V.A., *et al.*, *Vysokomol. Soedin., Ser. A*, 1988, vol. 30, no. 11, pp. 2345–2352.
16. Okhlopkova, A.A. and Sleptsova, S.A., *Mekh. Kompoz. Mater.*, 2003, vol. 39, no. 2, pp. 183–192.
17. Jiang, X.-l., Jordan, E., Shaw, L., and Gell, M., *Fiz.-Khim. Mekh. Mater.*, 2003, no. 2, p. 122.
18. Khozin, V.G., *Usilenie epoksidnykh polimerov* (Reinforcing of Epoxy Polymers), Kazan: Dom Pechati, 2004.

Russian Journal of Applied Chemistry, Vol. 78, No. 9, 2005, pp. 1512–1516. Translated from Zhurnal Prikladnoi Khimii, Vol. 78, No. 9, 2005, pp. 1537–1541.
Original Russian Text Copyright © 2005 by Ishkov, Sagalakov.

MACROMOLECULAR CHEMISTRY AND POLYMERIC MATERIALS

Effect of Active Fillers on Properties of Heat-Resistant Composites

A. V. Ishkov and A. M. Sagalakov

Altai State University, Barnaul, Russia

Received December 6, 2004

Abstract—The effect of active fillers such as titanium nitrides TiN_x, carbides TiC_x, and carbonitrides TiC_xN_y ($0.5 < x$ or $x + y \le 1.0$) on properties of polymeric composites based on thermostable binders PAIS-104, SFP-012 AK-30, and ED-20 is studied.

Active efforts are made today in developing new polymeric composites (PCs) representing both individual macromolecular compounds and polymer blends demonstrating not only additive, but also extraadditive properties [1].

Additives introduced into PCs to modify their physical and mechanical characteristics such as heat resistance, conductivity, strength, and plasticity are mostly referred to as active fillers.

The activity of one or another dispersed filler strongly depends on its specific surface area [1–3], since this characteristic controls the surface-modified fraction of the polymer. Additional contribution to the activity of the filler could be caused by the crystal-chemical defectiveness of its surface.

Introduction of many of the existing active fillers in a polymer matrix allows preparation of materials combining a number of useful performance characteristics. Such fillers are known as multifunctional [4].

Presently, one of the most widely spread techniques for preparation of active compounds is self-propagating high-temperature synthesis (SHS). The SHS technology allows simple and rapid synthesis of various classes of active compounds [5].

As active fillers for PCs, of some interest are inclusion compounds based on *d* elements of Groups IV–VI with nonmetals such as carbon, nitrogen, oxygen, boron, etc. In addition to high refractoriness (2800–3400 K), many of them are characterized by high strength and electrical conductivity. Therefore, their use allows preparation of novel advanced PCs.

In this study we examined the effect of active fillers on the properties of several heat-resistant composites.

EXPERIMENTAL

As multifunctional fillers we examined active Ti compounds with nitrogen and carbon, classified with inclusion phases.

Titanium nitrides TiN_x ($0.5 < x \le 1$) were prepared by the reaction of Ti powder (PTOM grade) with nitrogen gas in an autothermal flow reactor in the SHS mode at a controlled nitrogen consumption. Titanium carbides TiC_x ($0.5 < x \le 1$) were also prepared in the SHS mode by combustion of a mixture of Ti powder (PTK grade) with carbon black (PM-50 grade) under argon. Titanium carbonitrides TiC_xN_y ($x + y \le 1$) were synthesized by combustion of a mixture of Ti powder (PTK) with butadiene–acrylonitrile rubber of various grades under nitrogen. The composition of the products was determined by elemental and X-ray diffraction analyses. For synthesis of composites we used the <100-μm fraction of the active Ti compounds.

As a polymer matrix we used thermosetting polyaminoimide binder PAIS-104, rubber–resin binder SFP-012 AK-30, and epoxy–diphenylolpropane resin ED-20.

PAIS-104 binder (Karbolit Joint-Stock Company, Kemerovo, Russia) [TU (Technical Specifications) 6-05-231-192–79] is a powdered oligomer with a mean molecular weight of $(1–4) \times 10^3$, free amino group content ≤5%, dropping point 103°C, and gelation time 180 s. SFP-012 AK-30 binder was prepared at a pilot plant by combined coagulation of phenol–formaldehyde and rubber (SKN-26) latexes. ED-20 resin [GOST (State Standard) 10587–72] was cured with 2% polyethylenepolyamine (PEPA).

The composites were prepared by hot pressing of

1070-4272/05/7809-1512 © 2005 Pleiades Publishing, Inc.

a mixture of the filler and binder under the desired conditions.

The effects of active fillers on the polymerization of the binders as well as on the properties of the resulting heat-resistant composites were studied with an example of model binary mixtures.

As known, the presence of active fillers influences the parameters of the polymerization of a binder in PCs. For example, the curing of PAIS-104 occurs under heating through addition of free primary or secondary amino groups at the double bonds of the imide rings, which is accompanied by elongation of the chain and formation of a 3D polymer network. Cross-linking of SFP-012 AK-30 rubber–resin binder proceeds through the interaction of the reactive methylene, phenol, and nitrile groups, which is accompanied by liberation of low-molecular-weight by-products. Curing of epoxy–diphenylolpropane resins proceeds through opening of terminal epoxy groups under the action of PEPA with formation of cross-linked structures. Therefore, two former binders are cured through at least two competing processes, while a single reaction is responsible for polymerization of ED-20.

The lack of liberation of low-molecular-weight by-products in curing of PAIS-104 and ED-20 allows formation of compact monolithic structures with these binders, whose characteristics are controlled to a considerable extent by the kinetic parameters of the process. Introduction of the active filler increases the degree of polymerization (DP) of the binder in PCs, as demonstrated by sol–gel analysis and IR spectra.

Table 1 shows data on the degree of polymerization of PAIS-104 in the polymeric composite as influenced by the active filler ($TiC_{0.75}$ and $TiC_{0.5}N_{0.4}$) content.

Comparison of data from Table 1 with those on the conversion of free amino groups of PAIS in the course of polymerization, obtained photometrically upon azo couplingwith β-naphthol, reveals that the polymerization proceeds preferentially via the amino groups with formation of a 3D polymer network (Table 2), i.e., the filler has a specific effect on the process.

It is worth noting that this effect depends on the nature of filler and also on the stoichiometry of the process. Analysis of the rate constants of the competing reactions [polymerization–addition and autopolymerization (1)] in the absence and in the presence of active fillers $TiC_{0.75}$ and $TiC_{0.5}N_{0.4}$ shows that the fraction of structures formed by autopolymerization of dimaleimidodiphenylmethane (DMIDPM) increases

Table 1. Degree of polymerization of PAIS-104 in filled composites

Filler, %	DP		C=C bond conversion, %
	sol–gel analysis	IR spectroscopy	
$TiC_{0.75}$:			
0	77	73	29
50	80	77	42
60	89	86	55
70	91	93	70
80	94	94	75
90	95	94	79
$TiC_{0.5}N_{0.4}$:			
0	78	76	32
50	79	77	41
60	81	79	50
70	82	84	67
80	89	86	75
90	95	86	76

Table 2. Conversion of amino groups in polymerization of PAIS-104

Filler	Conversion of amino groups, %, at indicated filler content, %				
	50	60	70	80	90
$TiN_{0.5}$	12	26	44	50	56
$TiN_{0.95}$	8	16	30	44	50
$TiC_{0.5}$	18	32	42	50	54
$TiC_{0.75}$	20	30	40	54	54
TiC	10	16	24	30	38
$TiC_{0.5}N_{0.4}$	6	16	26	36	44
$TiC_{0.3}N_{0.2}$	14	28	42	50	54

in the polymer:

$$K = \frac{k(\text{–NH})}{k(\text{C=C})}, \quad (1)$$

where k(–NH) is the rate constant of polymerization–addition of DMIDPM and diaminodiphenylmethane (DADPM) and k(C=C), that of autopolymerization of DMIDPM.

The K values for PAIS-104 cured in the absence of a active filler range from 2.3 to 4.0 (for the samples studied K = 3.0). Introduction of $TiC_{0.75}$ decreases K to 1.4 [K was estimated by Eq. (1) from data on conversion of C=C bonds and amino groups (Tables 1

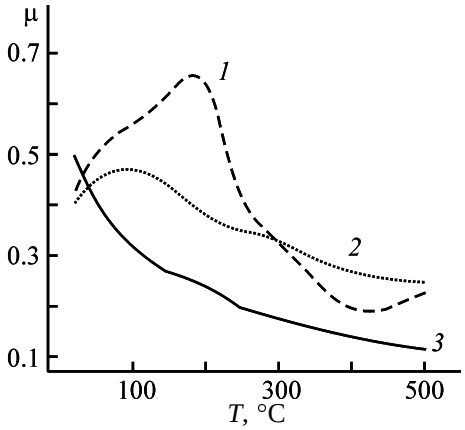


Fig. 1. Dry friction coefficient μ of PCs based on CFP-012 AK-30 as a function of the temperature *T*. Filler: (*1*) 5% $TiC_{0.75}$, (*2*) 5% $TiN_{0.5}$, and (*3*) no active filler.

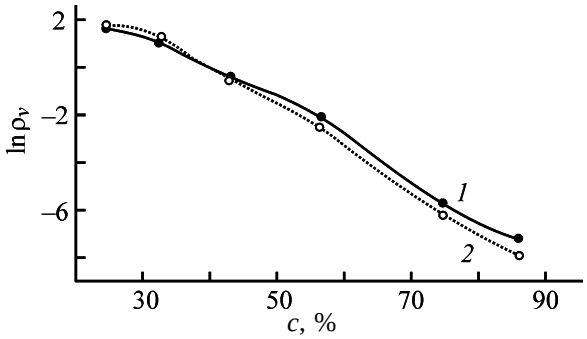


Fig. 2. Conductivity $\ln \rho_v$ of composites based on ED-20 resin as a function of the volume fraction of the active filler *c*: (*1*) $TiC_{0.5}$ and (*2*) $TiN_{0.95}$.

and 2)]. In the presence of $TiC_{0.5}N_{0.4}$ *K* decreased to 1.3.

The decrease in *K* by more than a half in the presence of active fillers suggests increasing cross-link density and rigidity of the 3D network in the cured polymers.

The increase in the cross-link density in PAIS cured in the presence of active fillers is supported also by TGA data. The heat resistance in air of the resulting composite increases by 45–55°C.

Similar effect of active fillers on the curing of polymers was observed also for SFP-012 AK-30 binder. Figure 1 shows the temperature dependences of the friction coefficient for the model friction material prepared on the basis of the indicated binder and dispersed and fibrous fillers with addition of active fillers in amount of up to 25% of the polymer weight. The results show that, for the materials obtained with the active fillers, the temperature dependence of the friction coefficient passes through a maximum, which is typical of friction materials cured through copolymerization of phenol–formaldehyde resins and nitrile rubbers. The material obtained without active filler is characterized by a regularly declined curve (Fig. 1, curve *3*) typical of other friction materials obtained with resinous binders [6]. Addition of the active binders increases the heat resistance in air of the composite prepared with SFP-012 AK-30 by 65–80°C.

The results obtained in this study on the specific effect of the investigated fillers on the polymerization of thermoreactive binders PAIS-104 and SFP-012 AK-30 in combination with TGA data for the resulting composites clearly show that these compounds are quite suitable as active fillers for the indicated plastics.

Introduction of these compounds into polymeric composites allows directed modification of physicochemical characteristics such as the heat resistance, cross-link density, and conversion of functional groups, and, therefore, performance characteristics of the resulting materials.

Since the investigated fillers are conducting materials characterized by high chemical and heat resistance [4], their use as a component of PCs allows not only modification of the materials, but also preparation of conducting composites.

We examined electrophysical characteristics of some of the PCs prepared in this study. Figure 2 shows the dependence of the conductivity of the material based on ED-20 resin, prepared with addition of nonstoichiometric titanium nitrides, $TiC_{0.5}$ and $TiN_{0.95}$, on the volume fraction of the filler. The curves demonstrate typical S-shaped behavior [7].

The results show that the resistance of PCs regularly decreases with increasing filler content; ρ_v is above unity at low filler contents. On passing to the surface-modified structure of composites, the resistance drops. The second transition is observed at a filler content of about 75% (highly filled composites). Such a behavior suggests formation of ordered structures in the bulk of the composite.

It is known that the formation of ordered structures from the particles of active fillers in polymer matrices can start even at a filler content as low as 5–10 vol % [8]. However, this is realized only for carbonaceous fillers. The metallic powders starts to form structures only when taken in amounts above 50%. In the case of fillers examined in this study, structurization starts at their content of 24–25 vol %. Therefore, they take an intermediate position between carbonaceous and

Table 3. Characteristics of friction composites

Characteristic	Filler-free material	Filler content		
		2.0	3.0	5.0
Bond resistance, MPa:				
without heating	4.7	9.5	7.2	10.4
after heat treatment (140 ± 10°C) for 1 ± 0.1 h	0.9	2.8	1.7	3.5
Friction coefficient	0.38	0.47	0.48	0.46
Energy wear, $cm^3\ kg^{-1}\ m^{-1}$:				
A	1.5	0.6	0.8	0.5
B	Failed	1.9	1.2	1.9

* Tested up to (A) 500°C and (B) 700°C.

metallic fillers, imparting high conductivity to composites at low content.

At a filler content of 24 vol %, stable conducting structures are formed from its particles coated with a film of the surface-modified polymer and linked to each other through bridging bonds.

Due to the electronic conductivity mechanism in Ti nitride, the overall conductivity of low-filled PCs is a resultant of the intrinsic conductivity of the filler and the conductivity of the thin surface film of the polymer, realized most likely by the tunneling mechanism.

In studying the temperature dependence of the conductivity for the PCs based on PAIS-104, we recognized the self-regulation effect. The materials containing from 50 to 70 wt % of the filler demonstrate nonlinear temperature dependence of the conductivity over the experimental temperature range. In the range 75–85°C, an abrupt increase in the conductivity is observed, which is reproduced in repeated heating–cooling cycles. These samples are characterized by high positive temperature coefficient of the resistance. These results suggest the self-regulation effect in PCs based on PAIS-104 containing from 50 to 70 wt % of active Ti nitrides (Fig. 3).

This can attributed to the fact that, in the heating–cooling cycle, reversible thermal relaxation occurs in the layers of the surface-modified polymer, accompanied by rearrangement of the conducting structures.

In highly filled samples, in the course of curing, the thermal stresses in the polymer dissipate throughout the bulk of the sample, which is reflected in monotonic dependences of the conductivity.

In view of the fact that the investigated fillers affect the polymerization mechanism and characteristics of the polymeric matrix, being also capable of forming ordered structures in the composite even at low content, we examined the effect of the active filler on the mechanical characteristics of the polymeric friction composite based on SFP-012 AK-30 binder and fibrous and mineral fillers.

The results show (Table 3) that addition of the active filler decreases the attrition wear and increases the friction coefficient and bond resistance.

To conclude, reactive compounds such as Ti nitrides, carbides, and carbonitrides show promise as active fillers for polymeric composite materials.

CONCLUSIONS

(1) Active fillers such as titanium nitrides TiN_x, carbides TiC_x, and carbonitrides TiC_xN_y ($0.5 < x$ or $x + y \le 1.0$) influence the polymerization of thermostable binders and properties of the resulting polymeric composites (heat resistance and strength).

(2) In binders cured through polymerization of single-type functional groups, e.g., ED-20, the degree of polymerization increases, while in those cured through reactions involving different functional

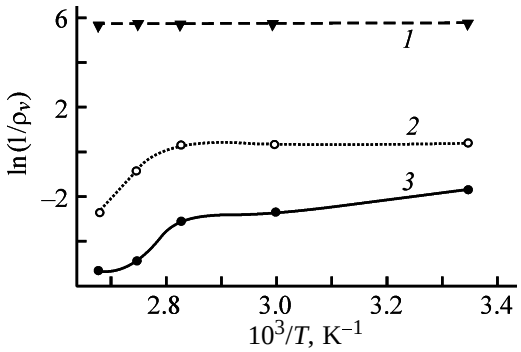


Fig. 3. Conductivity $\ln(1/\rho_v)$ of the PAIS-104-based composites containing (*1*) 90, (*2*) 70, and (*3*) 50 wt % of $TiN_{0.5}$ as a function of the temperature *T*.

groups (PAIS-104, SFP-012 AK-30), the active filler specifically influences the polymerization.

(3) In addition to the effects of reinforcing and increasing heat resistance, the reactive Ti compounds tend to structurization in the polymer matrix, allowing preparation of conducting polymeric composites.

REFERENCES

1. Bespalov, Yu.A. and Konovalenko, N.G., *Mnogokomponentnye sistemy na osnove polimerov* (Polymer-Based Multicomponent Systems), Leningrad: Khimiya, 1981.
2. Bobryshev, A.N., Avdeev, R.I., Zharin, D.E., *et al*., *Plast. Massy*, 2003, no. 1, pp. 15–17.
3. Balusov, V.A. and Tikhonov, A.N., *Klasternye materially – novyi klass plastmass s ul'tradispersnym napolnitelem* (Cluster Materials: A Novel Class of Plastics with a Superdispersed Filler), Leningrad: Leningr. Dom Nauch.-Tekh. Propagandy, 1988.
4. Gusev, A.I., *Fizicheskaya khimiya nestekhiometricheskikh tugoplavkikh soedinenii* (Physical Chemistry of Nonstoichiometric Refractory Compounds), Moscow: Nauka, 1991.
5. *Khimiya sinteza szhiganiem* (Chemistry of Combustion Synthesis), Koizumi, M., Ed., Moscow: Mir, 1998.
6. Zinov'ev, E.V. and Chichinadze, A.V., *Fiziko-khimicheskaya mekhanika treniya i otsenka asbofriktsionnykh materialov* (Physicochemical Mechanics of Friction and Characterization of Asbofrictional Materials), Moscow: Nauka, 1978.
7. Gul', V.E. and Shenfil', L.V., *Elektroprovodyashchie polimernye kompozitsii* (Conducting Polymeric Composites), Moscow: Khimiya, 1984.
8. Panova, L.G., Konovalenko, S.E., and Naumova, M.V., *Plast. Massy*, 2003, no. 7, pp. 10–11.

Russian Journal of Applied Chemistry, Vol. 78, No. 9, 2005, pp. 1517–1521. Translated from Zhurnal Prikladnoi Khimii, Vol. 78, No. 9, 2005, pp. 1542–1546.
Original Russian Text Copyright © 2005 by Chepik, Troshina, Golubkov.

MACROMOLECULAR CHEMISTRY AND POLYMERIC MATERIALS

Film-Forming Ability of Solutions Containing Products of Hydrolytic Polycondensation of Tetraethoxysilane

L. F. Chepik, E. P. Troshina, and V. V. Golubkov

Institute of Chemistry of Silicates, Russian Academy of Sciences, St. Petersburg, Russia

Received January 12, 2005

Abstract—Solutions containing products of hydrolytic polycondensation of tetraethoxysilane were studied by viscometry and small-angle X-ray scattering. The growth of polymer particles participating in formation of thin films was studied in relation to the solution composition and process conditions.

Processes with sol–gel transitions of the reaction mass are among the most intensively developed and promising methods of production of oxide materials. Variation of the conditions of sol–gel process opens up wide opportunities for preparation of oxide materials with given structure and characteristics [1–8]. One of the directions of using sol–gel synthesis, preparation of thin films on various surfaces, is based on the ability of oxygen-containing organoelemental compounds like metal alkoxides with the composition $M(OR)_n$ to undergo hydrolytic polycondensation to form polymers with M–O–M bonds. Deep hydrolytic polycondensation of oxygen-containing organoelemental compounds results in transition of a sol to a gel, i.e., in formation of inorganic polymer network structures, which transform to the oxide state on heating.

The hydrolytic polycondensation (HP) of tetraethoxysilane (TEOS) $Si(OC_2H_5)_4$ is used for preparing sols exhibiting film-forming characteristics. Thin silica films prepared from sols containing polymeric products of TEOS HP were used for production of antireflecting and beam-splitting coatings in optics [9] and as multifunctional coatings in microelectronics [10]. The noticeable drawback of these film-forming sols of TEOS is the instability of rheological characteristics. This is manifested in a regular increase in the viscosity of the initial low-viscous sol before its transformation to solid state, gel. The duration of the sol–gel transition and the time of manifestation of film-forming characteristics depend on the reaction conditions of TEOS HP. The increase in viscosity of sols is related to development of TEOS HP in time, and manifestation of film-forming characteristics, to the size of growing polymeric species formed from the initial TEOS. It was shown previously [11] that an increase in the viscosity of film-forming solutions is caused by an increase in the molecular weight of the polysiloxanes formed.

A wide use of sol–gel processes in preparation of oxide materials for industrial purpose stimulated active study of TEOS HP using various physical methods. In so doing, variations of physical characteristics and structure of sols are considered in relation to TEOS HP conditions. Among physical methods of studying sols and gels (^{29}Si NMR, DTA, X-ray fluorescence analysis), small-angle X-ray scattering (SAS) is one of the most informative methods. The use of this method for estimating changes in the size and shape of polymeric structures growing in the course of TEOS HP is described in numerous papers [12–19].

Here we made an attempt to study comprehensively using viscometry and SAS the dynamics of growth of polymer particles, whose presence governs the film-forming ability of TEOS sols in time.

The sols for preparing films were prepared by dissolving TEOS in aqueous alcohol at the molar ratio $TEOS : H_2O = 1 : 5.56$. The homogenizing medium was ethanol. The sol was acidified to pH 1–2.5 with HCl acting as acid catalyst. The amount of HCl (mol per mol of TEOS) in solutions was 5×10^{-4} (solution no. 2), 2×10^{-2} (solution no. 3), 0.14 (solution no. 4), or 0.7 (solution no. 5). In solution no. 1, no HCl was added. Variation of the amount of HCl affected the rate of increase in the solution viscosity and duration of film formation. HP of TEOS was performed at room temperature without stirring. The film-forming ability of TEOS sols was checked by casting of the solution onto plates of semiconductor-grade silicon with rotation on a centrifuge in the horizontal plane. With the expenditure of film-forming solution of

1070-4272/05/7809-1517 © 2005 Pleiades Publishing, Inc.

1–3 ml and the diameter of silicon plates from 70 to 90 mm, the thickness of films was 0.1–0.3 μm (n = 2000 rpm). We obtained a glassy film covering completely the plate, with no visual defects (cracks, fractures, uncovered areas, etc.) and standing thermal treatment at a temperature of 500–900°C without exfoliation from the support surface.

Preparation of oxide materials, including thin silica films, by sol–gel procedure involves TEOS HP. The TEOS HP proceeds in a solution under the action of acid catalyst in organic solvents in two steps:

(1) hydrolysis

$$\equiv Si{-}OC_2H_5 + HOH \xrightarrow{H^+,\ \text{organic medium}} \equiv Si{-}OH + C_2H_5OH;$$

(2) polycondensation

$$\equiv Si{-}OH + HO{-}Si\equiv \rightarrow \equiv Si{-}O{-}Si\equiv + H_2O,$$

$$\equiv Si{-}OC_2H_5 + HO{-}Si\equiv \rightarrow \equiv Si{-}O{-}Si\equiv + C_2H_5OH.$$

Thermal degradation of polyoxisilane results in formation of silica:

$$\equiv Si{-}O{-}Si\equiv \xrightarrow{\Delta} SiO_2.$$

In the course of TEOS HP, the molecular weight of polysiloxanes steadily increases owing to constantly arising siloxane bonds Si–O–Si. The inorganic structural network typical for the gel state is formed in the sol step, and then the sizes of the initial polymer particles increase. They are involved in side branching, cross-linking, and aggregation. The polymeric product of TEOS HP in the gel step is described by the formula

$$[Si(OC_2H_5)_a(OH)_bO_{0.5(4-a-b)}]_n,$$

with possible presence of certain amount of unchanged $-OC_2H_5$ and –OH groups in the final product [20].

The structural evolution of polymeric particles of TEOS sol, considered in relation to the synthesis conditions and aging time, is caused by variation of the sol rheology. Viscometry is one of the methods allowing estimation of the rate of TEOS HP. Here we used a Höppler viscometer with a falling ball rigidly connected to the balance beam.

In the initial step of existence of sol after combining all the components, the solution viscosity is an additive function of the viscosities of the initial substances and is approximately 2–3 cP (1 cP = 0.001 Pa s in the SI system). In this step called "ripening," film formation does not yet occur. With further development of TEOS HP in time, involving formation of polymers of more and more complicated structure up to three-dimensional skeleton of the gel, the solution viscosity increases. During aging of the solution in the range of viscosity from 3 to 7–8 cP, high-quality films can be produced. This period is termed the period of active film formation. At the viscosity above 7–8 cP, the film formation becomes practically impossible, although the solutions remain highly mobile and are far from transition into the gel state. These observations suggest that films can be prepared from sols at a certain size of polymeric products formed in the reactions involving TEOS.

Variation of the sizes of polymer formations in the course of TEOS HP was studied by small-angle X-ray scattering (SAS) on the installation described previously [21]. The SAS curves (dependence of X-ray scattering intensity on scattering angle) were measured at various ages of the solutions. The SAS data were compared with the viscosity data and manifestation of the film-forming characteristics of the solutions. Based on the SAS data, we determined the sizes of heterogeneity areas appearing as a result of development of TEOS HP in time. These sizes were determined in the approximation of scattering by spherical particles having a constant electron density by the Guinier method [22]. In the course of development of sol–gel process both in the initial steps and in the gel step up to its complete consolidation, a branched (fractal) structure is realized. The presence of a fractal structure results in appearance of a section in the SAS curves in which the angular dependence of the SAS intensity I can be presented in the form

$$I(\varphi) \sim \varphi^{-k},$$

where φ is the scattering angle. The parameter k depends on the structure type. For chain structures, k coincides with the fractal parameter (fractal dimension) D and relates the size and weight by

$$M \sim R^D,$$

where M is weight and R is radius.

It is well known that TEOS HP in acidic medium proceeds through formation of small (1.5–1.7 nm) polymer particles [7, 12]. This feature of the sol–gel process is of particular interest in design of materials with fine structure, such as thin-film coatings, mem-

branes, and microporous materials. The presence of these small particles in the sol in the early steps of TEOS HP should not noticeably affect the solution viscosity. Actually, irrespective of the amount of HCl per mole of TEOS, the viscosity of the solutions in this period is approximately 2–3 cP. This is equal to the additive value. The products of TEOS HP with gradually increasing the molecular weight do not noticeably contribute to this value (Fig. 1a). With development of TEOS HP, the viscosity of the solutions increases; in this case, aging of sols becomes dependent on the amount of HCl catalyzing TEOS HP. The variation of viscosity shown in Fig. 1a is restricted by the limiting viscosity equal to 15 cP, which can be measured on a Höppler viscometer with cell no. 0.01. The viscosities above 15 cP were not measured; the sol–gel transition was judged visually from the loss of the solution mobility.

In studying film-forming characteristics of sols, the range of viscosity variation from 2 to 7–8 cP, in which the solutions are able to form films, is of the most interest. The abrupt increase in viscosity for the solution without HCl and its transition to gel in 5 days did not allow us to evaluate the film-forming characteristics of this solution (Figs. 1a and 1b, curve *1*). For the other solutions, the period of film formation varied from 10 to 70 days, depending on the amount of HCl. The longest period of film formation (approximately 70 days) corresponded to the molar ratio HCl : TEOS = 0.03 : 1 (Figs. 1a and 1b, curve *3*). With increasing viscosity of the solutions, the film thickness tends to increase from 0.1 at the beginning of the process to 0.2–0.3 μm by the end of the film formation period. Increasing thickness of film applied from solutions with a viscosity higher than 8 cP makes these films not resistant to thermal treatment: they undergo fracture and exfoliate due to increasing mechanical stress. This period is associated with the loss of the film-forming ability of the sols. The viscometric method correlated with film-forming characteristics is quite reliable in indirect monitoring of TEOS HP and simplest estimation of the working life of the solutions.

The SAS method allows estimation of variations in the size of structural units in the course of TEOS HP, relating these variations to manifestation of the film-forming characteristics. From the X-ray scattering curves, we determined the size of heterogeneity areas appearing as a result of TEOS HP and confirming realization of the fractal structure in the step of the sol–gel transition. In the initial step, the heterogeneity size (radius), evaluated in the approximation of scattering with spherical particles with a constant electron density, is 4–5 Å. This value is close to the size of TEOS molecules entering into the process of chain growth. The variation of the size of polymer formations, obtained from SAS data, is shown in Fig. 2. For

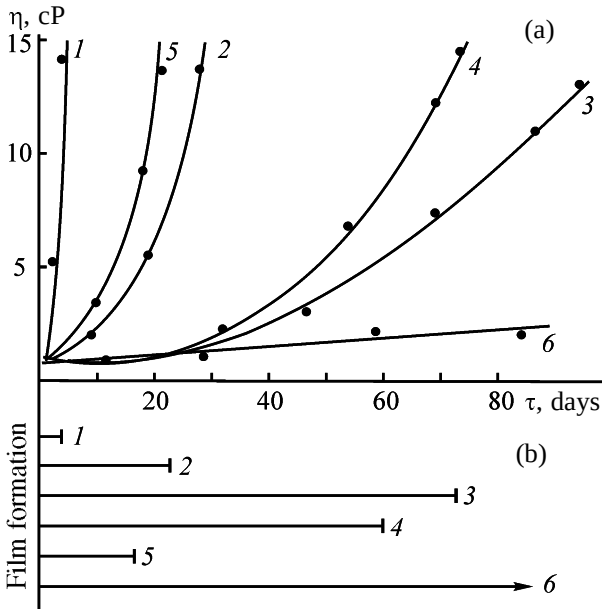


Fig. 1. (a) Variation of viscosity η and (b) film-forming ability of sols with time at various amounts of moles of HCl added. (τ) Process time. (*1*) Without acid; HCl content, mole per mole TEOS: (*2*) 0.0005, (*3*) 0.03, (*4*) 0.14, (*5*) 0.7, and (*6*) 0.7 (TEOS : TMEOS = 7 : 1 by volume); the same for Fig. 2.

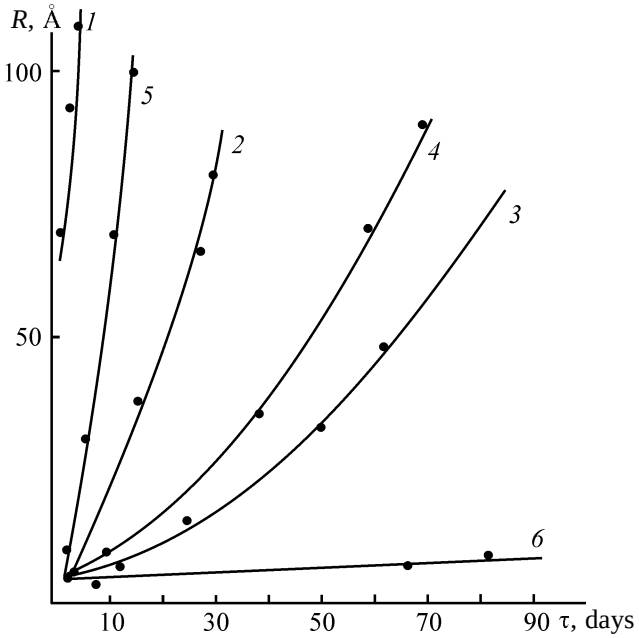


Fig. 2. Variation with time of the size of heterogeneity areas in sols at various amounts of HCl added (SAS data). (*R*) Radius of polymeric formation and (τ) time.

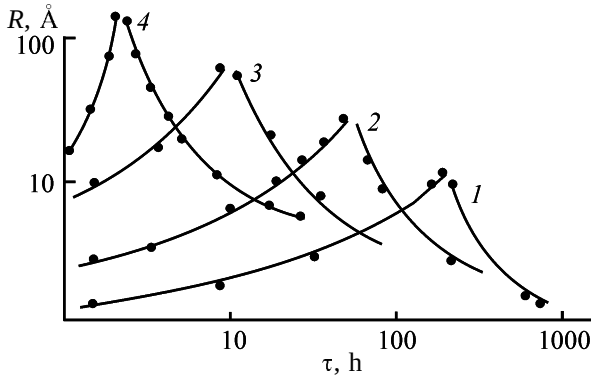


Fig. 3. Variation with time of the size of heterogeneity areas in sols at various temperatures (SAS data). (*R*) Radius of polymeric formation and (τ) process time. Temperature, °C: (*1*) 20, (*2*) 40, (*3*) 60, and (*4*) 80.

composition 1, in the absence of HCl, the SAS method revealed no variation in the scattering intensity in the first day, whereas for solutions containing HCl catalyst these variations were quite noticeable. Formally, this period can be considered as incubation period, as it is followed by abrupt increase in the sizes of polymer particles. On the fifth day, solution 1 transforms into a solid gel (Fig. 2, curve *1*). It can be suggested that, in composition 1, the areas of heterogeneity caused by more complete TEOS HP are denser. Comparison of the SAS data and film-forming characteristics suggests that the period of film formation corresponds to the presence of small particles in the solution with the size from 4–5 to 50–70 Å.

The duration of the film-forming period can be increased by adding trimethylethoxysilane (TMEOS) $(CH_3)_3Si(OC_2H_5)$. This monomer exerts a stabilizing effect on the polymeric reaction products. Cocondensation of TEOS and TMEOS results in termination of growing polysiloxanes chains due to blocking of the growth centers with methyl groups by the reaction

$$\equiv Si\text{–}OH + C_2H_5O\text{–}Si(CH_3)_3 \rightarrow \equiv Si\text{–}O\text{–}Si(CH_3)_3 + C_2H_5OH.$$

When cocondensation is performed at the volume ratio TEOS : TMEOS = 7 : 1 in a solution with the highest content of HCl, 0.7 mol per mol of TEOS, the lifetime of the solution can be increased from 5 days to 2 months and more (Figs. 1a and 1b, curve *6*). At a constant viscosity equal to approximately 3 cP within the observation period (more than 70 days), films of a constant thickness were obtained from the solution. The SAS data confirm constant size of heterogeneity areas in solution (Fig. 2, curve *6*).

Acceleration of aging of the sols and variations of the size of heterogeneity areas in the course of TEOS HP were studied by SAS (molar ratio HCl : TEOS = 0.03 : 1) at 80, 60, 40, and 20°C. As seen from Fig. 3, at each temperature the size of the scattering areas increases with time; at a certain instant of time, depending on temperature, the growth rate abruptly increases, the size becomes larger than the installation resolution, and then the size begins to decrease. The attainment of the largest size corresponds to formation of "infinite clusters" and sol–gel transition. It should be noted that the size grows in the step of polymerization. In this step, the size determined from the evidence of SAS data is an effective size of branched chains of silicon–oxygen tetrahedra randomly distributed in the liquid phase as matrix. After transition into the gel state, the silicon–oxygen skeleton becomes a matrix, and inclusions of the liquid phase become scattering areas. With further progress of the polymerization, the size of these inclusions decreases, i.e., the liquid phase is displaced. After evaporation of the liquid phase in the step of transition into the xerogel, the scattering areas are pores with the sizes of the order of 10–20 Å (radius in approximation of scattering with spherical particles with a constant density in the bulk).

The shapes of the dependences shown in Fig. 3 are typical of second-kind phase transitions and are in good agreement with the Flory–Stockmayer model [23, 24]. In this case, in deep steps of TEOS HP, an infinite cluster appears, which confirms irreversibility of the sol–gel transition. An increase in the temperature of TEOS HP results in acceleration of sol aging; with heating by 20°C, the time of attainment of a given particle size decreases by a factor of approximately 7. In this case, the SAS data also satisfactorily correlate with the period of manifestation of film formation properties. This fact suggests that the mechanisms of the influence of temperature and acid catalyst concentration on the TEOS HP are similar.

CONCLUSIONS

(1) Viscometric data give an insight into the rheology of hydrolytic polycondensation of tetraethoxysilane depending on the process conditions. The period of film formation corresponds to the variation of the sol viscosity from 2 to 8 cP.

(2) The results of analysis of sols by small-angle X-ray scattering allow the film-forming ability to be correlated with the presence of heterogeneity areas of the size from 4–5 to 50–70 Å in the solution.

(3) Data on the rheology of hydrolytic polycondensation of tetraethoxysilane, small-angle X-ray scattering, and film-forming ability reveal the similarity in the mechanism of development of hydrolytic polycondensation of tetraethoxysilane depending on the catalyst amount and temperature, consisting in gradual growth of the polymer from small primary particles to infinite cluster typical for sol–gel transition.

(4) Addition of trimethylethoxysilane as comonomer affects the rheology of tetraethoxysilane sols and their film-forming ability, with actually constant sizes of heterogeneity areas observed by small-angle X-rays scattering.

REFERENCES

1. Kindu, D., Biswas, P., and Yanguli, D., *J. Non-Cryst. Solids*, 1989, vol. 110, pp. 13–16.
2. Brautigam, H., Burger, H., and Vogel, W., *J. Non-Cryst. Solids*, 1989, vol. 110, pp. 163–169.
3. Kasoos, A., *J. Ceram. Soc. Jpn*, 1991, vol. 100, pp. 763–765.
4. MacKenzie, J.D., *J. Non-Cryst. Solids*, 1988, vol. 100, pp. 162–168.
5. Chul Ro, J. and Chung Ju Jae, *J. Non-Cryst. Solids*, 1989, vol. 110, pp. 26–32.
6. Chou Kan-Sen, *J. Non-Cryst. Solids*, 1989, vol. 110, pp. 122–124.
7. Brinker, C.J., Raman, N.K., Hua, D.-W., and Ward, T.Z., *J. Sol–Gel Sci. Technol.*, 1995, vol. 4, no. 2, pp. 117–133.
8. Kawaguchi, T. and Ono, K., *J. Non-Cryst. Solids*, 1990, vol. 121, pp. 383–388.
9. Suikovskaya, N.V., *Khimicheskie metody polucheniya tonkikh prozrachnykh plenok* (Chemical Methods of Preparing Thin Transparent Films), Leningrad: Khimiya, 1971.
10. Borisenko, A.I., Novikov, V.V., Prikhod'ko, N.E., *et al.*, in *Tonkie neorganicheskie plenki v mikroelektronike* (Thin Inorganic Films in Microelectronics), Leningrad: Nauka, 1972, pp. 1–144.
11. Suikovskaya, N.V., *Tr. Gos. Opt. Inst.*, 1956, vol. 24, no. 145, pp. 14–30.
12. Lange, R.S.A. de, Hekking, J.H.A., Keizer, K., and Burggraaf, A.J., *J. Non-Cryst. Solids*, 1995, vol. 191, nos. 1–2, pp. 1–7.
13. Chaumon, D., Craievich, A., and Zarzycki, J., *J. Non-Cryst. Solids*, 1992, vol. 147–148, pp. 127–134.
14. Kallala, M., Sanchez, C., and Cabane, B., *J. Non-Cryst. Solids*, 1992, vol. 147–148, pp. 189–193.
15. Blanko, E., Ramirez-del-Solar, M., and Rosa-Fox, N. de la, *J. Non-Cryst. Solids*, 1992, vol. 147–148, pp. 238–244.
16. Blanko, E., Rosa-Fox, N. de la, and Esquivias, L., *J. Non-Cryst. Solids*, 1992, vol. 147–148, pp. 296–302.
17. Hench, L.L. and Orcel, G., *J. Non-Cryst. Solids*, 1986, vol. 82, pp. 1–10.
18. Balley, J.K., *J. Non-Cryst. Solids*, 1989, vol. 109, pp. 198–210.
19. Himmel, B., Gerber, Th., and Burger, H., *J. Non-Cryst. Solids*, 1990, vol. 119, pp. 1–13.
20. Bechtold, M.F., Vest, R.D., and Plamberg, L., *J. Am. Chem. Soc.*, 1968, vol. 90, no. 17, pp. 1590–1597.
21. Golubkov, V.V., Titov, A.N., and Porai-Koshits, E.A., *Prib. Tekh. Eksp.*, 1975, no. 1, pp. 215–217.
22. Guinier, A. and Fournet, G., in *Small Angle Scattering of X-Ray*, New York: G.W.J.LLEU, 1955, pp. 268–270.
23. Flory, P.J., *Principles of Polymer Chemistry*, New York: Cornell Univ., 1953.
24. Korolev, S.V., Kuchanov, S.I., and Slin'ko, M.G., *Dokl. Akad. Nauk SSSR*, 1986, vol. 287, pp. 1157–1161.

Russian Journal of Applied Chemistry, Vol. 78, No. 9, 2005, pp. 1522–1525. Translated from Zhurnal Prikladnoi Khimii, Vol. 78, No. 9, 2005, pp. 1547–1550.
Original Russian Text Copyright © 2005 by A. Tereshatov, Fedchenko, Tereshatova, Makarova, V. Tereshatov.

MACROMOLECULAR CHEMISTRY AND POLYMERIC MATERIALS

Influence of the Chemical Structure of Flexible Blocks on the Mechanical Properties of Poly(Urethane–Ureas) in a Humid Atmosphere

A. V. Tereshatov, V. V. Fedchenko, E. N. Tereshatova, M. A. Makarova, and V. V. Tereshatov

Institute of Technical Chemistry, Ural Division, Russian Academy of Sciences, Perm, Russia

Received January 26, 2005

Abstract—Sorption of moisture on segmented poly(urethane–ureas) with flexible segments of various chemical structures and the effect of a humid atmosphere on the mechanical properties of these materials were studied. Poly(urethane–urea) prepared from mixtures of oligoethers shows advantages from the viewpoint of preservation of high strength in a humid atmosphere.

Block polyurethane elastomers, so-called segmented polyurethanes (SPUs), are widely used in various branches of industry thanks to their high strength, good deformation characteristics, and resistance to a number of solvents [1]. Depending on the destination, polyurethane items can operate in air or in direct contact with water (e.g., polyurethane coatings of squeeze rolls in paper-making industry).

Published data on the behavior of SPUs in moist media mainly concern the moisture transfer in these materials [2–5] and changes in the structure [2, 5, 6] and glass transition point [5, 6] of moistened polyurethanes. Experiments were performed with thin polyurethane films prepared from solution; in this case, correct estimation of changes in mechanical properties on moistening is complicated by intense moisture exchange with the surrounding medium. Data on the mechanical properties of the films are limited to the results of their mechanical tests before moistening [3]. Therefore, it is unclear to what extent the mechanical characteristics of various SPUs vary on moistening and how the extent of their variation depends on the polymer structure.

Studies in this direction are necessary for understanding how the mechanical characteristics of polyurethanes change on moistening and for choosing formulations of polyurethane materials suitable for operation in moist media.

In this study we examined the influence of the relative air humidity, varied in a wide range, on the mechanical properties of SPUs with various flexible segments. Our main goal was to reveal what structure of flexible blocks would provide the highest strength of the polyurethane material in a humid atmosphere.

EXPERIMENTAL

We used segmented poly(urethane–ureas) with poly(tetramethylene oxide) flexible blocks (SPUM-1), poly(propylene oxide) segments (SPUM-2), mixed polyether blocks (SPUM-3), and mixed polybutadiene–poly(tetramethylene oxide) flexible segments (SPUM-4). To prepare SPUMs, we took prepolymers based on oligo(tetramethylene oxide)diol (M ~1700), oligo(propylene oxide)diol Laprol 2102 (M ~1950), and polybutadienediol (M ~2100, SKU-DF-2 prepolymer). The molecular weight of the oligomeric diols was estimated from the content of hydroxy groups. The prepolymers were prepared by the reactions of appropriate diols with toluylene-2,4-diisocyanate. The prepolymers and their mixtures (in preparation of SPUMs with mixed flexible segments) were cured with 3,3'-dichloro-4,4'-diaminodiphenylmethane (Diamet Kh) by the procedure described in [7].

The molar ratio of the prepolymers (or their mixture) to Diamet Kh was 1.03, and the molar ratio of the NCO and OH groups in the synthesis of the prepolymers, 2.1.

The isotherms of the moisture sorption by SPUMs were obtained using the kinetic curves of the weight gain of the samples placed in atmospheres of different relative humidities φ (over appropriate solutions of

1070-4272/05/7809-1522 © 2005 Pleiades Publishing, Inc.

inorganic salts) at 22 ± 1.5°C. The control samples were kept over freshly calcined calcium chloride. As expected, the sample weights in this case were virtually the same as the initial weights of the samples taken from the molds. The weights of the dry and moistened samples were determined with an Ohaus AR-2140 analytical balance with an accuracy of $\pm 3 \times 10^{-7}$ kg.

For mechanical tests, SPUM samples were kept similarly in a dry or humid atmosphere to attain the equilibrium. The total time of the mechanical tests of a single sample did not exceed 120 s. In this time, the specific moisture content c changed by less than 4% relative to the equilibrium value.

The mechanical characteristics of SPUMs, strength f_b (breaking stress, or maximal stress calculated for actual sample cross section), relative critical strain ε_c, and nominal modulus E_{100} at 100% relative strain, were determined at 22 ± 1.5°C and an extension rate of 0.3 s^{-1}.

The molecular structures of the dry and moistened SPUM samples were studied by IR spectroscopy on a Bruker IFS-66/S Fourier spectrometer. Samples were prepared as films without solvents, by curing of the reaction mixture placed between two Teflon films. We checked that the Teflon film does not absorb in the range of carbonyl stretching vibrations (ν = 1620–1750 cm^{-1}). At moistening, one of the insulating Teflon films was removed. Before recording the spectrum, the sample surface was again covered with the Teflon film, and the sample was placed between KBr plates. The conversion of the isocyanate groups was also monitored by IR spectroscopy (disappearance of the absorption at ν = 2275 cm^{-1}). For the sake of convenient comparison, as in [8], the spectra of different samples were normalized with respect to the band at ν = 1575 cm^{-1}.

The results of the experiments showed that the equilibrium moisture content c of the samples was independent of whether it was reached from above (desorption from samples taken from a more humid atmosphere) or from below (sorption).

The reversibility of the moisture sorption and desorption and the shape of the curves in Fig. 1 indicate that the isotherms of the moisture sorption by the examined materials belong to type IV, according to the generally accepted classification. A significant difference in the moisture absorption by SPUM-1 and SPUM-2 (by a factor of 1.67–1.8) at $\varphi \geq 60\%$ may be caused not only by the different polarity of the flexible chains with different content of oxygen atoms.

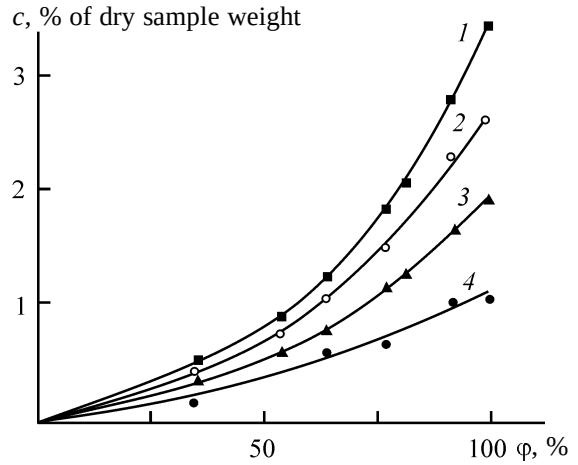


Fig. 1. Isotherms of moisture sorption by (*1*) SPUM-2, (*2*) SPUM-3, (*3*) SPUM-1, and (*4*) SPUM-4 at 22°C: (*c*) specific moisture content of the material and (φ) relative air humidity.

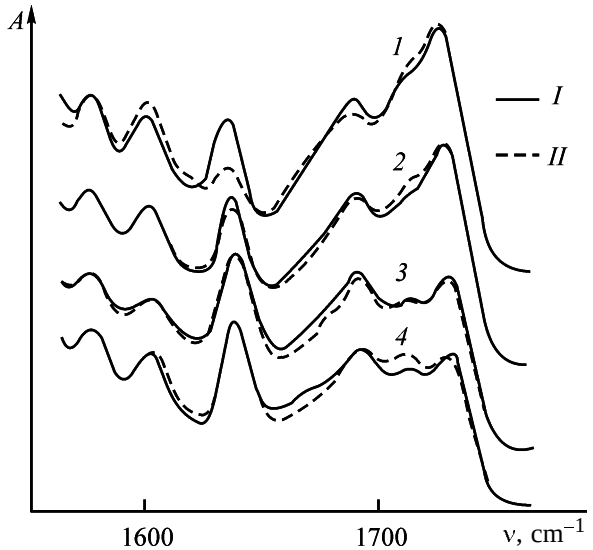


Fig. 2. IR spectra of (*I*) dry and (*II*) moistened (at φ = 92%) samples: (*1*) SPUM-2, (*2*) SPUM-3, (*3*) SPUM-1, and (*4*) SPUM-4. (*A*) Absorption and (ν) wave number.

On replacement of poly(tetramethylene oxide) flexible blocks by poly(propylene oxide) blocks, the degree of microphase segregation in poly(ether–urethane–urea) decreases; correspondingly, the amount of rigid polar blocks dissolved in the flexible phase of the polymer increases, and the volume of this phase grows [8]. Furthermore, the sorbed moisture breaks a part of self-associates of the urea groups localized in domains of rigid urethane–urea blocks. This is clearly seen from comparison of the intensities of the urea carbonyl absorption band (ν = 1640 cm^{-1}) in the IR spectra of the initial and moistened samples (Fig. 2, spectra *1*, dashed and solid lines). As shown in [2], an increase

Mechanical characteristics of dry and moistened SPUM samples

φ, %	SPUM-1		SPUM-2		SPUM-3		SPUM-4	
	E_{100}, MPa	ε_c, %	E_{100}, MPa	ε_c, %	E_{100}, MPa	ε_c, %	E_{100}, MPa	ε_c, %
0	7.7	700	3.6	1070	4.7	1060	7.3	680
35	7.6	710	3.4	1050	4.4	1040	7.1	680
54	7.3	700	2.9	1060	–	–	–	–
64	6.9	700	–	–	3.9	1080	6.6	–
77	6.7	700	2.4	1080	3.6	1090	6.3	660
82	6.6	690	–	–	–	–	–	–
92	6.5	680	2.0	1060	3.3	1080	5.9	680
100	6.3	670	1.8	1070	3.0	1080	5.9	680

in the volume accessible to water molecules and in the amount of polar groups capable of H bonding should increase the moisture absorption of the polyurethane material.

The structure of the rigid domains of the material with poly(tetramethylene oxide) flexible segments is less defective than that of SPUM-2 domains [8]. On moistening of SPUM-1, the amount of the strongest structural formations, self-associates of urea groups, remains essentially unchanged (Fig. 2, spectra *3*). As expected, the isotherm of moisture sorption by SPUM-3 containing mixed oligoether flexible blocks is intermediate between the isotherms of the moisture sorption by SPUM-1 and SPUM-2, and the specific moisture content of poly(urethane–urea) drastically decreases on partial replacement of polyether blocks by nonpolar polybutadiene flexible segments (Fig. 1, curve *4*).

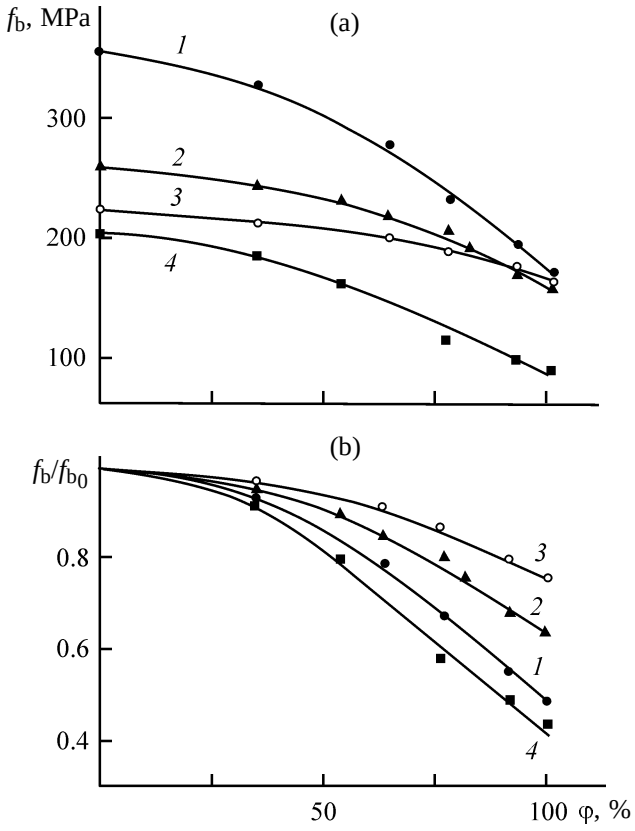


Fig. 3. (a) Strength f_b and (b) its relative change f_b/f_{b_0} on moistening of (*1*) SPUM-3, (*2*) SPUM-1, (*3*) SPUM-4, and (*4*) SPUM-2 samples, as functions of the relative air humidity φ.

The mechanical tests of SPUMs showed that the moistening exerted virtually no effect on the critical strain ε_c (see table). SPUM-2 sample with propylene oxide flexible segments is characterized by the lowest values of f_b and E_{100} and by their most pronounced decrease on moistening (by a factor of 2 at φ = 100%; Fig. 3, curves *4*). In the material containing 50% nonpolar flexible blocks, the decrease in the strength and nominal modulus was the least pronounced (Fig. 3, curves *3*). The curves of the relative change in the breaking stress upon SPUM moistening (Fig. 3b) are arranged in the order opposite to the sorption isotherms in Fig. 1.

The observed pattern of the mechanical behavior of SPUMs in a humid atmosphere is apparently caused by significant differences between the materials in the extent to which the domain structure and interchain interactions affect their density. The results of previous studies [8, 9] suggest that an increase in the intensity of the carbonyl absorption band belonging to urea self-associates (ν = 1640 cm^{-1}), observed in going from SPUM-2 to SPUM-3, SPUM-1, and SPUM-4, is indicative of an increase in the degree of segregation of rigid blocks in the same order. As the polarity of flexible chains decreases (and, as a result, the microphase segregation of rigid and flexible blocks in the polymer increases), the effect of the reinforcing filler

on the material strength (SPUM-1, SPUM-4) becomes stronger.

With an increase in the polarity of the flexible blocks and the corresponding increase in the solubility of the rigid segments in the SPUM flexible phase, the effect of the interchain interaction in the polymer matrix on the material strength is enhanced [1]. Correspondingly, weakening of this interaction upon water sorption should substantially decrease the strength of poly(ether–urethanes), which is the case. Partial break of urea self-associates in the presence of moisture also leads to a decrease in the elastomer strength (Fig. 3b, curve *4*).

It is noteworthy that, owing to high initial f_b of SPUM-3 (before moistening), the strength of the material with mixed flexible segments in a humid atmosphere is higher than f_b of the other materials, especially at moderate humidity ($\varphi = 50–75\%$) typical of industrial premises.

The fact that the strength properties of the SPUM containing nonpolar flexible segments are not significantly deteriorated in a humid atmosphere is of interest for developing materials preserving high strength in a moist medium.

CONCLUSIONS

(1) The dependence of the moisture absorption of poly(urethane–ureas) with various flexible blocks on the structural organization of the materials was elucidated.

(2) A correlation between the capability of poly(urethane–ureas) to sorb moisture and the decrease in their strength in a humid atmosphere was revealed.

(3) Moisture only weakly affects the mechanical characteristics of the material with mixed polyether and nonpolar polybutadiene flexible segments. The decisive effect on the properties of this material is exerted by the microdispersed rigid phase, which is not altered upon moistening of the polymer.

(4) To ensure high strength of poly(ether–urethane–urea) in a moist medium, it is appropriate to use for its synthesis a mixture or prepolymers derived from oligo(tetramethylene oxide)diol and oligo(propylene oxide)diol.

ACKNOWLEDGMENTS

The study was financially supported by the Russian Foundation for Basic Research and Administration of Perm oblast (project no. 04-03-97509).

REFERENCES

1. Lyubartovich, S.A., Morozov, Yu.L., and Tret'yakov, O.B., *Reaktsionnoe formirovanie poliuretanov* (Reactive Forming of Polyurethanes), Moscow: Khimiya, 1990.
2. Razumovskii, L.R., Iordanskii, A.L., Zolotova, E.V., *et al.*, *Vysokomol. Soedin., Ser. A*, 1991, vol. 33, no. 5, pp. 989–996.
3. Jeong, H.M., Ahn, B.K., and Kim, B.K., *Polym. Int.*, 2000, vol. 49, no. 12, pp. 1714–1721.
4. Schneider, N.S., Dusablon, L.V., Spano, H.B., *et al.*, *J. Appl. Polym. Sci.*, 1968, vol. 12, no. 3, pp. 527–532.
5. Kanapitsas, A., Pissis, P., Gomer Ribelles, J.L., *et al.*, *J. Appl. Polym. Sci.*, 1999, vol. 71, no. 8, pp. 1209–1221.
6. Pissis, P., Apekis, L., Christodoulides, C., *et al.*, *J. Polym. Sci., Part B: Polym. Phys.*, 1996, vol. 34, no. 9, pp. 1529–1539.
7. Tereshatov, V.V., Tereshatova, E.N., Makarova, M.A., and Tereshatov, S.V., *Vysokomol. Soedin., Ser. A*, 2002, vol. 44, no. 3, pp. 443–451.
8. Tereshatov, V.V., Makarova, M.A., and Tereshatova, E.N., *Vysokomol. Soedin., Ser. A*, 2004, vol. 46, no. 12, pp. 2019–2027.
9. Zharkov, V.V., Kopusov, L.I., and Kozlova, T.V., *Plast. Massy*, 1981, no. 12, pp. 41–45.

Russian Journal of Applied Chemistry, Vol. 78, No. 9, 2005, pp. 1526–1530. Translated from Zhurnal Prikladnoi Khimii, Vol. 78, No. 9, 2005, pp. 1551–1555.
Original Russian Text Copyright © 2005 by Puchkov, Turenko.

MACROMOLECULAR CHEMISTRY AND POLYMERIC MATERIALS

Blocked Diisocyanate as a Promoter of Rubber Adhesion to Brass-Plated Metal Cord

A. F. Puchkov and S. V. Turenko

Volgograd State Technical University, Volgograd, Russia
Volzhskii Polytechnic Institute, Volzhskii, Volgograd oblast, Russia

Received March 16, 2005

Abstract—Conditions for preparing boron-containing blocked diisocyanate in a melt of blocking agents at low temperatures in the absence of solvents were examined.

Variable-valence metal compounds, e.g., cobalt stearate and naphthenate, are effective promoters of rubber adhesion to brass-plated metal cord [1]. The main destination of promoters is to ensure not only the high initial adhesion strength in the rubber–brass-plated metal cord system, but also the stability of the strength under service conditions [1]. However, variable-valence metals catalyze oxidation of the rubber polymer [1] and therefore may decrease the durability of the items, e.g., of automobile tires. Also, these promoters are among the most expensive components of rubber stocks.

Various modifying systems, including blocked diisocyanates (BDs) [2], have been suggested as alternatives to cobalt-containing adhesion promoters. However, studies with BDs have not gone beyond laboratory trials. Probably, the advantages of BDs as adhesion promoters, as applied to a diversity of metal-reinforced elastomeric composites, require more evidences.

In this study, we proceed with the development of BDs ensuring high adhesion of rubber to brass-plated cord and the stability of the adhesion properties under the service conditions. We expect that an additional contribution to the adhesion properties will be made by high reactivity of diisocyanates regenerated by deblocking toward compounds containing labile hydrogen atoms.

EXPERIMENTAL

The source of labile hydrogen atoms in the brass coating of the metal cord can be zinc hydroxide. Its presence in the brass layer is very undesirable, because it not only causes formation of loose surface layers with a low mechanical strength, but also promotes excessive formation of copper and zinc sulfides [3]. Apparently, chemical bonds arising in the reaction of isocyanate groups with the OH groups of zinc hydroxide, on the one hand, and with rubber hydrogen, on the other hand, will prevent intense diffusion of copper and zinc ions toward the rubber–brass-plated layer contact zone. In turn, the density of the forming bonds will depend on the diffusion activity of BD. At a relatively low diffusion rate, the majority of the competing reactions of the diisocyanate with the rubber stock components and with rubber itself will occur beyond the adhesion contact zone. Therefore, to ensure fast supply of BDs to the boundary zones, these substances should have such specific properties as high dispersibility in the rubber bulk and high rate of diffusion to the adhesion zone.

To prepare such BDs, we proceeded from the process [4] involving synthesis in a melt of binary or ternary systems of blocking agents taken in an excess relative to the isocyanate groups and acting as a dispersion medium for BD particles proper. If the synthesis temperature does not exceed 90°C, the viscosity of the melt of the blocking agents, the melt with the added diisocyanate, and, finally, the reaction mixture up to complete conversion of the isocyanate groups is sufficiently low (at 80°C, 30–70 cP) to perform the process without solvent [5]. The products thus obtained are homogeneous compounds with a dropping point of 50–70°C and pronounced surface activity; they undergo no phase segregation in time [6]. In our case, to obtain a promoter of adhesion to brass-plated metal cord, we blocked a diisocyanate [brand D polyisocyanate, TU (Technical Specifications) 113-03-38-106–90, a (50–60) : (40–50) wt % mixture of diphenylmethane-4,4'-diisocyanate and its dimers] with

1070-4272/05/7809-1526© 2005 Pleiades Publishing, Inc.

the system ε-caprolactam–stearic acid, at the same component ratio as in [7].

A principally new approach to BD preparation is addition of boric acid (BA) to the BD formulation. It is noted [1] that boron-containing compounds favor preservation of the binding strength in the course of service, when the brass-plated metal cord is subjected to the action of water or sodium chloride diffusing to the surface of the metal cord in the tire belt through microcracks and cuts of the tread.

We found that BA added to BD in the step of the synthesis catalyzes the side reactions of branching and cross-linking which cause gelation of the reaction melt. Addition of BA to the BD melt after completion of the blocking reaction involves problems, as it becomes necessary to heat the reaction mixture to 120°C for melting of BA and homogenization of the formulation. Under these conditions, blocked diisocyanate catalyzes the deblocking–blocking reactions, which prevents obtaining a product with reproducible physicochemical properties and negatively affects the binding strength in the rubber–brass-plated cord system under the conditions of salt aging (Fig. 1).

Tests were performed with breaker rubbers based on SKI-3 polyisoprene rubber. Mother rubber stocks were prepared in a laboratory rubber mixer with a mixing chamber volume of 2 dm^3. The vulcanizing group and adhesion promoters were added to the mother stock on laboratory rollers. Vulcanization was effected with Kristeks polymeric sulfur in the presence of an accelerator, sulfenamide C, at 155°C for 25 min. The physicomechanical parameters of the vulcanized rubbers and samples of rubber with metal cord were determined in accordance with appropriate regulations: strength of vulcanized rubbers, according to GOST (State Standard) 270–75, and strength of binding of the rubber with 9L15/27 metal cord, according to GOST 23785.7–79 (H method). The salt aging of rubber samples with metal cord was performed in a boiling 5% NaCl solution, and exposure of the metal cord to a humid atmosphere, in a desiccator over water at 110°C.

It is known [8] that many substances form eutectic alloys. This phenomenon is typical both of substances whose alloys are mechanical mixtures of the individual components and of substances exhibiting limited mutual solubility of the components in the solid state. Therefore, we expected that the use of eutectic mixtures of BA with blocking agents would allow preparation of a boron-containing BD at temperatures as low as 80–90°C, thus eliminating gelation or premature deblocking–blocking reactions.

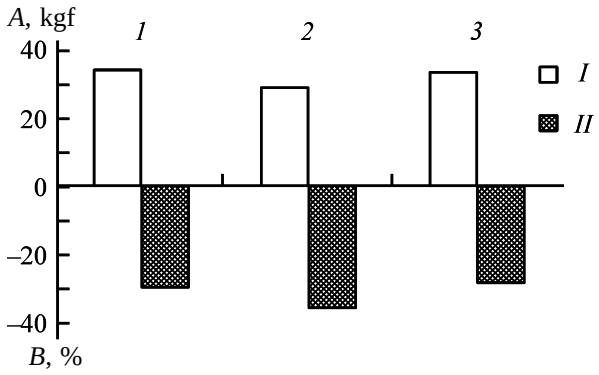


Fig. 1. (*I*) Initial strength *A* of binding of rubber with brass-plated metal cord (H method) as influenced by the kind of modifier and (*II*) change *B* in the binding strength after salt aging. (*1*) Cobalt stearate, (*2*) BD and BA (mechanical mixture), and (*3*) BD + BA in the form of an eutectic melt with ε-caprolactam.

We studied binary formulations of BA with ε-caprolactam and of BA with stearic acid. BA does not form an eutectic with stearic acid because of unlimited mutual solubility of the components in the solid state. A 8 : 2 (by weight) mixture of ε-caprolactam with BA forms an eutectic melt with a dropping point of 74°C.

Introduction of 2.0–2.5 wt % BA in the form of an eutectic alloy to the reaction mixture after complete conversion of isocyanate groups allows preparation of a BD compound with stable physical and colloidal properties. The properties of the compound in the initial state are, on the whole, virtually the same as in the absence of boron: It is highly soluble in toluene, the dropping point is 52 ± 2°C, and the surface tension isotherm obtained by the Kantor–Rebinder method coincides with that of an aqueous dispersion of BA–PIC [9]. The rubber–cord samples prepared with a boron-containing BD (BCBD) show relatively high strength in tests performed under normal conditions and in aggressive media (Fig. 1).

Thus, with BCBD used as adhesion promoter, zinc hydroxide in the brass layer exerts no negative effect on the binding strength in the rubber–metal cord system. Furthermore, preliminary exposure of the metal cord to a humid atmosphere, promoting formation of zinc hydroxide, decreases by 10% the strength of the adhesion contact when cobalt stearate is used as modifier and increases to the same extent the strength with the modifier we suggested.

The use of an ingredient with a relatively low dropping point in most cases involves problems because of possible agglutination of granules. To impart to the

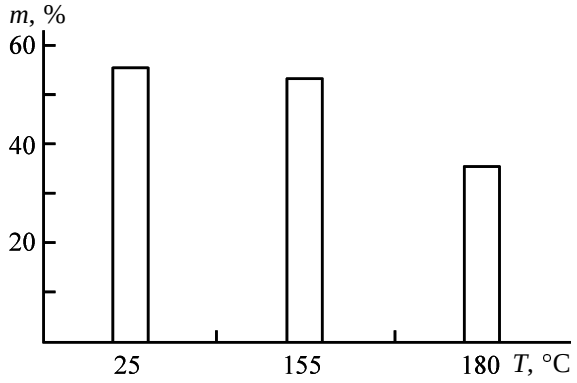


Fig. 2. Weight loss *m* of BCBD samples capsulated on BS-120 in extraction with toluene as a function of the heat treatment temperature *T*.

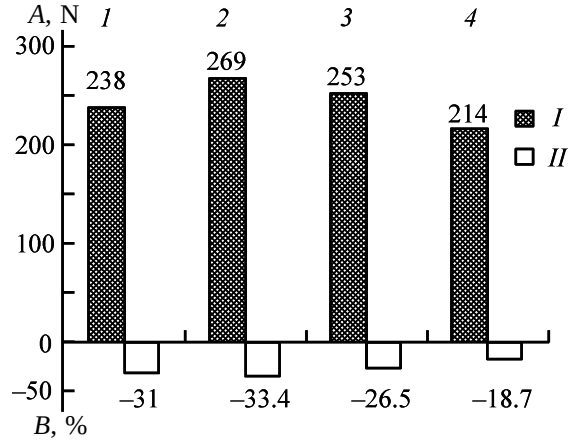


Fig. 3. (*I*) Initial strength *A* of binding of rubber with 9L15/27 brass-plated metal cord (H method) as influenced by the kind of modifier and (*II*) change *B* in the binding strength after thermal oxidative aging (100°C, 120 h). (*1*) Cobalt stearate, (*2*) BCBD capsulated on BS-120, (*3*) BCBD capsulated on BS-120 and heat-treated at 155°C, and (*4*) BCBD capsulated on BS-120 and heat-treated at 180°C.

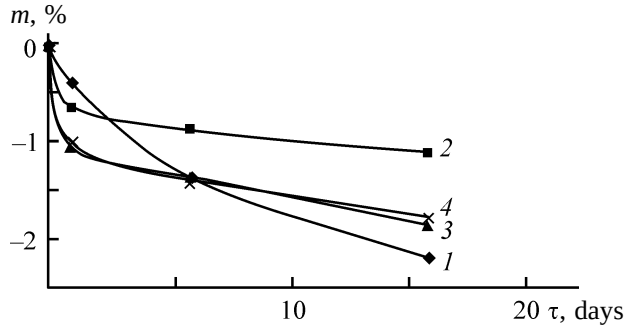


Fig. 4. Kinetics of weight loss *m* of rubber samples as influenced by the kind of the modifier. (τ) Time. (*1*) Cobalt stearate, (*2*) BKT-3, (*3*) BCBD capsulated with BS-120, and (*4*) BCBD.

products an acceptable technological shape, we used a previously developed procedure [10] involving capsulation of BD with colloidal silicic acid (white black, BS-100 or BS-120). The capsulation was performed in a ball mill. The BS-120 content in the examined modifiers was 35–38%.

It could be expected that a chemical reaction of the deblocked isocyanate groups with the silanol groups of white black and with adsorbed moisture would decrease the BD performance as adhesion promoter. Experiments on thermostating of the capsulated BDs at various temperatures and their subsequent extraction with toluene to remove the organic component show that the polyisocyanate reacts with the BS-120 surface only at 180°C. This is indicated by data shown in Fig. 2. From the samples that were not heat-treated or were heated at 155°C, the organic phase is extracted completely (52–55%), and from the samples heated at 180°C, only partially.

Hence, the adsorption interaction of BD with the surface of white black only slightly affects the modifying activity of the product heat-treated at 155°C (Fig. 3). The strength of rubber–metal cord samples obtained with this modifier is somewhat higher than that of the samples modified with cobalt stearate. It should be noted that, under the conditions of thermal oxidative aging, the rubber–metal cord samples modified with the heat-treated products show more stable binding strength parameters (Fig. 3). It is quite probable that, with non-heat-treated modifiers, the adsorbed moisture from silica causes hydrolytic degradation of the adhesion bonds in the contact zone. On the contrary, preliminary heat treatment of the products at 155°C results in removal of the adsorbed moisture and thus enhances the stability of the samples under the conditions of thermal oxidative aging. More severe heat treatment (180°C) causes not only removal of the adsorbed moisture, but also the reaction of the isocyanate groups with the silanol groups, as indicated by the results of the extraction of the organic component. As a result, the binding strength decreases.

It is interesting to compare the BDs that we suggested with the known BDs, in particular, with BKT-2 or BKT-3. The main differences in the physicochemical properties of these BDs are predetermined by the synthesis conditions. In the preparation of BKT-3, blocking of the diisocyanate is performed with a single blocking agent, ε-caprolactam, at relatively high temperatures, 145–150°C. The modifier is characterized by a branched structure owing to formation of biuret bonds and therefore has a relatively high dropping point (about 120°C).

Table 1. Interaction parameters and diffusion coefficients

Modifier	Interaction patameter χ	Diffusion coefficient $K_d \times 10^9$, $cm^2\ s^{-1}$
BKT-3	0.54	3.027
BCBD	0.51	6.005
BCBD capsulated with BS-120	–	5.490
Cobalt stearate	0.76	0.710

One of the conditions for formation of an adhesive joint is migration of the modifier to the rubber–cord boundary [11]. From the viewpoint of estimation of the distribution on the boundary, the boron-containing BD should be preferred because of its lower dropping point and better, compared to BKT-3, dispersibility in the rubber. These properties of the modifier are necessary but insufficient to ensure rapid modification of the boundary layer. Only the modifier with the high energy of egress to the surface [12] will be effective. Therefore, processes related to the diffusion of adhesion promoters to the polymer–brass-plated cord contact zone are of principal importance. The higher the diffusion rate, the more effective is the modifier [13].

We examined the diffusion activity of BCBD, BCBD capsulated with BS-120, BKT-3, and cobalt stearate. The diffusion processes were evaluated by the weight loss of rubber samples containing the modifiers being tested and stored between rubber samples containing no modifiers ("sandwich" system) [14]. We believed that the weight loss of the rubber samples was exclusively due to diffusion of the modifiers into the contacting rubber pieces. The diffusion coefficients were calculated by the procedure given in [14].

We found that BCBD and BCBD deposited onto BS-120 exhibit the highest diffusion rate in the initial period (24 h), as judged from the weight loss of the rubber samples (Fig. 4) and from the diffusion coefficients (Table 1).

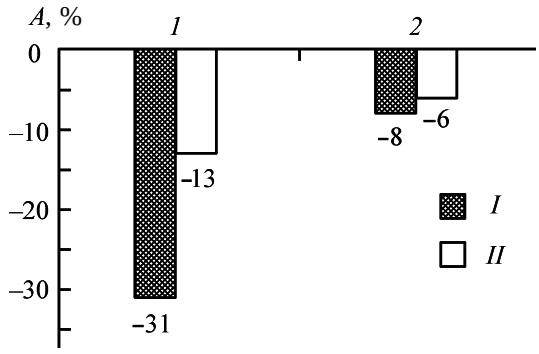


Fig. 5. Changes *A* in the strength of binding (H method) of rubber with 9L15/27 metal cord after (*I*) thermal oxidative aging (100°C, 72 h) and (*II*) salt aging (5% NaCl, 100°C, 6 h). Modifier: (*1*) BKT-3 and (*2*) BCBD capsulated with BS-120.

It should be noted that, despite close parameters of interaction with the polymer, the diffusion activity of BCBD is higher than that of BKT-3. The high diffusion coefficients of BCBD are most probably associated with its better dispersibility in the rubber matrix, which, in turn, is due to the fact that BD particles are surrounded with a surface-active dispersion medium. A BCBD particle capsulated with a silicic acid filler experiences no steric hindrance in migration toward the adhesive contact zone.

Under the conditions of thermal oxidative and salt aging (Fig. 5), BCBD compared to BKT-3 ensures more stable strength of the adhesive contact, which is consistent with the existing views [1] that the corrosion of brass-plated metal cord decelerates in the presence of boron compounds.

The physicomechanical properties of vulcanizates containing the modifiers under consideration are given in Table 2. The effect of BCBD on the strength of the vulcanizates is insignificant.

Table 2. Effect of modifiers on properties of vulcanizates

Parameter	Modifier* (1.00 wt % relative to rubber)			
	1	2	3	4
Nominal stress at 300% elongation, MPa	15.3	15.5	14.5	15.0
Nominal tensile strength, MPa	20.6	21.8	19.3	21.6
Relative elongation at break, %	407	445	397	446
Elongation set, %	27	31	24	28

* (1) Co stearate; (2–4) BCBD capsulated with BS-120, heat treatment: (2) none, (3) at 155°C, and (4) at 180°C.

CONCLUSIONS

(1) A boron-containing formulation imparting to rubber–metal cord samples high strength and stability under conditions of thermal oxidative and salt aging can be prepared by fusion of an eutectic alloy of boric acid and ε-caprolactam with blocked polyisocyanate having a dropping point of 50–70°C.

(2) Capsulation of the boron-containing blocked polyisocyanate with colloidal silicic acid, followed by heat treatment of the compounds at temperatures not exceeding 155°C, does not impair the strength of the rubber–metal cord samples.

(3) Good distribution in the rubber, low dropping point, and high diffusion activity ensure higher performance of the tested products as adhesion promoters, compared to the known blocked polyisocyanates.

REFERENCES

1. Salych, G.G., Sakharova, E.V., Shvarts, A.G., and Potapov, E.E., in *Tematicheskii obzor, Ser.: "Proizvodstvo shin"* (Topical Review, Ser.: Tire Production), Moscow: TsNIITEneftekhim, 1988, issue 8, pp. 15–49.
2. Shevtsova, K.V., Baranova, T.V., Vashchenko, Yu.M., and Pitsyk V.A., Abstracts of Papers, *IX nauchno-prakticheskaya konferentsiya "Rezinovaya promyshlennost': syr'e, materialy, tekhnologiya"* (IX Scientific and Practical Conf. "Rubber Industry: Raw and Auxiliary Materials, Technology"), Moscow, May 13–17, 2002, pp. 189–190.
3. Shmurak, I.L. and Matyukhin, S.A., in *Tematicheskii obzor, Ser.: "Proizvodstvo shin"* (Topical Review, Ser.: Tire Production), Moscow: TsNIITEneftekhim, 1989, issue 9, pp. 3–39.
4. RF Patent 2186059.
5. Puchkov, A.F., Turenko, S.V., Ogrel', A.M., and Reva, S.V., *Kauchuk Rezina*, 2002, no. 2, pp. 20–23.
6. Puchkov, A.F., Turenko, S.V., and Reva, S.V., *Kauchuk Rezina*, 2002, no. 3, pp. 16–18.
7. Turenko, S.V., Preparation of Blocked Poliisocyanate in Melts of Blocking Substances and Properties of the Resulting Compounds as Rubber Modifiers, *Cand. Sci. Dissertation*, Volgograd, 2002.
8. Kurnakov, M.S., *Izbrannye trudy* (Selected Works), Moscow: Akad. Nauk SSSR, 1961, vol. 2.
9. Puchkov, A.F., Turenko, S.V., and Reva, S.V., *Kauchuk Rezina*, 2002, no. 6, pp. 23–25.
10. Puchkov, A.F., Turenko, S.V., Ogrel', A.M., and Reva, S.V., *Kauchuk Rezina*, 2002, no. 2, pp. 23–25.
11. Tutorskii, I.A., Potapov, E.E., and Shvarts, A.G., *Khimicheskaya modifikatsiya elastomerov* (Chemical Modification of Elastomers), Moscow: Khimiya, 1993.
12. Vashchenko, Yu.N., Abstracts of Papers, *Mezhdunarodnaya konferentsiya po kauchuku i rezine* (Int. Rubber Conf.), Moscow, June 1–4, 2004, pp. 55–56.
13. Shmurak, I.L., Dedusenko, V.N., and Minyailova, V.P., *Kauchuk Rezina*, 1984, no. 2, pp. 16–17.
14. Kavun, S.M., Genkina, Yu.M., and Filippov, V.S., *Kauchuk Rezina*, 1995, no. 6, pp. 10–14.

Russian Journal of Applied Chemistry, Vol. 78, No. 9, 2005, pp. 1531–1537. Translated from Zhurnal Prikladnoi Khimii, Vol. 78, No. 9, 2005, pp. 1556–1562.
Original Russian Text Copyright © 2005 by Mamedov.

MACROMOLECULAR CHEMISTRY AND POLYMERIC MATERIALS

Sulfur-Free Vulcanization of Modified Butadiene–Acrylonitrile Rubber SKN-40PVKh-30, Aimed To Obtain Elastomeric Materials Resistant to Aggressive Media

Sh. M. Mamedov

Institute of Radiation Problems, National Academy of Sciences of Azerbaijan, Baku, Azerbaijan

Received November 17, 2004; in final form, April 18, 2005

Abstract—A study was made of the thermal, peroxide, and radiation vulcanization of modified butadiene–acrylonitrile rubber SKN-40PVKh-30 in the presence of a polyhalomethyl compound, 1,4-bis[(4-trichloromethylphenyl)dichloromethyl]benzene, with epoxy and phenol–formaldehyde resins and 4,4'-dithiobis-*N*-phenylmaleimide (a sensitizer) additionally included in the formulation with the aim to improve the technical properties of the vulcanizates and elastomeric materials. The parameters of the three-dimensional network of the vulcanizates were studied by sol–gel analysis; the total number of active chains of the network ($1/M_c$), number of cross-linked molecules ($1/M_{n_\tau}$), and gel fraction content were determined for the thermal, peroxide, radiation, and thermoradiation vulcanizates.

Sulfur-free vulcanizing systems find growing use in industry for preparing thermally stable vulcanized rubbers resistant to thermal oxidative aging and other effects. The most widely used are vulcanizing systems based on organic peroxides, synthetic resins, and polyhalo and other active additives capable of reacting with macromolecules to form three-dimensional elastomer structures based on C–C cross-links [1–5].

Depending on the conditions of elastomer vulcanization with low-molecular-weight additives, the reactions occurring in the system result in formation of not only cross-links but also groups that are located beyond the network points subsequently transforming into cross-links. These processes are considered as formation of heterogeneous vulcanization structures [6–8].

Recently there has been much interest in the formation of vulcanization structures using new organic cross-linking agents, modifiers, and sensitizers for butadiene–acrylonitrile rubbers (BNRs) [9].

When stored or used in chemically and physically aggressive media in contact with water, oil, oil-bearing fluids, clay suspensions, and fuel, elastomeric materials (EMs) prepared from SKN-40 and SKN-40M rubbers vulcanized with sulfur-containing cross-linking agents degrade because of the cleavage of chemical bonds [4, 10].

One of the major factors affecting the resistance to aggressive media and mechanical characteristics of EMs is formation of chemical structures, i.e., vulcanization bonds, in elastomers. The use of different cross-linking agents and procedures results in formation in the elastomer of different types of three-dimensional bonds, which, in turn, affects the service life of EMs [1, 10].

Effective additives in preparation of vulcanization structures are polyhalomethyl compounds (PHMCs) such as 1,4-bis[(4-trichloromethylphenyl)dichloromethyl]benzene, epoxy (ERs) and phenol–formaldehyde (PFRs) resins, dicumyl peroxide (DCP), and 4,4'-dithiobis-*N*-phenylmaleimide (DTBPMI) accelerating radiation-induced vulcanization of elastomers [8, 11]. It was also found [12, 13] that the service life of EMs operating under various conditions can be prolonged by varying the vulcanization structures. However, the role of PHMCs, ERs, DCP, and DTBPMI as cross-linking agents and sensitizers in radiation-induced processes is poorly understood, and the available data are scarce.

In this study we examined the vulcanization of a modified BNR, SKN-40PVKh-30, induced by heating and γ-irradiation with simultaneous introduction of a PHMC, 1,4-bis[(4-trichloromethylphenyl)dichloromethyl]benzene, as cross-linking agent, of epoxy and phenol–formaldehyde resins as modifiers, and of

1070-4272/05/7809-1531 © 2005 Pleiades Publishing, Inc.

Table 1. Main components and their contents in elastomer stocks based on SKN-40PVKh-30

Component	Content, wt % relative to elastomer in stock*				
	no. 1	no. 2	no. 3	no. 4	no. 5
SKN-40PVKh-30	100	100	100	100	100
PHMC	3.0	3.0	4.0	4.0	4.0
ZnO	5.0	5.0	5.0	5.0	5.0
DCP	–	4.0	–	–	–
PFR	1.0	–	–	1.0	–
Stearic acid (SA)	1.0	1.0	1.5	1.5	1.5
DTBPMI	–	–	3.0	3.0	3.0
ED-5 epoxy resin (ER)	6.0	–	6.0	6.0	6.0
P-324 carbon black	50	50	60	50	60

* Vulcanization mode: thermal (nos. 1, 2), peroxide (no. 3), radiation (no. 4), and thermoradiation (no. 5).

4,4'-dithiobis-*N*-phenylmaleimide (DTBPMI) as sensitizer. The formulation also contained dicumyl peroxide (DCP), zinc oxide, stearic acid, and P-324 carbon black, added to improve the technical properties of the vulcanizates and EMs.

EXPERIMENTAL

Elastomer stocks were prepared on rollers at 30–40°C and were vulcanized in a mold at 150–180°C (Table 1).

The radiation vulcanization was performed with a ^{60}Co γ-ray source [14]. The thermoradiation vulcanizates and elastomeric materials (EMs) were prepared by prebaking in a mold at 180°C for 5–7 min, followed by irradiation in air at 20°C to doses of 50–500 kGy at a dose rate of 6.9 Gy s^{-1}.

The sol–gel analysis was performed by the known procedure [13]. The degree of cross-linking was determined from the equilibrium swelling in toluene using the Flory–Renner equation.

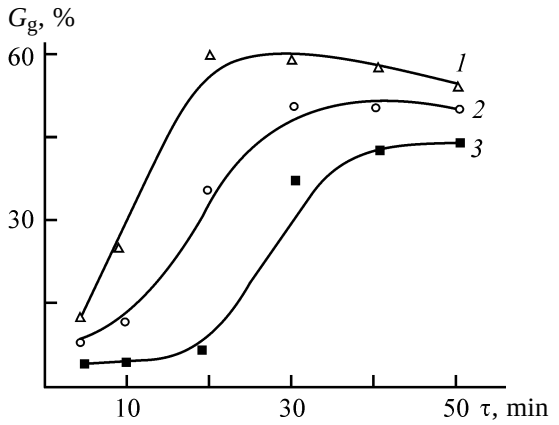


Fig. 1. Kinetic curves of gelation in elastomer mixtures based on SKN-40PVKh-30 and vulcanized by the (*1*) thermal, (*2*) sulfur, and (*3*) peroxide methods. (G_g) Gel fraction content and (τ) time.

The structural changes occurring in the rubber during vulcanization were estimated from the absorption spectra taken on an IKS-22 spectrometer.

Physicomechanical and rheological properties of the filled and unfilled rubbers were determined on samples vulcanized at elevated temperatures, by irradiation, and by combined thermoradiation treatment. The properties of the solutions were evaluated from the intrinsic viscosity, which was measured in benzene at 20°C on an Ubbelohde viscometer by the standard procedure. In calculations we used the Mark–Houwink equation with $K = 1.16 \times 10^5$ and $\alpha = 0.73$ [15].

The cross-links formed in the course of elastomer vulcanization consist of atomic groups of the vulcanizing system, or are simply the valence bonds between the atoms of the molecular chain of the elastomer. The structure of the vulcanization nodes depends on the composition of the vulcanizing system and the elementary reactions occurring between the cross-linking agent and elastomer.

The major vulcanization process is accompanied by chain degradation and internal addition of cross-linking agents and other reactive components. The formation of vulcanization networks depends on the relative reactivity of the elastomer in these processes.

The sol–gel analysis allows determination of the three-dimensional network parameters from the content of the gel (insoluble) fraction in the vulcanizate.

As expected, the gel content noticeably increases with the heating time (Fig. 1). The highest gel content in the model stocks indicates that the PHMC and ER

Table 2. Influence of the vulcanization mode (thermal, peroxide, radiation, thermoradiation) on the intrinsic viscosity [η] of SKN-40PVKh-30 rubber (VR-2 viscometer, benzene, 20°C) and the cross-linking rate*

Vulcanization	Vulcanizing system	[η]	τ_5, min	$\tau_{35} - \tau_5$
Sulfur (known)	Sulfur + Altax + SA + ZnO	1.72	1.8	5.6
Thermal	PHMC + ZnO + SA + ER	1.60	4.5	5.4
Peroxide (160°C, 25 min)	DCP + ZnO + SA + PFR + PHMC	1.58	5.0	5.9
Radiation (D = 300 kGy)	PHMC + ZnO + ER + SA + DTBPMI	1.45	5.7	6.8
Thermoradiation (180°C, 5 min, D = 400 kGy)	PHMC + ZnO + ER + SA + DTBPMI	1.69	3.5	4.2

* (τ_5) Time of vulcanization onset and ($\tau_{35} - \tau_5$) characteristic of the vulcanization rate.

participate in the cross-linking. As the measurements show, the gel fraction content in radiation and thermoradiation vulcanizates noticeably increases as the concentration of the vulcanizing systems in the elastomer bulk and the radiation dose are increased (Fig. 2). It should be noted that the initial gelation (100 kGy) corresponds to formation of one cross-linked polymeric unit per number-average rubber molecule. When insoluble fractions are formed at maximal doses (500 kGy), at a PHMC content of 4 wt % relative to the elastomer, the gel content in the radiation and thermoradiation vulcanizates reaches 58 and 80%, respectively.

One of the features of the elastomers is their high molecular weight, imparting to them unusual and valuable properties. Furthermore, the cross-linked elastomer consists of macromolecuels of different lengths, i.e., it is nonuniform in the molecular weight. The molecular weight of cross-linked elastomers was determined viscometrically. We evaluated the dependence of the viscosity of the unfilled vulcanizates on the heating time and irradiation dose.

The results of monitoring the intrinsic viscosity (Table 2) show that the molecular weights of the chemical and thermoradiation vulcanizates rapidly change. The elastomer stocks containing PHMC and ER give vulcanizates of higher molecular weights, compared to peroxide vulcanizates.

From the intrinsic viscosity we determined how the molecular weight of SKN-40PVKh-30 rubber varies in the course of vulcanization. In chemical vulcanization, it increases from 150.0 to 250.0 kDa within 25–35 min. With peroxide vulcanization, the pattern is different. Table 2 shows that the radiation vulcanization occurs more slowly than the thermal and peroxide vulcanization.

Interesting features are exhibited by thermoradiation vulcanizates in the presence of PHMC, ER, and DTBPMI. Additions of DTBPMI increase the degree of cross-linking by 15–20%. At a dose of 400 kGy, changes in the intrinsic viscosity of the thermoradiation vulcanizate are more pronounced compared to the thermal, peroxide, and radiation vulcanizates.

The rheological properties of vulcanizates are important service parameters of elastomers. We determined these properties viscometrically with a VR-2 Mooney viscometer. These properties are particularly sensitive to the molecular-weight distribution of a polymer.

The tendency of elastomer stocks to scorching was evaluated from the time in which the sample viscosity became higher than the initial value by 5 units.

The tendency to scorching is characterized by two parameters: (a) scorching onset time τ_5 in which the viscosity of the sample increased by unity and

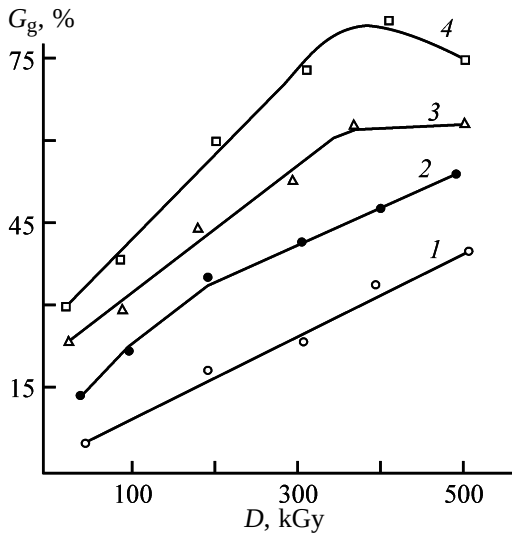


Fig. 2. Influence of the irradiation dose D on the gelation in (*1*, *2*) radiation and (*3*, *4*) thermoradiation vulcanizates based on SKN-40PVKh-30 rubber. (G_g) Gel fraction content. PHMC concentration, wt % relative to elastomer: (*1*, *3*) 2.0 and (*2*, *4*) 4.0.

Table 3. Influence of the vulcanization mode (thermal, peroxide, radiation, thermoradiation) on the total mumber of network chains $1/M_c$ and number of cross-linked molecules $1/M_{n_\tau}$ in SKN-40PVKh-30 vulcanizates

Vulcanization	Vulcanizing system	$1/M_c \times 10^5$	$1/M_{n_\tau} \times 10^5$
		mol cm^{-3}	
Sulfur (known)	Sulfur + Altax + SA + ZnO	11.2	4.7
Thermal	PHMC + ZnO + SA + ER	10.1	2.5
Peroxide (160°C, 25 min)	DCP + ZnO + SA + PFR + PHMC	11.5	2.2
Radiation (D = 300 kGy)	PHMC + ZnO + ER + SA + DTBPMI	6.7	0.92
Thermoradiation (180°C, 5 min, D = 400 kGy)	PHMC + ZnO + ER + SA + DTBPMI	12.3	4.0

(b) cross-linking rate evaluated as ($\tau_{35} - \tau_5$), where τ_{35} is the time in which the sample viscosity became higher than the initial value by 35 units. Both these quantities were taken as average values from tests of no less than two samples.

Examination of the influence of the PHMC, ER, DTBPMI, and PFR concentrations on the properties of rubber stocks and vulcanizates revealed an interesting trend. In contrast to common sulfur-containing cross-linking systems, on adding 3–4 wt % PHMC as cross-linking agent, 6.0 wt % epoxy compounds, and DTBPMI, the cross-linking induction period increased and not decreased, which reflects the higher resistance of these stocks to scorching.

At the same time, an increase in the PHMC content from 3.0 to 5.0 wt % relative to elastomer significantly affected the vulcanization activity of the system.

Also, an increase in the PHMC concentration in the peroxide and radiation vulcanizates does not noticeably affect the Mooney viscosity. All these results show that the vulcanizing group given in Table 1 should be considered as optimal for the stocks based on modified SKN-40PVKh-30.

As judged from the cross-linking rate, the thermoradiation and thermal vulcanization with the examined systems are the most efficient for SKN-40PVKh-30.

The calculation of structural parameters of unfilled rubbers from the results of sol–gel analysis is based on the use of quantitative relationships of the statistical theory of the structure of polymer networks, which does not take into account the physical state of molecular chains. According to this theory, the network structure is determined by the molecular weight of the elastomer, functionality of the forming network points, and molecular-weight distribution of the polymer.

The use of sol–gel analysis for determining structural parameters of the vulcanization network formed under the action of sulfur, PHMC, ER, and DCP allows more comprehensive characterization of the properties of the vulcanizates obtained using cross-linking agents.

Table 3 shows that the total number of active chains ($1/M_c$) in vulcanizates obtained with the examined system increases in accordance with the activity of the system. Higher concentration of these chains in thermoradiation and thermal vulcanizates obtained with the examined cross-linking systems, as compared to the traditional and peroxide vulcanizates, suggests more efficient cross-linking in the presence of PHMC and ER. In the radiation vulcanizates, on the contrary, the three-dimensional network is less thick than in peroxide and other examined vulcanizates.

To confirm the assumptions concerning the reactions of SKN-40PVKh-30 and PHMC in the course of cross-linking, we made a number of additional experiments.

After heating and irradiation for various times, we determined the content of total and bound chlorine in the vulcanizate and the content of chlorine in the form of $ZnCl_2$ (in both cases, relative to the amount added with the cross-linking agent). From these quantities, we calculated the number of incorporated PHMC molecules per cross-link. The results are given in Table 3.

With all the vulcanizing systems tested, the total content of chlorine somewhat decreases with increasing vulcanization time, and the content of bound chlorine increases. In particular, the amount of chlorine that has reacted with ZnO to form $ZnCl_2$ increases. This fact suggests simultaneous occurrence of the chlorine elimination from cross-linking agent molecules, evolution of volatile chlorine compounds, reaction with ZnO to form $ZnCl_2$, and addition of the organochlorine molecules to the rubber molecules, up

Table 4. Physicomechanical properties of vulcanizates based on modified SKN-40PVKh-30 rubber

Parameter	Cross-linking				
	with sulfur (C–S_x–C)	thermal (C–C)	peroxide (C–C)	radiation (C–C)	thermoradiation (C–C)
Stress at 300% elongation, MPa	12	14	9	8	15
Tensile strength f_t, MPa	25	26	22	21	27
Relative elongation ε_b, %	510	500	480	480	460
Rebound elasticity, %	26	27	29	29	31
TM-2 hardness, arb. units	61	63	65	65	57
Residual compression strain (20%, 150°C, 72 h), %	68	62	60	52	54
Dynamic endurance at repeated extension N (150%, 500 cycles per minute), thousands of cycles	21	18	22	20	23
Thermal aging coefficient (150°C, 144 h):					
for f_t	0.53	0.69	0.62	0.84	0.89
for ε_b	0.34	0.41	0.52	0.61	0.66
for N	0.51	0.60	0.71	0.78	0.82
Weight gain upon swelling in benzine–benzene mixture (3 : 1, 80°C, 24 h), wt %	54	46	40	30	35

to complete binding of the cross-linking agent with the elastomer, as indicated by a decrease in the PHMC content in the toluene extract. At longer heating and irradiation, the concentration of cross-links in the bulk of the vulcanizate increases and the number of incorporated PHMC molecules per cross-link decreases.

It should be noted, however, that calculation of this parameter, as we have done and as is done commonly, does not afford an informative result. Indeed, in our calculations we neglect the fact that, after partial elimination of chlorine, the molecular weight of the fragments bound to the elastomer becomes appreciably lower than that of the PHMC molecule as a whole. Also, PHMC molecules apparently decompose into two fragments, each capable of reacting with the elastomer; this fact is not taken into account either. Therefore, the number of cross-linking agent molecules per cross-link may be appreciably underestimated.

The molecular structure of the rubber changes similarly in the course of heating and irradiation. However, the background substantially increases under irradiation, which prevents quantitative determinations. Comparison of the IR spectra of the vulcanizates prepared by thermal and thermoradiation treatment in the presence of PHMC + ER + ZnO allows the following conclusions. Some trends are similar in both cases. The intensities of the bands at 1440 cm^{-1}, assignable to the C–H bending vibrations in $–CH_2–$ groups [7], and at 1340 cm^{-1}, assignable to the out-of-plane C–H bending vibrations in *trans*-CH=CH groups [6], decrease. A new band appearing at about 2240 cm^{-1} is assigned by some authors to complexes formed by metal chlorides with the –C≡N groups of the rubber [15]. The band at 740 cm^{-1} belonging to C–C vibrations noticeably decreases in the intensity [14]. This fact suggests that the cross-linking agent eliminates chlorine under the action of elevated temperatures and irradiation; this fact is apparently responsible for a decrease in the intensity of the band at 1230 cm^{-1}. Hence, addition of PHMC and ER to SKN-40PVKh-30-based stocks appreciably affects the cross-linking under various treatment modes.

It is known that the optimal structure of the vulcanization network of acrylonitrile rubbers, combining sufficient resistance to petroleum products, aggressive media, and thermal oxidation with the high performance under repeated strains and shear, should contain cross-links of different types, both polysulfide and those containing small amounts of sulfur or no sulfur, including C–C bonds [4].

Therefore, the physicomechanical properties of rubbers based on SKN-40PVKh-30 are of interest (Table 4). We found that PHMC and ER are reactive in all the vulcanization modes, especially in the presence of DTBPMI.

The radiation vulcanizates are inferior to thermoradiation vulcanizates in the strength but surpass thermal vulcanizates in the resistance to heat and solvents.

To elucidate the effect of temperature and service

Table 5. Changes in the performance characteristics of elastomeric materials based on SKN-40PVKh-30 in aggressive media* (treatment at 150°C for 72 h)

Parameter	Vulcanization				
	with sulfur	thermal	peroxide	radiation	thermoradiation
Nomonal tensile strength f_t, MPa					
I	15	13	10	9	18
II	14	16	13	10	21
III	15	18	14	10	20
Thermal aging coefficient (I/II):					
for f_t	0.46/0.57	0.61/0.72	0.53/0.66	0.69/0.73	0.73/0.79
for ε_b	0.52/0.65	0.63/0.77	0.64/0.72	0.80/0.76	0.87/0.81
Accumulation of residual compression strain, %					
I	67	57	60	53	53
II	56	44	53	47	42
III	60	42	51	45	40
Weight gain upon swelling, wt %					
I	147	127	125	103	108
II	94	88	84	68	64
III	72	66	62	54	50

* Medium: (I) seawater, (II) oil-bearing fluid, and (III) clay suspension.

conditions on the EM properties, we tested the EM samples at 150°C in aggressive media (Table 5). We found that the experimental EMs containing PHMC, ER, and DTBPMI, compared to the traditional (sulfur) vulcanizates, show lower swelling and residual compression strain and higher thermal aging coefficient in seawater and oil-bearing fluids. The tensile strength of the radiation vulcanizates after the contact with the aggressive medium decreased to a greater extent than that of the thermal and thermoradiation vulcanizates.

Thus, SKN-40PVKh-30-based thermal vulcanizates prepared by the radiation-chemical process in the presence of PHMC, ER, and DTBPMI surpass the vulcanizates prepared by the traditional procedures (sulfur, peroxide) in the resistance to thermal aging and in the dynamic endurance at repeated extension in aggressive media. All the examined stocks and cross-linking agents were recommended for use in EM formulations for fabricating sealing parts resistant to aggressive media for petroleum industry, using the radiation-chemical technology.

CONCLUSIONS

(1) The action of PHMC as a cross-linking agent in thermal, peroxide, radiation, and thermoradiation vulcanization of SKN-40PVKh-30 rubber in the presence of certain organic compounds (ER, PFR, DTBPMI) was studied.

(2) Structural changes occurring in SKN-40PVKh-30-based vulcanizates under the action of elevated temperatures and irradiation were examined.

(3) The IR spectra and data on the intrinsic viscosity, on the rates of reactions involving PHMC and the examined organic compounds, and on the structural parameters of the vulcanization networks allowed certain conclusions on the nature of the vulcanizing effect of the cross-linking systems tested and on their influence on the rheological and physicomechanical properties of the vulcanizates.

(4) The elastomeric materials prepared by the thermochemical and thermoradiation procedures are characterized by a medium ultimate strength and increased thermal aging coefficient, accumulation of residual strain, and weight gain; they surpass sulfur vulcanizates in the resistance to aggressive media.

(5) A formulation based on modified SKN-40PVKh-30 rubber and a procedure based on radiation-chemical technology were developed. The elastomeric materials resistant to aggressive media were recommended for use in oil well drilling.

REFERENCES

1. Mamedov, Sh.M., Yadreev, F.I., and Rivin, E.M., *Butadien-nitril'nye kauchuki i reziny na ikh osnove* (Butadiene–Acrylonitrile Rubbers and Vulcanizates Based on Them), Baku: Elm, 1991.

2. Mamedov, Sh.M., Abstracts of Papers, *The Third Eurasian Conf. on Nuclear Science and Its Application*, Tashkent, October 5–8, 2004, p. 127.
3. Mamedov, Sh.M., *Azerb. Khim. Zh.*, 2003, no. 4, pp. 103–107.
4. Mamedov, Sh.M., *Prots. Neftekhim. Neftepererab.*, 2004, no. 2, pp. 48–56.
5. Mamedov, Sh.M., *Kauchuk Rezina*, 2001, no. 3, pp. 5–8.
6. Schaal, S., Coran, A.Y., and Mowdood, S.K., *Rubber Chem. Technol.*, 2000, vol. 73, no. 2, p. 2463.
7. Mamedov, Sh.M., *Azerb. Khim. Zh.*, 2000, no. 3, pp. 46–50.
8. USSR Inventor's Certificate no. 1399311.
9. Mamedov, Sh.M., Abstracts of Papers, *Vsesoyuznaya konferentsiya po teoreticheskoi i prikladnoi radiatsionnoi khimii* (All-Union Conf. on Theoretical and Applied Radiation Chemistry), Obninsk, September 22–25, 1985, pp. 279–280.
10. Ponamarev, A.N., *Zh. Vses. Khim. O–va.*, 1986, vol. 31, no. 1, pp. 84–86.
11. Mamedov, Sh.M., *Khim. Neftekhim.*, 2001, no. 2, pp. 34–38.
12. Breger, A.Kh., Vainshtein, B.I., and Syrkus, N.P., *Osnovy radiatsionno-khimicheskogo apparatostroeniya* (Principles of Radiation-Chemical Apparatus Making), Moscow: Atomizdat, 1967.
13. Kuznetsov, E.V., Divgun, S.M., and Budarina, L.A., *Praktikum po khimii i fizike polimerov* (Practical Course of Polymer Chemistry and Physics), Moscow: Khimiya, 1977.
14. Bellamy, L.J., *The Infra-Red Spectra of Complex Molecules*, New York: Wiley, 1957.
15. Zakharov, N.D. and Kuznetsov, V.A., *Vysokomol. Soedin., Ser. A*, 1978, vol. 10, no. 1, pp. 331–338.

Russian Journal of Applied Chemistry, Vol. 78, No. 9, 2005, pp. 1538–1539. Translated from Zhurnal Prikladnoi Khimii, Vol. 78, No. 9, 2005, pp. 1563–1564.
Original Russian Text Copyright © 2005 by Nikandrov, Mikhailov.

BRIEF COMMUNICATIONS

Density and Viscosity of Sodium Phosphate Solutions

M. I. Nikandrov and Yu. I. Mikhailov

Dzerzhinsk Branch, Nizhni Novgorod State University, Dzerzhinsk, Nizhni Novgorod oblast, Russia

Received December 6, 2004

Abstract—The density and viscosity of sodium phosphate solutions with a concentration of 30–41.6 wt % at 70–100°C were determined.

In preparation of $Na_2HPO_4 \cdot 7H_2O$ and $Na_3PO_4 \cdot 10H_2O$, the polythermal precipitation is performed from more concentrated solutions than in preparation of the dodecahydrates. Data on properties of sodium phosphate solutions are available for concentration of up to 26–30 wt % [1, 2]; data on the properties of more concentrated solutions, which are necessary for process calculations and choice of the equipment, are lacking.

In this study we determined pycnometrically the density of the binary solutions of sodium hydrophosphate and orthophosphate and of mutual solutions of sodium carbonate and hydrophosphate at 70–100°C and measured their viscosity with a VPZh-3 viscometer (see table). Solutions were prepared from the analytically pure grade salts.

The results obtained show that the density of the sodium phosphate solutions increases with the number of sodium atoms in the phosphate formula unit (see figure). For example, the density of the solution at 80°C changes from 1105 kg m^{-3} (phosphoric acid) to 1172 (NaH_2PO_4), 1220 (Na_2HPO_4), and 1427 kg m^{-3} (Na_3PO_4). This is due to the fact that increasing fraction of sodium ions, and, consequently, charge of the phosphate ions in the solution causes a corresponding decrease in the fraction of "free" water molecules and thus results in the ordering of the solution structure.

The fact that the rate of the density growth somewhat decreases as the number of substituted hydrogen ions in the phosphate increases is likely due to partial occurrence of the reactions

$$Na_3PO_4 + H_2O \rightleftarrows Na_2HPO_4 + NaOH,$$

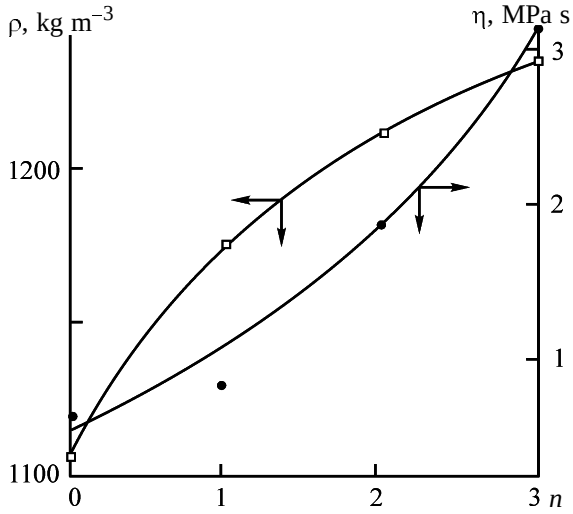
$$Na_2HPO_4 + H_2O \rightleftarrows NaH_2PO_4 + NaOH,$$

altering the true composition of the solution.

Density and viscosity of sodium phosphate solutions

Solution composition, wt %			Density ρ, kg m^{-3}, and viscosity η, mPa s, at indicated temperature °C							
Na_2CO_3	Na_2HPO_4	Na_3PO_4	70		80		90		100	
			ρ	η	ρ	η	ρ	η	ρ	η
32.0	–	–	1330	2.60	1319	2.04	1308	1.58	1301	1.33
31.0	6.2	–	1316	3.41	1312	2.72	1307	2.15	1299	1.75
31.4	13.0	–	1337	4.24	1326	3.40	1320	2.61	1315	2.13
–	30.0	–	1232	1.74	1227	1.27	1220	0.86	1211	0.63
–	32.6	–	1258	2.70	1252	2.01	1240	1.51	1228	1.03
–	36.3	–	1290	4.23	1280	2.98	1271	2.25	1262	1.50
–	41.6	–	1332	5.82	1313	4.76	1304	3.70	1297	3.21
–	–	25.8	1211	1.86	1208	1.53	1206	1.20	1204	0.87
–	–	31.1	1254	3.62	1246	2.64	1236	2.06	1225	1.55
–	–	36.6	1282	4.70	1274	3.42	1264	2.95	1253	2.40

1070-4272/05/7809-1538© 2005 Pleiades Publishing, Inc.



Density ρ and viscosity η of the solutions at 80°C as functions of the number of sodium atoms in the phosphate formula unit *n*.

The viscosity of the phosphate solutions as a function of temperature in the coordinates $\log\eta - 1/T$ is a linear dependence, which allows determination of the entropy of viscous flow (94.6 J mol^{-1} K^{-1} for Na_2HPO_4 solution and 97.1 J mol^{-1} K^{-1} for Na_3PO_4 solution). The activation energies of the viscous flow are 16.7 and 16.1 kJ mol^{-1}, respectively.

The viscosity of the solutions with the same mole fractions of phosphates (2.4–2.6 kmol m^{-3}) increases also proportionally to the number of sodium atoms in the phosphate. It should be noted that the viscosities of NaH_2PO_4 solutions and phosphoric acid differ only slightly.

The results obtained will be useful for engineering calculations in the sodium phosphate technology.

REFERENCES

1. *Termicheskaya fosfornaya kislota, soli i udobreniya na ee osnove* (Thermal Phosphoric Acid and Salts and Fertilizers on Its Basis), Postnikov, N.M., Ed., Moscow: Khimiya, 1976.
2. Zaitsev, I.D., and Aseev, G.G., *Fiziko-khimicheskie svoistva binarnykh i mnogokomponentnykh rastvorov neorganicheskikh veshchestv. Spravochnoe izdanie* (Physicochemical Properties of Binary and Multicomponent Solutions of Inorganic Substances: Handbook), Moscow: Khimiya, 1988.

Russian Journal of Applied Chemistry, Vol. 78, No. 9, 2005, pp. 1540–1542. Translated from Zhurnal Prikladnoi Khimii, Vol. 78, No. 9, 2005, pp. 1565–1567.
Original Russian Text Copyright © 2005 by Demidov, Markelov.

BRIEF COMMUNICATIONS

Thermodynamics of Fuel Combustion at Tuyeres of a Blast Furnace

A. I. Demidov and I. A. Markelov

St. Petersburg State Polytechnic University, St. Petersburg, Russia

Received June 16, 2005

Abstract—A thermodynamic analysis of fuel (carbon and methane) combustion at tuyeres of a blast furnace is made.

As is known [1], coal coke and natural gas are used as fuel in manufacture of cast iron. The combustion of coke and natural gas in the tuyere zone of a blast furnace strongly affects the entire run of a melting in a blast furnace and is highly important for control over the operation of a blast furnace. Methane, the main component of natural gas, virtually completely decomposes at temperatures exceeding 1273 K into carbon and hydrogen [2]:

$$CH_4 = C + 2H_2. \quad (1)$$

The reaction space at tuyeres of a blast furnace can be conventionally divided into two zones, oxidative and reductive. In combustion of carbon and methane in the oxidative zone, the following reactions are possible [3, 4]:

$$2C + O_2 = 2CO, \quad (2)$$

$$C + O_2 = CO_2, \quad (3)$$

$$2CO + O_2 = 2CO_2, \quad (4)$$

$$CH_4 + 3/2O_2 = CO + 2H_2O, \quad (5)$$

$$CH_4 + 2O_2 = CO_2 + 2H_2O, \quad (6)$$

$$CH_4 + 1/2O_2 = CO + 2H_2, \quad (7)$$

$$CH_4 + O_2 = CO_2 + 2H_2, \quad (8)$$

$$H_2 + 1/2O_2 = H_2O. \quad (9)$$

The combustion of carbon and methane in the reductive zone is accompanied by reactions of carbon and methane with carbon(IV) oxide and water in a gaseous state:

$$C + CO_2 = 2CO, \quad (10)$$

$$CH_4 + CO_2 = 2CO + 2H_2, \quad (11)$$

$$C + H_2O = CO + H_2, \quad (12)$$

$$CH_4 + H_2O = CO + 3H_2. \quad (13)$$

The forming carbon(II) oxide undergoes conversion:

$$CO + H_2O = CO_2 + H_2. \quad (14)$$

Here we made a comparative analysis of the standard Gibbs energies of the reactions of fuel combustion at tuyeres of a blast furnace. The standard Gibbs energies of the reactions were calculated per mole of atoms of the starting substances, as it was done in [5]. The input data for calculating the standard Gibbs energies of the reactions were taken from the reference book [6]. The results of the calculations are presented in Tables 1, 2 and Figs. 1, 2.

As seen in Fig. 1, the largest negative changes in the standard Gibbs energy in the oxidative zone at

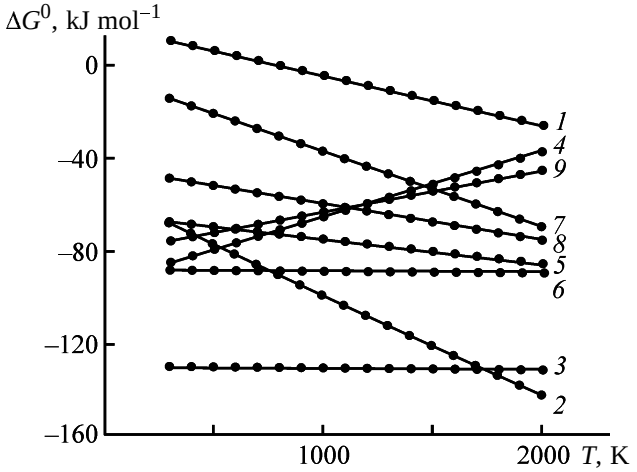


Fig. 1. Standard Gibbs energies ΔG^0 of reactions (1)–(9) vs. temperature T. Digits at curves are numbers of reactions; the same for Fig. 2.

1070-4272/05/7809-1540 © 2005 Pleiades Publishing, Inc.

Table 1. Standard Gibbs energies of reactions (1)–(9) in the temperature range 298–2000 K

T, K	ΔG^0, kJ mol^{-1}, for indicated reaction								
	(1)	(2)	(3)	(4)	(5)	(6)	(7)	(8)	(9)
298	10.2	–68.6	–131.5	–85.8	–68.2	–89.2	–14.4	–49.1	–76.5
300	10.1	–68.7	–131.5	–85.7	–68.2	–89.2	–14.5	–49.1	–76.4
400	8.4	–73.2	–131.6	–82.8	–69.2	–89.1	–17.4	–50.4	–74.9
500	6.6	–77.8	–131.7	–79.9	–70.3	–89.1	–20.5	–51.8	–73.3
600	4.6	–82.3	–131.8	–77.0	–71.4	–89.1	–23.6	–53.2	–71.6
700	2.6	–86.8	–131.9	–74.0	–72.5	–89.1	–26.8	–54.7	–69.9
800	0.5	–91.3	–132.0	–71.1	–73.6	–89.1	–30.1	–56.2	–68.1
900	–1.7	–95.8	–132.0	–68.2	–74.7	–89.2	–33.3	–57.8	–66.3
1000	–3.8	–100.2	–132.1	–65.3	–75.8	–89.2	–36.6	–59.4	–64.5
1100	–6.0	–104.6	–132.1	–62.4	–76.9	–89.2	–39.9	–60.9	–62.6
1200	–8.3	–109.6	–132.1	–59.5	–78.0	–89.2	–43.2	–62.5	–60.8
1300	–10.5	–113.4	–132.1	–56.6	–79.1	–89.1	–46.5	–64.1	–58.9
1400	–12.7	–117.7	–132.2	–53.7	–80.1	–89.1	–49.8	–65.7	–57.0
1500	–14.9	–122.0	–132.2	–50.8	–81.1	–89.1	–53.1	–67.3	–55.1
1600	–17.2	–126.2	–132.1	–48.0	–82.2	–89.0	–56.4	–68.9	–53.2
1700	–19.4	–130.5	–132.1	–45.1	–83.2	–89.0	–59.7	–70.5	–51.2
1800	–21.6	–134.7	–132.1	–42.3	–84.2	–88.9	–62.9	–72.1	–49.3
1900	–23.9	–138.9	–132.1	–39.5	–85.2	–88.9	–66.2	–73.7	–47.4
2000	–26.1	–143.1	–132.1	–36.7	–86.2	–88.8	–69.5	–75.3	–45.4

high temperatures are characteristic of reactions (2) and (3). Straight line *2* [reaction (2)] intersects straight line *3* [reaction (3)] at 1750 K. To the right of the intersection point, straight line *2* runs lower than straight line *3*. This means that the chemical affinity of carbon for oxygen under the conditions of CO formation is the highest at high temperatures (above 1750 K). As temperature increases, the equilibria of reactions (4) and (9) are shifted toward formation of carbon(II) oxide and oxygen, and hydrogen and oxygen.

The standard Gibbs energy of the methane dissociation becomes negative at temperatures above 800 K, i.e., the equilibrium of reaction (1) increasingly shifts toward formation of carbon and hydrogen as temperature becomes higher. Of all the reactions of methane oxidation [reactions (5)–(8)], reaction (6), which yields carbon(IV) oxide and water, has the most negative values of the standard Gibbs energy. At low temperatures (< 700 K), the standard Gibbs energy of reaction (6) becomes even more negative than thate for reaction (2).

The results obtained in calculating the standard Gibbs energies of the reactions of carbon and methane combustion in the reductive zone of the furnace [reactions (10)–(13)] indicate that the values of ΔG^0 for

Table 2. Standard Gibbs energies of reactions (1)–(9) in the temperature range 298–2000 K

T, K	ΔG^0, kJ mol^{-1}, for indicated reaction				
	(10)	(11)	(12)	(13)	(14)
298	30.0	21.4	23.0	17.9	–5.6
300	30.0	21.3	23.0	17.8	–5.6
400	25.5	18.0	19.6	15.0	–4.8
500	21.0	14.6	16.1	12.1	–4.0
600	16.6	11.2	12.6	9.2	–3.2
700	12.1	7.7	9.0	6.1	–2.5
800	7.7	4.1	5.4	3.0	–1.8
900	3.2	0.6	1.9	–0.1	–1.1
1000	–1.2	–3.0	–1.7	–3.3	–0.5
1100	–5.5	–6.6	–5.3	–6.4	0.2
1200	–9.9	–10.1	–8.9	–9.6	0.8
1300	–14.2	–13.7	–12.5	–12.8	1.4
1400	–18.6	–17.2	–16.1	–16.0	2.0
1500	–22.9	–20.8	–19.7	–19.2	2.6
1600	–27.1	–24.3	–23.2	–22.4	3.1
1700	–31.4	–27.8	–26.8	–25.5	3.7
1800	–35.6	–31.3	–30.4	–28.7	4.2
1900	–39.8	–34.8	–33.9	–31.9	4.7
2000	–44.1	–38.3	–37.5	–35.1	5.3

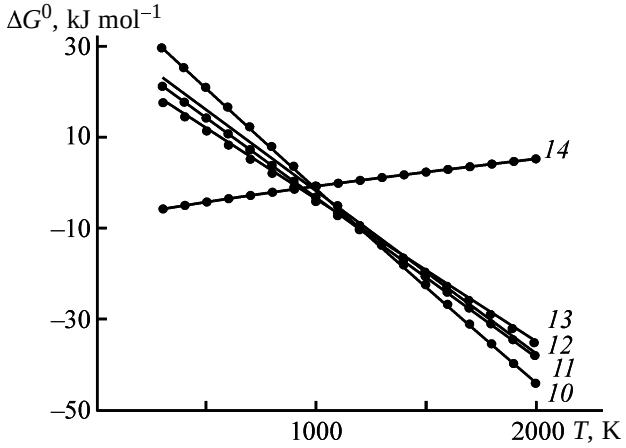


Fig. 2. Standard Gibbs energies ΔG^0 of reactions (10)–(14) vs. temperature T.

these reactions are close. At temperatures exceeding 1000 K, reactions (10)–(13) have negative standard Gibbs energies. As temperature becomes higher, the equilibria of these reactions increasingly shift toward formation of carbon(II) oxide and hydrogen. At high temperatures, reaction (14) of carbon(II) oxide conversion has positive standard Gibbs energy, i.e., gives a low yield of the reaction product [7].

Thus, thermodynamic analysis of fuel (carbon and methane) combustion at tuyeres of a blasting furnace shows that carbon(II) oxide and hydrogen must predominate in gases leaving the furnace. The experiments carried out in [8] confirm this conclusion. As a result of fuel combustion in the tuyere zone of the blasting furnace, the temperature of the gas reaches 2300 K. In this case, the content of methane and water vapor in the gas decreases nearly to zero. Carbon(II) oxide and hydrogen predominate in the reductive zone of the blasting furnace.

CONCLUSION

Thermodynamic analysis of fuel (carbon and methane) combustion at tuyeres of a blasting furnace and results of experimental studies show that carbon(II) oxide and hydrogen predominate in gases leaving the furnace.

REFERENCES

1. *Domennoe proizvodstvo: Spravochnoe izdanie* (Blast-Furnace Steel Production: Reference Book), vol. 1: *Podgotovka rud i domennyi protsess* (Ore Pretreatment and Blast-Furnace Process), Vegman, E.F., Ed., Moscow: Metallurgiya, 1989, vol. 1.
2. Chichibabin, A.E., *Osnovnye nachala organicheskoi khimii* (Fundamentals of Organic Chemistry), Sergeev, P.G., Ed., Moscow: Goskhimizdat, 1954, vol. 1.
3. Vvedenskii, A.A., *Termodinamicheskie raschety protsessov toplivnoi promyshlennosti* (Thermodynamic Calculations of Processes in Fuel Industry), Leningrad: Gostoptekhizdat, 1949.
4. Lavrov, N.V., *Fiziko-khimicheskie osnovy protsessa goreniya topliva* (Physicochemical Foundations of Fuel Combustion), Moscow: Nauka, 1971.
5. Demidov, A.I. and Markelov, I.A., *Zh. Prikl. Khim.*, 2005, vol. 78, no. 4, pp. 721–724.
6. Barin, I., Knacke, O., and Kubaschewski, O., *Thermochemical Properties of Inorganic Substances*. New York: Springer, 1973.
7. Gerasimov, Ya.I., Dreving, V.P., Eremin, E.N., *et al.*, *Kurs fizicheskoi khimii* (Course of Physical Chemistry), Gerasimov, Ya.I., Ed., Moscow: Khimiya, 1969, vol. 1.
8. Chaika, A.L., Ruchaevskii, A.L., Vasil'ev, A.P., *et al.*, *Chern. Met.*, 2003, December, pp. 8–14.

Russian Journal of Applied Chemistry, Vol. 78, No. 9, 2005, pp. 1543–1545. Translated from Zhurnal Prikladnoi Khimii, Vol. 78, No. 9, 2005, pp. 1568–1570.
Original Russian Text Copyright © 2005 by Morachevskii, Kuznetsova, Kal'ko.

BRIEF COMMUNICATIONS

Reaction of Calcium Hydroxide with the Oxide–Sulfate Fraction of Lead Battery Scrap

A. G. Morachevskii, Yu. S. Kuznetsova, and O. A. Kal'ko

St. Petersburg Polytechnic University, St. Petersburg, Russia
Cherepovets State University, Cherepovets, Vologda oblast, Russia

Received August 18, 2005

Abstract—The reaction of oxide–sulfate fraction of lead battery scrap with an aqueous suspension of calcium hydroxide was studied experimentally.

The up-to-date technologies intended for recycling lead battery scrap involve separation of scrap onto metallic, oxide–sulfate, and organic fractions and their subsequent reprocessing [1, 2]. In this utilization procedure, extraction of lead from the oxide–sulfate fraction into which the active masses of the positive and negative plates pass is an important problem. After washing with water and drying, the oxide–sulfate fraction contains, on the average, wt %: Pb 73.5, Sb up to 1.3, As up to 0.04, Cu 0.1, Fe 0.05, and SO_4^{2-} 16.7 (the remainder oxygen) [3]. A study of the mineralogical composition revealed PbO_2 and $PbSO_4$ as major components [3]. X-ray diffraction analysis also revealed the presence of PbO_2 (plattnerite, tetragonal modification) and $PbSO_4$ (anglesite) in comparable concentrations. According to the Rusin and Dasoyan's study [5], compounds of even more complex composition, $3PbO \cdot PbSO_4 \cdot H_2O$ and $4PbO \cdot PbSO_4$, can also be present in active masses.

Taking into account that lead oxides, unlike sulfates, are fairly easily reduced with carbon or carbon-containing materials at 720–740°C, it is reasonable to transform $PbSO_4$ into the carbonate, hydroxide, or hydrocarbonate, which decompose on heating with formation of lead monoxide PbO [6, 7]. The environmental advantages of this operation are doubtless. In a number of flowsheets at plants beyond Russia, sodium carbonate is mainly used for desulfation. As a result, cerussite $PbCO_3$ and relatively small amount of hydrocerussite $2PbCO_3 \cdot Pb(OH)_2$ are formed in the solid phase [4]. The possible materials for desulfation are also NaOH and K_2CO_3 [9].

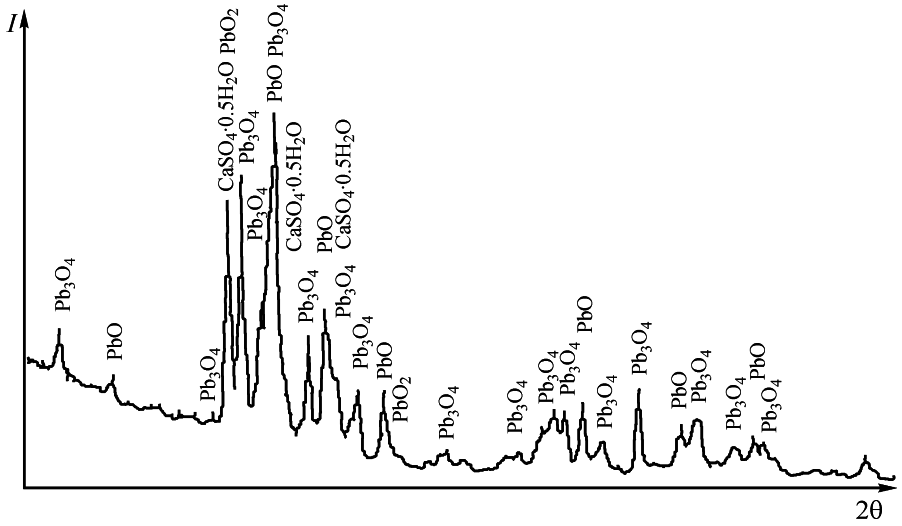
The desulfation is based on different solubility products (SPs) of lead compounds. According to handbook [10], SP of $PbSO_4$ at 25°C is 1.58×10^{-8}. At the same time, the SPs of the desulfation products are considerably smaller: 7.41×10^{-14} for $PbCO_3$ and 1.99×10^{-20} for $Pb(OH)_2$. According to an approximate estimate, SP for $2PbCO_3 \cdot Pb(OH)_2$ is 3.5×10^{-46} [11].

Along with sodium or potassium carbonate and sodium hydrocarbonate, a considerably cheaper chemical, calcium hydroxide, can be used for converting lead into a compound more convenient for the reduction [12, 13]. In this study we examined the reaction of an aqueous suspension of $Ca(OH)_2$ (SP at

Results of experiments. Initial mass 50 g, SO_4^{2-} content 14.5%, antimony content 1.17%

Dry solid phase			Initial filtrate			
mass, g	SO_4^{2-}	Sb	volume, cm^3	SO_4^{2-}	Pb^{2+}	Sb^{3+}, mg l^{-1}
	wt %			g l^{-1}		
53.9	11.0	1.06	98	1.71	3.8	<0.013
52.0	11.7	1.07	100	1.71	3.6	<0.013
53.0	11.0	1.06	112	1.71	3.9	<0.013

1070-4272/05/7809-1543 © 2005 Pleiades Publishing, Inc.



X-ray diffraction pattern of the products of reaction of oxide–sulfate fraction with aqueous suspension of calcium hydroxide, taken after keeping for 1 h at 480°C. (*I*) Reflection intensity and (2θ) Bragg angle.

25°C 7.94×10^{-6}) with the oxide–sulfate fraction from utilization of lead battery scrap. The solution was prepared from chemically pure grade CaO. The initial solution contained 0.025 g cm^{-3} CaO. pH of the initial solutions was within 12.2–12.4.

The necessary amount of CaO was calculated by the equation

$$PbSO_4 + Ca(OH)_2 + 2H_2O = Pb(OH)_2 + CaSO_4 \cdot H_2O.$$

In the experiments, CaO was in 10% excess relative to the calculated value.

The solid-to-liquid ratio (s : l) was 1 : 4 and temperature, 50°C. The pH was recorded continuously. The content of sulfate ions and antimony in the oxide–sulfate mass (50 g) was determined. After the experiment was complete, the precipitate was filtered off, washed, and dried at 130–140°C for 2 h. The reaction of the active mass with calcium hydroxide essentially differs from its desulfation with alkali metal carbonate or hydrocarbonate. The reaction products, $Pb(OH)_2$ and $CaSO_4 \cdot 2H_2O$, are in the solid phase, since SP of gypsum at 50°C is 3.89×10^{-5} [10]. The method is based on the fact that heating to the reduction temperature (720–740°C) yields PbO and $CaSO_4$ in the solid phase. With a NaCl–KCl mixture as flux, a rather readily fusible mixture is formed (equiv. %): KCl 38.5, $CaSO_4$ 19, $(NaCl)_2$ 42.5, melting point 605°C [15, 15]. The presence of a liquid flux facilitates the main reaction, reduction of lead(II) oxide.

A series of the experiments showed that the solution pH is stabilized at a level of 8.4–8.5 even within 20 min after the aqueous suspension starts to react with the solid phase, which indicates that the process is complete. Typical experimental results are presented in the table.

The presence of lead ions in the filtrate is associated with the relatively high pH values and amphoteric nature of lead hydroxide. The neutralization of the solution with sulfuric acid results in the precipitation of Pb^{2+} ions. In the process, antimony from the active mass is not noticeably dissolved. The X-ray diffraction analysis of the mass revealed the presence of $CaSO_4 \cdot 2H_2O$, PbO, and Pb_3O_4; $Pb(OH)_2$ being formed was amorphous. Only lead oxides, mainly Pb_3O_4, and $CaSO_4 \cdot 2H_2O$ were detected after keeping at 480°C for 1 h (see figure).

The reaction of CaO aqueous suspension with the oxide–sulfate fraction of lead battery scrap allows difficultly reducible lead(II) sulfate to be converted into lead hydroxide or lead monoxide PbO as the final product. PbO is reduced with carbon or carbon materials in the solid phase at 720–740°C.

REFERENCES

1. Morachevskii, A.G., *Zh. Prikl. Khim.*, 1997, vol. 70, no. 1, pp. 1–15.
2. Morachevskii, A.G., *Zh. Prikl. Khim.*, 2003, vol. 76, no. 9, pp. 1467–1476.
3. Chen, T.T., and Dutrizac, J.E., *Hydrometallurgy*, 1996, vol. 40, pp. 223–245.
4. Morachevskii, A.G., Bochagina, E.V., and Khabachev, M.N., *Zh. Prikl. Khim.*, 2003, vol. 76, no. 10, pp. 1748–1750.

5. Rusin, A.I., and Dasoyan, M.A., *Zh. Prikl. Khim.*, 1973, vol. 46, no. 12, pp. 2643–2646.
6. Yamaguchi, J., Sawada, Y., Sakurai, O., *et al*., *Thermochim. Acta*, 1980, vol. 35, no. 3, pp. 307–313.
7. Yamaguchi, J., Sawada, Y., Sakurai, O., *et al*., *Thermochim. Acta*, 1980, vol. 37, no. 1, pp. 79–88.
8. Morachevskii, A.G., Vaisgant, Z.I., Bochagina, E.V., and Khabachev, M.N., *Tsvetn. Met.*, 2002, no. 8, pp. 34–7.
9. Morachevskii, A.G., *Zh. Prikl. Khim.*, 1998, vol. 71, no. 6, pp. 881–890.
10. Kumok, V.N., Kuleshova, O.M., and Karabin, L.A., *Proizvedeniya rastvorimosti* (Solubility Products), Novosibirsk: Nauka, 1983.
11. Auerbach, F., and Pik, H., *Arb. Kaiserlichen Gesundheitsamte*, 1914, vol. 45, no. 2, pp. 113–165.
12. Sittig, M., *Metal and Inorganic Waste Reclaiming. Encyclopedia*, New York: Park Ridge, 1980.
13. Morachevskii, A.G., Vaisgant, Z.I., and Demidov, A.I., *Pererabotka vtorichnogo svintsovogo syr'ya* (Reprocessing of Secondary Lead Raw Materials), St. Petersburg: Khimiya, 1993.
14. Rubleva, V.V., and Bergman, A.G., *Zh. Obshch. Khim.*, 1956, vol. 20, no. 3, pp. 651–654.
15. *Diagrammy plavkosti solevykh sistem: Mnogokomponentnye sistemy* (Melting Diagrams of Salt Systems: Multicomponent Systems), Posypaiko, V.N., and Alekseeva, E.A., Eds., Moscow: Khimiya, 1977.

Russian Journal of Applied Chemistry, Vol. 78, No. 9, 2005, pp. 1546–1548. Translated from Zhurnal Prikladnoi Khimii, Vol. 78, No. 9, 2005, pp. 1571–1573.
Original Russian Text Copyright © 2005 by Lisitskii, Alekhina, Amineva.

BRIEF COMMUNICATIONS

Effect of Substituents in 1,2-Disubstituted Imidazolines on Properties of Concrete Mixtures

V. V. Lisitskii, I. E. Alekhina, and N. A. Amineva

Bashkir State University, Ufa, Bashkortostan, Russia

Received March 30, 2005

Abstract—Physicochemical properties of concrete mixtures and concretes was studied as influenced by the structure of salts of 1,2-disubstituted imidazolines with C_1–C_4 monocarboxylic saturated acids.

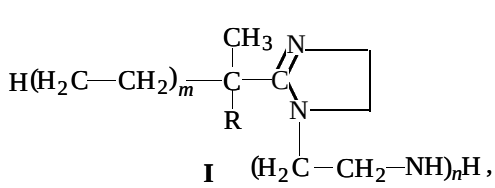
The products of condensation of higher carboxylic acids and polyethylenepolyamines are widely used in production of building materials. The hydrophobic properties of concrete mixtures are improved by modifying agents prepared by condensation of synthetic carboxylic acids with polyethylenepolyamines [1, 2]. The strength properties are enhanced by the products of reaction of 1-polyethylenepolyaminoethyl-2-alkyl-(C_6–C_{25})-2-imidazoline with orthophosphoric, sulfuric, or acetic acid [3–5]. *N*,*N*-Bis(2-hydroxyethyl)-2-alkyl-2-imidazoline [6] or polyamidoimidazoline resin [7] decrease water adsorption and permeability and increase the resistance of the concrete.

However, the products of cyclocondensation of linear carboxylic acids with polyethylenepolyamines are hydrolytically unstable (in contrast to 1,2-disubstituted imidazolines containing branched substituents in position 2 of the imidazoline ring [8–10]), and thus they are inefficient.

In this study we examined the mobility and water separation of concrete mixtures and strength properties of the concrete monolith as influenced by the nature of substituents in positions 1 and 2 of the imidazoline ring.

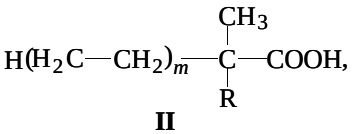
EXPERIMENTAL

1,2-Disubstituted imidazolines of the general formula



I

where R is ethyl, butyl; n = 1–3; m = 0–22, were prepared by heating in a nitrogen atmosphere of α,α'-branched monocarboxylic saturated acids of the general formula



II

where R is ethyl, butyl; n = 1–3; m = 0–22, with diethylenetriamine (DETA), triethylenetetramine (TETA), and polyethylenepolyamine (PEPA) at 280 ± 10°C for 10–12 h at the acid : polyamine molar ratio of 1 : 2 with subsequent vacuum treatment at 180–200°C. The salts of 1,2-disubstituted imidazolines (**I**) with formic, acetic, propionic, and butyric acids were prepared by heating of the equimolar amounts of imidazoline and acid in ethanol at 60–78°C for 1–2 h, followed by subsequent evaporation of solvents and vacuum drying of the salt at 80–90°C on a 350 R rotary evaporator (Poland).

The concrete mixture was prepared from a Portland cement and carbonate stone with coarseness of 5–10 and 10–20 mm (1 : 1.5 weight ratio). The salt was added to the concrete mixture with water. The concrete samples were hardened in the 4 + 3 + 6 + 2 mode (preliminary setting + heating + isothermal heating at 80 ± 3°C + cooling). The properties of the concrete mixtures and concrete monoliths were evaluated by the standard procedures.

In all the cases, addition of the salts of 1,2-disubstituted imidazolines with C_1–C_4 carboxylic acids increases their mobility and decreases the water separation (Table 1); the compression strength also increases.

1070-4272/05/7809-1546 © 2005 Pleiades Publishing, Inc.

Table 1. Properties of concrete mixtures and concrete monoliths as influenced by 1,2-disubstituted imidazolines

Composition of concrete mixtures	Content of components in sample, wt %								
	1	2	3	4	5	6	7	8	9
Portland cement	10.40	14.20	17.50	14.20	10.40	14.20	17.50	14.20	14.20
Filler	82.60	78.80	75.50	78.76	78.78	78.76	78.74	78.76	78.76
Water	7.00	7.00	7.00	7.00	7.00	7.00	7.00	7.00	7.00
Salt of 1-[2-(2-aminoethyl)aminoethyl]-2-alkyl(C_8–C_{18})-2-imidazoline with acids:									
formic	–	–	–	0.04	–	–	–	–	–
acetic	–	–	–	–	0.02	0.04	0.06	–	–
propionic	–	–	–	–	–	–	–	0.04	–
butyric	–	–	–	–	–	–	–	–	0.04
Properties of concrete mixtures									
Mobility from cone draft, cm	3	3	3	14	12	14	16	14	13
Water separation, g l^{-1}	20.0	15.0	7.0	3.0	4.5	2.0	0	2.0	0
Ultimate compression resistance, MPa	18.8	25.4	32.4	28.2	22.4	29.6	34.6	26.8	27.6

Table 2. Properties of concrete mixtures and concrete monoliths as influenced by the structure of 1,2-disubstituted imidazolines

Composition of concrete mixtures	Content of components in sample, wt %						
	1	2	3	4	5	6	7
Portland cement	14.20	14.20	14.20	14.20	14.20	14.20	14.20
Filler	78.76	78.76	78.76	78.76	78.76	78.76	78.76
Water	7.00	7.00	7.00	7.00	7.00	7.00	7.00
Salt of 1-(2-aminoethyl)-2-alkyl(C_4–C_8)-2-imidazoline with acetic acid	0.04	–	–	–	–	–	–
Salt of 1-[2-(2-aminoethyl)aminoethyl]-2-alkyl-(C_4–C_8)-2-imidazoline with acetic acid	–	0.04	–	–	–	–	–
Salt of 1-(polyethylenepolyaminoethyl)-2-alkyl-(C_4–C_8)-2-imidazoline with acetic acid	–	–	0.04	–	–	–	–
Salt of 1-(2-aminoethyl)-2-alkyl(C_8–C_{18})-2-imidazoline with acetic acid	–	–	–	0.04	–	–	–
Salt of 1-[2-(2-aminoethyl)aminoethyl]-2-alkyl-(C_8–C_{18})-2-imidazoline with acetic acid	–	–	–	–	0.04	–	–
Salt of 1-polyethylenepolyaminoethyl-2-alkyl-(C_8–C_{18})-2-imidazoline with acetic acid	–	–	–	–	–	0.04	–
Salt of 1-[2-(2-aminoethyl)aminoethyl]-2-alkyl-(C_{20}–C_{50})-2-imidazoline with acetic acid	–	–	–	–	–	–	0.04
Properties of concrete mixtures							
Mobility from cone draft, cm	8.0	9.0	9.6	12.8	14.0	14.8	14.6
Water separation, g l^{-1}	6.0	5.4	5.0	2.8	2.0	0.0	0.0
Decrease in water demand, %	13.9	14.8	16.0	18.6	20.2	20.0	21.6
Ultimate compression resistance, MPa	26.8	26.4	27.0	28.4	29.6	29.8	28.0
Resistance to type I corrosion (content of Ca^{2+} ions, g l^{-1})	0.20	0.25	0.22	0.18	0.16	0.20	0.18

It should be noted that the length of the C_1–C_4 alkyl substituent of saturated monocarboxylic acids does not affect the properties of the concrete mixtures. This indicates that the performance of the additive is determined by the structure of 1,2-disubstituted imidazoline. Our experimental results show that the increase in the length of the aminoethyl radical in position 1 of the imidazoline ring only slightly changes the mobility of concrete mixtures and water separation and does not noticeably affect the strength properties of the concrete monolith (Table 2).

With increasing length of alkyl substituents in position 2 of the imidazoline ring, the mobility of concrete mixtures sharply increases, whereas their water separation decreases (Table 2). The strength properties of the concrete also increase. Thus, the salts of 1,2-disubstituted imidazolines **I** with C_1–C_4 saturated monocarboxylic acids are efficient cationic surfactants, which, being adsorbed on the surface of Portland cement clinker, exert the plasticizing effect. Steaming of the concrete mixtures causes degradation of the concrete–additive complexes, but the rates of formation of hydroaluminates and hydrosilicates do not decrease, and the strength properties of the concrete are preserved.

It should be noted that addition of salts of 1,2-disubstituted imidazolines increases the resistance of concretes with respect to aggressive solutions that cause leach corrosion (Table 2).

CONCLUSION

(1) Salts of 1,2-disubstituted imidazolines with C_1–C_4 saturated monocarboxylic acids, when added to a concrete mixture, increase its mobility and decrease the water separation, which allows transportation of the concrete mixture at long distances without deterioration of its quality.

(2) Longer alkyl substituents in position 2 of the imidazoline ring strongly enhance the plasticizing effect of the salts of 1,2-disubstituted imidazolines.

REFERENCES

1. USSR Inventor's Certificate no. 0 638 564.
2. USSR Inventor's Certificate no. 0 727 591.
3. USSR Inventor's Certificate no. 0 908 764.
4. USSR Inventor's Certificate no. 0 958 374.
5. USSR Inventor's Certificate no. 01 030 334.
6. USSR Inventor's Certificate no. 0 931 278.
7. USSR Inventor's Certificate no. 0 962 253.
8. Kolomiets, B.S., German, V.K., Suchkov, V.V., and Kudryavtseva, M.I., *Zh. Prikl. Khim.*, 1978, vol. 51, no. 12, pp. 2758–2762.
9. Savignac, A., Kabbage, T., Dupin, P., and Calmon, M., *J. Heterocyclic Chem.*, 1978, vol. 15, no. 5, p. 897.
10. Bondareva, S.O., Lisitskii, V.V., Yakovtseva, N.I., and Murinov, Yu.I., *Izv. Ross. Akad. Nauk, Ser. Khim.*, 2004, no. 4, pp. 767–771.

Russian Journal of Applied Chemistry, Vol. 78, No. 9, 2005, pp. 1549–1551. Translated from Zhurnal Prikladnoi Khimii, Vol. 78, No. 9, 2005, pp. 1574–1576.
Original Russian Text Copyright © 2005 by Shoinbekova, Nikitina, Zhunusova, Mukhitdinova, Ergozhin.

BRIEF COMMUNICATIONS

Effect of Initiator on the Microstructure of Copolymers of Acrylic Acid with a Disubstituted Derivative of Monoethanolamine Vinyl Ether and Chloranil

S. A. Shoinbekova, A. I. Nikitina, G. N. Zhunusova, B. A. Mukhitdinova, and E. E. Ergozhin

Bekturov Institute of Chemical Sciences, Ministry of Education and Science of Kazakhstan Republic, Almaty, Kazakhstan

Received June 7, 2005

Abstract—The influence of the initiator on the copolymerization of acrylic acid with a disubstituted derivative of monoethanolamine vinyl ether and chloranil was examined.

The structure and properties of copolymers depend on the synthesis conditions, in particular, on the initiator used [1]. Numerous studies concern the relative activity of various monomers in copolymerization, but the effect of initiator on these parameters is considered only in a few of them [2, 3]. In this connection, it is interesting to study the reactivity of a new monomer derived from monoethanolamine vinyl ether and chloranil (MEAVE–CA–MEAVE) [4] in the reaction with acrylic acid (AA) in the presence of various initiators. The copolymers thus obtained exhibit redox, complexing, and ion-exchange properties and show promise as ion exchangers.

In this study we examined how the initiator affects the relative activity of the monomers and the composition and microstructure of the copolymers in the copolymerization of MEAVE–CA–MEAVE with acrylic acid.

EXPERIMENTAL

MEAVE–CA–MEAVE was prepared as described in [4]. Dimethylformamide (DMF) was purified by the standard procedure [5]. The initiators, azobis(isobutyronitrile) (AIBN, mp 102–103°C) and potassium persulfate (PP), were recrystallized from absolute methanol and water, respectively [6].

The copolymerization was performed by an ampule method. The starting components were loaded in one portion. The mixture contained 6 wt % initiator (AIBN or PP) relative to the sum of the monomers. The reaction was performed at 78°C. The MEAVE–CA–MEAVE concentration was 20 g l^{-1}. The solvent was DMF in the case of AIBN and DMF : water (2 : 3 by volume) in the case of PP. The molar ratio of the monomers was varied from 20 : 80 to 80 : 20. The conversion was estimated from the concentrations of the unchanged monomers, which were determined polarographically (MEAVE–CA–MEAVE) and by titration (AA).

The polarograms were taken in 25% DMF, with phosphate buffer solution (pH 7.4) as supporting electrolyte, at 25 ± 0.5°C on a PU-1 polarograph with a mercury dropping electrode (open-circuit capillary characteristic $m^{2/3}t^{1/6}$ = 4.38 $mg^{2/3}\,s^{-1/2}$. As reference electrode we used saturated calomel electrode. The solutions were deoxygenated by bubbling with argon.

The polymer structure is primarily determined by the initiation procedure and by chain propagation and termination reactions [1]. The initiation affects the copolymer composition and the configuration of monomeric units. The choice of the initiator is most frequently governed by its solubility in the monomer or in the solvent and by the temperature at which the required rate of generation of free radicals can be attained. The initiators usually used for preparing copolymers of vinyl ethers with styrene and acrylic and other monomers are peroxides and azo compounds [7]. In copolymerization of MEAVE–CA–MEAVE with acrylic acid, we used AIBN and PP inducing the polymerization by the free-radical mechanism.

Using the Mayo–Lewis integral equation of the copolymer composition [1], we calculated the copoly-

1070-4272/05/7809-1549 © 2005 Pleiades Publishing, Inc.

Table 1. Copolymerization constants and Alfrey–Price parameters for the system MEAVE–CA–MEAVE (M_1) : AA (M_2) in the presence of various initiators

Constant, parameter	Initiator	
	AIBN	PP
P	–0.52	–0.53
r_1	0.58	1.34
r_2	1.80	0.36
r_1r_2	1.044	0.482
$1/r_1$	1.72	0.75
$1/r_2$	0.56	2.78
Q_1	0.59	1.65
e_1	0.56	–0.08
Δe	0.21	0.85

merization constants r_1 and r_2 (the coefficient p was determined by the Shtraikhman method [8]), and from these quantities we determined the Alfrey–Price parameters Q_1 and e_1 [2] for MEAVE–CA–MEAVE (for AA, Q_2 = 1.15, e_2 = 0.77). The results are given in Table 1.

Comparison of the copolymerization constants, $1/r_2$, and Q_1 shows that MEAVE–CA–MEAVE is more active in the presence of PP than with AIBN. With PP, the copolymers of the more regular structure are formed, as indicated by the value of r_1r_2 = 0.482.

The microstructure of the copolymers largely depends on the inital monomer ratio and their reactivity, as shown above, depends on the initiator used. From the copolymerization constants and data on the composition of the monomer mixture, we calculated the probabilities of formation of various diads $f_{M_1–M_1}$, $f_{M_1–M_2}$, $f_{M_2–M_2}$, the statistical mean block lengths in the copolymer chains L_{M_1} and L_{M_2}, and the Harwood parameter of the block structure R [9, 10] with both initiators (Table 2).

Table 2 shows that, at any MEAVE–CA–MEAVE content in the starting mixture, the copolymers obtained in the presence of PP are enriched in units of this monomer, and those obtained with AIBN, in units of acrylic acid. Copolymers with more regular alternation of the monomeric units in the macromolecular chain are formed at MEAVE–CA–MEAVE : AA molar ratios of 58 : 42 (AIBN) or 40 : 60 (PP). At these ratios, the Harwood parameter reaches a maximum, which corresponds to the presence of short monomer blocks in the copolymers.

One of the factors responsible for major differences in the behavior of MEAVE–CA–MEAVE in the presence of AIBN and PP may be formation of HSO_4^- ions [11], along with $OH^\bullet$ radicals, in decomposition of PP, as it is known that acids accelerate polymerization of vinyl ethers [12]. Another factor may be different rates of decomposition of AIBN and PP. In particular, it is known [13] that PP in solutions of quaternary ammonium salts decomposes even at room temperature.

CONCLUSIONS

(1) Copolymerization of a disubstituted derivative of monoethanolamine vinyl ether and chloranil with acrylic acid was studied in the presence of two differ-

Table 2. Influence of the comonomer ratio on the composition and microstructure of copolymers prepared by copolymerization of MEAVE–CA–MEAVE (M_1) with acrylic acid (M_2) in the presence of various initiators

Initiator	Composition, mol %				Copolymer microstructure							
	initial mixture		copolymer		$f_{M_1–M_1}$	$f_{M_1–M_2}$	$f_{M_2–M_2}$	[9]		[10]		R
	M_1	M_2	m_1	m_2				L_{M_1}	L_{M_2}	L_{M_1}	L_{M_2}	
AIBN	78.77	21.23	74.73	25.27	0.461	0.216	0.106	3.13	1.49	3.08	1.50	43.62
	58.38	41.62	49.52	50.48	0.202	0.244	0.309	1.83	2.27	1.82	2.28	48.85
	47.62	52.38	36.11	63.89	0.121	0.224	0.431	1.54	2.92	1.53	2.98	44.38
	38.08	61.51	25.92	74.08	0.069	0.191	0.549	1.36	3.87	1.36	3.93	37.85
	19.84	80.16	10.92	89.18	0.016	0.109	0.765	1.15	8.02	1.14	8.27	21.24
PP	77.21	22.79	95.22	4.78	0.681	0.151	0.016	5.51	1.11	5.54	1.11	30.09
	60.38	39.62	89.39	10.61	0.473	0.235	0.056	3.01	1.24	3.04	1.24	46.75
	49.23	50.77	78.63	21.37	0.353	0.273	0.102	2.29	1.37	2.30	1.37	54.50
	39.78	60.22	61.43	38.57	0.255	0.292	0.161	1.87	1.55	1.88	1.54	58.31
	20.32	79.68	28.52	71.48	0.090	0.266	0.379	1.34	2.43	1.34	2.41	53.29

ent initiators: azobis(isobutyronitrile) and potassium persulfate. In the presence of potassium persulfate initiator, the activity of the redox monomer is higher than with azobis(isobutyronitrile).

(2) The microstructure of the copolymers can be controlled not only by varying the monomer ratio in the initial mixture but also by using different initiators. Potassium persulfate not only enhances the reactivity of the disubstituted derivative of monoethanolamine vinyl ether and chloranil, but also ensures formation of more compositionally uniform copolymers.

ACKNOWLEDGMENTS

The study was financially supported by ISTC (project K-604).

REFERENCES

1. *Copolymerization*, Ham, G.E., Ed., New York: Interscience, 1964.
2. Lavrov, N.A., Pisarev, A.G., and Sivtsov, E.V., *Plast. Massy*, 2004, no. 3, pp. 31–35.
3. Lavrov, N.A., Nikolaev, A.F., and Solomatin, Yu.V., *Izv. Vyssh. Uchebn. Zaved., Khim. Khim. Tekhnol.*, 1988, vol. 31, no. 12, pp. 113–115.
4. Kazakhstan Patent 8813.
5. Weissberger, A. and Proskauer, E.S., *Organic Solvents. Physical Properties and Methods of Purification*, Riddick, J.A. and Toops, E.E., Eds., New York: Interscience, 1955.
6. Toroptseva, A.M., Belogorodskaya, K.V., and Bondarenko, V.M., *Laboratornyi praktikum po khimii i tekhnologii vysokomolekulyarnykh soedinenii* (Laboratory Course of Chemistry and Technology of Macromolecular Compounds), Leningrad: Khimiya, 1972.
7. Nikolaev, A.F., *Tekhnologiya plasticheskikh mass* (Technology of Plastics), Leningrad: Khimiya, 1977.
8. Shtraikhman, G.A., Vanshteidt, A.A., and Petrova, G.A., *Zh. Fiz. Khim.*, 1958, vol. 32, no. 3, pp. 512–519.
9. Ushakov, S.N., Mitsengendler, S.P., and Shtraikhman, G.A., *Usp. Khim.*, 1950, vol. 19, no. 3, pp. 265–291.
10. Zil'berman, E.N., *Vysokomol. Soedin., Ser. B*, 1979, vol. 21, no. 1, pp. 33–36.
11. *Praktikum po khimii i fizike polimerov* (Practical Course of Polymer Physics and Chemistry), Kurenkov, V.F., Ed., Moscow: Khimiya, 1990.
12. Nikolaev, A.F., *Sinteticheskie polimery i plasticheskie massy na ikh osnove* (Synthetic Polymers and Plastics Based on Them), Moscow: Khimiya, 1966.
13. Pameditite, V.V., Makushka, R.Yu., and Baeras, G.I., *Vysokomol. Soedin., Ser. A*, 1992, vol. 34, no. 9, pp. 130–138.

Russian Journal of Applied Chemistry, Vol. 78, No. 9, 2005, pp. 1552–1554. Translated from Zhurnal Prikladnoi Khimii, Vol. 78, No. 9, 2005, pp. 1577–1579.
Original Russian Text Copyright © 2005 by Mamedov.

BRIEF COMMUNICATIONS

Acetylenic Esters of Polychlorobicyclo[2.2.1]hept-2-ene-5-carboxylic Acids

E. G. Mamedov

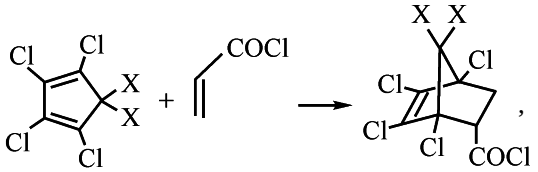
Institute of Petrochemical Processes, National Academy of Sciences of Azerbaijan, Baku, Azerbaijan

Received June 18, 2005

Abstract—Acetylenic esters of polychlorobicyclo[2.2.1]hept-2-ene-5-carboxylic acids were prepared from the corresponding acid chlorides and acetylenic alcohols.

Polyhalonorbornenes are widely used in production of synthetic polyester resins with enhanced heat and flame resistance, epoxy resins, and additives to lubricating oils, and also as starting compounds in organic synthesis [1–3]. They exhibit fungicide, insecticide, and hebricide power and other kinds of biological activity. Modification with reactive acetylenic fragments enhances these properties. Interest in polyhalonorbornene derivatives is steadily growing, and new compounds of this class are being synthesized [4, 5]. The presence of heavy halogen atoms extends the possibilities of structural studies of these compounds by IR and NMR spectroscopy and X-ray diffraction analysis [6–8].

Acetylenic esters of bicyclo[2.2.1]hept-2-ene-5-carboxylic acids were studied in [9–11]. In this study we developed preparation procedures and examined the structures of acetylenic esters of polychlorinated norbornenecarboxylic acids. These esters are prepared by the reactions of polychlorobicyclo[2.2.1]hept-2-ene-5-carboxylic acid chlorides with acetylenic alcohols. The starting chlorides **V**–**VII** were prepared by [4+2]-cycloaddition of chlorinated cyclopentadienes **I**–**III** to acryloyl chloride **IV**:



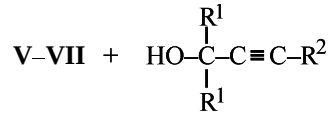
I–**III** **IV** **V**–**VII**

where X = Cl (**I**, **V**), H (**II**, **VI**), OCH_3 (**III**, **VII**).

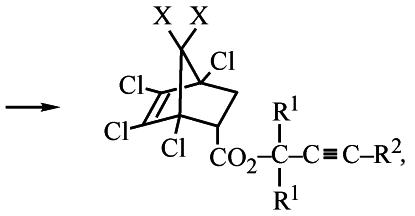
The condensation of **I**–**III** with **IV** was performed at 100–150°C for 10–15 h. The best results were obtained at 140°C, reaction time 10 h. Replacement of the geminal chlorine atoms by methoxy groups and hydrogen atoms favorably affects the reaction course; the yield of **V**–**VII** increases (see table).

The ^{1}H NMR spectra show that compounds **V**–**VII** prepared under these conditions are exclusively *endo* isomers.

Reactions of acid chlorides **V**–**VII** with alkynes **VIII**–**X** yielded the corresponding acetylenic esters of polychlorinated norbornenecarboxylic acids, **XI**–**XIX**:



VIII–**X**



XI–**XIX**

where $R^1 = R^2 = H$ (**VIII**); $R^1 = CH_3$, $R^2 = H$ (**IX**); $R^1 = CH_3$, $R^2 = CH{=}CH_2$ (**X**); $R^1 = R^2 = H$, X = Cl (**XI**); $R^1 = CH_3$, $R^2 = H$, X = Cl (**XII**); $R^1 = CH_3$, $R^2 = CH{=}CH_2$, X = Cl (**XIII**); $R^1 = R^2 = X = H$ (**XIV**); $R^1 = CH_3$, $R^2 = X = H$ (**XV**); $R^1 = CH_3$, $R^2 = CH{=}CH_2$, X = H (**XVI**); $R^1 = R^2 = H$, X = OCH_3 (**XVII**); $R^1 = CH_3$, $R^2 = H$, X = OCH_3 (**XVIII**); $R^1 = CH_3$, $R^2 = CH{=}CH_2$, X = OCH_3 (**XIX**).

The reaction was performed in organic solvents (diethyl ether, benzene) in the presence of tertiary amines (triethylamine, pyridine).

The use of chlorides **V**–**VII** as starting compounds allows preparation of esters **XI**–**XIX** of high purity

1070-4272/05/7809-1552 © 2005 Pleiades Publishing, Inc.

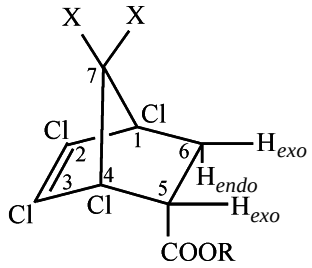
Yields, constants, and elemental analyses of **V**–**VII** and **XI**–**XIX**

Compound	bp (*p*, mm Hg) or mp, °C	Yield, %	Found, %			Formula	Calculated, %		
			C	H	Cl		C	H	Cl
V*	125–126 (2)	90	26.64	1.10	67.85	$C_8H_3Cl_7O$	26.41	0.83	68.32
VI*	120–121 (2)	93	32.10	1.59	61.04	$C_8H_5Cl_5O$	32.60	1.70	60.93
VII*	118–119 (2)	94	33.11	2.41	61.16	$C_{10}H_9Cl_5O_3$	33.38	2.50	50.76
XI	84–85	90	34.12	1.59	54.93	$C_{11}H_6Cl_6O_2$	34.46	1.57	55.61
XII	79–80	88	36.28	2.25	50.51	$C_{13}H_{10}Cl_6O_2$	37.16	2.43	51.72
XIII	87–88	87	41.91	2.62	47.55	$C_{15}H_{12}Cl_6O_2$	41.19	2.75	48.79
XIV	63–65	91	41.93	2.09	44.96	$C_{11}H_8Cl_4O_2$	42.03	2.55	45.22
XV	66–68	89	44.55	2.93	40.59	$C_{13}H_{12}Cl_4O_2$	45.61	3.23	41.52
XVI	64–68	88	47.11	3.85	39.42	$C_{15}H_{14}Cl_4O_2$	48.91	3.80	38.59
XVII	53–55	92	42.19	3.60	36.12	$C_{13}H_{12}Cl_4O_4$	41.72	3.20	37.96
XVIII	57–59	89	43.15	3.13	34.96	$C_{15}H_{16}Cl_4O_4$	44.78	3.78	35.32
XIX	49–52	88	47.11	4.62	31.95	$C_{17}H_{18}Cl_4O_4$	47.66	4.20	33.17

* **V**: d_4^{20} = 1.7974, n_D^{20} = 1.5620; **VI:** d_4^{20} = 1.6809, n_D^{20} = 1.5415; **VII**: d_4^{20} = 1.6989, n_D^{20} = 1.5460.

in almost quantitative yields. With propargyl alcohol **VIII**, the reaction occurs at room temperature with the heat release within 0.5 h; with alcohols **IX** and **X**, the reaction requires heating at 80°C for 5 h. In all the cases, the configuration of the starting acid chlorides **V**–**VII** remains unchanged, and the resulting esters are exclusively *endo* isomers. The structures of the compounds prepared were proved by IR and ^{1}H NMR spectroscopy and by elemental analysis (see table).

In the ^{1}H NMR spectra of **V**–**VII** and **XI**–**XIX**, the H^6_{endo} and H^6_{exo} protons give signals at 2.15–2.10 and 2.35–2.40 ppm, respectively, with the geminal coupling constant $J_{6,6}$ = –12–13 Hz and vicinal coupling constant $J_{5,6}$ = 4.50–4.60, $J_{5,6}$ = 6.10–6.20 Hz:



In the ^{1}H NMR spectra of **VII** and **XVII**–**XIX**, the protons of geminal OCH_3 groups give two singlets at 3.65–3.70 ppm.

The IR spectra of **V**–**VII** and **XI**–**XIX** contain characteristic bands at 1730 (C=O), 1620–1630 (C=C), and 750–760 cm^{-1} (C–Cl).

EXPERIMENTAL

The IR spectra were recorded on a UR-20 spectrometer, and the ^{1}H NMR spectra, on a Tesla BS-48 spectrometer (80 MHz) in CCl_4, internal reference TMS.

Hexachlorocyclopentadiene **I** was prepared according to [12], bp 109–111°C (11 mm Hg), n_D^{20} = 1.5654, d_4^{20} = 1.7210 {published data [12]: bp 110–111°C (11 mm Hg), n_D^{20} = 1.5652, d_4^{20} = 1.7213}. Tetrachlorocyclopentadiene **II** was prepared from hexachlorocyclopentadiene [13], mp 62–63°C (from petroleum ether). Dimethoxytetrachlorocyclopentadiene **III** was prepared from hexachlorocyclopentadiene [14], bp 109–111°C (11 mm Hg), n_D^{20} = 1.5268, d_4^{20} = 1.5012 {published data [14]: bp 108–110°C (11 mm Hg), n_D^{20} = 1.5288, d_4^{20} = 1.5010}. Acryloyl chloride **IV** was prepared according to [15], bp 75–76°C.

Polychlorobicyclo[2.2.1]hept-2-ene-5-carboxylic acid chlorides V–VII. A mixture of 0.05 mol of **I**–**III** and 0.05 mol of **IV**, containing 0.01 g of hydroquinone, was heated in a sealed ampule at 140°C for 10 h. The products were isolated by vacuum distillation.

Polychlorobicyclo[2.2.1]hept-2-ene-5-carboxylic acid propargyl esters XI, XIV, and XVII. To a stirred solution of 0.1 mol of propargyl alcohol **VIII** and 0.1 mol of triethylamine in 50 mol of absolute ether, we added dropwise with stirring 0.1 mol of **V**–**VII** at room temperature. An exothermic reaction was observed. After the reaction completion, the ammonium salt was filtered off, the solvent was distilled off, and the residue was recrystallized from *n*-heptane.

Polychlorobicyclo[2.2.1]hept-2-ene-5-carboxylic acid acetylenic esters XII, XIII, XV, XVI, XVIII, and XIX. A solution of 0.05 mol of **V**–**VII** in 15 ml

of benzene was added dropwise with stirring at 80°C to a solution of 0.05 mol of triethylamine in 15 ml of benzene. The mixture was stirred at 80°C for 5 h, after which it was worked up as described above.

CONCLUSIONS

(1) Acetylenic esters of polychlorinated bicyclo-[2.2.1]hept-2-ene-5-carboxylic acids were prepared in almost quantitative yields (87–92%) by reactions of acetylenic alcohols with the corresponding acid chlorides. The products are exclusively *endo* isomers.

(2) The primary alcohol reacts with the acid chlorides at 20°C within 0.5 h, and the tertiary alcohols, at 80°C.

REFERENCES

1. Mamedov, E.G., *Zh. Prikl. Khim.*, 2004, vol. 77, no. 8, pp. 1331–1335.
2. *Reaktsii i metody issledovaniya organicheskikh soedinenii* (Reactions and Methods of Investigation of Organic Compounds), Kazanskii, B.A., Ed., Moscow: Goskhimizdat, 1962.
3. Zefirov, N.S., Shestakova, T.P., and Kirpichenok, M.A., *Khimiya geksakhlortsiklopentadiena i rodstvennykh soedinenii* (Chemistry of Hexachlorocyclopentadiene and Related Compounds), Moscow: Mosk. Gos. Univ., 1985.
4. Veliev, M.G., Shatirova, M.I., Mamedov, El.Sh., *et al.*, *Azerb. Khim. Zh.*, 2001, no. 2, pp. 79–85.
5. Mamedov, E.G., Gasanov, A.G., Azizov, A.G., *et al.*, *Dokl. Nats. Akad. Nauk Azerb.*, 2002, nos. 5–6, pp. 183–192.
6. Mustafaev, A.M., Alekperov, N.A., and Guseinov, M.M., *Zh. Org. Khim.*, 1989, vol. 25, no. 9, pp. 1908–1915.
7. Akhmedov, I.M., Peynircioglu, B., Mamedov, E.G., *et al.*, *Tetrahedron*, 1994, vol. 50, no. 7, pp. 2099–2106.
8. Ho, K.F., Fungs, D.C.W., and Chan, W.H., *Tetrahedron Lett.*, 2001, vol. 42, no. 32, pp. 3121–3124.
9. Akhmedov, I.M., Mamedov, E.G., and Kyazimov, E.A., *Azerb. Khim. Zh.*, 1980, no. 5, pp. 51–54.
10. Mamedov, E.G., Abstracts of Papers, *III Bakinskaya Mezhdunarodnaya Mamedalievskaya neftekhimicheskaya konferentsiya* (III Baku Int. Mamedaliev Petrochemical Conf.), Baku, October 5–8, 1998, Baku: Nats. Akad. Nauk Azerb., 1998, p. 109.
11. Mamedov, E.G., *Azerb. Khim. Zh.*, 2001, no. 2, pp. 60–64.
12. Mamedaliev, Yu.G., Guseinov, M.M., and Mamedov, S.M., *Dokl. Akad. Nauk SSSR*, 1960, vol. 139, no. 2, pp. 379–382.
13. Nevcomer, J.C., and McBee, E.T., *J. Am. Chem. Soc.*, 1955, vol. 77, no. 1, p. 86.
14. McBee, E.T., Meyers, R.K., and Baranauskas, C.G., *J. Am. Chem. Soc.*, 1955, vol. 77, no. 1, pp. 86–91.
15. Hempel, G.H., Cross, R.P., and Marilla, R.P., *J. Am. Chem. Soc.*, 1950, vol. 72, no. 6, pp. 2299–2305.

Russian Journal of Applied Chemistry, Vol. 78, No. 10, 2005, pp. 1555–1558. Translated from Zhurnal Prikladnoi Khimii, Vol. 78, No. 10, 2005, pp. 1585–1588.
Original Russian Text Copyright © 2005 by V. Ukraintsev, Matsura, I. Ukraintsev.

INORGANIC SYNTHESIS AND INDUSTRIAL INORGANIC CHEMISTRY

On the Dissolution Mechanism of Powdered Noble Metals in Cyanide Solutions under Aerobic and Anaerobic Conditions

V. B. Ukraintsev, V. A. Matsura, and I. V. Ukraintsev

St. Petersburg State Technological Institute, St. Petersburg, Russia

Polimetall Inzhiniring (Polymetal Engineering) Private Company, St. Petersburg, Russia

Received June 9, 2005

Abstract—A possible mechanism of anaerobic dissolution of powdered palladium and gold is suggested.

At present, the main technique used to recover gold and silver from ores is their treatment with aqueous solutions of sodium cyanide in the presence of atmospheric oxygen. The world's output of gold recovered by this method in the early 1990s was as large as 70% [1]. This hydrometallurgical technique has been well developed and described in detail in the literature [1–6].

It is believed that silver and gold (M) dissolve in cyanide solutions in the presence of an oxidizing agent, atmospheric oxygen, in accordance with Elsner's equation

$$4M + 8CN^- + O_2 + 2H_2O = 4[M(CN)_2]^- + 4OH^-. \quad (1)$$

At the same time, the classical electrochemical mechanism of gold dissolution includes an anodic (2) and a cathodic (3) processes at the surface of a metallic particle and is described by the overall Bodlander equation (4):

$$Au + 2CN^- = [Au(CN)_2]^- + e, \quad (2)$$

$$O_2 + 2H_2O + 2e = H_2O_2 + 2OH^-, \quad (3)$$

$$2Au + 4CN^- + O_2 + 2H_2O = 2[Au(CN)_2]^- + H_2O_2 + 2OH^-. \quad (4)$$

It follows from Eqs. (1)–(4) that presence of oxygen in the reaction system is a necessary condition for dissolution of gold in cyanide solutions.

However, an important factor to be taken into account in studying the dissolution of gold is that its properties depend on particle size. A compact metal is chemically a very inert material, but, as its particles become smaller, not only the physical properties of the metal, but also its chemical activity start to change [7]. Metallic gold may be present in ores both in the form of rather large metallic particles and as colloid-dispersed particles, part of which have a size close to that of gold nanoclusters. Accordingly, it may be assumed that the conventional chemistry can somewhat change for gold particles of this kind.

Previously, the dissolution kinetics of powdered palladium and gold has been studied in relation to the concentration of sodium cyanide and composition of the gas atmosphere (oxygen, oxygen–argon, oxygen–hydrogen) [8].

As established in [8], the dissolution rate of powdered gold and palladium is first-order with respect to the concentration of a metal and cyanide ions, but zero-order with respect to the concentration of oxygen (partial pressure in the gas mixture). As the concentration of the cyanide ion increases, the dissolution rate of the metals grows and so does the amount of absorbed oxygen per mole of the metal. The dissolution rate of the metals also grows with temperature. However, the rate of oxygen uptake changes only slightly and even falls at comparatively high temperatures (40–60°C). In this case, the amount of deceases oxygen consumed for complete dissolution increases dramatically.

This communication reports on a study proceeding with these investigations in order to refine the possible pathways of dissolution of noble metals. On the whole, the experimental data obtained suggest that another oxidizing agent, water, is present in the system together with oxygen.

1070-4272/05/7810-1555 © 2005 Pleiades Publishing, Inc.

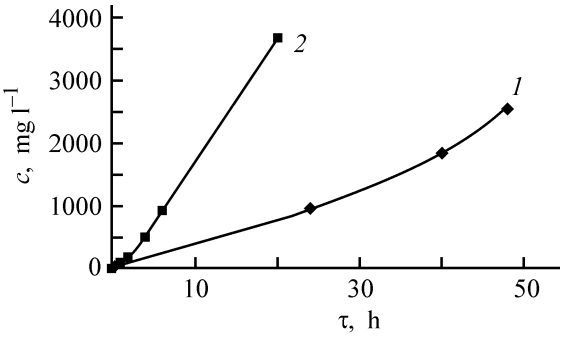


Fig. 1. Effect of the preparation procedure (dispersity) of gold on its solubility in aqueous cyanide solutions under anaerobic conditions. (*c*) Concentration of gold and (τ) time. (*1*) Gold produced by method 1 and (*2*) that produced by method 2.

EXPERIMENTAL

To study the influence exerted by the degree of dispersity on the solubility of gold under anaerobic conditions, it was obtained in two ways.

Method 1. A 2-g portion of metallic gold was dissolved in 200 ml of aqua regia, the excess of nitric acid was distilled off, the volume of the solution was brought to 100 ml by successive addition of hydrochloric acid and water, and it was cooled to room temperature. A 100-ml portion of an iron(II) sulfate solution with a concentration of 20 g l^{-1} was added to the resulting solution. The mixture obtained was allowed to stand until precipitation of metallic gold (for 24 h). The precipitate (finely dispersed brown powder) was filtered off, washed with distilled water to pH 6–7, and dried in a vacuum-desiccator over an alkali for 1 day.

Method 2. A 1-g portion of metallic gold was dissolved in 100 ml of aqua regia, the excess of nitric acid was distilled off, the volume of the solution was brought to 1000 ml by successive addition of hydrochloric acid and water and cooled to room temperature. A 50-ml portion of an iron(II) sulfate solution with a concentration of 20 g l^{-1} was added to the resulting solution. The mixture obtained was allowed to stand until precipitation of metallic gold (for 48 h). The precipitate (finely dispersed brown-violet powder) was filtered off, washed with distilled water to pH 6–7, and dried in a vacuum-desiccator over an alkali for 1 day.

Gold was dissolved at room temperature in a 150-ml three-necked round-bottom flask, into which 100 ml of a sodium cyanide solution with a concentration of 5 g l^{-1} (pH 11.5–11.8) was introduced. A 400-mg portion of gold was introduced into the extractor. After the system was purged with an inert gas of VCh grade (nitrogen, argon, helium) for 1 h, the weighed portion of gold was transferred into the solution. The dissolution was performed under continuous agitation and gas bubbling in order to prevent ingress of atmospheric oxygen into the system. To remove trace amounts of oxygen from the inert gas, it was preliminarily passed through a Drexel vessel filled with an alkaline solution of pyrogallol. To prevent loss of hydrogen cyanide, a Drexel vessel with a 10 wt % solution of an alkaline, was mounted at the outlet of the system. This made it possible to establish the balance for NaCN consumption.

Figure 1 shows kinetic curves for dissolution, under anaerobic conditions, of gold obtained in different ways. Approximately 50% of the gold produced by method 1 was dissolved in 2 days, whereas in the case of method 2, the metal virtually completely dissolved in 24 h. It can be seen from the results presented that, compared with method 1, gold produced by method 2 dissolves nearly five times faster. Apparently, this is due to its higher dispersity. The final concentration of NaCN was 3.3 g l^{-1} in the first case and 2.6 g l^{-1} in the second. This corresponds to consumption of 2.7 mol of sodium cyanide per mole of gold.

For explaining the results obtained, the authors made the following assumptions. As is known, the following equilibrium takes place at the interface between a powdered metal and water:

$$M + H_2O \rightleftarrows M_{aq}^{m+} + e_{aq}. \quad (5)$$

The equilibrium in reaction (5) is shifted toward the reverse reaction, for which $\log k_1 = 10$ [9] (where k_1 is the reaction rate constant) in the case of dissolution of gold. To shift the equilibrium toward the forward reaction, it is necessary to bind an electron. In the presence of oxygen in the reaction system, the following reaction must occur

$$O_2 + e_{aq} \rightleftarrows O_2^-. \quad (6)$$

For this reaction, $\log k$ is 10.3 at 23°C in an aqueous solution [9]. Indeed, a process of this kind does occur at the surface of gold nanoparticles [10].

The rates of the reverse reaction of (5) and forward reaction of (6) are comparable. However, compact noble metals virtually do not dissolve because $E^0_{O_2/O_2^-} = -0.563$ V [11] and there occurs the process

$$M_{aq}^{m+} + O_2^- \rightleftarrows M + O_2. \quad (7)$$

The presence of the CN^- ion, whose concentration in the solution commonly exceeds by several orders of magnitude the concentration of all other ingredients of the reaction system, leads to formation of the cyanide complexes $M(CN)_n^{m-n}$. This leads to dissolution of the corresponding noble metals.

Because powdered gold dissolves in the absence of oxygen in the reaction mixture under anaerobic conditions, the only compound that can act as an oxidizing agent in the reaction system is water:

$$e_{aq} + H_2O \rightleftarrows H^{\cdot} + OH^- \quad (8)$$

($\log k_3 = 1.2$, equilibrium constant $K_{eq} = 10^{-5}$ [9]).

A condition for a shift of the equilibrium (8) toward the reaction products and for the subsequent dissolution of the noble metal is that a high-power acceptor of atomic hydrogen should be present in the reaction system. This part can be played under anaerobic conditions by the cyanide ion only. It is known from the literature [9] that the rate constant of the reaction

$$H^{\cdot} + CN^- \rightarrow \text{(products not specified)} \quad (9)$$

is $10^{9.6}$. As mentioned above, the concentration of NaCN markedly exceeds that of all the other components of the reaction system. Therefore, process (9) can also shift reactions (5) and (8) toward forward reactions. However, even if this is the case, this occurs only to an exceedingly small extent.

In the presence of oxygen in an aqueous cyanide solution, it can be bound not only by reaction (6), but also by that with atomic hydrogen in accordance with the equations

$$H^{\cdot} + O_2 \rightarrow HO_2^{\cdot} \ (\log k_4 = 10.3 \ [9]), \quad (10)$$

$$H^{\cdot} + O_2^- \rightarrow HO_2^-. \quad (11)$$

Presumably, reactions (9)–(11) can proceed simultaneously. In this case, the products of reactions (10) and (11) can interact both with Au(0) and with the anion CN^-. If the fact that oxygen can also react with the cyanide ions and the products of reaction (9) is taken into account, it becomes clear why the consumption of oxygen grows with the concentration of the cyanide and the reaction order with respect to the concentration of oxygen is zero. In addition to reactions (9)–(11), hydrogen can also form H_2 molecules. An indirect evidence in favor of the mechanism suggested for dissolution of gold in aqueous cyanide solutions under anaerobic conditions is the well-known fact that dissolution of metallic copper is accompanied by vigorous evolution of hydrogen even if the process occurs in air. The rates of the processes considered here are the higher, the greater the reactivity of metallic gold, i.e., the closer the dimensions of its particles to nanoparticles.

It should be noted that the anion radical O_2^- formed can undergo disproportionation in aqueous solutions [12]:

$$2O_2^- + H_2O \rightleftarrows O_2 + OOH^- + OH^-. \quad (12)$$

Possibly, it is with the shift of equilibrium in Eq. (12) to the left that the above-described hindrance to dissolution of gold both at an excess of hydrogen peroxide and high concentrations of dissolved oxygen and at high pH values is associated [6].

It is known [13] that a qualitative reaction for the anion radical O_2^- in solution is the reduction by this anion of Nitro Blue Tetrazolium Chloride dye (Nitro BT), which is yellow in aqueous solutions, to red-brown diformazan, well soluble in chloroform. Indeed, introduction of several drops of chloroform into a solution that contains powdered gold being dissolved, sodium cyanide, and Nitro BT results in that the organic solvent first turns pink and then the color becomes more intense to the point of violet. This fact indicates that the solution contains O_2^- species, whose formation accompanies the dissolution of metallic gold. No coloration of this kind is observed in NaCN solutions in the absence of gold.

In order to confirm experimentally the possibility that noble metals can dissolve in aqueous cyanide solutions by the mechanism described by reactions (5) and (8)–(11), the kinetics of interaction between oxygen and hydrogen in the presence of a palladium black in an aqueous solution of sodium cyanide was studied.

Previously, the kinetics of this reaction in the absence of the cyanide ion was studied in [14–19]. It was established that, in the aqueous phase too, this reaction occurs by the radical-chain mechanism, with atomic hydrogen involved. It is important to note that the rates of the homolytic reactions between radicals in the gas phase or in water: $H^{\cdot} + H^{\cdot}$, $H^{\cdot} + OH^{\cdot}$, $H^{\cdot} + O_2$, $H^{\cdot} + HO_2^{\cdot}$, $H^{\cdot} + H_2O_2$, have second-order rate constants with values of about 10^{10} $M^{-1}\,s^{-1}$ [9, 20], which are comparable with the rate of reaction (9). Therefore, if the process goes via intermediate formation of the $H^{\cdot}$ radical, introduction of the cyanide ion into the system must lead to a sharp decrease in the rate of the reaction between hydrogen

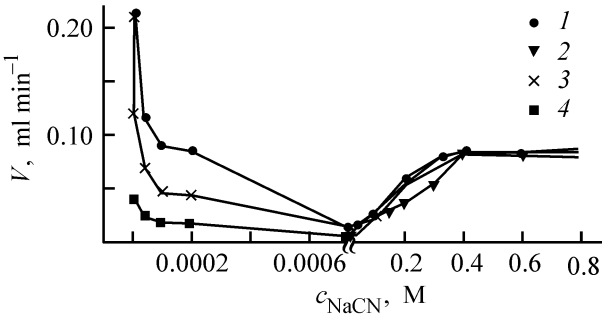


Fig. 2. Rate of uptake of oxygen or an oxygen–hydrogen mixture, *V*, vs. the concentration of sodium cyanide, c_{NaCN}, in the presence of a palladium black (m_{Pd} = *10 mg). (1)* 50% H_2 + 50% O_2, (*2*) 50% Ar + 50% O_2, (*3*) 25% O_2 + 50% H_2 + 25% Ar, and (*4*) 50% O_2 + 10% H_2 + 40% Ar.

and oxygen and must have no effect on the kinetics of palladium dissolution in aqueous cyanide solutions.

Figure 2 shows how the rate of uptake of an oxygen–hydrogen mixture in water depends on the concentration of sodium cyanide in the presence of a palladium black (the experimental procedure was described in [8]). Three regions can be distinguished in these dependences in going from low to higher concentrations of the cyanide ion: (1) steep decrease in the rate of uptake of the gas mixture at low concentrations of the cyanide ion (1×10^{-6}–1×10^{-3} M), (2) linear increase in the rate of uptake of the gas mixture at concentrations of the cyanide ion in the range 0.04–0.32 M, and (3) constant rate in the range 0.34–0.80 M. The steep decrease in the reaction rate in the first region, in which hydrogen reacts with oxygen, confirms experimentally that the cyanide ion is a kind of a trap for the $H^{\cdot}$ radical in the case of reactions that occur in water. The increase in the reaction rate in the second region is due to the dissolution of palladium and formation of a complex ion $[Pd(CN)_4]^{2-}$. In this region, only oxygen is absorbed from the gas phase and the reaction rate is first-order with respect to the concentration of the cyanide ion. In the third region, the reaction system is saturated with the cyanide ion and the reaction rate becomes independent of its concentration. At the same time, a decrease in the concentration of oxygen has no significant effect on the rate of oxygen uptake in portions 2 and 3 of the kinetic curves.

CONCLUSION

It was established that powdered palladium and gold can dissolve in aqueous solutions of sodium cyanide under anaerobic conditions.

REFERENCES

1. Marsden, J. and House, I., *The Chemistry of Gold Extraction*, New York: Ellis Horwood, 1992.
2. Meretukov, M.A. and Strizhko, L.V., *Sovremennoe sostoyanie proizvodstva zolota za rubezhom* (The Present-Day State of Gold Recovery Abroad), Moscow: Tsvetmetinformatsiya, 1985.
3. Maslenitskii, I.N., Chugaev, L.V., Borbat, V.F., *et al.*, Metallurgiya blagorodnykh metallov (Metallurgy of Noble Metals), Moscow: Metallurgiya, 1987.
4. Meretukov, M.A. and Orlov, A.M., *Metallurgiya blagorodnykh metallov: Zarubezhnyi opyt* (Metallurgy of Noble Metals: Foreign Experience), Moscow: Metallurgiya, 1990..
5. Plaksin, N.N., *Gidrometallurgiya: Izbrannye trudy* (Hydrometallurgy: Selected Works), Moscow: Nauka, 1972.
6. Larösch, J., *Process and Environmental Chemistry of Cyanidation*, Frankfurt am Main: Degussa AG, 2001.
7. Cortie, M.B., *Gold Bulletin*, 2004, vol. 37, nos. 1–2, pp. 12–19.
8. Brovin, K.G., Matsura, V.A., Potekhin, V.V., *et al.*, *Zh. Prikl. Khim.*, 2000, vol. 73, no. 7, pp. 1057–1062.
9. Denisov, E.T., *Konstanty skorosti gomoliticheskikh zhidkofaznykh reaktsii* (Rate Constants of Homolytic Liquid-Phase Reactions), Moscow: Nauka, 1971.
10. Zhang, Z., Berg, A., Levanon, H., *et al.*, *J. Am. Chem. Soc.*, 2003, vol. 125, no. 26, pp. 7959–7963.
11. Huheey, J.E., *Inorganic Chemistry, Principles of Structure and Reactivity*, New York: Harper and Row, 1983.
12. Sawyer, D.T. and Gibian, M.J., *Tetrahedron*, 1979, vol. 35, no. 3, pp. 1471–1481.
13. Fridovich, I., in *Svobodnye radikaly v biologii* (Free Radicals in Biology), Pryor, W.A., Ed., Moscow: Mir, 1979, vol. 1, pp. 272–314.
14. Potekhin, V.V., Matsura, V.A., and Ukraintsev, V.B., *Zh. Obshch. Khim.*, 2000, vol. 70, no. 6, pp. 886–890.
15. Matsura, V.A., Potekhin, V.V., and Ukraintsev, V.B., *Zh. Obshch. Khim.*, 2002, vol. 72, no. 1, pp. 113–117.
16. Matsura, V.A., Potekhin, V.V., Platonov, V.V., *et al.*, *Zh. Obshch. Khim.*, 2003, vol. 73, no. 12, pp. 2009–2012.
17. Potekhin, V.V., Matsura, V.A., Solov'eva, S.N., and Potekhin, V.M., *Kinet. Kataliz*, 2004, vol. 45, no. 3, pp. 407–411.
18. Potekhin, V.V., Solov'eva, S.N., and Potekhin, V.M., *Zh. Obshch. Khim.*, 2004, vol. 74, no. 5, pp. 709–713.
19. Matsura, V.A., Panina, N.S., Potekhin, V.V., *et al.*, *Zh. Obshch. Khim.*, 2004, vol. 74, no. 7, pp. 1057–1062.
20. Kondrat'ev, V.N., *Konstanty skorosti gazofaznykh reaktsii* (Rate Constants of Gas-Phase Reactions), Moscow: Nauka, 1970.

Russian Journal of Applied Chemistry, Vol. 78, No. 10, 2005, pp. 1559–1565. Translated from Zhurnal Prikladnoi Khimii, Vol. 78, No. 10, 2005, pp. 1589–1595.
Original Russian Text Copyright © 2005 by Kogut, Voronov, Kislenko, Peukert.

INORGANIC SYNTHESIS AND INDUSTRIAL INORGANIC CHEMISTRY

Effect of Functionalization of Colloidal Gold on Controlled Flocculation by the Ligand–Receptor Mechanism

A. M. Kogut, A. S. Voronov, V. N. Kislenko, and W. Peukert

Lvivska Politekhnika National University, Lviv, Ukraine

Friedrich-Alexander University, Erlangen–Nuremberg, Erlangen, Germany

Received June 16, 2005

Abstract—Modification of colloidal gold particles with octadecanthiol and alkyl biotin, with the subsequent flocculation of these particles via introduction of a tetramer protein avidin, was studied.

Studies of the controlled organization of colloid nanoparticles into two- or three-dimensional (2*D* or 3*D*) structures open up wide prospects for their use in optics, electronics, and medicine. It has been shown that gold nanoclusters show high potentialities for use in nanoelectronics and for fabrication of biosensors [1, 2]. The surface functionalization of gold nanoparticles as objects of study and "building blocks" for organized structures is being studied extensively [3–5].

The surface of colloidal gold particles is commonly modified by self-organized monolayers of alkanethiols [6] and aromatic thiols [7]. All gold modifiers are chosen in these cases in view of the strong binding of the modifier to the surface by the Au–S bond. Biologically important molecules can also be fixed on the surface of colloidal gold particles, with nanoparticles of this kind finding use in development of ensembles of required size and configuration [8, 9], biodiagnostics, immunoassays [10], and manufacture of luminescent bioconjugates [11]. This approach is, as a rule, based on biomolecular recognition of the components of the known specific reaction model on the ligand–receptor principle. Nevertheless, the pattern of the surface functionalization of gold particles and the mechanism of aggregate formation in systems of this kind remain insufficiently studied.

This study is devoted to the fundamental aspects of the controlled organization of gold nanoparticles into 2*D* structures (aggregates) via successive modification of the surface of the particles with octadecanethiol (ODT) and alkyl biotin, with their subsequent flocculation with a tetramer protein, avidin, by the ligand–receptor mechanism.

In this case, the hydrophobic interaction between alkyl fragments of biotin with the hydrocarbon moiety of ODT apparently leads to biotinylation of colloidal gold particles. The thus modified gold particles can be bound with avidin via specific biomolecular recognition [12].

Commonly, colloid gold solutions have, depending on the particle size, a certain color and change their coloration as the dispersity increases [13, 14]. First, the size of nanoparticles of "citrate-reduced" gold and the absorption of visible light by these nanoparticles were studied in relation to a widely varying concentration of ODT molecules fixed on the surface of the particles (Figs. 1–3). It was found that the absorption spectra of the gold sol, measured immediately after synthesis of particles and four months later virtually, completely coincide. This points to a high stability of the gold sol stabilized by negatively charged ions of ketodicarboxylic acids, because, as follows from published data [15, 16], the process of gold sol formation apparently occurs in three stages.

In the first stage, in boiling of hydrogen tetrachloroaurate(III), it is partly hydrolyzed with the simultaneous partial removal of HCl from the reacting mixture:

$$H[AuCl_4] + H_2O \rightarrow H[Au(OH)_xCl_{4-x}] + HCl\downarrow,$$

where $x = 0-4$; {$[H(AuCl_4)]$, $H[AuCl_3OH]$, $H[Au(OH)_4]$, etc.}.

1070-4272/05/7810-1559 © 2005 Pleiades Publishing, Inc.

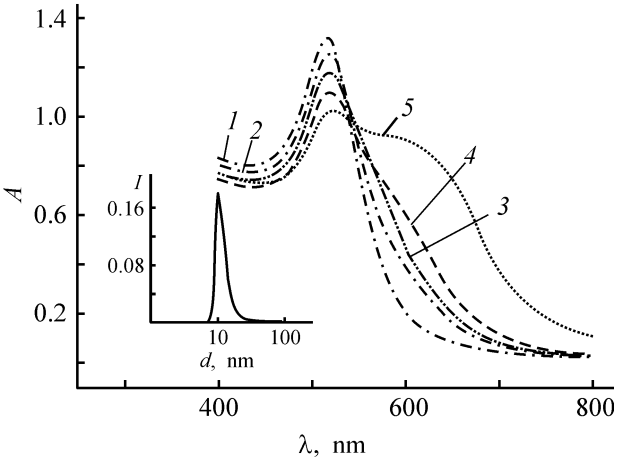
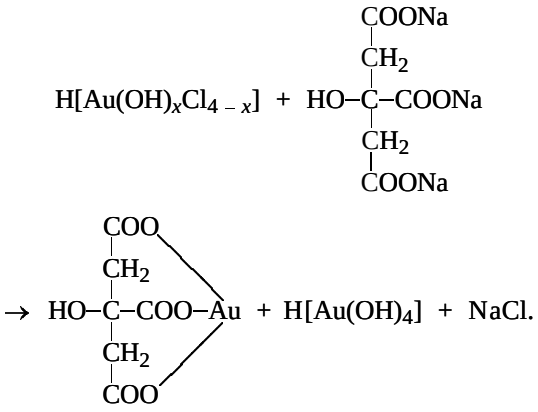
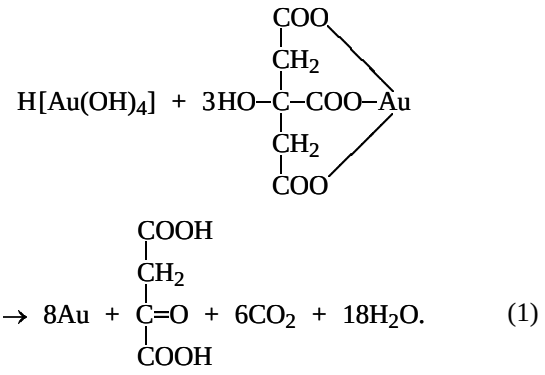


Fig. 1. (*1*) Spectrum of the initial gold sol and (*2*–*5*) its variation with time. Inset: particle size distribution of the initial gold sol. ODT concentration 1×10^{-5} M. (*A*) Optical density, (λ) wavelength, (*d*) particle diameter, and (*I*) signal intensity in measurements of dynamic light scattering. Time (min): (*2*) 15, (*3*) 3, (*4*) 6, and (*5*) 120.

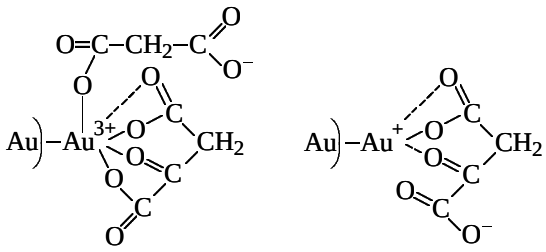
In the second stage, after a sodium citrate solution is added, $H[AuCl_4]$ rapidly hydrolyzes further to give NaCl and complexes of gold(III) with the ion of citric acid and hydroxy ions:



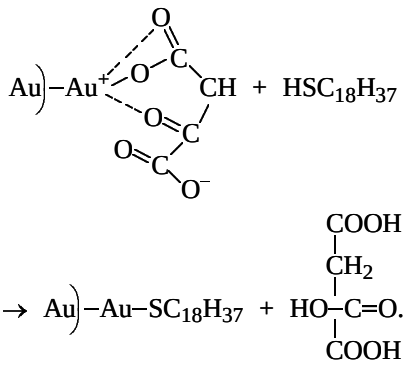
In the third stage, the Au(III) complexes obtained are reduced by citric acid to give gold particles and ketodicarboxylic acid:



The excess amount of A(III) and Au(I) ions bound into a complex with ketodicarboxylic acid is adsorbed on the surface of gold particles to form a double electric layer, which stabilizes the gold hydrosol by the scheme



If it is assumed that gold particles are formed by reaction (1), the residual concentration of gold complexes with ketodicarboxylic acids is $(0.5–1.5) \times 10^{-4}$ M. The average particle diameter of the gold sol obtained is 18 ± 2 nm, to which corresponds absorption at a wavelength of 519.3 nm (Fig. 1, inset). The particle size distribution is rather narrow. A particle contains, on the average, 2×10^5 gold atoms, on which $(2–5) \times 10^3$ gold ions bound into a complex with ketodicarboxylic acids are adsorbed. The number of particles in a unit volume of gold is 1.4×10^{16} l^{-1}. The sol has a bright red coloration. According to the data obtained by Mie [17], the effect of the particle size on the characteristic coloration of the gold sol is due both to the true absorption of light by the particles and to a "fictitious" absorption associated with light scattering. The gold sol, whose particles have a radius of 20 nm, absorbs in the green spectral range (~530 nm) and, therefore, has a bright red coloration enhanced by multiple scattering [13, 14]. The strongest coloration intensity of gold hydrosols corresponds to particles sizes in the range from 20 to 37 nm [14]. When light passes through a sol with different particle sizes, absorption peaks appear in the absorption spectra. The position of these peaks is determined by the particle size: as the particles become larger, the absorption peaks shift to longer wavelengths. Apparently, modification of the surface of gold particles with biotin molecules, with the subsequent addition of a tetramer protein avidin, will lead to particle aggregation and to changes in the absorption spectra. The concentrations of the reagents used to form an ODT coating on the particle surface were chosen so as to prevent their aggregation via substitution of ketodicarboxylic acids bound to gold ions on the surface of the particles by ODT molecules forming stronger bonds with gold ions by the reaction



As a result of the reaction, the surface charge of the particles decreases and their hydrophobicity becomes higher (Fig. 1). For example, a pronounced aggregation of gold particles occurs in the system at an ODT concentration of 1×10^{-5} M, which is indicated by a change in the absorption spectrum of the sol. The decrease in the height of the peak at 519 nm points to a fall in the concentration of primary particles in the sol, and its shift to longer wavelengths, to a gradual increase in the size of the aggregates. After 120 h, the absorption peak shifted into the range 600–630 nm, which can be attributed to a collective resonance of electrons in densely packed gold particles. It should be noted that, even at a sufficiently high concentration of aggregates, the concentration of the initial gold particles remains high, which is indicated by the peak in curve *5*. At a concentration of ODT in the system equal to 1×10^{-5} M, it binds up to 20% of gold ions adsorbed on the particle surface, which affects the total charge of the particles only slightly, but enhances the hydrophobicity of certain parts of a particle. With account of the fact that ODT is unevenly distributed over all the particles, only part of them, with the largest number of reacted gold ions, is capable of aggregation. It would be expected that a decrease in the ODT concentration in the system will only lead to a partial hydrophobization of the particles, without their subsequent aggregation. It is important for further studies that, at an ODT concentration of 1×10^{-7} M in the system, chemisorption does not lead to any significant disruption of the colloid stability of the gold sol (Fig. 2, curve *1*). The absorption spectrum of the mixture virtually coincides in the given case with that of the initial sample (Fig. 4). A study of how the gold particle size varies with time (Fig. 2) demonstrated that, at an ODT concentration of 1×10^{-7} M, their average size changes only slightly, whereas at 1×10^{-5} M, the average size of aggregates markedly increases already 15 min after the mixing of the reagents. In the latter case, aggregates containing up to several hundred primary gold particles can be formed. TEM

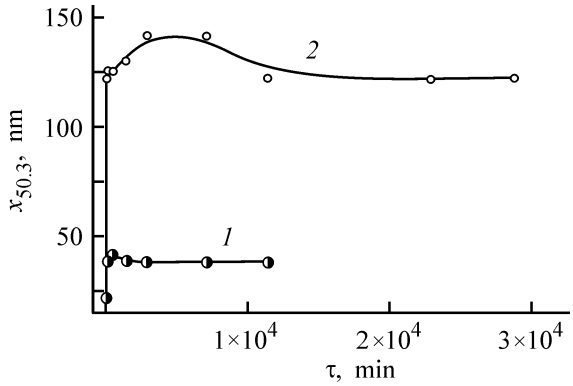


Fig. 2. Variation of the size $x_{50.3}$ of gold particles with time τ. ODT concentration (M): (*1*) 1×10^{-7} and (*2*) 1×10^{-5}.

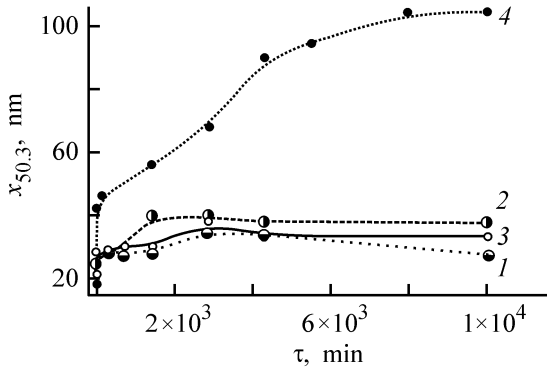


Fig. 3. Variation of the size $x_{50.3}$ of gold particles with time τ upon addition of (*1*) avidin, (*2*) alkyl biotin, (*3*) mixture of *1* and *2*, and (*4*) ODT, alkyl biotin, and avidin in accordance with the scheme. Concentration (M): (*1*, *2*, *4*) avidin, 1×10^{-8}; (*2*, *3*, *4*) alkyl biotin, 1×10^{-6}; and (*4*) ODT, 1×10^{-7}.

micrographs of a gold sol mixed with ODT demonstrated that, at an ODT concentration of 1×10^{-7} M, aggregates composed of three to five densely packed initial gold particles are formed, with a considerable fraction of the initial gold particles preserved.

Prior to studying the aggregation of gold particles in the system constituted by ODT, alkyl biotin, and avidin, it was appropriate to determine how addition of alkyl biotin or avidin molecules, or a mixture of these, affect the optical properties and particle size of the gold sol. As can be seen in Fig. 3, avidin and alkyl biotin present in the system in concentration of 1×10^{-8} and 1×10^{-6} M, respectively, lead to an only slight increase in the size of gold aggregates. This is apparently due to the fact that, under the experimental conditions, the adsorption of these reagents on gold particles stabilized with gold complexes with ketodicarboxylic acids is low. The absorption spectrum of

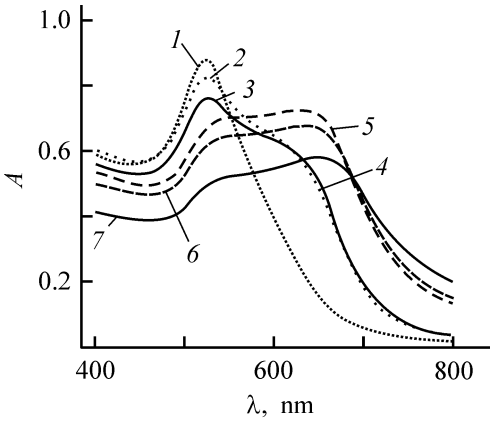


Fig. 4. Absorption spectra of (*1*) initial gold sol modified with ODT, (*2*, *3*) gold sol + ODT + alkyl biotin (*2*) 15 min and (*3*) 1 h after the introduction of alkyl biotin, and (*4*–*7*) gold sol + ODT + alkyl biotin + avidin (*4*) 5, (*5*) 5.5, (*6*) 9, and (*7*) 18 h after the introduction of avidin. (*A*) Optical density and (λ) wavelength. Concentration (M): (*1*–*7*) ODT, 1×10^{-7}; (*2*–*7*) alkyl biotin, 1×10^{-6}; and (*4*–*7*) avidin, 1×10^{-8}.

the gold sol remains virtually unchanged (Fig. 4). Successive introduction of alkyl biotin and avidin into the gold sol does not lead to its significant aggregation, either (Fig. 3, curve *3*), despite the reaction between alkyl biotin and avidin [11].

Introduction of alkyl biotin into a mixture containing the gold sol and 1×10^{-7} mol ODT leads to a slight decrease in the concentration of primary gold particles in the system and to formation of aggregates. This is indicated by a decrease in the height of the peak at 519 nm in the absorption spectrum of the gold sol and by the appearance of a new peak at 640 nm (Fig. 4, curves *1*–*3*). At an alkyl biotin concentration of 1×10^{-6} M, the spectrum of the mixture strongly varies during 1 h (Fig. 4, curves *1*–*3*) and then remains virtually unchanged. The last fact apparently indicates that alkyl biotin is adsorbed on hydrophobic parts of gold particles coated with ODT and there occurs partial aggregation of the particles via formation of bridge bonds between them. Apparently, the adsorption of alkyl biotin on the uncoated (with ODT) surface of gold particles is unimportant, which is indicated by only a slight change in the spectrum of the gold sol in the presence of alkyl biotin in the same concentration and by the insignificant increase in the number of aggregates in the system (Fig. 3, curve *2*). It may be assumed that alkyl biotin unbound to the surface of gold particles is present in the system in a considerable concentration.

Introduction of avidin, a tetramer protein with a molecular weight of 66 000, into a gold sol modified with ODT and alkyl biotin leads to an instantaneous change of the color of the gold sol in the system studied, which points to a noticeable flocculation of particles. The absorption spectrum of the gold sol markedly changes (Fig. 4, curves *4* and *5*). The height of the peak at 519 nm, associated with primary gold particles, dramatically decreases and a peak at 640 nm appears and grows in intensity during several hours. After 5–6 h, the heights of both peaks, at 519 and 640 nm, decrease. This indicates that coarse aggregates or floccules are formed. The conclusion is confirmed by measurements of the sizes of the aggregates (Fig. 3, curve *4*). During the first minutes after the mixture is formed, the particle size increases twice. After that the aggregates start to noticeably grow and reach the maximum size of 100–110 nm in 8×10^3 min. If the concentration of avidin is varied with the amount of the biotin "anchor" simultaneously raised, the rate of aggregate formation changes. This indicates that the aggregation rate can be controlled by varying the relative concentrations of the ligand and receptor. As already noted, the optical properties and size of gold particles modified with alkyl biotin apparently change upon the reaction with the protein because of the aggregation of gold particles, which results from "cross-linking" of the alkyl biotin adsorbed on their surface by the tetramer protein. In order to determine the efficiency of cross-linking and evaluate the change in the size and number of gold particle aggregates in a study of the absorption spectra of the sol in the visible range, a semiempirical spectroscopic flocculation parameter has been introduced [18], which can be used in evaluating the degree of aggregation of colloid particles. The flocculation parameter was defined as the integral area under the absorption curve in the range between 600 and 800 nm. In the course of flocculation and simultaneous aggregation of particles, the component determining the absorption at a longer wavelength grows in intensity. Thus, determining the area under the spectrum in the range between 600 and 800 nm must directly characterize the flocculation process. All the optical spectra presented in the figure (including that of unmodified gold) were normalized to the intensity of absorption at the wavelength of the surface resonance. The flocculation parameter was calculated for all the spectra obtained in the range between 600 and 800 nm. The calculations were carried out by subtracting spectrum of pure unmodified gold for the same range.

Figure 5 shows the plot of the flocculation parameter calculated for the experimental system against the time of experiment. It was found that the flocculation parameter can be neglected in experimental sys-

tems containing no avidin; the figure shows only the values calculated before and after the addition of the protein and in its presence. Apparently, aggregation occurs in the system after the addition of avidin, which is indicated by a steep rise in the flocculation parameter after the addition of the protein.

To obtain additional quantitative information about specific features of flocculation, the inset of Fig. 5 shows a typical curve describing the variation with time of the intensity of absorption by the initial particles at 519 nm (which is characteristic of pure gold particles). The decrease in the height of the peak at 519 nm in the absence of avidin from 1.3 to 1.0 points to an insignificant aggregation, which leads to disappearance of up to 20% of the initial particles to give aggregates constituted by 3–5 primary particles of the gold sol. This is demonstrated by the shift of the peak to longer wavelength. In the process, the flocculation parameter remains virtually constant.

Upon addition of an avidin solution to the system, the absorption peak substantially shifts to longer wavelengths (640 – 650 nm). Also, the height of the peak at 519 nm abruptly decreases, which points to a virtually instantaneous flocculation of primary particles to form aggregates.

In the first stage of flocculation, during the first minutes, primary gold particles are adsorbed on swollen globules of avidin macromolecules to give aggregates 45–50 nm in diameter (Fig. 3, curve *4*). In this case, there apparently occurs a reaction of specific addition of alkyl biotin adsorbed on the surface of primary gold particles to active groups on the surface of a swollen avidin globule. It should be noted that aggregates composed of 3–5 primary gold particles, which are formed upon addition of ADT and alkyl biotin, are also apparently adsorbed on avidin globules. The SEM micrographs in Fig. 6 clearly demonstrate rings of primary particles forming a shell on avidin globules. The number of aggregates composed of 3–5 primary particles in the SEM micrograph is insignificant, compared with chains of primary particles. This fact also points to an insignificant aggregation of primary particles upon their mixing with ODT and alkyl biotin. Apparently, the concentration of the avidin introduced affects the degree of adsorption saturation of the surface of globules of swollen avidin with primary gold particles and, accordingly, the flocculation rate. It should, however, be noted that dissolved alkyl biotin molecules favor cross-linking of avidin macromolecules and aggregation of its globules during the entire process. In the second, slow stage of flocculation, avidin globules undergo a slow aggregation because of the interaction of active groups

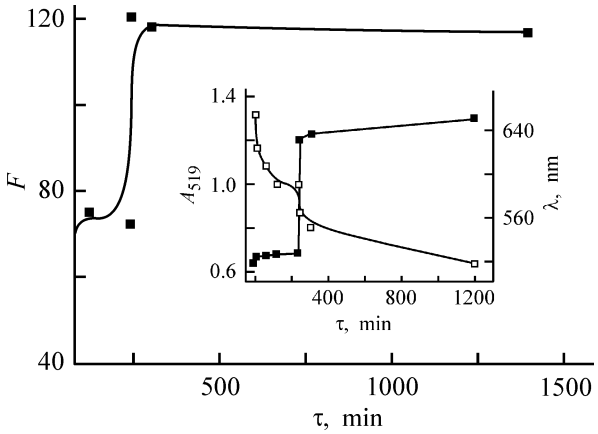


Fig. 5. Variation of the flocculation parameter *F* calculated for the experimental system described with time τ. Inset: variation of the light absorption at a wavelength of 519 nm, A_{519}, (synthesized colloid gold) and the shift of the absorption peak for a mixture of gold sol with ODT and biotin upon addition of avidin at 210th minute of the experiment.

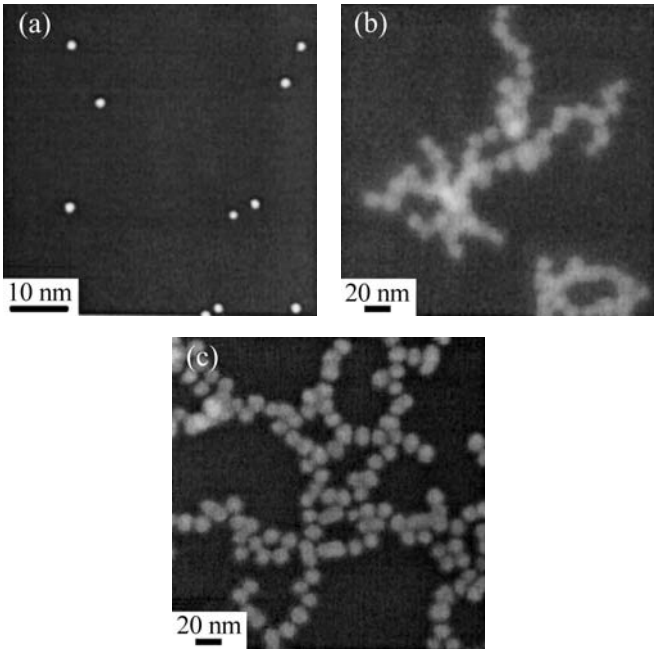


Fig. 6. SEM micrographs of (a) unmodified gold particles and of gold colloids containing alkyl biotin and 1×10^{-8} M avidin after (b) 1 and (c) 5 h of aggregation.

on the surface of avidin globules, which are not covered with primary gold particles, with free alkyl biotin molecules on gold particles adsorbed on avidin globules. This process yields aggregates more than 100 nm in diameter (Fig. 3, curve *4*). SEM micrographs (Fig. 6c) reveal the formation of a network constituted by chains of primary particles, with a pore size of 45–50 nm and more. Larger pores are appar-

ently formed by two or more avidin globules cross-linked by alkyl biotin molecules that were not adsorbed on gold particles before the introduction of avidin. It would be expected that the pore size will depend on the relative concentrations of avidin and primary gold particles and grow with the concentration of avidin and alkyl biotin in the system. The pore sizes will apparently be multiples of the size of the avidin globule, which is, to a certain extent, reflected by the SEM micrograph in Fig. 6c, obtained after 5 h of a specific interaction between biotin and avidin.

EXPERIMENTAL

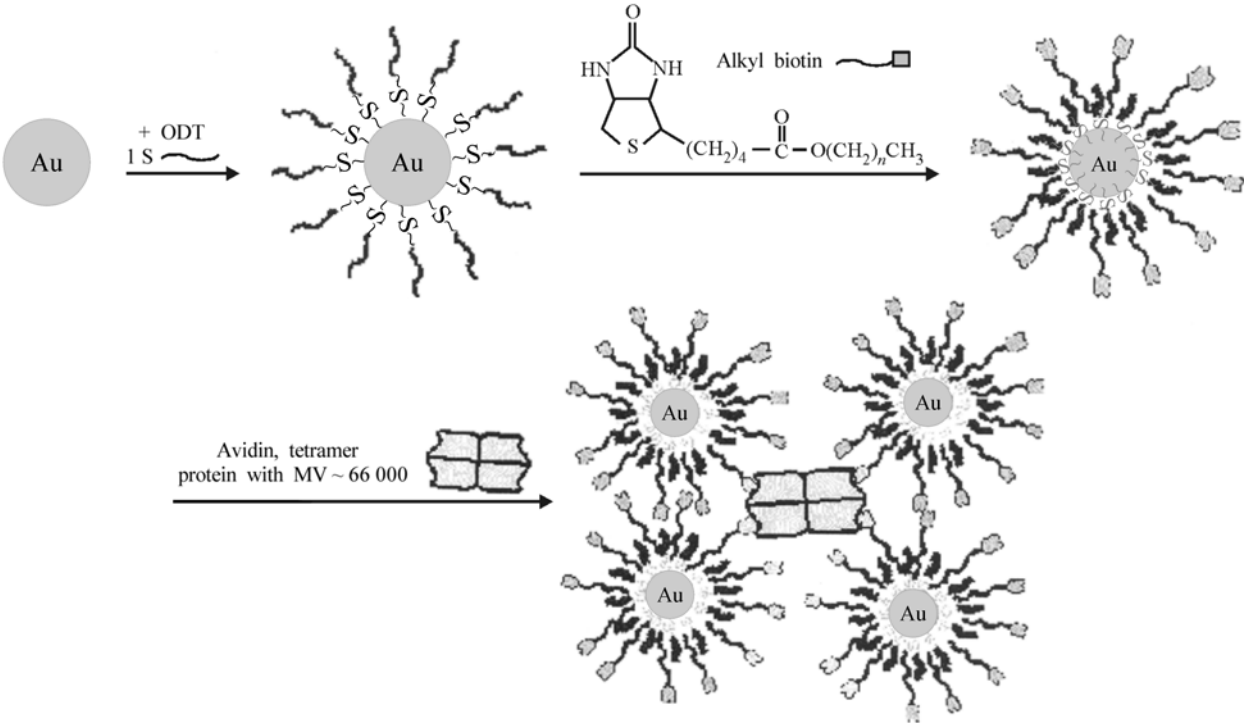
Sodium citrate dihydrate, $HAuCl_4$, 1-octadecanethiol, ethanol, 1-hexadcanol, 1-propanol, avidin (egg protein), and biotin (Aldrich) were used without additional purification.

A colloid gold solution was synthesized by reduction of hydrogen tetrachloroaurate(III) with sodium citrate. Prior to use, all the glassware was thoroughly washed and rinsed with water purified by filtration through a Millipore-Q filter. A 120-ml portion of an $HAuCl_4$ solution was charged into a 250-ml vessel and brought to boiling, after which 12.5 ml of a 0.5% sodium citrate solution was rapidly added. The mixture was boiled for 3–5 min, until it turned red. The average diameter of colloidal gold particles was measured by the method of dynamic light scattering (Zetasizer Nano ZS) and by transmission electron microscopy.

Cetyl and propyl esters of biotin were synthesized by reacting, respectively, 1-hexadecanol and 1-propanol by the procedure described in [20]. The products were purified by flash chromatography with MeOH : CH_2Cl_2 = 5 : 95 as eluent. The yield of the target products was 40 and 70%, respectively.

The functionalization of colloid particles and the reaction with avidin were studied by spectroscopy in the visible range, using a Varian Cary 100 Scan spectrometer with a resolution of 2 nm, as well as by the method of dynamic light scattering on a Zetasizer Nano ZS instrument.

Self-organizing ODT monolayers were fixed on the surface of colloidal gold particles from 1×10^{-7} and 1×10^{-5} M solutions of 1-octadecanethiol in ethanol, after which alkyl biotin molecules were attached to these layers. In the following stage, addition of biotinylated gold particles to avidin molecules was performed by the scheme described in [19].



The stability of gold hydrosols was examined in the presence of alkyl biotin at concentrations used in the experiments described above, and in the presence of a mixture of both components. To analyze the interaction between gold sol particles with ODT and the consecutive reaction with alkyl biotin and avidin

in the first stage, 0.1 ml of a 1×10^{-4} or 1×10^{-6} solution of ODT in ethanol, respectively, was added to 1 ml of a gold sol synthesized. Thus, the content of ODT in the reaction solution was 1×10^{-5} and 1×10^{-7} M. The mixture obtained was allowed to stand for 2 h. To a sample with a total ODT concentration of 1×10^{-7} was added 0.1 ml of a 1×10^{-5} M solution of alkyl biotin in a 1 : 1 mixture of ethanol and water. The resulting solution was allowed to stand for 48 h, after which 0.1 ml of a 4.5×10^{-7} M solution of avidin was added and the kinetics of formation of gold aggregates was studied.

Self-organizing layers of gold particles were obtained on the surface of quartz plates by using an apparatus with a step motor, intended for deposition of coatings at a constant temperature and humidity by means of immersion. The motion velocity of the quartz plate was varied within the range 0.l–1 m min^{-1}. The plates were washed with water purified with a Millipore filter and with ethanol immediately before use, after which they were immersed in a gold sol aggregated for a certain time, kept there for 60 s, and then dried. The kinetics of aggregation of colloidal gold particles were compared by field-emission scanning electron microscopy on an LEO 1530 microscope with enhanced resolution (down to 5 nm).

CONCLUSIONS

(1) The changes observed in the absorption spectra of a gold sol mixed with octadecanethiol, alkyl biotin, and avidin indicate that gold particle aggregates with a controllable size are formed.

(2) The aggregation of god particles and their structure can be controlled by varying the concentrations of the reagents used in the mixture and the order of their introduction into the system.

(3) The adsorption of aggregates of gold particles bound to avidin makes it possible to obtain organized 2*D* structures.

ACKNOWLEDGMENTS

Ananii Kogut thanks the DAAD Foundation for the financial support of his stay at the Erlangen-Nuremberg University. The authors are grateful to Clarissa Abetz (University of Bayreuth) for technical assistance in SEM measurements.

REFERENCES

1. Templeton, A.C., Wuelfing, W.P., and Murray, R.W., *Acc. Chem. Res.*, 2000, vol. 33, pp. 27–36.
2. Hostetler, M.J., Templeton, A.C., and Murray, R.W., *Langmuir*, 1999, vol. 15, pp. 3782–3789.
3. Nam, J.M., Park, S.J., and Mirkin, C.A., *J. Am. Chem. Soc.*, 2002, vol. 124, pp. 3820–3821.
4. Sato, K., Hosokawa, K., and Maeda, M., *J. Am. Chem. Soc.*, 2003, vol. 125, pp. 8102–8103.
5. Elghanian, V., Storhoff, J.J., Mucic, R.C., *et al.*, *Science*, 1997, vol. 277, pp. 1078–1080.
6. Brust, M., Walker, D., Bethell, D.J., *et al.*, *J. Chem. Soc. Chem. Commun.*, 1994, pp. 801–802.
7. Mayya, K.S., Patil, V., and Sastry, M., *Langmuir*, 1997, vol. 13, pp. 3944–3947.
8. Mirkin, C.A., Letsinger, R.L., Mucic, R.C., and Storhoff, J.J., *Nature*, 1996, vol. 382, pp. 607–609.
9. Li, V., Wong, K.K.W., and Mann, S., *Chem. Mater.*, 1999, vol. 11, pp. 23–26.
10. Sastry, V, Lala, N., Patil, V., *et al.*, *Langmuir*, 1998, vol. 14, pp. 4138–4142.
11. Chan, W.C.W. and Nile, S., *Science*, 1998, vol. 281, pp. 2016–2018.
12. Patil, V., Malvankar, R.D., and Sastry, M., *Langmuir*, 1999, vol. 15, pp. 8197–8206.
13. Shchukin, E.D., Pertsov, A.V., and Amelina, E.A., *Kolloidnaya khimiya* (Colloid Chemistry), Moscow: Mos. Gos. Univ., 1982.
14. Frolov, Yu.G., *Kurs kolloidnoi khimii: Poverkhnostnye yavleniya i dispersnye sistemy* (A Course of Colloid Chemistry: Surface Phenomena and Dispersed Systems), Moscow: Khimiya, 1988.
15. Turkevich, J., Stevenson, P.C., and Hillier, J., *Discuss. Faraday Soc.*, 1951, vol. 11, pp. 55–75.
16. Cotton, F.A. and Wilkinson, G., *Advanced Inorganic Chemistry*, New York: Interscience, 1966.
17. Mie, G., *Ann. Phys.*, 1908, vol. 25, pp. 377–345.
18. Weisbecker, V., Merritt, M.V., and Whitsides, G.M., *Langmuir*, 1996, vol. 12, pp. 3763–3772.
19. Lala Neeta, Chittiboyina, A.G., Chavan, S.P., and Sastry Murali, *Colloid Surfaces, A: Physicochem. Engineer. Aspects*, 2002, vol. 205, pp. 15–20.

Russian Journal of Applied Chemistry, Vol. 78, No. 10, 2005, pp. 1566–1570. Translated from Zhurnal Prikladnoi Khimii, Vol. 78, No. 10, 2005, pp. 1596–1599.
Original Russian Text Copyright © 2005 by V. Maiorov, Avsaragov, Kopkov, Popova, D. Maiorov, Nikolaev.

INORGANIC SYNTHESIS AND INDUSTRIAL INORGANIC CHEMISTRY

Recovery of Thorium(IV) and Radium(II) from Chloride Solutions

V. G. Maiorov, Kh. B. Avsaragov, V. K. Kopkov, T. V. Popova, D. V. Maiorov, and A. I. Nikolaev

Tananaev Institute of Chemistry and Technology of Rare Elements and Mineral Raw Materials, Kola Scientific Center, Russian Academy of Sciences, Apatity, Russia

Received March 28, 2005

Abstract—Recovery of thorium(IV) and radium(II) by precipitation methods in the chloride technology of perovskite processing was studied.

An efficient technique for breakdown of rare-metal raw materials is their decomposition with hydrochloric acid [1, 2]. Processing of concentrates containing radionuclides poses a problem of removal of these admixtures from chloride solutions. In this communication, we consider the recovery of thorium(IV) and radium (II) in the chloride technology of perovskite processing.

Perovskite from the Afrikanda deposit (best prepared for industrial processing) was used. The material contained (wt %): $(Nb + Ta)_2O_5$ 0.64–2.50, TiO_2 50.8–56.8, SiO_2 0.12–1.93, Al_2O_3 0.15–1.30, Fe_2O_3 0.43–2.00, FeO up to 1.44, Ln_2O_3 2.18–10.7 (here and hereinafter Ln_2O_3 is the sum of oxides of rare earth elements), CaO 26.3–38.1, Na_2O 0.10–2.35, ThO_2 0.07–0.14, and UO_3 ~0.01. Various alternative integrated technologies for perovskite processing to give tantalum and niobium pentaoxides, pigmentary titanium dioxide, and a rare-earth concentrate have been developed at the Institute of Chemistry, Kola Scientific Center, Russian Academy of Sciences. A promising variant is perovskite breakdown with hydrochloric acid, in which calcium(II), rare-earth elements(III), and thorium(IV) pass into a solution, and titanium(IV), niobium(V), and tantalum(V), into a precipitate, which is further processed into a commodity output by the known schemes [1, 2]. The chloride solutions obtained upon hydrolytic precipitation of titanium(IV), niobium(V), and tantalum(V) contained (g l^{-1}): HCl 100–200, $CaCl_2$ 100–150, ThO_2 0.1–0.2, Ln_2O_3 6–10, Fe_2O_3 [Fe(II) + Fe(III) in terms of Fe_2O_3], and TiO_2 1–10. In addition, sodium(I), aluminum(III), vanadium(V), manganese(II), and compounds of other elements were present in the solutions. The system has a complex multicomponent composition, with strongly different properties of chemical elements and a high salt content. It has been poorly investigated, which, on the whole, considerably complicates attacking the problem to be solved, specifically, the recovery of radionuclides from technological solutions.

Earlier [3, 4], we have studied the utilization of solutions produced in perovskite breakdown with hydrochloric acid, with thorium(IV) recovered by extraction with tributyl phosphate (TBP). The suggested variant of the technique enables efficient recovery of thorium(IV) from chloride solutions. A drawback of this procedure is a considerable flow rate of the extracting agent (1 : 1 volume ratio of organic and aqueous phases in the extraction process), which, in the end, adversely affects the economical characteristics of the technology. Furthermore, TBP is subjected to hydrolysis when brought in contact with acid (especially chloride) solutions, which requires that special operations should be introduced for removal of decomposition products from TBP and leads to an increased loss of the extracting agent [5].

This communication reports the results obtained in studying the purification of technological solutions to remove thorium(IV) and radium(II) by precipitation. In the experiments, we used solutions of the composition specified above and (for the most part) the same solutions concentrated by evaporation to a $CaCl_2$ concentration of 300 g l^{-1} and higher. The evaporation was performed to diminish the process flows and to regenerate (distill off) HCl, recycled into the stage of perovskite breakdown.

1070-4272/05/7810-1566 © 2005 Pleiades Publishing, Inc.

Table 1. Distibution of thorium(IV) and rare earth elements(III) upon neutralization of solutions with lime milk (20 wt % CaO)*

Run no.	Dilution of the starting solution with water	1st precipitation		2nd precipitation		Filtrate upon solution neutralization					
		pH	ThO_2 content of precipitate, wt %	pH	La_2O_3 content of precipitate, wt %	content, g l^{-1}		total degree of precipitation, %		activity, Bq l^{-1}	
						ThO_2	La_2O_3	ThO_2	Ln_2O_3	α	β
1	1.2	9.0	–	–	–	<0.0001	0.0035	>99.94	99.95	2940 ± 730	4020 ± 190
2	3	2.5	~0.6	9.3	50.3	<0.001	<0.001	>98.3	>99.9	–	–
3	1	4.4	0.44	8.5	53.3	″	″	>99.4	>99.99	3600 ± 210	3370 ± 200
4	1	5.1	0.48	8.0	66.3	″	″	>99.6	>99.99	–	–

* With a NaOH solution (330 g l^{-1}) in run no. 3.

The purification of solutions to remove radionuclides was monitored by measuring the alpha and beta activities (α and β) and by chemical analysis for the ThO_2 content. The activity of the solutions is determined by the presence of natural thorium(IV) and uranium(IV) radionuclides and products of their decay, predominantly radium(II). To determine the values of α and β, a sample of a solution was evaporated to dryness; preliminarily it was found that radionuclides do not pass into the condensate in evaporation. The alpha and beta activities of a solid product were measured on a UMF 1500 D low-background installation, with the data obtained recalculated to the activity of a filtrate in becquerels per liter. A standard composed of the perovskite concentrate was used as reference. The values of α and β, presented in the paper, were calculated from the results of 5–10 (depending on the activity of solutions) parallel measurements of a sample and the background. The determination error was ±75 Bq l^{-1} for low-active samples and increased with a rise in the activity of the solutions studied to ±(500–1000) Bq l^{-1}. Other specific features of the experimental procedure and analytical monitoring technique were reported in [3].

Table 1 lists data on the extraction of thorium(IV) and rare earth elements(III) by neutralization of a solution containing (g l^{-1}): ThO_2 0.38, Ln_2O_3 20.2, Fe_2O_3 22.9, TiO_2 5.2, HCl 105, and $CaCl_2$ 314. It was assumed that precipitation of Th(IV) and U(VI) [6, 7] and coprecipitation of Ra(II) [8] on hydroxides of Ti(IV) and other elements will give filtrates containing no radionuclides. In run nos. 2–4, a two-stage neutralization gave a precipitate containing most of thorium(IV) (precipitation at pH 4.4–5.1) and a concentrate of rare earth elements(III) (neutralization to pH 8.0–9.3 [9]). Further processing of the precipitates could be carried out by the known techniques [3, 4, 10]. However, the activity of filtrates for all the variants of neutralization represented in Table 1 considerably exceeds sanitary norms for waste solutions. As Th(IV) and U(VI) are readily precipitated (see [6, 7] and Table 1: the ThO_2 content of the filtrates, found by chemical analysis, is less than 0.0001–0.001 g l^{-1}) we can conclude that the high activity of the filtrates is mainly determined by the presence of Ra(II) and products of its decay. In this context, we further paid the main attention to removal of radium(II) from solutions by its precipitation on $BaSO_4$. This method is successfully applied in both analytical [8] and industrial practice [13].

We used two starting solutions containing (g l^{-1}): ThO_2 0.06, Ln_2O_3 24.7, HCl 44, and $CaCl_2$ 290 with the α and β activity of 710 ± 90 and 1640 ± 80 Bq l^{-1}, respectively, (Figs. 1, 2) and ThO_2 0.08, Ln_2O_3 28.2, HCl 29, $CaCl_2$ 376 with the α and β activity of 10460 ± 1280 and 10560 ± 410 Bq l^{-1}, respectively,

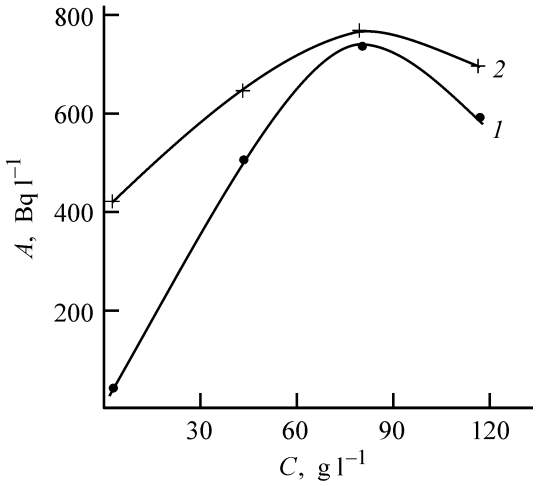


Fig. 1. (*1*) Alpha and (*2*) beta activities of filtrate vs. the concentration of BaCl in solution before recovery of radium(II). (*A*) Activity and (*C*) concentration of HCl.

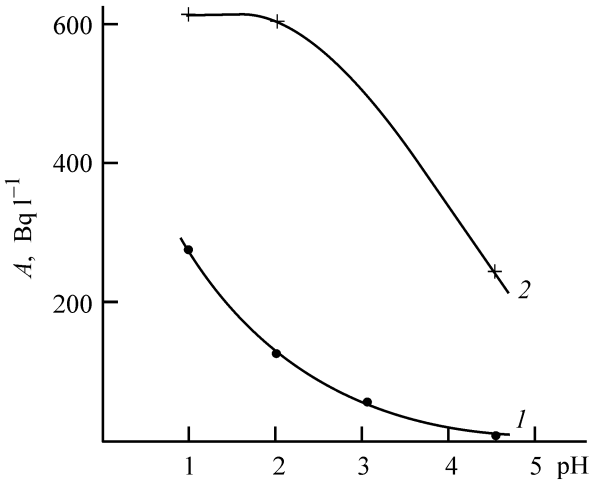


Fig. 2. (*1*) Alpha and (*2*) beta activities of the filtrate vs. the solution pH before recovery of radium(II). (*A*) Activity.

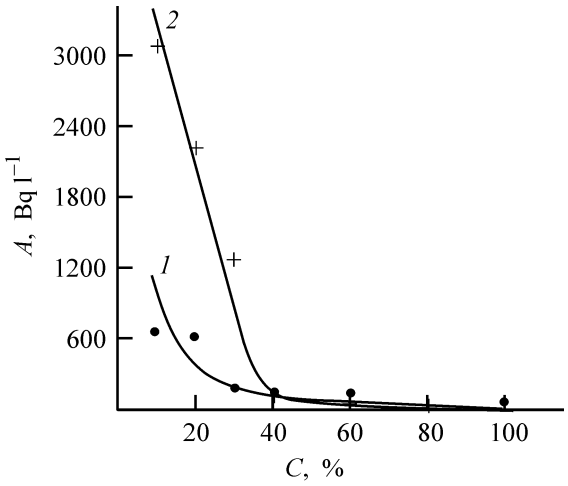


Fig. 3. (*1*) Alpha and (*2*) beta activities of the filtrate vs. the $BaCl_2$ expenditure. (*A*) activity and (*C*) $BaCl_2$ expenditure.

(Fig. 3, Table 2). The experimental results describing the influence of the acidity of a medium on the purification to remove radionuclides are presented in Figs. 1 and 2. Hydrochloric acid or lime milk was added to 25 ml of a solution of the above-mentioned composition to reach the required pH value or HCl content, and the solution was allowed to stay for at least 12 h. Further, a $BaCl_2$ solution (200 g l^{-1}) was added, the mixture was heated to a prescribed temperature (70°C), a Na_2SO_4 solution (180 g l^{-1}) was added, and the pulp was kept at a prescribed temperature for 60 min. After cooling to room temperature, the resulting precipitate was filtered off. A sample of the filtrate was evaporated to dryness and the alpha and beta activities were determined by the above-described technique. The amounts of $BaCl_2$ and Na_2SO_4, used in this set of experiments, were taken with regard to the experience of industrial processing of the loparite concentrate: 4 ml of the $BaCl_2$ solution per 25 ml of the technological solution (conditionally taken for 100%); the expenditure of the Na_2SO_4 solution was 400% relative to the stoichiometric amount required for $BaSO_4$ to be formed.

Table 2. Precipitation of radium(II) at the 100% $BaCl_2$ expenditure and varied solution pH values, Na_2SO_4 expenditure, and temperature

Solution pH before recovery of radium(II)	Na_2SO_4 expenditure, %	Temperature, °C	Filtrate activity, Bq l^{-1}	
			α	β
Effect of pH in the range 4.5–9.1				
4.5	400	70	150	429
5.5	〃	〃	118	334
6.5–9.1	〃	〃	<75	<75
Effect of Na_2SO_4 expenditure				
7.0	180–400	70	<75	<75
Effect of temperature				
7.0	180	20–70	<75	<75

It is known from the analytical practice [8] that Ra(II) is precipitated on $BaSO_4$ most completely from acid solutions. However, this is not confirmed for the system under study, which has a high calcium(II) content: by contrast, it is necessary to make lower the solution acidity to reach the minimum alpha and beta activities of solutions. It has been noted [8] that, in the case of joint crystallization of isomorphous compounds, the degree of precipitation of a microcomponent is the higher, the more completely it is precipitated. We can conclude that the solubility of $BaSO_4$ [and $CaSO_4$, on which Ra(II) is also partly coprecipitated in systems with a high $BaCl_2$ concentrations] is at a minimum at pH close to 7. Accordingly, a higher degree of Ra(II) removal is observed in this pH range. Additional studies of the mechanism of Ra(II) coprecipitation on $BaSO_4$ in systems with a high content of $BaCl_2$ and other salts are necessary.

The results of the experiments aimed to refine the conditions of Ra(II) precipitation are presented in Table 2 and Fig. 3. Raising the pH value further [before recovery of Ra(II)] improves the purification of the solution to remove radionuclides (Table 2) owing both to an increase in the degree of Ra(II) precipitation and to a more complete recovery of Th(IV) hydroxide.

However, carrying out the process at pH higher than 7 is inexpedient because of the precipitation of hydroxides of rare earth elements(III). We can also conclude that, in the technological range under study, a 180–400% variation of the Na_2SO_4 expenditure and a 20–70°C variation of temperature (Table 2) do not affect essentially the purification of solutions to remove radionuclides. Accordingly, the effect of $BaCl_2$ expenditure (Fig. 3) was studied at pH ~7, Na_2SO_4 expenditure of 180%, and temperature of ~20°C. It follows from the data obtained that the $BaCl_2$ expenditure can be lowered by at least a factor of 2. Calculations show that, with account of the decrease in the Na_2SO_4 expenditure from 400 to 180%, we can strongly (by a factor of 3.7) diminish the total weight of a $BaSO_4$ + $CaSO_4$ radioactive precipitate to be buried. In this case, the level of alpha and beta radiation from the solution (its composition is given above) decreased from ~10 000 to less than 75 Bq l^{-1} despite a decrease in the $BaCl_2$ and Na_2SO_4 expenditure. This means that the degree of removal of radiating elements was higher than 99%. It is necessary to note that not all the parameters affecting the purification of solutions to remove radium(II) in the complex system under study were investigated. For example, we found that keeping a pulp (before filtering-off the $BaSO_4$ precipitate) for no less than 12 h diminishes the alpha and beta activities in a filtrate by approximately factors of 9 and 3.8, respectively. This indicates that a further decrease in the activity of filtrates is possible. At present, we are carrying out investigations aimed to optimize the conditions at which technological solutions are purified to remove radionuclides and to improve the measurement accuracy, because nearly background values of α and β are to be determined.

The results obtained in testing the precipitating purification of a technological solution to remove radionuclides are listed in Table 3. Radium(II) was precipitated at 50 and 220% expenditures of $BaCl_2$ and Na_2SO_4, respectively, with the pulp allowed to stand before filtration for approximately 20 h. A high (> 99%) degree of purification to remove α- and β-radiating elements was reached; the content of ThO_2 and Ln_2O_3 in the filtrate after the recovery of a concentrate of rare earth elements(III) was less than 0.001 g l^{-1}. The precipitate obtained by neutralization with a lime milk to pH 2.5 is mainly composed of iron(III) hydroxide. After dissolution of the precipitate in HCl, iron(III) is readily removed by extraction with octanol at minimum process flows to give pure iron compounds [3, 4]; the aqueous solution purified to remove iron(III) and containing mainly titanum(IV) is directed to the operation of perovskite breakdown with hydrochloric acid to exclude loss of titanium(IV). The $BaSO_4$ + $CaSO_4$ precipitate obtained at pH 7 and containing Ra(II) and Th(IV) is buried, and the concentrate of rare earth elements(III) is processed by the known schemes (see [10] and G.V. Korpusov's works). The ways to process a solution freed from radionuclides and containing virtually only $CaCl_2$ were considered in [1–4].

Table 3. Precipitation of radionuclides from a solution containing (g l^{-1}): ThO_2 0.60, Ln_2O_3 29.2, Fe_2O_3 30.5, TiO_2 3.2, HCl 84, $CaCl_2$ 469 and having the activity α = 23 090 ± 2760 and β = 17 890 ± 670 (Bq l^{-1})

Solution	Activity, Bq l^{-1}	
	α	β
Filtrate upon precipitation of hydroxides (pH 2.5)	3610 ± 710	5110 ± 270
Filtrate upon recovery of Ra(II) (pH 7)	83 ± 200	120 ± 65
Filtrate upon precipitation of rare earth elements(III) (pH 9)	32 ± 180	52 ± 86

Thus, our studies revealed an efficient variant of utilization of chloride solutions in the perovskite technology. The variant is based on precipitating methods and has certain advantages over the recovery of thorium(IV) by extraction with tributyl phosphate (the procedure used is simpler and its technical and economic characteristics are improved).

CONCLUSIONS

(1) The precipitation of radium(II) on $BaSO_4$ was studied: namely, the influence exerted by the solution acidity [before Ra(II) isolation], $BaCl_2$ and Na_2SO_4 expenditure, and process temperature. It was found that radium(II) is most completely precipitated at pH ≥ 7. It was shown that, under the best conditions, the alpha and beta activities of the solutions studied decrease from approximately 10 000 to less than 75 Bq l^{-1}.

(2) A technological variant was suggested, which includes precipitation of hydroxides of Fe(III), Ti(IV), and other elements at pH ~2.5, precipitation of Ra(II) on $BaSO_4$ with the simultaneous precipitation of Th(IV) (pH ~7), and production of a concentrate of rare earth elements(III) (pH ~9).

REFERENCES

1. Nikolaev, A.I, Gerasimov, L.G., Maiorov, V.G., *et al.*, Abstracts of Papers, *XVII Mendeleevskii s'ezd po obshchei i priklandoi khimii* (XVII Mendeleev Congress on General and Applied Chemistry), vol. 3, *Materialy i nanotekhnologii* (Materials and Nanotechnologies), Kazan, 2003, p. 313.
2. Skiba, G.S., Voskoboinikov, N.B., Solov'ev, A.V., *et al.*, *Zh. Prikl. Khim.*, 2003, vol. 76, no. 10, pp. 1738–1739.
3. Maiorov, V.G., Nikolaev, A.I, Kopkov, V.K., *et al.*, *Zh. Prikl. Khim.*, 2004, vol. 77, no. 5, pp. 715–719.
4. Maiorov, V.G., Nikolaev, A.I, Kopkov, V.K., and Safonova, L.A., *Tsvet. Met.*, 2004, no. 2, pp. 15–20.
5. Babkin, A.G., Maiorov, V.G., and Nikolaev, A.I., *Ekstraktsiya niobiya, tantala i drugikh elementov iz ftoridnykh rastvorov* (Extraction of Niobium, Tantalum, and Other Elements from Fluoride Solutions), Leningrad: Nauka, 1988.
6. Ryabchikov, D.I. and Gol'braikh, E.K., *Analiticheskaya khimiya toriya* (Analytical Chemistry of Thorium), Moscow: Akad. Nauk SSSR, 1960.
7. Markov, V.K., Vernyi, E.A., Vinogradov, A.V., *et al.*, *Uran: Metody ego opredeleniya* (Uranium: Methods for Its Determination): Atomizdat, 1964.
8. Vdovenko, V.M. and Dubasov, Yu.V., *Analiticheskaya khimiya radiya* (Analytical Chemistry of Radium), Leningrad: Nauka, 1973.
9. Ryabchikov, D.I. and Ryabukhin, V.A., *Analiticheskaya khimiya redkozemel'nykh elementov i ittriya* (Analytical Chemistry of Rare Earth Elements and Yttrium), Moscow: Nauka, 1966.
10. Lebedev, V.N., Asseretskova, O.V., and Smirnova, I.P., *Khimiya i tekhnologiya mineral'nogo syr'ya Kol'skogo poluostrova* (Chemistry and Technology of Mineral Raw Materials of Kola Peninsula), St. Petersburg: Nauka, 1992, pp. 54–60.
11. Kosynkin, V.V., Makarov, V.D., and Shatalov, V.I., *Ochistka redkikh zemel' loparita ot radioaktivnykh primesei* (The Purification of Rare Earths of Loparite To Remove Radioactive Admixtures), Trudy IV nauchnoi *konferentsii Razvitie redkometal'noi promyshlennosti Rossii na baze loparita* (Proc. IV International Conf. Progress in Rare-metal Industry of Russia on the Basis of Loparite), St. Petersburg, 2001, pp. 153–158.

Russian Journal of Applied Chemistry, Vol. 78, No. 10, 2005, pp. 1571–1575. Translated from Zhurnal Prikladnoi Khimii, Vol. 78, No. 10, 2005, pp. 1600–1604.
Original Russian Text Copyright © 2005 by Litvinov, Poilov.

INORGANIC SYNTHESIS AND INDUSTRIAL INORGANIC CHEMISTRY

Reduction of Sulfates with Oil Coke in a Carnallite Melt

A. V. Litvinov and V. Z. Poilov

Perm State Technical University, Perm, Russia

Received April 7, 2005

Abstract—Purification of flotation carnallite to remove sulfates by their reduction in a melt was studied. The optimal parameters of the reduction and the effect of various factors on this process were determined. The mechanism of the process is suggested, and the results of industrial tests are given.

When passing to new raw materials for electrolytic production of metallic magnesium and, in particular, to flotation carnallite, brucite, or serpentinite, a necessity arises for additional purification of the molten magnesium electrolyte to remove sulfates. It is known that sulfate admixtures contained in the electrolyte substantially impair the current efficiency by magnesium and disrupt the operating mode [1, 2]. At a sulfate content in anhydrous carnallite exceeding 0.05 wt %, the current efficiency sharply decreases. A froth appears on the electrolyte surface and the electrolyte circulation is enhanced, which results in that the slime is stirred up and passivates the cathodes [3].

The procedures developed for purification of the molten magnesium electrolyte to remove sulfate admixtures by reduction with natural gas, carbon oxide, and magnesium [4–6] have been only implemented on laboratory installations. Their commercial use appeared to be unfeasible owing to the high fire and explosion hazard. In this study, we developed an efficient commercial procedure for removing sulfate admixtures from the melt of flotation carnallite.

We used as a raw material for laboratory studies four batches of flotation carnallite produced in laboratory by the flotation technique (VNIIG, St. Petersburg). They contained different amounts of calcium sulfate (0.07, 0.39, 0.55, and 0.68 wt %). We also used artificially contaminated halurgic carnallite containing 0.5–1.0 wt % sulfate ions.

When studying the removal of sulfate ions from an electrolyte melt, we simulated the processes occurring in the chambers of an industrial chlorinator: in the melting pot, in chlorinating chambers, and in the mixer (settling tank). We studied the removal of sulfate ions from the melt at 500–800°C (temperature profile of the chlorinator) in a reactor into which chlorine was fed to simulate the operation of chlorinating chambers, and argon, for a more complete mixing of the components. We determined the residual content of sulfate ions by photocolorimetry or gravimetry [7].

We used as reducing agents activated carbon and oil coke, and metallic magnesium for comparison. The data obtained for a model carnallite melt with various reducing additives are presented in Figs. 1 and 2.

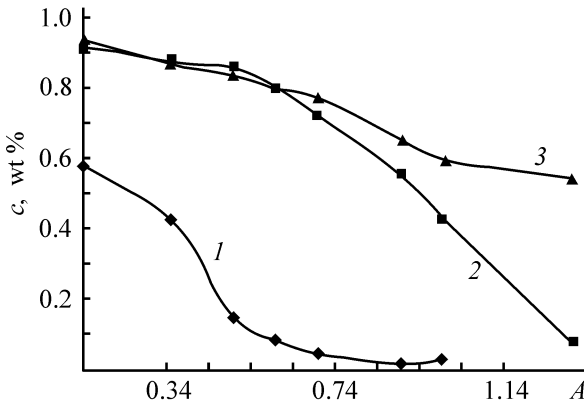


Fig. 1. Concentration c of sulfate ions in the carnallite melt vs. the weight ratio A between the amount of the reducing additive and $CaSO_4$. Process duration 1 h, T = 700°C, initial content of sulfate ions 1.0 wt %. Reducing agent: (*1*) oil coke, (*2*) metallic magnesium, (*3*) activated carbon; the same for Fig. 2.

1070-4272/05/7810-1571 © 2005 Pleiades Publishing, Inc.

Table 1. Degree of removal of sulfate ions from flotation carnallite, α, at a varied initial content of $CaSO_4$ in the carnallite melt

Content of $CaSO_4$ in carnallite, wt %		α, %
starting flotation-type	molten after removal of SO_4^{2-}	
0.070	0.020 ± 0.01	71.43
0.390	0.039 ± 0.01	90.00
0.550	0.049 ± 0.01	91.09
0.680	0.052 ± 0.01	92.35

Analysis of the curves in Figs. 1 and 2 shows that oil coke is the most effective additive. The maximum rate and degree of carnallite purification to remove sulfates are achieved with its help. In this case, the carnallite melt is not contaminated with carbon, whose content is strictly controlled in industry, because it is collected as a coke froth in the surface layer of the electrolyte melt. As can be seen, two other additives do not diminish the content of sulfate ions to the required value of 0.05 wt %. This fact predetermined the choice of oil coke as a reducing agent.

The effect of temperature on the reduction of sulfates with oil coke is shown in Fig. 3.

As can be seen from Fig. 3, the duration of purification of the electrolyte melt at 700–750°C to a residual concentration of sulfate ions of 0.02–0.05 wt % is 20–40 min. The obtained optimal parameters of the reduction of sulfate ions in the carnallite melt (700–750°C and process duration of 20–40 min) correspond to the working mode of the industrial chlorinator and to the residence time of the carnallite melt in the apparatus.

The procedure under study for removing sulfate ions was tested on four batches of dehydrated flotation carnallite with varied content of sulfates. The results obtained are listed in Table 1. The residual content of sulfate ions varied within the range 0.02–0.05 wt %. The content of sulfates in a dehydrated melt of halurgic carnallite at a working magnesium-manufacturing shop was 0.05–0.06 wt %. This suggests that the procedure developed for removal of sulfate ions from flotation carnallite can eliminate the main drawback of the flotation technology, the high content of sulfate ions.

The removal of sulfate ions from the carnallite melt was accompanied by vigorous gas evolution, which led to "boiling" of the melt. After the reduction was complete, the boiling stopped. At high initial concentrations of sulfates in carnallite, we observed blue tongues of flame on the surface of the "boiling" melt, which can be attributed to an additional oxidation of the products formed in the reduction of sulfate ions and in oil coke pyrolysis.

When bubbling methane, hydrogen, or propane through the melt, sulfate ions are reduced to give sulfur-containing gases [4]. The authors of [6] suggested that the products of pyrolysis of a hydrocarbon mixture make the greatest contribution to the reduction of sulfate admixtures in the carnallite melt.

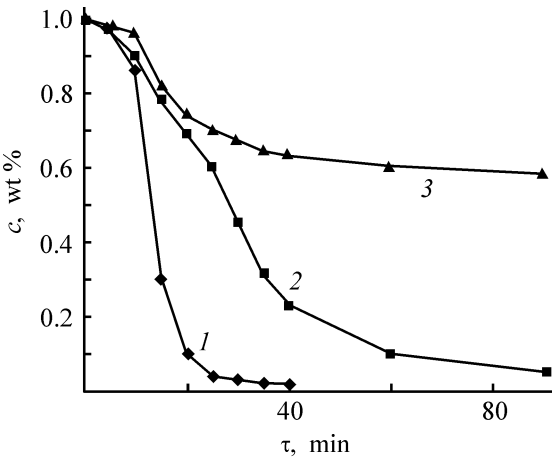


Fig. 2. Concentration c of sulfate ions in the carnallite melt vs. the process duration τ for different types of the reducing agent. The weight ratio between the amounts of the reducing agent and sulfate ions is 0.8.

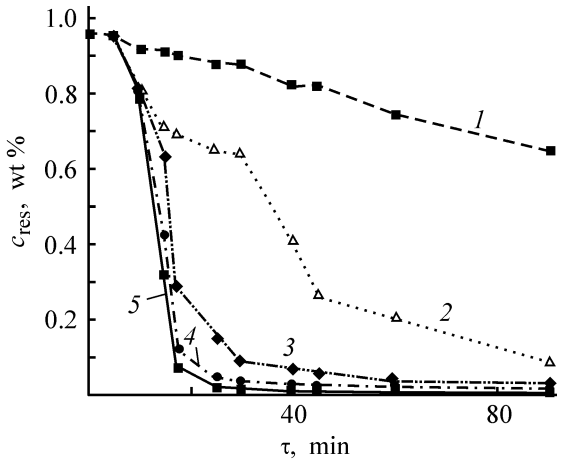


Fig. 3. Residual concentration c_{res} of sulfate ions in the carnallite melt vs. the duration of the reduction with oil coke, τ. Initial content of sulfate ions 1.0 wt %, weight ratio between the amounts of the reducing agent and sulfate ions 0.8; the same for Fig. 4. Reduction temperature (°C): (*1*) 550, (*2*) 675, (*3*) 710, (*4*) 750, (*5*) 790.

Experimental data obtained in the present study suggest that the reduction of sulfate ions in the carnallite melt has a more complicated character and cannot be accounted for exclusively by the reaction of sulfate ions with the reducing gases.

The mechanism of reduction of sulfate ions in a molten chloride medium can be represented as follows. Upon pyrolysis of the oil coke at 650–730°C, the bituminous part of the oil coke transforms into a carbonized solid and volatile substances H_2, CH_4, CO, CO_2, and H_2S [8]. At 670–730°C, the main part of the volatile products is evolved within the first 5 min of the process [9, 10]. Figure 4 shows the experimental time dependences of the rate of reduction of sulfate ions by oil coke in the carnallite melt.

Within the first 5 min of the process, sulfate ions are almost not removed from the melt (Figs. 3 and 4). Moreover, the total amount of gases evolved upon pyrolysis of the oil coke introduced as a reducing additive is substantially lower than that necessary for removing the admixtures from the melt [4]. We also emphasize that the oil coke is mostly distributed over the surface layer, and sulfate ions cannot be removed from the melt only via formation of volatile components of the oil coke and their reaction with sulfates, because the mixture of evolved gases passes through a minor upper part of the melt. The final evidence in favor of the "not-only-gaseous" mechanism of reduction of sulfate ions is that the oil coke calcined in the carnallite melt at 750°C and virtually freed of volatile components removes sulfate ions from the melt rather efficiently.

To determine the contribution of volatile reducing agents to the removal of sulfate ions from the melt, we carried out a thermal analysis of carnallite samples with fresh and calcined oil coke on an MOM Q-1500 derivatograph (Hungary). The sample weight was 200 mg, and the heating rate, 10 deg min^{-1}. The sample compositions are listed in Table 2.

The results of a differential thermal analysis of carnallite mixtures with oil coke (fresh and previously calcined in the carnallite melt) are presented in Fig. 5. In the range 550–750°C, a strong exothermic effect is observed for sample no. 1 (oil coke in the carnallite melt). This effect corresponds to oxidation of volatile components, primarily hydrogen and methane, by atmospheric oxygen [7, 8]. Owing to the superposition of this exothermic peak on the endothermic peak corresponding to reduction of sulfate ions by the oil coke (sample no. 2), the effect associated with the reduction is somewhat shifted and lies in the range 680–750°C, with the peak at 730°C.

Table 2. Compositions of samples for thermal analysis

Run no.	Sample composition, wt %			
	carnallite	oil coke		sulfate ions
		fresh	calcined	
1	97.5	2.5	–	–
2	95	2.5	–	2.5
3	97.5	–	2.5	–
4	95	–	2.5	2.5

In the case of pyrolysis of a calcined oil coke (sample no. 3), the peak of the endothermic effect is shifted to 630–720°C owing to changes in the composition of pyrolysis products and to an increase in the content of carbon monoxide and dioxide [7, 8]. Moreover, the total yield of volatile components decreases for

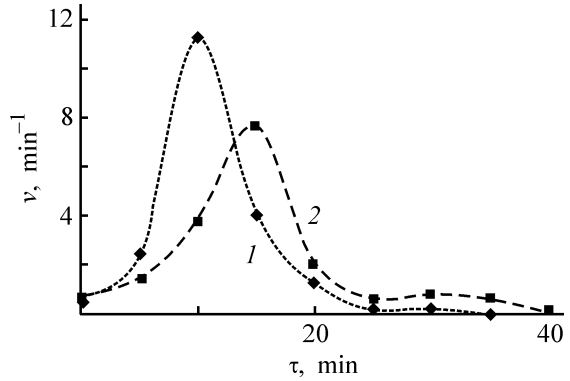


Fig. 4. Rate ν of removal of sulfate ions vs. time τ. T = 750°C. Reducing agent: (*1*) fresh oil coke; (*2*) oil coke calcined in the carnallite melt for 1 h.

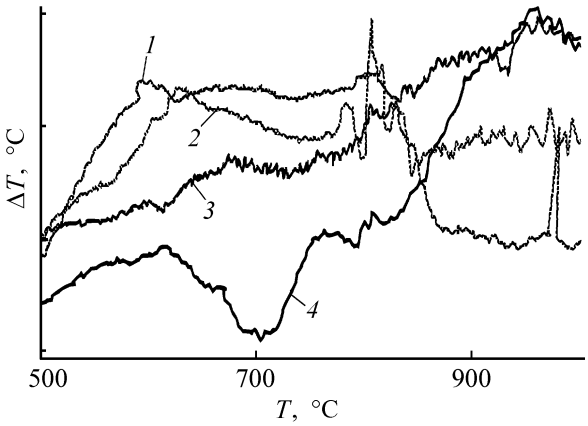


Fig. 5. DTA curves. (*T*) Temperature. (*1*) Pyrolysis of the oil coke in a carnallite melt containing no sulfates, (*2*) reduction of sulfates by a fresh oil coke, (*3*) pyrolysis of a calcined oil coke in the carnallite melt containing no sulfates, (*4*) reduction of sulfates by the calcined oil coke.

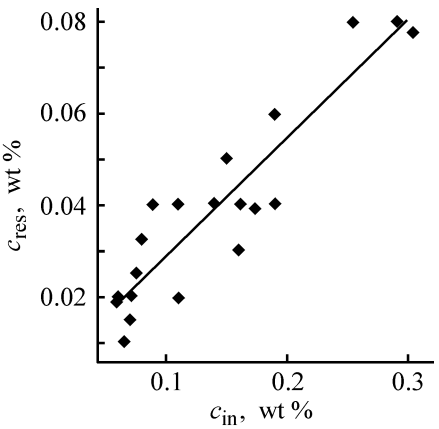


Fig. 6. Residual concentration c_{res} of sulfate ions in the carnallite melt in the mixer vs. the initial concentration c_{in} of sulfate ions in carnallite in the melting pot of the chlorinator.

this sample. For example, the loss of weight by sample no. 1 at 550–750°C was 3.6%, and that for the calcined sample, 1.7%. This fact is presumably responsible for the decrease in the rate of the process and for the shift of the peak of the maximum rate (Fig. 4). The reduction of sulfates in the carnallite melt by the calcined coke (Fig. 5, curve *4*) occurred in the range 660–750°C, with the maximum endothermic effect at 715°C. The difference between the peaks of endothermic effects in reduction with calcined and uncalcined coke is primarily due to the following: (i) pyrolysis of uncalcined oil coke releases a markedly greater amount of volatile components oxidized by atmospheric oxygen and (ii) the exothermic effect of oxidation of volatile products is superimposed on the endothermic effect of reduction of sulfate ions by carbon. In this case, the rate of reduction of sulfate ions by the preliminary calcined oil coke is significantly lower (Fig. 4) than that by the fresh coke. These data show that the reduction of sulfate ions by the oil coke also occurs via the reaction of oil coke components dispersed in the carnallite with sulfate ions.

Molecules of oil coke are a mixture of aromatic hydrocarbons with a π-electron system [9]. The high stability of molecular ions is a specific feature of aromatic hydrocarbons. When a C–C bond is formed, e.g., in the case when one macromolecule lies out of the plane of nearest neighbors, edge defects are formed. Foreign atoms, such as H, and groups like –OH, =O, –O–, =S, =N, and –N–, interact with the edge defects. On heating the oil coke, foreign atoms are removed from the carbon structure. For one or several carbon atoms, electrons appear to be unpaired near a defect. Such atoms have a trapped unpaired electron and rather stable C_M^-–C^+ groups are formed. As a result of evolution of a greater number of volatile components, the content of stable charged groups in a fresh oil coke is considerably higher, and, therefore, the rate of the reaction is higher in the case of a fresh oil coke (Fig. 4), compared with the oil coke calcined in the carnallite melt.

The reduction of sulfates, e.g., KSO_4^-, includes a primary act that consists in the attachment of a sulfate ion to certain points of the carbon network, in the first place to the edge defects, to give a transition complex C_M^-–C^+–O^-–SO_2–O^-–K^+. The stability of the complex and the composition of the products of its decomposition are determined by the temperature of the melt. At 650–750°C, the complex is unstable and decomposes.

Laboratory tests established that the oil coke can be used to reduce sulfates in the carnallite melt. It was shown that the reduction of sulfates by the oil coke also occurs via the reaction of oil coke components dispersed in the carnallite solution with sulfate ions.

Taking into account the requirements of cost saving and those of the current industrial scheme of magnesium production, we suggested to remove sulfates from the carnallite melt in a commercial chlorinator. The design of the chlorinator allows introduction of reducing additives of varied composition and enables purification to remove additionally introduced admixtures in a special chamber, the mixer.

We carried out tests on purification of a carnallite melt to remove sulfates in an indistrial chlorinator for magnesium production at the "Solikamsk magnesium plant" Joint-Stock Company. We tested the process of removal of sulfate ions from the carnallite melt for three ranges of sulfate ion concentrations in the carnallite melt (wt %): 0.07–0.16, 0.10–0.20, and 0.20–0.30. Sulfate ions were reduced in the chlorinator in the working mode in use at the electrolysis shop, with the only difference that a small amount of a reducing agent under study was introduced into the chlorinator mixer. We obtained a characteristic dependence of the residual content of sulfate ions in the carnallite melt at the chlorinator output on the content of sulfates in starting carnallite (Fig. 6).

It can be seen from Fig. 6 that the limiting content of sulfate ions in the starting carnallite, to which corresponds the permissible residual concentration of sulfate ions in the purified carnallite melt (0.05 wt %), is 0.15–0.18 wt %. The carnallite melt purified to this content of sulfate ions was further electrolyzed,

with no disturbance to the operation of electrolyzers observed.

CONCLUSIONS

(1) A procedure for purification of the flotation-type carnallite melt to remove sulfate admixtures was developed. The procedure ensures that the residual content of the admixtures decreases to 0.02–0.05 wt %.

(2) It was confirmed that a reducing agent dispersed in the carnallite melt, rather than that in the gaseous state, is involved in the reduction of sulfates by the oil coke.

(3) Industrial tests at an operating plant confirmed the high efficiency of the procedure developed for purification of the carnallite melt to remove sulfate ions.

REFERENCES

1. Ivanov, A.I., Lyandris, M.B., and Prokof'ev, O.V., *Proizvodstvo magniya* (Manufacture of Magnesium), Moscow: Metallurgiya, 1976.
2. Desyatnikov, O.G., *Trudy VAMI*, Leningrad: VAMI, 1960, no. 44, pp. 174–178.
3. Ivanov, A.B., Muzhzhavlev, K.D., and Yazev, V.D., *Tsvet. Met.*, 1972, no. 4, pp. 47–52.
4. Savinkova, E.I., Barsukova, G.A., and Vil'nyanskii, Ya.E., *Tsvet. Met.*, 1969, no. 6, pp. 61–66.
5. Savinkova, E.I., Kosnyrev G.T., and Partina, G.A., *Tsvet. Met.*, 1966, no. 4, pp. 56–61.
6. Shcheglov, V.I., Ivanov, A.B., Rudakov, V.A., and Andreeva, I.G., *Sovershenstvovanie tekhniki i tekhnologii proizvodstva legkikh metallov* (Improvement of the Technology of Manufacture of Light Metals), Trudy VAMI, Leningrad: VAMI, 1980, pp. 91–95.
7. Lur'e, Yu.Yu., *Spravochnik po analiticheskoi khimii* (Handbook of Analytical Chemistry), Moscow: Khimiya, 1979.
8. Ubbelode, A.R. and L'yus, F.A., *Grafit i ego kristallicheskie modifikatsii* (Graphite and Its Crystalline Modifications), Moscow: Prosveshchenie, 1969.
9. Shenfeld, B.E., Kon'shin, Yu.N., Ketov, A.N., and Sivkova, L.M., *Izv. Vyssh. Uchebn. Zaved.*, Tsvet. Metall., 1972, no. 3, pp. 77–79.
10. Shenfeld, B.E., Kon'shin, Yu.N., and Ketov, A.N., *Izv. Vyssh. Uchebn. Zaved.*, Tsvet. Metall., 1971, no. 5, pp. 54–57.

Russian Journal of Applied Chemistry, Vol. 78, No. 10, 2005, pp. 1576–1580. Translated from Zhurnal Prikladnoi Khimii, Vol. 78, No. 10, 2005, pp. 1605–1609.
Original Russian Text Copyright © 2005 by Evchuk, Musii, Makitra, Pristanskii.

PHYSICOCHEMICAL STUDIES OF SYSTEMS AND PROCESSES

Solubility of Polymethyl Methacrylate in Organic Solvents

I. Yu. Evchuk, R. I. Musii, R. G. Makitra, and R. E. Pristanskii

Litvinenko Institute of Physicoorganic and Coal Chemistry, National Academy of Sciences of Ukraine, Department of Physical Chemistry of Fuel Resources, Lviv, Ukraine

Received June 7, 2005

Abstract—Solubility of polymethyl methacrylate in 12 organic solvents at 30–70°C was studied.

The resistance of polymers to organic solvents is theoretically and practically important. At the same time, studies in this area are mainly concerned with swelling of polymers in various media. The dissolution process itself, despite its wide application in various technologies, has been studied to a considerably lesser extent.

According to the Nernst diffusion theory, the dissolution of low-molecular compounds in liquids occurs at the phase boundary rapidly and is limited by diffusion of components toward and away from the surface of a solid. The process rate v is determined by the diffusion coefficient D, boundary layer thickness l, and difference of the solute concentrations in the surface layer (c_0) and in the bulk (c):

$$v = \frac{D}{l}(c - c_0). \quad (1)$$

However, the process is considerably more complex in the case of polymers. Here, mention should be primarily made of studies by Ueberreiter *et al.* [1–4], who established for the example of polystyrene that the dissolution of a polymer is preceded by its swelling, with the subsequent formation of caoutchouc-like layer on the surface. Also, it was suggested that the overall rate of the process is determined by the rate of diffusion of a liquid into the polymer, in accordance with second Fick's law. It was found in [4] that the dissolution rate of polystyrene steadily decreases in the series of alkyl acetates as their molecular weight increases. However, attempts to relate the experimentally determined rate of polystyrene dissolution to the Einstein–Stokes coefficients

$$D = kT/6\pi\eta r \quad (2)$$

(D is the diffusion coefficient; η, viscosity; and r, radius of a solvent molecule) failed. This result is not surprising because no satisfactory correlation has been found until recently between the amount of adsorbed liquid S or the swelling rate and the physicochemical characteristics of solvents even for the first presumed stage of the dissolution, i.e., for swelling. The generally accepted Flory–Haggins theory, based on the Hildebrandt model of regular solutions, yields only semiquantitative relations and requires that an empirical correction interaction coefficient should be used [5]. Attempts to relate S to the electrophilicity E_T of solvents by Reichardt [6], their molal volume V_M [7], etc. have been no successful either.

At the same time, it was established in [8] that the only relationship between the limiting viscosity number of a polymer and the degree of its equilibrium swelling is that they behave in a similar way [8].

It was assumed that different types of interactions are involved in swelling of polymers and diffusion of solvents in these materials [9, 10]. Therefore, to obtain an adequate relation between S or D and solvent characteristics, it is necessary to take into account, in accordance with the linear free energies (LFE) principle, all mutually independent changes in the Gibbs energy of the components, associated with these parameters: $\Delta G = \Sigma \Delta g_i$.

To reveal the possible correlation between the physicochemical characteristics of organic solvents and the rate of polymer dissolution in them, we studied the dissolution of polymethyl methacrylate (PMMA) samples with an average molecular weight of 139 000 in 12 organic solvents. The dissolution rates at 30, 40, 50, and 70°C were determined gravimetrically.

1070-4272/05/7810-1576 © 2005 Pleiades Publishing, Inc.

Table 1. Degree Q of PMMA dissolution in organic solvents at 30°C

Solvent	Q, wt %, at indicated time, min							
	10	20	30	40	50	60	90	120
Benzene	10.4	18.9	25.2	29.2	34.7	38.6	49.9	68.5
Toluene	5.2	11.8	15.5	18.7	21.4	23.1	29.7	40.0
o-Xylene	3.1	4.9	6.1	7.3	8.7	9.2	11.3	15.5
m-Xylene	11.8	13.5	14.6	16.7	17.8	19.5	26.2	27.3
Trichloromethane	0.3	1.1	1.2	1.4	1.8	2.0	3.4	4.0
Trichloroethylene	35.8	65.7	88.4	96.0	–	–	–	–
1,4-Dioxane	5.3	10.6	14.4	17.2	19.7	21.6	27.2	37.9
Cyclohexanone	13.6	24.6	31.7	45.2	53.1	65.0	73.2	77.3
Acetophenone	8.0	14.0	18.1	21.0	23.1	25.8	31.9	45.6
Ethyl acetate	19.7	36.6	48.1	56.7	64.3	71.9	89.5	–
Pentyl acetate	2.2	3.2	4.5	4.8	5.4	6.1	7.2	8.5
Dimethylformamide	6.7	18.7	26.1	33.4	38.7	45.8	61.8	84.7

Table 2. Dissolution of PMMA samples in organic solvents at different temperatures

Solvent	Q, wt %, at indicated time, min														
	10			20			30			40			60		
	40°C	50°C	70°C	40°C	50°C	70°C	40°C	50°C	70°C	40°C	50°C	70°C	40°C	50°C	70°C
Benzene	24.4	33.3	47.8	38.1	57.3	90.3	60.0	77.6	–	73.0	90.7	–	88.9	–	–
Toluene	14.1	29.8	51.0	23.9	49.1	96.8	39.7	65.3	–	50.4	75.5	–	61.5	97.0	–
o-Xylene	5.0	13.5	24.6	6.8	22.3	50.4	13.6	26.2	58.7	19.1	31.4	80.0	23.6	47.6	–
m-Xylene	3.9	10.3	12.2	8.0	25.2	41.9	10.1	39.8	66.0	15.4	54.0	85.0	22.2	73.3	–
Trichloro-methane	9.5	2.8	5.7	11.5	9.7	11.4	12.6	12.3	29.5	14.2	25.8	42.0	16.7	33.9	63.0
1,4-Dioxane	11.5	18.7	31.9	18.3	39.6	74.0	31.1	55.1	93.8	44.0	72.8	97.8	60.0	96.8	–
Cyclohexanone	5.7	23.0	16.9	10.1	54.5	36.2	13.0	59.1	56.4	19.7	71.4	67.0	30.6	85.1	97.2
Acetophenone	13.3	21.3	45.9	14.0	28.5	34.3	43.7	53.9	96.9	53.4	65.9	–	69.6	94.6	–
Ethyl acetate	18.8	37.0	36.9	39.8	62.6	87.6	57.0	80.8	–	76.4	–	–	98.3	–	–
Pentyl acetate	4.6	8.5	7.7	9.5	26.9	27.3	12.5	41.9	42.7	17.6	54.2	66.8	26.9	74.1	82.3
Dimethylform-amide	12.5	19.6	35.1	25.2	28.1	66.8	35.8	48.5	96.6	56.0	67.9	–	75.0	–	–

The experimental results obtained are listed in Tables 1, 2. The data on the dissolution rate of PMMA at 30°C are analyzed in most detail (Table 1). As can be seen, there is no direct correlation between the dissolution rate and the structure or properties of a solvent, including its polarity. The best solvents for PMMA are partly substituted hydrocarbons, trichloromethane and trichloroethylene, in which polymer samples dissolve virtually completely in 30 min. At the same time, they nearly do not dissolve at all in trichloromethane. Good solvents are polar ethyl acetate and cyclohexanone. However, their ability to dissolve PMMA considerably decreases, as the molecular weight of esters increases, in agreement with the data of [4], and an even more polar dimethylformamide (DMF) dissolves PMMA even more slowly. Moreover, a strong difference in the dissolving power is even observed between aromatic hydrocarbons. At the same time, the curves describing the relative rate of the loss of mass by samples in the course of time, $Q = (w_0 - w_\tau)/w_0$, where w_0 is the initial mass of the sample and w_τ, its mass at an instant of time τ, are

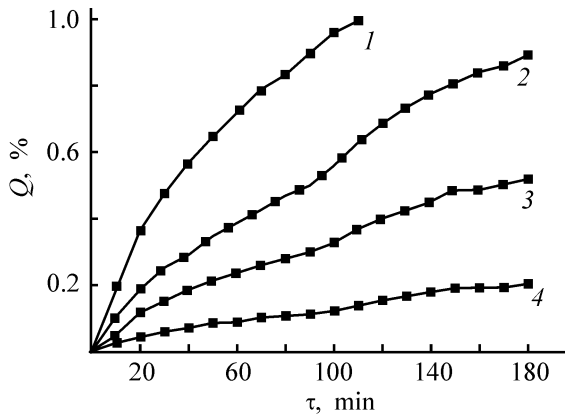


Fig. 1. Relative loss of mass by PMMA samples Q vs. time τ at 30°C in (*1*) ethyl acetate, (*2*) benzene, (*3*) toluene, and (*4*) *o*-xylene.

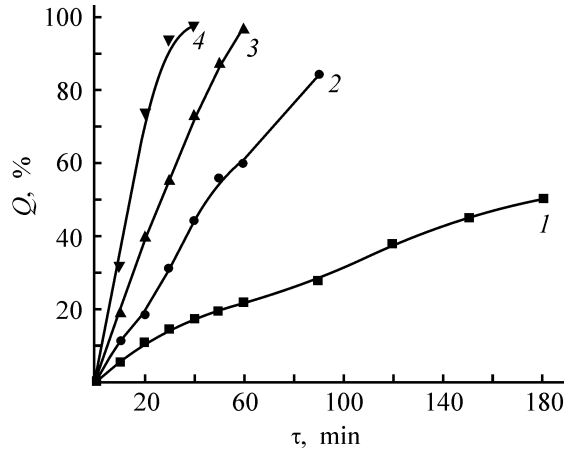


Fig. 2. Degree Q of PMMA dissolution in 1,4-dioxane vs. time τ. Temperature (°C): (*1*) 30, (*2*) 40, (*3*) 50, and (*4*) 70.

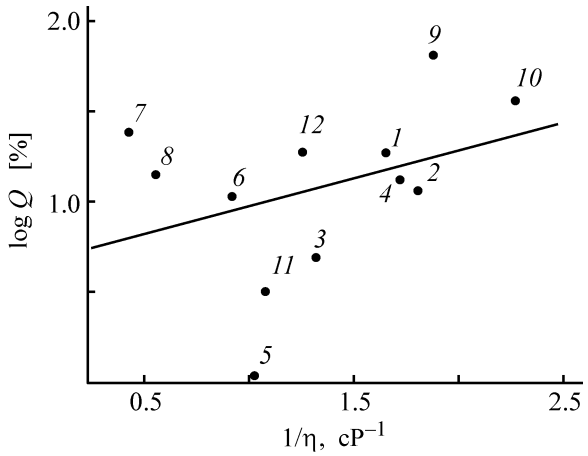


Fig. 3. Relationship between the degree Q of polymer dissolution in various solvents and their viscosity η (30°C, 20 min). (*1*) Benzene, (*2*) toluene, (*3*) *o*-xylene, (*4*) *m*-xylene, (*5*) trichloromethane, (*6*) 1,4-dioxane, (*7*) cyclohexanone, (*8*) acetophenone, (*9*) trichloroethylene, (*10*) ethyl acetate, (*11*) pentyl acetate, and (*12*) dimethylformamide.

always nearly linear, irrespective of the type of a solvent and temperature (Fig. 1).

Similarly to the rate of chemical reactions, the dissolution rate increases, on the average, twofold as the temperature is raised by 10°C (Table 2). A typical example of how the dissolution proceeds in the course of time at different temperatures is shown for dioxane in Fig. 2.

Attempts to describe the process in terms of the Einstein–Stokes dependence were unsuccessful. Figure 3 shows the relationship between the degree of PMMA dissolution (loss of mass in percent at 30°C in 20 min) and the parameter $1/\eta$ of this equation. It can be seen that these quantities exhibit to a certain extent opposite types of behavior: the degree of PMMA dissolution decreases as the solvent viscosity becomes higher, rather than a linear relationship. Especially strong deviations are observed for incompletely substituted hydrocarbons, trichloroethylene and chloroform.

Similar results were obtained for other time intervals (30, 40, and 60 min), with the deviations of experimental points from a straight line increasing with the extent of the process. This is not surprising, because the viscosity of the liquid phase gradually increases as it is saturated with the dissolved polymer. The deviations of the points also markedly increase with the temperature of the experiment, which can be attributed to dissimilar changes in viscosity with temperature for different solvents.

Somewhat better results were obtained with another parameter of the solvent, the molar volume V_M, which is directly related to the molecule radius r in formula (2). It was shown in [11] that the molar volume is an important parameter for generalization of data on the swelling rates for carbons in various solvents, with the process rate decreasing as this parameter becomes larger [11]. Similar results were obtained in the case in question. However, no clearly defined relationship could be obtained, either. Therefore, we attempted to find out whether the values obtained can be quantitatively generalized on the LFE principle by simultaneously taking into account the influence of both parameters in accordance with the dependence:

$$\log Q = a_0 + a_1\frac{1}{\eta} + a_2\frac{1}{V_M}, \qquad (3)$$

where Q is the relative loss of mass by the PMMA sample (%).

This attempt was unsuccessful too. Thus, the results obtained show that the dissolution kinetics of polymers is a complex process dependent on many

factors. Among them, mention should be made of the opposite directions of the following two processes. The first is the penetration (diffusion) of a solvent into the polymer, which is mainly determined by the size of its molecules. The second is that of a partial dissolution of a gel-like swollen surface layer of the polymer. This process is mainly dependent on the viscosity of the liquid phase, which, in addition, gradually increases in the course of its saturation with the polymer. Apparently, the second process will be also facilitated by agitation of the liquid, which makes its viscosity uniform throughout the polymer volume and prevents formation of highly viscous layers of a polymer solution on the surface of polymers.

Therefore, we attempted to generalize the data on the degree of polymer dissolution at different intervals of time (Tables 1, 2) by using the multiple-parameter Koppel–Palm equation [12], which takes into account different types of solvation, and supplementing this equation with terms that characterize self-association of solvents and their molar volume:

$$\log Q = a_0 + a_1\frac{n^2-1}{n^2-2} + a_2\frac{\varepsilon-1}{2\varepsilon+1} + a_3B + a_4E_T + a_5\delta^2 + a_6V_M. \quad (4)$$

Here n and ε are the refractive index and the dielectric constant of solvents, which determine the polarization and polarity and characterize the capacity of the solvents for nonspecific solvation; B and E_T, the Palm basicity and the Reichardt electrophilicity, which determine the specific solvation of the substrate; δ, Hildebrandt solubility, whose square is proportional to the cohesion energy of the medium; and V_M, molar volume of the solvent.

It was found that Eq. (4) adequately describes the dependence of the diffusion coefficients of solvents into the polymer on their physicochemical properties [9, 10]. Indeed, on excluding the most inconsistent data for trichloromethane, the degree of polymer dissolution attained at 30°C in 20 min (Table 1) is satisfactorily described by the following six-parameter equation

$$\log Q = 0.95 + (4.31 \pm 3.54)f(n) + (2.84 \pm 1.91)f(\varepsilon) - (0.95 \pm 0.93) \times 10^{-3}B + (0.088 \pm 0.107)E_T - (5.98 \pm 2.51) \times 10^{-3}\delta^2 - (26.1 \pm 4.32) \times 10^{-3}V_M, \quad (5)$$

$$N = 10,\ R = 0.987,\ S = 0.110.$$

On excluding the nonsignificant terms B and E_T, which characterize the specific solvation, we also obtain an adequate four-parameter equation:

$$\log Q = 3.35 + (4.11 \pm 1.48)f(n) + (4.41 \pm 0.63)f(\varepsilon) - (5.31 \pm 0.79) \times 10^{-3}\delta^2 - (26.2 \pm 2.59) \times 10^{-3}V_M, \quad (6)$$

$$R = 0.978,\ S = 0.109.$$

The above consideration shows that an increase in the size of solvent molecules (V_M) and in their self-association (δ^2) decelerates the dissolution of polymer in the solvents, which is presumably due to the hindrance to solvent diffusion into the polymer. At the same time, the nonspecific solvation of the chains of a polymer by the solvent favors its dissolution. However, particular interesting in this case is the conclusion that the possible specific solvation of PMMA is unimportant for the dissolution process, despite the presence of electron-donating carbonyl groups in its structure. Possibly, this is due to the fact that we studied nearly exclusively typical electron-donating solvents, and the electron-accepting trichloromethane is so active a solvent that it cannot be involved in the comparison.

It should be noted that Eq. (4) yields satisfactory results only for temperatures close to room temperature. Apparently, the effect of polymer diffusion into the liquid, which strongly depends both on the increase in viscosity upon saturation of the solution with the polymer and on the opposite effect of the decrease in the viscosity of the medium on raising the temperature, which is difficult to take into account, will be also the important factors under other conditions.

CONCLUSION

The dissolution rate of polymethyl methacrylate in various organic solvents cannot be described in terms of the Einshtein–Stokes dependence. Dissolution is a complex process dependent on the diffusion and solvation phenomena occurring in the system. The maximum dissolution rate is observed in trichloromethane and trichloroethylene. Dissolution in other solvents is determined, on the one hand, by the influence of their polarity and polarizability, which facilitate the process, and, on the other, by the energy density of cohesion and the molar volume, which act in the opposite direction.

REFERENCES

1. Ueberreiter, K. and Asmussen, F., *J. Polym. Sci.*, 1962, vol. 57, no. 165, pp. 187–198.

2. Asmussen, F. and Ueberreiter, K., *Koll. Z.*, 1962, vol. 185, no. 1, pp. 1–5.
3. Asmussen, F. and Ueberreiter, K., *J. Polym. Sci.*, 1962, vol. 57, no. 165, pp. 199–208.
4. Asmussen, F. and Ueberreiter, K., *Koll. Z.*, 1968, vol. 223, no. 1, pp. 6–13.
5. Flory, P J., *J. Chem. Phys.*, 1945, vol. 13, no. 6, pp. 453–465.
6. Jonquieres, A., Roizard, D., and Lochon, P., *J. Appl. Polym. Sci.*, 1994, vol. 54, no. 11, pp. 1673–1682.
7. Aminabhavi, T.M., Harogoppad, S.B., Khinnavar, R.S., and Balundgi, R.H., *JMS–Rev. Macromol. Chem. Phys.*, 1991, vol. 31, no. 4, pp. 433–498.
8. Bristow, G.M. and Watson, W.F., *Trans. Faraday Soc.*, 1958, vol. 54, no. 10, pp. 1567–1573.
9. Makitra, R.G., Zaglad'ko, O.A., Midyana, G.A., and Protsailo, L.V., *Zh. Fiz. Khim.*, 2001, vol. 75, no. 12, pp. 2283–2287.
10. Makitra, R.G., Pristanskii, R.E., Zagladko, E.A., *et al.*, *Russian Polymer News*, 2003, vol. 8, no. 3, pp. 24–29.
11. Makitra, R.G. and Pristanskii, R.E., *Khim. Tverd. Tela*, 2001, no. 5, pp. 3–16.
12. Koppel, I.A. and Palm, V.A., *Advances in Linear Free Energy Relationships*, Chapman, N.B. and Shorter, J., Eds., London: Plenum, 1972, pp. 203–280.

Russian Journal of Applied Chemistry, Vol. 78, No. 10, 2005, pp. 1581–1585. Translated from Zhurnal Prikladnoi Khimii, Vol. 78, No. 10, 2005, pp. 1610–1614.
Original Russian Text Copyright © 2005 by Grigorova, Semenova.

SORPTION AND ION-EXCHANGE PROCESSES

Effect of Various Treatment Methods on Sorption Properties of Antimony(V)-based Simple and Mixed Oxohydrates

N. S. Grigorova and Yu. Yu. Semenova

St. Petersburg State University, St. Petersburg, Russia

Received June 29, 2005

Abstract—A comparative study of the sorption characteristics of crystalline antimonic acid and a silicon-phosphorus-antimony cationite subjected to thermal treatment in air and in a molten sodium nitrate was carried out. The possibility of regeneration of these sorbents, which are used in ion-exchange strengthening of glasses, was analyzed.

Owing to their thermal stability and clearly pronounced selectivity, inorganic ionites occupy a prominent place in the ion-exchange practice. An interesting application field of inorganic sorbents is ion-exchange strengthening of glasses [1].

The strengthening process consists in that Na^+ and Ca^{2+} ions in the surface layer of a glass are substituted with K^+ cations from a KNO_3 melt. The strengthening is performed in stainless steel baths. An inorganic cationite placed in the melt absorbs products formed in bath corrosion (Fe^{3+}), impurities contained in a molten technical-grade KNO_3, and ions of sodium and alkaline-earth metals, displaced from the glass by K^+ ions. The contact with a KNO_3 melt having a temperature of about 400°C requires that the sorbents used should be highly temperature resistant [2]. The strength characteristics of the glasses obtained could be markedly improved by using inorganic cationites based on oxygen compounds of antimony(V) for purification of molten potassium nitrate [1, 2].

Cationites in the form of mixed Sb(V), P, and Si oxohydrates have been obtained and studied at the laboratory of ion exchange at the chemical faculty of St. Petersburg State University. The polymeric matrix of these sorbents is based on crystalline antimonic acid (CAA) [structural type of pyrochlore, space group *Fd*3*m*]. The unit cell of CAA consists of 16 antimony-oxygen octahedra $[SbO_{6/2}]^-$ jointed at vertices [3]. The excess charge of the lattice is neutralized by cations capable of exchange (H^+, Na^+, K^+, etc.). The substitution of antimony atoms in the pyrochlore structure by phosphorus atoms leads to rupture of the polymer chain, and, therefore, phosphorus can be contained in silicon-phosphorus-antimony cationites only in certain amounts (not exceeding 2 mg-at g^{-1}). Silicon, which can isomorphically substitute Sb(V) in the sorbent matrix under certain conditions, is contained in the ionites in the form of silicon-oxygen octahedra $[SiO_{6/2}]^{2-}$. An increase in the excess charge of the crystal lattice of a sorbent enhances the sorption of multiple-charge cations [5, 6]. The selectivity of each silicon-phosphorus-antimony ionites is determined by the relative amounts of Sb, P, and Si in a sample. Selectivity to single-, double-, or triple- charged ions can be formed by varying the chemical composition of SiPSb samples. In addition, raising the content of silicon improves the chemical and thermal stability of the sorbents [4–8].

A CAA sample and that of a silicon-phosphorus-antimony cationite (SiPSb) with the highest content of silicon [Sb : P : Si = 1.80 : 0.62 : 6.69 mg-at g^{-1}], both synthesized at the laboratory of ion exchange at St. Petersburg State University, were chosen for examination.

The aim of this study was to analyze transformations of cationites in molten KNO_3. In addition, it was necessary to determine whether these transformations are reversible.

1070-4272/05/7810-1581 © 2005 Pleiades Publishing, Inc.

Results of a chemical analysis of the samples studied

Sample no.	Sample	Sb(V) content, mg-at g^{-1}	Absorption of indicated ions, mg-equiv g^{-1}			
			Ag^+	Ca^{2+}	Cd^{2+}	Fe^{3+}
1	CAA	4.93	4.63	2.36	5.43	1.25
2	SiPSb	1.84	2.68	1.10	1.45	2.95
3	CAA(KNO_3)	2.28	0.34	0.24	0.39	1.75
4	SiPSb(KNO_3)	0.95	1.16	0.70	0.90	0.94
5	CAA(t)	3.28	0.45	0.31	0.37	0.87
6	SiPSb(t)	1.85	2.73	0.55	0.88	1.22
7	CAA(KNO_3)-r	5.00	4.75	0.6	1.83	1.0
8	SiPSb(KNO3)-r	1.95	1.82	1.10	1.25	2.0
9	CAA(t)-r	4.27	4.88	0.34	2.08	1.15
10	SiPSb(t)-r	1.93	1.93	1.19	1.46	1.95

The results of a chemical analysis of the samples are listed in the table. The content of Sb(V) in the samples was determined iodometrically [9], with starch as indicator. The determination error was about 4%.

The starting CAA and SiPSb sorbents were brought in contact with a KNO_3 melt (with the reagents taken in a 1 : 100 ratio by weight) at 450–550°C for 6 days and then washed to remove the excess amount of KNO_3 [the sorbents subjected to treatment are designated as CAA(KNO_3) and SiPSb(KNO_3)]. The treatment time was chosen on the basis of specific features of the technological process of strengthening. For comparison, the initial samples were calcined in air under similar conditions [designated as CAA(t) and SiPSb(t)]. Further, all the samples were treated with a 0.1 N HNO_3 solution ($g : V = 1 : 100$) under quasi-dynamic conditions (the acid solution was periodically renewed during 14 days), washed with water to remove the excess amount of the electrolyte, and dried at 70°C for 24 h [CAA(t)-r, CAA(KNO_3)-r and SiPSb(t)-r, SiPSb(KNO_3)-r]. The letter r in the sample designations means that they were subjected to regeneration with nitric acid. HNO_3 was used in this case not only to convert the sorbents into the H^+ form, but, to a greater extent, as a strong oxidizing agent.

Finished samples were subjected to chemical and X-ray phase analyses.[1]

[1] The X-ray phase analysis of the samples was carried out at the laboratory of X-ray diffraction analysis (St. Petersburg State University) by the powder method on a URS-50 instrument with Cu_{K_α} radiation.

As already mentioned, CAA has a well-defined structure of the pyrochlore type (space group *Fd*3*m*). The anionic skeleton of CAA is constituted by $[SbO_{6/2}]^-$ octahedra jointed at vertices. The octahedra bear an excess negative charge neutralized by cations that are capable of exchange (counter ions). A comparison of the results of X-ray phase analyses of the initial CAA samples and those calcined in air [10] demonstrated that, upon calcination in air, the crystal structure of the pyrochlore type is preserved, but reflections with odd *hkl* indices become extinct. As is known, the latter characterizes substitution of a proton [10] H^+ or a hydroxonium ion H_3O^+ in positions 16*d* by Sb(III) ions, which appear in the course of calcination of the initial CAA sample via dehydration of the structure and thermal reduction Sb(V) → Sb(III). According to the results of a chemical analysis (see table), about 30% of the whole amount of antimony(V) contained in the initial CAA was transformed into a triple-charged state in the course of thermal treatment in air.

Calcination of CAA in a KNO_3 melt led to amorphization of the structure, which is manifested in reflection broadening (Fig. 1b). In addition to the pyrochlore phase, a new phase (*A*) was clearly seen in the X-ray diffraction pattern. This phase is similar to the hexagonal form of KNO_2 and has an empirical formula K_3NO_3. It is apparently a product of thermolysis of the starting KNO_3. Both the initial SiPSb sample and that calcined in air are X-ray-amorphous [4]. Calcination of SiPSb in the melt yielded phase *A*.

The results obtained in a chemical analysis of samples treated after calcination with a 0.1 N HNO_3 solution (table, sample nos. 7–10) point to a quantitative

transformation of Sb(III) to Sb(V). However, the pyrochlore structure could be regenerated only for the CAA(KNO_3) sample, whereas the structural transformations of the CAA(t) sample were irreversible, which is due, as shown in [10], to the irreversibility of the dehydration process (Fig. 1c). Regeneration of a SiPSb(KNO_3) sample returned it into the initial X-ray-amorphous state (Fig. 2c), and the amount of Sb(V) in the sample structure increased from 0.95 to 1.95 mg-at g^{-1}.

The sorption capacity of the samples was evaluated by the amounts of absorption of metal ions (Ag^+, Ca^{2+}, Cd^{2+}, Fe^{3+}) from 0.1 N solutions of the respective solutions (see table) under static conditions ($g : V = 1 : 100$, time of contact 7 days). The exchange capacity of the samples was calculated from the loss of concentration of metal ions in equilibrium solutions. The ion concentrations were determined by trilonometry. [11].

The initial cationites well sorbed Ag^+ ions and doubly charged ions Ca^{2+} and Cd^{2+}. The sorption of triple-charged Fe^{3+} ions by CAA was approximately four times lower, which is characteristic of this ionite [7]. The superequivalent sorption of Cd^{2+} ions, observed for CAA, is due to the fact that this ion tends to be hydrolyzed and can be absorbed in the form of polynuclear complexes. On passing to a mixed oxohydrate SiPSb, a pronounced enhancement of the sorption of triple-charged Fe^{3+} ions was observed (see table).

Thermal treatment of CAA both in air and in a melt led to a dramatic decrease in the absolute sample capacities to 7–14% of the initial value. The only exception was sorption of Fe^{3+} ions. Depending on the type of treatment, it either somewhat decreased or even increased to 140% relative to the initial value. This fact is apparently due to the specific behavior of this ion in aqueous solutions, and primarily to its high susceptibility to hydrolysis. In the opinion of the authors of [12], calcination of CAA in air (T = 500°C) leads to a complete dehydration of the structure. This creates favorable conditions for incorporation of the Fe^{3+} ion, which exists in the form of exceedingly stable hydroxo complexes with a charge of +2, +1, and even 0 [12]. The increase in the exchange capacity (to 140%) for Fe^{3+} ions, observed for the CAA(KNO_3) sample, is probably due to a certain extent of amorphization of the structure.

After regeneration of CAA samples with a 0.1 N HNO_3 solution, the initial capacity for Ag^+ ions was restored and the anomalously high absorption of Fe^{3+} ions disappeared (see table, sample nos. 7 and 9).

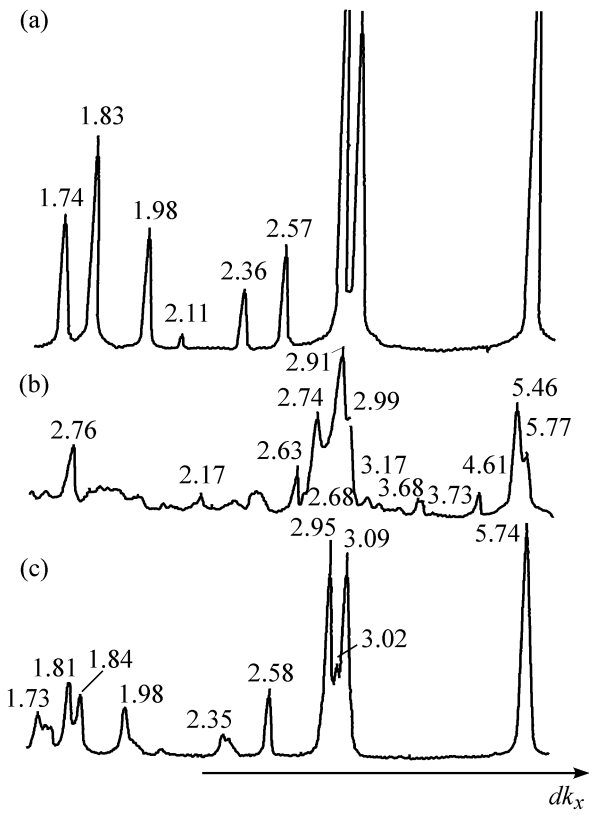


Fig. 1. X-ray diffraction patterns of CAA. (a) Initial CAA, (b) CAA(KNO_3), and (c) CAA(KNO_3)-r.

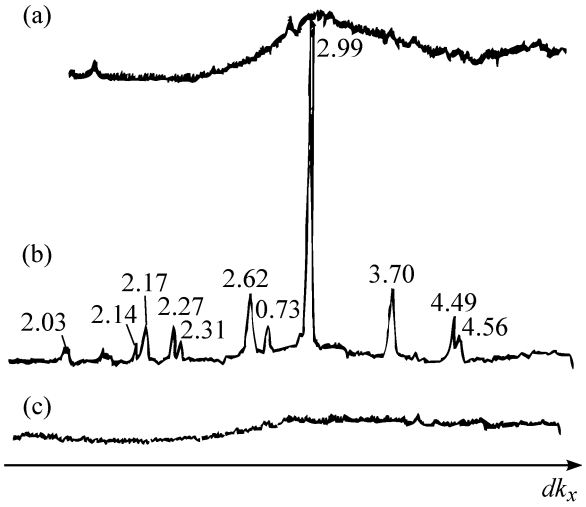


Fig. 2. X-ray diffraction patterns of SiPSb. (a) Initial SiPSb, (b) SiPSb(KNO_3), and (c) SiPSb(KNO_3)-r.

The sorption of doubly charged Ca^{2+} and Cd^{2+} ions remained virtually unchanged upon contact with HNO_3 and did not exceed 40% of the initial value.

Thermal treatment of SiPSb oxyhydrate did not lead to any pronounced fall in the sorption capacity of the ionites under study. In some cases, up to 100%

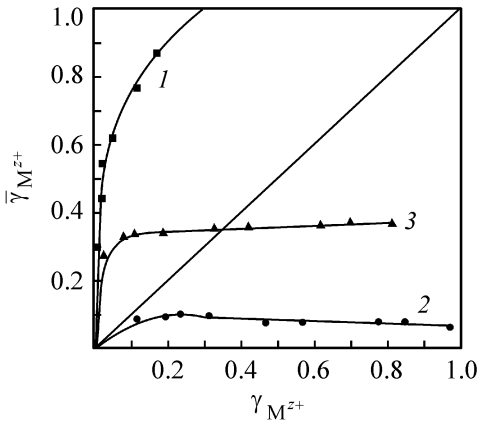


Fig. 3. Sorption isotherms for CAA(KNO_3). Sample: (*1*) CAA (init.), H^+ and Cd^{2+}; (*2*) CAA(KNO_3), K^+ and Cd^{2+}; and (*3*) CAA(KNO_3)-r, H^+ and Cd^{2+}. ($\bar{\gamma}_{M^{z+}}$, $\gamma_{M^{z+}}$) Equivalent fractions of the metal in the solid phase and in the equilibrium solution, respectively; the same for Figs. 4, 5.

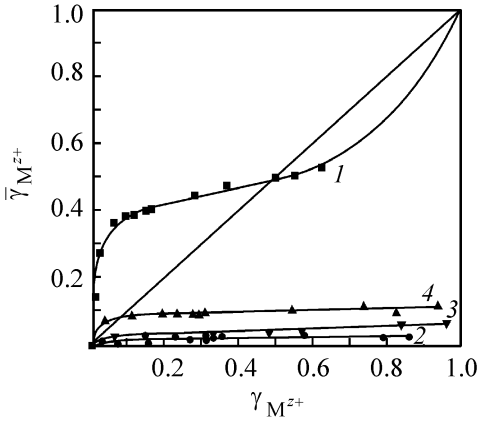


Fig. 4. Sorption isotherms for CAA(t). Sample: (*1*) CAA (init.), H^+ and Ca^{2+}; (*2*) CAA(t), H^+ and Ca^{2+}; (*3*) CAA(t)-r, H^+ and Ca^{2+}; and (*4*) CAA(KNO_3), H^+ and Ca^{2+}.

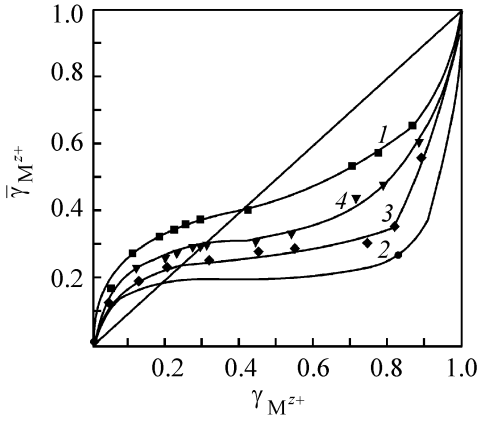


Fig. 5. Sorption isotherms for SiPSb. Sample: (*1*) SiPSb (init.), K^+ and Ca^{2+}; (*2*) SiPSb(KNO_3), K^+ and Ca^{2+}; (*3*) SiPSb(KNO_3)-r, K^+ and Ca^{2+}; and (*4*) SiPSb(t)-r, K^+ and Ca^{2+}.

of the exchange capacity was retained. SiPSb samples show a high degree of regeneration. After the regeneration, the capacity of the ionites for doubly charged ions was no less than 90% of the initial value, and that for Fe^{3+} and Ag^+ ions, about 70% (see table, sample nos. 8 and 10).

The sorption equilibrium on initial, calcined, and regenerated samples in mixed HCl–$CaCl_2$ and HNO_3–$Cd(NO_3)_2$ solutions was studied under static conditions by the method of separate samples (a weighed portion of a sample was poured over with a mixture of solutions of the acid and the corresponding salt of equal concentrations, taken in various ratios ($g : V$ = 1 : 100). Changes in the concentration of metal ions in equilibrium solutions were determined trilonometrically [11]. The results obtained in the form of exchange isotherms are represented as dependences of the equivalent fraction of a cation in the solid phase ($\bar{\gamma}_{M^{z+}}$) on the fraction of the same ion in the equilibrium solution ($\gamma_{M^{z+}}$) in Figs. 3–5. The determination error was 2–3%.

The initial CAA samples (Fig. 3, curve *1*) exhibited selectivity to the Cd^{2+} ion over the entire range of concentrations of the competing H^+ and Cd^{2+} ions in the equilibrium solution. As the solid phase was filled with Ca^{2+} ions, the selectivity of CAA was inverted (Fig. 4, curve *1*) in favor of H^+ ions, which is indicated by the S-like shape of the sorption isotherms.

For calcined CAA samples, all the isotherms (Fig. 3, curve *2*; Fig. 4, curves *2*, *3*) lie below the diagonal line K_{eq} = 1, which indicates that these samples have no selectivity to Ca^{2+} and Cd^{2+} ions. The general appearance of the isotherms points to a virtually complete loss of capacity by the sorbent. The regeneration of a CAA sample calcined in a melt was more complete than that for a sample calcined in air (Fig. 3, curve *3*; Fig. 4, curve *4*); however, it may be stated that the regeneration process leads to a minimum restoration of the sorption capacity of CAA.

The isotherms of sorption of Ca^{2+} ions on the initial SiPSb ionite are similar for thermally treated and regenerated samples, which indicates that, as the solid phase is filled, the selectivity to the metal ion is inverted in favor of H^+ ions (Fig. 5). The relative positions of the sorption isotherms demonstrate that thermal treatment affects the sorption characteristics of the SiPSb cationite to a considerably lesser extent, compared with the case of CAA, and regeneration is substantially more complete and efficient than that in CAA samples.

Some of the results of this study can be regarded as well expectable and coinciding with the available data.

This primarily refers to thermal transformations of CAA and SiPSb samples calcined in air. The data obtained confirm the conclusions [4] concerning the stabilizing effect of silicon on the thermal stability of the pyrochlore structure. The interaction between the sorbents studied and the melt is more complex. This process is accompanied by phase transformations, which lead to disintegration of the initial pyrochlore structure to give a new phase similar to the hexagonal lattice of the K_3NO_3 type.

The interaction of an amorphous mixed oxohydrate of SiPSb with a KNO_3 melt yields a clearly defined crystalline phase that does not belong to the pyrochlore type. The most interesting result obtained in regeneration with a HNO_3 solution of sorbents that were brought in contact with a KNO_3 melt is that the new phase disappears and the initial structure of pyrochlore is restored in CAA.

The data obtained in this study are practically important because they demonstrate the possibility of a complete restoration of the chemical composition, sorption properties, and initial structure of SiPSb oxohydrate after thermal treatment or exposure to a KNO_3 melt. The method developed can be suggested for regeneration of a valuable cationite that was used for a long time in ion-exchange strengthening of glasses.

CONCLUSIONS

(1) A comparative study of the behavior of a crystalline antimonic acid and silicon-phosphorus-antimony cationite in a KNO_3 melt revealed the following advantages of the silicon-containing sorbent: high thermal stability and increased selectivity to multiple-charge ions.

(2) Reversible phase transformations in an interaction between sorbents and a KNO_3 melt were found in an examination of the initial and modified sorbents based on oxygen compounds of Sb(V). These transformations lead to disintegration of the initial pyrochlore structure and give rise to a new crystalline phase.

(3) A new efficient method was suggested for regeneration of cationites based on oxygen compounds of antimony via a solid-phase transition Sb(III) $\rightarrow$ Sb(V). This method employs the oxidative capacity of nitric acid.

REFERENCES

1. Belinskaya, F.A., Grigorova, N.S., Militsina, E.A., *et al.*, Use of Inorganic Sorbents in the Technology of Ion-Exchange Strengthening of Glasses, *Vsesoyuznyi seminar "Khimiya i tekhnologiya neorganicheskikh sorbentov", Ashkhabad, 15–17 oktyabrya 1982 g* (All-Union Symp. "Chemistry and Technology of Inorganic Sorbents", Len. Gos. Univ., NITS, Ashkabad, October 15–17, 1982), Ashkhabad, 1982, p. 140.
2. Boguslavskii, I.A. and Mikulo, R.V., *Steklo Keram.*, 1979, no. 8, pp. 5–8.
3. Grigorova, N.S., in *Ionnyi obmen i ionometriya* (Ion Exchange and Ionometry), Belinskaya, F.A., Ed., St. Petersburg, 2000, issue 10, pp. 84–95.
4. Grigorova, N.S. and Veprinskaya, P.D., in *Ionnyi obmen i ionometriya* (Ion Exchange and Ionometry), 1996, issue 9, pp. 36–52.
5. Belinskaya, F.A., Grigorova, N.S., and Militsina, E.A., in *Ionnyi obmen i ionometriya* (Ion Exchange and Ionometry), 1976, issue 1, pp. 77–81.
6. Belinskaya, F.A., Grigorova, N.S., and Militsina, E.A., in *Ionnyi obmen i ionometriya* (Ion Exchange and Ionometry), 1976, issue 1, pp. 81–88.
7. Belinskaya, F.A. and Militsina, E.A., *Usp. Khim.*, 1980, no. 10, pp. 1904–1936.
8. Grigorova, N.S., Nikol'skii, B.P., Belinskaya, F.A., *et al., Vestnik Len. Gos. Univ.*, 1981, no. 10, no. 2, pp. 79–86.
9. Grigorova, N.S., A Physicochemical Study of Silicon-Phosphorus-Antomony Cationites, *Cand. Sci. Dissertation*, Leningrad, 1981.
10. Militsina, E.A., Malysheva, O.N., and Kozhina, I.I., *Vestnik Len. Gos. Univ., Ser. 4*, 1989, issue 3 (no. 18), pp. 40–47.
11. Schwarzenbach, G. and Flaschka, H., *Kompleksonometricheskoe titrovanie* (Complexonometric Titration), Moscow: Khimiya, 1970.
12. Militsina, E.A. and Orlova, O.A., *Vestnik Len. Gos. Univ., Ser. 4*, 1989, issue 4 (no. 25), pp. 48–54.

Russian Journal of Applied Chemistry, Vol. 78, No. 10, 2005, pp. 1586–1590. Translated from Zhurnal Prikladnoi Khimii, Vol. 78, No. 10, 2005, pp. 1615–1618.
Original Russian Text Copyright © 2005 by Grebennikov, Udal'tsova, Ustinov.

SORPTION AND ION-EXCHANGE PROCESSES

Porous Structure of Activated Carbon Fibers

S. F. Grebennikov, N. N. Udal'tsova, and E. A. Ustinov

St. Petersburg State University of Technology and Design, St. Petersburg, Russia
St. Petersburg State Technological Institute, St. Petersburg, Russia

Received February 14, 2005; in final form, July 2005

Abstract—The dependence of the microporous structure of activated carbon fibers on the carbonization temperature of hydrate-cellulose fibers was studied by BET, TVFMP, and Horvath and Kawazoe techniques and methods of the nonlocal density functional theory. The surface energy distribution function was obtained, together with the micropore size distribution curves. It was shown that the effective micropore sizes calculated by the TVFMP method are close to the maximum of the distribution function found in terms of the theory of the density functional.

Activated carbon fibers (ACF) differ from the conventional granulated adsorbents in that they make it possible to create adsorbents in the form of nonwoven structures, cardboard, fabrics, and other physical entities. The small geometric dimensions of elementary fibers lead to a substantial increase in the rate of internal mass transfer. Both the last parameter and the intensity of mass transfer in the course of adsorption depend on the size of micropores [1, 2]. At the same time, an objective analysis of the micropore volume distribution by pore size (MVDPS) is required in various areas of chemical technology, because this function determines the applicability fields and choice of an optimal adsorbent. Polymer precursors allow a sufficiently wide variation of the MVDPS. This study is concerned with one of ways to obtain ACF with various micropore volumes and sizes, which makes it possible to control the MVDPS in the existing industrial technology by somewhat modifying the carbonization mode of the starting precursor.

EXPERIMENTAL

As objects of study served samples of activated carbon fibers. A technical viscose thread was used as a precursor. Samples ACF-450, ACF-600, ACF-800, and ACF-1000 were obtained at different thermal treatment (carbonization) temperatures of 450, 600, 800, and 1000°C, respectively. The carbonization was performed in an industrial installation in nitrogen at the temperatures specified above for 36 min. Further, thermally treated carbon fibers were steam-activated at 800°C in an industrial furnace for 6 min. The resulting ACF had a mostly microporous structure with small-volume mesopores.

Isotherms of nitrogen adsorption were measured on a CAMO ERBA STRUMENTAZIONE MICROSTRUCTURE 85/02/04 instrument and SORTOMATIC-1900 installation. This was done at a temperature of –195.8°C at relative nitrogen pressures p/p_0 in the range from 1×10^{-4} to 0.85 (Fig. 1).

The adsorption isotherm reflects the porous structure of adsorbents and makes it possible to calculate

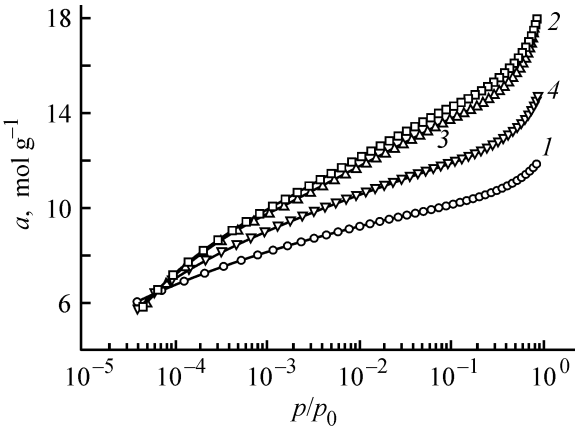


Fig. 1. Isotherms of nitrogen adsorption a (T = –195°C) on activated carbon fibers. (p/p_0) Relative pressure. (*1*) ACF-450, (*2*) ACF-600, (*3*) ACF-800, and (*4*) ACF-1000; the same for Fig. 2–4.

1070-4272/05/7810-1586 © 2005 Pleiades Publishing, Inc.

Parameters of the porous structure of activated carbon fibers

ACF	W_1/W_2	V_{me}	x, nm			S_{sp}, $m^2\ g^{-1}$	
	$cm^3\ g^{-1}$		TVFMP	HK	NLDFT	TVFMP	BET
450	$\frac{0.35}{0.02}$	0.04	$\frac{0.32}{3.1}$	0.30 – 0.34	0.25	$\frac{1090}{8}$	853
600	$\frac{0.48}{0.05}$	0.09	$\frac{0.48}{2.0}$	0.30 – 0.32	0.35	$\frac{1000}{23}$	1239
800	$\frac{0.47}{0.04}$	0.10	$\frac{0.48}{2.5}$	0.30 – 0.33	0.32	$\frac{985}{18}$	1201
1000	$\frac{0.41}{0.04}$	0.06	$\frac{0.40}{3.4}$	0.30 – 0.32	0.35	$\frac{1035}{11}$	1023

some of its characteristics in terms of various model concepts. This study used methods for linearization of experimental data in accordance with the BET equation [5] and the equation of theory of volume filling of micropores (TVFMP) [3] and in terms of the molecular approaches of Horvath and Kawazoe (HK) [4] and nonlocal density functional theory (NLDFT) [5].

The porous structure parameters obtained are listed in the table: W_1 and W_2, specific micropore volumes found using the two-term TVFMP equation ($cm^3\ g^{-1}$); V_{me}, mesopore volume ($cm^3\ g^{-1}$); x, halfwidth of slit-like micropores (nm); and S_{sp}, specific surface area of the pores ($m^2\ g^{-1}$). The conventional pore classification by sizes, adopted by IUPAC, is as follows: micropores, <2 nm; mesopores, 2–50 nm.

It can be seen from the table that ACF samples contain only a small volume of mesopores, and, therefore, are mostly microporous adsorbents. Their specific surface area was evaluated by the BET and TVFMP methods. From the formal standpoint, the isotherms of nitrogen adsorption on the samples studied can be well approximated by the linear form of the BET equation at p/p_0 in the range from 5×10^{-3} to 0.15, with the straight lines emerging virtually from the origin of coordinates, i.e., the constant C of the BET equation tends to infinity.

A thermodynamic analysis of the BET equation in [6] demonstrated that, in this case ($C \gg 100$), the value of another constant of the equation, a_m, must correspond to the monolayer capacity. This statement is valid if there is no steric hindrance in micropores to formation of monomolecular layers of the adsorbate on opposite walls [7]. It can be seen from the table that raising the carbonization temperature to 600 – 800°C leads to a substantial increase in the specific surface area, and as this temperature becomes even higher, S_{sp} somewhat decreases. This can be explained as follows. In the low-temperature stage of carbonization of carbon fibers, mostly a macroporous structure is developed because of the evolution of gaseous products and transport porosity is formed. Such a carbon structure is favorable for penetration of the activating agent and formation of a developed porous structure. The change in the properties of carbon-containing materials on elevating the carbonization temperature is due to the onset of structural transformations and to shrinking, which consists in that the bending of carbon layers decreases and ultramicropores become narrower and pass to the turbostrate state, which closes the mouths of micropores. In addition, the transport porosity decreases. These phenomena make the specific surface area of ACF smaller.

The size of micropores was calculated using the TVFMP method. The theory of volume filling of micropores is based on the fact that, irrespective of the nature of sorbate and adsorbent, the distribution function of the Gibbs energy over the amount of adsorption is described by the equation for the Weibull distribution. For active carbons with a bidisperse microporous structure [3], this equation has the form

$$a = \frac{W_1}{V}\exp\left[-\left(\frac{\Delta\mu_1}{\beta E_{01}}\right)^2\right] + \frac{W_2}{V}\exp\left[-\left(\frac{\Delta\mu_1}{\beta E_{02}}\right)^2\right], \qquad (1)$$

where $\Delta\mu_1 = RT\ln p/p_0$; β, similarity coefficient equal to 0.33 for nitrogen; V, molar volume of the adsorbate; W_1 and W_2, specific volumes of micropores I and II in the microporous structure; and p and p_0, equilibrium pressure and saturated vapor pressure of the adsorbate, respectively.

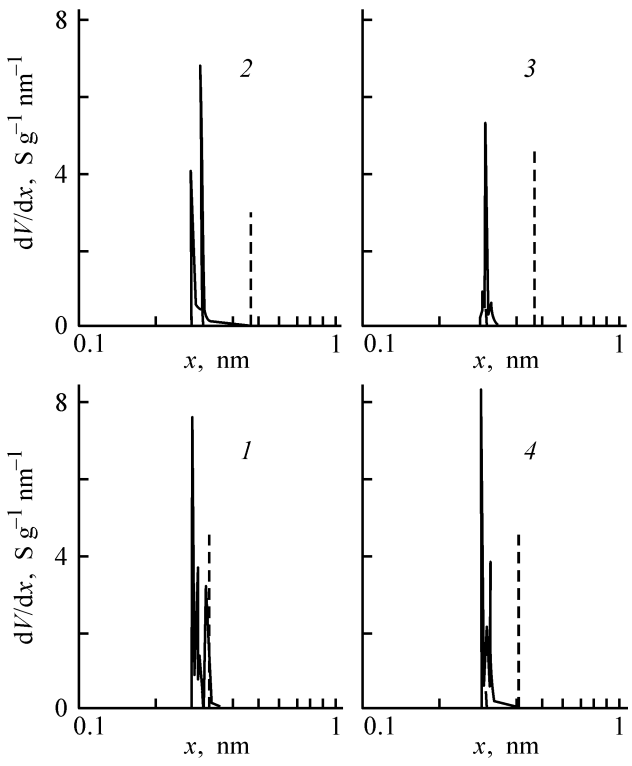


Fig. 2. Pore volume (V) distribution function by size x, calculated using the HK method.

The characteristic energy of benzene adsorption, E_0, is a function of the micropore size. The type of this function for active carbons was determined experimentally from small-angle X-ray scattering data and by the method of molecular probes [8]. It can be represented as

$$x = 5.4/(E_0 - 11.4), \quad (2)$$

where x is the micropore halfwidth (nm), and E_0 is the characteristic energy of benzene adsorption (kJ mol^{-1}). Simultaneously, a simpler expression $x = 12/E_0$ is used.

The following equation for calculating the specific surface area of micropores can be readily obtained in terms of the model of an infinite slitlike pore:

$$S = W/x. \quad (3)$$

In the given case, the experimental data are satisfactorily approximated by the two-term equation (1) in the range from $p/p_0 = 1 \times 10^{-4}$ [at lower pressures, the linear dependence $\ln a = f[\ln(p/p_0)]^2$ is not observed] to 0.04–0.05, which corresponded to the first basic microporous structure. To the second microporous structure corresponded a short linear portion that extended to $p/p_0 = 0.15$–0.2. The calculated values of W_1, W_2, x_1, x_2, and S_{sp} are listed in the table in the form of fractions, with the numerator corresponding to microporous structure I, and denominator, to structure II. Comparison of S_{sp} by TVFMP with that by BET shows that they are in a satisfactory agreement. However, TVFMP yields additional information about the porous structure: volume and size of micropores. The second porous structure has an order of magnitude smaller volume of micropores, and their size corresponds to the lower boundary of the range of mesopores (see table).

As the carbonization temperature is raised to 800°C (see table), the volumes of micro- and mesopores grow, with the size of micropores increasing simultaneously. Elevating the temperature further leads to a slight decrease in these parameters, which occurs in parallel with a similar change in the specific surface area of ACF for the reason described above.

Information about a finer structure of micropores is yielded by the HK and NLDTF methods. The starting point of the HK technique [4] is that the slitlike pore of the carbon adsorbent has only two states: empty or completely filled. A thermodynamic analysis and modeling of intermolecular interactions in a micropore led to steplike adsorption isotherms. To find the MVDPS, the authors of the HK technique calculated a set of local isotherms that could be used to describe any isotherm with a sufficiently high precision.

This analysis of the isotherms of nitrogen adsorption on ACF led to the distribution functions shown in Fig. 2. It can be seen that a rather uniform microporous structure is formed in ACF in the course of activation, with the TVFMP method (dashed line in Fig. 2) yielding closely similar results only for ACF-450 sample, and markedly overestimated results for the other samples.

The Nonlocal Density Functional Theory (NLDFT) was desribed in [5]. It starts from the fact that the adsorbate density varies across the width of a slit-like pore for the following two reasons. First, the intensity of intermolecular interactions varies under the conditions of superposition of the potentials of the opposite walls. Second, the energy of intermolecular interaction changes in formation of the second and subsequent layers, when the energies of the intermolecular interactions of an adsorbate molecule with the surface of the adsorbent and with the earlier adsorbed molecules are taken into account. In addition, the NLDFT theory can characterize the nonuniformity of the adsorbent sur-

face via the distribution function of the adsorbate–surface potential.

To determine the pore size ($dV/d\ln H$, where H is the width of micro- and mesopores) and surface energy distributions, the authors calculated a set of local isotherms at 70 values of ε_{sf}/k_B (20 to 90 K), 250 values of the pore width (up to 100 nm), and 500 values of the reduced pressure p/p_0 in the range 1×10^{-10}–1. The experimental isotherms were processed by Tikhonov's regularization method described in ample detail in [9]. In the NLDFT theory, the distribution function of the surface area of pores by energy is set in the form

$$\xi = \frac{dS/S_0}{d\varepsilon_{sf}/k_B}, \quad (4)$$

where S is the surface area of pores having a potential lower than ε_{sf}; S_0, total surface area of pores (thus, S/S_0 is the fraction of the surface area of the pores having a potential lower than ε_{sf}); ε_{sf}, potential of interaction between a carbon atom and a nitrogen molecule; and k_B, Boltzmann constant. The results obtained in the calculations are presented in Figs. 3, 4.

Comparison of the distribution curves produced by the HK and NLDFT methods shows that they are significantly different. This is a consequence of the nonrealistic steplike isotherm yielded by the HK technique. The NLDFT method seems to be more credible, because it postulates gradual filling of the adsorption volume, rather than a steplike filling of pores. Interestingly, the pore size by TVFMP falls in this case (if H is taken to be equal to $2x$) within the vicinity of the peaks in the pore distribution curves, even though do not coincide with these peaks.

As can be seen in Fig. 3, the carbonization temperature has virtually no effect on the distributions of mesopores (2.0–10 nm), but markedly shifts the peak for micropores to larger pore widths.

The surface energy distributions are shown in Fig. 4. It is of interest to compare them with the data of [5] for graphitized carbon black and activated kernel shell carbon, which have, similarly to ACF, a starting natural precursor based on cellulose.

The homogeneous graphitized carbon black studied in [5] shows a single peak at ε_{sf}/k_B = 58.01 K. ACF exhibit a strong scatter around this value, as also do the shell carbons Norit ROX and Ajax [5]. This can be attributed to a structural imperfection of the graphite lattice, especially for ACF, which are produced

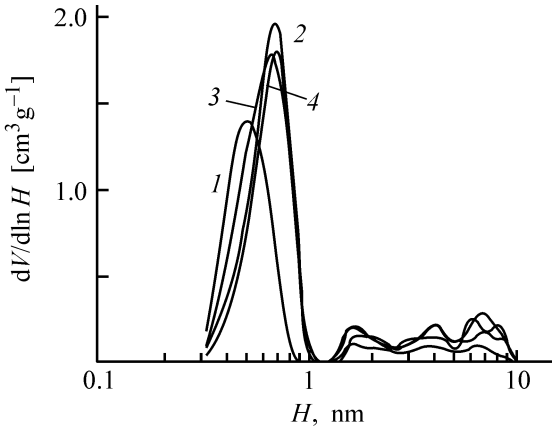


Fig. 3. Distribution function $dV/d\ln H$ of the volume V over pore width H by the NLDFT method.

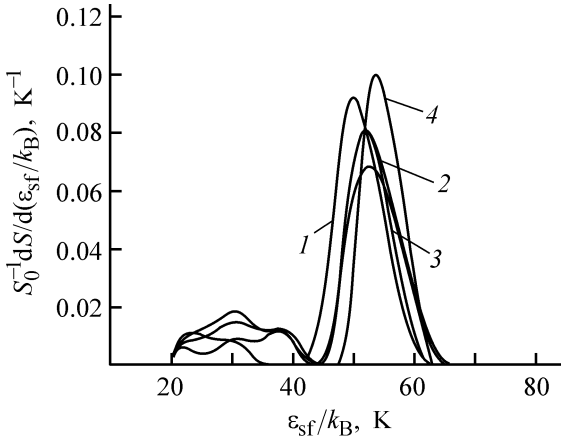


Fig. 4. Surface energy distributions $S_0^{-1}dS/d(\varepsilon_{sf}/k_B)$–$\varepsilon_{sf}/k_B$.

from an oriented precursor having no natural crystal structure.

Broadened peaks at lower energies are also present for kernel shell carbons. They can be attributed to a decrease in the interaction potential in blind pores (compared with the idealized infinite slitlike pores). It is interesting to note that the surface energy distribution curves for kernel shell carbons contain a peak at an energy exceeding 58.01 K. The authors of [5] attributed this peak to the presence of active centers of unsaturated carbon bonds at pore walls. Thus, ACF probably have a more energetically uniform surface than kernel shell carbons.

As the carbonization temperature increases, the structure of the ACF surface approaches that of graphite, because the peak of the curves is shifted toward 58 K, a value of ε_{sf}/k_B characteristic of pure graphitized carbon black.

CONCLUSIONS

(1) Activated carbon fibers have a mostly microporous structure, with the volume of mesopores not exceeding 0.1 $cm^3 g^{-1}$.

(2) As the carbonization temperature is elevated from 450 to 600–800°C, the volume of micropores increases from 0.37 to 0.51–0.53 $cm^3 g^{-1}$, with the pores simultaneously growing in size. At a carbonization temperature of 1000°C the volume of micropores somewhat decreases.

(3) The surface energy distribution curves were for the first time obtained for activated carbon fibers.

REFERENCES

1. Grebennikov, S.F., Pakhomov, Yu.I., Novinyuk, L.V., and Smirnova, M.V., *Zh. Prikl. Khim.*, 1984, vol. 57, no. 8, pp. 1710–1714.
2. Akulov, A.K., Pakhomov, Yu.I., and Grebennikov, S.F., *Zh. Prikl. Khim.*, 1986, vol. 59, no. 6, pp. 1236–1240.
3. Gregg, S.J. and Sing, K.S.W., *Adsorption, Surface Area and Porosity*, London: Academic, 1982. Translated under the titles *Adsorbtsiya, udel'naya poverkhnost', poristost'*, Moscow: Mir, 1984.
4. Horvath, G. and Kawazoe, K., *J. Chem. Eng. Japan*, 1983, vol. 16, no. 6, pp. 470–475.
5. Ustinov, E.A. and Do, D.D., *Langmuir*, 2004, vol. 20, pp. 3791–3797.
6. Klyuev, L.E., Grebennikov, S.F., and Yakubov, T.S., *Zh. Fiz. Khim.*, 1997, vol. 71, no. 6, pp. 1074–1076.
7. Grebennikov, S.F., Serpinskii, V.V., Grebennikova, O.D., and Pakhomov, Yu.I., *Izv. Akad. Nauk SSSR, Ser. Khim.*, 1983, pp. 498–503.
8. Rebstain, P., Ballorini, L., and Stoekli, H.F., *Carbon*, 1990, no. 6, pp. 907–909.
9. Ustinov, E.A. and Do, D.D., *Langmuir*, 2003, vol. 19, pp. 8349–8358.

Russian Journal of Applied Chemistry, Vol. 78, No. 10, 2005, pp. 1591–1595. Translated from Zhurnal Prikladnoi Khimii, Vol. 78, No. 10, 2005, pp. 1619–1624.
Original Russian Text Copyright © 2005 by Stavitskaya, Goba, Tomashevskaya, Kartel'.

SORPTION AND ION-EXCHANGE PROCESSES

Development of Procedures for Synthesis of Carbon Materials with Molecular-Sieve Properties

S. S. Stavitskaya, V. E. Goba, A. N. Tomashevskaya, and N. T. Kartel'

Institute of Sorption and Endoecology Problems, National Academy of Sciences of Ukraine, Kiev, Ukraine

Received December 30, 2004; in final form, April 2005

Abstract—New methods for synthesis of uniformly porous carbon materials with sieve properties and small apparent density from phenol-formaldehyde resins were developed; the optimal conditions of their synthesis were determined. New types of finely dispersed carbon powders were prepared using various treatment procedures at different stages; the structural and sorption properties of the resulting materials were studied.

Synthesis of sorption-active carbon materials with developed pores of molecular size is being intensively studied using both common procedures [e.g., progressive activation, which increases the content of micro- and mesopores in the polydispersed system of carbon material (CMs)] and new methods, which yield carbon particles (nanotubes) with controlled size of pore openings [1–9], which may exhibit a molecular-sieve effect.

Solution of various scientific and technological problems (such as sorption and separation of macromolecular compounds and preparation of chemosorbents, carbon-based conducting materials, electronic nanodevices, and molecular sensors) requires development of new special-purpose materials. Therefore, a search for new ultramicroporous carbon materials a topical task.

In this study, we examined the procedures for preparing new carbon materials with sieve properties: low-density nanosize carbon powders.

Carbon molecular sieves can be prepared from various carbon-containing materials: lignite and coal (including anthracite), lignin, wood, peat, synthetic and natural polymers, and other organic compounds. Carbonization and activation of these materials under appropriate conditions yield sorbents with a rather uniform pore structure containing micropores whose size is comparable with that of adsorbed molecules. For example, such low-density materials were prepared by carbonization of polymeric compounds pretreated by various procedures, including modification with inorganic additives [10–14]. In particular, carbon sorbents with exactly the prescribed structure were prepared using NaCl [15] and silicon [1] additives.

EXPERIMENTAL

Oxidation and activation of carbon sorbents as influenced by additives of alkali metal (including potassium) salts were studied in [16]. In the present study, we examined various procedures for synthesis of carbon sorbents with molecular-sieve properties (required porosity) from phenol-formaldehyde resins, using a finely dispersed KCl additive.

The samples were prepared by two procedures.

(1) The initial polymer was boiled in a saturated aqueous solution of potassium chloride for 2 h. The sample was stored in solution for 8 h at room temperature, recovered from the solution, and dried at 120°C. Then, the sample was annealed in a furnace in an argon atmosphere at 200°C for 1 h, at 600°C for 0.5 h, and at 1000°C for 0.5 h. After thermal treatment, KCl was washed out with hot distilled water.

(2) The initial resin was treated with saturated KCl solution for 2.5 h at room temperature, the solution was decanted, and the sample was dried at 120°C and annealed at 600°C in an argon atmosphere for 1.5 h. After thermal treatment, KCl was washed out with hot distilled water.

The parameters of the pore structure determined from benzene sorption at various P/P_s [17] and the calculated apparent densities d of the resulting

1070-4272/05/7810-1591 © 2005 Pleiades Publishing, Inc.

Table 1. Pore structure parameters and densities of carbon sorbents at various stages of treatment*

d, mg cm^{-3}		Structural parameters after carbonization				
before carbonization	after carbonization	V_s	V_{mi}	V_{me}	V_{ma}	S_g m^2 g^{-1}
		cm^3 g^{-1}				
Procedure I						
147** / 134	106 / 97	0.054 / 0.077	0.013 / 0.033	0.041 / 0.044	0.315 / 0.305	31.2 / 76.8
83 / 190	193 / 158	0.062 / 0.088	0.020 / 0.049	0.042 / 0.039	0.410 / 0.299	55.2 / 122.4
246 / 220	254 / 169	0.037 / 0.066	0.032 / 0.029	0.015 / 0.037	0.245 / 0.250	38.4 / 108.0
Procedure II						
40 / 91	28 / 54	0.170 / 0.190	0.160 / 0.180	0.010 / 0.010	0.805 / 0.765	37.0 / 98.0
122 / 246	100 / 190	0.220 / 0.360	0.200 / 0.340	0.020 / 0.020	0.650 / 0.559	104.0 / 80.0

* V_s is the limiting adsorption volume equal to $V_{mi} + V_{me}$; V_{mi}, V_{me}, and V_{ma} are the volumes of micro-, meso-, and macropores respectively; S_g is the geometric surface of micropores.

** The data for the initial polymer and sorbent treated with KCl are given in the numerator and denominator, respectively.

carbon sorbents before and after carbonization [18] are listed in Table 1. In this study, we used several samples of phenol-formaldehyde polymer [19], which were industrially prepared by polycondensation of various phenols and formaldehyde in the presence of catalysts. Both thermoplastic (novolak) and thermosetting (resol) resins [19] with a density of 40 to 250 mg cm^{-3} can be prepared, depending on the ratio of the initial compounds and their properties (e.g., the reactivities of mono- and bifunctional phenols are quite different), catalyst properties, solution pH, temperature and reaction time.

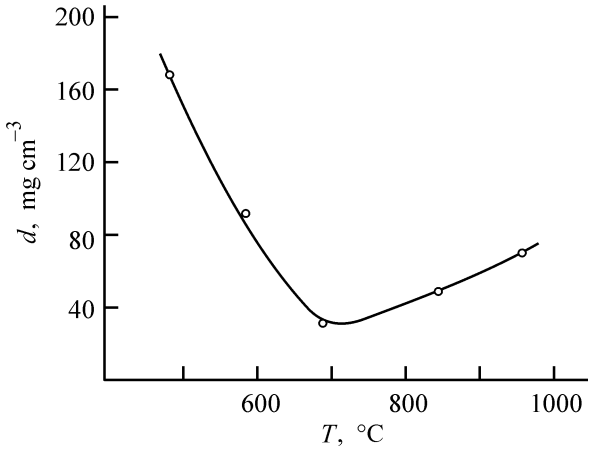


Fig. 1. Sample density d vs. temperature T of activation in a flow of carbon dioxide.

It can be seen from Table 1 that, after carbonization, the density of the samples treated with KCl by procedure 1 is significantly smaller as compared to the untreated samples. At the same time, the limiting adsorption volume V_s (equal to $V_{mi} + V_{me}$) is virtually independent of d and the ratio of micro- and mesopores varies in a relatively narrow range. Using procedure given in [18], we calculated the volume of macropores as the difference between the total pore volume determined from the moisture absorption capacity and the maximal volume of the adsorbed reference vapor (benzene). It should be noted that the structural parameters of the samples prepared by procedure 2 are significantly higher, which is probably due to worse removal of KCl from the pores in the samples prepared by procedure 1. However, both procedures yield uniformly microporous CMs.

We studied the reactivity and heat resistance of CMs under oxidation conditions (CO_2, O_2, HNO_3) at various temperatures to reveal the possibility of controlling the structure and chemical nature of the sorbent surface and imparting new properties to the resulting sorbents. To improve the microporosity and enhance the sorption capacity, the samples of various densities were exposed to high-temperature carbon dioxide activation [20]. The optimal activation parameters (namely, sample weight, time, temperature of thermal treatment and heating rate, and the flow rate of CO_2) were determined, and it was found how the density of CMs changes upon activation at 500–950°C (Fig. 1).

Table 2. Structural parameters of CMs as influenced by the temperature of carbon dioxide activation

T, °C	S_g, $m^2 g^{-1}$	W_0, $cm^3 g^{-1}$	E_0, kJ mol^{-1}	$B \times 10^6$	x, nm	T, °C	S_g, $m^2 g^{-1}$	W_0, $cm^3 g^{-1}$	E_0, kJ mol^{-1}	$B \times 10^6$	x, nm
400	367	0.15	25.5	0.56	0.70	700	220	0.15	16.6	1.18	0.47
500	418	0.22	23.6	0.66	0.53	850	235	0.19	15.6	1.50	0.80
600	370	0.22	21.2	1.40	0.76	950	265	0.14	23.6	0.66	0.59

Table 3. Structural and sorption parameters of oxidized carbon materials

Oxidant and oxidation time, h	CEC, mmol g^{-1}	Content of SFG,* mmol g^{-1}			V_s	V_{mi}	V_{me}	S_g, $m^2 g^{-1}$
		I	II	III	$cm^3 g^{-1}$			
HNO_3	4.00	2.70	0.50	1.40	0.071	0.053	0.010	120
O_2, 8	3.00	1.60	0.30	1.10	0.038	0.030	0.019	192
O_2, 12	3.25	1.75	0.36	1.15	0.036	0.030	0.006	144

* (I) Strongly acidic carboxy, (II) weakly acidic carboxy, and (III) phenol groups.

As can be seen in Fig. 1, the density of the samples first decreases as the most reactive amorphous fraction of carbon burns out with the subsequent development of a pore structure; however, d starts to grow with further increase in the treatment temperature.

This is probably related to changes in the texture of the carbon samples studied. Up to activation temperatures of 800–950°C, the initial carbonized organic materials consists of both an ordered fraction (carbon crystallites packed relatively irregularly) and an amorphous fraction (high-carbon radicals) bound with carbon atoms at the prismatic faces of the crystallites [20–22]. The diffusion of gaseous oxidants into the carbon pores in the course of activation at 750–950°C is accompanied by chemical reactions. First, less compact amorphous carbon is burnt out, which yields micropores of irregular structure. In further activation, partial or complete burning out of separate crystallites leads to formation of the main structure of micro- and supermicropores; the development of meso- and macropores proceeds simultaneously. The reactivity of carbon atoms located at the edges of the graphitelike crystal lattice toward gases is the highest.

Thus, thermal activation at 750–950°C in the presence of carbon dioxide involves not only side radicals of the polymer carbon chains but also the main fraction of the aromatic layers. As a result, the structure of carbon samples becomes more ordered, i.e., the linear dimensions of polymerized aromatic carbon networks increase, the interplanar spacings decrease, and the true density of the resulting CMs also grows (Fig. 1). This is confirmed by X-ray diffraction patterns recorded on a DRON-2 unit (Fig. 2), indicative of the increased content of crystalline carbon in the structure (diffraction peak 002 [23]).

The structural parameters of CMs prepared at various temperatures in the course of carbon dioxide activation and calculated from the sorption isotherms of water and benzene vapors [17] are listed in Table 2 (geometric surface S_g of micropores; micropore half-width x; structural constants of the Dubinin–Radushkevich equation W_0 and B, which are significant characteristics of micropores [17]; and specific adsorption energy E_0). Small values of the structural constants W_0 and B indicate that the resulting CMs possess a developed micropore structure with a half-width varying within the range 0.5–0.8 nm, which is typical of molecular-sieve sorbents [9].

We also studied the CM samples treated with oxygen at 450–500°C and with HNO_3 in the liquid phase [20]; the results obtained are listed in Table 3. In

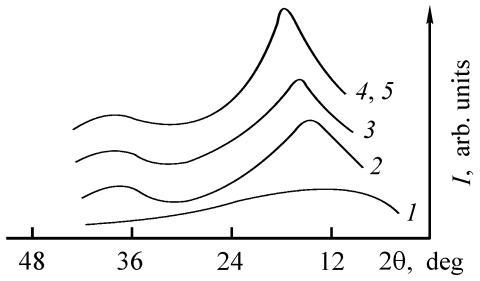


Fig. 2. X-ray diffraction patterns of carbon powders prepared by various procedures. Carbonized samples: (*1*) Initial, (*2*, *3*) after mechanical treatment for 15 and 150 min, and (*4*, *5*) after ultrasonic treatment for 60 and 720 min, respectively. (*1*) Peak intensity and (2θ) scattering angle.

Table 4. Apparent density and structural parameters of carbon powders prepared by ultrasonic treatment of CM samples carbonized during different intervals of time

Treatment time, min	d, mg cm^{-3}	W_0, cm^3 g^{-1}	S_g, m^2 g^{-1}	E_0, kJ mol^{-1}	$B\times10^6$
60	42.8	0.192	400	26.04	0.54
120	34.3	0.197	418	27.48	0.52
180	33.5	0.189	423	27.90	0.47
300	30.2	0.173	408	27.14	0.63
480	28.1	0.217	400	24.19	0.66
720	27.4	0.192	390	23.58	0.48

Table 5. Apparent density d and pore radius r of carbon powders as influenced by mechanical and ultrasonic treatment

Type of treatment	Treatment time, min	Procedure I		Procedure II	
		d, mg cm^{-3}	r, Å	d, mg cm^{-3}	r, Å
Mechanical	0	217	11	139	10
	15	250	12.6	135	11
	50	250	13.6	132	11.5
	150	250	14.7	132	11.6
	300	278	14.7	132	12.0
Ultrasonic	0	217	11	139	10.0
	60	208	11	122	12.0
	120	192	15.5	128	12.8
	180	192	16.5	135	13.0
	300	208	17	132	13.0
	480	178	17.7	128	15.1
	720	156	17.7	122	15.1

the first case, the sample in a quartz reactor was placed in an electric furnace heated to a required temperature and treated with oxygen at a flow rate of 5 l min^{-1}. As for carbons prepared from phenol-formaldehyde resin, the weight loss by materials studied was 25–30%, depending on the time of thermal oxidation (burning).

The cation-exchange capacity (CEC) of the resulting oxidized samples and the acid strength distribution of the surface functional groups (SFGs) formed in the course of oxidation were determined by titration with bases of various strengths ($NaHCO_3$, Na_2CO_3, and NaOH [20]). The structural and sorption parameters of the oxidized CMs are listed in Table 3.

As can be seen from Table 3, the surface of oxidized CMs primarily contains carboxy (especially strongly acidic with pK ~ 2 [20]) and phenol groups. Both meso- and micropores are formed in the course of oxidation; the limiting sorption volume V_s (which strongly depends on the oxidation procedure) of the samples prepared by liquid-phase oxidation with HNO_3 exceeds by a factor of 2 that of the samples oxidized with atmospheric oxygen; in all the samples studied the micropores are predominant.

Along with intercalation (filling of the initial phenol-formaldehyde resins with potassium chloride and their subsequent carbonization at various temperatures for different times, thermal activation, and oxidation with various oxidants), we studied the preparation of new microporous CMs by fine dispersion. It was expected that fine dispersion would provide breakdown of macro- and partially mesopores to give carbon nanoparticles with a micropore structure.

Carbon sorbents for dispersion were prepared by two procedures: (I) resins were carbonized and then dispersed or (II) powdered resin sample was carbonized. The carbonization was carried out in a furnace at 600°C for 1.5 in an inert gas. Along with mechanical grinding, the samples were subjected to ultrasonic treatment for 15–720 min. Analyses were performed using samples taken at certain intervals in the course of a continuous carbonization. The results are listed in Tables 4 and 5.

As a result, we obtained new carbon materials ("carbon powders"), i.e., finely dispersed powdered (nanosize) materials with a low apparent density (Table 4), whose structure and microstructure strongly differ from those of the known carbon sorbents, e.g., carbon black and carbon dust [21]. With increasing time of thermal activation, the apparent density d of the resulting carbon powders decreases (Table 4). These powders have a fairly high micropore surface area (about 400 m^2 g^{-1}), and the small W_0 and B constants suggest a developed micropore structure of the samples [17].

The X-ray diffraction patterns (Fig. 2, Table 5) show that the initial carbon material (d = 139–217 mg cm^{-3}) consists of irregular amorphous carbon (smooth curve without any peaks). The other diffraction patterns, obtained for dispersed samples, exhibit more or less pronounced diffraction peaks typical of crystalline carbon. It should be noted that, after mechanical grinding, the apparent density either remains unchanged or slightly increases, being almost independent of the grinding time. The size of micropores increases after both mechanical (from 12.6 to 14.7 Å) and ultrasonic (from 10.0 to 17.7 Å) treatments; in

the latter case, the pore size exceeds that in the samples prepared by mechanical grinding.

CONCLUSIONS

(1) Carbon materials with molecular-sieve properties and predominant content of micropores of certain size were prepared from phenol-formaldehyde resine and KCl additive, using mechanical and ultrasonic treatment of the initial resin and sorbents carbonized at various temperatures.

(2) It is possible to control the structure and chemical nature of the surface and to impart new properties to carbon sorbents by high-temperature activation or oxidation (O_2 and HNO_3).

(3) Fine dispersion (mechanical and ultrasonic) yielded nanosize carbon materials with a low density (d 27–43 mg cm^{-3}), which surpass in structural parameters the known carbon materials, such as carbon black or carbon dust.

REFERENCES

1. Ryoo R., Joo, S.H., and Jun, S., *J. Phys. Chem.*, 1999, vol. 102, no. 37, pp. 743–746.
2. Fenelonov, V.B., *Poristyi uglerod* (Porous Carbon), Novosibirsk: Inst. Kataliza, 1995.
3. Mukhin, V.M., Tarasov, A.V., and Klushin, V.N., *Aktivnye ugli Rossii* (Russian Activated Carbons), Moscow: Metallurgiya, 2000.
4. Fenelonov, V.B., *Vvedenie v fizicheskuyu khimiyu formirovaniya supramolekulyarnoi struktury adsorbentov i katalizatorov* (Introduction to Physical Chemistry of Formation of Supramolecular Structure of Adsorbents and Catalysts), Novosibirsk: Sib. Otd. Ross. Akad. Nauk, 2004, 2 ed.
5. Tel'biz, G.M., Gerda, V.I., Gun'ko, V.M., and Il'in, V.G., Abstracts of Papers, *NANSIS-2004*, Kiev, October, 12–14, 2004, p. 177.
6. Golovko, L.V., Povazhnyi, V.A., and Terent'ev, A.G., Abstracts of Papers, *NANSIS-2004*, Kiev, October, 12–14, 2004, p. 396.
7. Popov, A.P., Bazhin, I.V., and Boguslavskaya, E.S., Abstracts of Papers, *NANSIS-2004*, Kiev, October, 12–14, 2004, p. 33.
8. Ryabenko, A.G., Moroz, T.N., Kostrovskii, V.G., *et al.*, Abstracts of Papers, *NANSIS-2004*, Kiev, October, 12–14, 2004, p. 350.
9. Drozhalina, N.D., *Uglerodnye molekulyarnye sita na osnove torfa* (Carbon Molecular Sieves Based on Peat), Minsk: Nauka i Tekhnika, 1984.
10. Artemyanov, A.P., Khabarov, A.P., and Glushchenko, V.Yu., *Elektrokhimicheskie protsessy v vodnykh rastvorakh* (Electrochemical Processes in Aqueous Solutions), Vladivostok: Primorsk. TsNTI, 1987.
11. Wen Cui Li, An-Hui Lu, and Shu-Cai Gu, *Carbon*, 2001, vol. 39, no. 13, pp. 1989–2001.
12. Gnotong Qin and Shucai Guo, *Carbon*, 2001, vol. 39, no. 12, pp. 1935–1937.
13. Petricevic, R., Glora, M., and Fricke, J., *Carbon*, 2000, vol. 38, no. 5, p. 857–867.
14. Jamashita, J. Ojima, T., Shioya, M., *et al.*, *Carbon*, 2003, vol. 41, no. 2, pp. 285–295.
15. US Patent 4 806 290.
16. Gerasimenko, I.V., Stavitskaya, S.S., and Petrenko, T.P., *Teor. Eksp. Khim.*, 1998, vol. 34, no. 4, pp. 257–261.
17. Dubinin, M.M., *Usp. Khim.*, 1982, vol. 51, no. 7, pp. 1065–1074.
18. Kolyshkin, D.A. and Mikhailova, K.K., *Aktivnye ugli: Spravochnik* (Actavated Carbons: Handbook), Moscow: Khimiya, 1972.
19. Temkina, R.Z., *Sinteticheskie klei v drevoobrabotke* (Synthetic Adhesives in Wood Industry), Moscow: Lesnaya Prom–st., 1971.
20. Tarkovskaya, I.A., *Okislennyi ugol'* (Oxidized Carbon), Kiev: Naukova Dumka, 1981.
21. *Proizvodstvo i svoistva uglerodnykh sazh* (Production and Properties of Carbon Black), Surovikin, V.F., Ed., Tr. VNIISP, Omsk, 1972, no. 1, p. 407.
22. Kel'tsev, N.V., *Osnovy adsorbtsionnoi tekhniki* (Principles of Adsorption Technique), Moscow: Khimiya, 1984.
23. Spiridonov, E.P., Barykin, B.M., Drozdov, R.Ya., *et al.*, *Strukturnaya khimiya ugleroda i uglei* (Structural Chemistry of Carbon and Coals), Kasatochkin, V.I., Ed., Moscow: Nauka, 1969.

Russian Journal of Applied Chemistry, Vol. 78, No. 10, 2005, pp. 1596–1599. Translated from Zhurnal Prikladnoi Khimii, Vol. 78, No. 10, 2005, pp. 1625–1628.
Original Russian Text Copyright © 2005 by Shinkareva, Lazareva, Shchurevich, Kurakevich.

SORPTION AND ION-EXCHANGE PROCESSES

Effect of Synthesis Conditions of Magnetite on Its Water-Vapor Sorption Capacity

E. V. Shinkareva, T. G. Lazareva, O. A. Shchurevich, and L. A. Kurakevich

Institut Obshchei i Neorganicheskoi Khimii Natsional'noi Akademii Nauk Belorussii (Institute of General and Inorganic Chemistry, National Academy of Sciences of Belarus) State Research Institution, Minsk, Belarus

Received November 4, 2004; in final form, June 2005

Abstract—The water-vapor sorption capacity of magnetite obtained by precipitation with solutions of NaOH, $NH_3 \cdot H_2O$, and urea in a single stage was studied. It was found that the type of a precipitating agent, thermal treatment temperature, concentration of the starting $FeSO_4$ solution, and order in which the reagents are poured together affect the water-vapor sorption capacity of the magnetite obtained.

Most widely used as a magnetic component in manufacture of magnetorheological fluids and magnetic paints, fibers, and tapes [1, 2] are ferromagnetic materials based on iron oxides: magnetite (Fe_3O_4) and γ-Fe_2O_3 [3, 4]. Modern ferromagnetic materials should satisfy a number of requirements: have high magnetic characteristics, good sorption capacity (in the cases when the surface is to be modified), and a certain specific surface area (10–50 $m^2\ g^{-1}$) for dispersion in a binder.

Synthesis of magnetite is a rather complicated task performed in four successive stages: synthesis of goethite α-FeOOH, thermal decomposition of goethite to hematite α-Fe_2O_3, and reduction of hematite to magnetite Fe_3O_4 [5].

It is known that magnetite can be obtained by single-stage precipitation [6]. However, the characteristics of such a material strongly depend on synthesis conditions (type of a precipitating agent and washing reagent, thermal treatment temperature, concentration of the starting $FeSO_4$ solution, and order in which the reagents are poured together).

In this study, the influence exerted by conditions of a single-stage precipitation of magnetite on its water-vapor sorption capacity is assessed.

EXPERIMENTAL

The single-stage precipitation of magnetite was performed from a 0.1–1.0 M $FeSO_4$ solution with a 20% NaOH solution at 85°C and pH 10–11 or with a 25% $NH_3 \cdot H_2O$ solution at pH 8–9, as well as with a 10% urea solution at 100°C and pH 5–6 under vigorous stirring for 3 h; a 20% solution of the oxidizing agent, NH_4NO_3, was added at a molar ratio $Fe^{2+}/NO_3^- = 3$.

After the synthesis, the magnetite obtained was allowed to stand for 1 day under a layer of the mother liquor for the necessary structure of its crystals to be formed. Then the precipitate was washed by decantation with hot distilled water to negative reaction for the SO_4^{2-} ion in the washing water and filtered off. The washing process was monitored with a 2% $BaCl_2$ solution. The precipitate obtained was additionally washed with ethanol or acetone. Samples dried at room temperature for 12 h were thermally treated in nitrogen at temperatures of 100 to 200°C for 3 h. The samples were stored in quartz weighing bottles with ground-glass covers.

An X-ray phase analysis was performed on a DRF-2.0 diffractometer (Fe_{K_α} radiation).

The shape and dimensions of particles of magnetic powders were studied with an LEO 1420 scanning electron microscope at a magnification of 37000. A gold layer was deposited onto the surface of the samples in a VUP-2K vacuum-evaporation installation.

The sorption of water vapor by magnetite was carried out by keeping samples for 20 days (time of the most intense moisture absorption) in desiccators at

1070-4272/05/7810-1596 © 2005 Pleiades Publishing, Inc.

a water-vapor pressure of 0.8, 9.8, and 17.2 mm Hg, set by appropriate sulfuric acid solutions [7], at room temperature. The content of water in a sample was judged from the difference between the masses of the initial sample calcined at 100°C and that kept in the desiccator.

Raising the concentration of $FeSO_4$ in the starting solution for synthesis of magnetite precipitated with, e.g., NaOH makes higher the water-vapor sorption capacity of the final product washed with water and thermally treated at 100°C for 3 h (Table 1).

As can be seen from Table 1, the maximum sorption capacity for water vapor is observed for magnetite obtained from a 1.0 M $FeSO_4$ solution.

In studying the influence exerted by the nature of a precipitating agent (NaOH, $NH_3 \cdot H_2O$, urea) and washing reagents (hot water, ethanol, acetone) on the sorption capacity of magnetite for water vapor, the conditions of its synthesis were the same in all the experiments: a 1.0 M $FeSO_4$ solution introduced into the precipitating agent, washing of the final product with water, its thermal treatment at 100°C for 3 h. The highest sorption capacity for water vapor [28% at a water-vapor pressure of 17.2 mm Hg (Table 2)] was obtained for a magnetite precipitated with a NaOH solution. The moisture content of samples obtained with $NH_3 \cdot H_2O$ and urea as precipitating agents is lower at the same water-vapor pressure: 20 and 12%, respectively.

One of the main reasons why the structure and properties of the sorbents obtained with different precipitating agents vary is that the final product contains impurities, e.g., chemisorbed cations or anions, whose amount in the samples obtained commonly depends on the precipitation pH [8]. In the case in question, the possible impurities are, in particular, SO_4^{2-} anions and sorbed molecules of ammonia.

The effect of an additional treatment with ethanol or acetone of a freshly precipitated magnetite preliminarily washed with water on its sorption capacity for water vapor is illustrated in Table 3. An additional washing with organic reagents makes its sorption capacity higher, which presumably results from desorption of impurities.

Magnetite samples washed with water and treated with acetone have a better sorption capacity for water vapor, compared with those washed with ethanol.

The sorption capacity of magnetite powders was changed by their thermal treatment at 150 and 200°C. Raising the thermal treatment temperature from 100 to

Table 1. Effect of the concentration of $FeSO_4$ in the starting solution on the sorption capacity of magnetite precipitated with NaOH

Concentration of $FeSO_4$ solution, M	Water-vapor pressure, mm Hg	Moisture content, %
0.1	0.8	9
	9.8	11
	17.2	20
0.5	0.8	12
	9.8	14
	17.2	25
1.0	0.8	15
	9.8	19
	17.2	28

Table 2. Effect of a precipitating agent on the sorption capacity of magnetite

Precipitating agent	pH	Water-vapor pressure, mm Hg	Moisture content,
NaOH	10–11	0.8	15
		9.8	19
		17.2	28
$NH_3 \cdot H_2O$	8–9	0.8	10
		9.8	13
		17.2	20
Urea	5–6	0.8	8
		9.8	9
		17.2	12

Table 3. Effect of an additional treatment with reagents on the sorption capacity of magnetite

Precipitating agent	Reagent	Water-vapor pressure, mm Hg	Moisture content, %
NaOH (pH 10–11)	Ethanol	0.8	17
		9.8	22
		17.2	32
	Acetone	0.8	20
		9.8	25
		17.2	37
$NH_3 \cdot H_2O$ (pH 8–9)	Ethanol	0.8	11
		9.8	14
		17.2	22
	Acetone	0.8	13
		9.8	17
		17.2	24
Urea (pH 5–6)	Ethanol	0.8	9
		9.8	11
		17.2	13
	Acetone	0.8	12
		9.8	14
		17.2	18

Table 4. Sorption capacity of magnetite thermally treated at different temperatures (additional treatment with ace-tone, 0.1 M $FeSO_4$ solution, thermal treatment time 3 h)

Thermal treatment temperature, °C	Water-vapor pressure, mm Hg	Moisture content, %	Water-vapor pressure, mm Hg	Moisture content, %	Water-vapor pressure, mm Hg	Moisture content, %
	NaOH as recipitating agent		$NH_3 \cdot H_2O$ as recipitating agent		Urea as recipitating agent	
100	0.8	20	0.8	13	0.8	12
	9.8	25	9.8	17	9.8	14
	17.2	37	17.2	24	17.2	18
150	0.8	22	0.8	14	0.8	14
	9.8	27	9.8	19	9.8	16
	17.2	39	17.2	26	17.2	20
200	0.8	26	0.8	18	0.8	16
	9.8	33	9.8	23	9.8	19
	17.2	44	17.2	28	17.2	23

200°C leads to a pronounced increase in the sorption capacity of magnetite (Table 4).

As can be seen from Table 4, the sorption capacity of magnetite samples thermally treated at 200°C is considerably higher. An additional factor that affects the sorption capacity of magnetite is the order in which solutions are poured together in its synthesis.

Table 5. Sorption capacity of magnetite in relation to reagent mixing order (precipitating agent NaOH, additional treatment with acetone, thermal treatment temperature 200°C, treatment time 3 h)

Order of reagent mixing	Water-vapor pressure, mm Hg	Moisture content, %
$FeSO_4$ solution introduced into the precipitating agent	0.8	26
	9.8	33
	17.2	44
Precipitating agent introduced into the $FeSO_4$ solution	0.8	16
	9.8	20
	17.2	30

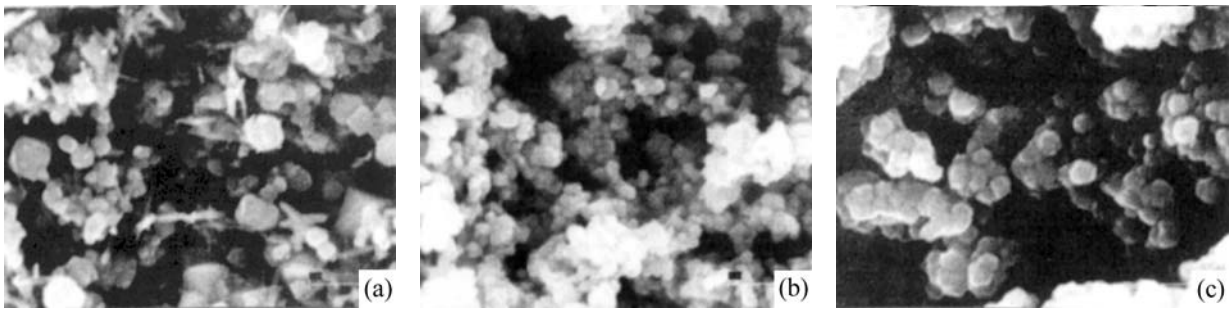
Table 6. Data of X-ray phase analysis

Data of the ASTM file (record no. 19-629)		Interplanar spacing *d*, nm, for magnetite samples precipitated with indicated solutions		
d, nm	Intensity	NaOH	$NH_3 \cdot H_2O$	urea
2.967	24	2.983	2.983	2.983
2.532	100	2.543	2.543	2.543
2.424	10	2.432	2.432	2.434
2.099	33	2.103	2.101	2.106
1.715	13	1.714	1.712	1.715
1.616	27	1.618	1.616	1.617
1.485	33	1.484	1.485	1.484

The sorption capacity of magnetite obtained by adding a $FeSO_4$ solution to the precipitating agent NaOH exceeds that in the case when these solutions are poured together in the inverse order (Table 5).

According to [8], introduction of a precipitating agent into a salt solution at a low pH of the medium yields gels whose particles are strongly hydrated and have a high aggregative stability. Gels of this kind, as a rule, undergo a strong shrinking in drying, under the action of capillary contraction forces, to give finely porous adsorbents. As the pH value increases, the structure of the adsorbents obtained is enriched with coarser pores and reaches the limiting value at a given pH, i.e., at the pH of complete precipitation. As a result, the structure of a sample is constituted by a variety of components that differ in structural parameters. The difference in the case of an inverse order of reagent mixing, i.e., at a slow pouring of a salt solution into that of the precipitating agent, consists in that the pH of the latter solution is markedly higher than the value corresponding to the complete precipitation of the gel. Therefore, the gelation occurs instantaneously and the structure of the resulting sample is coarsely porous.

It should be noted that, according to the results of an X-ray phase analysis, samples of magnetite synthesized by single-stage precipitation under the optimal conditions (1.0 M $FeSO_4$ solution; washing with hot water and, additionally, with acetone; thermal treatment of the final product at 200°C for 3 h) were virtually phase-clean and their composition corresponded to the theoretical ratio of the concentrations of Fe^{2+} and Fe^{3+} cations in Fe_3O_4 (Table 6).



Electron micrographs of magnetite precipitated with solutions of (a) NaOH, (b) $NH_3 \cdot H_2O$, and (c) urea. Magnification 37000.

It can be seen in the micrographs of magnetite samples obtained with various precipitating agents that particles of magnetite are rhombohedral and lamellar–needle-like in the case of precipitation with NaOH, and mostly spherical-rhombohedral in the case of $NH_3 \cdot H_2O$ and urea.

The average size of magnetite particles is 500–1200 nm in the case of precipitation with NaOH, <300 nm for $NH_3 \cdot H_2O$, and 300–800 nm for urea. Thus, the comparatively high sorption capacities for water vapor, achieved in the study, and the simplicity of synthesis make it possible to regard magnetite precipitated with a NaOH solution as a promising material for manufacture and modification of fluid formulations on its base and, in particular, magnetic paints.

CONCLUSIONS

(1) The highest sorption capacity for water vapor is observed for magnetite precipitated with a NaOH solution, compared with that precipitated with ammonia or urea. For example, magnetite samples precipitated with NaOH, washed with water and acetone, and then thermally treated at 200°C have a better sorption capacity for water vapor (44% at a water-vapor pressure of 17.2 mm Hg).

(2) Variation of the synthesis conditions of magnetite enables subsequent modification of its properties: water-vapor sorption capacity, structure and dispersity of particles).

REFERENCES

1. Lazareva, T.G., Shinkareva, E.V., and Prodan, S.A., *Zh. Prikl. Khim.*, 2001, vol. 74, no. 6, pp. 1002–1005.
2. Braginskii, G.N. and Timofeev, E.N., *Tekhnologiya magnitnykh lent* (Technology of Magnetic Tapes), Leningrad: Khimiya, 1987.
3. Turkin, S.N., Markvicheva, E.A., Lukin, Yu.V., *et al.*, *Trudy Mos. Khim.-Tekhnol. Inst. im. D.I. Mendeleeva, Biotekhnol. Promyshl. Ekol.*, 1986, no. 135, pp. 41–50.
4. Bibik, E.E., *Reologiya dispersnykh system* (Rheology of Dispersed Systems), Leningrad: Len. Gos. Univ., 1981.
5. Baenkevich, V.V., Gorbunov, A.I., Levina, E.F., *et al.*, *Magnitnye svoistva poroshkovykh nositelei magnitnoi zapisi i materialov dlya ikh proizvodstva* (Magnetic Properties of Magnetic Recording Media and Materials for Their Manufacture), Moscow: NIITEKhIM, 1988.
6. Popov, V.V., Levina, E.F., Gorbunov, A.I., and Shcherbinin, V.V., *Mekhanizm okisleniya soedinenii zheleza (II): Sintez oksigidroksidov zheleza (III)* [Oxidation Mechanism of Iron(II) Compounds: Synthesis of Iron(II) Oxyhydroxides], Moscow: NIITEKhIM, 1989.
7. *Kratkii spravochnik po khimii* (Concise Handbook of Chemistry), Goronovskii, I.T., Nazarenko, Yu.P., and Nekryach, E.F., Eds., Kiev: Naukova Dumka, 1974, pp. 810–811.
8. Komarov, V.S. and Dubnitskaya, I.B., *Fiziko-khimicheskie osnovy regulirovaniya poristoi struktury adsorbentov i katalizatorov* (Physicochemical Foundations of Control over the Porous Structure of Adsorbents and Catalysts). Minsk: Nauka i Tekhnika, 1981.

Russian Journal of Applied Chemistry, Vol. 78, No. 10, 2005, pp. 1600–1604. Translated from Zhurnal Prikladnoi Khimii, Vol. 78, No. 10, 2005, pp. 1629–1633.
Original Russian Text Copyright © 2005 by Ergozhin, Chalov, Rozhkova, Iskakova.

SORPTION AND ION-EXCHANGE PROCESSES

Epichlorohydrin-Based Polyfunctional Ion Exchangers

E. E. Ergozhin, T. K. Chalov, A. G. Rozhkova, and R. A. Iskakova

Bekturov Institute for Chemical Research, Ministry of Education and Science of the Republic of Kazakhstan, Almaty, Kazakhstan

Received May 3, 2005

Abstract—Polyfunctional polyelectrolytes were synthesized by polycondensation of epichlorohydrin oligomer in the presence of allyl bromide. The polycondensation conditions were optimized, and composition and the properties of the resulting ion exchangers were studied.

Thanks to their high reactivity toward aliphatic and aromatic amines, epoxy compounds are widely used for preparation of various high-performance ion-exchange materials [1–3]. However, synthesis of thermally and chemically resistant ion exchangers with advanced sorption characteristics mostly involves many steps, requiring rigorous conditions.

With epichlorohydrin oligomer (ECHO) containing functional groups with close reactivities used as a starting reagent, it is possible to prepare ion exchangers with a more regular structure and advanced mechanical characteristics.

In this study, we synthesized and characterized ECHO-based polyelectrolytes.

EXPERIMENTAL

Epichlorohydrin oligomers were obtained in the presence of 1 wt % M-14 catalyst, activated aluminosilicate ($H^+ + Al^{3+}$). The reaction mixture was heated for 2 h at 30–50°C and for 5–6 h at 60–80°C under continuous stirring, and then cooled. The product was dissolved in benzene, the solution was filtered, and the product was precipitated by adding a 1 : 2 water–alcohol mixture. The resulting brown viscous mass was vacuum-dried at room temperature to constant weight.

The polycondensation of ECHO with polyamines was performed in various solvents. The mixture was stirred for 6 h at 60–80°C to the onset of gelation. The gel was transferred into a porcelain bottle and cured for 14–24 h at 80–100°C. The polyamines used were polyethylenimine (PEI), hexamethylenediamine (HMDA), and polyethylenepolyamine (PEPA). Also poly-2-methyl-5-vinylpyridine (PMVP) was used.

The polycondensation of ECHO with allyl bromide (AB) and amines was carried out in DMF at 40–70°C for 3 h. The prepolymerization was performed at various component ratios. The resulting gel was cured in an oven, crushed, and washed with distilled water. Finally, the product was converted from the OH form to the Cl form.

The static exchange capacity (SEC) and moisture content W were determined by the standard procedures [4].

The infrared spectra were registered on a Specord M-80/M85 spectrophotometer (in pellets with KBr + 1 mg of substance).

It is known that the properties of ion-exchange polymers depend on the ratio of the starting reactants, their concentration in the reaction mixture, solvent, temperature, and reaction time.

Performing polycondensation in a solvent enables synthesis of polymers under considerably milder conditions. Without solvent, the process is very fast and yields an inhomogeneous product. Therefore, a proper selection of a solvent in modification of ECHO with polyamines enables polycondensation under homogeneous conditions before gelation.

The effect of a solvent on the conversion of ECHO, judged from the exchange capacity and chlorine content, is illustrated in Table 1. This effect appeared to

Table 1. Effect of a solvent on the properties of the polymers (ECHO : PEPA : solvent = 1.0 : 2.0 : 1.0 weight parts; τ = 4 h; and T = 80°C)

Solvent	SEC, mg-equiv g^{-1*}	Chlorine content, %	V_{sp}, ml g^{-1}
Hexane	7.4	5.3	4.2
DMF	8.8	4.6	4.4
Acetone	8.1	4.3	4.2

* Static exchange capacity in 0.1 N HCl; the same in Tables 2–6.

1070-4272/05/7810-1600 © 2005 Pleiades Publishing, Inc.

be insignificant: SEC ranged from 7.4 to 8.1 mg-equiv g^{-1} and the chlorine content in the products, from 4.6 to 5.3%. However, the gelation rate waried with the solvent. A homogeneous gel was formed in DMF, as providing sufficient solubility for both the initial and intermediate compounds, and good swellability for the final products.

The amount of the solvent varied from 1.0 to 5.0 weight parts relative to the oligomer. The effect of the ECHO : DMF ratio on the SEC of the polyelectrolytes based on PEPA and ECHO is illustrated in Table 2.

As can be seen, changes in this ratio only slightly affect the characteristics of the final products. However, the chlorine content appeared to be at a minimum at ECHO : DMF = 1.0 : 2.0, and further experiments were carried out in this system.

A study of the effect of the reagent ratio showed that the amount of the polyamine added influences the conversion of ECHO and the density of cross-links in the resulting polyelectrolyte.

Table 3 shows that cross-linking occurs even at the minimal polyamine : ECHO ratio (0.2 : 1.0). However, in this case, the resulting products are characterized by a low SEC, as demonstrated by the high chlorine content (25–33%) and low nitrogen content in the copolymer (3–6%).

The use of a double excess of the polyamine provides a deep conversion and, accordingly, high SEC.

When ECH is used instead of ECHO, the reaction conditions only slightly influence the properties of the ion exchangers, which is due to its high reactivity. In this case, despite the high conversion and the resulting high SEC of the ion exchanger, the products show a considerable swellability and low mechanical strength (Table 4). Therefore, it is advisable to use ECHO in synthesis of polyfunctional ion exchangers.

At the optimal component ratio, we studied the effect of the reaction temperature on the properties of the polyelectrolytes (Table 5). With the temperature increasing from 60 to 110°C, the SEC of the samples grows, reaching a maximum at 80–100°C, and the gelation time decreases from 6 to 4 h. To minimize the thermal degradation, it is advisable to perform the polycondensation of ECH or ECHO with PMVP at 80°C.

It is well known that the properties of polyelectrolytes are strongly influenced by the mode of gel curing. A study of this stage demonstrated (Table 6) that,

Table 2. Effect of the ECHO : DMF weight ratio on the properties of the ion exchangers based on PEPA and ECHO (τ = 6 h; T = 80°C)

ECHO : DMF	SEC, mg-equiv g^{-1}	Chlorine content, %
1.0 : 1.0	8.7	4.8
1.0 : 2.0	8.8	4.6
1.0 : 3.0	7.9	5.4
1.0 : 5.0	7.1	5.9

Table 3. Effect of the ECHO:polyamine weight ratio on the properties of the ion exchangers (τ = 6 h; T = 80°C)

ECHO : polyamine	SEC, mg-equiv g^{-1}	Chlorine content, %	Nitrogen content, %
PEI			
1.0 : 0.2	1.4	27.5	5.9
1.0 : 0.4	1.6	25.1	6.3
1.0 : 0.5	4.1	12.2	12.6
1,0 : 0.8	4.6	9.7	13.2
1.0 : 1.0	5.4	7.9	15.0
1.0 : 1.5	5.7	6.3	18.6
1.0 : 2.0	6.3	5.9	18.9
PEPA			
1.0 : 0.2	1.6	25.2	6.3
1.0 : 0.4	2.7	19.6	7.4
1.0 : 0.6	3.9	15.9	9.6
1.0 : 0.8	4.1	11.6	11.5
1.0 : 1.0	7.4	5.3	12.7
1.0 : 1.5	8.1	5.3	15.4
1.0 : 2.0	8.8	4.6	16.7

Table 4. Effect of the ECHO(ECH) : PMVP weight ratio on the properties of the ion exchangers (ECH: τ = 2 h, T = 40°C; OECH: τ = 4 h, T = 100°C)

Component ratio	SEC, mg-equiv g^{-1}	Nitrogen content, %	V_{sp}, ml g^{-1}	Strength, %
ECH : PMVP:				
1.0 : 1.0	5.9	6.2	4.0	83.4
1.0 : 2.0	5.4	5.8	3.5	88.2
1.0 : 3.0	5.5	5.8	3.5	88.1
1.0 : 5.0	5.7	6.0	3.7	87.7
ECHO : PMVP:				
1.0 : 1.0	3.0	4.8	2.0	99.8
1.0 : 2.0	5.1	5.7	2.6	98.4
1.0 : 3.0	4.8	5.0	2.4	99.6
1.0 : 4.0	4.7	5.4	2.4	99.6

Table 5. Static exchange capacity of the ECHO/polyamine ion exchangers at various polycondensation temperatures

Starting reagents	SEC, mg-equiv g^{-1}, at indicated *T*, °C					Starting reagents	SEC, mg-equiv g^{-1}, at indicated *T*, °C				
	60	70	80	100	110		60	70	80	100	110
ECHO : PEPA	4.3	6.4	8.1	7.9	7.2	ECHO : PMVP	2.8	4.1	4.5	5.1	5.3
ECHO : PEI	2.6	3.7	6.3	6.1	5.0	ECH : PMVP	5.4	5.5	5.6	5.8	5.9

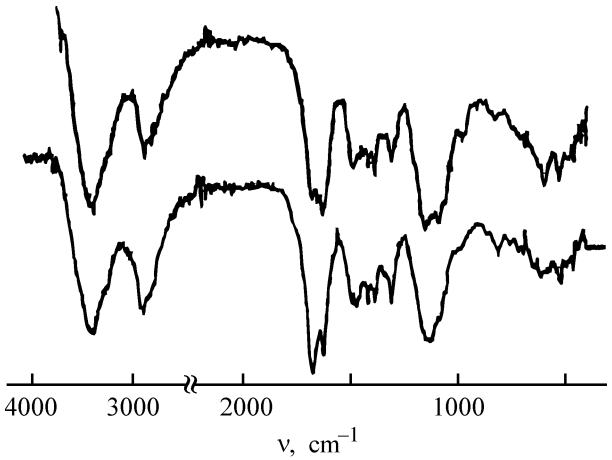
Table 6. (1) SEC and (2) swellability of the ion exchangers at various curing temperatures

Starting reagents	Temperature, °C							
	60		80		100		130	
	1	2	1	2	1	2	1	2
ECHO : PEPA	8.9	4.7	8.1	4.6	8.2	4.2	8.0	4.0
ECHO : PEI	5.7	4.8	6.3	4.4	5.8	4.3	5.2	4.0
ECHO : PMVP	4.1	2.2	5.1	2.6	5.4	2.7	5.5	2.7
ECH : PMVP	5.9	3.9	5.7	3.6	5.9	3.9	6.0	4.0

Table 7. Effect of the prepolymerization temperature on the swellability V_{sp} and SEC (ECHO : AB : PEPA = 1.0 : 1.0 : 1.0)

T, °C	Nitrogen content, %	V_{sp}, ml g^{-1}	SEC_{HCl}/SEC_{NaCl}	*T*, °C	Nitrogen content, %	V_{sp}, ml g^{-1}	SEC_{HCl}/SEC_{NaCl}
40	11.13	5.6	9.1 : 1.8	60	10.21	2.4	5.9 : 0.9
50	14.28	3.6	9.8 : 1.4	70	9.61	2.1	3.5 : 0.8

at 80–100°C, its duration should be at least 24 h, to avoid formation of mechanically unstable polymers as a result of low conversion. The observed high swellability of the samples obtained at an insufficient curing time suggests a low cross-link density in the ion exchanger. The static exchange capacity of the ion exchangers reaches a maximum at 80–100°C and decreases with a further increase in the reaction temperature.



Infrared spectra of ion exchangers based on ECHO, AB, and amines (PEPA and PEI). (ν) Wave number.

Finally, the optimal conditions for the synthesis of the ECHO-based polyelectrolytes are as follows: temperature 80°C, ECHO : polyamine = 1.0 : (1.0–3.0) (depending on the polyamine), DMF content (2.0 weight parts), curing at 100°C for 24 h; and for ECH/PMVP: 80°C and ECH : PMVP = 1.0 : 1.0.

The IR spectra of the polymers (see figure) demonstrate no absorption bands associated with stretching and bending vibrations of CH_2–Cl at 672 and 1270 cm^{-1}. The band at 1420 cm^{-1} is assigned to bending vibrations of the methylene group bound to the electron-donating nitrogen atoms. The spectra show characteristic bands of amino groups at 3400, 1670, and 1600 cm^{-1}.

Introduction of allyl groups into the polymer structure improves the strength and heat and chemical resistance of the ion exchangers [5]. Therefore, we synthesized samples based on ECHO, AB, and the amines. Data on the effect of the prepolymerization temperature on certain physicochemical properties of these polyelectrolytes are listed in Table 7. With

Table 8. Effect of the initial reagent ratio on properties of the polymers

Initial reagent ratio	T, °C	W, %	V_{sp}, ml g^{-1}	$SEC_{HCl} : SEC_{NaCl}$
AB : ECHO : PEPA:				
1.0 : 1.0 : 1.0	70	41.2	2.6	3.5 : 0.8
1.0 : 1.0 : 2.0		43.2	2.8	1.7 : 0.2
1.0 : 2.0 : 1.0		46.3	2.9	3.1 : 0.5
1.0 : 3.0 : 1.0		52.2	3.2	2.7 : 0.4
AB : ECHO : PEI:				
1.0 : 1.0 : 1.0	60	61.5	3.2	6.1 : 0.8
1.0 : 1.0 : 2.0		62.7	3.2	9.2 : 0.8
1.0 : 1.0 : 3.0		74.6	4.5	12.6 : 0.7
AB : ECHO : HMDA = 1.0 : 1.0 : 2.0	70	47.7	3.6	1.8 : 0.4

the temperature increasing from 40 to 70°C, the SEC passes through a maximum at 50°C and then decreases to 3.5 mg-equiv g^{-1}, and the swellability steadily decreases from 5.6 to 2.1 ml g^{-1}.

A study of the effect of the reagent ratio on properties of the resulting ion exchangers showed that, at 70°C, an increase in the PEPA concentration from 1.0 to 3.0 wt parts results in that a soluble product is formed (Table 8). With the ECHO concentration increasing within the range 1.0–3.0 wt parts, the density of cross-links in the copolymer grows, which hinders the access to the functional groups and, accordingly, leads to a decrease in the SEC in 0.1 N HCl from 3.5 to 2.7 mg-equiv g^{-1}.

Condensation of AB, ECHO, and PEI was carried out at 60°C. With the PEI concentration raised from 1.0 to 3.0 wt parts, SEC in 0.1 N HCl increased to 12.6 mg-equiv g^{-1}. A further increase in the concentration made higher the swellability of the resulting polymers because of a decrease in the fraction of the cross-linking agent. In the case of HMDA, cross-linked polymers could be obtained only at AB : ECHO : HMDA = 1.0 : 1.0 : 2.0.

Experiments with varied order of reagent introduction showed that cross-linked polymers are only formed if, initially, PEPA is condensed with AB, and then ECHO is added at 20°C. However, the sorbents synthesized under these conditions have a low SEC (3.0 mg-equiv g^{-1}). Condensation of PEPA with AB at room temperature, followed by elevation of the temperature to 70°C in the presence of ECHO, results in only a slight increase in the SEC from 3.0 to 3.3 mg-equiv g^{-1}. The low exchange capacities obtained using the indicated procedure can be attributed to the fact that the interaction of AB with PEPA raises the basicity of the nitrogen atom, which, in turn, makes lower the reactivity of the amino group [6].

Finally, the optimal condensation conditions of ECHO with AB and various amines are as follows: 50°C, ECHO : amine : AB = 1.0 : 1.0 : 1.0 for PEPA and 60°C, 1.0 : 3.0 : 1.0 for PEI. The ion exchangers synthesized under the optimal conditions contain increased concentrations of weakly and strongly acidic functional groups, which extends their application area as selective sorbents for transition and noble metal ions.

The IR spectra of these polymers exhibit the absorption bands due to stretching and bending vibrations of the amino groups at 3400, 1670, and 1600 cm^{-1} and of the C–N bond at 1275 cm^{-1}, but not the bands at 550 and 600 cm^{-1} characteristic of the stretching vibrations of the C–Br and C–Cl bonds (see figure).

CONCLUSIONS

(1) The optimal conditions for synthesis of polyelectrolytes based on epichlorohydrin oligomer and amines are as follows: temperature 80°C; oligomer : polyamine weight ratio 1.0 : (1.0–3.0) depending on the polyamine; solvent (DMF) concentration 2.0 wt parts; and curing at 100°C for 24 h. For epichlorohydrin with poly-2-methyl-5-vinylpyridine: 80°C and weight ratio 1.0 : 1.0. In the presence of allyl bromide: 50°C and weight ratio 1.0 : 1.0 : 1.0. For polyethyleneimine: 60°C and weight ratio 1.0 : 3.0 : 1.0.

(2) The polymers obtained exhibit enhanced ion-exchange properties, as demonstrated by physicochemical methods and IR and elemental analyses.

ACKNOWLEDGMENTS

The study was financially supported by the International Science and Technology Center (ISTC Project K-604).

REFERENCES

1. Nikagalina, V.N., Gembitskii, P.A., Kats, E.M., *et al.*, *Zh. Prikl. Khim.*, 2001, vol. 74, no. 9, pp. 1410–1412.
2. Lavnikova, I.V. and Zheltobryukhova, V.F., *Zh. Prikl. Khim.*, 2001, vol. 74, no. 12, pp. 2062–2064.
3. Ergozhin, E.E., Akimbaeva, A.M., and Bektenev, N.A., *Zh. Prikl. Khim.*, 2002, vol. 75, no. 3, pp. 398–400.
4. *GOSTs* (State Standards) *10 898–84, 10 898.2–84, and 10 898.5–84, Ion Exchangers: Methods for Physicochemical Testing.*
5. Vorob'eva, A.I., Prochukhan, Yu.A., and Monakov, Yu.B., *Vysokomol. Soedin., Ser. C*, 2003, vol. 45, no. 12, pp. 2118–2136.
6. Smirnov, Yu.N., Komarov, B.A., Kushch, P.P., *et al.*, *Zh. Prikl. Khim.*, 2002, vol. 75, no. 2, pp. 274–285.

Russian Journal of Applied Chemistry, Vol. 78, No. 10, 2005, pp. 1605–1609. Translated from Zhurnal Prikladnoi Khimii, Vol. 78, No. 10, 2005, pp. 1634–1637.
Original Russian Text Copyright © 2005 by Oshurkova, Nesterov.

APPLIED ELECTROCHEMISTRY AND CORROSION PROTECTION OF METALS

Synthesis of New Electrolytes in Solutions with dc Current

O. V. Oshurkova and V. P. Nesterov

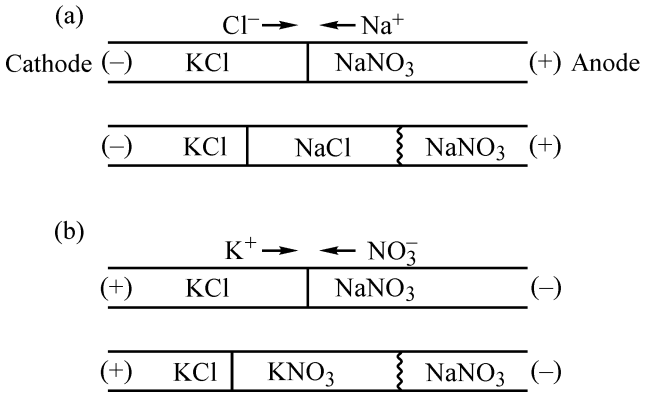
Sechenov Institute of Evolutionary Physiology and Biochemistry, Russian Academy of Sciences, St. Petersburg, Russia

Received June 18, 2005

Abstract—Conditions under which new pure electrolyte solutions can be obtained by passing dc electric current through contacting solutions with four different ions were considered. Electrolytes were synthesized in capillary columns by various procedures.

The study is concerned with synthesis of electrolytes in which a new solution is obtained by passing dc electric current through electrolytes brought in contact. The possibility of such a synthesis was mentioned by Kohlrauch [1], who wrote that, if electric current is passed across the interface between contacting electrolytes, one more electrolyte is to be formed. A review devoted to isotachophoresis [2] reported, with reference to [1], that such a synthesis of new electrolytes is possible. However, conditions for synthesis of a pure solution were not formulated, procedures for synthesis of new electrolytes were not systematized, and the synthesis itself was not carried out experimentally in [2].

According to Kohlrauch's concept, a new electrolyte can be obtained in interaction of two solutions containing four different ions. This condition is necessary, but not sufficient for obtaining a new pure electrolyte. Let us illustrate this with the following example. In scheme 1a, two electrolytes are represented: KCl (catholyte) and $NaNO_3$ (anolyte). These solutions contain K^+, Na^+, NO_3^-, and Cl^- ions. On applying an electric field, K^+ and Na^+ ions will move toward the cathode, and NO_3^- and Cl^- ions, toward the anode. In the course of electrolysis, a new NaCl solution is formed at the place of contact between the solutions. Because the mobility of the potassium ion (u_{K^+}) exceeds that of the sodium ion (u_{Na^+}), a stable interface moving toward the cathode is formed between the KCl and NaCl solutions [3, 4]. No stable boundary is formed at the other end of the column of the NaCl solution, because the mobility of chloride ions (v_{Cl^-}) exceeds that of nitrate ions ($v_{NO_3^-}$), which will lead to mixing of NaCl and $NaNO_3$ solutions (Scheme 1a). The width of the mixing zone will increase with the time of electrolysis.



Scheme 1. Motion of ions: (a) in interaction of KCl (catholyte) and $NaNO_3$ (anolyte) solutions; (b) upon a change of the polarity across the electrodes (*wavy lines* correspond to mixing of solutions).

In the case of a change of polarity across the electrodes, a KNO_3 solution will form at the place of contact between the solutions (Scheme 1b). However, the KNO_3 and $NaNO_3$ solutions will mix because $u_{K^+} > u_{Na^+}$. To synthesize from two electrolytes, C_1A_1 and C_2A_2, containing four different ions a pure electrolyte C_2A_1 not mixed with the starting solutions in the column, it is necessary that the following inequalities should be observed:

$$u^C_{C_1} > u^S_{C_2}, \quad (1)$$

$$v^S_{A_2} < v^A_{A_2}, \quad (2)$$

where $u^C_{C_1}$ and $u^S_{C_2}$ are the mobilities of the cations of the catholyte and the electrolyte being synthesized, respectively; $v^C_{A_1}$ and $v^A_{A_2}$, mobilities of the anions of

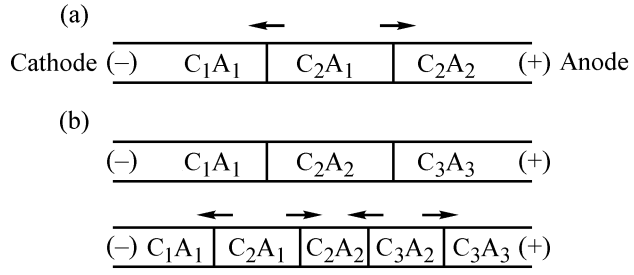
1070-4272/05/7810-1605 © 2005 Pleiades Publishing, Inc.

the anolyte and the electrolyte being synthesized, respectively.

The superscripts refer: *C* to the catholyte, *S* to the solution being synthesized, and *A* to the anolyte; the subscripts C_1, C_2, A_1, and A_2 denote the cations and anions of the respective solutions.

If inequalities (1) and (2) are observed, the boundaries between the solution being synthesized and the catholyte and anolyte are stable in an electric field and move in opposite directions. The boundary between the solution being synthesized and the catholyte will move toward the cathode, and that between the solution and the anolyte, toward the anode (Scheme 2a). The number of gram-equivalents of the substance being synthesized will be $I\tau$F, where I is the current (A); τ, time (s); and F, Faraday number (C g-equiv^{-1}). This formula follows from the fact that, if inequalities (1) and (2) are observed, only the anion passes across the boundary between the solution being synthesized and the catholyte, and only the cation, across the interface with the anolyte.

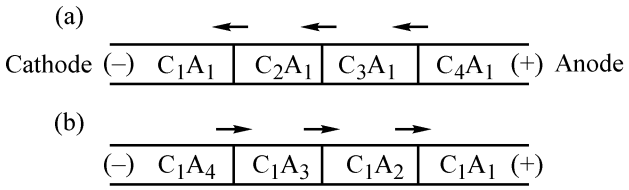
However, the potentialities of synthesis may markedly exceed that of the variant considered. Let us demonstrate this by the following example:



Scheme 2. (a) Synthesis of C_2A_1 solution from C_1A_1 (catholyte) and C_2A_2 (anolyte) in the case when inequalities (1) and (2) are observed; (b) simultaneous synthesis of two solutions, C_2A_1 and C_3A_2, from three solutions C_1A_1, C_2A_2, and C_3A_3. The *arrows* show the directions in which the boundaries of the electrolytes being synthesized move under the action of electric current.

Let us consider a column charged with three electrolytes. Let these be the following solutions: C_1A_1 (catholyte), C_2A_2 (middle solution), and C_3A_3 (anolyte) (Scheme 2b). If these solutions are chosen in such a way that, on passing an electric current, C_2A_1 solution is synthesized from the first pair of solutions (C_1A_1 and C_2A_2), and C_3A_2 solution from the second pair of solutions (C_2A_2 and C_3A_3), then two different substances will be simultaneously synthesized in the column. Such a synthesis is possible if inequalities (1) and (2) are observed for each pair of solutions (C_1A_1 and C_2A_2) and (C_2A_2 and C_3A_3) and for the solutions being synthesized (C_2A_1 and C_3A_2).

In this case, $I\tau$/F gram-equivalents of a new substance will be synthesized from each pair of solutions on passing $I\tau$ coulombs of electricity. The number of electrolyte pairs can be raised. In addition to the variants considered, replacement of one ion for another of the same sign in solution under the action of dc electric current should be regarded as synthesis of electrolytes. It is known that all the zones of the solutions acquire a common anion in the course of electrolyses in cationic isotachophoresis, and, by contrast, a common cation, in anionic isotachophoresis [3, 4]. The zones obtained in cationic and anionic isotachophoreses are shown schematically in Scheme 3. If C_2A_2 solution is placed instead of C_2A_1 solution in the column for cationic isotachophoresis, a stable zone of C_2A_1 solution will be obtained in the course of electrolysis. Thus, anion A_2 can be replaced with anion A_1 in the starting C_2A_2 solution. Similarly, one cation can be replaced with another in the starting solution by means of anionic isotachophoresis. One ion is frequently replaced with another in separation of electrolyte mixtures in practice of analytical capillary isotachophoresis [5, 6]. However, this method has not been regarded as synthetic and has not been used to synthesize new compounds.



Scheme 3. Distribution of zones in isotachophoresis. Variant: (a) capillary and (b) anionic.

To carry out this synthesis procedure experimentally, it is necessary to chose electrolytes and solution concentrations and to evaluate the ion mobilities. Let us describe a possible way to calculate the solution concentrations and ion mobilities for synthesizing a new electrolyte solution with the use of catholyte and anolyte (Scheme 2a).

This way can be put into effect only for the steady state (with the time-independent solution concentrations satisfying the controlling relation) [7]. To perform a calculation, it is necessary to know the catholyte concentration and have plots of the ion transference numbers with respect to the solvent against the solution concentrations for the catholyte, solution

being synthesized, and anolyte. With this information available, the calculation can be performed as follows.

(1) The cation transference number is found for the chosen catholyte concentration from the dependences of the ion transference numbers for the catholyte on its concentration.

(2) The concentration and the cation transference number of the electrolyte being synthesized are found graphically from the concentration dependence of the ion transference numbers of the catholyte and the electrolyte being synthesized [8].

(3) The anion transference number of this solution is found from the cation transference number of the catholyte being synthesized.

(4) The concentration and the anion transference number of the anolyte are found, also graphically, from the concentration and the anion transference number of the electrolyte being synthesized and from the concentration dependence of the ion transference numbers of the anolyte [8].

(5) The resulting solution concentrations and ion transference numbers can be used to find the mobilities appearing in relations (1) and (2).

(6) The ion mobility is calculated by the formula

$$u = T\chi/\mathrm{F}c, \tag{3}$$

where u is the ion mobility ($cm^2\ V^{-1}\ s^{-1}$); T, ion transference number; χ, electrical conductivity of the solution ($\Omega^{-1}\ cm^{-1}$); F, Faraday number ($C\ g\text{-}equiv^{-1}$); and c, solution concentration ($g\text{-}equiv\ l^{-1}$).

However, the above calculation procedure can be only used in very rare cases because of the complete lack of data on how the ion transference numbers depend on the solution concentration at high concentrations, for which such a synthesis is the most promising. In addition, the solution concentrations do not necessarily satisfy the steady-state conditions in syntheses of new substances.

Synthesis can be performed at equal solution concentrations. In this case, the choice of starting electrolytes is not difficult if the ion mobilities are only roughly estimated (higher or lower). The electrolytes are chosen by comparing the ion mobilities of solutions having equal concentrations ($g\text{-}equiv\ l^{-1}$) and a common ion. This evaluation method, suggested in [9], is worthwhile in practice in studying the separation of electrolyte mixtures in concentrated solutions by ion mobilities. Let us illustrate this technique by the following example.

Let there exist two electrolytes (C_1A_1 and C_2A_1) of equal concentrations. The equivalent electrical conductivity (λ) of C_1A_1 solution is given by

$$\lambda_{C_1A_1} = \mathrm{F}(u_{C_1} + v_{A_1}), \tag{4}$$

and that of C_2A_1 solution by

$$\lambda_{C_2A_1} = \mathrm{F}(u_{C_2} + v_{A_1}). \tag{5}$$

As the solutions have a common ion (anion) the mobility of the noncommon ion (cation) will be higher for that solution, which has a higher equivalent electrical conductivity. Therefore, a stable interface between the solutions will be formed if the electrolyte having a higher equivalent electrical conductivity is situated ahead of that with a lower electrical conductivity in the direction of motion of noncommon ions in the electric field. Hence follows that synthesis of a new solution on bringing in contact two solutions containing four different ions yields an electrolyte whose equivalent electrical conductivity is lower than that of each of these solutions at a concentration equal to that of the starting solutions. Let us consider, as an example, choice of electrolytes in interaction of two solutions containing four different ions: K^+, Na^+, Cl^-, and NO_3^-. Four different compounds can be formed from these ions: KCl, KNO_3, NaCl, and $NaNO_3$. The equivalent electrical conductivities of aqueous solutions of these compounds at a concentration of 2.0 $g\text{-}equiv\ l^{-1}$ and temperature of 18°C are as follows:

Substance	KCl	KNO_3	NaCl	$NaNO_3$
λ, $\Omega^{-1}\ g\text{-}equiv^{-1}\ cm^2$	92.3	69.0	66.6	54.4

It can be seen from the electrical conductivity data that the following compounds cannot be synthesized: (1) KCl, whose electrical conductivity is the highest; (2) KNO_3, whose electrical conductivity is lower than that of only a single solution; and (3) NaCl, whose electrical conductivity is lower than that of two solutions (KCl and KNO_3), but these solutions contain no sodium ions and, therefore, cannot be used in synthesis.

Only an $NaNO_3$ solution can be synthesized in pure form. As starting solutions for this synthesis can serve only KNO_3 and NaCl solutions containing four different ions and having an equivalent electrical conductivity exceeding that of the $NaNO_3$ solution. This principle of electrolyte selection was used when carrying out this synthesis in practice. In those cases when no data are available on the equivalent electrical conductivities of solution, the electrolytes can be chosen experimentally.

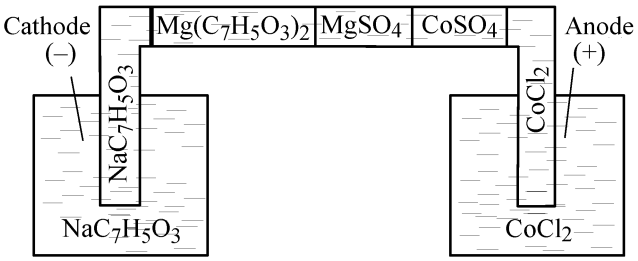
EXPERIMENTAL

Any of the synthesis variants considered above can be performed experimentally using devices for capillary isotachophoresis, described in [10, 11]. These devices have an extended detector that makes it possible to monitor the course of synthesis over a long part of the capillary column. ∏-shaped removable capillaries with an inner diameter of 0.05–0.8 mm can be used in the devices. The capillaries employed in this study had inner and outer diameters of 0.2–0.5 and 0.4–1 mm, respectively. The capillaries were 30 to 50 cm long, with a horizontal part of 20 to 30 cm. The ends of the capillaries were pointed as pipette tips, which made it possible to raise the hydrodynamic resistance of the capillaries and to virtually eliminate solution overflow. To carry out the synthesis, the capillaries were filled with the starting solutions and mounted in the device. This was done in such a way that like solutions at the capillary ends and in the electrode vessels came into contact. The synthesis was performed with aqueous electrolyte solutions. The following variants of synthesis were used.

(1) Synthesis of a solution (LiCNS) from a catholyte (2.0 N KCNS solution) and anolyte (2.0 N LiCl solution). The electrolysis was terminated when the solution being synthesized occupied a position in the horizontal part of the capillary between two marks. The marks were preliminarily deposited onto the capillary surface with a colored lacquer.

(2) Simultaneous synthesis of two new solutions. In this experiment, a 2.0 N solution of sodium salicylate ($NaC_7H_5O_3$) served as catholyte, and a 2.0 N $CoCl_2$ solution, as anolyte. A $MgSO_4$ solution was used as a middle solution. On passing an electric current, magnesium salicylate $Mg(C_7H_5O_3)$ was synthesized from $NaC_7H_5O_3$ and $MgSO_4$ solutions, and a $CoSO_4$ solution from $MgSO_4$ and $CoCl_2$ (Scheme 4). The electric current was switched off when the $MgSO_4$ solution completely disappeared. It should be noted that the interface between the $NaC_7H_5O_3$ and $Mg(C_7H_5O_3)$ solution, obtained in this case, was wider than those between other electrolytes. This is shown by a heavier line in Scheme 4.

(3) Replacement of the chloride ion for the rhodanide, acetate, and bromate ions in solutions of chlorides of rare-earth elements samarium(III), neodymium(III), and yttrium(III), respectively. $Sm(CNS)_3$ was synthesized from a 2.0 N KCNS solution (catholyte) and 1.5 N $NiCl_2$ solution (anolyte). In synthesis of $NdAc_3$, a 2.0 N KAc solution served as catholyte, and a 1.5 N $CdCl_2$ solution as anolyte. $Y(BrO_3)$ was obtained using a 2.0 N $KBrO_3$ solution as catholyte and a 1.5 N $CdCl_2$ solution as anolyte. In the cases mentioned in item 3, a steady state was attained in the capillary column. The lengths of the zones of the electrolytes synthesized were time-independent.



Scheme 4. Simultaneous synthesis of magnesium salicylate $Mg(C_7H_5O_3)$ and $CoSO_4$ solutions.

After an experiment was complete, the capillary in which synthesis was carried out was removed from the device and the zone of the solution synthesized was cut off at its boundaries. New electrolyte solutions with a prescribed chemical or isotopic composition can be synthesized in capillary columns not only in a free solution, but also in a transparent filler, e.g., agar-agar. It should be noted that the synthesis procedure under consideration can be easily made ecologically safe. However, only microscopic amounts of new electrolyte solutions can be synthesized in capillary columns. Special technological apparatus should be designed to synthesize larger amounts of electrolytes.

CONCLUSIONS

(1) Conditions for synthesis of a new electrolyte in interaction of two solutions containing four different ions were formulated.

(2) Various procedures for synthesis of new electrolytes were systematized.

(3) A rule for selection of starting electrolytes for syntheses was suggested.

(4) Various procedures for synthesis of electrolytes were carried out experimentally.

REFERENCES

1. Kohlrauch, F., *Annalen der Physik und Chemie*, 1897, vol. 62, no. 10. pp. 209–239.
2. Oshurkova, O.V. and Gorshkov, A.I., *Usp. Khim.*, 1993, vol. 62, no. 8, pp. 774–787.

3. Konstantinov, B.P. and Oshurkova, O.V., *Dokl. Akad. Nauk SSSR*, 1963, vol. 148, no. 5, pp. 1110–1113.
4. Everaerts, F.M., Beckers, J.L., and Verheggen, Th.P.E.M., *Isotachophoresis: Theory, Instrumentation and Applications*, Amsterdam: Elsevier, 1976.
5. Konstantinov, B.P., Oshurkova, O.V., and Starobina, I.Z., *Zh. Prikl. Khim.*, 1967, vol. 40, no. 6, pp. 1260–1265.
6. Oshurkova, O.V. and Gorshkov, A.I., *Zh. Prikl. Khim.*, 2001, vol. 74, no. 5, pp. 1393–1396.
7. Oshurkova, O.V., Lyadov, N.S., and Kozhurkina, I.A., *Zh. Prikl. Khim.*, 1973, vol. 46, no. 4, pp. 776–779.
8. Oshurkova, O.V., Gorshkov, A.I., and Nesterov, V.P., *Elektrokhimiya*, 1999, vol. 35, no. 1, pp. 125–127.
9. Konstantinov, B.P., Lyadov, N.S., and Oshurkova, O.V., *Elektrokhimiya*, 1970, vol. 6, no. 4, pp. 584–587.
10. Konstantinov, B.P. and Oshurkova, O.V., *Zh. Tekhn. Fiz.*, 1966, vol. 36, no. 5, pp. 942–957.
11. Bresler, P.I., Ivanova, I.A., Oshurkova, O.V, and Shtilerman, G.A., *Zh. Anal. Khim.*, 1981, vol. 36, no. 3, pp. 593–599.

Russian Journal of Applied Chemistry, Vol. 78, No. 10, 2005, pp. 1610–1614. Translated from Zhurnal Prikladnoi Khimii, Vol. 78, No. 10, 2005, pp. 1638–1642.
Original Russian Text Copyright © 2005 by Ivanova, Ivanov, Boldyrev, Stadnik.

APPLIED ELECTROCHEMISTRY AND CORROSION PROTECTION OF METALS

Electroreduction of Molybdate Ions in the Presence of Hydrofluoric Acid

N. D. Ivanova, S. V. Ivanov, E. I. Boldyrev, and O. A. Stadnik

Vernadskii Institute of General and Inorganic Chemistry, National Academy of Sciences of Ukraine, Kiev, Ukraine

National Aviation University, Kiev, Ukraine

Received February 9, 2005

Abstract—The electroreduction of molybdate ions in the presence of hydrofluoric acid was studied. The effective activation energy of the electroreduction of molybdate ions was determined using the Arrhenius equation.

The electrochemical reduction of molybdate ions has been extensively studied. It has been confirmed once again most recently that the refinement of the existing electrolytes and creation of new efficient ones is a necessary and topical task both for synthesis of nonstoichiometric molybdenum oxide compounds [1, 2] and for deposition of metallic molybdenum coatings [3] that would satisfy current ecological requirements.

The necessary condition for electrodeposition of transition metals is that a bifunctional electrochemical system electrode/film/electrolyte should be formed on the cathode [4]. At the electrolyte/film interface, the film itself is formed from nonstoichiometric oxide compounds through reduction of discharging metal ions to an intermediate degree of oxidation, whereas at the electrode/film interface, the material of the film is consumed through further reduction of these compounds to metal. The simultaneous occurrence of these processes results in that the film is in a permanent dynamic equilibrium. The electrode processes at the phase boundaries of the system electrode/film/electrolyte can be rather easily controlled in aqueous solutions containing hydrofluoric acid.

The study is concerned with the electrochemical reduction of molybdate ions from electrolytes containing hydrofluoric acid. The voltammetry with a linear potential sweep served as the main method for studying the electroreduction of ions in the presence of hydrofluoric acid. The voltammograms were recorded in the galvanodynamic mode with a PI-50-1.1 pulsed potentiostat and a PDA1-004 laboratory *X*–*Y* compensation self-recorder at a potential sweep rate of $0.002–0.5$ V s^{-1} with compensation of the *IR* error. The recording error did not exceed $\pm 0.5\%$. We used in the experiments a three-electrode cell made of high-pressure polyethylene. A platinum plate (4 cm^2) served as the auxiliary electrode and the edge of a molybdenum rod (0.78 mm^2 area) pressed into Teflon, as the working microelectrode. The current density was related to the geometrical surface area of the electrode. Prior to each measurement, the working electrode was trimmed with a fine emery paper, polished, degreased with Vienna lime, and activated in a dilute hydrofluoric acid, which provided well reproducible results. The Luggin capillary of the reference electrode (0.1 cm in diameter) was brought from below to a distance of 0.2 cm from the surface of the working electrode. This configuration made it possible to minimize the ohmic loss [5] and to preclude screening of the electrode surface. A saturated calomel electrode was used as reference. The potentials are given relative to a standard hydrogen electrode. All the experiments were performed at 20 ± 0.1°C.

The solutions used in the study contained 5–10 g l^{-1} chemically pure ammonium molybdate (in terms of metal) and 1–100 g l^{-1} hydrofluoric acid (or an equimolar amount of sulfuric acid) of special purity grade. The current density of electrodeposition was varied from 0.5 to 400 A dm^{-2}. The rate of deposition (g/A h) of the solid phase onto the cathode was determined by the standard electrochemical procedure from the gain of mass by the deposit during the preparative electrolysis.

1070-4272/05/7810-1610 © 2005 Pleiades Publishing, Inc.

The voltammograms of electroreduction of MoO_4^{2-} ions in the presence of HF and H_2SO_4 are shown in Fig. 1. The fact that more electronegative cathode potentials are possible in electrolytes containing hydrofluoric acid is due to the stronger complexing agent of the F^- ion and, accordingly, to formation of more stable complex compounds, compared with those constituted by sulfates.

The rise in the electroreduction rate of molybdate ions with hydrofluoric acid concentration shows that the concentration of nonelectroactive species of polymolybdate ions in the electrolyte decreases, whereas that of fluorine-containing electroactive complexes formed upon the decomposition of polymolybdate ions under the action of fluoride ions increases [6]. For example, rather stable complex species containing three fluoride ions (conditional stability constant $\log \beta_3 = 3.8 \pm 0.6$) are formed at small concentrations of hydrofluoric acid in the electrolyte. At large concentrations of the acid, a complex ion containing four F^- ions (conditional stability constant $\log \beta_4 = 3.0 \pm 0.5$) is formed. Thus, the increase in the number of similar ligands incorporated into a discharging species upon formation of molybdenum fluoride complexes is responsible for the decrease in the activation energy of charge transfer to this particle. In addition to doing so, it also prevents polymerization of metal ions in a solution, the effect known not only for molybdenum, but also for tungsten, titanium, and niobium. An increase in the polarization accelerates the electrode process by making higher the dissociation rate of the complex compounds.

A study of the cathodic polarization in this process showed that its character is determined by the concentration of hydrofluoric acid in the electrolyte. For example, at small concentrations of the acid (less than 5 g l^{-1}), the total rate of electroreduction of the molybdate ion is low, which is confirmed by the small slope of the initial portion of the voltammogram (Fig. 1a, curves *1*, *2*). Raising the concentration of hydrofluoric acid in the electrolyte considerably accelerates the overall process of MoO_4^{2-} reduction (Fig. 1a, curves *3*, *4*). With the concentration of hydrofluoric acid raised to 50 g l^{-1}, the cathode potential at a current density of 25 A dm^{-2} is shifted by 2–2.5 V toward the region of electropositive values. It should be noted that elevating the temperature also shifts the cathode potential to electropositive values, but this shift is considerably smaller than that observed on changing the acid concentration.

The presence of several portions on the voltammograms recorded in solutions containing hydrofluoric

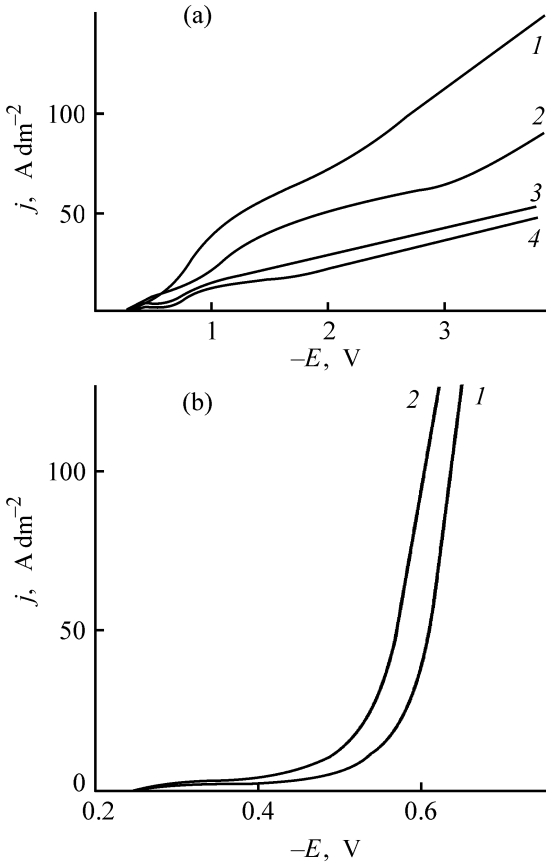


Fig. 1. Voltammograms of cathodic reduction of MoO_4^{2-} ions in electrolytes containing (a) HF and (b) H_2SO_4. Concentration (g l^{-1}): (a) Mo(VI) = 10, HF: (*1*) 5, (*2*) 10, (*3*) 25, and (*4*) 50; (b) Mo(VI) = 10, H_2SO_4: (*1*) 49 and (*2*) 123. (*j*) Current density, (*E*) potential; the same for Fig. 2.

acid confirms that different processes occur at the cathode. These data, along with the results of a microscopic study, suggest that each portion characterizes the formation of molybdenum oxide compounds with intermediate degrees of reduction, in which the average degree of oxidation of molybdenum decreases with increasing current density [3]. Colored films are formed on the cathode at a current density of 0.25–2.5 A dm^{-2}, dark deposits, at 2.5–15 A dm^{-2}, and black deposits, at current densities exceeding 25 A dm^{-2}. Light lustrous deposits of metallic molybdenum are formed at hydrofluoric acid concentrations higher than 25 g l^{-1} and current densities exceeding 50 A dm^{-2}.

The voltammograms characterizing the electroreduction of MoO_4^{2-} ions in a solution containing sulfuric acid are shown in Fig. 1b. The voltammograms have no extremal points and, compared with those recorded in solutions containing hydrofluoric acid, lie at more electropositive potentials. The deposits formed

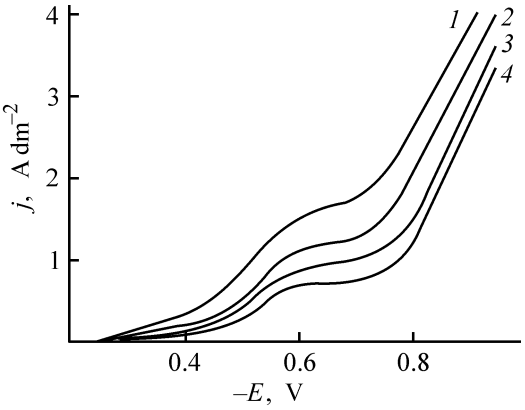


Fig. 2. Voltammograms of cathodic reduction of MoO_4^{2-} ions in the electrolyte at various potential sweep rates. Potential sweep rate (mV s^{-1}): (*1*) 100, (*2*) 50, (*3*) 20, and (*4*) 10. Concentration (g l^{-1}): Mo(VI) 10 and HF 10.

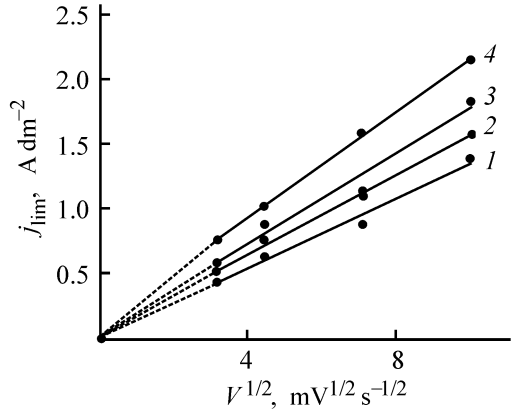


Fig. 3. Limiting current j_{lim} vs. potential sweep rate V in electrolytes containing (g l^{-1}): Mo(VI) 10, HF: (*1*) 5, (*2*) 10, (*3*) 25, and (*4*) 50.

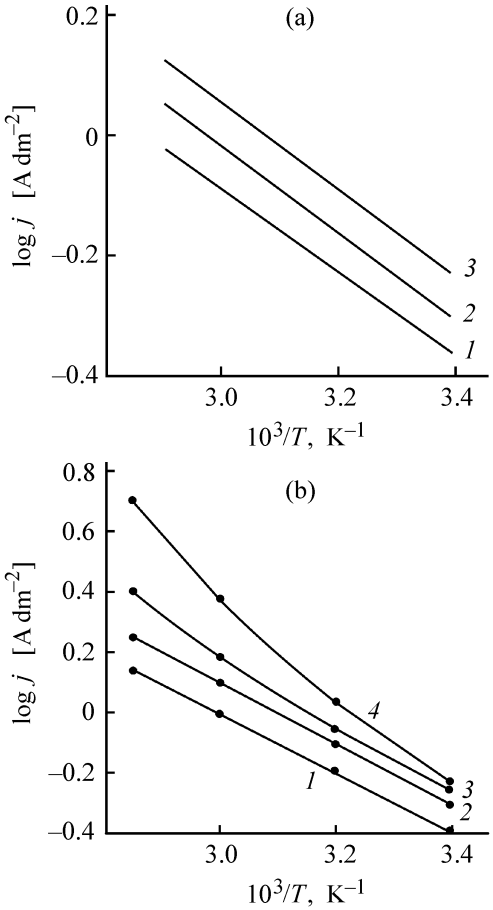


Fig. 4. Rate of the cathodic reduction of MoO_4^{2-} ions vs. temperature in electrolytes containing (a) 25 and (b) 5 g l^{-1} hydrofluoric acid. Potential (V): (a) (*1*) 2.0, (*2*) 2.2, and (*3*) 2.4; (*1*) 0.75, (*2*) 1.0, (*3*) 3 2.0, and (*4*) 3.0. Mo(VI) concentration 10 g l^{-1}. (*T*) Temperature.

at potentials of 0.7–0.8 V are sooty and strongly differ in structure from the black deposits formed from electrolytes containing hydrofluoric acid. It should be emphasized that we failed to obtain colored molybdenum-containing or metallic molybdenum coatings in H_2SO_4-containing electrolytes.

The voltammograms describing the reduction of molybdate ions in the solution containing hydrofluoric acid at various potential sweep rates are shown in Fig. 2. At potentials that precede the region of the limiting current, the electrode process depends on the potential sweep rate only slightly. All the voltammograms exhibit a characteristic delay up to a potential of approximately –0.45…–0.5 V, at which the current density is extremely low. As the polarization is raised further, the current density sharply increases up to a certain limiting value. Microscopic observations demonstrated that a film of molybdenum oxide compounds with intermediate degrees of reduction is formed on the cathode under these conditions. The plateau of this limiting current becomes narrower as the rate at which the polarization is varied increases.

At the highest variation rate of polarization, $|dE/d\tau|$, the ascending portion of the curve, which corresponds to reduction of molybdate ions, starts from less electronegative potentials. As the potential sweep rate decreases, the voltammogram shifts to the region of negative potentials, with the limiting current simultaneously decreasing. The dependences of the limiting current j_{lim} on the potential sweep rate V in the j_{lim}–$V^{1/2}$ coordinates are approximated by straight lines (Fig. 3), which confirms that these processes are diffusion-limited.

Raising the temperature makes considerably higher the rate of the above electrochemical process. The fact that the log j–1/T dependences (Fig. 4) are linear, i.e.,

formally similar to the Arrhenius equation, allows the effective activation energy to be determined from this equation. In this case, the behavior of the dependences obtained in the electrolytes containing more than 25 g l^{-1} hydrofluoric acid shows that the reduction of molybdate ion to metal is the diffusion-limited process (Fig. 4a). At low HF concentrations, when oxide compounds containing MoO_4^{2-} in an intermediate degree of reduction are formed, the process is limited by activated polarization (Fig. 4b) caused by the formation of a cathodic film [7]. The apparent disagreement between these results can be resolved on the assumption that the effective activation energy characterizes the diffusion limitation to the processes occurring in the film being formed on the electrode surface, because the polarization at the film/electrolyte phase boundary shows an activated behavior [8].

The effective activation energy of the electroreduction of molybdate ions in the presence of hydrofluoric acid strongly depends not only on the electrode potential (Fig. 5a), but also on the HF concentration in the electrolyte (Fig. 5b). This concentration determines the state of the metal surface in different portions of the polarization curve via redistribution of the rates of the processes occurring at the phase boundaries of a bifunctional electrochemical system electrode/film/electrolyte [9[. The effective activation energy of the MoO_4^{2-} electroreduction decreases in proportion to an increase in the potential, which electrostatically lowers the potential barrier for the reaction (Fig. 5a). This is especially clearly pronounced at low concentrations of hydrofluoric acid.

Thus, as the polarization potential and the rate of the electrode reaction increase, the contribution of the activated polarization gradually decreases, and that of the diffusion limitations grows. In the process, the effective activation energy gradually decreases to about 5 kJ mol^{-1}. Noteworthy is the fact that the effective activation energy remains virtually unchanged when the electrode potential is varied within 2–3 V at low HF concentrations in the electrolyte (Fig. 4a) and within 0.5–1.2 V at HF concentrations of 25–50 g l^{-1} (Fig. 5b). This may indicate that, not only the electrode process is diffusion-limited [7], but also the following two simultaneous processes cancel each other. The first is a decrease in the activation energy on raising the electrode potential, and the second, its increase with the derivative of current with respect to temperature in the Arrhenius equation. The second process is due to a rise in the diffusion permeability of the cathodic film, which acts as a kind of negative feedback. A similar effect

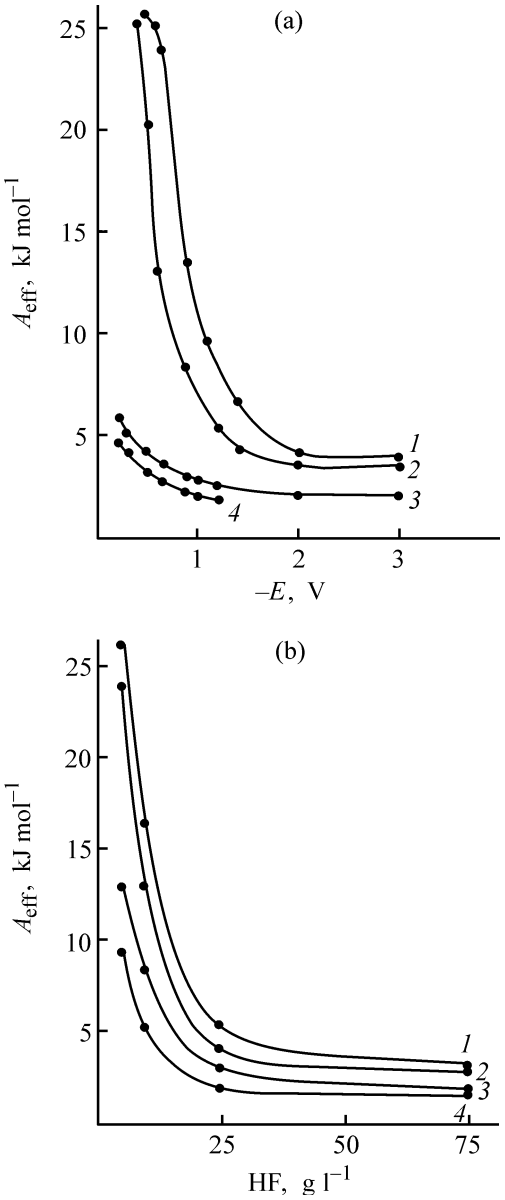


Fig. 5. Effective activation energy A_{eff} of cathodic reduction of MoO_4^{2-} ions in electrolytes vs. electrode potential E and HF concentration. (a) HF concentration (g l^{-1}): (*1*) 5, (*2*) 10, (*3*) 25, and (*4*) 50; (b) Electrode potential (V): (*1*) 0.5, (*2*) 0.6, (*3*) 0.9, and (*4*) 1.2. Mo(VI) concentration 10 g l^{-1}.

of a potential-independent effective activation energy has also been observed for the anodic dissolution of nickel [10, 11].

On the whole, the activation energy of the electroreduction of discharging molybdate ions considerably decreases as the concentration of hydrofluoric acid in the electrolyte becomes higher. This fact has been established previously in a study of how the activation energy varies with the ligand concentration and

the composition of the cathodic deposits formed in electroreduction of MoO_4^{2-} ion in the presence of hydrofluoric acid.

CONCLUSIONS

(1) A deeper electroreduction of molybdate ions occurs in electrolytes containing hydrofluoric acid, compared with those containing sulfuric acid. As a result, colored and black deposits of molybdenum oxide compounds containing molybdenum in a considerably lower degree of oxidation are formed at the cathode.

(2) Light lustrous deposits of metallic molybdenum can be obtained at current densities exceeding 50 A dm^{-2} and hydrofluoric acid concentrations higher than 25 g l^{-1}.

(3) The effective activation energy of the electroreduction of molybdate ions decreases as the polarization potential and rate of the electrode reaction become higher. This is accompanied by a decrease in the activation polarization and by enhancement of the diffusion limitations to the process occurring in a film composed of nonstoichiomertic molybdenum oxide compounds formed on the electrode surface.

REFERENCES

1. Kuznetsov, V.V., Pavlov, M.P., Zalmanov, D.I., *et al.*, *Elektrokhimiya*, 2004, vol. 40, no. 7, pp. 813–818.
2. Nagirnyi, V.M., Apostolova, R.D., and Baskevich, A.S., *Zh. Prikl. Khim.*, 2004, vol. 77, no. 1, pp. 75–77.
3. Ivanova, N.D., Ivanov, S.V., Boldyrev, E.I., *et al*, *Zashch. Met.*, 2005, vol. 41.
4. Ivanova, N.D. and Ivanov, S.V., *Usp. Khim.*, 1993, vol. 62, no. 10, pp. 963–974.
5. Thurgood, C.P., Kirk, D.W., Foulkes, F.R., and Graydou, W.F., *J. Electrochem. Soc.*, 1981, vol. 128, no. 8, pp. 1680–1687.
6. Ivanova, N.D. and Kladnitskaya, K.B., *Ukr. Khim. Zh.*, 1979, vol. 45, no. 11, pp. 1061–1064.
7. Gorbachev, S.V. and Nikich, V.I., *Trudy Mosk. Khim-Tekhnol. Inst.*, 1974, vol. 101, pp. 101–110.
8. Ivanov, S.V. and Ivanova, N.D., *Dokl. Ukr. Nat. Akad. Nauk*, 1992, no. 9, pp. 129–134.
9. Ivanova, N.D. and Ivanov, S.V., *Functional Materials*, 2000, vol. 7, no. 1, pp. 5–26.
10. Kozin, L.F., Manilevich, F.D., and Mashkova, N.V., *Zashch. Met.*, 2001, vol. 37, no. 2, pp. 178–183.
11. Grigor'ev, V.P., Kravchenko, V.M., and Gershanova, I.M., *Zashch. Met.*, 2004, vol. 40, no. 3, pp. 236–242.

Russian Journal of Applied Chemistry, Vol. 78, No. 10, 2005, pp. 1615–1619. Translated from Zhurnal Prikladnoi Khimii, Vol. 78, No. 10, 2005, pp. 1643–1647.
Original Russian Text Copyright © 2005 by Turaev.

APPLIED ELECTROCHEMISTRY AND CORROSION PROTECTION OF METALS

Use of Ion-Exchange Membranes in Chemical Power Cells

D. Yu. Turaev

Mendeleev Russian University of Chemical Technology, Moscow, Russia

Received March 28, 2005

Abstract—A chemical power cell is suggested, in which the positive and negative electrodes are placed each in its own electrolyte. This makes it possible to obtain the highest absolute value of the electrode potential of each electrode. The electromotive force and the maximum theoretical specific energy are calculated for an acid-alkaline-salt battery of the zinc-dioxide–lead system.

Chemical power cells employing aqueous electrolyte solutions can be divided into three groups: with salt, acid, and alkaline electrolytes. The active pastes of the positive and negative electrodes are spatially separated with a porous separator.

The active pastes are also separated with ion-exchange membranes [1]. An electrochemical cell [2] is a variant of an air–zinc system, with a partition permeable to only OH^- and H^+ ions and water molecules. The negative Zn electrode is placed in an acid electrolyte, and the positive electrode, in KOH. The charging and discharge voltages are 1.8 and 1.2–1.3 V, respectively.

The possibility of using bipolar ion-exchange membranes to produce electric power by back electrodialysis was demonstrated in [3]. The electric power is generated by feeding HCl and NaOH solutions into adjacent chambers. An acid (alkali) solution is in contact with the cationic (anionic) side of a bipolar ion-exchange membrane. Nickel, on which water decomposes in discharge of the power cell through an active load, is used as a material of the anode and cathode. At a zero load current, the algebraic sum of the electrode and membrane potentials of the cationite and anionite membranes is directed against the sum of membrane potentials of MB-24 bipolar membranes.

Highly important is the chemical resistance of an ion-exchange membrane serving to separate electrolytes with a strongly oxidizing power. For example, a sulfonate-polysulfocarbonate cation-exchange membrane has been developed for separation of two electrolytes and use in batteries containing a strong oxidizing electrolyte, e.g., for a zinc–ferrocyanide battery [4].

The parameters of perfluorinated cation-exchange membranes of foreign and domestic manufacture were reported in [5].

An anion-exchange ion-selective membrane has been used in a fuel cell employing an aqueous acid solution of chromium(II) chloride as a reducing agent, and an acid solution of iron(III) chloride as an oxidizing agent [6].

Thus, use of ion-exchange membranes makes it possible to obtain various chemical power cells, including fuel cells.

EXPERIMENTAL

If ion-exchange membranes that favor motion of only a single kind of ions are used to separate active pastes, chemical power cells can be designed taking into account the operation of each of the half-cells. Most of half-cells containing an oxidizing or reducing agent lie outside the thermodynamic stability region of H_2O, equal to 1.23 V (Purbet diagram for water) [7], specified by two boundary equations derived using the Nernst equation for the reactions

$$2H^+ + 2e = H_2, \quad (1)$$

$$E_{p,\,H^+/H_2} = E^0_{H^+/H_2} + \frac{RT}{nF}\ln\frac{a^2_{H^+}}{a_{H_2}} = -0.059\text{pH}, \quad (1a)$$

$$4H^+ + O_2 + 4e = 2H_2O, \quad (2)$$

$$E_{p,\,O_2/H_2O} = E^0_{O_2/H_2O} + \frac{RT}{nF}\ln\frac{a^2_{O_2}a^4_{H^+}}{a^2_{H_2O}} = 1.23 - 0.059\text{pH}. \quad (2a)$$

1070-4272/05/7810-1615 © 2005 Pleiades Publishing, Inc.

The electromotive force of the hydrogen-oxygen cell is given by

$$\text{emf} = \Delta E = E_{\text{p, O}_2/\text{H}_2\text{O}} - E_{\text{p, H}^+/\text{H}_2}$$
$$= 1.23 - 0.059\,\text{pH} - (-0.059\,\text{pH}) = 1.23\ \text{V}. \quad (3)$$

It can be seen from Eq. (3) that the electromotive force of the hydrogen-oxygen cell is 1.23 V at any solution pH. An electromotive force exceeding 1.23 V for a cell containing aqueous electrolyte solutions can be obtained if the reaction of water decomposition into hydrogen and oxygen is hindered. The electromotive force of a hydrogen-oxygen cell can be raised if two electrolytes are used, one with pH –2, and the other with pH 16:

$$\text{emf} = 1.23 - 0.059(-2) - (-0.059 \times 16) = 2.29\ \text{V}. \quad (4)$$

It can be seen from Eq. (4) that, if solutions with different pH values are used, the electromotive force of a hydrogen-oxygen cell increases by approximately a factor of 1.86, compared with that of a hydrogen-oxygen cell with a single electrolyte having any pH. The electromotive force can be raised to an even greater extent if a pair of half-cells is chosen, in which the active pastes have the highest absolute value of the electrode potential in acid and alkaline media. In the electrochemical system

$$\text{Pb}\,|\,\text{PbO}_2\,|\,\text{H}_2\text{SO}_4\,||\,\text{NaOH},\ \text{ZnO}\,|\,\text{Zn},$$

the following conjugated electrochemical reactions occur.

Cathodic reaction [8]:

$$\text{PbO}_2 + 4\text{H}^+ + \text{SO}_4^{2-} + 2\text{e} = \text{PbSO}_4 + 2\text{H}_2\text{O},$$
$$E^0_{\text{PbO}_2/\text{PbSO}_4} = 1.68\ \text{V}. \quad (5)$$

The dependence of the electrode potential of the half-cell constituted by the dioxide-lead electrode on the concentration of the H_2SO_4 solution (5 M) will be calculated by the Nernst equation similarly to the known calculation for a lead battery [9], using data from reference books [10, 11]:

$$E_{\text{p, PbO}_2/\text{PbSO}_4} = E^0_{\text{PbO}_2/\text{PbSO}_4} + \frac{RT}{nF}\ln\frac{a_{\text{PbO}_2}a^4_{\text{H}^+}a_{\text{SO}_4^{2-}}}{a_{\text{PbSO}_4}a^2_{\text{H}_2\text{O}}}$$
$$= 1.68 + \frac{8.314 \times 298}{2 \times 96\,500}\ln\frac{1(0.273 \times 2 \times 5)^4 \times 0.273 \times 5}{1 \times 0.579^2}$$
$$= 1.75\ \text{V}. \quad (6)$$

In the lead battery, the true potential of the positive electrode is +1.76 V [12].

Anodic reaction for the zinc-alkaline half-cell [11]:

$$\text{ZnO}_2^{2-} + 2\text{H}_2\text{O} + 2\text{e} = \text{Zn} + 4\text{OH}^-,$$
$$E^0_{\text{ZnO}_2^{2-}/\text{ZnO}} = -1.21\ \text{V}. \quad (7)$$

The dependence of the electrode potential of reaction (7) on the alkali concentration equal to 10 M is given by

$$E_{\text{p, ZnO}_2^{2-}/\text{Zn}} = E^0_{\text{ZnO}_2^{2-}/\text{Zn}} + \frac{RT}{nF}\ln\frac{a_{\text{ZnO}_2^{2-}}a^2_{\text{H}_2\text{O}}}{a_{\text{Zn}}a^4_{\text{OH}^-}}$$
$$= -1.21 + \frac{8.314 \times 298}{2 \times 96500}\ln\frac{a_{\text{ZnO}_2^{2-}} \times 0.45^2}{1(3.88 \times 10)^2}$$
$$= -1.42 + 0.02956\log a_{\text{ZnO}_2^{2-}}. \quad (8)$$

The solubility of zinc oxide in a concentrated alkali solution does not exceed 0.5–1 M, and the true potential of the zinc electrode in a concentrated alkali solution is –1.30 V [12]. At $0.02956\log a_{\text{ZnO}_2^{2-}} = 0$, we have

$$E_{\text{p, ZnO}_2^{2-}} = -1.42\ \text{V}. \quad (8a)$$

The theoretical electromotive force of a cell constituted by two half-cells, acid ($c_{\text{H}_2\text{SO}_4} = 5$ M) and alkaline ($c_{\text{NaOH}} = 10$ M), is given by

$$E = E_{\text{p, PbO}_2/\text{PbSO}_4} - E_{\text{p, ZnO}_2^{2-}/\text{Zn}}$$
$$= 1.75 - (-1.42) = 3.17\ \text{V}. \quad (9)$$

According to the calculation presented, the theoretical electromotive force of the compound cell exceeds 3.0 V, which is comparable with the electromotive force of some lithium chemical power cells and exceeds that of a chemical power cell using a compositionally homogeneous acid, alkaline, or salt aqueous electrolyte. In discharge of a compound cell into an active load, the following reactions occur:

$$\text{Zn} + 4\text{OH}^- = \text{ZnO}_2^{2-} + 2\text{H}_2\text{O} + 2\text{e}, \quad (10)$$

at the zinc electrode (anode), and

$$\text{PbO}_2 + 2\text{H}_2\text{SO}_4 + 2\text{e} = \text{PbSO}_4 + 2\text{H}_2\text{O} + \text{SO}_4^{2-}, \quad (11)$$

at the lead electrode (cathode), with the overall current-forming reaction:

$$\text{Zn} + 4\text{NaOH} + \text{PbO}_2 + 2\text{H}_2\text{SO}_4 \overset{2\text{e}}{=} \text{Na}_2\text{ZnO}_2$$
$$+ \text{Na}_2\text{SO}_4 + 4\text{H}_2\text{O} + \text{PbSO}_4. \quad (12)$$

In both half-cells, the electrolyte is involved in the electrochemical reaction and is simultaneously consumed. Reactions (10), (11) can be performed from right to left, i.e., the compound cell can act as a secondary power cell (membrane battery [13]). Charging from the neutral Na_2SO_4 solution by membrane electrolysis yields H_2SO_4 and NaOH solutions. Simultaneously, reactions (10), (11) occur at the electrodes in the reverse directions and yield the active paste of a battery. The maximum theoretical specific energy of the membrane battery, W_{th} (W h kg^{-1}), calculated by Eq. (12) for a cell voltage of 3.17 V [see Eq. (9)] constant in the course of discharge is given by

$$W_{th} = \frac{U_{th} nF}{\sum_{i=1}^{n} \nu_i M_i}, \quad (13)$$

where U_{th} is the electromotive force of the cell or the open-circuit (OC) voltage (V); n, number of electrons involved in the overall electrochemical reaction, $n = 2$; F, Faraday number; and $\sum_{i=1}^{n} \nu_i M_i$, sum of products of the molar mass of substances involved in the overall electrochemical reaction by their stoichiometric coefficients.

$$W_{th} = \frac{3.17 \times 2 \times 96500}{65.4 \times 1 + 4 \times 40 + 239.2 \times 1 + 2 \times 98} = 257.2 \text{ W h kg}^{-1}. \quad (14)$$

The resulting value $W_{th} = 257.2$ W h kg^{-1} exceeds the known value of W_{th} for the lead battery (175 W h kg^{-1}), calculated using $U_{th} = 2.1$ V and $c_{H_2SO_4} = 100\%$ [12].

For practical purposes, with 10 M NaOH solution and 5 M H_2SO_4 solution used, it is necessary to primarily take into account the mass of water serving as a solvent:

$$W_{th,1} = \frac{3.17 \times 2 \times 96500}{6.54 \times 1 + 4 \times 40 + 371.7 + 239.2 \times 1 + 2 \times 98 + 318.5} = 125.8 \text{ W h kg}^{-1}. \quad (15)$$

The value (15) is the theoretical limit and, similarly to the value (14), disregards the design features of a battery and conditions of its discharge into an active load. The electromotive force of a chemical power cell and, accordingly, W_{th} and $W_{th,1}$ can be raised by using more concentrated electrolyte solutions [Eqs. (6), (8)].

If a cation- or anion-exchange membrane is used, a process in which the acid can be neutralized by the alkali without passing an electric current is possible and this should be taken into account in designing and operating a membrane battery. A rational variant of its use is a standby battery. Upon a complete neutralization of the acid by the alkali to pH 7, the active pastes of the electrodes remain unchanged, but the electromotive force of the chemical power cell decreases dramatically. The electrode potential of the negative zinc electrode is

$$E_{p,\,Zn^{2+}/Zn} = E^0_{p,\,Zn^{2+}/Zn} + \frac{RT}{nF} \ln \frac{a_{Zn^{2+}}}{a_{Zn}} = E^0_{p,\,Zn^{2+}/Zn} + \frac{2.3RT}{2F} \log \frac{SP_{Zn(OH)_2}}{a^2_{OH^-}} = -0.764 + 0.05905(14 - 7) + 0.029521 \log (1.2 \times 10^{-17}) = -0.85 \text{ V}. \quad (16)$$

The potential of the dioxide-lead half-cell, calculated using Eq. (6) and data from reference book [10], is given by

$$E_{p,\,PbO_2/PbSO_4} = E^0_{PbO_2/PbSO_4} + \frac{RT}{nF} \ln \frac{a_{PbO_2} a^4_{H^+} a_{SO_4^{2-}}}{a_{PbSO_2} a^2_{H_2O}} = 1.68 + \frac{8.314 \times 298}{2 \times 96500} \ln \frac{1(10^{-7})^4 (0.14 \times 2.63)}{1 \times 0.88^2} = 0.842 \text{ V}, \quad (17)$$

at pH 7 and $c_{Na_2SO_4} = 2.63$ M. Then the electromotive force of the cell

$$E = E_{p,\,PbO_2/PbSO_4} - E_{p,\,Zn^{2+}/Zn} = 0.842 - (-0.85) = 1.69 \text{ V}. \quad (17a)$$

The value obtained exceeds the electromotive force of iron–nickel, cadmium–nickel, and cadmium–silver batteries with an alkaline electrolyte and is comparable with, or somewhat exceeds that of primary chemical power cells with an alkaline electrolyte. Upon mutual neutralization of two electrolytes and reduction of PbO_2 from the positive electrode to $PbSO_4$, the chemical power cell allows further discharge, with the following reaction possible at the lead electrode:

$$PbSO_4 + 2e = Pb\downarrow + SO_4^{2-}, \quad (18)$$

whose electrode potential at pH 7 and $c_{Na_2SO_4} = 2.63$ M

$$E_{p,\,Pb^{2+}/Pb} = E^0_{p,\,Pb^{2+}/Pb} + \frac{RT}{nF} \ln \frac{a_{Pb^{2+}}}{a_{Pb}} = E^0_{p,\,Pb^{2+}/Pb} + \frac{2.3RT}{2F} \log \frac{SP_{PbSO_4}}{a_{SO_4^{2-}}} = -0.126 + \frac{2.3 \times 8.314 \times 298}{2 \times 96500} \log \frac{1.6 \times 10^{-8}}{0.14 \times 2.63} = -0.343\text{V}, \quad (19)$$

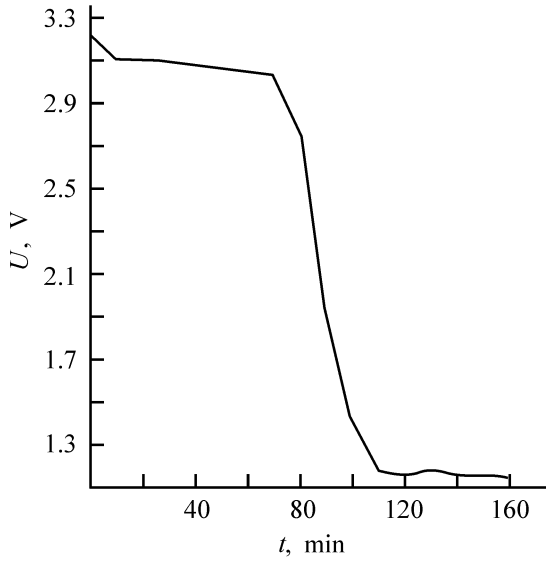


Fig. 1. Voltage U across the terminals of a chemical power cell vs. time t in discharge into an active load of 50 Ω at U_{OCin} = 3.25 V.

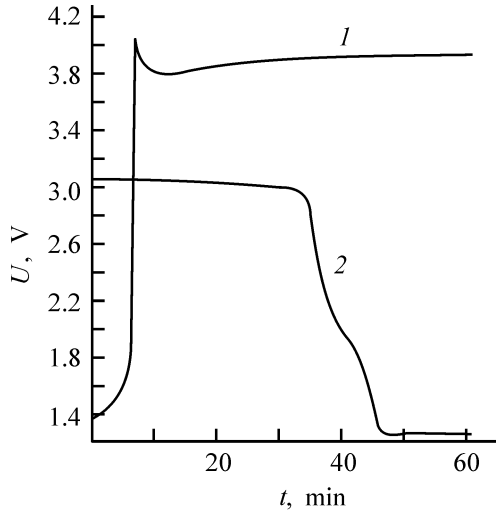


Fig. 2. Voltage U across the terminals of a chemical power cell vs. time t in (*1*) charging with a current of 0.25 A at U_{OCin} = 1.03 V and (*2*) discharge into an active load of 50 Ω at U_{OCin} = 3.13 V.

and then the electromotive force of the cell, found using Eqs. (19) and (16), is given by

$$E = E_{p,\,Pb^{2+}/Pb} - E_{p,\,Zn^{2+}/Zn} = -0.343 - (-0.85) = -0.507\ \text{V}. \quad (20)$$

Reaction (18) restores the working capacity of the dioxide-lead electrode, in contrast to the positive electrode in a lead battery, whose failure is due to disintegration of the Pb current lead of the positive electrode to $PbSO_4$.

The theoretical concepts were experimentally verified on a model chemical power cell, a two-chamber cell with a perfluorinated cation-exchange membrane of area 16 cm^2. A 25-ml portion of a 10 N NaOH solution was taken as a solution for the negative zinc electrode with S_{work} = 27 cm^2, and a 40-ml portion of a 10 N H_2SO_4 solution, for the positive electrode constituted by a PbO_2 layer on a smooth lead electrode with S_{work} = 35 cm^2. The potential difference across the electrodes was measured with an M830B digital multimeter. A PI-50-1.1 potentiostat served as a current source.

The results obtained in studying the time dependence of the voltage across the terminals of a chemical power cell are shown in Figs. 1, 2: discharge into an active load (Fig. 1), charging after 16 h in the idle state (with subsequent additional short-time discharge by short-circuiting) (Fig. 2, curve *1*), and subsequent discharge after 1.5 h (Fig. 2, curve *2*). The curve in Fig. 1 shows that the chemical power cell can be, in principle, used as a standby power source. The fact that a cell voltage exceeding 3.0 V is obtained confirms the theoretical calculations of the electromotive force, presented above. The decrease in the voltage is due to the complete reduction of the active paste of the positive electrode from PbO_2 to $PbSO_4$. In further discharge of the chemical power cell, the cell voltage is approximately 1.16 V and remains virtually unchanged, which can be attributed to occurrence of reduction reactions of lead sulfate to lead and of hydrogen ions to hydrogen gas. The possibility of using the chemical power cell as a battery is confirmed by its further charging (Fig. 2, curve *1*) and subsequent discharge (curve *2*). The rise in the voltage across the terminals of the cell to more than 4.0 V in its charging (Fig. 2, curve *1*) is due both to the formation of the active paste in the positive electrode (lead dioxide), with the corresponding shift of the electrode potential in the positive direction and its increasing contribution to the total electromotive force of the cell, and to a decrease in the voltage drop within the cell. The decrease in the voltage to 3.80 V is due both to an increase in the electrical conductivity of the solutions (via formation of additional amounts of the alkali and acid from Na_2SO_4) and to the formation of an electron-conducting PbO_2 film.

Further continuous rise in the cell voltage, which then tends to a constant value, is due to an increase in the concentrations of the alkali and acid and in the absolute value of the electrode potential of each of the electrodes. In the course of charging, sodium ions are species that carry the electric charge within the cell and do not change the intrinsic sign of the ion

charge on passing from the acid into the alkaline medium across the cation-exchange membrane. The subsequent discharge (Fig. 2, curve *2*) confirms the possibility of using the acid-alkaline-salt membrane battery as a secondary chemical power cell.

CONCLUSIONS

(1) Ion-exchange membranes can be used in various types of chemical power cells.

(2) The membrane chemical power cell has an electromotive force of more than 3.0 V, which exceeds that of cells using only a single aqueous electrolyte solution.

(3) The experimentally obtained charging-discharge curves demonstrate the possibility of using the membrane chemical power cell as an electric battery.

(4) Use of an ion-exchange membrane separating the electrolytes provides their regeneration in the course of electrolysis (cell charging).

REFERENCES

1. *Khimicheskie istochniki toka. Spravoschnik* (Chemical Power Cells: Reference Book), Korovin, V. and Skundin, A.M., Eds., Moscow: Mos. Energet. Inst., 2003.
2. Deutsches Patentamt DE 3324212.
3. Pivovarov, N.Ya., Greben', V.P., and Kovarskii, N.Ya., *Elektrokhimiya*, 1994, vol. 30, no. 6, pp. 785–789.
4. US Patent 4714663.
5. Mazanko, A.F., Kamar'yan, G.M., and Romashin, O.P., *Promyshlennyi membrannyi elektroliz* (Industrial Membrane Electrolysis), Moscow: Khimiya, 1989.
6. Ohya, H., Emori, K., Ohto, N., and Negishi, Y., *Membranes and Membrane processes: Proc. of the Europe-Japan Congress on Membrane Processes, June 18–22, 1984, Stresa, Italy*, New York, 1986.
7. *Spravochnik khimika* (Chemist's Handbook), Nikol'skii, B.P., Ed., Moscow: Khimiya, 1956, vol. 2, 2nd ed. supplemented and revised.
8. *Kratkii spravochnik po khimii* (Concise Handbook of Chemistry), Kurilenko, O.D., Ed., Kiev, Naukova dumka. 1974.
9. Stender, V.V., *Prikladnaya elektrokhimiya* (Applied Electrochemistry), Kharkov, 1961.
10. *Spravochnik po elektrokhimii* (Handbook of Electrochemistry), Sukhotin, A.M., Ed., Leningrad: Khimiya, 1981.
11. *Kratkii spravochnik po khimii* (Concise Handbook of Chemistry), Pilipenko, A.T., Ed., Kiev: Naukova Dumka, 1987.
12. *Prikladnaya elektrokhimiya* (Applied Electrochemistry), Tomilov, A.P., Ed., Moscow, 1984.
13. RF Patent 2131633.

Russian Journal of Applied Chemistry, Vol. 78, No. 10, 2005, pp. 1620–1624. Translated from Zhurnal Prikladnoi Khimii, Vol. 78, No. 10, 2005, pp. 1648–1652.
Original Russian Text Copyright © 2005 by Varentsov, Gnezdilova, Varentsova.

APPLIED ELECTROCHEMISTRY AND CORROSION PROTECTION OF METALS

Effect of Cathodic and Anodic Polarization in a Lithium Sulfate Solution on the Electrical Conductivity of Carbonized Fibrous Carbon Materials

V. K. Varentsov, L. A. Gnezdilova, and V. I. Varentsova

Institute of Solid-State Chemistry and Mechanochemistry, Siberian Division, Russian Academy of Sciences, Novosibirsk, Russia

Received July 20, 2005

Abstract—The effect of cathodic and anodic polarization of carbonized fibrous carbon materials of the KNM and NT-1 types in a Li_2SO_4 solution on their properties: electrical conductivity, steady-state electrode potential, electrical conductivity profile across the electrode thickness in relation to the electrolysis time, current density, Li_2SO_4 concentration, electrode thickness, and current reversal, was studied. The stability of the resulting electrical conductivity profile across the electrode thickness with time and in the course of the subsequent electrolysis was assessed. The reduction of Fe^{3+} in the ferri–ferrocyanide system on electrically iso- and nonisoconducting fibrous carbon electrode was considered.

The electrical conductivity of fibrous carbon materials (FCM) used in carrying out various redox processes in technical electrochemistry is an important parameter determining the efficiency of their use. The industrially manufactured FCM are electrically isoconducting across their thickness. At the same time, the efficiency of their use as flow-through 3*D* electrodes can be improved by creating a certain electrical conductivity profile across the electrode thickness. The possibility of fabrication of electrodes of this kind by cathodic and anodic polarization in solutions of acids and alkalis was first demonstrated in [1–3]. Of interest is to examine the possibility of obtaining electrodes with an electrical conductivity varying across their thickness in solutions of alkali metal salts whose dissolution does not change the solution pH.

The aim of this study was (i) to examine the influence exerted by conditions of electrode polarization of FCM in a Li_2SO_4 solution, Li_2SO_4 concentration, and electrode thickness on the electrical conductivity of FCM of the NT-1 and KNM types; (ii) to analyze the possibility of creating an electrical conductivity profile across the electrode thickness and its stability in storage of FCM and their use as electrodes; and (iii) to carry out comparative experiments in order to evaluate the efficiency of electroreduction processes for the example of Fe^{3+} reduction in the system $[Fe(CN)_6]^{3-}/[Fe(CN)_6]^{4-}$ on electrically iso- and nonisoconducting electrodes.

EXPERIMENTAL

The variation of the FCM properties was monitored by changes in the mass of samples, electrical conductivity, and steady-state electrode potential, determined by the procedures described in [1–3]. The study was carried out on carbonized low-electrical-conductivity materials of the NT-1 and KNM types, with electrical conductivities of 0.02–0.03 and 0.009 S cm^{-1}, respectively [4]. The choice of the materials was governed by the fact that the most pronounced changes upon polarization are observed for carbonized materials [1, 2], to which belong NT-1 and KNM. NT-1 is a combination of woven and nonwoven materials, which provides its mechanical strength and large reaction surface area. The experiments were performed with 2-cm^2 samples. The electrolysis was conducted with a B5-49 dc power source, with the solution circulated through the electrode volume at a rate of 0.2 ml s^{-1} cm^{-2} by a peristaltic pump in the installation described in [1]. After the electrode treatment, FCM samples were washed with distilled water and dried in air to constant mass. The electrical resistance of the samples was measured with a VM-509 ac bridge.

1070-4272/05/7810-1620 © 2005 Pleiades Publishing, Inc.

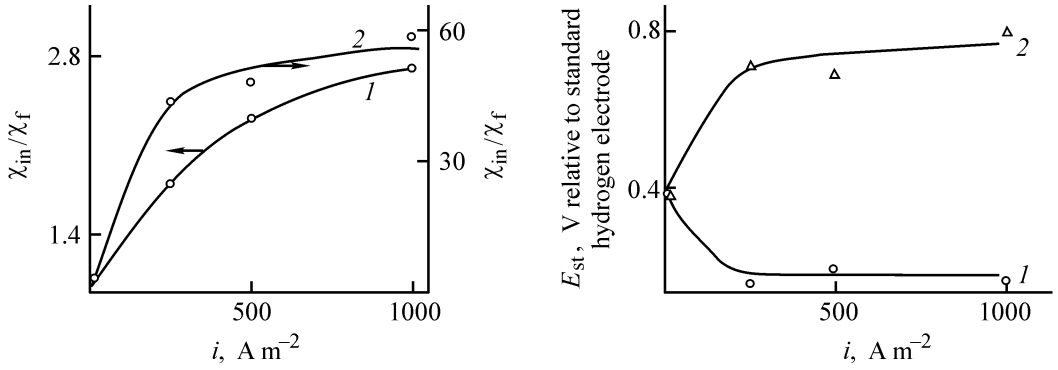


Fig. 1. (a) χ_{in}/χ_f and (b) steady-state electrode potential E_{st} of the NT-1 material vs. the polarization current density i. Polarization: (*1*) cathodic and (*2*) anodic. 0.1 M Li_2SO_4 solution, polarization time 1 h.

The electrical conductivity of FCM was calculated by the formula

$$\chi = l/RS, \quad (1)$$

where l is the sample thickness (cm); R, resistance (Ohm); and S geometric area of a sample (cm^2).

The steady-state electrode potential of FCM was measured relative to a silver chloride electrode and recalculated to the hydrogen scale. Dependences of the steady-state electrode potential of FCM ($E_{st.\ FCM}$) on the current density were plotted using potentials measured after keeping the FCM in solution for 1 h.

The working efficiencies of electrically iso- and nonisoconducting electrodes were compared for the example of electroreduction of iron(III) in the potassium ferri-ferrocyanide, with a 0.5 M KCl solution as a supporting electrolyte. The experiment was performed on the already mentioned installation in an electrochemical cell with electrode spaces separated by an MK-40 ion-exchange membrane. The cathodes were composed of several layers of the initial FCM and that subjected to an electrochemical pretreatment in such a way that a certain electrical conductivity profile was obtained. A solution of composition (M): $K_3[Fe(CN)_6]$ 0.02, $K_4[Fe(CN)_6]$ 0.02, KCl 0.5, was circulated in the cathode chamber; a 0.5 M K_2SO_4 solution served as anolyte. At regular intervals of time, 5-cm^3 samples were taken from the vessel with catholyte and analyzed for the content of Fe^{3+} by forward voltammetry with an electrode with surface renewed in solution [5].

Let us consider the influence exerted by some of the factored listed above (current density, anodic and cathodic polarization) on the electrical conductivity of a carbon material of the NT-1 type, because the effect of these factors has been studied in most detail just for this material. For convenience of comparison of the results obtained, the ratio of the electrical conductivities of NT-1 before (χ_{in}) and after (χ_f) its electrode polarization was plotted along the ordinate axis. Figure 1a shows how χ_{in}/χ_f depends on the current density. It can be seen that, first, the electrical conductivity of the material decreases as the current density grows, and, second, the anodic polarization leads to a more pronounced decrease in its value. For example, the electrical conductivity of FCM decreases at a current density of 1000 A m^{-2} by a factor of 55 in the case of anodic polarization (Fig. 1a, curve *2*) and only by a factor of 2.5 upon cathodic polarization (Fig. 1a, curve *1*).

The changes in the electrical conductivity in cathodic and anodic polarization are primarily due to modification of the surface chemical composition of fibers constituting an FCM and, in particular, to reduction (cathodic polarization) or formation of surface oxides (anodic polarization) [7]. This conclusion is also confirmed by the changes in the steady-state electrode potential of FCM ($E_{st.\ FCM}$). This potential shifts in the negative and positive directions upon cathodic and anodic polarization, respectively (Fig. 1b).

The results obtained in measuring the mass of FCM upon electrode polarization in a 0.1 M Li_2SO_4 solution are listed in the table.

It follows from the table that the mass of FCM changes only slightly upon cathodic polarization,

Change in the mass of NT-1, Δm, in relation to the current density i of electrode polarization (polarization time 1 h)

i, A m^{-2}	Δm, %	
	cathodic polarization	anodic polarization
250	+0.25	+11.5
500	–0.20	+15.4
1000	–0.70	+16.8

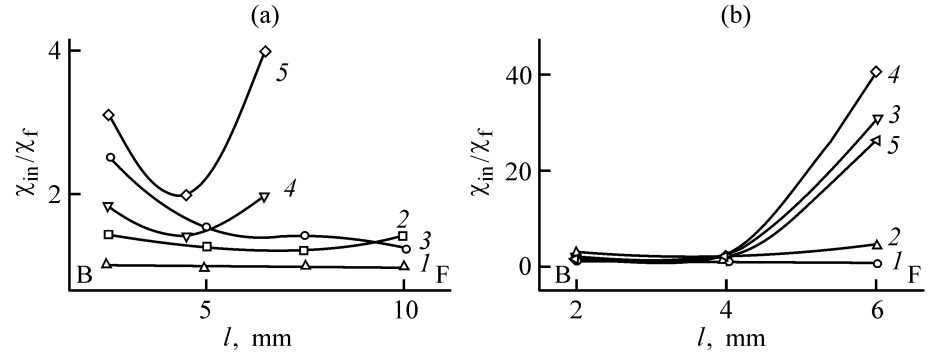


Fig. 2. χ_{in}/χ_f vs. the electrode thickness *l* after electrode polarization of NT-1 in a 0.1 M Li_2SO_4 solution. (a) cathodic polarization at current density (A m^{-2}): (*1*) 0.1, (*2*, *4*) 1000, and (*3*, *5*) 2500; polarization time (min): (*2*, *4*) 15 and (*3*, *5*) 5; (b) anodic polarization at current density (A m^{-2}): (*1*) 0, (*2*) 500, (*3*) 1000, (*4*) 1750, and (*5*) 2500; polarization time (min): (*5*) 5, (*4*) 10, and (*2*, *3*) 15.

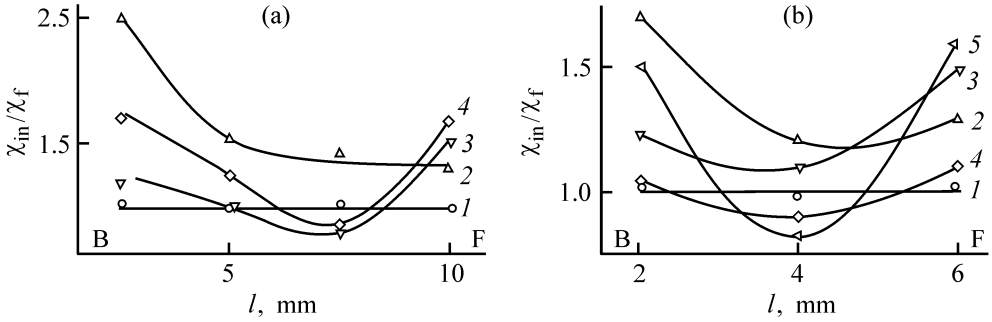


Fig. 3. χ_{in}/χ_f vs. the electrode thickness *l* after cathodic polarization of NT-1 at a current density of 2500 A m^{-2} at different (a) Li_2SO_4 solution concentrations and (b) polarization times. (a) Li_2SO_4 solution concentration (M): (*2*) 0.1, (*3*) 0.25, and (*4*) 5; polarization time (min): (*1*) 0 and (*2–5*) 5; (b) polarization time (min): (*1*) 0, (*2*) 2.5, (*3*) 5, (*4*) 10, and (*5*) 20; Li_2SO_4 solution concentration 0.1 M.

whereas that upon anodic polarization increases with the current density to reach a value of 17% at a current density of 1000 A m^{-2}. Such a significant increase in the FCM mass may be due to formation of oxide compounds and intercalation compounds of graphite [6, 7].

The results obtained served as a basis for a study of how electrolysis conditions affect the electrical conductivity profile across the electrode thickness. The possibility of formation of such a profile follows from the fact that the electrochemical process has a distributed nature and, consequently, the current density varies across the thickness of a 3*D* flow-through electrode, and from the data previously obtained for H_2SO_4 and NaOH (KOH) solutions [2].

The study revealed that an electrical conductivity profile across the electrode thickness is formed. The profile is dependent on the type of polarization, current mode, Li_2SO_4 concentration, and electrode thickness.

The results obtained are presented in the form of plots of the electrical conductivity distribution across the thickness of an FCM for different conditions of its polarization in a Li_2SO_4 solution; letters B and F designate the back (nearest to the current lead) and front (nearest to the anode) sides of the electrode, respectively (Figs. 2, 3).

The main factor that enables control over electrochemical processes is the current passed through the electrode. Therefore, the electrical conductivity profile across the electrode thickness can be strongly modified by changing the current (Figs. 2a, 2b). The experiments performed demonstrated that the type of polarization (cathodic or anodic) affects not only the quantitative characteristics of the electrical conductivity across the electrode thickness, but also the localization of regions with the minimum and maximum conductivity. In the case of a cathodic polarization in a 0.1 M Li_2SO_4 solution, the electrical conductivity decreases to the greatest extent at the backside of the electrode (Fig. 2a), and in the case of anodic polarization, at the front side (Fig. 2b). As the current density increases, the decrease in the electrical conductivity in the back and front surface layers of the electrode becomes more pronounced.

The electrical conductivity profile is noticeably affected by the electrode thickness. For a thinner electrode, a clearly defined profile with a minimum in the middle part of the electrode is observed. This leads to a more pronounced decrease in the electrical conductivity of FCM (Fig. 2a, curves *4*, *5*).

It was found that the Li_2SO_4 concentration affects the electrical conductivity profile across the electrode thickness (Fig. 3a). The electrical conductivity of the back and front sides of the electrode decreases. For solutions with a Li_2SO_4 concentration of ≥0.25 M, the electrical conductivity of the material increases upon cathodic polarization.

An increase in the electrical conductivity of FCM in the middle part of the electrode was also observed in the case of a cathodic polarization at a high current density (2500 A m^{-2}), depending on the electrolysis duration. At electrolysis times longer than 10 min, the electrical conductivity of FCM increases in the middle part of the electrode (Fig. 3b). A possible reason for this increase in the electrical conductivity of FCM is that intercalation compounds of graphite may be formed. Elucidation of why the electrical conductivity of FCM varies across the electrode thickness in this way requires an additional study, which is beyond the scope of this communication.

Interesting results were obtained in a study of the influence exerted by successive anodic and cathodic polarizations of FCM in a Li_2SO_4 solution on χ_{in}/χ_f (Figs. 4a, 4b). It can be seen from Fig. 4 that cathodic polarization of carbon materials (KNM and NT-1) preliminarily subjected to anodic polarization (curve *2*) restores the electrical conductivity of nearly all layers of the FCM electrode, with only the electrical conductivity of the front layer restored incompletely. The above results are in a good agreement with the data obtained in similar studies in H_2SO_4 and KOH solutions [3]. It may be assumed that oxide compounds formed on the surface of FCM fibers during anodic polarization are reduced in the subsequent cathodic polarization [7].

Further studies made it possible to compare the efficiencies of electrically nonisoconducting electrodes in reduction of Fe^{3+} to Fe^{2+} in the system $[Fe(CN)_6]^{3-}/[Fe(CN)_6]^{4-}$. The electrical conductivity of a potassium ferri-ferrocyanide solution (0.055 S cm^{-1}) exceeds $\chi_{NT\text{-}1}$ (0.02–0.03 S cm^{-1}). The distribution of the electrical conductivity across the electrode thickness will be the most favorable for the process of Fe^{3+} reduction in the case when the FCM conductivity is the highest at the backside, and the lowest at the front

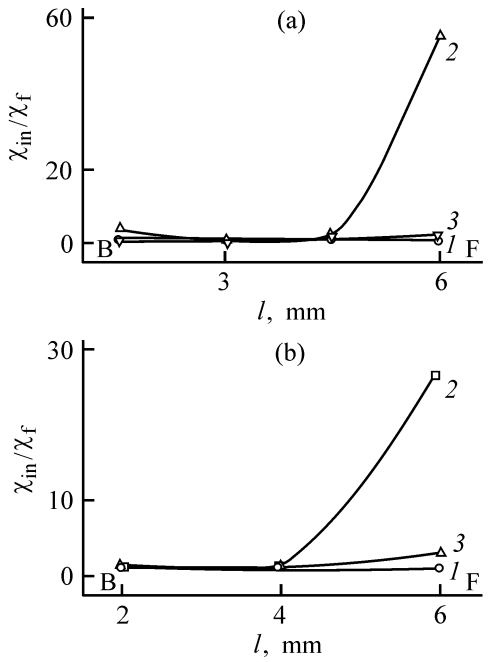


Fig. 4. χ_{in}/χ_f vs. the electrode thickness l after electrode treatment of (a) KNM and (b) NT-1 in a 0.1 M Li_2SO_4 solution. Current density 2500 A m^{-2}, polarization time 5 min. (*1*) Starting material, (*2*) anodic polarization, (*3*) anodic polarization followed by cathodic polarization.

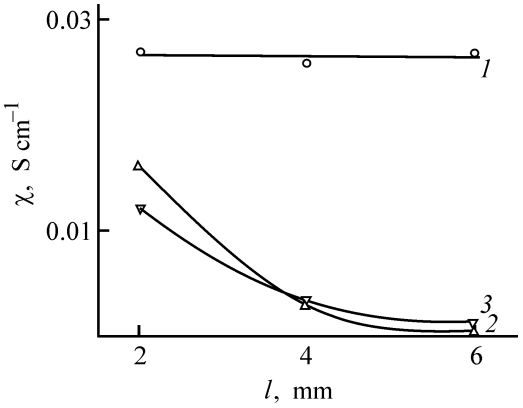


Fig. 5. Electrical conductivity χ vs. the electrode thickness l for NT-1. (*1*) Electrically isoconducting electrode made of the initial NT-1, (*2*) electrically nonisoconducting electrode composed of NT-1 subjected to electrode treatment in a 0.1 M Li_2SO_4 solution, and (*3*) electrode *2* upon reduction of Fe^{3+} to Fe^{2+}.

of the electrode. Therefore, two electrodes were chosen. The first was constituted by three layers of the starting material not subjected to any electrochemical pretreatment. The electrical conductivity profile of such an electrode is shown in Fig. 5 (curve *1*). The second was fabricated, to obtain the most favorable electrical conductivity profile (Fig. 5, curve *2*),

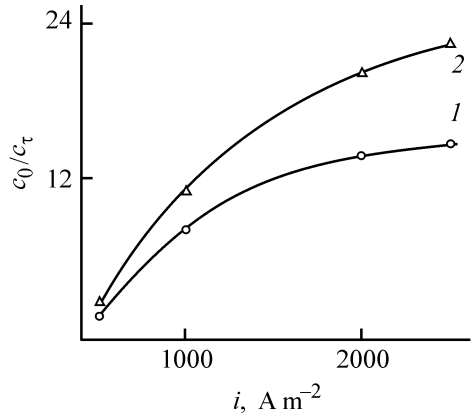


Fig. 6. Fe^{3+} to Fe^{2+} reduction ratio c_0/c_τ vs. the current density i. (*1*) Electrically isoconducting electrode and (*2*) electrically nonisoconducting electrode made of the NT-1 material.

from an FCM subjected to electrode pretreatment. The electrolysis was conducted, using the procedure described above, at different current densities for 30 min. After the electrolysis was complete, the solution was sampled and the concentration of Fe^{3+} was determined.

The data in Fig. 6 indicate that the Fe^{3+} reduction ratio c_0/c_τ increases with the current density for both the electrodes. At a current density of 500 A m^{-2} no significant difference in operation between the iso- and nonisoconducting electrodes is observed. At the same time, raising the current density to more than 500 A m^{-2} leads to a more efficient reduction of Fe^{3+} ions at the electrically nonisoconducting electrode. For example, at i = 2000 A m^{-2}, c_0/c_τ for the nonisoconducting electrode exceeds that for the isoconducting electrode by approximately a factor of 1.5.

A rather interesting and important result was that, if a target reaction not involving electrolysis of water occurs at the electrode, the electrical conductivity profile of a fibrous carbon electrode, produced by electrode treatment of FCM in a Li_2SO_4 solution, changes in the course of electrolysis only slightly (Fig. 5, curve *3*).

It should also be noted that the electrical conductivity of FCM, obtained by means of cathodic and anodic polarization, remains unchanged in storage for five to six months (measurements for longer periods of time were not performed).

CONCLUSIONS

(1) It was shown that cathodic or anodic polarization of carbonized FCM of the NT-1 and KNM types in a Li_2SO_4 solution can change their electrical conductivity, which depends on the current passed through the electrode.

(2) The most pronounced changes in the electrical conductivity of FCM were revealed upon anodic polarization. Successive anodic and cathodic polarizations can restore the electrical conductivity of FCM to nearly the initial value.

(3) The possibility of obtaining an FCM electrically nonisoconducting across its thickness by electrode polarization in a lithium sulfate solution was demonstrated. It was established that various electrical conductivity profiles across the electrode thickness can be obtained by varying such parameters as current density, electrode thickness, concentration of the Li_2SO_4 solution, and electrolysis time.

(4) It was demonstrated for the example of Fe^{3+} reduction in the $[Fe(CN)_6]^{3-}/[Fe(CN)_6]^{4-}$ system that electrically nonisoconducting electrodes produced by electrode treatment in a Li_2SO_4 solution enable a more efficient electroreduction, compared with the initial isoconducting FCM. The electrical conductivity profile of a fibrous carbon electrode remains unchanged in storage and upon its use in reduction of Fe^{3+} to Fe^{2+}.

REFERENCES

1. Varentsov, V.K. and Varentsova, V.I., *Zh. Prikl. Khim.*, 1999, vol. 72, no. 4, pp. 605–609.
2. Varentsov, V.K. and Varentsova, V.I., *Zh. Prikl. Khim.*, 1999, vol. 72, no. 4, pp. 609–613.
3. Varentsov, V.K. and Varentsova, V.I., *Elektrokhimiya*, 2001, vol. 37, no. 7, pp. 811–820.
4. Varentsov, V.K., *Intensifikatsiya elektrokhimicheskikh protsessov* (Intensification of Electrode Processes), Tomilov, A.P., Ed., Moscow: Nauka, 1988, pp. 94–118.
5. Kiryushov, V.N. and Kletenik, Yu.B., *Zavod. Lab.*, 1997, no. 12, pp. 13–16.
6. Fialkov, A.S., *Uglerod, mezhsloevye soedineniya i kompozity na ego osnove* (Carbon and Intercalation Compounds and Composites on Its Base), Moscow: Aspekt-press, 1997.
7. Varentsova, V.I. and Varentsov, V.K., *Zh. Prikl. Khim.*, 2005, vol. 78, no. 3, pp. 433–437.

Russian Journal of Applied Chemistry, Vol. 78, No. 10, 2005, pp. 1625–1630. Translated from Zhurnal Prikladnoi Khimii, Vol. 78, No. 10, 2005, pp. 1653–1658.
Original Russian Text Copyright © 2005 by Kolyagin, Kornienko, Kuznetsov, Chesnokov.

APPLIED ELECTROCHEMISTRY AND CORROSION PROTECTION OF METALS

Electrical Conductivity of Hydrophobized Electrodes Fabricated from Thermally Expanded Graphite and Their Activity in Electroreduction of Oxygen

G. A. Kolyagin, V. L. Kornienko, B. N. Kuznetsov, and N. V. Chesnokov

Institute of Chemistry and Chemical Technology, Siberian Division, Russian Academy of Sciences, Krasnoyarsk, Russia

Received July 15, 2005

Abstract—Intercalation compounds of GT-1 and GAK-3 graphites were electrically synthesized in concentrated sulfuric and nitric acids. Porous composite samples based on thermally expanded graphite produced from electrochemically synthesized GT-1 graphite hydrosulfate, chemically synthesized GSM-1 graphite nitrate, and fluoroplastic-4D (1–15 wt %), with a volume density of 650–1090 g l^{-2}, were fabricated and studied.

Studies concerned with power cells pay a considerable attention to development and testing of new materials for electrodes to be used, in particular, in fuel cells. It is known that thermally expanded graphite (TEG) and articles made of this material possess a number of unique properties: high porosity, electrical conductivity, corrosion resistance, and thermal stability; manufacturability and ductility; and possibility of fabrication of complex-shaped articles from this material [1–3]. This circumstance, combined with the comparatively low cost of TEG, makes it a promising material for electrochemical systems. For example, it has been suggested to use TEG for improving the distribution of gas reagents in electrodes of fuel cells [4]. It has been shown that making the current collector of TEG improves parameters of fuel cells [5]. Use of modified TEG in the electrodes of electrochemical sensors for methanol has been studied [6]. Oxidation of peroxide and glucose has been examined on an electrode made of TEG modified with cobalt phthalocyanine [7]. It has been demonstrated that the electrochemical parameters of TEG depend on whether or not oxygen functional groups are present on its surface [8]. The possibility of phenol electrooxidation on TEG has been analyzed [9].

Of interest in this context is to study a composite based on TEG and fluoroplastic, which shows a considerable hydrophobicity and chemical inertness at temperatures of up to 400°C. This composite can also be used to fabricate hydrophobized electrodes, which makes it possible to markedly raise the rate of electrochemical processes [10, 11].

The aim of the present study was to examine the influence exerted by the composition of a porous composite TEG–fluoroplastic on its electrical conductivity and electrochemical activity in oxygen reduction in aqueous electrolytes.

EXPERIMENTAL

Graphite intercalation compounds yielding TEG upon a thermal shock were obtained using electrochemical intercalation of acids. This method enables easy control over the degree of intercalation of acids into graphite and makes it possible to obtain intercalation compounds at lower acid concentrations without admixture of oxidizing agents [12]. For example, electrolysis in sulfuric [13–15], nitric [16], and formic [17] acids has been described.

The electrosynthesis was performed in a cylindrical glass electrolyzer with a thermostated jacket *1* and a horizontal position of the electrodes (Fig. 1). Onto the bottom electrode (anode) *2*, having the form of a fine-mesh platinum grid on a porous glass partition *3*, was placed a weighed portion *4* of graphite. A polypropylene diaphragm *5* made of a nonwoven material and then a fluoroplastic disc *6* with openings were placed on the graphite layer. A fluoroplastic cylinder *7* was put on the disc. A platinum

1070-4272/05/7810-1625 © 2005 Pleiades Publishing, Inc.

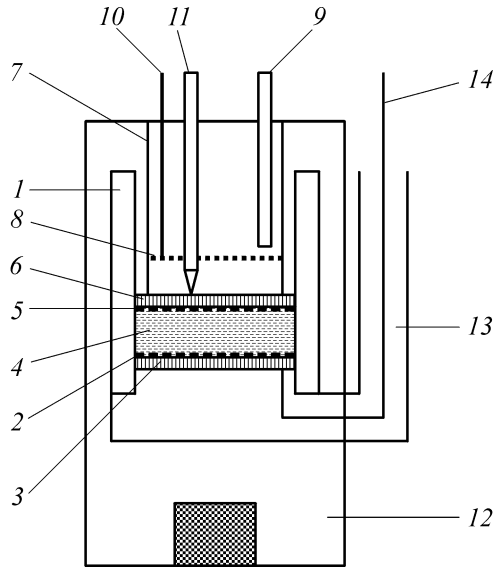


Fig. 1. Electrolyzer for synthesis of graphite intercalation compounds. For designations, see text.

cathode *8* was mounted in the middle of this cylinder, and a thermometer *9*, platinum current lead to the cathode *10*, and a capillary of the electrolytic switch *11* were fixed in its upper part. To improve the electric contact between graphite particles a load (20–30 g cm^{-2}) was applied to the cylinder by means of a rod *12*. An auxiliary vertical outlet *13*, through which the platinum current lead *14* to the anode passes and the electrolyte is poured-in (30 ml), was sealed-in in the lower part of the electrolyzer. The electrolysis was performed in the galvanostatic mode. The electrode potential was commonly varied within the range 1–3 V relative to a silver chloride reference electrode (EVL-1M1). The electrolysis conditions were as follows: weighed portion of graphite 4.5 g, area of the bulk electrode 7 cm^2 and its height 1.2 cm, electrolysis current 0.1 A per 1 g of graphite, temperature 20°C, electrolysis time 1.5–2.5 h, electrolytes 92% H_2SO_4 and 70% HNO_3. After electrolysis, graphite was washed to washing water pH 5–6 and dried in air at 100–120°C.

The possible influence exerted by the procedure used to prepare graphite intercalation compounds was examined using TEG obtained from graphite nitrate chemically synthesized from GSM-1 graphite and fuming HNO_3 [18]. Pd (2 wt %) was deposited onto this TEG by impregnation with an aqueous-alcoholic solution of H_2PdCl_2, with subsequent drying at 105°C and reduction in a flow of hydrogen at 100–250°C. The structural parameters of the resulting material and the size of Pd clusters on the graphite surface are similar to those for a G-Na TEG sample [19].

GT-1 and GAK-3 graphites manufactured by Uralgrafit Private Company, with bulk densities of 517 and 420 g l^{-1}, respectively, and particle size of 0.18–0.25 mm were used. The crucible graphite GT-1 contains 91.5 wt % graphite and ≤1.6 wt % Fe_2O_3 and has 90% of its particles more than 0.18 mm in size. The battery graphite GAK-3 contains 98 wt % graphite with 96% of its particles less than 0.25 mm in size and ≤0.5% Fe_2O_3. The special low-ash graphite GSM-1 has a bulk mass of 518 g l^{-1}, ash content of 0.08%, and 90% of its particles are 0.4–0.16 mm in size.

To obtain TEG, graphite compounds on a thin metallic tray were placed for several seconds in a furnace heated to 980°C and then transferred into a calibrated cylinder to measure the bulk density. The structural parameters of TEG were determined by measuring the nitrogen adsorption at 77 K [19].

The starting powder was obtained and articles were fabricated from it by the procedures used in [10, 11, 20]. Graphite was mixed with an aqueous suspension of fluoroplastic-4D (F-4D), which contained 2 wt % fluoroplastic, till complete coagulation of fluoroplastic on graphite particles. The resulting mass was transferred to a filter, washed with water and dried, first at 100–120°C and then at 310–320°C for 2.5 h. To make the powder loose, the mass was ground on a propeller-type mill and shaken in a closed space. To reveal the influence exerted by addition of two types of electrocatalysts, carbon blacks (of acetylene type, A437E, and of furnace type, P508E) and TEG with palladium were introduced into the electrode mass.

The samples were fabricated in the form of flat discs with a diameter of 3.5 cm, mass of 0.3–0.4 g, and thickness of 0.4–0.6 mm by compaction in a mold, and heated in air at 360°C for 5 min. When necessary, the samples were additionally compacted to a required thickness.

The electrical conductivity was measured by the four-probe potentiometric method [21]. The slope ratio of the dependence of voltage on current was used to find the resistance of a given sample, and then, using the known thickness and width of the sample, the electrical conductivity was calculated. The total porosity of the electrodes was measured by hydrostatic weighing; the electrolyte porosity was de-

Table 1. Parameters of products formed by electrochemical intercalation of sulfuric and nitric acids for different electrolysis times and graphite brands

Graphite	Acid	Amount of electricity, A h g^{-1}	Gain in graphite mass, %	Bulk density, g l^{-1}		TEG yield, %, in terms of graphite		S, $m^2 g^{-1}$	Pore volume, $cm^3 g^{-1}$	Average pore diameter, nm
				graphite compound	TEG	graphite compound	starting graphite			
GAK-3	HNO_3	0.15	10.8	268	4.2	81.5	90.3	–	–	–
		0.20	13.5	261	3.6	72.5	82.3	–	–	–
		0.25	15.2	272	3.4	74.0	85.2	70.0	0.407	23.1
	H_2SO_4	0.15	26.0	84.9	3.7	73.0	92.6	45.7	0.244	21.3
TG-1	HNO_3	0.15	10.2	331	4.2	84.0	92.5	–	–	–
		0.20	13.3	343	3.4	78.0	88.4	–	–	–
		0.25	15.0	371	1.8	79.0	90.9	68.5	0.554	32.3
	H_2SO_4	0.15	28.6	72.7	4.9	67.3	86.5	–	–	–
		0.2	29.5	59.8	4.4	69.7	90.2	40.6	0.216	21.3
GO-4/4,5–HNO_3 (industrial)	–	–	–	–	–	–	–	41.0	0.140	13.7

termined in a NaOH solution after the experiments were complete [22].

The electrochemical activity of the samples in the reaction of oxygen electroreduction was measured at 20°C in a glass electrolyzer [11]. The current density was calculated per unit visible frontal surface area (5 cm^2). The catholyte volume was 0.023 l. Oxygen was fed into the electrode from its backside under atmospheric pressure. The electrode potential was measured relative to a silver chloride reference electrode. Polarization curves were measured at a potential sweep rate of 4 mV s^{-1}.

Table 1 lists the results obtained in electrosynthesis of graphite intercalation compounds and the bulk densities of TEG powders prepared from them.

It can be seen from Table 1 that the TEG with the lowest bulk density and largest specific surface area and micropore volume were obtained upon graphite intercalation with nitric acid. The greater increase in the mass of graphite upon intercalation with sulfuric acid, compared with nitric acid, can be attributed to the larger molecular weight of the former and a higher residual amount of this acid and water in graphite. As the amount of electricity passed through a sample increases, the mass of graphite grows and the bulk density of expanded graphite decreases because of the stronger expansion of graphite by gaseous substances evolving in thermal treatment. Compounds of graphite with H_2SO_4 partly expand already in the stages of washing with water and drying, and, therefore, they have a lower bulk density than graphite with HNO_3. The compound formed in H_2SO_4 has a blue color disappearing on bringing the compound in contact with water or air, which indicates that a stage-one intercalation compound is formed [15]. A black compound with a bluish tint is formed in HNO_3, i.e., a mixture of stage-one and -two compounds is obtained. It should be noted that TEG samples with parameters exceeding those of commercial graphite can be prepared on passing an appropriate amount of electricity.

Table 2 lists data on the electrical conductivity of composite samples fabricated from TEG powders obtained from GT-1 (H_2SO_4, 0.2 A h g^{-1}) and GSM-1 graphite. Prior to fabricating a hydrophobic mass, the starting TEG was ground in a propeller-type mill, which led to an increase in the bulk density.

It should be noted that articles fabricated from TEG commonly possess a closed porosity [23], and, therefore, the true porosity will be higher. It can be seen from Table 2 that both brands of expanded graphite have the same bulk density. Introduction of 5 wt % fluoroplastic leads to a dramatic increase in the bulk density of TEG. A further increase in the concentration of fluoroplastic leads to a decrease in the bulk density, which is due to a loosening action of fluoroplastic particles. A more pronounced increase in the bulk mass is observed upon introduction of palladium into the TEG structure.

Table 2. Electrical conductivity of composites based on TEG and fluoroplastic-4D

Sample no.	Mass used (TEG + F4D), wt %	Density, g l^{-1}		Porosity of a sample, vol %	Presence of additional components, mg cm^{-2}	Electrical conductivity, S cm^{-1}
		bulk density of the mass	volume density of a sample			
1	100% GT-1	17.9	664	66	0	257
2	GT-1 + 5% F4D	31.1	770	57	0	124
3	GT-1 + 10% F4D	26.1	785	56	0	87
4	GT-1 + 15% F4D	23.3	727	60	0	65
5	100% GSM-1	17.8	1090	43	0	1090
6	GSM-1 + 5% F4D	38.9	977	49	0	436
7	GSM-1 + 10% F4D	32.4	1062	43	0	584
8	(GSM-1 + 2% Pd) + 10% F4D	94.8	843	56	Pd 0.80	8.6
9	1st layer: 60% [(GSM-1 + 2% Pd) + 5% F4D], 2nd layer: 40% (GSM-1 + 10% F4D)	–	753	60	Pd 0.45	62.3
10	1st layer: mixture [22% (GSM-1 + 5% F4D) + 22% (GSM-1 + 2% Pd)] 2nd layer: 56% (GSM-1 + 5% F4D)	–	1035	46	Pd 0.16	37.5
11	1st layer: mixture [40% (GSM-1 + 10% F4D) + 10% carbon black P805E] 2nd layer: [50% (GSM + 10% F4D)	–	845	56	Furnace-type carbon black P805E 4.1	197
12	1st layer: 52% (carbon black A437E + 8% F4D) 2nd layer: 48% (GSM-1 + 10% F4D)	–	654	67	Acetylene-type carbon black A437E 21.2	40.9
13	Carbon black A437E + 8% F4D	114	654	66	0	2.0

As can be seen from Table 2, the electrical conductivity of the materials strongly depends on their composition and porosity. Samples based on GSM-1 graphite have a higher electrical conductivity than those based on GT-1, which indicates that this parameter is affected by the synthesis procedure and nature of the starting graphite. The electrical conductivity of pure TEG samples has the same order of magnitude as that reported in the literature [21]: 150 S cm^{-1} at a density of 140 g l^{-2}. An increase in the concentration of fluoroplastic and in the porosity of the material makes its electrical conductivity lower, which is natural because the amount of the electrically conducting material decreases and the contact resistance between TEG particles increases through formation of nonconducting layers. The decrease in the conductivity of samples with Pd is presumably related to the procedure used to introduce Pd into the surface layer of TEG. Although the electrical conductivity decreases to 9 S cm^{-1}, it substantially exceeds that in materials with a carbon black. For example, the electrical conductivity is 1.28 S cm^{-1} for a material synthesized using a carbon black, with 12 wt % fluoroplastic, porosity of 58 vol %, and bulk density of 830 g l^{-1} [24], and 1.59 S cm^{-1} for a material with 30 wt % fluoroplastic and porosity of 55 vol % [20]. Approximately the same values have been obtained for materials containing a carbon black and high-pressure polyethylene and polyisobutylene [20]. Raising the content of the carbon black and Pd in the samples makes lower their electrical conductivity. Despite the high hydrophobicity of TEG [23], materials based on TEG exhibit a partial wettability with aqueous solutions (1.5–10.5 vol %), necessary for functioning of gas-diffusion electrodes.

Figure 2 shows polarization curves of oxygen electroreduction, obtained on electrodes fabricated from the materials listed in Table 2. In double-layer electrodes, the first layer was in contact with the electrolyte.

Hydrogen evolution occurs similarly to that on a carbon black with a high overvoltage. The evolution onsets at –1.6 V, i.e., the electroreduction of oxygen occurs till evolution of hydrogen. In the case of a vigorous gas evolution, there occurs relaxation of compacted TEG particles, they start to straighten, as if emerge to the surface, and regain their initial shape.

Addition of Pd and a carbon black enhances the activity of the electrodes. It should be noted that an increase in the Pd content by a factor of 2.8 (from 0.16 to 0.45 mg cm^{-2}) doubles the activity (at –0.45 V), whereas a further increase to 0.8 mg cm^{-2} has no effect on this parameter. This indicates that the internal surface of the electrodes is not equally accessible, which is also evidenced by the fact that the activities of electrodes with Pd and carbon black are virtually the same, although the activity of Pd in the reaction of oxygen electroreduction exceeds that of the carbon black. The electrode fabricated from a TEG electrochemically produced from GT-1 graphite has a higher activity than the electrode with TEG produced by the chemical method.

The best combination of an electrical conductivity and electric activity in reduction of oxygen was obtained for sample no. 11 (Table 2) with admixture of P805E carbon black. Electrode no. 12 has a lower activity than that of electrode no. 3, but exceeds the activity of a sample without admixture of carbon black. The increase in the activity of the electrode (Fig. 2, curves *2, 4*) on replacing the 0.5 M NaOH solution with 3 M KOH, i.e., on raising the electrical conductivity of the electrolyte, shows that the observed electrode polarization has a large ohmic component.

Curves *2* and *4* from Fig. 2 are plotted in the Tafel coordinates in Fig. 3. The slope of curve *2* varies from 0.33 to 1.52 V, and that of curve 4, from 0.082 to 1.0 V. It is known that, for porous electrodes, the slope of polarization curves measured in the kinetic mode and plotted in the Tafel coordinates is equal to a doubled slope of curves for an equally accessible electrode, and to a quadrupled slope for curves measured in the inner diffusion mode. An analysis of the polarization curves plotted in the Tafel coordinates demonstrated that, at noticeable current densities, the slope considerably exceeds a doubled slope (0.006 – 0.3 V [26]) of curves obtained in reduction of O_2 to H_2O_2 in alkaline solutions on electrodes

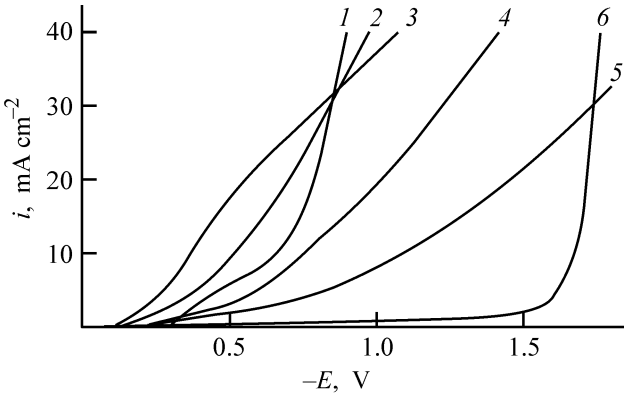


Fig. 2. Polarization curves for (*1–5*) electroreduction of oxygen and (*6*) hydrogen evolution on TEG-based electrodes in (*1*, *3–6*) a 5 M NaOH solution and (*2*) 3 M KOH solution. (*i*) Current density and (*E*) electrode potential. Electrodes from Table 2: (*1*) no. 11, (*2*, *4*, *6*) no. 3, (*3*) no. 8, and (*5*) no. 6.

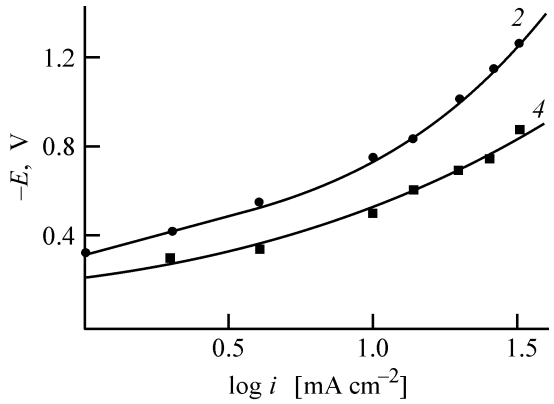


Fig. 3. Polarization curves *2* and *4* from Fig. 2, plotted in the Tafel coordinates.

fabricated from carbon graphite materials (no data on the kinetics of O_2 electroreduction on TEG can be found in the literature). This means that the electrodes probably operate in the inner-diffusion mode. Therefore, the rate of oxygen reduction on porous TEG-based electrodes can be raised if a three-phase boundary is developed and the diffusion and ohmic components of the process are diminished.

CONCLUSIONS

(1) Composites based on thermally expanded graphite and fluoroplastic-4D show a high electrical conductivity exceeding that of similar materials composed of carbon black.

(2) The rate of O_2 reduction in gas-diffusion electrodes fabricated from the materials under study is probably limited by inner diffusion.

(3) Deposition of palladium onto the surface of thermally expanded graphite enhances the activity of electrodes, but makes lower their electrical conductivity. A similar effect is produced by introduction of a carbon black into the electrode.

(4) Electrode fabricated from electrochemically produced thermally expanded graphite are more electrochemically active than electrodes fabricated from chemically obtained thermally expanded graphite, but have a lower electrical conductivity.

REFERENCES

1. Fialkov, A.S., *Uglerod, mezhsloevye soedineniya i kompozity na ego osnove* (Carbon and Intercalation Compounds abnd Composites on Its Base), Moscow: Aspekt Press, 1997.
2. Chung, D.D.L., *J. Mater. Sci.*, 1987, vol. 22, no. 16, pp. 4190–4198.
3. Chung, D.D.L., *J. Mater. Eng. Perform.*, 2000, vol. 9, no. 1, pp. 161–163.
4. US Patent 6 605 379.
5. Hentall, P.L., Lakeman, J.B., Mersted, G.O., *et al.*, *J. Power Sources*, 1999, vol. 80, nos. 1–2, pp. 235–241.
6. Ramesh, P., Sivakumar, P., and Sampath, S., *J. Electroanal. Chem.*, 2002, vol. 528, nos. 1–2, pp. 82–92.
7. Somashekarappa, M.P. and Sampath, S., *Anal. Chim. Acta*, 2004, vol. 503, no. 2, pp. 195–201.
8. Ramesh, P., Suresh, G.S., and Sampath, S., *J. Electroanal. Chem.*, 2004, vol. 561, no. 1, pp. 173–180.
9. Skowronski, J.M. and Krawczyk, P., *J. Solid State Electrochem.*, 2004, vol. 8, no. 6, pp. 442–447.
10. Kornienko, V.L., Kolyagin, G.A., and Kornienko, G.V., *Elektrokhimiya*, 1997, vol. 33, no. 8, pp. 971–978.
11. Kornienko, V.L., Kolyagin, G.A., and Saltykov, Yu.V., *Zh. Prikl. Khim.*, 1999, vol. 72, no. 3, pp. 353–361.
12. Noel, M. and Santhanam, R., *J. Power Sources*, 1998, vol. 72, no. 1, pp. 53–65.
13. Kang, F., Zheng, Y.-P., Wang, H.-N., *et al.*, *Carbon*, 2002, vol. 40, no. 12, pp. 1575–1581.
14. Apostolov, S.P., Krasnov, V.V., and Finaenov, A.I., *Zh. Prikl. Khim.*, 1997, vol. 70, no. 4, pp. 602–607.
15. Jnioui, A., Metrot, A., and Storck, A., *Electrochimica Acta*, 1982, vol. 27, no. 9, pp. 1247–1252.
16. Sorokina, N.E., Maksimova, N.V., and Avdeev, V.V., *Neorg. Mater.*, 2001, vol. 37, no. 4, pp. 441–447.
17. Kang, F., Leng, Y., and Zhang, T.-Y., *Carbon*, 1997, vol. 35, no. 8, pp. 1089–1096.
18. Yaroshenko, A.P., Popov, A.F., and Shapranov, V.V., *Zh. Prikl. Khim.*, 1994, vol. 67, no. 2, pp. 204–211.
19. Kuznetsov, B.N., Chesnokov, N.V., Mikova, B.M., *et al.*, *React. Kinet. Catal. Lett.*, 2003, vol. 80, no. 2, pp. 345–350.
20. USSR Inventor's ertificate, no. 500 557.
21. Gorshenev, V.G., Bibikov, S.V., and Novikov, Yu.N., *Zh. Prikl. Khim.*, 2003, vol. 76, no. 4, pp. 624–628.
22. Baranov, A.P., Shteinberg, G.V., and Bagotskii, V.S., *Elektrokhimiya*, 1971, vol. 7, no. 3, pp. 387–390.
23. Calas-Blanchard, C., Combat, M., Marty, J.-L., and Mauran, S., *Carbon*, 2003, vol. 41, no. 1, pp. 123–130.
24. Spalek, O. and Balej, J., *Collect. Czech. Chem. Commun.*, 1981, vol. 46, no. 9, pp. 2052–2059.
25. Chizmadzhev, Yu.A. and Chirkov, Yu.G., *Kinetika slozhnykh elektrokhimicheskikh reaktsii* (Kinetics of Complex Electrochemical REactins), Moscow: Nauka, 1981, pp. 240–305.
26. Tarasevich, M.R., *Itogi Nauki Tekhn., Elektrokhim.*, Moscow: VINITI, 1983, vol. 19, pp. 171–243.

Russian Journal of Applied Chemistry, Vol. 78, No. 10, 2005, pp. 1631–1635. Translated from Zhurnal Prikladnoi Khimii, Vol. 78, No. 10, 2005, pp. 1659–1663.
Original Russian Text Copyright © 2005 by Danilenko, Savel'ev, Yavorovskii, Khaskel'berg, Yurmazova, Shamanskii.

ENVIRONMENTAL PROBLEMS OF CHEMISTRY AND TECHNOLOGY

Water Purification To Remove As(V) by Electropulse Treatment of an Active Metallic Charge

N. B. Danilenko, G. G. Savel'ev, N. A. Yavorovskii, M. B. Khaskel'berg, T. A. Yurmazova, and V. V. Shamanskii

Research Institute of High Voltages, Tomsk, Russia
Tomsk Polytechnic University, Tomsk, Russia

Received June 7, 2005

Abstract—Power expenditure for water purification to remove arsenic(V) was determined. The processes and kinetics of purification in an electric-discharge reactor with a metallic (aluminum or iron) charge were investigated. The purification mechanisms based on the adsorption of arsenic(V) on a fresh surface of hydroxides formed through dispersion and subsequent oxidation of a charged metal were suggested. Rate equations corresponding to the experimental data and to these mechanisms were given.

One of problems accompanying many commercial processes, especially those in the metallurgical industry, is effective removal of arsenic and other toxic elements from wastewater. Methods for arsenic removal from wastewater can be combined in two groups: those with and without reagents. The second group includes galvanocoagulation, electrocoagulation, and electropulse water purification.

The reagent methods are mainly based on coprecipitation with calcium phosphate [1] and carbonate [2] or on precipitation of arsenic(V) in the form of iron arsenates [3]. These simple and reliable methods have an essential drawback: they permanently use expendable materials, which complicates the scheme of water purification.

As the same time, no-reagent methods are free of this disadvantage.

The galvanocoagulation method [4] is based on the use of short-circuited iron–carbon galvanic cells. The galvanic processes yield iron hydroxides, which adsorb arsenate ions. As well as reagent methods, this method does not consume reagents and electric energy from the outside; however, its drawbacks consist in a low rate of the purification process and necessity for a permanent stirring of the solution to oxidize As(III) to As(V) by hydrogen peroxide or by air bubbling.

In the electrocoagulation method, the electrodes dissolve on passing a current and impurities are bound with a precipitate of the forming metal hydroxide. This no reagent method is readily controlled. The process is characterized by consumption of electric energy per unit mass or one mole of the dissolved electrode. According to the data of different authors [5, 6], the energy expenditure is 20–40 kW h kg^{-1} of a coagulant. The electrodes are passivated during the electrolysis, which requires their periodic replacement. Furthermore, this method is characterized by low purification rates.

Recently electropulse water purification has gained a wide recognition. Water purification by these methods is characterized by a very high rate and efficiency. The energy consumption depends on the type of discharge and mode of its application. Data on the energy consumption for water purification (per unit volume) to remove various organic impurities by electric discharges (ED) in the mode of an electric breakdown of a liquid were reported in the review [7]. Depending on the nature of an admixture and on purification conditions, 10–100 J cm^{-3} (2.8–28 kW h m^{-3}) are consumed. The purification of solutions containing cobalt and strontium ions required 3×10^3–2×10^4 J cm^{-3} (0.84×10^3–0.56×10^4 kW h m^{-3}).

Pulsed nanosecond barrier discharges have been applied to purification of drinking water to remove admixtures. They demonstrated a high efficiency: the energy consumption was as low as 0.2–0.04 kW h m^{-3} [8].

We have shown previously [9, 10] that a highly efficient electroerosion occurs upon pulsed action of

1070-4272/05/7810-1631 © 2005 Pleiades Publishing, Inc.

Concentrations of As(III) and As(V) in model solutions after an ED treatment in a reactor with aluminum and iron charge ($c_{in[As(V)]}$ = 300, $c_{in[As(III)]}$ = 380 mg l^{-1})

Run no.	Charge	Solution	Concentration after treatment, mg l^{-1}	
			As(V)	As(III)
1	Al	As(III)	28	52
2		As(V)	15	0
3	Fe	As(III)	0	0
4		As(V)	0	0

electric current on an iron charge: in this case, the energy consumption for transfer of iron to a suspension is 0.067–0.142 kW h mol^{-1}.

The aim of this study was to determine the energy consumption in the electropulse water purification to remove arsenic compounds with the use of a chemically active metallic charge and to analyze the chemical mechanism of this method.

EXPERIMENTAL

The experimental installation consisted of a container with 200 g of metallic shavings (iron and aluminum) used as a reactive charge. The electrodes were lowered into the charge, and 950 ml of a solution under study was poured in. The electrodes were connected to a double-circuit source of pulsed currents, with the following characteristics: pulse duration τ_p = 10 μs, pulse repetition rate 100 Hz, voltage U = 500–1000 V, and current of the first half-period of a pulse, I = 250–400 A.

Solutions of As(III) and As(V) salts of various concentrations in distilled water were used. We used GSO (State Standard Sample) 7264–96 to prepare As(III) solutions and analytically pure NaH_2AsO_4, for As(V).

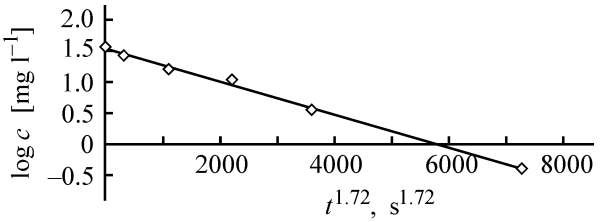


Fig. 1. Concentration of arsenic(V) ions, c, vs. the processing time t.

The concentration of As(III) was determined by inversion voltammetry with an STA-l instrument. The concentration of As(V) was found photometrically, in the form of arsenic-molybdenum blue [11] and also with the use of a QUICK As test-system (colorimetry on a sensitized paper by Gutzeit's technique) [12].

AsH_3 was qualitatively detected in the atmosphere over the surface of a solution treated with ED, using the QUICK As test-system at a sensitivity of 0.5 μg l^{-1}.

To compare the efficiencies of the aluminum and iron charges in water purification to remove arsenic compounds, we took equal volumes of solutions, with As(III) and As(V) concentrations of 380 and 300 mg l^{-1}, respectively, and treated them for 1.5 min with ED in the systems with iron and aluminum charges. Then the solutions were filtered ("blue-tape" filter) and the contents of both forms of arsenic were determined (see table).

It can be seen from the table that the efficiency of water purification with the iron charge is higher than that with the aluminum charge. Furthermore, As(III) is partially oxidized to As(V) in the case of an aluminum charge and incomplete water purification. In what follows, we studied in more detail the system with the iron charge, because it shows more promise for water purification to remove arsenic compounds.

To study the kinetics of arsenic(V) removal in an electric-discharge reactor with the iron charge, we carried out experiments on the kinetics of As(V) absorption. The concentration of the starting solution was 36.25 mg l^{-1}. In the course of the ED treatment, we sampled the filtrate at certain time intervals and determined its As(V) content:

t, s	$c_{As(V)}$, mg l^{-1}	t, s	$c_{As(V)}$, mg l^{-1}
0	36.25	120	3.958
30	27.395	180	0.521
60	16.18	240	0.208
90	11.31		

Processing of the experimental data demonstrated (Fig. 1) that the removal of arsenic(V) (mg s^{-1}) from water is described by equation(I).

$$\log c_{As(V)} = -0.0002 \log t^{1.72} + 1.5258, \quad (I)$$

The erosion of electrodes is described [10] by equation (II).

$$\log c_{Fe} = 0.72 \log t + 1.1331. \quad (II)$$

To study As(III) and As(V) adsorption on a solid erosion product after the ED treatment, we used As(III)

and As(V) solutions with the arsenic concentration of 51.92 and 38.01 mg l^{-1}, respectively. A solution was treated within 30 s in a reactor with an iron charge. The As(III) and As(V) contents of the treated solution (filtrate) were determined at certain time intervals. The results of the analyses are given in Fig. 2 in the coordinates: purification degree [$\alpha = (c_{in} - c)/c_{in}$]–logarithm of time.

It can be seen from Fig. 2 that, in both cases, the purification by ED is characterized by a very high rate and takes less than 30 s. Further, the concentrations of both As(III) and As(V) decrease insignificantly via the presumed adsorption.

In the course of the kinetic experiments, we made attempts to determine arsenic in the form of AsH_3 in the atmosphere over a solution with a charge. For this purpose, we tightly sealed a vessel with a polyethylene film and placed in it a strip of the QUICK test-system. The sensitivity of the test was 0.5 μg l^{-1}. At this sensitivity, the color of the strip remained unchanged upon complete purification of a solution with an As(V) concentration of 37 mg l^{-1}.

Mechanisms of water purification to remove admixtures of arsenic compounds. As(V) is present in water as $H_2AsO_4^-$ ions at pH 3–6 and as $HAsO_4^{2-}$ at pH 8–11; As(III) forms mainly H_3AsO_3 molecules at pH < 10 [13, 14]. As(III) and As(V) can be removed from water by an ED treatment through a reaction with iron(III) ions in solution and the subsequent precipitation of arsenates, e.g., by schemes (1) and (2).

$$Fe^{3+} + H_2AsO_4^- \rightarrow FeAsO_4\downarrow + 2H^+, \quad (1)$$

$$Fe^{3+} + H_3AsO_3 \rightarrow FeAsO_3\downarrow + 3H^+. \quad (2)$$

Such a scheme suggests that there is a functional relationship between the purification rate and the concentration of iron(III) ions in solution. As there is no relationship of this kind, these processes can be regarded as hardly probable.

A preliminary oxidation of As(III) by products of ED in water (OH, O_3, and H_2O_2) is also possible:

$$H_3AsO_3 + OH^- \rightarrow H_2AsO_4^- + 2H^+ \text{ etc.} \quad (3)$$

In the absence of oxygen or under oxygen-deficient conditions, oxidized arsenic can be also reduced to elementary arsenic or even to arsine by iron or atomic hydrogen [15]:

$$H_2AsO_4^- + Fe_H \text{ (or H)} + H_2O \rightarrow As\downarrow(AsH_3\uparrow) + Fe(OH)_2\downarrow + OH^-, \quad (4)$$

$$H_3AsO_3 + Fe_H \text{ (or H)} \rightarrow As\downarrow(AsH_3\uparrow) + (H_2O) + Fe(OH)_2\downarrow. \quad (5)$$

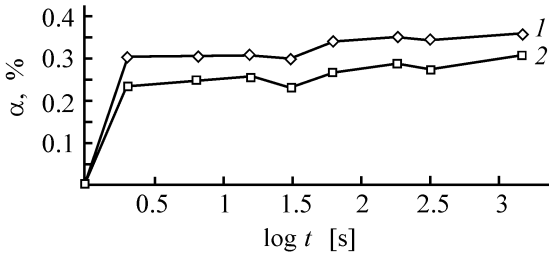


Fig. 2. Degree of extraction, α, of (*1*) As(III) and (*2*) As(V) from water (*1*) with the iron charge and (*2*) after the ED is switched off. (*t*) Treatment time.

The forming As^0 can be precipitated together with iron hydroxides, with arsine evolved as a gas. The possibility that this mechanism may be operative is supported by the data in Fig. 2: the degree of purification to remove As(III) is higher than that for As(V).

Our experiments did not confirm formation of arsine in water purification, i.e., reactions (4) and (5) yielding arsine do not take place. Furthermore, there are publications [15, 16] in which no elementary arsenic was detected on the surface of iron oxide and metal adsorbents by spectroscopic methods.

Therefore, the third mechanism is more probable, in which arsenic-containing ions are adsorbed on iron hydroxides (oxyhydroxides), e.g.,

$$=Fe(OH)_{solid} + H_2AsO_{4\,solution}^- \rightarrow (=Fe)_3AsO_{4\,solid} + H_2O + OH^-_{solution}, \quad (6)$$

$$=Fe(OH)_{solid} + H_3AsO_{3\,solution}^- \rightarrow (=Fe)_3AsO_{3\,solid} + H_2O. \quad (7)$$

Also possible is attachment of $H_2AsO_4^-$ anions to the surface [14].

We can assume that, under the action of ED, iron nanoparticles are removed from irregularities on the charge surface ("spikes") into solution, and dispersed particles of iron and a part of the metal in the resulting craters are partly or totally oxidized from the surface to give particles of Fe(II) hydroxides, which are rapidly oxidized further by dissolved oxygen. The resulting Fe(III) oxyhydroxide is the most efficient As(V) absorbent; as a result, the rate of its absorption is proportional to the total amount of corroded iron.

This method is rather efficient when ordinary iron-containing adsorbents are used [13]. In our case, its possibility is confirmed by the existence and type of functional *c*–*t* relationships for formation of iron hydroxide and water purification to remove arsenic (Figs. 1 and 2): the absolute values of the exponents

in these dependences differ by exactly unity. According to these data, the adsorption kinetics can be described as follows. The rate of absorption of arsenic compounds by the erosion product is given by

$$dc_1/dt = -k_i s c_{Fe} c_1, \quad \text{(III)}$$

Here c_1 is the concentration of the As impurity in water; s, specific surface area of the erosion product; and k_i, constant that accounts for the electric discharge characteristics and rate constants of chemical reactions.

As shown previously [10]:

$$c_{Fe} = (1 + m)kt^{1/(1+m)} = k_1 t^{1/(1+m)} = k_1 t^{\nu}, \quad \text{(IV)}$$

where $m = 1/3$ is the erosion index, which gives $\nu = 0.75$.

On substituting c_{Fe} into (III) and integrating, we obtain

$$\log c_i = \log c_{i,0} - \frac{k_1 k_i s}{2.3(1+\nu)} t^{\frac{m+2}{m+1}} = \log c_{i,0} - k_3 t^{1+\nu}, \quad \text{(V)}$$

where $c_{i,0}$ is the initial concentration of arsenic.

The experimental values $\nu = 0.72$ and $1 + \nu = 1.72$ are related to each other in complete correspondence with theoretical expressions (IV) and (V), being close to the theoretical value $\nu = 0.75$. Thus, the rate of the impurity absorption is proportional to the amount of dispersed metal.

It can be seen from Fig. 2 that the absorption proceeds very fast when the discharge is switched on, and nearly ceases when it is off. This means that absorption processes under ED conditions differ from the ordinary adsorption.

In this context, it is of interest to compare the experimental data on water purification to remove admixtures of arsenic compounds with the data on their adsorption on commercial adsorbents. Published data on the As(III) and As(V) adsorption on various adsorbents [17–19] are diverse, with the adsorption capacity for the most effective of them, $Fe(OH)_3$ and FeOOH, varying from 1 up to 250 mg g^{-1}. Such a wide scatter of the data is due to the dependence of the adsorption on numerous factors: dispersity and porosity of an adsorbent, adsorbate concentration, solution pH, adsorption duration, and stirring or the flow velocity of a solution relative to a layer. In the case of a complete (stoichiometric) reaction of iron oxyhydroxide with As(V), the capacity for As(V) would be 708 mg g^{-1}. Presumably, such a capacity is possible for a colloid solution of the hydroxide, but cannot be reached in the experiment because of the diffusion hindrances. Furthermore, practical use of colloids and suspensions presents serious difficulties associated with the necessity for separation of the dispersed phase from water.

The calculated capacity of an adsorbent monolayer for arsenic(V) is 0.004 mmol m^{-2} [14], i.e., 30 mg g^{-1} at a specific surface area of 100 m^2 g^{-1}.

For the process occurring under an electric discharge, the adsorption values were 96.1 and 156.7 mg g^{-1} for As(III) and As(V), respectively, at the specific surface area of the forming iron oxides equal to 105 m^2 g^{-1}. It is also important to note that these values were obtained under dynamic conditions within a very short time, which was considerably shorter than that required to obtain isotherms in [17, 18]. The capacity of the adsorbent in this case is 0.012 and 0.02 mmol m^2 for As(III) and As(V), respectively.

Thus, we see that the capacity in the electroerosion process approximately corresponds to the adsorption of three monolayers of As(III) and five monolayers of As(V). In all probability, this excess corresponds to a larger specific surface area at the instant of formation of a new phase, rater than to a multilayer adsorption (as it might be assumed). This specific surface area seems to be much larger than 105 m^2 g^{-1} at the beginning of the process, and then decreases to this value because of the cohesion and recrystallization of primary particles. If we assume that the surface is completely covered with arsenate ions, the specific surface area at the instant of adsorption will be 500 m^2 g^{-1} at the monolayer capacity of 0.004 mmol m^{-2} and As(V) adsorption of 156.7 mg g^{-1}. Such a surface area is physically well expected and corresponds to a size of FeO(OH) primary particles equal to 12 nm.

To gain insight into the purification mechanism, it is important to take into account the fact that the adsorption on a commercial adsorbent is limited by the diffusion of the adsorbate into micropores [18]. The capacity of the adsorbent formed in the ED purification exceeds by an order of magnitude that reached on commercial adsorbents (at a comparable sorption duration) and is close to the values corresponding to a complete monolayer on their surface. This indicates that, as expected, there is no diffusion hindrance in micro- and mesopores in adsorption at the instant when the adsorbent is produced, which ensures a higher rate and capacity.

CONCLUSIONS

(1) A study of the possibility of water purification to remove As(III) and As(V) by electric discharges with the use of an iron or aluminum charge demonstrated that the efficiency of the iron charge exceeds that of the aluminum charge. It was found in a study of the kinetics of arsenic(V) sorption that water is mostly purified during the electric discharge. The rate of water purification is proportional to the amount of dispersed iron; the subsequent adsorption on the erosion products is insignificant. The purification efficiency was 0.43 mol(As atoms) $(kW\ h)^{-1}$.

(2) Three possible mechanisms of water purification were considered. The results obtained in this study and published data made it possible to give preference to the mechanism in which an electric discharge acts upon the metal of the charge to form micro- and nanoparticles. Further, these particles are oxidized together with a part of the metal in the forming crater. At the instant when the oxides and hydroxides are formed, they sorb admixtures at a high rate, so that the adsorbent surface is completely filled.

REFERENCES

1. Nikolaev, A.V., Mazurova, A.A., Serdyuk, T.N., *et al.*, *Izv. Sib. Otd. Akad. Nauk SSSR, Ser. Khim.*, 1972, no. 12, issue 5, pp. 121–127.
2. Sedova, V.A., Kogan, B.I., and Vishnyakova, N.N., *Tsvet. Met.*, 1974, no. 8, pp. 27–29.
3. Panaiotov, Vl., *Elektron. Obrab. Mater.*, 1994, no. 2, pp. 41–45.
4. Chanturiya, V.A. and Solozhenkin, P.M., *Elektron. Obrab. Mater.*, 2004, no. 2, pp. 67–81.
5. Dedkov, Yu.M., *et al.*, *Vodosnabzh. San. Tekhn.*, 2003, no. 11, pp. 25–32.
6. RF Patent 2 220 110.
7. Goryachev, V.L., Rutberg, F.G., and Fedyukovich, V.N., *Izv. Ross. Akad. Nauk, Energetika*, 1998, no. 1, pp. 40–55.
8. RF Patent 2 136 600.
9. Shamanskii, V.V., Danilenko, N.B., and Gulak, N.V., *Trudy Nauchno-prakticheskoi Konferentsii "Osnovnye vodokhozyaistvennye problemy i puti ikh resheniya"* (Proc. Sci.-Pract. Conf. "Basic Hydroeconomic Problems and Ways to Their Solution"), Tomsk: Tomsk-vodokanal Open Joint-Stock Company, 2005, pp. 40–42.
10. Danilenko, N.B., Savel'ev, G.G., Yavorovskii, N.A., *et al.*, *Zh. Prikl. Khim.*, 2005, vol. 78, no. 9, pp. 1463–1468.
11. *Unifitsirovannye metody analiza vod* (Unified Methods for Analysis of Water), Lur'e, Yu.Yu., Ed., Moscow: Khimiya, 1973.
12. Charlot, G., *Les Methods de la Chemie Analytique. Analyse quantitative Minerale, Quatrieme Edition*, Paris: Masson, 1961.
13. Ashirov, A., *Ionoobmennaya ochistka stochnykh vod, rastvorov i gazov* (Ion-exchange Purification of Sewage, Solutions, and Gases), Leningrad: Khimiya, 1983.
14. Goldberg, S. and Johnston, C.T., *J. Colloid Interface Sci.*, 2001, vol. 234, pp. 204–216.
15. Meng, X., Bang, S., Johnson, M.D., and Korfiatis, G.P., Preprints of Extended Abstr. *ACS Nat. Meet. Am. Chem. Soc. Division of Environmental Chem.*, 2000, vol. 42 (2), pp. 484–487.
16. Farrell, J., Wang, J., and O'Day, P., *Environmental Sci. Technology*, 2001, vol. 35, pp. 2026–2033.
17. Galanov, A.I, Yurmazova, T.A., Danilenko, N.B., *et al.*, *Trudy III Vserossiskoi Nauchnoi Konferentsii "Khimiya i Khimicheskaya Tetekhnologiya na Rubeze Tysyacheletii"* (Proc. III All-Russian Sci. Conf. "Chemistry and Chemical Technology at the Turn of the Millenia"), Tomsk, 2004, pp. 149–151.
18. Savel'ev G.G., Yurmazova, T.A., Galanov, A.I, *et al.*, *Izv. Tomsk. Politekhn. Univ.*, 2004, vol. 207, no. 1, pp. 102–107.
19. Ahmed, F. and Jalil, M.A. The Effectiveness of Activated Alumina in Removing Arsenic from Groundwater: *Final Report of UNICEF-DPHE-BUET Res. Project*, 1999.

Russian Journal of Applied Chemistry, Vol. 78, No. 10, 2005, pp. 1636–1639. Translated from Zhurnal Prikladnoi Khimii, Vol. 78, No. 10, 2005, pp. 1664–1667.
Original Russian Text Copyright © 2005 by Ustinov, Yakunin, Polyanskii, Baluev, Shtutsa, Sukhanov.

ENVIRONMENTAL PROBLEMS OF CHEMISTRY AND TECHNOLOGY

Tests of Pilot and Industrial Pilot Installations for Catching of Nitrogen Oxides with Water Condensation Aerosols

O. A. Ustinov, S. A. Yakunin, A. I. Polyanskii, V. A. Baluev, M. G. Shtutsa, and L. P. Sukhanov

Bochvar All-Russia Research Institute of Inorganic Materials, Federal State Unitary Enterprise, Moscow, Russia

Chepetsk Mechanical Plant, Open Joint-Stock Company, Glazov, Udmurtiya, Russia

Received December 30, 2004; in final form, August 2005

Abstract—A pilot installation for catching of nitrogen oxides with water-condensation aerosols, with a throughput of 10 $m^3 h^{-1}$, was tested. A shell-and-tube industrial pilot installation for catching of nitrogen oxides with water-condensation aerosols, with a throughput of 1800 $m^3 h^{-1}$, was fabricated and tested.

Purification of gas flows to remove nitrogen oxides is an important issue of the environment protection. There exist various techniques for catching of nitrogen oxides: absorption by water or hydroxides, adsorption, catalytic reduction with ammonia, or thermal reduction with various reducing agents.

The conventional method of absorption by water is commonly used to catch nitrogen oxides of high concentration (approximately higher than 1 vol %), whereas catching of nitrogen oxides of lower concentrations by this technique requires a longer time of contact with the absorbing liquid. This, however, fails to ensure a high purification efficiency because of the low solubility of nitrogen oxide NO and low rate of its oxidation.

Absorption by aqueous solutions of alkali metal hydroxides is used for sanitary purification of exhaust gases; however, this does not solve the problem of NO catching, either, and, in addition, large volumes of salt-containing liquid waste are formed [1].

The more efficient adsorption methods of catching, which can also be used for sanitary purification to remove nitrogen oxides of low concentrations, operate in the batch mode, have a low sorbent capacity, involve a complex desorption procedure, and produce a large amount of liquid and solid wastes [2].

The selective catalytic method for detoxication of nitrogen oxides, with ammonia as a reducing agent [3], consumes ammonia, requires a careful adjustment of its feeding rate, fails to eliminate ammonia breakthrough, and is energy-intensive because the process occurs at 350°C with the use of expensive and deficient catalysts. It is appropriate to use this technique at low concentrations of nitrogen oxides (< 0.05 vol %, i.e., < 1 $g m^{-3}$).

A technique for reduction of nitrogen oxides without heating on carbamide supported by porous substrates (γ-Al_2O_3, zeolite, silica gel, activated carbon) has been developed [4]. The expenditure of carbamide is insignificant at low concentrations of nitrogen oxides in gases to be purified (<0.05 vol %, i.e., <1 $g m^{-3}$), but becomes unacceptably high as the concentration increases to 0.1–1.0 vol % (1–10 $g m^{-3}$) and more.

A method for catching of nitrogen oxides of these concentrations on water-condensation aerosols is suggested. Previously, it has been shown that the rate of absorption of nitrogen oxides by liquid aerosols is proportional to their surface area, i.e., substantially exceeds that in absorption by a film of a liquid [5]. Consequently, presence of liquid aerosols with a highly developed surface must accelerate the catching of nitrogen oxides and improve the efficiency of catching without use of expendable reagents. The results obtained in a laboratory study of the efficiency of purification of gas flows to remove nitrogen oxides by introduction of water-condensation aerosols have been published previously [6]. A patent on the corresponding technique for catching of nitrogen oxides has been obtained [7]. It was shown experimentally under laboratory conditions that the efficiency of catching of nitrogen oxides with concentrations of 0.2–30 $g m^{-3}$

1070-4272/05/7810-1636 © 2005 Pleiades Publishing, Inc.

increases upon introduction of water-condensation aerosols into a gas flow being purified. As gas flows with the above content of nitrogen oxides are commonly formed in dissolution of various products in nitric acid, the forming condensate of nitric acid should be returned to the dissolution reactor. The average volume of nitric acid is approximately 30–40 ml per gram of a caught nitrogen oxide. To reveal the potentialities of the method in more detail, tests were performed on pilot and pilot industrial installations.

EXPERIMENTAL

The pilot installation with a throughput of 10 $m^3 h^{-1}$ included a tube-in-tube cooler-condenser (diameter 120 mm, height 1000 mm) mounted over the cover of a working reactor in which wastes were dissolved in nitric acid. The installation was equipped with a rotameter and devices for gas sampling and was connected to the general ventilation system. To make larger the condensation surface area, a grating shelf comprising six discs placed one above another was introduced into the cooler-condenser.

NO_2 was determined by the accumulation method, which consisted in that nitrogen dioxide was reduced by passing the gas through an absorbing vessel filled with potassium iodide at a rate of 0.8 l min^{-1} and by titrating the forming iodine with sodium thiosulfate [8]. The determination of the sum NO + NO_2 was based on oxidation and absorption of nitrogen oxides by hydrogen peroxide to give nitric acid, whose amount was then found by titration with a sodium hydroxide solution [9].

Nitrogen oxide was determined by calculating the difference between the total content of NO and NO_2 and the content of NO_2.

The installation was tested under industrial conditions by passing through it a part of gases discharged from the reactor. The content of NO_2 in the exhaust gases was as high as 10 g m^{-3}, and that of NO, up to 1 g m^{-3} (maximum degree of oxidation 90%).

The efficiency of catching of nitrogen oxides was studied in relation to the time of gas passing and to the initial content of nitrogen oxides and water vapor. The last parameter was determined by the temperature maintained in the reactor. A study of the efficiency of NO and NO_2 catching in relation to the time of gas passing demonstrated that the efficiency remained virtually unchanged during 14 h.

The next set of experiments was concerned with the dependence of the efficiency of catching of nitrogen oxides on the amount of condensed water vapor, i.e., on the variation of the dissolution temperature. The efficiency of NO_2 catching increased from 63 to 83% as the temperature was raised from 40 to 70°C, i.e., as the content of water aerosols grew from 60 to 170 g m^{-3}, and remained unchanged (85%) in going from 80 to 90°C (content of aerosols 276 and 400 g m^{-3}, respectively). A similar pattern was observed for NO, with only the catching efficiency increasing to a lesser extent (Table 1).

Table 1. Efficiencies of NO_2 and NO catching in the condenser of the pilot installation in relation to the dissolution temperature (concentration of water aerosols) [initial concentration (g m^{-3}): NO_2 3, NO 0.55]

Reactor temperature, °C	Concentration of water aerosols, g m^{-3}	Catching efficiency, %	
		NO_2	NO
40	30	63	50
50	60	79	59
60	110	80	60
70	170	83	61
80	276	85	62
90	400	85	62

Table 2. Efficiencies of NO_2 and NO catching in the condenser of the pilot installation in relation to the initial concentration (reactor temperature 50°C)

Initial concentration, g m^{-3}		Catching efficiency, %		Residual concentration, g m^{-3}	
NO_2	NO	NO_2	NO	NO_2	NO
0.5	0.12	66	49	0.2	0.06
1.3	0.27	70	51	0.4	0.13
3.0	0.55	79	59	0.6	0.23
4.7	0.85	80	64	0.9	0.31
9.0	1.35	83	69	1.5	0.42

It was also established that the catching efficiency increases with the initial concentration of NO and NO_2 (Table 2).

The efficiency of NO_2 catching on the pilot installation is close to that previously published [6] for a laboratory installation.

Thus, it can be stated the process of water condensation can be used to catch NO_2 with a concentration in the range 0.5–9.0 g m^{-3} (and, possibly, higher) with

Table 3. Results obtained in testing the industrial pilot installation

Run no.	Throughput by gas, $m^3 h^{-1}$	NO_2 concentration at the inlet, $g m^{-3}$	NO_2 catching efficiency, %	Run no.	Throughput by gas, $m^3 h^{-1}$	NO_2 concentration at the inlet, $g m^{-3}$	NO_2 catching efficiency, %
1	1960	5.1	89	7	1960	6.0	93
2	1700	2.4	81	8	1960	4.0	89
3	1820	2.6	82	9	1700	1.5	73
4	1700	0.7	15	10	1820	3.1	85
5	1960	4.1	85	11	1960	4.3	91
6	1700	5.5	89	12	1700	1.6	74

a sufficiently high efficiency. Nitrogen oxide NO at degree of oxidation of about 90% is also caught under conditions in which condensed water aerosols are formed.

The results obtained in laboratory and pilot tests of the reagent-free method for purification of vent gases were used to design, fabricate, assemble, and test a industrial pilot installation with a gas flow throughput of 1800 $m^3 h^{-1}$. The installation has the form of a cooler-condenser (Fig. 1). A shell-and-tube variant is accepted for the design of the cooler-condenser, with 40 tubes 40 mm in diameter. The cooling water and the gas being cooled move in a counterflow. The cylindrical casing of the apparatus has two pipes on the side surface, which serve as inlet and outlet for cooling water *1*. The linear flow velocity of the gas is 2–4 $m s^{-1}$; calculated flow rate of cooling water, 45 $m^3 h^{-1}$; heat-exchange surface area, 2.2 m^2; apparatus height and diameter, 2500 and 950 mm, respectively; and the material of the apparatus, 12Kh18N10T steel. The apparatus is mounted directly onto the reactor in which the product is being dissolved.

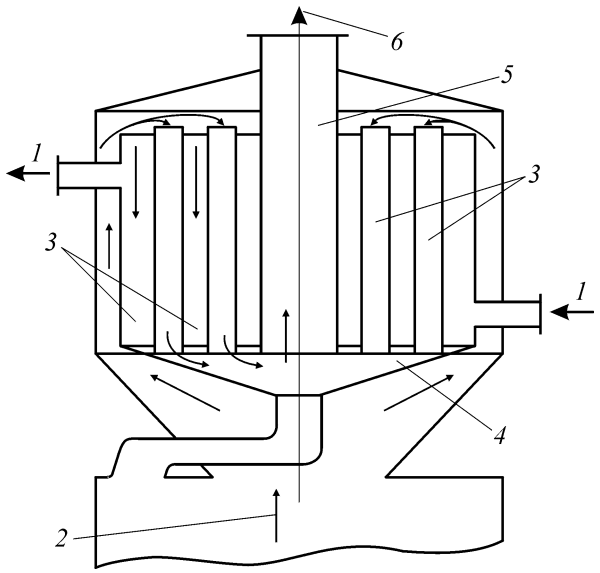


Fig. 1. 1 Schematic of the industrial pilot installation. (*1*) Cooling water, (*2*) inlet for vent gases, (*3*) tubes of the cooler-condenser, (*4*) condensate collector, (*5*) central tube, and (*6*) outlet for vent gases.

The gas flow is fed from the reactor into the cooler-condenser from below *2*, passes through the annular space between the outer wall and the shell-and-tube casing and turns down passing through the tube space *3*, where cooling mostly occurs. Swirling coils are inserted in each tube of the heat exchanger in order to improve the condensation. Arriving in the bottom part of the apparatus, where the condensate collector *4* is situated, the gas again changes its motion direction, passes through the central tube *5*, and is discharged into the atmosphere via the ventilation system *6*.

The condensate formed in film-type condensation and accumulated in the condensate collector flows down back into the reactor in which the waste is dissolved.

The industrial pilot installation was tested in waste processing. The tests were carried out in the following mode: the dissolution reactor was heated to 60–85°C, a portion of waste was introduced, the exhaust gases were passed through the cooled condenser, and the gas phase was sampled to determine the content of NO_2 (no analysis for NO was performed in the industrial tests) at the apparatus inlet and outlet. The results obtained are systematized and listed in Table 3.

It can be seen from Table 3 that the efficiency of nitrogen dioxide catching with water aerosols grows with the initial NO_2 concentration to reach 93–94% at an initial NO_2 concentration of 5.9–6.0 g m^{-3}. The low efficiency (15%) in run no. 4 is due to a decrease in the volume of cooling water, which resulted in that its temperature at the condenser outlet increased from 20 to 40°C and this made lower the concentration of condensation aerosols.

In addition, the poor efficiency is due to a lower initial concentration of NO_2. The dependence of

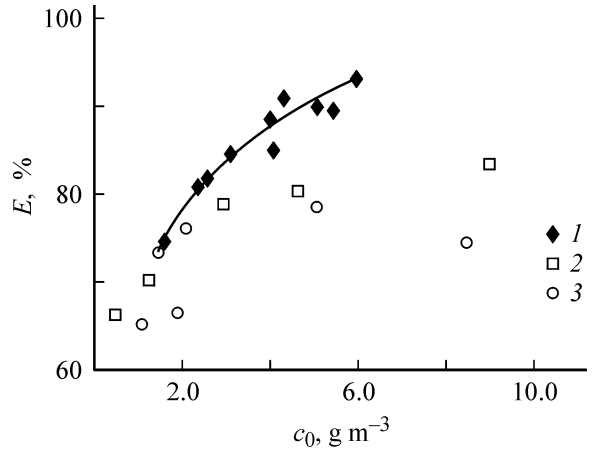


Fig. 2. Catching efficiency E vs. the initial NO_2 concentration c_0 in the gas flow being purified. Installation: (*1*) industrial pilot, (*2*) pilot, and (*3*) laboratory.

the efficiency on the initial NO_2 concentration is shown in Fig. 2, which also presents the results obtained on the pilot installation and in laboratory studies. Despite the different condensation conditions, a sufficiently good agreement is observed, with the higher efficiencies obtained on the industrial pilot installation.

CONCLUSIONS

(1) It was established in testing a pilot installation for catching of nitrogen oxides with water-condensation aerosols that the catching efficiency of NO_2 is 80% and more, and that of NO, 60% and more. The efficiency increases as the content of water aerosols is raised to 170 g m^{-3}. The catching efficiency remains constant within 14 h of operation.

(2) It was found in testing a shell-and-tube industrial pilot installation for catching of nitrogen oxides with water-condensation aerosols that the efficiency of NO_2 catching is 73–93% at a concentration of 1.5–6 g m^{-3}. It was demonstrated that the results obtained on the industrial pilot installation, pilot installation, and in laboratory studies coincide.

REFERENCES

1. Gladkii, A.V., Fedorova, S.K., and Artemova, E.N., *1Ochistka gazovykh vybrosov ot oksidov azota: Obzornaya informatsiya, Promyshlennaya i sanitarnaya o chistka gazov, Ser. KhM-14* (Purification of Discharged Gases To Remove Nitrogen Oxides: Review, Industrial and Sanitary Purification of Gases, Series KhM-14), Moscow: TsINTIkhimneftemash, 1989.
2. Ganz, S.N., *1Zh. Prikl. Khim.*, 1958, vol. 31, no. 1, pp. 138–139.
3. Rikhter, L.A. and Chernov, S.L., *Itogi Nauki Tekh. Ser. Tepl. Elektrostants., Teplosnabzh.*, VINITI, 1991, no. 6, pp. 3–157.
4. Ustinov, O.A., Yakunin, S.A., Polyanskii, A.I., and Baluev, V.A., *Zh. Prikl. Khim.*, 1999, vol. 72, no. 2, pp. 206–209.
5. Seigneur, Ch. and Saxena, P., *Atmos. Environ.*, 1984, vol. 18, no. 10, pp. 2109–2124.
6. Ustinov, O.A., Yakunin, S.A., Polyanskii, A.I., and Baluev, V.A., *Zh. Prikl. Khim.*, 1999, vol. 72, no. 11, pp. 1786–1789.
7 RF Patent 2 100 056.
8. Shustov, D.A. and Bakulina, L.A., Gig. Sanit. ,1975, no. 12, pp. 69–71.
9. Blazhennova, A.N., Il'inskaya, A.A., and Rapoport, F.M., *Analiz gazov v khimicheskoi promyshlennosti* (Analys of Gases in Chemical Industry), Moscow: Goskhimizdat, 1954.

Russian Journal of Applied Chemistry, Vol. 78, No. 10, 2005, pp. 1640–1645. Translated from Zhurnal Prikladnoi Khimii, Vol. 78, No. 10, 2005, pp. 1668–1673.
Original Russian Text Copyright © 2005 by Lebedev, Berenblit, Starobin, Gubanov.

ORGANIC SYNTHESIS AND INDUSTRIAL ORGANIC CHEMISTRY

Pyrolytic Decarboxylation of Some Derivatives of Perfluorinated Mono- and Dicarboxylic Acids

N. V. Lebedev, V. V. Berenblit, Yu. K. Starobin, and V. A. Gubanov

Lebedev Research Institute of Synthetic Rubber, Federal State Unitary Enterprise, St. Petersburg, Russia

Received July 7, 2005

Abstract—Pathways of pyrolysis of perfluorinated carboxylic acids are considered in relation to the structure of the acids and reaction conditions. The reaction mechanism is discussed.

As shown in [1, 2], pyrolytic decarboxylation of salts of linear perfluorinated carboxylic acids gives terminal fluoroolefins in high yields, reaching 90 mol % in the case of sodium salts:

$$C_nF_{2n+1}CF_2CF_2CO_2M \xrightarrow{250-300^\circ C} C_nF_{2n+1}CF{=}CF_2 + CO_2 + MF;\ (M = Na^+,\ K^+,\ ...,\ Ca^{2+}...).$$

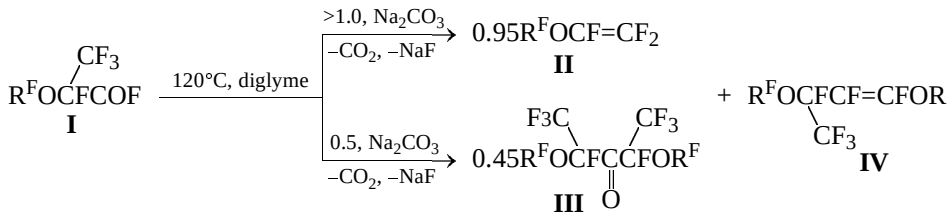
Similarly, terminal perfluoroalkoxyalkenes are formed in high yields by pyrolysis of sodium salts of perfluoro-ω-alkoxyalkanoic acids (from butyric to caproic) [3].

Perfluorinated alkyl vinyl ethers have also been obtained in high yields [4] by pyrolysis of solutions of perfluoro-2-alkoxypropionic acid salts in diglyme:

$$C_nF_{2n+1}OCF(CF_3)CO_2M \xrightarrow{120-160^\circ C,\ \text{diglyme}} C_nF_{2n+1}OCF{=}CF_2 + CO_2 + MF,$$

In this study, we examined in detail how the structure of perfluorinated carboxylic acid derivatives with various α- and β-substituents affects the pyrolysis pathway.

The pathway of pyrolysis of perfluoro-2-alkoxypropionyl fluorides in absolute diglyme at 120°C in the presence of anhydrous sodium carbonate depended on the ratio of perfluoroacyl fluoride and sodium carbonate:

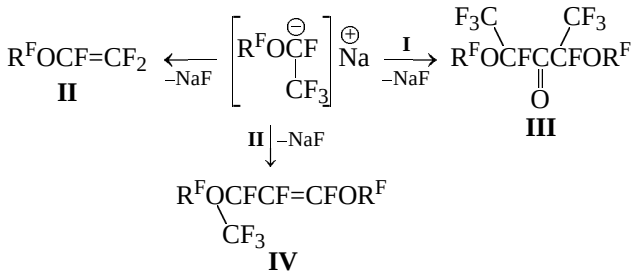


R^F = CF_3– (**a**), $CF_3CF_2CF_2$– (**b**), $CF_3O(CF_2)_3$– (**c**), $C_3F_7OCF(CF_3)CF_2$– (**d**).

The figure shows how the yields of perfluorinated alkyl vinyl ethers, their linear dimers, and the corresponding bis(perfluoro-1-methyl-2-oxaalkyl) ketones depend on the molar ratio of sodium carbonate and acyl fluoride.

The first step of the reaction involves formation of sodium perfluoro-2-alkoxypropionate along with NaF and CO_2. The pyrolytic decarboxylation proper presumably involves formation of the reactive intermediate carbanion:

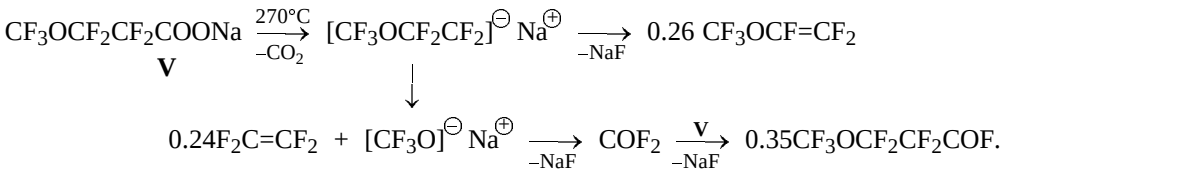
1070-4272/05/7810-1640 © 2005 Pleiades Publishing, Inc.



which, depending on the reactant ratio, can either eliminate the fluoride anion to form perfluorinated alkyl vinyl ether **II** or react with the initial substrate **I** to form ketone **III**. Also, we identified among the pyrolysis products small amounts of the dimers **IV** of perfluorinated alkyl vinyl ethers, which suggests the possibility of the reaction of the carbanion with **II**.

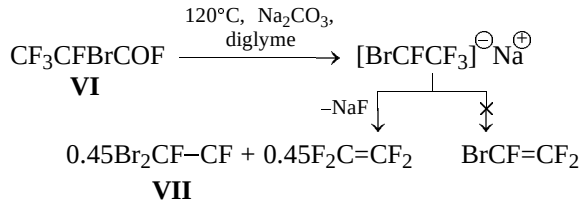
The structures of the products were confirmed by bromination across the double bond. The ^{19}F NMR data for the compounds identified are listed in the table.

Gubanov *et al.* [5] showed that dry pyrolysis of sodium perfluoro-3-methoxypropionate follows the scheme

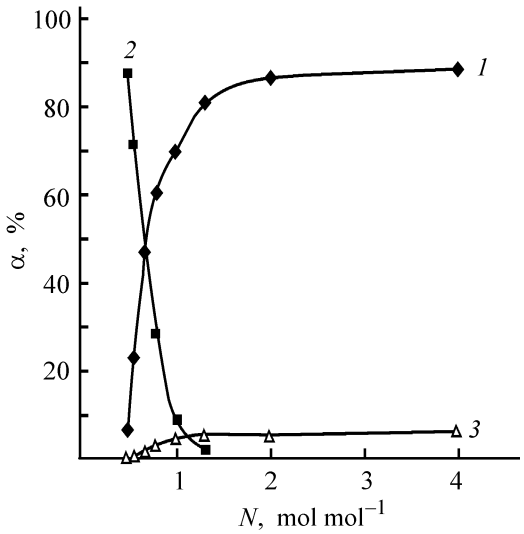


Experiments on pyrolysis of **V** in diglyme at 120°C showed that the perfluoro-3-oxaalkyl anion generated by decarboxylation can eliminate either the fluoride ion from the β-position or (major pathway) the perfluoromethoxide anion, with its subsequent transformation into carbonyl difluoride. The yields of perfluorinated methyl vinyl ether and tetrafluoroethylene were 30 and 60 mol %, respectively. With Na^+ replaced by K^+, the yield of tetrafluoroethylene increases from 60 to 95 mol %, suggesting stabilization of the trifluoromethoxide anion with the potassium ion, in agreement with the data of [5, 6].

An unexpected result was obtained in pyrolysis of 2-bromotetrafluoropropionyl fluoride **VI** in dry diglyme at 120°C in the presence of anhydrous sodium carbonate. Instead of the expected trifluorobromoethylene, we detected 1,1-dibromotetrafluoroethane **VII** in the reaction products by ^{19}F NMR (see table) and mass spectroscopy. Apparently, the bromotetrafluoroethyl anion generated by decarboxylation of the 2-bromotetrafluoropropionate anion is stabilized by abstraction of the bromine cation from the second substrate molecule, rather than by elimination of the fluoride or bromide anion:

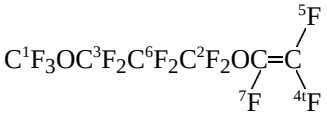
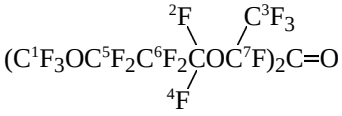
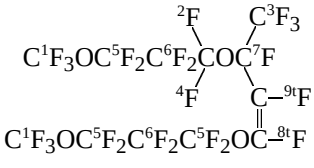
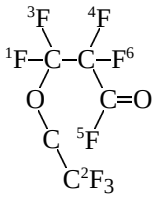


The formation of tetrafluoroethylene as the major product of pyrolysis of perfluoro-3-oxaalkanoic acid derivatives has been observed previously [7] in pyrolysis of sodium perfluoro-4-oxaheptanedioate at 250°C, when the monodecarboxylation product, perfluoro-3-vinyloxypropionyl fluoride, was obtained in a less than 2% yield. This product isomerized at room tem-

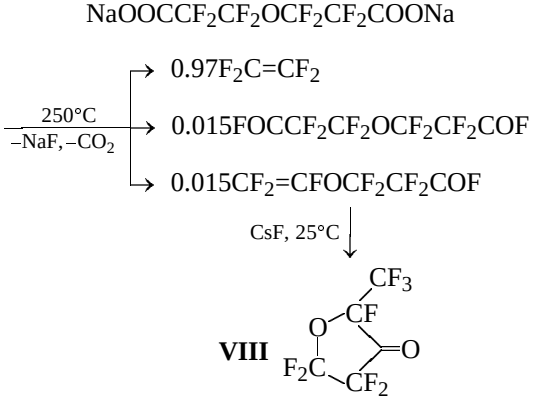


Yield α of pyrolysis products of perfluoro-2-alkoxypropionyl fluorides vs. the molar ratio *N* of sodium carbonate to acyl fluoride: (*1*) perfluorinated alkyl vinyl ether **II**, (*2*) perfluoro ketone **III**, and (*3*) dimer **IV** of perfluorinated alkyl vinyl ether.

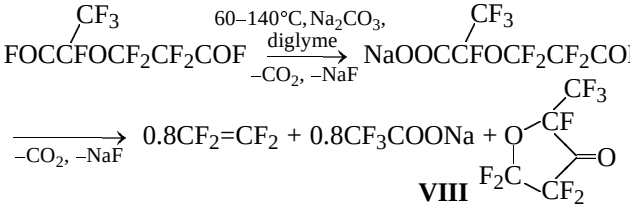
^{19}F NMR spectra of products formed in pyrolysis of perfluorinated carboxylic acid derivatives

Compound	Position	δ_{CCl_3D}, ppm	$J_{F^*-F^*}$, Hz	*n*F
Perfluorinated 4-oxaamyl vinyl ether **IIc** 	1	–55.5	F^1–F^3, 10	3
	2	–83.9	F^2–F^1, 10; F^2–$F^{5;\,7}$, 6	2
	3	–84.2	F^3–F^1, 10; F^3–F^2, 10	2
	4c	–114.2	F^4–F^5, 87; F^4–F^7, 67;	1
	5t	–121.5	F^5–F^7, 112; F^5–F^4, 87; F^5–F^2, 6	1
	6	–128.3	s	2
	7	–134.8	F^7–F^5, 111; F^7–F^4, 67; F^7–F^2,	6
Bis(perfluoro-1-methyl-2,6-dioxaheptyl) ketone **IIIc** 	1	–54.6	F^1–F^5, 10	3
	2	–76.5	F^2–F^4, 150	1
	3	–79.7	s	3
	4	–81.1	F^4–F^2, 150	1
	5	–84.6	F^5–F^1, 10	2
	6	–127.8	s	2
	7	–135.2	m	1
Perfluoro-9-methyl-2,6,10,14-tetraoxapentadec-7-ene **IVc** 	1	–55.0	m	6
	2	–76.7	F^2–F^4, 148	1
	3	–79.9	s	3
	4	–81.3	F^4–F^2, 150	1
	5	–84.5	m	6
	6	–127.8	m	4
	7	–130.5	m	1
	8t	–133.1	F^8–F^9, 120	1
	9t	–165.5	F^9–F^8, 120	1
1,1-Dibromotetrafluoroethane **VII** $C^2F_3C^1FBr_2$	1	–76.6	F^1–F^2, 10, q,	1
	2	–81.7	F^2–F^1, 10, d,	3
Perfluoro-2-methyloxalan-3-one **VIII** 	1	–79.1	F^1–F^3 125; F^1–F^5 10	1
	2	–81.0	s	3
	3	–92.5	F^3–F^1 125; F^3–F^4 8	1
	4	–120.2	F^4–F^6 280 F^4–F^3 8	1
	5	–120.9	s	1
	6	–129.8	F^6–F^4 280; F^6–F^1 10	1

perature under the action of CsF into a cyclic ketone, perfluoro-2-methyloxalan-3-one **VIII**:



Accordingly, we detected in the experiments on the pyrolysis of perfluoro-2-methyl-3-oxahexanedioic acid difluoride **IX** (its acyl moiety is isomeric to that of sodium perfluoro-4-oxaheptanedioate) in diglyme at 120°C in the presence of an equimolar amount of sodium carbonate, along with sodium trifluoroacetate and tetrafluoroethylene, also compound **VIII** formed in ~15 mol % yield:



The product was identified by the characteristic ^{19}F NMR signals of magnetically nonequivalent geminal fluorine atoms with coupling constants of 125 Hz for the CH_2O group and 280 Hz for the CF_2CO group. The ^{19}F NMR spectrum with the signals of the –OCF< and $–CF_3$ groups is given in the table; it is quite consistent with the data from [7].

EXPERIMENTAL

The pyrolysis products were analyzed chromatographically with an LKhM-8MD chromatograph [model 5, thermal conductivity detector, programmed heating from 30 to 200°C at a rate of 6 deg min^{-1}, 3000 × 3-mm columns, solid support Silokhrom-2 (0.16–0.2 mm, packing density 0.30 ± 0.01 g cm^{-3}), stationary phase 5F4E (15 wt %), carrier gas helium (40 ml min^{-1})].

The ^{19}F NMR spectra were recorded on a Bruker Spectrospin HX-90 spectrometer at a working frequency of 84.67 MHz; hexafluorobenzene or hexafluoro-*p*-xylene was used as internal reference. The ^{19}F chemical shifts were recalculated relative to CCl_3F.

The ^1H NMR spectra were recorded on the same device at 90 MHz, with hexamethyldisiloxane as external reference.

The mass spectra were recorded on a Chromass Varian CH-7M device.

Perfluoro-2-(4-oxaamyloxy)propionyl fluoride **Ic** was prepared by electrochemical fluorination of methyl 3-methoxypropionate [8], followed by condensation of the resulting perfluoro-3-methoxypropionyl fluoride with hexafluoropropene oxide on KF in diglyme.

The synthesis of perfluoro-2-methyl-3-oxahexanedioic acid difluoride **IX** has been described previously [9].

Perfluoro-2-methoxypropionyl fluoride **Ia** was prepared by condensation of COF_2 with hexafluoropropene oxide [10], and perfluoro-2-propoxypropionyl fluoride **Ib** and perfluoro-2-(2-methyl-3-oxahexyloxy)-propionyl fluoride **Id**, respectively, by dimerization and trimerization of hexafluoropropene oxide under similar conditions [11].

Perfluoro-2-bromopropionyl fluoride **VI** was prepared from 67 g (0.4 mol) of hexafluoropropene oxide and 43 g (0.42 mol) of dry NaBr in 75 ml of absolute diglyme at –30°C with stirring in a stainless steel autoclave. After warming up to room temperature, the lower organofluorine layer was separated, and 80 g of a product (yield 88 mol %) with bp ~20°C was obtained. It was identified as $CF_3CFBrCOOCH_3$ by the ^{19}F NMR [δ_F, ppm: 77.1 d (3F, CF_3, J 10 Hz), 134.1 q (1F, $CFBrCOOCH_3$, J 10 Hz] and mass spectra [m/z (I_{rel}, %): 209, 207 (5.4), $M^+ – OCH_3$; 181, 179 (30.5), $M^+ – 59$ (CF_3CFBr^+); 162, 160 (3.7), $C_2F_3Br^+$; 131, 129 (13.9), CF_2Br^+; 128 (4.8), $C_2F_4CO^+$; 109 (6.6), $C_2F_3CO^+$; 100 (7.2), $C_2F_4^+$; 81 (3.3), $C_2F_3^+$; 69 (119), CF_3; 59 (100) $COOCH_3^+$.

Pyrolysis of perfluoro-2-(4-oxaamyloxy)propionyl fluoride Ic. (a) A 250-ml four-necked round-bottomed glass flask equipped with a stirrer, thermometer, and water-cooled reflux condenser was charged with 31 g (0.3 mol) of dry Na_2CO_3 and 30 ml of diglyme dehydrated over CaH_2. The contents were heated on a water bath to 70°C, after which 50 g (0.15 mol) of **Ic** was added dropwise until the CO_2 evolution ceased. Then the reflux condenser was replaced with a descending condenser, the mixture [a suspension of Na_2CO_3 in a solution of sodium perfluoro-2-(4-oxaamyloxy)-propionate in diglyme] was heated to 120°C, and 40 g of the product was collected in the receiver. According to GLC, the product consisted of 97.5% per-fluorinated 4-oxaamyl vinyl ether **IIc** (92 mol %) and 2.5% perfluoro-4-oxaamyl 1,3,3,3-tetrafluoroethyl ether. The following products were isolated by fractional distillation and characterized: $CF_3OCF_2CF_2CF_2OCF=CF_2$, bp 64°C, d_4^{20} 1.636; mass spectrum, m/z (I_{rel}, %): 332 (0.37), $C_4F_{12}O_2^+ = M^+$; 169 (1.83), $C_3F_7^+$; 147 (1.92), $C_3F_5O^+$; 135 (1.39), $C_2F_5O^+$; 131 (0.9), $C_3F_5^+$; 119 (5.24), $C_2F_5^+$; 100 (2.2), $C_2F_4^+$; 97 (2.37), $C_2F_3O^+$; 81 (3.35), $C_2F_3^+$; 78 (4.29), $C_2F_2O^+$; 69 (100), CF_3^+; $CF_3OCF_2CF_2CF_2OCFHCF_3$, bp 71–72°C, d_4^{20} 1.622.

(b) Similarly, a mixture of 8 g (0.075 mol) of dry Na_2CO_3 and 30 ml of dry diglyme was heated to 60°C, and 50 g (0.15 mol) of **Ic** was added, after which the mixture was heated at 140–150°C for 2 h until the gas evolution ceased. Then the mixture was cooled to 80°C, the reflux condenser was replaced with the descending condenser, and the reaction products were distilled off in a vacuum (2–3 mm Hg). After the separation of the lower organofluorine layer, we obtained 43 g of the product containing, according to GLC, 93% bis(perfluoro-1-methyl-2,6-dioxaheptyl) ketone (90 mol %) and 7% of an impurity. We isolated by fractional distillation and characterized ketone **IIIc**, bp 74–75°C (18 mm Hg), d_4^{20} 1.757, n_D^{20} 1.2836. The impurity was identified by ^{19}F NMR as linear dimer **IVc** of perfluorinated 4-oxaamyl vinyl ether, $CF_3OCF_2CF_2CF_2OCFCF=CFOCF_2CF_2CF_2OCF_3$ (with CF_3 branch on the CF group).

bp 70–71°C (18 mm Hg), d_4^{20} 1.736, n_D^{20} 1.2805. Its structure was also confirmed by UV-induced bromination [characteristics of the dibromide: bp 73°C (2 mm Hg), d_4^{20} 1.9811, n_D^{20} 1.3443. The mass spectrum of the product was also consistent with the structure of the linear dimer, *m*/*z* (I_{rel}, %): 664 (6.4), $C_{12}F_{24}O_3$ = M^+; 595 (0.63), $M^+ - CF_3$; 579 (3.8), $M^+ - CF_3O$; 498 (0.6), $M^+ - C_3F_6O^+$; 479 (1.1), $M^+ - C_3F_7O$; 413 (7.7), 498 – CF_3O; 325 (2.4), $C_7F_{11}O_2^+$; 275 (2.3), $C_6F_9O_2^+$; 247 (2.7), $C_5F_9O^+$; 219 (1.1), $C_4F_9^+$; 178 (25.2), $C_4F_6O^+$; 169 (98.9), $C_3F_7^+$; 159 (33.0), $C_4F_5O^+$; 150 (5.9), $C_3F_6^+$; 147 (49.5), $C_3F_5O^+$; 135 (30.3), $C_2F_5O^+$; 119 (74.8), $C_2F_5^+$; 100 (37.3), $C_2F_4^+$; 69 (100), CF_3^+.

Similarly, we obtained by pyrolysis of perfluoro-2-methoxypropionyl fluoride **Ia**, perfluoro-2-propoxypropionyl fluoride **Ib**, and perfluoro-2-(2-methyl-3-oxahexyloxy)propionyl fluoride **Id** the corresponding symmetrical ketones **IIIa**, **IIIb**, and **IIId** with admixture of linear dimers **IV**.

Pyrolysis of perfluoro-3-methoxypropionyl fluoride. Similarly to the above-described procedure, a flask with the reflux condenser cooled by a dry ice/alcohol mixture was charged with 22.3 g (0.21 mol) of Na_2CO_3 and 40 ml of dry diglyme; 46 g (0.2 mol) of $CF_3OCF_2CF_2COF$ was fed through a siphon until the refluxing and CO_2 evolution ceased. The resulting suspension of NaF in a solution of sodium perfluoro-3-methoxypropionate **V** in diglyme was heated to 120°C, with fractional distillation of the pyrolysis products. Carbonyl fluoride was taken up by a sodium carbonate solution, perfluorinated methyl vinyl ether was condensed in a coil trap at –50°C, and tetrafluoroethylene was taken up by liquid bromine in a trap, with conversion into dibromotetrafluoroethane. We obtained 10 g of $CF_3OCF{=}CF_2$ (30 mol %) and 31 g of CF_2BrCF_2Br (60 mol %).

Pyrolysis of perfluoro-2-bromopropionyl fluoride VI. Similarly to the pyrolysis of perfluoro-3-methoxypropionyl fluoride, 45 g (0.2 mol) of **VI** was fed to a mixture of 22.3 g (0.21 mol) of Na_2CO_3 and 40 ml of dry diglyme, until the refluxing and CO_2 evolution ceased. Then the reflux condenser was replaced with a water-cooled descending condenser, the flask was heated to 120°C, and 23 g (45 mol %) of perfluoro-1,1-dibromoethane **VII** was distilled off; bp ~5°C, d_4^{20} 2.188, n_D^{20} 1.364; mass spectrum, *m*/*z* (I_{rel}, %): 262, 260, 258 (47.8), $C_2F_4^{79-81}Br_2^+ = M^+$; 193, 191, 189 (32.5), $M^+ - CF_3$; 181, 179 (100), $M^+ - Br$; 162, 160, 158 (17.5), $M^+ - C_2F_4 = Br_2^+$; 131, 129, $M^+ - CF_2Br$; 112, 110, $M^+ - CF_3Br = CFBr^+$. In low-boiling gases, after the uptake of CO_2 with an alkali, we identified tetrafluoroethylene and 1-hydro-1-bromotetrafluoroethane, which was also detected as impurity in the main product by ^{19}F NMR spectroscopy.

Pyrolysis of perfluoro-2-methyl-3-oxahexanedioic acid difluoride IX. A similar flask equipped with a water-cooled refluxed condenser was charged with 10.6 g (0.1 mol) of dry Na_2CO_3 and 50 ml of dehydrated diglyme. The mixture was heated on an oil bath to 60°C, and 31 g (0.1 mol) of **IX** was added dropwise from a dropping funnel over a period of 2 h. The mixture was stirred until the CO_2 evolution ceased. Then the mixture was gradually heated with stirring to 140°C, with collected the pyrolysis products in a trap cooled to –78°C. Low-boiling gases were passed through a trap with liquid bromine and then through an alkaline absorber. From the trap, we isolated 4 g (yield ~15%) of a product identified as perfluoro-2-methyloxolan-3-one **VIII** by comparison of the ^{19}F NMR and mass spectra with those reported in [6]; bp ~15°C. In the trap with bromine, 1,2-dibromotetrafluoroethane was obtained as a separate phase. The nonvolatile residue contained sodium trifluoroacetate.

CONCLUSIONS

(1) Depending on the pyrolysis conditions and structure of perfluorocarboxylic acid salts, the perfluoroalkyl carbanion generated by decarboxylation is stabilized not only by elimination of the fluoride anion to give the alkene, but also with that to give the corresponding ketones through both inter- and intramolecular attack at the acyl fluoride group.

(2) In the pyrolysis of potassium perfluoro-3-alkoxypropionates, the perfluorooxaalkyl anion is virtually quantitatively stabilized by elimination of the perfluoroalkoxide anion with the formation of tetrafluoroethylene.

(3) An attack of the bromotetrafluoroethyl anion at the bromine atom of another substrate molecule yields perfluoro-1,1-dibromoethane and tetrafluoroethylene.

REFERENCES

1. Hals, L.J., Reid, T.S., and Smith, G.H., *J. Am. Chem. Soc.*, 1951, vol. 73, p. 4054.

2. Haszeldine, R.N., *J. Chem. Soc.*, 1952, no. 11, pp. 4253–4254.
3. Berenblit, V.V., Zapevalov, A.Ya., Panitkova, E.S., *et al.*, *Zh. Org. Khim.*, 1979, vol. 15, no. 7, pp. 1417–1425.
4. US Patent 3114778.
5. Gubanov, V.A., Zevakin, I.A., Gurari, V.E., *et al.*, *Zh. Org. Khim.*, 1981, vol. 17, no. 8, pp. 1587–1590.
6. Redwood, M.E. and Willis, C.J., *Can. J. Chem.*, 1965, vol. 43, no. 7, pp. 1893–1898.
7. Ogden, P.H., *J. Chem. Soc. (C)*, 1971, no. 17, pp. 2920–2926.
8. Berenblit, V.V., Byzov, B.A., Grachev, V.I., *et al.*, *Zh. Prikl. Khim.*, 1975, vol. 48, no. 3, pp. 709–711.
9. Skoblikova, V.I., Sass, V.P., Ershov, A.E., *et al.*, *Zh. Org. Khim.*, 1973, vol. 9, no. 10, pp. 2021–2023.
10. UK Patent 998978.
11. US Patent 3250808.

Russian Journal of Applied Chemistry, Vol. 78, No. 10, 2005, pp. 1646–1650. Translated from Zhurnal Prikladnoi Khimii, Vol. 78, No. 10, 2005, pp. 1674–1678.
Original Russian Text Copyright © 2005 by Bazhin, Gorbunova, Zapevalov, Saloutin.

ORGANIC SYNTHESIS AND INDUSTRIAL ORGANIC CHEMISTRY

Synthesis of Polyfluorinated Ethers

D. N. Bazhin, T. I. Gorbunova, A. Ya. Zapevalov, and V. I. Saloutin

Postovskii Institute of Organic Synthesis, Ural Division, Russian Academy of Sciences, Yekaterinburg, Russia

Received November 10, 2004; in final form, June 2005

Abstract—Procedures for preparing polyfluorinated ethers $H(CF_2CF_2)_nCH_2OR$ by alkylation of the corresponding telomeric alcohols $H(CF_2CF_2)_nCH_2OH$ (n = 1–3) with alkyl halides and alkyl tosylates were examined.

The rising researchers' interest in synthesis of polyfluorinated ethers (PFEs) in the past decade is due to several factors. First, thanks to their physicochemical properties, compounds of this class are potential ozone-friendly substitutes of Freons [1]. Second, the majority of PFEs are inert low-freezing and, in some cases, relatively high-boiling liquids. These properties make them suitable as solvents, heat-transfer agents, and components of a new generation of power cells, improving the low-temperature characteristics of graphite electrodes [2]. An important property of PFEs is their adhesion to various materials, making these compounds promising as lubricants operating in a wide range of temperatures and loads.

Published procedures for PFE synthesis involve nucleophilic and radical addition of alcohols to polyfluoroalkenes, trifluoromethylation of polyfluorinated alcohols catalyzed by Lewis acids [3], alkylation of polyfluoroalkoxide anions with dimethyl sulfate [4] or polyfluoroalkyl chlorosulfites [5, 6], etc. Combinations of various reagents in PFE synthesis allow preparation of compounds of diverse structures. All the above-mentioned methods require anhydrous conditions, special equipment, and, frequently, difficultly available chemicals.

The classical route to ethers (Williamson reaction) involves the reaction of alcoholates with alkyl halides [7]. Among polyfluorinated alcohols commercially produced in Russia, telomeric alcohols of the general formula $H(CF_2CF_2)_nCH_2OH$ (n = 1–8) are the most readily available. However, conversion of telomeric alcohols into alcoholates for the Williamson reaction involves certain problems: reaction of these alcohols with alkali metals, developing with accumulation of the alcoholate or in the course of removal of excess alcohol, may cause self-ignition or even explosion of the reaction mixture; preparation of alcoholates using alkalis, followed by removal of water and excess alcohol, is not safe either [4]. At the same time, if the alcoholates are taken as solutions, the yields of the target compounds are low [8].

Within the framework of our study, the problem of raising the yields of PFEs derived from telomeric alcohols and alkyl halides is partially solved by performing the reaction in a DMSO + KOH mixture [see Experimental, method (a)] to enhance the basic and nucleophilic properties of the alcohol (n = 1):

$$HC_2CF_2CH_2OH + RX \xrightarrow{100^\circ C,\ 12\ h} HCF_2CF_2CH_2OR + HX,$$

I–**III**, 45–55%

where R = C_4H_9 (**I**), C_6H_{13} (**II**), $C_{10}H_{21}$ (**III**); X = Cl, Br.

However, even within the next telomeric alcohol (n = 2), this reaction yields no desired PFEs, apparently because of the formation of oligomeric products. The residue obtained after removing the excess KOH and solvent is undistillable in a rough vacuum.

Solov'ev *et al.* [9] reported on a one-step synthesis of fluorinated glycidol ethers under the conditions of phase-transfer catalysis. This method apparently facilitates the synthesis of a wide range of PFEs based on telomeric alcohols, but it is insufficiently versatile because of the different solubilities of the fluorine-containing components [10].

With the aim to raise the yields of PFEs, we chose appropriate solvent systems and prepared compound

1070-4272/05/7810-1646 © 2005 Pleiades Publishing, Inc.

IV–**IX** under relatively mild conditions [see Experimental, method (b)]:

$$H(CF_2CF_2)_nCH_2OH + RX \xrightarrow{A \text{ or } B,\ \text{catalyst, KOH}} H(CF_2CF_2)CH_2OR + HX,$$

IV–**IX**, 40–70%

conditions: (A) CH_2Cl, H_2O, 40°C, 5 h, n = 2; (B) THF, H_2O, 60°C, 5 h, n = 3. Catalyst: $[Et_3BzN]^+Cl^-$; X = Cl, Br; R = C_4H_9, n = 2 (**IV**); R = C_5H_{13}, n = 2 (**V**); R = $C_{10}H_{21}$, n = 2 (**VI**); R = C_4H_9, n = 3 (**VII**); R = C_6H_{13}, n = 3 (**VII**); R = $C_{10}H_{21}$, n = 3 (**IX**).

Comparative analysis of the two procedures for preparing PFEs **I**–**IX** shows that none of them ensures quantitative yields of the desired compounds, and no correlation can be revealed between the substrate structure and PFE yield.

The highest yields of PFEs (up to 90%) are attained when a two-step procedure is used: first a fluorinated alcohol is converted to a sulfonate (mesylate, tosylate, triflate) by the reaction with appropriate sulfonyl derivative [10], after which the sulfonate group is readily replaced by the alcoholate ion formed from a nonfluorinated alcohol *in situ*. According to [10], this two-step process can be schematically represented as follows:

$$R^fCH_2OH \xrightarrow{R'SO_2Cl,\ NEt_3} R^fCH_2OSO_2R' \xrightarrow{R''OH,\ NaH,\ 10\ h,\ 130^\circ C} R^fCH_2OR'',$$

where R^f = CF_3, C_6F_{13}; R' = CH_3, CF_3, *p*-$C_6H_4CH_3$; R'' = *p*-$C_6H_4NO_3$.

The key step in this reaction is nucleophilic replacement of the RSO_3^- group, which can be performed in a virtually quantitative yield. However, the reaction of sulfo derivatives with a fluorinated alcohol involves the loss of a valuable chemical in the first step. Furthermore, the use of NaH requires anhydrous conditions, and the reaction requires heating at 130°C for 10 h.

Among the examined routes to PFEs, the most promising is, apparently, introduction of a labile leaving group into the hydrocarbon component. The resulting derivative in the modified Williamson reaction is a more active alkylating agent than alkyl halides.

Comparison of the reactivity of mesylates, triflates, and tosylates, taking into account the reaction conditions, shows that tosylates are not inferior to the other reagents, but are preferable from the viewpoint of convenience in handling and availability.

Tosylation of common alcohols by the nucleophilic substitution mechanism occurs under relatively mild conditions; the subsequent reaction of the resulting derivatives with telomeric alcohols gives the desired compounds **IV**–**IX** in high yields and does not require any anhydrous medium [see Experimental, method (c)]:

$$ROH + TsCl \xrightarrow[-HCl]{KOH,\ H_2O} [ROTs]$$

$$\xrightarrow{H(CF_2CF_2)_nCH_2OH,\ KOH,\ THF,\ H_2O,\ \text{catalyst}} \textbf{IV}\text{–}\textbf{IX} + TsOK.$$

87–96%

It should be noted that isolation of the tosyl derivatives (ROTs) is not necessary for performing the second step of the synthesis successfully. Comparison of the yields of **IV**–**IX** in the processes whose second step was performed with isolated and crude ROTs shows that the difference in the yields is as small as 5–10%.

Thus, the latter procedure is the best from the viewpoint of conditions and results: reaction temperature 60°C, time (total of two steps) 8 h, and almost quantitative yields of the desired compounds.

The IR spectra of **I**–**IX** contain the following characteristic absorption bands, ν, cm^{-1}: 1111–1142 (C–F), 1200–1204 (C–O–C), and 2856–2879, 2927–2959, 2934–2966 (C–H).

The ^1H and ^{19}F spectra of all the PFEs prepared have common features.

EXPERIMENTAL

The IR spectra were recorded on a Perkin–Elmer Spectrum One Fourier spectrometer from thin films. The ^1H and ^{19}F NMR spectra were measured on a Bruker DRX-400 spectrometer in $CDCl_3$, internal references TMS and C_6F_6, respectively. The yields, boiling points, and elemental analyses of **I**–**IX** are given in Table 1, and the NMR data, in Table 2.

Synthesis of polyfluorinated ethers. Method (a). A mixture of 0.1 mol of alkyl halide, 0.25 mol of KOH, and 50 ml of DMSO was heated with vigorous stirring to 100°C to obtain a uniform mixture, and 0.1 mol of telomeric alcohol (n = 1) was added dropwise at this temperature over a period of 30 min. The mixture was stirred for 8 h at 100°C. Then 150 ml of water was added, and the mixture was neutralized with HCl. The resulting neutral solution was extracted with $CHCl_3$ (2 × 30 ml). The chloroform extracts were combined and dried over $CaCl_2$; the solvent was distilled off. The residue was subjected to fractional distillation to obtain 1-(1,1,3-trihydroperfluoroprop-

Table 1. Yields, boiling points, and elemental analyses of ethers **I**–**IX**, $H(CF_2CF_2)_nCH_2O(CH_2)_mH$ (n = 1–3, m = 4, 6, 10)

Compound	Yield, %	bp, °C/*p*, mm Hg	Found, %/Calculated, %			Formula
			C	H	F	
I	45	140–141	44.59/44.68	6.34/6.43	39.98/40.39	$C_7H_{12}F_4O$
II	49	170–171	50.15/49.99	7.40/7.46	34.93/35.15	$C_9H_{17}F_4O$
III	55	105–107/6	57.21/57.34	8.69/8.88	27.43/27.91	$C_{13}H_{24}F_4O$
IV	87	179–180	37.63/37.53	4.20/4.17	52.64/52.75	$C_9H_{12}F_8O$
V	89	196–198	41.58/41.67	5.28/5.36	47.05/47.43	$C_{11}H_{17}F_8O$
VI	94	195–196/30	48.56/48.42	6.56/6.45	40.39/40.83	$C_{15}H_{24}F_8O$
VII	89	201–202	34.35/34.05	3.12/3.09	58.24/58.73	$C_{11}H_{12}F_{12}O$
VIII	88	160–161/30	37.51/37.44	4.20/4.08	54.30/54.65	$C_{13}H_{17}F_{12}O$
IX	96	217–220/30	43.34/43.25	5.12/5.08	48.15/48.28	$C_{17}H_{24}F_{12}O$

Table 2. ^1H and ^{19}F NMR data for **I**–**IX**

Compound	Formula	^1H, δ, ppm (**I**)	^{19}F, δ, ppm	*J*, Hz
I	1 *b* *a* 2 3 4 5 6 $HCF_2CF_2CH_2OCH_2CH_2CH_2CH_3$	5.92 t.t (H^1), 3.76 t.t (H^2), 3.55 t (H^3), 1.57 m (H^4), 1.38 m (H^5), 0.92 m (H^6)	36.11 m (*a*), 21.52 d.m (*b*)	$J_{1,b}$ = 53.3, $J_{1,a}$ = 5.3, $J_{2,a}$ = 12.6, $J_{2,b}$ = 1.7, $J_{3,4}$ = 6.5
II	1 *b* *a* 2 3 4 5 6 7 $HCF_2CF_2CH_2OCH_2CH_2(CH_2)_2CH_2CH_3$	5.92 t.t (H^1), 3.79 t.t (H^2), 3.54 t (H^3), 1.58 m (H^4), 1.32 m (H^5, H^6), 0.89 t (H^7)	36.04 m (*a*), 21.51 d.m (*b*)	$J_{1,b}$ = 53.3, $J_{1,a}$ = 5.3, $J_{2,a}$ = 12.6, $J_{2,b}$ = 1.7, $J_{3,4}$ = 6.6, $J_{7,6}$ = 6.9
III	1 *b* *a* 2 3 4 5 6 7 $HCF_2CF_2CH_2OCH_2CH_2(CH_2)_6CH_2CH_3$	5.91 t.t (H^1), 3.79 t.t (H^2), 3.54 t (H^3), 1.57 m (H^4), 1.27 m (H^5, H^6), 0.88 t (H^7)	36.09 m (*a*), 21.49 d.m (*b*)	$J_{1,b}$ = 53.3, $J_{1,a}$ = 5.3, $J_{2,a}$ = 12.6, $J_{2,b}$ = 1.7, $J_{3,4}$ = 6.6, $J_{7,6}$ = 6.8
IV	1 *d* *c* *b* *a* 2 3 4 5 6 $HCF_2CF_2CF_2CF_2CH_2OCH_2CH_2CH_2CH_3$	6.06 t.t (H^1), 3.91 t (H^2), 3.59 t (H^3), 1.58 m (H^4), 1.39 m (H^5), 0.93 t (H^6)	41.94 m (*a*), 36.03 m (*b*), 31.38 m (*c*), 24.45 d.m (*d*)	$J_{1,d}$ = 52.0, $J_{1,c}$ = 5.5, $J_{2,a}$ = 13.8, $J_{3,4}$ = 6.5, $J_{6,5}$ = 6.8

Table 2. (Contd.)

Compound	Formula	^{1}H, δ, ppm (**I**)	^{19}F, δ, ppm	*J*,/Hz
V	1 *d* *c* *b* *a* 2 3 4 5 6 7 $HCF_2CF_2CF_2CF_2CH_2OCH_2CH_2(CH_2)_2CH_2CH_3$	6.06 t.t (H^1), 3.90 t (H^2), 3.58 t (H^3), 1.57 m (H^4), 1.33 m (H^5, H^6), 0.89 t (H^7)	41.91 m (*a*), 36.08 m (*b*), 31.34 m (*c*), 24.41 d.m (*d*)	$J_{1, d}$ = 52.0, $J_{1, c}$ = 5.5, $J_{2, a}$ = 13.9, $J_{3, 4}$ = 6.5, $J_{7, 6}$ = 6.9
VI	1 *d* *c* *b* *a* 2 3 4 5 6 7 $HCF_2CF_2CF_2CF_2CH_2OCH_2CH_2(CH_2)_6CH_2CH_3$	6.07 t.t (H^1), 3.91 t.t (H^2), 3.59 t (H^3), 1.57 m (H^4), 1.32 m (H^5, H^6), 0.89 t (H^7)	41.87 m (*a*), 35.83 t (*b*), 31.17 m (*c*), 24.32 d.m (*d*)	$J_{1, d}$ = 52.2, $J_{1, c}$ = 5.6, $J_{2, a}$ = 13.9, $J_{2, b}$ = 1.4, $J_{3, 4}$ = 6.5, $J_{7, 6}$ = 6.9, $J_{b, d}$ = 8.1
VII	1 *e* *d* *c* *b* *a* 2 3 4 5 6 $HCF_2CF_2(CF_2)_2CF_2CF_2CH_2OCH_2CH_2CH_2CH_3$	6.05 t.t (H^1), 3.92 t (H^2), 3.60 t (H^3), 1.57 m (H^4), 1.39 m (H^5), 0.93 t (H^6)	42.22 t.m (*a*), 39.58 m (*b*), 38.32 m (*c*), 32.22 m (*d*), 24.74 d.m (*e*)	$J_{1, e}$ = 51.9, $J_{1, d}$ = 5.2, $J_{2, a}$ = 13.9, $J_{3, 4}$ = 6.5, $J_{6, 5}$ = 7.2
VIII	1 *e* *d* *c* *b* *a* 2 3 4 5 6 $HCF_2CF_2(CF_2)_2CF_2CF_2CH_2OCH_2CH_2(CH_2)_3CH_3$	6.05 t.t (H^1), 3.92 t (H^2), 3.59 t (H^3), 1.58 m (H^4), 1.30 m (H^5), 0.89 m (H^6)	42.22 t.m (*a*), 39.44 m (*b*), 38.29 br.s (*c*), 32.20 br.s (*d*), 24.76 d.m (*e*)	$J_{1, e}$ = 51.9, $J_{1, d}$ = 5.2, $J_{2, a}$ = 14.0, $J_{3, 4}$ = 6.5
IX	1 *e* *d* *c* *b* *a* 2 3 4 5 6 7 $HCF_2CF_2(CF_2)_2CF_2CF_2CH_2OCH_2CH_2(CH_2)_6CH_2CH_3$	6.05 t.t (H^1), 3.92 t (H^2), 3.59 t (H^3), 1.60 m (H^4), 1.31 m (H^5,6), 0.88 t (H^7)	42.22 t.m (*a*), 39.58 m (*b*), 38.32 br.s (*c*), 32.22 m (*d*), 24.76 d.m (*e*)	$J_{1, e}$ = 51.9, $J_{1, d}$ = 5.2, $J_{2, a}$ = 13.9, $J_{3, 4}$ = 6.5, $J_{7, 6}$ = 6.8

oxy)butane **I**, 1-(1,1,3-trihydroperfluoropropoxy)hexane **II**, and 1-(1,1,3-trihydroperfluoropropoxy)decane **III**.

Method (b). A mixture of 50 ml of CH_2Cl_2 and 50 ml of 40% KOH (conditions A) [or 60 ml of THF and 30 ml of 50% KOH (conditions B)], 0.1 mol of telomeric alcohol [n = 2 (conditions A) or n = 3 (conditions B)], and 1 g of triethylbenzylammonium chloride was heated with vigorous stirring to 40°C (conditions A) or 60°C (conditions B). At this temperature, 0.1 mol of alkyl halide was slowly added over a period of 30 min, and the mixture was kept for 5 h. Then, for conditions A, the upper organic layer was separated, washed with dilute HCl (2 × 100 ml), and dried over $CaCl_2$; the solvent was distilled off. For conditions B, 150 ml of water was added, and the oil thus formed was extracted with $CHCl_3$ (2 × 30 ml). The combined chloroform extracts were dried over $CaCl_2$, and the solvent was distilled off. In both cases, the residue was subjected to fractional distillation to obtain 1-(1,1,5-trihydroperfluoropentoxy)butane **IV**, 1-(1,1,5-trihydroperfluoropentoxy)hexane **V**, 1-(1,1,5-trihydroperfluoropentoxy)decane **VI**, 1-(1,1,7-trihydroperfluoroheptoxy)butane **VII**, 1-(1,1,7-trihydroperfluoroheptoxy)hexane **VIII**, and 1-(1,1,7-trihydroperfluoroheptoxy)decane **IX**.

Method (c). A mixture of 0.15 mol of *p*-toluenesulfonyl chloride and 0.15 ml of ethanol was heated to 35–40°C, and 50 ml of 40% KOH was added dropwise over a period of 1 h with vigorous stirring. The resulting mixture was stirred for 3 h at 35–40°C and cooled, after which 200 ml of water was added. The oil thus formed was separated and treated under conditions A [method (b)].

CONCLUSION

The most efficient route to polyfluorinated ethers is a two-step process involving preparation of tosyl derivatives of alcohols, followed by their reaction with telomeric alcohols $H(CF_2CF_2)_nCH_2OH$ under the conditions of phase-transfer catalysis, which allows preparation of ethers $H(CF_2CF_2)_nCH_2OR$ (n = 2, 3) in high yields (87–96%).

ACKNOWLEDGMENTS

The study was financially supported by the Russian Foundation for Basic Research (project no. 04-03-96109).

REFERENCES

1. Sekiya, A. and Misaki, S., *J. Fluorine Chem.*, 2000, vol. 101, no. 2, pp. 215–221.
2. Nakajima, T., Dan, K.-I., Koh, M., *et al.*, *J. Fluorine Chem.*, 2001, vol. 111, no. 2, pp. 167–174.
3. Petrov, V.A., *J. Fluorine Chem.*, 2001, vol. 112, no. 1, pp. 167–121.
4. Bagnall, R.D., Bell, W., and Pearson, K., *J. Fluorine Chem.*, 1978, vol. 11, no. 2, pp. 93–107.
5. Rakhimov, A.I., Nalesnaya, A.V., and Vostrikova, O.V., *Zh. Org. Khim.*, 2003, vol. 39, no. 6, p. 949.
6. Rakhimov, A.I., Nalesnaya, A.V., and Vostrikova, O.V., *Zh. Obshch. Khim.*, 2004, vol. 74, no. 4, pp. 693–694.
7. Vatsuro, K.V. and Mishchenko, G.L., *Imennye reaktsii v organicheskoi khimii* (Named Reactions in Organic Chemistry), Moscow: Khimiya, 1976, p. 403.
8. Takada, N., Abe, T., and Sekiya, A., *J. Fluorine Chem.*, 1998, vol. 92, no. 2, pp. 167–171.
9. Solov'ev, D.V., Kolomenskaya, L.V., Rodin, A.A., *et al.*, *Zh. Obshch. Khim.*, 1991, vol. 61, no. 3, pp. 673–677.
10. Prescher, D., Thiele, T., and Ruhmann, R., *J. Fluorine Chem.*, 1996, vol. 79, no. 2, pp. 145–148.

Russian Journal of Applied Chemistry, Vol. 78, No. 10, 2005, pp. 1651–1655. Translated from Zhurnal Prikladnoi Khimii, Vol. 78, No. 10, 2005, pp. 1679–1683.
Original Russian Text Copyright © 2005 by Paleckiene, Sviklas, Šlinkšiene.

ORGANIC SYNTHESIS AND INDUSTRIAL ORGANIC CHEMISTRY

Reaction of Urea with Citric Acid

R. Paleckiene, A. Sviklas, and R. Šlinkšiene

Kaunas Technological University, Kaunas, Lithuania

Received May 12, 2005

Abstract—Reaction of urea with citric acid in aqueous solutions at molar ratios of 1 : 1, 1 : 2, and 2 : 1 and the solubility of urea citrate were studied. The data obtained can serve to optimize use of citric acid as a physiologically active substance or nitrification inhibitor and in production of liquid fertilizers containing urea.

Urea is a frequent component of many liquid integrated fertilizers. Interaction of urea with citric acid can affect phase equilibria in the systems constituting liquid complex fertilizers.

Urea is highly reactive. Many urea compounds obtained in reactions with mineral or organic acids are known [1–5]. Citric acid is a necessary component in the system of biochemical reactions of the cellular respiration. Along with other tricarboxylic acids, citric acid is contained in small amounts in mitochondria of all the cells. Another function of citric acid is to support the acid–base equilibrium and ionic composition in a living body. Citric acid is a typical chelate forming agent in reactions with metal ions. It can also inhibit nitrification [6] and hence is of interest as a component of liquid complex fertilizers.

There is no reliable information on how urea reacts with citric acid. Fragmentary tentative results have been published previously [7].

In this study, we examined the reaction of urea with citric acid in aqueous solutions and determined the main physicochemical properties of the reaction product.

Urea $CO(NH_2)_2$ and citric acid $C_6H_8O_7 \cdot H_2O$ were of chemically pure grade. The compositions of the substances were determined by chemical and physicochemical analyses. The nitrogen content was found in solutions and in the solid phase [8–10].

A thermal analysis of solids was performed on a Du Pont Instruments 990 Thermal Analyzer at a heating rate of 10 deg min^{-1}.

The IR spectra were recorded on a Spectrum GX (Perkin Elmer) FT-IR spectrometer in KBr pellets. An X-ray phase analysis was performed on a DRON-6 diffractometer with copper radiation and nickel filter within the 0°–166.5° range of diffraction angles with a relative error at no more than 0.5%.

Mixtures of urea (Ur) and citric acid (HCit), taken in molar ratios of 1 : 1, 2 : 1, and 1 : 2, were dissolved in water taken in amounts corresponding to the weight ratio of the sum of the reactants to water of 1 : 0.25, 1 : 0.5, 1 : 0.75, and 1 : 1. The solutions were prepared at room temperature and, in a number of cases, were heated, if required, for complete dissolution of the initial substances. The results are listed in Table 1.

As can be seen, a precipitate is formed at a 1 : 1 molar ratio; its chemical composition corresponds to urea citrate with a nitrogen content of 11.1 wt %. Practically no nitrogen remains in solution. At Ur : HCit = 2 : 1, a substance with ~11 wt % nitrogen content precipitates, but nitrogen remains in solution in

Table 1. Chemical composition of aqueous solutions containing urea and citric acid and of precipitate

Ur/HCit molar ratio	Weight ratio of Ur + HCit to water	Nitrogen content, wt %	
		precipitate	solution
1 : 1	1 : 0.50	11.0	–
	1 : 0.75	10.9	0.1
	1 : 1.00	11.1	–
2 : 1	1 : 0.50	10.9	12.1
	1 : 0.75	11.0	10.1
	1 : 1.00	–*	–**

* No precipitate formed.

** Not analyzed.

1070-4272/05/7810-1651 © 2005 Pleiades Publishing, Inc.

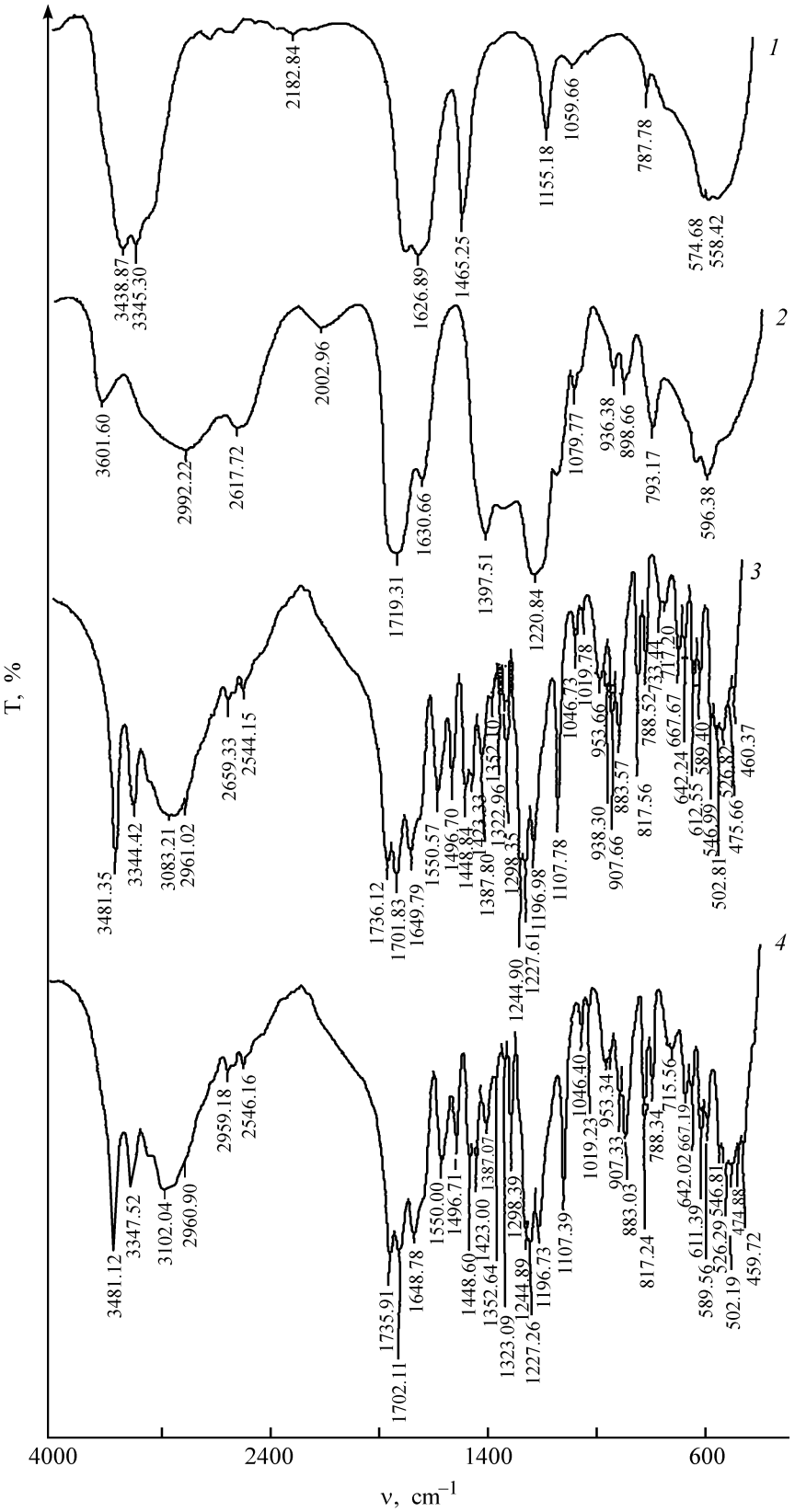


Fig. 1. IR spectra of (*1*) urea, (*2*) citric acid, and (*3*, *4*) Ur · HCit. Weight ratio of Ur + HCit to water: (*3*) 1 : 1 and (*4*) 1 : 0.5. (T) Transmission and (ν) wave number.

the amounts corresponding to 1 : 1 Ur : HCit molar ratio. All these facts suggest that urea citrate crystallizes.

In solutions with a Ur : HCit molar ratio of 1 : 2, no precipitate was formed within the range of weight ratios of the initial substances to water from 1 : 0.25 to 1 : 1. This shows that the compound Ur · HCit is not formed under the above conditions.

Interaction of urea with citric acid was studied by IR spectroscopy. Figure 1 shows the spectra of the starting urea (spectrum *1*) and citric acid (*2*) and of the 1 : 1 compound separated from the solutions with weight ratios of (Ur + HCit) to water of 1 : 1 (*3*) and 1 : 0.5 (*4*).

Changes in the spectrum of Ur · Hcit (Fig. 1, spectra *3*, *4*) relative to spectra of the starting urea (Fig. 1, spectrum *1*) and citric acid (Fig. 1, spectrum *2*) show that Ur reacts with HCit. The band of asymmetric stretching vibrations of the NH_2 group of Ur at 3480–3200 cm^{-1} is shifted to 3480–2500 cm^{-1} in the spectrum of the compound. In the spectrum of the compound, there is no well-defined band ν_{OH} within the range 3600–2500 cm^{-1}, in contrast to the spectrum of HCit.

In the region of bending vibrations of the urea amide group (1720, 1680, 1650 cm^{-1}), new narrow, well-defined bands, absent in the spectra of urea (Fig. 1, spectrum *1*) and HCit (Fig. 1, spectrum *2*), appear in the spectrum of the 1 : 1 compound (Fig. 1, spectra *3*, *4*). The bands of COO^- (1750–1600 cm^{-1}) and CH_2 (920–890, 855–735 cm^{-1}) groups and bands of the compound overlap with bands of urea CN (1604–1590 cm^{-1}) and CO (1700–1620 cm^{-1}) groups (Fig. 1, curve *1*). The presence of many new narrow, well-defined bands confirms that a compound of urea with citric acid is formed.

Figure 2 shows the curves obtained in differential thermal analysis (DTA) of urea (curve *1*), citric acid (*2*), and product of their reaction, prepared by crystallization from 1 : 1 aqueous solutions with a weight ratio of (Ur + HCit) to water of 1 : 1 (*3*) and 1 : 0.5 (*4*).

Well-defined endothermic effects are seen in the DTA curve of urea (Fig. 2, curve *1*). At 135°C, it melts and at 160–190°C, decomposes to give of biuret and cyanuric acid, which transforms at 220°C into cyanic acid with liberation of NH_3 and CO_2. At 370–470°C, cyanic acid undergoes a stepwise decomposition [1].

Under ordinary conditions, citric acid exists as a crystalline monohydrate, and the endothermic effect

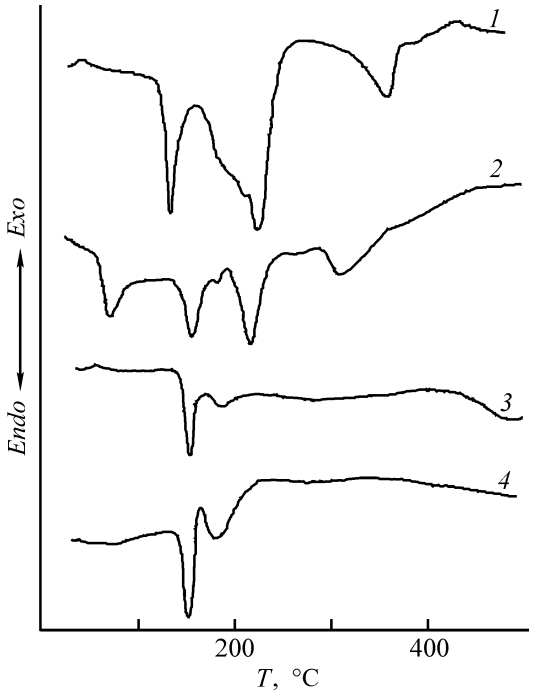


Fig. 2. DTA curves of (*1*) urea, (*2*) citric acid, and (*3*, *4*) Ur · HCit. Weight ratio of Ur + HCit to water: (*3*) 1 : 1 and (*4*) 1 : 0.5.

in the DTA curve at 60–93°C can be assigned to its dehydration (Fig. 2, curve *2*). At 148–160°C, anhydrous citric acid melts (this is in accordance with published data [11]). At temperatures higher than mp (180°C), citric acid transforms into an itaconic acid, which is reflected in the DTA curve by a large endothermic effect at 200°C. A diffuse endothermic effect at 310°C probably corresponds to itaconic acid decomposition [12].

Two endothermic effects are observed in DTA curves of the urea compound with citric acid (Fig. 2, curves *3*, *4*); a stronger effect at 160°c and a weaker effect at 200°C.

Comparison shows that urea, citric acid, and their compound have different DTA curves, and in the DTA curve of the compound, the effects characteristic of urea and citric acid are absent. This fact convincingly confirms that all the three compounds are individual. Thus, the DTA data confirm the existence of the Ur · HCit compound.

Figure 3 shows the X-ray powder patterns of urea (Fig. 1; *1*), citric acid (Fig. 1, *2*), and product of their reaction, prepared by crystallization from solutions with Ur to HCit molar ratio of 1 : 1 [Fig. 3, weight ratio of Ur + HCit to water: (*3*) 1 : 1 and (*4*) 1 : 0.5].

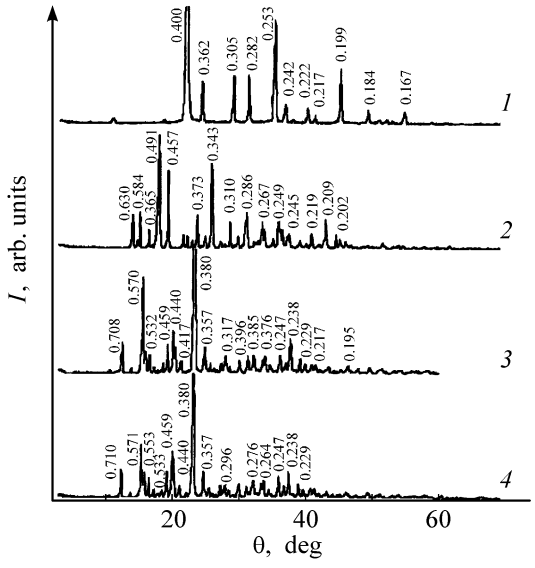


Fig. 3. X-ray powder patterns of (*1*) urea, (*2*) citric acid, and (*3*, *4*) Ur · HCit. Weight ratio of Ur + HCit to water: (*3*) 1 : 1 and (*4*) 1 : 0.5. (*I*) Intensity and (θ) Bragg angle.

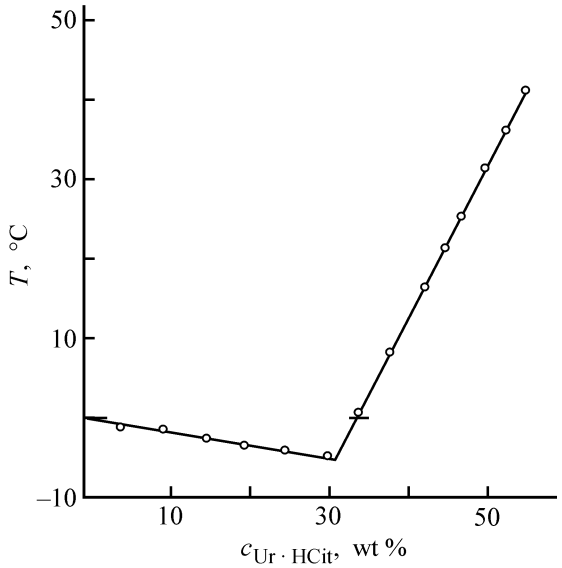


Fig. 4. Polytherm of Ur · HCit crystallization from water. (*T*) Temperature and ($c_{Ur \cdot HCit}$) Ur · HCit concentration.

The reflection intensities *I* and interplanar spacings *d* for Ur almost completely coincide with published data [13]. For HCit, certain discrepancies in *d* and *I* values between our and published data are observed, which may be caused by differences in methods of measurement and estimation of *I* and by the presence of an impurity of anhydrous HCit due to partial dehydration of $HCit \cdot H_2O$ in air.

A comparison of the powder patterns of the initial urea and citric acid and the product of their reaction showed that the product has an individual powder pattern, which contains no reflections belonging to Ur and $HCit \cdot H_2O$. This fact also convincingly confirms that the compound obtained is individual.

After recrystallization of Ur · HCit in ethanol and drying, we determined a solubility polytherm of the compound in water by the visual polythermal method [14] in the range from –5 to +40°C (Table 2, Fig. 4).

The solubility polytherm consists of two crystallization branches: those of ice (H_2O) and Ur · HCit. The eutonic point of the binary system corresponds to –5°C and to concentrations of the compound and water equal to 31.5 and 68.5%, respectively.

Thus, this study showed that urea reacts with citric acid to form a compound readily soluble in water.

Table 2. Physicochemical properties of the binary system Ur · HCit–H_2O

System composition, %		T_{cr}, °C	System composition, %		T_{cr}, °C	System composition, %		T_{cr}, °C
Ur · HCit	H_2O		Ur · HCit	H_2O		Ur · HCit	H_2O	
2.5	97.5	–0.5*	22.5	77.5	–3.7*	40.0	60.0	+11.8**
5.0	95.0	–0.9*	25.0	75.0	–4.0*	42.5	57.5	+16.0**
7.5	92.5	–1.2*	27.5	72.5	–4.5*	45.0	55.0	+21.2**
10.0	90.0	–1.7*	30.0	70.0	–4.9*	47.5	52.5	+26.2**
12.5	87.5	–2.0*	32.5	67.5	–3.2**	50.0	50.0	+31.5**
15.0	85.0	–2.4*	35.0	65.0	+1.8**	52.5	47.5	+36.2**
17.5	82.5	–2.7*	37.5	62.5	+8.0**	55.0	45.0	+41.0**
20.0	80.0	–3.2*						

* Solid phase ice (H_2O). ** Ur · HCit.

CONCLUSION

Urea reacts with citric acid in water at the 1 : 1 molar ratio to give urea citrate, which is readily soluble in water. Its solubility polytherm consists of two branches of crystallization: those of ice and urea citrate. The eutonic point of this binary system lies at –5°C and an urea citrate concentration of 31.5 wt %.

REFERENCES

1. Mel'nikov, B.P. and Kudryavtseva, I.A., *Proizvodstvo mocheviny* (Production of Urea), Moscow: Khimiya, 1965.
2. Kuznetsova, M.N. and Bergman A.G., *Zh. Obshch. Khim.*, 1956, vol. 26, pp. 1326–1329.
3. Bokhovina, I.M., Bokhovin, Yu.I., and Usplyanina, L.S., *Zh. Obshch. Khim.*, 1964, vol. 34, pp. 1375–1379.
4. Dalman, L.H., *J. Am. Chem. Soc.*, 1937, vol. 56, pp. 559–562.
5. Kucheryavyi, V.I. and Lebedev, V.V., *Sintez i primenenie mocheviny* (Synthesis and Use of Urea), Leningrad: Khimiya, 1970.
6. *Material Safety Data Sheet, Citric Acid; ACC*, no. 95374, Revision no. 1, Date 8/02/2000.
7. Sviklas, A.M., in *Neorganines chemijos ir technines elektrochemijos problemos, Kaunas, 1992 m. Resp. Conf. Medziaga*, Kaunas: Technologija, 1992, pp. 98–101.
8. *The Fertilizers (Sampling and Analysis) Regulations. Statutory Instruments. Agriculture*, London: HMSO, 1991, no. 973, p. 109.
9. Pokhodenko, L.A., *Metody opredeleniya razlichnykh form azota v mineral'nykh azotnykh udobreniyakh. Instruktsiya* (Methods of Determination of Various Nitrogen Forms in Mineral Nitrogen Fertilizers. Instruction), Lvov: LPI, 1986.
10. Williams, W.J., *Handbook of Anion Determination*, London: Butterworths, 1979.
11. Perel'man. V.I., *Kratkii spravochnik khimika* (Brief Chemist's Handbook), Moscow: Khimiya, 1964.
12. *Khimicheskii entsiklopedicheskii slovar'* (Chemical Encyclopaedia), Knunyants, I.L., Ed., Moscow: 1983.
13. McMurdie, H., Morris, M., Evans, E., *et al., Powder Diffraction*, 1986, no. 1, p. 345.
14. Eraizer, L.N. and Kaganskii, I.M., *Zavod. Lab.*, 1967, no. 1, p. 119.

Russian Journal of Applied Chemistry, Vol. 78, No. 10, 2005, pp. 1656–1658. Translated from Zhurnal Prikladnoi Khimii, Vol. 78, No. 10, 2005, pp. 1684–1686.
Original Russian Text Copyright © 2005 by Badalova, Mamedova, Alieva, Magerramov, Allakhverdiev.

ORGANIC SYNTHESIS AND INDUSTRIAL ORGANIC CHEMISTRY

Reaction of 1-Amino-3-propoxy-2-propanol with Aldehydes

K. K. Badalova, A. R. Mamedova, R. A. Alieva, A. M. Magerramov, and M. A. Allakhverdiev

Baku State University, Baku, Azerbaijan

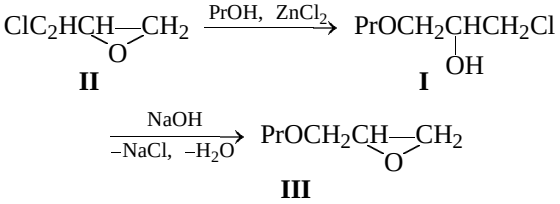
Received January 13, 2005

Abstract—The reaction of 1-amino-3-propoxy-2-propanol was examined as a route to the corresponding 1,3-oxazolidines.

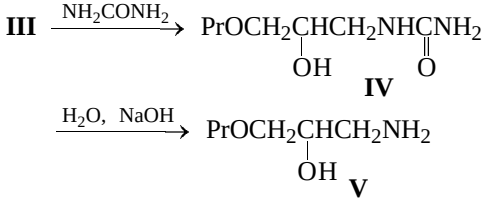
Condensation of 1,3-amino alcohols with carbonyl compounds yields 1,3-oxazolidines [1–7], which exhibit a wide spectrum of biological activity. They are used as starting compounds for preparing drugs against arrythmia and stenocardia [8]. Some oxazolidine derivatives exhibit antitumor activity [9]. 1,3-Oxazolidine derivatives are frequently effective as antimicrobial agents [10].

In this study, we examined the reaction of 1-amino-3-propoxy-2-propanol with aldehydes as a route to new substituted 1,3-oxazolidines.

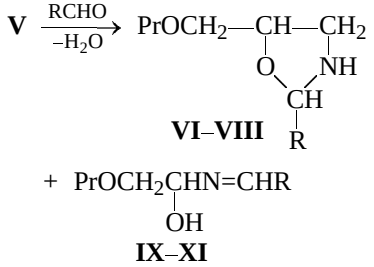
In the synthesis of 1-amino-3-propoxy-2-propanol, we started from compound **I** formed by reaction of 1-propanol with epichlorohydrin **II** in the presence of $ZnCl_2$ catalyst. Compound **I** was converted to 3-propoxy-1,2-epoxypropane **III** by treatment with NaOH:



Nucleophilic opening of the oxirane ring in **III** with urea, followed by hydrolysis of the resulting amide **IV** with aqueous NaOH, yielded 1-amino-3-propoxy-2-propanol **V**:



Then we studied the condensation of amino alcohol **V** with various aldehydes and obtained the corresponding 1,3-oxazolidines **VI**–**VIII**:

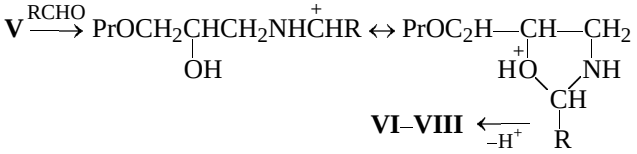


where R = Me (**VI**, **IX**), Pr (**VII**, **X**), Ph (**VIII**, **XI**).

The yield of **VI**–**VIII** largely depends on the reactant ratio and reaction conditions. Usually the reaction starts at low temperatures (25–30°C). On adding an aldehyde to **V**, the temperature rises to 90–100°C. Above 90–100°C, by-products are formed. The 1 : 1.2 ratio between amino alcohol **V** and aldehyde **VI**–**VIII** is optimal. The yield of oxazolidines increases when the reaction is performed in benzene with azeotropic distillation of the released water.

The reaction of **V** with aldehydes yields, along with oxazolidines **VI**–**VIII**, also propoxy-substituted azomethines **IX**–**XI**.

The ratio of oxazolidines **VI**–**VIII** and azomethines **IX**–**XI** depends on the substituent at the carbonyl group. Apparently, bulky substituents R hinder the heterocyclization:



1070-4272/05/7810-1656 © 2005 Pleiades Publishing, Inc.

The structures of **VI**–**VIII** were confirmed by NMR and IR spectroscopy.

In the ^{1}H NMR spectrum of oxazlidine **VI**, the methyl group gives a triplet at 0.85 ppm. The methine proton bonded to the CH_3 group gives a multiplet at 4.2 ppm. The two CH_2N protons give a doublet at 2.9 ppm. The methine group in the CH_2CHCH_2 fragment appears as a quintet at 4.1–4.4 ppm. The ^{1}H NMR spectra of **VII** and **VIII** are similar to that of **VI** and differ only in the signals of R.

The IR spectra of 1,3-oxazolidines **VI**–**VIII** contain an absorption band of the five-membered ring at 1381, 1355, and 1240 cm^{-1}, respectively. The N–H stretching vibrations are manifested at about 3150 cm^{-1}.

Compounds **VI**–**XI** were tested as antimicrobial additives to DS-11 oil [GOST (State Standard) 9.052–75]. The antimicrobial activity of these compounds was assessed by the zone diffusion method using microorganisms (GOST 9.052–75). The procedure is described below.

A culture medium (20–25 ml) was placed in a Petri dish, cooled, and seeded with microorganisms. Then four holes (10 mm in diameter, 4–5 mm deep) were made with sterile tools on the surface of the culture medium, and 0.3–0.4 ml of a 5% solution of a test compound in T-46 oil was introduced into these holes. The Petri dishes with bacteria were kept in a thermostat for 2 days at 28–30°C, and those with fungi, at the required humidity for 4 days.

We found that the compounds synthesized are readily soluble in oil, exhibit pronounced antimicrobial effect at low concentrations (0.5–1.0 mol %), and do not stimulate corrosion. With 0.5–1.0 mol % of **V**, the width of the suppression zone is 0.9–1.6 cm for bacteria and 1.1–1.3 cm for fungi. As a reference we chose the widely used sodium pentachlorophenolate; at its concentration of 0.5–1.0 mol %, the width of the suppression zone is 0.7–1.3 cm for bacteria and 0.7–1.4 cm for fungi.

The antimicrobial activities of oxazolidines **VI**–**VIII** and azomethines **IX**–**XI** are lower than that of amino alcohol **V**.

EXPERIMENTAL

1-Chloro-3-propoxy-2-propanol I. A three-necked flask equipped with a thermometer was charged with 10 g of 1-propanol, 18.5 g of epichlorohydrin **II**, and 0.5 g of $ZnCl_2$. The mixture was heated at 60–70°C for 4 h and then cooled to 20°C in a vacuum. Compound **I** was isolated by distillation; yield 25.6 g (90%), bp 93–94°C (20 mm Hg), n_D^{20} = 1.4398. Published data [11]: bp 97–98°C (20 mm Hg), n_D^{20} = 1.4378.

3-Propoxy-1,2-epoxypropane III. A three-necked flask was charged with 15.3 g of **I** and 50 ml of dry diethyl ether, after which 11.2 g of finely divided KOH was added in portions, and the mixture was heated on a water bath at 50°C for 1 h. After cooling, the precipitate was separated and washed with three portions of diethyl ether. The solvent was removed, and the product was distilled. Yield 7 g (60%), bp 147–148°C, n_D^{20} = 1.4716. Published data [12]: bp 63°C (11 mm Hg), n_D^{20} = 1.4691.

***N*-(3-Propoxy-2-hydroxypropyl)urea IV.** Compound **III** (23.2 g) was added dropwise to 12 g of molten (135–140°C) urea, and the mixture was heated at 135–140°C for 3 h, after which it was cooled and extracted with hot chloroform. The white crystalline substance that precipitated from chloroform was filtered off. Yield 5 g (14%), mp 121–122°C.

Found, %: C 47.53, H 9.29, N 15.71.
$C_7H_{16}N_2O_3$.
Calculated, %: C 47.71, H 9.15, N 15.90.

1-Amino-3-propoxy-2-propanol V. A flask equipped with a thermometer and a reflux condenser was charged with 8.8 g of **IV** and 2 g of 20% NaOH. The mixture was refluxed for 15 h, cooled, dried over KOH, and distilled in a vacuum. Yield 4 g (60%), bp 85–86°C (1 mm Hg), n_D^{20} = 1.4520.

2-Methyl-5-propoxymethyl-1,3-oxazolidine VI and 1-methylimino-3-propoxy-2-propanol IX. A three-necked flask equipped with a thermometer and a dropping funnel was charged with 13.3 g of **V** and 50 ml of benzene. Then 3.4 g of acetaldehyde was added with vigorous stirring from the dropping funnel. The stirring was continued for 1 h at room temperature and then for 2 h at 65–70°C. The solvent was distilled off on a water bath, and the residue was distilled in a vacuum. Two fractions were isolated: (i) 5.9 g (37%) of **VI** and (ii) 7.5 g (47%) of **IX**.

Compounds **VII**, **VIII**, **X**, and **XI** were obtained similarly. The physicochemical constants of **VI**–**XI** are listed in the table.

Yields, constants, and elemental analyses of **VI**–**XI**

Compound	Yield, %	bp, °C (*p*, mm Hg)	n_D^{20}	d_4^{20}	Found, %/Calculated, %			Formula
					C	H	N	
VI	59	67–68 (1)	1.4405	1.2577	59.98/60.35	10.61/10.76	8.96/8.79	$C_8H_{17}NO_2$
VII	50	81–82 (1)	1.4490	1.2433	64.47/64.14	11.06/11.30	7.92/7.48	$C_{10}H_{21}NO_2$
VIII	14	178–179 (1)	1.5510	1.5214	70.12/70.5	8.87/8.65	6.08/6.33	$C_{13}H_{19}NO_2$
IX	18	104–105 (1)	1.4670	1.2824	60.13/60.35	10.51/10.76	8.95/8.79	$C_8H_{17}NO_2$
X	28	132–133 (1)	1.4750	1.2724	63.88/64.14	11.43/11.30	7.61/7.48	$C_{10}H_{21}NO_2$
XI	36	140–141 (1)	1.5315	1.5410	70.62/70.56	8.19/8.65	6.08/6.33	$C_{13}H_{19}NO_2$

CONCLUSIONS

(1) A procedure was developed for preparing 1-amino-3-propoxy-2-propanol, from which the corresponding 1,3-oxazolidines were obtained in reasonable yields.

(2) 1-Amino-3-propoxy-2-propanol, when used as an additive to DS-11 oil, exhibits antimicrobial and fungicidal activity, exceeding that of sodium pentachlorophenolate.

REFERENCES

1. Rakhmankulov, D.L., Zorin, V.V., Latynova, F.N., *et al.*, *Khim. Geterotsikl. Soedin.*, 1982, no. 4, pp. 435–449.
2. Kukharev, B.F., Stankevich, V.K., Klimenko, G.R., and Lobanova, N.A., *Zh. Org. Khim.*, 2003, vol. 39, no. 11, pp. 1627–1630.
3. Keiko, N.A., Funtikova, E.A., Stepanova, L.G., *et al.*, *Zh. Org. Khim.*, 2003, vol. 39, no. 10, pp. 1546–1552.
4. Bulatova, O.F., Romanov, N.A., Chalova, O.B., and Rakhmankulov, D.L., *Zh. Org. Khim.*, 2001, vol. 37, no. 12, pp. 1834–1837.
5. Blancht, J., Bonin, M., Mecacum, L., and Husson, H., *J. Org. Chem.*, 2000, vol. 65, no. 20, pp. 6423–6426.
6. Zhang, I. and Ye, F., *Finne Chem.*, 2002, vol. 19, no. 81, pp. 493–495.
7. Sharma, S.D. and Bhaoluri, S., *J. Chem. Res. Synop.*, 2001, no. 8, pp. 321–323.
8. JPN Patent 21421, *Ref. Zh. Khim.*, 1973, 8N290P.
9. Banerjee, D., Mukerji, S., Dutta, N.L., and Mitra, B.N., *Indian J. Chem.*, 1971, vol. 9, no. 4, pp. 799–803.
10. Kalm, M.J., *J. Org. Chem.*, 1960, vol. 25, no. 11, pp. 1929–1936.
11. Flores-Gallardo, H. and Pollard, C.D., *J. Org. Chem.*, 1947, vol. 12, no. 6, pp. 831–833.
12. Ponomarev, F.G., *Zh. Obshch. Khim.*, 1952, vol. 22, no. 4, pp. 929–931.

Russian Journal of Applied Chemistry, Vol. 78, No. 10, 2005, pp. 1659–1661. Translated from Zhurnal Prikladnoi Khimii, Vol. 78, No. 10, 2005, pp. 1687–1690.
Original Russian Text Copyright © 2005 by Baranova, Bogdanova, Bandorin, Kostochko.

ORGANIC SYNTHESIS AND INDUSTRIAL ORGANIC CHEMISTRY

Energy and Acid–Base Characteristics of the Surface of Nitramine Fillers for Polymeric Composites

N. V. Baranova, S. A. Bogdanova, V. G. Bandorin, and A. V. Kostochko

Kazan State Technological University, Kazan, Tatarstan, Russia

Received March 25, 2005

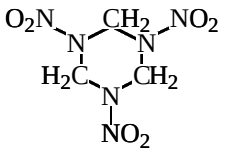
Abstract—Single crystals of nitramine fillers for special-purpose polymeric composites are characterized by the surface energy and its constituents and also by the acidity of their surface.

It is well known that mechanical properties of filled polymeric composites are governed by interactions at the interface between the polymer matrix and the filler. The structure and properties of the interfacial layers depend not only on the physicochemical characteristics of the polymer, but also on the surface properties of the filler. The major contribution to the development of the concepts of the interfacial interactions as the key factor governing the properties of filled polymers was made by Lipatov [1, 2], Fowkes [3], Berger [4], and Kinloch [5]. They have clearly demonstrated the necessity for studying the donor–acceptor and dispersion interactions at the polymer/filler interface. At the same time, the morphology of fillers, as a factor strongly affecting the surface energy and acid–base characteristics, has been considered insufficiently.

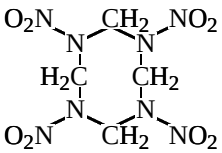
In preparation of energetic cellulose nitrate composites, it is necessary to ensure the adhesion of the polymer to crystalline nitramine fillers. We have determined previously the surface energy and its constituents in softened cellulose nitrates [6, 7]. In studying mechanism of interaction between the polymer and filler in order to improve the performance characteristics of such systems, it appeared advisable to estimate the surface energy and its constituents and also the surface acidity of crystalline fillers, nitro derivatives of heterocyclic amines.

EXPERIMENTAL

As objects of this study served single crystals of cyclotrimethylenetrinitramine (N3) and cyclotetramethylenetetranitramine (N4), prepared by the temperature drop method under free convection conditions in solution.



N3



N4

In this method, supersaturation was set by the temperature difference between the zone of dissolution of the polydisperse crystals and the zone of single-crystal growth.

As initial solutions we used the solution of N3 in an acetone–DMF mixture and the solution of N4 in an acetone–DMSO mixture, saturated at room temperature. The solvents were purified prior to use.

The surface energy (SE) of various faces of the samples (γ_S) and its polar (γ_S^p) and dispersion (γ_S^d) terms were determined from the contact angles with probe liquids whose surface tensions are listed in Table 1.

Table 1. Surface tension of probe liquids and its polar and dispersion terms

Liquid	γ_L^p	γ_L^d	γ_L
	mN m^{-1}		
Water	50.2	22.0	72.2
Glycerol	30.0	34.0	64.0
Formamide	26.0	32.3	58.3
5% Aqueous ammonia	33.8	31.9	65.7
Ethylene glycol	29.3	19.0	48.3
Methylene iodide	2.3	48.5	50.8

1070-4272/05/7810-1659 © 2005 Pleiades Publishing, Inc.

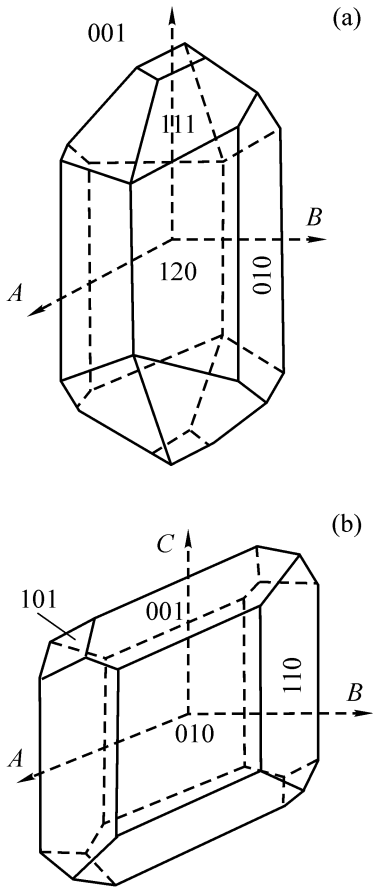


Fig. 1. Crystallographic orientation of single crystals of (a) cyclotrimethylenetrinitramine and (b) cyclotetramethylenetetranitramine.

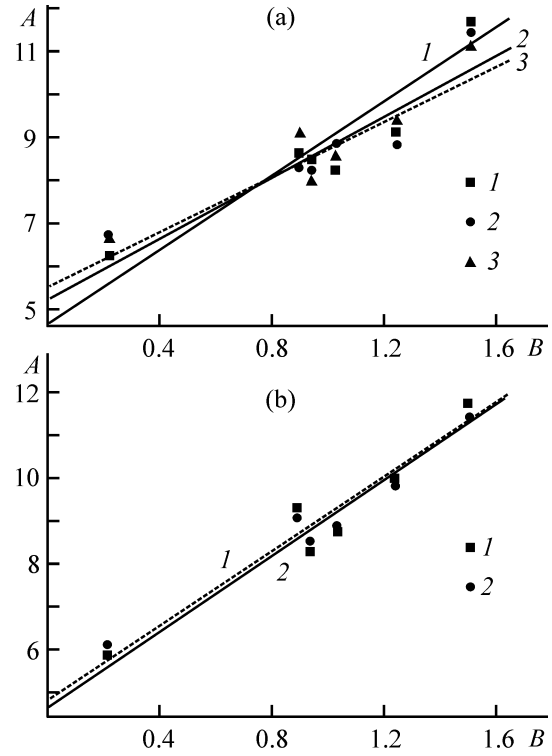


Fig. 2. Fowkes plots for determining the surface energy of (*1*) cyclotrimethylenetrinitramine and (*2*) cyclotetramethylenetetranitramine from data obtained with six probe liquids. Fowkes coordinates: (*A*) $W/(\gamma_L^d)^{0.5}$ and (*B*) $(\gamma_L^p/\gamma_L^d)^{0.5}$. (a) Face: (*1*) (120), (*2*) (010), and (*3*) (001). Fit parameters: (*1*) $Y = 4.68 + 4.29X$, (*2*) $Y = 5.24 + 3.53X$, and (*3*) $Y = 5.54 + 3.18X$. (b) Face: (*1*) (010) and (*2*) (110). Fit parameters: (*1*) $Y = 4.70 + 4.36X$ and (*2*) $Y = 4.84 + 4.31X$.

The contact angle was determined by the sessile drop method at 29 ± 1 K. The measurements were carried out in a cell with a water seal, using a KM-8 cathetometer equipped with a micrometer gauge. At least 10 drops of equal volume were placed onto the surface with a microsyringe. Preliminarily, the spread kinetics was studied, to determine the equilibrium value of $\cos\theta$.

Following to the Fowkes concept [3], the free surface energy was estimated graphically from the experimental contact angles using the Owens–Wendt equation. The dependence plotted in the coordinates $(\gamma_L^p/\gamma_L^d)^{0.5} - 0.5\gamma_L(1 + \cos\theta)/(\gamma_L^d)^{0.5}$ was represented by a straight line (correlation factor $r \geq 0.93$). Data were processed by the least-squares method.

The surface acidity parameter D was determined by Berger's method [4] from the polar and dispersion terms of the surface energy and contact angles with Lewis acids (ethylene glycol and glycerol) and Lewis bases (5% aqueous ammonia and formamide). For the surfaces bearing essentially acidic groups (proton donors), $D > 0$, and for proton-acceptor surfaces, $D < 0$.

The elementary fragments forming the single crystal of cyclotrimethylenetrinitramine are rhombic prism (120), bipyramid (111), and pinacoids (010) and (001) (Fig. 1a), and those in the cyclotetramethylenetetranitramine are rhombic prism (110), dihedrons (011), and pinacoids (010) and $(\bar{1}01)$ (Fig. 1b).

Contact angle measurements were carried out on the most developed faces of the single crystals. For N3 these are (120), (010), and (001); and for N4, (010) and (110). The surfaces to be studied were 1.0×0.7 cm.

Since the surface energy is mostly different for different faces [8], it was necessary to determine the energy characteristics of all the most developed surfaces in the crystals.

The dependences plotted in the Fowkes coordinates are shown in Figs. 2a and 2b. The experimental sur-

Table 2. Energy parameters of different faces in single crystals of the nitramine fillers

Filler	Face index	γ_S^p	γ_S^d	γ_S
		mN m^{-1}		
N3	(120)	18.40	21.90	40.30
	(010)	12.50	27.40	39.90
	(001)	10.10	30.70	40.80
N4	(010)	19.00	22.00	41.00
	(110)	18.60	23.40	42.00

face energy γ_S and its polar (γ_S^p) and dispersion (γ_S^d) terms are listed in Table 2.

The surface energy of the N4 crystal is somewhat higher than that of N3 (Table 2), which can be attributed to the presence of short intra- and intermolecular bonds in the structure of N4. Despite that the crystals of the nitramines studied are built up from polar molecules, they demonstrate orientation polarization in the solid state. The N4 molecules have some rotational freedom and, in the crystal, they demonstrate capacity for polarization, which is more clearly pronounced as compared to N3.

The results obtained show that, in the organic crystals studied, the dispersion term of the surface energy prevails over the polar term.

Presently, the adsorption (molecular) theory of adhesion is considered to be the most preferable tool for understanding of processes occurring in formation of polymer-based materials [5]. In the framework of this theory, an important part is played by the concept of acid–base interactions, since it is the acidity or basicity of polar molecules in the surface layer between the contacting condensed phases that controls the adhesion interaction (the effect of acidity or basicity on the adhesion contact is more significant than that of the surface energy). The Fowkes opinion [3] is that the work of adhesion could be considerably increased through acid–base interaction on the surface. Therefore, it is important to determine the acidity factor of both the polymer and surface centers of the filler.

The acidity factors of the nitramine fillers in hand, determined by Berger's method, are given in Table 3.

Analysis of these data shows that acid sites dominate on the surface of the fillers ($D > 0$). This is not surprising, since N3 and N4 molecules contain electropositive nitrogen of the nitro groups, which is a typical Lewis acid. It is noteworthy that the maximal D values correspond to the pinacoidal faces.

Table 3. Acid–base characteristics of the surfaces of single crystals of the nitramine fillers

Filler	Face index	Acidity factor D, (mN m^{-1})$^{0.5}$
N3	(120)	1.10
	(010)	3.64
	(001)	1.49
N4	(010)	2.88
	(110)	1.82

The results obtained show that the acidity factor depends on the type of the crystal surface, more so for N3, which is probably due to its more pronounced anisotropy.

To conclude, the surface energy and acid–base characteristics of the fillers should be necessarily taken into account in developing filled polymeric composites with advanced mechanical properties.

CONCLUSIONS

(1) The surface energy and its constituents were determined for various faces of the single crystals of nitramine fillers. It was shown that the surface energy characteristics depend on the crystal morphology.

(2) It was demonstrated Lewis acid groups dominate in the surface layer of the cyclotrimethylenetrinitramine and cyclotetramethylenetetranitramine crystals.

REFERENCES

1. Lipatov, Yu.S., *Fizicheskaya khimiya napolnennykh polimerov* (Physical Chemistry of Filled Polymers), Moscow: Khimiya, 1977.
2. Lipatov, Yu.S., *Fizikokhimicheskie osnovy napolneniya polimerov* (Physicochemical Principles of Filling Polymers), Moscow: Khimiya, 1991.
3. Fowkes, F., *J. Adhesion Sci. Tech.*, 1987, vol. 1, no. 1, pp. 7–27.
4. Berger, E.J., *J. Adhesion Sci. Tech.*, 1990, vol. 4, no. 5, pp. 373–391.
5. Kinloch, A.J., *Adhesion and Adhedsives: Science and Technology*, New York: Chapman & Hall, 1987.
6. Baranova, N.V., Bogdanova, S.A., Smola, E.B., *et al.*, *Fiz. Khim. Mikrosk.*, 2000, vol. 2, no. 2, pp. 187–195.
7. Baranova, N.V., Bogdanova, S.A., Smola, E.B., *et al.*, in *Vserossiiskaya konferentsiya "Energeticheskie kondensirovannye sistemy"* (All-Russian Conf. "Energetic Condensed Systems"), Moscow, 2002, pp. 114–115.
8. Adamson, A.W., *Physical Chemistry of Surfaces*, New York: Wiley, 1976.

Russian Journal of Applied Chemistry, Vol. 78, No. 10, 2005, pp. 1662–1667. Translated from Zhurnal Prikladnoi Khimii, Vol. 78, No. 10, 2005, pp. 1691–1696.
Original Russian Text Copyright © 2005 by Marinichev, Vyaz'min, Domnin.

MACROMOLECULAR CHEMISTRY AND POLYMERIC MATERIALS

A Spectrophotometric Study of Solid-Phase Topochemical Polymerization of Diyne Arylcarbamates and Logistic Representation of Results

A. N. Marinichev, S. Yu. Vyaz'min, and I. N. Domnin

St. Petersburg State University, St. Petersburg, Russia

Received April 27, 2005

Abstract—Application of a logistic regression to interpretation of results is illustrated by spectrophotometric data on solid-state polymerization of symmetric and asymmetric diyne carbamates.

Use of organic solvents in modern large-tonnage chemical industry may be a source of ecological problems because of the possible uncontrolled development of chemical processes performed. Therefore, chemical transformations in the solid phase have a clear advantage and development of methods for carrying out processes of this kind is a task of a rapidly developing, ecologically safe "green chemistry" [1]. The reaction of solid-state topochemical polymerization (STP) has been discovered by Wegner for the example of 2,4-hexadiyne-1,6-diol $HOCH_2C{\equiv}CC{\equiv}CCH_2OH$ [2]. STP of functionally substituted diacetylenes (DA) belongs to one of classes of topochemical reactions and consists in a diffusionless transition of monomer crystals into polymer crystals, with the centers of mass of monomer units retaining their crystallographic position. Such a stereospecific polymerization, governed by the monomer packing in the crystal lattice, yields a stereoregular polymer with a linear arrangement of molecules and small number of structural defects [3]. As is known, a key influence on the course of such STP is exerted by the long-range order in the crystal lattice of a monomer. STP to give polydiacetylenes (PDA) can be initiated by ultraviolet or gamma-ray irradiation, as well as by X-rays or a flow of beta-decay electrons. In some cases, STP is also possible upon heating of the starting monomers [4].

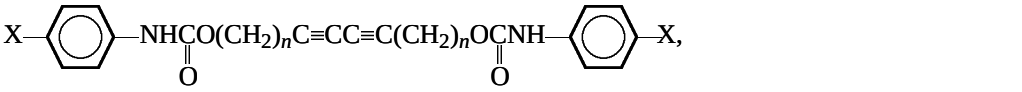
PDA find increasingly wide use as a chromatic element in biosensors [5–7]. However, of particular interest to researchers are their unique optical properties, because their third-order optical susceptibility coefficients $\chi^{(3)}$ reach, for this class, the most optimal values among all the known organic compounds. In this context, a study of PDA has become, from a particular area of the chemistry of polymers, an interdisciplinary field of intensive research including synthesis of new DA and PDA, analysis of the STP mechanism, spectroscopy, materials science, and even chemistry of biomimetics [8].

One of the most important tasks in studies of STP is to establish relationships between structural features of monomer DA and their activity in STP. The best studied, in this regard, monomer is bis(*p*-tolyl) hexa-2,4-diyne-1,6-diol sulfonate [9], for which an induction period and an autocatalytic stage have been observed in UV- and radiation-initiated STP. In the first case (UV irradiation), the rate of TPS markedly decreases as the conversion becomes higher, which can be attributed to transfer of the energy of the excited state of the monomer to the polymer chain [10]. As a rule, STP is only observed in those DA whose substituents contain groups that can form hydrogen bonds or be involved in a dipole–dipole interaction. In this context, DA that contain urethane groups as substituents in the side chain and can form intermolecular hydrogen bonds in neighboring stacks of diacetylene monomers are of particular interest [11]. As a continuation of the previous research in this field [12], 5 new symmetric diacetylene arylcarbamates and 27 new phenyl- and arylcarbamates of asymmetric structure were synthesized.

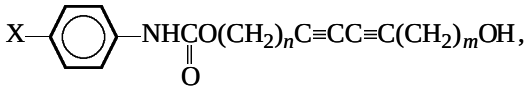
No detailed systematic data on the reactivity of diynes in relation to the number of methylene groups (*n*) between the system of conjugated triple carbon–carbon bonds and the carbamate function can be found in the literature. There are no data, either, on the influence exerted by a substituent in the aryl ring of diyne carbamates. This influence must apparently af-

1070-4272/05/7810-1662 © 2005 Pleiades Publishing, Inc.

fect the strength of the hydrogen bond and, consequently, the specific features of packing of diyne molecules in the crystal. For these reasons, the carbamate group was chosen as a functional group, and the following bis-arylcarbamates were selected among the simplest model compounds:



[X = H: n = 2 (**Ia**), n = 3 (**Ib**), n = 4 (**Ic**), n = 5 (**Id**). n = 6 (**Ie**), n = 7 (**If**), and n = 9 (**Ig**); X = OMe: n = 3 (**Ih**), n = 4 (**Ii**), and n = 5 (**Ij**)] and a number of diyne *N*-arylcarbamates of asymmetric structure, previously not described in the literature:



[X = H: n = 2, m = 2 (**IIa**); n = 2, m = 4 (**IIb**); n = 4, m = 4 (**IIc**); n = 5, m = 4 (**IId**); n = 6, m = 4 (**IIe**); and n = 9, m = 4 (**IIf**); X = OMe: n = 2, m = 2 (**IIg**); and n = 4, m = 4 (**IIh**)].

EXPERIMENTAL

The PMR and ^{13}C NMR spectra were measured on a Bruker DPX-300 instrument (300.13 MHz), with TMS as internal standard and $CDCl_3$, DMCO-d_6, and CD_3COCD_3 as solvents. The IR spectra were recorded on a Specord IR-75 spectrometer in $CHCl_3$ or KBr pellets. The electronic spectra were obtained on a Specord M40 UV-VIS spectrometer in DMF and CH_3CN. Analytical thin-layer chromatography was performed on Sulifol UV-254 plates, with development with UV light (λ_{max} = 254 nm) or a potassium permanganate solution. Preparative thin-layer chromatography was carried out on Silpearl silica gel with development with UV light, and column chromatography, on an M60 silica gel (manufactured by Merck). STP was performed under irradiation with UV light from BUV-15 low-pressure mercury lamps (λ_{max} = 254 nm). The polymerization was done under the standard conditions for all the diynes. A 5- to 20-mg portion of a diyne, dependent on the mass of the weighed portion necessary for recording the electronic spectrum, 3–5 ml of *n*-hexane, and a magnetic rabble were placed in a weighing bottle 21 mm in diameter. The bottle with the suspension was placed at a distance of 10 cm from the lamps. The irradiation was carried out with agitation at a constant rate at room temperature for a varied time recorded with a stopwatch. After that, the reaction mixture was allowed to stay for 1.5–2 h in an exhaust hood to remove *n*-hexane and then placed in a vacuum-desiccator for 24 h. Two samples were taken from each weighing bottle for a study of the STP by electron spectroscopy.

Changes in the system, caused by the STP of diyne arylcarbamates, are well recorded spectrophotometrically by measuring the analytical signal (AS), whose role can be played by the extinction coefficient ε (M^{-1} cm^{-1}), at different instants of time t. Tables 1, 2 list the experimental extinction coefficients obtained in this study for 10 symmetric and 8 asymmetric dyine carbamates.

The kinetic curves $\varepsilon(t)$ are monotonic lines bounded by the limiting value $\varepsilon(\infty)$, which can show a slowed-down variation of the extinction coefficient at the initial instants of time (so-called induction period).

Such dependences, both with an induction period and without it, are well described by logistic regression curves of the type:

$$\varepsilon(t) = c/[1 + a\exp(-bt)], \quad (1)$$

where a and c are constants relating the initial and final (limiting) values of AS:

$$\varepsilon(0) = c/(1 + a) \text{ and } \varepsilon(\infty) = c. \quad (2)$$

In addition, it can be readily shown that expression (1) is a solution to the differential equation

$$dy/dt = bt(1 - y), \quad (3)$$

in which $y = \varepsilon(t)/c$ is a dimensionless AS. Similarly to the rate constant of a first- or pseudo-first-order, the parameter b has dimension of a reverse time (min^{-1}). Thus, the single-parameter kinetic equation (3) can be accepted as a simplified description of the kinetics of a multistage chemical process, with the formation and accumulation of the product (poly-

Table 1. Experimental and calculated extinction coefficients of symmetric diyne carbamates in the course of STP

Substance			Experiment		Results of calculation				
					parameters of Eq. (1)				
no.	*n*	X	*t*, min	ε, M^{-1} cm^{-1}	*a*	*b*	*c*	ε_{calc}, M^{-1} cm^{-1}	Δε
Ia	2	H	10	1471, 1471	6.39	0.0938	4304	1228	380
			20	1731, 1675				2173	
			30	3583, 3517				3110	
			40	3402				3742	
Ib	3	H	10	1437, 1473	4.38	0.0702	4388	1380	195
			30	2332, 2973				2858	
			40	3421, 3913				3468	
			90	4370				4353	
Ic	4	H	30	137, 164	71.9	0.0702	879	90	35
			40	130, 132				165	
			50	243, 244				279	
			60	442, 469				426	
			90	770				778	
Id	5	H	30	96, 94	1.17	0.0594	108	90	4
			40	94, 101				97	
			90	106				107	
			120	109				108	
Ie	6	H	45	61, 75	40.1	0.0511	436	87	15
			60	158, 187				152	
			90	290				311	
			120	412, 397				401	
If	7	H	10	1933, 1892	3.41	0.0430	5921	1844	140
			30	2968, 2905				3058	
			60	4896				4708	
			90	5271, 5696				5529	
Ig	9	H	10	6024, 5733	1.03	0.0332	10196	5937	75
			20	6597, 6736				6731	
			60	8912, 8933				8972	
			70	9213, 9304				9287	
Ih	3	OMe	2	2249, 2254	0.67	0.218	3115	2144	130
			5	2347, 2380				2522	
			10	3062, 3030				2887	
			15	3144				3034	
			20	2936, 3038				3087	
Ii	4	OMe	2	2258, 2230	2.30	0.216	6251	2504	310
			5	3977, 3950				3510	
			10	4328				4941	
			15	5838				5734	
			20	6292, 5954				6065	
Ij	5	OMe	30	127	139.1	0.180	207	127	6
			40	180, 196				188	
			60	195, 206				206	
			90	205, 219				207	

Table 2. Experimental and calculated extinction coefficients of asymmetric diyne carbamates in the course of STP

Substance				Experiment		Results of calculation				
						parameters of Eq. (1)				
no.	*n*	*m*	X	*t*, min	ε, M^{-1} cm^{-1}	*a*	*b*	*c*	ε_{calc}, M^{-1} cm^{-1}	Δε
IIa	2	2	H	10	447, 495	0.51	0.0885	569	472	8
				20	550, 550				524	
				30	524				550	
				60	573, 563				568	
IIg	2	2	OMe	30	49, 44	28562	0.268	933	91	83
				40	576, 645				572	
				50	726, 751				894	
				54	1027, 1025				919	
				120	987				933	
IIh	4	4	OMe	45	136, 139	28124	0.211	423	87	7
				60	387				136	
				75	445, 417				388	
				120	413				421	
IIb	2	4	H	10	524, 520		0.101	1625	548	100
				20	939, 942				947	
				30	1404, 1428				1289	
				40	1197, 1397				1484	
				60	1782				1605	
IIc	4	4	H	45	46, 54	119.7	0.0700	249	41	15
				75	135, 135				153	
				90	226, 226				204	
				120	226				242	
IId	5	4	H	60	20, 16	59.9	0.0613	47	19	2
				80	34, 34				33	
				100	38, 44				42	
				120	42				45	
				180	48, 49				47	
IIe	6	4	H	25	84, 71	4.92	0.0522	202	87	7
				30	162, 164				100	
				60	197, 193				166	
				90	121				193	
IIf	9	4	H	45	64, 65	4.12	0.0352	113	61	6
				63	73, 74				78	
				75	75, 89				87	
				90	108, 107				96	
				120	102, 104				107	

diacetylene in the case in question) recorded via the AS. It is noteworthy that a nonzero value of ε(0) may, apparently, be due to the instrumental background of the AS being measured.

Previously [13], a logistic regression has been applied to description of a reversible decomposition of a substance into products, with direct monitoring of how the reagent concentration varies. The present com-

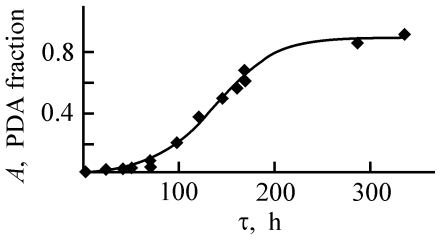


Fig. 1. Kinetic curve for polymerization of diyne at 75°C [15]. (*A*) PDA fraction and (τ) time. Here and in Fig. 2, the experimental data are represented by points, and the calculated dependence, by lines.

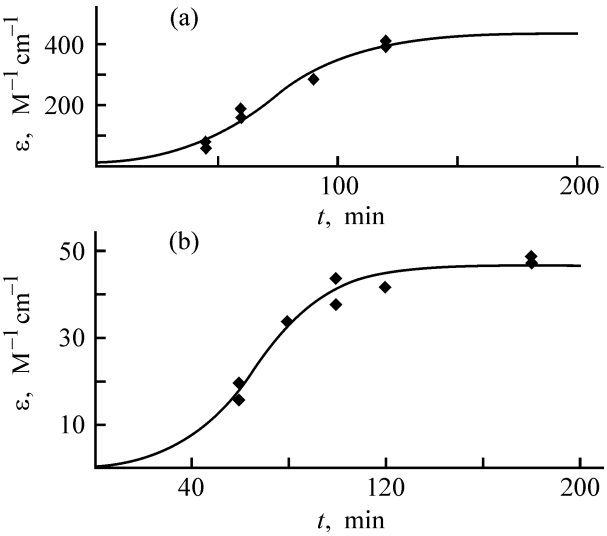


Fig. 2. Kinetic curve for STP of (a) 7,9-hexadecadiyne-1,16-diyl-bis-*N*-phenylcarbamate (**Ie**, n = 6, X = H) and (b) 13-hydroxy-6,8-tridecadiyne-1-yl-*N*-phenylcarbamate (**IId**, n = 5, m = 4, X = H). (ε) Extinction coefficient and (*t*) time.

munication discusses the cases when this monitoring is done with AS.

The parameters *a*, *b*, and *c* were calculated from the experimental data obtained, using the Logist 83 program from the freely accessible software package Statistics with List Editor (http://text.staticfree.info/statsle.pdf), which was transferred to a Texas Instruments TI-89 graphic calculator [14].

An equation of type (1) was tested for published data on [15] the STP of diyne to give PDA. Here, the PDA fraction x was regarded as the AS. The equation for calculating $x(t)$, obtained by processing of experimental data, has the form:

$$x(t) = \frac{0.900}{1 + 81.5\exp(-0.0323t)}.$$

The results obtained in the calculation (line) and the experimental points are shown in Fig. 1.

In a similar way, an expression of type (1) was used to describe the experimental data [ε(*t*)] obtained in this study (Tables 1, 2). The same tables list values of the parameters *a*, *b*, and *c*. To characterize the agreement between the calculated results and the experiment, the average value of Δε, the absolute value of the differences of the experimentally determined ε and ε_{calc} calculated by an equation of type (1), was determined. It can be seen from the values of Δε in Tables 1, 2 that the nonlinear equation (1), which reflects the logistic time dependence of the extinction, rather adequately reproduces the fundamental aspects of the STP: existence of a limiting value, and S-shaped time dependence. It should be noted that no *a priori* information (initial values) is necessary for finding the parameters of the nonlinear equation (1). The relative error of the parameter *b*, which is, in fact, the rate constant of STP in the brief kinetic description suggested here, did not exceed 10%, as a rule.

The error of *a* and *c*, which did not exceed five units of the last digit, was found by variation to obtain, wherever possible, stable smallest values of Δε.

Figure 2a shows calculated lines (kinetic curves of STP) and experimental points for a symmetric (**Ie**) and asymmetric (**IId**) diynes.

CONCLUSION

The data obtained make it possible to formulate some semiquantitative conclusions concerning the relative reactivities of diyne arylcarbamates. In particular, the rate of STP decreases in proportion to the increasing number n of methylene groups in series with both even and odd n. The rate of STP increases by approximately a factor of 3 on introducing a methoxy group into the aryl ring.

REFERENCES

1. Anastas, P.T. and Warner, J.C., *Green Chemistry: Theory and Practice*, New York: Oxford Univ., 1998.
2. Wegner, G., Z. *Naturforsch.*, 1969, vol. 24B, no. 7, pp. 824–832.
3. Vinogradov, G.A., *Usp. Khim.*, 1984, vol. 53, no. 1, pp. 135–175.
4. *Polydiacetylenes. Synthesis, Structure and Electronic Properties*, Bloor, D. and Chance, R.R., Eds., Dordrecht: Nijhof Publ., 1985.
5. Kolusheva, S., Kafri, R., Katz, M., and Jelinek, R., *J. Amer. Chem. Soc.*, 2001, vol. 123, no. 3, pp. 417–422.
6. Cheng, Q. and Stevens, R.C., *Langmuir*, 1998, vol. 14, no. 8, pp. 1974–1976.

7. Muller, W., Ringsdorf, H., Rump, E., *et al., Science*, 1933, vol. 262, pp. 1706–1708.
8. *Nelineinye opticheskie svoistva organicheskikh molekul i kristallov* (Nonlinear Properties of Organic Molecules and Crystals), Shemly, D. and Zyss, J., Eds., Moscow: Mir, 1989, vol. 2, pp. 5–130.
9. Misin, V M. and Cherkashin, M.I., *Usp. Khim.*, 1985, vol. 54, no. 6, pp. 956–1008.
10. Gross, H., Sixl, H., Krohnke, C., and Enkelmann, V., *Chem. Phys.*, 1980, vol. 45, no. 1, pp. 15–16.
11. *Crystallographically Ordered Polymers*, Sandman, D.J., Ed., *ACS Symposium series 337*, Washington: American Chemical Society, 1987, pp. 140–151.
12. Vyaz'min, S.Yu., Berezina, S.E., Remizova, L.A., Domnin, I.N., *et al., Zh. Org. Khim.*, 2002, vol. 38, no. 6, pp. 817–829.
13. Marinichev, A.N., *4-ya Vserossiiskaya nauchnaya internet-konferentsiya: Komp'yuternoe i matematicheskoe modelirovanie v estestvennykh i tekhnicheskikh naukakh (KMM-4)* [Fourth All-Russia Sci. Internet-Conf.: Computer and Mathematical Modeling in Natural and Technical Sciences (KMM-4)], Tambov: Tamb. Gos. Univ., 2002, issue 13, pp. 47–48.
14. *TI-89/TI-92 Plus. Guidebook for Advanced Mathematics Software, Version 2.0*, Texas Instruments Inc., 2001.
15. Galiotis, C., Young, R.J., Ando, D.J., and Bloor, D., *Makromol. Chem.*, 1983, vol. 184, no. 5, pp. 1083–1101.

Russian Journal of Applied Chemistry, Vol. 78, No. 10, 2005, pp. 1668–1673. Translated from Zhurnal Prikladnoi Khimii, Vol. 78, No. 10, 2005, pp. 1697–1702.
Original Russian Text Copyright © 2005 by Kurenkov, Zhelonkina, Meshcheryakova, Lobanov.

MACROMOLECULAR CHEMISTRY AND POLYMERIC MATERIALS

Copolymerization of Sodium 2-Acrylamido-2-Methylpropane-1-Sulfonate with *N*-Vinylpyrrolidone in Aqueous-Ethanol Solutions

V. F. Kurenkov, T. A. Zhelonkina, A. N. Meshcheryakova, and F. I. Lobanov

Kazan State Technological University, Kazan, Tatarstan, Russia

Degussa Evraziya Limited Liability Company, Moscow, Russia

Received February 25, 2005; in final form, June 2005

Abstract—The solvent effect on the kinetic parameters of synthesis and molecular characteristics of copolymers formed by homogeneous radical copolymerization of sodium 2-acrylamido-2-methylpropane-1-sulfonate with *N*-vinylpyrrolidone in aqueous-ethanol solutions at pH 9 and 60°C in the presence of potassium persulfate as an initiator was studied.

The reaction medium strongly affects the radical polymerization of water-soluble monomers [1, 2], which allows variation of the kinetic parameters and characteristics of the resulting polymers by changing the nature of a solvent. Here, we consider the influence of the composition of water–ethanol mixtures on homogeneous radical copolymerization of sodium 2-acrylamido-2-methylpropane-1-sulfonate (Na-AMS) with *N*-vinylpyrrolidone (VP), which has not been studied previously. The interest in these studies is caused by the features of radical polymerization of ionic monomers [1, 3] and VP [4, 5] and also by the practical significance of copolymers of Na-AMS with VP, which have valuable characteristics and show promise for industry and medicine.

EXPERIMENTAL

We used Na-AMS prepared by neutralization of H-AMS solutions [Lubrizol-2404 manufactured by the Lubrizol Corporation (UK), mp 185°C, main substance content more than 99%] with NaOH to pH 9. VP manufactured by Merck (Germany) was twice distilled in a vacuum in the presence of 0.1% KOH (63°C, 3 mm Hg), n_D^{20} = 1.5117, main substance content (GLC) more than 99%. Potassium persulfate (PP) was twice recrystallized from aqueous solution; the main substance content found by the redox method was 98.7%. Ethanol was purified by distillation, bp 78.3°C. All the solutions were prepared using distilled water; the other reagents were of chemically pure grade.

The procedures of copolymerization and dilatometric analysis and the experimental procedure have been described previously [6]. After copolymerization, the copolymers were recovered from the reaction mixture by precipitation in a large excess of acetone, washed with acetone, and dried in a vacuum at 50°C to constant weight. The yield of the copolymer was determined gravimetrically. The composition of copolymers of Na-AMS with VP was determined by elemental analysis for sulfur [7]. The molecular weight (MW) of the copolymer was judged from the intrinsic viscosity of the solutions [η], which was measured in 0.5 N NaCl at 30°C in a VPZh-3 capillary viscometer with d_c = 0.43 mm.

The copolymerization of Na-AMS (M_1) with VP (M_2) was carried out in 20% aqueous solutions and in water–ethanol mixtures (volume ratios 70 : 30, 50 : 50, and 30 : 70). The reaction was initiated by thermal decomposition of PP ([PP] = 7.4×10^{-4} M) at 60°C. To exclude phase separation, the content of ethanol in the solvent did not exceed 75 vol %. All the copolymerization runs were performed at pH 9 to prevent hydrolysis of VP [8] and to provide the efficiency of initiation with PP [9] and the constancy of the initiation rate with variation of the ionic strength of the solution (due to variation of Na-AMS concentration in the initial monomer mixture and in the course of copolymerization) [10]. In the absence of PP, no copolymers were formed under the experimental conditions. The process rate was monitored dilatometrically. The initial portions of the kinetic curves ob-

1070-4272/05/7810-1668 © 2005 Pleiades Publishing, Inc.

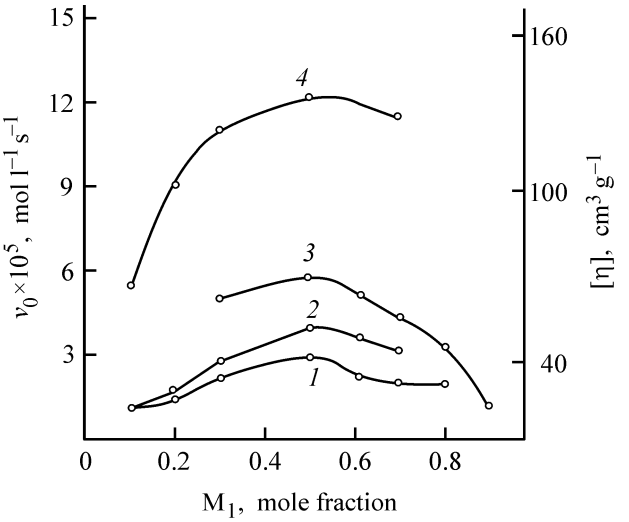


Fig. 1. (*1, 2*) Initial rate of copolymerization of Na-AMS with VP v_0 and (*3, 4*) [η] of copolymers vs. the mole fraction of Na-AMS in the initial monomer mixture M_1. Solvent: (*1, 3*) water–ethanol (1 : 1) and (*2, 4*) water.

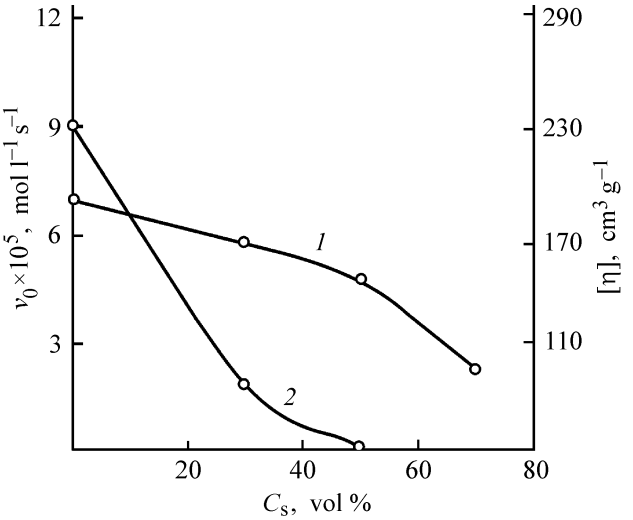


Fig. 2. (*1*) Initial rate of copolymerization of Na-AMS with VP v_0 and (*2*) [η] of copolymers vs. the content of ethanol in aqueous–ethanol mixture C_s. $[M_1] + [M_2] = 30\%$, $[M_1]/[M_2] = 1 : 1$.

tained from the dilatometric data were linear, and we found from their slopes the initial rates of copolymerization v_0 at low degrees of conversion ($\chi < 3\%$).

The dependence of v_0 on the mole fraction of Na-AMS in the initial monomer mixture (M_1) in copolymerization of Na-AMS with VP in water and in water–ethanol mixture (1 : 1) is shown in Fig. 1. The dependence $v_0 = f(M_1)$ passes through a maximum. As can be seen, the MWs of the resulting copolymers vary in parallel with v_0. The maximum values of v_0 and MWs of copolymers correspond to the equimolar ratio of the comonomers in the initial mixture ($M_1 = 0.5$). The IR data [11] showed that the maxima in the dependences $v_0 = f(M_1)$ and MW = (M_1) are caused by the donor–acceptor interaction between the comonomers (Na-AMS has a medium electron-acceptor power and VP, a medium electron-donor power).

The yields of the copolymer in copolymerization in water and in water–ethanol (1 : 1) mixture are listed in Table 1. It can be seen that the yield of the copolymer in these solvents increases with the content of Na-AMS in the initial monomer mixture.

The influence of the solvent composition on copolymerization of Na-AMS with VP is shown in Fig. 2. With increasing polarity of the solvents and with increasing water content in the water–ethanol mixture, v_0 grows. The MW of the copolymer increases in parallel with v_0 because of increasing influence of the chain transfer to alcohol molecules owing to labile hydroxyl hydrogen atoms. These trends can also be traced in Fig. 1 (curves *1*, *2* and *2*, *4* at M_1 = const). According to data on radical polymerization of other water-soluble monomers and, in particular, acrylamide [4] and VP [12], formation of hydrogen bonds between water molecules and C=O groups of both monomers is enhanced with increasing water content in the solvent, which lowers the electron density at the double bonds of the comonomers and raises their reactivity. As a result, v_0 values increase.

The running composition of the copolymer of Na-AMS with VP as a function of the composition of the initial monomer mixture at low conversions ($\chi < 3\%$) is shown in Fig. 3. The dependences $m_1 = f(M_1)$ in copolymerization in water and in a water–ethanol mixture (1 : 1 by volume) are S-shaped with

Table 1. Yield of copolymers of Na-AMS with VP in copolymerization in the water–ethanol (1 : 1) mixture and in water in 1 h

M_1, molar fraction	Yield in 1 h	
	water : ethanol (1 : 1)	water
0.1	–	26
0.2	–	37
0.5	44	45
0.6	51	52
0.7	–	53
0.8	52	60
0.9	59	–

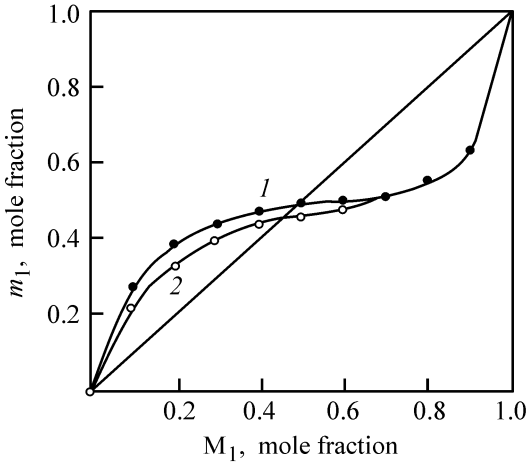


Fig. 3. Mole fraction of Na-AMS units in copolymer m_1 (at conversion χ < 3%) vs. Na-AMS mole fraction in the initial monomer mixture M_1 in copolymerization in (*1*) water–ethanol mixture (1 : 1) and (*2*) water.

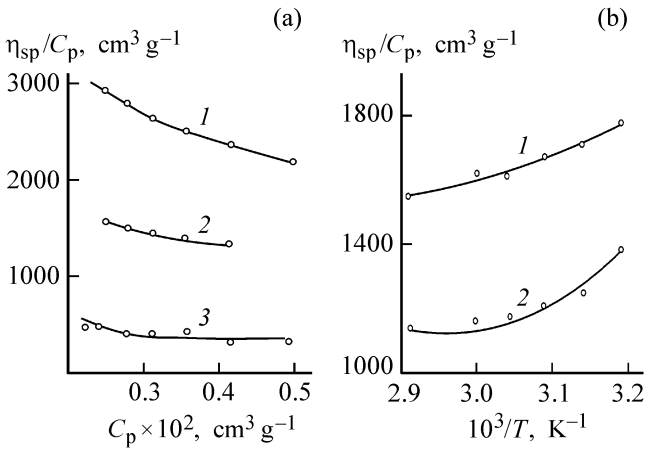


Fig. 4. Reduced viscosity of Na-AMS–VP copolymer η_{sp}/C_p ([η] = 265 cm^3 g^{-1}, content of Na-AMS units 42 mol %) (a) vs. copolymer concentration C_p at 30°C and (b) vs. temperature (T, K) (*1*) in water and (*2*, *3*) in a water–ethanol mixture, (*2*) 1 : 1 and (*3*) 1 : 3. C_p = 0.5 wt %.

an azeotropic point. The effective relative activities of the monomers in copolymerization, evaluated from data in Fig. 3, $r_1 = k_{11}/k_{12}$ (for Na-AMS) and $r_2 = k_{22}/k_{21}$ (for VP), are summarized in Table 2. It can be seen that that the r_1 and r_2 values determined by the Mayo–Lewis and Kelen–Tudos methods are in a good agreement with each other: In the solvents studied, $r_1 < 1$ and $r_2 < 1$, which suggests preferable reaction of macroradicals with the "foreign" monomer in comparison with the "own" monomer. In this case, $r_2 > r_1$, which confirms the higher reactivity of VP in comparison with Na-AMS. The product $r_1 r_2$ suggests formation of alternating copolymers of regular composition in the solvents studied.

Figure 3 shows that, in a wide range of compositions of the initial monomer mixture, the polymer is enriched with VP units on passing from the mixed solvent to water (from curve *1* to curve *2*). The above variation of the composition of the Na-AMS–VP copolymer is caused by an increase in r_2 (Table 2).

The copolymerization of Na-AMS with VP in the media under consideration is influenced not only by the solvation effect but also by ionization of the ionic groups of Na-AMS and its units in macroradicals. The latter factor governs the electrostatic interactions between the reacting particles and the conformation state of the macroradicals, which, in tern, affect the reactivity of Na-AMS and its macroradical in copolymerization. The significant role of electrostatic interactions in the system studied is indirectly suggested by the polyelectrolytic character of the concentration dependence of the reduced viscosity η_{sp}/C_p of the Na-AMS–VP copolymer of (Fig. 4a) in water (curve *1*) and in water–ethanol mixtures (curves *2* and *3*). With increasing polarity of the solvent, the ionization of the ionic groups of the macromolecules and the electrostatic repulsion between like fixed charges along the chain become stronger. As a result, the sizes of macromolecular globules and η_{sp}/C_p values at C_p = const increase (Fig. 4a). In copolymerization, an increase in the water content enhances the elec-

Table 2. Effective values of r_1 and r_2 in copolymerization of Na-AMS with VP in water and in a water–ethanol mixture (1 : 1 by volume)

Determination method*	r_1 (Na-AMS)	r_2 (VP)	$r_1 r_2$	Determination method*	r_1 (Na-AMS)	r_2 (VP)	$r_1 r_2$
Water				Water–ethanol (1 : 1)			
1	0.05 ± 0.01	0.25 ± 0.01	0.013	1	0.05 ± 0.01	0.14 ± 0.03	0.007
2	0.05 ± 0.03	0.26 ± 0.02	0.013	2	0.05 ± 0.08	0.14 ± 0.05	0.007

trostatic repulsion between Na-AMS and macroradical with terminal Na-AMS unit, which decreases the elementary constant of chain prolongation k_{11}. It can be assumed that a decrease in the activity of Na-AMS as a result of electrostatic interactions prevails over an increase in its activity as a result of hydrogen bonding with the solvent. This resulted in low r_1 values and their constancy in the solvents studied. An increase in the solvation power of the medium in substitution of water for a water–ethanol mixture (1 : 1 by volume) resulted in an increase in r_2 and caused enrichment of the copolymer with VP units, observed in Fig. 3 (passing from curve *1* to curve *2*).

The influence of conversion on the characteristics of the resulting copolymers was estimated in copolymerization of Na-AMS with VP in a water–ethanol mixture (1 : 1 by volume) for various compositions of the initial monomer mixture; the results are summarized in Table 3. As can be seen, the composition and MW of the copolymer do not noticeably vary in the course of the reaction. Similar data have been obtained in copolymerization of other water-soluble monomers in solutions [13, 14]. Gromov *et al.* [13, 14] believe that the constancy in the copolymer composition with variation of the degree of conversion is caused by the constancy of the comonomer ratio in the vicinity of the macroradicals due to formation of micellar associates selectively adsorbing monomers from aqueous solutions. In our case, penetration of Na-AMS molecules having bulky side substituent [–C(O)–N(H)–C$(CH_3)_2$–CH_2–SO_3Na] is more hampered, compared to VP, by steric hindrance. Therefore, the VP concentration in the vicinity of the macroradical will differ from its average concentration in the reaction mixture.

To determine the equations for the overall rate of copolymerization of Na-AMS with VP in the solvent studied, we performed experiments at varied concentrations of the monomers and initiator, with the other reaction conditions being constant. The log–log dependences of v_0 on the concentrations of Na-AMS, VP, and PP in copolymerization in the water–ethanol mixture (1 : 1 by volume) are shown in Fig. 5. In all cases, v_0 grows with increasing concentrations of comonomers and initiator. Data presented in Fig. 5 are well fitted by straight lines; from their slopes we determined the kinetic reaction orders with respect to the monomers and initiator and obtained the empiric equation for the total rate of copolymerization of Na-AMS with VP in water:

$$V = k_c[\text{Na-AMS}]_{0.9}[\text{VP}]_{0.6}[\text{PP}]_{0.8}, \qquad (1)$$

where k_c is the copolymerization rate constant.

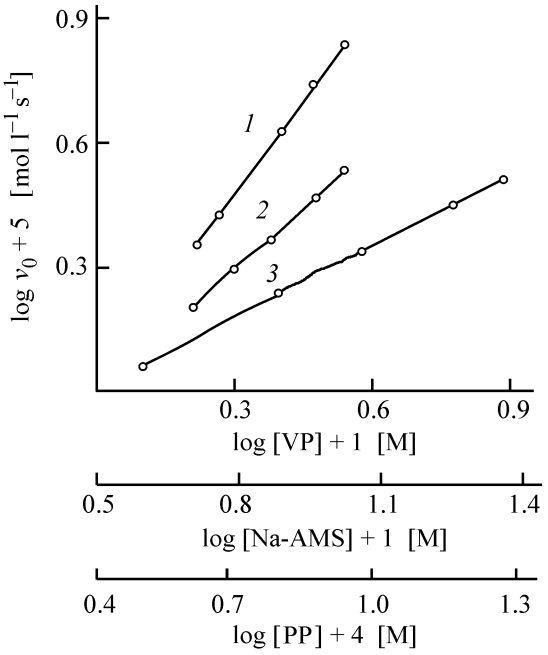


Fig. 5. Initial rate of copolymerization v_0 of (*1*) Na-AMS with VP in a water–ethanol mixture (1 : 1) vs. concentration of (*1*) Na-AMS, (*2*) VP, and (*3*) PP in log–log coordinates. (*1*) [VP] = 0.587, [PP] = 7.4×10^{-4} M; (*2*) [Na-AMS] = 0.587, [PP] = 7.4×10^{-4} M; and (*3*) [Na-AMS] = [VP] = 0.587 M.

For copolymerization of Na-AMS with VP in a water–ethanol mixture (1 : 1 by volume), the equation is as follows:

$$V = k_c[\text{Na-AMS}]_{1.5}[\text{VP}]_{0.6}[\text{AIBN}]_{1.0}. \qquad (2)$$

Comparison of Eqs. (1) and (2) shows that, in the case when ethanol is added to water, the reaction

Table 3. Dependence of [η] and composition of Na-AMS–VP copolymer on conversion *x* in copolymerization in the water–ethanol mixture (1 : 1)

M_1, molar fraction	*x*, %	[η], cm^3 g^{-1}	m_1, mol %
70	4	20	47
70	10	–	51
70	69	25	52
70	91	35	55
50	4	–	47
50	19	–	50
50	25	–	51
50	43	–	52
50	52	–	53
50	81	–	55

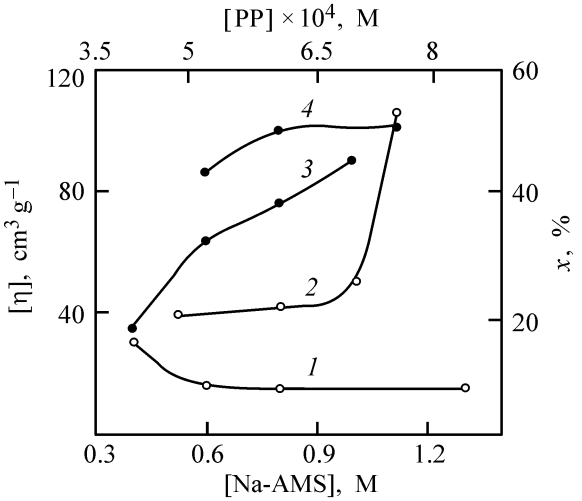


Fig. 6. (*1*, *2*) [η] and (*3*, *4*) copolymer yield *x* vs. the concentration of (*2*, *4*) Na-AMS and (*1*, *3*) PP in copolymerization in a water–ethanol mixture (1 : 1).

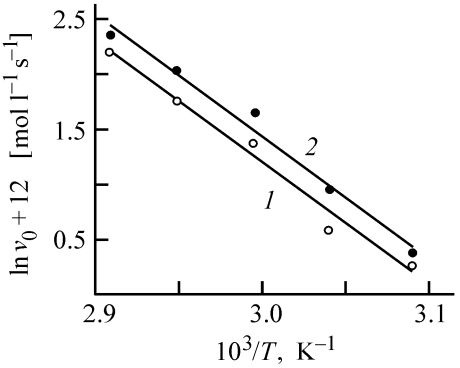


Fig. 7. Initial rate of copolymerization of Na-AMS with VP v_0 (*1*) in a water–ethanol mixture (1 : 1) and (*2*) in water vs. temperature *T* in the Arrhenius coordinates.

orders with respect to Na-AMS and PP somewhat increase. The above rise in the reaction order with respect to the initiator is apparently caused by increased contribution of monomolecular chain termination to the total chain termination in copolymerization in concentrated solutions. Low reaction orders with respect to VP are in a good agreement with published data [15, 16] and are usually observed in polymerization of this monomer in concentrated aqueous solutions.

The MW and copolymer yield in copolymerization of Na-AMS with VP in water–ethanol mixture (1 : 1 by volume) are plotted in Fig. 6 as functions of concentration of Na-AMS and PP. It can be seen that, the yield of the copolymer increases with the concentrations of Na-AMS and PP and MW grows with increasing concentration of Na-AMS and decreasing concentration of initiator, which agrees with the general pattern of radical polymerization.

The influence of temperature on the copolymerization of Na-AMS with VP in water and in a water–ethanol mixture (1 : 1 by volume) was studied in the range 40–70°C. The experimental results are plotted in the Arrhenius coordinates in Fig. 7. These data show that v_0 increases with temperature. The effective overall activation energies of copolymerization in the solvents studied are the same and equal to 99.6 kJ mol^{-1}. With variation of temperature, v_0 is affected by the conformational state of macroradicals, as suggested by data presented in Fig. 4. An increase in temperature results in a decrease in the sizes of macromolecular globules and in η_{sp}/C_p values at C_p = const (Fig. 4b) as a result of weakening of electrostatic repulsion between sulfonate anions along the chain, caused by a decrease in the degree of ionization of Na-AMS units. Therefore, a decrease in the chain charge makes higher local concentration of Na-AMS in the vicinity of macroradicals and causes v_0 to increase.

CONCLUSIONS

(1) With increasing water content in a water–ethanol mixture, v_0, MW, and the content of VP units in copolymer grow due to an increase in r_2 (at constant r_1). The composition and MW of the copolymer do not vary with conversion.

(2) The v_0 values increase with the concentrations of Na-AMS, VP, and PP and temperature and pass through a maximum (similar to MW of copolymer) with as the composition of the initial monomer mixture is varied (the maximum is reached at the molar ratio $[M_1]/[M_2] = 1 : 1$) due to complexation between the comonomers.

REFERENCES

1. Kabanov, V.A. and Topchiev, D.A., *Polimerizatsiya ionizuyushchikhsya monomerov* (Polymerization of Ionizable Monomers), Moscow: Nauka, 1975.
2. Kabanov, V.A., Zubov, V.P., and Semchikov, Yu.D., *Kompleksnoradikal'naya polimerizatsiya* (Complex-Radical Polymerization), Moscow: Khimiya, 1987.
3. Kurenkov, V.F. and Myagchenkov, V.A., *Zh. Prikl. Khim.*, 1999, vol. 72, no. 6, pp. 881–890.
4. Gromov, V.F., Bune, E.V., and Teleshov, E.N., *Usp. Khim.*, 1994, vol. 63, no. 6, pp. 530–541.
5. Sivtsov, E.V., Lavrov, N.A., and Nikolaev, A.F., *Plast. Massy*, 2001, no. 10, pp. 32–42.

6. Kurenkov, V.F., Sirotkin, R.O., Beryachkova, E.A., and Khairullin, M.R., *Zh. Prikl. Khim.*, 1999, vol. 27, no. 8, pp. 1533–1537.
7. Charlot, G., *Les methodes de la chimie analytique*, Paris: Masson, 1961. Translated under the title *Metody analiticheskoi khimii*, Moscow: Khimiya, 1969, pp. 988–989.
8. Sidel'kovskaya, F.P., *Khimiya N-vinilpirrolidona i ego polimerov* (Chemistry of *N*-Vinylpyrrolidone and Its Polymers), Moscow: Nauka, 1970.
9. Kholodnova, L.V., Pavlyuchenko, V.I., Alekseeva, Z.M., and Andreeva, A.I., in *Kataliticheskie i initsiiruyushchie sistemy dlya sinteza i modifikatsii polimerov* (Catalytic and Initiating Systems for Synthesis and Modification of Polymers), Leningrad: Plastpolimer, 1984, pp. 94–104.
10. Kolthoff, I.M. and Miller, I.K., *J. Am. Chem. Soc.*, 1951, vol. 73, no. 7, pp. 3055–3059.
11. Kurenkov, V.F., Zhelonkina, T.A., and Kovalenko, V.I., *Zh. Prikl. Khim.*, 2005, vol. 78, no. 2, pp. 301–305.
12. Karaputadze, T.M., Shumskii, V.I., and Kirsh, Yu.E., *Vysokomol. Soedin., Ser. A*, 1978, vol. 20, no. 8, pp. 1854–1859.
13. Barabanova, A.I., Gromov, V.F., Bune, E.V., *et al.*, *Vysokomol. Soedin., Ser. A*, 1994, vol. 36, no. 6, pp. 901–907.
14. Gromov, V.F., Bune, E.V., Barabanova, A.I., *et al.*, *Vysokomol. Soedin., Ser. A*, 1995, vol. 37, no. 11, pp. 1818–1822.
15. Topchiev, D.A., Martynenko, A.I., Kabanova, E.Yu., and Timofeeva, L.M., *Vysokomol. Soedin., Ser. A*, 1997, vol. 39, no. 6, pp. 1129–1139.
16. Nud'ga, L.A., Petrova, V.A., Klishevich, N.G., *et al.*, *Zh. Prikl. Khim.*, 2002, vol. 75, no. 10, pp. 1712–1716.

Russian Journal of Applied Chemistry, Vol. 78, No. 10, 2005, pp. 1674–1677. Translated from Zhurnal Prikladnoi Khimii, Vol. 78, No. 10, 2005, pp. 1703–1706.
Original Russian Text Copyright © 2005 by Starokadomskii, Fedorenko.

MACROMOLECULAR CHEMISTRY AND POLYMERIC MATERIALS

Physicomechanical Properties of Photocured Composites as Influenced by the Degree of Filling with Silica of Various Particle Sizes

D. L. Starokadomskii and O. M. Fedorenko

Institute of Surface Chemistry, Ukrainian National Academy of Sciences, Kiev, Ukraine

Received July 5, 2004; in final form, August 2005

Abstract—The strength of photocured composites as influenced by the concentration and specific surface area of a silica filler was studied.

Photocured composites used in various branches of industry are promising materials owing to their high quality and relatively simple curing procedures. Filling is the main procedure for integrated control over the polymer properties. Filled photocured composites are of particular interest in view of their expanding use in stomatology and microelectronics [1–8] and prospects for their use in other branches of industry (e.g., in automobile and aircraft building). Applicability of filled photocured composites is primarily determined by their strength. The compression strength, microhardness, and abrasion resistance are the main parameters characterizing photocured composites for stomatology [4]. The strength parameters also furnish certain information on the composite structure [9, 10].

In this study, we examined the strength of filled photocured composites as influenced by the concentration and specific surface area of the silica filler.

EXPERIMENTAL

The following chemicals were used: α,ω-bis(methacryloxyethyleneoxycarbonyloxy)ethylene-oxyethylene (OKM-2), triethylene glycol α,ω-dimethacrylate (TGM-3), and ethoxybisphenol α-dimethacrylate (EPO) [Dzerzhinsk, Russia] oligomers; Aerosils A-100, A-175, A-300, and A-455 [Kalush, Ukraine] (additionally calcined at 400°C for 1 h), silica gels were modified using K-2 and A-174 silane acrylates [Red'kino, Russia]; benzyl dimethyl ketal (BDK) [Ciba (Switzerland)] photoinitiating agent; and tris(dimethylaminomethyl)phenol (TMP), *N*,*N*,*N*,*N*-tetramethylehexamethylenediamine (THA), and *N*,*N*,*N*,*N*-tetramethylenethylenediamine (TMEDA) activators.

Oligomer OKM-2 containing 0.6 wt % DBK and 0.1–0.2 wt % TMP, THA, or TMEDA was used as a polymeric matrix for filled photocurable composites. This composition was filled with various amounts of A-175, A-300, A-380, and A-455 Aerosils. As a rule, we used in our experiments the composition consisting of OKM-2 + 0.6 wt % BDK + 0.1wt % TMP (hereinafter named as matrix).

The compositions were photocured using a DRUFZ-125 lamp (17.3 W m^{-2}, λ 300–400 nm) placed at distance of 10–20 cm from the sample. The physicomechanical propertiesof the resulting photopolymers were measured in conformity with the following GOSTs (State Standards): compression resistance σ_c (MPa), GOST 232026–78, 4651–82; abrasion wear $d = 1/\sigma_a$ (m mm^{-3}), GOST 110127–69; microhardness σ_m (MPa), GOST 4670–71; flexural strength σ_f (MPa), GOST 25604–82; and impact resilience F_i (MPa, GOST 9454–78).

In filling of oligomers, the limiting concentrations of silica can be attained, namely, the limiting filler concentration c_l and concentration of the fluidity loss, c_f. At silica concentration higher than c_l the composite loses stability (self-dispersion) and its strength properties decrease to zero, and at $c > c_f$ the viscous flow of the composite is terminated. Apparently, c_l and c_f should show an inverse correlation with the specific surface area *S* of silica. Indeed, as can be seen

1070-4272/05/7810-1674 © 2005 Pleiades Publishing, Inc.

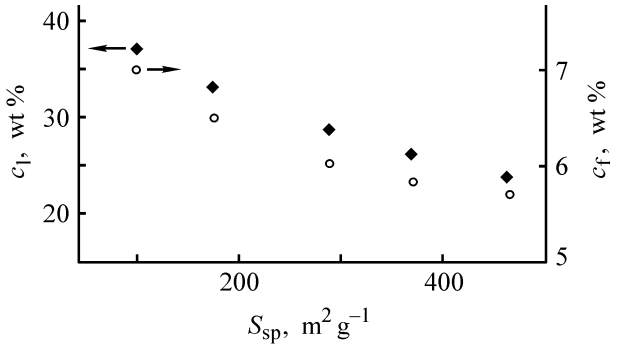


Fig. 1. Limiting concentration of the filler c_l and concentration of the fluidity loss, c_f, for OKM-2 oligomer vs. the silica specific surface area S_{sp}.

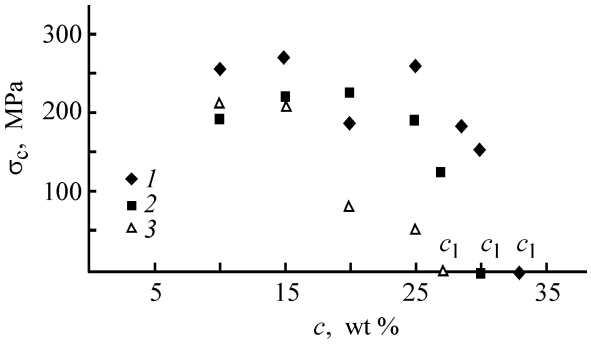


Fig. 2. Compression strength σ_c of the matrix [OKM-2 + 0.6 wt % BDK + 0.1 wt % TMP] vs. the concentration c of unmodified (*1*) A-175, (*2*) A-300, and (*3*) A-380 fillers.

from Fig. 1, c_l and c_f of OKM-2, TGM-3, and EPO oligomers nonlinearly decrease with increasing content and specific surface area of A-100, A-175, A-300, and A-455 fillers (numbers indicate the increasing specific surface area of Aerosils). It should be noted that the modification of the filler surface can affect these dependences and c_l can be raised by a factor of 1.2–1.5, using K-2 and A-174 modifying agents. For example, c_l = 28 wt % in the case of unchanged A-300, and c_l of the same filler modified with A-174 (10 wt %) reaches 45 wt %.

We also found that the strength properties (σ_c, σ_m, and d) are improved, with a decrease in the specific surface area of unmodified silica (Table 1).

For each silica we found the concentration range in which the compression strength σ_c of the photocured composites is higher as compared to the unfilled matrix. The typical dependences of σ_c on the silica content are shown in Fig. 2. It cab be seen that these dependences can be divided into two types. The dependences for highly dispersed A-300 and A-380 fillers pass a single maximum, after which the composites completely lose their strength. This maximum is indicative of the formation of the optimal three-dimensional silica skeleton (Shklovskiy-de Gennes model). As c_l is approached, the strength drastically decreases (Fig. 2) causing degradation of the system (overfilling).

In filling with A-175 silica, the dependences $\sigma_c = f(c)$, $F_i = f(c)$, $\sigma_f = f(c)$, and $\sigma_m = f(c)$ pass through two maxima (Figs. 2, 3; Table 2), which are preserved even upon replacement of the activator. This phenomenon can be explained as follows. The first maximum (which is absent with A-300 and A-350 fillers) is probably due to the maximum in the degree of conversion at an A-175 filler concentration of 10–12 wt % [11, 12], because σ_c directly depends on the conversion [13, 14]. As in the case of highly dispersed fillers, the second maximum indicates the formation of the optimal silica skeleton, because, with further increase in the filler content, the composite strength drastically decreases with its self-dispersion.

Table 1. Strength properties as influenced by the degree of filling with Aerosils of various particle size

Aerosil	Degree of filling, wt %				
	15	20	25	20	
	σ_c, MPa			σ_m, MPa	d, m mm^{-3}
–	(176)*	(176)	(176)	(382)	(0.2)
A-165	273	192	261	631	1.35
A-300	221	228	195	682	1.05
A-380	214	82	60	–	0.89

Table 2. Strength properties of OKM-2 + 0.6 wt % BDK + 0.1 wt % THA or 0.18 wt % TMEDA composites as influenced by the content c of A-175 Aerosil

c, wt %	σ_c, MPa		σ_m, MPa		d, m mm^{-3}	
	TMEDA	THA	TMEDA	THA	TMEDA	THA
0	94	143	–	335	–	1.1
15	145	–	675	605	0.8	–
16	230	160	460	445	0.7	0.8
17	–	260	475	–	0.6	0.5
18	250	255	560	510	0.6	0.5
19	210	215	575	710	0.5	1.1
20	120	172	630	700	0.95	1.4
21	142	–	650	630	0.7	1.0
22	180	200	–	–	1.5	–
24	150	175	520	–	–	–

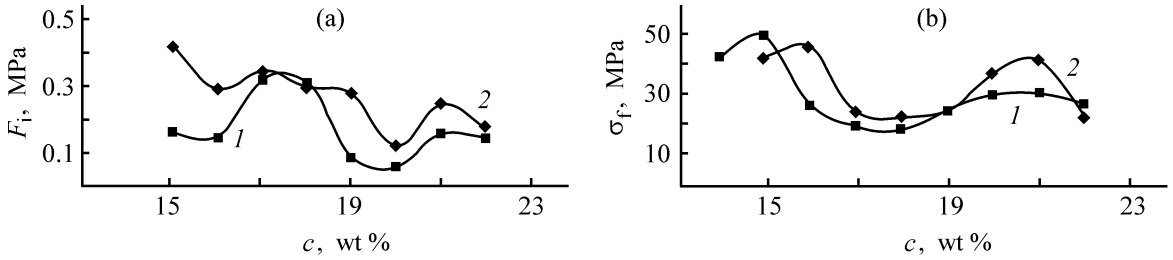


Fig. 3. (a) Impact resilience F_i and (b) flexural strength σ_f vs. the content of A-175 silica in OKM-2 + 0.6 wt % BDK + 0.1 TMEDA upon irradiation for (*1*) 8 and (*2*) 12 min.

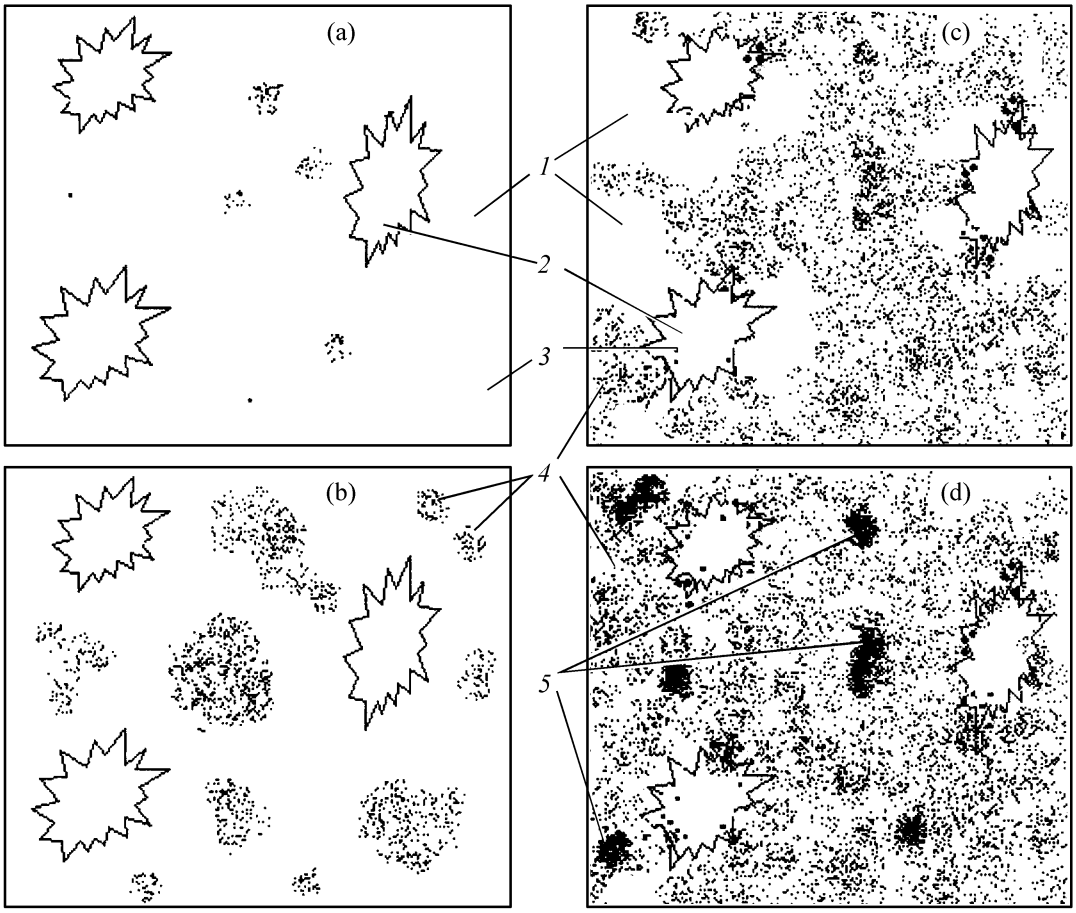


Fig. 4. Arrangement of silica particles and heterogeneous areas at different degrees of filling: (a) low filler concentrations, (b) moderate filler concentrations, (c) high and near-limiting filler concentrations, and (d) overfilled composites. (*1*) Free polymer, (*2*) heterogeneous areas, (*3*) separate filler particles, (*4*) particles and aggregates of filler surrounded by near-surface polymer layers, and (*5*) areas of degradation of the polymer structure and "dry" aggregates of silica filler.

To account for the maxima observed, we suggest the following scheme of changes in the polymer structure with increasing silica content, which is based on the tetra-component model of the filled polymer, suggested by Solomko [9] and Shklovskii-de Gennes model [15]. At low and moderate concentrations of the filler (e.g., up to 5–10 wt %), its particles are displaced in the course of polymerization to the less compact and poorly ordered areas of the polymer (Figs. 4a, 4b). With increasing concentration, these silica-structured areas expand, which raised up to a certain filler concentration increases the conversion [11, 12] and improves the polymer strength (Fig. 2, first maximum). With a further increase in the filler concentration, the silica-free polymer volume decreases (Fig. 4c, *1*). As a rule, these polymer areas are preserved near dense heterogeneous polymer areas, into which no silica particles can enter. The formation of

such heterogeneities was reported in [13, 16]. As a result, the polymer structure is reinforced by the silica particles. This accounts for the appearance of the second extremum in the dependences of the strength on the degree of filling (Fig. 2, Table 2). As of the limiting filler concentration is attained, separate silica particles are probably displaced into the dense heterogeneous areas of the polymer, causing their deformation and degradation (Fig. 4d). At the same time, the amount of the polymer phase with a broken structure and high internal stresses increases (Fig. 4d, *5*). As a result, the strength of the composite sharply decreases (Fig. 2).

CONCLUSIONS

(1) In c_l filling of oligomers with silica, the limiting concentration c_l of the filler, above which the composite undergoes mechanical breakdown (self-dispersion), should be taken into account. The values of c_l nonlinearly decrease with increasing specific surface area of silica and can be raised by modification of the filled surface.

(2) As a rule, addition of silica (A-175, A-300, and A-380 Aerosil) at concentrations of up to $c << c_l$ (10–20 wt %) significantly improves the compression strength, microhardness, and abrasion wear of the polymer. With decreasing specific surface area of silica, the strength properties of the resulting polymers are enhanced.

REFERENCES

1. Chung, C.M., Kim, J.C., and Choi, J.H., *J. Appl. Polym. Sci.*, 2000, vol. 77, no. 8, pp. 1802–1808.
2. Bland, M.H. and Peppas, N.A., *Biomaterials*, 1996, vol. 17, no. 11, pp. 1109–1114.
3. Makeeva, I.M., *Vosstanovlenie zubov svetootverzhdaemymi kompozitnymi materialami* (Tooth Restoration Using Photocurable Composites), Moscow: Stomatologiya, 1997.
4. Leinfel'der, K.F., *Kvintessentsiya*, 1996, no. 3, pp. 51–62.
5. Baikerikar, K.K. and Scranton, A.B., *Polymer*, 2001, vol. 42, no. 2, pp. 431–441.
6. Uhl, F.M., Davuluri, S.P., Wong, S.-C., *et al.*, Polymer, 2004, vol. 45, no. 18, pp. 6175–6187.
7. Ohe, Y., Kume, M., Taguchi, T., and Ichimura, K., *Appl. Optics*, 1999, vol. 38, no. 32, pp. 6722–6731.
8. Urano, T., Nagao, T., Takada, A., and Itoh, H., *Polym. Adv. Technol.*, 1999, vol. 10, no. 4, pp. 244–250.
9. Solomko, V.P., *Napolnennye kristallizuyushchiesya polumery* (Filled Crystallizing Composites), Kiev: Naukova Dumka, 1980.
10. Gede, I., *Kompoz. Polim. Mater.*, 1982, no. 2, pp. 10–16.
11. Starokadomskii, D.L. and Solov'eva, T.P., *Zh. Prikl. Khim.*, 2002, vol. 75, no. 1, pp. 138–141.
12. Starokadomskii, D.L. and Solov'eva, T.P., *Zh. Prikl. Spektrosk.*, 1999, no. 1, pp. 119–124.
13. Korolev, G.V., Mogilevich, M.M., and Golikova, I.V., *Setchatye polimery* (Network Polymers), Moscow: Khimiya, 1995.
14. Antonov, A.I., Maslyuk, A.F., and Mirontsov, L.I., Abstracts of Papers, *5 Respublikanskaya konferentsiya po vysokomolekulyarnym soedineniyam* (5 Republ. Conf. on Macromolecular Compounds), Donetsk, 1984, Kiev: Naukova Dumka, 1984, p. 13.
15. Bobryshev, A.I., Kozitsyn, V.S., Avdeev, R.I., *et al.*, *Plast. Massy*, 2003, no. 3, pp. 21–25.
16. Usmanov, S.M., Sivergin, Yu.M., and Monakov, Yu.B., *Vysokomol. Soedin., Ser. A*, 1999, vol. 41, no. 3, pp. 474–479.

Russian Journal of Applied Chemistry, Vol. 78, No. 10, 2005, pp. 1678–1682. Translated from Zhurnal Prikladnoi Khimii, Vol. 78, No. 10, 2005, pp. 1707–1711.
Original Russian Text Copyright © 2005 by Gurbanov, Chalabiev, Mamedov, Efendiev.

MACROMOLECULAR CHEMISTRY AND POLYMERIC MATERIALS

Epoxidation of Soybean Oil in the Course of Cooxidation with Hydrogen Peroxide in the Presence of Propanoic Acid and Chlorinated KU-2 × 8 Cation Exchanger

M. Sh. Gurbanov, Ch. A. Chalabiev, B. A. Mamedov, and A. A. Efendiev

Institute of Polymeric Materials, National Academy of Sciences of Azerbaijan, Sumgait, Azerbaijan

Received February 22, 2005; in final form, June 2005

Abstract—Pattern of soybean oil epoxidation catalyzed by chlorinated KU-2 × 8 cation exchanger in the presence of H_2O_2 and propanoic acid was studied. The epoxidation rate and the selectivity of formation and yield of the epoxidation product were studied as influenced by the concentration of H_2O_2, C_2H_5COOH, and the catalyst. Some kinetic and activation parameters of soybean oil epoxidation were determined.

Epoxidized unsaturated oils are used in paint-and-varnish industry and as a plasticizer-stabilizer of polyvinyl chloride [1]. Unsaturated compounds, including higher unsaturated acids are epoxidized by peroxy acids in organic solvents [2–6]. The process can be performed with peroxy acids generated *in situ* from the corresponding carboxylic acid and hydrogen peroxide in the presence of mineral (H_2SO_4, HNO_3, and H_3PO_4) and organic (*p*-toluenesulfonic acid and trichloroacetic acid) acids, transition metal salts [cerium(IV) sulfate and zirconium(IV) sulfate], KU-2 cation exchanger, and Mn(IV) complexes. Strong water-soluble acids can be readily converted into peroxy acids. However, cooxidation of carboxylic acid and epoxidation of unsaturated compounds in the presence of these catalysts is ineffective because of the difficult recovery of the catalysts from the final reaction products. At the same time, epoxidation of unsaturated compounds with peroxy acids prepared in advance is unfeasible, because peroxy acids are explosive and the process is performed in two steps. Ion-exchange catalysts are the most suitable both for preparation of peroxy acids [7, 8] and for epoxidation of unsaturated compounds with peroxy acids formed *in situ* [9, 10].

In this study we examined the pattern of epoxidation of soybean oil (SO) with peroxypropanoic acid formed *in situ* in the presence of a chlorinated KU-2 × 8 cation exchanger (CCE).

EXPERIMENTAL

Epoxidation was performed in a 250-ml three-necked flask equipped with a hydroseal, mechanical stirrer, and reflux condenser. The required amounts of propanoic acid, hydrogen peroxide, CCE, and toluene solution of SO were placed in the flask. The reaction was performed in the course of 8 h. Then the catalyst was filtered off on a Schott filter. The aqueous layer of the filtrate was separated from the organic layer. The organic solution was diluted with toluene and washed with distilled water to absence of H_2O_2 in the aqueous phase. Toluene was removed (323–328 K, 13.3 kPa) and the epoxidized oil was recovered. The physicochemical parameters of the epoxidized soybean oil (ESO) were determined.

The catalysts, chlorinated KU-2 × 8 cation exchanger with a 9.5 wt % chlorine content and an exchange capacity of 3.54 mg-equiv g^{-1}, was prepared by treatment of KU-2 × 8 cation exchanger with a mixture of HCl and H_2O_2 [11]. The efficiency and stability of this catalyst in synthesis of peroxy acids was shown in [12].

We used a 30 wt % solution of H_2O_2, freshly distilled propanoic acid (chemically pure grade, bp = 414.4 K, d = 0.9934 g cm^{-3}, n_D^{20} = 1.3865), and SO with an iodine number of 129. The content of epoxy groups and the iodine number were determined by the procedure described in [13]; the content of H_2O_2

1070-4272/05/7810-1678 © 2005 Pleiades Publishing, Inc.

Reaction conditions and some kinetic parameters of SO epoxidation in the presence of PA, H_2O_2, and CCE* ($[H_2O_2]$ = 2 M)

Run no.	[PA], M	[SO], M	CCE, % of $m(H_2O_2 + PA)$	T, K	$W_0 \times 10^4$, M s^{-1}	Content of epoxy groups, %	Iodine number	Degree of epoxidation, %	Selectivity, %	$k_1 \times 10^4$, M^{-1} s^{-1}
1	2.00	2.00	10	313	0.97	5.3	38.8	65.4	93.3	0.243
2	2.00	2.00	10	323	2.3	5.8	27.4	71.6	90.6	0.575
3	2.00	2.00	10	333	4.4	6.2	25.4	76.5	94.9	1.10
4	2.00	2.00	10	343	9.7	5.3	31.6	65.4	86.9	2.43
5	2.00	2.00	5	333	2.3	5.7	29.5	70.4	91.2	
6	2.00	2.00	15	333	6.8	6.5	23.2	80.2	95.2	
7	2.00	2.00	20	333	7.8	6.7	21.8	82.7	95.8	
8	1.00	2.00	10	333	2.6	6.9	20.4	85.2	95.5	
9	0.50	2.00	10	333	1.1	7.2	18.4	88.8	96.3	
10	2.00	1.00	10	333	4.8	6.0	26.5	74.1	87.2	
11	2.00	0.50	10	333	3.9	5.4	38.0	66.7	86.5	

* (1) Qualitative parameters were determined for the final products epoxidized for 8 h.
(2) Some epoxidation parameters: $A = 5.02 \times 10^5$ M^{-1} s^{-1}, E = 57.4 kJ mol^{-1}, ΔH^0 = 52.0 kJ mol^{-1}, $\Delta S^{\neq}$ = –152.5 J mol^{-1} K^{-1}, $\Delta G^{\neq}$ = 47.1 kJ mol^{-1}, k_1 (M^{-1} s^{-1}): 0.243×10^{-4} (313 K), 0.575×10^{-4} (323 K), 1.1×10^{-4} (333 K), 2.43×10^{-4} (343 K).

and peroxypropanoic acid, by the procedure in described [14]; and the viscosity of ESO, by the procedure in described [15]. Toluene (analytically pure grade, bp = 383.6 K, d = 0.8669 g cm^{-3}, n_D^{20} = 1.4969) was used as a solvent.

Samples of ESO are transparent green-yellow viscous liquids without mechanical impurities. The viscosity of these samples at 293 K is 0.0865–0.0890 N s cm^{-2}, and the acid number ranges from 0.3 to 0.4 mg (KOH), depending on the preparation conditions (see table). These parameters did not change after storage of these samples at room temperature for a year and after heating on an oil bath at 473 K for 20 min.

The selectivity of the CCE catalyst was estimated as the molar ratio of the epoxy groups in the products to the total number of SO double bonds that had reacted with H_2O_2 in the presence of PA.

Cooxidation of SO in the presence of PA, H_2O_2, and CCE is a consecutive two-step process. The first step is the reaction of PA with H_2O_2 in the presence of CCE to form peroxypropionic acid (PPA); the second step is oxidation of SO, with PPA being formed. It is known [16] that oxidation of carboxylic acids to peroxycarboxylic acids in the presence of acidic catalysts is reversible; both forward and reverse reaction are second-order. However, as PPA is consumed for SO oxidation, the overall process may be irreversible, depending on the ratio of the rate constants of the first and the second steps. Clearly, the epoxidation is the most efficient when the rate of the second step is equal to, or higher than, that of the first step. Hence, to provide simultaneous efficient generation of PPA and SO epoxidation and to prepare the target product with a high content of epoxy groups, the optimal range of the process parameters should be determined.

For this purpose, we studied the rate of H_2O_2 consumption and a change in the PPA concentration as influenced by the temperature and CCE amount. The kinetic curves of H_2O_2 consumption in SO oxidation in the presence of PA and CCE are shown in Fig. 1. It can be seen that the H_2O_2 consumption is accelerated on heating from 313 to 343 K (see table), and hence the time of SO oxidation decreases. For

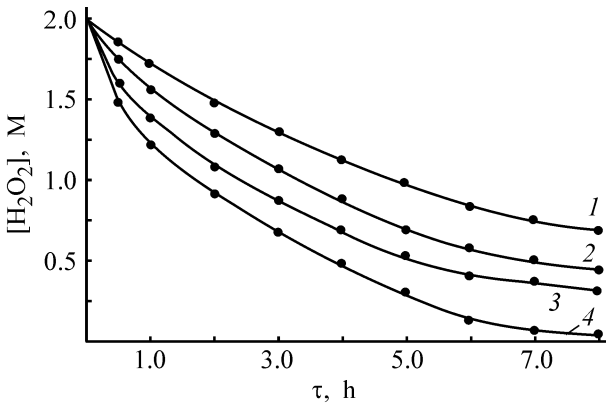


Fig. 1. Kinetic curves of $[H_2O_2]$ consumption in SO epoxidation at (*1*) 313, (*2*) 323 (*3*) 333, and (*4*) 343. Amount of CCE 10 wt % relative to the total amount of H_2O_2 and PA. $[H_2O_2]_0 = [PA]_0 = [SO]_0$ = 2 M. (τ) Time; the same for Figs. 2–4.

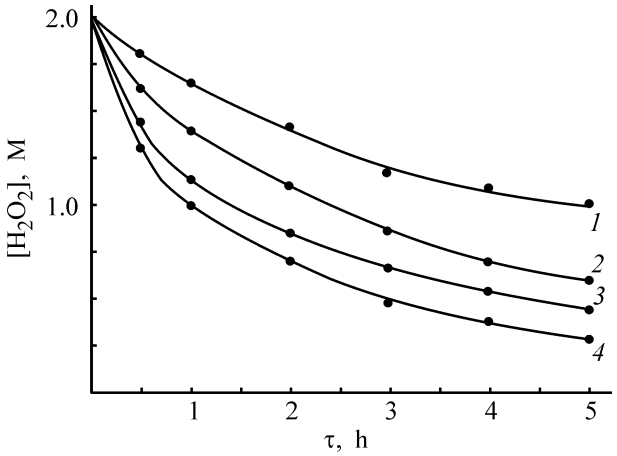


Fig. 2. Kinetic curves of $[H_2O_2]$ consumption in SO epoxidation in the presence of CCE. CCE amount, wt % relative to H_2O_2 + PA: (*1*) 5, (*2*) 10 (*3*) 15, and (*4*) 20. $[H_2O_2]_0 = [PA]_0 = [SO]_0 = 2$ M, T 333 K.

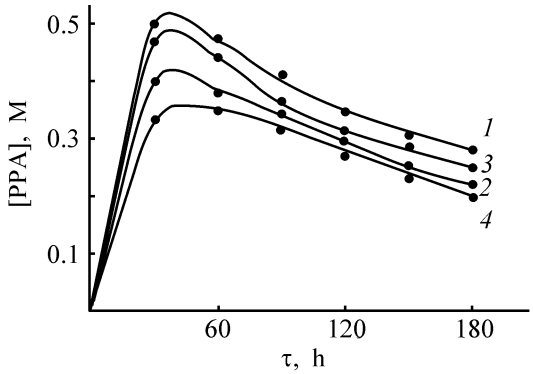


Fig. 3. Time dependence of [PPA] in SO epoxidation with hydrogen peroxide in the presence of PA and chlorinated KU-2 × 8 cation exchanger (10 wt % relative to H_2O_2 + PA) at (*1*) 343, (*2*) 333, (*3*) 323, and (*4*) 313 K. $[H_2O_2]_0 = [PA]_0 = [SO]_0 = 2$ M.

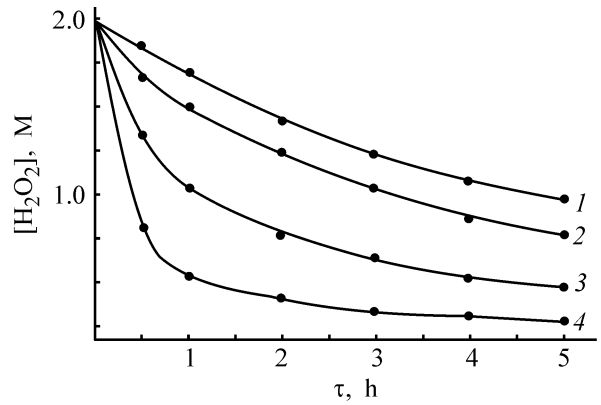


Fig. 4. Kinetic curves of $[H_2O_2]$ consumption in SO epoxidation at $[H_2O_2]_0 : [PA]_0 : [SO]_0$ (*1*) 1 : 0.25 : 1, (*2*) 1 : 0.5 : 1, (*3*) 1 : 1 : 1, and (*4*) 1 : 2 : 1. Amount of KU-2 × 8 cation exchanger 10 wt % relative to H_2O_2 + PA, T = 333 K, $[H_2O_2]$ = 2 M.

example, 50% of the H_2O_2 amount required for SO epoxidation is consumed at 343 K within 114 min, whereas at 313 K, thus takes 290 min. The first portions of the kinetic curves are well described by the kinetic equation of a second-order irreversible reaction, i.e., in this temperature range, the second step is faster than the first step and the SO oxidation becomes irreversible.

The kinetic curves of H_2O_2 consumption in SO oxidation in the presence of PA and different amounts of CCE are shown in Fig. 2. It can be seen that the H_2O_2 consumption is accelerated as the CCE content increases from 5 to 20%. The reaction is of the first order with respect to the catalysts at the CCE content of 15%. Previously, we have shown [3] that acid catalysts including KU-2 × 8 accelerate only the first step of cooxidation of unsaturated compounds in the presence of carboxylic acids and H_2O_2 and do not accelerate epoxidation of the double bond. To confirm the absence of the catalytic effect of CCE on SO epoxidation, we studied the oxidation of SO with PPA in the absence and in the presence (10 wt %) of CCE. No effect of CEE on the epoxidation rate was detected.

Hence, the effects of temperature and the CCE content on the rate of formation and consumption of the peroxy acid differ. The acceleration of the process with increasing catalyst content is due to a rise in the current PPA concentration. On heating, both the formation of peroxy acid and the oxidation of the double bond are accelerated (Fig. 1, 3).

The kinetic curves of H_2O_2 consumption in cooxidation of SO in the presence PA and CCE at different $[H_2O_2] : [PA] : [SO]$ molar ratios are shown in Fig. 4. The qualitative parameters of SO epoxidation are summarized in the table. These data show that the optimal are the equimolar $[H_2O_2] : [PA] : [SO]$ ratio, and CCE amount equal to 15% of the total weight of H_2O_2 and PA. When the molar ratio changes from 1 : 0.25 : 1 to 1 : 2 : 1 (an increase in the PA amount), the process is significantly accelerated but the quality of the target product is impaired, probably bacause of acceleration of side reactions, including the opening of the epoxy ring of PA. Hence, the reaction should be performed at 333 K, despite that the H_2O_2 consumption in the epoxidation at 343 K is faster.

It should be noted that SO oxidation is accelerated with increasing H_2O_2 content. However, the use of large amounts of hydrogen peroxide is inefficient owing to the high consumption of the oxidizing agent. In addition, the epoxy number of the target product increases insignificantly in this case. Some kinetic parameters of cooxidation of SO with H_2O_2 in the pres-

ence of PA and CCE are also listed in the table. It is seen that the rate and the rate constant of the first step are fairly high, the activation energy is low, and the negative activation entropy is fairly high.

Thus, SO epoxidation with hydrogen peroxide in the presence of PA and CCE is a complex process including consecutive and parallel steps. The first step is PA oxidation with hydrogen peroxide to PPA:

$$H_2O_2 + C_2H_5COOH \underset{k_2}{\overset{k_1,\ CCE}{\rightleftarrows}} C_2H_5COOOH + H_2O. \quad (1)$$

As PPA is formed in the aqueous phase (aq.ph) and the epoxidation occurs in the organic phase (org.ph), PPA is distributed between these phases

$$[C_2H_5COOOH]_{aq.ph} \rightleftarrows [C_2H_5COOOH]_{org.ph}, \quad (2)$$

$$\gamma_1 = [CH_3COOOH]_{org.ph}/[CH_3COOOH]_{aq.ph}. \quad (3)$$

The distribution of PA between the aqueous and organic phases occurs in a similar way

$$[C_2H_5COOH]_{aq.ph} \rightleftarrows [C_2H_5COOH]_{org.ph}, \quad (4)$$

$$\gamma_1 = [CH_3COOH]_{org.ph}/[CH_3COOH]_{aq.ph}. \quad (5)$$

The double bonds of SO are epoxidized mainly in the organic phase

$$\rangle C{=}C\langle + [C_2H_5COOOH]_{org.ph} \xrightarrow{k_3} \rangle C\text{--}C\langle\ (O) + [CH_3COOH]_{org.ph} \quad (6)$$

It should be noted that side reactions are possible. Propionic acid dissolved in the organic phase promotes opening of the epoxy ring to form ester:

$$\rangle C\text{--}C\langle\ (O) + [C_2H_5COOH]_{org.ph} \xrightarrow{k_4} \underset{HO\ \ OCOC_2H_5}{\rangle C(OH)\text{–}C(OCOC_2H_5)\langle} \quad (7)$$

The epoxidation kinetics can be described by the following set of differential equations:

$$-\frac{d[H_2O_2]}{dt} = \{k_1[C_2H_5COOH][H_2O_2] - k_2[C_2H_5COOOH][H_2O]\}[CCE], \quad (8)$$

$$-\frac{d[SO]}{dt} = k_3[SO][C_2H_5COOOH]_{org.ph}, \quad (9)$$

$$\frac{d[SOE]}{dt} = k_3[SO][C_2H_5COOOH]_{aq.ph}\gamma_1 - k_4[SOE][C_2H_5COOH]_{aq.ph}\gamma_2, \quad (10)$$

$$\frac{d[SOEst]}{dt} = k_4[SOE][C_2H_5COOH]_{aq.ph}\gamma_2. \quad (11)$$

In accordance with the mass balance, the components of the reaction mixture are related by the following equations

$$[H_2O_2]_t = [H_2O_2]_0 - [H_2O_2]_{cons.}, \quad (12)$$

$$[SO]_t = [SO]_0 - [SOE] - [SOEst], \quad (13)$$

$$[C_2H_5COOH]_t = [C_2H_5COOH]_0 - [C_2H_5COOOH] - [SOEst], \quad (14)$$

where $[H_2O_2]_0$ and $[H_2O_2]_t$ are the initial and current concentrations of H_2O_2, respectively; $[SO]_0$ and $[SO]_t$, initial and current concentrations of SO (or the double bond of SO), respectively; [SOE] and [SOEst], current concentrations of epoxidized SO and SO ester, respectively; $[C_2H_5COOH]_0$ and $[C_2H_5COOH]_t$, initial and current concentrations of PA, respectively.

The distribution coefficients of PA and PPA between the aqueous and organic phases at different temperatures are determined experimentally.

CONCLUSIONS

(1) Chlorinated KU-2 × 8 cation exchanger is highly active and stable catalyst for SO epoxidation in the presence of H_2O_2 and C_2H_5COOH.

(2) Chlorinated KU-2 × 8 cation exchanger catalyzes only the formation of peroxypropionic acid and has no effect on the rates of oxidation of the double bond of soybean oil and of the opening of the epoxy ring of the target product, which increases the selectivity and efficiency of epoxidation and improves the quality of the target product.

REFERENCES

1. Blagonravova, A.A. and Nepomnyashchii, A.I., *Lakovye epoksidnye smoly* (Varnish Epoxy Resins), Moscow: Khimiya, 1970.
2. US Patent 2 997 484.
3. Chalabiev, Ch.A., Guseinov, M.M., and Salakhov, M.S., *Zh. Prikl. Khim.*, 1978, vol. 51, no. 9, pp. 2036–2041.
4. Ermakov, O.A., Utkin, B.N., Yanova, N.A., and Makarcheva, T.V., *Zh. Prikl. Khim.*, 1976, vol. 49, no. 9, pp. 2059–2061.
5. Kozlov, Yu.N., Mandelli, D., Voitiski, K.B., and Shul'pin, G.B., *Zh. Fiz. Khim.*, 2004, vol. 78, no. 3, pp. 453–457.

6. Ermakov, O.A. and Yanova, N.A., *Kinet. Katal.*, 1975, vol. 16, no. 4, pp. 1100–1106.
7. Sadykhov, O.A., Guseinov, M.M., and Chalabiev, Ch.A., *Zh. Org. Khim.*, 1984, vol. 20, no. 8, pp. 1638–1645.
8. Chalabiev, Ch.A., Sadykhov, O.A., Guseinov, M.M., *Kinet. Katal.*, 1983, vol. 24, no. 6, pp. 1400–1405.
9. Kupysevich, O.Ya. and Pik, Z.G., *Zh. Org. Khim.*, 1996, vol. 32, no. 6, pp. 817–819.
10. Krylov, O.V., *Kinet. Katal.*, 2002, vol. 43, no. 2, pp. 310–316.
11. USSR Inventor's Certificate, no. 1728250.
12. USSR Inventor's Certificate, no. 1685932.
13. Houben-Weyl, *Methoden der organischen Chemie. Band 2. Analytische Methoden*, Stuttgart: Georg Tieme, 1953
14. Swern, D., *Organic Peroxyacids*, New York: Wiley, 1970, vol. 5, no. 1.
15. Toroptseva, A.M., Belogorodskaya, K.V., and Bondarenko, V.M., *Laboratornyi praktikum po khimii i tekhnologii vysokomolekulyarnykh soedinenii* (Laboratory Course of Chemistry and Technology of Macromolecular Compounds), Leningrad: Khimiya, 1972.
16. Chalabiev, Ch.A., Agabalaev, Sh.B., and Salakhov, M.S., *Zh. Prikl. Khim.*, 1978, vol. 51, no. 3, pp. 577–580.

Russian Journal of Applied Chemistry, Vol. 78, No. 10, 2005, pp. 1683–1686. Translated from Zhurnal Prikladnoi Khimii, Vol. 78, No. 10, 2005, pp. 1712–1715.
Original Russian Text Copyright © 2005 by Gileva, Kraikin, Sedova, Lobov, Kuznetsov, Salazkin.

MACROMOLECULAR CHEMISTRY AND POLYMERIC MATERIALS

Control over the Composition and Microstructure of Copoly(Arylene Phthalides)

N. G. Gileva, V. A. Kraikin, E. A. Sedova, M. S. Lobov, S. I. Kuznetsov, and S. N. Salazkin

Institute of Organic Chemistry, Ufa Scientific Center, Russian Academy of Sciences, Ufa, Bashkortostan, Russia

Nesmeyanov Institute of Organoelement Compounds, Russian Academy of Sciences, Moscow, Russia

Received March 28, 2005

Abstract—The possibility of controlling the composition, microstructure, and molecular weight of copoly(arylene phthalides) was examined.

One of promising lines in modern polymer chemistry is synthesis of heat-resistant polymers and materials based on them, [in particular, poly(arylene phthalides)], which exhibit, along with high heat resistance and high softening points, other valuable properties, such as solubility, film-forming ability, and chemical resistance [1–3]. Poly(arylene phthalides) possess not only a unique combination of physicomechanical characteristics, but also unusual electrical properties.

Understanding of the fundamental aspects of synthesis of copoly(arylene phthalides) would allow preparation of copolymers with a required composition, microstructure, and molecular weight.

Under the conditions of nonequilibrium binary copolycondensation, the microstructure and composition of the forming copoly(arylene phthalides) can be affected by such factors as the reactivity of the comonomers, order of introduction of the starting monomers and catalyst, concentration and ratio of the monomers, type and amount of the catalyst, and temperature and time of synthesis. We have shown previously that acid pseudomonochlorides *p*-(3-chloro-3-phthalidyl)diphenyl oxide and *p*-(3-chloro-3-phthalidyl)diphenyl sulfide are highly reactive, form the corresponding homopolymers [2, 3], and enter into copolycondensation to give macromolecular copoly(arylene phthalides) [4].

In this study, we examined how the kind and amount of the catalyst affect the microstructure, composition, and reduced viscosity of the forming copoly(arylene phthalides) and estimated the relative reactivities of the comonomers.

EXPERIMENTAL

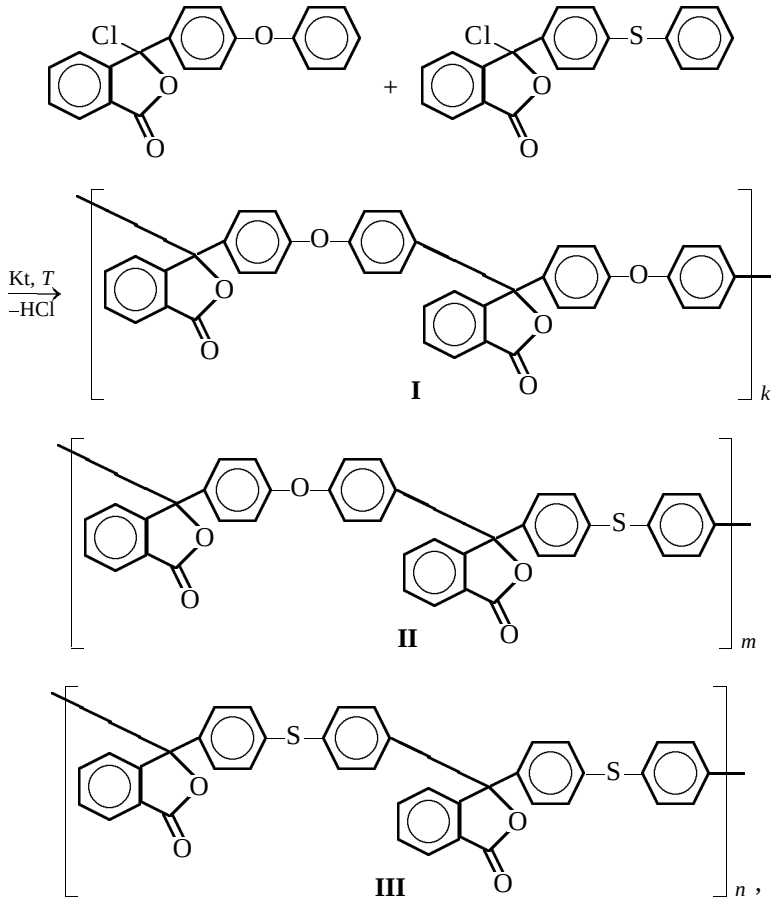
The starting compounds and solvents were purified according to [5–7]; their constants were consistent with published data [6, 7]. *p*-(3-Chloro-3-phthalidyl)diphenyl oxide and *p*-(3-chloro-3-phthalidyl)diphenyl sulfide were prepared according to [2]. The copolymerization was performed in the one-step mode; the comonomers were loaded in a single portion at the beginning of the process. An example of the procedure for preparing copoly(arylene phthalide) is given below. A four-necked flask equipped with a mechanical stirrer, an air-cooled reflux condenser, and a gas (Ar) bubble counter was charged with 4.206 g of *p*-(3-chloro-3-phthalidyl)diphenyl oxide and 4.406 g of *p*-(3-chloro-3-phthalidyl)diphenyl sulfide, after which 12.5 ml of nitrobenzene and 0.055 g of anhydrous $InCl_3$ were added. The synthesis was performed at 110°C for 10 h. Samples of the reaction mixture were taken at definite intervals (5, 10, 20, 40, 60, 90 min). The polymer from the samples and the final product were precipitated into methanol, reprecipitated from chloroform into methanol, washed with methanol and acetone, and dried in air at 180°C for 24 h.

The reduced viscosities η_r of the copolymers were measured in chloroform at 25°C and a polymer concentration of 0.5 g in 100 ml of the solvent.

The electronic absorption spectra of the solutions of copoly(arylene phthalides) were measured on a Shimadzu UV-3100 spectrophotometer at 20°C; the substrates were taken as $(0.1–1) \times 10^{-4}$ M solutions in 96 wt % sulfuric acid.

1070-4272/05/7810-1683 © 2005 Pleiades Publishing, Inc.

The reaction of equimolar amounts of *p*-(3-chloro-3-phthalidyl)diphenyl oxide and *p*-(3-chloro-3-phthalidyl)diphenyl sulfide in nitrobenzene in the presence of Lewis acids yields structures **I**–**III**;



where **I** is the diphenyl oxide phthalide (OO) homodiad; **II**, diphenyl oxide phthalide–diphenyl sulfide phthalide (OS) heterodiad; and **III**, diphenyl sulfide phthalide (SS) heterodiad; *k*, *m*, and *n* are the mole fractions of the OO, OS, and SS diads, respectively.

The mole fractions of the homo- (OO, SS) and heterodiads (OS) and the composition and microstructure of the copoly(arylene phthalides) were determined from the UV spectra (sulfuric acid solutions) of the copolymer samples taken in the course of the synthesis [8]. As catalysts for binary copolycondensation of the chloro phthalides we tested Lewis acids $InCl_3$, $GaCl_3$, and $SbCl_5$, which were taken in concentrations of 0.5–10 mol %. Figures 1a–1c show how the content of diads **I**–**III** in the copolymers varies in the course of the synthesis at various concentrations of $InCl_3$, $GaCl_3$, and $SbCl_5$. It is seen that, irrespective of the kind and concentration of the catalyst, OO diads are formed in the first minutes of the synthesis in larger amounts than SS diads. Only with 10 mol % $SbCl_5$, OO and SS diads are formed in the first minutes of the synthesis in equal amounts (Fig. 1c, curves *1*‴ and *3*‴). At $InCl_3$ and $GaCl_3$ concentrations of 0.5 mol %, the content of OO diads in the course of the synthesis exceeds that of SS diads by a factor of 25–50. The activity of $SbCl_5$ at its concentration of 0.5 mol % is low, and the copolymer is not formed. With an increase in the concentration of any of the catalysts tested and in the synthesis time, the amount of OO diads decreases, and that of SS diads increases. The content of heterodiads rapidly grows with the catalyst concentration, and their mole fraction approaches 0.55. Within 1 h, all the kinetic curves flatten out, and, in the subsequent process, the content of homo- and heterodiads varies insignificantly. The content

of OO and SS homodiads by the end of the synthesis varies with the catalyst used, whereas the content of heterodiads is about the same. With $InCl_3$, copoly(arylene phthalides) with almost equal content of OO and SS homodiads can be obtained. With $GaCl_3$, the resulting copolymers contain an appreciably larger amount of OO homodiads than that of SS homodiads, with the difference being the larger, the lower the $GaCl_3$ concentration. With $SbCl_5$ taken in concentrations of 1.0 mol % and higher, copolymers with the mole fraction of the heterodiads in the range 0.5–0.55 can be obtained, and the content of the homodiads depends on the catalyst concentration. With 1.0 mol % $SbCl_5$, the content of OO homodiads is higher than that of SS homodiads (mole fraction 0.35 and 0.12, respectively); the mean length of diphenyl oxide phthalide blocks, L_O, is 1.6, and that of diphenyl sulfide phthalide blocks, L_S, is 0. With 5 mol % $SbCl_5$, the content of OO and SS diads becomes close within 10 min (mole fraction 0.24 and 0.22, respectively; L_O = 1.9, L_S = 1.8). With 10 mol % $SbCl_5$, the content of the homodiads is the same in the first minutes of the synthesis, but then the content of OO diads tends to decrease, and that of SS diads, to increase. As a result, the polymer formed by the end of the synthesis is enriched in SS diads (mole fractions: OO 0.18 and SS 0.3; L_O = 1.6, L_S = 2.1).

The polymer chain structure can be quantitatively characterized by the microheterogeneity coefficient K_m and mean lengths of the oxide and sulfide blocks, L_O and L_S, which were calculated from the mole fractions of the homo- and heterodiads of copoly(arylene phthalides) [9]. With an increase in the concentration of any of the catalysts tested and in the synthesis time, K_m decreased from 1.27 at the beginning of the synthesis to 1.0 by its end (10 h). This means that, in the first minutes of the synthesis at low concentrations of the catalyst, the more active oxide comonomer forms oxide sequences which fairly regularly alternate with a single sulfide fragment (the most probable structure is ~OOSOOSOOOSOOO~, K_m = 1.27, L_O = 3.0, L_S = 1.0), with no sulfide homodiads. *p*-(3-Chloro-3-phthalidyl)diphenyl sulfide is incorporated exclusively in OS heterodiads **II**. With an increase in the catalyst concentration and synthesis time, the microheterogeneity coefficient tends to unity, which is indicative of the formation of random microblock copolymers enriched in oxide or sulfide fragments, depending on the kind and concentration of the catalyst.

The kind and concentration of the catalyst exert no significant influence on the molecular weight of copoly(arylene phthalides). This is illustrated by

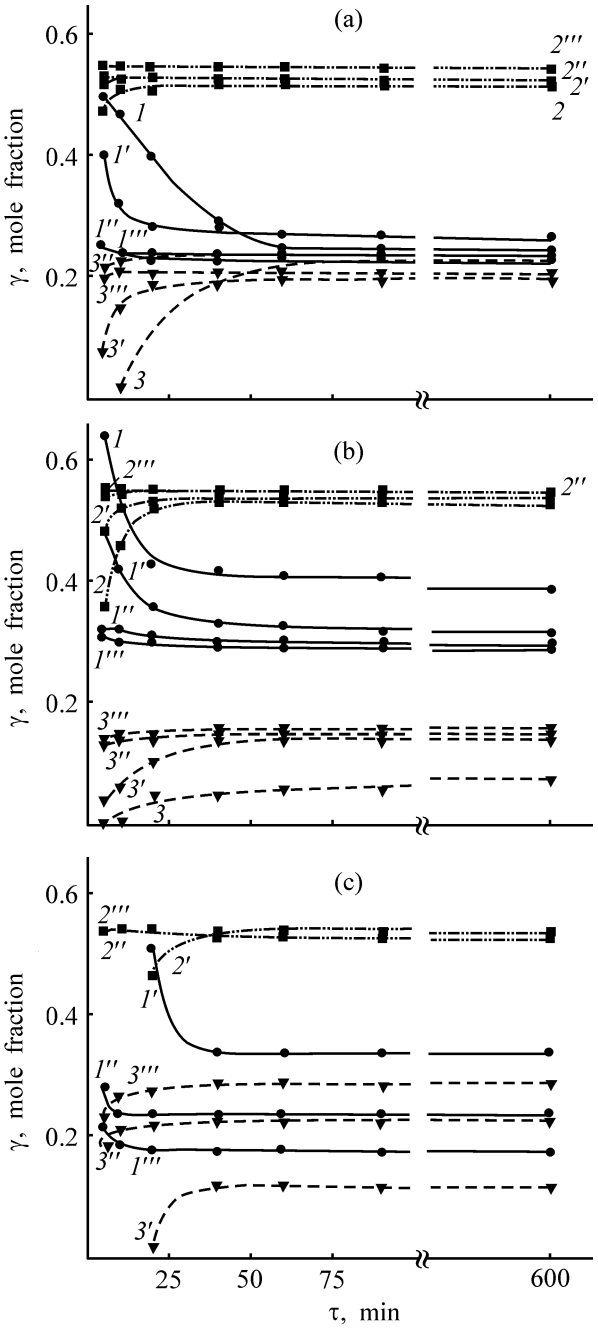


Fig. 1. Variation of the content of (*1*) OO, (*2*) OS, and (*3*) SS diads in the course of copolycondensation of *p*-(3-chloro-3-phthalidyl)diphenyl oxide and *p*-(3-chloro-3-phthalidyl)diphenyl sulfide in the presence of catalysts (a) $InCl_3$, (b) $GaCl_3$, and (c) $SbCl_5$. (γ) Mole fraction of diads and (τ) time. Catalyst concentration, mol %: (*1*–*3*) 0.5, (*1*′–*3*′) 1.0, (*1*″–*3*″) 5.0, and (*1*‴–*3*‴) 10.0.

Figs. 2a–2c. With an increase in the $GaCl_3$ concentration, the reduced viscosities of the copolymers steadily increase in the course of the synthesis. The highest reduced viscosity (0.75 dl g^{-1}) was obtained with 10 mol % $GaCl_3$ at a reaction time of 10 h (Fig. 2b).

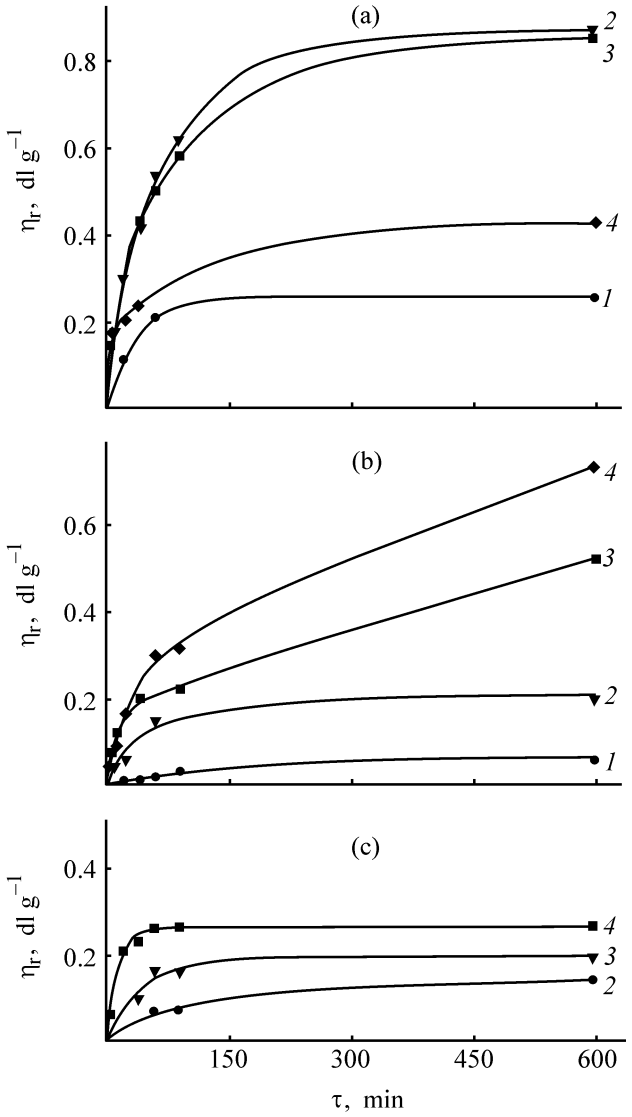


Fig. 2. Influence of the concentration of (a) $InCl_3$, (b) $GaCl_3$, and (c) $SbCl_3$ on the reduced viscosity η_r of copoly(arylidene phthalide) in the course of its synthesis. Catalyst concentration, mol %: (*1*) 0.5, (*2*) 1.0, (*3*) 5.0, and (*4*) 10.

With $InCl_3$, the copolymer with the highest reduced viscosity, 0.87 dl g^{-1}, was obtained at a 10 times lower catalyst concentration, compared to $GaCl_3$ (Fig. 2a). As can be seen from Fig. 2a, the optimal $InCl_3$ concentration is in the range 0.5–1.0 mol %. $SbCl_5$ is the least active among the catalysts tested. At an $SbCl_5$ concentration of 0.5 mol %, no copolymer is formed, and even at its concentration of 10 mol % the reduced viscosity of the copolymer is as low as 0.2 dl g^{-1}.

CONCLUSIONS

(1) A UV study of sulfuric acid solutions of copoly(arylene phthalides) formed by binary copolycondensation of equimolar amounts of *p*-(3-chloro-3-phthalidyl)diphenyl oxide and *p*-(3-chloro-3-phthalidyl)diphenyl sulfide revealed the influence of the kind and concentration of the catalyst on the composition, microstructure parameters (mole fractions of diads, microheterogeneity coefficient, mean block lengths), and molecular weight of the copolymers.

(2) The composition, microstructure, and molecular weight of the copoly(arylene phthalides) can be controlled by varying the kind and concentration of the catalyst.

(3) The catalysts tested allow preparation of both random copolymers and copolymers enriched in oxide or sulfide sequences of various lengths.

ACKNOWLEDGMENTS

The study was financially supported by the Russian Foundation for Basic Research (project no. 03-03–32 551).

REFERENCES

1. USSR Inventor's Certificate no. 704 114.
2. Salazkin, S.N., *Vysokomol. Soedin., Ser. B*, 2004, vol. 46, no. 7, pp. 1244–1269.
3. Salazkin, S.N., Rafikov, S.R., Tolstikov, G.A., *et al.*, *Dokl. Ross. Akad. Nauk*, 1982, vol. 262, no. 2, pp. 355–359.
4. Kraikin, V.A., Gileva, N.G., Sedova, E.A., *et al.*, *Dokl. Ross. Akad. Nauk*, 2002, vol. 385, no. 3, pp. 363–366.
5. Weissberger, A. and Proskauer, E.S., *Organic Solvents. Physical Properties and Methods of Purification*, Riddick, J.A. and Toops, E.E., Eds., New York: Interscience, 1955.
6. Gordon, A.J. and Ford, R.A., *The Chemist's Companion. A Handbook of Practical Data, Techniques, and References*, New York: Wiley, 1972.
7. *Dictionary of Organic Compounds*, Heilborn, I. and Banbury, H.M., Eds., London: Eyre and Spottiswoode, 1946, vol. 3.
8. Kraikin, V.A., Kuznetsov, S.I., Gileva, N.G., *et al.*, *Dokl. Ross. Akad. Nauk*, 2002, vol. 387, no. 2, pp. 213–218.
9. Vasnev, V.A. and Kuchanov, S.I., *Usp. Khim.*, 1973, vol. 42, no. 12, pp. 2194–2220.

Russian Journal of Applied Chemistry, Vol. 78, No. 10, 2005, pp. 1687–1690. Translated from Zhurnal Prikladnoi Khimii, Vol. 78, No. 10, 2005, pp. 1716–1720.
Original Russian Text Copyright © 2005 by Ergozhin, Mukhitdinova, Chalov, Iskakova.

MACROMOLECULAR CHEMISTRY AND POLYMERIC MATERIALS

Polymers Based on Polyglycidyl Aromatic Amines

E. E. Ergozhin, B. A. Mukhitdinova, T. K. Chalov, and R. A. Iskakova

Bekturov Institute for Chemical Research, Ministry of Education and Science of Kazakhstan Republic, Almaty, Kazakhstan

Received May 3, 2005

Abstract—Synthesis of cross-linked polyfunctional polyelectrolytes based on polyglycidyl aromatic amines is optimized, and the composition and physicochemical properties of the products are studied.

The three-membered ring in epoxy monomers is reactive toward both electrophilic and nucleophilic reagents. Similarly to compounds with unsaturated bonds, α-oxides are typically involved in reactions of addition and polymerization, and they are widely used in synthesis of soluble and solid polyelectrolytes [1–4].

Polyglycidyl aromatic compounds show the greatest promise for preparation of ion exchangers by polycondensation. These compounds exibit high reactivity and enhanced heat and chemical resistance. Furthermore, it is possible to control the density of cross-links in the resulting ion exchanger by varying the distance between the three-membered rings in the monomers.

The goal of this study was to develop procedures for synthesis of highly permeable polyelectrolytes on the basis of polyglycidyl aromatic diamines and to characterize their properties.

EXPERIMENTAL

Polyglycidyl diamines were synthesized according to the procedure described in [5].

Condensation of the resulting epoxy compounds with amines was carried out in the presence of acetone, DMF, toluene, or cyclohexanone (CH) for 0.5–2 h. Then the homogeneous mass was transferred into a porcelain bottle and cured in an oven for 14 h at 80–110°C. The gel was crushed and screened, to obtain the 0.25–1.0-mm fraction.

Pretreatment of the resulting products and determination of the relevant physicochemical characteristics were performed using the procedures described in [6].

The infrared spectra of the initial, intermediate, and final products were recorded on a Specord M-80/M85 spectrophotometer in KBr (1 mg of substance per 200 mg of KBr) and in a thin layer.

As starting reagents in synthesis of the polyelectrolytes we used polyglycidyl aromatic compounds obtained by condensation of epichlorohydrin with aromatic diamines [4,4'-diaminodiphenyl (DADP), 4,4'-diaminodiphenylmethane (DADPM), 4,4'-diaminodiphenyl oxide (DADPO), 4,4'-diaminodiphenyl sulfide (DADPS), and 4,4'-diamino-3,3'-dimethyldiphenyl (DADMDP)] (Table 1) or aliphatic di- and polyamines

Table 1. Characteristics of polyglycidyl aromatic amines

Compound	Content, %							
	epoxy groups		C		H		N	
	calculated	found	calculated	found	calculated	found	calculated	found
DADP	42.8	42.6	70.59	69.92	6.86	7.21	6.86	6.93
DADPM	40.8	39.0	71.10	72.30	7.10	7.02	6.64	6.80
DADPO	40.7	39.7	67.90	67.63	6.60	6.69	6.60	6.71
DADPC	27.6	27.4	65.90	64.38	6.10	7.18	8.54	8.23
DADMDP	39.4	39.2	71.60	71.00	7.34	7.26	6.42	6.28

1070-4272/05/7810-1687 © 2005 Pleiades Publishing, Inc.

Table 2. Effect of solvent and amine on SEC of ion exchangers synthesized on the basis of various PGAs (T = 80°C, τ = 2 h)

Starting aromatic diamine	SEC_{HCl}, mg-equiv g^{-1}			
	acetone	DMF	toluene	CH
	PEI			
DADP	10.2	10.5	10.1	9.4
DADPM	11.8	10.9	9.4	7.7
DADPO	11.8	10.8	8.9	8.7
DADPS	10.5	10.6	–	9.3
DADMDP	10.4	10.7	9.6	9.3
	PEPA			
DADP	9.8	9.6	8.3	8.0
DADPM	8.8	9.5	8.3	6.6
DADPO	8.5	9.4	7.8	6.8
DADPS	8.6	8.9	–	8.1
DADMDP	9.6	9.8	8.4	8.4
	HMDA			
DADP	5.9	6.4	6.0	4.4
DADPM	6.4	6.0	6.4	4.3
DADPO	6.0	5.7	5.7	4.2
DADPS	5.5	–	–	4.2
DADMDP	5.9	5.4	5.4	4.2

Table 3. Effects of temperature and PGA : HMDA weight ratio on SEC of the ion exchangers

Starting aromatic diamine	SEC_{HCl}, mg-equiv g^{-1}, at indicated temperature, °C			
	60	80	100	120
	PGA : HMDA = 1.0 : 0.5			
DADP	4.2	3.4	2.8	2.6
DADPM	s*	5.0	6.2	4.5
DADPO	5.5	4.6	3.3	2.2
DADPS	5.0	3.4	3.2	2.5
DADMDP	4.0	3.5	2.6	2.5
	PGA : HMDA = 1.0 : 1.0			
DADP	5.3	4.8	4.6	4.3
DADPM	s	6.6	6.4	6.3
DADPO	s	s	6.0	6.3
DADPS	s	s	4.1	3.1
DADMDP	4.6	4.8	4.2	4.2
	PGA : HMDA = 1.0 : 1.5			
DADP	5.5	6.1	6.0	4.8
DADPM	s	s	s	7.0
DADPO	s	s	6.5	6.7
DADPS	s	s	s	s
DADMDP	5.2	6.0	5.3	4.8
	PGA : HMDA = 1.0 : 2.0			
DADP	s	6.4	6.1	5.5
DADPM	s	s	s	s
DADPO	s	s	6.6	6.9
DADPS	s	s	s	s
DADMDP	s	6.2	5.9	5.4

* (s) Soluble product.

[hexamethylenediamine (HMDA), polyethylenepolyamine (PEPA), and polyethyleneimine (PEI)].

It is known [5–7] that properties of ion exchangers are primarily characterized by the static exchange capacity (SEC), which, in turn, depends on such factors as the nature of a solvent, proportion of the initial components, temperature, and curing time.

The effect of a solvent on SEC of the ion exchangers was examined with acetone, DMF, toluene, and cyclohexanone (Table 2). DMF and acetone were found to be the most appropriate solvents providing a sufficient solubility of the starting reagents and good swellability of the final products. The static exchange capacity of PEI/DADPM copolymers prepared in acetone and DMF is 11.8 and 10.9 mg-equiv g^{-1}, respectively, while that in cyclohexanone, only 7.7 mg-equiv g^{-1}. Similar trends were observed for the other amines. In the absence of a solvent, the condensation is too fast, producing an inhomogeneous gel. Additionally, the use of a solvent eliminates a local overheating which could occur as a result of exothermic opening of the epoxy groups. Therefore, we used as a reaction medium DMF or acetone (50 wt % solutions).

Previously, we have shown [8] that the SEC of the polymers based on polyglycidyl aromatic diamines (PGAs) and aliphatic diand polyamines increases in the order HMDA < PEPA < PEI. Table 2 demonstrates that high-molecular-weight amines are more efficient in synthesis of ion exchangers with a high SEC as compared to the monomeric diamines. Use of PEPA and PEI enables preparation of ion exchangers with an SEC of 8–12 mg-equiv g^{-1}.

In the synthesis of polyfunctional compounds by polycondensation, unchanged active groups could remain in the product, which is caused by differences in their reactivity and also by steric and concentration factors. Therefore, it is necessary to determine the optimal curing temperature, at which all the functional groups of the initial monomer are involved in the reaction.

The results obtained in a study of how the curing temperature and the composition of the starting mixture affect the SEC of the resulting HMDA-based ion exchangers are listed in Table 3. An increase in tem-

perature from 60 to 120°C makes the SEC smaller, which can be attributed to a considerable compaction of the polyelectrolyte structure and to its possible deamination and degradation under these conditions. At temperatures below 60°C the prepolymer is not cured because of the formation of soluble products.

A study of the effect of the reagent ratio revealed that the amount of amine introduced into the copolymer strongly affects the properties of the final products. A significant increase in the SEC was observed as the amine content in the reaction mass was raised up to a two-fold excess of the polyamine by weight (Table 3), and further increase only slightly changed the SEC. In the case of HMDA, essentially soluble products are formed.

As for the effect of the curing time, the SEC increases significantly in the first 1.5–2.0 h and then slightly decreases. For DADPM/HMDA ion exchangers, the SEC decreased from 6.3 to 6.1 mg-equiv g^{-1} as the curing time increased from 2 to 8 h. A similar trend was observed for the rest of the aromatic diamines studied.

The IR spectra of PGAs demonstrate characteristic absorption bands due to symmetric (1260 and 1280 cm^{-1}) and antisymmetric (745, 865, 935, and 970 cm^{-1}) stretching vibrations of the C–O bonds in the epoxy ring. The bands at 1650–1550 m^{-1} confirm the presence of the amino groups. The bands at 1300–1350 m^{-1} are assigned to stretching vibrations of the C–N bonds in the aromatic amines. No characteristic absorption bands of the epoxy rings are found in the spectra of the final products.

The acid–base behavior of the solid polyelectrolytes was studied by potentiometric titration. The shape of the potentiometric curves is controlled by the nature of di- and polyamines, and also by the set of functional groups of the ion exchanger. For the PEI- and PEPA-based products, the shape of the curves is more distinct as compared to that for the HMDA-based copolymer. From the potentiometric curves we estimated the dissociation constants pK_a and empirical coefficients m reflecting the strength of electrostatic interaction between the functional groups in the polymer (Table 4).

Data on the chemical resistance of the ion exchangers are summarized in Table 5. The ion exchangers studied demonstrate a high stability in alkaline and acid solutions, but are less resistant to strong oxidizing agents. Analysis of the chemical resistance data in relation of the nature of a polyamine shows that the PEI-based samples are relatively more stable in aggressive media.

Table 4. pK_a and m of the ion exchangers based on PEI and PEPA with a series of polyglycidyl amines

Starting aromatic diamine	PEI		PEPA	
	pK_a	m	pK_a	m
DADP	8.53	2.17	8.42	2.60
DADPM	8.56	1.85	8.17	2.32
DADPO	8.11	2.70	8.23	2.40
DADPS	8.02	2.56	8.05	2.30
DADMDP	8.53	2.51	8.24	2.09

Table 5. Chemical resistance of the ion exchangers in NaOH, H_2SO_4, and H_2O_2 solutions

Starting aromatic diamine	SEC_{HCl}, mg-equiv g^{-1}, before/after treatment loss, %		
	5 N NaOH	5 N H_2SO_4	10% H_2O_2
	PEI		
DADP	11.60/11.59 0.10	11.60/11.58 0.17	11.60/11.43 0.95
DADPM	11.82/11.81 0.10	11.82/11.80 0.17	11.82/11.64 1.52
DADPO	11.90/11.89 0.10	11.90/11.88 0.17	11.90/11.72 1.51
DADPS	11.59/11.58 0.10	11.59/11.51 0.17	11.59/11.29 2.59
DADMDP	10.86/10.86 0	10.86/10.86 0	10.86/10.52 3.13
	PEPA		
DADP	10.80/10.80 0	10.80/10.80 0	10.80/10.61 1.76
DADPM	9.40/9.40 0	9.40/9.38 0.21	9.40/9.18 2.34
DADPO	8.80/8.79 0.12	8.80/8.76 0.45	8.80/8.32 5.45
DADPS	9.09/9.08 0.10	9.09/9.05 0.44	9.09/8.86 2.53
DADMDP	10.48/10.47 0.10	10.48/10.48 0	10.48/10.04 4.20
	HMDA		
DADP	6.36/6.35 0.16	6.36/6.36 0	6.36/6.02 5.35
DADPM	6.42/6.41 0.16	6.42/6.41 0.16	6.42/6.11 4.83
DADPO	6.30/6.28 0.32	6.30/6.30 0	6.30/6.01 4.29
DADPS	4.13/4.10 0.73	4.13/4.12 0.24	4.13/4.00 3.14
DADMDP	4.82/4.79 0.62	4.82/4.81 0.21	4.82/4.52 6.28

Table 6. Heat resistance of the ion exchangers

Starting aromatic diamine	SEC_{HCl}, mg-equiv g^{-1}, after treatment loss, %				
	SEC*	2 h	4 h	6 h	8 h
			PEI		
DADP	11.60	11.59 0.10	11.59 0.10	11.50 0.86	11.42 1.55
DADPM	11.82	11.82 0	11.77 0.42	11.72 0.85	11.55 2.28
DADPO	11.90	11.90 0	11.86 0.34	11.81 0.76	11.43 3.95
DADPS	10.58	10.56 0.10	10.56 0.28	10.52 0.66	10.21 3.59
DADMDP	10.86	10.84 0.18	10.81 0.46	10.77 0.83	10.39 4.33
			PEPA		
DADP	10.80	10.79 0.10	10.72 0.74	10.65 1.39	10.43 3.43
DADPM	9.40	9.39 0.11	9.31 0.96	9.26 1.49	9.14 2.77
DADPO	8.80	8.80 0	8.76 0.45	8.64 1.82	8.48 3.64
DADPS	9.09	9.08 0.10	9.01 0.82	8.94 1.66	8.85 2.64
DADMDP	10.48	10.46 0.19	10.42 0.57	10.36 1.14	10.18 2.86
			HMDA		
DADP	6.36	6.36 0	6.31 0.79	6.28 1.28	6.14 3.46
DADPM	6.42	6.41 0.16	6.10 0.31	6.32 1.56	6.26 2.49
DADPO	6.30	6.30 0.32	6.26 0.63	6.18 1.90	6.03 4.29
DADPS	4.13	4.13 0	4.08 1.21	4.02 2.64	3.99 3.39
DADMDP	4.82	4.82 0	4.80 0.41	4.74 1.66	4.62 4.15

* Initial SEC.

The heat resistance of polyelectrolytes is governed not only by the nature of functional groups, but also by the network structure. However, thermal degradation of the ion exchangers first involves the active groups, being primarily reflected in a decrease in the SEC. Heat resistance tests were carried out by boiling the products in distilled water for a long time. The maximal decrease in the SEC was 4.33, 3.64, and 4.29% for PEI-, PEPA-, and HMDA-based polyelectrolytes, respectively.

Such a high heat resistance (Table 6) is probably due to the cross-linked structure of the polymers and also to the presence of thermally stable aromatic fragments in them. Depending on the structure of the starting amines used, the heat resistance of the products increases in the order tetraglycidyl derivatives of aromatic diamines < DADPS < DADP <DADPM, and decreases in the series of aliphatic polyamines HMDA > PEI > PEPA.

CONCLUSIONS

(1) The optimal synthesis conditions of polyfunctional anion exchangers by condensation of polyglycidyl aromatic diamines with aliphatic di- and polyamines are as follows: curing temperature 80–100°C, curing time 1.5–2.0 h, solvents: DMF and acetone, and glycidyl amine : hexamethylenediamine weight ratio 1.0 : 1.0; glycidyl amine : polyethylenepolyamine = 1.0 : (1.5–2.0); and glycidyl amine : polyethyleneimine = 1.0 : (2.0–3.0).

(2) The acid–base dissociation constants of the functional groups of the polymer and the empirical coefficient characterizing the interchain interaction suggest that weakly basic anion exchangers with high chemical resistance are formed.

ACKNOVLEDGMENTS

The study was financially supported by the International Science and Technology Center (ISTC Project K-604).

REFERENCES

1. Ergozhin, E.E. and Menligaziev, E.Zh., *Polifunktsional'nye ionoobmenniki* (Polyfunctional Ion Exchangers), Alma-Ata: Nauka, 1986.
2. Molochnikov, L.S., Sultanov, Yu.M., Il'ichev, S.A., *et al., Vysokomol. Soedin., Ser. A*, 1989, vol. 31, no. 5, pp. 1062–1065.
3. Smirnov, Yu.N., Komarov, B.A., Kushch, P.P., *et al., Zh. Prikl. Khim.*, 2002, vol. 75, no. 2, pp. 274–285.
4. Ostanina, N.Yu., Dul'tseva, L.D., Suvorov, A.L., and Chupakhin, O.N., *Zh. Prikl. Khim.*, 2002, vol. 75, no. 5, pp. 832–835.
5. US Patent 2951822.
6. *GOSTs* (State Standards) *10898–84, 10898.2–84, and 10898.5–84: Ion Exchangers: Methods for Physicochemical Testing.*
7. Korshak, V.V., *Khimicheskoe stroenie i temperaturnye kharakteristiki polimerov* (Chemical Structure and Temperature Characteristics of Polymers), Moscow: Nauka, 1970.
8. Chalov, A.K., Chukenova, T., and Ergozhin, E.E., *Izv. Min. Nauki Vyssh. Obraz. Resp. Kaz., Ser. Khim.*, 1999, no. 4, pp. 34–63.

Russian Journal of Applied Chemistry, Vol. 78, No. 10, 2005, pp. 1691–1694. Translated from Zhurnal Prikladnoi Khimii, Vol. 78, No. 10, 2005, pp. 1721–1724.
Original Russian Text Copyright © 2005 by Mudarisova, Badykova, Tolstikova, Aleksandrova, Borisov, Monakova.

MACROMOLECULAR CHEMISTRY AND POLYMERIC MATERIALS

Modification of Arabinogalactan and Its Oxidized Fractions with 5-Aminosalicylic Acid

R. Kh. Mudarisova, L. A. Badykova, T. G. Tolstikova, G. P. Aleksandrova, I. M. Borisov, and Yu. B. Monakova

Institute of Organic Chemistry, Ufa Research Center, Russian Academy of Sciences, Ufa, Bashkortostan, Russia
Bashkir State University, Ufa, Bashkortostan, Russia
Novosibirsk Institute of Organic Chemistry, Novosibirsk, Russia
Irkutsk Institute of Organic Chemistry, Irkutsk, Russia

Received June 2, 2005

Abstract—Modification of arabinogalactan of Siberian larch and of its oxidized oligomers with 5-aminosalicylic acid was studied. The chemical composition, some physicochemical properties of the modification products, and the optimal modification conditions were determined.

Modification of macromolecular compounds (MMCs) with pharmaceuticals is a promising approach to improvement of the pharmaceutical properties of drugs [1].

Macromolecular pharmaceuticals should meet the following requirements: (i) the molecular weight of water-soluble MMCs should be optimal, (ii) a polymer (or oligomer) should contain functional groups binding drugs, and (iii) elimination of the polymeric or oligomeric matrix from the body after completion of the drug action should occur readily. Natural polysaccharide, arabinogalactan (AG), prepared by extraction of Siberian larch (*Larix sibirica L*) with water, meets these requirements [2–4]. This water-soluble polymer exhibits membrane-acting, gastroprotecting, and immunomodulatory properties and undergoes receptor intermediate endocytosis [4–6], which makes it promising as a nontoxic carrier of molecular and ionic drugs in preparation of biologically active compounds of prolonged action. In this study, we modified polymeric (AG_{pol}) and oligomeric (AG_{ol}) fractions of AG prepared by oxidative functionalization and degradation of AG under the action of $H_2O_2 + O_2$.

Polysaccharides form complexes with various metal ions [7–9]. Data on complexation of AG with compounds exhibiting therapeutic properties are scarce [10].

In this study, we examined modification of AG and its oxidized fractions with 5-aminosalicylic acid (5-ASA), which inhibits prostaglandin synthesis [11].

EXPERIMENTAL

We used natural AG (M 40 000) recovered from Siberian larch by extraction with water [12]. Water-soluble phenols including dihydroquercetin were removed from AG on a polyamide sorbent. The resulting aqueous solutions contained trace amounts of flavonoids. The weight ratio of the galactose and arabinose residues was 5.6 : 1 [13]. Oxidative functionlization of natural AG and synthesis of its oxidized oligomers were performed by oxidation of aqueous hydrogen peroxide solutions of AG with molecular oxygen in a glass bubbling reactor. The volume of the reaction mixture was 10 ml. After the reaction was complete, the fraction of oxidized AG polymers was separated from the oligomer fraction by precipitation with acetone at a reaction mixture to acetone volume ratio of 1 : 5. To recover the oligomer fraction from the supernatant, acetone and water were removed and the residue was dried in a vacuum. The functional groups of natural AG and the polymer and oligomer fractions were analyzed in our previous study [14]. The IR spectra of the samples (Nujol mulls) were recorded on a UR-20 spectrophotometer. The UV spectra of 0.1% aqueous solutions of the compounds were recorded on a Specord M-40 spectrophotometer. The pH of aqueous solutions was measured on a ANION-4100 pH meter and adjusted with 0.1 M NaOH. The optical rotatory power was measured on a Perkin-Elmer-141 polarimeter. The intrinsic viscosity of solutions of

1070-4272/05/7810-1691 © 2005 Pleiades Publishing, Inc.

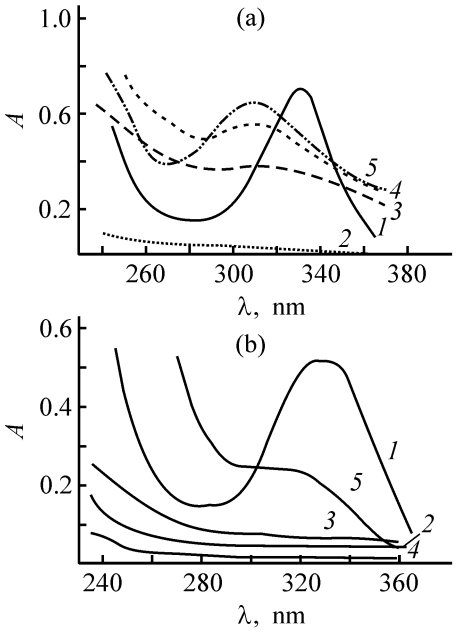


Fig. 1. UV spectra of aqueous solutions of (a) (*1*) 5-ASA, (*2*) AG, (*3*) AG–5-ASA, (*4*) AG_{pol}–5-ASA, and (*5*) AG_{ol}–5-ASA, and of (b) (*1*) 5-ASA (*2*) PVA, (*3*) PVA–5-ASA, (*4*) GA, and (*5*) GA–5-ASA. Concentration (g l^{-1}): (*1*) 0.01 and (*2–5*) 1; *l* = 1 cm.

AG, its oxidized fractions, and modified compounds was measured at 30 ± 1°C on an Ubbelode viscometer with a suspended level [15].

To remove unchanged 5-aminosalicylic acid (5-ASA), the products were twice precipitated from an aqueous solution with ethanol. As determined by TLC, the resulting product did not contain 5-ASA. A thin-layer chromatographic analysis of the compounds was performed on Silufol plates using a 1-butanol–pyridine–water mixture (6 : 4 : 5) as an eluent. The chromatograms were developed with ninhydrin.

The main functional groups of AG macromolecules are hydroxy groups and ether bonds. Natural AG also contains a small amount of carboxy groups of uronic acids. Arabinogalactan can be modified by reaction of these functional groups with drugs. Arabinogalactan macromolecules undergo oxidative functionalization and degradation during treatment of AG with hydrogen peroxide [16]. The oxidized polymers and oligomers contain additional carboxy and carbonyl groups, offering an additional potential for the chemical modification.

Natural AG and AG_{pol} and AG_{ol} fractions of oxidized AG were modified with 5-ASA containing carboxy, hydroxy, and amino groups. 5-Aminosalicylic acid, as well as salicylic acid, is weak and partially dissociates in water. We determined what form of 5-ASA (molecular or ionic) reacts with AG. The dissociation constants of carboxy and hydroxy groups of salicylic acid are 10^{-3} and 1.5×10^{-14}, respectively [17]. Probably, these functional groups of 5-ASA also weakly dissociate. The amino groups of 5-ASA can bind protons formed in dissociation, thus increasing the degree of dissociation of the carboxy groups. Hence, not only acid molecules, but also zwitterions $^{+}H_3NC_6H_3(OH)COO^{-}$ should be present in aqueous solutions of 5-ASA. In neutral solutions of the sodium salt of this acid prepared by neutralization with NaOH, $H_2NC_6H_3(OH)COO^{-}$ also exists. In an acidic solution, $^{+}H_3NC_6H_3(OH)COOH$ ions prevail, whereas in a basic solution, the main species is $H_2NC_6H_3(OH)COO^{-}$. The electronic absorption spectrum of a 5×10^{-4} M aqueous solution of 5-ASA with pH 7 contains a single band at 333 nm. At pH < 7, the sorption peak is shifted to 304 nm. Modification products of arabinogalactan and its oxidized species AG_{pol} and AG_{ol} containing 5-ASA absorb at 315–317 nm (Fig. 1a). Since polysaccharide solutions do not absorb in this range, the band with λ_{max} = 315–317 nm can be assigned to the reaction product of 5-ASA with the examined biopolymers. This product is not formed in acidic solutions. Therefore, all the subsequent reactions of AG, AG_{pol}, and AG_{ol} were performed at pH 7.0–7.1.

To determine the type of functional groups of 5-ASA reacting with AG and AG_{pol} and AG_{ol}, we performed a model experiment with polyvinyl alcohol (PVA) and hyaluronic acid, instead of the biopolymer. The product of the reaction of PVA with an equimolar amount of 5-ASA does not absorb in the range 220–350 nm (Fig. 1b). Hence, the hydroxy groups of PVA (and hence those of AG and AG_{pol} and AG_{ol}) do not react with 5-ASA. Since sodium salts of AG and AG_{pol} and AG_{ol}, formed in neutral solutions, dissociate into carboxylate anions, modification of the polymers and oligomers involves these functional groups. Indeed, the reaction product of 5-ASA and GA absorbs at λ_{max} = 317 nm (Fig. 1b). Thus, our model experiments showed that the most possible modification mechanism is the reaction of the protonated amino group of 5-ASA with the carboxy groups of GA, AG and AG_{pol} and AG_{ol} by the following scheme:

$$\text{AG–COOH} + \text{H}_2\text{N–C}_7\text{O}_3\text{H}_5 \rightarrow \text{AG–COO}^{-}\,^{+}\text{H}_3\text{N–C}_7\text{O}_3\text{H}_5,$$

where AG–COOH is AG, AG_{pol}, or AG_{ol} and $H_2N–C_7O_3H_5$ is 5-ASA.

The 5-ASA content of the modified product decreased by 0.15 wt % after treatment with hydrochlor-

ic acid (pH 2) for 48 h. Hence, this product is fairly stable in acidic solutions.

The reaction products of 5-ASA with AG and AG_{pol} and AG_{ol} were isolated, purified, and characterized by IR and UV spectroscopy and TLC. The optical rotatory power of these products was determined. All these compounds are water-soluble, but insoluble in acetone, alcohol, and diethyl ether. Their intrinsic viscosity η is close to that of the initial polysaccharide fractions, suggesting that the biopolymer chains do not degrade during modification. After addition of 5-ASA to the initial and oxidized AG, the rotatory power increases: $[\alpha]_D^{25}$: +11.9 (AG), +8.4 (AG_{pol}), +5.3 (AG_{ol}), and +12.0 (AG–5-ASA), +13.0 (AG_{pol}–5-ASA), and +16.0 (AG_{ol}–5-ASA). The maximal change in $[\alpha]_D^{25}$ is observed after modification of the oligomeric and polymeric fractions of oxidized AG.

The IR spectra of the modified samples of initial and oxidized AG contain and additional band at 1580 cm^{-1}, which is due to stretching vibrations of the benzene ring of the 5-ASA residue. This fact also suggests that the modified samples contain 5-ASA. The compositions of the modification products prepared under different conditions are listed in the table.

These data allow the following conclusions. The 5-ASA content of the products prepared at 20°C in 24 h increases as the [5-ASA] : [AG] molar ratio is raised by a factor of 10. An increase in the reaction time at 20°C and [5-ASA] : [AG] molar ratio = 1 : 1 has a similar effect. The 5-ASA content of the reaction products prepared in 3 h at the [5-ASA] : [AG] molar ratio of 1 : 1 increases with temperature. The relative increase in the 5-ASA content in the modified compounds in going from AG to AG_{pol} and AG_{ol} is clearly due to the higher content of carboxy groups in the oxidized samples. The content of carboxy groups per 100 polysaccharide molecules in AG is 4.7, whereas in AG_{pol} and AG_{ol} it is 12 and 76, respectively. Hence, the content of carboxy groups in the oligomeric and polymeric fraction exceeds that in the initial AG by a factor of 15 and 3, respectively, which agrees well with the 5-ASA content of these compounds.

The acute toxicity of the examined compounds is more than 5000 mg kg^{-1}. Hence, these compounds are moderately and low-toxic.

Drug content in AG, AG_{pol}, and AG_{ol} modified with 5-ASA under different conditions

Molar ratio AG : 5-ASA	τ, h	*T*, °C	Content of 5-ASA, mol mol^{-1} in AG, AG_{pol}, and AG_{ol}
AG + 5-ASA ([COOH] : [AG] = 0.043 mol mol^{-1})			
1 : 1	0.5	20	0.012
1 : 1	1	20	0.016
1 : 1	2	20	0.013
1 : 1	3	20	0.012
1 : 1	4	20	0.016
1 : 1	6	20	0.025
1 : 1	24	20	0.017
1 : 0.5	24	20	0.016
1 : 0.1	24	20	0.012
1 : 1	3	40	0.018
1 : 1	3	60	0.021
AG_{pol} + 5-ASA ([COOH] : [AG_{pol}] = 0.12 mol mol^{-1})			
1 : 1	1	20	0.035
1 : 1	3	20	0.036
1 : 1	6	20	0.040
1 : 1	10	20	0.050
1 : 1	24	20	0.048
1 : 0.5	24	20	0.028
1 : 0.1	24	20	0.017
1 : 1	3	40	0.037
1 : 1	3	60	0.047
AG_{ol} + 5-ASA ([COOH] : [AG_{ol}] = 0.75 mol mol^{-1})			
1 : 0.1	24	20	0.12
1 : 1	24	20	0.34
1 : 1	3	60	0.21

COMCLUSIONS

(1) Arabinogalactan and its oxidized polymeric and oligomeric fractions were modified with 5-aminosalicylic acid. Modified compounds with the drug content ranging from 1 to 29%, depending on the type of the polysaccharide fraction, were prepared. The modification involves reaction of the protonated amino groups of 5-aminosalicylic acid with carboxylate anions.

(2) The modified compounds are low-toxic, with the polymers and oligomers being synergists of 5-aminosalicylic acid.

ACKNOWLEDGMENTS

This study was financially supported in part by the Foundation for Support of Leading Research Schools (project NSh 728.2003.3), Research Program of the Federal Education Agency “Development of Research Potential of the Higher School” (project UR.05.01.008), and State Research Program of Bashkortostan Republic for the years of 2005–2007 (contract 419-Kh).

REFERENCES

1. Plate, N.A. and Vasil'ev, A.E., *Fiziologicheski aktivnye polimery* (Physiologically Active Polymers), Moscow: Khimiya, 1986.
2. Ovodov, Yu.S., *Bioorg. Khim.*, 1998, vol. 24, no. 7, pp. 483–501.
3. Arifkhodzhaev, A.O., *Khim. Prirodn. Soedinin.*, 2000, no. 3, pp. 185–197.
4. Antonova, G.F. and Usov, A.I., *Bioorg. Khim.*, 1984, vol. 10, pp. 1664–1669.
5. Kiyohara, H. and Yamada, H., *Carbohydrate Res.*, 1989, vol. 193, no. 10, pp. 173–192.
6. Ovodov, Yu.S., Ovodova, R.G., and Loenko, Yu.N., *Khim. Prirodn. Soedin.*, 1983, no. 6, pp. 675–694.
7. Medvedeva, S.A., Aleksandrova, G.P., Grishchenko, L.A., and Tyukavkina, N.A., *Zh. Obshch. Khim.*, 2002, vol. 72, no. 9, pp. 1569–1573.
8. Groman, E.V., Enriquez, P.M., Jung, C., and Josephson, L., *Bioconjugate Chem.*, 1994, vol. 5, no. 6, pp. 547–556.
9. Tolmachev, V.N., Lugovaya, Z.A., Ishchenko, I.K., *et al.*, *Vysokomol. Soedin., Ser. A*, 1975, vol. 17, no. 2, pp. 419–422.
10. Medvedeva, S.A., Aleksandrova, G.P., and Babkin, V.A., *Khim. Drev.*, 1998, no. 1, pp. 6–7.
11. Mashkovskii, M.D., *Lekarstvennye sredstva* (Pharmaceuticals), Kharkov: Torsing, 1997, vol. 2.
12. Antonova, G.F. and Tyukavkina, N.A., *Khim. Drev.*, 1976, no. 4, pp. 60–62.
13. Tyukavkina, N.A. and Antonova, G.F., *Izv. Sib. Otd. Akad. Nauk SSSR*, 1969, no. 9, no. 4, pp. 112–116.
14. Borisov, I.M., Shirokova, E.N., Mudarisova, R.Kh., *et al.*, *Izv. Ross. Akad. Nauk, Ser. Khim.*, 2004, no. 2, pp. 305–311.
15. Rafikov, S.R., Budtov, V.T., and Monakov, Yu.B., *Vvedenie v fiziko-khimiyu rastvorov polimerov* (Introduction to Physical Chemistry of Polymer Solutions), Moscow: Nauka, 1978.
16. Borisov, I.M., Shirokova, E.N., Babkin, V.A., *et al.*, *Dokl. Ross. Akad. Nauk*, 2002, vol. 383, pp. 774–777.
17. Rabinovich, V.A. and Khavin, Z.Ya., *Kratkii khimicheskii spravochnik* (Brief Chemical Handbook), Moscow: Khimiya, 1977.

Russian Journal of Applied Chemistry, Vol. 78, No. 10, 2005, pp. 1695–1698. Translated from Zhurnal Prikladnoi Khimii, Vol. 78, No. 10, 2005, pp. 1725–1728.
Original Russian Text Copyright © 2005 by Ramazanov, Shakhnazarova, Guliev.

MACROMOLECULAR CHEMISTRY AND POLYMERIC MATERIALS

Synthesis and Properties of Functionally Substituted Unsaturated Polysulfones

G. A. Ramazanov, R. Z. Shakhnazarova, and A. M. Guliev

Institute of Polymeric Materials, National Academy of Sciences of Azerbaijan, Sumgait, Azerbaijan

Sumgait State University, Sumgait, Azerbaijan

Received May 12, 2005

Abstract—High-temperature copolymerization of ethyl esters of vinyl- or isopropenylcyclopropanecarboxylic acids with SO_2 was studied as a route to functionally substituted unsaturated polysulfones. The composition, structure, and some properties of the polysulfones obtained were studied. The copolymerization mechanism was considered.

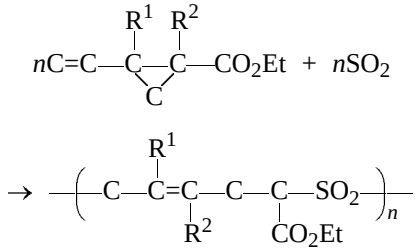
Copolymers of olefins with SO_2, polysulfones (PSs), show much promise for practice [1–3]. In particular, they can be used as plastics, materials for concentrating sulfuric acid solutions [1], and coatings for fabrics, paper, and wood [2]. Polysulfone materials are used for insulation and soundproofing. Polysulfones prepared from SO_2 and higher olefins improve the viscosity index of hydrocarbon lubricants [3].

One of the main application fields of PSs is microelectronics. The fact that PSs degrade to monomers under high-energy irradiation allows their use as sensitive components in positive resists [4]. At the same time, it is known that the properties of resists largely depend on the conditions of their synthesis and on the structure of an olefin used [5].

The physicochemical characteristics of the existing polysulfones do not meet the growing requirements to polymers used in photolithographic processes. Therefore, it is necessary to develop new high-performance reactive materials of this type.

In this study, we examined copolymerization of SO_2 with functionally substituted vinylcyclopropanes (VCPs). Copolymerization of VCPs with SO_2 was performed at low temperatures in the presence of *tert*-butyl hydroperoxide (TBH). To examine the reaction features, the reaction was performed at different temperatures.

Experiments showed that VCPs react with SO_2 in the presence of TBH according to the scheme



where R^1, R^2 = H, Me.

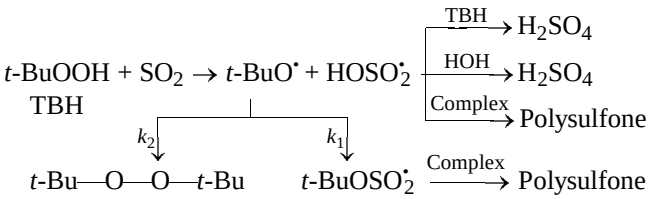
The reaction occurs spontaneously and is complete in a short time. However, after thorough purification of the components, the spontaneous copolymerization of VCPs with SO_2 does not occur. The yield of the polysulfones does not exceed 5% in 1 h, being essentially independent of the copolymerization temperature.

Introduction of O_2 substantially raises the final yield of the polysulfone. Similar effect was observed in copolymerization of cyclopentene with SO_2 in the bulk [6].

Further experiments showed that the VCP activity in the copolymerization depends on the time of its contact with air: The longer the contact with air (or oxygen), the higher the activity. Hence, the copolymerization is initiated by a substance formed from VCP and O_2, i.e., by a hydroperoxide. In the presence of a hydroperoxide, the copolymerization rate is high and the transformation of VCP to PS can be apparently brought to completion. Upon contact with O_2, VCP copolymerizes with SO_2 in the absence of TBH.

1070-4272/05/7810-1695 © 2005 Pleiades Publishing, Inc.

Thus, the copolymerization occurs in the redox system TBH–SO_2 [7]. The reaction of the two components of the redox system generates free radicals:



where $k_1 >> k_2$.

According to elemental analysis, the VCP : SO_2 ratio in the repeating unit of the copolymer is 1 : 1. When the copolymerization is performed in solution, the reaction rate is the highest at the equimolar ratio of the monomers. The yield of PS considerably decreases with increasing temperature.

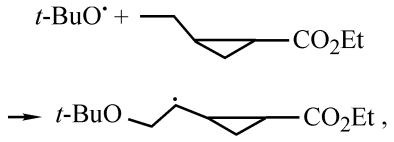
The copolymerization is fast and occurs without an induction period typical of radical reactions. The highest yield of PS is attained in 10–15 min. A longer reaction does not result in a higher yield. The structure of PSs was determined by spectroscopic methods. The IR spectra suggest that VCP is incorporated into the polymer chain, with simultaneous opening of the double bond and three-membered ring, as indicated by the presence of a medium-intensity band at 1630 cm^{-1} (stretching vibrations of internal C=C bond), two strong bands at 1320 and 1130 cm^{-1} assignable to the antisymmetric and symmetric stretching vibrations of SO_2, and a weak band at 3020 cm^{-1} (C–H stretching vibrations of VCP molecule). Also, bands corresponding to the *cis* (730 cm^{-1}) and *trans* (970 cm^{-1}) configurations of the C=C bond are present. Thus, we can conclude that VCP reacts at the 1,5-positions, i.e., with simultaneous opening of the double bond and three-membered ring. The ^1H NMR spectra are also indicative of the formation of a linear PS.

The copolymerization apparently involves intermediate formation of a π complex of SO_2 with the C=C bond of the VCP molecule [8]. This follows from changes in the chemical shift of olefinic protons in the ^1H NMR spectra, from the shift of the absorption peak in the UV spectra, and from the facts that the copolymer composition is independent of the composition of the starting mixture and that the reaction virtually does not occur in some solvents. Both the free and complexed VCP molecules may be involved in the process, although the complexation should enhance the susceptibility of VCP to attack by free radicals. The complexation of VCP and SO_2 follows from a downfield shift of the olefinic proton signals in the ^1H NMR spectra in the presence of SO_2.

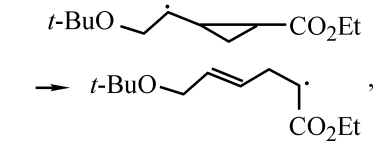
The copolymerization mechanism involves homolytic cleavage of TBH into free radicals, induced by SO_2:

$$t\text{-BuOOH} + SO_2 \rightarrow t\text{-BuO}^{\bullet} + HOSO_2^{\bullet}.$$

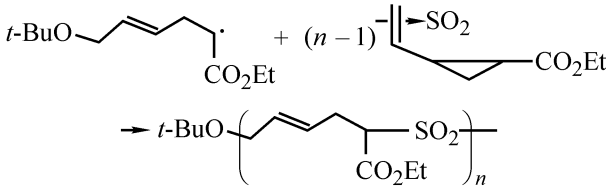
These radicals initiate the copolymerization, which consists of the following elementary steps [9]: initiation to give intermediate cyclopropylcarbinyl radicals



rearrangement of these radicals into allylcarbinyl radicals



and chain propagation on allylcarbinyl radicals, involving the donor–acceptor complexes:



The copolymerization occurs at a high rate even at low temperatures. Hence, the initiator is rapidly consumed. The radicals are generated in a large amount, which results in their recombination and formation of low-molecular-weight products. To obtain high-molecular-weight copolymers in high yield, it is necessary to prolong the effect of the initiator. This can be done by performing the copolymerization under heterogeneous conditions (in the bulk, so as to exclude dissolution of the forming PS). Another alternative is to perform homogeneous copolymerization at low temperatures (so as to raise the viscosity of the system, thus complicating the diffusion of macroradicals and lowering the termination rate).

The thermal stability of the PSs obtained was evaluated by differential thermal analysis. We found that the polysulfones are stable up to 200°C. Analysis of the gas phase shows that intense degradation of PS

starts above 200°C and is accompanied by SO_2 evolution. Kinetic analysis shows that the degradation occurs in a single step. The calculated activation energy (E_a = 34.3–76.2 kJ mol^{-1}) and reaction order (n = 1.1–1.3) suggest the chain mechanism of PS degradation [10].

A GPC analysis of PSs showed that, despite relatively low polydispersity, they are nonuniform in molecular weight (the chromatograms are bimodal). The number-average and weight-average molecular weights of the synthesized PSs, determined with PEG as reference, are as follows: $\overline{M}_n \sim (350-470) \times 10^3$ and $\overline{M}_w \sim (500-760) \times 10^3$. A characteristic feature of PS is the presence of active functional groups. Therefore, irradiation of thin PS films causes structural changes. The prevalent process is photodegradation, as indicated by a decrease in the intrinsic viscosity [η] of solutions of the irradiated PSs, by an increase in the precipitation threshold in their turbidimetric titration due to decreased content of high-molecular-weight fractions, by a decrease in the slope of the integral curve (and the resulting broadening of the peak in the differential curve), and by a decrease in the quantum yield of degradation.

Thus, the copolymerization of VCPs with SO_2 can be regarded as spontaneous copolymerization of donor–acceptor complexes formed by the comonomers in the initial mixture. After thorough removal of hydroperoxides and instantaneous degassing of all the components, the copolymerization of VCP with SO_2 is insignificant. To obtain high-molecular-weight PSs suitable for use in microelectronics, it is necessary to perform the process at low temperatures in the presence of TBH.

EXPERIMENTAL

The IR spectra of PSs were recorded on a Specord M80 spectrometer, and the ^{1}H NMR spectra, on a Tesla BS-487B spectrometer (80 MHz, reference HMDS). The thermograms were measured on an MOM derivatograph (Hungary) in air at a heating rate of 5 deg min^{-1}.

The molecular weight was determined by gel permeation chromatography (GPC) and viscometry. Chromatographic analysis of PSs was performed on Covo (Czechia) and KhZh-1309 high-performace liquid chromatographs. The columns were packed, respectively, with microspherical silica gel Separon SGX and microspherical macroporous silica gel with grafted octadecyl groups Separon C-18; eluent DMF.

Turbidimetric titration of PSs was performed on an FEK-56M photoelectron colorimeter.

VCPs were prepared as described in [6] and were distilled before use from freshly calcined $CaCl_2$; SO_2 was dried by passing through a column packed with $CaCl_2$ and bubbling through H_2SO_4.

The monomers were washed first with 10% NaOH and then with 3% $FeSO_4$ to remove hydroperoxides, after which they were treated with water, dried over $CaCl_2$, and vacuum-distilled.

Copolymerization was performed in the bulk and in toluene or acetone by the following procedure. The required amount of SO_2 was condensed in a flask cooled with a dry ice–acetone mixture. Then the required amount of VCP containing the required amount of TBH was added to the cooled flask. The copolymerization was performed at temperatures of –10 to 0°C; the VCP : SO_2 molar ratio was 1 : 1.2.

After a certain time, the copolymers were precipitated, purified by reprecipitation from acetone into diethyl ether, and dried at 30–40°C in air.

The compositions of the copolymers were determined from the sulfur content, and the structures, by IR and ^{1}H NMR spectroscopy.

The viscosity of PSs was measured on an Ubbelohde viscometer at 25°C in cyclohexanone. All the PSs were tested for solubility in acetone, DMF, DMSO, cyclohexanone, 1,2-dichloroethane, toluene, and dioxane.

CONCLUSIONS

(1) Reactions of ethyl esters of vinylcyclopropanecarboxylic acids with SO_2 in the presence of tert-butyl hydroperoxide yield unsaturated polysulfones with equimolar ratio of the comonomer units. In the course of the copolymerization, both the double bond and the cyclopropane ring in vinylcyclopropane monomers are opened simultaneously; the copolymerization involves formation of a complex by the comonomers.

(2) The polysulfones prepared are thermally stable up to 200°C. Above this temperature, they decompose with evolution of SO_2. The polysulfones can be used as resists in microelectronics.

REFERENCES

1. French Patent 1 060 886.
2. Goethals, E.J., *J. Macromol. Sci., Ser. C2: Rev. Macromol. Chem.*, 1968, no. 1, pp. 105–110.

3. US Patent 2 853 373.
4. Moreau, M.W., *Semiconductor Lithography. Principles, Practices, and Materials*, New York: Plenum, 1988.
5. Tsonis, C.P., Ali, S.A., and Wazeer, M.T.M., *Polymer*, 1986, vol. 27, no. 12, pp. 1991–1998.
6. Budris, S.V., Chikhacheva, I.P., Stavrova, S.D., *et al.*, *Vysokomol. Soedin., Ser. B*, 1995, vol. 37, no. 6, pp. 1104–1106.
7. Dolgoplosk, B.A. and Tinyakova, E.I., *Generirovanie svobodnykh radikalov i ikh reaktsii* (Generation of Free Radicals and Their Reactions), Moscow: Nauka, 1982.
8. Ratzsch, M. and Bormann, G., *Plast. Kautsch.*, 1975, vol. 22, no. 12, pp. 937–942.
9. Guliev, A.M., Ramazanov, G.A., Guliev, M.F., and Gasanova, S.S., *Vysokomol. Soedin., Ser. B*, 1987, vol. 29, no. 8, pp. 581–584.
10. Kiran, E., Gillham, J., and Gipstein, E., *J. Appl. Polym. Sci.*, 1977, vol. 21, no. 5, pp. 1159–1176.
11. Guliev, A.M., Kasimova, S.P., Lemeshev, A.N., and Nefedov, O.M., *Zh. Org. Khim.*, 1990, vol. 26, no. 6, pp. 1261–1269.

Russian Journal of Applied Chemistry, Vol. 78, No. 10, 2005, pp. 1699–1702. Translated from Zhurnal Prikladnoi Khimii, Vol. 78, No. 10, 2005, pp. 1729–1732.
Original Russian Text Copyright © 2005 by Chursin.

MACROMOLECULAR CHEMISTRY AND POLYMERIC MATERIALS

Fat-Polymeric Fillers: Synthesis, Properties, and Application

V. I. Chursin

Central Research Institute of Leather-Shoe Industry, Federal State Unitary Enterprise, Moscow, Russia

Received March 24, 2005

Abstract—Properties of the copolymerization products of acrylic monomers and esters of polyethylene glycol and unsaturated fatty acids were studied. The complexing power and leather-technological properties of fat-polymeric systems were analyzed as influenced by the acidity of the medium and the type of the monomer.

Polymeric products modified with fat-liquoring materials find increasingly growing application in leather production [1]. One of the methods for preparing these products is mixing of individual components yielded by dispersion into aqueous medium of fat-polymeric compositions. Among the drawbacks of such products are different resistances of the system components to changes in pH, rise in temperature, and exposure to chemicals. Depending on the treatment conditions, chemical compounds entering into the fat-polymeric composition are sorbed by the structural elements of the derma to different extents, which gives no way attaining uniform properties across the thickness and over the area of the ready-for-use leather. In our opinion, the greatest promise is offered by synthesis of the polymers in the presence of fats containing unsaturated groups that can be involved in copolymerization.

In this study, we examined the properties of fat-polymeric filling materials (Fetan) synthesized from acrylic monomers and esters of polyethylene glycol and unsaturated acids (OPEGs) with a high degree of unsaturation.

EXPERIMENTAL

We studied how the amount of the acid catalyst affects the properties of the products synthesized from acrylamide (AA) (Fetan 8, Fetan 16, and Fetan 30; the figures indicate the amount of sulfuric acid in units of 0.1% of the mass of the reaction system), as well as those based on glycidyl methacrylate (GMA), Fetan GMA. The copolymerization was done at 25°C at the monomer : OPEG : water volume ratio of 1 : 1 : 4.

The resulting products are viscous light yellow systems with the following characteristics: content of the base substance and substances extractable with organic solvents 24–26 and 7–9 wt %, respectively, and pH of the 5% (by weight) solution 3.0–4.0.

The fat-polymeric filler Fetan was examined spectrophotometrically, viscometrically, and turbidimetrically. The viscometric measurements were made on a capillary viscometer (d = 0.56 mm) at 20°C. The viscosity-average molecular weight $\bar{M}_\eta$ was calculated from the intrinsic viscosity [η] by the formula $[\eta] = 0.63 \times 10^{-4} M_\eta^{0.8}$, suggested for aqueous solutions of polyacrylamide (PAA) [2], since in both cases the initial monomer is AA.

We found that polymerization yields macromolecular compounds with $\bar{M}_\eta = (250-400) \times 10^3$. When Fetan is prepared in the presence of a large amount of H_2SO_4, the parameters [η] and $\bar{M}_\eta$ increase. Kritskaya and Ponomarev [3] reported that an increase in $\bar{M}_\eta$ during nonisothermal polymerization of AA may be due to enhanced activation in the presence of H_2SO_4. The $H^\bullet$ atoms, which are free radicals, can add at the double bond of the monomer molecule, thereby initiating copolymerization. Such initiation is not associated with decomposition of peroxides, since they were not used in the polymerization. The $\bar{M}_\eta$ of the fat-polymeric fillers under study increases in the order: Fetan 8 < Fetan 16 < Fetan 30. These results were confirmed by the turbidimetric data. We showed that the precipitation threshold for Fetan 8 is 1.5 times that of Fetan 30.

The structure and molecular-weight distribution (MWD) of the polymer are strongly affected by its ability to penetrate deep inside the derma and get bound to the functional groups of collagen. In the presence of a large amount of an acid catalyst, the polymer chain propagates more actively, which yields

1070-4272/05/7810-1699 © 2005 Pleiades Publishing, Inc.

Table 1. IR spectra of the initial components and copolymerization products

Acrylamide	OPEG	Fetan 8	Fetan 16	Fetan 30
709 δ(C–H)	–	–	676	600
–	–	789	–	–
960 δ(–C–H)	952	–	–	–
1109	–	–	1098	1120
–	1131 (CH_3)	1169	1197	–
1283	–	–		
1355 δ(C–H)	–	–	–	1300
1435 δ(CH_2)	–	–	1494	1470
1590 δ(N–H)	–	–	–	–
1687 δ(C=O)	–	1669	1670	1650
–	1738 ν(C=O)	–	–	–
–	2848 ν_s(CH)	–	–	–
–	2910 ν_{as}(CH_2)	–	2900	2920

fillers with high $\bar{M}_\eta$. It should be remembered that diffusion of the polymeric filler with a high $\bar{M}_\eta$ deep into the leather will be hindered, and Fetan 30 will be mostly deposited in loose layers and on the surface of the semifinished product. The particle size of the polymeric filler was estimated from the absorption intensity of the Fetan solution at various wavelengths, i.e., from the turbidity spectrum [4]. We found that the particle size is the largest for Fetan 30 (160–170 nm), and the smallest, for Fetan GMA (110 nm). The particle size for Fetan 8 and Fetan 16 lies within 140–160 nm.

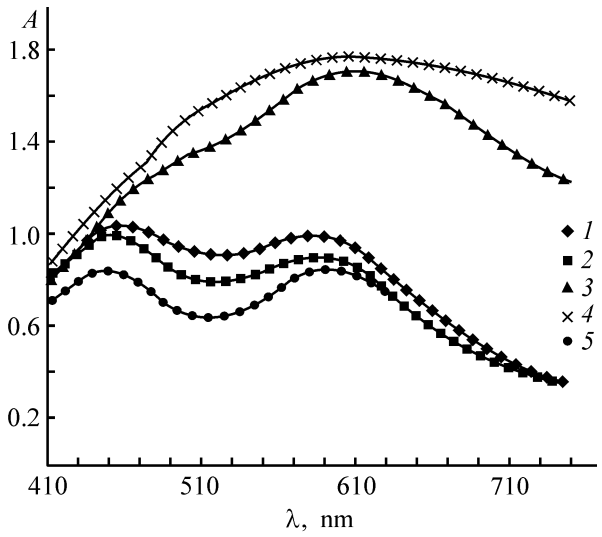


Fig. 1. Electronic absorption spectra of the solutions of the filler in the presence of CTA. (*A*) Optical density and (λ) wavelength. (*1*) CTA, (*2*) Fetan 8, (*3*) Fetan 16, (*4*) Fetan 30, and (*5*) Fetan GMA.

Additional information about copolymerization was derived from the absorption spectra of the initial components and end products. Table 1 shows that OPEG is characterized by an intense absorption band corresponding to stretching vibrations of the C=O bond of the ester group at 1738 cm^{-1}, as well as a band at 952 cm^{-1} corresponding to out-of-plane bending vibrations of the C–H bond in the >C=CH– group of oleic acid. It can be stated that the copolymerization is rather fast, because already 15 min after mixing of the initial components the spectra contain no absorption bands characteristic of the double bonds of AA and OPEG. Polymerization goes to high conversions of the initial components and is mostly complete within 1 h. In the spectra of the polymerization products, the intensity of absorption near 1650–1670 cm^{-1}, characteristic of the COO– groups, is enhanced, and a new band corresponding to sulfurcontaining groups of H_2SO_4 appears at 600–680 cm^{-1}. The absorption bands at 1095 and 1197 cm^{-1}, characteristic of the ester moieties, become more prominent. Thus, the absorption spectrum of the resulting products is similar to that of PAA (1110, 1340, 1450, 1670 cm^{-1}) [5], except for the presence of a broad band at 670 and the lack of a band at 1340 cm^{-1}.

In view of the fact that fat-polymeric fillers are used in the stage of the dye-fat liquoring processes, following the chrome aftertanning, it was of interest to study their interaction with the chrome tanning agent (CTA). Technologically, our results should be taken into account in substantiating the expediture of the CTA for fixing of fats and dyes in the final stage of fat liquoring. The interaction of Fetan with CTA was studied photometrically [6]. The absorption spectrum of the CTA solution contains two bands with characteristic peaks at 420 and 580 nm. Figure 1 shows the absorption spectra of the solutions containing Fetan and CTA in certain proportions. It is seen that, upon introduction of the CTA into a solution of fat-polymeric fillers Fetan 16 and Fetan 30, the optical density *A* strongly increases. The spectrometric curves do not contain the peak at 420 nm, characteristic of the CTA. This suggests that, upon increasing molecular weight of the filler in the presence of a larger amount of H_2SO_4, CTA can react with the carboxy groups of the polymer, yielded by acid hy-

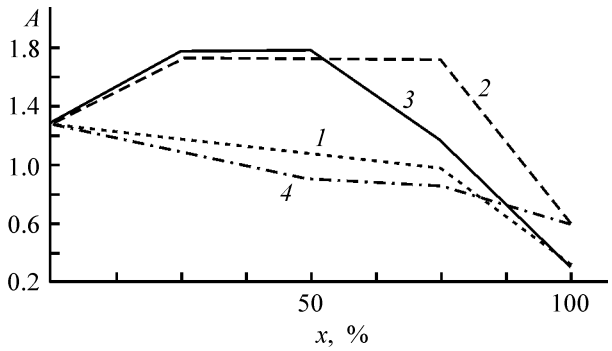


Fig. 2. Optical density A of the solution vs. the weight fraction of Fetan x, %: (*1*) Fetan 8, (*2*) Fetan 16, (*3*) Fetan 30, and (*4*) Fetan GMA.

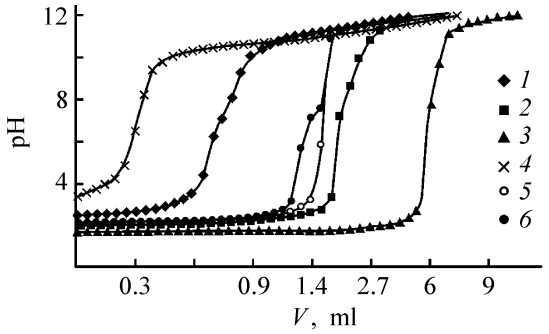


Fig. 3. Potentiometric titration of the initial components and copolymerization products. (V) Volume of the 0.5 N NaOH solution added. (*1*) Fetan 8, (*2*) Fetan 16, (*3*) Fetan 30, (*4*) Fetan GMA, (*5*) OPEG, and (*6*) AA.

drolysis of Fetan. Figure 2 shows that there is no complexing in the case of Fetan GMA. For Fetan 8, complexing can be observed even at the filler : CTA weight ratio of 75 : 25. Introduction of CTA into a Fetan 16 solution yields fairly stable complexes at the identical ratio of the components. This conclusion is of technological importance, as this allows optimization of the amount of CTA required for fixing of Fetan in leather. As the content of the carboxy groups increases due to acid hydrolysis, stable complexes are formed in the case when the weight fraction of Fetan 30 is 50%.

The potentiomatric titration curves of the initial components and copolymerization products (Fig. 3) show that, with increasing amount of the H_2SO_4 spent, the alkaline capacity of Fetan tends to grow. The identical runs of the curves suggest that polymerization of Fetan proceeds at the double bonds of AA and OPEG, without involving the functional groups of the initial components. A similar effect has been revealed earlier by Averina *et al.* [7] in a study of copolymers of MMA and triglycerides.

Thus, we confirmed the feasibility of preparation of fat-polymeric fillers based on acryl monomers and polyethylene glycol esters of unsaturated acids. With increasing acidity of the reaction system, the molecular weight and particle size of the polymer tend to grow, which suggests that this factor can be used in preparation of polymerization products with desired molecular weights. We carried out technological tests of the filler with a semifinished product intended for manufacturing of leathers for shoe top. With the Fetan fat-polymeric filler used in dye and fat liquoring processes in amount of 3% relative to the mass of the semifinished product, the amount of the CTA was, in accordance with the previously revealed relationships, 1% for Fetan 8 and Fetan 16 and 1.5% for Fetan 30. The technological tests of the new fat-polymeric filler in production of leathers for the shoe top (Table 2) showed that treatment with Fetan filler yields filled elastic leathers and affords a growth of the leather sample area relative to the reference sample. The largest gain in the thickness and area of the leather samples was exhibited by the samples filled with Fetan GMA and Fetan 30. The use of the fat-polymeric fillers in dye and fat liquoring processes decreases the amounts of the corresponding filling and fat liquoring materials by 20–30%, favors uniform distribution of fats, and ensures manufacture of high-quality competitive leathers.

Table 2. Characteristics of the leathers manufactured with the use of Fetan fat-polymeric fillers

Characteristic	Reference sample	Fetan 8	Fetan GMA	Fetan 16	Fetan 30
Gain, %:					
thickness	4.5	6.8	7.7	7.0	7.6
area	0.65	1.0	1.22	1.0	1.4
Elongation at a stress of 9.8 MPa, %	22.0	19.0	24.0	17.5	18.4
Elongation at break, %	48.0	39.0	39.0	42.0	41.0
Ultimate strength, MPa	28.0	23.5	25.5	26.5	26.0

CONCLUSIONS

(1) Raising in the amount of H_2SO_4 spent for polymerization during synthesis of fat-polymeric tanning agents based on acrylic monomers and esters of polyethylene glycol and unsaturated acids leads to an increase in the viscosity-average molecular weight of the polymer.

(2) Spectral studies showed that the expenditure of H_2SO_4 affects the ratio of the components during complexing in the copolymer–chrome tanning agent system.

REFERENCES

1. Kneip, M., *Leder*, 1995, no. 5, pp. 106–109.
2. Chimarityan, Dzh. G., Arutyunyan, L.R., Grigoryan, M.V., *et al.*, *Fiziko-khimiya polimerov: Sintez, svoistva i primenenie: Sbornik nauchnykh trudov* (Physical Chemistry of Polymers: Synthesis, Properties, and Application: Coll. of Scientific Works), Tver, 2002, issue 8, pp. 195–200.
3. Kritskaya, D.A. and Ponomarev, A.M., *Vysokomol. Soedin., Ser. A*, 2002, vol. 44, no. 6, pp. 910–915.
4. Klenin, V.I., Shchegolev, S.Yu., and Lavrushin, V.I., *Kharakteristicheskie funktsii rasseyaniya dispersnykh sistem* (Characteristic Functions of Light Scattering in Dispersed Systems). Saratov: Saratov. Gos. Univ., 1977.
5. Karapetyan, F.O., Sarukhanyan, E.R., and Beileryan, N.M., *Fiziko-khimiya polimerov: Sintez, svoistva i primenenie: Sbornik nauchnykh trudov* (Physical Chemistry of Polymers: Synthesis, Properties, and Application: Coll. of Scientific Works), Tver, 2002, issue 8, pp. 186–194.
6. Deryabkina, E.V. and Galashina, V.N., *Izv. Vyssh. Uchebn. Zaved., Khim. Khim. Tekhnol.*, 2001, vol. 44, no. 5, pp. 8–12.
7. Averina, E.S., Radnaeva. L.D., and Vasnev, V.A., *Plast. Massy*, 2002, no. 11, pp. 31–32.

Russian Journal of Applied Chemistry, Vol. 78, No. 10, 2005, pp. 1703–1708. Translated from Zhurnal Prikladnoi Khimii, Vol. 78, No. 10, 2005, pp. 1733–1738.
Original Russian Text Copyright © 2005 by Dubovyi.

MACROMOLECULAR CHEMISTRY AND POLYMERIC MATERIALS

Binding in Paper-Like Composites Based on Mineral Fibers

V. K. Dubovyi

St. Petersburg State Forestry Engineering Academy, St. Petersburg, Russia

Received May 24, 2005

Abstract—The structural and physical parameters of paper-like composites based on mineral fibers with aluminum polyhydroxo complexes as binders were determined and analyzed. Samples of the composites based on mineral fibers differing in the content of binders were analyzed by IR spectroscopy and electron microscopy. Formation of interfiber bonds in the materials studied was hypothesized.

The use of inorganic, mainly artificially prepared, mineral fibers as the base component of composites is one of the most intensively developed lines in modern paper technology. Paper-like composites based on mineral fibers exhibit a set of properties unachievable in principle for conventional paper and pressboard types based on plant fibers. Specifically, they are characterized by high thermal, chemo-, and biostability and resistance to various, in particular, hard radiations, as well as high filtration power, which allows a low aerodynamic resistance to be combined with a high coefficient of entrapment of submicron particles [1, 2].

However, despite these properties, applications of materials based on mineral fibers are yet limited. Mineral fibers are used in noticeable amounts in production of insulation materials and, to a lesser extent, of filtration materials. The reason is that, unlike plant fibers, mineral fibers cannot form interfiber bonds in paper sheets. Thus, the conventional paper production technology should be supplemented with introduction of special binders in order to obtain materials combining the advantages offered by the sheet form with unique properties of mineral fibers. The use of organic binders limits application of materials based on mineral fibers, since, at high temperatures and under exposure to aggressive media, binding additives degrade, which leads to degradation of the material as a whole. The properties of composites based on mineral fibers are manifested to the full extent when inorganic substances, in particular, aluminum compounds, are introduced as binders.

Theoretical concepts of how aluminum compounds exert their reinforcing effect on cellulose-based materials suggest that similar mechanisms are applicable to certain kinds of mineral fibers as well. In this study, we used $Al_2(SO_4)_3$ as a compound of this kind. This chemical is readily available and is widely used in paper production [3]. Aluminum sulfate proper is not a binder; rather, reinforcing effect is exerted by the products of its hydrolysis at a pH adjusted by a NaOH solution. Presumably, the resulting polynuclear acido complexes of aluminum can attract into their structure various ligands and, in particular, hydroxy ions occurring on the mineral fiber surface [4].

We examined glass fibers with average diameters of 0.2 and 0.7 μm, as well as kaolin and basalt fibers with diameters of 1.9 and 1.1 μm, respectively. A paper casting apparatus produced laboratory paper sheets (sheet-cast paper) from mineral fibers without and with $Al_2(SO_4)_3$. In the latter case, $Al_2(SO_4)_3$ was added in amounts of 20, 40, 60, and 80% relative to the fiber mass (recalculated for Al_2O_3). Casting was conducted at pH 7.0–7.5. The surface density of the cast paper varied from 15 to 80 g m^{-2}.

The strength and deformation properties of the cast paper were derived from the results of mathematical processing of the stress (σ)-vs.-strain (ε) curves.

The stress–strain curve obtained by processing the load (F)-vs.-elongation (ΔL) indicator diagram demonstrating the results of the static tensile tests allows analysis of the deformation process and is widely used in materials science as an integrated characteristic of the mechanical properties. Such a diagram was obtained for sheet paper-like materials based on mineral fibers, tested on tensile-testing machines equipped with a unit recording variations of the load and strain for the sample during the tests.

1070-4272/05/7810-1703 © 2005 Pleiades Publishing, Inc.

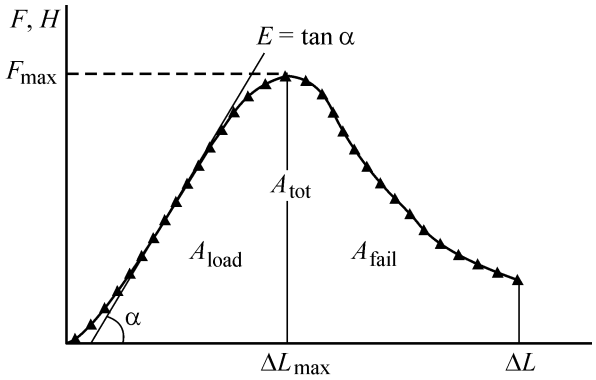


Fig. 1. Technique for calculation of the deformation characteristics.

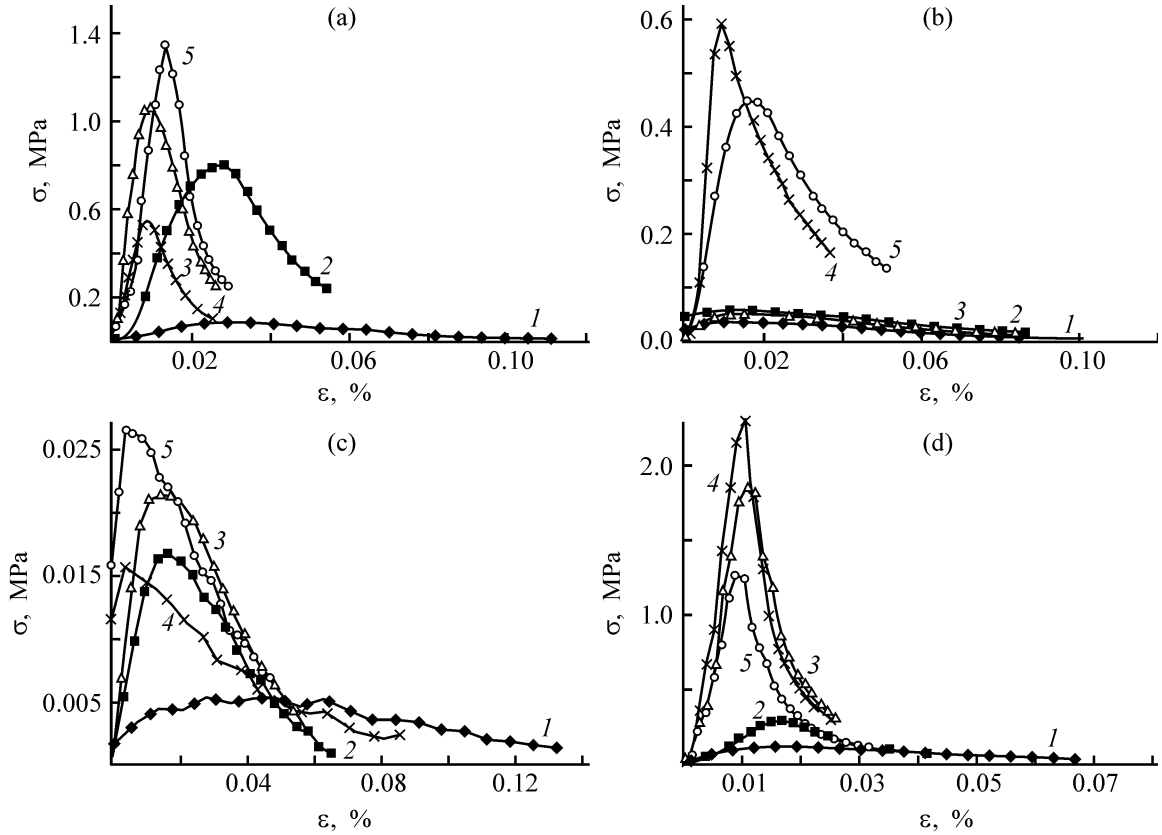


Fig. 2. Stress (σ) vs. strain (ε) curves for samples of the sheet materials from mineral fibers with a surface density of 50 g m^{-2}, differing in the content of aluminum sulfate (recalculated for Al_2O_3). $Al_2(SO_4)_3$ content, wt %: (*1*) 0, (*2*) 20, (*3*) 40, (*4*) 80, and (*5*) 100. Sample: (*1*) glass fiber 0.2 μm in diameter, (b) glass fiber 0.7 μm in diameter, (c) kaolin, and (d) basalt; the same for Figs. 6, 7.

In this study, we carried out measurements on a laboratory test complex comprising a Testosistema-105 tensile-testing machine and a PC.

Each sample tested was characterized by the length *L*, width *b*, and thickness δ, averaged over the measurements taken at several points. After testing each sample, the information about the characteristics of the sample and the testing results were transferred from the Testosistema-105 machine to the PC.

Mathematical processing of the results was carried out using the MS Excel table processor by a specially developed routine according to the scheme shown in Fig. 1. Mathematical processing on the PC of the experimental load–elongation curves, obtained in replicate runs, yielded an average curve consisting of 21 points, for each of which the following characteristics are calculated: force *F*; *H*; elongation Δ*L*, mm; stress σ, MPa,

$$\sigma = F/b\delta;$$

and strain ε, %,

$$\varepsilon = \Delta L/L.$$

The curve in Fig. 1 clearly exhibits two portions: up to the point corresponding to the maximal load (F_{max}, ΔL_{max}), when the sample preserves integrity, and after applying the maximal load, when the sample fails. There is no instantaneous failure; rather, the fibers are pulled apart, which requires applying certain force to overcome the friction forces [5].

Figure 2 shows the strain dynamics of the materials in the form of the stress–strain curves.

The rigidity in extension of a sheet material is estimated from the modulus of elasticity (E) characterizing the slope of the initial section of the stress–strain curve, i.e., the response of the material to the force applied.

Without binder, all the samples under study exhibit an extremely low strength, which could be enhanced by increasing the mass per square meter, which will yield more reliable results. The poorest strength and strain characteristics were exhibited by a sheet material prepared from kaolin fibers, and the best strength and rigidity, by basalt fiber materials and small-diameter glass fibers. An increase in the diameter of glass fibers deteriorates the properties by decreasing the number of the fibers per unit volume and, accordingly, that of interfiber contacts.

The σ–ε curves of the kaolin fiber samples and of the glass fiber samples with the diameter of 0.7 μm are flat near the peak, i.e., a very weak structure breaks very smoothly, and the fibers virtually do not resist pulling apart.

By contrast to paper and pulp materials, the σ–ε curves of the mineral fiber sample exhibit a pronounced reverse branch after passing the peak. This suggests that the material does not fail instantaneously, and the fibers being pulled apart exhibit a certain resistance by virtue of the friction forces. The relative fraction of the total area under the curve for the area after failure is about the same.

The binder not only improves the deformation and strength characteristics, but also affects the character of deformation of the sheet material under extension (Fig. 2). We showed that the material gets not only stronger but also more rigid, which is accompanied by a decrease in the extensibility of the material: the peak in the curves shifts toward the ordinate.

In extension of a fibrous material containing a binder, interfiber binding forces are specifically responsible for the increasing rigidity of the structure and its response to the force applied. This follows from the stress–strain curves: a steeper portion of the curves in the loading branch corresponds to the samples containing a larger amount of the binder. The reverse runs of the curves after the peak are similar in length and slope for most of the samples; they characterize the resistance of the fibers to pulling apart, when the interfiber contacts are broken.

The reinforcing effect in the presence of the binder varies between different materials. For example, for paper cast from the glass fiber with the diameter of 0.2 μm, the reinforcing effect is manifested even with 20% $Al_2(SO_4)_3$ (recalculated to Al_2O_3), and for the paper cast from glass fiber with a diameter of 0.7 μm, a comparable effect requires introduction of 60–80% additive.

The nature of the mineral fibers also affects the deformation and strength characteristics of the samples prepared using a binder. Even with the binder, the kaolin fiber material remains very weak. The strength of the samples increases in the order kaolin < glass fiber 0.7 μm in diameter < glass fiber 0.2 μm in diameter < basalt.

The deformation characteristics of the materials based on mineral fibers suggest that the strength and rigidity of the samples increase upon introduction of $Al_2(SO_4)_3$ and adjustment of pH to 7.0–7.5. This confirms formation of interfiber bonds, which are stronger than the permanently acting friction forces and intermolecular interaction forces.

To elucidate the nature of the interfiber bonds formed, we carried out an IR study of the samples. They were prepared from a formulation similar to that used for studying the deformation characteristics, though with a surface density of 5–15 g m^{-2} to ensure the required IR transmission.

The transmission spectra of the samples were measured on a Specord IR spectrometer in the range 2700–3800 cm^{-1}, corresponding to the vibrational frequencies of the hydrogen-bonded OH groups. The spectra were recorded with a resolution of 2 cm^{-1}.

The characteristic lengths of the hydrogen bond in the samples under study were estimated by the band shape analysis.

The analysis of the shape of the OH absorption band was based on the previously used [6] ratio of the hydrogen bond length d to the OH absorption

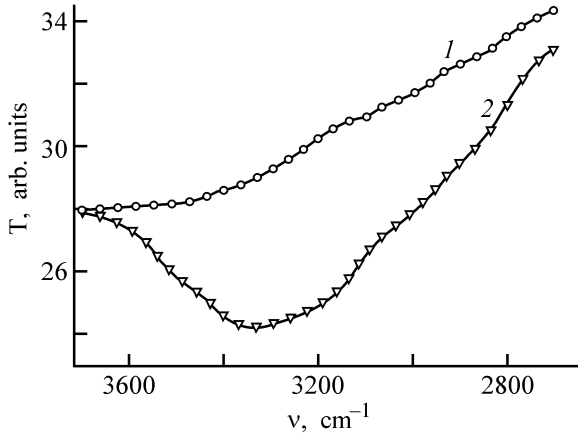


Fig. 3. Fragments of the IR spectra of the samples in the region of the OH vibrational frequencies. (*1*) with binder and (*2*) without binder. (T) Transmission, and (ν) wave number.

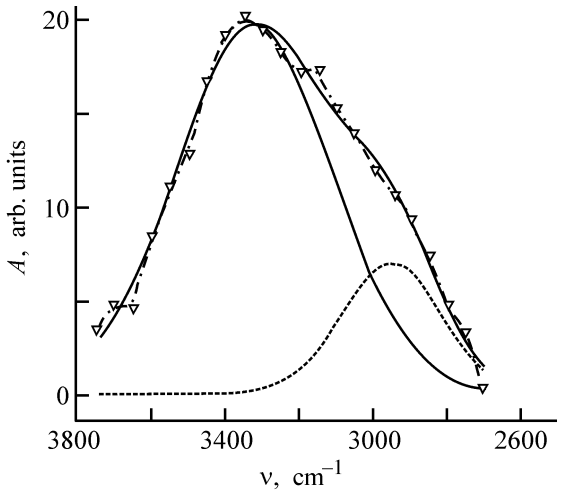


Fig. 4. An example of decomposition into Gaussians. (*A*) Absorption, and (ν) wave number.

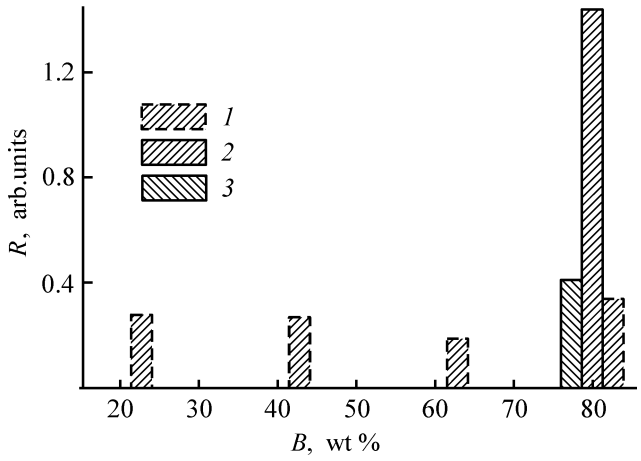


Fig. 5. Ratio of strong to weak H bonds, *R*, vs. the amount of the binder *B* (recalculated to Al_2O_3). (*1*) Fiber glass 0.2 μm in diameter, (*2*) kaolin fiber, and (*3*) basalt fiber.

frequency. Using this approach, we studied formation of the composites based on mineral fibers and aluminum hydroxo complexes as influenced by the hydrogen bond.

The shape of the OH absorption band was analyzed using the empirical ratio of the frequency ν of vibrations of the proton in the OH groups to the distance *d*, Å, separating the proton from the nearest oxygen atom.

$$\nu = A - B\exp(-d/C).$$

Here, *A*, *B*, and *C* are numerical coefficients calculated using published data [7], $A = 3590$ cm^{-1}, $B = 3.04 \times 10^{11}$ cm^{-1}, and $C = 0.13$ Å.

Figure 3 shows fragments of the IR transmission spectra of the basalt fiber samples in the range corresponding to stretching vibrations of the OH group. It is seen that 80% of the $Al_2(SO_4)_3$ binder introduced (recalculated to Al_2O_3) gives rise to a broad asymmetric absorption band. To analyze the shape of the absorption band, it was decomposed into Gaussians (see an example of decomposition into two Gaussians in Fig. 4). It is seen that such a decomposition fairly satisfactorily describes the experimental absorption band for the basalt fiber. The Gaussian with a maximum at 2950 cm^{-1} corresponds to a stronger hydrogen bond [a smaller distance to the nearest oxygen atom (d = 2.65 Å)], and the Gaussian with a maximum at 3320 cm^{-1}, to a weaker hydrogen bond [(d = 2.77 Å)]. The accuracy of resolution over the curve area was ca. 1%. In the frequency range under study, the shape of the absorption band varied with the kind of the mineral fibers and with the percentage of the $Al_2(SO_4)_3$ introduced, which can be interpreted in terms of the change in the strength of the hydrogen bond. To quantitatively estimate the ratio of the strong to weak hydrogen bonds, we determined the ratio of the areas of the corresponding Gaussians. Figure 5 demonstrates how the ratios of the strong to weak hydrogen bonds are influenced by the amount of $Al_2(SO_4)_3$ introduced.

Our results show that the samples under study contain interfiber bonds which, according to their nature, can be categorized as hydrogen bonds, i.e., those involving OH groups.

The strength of the hydrogen bond as determined by the distance between the hydrogen and oxygen atoms does not fully characterize the efficiency of the interfiber binding, since integrated assessment requires information about the area of the contacts. It should also be noted that the materials prepared for

IR spectroscopy had a low mass per square meter. The degree of retention of the binder in them is very low. Moreover, it is necessary to take into account the possibility of incorporation into the sphere of aluminum polyhydroxo complexes of other ligands in addition to the surface OH groups entering into the composition of mineral fibers. Thus, the IR data can be regarded as a qualitative confirmation of the occurrence of bonding via OH groups.

To understand more clearly the nature of binding in the presence of binders, we carried out optical- and electron-microscopic studies of the samples based on mineral fibers.

The surface and the internal structure of the samples were examined on an MBB-1 microscope in the ordinary white transmitted light using ×20 lenses and ×40 and ×70 water-emulsion lenses, as well as in the phase contrast mode with ×10f, ×20f, and ×40f lenses. The micrographs of the samples were obtained with an optical microscope using an MFNE-1U4,2 automatic microphotographic attachment.

The surface of the samples was examined at ×620 to ×7200 magnifications in a JSM-32C (Jeol) scanning electron microscope.

The samples were preliminarily mounted on stages and then coated with a Pd + Au alloy film on a JFC-100 (Jeol) ion sputtering setup. Stereo images were obtained with a Mantya 6 × 7-cm photo camera.

It is seen from the micrographs that the glass fibers 0.2 μm in diameter (Fig. 6a) have a smooth surface and a uniform internal structure. In the sheet, fibers are bent and curved, and thinner fibers are roundly bent into loops 5–6 μm in diameter. The glass fibers 0.7 μm in diameter are more linear, though slightly curved (Fig. 6b). The basalt fibers have a smooth surface, and their diameter varies along their length. The internal structure of the fibers is uniform (Fig. 6c). The kaolin fibers have a smooth, clean surface; they occur in a bent state over a wide thickness range. They have a uniform internal structure and are virtually transparent (Fig. 6d). The smooth surface of the mineral fibers suggests insignificant influence of the friction forces on the interfiber binding in the paper-like materials under study.

With increasing amount of the $Al_2(SO_4)_3$ introduced, the binder starts to deposit in the form of "lumps" growing in size (Figs. 7a–7d). At the maximal amount of $Al_2(SO_4)_3$ (80% relative to the mass of the fiber) (recalculated to Al_2O_3), the interfiber contacts are covered with the binder, which creates structures typical of the paper-like composites with the nodal

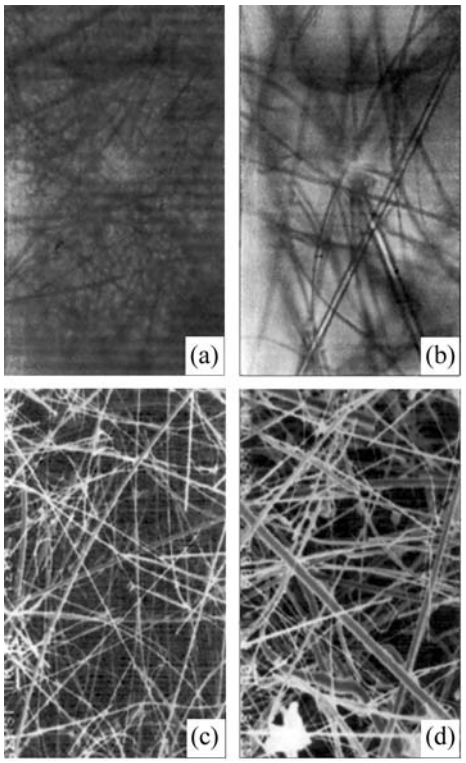


Fig. 6. Electron micrographs of the samples based on mineral fibers without binder.

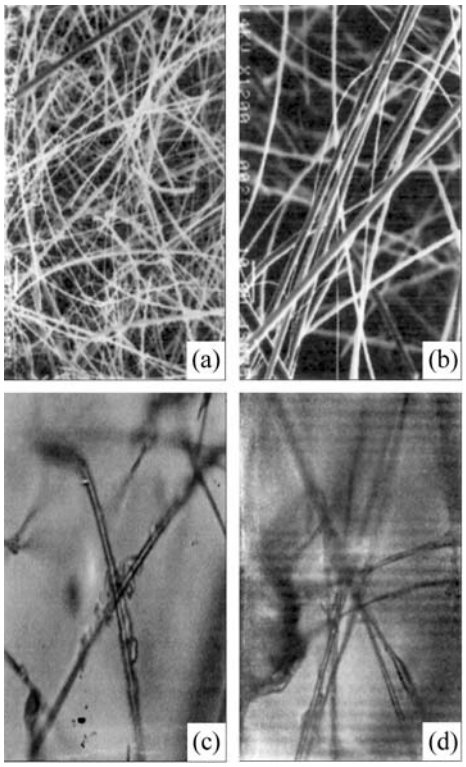


Fig. 7. Electron micrographs of the samples based on the mineral fibers with the binder (80% relative to the fiber mass, recalculated to Al_2O_3).

localization of the binder and fairly large pores [8]. The stress–strain curves (Fig. 2) correspond specifically to this type of the structure.

CONCLUSIONS

(1) A comprehensive study of the binding in materials based on mineral fibers containing inorganic binder, such as aluminum polyhydroxo complexes, showed that, upon introduction of this binder into a formulation based on mineral fibers, the strength of the paper-like composites prepared by wet molding increases.

(2) Formation of hydrogen bonds (presumably, via incorporation of the surface OH groups of the mineral fibers into the sphere of aluminum polyhydroxo complexes) was confirmed.

(3) It was demonstrated that the structure of the materials based on the mineral fibers studied can be characterized as a porous composite with the binder occurring at the interfiber contact sites.

ACKNOWLEDGMENTS

The author is grateful to V.I. Ivanov-Omskii (Ioffe Physicotechnical Institute, St. Petersburg), V.B. Skupchenko (Kirov State Forestry Engineering Academy, St. Petersburg), and Ya.V. Kazakov (Arkhangelsk State Technical University) for assistance in conducting the experiments and useful discussions.

REFERENCES

1. Dubovyi, V.K., *Steklyannye volokna: Svoistva i primenenie* (Fiber Glasses: Properties and Application), St. Petersburg, Nestor, 2003.
2. Karoll-Porchinskii, Ts., *Material budushchego* (Future Material), Moscow: Khimiya, 1996.
3. Flyate, D.M., *Svoistva bumagi* (Properties of Paper), St. Petersburg: Interlain, 1995.
4. Chizhov, G.I., *Tsellyuloza, bumaga, karton: Obzorhaya informatisya* (Cellulose, Paper, Pressboard: Review), Moscow: VNIPIEIlesprom, 1984.
5. Komarov, V.I., *Deformatsiya i razrushenie voloknistykh tsellyulozno-bumazhnykh materialov* (Strain and Failure of Fibrous Paper and Pulp Materials), Arkhangelsk: Arkhangel'sk. Gos. Tekh. Univ., 2002.
6. Ivanov-Omskii, V.I., *Pis'ma Zh. Tekh. Fiz.*, 2000, vol. 26, no. 12, p. 30.
7. Libowitzky, M.N., *Monatsh. Chem.*, 1999, vol. 130, p. 1047.
8. Frolov, M.V., *Strukturnaya mekhanika bumagi* (Structural Mechanics of Paper), Moscow: Lesn. Prom–st., 1982.

Russian Journal of Applied Chemistry, Vol. 78, No. 10, 2005, pp. 1709–1711. Translated from Zhurnal Prikladnoi Khimii, Vol. 78, No. 10, 2005, pp. 1739–1741.
Original Russian Text Copyright © 2005 by Kononov, Golounin, Pashkov, Kuklina, Mikhailenko, Tsupinin.

BRIEF COMMUNICATIONS

Sorptive Recovery of Gold(I) from Cyanide-containing Aqueous Alkali with Resins Containing Guanidinium Sorption Sites

Yu. S. Kononov, A. V. Golounin, G. L. Pashkov, U. F. Kuklina, M. A. Mikhailenko, and D. V. Tsupinin

Institute of Chemistry and Chemical Technology, Siberian Division, Russian Academy of Sciences, Krasnoyarsk, Russia

Purolite Int. Ltd. Agency, Moscow, Russia

Received June 9, 2005

Abstract—A technique was developed for desorption of gold(I) from a strongly basic resin containing guanidinium sorption sites with aqueous-organic alkalis.

Strongly basic resins containing quaternary ammonium cations as sorption sites are widely used for industrial recovery of gold(I) from cyanide-containing aqueous alkalis. Gold(I) is desorbed from these resins with acidic aqueous thiourea. This procedure is hazardous and expensive. Furthermore, these resins must be treated before sorption with acid to remove cyanide complexes of nonferrous metals and iron [1].

Anion exchangers containing basic nitrogen sorption sites, among them guanidine derivatives, sorb gold(I) from cyanide-containing aqueous alkalis. However, desorption of Au(I) from these sorbents with aqueous alkali is inefficient. For example, in eluting Au(I) from a resin containing *N*-(6-aminohexyl)-*N*′-butylguanidinium sorption sites ($pK_a \sim 12$) with 10% aqueous alkali, only 40% of gold passes into the eluate. Under the same conditions, the degree of gold desorption from a resin containing 1,5,7-triazabicyclo-[4.4.0]decene-5 sorbing groups ($pK_a \sim 16$) is only 1%. From resins with different sorbing amino groups separated by di- and triatomic hydrocarbon bridges containing alcoholic groups, 35–65% of gold is desorbed with 0.01–4 M aqueous alkali [2].

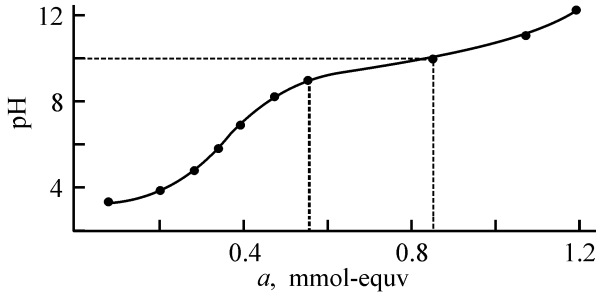
These data show that a significant fraction of gold(I) sorbed on resins under consideration cannot be eluted from them with aqueous alkali.

It is known that the acid ionization constants of organic compounds depend on the solvent. For example, pK_a of ammonium salts in water–alcohol mixtures decreases linearly with increasing alcohol concentration and sharply decreases (by two pK_a units) at alcohol concentrations of 60–70% [3]. Assuming that similar correlations occur for resins containing guanidinium cations, we can expect that, in going from aqueous alkali to solutions of alkali in water–alcohol mixtures or other appropriate aqueous-organic solvent with relatively low permittivity, the pK_a of the resin sorption sites decreases and, as a result, the desorption of gold(I) from the resins is facilitated.

EXPERIMENTAL

In our experiments, we used a strongly basic anion exchanger Purolite A-180 widely accepted in the hydrometallurgy of gold. This resin has the form of a poly(styrene–divinylbenzene) matrix modified with guanidinium cation as sorbing groups. To elucidate the acid–base behavior of Purolite in aqueous alkali, we carried out its potentiometric titration with aqueous NaOH.

The potentiometric titration curve (see figure) shows that, in alkaline medium, guanidinium cations



Potentiometric titration curve of Purolite A-180 resin with aqueous alkali. (*a*) NaOH consumption.

1070-4272/05/7810-1709 © 2005 Pleiades Publishing, Inc.

Table 1. Counterflow sorptive leaching of gold(I) with Purolite A-180 resin from a pulp containing 3.5 mg l^{-1} Au on a device consisting of 10 series-connected pulp agitators (mixing time in each stage 6 h, resin amount 0.2–0.4% of pulp volume, ore grain size <74 μm (90%), initial NaCN concentration 1–2 g l^{-1})

Pulp agitator no.	Gold content		
	in the solid phase of the pulp, g t^{-1}	in the liquid phase of the pulp, g t^{-1}	in resin, %
1	1.9		
2	1.0		
3	0.5		
4	0.3		0.92–1.33
5	–	–	
6		0.1	
7		0.1	
8		Traces	
9	–	″	
10	0.07–0.13	″	

Table 2. Desorption of gold from Purolite A-180 after four successive desorption stages without stirring (solid-to-liquid phase ratio s : l = 1 : 5; desorption time 24 h; temperature 45°C; desorbing solution: organic solvent 20–96%, 1 M NaOH; initial Au content in the resin 1.33%)

Solvent, %	Au content in eluate after first desorption stage, mg l^{-1}	Residual Au content in resin	
		%	% relative to the initial value
10% aqueous NaOH	125	0.427	32.1
Ethanol:			
20	700	0.33	24.8
40	900	0.149	11.2
60	1300	0.053	4.0
80	1300	0.037	2.8
96	1395	0.01	0.75
1,2-Ethanediol:			
20	1000	0.15	14
40	1500	0.039	3.6
60	1800	0.037	3.5
96	2350	0.019	1.3
Dimethylacetamide:			
40	900	0.14	13
60	1300	0.018	1.7
96	1530	0.007	0.5

in Purolite are formed at pH up to 12. This means that the resin can sorb anions from aqueous alkali. The total anion-exchange capacity of Purolite is 1.2 mg-equiv g^{-1}. The inflection point in the potentiometric titration curve is due to the presence of foreign protonated species in the resin. The sorption capacity of the resin, calculated from the portion of the potentiometric titration curve in the pH range 9–12 corresponding to deprotonation of guanidinium cations, is 0.65 mg-equiv g^{-1}. This value shows that guanidinium groups in Purolite can efficiently recover anions from aqueous alkali.

Gold was recovered from the pulp in an counterflow device consisting of 10 series-connected pulp agitators. The resin was fed into the tenth and discharged from the fourth agitator. As pulp passed through agitator nos. 1–3, gold was leached from the ore with aqueous sodium cyanide. The results of these experiments are listed in Table 1.

Table 1 shows that after seven successive stages of sorptive leaching of gold with Purolite A-180, tailings containing 0.07–0.13 g Au/t are formed. Under these conditions, the resin capacity for gold recovery is 1%, which is sufficient for preparing a commercially acceptable final eluate.

As can be seen from Table 2, desorption of gold with 10% aqueous NaOH is inefficient, since more then 30% of gold remains on the resin.

We also studied desorption of gold from Purolite A-180 anion exchanger with 0.1 M NaOH solution in an aqueous–organic mixture. In these experiments, a weighed portion of the resin was contacted with the desorbing solution for 24 h at 45°C without stirring. After the first desorption stage was complete, the liquid phase was separated from the resin and analyzed for gold. The desorption procedure was repeated four times. After the fourth desorption treatment was complete, the resin was analyzed for gold. The results of these experiments are listed in Table 2.

Table 2 shows that solutions of alkali in aqueous–organic mixtures efficiently desorb gold(I) from the resin. After four successive desorption stages the residual gold content in the resin was 0.007–0.05%. Under these conditions, the gold content in the first eluate fractions was sufficiently high to use them for recovery of gold by electrolysis. The gold content in the final eluate was 1–2 g l^{-1}. After desorption of gold with aqueous alkali, the resin can be reused without regeneration.

CONCLUSIONS

(1) In recovery of gold from cyanide-containing leachates with Purolite A-180 anion exchanger, the tailings contain 0.07–0.13 g Au/t.

(2) Desorption of gold from Purolite A-180 containing approximately 1% dicyanoaurate(I) complex with solutions of alkali in aqueous–organic mixtures allows preparation of eluates with a gold content as high as 1–2 g l^{-1}.

REFERENCES

1. Strizhko, L.S., *Metallurgiya zolota i serebra* (Metallurgy of Gold and Silver), Moscow: Mosk. Inst. Stali i Splavov, 2001.
2. Hainay, P. and Sherrington, D.C., *React. and Funct. Polym.*, 2000, vol. 43, pp. 195–210.
3. Reutov, O.A., Kurts, A.L., and Butin, K.P., *Organicheskaya khimiya* (Organic Chemistry), Moscow: Mosk. Gos. Univ., 1999, part 1.

Russian Journal of Applied Chemistry, Vol. 78, No. 10, 2005, pp. 1712–1714. Translated from Zhurnal Prikladnoi Khimii, Vol. 78, No. 10, 2005, pp. 1742–1744.
Original Russian Text Copyright © 2005 by Golounin, Larionova.

BRIEF COMMUNICATIONS

Extractive Recovery of Gold(I) from Cyanide-containing Aqueous Alkali with Guanidine Derivatives

A. V. Golounin and I. A. Larionova

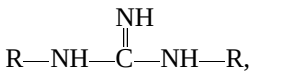
Institute of Chemistry and Chemical Technology, Siberian Division, Russian Academy of Sciences, Krasnoyarsk, Russia

State University of Nonferrous Metals and Gold, Krasnoyarsk, Russia

Received April 27, 2005

Abstract—Extractive recovery of gold(I) from cyanide-containing aqueous alkali with guanidine dialkyl and diaryl derivatives was studied.

According to recent studies, alkyl guanidines show promise for extraction and sorption of dicyanoaurate(I) anions from aqueous solutions [1, 2]. To elucidate how the guanidine structure affects the efficiency of extractive recovery of gold(I) from aqueous cyanide solutions, we prepared and tested several guanidine derivatives



where R is isopropyl, isobutyl, octyl, cyclohexyl, phenyl, or benzyl.

Taking into account that alkylguanidines are poorly soluble in the solvents commonly used in extraction (benzene, toluene, xylene, hexane, kerosene), we tested some other solvents. We found that the best solvent for guanidine derivatives are aromatic and aliphatic amines.

EXPERIMENTAL

In our experiments, gold(I) was recovered from aqueous solutions containing dicyanoaurate(I) $[Au(CN)_2]^-$ (50 mg l^{-1}, 0.01 M) with solutions of dialkyl- and diphenylguanidines in both dichloroethane and 0.02 M amine–dichloroethane mixture. Gold was determined by atomic absorption technique on an AAS-30 device.

Disubstituted guanidines used in our experiments were as follows:

Guanidine	Yield, %	mp, °C
N,*N*'-dioctyl	53	98–160
N,*N*'-dicyclohexyl	62	157–158
N,*N*'-dibenzyl	94	176–178
N,*N*'-diisopropyl	99	62–64
N,*N*'-diisobutyl	99	153–154
N,*N*'-diphenyl	chemical pure	148–148.5

It is known that amines, among them aromatic amines, are capable of extracting gold(I) from cyanide solutions [3]. For example, on bringing 2,4-xylidine in contact with aqueous $[Au(CN)_2]^-$ at pH 8, approximately 20% of gold passes into the organic phase. On contact of 0.01 M *N*,*N*'-diisoropylguanidine in dichloroethane with Au(I) cyanide complexes in aqueous alkali at pH 9, 10.5, 11.4 and 12.5, gold is recovered to 99, 80, 43 and 20%, respectively. The extraction of gold from cyanide-containing aqueous alkali with alkylguanidine slightly increases with lengthening of alkyl substituents. For example, on contact of *N*,*N*'-diisobutyl- and *N*,*N*'-dioctylguaniine in dichloroethane with a solution of gold(I) in cyanide-containing aqueous alkali at pH 9, 10.6 and 12.3, the percentage of gold that passes into the organic phase is 93, 78, 41 and 96, 87 and 51 for the former and latter guanidine derivatives, respectively.

In going from 0.01 M *N*,*N*'-diisobutylguanidine in dichloroethane to its solution in 2,4-xylidine, the degree of gold recovery is 99% up to pH 12.5 at the contact time shorter than 5 min. A similar pattern is observed in extraction of Au(I) with *N*,*N*'-diisobutyl

1070-4272/05/7810-1712 © 2005 Pleiades Publishing, Inc.

and *N,N'*-dioctylguanidine in 2,4-xylidine. The results obtained in extraction of gold(I) with solution of *N,N'*-dicyclohexylguanidine in multicomponent organic solvents are listed in Table 1.

We believe that the synergistic effect in extraction of Au(I) with guanidine–amine mixtures is caused by the fact that the guanidinium cation–$[Au(CN)_2]^-$ ion pairs dissolve in the amine. In the presence of an amine, the guanidine basicity significantly increases, and, as a result, so does the stability of the ion pairs in the alkaline media (up to pH 12). Under these conditions amine molecules solvate dicyanoaurate complexes.

Taking into account the fact that the addition of amines to guanidines improves the extraction of gold(I) from alkaline solutions, it was of interest to elucidate how the amine structure influences the recovery of gold(I) from cyanide-containing aqueous alkali. For this purpose, we studied the extraction of $[Au(CN)_2]^-$ with *N,N'*-diisobutylguanidine in the presence of both aliphatic and aromatic amines.

The figure shows the curves of gold(I) extraction from cyanide-containing aqueous alkali with *N,N'*-diisobutylguanidine–amine mixtures.

It is seen that, depending on their structure, amines either enhance or suppress extraction of gold with alkylguanidine. For example, in the presence of di- and tributylamines, the extraction of gold with *N,N'*-diisobutylguanidine decreases (curves *1*, *2*). This negative effect can be attributed to dissolution of guanidinium cation–$[Au(CN)_2]^-$ ion pairs in the aqueous phase. This assumption is confirmed by the fact that, on adding trioctylamine instead of tributylamine, gold(I) is completely extracted even at pH 13 (curve *4*).

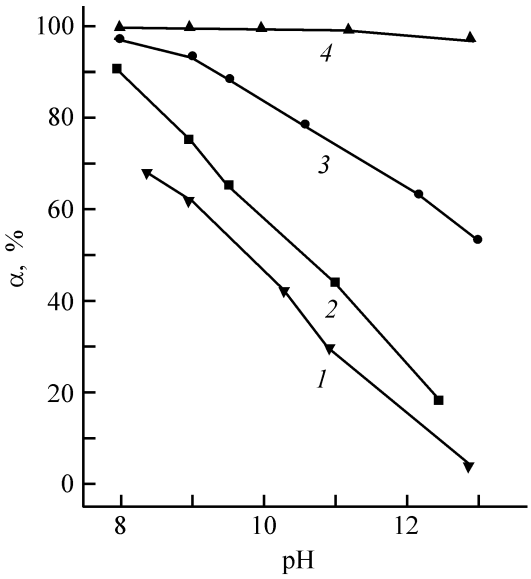
We found that, in extraction of gold with guanidine derivatives in the presence of amines, the phase separation is decelerated in going from lower to higher amines. Thus, the organic phase composition can be chosen so as to ensure both the efficient extraction of gold(I) from cyanide-containing aqueous alkali and fast phase separation. One of extractants meeting these requirements is a solution of *N,N'*-diisobutylguanidine in trioctyamine–xylene mixture.

It was noted above that alkylguanidines with long-chain substituents show limited solubility even in amines. We found that, as opposed to alkylguanidines, their aromatic derivatives are readily soluble in amines.

Table 1. Extraction of gold(I) with 0.01 M *N,N'*-dicyclohexylguanidine in multicomponent solvent (50% 2,4-xylidine, 30% decanol, and 18% xylene

pH	Gold content, mg l^{-1}		Degree of gold recovery, %
	aqueous phase	organic phase	
8.0	0.5	68.2	99.3
9.4	0.6	68.1	99.1
10.2	0.6	68.1	99.1
11.7	0.6	68.1	99.1
13.0	0.6	63.1	91.8

Aromatic *N,N'*-diphenyl- and *N,N'*-dibenzylguanidines are fairly readily soluble in aromatic hydrocarbons and, in particular, in xylene. Therefore, we studied the extraction of gold(I) with solutions of aromatic guanidines in amine–xylene mixtures. Although 0.01 M *N,N'*-diphenylguanidine in aniline efficiently extracts gold(I) from aqueous alkali (pH 10–11), a significant fraction of the extractant dissolves in the aqueous phase. This drawback is absent in extraction with mixture of *N,N'*-dibenzylguanidine with higher amines, which are poorly soluble in water. The data on extraction of gold(I) from cyanide-containing aqueous alkali at different pH with *N,N'*-dibenzylguanidine in vari-



Degree of gold(I) extractive recovery α from cyanide-containing aqueous alkali with 0.01 M *N,N'*-diisobutylguanidine + 0.02 M amine in xylene. Amine: (*1*) dibutylamine, (*2*) tributylamine, (*3*) no amine and (*4*) trioctylamine.

Table 2. Extraction of gold(I) with 0.01 M *N,N'*-dibenzylguanidine in multicomponent organic solvents

Amine	Solvent	Degree of gold(I) recovery, %, at indicated pH				
		8.4	10.5	11.8	12.6	13
	$C_2H_4Cl_2$	99	72	43	24	–
Aniline	Aniline	99	98	97	95	–
2,4-Xylidine	2,4-Xylidine	99	99	99	99	97
Trioctylamine*	Xylene	99	99	99	98	97
N-Hexylaniline*	"	99	99	99	99	98
N-Octylaniline*	"	99	99	99	99	99
N-Decyl-2,4-xylidine	"	99	99	99	99	99

* In the presence of trioctylamine (0.02 M).

ous solvents are listed in Table 2. These results show that gold(I) is quantitatively extracted with a solution of *N,N'*-dibenzylguanidine in 2,4-xylidine and trioctylamine–xylene mixture.

These data also show that *N*-alkyl aromatic amines can be used instead of trioctylamine as additives ensuring virtually complete extractive recovery of gold(I).

CONCLUSIONS

(1) Disubstituted guanidines efficiently extract gold(I) dicyanide complexes from aqueous alkali.

(2) Gold(I) is quantitatively extracted from cyanide-containing aqueous alkali with guanidine derivatives in combination with aliphatic and aromatic amines at widely varied alkali concentration.

REFERENCES

1. US Patent 5 198 021.
2. USSR Patent 1 831 508.
3. Alguacil, F.J., Hernandez,A., and Luis, A., *Hydrometallurgy*, 1999, vol. 24, no. 2, pp. 245–261,

Russian Journal of Applied Chemistry, Vol. 78, No. 10, 2005, pp. 1715–1717. Translated from Zhurnal Prikladnoi Khimii, Vol. 78, No. 10, 2005, pp. 1745–1747.
Original Russian Text Copyright © 2005 by Shteinberg.

BRIEF COMMUNICATIONS

Catalysis of the Reaction between 4-Nitrobenzoic Acid and Ammonia by Boric Acid + Polyehylene Glycol-400

L. Ya. Shteinberg

Institute of Chemical Technology and Industrial Ecology, Rubezhanskii Krasitel' Limited Liability Company, Rubezhnoe, Lugansk oblast, Ukraine

Received April 13, 2005

Abstract—Solvent effect on the synthesis of 4-nitrobenzamide by the reaction of 4-nitrobenzoic acid with ammonia in the presence of the catalytic system constituted by boric acid and polyethylene glycol-400 was studied.

4-Nitrobenzamide is the synthetic precursor of 4-aminobenzamide used for preparing a numbers of dyes [1].

In [2], we showed that the system constituted by boric acid and polyethylene glycol (PEG-400) effectively catalyzes the synthesis of 4-nitrobenzamide (NBA) by the reaction of 4-nitrobenzoic acid (NBAc) with ammonia in a mixture of 1,2,4-trichlorobenzene with *o*-xylene. It was noted that PEG-400 favors dissolution of boric acid and homogenization of the reaction mixture. In this study, we examined this catalytic reaction in various media:

$$\underset{\text{NBAc}}{4\text{-}NO_2C_6H_4COOH} + NH_3 \xrightarrow{H_3BO_3 + \text{PEG-400}} \underset{\text{NBA}}{4\text{-}NO_2C_6H_4CONH_2} + H_2O.$$

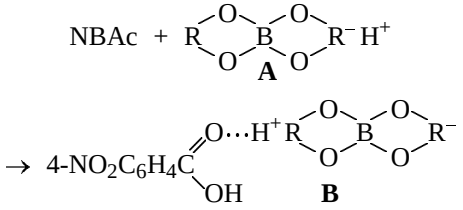
Catalysis by boron compounds of amidation reactions performed in aromatic and aliphatic hydrocarbons, including hexane, benzene, toluene, cumene, isomeric xylenes, and trichlorobenzene, was considered in [3–5]. To carry out the reaction of NBA with ammonia, we took protic and aprotic solvents differing in the polarity and boiling point. The results obtained and dielectric constants of the solvents ε are listed in the table.

As seen, the reaction readily proceeds in various aromatic and aliphatic aprotic solvents and their mixtures. With an increase in the reaction time and catalyst amount, the NBA yield grows becoming almost quantitative (run nos. 4, 7, 8).

In the series of solvents with low (and similar) polarity, the yield of the target product varies in parallel with the reaction temperature (run nos. 1–3, 5, 12): *p*-cymene (177°C) > decane (174°C) > white spirit (155–162°C) > *o*-chlorotoluene (155°C) > *o*-xylene (145°C). At close temperatures, the NBA yield varies in parallel with the solvent polarity in the order (run nos. 6, 7, 9) *o*-dichlorobenzene > 1,2,4-trichlorobenzene > decane. The same influence of the solvent polarity on the NBA yield is observed in amidation under similar conditions in binary mixtures *p*-cymene–nitrobenzene (run nos. 13–17). As can be seen, the NBA yield steadily grows with increasing nitrobenzene content, and accordingly, solvent polarity.

The highest NBA yields were attained in *o*-dichlorobenzene and 1,2,4-thichlorobenzene even without refluxing of the reaction mixture and distillation of the water released, which is evidently removed from the reaction zone with excess ammonia (previously, in catalysis by titanium and boron compounds, intense azeotropic distillation of the released water was necessary for obtaining benzanilide [9]).

As known [10], boric acid readily reacts with various alcohols, including glycols, and polyethylene glycols (HOROH), to give complexes **A** exhibiting elevated acidity. Such compounds can serve as acid catalysts in amidation. An increase in solvent polarity can favor stabilization of transition state **B** and acid catalysis:



B + NH_3 → NBAm + H_2O + **A**.

1070-4272/05/7810-1715 © 2005 Pleiades Publishing, Inc.

Synthesis of NBAc in various solvents*

Run no.	Solvent	ε**	*T*, °C	τ, h	H_3BO_3, mol % relative to NBAc	Yield of NBA, %
1	*o*-Xylene	2.57	145	6.0	5	2
2	*o*-Chlorotoluene	4.45	155	6.0	5	3
3	White spirit	–	155–162	6.0	5	4
4	〃	–	155–162	6.5	34	70
				10.0	34	95
5	Decane	1.99	174	6.0	5	10
6	〃	1.99	174	6.0	34	63
7	*o*-Dichlorobenzene	9.93	162–164	6.0	34	92
8	1,2,4-Trichlorobenzene	3.98	170–175	6.0	2	66
				10.0	2	93
9	〃	3.98	170–175	6.0	34	79
				9.0	34	96
10	Decane***	1.99	174	6.0	0	Traces
11	1,2,4-Trichlorobenzene****	3.98	170–175	7.0	0	49
12	*p*-Cymene	2.24	177	6.0	5	13
13	〃	2.24	177	8.0	2	13
	p-Cymene : nitrobenzene :					
14	10 : 1	5.21	177	8.0	2	40
15	8 : 1	5.89	177	8.0	2	59
16	5 : 1	7.68	177	8.0	2	67
17	3.5 : 1	9.51	177	8.0	2	72
18	Ethylene glycol	38.66	175–180	6.0	33	0
19	Diethylene glycol	31.69	175–180	6.0	33	0
20	Triethylene glycol	23.19	175–180	6.0	33	0

* In all the experiments, the PEG-400 amount was taken as a half (in moles) of that of boric acid.

** The values of ε were taken from [6, 7]; for the mixture of *n*-cumene with nitrobenzene, the ε values were calculated using an additive scheme from the volume fractions of the components [8] (listed in table).

*** Filtrate from run no. 6 was taken as a solvent.

**** Filtrate from run no. 8 was taken as a solvent.

However, an attempt to obtain NBA in more polar solvents, glycols, failed (run nos. 18–20). A TLC analysis of the reaction mixture showed that NBAc rapidly (during 1 h) disappeared, but there was no NBA among the reaction products. Probably, in glycols, NBAc in the presence of boric acid forms glycol esters, which then do not react with ammonia.

A high polarity of the solvent may also favor homogenization of the reaction mixture. We found that, in amidation in low-polar decane (run nos. 5, 6), crystalline NBA precipitates already within 2 h. In more polar *o*-dichlorobenzene and 1,2,4-trichlorobenzene, the reaction mixture is homogeneous, amidation proceeds faster, and crystalline NBA precipitates only after cooling the reaction mixture to room temperature after the reaction is complete (run nos. 7–9).

Thus, with decane as a solvent, the reaction proceeds in the heterogeneous system gas–liquid–solid, formed within 2 h after the beginning of the reaction. Probably, the crystalline NBA precipitate is bound with a part of the catalyst, which may hinder its interaction with the reactants and the catalytic reaction as a whole.

To study the catalyst distribution in the reaction mixture, we performed experiment nos. 10 and 11, using as solvents the filtrates from separation of the solid target product in experiment nos. 6 and 8, respectively, without adding the catalytic system. It was found that the filtrate showed no catalytic power in decane (run no. 10), i.e., the whole amount of the catalyst was probably removed from the filtrate with NBA. In 1,2,4-trichlorobenzene, the filtrate showed fairly high catalytic power (run no. 11), thus confirming the uniform distribution of the catalyst. The degree of NBAc binding with ammonia can vary with the solvent polarity. As known, carboxylic acids form salts with amines. The reactivity of carboxylate anions and protonated amines in nucleophilic substitution at

the carbonyl carbon atom may be substantially lowered [11, 12].

Since NBA is not formed from NBAc ammonium salt in the presence of the catalytic system [2], it was of interest to test the stability of this salt under the reaction conditions.

We found that the NBAC ammonium salt undergoes no changes on heating to 120°C for 20 h without solvents or on washing with *o*-xylene or *o*-chlorobenzene at room temperature, followed by filtration and drying: its melting point remains unchanged. However, on heating of the suspension of NBAc ammonium salt in these solvents to 60–80°C, it decomposes with liberation of ammonia. Heating of such a suspension in *o*-xylene at 145°C for 10 min causes complete decomposition of the ammonium salt: after cooling, only NBAc is recovered from the reaction mixture. Probably, NBAc reacts in the free state but not as ammonium salt under the reaction conditions, even in the presence of a large excess of ammonia.

EXPERIMENTAL

Boric acid, NBAC, PEG-400, *o*-xylene, decane, 1,2,4-trichlorobenzene, *o*-dichlorobenzene, and nitrobenzene were of the same quality as in [2, 9, 13]. *o*-Chlorotoluene and white spirit were vacuum-distilled. Ethylene glycol, diethylene glycol, and triethylene glycol were dried over sodium sulfate and vacuum-distilled. *n*-Cymene was washed with sulfuric acid, water, solutions of potassium permanganate, sodium hydroxide, and again water, dried over sodium sulfate, and vacuum-distilled. NBA and ammonium salt of NBAc were prepared, the mixtures were analyzed, and the purity of the products was determined as in [2] with separation of an additional amount of the target product and vacuum distillation of the solvent from the reaction mixture.

CONCLUSIONS

(1) The catalytic system constituted by boric acid and polyethylene glycol-400 is the most efficient in synthesis of 4-nitrobenzamide from 4-nitrobenzoic acid and ammonia in aprotic solvents at 145–177°C. Under the reaction conditions, ammonium salt of 4-nitrobenzoic acid rapidly decomposes, with ammonia liberated and no 4-nitrobenzamide formed.

(2) In polar proton-donor glycols, 4-nitrobenzoic acid rapidly transforms into unidentified products without formation of 4-nitrobenzamide.

REFERENCES

1. *The Chemistry of Synthetic Dyes*, vol. 5, Venkataraman, K., Ed., New York: Academic, 1971.
2. Shteinberg, L.Ya., *Zh. Org. Khim.*, 2003, vol. 39, no. 7, pp. 1033–1036.
3. Swiss Patent 367 509.
4. Nelson, P. and Pelter, A., *J. Chem. Soc.*, 1965, no. 9, pp. 5142–5144.
5. Pelter, A. and Levitt, T.E., *Tetrahedron*, 1970, vol. 26, no. 6, pp. 1545–1553.
6. Weissberger, A. and Proskauer, E.S., *Organic Solvents. Physical Properties and Methods of Purification*, Riddig, J.A. and Toops, E.E., Eds., New York: Interscience, 1955.
7. Akhadov, Ya.Yu., *Dielektricheskie svoistva chistykh zhidkostei* (Dielectric Properties of Pure Liquids), Moscow: Khimiya, 1989.
8. Fialkov, Yu.Ya., *Rastvoritel' kak sredstvo upravleniya khimicheskim protsessom* (Solvent as a Means for Controlling a Chemical Process), Leningrad: Khimiya, 1990.
9. Shteinberg, L.Ya, Kondratov, S.A., and Shein, S.M., *Zh. Org. Khim.*, 1988, vol. 24, no. 9, pp. 1968–1972.
10. Shvarts, E.M., *Vzaimodeistvie bornoi kisloty so spirtami i oksikislotami* (Reaction of Boric Acid with Alcohols and Hydroxy Acids), Riga: Zinatne, 1990.
11. Temnikova, T.I., *Kurs teoreticheskikh osnov organicheskoi khimii* (Course of Theoretical Foundations of the Organic Chemistry), Leningrad: Khimiya, 1968.
12. Litvinenko, L.M. and Oleinik, N.M., *Organicheskie katalizatory i gomogennyi kataliz* (Organic Catalysts and Homogeneous Catalysis), Kiev: Naukova Dumka, 1981.
13. Shteinberg, L.Ya, Kondratov, S.A., and Shein, S.M., *Zh. Org. Khim.*, 1989, vol. 25, no. 9, pp. 1945–1949.

Russian Journal of Applied Chemistry, Vol. 78, No. 10, 2005, pp. 1718–1719. Translated from Zhurnal Prikladnoi Khimii, Vol. 78, No. 10, 2005, pp. 1748–1749.
Original Russian Text Copyright © 2005 by Protopopov, Kon'shin, Chemeris.

BRIEF COMMUNICATIONS

Acylation of Aspen Wood and Cellulose with *p*-Aminobenzoic Acid in Trifluoroacetic Acid and Thionyl Chloride

A. V. Protopopov, V. V. Kon'shin, and M. M. Chemeris

Polzunov Altai State Technical University, Barnaul, Russia

Received November 15, 2004; in final form, September 2005

Abstract—Cellulose esters with *p*-aminobenzoic acid were prepared.

Cellulose esters find growing use in industry due to their characteristics (e.g., light and weather resistance, hydrophobicity, and low processing temperature) and the renewability of raw materials for their production [1]. Esters of cellulose with aromatic amino acids (e.g., *p*-aminobenzoic acid) may exhibit biological activity; it is well known that all amino acids and their derivatives are biologically active substances. Cellulose by itself, as a matrix-carrier, is biologically inert and has sorption characteristics [2]. Therefore, new methods for synthesis of cellulose esters are of interest.

Synthesis and characteristics of cellulose esters containing aromatic substitutes have not been systematically studied, although some representatives (cellulose benzoate and phenylacetate) have been synthesized using chlorides of the corresponding acids [3] and trifluroacetic anhydride [4] as acylating agents.

Here, we suggest a method for preparing cellulose derivatives with the use of *p*-aminobenzoic acid (*p*-ABA), starting directly from pretreated aspen wood [lignocellulose material (LCM)], and describe the procedures of analysis for the content of the bound amino acid.

EXPERIMENTAL

Acylated derivatives of LCM (ALCM) were formed by the reaction of LCM with an acylating mixture containing *p*-ABA, trifluoroacetic acid (TFAA), and thionyl chloride (TC), with continuous stirring at constant temperature. Synthesis of ALCM can be represented by the scheme

$$p\text{-}NH_2C_6H_4CO_2H + CF_3COOH + SOCl_2 \rightarrow [p\text{-}NH_3C_6H_4COCl]^+CF_3CHCOO^- + ROH \xrightarrow[-CF_3CO_2H]{} p\text{-}NH_2C_6H_4CO_2R,$$

where ROH is cellulose or LCM.

ALCM was synthesized in a round-bottomed flask, into which *p*-ABA and TFAA were introduced. The mixture was kept at a required temperature, after that TC was added and the mixture was kept at the same temperature *p*-ABA chloride was formed. To the resulting acylating mixture we added air-dry aspen wood (content of α-cellulose 64.8, lignin 35.2 wt %), which was preliminarily extracted and prehydrolyzed to remove extractive substances and hemicelluloses. The reaction product, ALCM, was precipitated into ethanol, washed, and dried to air-dry state. Cellulose produced by the Priozersk Paper and Pulp Plant (content of α-cellulose 96 wt %) was acylated under the similar conditions to obtain acylated cellulose (AC).

Bound *p*-ABA was determined by the Kjeldahl method [5].

The degree of substitution of hydroxyls by *p*-ABA in the resulting products was evaluated by chemical analysis for nitrogen in percent relative to the cellulose weight; the amount of converted hydroxy groups of cellulose c_a was also evaluated:

$$c_a = \frac{N \times 8.571n \times 100}{M}, \quad (1)$$

$$c_{OH} = \frac{17n \times 100}{M - 1.19n}, \quad (2)$$

where N is the content of bound nitrogen (wt %); $c_a = 8.571N$, content of *p*-aminobenzoate groups (wt %); 8.571, coefficient equal to the ratio of molecular weight of *p*-aminobenzoate group to the atomic weight of nitrogen; n, number of acyl groups in *p*-ABA, $n = 1$; c_{OH}, amount of acylated hydroxyl groups (wt %); and M, molecular weight of LCM or cellulose.

1070-4272/05/7810-1718 © 2005 Pleiades Publishing, Inc.

Content of bound nitrogen N in ALCM and AC (the amount of converted OH groups c_{OH} is given in parentheses)

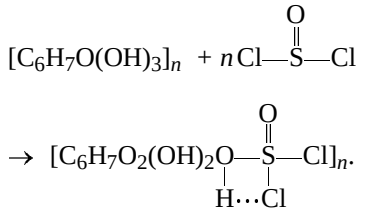
Synthesis duration, h	Content of N (c_{OH}, wt %) at indicated synthesis temperature, °C				
	25	35	45	55	65
ALCM:					
1	3.82 (7.01)	3.95 (7.22)	3.34 (5.66)	3.66 (6.45)	2.34 (3.55)
2	5.57 (12.84)	4.70 (9.50)	3.56 (6.20)	3.31 (5.59)	3.02 (4.93)
3	5.93 (14.52)	5.42 (12.20)	5.01 (10.59)	5.36 (11.95)	5.24 (11.47)
5	6.86 (19.98)	6.14 (15.59)	6.10 (15.38)	5.18 (11.24)	–
AC:					
1	1.65 (2.32)	1.52 (2.12)	0.98 (1.30)	0.15 (1.18)	–
2	2.44 (3.75)	2.06 (3.05)	1.02 (2.36)	0.28 (1.35)	–
3	2.52 (3.87)	2.31 (3.51)	1.75 (2.50)	0.88 (2.15)	–
5	4.50 (5.81)	3.20 (5.32)	3.16 (5.26)	3.07 (5.04)	–

Solving jointly Eqs. (1) and (2), we find c_{OH}:

$$c_{OH} = \frac{17n \times 8.571/120}{1 - 1.19N \times 8.571/120}. \quad (3)$$

The analytical data for acylation products are listed in the table.

The data obtained show that acylation of *p*-ACA proceeds better at room temperature. With increasing synthesis duration, the content of bound nitrogen in the acylation products grows. The data suggest that acylation of LCM with the above mixture proceeds more completely than the similar acylation of cellulose. In this case, acylation of LCM proceeds predominantly at the OH groups of cellulose, since lignin contains 9–11% hydroxy groups, among which 3–4% are phenolic hydroxyls, which are not acetylated under these conditions. As shown previously [6, 7], TC forms a stable adduct with OH groups of cellulose at the crystallite surface, thus hampering the catalytic function of the solvent, TFAA. The presence of branched network of lignin in LCM retards the formation of the adduct with TC:



An IR analysis of ALCM and AC revealed the absorption bands in the ranges 3500–3000 (stretching vibrations of OH and NH_2 groups and the C–H bond of aromatic ring), 1730–1750 (stretching vibrations of CO groups in esters), and 1610–1450 cm^{-1} (weak bands caused by vibrations of aromatic ring).

CONCLUSION

In acylation of a lignocellulose material and cellulose with *p*-aminobenzoic acid in trifluoroacetic acid in the presence of thionyl chloride, the process is more complete with the lignocellulose material at 25°C.

REFERENCES

1. Manushin, V.I., Nikol'skii, K.S., Minsker, K.S., *et al.*, *Tsellyulozy i plasticheskie massy na ikh osnove* (Cellulose, Cellulose Esters, and Plastics Based on Them), Vladimir: Polimersintez, 2002.
2. Grigor'yants, I.K. and Trikhanova, G.A., *Plast. Massy*, 1995, no. 3, pp. 47–52.
3. Revel'skaya, L.G., Khripunov, A.K., Purkina, A.V., *et al.*, *Khim. Drev.*, 1980, no. 4, pp. 32–36.
4. Eur. Patent 1215216.
5. Klimova, V.A., *Osnovnye mikrometody analiza organicheskikh soedinenii* (The Main Micromethods of Analysis of Organic Compounds), Moscow: Khimiya, 1967.
6. Shabalin, V.G., Acylation of Wood with Carboxylic Acids in the Presence of Thionyl Chloride and Trifluroacetic Acid, *Cand. Sci. Dissertation*, Barnaul, 2001.
7. Kon'shin, V.V., Shabalin, V.G., Chemeris, M.M., *et al.*, *Lesn. Zh.*, 2003, no. 4, pp. 92–98.

Russian Journal of Applied Chemistry, Vol. 78, No. 10, 2005, pp. 1720–1722. Translated from Zhurnal Prikladnoi Khimii, Vol. 78, No. 10, 2005, pp. 1750–1752.
Original Russian Text Copyright © 2005 by Gankov, Nenov, Radenkov.

BRIEF COMMUNICATIONS

Influence of the Caprolactam Quality on the Characteristics of Polycaproamide Thereof

N. P. Gankov, D. P. Nenov, and F. D. Radenkov

Ekomedbio EAD Business-Innovation Center, Sofia, Bulgaria
Technical University, Sofia, Bulgaria

Received March 2, 2005

Abstract—The influence of the caprolactam quality on the characteristics of polycaproamide thereof was elucidated.

Among the main factors governing the quality of polycaproamide (PCA) is the quality of the raw material, caprolactam (CL) [1].

We have found earlier [2] that caprolactam undergoes major changes during preparation for polymerization. Accumulation of the oxidation products begins even during transportation of liquid CL, as well as during melting of crystalline CL and storage of CL in the liquid state [3].

It was of interest to elucidate how the quality of commercial CL[1] satisfying the requirements imposed by the appropriate standard affects the characteristics of PCA thereof, using high-sensitive instrumental methods of analysis along with the conventional techniques.

First, we examined samples of commercial crystalline caprolactam, CL-1, prepared using phenol[2]: reference CL-2 sample prepared by recrystallization of CL-1 from dilute aqueous solution at room temperature; and sample of preoxidized caprolactam, CL-3, prepared by heat treatment of CL-1 in air at 90°C for 24 h.

The CL samples were polymerized at 260 ± 1°C in sealed glass ampules heated in an aluminum unit for 24 h. This time is sufficient equilibrium in molecular weight to be attained. Before being sealed the ampules containing CL were purged with nitrogen for a long time. The AG salt (3%) was added to the samples as a polymerization activator. No H_2O was introduced as activator and no acid, as chain-terminating agent, since they create superpressure and cause ampules to break. After polymerization was the complete, the ampules were cooled, and the polymer was crushed manually.

The CL samples under study were characterized by such parameters as compliance with the BDS 10780–88 requirements, content of carbonyl compounds (CCs) [4], and fluorescence intensity. The PCA samples werecharacterized by relative viscosity, Huggins constant K_H [5] characterizing the content of branched and cross-linked PCA structures, content of the abnormal acylation product (1,11-diamino-6-ketoundecane, DAKU) [6] and of carbonyl compounds, optical density [7], fluorescence intensity, and content of terminal carboxy groups.

We measured the relative viscosity of a 1% (by weight) PCA solution in H_2SO_4 (95.6 wt %) at 25°C using an Ubbelohde viscometer at the solvent outflow time of over 100 s. The CC and DAKU content in CL and PCA was determined polarographically [7]. The optical density of the solutions was measured on an SF-16 spectrophotometer (according to BDS 10780–88), and the fluorescence intensity, on a KFL-2-1 instrument. The optical density of the sulfuric acid solutions of PCA was measured by the modified Sbrolli technique [7] (300 mg PCA per 25 ml of 60 wt % H_2SO_4, wavelength 245 nm, rectangular cell with the absorbing layer thickness of 10 mm). The results obtained are listed in the table.

The table shows that the samples of commercial and additionally crystallized CL contain no carbonyl compounds. The freshly prepared CL should not contain oxidation products [8]. If these compounds are

[1] Bulgarian State Standard BDS 10780–88.
[2] Agrobiokhim Company, EAD, Stara Zagora.

1070-4272/05/7810-1720 © 2005 Pleiades Publishing, Inc.

Characteristics of the samples of CL and PCA thereof

Sample	CC content, mg-equiv g^{-1}		Optical density		Fluorescence intensity, arb. units		PCA characteristics			
	in CL	in PCA	CL, λ = 290 nm	PCA, λ = 245 nm	CL	PCA	DAKU content mg-equiv g^{-1}	η_{rel}	content of terminal carboxy groups, mg-equiv g^{-1}	K_H
CL-1	Traces	Traces	0.012	0.070	15.5	16.2	0.10	2.38	62.2	0.27
CL-2	〃	〃	0.005	0.045	14.2	15.8	0.22	2.39	63.6	0.25
CL-3	0.44	0.36	0.034	0.130	21.2	28.9	0.18	2.26	68.6	0.36

formed during synthesis of CL, they are removed in the course of the final purification by rectification and distillation.

We have reported earlier [1, 9] that the oxidation products and, in particular, carbonyl compounds are accumulated in commercial CL only during its transportation and storage, especially in the molten state in the presence of atmospheric oxygen.

We found that special preoxidation of the initial caprolactam (CL-3) modifies its properties and the properties of the resulting PCA: the content of the carbonyl compounds increases to 0.44 in CL-3 and to 0.36 mg-equiv g^{-1} in PCA, and the fluorescence intensity and optical density become higher.

Interestingly, the content of CC in PCA is lower than that in the initial oxidized CL. This is consistent with the previously revealed relationship: The CC content in the polymer is independent of the degree of oxidation of CL, while the fluorescence intensity of the polymer correlates well with the degree of oxidation of the initial caprolactam. This is presumably due to the fact that the fluorescence of the polymer solution is associated with compounds that possess conjugated double bonds [10], which are formed by polyamidation of the oxidized CL. In polyamidation at high temperatures, hydroperoxides and their decomposition products contained in CL decompose to compounds having no aldehyde groups [11], which prevents their polarographic detection. This led to a conclusion that only a combination of the fluorescence and polarographic analysis can furnish true information about the thermooxidative processes in PCA.

We also found that oxidation of CL is essential for synthesis of polymers and deteriorates the quality of PCA, except for such a parameter as the DAKU content. By contrast, the DAKU content in the PCA obtained from oxidized CL-3 is lower than that in the PCA prepared from recrystallized CL-2. This may be due to the inhibiting effect exerted on the abnormal acylation by water released in side reactions that occur during the synthesis of PCA. The table shows that, with oxidized CL, the relative viscosity of the polymer solution decreases, and the content of the terminal carboxy groups increases, which suggests a decrease in the molecular weight. This is accompanied by a major increase in the Huggins constant (K_H = 0.36), which suggests the presence of branched and cross-linked structures in the polymer. For the PCA samples prepared from the oxidized caprolactam (CL-3) the Huggins constants exceed 0.25. This specific value of the Huggins constant in the absence of DAKU is due to the disturbance of the chemical homogeneity of PCA by side thermooxidative reactions proceeding during synthesis [12, 13].

Apparently, there is a complex correlation between the characteristics of the initial caprolactam and the quality of the resulting PCA. Undoubtedly, a major role is played by the degree of oxidation of the initial CL, but this parameter is not stipulated by the BDS 10 780 – 88 and, thus, is not monitored manufacture of Vidlon fibers.

CONCLUSIONS

(1) There exists a complex correlation between the characteristics of the initial caprolactam and polycaproamide thereof, on the one hand, and the degree of oxidation of caprolactam, on the other. This correlation is governed, above all, by the polyamidation conditions.

(2) True information about the thermooxidative processes occurring during synthesis of polycarpoamide can be furnished by combined fluorescence and polarographic analyses only.

(3) The content of 1,11-diamino-6-ketoundecane in polycaproamide prepared from oxidized caprolactam is lower than that in the polycaproamide prepared from recrystallized caprolactam. This is due to the in-

hibiting effect exerted on the abnormal acylation by water released in the side reactions that occur during synthesis of polycaproamide.

REFERENCES

1. Gankov, N.P., *Zh. Prikl. Khim.*, 1998, vol. 71, no. 5, pp. 870–872.
2. Pishev, D., Gankov, N., Garvanska, R., *et al.*, *Khim. Industr.*, 1982, no. 1, pp. 14–16.
3. Gankov, N.P., *Zh. Prikl. Khim.*, 1998, vol. 71, no. 5, pp. 861–864.
4. Ignat'ev, Yu.S., Al'tshuler, O.S., Kvasha, N.M., *et al.*, *Khim. Volokna*, 1978, no. 4, pp. 71–73.
5. Sbrolli, W. and Capaccioli, T., *Chim. Ind.*, 1960, vol. 42, no. 3, pp. 243–244.
6. Ignat'ev, Yu.S., Al'tshuler, O.S., and Gyulkhandan'yan, E.M., *Khim. Volokna*, 1980, no. 3, pp. 51–52.
7. Sbrolli, W., Capaccioli, T., and Bertotti, E., *Chim. Ind.*, 1960, vol. 42, no. 4, pp. 357–363.
8. Nikonov, I.T., Smirnova, E.I., *et al.*, *Khim. Volokna*, 1982, no. 1, pp. 29–30.
9. Gankov, N.P. and Penchev, I.P., *Zh. Prikl. Khim.*, 1999, vol. 72, no. 4, pp. 697–698.
10. Smirnova, E.I., Vechkanov, G.N., and Kremer, E.B., Abstracts of Papers, *Vsesoyuznaya konferentsiya "Problemy povysheniya kachestva khimicheskikh volokon i nitei"* (All-Union Conf. "Problems of Improvement of the Quality of Chemical Fibers and Threads"), Kalinin, 1977, pp. 45–48.
11. Dege, G.J. and Reimschuessel, V.K., *J. Polym. Sci.*, 1973, no. 4, pp. 875–896.
12. Stein, G. and Adams, H., *Chemiefas. Text. Ind.*, 1977, no. 6, pp. 534–536.
13. Klare, G. *et al.*, *Khim. Volokna*, 1974, no. 6, pp 34–36.

Russian Journal of Applied Chemistry, Vol. 78, No. 10, 2005, pp. 1723–1725. Translated from Zhurnal Prikladnoi Khimii, Vol. 78, No. 10, 2005, pp. 1753–1755.
Original Russian Text Copyright © 2005 by Morachevskii.

Professor Petr Petrovich Budnikov (To 120th Anniversary of His Birthday)

Petr Petrovich Budnikov, a prominent scientist and pedagogue, made an outstanding contribution to the development of chemistry and technology of silicates, binders, and construction materials. During many years, he had been a member of the Editorial Board of *Zhurnal Prikladnoi Khimii* (Russian Journal of Applied Chemistry) and was actively involved in its work.



P.P. Budnikov was born on October 21, 1885, in Smolensk. In 1906, he finished Smolensk secondary school and entered the chemical department of Riga Polytechnic Institute (RPI). This institute, founded in 1862, was the first polytechnic institute in Russia. The teaching level of chemical disciplines at the institute and its research activities were strongly affected by the already well-known, by that time, physical chemist W. Ostwald (1853–1932, 1909 Nobel Prize in Chemistry), who was a professor at Riga Polytechnicum in 1881–1887 [1]. In 1903, Ostwald was elected the first honorary member of Riga Polytechnic Institute. Budnikov mentioned, among his teachers, professor of inorganic and physical chemistry and department dean P.I. Walden (1863–1957), professor of organic chemistry K.A. Bischoff (1855–1908), and talented physical chemist M.G. Centnerschwer (1874–1944). Technological disciplines were taught by professors M. Witlich (1866–1933), E.W. Britzke (1877–1953), M. Glasenapp (1845–1923), and S.G. Shimanskii (1867–1931) [1–3].

In May 1911, Budnikov graduated with excellence from RPI and worked during a certain time at the dye-and-paint laboratory of the Institute under the supervision of professor Shimanskii. In 1912, Budnikov became an engineer at the electrocarbon plant at Kudinovo (Moscow Province), but soon moved to Lodz (Poland), where he started teaching chemistry and chemical technology at Lodz textile industrial college. At the beginning of World War I, in 1914, the college was evacuated to Moscow. In 1915–1918, together with teaching at the college, he headed a shop at a chemical plant in Moscow. In 1915, RPI was also evacuated to Moscow. After having graduated from this institute, Budnikov continued to maintain close relationships with a number of professors from RPI. The Brest peace treaty (March 1918) envisaged re-evacuation of RPI with the entire teaching staff, equipment, and library. However, a part of teachers and students decided not to return to Riga occupied by German troops. The remaining part of RPI served as a basis for organization of Polytechnic Institute in the town of Ivanovo-Voskresensk (now Ivanovo). The decree on founding the Institute was signed by V.I. Lenin on August 10, 1918. Budnikov was actively involved in the organization of the new institute and was elected first a docent, and in 1919, a professor of Ivanovo-Voznesensk Polytechnic Institute and headed the chair of chemical technology of mineral substances.

In 1926, Budnikov moved to Kharkov and was elected a professor of the chair of technology of mineral substances and technology of silicates at Kharkov Technological Institute. In 1927–1932, he also held a professorship at the chair of chemical technology of inorganic substances at Kharkov Engineering-Economical Institute. Budnikov was dean of the faculty of chemical engineering at Kharkov Technological Institute in 1934–1938, and dean of the faculty of silicate technology at the same institute in 1938–1941). In 1936–1939, Budnikov headed the chair of silicate technology at the Industrial Academy (Kharkov).

1070-4272/05/7810-1723 © 2005 Pleiades Publishing, Inc.

Together with being involved in intensive pedagogical and research activities at higher-school institutions of Kharkov (in 1926–1941), Budnikov paid a considerable attention to engineering, scientific-organizational, and public issues. In 1926–1928, he was chief engineer of the silicate plants ?managed by Kharkov City Council; in 1932–1941, he headed the department of chemically resistant ceramic materials at the Reasearch Institute of Silicates (Kharkov). In 1932–1941, he was chairman of the Kharkov branches of the Mendeleev All-Union Chemical Society and All-Union Scientific, Engineering, and Technological Society of the silicate industry. Beginning in 1935, Budnikov had long been a member of the Expert commission on chemical technology at the Higher Qualification Commission of the USSR.

In 1934, the degree of a doctor of technical science was conferred on Budnikov; in 1939, he was elected an academician of the Department of physicomathematical, chemical, and geological sciences, Academy of Sciences of the Ukrainian Soviet Socialist Republic. In the same year, Budnikov was elected a corresponding member of the Department of chemical sciences, Academy of Sciences of the USSR.

In 1941–1943, Budnikov lived in Ufa (Bashkir Autonomous SSR), where institutions of the Academy of Sciences of the Ukrainian SSR were evacuated. During this period of time, he was chairman of the Department of physicomathematical, chemical, and geological sciences, Academy of Sciences of the Ukrainian SSR.

Beginning in the autumn of 1943 and till the end of his life, Budnikov was a professor at Mendeleev Institute of Chemical Engineering in Moscow and headed the chair of general silicate technology.

Budnikov's scientific legacy is vast. The evidence concerning his published works and numerous inventor's certificates can be found in a publication from the series "Materials on Biobibliographies of Scientists from the USSR," devoted to Budnikov [5]. The same book, as well as other publications [6–8], makes a brief analysis of his scientific, pedagogical, and public activities. Budnikov has been the subject of numerous journal publications, listed (till 1965 inclusive) in [5].

The following principal areas of scientist's research can be distinguished: physicochemical properties of oxide and silicate systems, refractory and highly refractory materials and compounds, ceramic materials, binders and cement, methodological issues.

In the first of the areas mentioned, Budnikov paid a considerable attention to analysis of reactions in liquid and solid phases; mechanism, thermodynamics, and kinetics of reactions in solids; and control over reaction rates. Investigations of this kind are important for solving a large number of problems in inorganic materials science. These studies were partly summarized in the monograph *Reaktsii v smesyakh tverdykh veshchestv* (Reactions in Solid Mixtures), in coauthorship with A.M. Gistling, Moscow: Gostroizdat, 1961, 423 pp.). Budnikov with co-workers studied, using various methods, phase diagrams of a large number of oxide systems, including those containing oxides of rare and rare-earth metals, and refined to a substantial extent the state diagrams of systems that are the most important for the technology of silicate systems. The scientist performed extensive studies of high-temperature sintering of systems of interest for nuclear power engineering.

Widely known and highly practically important were Budnikov's studies of the physicochemical properties of gypsum and its varieties. His monograph, *K issledovaniyu gipsa* (To a Study of Gypsum, Leningrad: Akad. Nauk SSSR, 1930, 180 pp.), was reprinted with supplements in 1933 and 1943. These studies served as basis for the development of quite a number of cement brands with various properties.

Numerous studies of refractories, including their new types, were concerned with thermal apparatus for widely diverse fields of industry: metallurgy, power engineering, and cement, glass, and chemical industries. Budnikov was the first to obtain and study new highly refractory materials, made an important contribution to the development of scientific foundations for manufacture of articles with an mp > 2000°C from pure beryllium, zirconium, and aluminum oxides, and developed the technology of hot compaction of metal oxides to obtain complex-shaped articles.

Budnikov paid a considerable attention to the most important ceramic material, porcelain. He demonstrated the possibility of improving the working parameters of insulating porcelain by introduction of various additives. His studies devoted to use of zirconium dioxide favored the improvement of domestic brands of ceramic materials. His works in the field of ceramics (including those chemically resistant), glasses, and enamels led to a pronounced improvement of the technology of their manufacture and to expansion of their application fields. The book published by a group of authors headed by Budnikov, *Tekhnologiya keramiki i ogneuporov* (Technology of Ceramics and Refractories), Moscow: Izd. Lit.

Stroit. Mater., 1950, 575 pp., was later reprinted and strongly affected the training of specialists in this field.

Studies of the physicochemical foundations and manufacture technology of binders and cement were widely represented among Budnikov's works. According to the available data [8], the number of his printed publications exceeds 1600. Budnikov was the author of a number of monographs, textbooks, manuals, original studies, and 80 inventions. He was many times a participant of international congresses and conferences, studied the organization of higher education in countries of Western Europe and in the United States, and visited a large number of foreign plants. Budnikov was elected a member of the American Ceramic Society (1924), member of the German Ceramic Society (1929), honorary member of the Czechoslovak Ceramic and Glass Society (1934), and academician of the Polish Academy of Sciences (1956).

Budnikov was awarded honorary titles of the Honored Scientist and Technologist of the Ukrainian SSR (1943) and Russian Soviet Federative Socialist Republic (1961), and, three times, the State Prize of the USSR. Budnikov's scientific, pedagogical, and public activities were honored with the highest State awards.

Petr Petrovich Budnikov died on December 6, 1968, at the age of 83.

REFERENCES

1. Stradyn', Ya., *Uchen. Zap. Latv. Gos. Univ.*, 1958, vol. 22, *Khim. Fakul't.*, no. 6, pp. 307–325.
2. Budnikov, P.P., *Uchen. Zap. Rizh. Politekhn. Inst.*, 1962, vol. 6, *Khim. Fakul't.*, no. 8, pp. 275–286.
3. Eiduk, Yu.Ya. and Grosvald, I.Ya., *Iz istorii estestvoznaniya i tekhniki Pribaltiki* (Excerpts from the History of Natural Science and Technology in Baltic Countries), Riga: Zinatne, 1972, vol. 4, pp. 175–182.
4. Stradyn', Ya.P. and Solov'ev, Yu.I., *Pavel Ivanovich (Paul) Walden*, Moscow: Nauka, 1988.
5. *Petr Petrovich Budnikov: Materialy k biobibliografii uchenykh SSSR: Seriya Khimicheskikh Nauk* (Petr Petrovich Budnikov: Materials on Biobibliography of Scientists from the USSR), Moscow: Nauka, 1967, issue 40.
6. Kukolev, G.V. and Budnikov, P.P., *Izbrannye trudy* (Selected Works), Kiev: Akad. Nauk USSR, 1960, pp. 3–10.
7. Ovcharenko, F.D. and Budnikov, P.P., *Khimiya i tekhnologiya silikatov* (Chemistry and Technology of Silicates), Kiev: Naukova Dumka, 1964, pp. 3–12.
8. Kukolev, G.V. and Ved', E.I., *Geroi sotsialisticheskogo truda P.P.Budnikov* (Hero of Socialist Labor P.P. Budnikov), Kharkov: Kharkov Univ., 1973.

A. G. Morachevskii

Russian Journal of Applied Chemistry, Vol. 78, No. 11, 2005, pp. 1727–1744. Translated from Zhurnal Prikladnoi Khimii, Vol. 78, No. 11, 2005, pp. 1761–1779.
Original Russian Text Copyright © 2005 by Kalnin'sh.

REVIEWS

Electron–Proton Effect in Catalysis

K. K. Kalnin'sh

Institute of Macromolecular Compounds, Russian Academy of Sciences, St. Petersburg, Russia

Received October 24, 2005

Abstract—The essence of the electron–proton effect is described with donor–acceptor complexes of quinones with hydroquinones as example. It is shown that this effect frequently occurs in organic chemistry and plays an important role in noncatalytic and catalytic reactions.

INTRODUCTION

Catalytic processes play an enormous role in organic and bioorganic chemistry. The essence of the catalytic effect is a decrease in the energy barrier of a chemical reaction, resulting in acceleration of the reaction. Thanks to the catalysis, many reactions can be carried out at common temperatures and pressures. Particularly high performance and striking specificity are shown by natural catalysts, enzymes, ensuring concerted occurrence of numerous biochemical reactions at very high rates.

In this review we discuss a new phenomenon that we discovered, the electron–proton effect underlying the acid–base catalysis. It is impossible to adequately account for a catalytic decrease in the energy barrier of chemical reactions without considering this effect. The electron–proton effect is a physical phenomenon arising from concerted interaction of the fast motion of electrons and slow motion of protons. The effect is manifested in a considerable decrease in the energy of the excited levels of an electron donor–acceptor (EDA), or charge-transfer, complex under the action of an intra- or intermolecular hydrogen bond.

The EDA interactions and H bonds are so-called specific intermolecular interactions. Their energy is usually low compared to the energy of chemical bonds (~100 kcal mol^{-1}), being as low as 3–5 kcal mol^{-1}. The EDA interactions are associated with an overlap of the electronic shells of molecules (frontier orbitals) and are characterized in the ground state by a small shift of the electron density from the donor molecule to the electron-acceptor molecule. Under thermal, electrical, or photochemical excitation of sufficient energy, EDA complexes can pass to an electronically excited state in which an electron is fully transferred from the donor to acceptor. A characteristic feature of EDA complexes is that their electronic spectra contain absorption bands corresponding to the intermolecular electron transfer. The frequency of this band is unambiguously determined by the ionization potential of the donor I_D and electron affinity of the acceptor E_A.

In the excited state, an EDA complex transforms into a neutral or charged chemically active radical pair (or biradical), which subsequently undergoes radiative (luminescence) or nonradiative (chemical reaction or energy dissipation) deactivation. From the chemical viewpoint, EDA interactions are redox reactions, also characterized as electron transfer reactions.

In a hydrogen bond, a proton donor DH interacts with electron-donor groups of a proton acceptor A; depending in the extent of this interaction, the proton H^+ is either localized at the donor molecule DH and only slightly shifted along the hydrogen bond D–H···A toward the acceptor A, or fully transferred to the acceptor A: $D^-\cdots H-A^+$. The latter case is a proton transfer reaction occurring in the vibrationally excited state of a hydrogen bond. Hydrogen bonding is a kind of acid–base interactions.

Charge-transfer complexes and hydrogen bonds are traditionally studied independently from each other and not in connection with each other, although it is quite obvious that these two kinds of intermolecular interactions should exert a certain influence on each other, and their effect on physical and chemical processes should be combined. In terms of the electronic states, the effect of an H bond on EDA complexes consists in a decrease in the energy and lifetime of the lowest excited levels corresponding to charge (electron) transfer; however, only in a few separate papers we can find experimental evidence for this conclusion. Published facts of the mutual influence of charge-transfer complexation and H bonding are not summarized and correlated, and they give no grounds for any far-reaching conclusions. No attempts were made to evaluate this influence quantitatively, which could

1070-4272/05/7811-1727 © 2005 Pleiades Publishing, Inc.

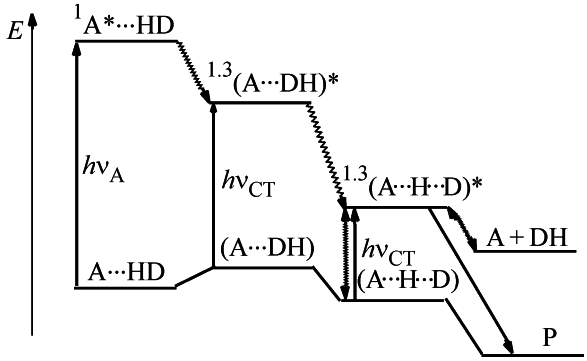


Fig. 1. Scheme of energy levels for photochemical and thermal processes.

impart predictive power to reasoning about the role of hydrogen bond in electron-transfer processes.

In this connection, discovery of the electron–proton effect [1–10] is of principal importance. This discovery reveals a fundamental relationship between the electron donor–acceptor and proton donor–acceptor (PDA) interactions of molecules. The spectral manifestation of the effect is an appreciable (by 1.5 eV and more) decrease in the energy of excited levels of an EDA complex upon H bonding. This effect underlies such physical phenomena as luminescence quenching with hydrogen bond or paramagnetism of hydrogen-bonded compounds; it accounts for the occurrence of numerous and diverse reactions involving transfer of an electron and a proton (a hydrogen atom in total). The electron–proton effect plays an extremely important role in acid–base enzymatic catalysis.

1. ENERGY DIAGRAM FOR PHOTOCHEMICAL AND THERMAL PROCESSES

Several types of catalysis are considered in the literature: acid and base (usually termed acid–base), bifunctional, coordination, organometallic, etc. In each case, the corresponding specific interactions (e.g., hydrogen bonding, interactions involving donor and vacant orbitals of a transition metal catalyst) ensure the main and the most important catalytic effect (in accordance with our concept [1]): a decrease in the energy of the electronically excited state of the catalytic reaction complex to the level corresponding to thermal energy.

Since the probability of occurrence or the rate of a chemical process is determined by the energy of the excited complex, the lower this level lies (Fig. 1), the higher its population and the larger the number of elementary reaction events occurring in unit time, and hence the higher the reaction rate. The vertical straight lines in Fig. 1 show transitions from the ground state to an excited level of an H-bonded complex A···HD and to electronically excited levels of an electron donor–acceptor complex (A···DH)* and $^{1.3}$(A···H···D)*, shifted toward lower energies. The energy gap between the latter level characterizing an EDA complex with a hydrogen bond and the level of the free reactants in solution A + DH is narrow and can be readily overcome in the course of thermal excitation of molecules under common conditions.

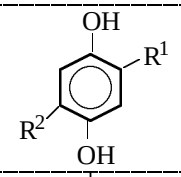
The scheme in Fig. 1 illustrates the simplest case of catalysis by a hydrogen bond in an excited state of an EDA complex. It is important that here we deal with the excitation of an electron donor–acceptor complex and not of a hydrogen-bonded complex. If the labile hydrogen atom in the electron-donor molecule DH will be replaced by the CH_3 group, the hydrogen bond between the donor D–CH_3 and acceptor A will not be formed, and the catalytic decrease in the energy levels in this system will not take place. Within the traditional concept, the two above-considered cases (with a hydrogen bond between the electron donor and acceptor and without it) are considered as different classes of chemical compounds, so that the relationship between the above example (when hydrogen bonding decreases the energy levels) and acid–base catalysis is lost. At the same time, acid–base catalysis is essentially based on the effects of a hydrogen bond in an excited state of a catalytic reaction complex.

Let us consider a simple but frequent case of interaction of two molecules one of which (DH) is an electron and proton donor and the other (A), an electron and proton acceptor. The electron transfer (electronic excitation) between the electron donor and acceptor in the case when the components contain labile hydrogen atoms should be considered in combination with the proton transfer.

2. ELECTRON DONOR–ACCEPTOR AND PROTON DONOR–ACCEPTOR PROPERTIES OF QUINONES AND HYDROQUINONES

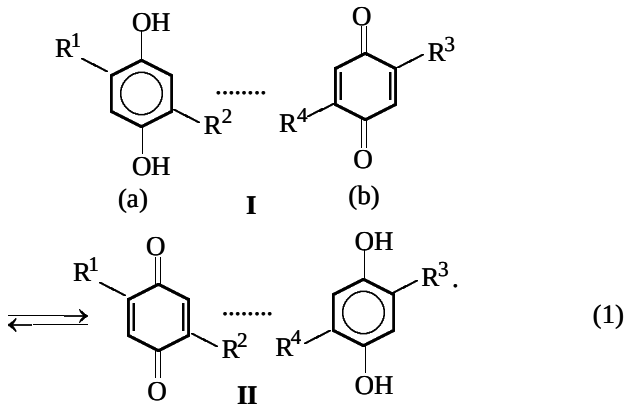
Convenient objects for experimental studies of the electron–proton effect are crystalline complexes of quinones with hydroquinones, so-called quinhydrones, which are a particular case of π complexes with a hydrogen bond. The excited states of such complexes are responsible for the thermal transfer of the hydrogen atom [5], an elementary step of many organic reactions. The specific crystal structure of quinhydrones is constructed by the donor–acceptor bond and a chain

Table 1. Electron-donor and proton-donor power of substituted hydroquinones

Compound			I_D	I_D^{calc}	pK_a	ν_{OH}	$\Delta\nu_{OH}$
	R^1	R^2	eV			cm^{-1}	
2a	CH_3	H	7.70	8.15	10.05	3618	251
3a	OCH_3	H	7,65	8.05	9.91	3617, 1569	259
1a	H	H	7.83	8.23	9.91	3617	278
4a	Cl	H	7.96	8.41	8.09	3614, 3559	327
5a	Br	H	7.90	8.42		3612, 3543	318
6a	Cl	Cl	8.16		7.90	3553	375
7a	C_6H_5	H		8.10			

system of hydrogen bonds [11–13]. Unusual spectral and chemical properties of quinhydrones are caused by the stabilizing effect of the hydrogen bond on the excited states of the complexes. No more than 30 quinhydrones are known; in most cases, these are complexes of 1,4-naphthoquinone and *p*-benzoquinone derivatives with the corresponding reduced species [13, 14].

In our studies we used *p*-benzoquinone and its derivatives, differing in the electron-acceptor and proton-acceptor power. The electron- and proton-donor power of the corresponding hydroquinones can be changed by varying the substituents. For any quinhydrone complex **I**, there exists the conjugated complex **II** arising from the transfer of two hydrogen atoms:



(1)

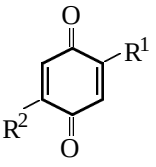
Four characteristics are decisive in the formation of a quinhydrone: electron-donor and proton-donor power of hydroquinone derivatives and electron-acceptor and proton-acceptor power of the corresponding quinone derivatives; the steric effects of substituents are also significant. To understand the nature of the electron–proton effect, it is necessary to reveal the relationship between these four EDA and PDA characteristics; to do this, it is appropriate to use a series of hydroquinones and the corresponding oxidized species as example.

The proton-donor power of substituted hydroquinones can be evaluated by the shift of the OH stretching vibration frequency, $\Delta\nu_{OH}$, upon formation of a hydrogen bond with a reference proton acceptor, tetrahydrofuran (Table 1). The IR spectra of hydroquinone **1a** and methylhydroquinone **2a** in the isolated (monomeric) form contain single OH bands whose frequencies ν_{OH} are close to those of the corresponding phenols [15]. In methoxy, chloro, and bromo derivatives of hydroquinone (**3a**–**5a**), the hydroxy group vicinal to the substituent forms an intramolecular hydrogen bond (IHB), which results in a low-frequency shift of ν_{OH} (Table 1). The vibration frequencies of these groups in the free state are unknown and were assumed to be equal to those of the corresponding *meta*-substituted phenols.

In tetrahydrofuran, all the examined hydroquinone derivatives in a concentration less than 0.05 M give single bands corresponding to the hydrogen-bonded species O–H···O. The spectral shifts relative to the band of the corresponding monomeric form, $\Delta\nu_{OH}$, linearly correlate with the acidity constants pK_a; with respect to the acidity, the hydroquinone derivatives can be ranked in the following order: **2a** ≈ **3a** < **1a** < **5a** < **4a** ≈ **6a**.

The proton-acceptor power of quinones is characterized by the shift $\Delta\nu_{OH}$ of the OH stretching frequency of a reference proton donor ROH upon formation of a hydrogen bond C=O···H–OR. The spectral shifts $\Delta\nu_{OH}$ (Tables 1, 2) show that substituents oppositely affect the proton-donor power of hydroquinones

Table 2. Electron- and proton-acceptor power of quinones

Compound			E_A	E_A^{calc}	$\Delta\nu_{OH}$, cm^{-1}
	R^1	R^2	eV		
2b	CH_3	H	1.79	2.03	109
3b	OCH_3	H	1.60	2.04	96
1b	H	H	1.88	2.06	93
4b	Cl	H	2.10	2.29	69
5b	Br	H	2.15	2.34	
6b	Cl	Cl	2.26	2.50	54
7b	C_6H_5	H		2.58	

1a–**6a** and the proton-acceptor power of the corresponding oxidized species **1b**–**6b**. In particular, methylhydroquinone is the weakest proton donor in the examined series, whereas the corresponding oxidized species, methylbenzoquinone, is a good proton acceptor. The electron-withdrawing Cl substituent enhances the proton-donor power of hydroquinones but decreases the proton-acceptor power of the oxidized species.

The electron-donor power of **1a**–**6a**, characterized by the ionization potential I_D, can be evaluated either theoretically or from the charge-transfer (CT) bands of the complexes of these compounds with a reference electron acceptor, 1,3,5-trinitrobenzene (Table 1). For a group of electron donors with known ionization potentials [16] and energies E_{CT}, a linear correlation

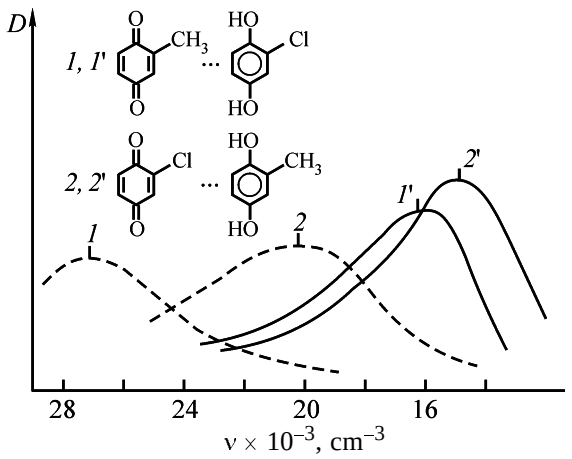


Fig. 2. Absorption spectra of complexes (*1*, *1*') methylbenzoquinone (MBQ)–chlorohydroquinone (CHQ) and (*2*, *2*') chlorobenzoquinone (CBQ)–methylhydroquinone (MHQ) in (*1*, *2*) acetonitrile and (*1*', *2*') KBr. (*D*) Optical density and (ν) wave number; the same for Figs. 4–6 and 18.

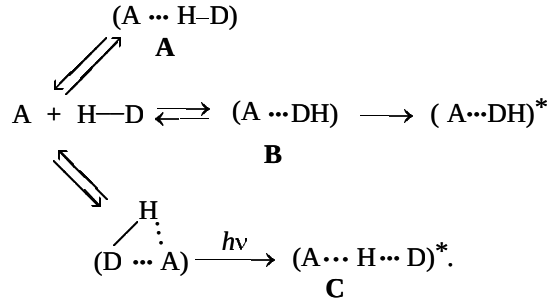
is observed:

$$I_D = 1.31 \times 10^{-4} E_{CT} + 4.49 \text{ eV}. \quad (2)$$

Equation (2) was used to find the ionization potentials of substituted hydroquinones **1a**–**6a**; for **1a**, the value we obtained, I_D = 7.83 eV, is close to that reported previously, I_D = 7.86 eV [16]. The electron affinities E_A of **1b**–**6b** were determined by Briegleb [17] and later refined by Farragher and Page [18]. The E_A values slightly corrected using the CT energies for various compounds are listed in Table 2.

On the whole, it can be concluded that the enhancement of the electron-donor power of hydroquinones is accompanied by weakening of their proton-donor power. The similar conclusion is valid for the electron-acceptor and proton-acceptor power of quinones. The experimental dependences obtained express the universal inverse correlation between the electron and proton affinities of molecules.

The interaction of a quinone (electron and proton acceptor) A and hydroquinone (electron and proton donor) H–D involves the following steps:



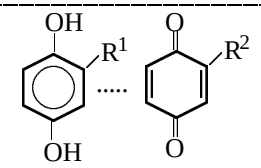
where (A···H–D) is a hydrogen-bonded complex; (A···DH), π complex; and  , a hydrogen-bonded π complex.

Structures **A** and **B** can be formed both in solution and in the crystal, whereas structure **C** in the ground electronic state predominantly exists only in the crystal.

A compromise between the donor–acceptor interaction requiring the planar orientation of the molecules and the hydrogen bond O–H···O=C results in a specific structure of the crystal; for example, in the complex **1a**–**1b**, the distance between the molecular planes is 3.16 Å, at a hydrogen bond length of 2.72 Å [11].

The most significant feature of quinhydrone complexes is a considerable decrease in the CT energy in going from a solution to a crystal (Fig. 2, Table 3), depending on the kind of substituent and procedure for preparing the complex and the sample. For exam-

Table 3. Spectral and thermochemical characteristics of quinhydrones

Complex			E_{CT}, cm^{-1}		ΔE_{CT}	$\Delta\nu_{OH}$	E_a	Preexponential term
	R^1	R^2	solution	crystal, in KBr	cm^{-1}			
1a–**1b**	H	H	24000	16800	7200	390	17400	31 [19]
1a–**2b**	H	CH_3	25000	18200	6800	460, 360, 320		
2a–**1b**	CH_3	H	23000	17200	6900	350	14300	24
2a–**2b**	CH_3	CH_3	24100	16400	7700	320		
1a–**4b**	H	Cl	22100	16600	5500	360	14400	22.9
4a–**1b**	Cl	H	26000	17900	8100	370		
4a–**4b**	Cl	Cl	23500	18100	6400	360, 225		
2a–**4b**	CH_3	Cl	21200	15600	5600	380	12200	20
4a–**2b**	Cl	CH_3	26800	17400	9400	360		

ple, trituration of the crystalline complex with mineral oil results in lower E_{CT} (by 1000–1500 cm^{-1}) than pelletizing with KBr. These factors ultimately affect the state of the hydrogen bond whose effect on E_{CT} is the most significant. The major contribution to this spectral shift is made, along with the effects associated with the phase transition, by stabilization of the excited state of the π complex (A···DH)* due to hydrogen bonding; therefore, the difference E_{CT}(soln) – E_{CT}(cr) is the measure of participation of the hydrogen bond in the formation of a quinhydrone.

Quinhydrones are characterized by large shifts of the OH stretching vibration frequencies, $\Delta\nu_{OH}$, in the crystal compared to solution; for example, for complex **4a**–**4b** in the crystal $\Delta\nu_{OH}$ = 360 cm^{-1}, whereas in solution $\Delta\nu_{OH}$ is as small as 90 cm^{-1}. This fact indicates that the hydrogen bond in the crystal is considerably stronger. At the same time, the relative shift in going from one complex to another, $\Delta(\Delta\nu_{OH})/\Delta\nu_{OH}$, in the crystal is several times smaller than in solution. For example, for the pair of complexes **2a**–**4b** (weak proton donor and strong electron acceptor) and **4a**–**2b** (strong proton donor and weak electron acceptor), the relative shift is 0.2 in the crystal and 1.0 in solution. These features of quinhydrones are caused by the fact that in the crystal the hydrogen bond coexists with the donor–acceptor bond.

The IR spectrum of complex **1a**–**2b** contains several relatively narrow OH stretching vibration bands, suggesting the presence of several hydrogen bonds of different energy in the unit cell. Also, the strength of hydrogen bonds in the crystal is subject to the steric effect of bulky substituents. For example, the methyl group in the acceptor fragment of the complex produces steric hindrance in formation of crystalline quinhydrone. This fact may be responsible for weaker H bonding in complex **1a**–**2b** compared to **1a**–**1b** (Table 3), despite the fact that methylbenzoquinone **2b** is a stronger proton acceptor than *p*-benzoquinone **1b**.

3. COMPENSATION EFFECT

Pair complexes of quinones with hydroquinones in solution are common EDA complexes without hydrogen bonds, as indicated by a linear correlation between the CT energy and the difference $I_D - E_A$, with a slope close to unity (Fig. 3, straight line *A*). Similar correlations were obtained for a large number of EDA complexes without hydrogen bond in solution [20, 21]; passing to the solid phase causes only a slight decrease in E_{CT} (by no more than 0.3 eV). On the contrary, the CT bands of complexes of quinones with hydroquinones undergo a considerable bathochromic shift, depending on the structure of the components, in going from solution to the solid phase. For a group of structurally related complexes we obtain straight line *B* with a slope of 0.6 (Fig. 3), and the lowest values of E_{CT} are approximated by straight line *C*.

The largest shift, ΔE_{CT} = 9400 cm^{-1}, is observed for a complex of a weak electron acceptor, methyl-*p*-benzoquinone **2b**, with a relatively weak electron donor, chlorohydroquinone **4a**, whereas for the conjugated complex **4b**–**2a** the shift is as small as 5600 cm^{-1}. In the other complexes, the shifts range from 5000 to 10000 cm^{-1} (Table 3), with the following regular trend: In a pair of conjugated complexes,

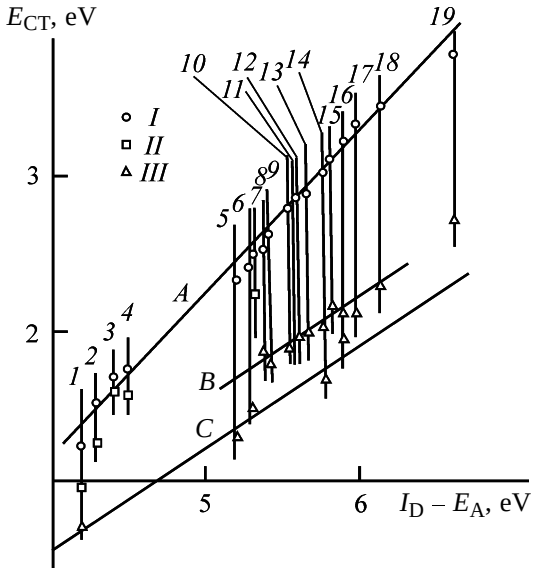


Fig. 3. Correlation of the charge-transfer energy E_{CT} with the difference $I_D - E_A$ for (*I*) complexes in solution, (*II*) crystals without hydrogen bond, and (*III*) crystals with hydrogen bond. (*1*) Tetracyanoquinodimethane–benzidine, (*2*) dichloro-PM–TMPD, (*3*) chloro-BQ–TMPD, (*4*) PM–TMPD, (*5*) BQ–*p*-PD, (*6*) BQ–bromo-*p*-PD, (*7*) 1,3,5-trinitrobenzene–*p*-PD, (*8*) BQ–2,6-dichloro-*p*-PD, (*9*) bromo-BQ–methyl-HQ, (*10*) bromo-BQ–HQ, (*11*) chloro-BQ–HQ, (*12*) BQ–methyl-HQ, (*13*) methyl-BQ–methyl-HQ, (*14*) BQ–HQ, (*15*) methyl-BQ–HQ, (*16*) BQ–chloro-HQ, (*17*) methyl-BQ–chloro-HQ, (*18*) methyl-BQ–2,5-dichloro-HQ, and (*19*) BQ–phenol, where PM is pyromellitic anhydride; TMPD, *N,N,N′,N′*-tetramethyl-*p*-phenylenediamine; *p*-PD, *p*-phenylenediamine; BQ, *p*-benzoquinone; and HQ, hydroquinone.

the complex exhibiting weaker EDA characteristics is characterized by the larger shift.

Among the complexes given in Table 3, the crystal structure was determined only for **1a**–**1b** [11]; the crystal consists of stacks of alternating 1,4-benzoquinone and 1,4-hydroquinone molecules. The crystal structures have also been determined for two more quinhydrones: the complex of 1,4-naphthoquinone with hydroquinone [22] and the complex of 2-phenyl-1,4-hydroquinone with *p*-chlorobenzoquinone [23]. The spectral data suggest that the other crystalline quinone–hydroquinone complexes have a similar characteristic quinhydrone structure.

Among two conjugated complexes, e.g., **2a**–**4b** and **4a**–**2b**, the shift of the CT band in going from solution to the crystal is larger for a weak donor–acceptor pair, in this case for **4a**–**2b**. Since thermochemical transformations of quinhydrones occur in the direction of increasing difference $I_D - E_A$ [10], e.g., **2a**–**4b** → **4a**–**2b**, the EDA properties weaken and the PDA properties are enhanced in the course of the reaction. Strong electron donors and acceptors are, respectively, weak proton donors and acceptors. Hence, the strength of EDA interactions inversely correlates with the strength of hydrogen bonding in complexes in which both kinds of interactions are realized. Crystalline quinhydrones and some other EDA complexes with hydrogen bonding are just such complexes.

The combined but oppositely directed effect of EDA and PDA properties of quinones and hydroquinones levels off the CT energy in the series of complexes, so that it becomes only weakly dependent on the difference $I_D - E_A$, whereas for the same complexes without hydrogen bond in solution the correlation $E_{CT} \sim I_D - E_A$ is linear with the slope close to unity. In other words, the H bond compensates to a certain extent the variation of the EDA properties of interacting molecules; as a result, in the solid state strong and weak donor–acceptor pairs have close E_{CT}.

The strength of the hydrogen bond can be estimated from the shift of the OH stretching vibration frequency ν_{OH}, using an empirical formula

$$E_H = 0.33(\Delta\nu_{OH} - 40)^2 \text{ kcal mol}^{-1}. \quad (3)$$

Estimations show that, the stronger the H bond, the larger the shift of the CT band upon H bond formation; this fact confirms the regular correlation between these two quantities. For two conjugated complexes **4a**–**2c** and **2a**–**4c**, the difference in the H bond energy is 0.6 kcal mol^{-1}, which amounts to approximately 10% of ΔE_{CT}. Hence, small changes in the H bond energy in the ground state can cause significant shifts of CT bands.

4. CRYSTALLINE QUINHYDRONES WITH INCLUDED SOLVENT MOLECULES

The CT energies (Table 3) were determined for solid quinhydrones pelletized with KBr; in these samples, the complexes mainly preserve the crystalline structure [14]. Since E_{CT} strongly depends on the state of the H bond, a question arises: Is it possible to affect the H bond strength by modifying the crystal structure? One of the modification procedures is inclusion of foreign molecules in the crystal lattice to obtain host–guest structures. The incorporated molecules alter the interstack and interplanar spacings and thus affect the H bond strength. Examples of such structures are complexes of tetracyanoquinodimethane (TCQ) with benzidine [24]. Experiments on preparation of inclusion complexes from quinhydrones failed, because such complexes appeared to be unstable in the crystalline form.

We succeeded in growing the crystals of the complexes at low temperature. By slow cooling of a solution of BQ–HQ to a temperature from –40 to –60°C in a mixture of acetonitrile with chloroform or methylene chloride at a definite ratio of the polar and nonpolar components (1 : 1.5 to 1 : 2), we obtained a finely crystalline blue suspension which did not settle within several hours. The crystals are so small that are not observed visually, and their formation is judged only from certain turbidity of the mixture.

The absorption spectrum of the finely crystalline suspension (Fig. 4) depends on the composition of the solvent mixture and kind of the inert component: $CHCl_3$ or CH_2Cl_2. With an increase in the content of the nonpolar component (e.g., methylene chloride), the frequency of the CT band decreases. The decolorization of the solution on heating and its coloring on cooling are fully reversible; however, we failed to isolate blue crystals. The lowest-frequency position of the CT band of the crystalline complex, 13000 cm^{-1}, is shifted relative to E_{CT} of the solid complex by 4000 cm^{-1} and relative to the solution in which the EDA complexes exist as non-hydrogen-bonded pairs by a value as large as 11000 cm^{-1}.

Presumably, in crystallization from a mixed solvent a structure incorporating solvent (e.g., chloroform) molecules is formed, favoring formation of a strong hydrogen bond and hence decreasing the CT energy. The energies of the charge-transfer excited states (13000 cm^{-1}) are very low for relatively weak electron donors and acceptors, BQ and HQ, which suggests that the CT states are stabilized by certain specific mechanisms.

Thus, the EDA and PDA characteristics of quinones and hydroquinones show inverse correlation with each other, i.e., the higher the electron affinity of a quinone, the lower its proton affinity (capability for H bonding), and the higher the electron-donor power of a hydroquinone, the lower its proton-donor power. This correlation is quite obvious, as it is associated with the opposite signs of charges of electron and proton, and has profound chemical consequences, the main of which is a considerable decrease and leveling of the energies of excited levels of the complexes, determining the reaction rates.

5. PICOSECOND TRANSIENT ABSORPTION SPECTRA

The product of hydrogen transfer in quinhydrones is the conjugated crystalline complex; the activation

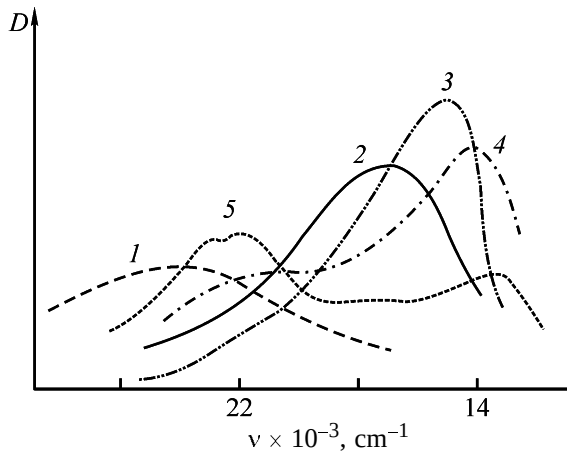


Fig. 4. Absorption spectra of *p*-benzoquinone–hydroquinone complex: (*1*) solution in acetonitrile, 25°C; (*2*) crystalline complex in KBr; and (*3*–*5*) microcrystalline suspension in mixed solvents, –50°C: (*3*, *4*) acetonitrile–methylene chloride, 1 : 1.5 and 1 : 2, respectively, and (*5*) acetonitrile–chloroform, 1.5 : 1.

energy of the thermochemical reaction is comparable with the CT energy [5]. These data suggest that the excited state of hydrogen-bonded complexes participates in chemical transformations of quinhydrones, but the lifetime and deactivation pathways of these two states are studied insufficiently. The excited states of the complexes can be formed along two pathways: (1) photoexcitation of a molecule of one of the components, followed by formation of an exciplex with a molecule of the other component in the ground state (luminescence quenching), and (2) excitation of the complex in the ground state. The first pathway was examined in basic studies [25–28] and other papers. However, with this excitation pathway it is impossible to determine the energies of the excited states (exciplexes), which is necessary for evaluating the probability of thermal transformations.

The second pathway yields the same excited species as does the first pathway, but it allows determination of the energies of the levels and hence evaluation of the probability of their thermal population. In this connection, it is very interesting to examine the transient spectra in excitation of solid quinhydrones in the CT band in the ground state.

The time-resolved transient absorption spectra in the range 420–765 nm were recorded on a picosecond spectrometer [29]. The optical paramagnetic generator used allowed continuous adjustment of the excitation wavelength in the whole visible range. The excitation pulse energies were about 0.05 mJ at λ_{exc} = 500–530 nm and 0.3 mJ at λ_{exc} = 532 nm; the pulse width

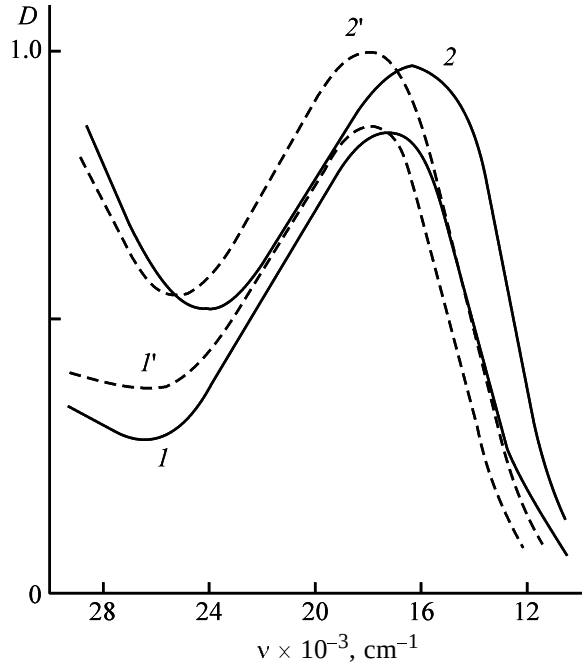


Fig. 5. Absorption spectra of complexes (solid-phase mixing) in KBr: (*1*) MHQ–BQ (**2a**–**1b**), (*2*) MHQ–CBQ (**2a**–**4b**), and (*1'*, *2'*) respective conjugated complexes HQ–MBQ (**1a**–**2b**) and CHQ–MBQ (**4a**–**2b**) after heating.

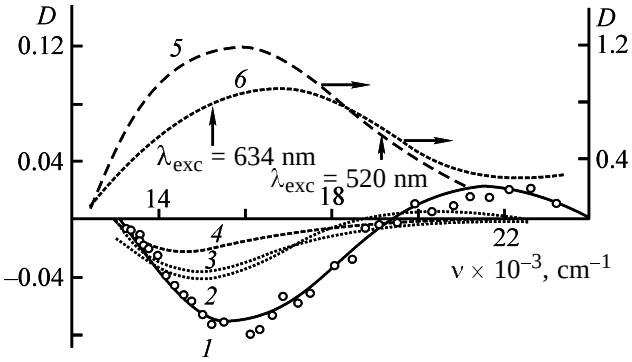


Fig. 6. (*1*–*4*) Transient spectra and (*5*, *6*) stationary absorption spectra of complexes **7a**–**1b** and **1a**–**7b**, respectively, in KBr pellets (solid-phase mixing). Excitation of (*1*, *2*) complex **7a**–**1b** at λ = 634 nm and (*3*, *4*) complex **1a**–**7b** at λ = 520 nm. Delay, ps: (*1*, *3*) 0 and (*2*, *4*) 600; experimental points in spectra *2*–*4* are omitted.

was 20 ps. The fluctuation of the laser beam on microcrystals of the sample pelletized with KBr caused scattering of the measured optical densities; therefore, the observed spectral curves were subjected to mathematical treatment. The kinetic curves were approximated by a sum of several (usually two) exponents:

$$A(t) = A_{10}\exp(-t/t_1) + A_{20}\exp(-t/t_2). \quad (4)$$

Conjugated complex **II** absorbs at higher frequencies compared to **I** [Eq. (1)], but the shift does not exceed 1000–2000 cm^{-1}; e.g., for the transformations **2a**–**1b** → **1a**–**2b** and **2a**–**4b** → **4a**–**2b**, the shifts are 1000 and 1800 cm^{-1}, respectively (Fig. 5). The CT bands of the initial (**I**) and conjugated (**II**) complexes noticeably overlap because of their large width (5000–7000 cm^{-1}); therefore, both complexes are excited by laser irradiation in the CT band. This fact is one of the causes of low photochemical activity of quinhydrones.

The large width of the CT bands may be caused both by the structural nonuniformity of the polycrystalline sample and by the distribution of the electronic transition energies in the ordered system of the hydrogen-bonded complex. Two elucidate the broadening mechanism, two wavelengths were chosen on the low- and high-frequency wings of the CT band. Figure 6 shows the stationary and transient spectra of crystalline complexes **7a**–**1c**. Similar pattern is observed with the other complexes **1a**–**1b** and **1a**–**2b**.

The decolorization curve (decrease in the optical density) of the ground state is similar to the charge-transfer band in the stationary spectrum, and at the delay τ = 0 ps both bands have the same frequency, 15800 cm^{-1}. Comparison of the optical densities in the stationary and induced spectra shows that each laser pulse causes excitation of 5–15% of the molecules of the complex. Hence, during recording of the spectrum (more than 1000 laser pulses), each molecule of the complex undergoes repeated excitation to the charge-transfer state. In the range of positive absorption, 20000–24000 cm^{-1}, despite high noise level, two weak bands were detected at 21000 and 23000 cm^{-1}. The nature of these bands, which were assigned to radical species, will be considered below.

6. KINETICS OF TRANSIENT SPECTRA

The deactivation kinetics of the excited state (Fig. 7, curve *1*) can be approximated by two exponents with characteristic times of 80 and 3500 ps. A change in the sign of the optical density at about 200 ps indicates that the positive absorption associated with radical ions disappears faster than the induced absorption assigned to the complex in the excited state. Hence, in the time interval between the primary event of the electron transfer due to photoexcitation and the restoration of the absorption of the ground state of the initial complex, relaxation processes occur in the excited charge-transfer state. These processes are associated with the proton transfer and can be monitored only kinetically. Similar kinetic curve was obtained for the conjugated complex **7a**–**1b**.

The kinetic curve of the decrease in the induced absorption at 17212 cm^{-1} (591 nm) in the region of the CT band [ν_{exc} = 19230 cm^{-1} (λ_{exc} = 520 nm)] (Fig. 7, curve *3*) also consists of two portions: fast decay with a rate constant of 7×10^9 s^{-1} and slow decay (1.85×10^8 s^{-1}). Excitation on the long-wave wing of the CT band [ν_{probe} = 15780 cm^{-1} (λ_{probe} = 610 nm)] gives rise to similar kinetic curves. Hence, the kinetics of the photochemical states is independent of the excitation wavelength in the region of the CT band, and the excited states of these samples obtained by solid-phase mixing are deactivated in two steps with the rates differing by a factor of 40.

An essentially different pattern was observed with the complexes prepared by crystallization from CH_2Cl_2. In this case, the decay curves can be approximated by a monoexponential kinetic curve with a lifetime of 1700 ps (Fig. 7, curve *2*), and the contribution of the initial fast step is insignificant. The kinetics depends not only on the sample preparation procedure (solid-phase mixing or crystallization) but also on the degree of grinding the crystals prior to pelletizing with KBr. Intense grinding of the crystals leads to a two-step kinetics characteristic of solid-phase mixing.

Coincidence of the maximum (15800 cm^{-1}) and shape of the band in the stationary and transient spectra at $\tau = 0$ and weak dependence of these characteristics on the excitation wavelength (Fig. 6) indicate that broadening of the CT band is caused by the nature of the electronic transitions in the crystalline phase of the sample, rather than by its structural nonuniformity.

At a long delay time of the probing pulse, the absorption band in the transient spectrum is shifted toward lower frequencies (Fig. 6). This shift is characteristic of all the examined samples and is caused by rapidly growing negative absorption at 13000 cm^{-1}, whose summation with the induced absorption causes the shift of the band maximum. As the probing frequency is decreased, the maximum of the kinetic curve shifts from 300 (472 nm) to 800–1000 ps (974 nm). The induced absorption is of low intensity in this spectral range; therefore, the negative absorption should be assigned to emission of the complex. Its summation with the induced absorption causes a shift of the band maximum. The luminescence band of the crystalline complex arising from the recombination of radical ions is very broad; its maximum is apparently in the range 10000–13000 cm^{-1}.

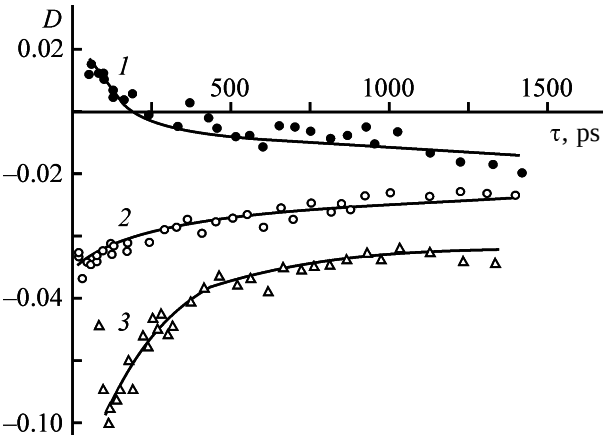


Fig. 7. Kinetic curves of transient absorption of complex **7a**–**1b** at probing wavelengths. (*D*) Optical density and (τ) time. λ, nm: (*1*) 438 (λ_{exc} = 532 nm), (*2*) 586 (λ_{exc} = 512 nm), and (*3*) 581 (λ_{exc} = 520 nm). The complexes were prepared by (*1*, *2*) crystallization and (*3*, *4*) solid-phase mixing.

7. THERMOCHEMICAL AND PHOTOCHEMICAL TRANSFER OF A HYDROGEN ATOM

The hydrogen atom transfer as an elementary chemical process consists of successive steps of electron and proton transfer, which are observed separately in time-resolved photophysical experiments [25–27, 30] or in thermochemical reactions at sufficient stability of the intermediate radical ion species [31]. However, in the majority of chemical reactions the steps of the electron and proton transfer are not registered separately and merge into a common process of hydrogen atom transfer. Therefore, chemical reactions are usually considered in terms of the traditional concept of the transition state [32], without considering the electron transfer as a necessary and essential step of the reaction.

Quinhydrones are a convenient model for studying the mechanism of the hydrogen atom transfer [33], since redox transformations occur in an ordered crystalline phase, and the measured thermodynamic characteristics can be correlated with definite electronic states of the crystal. In the course of the reaction, the crystalline state is preserved, with only slight changes in the unit cell parameters; therefore, the transfer of the hydrogen atom (electron + proton) can be studied in the purest form.

In [8–10] we used the procedure of solid-phase mixing, which allows preparation of finely crystalline samples, apparently with a fairly high content of lattice defects. The reaction progress was monitored by

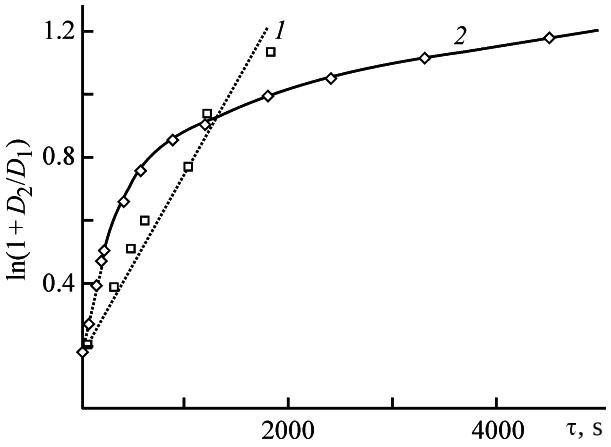


Fig. 8. Thermokinetic curves of transformations of quinhydrone **7a**–**1b**. (D_1, D_2) Optical densities of absorption bands at 872 (*p*-benzoquinone) and 900 cm^{-1} (phenylbenzoquinone).

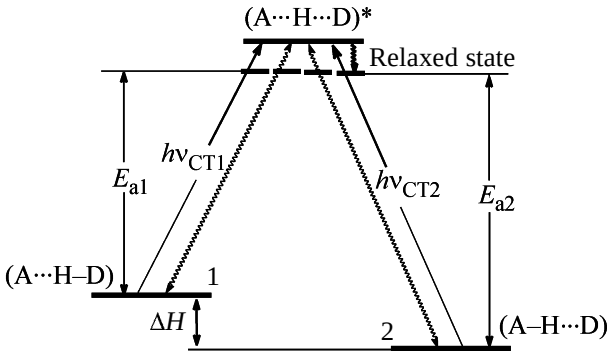


Fig. 9. Energy diagram of the thermal transfer of hydrogen atom in crystalline complexes.

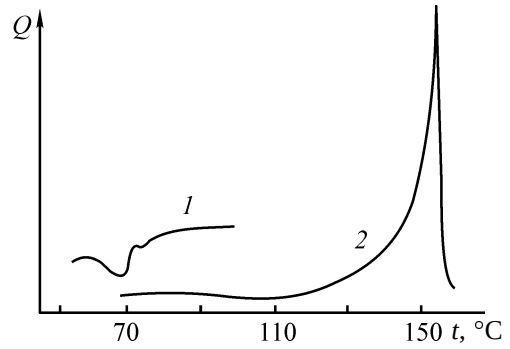


Fig. 10. Calorimetric curves (2 deg min^{-1}) of solid-phase complexes: (*Q*) endothermic effect and (*t*) temperature. (*1*) MHQ–BQ (solid-phase mixing) and (*2*) HQ–BQ (crystallization).

IR spectroscopy, by absorption bands of one of the components. This procedure is inapplicable to symmetrical complexes such as *p*-benzoquinone–hydroquinone with mutual transformations of the components. As far as we know, only in a single paper [19] the deuterated components were used, which allowed the reaction monitoring; however, the results of that study were interpreted using the traditional scheme.

In the case of the ideal structure of a complex, transformation (1) can be considered as a first-order reaction, which is described by the equation

$$-\ln(1 - x/x_0) = kt \quad (5)$$

at $k_{-1} = 0$. In a real crystal, the presence of several structural modifications complicates the reaction kinetics, and it becomes multistep rather than monoexponential (Fig. 8).

An important feature of these systems is that the transformation **I** → **II** is strictly equimolar, with the crystal structure of the complex remaining essentially unchanged. Therefore, the kinetic curves can be constructed from variations in the concentration of any of the four system components. However, to calculate the thermokinetic characteristics, it is appropriate to use the initial portions of the kinetic curves (Fig. 8). Thermochemical reaction (1) in the sollid phase goes virtually to completion in a narrow temperature range, whereas in solution an equilibrium [8] is attained.

The spectral and thermochemical characteristics of the complexes prepared by solid-phase mixing are listed in Table 3. The measurement procedure can be considered using as examples two complexes containing the same donor, MHQ (**2a**), and two different acceptors, BQ (**1b**) and CBQ (**4b**). For MHQ–BQ, the activation energy is 41 kcal mol^{-1} (14300 cm^{-1}), with the preexponential term of $10^A = 10^{24}$ s^{-1}; its large value suggests the cooperative character of the reaction. The activation energy of the thermal reaction, 41 kcal mol^{-1}, is close to the CT energy in the crystal, 48 kcal mol^{-1}. In the case of MHQ–CBQ, the activation energy is 35 kcal mol^{-1} at $A = 21$. Comparison of two structurally related complexes HQ–CBQ and MHQ–CBQ reveals a clear correlation between the variations in E_{CT} and E_a (Table 3).

Figure 9 shows the energy scheme of solid-phase transformations of quinhydrones, with the pathways of photochemical and thermal transformations (zigzag lines). Neglecting the entropy of the reaction, the difference between the energies of the optical charge-transfer transitions for the final (2) and initial (1) complexes should be equal to the heat of the reaction:

$$\Delta H = E_{CT2} - E_{CT1}. \quad (6)$$

We were able to check this important conclusion experimentally. The thermal effect of the reaction MHQ–BQ → HQ–MBQ (Fig. 10), determined to be $\Delta H = -9$ kJ mol^{-1} by integration of curve *1*, reas-

onably agrees with the difference $E_{CT2} - E_{CT1} = -12$ kJ mol^{-1}.

It is of interest to study redox transformations of quinhydrone crystals prepared from solution. Only two complexes containing phenylhydroquinone, **7a**–**1b** (PHQ–BQ) and **7a**–**4b** (PHQ–CBQ), appeared to be suitable for this purpose. Their crystals were grown from methylene chloride at low temperature. Platelike crystals of complex **7a**–**1b** are stable in air for several months. CBQ is a stronger electron acceptor than BQ (E_A^{calc} = 2.28 and 2.06 eV, respectively), which accounts for the low-frequency shift of the CT band of the complexes in the solid phase (from 16000 cm^{-1} for **7a**–**1b** to 15400 cm^{-1} for **7a**–**4b**) and for an increase in the reactivity of the corresponding quinhydrones. Crystalline complex **7a**–**4b** at room temperature slowly transforms into the conjugated complex **4a**–**7b**.

In contrast to the complexes studied in pressed KBr pellets (solid-phase mixing), in this case the crystals of the quinhydrones were heated in special ampules without mechanical treatment, so as to avoid formation of crystal defects. The procedure for preparing the complex significantly affects the reaction kinetics. In solid-phase mixing of the components, the kinetics is clearly two-step (Fig. 8), whereas for quinhydrones prepared by crystallization from solution the kinetics is strictly one-step, indicating that the chemical process occurs by a single mechanism.

The kinetic curves show that the reaction **7a**–**1b** → **1a**–**7b** with the crystalline complex in the narrow temperature range 115–130°C is strictly monomolecular, with the reaction rate being independent of the conversion (Fig. 8). It is interesting that the reaction onset temperature in crystalline quinhydrones is 5–10°C higher than the melting point of one of the components. The first, fast step of the reaction of complex **7a**–**1b** prepared by solid-phase mixing occurs at 50°C lower temperatures, and this acceleration of the reaction is apparently due to the defectiveness of the complex.

A kinetic study of the reaction **7a**–**1b** → **1a**–**7b** with the crystals grown from solution gives the activation energy E_a = 42.2 kcal mol^{-1} (Fig. 11). The reaction rate is described by the equation

$$k\ (s^{-1}) = 10^{20} \exp(-176/RT).$$

The fact that the activation energy of the thermochemical reaction (14800 cm^{-1}) is close to the CT energy (16000 cm^{-1}) confirms the previous conclusion [5] that the thermal electronic excitation of the complex of the reagents is the primary elementary step of the reaction.

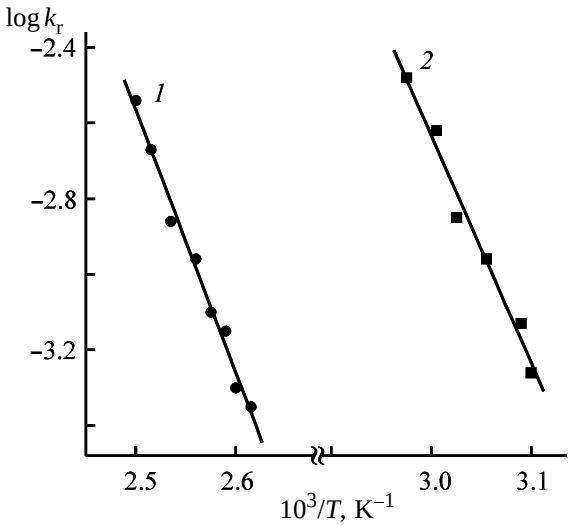


Fig. 11. Rate constant k_r of the reaction of quinhydrone **7a**–**1b** as a function of temperature T: (*1*) crystals grown from solution and (*2*) solid-phase mixing of components.

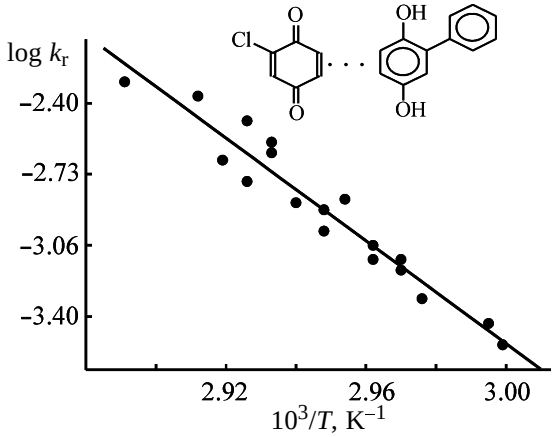


Fig. 12. Rate constant k_r of the reaction **7a**–**4b** → **4a**–**7b** as a function of temperature T (crystals grown from CH_2Cl_2 solution).

In solid-phase mixing, compared to the crystallization from solution, the rate of the redox transformation of complex **7a**–**1b** sharply increases (Fig. 11), apparently owing to the defectiveness of the crystal structure:

$$k\ (s^{-1}) = 10^{21} \exp(-155/RT).$$

the reaction acceleration is mainly due to a decrease in the activation energy to 37.3 kcal mol^{-1}.

In the case of very reactive complex **7a**–**4b** prepared by crystallization from CH_2Cl_2, the kinetic curves of the reaction **7a**–**4b** → **4a**–**7b** are linearized in the coordinates $\ln(1 + D_2/D_1)$–τ, as in the case of **7a**–**1b**, indicating that the reaction is strictly monomolecular. Certain scatter of the rate constant (Fig. 12) is caused by partial decomposition of the complex due

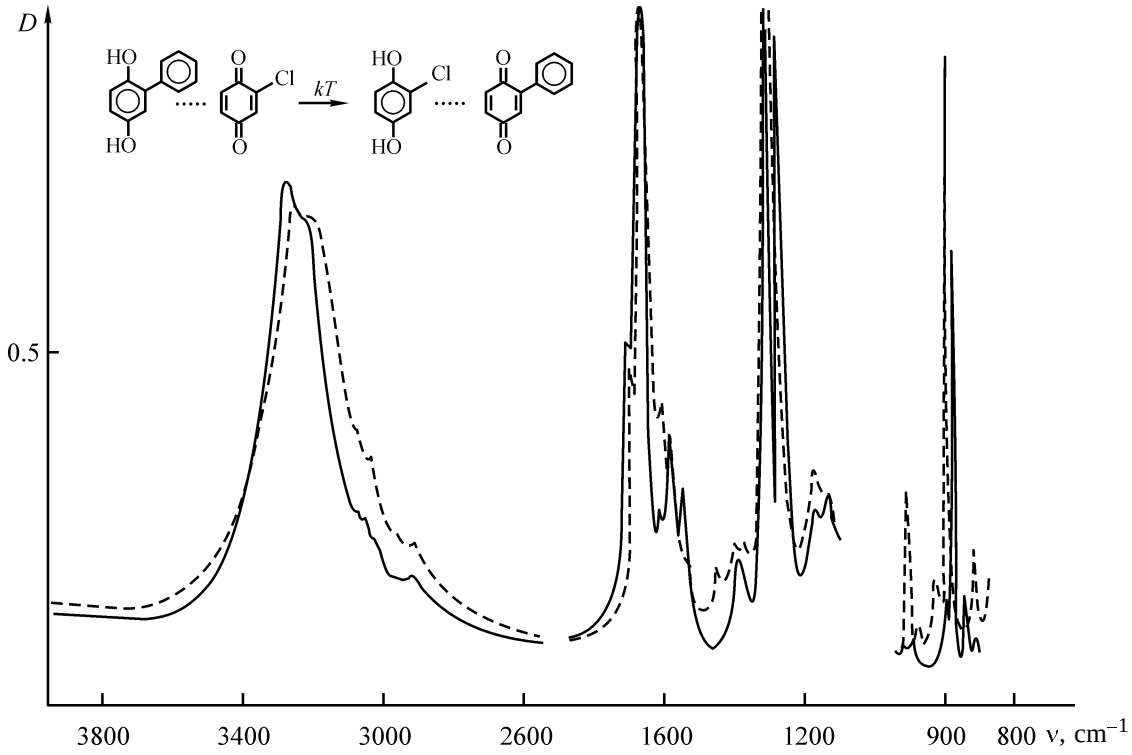


Fig. 13. IR absorption spectra of the (solid line) crystalline complex **7a**–**4b** grown from CH_2Cl_2 and (dashed line) reaction product **4a**–**7b** prepared by heating the initial complex at 79°C. (*D*) Optical density and (ν) wavenumber.

to sublimation of chlorobenzoquinone **4b** at high temperatures ($t^0 > t_m$ = 56°C). The activation energy of the reaction is 37.4 kcal mol^{-1} (13000 cm^{-1}), which is close to the CT energy of the complex, 15400 cm^{-1}.

Thus, a study of two quinhydrone complexes prepared by crystallization from solution confirmed our conclusions [8–10] that the activation energy of the thermal reaction is close to the energy of the optical charge-transfer transition; owing to the strictly monomolecular character of the reaction, the kinetic characteristics can be determined more accurately. The high preexponential term, 10^{20}–10^{21}, is indicative of the cooperative character of the electron and proton transfer in an ordered crystal lattice of the complex.

The IR spectra of the initial (**7a**–**4b**) and conjugated (**4a**–**7b**) complexes (Fig. 13) contain extremely narrow bands characteristic of the crystalline states. Each of the two OH stretching vibration bands, 3275 and 3230 cm^{-1}, belonging to two nonequivalent hydroxy groups, has the width as small as ~100 cm^{-1}. The conjugated complex **4a**–**7b** absorbs at lower frequencies, 3250 and 3200 cm^{-1}, suggesting stronger H bonding between strong proton donor CHQ (**4a**) and strong proton acceptor PBQ (**7b**), compared to the components of the initial complex, **7a** and **4b**. The redox transformation **7a**–**4b** → **4a**–**7b** is accompanied by an increase in the CT energy from 15400 to 16000 cm^{-1} as a result of weakening of the EDA properties of the components and of a 50 cm^{-1} decrease in the OH stretching vibration frequency, suggesting strengthening of the hydrogen bond.

The primary event in the laser excitation at the CT band,

$$(Q\cdots H_2Q) \xrightarrow{h\nu} {}^1(Q^{\bullet-}\cdots H_2Q^{\bullet+}), \qquad (7)$$

is the electron transfer yielding radical species responsible for the absorption at 20000–24000 cm^{-1} in the transient spectra (Fig. 6). In the case of a thermodynamically favorable reaction, e.g., **7a**–**1b** → **1a**–**7b**, enhancement of the PDA properties caused by the electron transfer stimulates the proton transfer giving rise to semiquinone radicals, which is followed by the transfer of the second proton with the formation of the conjugated complex **1a**–**7b**:

$$(Q_1)\cdots(H_2Q_2) \underset{h\nu^f}{\overset{h\nu^a}{\rightleftarrows}} {}^1[(Q^{\bullet-})_1\cdots(H_2Q^{\bullet+})_2]$$

$$\rightleftarrows [(HQ^{\bullet})_1\cdots(HQ^{\bullet})_2 \rightleftarrows [H_2Q^{\bullet+})_1\cdots(Q^{\bullet-})_2]$$

$$\xrightarrow{h\nu^f} (H_2Q)_1\cdots(Q)_2. \qquad (8)$$

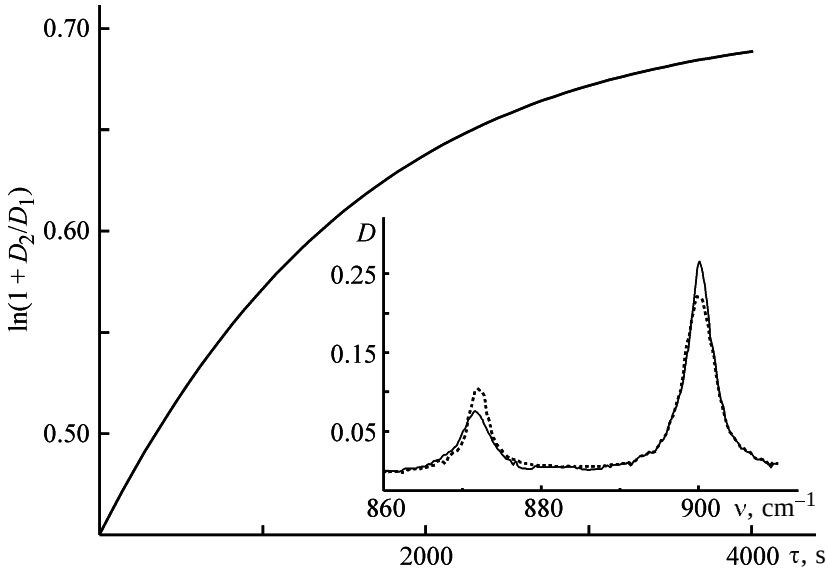


Fig. 14. Photochemical reaction **7a**–**1b** → **1a**–**7b** in a KBr pellet upon irradiation with a 1 W argon laser. Insert: IR spectra of the complexes. (*D*) Optical density and (τ) time; (ν) wavenumber.

It is difficulty to detect semiquinone radicals in the transient spectra because of the low intensity of the absorption bands; however, their formation is confirmed by the kinetic data. In particular, faster decrease in the absorption of radical ions $(H_2Q^{\cdot+})_1\cdots(Q^{\cdot-})_2$ compared to the decrease in the induced absorption (Fig. 6) suggests the presence of an intermediate step associated with the proton transfer. The radicals arising in the process are unstable and rapidly transform into the conjugated complex upon transfer of the second proton.

Because of the high rate of the thermal redox reaction, it is very difficult to detect the photochemical transfer of the hydrogen atom. Nevertheless, it is possible to monitor the slow photochemical reaction **7a**–**1b** → **1a**–**7b**, occurring upon irradiation of a sample of complex **7a**–**1b** with a defocused beam of a continuous 1 W argon laser (Fig. 14). A considerably weaker effect is attained by irradiation with a harmonic of a pulse garnet laser (532 nm, 1 mW); during the irradiation (several hours), the crystalline complex undergoes repeated excitation to the CT state. Hence, the photochemical reaction [Eq. (8)] occurs with a low efficiency, probably because of the strong overlap of the CT bands of the initial and final complexes.

8. HYDROGEN BOND IN THE ELECTRONICALLY EXCITED STATE OF AN EDA COMPLEX IN SOLUTION

The electron–proton effect is manifested to the greatest extent in crystalline quinhydrone complexes; however, this phenomenon is general and should be manifested in diverse systems, including complexes in solution. For pair complexes A···H–D, the coexistence of an electron donor–acceptor bond and an H bond is improbable at plane-parallel arrangement of the molecules but can be realized in ternary and more complex structures. Ternary complexes A···D–H···X were studied in [6, 34–37].

Stabilization of the excited states of the complexes by H bonding can be estimated theoretically; however, the nature of this interesting phenomenon remained incompletely understood. The shifts of the absorption and luminescence bands of molecules upon H bond formation usually do not exceed 0.04–0.07 eV [38, 39], which is an order of magnitude lower than the effects observed in the complexes. In this connection, it is interesting to consider EDA complexes in which the electron donor (e.g., phenol) is also a proton donor and hence can form a hydrogen bond with the third component, e.g., a solvent molecule.

The EDA complex of chloranil with anisole (I_D = 8.22 eV, I_D^{calc} = 8.45 eV), which is an analog of phenol (I_D = 8.5 eV, I_D^{calc} = 8.76 eV) but contains no labile hydrogen atoms, is characterized by a charge-transfer band at 21800 cm^{-1} with the intensity f = 0.014 in CCl_4 (calculation: 25250 cm^{-1}, f = 0.003). For this complex, the CT band is not noticeably shifted on adding to CCl_4 aprotic solvents (0.1 M) acting as proton acceptors, but somewhat increases in neat aprotic solvents; for example, in tetrahydrofuran (THF), the chloranil–anisole complex absorbs at 23200 cm^{-1}.

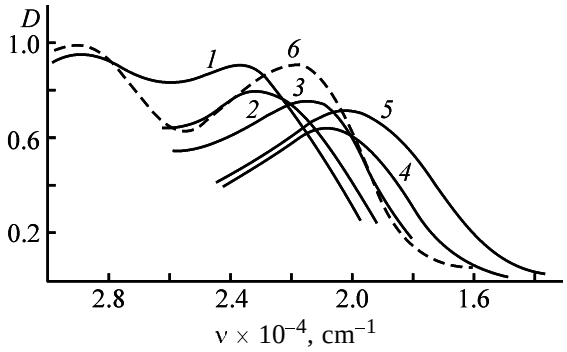


Fig. 15. Absorption spectra (*1*, ×40; *2*–*5*, ×10) of complexes of chloranil (0.002 M) with phenol in CCl_4 containing various additives. Additive: (*1*, *2*) none, (*3*) acetonitrile, (*4*) THF, and (*5*) dimethylacetamide. Phenol concentration, M: (*1*) 0.005 and (*3*–*5*) 0.035. (*6*) Absorption spectrum of the chloranil–anisole complex.

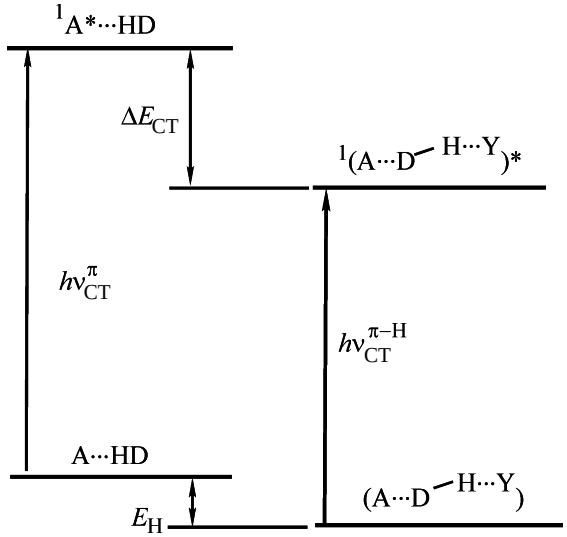


Fig. 16. Scheme of the energy levels of an EDA complex upon formation of an H bond.

The enthalpy of formation of the chloranil–anisole complex in CCl_4 was found to be 3.2 kcal mol^{-1}.

In the absorption spectrum of the complex chloranil (Cl)–phenol (Ph) (Fig. 15), at a low phenol concentration (0.005 M), new bands at 24000 and 29000 cm^{-1} appear along with the intrinsic bands of Cl and Ph. The first of these bands is shifted relative to the CT band of the Cl–anisole complex by 0.28 eV, which is equal to the difference between the ionization potentials of phenol and anisole; hence, this is the CT band. The band at 29000 cm^{-1} is assigned to the n–π^* transition in the Cl molecule perturbed by the effect of the electron donor (for the free molecule in CCl_4, the frequency is 26800 cm^{-1}).

Small (1–3 vol %) additions to CCl_4 of proton-acceptor solvents ensuring complete binding of phenol cause a considerable shift of the CT band of the Cl–Ph complex, but exert no effect on the position of the CT band of the Cl–anisole complex. The shifted bands of the Cl–Ph complex, as a rule, are symmetrical (Fig. 15) and undergo reversible changes with temperature, which confirms their assignment as CT bands.

The shift of the CT band unambiguously correlates with the energy of the hydrogen bond between phenol and the proton-acceptor solvent. For the ground electronic state, this energy was estimated from the low-frequency shift of the OH stretching vibration frequency using empirical relationship (9):

$$E_H = 0.33(\Delta\nu_{OH} - 40)^{1/2}. \quad (9)$$

For the selected solvent series, E_H does not exceed 0.3 eV and is close to the energy of the H bond in the ground state of the EDA complex. Neglecting the entropy of the electronic transition, the level of the excited state of the complex will decrease upon H bond formation by the value

$$E_{CT} = h\nu_{CT}^{\pi} - h\nu_{CT}^{\pi-H} + E_H, \quad (10)$$

where $h\nu_{CT}^{\pi}$ and $h\nu_{CT}^{\pi-H}$ are the transition frequencies for the complexes without and with H bond, respectively (Fig. 16).

The stabilization energy ΔE_{CT}, which is essentially the H bond energy in the excited state of the complex, linearly correlates with the H bond energy in the ground state, with a slope of 2.6 (Fig. 17, line *A*). Hence, in the Franck–Condon excited state the H bond energy increases by a factor of 2.6 compared to the ground state.

Figure 17 also shows the spectral shifts for the complex of chloranil with 2,4-dichlorophenol, which are close to the corresponding shifts for the chlorophenol complexes [34]. The calculation gives equal ionization potentials for phenol and chlorophenol (8.76 eV), and for anisole and chloroanisole (8.45 eV), but the proton-donor properties of phenol are stronger (pK_a of chlorophenol and phenol 9.38 and 9.98, respectively), which accounts for the higher energy of the H bond in the ground state of chlorophenol, compared to phenol. The correlations of ΔE_{CT} with E_H appeared to be common for the complexes Cl–Ph and Cl–chlorophenol [34]. Similar correlations are observed with a number of other complexes.

A considerable difference in the spectral shifts for the two cases, excitation at the CT band of the EDA complex and excitation at the phenol band of the

Table 4. Heats of formation of an H bond of phenol with THF $-\Delta H$, H bond lengths R, ionization potentials I_D, and atomic charges q_O and q_H

Molecule, complex	State	$-q_O$	q_H	I_D	R, Å	$-\Delta H$, kcal mol^{-1}
Ph	S_0	0.228	0.196	9.17		
Ph⋯THF		0.256	0.227	8.84	2.77	2.73
Ph	T_1	0.145	0.197	2.57		
Ph⋯THF		0.170	0.229	2.25	2.72	2.83
Ph	S_1	0.140	0.198	2.50		
Ph⋯THF		0.172	0.230	2.20	2.76	4.11
$Ph^{\bullet+}$		0.075	0.258	14.93		
$Ph^{\bullet+}$⋯THF		0.106	0.290	14.44	2.71	12.56

H-bonded complex, is caused by the charge distribution in the phenol molecule in the excited state. In the first case, the excitation results in the electron transfer between the phenol and chloranil molecules, and the hydrogen bond is formed between the proton acceptor (dioxane, DME) and phenol radical cation whose proton-donor power is considerably enhanced by the loss of an electron. In the second case, the electron density is redistributed within the phenol molecule, and the enhancement of the proton-donor power should be less significant.

Hence, the effects of H bond in the excited state of an EDA complex consist in that the electron transfer considerably enhances the proton donor–acceptor properties of the molecules constituting the complex.

Experimental study of hydrogen bonding of components of the EDA complex in the excited state, radical anion $A^{\bullet-}$ and radical cation $DH^{\bullet+}$, involves considerable problems due to the short lifetime and low concentration of these species.

The energy of hydrogen bonding of the phenol radical cation $Ph^{\bullet+}$ with the THF molecule was calculated theoretically; the results were compared to the experimental shifts of the charge-transfer bands (Table 4).

The proton-donor power of Ph (its capability for hydrogen bonding) depends on the electronic state [40]: $S_0 \approx T_1 < S_1$. The charge on the hydroxy group increases in the same direction (Table 4); the change is the most significant in going to the radical cation $Ph^{\bullet+}$. The calculated heat of formation of an H bond of Ph with THF (2.73 kcal mol^{-1}) reasonably agrees with experimental data (3–4 kcal mol^{-1}) for such hydrogen bonds [43]. To calculate the heat of H bond of Ph with THF in the singlet excited state ($-\Delta H^*$), we took the optimized geometric parameters for the S_1 state. The value obtained, 4.11 kcal mol^{-1}, somewhat exceeds the corresponding value for the ground state (2.73 kcal mol^{-1}), which is consistent with the experimental data for the H bond of phenol with dioxane [41]: $-\Delta H(S_0) = 5.5$, $-\Delta H(S_1) = 6.5$ kcal mol^{-1}.

A PM3 calculation for ohenol in the triplet state gives the H bond energy coinciding with that for the ground state (Table 4).

The calculated potential curves of H bonds of phenol and $Ph^{\bullet+}$ radical cation with tetrahydrofuran (Fig. 18) differ essentially in both the depth and position of the minimum, which is due to the considerably enhanced proton-donor power of $Ph^{\bullet+}$ compared to phenol, and also to the contribution of the ion–dipole interactions to the total heat of H bond formation.

The correlation between the calculated heats of formation of H bonds of phenol in the radical cation

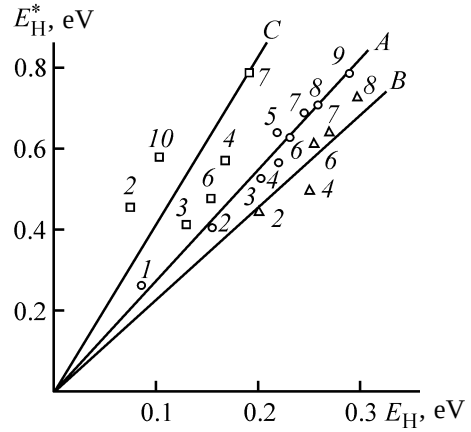


Fig. 17. Correlation between the H bond energies in the excited (E_H) and ground (E_H) states of EDA complexes of (*A*) Ph and (*B*) DCP with chloranil. Proton acceptors: (*1*) nitromethane, (*2*) acetonitrile, (*3*) dioxane, (*4*) diethyl ether, (*5*) dimethylformamide, (*6*) THF, (*7*) dimethylacetamide, (*8*) DMSO, (*9*) hexamethylphosphoramide, and (*10*) dimethyl ether. (*C*) Correlation between the calculated heats of the H bond formation of phenol radical cation with proton acceptors and the respective quantities for molecular phenol.

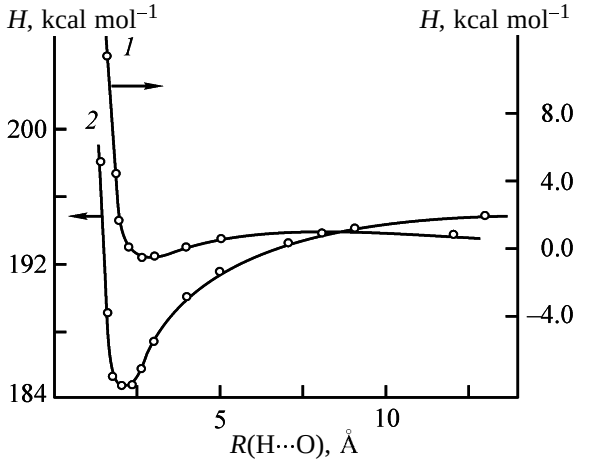


Fig. 18. Calculated heats *H* of formation of an H bond of (*1*) phenol and (*2*) phenol radical cation with THF, as functions of the H···O distance *R*.

($Ph^{\bullet+}$) and ground (Ph) states (Fig. 17, curve *C*), at a certain scatter, can be, on the whole, approximated by a straight line with a slope of 4.1, which is comparable with the slope (2.6) of the linear correlation between the H bond energies in the excited and ground states of the EDA complex (Fig. 17, curve *A*).

The calculations confirm the qualitative conclusion that considerable low-frequency shifts of the charge-transfer bands of EDA complexes in the presence of proton acceptors are caused by H bonding between the electron donor (in our case, phenol in the radical cation form) and a proton acceptor acting as a third component. The second component of the EDA complex, electron acceptor chloranil (Cl), in the excited CT state becomes a radical anion; therefore, it can also be expected to form a stronger H bond compared to the ground state. The calculation results confirm this assumption: The heat of formation of an H bond of Cl with formic acid (13.7 kcal mol^{-1}) exceeds by a factor of more than 4 the corresponding value for chloranil in the ground state (3.0 kcal mol^{-1}).

Table 5. CT energy of EDA complexes in CCl_4 (E_{CT}) and in CCl_4 with addition of DMSO (E^{H}_{CT})

Complex	E_{CT}	E^{H}_{CT}	$(E_{CT} - E^{H}_{CT})/E_{CT}$
	cm^{-1}		
Cl–Ph	24060	20400	0.152
Cl–NPT	18500	16900	0.086
TCE–Ph	20800	18900	0.091
TCE–Ph*	20800	19500	0.63
TCE–NPT	15900	14600	0.082
TCE–anisole	19500	19500	0.000
TCQ–Ph	20500	18500	0.098
TNB–Ph	30500	27200	0.108

Replacement of phenol by a stronger electron donor, α-naphthol (NPT; I_D = 7.78 eV [16], I_D^{calc} = 8.13 eV), decreases the absolute value of the shift of the CT band upon formation of an H bond Ph···DMSO by a factor of more than 2 (Table 5), although phenol and α-naphthol differ in the proton-donor power insignificantly ($\Delta\nu_{OH}$ 371 and 390 cm^{-1}, respectively). Passing to a stronger electron acceptor, TCE (E_A 2.8 eV), is accompanied by a further decrease in the shift of the CT bands. These data show that enhancement of EDA interactions, evaluated by the difference $I_D - E_A$, causes a decrease in the shift of the CT band due to H bonding.

CONCLUSION

Thus, interaction of an electron and proton donor DH with an electron and proton acceptor A in a typical case involves formation of specific electronically excited states denoted as (D···H···A)*, which are characterized by the conjugation of two fundamental processes, electron transfer (excitation) and proton transfer. The energy of this state is determined, on the one hand, by the electron donor–acceptor properties of the components DH and A and, on the other hand, by the proton donor–acceptor processes of DH and A. The characteristics of the two coexisting and conjugated interactions, EDA complexation and H bonding, show inverse correlation: The stronger the EDA interaction between DH and A, i.e., the lower the charge-transfer energy, the weaker the H bond D–H···A. Owing to the effect of the hydrogen bond in the excited state of the EDA complex, the CT energy decreases relative to the complex without H bonding by a value as large as 1.5 eV and more, falling in the range characteristic of thermal excitations (<1 eV). Such low-lying electronic states (D···H···A) are efficiently populated at room temperature; hence, they are responsible for the thermal transfer of a hydrogen atom, which is involved in many organic catalytic reactions.

The interrelation between the two fundamental processes, electron transfer (excitation) and proton transfer, is determined by the electron–proton effect underlying many physical (luminescence quenching with hydrogen bond, electrical conductivity of hydrogen-bonded systems) and chemical (hydrogen atom transfer, acid–base catalysis) phenomena. Any factor decreasing the energy of the electronically excited level of the complex of the reactants and hence increasing the reaction rate should be considered as an

element of catalysis. In this sense, the electron–proton effect that we discovered makes the most powerful catalytic action. The classical catalytic system reactant 1 + reactant 2 + catalyst is only a particular case of catalysis. Considerably more widespread are bimolecular reactions of the type reactant 1···interaction 1 + interaction 2···reactant 2 in which the reactant molecules form several types of bonds with each other, e.g., a charge-transfer complex and an H bond. In the process, the catalytic effect is exerted not by an external agent (catalyst) but by a specific interaction between the reactant molecules, e.g., by a hydrogen bond. In ternary complexes A···D–H···X, in which the EDA interaction A···DH is supplemented by a hydrogen bond with a third component X, the effect of the external hydrogen bond D–H···X is also very significant: a decrease in the CT energy exceeds several times the H bond energy in the ground electronic state. As expected, in such complexes the catalytic effect of the H bond decreases with a decrease in the absolute value of the CT energy, i.e., in going to strong EDA pairs absorbing in the IR range.

The experimental data presented in this paper allowed us not only to develop a new approach to the phenomenon of catalysis, based on the electron–proton interaction, but also to disclose the nature of elementary chemical processes. The so-called noncatalytic reactions actually involve an element of catalysis associated with hydrogen (or other) bonds arising between the reactant molecules in the excited electronic state.

REFERENCES

1. Kalnin'sh, K.K., *Elektronnoe vozbuzhdenie v khimii* (Electronic Excitation in Chemistry), St. Petersburg: Sankt-Peterb. Gos. Univ. Tekhnologii i Dizaina, 1998.
2. Kalninsh, K.K., *J. Chem. Soc., Faraday Trans. 1*, 1981, vol. 77, pp. 227–238.
3. Kalninsh, K.K., *Chem. Phys. Lett.*, 1981, vol. 79, no. 3, pp. 427–431.
4. Kalninsh, K.K., *J. Chem. Soc., Faraday Trans. 2*, 1982, vol. 78, pp. 327–338.
5. Kalninsh, K.K., *J. Chem. Soc., Faraday Trans. 2*, 1984, vol. 80, no. 12, pp. 1569–1538.
6. Kalnin'sh, K.K. and Bursian, A.E., *Zh. Fiz. Khim.*, 1996, vol. 70, no. 12, pp. 2214–2219.
7. Kalninsh, K., Gadonas, R., Krasauskas, V., and Pugzlys, A., *Chem. Phys. Lett.*, 1993, vol. 209, nos. 1–2, pp. 63–66.
8. Kalnin'sh, K.K., *Zh. Fiz. Khim.*, 1990, vol. 64, no. 8, pp. 2081–2086.
9. Kalnin'sh, K.K., *Zh. Fiz. Khim.*, 1982, vol. 56, no. 5, pp. 1125–1128.
10. Kalnin'sh, K.K. and Shchukareva, V.V., *Izv. Akad. Nauk SSSR, Ser. Khim.*, 1985, no. 1, pp. 95–102.
11. Matsuda, H., Osaki, K., and Nitta, J., *Bull. Chem. Soc. Jpn.*, 1958, vol. 31, pp. 611–626.
12. Sakurai, T., *Acta Crystallogr.*, 1965, vol. 19, no. 3, pp. 320–331.
13. Shipley, G.G. and Walwork, S.C., *Acta Crystallogr.*, 1967, vol. 22, no. 5, pp. 585–600.
14. Patial, A.O. and Curtin, D.Y., *J. Am. Chem. Soc.*, 1984, vol. 106, no. 2, pp. 348–353.
15. Lutz, E.T.G. and Van der Maas, J.H., *Spectrochim. Acta (A)*, 1983, vol. 39, no. 11, pp. 1007–1018.
16. *Energii razryva khimicheskikh svyazei. Potentsialy ionizatsii i srodstvo k elektronu* (Dissociation Energies of Chemical Bonds. Ionization Potentials and Electron Affinities), Kondrat'ev, V.I., Ed., Moscow: Nauka, 1974.
17. Briegleb, G., *Angew. Chem.*, 1964, vol. 76, no. 4, pp. 326–336.
18. Farragher, A.F. and Page, F.A., *Trans. Faraday Soc.*, 1966, vol. 62, pp. 3072–3080.
19. Brodskii, A.I. and Gragerov, I.P., *Dokl. Akad. Nauk SSSR*, 1951, vol. 79, pp. 277–281.
20. Foster, R., *Organic Charge Transfer Complexes*, New York: Academic, 1969, p. 40.
21. Kampar, V.E., *Izv. Akad. Nauk Latv. SSR, Ser. Khim.*, 1984, no. 5, pp. 585–601.
22. Thozet, A. and Gaultier, J., *Acta Crystallogr., Sect. B*, 1977, vol. 33, pp. 1052–1065.
23. Desiraju, G.R., Curtin, D.Y., and Paul, I.C., *Mol. Cryst. Liq. Cryst.*, 1979, vol. 52, pp. 259–266.
24. Yakushi, K., Iguchi, M., and Kuroda, H., *Bull. Chem. Soc. Jpn.*, 1979, vol. 52, pp. 3180–3191.
25. Ikeda, N., Miyasaka, H., Okada, T., and Mataga, N., *J. Am. Chem. Soc.*, 1983, vol. 105, pp. 5206–5220.
26. Miyasaka, H., Tabata, A., Kamada, K., and Mataga, N., *J. Am. Chem. Soc.*, 1993, vol. 115, pp. 7335–7350.
27. Okada, T., Tashita, N., and Mataga, N., *Chem. Phys. Lett.*, 1980, vol. 75, no. 2, pp. 220–225.
28. Martin, M., Miyasaka, H., Karen, A., and Mataga, N., *J. Phys. Chem.*, 1985, vol. 89, no. 1, pp. 182–198.
29. Gadonas, R., Danielius, R., and Piskarskas, A., *Quantum Electron.*, 1981, vol. 8, pp. 669–680.
30. Miyasaka, M., Morita, K., Kamada, K., *et al.*, *Bull. Chem. Soc. Jpn.*, 1991, vol. 64, pp. 3229–3244.
31. Kalnin'sh, K.K. and Lyubimova, G.V., *Vysokomol. Soedin.*, 1982, vol. 24, no. 7, pp. 1446–1455.
32. Dewar, M.J.S. and Dougherty, R.C., *Orbital Topology*

and Elementary Processes, New York: Wiley–Interscience, 1976.

33. Takahashi, N., Yakushi, K., Ishii, K., and Kuroda, H., *Bull. Chem. Soc. Jpn.*, 1976, vol. 49, pp. 182–187.
34. Kalnin'sh, K.K., *Zh. Fiz. Khim.*, 1990, vol. 64, no. 8, pp. 2081–2086.
35. Kalnin'sh, K.K., Bedrina, M.E., Semenov, S.G., and Glebovskii, D.N., *Zh. Fiz. Khim.*, 1988, vol. 62, no. 6, pp. 1563–1568.
36. Kalnin'sh, K.K. and Bursian, A.E., *Zh. Fiz. Khim.*, 1992, vol. 66, no. 4, pp. 1007–1013.
37. Kalnin'sh, K., *Vysokomol. Soedin., Ser. A*, 1988, vol. 30, no. 3, pp. 521–527.
38. Babe, N. and Suzuki, S., *J. Chem. Phys.*, 1961, vol. 35, no. 3, pp. 1118–1127.
39. Suzuki, S. and Babe, H., *J. Chem. Phys.*, 1964, vol. 38, no. 2, pp. 349–353.
40. Ireland, J.F. and Wyatt, R.A.H., *Adv. Phys. Org. Chem.*, 1976, vol. 12, p. 131.
41. Pimentel, G.C. and McClellan, A.L., *The Hydrogen Bond*, San Francisco: Freeman, 1960.

Russian Journal of Applied Chemistry, Vol. 78, No. 11, 2005, pp. 1745–1752. Translated from Zhurnal Prikladnoi Khimii, Vol. 78, No. 11, 2005, pp. 1780–1787.
Original Russian Text Copyright © 2005 by Vydysh, Naftal', Batsunova, Petrov.

INORGANIC SYNTHESIS AND INDUSTRIAL INORGANIC CHEMISTRY

Specific Features of Chemical Interactions in Double-Stage Leaching of a Solid Target Product Formed in Processing of High-Copper Converter Matte

A. V. Vydysh, M. N. Naftal', I. V. Batsunova, and A. F. Petrov

Norilsk Nickel Mining and Metallurgical Open Joint-Stock Company, Norilsk, Taimyr autonomous okrug, Russia

Received August 18, 2005

Abstract—Oxidative leaching of a solid product of copper refining was studied in a laboratory, with autoclave oxidation replaced with that in the atmosphere. The extent of the chemical reactions that occur in atmospheric oxidative leaching and autoclave refining in the technology of sulfate leaching of high-copper converter matte was determined.

In 1998–2003, specialists from the Norilsk Nickel Mining and Metallurgical Open Joint-Stock Company developed a process for sulfate leaching of high-copper converter matte and carried out semicommercial tests in the continuous mode. The scheme of processing by leaching includes atmospheric copper refining (ACR) with the starting converter matte and autoclave-oxidative leaching (AOL) of the ACR cake, with the subsequent autoclave refining (AR). The process developed makes it possible to obtain high-quality target products: nickel–cobalt solution containing no more than 1 mg dm^{-3} metal impurities and a copper sulfide product (CSP) containing no more than 0.5% nickel and iron [1]. The technology of hydrometallurgical processing of converter matte is to be implemented at the Nadezhdinskii metallurgical plant (NMP) of the Norilsk Nickel Mining and Metallurgical Company.

The process of autoclave leaching of converter matte is accompanied by oxidation of 9.4% of the sulfide sulfur to the sulfate form [2]. Depending on the conditions of the oxidation stage, the overall recovery of sulfur into solution in AR (in processing of the ACR cake) is 18–25%. The accumulation of sulfate ions in reusable solutions makes necessary control over the sulfur balance. The excess sulfur is removed in the form of sulfate ions with technical-grade soda, whose gross expenditure impairs the technical and economical parameters of the process.

To diminish the overall recovery of sulfur into an AR solution, it was suggested to modify the conditions of the oxidative leaching stage: to pass from the autoclave version to the atmospheric process (see scheme). The lowering of the parameters of the oxidative leaching stage makes it possible to reduce the formation intensity of sulfate sulfur through kinetic hindrance to side reactions of direct oxidation of sulfides.

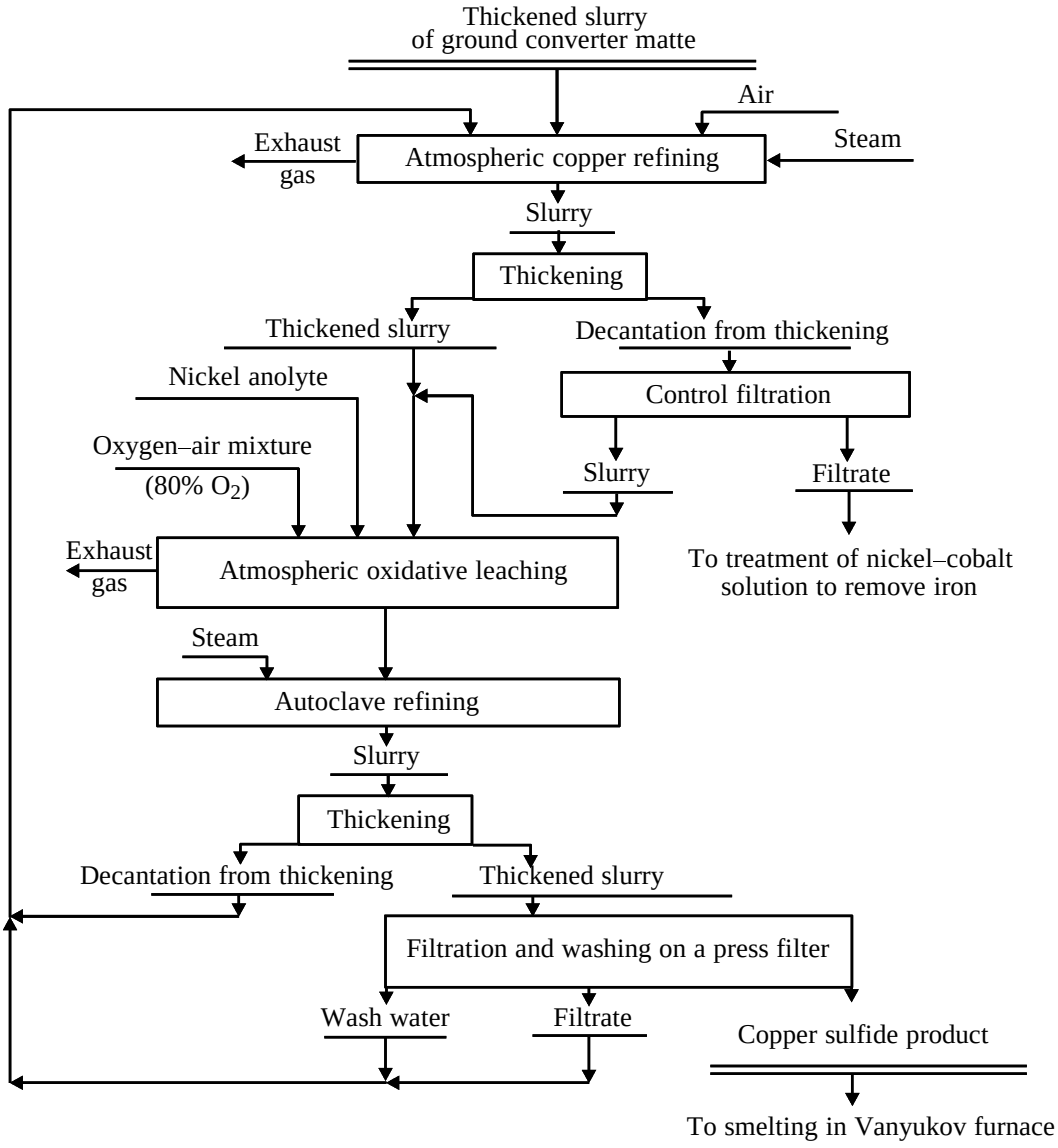
At the same time, in passing from the autoclave process to atmospheric oxidative leaching (AtOL), the presence of soluble copper forms is insufficient for effective refining of CSP to remove nickel. To make up for this deficit, it was suggested to introduce into the AR procedure an additional amount of copper sulfate in the form of a preliminarily prepared copper-containing solution. The specific expenditure of the copper-containing solution in the AR procedure was determined from the occurrence conditions of the classical reaction of refining [3]

$$M + CuSO_4 \rightarrow MSO_4 + Cu, \qquad (1)$$

where M is Ni, Fe, or Co. This parameter was found to be 1.1–1.5 g Cu/g Ni contained in the AtOL cake.

To determine more precisely the parameters of atmospheric leaching of high-copper converter matte, a laboratory search was conducted, primarily aimed (i) to determine whether it is possible in principle to replace the autoclave oxidation stage with the atmospheric process, provided that a CSP with Ni content less than 0.5% is obtained; (ii) to find the optimal conditions of converter matte leaching in performing the oxidation stage under atmospheric conditions; and (iii) to determine the degree of sulfur oxidation in

1070-4272/05/7811-1745 © 2005 Pleiades Publishing, Inc.



Flowsheet of atmospheric and autoclave leaching of high-copper converter matte.

AtOL and AR processes carried out in the optimal mode.

EXPERIMENTAL

Solid products obtained in ACR under semicommercial conditions and model solutions with a composition reproducing that of the nickel anolyte formed upon electroextraction of nickel were used in the study. The laboratory analysis of the stage of atmospheric leaching was made in a 1.0 dm^3 laboratory autoclave equipped with a stirrer and a temperature control system. Technical-grade oxygen fed from a cylinder served as an oxidizing agent. Its flow rate was controlled using the readings of a rotameter. In the laboratory studies, the autoclave was not sealed hermetically, with the line for the exhaust gas opened and no excess pressure created in the system. The stirring rate was about 2800 rpm. The temperature was controlled in the automatic mode.

The autoclave was charged with a model solution and then stirring and heating were switched on. After a temperature of 90–95°C was reached, the starting solid material was introduced and supply of oxygen was commenced at a flow rate of 1.0 $dm^3\,min^{-1}$ per 1 dm^3 of slurry during the entire experiment. The time of an experiment was measured from the beginning of

feeding of the oxidizing agent. After AtOL was complete, the oxygen feeding was terminated and the slurry was sampled for chemical analysis. After that, the autoclave was hermetically sealed and purged with nitrogen, and the AR procedure was performed. After the experiment was over, the autoclave was cooled and discharged. The resulting slurry was filtered and then necessary weight and volume measurements were made and the chemical composition of the solid and liquid phases was determined.

It was found previously that the optimal specific expenditure of the acid in AOL is 30–36.3 wt % [4]. At the same time, chemical transformations that occur when the oxidation stage is performed in autoclave and atmospheric conditions may have different mechanisms. For example, the optimal specific expenditure of the acid in atmospheric leaching of a copper concentrate obtained in flotation separation of converter matte, calculated taking into account the chemical reactions and confirmed by experiment, was 24 wt % [5]. With account of the available data, the specific expenditure of the acid in AtOL was, originally, 27–28%, which corresponded to a liquid-to-solid phase ratio l : s = 3.5 : 1.

In the first stage of the study, a set of laboratory experiments aimed to determine the optimal duration of the AtOL procedure were carried out. The autoclave refining of the slurry formed in the atmospheric stage was performed under the standard conditions (T = 150°C, τ = 2 h). It was found that the optimal duration of the atmospheric oxidation stage is 150 min. In this case, the residual content of nickel in the sulfide copper product was 4.2% at an overall recovery of copper equal to 8.9% (Table 1, procedure no. 1).

In a search for ways to diminish the residual content of nickel in the CSP, a set of experiments concerned with the influence exerted by parameters of the autoclave refining on this quantity were performed. The results obtained are listed in Table 1 (procedure nos. 1–4), whence follows that elevating to 190°C the temperature at which the autoclave refining is carried out lowered the concentration of nickel in the CSP to 1.93%, and making longer (3 h) the duration of the AR stage at 190°C diminished the residual content of nickel in the CSP to 1.74% at the overall recovery of sulfur into solution equal to 11.2%.

It was decided that there is no point in improving the parameters of the autoclave refining, and, therefore, the efforts in a search for ways to diminish the residual concentration of nickel in CSP were concentrated in optimization of parameters of the AtOL technique.

The main goal of further research was to determine the liquid-to-solid phase ratio l : s in the feed for AtOL (Table 1, procedure nos. 3, 5–7). It follows from Table 1 that the optimal ratio for AtOL is l : s = 5 : 1, at which the content of nickel in the CSP was 0.76%, and the overall recovery of sulfur into solution, 15.1%. On raising the initial l : s ratio to 5.0 : 1, the amount of the acid consumed in leaching of sulfides increases from 28 to 40.5% relative to the mass of the starting solid phase. The curves describing how the compositions of the solid and liquid phases of the slurry formed in autoclave refining depend on the specific expenditure of the acid in AtOL (see figure) show an extremum: if the amount of acid involved in the process exceeded the optimal value (~41%), the quality of the CSP was impaired.

The minimum residual content of nickel in the modes studied was 0.76%. However, implementation of the AR mode developed by the authors (190°C) requires that a new autoclave equipment with enhanced process characteristics should be installed at NMP. The working temperatures of the 50 stills at NMP is 150°C, which makes impossible carrying out AR at 190°C. In order to determine whether the temperature parameters can be lowered, an experiment was carried out with the AtOL stage at l : s = 5 : 1 and AR temperature of 150°C (Table 1, procedure no. 8). The results obtained indicate that lowering the AR temperature to 150°C at the optimal expenditure of the acid leads to an increase in the overall recovery of sulfur to 13.9%, and in the residual content of nickel in the CSP, to 0.93%.

Comparison of the parameters of the atmospheric leaching technique with those of the autoclave method shows that the overall recovery of sulfur into solution is higher in autoclave oxidation. However, oxidation under atmospheric conditions failed to ensure a nickel content of CSP lower than 0.5%.

To determine the phase composition and structure of the starting and final solid products of ACR, AtOL, and AR, a mineralogical study was carried out.[1]

A study of the solid product of ACR revealed that the main phase component of a sample was relict

[1] The mineralogical study was carried out at Gipronikel' Institute Open Joint-Stock Company (St. Petersburg) by L.N. Ertseva by means of X-ray diffraction and optical analyses, scanning electron microscopy, and X-ray fluorescence microprobe analysis.

Table 1. Results of a laboratory study of the atmospheric oxidative leaching and autoclave refining

Procedure no.	AR		l : s in AOL	Specific expenditure of acid, wt %	Procedure	Content of indicated element after leaching, %/g dm^{-3}					Yield of solid product, wt %	Overall recovery into solution			
	τ, h	*T*, °C				Ni	Cu	Co	Fe	S_{tot}		Ni	Co	Fe	S_{tot}
1	2	150	3.5 : 1	28.3	AtOL	14.2*	50.9	0.26	2.20	26.0	78.4	85.7	40.7	86.9	8.9
						93.0	23.8	0.17	0.01	77.8					
					AR	4.2	67.2	0.21	0.30	25.1	76.2				
						108.2	32.4	0.18	3.90	97.8					
2	2	170	3.5 : 1	28.3	AtOL	14.5	50.2	0.31	2.28	26.5	75.9	86.2	47.0	88.9	9.5
						95.9	29.5	0.12	0.06	83.1					
					AR	3.7	67.2	0.17	0.23	22.6	84.1				
						106.0	15.7	0.33	4.20	100.3					
3	2	190	3.5 : 1	28.3	AtOL	14.2	51.1	0.29	2.09	25.8	79.0	92.7	52.8	95.6	10.5
						82.8	21.6	0.10	0.004	72.8					
					AR	0.93	71.9	0.15	0.09	22.1	85.0				
						108.2	11.7	0.46	4.61	99.0					
4	3	190	3.5 : 1	28.3	AtOL	14.1	50.5	0.29	2.17	26.2	75.7	93.4	65.5	95.1	11.2
						98.8	27.9	0.14	0.06	86.5					
					AR	1.74	70.0	0.11	0.10	22.0	84.8				
						107.5	9.8	0.50	4.30	101.1					
5	2	190	4 : 1	32.4	AtOL	14.5	48.3	0.28	2.03	26.2	78.3	94.6	57.9	95.8	13.1
						100.3	32.6	0.12	0.01	94.4					
					AR	1.50	72.7	0.14	0.09	22.6	81.1				
						124.1	10.2	0.47	4.90	114.4					
6	2	190	5 : 1	40.5	AtOL	16.3	43.7	0.30	1.97	27.9	76.3	97.3	70	94.9	15.1
						85.7	37.6	0.11	0.12	81.6					
					AR	0.76	72.0	0.10	0.11	22.0	81.0				
						105.7	6.6	0.43	3.50	97.4					
7	2	190	6 : 1	48.6	AtOL	18.0	42.2	0.31	2.20	31.2	68.7	90.8	83.2	94.8	9.9
						77.0	40.9	0.12	0.37	78.2					
					AR	2.27	68.3	0.05	0.10	20.8	90.9				
						95.9	8.9	0.41	2.91	102.4					
8	2	150	5 : 1	40.5	AtOL	14.4	48.34	0.30	1.26	26.31	78.3	96.2	65.0	91.5	13.9
						78.47	26.31	0.20	1.72	84.9					
					AR	0.93	73.25	0.11	0.16	21.3	86.31				
						75.2	5.98	0.40	2.60	80.19					

* Numerator, content in the solid phase; denominator, that in solution.

djurleite $Cu_{1.96}S$ with virtually zero content of iron. The finely dispersed part of the residue was mainly composed of copper sulfide (mostly of secondary origin). The sample of the solid residue contained both particles containing all the three components and particles containing no metallic phase, whose dissolution led to a decrease in the total content of iron and cobalt in the solid residue, compared with the starting converter matte. The decrease in the content of iron in the solid phase is also due to its leaching-out also from the bornite component of copper sulfide, with probable formation of a secondary copper sulfide. The phase component of nickel sulfide contained a considerable amount of copper impurity and had a formula close to $Ni_{50}Cu_{10}S_{40}$, which stoichiometrically corresponded to a mixture of $Cu_{2-x}S$ and Ni_3S_2. A minor part of nickel sulfide was in the form of millerite.

According to the results of an X-ray diffraction analysis, a sample of the solid product of AtOL was mainly composed of digenite $Cu_{1.765}S$ and covelline CuS; the sample also contained an appreciable amount of millerite γ-NiS and trace concentrations of polydymite Ni_3S_4. The sample contained no oxygen or oxygen-containing phases. No elementary sulfur in the AtOL cake was detected either.

The metallic phase was completely absent, which pointed to the large extent of its leaching-out by the reaction [6]

$$M + H_2SO_4 + 0.5O_2 \rightarrow MSO_4 + H_2O, \quad (2)$$

where M = Ni, Fe, Cu, or Co.

The recovery of cobalt into solution in AtOL quantitatively corresponded to that in the case of a complete dissolution of the metallic phase. Consequently, cobalt sulfides were not leached-out when the oxidation stage was performed under atmospheric conditions.

The matrix component had the form of a mixture of dispersed phases of composition $Cu_{15}Ni_{40}S_{46}$, which was identified as a mixture of digenite and millerite. Compared with the ACR cake, the Ni/Cu ratio in nickel sulfide decreased to 2.7. In view of the above-mentioned increase in the content of copper in the nickel matrix, the formation of millerite and digenite is probably provided by parallel occurrence of two processes: "cementation" of copper on heazlewoodite [reaction (3)] and acid dissolution of the forming chalcosine [reaction (4)]:

$$Ni_3S_2 + 2CuSO_4 \rightarrow NiS + 2NiSO_4 + Cu_2S \quad (3)$$

$$Cu_2S + 0.2H_2SO_4 + 0.1O_2 \rightarrow Cu_{1.8}S + 0.2CuSO_4 + 0.2H_2O \quad (4)$$

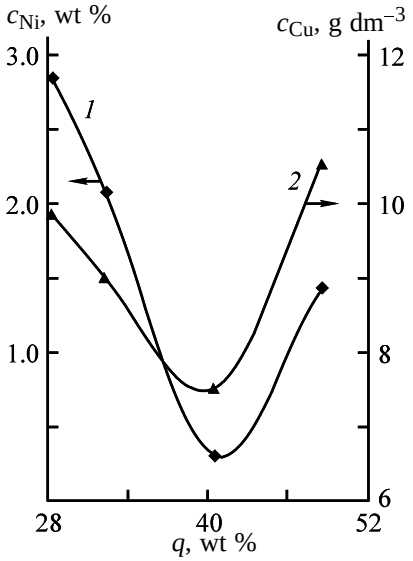
$$Ni_3S_2 + 0.2H_2SO_4 + 1.8CuSO_4 + 0.1O_2 \rightarrow NiS + 2NiSO_4 + Cu_{1.8}S + 0.2H_2O. \quad (5)$$

The extent of this reaction with respect to heazlewoodite was determined by the Ni/Cu ratio in nickel sulfide, reaching a value of 2.7.

The formation of trace amounts of polydymite is presumably due to acid dissolution of millerite [6]

$$4NiS + H_2SO_4 + 0.5O_2 \rightarrow Ni_3S_4 + NiSO_4 + H_2O. \quad (6)$$

A part of the acid contained in the starting solution was spent for dissolution of nickel from heazlewoodite



Residual content of nickel in CSP, c_{Ni}, and concentration of copper in the AR solution, c_{Cu}, vs. the specific expenditure of the acid in the AtOL procedure, q.

and of iron isomorphically present in heazlewoodite, by the reaction

$$M_3S_2 + H_2SO_4 + 0.5O_2 \rightarrow MSO_4 + 2MS + H_2O, \quad (7)$$

where M is Ni and Fe contained in heazlewoodite.

Further dissolution of iron occurred by the reaction [7]

$$Ni_3S_2 \cdot FeS + 2H^+ + 0.5O_2 \rightarrow 3NiS + Fe^{2+} + H_2O. \quad (8)$$

The extent of reactions (7) and (8) was determined by the recovery of nickel and iron into solution.

Chalcosine contained in the copper sulfide phase and in the nickel sulfide matrix was completely oxidized to digenite in accordance with Eq. (9), with a part of digenite reacting with oxygen to give covelline [6]:

$$5Cu_2S + 0.5O_2 + H_2SO_4 \rightarrow 5Cu_{1.8}S + CuSO_4 + H_2O, \quad (9)$$

$$5Cu_{1.8}S + 4H_2SO_4 + 2O_2 \rightarrow 5CuS + 4CuSO_4 + 4H_2O. \quad (10)$$

The recovery of sulfur into solution in the experiment was 3.78%, which was due to the occurrence of direct oxidation of a certain amount of covelline [3]:

$$CuS + 2O_2 \rightarrow CuSO_4. \quad (11)$$

The main chemical reactions in AtOL and their extents are listed in Table 2.

Table 2. Calculated extents of the main chemical reactions in AtOL

Reaction	Recovered or precipitated M	Total recovery of M into solution, %	Extent of reaction in terms of leached-out sulfide, %	Recovery of M into solution by reaction, %	Share of reaction in total recovery of component, %
$Ni^0 + H_2SO_4 + 0.5O_2 = NiSO_4 + H_2O$	Ni	47.01	100.0	3.31	9.14
$Ni_3S_2 + 0.2H_2SO_4 + 1.8CuSO_4 + 0.1O_2 = NiS + 2NiSO_4 + Cu_{1.8}S + H_2O$			44.3	26.88	74.30
$Ni_3S_2 + H_2SO_4 + 0.5O_2 = NiSO_4 + 2NiS + H_2O$			52.4	15.89	43.92
$Ni_3S_2 \cdot FeS + H_2SO_4 + 0.5O_2 = 3NiS + H_2O$			3.3	–	–
$4NiS + H_2SO_4 + 0.5O_2 = Ni_3S_4 + NiSO_4 + H_2O$			6.9	0.94	2.99
$Co^0 + H_2SO_4 + 0.5O_2 = CoSO_4 + H_2O$	Co	8.66	100.0	8.66	100.00
$Fe^0 + H_2SO_4 + 0.5O_2 = FeSO_4 + H_2O$	Fe	40.10	100.0	5.52	7.90
$Fe_3S_2 + H_2SO_4 + 0.5O_2 = FeSO_4 + 2FeS + H_2O$			100.0	22.12	28.09
$FeS \cdot Ni_3S_2 + H_2SO_4 + 0.5O_2 = FeSO_4 + 3NiS + H_2O$			28.2	12.47	15.83
$Cu^0 + H_2SO_4 + 0.5O_2 = CuSO_4 + H_2O$	Cu	21.35	100.0	0.19	0.84
$Ni_3S_2 + H_2SO_4 + CuSO_4 + 0.5O_2 = NiS + 2NiSO_4 + CuS + H_2O$			–	–11.53	–51.72
$5Cu_2S + 0.5O_2 + H_2SO_4 = 5Cu_{1.8}S + CuSO_4 + H_2O$			100.0	9.40	42.14
$5Cu_2S + 4H_2SO_4 + 2O_2 = 5CuS + 4CuSO_4 + 4H_2O$			53.1	19.96	89.51
$CuS + 2O_2 = CuSO_4$			10.8	3.34	14.96

According to the results of mineralogical studies, a sample of the solid product of AR was composed of a mixture of particles bound into conglomerates by the disperse mass of virtually nickel-free copper sulfide.

Under the conditions of the AR procedure, copper sulfide contained in the starting solution and additionally introduced into the copper-containing solution entered into reactions with nickel, iron, and cobalt sulfides [8]:

$$6NiS + 9CuSO_4 + 4H_2O \rightarrow 5Cu_{1.8}S + 6NiSO_4 + 4H_2SO_4, \quad (12)$$

$$8Co_3S_2 + 27CuSO_4 + 4H_2O \rightarrow 15Cu_{1.8}S + 24CoSO_4 + 4H_2SO_4, \quad (13)$$

$$6CoS + 9CuSO_4 + 4H_2O \rightarrow 5Cu_{1.8}S + 6CoSO_4 + 4H_2SO_4, \quad (14)$$

$$6FeS + 9CuSO_4 + 4H_2O \rightarrow 5Cu_{1.8}S + 6FeSO_4 + 4H_2SO_4. \quad (15)$$

In this case, reactions (12), (13), and (15) were complete, and the extent of reaction (14) was determined by the recovery of cobalt into the AR solution.

It was established by means of X-ray fluorescence microprobe analysis and scanning electron microscopy that the matrix component was a mixture of several phases of average composition $Cu_{18}Ni_{30}S_{50}$, which best corresponded to a mixture of digenite and polydymite. The presence of polydymite in the sample was also confirmed by diffraction methods. No other nickel sulfides were detected in the sample. Thus, the volume of polydymite in the sample of the AR cake somewhat increased, compared with the AtOL sample, on the background of a decrease in the total amount of nickel in the former, which indicates that millerite recrystallizes into polydymite [9]:

$$3.2NiS + 0.8CuSO_4 + CuS \rightarrow 0.8Ni_3S_4 + Cu_{1.8}S + 0.8NiSO_4. \quad (16)$$

Table 3. Calculated extents of the main chemical reactions in autoclave refining of the solid product of AtOL

Reaction	Recovered or precipitated M	Recovery of M into solution, %		Extent of reaction in terms of leached-out sulfide, %	Recovery of M into solution by reaction, %	Share of reaction in total recovery of component, %	
		during AR	AtOL + AR			during AR	AtOL + AR
(12)	Ni	49.52	96.53	97.40	48.88	98.71	50.64
(16)				2.60	0.64	1.29	0.66
(13)	Co	56.34	96.53	100.00	34.76	61.70	53.48
(14)				38.14	21.58	38.30	33.19
$Fe_2S_3 + 3CuSO_4 = Fe_2(SO_4)_3 + 3CuS$	Fe	51.40	91.50	100.00	28.13	54.73	30.74
(15)				49.26	23.27	45.27	25.43
(19)	Cu	–52.62	–31.27	2.40	0.55	–1.04	–1.75
$6FeS + 9CuSO_4 + 4H_2O = 5Cu_{1.8}S + 6FeSO_4 + 4H_2SO_4$	Cu			–	–1.35	2.57	4.33
$6FeS + 9CuSO_4 + 4H_2O = 5Cu_{1.8}S + 6FeSO_4 + 4H_2SO_4$				–	–1.64	3.11	5.24
$6NiS + 9CuSO_4 + 4H_2O = 5Cu_{1.8}S + 6NiSO_4 + 4H_2SO_4$				–	–34.96	66.43	111.78
$3.2NiS + 0.8CuSO_4 + CuS = 0.8Ni_3S_4 + Cu_{1.8}S + 0.8NiSO_4$				–	–0.16	0.30	0.50
$8Co_3S_2 + 27CuSO_4 + 4H_2O = 15Cu_{1.8}S + 24CoSO_4 + 4H_2SO_4$				–	–0.23	0.44	0.73
$6Co_3S_2 + 9CuSO_4 + 4H_2O = 5Cu_{1.8}S + 6CoSO_4 + 4H_2SO_4$				–	–0.19	0.36	0.61
(17)				99.00	–14.64	27.83	46.82

Copper sulfide had a composition $Cu_{1.77}S$, corresponding to digenite formed by the reaction [3, 6, 8, 9]:

$$6CuS + 3CuSO_4 + 4H_2O \rightarrow 5Cu_{1.8}S + 4H_2SO_4. \quad (17)$$

The extent of this reaction was determined by the experimentally determined transfer of sulfur into solution.

The recovery of iron in AR also occurred via decomposition of the "iron" component of bornite ($Cu_4^+Cu_{0.5}^{2+}Fe^{3+}S_4 \overrightarrow{\leftarrow} 2Cu_2S + 0.5CuS + 0.5Fe_2S_3$), with digenite acting as a reducing agent for iron(III). The overall reaction can be written as

$$4Fe_2S_3 + 12CuSO_4 \rightarrow 4Fe_2(SO_4)_3 + 12CuS \quad (18)$$

$$5Cu_{1.8}S + 4Fe_2(SO_4)_3 \rightarrow CuSO_4 + 5CuS + 8FeSO_4 \quad (19)$$

$$4Fe_2S_3 + 8CuSO_4 + 5Cu_{1.8}S \rightarrow 12CuS + 8FeSO_4 \quad (20)$$

The main chemical reactions of the AR procedure and their extents are listed in Table 3.

CONCLUSIONS

(1) In the oxidation stage of leaching under atmospheric conditions, the content of nickel in the copper sulfide product is less than 1.0%. The key condition for a decrease in the residual content of nickel is that the atmospheric oxidative leaching should be performed at l : s = 5 : 1, which corresponds to a specific expenditure of the acid equal to about 41% relative to the mass of the solid phase.

(2) The optimal conditions of the successive procedures of atmospheric oxidative leaching and autoclave refining are as follows: leaching temperature, 90–95°C; oxygen flow rate, 1.0 $dm^3\,min^{-1}$ per 1 dm^3 of slurry; stirring rate, ~2800 rpm; l : s ratio in the feed for atmospheric oxidative leaching, 5 : 1

(acid expenditure ~41 wt %); duration of leaching, 150 min; refining temperature, 150°C; duration of refining, 120 min; specific expenditure of the copper-containing solution in refining, 1.1–1.5 g Cu/g Ni in the solid product of atmospheric oxidative leaching.

(3) The amount of dissolved sulfides of nonferrous metals and the degree of oxidation of the sulfide sulfur to the sulfate form are lower in atmospheric oxidation, compared with the autoclave process. The overall recovery of sulfur into solution in atmospheric oxidative leaching in the optimal mode was 13.9%, which is considerably lower than that in the oxidation stage carried out under autoclave conditions.

(4) Basic copper sulfates and oxide compounds of iron are not precipitated in atmospheric oxidative leaching. No elemental sulfur is detected in leaching cakes.

(5) A specific feature of the copper sulfide product obtained in the oxidation stage performed under atmospheric conditions is that it contains polydymite in an amount exceeding that formed in the leaching stage. The formation of polydymite gives no way of recommending the atmospheric oxidation mode for processing of nickel-containing converter mattes, because even introduction of considerable amounts of copper sulfate fails to ensure deep refining of the copper sulfide product to remove nickel.

(6) The choice of an oxidative leaching mode for high-copper converter matte will be determined by the technology of further processing of the copper sulfide product. In the case of a hydrometallurgical processing scheme, which involves autoclave leaching, it is advisable to use the atmospheric oxidative leaching mode. The pyrometallurgical mode requires a greater extent of nickel removal from the copper sulfide product (to <0.5%), which makes it necessary to carry out the oxidative leaching procedure in the autoclave mode.

REFERENCES

1. Naftal', M.N., Shestakova, R.D., Galantseva, T.V., *et al*., *Tsvetn. Met*., 2000, no. 6, pp. 44–49.
2. Vydysh, A., Naftal, M., Petrov, A., and Batsunova, I., in *ALTA 2005: Nickel/Cobalt and Copper Conference*, Hyatt Hotel, Perth, Western Australia, May 1–20, 2005.
3. Naboichenko, S.S., Ni, L.P., Shneerson, Ya.M., and Chugaev, L.V., *Avtoklavnaya gidrometallurgiya tsvetnykh metallov* (Autoclave Hydrometallurgy of Nonferrous Metals), Yekaterinburg, 2002.
4. Vydysh, A.V., Naftal', M.N., and Batsunova, I.V., in *Dobycha i pererabotka rud Noril'skogo promyshlennogo raiona: Sbornik nauchnykh trudov* (Mining and Processing of Ores in the Norilsk Industrial Region: Coll. of Scientific Works), Norilsk: Noril'skii Industrial'nyi Inst., 2005, pp. 92–96.
5. Chugaev, L.V., Shneerson, Ya.M., and Berezkina, N.A., *Khim. Tekhnol*., 2003, no. 12, pp. 18–24.
6. Knuutila, K., Hultholm, S.-E., Saxen, B., and Rosenback, L., in *ALTA 1997: Nickel/Cobalt Pressure Leaching and Hydrometallurgy Forum*, Hyatt Hotel, Perth, Western Australia, May 19–20, 1997.
7. Rademan, J.A.M., Lorenzen, L., and Deventer, J.S.J. van, *Hydrometallurgy*, 1999, vol. 52, pp. 231–252.
8. Hofirek, Z. and Kerfoot, D.G.E., *Hydrometallurgy*, 1992, vol. 29, pp. 357–381.
9. Chugaev, L.V., Berezkina, N.A., and Shneerson, Ya.M., *Tsvetn. Met*., 2004, no. 12, pp. 87–90.

Russian Journal of Applied Chemistry, Vol. 78, No. 11, 2005, pp. 1753–1756. Translated from Zhurnal Prikladnoi Khimii, Vol. 78, No. 11, 2005, pp. 1788–1791.
Original Russian Text Copyright © 2005 by Kolyshkin, Poilov.

INORGANIC SYNTHESIS AND INDUSTRIAL INORGANIC CHEMISTRY

Production of Complex Nitrogen–Potassium and Nitrogen–Magnesium Fertilizers from Substandard Urea Fractions

A. S. Kolyshkin and V. Z. Poilov

Perm State Technical University, Perm, Russia

Received May 4, 2005

Abstract—The production of NK and NMg fertilizers of various compositions from urea and finely crystalline potassium sulfate or urea and caustic magnesite powder was optimized. The commercial characteristics (qualitative composition, hygroscopicity, and strength) of the granulated NK and NMg fertilizers obtained were studied. The possibility of undesirable chemical reactions occurring on fusing potassium sulfate or magnesium oxide with urea in the fertilizer mixture was studied by X-ray phase analysis and IR spectroscopy.

Presently granulated urea produced at the nitrogen industry plants by the method of prilling (spraying the melt in a granulation tower) has insufficient mechanical strength of the granules, which results in the formation of a significant part (2–5 wt %) of substandard product, which is returned to the starting point of the process (into a urea melt). As a result, the net cost of commercial urea increases. Moreover, on storage, transportation, and reloading of urea, its consumer quality decreases owing to mechanical crushing of urea granules. The problem is aggravated also by the fact that the market of prilled urea is narrowing progressively in the last few years [1].

At the same time, substandard urea fractions with a high content of nitrogen would be most appropriate for use as a nitrogen-containing component of complex fertilizers being in the greatest consumer demand. The second component of fertilizers could be substandard finely crystalline products containing potassium and magnesium components in the form taken up by plants. These products are not in demand as individual fertilizers owing to extremely small size of the particles.

By their availability, harmlessness, and correspondence to the claimed characteristics of the end product, finely crystalline technical-grade K_2SO_4 can be used as a potassium-containing component of NK fertilizers, and magnesite caustic powder containing 85 wt % MgO, as a magnesium-containing component of NMg fertilizers. However, a mechanical mixture of nutritive components will not have the required commercial characteristics. Therefore, we have suggested a process for fusing powdered K_2SO_4 and MgO with substandard fractions of urea.

Understanding of physicochemical features of processes occurring in a urea melt is very important for successful promotion of this technology. Thus, when obtaining mixed complex fertilizers, it is necessary to take into account the fact that some starting salts and end products must not be mixed, since undesirable chemical reactions can occur upon their contact. These reactions can result in losses of nutritive materials and in deterioration of the physical properties of the fertilizers [2].

Pozin [3] indicates that the problem of fertilizer antagonism has not been studied adequately; however, he points to a possibility of mixing K_2SO_4 with urea. According to [4, 5], complex compounds of the compositions $MSO_4 \cdot CO(NH_2)_2$, $MSO_4 \cdot 2CO(NH_2)_2$, $MSO_4 \cdot 4CO(NH_2)_2$, and $MSO_4 \cdot 6CO(NH_2)_2$ are formed in aqueous solutions of alkali (or alkaline-earth) metal sulfates and urea. Such compounds may also be formed in the reaction of molten urea with K_2SO_4 dissolved in it.

The suspension of MgO in water has a weakly basic reaction. Hence, urea can be hydrolyzed to give as the final product the corresponding carbonate and ammonia [6]:

$$2CO(NH_2)_2 + Mg(OH)_2 \rightarrow Mg(OCN)_2 + 2NH_3 + 2H_2O, \quad (1)$$

$$Mg(OCN)_2 + 3H_2O \rightarrow MgCO_3 + 2NH_3 + CO_2. \quad (2)$$

1070-4272/05/7811-1753 © 2005 Pleiades Publishing, Inc.

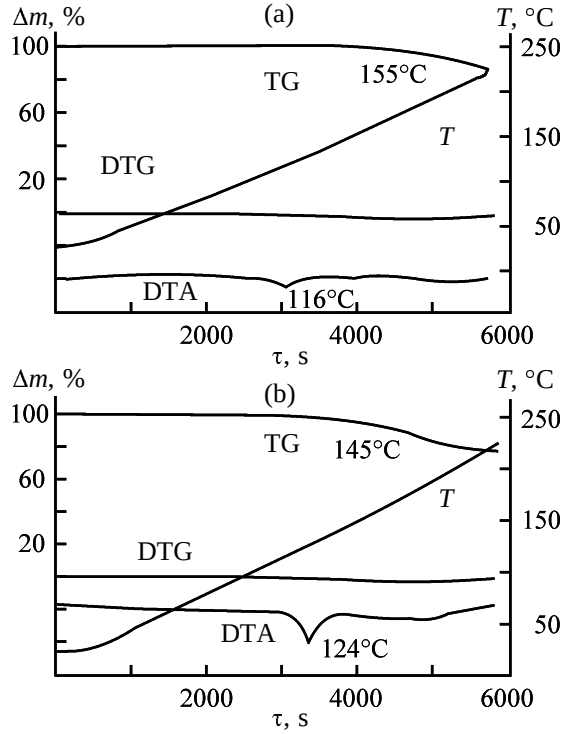


Fig. 1. Derivatogram of a urea fertilizer mixture containing (a) 70% K_2SO_4 and (b) 50% caustic magnesite powder. (Δm) Weight loss, (T) temperature, and (τ) time.

Moreover, reaction (3) is possible:

$$Mg(OCN)_2 + 2H_2O \rightarrow MgCO_3 + CO(NH_2)_2. \quad (3)$$

These reactions must inevitably result in losses of the nutritive component, nitrogen.

Therefore, one of our goals was to study the physicochemical processes occurring on fusing urea with finely crystalline additions, and primarily the processes that can result in the loss of nitrogen.

The most important commercial characteristics of any fertilizer are also hygroscopicity and strength of granules. The capability of polycrystalline products for agglutination and clotting in storage is associated with their hygroscopicity. The content of hygroscopic moisture in a substance affects its friability and capability for thermal decomposition, freezing together, etc. The technology of further treatment and storage of a substance depends on its hygroscopicity.

Therefore, another goal of our study was to optimize the process of fusing urea with finely crystalline additions with the aim of improving commercial characteristics (qualitative composition, hygroscopicity, and strength) of the resulting fertilizers.

The synthesis of complex NK and NMg fertilizers included the following stages: preparation of a fertilizer mixture of a varied composition, its melting at 140°C in an isothermal reactor, solidification of the fertilizer mixture melt on a cooled surface, grinding of the resulting slab, and the separation of the complex fertilizer granules with segregating the commercial fraction.

The qualitative composition of complex fertilizers was determined by IR spectroscopy. The IR spectra were recorded on a Specord 75-IR spectrometer. The samples were prepared as KBr pellets. We determined the parameters of thermal stability of the samples of NK and NMg fertilizers with a Q 1500 D derivatograph (Hungary) in the range 20–600°C at a heating rate of 2.5 and 5 deg min^{-1}. Calcined Al_2O_3 was used as a reference.

We carried out the X-ray analysis on a DRON-3M diffractometer with a monochromator on a primary beam and CuK_α radiation. We set the rate of the sample rotation at 2 or 4 deg min^{-1}. The samples of the materials to be analyzed were prepared as powders. The diffraction patterns were treated by the standard procedure [7].

To study the hygroscopicity of the fertilizers, we used Pestov's method consisting in the estimation of the critical humidity [8]. We estimated the strength of the samples of solidified melt of complex fertilizers with a 2054 P-5 device. Samples in the form of cylindrical pellets 12 mm in diameter and 16–36 mm long were tested for the critical compression stress. We calculated the critical strength as the ratio of the sample failure stress to the area of its failure (area of the longitudinal section of the cylindrical sample).

The first effect (endothermic) corresponding to urea melting is observed in the derivatograms of the $CO(NH_2)_2$–K_2SO_4 and $CO(NH_2)_2$–MgO fertilizer mixtures (Figs. 1a, 1b) at the temperature approximately 10–15°C lower than the melting point of pure urea (132°C). The reaction with a weight loss (urea decomposition) starts at temperatures higher than 145°C for the mixture of urea with magnesium oxide and higher than 150–155°C for urea and for the mixture of urea with potassium sulfate. A decrease to 145°C in the temperature of the onset of urea decomposition may be due to a catalytic effect of pulverized MgO particles on the urea decomposition, as they represent a ready seed for the primary nucleation of a solid phase of urea decomposition products. Nevertheless, the DTA data show that the systems under study are stable up to the temperatures 10–20°C higher than the melting point, which allows melting of fertilizer mixtures without losing nitrogen.

The IR spectra and the X-ray and thermographic data for these mixtures showed that no specific reactions occur when K_2SO_4 is added to a urea melt at 140°C.

However, the IR spectra of NMg fertilizers prepared at the same temperature contain a weak absorption band at 2170 cm^{-1} indicative of the presence of cyanate ions in the granulate [9]. This fact suggests that urea in the melt reacts with finely dispersed MgO to give magnesium cyanate by reaction (1). The intensity of the absorption band of cyanate ions does not depend on the MgO content in the mixture.

The differential thermal analysis of $CO(NH_2)_2$–MgO mixtures (Fig. 1b) revealed no effect corresponding to reaction (1), probably because this effect is obscured by a strong endothermic effect of urea melting. The X-ray analysis confirms the fact that the NMg fertilizer basically consists of the phases of urea and magnesium oxide; the phase of magnesium cyanate was not detected.

Hence, the content of magnesium cyanate in the granulate is low, and the nitrogen loss due to its formation is insignificant. The mechanism of magnesium cyanate formation remains to be elucidated. However, apparently, the minor content of magnesium cyanate is associated with the low solubility of MgO in the urea melt and with the short time of MgO contact with the urea melt.

The X-ray phase analysis showed that a substantial part of the pure urea melt solidifies in the amorphous state. As solid finely dispersed particles of K_2SO_4 or MgO are introduced into the melt, the urea structure becomes considerably less amorphous. This is associated with an increase in the crystallization rate, since the crystallization is possible on ready nuclei of a solid phase with a minimal overcooling of the melt.

Thus, we found by the physicochemical methods of analysis that undesirable chemical reactions in the fertilizer mixture melt resulting in significant losses of precious nutritive components do not proceed when K_2SO_4 or MgO is melted together with urea.

The laboratory studies of the synthesis of nitrogen–potassium (or nitrogen–magnesium) fertilizers have shown that the N : K_2O ratio in the NK fertilizer must be no less than (1.2–1.3) : 1, and the N : MgO ratio in the NMg fertilizer, no less than (1.0–1.1) : 1.5. A lower content of urea results in a decrease in the fluidity of the melt, which complicates its unloading from the melting pot and forming of a melt layer of the desired thickness on a cooled crystallizer surface.

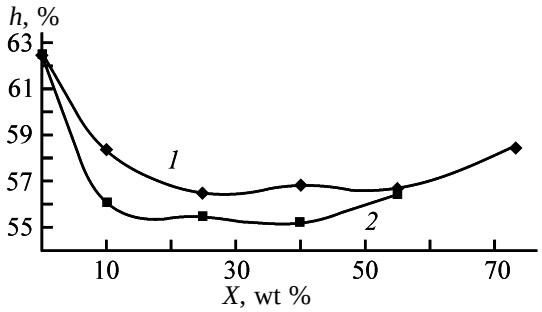


Fig. 2. Plot of hygroscopic point of (*1*) NK and (*2*) NMg fertilizers vs. content *X* of (*1*) K_2SO_4 and (*2*) MgO. (*h*) Relative humidity.

The N : K_2O ratio exceeding 3 : 1 results in obtaining nonuniform granules owing to the melt segregation in the course of its slow solidification.

We studied the hygroscopicity of the fertilizers using samples of the commercial fraction from 2 to 5 mm. The results of replicate experiments are summarized in Fig. 2.

The hygroscopicity of the complex NK and NMg fertilizers is higher than that of granulated urea, since two different crystal phases are present in their granules. Figure 2 shows that the critical humidity passes through a minimum and then starts to increase as the N : K_2O or N : MgO ratio in the fertilizer increases, i.e., as the content of urea increases, the fertilizer initially becomes less hygroscopic. This can be accounted for by the fact that the probability of the formation of fractures in the bulk and on the surface of the granules decreases as the amount of urea in the fertilizer increases. The granules have a more monolithic structure, which results in a decrease in the adsorbing surface area of the material.

With regard to the fact that the critical air humidity for the granules of the fertilizers obtained is low, it is necessary to make provisions for packaging the product in the production process.

We also studied the indices of strength of solidified melt of complex fertilizers based on urea. In the general case, the influence of dispersed particles of K_2SO_4 and MgO on the strength of the granules seems to be associated with changes in the kinetics of the structure formation, with the formation of dendritic crystals piercing the granule volume, and with the changes in the strength of single phase contacts and in their concentration. Insoluble finely dispersed modifying additives introduced into the urea melt create a large surface area of phase contact, which accelerates the nucleation of urea particles adsorbed on the nuclei of the solid phase. An increase

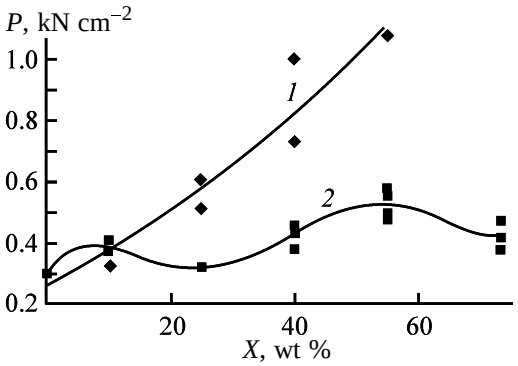


Fig. 3. Plot of mechanical strength *P* of samples vs. composition of the crystallized melt of fertilizer mixture. (*X*) Content of (*1*) MgO and (*2*) K_2SO_4.

in the strength of such a microheterogeneous structure is defined by a large number of forming bonds and contacts between two crystal phases.

In such materials, the matrix takes the whole load, and dispersed particles of a reinforcing filler inhibit the development of plastic deformation offering a resistance to the movement of both single dislocations and dislocation formations (subinterfaces and grain boundaries) [10].

The strength of NK fertilizer pellets is slightly higher than the strength of pure urea pellets (Fig. 3). A maximal strength is attained at the 55 wt % content of K_2SO_4 in the melt. The further increase in the K_2SO_4 concentration in the melt results in a minor decrease in the strength of the pellets, which seems to be associated with a decrease in the number of single interfacial contacts and with poor wetting of the solid phase particles owing to a deficiency of the liquid phase in the suspension consisting of molten urea and solid potassium sulfate. Presumably, at a low content of urea, the interfacial contacts are weakened, and at a high content of urea, the strength decreases owing to a lower strength of urea crystals compared to the crystallizate obtained by fusing urea with potassium sulfate.

The strength of NMg fertilizer pellets increases over the whole interval of the suspension fluidity as the MgO concentration in the fertilizer increases (Fig. 3). This is due to the better wetting of MgO particles (caustic magnesite powder) owing to their smaller size compared to the K_2SO_4 particles. As a result, MgO particles form a larger number of crystallization centers with a larger interface surface in the urea melt, which is accompanied by a stronger reinforcing effect.

CONCLUSIONS

(1) It was found by physicochemical methods that, when potassium sulfate is fused with urea at 140°C, no undesirable chemical reactions occur in the fertilizer mixture melt and the loss of valuable nutritive components is negligible.

(2) Finely dispersed magnesium oxide dissolved in the urea melt forms magnesium cyanate. However, the rate of this reaction is low; therefore, the amount of forming magnesium cyanate is on the impurity level.

(3) Owing to relatively high hygroscopicity of the resulting fertilizers, the product must be packaged. The optimal compositions providing the maximal strength of the samples of NK and NMg fertilizers have been determined.

(4) A substantial part of the melt of pure urea crystallizes in an amorphous state. The introduction of solid finely dispersed particles of potassium sulfate or magnesium oxide into the melt decreases the amorphization of its structure, promoting the crystallization and reinforcement of the structure of the solidified melt.

REFERENCES

1. Aleinov, D.P., *Khim. Prom-st.*, 2001, no. 4, pp. 3–10.
2. Pozin, M.E., *Tekhnologiya mineral'nykh solei* (Technology of Mineral Salts), Leningrad: Khimiya, 1970.
3. Pozin, M.E., *Tekhnologiya mineral'nykh udobrenii* (Technology of Mineral Fertilizers), Leningrad: Khimiya, 1983.
4. Tudorovskaya, G.L. and Margolis, F.G., *Usp. Khim.*, 1965, vol. 34, no. 12, pp. 2124–2143.
5. Kucheryavyi, V.I. and Lebedev, V.V., *Sintez i primenemie karbamida* (Synthesis and Application of Urea), Leningrad: Khimiya, 1970.
6. Zotov, A.T., *Mochevina* (Urea), Moscow: Goskhimizdat, 1963.
7. Lipson, H. and Steeple, H., *Interpretation of X-ray Powder Diffraction Patterns*, London: MacMillan, 1970.
8. Kuvshinnikov, I.M., *Mineral'nye udobreniya i soli: svoistva i sposoby ikh uluchsheniya* (Mineral Fertilizers and Salts: Properties and Methods of Their Improvement), Moscow: Khimiya, 1987.
9. Nakamoto, K., *Infrared and Raman Spectra of Inorganic and Coordination Compounds*, New York: Wiley, 1986.
10. Karpman, M.G., Fetisov, G.P., and Matyunin, V.M., *Materialovedenie i tekhnologiya metallov* (Materials Science and Technology of Metals), Moscow: Vysshaya Shkola, 2002.

Russian Journal of Applied Chemistry, Vol. 78, No. 11, 2005, pp. 1757–1760. Translated from Zhurnal Prikladnoi Khimii, Vol. 78, No. 11, 2005, pp. 1792–1795.
Original Russian Text Copyright © 2005 by Gudkova, Kienskaya, Nazarov, Kim, Mukhtarova.

INORGANIC SYNTHESIS AND INDUSTRIAL INORGANIC CHEMISTRY

Synthesis and Use of Highly Dispersed Zinc Oxide

A. V. Gudkova, K. I. Kienskaya, V. V. Nazarov, V. Kim, and S. E. Mukhtarova

Mendeleev Russian University of Chemical Engineering, Moscow, Russia
Tekhkon Research and Production Company, Moscow, Russia

Received August 2, 2005

Abstract—Methods for synthesis of zinc oxide hydrosols by peptization and condensation were developed. The basic colloid-chemical properties of the sols were determined: electrokinetic properties, size and phase composition of particles, and stability of hydrosols against introduction of electrolytes. The possibility of obtaining antibacterial and UV-protecting cosmetic preparations from the hydrosols obtained was demonstrated.

Owing to the combination of diverse physical and chemical properties (high melting point and heat conductivity, ability to effectively absorb UV light, high photosensitivity, largely unique piezo- and pyroeffects, rather strong luminescence, etc.), zinc oxide ZnO is extensively used in a wide variety of industries. In particular, introduction of zinc oxide into cosmetic creams and gels makes them sunlight-protective and antibacterial [1]. The efficiency of their action largely depends not only on the concentration of the active substance, zinc oxide, but also on the size of its particles, their modification, and degree of polydispersity. In particular, the higher the dispersity of the particles, the more effective a preparation on their basis [2]. This means that the task of obtaining as fine particles of this oxide as possible is a matter of current interest.

Here we demonstrate the possibility of synthesizing highly dispersed zinc oxide by the sol–gel method. This technique was chosen because it can yield nanomaterials with controlled polydispersity and prescribed particle size.

We chose zinc nitrate as a precursor owing to its ready availability and nontoxicity. It should be noted that synthesis of nanodispersed ZnO by the sol–gel method has already been described in the literature [3, 4], but the synthesis was performed from other materials (zinc alkoxides or organometallic compounds), whose use in cosmetology is prohibited. As for other ways to obtain zinc oxide, which are not based on the sol–gel technology, they can also be found in the literature, but are rather complicated and exotic (decomposition in an electric arc, laser evaporation of a target, etc. [5, 6]). In view of the aforesaid, we suggest a rather easy procedure for preparing highly dispersed ZnO (in the form of a sol) by hydrolysis of $Zn(NO_3)_2$.

EXPERIMENTAL

The hydrosol was synthesized by two methods, peptization and condensation. The concentration of all the sols was determined gravimetrically, both in a sol itself and in the ultrafiltrate obtained from the sol. The ultrafiltration was done in a standard cell equipped with polysulfone membranes. The size of sol particles was monitored by photon-correlation spectroscopy (PCS), using the known procedure [7]. The phase composition of sol particles was determined by X-ray diffraction analysis on a DRON-3 diffractometer with CuK_α radiation (1.54051 Å).

In the peptization method, a hydroxide freshly precipitated from a nitrate solution with ammonia was washed with distilled water and then peptized either with an electrolyte (zinc nitrate) solution or with dilute nitric acid. It should be noted that heating of a freshly precipitated and washed zinc hydroxide in distilled water (without any peptizing agent) to 90°C also yields a stable hydrosol.

To develop a technique based on the condensation method, we used as a basis the procedure described for hydrosols of Fe(III) and La(III) [8]. In this method, a certain amount of a $Zn(NO_3)_2$ solution is introduced with vigorous stirring into a boiling aqueous ammonia solution of a known concentration. The resulting suspension is subjected to an ultrasonic treatment for 2 min. On cooling, a transparent opalescent hydrosol is obtained. However, the concentration of such sols is not high (about 0.03 wt %), which is considerably lower than the value provided by the peptization

1070-4272/05/7811-1757 © 2005 Pleiades Publishing, Inc.

Table 1. Synthesis conditions and main parameters of hydrosols

Peptization method							Condensation method			
Sol no.	PA*	ZnO/PA, mol/mol	*c*, wt %	*T*, °C	pH	*r*, nm	Sol no.	pH	ZnO/NH_4OH, mol/mol	*r*, nm
1	$Zn(NO_3)_2$	1 : 0.7	0.12	20	7.2	45	1	7.2	1 : 3.5	35
2	$Zn(NO_3)_2$	1 : 1	0.35	100	6.8	75	2	7.5	1 : 2.0	40
3	–	–	0.08	40	7.5	50				
4	–	–	0.18	100	7.0	65				
5	HNO_3	1 : 0.05	0.20	100	6.5	65				

* PA, peptizing agent.

method. When speaking about the concentration, we should specify that the content of Zn(II) in the ionic form (in the ultrafiltrate) is virtually zero, i.e., the sols produced by peptization and condensation contain virtually no electrolyte.

The main parameters of the hydrosols obtained and the conditions of their synthesis are listed in Table 1. It can be seen that the region of aggregative stability of all the hydrosols lies within the range of pH 6.0–7.5. The virtually neutral medium does not hinder their use in cosmetology and medicine. We established by X-ray diffraction analysis that, irrespective of the synthesis procedure, particles of all the hydrosols are particles of ZnO with a hexagonal structure of the wurtzite type.

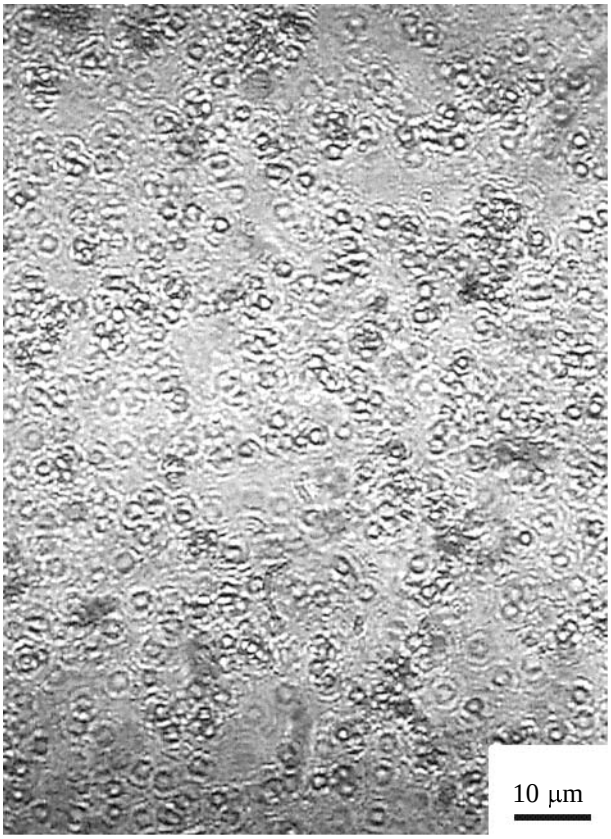


Fig. 1. Micrograph of particles of a dried hydrosol.

We chose for further studies, aimed to determine the basic colloid-chemical properties of the hydrosols obtained, hydrosol no. 2 synthesized by peptization (Table 1), because the concentration of its dispersed phase is the highest. A visual inspection under a microscope revealed that all of its particles are spheres with a nearly monodisperse size distribution (Fig. 1).

Here, we should mention the fact that a sol dried on a glass substrate was used in the microscopic studies. In the course of drying, particles aggregate, so that their size in micrographs considerably exceeds that determined by the PCS method in the dispersion medium (Table 1). To evaluate the aggregative stability of the hydrosol, the ζ potential and coagulation thresholds in the presence of certain electrolytes were determined by macroelectrophoresis and turbidimetry, respectively.

Figure 2 shows how the optical density and ζ potential of the hydrosol depend on pH of the dispersion medium. The ζ potentials were calculated by the Helmholtz–Smoluchowski equation. As seen from Fig. 2, the electrokinetic potential is not high ($\leq$37 mV), with the particles positively charged. However, these rather low values are in good agreement with published data for other hydrosols, which are stable in weakly acidic or weakly alkaline media [8, 9]. The data in Fig. 2 are rather consistent. As already noted, the region of aggregative stability of this hydrosol lies at pH 6.5–7.5. It is in this pH range that the minimum optical density (smallest particle size) and highest ζ potential, corresponding to the largest electrostatic component of the disjoining pressure, are observed. At pH < 6, the hydrosol particles dissolve, and at pH > 10 the excess amount of the electrolyte causes phase separation in the system.

Additional information about the aggregative stability is yielded by the coagulation thresholds with respect to electrolytes. Furthermore, the knowledge of these values is also highly advantageous in development of cosmetic formulations in which this hydrosol is to be used, because most of cosmetic formulations contain an electrolyte. The role of electrolyte in such formulations is rather diverse, from viscosity and pH adjustment to introduction of the required amount of microelements. The most widely used electrolyte is sodium chloride, and, therefore, we studied the behavior of the sol in its presence, as well as upon introduction into the system of other sodium salts: nitrate and sulfate.

The coagulation thresholds for sodium nitrate and chloride coincide (7.5 mM), and that for sodium sulfate is 0.14 mM. Knowing the coagulation thresholds, we can find by what mechanism, concentration or neutralization, coagulation occurs. This can be done in several ways, the simplest of which is the Schulze–Hardy rule. According to this rule, in the case of the concentration mechanism, the coagulation thresholds (C_c) associated with electrolytes with a charge of counterions (z) equal to 1 (chloride and nitrate, in the case in question) and 2 (sulfate) relate as 1 : 1/64, i.e., $C_c = \text{const}/z^6$. In our case, the coagulation thresholds relate as 1 : 1/54, which reasonably agrees with the value given by the rule and suggests that the coagulation occurs by the concentration mechanism.

The rather high coagulation thresholds and low ζ potentials suggest that the aggregative stability of the given hydrosol is provided not only by the electrostatic factor of the disjoining pressure. In all probability, a developed hydrated layer is formed on zinc oxide particles by bulky complex ions $[Zn(H_2O_4)]^{2+}$. This layer ensures the stability of the sol also via the structural component. The presence of this layer has been confirmed for numerous hydrosols including, in particular, sols of basic copper salts in a virtually neutral medium [10].

Thus, the set of studies we performed yielded an aggregatively stable zinc oxide hydrosol and data on its basic properties.

The goal of the second stage of our research was to obtain some cosmetic formulations based on the given sol. In the process, it was of interest to reveal whether they are antibacterial and(or) sunlight-protective and how high is their efficiency, compared to formulations containing macrodispersed zinc oxide.

Preliminary studies revealed that the zinc oxide hydrosol is stable in the presence of such surfactants and polymers frequently used in cosmetics as cremophors and hydroxyethyl cellulose (HEC). Because cremophors are nonionic surfactants and HEC is a weak polyelectrolyte, they do not cause coagulation of sol particles. Moreover, HEC is a rather efficient stabilizer. Therefore, we took as a model system the formulation of a cosmetic cream given in Table 2. In introduction of nanodispersed zinc oxide into this formulation, water was replaced with a 0.25% hydrosol.

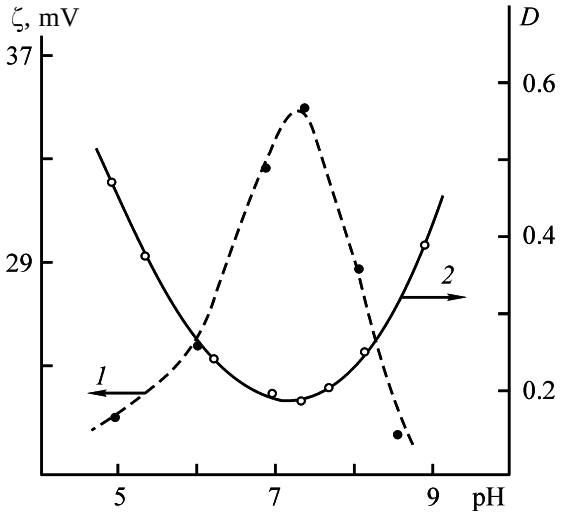


Fig. 2. (*1*) Electrokinetic ζ potential and (*2*) optical density D vs. pH of the dispersion medium of the hydrosol. Concentration of the dispersed phase 0.35 wt %.

The formulation is a homogeneous white system, fairly well absorbed by skin. It is thermally stable and resistant to phase separation during centrifugation. From the standpoint of rheology, this system is a typical pseudoplastic that is well deposited onto skin and distributed over its surface.

To study the antibacterial activity, a formulation

Table 2. Basic composition of a cosmetic formulation

Ingredient*	Content, wt %
Mixture of oxyethylated derivatives of cetearyl and stearyl alcohols (Cremophor A-25)	5.0
Cetearyl alcohol	3.5
Paraffin oil	10.0
HEC	0.05
Vaseline oil	2.0
Conserving agent	0.05
Water (or zinc oxide hydrosol, 0.25 wt %)	Up to 100

* To obtain a homogeneous mass, the finished formulation was subjected to homogenization at a rabble rotation rate of 2000 rpm for 5 min.

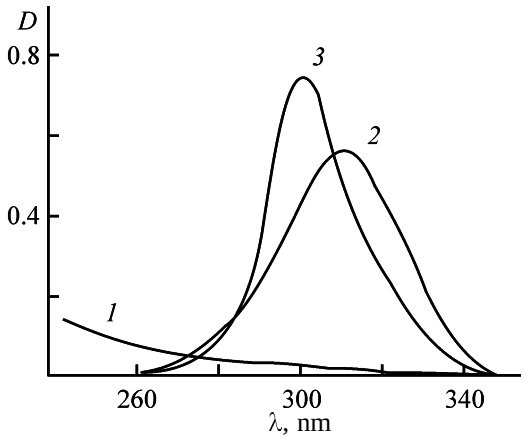


Fig. 3. Absorption spectra of cosmetic formulations: (*1*) without zinc oxide, (*2*) in the presence of macrodispersed zinc oxide, and (*3*) in the presence of zinc oxide hydrosol. (*D*) Optical density and (λ) wavelength.

containing nanodispersed zinc oxide was subjected to a standard test. In this method, growth of test strains of microorganisms is suppressed by a preparation subjected to testing. Bacterial cultures were cultivated for 18–20 h at 37°C on a blood agar with subsequent staining (prior to analysis) by Grumm [11]. We introduced dropwise into a Petri dish with a bacterial cultures of the Streptococcus agelactae family, *Staphylococcus aureus sp*., and *Pseudomonas aeruginosa* 2 ml of zinc oxide hydrosol (0.25 wt %) or the same amount of a 10-fold diluted cosmetic formulation. As controls served Petri dishes with growth media and the corresponding test strains, into each of which 2 ml of distilled water was introduced. The inoculations were incubated for 48 h and then a microscopic analysis was made. It was found that, in the presence of both a pure hydrosol and a cosmetic formulation based on it, the abundance of colonies significantly decreases. Raising the concentration of the hydrosol in the formulation by a factor of 2 completely suppresses the growth of the microorganisms.

The method for determining the sunlight-protective properties of a cosmetic formulation is based on absorption of the UV light by the formulation deposited as a thin layer on a solid surface [11]. The tests were performed as follows. The formulation was deposited onto a quartz plate in such a way that no air bubbles appeared. The sample was covered from above with an identical quartz plate and the layer thickness was brought to 0.01 mm. Clean plates of exactly the same thickness served as reference. The UV spectra of the sample were recorded in the 260–350 nm range. The spectra obtained are shown in Fig. 3. The optical density increases in the presence of the hydrosol, with the effect for the hydrosol being more pronounced than that in the presence of a macrodispersed zinc oxide. This may be due to a more uniform distribution of nanoparticles in the formulation and to a higher monodispersity of the dispersed phase. In addition, a tendency is observed for the absorption peak to be shifted to longer wavelengths, which indicates that the sunlight-protective effect is enhanced. Additional studied revealed that introduction of the hydrosols into the sunlight-protective complex TiO_2 + Al_2O_3 + SiO_2 + *N*-acrylate markedly enhances its efficiency.

CONCLUSIONS

(1) Zinc oxide hydrosols stable in a neutral medium were synthesized by hydrolysis of zinc nitrate. Suggestions were made concerning the factors providing the aggregative stability of these sols (electrostatic and structural components of the disjoining pressure).

(2) It was found that introduction of these hydrosols into cosmetic creams enhances their antibacterial and sunlight-protective activity, compared to formulations based on macrodispersed zinc oxide.

REFERENCES

1. Arct, J. and Frydrych, A., *Syr'e Upak.*, 2004, vol. 1, no. 1, pp. 21–23.
2. Dvoryankova, E.A., *Cosmetic Int.*, 2004, vol. 1, pp. 22–26.
3. Corrie, L. and Kenneth, J., *Langmuir*, 2000, vol. 16, pp. 3764–3772.
4. Rataboul, F. and Casanove, M., *J. Organomet. Chem.*, 2002, vol. 643, pp. 307–312.
5. Cheng Jing-quan, Yan Hui-jian, and Wei Yu, *J. Hebei Norm. Univ.*, 2000, vol. 24, no. 4, pp. 509–512.
6. Marshall, B., Telford, I., and Wood, R., *Analyst*, 1971, vol. 96, pp. 569–578.
7. Finsy, R., *Adv. Colloid Interface Sci.*, 1994, vol. 52, no. 1, pp. 79.
8. Dibtseva, N.M., Kienskaya, K.I., and Nazarov, V.V., *Kolloidn. Zh.*, 2001, vol. 63, no. 2, pp. 27–34.
9. Antonova, A.A., Kagramanov, G.G., Nazarov, V.V., *et al*., *Kolloidn. Zh.*, 2001, vol. 63, no. 6, pp. 431–440.
10. Nazarov, V.V., Yarovaya, O.V., and Kienskaya, K.I., *Kolloidn. Zh.*, 2004, vol. 66, no. 3, pp. 117–125.
11. *Praktikum po tekhnologii kosmeticheskikh sredstv: Analiz syr'ya i gotovoi produktsii: Mikrobiologicheskii kontrol'* (Manual of Technology of Cosmetic Preparations: Analysis of Raw Materials: Microbiological Monitoring), Kim, V., Zil'berg, L.L., and Puchkova, T.V., Eds., Moscow: Shkola Kosmeticheskikh Khimikov, 2005.

Russian Journal of Applied Chemistry, Vol. 78, No. 11, 2005, pp. 1761–1766. Translated from Zhurnal Prikladnoi Khimii, Vol. 78, No. 11, 2005, pp. 1796–1800.
Original Russian Text Copyright © 2005 by Lokshin, Ivlev, Tareeva.

INORGANIC SYNTHESIS AND INDUSTRIAL INORGANIC CHEMISTRY

Leaching-out of Lanthanides from Waste Phosphosemihydrate with Sulfuric Acid Solutions of Increased Concentration

E. P. Lokshin, K. G. Ivlev, and O. A. Tareeva

Tananaev Institute of Chemistry and Technology of Rare Elements and Mineral Raw Materials, Kola Scientific Center, Russian Academy of Sciences, Apatity, Murmansk oblast, Russia

Received January 26, 2005

Abstract—Leaching-out of lanthanides from waste phosphosemihydrate with 20–30% sulfuric acid solutions was studied.

Upon processing of the Khibiny apatite concentrate by the semihydrate technology to obtain wet-process phosphoric acid, the main part of lanthanides is contained in calcium sulfate semihydrate [technical name of the product: phosphosemihydrate (PSH)] [1, 2]. Sulfuric acid leaching can be used for recovery of lanthanides [3, 4].

In [3, 4], the sulfuric acid leaching was performed with low-concentration solutions ($c_{H_2SO_4} \le 10$ wt %) at high l : s = (5–10) : 1. A high degree of recovery of lanthanides into solution was achieved (up to 84%), but the concentration of lanthanides in solution, $c_{\Sigma Ln_2O_3}$, did not exceed 1 g l^{-1}. All attempts to raise $c_{\Sigma Ln_2O_3}$ in leaching solutions failed.

In the process, it was established that, in leaching of several portions of PSH with the same sulfuric acid solution at l : s = 3 : 1, leaching time of 2–3 h, and $c_{H_2SO_4}$ subsequently raised to 12–24 wt %, the concentration of lanthanides in solution increased to 3 g l^{-1} and more, but the recovery of lanthanides in each stage did not exceed 30–40% and decreased as $c_{\Sigma Ln_2O_3}$ became higher [3]. With a solution with $c_{H_2SO_4}$ = 25 wt % and l : s = 5 : 1, the recovery of lanthanides into solution was 30% at $c_{\Sigma Ln_2O_3}$ = 0.34 g l^{-1} [5].

The experimentally determined concentration of lanthanides in leaching solutions is considerably lower than the solubility of lanthanide sulfates in sulfuric acid solutions. However, the reason for this fact has not been established.

The large volumes of the solutions involved and low concentration of lanthanides in them strongly hinder their processing to recover lanthanides and subsequent utilization in manufacture of wet-process phosphoric acid. This makes studies aimed to improve the leaching technology a matter of current interest.

The goal of this study was to examine leaching-out of lanthanides from waste PSH with sulfuric acid solutions of medium concentrations (20–32 wt %) and to reveal the factors limiting the accumulation of lanthanides in leaching solutions.

EXPERIMENTAL

Experiments were carried out with waste PSH[1] with a moisture content of 20 wt %. It contained 0.56 wt % ΣLn_2O_3 in terms of a dry product.

The influence exerted by the conditions of leaching with sulfuric acid solutions of medium concentration ($c_{H_2SO_4}$ = 20–32 wt %) on the processing efficiency was analyzed. The leaching time was 1 h, because this time is sufficient according to [6]. After the leaching was complete, the solid phase was separated from the solution by filtration. In some of the experiments, the same portion of the sulfuric acid solution was used to successively process two portions of the starting PHS (double-stage leaching). The concentration of the sum of lanthanides $c_{\Sigma Ln_2O_3}$ and c_{CaO} were determined by the oxalate gravimetric technique, in which the relative determination error was 0.3 rel % and more for the lanthanide concentrations in the range under study [7]. The concentrations of individual oxides were determined by atomic-emission spectrometry with inductively coupled plasma on a Perkin–Elmer Plasma 400 instrument. The sums of lanthanides determined by different methods were in good agreement.

[1] Produced by Ammofos Open Joint-Stock Company (Cherepovets).

1070-4272/05/7811-1761 © 2005 Pleiades Publishing, Inc.

Table 1. Efficiency of leaching-out of lanthanides with sulfuric acid from PSH at 20°C

Run no.	l : s	$c_{H_2SO_4}$, wt %	Concentration in solution, g l^{-1}		ΣLn_2O_3 recovered into solution, %
			ΣLn_2O_3	CaO*	
1	2	20	1.87	0.90	66.8
2	2	22	1.74	0.78	62.0
3	2	24	1.74	0.64	62.0
4	2.5	24	1.95	0.55	87.0
5	2	25	1.81	0.43	64.7
6	2.5	25	1.84	0.42	82.0
7	2.5	26	1.71	0.36	76.0
8	2.5	27	0.45	0.31	20.1
9	2.5	28	0.76	0.27	30.0
10	2.5	30	1.29	0.20	57.7
11	2.5	30	0.35	0.26	15.7

* The small amount of SrO was neglected; the same in Tables 2, 3.

Table 2. Efficiency of leaching-out of lanthanides with sulfuric acid from PSH at different temperatures and l : s = 2.5

Run no.	*T*, °C	$c_{H_2SO_4}$, wt %	Concentration in solution, g l^{-1}		ΣLn_2O_3 recovered into solution, %
			ΣLn_2O_3	CaO	
1	20	28	0.67	0.27	30.0
2	30	28	0.86	0.41	38.6
3	40	28	0.78	0.48	34.6
4	30	31	0.60	0.32	26.8
5	40	31	0.64	0.38	28.4

Table 1 lists the results obtained in determining how the efficiency of leaching-out of lanthanides from PSH depends on $c_{H_2SO_4}$ in the leaching solution at 20°C. It can be seen that it is fairly high at $c_{H_2SO_4}$ = 20–25 wt % and grows as the l : s ratio increases from 2 to 2.5. As $c_{H_2SO_4}$ is raised further to 30 wt %, the recovery of lanthanides into solution decreases even at a larger ratio l : s = 2.5.

The anomalous results of run nos. 8–11 can probably be accounted for by dissolution, in leaching-out of lanthanides with solutions with $c_{H_2SO_4} \geq 25$ wt %, of lanthanide compounds (primarily hydrated orthophosphates) by the reaction

$$LnPO_4 \cdot nH_2O + H_2SO_4 = Ln_2(SO_4)_3 + H_3PO_4 + gH_2O \quad (1)$$

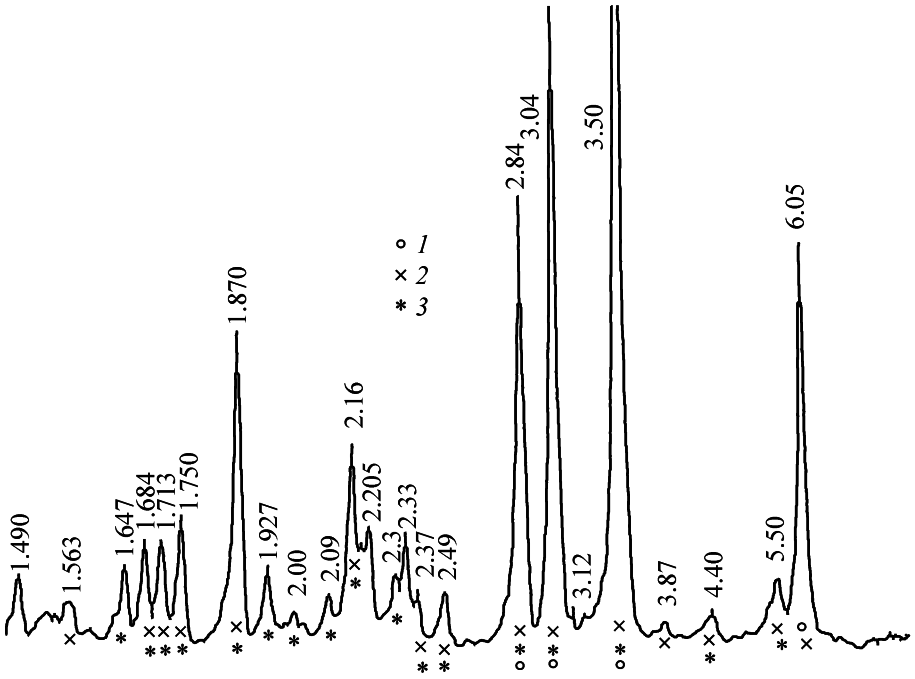
and their precipitation from solution via secondary formation of sparingly soluble lanthanide compounds by the reaction

$$Na_2SO_4 + Ln_2(SO_4)_3 + 2H_2O = 2NaLn(SO_4)_2 \cdot H_2O. \quad (2)$$

Indeed, solutions obtained in leaching-out with sulfuric acid of medium concentrations are metastable and form precipitates in storage. The solution obtained in run no. 10 was somewhat more stable and did not have enough time to decompose during the experiment.

A study of the precipitates demonstrated that they poorly dissolve in a large excess of water. The composition of a typical precipitate is as follows (wt %): Na_2O 3.98, K_2O 0.22, ΣLn_2O_3 31.4, CaO 13.4. The most probable main phase is a solid solution of double sulfates $Na_xK_{1-x}La(SO_4)_2 \cdot nH_2O$, in which about 70% of ΣLn_2O_3 is bound. About 30% of ΣLn_2O_3 cocrystallizes with calcium compounds at a molar ratio ΣLn_2O_3 : CaO = 0.123. Data of an X-ray phase analysis (see figure) confirm that the main phases of the precipitate are hydrated calcium sulfate $CaSO_4 \cdot 0.67H_2O$ and double sulfate of lanthanides and sodium.

If solutions with $c_{H_2SO_4}$ = 28–31 wt % are used for leaching, elevating the leaching temperature to 40°C has virtually no effect on the recovery of lanthanides into the leaching solution, which remains low, but somewhat raises c_{CaO} (Table 2).



X-ray diffraction pattern of a precipitate from the leaching solution. (*1*) $CaSO_4 \cdot 0.67H_2O$, (*2*) $NaCe(SO_4)_2 \cdot H_2O$, and (*3*) $NaLa(SO_4)_2 \cdot H_2O$. Interplanar spacings, Å, are indicated.

The recovery in the second stage of double-stage leaching in all the runs (Table 3) was somewhat lower than that in the first stage, but acceptable, except for the solution containing 25 wt % H_2SO_4. Virtually no accumulation of lanthanides was observed. With $c_{H_2SO_4}$ raised at a constant temperature, the content of CaO in the leaching solution decreased. Thus, effective accumulation of lanthanides in sulfuric acid leaching of PSH is possible if $c_{H_2SO_4} \leq 24$ wt %.

The relative content of most of individual lanthanides in leaching solutions is largely similar to their relative content in the apatite concentrates; however, accumulation of holmium, erbium, and ytterbium is observed (Table 4).

The lower content of yttrium in solution is due to its lower content in the starting PSH, the latter being probably associated with the loss in PSH washing with water to remove phosphoric acid. In the second stage of leaching, the relative, with respect to cerium, concentrations of all the lanthanides increase, i.e., the recovery of lanthanides into solution is largely determined by the difficulty of cerium transfer to solution.

Use of sulfuric acid solutions with concentrations exceeding those used in earlier studies [3, 4] may make the leaching time shorter. Therefore, we examined the effect of the leaching time on the recovery of lanthanides (Table 5).

Table 3. Efficiency of two-stage leaching-out* of lanthanides from PSH with sulfuric acid solutions with $c_{H_2SO_4}$ = 20–25 wt %. Temperature 20°C, l : s = 2

Run no.	$c_{H_2SO_4}$, wt %	Concentration in solution, g l^{-1}		Recovered ΣLn_2O_3, %	
		ΣLn_2O_3	CaO	in a stage	average
1	20	1.87/3.145	0.895/0.86	66.8/45.5	56.15
2	22	1.736/2.936	0.785/0.58	62.0/42.8	52.4
3	24	1.736/3.012	0.636/0.608	62.0/45.6	53.8
4	25	1.81/1.98	0.43/0.48	64.7/6.1	35.4

* Numerator, leaching in the first stage; denominator, in the second stage.

Table 4. Content of Ln_2O_3 relative to Ce_2O_3 in the apatite concentrate and in solutions obtained in sulfuric acid leaching of PSH

Oxide	Relative content of oxide		
	in apatite concentrate [8]	in solution in the indicated stage	
		first	second
Y_2O_3	0.092	0.065	0.00715
La_2O_5	0.485	0.698	0.66
Ce_2O_3	1	1	1
Pr_2O_3	0.137	0.141	0.167
Nd_2O_3	0.337	0.348	0.389
Sm_2O_3	0.0448	0.05	0.0576
Eu_2O_3	0.0118	0.013	0.014
Gd_2O_3	0.0424	0.0271	0.030
Tb_2O_3	0.0047	0.0033	0.0041
Dy_2O_3	0.0165	0.0187	0.0191
Ho_2O_3	–	0.0022	0.0021
Er_2O_3	0.0035	0.005	0.0056
Yb_2O_3	–	0.0037	0.004

As can be seen from Table 5, the maximum $c_{\Sigma Ln_2O_3}$ in solution, corresponding to a recovery of 85.3–96.4%, is reached in 20–25 min with solutions with $c_{H_2SO_4}$ = 24–30 wt% used to leach PSH at Ammofos Company. Further increase in the leaching time led to a decrease in $c_{\Sigma Ln_2O_3}$ in solution. With $c_{H_2SO_4}$ raised to 32 wt % and more, the maximum recovery is reached during the first 5 min and then $c_{\Sigma Ln_2O_3}$ starts to gradually decrease.

The optimal leaching time and the maximum achievable degree of recovery decreased as $c_{H_2SO_4}$ was raised from 24 to 30 wt %. Elevating the temperature to 40°C affected the recovery efficiency of lanthanides only slightly. The maximum recovery of lanthanides into solution (96.4%) was reached with a sulfuric acid solution with $c_{H_2SO_4}$ = 24 wt % used in leaching.

The variation of c_{CaO} in the leaching solution (Table 6) had a more complicated nature; however, c_{CaO} also decreased by the end of the process, which is due to cocrystallization of a part of calcium sulfate with precipitated lanthanide compounds.

In sulfuric acid leaching of waste PSH, phosphorus, sodium, and potassium impurities pass into solution in addition to lanthanides. The solubility of hydrated orthophosphates, fluorides, and double sulfates of lanthanides with sodium and potassium, in which form lanthanides may be present in PSH and in leaching solutions, changes only slightly in the presence of

Table 5. Kinetics of leaching-out of lanthanides from waste PSH at Ammofos Company

$c_{H_2SO_4}$, wt %	l : s	*T*, °C	($c_{\Sigma Ln_2O_3}$ in solution, g l^{-1})/(recovered, %, during indicated leaching time, min)								
			5	10	15	20	25	30	35	45	60
24	1 : 2	20	1.87 66.9	2.12 75.6	2.14 76.4	2.19 78.1	2.70 96.4	–	2.50 89.3	2.02 72.1	1.72 61.4
24	1 : 2	40	–	2.15 76.8	2.32 82.9	2.45 87.5	2.58 92.1	1.85 66.1	1.77 63.2	1.66 59.3	1.59 56.8
28	1 : 2	20	1.07 38.2	1.52 54.3	1.70 60.6	2.09 74.6	2.50 89.3	1.58 56.4	1.45 51.7	–	–
30	1 : 2.5	20	–	1.60 71.4	1.82 81.2	1.91 85.3	1.76 78.6	1.71 76.3	1.63 72.8	1.57 70.1	1.46 65.2
30	1 : 2.5	40	–	1.71 76.3	1.92 85.7	2.01 89.7	1.81 80.8	1.75 78.1	1.60 71.4	1.54 68.7	1.32 58.9
32	1 : 2.5	48 ± 1	1.32 58.9	0.92 41.1	0.65 29.0	0.57 25.4	0.47 21.0	0.43 19.2	–	0.44 19.6	–

Table 6. Variation of the calcium concentration in leaching-out of lanthanides from waste PSH at Ammofos Company

$c_{H_2SO_4}$, wt %	l : s	*T*, °C	c_{CaO}, g l^{-1}, after indicated leaching time, min								
			5	10	15	20	25	30	35	45	60
24	1 : 2	20	–	0.45	0.44	0.46	0.51	0.51	0.52	0.59	0.40
24	1 : 2	40	–	0.65	0.60	0.52	0.54	0.58	0.56	0.49	0.44

Table 7. Effect of the content of sodium in the sulfuric acid leaching solution on the recovery of lanthanides into solution ("stale" waste PSH, leaching time 25 min, l : s = 2)

Run no.	Content in solution				Recovered ΣLn_2O_3, %
	starting		after leaching		
	$c_{H_2SO_4}$, wt %	c_{Na_2O}, g l^{-1}	c_{Na_2O}, g l^{-1}	$c_{\Sigma Ln_2O_3}$, g l^{-1}	
1	24*	0.0	0.25	2.70	96.4
2	26	0.0	0.85	1.97	77.2
3	26	1.0	1.85	1.61	63.1
4	26	2.0	2.45	1.16	45.5
5	26	3.0	3.2	1.07	42.0

* PSH batch no. 1; run nos. 2–4 with PSH batch no. 2.

minor concentrations of PO_4^{3-} ions. These ions may pass from waste PSH into leaching solutions [9–11].

The solubility of double sulfates of lanthanum and cerium with sodium in sulfuric acid and sulfuric–phosphoric acid solutions of medium concentrations is low [10]. Therefore, even a small excess of sodium in the solutions must hinder leaching-out of lanthanides by decreasing the solubility of their double sulfates with sodium to an even greater extent. Therefore, we examined the influence exerted by the sodium concentration c_{Na_2O} in leaching solutions on the efficiency of recovery of lanthanides. As seen from Table 7, an increase in c_{Na_2O} (upon addition of Na_2SO_4) leads to a pronounced decrease in the recovery of lanthanides into solution.

Thus, it may be assumed that the transfer of lanthanides to solution in leaching of waste PSH with H_2SO_4 solutions of medium concentration is governed by simultaneous occurrence of two processes: (i) dissolution of hydrated orthophosphates and (ii) formation and precipitation of double sulfates with sodium. The solubility of double sulfates of lanthanum and cerium, which constitute the most part of lanthanides present in the apatite concentrate, is the highest at $c_{H_2SO_4}$ = 10–12 wt % [9]. Therefore, raising the concentration $c_{H_2SO_4}$ not only accelerates the dissolution of hydrated orthophosphates, but also makes faster the secondary precipitation of double sulfates. The secondary precipitation of double sulfates is also enhanced on raising the concentration of sodium cations.

CONCLUSIONS

(1) A primary process of dissolution of hydrated orthophosphates and a secondary process of precipitation of double sulfates of lanthanides with sodium occur in leaching-out of lanthanides from waste phosphosemihydrate with H_2SO_4 solutions. The former leads to an increase in the concentration of lanthanides, and the latter, to a decrease in the recovery of lanthanides into solution.

(2) Raising the sodium concentration in a leaching solution impairs the efficiency of leaching-out of lanthanides because of the formation of double sulfates of lanthanides with sodium, which are sparingly soluble in H_2SO_4 solutions of medium concentrations.

(3) Lanthanides are effectively leached-out from waste phosphosemihydrate with sulfuric acid solutions of medium concentrations (20–24 wt %) at l : s = (2–2.5) : 1. Use of the same sulfuric acid solution for successive leaching-out of lanthanides from two PSH batches yields solutions with a concentration of lanthanides of about 3 g l^{-1} at a medium l : s = 1 and recovery of lanthanides into solutions of up to 56%.

(4) The relative amounts of lanthanides in leaching solutions approximately correspond to those in the starting apatite concentrate, with, however, a tendency toward accumulation of holmium, erbium, and ytterbium.

ACKNOWLEDGMENTS

The study was financially supported by the Program "Leading Scientific Schools" (project no. NSh-1616-2003.03).

REFERENCES

1. Lebedev, V.N., Masloboev, V.A., Popova, L.A., and Serkova, R.P., in *Problemy effektivnogo ispol'zovaniya mineral'nogo syr'ya Kol'skogo poluostrova: Sbornik*

nauchnykh trudov (Problems of Effective Use of the Mineral Resources of the Kola Peninsula: Coll. of Scientific Works), Apatity: Kol'sk. Nauchn. Tsentr Ross. Akad. Nauk, 1993, pp. 43–49.

2. Kazak, V.G., Angelov, A.I., and Zaitsev, P.M., *Khim. Prom-st.*, 1995, no. 9, pp. 11–19.
3. Lokshin, E.P., Vershkov, A.V., and Vershkova, Yu.A., *Metally*, 2001, no. 1, pp. 42–50.
4. Malikov, V.A. and Krylova, O.K., *Tsvetn. Met.*, 2003, no. 4, pp. 63–64.
5. Lebedev, V.N., Smirnova, I.P., Masloboev, V.A., and Mikhlin, E.B., in *Fiziko-khimicheskie i tekhnologicheskie problemy pererabotki syr'ya Kol'skogo poluostrova* (Physicochemical and Technological Problems in Processing of Raw Materials from the Kola Peninsula), St. Petersburg: Nauka, 1993, pp. 56–60.
6. Jarosinski, A., Kijkowska, R., Kovalczyk, J., *et al.*, *Pr. Nauk AE Wroclawiu*, 1990, no. 526, pp. 129–133.
7. Ryabchikov, D.I. and Ryabukhin, V.A., *Analiticheskaya khimiya redkozemel'nykh elementov i ittriya* (Analytical Chemistry of Rare-Earth Elements and Yttrium), Moscow: Nauka, 1966.
8. Lebedev, V.N., Belokoskov, V.I., Smirnova, I.P., *et al.*, *Khimicheskaya tekhnologiya redkikh elementov i mineral'nogo syr'ya* (Chemical Technology of Rare Elements and Mineral Raw Materials), Apatity, 1986, pp. 28–32.
9. Lokshin, E.P., Ivlev, K.G., and Tareeva, O.A., *Materialy Mezhdunarodnoi nauchno-tekhnicheskoi konferentsii* (Proc. Int. Scientific and Technical Conf.), Murmansk: Murm. Gos. Tekh. Univ., 2004, part 4, pp. 120–121.
10. Lokshin, E.P., Vershkova, Yu.A., Ivlev, K.G., and Tareeva, O.A., *Zh. Neorg. Khim.*, 2004, vol. 49, no. 4, pp. 707–710.
11. Lokshin, E.P., Vershkova, Yu.A., Ivlev, K.G., and Tareeva, O.A., Abstracts of Papers, *XVII Mendeleevskii s''ezd po obshchei i prikladnoi khimii* (XVII Mendeleev Congr. on General and Applied Chemistry), Kazan, 2003, vol. 2, p. 35.

Russian Journal of Applied Chemistry, Vol. 78, No. 11, 2005, pp. 1767–1771. Translated from Zhurnal Prikladnoi Khimii, Vol. 78, No. 11, 2005, pp. 1801–1805.
Original Russian Text Copyright © 2005 by Perevislov, Panteleev, Ordan'yan.

INORGANIC SYNTHESIS AND INDUSTRIAL INORGANIC CHEMISTRY

Synthesis of Complex Tungsten–Zirconium Carbonitrides

S. N. Perevislov, I. B. Panteleev, and S. S. Ordan'yan

St. Petersburg State Technological Institute, St. Petersburg, Russia

Received September 23, 2005

Abstract—The process parameters (temperature, atmosphere, and composition) of the synthesis of complex carbonitrides $W_{1-x}Zr_xC_{1-y}N_y$ were determined. The area of formation of homogeneous carbonitrides in synthesis from refractory compounds and from WC and zirconium oxide was found. The conditions of appearance of the hemicarbide W_2C were elucidated. The possibility of fabricating homogeneous carbonitrides (CNs) at the lower temperature of the synthesis by increasing fineness of the starting components by vibrogrinding was examined.

Nitrogen-containing compounds, and carbonitrides of the Group IV–VI metals in particular, can be considered as very promising components of hard alloy cutting tools based on tungsten carbide. Carbonitrides occupy the intermediate place between carbides and nitrides and possess a complex of physicochemical properties including high hardness, high heat conductivity, and ability to sustain low-temperature microplastic deformation. At the same time, they are free from the main drawback typical of nitrides consisting in that the angle of wetting of a metal binder with the melts is close to zero. At the same time, the presence of nitrogen largely decreases the friction coefficient and adhesion to the treated metal, which enhances the cutter performance.

The cubic carbonitrides in a mixture with tungsten carbide can partially dissolve it with the formation of carbonitrides of a complex composition. Such processes should inevitably lead to the appearance of diffusion porosity (Frenkel–Kirkendall effect) and result in the deterioration of mechanical properties (bending strength and hardness). To eliminate this drawback, preliminary synthesis of complex carbonitrides may be suggested. To obtain high-purity stoichiometric preparations, it is the most reasonable to use carbides and nitrides of tungsten and of Group IV–VI transition metals.

The reaction of WC with zirconium nitride and zirconium carbide can yield a new interstitial phase, a solid solution of complex carbonitride (CN) of the general formula $(W_{1-x}Zr_x)(C_{1-y-z}N_y\square_z)$, where $\square$ designates the vacancies in the nonmetal sublattice. For stoichiometric compositions, the area in which such compounds can exist can be presented by the section in the four-component system W–Zr–C–N (Fig. 1), formed by the binary compounds WC and WN (hexagonal crystal system), and by ZrC and ZrN (cubic crystal system).

Tungsten nitride WN decomposes above 600°C. This restricts the choice of compositions and makes carbonitride synthesis feasible only for compositions in the WC–ZrC–ZrN pseudoternary system. Thus, the dashed line in Fig. 1 is the conventional boundary of the area of compositions wherein the complex carbonitrides can be synthesized from carbides and nitrides without participation of WN.

The mutual solubility of WC and ZrC was studied elsewhere [1–6]. The results are summarized in Table 1.

Data on the solubility of WC in zirconium nitride are lacking. Zirconium carbide and zirconium nitride form a continuous series of solid solutions over the entire concentration range [7].

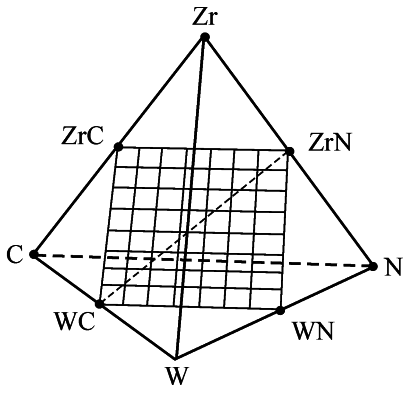


Fig. 1. The WC–ZrC–ZrN–WN section in the quaternary system W–Zr–C–N.

1070-4272/05/7811-1767 © 2005 Pleiades Publishing, Inc.

Table 1. Data of various authors on the mutual solubility of WC and ZrC

Solubility, mol %	*T*, °C
ZrC in WC:	
0	1800–2250 [6]
< 5	1900–2100 [1]
34	1500 [2]
40	1950 [2]
WC in ZrC:	
15–20	1600 [5]
25	1800 [6]
26	1600 [4]
30	2000 [3]
35	2100 [5]
50	2500 [3]
58	2100 [4]
65	2550 [6]

To elucidate the mechanism and parameters of the synthesis, we used in this study pure grade WC, ZrC, and ZrN powders produced by the Donetsk Plant of Chemicals (fineness 10–30 μm). The components were triturated in a titanium mortar with ethanol, and the mixture was dried and pressed. The heat treatment was done within 1300–1900°C. The samples were kept at constant temperature for different times under a pressure of 1.2 atm in ultrapure argon. The phase analysis of the synthesis products was performed with a DRON-3 diffractometer (copper anode, Ni-filter). To control the stoichiometry, the samples of homogeneous carbonitrides were selected and the content of carbon and nitrogen in them was determined by chemical analysis. The loss of carbon and nitrogen did not exceed 5 at. %.

The phase composition of the samples heat-treated at 1700°C for 1 h is presented in Fig. 2a. The homogeneous zirconium carbonitride was formed for compositions along the ZrC–ZrN line, in good agreement with the data from [7]. Two phases, tungsten carbide and cubic complex carbonitride, were detected in the heat-treated WC–ZrC–ZrN ternary mixtures. The X-ray diffraction patterns of the samples heated within 1300–1800°C for 10–60 min were recorded at a lower scanning rate to analyze the shape of reflections. The analysis shows that zirconium carbonitride is formed first and solvent may be ZrC, with its crystal lattice being a basis for the formation of zirconium carbonitride. Because ZrC and ZrN are isostructural compounds, diffusion of nonmetal ions becomes of decisive importance. The radius of the carbon atom (R_C = 0.077 nm) is somewhat larger than of the nitrogen atom (R_N = 0.070 nm). Therefore, we can state that ZrN dissolves in ZrC. As the synthesis temperature is increased, the forming ZrCN intensely dissolves tungsten carbide to yield a complex carbo-

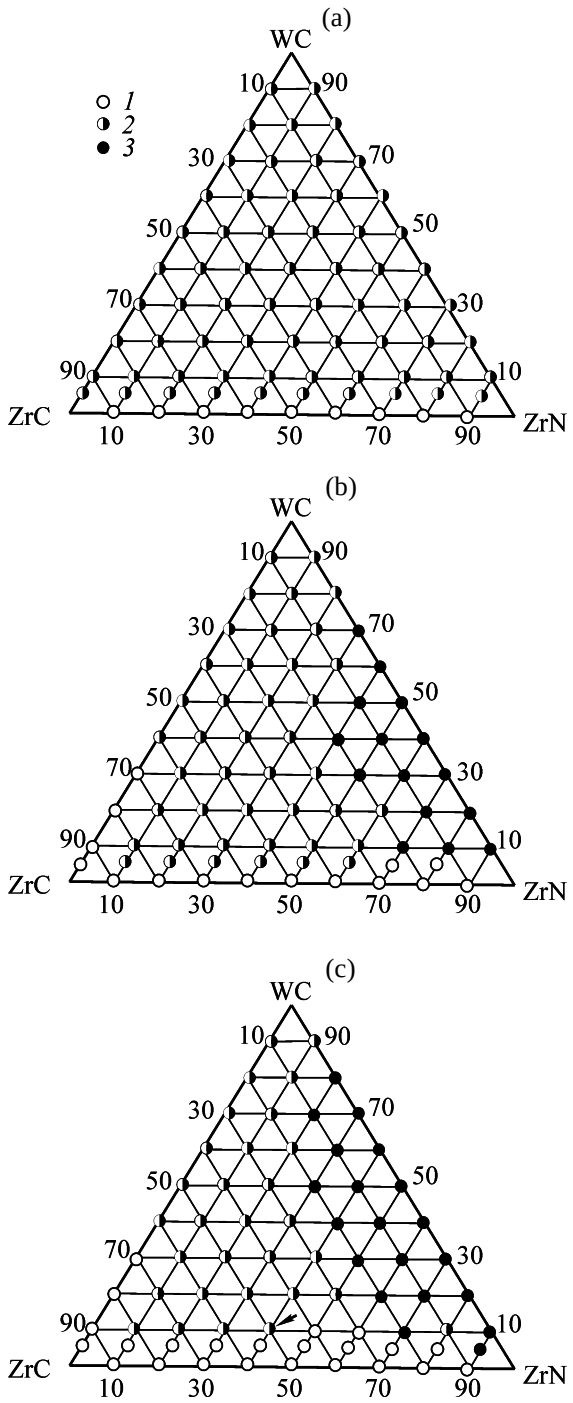


Fig. 2. Phase composition of samples of the WC–ZrC–ZrN system heat-treated at various temperatures. *T*, °C: (a) 1700, (b) 1800, and (c) 1900. (*1*) Carbonitride, (*2*) carbonitride + tungsten carbide WC, and (*3*) carbonitride + tungsten carbide WC + W_2C.

nitride $(W_{1-x}Zr_x)(C_{1-y-z}N_{yz})$. This procedure is reasonable, because ZrC and ZrN have the face-centered cubic (fcc) structure with close unit cell parameters (a_{ZrC} = 0.4683, a_{ZrN} = 0.4537 nm). Moreover, for the formation of ZrCN only redistribution of carbon and nitrogen atoms, whose atomic radii are considerably smaller than those of metals (R_{Zr} = 0.160, R_W = 0.139 nm), is sufficient. At the same time, in formation of a solid solution of hexagonal WC in carbonitride with the fcc lattice, large energies (and high temperatures) are required for the redistribution of metal atoms by diffusion.

At the heat-treatment temperature increased to 1800°C (Fig. 2b), the third phase, tungsten semicarbide W_2C, is detected in a number of compositions. Probably, WC is formed by thermal dissociation of zirconium nitride followed by decarbonization of excess WC owing to the diffusion of carbon atoms into the crystal lattice of defective ZrN_x.

For the compositions located along the WC–ZrC line on the side of zirconium carbide, the $W_{1-x}Zr_xC$ solid solutions are formed, in agreement with the data of [3, 4, 6]. At the same time, on the side of WC, the solubility process was not detected, as in [2, 6].

The homogeneous tungsten–zirconium carbonitride free from the impurities of starting components and W_2C is formed only for two compositions having a low concentration of tungsten and high concentration of nitrogen. The low solubility of WC in the nitrogen-containing zirconium phases is likely due to the difficulty of incorporation of W atoms into the stressed lattice of the forming carbonitride $ZrC_{1-x}N_x$. It appears to be lower than solubility in pure zirconium carbide. However, in the case of the WC–ZrN compositions, the solubility is virtually lacking (at the indicated heat-treatment temperature and component fineness).

At heat-treatment temperature raised to 1900°C (Fig. 2c), the homogeneous CNs are formed for all the compositions along the $W_{0.05}Zr_{0.95}C_xN_y$ line and for a number of compositions along the $W_{0.1}Zr_{0.9}C_xN_y$ line. At the same time, owing to possible loss of nitrogen from zirconium nitride, the carbon redistribution results in the appearance of W_2C in even larger number of compositions, predominantly in those formed from the stocks with a low concentration of ZrC.

The probability of appearance of tungsten semicarbide and the pathway of the solid-phase reactions can be described by the method in which equations of equilibrium thermodynamics are used to simulate the chemical and phase transformations. We used a complex of methods involving the computer algorithms for solving equations and the chemical thermodynamic database [8]. The feature of this system is that the program complex, depending on the parameters of state (temperature, pressure, and composition), calculates the whole set of interconnected reactions and substances.

In this study, the chemical and phase transformations for an arbitrarily chosen composition $W_{0.1}Zr_{0.9}\cdot C_{0.4}N_{0.6}$ (indicated by the arrow in Fig. 2c) were simulated and calculated on the basis of the Gibbs energy minimization.

The main conclusion made from the results of the calculation is that, theoretically, W_2C can appear starting from 1500°C, irrespective of the WC concentration in the starting mixture in the presence of ZrN.

The calculated variations with temperature of the composition of the starting mixture and reaction products present in the condensed phase show that the most temperature-sensitive compound is tungsten carbide, whereas zirconium compounds are virtually insensitive.

The results of the thermodynamic calculations and practical syntheses show that the probability of formation of tungsten semicarbide increases with increasing synthesis temperature, which is confirmed by the experiment.

The synthesis of complex carbonitrides from expensive refractory compounds is very expensive and, in all probability, unacceptable for industry. An alternative is the carbothermal synthesis of carbonitrides in argon with oxides as starting materials and carbon as reducing agent. With zirconium oxide as starting material, the net cost of the product is lower and the range of CN compositions can be somewhat extended toward higher concentrations of tungsten and nitrogen.

The practical fabrication of refractory carbide alloys shows that the synthesis of complex titanium–tungsten carbide from oxides WO_3 + TiO_2 involves problems with keeping the prescribed carbon concentration, and appearance of free carbon is possible [9]. It is recommended to perform the synthesis from a mixture WC + TiO_2 + C, and this is widely used in industry.

In view of these recommendations, we decided to perform a pilot synthesis of complex zirconium–tungsten carbonitride by the reaction

$$WC + ZrO_2 + C + N_2 \rightarrow (W, Zr)CN + CO\uparrow$$

Table 2. Phase composition of products synthesized at various temperatures

Phase composition no.	Carbonitride formula	*T*, °C	Phase composition after synthesis
1	$W_{0.1}Zr_{0.9}C_{0.6}N_{0.4}$	1600	SC*
		1700	CN
		1800	CN
2	$W_{0.3}Zr_{0.7}C_{0.8}N_{0.2}$	1600	SC
		1700	CN
		1800	CN + W_2C
3	$W_{0.3}Zr_{0.7}C_{0.6}N_{0.4}$	1600	SC
		1700	CN
		1800	CN + W_2C
4	$W_{0.3}Zr_{0.7}C_{0.3}N_{0.7}$	1600	SC
		1700	CN
		1800	CN + W_2C
5	$W_{0.5}Zr_{0.5}C_{0.8}N_{0.2}$	1600	SC
		1700	CN
		1800	CN + W_2C
6	$W_{0.5}Zr_{0.5}C_{0.5}N_{0.5}$	1600	SC
		1700	CN + WC
		1800	CN + WC + W_2C
7	$W_{0.7}Zr_{0.3}C_{0.7}N_{0.3}$	1600	SC
		1700	CN + WC
		1800	CN + WC + W_2C
8	$W_{0.7}Zr_{0.3}C_{0.5}N_{0.5}$	1600	SC
		1700	CN + WC
		1800	CN + WC + W_2C

* Starting components.

in the temperature range from 1600 to 1800°C in nitrogen.

Needless to say, the synthesis in this system proceeds by somewhat different mechanism, apparently involving reduction of zirconium oxide to metallic zirconium and then joint filling of the metalloid sub-

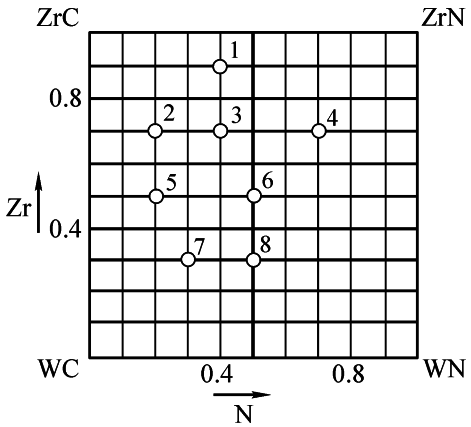


Fig. 3. Choice of compositions in CN synthesis with zirconium oxide. Point nos. are nos. of compositions in Table 2.

Table 3. Phase composition of the products synthesized under various conditions

Carbonitride formula	Vibrogrinding time, h	*T*, °C	Phase composition of synthesis products
$W_{0.3}Zr_{0.7}C_{0.8}N_{0.2}$	0*	1600	CN, WC, C, ZrO_2
		1700	CN, WC
	0.5	1600	CN, WC, C, ZrO_2
		1700	CN, WC, C
	1	1600	CN, WC, C
		1700	CN, WC, C
	3	1600	CN
		1700	CN
	5	1600	CN, WC, C, ZrO_2
		1700	CN, WC, C
$W_{0.3}Zr_{0.7}C_{0.6}N_{0.4}$	0*	1600	CN, WC, C, ZrO_2
		1700	CN, WC
	0.5	1600	CN, WC
		1700	CN, WC, C
	1	1600	CN, WC
		1700	CN, WC, C
	3	1600	CN, WC
		1700	CN
	5	1600	CN, WC, C
		1700	CN, WC, C, W_2C
$W_{0.5}Zr_{0.5}C_{0.8}N_{0.2}$	0*	1600	CN, WC, C
		1700	CN, WC
	0.5	1600	CN, WC, C, ZrO_2
		1700	CN, WC, C
	1	1600	CN, WC, C, ZrO_2
		1700	CN, WC, C, W_2C
	3	1600	CN, WC
		1700	CN
	5	1600	CN, WC, C
		1700	CN, WC, C, W_2C
$W_{0.5}Zr_{0.5}C_{0.5}N_{0.5}$	0*	1600	CN, WC, C
		1700	CN, WC, W_2C
	0.5	1600	CN, WC, C, ZrO_2
		1700	CN, WC
	1	1600	CN, WC, C, ZrO_2
		1700	CN, WC, C, W_2C
	3	1600	CN, WC
		1700	CN
	5	1600	CN, WC, C
		1700	CN, WC, W_2C

* Agitation in a mortar.

lattice with carbon and nitrogen with the formation of ZrCN. Then, tungsten carbide will be dissolved in it to yield the homogeneous cubic phase of complex zirconium–tungsten carbonitride $W_{1-x}Zr_xC_{1-y}N_y$.

The compositions chosen for the study are shown in Fig. 3. The phase composition of the samples heat-treated at different temperatures is given in Table 2.

The synthesis of homogeneous carbonitride at 1600°C is incomplete for all the compositions, whereas that at 1700°C is complete in almost all the cases. This temperature is considerably lower than the temperature of CN formation from refractory compounds, which is associated with high fineness of ZrO_2 (about 1 μm).

To form a homogeneous CN from compositions containing 50 at. % W and more, it is necessary to increase the time of the isothermal annealing, or, which is more reasonable, to increase the WC fineness, e.g., by vibrogrinding of the starting material.

Grinding to a fineness of 0.5–1.0 μm, a value commonly used in the hard-alloy technology, results in the activation of interdiffusion processes in the CN synthesis. The experiment was performed with four compositions (nos. 2, 3, 5, and 6) differing in the component ratios. The starting components were ground in a vibration mill in ethanol for 0.5, 1, 3, and 5 h. The synthesis temperature was 1600 and 1700°C, and the time of the isothermal annealing, 1 h. The results of the phase analysis of the carbonitride samples of the prescribed composition are summarized in Table 3. To obtain a homogeneous CN, mixing of the starting components and their grinding in a vibration mill for 3 h, followed by the synthesis at 1700°C, are optimal.

CONCLUSIONS

(1) To prepare complex carbonitrides $W_{1-x}Zr_x \cdot C_{1-y}N_y$, a temperature of 1700°C, nitrogen atmosphere, and isothermal annealing for 1 h at the final temperature are the optimal parameters.

(2) The region in which homogeneous carbonitrides are synthesized from refractory compounds is limited by the tungsten concentration of 20 mol %, and the region in which they are synthesized from WC and zirconium oxide, by the W concentration of 60 mol %.

(3) Theoretically, W_2C can appear starting from 1500°C, irrespective of the WC concentration in the starting mixture.

(4) From the starting components ground in a vibration mill for 3 h to increase fineness, the homogeneous CNs are formed at a lower temperature of the synthesis.

REFERENCES

1. Vil'k, Yu.N., Ordan'yan, S.S., and Avgustinik, A.I., *Izv. Akad. Nauk SSSR, Neorg. Mater*., 1972, vol. 8, no. 7, pp. 1245–1248.
2. Kuz'ma, Yu.B., Fedorov, T.F., and Shvets, E.A., *Poroshk. Metall*., 1965, vol. 2, p. 22.
3. Umanskii, Ya.S., *Izv. Sekt. Fiz.-Khim. Anal. Inst. Obshch. Neorg. Khim. Akad. Nauk SSSR*, 1948, vol. 16, p. 127.
4. Tombrel, M.T., Abstracts of Papers, *The 2nd Plansee Seminar*, Reutte, Wien: Springer, 1955, p. 205.
5. Nowotny, H. and Kieffer, R., in *Metallforschung*, Springer, 1947, vol. 2, p. 257.
6. Brun, M., and Stubican, V.S., *J. Am. Ceram. Soc*., 1974, vol. 57, no. 3, pp. 117–119.
7. Shveikin, G.P., Alyamovskii, S.I., Zainulin, Yu.G., *et al*., *Soedineniya peremennogo sostava i ikh tverdye rastvory* (Compounds of Variable Composition and Their Solid Solutions), Sverdlovsk: Ural. Nauchn. Tsentr, Akad Nauk SSSR, 1984.
8. Slobodov, A.A., Zarembo, A.V., Zarembo, V.I., and Domanin, D.V., Abstracts of Papers, *Mezhdunarodnaya konferentsiya "Khimicheskoe primenenie nevodnykh rastvorov"* (Int. Conf. "Chemical Application of Nonaqueous Solutions"), Ivanovo: Inst. Khim. Nevodn. Rastvorov, 1995, pp. 35–36.
9. Tret'yakov, V.I., *Osnovy metallovedeniya i tekhnologii proizvodstva spechennykh tverdykh splavov* (Principles of Metal Science and Production of Sintered Hard Alloys), Moscow: Metallurgiya, 1978.

Russian Journal of Applied Chemistry, Vol. 78, No. 11, 2005, pp. 1772–1774. Translated from Zhurnal Prikladnoi Khimii, Vol. 78, No. 11, 2005, pp. 1806–1808.
Original Russian Text Copyright © 2005 by Lebedev.

INORGANIC SYNTHESIS AND INDUSTRIAL INORGANIC CHEMISTRY

Extraction of Nitric Acid from Chloride–Nitrate Solutions

V. N. Lebedev

Tananaev Institute of Chemistry and Technology of Rare Elements and Mineral Raw Materials, Kola Scientific Center, Russian Academy of Sciences, Apatity, Murmansk oblast, Russia

Received March 25, 2005; in final form, September 2005

Abstract—The extraction of nitric acid from chloride–nitrate solutions simulating solutions that result from eudialyte breakdown with hydrochloric acid after extractive recovery of rare-earth elements was studied. A general flowsheet was suggested for the extraction of rare-earth elements from chloride solutions and utilization of nitrate ions as concentrated solutions of nitrates used in recycling.

Hydrochloric acid is used in processing rare-metal raw materials to transfer main components into solution. When concentrates contain rare-earth elements (REEs) with a considerable amount of acid-soluble impurities, problems arise with the recovery of REEs from solution, as REEs do not form extractable chloride complexes. One of possible alternatives of their recovery is extraction with neutral agents after adding nitrate ions to the solution. Such procedures for their recovery during processing perovskite and eudialyte using HCl were suggested in [1, 2]. However, in view of the inadmissibility of dumping nitrate ions and high cost of nitric acid, nitrates should be recoveed from chloride–nitrate solutions.

Nitric acid is extracted with tributyl phosphate much better than hydrochloric acid. It was found that HNO_3 suppresses the extraction of HCl from a mixture of acids. In turn, hydrochloric acid and $CaCl_2$ are salting-out agents for HNO_3 [3–5]. This study concerns systems containing simultaneously a mixture of various chlorides and nitrates. Conditions for applying the extraction to recovery of nitrate ions from such solutions are considered.

EXPERIMENTAL

The experiments were carried out with a solution simulating a raffinate of REE extraction in the technology of processing eudialyte using hydrochloric acid [1]. The solution contained (M): $CaCl_2$ 0.9, $AlCl_3$ 1.0, $MnCl_2$ 0.25, and $NaNO_3$ 2.8. To carry out the extraction of HNO_3, an equivalent (with respect to nitrate ions) amount of hydrochloric acid was added to a chloride–nitrate solution. A solution containing 80% TBP in dodecane was used as extractant. The mixtures were shaken in separatory funnels for 3 min. After separating the phases, the total acidity was determined; in the organic phase, the content of Cl^- ions was determined by titration with silver nitrate and the content of CaO and MnO, by flame photometry. The data on the HNO_3 distribution are given in Table 1.

Table 1. Extraction of nitric acid from a mixed electrolyte solution

Phase volume ratio o : aq	Phase	Content in phase, M				HNO_3 distribution coefficient D
		HNO_3	Cl^-	$CaCl_2$	$MnCl_2$	
5 : 1	o	0.5	0.085	0.007	0.003	1.67
	aq	0.3				
2.5 : 1	o	0.85	0.057	0.005	0.002	1.3
	aq	0.65				
1 : 1	o	1.43	0.075	0.006	0.003	0.97
	aq	1.47				
1 : 2.5	o	1.72	0.13	0.01	0.0043	0.81
	aq	2.11				
1 : 5	o	1.89	0.1	0.009	0.0038	0.78
	aq	2.42				

1070-4272/05/7811-1772 © 2005 Pleiades Publishing, Inc.

It follows from Table 1 that HNO_3 is selectively extracted from the mixed solution of salts and acids. The presence of chloride salts in total of up to 5 M considerably increases the distribution coefficients; therefore, HNO_3 is extracted much better compared to the published data [3–5]. Chloride ions are extracted insignificantly, mainly in the form of the acid, because the extraction of $CaCl_2$ and $MnCl_2$ is suppressed in the presence of nitrate ions, as it was found earlier [1]. The extraction of hydrochloric acid, Ca^{2+}, and Mn^{2+} is minimal at the acidity of 0.6–1.5 M.

As HNO_3 is extracted, the concentration of nitrate ions in the aqueous phase decreases, and an increase in the extraction of $CaCl_2$, $MnCl_2$, and also of hydrochloric acid owing to the salting-out effect of chlorides should be expected [6]. Therefore, the conditions for complete extraction of HNO_3 from the solution of chlorides and nitrates were studied in more detail by the exhaustive extraction at the volume ratio of the organic and aqueous phases o : aq = 1 : 1. Hydrochloric acid was introduced in the stoichiometric (with respect to nitrate ions) amount and in excess of 0.5 M. The solution contained Ca^{2+}, Mn^{2+}, and Al^{3+} in the above-mentioned amounts, and up to 1 M $NaNO_3$. The results of the extraction are given in Table 2.

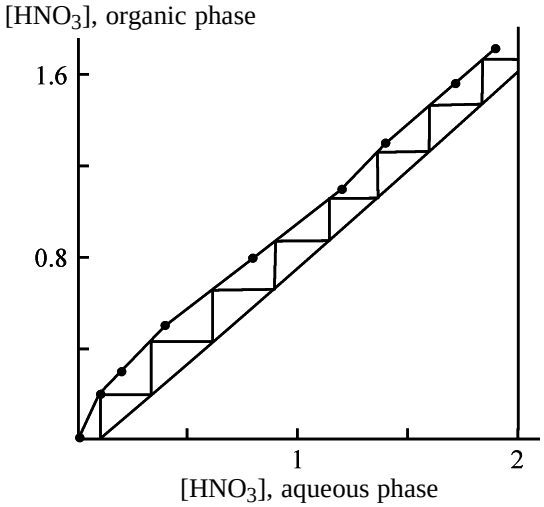
It follows from Table 2 that 93–97% of nitric acid is recovered into the organic phase in 3–4 steps of the exhaustive extraction. An excess of hydrochloric acid considerably increases the HNO_3 distribution coefficient. The amount of coextracted chloride ions increases as the concentration of nitrate ions decreases. The isotherm of the nitric acid extraction with 80% TBP and the calculated number of steps required for its isolation are given in the figure. It is seen from the figure that the extraction of HNO_3 is possible at o : aq = 1 : 1.1; in this case, the concentration of HNO_3 in the extract cannot exceed 1.65 M, and therefore it will be approximately the same in the backwash. The utilization of dilute HNO_3 involves certain problems, as it is unlikely that the evaporation can be economically feasible. However, the process of HNO_3 extraction can become feasible in the case when sodium and calcium nitrates are obtained in the backwash. Their concentration in the backwash can be brought to 6–8 M, which is sufficient for using them in a recycle, by applying lime milk or an alkali of the required concentration in equivalent amounts for the backwashing.

The process involves the addition of $NaNO_3$ or $Ca(NO_3)_2$ to 2–3 M in productive solutions from the breakdown of rare-earth concentrates with hydrochloric acid, the extraction of REE nitrates with a neutral organophosphorus extractant, the addition of an equivalent (with respect to nitrate ions) amount of hydrochloric acid to chloride–nitrate raffinate-1, the extraction of HNO_3 with a neutral organophosphorus extractant, and the backwashing of nitric acid with NaOH or CaO to obtain concentrated solutions of $NaNO_3$ or $Ca(NO_3)_2$ used in recycling. The extraction of REEs with TBP from chloride solutions

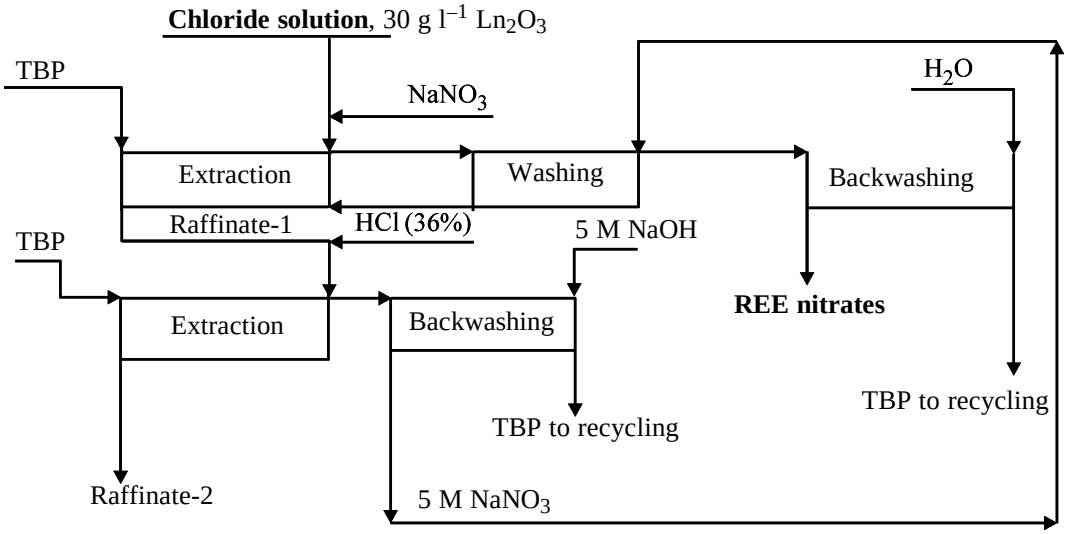
Table 2. Exhaustive extraction of nitric acid from a chloride–nitrate solution

Cycle no.	Phase	Concentration, M			HNO_3 distribution coefficient D
		H	NO_3^-	Cl^-	
1*	o	0.53	0.52	0.07	1.06
	aq	0.48	0.49	N.d.**	
2	o	0.26	0.25	0.08	1.04
	aq	0.24	0.24	N.d.	
3	o	0.12	0.11	0.086	0.85
	aq	0.12	0.13	N.d.	
4	o	0.06	0.06	0.1	0.85
	aq	0.06	0.07	N.d.	
1***	o	0.68	0.67	0.083	2.2
	aq	0.83	0.32	N.d.	
2	o	0.27	0.26	0.09	3.2
	aq	0.55	0.08	N.d.	
3	o	0.07	0.05	0.11	1.67
	aq	0.46	0.03	N.d.	

* Stoichiometric amount of HCl.
** Not determined.
*** Excess of HCl 0.5 M.



Isotherm of nitric acid extraction with 80% TBP from a chloride–nitrate solution.



Scheme of REE extraction from a solution resulting from eudialyte breakdown wiht hydrochloric acid.

with the utilization of the added nitrate ions can be presented by the flowsheet shown in the scheme.

CONCLUSION

The extraction of nitric acid from chloride–nitrate solutions simulating solutions that result from the breakdown of eudialyte with hydrochloric acid after the extractive recovery of rare-earth elements was studied. The recovery is attained by introducing hydrochloric acid into solution in an amount equivalent to nitrate ions. Higher distribution coefficients were obtained when an excess of the acid over the stoichiometric amount of nitrate ions was introduced. The nitrate ions can be backwashed with alkaline reagents to obtain concentrated solutions used in recycling.

REFERENCES

1. Lebedev, V.N. and Masloboev, V.A., *Khim. Tekhnol.*, 2004, no. 3, pp. 26–30.
2. Lebedev, V.N., Asseretskova, O.V., and Smirnova, I.P., in *Khimiya i tekhnologiya mineral'nogo syr'ya Kol'skogo poluostrova* (Chemistry and Technology of Mineral Raw Materials of Kola Peninsula), Leningrad: Nauka, 1991, pp. 54–60.
3. Rozen, A.M., Reznik, A.M., Korovin, S.S., *et al.*, *Zh. Neorg. Khim.*, 1963, vol. 8, no. 4, pp. 1003–1010.
4. Apraksin, I.A., Korovin, S.S., Musorin, V.A., *et al.*, *Zh. Fiz. Khim.*, 1966, vol. 40, pp. 1292–1297.
5. Korovin, S.S., *Izv. Vyssh. Uchebn. Zaved., Khim. Khim. Tekhnol.*, 1968, no. 7, pp. 752–757.
6. Korovin, S.S., Berezhko, L.B., Kol'tsov, Yu.I., and Reznik, A.M., *Izv. Vyssh. Uchebn. Zaved., Khim. Khim. Tekhnol.*, 1968, no. 4, pp. 420–425.

Russian Journal of Applied Chemistry, Vol. 78, No. 11, 2005, pp. 1775–1778. Translated from Zhurnal Prikladnoi Khimii, Vol. 78, No. 11, 2005, pp. 1809–1812.
Original Russian Text Copyright © 2005 by Voropanova, Yakovleva.

INORGANIC SYNTHESIS AND INDUSTRIAL INORGANIC CHEMISTRY

Extraction Kinetics of Copper Ions from Aqueous Solutions with a Mixture of Oleic Acid and Triethanolamine

L. A. Voropanova and V. N. Yakovleva

North-Caucasian Mining and Metallurgical Institute, State Technological University, Vladikavkaz, North Ossetia, Russia

Received March 2, 2005; in final form, September 2005

Abstract—Solvent extraction of copper(II) ions from aqueous solutions with a mixture of oleic acid and triethanolamine in kerosene is studied.

Selective extraction of copper(II) from aqueous solutions containing other metals was studied, e.g., in [1–3]. In our previous papers we reported on the extraction of Cu(II) from aqueous solutions with a mixture of oleic acid and triethanolamine in benzine or kerosene and also in industrial lubricating oil (SP-3 grade) [4–6]. The best extraction characteristics were obtained in the pH range corresponding to hydration of Cu(II) in aqueous solutions.

In this study we examined the kinetics of solvent extraction of copper(II) from aqueous solutions with a mixture of oleic acid and triethanolamine in kerosene at pH 7.

The initial solutions were prepared from $CuSO_4 \cdot 5H_2O$ (chemically pure grade). Since pH changed in the course of extraction, the desired pH 7 was maintained by adding sulfuric acid with continuous stirring during the first 2 h. Then pH changed only slightly, i.e., 2 h is the time sufficient for establishing the extraction equilibrium. In the experiments, pH was determined with a pH-121 pH-meter.

The Cu(II) concentration in the initial solution and raffinate was determined by volumetric titration and on a KFK-3 photocolorimeter, and that in the extract, as the difference.

As an extractant we used a mixture of oleic acid (10–12 wt %) and triethanolamine (4.5–6.0 wt %) in kerosene.

It was demonstrated previously [4–6] that, in the course of extraction, the volumes of the organic (o) and aqueous (aq) phases change insignificantly.

As extraction characteristics we used the distribution coefficient D [ratio of Cu(II) concentrations in the extract and raffinate] and the degree of recovery E (weight ratio of copper in the extract and initial solution, %).

Data on the extraction of copper(II) at various initial solution concentrations c_0 are given in Table 1.

Table 1. Extraction of Cu(II) from aqueous solutions at o : aq = 1 : 19

τ, min	Cu(II) concentration c, mM, at indicated temperature, K								
	273							303	
0	71.09	54.80	40.44	31.31	24.14	15.94	8.06	23.47	8.30
5	69.14	48.27	32.61	30.00	23.25	15.39	6.45	14.28	2.36
10	66.53	43.05	30.00	26.09	20.83	13.03	4.55	8.47	1.83
15	63.92	36.53	28.70	20.88	13.89	7.83	3.58	7.81	1.42
20	62.63	31.31	27.39	16.95	12.50	6.56	2.86	6.53	1.11
30	56.09	28.70	16.95	13.05	8.33	3.91	2.50	5.00	0.91
40	48.27	24.78	10.44	9.78	6.53	3.27	2.02	3.91	0.84
50	41.75	22.17	8.48	6.59	5.16	2.61	1.13	3.13	
60	37.83	18.05	6.52	5.19	3.91	2.03	0.81		
90	34.34	16.95	5.22	3.44	2.61	1.56	0.78		
120	33.92	16.95	5.22	3.44	2.61	1.56	0.78		
1 day	33.92	16.95	5.22	3.44	2.61	1.56	–		

1070-4272/05/7811-1775 © 2005 Pleiades Publishing, Inc.

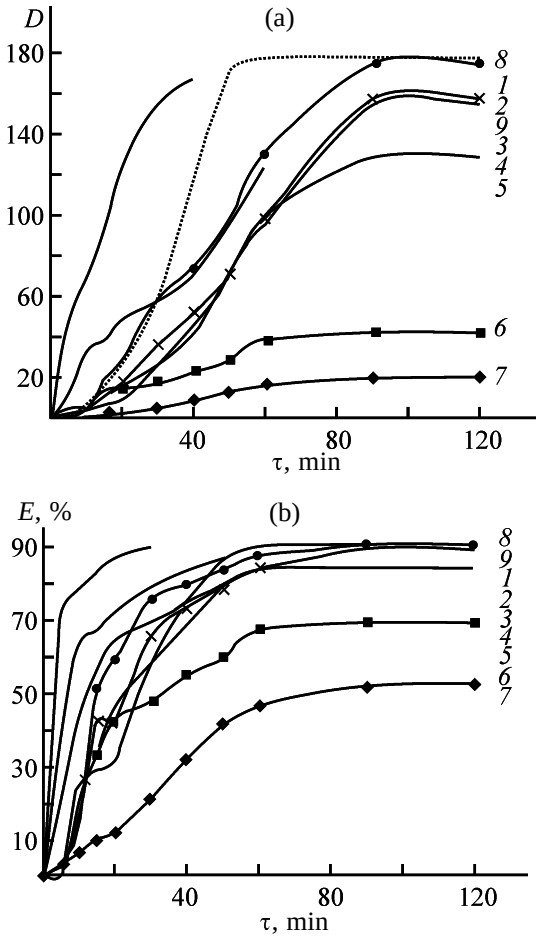


Fig. 1. (a) Distribution coefficient D and (b) degree of recovery E as functions of the time τ. Temperature, K: (*1–7*) 293 and (*8, 9*) 303. Initial Cu(II) concentration c_0 (mM): (*1*) 8.06, (*2*) 15.94, (*3*) 24.14, (*4*) 31.31, (*5*) 40.44, (*6*) 54.80, (*7*) 71.09, (*8*) 8.30, and (*9*) 23.47.

Figures 1a and 1b show the distribution coefficient D and degree of recovery E as functions of the time and initial Cu(II) concentration.

The results show that D and E increase with increasing c_0, temperature, and extraction time.

Table 2 shows the effects of the o : aq ratio and extraction time on the extraction of Cu(II) at c_0 = 23.56 mM. The corresponding data on D and E are plotted in Figs. 2a and 2b as functions of the time and o : aq ratio.

As seen, with increasing o : aq ratio, the extraction of copper(II) into the organic phase and extraction rate increase, and the equilibrium distribution coefficient passes through a minimum.

Figure 3 shows the distribution coefficient D as a function of the o : aq ratio at τ = 90 min. The experimental dependence can be fit by Eq. (1):

Table 2. Extraction of Cu(II) as a function of the o : aq ratio and extraction time (c_0 = 23.56 mM)

τ, min	c_{raf}, mM	c_{extr}, mM	τ, min	c_{raf}, mM	c_{extr}, mM
o : aq = 1 : 19			o : aq = 1 : 4		
0	24.14	0	0	23.56	0
5	23.25	17.81	5	10.42	52.56
10	20.83	66.25	10	5.34	72.88
15	13.89	205.00	15	3.09	81.88
20	12.50	232.81	20	2.09	85.88
30	8.33	316.25	30	1.38	88.75
40	6.53	352.19	40	1.38	88.75
50	5.16	379.69			
60	3.91	404.69			
90	2.61	430.63			
120	2.61	430.63			
o : aq = 1 : 9			o : aq = 1 : 3		
0	23.56	0	0	23.56	0
5	16.95	59.48	5	7.58	47.95
10	11.23	110.95	10	4.47	57.28
15	5.31	164.25	15	2.09	64.41
20	3.05	184.64	20	1.69	65.63
30	2.61	188.58	30	1.02	67.64
40	2.09	193.22	40	1.02	67.64
50	2.09	193.22			
o : aq = 3 : 17			o : aq = 3 : 7		
0	23.56	0	0	23.56	0
5	13.05	59.59	5	5.34	42.52
10	10.42	74.47	10	1.64	51.16
15	4.38	108.73	15	1.38	51.77
20	2.61	118.73	20	0.06	53.30
30	2.09	121.66	30	0.06	53.30
40	1.69	123.95			
50	1.69	123.95			

$$D = -1766.7(\text{o : aq})^3 + 2158.7(\text{o : aq})^2 - 790.98(\text{o : aq}) + 155.66. \quad (1)$$

By solving Eq. (1) for the minimal D we obtain: D_{min} = 58.6430, o : aq = 0.27826 = 1 : 3.5938, and τ = 90 min.

The occurrence of a minimum suggests that the extraction at o : aq = 1 : 3.5938 is accompanied by formation of a well-defined Cu(II) complex with extractant and water.

According to [4], the mechanism of extraction can be represented by complexation equation (2):

$$4(Cu^{2+})_{aq} + 5(RCOOH \cdot R'_3N)_o + x(OH^-)_{aq} + y(H_2O)_{aq} = [Cu_4(OH)_x(RCOOH \cdot R'_3N)_5 \cdot y'H_2O]_o + y''(H_2O)_{aq}. \quad (2)$$

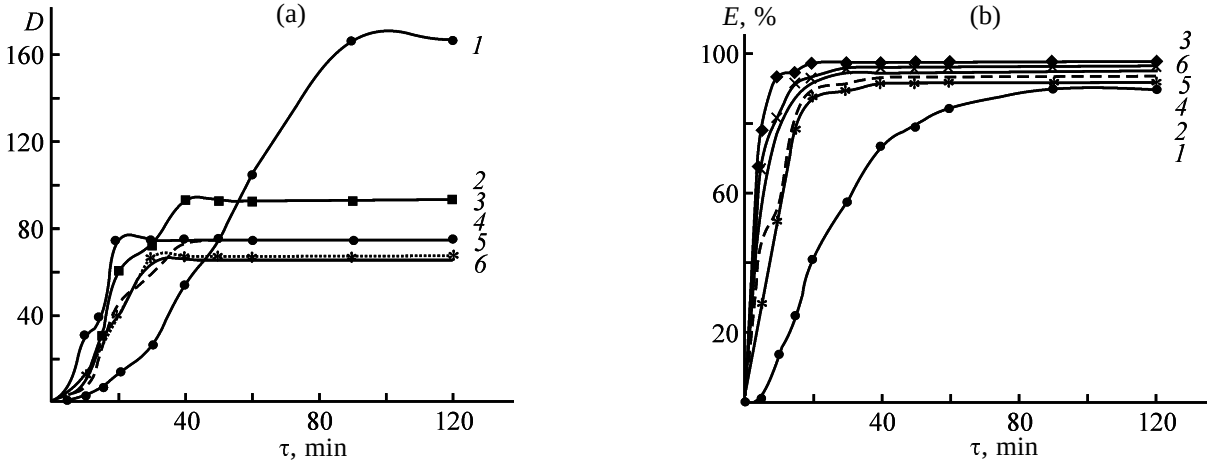


Fig. 2. (a) Distribution coefficient D and (b) degree of recovery E as functions of the time τ at c_0 = 23.56 mM. o : aq: (*1*) 1 : 19, (*2*) 1 : 9, (*3*) 3 : 7, (*4*) 3 : 17, (*5*) 1 : 4, and (*6*) 1 : 3.

It was experimentally demonstrated that, in settling the emulsion after extraction, the mean floating rate of the drops of the oil phase is $U = 0.014129$ cm s^{-1}. Using the Stokes equation

$$U = 2g(\rho - \rho_0)r^2/(9\eta), \quad (3)$$

where $g = 9.8$ m s^{-2} is the acceleration of gravity; $\rho = 0.86$ and $\rho_0 = 1.0$ g cm^{-3} are the densities of the extract and raffinate, respectively; r is the mean radius of the dispersed extract particles (cm); $\eta = 1.005$ cP is the viscosity of the raffinate; and $U = 0.014129$ cm s^{-1} is the floating rate of the drops of the oil phase in settling the emulsion, the mean radius of the extract particles was estimated to be $r = 0.02158$ cm.

Using the least-squares method, we analyzed the experimental kinetic parameters of the process by the film kinetics equation [2], corresponding to the stage of diffusion in the layer around the extract particle:

$$F(\tau) = Q/Q_\infty = 1 - \exp(-K\tau) \quad (4)$$

or

$$\ln(1 - F) = -K\tau \quad (5)$$

and also by the gel kinetics equation, corresponding to diffusion in the interior of the extract particle:

$$F(\tau) = Q/Q_\infty = 1 - (6/\pi^2)\sum_{n=1}^{\infty}(1/n^2)\exp(-n^2B\tau), \quad (6)$$

where $F(\tau)$ is the current degree of extraction (against the limiting value); Q, current extraction; Q_∞, limiting extraction; and K, constant in the kinetic equation

$$B = \pi^2 D/r^2, \quad (7)$$

where D is the diffusion coefficient (cm^2 s^{-1}); r, mean grain size of the anion exchanger (cm); τ, time (s); and n, natural integers.

According to Eq. (5), in the case of film kinetics, $\ln(1 - F)$ should be in direct proportion to τ. In the case of gel kinetics, the argument of the function $X = B\tau$ depends linearly on the time. This argument can be determined using the Boyd, Adamson, and Myers' Tables.

In Table 3 we present the results of kinetic analysis using Eqs. (4)–(6).

The results show that the process kinetics is controlled by the external diffusion of copper(II) to the surface of a drop of the extractant (film kinetics), while elevated temperature, higher o : aq ratio, and vigorous stirring favor transition to the internal-diffusion control.

The mean diffusion coefficient of Cu(II) in the

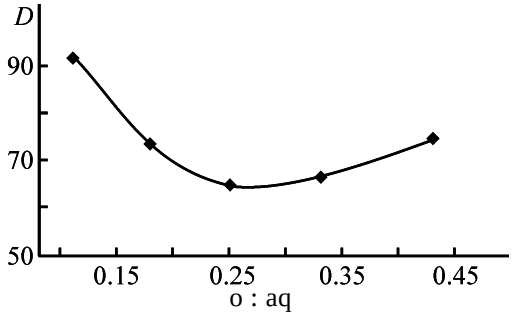


Fig. 3. Distribution coefficient D as a function of the o : aq ratio (extraction time 90 min).

Table 3. Results of kinetic analysis by Eqs. (4)–(6)

c_0, mM	T, K	o : aq	R^2	
			film kinetics	gel kinetics
71.09	273	1 : 19	0.9490	0.9633
54.80	273	1 : 19	0.9033	0.9350
40.44	273	1 : 19	0.9236	0.8900
31.31	273	1 : 19	0.9666	0.9522
24.14	273	1 : 19	0.9473	0.9910
15.94	273	1 : 19	0.9417	0.9857
8.06	273	1 : 19	0.9509	0.9416
23.56	273	1 : 9	0.9445	0.9934
23.56	273	3 : 17	0.9998	0.9975
23.56	273	1 : 4	0.9783	0.9790
23.56	273	1 : 3	0.9754	0.9459
23.56	273	3 : 7	0.8759	0.9048
23.47	303	1 : 19	0.9510	0.9742
8.30	303	1 : 19	0.6684	0.9581

oil phase was found by Eq. (7) to be $D = 2.361 \times 10^{-6}$ cm^2 s^{-1} (o : aq = 1 : 4, τ = 20 min, B = 3.0, and r = 0.02158 cm).

CONCLUSIONS

(1) The extraction rate of copper(II) with a mixture of oleic acid and triethanolamine in kerosene depends on the initial solution concentration, stirring rate, organic to aqueous phase ratio, temperature, and extraction time.

(2) The distribution coefficient D and the degree of recovery E increase with increasing initial solution concentration, temperature, and extraction time.

(3) With increasing o : aq ratio, the extraction of copper(II) into the organic phase and extraction rate increase, and the equilibrium distribution coefficient passes through a maximum.

(4) The extraction kinetics is controlled by the external diffusion of copper(II) to the surface of a drop of the extractant (film kinetics), while elevated temperature, higher o : aq ratio, and vigorous stirring favor transition to the internal-diffusion control.

REFERENCES

1. Naboichenko, S.S. and Smirnov, V.N., *Gidrometallurgiya medi* (Hydrometallurgy of Copper), Moscow: Metallurgiya, 1974.
2. Vol'dman, G.M. and Zelikman, A.N., *Teoriya gidrometallurgicheskikh protsessov* (Theory of Hydrometallurgical Processes), Moscow: Metallurgiya, 1993.
3. Laskorin, B.N., Popov, I.F., Ul'yanov, V.S., *et al.*, in *Ekstraktsiya i sorbtsiya v metallurgii tsvetnykh metallov: Nauchnye trudy* (Extraction and Sorption in Metallurgy of Nonferrous Metals: Scientific Works), Alma-Ata: Nauka, 1975, pp. 16–21.
4. Voropanova, L.A., *Izv. Vyssh. Uchebn. Zaved., Tsvetn. Metall.*, 2001, no. 5, pp. 32–38.
5. Voropanova, L.A. and Velichko, L.N., *Zh. Prikl. Khim.*, 1999, vol. 72, no. 11, pp. 1858–1863.
6. Voropanova, L.A. and Velichko, L.N., *Zh. Prikl. Khim.*, 1999, vol. 72, no. 3, pp. 450–454.

Russian Journal of Applied Chemistry, Vol. 78, No. 11, 2005, pp. 1779–1785. Translated from Zhurnal Prikladnoi Khimii, Vol. 78, No. 11, 2005, pp. 1813–1818.
Original Russian Text Copyright © 2005 by Kirsanov.

INORGANIC SYNTHESIS AND INDUSTRIAL INORGANIC CHEMISTRY

Combustion of a Layered System Based on Sodium Chlorate

O. N. Kirsanov

Prikladnaya Khimiya Russian Scientific Center, Federal State Unitary Enterprise, St. Petersburg, Russia

Received December 29, 2003

Abstract—The velocity of combustion under atmospheric conditions in a constant-volume bomb of formulations based on sodium chlorate and polyethylene in the form of tubes (layered system) was subjected to a comparative study in relation to the type of additive, layer porosity, and fraction composition of sodium chlorate.

This study, proceeding with the previously commenced investigations, mostly served needs of the mining and building industries [1]. Our primary goal was to search for additives that affect the combustion velocity of the basic formulation. This is necessary if the geology of the rock being mined is taken into account. It is known [2] that the combustion of heterogeneous condensed systems is affected by such factors as the type of additives and their fraction composition and porosity. In studying the process mechanism, it is of primary importance to find out whether a chemical reaction in question is autocatalytic. According to [3], the thermal decomposition of $KClO_3$ mainly occurs in accordance with the equation

$$2KClO_3 \rightarrow 2KCl + 3O_2 \quad (1)$$

to give O_2 and KCl and is autocatalytic (KCl is the decomposition catalyst).

In the process under study, combustion of $NaClO_3$ + polyethylene (PE), the decomposition of $NaClO_3$ is one of the first stages. It could be assumed that this reaction is also autocatalytic and affects the overall process. Therefore, it was necessary to primarily study the influence exerted on the process by the NaCl additive. Other additives were considered also: SiO_2, $NaHCO_3$, Na_2CO_3, KCl, Al_2O_3, Co_3O_4, CuO, Ni_2O_3, and MnO_2. Silica and alumina were assumed to be inert additives diminishing the combustion velocity in proportion to the mass introduced. $NaHCO_3$ and Na_2CO_3 were used as additives because of their low thermodynamic stability in a flame ($NaHCO_3$ decomposes with heat absorption at 100–150°C; Na_2CO_3 does so above 851°C, also with an endothermic effect [4]). According to [5], MnO_2 lowers the decomposition temperature of $NaClO_3$ from 350 to 160°C. The effect of KCl on the process was expected to be similar to that of NaCl.

EXPERIMENTAL

The combustion of the formulation composed of $NaClO_3$ and PE was experimentally studied on a setup similar to that used in [1]. We measured the time of propagation of the combustion front between two reference points spaced by l = 40 mm and each situated at a distance of 10 mm from the vessel edge to preclude any influence of nonstationary conditions on the measurement results. The measuring system included two electric circuits with a single dc power source (V = 25 V) connected to the electrically conducting case. Each circuit had an electric contact inserted through a ceramic insulating channel into the case. The instants of time at which the combustion front passed the reference points were recorded as successive closures of the contacts of the two electric circuits connected to a P14M electric stopwatch. The tests were performed under atmospheric pressure at ambient temperature. All the additives except SiO_2 were of chemically pure grade. We used as oxidizing agent $NaClO_3$ of a 25–150-μm fraction (60% 25–65-μm fraction). The mass of $NaClO_3$ in a run was varied within 20–24 g. The mass of the experimental vessel was measured. In studying the layered system, we first charged the vessel case (∅25 × 2.0, Cr19Ni9Ti steel) with tubes of required dimensions in an amount (mass) necessary according to a calculation. A preliminarily prepared mixture of $NaClO_3$ with an additive of the required composition was charged to a height of 60 mm into the assembly weighed on a VLK-500 balance in several stages with tapping at the case (manual vibrational compaction). The scatter

1070-4272/05/7811-1779 © 2005 Pleiades Publishing, Inc.

Table 1. Relative changes in the linear combustion velocity Z upon introduction of additives into $NaClO_3$

Additive, wt %	Z upon introduction of indicated additive									
	NaCl	KCl	SiO_2	$NaHCO_3$	Na_2CO_3	Al_2O_3	Ni_2O_3	Co_3O_4	CuO	MnO_2
1.3							0.98	1.04	1.04	1.1
2.4										1.15
4.8	1.0	0.77								1.35
9.1	0.96	0.93	0.85	0.62	0.67	0.94				1.43

in the bulk density did not exceed ±7% in this case. The fuel formulation was ignited by setting fire to a weighed portion (~1 g) of a PTT paste with a Nichrome coil (V = 12 V, R = 1 Ω). To obtain more reliable results, we performed each test at least twice. The linear combustion velocity of a formulation (mm s^{-1}) was found as

$$U = l/t_c^{-1}, \quad (2)$$

where l is the distance between the reference points (mm), and t_c is the time of formulation combustion between these points (s). The total relative measurement error of the linear combustion velocity did not exceed ±3%.

The relative change in the linear combustion velocity Z was found using the formula

$$Z = U/U_t, \quad (3)$$

where $U_t = 2.211x\exp(-0.78x)$ (mm s^{-1}) is the combustion velocity calculated from the oxidant excess factor x found in a given experiment.

The basic results we obtained in a study of the effect of additives on the linear combustion velocity are listed in Table 1.

Table 1 shows that the linear combustion velocity decreases to the greatest extent for formulations with addition of $NaHCO_3$ and Na_2CO_3, and the maximum increase in the combustion velocity is observed with the MnO_2 additive. The effect of nickel, cobalt, and copper oxides on the linear combustion velocity in the range studied is less pronounced than that of MnO_2. The decrease in the linear combustion velocity upon addition of Al_2O_3 was smaller than that in the presence of SiO_2. In both cases, a conglomerate was formed. If SiO_2 was introduced in the form of a sand, this conglomerate concentrated at the vessel outlet, whereas in the case of Al_2O_3 it was formed throughout the vessel.

According to [2], introduction of an inert additive may either raise the mass rate of combustion, or reduce it, but by a factor of no more than 1.11 or 1.25 upon introduction of the additive in an amount of 10 or 20%, respectively. The discrepancy between these and our results is insignificant. Introduction of 4.8 wt % NaCl into the formulation had no effect on the linear combustion velocity, whereas introduction of 9.1 wt % led to a change considerably smaller than the expected value (estimated assuming NaCl to be an inert additive). Thus, we may conclude that the combustion of the $NaClO_3$ + hydrocarbon formulation is an autocatalytic process, i.e., the NaCl additive acts as an initiator. As already noted, MnO_2 leads to an increase in the linear combustion velocity of the layered $NaClO_3$ + PE formulation, and this increase is the more pronounced, the higher the fraction of the additive introduced into the formulation. This relationship can be expressed for the range under study (with a correlation coefficient of 0.95) as

$$U = 1.4c^{0.5} + 1.01, \quad (4)$$

where c is the MnO_2 content relative to its sum with $NaClO_3$ (mass fraction).

The insignificant influence of the Al_2O_3 additive on the linear combustion velocity could be attributed to a pressure buildup within the vessel because of the increased resistance (conglomerate formation). In view of this circumstance, we carried out additional experiments. For this purpose, a pipe was welded-in into the lower part of the vessel, and a TNMP-100 vacuum gage [GOST (State Standard) 2648–78] was connected to this pipe. Measurements demonstrated that there is no rarefaction observed in [6] in a study of the combustion of pyroxylin and NH_4ClO_4 with combustible additives. By contrast, a rise in pressure (10 kg m^{-2}) was observed both for a pure layered system and for that with additives. The absence of scatter in the pressure difference can probably be understood as follows: the hydraulic resistance of the formulation layer is mostly determined by the presence of a large number of tubes, rather than by the powdered mass of $NaClO_3$ with or without additives.

Table 2. Effect of the fraction composition on the linear combustion velocity

Fraction, mm	ρ, g cm^{-3}	x	U_t	U	Z	U_m, g cm^{-2} s^{-1}
			mm s^{-1}			
>0.4	1.25	0.82	0.96	1.04	0.92	0.13
0.1–0.16	1.37	0.90	0.99	1.01	1.02	0.14
<0.05	1.48	0.84	0.97	1.01	1.04	0.15

Table 3. Basic parameters of the process in the bomb

Formulation	BP	$NaClO_3$ + PEP	$NaClO_3$ + DF	$NaClO_3$ + PET	$NaClO_3$ + PET + NaCl
m, g	40	60	48.6	68.7	61.28
x		1.0	1.0	1.02	0.92
P_{max}, mPa	55	127	91	121	105
t_{max}, s	0.016	0.010	0.036	0.34	0.28

In charging a layered system, it is necessary that the density (or porosity) of the layer as a whole and intertube spaces in particular should be the same. The porosity of the main layer can be evaluated by varying the fraction composition of the oxidizing agent. The influence exerted by the intertube space was studied both by charging the vessel with tubes separately filled with $NaClO_3$ or by sealing the intertube space with technological plugs (wires, rods). The tests we performed demonstrated an insignificant drop in the linear combustion velocity in the case of such a change in the porosity of the intertube space (within the measurement error). This is apparently due to a decrease in the combustion surface area and to a change in the oxidant excess coefficient. In this case, the relative fall of the linear combustion velocity (found using the procedure described above) was by a factor of no more than 1.03.

The effect of the fraction composition of the oxidizing agent on the linear combustion velocity is illustrated by Table 2.

Table 2 shows that, as the grain size decreases, the charge density becomes higher. As for the oxidant excess factor x and the linear velocity U, the effect of the fraction composition on these parameters is ambiguous. As the $NaClO_3$ grain size is decreased, the mass rate of combustion, $U_m = U\rho$, tends to grow. The rise in the mass rate of combustion with increasing density is characteristic of secondary explosives (hexogen, Tetryl), nitroglycerol powder, thermite formulations, etc. [2, 6]. In combustion of the formulation in question, $NaClO_3$ melts (mp 255°C), liquefies, and decomposes with heat release (54.76 J mol^{-1}) [5]. Thus, it would be expected that the contribution of the exothermic reaction in the condensed phase to the overall reaction is quite apparent for the formulation in question.

In order to make sure that the combustion of a layered system constituted by $NaClO_3$ mixed with hydrocarbons occurs in the nondetonation mode and the reaction is autocatalytic, we performed tests in a constant-volume bomb (V = 338 cm^3). The pressure was measured with a DD-10 pressure gage (natural frequency 10 kHz) with the signal recorded by an H-117 loop oscillograph (working frequency range of the measuring loop 1200 Hz). The maximum admissible measurement error was ±10%. The formulations studied were charged into textolite vessels with inner diameter of 38 mm, placed on the bottom of the bomb. The ignition was done by setting fire to a weighed portion (2 g) of black powder (BP).

Table 3 lists the charge mass m, combustion time t_{max}, and maximum pressure P_{max} developed in combustion of the formulations: BP, $NaClO_3$ + PE as powder ($NaClO_3$ + PEP), $NaClO_3$ + diesel fuel ($NaClO_3$ + DF), $NaClO_3$ + PE as tubes (layered system $NaClO_3$ + PET), and $NaClO_3$ with 9.1% NaCl + PE as tubes (layered system $NaClO_3$ + PET + NaCl).

Among the results not represented in Table 3, we should mention an increase in the induction period for chlorate formulations subjected to prolonged storage in open air. However, this circumstance invites further investigation.

Figure 1 shows superposed oscillograms obtained in recording the reduced (to the maximum value) pressure in the bomb and computer processing of the results for the $NaClO_3$-based formulations under

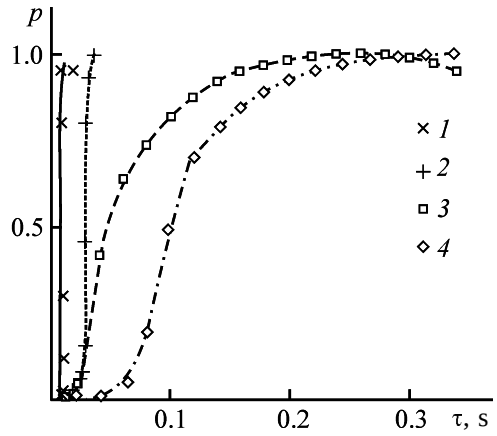


Fig. 1. Reduced pressure p in combustion in a bomb vs. time τ at different compositions. Formulation: (*1*) $NaClO_3$ + PE as a powder, (*2*) $NaClO_3$ + DF, (*3*) $NaClO_3$ + PE as tubes (layered system), and (*4*) $NaClO_3$ + PE as tubes (layered system) with addition of 9.1 wt % NaCl to sodium chlorate (1 : 10).

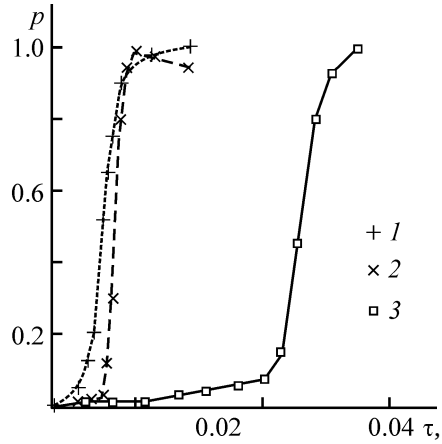


Fig. 2. Reduced pressure p in combustion of different formulations in the bomb vs. time τ for fast processes. Formulation: (*1*) black powder, (*2*) $NaClO_3$ + PE as a powder, and (*3*) $NaClO_3$ + DF

study. Figure 2 shows on another scale pressure records for the first three formulations in Table 3, whose combustion velocity is the highest. The specific working capacity of combustion products, RT, was calculated for the first two formulations for the conditions of the bomb used. It was ~392.7 kJ kg^{-1} for black powder and ~626.5 kJ kg^{-1} for $NaClO_3$ with a PE powder. The latter value is somewhat different from the value of 717.7 kJ kg^{-1} found by preliminary calculation (NaCl in the vapor state). The critical temperature found for NaCl by the Liedersen method [7] from the boiling point of 1440°C [4] was 2933 K. Analysis of the values obtained shows that the extent of the process for $NaClO_3$ with a PE powder does not exceed 0.87. The oscillograms in Fig. 1 show the difference in the rate of pressure buildup in the bomb. The duration of the main combustion process is milliseconds to hundredths of a second for black powder and $NaClO_3$ mixed with diesel fuel of PE powder (Fig. 2) and is approximately an order of magnitude longer for a layered system ($NaClO_3$ + PE tubes). This indicates that the combustion of the layered system is of nondetonation nature. It should be noted that the combustion time of a layered system with addition of 9.1% NaCl is considerably shorter than that without the additive, mostly because of a decrease in the duration of the induction period, i.e., the NaCl additive has a catalytic effect in the initial stage of the reaction. In their main (as regards time) part, the curves run virtually in parallel. Thus, there is good reason to describe the combustion of the formulation under consideration in the bomb in terms of autocatalytic reactions [8]. The same results could be obtained using the Erofeev equation [9] for describing the process; however, physicochemical interpretation of the equation coefficients obtained in this case is difficult (the exponent for some of the runs exceeds 30). Consequently, it is preferable to use in deriving the process equation the description scheme considered in [8]. If we assume that the final pressure in the bomb is determined by the mass of the charge (initial concentration [A], initiator concentration [B]), the modified starting expression for the autocatalytic reaction in terms of the extent of the process, equal to the ratio between the pressure and the maximum pressure, can be represented as

$$d\alpha/dt = k_1(1 - \alpha)(\beta + \alpha), \quad (5)$$

where α is the extent of the process (reduced pressure in the bomb); β = [A]/[B], fraction of the initiator in the total mass; and $k_1 = k$[A].

The solution to this differential equation has the form

$$\alpha = \beta\frac{e^{(\beta+1)k_1t} - 1}{1 + \beta e^{(\beta+1)k_1t}}. \quad (6)$$

The results of processing of the oscillograms obtained in studying the combustion processes in a constant-volume bomb using the Mathcad software package are listed in Table 4 for formulations based on $NaClO_3$.

Table 4. Equation coefficients

Coefficient	PE powder	Diesel fuel	Tubes	
			PE	PE + NaCl
β	0.03	0.003	0.003	0.091
k_1	875	1050	55	43

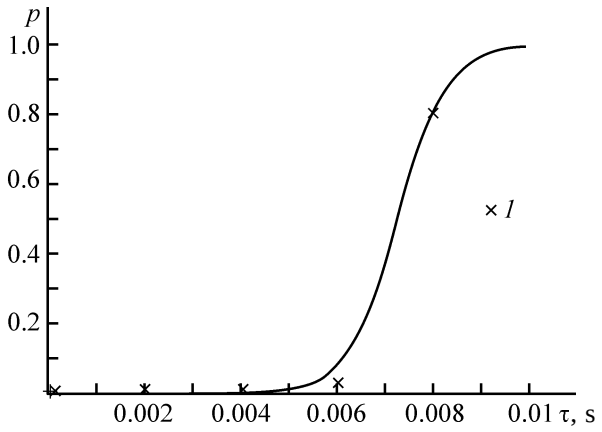


Fig. 3. Comparison of the experiment (point 1) with the calculation for a formulation composed of sodium chlorate with powdered polyethylene at the equation coefficients $\alpha = 10^{-6}$ and $k_1 = 1900$ (solid line).

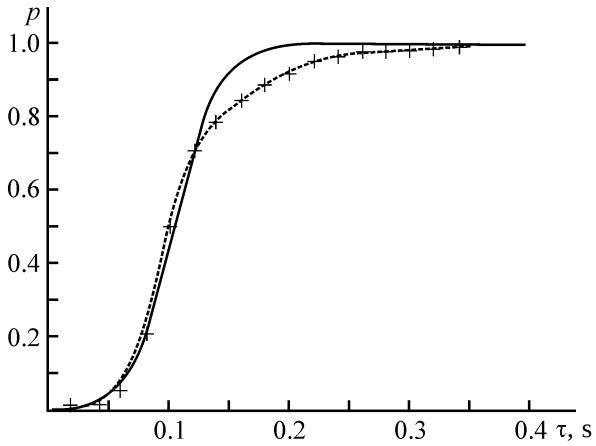


Fig. 4. Comparison of the experiment (dashed line) with the calculation (solid line) for the layered system. Equation coefficients $\beta = 0.003$, $k_1 = 55$.

The first row in Table 4 lists values of β, the fraction of NaCl initiator in $NaClO_3$. For the first three compositions, the NaCl content β is at the level required by GOST, 0.3%. For the last composition, we indicate the real fraction of NaCl specially introduced into $NaClO_3$ to verify the autocatalytic nature of the combustion of $NaClO_3$ mixed with hydrocarbons. For the first two compositions with explosive pressure buildup in the bomb, we obtained large values of k_1, whereas for the last two compositions, they are approximately 15–25 times smaller. The correlation coefficient is no less than 0.95 for all the cases. The coincidence with the experiment is nearly complete for extents of the process of up to 0.8. Further, the calculated curve runs more steeply than the experimental one. Such a deviation of the calculated curve from the experiment for large conversions has been reported extensively [2, 6, 9]. Figures 3 and 4 compare experimental data with results of calculations by Eq. (6) for a PE powder mixed with $NaClO_3$ and PE tubes with $NaClO_3$ (layered system), respectively. The deviation of the calculated curve from the experimental one in the final stage is due to the nonadiabatic nature of the process. There are two ways to obviate this difficulty. The first is to take into account the change in temperature in the equation for the reaction rate and to supplement it with a heat loss equation. This yields a system of two nonlinear differential equations, which cannot be integrated by quadratures. The second, suggested by Ya.B. Zel'dovich, consists in selecting the law of heat loss variation (cooling of the system constituted by the bomb and combustion products) for the given conditions of the experiment. Following the second way, we take the law of variation of the reduced rate constant k_1 with account of changes in the temperature of the system in the form

$$k_1(t) = 1/(a/T_0 + bt), \quad (7)$$

where T_0 is the initial (calculated adiabatic) temperature of the system; t, time; and a, b, coefficients to be determined.

The equation of the autocatalytic reaction can be written with account of the cooling law as follows:

$$\alpha(t) = \frac{\beta[\exp(\beta + 1)k_1(t)t - 1]}{1 + \beta\exp(\beta + 1)k_1(t)t}. \quad (8)$$

Figure 5 compares the experimental dependence of the extent of the process for the layered system with account of nonadiabaticity ($a = 33.2$, $b = 0.07$). It can

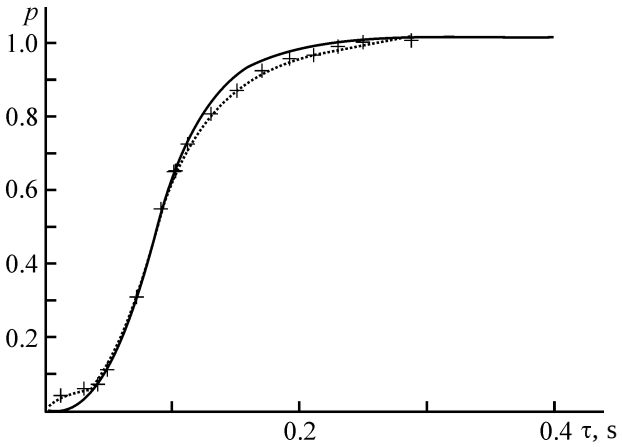


Fig. 5. Variation of the extent of the process with time τ for the layered system. Comparison of the results of a calculation that takes into account the nonadiabatic nature of the system (solid line) with the experiment (dashed line).

be seen that the calculated curve virtually coincides in this case with the experimental value, especially after the extent of the process reaches a value of 0.5, with a correlation coefficient of 0.99. At the same time, if we take an initiator fraction of 10^{-6} and k_1 = 1900 for a PE powder mixed with $NaClO_3$, we achieve a nearly complete coincidence with the experiment (Fig. 3, correlation coefficient 0.99). A similar result is also obtained for a diesel fuel with $NaClO_3$ at $\beta = 10^{-8}$ and k_1 = 950. With these assumptions made, we should accept that the role played by the initiator is minimized and the process is probably initiated by another mechanism (in all probability, of the chain-thermal type). Naturally, the equation coefficients will have other values for a bomb with other parameters, but these values will be of the same order of magnitude. Without pretending to be of metrological importance, the values of the equation coefficients presented here can be used as additional evidence in favor of the hypothesis that the combustion of the layered system is of nondetonation nature.

We use an analytical description because mathematical simulation of processes is considerably less expensive than full-scale experiments. In our case, it allows determination of the influence exerted by such parameters as the charge length, charging density, formulation composition, etc. on the combustion velocity of the system, evaluation of the outflow velocity of combustion products from the burning surface, and its comparison with the critical value at which the combustion mode changes from deflagration- to detonation-type.

CONCLUSIONS

(1) The dependence of the linear combustion velocity of formulations based on sodium chlorate and polyethylene tubes (layered system) with NaCl, KCl, $NaHCO_3$, Na_2CO_3, CuO, Co_3O_4, NiO, and MnO_2 additives was analyzed under atmospheric conditions.

(1.1) Introduction of the above additives in an amount of 9.1 wt % makes it possible to either reduce the linear combustion velocity by a factor of 15–1.6 (with $NaHCO_3$ and Na_2CO_3) or to raise it by a factor of approximately 1.4 (with MnO_2).

(1.2) The effect of SiO_2 is close to the theoretical value for an inert additive: addition of 9.1 wt % diminishes the linear velocity by a factor of 1.18. Addition of the same amount of Al_2O_3 has a weaker effect (decrease by a factor of 1.06).

(1.3) CuO, Co_3O_4, and NiO have virtually no effect of the combustion velocity (an increase by a factor of no more than 1.04).

(1.4) Addition of up to 9.1 wt % NaCl has virtually no effect of the linear combustion velocity of the layered system. This fact can be interpreted as evidence in favor of the autocatalytic nature of combustion of the formulation under consideration.

(1.5) The effect of KCl on the whole process is close to that of Al_2O_3, but without formation of the conglomerate typically formed in combustion of formulations with SiO_2 and Al_2O_3 additives.

(2) The "artificial" porosity of the intertube space has virtually no effect on the linear combustion velocity.

(3) The dynamic pressure developed in combustion of a layered system is about 10 kg m^{-2} for the compositions studied.

(4) The combustion in a constant-volume bomb in textolite vessels with an inner diameter of 38 mm has explosive nature for black powder and formulations composed of sodium chlorate with diesel fuel or powdered polyethylene. The combustion time of a layered system exceeds by one to two orders of magnitude that for the systems considered above, which clearly points to a nondetonation combustion mode.

(5) In the case of combustion of a layered system in the bomb, introduction of 9.1 wt % NaCl into $NaClO_3$ makes the induction period shorter, which also confirms the autocatalytic nature of the combustion of formulations based on sodium chlorate and hydrocarbons.

(6) An equation for autocatalytic reactions, with the nonadiabatic nature of the process taken into account as suggested by Ya.B. Zel'dovich, can be used to describe with a sufficient reliability the combustion of a layered system based on sodium chlorate in a closed space.

(7) The best agreement between the experiment and calculation for explosive processes with sodium chlorate as oxidizing agent and powdered polyethylene or diesel fuel as combustible is achieved when the NaCl concentration in the equation is minimized (10^{-6}–10^{-8} mass fraction instead of the value of 0.003 recommended by GOST).

ACKNOWLEDGMENTS

The author is sincerely grateful to V.B. Ulybin for permanent support of the study and a number of valuable remarks taken into account in preparing the manuscript.

REFERENCES

1. Kirsanov, O.N., Berezuev, Yu.A., Ostrovskii, V.I., and Tyminskii, V.N., *Zh. Prikl. Khim.*, 2003, vol. 76, no. 5, pp. 734–737.
2. Bakhman, N.N. and Belyaev, A.F., *Gorenie geterogennykh kondensirovannykh system* (Combustion of Heterogeneous Condensed Systems), Moscow: Nauka, 1967.
3. Glasner, and Weidenfeld, *J. Am. Chem. Soc*., 1952, vol. 74, pp. 2465–2467.
4. Goronovskii, I.T., Nazarenko, Yu.P., and Nekryach, E.F., *Kratkii spravochnik po khimii* (Concise Handbook of Chemistry), Kiev: Akad. Nauk Ukr. SSR, 1962.
5. Blinov, I.F., *Khloratnye i perkhloratnye vzryvchatye veshchestva* (Chlorate and Perchlorate Explosives), Moscow: Oborongiz, 1941.
6. Belyaev, A.F., Bobolev, V.K., Korotkov, A.I., *et al*., *Perekhod goreniya kondensirovannykh sistem vo vzryv* (Transition from Combustion of Condensed Systems to Explosion), Moscow: Nauka, 1973.
7. Reid, R.G. and Sherwood, T.K., *The Properties of Gases and Liquids*, New York: McGraw-Hill, 1966.
8. Emanuel', N.M. and Knorre, D.G., *Kurs khimicheskoi kinetiki* (Chemical Kinetics), Moscow: Vysshaya Shkola, 1974.
9. Rozovskii, A.Ya., *Kinetika topokhimicheskikh reaktsii* (Kinetics of Topochemical Reactions), Moscow: Khimiya, 1974.

Russian Journal of Applied Chemistry, Vol. 78, No. 11, 2005, pp. 1786–1790. Translated from Zhurnal Prikladnoi Khimii, Vol. 78, No. 11, 2005, pp. 1819–1823.
Original Russian Text Copyright © 2005 by Shkol'nikov.

PHYSICOCHEMICAL STUDIES OF SYSTEMS AND PROCESSES

Thermodynamic Characteristics of the Amphoterism of $M(OH)_2$ Hydroxides in Aqueous Media

E. V. Shkol'nikov

St. Petersburg State Forestry Engineering Academy, St. Petersburg, Russia

Received April 7, 2005

Abstract—Dependences of the molar solubility of amorphous and crystalline hydroxides $M(OH)_2$ on pH of aqueous alkaline nonoxidizing medium at 25°C, and also step constants of basicity and acidity of amphoteric hydroxides $M(OH)_2$ (M = Be, Mn–Zn, Cd, Sn, Pb) were calculated by the thermodynamic method.

The effects of pH on the molar solubility of solid hydroxides of Group II elements in aqueous–alkaline media was calculated earlier [1] by the thermodynamic method. Of interest is the thermodynamic calculation of the solubility of amphoteric hydroxides $M(OH)_2$ for M = Sn, Pb, and 3*d* elements from Mn to Cu. The results of such calculations can be used in the potentiometric analysis and in the determination of conditions for hydrolysis and for practically complete precipitation or efficient masking of cations in the form of soluble hydroxo complexes [2–5]. The amphoterism of hydroxides has been studied insufficiently, and quantitative data on the solubility in aqueous media and on the acid–base properties of ampholytes $M(OH)_2$ are scanty and often contradictory. Thus, according to [3], freshly precipitated hydroxides $M(OH)_2$ are practically water-insoluble, have indications of amphoterism, start to dissolve in alkalis at pH from 10–10.5 (M = Sn, Zn, Pb) to 13.2–14.1 (M = Ni, Be, Fe, Cd, Cu, Mn, Co), and dissolve completely at pH 12–13.5 (M = Zn, Sn). According to [6], $Mn(OH)_2$ and $Fe(OH)_2$ are practically insoluble, and $Ni(OH)_2$ is difficultly soluble in alkalis. According to [7], amorphous precipitates $Cu(OH)_2$ and $Fe(OH)_2$ are soluble in concentrated alkalis; $Co(OH)_2$ is formed as a finely dispersed blue precipitate transforming upon aging into a pink modification soluble in boiling concentrated alkali. No data on the amphoterism of $Mn(OH)_2$ and $Ni(OH)_2$ are given in [7]. According to [2, 7, 8], ampholytes $M(OH)_2$ have weak basic properties, which dominate over acid properties.

Using the procedure from [1], we continued the thermodynamic calculation of the solubility of amorphous and crystalline hydroxides $M(OH)_2$ in pure water and in aqueous–alkaline medium (with additions of NaOH) at pH 7–15 and 25°C. The standard free energies ΔG_f^0 of formation of ions in aqueous solutions, which are necessary for calculating the thermodynamic solubility constants K_s^0 (SP^t), were taken from [9], and the free energies ΔG_f^0 of formation of solid hydroxides at 298 K, from handbooks [10, 11] or were calculated [12]. The molar solubilities of $M(OH)_2$ in pure water and in aqueous NaOH solutions were calculated taking into account the solution ionic strength and the formation of mononuclear hydroxo complexes using the data of [2], and, for the case of nickel(II) and tin(II), the data from the handbook [3]. The calculations were carried out by the generalized equation

$$S = \frac{K_s^0}{f_{M^{2+}} f_{OH^-}^2} \sum_{i=0}^{n} \beta_i [OH^-]^{i-2},$$

where the constant K_s^0 characterizes heterogeneous chemical equilibrium (2); $f_{M^{2+}}$ and f_{OH^-} are molar activity coefficients of M^{2+} and OH^- ions; $\beta_0 = 1$; β_1, β_2, β_3, and β_4 are overall stability constants of the hydroxo complexes MOH^+, $M(OH)_2$, $M(OH)_3^-$, and $M(OH)_4^{2-}$.

The molar solubility of $M(OH)_2$ in 1 M NaOH solution was calculated by the simplified formula $s = 1.06 K_s^0 \Sigma \beta_i$.

We found the equilibrium concentration of free OH^- anions and pH of saturated solutions of hydroxides in pure water (shown in the figure by arrows) by solving a system, as a rule, of three equations [1] using Cardano's method for the reduced cubic equation. For tin(II) and copper(II) hydroxides, we solved systems of four equations taking into account the formation of the complexes $Sn(OH)_3^-$ and $Cu_2(OH)_2^{2+}$,

1070-4272/05/7811-1786© 2005 Pleiades Publishing, Inc.

Table 1. Thermodynamic parameters of dissolution of amorphous and crystalline hydroxides in water and alkali at 25°C

Composition	pK_s^0		H_2O			NaOH		s, M, in 1 M NaOH	A*
	calculation	[3]	$x^0_{M^{2+}}$, mol %	pH^0	s^0, M	pH_{opt}	ps_{min}		
$Mn(OH)_2$**	11.25	–	60	10.4	1.6×10^{-4}	11.5	4.85	2.2×10^{-3}	98
$Mn(OH)_2$	12.76	12.72	84	9.9	4×10^{-5}	11.5	6.36	6.7×10^{-5}	15
$Fe(OH)_2$*	15.10	15.15	72	9.1	7×10^{-6}	10.8	6.88	9×10^{-5}	81
$Fe(OH)_2$	16.38	–	88	8.7	2.4×10^{-6}	10.8	8.16	5×10^{-6}	12
α-$Co(OH)_2$	14.20	14.20	33	9.4	3×10^{-5}	10.9	4.78	3×10^{-4}	73
$Co(OH)_2$**	14.96	14.80	57	9.1	1.1×10^{-5}	10.9	5.54	6×10^{-5}	36
β-$Co(OH)_2$	15.64	15.70	79	8.8	7×10^{-6}	10.9	6.22	1.2×10^{-5}	13
$Ni(OH)_2$**	14.90	14.89	73	9.1	1×10^{-5}	10.2	5.78	1.4×10^{-3}	6×10^2
$Ni(OH)_2$	17.19	17.20	96	8.4	1.2×10^{-6}	10.2	8.10	7×10^{-6}	26
$Cu(OH)_2$**	18.82	19.08	45	7.9	5.8×10^{-7}	9.9	7.96	4×10^{-3}	1×10^5
$Cu(OH)_2$	19.55	19.66	65	7.6	2.6×10^{-7}	9.9	8.67	7×10^{-4}	6×10^4
$Sn(OH)_2$**	25.40	–	10^{-5}	7.06	4×10^{-5}	7.11	4.46	1.0	1.4×10
$Sn(OH)_2$	26.21	26.20	10^{-5}	7.02	6×10^{-6}	7.11	5.26	0.16	1.3×10
$Pb(OH)_2$	19.64	–	60	7.6	2.5×10^{-7}	10.2	8.69	1×10^{-3}	8×10^4

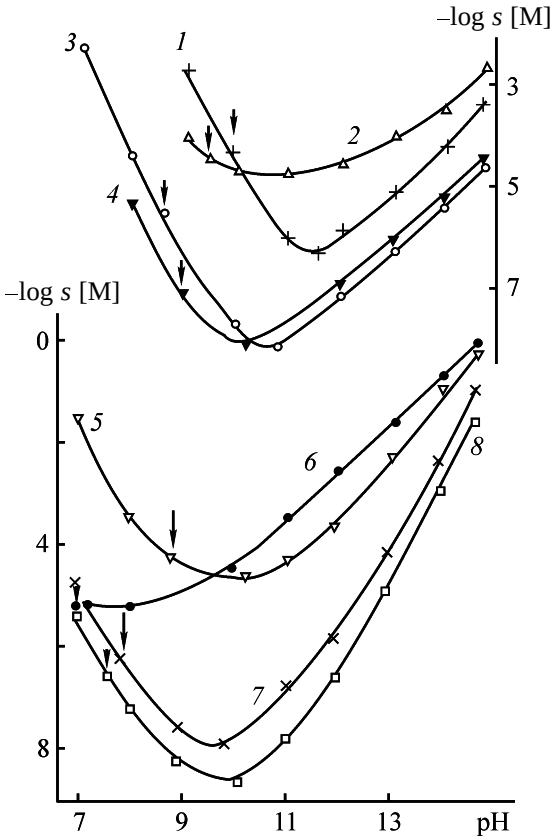
* A is amphoterism parameter.
** Freshly precipitated amorphous.

respectively [2]. The mole fraction $x^0_{M^{2+}}$ of free M^{2+} cations in saturated aqueous solutions of $M(OH)_2$ was calculated similarly to [1] using data of [2, 3].

The calculated results are given in Table 1, where $pK_s^0 = -\log K_s^0$; s^0 and pH^0 are molar solubilities of solid hydroxides in water and pH of saturated aqueous solutions at 25°C, respectively.

Table 1 shows that the pK_s^0 values calculated by the thermodynamic method satisfactorily agree with the reference data [3]. The K_s^0 values for certain modifications of the hydroxides were unknown previously. The solubility of freshly precipitated amorphous hydroxides is higher than that of crystalline modifications. Free M^{2+} cations dominate ($x^0_{M^{2+}} > 0.5$) in saturated aqueous solutions of solid hydroxides (pH^0 7.6–10.4), except for α-$Co(OH)_2$ and amorphous $Cu(OH)_2$ (Table 1). Free Sn^{2+} cations dominate in acid solutions (pH < 3) where they can be determined by potentiometric methods, as well as other M^{2+} cations. The calculated average numbers of ligand $\bar{n}$ in hydroxo complexes (Bjerrum's function) at pH 15 lie in the interval 3–4 for all the hydroxides in Table 1, i.e., the amphoterism conditions $\bar{n} > 2$ are met [1]. The minimal solubility of $M(OH)_2$ precipitates is observed at the optimal concentration of OH^- ions when neutral complexes $M(OH)_2$ dominate in solution among equilibrium species. We found pH_{opt} and then s_{min} from the condition of the maximal mole fraction $x_{M(OH)_2}$, as it was done in [1]. The values of $ps_{min} = -\log s_{min}$ at 25°C are given in Table 1 and partly in the figure, where a strong negative effect of common OH^- ions on the solubility of $M(OH)_2$ in alkali is seen, except for $Sn(OH)_2$, α-$Zn(OH)_2$, and α-$Co(OH)_2$. The effect of common OH^- ions is virtually absent with $Sn(OH)_2$ and HgO [1] (see figure, curve *6*). The analysis shows that high stability constants β_2 of neutral complexes $M(OH)_2$ and their high mole fractions in aqueous solution ($x_{M(OH)_2} \geq 0.9$) are the conditions for the absence of this effect. In the cases of α-$Co(OH)_2$ and α-$Zn(OH)_2$, the common ions decrease by a factor of 2 the solubility in alkali (see figure, curves *2* and *5*), and with the crystalline hydroxide $Fe(OH)_2$ (curve *3*) the effect is the strongest (by a factor of 350).

To estimate quantitatively the amphoterism of hydroxides, we used the ratio ($A > 1$) of their molar solubilities in an alkaline medium with pH 14.7 (5 M NaOH solution) and in pure water. As follows from Table 1 and the calculations [1], the amphoterism parameter A of crystalline hydroxides $M(OH)_2$ decreases in the series Sn > Pb ~ Zn > Cu > Be > Ni > Mn > Co ~ Fe > Cd. The results of the calculations basically agree with scanty experimental data on the solubility of solid hydroxides $M(OH)_2$ in water and alkalis [3–8]. Unlike the data of [6], our calculation shows a 12–15-fold increase in the solubility of $Fe(OH)_2$ and $Mn(OH)_2$ crystals upon the replacement



Solubility *s* of solid hydroxides as a function of pH of aqueous-alkaline medium at 25°C. Hydroxide: (*1*) $Mn(OH)_2$, (*2*) α-$Co(OH)_2$, (*3*) $Fe(OH)_2$, (*4*) $Ni(OH)_2$, (*5*) α-$Zn(OH)_2$, (*6*) $Sn(OH)_2$, (*7*) freshly precipitated $Cu(OH)_2$, and (*8*) $Pb(OH)_2$.

of water by a 5 M NaOH solution (Table 1). Polycondensation, polymerization, and crystallization processes occurring on aging amorphous precipitates considerably decrease the solubility of the hydroxides in water and alkalis [7, 8] with decreasing *s* and *A* (Table 1). Stable crystalline $M(OH)_2$ modifications have the lowest values of these parameters. Their molar solubility in 5 M NaOH solution at 25°C decreases in the order $Sn(OH)_2$ > α-$Zn(OH)_2$ > $Pb(OH)_2$ > $Cu(OH)_2$ > β-$Be(OH)_2$ > $Mn(OH)_2$ > β-HgO > β-$Co(OH)_2$ > β-$Cd(OH)_2$ > $Ni(OH)_2$ > $Fe(OH)_2$ from 0.76 to 3.1×10^{-5} M, respectively, for $Sn(OH)_2$ and $Fe(OH)_2$. Under these conditions, the solubility of the hydroxides does not exceed 0.05 g l^{-1} (starting from β-$Be(OH)_2$); therefore, for its increase, heating in more concentrated alkalis is necessary, whereas in the case of the readily oxidizable hydroxides $Fe(OH)_2$, $Mn(OH)_2$, and $Co(OH)_2$ a reducing atmosphere is also required [7, 8]. Despite high values of amphoterism parameter *A*, the solubility of beryllium and copper(II) hydroxides in 5 M NaOH solution is low (10^{-3} and 0.015 M) because of low values of K_s^0 and s^0 (Table 1).

Amphoteric electrolytes (ampholytes) in which the M–O bonds are similar to O–H bonds in the ionicity [1] are capable of donating or accepting hydroxide ions and protons, transforming into the corresponding ions. Therefore, we supplemented the comparative characteristics of acid–base properties of stable crystalline hydroxides by a calculation of the thermodynamic parameters ΔG_{298}^0 and pK_{298} (*K* is an equilibrium constant) of heterogeneous reactions (1) and (2) in saturated aqueous solution:

$$M(OH)_2(cr) \rightleftarrows MOH^+(sol) + OH^-(sol), \quad (1)$$

$$M(OH)_2(cr) \rightleftarrows M^{2+}(sol) + 2OH^-(sol), \quad (2)$$

$$M(OH)_2(cr) \rightleftarrows H^+(sol) + HMO_2^-(sol), \quad (3)$$

$$M(OH)_2(cr) \rightleftarrows 2H^+(sol) + MO_2^{2-}(sol). \quad (4)$$

The values of pK_{298} calculated using data of [2, 3, 9–11] are given in Table 2, which shows that the basic properties of amphoteric hydroxides $M(OH)_2$, except for $Sn(OH)_2$, dominate over the acid properties. This conclusion is also proved by the calculation of pK_{298} for chemical equilibria (5)–(7) in alkaline and acidic media.

$$M(OH)_2(cr) + OH^-(sol) \rightleftarrows M(OH)_3^-(sol), \quad (5)$$

$$M(OH)_2(cr) + 2OH^-(sol) \rightleftarrows M(OH)_4^{2-}(sol), \quad (6)$$

$$M(OH)_2(cr) + H(sol) \rightleftarrows MOH^+(sol) + H_2O(l), \quad (7)$$

$$M(OH)_2(cr) + 2H^+(sol) \rightleftarrows M^{2+}(sol) + 2H_2O(l). \quad (8)$$

It is seen from Table 2 that zinc and tin(II) hydroxides are the most readily soluble in alkalis, whereas $Mn(OH)_2$, $Cd(OH)_2$, $Co(OH)_2$, and $Zn(OH)_2$ are the most readily soluble in acids.

Thermodynamic constants of basicity ($K_{b,1}$, $K_{b,2}$) and acidity ($K_{a,1}$, $K_{a,2}$) of the ampholytes $M(OH)_2$ dissolved in water as neutral complexes are given in Table 3. Along with the values calculated on the basis of the data form [2, 3, 9], p*K* values from the monograph [8] are also presented.

Table 3 shows that $K_{a,1}$ is higher than $K_{b,1}$ only for $Sn(OH)_2$ molecules in solution. For all the other dissolved ampholytes $M(OH)_2$, the base properties dominate ($K_{b,1} > K_{a,1}$), being the most pronounced

Table 2. Thermodynamic constants of heterogeneous equilibria for stable crystalline hydroxides in water [(1)–(4)], alkaline [(5), (6)], and acidic [(7), (8)] media

Hydroxide	pK_{298} for indicated equilibria							
	(1)	(2)	(3)	(4)	(5)	(6)	(7)	(8)
$Sn(OH)_2$	15.61	26.21	14.28	–	0.84	–	1.62	–1.77
ε-$Zn(OH)_2$	11.45	16.48	–	29.18	2.90	1.77	–2.54	–11.50
$Pb(OH)_2$	13.42	19.64	19.65	–	5.80	3.02	–0.57	–8.35
$Cu(OH)_2$	13.52	19.55	18.17	31.29	4.34	3.21	–0.46	–8.42
β-$Be(OH)_2$	13.11	22.39	–	29.49	2.98	3.16	–0.88	–5.58
$Ni(OH)_2$	12.95	17.19	–	–	5.10	3.91	–1.04	–10.76
$Fe(OH)_2$	11.88	16.38	20.37	–	5.38	6.38	–2.11	–11.60
$Mn(OH)_2$	9.36	12.76	19.0	–	4.27	5.08	–4.63	–15.21
β-$Co(OH)_2$	11.23	15.64	–	–	5.10	5.90	–2.76	–12.27
β-$Cd(OH)_2$	10.37	14.27	18.70	–	5.93	5.67	–3.62	–13.70

Table 3. Thermodynamic step constants of basicity $K_{b,1}$, $K_{b,2}$ and acidity $K_{a,1}$, $K_{a,2}$ of amphoteric hydroxides $M(OH)_2$ in water at 25°C

Compound	$pK_{b,1}$	$pK_{b,2}$	$pK_{a,1}$	$pK_{a,2}$
$Sn(OH)_2$	9.8 ± 0.5	11.1 ± 0.5 12.0 [8]	9.0	–
$Zn(OH)_2$	6.05	5.02 4.4 [8]	11.5 [8]	12.7 [8] 12.3
$Pb(OH)_2$	3.9 ± 0.6	6.9 ± 0.6 7.7 [8]	10.8 11.0 [8]	–
$Cu(OH)_2$	5.68	6.03 6.5 [8]	10.33 10 [8]	13.12 13 [8]
$Be(OH)_2$	5.75	9.27 7.5 [8]	10.5	11.6
$Ni(OH)_2$	4.86	4.27	–	–
$Fe(OH)_2$	2.90	4.49	11.39	–
$Mn(OH)_2$	2.38	3.41	11.97	–
$Co(OH)_2$	4.84	4.47 4.4 [8]	–	–
$Cd(OH)_2$	3.72	3.91 4.2 [8]	12.06	–
$Hg(OH)_2$	11.22	10.59 10.4 [8]	14.80	–

for $Mn(OH)_2$, $Fe(OH)_2$, and $Cd(OH)_2$ and the weakest for $Hg(OH)_2$.

CONCLUSIONS

(1) The molar solubility of hydroxides $M(OH)_2$ in water decreases as the thermodynamic stability of solid hydroxides and hydroxo complexes in aqueous solution increases. It decreases also on passing from amorphous to stable crystalline modifications.

(2) The effect of pH of an aqueous-alkaline nonoxidizing medium on the molar solubility of solid hydroxides $M(OH)_2$ (M = Sn, Pb, and 3*d* elements Mn–Cu) was calculated by the thermodynamic method. It was found that these hydroxides meet the amphoterism condition (the average ligand number in the hydroxo complexes $\bar{n} > 2$ at pH 14–15). The amphoterism was assessed quantitatively [parameter *A* increases in the range from 12 for $Fe(OH)_2$ to 1.4×10^5 for $Sn(OH)_2$].

(3) The minimal solubility and the values of pH corresponding to the most complete precipitation of the amphoteric hydroxides $M(OH)_2$ were calculated in view of the formation of hydroxo complexes.

(4) The calculation of the thermodynamic constants for heterogeneous acid–base equilibria in aqueous media and also of basicity and acidity step constants of neutral complexes $M(OH)_2$ shows that their base properties dominate. Such properties are the most noticeable in case of the ampholytes $Mn(OH)_2$, $Fe(OH)_2$, and $Cd(OH)_2$ and are the weakest in the case of $Hg(OH)_2$. Only in the case of $Sn(OH)_2$ weak acid properties noticeably dominate over weak base properties.

REFERENCES

1. Shkol'nikov, E.V., *Zh. Prikl. Khim.*, 2004, vol. 77, no. 8, pp. 1271–1274.
2. Fishtik, I.F. and Vataman, I.I., *Termodinamika gidroliza ionov metallov* (Thermodynamics of the Hydrolysis of Metal Ions), Chisinau: Shtiintsa, 1988.
3. Lur'e, Yu.Yu., *Spravochnik po analiticheskoi khimii* (Handbook on Analytical Chemistry), Moscow: Khimiya, 1989.

4. Kumok, V.N., Kuleshova, O.M., and Karabin, L.A., *Proizvedeniya rastvorimosti* (Solubility Products), Novosibirsk: Nauka, 1983.
5. Nazarenko, V.A., Antonovich, V.P., and Nevskaya, E.M., *Gidroliz ionov metallov v razbavlennykh rastvorakh* (Hydrolysis of Metal Ions in Dilute Solutions), Moscow: Atomizdat, 1979.
6. Efimov, A.I. *et al.*, *Svoistva neorganicheskikh soedinenii: Spravochnik* (Properties of Inorganic Compounds: Handbook), Leningrad: Khimiya, 1983.
7. Remy, H., *Lehrbuch der Anorganischen Chemie*, Leipzig: Geest und Portig, 1961, vol. 2.
8. Nekrasov, B.V., *Osnovy obshchei khimii* (Foundations of General Chemistry), St. Petersburg, 2003, vols. 1, 2.
9. Vasil'ev, V.P., *Termodinamicheskie svoistva rastvorov elektrolitov* (Thermodynamic Properties of Electrolyte Solutions), Moscow: Vysshaya Shkola, 1982.
10. Karapet'yants, M.Kh. and Karapet'yants, M.L., *Osnovnye termodinamicheskie konstanty neorganicheskikh i organicheskikh veshchestv* (Basic Thermodynamic Constants of Inorganic and Organic Substances), Moscow: Khimiya, 1968.
11. *Termodinamicheskie svoistva individual'nykh veshchestv: Spravochnik* (Thermodynamic Properties of Individual Substances: Handbook), Glushko, V.P., Ed., Moscow: Nauka, 1979–1981, vols. 1–4.
12. Shkol'nikov, E.V., Naraev, V.N., and Fomicheva, T.I., *Osnovy khimicheskoi termodinamiki* (The Foundations of Chemical Thermodynamics), St. Petersburg: Sankt-Peterb. Gos. Lesotekh. Akad., 2002.

Russian Journal of Applied Chemistry, Vol. 78, No. 11, 2005, pp. 1791–1794. Translated from Zhurnal Prikladnoi Khimii, Vol. 78, No. 11, 2005, pp. 1824–1826.
Original Russian Text Copyright © 2005 by Tseluikin, Solov'eva.

PHYSICOCHEMICAL STUDIES OF SYSTEMS AND PROCESSES

Viscous Flow of Concentrated Aqueous Solutions of $NiCl_2$ + $FeCl_2$

V. N. Tseluikin and N. D. Solov'eva

Technological Institute, Saratov State Technical University, Engels, Saratov oblast, Russia

Received February 17, 2005; in final form, September 2005

Abstract—The dynamic viscosity, apparent molar volume, enthalpy, and Gibbs energy of activation of a viscous flow of concentrated aqueous solutions of $NiCl_2$ + $FeCl_2$ were calculated. The concentration dependences of these parameters were analyzed in terms of structural transformations. A polynomial approximation of the concentration dependences of the dynamic viscosity of the solutions under study was performed using MATLAB 6.1 software package.

The internal friction in a fluid, the energy of interaction between particles, and structural transformations occurring when the concentration and temperature of a solution are changed can be characterized by analyzing the dynamic viscosity [1–3]. Previously we studied the viscous flow of $NiSO_4$ and $NiCl_2$ solutions [4]. The aim of this study was to examine the concentration dependences of the dynamic viscosity of a two-component solution of $NiCl_2$ + $FeCl_2$ with a constant concentration of iron(II) chloride (1.20 M). These salts are the main components of chloride electrolytes used in deposition of the iron–nickel alloy.

EXPERIMENTAL

The dynamic viscosity η (cP) was calculated using the relation

$$\eta = \nu\rho,$$

where ν is the kinematic viscosity (cSt), and ρ is density (g cm^{-3}).

The kinematic viscosity was determined using a VPZh viscometer with a capillary diameter of 0.56 mm [GOST (State Standard) 10028–81]. The density was measured pycnometrically. The measurement error was 0.2–0.4%. The reproducibility of the experimental results was confirmed by calculating the Cochran test [5].

The competitive action of disrupting and stabilizing factors leads to a nonmonotonic run of the concentration dependences of the dynamic viscosity of the solutions under study (Fig. 1). It is known [6, 7] that, when penetrating into structural voids of water, ions with crystallographic radii exceeding 0.130 nm (void size) deform these voids and rupture hydrogen bonds between molecules. The radius of the Cl^- ion is 0.181 nm [8], and, apparently, chloride ions characterized by negative hydration will disrupt the structure of the solvent. However, Ni^{2+} and Fe^{2+} ions, whose radii are 0.074 and 0.080 nm, respectively, will stabilize the solution structure by being freely accommodated in the voids and binding free water molecules into hydrate complexes. The considerable increase in the viscosity of two-component solutions at $NiCl_2$ concentrations of 3.10–3.86 M (Fig. 1) is probably due to formation of a new structure of the solution, constituted by hydrated ions bound together by hydrogen bonds.

The significant changes in the structure of $NiCl_2$ + $FeCl_2$ solutions are indicated by the nonlinear concentration dependence of the apparent molar volume Φ_V

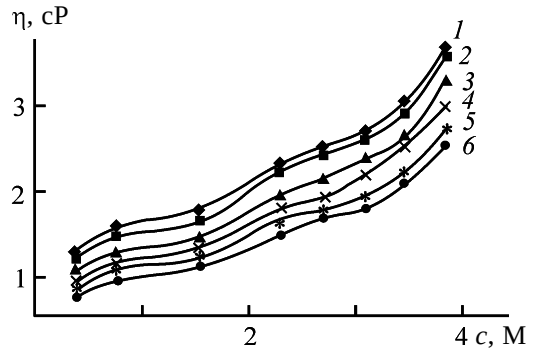


Fig. 1. Dynamic viscosity η vs. the concentration c of $NiCl_2$ in a solution with 1.20 M $FeCl_2$. T (°C): (*1*) 20, (*2*) 30, (*3*) 40, (*4*) 50, (*5*) 60, and (*6*) 70.

1070-4272/05/7811-1791 © 2005 Pleiades Publishing, Inc.

Table 1. Activation energy of viscous flow, ΔG_η^*, for aqueous solutions of $NiCl_2$ + $FeCl_2$. $FeCl_2$ concentration 1.20 M

T, °C	ΔG_η^*, kJ mol^{-1}, at indicated c_{NiCl_2}, M							
	0.39	0.77	1.54	2.30	2.70	3.10	3.47	3.86
20	94.2	94.7	95.1	95.9	96.2	96.4	96.7	97.3
30	97.2	97.8	98.2	99.0	99.4	99.7	99.9	100.5
40	100.1	100.7	101.1	102.0	102.4	102.7	103.0	103.6
50	103.0	103.6	104.1	105.0	105.4	105.8	106.2	106.7
60	105.9	106.6	107.1	108.1	108.4	108.7	109.1	109.8
70	108.8	109.5	110.0	111.0	111.6	111.8	112.2	112.8

(Fig. 2). Φ_V was calculated in terms of the approach suggested by Onori [9]:

$$\Phi_V = (V - X_1V_1)/X_2,$$

where V is the average molar volume of the solution, defined by

$$V = (X_1M_1 + X_2M_2)/\rho,$$

X_1, X_2, M_1, M_2, mole fractions and molecular weights of the solvent and solute; and V_1 is the volume of 1 mol of free molecules of water. This volume can be calculated by the formula

$$V_1 = (1 - x)V_s,$$

where x is the mole fraction of water molecules in the voids, and V_s is the molar volume of the skeleton.

The apparent molar volume of ions increases through a decrease in the amount of water subjected to electrostriction and is complete when no water remains in the solution outside the coordination sphere of the cations. The deviation from linearity of the Φ_V–$c^{1/2}$ dependence for the solutions under study (Fig. 2) may indicate that the limit of complete hydration is reached. The increase in the apparent molar volume on raising the temperature from 40 to 50°C is probably due to deformation and rupture of hydrogen bonds in the structure of the solvent and to simultaneous binding of free water molecules into hydrate complexes.

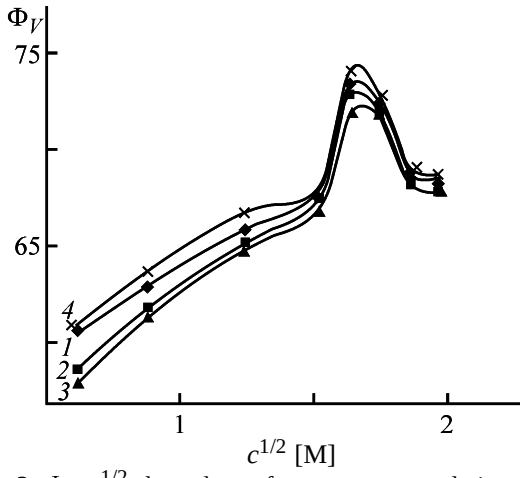


Fig. 2. Φ_V–$c^{1/2}$ dependence for an aqueous solution containing $NiCl_2$ and 1.20 M $FeCl_2$. (c) $NiCl_2$ concentration. T (°C): (*1*) 20, (*2*) 30, (*3*) 40, and (*4*) 50.

As water is an associated fluid, the viscous flow is accompanied by a structural deformation, which requires energy expenditure. The energy expenditure for a viscous flow can be evaluated using the Eyring theory [10]. The Gibbs energy of the solutions under study was calculated in terms of this theory by the formula

$$\Delta G_\eta^* = RT\ln(\nu\overline{M}/hN_A),$$

where R is the universal gas constant; T, absolute temperature; $\overline{M}$, average molecular weight ($\overline{M} = \Sigma M_iN_i$, M_i and N_i, molecular weights and mole fractions of solution components); h, Planck constant; and N_A, Avogadro number.

The Gibbs energy of activation of a viscous flow of $NiCl_2$ + $FeCl_2$ solutions (Table 1) markedly exceeds ΔG_η^* of single-component $NiSO_4$ and $NiCl_2$ electrolytes [4]. This indicates that the structure of two-component solutions is more ordered.

The equation [10]

$$\Delta H_\eta^* = R\frac{d\log\nu}{d(1/T)}$$

was used to calculate the enthalpy of activation of a viscous flow in the solutions under study at T = 20–70°C.

Table 2. Coefficients of the dependences of the dynamic viscosity of aqueous solutions of $NiCl_2$ + $FeCl_2$ on the $NiCl_2$ concentration at different temperatures: $\eta = A + Bc + Cc^2 + Dc^3 + Fc^4 + Hc^5 + Kc^6 + Lc^7$. $FeCl_2$ concentration 1.20 M

T, °C	*A*	*B*	*C*	*D*	*F*	*H*	*K*	*L*
20	0.1058	5.0845	–6.3755	3.2639	–0.2081	–0.3520	0.1107	–0.0099
30	–2.0366	16.9794	–31.3670	28.5410	–14.0150	3.8315	–0.5520	0.0329
40	–2.3925	18.7287	–36.4859	35.3083	–18.6074	5.4812	–0.8501	0.0542
50	–3.5413	24.6658	–49.0094	47.9628	–25.3943	7.4499	–1.1401	0.0711
60	–1.8370	13.9137	–25.6536	23.5105	–11.6640	3.2156	–0.4649	0.0276
70	3.2809	–15.7905	36.3661	–39.7843	23.3536	–7.5131	1.2474	–0.0835

Enthalpy of activation of a viscous flow, ΔH_η^*, for aqueous solutions of $NiCl_2$ + 1.20 M $FeCl_2$

c_{NiCl_2}, M	ΔH_η^*, kJ mol^{-1}
0.39	9.0
0.77	8.4
1.54	7.8
2.39	7.5
2.70	7.1
3.10	7.0
3.49	6.4
3.86	6.4

The values of ΔH_η^* for $NiCl_2$ + $FeCl_2$ solutions are lower than the enthalpies of activation of a viscous flow of water (ΔH_η^* for water is 16.26 kJ mol^{-1} [7]), which indicates that the process can easily pass from one equilibrium position to another, and, consequently, the structure of the solution is disordered. The decrease in the height of the potential barrier with increasing viscosity can be understood if it is assumed that a new polyion structure, whose elements are hydrated ions of the solution and water molecules, is formed in concentrated solutions close to saturation. The structure being formed is less stable than the water skeleton.

Representation of the concentration dependence of the dynamic viscosity in the form of a polynomial allows its adequate mathematical description [7]. The functions polyfit(*x*, *y*, *n*) and polyval(*x*, *y*) of the MATLAB 6.1 software package [11] were used to perform a polynomial approximation of experimental data at concentrations in the range 0.3–4 M, using the least-squares method. The approximating polynomial has the form

$$\eta = a_0 + \sum_{i=1}^{n} a_i c^i,$$

where *a* is a coefficient and *c* is the electrolyte concentration (M).

An analysis of the experimental data with approximating polynomials of the order *n* = 3–10 demonstrated that, as in the case of single-component $NiSO_4$ and $NiCl_2$ electrolytes [4], the adequate mathematical model of the dynamic viscosity of $NiCl_2$ + $FeCl_2$ solutions is a 7th-order polynomial (Table 2).

CONCLUSIONS

(1) The behavior of the dynamic viscosity, activation characteristics of the viscous flow, and apparent molar volume of $NiCl_2$ + $FeCl_2$ electrolytes with increasing concentration and temperature indicates that complex structural transformations occur in these electrolytes, which are accompanied by disintegration of the structure of the solvent, hydration of ions, and formation of a new polyion structure in concentrated solutions close to saturation.

(2) The resulting polynomial models of the dynamic viscosity of the solutions studied make it possible to calculate this parameter at concentrations in the range 0.3–4 M. A 7th-order polynomial was accepted as an adequate mathematical model.

REFERENCES

1. Krestov, G.A., *Termodinamika ionnykh protsessov v rastvorakh* (Thermodynamics of Ionic Processes in Solutions), Leningrad: Khimiya, 1984.
2. Krestov, G.A., Novoselov, I.P., Perelygin, I.S., *et al*., *Ionnaya sol'vatatsiya* (Ionic Solvation), Moscow: Nauka, 1987.
3. Abrosimov, V.K., Krestov, A.G., Al'per, G.A., *et al*., *Dostizheniya i problemy sol'vatatsii: strukturno-termodinamicheskie aspekty* (Advances and Problems of Solvation: Structural and Thermodynamic Aspects), Moscow: Nauka, 1998.
4. Solov'eva, N.D., Klinaev, Yu.V., and Tseluikin, V.N., *Zh. Fiz. Khim.*, 2003, vol. 77, no. 3, pp. 459–462.

5. Tyurin, Yu.N. and Makarov, A.A., *Statisticheskii analiz dannykh na komp'yutere* (Statistical Analysis of Data on a Computer), Moscow: Infra-M, 1998.
6. Voloshin, V.P., Zheligovskaya, E.A., Malenkov, G.G., *et al*., *Ross. Khim. Zh.*, 2001, vol. 45, no. 3, pp. 31–37.
7. Erdey-Gruz, T., *Transport Phenomena in Aqueous Solutions*, Budapest: Akad. Kiado, 1974.
8. Rabinovich, V.A. and Khavin, Z.Ya., *Kratkii khimicheskii spravochnik* (Concise Handbook of Chemistry), Leningrad: Khimiya, 1977.
9. Onori, G., *J. Chem. Phys.*, 1988, vol. 69, no. 1, pp. 510–516.
10. Glasstone, S., Laidler, K.J., and Eyring, H., *The Theory of Rate Processes. The Kinetics of Chemical Reactions, Viscosity, Diffusion and Electrochemical Phenomena*, New York: McGraw-Hill, 1941.
11. D'yakonov, V.P., *MATLAB: uchebnyi kurs* (MATLAB: Student's Manual), St. Petersburg: Piter, 2001.

Russian Journal of Applied Chemistry, Vol. 78, No. 11, 2005, pp. 1795–1800. Translated from Zhurnal Prikladnoi Khimii, Vol. 78, No. 11, 2005, pp. 1827–1832.
Original Russian Text Copyright © 2005 by Rubtsov, Kazakov, Rustambekov, Starshinov.

PHYSICOCHEMICAL STUDIES OF SYSTEMS AND PROCESSES

Kinetic Aspects and Heats of Reaction between Components in Thermal Decomposition of Ammonium Nitrate–Calcium (Magnesium) Carbonate Mixtures

Yu. I. Rubtsov, A. I. Kazakov, M. K. Rustambekov, and M. S. Starshinov

Institute for Problems of Chemical Physics, Russian Academy of Sciences, Chernogolovka, Moscow oblast, Russia

Received February 22, 2005

Abstract—The kinetics of heat absorption in thermal decomposition of commercial ammonium nitrate–calcium (magnesium) carbonate mixture and a model mixture of ammonium nitrate and calcium carbonate was studied. Rate equations of the processes and temperature dependences of constants in these equations were determined. The heats of these reactions were calculated.

It is known that manufacture, transportation, and storage of a nitrogen fertilizer, ammonium nitrate (AN), is associated with a certain danger of its explosive transformation. This transformation may result from a detonation explosion of AN, initiated by an external shock wave, or be caused by its spontaneous thermal ignition upon violation of the required temperature mode of storage or in a fire during transportation or storage. More than 80 major accidents caused by explosive transformations of AN have been described; these reports are reviewed in [1]. Most frequently, such explosions are caused by spontaneous thermal ignition of AN in fires in storehouses and cars.

That is why the possible reasons for such explosions of AN and, in particular, for its spontaneous thermal ignition have been studied extensively [2–5]. A considerable attention has been given to analysis of the kinetic aspects of heat release in thermal decomposition of AN and to the influence exerted by various factors on its rate, because the main cause of thermal explosions is the disturbance of the equilibrium between heat release and heat removal across the boundaries of the system [5]. It was established that the rate of heat release is determined by the content of HNO_3 molecules in the system and an increase in this rate in the course of decomposition is due to accumulation of HNO_3. Accordingly, introduction of minor amounts of additives that can bind HNO_3 makes lower the rate of heat release.

As a main way to diminish the detonation capacity of AN, it is recommended to lower its nitrogen content to below 28% by introducing various additives, primarily ammonium carbonates and phosphates. At present use of AN with nitrogen content higher than 28% in agriculture is either prohibited or strictly limited in some countries (pure AN contains more than 34.8% nitrogen). This goal is achieved in production of ammonium nitrate–calcium (magnesium) carbonate (CAN; AN with addition of 20–40% limestone, chalk, or dolomite), whose manufacture is being set-up in Russia now. In doing so, a question arises as to whether granulation of mixtures of this kind is safe, compared with pure AN. The possible difference in safety is primarily determined by that in rates of heat release in thermal decomposition of these fertilizers. The aim of this study was to find the rates of thermal decomposition of CAN and to compare the data obtained with the rates for ordinary AN. It has been established previously [6] that introduction of less than 1% ammonium phosphates into AN markedly reduces the rate of heat release in thermal decomposition and slows down the self-acceleration of the reaction. The latter occurs through a decrease in the excess amount of HNO_3 both in model mixtures of AN with phosphates and in a commercial sample of ammonium nitrate with a phosphate-sulfate additive. Introduction of carbonates into AN must, in principle, exert a similar influence, but a markedly larger amount of the additive may lead not only to quantitative, but also to fundamental changes.

EXPERIMENTAL

We studied the kinetics of heat release on a DAK-1-2 automated differential calorimeter [7]. Commonly, AN is decomposed in a sealed ampule, as

1070-4272/05/7811-1795© 2005 Pleiades Publishing, Inc.

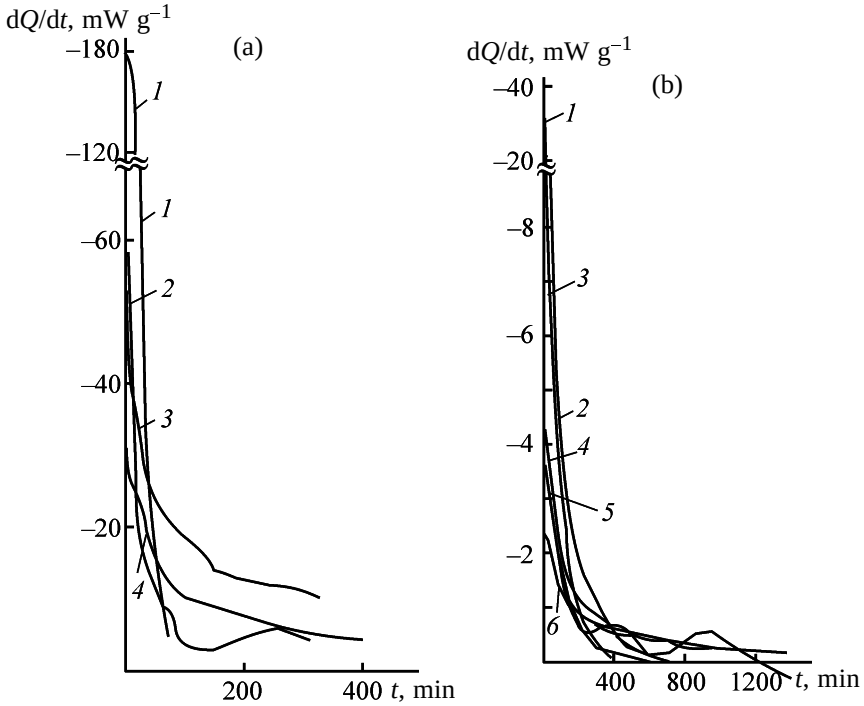


Fig. 1. Heat absorption rate dQ/dt vs. time t in thermal decomposition of (a) a mixture of AN and $CaCO_3$ and (b) CAN. Decomposition temperature, °C: (a) (*1*) 222.5, (*2*) 211.0, (*3*) 202.4, and (*4*) 192.7; (b) (*1*) 234.7, (*2*) 219.5, (*3*) 207.3, (*4*) 202.8, and (*5*) 188.1.

it was done in [6]. However, a certain amount of NH_3 and CO_2 is evolved in mixing of components in manufacture of CAN, and, therefore, the mixer is equipped with an outlet for their discharge. Therefore, to approach the industrial conditions, we used long glass ampules that extended beyond the limits of the calorimeter and allowed discharge of gaseous reaction products into the atmosphere. The gas pressure within the ampule is always equal to the atmospheric pressure. Under these conditions, too, the ampule will always contain a certain amount of NH_3, which will shift the equilibrium of AN dissociation and make lower the concentration of HNO_3 in the melt, but ammonia will not be accumulated and its content in the gas and, accordingly, in the AN melt will decrease as the reaction rate will become lower. These conditions are rather close to those of the real industrial process.

We studied the thermal behavior of a model mixture of analytically pure grade AN with calcium carbonate of the same grade in the temperature range 192.7–222.0°C, with mechanical mixtures of the components taken in a 50 : 50 mass ratio at a total mass of 0.5 g. The absence of the granulation operation in this case is of no importance because the study was performed at temperatures above the melting point of AN and grains would anyway melt. The system under study had the form of molten AN melt with $CaCO_3$ particles embedded in the melt.

It was established that, in contrast to any of the previously studied AN-based fertilizer samples, in which heat release was always observed at all temperatures exceeding the melting point of AN, heat absorption occurs in the model samples under study during a rather long time. The obtained heat absorption curves are shown in Fig. 1. The initial portion of these curves is described by a first-order kinetic equation, and the temperature dependence of the initial rate of heat absorption, k_1 (W g^{-1}), has the form

$$k_1 = -8.1 \times 10^{12} \exp(-129.5 \times 10^3/RT).$$

An analysis of published data on CAN properties [8] demonstrated that, in mixing of an AN melt with $CaCO_3$, there occurs a rather slow exchange reaction between these salts to give ammonium carbonate, which, in turn, decomposes into NH_3, CO_2, and H_2O. Ammonia and carbon dioxide are mostly released into the gas phase, and H_2O may be partly retained in the melt in the form of calcium nitrate hydrate. The evolving gaseous products agitate the mixture. This process occurs with absorption of heat (for a thermodynamic calculation of the heat of this reaction, see below) and its rate under the experimental conditions is higher than that of heat release in decomposition of AN, which predetermines the overall absorption of heat in the system.

We paid primary attention to a study of experimental CAN samples based on dolomite. Compared with limestone and chalk, this mineral is a considerably less reactive toward acid products and does not dissolve in dilute acids under ordinary conditions [8]. Therefore, it was important to find out whether the heat absorption effect, observed in examination of the model mixture of AN and $CaCO_3$, will be manifested for a fertilizer with dolomite. The formation and decomposition of ammonium carbonate in a mixture of this kind will be governed by the reaction of dolomite with HNO_3, but at a temperature markedly exceeding room temperature.

We examined the kinetics of heat absorption in thermal decomposition for two experimental samples of a calcium–ammonium fertilizer of the following composition (%): sample no. 1: AN 75, dolomite 25, and SO_4^{2-} 0.5; sample no. 2: AN 75, dolomite 25, SO_4^{2-} 0.5, and lilamine AS-6/2 0.08. The samples only differ in that sample no. 2 contains a lilamine-based anticaking coating on the grain surface. In both samples, we used dolomite of the following chemical composition (%): CaO(tot) 29.9, MgO(tot) 19.3, SiO_2 5.4, Fe_2O_3 0.42, Al_2O_3 0.45, and H_2O 0.2; and granulometric composition (%) >3 mm 0, >1 mm 0.2, 1–0.63 mm 0.1, 0.63–0.25 mm 1.2, 0.25–0.1 mm 67.2, and <0.1 mm 31.3.

We analyzed the kinetics of heat absorption in decomposition of sample nos. 1 and 2 in the temperature range 188.1–234.0°C. The curves of heat absorption rates for sample no. 1 are shown in Fig. 1b. For sample no. 2, they are for the most part similar, with minor quantitative differences. It can be seen that, at all temperatures, heat absorption occurs during a rather long time from the very beginning of the experiment, and the rate of this heat absorption gradually decreases to about 0.1–0.2 mW g^{-1}. Only at 234°C a minor heat release is observed after 20–23 h, whereas at lower temperatures there is virtually no significant heat release from sample nos. 1 and 2 during 24 h. The reproducibility of the rates of heat absorption or release, obtained in the final stages of the experiments, is low, which is probably due to very small absolute values of these rates and to an insufficient compositional homogeneity of technical-grade samples. Solid dolomite particles in the AN melt are agitated, as in the case of calcium carbonate, by the evolving gaseous products.

The heat absorption is the highest at the beginning of the process and then decreases, which is apparently due to consumption of the components and passivation of the surface of dolomite particles by products of the exchange reaction. As temperature increases, the rate of heat absorption grows, as it should be for the rate of a chemical reaction. The resulting heat absorption curves can be described, in their initial portions, by a first-order kinetic equation:

$$dQ/dt = k_1(1 - Q/Q_1),$$

where dQ/dt is the rate of heat absorption (mW g^{-1}); k_1, rate constant (mW g^{-1}); and Q and Q_1, running and final heats of the process in the initial stage, respectively (J g^{-1}).

Selected numerical parameters of the heat absorption curves are listed in Table 1; the decomposition heat was calculated by integrating the experimental curves for heat absorption rates. The quantity Q_- (J g^{-1}) in the table is the overall heat absorption measured during the experiment, which is the sum of heat absorption in the initial stage (Q_1) and of that in the subsequent stages. The quantity Q_{tot} (J g^{-1}) is an algebraic sum of the absorbed and released heat, recorded during the time of the experiment (t_{fin}, h). In the runs in which no heat was released at the end of the process, Q_{tot} is equal to the overall heat absorption Q_- during the experiment, in which case the figures in columns 5 and 6 coincide. In those runs in which $Q_- < Q_1$, the process was terminated before the completion of the final stage, and Q_1 was found by interpolation of the linear dependence of dQ/dt on Q to zero rate. The quantity $(dQ/dt)_{fin}$ (mW g^{-1}) corresponds to the rate at the end of the run.

The temperature dependence of the rate constants k_1 for sample nos. 1 and 2 has the following form: sample no. 1: $k_1 = -8.1 \times 10^{11} \exp(-129.5 \times 10^3/RT)$; sample no. 2: $k_1 = -9.6 \times 10^{12} \exp(-140.3 \times 10^3/RT)$.

The heat absorption rates obtained in the case of CAN (sample no. 1) decomposition are approximately an order of magnitude lower than those in decomposition of a mixture of AN with $CaCO_3$, which is primarily due to the lower reactivity of dolomite. The heat absorption rates in decomposition of sample no. 2 are, on the average, somewhat lower than those for sample no. 1, which is due to presence of an organic coating on grains of sample no. 2. This coating is oxidized by the AN melt with heat release. Because the share of this coating in the sample is only 0.08%, the contribution of its oxidation to the overall process is small and it can only somewhat reduce the observed rate of heat release. The oxidation leads to formation on the sample surface of a well-noticeable thin polymeric film, which hinders pouring-out of the molten mixture from the ampule, and this confirms that the

Table 1. Heat absorption rates and heat effects in decomposition of CAN samples

Sample no.	T, °C	k_1, mW g^{-1}	Q_1	Q_-	Q_{tot}	t_{fin}, h	$(dQ/dt)_{fin}$, mW g^{-1}
			J g^{-1}				
1	188.1	–2.3	–35.5	–35.5	–35.5	23.2	–0.13
2	188.1	–1.2	–50.5	–43.5	–43.5	22.0	–0.46
1	194.1	–1.7	–56.4	–53.1	–53.1	23.0	–0.71
2	194.1	–1.4	–54.3	–52.3	–52.3	30.8	–0.26
1	207.3	–7.7	–29.3	–42.6	–42.6	19.2	–0.6
2	207.3	–6.3	–30.5	–61.4	–61.4	20.8	–0.21
1	219.5	–12.8	–59.4	–59.4	–59.4	22.5	–0.04
2	219.5	–9.4	–47.7	–78.6	–78.6	22.8	–1.17
1	234.7	–42	–60.2	–114	–113	23.3	1.13
2	234.7	–32.5	–64.4	–106	–102	22.5	1.93

oxidation reaction does occur. In a melt of granulated AN, this reaction is very fast and is manifested in an increase in the initial rate of heat release, which makes shorter the calculated adiabatic induction period of ignition. In the mixture in question, this heat release proceeds at a considerably lower rate because of the lower concentration of nitric acid. It is compensated by a stronger heat absorption in the exchange reaction, so that the safety of the process is virtually not changed at all by the presence of an organic coating and there is no overall heat release with the organic coating, too.

The kinetic data presented above were obtained for an open ampule and small (0.5–1 g) sample masses. Under industrial conditions, gas discharge is more difficult, primarily because of the large mass of a mixture being processed. To determine whether this circumstance can affect the fundamental aspects of heat absorption, we performed an experiment at 234°C in a sealed ampule, in which all products are retained and accumulated in the gas over the sample. The initial rate of heat absorption under these conditions is 2–3 times lower, compared with an open ampule, which is probably due to hindered evolution of NH_3 and H_2O into the gas phase, but all the fundamental aspects of heat absorption are preserved: there is no heat release under these conditions during the first 10–20 h.

We performed a thermodynamic calculation of the reactions

$$CaCO_3 + 2NH_4NO_3 = Ca(NO_3)_2 + 2NH_3 + CO_2 + H_2O, \quad (1)$$

$$CaCO_3 \cdot MgCO_3 + 4NH_4NO_3 = Ca(NO_3)_2 + Mg(NO_3)_2 + 4NH_3 + 2CO_2 + 2H_2O \quad (2)$$

on the basis of the standard enthalpies of formation of the reactants, taken from the handbook [9]. Instead of the unknown standard enthalpy of dolomite formation, we took the sum of the standard enthalpies of formation of calcium and magnesium carbonates and the calculation was performed for formation of both liquid and gaseous water. The following heats were obtained: reaction (1): –435 kJ mol^{-1} $CaCO_3$ for water in the melt and –481 kJ mol^{-1} $CaCO_3$ for water in the gas; reaction (2): –715 kJ mol^{-1} dolomite for water in the melt and –807 kJ mol^{-1} dolomite for water in the gas. If these values are used and the excess, over the equivalent composition, amount of AN in the fertilizer is considered an inert constituent, the following maximum possible amounts of heat absorption can be obtained per gram of sample nos. 1 and 2: –982 J g^{-1} for water in the melt and –1104 J g^{-1} for water in the gas.

The heats for liquid and gaseous water are not strongly different, both being several times the heats obtained in experiments for sample nos. 1 and 2. Surely, the heat absorption may somewhat decrease because of the heat release in decomposition of AN, but this rate cannot be significant in the presence of a major excess of NH_3. Comparison of the calculated heats with the experimental values (Table 1) shows that the extent of the exchange reaction reaches during the experiment a comparatively small value of no more than 15%. In principle, a reaction with heat absorption may proceed for a very long time. During our experiments, the rate of heat absorption decreases very strongly, to virtually zero, despite the comparatively small extent of the reaction. This is apparently caused by the following two factors. The first is hindrance to the reaction of molten AN with solid dolomite, caused by formation and growth on the dolomite surface of a

layer constituted by reaction products and impurities in dolomite, which do not react with AN. The second is an increase in the relative role of heat release via thermal decomposition of AN, which occurs at a small, but gradually increasing rate.

The decrease in the rate of the exchange reaction will also automatically lead to a decrease in the rate of NH_3 formation, which, in an open ampule, will make smaller the content of NH_3 in the melt. To a first approximation, it can be considered that there exists equilibrium between ammonia in the gas and that in the melt. For this reason, the content of HNO_3 molecules in the AN melt will gradually increase, thus accelerating the thermal decomposition of AN, which occurs with heat release: about 1450–1650 J per gram of decomposed AN. Therefore, it would be expected that the rate of heat release via decomposition of AN will become, even before the completion of the exchange reaction, higher than the rate of heat absorption in the exchange reaction. As a result, an overall heat release will be observed, which is probably the case in our experiments, especially at 234°C. While the exchange reaction proceeds, the decomposition cannot be self-accelerating, because the increase in the rate of thermal decomposition of AN is determined by accumulation of HNO_3 in AN, and the released NH_3 will primarily neutralize the excess HNO_3 and thereby eliminate the acceleration of the process. About 0.1 mol HNO_3 is released in decomposition from 1 mol AN, and 1 mol NH_3 per mole of AN that entered into the reaction is released in the exchange reaction. Consequently, a 10 times slower rate of the exchange reaction involving AN, compared with that of thermal decomposition, is sufficient for neutralizing the excess HNO_3. In this case, the absorption of heat in the exchange reaction will decrease by the heat of neutralization of nitric acid by ammonia. A direct reaction of the excess HNO_3 with dolomite to give the corresponding metal nitrates, carbon dioxide, and water is quite possible. In the end, we can make a rather reliable conclusion that, even when the rate of heat release in AN decomposition will exceed the rate of heat absorption in the exchange reaction, the rate of the observed heat release will be lower than the initial rate of heat release for pure AN. Only after the main part of dolomite is consumed, accumulation of nitric acid and acceleration of the AN decomposition proper will become possible, with no more than a third of the initial amount of AN remaining, and the time in which this situation is reached will be many times the duration of our experiments.

For the heat release rates of about 1.13–1.93 mW g^{-1}, experimentally obtained at 234°C, the calculated duration of the adiabatic induction period is 21–12 h, respectively. For pure AN the value at the same temperature is 0.56 h. Approximately the same ratio between the adiabatic induction periods of pure AN and the fertilizers under study must be preserved at lower temperatures, because the variation of these values is governed by the activation energy of AN decomposition. The adiabatic induction period should be counted-off for CAN from the instant of transition to heat release, which was not reached at lower temperatures. Because data on the rates of heat release are lacking, it is impossible to calculate the adiabatic induction periods for lower temperatures, and there is no warming-up of the system upon heat absorption.

Table 2. Initial heat absorption rates and times of completion of the first stage at temperatures of CAN granulation

Sample no.	T, °C	k_2, mW g^{-1}	t, h
1	170	–0.42	100
2	170	–0.23	210
1	180	–0.89	48.3
2	180	–0.53	92.0
1	190	–1.8	24.0
2	190	–1.2	41.6

From the experimental curves describing the time dependence of the heat absorption rates, we determined the reaction times (s) in which the heat absorption in the initial stage reached a value Q_1 and found the temperature dependences of these times: $t = 1.6 \times 10^{-9} \exp(121.5 \times 10^3/RT)$ for sample no. 1 and $t = 4.0 \times 10^{-11} \exp(138.2 \times 10^3/RT)$ for sample no. 2. Using the temperature dependences of the rate constant of heat absorption and of the time in which heat Q_1 is absorbed, we calculated the initial rate of heat absorption (mW g^{-1}) and the time in which the first stage of heat absorption is complete (h) for the technological granulation temperatures of 170–190°C (Table 2). It should be noted that the completion of the first stage of heat absorption does not mean that there is no more heat absorption at all, it continues for a long time and obeys another kinetic law.

To confirm the above conclusion that accelerated decomposition of AN in the presence of dolomite is impossible, we performed at 209.8°C an experiment on thermal decomposition of a 50 : 50 (by mass) mixture consisting of a sample of technical-grade AN, in which a strong self-acceleration of its decomposition is observed with the corresponding heat release, and sample no. 1 containing 25% dolomite. Heat absorption was observed during the entire experiment, with

the rate curve qualitatively similar to those shown in Fig. 1b. The heat absorption rate in the mixture was lower than that in sample no. 1, but the content of dolomite in the mixture was smaller, too. During the time of the experiment, a fast decomposition process with heat release should have developed in the AN sample in accordance with the pattern of its thermal decomposition [5]. However, this is not the case because both dolomite and NH_3 released in the exchange reaction bind the excess HNO_3, and, accordingly, the decomposition is not accelerated.

All the above experimental data on the kinetics of heat absorption, combined with the results obtained in calculating the heats of the processes and in assessing the possibility of transition to the overall heat release, unambiguously demonstrate that the safety of processing of CAN is considerably better than that for technical-grade AN. In the process temperature range 170–190°C, and even at substantially higher temperatures of up to 219°C, any substantial warming-up of sample nos. 1 and 2 studied, and the more so the spontaneous thermal ignition are impossible under these conditions, at least during the first 24 h of decomposition. In further development of the process, there occurs transition to heat release, but the heat release rates are low and the calculated adiabatic induction periods markedly exceed the corresponding values for AN.

It should be noted that, in manufacture of CAN, a mixture of AN with dolomite is force agitated in granulation. Because the mass in the apparatus is rather large, the gases released in the exchange reaction upon termination of the process cannot prevent the process suspension from settling. This may result in that, in the end, AN containing no filler and consequently corresponding to technical-grade AN as regards the thermal decomposition criteria may remain in the upper layer. Thus, a better safety of industrial manufacture of CAN is provided under conditions of a working shop only when the production regulations are observed.

CONCLUSIONS

(1) In heating of a model mixture of AN with calcium carbonate and of CAN samples at temperatures lower than 219°C for at least 24 h, there occurs an overall heat absorption, with warming-up of the substance and its spontaneous thermal ignition being impossible.

(2) Heat absorption occurs in the exchange reaction between calcium carbonate or dolomite and AN.

(3) The release of ammonia in the exchange reaction makes lower the rate of thermal decomposition of AN via binding of nitric acid, and, therefore, presence of a limestone additive virtually eliminates the self-acceleration of the AN decomposition.

(4) The whole set of the data obtained demonstrates that, under conditions of a working shop, the safety of high-temperature processing of CAN considerably exceeds that for AN manufactured as a fertilizer.

REFERENCES

1. Chernyshev, A.K., Levin, B.V., and Konvisar, L.V., *Ammiachnaya selitra i udobreniya na ee osnove* (Ammonium Nitrate and Fertilizes Based on It), Moscow: Infokhim, 2003.
2. Rubtsov, Yu.I., Kazakov, A.I., Morozkin, S.Yu., *et al*., *Zh. Prikl. Khim.*, 1984, vol. 57, no. 9, pp. 1926–1929.
3. Pubtsov, Yu.I., Samoilenko, N.G., Kazakov, A.I., and Manelis, G.B., *27th Int. Annual Conf. ICT "Energetic Materials: Technology, Manufacturing and Prosessing,"* Karlsruhe, June 25–28, 1996, pp. 106.1–106.11.
4. Strizhevskii, I.I., *Bezopasn. Tr. Prom–sti*., 1984, no. 5, pp. 49–51.
5. Manelis, G.B., Nazin, G.M., Rubtsov, Yu.I., and Strunin, V.A., *Termicheskoe razlozhenie i gorenie vzryvchatykh veshchestv i porokhov* (Thermal Decomposition and Combustion of Explosives and Powders), Moscow: Nauka, 1996.
6. Rubtsov, Yu.I., Strizhevskii, I.I., Kazakov, A.I., *et al*., *Zh. Prikl. Khim.*, 1989, vol. 62, no. 10, pp. 2169–2174.
7. Gal'perin, L.N., Kolesov, Yu.R., Mashkinov, L.B., *et al*., *VI Vsesoyuznaya konferentsiya po kalorimetrii* (VI All-Union Conf. on Calorimetry), Tbilisi, September 17–19, 1973, pp. 539–543.
8. *Tekhnologiya ammiachnoi selitry* (Technology of Ammonium Nitrate), Olevskii, V.M., Ed., Moscow: Khimiya, 1978, p. 240.
9. *Termicheskie konstanty veshchestv: Spravochnik* (Thermal Constants of Substances: Handbook), Glushko, V.P., Ed., Moscow: VINITI, 1979, vol. 9.

Russian Journal of Applied Chemistry, Vol. 78, No. 11, 2005, pp. 1801–1805. Translated from Zhurnal Prikladnoi Khimii, Vol. 78, No. 11, 2005, pp. 1833–1837.
Original Russian Text Copyright © 2005 by Anpilogova, Murinov.

SORPTION AND ION-EXCHANGE PROCESSES

Selective Sorption of Pd(II) from Nitric–Nitrous Acid Solutions Simulating PUREX Raffinates with Polymethylene Monosulfide

G. R. Anpilogova and Yu. I. Murinov

Institute of Organic Chemistry, Ufa Scientific Center, Russian Academy of Sciences, Ufa, Bashkortostan, Russia

Received June 8, 2005

Abstract—Static sorption of Pd(II) from nitric and nitric–nitrous acid solutions, simulating PUREX raffinates, with laboratory and semicommercial samples of polymethylene monosulfide is studied. The selectivity of Pd(II) recovery from the simulated solutions is determined.

Currently there is a need in developing hydrometallurgical methods for selective recovery of fission palladium from high-level raffinates, generated in the course of reprocessing of spent nuclear fuel using PUREX process [1, 2]. These aqueous solutions contain 2–3.5 M HNO_3, up to 5 mM Pd(II), and also up to 10 mM radiolytic HNO_2 [2–4]. Tatarchuk *et al*. [2] have demonstrated that, because of strong effect of nitrous acid in the raffinates, nitric acid solutions cannot be considered as an adequate model in studying sorption recovery of Pd(II). In simulated nitric–nitrous acid solutions containing 5 mM Pd(II), 2–3 M HNO_3, and up to 10 mM HNO_2, the dominating Pd(II) species are Pd^{2+} aqua cation, $[PdNO_2]^+$ (<20%), and $[Pd(NO_2)_2]$. The rate of Pd(II) extraction from such solutions with organic sulfides is considerably higher than that from nitrate and chloride solutions [2].

Since polymethylene monosulfide (PMS), complexing heterochain sorbent, demonstrates high efficiency and selectivity in recovering Pd(II) from highly saline nitric acid solutions at room temperature over a wide range of HNO_3 concentrations (0–5 M) [5], it was advisable to examine the applicability of this sorbent for selective recovery of Pd(II) from acidic nitrate–nitrite solutions simulating PUREX raffinates.

Therefore, in this study we examined the efficiency and selectivity of the sorption of Pd(II) from such simulated solutions with laboratory and semicommercial samples of PMS.

EXPERIMENTAL

In this study we used two different PMS samples: PMS1 synthesized under laboratory conditions and PMS2, semicommercial sample partially oxidized as a result of long-term storage (for several years), as an aqueous paste (22% H_2O). PMS1 was used as prepared. PMS2 was conditioned as described in [5]. The samples were screened to obtain the 0.010–0.020-cm fraction. The composition of the samples, bulk density *d*, and the terminal acidic group concentration are given in Table 1. The static exchange capacity ($SEC_{0.1\ N\ NaOH}$) was determined by the procedure described in [6].

The sorption characteristics of the samples with respect to Pd(II), Fe(III), and Pr(III) were determined in the static mode at s : l = 1 : 200 at room temperature (19 ± 1°C) or in temperature-controlled cells at 20 ± 0.5°C (UH-4 thermostat). The contacting time was 4 h, and the stirring rate, 800 rpm (magnetic stirrer). Sorption of the metals from nitrate–nitrite solutions was studied in the dark.

To prepare the working solutions, we used commercial aqueous palladium(II) nitrate (5 M, pure grade), HNO_3 and $NaNO_3$ (analytically pure grade), $NaNO_2$ and $Fe(NO_3)_3 \cdot 9H_2O$ (chemically pure grade), $Pr(NO_3)_3 \cdot 6H_2O$ (pure grade), and also 25% aqueous ammonia (ultrapure grade) and NH_4NO_3 (pure grade) for preparation of the eluents. The Pd(II) solution was activated prior to use according to the procedure described in [5]. In the experiments we used nitrate and nitrate–nitrite solutions containing 5.1 ± 0.1 mM Pd(II) and 2–4 M HNO_3, simulating PUREX raffinates in the concentrations of a series of components: Pr(III) 0.0177, Fe(III) 0.0210, and $NaNO_3$ 0.0754 M in mixed nitrate solutions and 0.010 M $NaNO_2$ in nitrate–nitrite solutions. Also we used individual Pr(III) nitric and nitric–nitrous acid solutions.

1070-4272/05/7811-1801 © 2005 Pleiades Publishing, Inc.

Table 1. Characteristics of PMS samples

Sample	Content, %					$SEC_{0.1\ N\ NaOH}$, mg-equiv g^{-1}	d, g cm^{-3}
	C	H	S	Cl	ash		
PMS1	26.1	4.1	69.7	0	0.0	0.6	0.129
PMS2	25.8	4.4	64.2	0	3.0	1.4	0.333

The electronic absorption spectra of the nitrate and nitrate–nitrite solutions of Pd(II) in the range 350–500 nm were recorded on a Specord M40 spectrophotometer using 1- and 0.2-cm quartz cells, respectively, relative to water or a mixed solution containing 2 M HNO_3 as a reference. A day after preparation, the extinction coefficients ε of the individual and mixed nitrate solutions of Pd(II) were 104–113 at 401–411 nm and 102–112 at 397–406 nm, respectively, in the HNO_3 concentration range 2–4 M, suggesting that no polynuclear species of Pd(II) are formed [5] and also that similar Pd(II) complexes are formed in both individual and mixed nitrate solutions. According to the visible spectra, the nitric acid solutions of Pd(II) are stable for at least a month. The extinction coefficients of the nitrate–nitrite solutions at λ = 388–389 nm {absorption band of the mono- and dinitroaqua complexes of Pd(II) [4]} slowly decreases with time as a result of decomposition of HNO_2 and decrease in the concentration of the nitrite complexes of Pd(II) [2]. The nitrate–nitrite solutions were used a day after preparation.

The Pd(II) concentration in the nitrate and nitrate–nitrite solutions was determined spectrophotometrically with tin chloride [7] on a Specord M40 spectrophotometer. The presence of Pr(III) and Fe(III) did not interfere with determination of Pd(II) in mixed solutions. The Fe(III) concentration in the mixed solutions was determined chelatometrically with Na_2EDTA in 0.1 M HCl in the presence of sulfosalicylic acid [8] to within 1.4%. In this case, Pr(III) and Pd(II) did not interfere. Pr(III) in the individual solutions was determined by EDTA titration at pH 5.8 (acetate buffer) with Xylenol Orange [8] to within <0.6%. Pd(II) in aqueous ammonia eluates was determined by atomic absorption spectroscopy on a Hitachi 508 instrument.

The IR spectra of the sorbents in the ranges 200–4000 and 1300–1500 cm^{-1} were recorded on a Specord M80 spectrophotometer in Nujol and hexachlorobutadiene, respectively.

The higher concentration of the terminal acidic groups in PMS2 (Table 1) is an indication of lower molecular weight of this sample. The IR spectra of the sorbents demonstrate the differences in the qualitative and quantitative compositions of the terminal groups and also in the degree of oxidation of the sulfide groups in the samples. In PMS1, the terminal groups are sulfhydryl groups, as demonstrated by the absorption band at 2550 cm^{-1} {ν(SH) [9, 10]}, and also small amount of the sulfonate groups in the hydroxonium form $RSO_2O^-H_3O^+$ {medium-intensity band $\nu_{as}(SO_2)$ at 1174 cm^{-1}; weak band $\nu_s(SO_2)$ at 1012 cm^{-1} [9, 10]; to vibration bands of hydroxonium we could assign the broad weak band in the range 3100–3600 cm^{-1} with a maximum at 3440 cm^{-1} [$\nu_1(A_1)$, $\nu_3(E)$], the band at 1174 cm^{-1} [$\nu_2(A_1)$, and weak bands at 1632 and 1600 cm^{-1} [$\nu_4(E)$] [11]}. The sample PMS1 contains small amount of the oxidized groups: sulfoxide {very weak band ν(S=O) at 1060 cm^{-1} [9, 10]} and sulfonic groups {weak band $\nu_{as}(SO_2)$ at 1368 cm^{-1} and the band $\nu_s(SO_2)$ at 1174 cm^{-1} [9, 10]}. In PMS2, the terminal groups are primarily sulfonate groups in the hydroxonium form, as demonstrated by the medium-intensity bands $\nu_{as}(SO_2)$ and $\nu_2(A_1)$ of hydroxonium at 1176 cm^{-1} and ν(S–O) at 706 cm^{-1} [12], the strong band $\nu_s(SO_2)$ at 1012 cm^{-1}, and also by more intense (as compared to PMS1) absorption bands of hydroxonium at 3368 [$\nu_1(A_1)$], 3310 [$\nu_3(E)$], and 1640 and 1600 cm^{-1} [$\nu_4(E)$]. The low intensity of the bands of the sulfoxide groups ν(S=O) suggests low content of these groups in PMS2. The medium intensity of the bands of the sulfonic groups $\nu_{as}(SO_2)$ at 1368 cm^{-1} and $\nu_s(SO_2)$ at 1176 cm^{-1} is indicative of higher content of these groups in PMS2 as compared to PMS1.

The study of the chemical stability of PMS in 2–4 M HNO_3 showed that, at s : l = 1 : 200, contacting of PMS1 for 4 h increases the content of the sulfonic groups and, to smaller extent, of the sulfoxide groups. In the IR spectra of the sample, the relative intensity of the bands of sulfonic groups increased with increasing HNO_3 concentration. The lower molecular weight and higher concentration of the oxidized groups in PMS2 cause larger loss through oxidative oligomeri-

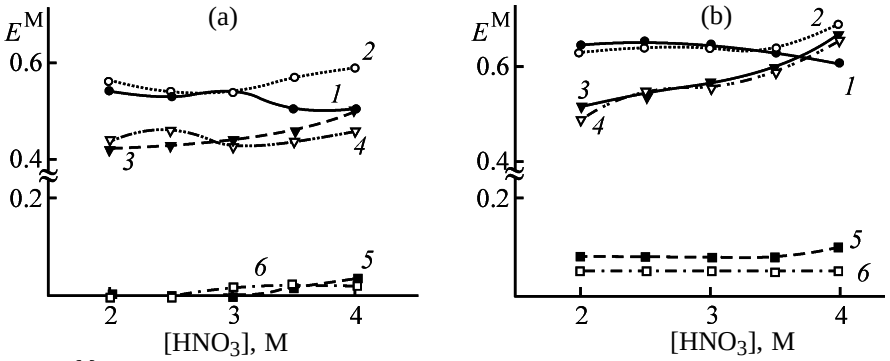


Fig. 1. Sorption capacity E^M of (a) PMS1 and (b) PMS2 samples with respect to (*1–4*) Pd(II) and (*5, 6*) Fe(III) as a function of the composition of nitrate and nitrate–nitrite solutions: (*1*) individual Pd(II) nitrate solutions, (*2, 5*) mixed nitrate solutions, (*3*) individual Pd(II) nitrate–nitrite solutions, and (*4, 6*) mixed nitrate–nitrite solutions.

zation upon long-term contacting with strong HNO_3 solutions. The loss in PMS1 and PMS2 in 8 h of contacting with 4 M HNO_3 was <8 and 10%, respectively. Therefore, we have not studied the equilibrium sorption characteristics, as requiring prolonged contact (about 30 days [5]) of the phases.

The dependences of the nonequilibrium sorption capacity for Pd(II) on the solution composition are generally similar for both samples (Fig. 1). In this case, E^{Pd} of PMS2 is somewhat higher in all the solutions studied, as compared to less hydrophilic PMS1. Increased concentration of strongly hydrophilic sulfonic and sulfonate groups in PMS2 is reflected in higher wettability and swellability, enabling us to expect better kinetic characteristics of sorption of Pd(II) as compared to PMS1 [9]. The dependence of the sorption capacity of the samples for Pd(II) on the acid concentration in the individual Pd(II) solutions in nitric acid (Figs. 1a and 1b, curves *1*) is similar to that presented in [5]. The decrease in the sorption of Pd(II) at a nitric acid concentration above 3 M is caused by partial dissolution of the sorbents through oxidative oligomerization. Increasing salinity in the mixed nitrate solutions has no effect on the sorption of Pd(II) at a nitric acid concentration below 3 M (Figs. 1a and 1b, curves *1, 2*). The increase in E^{Pd} with increasing HNO_3 concentration to above 3 M is probably due to increase in the permeability of the sorbents because of increasing concentration of the oxidized groups, and also to decrease in the solubility of the resulting oligomers and their Pd(II) complexes with increasing salinity, which is caused by decreasing activity of the solvent and dielectric constant of the solution [13, 14]. Further reason could be sorption of Fe(II) on the oxidized groups of PMS (curves *5*). Evidently, the complexation of Fe(III) with the sulfoxide and sulfonic groups eliminates their further oxidation to sulfonate, thus preventing break of the polymer chain.

The Pd(II) recovery from the individual and mixed nitrate–nitrite solutions regularly increases with increasing acid concentration. In this case, increase in the salinity has no significant effect on the sorption of Pd(II) (Fig. 1, curves *3, 4*). The nonequilibrium sorption capacity of the samples with respect to Pd(II) is lower in the nitrate–nitrite solutions, especially, at low acid concentrations (Fig. 1), which can be attributed to different rates of sorption of Pd(II) complexes from nitrate and nitrate–nitrite solutions.

The lack of the effect of the stirring rate above 600 rpm on the rate of Pd(II) recovery from all the solutions studied, and also the observed linearity of the initial sections of the kinetic curves linearized in the coordinates E^{Pd}–$\tau^{1/2}$ suggest pore-diffusion-controlled kinetics of the sorption of Pd(II) from nitrate and nitrate–nitrite solutions [6]. We have demonstrated previously [5] that the sorption kinetics of $[Pd(H_2O)_4]^{2+}$ from 1 M HNO_3 with PMS is controlled by pore diffusion with a mobile front of sorption and variable coefficient of the inner diffusion. It was demonstrated by X-ray photoelectron spectroscopy that chloro complexes of platinum metals (Pd, Pt) labile with respect to inner-sphere substitution are sorbed primarily in the PMS surface layer, while sorption of inert Rh and Ir chloro complexes results in more uniform distribution of the metals throughout the bulk of the sorbent [15]. Data on extraction of Pd(II) from nitrate–nitrite solutions with dialkyl sulfides [2] show that the extraction rate of Pd(II) complexes increases in the order $Pd^{2+} \ll [Pd(NO_2)_2] < [PdNO_2]^+$. Therefore, it may be suggested that the rate of interaction of Pd(II) mono- and dinitro complexes with the sulfide groups of PMS is considerably higher than for $[Pd\cdot(H_2O)_4]^{2+}$, and, in sorption of nitro complexes, a com-

Table 2. Distribution coefficients of Pd(II) and Fe(III) and $K_{Pd/Fe}$ partition coefficients in sorption from mixed nitrate and nitrate–nitrite solutions (s : l = 1 : 200, τ = 4 h)

Solution (2–4 M HNO_3)	PMS1			PMS2		
	K_d^{Pd}	K_d^{Fe}	$K_{Pd/Fe}$	K_d^{Pd}	K_d^{Fe}	$K_{Pd/Fe}$
	ml g^{-1}			ml g^{-1}		
Nitrate	235–288	0–2.0	∞–146	341–445	4.0–5.0	86–91
Nitrate–nitrite	147–161	0–1.2	∞–131	178–357	2.4–2.5	74–144

pact surface layer of sorption complexes is rapidly formed, thus decreasing the effective coefficient of inner diffusion. The evidence in favor of this suggestion is that the Pd(II) sorption rate decreases on passing from the nitrate solution (Fig. 2, curve *3*) to the nitrate–nitrite solutions (curves *1*, *2*) and also with increasing concentration of nitro complexes in the initial solution (curves *2* and *1*). Whereas in the initial sections of the kinetic curves (τ ≤ 5 min) the sorption rate from the indicated kinds of solutions is characterized by close $dE^{Pd}/d\tau$ values of about $(1.3–1.6) \times 10^{-2}$ mmol g^{-1} min^{-1} (determined by graphical differentiation of the kinetic curves shown in Fig. 2), already at τ = 30 min $dE^{Pd}/d\tau$ decreases considerably in the order nitrate solution > nitrate–nitrite solution (ε_{388} = 836) > nitrate–nitrite solution (ε_{388} = 1010), being 2.1×10^{-3}, 1.4×10^{-3}, and 9.5×10^{-4} mmol g^{-1} min^{-1}, respectively.

The decrease in $\varepsilon_{388–389}$ of the nitrate–nitrite solutions with increasing HNO_3 concentration from 2 to 4 M (for example, from 1003 to 736 for mixed solutions a day after preparation) and also the appearance

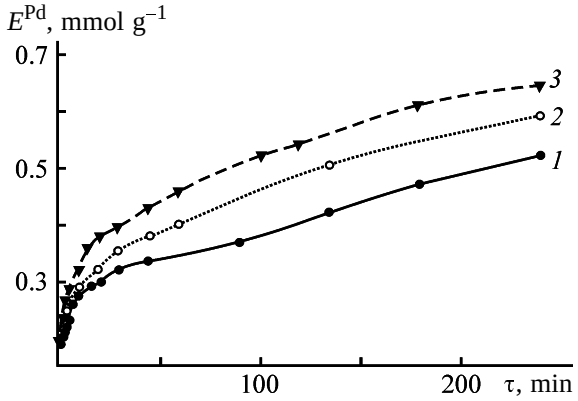


Fig. 2. Kinetic curves of sorption of Pd(II) from (*1*, *2*) individual nitrate–nitrite and (*3*) nitrate solutions on PMS at [HNO_3] = 2 M. (E^{Pd}) Sorption capacity and (τ) time. (*1*) Nitrate–nitrite solution a day after preparation (ε_{388} = 1010) and (*2*) same solution 7 days after preparation (ε_{388} = 836).

of a new band at 372 nm (as a shoulder at the band with a maximum at 388 nm) in the UV spectra at HNO_3 concentration above 3 M suggest that the concentration of nitro complexes decreases and free HNO_2 is formed [4], which corresponds to the shift of the complexation equilibrium to the left [2]:

$$Pd^{2+} + HNO_2 \rightleftarrows [Pd(NO_2)]^+ + H^+,$$

$$[Pd(NO_2)]^+ + HNO_2 \rightleftarrows [Pd(NO_2)_2] + H^+.$$

Therefore, the increase in the Pd(II) recovery from nitrate–nitrite solutions with increasing acid concentration is caused by both increase in the hydrophilicity of the sorbent as a result of increasing concentration of oxidized groups and decrease in the concentration of nitro complexes in the initial solution.

It was demonstrated that Pr(III) is not sorbed from individual nitrate and nitrate–nitrite solutions of praseodymium nitrate over the HNO_3 concentration range 2–4 M with PMS1 and PMS2. Iron(III) is sorbed from simulated solutions with a low distribution coefficient K_d^{Fe}. Therefore, Pd(II) can be separated from iron with a fairly high partition coefficient $K_{Pd/Fe}$ (Tables 2, 3). Increase in the content of oxidized groups in PMS during storage as an aqueous paste, and also with increasing acid concentration and contacting time decreases the selectivity of Pd(II)–Fe(III) separation (Fig. 1; Tables 2, 3).

At s : l = 1 : 100, Pd(II) can be fully recovered from mixed nitrate and nitrate–nitrite solutions by sorption on PMS2 in 4 and 5 h, respectively, at high distribution and partition coefficients. The degree of Pd(II) recovery by single-step sorption on PMS1 is insufficient (Table 3).

In view of the fact that, in extractive recovery of Pd(II) from chloride and nitrite solutions with dialkyl sulfides, Pd(II) can be fully backwashed with ammonia solutions [14], it was advisable to study the possibility of desorption of Pd(II) sorbates on

Table 3. Recovery of Pd(II) from mixed nitrate and nitrate–nitrite solutions ([HNO_3] = 2 M; s : l = 1 : 100)

Solution	Sample	τ, h	Pd(II) recovery, %	K_d^{Pd}	K_d^{Fe}	$K_{Pd/Fe}$
				ml g^{-1}		
Nitrate	PMS1	4	95	1900	0.5	3876
	PMS2	4	100	∞	1.0	∞
Nitrate–nitrite	PMS1	4	76	316	0.5	645
	PMS1	5	82	453	2.2	204
	PMS2	4	94	1650	0.6	2723
	PMS2	5	99	10 400	2.5	4211

PMS2 obtained after sorption from individual nitrate (E^{Pd} = 0.52 mmol g^{-1}) and nitrate–nitrite (E^{Pd} = 0.42 mmol g^{-1}) solutions at [HNO_3] = 2 M using ammonia solutions. The desorption of Pd(II) with 6 and 12 M NH_4OH solutions containing 0.1 M NH_4NO_3 at s : l = 1 : 100 and τ = 4 h was determined to be 6.7 and 11.5% and 11.6 and 11.4% for the sorbates obtained from the nitrate and nitrate–nitrite solutions, respectively.

CONCLUSIONS

(1) Polymethylene monosulfide efficiently sorbs Pd(II) at room temperature from nitrate–nitrite solutions simulating PUREX raffinates. Over the practically significant HNO_3 concentration range (2–3.5 M), Pd(II) can be completely separated from lanthanides [Pr(III)] and, at sufficiently high partition coefficients, from Fe(III).

(2) Increase in the content of oxidized sulfonic and sulfonate groups in the sorbent as a result of long-term storage in the form of an aqueous paste and also with increasing acid concentration in the solution and contacting time makes the sorbent more hydrophilic, thus increasing the sorption rate and Pd(II) recovery. At the same time, the separation of Pd(II) from Fe(III) becomes less efficient.

(3) Decrease in the concentration of Pd(II) nitro complexes in the course of storage of the nitrate–nitrite solution and also with increasing acid concentration increases the sorption rate and nonequilibrium sorption capacity of the sorbent for Pd(II).

REFERENCES

1. Kolarik, Z. and Renard, E.V., *Platinum Met. Rev.*, 2003, vol. 47, no. 2, pp. 74–87.
2. Tatarchuk, V.V., Druzhinina, I.A., Korda, T.M., and Torgov, V.G., *Zh. Neorg. Khim.*, 2002, vol. 47, no. 12, pp. 2082–2086.
3. Zilberman, B.Ya., in *Sovremennye problemy khimii i tekhnologii ekstraktsii: Sbornik statei* (Modern Problems in Extraction Chemistry and Technology: Coll. of Papers), Moscow: Ross. Akad. Nauk, 1999, vol. 1, pp. 271–289.
4. Vladimirova, M.V. and Kalinina, S.V., *Radiokhimiya*, 1989, vol. 31, no. 5, pp. 95–100.
5. Anpilogova, G.R., Kondrat'eva, E.V., Afzaletdinova, N.G., *et al.*, *Zh. Neorg. Khim.*, 1996, vol. 41, pp. 447–452.
6. Saldadze, K.I. and Kopylova-Valova, V.D., *Kompleksoobrazuyushchie ionity* (Complexing Ion Exchangers), Moscow: Khimiya, 1980.
7. Ginzburg, E.G., Ezerskaya, N.Z., Prokof'eva, S.M., *et al.*, *Analiticheskaya khimiya platinovykh metallov* (Analytical Chemistry of Platinum Metals), Moscow: Nauka, 1972.
8. Markov, V.K., Vernyi, E.A., Vinogradov, A.V., *et al.*, *Uran. Metody ego opredeleniya* (Uranium: Methods for Its Determination), Moscow: Atomizdat, 1964.
9. Shriner, R.L., Fuson, R.C., and Curtin, D.Y., *The Systematic Identification of Organic Compounds: A Laboratory Manual*, New York: Wiley, 1980.
10. *Comprehensive Analytical Chemistry*, Amsterdam: Elsevier, 1976, vol. 6.
11. Nakamoto, K., *Infrared and Raman Spectra of Inorganic and Coordination Compounds*, New York: Wiley, 1986.
12. Nakanishi, K., *Infrared Absorption Spectroscopy*, San Francisco: Holden-Day, 1962.
13. Fridrikhsberg, D.A., *Kurs kolloidnoi khimii* (Course of Colloid Chemistry), Moscow: Khimiya, 1984.
14. Chekushin, V.S. and Borbat, V.F., *Ekstraktsiya blagorodnykh metallov sul'fidami i sulfoksidami* (Extraction of Noble Metals with Sulfides and Sulfoxides), Moscow: Nauka, 1984.
15. Petrukhin, O.M., Malofeeva, G.I., Nefedov, V.I., *et al.*, *Zh. Anal. Khim.*, 1983, vol. 38, no. 2, pp. 250–255.

Russian Journal of Applied Chemistry, Vol. 78, No. 11, 2005, pp. 1806–1812. Translated from Zhurnal Prikladnoi Khimii, Vol. 78, No. 11, 2005, pp. 1838–1844.
Original Russian Text Copyright © 2005 by Ovchinnikova, Glazunov, Starkov, Chernyak.

SORPTION AND ION-EXCHANGE PROCESSES

Sorption of Silver and Chemiluminescent Activity of Clinoptilolite

O. V. Ovchinnikova, O. O. Glazunov, E. N. Starkov, and A. S. Chernyak

Vinogradov Institute of Geochemistry, Siberian Division, Russian Academy of Sciences, Irkutsk, Russia
Irkutsk State University, Irkutsk, Russia

Received March 16, 2005

Abstract—Sorption conditions of ions and colloidal particles of silver by a zeolite (clinoptilolite) and clays, and specific features of distribution of absorbed silver in clinoptilolite grains were studied. Temperature dependences of the intensity of heterogeneous chemiluminescence from samples of natural clinoptilolite and its modified forms were obtained. The activation energies of the luminescence-active chemisorption of oxygen on electron-donor centers of the zeolite surface and relative amount of centers were determined.

Active search for effective means for concentrating noble metals and ways to diminish their loss in their secondary absorption by minerals in the slurry during leaching, and also the need to elucidate the mechanism of sorption processes that occur in nature make urgent a study of sorption of ions and colloidal particles of gold and silver on inorganic ion exchangers and minerals [1, 2]. A known mineral sorbent is a natural zeolite, clinoptilolite, whose deposits widely occur in Russia and other countries [3]. The considerable resources of the zeolite, simplicity of its mining, and its unique properties (acid resistance, selectivity, thermal stability, etc.) promote studies of its structure [4] and properties, aimed to reveal the possibility of modifying this zeolite and extending its application areas [3, 5, 6].

Previously we studied the absorption of complex cations of gold and silver from acid thiourea solutions by clinoptilolite from the Dzegvi deposit (Georgia) [7]. Later, data on the mechanism and kinetics of gold sorption in the form of complex anions from hydrochloric acid solutions were reported [8]. Further, studies of the physicochemical parameters of zeolite samples from deposits of Eastern Siberia and Far East and the concentration of noble metals by these zeolites were continued [9–11].

The aim of this study was to examine sorption of ions and colloidal particles of silver by a natural zeolite (clinoptilolite) and clays and to reveal possibilities of using heterogeneous chemiluminescence for analysis of the chemiluminescent activity of the surface of clinoptilolite, its modified forms, and products of silver sorption.

The clinoptilolite from the Shivyrtuiskoe deposit (Transbaikalia) with grain size from 0.4 to 2.8 mm was studied.[1]

The chemical composition of the clinoptilolite (%) is presented below: SiO_2 61.90, Al_2O_3 11.50, Fe_2O_3 2.20, FeO 0.10, CaO 4.20, $CaCO_3$ 1.10, CaF_2 3.30, MgO 1.50, K 2.68, Na 0.76, Mn 0.12, calcination loss 10.64.

In addition to clinoptilolite, the zeolite tuff contains an admixture (up to 20%) of clayey minerals (montmorillonite, kaolinite, etc.), micas, quartz, and iron oxides. In the composition of the crystalline phase, the sample is close to clinoptilolite from the Tedzami deposit (Georgia) [9].

As a major part of impurity minerals in clinoptilolite tuffs is, as a rule, constituted by clays, which also exhibit sorption properties, we studied also the sorption of silver by the most typical samples of clays from deposits of Irkutsk oblast and by palygorskite (Cherkassy deposit, Ukraine). Data on the chemical composition of the clays are listed in Table 1.

The Bulusinsk clay is a mixture of kaolinite and montmorillonite, and the Novorazvodninsk clay, a mixture of silicon oxide with montmorillonite, albite, and kaolinite.

Silver(I) solutions were obtained by dissolving a precisely weighed portion of silver nitrate of chemically pure grade in double-distilled water (pH 6.9).

[1] The zeolite and data on its chemical composition were placed at authors' disposal by Priargunskii Mining and Chemical Combine, Joint-Stock Company.

1070-4272/05/7811-1806 © 2005 Pleiades Publishing, Inc.

Silver colloidal solutions were prepared by the known procedure [12]; the pH value of these solutions was 7.5. Emission of light from colloidal particles in the solutions obtained was observed in a dark-field condensing lens. It was found, using the electrophoresis technique, that silver particles are positively charged under the experimental conditions.

Experiments on sorption of ions and colloidal particles of silver were carried out in the dark under static conditions with agitation for 24 h; the weighed portion of the zeolite was 0.1 g, and the volume of the silver solution, 20 ml. We examined the influence exerted by the duration of sorption, $V:m$ ratio (V, solution volume, ml; m, weighed portion of the sorbent, g), and content of silver in the initial solutions on the sorption of silver colloidal particles and silver ions by clinoptilolite. The content of silver in solutions after separation of the minerals was determined by the atomic-absorption method on a Saturn spectrometer. The sorption parameters were calculated from the difference of silver concentrations in solution before and after sorption.

The sodium and hydrogen forms of clinoptilolite were obtained by treating a starting sample with 1 M solutions of NaCl and HCl, respectively, with the subsequent washing to remove chloride ions; silver-containing samples were produced by sorption of Ag^+ from 2.39 mM $AgNO_3$ solutions.

The mechanochemical activation of the zeolite was performed by ultrafine grinding in an AI-2.30 high-energy-intensity planetary centrifugal mill in dry air at an acceleration of $40g$ (g = 9.8 m s^{-2}). The grinding was done for 1, 5, 15, and 30 min in 80 cm^3 feldspar drums. Feldspar balls 7 mm in diameter were used as grinding bodies. The mass of the clinoptilolite charge was 5 g, and that of the balls, 50 g.

To study the luminescent properties of clinoptilolite, its weighed portions (0.2 g) were thoroughly ground in a mortar and compacted into pellets. The luminescence from the samples was recorded with a photomultiplier in the blue-green spectral range selected with an SZS-22 glass light filter, with heating in air at a rate of 2 deg s^{-1}.

An X-ray fluorescence microprobe analysis of cross sections of clinoptilolite grains and of samples after sorption of silver from colloidal and true solutions was performed on a Camebax SX-50 X-ray fluorescence microanalyzer. Zeolite grains were preliminarily embedded in epoxy resin, ground, and polished.

It was preliminarily found that clinoptilolite effectively absorbs silver colloidal particles and silver ions, which are recovered to a greater extent. The sorption is accompanied by an increase in pH, as a rule by 0.5, both in colloidal and true ionic solutions. To determine why the pH changes, the following experiment was carried out: 0.1-g portions of the zeolite were poured over with 20 ml of distilled water. During the time of contact (24 h), the pH of water increased from 7.0 to 7.5. It may be assumed that in sorption of silver by clinoptilolite, too, the increase in the solution pH occurs not only upon absorption of silver, but also through hydrolysis of the zeolite surface.

Table 1. Chemical composition of clay samples

Component	Clay composition, wt %		
	Novorazvodninsk deposit	Bulusinsk deposit	palygorskite
SiO_2	64.30	53.60	55.40
Al_2O_3	12.60	27.00	10.80
Fe_2O_3	5.50	3.90	6.10
CaO	3.60	0.30	0.90
MgO	2.60	0.50	7.50
Na_2O	6.05	0.12	0.27
K_2O	0.22	1.20	1.00
TiO_2	0.17	0.65	–
H_2O	3.60	3.90	1.30
Calcination loss	1.36	8.83	16.73

The dependences of silver sorption by clinoptilolite on the process duration (Fig. 1a) indicate that the sorption equilibrium in the system constituted by the zeolite and the silver solution is attained in 6 h. Raising the sorption duration to 48 h does not lead to any improvement of the sorption parameters. The time of half-sorption is 40 min in both cases.

The effect of the V/m ratio on the parameters of silver sorption by clinoptilolite was studied in solutions with a silver concentration of 50 mg l^{-1} (Table 2). The contact duration was 24 h.

Under the conditions studied, silver ions are absorbed more effectively; making smaller the V/m ratio favors more complete recovery of colloidal silver(I).

The influence exerted by the content of silver on its absorption by clinoptilolite was studied with the silver concentration varied from 10 to 160 mg l^{-1} at V/m = 200 and sorption duration of 24 h (Fig. 1b). In the concentration range studied, the capacity of clinoptilolite for silver ions exceeds that for colloidal particles. An analysis of silver solutions for the content of alkali

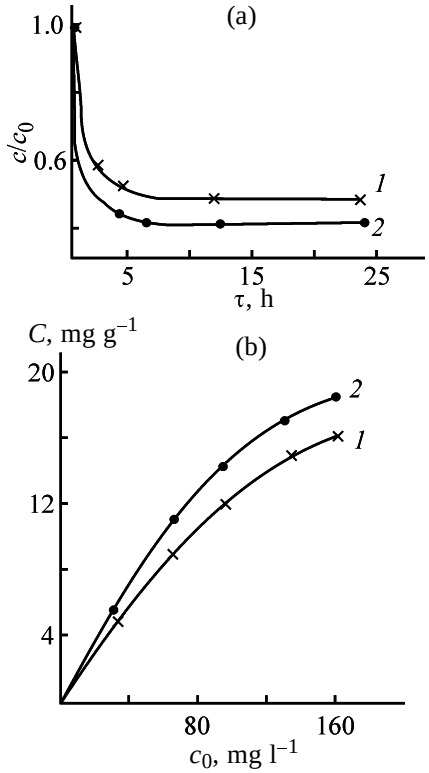


Fig. 1. Effect of (a) sorption duration and (b) silver concentration in solutions on the silver sorption parameters. (c_0) Silver concentration in the starting solutions, (c) that in solutions after sorption, (τ) sorption duration, and (C) sorption capacity of clinoptilolite. (*1*) Colloidal silver and (*2*) silver ions.

Table 2. Effect of the *V*/*m* ratio on the recovery of silver by clinoptilolite

Solution	Recovery of silver, %, at indicated *V*/*m*			
	50	100	200	400
Colloidal	85.3	72.5	50.8	37.2
Silver(I)	93.4	81.1	58.6	45.5

Table 3. Leaching-out of metal ions from the clinoptilolite structure in silver sorption

Silver	Sorption capacity of mineral, mg g^{-1}	Amount of leached-out ions (relative to their content in zeolite), wt %				
		Na	K	Ca	Mg	Fe
Colloidal	10.8	51.3	3.7	2.3	1.7	0.9
Truly dissolved	14.8	64.7	3.7	0.6	0.4	0.6

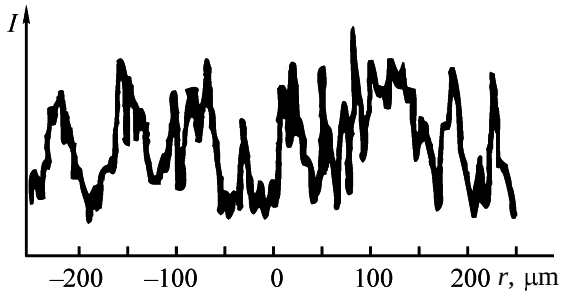


Fig. 2. Distribution of absorbed silver within a grain of the starting clinoptilolite. Scanning range 500 μm, scanning step 50 μm. (*I*) Intensity and (*r*) distance.

and alkaline-earth metal ions after their contact with the zeolite demonstrated that the absorption of silver is accompanied by transfer of a considerable amount of sodium ions, as well as those of potassium, calcium, magnesium, and iron, into solution from the structure of the mineral (Table 3). However, part of sodium and potassium ions can also be leached out from the zeolite structure when clinoptilolite is brought in contact with water. For example, upon a 24-h contact of clinoptilolite with water, sodium and potassium ions pass into solution in amounts of up to 19.2 and 0.7 wt %, respectively, relative to their content in the mineral.

It should be noted that, in sorption of silver from both true and colloidal solutions, sodium ions are more intensively leached out from the zeolite structure, compared with potassium ions, and a larger amount of sodium ions that passed into solution corresponds to a larger amount of sorbed silver. The absorption of colloidal silver particles is accompanied by an increase in the amount of calcium, magnesium, and iron ions that passed into solution from the zeolite structure, compared with sorption of silver ions. The clinoptilolite under study contains a nearly three times larger amount of potassium ions, compared with sodium (Table 1); however, sodium ions most actively pass into solution in sorption of silver.

Examining the grains of silver-containing samples of the starting and modified clinoptilolite by X-ray fluorescence microanalysis revealed the presence of silver throughout the zeolite grains and its nonuniform distribution in the grains. Figure 2 shows as an example a typical distribution of absorbed silver ions in a clinoptilolite grain. A similar distribution is observed in sorption of colloidal silver, i.e., the distribution of this kind is characteristic of all the samples studied, irrespective of the nature of solutions from which it is recovered. A considerable part of absorbed silver is contained in those microregions of the grains

which contain impurity minerals. Figure 3 shows a typical energy spectrum of a microscopic part of the cross section of a grain. The spectrum shows, in addition to the lines of silicon and absorbed silver, those of iron and titanium, contained in the corresponding oxides. It may be assumed that impurity minerals, primarily iron and titanium oxides, are involved in absorption of ions and colloidal particles of silver by clinoptilolite tuff. In our previous study [7] in which the sorption of complex silver cations by clinoptilolite from thiourea solutions was examined by X-ray fluorescence microanalysis, we also noted that regions in which sorbed silver and iron of impurity minerals are distributed coincide. The revealed involvement of iron and titanium oxides in sorption makes it possible to explain the nature of the anion-exchange properties of clinoptilolite, because the ability of clinoptilolite to absorb complex metal anions is known [8]. The anion-exchange properties of clinoptilolite may be accounted for by the involvement in sorption of oxides and hydrated oxides of iron, titanium, and other transition metals, which are contained in clinoptilolite tuff.

It was found in studying the sorption of silver by clays that clayey minerals absorb silver ions from nitrate solutions (Fig. 4). Similar data were obtained in concentration of silver from colloid solutions. Comparison of the parameters of silver sorption by clays and clinoptilolite shows a considerable advantage of clinoptilolite. The results obtained suggest that the contribution of clayey components to the parameters of silver sorption by clinoptilolite tuff does not exceed 10%.

To obtain evidence concerning active centers on the surface of clinoptilolite and its modified forms, the chemiluminescent properties of the zeolite were studied. It is known that heating of inorganic substances in air is accompanied by heterogeneous chemiluminescence (HCL), which occurs upon luminescence-active chemisorption of atmospheric oxygen [13–15]. In this case, oxygen acts as electron acceptor, and, therefore, data obtained in analysis of HCL curves furnish information about the amount and energy state of electron-donor centers on the surface of a substance. The fundamental aspects of HCL from alkali halide crystals have been rather well studied, with the relationship between their chemiluminescent properties and surface defectiveness revealed [13, 14]. The luminescence appearing upon chemisorption of oxygen by electron-donor centers on the surface of inorganic ion exchangers (titanium, zirconium, and aluminum oxides) and products of sorption of metal ions by these ion exchanges was studied previously

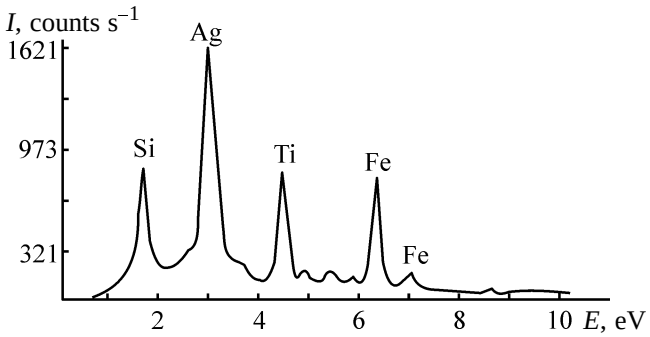


Fig. 3. Energy spectrum of a microregion on the cross section of a grain of the starting clinoptilolite after sorption of colloidal silver. (*I*) Intensity and (*E*) energy.

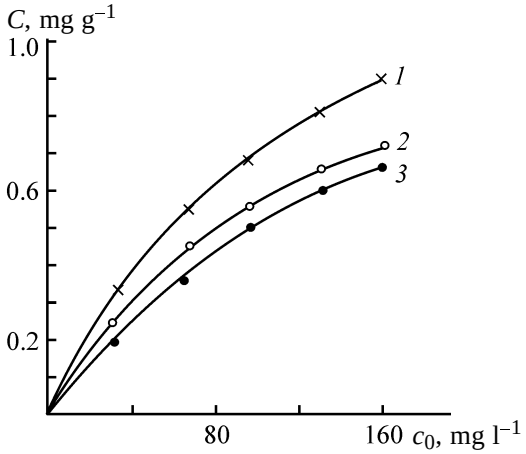


Fig. 4. Effect of the concentration of silver in solutions on the parameters of its sorption by clays. Clay: (*1*) Novorazvodninsk deposit, (*2*) Bulusinsk deposit, and (*3*) palygorskite. (*C*) Sorption capacity of a clay and (c_0) concentration of silver in the starting solutions.

[15]. It was found that heating of a natural zeolite, clinoptilolite, in air also gives rise to luminescence [10, 11].

The temperature dependences of the intensity of luminescence from clinoptilolite lie in the range 500–700 K and show two overlapping peaks with maxima at 545 and 665 K (Fig. 5, curve *1*). As the clinoptilolite under study is a natural mineral, the observed thermally stimulated luminescence may be due not only to chemisorption of oxygen on its surface, but also to release of the stored natural radiative energy. In view of the irreversibility of the luminescence-active chemisorption of oxygen, repeated heating of the sample is not accompanied by luminescence in both cases. At the same time, it is known that HCL appears again upon treatment of the sample surface with water vapor.

To reveal the nature of the observed luminescence from clinoptilolite, the following experiments were

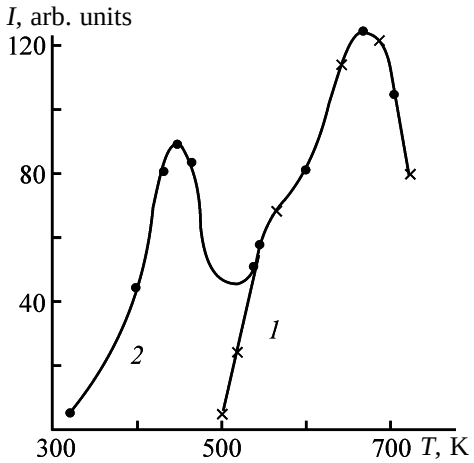


Fig. 5. Thermally stimulated luminescence from the starting clinoptilolite: (*1*) without irradiation and (*2*) after irradiation. (*I*) Relative intensity and (*T*) temperature; the same for Fig. 6.

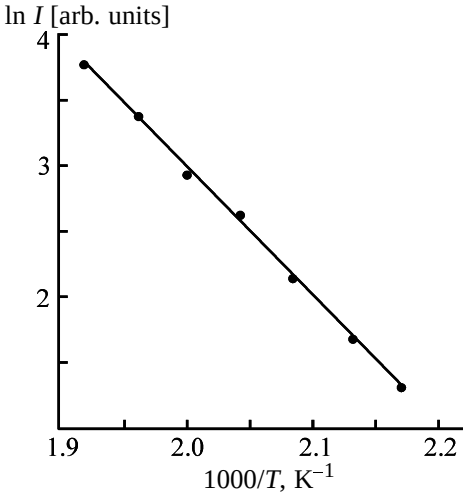


Fig. 6. Linearization of the initial portion of the curve of chemiluminescence from the starting clinoptilolite.

performed. On being heated to 700 K, a sample that lost its chemiluminescent activity was exposed to water vapor. In a repeated heating, the luminescence at 500–700 K was partly restored. Also, the initial sample was subjected to X-ray irradiation. Upon this irradiation, a thermally stimulated luminescence peaked at 450 K (Fig. 5, curve *2*), not observed in unirradiated samples, appeared in addition to the luminescence at 500–700 K.

These experiments give reason to believe that the luminescence observed on heating the starting clinoptilolite in air is HCL.

Formally, the generation of HCL can be represented as

$$L_m + O_2 \rightarrow (L_mO_2) + h\nu,$$

where L_m is a surface center at which luminescence-active chemisorption of oxygen occurs.

Because the concentration of atmospheric oxygen in the experiments is many times that of the L_m centers, its change in HCL can be neglected. In this approximation, the kinetics of HCL is only determined by the rate of variation of the concentration of L_m centers, i.e., will correspond to a first-order kinetics. Therefore, the HCL curves were analyzed using the known methods applied in processing of thermoluminescence curves [16].

Modification of the clinoptilolite surface leads to a change in the HCL intensity and to a redistribution of intensity among the peaks. The initial portion of the first HCL peak is well linearized in the $\ln I$–$1/T$ coordinates (I is the luminescence intensity, arb. units). Figure 6 shows as an example the result obtained in linearization of the initial portion of the chemiluminescence curve for a sample of the starting clinoptilolite. The absolute value of the slope of the thus obtained straight line is ε/k, where ε is the activation energy, and k, Boltzmann constant. Similar data were obtained for clinoptilolite samples in the sodium, hydrogen, and silver-containing forms. For all the samples, the activation energy of luminescence-active chemisorption of oxygen at centers of the "first type" is 0.6 eV.

These results made it possible to approximate the temperature dependence of the intensity of the first HCL peak. The integral HCL curve was decomposed into two peaks and the full width at half-maximum ΔT of the second HCL peak was used to determine the activation energy of luminescence-active chemisorption of oxygen at L_m centers of the "second type":

$$\varepsilon = 2.5kT_m^2/\Delta T - 2kT_m,$$

where T_m is temperature at which the second HCL peak lies.

For all of the samples studied, the activation energy is 0.7 eV.

The fact that the activation energy is invariable for centers of each type indicates that the chemical modification of the surface of the starting clinoptilolite does not give rise to L_m luminescence centers of a new type. As the HCL intensity is proportional to the chemisorption rate, the area delimited by the HCL curve can be used to determine the relative amount of L_m centers of each type. The results of calculations of this kind are listed in arbitrary units in Table 4.

Our results show that chemical treatment of clinoptilolite, leading to a change in the composition and

Table 4. Concentration of L_m centers in samples of zeolite of various forms

Type of center	Concentration of L_m centers, arb. units, in a zeolite of indicated form			
	starting	Na form	H form	Ag form
First, T_m = 545 K, ε = 0.6 eV	54	43	32	31
Second, T_m = 665 K, ε = 0.7 eV	130	140	23	46

amount of exchangeable metal ions in its structure, differently affects the amount of L_m centers. Introduction into the zeolite of an additional amount of sodium ions (sodium form) that substitute part of potassium ions in the zeolite lattice virtually does not change the total concentration of L_m centers and only leads to their redistribution in favor of centers of the second type. Treatment of samples with an HCl solution (hydrogen form), which leads to substitution of a part of sodium and potassium ions in the zeolite structure by hydroxonium ions, makes lower the concentrations of centers of both types, with the amount of centers of the second type decreasing to a greater extent. The amount of L_m centers changes in a similar way upon partial substitution of sodium and potassium ions by silver ions. However, centers of the second type are less sensitive to treatment of zeolite samples with $AgNO_3$, compared with the H form of the zeolite.

These results give reason to believe that L_m centers are formed in clinoptilolite under the action of alkali metal ions. Possibly, these ions are themselves incorporated in L_m centers. This statement is supported by the results obtained in measuring the HCL from clinoptilolite samples subjected to mechanochemical activation. It is known [5] that mechanochemical activation of aluminosilicates primarily affects the structure and properties of their lattice frameworks and leaves unchanged the concentration and activity of exchanging alkali metal ions. Experiments show that, after a mechanochemical activation of clinoptilolite for 1 to 30 min, the HCL curves of activated and initial samples coincide, i.e., mechanochemical activation of clinoptilolite does not lead to any significant changes in the luminescent properties of clinoptilolite samples.

Table 5. Changes in the concentrations of silver, potassium, and sodium ions in solutions upon sorption of silver(I) by the starting clinoptilolite*

c_0(Ag)	c_s(Ag)	c_s(Na)	c_s(K)
mM			
0.37	0.06	0.43	0.10
0.72	0.15	0.74	0.12
1.61	0.61	0.89	0.11
2.39	1.10	1.00	0.12

* c_0, concentration of ions in the starting solutions; c_s, that in solutions upon their contact with clinoptilolite.

It should be noted that, in sorption of silver ions by clinoptilolite, mostly sodium ions, and to a lesser extent potassium ions, are washed out from its structure (Table 5).

Analysis of the whole set of results obtained in studying the sorption of silver and the chemiluminescent activity of the initial and modified clinoptilolites suggests that the first peak in the HCL curve is due to presence of exchange potassium ions in the zeolite structure, and the second peak is associated with presence of sodium ions.

CONCLUSIONS

(1) A study of the sorption of ions and colloidal particles of silver by clinoptilolite and clays demonstrated that the parameters of silver sorption by clinotilolite markedly exceed those for clays. Specific features of the distribution of absorbed silver in clinoptilolite grains were examined: silver is nonuniformly distributed in grains and is more effectively absorbed by those microscopic regions of grains which contain iron and titanium oxides.

(2) Centers of luminescence-active adsorption of oxygen on the surface of the clinoptilolite zeolite were detected. Temperature dependences of the intensity of heterogeneous chemiluminescence from samples of natural clinoptilolite and its modified forms were measured.

(3) The activation energies of luminescence-active chemisorption of oxygen on electron-donor centers on the zeolite surface were evaluated, and relative amounts of these centers were determined. The chemiluminescent properties of clinoptilolite are determined by the nature of exchangeable cations in its structure.

ACKNOWLEDGMENTS

The authors are grateful to Yu.V. Shchegol'kov, S.L. Vasin, L.M. Dimova, and V.G. Barankevich for the assistance in the experimental part of the study.

The study was supported by the Integration Program "Nanomineralogy of Noble Metals" (project no. 6.4.1) of the Presidium of the Siberian Division of the Russian Academy of Sciences and completed with the support of the Russian Foundation for Basic Research (project no. 05-05-65250).

REFERENCES

1. Ovchinnikova, O.V. and Chernyak, A.S., in *Ionnyi obmen i ionometriya* (Ion Exchange and Ionometry), Leningrad: Leningr. Gos. Univ., 1988, issue 6, pp. 61–78.
2. Mullov, V.N. and Lodeishchikov, V.V., *Gidrometallurgiya zolota* (Hydrometallurgy of Gold), Moscow: Nauka, 1980, pp. 97–102.
3. Chelishchev, N.F., Volodin, V.F., and Kryukov, V.L., *Ionoobmennye svoistva prirodnykh vysokokremnistykh tseolitov* (Ion-Exchange Properties of High-Silica Zeolites), Moscow: Nauka, 1988.
4. Moroz, I.K., Seretkin, Yu.V., Afanas'ev, I.S., and Bakakin, V.V., *Zh. Strukt. Khim.*, 2002, vol. 43, no. 4, pp. 642–648.
5. Lapteva, E.S., Yusupov, T.S., and Berger, A.S., *Fiziko-khimicheskie izmeneniya sloistykh silikatov v protsesse mekhanokhimicheskoi aktivatsii* (Physicochemical Changes in Properties of Silicates in Mechanochemical Activation), Novosibirsk: Nauka, 1981.
6. Nikashina, V.A., Gembitskii, P.A., Kats, E.M., *et al.*, *Zh. Prikl. Khim.*, 2001, vol. 74, no. 9, pp. 1410–1412.
7. Chernyak, A.S., Ovchinnikova, O.V., and Zav'yalova, L.L., *Zh. Prikl. Khim.*, 1978, vol. 51, no. 6, pp. 1243–1246.
8. Zonkhoeva, E.L. and Belomestnova, N.V., *Zh. Prikl. Khim.*, 1996, vol. 69, no. 2, pp. 232–237.
9. Ovchinnikova, O.V., Chernyak, A.S., Foroshcha, G.I., *et al.*, *Obogashchenie rud* (Ore Dressing), Irkutsk: Irkutsk. Gos. Tekh. Univ., 1994, pp. 113–125.
10. Starkov, E.N., Ovchinnikova, O.V., Chernyak, A.S., and Glazunov, O.O., Abstracts of Papers, *Mezhdunarodnaya konferentsiya "Spektroskopiya, rentgenografiya i kristallokhimiya mineralov"* (Int. Conf. "Spectroscopy, X-ray Diffraction Analysis, and Crystal Chemistry of Minerals"), Kazan: Kazan. Univ., 1997, pp. 157–158.
11. Ovchinnikova, O.V., Glazunov, O.O., and Chernyak, A.S., Abstracts of Papers, *17-yi Mendeleevskii s''ezd po obshchei i prikladnoi khimii: Materialy i nanotekhnologii* (17th Mendeleev Congr. on General and Applied Chemistry: Materials and Nanotechnologies), Kazan, 2003, p. 319.
12. *Handbuch der präparativen anorganischen Chemie*, Brauer, G., Huber, F., *et al.*, Eds., Stuttgart: Enke, 1978, vol. 2.
13. Glazunov, O.O. and Karnaukhova, V.K., *Izv. Akad. Nauk SSSR, Neorg. Mater.*, 1991, vol. 27, no. 11, pp. 2455–2456.
14. Glazunov, O.O., *Izv. Ross. Akad. Nauk, Neorg. Mater.*, 1994, vol. 30, no. 5, pp. 672–674.
15. Ovchinnikova, O.V., Glazunov, O.O., Chernyak, A.S., *et al.*, Abstracts of Papers, *III Vsesoyuznoe soveshchanie po khemilyuminestsentsii* (III All-Union Meet. on Chemiluminescence), Riga, 1990, pp. 222–223.
16. Chen, R. and Kirsh, Y., *Analysis of Thermally Stimulated Processes*, Oxford: Pergamon, 1981.

Russian Journal of Applied Chemistry, Vol. 78, No. 11, 2005, pp. 1813–1815. Translated from Zhurnal Prikladnoi Khimii, Vol. 78, No. 11, 2005, pp. 1845–1847.
Original Russian Text Copyright © 2005 by Lavnikova, Bakhtina, Zheltobryukhov.

SORPTION AND ION-EXCHANGE PROCESSES

Sorption Properties of Materials Based on Graft Polycaproamide Copolymers

I. V. Lavnikova, G. D. Bakhtina, and V. F. Zheltobryukhov

Volgograd State Technical University, Volgograd, Russia

Received December 16, 2004; in final form, September 2005

Abstract—Sorption of metal ions with a cation exchanger based on a graft polycaproamide copolymer was studied, and the sorption power of the material was evaluated.

Polymer-analogous transformations in grafted copolymer chains are a promising route for introducing new functional groups into pendant chains of polymeric materials [1, 2]. A characteristic example is phosphorylation of grafted polycaproamide (PCA) chains. Increased interest in this procedure for preparing ion-exchange materials is caused by the fact that phosphorylation of pendant chains of polymer macromolecules allows not only improvement of the properties of the starting polymers but also preparation of fibrous polymers capable of ion exchange and complex formation depending on the functional groups introduced.

Ion-exchange fibrous materials have developed surface and better kinetic characteristics than granular ion exchangers. Their exchange capacity is sufficiently high for practical applications and does not decrease in repeated cycles of regeneration with acids and bases. One of advantages of fibrous materials is the possibility of preparing from them articles of any shape: threads, porous plates, woven and nonwoven fabrics, which is especially valuable when the traditional process implementation is unacceptable [3].

Modified polycaproamide fibers with P–OH groups based on graft copolymers of polycaproamide and poly(glycidyl methacrylate) (PGMA) [4] were prepared by phosphorylation of grafted chains with 1-hydroxyethylidenediphosphonic acid (HEDP) [5]. As shown in [6], modification of glycidyl methacrylate (GMA) copolymers at the epoxy group with the aim to prepare a phosphorus-containing sorbent is a promising procedure.

The major factor governing the sorption capacity of fibrous cation exchangers is the presence of a sufficient amount of sterically accessible functional groups capable of ion exchange.

In this study we examined how the phosphorylation conditions affect the composition and sorption properties of fibrous materials based on PCA–PGMA graft copolymers. The degree of phosphorylation was estimated from the phosphorus content in the modified polymer. Because of possible hydrolysis of the ester group in the grafted PGMA, we performed an experiment on determining the static exchange capacity (SEC) of unmodified PCA–PGMA and obtained the value of 0.4 mg-equiv g^{-1}. The influence of the phosphorus content on the sorption properties of the fibers is illustrated by Table 1.

Table 1 shows that SEC depends on the content of phosphoric acid groups in PGMA, which, in turn, is determined by the structure of the modified PCA and phosphorylation conditions. It should be noted that the phosphorylation of fibers containing 43–50% PGMA under the chosen conditions yields a polymer containing 2.9% P, with SEC of 3.9 mg-equiv g^{-1}.

Table 1. Influence of the phosphorus content on the sorption properties of PCA–PGMA copolymer. Graft polymerization: τ = 60 min, T = 80°C, [GMA] = 2.35 M; phosphorylation: τ = 300 min, T = 90°C, [HEDP] = 4.04 M

Content in graft copolymer, wt %		SEC, mg-equiv g^{-1}
PGMA	P	
10	0.5	2.5
16	1,0	2.9
20	1,4	3.3
41	2.9	3.9
43	2.9	3.9
45	2.9	3.9
48	2.9	3.9
50	2.9	3.9

1070-4272/05/7811-1813 © 2005 Pleiades Publishing, Inc.

Table 2. Influence of HEDP concentration on the amount of P in the graft copolymer (c_P) and SEC; [PGMA] = 43%, τ = 300 min, bath ratio 30, T = 90°C

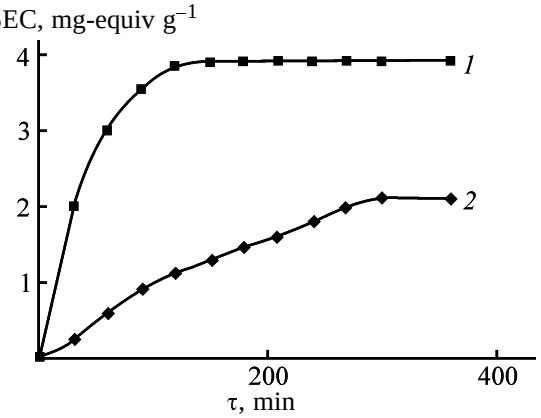
HEDP, M	c_P, %	SEC, mg-equiv g^{-1}
0.81	0.7	2.8
1.62	0.87	2.9
2.43	1.2	3.0
3.24	2.0	3.5
4.04	2.9	3.9
4.83	2.8	3.7

Table 3. Degree of recovery of metal ions. Sorption conditions: SEC = 3.9 mg-equiv g^{-1}, initial concentration of metal ions in solution 5 mg l^{-1}, bath ratio 100

Metal ion	Degree of recovery of metal ions, %, in indicated time τ, min					
	30	60	90	120	180	720
Cu^{2+}	25	36	68	80	80	80
Ni^{2+}	21	27	58	68	68	68
Ca^{2+}	19	23	44	56	56	56

An increase in the SEC may be caused by increasing content of P–OH groups capable of ion exchange and complexation. Our results show (Table 2) that it is appropriate to take HEDP as 4.04 M solution. This concentration is sufficient to obtain the maximal content of phosphorus in the copolymer, 2.9% (SEC = 3.9 mg-equiv g^{-1}). Although the phosphorylation is a heterogeneous process, it occurs at a high rate (1.6×10^{-4}–2.2×10^{-4} mol l^{-1} s^{-1}) [5].

The figure shows the kinetic curves of sorption with the ion-exchange material obtained, in comparison with GMF-1 granular sorbent. GMF-1 cation exchanger is prepared by phosphorylation of cross-linked GMA copolymers in the H^+ form [7]. The fibrous sorbent showed higher rate of Na^+ sorption. The equilibrium in the solution–fiber system was attained within 120 min, against 300 min required for GMF-1.



Kinetic curves of sorption of Na^+ cations from 0.1 M aqueous NaOH (20°C, bath ratio 30). (τ) Time. (*1*) Fibrous sorbent prepared in this study and (*2*) GMF-1 granular sorbent.

Data on recovery of the Cu^{2+}, Ni^{2+}, and Ca^{2+} ions from aqueous solutions with the phosphorylated fibrous sorbent are given in Table 3. The degree of recovery of metal ions in 120 min is as follows (%): Cu^{2+} 80, Ni^{2+} 68, and Ca^{2+} 56. The content of the metal ions in solutions before and after sorption was determined compexometrically (see Experimental).

It should be noted that the fibrous ion-exchange sorbent prepared by the above procedure has satisfactory physicomechanical properties (Table 4). A small decrease in the strength parameters is caused by the distortion of the fiber structure by the forming pendant chains, which is consistent with the results of a detailed study [8] of the effect exerted by a graft copolymer on the physicomechanical properties of the modified fiber.

Thus, the suggested sorbent shows promise for recovery of metal ions from aqueous solutions.

EXPERIMENTAL

Phosphorylation of the graft copolymer was performed as follows: The copolymer was treated with a 0.84–4.86 M solution of HEDP for 50–300 min at 70–90°C in a flask equipped with a reflux condenser. After the reaction completion, the resulting copolymer was thoroughly washed with distilled water and dried to constant weight.

The SEC of the cation exchanger was determined as follows [9]. A flask was charged with a 1-g fiber portion, 200 ml of 0.1 N NaOH was added, and the mixture was allowed to stand for 24 h with intermittent shaking. Then the ion exchanger was filtered off, and a 25-ml aliquot of the filtrate was taken and titrated with 0.1 N HCl in the presence of phenolphthalein.

In experiments on recovery of metal ions from aqueous solutions, 25 ml of 5% $CaCl_2$ was added with continuous stirring to a 1-g portion of the fiber, and the system was allowed to stand for 24 h. Then the sorbent was filtered off. To obtain a control solution, 5 ml of the filtrate was taken and diluted with distilled water to a volume of 100 ml. Then 10 ml of a test solution (pH 10) was transferred into a titration flask and titrated in the presence of Eriochrome Black T indicator. After the filtration, the residual amount

Table 4. Physicomechanical properties of fibers

Parameter	Initial PCA	PCA–PGMA	
		grafted	modified
Linear density, tex	1.15	1.23	1.03
Cutting length, mm	66	66	67
Number of tortuosities, cm^{-1}	3.6	3.8	4.0
Moisture content, %, at 65% humidity	3.0	3.6	3.59
Elongation at break, %	46.2	36.9	34.9
Relative breaking load, cN tex^{-1}	32.7	25.6	24.3

of the metal in the aqueous solution was determined by complexometric titration of a solution aliquot with 0.1 N Na_2EDTA in the presence of Eriochrome Black T indicator until a violet color appeared.

CONCLUSION

A fibrous corbent with a static exchange capacity of 3.9 mg-equiv g^{-1} was prepared from graft copolymers by polymer-analogous transformations. The sorbent is active toward Cu^{2+}, Ni^{2+}, and Ca^{2+} ions; the degree of their recovery from dilute solutions reaches 56–80%.

REFERENCES

1. Druzhinina, T.V,, Nazar'ina, L.A., and Kargash, K.V., *Khim. Volokna*, 2000, no. 6, pp. 18–21.
2. Epifanova, N.Yu. and Druzhinina, T.V., *Khim. Volokna*, 1998, no. 6, pp. 41–43.
3. Zubankova, L.V., Tevlina, A.S., and Davankov, A.B., *Sinteticheskie ionoobmennye materialy* (Synthetic Ion-Exchange Materials), Moscow: Khimiya, 1978.
4. Lavnikova, I.V. and Zheltobryukhov, V.F., *Zh. Prikl. Khim.*, 2001, vol. 74, no. 4, pp. 657–659.
5. Lavnikova, I.V. and Zheltobryukhov, V.F., *Zh. Prikl. Khim.*, 2001, vol. 74, no. 12, pp. 2062–2064.
6. Bakhtina, G.D., Zauer, E.A., Kochnov, A.B., *et al.*, *Zh. Prikl. Khim.*, 2000, vol. 73, no. 10, pp. 1652–1655.
7. *Ionoobmennye materialy dlya protsessov gidrometallurgii, ochistki stochnykh vod i vodopodgotovki: Spravochnik* (Ion-Exchange Materials for Hydrometallurgy and Wastewater and Water Treatment), Laskorin, B.N., Ed., Moscow: Vses. Nauchno-Issled. Inst. Khim. Tekhnol., 1989.
8. Zheltobryukhov, V.F., Development of Process Principles and Semicommercial Implementation of a Process for Preparing Graft Polycaproamide Copolymers, *Doctoral Dissertartion*, Volgograd, 1987.
9. Toroptseva, A.M., Belogorodskaya, K.V., and Bondarenko, V.M., *Laboratornyi praktikum po khimii i tekhnologii vysokomolekulyarnykh soedinenii* (Laboratory Course of Chemistry and Technology of Macromolecular Compounds), Leningrad: Khimiya, 1972.

Russian Journal of Applied Chemistry, Vol. 78, No. 11, 2005, pp. 1816–1820. Translated from Zhurnal Prikladnoi Khimii, Vol. 78, No. 11, 2005, pp. 1848–1852.
Original Russian Text Copyright © 2005 by Khomutov, Klushin, Mukhin.

SORPTION AND ION-EXCHANGE PROCESSES

Variation of the Technical Parameters of Steam-Activated Carbons Based on Peat and Polyurethane–Polyamide Fiber Waste

A. N. Khomutov, V. N. Klushin, and V. M. Mukhin

Mendeleev Russian University of Chemical Engineering, Moscow, Russia
Neorganika Research and Production Association, State Unitary Enterprise, Elektrostal, Moscow oblast, Russia

Received November 25, 2004; in final form, July 2005

Abstract—The wear resistance, porosity, and ion-exchange properties of steam-activated cokes in the form of cylindrical granules, obtained from Dorlastan polyurethane–polyamide fiber waste and cotton grass–sphagnum peat under conditions of purely kinetic control were studied at the combustion loss increased to 50%.

Of much practical importance are such technical parameters of activated carbons as wear resistance, micro-, meso-, and macropore volume, and the total porosity as estimated using various pycnometric liquids [1].

Mechanical resistance is one of the basic properties of carbon adsorbents, decisive in assessing their applicability in processes run in intensive hydrodynamic regimes. Activated carbons with wear resistance above 89%, as estimated by the MIS (sorbent testing procedure) 60-8 [1], are indispensable in hydrometallurgy of noble and rare metals, especially in sorption of platinum group metals from cyanide pulps (according to [2], 89% is the minimal wear resistance for carbon adsorbents to be suitable for application in gold recovery from pulps). High-strength carbon adsorbents with developed micropore structure are typically prepared worldwide using various expensive carbon-containing raw materials. In the former Soviet Union and in the Russian Federation, such activated carbons were based on furfural [3], 2CC coal and phosphoric acid [4], vinylpyridine ion exchangers [5], brown coal raw material [6], and shale phenols and resins [7].

The new technology of preparation of activated carbons with enhanced strength[1] implies the use of polymer wastes with low (virtually zero) coke residue and powdered carbon-containing plant raw materials for preparing molded cokes in a high (35–45%) yield with a mechanical compression strength of up to 400 kgf cm^{-2}, wear resistance of up to 99–99.5% (according to MIS 60-8), and open micropore volume of 0.2–0.25 $cm^3\ g^{-1}$ [8].

In this study we prepared molded carbons from a formulation made of Dorlastan polyurethane–polyamide fiber waste and cotton grass–sphagnum peat. The weight ratios of the components of the formulation and its heat treatment regimes were identical to those required for preparation of carbonizate (a solid carbonized residue from high-temperature heat treatment of the raw material formulation) with the maximal compression strength [8]. When nitrogen-containing polymers are introduced into the raw formulation prepared by the method from [8] in amounts ensuring the maximal strength of the carbonizates, the content of nitrogen in the pyrolysis products increases to 10–14%, and the anion-exchange power of the carbons is enhanced.

The anion-exchange centers in activated carbons arise from hydration of the heteroatoms of nitrogen and oxygen, incorporated in graphite-like networks of carbon matrices. As shown by previous studies of activated carbons, carried out in different times and by different methods, they comprise diverse oxygen- and nitrogen-containing surface functional groups. By contrast to conventional anion-exchange resins, these are electroconducting media with a low electrical resistivity ($\rho \approx 10^{-2}$–$10^{-4}\ \Omega$ cm) [9].

When the surface functional groups dissociate, the charge is delocalized over the entire activated carbon surface. Hence, ion exchange occurs not only at the

[1] Developed at the Chair of Biosphere Protection Technologies, Mendeleev Russian University of Chemical Engineering.

1070-4272/05/7811-1816 © 2005 Pleiades Publishing, Inc.

location sites of the heteroatoms but also over the entire surface, by replacement of the anions from the internal plate of the electrical double layer. According to the second law of thermodynamics, the equilibrium constant for such a process is a function of the difference between the stationary electrode potential and the zero-charge potential of activated carbon [9, 10]. In air, activated carbons immersed in water behave like reversible oxygen electrodes (the electrode potential of activated carbons linearly varies with pH) [9]. Therefore, calculations of the dissociation constants for the surface functional groups by the Henderson–Hasselbach equation, based on the results of direct potentiometric titration of activated carbons, do not make as much sense as those for ion exchangers [11]. The exact number of oxygen-containing functional groups in activated carbons is determined by the Boehm titration procedure [12], polarographically [13], and by cyclic voltammetry [14]. The number of strongly basic nitrogen-containing functional groups is estimated by direct potentiometric titration of the carbons [5].

Steam activation, along with development of the pore structure of carbons, typically decreases the mechanical strength of the end product [15]. Although carbons are activated under conditions of purely kinetic control (under hydrodynamic conditions such that the steam concentration gradient in the bulk of the carbon grain is insignificant, and the steam concentration at the centre of the carbon particle is no less than 90% of the steam concentration on the grain surface), an increase in the combustion loss (a relative loss of the carbon weight due to carbon burnup) during steam activation differently affect the strength of different brands of activated carbons. Activated carbons with a regular structure such as, e.g., FAS-3, AG-95, and coal adsorbents prepared with the use of binders based on shale resins virtually preserve their strength up to combustion losses $\alpha = 50-60\%$ [7, 15]. The volume of macropores and large transient pores (sites at which the failure of sorbents is the most probable) for this type of carbons under the conditions of purely kinetic control cannot substantially increase [16], and they begin to lose their strength during burnup of the micropore walls. Carbons prepared from pressed finely ground plant material wastes lose their strength at lower combustion losses [17, 18], since specific carbon layers are the first to burn up, being replaced by large pores. Published data [17, 18] suggest that, in contrast to carbonizates of FAS or AG carbons, the strongest peat cokes have irregular structure, and the main failure sites in their activated products are extended wedge-shaped or flat mesopores [19]. Nitrogen-containing carbons typically lose certain amount of nitrogen by activation, which affects their strength and ion-exchange power [5].

In standard industrial activation furnaces, the temperature varies within the range corresponding to purely kinetic control. This makes of practical importance monitoring of the technical parameters of carbons under increasing combustion loss throughout this region rather than at specific temperatures.

Therefore, we studied the changes in the total porosity, volumes of the sorbing pores, numbers of strongly basic surface functional groups, and the wear resistance of the molded carbon during steam activation of its carbonizate at different temperatures in the range of purely kinetic control, as estimated by MIS 60-8. The boundaries of the areas of heterogeneous reactions of steam with the carbon material prepared from Dorlastan fiber waste and cotton grass–sphagnum peat were determined earlier [20].

EXPERIMENTAL

Samples of carbonizates were prepared in the form of cylindrical granules with the cross-section diameter of 1 mm [8]. Steam activation was run at the specific consumption of 3 g of steam per gram of the end product at 800, 840, 880, and 900°C in a stainless steel vertical reactor, placed into a SUOL-4 tubular furnace. The combustion loss during activation was increased via increasing the time of keeping of the carbonizates in the reactor. Development of their pore structure was monitored by determining the total pore volumes with respect to water $V_{\Sigma H_2O}$ and carbon tetrachloride $V_{\Sigma CCl_4}$, as well as the total volume of the sorbing pores with respect to benzene V_{sorb} at $p/p_s = 1$ and the micropore volume V_{mi} at $p/p_s = 0.83$ by the standard procedures [1, 19]. The ion-exchange properties of the resulting activated carbons were studied by direct potentiometric titration by the method of many weighed portions [20]. The carbons were titrated in the neutral form, as their conversion into the OH^- form involves capture of significant amounts of the equilibrium solution of alkali with transport pores (comparable with the anion-exchange capacity of the sorbent). To this end, 1-g weighed portions of the freshly cooled carbon were poured over with 50 ml of an aqueous KCl solution (concentration 1 M, $2 < pH < 10$). The pH of the initial solutions was adjusted with HCl or KOH. The molar concentration of the supporting electrolyte during titration was 100 and over times that of the anion of the acid residue or the cation of the base used for adjusting pH. Hence, fluctuations of the concentration of the supporting

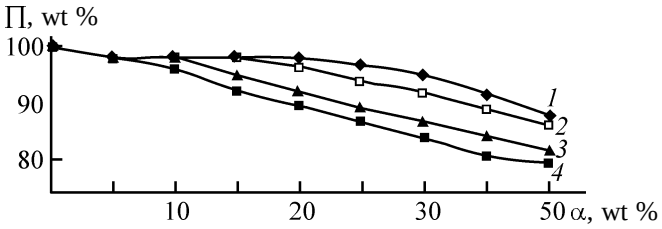


Fig. 1. Wear resistance ∏ estimated by MIS 60-8 as a function of the combustion loss α of the activated carbons obtained at different temperatures. Activation temperature, °C: (*1*) 800, (*2*) 840, (*3*) 880, and (*4*) 900.

electrolyte anions and cations were considered to exert no effect on the equilibrium capacity. The equilibrium was judged from invariance of pH of the solution within 3 days and over. The anion-exchange capacity was estimated from the change of the concentration of the hydrogen ions during establishment of the equilibrium, using the initial and equilibrium pH of the solutions. The data represented as $\Delta A/\Delta\text{pH} = f(\text{pH})$ were processed on a PC into $A = f(\text{pH})$ integrated dependences.

Table 1. Parameters of the pore structure of the activated carbons with different combustion losses, obtained at different temperatures

T, °C	α, wt %	$V_{\Sigma H_2O}$	$V_{\Sigma CCl_4}$	V_{sorb}	V_{mi}
		$cm^3\ g^{-1}$			
800	0	0.24	0.06	0.14	0.14
	10	0.33	0.20	0.23	0.23
	20	0.42	0.28	0.32	0.32
	30	0.59	0.49	0.41	0.41
	40	0.7	0.64	0.51	0.51
	50	0.8	0.8	0.6	0.6
840	0	0.24	0.06	0.14	0.14
	10	0.33	0.21	0.22	0.22
	20	0.44	0.30	0.3	0.3
	30	0.62	0.52	0.4	0.4
	40	0.73	0.66	0.5	0.5
	50	0.82	0.82	0.58	0.58
880	0	0.24	0.06	0.14	0.14
	10	0.33	0.22	0.22	0.22
	20	0.45	0.31	0.28	0.28
	30	0.63	0.53	0.38	0.38
	40	0.77	0.69	0.48	0.48
	50	0.84	0.84	0.54	0.54
900	0	0.24	0.06	0.14	0.14
	10	0.34	0.24	0.19	0.19
	20	0.46	0.33	0.27	0.27
	30	0.64	0.54	0.36	0.36
	40	0.8	0.73	0.52	0.52
	50	0.84	0.84	0.53	0.53

Figure 1 presents the plots of the wear resistance vs. the combustion loss at different temperatures; it shows that the combustion loss at different temperatures differently affects the strength of the activated samples.

It is seen from Fig. 1 that, at α = 10%, the strength of the activated carbons virtually does not tend to decrease and fluctuates around 98% irrespective of the activation temperature. At 800°C, a decrease in the strength with increasing combustion loss is at a minimum. At α = 20–30%, it decreases the stronger, the higher the temperature. At α = 40–50% and temperature of 880–900°C, the strength decreases more prominently but does not drop below 80%, which strongly exceeds the strength of ordinary activated carbons BAU, SKT, and AG. At the combustion loss of 50% and activation temperatures of 800–840°C, the strength does not drop below 90%.

Table 1 presents the pore volumes of the activated carbons with different combustion losses, obtained at different temperatures. It is seen that micropores are the basic type of the sorbing pores for the activated carbons under study. The measured volumes of the micropores and sorbing pores are identical, which suggests that mesopores are virtually lacking. The difference in the total pore volumes, estimated with water and CCl_4 at small combustion losses, suggests that the carbons contain thin pores, accessible to water molecules and inaccessible to CCl_4 molecules.

At the same time, this difference at small combustion losses exceeds V_{mi}, which suggests that the carbon samples with small combustion losses contain ultrathin micropores accessible to water molecules and inaccessible to benzene molecules. With increasing combustion loss, the situation changes: The total pore volumes as estimated with H_2O and CCl_4 are leveled, which, along with increase in V_{mi}, suggests an increase in the micropore size. At α = 40–50%, the parameters $V_{\Sigma H_2O}$ and $V_{\Sigma CCl_4}$ are virtually identical and exceed V_{mi}, which, in the absence of mesopores, suggests that the carbons contain macropores. In this connection, we can state that the pore structure of the carbonizate is also represented by micro- and macropores only. Increase in the volume of the macropores with increasing combustion loss is more prominent at higher activation temperatures (Table 1). These conditions do not favor development of large-volume micropores, in contrast to lower activation temperatures. Figure 1 shows that, at higher activation temperatures, the decrease in the strength of the carbons

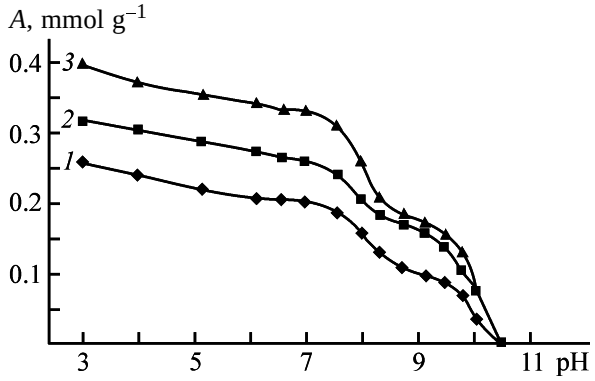


Fig. 2. Equilibrium anion-exchange capacity *A* of activated carbons obtained at 840°C as a function of pH. α, %: (*1*) 10, (*2*) 30, and (*3*) 50.

with increasing combustion loss is more prominent. This does not contradict the published data [6, 9, 21] and suggests that a decrease in the strength of the carbons during activation is mostly due to formation of macropores. It should be noted that steam activation makes it possible to increase the micropore volume of the material under study to 0.4–0.5 $cm^3 g^{-1}$, with the wear resistance of the sample of over 95% being preserved. Such parameters are exhibited by the best domestic carbons AG-95 and FAS-3 utilized in gold mining.

Samples of activated carbons with combustion losses of 10, 30 and 50%, obtained at 840°C, were decalcified by the procedure from [22], washed with distilled water to negative reaction for the chloride ions, and, after calcination under nitrogen at 850°C, subjected to direct potentiometric titration (Fig. 2). Figure 2 shows that the titrated samples of the activated carbons have two types of strongly basic ion-exchanging groups, dissociating at pH 8.5–10 and 7–8.2. The manifestation of the ion-exchanging groups dissociating at pH 8–10 and 6–8 can be due to the pyridine nitrogen and phenolic hydroxy group, occurring in the carbons [22]. Table 2 presents the total number of the ion-exchange centers, dissociating at pH 8.5–10 and 7–8.5, calculated by integration of the titration curves. It is seen that, under increasing combustion loss, the ion-exchange properties of the carbon vary differently from those of the carbons studied in [23]. The reason is that, when the combustion loss decreases to 30%, the number of the ion-exchange centers dissociating at pH 8.2–10 (these centers are due to the presence of nitrogen in the carbon) increases rather than decreases, while the number of those dissociating at pH 7–8.2 (due to the presence of the phenolic hydroxyls in the carbon) remains constant. Further activation to combustion losses of 50% increases the number of the ion-exchanging centers with p*K* 7–8.2 by 0.06 mmol g^{-1}, while the number of strongly basic groups increases by 0.01 mmol g^{-1} only.

Table 2. Total amount *A* of ion-exchanging groups dissociating at pH 7–8.2 and 8.2–10

α, %	*A*, mmol g^{-1}, at indicated pH	
	8.2–10	7–8.2
10	0.12	0.08
30	0.18	0.08
50	0.19	0.14

We checked the adsorption power of the activated carbon sample with α = 40%, obtained at 840°C, with gold cyanide complexes (Central Scientific Research Institute for Geological Exploration). The equilibrium adsorption capacity with respect to the gold ions at the gold residual concentration in solution of 1 mg l^{-1} and pH 10.5 was 22 mg g^{-1}; the wear resistance of this sample, estimated by MIS 60-8, was 98%, while the analogous parameters of the AG-95 commercial sample were 19 mg g^{-1} and 95%, respectively. Thus, the parameters of the activated carbon that we prepared make it suitable for gold mining applications and surpass the corresponding parameters of the commercial sample of activated carbon AG-95.

CONCLUSIONS

(1) Steam activation of carbon material based on polyurethane–polyamide fiber waste and peat yields activated carbons suitable for gold mining applications (wear resistance, as estimated by MIS 60-8, is over 89%, and equilibrium capacity with respect to the gold ions, over 8 mg g^{-1} in adsorption of aurocyanide until the residual concentration of 1 mg l^{-1}).

(2) The wear resistance, estimated by MIS 60-8, and microporosity of the resulting activated carbons correspond to those of the best domestic commercial samples of activated carbons AG-95 and FAS-3, intended for gold mining applications.

(3) Decrease in the wear resistance of the activated carbons based on polyurethane–polyamide fiber waste and peat with increasing combustion loss is associated with increase in the macropore volume.

(4) The anion-exchange centers of activated carbons based on polyurethane–polyamide fiber waste and peat are represented by two types of functional groups dissociating at pH 7–8.2 and 8.2–10.

(5) The number of the ion-exchanging groups of activated carbons based on polyurethane–polyamide fiber waste and peat varies with increasing combustion losses differently from that of activated carbons based on vinylpyridine resins and other nitrogen-containing polymers.

REFERENCES

1. Kolyshkin, D.A. and Mikhailova, K.K., *Aktivnye ugli: svoistva i metody ispytanii: spravochnik* (Activated Carbons: Properties and Testing Methods: Reference Book), 1972.
2. Voiloshnikov, V.I., Sorption Recovery of Noble Metals from Cyanide Solutions and Pulps, *Cand. Sci. Dissertation*, Irkutsk, 1989.
3. RF Patent Appl. 94020452/26.
4. Mukhin, V.M., Zimin, N.A., Zubova, I.D., and Labun', A.N., Abstracts of Papers, *IX Mezhdunarodnaya konferentsiya po teoreticheskim voprosam adsorbtsii i adsorbtsionnoi khromatografii "Sovremennoe sostoyanie i perspektivy razvitiya teorii adsorbtsii", k 100-letiyu so dnya rozhdeniya akad. M.M. Dubinina* (Int. Conf. on Theoretical Problems of Adsorption and Adsorption Chromatography "Current State and Prospects for Development of the Theory of Adsorption", Dedicated to the Centennial of Acad. M.M. Dubinin), Moscow, April, 24–28, 2001, Moscow: Inst. Fiz. Khim. Ross. Akad. Nauk, 2001, p. 67.
5. Nikolaev, V.G. and Strelko, V.V., *Gemosorbtsiya na aktivnykh uglyakh* (Hemosorption on Activated Carbons), Kiev: Naukova Dumka, 1979.
6. Dudarev, V.I., Carbon Adsorbents for Metal Recovery from Solutions and Pulps, *Doctoral Dissertation*, Moscow, 2001.
7. Pokonova, Yu.V., *Khim. Tverd. Topl.*, 2001, no. 2, pp. 24–34.
8. Khomutov, A.N., Klushin, V.N., and Mukhin, V.M., *Sb. Nauchn. Tr. Ross. Khim.-Tekhnol. Univ. im D.I. Mendeleeva: Usp. Khim. Khim. Tekhnol.*, 2004, vol. 18, no. 6 (46), part 1, pp. 94–95.
9. Tarasevich, M.R., *Elektrokhimiya uglerodnykh materialov* (Electrochemistry of Carbon Materials), Moscow: Nauka, 1984.
10. Golub, D., Soffer, A., and Oren, Y., *J. Electroanal. Chem.*, 1989, vol. 260, pp. 383–392.
11. Tarkovskaya, I.A., *Okislennyi ugol'* (Oxidized Carbon), Kiev: Naukova Dumka, 1981.
12. Boehm, H.P., *Adv. Catal. Relat. Subj.*, 1966, vol. 16, pp. 179–274.
13. Glushchenko, V.Yu., *Adsorbtsiya i poristost': Trudy Chetvertoi vsesoyuznoi konferentsii po teoreticheskim voprosam adsorbtsii* (Adsorption and Porosity: Proc. Fourth All-Union Conf. on Theoretical Problems of Adsorption), Moscow: Nauka, 1976, pp. 35–40.
14. Gunasingham, H. and Fleet, B., *Analyst*, 1982, vol. 107, pp. 896–902.
15. Mukhin, V.M., Klushin, V.N., and Tarasov, A.V., *Aktivnye ugli Rossii* (Activated Carbons of Russia), Moscow: Metallurgiya, 2000.
16. Gur'yanov, V.V., Polyakov, N.N., and Petukhova, G.A., *Izv. Ross. Akad. Nauk, Ser. Khim.*, 2001, no. 6, pp. 933–937.
17. Besedina, I.N., Simkin, Yu.Ya., and Petrov, V.S., *Khim. Rast. Syr'ya*, 2001, no. 2, pp. 71–74.
18. Honyak, V.P., Mazina, O.I., and Drozhalina, N.D., *Khim. Tverd. Topl.*, 1990, no. 3, pp. 74–77.
19. Drozhalina, N.D., *Uglerodnye molekulyarnye sita na osnove torfa* (Peat-Based Carbon Molecular Sieves), Minsk: Nauka i Tekhnika, 1984.
20. Khomutov, A.N., Klushin, V.N., and Mukhin, V.M., *Sb. Nauchn. Tr. Ross. Khim.-Tekhnol. Univ. im D.I. Mendeleeva: Usp. Khim. Khim. Tekhnol.*, 2004, vol. 18, no. 6 (46), part 2, pp. 95–97.
21. Cheremskoi, G.P., *Metody issledovaniya poristosti tverdykh tel* (Methods of Studying the Porosity of Solids), Moscow: Energoizdat, 1985.
22. Polyanskii, N.G., Gorbunov. G.V., and Polyanskaya N.L., *Metody issledovaniya ionitov* (Methods of Studying Ion Exchangers), Moscow: Khimiya, 1976, pp. 159–163.
23. Velikii, E.M. and Alifanova, N.N., *Aktual'nye problemy adsorbtsionnykh protsessov: Materialy 4 Vserossiiskogo simpoziuma* (Urgent Problems of Adsorption Processes: Proc. 4th All-Russia Symp.), Moscow, 1997 (publ. 1998), p. 145.

Russian Journal of Applied Chemistry, Vol. 78, No. 11, 2005, pp. 1821–1826. Translated from Zhurnal Prikladnoi Khimii, Vol. 78, No. 11, 2005, pp. 1853–1858.
Original Russian Text Copyright © 2005 by Ledenev, Zorin, Prikhod'ko, Sychev, Astrelin.

SORPTION AND ION-EXCHANGE PROCESSES

The Role of the Nature of Active Centers in Chemisorption of Iron Acetylacetonate on the Surface of Amorphous Aluminosilicates and Aluminum Oxide

I. A. Ledenev, V. E. Zorin, R. V. Prikhod'ko, M. V. Sychev, and I. M. Astrelin

Kiev Polytechnic Institute, National Technical University of Ukraine, Kiev, Ukraine
Dumansky Institute of Colloidal Chemistry and Chemistry of Water, National Academy of Sciences of Ukraine, Kiev, Ukraine
Department of Chemistry, University of Durham, Durham, the United Kingdom
Siberian State Technological University, Krasnoyarsk, Russia

Received May 12, 2005

Abstract—γ-Al_2O_3 and amorphous and structured aluminosilicates were modified with iron acetylacetonate $Fe(acac)_3$ in a liquid medium.

One of the most efficient procedures of preparing supported catalysts is atomic layer deposition [1], which allows formation of superfine and uniformly distributed oxide phase [2, 3]. This procedure is based on chemisorption of metal acetylacetonate on the support surface and subsequent thermal decomposition of the complex in an oxygen-containing medium. This process occurs either through formation of hydrogen bonds between acetylacetonate ligand and surface hydroxyls or through substitution of this hydroxyl, which results in formation of a covalent bond between the metal atom and oxygen atom of the support surface [2–4]. Heterogeneity in the distribution of active centers on the support surface can significantly affect the mechanism of chemisorption of the acetylacetonate complex and thus affect the dispersity of the catalytically active phase. For aluminosilicates, the pattern is sophisticated since on their surface there are acidic, neutral, and basic hydroxy groups and also coordination-unsaturated centers formed by Al^{3+} cations [4–6]. Although atomic layer deposition shows much promise for preparing Fe-containing catalysts, which are of particular interest for catalysis [7–10], the possibility of its use for this purpose was not adequately studied.

Therefore, in this study we examined in detail the role of the nature of active centers in chemisorption of iron acetylacetonate on the surface of a series of supports.

EXPERIMENTAL

As supports we used amorphous aluminosilicates with the atomic ratio Si^{4+}/Al^{3+} 6.0 and 7.6, synthesized by coprecipitation or by the sol–gel method similar to that described in [11]. In the first case, 10.75 g of $AlCl_3 \cdot 6H_2O$ and 60 g of $Na_2SiO_3 \cdot 9H_2O$ were dissolved in 400 cm^3 of H_2O, 35 cm^3 of glacial acetic acid was added, and then 25% NH_4OH in the amount required for keeping pH 7.1 was added dropwise with vigorous stirring. The resulting gel was stirred for 1 h, filtered, washed 5 times with hot (363 K) 0.25 M CH_3COONH_4, and dried at 343 K for 24 h. Thus prepared precursor of amorphous aluminosilicate was calcined in an air flow at 923 K for 7 h. The resulting material was denoted as AAS. Partially dealuminated amorphous aluminosilicate, denoted as AAS(D), was prepared by treatment of AAS with 0.5 M $H_2C_2O_4$ for 12 h at 295 K with subsequent washing with deionized water. To remove possible impurities of amorphous SiO_2, air-dry precursor of AAS was treated with 0.5 M Na_2CO_3 for 20 min at 378 K and then the ammonium form of the resulting sample was calcined for 5 h at 923 K. This sample was denoted as AAS(S).

In sol–gel synthesis of structured aluminosilicstes (SASs), we used tetraethyl orthosilicate $Si(OC_2H_5)_4$ and $Al(NO_3)_3 \cdot 9H_2O$ as sources of silicon and aluminum, respectively. Polyethylene glycol (PEG) with a molecular weight of 4400 served as a reagent forming porous structure of SAS, and HNO_3, as a catalyst of hydrolysis and polycondensation of $Si(OC_2H_5)_4$ [11]. To prepare SAS, $Si(OC_2H_5)_4$ was gradually added with vigorous stirring to a solution containing HNO_3, PEG, and $Al(NO_3)_3$. The molar composition of the mixture was $Si(OC_2H_5)_4 : Al(NO_3)_3 \cdot 9H_2O : PEG : HNO_3 : H_2O = 1 : 0.132 : 0.01 : 0.41 : 14.27$. This

1070-4272/05/7811-1821 © 2005 Pleiades Publishing, Inc.

Table 1. Atomic ratio Si^{4+}/Al^{3+}, specific surface area, and pore size of the synthesized materials

Sample	Si^{4+}/Al^{3+}	S_{BET}, $m^2\ g^{-1}$	D_{por}, nm
AAS	6.0	411	3.6–4.2
AAS(D)	6.3	420	3.6–4.6
AAS(S)	5.6	425	3.4–4.8
SAS	7.6	429	2.6

mixture was kept in a hermetically sealed autoclave for 20 h at 323 K without stirring. Then, the resulting gel was dried at the same temperature for 170 h, after which PEG was removed by calcination at 873 K for 3 h and a heating rate of 5 K min^{-1}. The NH_4^+ form of SAS was prepared by its threefold treatment with 1.0 M NH_4Cl solution (the ratio solid : liquid = 1 : 20, contact time 12 h) at 298 K, followed by washing with deoinized water to negative reaction for Cl^- ions and drying at 383 K for 18 h. The H^+ form of this aluminosilicate was obtained by calcination of the NH_4^+ form in a thin layer at 773 K for 5 h at a heating rate of 5 K min^{-1}. These materials are denoted as NH_4^+–SAS and H^+–SAS, respectively.

Before modification of the supports with iron acetylacetonate $Fe(acac)_3$, they were heated in a vacuum (1.2 kPa) at 423 K for 2 h. The reaction vessel was cooled to 298 K and filled with dry argon; a solution of $Fe(acac)_3$ in toluene was added, and the resulting mixture was kept with stirring for 3 h. The solid phase was separated by centrifugation and in some cases washed with the fresh solvent and dried in a vacuum at 373 K. The samples were treated with acetylacetone in a similar way. The concentration of the adsorbed complex was determined photometrically using calibration plots (Specord UV-VIS M 40 spectrometer, Carl Zeiss, Jena).

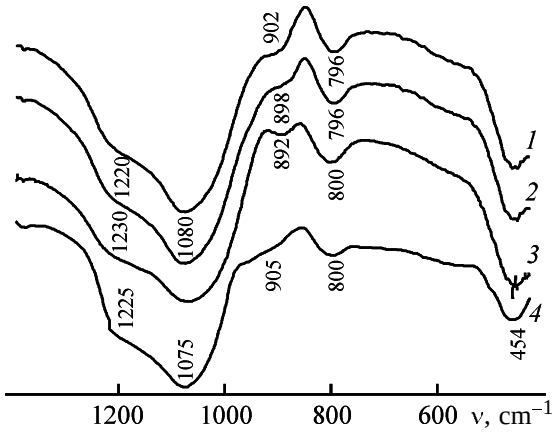


Fig. 1. IR spectra of synthesized aluminosilicates. (ν) Wave number. (*1*) AAS, (*2*) AAS(D), (*3*) AAS(S), and (*4*) SAS.

The isotherms of nitrogen adsorption–desorption (77 K) on the samples preliminarily evacuated at 473 K for 5 h were obtained with a Micromeritics ASAP 2010 adsorption installation. The pore size distribution was determined from the desorption isotherm by the Barrett–Joyner–Halenda (BJH) method [12].

The IR spectra were recorded on a Nicolet Avatar 360 FT-IR spectrophotometer; samples were pelletized with thoroughly dried KBr (1 : 60 ratio).

High-resolution NMR spectra with magic-angle spinning (MAS) and two-dimensional multi-quantum NMR spectra with magic-angle spinning (MQMAS) for ^{27}Al nuclei were recorded on a Bruker Avance 500 spectrometer at 130 MHz and magic-angle spinning rate of 28 kHz. To suppress artefacts of the baseline in unidimensional NMR spectra, we used a two-pulse spin-echo sequence. The pulse frequency was 50 kHz; pulse lengths, 2 and 4 μs; and spin echo delay, 10 μs. The spectrum acquisition number was from 256 to 1024. ^{27}Al chemical shifts were determined relative to saturated $Al(NO_3)_3$ solution. In processing of the MQMAS spectra we used the shearing procedure to obtain the isotropic chemical shift in the second dimension of the two-dimensional spectrum. The NMR spectra were processed using the Xwin-NMR software (Bruker).

The exchange capacity of the synthesized materials was determined at pH 7.0 using their Na^+ forms by the procedure described in [13]. The contact time of the samples with the complex $Cu(EDA)_2^{2+}$ was 30 min, after which they were recovered from the solution by centrifugation. The residual concentration of the complex in the liquid phase was determined by iodometric titration. Then, the exchange capacity was determined by subtracting the residual concentration from the concentration of the complex in the initial solution.

Chemical analysis shows that treatment of amorphous aluminosilicate (AAS) with $H_2C_2O_4$ or Na_2CO_3 solution results in partial removal of Al^{3+} and Si^{4+} ions, respectively (Table 1). However, in so doing, the parameters of the pore structure of this material (Table 1), which, similar to structured aluminosilicate (SAS), is predominantly mesoporous, change insignificantly. This follows from the shapes of isotherms of N_2 adsorption (type IV according to the IUPAC classification [14]) and from the pore size distribution found from these isotherms (Table 1). The IR spectrum of AAS (Fig. 1) contains absorption bands at 1215, 1070, 890, 800, and 454 cm^{-1} corresponding to

Table 2. Adsorption of $Fe(acac)_3$ on various supports

Sample	Total sorption capacity of complex	Content of physically sorbed complex	Content of chemisorbed complex	
	mmol g^{-1}		mmol g^{-1}	μmol m^{-2}
γ-Al_2O_3	0.22	0.14	0.08	0.42
AAS	0.48	0.05	0.43	1.00
AAS*	0.25	0.03	0.22	0.51
AAS(D)	0.61	0.31	0.30	0.68
AAS(D)*	0.36	0.28	0.08	0.19
AAS(S)	0.46	0.12	0.34	0.78
AAS(S)*	0.18	0.11	0.07	0.16
H^+-SAS	0.24	0.18	0.06	0.14
H^+-SAS*	0.10	0.06	0.04	0.09
NH_4^+-SAS	0.06	0.04	0.02	0.04

* Samples pretreated with acetylacetone.

vibrations of the =Si–O–Si≡, ≡Si–O–, ≡Si–O–Al=, ≡Si–OH, and ≡Si–O– bonds typical for aluminosilicates [15]. Treatment of this material with $H_2C_2O_4$ solution decreases the intensity of absorption bands corresponding to vibrations of the structural fragments ≡Si–O–Al= (890 cm^{-1}), which suggests their partial decomposition. Comparison of the IR spectra of the initial AAS and the sample treated with Na_2CO_3 solution (Fig. 1) shows that in the latter case the intensities of the shoulder at 1210–1230 cm^{-1} and absorption band at 800 cm^{-1} significantly decrease. This suggests the presence of free SiO_2 in the sample, which can be removed to a large extent by treatment of AAS with a soda solution. However, it is not improbable that in parallel some amount of structure-forming Si^{4+} ions is leached out, which can result in formation of additional active centers formed by coordination-unsaturated aluminum.

The IR spectrum of structured aluminosilicate (SAS) AAS (Fig. 1) also contains absorption bands typical for aluminosilicates [15]. However, contrary to AAS, in this case the absorption band of the structural fragments ≡Si–O–Al= at 890 cm^{-1} is weaker. This may be due to the fact that only a part of oxygen atoms coordinated to aluminum [11] form a chemical bond with Si^{4+}.

The ^{27}Al NMR spectrum of γ-Al_2O_3 contains the signals of Al^{3+} ions with tetrahedral and octahedral coordination [16, 17] with chemical shifts of 70.0 and 5.0 ppm, respectively (Fig. 2). For AAS, along with these signals, there is a signal at approximately 30 ppm, which can be assigned to five-coordinate aluminum [18]. This assumption was checked by two-dimensional multi-quantum (MQMAS) NMR allowing exclusion of erroneous signals arising, e.g., from

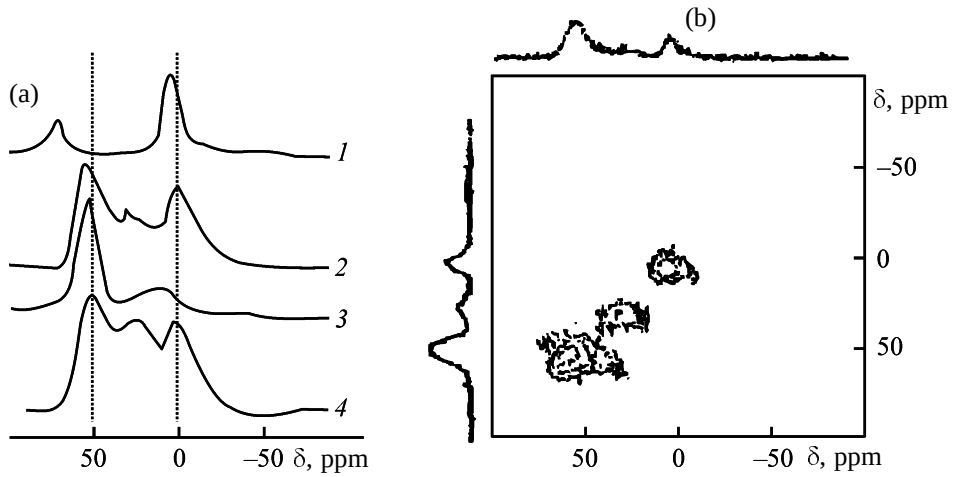


Fig. 2. ^{27}Al NMR spectra of the materials studied. (δ) Chemical shift. (a) (*1*) γ-Al_2O_3, (*2*) AAS, (*3*) SAS, and (*4*) AAS(S) (MAS); (b) AAS (MQMAS).

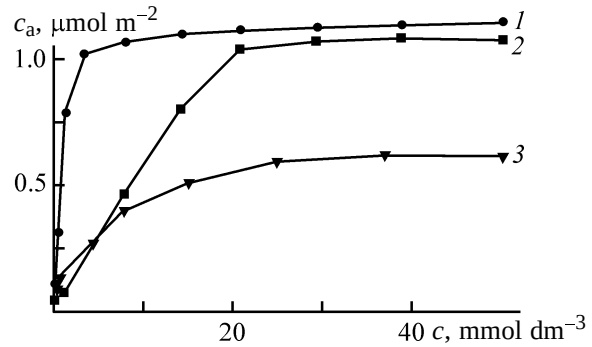


Fig. 3. Isotherms of $Fe(acac)_3$ adsorption on the surface of the supports studied. (c_a) Amount of adsorbed $Fe(acac)_3$ and (c) concentration of $Fe(acac)_3$ in solution. (*1*) γ-Al_2O_3, (*2*) AAS, and (*3*) SAS.

superposition of satellite signals [19]. In the MQMAS spectrum of the AAS sample (Fig. 2) there is a pronounced signal with a chemical shift of approximately 31 ppm, which is absent in the spectra of SAS or γ-Al_2O_3 [15]. Hence, the signal, indeed, reflects the presence of a fraction of Al^{3+} ions with coordination number 5 in this material. In the ^{27}Al NMR spectrum of AAS the signal of aluminum with coordination number 4 is downfield shifted in comparison with γ-Al_2O_3 (Fig. 2). This may be due to the influence of Si^{4+} ions forming fragments ≡Si–OH–Al=, whose presence in the structure of AAS was shown by IR spectroscopy. It is likely that treatment of this material with a Na_2CO_3 solution results in decomposition of a part of these fragments, as suggested by certain change in the ratio of intensities of signals in the ^{27}Al NMR spectrum.

As seen from Fig. 3, the amount of iron acetylacetonate complex adsorbed on the support surface depends on its concentration in solution, due to equilibrium character of protonation of acid-sensitive $Fe(acac)_3$ [3, 20]:

$$Fe(acac)_3 + 3H^+ \rightleftarrows [Fe(acacH)_3]^{3+}. \quad (1)$$

Formation of protonated complex of the $[Fe(acacH)_3]^{x+}$ type (x = 1–3) is favorable for its adsorption [21]; in this case, the degree of fixation depends on the strength and amount of surface acidic groups. Washing of modified γ-Al_2O_3 with toluene removed the most part of sorbed $Fe(acac)_3$ from the support surface (Table 2). This can be explained as follows. As known, $Fe(acac)_3$ is fixed on the γ-Al_2O_3 due to its reaction with coordination-unsaturated centers formed by aluminum cations (c.u.c. Al^{3+}) and also acidic hydroxy groups [3, 21]. As OH groups of γ-Al_2O_3 are weakly acidic and hence show low protonation power, their contribution to this process is hardly significant. Aluminum ions in c.u.c. participating in adsorption of $Fe(acac)_3$ on the surface of this support are in various coordination states: tetrahedral Al^{3+}(tetr) and octahedral Al^{3+}(oct) [3]:

$$Fe(acac)_3 + \text{c.u.c. } Al^{3+} \rightarrow Al(acac)_3 + [Al(acac)_x]_s^{(3-x)+} + Fe_s^{3+} + [Fe(acac)_{3-x}]^{x+}. \quad (2)$$

High extent of coordination unsaturation of Al^{3+}(tetr) [5] is favorable for formation of the delocalized complex $Al(acac)_3$ readily removable from the surface. Its transition to the liquid phase results in appearance of a vacancy, which then participates in chemisorption of Fe^{3+} ions formed as a result of elimination of acetylacetonate ligands. The reaction of $Fe(acac)_3$ with less coordination-unsaturated Al^{3+}(oct) [5] yields localized surface compounds $[Al(acac)_x]_s^{(3-x)+}$, which can block adsorption centers and thus hinder fixation of $[Fe(acac)_{3-x}]^{x+}$ and Fe^{3+} ions [3]. Hence, chemisorption of $Fe(acac)_3$ on the surface of γ-Al_2O_3 predominantly involves c.u.c. Al^{3+}(tetr), whereas c.u.c. Al^{3+}(oct) and weakly acidic hydroxy groups participate in physical adsorption of the complex. However, this interpretation does not consider the role of proton-donor structural fragments ≡Si–O–Al= (Brønsted centers) and silanol groups on the surface of aluminosilicates [5, 6], participating in protonation of the complex. The contribution of proton–donor groups to chemisorption of $Fe(acac)_3$ can be estimated by excluding the influence of other active centers. This can be realized by pretreating the samples with acetylacetone, whose reaction with c.u.c. Al^{3+} results in their selective blocking [3, 4]. Table 2 shows that washing of AAS modified by this procedure with toluene results in removal of only insignificant part of the adsorbed complex. This suggests that its reaction with proton of the structural fragments ≡Si–O–Al= yields tightly fixed chemisorbed surface compounds. It should be noted that the amount of Brønsted centers participating in this process (0.22 mmol g^{-1}) practically coincides with the exchange capacity of AAS (0.26 mmol g^{-1}). C.u.c. Al^{3+} make the same contribution to adsorption of $Fe(acac)_3$, which follows from comparison of the amounts of the chemisorbed complex on the initial AAS and on the sample treated with acetylacetone (Table 2). The significant role of these centers may be due to the fact that, along with c.u.c. Al^{3+}(tetr), AAS contains Al^{3+} with coordination number 5 (Fig. 2, ^{27}Al NMR spectrum). These cations can also form delocalized

$Al(acac)_3$ and thus assist to fixation of $Fe(acac)_3$ in its adsorption.

Insignificant amount of $Fe(acac)_3$ physically sorbed on AAS suggests insignificant contribution of c.u.c. Al^{3+}(oct) and silanol groups to this process. Nevertheless, these groups can promote elimination of acetylacetonate ligands in adsorption of the complex on other centers due to its partial protonation. The amount of the complex adsorbed on dealuminated sample, AAS(D), is somewhat higher than that on the initial amorphous aluminosilicate (Table 2). It is most likely that this is caused by formation of structural defects; however, in this case, the strength of bonding of adsorbed complex with the surface is small. In addition, the role of Brønsted centers and c.u.c. Al^{3+}(tetr, pent) is considerably smaller than that for AAS (Table 2). Hence, decomposition of the structural fragments ≡Si–O–Al= in dealumination of AAS results in formation of considerable amount of silanol groups weakly reactive with respect to $Fe(acac)_3$.

Table 2 shows that treatment of AAS with a Na_2CO_3 solution results in increasing contribution of c.u.c. Al^{3+}(tetr, pent) and acidic ≡Si–OH groups to adsorption of $Fe(acac)_3$ (approximately 0.29 and 0.11 mmol g^{-1}, respectively); in the process, the role of Brønsted centers significantly decreases. This is caused by formation of a large amount of coordination vacancies on aluminum ions and formation of silanol groups due to decomposition of ≡Si–O–Al= and ≡Si–O–Si≡ fragments, respectively. Thus, in treatment of amorphous aluminosilicate with Na_2CO_3 solution the Brønsted centers transform into c.u.c. Al^{3+}(tetr, pent), which is also suggested by variation of the relative intensities of the signals in the ^{27}Al NMR spectrum (Fig. 2).

The amount of the complex adsorbed on structured aluminosilicate (SA) is significantly smaller than that in the case of AAS (Fig. 3, Table 2). This is most probably due to the absence of aluminum with coordination number 5 in this material (Fig. 2). In the ^{27}Al NMR spectrum of SAS, the signal of octahedral aluminum is significantly upfield shifted (13 ppm), which suggests the presence of significant amount of c.u.c. Al^{3+}(oct). This is also suggested by their significant contribution to adsorption of $Fe(acac)_3$ (0.12 mmol g^{-1}, ±50%). It should be noted that at relatively high content of aluminum with coordination number 4 in SAS (Fig. 2, ^{27}Al NMR spectrum) Brønsted centers and c.u.c. Al^{3+} present in this material play an insignificant role in chemisorption of $Fe(acac)_3$ on its surface. This can be explained as follows. As shown previously [11, 12], during formation of SAS the reaction gel contains aluminum ions exclusively in the octahedral coordination state. In removal of the structure-forming agent, these ions are incorporated into the silicate matrix, with their coordination becoming tetrahedral. These Al^{3+}(tetr) ions are surrounded predominantly by oxygen atoms that do not form covalent bonds with silicon atoms. Therefore, Brønsted centers have weak acidity, and $Fe(acac)_3$ molecules sorbed on these centers are readily removed from the surface by washing with toluene. This explanation is confirmed by the significantly lower, compared to H^+-SAS, total sorption capacity of the NH_4^+-SAS sample, which does not contain proton-donor centers (Table 2).

CONCLUSION

Our results suggest that the nature of the active surface centers critically affects the chemisorption of iron acetylacetonate on the surface of aluminum oxide and amorphous aluminosilicates. In the case of amorphous aluminosilicates, the centers with high extent of coordination unsaturation, formed by Al^{3+} ions with coordination number 4 and 5, and also acidic bridging hydroxyls of ≡Si–OH–Al≡ are the dominating centers of $Fe(acac)_3$ chemisorption. Adsorption of this complex on weakly acidic hydroxyls and c.u.c. formed by Al^{3+} ions with octahedral coordination does not result in its fixation on the surface of Al-containing materials.

ACKNOWLEDGMENTS

This study was financially supported by the Ministry of Education and Science of Ukraine (grant no. 0104U000999).

The authors are grateful to J.A.R. van Veen (Shell International Chemicals, B.V., Amsterdam, Netherlands) for fruitful discussion and useful advices.

REFERENCES

1. Puurunen, R.L., Zeelie, T.A., and Krause, A.O.I., *Catal. Lett.*, 2002, vol. 83, nos. 1–2, p. 27.
2. Baltes, M., Voort, P. van der, Cillart, O., and Vansant, E.F., *J. Porous Mater.*, 1998, vol. 5, nos. 3–4, p. 317.
3. Veen, J.A.R. van, Jonkers, G., and Hesselink, W.H., *J. Chem. Soc., Faraday Trans. 1*, 1989, vol. 85, no. 2, pp. 389–413.
4. Baltes, M., Voort, P. van der, Weckhuysen, B.M., *et al.*, *Phys. Chem. Chem. Phys.*, 2000, vol. 2, no. 11, p. 2673.

5. Knozinger, H. and Ratnasamy, P., *Catal. Rev.–Sci. Eng*., 1978, vol. 17, no. 1, pp. 31–70.
6. Bremer, H. and Wendlandt, K.-P., *Heterogene Katalyse: Eine Einführung*, Berlin: Akademie, 1978.
7. Perez-Ramirez, J., Kapteijn, F., Scoffel, K., *et al*., *Appl. Catal. B: Environ*., 2003, vol. 44, pp. 117–151.
8. Romonis, P., Vattis, D., and Lycourghiotis, A., *J. Chem. Soc., Faraday Trans. 1*, 1985, vol. 81, pp. 2043–2051.
9. Shen, J., Guang, B., Tu, M., and Chen, Yi., *Catal. Today*, 1996, vol. 30, pp. 77–82.
10. Neamtu, M., Zaharia, C., Catrinescu, C., *et al*., *Appl. Catal. B: Environ*., 2004, vol. 48, pp. 287–294.
11. Yabuki, M., Takahashi, R., Sato, S., *et al*., *Phys. Chem. Chem Phys*., 2004, vol. 4, pp. 4830–4837.
12. Barrett, E.P., Joyner, L.G., and Halenda, P.P., *J. Am. Chem. Soc*., 1951, vol. 73, p. 373.
13. Bergaya, F. and Vayer, M., *Appl. Clay Sci*., 1977, vol. 12, p. 275–280.
14. Rouquerol, F., Rouquerol, J., and Sing, K., *Adsorption by Powder and Porous Solids: Principles, Methodology and Applications*, San Diego: Academic, 1999, pp. 439–441.
15. Farmer, V.C., *The Infrared Spectra of Minerals*, London: Mineral Soc., 1974.
16. Shen, J., Tu, M., Hu, C., and Chen, Yi., *Langmuir*, 1998, vol. 14, no. 10, p. 2756.
17. Rocha, J. and Klinovski, J., *Phys. Chem. Miner*., 1990, vol. 17, pp. 179–186.
18. Yan, Z., Ma, D., Zhuang, J., *et al*., *J. Mol. Catal., Ser. A*, 2003, vol. 194, nos. 1–2, p. 153.
19. Frydman, L. and Harwood, J.S., *J. Am. Chem. Soc*., 1995, vol. 117, no. 19, p. 5367.
20. Skopenko, V.V. and Savranskii, L.I., *Koordinatsionnaya khimiya* (Coordination Chemistry), Kiev: Libid', 1997.
21. White, M., *Catal. Today*, 1993, vol. 18, pp. 73–109.
22. Corma, A., *Chem. Rev*., 1995, vol. 95, pp. 559–614.

Russian Journal of Applied Chemistry, Vol. 78, No. 11, 2005, pp. 1827–1831. Translated from Zhurnal Prikladnoi Khimii, Vol. 78, No. 11, 2005, pp. 1859–1863.
Original Russian Text Copyright © 2005 by Shashkova, Mil'vit, Rat'ko.

SORPTION AND ION-EXCHANGE PROCESSES

Selective Sorption of Fe(III) Ions from Ni(II)–Fe(III) Mixtures with Chemisorbents

I. L. Shashkova, N. V. Mil'vit, and A. I. Rat'ko

Institute of General and Inorganic Chemistry, Belarussian National Academy of Sciences, Minsk, Belarus

Received June 15, 2005

Abstract—Selective recovery of Fe(III) ions from two-component nitrate solutions of Fe(III) and Ni(II) with synthetic nickel phosphate, natural chalk, and natural tripoli were studied. The mechanism of selective action of chemisorbents was considered, and high efficiency of the materials considered was demonstrated.

Ion exchange and chemisorption are traditionally used to sorb metal ions. In the latter case, sorbents chemically bind metal ions. Unlike ion exchange, chemisorption is characterized by substantial selectivity.

The capability of inorganic substances for selective chemisorption is caused by formation of new chemical compounds with lower Gibbs energy as compared to the initial state (e.g., less soluble compound), possibility of redox reactions, and other effects [1].

Poorly soluble sulfides, hydroxides, carbonates, and phosphates of some rare-earth and other bivalent metals exhibit chemisorption power with respect to heavy and nonferrous metals. The compounds formed in the process are less soluble than the initial compounds [1–3]. The chemisorption power depends on a number of factors; the major factor is the difference between the solubility products of the initial sorbent and compound formed, ΔSP.

A sorbent suitable for chemisorption of definite ions from mixtures can be found by considering the solubility series of phosphates, carbonates, and hydroxides of double and triple-charged metals.

Chemisorption can be a promising procedure for selective recovery of some nonferrous metal ions from two- and multicomponent solutions.

After deposition of nonferrous metal hydroxides from electroplating waste, filtrates (aqueous solutions containing from 2 to 25 g l^{-1} of alkali, alkaline-earth, and nonferrous metal salts) are formed; with the nonferrous metal fraction being 5–6% of the total metal content [4]. The composition of filtrates depends on the waste processing technology. Such solutions may contain ions of 2–10 nonferrous metals in amounts from 20–30 to 600–800 mg l^{-1}.

Dilute solutions containing nonferrous metals are concentrated using nonselective and selective ion-exchange materials. In the first case, all above metals and in the second case, only nonferrous metals are sorbed [4]. In contrast to selective ion-exchange materials, selective chemisorbents can be used not only for group concentration of nonferrous metals, but also for their separation.

In this study, we used synthetic nickel(II) orthophosphate and natural carbonates for selective sorption of iron(III) from binary solutions containing Fe(III) and Ni(II). Two-component dilute Fe^{3+}–Ni^{2+} aqueous solutions are formed during processing waste from nickel–iron battery electrodes [5] and from electrolytic baths for iron nickel-plating.

EXPERIMENTAL

Amorphous $Ni_3(PO_4)_2 \cdot 8H_2O$ was synthesized as in [6]. A hydrochloric (pH 5) solution of $(NH_4)_2HPO_4$ (5 g) in 100 ml of water was added dropwise to a solution of $NiCi_2 \cdot 6H_2O$ (100 g) in 100 ml of water with stirring at room temperature. The light green precipitate obtained was stored under the mother liquor for 2 h, filtered through a Büchner funnel, washed several times with distilled water, and dried in air and then over P_2O_5.

Tripoli with 30–65 wt % $CaCO_3$ content and chalk[1] were taken as natural sorbents. Chalk and tripoli were ground, and the fraction < 0.025 mm was sifted out before use.

The iron(III) sorption from two-component solutions [iron(III) and nickel(II) nitrates] was studied

[1] Tripoli from Stal'noe deposit (Mogilev oblast) and chalk from Volkovskoe deposit.

1070-4272/05/7811-1827 © 2005 Pleiades Publishing, Inc.

under static conditions at room temperature. The starting solutions were prepared from chemically pure and analytically pure grade crystal hydrates of iron(III) and Ni(II) nitrates. For comparison, sorption of iron(III) from one-component solutions of iron(III) nitrate was also studied. The experiment was performed at the constant bath rario (s : l = 1 : 250). The sorbent sample (0.1 g) was added to 25 ml of the solution studied and stored for a day with intermittent stirring. Then, the solid phase was filtered off, and the iron(III) and nickel(II) contents in the liquid were determined by atomic-absorption spectroscopy on an AAS-220 spectrometer. The concentrations of the initial solutions were varied within the 5–500 mg l^{-1} range.

The solubility product of $Ni_3(PO_4)_2$ was estimated by us at 1×10^{-7}, and that of $FePO_4$ is 10^{-23} in accordance with the reference data [7]. The difference between these SP values is substantial. Therefore, the contact of solid $Ni_3(PO_4)_2$ with a $Fe(NO_3)_3$ solution should lead to the substitution with formation of the less soluble compound

$$Ni_3(PO_4)_2 \cdot 8H_2O\downarrow + 2Fe^{3+} \rightleftarrows 2(FePO_4 \cdot yH_2O)\downarrow + 3Ni^{2+}. \quad (1)$$

As a result, nickel(II) ions pass into the solution, whereas the solid phase transforms into iron(III) phosphate, and hence nickel(II) phosphate can be used for selective sorption of Fe^{3+} ions from Fe^{3+}–Ni^{2+} mixtures.

The capacity of nickel phosphate for iron(III) ions in accordance with Eq. (1), corresponding to complete transformation of nickel phosphate into iron(III) phosphate, amounts to 11.8 mg-equiv g^{-1} (220 mg g^{-1}).

In addition to nickel phosphate, $CaCO_3$ can also be used as selective sorbent of Fe(III) ions from Fe^{3+}–Ni^{2+} mixtures. SPs of $CaCO_3$, $Ni_3(PO_4)_2$, and $FePO_4$ are 4.8×10^{-9}, 6.6×10^{-9}, and 3.47×10^{-11}, respectively. Thus, $CaCO_3$ should selectively sorb iron(III) ions from Fe^{3+}–Ni^{2+} mixtures.

Since iron(III) and aluminum(III) carbonates are instable hydrolytically and undergo hydrolytic decomposition to hydroxides [8], chemisorption of iron(III) ions can be described by scheme (2):

$$3CaCO_3\downarrow + Fe^{3+} \rightarrow FeCO_3\downarrow + 3Ca^{2+} \rightarrow 2Fe(OH)_3\downarrow + 3Ca^{2+} + CO_2. \quad (2)$$

The experimental data obtained are well consistent with the above theoretical consideration and confirm the possibility of using nickel phosphate and calcium carbonate for selective recovery of iron(III) ions from Fe^{3+}–Ni^{2+} mixtures.

The concentrations of metal ions in one-component (Fe^{3+}) and two-component (Fe^{3+}–Ni^{2+}) solutions before and after sorption, pH of the initial and equilibrium solutions, calculated amounts of adsorbed and released into the solution ions (mg-equiv g^{-1}), and the degree of Fe(III) recovery from solutions with various concentrations (%) are listed in the table. The amount of ions adsorbed was calculated by the formula

$$S_{M^{n+}} = \frac{(c_0 - c_s)V}{1000mE_{M^{n+}}},$$

where $S_{M^{n+}}$ is the amount of the metal ion sorbed per gram of the sorbent (mg-equiv g^{-1}); c_0 and c_s, concentrations of the solution before and after sorption (mg l^{-1}); V, solution volume (ml); m, sorbent weight (g); and $E_{M^{n+}}$, equivalent weight of metal ion (mg) equal to 18.67 and 29.35 mg for iron(III) and nickel(II), respectively.

When calculating the amount of nickel(II) transferred into the solution, instead of the difference between the solution concentrations before and after sorption ($c_0 - c_s$) we used the opposite quantity.

Figures 1–3 show the dependences of the Fe(III) sorption capacities for (a) one-component and (b) two-component solutions as functions of Fe(III) concentration for three sorbents: nickel phosphate (Figs. 1a, 1b), natural chalk (Figs. 2a, 2b), and carbonate tripoli (Figs. 3a, 3b).

Nickel phosphate completely recovers iron(III) from solutions with the initial iron concentration of up to 490 mg l^{-1} (one-component solution) and up to 242 mg l^{-1} (two-component solution). The amount of iron(III) sorbed (S_{Fe}) is a virtually linear function of its concentration in the initial solution ($c_0^{Fe^{3+}}$) both for one-component and two-component solutions. The sorption capacities of nickel phosphate for iron(III), S_{Fe}, in one-component and two-component solutions with equal $c_0^{Fe^{3+}}$ are very close. This means that Ni(II) does not interfere with the Fe(III) adsorption from the solution.

As seen from the table, the Ni(II) concentration in the solution after the contact with nickel phosphate increases. This confirms iron sorption in accordance with Eq. (1).

However, the amount of Fe(III) ions sorbed

Metal ion concentrations and pH of solutions before and after sorption

Metal ion concentration, mg l^{-1}				Fe(III) sorbed	Ni(II) sorbed or released	Degree of Fe(III) recovery from solution, %	Solution pH	
Ni(II)		Fe(III)						
in the initial solution	after sorption	in the initial solution	after sorption	mg-equiv^{-1}			before sorption	after sorption
Sorbent $Ni_3(PO_4)_2 \cdot H_2O$, $Fe(NO_3)_3$ solution								
–	6.1	6.8	0	0.1	0.05	100	3.28	6.91
–	62	69	0	0.9	0.5	100	3.01	6.90
–	132	140	0	1.9	1.1	100	2.65	6.87
–	229	232	0	3.1	2.0	100	2.62	6.78
–	303	312	0	4.2	2.6	100	2.52	6.53
–	472	484	0	6.5	4.0	100	2.44	5.57
Sorbent $Ni_3(PO_4)_2 \cdot H_2O$, $Fe(NO_3)_3$–$Ni(NO_3)_2$ solution								
14	26	10	0	0.1	0.02	100	3.19	6.95
82	122	60	0	0.8	0.4	100	2.85	6.86
165	234	121	0	1.6	0.8	100	2.74	6.56
330	466	300	0	4.0	1.7	100	2.55	6.34
465	667	490	4	6.4	2.2	99	2.41	5.38
Sorbent $CaCO_3$, $Fe(NO_3)_3$ solution								
–	–	6.8	0	0.09	–	100	3.28	7.70
–	–	69	0	0.9	–	100	3.01	6.90
–	–	140	0	1.9	–	100	2.65	7.61
–	–	232	0	3.1	–	100	2.62	7.97
–	–	312		4.2	–	100	2.52	7.36
–	–	484	0	6.4	–	100	2.44	7.51
Sorbent $CaCO_3$, $Fe(NO_3)_3$–$Ni(NO_3)_2$ solution								
14	3	10	0	0.1	0.09	100	3.19	7.40
82	59	60	0	0.8	0.2	100	2.85	7.32
165	125	121	0	1.6	0.3	100	2.74	7.10
330	256	300	0.5	4.0	0.6	99.8	2.55	7.58
465	365	490	0.6	6.6	0.9	99.9	2.41	7.34
Sorbent carbonate tripoli, $Fe(NO_3)_3$ solution								
–	–	6.8	0	0.09	–	100	3.28	7.62
–	–	69	0	0.9	–	100	3.01	6.90
–	–	140	0	1.9	–	100	2.65	7.51
–		232	0	3.1	–	100	2.62	8.26
–		312	0	4.2	–	100	2.52	8.31
–		484	0	6.4	–	100	2.44	8.40
Sorbent carbonate tripoli, $Fe(NO_3)_3$–$Ni(NO_3)_2$ solution								
14	12	10	0	0.1	0.02	100	3.19	7.60
82	60	60	0	0.8	0.2	100	2.85	7.46
165	129	121	0	1.6	0.3	100	2.74	7.24
330	214	300	64	3.2	0.7	79	2.55	7.10
465	369	490	226	6.5	0.8	54	2.41	5.62

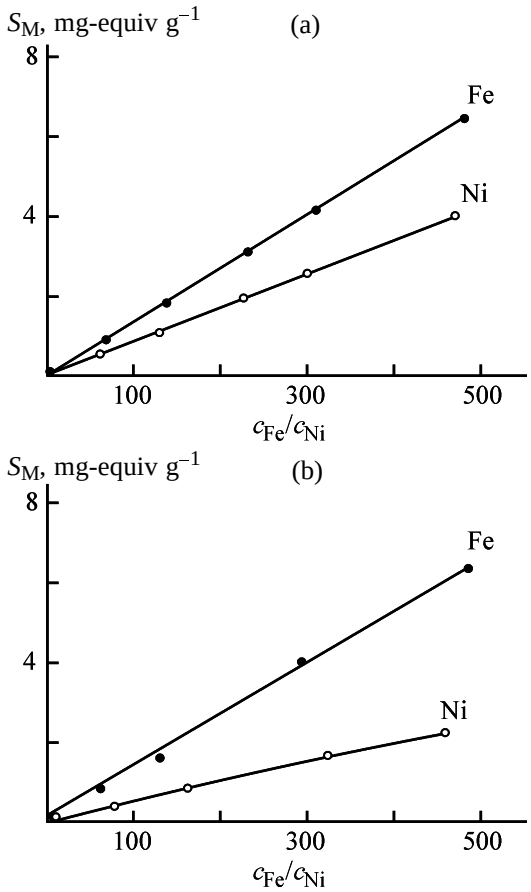


Fig. 1. Sorption of Fe^{3+} ions and release of Ni^{2+} ions S_M in the systems (a) [$Ni_3(PO_4)_2 \cdot 8H_2O_s$ (sorbent)–$Fe(NO_3)_3$ solution] and (b) [$Ni_3(PO_4)_2 \cdot 8H_2O_s$ (sorbent)–$Fe(NO_3)_3$ + $Ni(NO_3)_2$ solution] as a function of c_{Fe}/c_{Ni} ratio, where c_{Fe} and c_{Ni} are concentrations of Fe^{3+} and Ni^{2+} ions in the initial solution (mg l^{-1}), respectively.

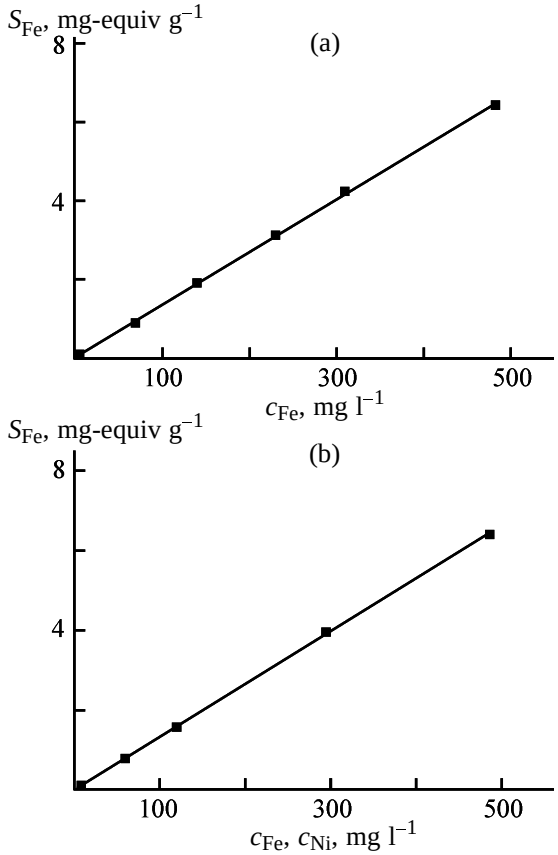


Fig. 2. Sorption of Fe^{3+} ions S_{Fe} with natural chalk as a function of iron(III) ion concentration c_{Fe} in (a) one-component and (b) two-component solutions of $M(NO_3)_n$ (M = Fe, Ni).

(mg-equiv) exceeds the amount of Ni(II) ions transferred into the solution (see table). Correspondingly, the line for nickel transferred into the solution lies lower than the line of iron sorption. Nonequivalent ratio of the sorbed and released ions suggests the occurrence of an additional process not described by Eq. (1).

Phosphates of double-charged metal ions, including Ni^{2+}, form alkaline solutions on contact with water, e.g., pH of aqueous extract of $Ni_3(PO_4)_2 \cdot 8H_2O$ is 7.79. Hence, pH of equilibrium solutions increases after their contact with the sorbent (see table). For instance, the pH values of the initial two-component solutions with iron(III) concentrations from 10 to 490 mg l^{-1} before sorption are 2.45–3.28, and after sorption they become 5.57–6.91. It should be noted that chemisorption and heterogeneous precipitation occur in the near-surface layer of the sorbent, where the ionic concentration and, correspondingly, pH are still higher. pH 6–7 is favorable for $Fe(OH)_3$ precipitation from dilute solutions. Probably, reaction (1) is accompanied by precipitation of $Fe(OH)_3$, and the product of chemisorption is a mixture of iron(III) phosphate and hydroxide. The X-ray phase analysis of this product calcined at 900°C confirms this suggestion. The powder pattern of the product contains iron(III) phosphate and iron(III) oxide reflections.

The S_{Fe}–$c_0^{Fe^{3+}}$ dependences for iron sorption from one-component and two-component solutions with carbonate sorbents are shown in Figs. 2 and 3. They are similar to those of nickel phosphate, except the tripoli–two-component solution system. At the concentration of the initial solution higher than 200 mg l^{-1}, the S_{Fe}–$c_0^{Fe^{3+}}$ curve flattens out, i.e., iron(III) sorption at its concentration higher than 300–400 mg l^{-1} stops. This is caused by the limited content (45%) of the sorbing component, calcium carbonate, in the natural tripoli studied.

The degree of iron(III) recovery with natural car-

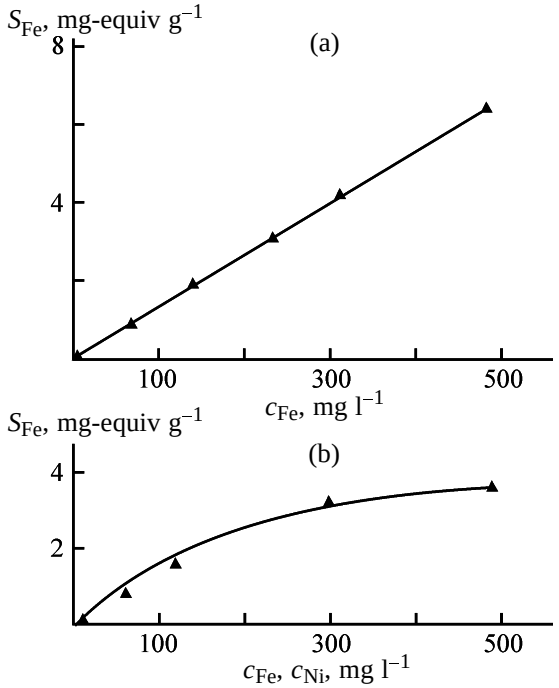


Fig. 3. Sorption of Fe^{3+} ions S_{Fe} with natural tripoli as a function of iron(III) ion concentration c_{Fe} in (a) one-component and (b) two-component solutions of $M(NO_3)_n$ (M = Fe, Ni).

bonate sorbents from one-component solutions is 100% within the entire range of solution concentrations (c_0 < 484 mg l^{-1}). In the case of two-component solutions with the initial iron(III) concentration higher than 240 mg l^{-1}, the solutions after sorption contain small amounts of iron (0.5–0.9 mg l^{-1}).

Similarly to phosphate sorbents, carbonate sorbents exhibit base properties. The pH of aqueous extracts for chalk and tripoli is 7.46 and 8.18, respectively. These high pH values provide a high degree of iron(III) recovery from solutions within the iron concentration range studied. The results of our study are consistent with previous data [9, 10] that the complete deironing of dilute iron(III) solutions with carbonate sorbents is possible at pH > 7. In particular, Shanina *et al.* [9] found that solutions are completely deironed with calcium carbonate at pH 3.5, when the iron(III) concentration is 0.15 g-equiv l^{-1}, whereas in accordance with data of Batalova *et al.* [10] this result is attained at pH > 7 when the iron(III) concentration is 0.005 g-equiv l^{-1}.

CONCLUSIONS

(1) Nickel(II) phosphate, natural chalk, and carbonate tripoli can be used as sorbents for selective sorption of iron(III) ions from two-component Fe^{3+}–Ni^{2+} solutions.

(2) Selective recovery of iron(III) ions from two-component Fe^{3+}–Ni^{2+} solutions with nickel(II) phosphate is caused by heterogeneous exchange reaction with formation of less soluble iron(III) phosphate and deposition of iron(III) hydroxide. Carbonate and phosphate chemisorbents provide 100% recovery of iron(III) ions within a wide range of iron concentrations.

(3) The use of calcium carbonate for selective iron(III) chemisorption is promising because it is a widespread and cheap natural raw material.

REFERENCES

1. Aleksandrov, S.T., *Zh. Anal. Khim.*, 1975, vol. 30, no. 3, pp. 528–534.
2. Shashkova, I.L., *Zh. Neorg. Khim.*, 2001, vol. 46, no. 4, pp. 592–598.
3. Shashkova, I.L., Rat'ko, A.I., Mil'vit, N.V., *et al.*, *Zh. Prikl. Khim.*, 2000, vol. 73, no. 6, pp. 914–919.
4. Kargman, V.B., Sokolova, L.P., Saldadze, G.K., *et al.*, *Zh. Prikl. Khim.*, 2001, vol. 74, no. 11, pp. 1803–1808.
5. Demidov, A.I. and Krasovitskaya, O.A., *Zh. Prikl. Khim.*, 2000, vol. 73, no. 10, pp. 1656–1660.
6. Klement, R. and Haselbeck, H., *Z. Anorg. Allg. Chem.*, 1964, vol. 334, nos. 1–2, pp. 27–36.
7. Lur'e, Yu.Yu., *Spravochnik po analiticheskoi khimii* (Handbook on Analytical Chemistry), Moscow: Khimiya, 1967.
8. *Obshchaya khimiya v formulakh, opredeleniyakh, skhemakh* (General Chemistry in Formulas, Definitions, and Schemes), Tikavyi, V.F., Ed., Minsk: Universitetskoe, 1987.
9. Shanina, T.P., Poladyan, V.E., Marants, I.S., *et al.*, *Kompl. Ispol'z. Miner. Syr'ya*, 1992, no. 4, pp. 87–89.
10. Batalova, Sh.B., Pak, N.D., Duimagambetova, S.D., *et al.*, *Kompleks. Ispol'z. Miner. Syr'ya*, 1979, no. 10, pp. 56–59.

Russian Journal of Applied Chemistry, Vol. 78, No. 11, 2005, pp. 1832–1835. Translated from Zhurnal Prikladnoi Khimii, Vol. 78, No. 11, 2005, pp. 1864–1867.
Original Russian Text Copyright © 2005 by Mishutkin, Momot.

SORPTION AND ION-EXCHANGE PROCESSES

A New Technique for Determining Coproporphyrin III Content in Culture Broth

S. N. Mishutkin and N. N. Momot

Elest Limited Liability Company, St. Petersburg, Russia

Received August 11, 2005

Abstract—A new technique for spectrophotometric determination of coproporphyrin III in culture broth, based on its preliminary separation from impurities, was developed. This technique ensures higher accuracy of coproporphyrin III determination than the commonly used method based on sorption of coproporphyrin III on talc.

Porphyrins belong to a vast group of aromatic tetrapyrrole compounds containing four pyrrole rings bound by monocarbon bridges. Most of biologically active tetrapyrroles are metal complexes. For example, heme and siroheme contain iron, chlorophylls and bacteriochlorophylls contain magnesium, etc. [1].

It is known that cancerous growths selectively accumulate coproporphyrin III. On laser irradiation of coproporphyrin III-containing cancerous growth at 401 nm, which corresponds to the maximum of coproporphyrin III absorption [2], a tumor is destroyed by free radicals photochemically generated in the living tissues saturated with oxygen. Thus, in the course of photodynamic therapy of cancerous growth, coproporphyrin III is a photosensitizer. Coproporphyrin III is a low-toxic drug exhibiting broad antitumor effects exceeding those of other antitumor drugs [3].

Coproporphyrin III is a metabolite of *Artrobacter globiformis* microorganisms. In recovery of coproporphyrin III from both culture broth and native solution, its quantitative determination in these media is required. In this study we developed a new technique for determining coproporphyrin III content in culture broth ensuring higher accuracy than the commonly used methods.

A technique for determining proporphyrin III in culture broth based on its sorption on talc powder was described in [2]. According to this method, the initial culture broth is centrifuged to obtain a native solution, and then a weighed portion of talc is added to them. The resulting suspension is stirred and allowed to stand for 24 h in the dark. Thereafter, the talc is filtered off and washed with acidified water with pH 3.5–4.0 at which coproporphyrin III is poorly soluble in water [2]. The coproporphyrin III accumulated on the talc surface is desorbed with a solution of HCl in aqueous acetone. The coproporphyrin-containing desorbate is diluted with 5% aqueous hydrogen chloride, and its optical absorption is recorded at wavelengths 380, 401, and 430 nm. The coproporphyrin III content in the initial culture broth X is calculated by the equation

$$X = [2D_{401} - (D_{430} + D_{380})](V_{el}P)(E \times 1.835V_{cb})^{-1}, \quad (1)$$

where D_{430}, D_{380} and D_{401} are the optical densities of the desorbate diluted with 5% aqueous HCl at 430, 380 and 401 nm, respectively; V_{el}, desorbate volume, ml; V_{cb}, culture broth volume used for preparing native solution; P, dilution factor of desorbate before spectrophotometric determination; $E = 0.667$, specific absorption coefficient; and 1.835, correction factor.

Taking into account that talc has poor sorption selectivity to coproporphyrin III, we expected that the desorbate can contain not only coproporphyrin III but also some foreign species present in culture broth. To check this assumption, the desorbate was subjected to chromatographic separation. Before chromatographic analysis, acetone was removed from the desorbate by evaporation and the remaining solution (15 ml) was applied to a 100-ml column 2 cm in diameter, packed with KSK silica gel. On washing the column with 5% aqueous HCl, three sorption bands were formed. The first sorption band of light brown color, related to impurities, was eluted with 5% HCl and collected as a separate fraction. The middle sorption band of pink color containing coproporphyrin III was also eluted with 5% HCl and collected. The uppermost sorption band of brown color, related to impurities,

1070-4272/05/7811-1832 © 2005 Pleiades Publishing, Inc.

Table 1. Sorbent characteristics

Sorbent brand	Average pore diameter, μm	Porosity (specific pore volume), $cm^3\ g^{-1}$	Specific surface area, $m^2\ g^{-1}$	Specific volume of sorbent in column, $cm^3\ g^{-1}$
Sephadex G-15	–	–	–	2.5–3.5
Silokhrom S-80	0.06–0.08	0.7–1.3	70–90	–
Silokhrom S-120	0.03–0.05	0.8–1.2	110–130	–
Silokhrom SKh-2.5	0.066–0.12	1.5–2.0	60–89	
KSK silica gel	0.02–0.05	1.00–1.25	250	–
L silica gel	0.008	0.6–0.75	600–750	–

could not be eluted with 5% aqueous HCl. To elute these impurities, the column was washed with 0.5% aqueous ammonia and the resulting eluate was collected. The residual foreign species remaining in the column were washed off with acidified acetone and also collected. The four fractions eluted from the chromatographic column were diluted to the required volume, and the electronic absorption spectra of the resulting solutions were recorded on an SF-26 spectrophotometer in the wavelength range 360–450 nm with a wavelength step from 2 to 5 nm (Fig. 1). The comparison of the absorption spectra of the fractions obtained by chromatographic separation of the desorbate from talc shows that the maxima of absorption bands of coproporphyrin III and the first fraction of impurities almost coincide. Therefore, the calculation of coproporphyrin III content by the expression $2D_{401} - (D_{430} + D_{380})$ [Eq. (1)] accepted in the technique based on recovery of coproporphyrin III from culture broth by sorption on talc is inaccurate. We found that the technique based on sorption on talc overestimates the coproporphyrin III content in the culture broth by approximately 10%.

In this connection, we developed a more accurate technique for determining the coproporphyrin III content in culture broth. According to this technique, coproporphyrin III is selectively recovered from culture broth by sorption chromatography. To choose a sorbent exhibiting the required selectivity to coproporphyrin III, we tested sorbents of various brands: Sephadex G-15, Silokhrom S-120, Silokhrom S-80, KSK silica gel, and L silica gel. The characteristics of these sorbents are listed in Table 1 [4, 5].

In our experiments, a chromatographic column was packed with sorbent grains 100–200 μm in diameter. The sorbent was preliminarily immersed in water and then loaded into a 100-ml column 2 cm in diameter. A portion of native solution (15 ml) was applied to the column packed with the sorbent. All the native solutions used in our experiments were prepared from the same culture broth sample. The column was successively washed with 5% aqueous HCl, 0.5% aqueous ammonia, and acidified acetone. In the course of washing, the separation of sorption bands was visually observed. We found that species present in the tested native solution are not separated on Sephadex G-15 and Silokhrom S-120. Therefore, these sorbents were discarded. In going to Silokhrom-80, KSK silica gel, and L silica gel, partial separation of coproporphyrin III from impurities was reached. We repeated the chromatographic separation of the components present in the native solution using three above-chosen sorbents. In these experiments, the eluate fractions (5–70 ml) were collected and coproporphyrin III content in them was determined spectrophotometrically. Before analysis, the eluate fractions were diluted with 5% aqueous HCl by a factor of 10–25 depending on their coproporphyrin III content. The optical density of these fractions was measured and the output elution curves were built (Fig. 2). As with 15-ml portions

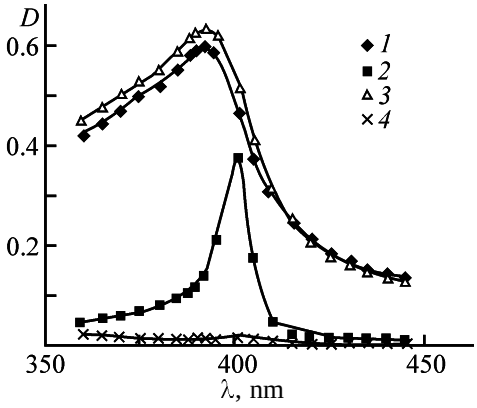


Fig. 1. Electronic absorption spectra of species desorbed from talc and then separated on column packed with KSK silica gel. (*D*) Optical density and (λ) wavelength. Spectra: (*1*) fraction eluted before coproporphyrin III (fraction 1), (*2*) fraction of coproporphyrin III (fraction 2), (*3*) fraction of impurities eluted with 0.5% aqueous ammonia (fraction 3), and (*4*) fraction of impurities eluted with acidified acetone.

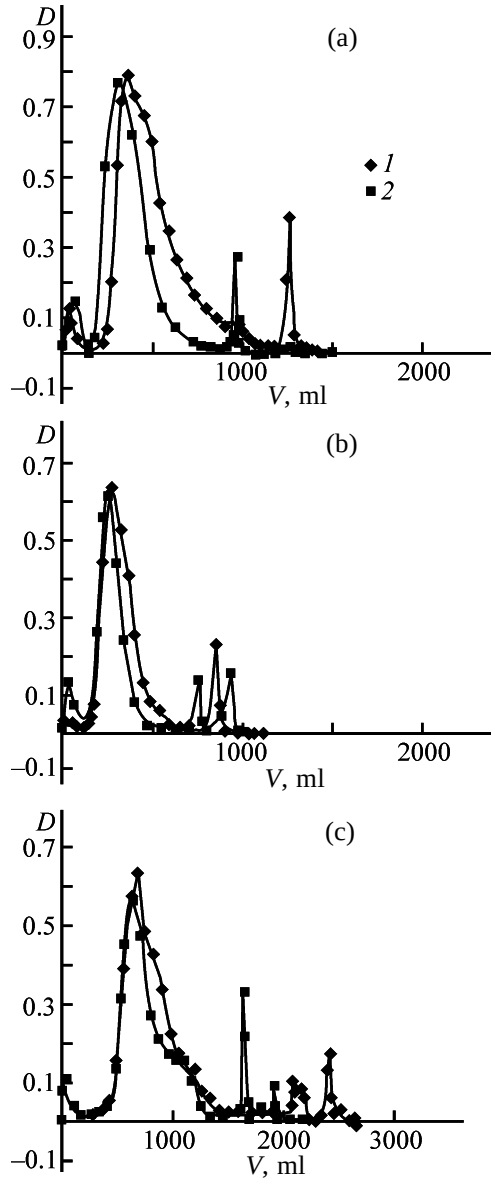


Fig. 2. Elution curves of components of native solution from a column 2 cm in diameter packed with 100 ml of (a) Silokhrom S-80, (b) KSK silica gel, and (c) L silica gel in successive washing with 5% aqueous HCl, 0.5% aqueous ammonia, and acidified acetone. Elution rate 50–70 ml $(h\ cm^2)^{-1}$. (*D*) Eluent optical density at λ = 401 nm and (*V*) eluent volume. Native solution volume applied to column: (*1*) 15 ml and (*2*) 10 ml.

the separation was incomplete, the sample volume was decreased to 10 ml, and better separation was attained on all the three sorbents (Fig. 2).

Taking into account that coproporphyrin III fractions were diluted to different extents, the sorption selectivity of the tested sorbents to coproporhhyrin III was estimated by the optical density of an intermediate undiluted fraction eluted with 5% aqueous HCl between coproporphyrin III and impurity fractions. The optical densities of these intermediate fractions eluted from columns packed with three different sorbents are compared in Table 2.

Table 2. Optical density of intermediate fraction of native solution eluted between coproporphyrin III and impurity fractions

Sorbent	Optical density of intermediate fraction	Native solution volume applied to column, ml
Silokhrom S-80	0.090	10
KSK silica gel	0.150	10
L silica gel	0.190	10

Table 2 shows that in the series of tested sorbents the intermediate fraction eluted from Silokhrom S-80 has the lowest optical density, i.e., this sorbent is the most selective. Along with the sorbents under consideration, we tested Silokhrom SKh-2.5 sorbent whose characteristics, according to published data, are close to those of Silokhrom S-80 (Table 1). This sorbent was used for separating the native solution applied to the column in an amount of 10 ml. The elution curve was obtained, and the optical density of the intermediate fraction was found to be 0.120. Thus, among the sorbents tested Silokhrom S-80 exhibits the highest selectivity to coproporphyrin III.

Our results show that the sorption chromatography is a more efficient technique for recovery of coproporphyrin II from native solution than sorption on talc and can be used for accurate determination of the coproporphyrin III content in culture broth. To perform the chromatographic separation of native solution, the following equipment is required: volumetric flask, column 2 cm in diameter packed with Silokhrom S-80 (100 ml) with a grain size of 100–200 μm, and a spectrophotometer.

The chromatographic separation of native solution was carried out as follows.

A portion of native solution (10 ml) was applied to the column and then the column was washed with 5% aqueous HCl to separate coproporphyrin III from impurities. The coproporphyrin III fraction was collected and its volume was measured. This fraction was diluted to a concentration required for determining the optical density at 380, 401 and 430 nm. Based on these data, the coproporphyrin III content in culture

Table 3. Comparison of coproporphyrin III content in culture broth as determined by chromatographic separation and sorption on talc

Culture broth volume, ml	Coproporphyrin III content in culture broth, mg l^{-1}		$(c_2 - c_1)C_1^{-1} \times 100\%$
	chromatographic method	sorption on talc	
2340	215	235	9.3
3570	348	376	8.0
3820	327	370	13.1

broth was calculated by formula (1), where V_{el} is the volume of coproporphyrin III fraction obtained in eluting 10-ml sample of native solution applied to column, and V_{cb} is the culture broth volume required for preparing 10 ml of native solution.

The following factors contribute to the total error of coproporphyrin III determination by our technique: (1) error in sampling native solution with 10-ml pipette (0.6%), (2) error caused by incomplete separation of coproporphyrin from impurities (0.5%), (3) error in determining the volume of eluted fraction with a volumetric cylinder (0.8%) and (4) error in determining the optical density on an SF-26 spectrophotometer (1%).

The total error of determining coproporphyrin III content in culture broth did not exceed 3%.

Three different samples of culture broth were analyzed for coproporphyrin III by methods based on sorption of coproporphyrin III on talc and chromatographic techniques. The results of these analyses are compared in Table 3.

These data show that the method of coprporphyrin determination based on sorption of coproporphyrin III on talc overestimates the coproporphyrin III content in culture broth by 10% as compared to chromatographic technique. This discrepancy is caused by the fact that talc sorbs not only coproporphyrin III but also foreign components present in the culture broth.

CONCLUSION

To ensure correct spectrophotometric determination of coproporphyrin III content in culture broth, this compound must be separated from impurities. This problem is successfuully solved by sorption chromatography. In recovery of coproporphyrin III by sorption on talc, the overestimated results are obtained due to sorption of impurities. In this case, the coproporphyrin III content can be corrected by multiplying by a factor of 0.9.

REFERENCES

1. Bykhovskii, V.Ya., Zaitseva, N.I., and Polulyakh, O.V., *Mikrobiologicheskii sintez porfirinov* (Microbiological Synthesis of Porphyrins), Moscow: VNIISENTI, 1985.
2. Falk, G.E., *Porphyrins and Metalloporphyrins*, Amsterdam: Elsevier, 1964.
3. Malkov, M.A., Mel'nikov, A.S., and Petrishchev, N.N., *Lazern. Med.*, 2004, vol. 3, no. 8, p. 144.
4. Lur'e, A.A., *Sorbenty i khromatograficheskie nositeli* (Sorbents and Chromatographic Supports), Moscow: Khimiya, 1972.
5. Kolikov, V.M. and Mchedlishvili, B.V., *Khromatografiya biopolimerov na makroporistykh kremnezemakh* (Chromatography of Biopolymers on Macroporous Silicas), Leningrad: Nauka, 1968.
6. Goronovskii, I.T., Nazarenko, Yu.P., and Nekryach, E.F., *Kratkii spravochnik po khimii* (Concise Chemical Handbook), Kiev: Akad. Nauk Ukr. SSR, 1963.

Russian Journal of Applied Chemistry, Vol. 78, No. 11, 2005, pp. 1836–1839. Translated from Zhurnal Prikladnoi Khimii, Vol. 78, No. 11, 2005, pp. 1868–1871.
Original Russian Text Copyright © 2005 by Yudilevich, Kolikova.

APPLIED ELECTROCHEMISTRY AND CORROSION PROTECTION OF METALS

Influence of Fabric-Enclosed Positive Electrodes on Self-Discharge Mechanism of Active Masses of Lead Batteries

S. R. Yudilevich and G. A. Kolikova

Istochnik Research Battery Institute, Joint-Stock Company, St. Petersburg, Russia

Received August 8, 2005

Abstract—The self-discharge of lead batteries with fabric-enclosed positive electrodes was studied. The self-discharge mechanism was proposed.

On storage of charged lead batteries, the active materials of electrodes spontaneously react with the electrolyte. On the positive electrode, lead dioxide reacts with sulfuric acid:

$$PbO_2 + H_2SO_4 \rightarrow PbSO_4 + H_2O + 1/2O_2, \quad (1)$$

and alloy components used for fabricating a current lead are oxidized with lead dioxide. In the overall self-discharge balance, the alloy oxidation is not predominant.

The self-discharge of a negative electrode is determined by two reactions: reaction of lead with sulfuric acid

$$Pb + H_2SO_4 \rightarrow PbSO_4 + H_2 \quad (2)$$

and oxidation of lead with oxygen formed by the reduction of lead dioxide

$$Pb + 1/2O_2 + H_2SO_4 \rightarrow PbSO_4 + H_2O. \quad (3)$$

It was estimated in [1] that, in the overall self-discharge balance of the negative electrode, reaction (3) is insignificant, since lead sulfate formed on the surface of active material impedes access of oxygen molecules toward the surface of spongy lead. Reactions (1) and (2) proceed on electrodes independently. The capacity losses by a battery owing to the self-discharge of active materials can differ, because even the same factors, such as, e.g., the electrolyte density, differently affect self-discharge of lead and lead dioxide.

The modern alloys used for fabricating current leads of positive electrodes contain considerably less antimony and other alloying additives. This results in a weaker transfer of corrosion products toward negative active mass and, as a result, in the decreased rate of spontaneous dissolution of lead.

It was established that, with the positive electrode covered by a fabric, the self-discharge of a lead battery can be decreased several-fold [2]. This is partly due to the fact that the antimony transfer from positive to negative electrode is weaker [3].

We studied how fabric envelope affects the loss of capacity by stationary TB-M batteries and by high power (HP) traction batteries in the course of storage.

The current leads to positive electrode of TB-450M batteries were fabricated from the US-1M alloy containing small amount (1.5%) of antimony, and those to the pilot samples of HP traction batteries, from the alloy containing 4% antimony.

The TB batteries were tested from the beginning of the life till the 40th cycle inclusive.

The results of the tests (Table 1) show that not loss, but some increase in capacity is observed for TB-450M batteries stored for 15 days, i.e., within the period of time imposed on TB batteries by GOST [(State Standard) 26881–86] and TU (Technical Specification). The same results were obtained for batteries stored for 18 and 20 days. The loss of capacity by a reference TB-600 battery whose positive electrodes were not enclosed with a fabric and current leads were also fabricated from the US-1M alloys was about 0.4% day^{-1}.

The fact that the fabric-enclosed positive electrodes largely affect the self-discharge rate was also confirmed on pilot HP batteries tested on the 21–22nd and 81–82nd cycles. The HP batteries with positive electrodes made of the same materials without fabric envelope were tested as reference. The capacity of the pilot batteries stored without current for 10 days was

1070-4272/05/7811-1836© 2005 Pleiades Publishing, Inc.

Table 1. Comparative results on self-discharge of TB batteries

Testing time, day	Discharge no.	Discharge parameter	Discharge parameter value for indicated battery	
			TB-450M	TB-600
15	16th	Capacity, A h	501.6	617.6
	17th	Capacity, A h	513.0	577.4
		Change in capacity	–11.4*/–0.15	40.2/0.43
18	27th	Capacity, A h	477.7	643.9
	28th	Capacity, A h	499.4	592
		Change in capacity	–21.7/–0.25	51/0.44
20	32nd	Capacity, A h	515.5	639.0
	33rd	Capacity, A h	532.2	588.4
		Change in capacity	–16.7/–0.16	50.6/0.40

* The quantities in the numerator are in A h, and those in the denominator, in % day^{-1}.

higher by 7% on 22nd cycle and by 3% on 82nd cycle than the capacity attained during the previous discharge. The loss of capacity by the reference batteries for the same time was 4 and 16%, respectively.

The degree of self-discharge (capacity loss) η (%) was calculated by the equation

$$\eta = \frac{C_1 - C_2}{C_1 n} \times 100, \quad (4)$$

where C_1 is the battery capacity immediately after charging (A h); C_2, battery capacity after storage (A h); and n, storage time (days).

Because alloys for preparing current leads to positive electrodes of pilot and reference TB batteries are the same and materials used for fabricating negative electrodes of each battery are the same also, we can conclude that difference in the self-discharge rate is due to the presence of the fabric envelope entirely enclosing the positive electrode.

Anomalous increase in the capacity observed for TB-450M batteries and for pilot BM batteries discharged after the storage without current is likely due to the fact that oxygen escape from the positive electrode immediately after charging is decelerated owing to the presence of fabric envelope. This can cause some increase in the inner resistance of the battery and, as a consequence, some decrease in the discharge capacity. The discharge was performed after 10–20 days of storage, when all the gas from the interelectrode space escaped. Despite the fact that some loss of capacity by the active masses could take place, its value did not exceed the gas-filling effect during the first discharge.

To determine the daily average loss of capacity (self-discharge) of the batteries with fabric-enclosed positive electrodes, the storage time of the TB-450M batteries was increased to 6 months (183 days). The TB-600 reference batteries were tested for comparison. The results of the tests are collected in Table 2. The capacity values of the stored battery before and after the test were reduced to 20°C and the actual degree of self-discharge was calculated. The final self-discharge value with due regard for the battery temperature averaged throughout the storage period

Table 2. Results obtained in testing the self-discharge of TB batteries stored for a long time

Parameter	Battery type	
	TB-450M	TB-600
38th discharge		
Actual capacity, A h	486.5	556.7
Average temperature of discharge, °C	22.5	14.0
Capacity reduced to 20°C, A h	483.4	576.7
Storage time, day	183	165
Average temperature of storage, °C	19.6	16.1
39th discharge		
Actual capacity, A h	400.5	402.6
Average temperature of discharge, °C	24.5	22.5
Capacity reduced to 20°C, A h	395.4	400.0
Change in capacity, A h	88.0	176.7
Actual self-discharge, % day^{-1}	0.10	0.19
Self-discharge (reduced to storage temperature of 20°C), % day^{-1}	≈0.10	0.23

Table 3. Results obtained in testing the self-discharge of positive electrodes of a lead–copper battery

Test conditions		Cell type	$PbSO_4$ amount in active mass of positive electrodes, %
τ, days	*T*, °C		
109	20	Sealed	30.1
109	20	Open	20.5
105	40	Sealed	57.0
105	40	Open	42.6

was determined from the equation

$$\eta_{20} = \eta_{act}[1 + (20 - T_{av})K], \quad (5)$$

where η_{20} is the self-discharge value reduced to a storage temperature of 20°C; η_{act} is the actual self-discharge calculated for a storage temperature T_{av}; K is the correction coefficient calculated for the stationary lead batteries stored for 180 days in the temperature range 15–20°C by data of the Varta Company, and $K = 0.06$.

Thus, after 6 months of storage, the capacity loss is 18% (0.1% day^{-1}) for pilot batteries and 41.4% (0.23% day^{-1}) for reference batteries.

To explain the results obtained, we used data of [4] obtained in studying the self-discharge of the lead–copper battery whose operation is described by the reaction

$$PbO_2 + Cu + 2H_2SO_4 \rightleftarrows PbSO_4 + CuSO_4 + 2H_2O. \quad (6)$$

Unlike lead battery, in this case a well soluble compound, copper sulfate, is formed on the negative electrode. In the limits of solubility of this reaction product, a copper electrode can actively facilitate oxygen depolarization.

It was shown that the self-discharge of sealed lead–copper batteries of SM-330 type is more intense than that of the same batteries with the inner volume accessible to the atmosphere. In the sealed batteries tested during 8 months, the gas pressure in the volume below the lid was monitored. The pressure inside the battery decreased by 40 mm H_2O during two days elapsed from the beginning of the test and then remained constant. The loss of capacity by the sealed SM-330 batteries during the test was 50%, i.e., 0.21% day^{-1} [4].

The self-discharge of a lead–copper power source is described by two reactions. These are reduction of Pb^{4+} to the bivalent state and oxygen evolution [reaction (1)] on the positive electrode and oxidation of copper with the formation of copper sulfate on the negative electrode:

$$Cu + 1/2O_2 + H_2SO_4 \rightarrow CuSO_4 + H_2O. \quad (7)$$

As copper oxidant in reaction (7) serves oxygen formed by reaction (1) and oxygen that appeared in the volume below the lid at the moment of sealing the battery. The decreased pressure is explained by the fact that the rate of the copper oxidation is higher than the rate at which oxygen is formed owing to the lead dioxide reduction.

To ascertain the mechanism of self-discharge of the positive electrode of a lead–copper power source, a test was performed in the cells equipped with copper and lead dioxide electrodes. The cells were tested at 20 and 40°C. Half of cells was sealed, and half was left accessible to the atmosphere. Three cells were tested for each type, i.e., the total number of the tested cells was 12. The self-discharge of the dioxide electrode was estimated from the amount of lead sulfate formed in the active mass of the electrodes after the test (Table 3).

The analysis of the active materials of the positive electrodes shows that sealing of cells accelerates accumulation of lead sulfate, whose amount is 1.5 times larger than that in the electrodes withdrawn from the open-type cells. Increasing the temperature from 20 to 40°C increases approximately twofold the amount of lead sulfate for both sealed and open-type cells.

The influence of sealing on the intensification of self-discharge of the dioxide electrode is likely due to the fact that oxygen formed by reaction (1) is in equilibrium with that dissolved in the electrolyte. The sealed cells, like the sealed batteries, can be considered as systems isolated from the environment. Owing to the reaction of dissolved oxygen with copper, the oxygen concentration in the electrolyte decreases and reaction (1) shifts to the right.

In the open-type cells, the concentrations of gases (nitrogen and oxygen) dissolved in the electrolyte remain virtually unchanged. Therefore, the self-discharge of lead dioxide proceeds at a lower rate, and the analysis of the active materials confirms this conclusion (Table 3).

The self-discharge mechanism considered here for lead–copper batteries suggests the following mechanism of the influence of the fabric envelope on the decrease in the self-discharge rate of the battery. The fabric envelope enclosing the positive electrode

creates a space in a near-electrode layer in which the electrolyte is saturated with oxygen. In accordance with the Le Chatelier principle, the equilibrium of reaction (1) shifts to the left, i.e., the lead dioxide reduction (a process opposite to the self-discharge of sealed lead–copper battery) is decelerated. Moreover, the presence of the fabric envelope in a stored lead battery impedes diffusion of electrolyte with dissolved oxygen toward the negative electrode, which also decreases the self-discharge caused by the oxidation of the active mass of the negative electrode by reaction (3).

Thus, the results obtained show that the decrease in the self-discharge of batteries equipped with a fabric-enclosed positive electrode is due not only to a weaker transfer of antimony [3], but also to decelerated lead dioxide reduction owing to saturation of the near-electrode layer of the electrolyte with dissolved oxygen, and also to decreased oxygen transfer to the negative electrode.

CONCLUSIONS

(1) The self-discharge mechanism was suggested and the increase in the discharge capacity was explained for batteries stored for 10–20 days without current.

(2) In studying the self-discharge of lead batteries with a fabric-enclosed positive electrode, additional factors markedly affecting the electrical characteristics of batteries in the course of exploitation were determined.

(3) The results obtained open prospects for the long-term storage of batteries without intermediate chargings and for a decrease in the exploitation cost of batteries.

REFERENCES

1. Dasoyan, M.A., and Aguf, I.A., *Sovremennaya teoriya svintsovogo akkumulyatora* (Modern Theory of Lead Battery), Leningrad: Energiya, 1975.
2. Kolikova, G.A., Bayunov, V.V., Barsukova, M.M., *et al*., *Prom. Energet*., 2002, no. 11, pp. 18–22.
3. Barsukova, M.M., Prospects toward Improvement of Performance of Lead Dioxide Electrode of a Lead Battery, *Cand. Sci. Dissertation*, St. Petersburg, 2002.
4. Rusin, A.I., Yudilevich, S.R., Nikol'skii, V.A., and Batin, A.P., in *Sbornik rabot po khimicheskim istochnikam toka* (Coll. of Works on Chemical Power Sources), Leningrad: Energiya, 1975, no. 10, pp. 110–115.

Russian Journal of Applied Chemistry, Vol. 78, No. 11, 2005, pp. 1840–1843. Translated from Zhurnal Prikladnoi Khimii, Vol. 78, No. 11, 2005, pp. 1872–1874.
Original Russian Text Copyright © 2005 by Malyshev, Duda, Shevchenko.

APPLIED ELECTROCHEMISTRY AND CORROSION PROTECTION OF METALS

Effect of High-Temperature Electrochemical Deposition of Mo_2C Coatings on the Corrosion and Electrochemical Behavior of Titanium

V. V. Malyshev, T. I. Duda, and V. M. Shevchenko

Kiev Polytechnic Institute, National Technical University of Ukraine, Kiev, Ukraine

Received May 12, 2002; in final form, May 2005

Abstract—The possibility of increasing the corrosion resistance of titanium by electroplating molybdenum carbide coatings from the melts was studied.

Molybdenum and molybdenum carbide are widely used as components of corrosion-resistant steels and alloys and of coatings for surface modification. Therefore, the corrosion and electrochemical behavior of molybdenum and molybdenum carbide in aggressive media attracts growing researchers' attention. Various methods are used for surface modification of titanium. For example, the deposition of platinum-group metals increases the corrosion resistance of titanium in hot solutions of acids by several orders of magnitude [1, 2]. However, noble metals are expensive, which makes application of this protection method limited. Alloying titanium with molybdenum shows promise [1, 3, 4]. At the same time, the level of alloying ensuring high corrosion resistance should be no less than 20–25%. This level is successfully attained when, for example, the method of diffusion saturation from solid mixtures with the oxide activator in a vacuum or under argon at 1100–1200°C is used for surface alloying of titanium samples with molybdenum [5]. The method of the high-temperature electrochemical synthesis (HTES) from ionic melts allows the temperature of alloying of titanium with molybdenum, tungsten, and their carbides to be decreased to 800–900°C and alloying time to be shortened considerably. In this case, the corrosion resistance of St.3 and St.45 steels in sodium chloride solutions and in hot concentrated and dilute solutions of hydrochloric, sulfuric, and phosphoric acids considerably increases.

In this study we examined the electrochemical and corrosion behavior of titanium, onto which molybdenum carbide coating was deposited by HTES, in a sulfuric acid solution. Because Mo_2C is in short supply and is brittle at room temperature, it has not found wide application in industry as structural material [1, 8]. At the same time, it is an important alloying component for coating deposition.

Molybdenum carbide was plated onto VT 1–0 titanium by the HTES method from the melts of composition (mol %): 85 Na_2WO_4, 5 MoO_3, and 10 Li_2CO_3 at 800–900°C and a cathodic current density of 0.04–0.12 A cm^{-2} in air. The maximum thickness of the coatings was 50 μm.

An important condition for the successful coating deposition is that the corrosion potential of titanium should be more positive than that of carbide (–1.60 to –1.90 V vs. the reference electrode $(O_2)Pt \mid Na_2WO_4$–0.2 WO_3 in the alloy studied). Therefore, we measured the stationary potentials of titanium in a Na_2WO_4–5 mol % MoO_3 melt containing different amounts of Li_2CO_3 and estimated whether molybdenum carbide coatings with good adhesion to the substrate can be deposited. The stationary potentials were not established for a long time and varied jumpwise. Apparently, this is associated with dissolution of oxygen-containing phases in the surface layer of the electrode. After measuring the potentials, we studied the composition of surface layers formed on titanium and confirmed the presence of oxide phases weakly adherent to the surface. The X-ray phase analysis of the surface layers revealed Ti, TiO, and TiO_2.

To form coatings strongly adherent to the support, it was necessary to remove the oxide phases of titanium. Therefore, prior to the molybdenum carbide deposition, titanium was nickel-plated in aqueous solutions or subjected to surface nitriding at 600–700°C. The stationary potential of nickel at 900°C in the range of the Li_2CO_3 concentrations 5–10 mol % was 0.89–1.07 V, the value considerably more positive than the deposition potential of carbide.

1070-4272/05/7811-1840 © 2005 Pleiades Publishing, Inc.

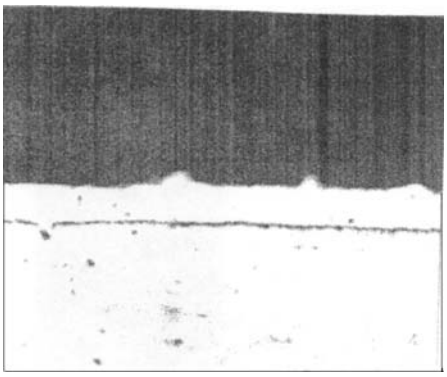


Fig. 1. Photomicrograph of the cross section of the nitrided titanium sample with molybdenum carbide coating electroplated at a cathodic current density of –0.07 A cm^{-2} for 1 h. Magnification ×400.

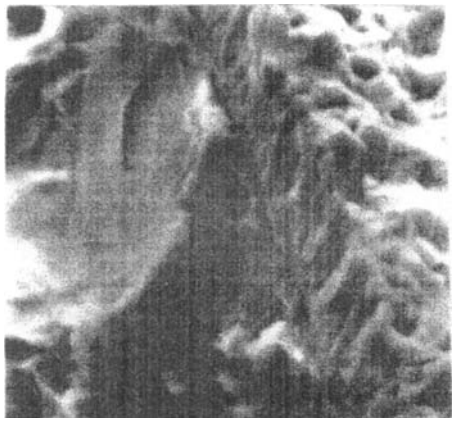


Fig. 2. Stereoscopic scanning image of the chip of a titanium sample plated with molybdenum carbide (magnification ×800 and ×1600).

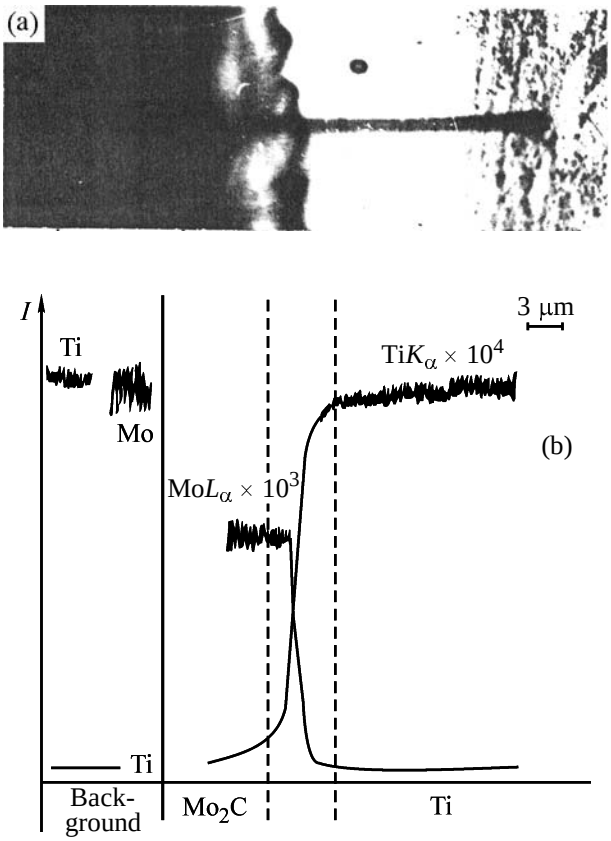


Fig. 3. (a) Electron probe profile and (b) concentration distribution curves of (*1*) titanium and (*2*) molybdenum in the diffusion zone between substrate and coating. (*I*) Radiation intensity.

The photomicrograph of the cross section of the titanium sample coated with molybdenum carbide is shown in Fig. 1. Continuous coatings are clearly observed on chips of the coated samples (Fig. 2). The phase analysis of the surface layer of the coated samples revealed strong reflections associated with molybdenum. The microhardness of molybdenum carbide was 1800–1900 kgf mm^{-2}. In the surface layers adjacent to the support, the microhardness increases, which confirms the mutual diffusion of their elements. The existence of diffusion zone ensuring adhesion between the coating and the support is also confirmed by the analysis of sections on an MS-46 X-ray microanalyzer (Cameca) (Fig. 3). The diffusion zone extends to 5–6 μm.

The corrosion was tested in a 9.5 M solution of sulfuric acid at 70–80°C by recording variations with time of potential and diffusion rate. The corrosion rate was determined from the amount of titanium and molybdenum in the solution, evaluated photocolorimetrically [9]. Also, the anodic and cathodic polarization curves on titanium, molybdenum carbide, and on titanium coated with molybdenum carbide were recorded (potential sweep rate 50 mV s^{-1}). All potentials were recalculated relative to standard hydrogen electrode.

The corrosion potential of titanium coated with molybdenum carbide considerably increases with time, from –(0.59–0.61) to 0.26–0.31 V, going into the passive/active region of titanium (Fig. 4) to a value lower than the corrosion potential of molybdenum carbide by only 0.02–0.04 V. The photocolorimetric analysis of the solution was performed after 5, 10, 15, and 30 h of tests. The average rate of the titanium dissolution calculated after these time intervals for the coated sample was constant (0.005–0.01 g m^{-2} h^{-1}). At the same time, the dissolution rate of titanium at the free corrosion potential is 19.1–19.3 g m^{-2} h^{-1}. Depositing the coatings decreases the rate of the titanium dissolution by a factor of

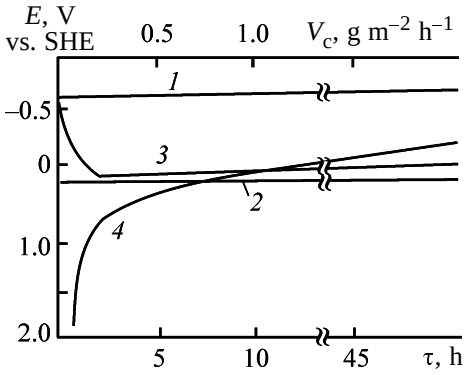


Fig. 4. Variations with time τ of corrosion potential E of (*1*) titanium, (*2*) molybdenum carbide, and (*3*) titanium coated with molybdenum carbide; (*4*) dependence of dissolution rate V_c of titanium on potential.

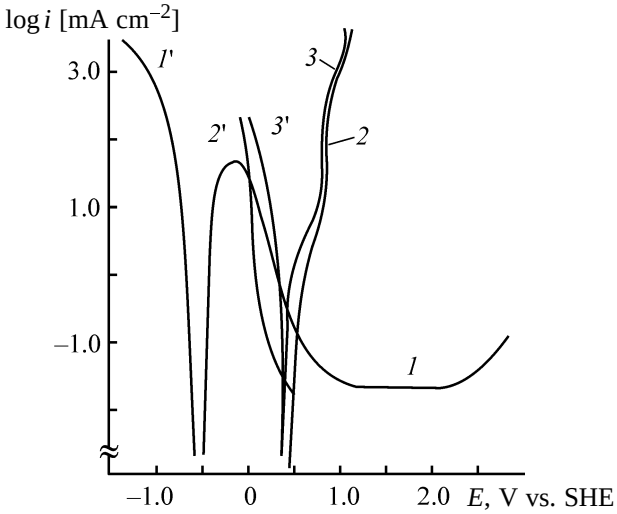


Fig. 5. log i–E curves of (*1*–*3*) anodic and (*1*'–*3*') cathodic polarization of (*1*, *1*') titanium, (*2*, *2*') molybdenum carbide, and (*3*, *3*') titanium coated with molybdenum carbide in 9.5 M sulfuric acid at 75°C. (E) Potential and (i) current density. Polarization rate 50 mV s^{-1}.

2000–4000. The dissolution rate of free titanium at a potential established on the samples coated with molybdenum carbide (300–310 mV) was 0.41–0.50 g m^{-2} h^{-1} (Fig. 4).

For longer corrosion tests, the average rate of the dissolution of molybdenum from the molybdenum carbide coating decreased from 0.03–0.04 g m^{-2} h^{-1} after the first five hours to 0.007–0.011 g m^{-2} h^{-1} after 30 h. Similar change in the average corrosion rate with time was also observed for molybdenum in sulfuric and hydrochloric acid solutions of different concentrations in [10].

According to the anodic polarization curves (Fig. 5), the free corrosion potential of titanium in experimental conditions is from –0.59 to –0.61 V. Titanium is characterized by the narrow region of active dissolution, rather negative passivation potential (from –0.27 to –0.29 V), and large critical passivation current. For molybdenum carbide, the region of the active dissolution does not exist and therefore it is passive up to the overpassivation potential. The anodic polarization curve obtained on titanium coated with molybdenum carbide is similar to that on molybdenum carbide and virtually coincides with it at a polarization potential exceeding 1.0 V. The potential of the coated titanium is close to the overpassivation potential of molybdenum carbide. The molybdenum carbide dissolution with the formation of molybdate ions is the main process responsible for the anodic current in the passive and transpassive regions.

The cathodic polarization curves show that the efficiency of the cathodic processes on molybdenum carbide and on titanium coated with Mo_2C is considerably higher than on pure titanium (Fig. 5). The cathodic curve taken on molybdenum carbide intersects the anodic curve taken on titanium virtually in the very beginning of the active/passive region. Therefore, at comparable areas, the molybdenum cathode cannot provide complete passivation of the titanium anode. The cathodic curve taken on molybdenum carbide coating intersects the anodic curve of titanium just near the passivation region. Therefore, this material as cathodic coating is more efficient.

CONCLUSIONS

(1) The electroplated molybdenum carbide coating transfers titanium into the passive state and decreases the rate of its corrosion in a 9.5 M H_2SO_4 solution at 70–80°C by a factor of 2000–4000.

(2) The anodic and cathodic behavior of titanium coated with molybdenum carbide is determined by the electrochemical properties of molybdenum carbide. The efficiency of the cathodic process on the coating plated onto titanium is somewhat higher than that on molybdenum carbide. This enables transfer of titanium into the passive state and ensures its electrochemical protection.

REFERENCES

1. Tomashov, N.D. and Chernova, G.P., *Teoriya korrozii i korrozionnostoikie konstruktsionnye splavy* (Corrosion Theory and Corrosion-Resistant Structural Alloys), Moscow: Metallurgiya, 1993.
2. Tomashov, N.D., Chernova, G.P., and Kornienko, L.P., in *Sbornik nauchnykh trudov "Korrozionnaya stoikost'*

titana v tekhnologicheskikh sredakh khimicheskoi promyshlennosti" (Coll. of Scientific Woks on Corrosion Resistance of Titanium in Process Media of Chemical Industry), Moscow: NIITEKhim, 1982, pp. 18–25.

3. Shcherbakov, A.I., Dorofeeva, V.N., and Plavnik, G.M., *Zashch. Met*., 1992, vol. 28, no. 3, pp. 364–368.
4. Shcherbakov, A.I., Kasatkina, I.V., and Tomashov, N.D., *Zashch. Met*., 1990, vol. 26, no. 6, pp. 992–996.
5. Kasatkin, A.V., Kornienko, L.P., Chernova, G.P., and Andryushin, S.G., *Zashch. Met*., 1998, vol. 34, no. 1, pp. 21–25.
6. Malyshev, V.V. and Shapoval, V.I., *Rasplavy*, 1998, no. 4, pp. 86–91.
7. Malyshev, V.V. and Shapoval, V.I., *Fiz.-Khim. Mekh. Mater*., 1998, vol. 64, no. 6, pp. 96–102.
8. Malyshev, V.V., Novoselova, I.A., and Shapoval, V.I., *Zh. Prikl. Khim*., 1996, vol. 69, no. 8, pp. 1233–1247.
9. Ponomarev, A.I., Bykovskaya, Yu.I., and Veselago, L.I., *Analiz splavov na osnove niobiya, titana, khroma* (Analysis of Niobium, Titanium, and Chromium Base Alloys), Moscow: Nauka, 1979.
10. Neiman, N.S., Kolotyrkin, Ya.M., and Knyazheva, V.M., *Dokl. Akad. Nauk SSSR*, 1974, vol. 216, no. 6, pp. 1331–1334.

Russian Journal of Applied Chemistry, Vol. 78, No. 11, 2005, pp. 1844–1848. Translated from Zhurnal Prikladnoi Khimii, Vol. 78, No. 11, 2005, pp. 1875–1880.
Original Russian Text Copyright © 2005 by Boyarskii, Zhesko, Lanina.

APPLIED ELECTROCHEMISTRY AND CORROSION PROTECTION OF METALS

Synthesis of Aromatic Carboxylic Acids by Carbonylation of Aryl Halides in the Presence of Epoxide-Modified Cobalt Carbonyls as Catalysts

V. P. Boyarskii, T. E. Zhesko, and S. A. Lanina

VNIINeftekhim Joint-Stock Company, St. Petersburg, Russia
Galar Research and Production Limited Liability Company, St. Petersburg, Russia

Received July 19, 2005

Abstract—A new procedure was developed for synthesis of aromatic and heteroaromatic acids and their derivatives (esters, salts) by carbonylation of the corresponding aryl halides. The acids are selectively formed in a high yield under very mild conditions. Highly active catalytic systems, base-containing alcoholic solutions of cobalt carbonyl modified with epoxides, were used to activate aryl halides.

Aromatic acids and their derivatives (esters and salts) are widely used both in preparative organic chemistry and as commercial raw materials to produce pharmaceuticals, plant protecting agents, paint and varnish materials, lubricants, and corrosion inhibitors. In addition, aromatic carboxylic acids are used as the base of modern liquid-crystal materials. Di- and polyaryl carboxylic acids are used in production of polyester fibers and liquid-crystal thermoplastics as well as electroluminophores in development of new equipment.

The conventional methods for preparing aromatic acids under industrial and laboratory conditions are different and involve classical organic reactions: alkylation, acylation, oxidation, and cyanidation. The disadvantages of these methods are their low selectivity and high consumption of raw materials. The synthesis is multistep and requires complex process schemes. Many of these methods are environmentally hazardous.

Recently, researchers turned attention to an alternative one-step selective procedure for preparing aromatic carboxylic acids: carbonylation of the corresponding aryl halides. Aryl halides are readily available and cheap. However, these compounds, especially the cheapest aryl chlorides, have low reactivity.

Originally, "soft" aryl halides (iodides and bromides) were used for this purpose. These compounds can be activated by oxidative addition to complexes of palladium in a low oxidation state [1–3].

At the same time, alkylaromatic halides are carbonylated under extremely mild conditions in alcohols in the presence of a base and conventional catalyst of oxosynthesis, octacarbonyldicobalt [1, 4, 5].

Alkylcobalt carbonyl complexes are formed *in situ* by the reaction of alkyl halides reactive in nucleophilic substitution (e.g., methyl chloroacetate) with dicobalt octacarbonyl in alcoholic solutions containing a base. These complexes can activate weakly active aryl halides, involving them in carnolylation [6]. In this case, alkyl halides are cocatalysts (activators) of cobalt carbonyl in carbonylation of aryl halides:

$$\mathrm{ArHal + CO} \xrightarrow[\mathrm{ROH + B}]{\mathrm{Co_2(CO)_8 + A}} \mathrm{ArCOOR},$$

where A and B are cocatalyst and base, respectively.

The facts that acceptor substituents accelerate carbonylation of substituted bromobenzenes and one-electron acceptors (nitrobenzene and anthraquinone) inhibit carbonylation of aryl halides suggests radical anion mechanism of aryl halide activation ($S_{RN}1$). The actual carbonylation catalyst is, apparently, the anionic complex $[RCo(CO)_3COOCH_3]^-$ formed by the nucleophilic attack of the carbon atom of one of the carbonyl groups by the methylate anion. The nucleophilic power of this complex is high. Since benzyl chloride is also carbonylated under these conditions, its was gradually fed by a special procedure to the reaction mixture to maintain the catalyst in the active form and to increase the conversion (see figure). A series of valuable aromatic acids were prepared by carbonylation of the corresponding aryl halides in

1070-4272/05/7811-1844© 2005 Pleiades Publishing, Inc.

methanol in the presence of cobalt carbonyl–benzyl chloride–base catalytic system. This system is the most suitable for carbonylation of 5,6-dichloroacenaphthene to acenaphthene dicarboxylic acid used for preparing a valuable commercial product, 1,4,5,8-naphthalenetetracarboxylic acid [9].

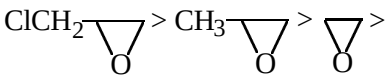
To prepare more efficient catalytic systems for carbonylation of aryl halides, dicobalt octacarbonyl was modified.

Since aryl halides are activated by strongly nucleophilic anionic cobalt complexes, we examined catalytic systems generating new reactive intermediate anionic cobalt complexes.

It is known [10] that $Co(CO)_4^-$ in alcoholic solutions containing a base undergoes nucleophilic attack of epoxides to form immediately anionic alkylcobalt carbonyl complexes in which the negative charge is localized on the alkyl group. We suggest that catalytic properties of these complexes will differ from those of the anionic complexes formed with alkyl halides after attack of methylate anion on the carbonyl group of the neutral alkylcobalt carbonyl complex. Indeed, as seen from the figure, the cobalt carbonyl–olefin oxide system is more active by a factor of approximately 2 than our most active alkylcobalt carbonyl catalytic system containing benzyl chloride [7–9]. Based on these results, we developed a series of highly active catalytic systems [8, 11, 12] containing olefin oxides, epichlorohydrin, and ethylenechlorohydrin as cocatalysts (see figure). All these cocatalysts, as well as epoxides, form intermediate anionic complexes, with epichlorohydrin being more active owing to the presence of two functional groups. These cocatalysts are not consumed by the parallel pathway of self-carbonylation (as does benzyl chloride). These compounds may undergo methanolysis but this reaction is insignificant in the presence of weak bases such as alkali metal carbonates. The methanolysis products, monomethyl ethers of glycols can be readily separated from the target products, arylcarboxylic acids.

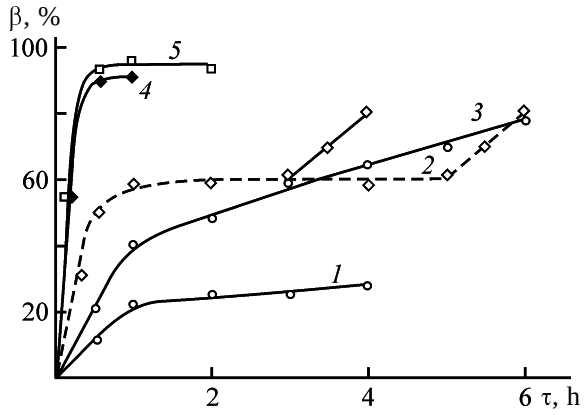
An important advantage of epoxide cocatalysts is the absence of halogen atom in their composition. Hence, the base is not consumed for binding the halogen. Propylene oxide is the most available, cheap, and convenient in use.

The activity of the examined cocatalysts decreases in the following order:



$> CH_3$$> $$> OHCHRCH_2Cl >$

$PhCH_2Cl > p\text{-}ClC_6H_4CH_2Cl > CH_3I > C_2H_5I > C_2H_5Br > n\text{-}C_8H_{17}Br > ClCH_2COOCH_3$.



Conversion β of α-chloronaphthalene in the presence of different cocatalysts: (*1*) $ClCH_2COOCH_3$, (*2*) $PhCH_2Cl$ (dashed line reflects the reaction course after introduction of additional portion of benzyl chloride), (*3*) $C_8H_{17}Br$, (*4*) $ClCH_2CH_2OH$, and (*5*) $CH_3CH\!-\!CH_2$ (O) as a function of time τ. T = 60°C, P_{CO} = 1 atm, $[Co_2(CO)_8]$ = 0.017 M.

The mechanism of carbonylation of aryl halides in the presence of $Co_2(CO)_8$–epoxide catalytic system is similar to that of the reaction catalyzed by cobalt carbonyl modified with benzyl chloride [4, 8]. The mechanism of carbonylation of aryl halides in the presence of cobalt carbonyl–epoxide–base catalytic system can be described by a catalytic cycle (see scheme).

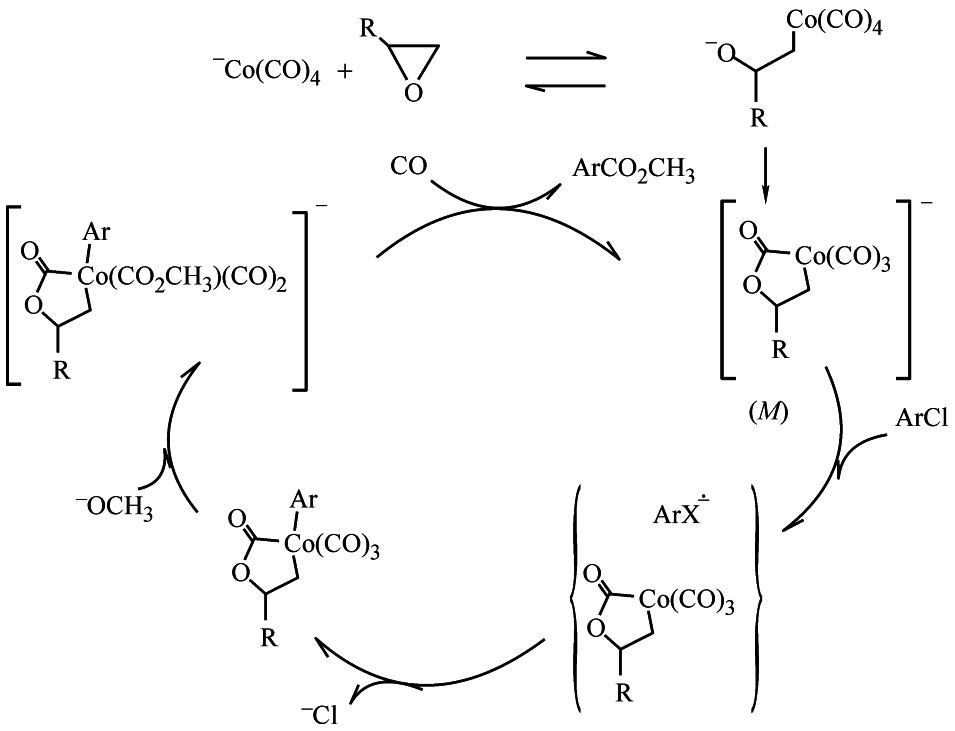
In this system, $Co(CO)_4^-$ anion reacts with epoxide with opening of the three-membered epoxy ring to form intermediate anionic complex. Probably, this complex is subjected to cyclization into negatively charged metallalactone M which is a "true" catalyst of aryl halide carbonylation.

This complex is highly nucleophilic and activates ArHal by the $S_{RN}1$ mechanism (which is confirmed by the fact that this reaction is inhibited by aromatic nitro compounds and other one-electron acceptors) via formation of arylalkylcobalt carbonyl complex. Formation of metallalactones from metal carbonyls has been demonstrated with an example of alkylcobalt carbonyl complexes of iron [13].

The main examples of highly efficient synthesis of mono- and polyaromatic acids performed for the first time by carbonylation of the corresponding aryl halides in methanol in the presence of $Co(CO)_4^-$–propylene oxide–K_2CO_3 catalytic system are presented in Tables 1 and 2.

As seen from Tables 1 and 2, $Co(CO)_4^-$–propylene oxide–K_2CO_3 catalytic system can be used for selective synthesis of aromatic mono- and dicarboxylic acids in a high yield in methanol under very mild

Catalytic cycle of ArHal carbonylation



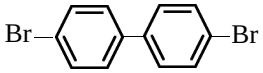
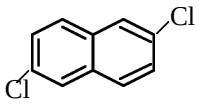
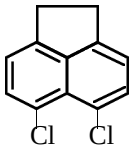
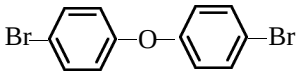
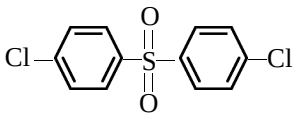
conditions. This method is suitable for both laboratory preparation and industrial production of aromatic carboxylic acids. It should be noted that a large amount of the activator (epoxide) should be used to prepare the target product in a high yield. This is due to consumption of the epoxide by its methanolysis with the solvent in the presence of a weak base. However, this fact does not minimize the importance of both the laboratory and industrial procedures. Methanolysis of propylene oxide and ethylene oxide (more convenient

Table 1. Carbonylation of aryl monohalides

Run no.[a]	Aryl halide	Molar ratio[b]	Reaction time, h	Aryl halide conversion,[c] %	Yield,[d] %
1	PhBr	30 : 1 : 30 : 90	6.0	89	82 (92)
2	*p*-FC_6H_4Br	50 : 1 : 40 : 120	6.0	94	89 (95)
3	*o*-$CF_3C_6H_4Br$	133 : 80 : 311	8.0	98	92 (94)
4	*m*-$CF_3C_6H_4Br$	123 : 1 : 86 : 307	7.0	100	96 (96)
5	*p*-BuC_6H_4Br	15 : 1 : 30 : 40	3.5	83	80 (96)
6	4-F-2-$CH_3C_6H_3Br$	143 : 1 : 106 : 394	10.0	60	58 (97)
7	*p*-(cyclo-C_6H_{11})C_6H_4Br	20 : 1 : 40 : 60	4.0	90	87 (97)
8	α-$C_{10}H_7Cl$	25 : 1 : 20 : 70	2.5	96	92 (96)
9	6-MeO-2-Br-$C_{10}H_6$	67 : 1 : 100 : 220	10.5	100	100 (100)
10	5-Br-acenaphthene	130 : 1 : 157 : 260	6.0	70	50 (71)[e]
11	*p*-$CH_3COC_6H_4Br$	290 : 1 : 153 : 447	6.0	78	74 (95)
12	4-MeO-3-BrC_6H_3CHO	81 : 1 : 67 : 193	9.0	95	80 (84)
13	4-BnO-3-BrC_6H_3CHO	97 : 1 : 104 : 245	10.0	74	64 (86)
14	2-EtO-5-BrC_6H_3CHO	43 : 1 : 50 : 104	9.0	26	20 (77)

[a] T = 60°C, P_{CO} = 1 atm, $[Co_2(CO)_8]$ = 2.7 g l^{-1} (0.008 mol). [b] Aryl halide : cobalt carbonyl : propylene oxide : potassium carbonate molar ratio. [c] Determined by GLC. [d] Preparative yield of the corresponding arenecarboxylic acid (in parentheses, the yield determined taking into account isolated unchanged aryl halide). [e] Unchanged aryl halide recovered from the reaction mixture contains 25% acenaphthene formed by reduction of the initial 5-bromoacenaphthene (9% of the initial aryl halide).

Table 2. Carbonylation of aryl dihalides

Run no.[a]	Aryl halide	Molar ratio[b]	Reaction time, h	Aryl halide conversion,[c] %	Content of dicarboxylic acid in the reaction product,[d] %
1		41 : 1 : 20 : 125	7.0	99	95
2		50 : 1 : 50 : 220	7.0	94	94
3		35 : 1 : 30 : 100	4.0	81	87
4		24 : 1 : 30 : 90	4.0	99	93
5		10 : 1 : 20 : 60	4.5	96	82

[a] T = 60°C, P_{CO} = 1 atm, $[Co_2(CO)_8]$ = 2.7 g l^{-1} (0.008 mol). [b] Aryl halide : cobalt carbonyl : propylene oxide : potassium carbonate molar ratio. [c] Determined by GLC. [d] Reaction mixture contained not only dicarboxylic acids but also the corresponding monohaloarenecarboxylic acids. Base is KOH.

for industrial purposes) yields monomethyl ether of propylene glycol and methyl Cellosolve, respectively. These compounds are quite compatible as solvents with methanol and can be readily separated from the aromatic carboxylic acid (the main reaction product). If necessary, they can be recovered separately in the step of methanol regeneration.

A number of aromatic carboxylic acids were successfully prepared from the corresponding aryl halides by this procedure in a 100-l pilot reactor. This method was also tested for dechlorination of environmentally hazardous highly heat-resistant dielectrics prepared from polychlorobiphenyls (PCB). These compounds belong to the family of dioxin-like stable organic pollutants. For this purpose, we tested the new catalytic systems. Previously we found that the least reactive aryl chlorides, chlorobenzene, chlorodiphenyl, and 4,4'-dichlorodiphenyl, are not carbonylated. At the same time, model PCB (congeners) containing 3–4 chlorine atoms are carbonylated under these conditions to form various polychlorobiphenylcarboxylic acids (Table 3).

We found that from 1 to 4 halogen atoms can be involved in the carbonylation. Carbonylation of individual PCBs is a new procedure for preparing a series of polyaromatic and polyhaloaromatic carboxylic acids which can be used for both laboratory synthesis and industrial production of a number of unique chemical products for preparing new (e.g., electroluminescent) materials. It should be noted that many of these compounds were prepared for the first time by the above procedure. Thus, we proposed a new procedure for processing PCBs under mild conditions in the presence of available catalytic systems [14].

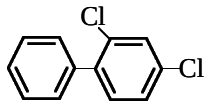
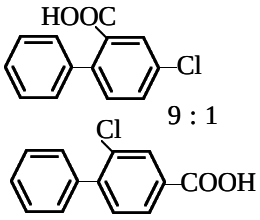
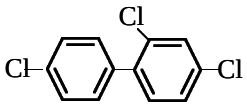
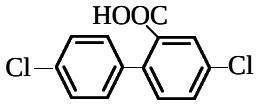
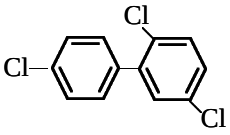
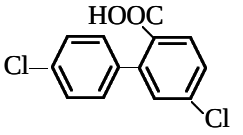
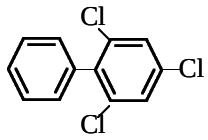
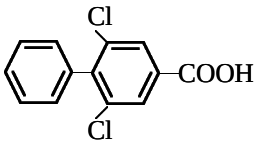
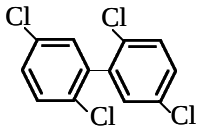
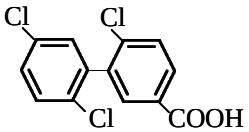
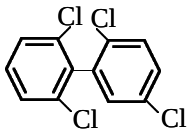
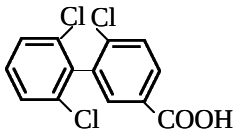
EXPERIMENTAL

Carbonylation was performed in laboratory temperature-controlled glass reactors in a CO flow under vigorous stirring at atmospheric pressure. The reaction products were analyzed by GLC and ^{1}H NMR spectroscopy. The products were identified by NMR (PFG, DQF ^{1}H, ^{1}H COSY; PFG ^{1}H, ^{13}C HMQC; PFG ^{1}H, ^{13}C HMBC) spectroscopy and mass spectrometry.

CONCLUSIONS

(1) A new procedure was developed for preparing aromatic and heteroaromatic carboxylic acids and their

Table 3. Carbonylation products of individual PCBs

Initial PCB	Reaction products
	
	
	
	
	
	

derivatives (esters and salts) by carbonylation of the corresponding aryl halides in the presence of new catalytic systems containing cobalt carbonyl modified with epoxides.

(2) Carbonylation occurs in a high yield and with a high selectivity under mild conditions (CO pressure of 1–3 atm) in alcoholic solutions containing a base.

(3) A series of mono- and dicarboxylic aromatic acids were prepared for the first time by this procedure.

REFERENCES

1. Sheldon, R.A., *Chemicals from Synthesis Gas: Catalytic Reactions of CO and H_2*, Dordrecht: Reidel, 1983. Translated under the title *Khimicheskie produkty na osnove sintez-gasa*, Moscow: Khimiya, 1987, pp. 111–120.
2. Zhesko, T.E., Shygalevsky, V.A., and Novikova, E.G., *Fundamental Research in Homogeneous Catalysis*, New York: Gordon and Breach, 1986, vol. 3, pp. 1141–1152.
3. Magerlein, W., Indolese, A., and Beller, M., *J. Organomet. Chem.*, 2002, vol. 641, pp. 30–40.
4. Zhestko, T.E., Boyarskii, V.P., Nikitina, A.G., and Novikova, E.G., *Protsessy neftepererabotki i neftekhimii* (Processes of Oil Refining and Petrochemistry), Moscow: TNIITEneftekhim, 1989, vol. 1, pp. 121–132.
5. RF Patent 2047592.
6. Foa, M. and Francalanci, F., *J. Mol. Catal.*, 1987, vol. 41, nos. 1–2, pp. 89–107.
7. Zhesko, T.E., Boyarskii, V.P., and Beletskaya, I.P., *Metalloorg. Khim.*, 1989, vol. 2, no. 2, pp. 385–387.
8. Zhesko, T.E., Boyarskii, V.P., and Nikitina, A.G., *Zh. Obshch. Khim.*, 1998, vol. 68, no. 1, pp. 85–89.
9. RF Patent 1825488.
10. *Organic Synthesis via Metal Carbonyls*, Wender, I. and Pino, P., Eds., New York: Interscience, 1968, vol. 1. Translated under the title *Organicheski sintez cherez karbonily metallov*, Nesmeyanov, A.N., Ed., Moscow: Mir, 1970, p. 296.
11. Zhesko, T.E. and Boyarskii, V.P., *Kinet. Katal.*, 1994, vol. 35, no. 2, p. 320.
12. RF Patent 2064921.
13. Carbon, P. and Sellin, M., *Organometallics*, 2002, vol. 21, no. 11, pp. 2196–2202.
14. RF Patent 2215729.

Russian Journal of Applied Chemistry, Vol. 78, No. 11, 2005, pp. 1849–1853. Translated from Zhurnal Prikladnoi Khimii, Vol. 78, No. 11, 2005, pp. 1881–1885.
Original Russian Text Copyright © 2005 by Danilov, Melezhik, Danilenko.

CATALYSIS

Carbon Nanotubes as Catalyst Supports for Oxygen Electrodes

M. O. Danilov, A. V. Melezhik, and N. I. Danilenko

Institute of General and Inorganic Chemistry, National Academy of Sciences of Ukraine, Kiev, Ukraine
Spetsmash Limited Liability Company, Kiev, Ukraine
Institute of Problems of Materials Science, National Academy of Sciences of Ukraine, Kiev, Ukraine

Received August 9, 2005

Abstract—Carbon nanotubes modified with manganese dioxide were prepared. Manganese dioxide was deposited by reduction of $KMnO_4$ in solution using formic acid or nanotube carbon. The electrochemical properties of oxygen electrodes containing nanotubes modified with manganese dioxide were studied.

Since oxygen or air electrodes can be used in fuel cells and metal–air power sources, their utilization in chemical power sources seems very promising. These electrodes produce no environmental problems, save rare materials, and decrease the cost and increase the capacity of power sources.

Electrochemical reduction of oxygen is a rather complex process [1–5], and it strongly depends on catalysts. At present, a wide series of catalysts are used for oxygen reduction, including platinum, rhodium, iridium, silver, La_xMnO_3, MnO_2, activated carbons, nickel oxides, spinels ($NiCo_2O_4$, $MnCo_2O_4$, $CoAl_2O_4$), perovskites ($LaCoO_3$, $La_{1-x}Sr_xCoO_3$, $La_{1-x}Sr_xMnO_3$, $La_{1-x}Ca_xCoO_3$, etc.), macrocyclic complexes, their polymers, and pyropolymers [6].

Discovery of carbon nanomaterials, in particular, nanotubes (NTs) opens up possibilities for preparing new catalyst materials by applying known catalysts to the surface or intercalating them inside carbon NTs. In this case, we can expect synergistic affect (owing to interaction of the catalyst particles with carbon nanostructures) and thus formation of catalysts with better characteristics than those of the carbon materials and metal-containing catalysts used separately [7, 8]. It is known that activated carbons can interact with some metal ions with the deposition of the metal on carbon [9]. In the reaction of metal ions and oxidized carbon (OC), carbon is oxidized and thus acts as reducing agent. The resulting metal–carbon composites can be effective catalysts.

Since carbon NTs exhibit high electrical conductivity and developed specific surface area and can form mesoporous three-dimensional structures, their use as catalyst supports shows promise. It is known that weakly ordered carbon is first consumed in oxidation of carbon NT in aqueous solutions with various reagents [10]. Hence, oxidative atmosphere would allow precipitation of metals on the carbon NTs with their simultaneous treatment to remove weakly ordered carbon.

In this paper we examined the effect of interaction between the catalyst and support (nanotubes) on the electrochemical properties of oxygen electrodes prepared from the resulting material. This interaction was studied using carbon NTs modified with manganese dioxide.

EXPERIMENTAL

As supports we used multilayer carbon NTs; these NTs were modified with MnO_2 prepared by reduction of potassium permanganate in solution using formic acid or nanotube carbon, according to the following reactions:

$$2KMnO_4 + 3HCOOH \rightarrow 2MnO_2(aq) + 2KHCO_3 + CO_2 + 2H_2O, \quad (1)$$

$$4KMnO_4 + 3C + H_2O \rightarrow 4MnO_2(aq) + 2KHCO_3 + K_2CO_3. \quad (2)$$

It should be noted that the above equations do not take into account the possibility of formation of the hydroxy and carboxy groups bound with nanotubes. With this fact taken into account, the loss of nanotube carbon in the course of MnO_2 deposition in accordance with Eq. (2) should be smaller than at complete oxidation of carbon to carbonate.

The multilayer carbon NTs were obtained by catalytic pyrolysis of ethylene on a catalyst prepared by precipitation of metal hydroxides with ammonia from solutions of aluminum nitrate, iron acetate, and am-

1070-4272/05/7811-1849 © 2005 Pleiades Publishing, Inc.

monium molybdate at Al : Fe : Mo atomic ratio of 1 : 1 : 0.07. To decrease agglomeration of NTs, Aerosil A-300 (pyrogenic silicon dioxide) was supplied into the reactor [11]. As a result, we obtained a black powdered product with a bulk density of 25–30 g dm^{-3}. The external diameter of carbon NTs varied from 10 to 30 nm, their specific surface area was 230 m^2 g^{-1}, and the content of mineral impurities in the crude product was 15–20%. Nanotubes were treated with a solution of hydrofluoric acid to remove the impurities of catalysts and Aerosil and then were used in further experiments as aqueous paste without drying.

In the course of deposition of manganese dioxide on the NT surface, the amount of $KMnO_4$ was determined so as to provide the content of MnO_2 in the NT + MnO_2 composite of 9, 16.7, 50, and 80 wt % (recalculated to anhydrous MnO_2). Actually, under given conditions hydrated MnO_2 was deposited.

Manganese dioxide was deposited on NTs by two procedures. In the first procedure, $KMnO_4$ was reduced with formic acid in the presence of NT suspension in accordance with Eq. (1). It was found that at mixing of the aqueous solution of potassium permanganate with NT suspension without heating the reduction of $KMnO_4$ proceeds to some extent, and then the reaction sharply decelerates. It should be noted that, with increasing $KMnO_4$ charge, the fraction of permanganate participating in the reaction with NT suspension without heating decreases. Probably, only certain sections of the NT surface with a defective structure participate in the reaction under the above conditions. The reaction can be activated with formic acid. The aqueous paste of purified NTs (73.5 g, 6.8 wt % dry matter) was placed into a beaker and diluted with water (430 ml) with stirring. The solution of potassium permanganate (1.82 g) in water (50 ml) was added to the solution of NT suspension with stirring, and the mixture was stirred with a mechanical stirrer for 1 h at room temperature. Then, formic acid [64% of stoichiometric amount calculated from Eq. (1)] was added to the reaction mixture over a period of 20 min with continuous stirring. The color of potassium permanganate disappeared within 50 min. The resulting reaction mixture consisted of coarse NT aggregates and colloidal brown suspension of hydrated MnO_2; it was boiled for 1 h, and in this time all colloidal particles of manganese dioxide were adsorbed on the nanotubes. After coagulation, we observed black flakes in the transparent colorless liquid. The product was filtered off, washed with water, and dried at 120°C in air; the yield of the product, designated as M-16.7MC, was 6.1 g. The calculated content of MnO_2 (recalculated to the anhydrous compound) was 16.7% relative to MnO_2 + NT total weight.

The materials with 50 and 80% content of MnO_2 relative to MnO_2 + NT total weight (M-50MC and M-80MC samples) were prepared by similar procedures. In these cases, the charge of $KMnO_4$ was increased to obtain the required content of MnO_2, whereas the amount of formic acid for complete reduction of $KMnO_4$ (disappearance of a rose halo around the sample drop on a paper filter) was 80 and 89% of stoichiometry for M-50MC and M-80MC, respectively. Thus, only a small amount of $KMnO_4$ was reduced with NT carbon before addition of formic acid. In these experiments, complete adsorption of MnO_2 particles on NTs after reduction with formic acid and subsequent boiling of the reaction mixture was not attained. The products were mechanical mixtures of NTs coated with unknown amount of MnO_2 and excess MnO_2 as a separate phase.

The second procedure of NT modification with manganese dioxide is based on reduction of $KMnO_4$ solution with NT carbon on boiling. As seen from Eq. (2), 1 g of MnO_2 is formed at consumption of 0.1036 g of carbon. Thus, significant amount of MnO_2 can be deposited with consumption of a relatively small amount of NT carbon (especially weakly ordered fraction). In these experiments, NT suspension was mixed with a solution of $KMnO_4$ and boiled with stirring up to disappearance of the permanganate color. For example, 40.6 g of purified NT paste (6.8 wt % of dry matter) was diluted with water (250 ml), and a solution of $KMnO_4$ (4.55 g in 250 ml H_2O) was added with stirring. The mixture was heated and boiled with stirring for 40 min up to complete disappearance of the permanganate color. The reaction yielded black flaky precipitate and a brownish transparent solution (probably due to the formation of MnO_2 sol). To prevent transition of adsorbed MnO_2 into the sol, the product was washed with NH_4HCO_3 and dried in air at 120°C. The yield of the product, designated as M-50C, was 5.20 g. The calculated content of MnO_2 (recalculated to the anhydrous compound) was 50%. In our calculations we took into account that certain fraction of NT carbon was consumed in the reaction [Eq. (2)].

Samples with other contents of manganese oxide were prepared by the similar procedure, and the time of boiling required for complete reduction of $KMnO_4$ for samples M-9C, M-16.7C, M-50C, and M-80C was 5, 20, 40, and 75 min, respectively.

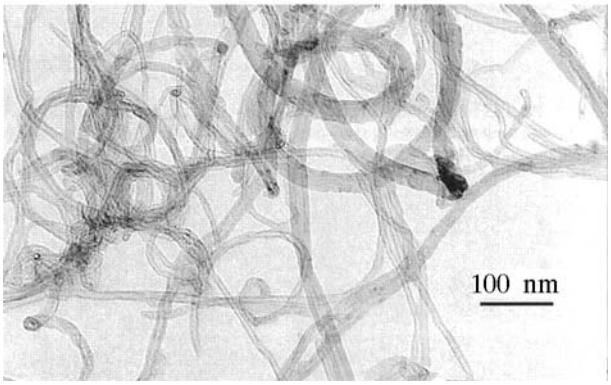


Fig. 1. Electron microscopic pattern of initial carbon nanotubes.

The oxygen electrodes were prepared by pressing. The hydrophobic layer consisted of acetylene black (0.07 g cm^{-2}) containing polytetrafluoroethylene (25%) and the active layer, 0.02 g cm^{-2} NT modified with manganese dioxide and containing 5% polytetrafluoroethylene. The measurements were carried out on a model of zinc–oxygen current cell [12] with analytically pure grade 5 M KOH as electrolyte. In our measurements we used zinc auxiliary electrode and silver chloride reference electrode. All the potentials are given with respect to the silver chloride reference electrode. The electrochemical characteristics were recorded in the galvanostatic mode. Oxygen was produced using a U-shaped electrolyzer with alkali electrolyte; it was supplied to the oxygen electrode under an excess pressure of 0.1 atm. Before operation, the electrode was purged with oxygen for 1 h. In the course of measurements, the current in the electrolyzer was higher than the current at the oxygen electrode by a factor of 3.

The microscopic patterns were recorded on a JEM-100 CXII transmission electron microscope.

The microscopic patterns of the initial NT and NT modified with MnO_2 are shown in Fig. 1 and Figs. 2a and 2b, respectively. As seen from Fig. 2a, modified NTs prepared by reduction of $KMnO_4$ with NT carbon (50% MnO_2 in the MnO_2 + NT composite recalculated to the dry components) contain fine particles (probably MnO_2) covering the nanotube surface. If the reduction was performed with formic acid (Fig. 2b), the surface of nanotubes is clean, and the sample consisted of a mixture of coarser particles and nanotubes. It should be noted that the reduction of $KMnO_4$ with NT carbon on boiling yields a black product with a MnO_2 content of 80%, whereas reduction with formic acid yields brown Mn(IV) hydroxide; this product is probably amorphous.

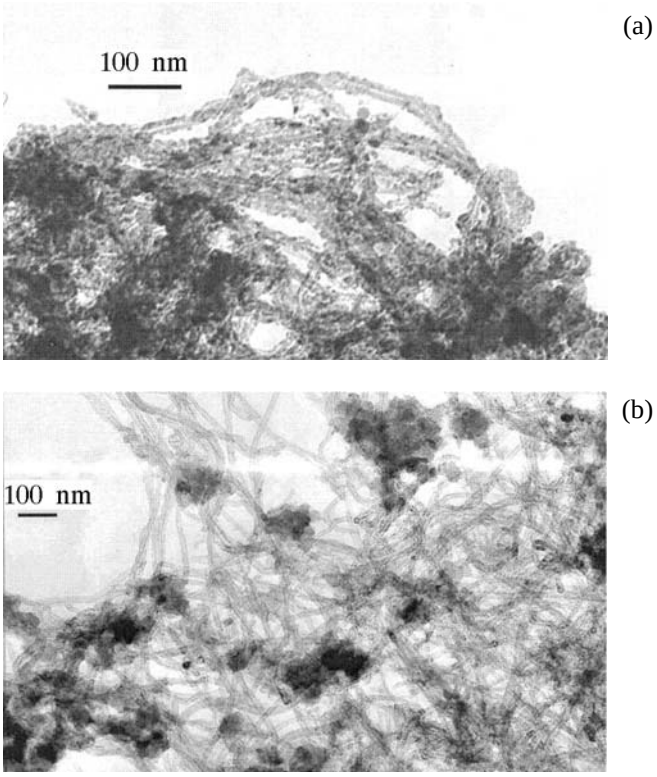


Fig. 2. Electron microscopic patterns of carbon nanotubes modified with 50% MnO_2 and prepared by reduction of $KMnO_4$ with (a) NT carbon and (b) formic acid.

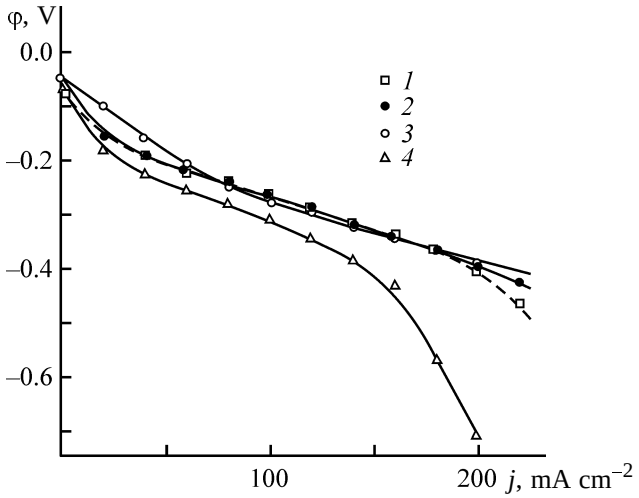


Fig. 3. Voltammetric curves of oxygen electrodes containing carbon nanotubes modified with different content of MnO_2. MnO_2 content, %: (*1*) 9 (M-9C), (*2*) 16.7 (M-16.7MC), (*3*) 50 (M-50C), and (*4*) 80 (M-80C). (φ) Potential and (*j*) current density; the same for Fig. 4.

The dependence of the electrochemical characteristics of the oxygen electrode containing NTs modified with manganese dioxide as influenced by the content of MnO_2 is shown in Fig. 3. The increase in the

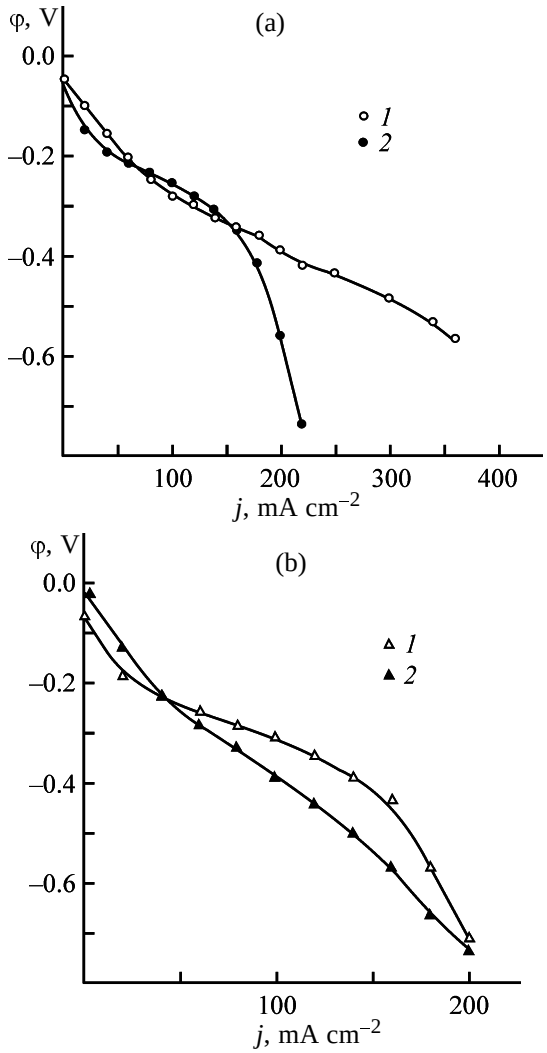


Fig. 4. Voltammetric curves of oxygen electrodes containing carbon nanotubes modified with (a) 50 and (b) 80% MnO_2 prepared by different procedures. $KMnO_4$ was reduced with (*1*) NT carbon and (*2*) formic acid.

electrochemical characteristics of electrodes with increasing MnO_2 content from 9 to 16.6 and 50% (Fig. 3, curves *1*–*3*) is probably due to the formation of uniformly distributed MnO_2 with the optimal structure. The decrease in these characteristics with increasing MnO_2 content to 80% is due to the nonoptimal structure and formation of excess manganese dioxide as a separate phase, which has no contact with NTs.

The effect of the procedure of MnO_2 preparation on the electrochemical properties is also of particular importance. The voltammetric curves of the electrodes containing NTs modified with 50% MnO_2 and prepared by reduction of NT suspension with formic acid and with NT carbon without formic acid are shown in Fig. 4a (curves *2* and *1*, respectively). The corresponding curves for the electrodes containing NTs modified with 80% MnO_2 and prepared by reduction of NT suspension with formic acid and NT carbon are shown in Fig. 4b (curves *2* and *1*, respectively). As seen from Figs. 4a and 4b, the electrochemical parameters of the electrodes prepared by reduction of $KMnO_4$ with NT carbon are higher than those of the electrodes prepared by reduction with formic acid. This is probably due to the fact that the reduction of $KMnO_4$ with NT carbon yields nanosize MnO_2 which coated directly the NT surface (Fig. 2a) and did not accumulate as a separate phase having no contact with the NT surface. In the case of reduction of $KMnO_4$ with formic acid, colloidal manganese dioxide particles are absorbed by NT to a certain limit (in our experiments up to 16.7% MnO_2). However, with the subsequent increase in the $KMnO_4$ content, excess MnO_2 is formed, which is not bound to the NT surface and thus deteriorates the electrode properties (Fig. 4b).

CONCLUSIONS

(1) Carbon nanotubes coated with the catalyst can be used as materials for fuel cells.

(2) Manganese dioxide deposited on the nanotube surface exhibits better electrochemical characteristics as a component of oxygen electrodes than does pure manganese dioxide.

(3) Oxygen electrodes prepared using nanotubes modified with 50% manganese dioxide exhibit the best voltammetric characteristics.

REFERENCES

1. Bagotskii, V.S. and Skundin, A.M., *Khimicheskie istochniki toka* (Chemical Power Sources), Moscow: Energoizdat, 1981.
2. Tarasevich, M.R., *Elektrokhimiya uglerodnykh materialov* (Electrochemistry of Carbon Materials), Moscow: Nauka, 1984.
3. *Toplivnye elementy* (Fuel Cells), Bagotskii, V.S., Ed., Moscow: Nauka, 1988.
4. Hoar, J.P., *The Electrochemistry of Oxygen*, New York: Interscience, 1968.
5. Iliev, J., Gamburzev, I., Kaisherva, A., and Mrha, J., *J. Appl. Chem.*, 1975, vol. 5, p. 291.
6. Korovin, N.V., *Elektrokhim. Energ.*, 2001, vol. 1, nos. 1–2, pp. 16–23.
7. Kublanovskii, V.S., Danilov, M.O., and Antonov, S.M.,

in *Elektrokataliz i elektrokhimicheskie protsessy. Sbornik nauchnykh trudov* (Electrocatalysis and Electrochemical Processes. Coll. of Scientific Papers), Kiev: Naukova Dumka, 1986.

8. Boudart, M., Aldag, A.W., and Vannice, M.A., *J. Catal.*, 1970, vol. 18, no. 1, pp. 46–51.
9. Tarkovskaya, I.A., *Okislennyi ugol'* (Oxidized Coal), Kiev: Naukova Dumka, 1982.
10. Shpak, A.M., Kunitskii, Yu.A., and Karbovskii, V.L., *Klasternye i nanostrukturnye materialy* (Cluster and Nanosize Materials), Kiev: Akademkniga, 2001.
11. Melezhik, A.V., Sementsov, Yu.I., and Yanchenko, V.V., *Zh. Prikl. Khim.*, 2005, vol. 78, no. 6, pp. 938–944.
12. Danilov, M.O., Kolbasov, G.Ya., and V'yunova, N.V., *Zh. Prikl. Khim.*, 2004, vol. 77, no. 10, pp. 1663–1666.

Russian Journal of Applied Chemistry, Vol. 78, No. 11, 2005, pp. 1854–1858. Translated from Zhurnal Prikladnoi Khimii, Vol. 78, No. 11, 2005, pp. 1886–1890.
Original Russian Text Copyright © 2005 by Agaeva, Dadashev, Tagiev, Abasov.

CATALYSIS

Increase in Selectivity of Toluene Disproportionation and in *p*-Xylene Yield by Optimization of Zeolite Microporous Structure

S. B. Agaeva, B. A. Dadashev, D. B. Tagiev, and S. I. Abasov

Mamedaliev Institute of Petrochemical Processes, National Academy of Sciences of Azerbaijan, Baku, Azerbaijan

Received September 20, 2004

Abstract—The possibility of increasing the yield of target products and *para*-selectivity of toluene disproportionation on modified zeolites by optimization of their microporous structure was studied.

Benzene and xylenes (especially *p*-xylene) are widely used in industry. The main method of the synthesis of the above compounds is alkene dehydrocyclization. In the process, benzene (BZ) and xylenes (XLs) are formed together with large amounts of toluene (TL). Disproportionation of TL allows an increase in the production of BZ and XLs.

The TL disproportionation (TD) is an acid-type reaction and is catalyzed by H forms of zeolites [1, 2]. A study of TD on Y and M type zeolites and on pentasils showed that TD proceeds with the highest efficiency but with low selectivity on HY and on catalysts based on Y, with rapid deactivation of the catalysts. The catalysts based on mordenite are less active but more selective and stable than Y-based catalysts. The pentasil-based catalysts (ZSM-5) are less active but very selective and stable. They are also characterized by high selectivity for *p*-xylene (*p*-XL).

Thus, development of new zeolite catalysts of TD should involve either Y- and M-based zeolite catalysts or enhancing the activity of ZSM-5. Taking into account that mordenite catalysts are highly active, selective [3–5], have commercial application [6], and are more stable with respect to modification than Y, we believe that the synthesis of more selective and active M-based catalysts for TD is possible.

In this study, we examined the effects of modifying synthetic mordenite on the selectivity of TD and *p*-XL yield.

EXPERIMENTAL

Na-exchanged zeolites Y (Y), synthetic mordenite M (M), ZSM-5, and natural mordenite (NM) from Chananab deposit (Azerbaijan) were initial materials for the catalyst synthesis. The samples were synthesized by decationization of the initial zeolites by ion exchange with 2 M NH_4Cl followed by calcinations at 823 K and dealumination with 2.5 M HCl [7]. After these procedures, the SiO_2/Al_2O_3 ratio for M was determined by the method suggested in [8]. Then, the zeolites obtained were modified with a rare-earth element (REE) (Gd) by the ion-exchange procedure (0.5 mol % Gd_2O_3) and with a transition metal (Co) by ion-exchange impregnation (2.5 wt %). The modified zeolites were molded with a binding agent, alumina gel, taken in the amount of 25 g of Al_2O_3 per 100 g of dry catalyst.

The catalytic conversion of TL was studied at atmospheric pressure in a flow-type catalytic apparatus equipped with an adiabatic reactor. Experiments were performed within the 673–748 K range at the space velocity of 1 h^{-1} and H_2/toluene ratio of 3.

The products of TL conversion were analyzed chromatographically on a capillary column (50 × 0.25 mm) coated with liquid-crystalline phase, methoxyethoxyazobenzene (T = 360 K; carrier gas argon).

Adsorption properties of the catalysts were studied gravimetrically on a vacuum device equipped with a McBain quartz balance. Benzene was used as an adsorbate. Experiments were performed at 293 K within the range of relative pressures p/p_0 0–0.3. Isotherms of benzene adsorption on zeolites used as catalysts are related to type I isotherms in accordance with Brunauer classification and are well described by the Dubinin–Radushkevich equation [9]

$$\ln a = \ln W_0\rho - K[RT\ln(p_0/p)]^2,$$

where a is the amount of the adsorbate sorbed

1070-4272/05/7811-1854© 2005 Pleiades Publishing, Inc.

Table 1. Distribution of products of TL conversion on modified zeolite catalysts

Catalyst, Co/zeolite	SiO_2/Al_2O_3	T, K	Product composition,* wt %							
			BZ	TL	*o*-XL	*m*-XL	*p*-XL	EBZ	PMBZ	AN
Co/HM_{10}	10	673	18.2	60.8	2.1	9.4	6.0	0.3	2.3	0.9
Co/HM_{25}	25		21.3	54.7	2.8	11.5	6.2	0.4	2.1	1.0
Co/HM_{30}	30		22.3	52.5	3.2	13.2	5.4	0.3	2.2	0.9
Co/HM_{10}	10	723	20.9	56.2	2.2	10.6	6.6	0.4	2.5	0.6
Co/HM_{25}	25		22.4	52.2	3.0	12.0	6.5	0.3	2.9	0.5
Co/HM_{30}	30		23.7	51.3	3.2	12.7	5.4	0.2	3.1	0.4
Gd/HM_{25}	25	723	22.7	52.8	2.3	13.0	4.8	0.3	3.4	0.7
$GdCo/HM_{25}$	25	723	21.5	54.0	2.8	6.7	11.2	0.4	2.9	0.5
GdCo/HZSM-5	61	748	19.5	59.3	2.0	7.0	8.7	0.4	2.5	0.6
GdCo/HNM	10	723	17.4	65.0	4.0	7.6	4.3	0.2	1.0	0.5
GdCo/HY	5	673	24.1	49.3	4.6	9.9	4.9	0.7	5.7	0.8

* (EBZ) Ethylbenzene, (PMBZ) polymethylbenzene, and (AN) alkanes C_1–C_2.

(mg g^{-1}); ρ, adsorbate density (g cm^{-3}); and W_0, the volume of adsorption area (cm^3 g^{-1}), which is found by extrapolation of the isotherms obtained to $p_0/p = 1$.

In accordance with the theory of micropore volume filling TMVF [9], the parameter K related to the cross section of zeolite micropore inlets is calculated from the shapes of the Dubinin–Radushkevich isotherms obtained. The results listed in Table 1 show that BZ and XL are the main products of TD.

We also detected among the products ethylbenzene (EBZ), polymethylbenzene (PMBZ), and alkanes C_1–C_2 (AN). Formation and distribution of these products indicate that toluene transforms along different pathways. Large amounts of BZ and XL formed show that TD makes the prevalent contribution to TL transformations; other arenes and AN are formed by side reactions: XL disproportionation, realkylation, hydrodealkylation, etc., which are also acid-catalyzed reactions. As a result, the selectivity is an ambiguous quantity. For instance, when determining the selectivity for TD products found as the weight ratio of BZ + XL to converted TL, the fraction of benzene formed by TD and the conversion of TL are not quite clear because of the occurrence of XL disproportionation and hydrodemethylation, which is confirmed by the presence of the above-mentioned compounds among the conversion products. However, taking into account small amounts of trimethylbenzenes formed, whose participation in BZ and TL transalkylation is insignificant, we can consider the XL mole fraction in the product mixture as the initial value characterizing the TD selectivity.

Thus, the yields of toluene conversion products can be characterized by selectivities for target products, namely, for BZ and XL sum, and for TD. Taking also into account that *p*-XL is of particular significance among XLs [10], the selectivity for *p*-XL should be considered separately. The experimental yields of particular products are listed in Table 1, and quantities reflecting the selectivity for target products (BZ + ΣXL/TL conversion), for TD (molar ratio ΣXL/BZ), and for *p*-XL (γ = *p*-XL/ΣXL), in Table 2.

As follows from Table 2, the activity of cobalt–mordenite (CoM) catalysts weakly depends on the zeolite dealumination (5–8%). The same conclusion follows from the comparison of the selectivities of these catalysts. Such a behavior of Co–M systems is caused by the diffusion control of the TL conversion. This is confirmed by the independence of the catalyst activity in TD from temperature within the 673–748 K range. Hence, the TL conversion and product yields are, to a first approximation, limited by thermodynamic features of TL transformations and by the probable subsequent transformations of the molecules formed. The process control by diffusion of the reactant to active centers and of the reaction products from the reaction zone can be associated with molecular-sieve properties of zeolites. Such a dependence is known for H forms of the zeolites used [11].

It follows from Table 2 that the mole ratio of XL and BZ formed at 673 K is practically independent of the SiO_2/Al_2O_3 ratio in mordenite catalysts. As temperature is increased from 673 to 723 K, $\beta = \Sigma$XL/BZ corresponding to HM_{10} and HM_{30} samples decreases, whereas for HM_{25} it remains constant. It is interesting that γ characterizing *para*-selectivity for all these samples remains unchanged. Thus, in TL conversion, the distribution of disproportionation products weakly

Table 2. Adsorption and catalytic parameters of Co-containing zeolite catalysts of TD

Parameter	Co/HM_{10}		Co/HM_{25}		Co/HM_{30}		Co/HM_{25} (I)	Co/HM_{25} (II)	HY	HZM	HNM
T, K	673	723	673	723	673	723	723	723	673	748	748
α,* %	39.2	43.8	45.3	47.8	47.5	48.7	47.2	46.0	50.7	40.7	35.0
S,** %	91	92	92	92	93	92	92	92	86	91	95
β = Σ XL/BZ, M	0.71	0.68	0.71	0.71	0.72	0.66	0.71	0.82	0.59	0.67	0.67
γ = *p*-XL/Σ XL	0.34	0.34	0.30	0.30	0.25	0.25	0.24	0.54	0.25	0.49	0.27
Adsorption parameters of Dubinin–Radushkevich equation											
W_0, $cm^3\ g^{-1}$	0.0747		0.0903		0.0895		0.0995	0.1005	0.1650	0.0786	0.0210
K	0.0255		0.0295		0.0305		0.0250	0.0270	0.0310	0.0260	

* (α) Toluene conversion. ** (S) Selectivity to BZ and XL.

depends on the temperature. Modifying HM_{25} with REE [M_{25}(I)] does not affect the TD selectivity. The TD selectivity increases by 10–11% only when HM_{25} is modified with Co and REE. At similar modifications of different zeolites, the TD selectivity depends on their nature (Table 2), similarly to unmodified zeolites [11]. These results demonstrate the influence of molecular-sieve properties of zeolites studied on the selectivity of TL conversion. However, whereas in the series of unmodified zeolites ZSM-5, HM, HY ZSM-5 is the most selective, after modifying with Co and REE the selectivity of this zeolite decreases and that of HM_{25}(II) increases. Then, the selectivity series becomes as follows: HM_{25}(II) > ZSM > HY.

The most substantial changes are observed for γ. As seen, the *p*-XL yield decreases with dealumination of the synthetic mordenite with other catalyst parameters remaining practically constant. Modifying of HM_{25} with REE also decreases *p*-XL yield. The modifications performed do not affect the activity of M catalysts, but favor attaining equilibrium distribution of isomeric XLs in TD [12]. Taking into account that enrichment of TD products with the "narrowest" XL isomer (i.e., *p*-XL) is associated with a decrease in size of zeolite micropores [11], the above-mentioned decrease in γ in the series of M catalysts can be attributed to an increase in the cross section of micropore inlets. In this case, modification of HM_{25} with Co and REE simultaneously gives an opposite effect. Hence, the substantial increase in the selectivity for TD and *p*-XL is associated with a decrease in the inlet cross section in modified HM_{25} as compared to the other HMs.

Table 2 allows comparison of the catalytic properties of zeolite samples in TL conversion in relation to the micropore inlet cross sections for various types of zeolites identically modified with Co and REE. It should be noted that, in the series HY, HM_{25}(II), HZSM-5, and HNM, the cross sections of the inlets to wide micropores of zeolites decrease. The comparison of the catalytic properties of samples prepared from these zeolites shows that only their activity in TL conversion varies in the same order. The other catalytic parameters listed in Table 2, in contrast to [11], show different trends. Thus, modifying with Co and REE substantially promotes only HM_{25}.

Previously Gnep *et al*. [13] suggested to use the sensitivity of XL transformation to zeolite microporous structure for identification of the nonmodified zeolite type. As mentioned above, the major pathway of TL transformation is disproportionation complicated by the further transformations of XLs formed. Therefore, ambiguous influence of the modification on the selectivity of TL conversion may be due to changes in microporous structure of the zeolites considered.

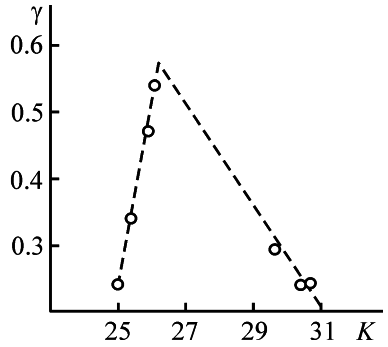
To estimate the effect of modification on the zeolite microporous structure, we studied the adsorption properties of the TD catalysts synthesized for BZ. The isotherms measured are well described by the Dubinin–Radushkevich two-parameter adsorption equation. The values of parameters are listed in Table 2 and can be interpreted in terms of TMVF [9]. In accordance with these data, only within the range of SiO_2/Al_2O_3 ratios from 10 to 25 the volume of adsorption space W_0 noticeable changes, with an increase in the catalyst activity by 4%. The further dealumination of HM_{25} to SiO_2/Al_2O_3 = 30 and modification with REE or REE + Co affects W_0 insignificantly; however, it should be noted that the catalyst

activities and W_0 vary similarly. Such a sensitivity of TL conversion to W_0 is an evidence of reactant interaction with active centers located in micropores. At the same time, whereas the selectivities S for the target products remains practically constant, i.e., independent of W_0, the HM_{25}(II) sample, in contrast to the other catalysts of HM series, exhibits higher selectivity for TD. The elevated selectivity for TD of this sample cannot by the result of somewhat elevated W_0 (Table 2).

In contrast to the quantities characterizing the selectivity of TD, the β-γ selectivity for *p*-XL is more sensitive to modification. High sensitivity of γ to modification is attributable to substantial difference between the kinetic diameters of *p*-XL (0.66 nm) and *o*-XL and *m*-XL (0.76 nm) [14]. Taking into account closeness of the kinetic diameters of BZ, TL, and *p*-XL, we can suggest that the diffusion of the reactant to active centers and of products (*p*-XL and BZ) from the reaction zone follows the same relationships, whereas large kinetic diameters of *o*-XL and *m*-XL can complicate removal of these products from the reaction zone. Hence, the yield of products of TL transformations on zeolite catalysts depends on the cross section of zeolite micropore inlets. Also, apparently, depending on inlet cross sections, the cases are possible when the internal space of micropores is inaccessible to reactant (HNM), or, vice versa, *o*-XL and *m*-XL will freely escape from the reaction zone (zeolite of HY type).

Table 2 shows that modification of HMs affects the adsorption parameter *K*. This parameter, related to the diameter of zeolite micropore and channel inlets, increases with dealumination and decreases with introduction of REE. At the same time, introduction of Co into the sample containing REE increases *K*. However, in this case, *K* (0.027) is less than in the absence of REE (0.029). The comparison of the adsorption parameter *K* with the catalytic parameter γ shows that *K* corresponding to maximal γ has an intermediate value in the series of modified HMs studied. This indicates that there is some optimal diameter of micropore inlet, favoring selective TD and elevated yield of *p*-XL.

To comment upon this suggestion, let us consider the results of TL transformation on a series of catalysts prepared from various types of zeolites. In the series HY, HZSM, and HNM, the highest *para*-selectivity γ is shown by HZSM. At the same time, wide-pore zeolite HY (W_0 = 0.165 $cm^3\ g^{-1}$) and narrow-pore HNM (W_0 = 0.021 $cm^3\ g^{-1}$) exhibit approximately equal *para*-selectivity. Obviously, in this case,



para-Selectivity of toluene transformation γ as a function of the parameter *K* of Dubinin–Radushkevich adsorption equation.

the above effect of the loss of molecular-sieve properties takes place because of *o*-XL and *m*-XL free diffusion from the reaction zone (for HY) or, vice versa, inaccessibility of the inner pore space to TL (for HNM). On the one hand, due to this effect the HY activity is the highest and that of HNM is the lowest. On the other hand, the *para*-selectivity of HNM is close to that of HY, and selectivity for TD, to that of HZSM. The above-mentioned coincidence of HNM an HZSM properties in TD and the difference in the behavior of the HY sample may be due to features of the subsequent XL transformations on these catalysts. As shown in [15–17], TD proceeds on HNM and HZSM in the surface layer and on HY, inside micropores.

In the series of catalysts prepared from various types of zeolites, an HM_{25}(II) sample stands out by higher selectivity in TD and *p*-XL formation, and in the activity it is inferior only to HY. In view of the above reasonings, high activity of this sample can be associated with accessibility of the inner volume of mordenite micropores. It is seen from the comparison of W_0 values that these pores are larger than the pores of HZSM and smaller than the pores of HY. Probably, the structure of HM_{25} pores is such that side transformations of TL are sterically hindered and diffusion of BZ and *p*-XL is easier compared to HZSM. Indeed, the adsorption parameter *K* of of Dubinin–Radushkevich equation occupies an intermediate position between the values of this parameter for HY and HZSM (Table 2). Thus, the selectivity in *p*-XL formation is governed by the size of inlets to wide pores of zeolites and thus can be characterized by the parameter *K* of Dubinin–Radushkevich adsorption equation. The dependence of the parameter γ on *K* is shown in the figure. As seen, the γ–*K* curve consists of two branches. The left branch corresponds to worsening of molecular-sieve properties due to a decrease in accessibility of zeolite micropores to the reactant, and the right

branch corresponds to worsening of molecular-sieve properties because of easier diffusion of large molecules of products (*o*-XL and *m*-XL) from the reaction zone in micropores. Intersection of these branches corresponds to the maximum possible *para*-selectivity and hence to the optimal microstructure of zeolite catalyst for TD.

CONCLUSIONS

(1) The selectivity of toluene conversion is governed by two cross sections of micropore inlets in zeolite catalysts: the lower limit is dictated by diffusion of the reactant to active centers located in micropores, and the upper limit, by removal of larger products from the reaction zone.

(2) The yield of the target products of toluene conversion and selectivity of TD on modified zeolites can be increased by optimization of their microporous structure.

REFERENCES

1. Jacobs, P.A., *Carboniogenic Activity of Zeolites*, Amsterdam: Elsevier, 1977.
2. Isakov, Ya.I., *Neftekhimiya*, 1998, vol. 38, no. 6, pp. 409–412.
3. Agaeva, S.B., Dadashev, B.A., Nasirova, F.M., *et al.*, *Azerb. Khim. Zh.*, 2000, no. 3, pp. 19–22.
4. Agaeva, S.B., Dadashev, B.A., Nasirova, F.M., *et al.*, *Azerb. Khim. Zh.*, 2000, no. 4, pp. 36–39.
5. Agaeva, S.B., Dadashev, B.A., Tagiev, D.B., *et al.*, *Neftekhimiya*, 2004, vol. 44, no. 1, pp. 42–46.
6. *ACS Symp. Ser.*, 1984, no. 248, p. 15.
7. Tsybulevskii, A.M., Klyachko, A.L., Brueva, T.R., *et al.*, *Izv. Akad. Nauk SSSR, Ser. Khim.*, 1980, no. 12, pp. 2690–2694.
8. Ponomarev, A.I., *Metody khimicheskogo analiza silikatnykh i karbonatnykh gornykh porod* (Methods of Chemical Analysis of Silicate and Carbonate Rocks), Moscow: Akad. Nauk SSSR, 1961, pp. 18–19.
9. Belen'kaya, I.M., Dubinin, M.M., and Kristofori, I.I., *Izv. Akad. Nauk SSSR, Ser. Khim.*, 1971, no. 7, pp. 1391–1397.
10. *Neft', Gaz Neftekhim. Rubezhom*, 1989, no. 11, pp. 100–101.
11. Penchev, V., Mavrodinova, V., and Minchev, Khr., *Izv. Akad. Nauk SSSR, Ser. Khim.*, 1982, no. 5, pp. 1168–1171.
12. Zhorov, Yu.M., in *Termodinamika khimicheskikh protsessov* (Thermodynamics of Chemical Processes), Moscow: Khimiya, 1985, p. 223.
13. Gnep, N.S., Tejada, J., and Guisnet, M., *Bull. Soc. Chim. Fr., Part 1*, nos. 1–2, pp. 5–8.
14. Breck, D.W., *Zeolite Molecular Sieves*, New York: Wiley, 1974.
15. Dadashev, B.A., Popova, E.N., Abasov, S.I., *et al.*, *Zh. Fiz. Khim.*, 1988, vol. 62, no. 2, pp. 315–319.
16. Agaeva, S.B., Dadashev, B.A., Abasov, S.I., and Tagiev, D.B., *Proc. 13 Int. Zeolite Congr.*, Montpellier (France), 2001, 23-P-15.
17. Agaeva, S.B., *Proc. Petrochem. Oil Refining*, 2003, no. 2, pp. 61–65.

Russian Journal of Applied Chemistry, Vol. 78, No. 11, 2005, pp. 1859–1863. Translated from Zhurnal Prikladnoi Khimii, Vol. 78, No. 11, 2005, pp. 1891–1894.
Original Russian Text Copyright © 2005 by Vasil'eva, Rudnev, Tyrina, Kondrikov, Budina.

CATALYSIS

Composition and Catalytic Activity of Plasma-Electrolytic Manganese Oxide Films on Titanium, Modified with Silver Compounds

M. S. Vasil'eva, V. S. Rudnev, L. M. Tyrina, N. B. Kondrikov, and A. N. Budina

Far-Eastern State University, Vladivostok, Russia
Institute of Chemistry, Far-Eastern Division, Russian Academy of Sciences, Vladivostok, Russia

Received August 18, 2005

Abstract—The effect of impregnation in aqueous solutions of $AgNO_3$ and subsequent calcination of manganese oxide surface structures produced on a titanium substrate by plasma-electrolytic oxidation on their catalytic activity in oxidation of CO was studied.

The most efficient catalysts for catalytic oxidation of CO are precious metals [1]. However, these metals are expensive and their pretreatment is complicated. Therefore, a considerable attention is given to formation processes and properties of catalysts based on compounds of nonprecious metals and, in particular, oxides [2]. Recently, composite structures containing a metal with a deposited oxide layer and a catalytically active additive have been finding increasing use [3, 4]. An important advantage of the composites of this kind is the high thermal and electrical conductivity of the substrate.

Manganese oxides are among the most active oxidation catalysts [5, 6]. Manganese oxides are, as a rule, deposited onto metals by pyrolytic and electrochemical methods [7, 8].

Oxide systems of various compositions with a developed surface can be formed on metals by plasma-electrolytic treatment (PET) [9]. A specific feature of this technique is that high-temperature reactions occur on local areas of the surface under the action of electric discharges. These reactions include thermolytic transformations of solution components at the anode and incorporation of the forming insoluble compounds into the surface structures. In many cases, the film thus formed is a "sandwich" constituted both by oxides of a metal being treated and by compounds based on electrolyte components.

Recently, conditions (electrolytes, modes) have been suggested under which layers containing compounds of bi-, tri-, and polyvalent metals can be formed by plasma-electrolytic oxidation on rectifying metals [10–12]. In particular, manganese oxide layers with a layered structure ($Ti/TiO_2/Mn_2O_3–Mn_3O_4$) have been obtained on titanium in aqueous electrolytes containing $Na_2B_4O_7$ and $Mn(CH_3COO)_2$ [10–12]. The content of manganese in the surface layer (2 to 60 wt %) and the morphology of the resulting oxide structures depend both on the concentration of manganese acetate in the electrolyte and on the formation conditions. These PET films on titanium catalyze CO oxidation at temperatures in the range 200–350°C [13]. The catalytic activity of structures of this kind compares well with that of manganese oxide layers obtained on the surface of titanium by the conventional pyrolytic method. The rate of CO conversion by the anodic structures formed depends on their content of manganese.

It is known [14–17] that addition of silver to certain metal oxides markedly improves their catalytic properties. In addition, silver is relatively accessible, compared with other precious metals. In this study we examined the influence exerted by silver additives on the composition and catalytic properties of manganese oxide films formed on titanium by plasma-electrolytic oxidation.

EXPERIMENTAL

Oxide layers were formed on $0.5 \times 2.5 \times 0.08$ cm^3 titanium (VT1-0) plates. The samples were preliminarily chemically polished in a mixture of concentrated acids ($HF : HNO_3 = 1 : 3$) at 60–80°C for 2–3 s, washed with distilled water, and dried in air.

The oxidation was done in an electrochemical cell in the form of a 0.5-l glass vessel. A hollow stainless

1070-4272/05/7811-1859 © 2005 Pleiades Publishing, Inc.

Composition and catalytic activity of Ag,MnO_x oxide layers on titanium

Sample no.	c_{AgNO_3}, M	T_{cal}, °C	Elemental composition, at. %	Phase composition	Maximum conversion α_{CO}, %	T_{50}, °C
1	–	300	17.3 Mn, 1.9 Ti	Mn_3O_4	97 (350°C)	218
2*	1×10^{-4}	300	0.2 Ag, 17.4 Mn, 26.7 Ti	Mn_3O_4	58 (400°C)	319
3	1×10^{-3}	300	1.0 Ag, 26.0 Mn, 35.0 Ti	Mn_3O_4**	64 (350°C)	260
4	1×10^{-2}	300	0.8 Ag, 17.8 Mn, 8.1 Ti	Mn_3O_4**	80 (350°C)	250
5	1×10^{-1}	300	4.6 Ag, 15.0 Mn, 3.2 Ti	Mn_3O_4**	100 (215°C)	180
6	1×10^{-1}	300	7.1 Ag, 20.0 Mn, 1.7 Ti	Mn_3O_4**	100 (200°C)	162
7	1×10^{-1}	400	0.3 Ag, 21.0 Mn, 14.0 Ti	Mn_2O_3	77 (450°C)	388
8	1×10^{-1}	500	2.8 Ag, 17.2 Mn, 10.6 Ti	Mn_2O_3	70 (450°C)	378

* Kept in an $AgNO_3$ solution for 1 h (sample nos. 2–5, 7, 8) and 24 h (sample no. 6).
** Presence of the indicated phase is possible.

steel cathode, fabricated in the form of a coil simultaneously serving as a condenser, was placed within the vessel. The electrolyte composed of 0.1 M $Na_2B_4O_7$ and 28.8×10^{-3} M $Mn(CH_3COO)_2$ was agitated with a magnetic stirrer. The electrolytes were prepared from commercial chemicals of chemically pure grade and distilled water.

The oxide structures were formed under galvanostatic conditions at a constant current density I = 0.2 A cm^{-2} in the course of 4 min, with a thyristor power source of the TEP4-100/460H type with unipolar current pulses. After the PET treatment, the samples were washed with distilled water and dried in air at room temperature.

Silver was introduced by impregnating the manganese oxide layers obtained in 0.0001–0.1 M aqueous solutions of $AgNO_3$ for 1 h. After the impregnation, the samples were calcined in air in a muffle furnace at 300 to 500°C for 4.5 h.

Data on the phase composition of the surface structures were obtained with a DRON-2.0 X-ray diffractometer (CuK_α radiation), and the elemental composition was determined with a JXA-5A X-ray fluorescence microanalyzer (Japan).

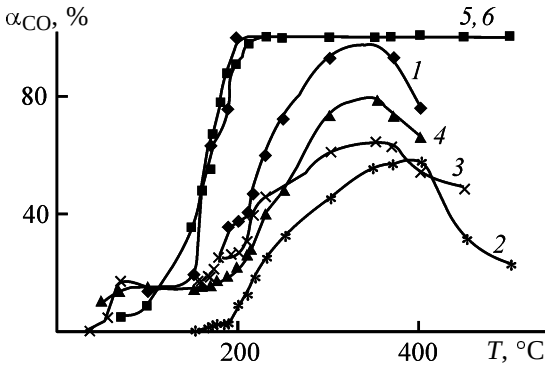


Fig. 1. CO conversion α_{CO} vs. the reaction temperature T in the presence of $Ti/TiO_2/MnO_x,Ag$ structures. Silver content c_{Ag}, at. %: (*1*) 0, (*2*) 0.2, (*3*) 1.0, (*4*) 0.8, (*5*) 4.6, and (*6*) 7.1.

The catalytic activity of the samples was determined on a BI-CATflow universal flow-through catalytic installation (manufactured by the Institute of Catalysis, Siberian Division, Russian Academy of Sciences). Finely cut samples (~$1.0 \times 1.0 \times 0.8$ mm^3) with a total area before cutting of 16 cm^2 were placed in the active zone (d = 0.9 cm, h = 3 cm) of a tubular quartz reactor. The gas flow rate was 50 ml min^{-1}. The starting reaction mixture contained (%) Ar 75, O_2 20, and CO 5.

The content of CO at the reactor outlet was determined with an LKhM-8MD chromatograph with a thermal conductivity detector. Analysis parameters: length of a column with Ca5A molecular sieves, 1 m; inner diameter of the column, 3 mm; detector current, 75 mA; flow rate of the carrier gas, 20 ml min^{-1}.

The table and Fig. 1 present data on the phase and elemental compositions and the results obtained in a study of the catalytic activity of TiO_2/MnO_x structures formed by the PET method on titanium, impregnated with $AgNO_3$ solutions, and then calcined. The catalytic activities of the samples were compared on the basis of temperatures of 50 and 100% conversions of CO into CO_2, T_{50} and T_{100}, respectively. It can be seen that the elemental composition of calcined oxide layers depends on the concentration of $AgNO_3$ used to impregnate the samples. A considerable difference in the titanium content is observed between the surface layers being analyzed in the samples under study: starting sample (no. 1, without calcination) and those impregnated in dilute solutions and calcined (nos. 2, 3). As the concentration of $AgNO_3$ increases, the con-

tent of titanium in the layers decreases and approaches that in the starting sample, whereas the content of silver grows. In all of the samples studied, the concentration of manganese does not change so significantly (within 15–26 at. %). According to the results of an X-ray phase analysis, the oxide films contain crystalline manganese oxide and no crystalline compounds of silver and titanium.

The table and Fig. 1 show that impregnation of the samples in dilute silver nitrate solutions, followed by calcination, impairs their catalytic activity. For example, the half-conversion temperature T_{50} is 218°C for the starting sample (no. 1) and increases to 319°C for samples containing a minor amount of silver. If the concentration of the impregnating solution is raised further, with the corresponding increase in the content of silver and decrease in that of titanium in surface structures, the catalytic activity increases. For example, T_{50} is 180°C at a silver content of 4.6 at. %.

The type of the temperature dependence of the CO conversion α_{CO} is also determined by the content of silver, c_{Ag}, in the manganese oxide layers (Fig. 1). The conversion of CO into CO_2 reaches 100% at 200°C for a sample with c_{Ag} = 7.1 at. % and at 215°C for that with c_{Ag} = 4.6 at. % and remains at this level up to 500°C. At a lower c_{Ag} (0.2–1.0 at. %) in the manganese oxide layers, 100% conversion is not reached in the temperature range under study under the given experimental conditions. Moreover, the maximum CO conversion α_{CO} decreases as the reaction temperature becomes higher. It should be noted that the dependence $\alpha_{CO} = f(T)$ exhibits a similar behavior for a manganese oxide catalyst without silver additives (Fig. 1, curve *1*).

The effect of the calcination temperature on the phase and elemental composition and the catalytic activity was studied for TiO_2/MnO_x, Ag layers (see table, sample nos. 5, 7, and 8; Fig. 2). Raising the calcination temperature from 300 to 500°C leads to changes in the phase composition: layers calcined at high temperatures contain crystalline Mn_2O_3, rather than Mn_3O_4. In addition, the content of titanium in the surface part of the layers, which is analyzed, increases, that of silver decreases, and that of manganese changes only slightly. Simultaneously with the increase in the amount of titanium in the surface layer, the catalytic activity of the systems under study decreases, as it also does when the amount of titanium increases because of changes in the impregnation conditions (sample nos. 2–6). Consequently, raising the calcination temperature of TiO_2/MnO_x, Ag layers on titanium from 300 to 500°C impairs their catalytic activity.

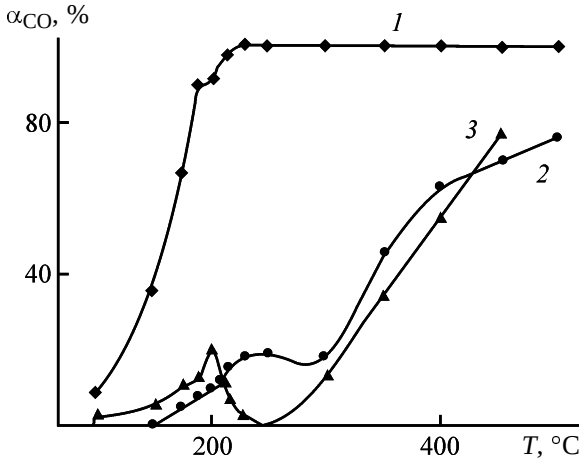


Fig. 2. CO conversion α_{CO} vs. the reaction temperature T in the presence of $Ti/TiO_2/MnO_x$, Ag structures calcined at (*1*) 300, (*2*) 400, and (*3*) 500°C. Concentration of the impregnating solution 0.1 M.

The results obtained demonstrate that introduction of silver affects the catalytic properties of the manganese-containing oxide structures on titanium, studied here. However, the nature of this influence differs from the known dependences for bulk oxide catalysts of the MnO_x type.

It is known [14–17] that introduction of silver into transition metal oxides improves their catalytic properties. In particular, bulk samples obtained by coprecipitation of manganese and silver nitrates were studied in [17]. It was shown that addition of minor amounts of silver (up to 5 mol %) enhances the catalytic activity of MnO_x in CO oxidation. For example, the half-conversion temperature of CO, T_{50} is 430°C for silver and 180°C for MnO_x, being as low as 73°C for Ag(5%)/MnO_x. However, raising the silver content to 10–20 mol % impairs the activity of the catalyst. Lin *et al.* [17] believe that, at a low content of silver, it interacts with manganese oxide with a synergistic effect, which is responsible for the high activity of this system at low temperatures.

Introduction of minor amounts of silver (0.2–1.0 at. %) into preliminarily formed manganese oxide layers on titanium leads to a decrease in the catalytic activity. This is manifested in that the half-conversion temperature increases from 218 to 319°C.

Introduction of silver improves the catalytic properties and leads to a decrease in T_{50} and to a change in the run of the $\alpha_{CO} = f(T)$ curves beginning at its content in the surface layer exceeding 4 at. % (see table,

Fig. 1). This is presumably due to the fact that the structures under study are complex systems containing not only catalytically active compounds, but also compounds of titanium and, in particular, TiO_2, which is low-active in oxidation of CO [18].

As the characteristic feature of most of silver compounds is that they are readily reduced to metal [19], silver is, in all probability, present in the surface layers studied in the form of metal particles. The radii of both the Ag atom (0.1445 nm) and Ag^+ ion (0.1011 nm) rather strongly differ from those of manganese ions (Mn^{2+}, 0.083 nm; Mn^{4+}, 0.052 nm [20]), and, therefore, formation of solid solutions is unlikely. Formation of silver oxide Ag_2O via decomposition of silver nitrate is virtually impossible, because this oxide is unstable an readily decomposes at temperatures exceeding 100°C [19].

It follows from the data obtained (see table) that the variation of the catalytic properties correlates with that of the titanium content in the surface layer: as the titanium content increases, the catalytic activity falls. The amount of titanium depends on the annealing temperature and on the concentration of the impregnating solution. The content of titanium in the oxide layers presumably changes as a result of impregnation and the subsequent annealing because of the thermal diffusion of titanium from deep in the film toward its surface. It is noteworthy that an increase in the content of titanium was also observed on annealing the starting, unimpregnated, samples [13]. In addition, raising the annealing temperature also leads (see table, sample nos. 5, 7, 8) to an increase in the content of titanium in the surface layers. Simultaneously, the content of silver in the surface layers tends to decrease, i.e., silver moves deeper into the layer. Thereby, the number of catalytically active centers on the surface of the structures under study becomes smaller.

Because the concentration of manganese in the surface layer changes only slightly, the diffusion of titanium and silver presumably occurs mainly via pores and cracks. However, it is unclear in this case why the surface part of the films is not enriched with titanium after their impregnation in concentrated $AgNO_3$ solutions. In addition, it is not improbable that the surface layer dissolves in dilute silver nitrate solutions, with areas of metallic titanium appearing on the surface. Also, partial deactivation of the catalysts may be due to the possible formation (crystallization), upon annealing, of spinel compounds of the Mn_2TiO_4 type in the surface layer. Compounds of this kind have been found in manganese oxide structures formed on titanium by the PET method in electrolytes containing manganese polyphosphate and acetate [21], sodium tetraborate and manganese sulfate [12], and sodium sulfate and manganese acetate [22].

CONCLUSIONS

(1) Silver introduced in minor amounts (up to 1 at. %) impairs the catalytic activity in CO oxidation of manganese oxide layers formed on titanium by plasma-electrolytic treatment, and that present in larger amounts (4–7 at. %) enhances the catalytic activity of these layers.

(2) At an approximately invariable content of manganese, the activity of the catalyst depends on the silver/titanium ratio in the surface layer: the larger this ratio, the higher the catalytic activity.

(3) The maximum activity was found for Ti/TiO_2, MnO_x, Ag structures fabricated by impregnation of manganese oxide layers in 0.1 M $AgNO_3$ with subsequent annealing at 300°C.

REFERENCES

1. Boreskov, G.K., *Geterogennyi kataliz* (Heterogeneous Catalysis), Moscow: Nauka, 1988.
2. Sadykov, V.A., *Oksidnye katalizatory: Sbornik lektsii* (Oxide Catalysts: Coll. of Lectures), Noskov, A.S., Ed., Ser.: *Kursy povysheniya kvalifikatsii po katalizatoram i kataliticheskim protsessam* (Professional Courses on Catalysts and Catalytic Processes), Novosibirsk, 2002.
3. Tikhov, S.F., Chernykh, G.V., Sadykov, V.A., *et al.*, *Mater. Res. Soc. Symp. Proc.*, 1998, vol. 497, pp. 71–78.
4. Tikhov, S.F., Chernykh, G.V., Sadykov, V.A., *et al.*, *Catal. Today*, 1999, vol. 53, pp. 639–646.
5. Roginskii, S.Z., *Adsorbtsiya i kataliz na neodnorodnykh poverkhnostyakh* (Adsorption and Catalysis on Heterogeneous Surfaces), Moscow: Akad. Nauk SSSR, 1948.
6. Zaki, M.I., *Thermochim. Acta*, 1997, vol. 311, pp. 97–103.
7. Nohman, A.K., *Thermochim. Acta*, 1992, vol. 210, pp. 103–121.
8. Zaki, M.I., *Thermochim. Acta*, 1997, vol. 303, no. 2, pp. 171–191.
9. Gordienko, P.S., Rudnev, V.S., Gnedenkov, S.V., *et al.*, *Zh. Prikl. Khim.*, 1995, vol. 68, no. 6, pp. 971–974.
10. RF Patent 2 241 541.
11. Vasil'eva, M.S., Rudnev, V.S., Tyrina, L.M., *et al.*, *Izv. Vyssh. Uchebn. Zaved., Khim. Khim. Tekhnol.*, 2003, vol. 46, no. 5, pp. 164–165.

12. Rudnev, V.S., Vasil'eva, M.S., Tyrina, L.M., *et al*., *Zh. Prikl. Khim*., 2003, vol. 76, no. 7, pp. 1092–1098.
13. Vasil'eva, M.S., Rudnev, V.S., Kondrikov, N.B., *et al*., *Zh. Prikl. Khim*., 2004, vol. 77, no. 2, pp. 222–225.
14. Luo, M.-F., Yuan, X.-X., and Zheng, X.-M., *Appl. Catal*., 1998, vol. 175, no. 1–2, pp. 121–129.
15. Wang, X. and Xie, Y., *React. Kinet. Catal. Lett*., 2000, vol. 71, no. 1, pp. 121–128.
16. Gulari, E., Guldur, C., Srivannavit, S., and Osuwan, S., *Appl. Catal. A*, 1999, vol. 182, pp. 147–163.
17. Lin, R., Liu, W.P., Zhong, Y.J., and Luo, M., *React. Kinet. Catal. Lett*., 2001, vol. 72, no. 2, pp. 289–295.
18. *Kataliticheskie svoistva veshchestv: Spravochnik* (Catalytic Properties of Substances: Handbook), Gorokhovskii, Ya.B., Ed., Kiev: Naukova Dumka, 1977, vol. 4, pp. 225–226.
19. Nekrasov, B.V., *Osnovy obshchei khimii* (Fundamentals of General Chemistry), Moscow: Khimiya, 1973, vol. 2.
20. *Kratkii spravochnik fiziko-khimicheskikh velichin* (Concise Reference Book of Physicochemical Quantities), Ravdel', A.A. and Ponomareva, A.M., Eds., Leningrad: Khimiya, 1983, 8th ed.
21. Tyrina, L.M., Rudnev, V.S., Abozina, E.A., *et al*., *Zashch. Met*., 2001, vol. 37, no. 4, pp. 366–369.
22. Khrisanfova, O.A., Volkova, L.M., Gnedenkov, S.V., *et al*., *Zh. Neorg. Khim*., 1995, vol. 40, no. 4, pp. 558–562.

Russian Journal of Applied Chemistry, Vol. 78, No. 11, 2005, pp. 1864–1868. Translated from Zhurnal Prikladnoi Khimii, Vol. 78, No. 11, 2005, pp. 1895–1899.
Original Russian Text Copyright © 2005 by Rutkoviene, Grazuliaviciene, Cesoniene, Kusta.

ENVIRONMENTAL PROBLEMS OF CHEMISTRY AND TECHNOLOGY

Determination of Nitrate Concentration in Natural Waters

V. Rutkoviene, V. Grazuliaviciene, L. Cesoniene, and A. Kusta

Lithuanian Agricultural University, Kaunas region, Lithuania

Received August 11, 2005

Abstract—Three methods of determining nitrate ion concentration in natural waters, namely, the potentiometric method, the spectrophotometric method using sodium salicylate, and the spectrophotometric method using 4-fluorophenol after distillation, are compared. Factors influencing the accuracy and reproducibility of the measurements are determined, and the statistical evaluation of the results obtained is given.

Nitrates are an inherent component of natural water. The amount of nitrates in surface waters is usually insignificant, but their concentration in subsoil waters is high [1]. In rural places, the inhabitants most often use water from dugout wells. Water enters dugout wells from subsoil aquifers which are the least protected from the surface pollution. Therefore, it is extremely susceptible to chemical and microbiological pollution [2]. The subsoil water is most often polluted with nitrates, and their concentration exceeds the background concentration in the nature [3–5].

An increase in the water pollution with nitrates makes it necessary to monitor the quality of potable water, to estimate the influence of the environmental factors on the water quality, and to determine how these compounds enter the natural water sources. Reliable and efficient methods of determining the nitrate concentration in water are necessary for these studies. Since the concentrations of nitrates in natural waters are essentially different, it is important to select procedures suitable for a wide concentration range. Potentiometric, voltammetric, polarographic, and spectrophotometric methods are used for determining nitrate concentrations [6, 7]. The spectrophotometric methods are based on the reaction of nitrates with certain reagents and on the measurement of the optical density of a light-absorbing solution of a colored compound formed in the reaction. Phenoldisulfonic acid, sodium salicylate, 4-fluorophenol, and 2,6-dimethylphenol are used to obtain colored compounds [8–11]. The spectrophotometric methods of determining nitrate concentrations with phenoldisulfonic acid and sodium salicylate are used in the analysis of potable and surface waters. These methods allow the nitrate concentrations of 2.0 and 25 mg l^{-1}, respectively, to be determined in an undiluted sample. In the case of high nitrate concentrations, samples must be diluted, which can affect the accuracy of the measurements. The nitrate concentrations of up to 250 mg l^{-1} in water are determined by the spectrophotometric method using 4-fluorophenol without diluting a water sample.

When selecting a method, we must take into account not only the nitrate concentration, but also the presence of other ions in water under study. The presence of chlorides, nitrites, sulfates, and other ions can affect the accuracy of the measurements.

The accuracy of the method depends on the characteristics of devices in use. For example, when determining the nitrate ion concentration potentiometrically, the sensitivity and selectivity of the electrodes in use determine the accuracy of the measurements to a large extent.

The aim of this study was to assess the expediency of using various methods of determining nitrate concentrations in natural waters and to examine how specific features of a particular method and concomitant ions affect the accuracy and reproducibility of the results.

EXPERIMENTAL

We determined nitrate concentrations by the following methods.

(I) Spectrophotometric method with sodium salicylate [6, 8]. To construct a calibration plot, we used reference solutions with nitrate concentrations from 0.1 to 10 mg l^{-1}. We measured the optical density of the solutions using a Genesys 5 spectrophotometer at a wavelength of 410 nm. We used cells with a layer thickness of 1 and 5 cm.

1070-4272/05/7811-1864© 2005 Pleiades Publishing, Inc.

Table 1. Results of determining nitrate ion concentration in model solutions

Actual concentration, mg l^{-1}	Method	Dilution of sample (multiplicity)	Arithmetic mean, mg l^{-1}	Confidence interval (95%)	Standard deviation	Relative error with respect to actual concentration, %
12.0	I	10	12.2	12.1–12.3	0.19	1.82
	II	–	12.8	12.3–13.4	1.02	6.99
	III	–	11.0	–	0	8.33
54.7	I	50	53.8	53.4–54.1	0.6	–1.71
	II	–	54.6	54.0–55.0	0.9	–0.27
	III	–	52.0	–	0	–4.94
77.0	I	50	77.6	77.3–77.9	0.5	0.81
	II	–	75.6	75.1–76.1	0.9	–1.82
	III	–	73.4	72.4–74.1	0.5	–4.68
1100.0	I	50	99.1	98.8–99.4	0.5	–0.91
	II	–	100.5	100.0–100.9	0.8	0.46
	III	–	100.0	–	0	0
147.0	I	100	147.2	145.9–148.4	2.2	0.13
	II	–	147.1	146.2–147.9	1.4	0.04
	III	–	133.8	126.1–141.4	4.8	–9.01

(II) Spectrophotometric method with 4-fluorophenol after distillation [9]. To construct a calibration plot we used reference solutions with nitrate concentrations from 8 to 200 mg l^{-1}. We measured the optical density at a wavelength of 430 nm. We used cells with a layer thickness of 1 cm. We uased a UDK 130 D apparatus for steam distillation and a Genesys 5 spectrophotometer. Chloride and nitrite ions interfere with the determination of nitrate concentrations by the above methods.

(III) Potentiometric method [7]. To calibrate the device, we used solutions with nitrate concentration from 5 to 250 mg l^{-1}. We used 1 M solution of ammonium sulfate to support a constant ionic strength of the solution. Measurements were made with a 692 METROHM AG CFH-9101 Herisau pH-meter. Chlorides, nitrites, sulfates, and bromides are interfering ions.

As the subjects of the study we used model solutions and water of the dugout wells. We used sodium nitrate (analytically pure grade) dried at 110°C for 2 h to prepare model solutions containing 12.0, 54.7, 77.0, 100.0, and 147.0 mg l^{-1} nitrate ions. For each water sample we carried out five replicate determinations.

We determined the concentration of interfering ions by the following methods: the concentration of nitrites, by the spectrophotometric method and the concentration of chlorides, by titration with a silver nitrate solution [12, 13].

Studies with model solutions free from foreign ions make it possible to evaluate more accurately the effects exerted on the measurement accuracy by the cell nonuniformity, dilution, and other factors associated with the sample preparation.

The statistical evaluation of the determination results, performed using the Statistica program, is given in Table 1. It is seen that the most reproducible results were obtained in the potentiometric determination of the nitrate concentrations. This is due to the simplicity of the method and of the technique of the water sample preparation. Spectrophotometric methods are characterized by larger standard deviations, because of the errors introduced during the preparation of water samples for the analysis (dilution, distillation) and in measurement of the optical density.

When using spectrophotometers with holders for several cells, the optical density of several samples can be determined simultaneously (seven samples in the case of Genesys 5). In this case, the measuring errors may arise from the nonuniformity of the cells: although they are of the same thickness, they are not identical. To reveal the influence of the cell nonuniformity on the measurement accuracy, we measured the optical density of each water sample in seven different cells of the same length. We used cells with a layer thickness of 1 cm. Thus found nitrate concentrations are given in Fig. 1, and standard deviations for these measurements, in Fig. 2. The greatest scattering of the results is observed when determining nitrate

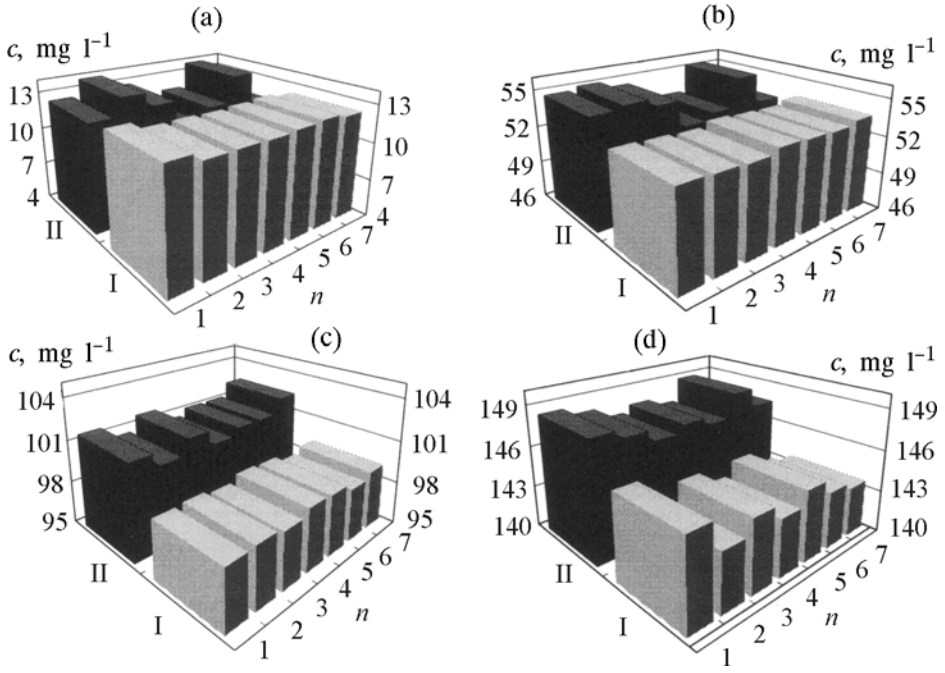


Fig. 1. Nitrate concentrations determined by measuring optical density with seven different cells, *n*, with a layer thickness of 1 cm. (*c*) Measured concentration of nitrates in model solutions. Actual concentration, mg l^{-1}: (a) 12.0, (b) 54.7, (c) 100.0, and (d) 147.0; the same for Fig. 2. Method: (I) with sodium salicylate and (II) with 4-fluorophenol after distillation.

concentrations with 4-fluorophenol. When determining the nitrate concentration with sodium salicylate, the nonuniformity of the cells affects the reproducibility of the results only slighly.

The difference between the standard deviations given in Table 1 and in Fig. 2 for the method using sodium salicylate demonstrates the effect of dilution on the reproducibility of the results, since we diluted water samples by factors of 10, 50, and 100 when determining of concentration of nitrate ions by this method. The largest standard deviation was obtained at 100-fold dilution of the sample.

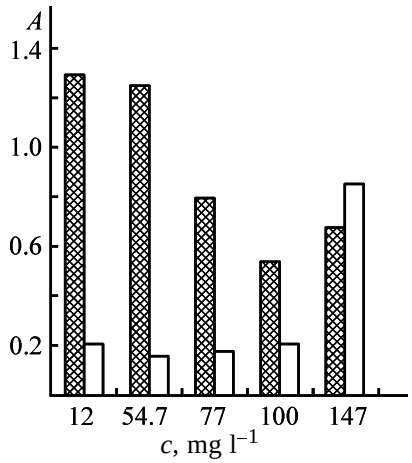


Fig. 2. Standard deviations *A* of nitrate concentrations *c* determined in seven different cells with a layer thickness of 1 cm: (left bars) with 4-fluorophenol and (right bars) with sodium salicylate.

As seen from these data, the spectrophotometric method is the most accurate. However, when selecting a reagent, we must take into account the concentration of nitrates in water. At relatively high nitrate concentrations in water, the most reliable results are obtained with 4-fluorophenol. The spectrophotometric method with sodium salicylate is also suitable for the determinations in a wide concentration range. In this case, the choice of the optimal procedure for the sample dilution substantially increases the reproducibility of the measurements.

The largest deviations of the found concentrations from the actual values are observed with the potentiometric method.

The results of determining nitrate concentrations in water of ten dugout wells and the concentrations of interfering ions (nitrites and chlorides) are given in Table 2. The concentrations of nitrate ions in water of dugout wells lie in the range 4–200, and the concentrations of nitrites, in the range 0.013–0.225 mg l^{-1}. Such a ratio of nitrate and nitrite concentrations is typical for the most part of natural waters, including also water from dugout wells. This is confirmed by the results of long-term studies [14]. The determina-

Table 2. Results of determining nitrate concentrations in water of dugout wells

Sample no.	Content in sample, mg l^{-1}		Method	Sample dilution (multiplicity)	Arithmetic mean	Confidence interval (95%)	Standard deviation
	chlorides	nitrites					
1	142	0.076	I	40	81.3	79.9–82.7	2.6
			II	–	82.7	81.8–83.6	1.6
			III	–	72.3	70.9–73.8	0.6
2	48	0.013	I	20	20.2	20.0–20.3	0.3
			II	–	19.7	19.3–20.0	0.7
			III	–	18.0	17.9–18.1	0.02
3	62	0.028	I	20	19.9	19.8–20.0	0.2
			II	–	19.4	18.8–20.1	0.9
			III	–	17.0	–	0
4	67	0.214	I	100	162.8	161.3–164.4	2.8
			II	–	172.5	171.4–173.6	1.9
			III	–	159.7	158.2–161.1	0.6
5	53	0.005	I	10	6.6	6.5–6.7	0.2
			II	–	6.8	6.1–7.5	1.3
			III	–	6.3	6.1–6.4	0.1
6	124	0.225	I	20	42.9	42.7–43.1	0.30
			II	–	36.7	35.9–37.5	1.6
			III	–	36.0	–	0
7	87	0.049	I	100	207.4	205.5–209.2	3.3
			II	–	206.2	204.4–207.9	3.2
			III	–	191.7	184.5–198.8	2.9
8	39	0.038	I	5	4.1	4.05–4.1	0.04
			II	–	5.8	5.1–6.5	1.3
			III	–	4.2	4.02–4.3	0.06
9	37	0.030	I	5	5.3	5.2–5.4	0.1
			II	–	4.5	4.0–4.9	0.7
			III	–	3.9	3.8–4.1	0.06
10	28	0.034	I	5	8.4	8.3–8.4	0.07
			II	–	6.2	5.9–6.5	0.7
			III	–	6.4	6.2–7.2	0.2

tion of the nitrate ion concentration by spectrophotometric methods gives overestimated results when the content of nitrites is higher than 0.7 mg l^{-1} [8]. Thus, the presence of nitrites in the amounts typical for natural waters does not affect the accuracy of determining nitrates.

The concentration of chlorides in waters under study is 28–142 mg l^{-1}. When determining the concentration of nitrates (by the method using 4-fluorophenol), we added a solution of tin(II) sulfate to water samples to neutralize the influence of chlorides. For the method using sodium salicylate, the presence of chlorides has no effect on the measurement results.

The concentrations of nitrates measured potentiometrically appeared to be lower than the concentrations determined by the spectrophotometric methods, which is also the case with model solutions.

CONCLUSIONS

(1) Concentration of nitrates in water under study must be taken into account when selecting a method for determining the nitrate concentration in natural waters.

(2) The spectrophotometric method using 4-fluorophenol after distillation is acceptable for determining high nitrate concentrations (>20 mg l^{-1}). However, attention must be paid to the factor of nonuniformity of cells when using spectrophotometers with multicell holders.

(3) The spectrophotometric method using sodium salicylate is more versatile, but it is necessary to select the optimal procedure for diluting a water sample.

(4) The potentiometric method is less reliable, but it gives the most reproducible results; this method is

appropriate for measurements requiring no special accuracy.

(5) The presence of chlorides and nitrites in natural water does not substantially affect the measurement accuracy.

REFERENCES

1. Clawges, R.M. and Vowinkel, E.F., *Water Resources Bull.*, 1996, vol. 32, no. 5, p. 1055.
2. Noland, V.T. and Stoner, J.D., *Environ. Sci. Technol.*, 2000, vol. 34, p. 1156.
3. Pacheco, J.A. and Cabrera, A.S., *Hydrogeol. J.*, 1997, vol. 5, no. 2, p. 47.
4. Roux, J.C., *Sci. Total Environ.*, 1995, vol. 171, nos. 1–3, p. 3.
5. Whitsell, W.J. and Hutchinson, G.D., *Trans. ASAE*, 1973, vol. 16, p. 777.
6. Lur'e, Yu.Yu., *Unifitsirovannye metody analiza vod* (Unified Methods for Analysis of Waters), Moscow: Khimiya, 1971.
7. Determination of Nitrate with an Ion-Selective Electrode, *Application Bulletin of Environment Protection Laboratories*, 2000, no. 121/1e.
8. *GOST* (State Standard) *18826–73: Potable Water: Methods of Determining Nitrate Content.*
9. *ISO 7890-2:1998(E): Water Quality: Determination of Nitrate*, part 2: *4-Fluorophenol Spectrometric Method after Distillation*.
10. *ISO 7890-3:1998(E): Water Quality: Determination of Nitrate*, part 3: *Spectrometric Method using Sulfosalicylic Acid*.
11. *ISO 7890-1:1998: Water Quality: Determination of Nitrate*, part 1: *2,6-Dimethylphenol Method*.
12. *ISO 6777:1984: Water Quality: Determination of Nitrite: Molecular Absorption Spectrometric Method.*
13. *ISO 9297:1989: Water Quality: Determination of Chloride: Silver Nitrate Titration with Chromate Indicator (Mohr's Method).*
14. Cesoniene, L., Influence of Factors of Environment on the Dynamics of Pollution of Dugout Wells, *Cand. Sci. Dissertation*, Kaunas, 2004.

Russian Journal of Applied Chemistry, Vol. 78, No. 11, 2005, pp. 1869–1871. Translated from Zhurnal Prikladnoi Khimii, Vol. 78, No. 11, 2005, pp. 1900–1902.
Original Russian Text Copyright © 2005 by Levichev, Lobacheva.

ENVIRONMENTAL PROBLEMS OF CHEMISTRY AND TECHNOLOGY

Foam Separation of Nickel and Copper Ions from Dilute Aqueous Solutions

S. A. Levichev and O. L. Lobacheva

St. Petersburg State University, St. Petersburg, Russia
St. Petersburg State Mining Institute, St. Petersburg, Russia

Received June 3, 2005

Abstract—The minimal expenditure of anionic surfactant, sodium dodecyl sulfate, required for decreasing concentrations of nickel and copper ions to the maximum permissible concentration was determined experimentally. A possibility of selective recovery of nickel ions by foam separation with sodium dodecyl sulfate under conditions of complex formation of copper cations with thiosulfate anions was studied.

The maximum permissible concentrations (MPCs) for nickel and copper cations in water are steadily decreased. Fairly recently they were 0.1 mg l^{-1} for nickel and 1.0 mg l^{-1} for copper [1]. The problems of recovery of salts of these metals from wastewaters were solved by precipitation flotation [2–5], flotation with a carrier [6], and foam separation [7–9].

Here we present the results of experiments on foam separation of dilute aqueous solutions containing copper and nickel salts both separately and in combination, aimed to determine the expenditure of surfactant, sodium dodecyl sulfate (SDS), and assess the possibility of separate recovery of these cations.

One of the mechanisms of foam recovery of ions from dilute aqueous solutions is ion exchange [10, 11]. Due to adsorption on the bubble walls, a layer of surface-active ions is formed. In the case of anionic surfactants these are anions and in the case of cationic surfactants, cations. These adsorption layers attract counterions. As a result, diffusion layers of counterions held by Coulomb interaction are formed. The content of a certain type of counterion is governed by its valence and concentration in the solution. The experimental data on the influence of ions on the surface tension of aqueous solutions of SDS far from critical micellization concentration (CMC) showed that, with increasing valence of ion, the surface activity of cations increases [12]. For ions of the same valence, the activity is approximately the same. The increase in the probability of penetration into the diffusion layer due to a high concentration of SDS in solution suggests that in foam separation it is necessary to decrease the SDS concentration.

To check this assumption, the foam recovery of copper and nickel cations was carried out as follows. A glass vessel was charged with 700 ml of a 0.001 M solution of copper or nickel sulfate or both salts. The solutions were prepared gravimetrically from crystal hydrates of analytically pure grade; the concentrations of the solutions were checked by EDTA titration. A disc-shaped bubbler presenting a porous plate from microporous plastic with a pore size of 33 μm was placed on the vessel bottom. Air (or nitrogen) was passed through this plate into the solution; the flow rate was controlled with a fine adjustment valve. A 0.05 M SDS solution was fed into the solution in 5-ml portions, so that the highest concentration of surfactant in the solution to be treated did not exceed 0.005 M, i.e., it was lower than the CMC. The next portion of SDS solution was added only after the solution lost the ability to form stable foam as a result of transition of the surfactant to the foam. The resulting foam was subjected to drainage in a glass vertical tube 30 mm in diameter, to avoid the loss of the "outgoing" solution. Due to gravity drainage, the dry transparent foam was withdrawn; in so doing, the solution weight did not change noticeably. With decreasing foam-forming power of the solution, the height of the drainage column was decreased removing its separate units. After addition of SDS to the solution in the equimolar amount relative to the salt in the solution, the solution was analyzed for content of SDS and copper and nickel ions.

The SDS concentration was determined by potentiometric titration with an ion-selective electrode for ionic surfactants. A 1.2×10^{-4} M solution of a cationic surfactant, cetyltrimethylammonium bromide of

1070-4272/05/7811-1869 © 2005 Pleiades Publishing, Inc.

Experimental data on foam separation in solutions containing copper and nickel cations. Solution volume 650 ml

Initial concentration, $c \times 10^4$, M		Volume of $Na_2S_2O_3$ added, ml	Expenditure of surfactant, ml, 5×10^{-2} M	Degree of Ni^{2+} recovery, %	Residual concentration, $c \times 10^4$, M	
Cu^{2+}	Ni^{2+}				Cu^{2+}	Ni^{2+}
5.00	5.00	37	30	93.0	4.14	36.0
5.00	5.00	37	30	93.0	4.67	36.0
2.50	2.50	22	15	92.2	2.67	39.0
2.50	2.50	22	15	90.2	2.80	49.0
2.50	2.50	0	40	~100.0	~0	~0
2.50	2.50	0	40	~100.0	~0	~0

pure grade produced by Chemapol, was used as a titrant. The relative titration error was 2%.

The concentration of cations was determined by atomic adsorption spectroscopy (AAS). The measurements were carried out on an AASIN atomic adsorption spectrometer. Lamps with hollow cathodes were used as a source of radiation. The operating wavelength for copper was 324.75 nm, and the sensitivity, 0.1 mg l^{-1}. The wavelength for nickel was 232.0 nm, and the sensitivity, 0.12 mg l^{-1}. The determination error was 15%. The average nitrogen flow rate was 3.3×10^{-4} m^3 h^{-1}. The foaming process was carried out for 60 h.

Since the MPC for nickel is 10 times lower than that for copper, in its recovery we used the double amount of SDS relative to the salt (on the molar scale).

The long duration of the process was caused by the need to lose no solution as a result of foaming, which was provided by prolonged gravity drainage. Compulsory drainage by suction of the liquor from the foam can undoubtedly make the process shorter. The MPC was reached for both copper and nickel. The residual concentration of copper was approximately 1.0 mg l^{-1}, and that of nickel, approximately 0.1 mg l^{-1}. Both concentrations lie at the boundary of applicability of atomic adsorption spectrometry. With a further increase in the concentration of SDS added and in the foaming duration we can reach such concentrations of cations that are governed by their content in the solution used.

As a result of foaming, the solution gets salinized with sodium sulfate. The concentration of this salt in the final solution was not determined. The residual concentration of SDS in this method cannot be lower than the boundary of foaming and was 10 mg l^{-1}. The experiments showed that the expenditure of SDS expressed in moles for recovery of 1 mol of copper was 1.5, and for 1 mol of nickel, 2. The residual concentration of SDS and its expenditure can be undoubtedly reduced using flotation extraction with an organic layer incapable to absorb SDS [13, 14]. In this process, foaming is not required and one portion of SDS is repeatedly used as ion exchanger at the walls of gas bubbles.

The study of surface characteristics and foam separation of the solutions of the mutual system [12]

$$Na^+,\ Co^{2+},\ Ni^{2+} \parallel DS^-,\ SO_4^{2-} - H_2O$$

(DS^- is dodecyl sulfate ion) showed that both surface characteristics and ability to pass into foam for bivalent cobalt and nickel cations do not differ. Foaming did not affect the concentration ratio of cations in the solution. Of course, the concentrations decreased down to the MPC; however, no selectivity of recovery was found. Therefore, in solving problem of selective recovery of nickel, we used a well-known method: masking of one of the cations by complex formation [15].

It is well known that copper cation is able to form complex anion in the reaction with sodium thiosulfate. It was shown previously [15] that copper(II) ions can form with thiosulfate ions three stable complexes of different compositions. The copper thiosulfate complex is stable in the region of pH 4.5. However, when a solution contains a large amount of ammonium chloride or nitrate, the stability of the complex decreases and even at pH 8–9 copper(II) ammoniate is formed and thiosulfate begins to decompose to release sulfur. It was noted that, when borate or ammonium acetate buffer solution is used, the copper thiosulfate complex is stable for several hours.

In one series of the solutions copper and nickel ions were recovered simultaneously without separation. In foaming of other series of the solutions containing copper(II) and nickel(II) ions, we attempted

to recover only nickel ions and retain copper ions in the solution in the form of a thiosulfate complex. Before foaming, ammonium acetate buffer solution (to obtain pH 8.5–9.5) and $Na_2S_2O_3$ were added to the solution. To 650 ml of the solution containing 5×10^{-4} M copper, 33 ml of 540 g l^{-1} $Na_2S_2O_3$ was added. Addition of the buffer solution stabilizes the copper thiosulfate complex. The total amount of SDS added to the column for foaming was 2 times greater than that required for complete recovery of nickel. Foaming was carried out at the average gas flow rate of 3.3×10^{-4} m^3 h^{-1} for 3 days. After foaming, the solutions were analyzed by AAS for the content of copper and nickel ions. The experimental data are listed in the table.

It is evident that the complex formation allows the initial concentration of copper to be kept constant within the limits of experimental error. Without complex formation, both bivalent ions are removed from the solution during foaming.

CONCLUSIONS

(1) The expenditures of surfactant, sodium dodecyl sulfate, required for recovery of copper and nickel cations from dilute aqueous solutions are 1.5 and 2.0 mol per mole of cations, respectively.

(2) Transformation of one of the cations to an anionic complex allows selective recovery of nickel ions by foam separation.

REFERENCES

1. Glushko, Ya.M., *Yadovitye metally i ikh neorganicheskie soedineniya v promyshlennykh stochnykh vodakh* (Toxic Metals and Their Inorganic Compounds in Industrial Wastewaters), Moscow: Meditsina, 1972.
2. Almanov, K.V. and Skrylev, L.D., *Izv. Akad. Nauk Turkm. SSR, Ser. Fiz.-Tekh. Khim. Geol.*, 1975, no. 1, pp. 96–99.
3. Baarson, R.E. and Ray, C.L., *Hydrometallurgy*, New York: Gordon and Breach, 1964.
4. Poltoranina, T.F., *Zap. Leningr. Gorn. Inst.*, 1963, vol. 42, issue 2, pp. 78–84.
5. Poltoranina, T.F. and Razumov, K.A., *Obogashch. Rud*, 1964, no. 3, pp. 11–15.
6. Safaa Al Abrash, Physicochemical Features of Flotation Recovery of Nickel and Copper Ions Using Fatty Acid Collectors, *Cand. Sci. Dissertation*, Odessa, 1989.
7. Lobacheva, O.L., Levichev, S.A., and Rusanov, A.I., *Zh. Prikl. Khim.*, 1988, vol. 61, no. 1, pp. 102–105.
8. Lobacheva, O.L. and Levichev, S.A., *Zh. Obshch. Khim.*, 1994, vol. 65, pp. 1242–1245.
9. Lobacheva, O.L., Levichev, S.A., and Rusanov, A.I., *Mendeleev Commun.*, 1994, no. 4, pp. 215–216.
10. Sviridov, V.V., Golupkov, A.I., and Mudretsov, A.I., *Izv. Vyssh. Uchebn. Zaved., Khim. Khim. Tekhnol.*, 1981, vol. 24, no. 9, pp. 1117–1121.
11. Sviridov, V.V. and Golupkov, A.I., *Zh. Fiz. Khim.*, 1980, vol. 54, no. 8, pp. 2113–2116.
12. Lobacheva, O.L. and Levichev, S.A., *Vestn. Sankt-Peterb. Gos. Univ., Ser. 4*, 2002, issue 1, no. 4, pp. 117–119.
13. *Adsorptive Bubble Separation Techniques*, Lemlich, R., Ed., New York: Academic, 1972.
14. Rusanov, A.I., Levichev, S.A., and Zharov, V.T., *Poverkhnostnoe razdelenie veshchestv* (Surface Separation of Substances), Leningrad: Khimiya, 1981.
15. Schwarzenbach, G. and Flaschka, H., *Die komplexometrische Titration*, Stuttgart: Ferdinand Enke, 1965.

Russian Journal of Applied Chemistry, Vol. 78, No. 11, 2005, pp. 1872–1875. Translated from Zhurnal Prikladnoi Khimii, Vol. 78, No. 11, 2005, pp. 1903–1906.
Original Russian Text Copyright © 2005 by Kurenkov, Shatokhina, Hartan, Lobanov.

ENVIRONMENTAL PROBLEMS OF CHEMISTRY AND TECHNOLOGY

Sedimentation of Kaolin Suspension in the Presence of Praestol Anionic Flocculant and Aluminum Polyoxychloride and Sulfate Coagulants

V. F. Kurenkov, E. V. Shatokhina, H.-G. Hartan, and F. I. Lobanov

Kazan State Technological University, Kazan, Tatarstan, Russia
Stockhausen GmbH Company, Krefeld, Germany
Degussa Eurasia Joint-Stock Company, Moscow, Russia

Received September 19, 2005

Abstract—The kinetics of sedimentation of kaolin suspension in the presence of coagulants (aluminum polyoxychloride and sulfate) and Praestol anionic flocculant was studied, as influenced by the concentrations of coagulants and flocculant, mode and time of their addition into the suspension, composition of the coagulant mixture, and chemical structure and conformation of flocculant macromolecules.

Simultaneous use of coagulants and flocculants can make the treatment of natural and waste waters much more efficient, and the most common reagents are aluminum sulfate coagulant and polyacrylamide flocculants [1, 2]. As a new aluminum polyoxychloride coagulant becomes commercially available, the data on its performance in water treatment as compared to aluminum sulfate are required. Previously we studied treatment of natural waters using aluminum sulfate and partially hydrolyzed polyacrylamide [3] and copolymers of acrylamide with sodium acrylate [4] and compared the efficiency of water treatment with aluminum sulfate and aluminum polyoxychloride in the presence of polyacrylamide [5]. Here we report on the sedimentation kinetics of kaolin suspension in the presence of aluminum sulfate and polyoxychloride and anionic Praestol as influenced by the concentrations of coagulant (C) and flocculant (F), mode and time of addition of the reagent mixture (C + F), composition of the coagulant mixture, and chemical structure and conformation of the flocculant macromolecules.

EXPERIMENTAL

In the tests we used Akva-Aurat-30 brand aluminum polyoxychloride $[Al(OH)_xCl_y]_m$ (APOC, x = 1.33, y = 1.67) [TU (Technical Specifications) 6-09-05-1456–96] with 30 wt % content of Al_2O_3 and technical-grade aluminum sulfate (AS) [GOST (State Standard) 12966] with 16.4 wt % content of Al_2O_3. We also used anionic Praestols [copolymers of acrylamide (AA) with sodium acrylate (Na-AA)] produced by Moscow–Stockhausen–Perm Russian–German Joint-Stock Company; the properties of Praestol flocculants are listed in the table. The tests were performed with KE-1 brand kaolin (TU 21-5494-310-001–92), because this dispersion system with uniform particle size distribution (average particle size 0.2×10^{-6} m) is widely used to evaluate the flocculation properties of water-soluble polymers. All solutions were prepared in distilled water.

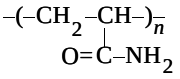
The sedimentation kinetics was studied using 0.15% kaolin suspensions on a sedimentometric unit equipped with a VT-500 torsion balance. The sedi-

Properties of Praestol flocculants*

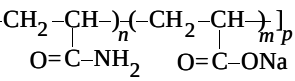
Sample no.	Praestol brand	$[\eta]$, $cm^3\ g^{-1}$	$\bar{M}_\eta \times 10^{-6}$	Content of indicated units, mol %	
				AA	Na-AA
1	2500	1550	8.7	97	3
2	2515	1500	4.6	89	11
3	2530	1800	4.4	80	20
4	2540	1600	4.5	72	28

* Structure of units in macromolecule;

sample no. 1



sample nos. 2–4



1070-4272/05/7811-1872 © 2005 Pleiades Publishing, Inc.

mentation rate was determined from the weight of precipitate accumulated on the balance dish in time t after tenfold stirring of the suspension using a perforated disk stirrer.

The content of the ionic units α in AA–Na-A copolymers was determined by potentiometric titration [6]. The intrinsic viscosity [η] of copolymer solutions was measured in a 0.5 M NaCl solution at 30°C on a VPZh-3 viscometer (d_c = 0.56 mm). The [η] values were determined from the experimental linear dependence of the reduced viscosity $\eta_{sp}/c_p = f(c_p)$, where c_p is the copolymer concentration:

$$[\eta] = \lim(\eta_{sp}/c_p) \text{ at } c_p \to 0.$$

The viscosity-average molecular weight $\overline{M}_\eta$ of AA–Na-A copolymer was calculated with the Mark–Houwink equation

$$[\eta] = k\overline{M}_\eta^a,$$

where the factors K and a varied with the concentration of the ionic units in the copolymer; the numerical values K and a were taken from [7].

The effective size of the flocculant macromolecules $(\bar{r}^2)^{1/2}$ was evaluated from the reduced viscosity of solutions η_{sp}/c_p at constant flocculant concentration c_p; in accordance with the Flory–Fox equation $\eta_{sp}/c_p \sim (\bar{r}^2)^{3/2}$ [8].

The effect of concentration of the dispersed phase c_d in the kaolin suspension on sedimentation was evaluated in the 0.1–0.2 wt % range in the absence of flocculant and coagulants. As seen from Fig. 1, with increasing c_d under the conditions of unhindered sedimentation of the kaolin particles the rate of precipitate accumulation on the balance dish increases (Fig. 1, passing from curve *1* to curve *4*). This is obviously due to a decrease in the distances between the kaolin particles, which increases their van der Waals interaction. Since this interaction exceeds the electrostatic repulsion between the negatively charged kaolin particles (–4.2 mV ζ potential), the rates of aggregation and precipitation increase.

The simultaneous effect of coagulant and flocculant on the stability of the kaolin suspension was studied at various modes of their addition. The dependences of the rate of precipitate sedimentation V as influenced by simultaneous and successive (when second coagulant is added 1 min after the first coagulant) addition of the reagents are shown in Fig. 2. As seen, successive addition of the reagents provides higher V as compared to their simultaneous addition into the suspension, and this trend is observed with both APOC (Fig. 2, passing from curves *1*, *2* to curve *4*) and AS (Fig. 2, passing from curves *3*, *5* to curve *6*). The flocculant, when added before the coagulant, hinders coagulation and thus decreases the sedimentation rate. At the same time, when the coagulant is added before the flocculant, the sedimentation rate increases as compared to the above case (Fig. 2, passing from curve *2* to curve *1* for APOC and from curve *5* to curve *3* for AS). This suggests certain differences in adsorption of the flocculant macromolecules on the kaolin particles and irreversibility of the process. When the coagulant is added first, the coagulant hydrolysis is completed before the flocculant addition and the resulting positively charged particles of hydroxo complexes neutralize negatively charged kaolin

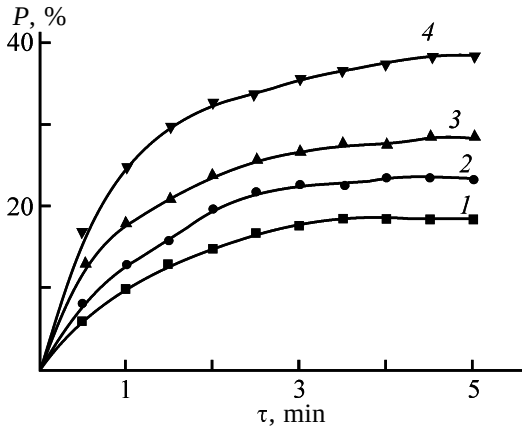


Fig. 1. Degree of precipitate sedimentation P as a function of time τ at various kaolin concentrations in the suspension c_d, %: (*1*) 0.1, (*2*) 0.12, (*3*) 0.15, and (*4*) 0.2.

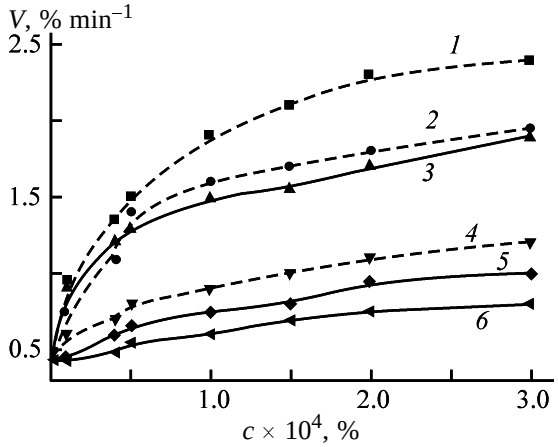


Fig. 2. Sedimentation rate of a kaolin suspension V as influenced by the concentration of Al_2O_3 c in (*1*, *2*, *3*) APOC and (*3*, *5*, *6*) AS in the presence of Praestol 2530; c_p 2×10^{-3}%. Mode of addition: (*1*, *3*) C + F, (*2*, *5*) F + C, and (*4*, *6*) mixture of F and C.

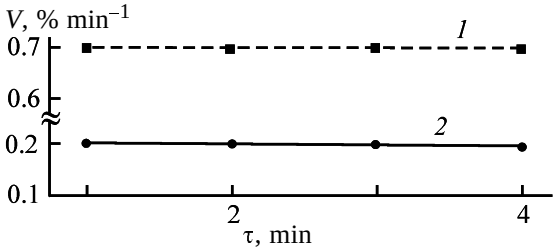


Fig. 3. Sedimentation rate of the kaolin suspension *V* as influenced by the time of addition of Praestol 2530 flocculant after coagulants (*1*) APOC and (*2*) AS; c_p 1.8×10^{-4}% and c_c 0.5×10^{-4}%.

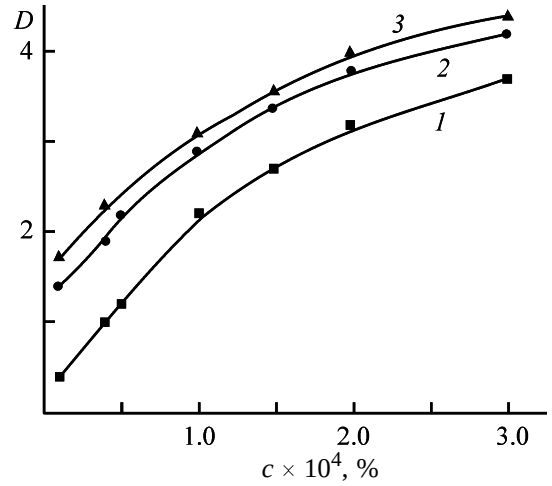
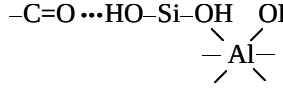


Fig. 4. Flocculation parameter *D* as a function of the concentration of Al_2O_3 *c* in APOC at various concentrations of Praestol 2530. c_p, %: (*1*) 4×10^{-4}, (*2*) 2×10^{-3}, and (*3*) 3×10^{-3}.

particles, causing their sedimentation. The flocculant macromolecules added successively are adsorbed on the precipitated kaolin particles. It is known [9] that the kaolin ($Al_2O_3 \cdot 2SiO_2 \cdot 2H_2O$ with impurities of Fe_2O_3, MnO, Na_2O, K_2O, and TiO_2) particles form hexagons, whose basal surfaces are charged negatively at various pH, whereas lateral faces can be either neutral or positively and negatively charged depending on the solution pH. Obviously, anionic Praestol can be adsorbed due to the formation of the hydrogen bonds between the carbonyl groups of the flocculant macromolecules and hydroxy groups on the lateral faces of the kaolin particles:



Formation of the coarse aggregates accelerates their sedimentation. In all further tests we used the successive C + F mode of the reagent addition, as providing better results.

The effect of the lag between addition of the coagulant and flocculant on the stability of kaolin suspension is shown in Fig. 3. As seen from these data, no changes in the sedimentation rate are observed at time >1 min, and in our further tests the flocculant was added into the suspension 1 min after coagulant addition.

Figure 2 also shows that at c_p = const *V* increases with increasing concentrations of APOC (Fig. 2, curves *1, 2, 4*) and AS (Fig. 2, curves *3, 5, 6*), which is due to acceleration of coagulation of the kaolin suspension, enhancing the resulting flocculation effect. As seen from these experimental data at fixed concentrations of Al_2O_3 in the coagulants, *V* increases on substitution of APOC for AS (Fig. 2, passing from curves *3, 5, 6* to curves *1, 2, 4*); this fact well agrees data in Fig. 3 (passing from curve *2* to curve *1*).

The effect of the flocculant concentration on the kaolin suspension sedimentation was studied in the $(4–30) \times 10^{-6}$% range, the other conditions being constant. The flocculating power of polymers can be evaluated using the parameter *D*:

$$D = (V - V_0)/V_0,$$

where *V* and V_0 are the sedimentation rates of the kaolin suspension in the presence of the flocculant and without it. The dependences of *D* on the concentration of Al_2O_3 in APOC at different c_p are shown in Fig. 4. Comparison of experimental data (Fig. 4) at $[Al_2O_3]$ = const shows that *D* increases with increasing c_p. Apparently, increasing additions of the flocculant increase the concentration of macromolecular bridges between the kaolin particles, providing formation of coarse floccules and thus accelerating their sedimentation.

The dependence of the flocculation parameter *D* on the chemical composition of the flocculant macromolecules is illustrated in Fig. 5. The dependences pass through a maximum (Fig. 5, curves *1, 2*), which agrees with the dependence of η_{sp}/c_p (Fig. 5, curve *3*). These data show that the highest *D* corresponds to the content of ionic units in the flocculant macromolecule of about 30 mol %. We assumed that in this case the macromolecules are characterized by the optimal ratio of the charge density and chain flexibility, providing the highest $(\bar{r}^{-2})^{1/2}$ values. With increasing $(\bar{r}^{-2})^{1/2}$, macromolecules can bind the larger number of the kaolin particles, which increases the flocculation effect. As seen, *D* increases with increasing c_p (Fig. 5, passing from curve *2* to curve *1*), which agrees with the data given in Fig. 4.

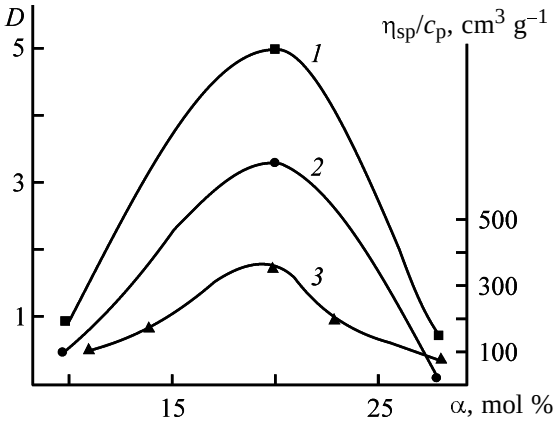


Fig. 5. (*1*, *2*) Flocculation parameter *D* and (*3*) reduced viscosity η_{sp}/c_p as functions of the content of ionic units α in the Praestol flocculant. c_c (APOC) 0.15×10^{-4}%. c_p, %: (*1*) 6×10^{-3} and (*2*, *3*) 2×10^{-3}.

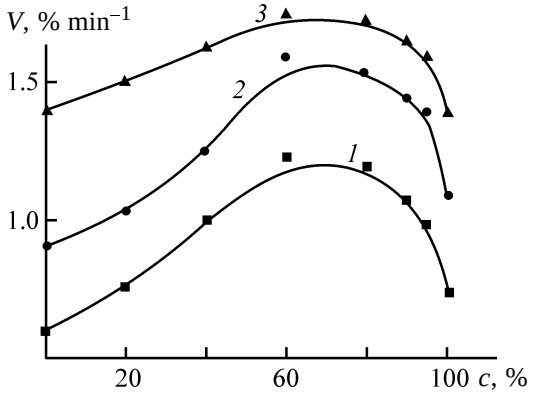


Fig. 6. Sedimentation rate of the kaolin suspension *V* as a function of the APOC content in the mixture [APOC]/[([APOC] + [SA]) *c* at various concentrations of Praestol 2530. c_p, %: (*1*) 1×10^{-3}, (*2*) 2×10^{-3}, and (*3*) 6×10^{-3}.

It is known [10] that polydispersion coagulant aggregates are formed at successive addition of various coagulants and, owing to an increase in the time of their hydrolysis, coagulation is accelerated. We also studied sedimentation of the kaolin suspension as influenced by successive addition of a mixture of APOC and AS coagulants at c_p = const. The results are shown in Fig. 6. As seen, with increasing APOC content in the APOC + SA mixture *V* first increases and then decreases, and the highest sedimentation rates are observed at APOC content of about 60%. Similar dependences of *V* on the composition of the coagulant mixture were determined for various c_p. We found that *V* increases with increasing c_p (Fig. 6, passing from curve *1* to curve *3*), which agrees with the data given in Fig. 4.

CONCLUSIONS

(1) The sedimentation rate increases with increasing concentration of coagulants (aluminum polyoxychloride and sulfate) and Praestol flocculant; it also increases on substitution of aluminum polyoxychloride for aluminum sulfate, on passing from simultaneous to successive addition of coagulants and flocculant, and on passing from flocculant + coagulant to coagulant + flocculant addition modes.

(2) The dependences of the flocculation parameter and reduced viscosity on the chemical nature of the flocculant macromolecules at constant polymer concentration are similar, as both are associated with the effective size of macromolecules in solutions.

(3) The dependence of the flocculation parameter on the content of aluminum polyoxychloride in the mixture of coagulants at their simultaneous use with the flocculant passes through a maximum.

REFERENCES

1. Veitser, Yu.I. and Mints, D.M., *Vysokomolekulyarnye flokulanty v protsessakh ochistki prirodnykh i stochnykh vod* (Macromolecular Flocculants in Treatment of Natural and Waste Waters), Moscow: Stroiizdat, 1984.
2. Kurenkov, V.F., Hartan, H.-G., and Lobanov, F.I., *Khim. Komp'yut. Model. Butlerovsk. Soobshch*., 2002, vol. 3, no. 11, pp. 31–40.
3. Kurenkov, V.F., Churikov, F.I., and Snigirev, S.V., *Zh. Prikl. Khim*., 1999, vol. 72, no. 9, pp. 1485–1489.
4. Kurenkov, V.F., Churikov, F.I., and Snigirev, S.V., *Vest. Kazansk. Tekhnol. Univ*., 1998, no. 2, pp. 104–108.
5. Kurenkov, V.F., Churikov, F.I., and Snigirev, S.V., *Zh. Prikl. Khim*., 2000, vol. 73, no. 8, pp. 1346–1349.
6. Kurenkov, V.F., Baiburdov, T.A., and Stupen'kova, L.L., in *Fiziko-khimicheskie osnovy sinteza i pererabotki polimerov* (Physicochemical Bases of Synthesis and Processing of Polymers), Gor'kii: Gor'k. Gos. Univ., 1985, pp. 79–86.
7. Klein, J. and Conrad, K.-D., *Makromol. Chem*., 1978, vol. 179, no. 6, pp. 1635–1638.
8. Fox, T.G. and Flory, P.I., *J. Am. Chem. Soc*., 1957, vol. 73, pp. 1904–1909.
9. Hocking, M.B., Klimchuk, K.A., and Lowen, S., *J.V.S.–Rev. Macromol. Chem. Phys*., 1999, vol. 39, no. 2, pp. 177–203.
10. Zapol'skii, A.K. and Baran, A.A., *Koagulyanty i flokulyanty v protsessakh ochistki vody* (Coagulants and Flocculants in Water Treatment), Leningrad: Khimiya, 1987.

Russian Journal of Applied Chemistry, Vol. 78, No. 11, 2005, pp. 1876–1879. Translated from Zhurnal Prikladnoi Khimii, Vol. 78, No. 11, 2005, pp. 1907–1911.
Original Russian Text Copyright © 2005 by Zarochentsev, Shvydko, Voropanova.

ENVIRONMENTAL PROBLEMS OF CHEMISTRY AND TECHNOLOGY

Treatment of Spent Oil-Based Cutting Fluid

V. M. Zarochentsev, A. S. Shvydko, and L. A. Voropanova

North-Caucasian Mining and Metallurgical Institute, Vladikavkaz, North Ossetia, Russia

Received June 16, 2005

Abstract—Treatment of spent oil-based cutting fluid was studied and simulated to identify the optimal treatment conditions.

Units manufactured from very hard and wear-resistant materials prepared from technical stone, e.g., agate, find wide technical application, in particular, in instrument making. The flowsheet for manufacturing such articles includes cutting and abrading. Virtually all the flowsheet operations involve the use of oil-based cutting fluids (CFs). When the radius of the particles based on SiO_2 is small, their gravity sedimentation is very slow. For example, in the system under study, the time of sedimentation of the particle by 1 cm was 3 days. By taking this into account and using the Stockes' law for spherical particles in the form

$$v = \frac{2g(\rho - \rho_0)r^2}{9\eta}, \quad (1)$$

it was possible to estimate the sedimentation rate v at 3.858×10^{-6} cm s^{-1}. Here, v is the particle sedimentation rate; ρ and ρ_0, density of the particle and medium, respectively; r, particle radius; η, viscosity of the medium; and g, acceleration of gravity.

The known procedures for treatment of spent oils, involving sedimentation, filtration, adsorption, treatment with chemicals, distillation of the combustible, centrifugation, pressure variation, etc., involve many operations and are inefficient.

Earlier experiments [1] allowed development of a procedure for treatment of spent oil-based CF, consisting in the following. The pulp is treated with 2–10% aqueous NaOH in amount of 3–17% of the pulp volume under continuous stirring and heating to 313–338 K, which is followed by keeping the warm mixture until degradation of the colloid structure of the gel. Next, phases are separated in accordance with the specific weight, without heating, under intermittent slow stirring of the bottom phase of the silica residue, and the CF after sedimentation is decanted.

Technical and economic calculations showed the promise of a change from alkali to sodium carbonate, which enhances foaming during the pulp aeration. Sodium carbonate is a less expensive chemical; it is widely used in various processes and is less reactive. The use of sodium carbonate in the process of interest is beneficial from both economic and environmental viewpoints and also affords a slightly greater technological effect.

According to the procedure proposed in [2], the pulp is treated at 40–70°C with an aqueous solution containing 0.1–17.7 wt % Na_2CO_3 in the amount corresponding to 3.3–23.3% of the volume of the initial oil-based CF and kept at room temperature, while the oil phase is removed as it separates out.

The table presents the main process parameters of the tests on treatment of the CF. The experiments were run under the following conditions: heating over a period of 1 h and keeping at 293–363 K for 0.5–5.0 h. The spent pulp of the CF was treated with alkaline chemicals NaOH and Na_2CO_3 to remove impurities, and I-20A grade oil served as the initial CF.

Tests of the treated CF in cutting technical stone did not reveal any departures from the ordinary run of the process.

The experimental data were processed using the MathCAD program [3]. The experimental conditions (see table) were set in the form of the $x_{(19.3)}$ matrix, and the degrees of recovery, in the form of the $y_{(19.5)}$ matrix. Block 1 of the program transforms the matrices, taking account of the time of the experiment (0.5, 1.0, 1.1, 3.0, and 5.0 h), and yields matrices of experimental conditions $X_{(95.4)}$ and observations $Y_{(95.1)}$.

We developed a mathematical model describing the recovery of oil from CF as a function of a set of in-

1070-4272/05/7811-1876 © 2005 Pleiades Publishing, Inc.

Main process parameters of CF treatment

Run no.	$c_{Na_2CO_3}$, wt %	$V_{Na_2CO_3}/V_{pulp}$, %	T, K	Degree of recovery of oil from CF, % of the CF volume in pulp being treated at indicated sedimentation time, h				
				0.5	1.0	1.5	3.0	5.0
1	17.7	3.3	333	21	31	61	64	65
2	17.7	7.0	333	25	35	62	64	65
3	17.7	10.0	333	28	39	63	67	70
4	17.7	16.7	333	30	42	64	78	82
5	17.7	23.3	333	32	46	65	80	85
6	5.0	3.3	333	0	7	18	28	35
7	5.0	7.0	333	16	28	37	56	62
8	5.0	10.0	333	32	49	56	61	67
9	5.0	16.7	333	33	58	68	73	80
10	5.0	23.3	333	35	67	80	81	82
11	0.1	23.3	333	0	37	58	59	61
12	0.5	23.3	333	0	42	63	64	65
13	1.0	23.3	333	0	44	65	66	67
14	1.5	23.3	333	30	50	64	65	68
15	2.0	23.3	333	34	55	62	70	75
16	5.0	23.3	313	13	25	30	35	40
17	5.0	23.3	323	28	42	45	55	64
18	5.0	23.3	348	36	68	72	84	87
19	5.0	23.3	353	45	74	75	87	92

* $V_{Na_2CO_3}$ is the volume of the sodium carbonate solution added, and V_{pulp} is the volume of the initial pulp.

dependent parameters, set in the table:

$$E(X) = a_0 + a_1x_0 + a_2x_1 + a_3x_2 + a_4x_3 + a_5x_0^2 + a_6x_1^2 + a_7x_2^2 + a_8x_3^2 + a_9x_1^3 + a_{10}x_1x_3, \quad (2)$$

where $E(x)$ is the degree of recovery of the oil into solution; x_0, content of sodium carbonate in the solution added; x_1, volume of the Na_2CO_3 solution added; x_2, temperature; and x_3, process time.

The coefficients in the mathematical model were calculated by the least-squares method for a linear combination of arbitrary functions [4]. The matrix X is transformed into the matrix of the $U_{(95.11)}$ functions, corresponding to the form of model (2), in program block II.

The coefficients in regression equation (2) are calculated by the least-squares method in the matrix form [4] (block III).

Technologically preferable option consists in carrying out the process at 333 K (at higher temperatures, thermal degradation of oil becomes more probable) and at the sodium carbonate concentration $c_{Na_2CO_3}$ = 5%. It is convenient to present regression equation (2) in the reduced form as $E = f(V, \tau)$ at fixed $c_{Na_2CO_3}$ and T:

$$E(V, \tau) = s + a_2V + a_4\tau + a_6V^2 + a_8\tau^2 + a_9V^3 + a_{10}V\tau, \quad (3)$$

where $E(V, \tau)$ is the degree of recovery of oil into solution; V, volume of the Na_2CO_3 solution added; τ, process time; and s, sum of the fixed terms in Eq. (2).

Figure 1 presents the response surface for function (3), calculated using MathCAD. It is seen that

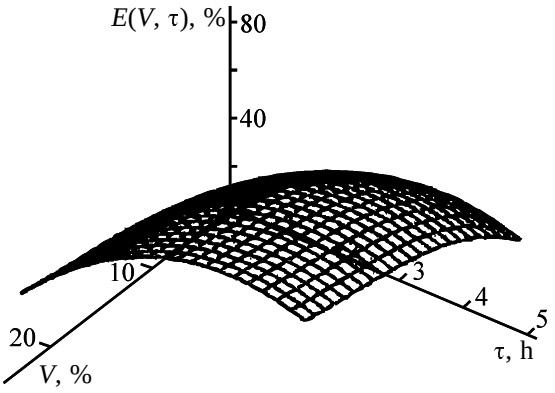


Fig. 1. Response surface for the degree of recovery $E(V, \tau)$, as a function of the reagent volume V and the process time τ.

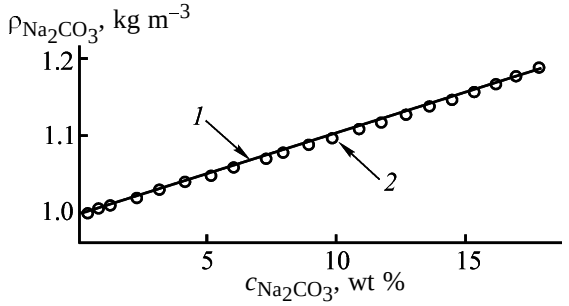


Fig. 2. Sodium carbonate solution density $\rho_{Na_2CO_3}$ as a function of the sodium carbonate content in solution $c_{Na_2CO_3}$. (*1*) (Line) Calculation by Eq. (5) and (*2*) experimental points.

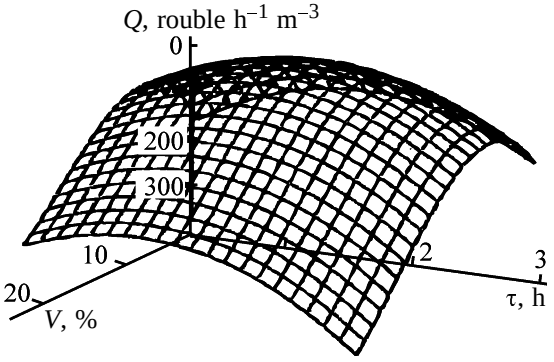


Fig. 3. Response surface of the function of the cost optimization criterion Q with respect to time τ and reagent volume.

the optimal values of the process parameters lie within the region under study. Technologically justified option implies the process time of 1.5–2.5 h and volume of 5% Na_2CO_3 solution of 7–23% relative to the volume of the initial pulp.

To determine the optimal parameters of the process, based on mathematical model (3), we formed a function of the optimization criterion Q, which gives the profit from oil recycling, depending on the operation costs, separation time, and cost of the oil recycled:

$$Q = Eq_0 - G_{Na_2CO_3} q_{Na_2CO_3} - V_r \tau q_v, \quad (4)$$

where q_0 is the cost of the oil recycled; $G_{Na_2CO_3}$, weight of water added during the process; $g_{Na_2CO_3}$, cost of 1 kg of sodium carbonate; V_r, volume of the reactor, required for treatment of 1 m^3 of the CF; and q_v, operation costs for 1 m^3 of the reactor volume in 1 h of the work.

The degrees of recovery in Eq. (4) were calculated by Eq. (3), and the volume of the reactor was composed from those of the CF pulp and the sodium carbonate solution added; the amount of the sodium carbonate added was calculated on the basis of the density and volume of the solution added: $G_{Na_2CO_3} = V\rho_{Na_2CO_3}$.

To estimate the density of the sodium carbonate solution as dependent on the concentration, we determined the $\rho_{Na_2CO_3} = f(c_{Na_2CO_3})$ dependence in the form of the

$$\rho_{Na_2CO_3}(x) = b_0 + b_1 x + b_2 x^2 \quad (5)$$

polynomial, where x is the sodium carbonate concentration in solution.

Coefficients b_0, b_1, and b_2 is Eq. (5) were determined using the linfit (RoNa$^{\langle 1\rangle}$, RoNa$^{\langle 0\rangle}$, FRo) function, processing the concentration vector RoNa$^{\langle 1\rangle}$ and its corresponding density vector RoNa$^{\langle 0\rangle}$ by the least-squares method [4]; the regression equation is set as a linear combination of the functions in the FRo matrix (block IV).

The solution densities were taken from [5] in the concentration range 0.19–17.7 wt %. Figure 2 shows the concentrations calculated by Eq. (5), which agree well with the experimental data.

For transformation of the optimization criterion (4), we substituted the function (3) of the degree of oil recovery and calculated the sodium carbonate solution density by Eq. (5) for the concentration of 5 wt %, which yielded

$$Q(V,\tau) = 10E(V,\tau)q_0 - (Vc_{Na_2CO_3}\rho_{Na_2CO_3}q_{Na_2CO_3}) \times 10^{-1} - (1 + V_r \times 10^{-2})\tau q_v, \quad (6)$$

where $Q(V,\tau)$ is the profit in the separation process (rouble h^{-1} m^{-3} of the CF).

By substituting q_0 = 1.7 rouble l^{-1} and q_v = 280 rouble m^{-3} h^{-1}, as suggested by practical experience, we calculated function (6) in the region of independent parameters studied. The resulting surface has a prominent maximum (Fig. 3).

The region of the optimal values, corresponding to the largest benefit from the CF treatment, was determined using the Maximize function, built in MathCAD, in which the extremum is searched by the Newton method [3] (block V).

The first row in block V sets the initial v and t parameters for the search of the maximum of function (6), which is set in the calculation as $Q(V,\tau)$. We

obtained the following optimal conditions: volume of the sodium carbonate solution added 9.14 l and time of separation 1.63 h (the first and second rows in the P_{opt} matrix); the conditions chosen correspond to the largest profit from the process of 65.6 rouble h^{-1} m^{-3} of the CF.

The experimental data tabulated and the response surface $Q(V, \tau)$ in Fig. 3 confirm that the most economically profitable option is treatment of the CF for 1.5–2 h at the reagent volume of 5% of the volume of the initial pulp and at a temperature no higher than 333 K.

Block I

$n := \text{rows}(x)$ $n = 19$ $N := 5n$ $j := 0..\ N-1$ $N = 95$

$X :=$ for $k \in 0..\ 4$
  $t \leftarrow \text{tau}_{0,k}$
  for $i \in 0..\ n-1$
    $u_{i+nk,\,3} \leftarrow t$
    for $j \in 0..\ 2$
      $u_{i+nk,\,j} \leftarrow x_{i,j}$
u

$Y :=$ for $k \in 0..\ 4$
  for $i \in 0..\ n-1$
    $u_{i+nk} \leftarrow y_{i,k}$
u

$X =$

	0	1	2	3
0	17.7	3.3	333	0.5
1	17.7	7	333	0.5
2	17.7	10	333	0.5
3	17.7	16.7	333	0.5
4	17.7	23.3	333	0.5
5	5	3.3	333	0.5
6	5	7	333	0.5
7	5	10	333	0.5
8	5	16.7	333	0.5
9	5	23.3	333	0.5
10	0.1	23.3	333	0.5
11	0.5	23.3	333	0.5
12	1	23.3	333	0.5

$Y =$

	0
0	21
1	25
2	26
3	30
4	32
5	0
6	16
7	32
8	33
9	35
10	0
11	0
12	0

Block II

$U_{j,0} := 1$ $U_{j,1} := X_{j,0}$ $U_{j,2} := X_{j,1}$ $U_{j,3} := X_{j,2}$
$U_{j,4} := X_{j,3}$ $U_{j,5} := (X_{j,0})^2$ $U_{j,6} := (X_{j,1})^2$ $U_{j,7} := (X_{j,2})^2$
$U_{j,8} := (X_{j,3})^2$ $U_{j,9} := (X_{j,1})^3$ $U_{j,10} := X_{j,1} X_{j,3}$

Block III

$A := (U^T U)^{-1} U^T Y$ $A =$

$$\begin{pmatrix} -3.772 \times 10^{3} \\ 4.168 \\ 5.851 \\ 21.294 \\ 31.477 \\ -0.163 \\ -0.267 \\ -0.03 \\ -4.146 \\ 4.586 \times 10^{-3} \\ 4.057 \times 10^{-3} \end{pmatrix}$$

Block IV

$$\text{ERo}(c) := \begin{pmatrix} 1 \\ c \\ c^2 \end{pmatrix}$$

$b := \text{linfit}(\text{RoNa}^{\langle 1 \rangle}, \text{RoNa}^{\langle 0 \rangle}, \text{FRo})$ $b = \begin{pmatrix} 0.999 \\ 9.957 \times 10^{-3} \\ 4.481 \times 10^{-3} \end{pmatrix}$

Block V

$v := 15$ $t := 2$

$P_{opt} := \text{Maximize}(O, v, t)$ $P_{opt} = \begin{pmatrix} 9.136 \\ 1.633 \end{pmatrix}$

$Q_{opt} := Q(P_{opt_0}, P_{opt_1})$ $Q_{opt} = 65.594$

CONCLUSIONS

(1) Procedures for mineral oil recovery through utilization and recycling of the treatment products and chemicals were developed.

(2) A mathematical model was developed for treatment of the oil-based cutting fluid using 5% sodium carbonate solution.

(3) Optimal process and economic parameters for treatment of the cutting fluid were determined.

REFERENCES

1. RF Patent 2 036 960.
2. RF Patent 2 062 294.
3. *Mathcad 6.0 PLUS. Financial, Engineering, and Scientific Calculations in the Windows 95 Environment*, Moscow: Filin", 1996.
4. Adler, Yu.P., Mrakova, E.V., and Granovskii, Yu.V., *Planirovanie eksperimenta pri poiske optimal'nykh uslovii* (Experiment Designing in the Search of the Optimal Conditions), Moscow: Nauka, 1976.
5. Rabinovich, V.A. and Khavin, Z.Ya., *Kratkii khimicheskii spravochnik* (Concise Chemical Handbook), Leningrad: Khimiya, 1977, pp. 258–259.

Russian Journal of Applied Chemistry, Vol. 78, No. 11, 2005, pp. 1880–1883. Translated from Zhurnal Prikladnoi Khimii, Vol. 78, No. 11, 2005, pp. 1912–1916.
Original Russian Text Copyright © 2005 by Belaya, Ovcharova, Filippenko, Nikolaevskii, Palagushkina.

ORGANIC SYNTHESIS AND INDUSTRIAL ORGANIC CHEMISTRY

Aminophenols as Inhibitors of Oxidation of Nujol

N. I. Belaya, O. Yu. Ovcharova, T. A. Filippenko, A. N. Nikolaevskii, and L. A. Palagushkina

Donetsk National University, Donetsk, Ukraine

Received May 4, 2005

Abstract—Antioxidant properties of aminophenols in initiated oxidation of Nujol were studied by a chemiluminescence procedure.

Polyfunctional antioxidants (AO) with several reactive groups can be used to stabilize fats and oils. Among these compounds are aminophenols (APs)[1]. To assess practical applicability of APs for inhibition of radical chain oxidation of organic compounds, their antioxidant power (AOP) with respect to model systems should be determined and features of the behavior of APs in complex substrates (liquid fuels, mineral oils, etc.) should be taken into account.

In this study we examined the antioxidant power of aminophenol with respect to Nujol by chemiluminescence (CL) observed during the oxidation.

EXPERIMENTAL

We used Nujol (Merck) as received. Azobisisobutyronitrile (AIBN) (pure grade) double-recrystallized from absolute ethanol was used as the free radical source [2]. CL activator, 9,10-dibromoanthracene (DBA), was prepared and purified by the procedure described in [3]. Aminophenols were prepared by the procedures described in [4, 5]. These compounds were identified and characterized by thin-layer chromatography, IR spectroscopy, and elemental analysis. The CL kinetics in the course of initiated oxidation of Nujol in the presence and in the absence of AO was monitored with a chemiliminesecnce unit described in [6].

The reactivity of aminophenols (InH) in reaction with peroxy radicals of Nujol (ROO) (2) was characterized by the ratio $k_2/k^{1/2}$ and stoichiometric coefficient of inhibition (f).

$$ROO^{\bullet} + ROO^{\bullet} \xrightarrow{k_1} \text{Products}, \quad (1)$$

$$ROO^{\bullet} + PhOH \xrightarrow{k_2} ROOH + PhO^{\bullet}. \quad (2)$$

Since the composition of the substrate being oxidized is complex and variable, the rate constant (k_1) of recombination of peroxy radicals (1) is unknown and hence the quantity $k_2/k^{1/2} = k_{app}$ is apparent.

Oxidation of Nujol initiated by AIBN was performed at 333 K in chlorobenzene at a volume ratio of 1 : 1. The initiation rate (v) of Nujol oxidation was calculated from Eq. (3). For this purpose, the induction period of Nujol oxidation in the presence of a reference inhibitor (Ionol) was determined. The inhibition coefficient (f) of Ionol is 2 [7].

$$v_i = f[InH]_0/\tau, \quad (3)$$

where $[InH]_0$ is the initial Ionol concentration, M.

To determine this parameter, the chemiluminescence kinetic curves were linearized in the coordinates of Eq. (4):

$$(I_0/I)^{1/2} = 1 + 1.1k_2[InH](v_i k_1)^{-1/2}, \quad (4)$$

where I_0 and I are the chemiluminescence intensities in the absence and in the presence of AO, respectively.

The apparent rate constant k_{app} was calculated from the slope of the linearized kinetic curves of CL (φ) (Fig. 1b) by the equation

$$k_{app} = k_2/(k_1)^{1/2} = \tan\varphi\,(v_i)^{1/2}/1.1. \quad (5)$$

The number of radicals decaying on a single AO molecule was calculated from the experimental induction period of oil oxidation (τ) in the presence of AP by Eq. (3).

After addition of the examined AOs into the system, the CL intensity (I) decreases as compared to that

1070-4272/05/7811-1880 © 2005 Pleiades Publishing, Inc.

Table 1. Antioxidant properties of AP (k_{app} and f) in initiated oxidation of ethylbenzene and Nujol and N–H and O–H bond strengths in their molecules

Compound	Ethylbenzene, T = 333 K, $v_i = 4.9 \times 10^{-7}$ mol l^{-1} s^{-1}		Nujol, T = 333 K, $v_i = 3 \times 10^{-7}$ mol l^{-1} s^{-1}		D_{N-H}	D_{O-H}
	k_{app}	f	k_{app}	f	kJ mol^{-1}	
N,*N*'-Bis(4-hydroxy-3-methoxybenzyl)-*o*-phenylenediamine (**I**)	545	2.7	571	3.8	288	310
N,*N*'-Bis(2-hydroxybenzyl)-*o*-phenylenediamine (**II**)	263	1.2	329	3.6	289	350
N,*N*'-Bis(2-hydroxy-3,5-di-*tert*-butylphenyl)-ethylenediamine (**III**)	326	1.6	1318	3.0	293	286
N,*N*'-Bis(2-hydroxybenzyl)-*p*-phenylenediamine (**IV**)	28.7	2.1	256	3.8	310	320
2,6-Di-*tert*-butyl-4-methylphenol (Ionol) (**V**)	4.9	2.0	11	2.0	–	306

in their absence (I_0) owing to a decrease in the concentration of peroxy radicals (Fig. 1a). As seen from Table 1, compounds **I**–**IV** actively react with ROO$^{\bullet}$BM and hence have a high AO power with respect to Nujol oxidation.

As seen from Table 1, the constants k_{app} of the APs are higher than that of the known AO, Ionol, and depend on the structure of these antioxidants. The AOP of the all examined APs in Nujol oxidation is higher than that in ethylbenzene oxidation. This is due to higher oxidation stability of Nujol (which is a mixture of aliphatic and naphthene hydrocarbons) and different reactivity of peroxy radicals of Nujol and ethylbenzene.

The main structural feature of APs affecting their AOP is the presence of two reactive sites (NH and OH groups). Experimental data on the strength of N–H (D_{N-H}) and O–H (D_{O-H}) bonds in the molecules of the APs in question are lacking. We calculated these parameters by AM1 semiempirical quantum chemical method using MOPAC-97 software [8]. The results are presented in Table 1.

Since the strengths of OH and NH bonds in AP molecules differ, the antioxidant activities of these groups should also differ. The amino groups in *ortho* position to each other are directly conjugated and hence the N–H bonds are weakened. Since the electronegativity of an oxygen atom is higher than that of a nitrogen atom, $D_{O-H} > D_{N-H}$. Hence, under the action of peroxy radical the amino group of AP will lose the H atom first. The AOP of *N*,*N*'-bis(2-hydroxybenzyl)-*o*-phenylenediamine is determined by the activity of its amino group. The apparent rate constant k_{app} of the *para* isomer of **II** (Table 1, compound **IV**) is low, since the strength of its N–H bond is comparable with that of the O–H bond. The O–H bond of *N*,*N*'-bis-(4-hydroxy-3-methoxybenzyl)-*o*-phenylenediamine is weakened by the electron-donor methoxy group and can be involved, along with the NH group, in the peroxy radical deactivation.

Compound III is the most reactive (k_{app}) with respect to peroxy radicals of Nujol (Table 1). This is due to the presence in its molecule of two fragments which can be independently involved in chain termination. The reaction sites of this compound are labile OH groups.

Comparison of the AOP of the APs with that of Ionol shows that APs are more reactive AOs with respect to both substrates. The apparent rate constant k_{app} determined from the CL data characterizes the

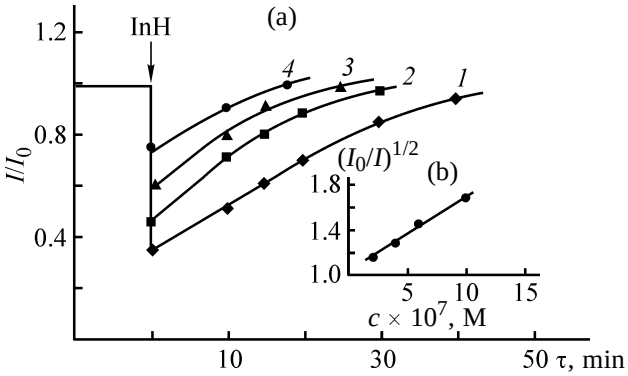


Fig. 1. (a) Kinetic curves of CL intensity in initiated oxidation of Nujol in a mixture with CB (1 : 1) in the presence of (*1*) 1×10^{-6}, (*2*) 6×10^{-7}, (*3*) 4×10^{-7}, and (*4*) 2×10^{-7} M *N*,*N*'-bis(2-hydroxybenzyl)-*o*-phenylenediamine; and (b) linearization of the kinetic curves in the coordinates $(I_0/I)^{1/2}$ vs. *N*,*N*'-bis(2-hydroxybenzyl)-*o*-phenylenediamine concentration {T = 333 K, $v_i = 3 \times 10^{-7}$ mol l^{-1} s^{-1}, [DBA] = 1×10^{-3} M} (I_0) CL intensity without AO, (I) CL intensity in the presence of AO, (c) concentration, and (τ) time.

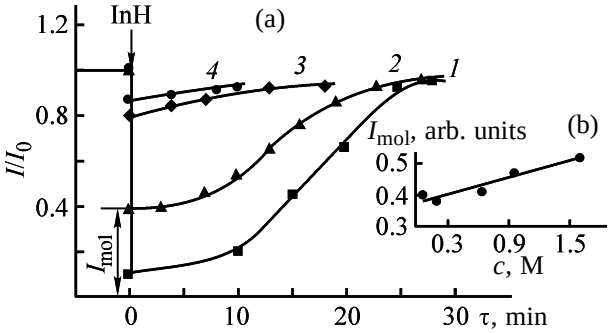


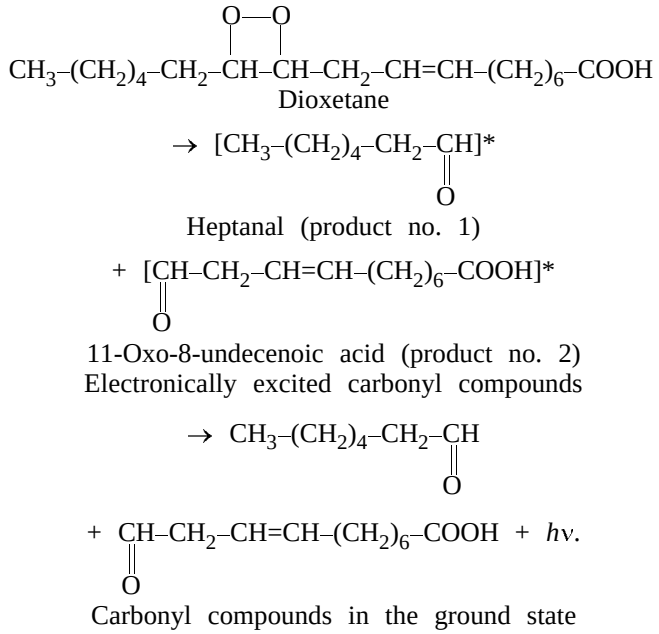
Fig. 2. (a) Time dependence of I/I_0 for a Nujol : CB (1 : 1) mixture containing 1×10^{-4} M Ionol and (*1*) 0. (*2*) 0.1, (*3*) 1.5, and (*4*) 2.5 ml of LA; (b) intensity of molecular CL (I_{mol}) as a function of the LA concentration [T = 333 K, $V_i = 3 \times 10^{-7}$ M, [DBA] = 1×10^{-3} M]. (*c*) Concentration and (τ) time.

activity of the group with minimal bond strength. The stoichiometric coefficient of inhibition (f) characterizes the total AOA of a compound under these conditions. This parameter depends on the number and reactivity of all groups involved in oxidation inhibition. Hence, these is no correlation between k_{app} and f (Table 1).

Our study of AOP of APs in initiated oxidation of Nujol showed that Nujol oxidation, unlike that of vegetable oils (sunflower-seed and cotton-seed oils) [10], has no induction period. As shown previously [10, 11], the induction period in Nujol oxidation is due to the presence of AOs added to the oil in the course of its preparation from petroleum. The absence of the induction period in our experiments is due to the fact that we used Nujol of high purity, containing no inhibiting impurities.

We did not observed the CL features in Nujol oxidation found in [10, 11]. These authors reported that, after addition of various inhibitors to Nujol being oxidized, the CL intensity decreases to a definite value I_{mol} which is independent of the concentration and nature of AO at the instant of its introduction. This is caused by the fact that the CL signal consists of two components: the radical constituent (I_{rad}) which is generated in recombined atom of peroxy radicals and is quenched by AO, and the molecular constituent (I_{mol}) which is generated in nonradical reactions and is quenched by AO.

Our study performed under the similar conditions showed that the molecular constituent of CL is absent in oxidation of pure Nujol. This fact agrees with the results of detailed studies [12, 13] where it was found that molecular CL is observed only in oxidation of unsaturated compounds. Molecular CL is generated by electronically excited carbonyl compounds formed in degradation of dioxetanes, oxidation products of unsaturated compounds.



To check this assumption, we added a small amount of unsaturated compound (linoleic acid, LA) to Nujol (Fig. 2a). The CL intensity increased with increasing the LA content in Nujol (Fig. 2b).

To confirm the feasibility of formation of electronically excited species by nonradical degradation of dioxetanes in initiated oxidation of LA, we calculated thermodynamic parameters of reaction (6) by AM1 method.

The enthalpy of this reaction is determined by the following equation:

$$\Delta H_r = (\Delta H^0_{pr.1} + \Delta H^0_{pr.2}) - \Delta H^0_d,$$

where ΔH_r is the standard enthalpy of reaction (6); $\Delta H^0_{pr.1}$ and $\Delta H^0_{pr.2}$ are the standard enthalpies of formation of electronically excited products; and ΔH^0_d is the standard enthalpy of formation of dioxetane.

$$\Delta E_{S_0 \to S_1} = \Delta H^0_{S_1} - \Delta H^0_{S_0},$$

where $\Delta E_{S_0 \to S_1}$ is the transition energy of carbonyl compounds from the ground state to singlet excited state; $H^0_{S_0}$ and $H^0_{S_1}$ are the standard heats of formation of the molecular products in the ground and singlet excited states, respectively.

$$\Delta E_{T_1 \to S_0} = H^0_{S_0} - H^0_{T_1},$$
$$\Delta E_{S_1 \to S_0} = H^0_{S_0} - H^0_{S_1},$$

where $\Delta E_{T_1 \to S_0}$ and $\Delta E_{S_1 \to S_0}$ are the transition ener-

Table 2. Thermodynamic parameters of degradation of dioxetanes formed by initiated (AIBN, 333 K) oxidation of LA [reaction (6)]

Parameter	Heptanal	11-Oxo-8-undecenoic acid
$H^0_{S_0}$, kJ mol^{-1}	–315	–662
$H^0_{S_1}$, kJ mol^{-1}	–30	–377
$H^0_{T_1}$, kJ mol^{-1}	–108	–454
$\Delta E_{S_0 \to S_1}$, kJ mol^{-1}	285	285
$\Delta E_{S_1 \to S_0}$, kJ mol^{-1}	–285	–285
$\Delta E_{T_0 \to S_0}$, kJ mol^{-1}	–207	–208
H_r, kJ mol^{-1}	–364	
λ_S, nm	420	
λ_T, nm	573	

gies of carbonyl compounds from the triplet and from the singlet excited states to ground state, respectively; $H^0_{S_0}$ and $H^0_{T_1}$ are the standard heats of formation of the molecular products in the ground and triplet excited state, respectively.

The results are summarized in Table 2. It is known [6] that electronically excited products can be formed in exothermic chemical reactions. As seen from Table 2, ΔH_r is higher than the transition energy of the carbonyl compounds from the ground to electronically excited states ($\Delta H_r > \Delta E_{S_0 \to S_1}$). Hence, molecular CL ($I_{mol}$) in oxidation of LA is caused by degradation of deoxetanes to form electronically excited products whose transition to the ground state is accompanied by CL.

Transition to the ground state from both singlet and triplet electronically excited states is possible [6]. To determine the type of the excited state of the carbonyl compounds, we calculated from the transition energies ($\Delta E_{S_1 \to S_0}$, $\Delta E_{T_1 \to S_0}$) the wavelengths of emission in the transition to the ground state by the following equations:

$$\lambda_S = \frac{\nu N_A h}{\Delta E_{S_1 \to S_0}}, \qquad \lambda_T = \frac{\nu N_A h}{\Delta E_{T_1 \to S_0}},$$

where v is the velocity of light, N_A is the Avogadro constant, h is the Planck constant, λ_S is the emission wavelength in the transition from the singlet to the ground state, and λ_T is the emission wavelength in the transition from the triplet to the ground state.

The calculated wavelengths λ_S and λ_T are in the visible range, which agrees with the experimental data. Since the maximal spectral sensitivity of the photcathode of FEU-29 photomultiplier of the CL unit lies in the range 420–430 nm, which almost coincides with λ_S, the molecular component of CL of linoleic acid being oxidized is due to the products in singlet electronically excited state.

CONCLUSION

(1) The molecular component of CL appears only in oxidation of unsaturated compounds. This component is absent in initiated oxidation of Nujol (saturated compound) in the presence of aminophenols.

(2) Among examined AOs, *N,N'*-bis(2-hydroxy-3,5-di-*tert*-butylphenyl)-*o*-ethylenediamine and *N,N'*-bis(4-hydroxy-3-methoxybenzyl)-*o*-phenylenediamine are the most efficient in Nujol oxidation.

REFERENCES

1. Denisov, E.T. and Kovalev, G.I., *Okislenie i stabilizatsiya reaktivnykh topliv* (Oxidation and Stabilization of Propellants), Moscow: Khimiya, 1983.
2. Toroptseva, A.M., Belgorodskaya, K.V., and Bondarenko, V.M., *Laboratornyi praktikum po khimii i tekhnologii vysokomolekulyarnykh soedenenii* (Laboratory Course on Chemistry and Technology of Macromolecular Compounds), Leningrad: Khimiya, 1972.
3. *Organic Synthesis*, Blatt, A.H., Ed., New York: Wiley, 1944, 2nd ed., coll. vol. 1.
4. Busev, A.I., *Sintez novykh organicheskikh reagentov dlya neorganicheskogo analiza* (Synthesis of New Organic Reagents for Inorganic Analysis), Moscow: Mosk. Gos. Univ., 1972.
5. Citterio, A., Minisci, F., Parta, O., and Sesana, G., *J. Am. Chem. Soc.*, 1977, vol. 99, no. 24, pp. 7667–7960.
6. Shlyapintokh, V.Ya., Karpukhin, O.N., Postnikov, L.M., *et al.*, *Khemilyuminestsentnye metody issledovaniya medlennykh khimicheskikh protsessov* (Chemiluminescent Methods for Studying Slow Chemical Procersses), Moscow: Nauka, 1966.
7. Denisov, E.T., *Usp. Khim.*, 1973, vol. 42, no. 10, p. 361.
8. Steward, J.J.P., *MOPAC-93 Manual*, Oxford, 1993.
9. Gol'denberg, V.I. and Shmulovich, V.G., *Neftekhimiya*, 1979, vol. 19, no. 2, pp. 208–213.
10. Belaya, N.I., Filippenko, T.A., Nikolaevskii, A.N., *et al.*, *Zh. Prikl. Khim.*, 2004, vol. 77, no. 8, pp. 1351–1355.
11. Shmulovich, V.G. and Gol'denberg, V.I., *Neftekhimiya*, 1979, vol. 19, no. 6, pp. 912–920.
12. Belyakov, V.A., Vasil'ev, R.F., and Fedorova, G.F., *Izv. Akad. Nauk SSSR, Ser. Khim.*, 1983, no. 12, pp. 2709–2717.
13. Vasil'ev, R.F., *Kinet. Katal.*, 1999, vol. 40, no. 2, pp. 192–200.

Russian Journal of Applied Chemistry, Vol. 78, No. 11, 2005, pp. 1884–1887. Translated from Zhurnal Prikladnoi Khimii, Vol. 78, No. 11, 2005, pp. 1917–1920.
Original Russian Text Copyright © 2005 by Galibeev, Mukhametzyanova, Kochnev, Arkhireev, Gnezdilov.

MACROMOLECULAR CHEMISTRY AND POLYMERIC MATERIALS

Copolymerization of Chlorine-Substituted Monoisocyanates with ε-Caprolactone in the Presence of Sodium Caprolactamate

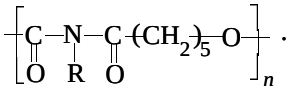
S. S. Galibeev, A. M. Mukhametzyanova, A. M. Kochnev, V. P. Arkhireev, and O. I. Gnezdilov

Kazan State Technological University, Kazan, Tatarstan, Russia

Received August 17, 2005

Abstract—Copolymerization of ε-caprolactone with a series of aromatic chlorine-substituted monoisocyanates in the presence of catalytic amounts of sodium caprolactamate was performed. The structures of the products obtained and their macromolecular characteristics were determined by IR and ^{1}H NMR spectroscopy and by gel permeation chromatography; kinetic and thermodynamic relationships of the process were found.

Previously we demonstrated the possibility of copolymerization of phenyl isocyanate (PIC) with ε-caprolactone (ε-CLN) in the presence of a catalyst (sodium caprolactamate, Na-CL) and an activator (2,4-toluylene diisocyanate, TDI) [1]. The reaction mainly yielded alternating copolymers, and its rate largely depended on the comonomer ratio, growing with an increase in the content of the isocyanate component. Our IR and ^{1}H NMR study [2] showed that the copolymerization of ε-CLN with isocyanates occurs via cleavage of the N=C bond in isocyanates and acyl bond in the lactone; the resulting copolymer has the following structure:



To extend the range of the isocyanates used and confirm the possibility of preparing alternating copolymers, we performed in this study the copolymerization of ε-CLN with chlorine-substituted monoisocyanates: 3-chlorophenyl isocyanate (3-CPI) and 4-chlorophenyl isocyanate (4-CPI).

EXPERIMENTAL

ε-CLN and 3-CPI (Fluka) were vacuum-distilled before use; 4-CPI (Fluka) was used without additional purification.

As catalyst we used sodium caprolactamate (Na-CL) prepared by the reaction of sodium metal with ε-caprolactam (ε-CL) in the bulk at 110–120°C. The product was stored in a desiccator under an inert gas. The Na-CL content in the product was 25 wt %.

The syntheses of the copolymers were performed in an argon flow in a three-necked flask equipped with a reflux condenser and a stirrer. The polymerization was carried out as follows: 1 wt % Na-CL was dissolved in ε-CLN at 80°C, after which the calculated amount of isocyanate was added with continuous stirring, and 1 wt % activator (TDI) was added. The products were purified by tenfold reprecipitation with hexane from acetone.

The chemical structures of the products formed in the reactions of monoisocyanates with ε-CLN were studied by IR Fourier spectroscopy on a Perkin–Elmer PC-16 spectrometer and by ^{1}H NMR spectroscopy on a Bruker MSL-400 spectrometer (400 MHz) with $CDCl_3$ as solvent and reference.

Gel chromatographic studies were performed with a Waters 150C gel chromatograph equipped with Ultrastyrogel HR 10^3 Å columns; the solvent was DMF, and the reference, polystyrene.

The content of isocyanate groups was determined by potentiometric titration according to [3]. The reaction rate constants and the activation energy and entropy were determined according to [4]. The copolymerization constants were calculated by the Fineman–Ross method [5].

As compared to the spectra of the starting monomers, the ^{1}H NMR spectrum of the product of copolymerization of ε-CLN with 3-CPI contains a signal at 2.4–2.2 ppm corresponding to the α-CH_2 protons relative to the carbonyl group of the opened lactone ring and a signal at 4.3–3.9 ppm corresponding to the α-CH_2 protons relative to the ester oxygen atom. The

1070-4272/05/7811-1884© 2005 Pleiades Publishing, Inc.

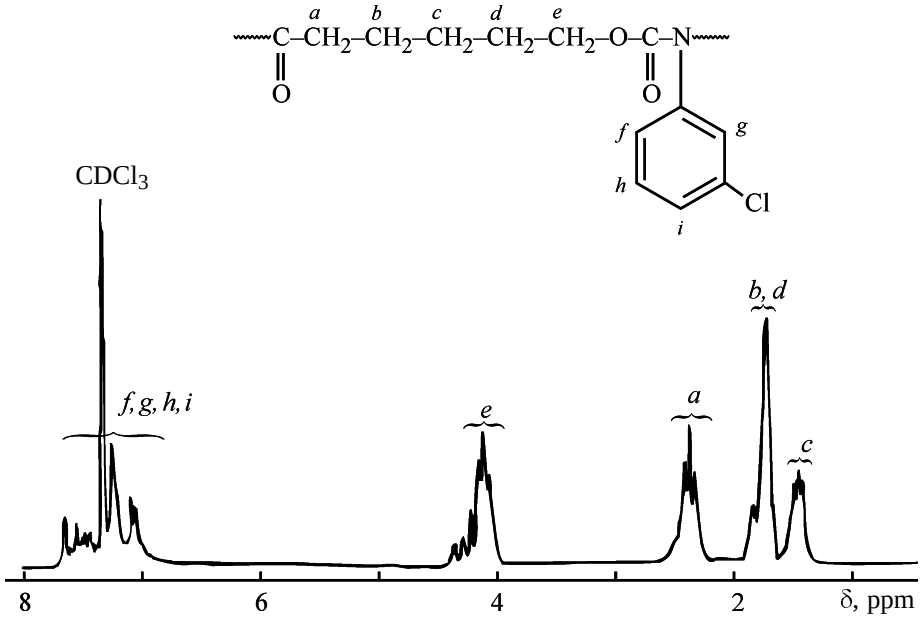


Fig. 1. ^{1}H NMR spectrum of ε-CLN–3-CPI copolymer. (δ) Chemical shift.

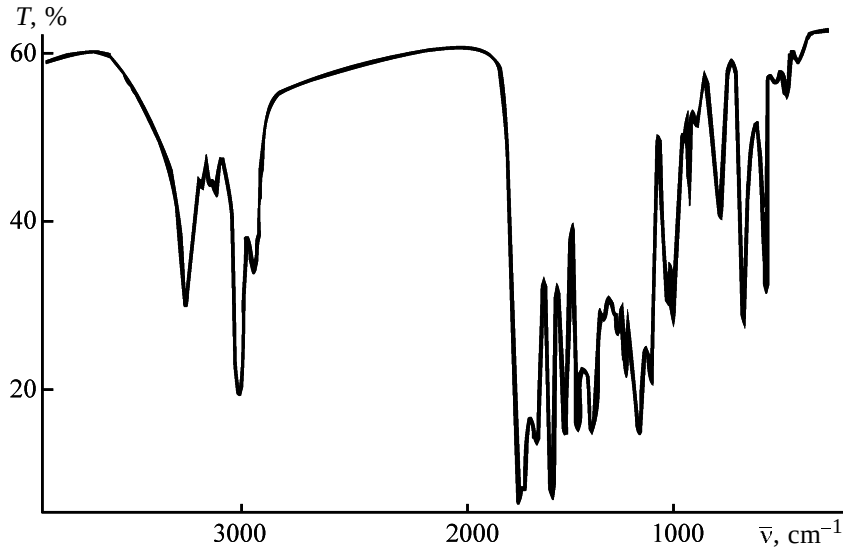


Fig. 2. IR spectrum of ε-CLN–3-CPI copolymer. (*T*) Transmission and ($\bar{\nu}$) wavenumber.

isocyanate component gives rise to sugnals at 7.9–6.9 ppm (benzene ring protons) (Fig. 1). The similar signals are present in the spectra of the copolymers of ε-CLN with 4-CPI and PIC.

The IR spectrum of the ε-CLN–3-CPI copolymer (Fig. 2) contains absorption bands at 1700 (C=O group in amides), 1599 (C=C stretching vibrations of aromatic rings), and 1540 cm^{-1} (C–N stretching vibrations). Also present are bands at 1730 (C=O stretching vibrations in aliphatic esters), 2866, and 2934 cm^{-1} (symmetric and antisymmetric vibrations of aliphatic methylene groups, respectively) [6].

By analytical titration we determined the rates of consumption of isocyanate groups in the course of copolymerization at various ε-CLN : isocyanate ratios (from 90 : 10 to 50 : 50 mol %). Processing of the kinetic data showed that the reaction order was close to 2 at any reactant ratio; therefore, the calculated rate constants were determined with second-order dimensions. We found that the reaction appreciably accelerated with an increase in the isocyanate content in the starting monomer mixture (Table 1). The polymer yield reached a maximum at equimolar ratio of the comonomers (Fig. 3). The same trend was observed with the PIC copolymers [1].

Table 1. Rate constants of copolymerization of ε-CLN with monoisocyanates at various molar ratios of comonomers*

Monomer content, mol %		$k \times 10^3$, l mol^{-1} s^{-1}		
ε-CLN	IC	PIC**	3-CPI	4-CPI
80	20	1.20	0.07	0.07
70	30	1.70	0.10	0.22
60	40	2.70	0.12	0.25

* Temperature: with PIC, 170°C; with 3-CPI and 4-CPI, 80°C.
** Data from [1].

Table 2. Rate constants of copolymerization of ε-CLN with monoisocyanates at various temperatures*

Isocyanate	T, °C	$k \times 10^3$, l mol^{-1} s^{-1}
3-CPI	80	0.12
	100	0.13
	120	0.17
4-CPI	80	0.25
	100	0.39
	120	0.43

* Molar ratio ε-CLN : isocyanate = 60 : 40.

Table 3. Activation energies and entropies of the reaction of ε-CLN with various isocyanates

Isocyanate	E_a, kJ mol^{-1}	ΔS, kJ K^{-1} mol^{-1}
PIC*	21.6	–0.25
3-CPI	35.1	–0.23
4-CPI	22.3	–0.18

* For PIC, data from [1]; the same for Table 4.

Table 4. Copolymerization constants for the system ε-CLN–isocyanate

Isocyanate	r_1	r_2
PIC*	0.67 ± 0.07	0.55 ± 0.06
3-CPI	0.63 ± 0.06	0.61 ± 0.06
4-CPI	0.50 ± 0.05	0.50 ± 0.05

The process was also appreciably intensified by raising temperature. In particular, with increasing temperature from 80 to 120°C, the rate constants of the copolymerization of ε-CLN with 4-CPI increased from 0.25×10^{-3} to 0.43×10^{-3} l mol^{-1} s^{-1} (Table 2).

The activation energy of the process (E_a) was the lowest (21.5 kJ mol^{-1}) with PIC and the highest (35.1 kJ mol^{-1}) with 3-CPI, which is apparently due

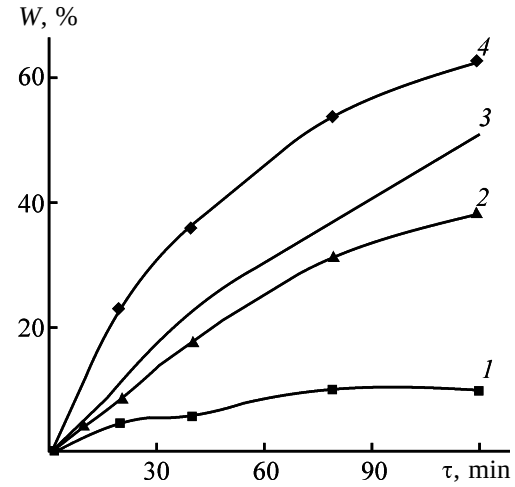


Fig. 3. Copolymer yield W as a function of time τ at various molar ratios of ε-CLN and 4-CPI in the initial mixture: (*1*) 80 : 20, (*2*) 70 : 30, (*3*) 60 : 40, and (*4*) 50 : 50. T = 120°C.

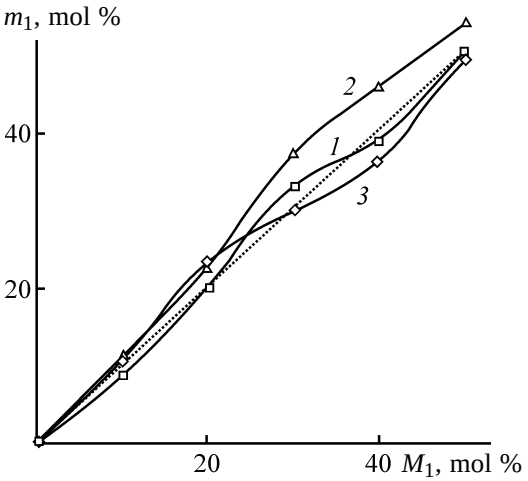


Fig. 4. Content of amide units in polymer m_1 vs. content of isocyanates M_1 in the initial mixture: (*1*) PIC, (*2*) 3-CPI, and (*3*) 4-CPI.

to the lower reactivity of 3-CPI. The negative activation entropies ΔS (Table 3) suggest decreased number of degrees of freedom of the reacting system in the transition state.

As aready noted, with PIC mainly random copolyamido esters were obtained, showing some tendency to alternation of the units, as indicated by the copolymerization constants of 0.67 for ε-CLN and 0.55 for isocyanates. For the copolymers derived from 3- and 4-CPI, r_1 and r_2 are also approximately equal, and their product is less than unity (Table 4). This fact also indicates that the copolymers are mainly alternating. The same conclusion follows from the dependence of the copolymer composition on the monomer ratio in the initial mixture (Fig. 4).

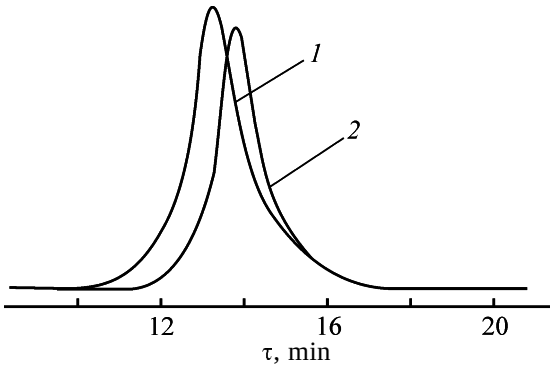


Fig. 5. Gel chromatograms of isocyanate–ε-CLN copolymers. (τ) Retention time. (*1*) 4-CPI–ε-CLN ($\overline{M}_w$ = 7500) and (*2*) 3-CPI–ε-CLN ($\overline{M}_w$ = 3200). Molar ratio isocyanate : ε-CLN: (*1*) 70 : 30 and (*2*) 60 : 40.

In view of the high reactivity of the monoisocyanates and ε-CLN and their tendency to homopolymerization under the reaction conditions, formation of the homopolymers along with the copolymers cannot be ruled out. However, actually the products have unimodal and fairly narrow molecular-weight distribution (Fig. 5) suggesting their uniform composition.

The molecular weights of the copolymers were relatively low. The weight-average molecular weights $\overline{M}_w$ varied in the range 3000–8000 depending on the comonomer ratio and isocyanate used; higher-molecular-weight products were obtained with 4-CPI.

CONCLUSIONS

(1) Copolymerization of ε-caprolactone with chlorinated aromatic monoisocyanates yields copolymers with predominant alternation of units.

(2) The trends revealed previously with phenyl isocyanate are also observed with chlorinated aromatic monoisocyanates.

REFERENCES

1. Mukhametzyanova, E.A., Galibeev, S.S., Arkhireev, V.P., *et al.*, *Izv. Vyssh. Uchebn. Zaved., Khim. Khim. Tekhnol.*, 2005, vol. 48, no. 4, pp. 133–135.
2. Mukhametzyanova, E.A., Galibeev, S.S., Yakimov, R.V., and Kochnev, A.M., *Vysokomol. Soedin., Ser. B*, 2005, vol. 47, no. 9, pp. 1750–1754.
3. *Praktikum po khimii i fizike polimerov* (Practical Course of Polymer Chemistry and Physics), Kurenkov, V.F., Ed., Moscow: Khimiya, 1995.
4. Samuilov, Ya.D. and Cherezova, E.N., *Reaktsionnaya sposobnost' organicheskikh soedinenii* (Reactivity of Organic Compounds), Kazan: Kazan. Gos. Tekhnol. Univ., 2003.
5. Sutyagin, V.M., *Eksperimental'nye metody issledovaniya polimerizatsii i sopolimerizatsii* (Experimental Methods for Studying Polymerization and Copolymerization), Tomsk: Tomsk. Politekh. Univ., 1988.
6. Kuptsov, A.Kh. and Zhizhin, G.N., *Fur'e-KR i Fur'e-IK spektry polimerov* (Fourier Raman and Fourier IR Spectra of Polymers), Moscow: Fizmatlit, 2001.

Russian Journal of Applied Chemistry, Vol. 78, No. 11, 2005, pp. 1888–1890. Translated from Zhurnal Prikladnoi Khimii, Vol. 78, No. 11, 2005, pp. 1921–1923.
Original Russian Text Copyright © 2005 by Zoolshoev, Bel'nikevich, Nud'ga, Petrova.

MACROMOLECULAR CHEMISTRY AND POLYMERIC MATERIALS

Behavior of Methyl and Propyl Methyl Cellulose Solutions in Longitudinal and Convergent Flows

Z. F. Zoolshoev, N. G. Bel'nikevich, L. A. Nud'ga, and V. A. Petrova

Institute of Macromolecular Compounds, Russian Academy of Sciences, St. Petersburg, Russia

Received April 12, 2005

Abstract—A mixed ether, propyl methyl cellulose with varied number of propyl groups, was synthesized from commercial water-soluble methyl cellulose. The effect of the number of side propyl groups on the dynamics of aqueous methyl and propyl methyl cellulose solutions in longitudinal and convergent flows was studied. The conditions under which solutions transform into the induced anisotropic state were determined.

Environmentally safe and biodegradable polymeric systems based on natural polymers attract a considerable interest of researchers. For example, certain water-soluble derivatives of cellulose, which show reversible gelation and lyotropic mesomorphism, have found wide application in medicine, food and textile industries, some fields of technology, well drilling, and oil production [1–4]. To this group of polymers belong methyl cellulose (MC), hydroxypropyl cellulose (HPC), hydroxypropyl methyl cellulose (HPMC), and some other cellulose ethers. The unique properties of these polymers invite a detailed study of their molecular characteristics.

In [5], gelation conditions of solutions were studied and it was shown that introduction of propyl groups into the MC macromolecule depresses the points of gelation (T_{gel}) and phase separation (T_{tur}) of solutions. Kalinina *et al.* [6] quantitatively described how the supramolecular associative structure of moderately concentrated aqueous solutions of MC and of propyl methyl cellulose (PMC) varies with the number of propyl groups introduced.

In this study we examined the influence of the number of propyl groups on the dynamics of PMC solutions in longitudinal and convergent flows. It should be noted that just flows of this kind are formed in fabrication of polymeric films or fibers, when the solution is forced through spinnerets of various shapes or in those cases when polymer solutions are used to enhance the productivity of oil-bearing strata.

EXPERIMENTAL

Semidilute aqueous MC and PMC solutions (degree of substitution by propyl groups, DS_{pg} = 0.1, 0.25, 0.3), with a polymer concentration C_p = 0.3 g dl^{-1}, were studied.

A mixed cellulose ether was synthesized from a commercial water-soluble MC of MTs-100 brand, with a degree of polymerization (DP) of 830 and degree of substitution (DS) of 1.62 (by methoxy groups). The synthesis of water-soluble PMC was described in [5]. As MC is a cellulose ether, the propylation occurs at free hydroxy groups without elimination of methoxy groups. Therefore, the DS by methoxy groups is constant and equal to 1.62 (DS of the starting MC) for all of the PMC samples synthesized. Both the degree of substitution by propyl groups (DS_{pg}) and the total degree of substitution (DS_{tot}) change during synthesis. The values of DS_{tot} were calculated using the expression $DS_{tot} = 1.62 + DS_{pg}$. The values of DS_{pg} were found by elemental analysis.

The choice of PMC samples is determined by the fact that the solubility of PMC in water becomes zero at $DS_{pg} > 0.30$. At the same time, it is known that trisubstituted MC remains soluble in water [4, 7]. Consequently, introduction of propyl substituents in an amount exceeding 0.30 per monomer unit substantially shifts the hydrophilic–hydrophobic balance of macromolecules toward their hydrophobization, which leads to the loss of PMC solubility in water at $DS_{tot} > 1.92$.

The intrinsic viscosity [η] of the solutions was determined using an Ubbelohde viscometer with a suspended level. The measurements were performed at T = 25°C. The data obtained are listed in the table. It can be seen that [η] grows with an increase in the number of propyl groups in the chain, DS_{pg}.

1070-4272/05/7811-1888 © 2005 Pleiades Publishing, Inc.

Parameters and results of an experimental study of MC and PMC solutions

Object of study	DS_{pg}	DS_{tot}	$[\eta]$, dl g^{-1}	$[\eta]c$	g_{cr}, s^{-1}	$\tau \times 10^{-4}$, s
MC	0	1.62	3.8	1.14	3200	1.6
PMC	0.1	1.72	3.95	1.19	4100	1.2
PMC	0.25	1.87	4.25	1.28	5200	0.9
PMC	0.30	1.92	4.4	1.32	8400	0.6

The absorption of light by MC and PMC solutions in the UV and visible ranges was studied with a Specord M-40 spectrophotometer. The dependence of the optical density D on the wavelength λ was used to evaluate the absorption of light by MC and PMC solutions at a varied number of propyl groups in the chain (Fig. 1). It can be seen that the optical densities D are the lowest for the MC solution, and raising the number of propyl groups in the chain leads to an increase in the optical density and, accordingly, to a stronger absorption of light by PMC solutions.

The birefringence method was used to study the dynamics of aqueous MC and PMC solutions with a varied number of propyl groups in a longitudinal flow. The study was carried out on a setup in which the hydrodynamic field is generated in the gap between coaxial capillaries (Frank–Keller method) [8]. When the solution is drawn in the capillaries, an optically anisotropic region in the form of a "filament" appears along their axis at a certain critical velocity gradient g_{cr}. The velocity gradient was found from the flow rate of the fluid, Q, through a capillary:

$$g = Q/\pi r^2 (l/2), \quad (1)$$

where r is the capillary radius, and l is width of the gap between the edge surfaces of the capillaries.

The critical velocity gradient g_{cr}, corresponding to the onset of unfolding of polymer chains and to transition of the solutions to the anisotropic state, was recorded. According to theory of dynamics of macromolecules in a strong longitudinal field, the value of g_{cr} is related to the time τ of orientation-deformation relaxation of the chain as a whole by

$$g_{cr}\tau = 0.5. \quad (2)$$

The effect of the longitudinal flow on the MC and PMC solutions is shown in Fig. 2 in the form of a dependence of g_{cr} on the number of propyl groups in the chain, DS_{pg}. It can be seen that an increase in the number of propyl groups shifts the region in which PMC solutions pass into the anisotropic stage toward larger values of g_{cr}. This result is accounted for by the fact that substitution of a part of hydroxy groups of methyl cellulose with propyl groups makes higher the equilibrium rigidity of macromolecules [9].

To evaluate the resistance of the solutions to longitudinal deformation, the effective viscosity was determined in a convergent flow of the solutions through a short capillary, whose diameter is two times its length (d/l = 2). To stabilize the convergent flow, a cylindrical obstacle was mounted in the entrance zone of the capillary. In the case of such a flow, a unit volume of the solution at the axis of the capillary axis, between its inlet and the obstacle plane, experiences

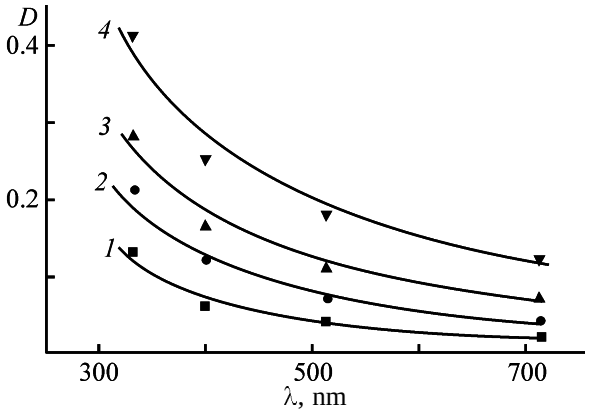


Fig. 1. Optical density D vs. wavelength λ of incident light for MC and PMC solutions. DS_{pg}: (*1*) 0, (*2*) 0.1, (*3*) 0.25, and (*4*) 0.30; the same for Fig. 2. Polymer concentration in solution C = 0.3 g dl^{-1}; the same for Figs. 2, 3.

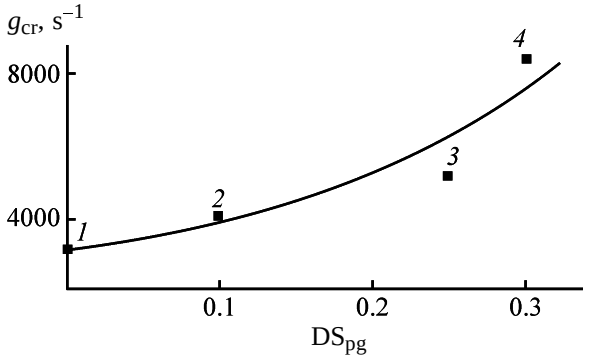


Fig. 2. g_{cr} vs. DS_{pg} for solutions in a longitudinal flow.

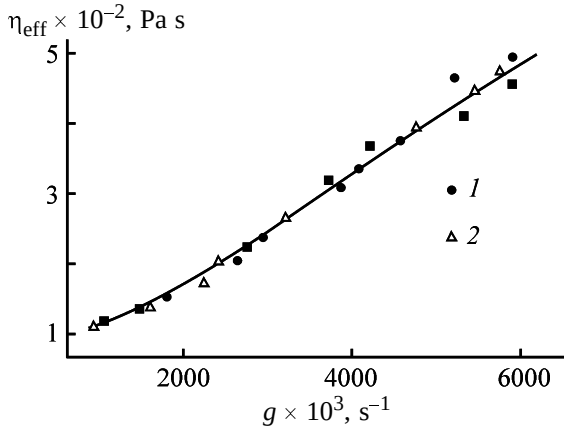


Fig. 3. Effective viscosity η_{eff} of the solutions in a convergent flow vs. the rate gradient *g*. (*1*) MC and (*2*, *3*) PMC; DS_{pg}: (*2*) 0.1 and (*3*) 0.30.

both longitudinal and shear deformations [10]. The effective viscosity η_{eff} in a convergent flow was found using calibration dependences of $\Delta P t$ against η and Re, determined in a flow of water–glycerol solutions through the short capillary. Here, ΔP is the pressure head that causes the flow, and *t* is the time in which a prescribed volume of the solutions flows through.

The gradient dependences of the effective viscosity of MC and PMC solutions in a convergent flow are shown in Fig. 3. It can be seen that, as the velocity gradient *g* becomes higher, η_{eff} grows for all the solutions. The increase in the viscosity is due, in the given case, to unfolding of chains and strengthening of interchain contacts with increasing *g*. The reverse run of the η_{eff} vs. *g* dependence completely repeats the forward run. The viscosities of the solutions, measured before and after the experiment, also coincide. This indicates that there is no degradation of macromolecules and the structure of the solutions under study is stable against the action of both converging and longitudinal flows. It should be noted that variation of the number of propyl groups in the chain does not cause any change in η_{eff} and the gradient dependences of the effective viscosity are approximately the same for all the solutions (Fig. 3). This is due to the fact that the converging flow exerts a weaker influence on polymer chains, compared to the longitudinal flow in coaxial capillaries, because, in the former case, a shear deformation occurs in addition to the longitudinal flow. Extension of a chain periodically alternates with compression, and the deforming action of the flow is weakened. In addition, the results obtained indicate that, in a longitudinal flow, the birefringence method is more sensitive to structural changes in the solution, compared to the rheology of a convergent flow in short capillaries.

CONCLUSIONS

(1) A study of the dynamics of aqueous MC and PMC solutions demonstrated that an increase in the number of propyl groups in the chain shifts the region in which macromolecules pass into the unfolded state toward higher values of the velocity gradient.

(2) A high-intensity longitudinal flow in the space between coaxial capillaries is more sensitive to structural and conformational changes in the polymer chain, compared to a converging flow through a short capillary.

(3) The structure of the solutions studied is stable against the action of both converging and high-intensity longitudinal flows.

REFERENCES

1. Werbowyi, R.S. and Gray, D.G., *Macromolecules*, 1980, vol. 13, no. 1, pp. 69–74.
2. Hague, A. and Moris, E., *Carbohydr. Polym.*, 1993, vol. 22, pp. 161–165.
3. Rogovin, Z.A., *Khimiya tsellyulozy* (Chemistry of Cellulose), Moscow: Khimiya, 1972.
4. Petropavlovskii, G.A., *Gidrofil'nye chastichno-zameshchennye efiry tsellyulozy i ikh modifikatsiya putem khimicheskogo sshivaniya* (Hydrophilic Partly Substituted Cellulose Ethers and Esters and Their Modification by Cross-Linking). Leningrad: Nauka, 1980.
5. Bochek, A.M., Nud'ga, L.A., Petrova, V.A., *et al.*, *Zh. Prikl. Khim.*, 2000, vol. 73, no. 2, pp. 304–308.
6. Kalinina, N.A., Bochek, A.M., Silinskaya, I.G., *et al.*, *Zh. Prikl. Khim.*, 2001, vol. 74, no. 9, pp. 1522–1525.
7. Petropavalovskii, G.A., Krunchak, M.M., and Vasil'eva, G.G., *Cellulose Chem. Technol.*, 1972, vol. 6, no. 2, pp. 135–144.
8. Brestkin, Yu.V., Zoolshoev, Z.F., Agranova, S.A., *et al.*, *Vysokomol. Soedin., Ser. A*, 1995, vol. 37, no. 8, pp. 1319–1324.
9. Tsvetkov, V.N., *Zhestkotsepnye polimernye molekuly* (Rigid-Chain Polymer Molecules), Leningrad: Nauka, 1986.
10. Brestkin, Yu.V., Frenkel', S.Ya., Zoolshoev, Z.F., *et al.*, *Vysokomol. Soedin.* 1994, vol. 36, no. 8, pp. 1281–1286.

Russian Journal of Applied Chemistry, Vol. 78, No. 11, 2005, pp. 1891–1892. Translated from Zhurnal Prikladnoi Khimii, Vol. 78, No. 11, 2005, pp. 1924–1925.
Original Russian Text Copyright © 2005 by A. Sokol'skii, Barulin, Kruchinin, S. Sokol'skii.

BRIEF COMMUNICATIONS

Thermal Treatment of AK-215 Acryl Dispersion in Manufacture of Heat-Insulating Coatings

A. I. Sokol'skii, E. P. Barulin, M. I. Kruchinin, and S. A. Sokol'skii

Ivanovo State University of Chemical Engineering, Ivanovo, Russia

Received March 28, 2005

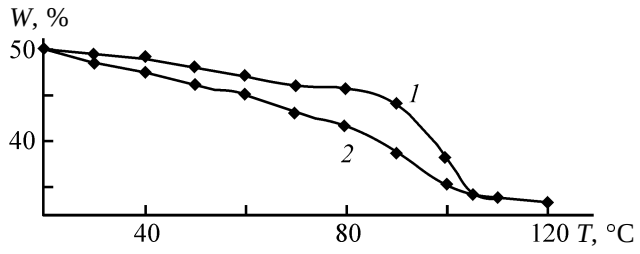
Abstract—Experimental and theoretical data on thermal treatment of latex in a conductive-infrared drier for manufacture of heat-and-noise insulation for automobiles are presented.

AK-215 acryl dispersion is an aqueous solution of a polymer of the acryl series. The mass transfer in polymeric systems is determined by the intensity of molecular motion, which can be characterized by the mass conductivity coefficient. In colloid capillary-porous materials, a substance being distributed is bound by absorption, adsorption, and capillary forces. The sorption hysteresis covers the whole range of relative humidities of the medium. A latex contains both an osmotic moisture within grains and a capillary-bound moisture, which fills spaces between the grains [1]. In the course of drying, the volume of the latex film changes, with the decrease in the volume of the latex film at $C > C_r$ equal to the volume of evaporated moisture. This can be explained as follows. When the capillary moisture is removed from a latex film in drying, the high elasticity of the skeleton of the body leads to its contraction, to the point of complete coalescence of grains and elimination of the porosity, i.e., the process of drying of this material is accompanied by continuous modification of its porous structure. At a high content of moisture, it is transported by the capillary flow. As the film reaches a certain moisture content in the course of drying, the intergrain free space vanishes and removal of the swelling moisture begins in the already nonporous material. In this case, the process of drying should be performed in two steps; in the first step, heat should by delivered to the film in the conductive way, and in the second, the film should by exposed to IR light with a wavelength corresponding to the maximum absorption of the glue formulation.

EXPERIMENTAL

To determine the influence exerted by the temperature of the heat-transfer surface on the rate of moisture removal from the glue formulation, a latex layer was deposited onto a polyethylene terephthalate film in an amount of 250 g m^{-2}. The sample was weighed on an analytical balance and placed on the heat-transfer surface. The heating time was 15 and 50 s. After that the sample was weighed and the moisture content of the glue formulation was calculated. The figure shows how the humidity of a film depends on the temperature of the heat-transfer surface. Analysis of the curves obtained shows that the removal of the capillary moisture continues until the latex moisture content reaches 33.8% and the optimal temperature of the heat-transfer surface is 105°C. At higher temperatures, the curves merge and moisture removal becomes insignificant, i.e., grains coalesce and the porosity disappears. At a temperature of the heat-transfer surface equal to 120°C, the glue formulation boils up. Consequently, some other type of heat delivery is necessary for further moisture removal.

An analytical calculation of the time necessary for removal of the capillary and adsorption moisture, with the use of the dependence of the mass conductivity coefficient on the moisture content of the latex [2], made it possible to determine more precisely the time of thermal treatment in the conductive- and infrared-heating zones of the installation.



Effect of the temperature of the heat-transfer surface on the final moisture content of a latex film. τ (s): (*1*) 15 and (*2*) 50.

1070-4272/05/7811-1891 © 2005 Pleiades Publishing, Inc.

The mathematical formulation of the problem of the nonstationary mass conductivity of bodies of unlimited dimensions includes a differential equation, as well as initial and boundary conditions:

$$\partial C/\partial\tau = k\partial^2 C(r,\tau)/\partial r^2, \quad \tau > 0, \quad 0 < r < R, \qquad (1)$$

$$C(r,0) = C_0, \qquad (2)$$

$$\partial C(0,\tau)/\partial r = 0, \qquad (3)$$

$$\beta[C_e - C(R,\tau)] = -k[\partial C(R,\tau)/\partial r]. \qquad (4)$$

In these equations, R is the film thickness (m); r, running coordinate; C, concentration of the component being distributed (kg kg^{-1}); τ, time (s); and k, mass conductivity coefficient (m^2 s^{-1}).

The analytical solution to this system of equations has the form

$$\frac{C(r,\tau) - C_e}{C_{in} - C_e} = 2\sum_{m=1}^{\infty} (\mu_m)^{-1}(-1)^{m+1}\cos(\mu_m \bar{r})\exp(-\mu_m^2 \mathrm{Fo}_m), \qquad (5)$$

where $\mu_m = (2m - 1)\pi/2$ are roots of the characteristic equation $\tan\mu_m = \mu_m/(1 - \mathrm{Bi}_m)$; Bi, Biot number; $\mathrm{Fo}_m = k\tau/R^2$, Fourier mass-exchange criterion; and $m = 1, 2, 3, \ldots$, number of terms in the series.

The results of the calculation show that the time necessary for removal of the capillary moisture in the case of a conductive heat supply virtually coincides with experimental data and is equal to 14.25 s. The discrepancy between the experimental and calculated data is within ±5%, i.e., the convergence of the results is fairly good. The calculated residence time in the infrared-heating zone is 91 s.

The main geometric parameters of the drying installation were determined using balance relations with account of the experimental and calculated data. In this way, the lengths of the heat supply zones were found to be 2 m in the case of a conductive heat supply and 10 m for the infrared-heating zone. Also, the necessary power characteristics of electric heaters and their temperatures were calculated. With the calculated values taken, the amount of heat required to remove the capillary moisture is 33 kW. In this case, the calculated temperature of the outer surface of the latex film is 90°C, and that of the heat-transfer surface, 105°C, at an infrared radiator temperature of 800°C.

The amount of heat needed to remove the adsorption moisture in the radiator zone is 29 kW. The temperature of infrared radiators is 400°C, and the calculated distance to the film surface, 113 mm. The experimental and theoretical data obtained were used in designing a conductive-infrared drier for latex drying in manufacture of heat-and-noise insulation for the interior of automobiles at Standartplast Ltd., Ivanovo.

CONCLUSIONS

(1) It was experimentally determined that 15 s is necessary for removal of the capillary moisture from latex at a temperature of the heat-transfer surface equal to 105°C.

(2) The residence time of a latex film in the zone of infrared drying is 91 s, and the temperature of radiator surfaces, 400°C.

(3) The main geometric parameters of the drying chamber were determined.

REFERENCES

1. Neiman, R.E., *Koagulyatsiya sinteticheskikh lateksov* (Coagulation of Synthetic Latexes), Voronezh: Voronezh. Gos. Univ., 1967.
2. Rudobashta, S.P., *Massoperenos v sistemakh s tverdoi fazoi* (Mass Transfer in Systems with a Solid Phase), Moscow: Khimiya, 1980.

Russian Journal of Applied Chemistry, Vol. 78, No. 11, 2005, pp. 1893–1897. Translated from Zhurnal Prikladnoi Khimii, Vol. 78, No. 11, 2005, pp. 1926–1930.
Original Russian Text Copyright © 2005 by Morachevskii.

HISTORY OF CHEMISTRY AND CHEMICAL TECHNOLOGY

Academician Vladimir Aleksandrovich Kistyakovskii (to 140th Anniversary of His Birthday)

Vladimir Aleksandrovich Kistyakovskii is among the prominent Russian natural scientists of the late XIX and early XX centuries. He made a major contribution to the understanding of the nature of electrolyte solutions and to the theory of corrosion and metal protection; he was a versatile physical chemist and electrochemist. In 1904–1905, he organized at St. Petersburg Polytechnic Institute the first Russia's laboratory of physical chemistry and theoretical electrochemistry, which was excellently equipped for that time.

V.A. Kistyakovskii was born on September 30 (October 12), 1865, into the family of a known lawyer, professor of criminal law at Kiev University, Aleksandr Fedorovich Kistyakovskii (1833–1885). A.F. Kistyakovskii descended from a clergyman from Chernigov province. He received his secondary education at Chernigov theological seminary and graduated from the department of law of Kiev University in 1857. In 1970, he became doctor of criminal law and ordinary professor. As more than once evidenced by his contemporaries, he was among outstanding Russia's criminologists.

In 1883, V.A. Kistyakovskii finished Second Kiev Gymnasium and entered the natural department of the physicomathematical faculty of Kiev University. In 1884, the university was temporarily closed because of students' disturbances and the students had to pass again the entrance procedure. In this situation, V.A. Kistyakovskii decided to enter a similar department of St. Petersburg University, where quite a number of known scientists were in the teaching staff at that time [1, 2]. When at senior courses, V.A. Kistyakovskii worked under supervision of Professor M.D. L'vov (1848–1899), an organic chemist and a disciple of A.M. Butlerov (1828–1886). An experimental study of the action of arsenic acid on some organic compounds, reported already in 1889 at a meeting of the Russian Physicochemical Society, was the only V.A. Kistyakovskii's work in the field of organic chemistry. Further, his scientific interests shifted to physical chemistry under the influence of works by West-European scientists J. van't Hoff (1852–1911), M. Planck (1858–1947), and S. Arrhenius (1859–1927). The young V.A. Kistyakovskii accepted with a considerable interest new approaches to the nature of electrolyte solutions and presented as a graduation thesis a review paper "Arrhenius–Planck Hypothesis." This was one of the first papers in Russia in which concepts of dissociation processes in solutions were presented [3]. In the final part of the paper, V.A. Kistyakovskii discussed the possibility of making closer different views concerning the nature of solutions, using the concept of hydration of ions.



At the end of January in 1889, V.A. Kistyakovskii successfully graduated from the natural department of the physicomathematical faculty of St. Petersburg University with a degree of a candidate. After that, in 1889–1890, he continued, on his own initiative, his education at the laboratory of Professor W. Ostwald (1853–1932) in Leipzig (Germany), which, in those years, was a center of newly born scientific disciplines, physical chemistry and electrochemistry. Together with W. Ostwald, W. Nernst (1864–1941) and S. Arrhenius worked at the laboratory during the same period of time. All the three scientists were Nobel Prize winners at different times: in 1909, 1920, and 1903, respectively. In publication of the first

1070-4272/05/7811-1893 © 2005 Pleiades Publishing, Inc.

world's journal specialized in physical chemistry and in studies of solutions, Ostwald had a close associate, van't Hoff. Van't Hoff was a professor of chemistry, mineralogy, and geology at Amsterdam University; later, a professor of Berlin University and one of the first scientists who received the 1901 Nobel Prize in chemistry for the discovery of laws of chemical dynamics and osmotic pressure in solutions [4, 5].

The work at Ostwald's laboratory and personal contacts with prominent physical chemists and electrochemists strongly affected all the subsequent V.A. Kistyakovskii's scientific activities. After his work in Leipzig, the young scientists attended a course of lectures on physics in Paris University. In 1890, V.A. Kistyakovskii summarized the results obtained at Ostwald's laboratory in an important publication on the nature of aqueous solutions of double salts, in which he also considered complicated cases of electrolytic dissociation and introduced the concept of complex compounds into the Russian literature. In November 1890, at the age of 25, V.A. Kistyakovskii returned to Russia.

The last decade of the XIX century was a very difficult time for the young scientist. His attempts to obtain a grant to prepare for professorship at St. Petersburg University failed, and there were no vacant positions at higher-school institutions of the city. V.A. Kistyakovskii had to earn his living in various ways, simultaneously performing experiments as a supernumerary researcher at the chemical laboratory of the university. In 1894–1896, he published in two parts the paper "On Chemical Transformations in a Homogeneous Medium," in which he summarized the results of his experimental studies in the field of kinetics of esterification in aqueous-alcoholic solutions. After having passed his master's examination and delivering test lectures, V.A. Kistyakovskii was allowed to teach at St. Petersburg University as a privatdocent beginning on October 15, 1896. In the same year, he submitted to the Council of the physicomathematical faculty of St. Petersburg University his master's dissertation in chemistry. However, the defense of the dissertation did not take place because rather authoritative chemists, D.P. Konovalov (1856–1929), N.A. Menshutkin (1842–1907), and A.E. Favorskii (1860–1945), and a mathematician K.A. Posse (1847–1928) gave negative referees' comments to the work [6]. From January 1, 1897, till September 1, 1901, V.A. Kistyakovskii taught physics at Peter the Great women's gymnasium in St. Petersburg. Simultaneously he delivered facultative courses of lectures on physical chemistry and photochemistry as a privatdocent of the university. A considerable attention of the scientific community was attracted by V.A. Kistyakovskii's report "Analysis of Objections to the Theory of Electrolytic Dissociation" at the XI Congress of Natural Scientists in 1901 [7]. The scientist emphasized that "it will become possible in the future to find a direct relationship between the chemical nature and electrolytic dissociation."

On August 1, 1902, later than others, after a personal address to Menshutkin, V.A. Kistyakovskii was invited to occupy the position of a senior laboratory assistant at the opening Emperor Peter the Great Polytechnic Institute in St. Petersburg. The institute had, from the time of its foundation, a metallurgical department and electrochemical subdepartment, in whose curricula chemical disciplines occupied the central place. The curricula were composed with the participation of such known chemists as D.I. Mendeleev (1834–1907), P.I. Walden (1863–1957, academician since 1910), and a prominent metallurgist D.K. Chernov (1839–1921). After Walden refused to occupy the position of dean of the metallurgical department, Menshutkin was appointed, and then elected the dean and formed the teaching staff.

Already at the beginning of 1903, V.A. Kistyakovskii submitted to Moscow University a new version of his master's dissertation with a brief title "Physicochemical Studies." The author summarized his previously performed and published studies, largely devoted to substantiation and development of the concept of electrolytic dissociation. The choice of Moscow University was not accidental because I.A. Kablukov (1857–1942), who actively supported ideas of Arrhenius and Ostwald, worked there. In May 1903, V.A. Kistyakovskii's master's degree was approved.

On June 15, 1903, V.A. Kistyakovskii was appointed extraordinary professor of Polytechnic Institute and organized the first Russia's laboratory and chair of physical chemistry and theoretical electrochemistry, which possessed a first-class, for that time, equipment [8, 9]. V.A. Kistyakovskii delivered lectures on physical chemistry and electrochemistry, supervised graduation works, and, in the first years, himself conducted laboratory studies with students. At that time, studies of the electrochemical behavior of metals in aqueous media started to occupy the central place among quite a number of V.A. Kistyakovskii's research areas. Being himself an excellent experimenter, V.A. Kistyakovskii had an opportunity to perform a wide variety of electrochemical studies.

Already in 1901, when determining the electrode potential of magnesium in a solution of potassium cyanide, V.A. Kistyakovskii observed the phenome-

non of passivity for the first time for this metal. The electrochemical behavior of magnesium in various media was studied by him in more detail in 1907. Originally, the passive state of magnesium had been attributed only to formation of an invisible film of the metal oxide. Later, the scientist interpreted this process as formation of magnesium oxide hydrate. This gave rise to examination of thin films from the colloidal-electrochemical standpoint. Beginning in 1909, V.A. Kistyakovskii developed his own original film theory of passivity and corrosion of metals, primarily as applied to magnesium, iron, chromium, and, in part, aluminum. The results obtained were summarized in V.A. Kistyakovskii's doctoral dissertation [10], which was published as a separate book in conformity with the regulations of that time. The concepts of passivity and corrosion of metals, developed by V.A. Kistyakovskii, were put into final shape only in the second half of the 1920s.

Having defended his dissertation for the degree of a doctor of chemistry at Moscow University in May 1910, V.A. Kistyakovskii was elected an ordinary professor at St. Petersburg Polytechnic Institute. In 1912–1916 was, in parts, published the full course of electrochemistry written by the scientist. This course also included the basic concepts of the film theory of passivity of metals. The time from 1903 to 1917 was the most fruitful during the whole period of V.A. Kistyakovskii's scientific activities.

In the summer of 1918, in view of the unfavorable living conditions in Petrograd, V.A. Kistyakovskii went to a long business trip to southern Russia. He first went to Kiev, where his mother and other relatives lived. As is known, German troops were brought into the Ukraine, including Kiev, in early April 1918, in accordance with the Brest peace treaty. On April 29, 1918, the supreme power was handed over to the Ukrainian hetman, to which position was elected P.P. Skoropadskii (1873–1945), a former general of the Russian army. High official positions (Secretary of State, Minister of the Interior) were occupied by I.A. Kistyakovskii (1876–1940), V.A. Kistyakovskii's brother, a prominent lawyer and an active member of the party of constitutional democrats, who later emigrated [11]. After the hetman's rule was established, a group of scientists raised the question of organization of the Ukrainian Academy of Sciences. A Russian academician V.I. Vernadsky (1863–1945, academician since 1912), a prominent natural scientist, geochemist, mineralogist, public figure, and one of leaders of constitutional democrats, who was in the Ukraine at that time, was invited to chair the Commission for organization of the Ukrainian Academy of Sciences. At the ceremony devoted to the beginning of work of the Commission in July 1918, Vernadsky delivered a speech "To organization of the Ukrainian Academy of Sciences." on November 27, 1918, Vernadsky was unanimously elected its president. Among other scientists who was in the Ukraine at that time, V.A. Kistyakovskii and his brother B.A. Kistyakovskii (1868–1920), a lawyer and philosopher, and an ordinary professor of state law at Kiev University, were actively involved in the preparatory work on the draft law concerning foundation of the Academy of Sciences and on its statute [8, 12]. In Vernadsky's opinion, organization of the Ukrainian Academy of Sciences should have promoted the national revival of the Ukraine, rise in its science and culture, and development of economy. It was presumed that intensive exchange of scientific achievements between the Academies of Sciences of Russia and Ukraine would strengthen their union within a common federal state.

In January 1920, V.A. Kistyakovskii's health deteriorated and he went to the North Caucasus for medical treatment. His stay there was described in detail in scientist's autobiography [13]. In view of V.A. Kistyakovskii's departure from the Ukraine, V.A. Plotnikov (1873–1947), a graduate from Moscow University (1895) and a professor of Kiev Polytechnic Institute, who was known for his studies in the field of electrochemistry of nonaqueous solutions, was elected to fill his position as head of the chair of chemistry at the Ukrainian Academy of Sciences. V.A. Kistyakovskii became a supernumerary academician of the Ukrainian Academy of Sciences [14]. Only in the autumn of 1922, he managed to return to Petrograd and resume, after a four years' interruption, his teaching and scientific activities at the Polytechnic Institute, which then continued until he moved to Moscow with Academy's institutions in 1934.

Beginning in 1925, the concepts of the film theory of passivity were fully formulated and its relationship with metal corrosion processes was emphasized in V.A. Kistyakovskii's papers [8, 15–17]. In those years, the film theory of passivity was a major contribution to the theory of electrode potentials and served as a basis for the development of the theory of corrosion of metals [18]. V.A. Kistyakovskii's many-years' comprehensive research activities were highly appreciated in our country and abroad. In 1925, he was elected a corresponding member, and in 1929, an academician of the Academy of Sciences of the USSR. He also was a full member of the Paris Physicochemical Society and Electrochemical Society in New York. It would be incorrect to believe that, beginning in 1907, the whole attention of the scientist was concen-

trated on problems of the electrochemistry of metals, development of the theory of the passive state, and analysis of the nature of passive films. It is clear from V.A. Kistyakovskii's publications and correspondence that in the following years, too, he paid a considerable attention to other issues. In response to a suggestion by Arrhenius to deliver at the Nobel Institute in Stockholm a number of lectures on his works, V.A. Kistyakovskii wrote on September 1, 1923: "... I divided my studies into three series: (1) Theory of heat and the liquid state; here, seven papers were already published in Russian in 1915–1923 and several works remain unpublished. (2) Colloid chemistry and related areas. (3) Miscellaneous. Here belong studies of passivity, periodic phenomena, and motochemical and other observations in the field of electrochemistry" [19].

Already in 1904, V.A. Kistyakovskii established the relationship between the molecular weight of a fluid, its capillary head, and boiling point under atmospheric pressure (Kistyakovskii rule). This relationship was theoretically substantiated in another his work in 1913 and confirmed by a vast body of experimental data. The Kistyakovskii rule can be used to determine the molecular weight of fluids and the degree of their association at the boiling point. In 1923, V.A. Kistyakovskii established an empirical relationship between the molar heat of vaporization of an unassociated fluid and its boiling point at atmospheric pressure (Kistyakovskii formula). The heats of vaporization, calculated by this formula, are in good agreement with experimental data. The scientist's studies in this area are considered in detail in a textbook *Prikladnaya fizicheskaya khimiya* (Applied Physical Chemistry) (part 1, Leningrad, 1926), written by him.

In 1930, V.A. Kistyakovskii organized the Leningrad Colloid-Electrochemical Laboratory of the Academy of Sciences of the USSR (LAKE). Originally, the laboratory had the minimum number of staff members and several postgraduate students. Later, the laboratory was transferred to Moscow, together with a number of other institutions of the Academy. After that the laboratory was, on V.A. Kistyakovskii's initiative, substantially expanded and transformed into the Colloid-Electrochemical Institute of the Academy of Sciences of the USSR (KEIN), where quite a number of prominent scientists worked afterwards [20]. The institute was concerned with a wide variety of problems. In 1939, Academician A.N. Frumkin (1895–1976) became director of KEIN. In 1945, V.A. Kistyakovskii's 80th birthday was celebrated [8].

The more than half a century of V.A. Kistyakovskii's vigorous scientific and pedagogical activities substantially enriched the chemical science with valuable generalizations and laws, new approaches and ideas. V.A. Kistyakovskii luckily combined qualities of a pedagogue, theoretician, experimenter, and organizer. The experimental studies personally carried out by the scientist in the field of physical chemistry and electrochemistry can be rightfully regarded as classical.

For his activities, Academician V.A. Kistyakovskii was decorated with high state awards.

Vladimir Aleksandrovich Kistyakovskii died on October 19, 1952, at the age of 87 after a long illness. The last period of his life was aggravated by the fact that, because of a serious injury, from which he suffered during evacuation to Kazan, he lost, despite prolonged medical treatment, ability to move by himself. Nevertheless, his relationships with the institute and industrial organization survived till the last years of his life [6].

According to recollections of his contemporaries, V.A. Kistyakovskii was a broadly educated scientist, was connoisseur of literature, took interest in theater, and wrote poetry. He was known not only in our country, but also among foreign scientists, and maintained friendly relationships with Arrhenius, Nernst, Bredig, and other colleagues. The scientific and pedagogical activities of V.A. Kistyakovskii constitute an entire epoch in the origination and development of physical chemistry, electrochemistry, and theory of metal corrosion.

An outstanding lawyer Aleksandr Fedorovich Kistyakovskii and his sons were typical representatives of Russian liberal intelligentsia, whose fate is inseparable from the political events in Russia in the first quarter of the XX century. B.A. Kistyakovskii's son, G.B. Kistyakovskii (1900–1982), was educated in Germany and worked in the United States since 1926, at Princeton and Harvard Universities. He was a known physical chemist, special advisor for science and technology of the President of the United States (1959–1968), and bearer of higher scientific and state awards of the United States and other countries [8].

REFERENCES

1. Kapustinskii, A.F., *Ocherki po neorganicheskoi i fizicheskoi khimii v Rossii* (Essays on Inorganic and Physical Chemistry in Russia), Moscow: Akad. Nauk SSSR, 1949.
2. Solov'ev, Yu.I., *Istoriya khimii v Rossii* (History of Chemistry in Russia), Moscow: Nauka, 1985.

3. Solov'ev, Yu.I., *Zh. Fiz. Khim.*, 1956, vol. 30, no. 8, pp. 1910–1915.
4. Morachevskii, A.G., *Zh. Prikl. Khim.*, 2001, vol. 74, no. 7, pp. 1205–1210.
5. Morachevskii, A.G., *Zh. Prikl. Khim.*, 2003, vol. 76, no. 10, pp. 1751–1755.
6. Figurovskii, N.A. and Roman'kov, Yu.I., *Vladimir Aleksandrovich Kistyakovskii*, Moscow: Nauka, 1967.
7. Kistyakovskii, V.A., *Zh. Ross. Fiz.-Khim. O–va.*, 1902, vol. 34, no. 1, chemical part, section 2, pp. 19–33.
8. *Akademik Vladimir Aleksandrovich Kistyakovskii: Sbornik materialov* (Academician Vladimir Aleksandrovich Kistyakovskii: Coll. of Works), Morachevskii, A.G. and Demidov, A.I., Compilers, St. Petersburg: Politekh. Univ., 2005.
9. *Sankt-Peterburgskii politekhnicheskii institut Imperatora Petra Velikogo: Metallurgicheskoe otdelenie* (Emperor Peter the Great Polytechnic Institute in St. Petersburg: Metallurgical Department), St. Petersburg: Tipolit. Shredera, 1914.
10. Kistyakovskii, V.A., *Elektrokhimicheskie reaktsii i elektrodnye potentsialy nekotorykh metallov* (Electrochemical Reactions and Electrode Potentials of Some Metals), St. Petersburg: Tipolit. Shredera, 1910.
11. *Nezabytye mogily: Rossiiskoe zarubezh'e: Nekrologi. 1917–1999* (Unforgotten Graves: Russians Abroad: Obituaries, 1917–1999), in 6 vols., Moscow: Ross. Gos. Biblioteka, 2001, vol. 3, I–K.
12. Sapov, V.V., *Vestn. Ross. Akad. Nauk*, 1994, vol. 64, no. 3, pp. 248–252.
13. Solov'ev, Yu.I., *Vestn. Ross. Akad. Nauk*, 1995, vol. 65, no. 12, pp. 1130–1134.
14. Turchenko, Ya.I., *Osnovnye puti razvitiya obshchei, neorganicheskoi i fizicheskoi khimii na Ukraine* (Main Ways of Development of General, Inorganic, and Physical Chemistry in the Ukraine), Kiev: Kiev. Gos. Univ., 1957.
15. Kistyakovskii, V.A. and Krotov, I.V., *Izv. Akad. Nauk SSSR, VII Ser., Otd. Fiz.-Mat. Nauk*, 1930, no. 8, pp. 715–726.
16. Kistyakovskii, V.A., *Trudy Noyabr'skoi yubileinoi sessii Akademii Nauk SSSR, 12–19 noyabrya 1932 g.* (Proc. November Jubilee Session of the Academy of Sciences of the USSR, November 12–19), Leningrad: Akad. Nauk SSSR, 1933, pp. 253–265.
17. Kistyakovskii, V.A., *Usp. Khim.*, 1933, vol. 2, no. 2, pp. 237–248.
18. Dankov, P.D., *Izv. Akad. Nauk SSSR, Otd. Khim. Nauk*, 1946, no. 2, pp. 137–142.
19. Solov'ev, Yu.I. and Figurovskii, N.A., *Svante Arrhenius, 1859–1959*, Moscow: Akad. Nauk SSSR, 1959.
20. Morachevskii, A.G., *Ocherki ob uchenykh-khimikakh Sankt-Peterburgskogo politekhnicheskogo instituta* (Essays on Chemists from St. Petersburg Polytechnic Institute), St. Petersburg: Sankt-Peterb. Gos. Politekh. Univ., 2002.

A. G. Morachevskii

Russian Journal of Applied Chemistry, Vol. 78, No. 11, 2005, pp. 1898–1899. Translated from Zhurnal Prikladnoi Khimii, Vol. 78, No. 11, 2005, pp. 1931–1932.
Original Russian Text Copyright © 2005 by Morachevskii, Beloglazov.

BOOK REVIEWS

Kobayashi, N., *Vvedenie v nanotekhnologiyu* (Introduction to Nanotechnology),

Russian translation from Japanese by Khachoyan, A.V.; Patrikeev, L.N., Ed. of translation; Moscow: BINOM, 2005, 134 pp.

A brief and well-published book in the popular form introduces the reader to advances in nanotechnology in Japan and other countries in the late XX and early XXI centuries. The authors demonstrate the exceedingly wide opportunities of nanotechnologies in such fields of technology as electronics and power engineering, as well as in biology and medicine.

The brief preface by translator and editor (pp. 7, 8) emphasizes that the book is neither a scientific monograph nor a textbook on nanotechnology. Its purpose is to give to a wide audience of readers a notion of the rapid present-day development of nanotechnologies and prospects for their application. The nanoscience develops before our eyes at the interface between quite a number of independent fields of science and technology and has a largely interdisciplinary nature. The preface also notes that the state of development of nanotechnologies in our country was described in an issue of *Rossiiskii khimicheskii zhurnal* (Russian Chemical Journal) (2002, vol. 46, no. 5) devoted to this subject. In recent years, the research in nanotechnology at the leading scientific centers of Russia has become considerably more intensive.

In the introduction of the Japanese edition of the book (pp. 9, 10), its author, N. Kobayashi, notes that the first country that understood the opportunities furnished by nanotechnology and devised a long-term strategy of development of this area was the United States, where an extensive scientific and technological program was adopted already in February 2000.

The material of the book is presented in seven small chapters. Chapter 1 (pp. 11–20) gives a general notion of what is nanotechnology. The author defines it as a set of technologies or methods based on manipulations with separate atoms or molecules on a scale of 1 to 100 nm. Passing to the nanometer scale (to objects less than 10 nm in size) leads to changes in quite a number of highly important parameters of a substance.

Chapter 2 (pp. 21–30) briefly describes the most important scientific achievements that gave rise to nanotechnology. Particularly prominent among these is the idea put forward in 1959 by R. Feynman, an American physicist and Nobel Prize winner, that substances and objects can be created by piece-by-piece "atomic" assembly. Chapter 3, "Nanotechnology World" (pp. 31–70), occupies the central place in the book. The author describes practical applications of the tunneling effect, gives notion of how microscopy develops, traces the transition from optical to electron microscopes, and further to scanning probe microscopes, and explains the principle of their operation. Special attention is given in the chapter to carbon nanotubes and prospects for their use.

Chapter 4 (pp. 71–103) prognosticates economical and social consequences of the introduction of nanotechnologies. The author, in particular, notes that the main difficulty in industrial implementation of nanotechnologies consists in that it is necessary to develop methods for processing of new materials, rather than in their synthesis. The chapter describes methods for measurements, processing, and modeling, to be used to obtain and use nanomaterials. It discusses the relationship between nanotechnologies, on the one hand, and problems of conservation and power engineering, development of science and life, and problems of agriculture, on the other. Also, the possibility of application of nanotechnologies in aerospace engineering and prospects for creation of ultralight and ultrastrong materials are considered.

The small Chapter 5 (pp. 104–115) is devoted to the development of nanotechnologies in the United States, some West-European countries, and Japan. According to the author's prognoses based on budget allocations, the main competition in the field of nanotechnologies will occur in the nearest future between the United States and Japan. In accordance with the Basic plan of development of the Japanese science, the government of the country will spend on the scientific and technological research as a whole 1% of the national income, which will constitute in five years (beginning in 2001) a sum equivalent to about 200 bil-

1070-4272/05/7811-1898 © 2005 Pleiades Publishing, Inc.

lion dollars. To the four research areas that are the most important for Japan belong medicine and public health, information technologies, ecology, and nanotechnology.

Chapter 6 (116–128) is fully devoted to the development of nanotechnologies in Japan. According to the author's prognoses, nanotechnologies will become the base of the industry and will fundamentally change the economy and social life in 10–20 years. In this context, it is necessary to devise a state strategy for development of this field of science. The development of nanotechnologies must improve the competitiveness of Japanese companies and preserve their leadership in key areas of science and technology. The priorities in financing of nanotechnological studies are considered.

Chapter 7 (pp. 129–134) discusses the problems of organization of nanotechnological industries.

The book contains a large number of informative illustrations, schemes, and tables; the presentation is very simple and easily understandable. According to the author's intention, the book will be of use for businesspersons, economists, and sociologists who wish to get an, at least, general notion of the new and rather promising area of science and technology. In the referees' opinion, the audience may be even wider. A popular presentation of the fundamentals of nanotechnology will be of use for teachers of chemistry and physics in senior classes of schools, especially those specialized in physics and mathematics, and teachers of chemical and physical disciplines at junior courses of higher-school institutions.

A. G. Morachevskii and I. N. Beloglazov

Russian Journal of Applied Chemistry, Vol. 78, No. 11, 2005, pp. 1900–1901. Translated from Zhurnal Prikladnoi Khimii, Vol. 78, No. 11, 2005, pp. 1933–1934.
Original Russian Text Copyright © 2005 by Zaikov, Artsis, Madyuskina.

INFORMATION

11th International Conference on Renewable Resources and Plant Biotechnology NAROSSA 2005

The 11th International Conference on Renewable Resources and Plant Biotechnology was held on June 6–7, 2005 at the head office of the Institute of Natural Fibers (Poznan, Poland). The Conference was organized under patronage of the Department of Agriculture of Saxony-Anhalt (Germany). The sponsors of the Conference were Pilot Pflanzeneöltechnologie Magdeburg e.V. (PPM), Dr. Wiegel, Anlagenbau GmbH (Germany), BMD (BIO Mitteldeutschland GmbH, Halle-Saale, Germany), OHMI-Consulting GmbH (Magdeburg, Germany), and "Cellubast" (Center of Excellence on Natural Lignocellulosic Fibrous Raw Materials, INF). The conference was organized by Innoplanta e.V. (Gatersleben, Germany), INF, BioPro AG (Biological Products, Magdeburg, Germany), Forschungs- und Beratungszentrum für Maschinen- und Energiesysteme e.V. (FBZ), and An-Institut an der Hochschule Merseburg (FH) (Germany).

The conference organizers were Prof. Ryszard Kozlowski (Director of INF) and Dr. Frank Pudel (OHMI, Magdeburg). The members of the Scientific Committee were experts from Belarus, Bulgaria, Canada, Estonia, France, Germany, Hungary, Latvia, Poland, Romania, Russia, the United Kingdom, and the United States (a total of 29 persons). Researchers and industry representatives from these countries and also from Czech Republic, Switzerland, and Vietnam have delivered presentations at the Conference.

The Conference Program covered four plenary lectures and 34 brief presentations, which were delivered at two sections.

At the opening ceremony, Prof. Kozlowski outlined the topicality of the Conference for theoretical and applied chemistry. The ceremony also included speeches by Mr. B. Mackoviak (The Office of the Marshal of Wielkopolskie Voivodeship, Poland), Mrs. Anne-Maria Keding (Ministry of Agriculture and Environment of Saxony-Anhalt, Germany), and Marek Beer (The Wielkopolska Voivodeship Office, Poland).

The plenary lectures covered the most topical areas of science presented at the Conference. Prof. Melvyn F. Askew (Central Science Laboratory, York, England, the United Kingdom) in his lecture considered potentialities and limitations in using bioresources in Europe. The problem of renewable resources and their food and nonfood applications in Poland was analyzed in the lecture given by Ryszard Kozlowski, Maria Mackiewicz-Talarczyk, and Przemyslaw Baraniecki (Institute of Natural Fibres, Poznan, Poland). Dr. Detlef Wilke (Inno Planta e.V., Gatersleben, Germany) told about why we have a need in plant biotechnology. Prof. G.E. Zaikov (Emanuel Institute of Biochemical Physics, Russian Academy of Science, Moscow, Russia) gave a lecture on quantitative prediction of the behavior of polymers in living bodies including human beings.

The presentations delivered at the First Section covered the topics concerning understanding of the strategic potentialities of natural genetic engineering: renewable resources; cultivation of wheat; cultivation of rye for bioethanol production; new quality of potato starch—a novel product produced from the renewable raw material using plant biotechnology; transgenic oil-producing crops as a renewable resource for production of long-chain polyunsaturated fatty acids; interaction of polymers with atmospheric pollutants, utilization of wastes from farming and textile industry; hemp production, processing, and market in the Europe; research on flax in the United States (production and standards); from hemp to textile—some ideas concerning yield, processing, and storage; properties of fibers produced from hail-damaged hemp, recent data on fiber production by biotreatment, and study of the stability of hempseed oil; low-temperature drying of plants in air-fluidized bed; microbial impact on the yield and composition of oils produced from marjoram (*Majorana hortensis*), caraway (*Carum carvi L.*), and common thyme (*Thymus vulgaris L.*); cultivation and production of mulberry-tree (*Bombyx mori L.*); the use of biotechnology in cultivation of flax in Czech Republic; current progress in cultivation of hemp in Poland; *in vitro* methods in production of flax; effect of micro- and macroelements on the yield of flax seed and performance of flax fiber; and some aspects of the effect of sodium ions on flax growing.

The presentations delivered at the Second Section covered the following topics: enzymatic processing in

1070-4272/05/7811-1900 © 2005 Pleiades Publishing, Inc.

fiber production; cotton yarn with high fiber density produced using enzymatic processing; application of hemp fibers obtained by enzymatic processing; protection of flax fabrics against UV rays using natural dyes; new (heterogeneous–heterophase) model for oxidation of carbochain polymers; and improvement of the quality of herbicides using linseed-oil, to meet the European Community standards.

In the Closing Plenary Section, Prof. Ryszard Kozlowski and Dr. Frank Pudel noted that this Conference contributed significantly to both theory and practice. Close interlinks are seen in the Conference contributions between the chemistry, physics, biochemistry, biology, agriculture, and chemical industry.

The next 12th Conference will be held at the University of Magdeburg (Germany) on June 5–7, 2006.

G. E. Zaikov, M. I. Artsis, and L. L. Madyuskina

Russian Journal of Applied Chemistry, Vol. 78, No. 12, 2005, pp. 1903–1912. Translated from Zhurnal Prikladnoi Khimii, Vol. 78, No. 12, 2005, pp. 1937–1946.
Original Russian Text Copyright © 2005 by Lokshin, Ivlev, Tareeva.

INORGANIC SYNTHESIS AND INDUSTRIAL INORGANIC CHEMISTRY

Synthesis of Lanthanide Nitrates from Phosphosemihydrate

E. P. Lokshin, K. G. Ivlev, and O. A. Tareeva

Tananaev Institute of Chemistry and Technology of Rare Elements and Mineral Resources, Kola Scientific Center, Russian Academy of Sciences, Apatity, Murmansk oblast, Russia

Received January 26, 2005; in final form, May 2005

Abstract—A technological scheme for the recovery of lanthanides from phosphosemihydrate to obtain a nitrate solution was suggested. This scheme does not violate the balance of sulfuric acid and water, adopted in manufacture of extraction phosphoric acid.

Sulfuric acid leaching-out of lanthanides (Ln) from calcium sulfate semihydrate [technical name, phosphosemihydrate (PSH)] yields solutions containing 0.4–3.25 g l^{-1} Σ Ln_2O_3 [1–3]. Lanthanides are commonly recovered from sulfuric-phosphoric acid leaching solutions by a number of methods. It was shown in [5, 6] that neutralization of leaching solutions with ammonia produces water-enriched, difficultly filterable concentrates containing up to 40 wt % lanthanides. The filtration can be improved as follows: by performing neutralization before the onset of precipitation, with the solutions then evaporated to obtain crystalline precipitates of lanthanide phosphates [7]; by lowering the neutralization rate by using a mixture of gaseous ammonia and air, taken in a 1 : (2–4) ratio [8]; and by using magnesium oxide or carbonate for neutralization [9].

Calculations show that the expenditure for evaporation of solutions may exceed the price of the lanthanide concentrate obtained. No technology has been developed for utilization of low-concentration solutions based on ammonium sulfate and phosphate, contaminated with a number of impurities. Processing of phosphate concentrates of lanthanides is a complicated task involving a gross expenditure.

Lanthanides can be precipitated from sulfuric acid leaching solutions in the form of sparingly soluble fluorides [10, 11]. Upon introduction of hydrofluoric acid into a leaching solution containing 10 wt % sulfuric acid, the fluoride concentrate contains 40–42 wt % lanthanides [10].

Lanthanide fluorides, and especially the most valuable fluorides of yttrium-group lanthanides, are well soluble in sulfuric acid solutions [12]. Therefore, precipitation is commonly carried out using a large excess of hydrofluoric acid, whose main part remains in a solution after the separation of lanthanides. Consequently, it is unlikely that the mother liquor can be used for leaching-out of lanthanides from subsequent batches of PSH. In addition, accumulation of alkaline elements in reused leaching solutions will impair the efficiency of precipitation of lanthanides because of the formation of better soluble double fluorides [13]. Similarly to that of phosphate concentrates, processing of fluoride concentrates of lanthanides is a complicated task involving a gross expenditure. Hydrofluoric acid is expensive and its use can be economically justified only if the resulting fluoride concentrate is used without further processing. However, yttrium and lanthanides of the medium group, which largely predetermine the necessity for recovery of lanthanides from the apatite concentrate, cannot be recovered into separate products in this case.

In [14], it was suggested to recover a lanthanide concentrate from sulfuric acid leaching solutions containing 10–20 wt % sulfuric acid by evaporating a solution to a sulfuric acid concentration exceeding 30 wt %. The thus obtained sulfate concentrates of lanthanides contain up to 25 wt % Ln_2O_3 [1]. Their processing into target products is less expensive and simpler than that in the case of phosphate or fluoride concentrates. However, evaporation of sulfuric acid solutions is expensive. In addition, the possibility of recycling a sulfuric acid solution after recovery of a lanthanide concentrate into leaching of subsequent PSH batches has not been analyzed.

Lanthanides can be extracted from sulfuric acid solutions for PSH leaching with solutions in a hydro-

1070-4272/05/7812-1903 © 2005 Pleiades Publishing, Inc.

carbon stock for manufacture of polyalkylnitrile-phosphoric acid (10% solution). Re-extraction can be done with an aqueous solution of ammonium carbonate to give solid lanthanide carbonates [15]. However, this process cannot be used because there is no industrial manufacture of the extracting agent suggested and its cost is high. The low concentrations of lanthanides and the resulting large volumes of solutions being processed lead to an increased loss of the extracting agent and solvents and to contamination of reused solutions and waste phosphogypsum with hydrocarbon solvents.

Lanthanides can be recovered from sulfuric acid solutions containing ≤20 wt % H_2SO_4 by ionic flotation, with dialkylphosphoric acids as a surfactant, with the subsequent nitric or hydrochloric acid processing of the resulting sublate to regenerate the surfactant and obtain a solution of lanthanide nitrates or chlorides. It has been shown that the surfactant can be introduced without its preliminary dissolution in organic solvents, which makes this method feasible [4]. The implementation of the process is hindered by the necessity for development of a nonstandard industrial equipment for ionic flotation and conversion of the surfactant and by the fact that this surfactant is not manufactured in Russia.

Thus, there still exists no efficient technology for processing of large volumes of lanthanide-containing sulfuric acid leaching solutions with a high content of ecologically hazardous impurities.

In developing methods for recovery of lanthanides from leaching solutions, it necessary to provide their complete utilization and recovery of lanthanides in the form of products convenient for further processing.

The aim of this study was to develop a technique for recovery of lanthanides from sulfuric acid solutions for PSH leaching to obtain conveniently processed lanthanide concentrates and spent sulfuric acid solutions that can be used in manufacture of mineral fertilizers.

EXPERIMENTAL

The solutions used were prepared from waste PSH produced at Ammofos Open-Joint-Stock Company (Cherepovets), which contained 0.56 wt % ΣLn_2O_3 in terms of dry product.

PSH was leached with a sulfuric acid solution for 1 h at 20°C. Then, PSH was separated from the solution and washed with water. A single portion of a sulfuric acid solutions with varied concentration was used to treat successively two batches of the starting PSH, to reach a concentration of ΣLn_2O_3 of about 3 g l^{-1}. Preliminary experiments demonstrated that the optimal leaching conditions are as follows: $c_{H_2SO_4}$ = 20–25 wt %, $V_l : S$ = 2–2.5, temperature 20°C. The concentration of ΣLn_2O_3 and CaO was analyzed by the oxalate gravimetric method, whose relative error for the lanthanide concentrations in the range being analyzed was 0.3 rel % and less [16]. The small amount of SrO, determined together with CaO, was not taken into account separately. The concentrations of individual lanthanides were determined by atomic-emission spectrometry with inductively coupled plasma on a Perkin Elmer Plasma 400 instrument. A good agreement between the results obtained by different methods was observed.

The possibility of precipitation of lanthanides from leaching solutions was analyzed. A 93.5 wt % H_2SO_4 was introduced and its concentration in solution was raised to a prescribed value. The solution was kept with occasional agitation for, as a rule, 12 h. During this time, the rare-earth concentrate crystallized. The mother liquor was separated from the precipitate, diluted to a concentration of 20 wt %, and partly used to process further batches of PSH. The experiments were carried out at $V_l : S$ = 2.5 and 2.0 (Table 1). In determining the recovery, the increase in the solution volume upon addition of concentrated H_2SO_4 was taken into account.

It follows from the data in Table 1 that repeated use of recycled mother liquors obtained upon spontaneous precipitation of the lanthanide concentrate from them provides a satisfactory leaching-out of lanthanides from PSH. A decrease in $V_l : S$ to 2.0 has virtually no effect on the average recovery of lanthanides into a leaching solution. In separate experiments, the concentration of lanthanides in solutions could be raised to $c > 4$ g l^{-1}; however, the significant decrease in recovery in the second stage of each cycle demonstrates that further accumulation of, at least, some of lanthanides in solution is impossible. Although a major part of lanthanides crystallized on raising the H_2SO_4 concentration to 30 wt %, their concentration in the mother liquor remained rather high.

An increase in the initial concentration of lanthanides in solution on lowering $V_l : S$ from 2.5 to 2.0, introducting seed crystals, making longer the crystallization time, and agitating the solutions (Table 1, run nos. 6–10) favored a rise in the completeness of precipitation and, consequently, led to a higher recovery of lanthanides into the concentrate.

However, an insufficient reproducibility of the degree of precipitation of lanthanides was observed.

Table 1. Recovery of lanthanides from PSH by sulfuric acid leaching and crystallization*

Run no.	Stage	$c_{H_2SO_4}$, wt %	Concentration in solution, g l^{-1}		Recovery of ΣLn_2O_3 from PSH, %	
			ΣLn_2O_3	CaO	in a stage	average
			$V_l : S = 2.5$			
1	Leaching solution	20	0	0		
	Stage 1.1	20	1.74	0.74	77.7	65.6
	Stage 1.2	20	2.94	0.69	52.6	
	Mother liquor 1	–	1.75	0.49	–	39.1
	Concentrate 1	–	–	–	–	26.5
2	Leaching solution	20	1.17	0.33		
	Stage 2.1	20	2.74	0.73	70.1	55.1
	Stage 2.2	20	3.64	0.82	40.1	
	Mother liquor 2	30	1.87	0.36	–	15.6
	Concentrate 2	–	–	–	–	39.5
3	Leaching solution	20	1.25	0.24		
	Stage 3.1	20	2.04	0.80	35.3	40.4
	Stage 3.2	20	3.06	0.68	45.5	
	Mother liquor 3	30	0.89	0.13	–	–8.0
	Concentrate 3	–	–	–	–	48.4
4	Leaching solution	20	0.59	0.09		
	Stage 4.1	20	2.41	0.86	81.2	60.7
	Stage 4.2	20	3.31	0.78	40.2	
	Mother liquor 4	30	1.81	0.16	–	27.2
	Concentrate 4	–	–	–	–	33.5
5	Leaching solution	20	1.21	0.11		
	Stage 5.1	20	2.56	0.82	60.3	48.9
	Stage 5.2	20	3.40	0.66	37.5	
	Mother liquor 5	30	1.38	0.55	–	3.0
	Concentrate 5	–	–	–	–	36.1
Average recovery of lanthanides into a leaching solution 54.2						
Average recovery of lanthanides into concentrate 36.8						
			$V_l : S = 2.0$			
6	Leaching solution	20	0	0		
	Stage 6.1	20	2.49	0.685	88.9	68.5
	Stage 6.2	20	3.84	0.415	48.2	
	Mother liquor 6	–	2.49	0.335	–	44.4
	Concentrate 6	–	–	–	–	24.1
7	Leaching solution	20	1.66	0.41		
	Stage 7.1	20	3.52	0.61	66.4	43.4
	Stage 7.2	20	4.09	0.63	20.3	
	Mother liquor 7	30	1.85	–	–	3.4
	Concentrate 7	–	–	–	–	40.0
8	Leaching solution	1.23	–			
	Stage 8.1	20	3.53	1.03	82.1	64.6
	Stage 8.2	20	4.85	0.395	47.1	
	Mother liquor 8	30	1.035	0.195	–	–3.5
	Concentrate 8	–	–	–	–	68.1

* Crystallization time (h): (run nos. 1, 2, 4, 6–10) 12 and (run no. 3) 84.

Table 1. (Contd.)

Run no.	Stage	$c_{H_2SO_4}$, wt %	Concentration in solution, g l^{-1}		Recovery of ΣLn_2O_3 from PSH, %	
			ΣLn_2O_3	CaO	in a stage	average
9	Leaching solution	0.69	0.13			
	Stage 9.1	20	2.43	0.74	62.1	
						47.6
	Stage 9.2	20	3.355	0.615	33.0	
	Mother liquor 9	30	0.855	0.405	–	3.0
	Concentrate 9	–	–	–	–	44.6
10	Leaching solution	0.57	0.27			
	Stage 10.1	20	2.475	1.015	68.0	
						51.6
	Stage 10.2	20	3.465	0.795	35.4	
	Mother liquor 10	30	0.975	0.435	–	7.2
	Concentrate 10	–	–	–	–	44.5
Average recovery of lanthanides into a leaching solution 55.2						
Average recovery of lanthanides into concentrate 44.3						

Table 2. Relative amounts of individual lanthanides in ΣLn_2O_3 (solution numbering coincides with that in Table 1)

Product*	Ratio of molar concentrations of lanthanide oxides in solution, Ln_2O_3/Ce_2O_3						
	Y_2O_3	La_2O_3	Ce_2O_3	Pr_2O_3	Nd_2O_3	Sm_2O_3	Eu_2O_3
Concentrate produced from apatite [17]	0.092	0.485	1	0.137	0.337	0.0448	0.0118
Solution 1.1	0.0794	0.446	1	0.086	0.246	0.0400	0.0106
Solution 1.2	0.109	0.518	1	0.162	0.304	0.0464	0.0145
Solution 2.1	0.0787	0.453	1	0.116	0.295	0.0410	0.0122
Solution 2.2	0.155	0.556	1	0.193	0.311	0.0556	0.0181
Solution 3.1	0.108	0.471	1	0.124	0.294	0.0426	0.0137
Solution 3.2	0.0864	0.450	1	0.120	0.300	0.0400	0.0116
Solution 4.1	0.0994	0.470	1	0.105	0.253	0.0434	0.0125
Solution 4.2	0.0842	0.436	1	0.099	0.297	0.0416	0.0126
Solution 5.1	0.109	0.480	1	–	0.299	0.0468	0.0135
Solution 5.2	0.218	0.564	1	0.126	0.308	0.0590	0.0266

Product*	Ratio of molar concentrations of lanthanide oxides in solution, Ln_2O_3/Ce_2O_3					
	Gd_2O_3	Tb_2O_3	Dy_2O_3	Ho_2O_3	Er_2O_3	Yb_2O_3
Concentrate produced from apatite [17]	0.0424	0.0047	0.0165	0.0035	–	
Solution 1.1	0.020	0.0015	0.0106	< 0.0018	0.0126	< 0.0017
Solution 1.2	0.0446	0.0054	0.0225	0.0021	0.0206	0.0041
Solution 2.1	0.0326	0.0042	0.0193	0.0037	0.0144	0.0024
Solution 2.2	0.0667	0.0089	0.0408	0.0077	0.033	0.0050
Solution 3.1	0.0426	0.0044	0.0236	0.0033	0.0218	0.0033
Solution 3.2	0.031	0.0040	0.0184	0.0034	0.0172	0.0023
Solution 4.1	0.0361	0.0048	0.0222	0.0041	0.0372	0.0027
Solution 4.2	0.0396	0.0040	0.0193	0.0023	0.0272	0.0034
Solution 5.1	0.0442	0.0052	0.0268	0.0030	0.0327	0.0030
Solution 5.2	0.0769	0.0102	0.0530	0.0059	0.0645	0.0058

* Solution nos. 1.2, 2.2, and 4.2 contain a solid phase.

This is probably due to existence of additional factors affecting the process of their crystallization, in addition to the supersaturation by lanthanides, which appears on raising the H_2SO_4 concentration. The most probable of these are fluctuations of the induction period in crystallization or of sodium and potassium concentrations in comparatively small PSH samples used in different experiments. It should be noted that precipitates enriched in lanthanides were formed upon prolonged storage from some solutions obtained in the second stages of leaching and containing, according to a calculation, 20 wt % H_2SO_4.

Table 2 compares the Ln_2O_3/Ce_2O_3 ratio in leaching solutions with that in the apatite concentrate. It can be seen that, in the case of a multiple use of recycled mother liquors, the relative concentrations of most of individual lanthanides that passed into solution are close to those in the apatite concentrate, with, however, a tendency toward accumulation of holmium, erbium, and ytterbium observed.

The Ln_2O_3/Ce_2O_3 ratio in solutions from which precipitates were formed (Table 2, solution nos. 1.2, 2.2, and 4.2) exceeds that in undecomposed solutions. This suggests that precipitates formed in storage are enriched in cerium. However, the fact that there is no noticeable accumulation of lanthanides of the medium group in solutions shows that they also pass in noticeable amounts into concentrates.

The change in the concentrations of ΣLn_2O_3 and CaO in solutions before and after crystallization (Table 1) was used to evaluate their ratio in the concentrates obtained (Table 3).

It can be seen from Table 3 that 71.9–78.6% of lanthanides can be precipitated from leaching solutions obtained at $V_l : S = 2.0$ is. Further increase in the H_2SO_4 concentration markedly raises the completeness of crystallization of lanthanides from leaching solutions (Table 4).

The behavior of individual lanthanides in the course of sulfuric acid precipitation was analyzed using model sulfuric acid solutions containing prescribed concentrations of individual lanthanides. The efficiency of precipitation of yttrium, cerium, and gadolinium was evaluated. The results of the experiments are listed in Table 5, whence it can be seen that raising the H_2SO_4 concentration to 40–42.7 wt % provides precipitation of cerium to an extent of 96% and more; however, an acceptable extent of precipitation was reached for yttrium and gadolinium only at a H_2SO_4 concentration of 50 wt % and more. As can be seen in Table 4, cocrystallization makes greater the extent of precipitation of more soluble lanthanides.

Table 3. Characterization of the precipitate formed in crystallization of lanthanides and calcium from 30 wt % H_2SO_4 leaching solutions

Run no.	Passed into precipitate, %		Ln_2O_3/CaO in the precipitate, g/g
	ΣLn_2O_3	CaO	
1	40.5	29.0	5.95
2	48.6	56.1	3.85
3	70.9	80.9	3.95
4	45.3	72.1	2.42
5	59.4	16.7	18.4
6	35.2	39.4	5.00
7	54.8	–	–
8	78.6	50.6	19.0
9	74.5	34.1	11.9
10	71.9	45.3	6.9

Table 4. Recovery of lanthanides from PSH by two-stage sulfuric acid leaching and crystallization at an increased concentration $c_{H_2SO_4}$ ($V_l : S = 2.0$, crystallization time 2 h)

Run no.	$c_{H_2SO_4}$, wt %	ΣLa_2O_3	CaO	Recovery of ΣLn_2O_3 into concentrate
		g l^{-1}		
1	22* 43.8	2.936 0.28	0.58 0.208	88.6
2	24 45.1	3.012 <0.05	0.608 <0.05	>98.0

* Concentration in solution: numerator, initial solution; denominator, final solution.

Table 5. Results of experiments of precipitation of lanthanides with sulfuric acid

H_2SO_4 content in solution, wt %	Concentration in solution, g l^{-1}			Recovery into precipitate, %		
	Y_2O_3	Ce_2O_3	Gd_2O_3	Y_2O_3	Ce_2O_3	Gd_2O_3
20.0*	0.130	1.780	0.050	–	–	–
40.0	0.093	0.060	0.017	28.5	96.6	66
42.7	0.084	0.038	0.014	35.4	97.9	72
50.0	0.065	0.023	0.007	50	98.7	86
61.0	0.050	0.077	0.0036	61.5	96	92.8
22.0*	0.126	1.39	0.047	–	–	–
43.8	0.086	0.045	0.016	31.7	96.8	66.0
45.0	0.076	0.032	0.009	39.7	97.7	80.9

* Starting solution.

Table 6. Composition of some lanthanide concentrates precipitated from a sulfuric acid solution*

Lanthanide concentrate	Content, wt %						
	Al_2O_3	SO_4^{2-}	P_2O_5	CaO	Fe_2O_3	SiO_2	ΣLn_2O_3
Precipitation:							
on a seed	0.14	56.2	0.19	8.00	0.03	–	35.5
without seed	0.08	54.4	0.3	–	0.37	0.47	29.1

* Concentrate not washed to remove mother liquor.

Table 7. Data on conversion of the sulfate concentrate of lanthanides

τ, min	Concentration in solution, g l^{-1}		Recovery of ΣLn_2O_3 into solution, %	τ, min	Concentration in solution, g l^{-1}		Recovery of ΣLn_2O_3 into solution, %
	ΣLn_2O_3	CaO			ΣLn_2O_3	CaO	
10	35.8	11.1	79.5	50	41.0	9.5	91.1
20	36.9	10.8	82.0	60	41.3	9.5	91.7
30	38.1	10.4	84.7	90	41.3	9.4	91.8
40	39.6	10.4	88.1	120	41.4	9.4	92.0
				180	41.4	9.4	92.1

An analysis of lanthanide concentrates demonstrated (see Table 6) that lanthanides are precipitated in the form of sulfates. The main impurity is calcium sulfate, and the content of P_2O_5 and a number of other impurities in the concentrates is low.

The conversion of sulfate concentrates of lanthanides, recovered by filtration from sulfuric acid leaching solutions, into nitrates by treatment with a solution of calcium nitrate was studied. A concentrate containing (wt %): Ln_2O_3 45 and Ca 12.8, was used in the experiments. The conversion was performed at $V_l : S = 10$. The expenditure of $Ca(NO_3)_2$ exceeded by 5% the amount stoichiometrically necessary for lanthanide nitrates to be formed by the reaction

$$Ln_2(SO_4)_3 + 3Ca(NO_3)_2 = 2Ln(NO_3)_3 + 3CaSO_4. \quad (1)$$

The excess was consumed for the reaction of the mother liquor with sulfuric acid:

$$H_2SO_4 + Ca(NO_3)_2 = CaSO_4 + 2HNO_3. \quad (2)$$

As indicated by the data in Table 7, the conversion is rather fast and complete. A part of "loss" is presumably associated with cocrystallization of lanthanides with $CaSO_4 \cdot 2H_2O$. Calculations show that the content of ΣLn_2O_3 in the $CaSO_4 \cdot 2H_2O$ precipitate is no less than 6 wt %.

To accumulate lanthanides in the nitrate solution, the $V_l : S$ ratio was lowered and the primary nitrate solution was used for conversion of subsequent portions of the sulfate concentrate of lanthanides.

Introduction of additional amounts of $Ca(NO_3)_2$ and a sulfate rare-earth concentrate into a solution containing 41.4 g l^{-1} ΣLn_2O_3 yielded, without any decrease in recovery during 1 h at $V_l : S = 4$, solutions containing 106.5 g l^{-1} ΣLn_2O_3 and 13.9 g l^{-1} CaO.

Conversion of leaner concentrates (35 wt % Ln_2O_3 and 12.8 wt % CaO), performed in the course of 1 h at $V_l : S = 4$ and a 5% excess of $Ca(NO_3)_2$ in two stages, yielded a solution containing 137.1 g l^{-1} ΣLn_2O_3 and 22.0 g l^{-1} CaO at a 83.5% recovery of lanthanides.

The increased content of CaO in the nitric acid solution of lanthanides is due to the noticeable solubility of $CaSO_4 \cdot 2H_2O$ in the nitric acid solution [18] and can be diminished by neutralization of the free nitric acid formed in solution by reaction (2).

If an unwashed PSH is used to recover lanthanides, water spent for its washing to remove extraction phosphoric acid can be delivered to washing of PSH after a sulfuric acid treatment. This will preserve the balance for water of the main production process. Therefore, leaching of PSH with model sulfuric acid solutions, into which H_3PO_4, Na_2SiF_6, and

Table 8. Leaching-out of lanthanides from PSH with sulfuric-phosphoric acid solutions with addition of silicofluorides at 20°C

Run no.	Leaching conditions		Composition of the leaching solution, g l^{-1}				Concentration in solution, g l^{-1}		Recovery of ΣLn_2O_3, %	
	$V_l:S$	τ, h	H_2SO_4	H_3PO_4	Na_2SiF_6	K_2SiF_6	ΣLn_2O_3	CaO	in a stage	average
1	2.5*	1	237	106	–	–	2.03	0.47	90.6	71.4
	2.5	1	220	212	–	–	3.20	0.47	52.2	
2	2.5	1	237	106	1.32	–	2.05	0.34	91.5	71.9
	2.5	1	220	212	2.64	–	3.22	0.36	52.2	
3	2.5	1	237	106	–	1.55	1.31	0.47	58.5	50.7
	2.5	1	220	212	–	3.10	2.27	0.40	42.9	
4	2.0	1	237	106	1.00	0.39	1.93	0.36	68.9	48.4
	2.0	1	220	212	2.00	0.78	2.71	0.47	27.9	
5	2.5	1	237	106	1.00	0.39	1.60	0.48	71.3	54.2
	2.5	1	220	212	2.00	0.78	2.43	0.36	37.1	
6	2.5	2	237	106	1.00	0.39	1.76	0.48	78.6	51.3
	2.5	2	220	212	2.00	0.78	2.30	0.48	24.1	

* Numerator, conditions and results of leaching in the first stage; denominator, those in the second stage.

K_2SiF_6 were preliminarily introduced, was studied. The amount of the additives to be introduced was evaluated on the assumption that extraction phosphoric acid remaining in PSH after filtration completely passes, together with Na_2SiF_6 and K_2SiF_6 it contains, into solution.

When the same solution was used for successive leaching of two weighed portions of PSH, the efficiency of leaching in the second stage decreased under any experimental conditions (Table 8). The basic dependences obtained in the case of single-stage leaching were preserved: presence of orthophosphoric acid in a leaching solution improves the efficiency of two-stage leaching-out of lanthanides (run no. 1), presence of Na_2SiF_6 has virtually no effect (run no. 2), and K_2SiF_6 leads to a decrease in the recovery into solution (run no. 3). In the case of a solution with a molar ratio $Na_2SiF_6:K_2SiF_6 = 3$, $V_l:S$ ratio lowered from 2.5 to 2 (run nos. 4 and 5), and leaching time increased to 2 h (run no. 6), the recovery in the second stage decreased.

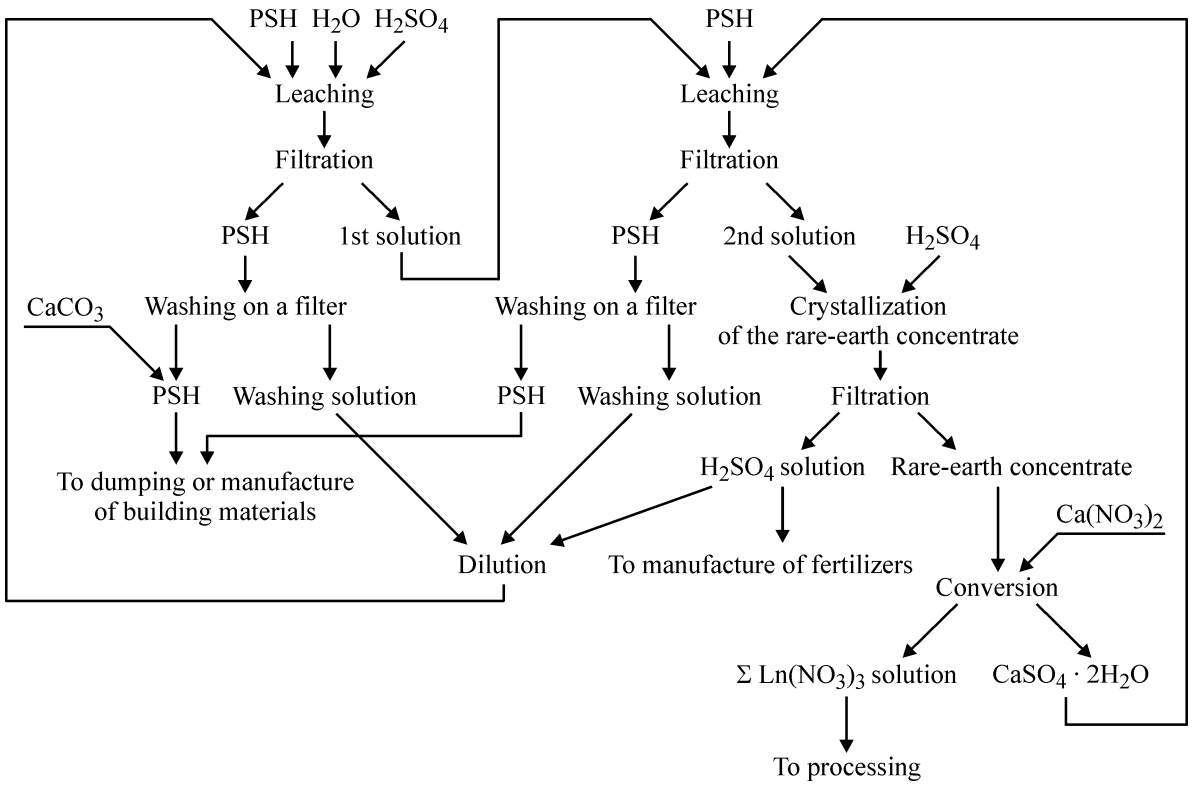
The results of the study made it possible to suggest [19] a new technological scheme for recovery of lanthanides from PSH (see Scheme). It includes leaching-out of lanthanides with 20–24% sulfuric acid at 20°C and $V_l : S = 2$ for 1 h, crystallization of the lanthanide concentrate by raising the concentration of H_2SO_4 in the leaching solution, separation of the solution from the lanthanide concentrate, and conversion of lanthanide sulfides into nitrates with calcium nitrate. With calcium chloride used for conversion, solutions of lanthanide chlorides can be obtained.

The sulfuric acid solution obtained upon recovery of lanthanides can be used in the main technology of manufacture of extraction phosphoric acid. In the semihydrate process, 0.924 tons of 93.5% H_2SO_4 is consumed per ton of the apatite concentrate [20]. In principle, it can be used to precipitate the lanthanide concentrate from PSH leaching solutions, with the resulting solutions delivered to processing of the apatite concentrate.

Table 9 lists the limiting H_2SO_4 concentrations in recycled solutions in relation to the acid concentration in the solution used to leach PSH, which can

Table 9. Maximum possible H_2SO_4 concentration in recycled solution in relation to acid concentration in the solution used to leach PSH

H_2SO_4 content in the leaching solution, wt %	H_2SO_4 content in recycling solution, wt %	
	$V_l : S = 2$	$V_l : S = 2.5$
20	46.4	42.7
22	47.4	43.8
24	48.5	45.1



Scheme.

be reached in this case. The calculations disregarded the increase in the concentration of the sulfuric acid solution by the reaction that occurs in PSH leaching:

$$CaSO_4 \cdot 0.5H_2O + 1.5H_2O = CaSO_4 \cdot 2H_2O. \quad (3)$$

As can be seen in Tables 4, 5, and 9, the maximum possible H_2SO_4 concentration in the recycled solution will provide a sufficiently complete precipitation of lanthanides. When necessary to make higher the degree of precipitation, the concentration of H_2SO_4 can be raised if not the whole amount of PSH formed on the technological line is to be processed.

An important issue determining the possibility of application of the technology suggested is to maintain the water balance in manufacture of mineral fertilizers, which is achieved when unwashed PSH is used. In this case, phosphoric acid is not lost and is returned with the recycled sulfuric acid solution into the technological process in which extraction phosphoric acid is manufactured.

The sulfate rare-earth concentrate is converted into a concentrated nitric acid solution, which can be used for extractive production of group concentrates or individual compounds by the known techniques [21] or without processing in manufacture of catalysts. The concentration of lanthanides in a minor amount of gypsum formed in conversion of lanthanide sulfates is rather high, and it is advisable to recycle it into the stage of sulfuric acid leaching.

The direct recovery of lanthanides, achieved in laboratory experiments with a 45% H_2SO_4 solution used for precipitation, will be no less than $0.55 \times 0.9 \times 0.917 \times 100 = 45.4\%$ relative to their content in PSH or 37.8% relative to that in the apatite concentrate. In the calculation, the recovery of lanthanides is taken to be 55% in leaching (the lower recovery in the modeling of leaching from an unwashed PSH is compensated by the higher initial content of $\Sigma\ Ln_2O_3$ in this PSH), 90% in precipitation into a sulfide concentrate, and 91.7% in conversion into a nitric acid solution. In further development of the technology, the recovery may increase because lanthanides are returned with the washing solution into the process for manufacture of extraction phosphoric acid and may pass into PSH, a more complete precipitation of lanthanides into the sulfate concentrate is possible, and additional recovery of a part of lanthanides from gypsum formed in conversion of lanthanide concentration is probable.

Table 10. Content of radionuclides in the apatite concentrate and products of PSH processing*

Product	Activity of radionuclides, Bq kg^{-1}			Content of nuclides, wt % (PSH) or g l^{-1} (solution)		A_{eff}, Bq kg^{-1}
	^{40}K	^{226}Ra	^{232}Th	^{238}U	^{232}Th	
PSH:						
starting	16 ± 13	20 ± 3	54 ± 7	0.00016 ± 0.00002	0.0013 ± 0.0002	92 ± 14
leached	18	12 ± 5	36 ± 6	0.00009 ± 0.00004	0.0009 ± 0.0001	60 ± 4
$Ln(NO_3)_3$ solution	<22	<6	5.4–	<0.0006	0.0016 ± 0.0008	10 ± 2

* Data obtained by N.A. Mel'nik.

A study of the behavior of radionuclides (Table 10) demonstrated that the main part of radionuclides find their way into extraction phosphoric acid. ^{238}U and, especially, ^{232}Th are leached-out to a considerably lesser extent than lanthanides. Analysis of data on the radioactivity of a solution of lanthanide nitrates suggests that the activity A_{eff} of ΣLn_2O_3 recovered from a nitric acid solution will not exceed 250 ± 50 Bq kg^{-1}, i.e., further processing of the lanthanide concentrate or its use are possible without limitations by the radiation factor.

The technology suggested does not produce waste and virtually does not use reagents alien to manufacture of extraction phosphoric acid. Calcium nitrate is converted in the process into gypsum. Typical chemical equipment can be used in all the procedures involved.

CONCLUSIONS

(1) At room temperature, raising the H_2SO_4 concentration in leaching solutions containing 20–24 wt % H_2SO_4 and about 3 g l^{-1} ΣLn_2O_3 to 30 wt % and more causes crystallization of a lanthanide concentrate. The extent of precipitation of lanthanides increases with the H_2SO_4 concentration in solution. It is shown that mother liquors remaining upon crystallization of the lanthanide concentrate can be repeatedly used for effective leaching-out of lanthanides from phosphosemihydrate.

(2) The relative concentrations of lanthanides in the leached-out sum for the most part correspond to those in the starting apatite concentrate; however, there is a tendency toward accumulation of holmium, erbium, and ytterbium. Sulfate concentrations of lanthanides are converted into nitrates by treatment with calcium nitrate solutions to give solutions containing (g l^{-1}): ΣLn_2O_3 137 and CaO 22.

(3) A technological scheme is suggested for recovery of lanthanides from phosphosemihydrate produced from the Khibiny apatite concentrate. The scheme includes sulfuric acid leaching-out of lanthanides with 20–24% sulfuric acid, precipitation of lanthanides in the form of double sulfates with alkali metals by raising the concentration of H_2SO_4 to 30 wt % and more, and conversion of the sulfide concentrate of lanthanides into a nitric acid solution by treating the concentrate with a calcium nitrate solution.

(4) No radioactive products or wastes are formed in recovery of lanthanides by the technological scheme suggested, which is an exceptional situation for the rare-earth production processes.

ACKNOWLEDGMENTS

The study was financially supported by the Program "Leading Scientific Schools" (project no. NSh-1616-2003.03.

REFERENCES

1. Jarosinski, A., Kijkowska, R., Kowalczyk, J., *et al.*, *Pr. Nauk AE Wroclawin.*, 1990, no. 526, pp. 129–133.
2. Ciurla, Z. and Grudzewski, W., *Gosp. Surow. Miner.*, 1990, vol. 6, no. 4, pp. 819–828.
3. Lebedev, V.N., Smirnova, I.P., Masloboev, V.A., and Mikhlin, E.B., *Fiziko-khimicheskie i tekhnologicheskie problemy pererabotki syr'ya Kol'skogo poluostrova* (Physicochemical and Technological Problems in Processing of Raw Materials from the Kola Peninsula), St. Petersburg: Nauka, 1993, pp. 56–60.
4. Lokshin, E.P., Vershkov, A.V., and Vershkova, Yu.A., *Metally*, 2001, no. 1, pp. 42–50.
5. Lokshin, E.P., Lebedev, V.N., Vershkov, A.V., *et al.*, Abstracts of Papers, *XVI Mendeleevskii s'ezd po obshchei i prikladnoi khimii, S.-Peterburg, 1998 g.* (XVI Mendeleev Congress on General and Applied Chem-

istry, St. Petersburg, 1998), Moscow, 1998, vol. 2, pp. 378–379.

6. USSR Inventor's Certificate, no. 1818304.
7. RF Patent 21118613.
8. RF Patent 2104938.
9. RF Patent 2158317.
10. Jarosinski, A. and Mazanek, Cr., *Fizykochem. Probl. Mineralurg.*, 1992, no. 25, pp. 91–96.
11. RF Patent 2109686.
12. Lokshin, E.P., Vershkova, Yu.A., Ivlev, K.G., and Tareeva, O.A., *Zh. Neorg. Khim.*, 2004, vol. 49, no. 4, pp. 707–710.
13. Butler, J.R. and Hall, R.A., *J. Soc. Anal. Chem.*, 1960, vol. 85, no. 2, pp. 149–150.
14. Polish Patent Appl. 272533.
15. Kosynkin, V.D., Shatalov, V.V., Selivanovskii, A.K., *et al., Khim. Tekhnol.*, 2001, no. 1, pp. 27–36.
16. Ryabchikov, D.I. and Ryabukhin, V.A., *Analiticheskaya khimiya redkozemel'nykh elementov i ittriya* (Analytical Chemistry of Rare-Earth Elements and Yttrium), Moscow: Nauka, 1966.
17. Lebedev, V.N., Belokoskov, V.I., Smirnova, I.P., *et al., Khimicheskaya tekhnologiya redkikh elementov i mineral'nogo syr'ya* (Chemical Technology of Rare Elements and Mineral Resources), Apatity, 1986, pp. 28–32.
18. Vershkova, Yu.A., Tareeva, O.A., Ivlev, K.G., and Lokshin, E.P., *Zh. Prikl. Khim.*, 2003, vol. 76, no. 1, pp. 162–163.
19. RF Patent 2225892.
20. Pozin, M.E., *Tekhnologiya mineral'nykh solei* (Technology of Mineral Salts), Leningrad: Khimiya, 1970, part 2, pp. 801–1556.
21. Mikhaylichenko, A.I., Mikhlin, E.B., and Patrikeev, Yu.B., *Redkozemel'nye metally* (Rare-Earth Metals), Moscow: Metallurgiya, 1987.

Russian Journal of Applied Chemistry, Vol. 78, No. 12, 2005, pp. 1913–1916. Translated from Zhurnal Prikladnoi Khimii, Vol. 78, No. 12, 2005, pp. 1947–1949.
Original Russian Text Copyright © 2005 by Lokshin, Tareeva, Ivlev, Levin.

INORGANIC SYNTHESIS AND INDUSTRIAL INORGANIC CHEMISTRY

A Study of the Solubility of Hydrated Orthophosphates of Yttrium, Lanthanum, Cerium, and Neodymium in Sulfuric-Phosphoric Acid Solutions at 20°C

E. P. Lokshin, O. A. Tareeva, K. G. Ivlev, and B. V. Levin

Tananaev Institute of Chemistry and Technology of Rare Elements and Mineral Resources, Kola Scientific Center, Russian Academy of Sciences, Apatity, Murmansk oblast, Russia

Fosagro Open Joint-Stock Company, Moscow, Russia

Received April 5, 2005

Abstract—The solubility of $YPO_4 \cdot 2H_2O$, $LaPO_4 \cdot 1.5H_2O$, $CePO_4 \cdot 1.5H_2O$, and $NdPO_4 \cdot H_2O$ 10–60 wt % in sulfuric-phosphoric acid solutions containing 10–60 wt % H_2SO_4 and 13.8–41.4 H_3PO_4 was studied.

The Khibiny apatite concentrate is a promising source of lanthanides. It is mostly processed by the semihydrate sulfuric acid technology, with the main part of lanthanides concentrated in the phosphosemihydrate [1, 2]. It has been shown previously that the main part of lanthanides is present in the phosphosemihydrate in the form of hydrated orthophosphates [3, 4]. The content of yttrium, lanthanum, cerium, and neodymium oxides in the sum of lanthanide oxides in the apatite concentrate is about 90 wt % [5]. Therefore, data on the solubility of their hydrated orthophosphates in mineral acids are particularly important for development of processes for acid leaching-out of lanthanides from the phosphosemihydrate. In addition, data on the solubility of $YPO_4 \cdot 2H_2O$ make it possible to indirectly evaluate the solubility of hydrated orthophosphates of lanthanides of the yttrium group.

The solubility of hydrated lanthanum, cerium, and neodymium orthophosphates in nitric acid solutions containing 1–5 M HNO_3 has been examined [6]. It was found that, for the compounds studied, it increased with the HNO_3 concentration, to reach a value of 70–100 g l^{-1} (in terms of oxides) at 20°C. The solubility varied in the order Ce ≈ Nd > La; however, the solubility of hydrated lanthanum orthophosphate at 100°C markedly exceeded that of hydrated neodymium orthophosphate.

The most promising method for recovery of lanthanides from phosphogypsum and phosphosemihydrate formed in sulfuric acid processing of the apatite concentrate into extraction phosphoric acid is their leaching-out with sulfuric acid [7, 8]. However, the solubility of hydrated lanthanide orthophosphates in sulfuric acid solutions has been insufficiently studied.

It has been found that the solubility of yttrium, lanthanum, and cerium hydrophosphates in sulfuric acid solutions containing 2–10 wt % H_2SO_4 and 2.76 g l^{-1} H_3PO_4 increases with the H_2SO_4 concentration, to reach values of 11.8, 11.1, and 10.7 g l^{-1}, respectively (in terms of Ln_2O_3). In a H_2SO_4 solution with a concentration of 2 wt %, their solubility decreased by a factor of 1.8–2.0 as the H_3PO_4 concentration was raised from 0 to 14 g l^{-1}.

The aim of this study was to determine how the solubility of $YPO_4 \cdot 2H_2O$, $LaPO_4 \cdot 1.5H_2O$, $CePO_4 \cdot 1.5H_2O$, and $NdPO_4 \cdot H_2O$ at 20°C depends on the concentration of sulfuric acid solutions with $c_{H_2SO_4}$ = 10–60 wt % and minor additions of orthophosphoric acid ($c_{H_3PO_4}$ = 13.8–41.4 g l^{-1}).

EXPERIMENTAL

Reagents of analytically pure grade were used in the study. The hydrated phosphates were synthesized by the procedures described in [9–12]. It was established, using thermogravimetric and X-ray phase analyses, that the phosphates synthesized corresponded to $YPO_4 \cdot 2H_2O$ and $LnPO_4 \cdot 1.5H_2O$ (Ln = La, Ce) and $NdPO_4 \cdot H_2O$.

1070-4272/05/7812-1913 © 2005 Pleiades Publishing, Inc.

Equilibrium concentrations of lanthanides (in terms of oxides) in sulfuric-phosphoric acid solutions of their hydrated orthophosphates at 20°C

$c_{H_2SO_4}$, wt %	Concentration, g l^{-1}, of a lanthanide oxide at indicated $c_{H_3PO_4}$ in solution, g l^{-1}											
	13.8	27.6	41.4	13.8	27.6	41.4	13.8	27.6	41.4	13.8	27.6	41.4
	Y_2O_3			La_2O_3			Ce_2O_3			Nd_2O_3		
10	37.4	35.9	35.6	14.4	12.8	11.8	12.1	9.64	7.68	4.25	3.94	3.21
15	37.7	36.9	35.8	21.8	19.1	19.0	27.0	24.2	23.4	6.79	6.56	5.77
20	25.5	24.8	24.1	12.2	11.8	11.8	42.8	40.3	36.5	10.8	10.6	10.5
25	12.9	12.6	12.4	7.85	7.95	8.29	25.9	25.3	25.3	12.6	12.2	11.2
30	8.05	7.77	7.35	5.53	5.47	5.94	18.2	18.0	17.6	11.2	9.83	9.88
35	3.18	3.55	3.80	3.78	3.75	4.43	9.06	8.77	8.58	5.74	5.9	6.16
40	1.72	1.95	2.12	3.09	3.35	3.48	6.92	7.89	8.39	3.34	3.69	3.89
45	1.15	1.16	1.18	2.72	2.81	3.3	4.23	4.35	3.85	2.9	2.9	3.12
50	0.96	0.80	0.91	2.27	2.51	2.55	3.07	3.09	3.04	2.74	2.66	2.73
55	0.53	0.55	0.60	1.79	1.85	1.82	2.36	2.40	2.13	1.54	1.53	1.59
60	0.41	0.51	0.67	1.6	1.66	1.72	1.71	1.67	1.89	1.46	1.43	1.54

Sulfuric-phosphoric acid solutions were prepared by introducing minor additions of concentrated (85 wt %) H_3PO_4 into a solution with a prescribed concentration of H_2SO_4. In doing so, changes in $c_{H_2SO_4}$ were neglected. The range of variation of $c_{H_3PO_4}$ in solutions corresponded to the possible content of H_3PO_4 in technological solutions produced in sulfuric acid leaching of a waste phosphosemihydrate.

The concentration of lanthanides in solutions was determined by the oxalate gravimetric method [13].

The solubility was studied by the isothermal method. An excess amount of hydrated lanthanides orthophosphates was introduced into starting solutions with a prescribed concentration. The mixtures were kept with agitation in hermetically sealed vessels at 20 ± 0.5°C until equilibrium was established (≥720 h). The attainment of equilibrium was judged from the invariability of the results obtained in analysis of samples of the liquid phase. The experimental data obtained are listed in the table.

As can be seen from the data in the table, the solubility of the hydrated lanthanide orthophosphates studied in sulfuric-phosphoric acid solutions strongly differs from their solubility in nitric acid solutions. An increase in $c_{H_2SO_4}$ first leads to a rise in solubility, but then it markedly decreases for all of the orthophosphates studied. The highest solubility is observed at different $c_{H_2SO_4}$ (wt %): 15 for yttrium and lanthanum orthophosphates, 20 for cerium orthophosphate, and 25 for neodymium orthophosphate. The solubility in sulfuric-phosphoric acid solutions of the same composition decreases in the order Ce > La > Nd, with the exception of solutions with $c_{H_2SO_4} = 10$ wt %, in which the solubility of hydrated lanthanum orthophosphate exceeds that of cerium orthophosphate. The solubility of yttrium orthophosphate exceeds that of cerium orthophosphate at $c_{H_2SO_4} \leq 15$ wt %; however, as $c_{H_2SO_4}$ increases further, it steeply decreases, to become lower than that of orthophosphates of other lanthanides under study at $c_{H_2SO_4} \leq 35$ wt %.

It was found by X-ray phase analysis that the equilibrium phases were $Y_2(SO_4)_3 \cdot 8H_2O$, $La_2(SO_4)_3 \cdot 9H_2O$, $Ce_2(SO_4)_3 \cdot 9H_2O$, and $Nd_2(SO_4)_3 \cdot 8H_2O$. The composition of the solid phase indicates that the hydrated orthophosphates of the lanthanides under study dissolve in sulfuric-phosphoric acid solutions, with their preliminary conversion into sulfates by the reaction

$$2LaPO_4 \cdot kH_2O + 3H_2SO_4 + (m - 2k)H_2O \rightarrow Ln_2(SO_4)_3 \cdot mH_2O + 2H_3PO_4. \quad (1)$$

At the same time, their solubility both in nitric acid and in sulfuric-phosphoric acid solutions is only qualitatively determined (solubility was a maximum as $c_{H_2SO_4}$ becomes higher) by the salting-out action of main acids. This is so because the solubilities of lanthanide nitrates in nitric acid [14] and sulfates in sulfuric acid [15] of about the same concentrations is many times higher. This indicates that presence of phosphate ions in acid solutions noticeably affects the solubility. It should be noted that, because of the occurrence of reaction (1), the $c_{H_2SO_4}$ in equilibrium solutions in fact exceeded that in the starting

solutions and could not be precisely determined because of the variable amount of the solid phase.

An increase in $c_{H_3PO_4}$ in sulfuric acid solutions with lowered $c_{H_2SO_4}$ leads to a decrease in solubility. This is observed at $c_{H_2SO_4} \le 30$ wt % for yttrium and neodymium orthophosphates, ≤ 20 wt % for lanthanum, and ≤ 35 wt % for cerium. The extent of the decrease becomes lower as $c_{H_2SO_4}$ increases. On raising $c_{H_2SO_4}$ further, to 40–45 wt %, making $c_{H_3PO_4}$ higher at a constant $c_{H_2SO_4}$, as a rule, leads to a slight increase in the solubility of hydrated orthophosphates. Finally, upon a further increase in $c_{H_2SO_4}$, introduction of orthophosphoric acid into leaching solutions has virtually no effect on the solubility, whose value becomes rather low.

The decrease in the solubility of hydrated orthophosphates in solutions with a constant comparatively low concentration of H_2SO_4, observed on raising the $c_{H_3PO_4}$, can be attributed to a noticeable decrease in the actual $c_{H_2SO_4}$ because of the occurrence of reaction (1). At higher $c_{H_2SO_4}$, the influence exerted by reaction (1) on the actual value of $c_{H_2SO_4}$ becomes less important, and an increase in $c_{H_3PO_4}$ in solutions of this kind possibly leads to formation of more soluble acid phosphates of lanthanides or of their salts with a mixed sulfate–phosphate anion. The formation of acid phosphates of lanthanides, including those studied here, was observed on raising the concentration of phosphoric acid solutions [6–9]. Raising the concentration of phosphoric acid to ≥75 wt % led to a considerable increase in the solubility of hydrated acid phosphates in this acid at 20–25°C. At low $c_{H_3PO_4}$, the bottom phase was composed of hydrated phosphates. On being kept in more concentrated phosphoric acid solutions these phosphates were converted into $YPO_4 \cdot H_3PO_4 \cdot 2H_2O$ at $c_{H_3PO_4}$ = 44.7–70.2 wt %, $Y(H_2PO_4)_3 \cdot 2.5H_2O$ at $c_{H_3PO_4}$ = 73.1–89 wt %, $3LaPO_4 \cdot H_3PO_4 \cdot H_2O$ at $c_{H_3PO_4}$ = 6.73–77.8 wt %, and $CePO_4 \cdot xH_3PO_4 \cdot yH_2O$ at $c_{H_3PO_4}$ = 1.42–84.8 wt %. Only for hydrated neodymium phosphate in phosphoric acid solutions, no acid phosphate was formed at $c_{H_3PO_4}$ = 8.91–80.50 wt %. Possibly, the less pronounced tendency toward formation of acid salts by hydrated neodymium phosphate predetermines its lowest solubility in sulfuric-phosphoric acid solutions.

To conclude, it should be noted that the hydrated lanthanide orthophosphates studied determine the composition of lanthanides in the apatite concentrate and in phosphogypsum obtained in its processing. Their solubility is sufficiently high and does not limit the accumulation of lanthanides in sulfuric-phosphoric acid solutions for leaching of phosphogypsum at the sulfuric acid concentrations used in this study.

CONCLUSIONS

(1) The dependence of the solubility of $YPO_4 \cdot 2H_2O$, $LaPO_4 \cdot 1.5H_2O$, $CePO_4 \cdot 1.5H_2O$, and $NdPO_4 \cdot H_2O$ at 20°C on the concentration of the acids in sulfuric–phosphoric acid solutions containing 10–60 wt % H_2SO_4 and 13.8–41.4 g l^{-1} H_3PO_4 was determined.

(2) It was established that, for the phosphates studied, the solid phase is composed of hydrated sulfates of the corresponding lanthanide.

(3) It was shown that, as the concentration of sulfuric acid is raised, the solubility of the hydrated lanthanide phosphates studied first increases and then falls.

(4) It was demonstrated that the solubility of the hydrated lanthanide phosphates under study in sulfuric-phosphoric acid solutions is sufficiently high and does not limit the accumulation of lanthanides in sulfuric–phosphoric acid solutions for leaching of phosphogypsum at the sulfuric acid concentrations used in the study.

ACKNOWLEDGMENTS

The study was financially supported by the Program “Leading Scientific Schools” (Project no. HSh-1616–2003.03).

REFERENCES

1. Lebedev, V.N., Masloboev, V.A., Popova, L.A., and Serkova, R.P., *Problemy effektivnogo ispol’zovaniya mineral’nogo syr’ya Kol’skogo poluostrova* (Problems of Efficient Use of Mineral Resources of the Kola Peninsula), Apatity: Kol’sk. Nauch. Tsentr Ross. Akad. Nauk, 1993, pp. 43–49.
2. Kazak, V.G., Angelov, A.I., and Zaitsev, P.M., *Khim. Prom–st.*, 1995, no. 9, pp. 11–19.
3. Lokshin, E.P., Vershkov, A.V., Vershkova, Yu.A., *et al.*, Abstracts of Papers, *Nauchnaya konferetsiya “Khimiya i khimicheskaya tekhnologiya v osvoenii prirodnykh resursov Kol’skogo poluostrova”* (Sci. Conf “Chemistry and Chemical Technology in Use of Natural Resources of the Kola Peninsula), Apatity: Kol’sk. Nauch. Tsentr Ross. Akad. Nauk, 1998, pp. 31–32.
4. Lokshin, E.P., Lebedev, V.N., Masloboev, V.A., *et al.*, *Mineral’n. Syr’e*, 2000, no. 7, pp. 122–126.
5. Mineev, D.A., *Lantanoidy v rudakh* (Lanthanides in Ores), Moscow: Nauka, 1974.
6. Kuzina, T.P., Slivko, T.A., Zimina, G.V., and

Komissarova, L.N., *Izv. Vyssh. Uchebn. Zaved. RF, Tsvet. Metall.*, 1994, nos. 1–2, pp. 68–70.

7. Lokshin, E.P., Vershkov, A.V., and Vershkova, Yu.A., *Metally*, 2001, no. 1, pp. 42–50.
8. Malikov, V.A. and Krylova, O.K., *Tset. Met.*, 2003, no. 4, pp. 63–64.
9. Tananaev, I.V., Davitashvili, E.G., Dzhabishvili, N.A., and Landiya, M.V., *Izv. Akad. Nauk SSSR, Neorg. Mater.*, 1973, vol. 9, no. 12, pp. 2174–2177.
10. Tananaev, I.V. and Vasil'eva, V.P., *Zh. Neorg. Khim.*, 1964, vol. 9, no. 9, pp. 213–214.
11. Ul'yanov, A.I. and Kazakova, T.I., *Izv. Akad. Nauk SSSR, Ser. Khim.*, 1963, no. 7, pp. 1157–1164.
12. Tananaev, I.V. and Dzhabishvili, N.A., *Izv. Akad. Nauk SSSR, Neorg. Mater.*, 1969, vol. 5, no. 8, pp. 1402–1405.
13. Laitinen, G.A. and Harris, E., *Himicheskiy analiz* (Chemical Analysis) Russian translation, Moscow: Khimiya, 1979.
14. Protsenko P.I., Razumovskaya, O.N., and Brykova, N.A., *Spravochnik po rastvorimosti nitritnykh i nitratnykh solevykh system* (Reference Book of Solubilities of Nitrite and Nitrate Salt Systems), Leningrad: Khimiya, 1971.
15. Wirth, F., *Z. Anorg. Chem.*, 1912, vol. 76, pp. 174–180.

Russian Journal of Applied Chemistry, Vol. 78, No. 12, 2005, pp. 1917–1920. Translated from Zhurnal Prikladnoi Khimii, Vol. 78, No. 12, 2005, pp. 1950–1953.
Original Russian Text Copyright © 2005 by Kopilevich, Zhilyak, Voitenko.

INORGANIC SYNTHESIS AND INDUSTRIAL INORGANIC CHEMISTRY

Synthesis and Thermal Transformations of Hydrated Ammonium Copper(II) Zinc Diphosphate

V. A. Kopilevich, I. D. Zhilyak, and L. V. Voitenko

National Agrarian University, Kiev, Ukraine

Received July 26, 2005

Abstract—Synthesis of hydrated ammonium copper(II) zinc diphosphate was described. Its thermal properties were studied and schemes of thermal transformations were suggested.

Synthesis of phosphates containing cations of various *d*-metals [1–5] with ammonium coordinated to them [6–8] is of potential interest from the viewpoint of their possible catalytic or biological activity [9–11]. We have not found any published information on the synthesis and thermal behavior of ammonium copper(II) zinc diphosphate.

The aim of this study was to prepare hydrated ammonium copper(II) zinc diphosphate and to study its thermal properties.

EXPERIMENTAL

Hydrated ammonium copper(II) zinc diphosphate was prepared by its salting out from an ammonia solution with an organic solvent [8]. As starting reagents we used a mechanical mixture of copper and zinc diphosphates, which were synthesized according to the procedures [12, 13] and taken in a prescribed molar ratio, a concentrated aqueous solution of ammonia (23–25 wt %), and acetone. The mechanical mixture of copper and zinc diphosphates with a prescribed Cu : Zn mole ratio was dissolved in concentrated aqueous ammonia. The resulting solution was poured into acetone. In the process, a bottom phase, i.e., an oily liquid of intense blue color, was separated. The mother liquor was removed by decanting, and the bottom phase was kept in air at 15–25°C to complete solidification and constant weight.

For ammonium copper(II) zinc diphosphate of the composition $CuZnP_2O_7 \cdot 3.0NH_3 \cdot 2.5H_2O$ (**I**)

Found (%): CuO 20.20, ZnO 20.50, P_2O_5 35.30, NH_3 12.72, H_2O 11.28.
Calculated (%): CuO 19.94, ZnO 20.40, P_2O_5 35.58, NH_3 12.80, H_2O 11.28.

The anionic composition of the compound synthesized (in terms of P_2O_5), determined by quantitative paper chromatography [14], is as follows (%): $P_2O_7^{4-}$ 92.30 and PO_4^{3-} 7.70. The starting copper and zinc diphosphates contained 6.00 rel % P_2O_5 in the form of PO_4^{3-}.

The contents of the components were determined as follows: Zn^{2+} by trilonometry [15], with copper masked by thiosulfate; copper(II) by iodometry; P_2O_5 by gravimetry [16]; and ammonia by evaporation on a Seren'ev apparatus [16]. The contents of water and ammonia were determined from the loss of mass upon heating for 2 h at 750°C. The anionic composition of synthesis products was analyzed by quantitative paper chromatography [14].

An X-ray analysis was carried out on a DRON-UM1 diffractometer (Cu_{K_α} radiation). A graphite single crystal placed in the diffracted beam was used as a monochromator. X-ray diffraction patterns were obtained by the step scanning method at angles 2θ = 4°–80°. The scanning step was 0.05°, and the exposure time at a point, 3–9 s. The experimental diffraction peaks were approximated with Voight's pseudo-function, with the K_{α_1} component isolated. The IR spectra were recorded with a Specord 75-IR spectrophotometer. The samples for measurements were fabricated in the form of pellets with KBr, the concentration of a substance under study was 0.2–0.3 wt %.

The transformations of compound **I** upon heating to 20–815C were studied by thermal analysis on a Q-1500D derivatograph. In the dynamic mode of temperature rise, we used cylindrical platinum crucibles with lids; weighed portions of compound **I** were 0.400–0.500 g. The final decomposition prod-

1070-4272/05/7812-1917 © 2005 Pleiades Publishing, Inc.

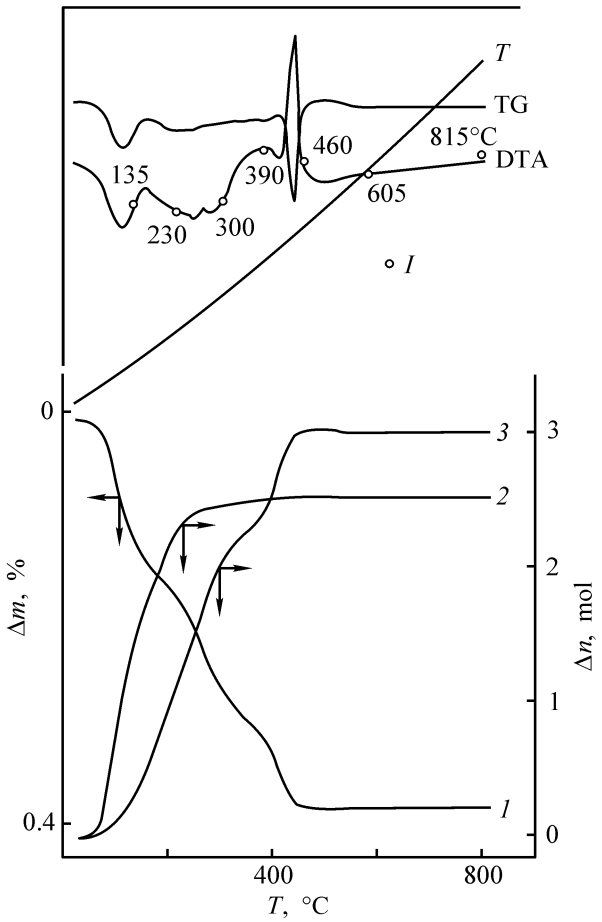


Fig. 1. DTA and TG curves of $CuZnP_2O_7 \cdot 3.0NH_3 \cdot 2.5H_2O$. ($\Delta m$) Change in mass, ($T$) temperature, and ($\Delta n$) change in amount of substance. *I* are sampling points. (*1*) Dynamic heating at a rate of 2.5 deg min^{-1}; (*2*, *3*) loss of (*2*) NH_3 and (*3*) H_2O from the substance on heating.

ucts and all the intermediates were obtained at a sample heating rate of 5 deg min^{-1}.

According to the results of the X-ray analysis, compound **I** has a rhombic crystal lattice with the following lattice constants: a = 6.860(1) Å, b = 15.720(1) Å, c = 18.761(2) Å, and V = 2018.2 Å^3.

According to the results of the thermal analysis (Fig. 1), the thermolysis of the synthesized compound proceeds in the dynamic heating mode in a wide temperature range (70–815°C) and is accompanied (according to the DTA curve) by endothermic effects with dips at 115, 255, 280, and 410°C. At 460°C, a peak associated with an exothermic effect is observed, which is superimposed on an endothermic effect, which is indicated, in particular, by an abrupt change in the weight loss by the sample in the DTG and TG curves.

The TG curve shows a weight loss by the sample at 70–460°C. An analysis of the products formed on heating of compound **I** (Fig. 1, curves *2* and *3*) shows that, in the range 70–135°C, $CuZnP_2O_7 \cdot 3.0NH_3 \cdot 2.5H_2O$ loses 1.43 mol of H_2O and 0.30 mol of NH_3. According to chromatographic data, a sample taken at 135°C, contains 14.00 rel % of P_2O_5 in the form of PO_4^{3-} and 86% in the form of $P_2O_7^{4-}$ (see table). These results indicate that, in the first stage, water is predominantly removed from compound **I** without any essential change of the diphosphate anion:

$$[(CuZn)_2(NH_3)_6(H_2O)_3(P_2O_7)_2] \cdot 2H_2O \xrightarrow{70\text{–}135^\circ C} 2.9H_2O + 0.6NH_3 + [(CuZn)_2(NH_3)_{5.4}(H_2O)_{2.1}(P_2O_7)_2].$$

The results of quantitative chromatography (see table) indicate that a part of diphosphate anions (~45%) are transformed in accordance with the scheme

$$[(CuZn)_2(NH_3)_6(H_2O)_3(P_2O_7)_2] \cdot 2H_2O \xrightarrow{70\text{–}230^\circ C} (CuZn)_2(NH_3)_{3.6}(H_2O)_{0.24}(PO_4)_2(P_2O_7).$$

Variation of the elemental and chemical composition of ammonium zinc diphosphate upon thermolysis in the dynamic mode

T, °C	Composition, as indicated by chemical analysis	Distribution of P_2O_5, rel %			Removed from the starting compound, mol	
		PO_4^{3-}	$P_2O_7^{4-}$	$P_3O_{10}^{5-}$	NH_3	H_2O
Starting	$CuO \cdot ZnO \cdot P_2O_5 \cdot 3.00NH_3 \cdot 2.50H_2O$	7.7	92.3	–	0	0
135	$CuO \cdot ZnO \cdot P_2O_5 \cdot 2.70NH_3 \cdot 1.07H_2O$	14.0	86.0	–	0.30	1.43
230	$CuO \cdot ZnO \cdot P_2O_5 \cdot 1.79NH_3 \cdot 0.12H_2O$	44.9	55.1	–	1.21	2.38
300	$CuO \cdot ZnO \cdot P_2O_5 \cdot 1.00NH_3 \cdot 0.06H_2O$	36.1	52.8	11.1	2.00	2.44
390	$CuO \cdot ZnO \cdot P_2O_5 \cdot 0.59NH_3 \cdot 0.02H_2O$	28.0	60.0	12.0	2.41	2.48
465	$CuO \cdot ZnO \cdot P_2O_5$	9.8	81.2	–	3.00	2.50
605	$CuO \cdot ZnO \cdot P_2O_5$	8.8	91.2	–	3.00	2.50
815	$CuO \cdot ZnO \cdot P_2O_5$	7.8	92.2	–	3.00	2.50

According to the X-ray data (Fig. 2), the substance undergoes amorphization already at 135°C, which points to the active role of water in the crystal structure of the compound. The X-ray-amorphous state of the substance is preserved up to 390°C.

A further increase in temperature in the range 230–390°C results in the condensation of monophosphate and diphosphate ions into tripolyphosphate ions, which is accompanied by removal of additional 2.4 mol of ammonia and 2.5 mol of water. In this case, according to the chromatographic data, the anionic composition of the product of thermolysis at 300–390°C is as follows: 36–28% of P_2O_5 in the form of PO_4^{3-}, 53–60% in the form of $P_2O_7^{4-}$, and 11–12% in the form of $P_3O_{10}^{5-}$. Taking into account the known concepts of thermal transformations of hydrated phosphates [17], we can represent such a distribution of P_2O_5 over oligomeric forms by the following scheme of this stage of thermolysis:

$$(CuZn)_2(NH_3)_{3.60}(H_2O)_{0.24}(PO_4)_2(P_2O_7) \xrightarrow{230–390°C} 2.40NH_3 + 0.20H_2O$$
$$+ (CuZn)_2(NH_3)_{1.20}(H_2O)_{0.04}(PO_4)_{1.12}(P_2O_7)_{1.20}(P_3O_{10})_{0.16}.$$

At 460°C, a new phase is crystallized from the X-ray-amorphous thermolysis products (Fig. 2), and its structure remains unchanged upon further heating up to 815°C. This process is accompanied by a strong exothermic effect and by simplification of the anionic composition of samples, which results from a decrease in the content of tri- and monophosphate ions. The following scheme corresponds to this stage of transformation:

$$(CuZn)_2(NH_3)_{1.20}(H_2O)_{0.04}(PO_4)_{1.12}(P_2O_7)_{1.20}(P_3O_{10})_{0.16} \xrightarrow{460°C} 1.20NH_3 + 0.04H_2O + 2CuZnP_2O_7.$$

According to the X-ray data (Fig. 2), the final thermolysis product is anhydrous copper zinc diphosphate formed at 460°C. According to the results of a full-profile analysis, it has a monoclinic crystal lattice (space group C1 2/*m*1), with the following lattice constants: a = 6.734(1) Å, b = 8.203(4) Å, c = 4.547(2) Å, β = 107.5°, V = 239.53 Å^3, and Z = 2, which is in a good agreement with the known structural data for $CuZnP_2O_7$ [18].

The order in which water and ammonia are removed from the substance is accounted for by the different strengths of H_2O and NH_3 bonds with ions of *d*-metals and by the formation of hydrogen bonds

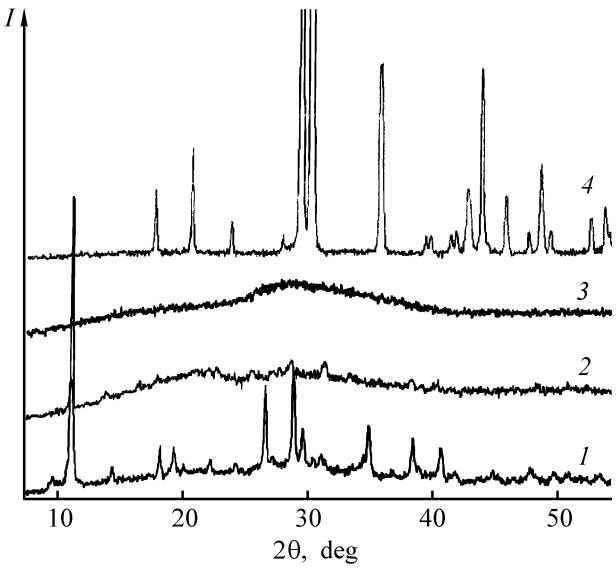


Fig. 2. X-ray diffraction patterns of (*1*) $CuZnP_2O_7 \cdot 3.0NH_3 \cdot 2.5H_2O$ and products of calcination at (*2*) 135, (*3*) 230–390, and (*4*) 815°C. (*I*) Intensity and (2θ) Bragg angle.

in the $M\begin{matrix}\swarrow NH_3 \\ \nwarrow OH_2\end{matrix}\cdots O_3P–O–PO_3$ chain (M = Cu, Zn) with averaging of the electron density [19].

This is confirmed by the results of an IR spectroscopic study of the products formed in thermolysis of the compound, which reveal the presence of bending asymmetric and symmetric vibrations of ammonia molecules at 1595 and 1410 cm^{-1}, respectively, up to 390°C, when vibrations of water molecules are no longer observed.

CONCLUSION

An individual crystalline hydrated ammonium copper(II) zinc diphosphate $CuZnP_2O_7 \cdot 3.0NH_3 \cdot 2.5H_2O$ was isolated from an aqueous ammonia solution. Its thermal properties were studied in the range 20–815°C. It was found that the final product of its thermolysis is anhydrous crystalline copper zinc diphosphate and the process occurs stepwise.

REFERENCES

1. Lavric, R.V., Synthesis and Study of Aqueous Phosphates of Alkali and 3*d*-Metals (Mn, Co, Ni), *Cand. Sci. (Chem.) Dissertation*, Kiev, 2003.
2. Viter, V.M., Synthesis and Properties of Solid Substitution Products Based on Hydrated Phosphates of Divalent 3*d*-Metals and Mg, *Cand. Sci. (Chem.) Dissertation*, Kiev, 2005.

3. Boukhari, A., Moqine, A., and Flandroids, S., *J. Solid State Chem.*, 1990, vol. 87, no. 2, pp. 251–256.
4. Belghiti, E., Alaoui, A., Elmarzouki, A., *et al., J. Solid State Chem.*, 1994, vol. 109, no. 2, pp. 333–337.
5. Voitenko, L.V., Zhilyak, I.D., and Kopilevich, V.A., *Zh. Prikl. Khim.*, 2004, vol. 77, no. 9, pp. 1421–1424.
6. Voitenko, L.V., Zhilyak, I.D., and Kopilevich, V.A., *Zh. Prikl. Khim.*, 2005, vol. 78, no. 3, pp. 369–372.
7. Acharyya, H. and Roy, H., *Technology* (India), 1972, vol. 9, no. 4, pp. 273–277.
8. UA Patent 62782, AC 01 B 25/26.
9. Knyazeva, A.A., Oxidation of C_2–C_4 Alcohols on Copper Catalysts, *Cand. Sci. (Chem.) Dissertation*, Tomsk, 2004.
10. Kopilevich, V.A., Kokhan, S.S., and Voitenko, L.V., *Proc. 11th World Ferti1izer Congress of CIEC*, Belgium, Ghent, 1997, vol. 2. p. 296.
11. Voitenko, L.V., Hydrated Ammonium Phosphates of Cobalt(II), Copper(II), and Zinc, *Cand. Sci. (Chem.) Dissertation*, Kiev, 1994.
12. Kokhanovskii, V.V. and Zemtsova, Z.N., *Vestsi Akad. Nauk BelSSR*, 1981, no. 5, pp. 5–9.
13. Kokhanovskii, V.V., *Zh. Neorg. Khim.*, 1995, vol. 40, no. 1, pp. 173–176.
14. Shchegrov, L.N., *Fosfaty dvukhvalentnykh metallov* (Phosphates of Divalent Metals), Kiev: Naukova Dumka, 1987.
15. Umland F., Janssen A., Thierig D., Wunsch, G., *Theorie und Praktische Anwendung von Komplex-bildnern*, Frankfurt am Main: Akademische, 1971.
16. *GOST* (State Standard) *20851.2–75 (ST SEV 2531–80, ST SEV 2532–80, ST SEV 3369–81), GOST 20851.2–75–GOST 20851.4–75. Mineral Fertilizers: Methods of Analysis*, 1983.
17. Voitenko, L.V., Kopilevich, V.A., and Shchegrov, L.N., *Zh. Neorg. Khim.*, 1992, vol. 37, no. 9, pp. 2055–2060.
18. El Maadi, Boukhari, A., Holt, E.M, and Flandrois, S., *Ref. J. Alloys Compd.*, 1994, vol. 205, pp. 243–247.
19. Shevchenko, Yu. N., Coordination Compounds of 3*d*-Transition Metals with Hydroborate Anions, *Doctoral (Chem.) Dissertation*, Moscow, 1991.

Russian Journal of Applied Chemistry, Vol. 78, No. 12, 2005, pp. 1921–1924. Translated from Zhurnal Prikladnoi Khimii, Vol. 78, No. 12, 2005, pp. 1954–1957.
Original Russian Text Copyright © 2005 by Kozyrev, Shvartsman, Mnukhin.

INORGANIC SYNTHESIS AND INDUSTRIAL INORGANIC CHEMISTRY

On the Mechanism of Nickel Recovery from the Sulfide Component in the Ni–Cu–S System in Carbonylation

V. F. Kozyrev, R. A. Shvartsman, and A. S. Mnukhin

Institut Gipronikel' Open Joint-Stock Company, St. Petersburg, Russia

Received July 26, 2005

Abstract—A mechanism of a solid-phase interaction between metallic copper released from the copper–nickel alloy in nickel recovery into the carbonyl gas phase with nickel sulfide in carbonylation of copper-nickel metallurgical half-products is suggested. Experimental data on carbonylation of the magnetic fraction of converter matte in a horizontal rotating reactor at a pressure of 70 gage atm and reaction zone temperature of 180°C are used to determine the coefficient of volume heterodiffusion of copper across a copper sulfide layer.

It is expected that the domestic carbonyl industry will be transferred to synthesis of nickel carbonyl in a horizontal rotating reactor at a pressure of 70 gage atm. In this context, it seems appropriate to consider processes that occur in the course of carbonylation in the Ni–Cu–S system under conditions markedly differing from those in the presently used industrial processes, in which the carbonylation is performed in vertical columns with a fixed bed of a material being carbonylated under a pressure of 200–250 gage atm.

The study was carried out on a laboratory installation, in a horizontal rotating reactor at a pressure of 70 gage atm and reaction zone temperature of 180°C. The magnetic fraction of converter matte, one of the most promising materials for industrial synthesis of nickel carbonyl, was used as the starting raw material. The residue formed in carbonylation, with various techniques used for nickel recovery, was studied by methods of metallography and X-ray fluorescence microanalysis.

One of the main factors governing the rate and extent of nickel recovery in carbonylation of half-products formed in metallurgical processing of sulfide copper-nickel raw materials is recovery of nickel from its sulfide.

This study is concerned with solid-phase interaction of nickel sulfide released from a copper-nickel solid solution after removal of nickel into the gas phase in accordance with the equation

$$Ni_3S_2 + 4Cu = 2Cu_2S + 3Ni. \quad (1)$$

The characteristic structure of a part of a polished section of the residue formed in carbonylation of the magnetic fraction of converter matte produced in solid-phase interaction between metallic copper and nickel sulfide by reaction (1) is shown in Fig. 1. It can be seen that copper sulfide Cu_2S is formed as a continuous fringe at the interface between metallic copper released from grains of a copper-nickel solid solution after removal of nickel from this solution, and grains of nickel sulfide. In this case, copper sulfide reproduces the shape of grains of nickel sulfide it sub-

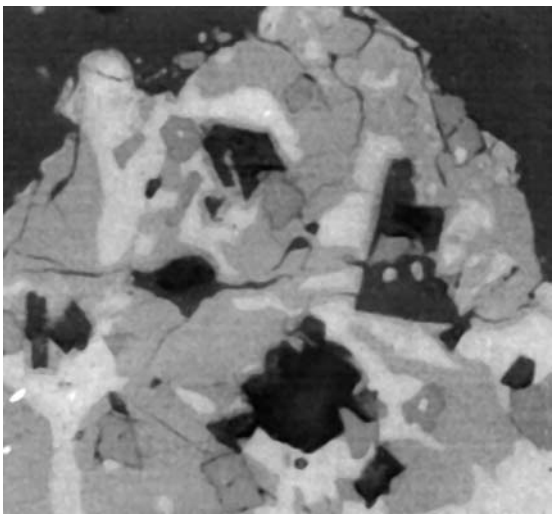


Fig. 1. Formation of Cu_2S at the Cu–Ni_3S_2 phase boundary. *Dark field*, metallic copper released from the Cu–Ni alloy; *light field*, Ni_3S_2; gray fringe at the phase boundary, newly formed copper sulfide Cu_2S.

1070-4272/05/7812-1921 © 2005 Pleiades Publishing, Inc.

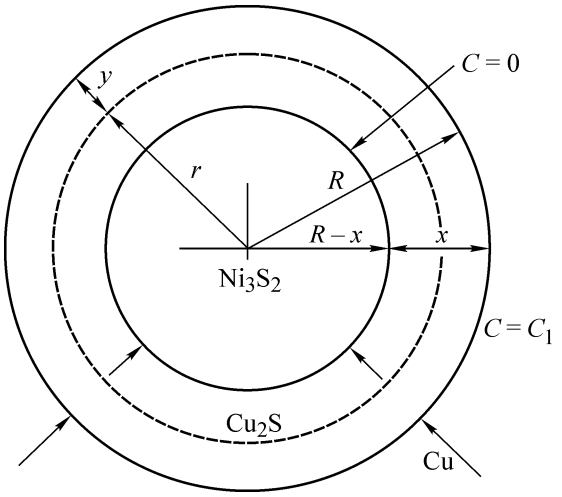


Fig. 2. Model of interaction between metallic copper and nickel sulfide.

stitutes, with the rectilinear contour at the interface between the sulfide and the solid solution, characteristic of nickel sulfide.

In manufacture of nickel from a copper-nickel solid solution, a concentration gradient arises in a layer of the remaining metallic copper. This gradient gives rise to a diffusion flow of its atoms toward the surface of a nickel sulfide grain. The change in the concentration of copper in regions adjacent to nickel sulfide can be rather clearly seen in the same micrograph.

The observed course of the solid-phase reaction of nickel substitution in its sulfide with metallic copper can be understood in terms of the electronic structure of the material being carbonylated. The reactivity of double copper-nickel alloys depends on the number of vacancies in the 3-*d* band of the alloy [1]. The change in the number of vacancies in the 3-*d* band in carbonylation of sulfide copper-nickel materials is due not only to the chemical composition of the metallic phase, which varies as nickel is recovered into carbonyl, but also to contact phenomena that occur at the interface between the solid solution and copper sulfide. A quantitative X-ray fluorescence microanalysis demonstrated that copper sulfide formed by reaction (1) corresponds to a stoichiometry $Cu_{2-x}S$, where $0 < x < 0.22$. This sulfide is a semiconductor with a predominantly *p*-type conduction [2]. The existence of a contact between $Cu_{2-x}S$ and the copper-nickel solid solution in the course of carbonylation leads to redistribution of electrons among the contacting phases because of the different positions of the Fermi level [3]. It may be assumed here that the motion of electrons is directed toward copper sulfide away from the copper-nickel solid solutions, which has a higher lying Fermi level. This is so because, in any system with two condensed phase brought in contact, electrons pass from a subsystem with a higher-lying Fermi level to that with a lower Fermi level. The condition for the attainment of equilibrium is the alignment of the Fermi levels, i.e., equality of the chemical potentials. It is known [4] that, upon chemisorption of gases on ferromagnetic metals and alloys, the magnetic moments of surface atoms change because of the redistribution of the electron density among the adsorbate and adsorbent. Chemisorption of carbon oxide on the surface of ferromagnetic bodies leads to a decrease in the magnetic moments of surface atoms, which is due to filling of holes (vacancies) in the 3-*d* band of the adsorbate by electrons of chemisorbed carbon oxide molecules. The chemisorption capacity of the copper-nickel solid solution for electron-donor species, whose role is played in carbonylation by carbon oxide molecules, grows as the Fermi level moves downwards.

Therefore, the existence of a contact between the copper-nickel solid solution and copper sulfide $Cu_{2-x}S$ in synthesis of nickel carbonyl and the change in the concentration of electrons, which is due to their outflow into copper sulfide, make larger the number of vacancies in the 3*d* band of the metallic alloy and depress the Fermi level. This, in turn, leads to an increase in the chemisorption capacity and reactivity of the copper-nickel solid solution in the near-contact zone.

Copper sulfide Cu_2S is formed as a continuous fringe at the interface between metallic copper released from grains of a copper-nickel solid solution upon removal of nickel. Simultaneously, a concentration gradient arises in a layer of metallic copper. This gradient gives rise to a diffusion flow of its atoms toward the surface of a nickel sulfide grain.

Three main stages can be distinguished when the mechanism of interaction between metallic copper and nickel sulfide by reaction (1) is considered (Fig. 2). The first is migration of copper released from the copper-nickel solid solution after removal of nickel into the carbonyl gas phase toward the surface of nickel sulfide grains (bulk self-diffusion). The second is the bulk heterodiffusion of copper atoms toward the surface of nickel sulfide grains across the copper sulfide layer, which is formed in the course of the reaction and has a continuously growing thickness. The third is bulk heterodiffusion or diffusion along the grain boundaries of nickel released from the sulfide.

If the process of copper migration is considered in terms of the bulk self-diffusion mechanism (stage 1), the diffusion rate can be expressed as

$$\frac{\partial c}{\partial \tau} = \frac{\partial}{\partial x}\left(D\frac{\partial c}{\partial x}\right), \quad (2)$$

whence follows

$$D = \frac{1}{2\tau}\frac{\partial c}{\partial x}\int_{c=c_1}^{c=0} x\partial x, \quad (3)$$

where D is the bulk self-diffusion coefficient of copper ($cm^2\ h^{-1}$).

The rate of nickel migration along crystal faces (stage 3) can be represented as the expression suggested by Hauffe [5]:

$$C_m = \Phi\left(\frac{\eta}{2}\sqrt{D_c t}\right), \quad (4)$$

where $\Phi = \frac{2}{\sqrt{\pi}}\int_0^x e^{-z^2}dz$ is the symbol representing the Gauss error integral.

The problem of bulk heterodiffusion of components in polycrystalline media has been the object of study by domestic and foreign researchers [5–7]. If the model presented in Fig. 2 is adopted as a basis and the Fick equation for spherical coordinates with the boundary and initial conditions

$$C = C_1,\ r = R,\ \tau > 0; \quad (5)$$

$$C = 0,\ r = R - x, \quad (6)$$

is used, the rate of bulk heterodiffusion of copper across the copper sulfide layer (stage 2) can be represented as

$$\frac{\partial x}{\partial \tau} = \frac{D}{B}\left(\frac{\partial c}{\partial r}\right)_{r=R-x}, \quad (7)$$

Here $B = \rho_s/\mu$ is a proportionality factor; ρ_s = 5.7 g cm^{-3}, density of Cu_2S; μ = 159 g mol^{-1}, molecular weight of Cu_2S; c, concentration of metallic copper in the Cu_2S layer; c_1, concentration of copper at the Cu–Cu_2S interface; c_y, concentration of copper on the surface of an arbitrary sphere at a distance of y from the Cu–Cu_2S interface.

Hence, the bulk heterodiffusion coefficient of copper is given by

$$D = \frac{x^2(1 - 2x/3R)B}{2\tau c_1}, \quad (8)$$

Results obtained in measurements of R and x and in calculation of the coefficient D (P = 70 atm, T = 180°C)

Measurement no.	$R\times10^{-4}$, cm	$x\times10^{-4}$, cm	$D\times10^{-8}$, $cm^2\ h^{-1}$
1	9.25	1.85	0.683
2	5.55	0.92	0.173
3	13.90	1.85	0.720
4	6.02	1.38	0.370
5	9.25	1.85	0.638
6	9.25	1.38	0.393
7	2.78	0.92	0.152
8	6.94	1.38	0.379
9	3.70	0.92	0.162
10	4.63	0.92	0.169
11	6.48	0.92	0.175
12	9.25	1.38	0.394
Average	7.25	1.31	0.373

and the transformation rate of nickel sulfide grains, by

$$\frac{\partial \varepsilon}{\partial \tau} = K\frac{(1-\varepsilon)^{1/3}}{1-(1-\varepsilon)^{1/3}}, \quad (9)$$

where $K = 2Dc_1/B$.

Experimental data necessary for calculating the bulk heterodiffusion coefficient of copper were obtained by direct measurement of R and x under a microscope at magnification of 1080.

The measurements were made on polished sections of the residues obtained upon carbonylation of the magnetic fraction of the nickel concentrate produced in separation of converter matte, for which the mass recovery of nickel was about 50%.

The results obtained in experiments and in calculating the coefficient D are listed in the table.

Metallographic studies of the x : R ratio in residues formed in carbonylation of various materials at different process durations made it possible to determine the coefficient of bulk heterodiffusion of copper across the newly formed layer of copper sulfide, which was found to be 3.73×10^{-9} $cm^2\ h^{-1}$ at 180°C. For nickel sulfide grains of size not exceeding 10 μm, the rate of their transformation is well comparable with that of nickel recovery from a copper-nickel solid solution.

CONCLUSION

It was shown that, for the recovery of nickel into carbonyl from the sulfide component of the alloy to

be more complete, it is necessary that the structure formed in metallurgical preparation of the material for carbonylation should have grains of the phase constituents of size not exceeding 10–15 μm.

REFERENCES

1. Shvartsman, R.A., Kipnis, A.Ya., and Krinchik, G.S., *Zh. Fiz. Khim.*, 1973, vol. 47, no. 6, pp. 1570–572.
2. Dekhtyar, I.Ya. *Elektronnaya struktura i svoystva perekhodnyh metallov i ikh splavov* (Properties of Transition Metals and Their Alloys), Kiev: Naukova Dumka, 1974.
3. Bader, V.I. and Mnukhin, A.S., *Metally*, 1979, no. 4, pp. 42–48.
4. Krinchik, G.S., Shvartsman, R.A., and Kipnis, A.Ya., *Fiz. Tverd. Tela*, 1974, no. 16, pp. 193–195.
5. Hauffe, K., *Reaktionen in und an festen Stoffen*, Berlin: Springer, 1955, Bd. 2. Translated under the title *Reakcii v tverdy'h telah i na ih poverhnosti*, Moscow: Inostrannaya Literatura, 1962.
6. Ginstling, A.M., *Fiziko-khimicheskie osnovy keramiki* (Physicochemical Foundations of Ceramics), Moscow: Promstroyizdat, 1956, pp. 212–224.
7. Ginstling, A.M. and Brounshtein, B.I., *Zh. Prikl. Khim.*, 1950, vol. 23, pp. 1249–1251.

Russian Journal of Applied Chemistry, Vol. 78, No. 12, 2005, pp. 1925–1929. Translated from Zhurnal Prikladnoi Khimii, Vol. 78, No. 12, 2005, pp. 1958–1962.
Original Russian Text Copyright © 2005 by Kozyrev, Shvartsman, Mnukhin.

INORGANIC SYNTHESIS AND INDUSTRIAL INORGANIC CHEMISTRY

A Study of the Behavior of Cobalt in Carbonylation of Copper-Nickel Metallurgical Half-Products at Medium Pressure of the Reaction Gas

V. F. Kozyrev, R. A. Shvartsman, and A. S. Mnukhin

Institut Gipronikel' Open Joint-Stock Company, St. Petersburg, Russia

Received July 26, 2005

Abstract—Dependences of the cobalt recovery into the carbonyl gas phase on the content of sulfur and carbon in sulfidized copper-nickel metallurgical half-products subjected to carbonylation were studied at a medium pressure of the reaction gas (70 gage atm). The behavior of cobalt was examined by means of metallographic analysis of the residue formed in carbonylation. A mechanism of solid-phase interaction of cobalt with copper sulfide and a method for calculation of the volume self-diffusion coefficient of cobalt in the crystal lattice of metallic copper deformed after removal of nickel were suggested.

One of the most complicated and capital-intensive conversion techniques in the carbonyl metallurgy of nickel is synthesis of nickel tetracarbonyl. At present, both the technology of this conversion, carried out at a high pressure of the reaction gas (200–250 gage atm) in vertical columns with a fixed bed of the material being carbonylated, and the equipment used in the process have become physically outdated and obsolescent and require a fundamental reconstruction [1].

A new, highly efficient technique for carbonylation of nickel-containing metallurgical half-products formed in processing of sulfide raw materials at a medium pressure of the reaction gas (70 gage atm) in a horizontal rotating reactor has been developed [2, 3]. Industrial implementation of this technology will markedly raise the output capacity of the process, diminish its capital- and energy-intensity, and improve the ecological situation in manufacture of carbonyl nickel.

Of key importance among a number of problems to be solved in developing the new technology was the choice and preparation of a starting raw material for carbonylation that would ensure the maximum selectivity of separation of carbonyl-forming metals, including cobalt.

The behavior of cobalt in the course of carbonylation is largely determined by the ratio of its content in the metallic solid solution to that in the alloy of nickel and cobalt sulfides, because the sulfide cobalt does not react with carbon oxide and its whole amount is preserved in the residue formed in the synthesis [4].

To study the influence exerted by the content of sulfur on the recovery of cobalt in carbonylation, synthetic cobalt-containing sulfur-enriched nickel alloys were prepared. This was done using the most chemically pure materials: carbonyl nickel, electrolytic cobalt, and purified sulfur. The smelting was performed in a corundum crucible placed in a high-frequency induction furnace in a protective argon atmosphere. The compositions of the alloys, recovery of cobalt into carbonyl, and dependence of the cobalt recovery on the content of sulfur in the alloy are listed in Table 1 and shown in Fig. 1a.

Table 1. Chemical composition of cobalt-containing sulfur-enriched nickel alloys

Alloy no.	Mass content in an alloy, %		Mass recovery of Co, %
	Co	S	
1	2.00	0.03	45.3
2	2.01	0.49	36.2
3	2.00	0.86	30.4
4	2.0	1.33	23.8
5	2.00	1.53	18.9
6	2.00	2.00	17.5
7	2.00	3.13	8.5
8	2.00	4.02	4.8
9	2.01	4.66	5.0
10	2.01	6.32	2.6

1070-4272/05/7812-1925 © 2005 Pleiades Publishing, Inc.

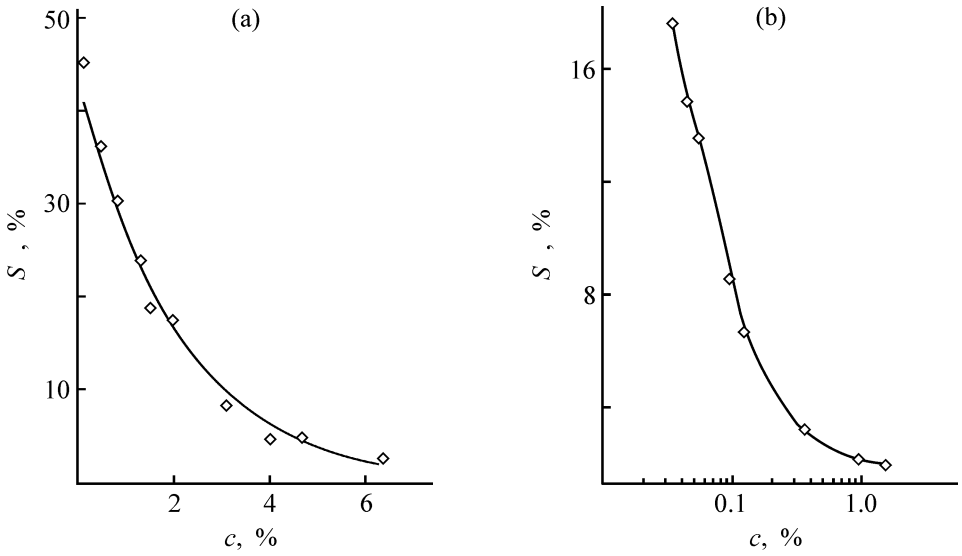


Fig. 1. Mass recovery *S* of cobalt into carbonyl vs. the mass content *c* in the alloy of (a) sulfur and (b) carbon.

Nickel alloys were carbonylated at a pressure of 70 gage atm and temperature of 180°C on a laboratory kinetic installation. The recovery of cobalt was determined from its content in the solid residue formed in the synthesis. The experimental data obtained indicate that, as the mass content of sulfur in the alloy increases from 0.03 to 6.32%, the recovery of cobalt into the carbonyl decreases from 45 to 2%.

Carbon additives introduced to deoxidize the melt in the course of smelting into a raw material to be carbonylated inevitably affect the behavior of cobalt. In order to study the influence exerted by carbon on the recovery of cobalt into the carbonyl, synthetic cobalt-containing carbon-enriched nickel alloys were prepared. Graphite was introduced into the stock as a carbon-containing material. The compositions of the alloys under study, recovery of cobalt into carbonyl, and dependence of the recovery on the content of carbon in the alloy are listed in Table 2 and shown in Fig. 1b.

Table 2. Chemical composition of cobalt-containing carbon-enriched nickel alloys

Alloy no.	Mass content in an alloy, %		Mass recovery of Co, %
	Co	C	
1	2.86	0.035	17.5
2	2.94	0.046	14.8
3	2.54	0.056	12.5
4	2.85	0.098	9.8
5	2.92	0.126	6.7
6	2.68	0.254	2.5
7	2.88	0.368	3.2
8	2.70	0.950	2.2
9	2.43	1.56	2.0

Raising the concentration of carbon in the alloy leads to a dramatic decrease in the cobalt recovery, with this change being the most pronounced when the mass content of carbon is varied within the range from 0.035 to 0.126%. The passivating effect of carbon on the reaction of cobalt carbonylation is accounted for by the overlapping of the "magnetic" band of cobalt in the alloy. In this case, the limited solubility of carbon in cobalt leads, as carbide is formed, to a pronounced decrease in the cobalt recovery just in the range mentioned above, because a carbon atom introduces six electrons into the magnetic matrix of cobalt.

A further increase in the content of carbon has only a slight effect on the recovery of cobalt, which is due to the formation of a separate phase (sooty carbon) at a content of carbon in the alloy that exceeds its solubility limit in both nickel and cobalt. The presence of such a phase does not lead to overlapping of the magnetic band in the ferromagnetic material.

The mass recovery into the carbonyl phase of metallic cobalt contained in the copper-nickel solid solution varies, depending on the composition of the starting raw material and technological parameters of the carbonylation process, from 2 to 40%.

Apparently, the efficiency of the industrial application of the carbonyl process to nickel-containing raw

materials is largely determined by the selectivity of separation of metals. This primarily refers to cobalt and platinum-group metals, because even partial transfer of these metals into the carbonyl phase causes, in further processing, a virtually irrecoverable additional loss.

In order to examine the behavior of cobalt in synthesis of nickel carbonyl, the residue formed in carbonylation of copper-nickel metallurgical half-products was subjected to a metallographic and X-ray fluorescence microprobe analyses. In doing so, a newly formed bright light yellow phase was observed. This phase is formed as a fine fringe at the interface between partly processed grains of the metallic solid solution and copper sulfide. The characteristic appearance of this phase is shown in metallographic micrographs of the residue formed in carbonylation (Fig. 2).

X-ray diffraction and fluorescence microprobe analyses demonstrated that this phase is composed of cobalt sulfide.

Being originally uniformly distributed throughout grains of the solid solution, cobalt concentrates in the course of carbonylation at grain boundaries and forms, after partial or complete removal of nickel into carbonyl, finely dispersed inclusions, now in the form of sulfide in a copper sulfide matrix.

Analysis of the data obtained convincingly demonstrates that the nature of bonds of metallic cobalt in the crystal lattice of the copper-nickel solid solution is of particular importance for the carbonylation process. According to the phase diagrams of the Co–Ni and Co–Cu systems, it can be stated with certainty that, owing to a virtually zero solubility of cobalt in copper, cobalt atoms are associated in the alloy structure exclusively with nickel atoms.

As nickel is recovered into carbonyl, cobalt is liberated from the lattice of the remaining metallic copper and either undergoes carbonylation:

$$2Co + 8CO \rightleftarrows Co_2(CO)_8, \quad (1)$$

or migrates. In the latter case, cobalt migration in the copper lattice may occur in two directions:

(a) from the reaction zone across the layer of metallic copper to the boundary with the newly formed copper sulfide, with the subsequent reaction in accordance with the equation:

$$Co + Cu_2S \rightleftarrows CoS + 2Cu, \quad (2)$$

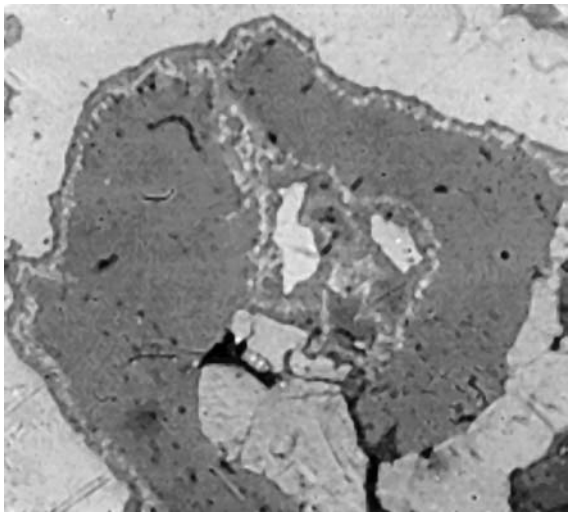


Fig. 2. Characteristic appearance of the residue produced in carbonylation with the formation of a cobalt-containing sulfide phase.

(b) from the reaction zone into as yet unprocessed grains of the copper-nickel solid solution.

The reaction of cobalt sulfide formation goes successfully if copper formed upon removal of nickel is continuously consumed by the reaction with nickel(III) sulfide, which, in turn, is initiated by removal of reduced nickel into the carbonyl phase:

$$Ni_3S_2 + 4Cu \rightleftarrows 2Cu_2S + 3Ni, \quad (3)$$

$$Ni + 4CO \rightleftarrows Ni(CO)_4. \quad (4)$$

Upon the removal of nickel and partial consumption of copper by reaction (3), the crystal lattice is markedly strained and contains a large number of defects. Therefore, the diffusion flux of cobalt across the interface will considerably exceed that in the case of compact metallic copper because of the higher concentration of vacancies and a significant contribution of the surface diffusion.

Let us consider the mechanism of this process for the case of carbonylation of a spherical grain of the copper-nickel solid solution, which has a radius R, contains cobalt, and is embedded in nickel sulfide.

Cobalt released from the crystal lattice after the removal of nickel into carbonyl diffuses from the reaction zone across a layer of metallic copper of thickness $R - \rho = x$. Copper interacts with nickel sulfide and substitutes the latter at the outer contour of the alloy grain, to form a layer of copper sulfide. The scheme of interaction between the phases in

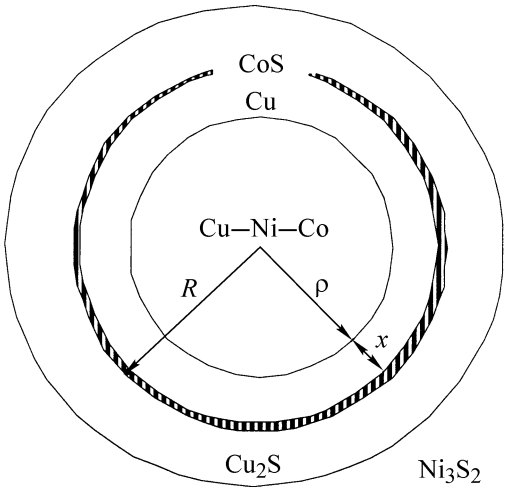


Fig. 3. Scheme of the solid-phase interaction to give cobalt sulfide.

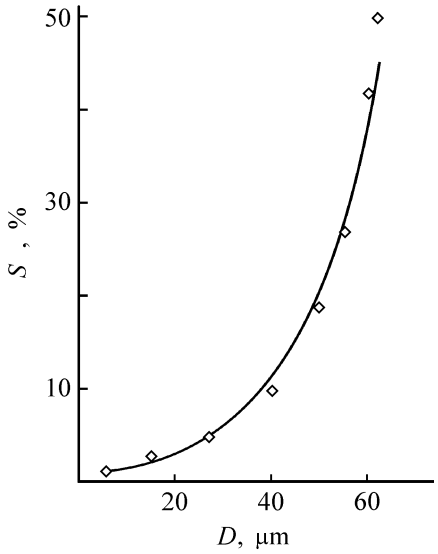


Fig. 4. Mass recovery *S* of cobalt into carbonyl vs. the grain size *D* of the phase constituents of the raw material being carbonylated.

the process under consideration is shown in Fig. 3. The rate of this process is limited by the rate of volume self-diffusion of cobalt across a porous layer of metallic copper. With account of the comparatively low content of cobalt in the initial solid solution, the volume heterodiffusion of cobalt across the layer of its sulfide, formed in the reaction, can be neglected.

To describe the process of cobalt migration across the layer of porous metallic copper, we use the equation of unidimensional spherical diffusion

$$\varepsilon \frac{\partial c}{\partial t} = -D\left(\frac{\partial^2 c}{\partial r^2} + \frac{2\partial c}{r\partial r}\right), \quad (5)$$

where ε is the porosity of the copper layer; *D*, effective diffusion coefficient; and *c*, cobalt concentration at a distance *r* from the particle center, numerically equal to the mass content of cobalt in a unit volume.

We assume that the diffusion process is quasi-stationary, which is justified if the radius of the unprocessed core varies at a sufficiently low rate and the concentration of cobalt in the initial alloy is not high. This assumption can be fully referred to cobalt. Then, integrating the equation

$$\frac{\partial^2 c}{\partial r^2} + \frac{2\partial c}{r\partial r} = 0$$

we obtain

$$\frac{dc}{dr} = \frac{A}{r^2}, \quad (6)$$

where *A* is a numerical coefficient.

Repeated integration yields $c = -A/r + B$.

Taking into account the boundary conditions $r = R$, $r = \rho$, $c = c_r$, and $c = c_\rho$, we find *A*

$$A = \frac{c_\rho - c_R}{1/R - 1/\rho}. \quad (7)$$

Consequently,

$$\frac{dc}{dr} = \frac{c_\rho - c_R}{(1/R - 1/\rho)r^2}. \quad (8)$$

To provide a successful binding of cobalt into sulfide, the diffusion flux across any spherical surface $4\pi r^2$ ($\rho < r < R$) should be no less than the flux of the same metal into the unprocessed core of the metallic solid solution. In view of this fact, we equate both the diffusion fluxes

$$D\frac{c_\rho - c_R}{1/R - 1/\rho} = \gamma_0 \rho^2 \frac{d\rho}{dt}. \quad (9)$$

where γ_0 is the initial mass content of cobalt in a unit volume of the metallic solid solution.

On integrating, we find the time necessary for cobalt released in processing of a grain of the alloy to be bound into sulfide, during which the radius of the grain decreases from *R* to ρ.

$$t = \frac{\gamma_0}{6D(c_\rho - c_R)}[2/R(\rho^3 - R^3) - 3(\rho^2 - R^2)]. \quad (10)$$

The time τ of complete processing of a grain of the cobalt-containing solid solution is found from the condition $\rho = 0$:

$$\tau = \frac{\gamma_0 R^2}{6D(c_\rho - c_R)}. \quad (11)$$

We assume that $c_R = 0$, because cobalt is completely bound into sulfide at the outer surface of the grain and equate c_ρ to the density of cobalt, because being released from the copper-nickel solid solution it virtually does not dissolve in porous metallic copper. Having done so, we can obtain from Eq. (11) the diffusion coefficient of cobalt under carbonylation conditions.

Using the conversion time of a grain of the solid solution of radius R in carbonylation, we calculated the coefficient D_c of volume self-diffusion of cobalt: $D_c = 2.75 \times 10^{-8}$ cm^2 h^{-1} in carbonylation of a granulated nickel alloy at 70 gage atm and a temperature of 180°C.

This value of the diffusion coefficient of cobalt indicates that the diffusion rate and, consequently, the rate of sulfide formation are well comparable with the carbonylation rate of this metal, and the conversion time is directly proportional to the grain size of the phase constituents. The dependence of the recovery of cobalt into the carbonyl phase on the grain size of the phase constituents is shown in Fig. 4.

Thus, an as finely dispersed structure as possible should be formed in the course of a metallurgical preparation of the starting metallurgical half-products for carbonylation in order to improve the selectivity of separation of metals (nickel and cobalt, in particular).

CONCLUSIONS

(1) The behavior of cobalt was studied using methods of metallographic analysis of a residue formed in carbonylation and it was shown that cobalt sulfide appears as a newly formed phase at the boundary between grains of the copper-nickel solid solution and copper sulfide.

(2) An as finely dispersed structure as possible should be formed in metallurgical preparation of the starting metallurgical half-products for carbonylation in order to improve the selectivity of separation of nickel and cobalt in carbonylation.

REFERENCES

1. Shvartsman, R.A., Semenov, B.M., Vigdorchik, E.M., *et al.*, *Tsvet. Met.*, 2004, no. 12, pp. 110–114.
2. Zaitsev, A.Yu., Biketova, L.V., Mnukhin, A.S., and Shvartsman, R.A., *Tsvet. Met.*, 1995, no. 5, pp. 17–20.
3. Zaitsev, A.Yu., Mnukhin, A.S., Ginzburg, A.A., and Shvartsman, R.A., *Tsvet. Metall.*, 1994, nos. 4–5, pp. 12–14.
4. Verblovskii, A.M., Mnukhin, A.S., and Vereshchagina, A.I., *Tr. In–ta Gipronikel'*, 1972, issue 51, pp. 72–76.

Russian Journal of Applied Chemistry, Vol. 78, No. 12, 2005, pp. 1930–1933. Translated from Zhurnal Prikladnoi Khimii, Vol. 78, No. 12, 2005, pp. 1963–1966.
Original Russian Text Copyright © 2005 by Morachevskii, Kolosova, Tsymbulov, Tsemekhman

PHYSICOCHEMICAL STUDIES OF SYSTEMS AND PROCESSES

Activity of Components in Liquid Alloys of the Iron–Cobalt–Nickel System

A. G. Morachevskii, E. Yu. Kolosova, L. B. Tsymbulov, and L. Sh. Tsemekhman

St. Petersburg State Polytechnic University, St. Petersburg, Russia
Institut Gipronikel' Joint-Stock Company, St. Petersburg, Russia

Received November 15, 2005

Abstract—Data on the thermodynamic properties of boundary binary systems were used to calculate the activities of components in liquid alloys of the iron–cobalt–nickel ternary system at a temperature of 1600°C.

Calculational methods have gained wide acceptance in the thermodynamics of liquid three-component metallic systems [1–7]. As rule, the calculations are based on data on thermodynamic properties of boundary binary systems. Using various comparatively simple geometric models, it is possible to describe the surface of an integral thermodynamic property of a ternary system on the basis of the corresponding property of boundary binary systems. Together with geometric models, polynomial expressions for a ternary system are used. The coefficients of these polynomials are found using data on boundary binary systems.

Previously, the integral molar excess Gibbs energy (ΔG^{ex}) and the enthalpy of mixing (ΔH) of alloys of the Fe–Co–Ni system at a temperature of 1600°C were calculated in [8]. The agreement between the results of calculations performed in terms of six different geometric models and those obtained using polynomial dependences reflecting the contribution of binary systems is quite satisfactory. This indirectly confirms that the real shape of the surface of thermodynamic properties of the ternary system is adequately described. The choice of thermodynamic characteristics for the binary boundary systems Fe–Co, Co–Ni, and Ni–Fe was substantiated in detail in [8]. In evaluating the excess Gibbs energy of the binary systems, preference was given to studies carried out using the effusion Knudsen method combined with a mass-spectrometer. Also, the recommendations given in reviews [9–13] were taken into account.

Until recently, data on the thermodynamic properties of the Fe–Co–Ni system have been rather scarce. Velisek and co-authors [13] determined the activities of the components of the ternary system in a limited range of compositions by measuring the saturated vapor pressure at 1227°C, i.e., in the solid state. In [14], the activity of each of the components of the Fe–Co–Ni system was determined at 1200–1650°C, using a Knudsen cell combined with a mass-spectrometer. However, the authors did not intend to make a complete thermodynamic description of the system, and they only studied the Fe–Ni binary system and an adjacent section of the ternary system, with a constant ratio $x_{Fe} : x_{Ni} = 9 : 1$ (x_i, molar fraction of a component in an alloy). In [15, 16], the liquid–vapor equilibrium was studied for eight compositions of the Fe–Co–Ni ternary system at 1600°C. Based on the data obtained and the evidence concerning the boundary binary systems, the authors derived, by means of statistic processing, equations describing how the composition of the vapor phase depends on that of the liquid phase and evaluated the activity coefficients of the components.

Recently, Tomiska studied, using a method modified by him, which employed a Knudsen cell and a mass-spectrometer, the thermodynamic properties of

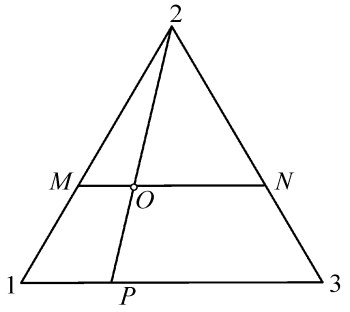


Fig. 1. Scheme illustrating the calculation of the activity coefficient of a component in a ternary system. For explanations, see text.

1070-4272/05/7812-1930 © 2005 Pleiades Publishing, Inc.

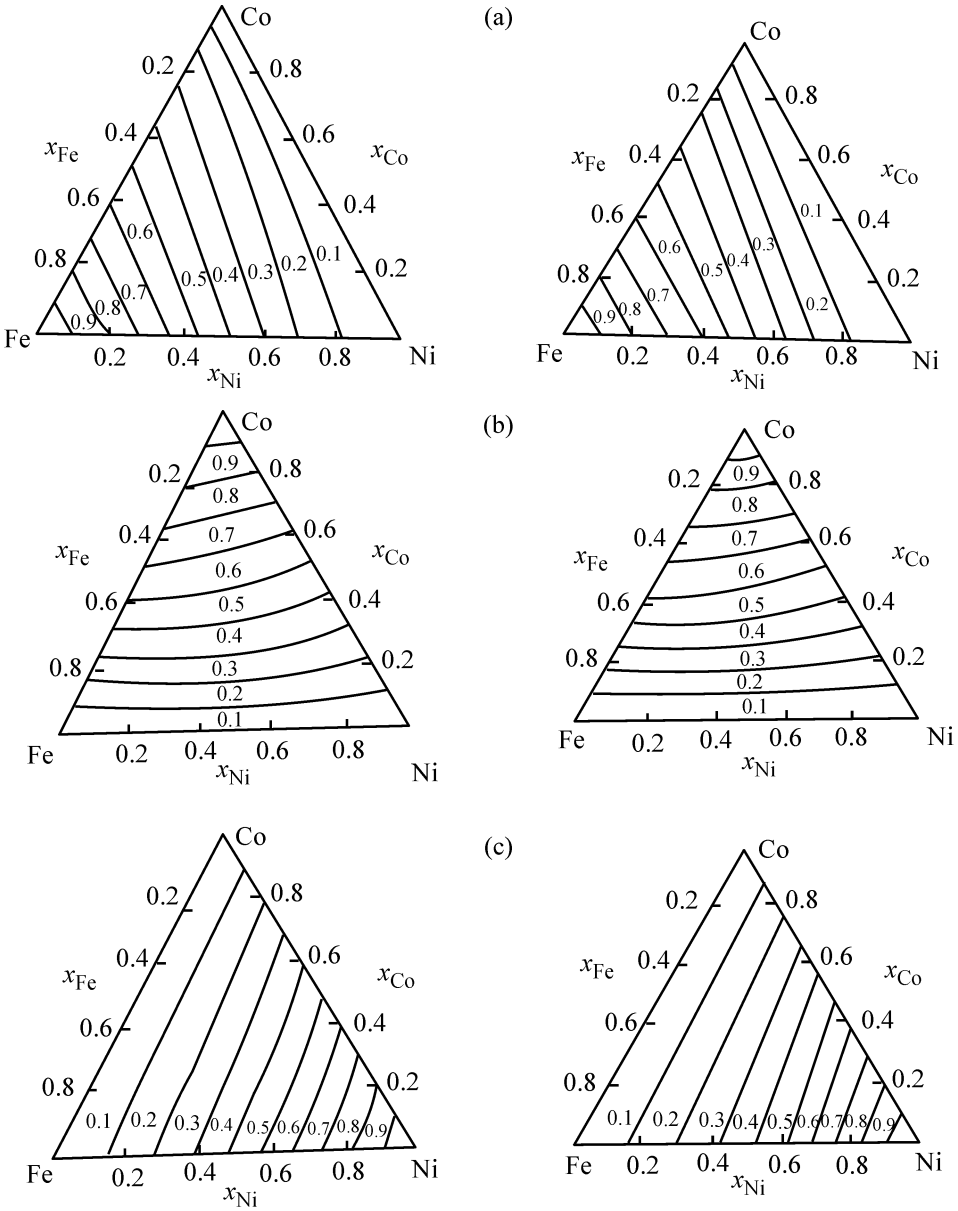


Fig. 2. Isoactivity lines of (a) iron, (b) cobalt, and (c) nickel in liquid alloys in the Fe–Co–Ni system, plotted using experimental (left-hand, 1577°C, data from [18]) and calculated (right-hand, 1600°C) data.

the Fe–Co–Ni system in both the solid (1327°C) [17] and liquid states. Doing so makes it possible to compare the calculated activities of the components in liquid alloys of the Fe–Co–Ni system with the results of an experimental study. As before [19], an equation following from the Toop method was used in calculations. For example, for component 2

$$\log \gamma_2 = \left[\frac{x_1}{1-x_2}\log \gamma_{2(1)} + \frac{x_3}{1-x_2}\log \gamma_{2(3)}\right]_{x_2} + (1-x_2)^2\left[\frac{\Delta G_{13}^{ex}}{2.303\,RT}\right]_{x_1/x_3},$$

where γ_2 is the activity coefficient of component 2 for a composition defined by molar fractions x_1, x_2, and x_3 (Fig. 1, point O); $\gamma_{2(1)}$ and $\gamma_{2(3)}$, activity coefficients of component 2 in boundary binary systems 1–2 and 2–3 at a prescribed value of x_2 (Fig. 1, points M and N); and ΔG_{13}^{ex}, integral molar excess Gibbs energy of the boundary binary system 1–3 at a prescribed $x_1 : x_3$ ratio (Fig. 1, point P).

Similar equations and constructions can be also written for the two other components of the ternary system. The activity coefficients of the boundary binary systems, taken for the calculation, a listed in

Table 1. Activity coefficients of the components in the boundary binary systems at 1600°C,* taken for calculation

x_2^{**}	Fe–Co		Co–Ni		Ni–Fe		x_2^{**}	Fe–Co		Co–Ni		Ni–Fe	
	γ_{Fe}	γ_{Co}	γ_{Co}	γ_{Ni}	γ_{Ni}	γ_{Fe}		γ_{Fe}	γ_{Co}	γ_{Co}	γ_{Ni}	γ_{Ni}	γ_{Fe}
0.10	1.43	1.15	0.88	0.88	0.67	0.46	0.50	1.03	1.15	0.96	0.96	0.76	0.92
0.20	1.29	1.22	0.90	0.90	0.67	0.60	0.60	0.99	1.10	0.97	0.98	0.81	0.97
0.30	1.18	1.23	0.92	0.92	0.68	0.74	0.70	0.98	1.06	0.98	0.99	0.87	0.99
0.40	1.09	1.20	0.94	0.94	0.71	0.85	0.80	0.98	1.02	0.99	0.99	0.93	1.00
							0.90	0.99	1.01	1.00	1.00	0.98	1.00

* Standard state: pure liquid metals. ** Molar fraction of the second component.

Table 2. Results obtained in calculating the activity coefficients of the components of liquid alloys in the Fe–Co–Ni system (1600°C)*

x_{Fe}	$x_{Co} : x_{Ni} = 3 : 1$		$x_{Co} : x_{Ni} = 1 : 1$			$x_{Co} : x_{Ni} = 1 : 3$	
	a_{Fe}	γ_{Fe}	a_{Fe}	a_{Fe}^{exp}	γ_{Fe}	a_{Fe}	γ_{Fe}
0.10	0.11	1.10	0.08	0.10	0.80	0.06	0.60
0.20	0.22	1.10	0.18	0.20	0.90	0.15	0.75
0.30	0.32	1.07	0.29	0.29	0.97	0.25	0.83
0.40	0.41	1.03	0.39	0.38	0.98	0.36	0.90
0.50	0.50	1.00	0.49	0.48	0.98	0.48	0.96
0.60	0.60	1.00	0.59	0.58	0.98	0.59	0.98
0.70	0.69	0.99	0.69	0.68	0.99	0.70	1.00
0.80	0.79	0.99	0.79	0.79	0.99	0.80	1.00
0.90	0.90	1.00	0.90	0.90	1.00	0.90	1.00
x_{Co}	$x_{Ni} : x_{Fe} = 3 : 1$		$x_{Ni} : x_{Fe} = 1 : 1$			$x_{Ni} : x_{Fe} = 1 : 3$	
	a_{Co}	γ_{Co}	a_{Co}	a_{Co}^{exp}	γ_{Co}	a_{Co}	γ_{Co}
0.10	0.11	1.10	0.10	0.14	1.00	0.12	1.20
0.20	0.22	1.10	0.22	0.26	1.10	0.24	1.20
0.30	0.32	1.07	0.33	0.37	1.10	0.36	1.20
0.40	0.43	1.08	0.43	0.46	1.80	0.47	1.18
0.50	0.52	1.04	0.53	0.56	1.06	0.56	1.12
0.60	0.62	1.03	0.63	0.64	1.05	0.65	1.08
0.70	0.71	1.01	0.72	0.73	1.03	0.73	1.04
0.80	0,81	1.01	0.81	0.81	1.01	0.82	1.03
0.90	0.90	1.00	0.90	0.90	1.00	0.90	1.00
x_{Ni}	$x_{Fe} : x_{Co} = 3 : 1$		$x_{Fe} : x_{Co} = 1 : 1$			$x_{Fe} : x_{Co} = 1 : 3$	
	a_{Ni}	γ_{Ni}	a_{Ni}	a_{Ni}^{exp}	γ_{Ni}	a_{Ni}	γ_{Ni}
0.10	0.07	0.70	0.07	0.08	0.70	0.08	0.80
0.20	0.14	0.70	0.15	0.15	0.75	0.16	0.80
0.30	0.22	0.73	0.23	0.24	0.77	0.15	0.83
0.40	0.30	0.75	0.32	0.33	0.80	0.34	0.85
0.50	0.40	0.80	0.42	0.43	0.84	0.44	0.88
0.60	0.51	0.85	0.53	0.54	0.88	0.55	0.92
0.70	0.63	0.90	0.65	0.66	0.93	0.67	0.96
0.80	0.76	0.95	0.77	0.78	0.96	0.78	0.98
0.90	0.89	0.99	0.89	0.89	0.99	0.89	0.99

* Experimentally determined, from the data obtained by Tomiska [18] (1577°C), activities of one of the components are given for the $x_i : x_j = 1 : 1$ sections. For other sections, no numeric data were presented in the original paper.

Table 1, and values of ΔG^{ex} can be found in [8]. The results of the calculation are listed in Table 2.

Figure 2 compares the isoactivity lines of the componentsin the Fe–Co–Ni system, plotted using experimental and calculated data, and shows a rather satisfactory agreement. In the Fe–Co–Ni system, only very small deviations from ideal behavior are observed for all of the three components.

REFERENCES

1. Toop, G.W., *Trans. Met. Soc. AIME*, 1965, vol. 233, May, pp. 850–855.
2. Sharkey, R.L., Pool, M.J., and Hoch, M., *Met. Trans.*, 1971, vol. 2, November, pp. 3039–3049.
3. Hillert, M., *CALPHAD*, 1988, vol. 12, no. 3, pp. 257–259.
4. Chou, K.-Ch. and Chang, Y.A., *Ber. Bunsengesell. Phys. Chem.*, 1989, vol. 93, no. 6, pp. 735–741.
5. Li, R.-Y, *CALPHAD*, 1989, vol. 13, no. 1, pp. 61–65.
6. Luck, R., Wang, H., and Predel, B., *J. Non-Cryst. Solids*, 1990, vol. 117/118, pp. 529–532.
7. Morachevskii, A.G., Voronin, G.F., Geyderikh, V.A., and Kutsenok, I.B., *Elektrokhimicheskie metody issledovaniya v termodinamike metallicheskikh sistem* (Electrochemical Methods of Study in Thermodynamics of Metallic Systems), Moscow: Akademkniga Izd. Kul't. Tsentr, 2003.
8. Morachevskii, A.G., Tsemekhman, L.Sh., Tsymbulov, L.B., and Fedorova, N.A., *Zh. Prikl. Khim.*, 2003, vol. 78, no. 11, pp. 1779–1784.
9. Batalin, G.I., *Termodinamika jidkikh splavov na osnove zheleza* (Thermodynamics of Iron-based Liquid Alloys), Kiev: Vyshcha Shkola, 1982.
10. Lee, B.J., *CALPHAD*, 1993, vol. 17, no. 3, pp. 251–268.
11. Fernandez Guillermet, A., *High Temper.–High Pressures*, 1987, vol. 19, no. 5, pp. 477–499.
12. Fernandez Guillermet, A., *Z. Metallkunde*, 1987, vol. 78, no. 9, pp. 636–647.
13. Velisek, J., Vrestal, J., and Stransky, K., *Kovove Mater.*, 1976, vol. 14, no. 2, pp. 121–136.
14. Fraser, J. and Rammensee, W., *Geochim. Cosmochim. Acta*, 1982, vol. 46, pp. 549–556.
15. Tsemekhman, L.Sh., Alekseeva, N.N., and Parshukova, L.N., *Metally*, 2000, no. 1, pp. 26–29.
16. Tsemekhman L.Sh., Alekseeva, N.N., and Parshukova, L.N., *Novye processy v metallurgii nikelya, medi i kobal'ta* (New Processes in Metallurgy of Nickel, Copper, and Cobalt), Moscow: Izd. Dom Ruda i Metally, 2000, pp. 205–213.
17. Tomiska, J., *Z. Metallkunde*, 2004, vol. 95, no. 3, pp. 136–141.
18. Tomiska, J., *J. Alloys Compounds*, 2004, vol. 373, pp. 142–150.
19. Morachevskii, A.G., Tsymbulov, L.B., and Kolosova, E.Yu., *Zh. Prikl. Khim.*, 2004, vol. 77, no. 9, pp. 1438–1441.

Russian Journal of Applied Chemistry, Vol. 78, No. 12, 2005, pp. 1937–1943. Translated from Zhurnal Prikladnoi Khimii, Vol. 78, No. 12, 2005, pp. 1970–1976.
Original Russian Text Copyright © 2005 by Rubtsov, Kazakov, Lempert, Manelis.

PHYSICOCHEMICAL STUDIES OF SYSTEMS AND PROCESSES

Kinetics and Mechanism of Thermolysis of Mixtures of Ammonium Nitrate with Polynitro Compounds

Yu. I. Rubtsov, A. I. Kazakov, D. B. Lempert, and G. B. Manelis

Institute for Problems of Chemical Physics, Russian Academy of Sciences, Chernogolovka, Moscow oblast, Russia

Received May 12, 2005

Abstract—Kinetics of heat release in thermolysis of mixtures of ammonium nitrate with bis(2,2,2-trinitroethyl) succinate, tetrakis(2,2,2-trinitroethyl) orthocarbonate, technical-grade trinitrotoluene and of the individual polynitro compounds was studied. The temperature dependences of the initial rates of the processes and the time required to attain the maximal rate were determined. A thermolysis mechanism of these mixtures was suggested and the dependence of the thermolysis rate on the properties of the polynitro compounds was accounted for.

Mixtures of ammonium nitrate (AN) with nitro compounds (primarily, with trinitrotoluene [1]) are widely used as industrial explosives. New compositions containing AN are being developed and studied as gas-generating fuels, including those with low combustion temperature. Nitro compounds with low enthalpy of formation show promise in this regard. Fast heat release in these mixtures may result in their self-ignition.

Previously we have studied the kinetic features of heat release in thermolysis of an AN–pyroxylin mixture [2]. Under certain conditions, the reaction between these compounds and their thermolysis products is vigorous and results in a sharp spontaneous acceleration of the thermolysis. As the temperature increases, the process initially accelerates weakly, and then, at a certain temperature, the acceleration becomes sharp. This transition may result in thermal ignition of the mixture if its amount is sufficiently large. The sharp acceleration of heat release is mainly due to fast reaction of AN with nitrogen dioxide liberated in thermolysis of pyroxylin. Nitrogen dioxide oxidizes the ammonium ion to form nitric acid, which, in turn, initiates fast decomposition of pyroxylin to form nitrogen dioxide. Thermolysis of the mixture is sharply accelerated when the steady-state balance between the formation and consumption of nitrogen dioxide is disturbed. Similar reactions should occur in mixtures of AN with other nitro compounds, since their thermolysis also yields large amounts of nitrogen dioxide, which will oxidize AN. However, the catalytic effect of nitric acid on thermolysis of nitro compounds is substantially weaker than that on pyroxylin.

Diverse polynitro compounds are known. The thermal stability of these compounds depends on their molecular structure (primarily, on the number of nitro groups at a carbon atom) and varies widely. Compounds containing the trinitromethyl group exhibit the highest thermolysis rate. The main features of thermolysis of nitro compounds are described in [3].

Here, we studied thermolysis of nitro compound–AN mixtures, direct reactions of these compounds, and reactions of these compounds with their thermolysis products. We studied nitro compounds strongly differing in thermal stability and oxidizing properties. The thermolysis of the individual compounds was examined to a lesser extent; only some quantitative data on their thermolysis were obtained.

EXPERIMNETAL

The critical factor for spontaneous ignition or explosion in chemically reacting systems is deterioration of the thermal balance between the rates of heat release and heat removal. The rate of heat release and its kinetic features determine the possibility of spontaneous ignition of a system under certain conditions of heat removal in any chemical reactor. To study the rate of AN reaction with other components of the mixture, we determined the rate and features of heat

1070-4272/05/7812-1937 © 2005 Pleiades Publishing, Inc.

release (DAK-1-2 calorimeter) [4]. The rate of heat release was measured with a relative error of about 1%. In most of our experiments, we used sealed glass ampules which can be fully accommodated in the working cell of the calorimeter. Their inner volume was about 2 ml. Under these experimental conditions, all the components of the system remain in the ampule and the volatile compounds are in the condensed state. This is of particular importance when studying AN-containing mixtures, since ammonia and nitric acid formed in equilibrium dissociation of AN in the gas phase in an open system can escape from the reaction zone, thus changing the composition of the system. Under these conditions, the pressure of the gaseous products in an ampule may be as high as 1 MPa and more, and the influence of these products on the thermolysis kinetics is usually considerably more significant than that at a pressure lower than 0.l MPa.

We studied the kinetics of heat release in thermolysis of three individual nitro compounds and their mixtures with AN: bis(2,2,2-trinitroethyl) succinate $(NO_2)_3C–CH_2–OC(O)–CH_2–CH_2–C(O)–OCH_2C(NO_2)_3$ (**I**), mp = 125°C; tetrakis(2,2,2-trinitroethyl) orthocarbonate $C(–O–CH_2–C(NO_2)_3)_4$ (**II**), mp = 162°;, and technical-grade trinitrotoluene (TNT) $C_6H_2CH_3(NO_2)_3$, mp ~80°C.

Compounds **I** and **II** were prepared at the Institute of Organic Chemistry by the procedures described in [5, 6]. Ammonium nitrate (analytically pure grade) was dried over P_2O_5, ground in an agate mortar, and mixed manually with an appropriate nitro compound. The AN-to-nitro compound weight ratio was 1 : 1. The weight of each component was about 30 mg.

Liquid trinitrotoluene decomposes at an appreciable rate on being heated to above 190°C. The kinetics of its thermolysis is reviewed in [3]. The thermolysis in the liquid phase is a multistep process which is considerably faster than that in the gas phase. To compare the rate of heat release in TNT and its mixtures with AN, we performed several experiments in the temperature range from 192.7 to 222.5°C. Thermolysis of TNT is an autocatalytic process of approximately the first order. The thermolysis rate increases by a factor of 25–30. The initial thermolysis rates were substantially higher than the published values [3].

Thermolysis of compounds **I** and **II** containing trinitromethyl groups is substantially faster than that of TNT. The rate of heat release in decomposition of compound **I** in the liquid phase at a temperature of 143.3 to 167.1°C was studied. This is a complex autocatalytic process characterized by two rate maximums. However, the rate of the overall process increases by only a factor of 3–6. The total heat of thermolysis of compound **I** is about 3600 J g^{-1}. The experimental initial rates of heat release $(dQ/dt)_{t=0}$ (W g^{-1}) in decomposition of **I** are given below:

T, °C	143.3	155.6	162.5	167.1
$(dQ/dt)_{t=0} \times 10^2$	0.76	2.3	6.5	7.5

The temperature dependence of $(dQ/dt)_{t=0}$ for compound **I** is described by the following equation

$$(dQ/dt)_{t=0} = 10^{17 \pm 2}\exp[(-15 \pm 2) \times 10^4/RT].$$

The kinetics of thermolysis of **II** was studied in the temperature range 145.8–167.1°C. At higher temperatures, the thermolysis is fast and isothermal conditions cannot be provided. At temperatures lower than 162°C, the major portion of the substance is in the solid state. Thus, thermal degradation of **I** in the single-phase liquid state was studied at 162.5–167.1°C. The reaction is autocatalytic and occurs mainly in the liquid phase. The autocatalytic effect is manifested both in acceleration of the reaction and in an increase in the fraction of the liquid phase owing to dissolution of **II** in the thermolysis products. This impairs the true kinetic law for thermolysis rate of liquid **II**, since the thermolysis in the solid state is usually slower than that in the liquid state. In particular, thermolysis, especially at lower temperatures, reaches the maximal rate within a longer time, virtually simultaneously with complete melting of the compound. At 167.1°C, when compounds **I** and **II** are completely in the liquid state, the initial and maximal rates of heat release in thermolysis of compound **II** are higher by factors of 2.5 and 4.5, respectively, than those of compound **I**. The heat of thermolysis of **II** is about 3700 J g^{-1}. The initial rates of heat release $(dQ/dt)_{t=0}$ (W g^{-1}) in thermolysis of **II** are as follows:

T, °C	145.8	155.6	162.5	167.1
$(dQ/dt)_{t=0} \times 10^2$	0.56	3.1	7.7	19.0

The temperature dependence of $(dQ/dt)_{t=0}$ for **II** is described by the following equation:

$$(dQ/dt)_{t=0} = 10^{29 \pm 1}\exp[(-25 \pm 1) \times 10^4/RT]$$

At temperatures lower than the melting point, the system is two-phase owing to partial melting of an eutectic mixture with impurities. The fraction of the liquid phase increases with temperature. Above 162°C the compound is liquid.

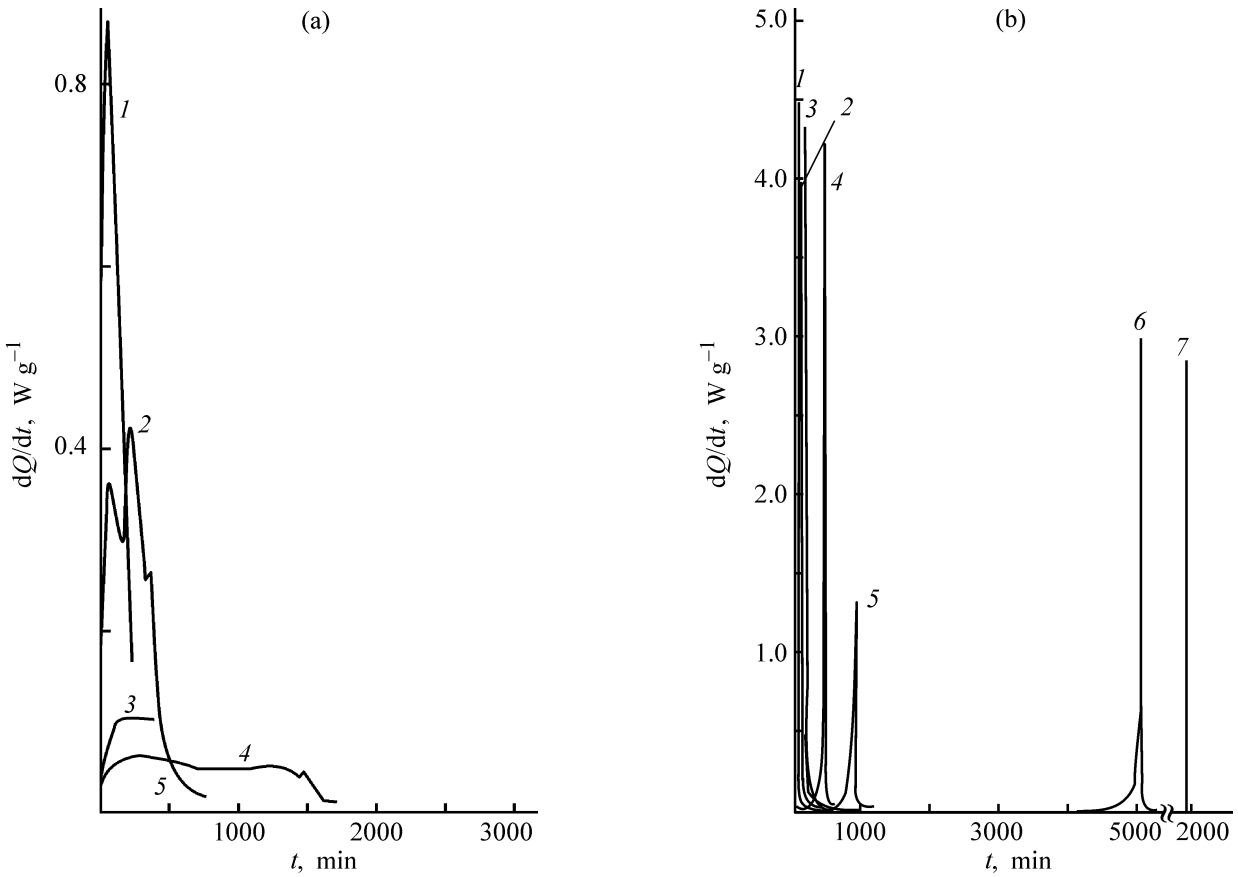


Fig. 1. Rate of heat release, dQ/dt, in thermolysis of mixtures of AN with (a) TNT and (b) compound **I** vs. time t. Thermolysis temperature, °C: (a) (*1*) 222.5, (*2*) 211, (*3*) 192.7, (*4*) 180.7, and (*5*) 144.3 (b) (*1*) 167.1, (*2*) 162.5, (*3*) 155.6, (*4*) 143.3, (*5*) 134.8, (*6*) 121.5, and (*7*) 112.6.

Our study of the kinetics of heat release in thermolysis of mixtures of all the nitro compounds examined with AN showed that the critical factors of this reaction are the thermolysis rate of the nitro compound and the susceptibility to oxidation with nitric acid and nitrogen oxides. Themolysis of AN–TNT mixtures was studied in the temperature range from 143.3 to 222.5°C. The kinetic curves of heat release are shown in Fig. 1a. The initial and maximal rates of heat release are higher by a factor of 10–15 and 1.5–2.5, respectively, than those in thermolysis of individual trinitrotoluene. The overall acceleration is substantially smaller owing to the stronger acceleration in the initial steps. The initial portion of the dependence of the hear release rate on the heat release by this time and proportional to the degree of conversion at $Q <$ 800 J g^{-1} of TNT is fitted by the equation

$$\mathrm{d}Q/\mathrm{d}t = k_1 Q_{\mathrm{tot}} + k_2 Q. \qquad (1)$$

The rate constants of the initial (k_1, s^{-1}) and autocatalytic (K_2, s^{-1}) steps in Eq. 1 are presented below:

T, °C	143.3	180.7	192.7	202.5	211	222.5
$k_1 \times 10^6$	0.19	3.5	5.5	10	17	35
$k_2 \times 10^6$	6.9	83	110	270	300	630

The temperature dependences of k_1 and k_2 are described by the following equations:

$$k_1 = 10^{7.2 \pm 0.4}\exp[(-111 \pm 4) \times 10^3/RT]$$

$$\text{at } Q_{\mathrm{tot}} = 9000 \text{ J g}^{-1} \text{ TNT},$$

$$k_2 = 10^{6.9 \pm 0.5}\exp[(-96 \pm 5) \times 10^3/RT].$$

The mixture is two-phase in the whole temperature range examined. Ammonium nitrate melts at 169.6°C. At higher temperatures, the mixture consists of two liquid phases: AN melt and TNT melt. These liquids are partially soluble in each other. As in the case of AN–pyroxylin mixtures, nitrogen dioxide formed in thermolysis of TNT rapidly oxidizes AN to form nitric acid. As a result, the total enthalpy of thermolysis increases from 3000 for pure TNT to 9000 J g^{-1} for an AN–TNT mixture. The increase in the total

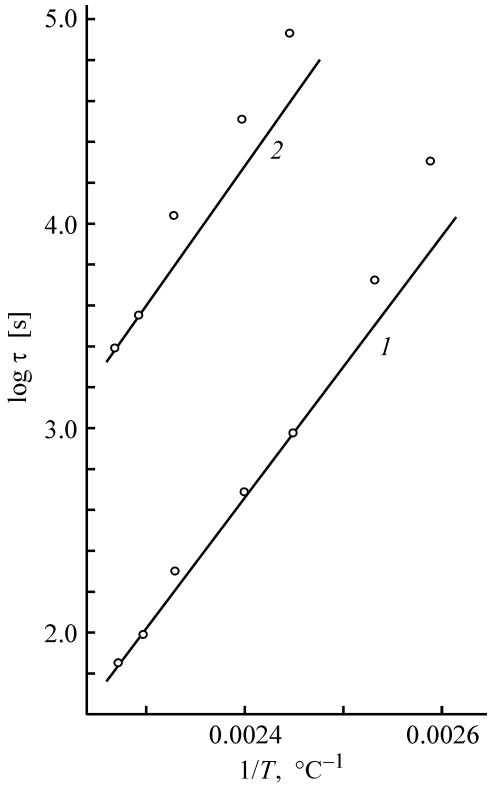


Fig. 2. Logarithm of the time τ required to reach the maximal rate of heat release in thermolysis of compounds (*1*) **I** and (*2*) **II** vs. temperature *T*.

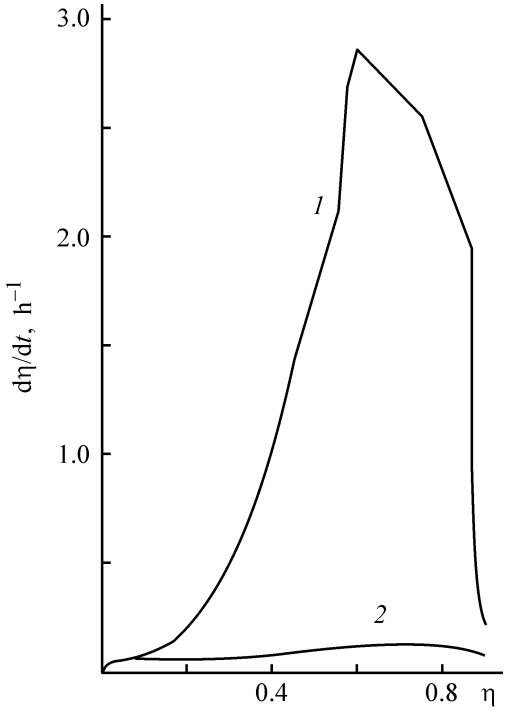


Fig. 3. Thermolysis rate dη/d*t* of (*1*) AN–compound **I** mixture and (*2*) pure **I** at 155.6°C vs. conversion η.

enthalpy of the process accelerates the heat release in the mixture. The increase in the maximal rate of heat release is determined by the growth of the enthalpy of thermolysis. On being heated to above 180°C, liquid AN decomposes at a noticeable rate and the nitric acid released in the process can oxidize TNT. This fact is apparently responsible for the additional increase in the initial rate of heat release. At the same time, it is known [7] that the hydrogen atoms of the benzene ring are difficultly oxidized (especially in the presence of adjacent nitro groups). Hence, the cross influence of thermolysis products of TNT and AN is substantially weaker than that of the products formed in thermolysis AN-pyroxylin mixtures. The sharp maximum of heat release and the jumpwise acceleration of heat release are not observed in thermolysis of AN–TNT mixtures in the temperature range examined. The rate of heat release gradually increases up to a conversion of 0.25–0.3 and then decreases after reaching a maxim (in some cases, two close maxima). It is possible that the sharp acceleration of the thermolysis of an AN–TNT mixture, as in the case of an AN–pyroxylin mixture, will be observed at higher temperatures. This acceleration on heating above 220°C is not of practical importance.

The kinetic features of thermolysis of mixtures of AN with compounds **I** and **II** somewhat differ. The kinetics of thermolysis of an AN–compound **I** mixture was studied in the range 112.6–167.1°C. At these temperatures, thermal decomposition of AN can be neglected. The kinetic curves are shown in Fig. 1b. It is clearly seen that a relatively long period of slow heat release at a rate exceeding by only a factor of 1.5–2 the rate of thermolysis of pure compound **I** is followed by a sharp acceleration of the process. About 30–35% of the total heat of reaction is liberated within 5–10 min. The maximal rate of heat release is higher by a factor of 13–1000 than the initial rate. This ratio decreases with increasing temperature. The temperature dependence of the time τ (s) required to reach the maximal rate at temperatures from 134.8 to 167.1°C, when compound **I** is completely molten, is described by the equation

$$\tau = 10^{-11 \pm 2}\exp[(-119 \pm 5) \times 10^3/RT].$$

This dependence is shown in Fig. 2 in comparison with the similar dependence for solid **I**.

The initial rates of heat release $(dQ/dt)_{t=0}$ (W g^{-1}) in thermolysis of AN–compound **I** mixture are presented below:

T, °C	134.8	143.3	155.6	162.5	167.1
$(dQ/dt)_{t=0} \times 10^2$	0.92	2.4	3.7	18	36

The temperature dependence of $(dQ/dt)_{t=0}$ for a compound **I**–AN mixture is described by the equation

$$(dQ/dt)_{t=0} = 10^{18 \pm 3}\exp[(-16 \pm 3) \times 10^4/RT].$$

The total enthalpy of thermolysis of a compound **I**–AN mixture is about 5400 J g^{-1} of compound **I**. The ratio of the initial rate to the enthalpy of thermolysis of compound **I**–AN mixture is close to that of compound **I**. However, the autocatalytic effect in the mixture is substantially stronger. The dependences of the rate of thermolysis of compound **I** and its mixture with AN $d\eta/dt = (dQ/dt)/Q_{tot})$ h^{-1}) on the conversion $\eta = Q/Q_{tot}$ at 155.6°C are shown in Fig. 3.

At 112.6 and 121.5°C only a small portion of **I** melts owing to the formation of a eutectic with impurities. In the course of the thermolysis, compound **I** melts further owing to its dissolution in the accumulated thermolysis products. The kinetic features of thermolysis under these conditions are considered in [8]. In all cases, the process additionally autocatalytically accelerates owing to an increase in the content of the liquid phase; the maximal rate is attained in the final reaction steps by the end of melting of the compound. In the first steps of the process, compound **I** is only partially in the liquid state, the initial rates of the heat release are lower, and the time required to attain the maximal rate is substantially longer, compared with the values determined from the temperature dependences. The initial rate in the binary mixture at 112.6°C is below the sensitivity limit of the calorimeter. At 121.5°C it is lower by a factor of 2.3 than the rate determined by extrapolation of the temperature dependence of $(dQ/dt)_{t=0}$. The time τ measured at 112.6 and 121.5°C is longer by a factor of 2.6 and 1.6, respectively, than the extrapolated values. This difference confirms our assumption that the thermolysis of the mixture is controlled by thermal degradation of **I** in the liquid phase, since the process is slower in the presence of solid **I**.

The features of thermolysis of AN–compound **II** mixtures are similar. In this case, the rate of heat release in the presence of solid **II** is lower since the melting point of this compound is higher. A sharp acceleration of the heat release is observed on heating to 143°C and higher. The heat release accelerates by only a factor of 5–10 and becomes maximal in the final thermolysis steps. The enthalpy of thermolysis of this mixture is 5700 J g^{-1} of compound **II**. At temperatures below 143°C, the heat is released slowly with slight self-acceleration. The temperature dependence of the time required to reach the maximal rate τ (s), determined from two points in the temperature range 162.5–167.1°C when compound **II** is completely in the liquid state, is described by the equation

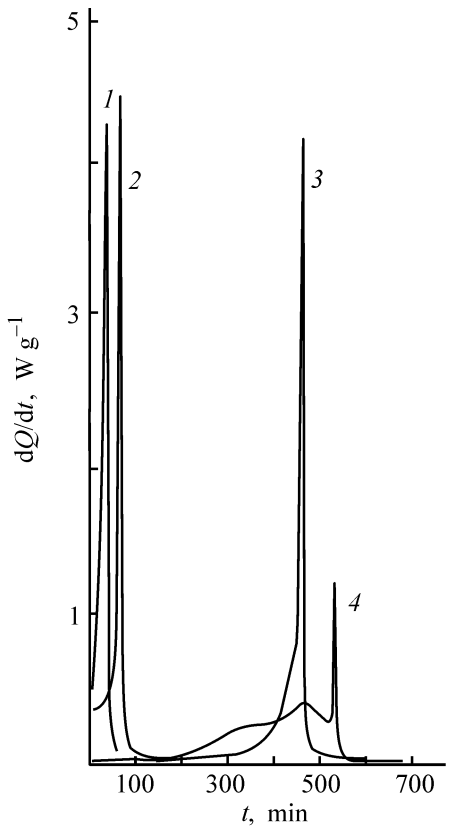


Fig. 4. Rate of heat release, dQ/dt, in thermolysis of mixtures of AN with (*2*, *3*) compound **I** and (*1*, *4*) compound **II** vs. time *t*. Thermolysis temperature, °C: (*1*, *2*) 167.1 and (*3*, *4*) 143.3.

$$\tau = 6 \times 10^{-13}\exp(130 \times 10^3/RT).$$

This dependence in comparison with the similar dependence for solid **II** is shown in Fig. 2.

The initial rates of heat release $(dQ/dt)_{t=0}$ (W g^{-1}) in thermolysis of AN–compound **II** mixture are presented below:

T, °C	134.8	143.3	155.6	162.5	167.1
$(dQ/dt)_{t=0} \times 10^2$	0.33	0.93	5.2	19	54

The temperature dependence of $(dQ/dt)_{t=0}$ for a compound **II**–AN mixture at 134.8–167.1°C is described by the equation

$$(dQ/dt)_{t=0} = 10^{27 \pm 2}\exp[(-23 \pm 2) \times 10^4/RT].$$

At 167.1 °C, when compounds **I** and **II** are completely molten, the initial and maximal rates of heat release for both mixtures are close, but the time in which the maximal rate is attained in the mixture with **II** is shorter by almost a factor of 2 (Fig. 4). In

the case of AN–compound **II** mixture, the maximal rate is higher than the initial rate by only a factor of 12–13. The thermolysis of this mixture in the liquid state is a true autocatalytic process. At lower temperatures, the increase in the fraction of the liquid phase additionally accelerates the process.

To confirm the strong influence of transfer of the nitro compound into the liquid phase on the thermolysis, we studied the kinetics of heat release in the ternary system compound **I** (or **II**)–TNT–AN at 122.1°C. At this temperature, compound **I** is partially molten and melting of **II** is insignificant; at the same time, TNT is liquid at 122.1°C, and nitro compounds are readily soluble in liquid TNT, so that compounds **I** and **II** are completely in the liquid phase. The thermolysis of TNT at this temperature is very slow. Introduction of TNT into an AN–compound **I** mixture shortens the time of attainment of the maximal rate by a factor of 1.75. This value corresponds to the above temperature dependence of this time for a mixture of AN with molten **I**. The thermolysis of the ternary mixture, as well as that of the AN-compound **I** mixture, is characterized by sharp acceleration of the heat release, followed by its deceleration. The maximal rate is higher by a factor of 1000 than the initial rate. Thus, the rate peak is observed in the whole temperature range for the mixture of AN with liquid **I**. The kinetic curve of thermolysis of AN-compound **II** binary mixture at 122.1°C was not measured, since the heat release in this process is very small. In the presence of TNT, the rate of heat release becomes measurable; the initial rate is higher by a factor of 1.5 than that in the ternary mixture with compound **I**. The rate of heat release increases more gradually, reaching a maximum in 67.5 h. The maximal rate is a factor of 18–20 smaller than that with compound **I**. Probably, for a mixture of AN with **II** there may be a sharp jump of the rate of heat release at temperatures from 122 to 143°C; however, an additional study is required to confirm this assumption.

Thus, transition of relatively unstable nitro compounds into the liquid state is a critical factor for thermolysis of their mixtures with AN. To obtain stable mixtures with compounds containing trinitromethyl groups, relatively high-melting compounds should be used. Aromatic nitro compounds like TNT, which are relatively resistant to heat and oxidation, weakly react with AN even after their melting.

Based on our kinetic data and the results of [2], we can elucidate the reaction mechanism in the mixtures in question. As noted above, the first step is thermolysis of the nitro compound or nitrate to form nitrogen dioxide. This is the rate-determining reaction in the initial steps of thermolysis. The rate of thermolysis of aliphatic nitro compounds is determined mainly by the number of nitro groups at the carbon atom and by the influence of adjacent substituents [3] and can vary widely. The thermolysis rate of trinitromethyl-containing compounds in the liquid state is the maximal. The functional groups of **I** and **II** substantially accelerate their thermolysis as compared to aliphatic nitro compounds containing no other functional groups. The liberated nitrogen dioxide rapidly reacts with AN in accordance with the equation

$$4NH_4NO_3 + 3NO_2 = 4HNO_3 + 6H_2O + 3.5N_2.$$

The heat of this reaction is about 1700 J g^{-1} of the equivalent mixture and is higher than the heat of thermolysis of pure AN.

The kinetic features of the final steps of thermolysis somewhat differ. In this case, the fast reaction of the nitro compounds with nitric acid to form nitrogen dioxide plays an important role. This reaction is responsible for the sharp acceleration of the process and the rapid attainment of high heat release rates. The reaction of pyroxylin with nitric acid is the most intense and results in a strong autocatalytic acceleration of the thermolysis. The contribution of this reaction to thermolysis of an AN–TNT mixture is insignificant. In this case, the autocatalytic effect is weaker that that in thermolysis of the initial TNT. The reactivity of the examined esters of 2,2,2-trinitroethanol with respect to nitric acid is intermediate. Compounds **I** and **II** can both be oxidized by nitric acid and undergo acid hydrolysis with subsequent oxidation of the hydrolysis products. These reactions are slower than hydrolysis of cellulose nitrate and oxidation of cellulose with nitric acid. Previously, we have shown that in AN–pyroxylin mixtures nitrogen dioxide is completely taken up by additions of diphenylamine or urea [2]. No autocatalytic effect is observed until these additives are completely spent in reaction with nitrogen dioxide. This fact confirms the proposed thermolysis mechanism. The behavior of these additives in the AN–nitro compound mixtures should be similar.

CONCLUSIONS

(1) The temperature dependences of the specific initial rates of heat release in thermolysis of individual bis(2,2,2-trinitroethyl) succinate and tetrakis(2,2,2-trinitroethyl) orthocarbonate and of their mixtures with ammonium nitrate are described by similar equations. The difference in the initial rates of heat release in

thermolysis of these mixtures and individual bis(2,2,2-trinitroethyl) succinate and tetrakis(2,2,2-trinitroethyl) orthocarbonate is due to different total heats of thermolysis.

(2) The degree of autocatalytic acceleration of thermolysis of mixtures of ammonium nitrate with bis(2,2,2-trinitroethyl) succinate and tetrakis(2,2,2-trinitroethyl) orthocarbonate is higher than that in thermolysis of the individual nitro compounds. The reactive compound of the autocatalytic step is nitrogen dioxide. Nitrogen dioxide rapidly reacts with ammonium nitrate to form an equimolar amount of HNO_3, which catalyzes thermolysis of the polynitro compounds.

(3) The rate of reaction of ammonium nitrate with relatively unstable compounds is controlled by transfer of these compounds into the liquid phase.

ACKNOWLEDGMJENTS

This study was financially supported by the International Science and Technology Center (project no. 1882-2001).

REFERENCES

1. Gorst, A.G., *Porokha i vzryvchatye veshchestva* (Gunpowders and Explosives), Moscow: Mashinostroenie, 1972.
2. Rubtsov, Yu. I., Kazakov, A.I., Kirpichev, E.P., *et al.*, *Zh. Prikl. Khim.*, 2005, vol. 78, no. 6, pp. 891–900.
3. Manelis, G.B., Nazin, G.M., Rubtsov, Yu.I., *et al.*, *Thermal Decomposition and Combustion of Explosives and Propellants*, London: Taylor & Francis Group, 2003.
4. Galyuk, O.S., Rubtsov, Yu.I., Malinovskaya, G.F., *et al.*, *Zh. Fiz. Khim.*, 1965, vol. 39, no. 9, pp. 2319–2322.
5. Kochoy, R.E. and McGuire, R.R., *J. Org. Chem.*, 1972, vol. 37, pp. 3041–3042.
6. US Patent 3 306 939.
7. Emanuel', N.M., Denisov, E.T., and Maizus, Z.K., *Tsepnye reaktsii okisleniya uglevodorodov v zhidkoi faze* (Chain Reactions of Hydrocarbon Oxidation in the Liquid Phase), Moscow: Nauka, 1965.
8. Manelis, G.B. and Dubovitskii, F.I., *Dokl. Akad. Nauk SSSR*, 1959, vol. 126, pp. 813–816.

Russian Journal of Applied Chemistry, Vol. 78, No. 12, 2005, pp. 1944–1947. Translated from Zhurnal Prikladnoi Khimii, Vol. 78, No. 12, 2005, pp. 1977–1980.
Original Russian Text Copyright © 2005 by Alekseev, Arapov, Belozerov, Osipov, Semenov, Polovtsev, Charykov, Izotova.

APPLIED ELECTROCHEMISTRY AND CORROSION PROTECTION OF METALS

Formation of Carbon Nanostructures in Electrolytic Production of Alkali Metals

N. I. Alekseev, O. V. Arapov, I. M. Belozerov, Yu. G. Osipov, K. N. Semenov, S. V. Polovtsev, N. A. Charykov, and S. G. Izotova

Innovations of Leningrad Institutes and Enterprises Closed Joint-Stock Company, St. Petersburg, Russia

Ioffe Physicotechnical Institute, Russian Academy of Sciences, St. Petersburg, Russia

St. Petersburg State University, St. Petersburg, Russia

State Institute of Applied Chemistry, St. Petersburg, Russia

Received May 25, 2005

Abstract—Carbon-based solid phase containing open and closed multiwalled carbon nanotubes (up to 5% of the total carbon) was found in the waste from industrial production of metallic lithium by electrolysis of lithium chloride melt with graphite electrodes.

The electrochemical method of preparation of carbon nanostructures [1, 2] and, in particular, carbon nanotubes (CNTs) was developed and studied somewhat later than the electric arc method [3] and virtually simultaneously with that CVD method (chemical vapor deposition, i.e., chemical decomposition of volatile carbon-containing substances in the presence of catalysts [4, 5]) and HIPCO [6]. Chen *et al.* [2] studied the structure of a nanomaterial in relation to a salt used in the electrolysis, and Bai *et al.* [7] considered in detail this process with the most readily available salt in the CNT synthesis, sodium chloride. It was found that, under definite conditions, the carbon constituent of the product accumulating in the electrolytic tank may contain up to 50% nanocarbon material. The quality of the thus obtained CNTs may be close to that of nanotubes synthesized in the arc, and their amount is substantially larger than that of multiwalled nanotubes generated in the arc without catalysts [3] and comparable with the CNT content in "cobweb" prepared in the arc, using catalysts. However, in contrast to the latter process, both multiwalled nanotubes (MNT) and single-walled nanotubes (SNT) by electrolysis can be successfully synthesized without catalyst, and hence its subsequent removal is not required.

Unfortunately, the electrolysis as a method of purposeful synthesis of CNTs has not been developed. This is caused by the fact that it is difficult to organize the electrolysis as a continuous process similar to arc synthesis [8]. Coking of an electrolytic tank with the products of graphite electrode degradation rapidly causes breakdown, and tank cleaning is required, so that, e.g., under laboratory conditions, the working time of the electrolyzer (actually, electrochemical cell) was no more than 10–15 min.

In this context, the goal of our study was to examine the possibility of CNT synthesis in the course of industrial production of alkali metals by electrolysis of their salts. In this case, the problem of coking of the electrolytic tank becomes less pressing, because all dimensions of the apparatus are larger by two to three orders in magnitude as compared to the laboratory device. An idea of CNT synthesis under such conditions was published in [1], however, we could find no information on its implementation.

EXPERIMENTAL

In production of alkali metals (lithium), a eutectic melt of lithium and potassium chlorides (Khimkontsentrat plant, Novosibirsk, Russia) serves as a starting material. The anode consisted from four $30 \times 30 \times 180$-cm graphite blocks immersed in the melt approximately to a depth of 1 m. The direct current was 25 kA. The total surface area of the graphite anode was about $2 \times 0.3 \times 1 \times 4 = 2.4$ m^2. The electrolyzer operates for 1–1.5 years. During this time, each graphite block wears out approximately by half.

1070-4272/05/7812-1944 © 2005 Pleiades Publishing, Inc.

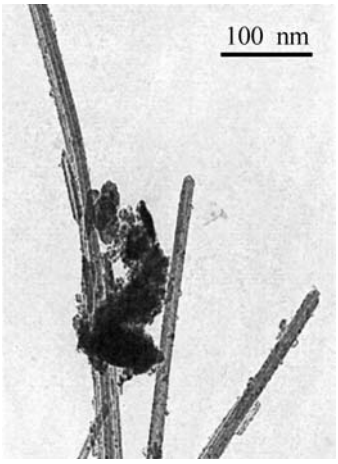


Fig. 1. Electron micrograph of MNT with d = 10–40 nm in a waste from electrolytic production of lithium.

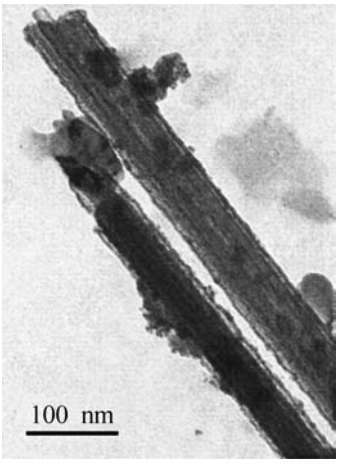


Fig. 2. Electron micrograph of partially open MNTs with d = 50–70 nm in a waste from electroltic production of lithium.

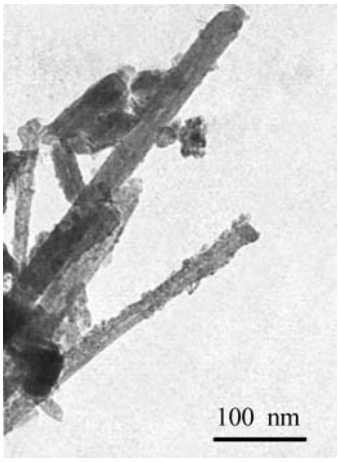


Fig. 3. Electron micrograph of partially open (including "short" tubes) MNTs in a waste from electrolytic production of lithium.

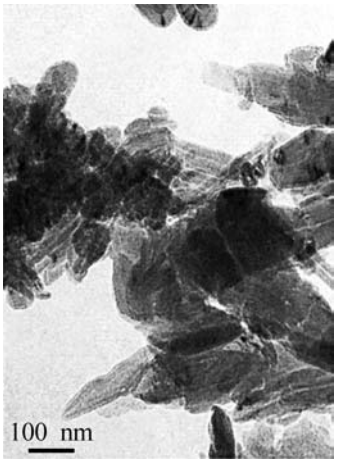


Fig. 4. Electron micrograph of carbon nanobarrels and nanobulbs in a deposit from fullerene production.

A steel cathode is used under the industrial conditions. During the electrolysis, the anode material rapidly converts into a graphitized coke.

We took 5–100-g coke samples from different points of the tank and found that they contain up to 20–30 wt % lithium and potassium chlorides and 30–40 wt % lithium and barium carbonates. To eliminate soluble chlorides, the coke was treated with water for 1 h at 60°C under stirring with a magnetic stirrer and filtered through a "blue tape" paper filter. To separate carbonates insoluble in water, the residue was treated with dilute hydrochloric acid (10 wt %) for 13 h with stirring at room temperature, or boiled in concentrated HCl (36 wt %) for 2h. The weight of the residue thus obtained amounted to 12–20% of the initial slime.

The samples obtained were examined with a JEM-100S (JEOL) transmission electron microscope at 10 000–100 000 magnification after ultrasonic disintegration in toluene.

A typical TEM image of the sample is shown in Fig. 1. MNT bundles 50–70 nm in diameter (d) and separate MNTs 10–40 nm in diameter and 1–2 μm long (L) are clearly seen. In contrast to electron micrographs shown in [1, 2, 7], a substantial part of CNTs have open ends, e.g., MNT with $d \approx 20$ nm projecting from MNT bundle (Fig. 2). The formation of open CNTs is of interest, since, in accordance with reference data, no opening of CNT is observed when a CNT-containing material is treated with dilute acid at room temperature. This fact suggest that at least a part of nanotubes remain open during growth.

The length L of CNTs shown in Figs. 1 and 2 is 1–2 μm. At the same time, short nanotubes with $L \approx$ 100 nm are also seen (Fig. 3). Their number is relatively low. Single-walled CNTs were not observed.



Fig. 5. Electron micrograph of carbon nanobarrels and nanobulbs in modified natural schungites-III.

We did not observe, either, any spiral structures described in [1, 2, 7]. The morphology of nanotubes was similar to that of CNT of crumbled cathodic deposit prepared without a catalyst [3]. The similarity with the crumbled deposit is also observed in the content of nanotubes (~5 wt %) relative to the carbon constituent of the slime. However, in contrast to the deposit[1], we did not observe nanobulbs, nanobarrels, and other concomitant particles in the slim. A typical electron micrograph of the deposit is shown in Fig. 4. The same concerns the nanocarbon constituent of natural schungites (I, II, III, etc.). Schungites always contain, along with nanotubes, noticeable amounts of other hollow and nonhollow nanoparticles (Fig. 5) [11].

Both the properties mentioned above make the carbon constituent of the slimes from alkali metal production (after separation of soluble and insoluble impurities, graphite fraction, and amorphous carbon) fairly precious material for production of emitting coatings, heterogeneous catalysis, etc., when high quality of a separate nanotube and its ideal reproducibility are not required.

The fact that the carbon constituent of the slime from alkali metal production is essentially a waste makes the suggested process commercially attractive. In contrast to a laboratory electrolyzer, the working life of an industrial salt tank into which fresh portions of salts are regularly added can reach 1.5 years. In this time, about 300 kg of the carbon constituent containing several kilograms of nanotubes is accumulated.

[1] Deposit is the product formed on a cathode during recrystallization of carbon that evaporated from the anode surface.

The electrochemical synthesis of CNT is of scientific interest because it proceeds without any catalyst, which is unusual from the viewpoint of the theory. Although iron group metals are inevitably present under conditions of an industrial salt tank (at least at a level of 10–100 ppm), the synthesis of CNT proceeds with the same success as in the chemically pure electrolyte. At the same time, in the case of cathodic deposit, when the CNT synthesis proceeds without the catalyst, the CNTs undoubtedly associated with the cathode [9]. In particular, a model exists in which CNTs are formed by high-temperature solid-phase transformation of fullerenes [10]. In the case of electrolytic CNT with similar morphology, such an association is not obvious.

Another interesting feature (which has not been mentioned in publications devoted to nanotube synthesis) is the formation of a substantial fraction of open tubes. This fact suggests that an unusual mechanism of CNT synthesis under the conditions of the salt tank is operative (this mechanism will be considered in our subsequent paper).

The fact of high CNT content in the electrolytic slime is also of interest. In spite of the apparent similarity of the conditions of laboratory and industrial syntheses, there are substantial differences. In all laboratory experiments, the depth of the electrode immersion into the salt melt was less than 1 cm and substantially affected the nanomaterial structure: at larger immersion depths no CNT or other nanoparticles were formed [1]. In the industrial tank, the depth of electrode immersion was about 1 m.

As for temperature, the conditions of the laboratory device and industrial tank are closer: in the interelectrode area, the temperature in the tank did not exceed 500°C; at this temperature, the CNT yield in the laboratory experiment decreases to several percent relative to the yield at 900°C.

CONCLUSIONS

(1) In the electrolytic tank for the industrial production of alkali metals, small amounts of carbon nanotubes are formed (about 1–2 wt % relative to the total amount of the slime and 5 wt % relative to the slime carbon constituent).

(2) The morphology of nanotubes formed mainly corresponds to that of particles formed in laboratory electrolysis. However, differences also exist: there are no spiral structures and single-walled CNTs, but large amounts of open nanotubes occur.

(3) The latter fact suggests that the growth of open-end CNTs is possible.

REFERENCES

1. Hsu, W.K., Terrones, M., Hare, J.P., *et al.*, *Chem. Phys. Lett.*, 1996, vol. 262, pp. 161–166.
2. Chen, G.Z., Fan, X., Luget, A., *et al.*, *J. Electroanal. Chem.*, 1998, vol. 446, pp. 1–6.
3. Ebbesen, T.W., *Carbon Nanotubes: Preparation and Properties*, Ebbesen, T.W., Ed., Boca Raton: CRC, 1997.
4. Li, W.Z., Xie, S.S., Qain, L.X., *et al.*, *Science*, 1996, vol. 274, pp. 1701–1703.
5. Fan, S., Chapline, M.G., and Franklin, N.R., *Science*, 1996, vol. 283, pp. 512–534.
6. Dai, H., Rinzler, A.G., Nicolaev, P., *et al.*, *Chem. Phys. Lett.*, 1996, vol. 262, pp. 161–166.
7. Bai, J.B., Hamon, A.L., and Marraud, A., *Chem. Phys. Lett.*, 2002, vol. 365, pp. 184–188.
8. Dyuzhev, G.A., Basargin, I.V., Filippov, B.M., Alekseev, N.I., *et al.*, *Int. Appl. Publ. under PCT*, WO 02/096800, PCTRU02/00083.
9. Harris, P.J., *Carbon Nanotubes and Related Structures. New Materials for the Twenty First Century*, Cambridge Univ. Press, 1999.
10. Harris, P.J., Tsang, S.C., Claridge, J.B., and Green, L.N., *J. Chem. Soc., Faradey Trans.*, 1994, vol. 90, pp. 2799–2803.
11. Charykov, N.A., Alekseev, N.I., Arapov, O.V., *et al.*, *Zh. Prikl. Khim.*, 2005, vol. 78, no. 6, pp. 887–890.

Russian Journal of Applied Chemistry, Vol. 78, No. 12, 2005, pp. 1948–1952. Translated from Zhurnal Prikladnoi Khimii, Vol. 78, No. 12, 2005, pp. 1981–1984.
Original Russian Text Copyright © 2005 by Daminova, Novokreshchenova, Yukhin.

APPLIED ELECTROCHEMISTRY AND CORROSION PROTECTION OF METALS

Precipitation of Bismuth(III) Oxochloride from Nitrate Solutions

T. V. Daminova, M. N. Novokreshchenova, and Yu. M. Yukhin

Institute of Solid-State Chemistry and Mechanochemistry, Siberian Division, Russian Academy of Sciences, Novosibirsk, Russia

Received June 3, 2005

Abstract—X-ray phase analysis, thermogravimetry, IR spectroscopy, and chemical analysis were used to study precipitation of bismuth from nitrate solutions upon addition of aqueous solutions of hydrochloric acid or ammonium chloride. The conditions in which bismuth(III) oxochloride of BiOCl composition is formed and the possibility of obtaining a high-purity product were determined.

Bismuth(III) oxochloride is used in medicine, for fabrication of polymeric X-ray contrast media, and in cosmetics for imparting pearly luster to lipstick, nail lacquers, and eyeshades. There is evidence that bismuth oxochloride us used for dyeing of lacquers and plastics, in manufacture of paints, in production of light-sensitive photographic films with nonsilver image development, and as a catalyst for cracking of hydrocarbons [1]. This compound is commonly synthesized by precipitation of bismuth from chloride solutions prepared by dissolution of a reagent-pure oxide in hydrochloric acid, with the subsequent ~10-fold dilution of the bismuth-containing solution with water [2, 3]. A method is known for preparing bismuth(III) oxochloride by its precipitation from solutions containing 5–35% nitric acid and 10–400 g l^{-1} bismuth by addition of chlorides of alkali metals or ammonium, or hydrochloric acid in an amount of 70–150% relative to stoichiometry [4].

Compounds of bismuth(III) are, as a rule, prepared from the metal of Vi1 brand, which contains no less than 98.0% bismuth, with lead and silver present as the main impurities (no more than 1.8 and 0.12%, respectively). Metallic bismuth slowly dissolves in hydrochloric acid. For example, in treatment of metal grains at 60°C for 36 h, the bismuth concentration in solution is only 1.88 and 2.85 g l^{-1} when hydrochloric acid with a concentration of 6 and 12 M, respectively, is used. In this connection, compounds of bismuth are commonly synthesized by dissolving its grains in nitric acid with a concentration of 9 M, with the subsequent hydrolytic purification of bismuth to remove impurity metals at pH 1.5–2.0 [5]. Among disadvantages of this method is evolution of toxic nitrogen oxides into the gas phase in the stage of preparation of bismuth nitrate solutions, because the dissolution process occurs in accordance with the equation

$$Bi + 6HNO_3 = Bi(NO_3)_3 + 3NO_2\uparrow + 3H_2O. \quad (1)$$

It has been shown [6] that preliminary oxidation of metallic bismuth to obtain a technical-grade oxide makes it possible to diminish by half the expenditure of nitric acid and to preclude evolution of nitrogen oxides into the atmosphere in the stage of preparation of bismuth nitrate solutions, because, in the given case, the dissolution process is described by the equation

$$Bi_2O_3 + 6HNO_3 = 2Bi(NO_3)_3 + 3H_2O. \quad (2)$$

Together with nitric acid, hydrochloric acid also well dissolves bismuth oxide, and the dissolution reaction has the following form:

$$Bi_2O_3 + 6HCl = 2BiCl_3 + 3H_2O. \quad (3)$$

Of practical interest in this context is a study of the synthesis of bismuth(III) oxochloride directly from solutions obtained upon dissolution of technical-grade bismuth oxide in hydrochloric or nitric acid.

This communication reports the results obtained in a study of how the concentration of chloride ions and process temperature affect the purity and extent of precipitation of bismuth(III) oxochloride from ni-

1070-4272/05/7812-1948 © 2005 Pleiades Publishing, Inc.

Hydrolytic processing of technical-grade bismuth oxide **I** to give oxochlorides **II**–**VI**

Composition	Content of indicated impurity, %					
	Pb	Cu	Ag	Fe	Zn	Cd
I	1.08	8.7×10^{-3}	5.0×10^{-2}	5.6×10^{-3}	5.8×10^{-4}	2.7×10^{-3}
II	0.36	4.0×10^{-5}	2.3×10^{-2}	4.0×10^{-4}	6.0×10^{-5}	1.0×10^{-5}
III	0.40	6.0×10^{-5}	2.5×10^{-2}	$<1.0 \times 10^{-4}$	6.0×10^{-5}	3.0×10^{-5}
IV	0.22	2.0×10^{-5}	2.3×10^{-2}	$<1.0 \times 10^{-4}$	1.0×10^{-5}	6.0×10^{-6}
V	0.15	2.0×10^{-5}	2.6×10^{-2}	$<1.0 \times 10^{-4}$	1.0×10^{-5}	5.0×10^{-6}
VI	1×10^{-4}	1.0×10^{-6}	3.0×10^{-4}	$<1.0 \times 10^{-4}$	1.0×10^{-5}	5.0×10^{-6}

trate and chloride solutions prepared by dissolving technical-grade bismuth oxide in solutions of these acids.

The metal was oxidized in a stainless steel reactor equipped with a worm for agitation of the melt. A single charge of metallic bismuth into the oxidation reactor was 150–160 kg. The metal was melted at a temperature of 350°C and bismuth oxide from the preceding stage of oxidation of metallic bismuth was added to the melt (20%) under stirring. The temperature was raised to 600°C and the powder was agitated for 6 h. Technical-grade oxide contained 88.4% bismuth, its composition **I** as regards impurity metals is listed in the table. A bismuth(III) nitrate solution of composition (g l^{-1}): Bi(III) 380 and nitric acid 110, was obtained by dissolving technical-grade oxide in 6 M HNO_3. The composition corresponded to that of solutions commonly used in the technology of bismuth compounds. The ratio between the volumes of the initial and final bismuth-containing solutions was 1 : 10. On adding hydrochloric acid or a solution of ammonium chloride to the solution of bismuth nitrate it was adjusted by addition of distilled water. A solution of bismuth chloride, prepared by dissolving technical-grade oxide in 6 M HCl, had the following composition (g l^{-1}): Bi(III) 230 and free hydrochloric acid 70. The bismuth-containing chloride solution was processed by its dilution with distilled water (1 : 9). This was done in fluoroplastic vessels with rabbles. The mixture was agitated for 1 h. After a 1-h settling, the precipitate formed was filtered off in a vacuum, washed with distilled water on a filter, and dried in air. An X-ray phase analysis of the precipitation products was carried out with a DRON-3 diffractometer with Cu_{K_α} radiation, counter rotation rate of 0.5 deg min^{-1}, and I = 4000. Differential-thermal and thermogravimetric analyses of the samples studied were made on an MOM derivatograph (Hungary) at a heating rate of 10 deg min^{-1}. Electron micrographs of the products were obtained on a JSMT-20 scanning electron microscope with a resolution of 200 Å. The specific surface area of the samples obtained was measured by the chromatographic method of thermal desorption of argon. Macroscopic amounts of bismuth(III) in the liquid and solid phases were determined by titration with a solution of Complexone III, with Xylenol Orange as indicator; microscopic amounts were determined by photocolorimetry in the presence of KI. The concentrations of metals (Bi, Pb, Ag, Cu, Fe, Zn) were found by the atomic-absorption method on a Saturn 2M spectrophotometer. The precipitation products were preliminarily dissolved in nitric acid (1 : 1). The concentration of nitrate ions was determined by voltammetry on a renewed copper electrode [7], and that of chloride ions, on a silver electrode [8], after transferring these ions to solution by preliminary treatment of the precipitates with a sodium hydroxide solution (2 M) at 70–90°C.

A study of the hydrolytic processing of bismuth-containing chloride solutions demonstrated that, at their dilution with distilled water (1 : 9) and process temperatures of 25 and 65°C, the recovery of bismuth into oxochloride is 95.2 and 90.1%, respectively. A precipitate obtained at a process temperature of 65°C was washed with a hydrochloric acid solution with a concentration of 0.25 M and twice with water at 65 ± 5°C, with subsequent drying of the product at 110 ± 10°C, to give bismuth(III) oxochloride, whose composition **II** is listed in the table. The results obtained in analyzing this product indicate that processing of bismuth-containing solutions fails to provide an effective purification of bismuth to remove lead and silver. In view of this circumstance, the possibility of obtaining bismuth oxochloride from nitrate

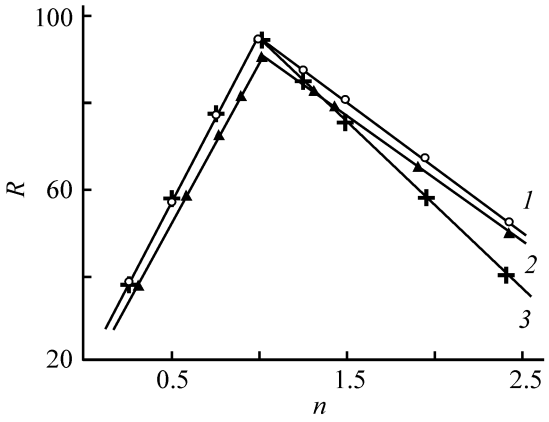


Fig. 1. Degree of bismuth precipitation, *R*, vs. the molar ratio of chloride ions to bismuth (Cl/Bi), *n*, in the system. (*1*, *3*) NH_4Cl and (*2*) HCl. Process temperature (°C): (*1*, *2*) 20 and (*3*) 60.

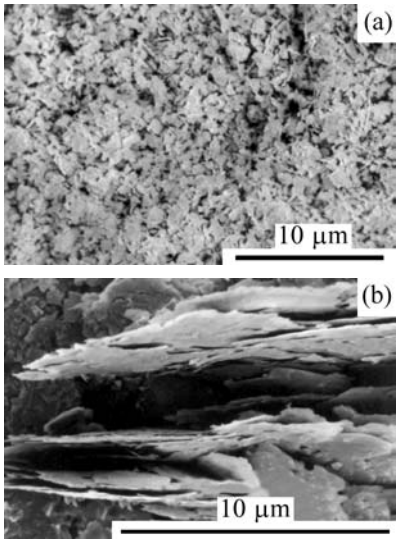


Fig. 2. Electron micrographs of hydrolysis products obtained upon addition of a bismuth-containing nitrate solution to a hydrochloric acid solution. Temperature (°C): (a) 23 and (b) 90.

solutions commonly used in synthesis of bismuth compounds was studied.

In precipitation of bismuth from nitrate solutions by addition of a solution of ammonium chloride or hydrochloric acid, the dependence of the degree of bismuth precipitation, *R*, on the molar ratio of chloride ions to bismuth in solution, *n*, passes through a maximum at 1.0–1.1 (Fig. 1). The decrease in *R* at $n > 1$ is due to the formation in solution of chloride complexes of the type Bi_xCl_{3-x}, which hinders precipitation of bismuth in the form of oxochloride. It can also be seen in Fig. 1 that solutions of both ammonium chloride and hydrochloric acid can be used for quantitative precipitation of bismuth, whereas raising the process temperature leads to a decrease in the degree of bismuth recovery into a precipitate. This is due to the fact that complexation of bismuth with chloride ions mainly occurs via endothermic reactions [9]. As a result, the extent of bismuth complexation with chloride ions in solution increases with temperature, and, accordingly, the degree of its recovery into precipitate decreases. When hydrochloric acid is used as donor of chloride ions, the degree of bismuth recovery into precipitate also somewhat decreases, which is due to an increase in the solubility of bismuth oxochloride as the concentration of hydrogen ions in solution becomes higher.

Bismuth oxochloride shows clearly pronounced characteristic diffraction peaks with d = 7.38, 3.69, 3.442, 2.753, 2.677, 2.205, 1.946, 1.694, and 1.574 Å [10]. It follows from X-ray diffraction analysis that the positions of these peaks remain virtually the same in precipitation of bismuth from both chloride and nitrate solutions upon addition of chloride ions, irrespective of the nature of the solutions used. This fact confirms that bismuth precipitates from these solutions in the pH range studied (0–3) in the form of the oxochloride BiOCl.

The results of differential-thermal and thermogravimetric analyses of bismuth oxochloride samples obtained in processing of bismuth-containing chloride and nitrate solutions indicate that the product has a homogeneous composition and is stable in a wide temperature range. When bismuth oxochloride is heated, loss of mass begins at temperatures above 600°C, which is due to sublimation of bismuth in the form of a chloride to form oxochlorides with a bismuth : chlorine molar ratio exceeding unity [11].

Electron micrographs of hydrolysis products indicate that bismuth oxochloride obtained at 25±5°C by adding water to a hydrochloric acid solution, or a chloride containing solution to a nitrate solution, are, in both cases, aggregates of micrometer microcrystals, presumably of planar-prismatic type, with a poor morphology (Fig. 2a). The product obtained in precipitation of bismuth oxochloride at an elevated temperature, 90±5°C, has the form of aggregates of fine-lamellar crystals with metallic shine and the following dimensions (μm): 20–100 in the basal plane and about 0.1–0.3 in thickness (Fig. 2b). In this case, the specific surface area of bismuth(III) oxochlorides obtained at a process temperature of 25°C varies within 9.6–12.4 $m^2 g^{-1}$, and that of products synthesized at 90°C, within 1.1–1.4 $m^2 g^{-1}$.

To synthesize bismuth oxochloride of increased purity, the possibility of its purification to remove the main impurity metals in precipitation from nitrate solutions was analyzed. The study performed demonstrated that, in precipitation of bismuth from nitrate solutions in the form of oxochloride at a molar ratio of chloride ions to bismuth equal to 1.05, as also in its precipitation from chloride solutions, there is no effective purification of bismuth to remove lead and silver [see table, compositions **III** and **IV**]. In this case, raising the process temperature leads to synthesis of a purer product [**III** at 25°C and **IV** at 65°C]. This result agrees with previously obtained data on bismuth precipitation from hydrochloric acid solutions [12]. The results of the present study demonstrate that, even at a molar ratio of chloride ions to bismuth in solution equal to 0.9, there is no effective purification of bismuth to remove lead and silver at the process temperature of 65°C [product **V**].

Precipitation of bismuth from nitrate solutions in the form of a compound of composition $[Bi_6O_5(OH)_3](NO_3)_5 \cdot 3H_2O$ allows its effective purification to remove impurity metals, and this process is used in synthesis of special-purity bismuth(III) oxide [13]. In this context, it is advisable, in order to obtain high-purity bismuth oxochloride, to preliminarily purify bismuth nitrate solutions to remove accessory metals, with subsequent precipitation of bismuth in the form of oxochloride.

In view of the aforesaid, a variant in which bismuth oxochloride is synthesized by precipitation from oxochloride solutions was chosen for enlarged-scale tests. The advantage of this process is that solutions with a higher concentration of bismuth are obtained in the stage of dissolution of technical-grade oxide and the stainless steel apparatus, used in syntheses of other bismuth compounds, can be used in this case. High-purity bismuth(III) oxochloride was synthesized as follows: metallic bismuth of Vi1 brand was melted at 350°C and 20% bismuth oxide from the preceding stage of oxidation of metallic bismuth was added to the melt with stirring. The temperature was raised to 600°C and the powder was agitated for 6 h. The resulting bismuth oxide was dissolved in a 6 M solution of nitric acid. Bismuth was precipitated from a solution containing 380 g l^{-1} Bi and 110 g l^{-1} free nitric acid by addition, under stirring, of a 2.5 M ammonium carbonate solution at 60°C. The mother liquor was separated by decantation, and the precipitate was washed, under stirring, with a 0.1 M nitric acid solution and then distilled water at 60°C. The filtered-off precipitate of bismuth oxohydroxonitrate was dissolved in 6 M nitric acid, and bismuth was precipitated from the solution in the form of oxochloride by adding a hydrochloric acid solution at a molar ratio of chloride ions to bismuth equal to unity and process temperature of 60°C. The precipitate was washed with a 0.1 M solution and twice with distilled water, and then dried at 100°C. The enlarged-scale tests yielded bismuth(III) oxochloride containing (%): bismuth 80.25 and nitrate ions $<5 \times 10^{-3}$. The content of impurity metals in product (VI) is listed in the table. The degree of bismuth recovery into oxochloride is 89.8%.

CONCLUSIONS

(1) Precipitation of bismuth from both chloride and nitrate solutions upon addition of chloride ions was examined and it was shown that bismuth is precipitated from these solutions in the pH range studied (0–3) in the form of oxochloride BiOCl and the specific surface area of the product decreases from 12.4 to 1.1 $m^2 g^{-1}$ as temperature is raised from 25 to 90°C.

(2) It was demonstrated that, in preparing bismuth-containing chloride solutions from metallic bismuth, it is advisable to preliminarily convert bismuth into oxide by introduction of 20–30 wt % bismuth oxide into its melt at 350 ± 50°C under agitation, with the process temperature subsequently raised to 600 ± 50°C.

(3) It was shown that, to obtain high-purity bismuth oxochloride from technical-grade products, it is necessary to preliminarily purify bismuth to remove accessory metals by its precipitation from nitrate solutions in the form of a compound of composition $[Bi_6O_5(OH)_3](NO_3)_5 \cdot 3H_2O$.

REFERENCES

1. Yukhin, Yu.M. and Mikhailov, Yu.I., *Khimiya vismutovykh soedinenii i materialov* (Chemistry of Bismuth Compounds and Materials). Novosibirsk: Sib. Otd. Ross. Akad. Nauk, 2001.
2. *Rukovodstvo po neorganicheskomu sintezu* (Manual of Inorganic Synthesis), 6 vols., Translated from German, Brauer, G. Ed., Moscow: Mir, 1985, vol. 2.
3. Klyuchnikov, N.G., *Neorganicheskii sintez* (Inorganic Synthesis), Moscow: Prosveshchenie, 1988.
4. RF Patent 2049731.
5. Karyakin, Yu.V. and Angelov, I.I., *Chistye khimicheskie veshchestva* (Pure Chemical Substances), Moscow: Khimiya, 1974.

6. Yukhin, Yu.M., Daminova, T.V., and Smirnov, V.I., *Khim. Interes. Ustoich. Razv.*, 1999, vol. 7, pp. 745–749.
7. Aleksandrova, T.P. and Kletenik, Yu.B., *Zh. Anal. Khim.*, 1994, vol. 49, pp. 615–619.
8. Kletenik, Yu.B., Tarasova, V.A., and Bek, R.Yu., *Zh. Anal. Khim.*, 1987, vol. 42, pp. 891–896.
9. Mironov, V.E., Kul'ba, F.Ya., Fedorov, V.A., and Nikitenko, T.F., *Zh. Neorg. Khim.*, 1963, vol. 8, pp. 1852–1856.
10. Powder Diffraction File, *J.C.P.D.S.*, USA, Pennsylvania, 1985.
11. Nurgaliev, B.Z., Popovkin, B.A., and Stefanovich, S.Yu., *Zh. Neorg. Khim.*, 1983, vol. 28, pp. 2207–2211.
12. Yukhin, Yu.M., Vorsina, I.A., and Danilova, L.E., *Zh. Neorg. Khim.*, 1995, vol. 40, pp. 229–233.
13. Yukhin, Yu.M., Mikhailov, Yu.I., Afonina, L.I., and Podkopaev, O.A., *Vysokochist. Veshchestva*, 1996, no. 4, pp. 62–71.

Russian Journal of Applied Chemistry, Vol. 78, No. 12, 2005, pp. 1953–1960. Translated from Zhurnal Prikladnoi Khimii, Vol. 78, No. 12, 2005, pp. 1985–1992.
Original Russian Text Copyright © 2005 by Turaeva, Tarasenkova, Vasilevskii.

APPLIED ELECTROCHEMISTRY AND CORROSION PROTECTION OF METALS

Molybdenum Indicator Electrode for Potentiometric Sensor for Dissolved CO_2

M. S. Turaeva, I. V. Tarasenkova, and V. L. Vasilevskii

Agrophysical Research Institute, St. Petersburg, Russia

Received June 16, 2005

Abstract—Formation of an indicator layer sensitive to dissolved CO_2 on a molybdenum electrode was studied, as influenced by the solution composition, by potentiometry and voltammetry with continuous voltage variation. Kinetic dependences of the potentiometric response and stationary potential of prototype carbon dioxide sensors based on these electrodes were analyzed.

Possible climate changes related to very complex physicochemical and biological processes in the atmosphere, lithosphere, and hydrosphere and to emission of anthropogenic greenhouse gases stimulate studies of indicator structures sensitive to gases. Carbon dioxide is the main climate-affecting gas, and development of compact and reliable CO_2 sensors capable of monitoring an object in its interaction with the environment without damaging the object or affecting the composition of the medium is a topical problem [1, 2].

Since being created, the potentiometric sensor for dissolved CO_2 of the Stone-Severinghaus type [3] has been modified many times. The need for low-resistantce, compact, and mechanically strong devices initiated the use of metal oxide [4–6] and polymeric [7–9] electrodes, instead of glass electrodes, in potentiometric sensors for dissolved CO_2. In most cases, the indicator surface of metal oxide electrodes was prepared by high-temperature oxidation or by chemical or electrochemical oxidation in single-component aqueous solutions [10]. The molybdenum electrode has not been used previously in CO_2 sensors. It has been found [11] that the potential of air-oxidized molybdenum electrode gradually shifts as the solution pH changes and exhibits a hysteresis of the E–pH function. At the same time, molybdenum exhibits stable passivity in aqueous solutions [12–14].

In this study, we examined the formation of an indicator layer sensitive to dissolved CO_2 on a molybdenum electrode and the sensor properties of the indicator electrode for potentiometric CO_2 sensor as influenced by the solution composition.

EXPERIMENTAL

The molybdenum electrode with a front working surface was made of the 99.96% molybdenum wire (0.5 mm in diameter) sealed in molybdenum glass. The inactive surface of the electrode should be reliably insulated, because the contact between the electrolyte and the side surface of the electrode can give rise to additional uncontrollable voltaic cells and cause potential relaxation disturbing the sensor response.

First, the sensor layer on a molybdenum electrode was formed in solutions of various compositions, and then the effect of the preparation conditions on the properties of this layer with respect to H^+ ion exchange and on the stationary potential and potentiometric response to dissolved CO_2 was analyzed. The open-circuit voltage was measured with an I-115 pH-meter (input resistance 10^{12} Ω) or an ITN-7 ion meter (input resistance 10^{16} Ω) and a KSP-4 recording potentiometer. The open-circuit voltage was monitored from the instant of immersion of the molybdenum electrode in the solution of a certain composition until the attainment of the stationary state E_{st}. The measurements were performed with an EVL-3M reference electrode. Before experiments, the working molybdenum electrode was polished, rinsed with water, and dried in air.

The electrolytes for preparing sensor layer were preliminarily selected by analyzing dynamic voltammograms recorded in a three-electrode cell with a Pt auxiliary electrode and a silver chloride reference electrode (with a Luggin capillary), using a PU-1 polarograph and an LKD 4-003 X–Y potentiometer.

1070-4272/05/7812-1953 © 2005 Pleiades Publishing, Inc.

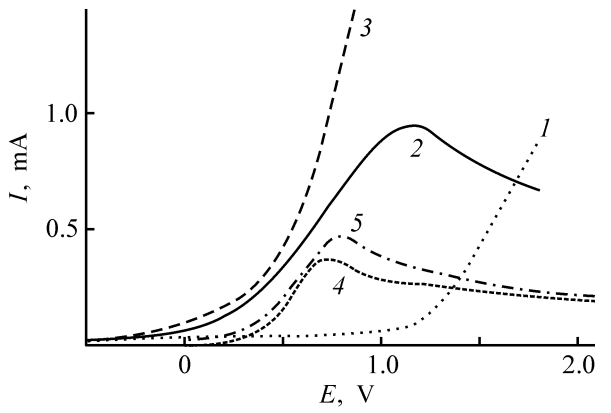


Fig. 1. Polarization curves of the molybdenum electrode as influenced by the solution composition; potential sweep rate 0.02 V s^{-1}. Solution composition, M: (*1*) 0.01 NaOH, (*2*) 0.1 NaOH, (*3*) 1 NaOH, (*4*) 1 $K_4Fe(CN)_6$, and (*5*) 1 $K_4Fe(CN)_6$ + 0.1 sodium citrate.

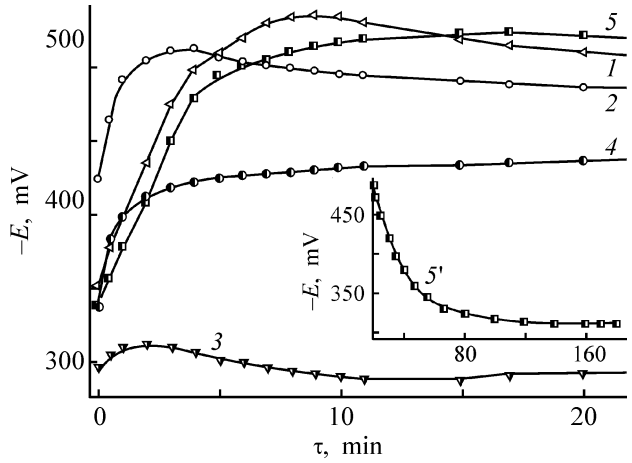


Fig. 2. Open-circuit voltage E vs. time τ of formation of the indicator molybdenum electrode. Solution composition, M: (*1*) 0.1 NaOH, (*2*) 0.1 LiOH, (*3*) 0.1 NaOH + 0.1 $K_3Fe(CN)_6$, (*4*) 0.1 NaOH + 0.1 $K_4Fe(CN)_6$, (*5*) 0.1 NaOH + 1.0 $K_4Fe(CN)_6$ + 0.1 sodium citrate, and (*5′*) the same solution (insert).

Appearance of the area of molybdenum passivation in the voltammogram was a criterion of the solution suitability. It is known that the passivation and corrosion behavior of molybdenum are determined by the composition and pH of the forming solution [15], and stable passive films on the metal surface are formed in alkaline solutions. In our study, we used solutions with pH ≥ 10, because the effect of molecular oxygen is more pronounced in alkaline solutions, compared with that in the acidic medium. An anodic polarization of the molybdenum electrode in alkaline solutions showed that the formation of the surface layer depends on the alkali concentration. For example, the current sharply increases in 1 M NaOH at continuous change in the potential of the molybdenum electrode at a sweep rate V 0.05 V s^{-1}. In the process, the working face of the electrode "sinks" deeper into the glass shell owing to intensive dissolution of molybdenum. In 0.1 M NaOH solutions, the anodic polarization curves recorded in the 0–2.5 V range at a sweep rate V 20 mV s^{-1} can be divided in three portions of (1) slow rise in the current at potentials of 0 to 0.5 V, related to the overvoltage of metal; (2) active dissolution of the metal (from 0.5 to 1.2 V), and (3) passivation (from 1.2 to 2.0 V) (Fig. 1). As the potential increases above 2.5 V, the current grows owing to degradation of the passive layer and pitting. The voltammogram recorded in 0.01 M NaOH shows that, in this case, the passivation potential of the molybdenum electrode shifts toward more positive values.

We found that, at passivation potentials of 2.2 V (0.01 M NaOH) and 1.4 V (1 M NaOH), the electrode surface is coated with a black film. Similar changes in the voltammetric curves were observed in KOH solutions.

The sensitivity $S = dE/d\log[CO_2]$ of the electrodes prepared to dissolved CO_2 and the stability of the stationary potential E_{st} were studied in an open electrochemical system in carbonate-bicarbonate buffers (CBCBs) simulating solutions with a fixed content of carbon dioxide within the 0.998–0.005 vol % range [16], with an EVL-3M silver chloride reference electrode and ESL-43-07 glass pH electrode (to monitor the solution pH). These studies allowed selection of prototype CO_2 sensors.

A study of the potentiometric response showed that the formation of the sensor layers at potentials corresponding to the passivation caused a significant scatter E_{st} of the electrodes (±20 mV), even in the same electrolyte. Initially, the response of freshly prepared electrodes was 55 ± 4 mV per pH unit. However, due to dissolution of the surface film, the sensor electrodes loss their sensitivity.

Stronger films were formed on keeping the molybdenum electrodes in solutions, i.e., when they were prepared by chemical passivation. The changes in the open-circuit voltage after immersion of the molybdenum electrode in 0.1 M NaOH and LiOH solutions are shown in Fig. 2.

In the initial period, the rate of molybdenum dissolution in 0.1 M LiOH is rather high. As the treatment time is rised, mostly passive films are formed after keeping for 3 and 8 min in 0.1 M LiOH and NaOH, respectively. Similar E–t curves are obtained

in passivation of the molybdenum electrode in 0.1 M KOH (with a maximum at ~6 min). The stationary potentials of about –480 mV were attained in 30 (LiOH) or 50 min (NaOH, KOH) after immersion of the electrodes in 0.1 M alkaline solutions.

The electrodes formed in 0.1 M NaOH or KOH in 3 days show a linear E_{st}–pH dependence at pH 2.0–12.5 in various buffer systems, such as oxalate (pH 1.5–2.2), hydrophthalate (pH 2.2–6.0), phosphate (pH 6.8–8.0), tetraborate (pH 8.0–10.6), tris(hydroxy)aminomethane (pH 10.4–11.0), carbonate–bicarbonate (pH 8.5–10.4), and glycine (pH 11.3–12.6) solutions (Fig. 3). The pH dependence of E_{st} of the molybdenum electrode with a deposited sensor layer relative to the silver chloride reference electrode can be described by approximation equations:

$$E_{st} = (0.235 \pm 0.008) - (0.055 \pm 0.005)\text{pH}, \text{ (NaOH 0.1 M)},$$

$$E_{st} = (0.238 \pm 0.009) - (0.052 \pm 0.007)\text{pH}, \text{ (KOH 0.1 M)}.$$

For comparison, we measured the open-circuit voltage (E_{st}–pH) of the molybdenum electrode oxidized in air at 25–60°C. In the pH range 1.0–2.1, the stationary potential remains constant. With the pH increasing to 12.5, linear portions were observed, but, in the case of a hydrophthalate buffer, the linear portion in the pH range 5.50–6.24 shifted by –10 mV, whereas the slope of the dependence increased by +10 mV. On changing the phosphate buffer system for tris(hydroxy)aminomethane in the pH range 7.26–8.40, the stationary potential shifted by –20 mV, whereas the slope dE/dpH remained unchanged.

A study of the time dependence of the open-circuit voltage of the indicator electrodes formed in the alkaline solution and stored in a CBCB (pH 9.4) + KCl (0.001 M) with a CO_2 content of 1.18×10^{-4} M showed that the E_{st} values are unstable. The electrode sensitivity $\Delta E/\Delta$pH changes irregularly (Fig. 4a) with the dependence $E_{st} = f(\text{pH})$ remaining linear. At the same time, the pH function of the indicator electrodes formed in 0.1 M NaOH remains stable in CBCB for more than a month within 50 ± 10 mV. It was found that the reproducibility of the stationary potentials was ±20 mV for a set of 20 electrodes. The function of electrodes formed in 0.1 M NaOH is close to the Nernst dependence, its reproducibility is higher, and the scatter of the stationary potentials is narrower than that of the sensor electrodes formed in 0.1 M KOH (±26 mV for 20 electrodes). Taking these facts into account we used 0.1 M NaOH (S1) as a supporting electrolyte in our further tests of

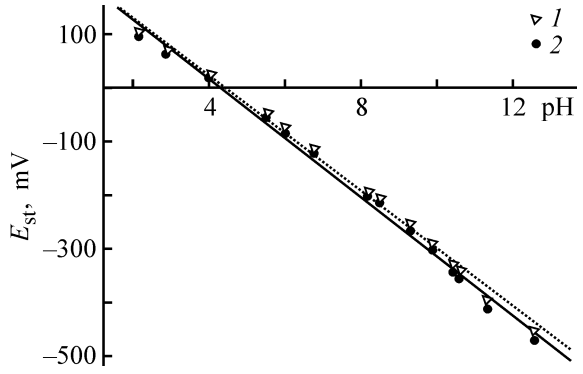


Fig. 3. Potential E_{st} of the molybdenum electrode vs. the solution pH in various buffer solutions after keeping for 3 days in (*1*) 0.1 M NaOH and (*2*) 0.1 M KOH; for explanations see text.

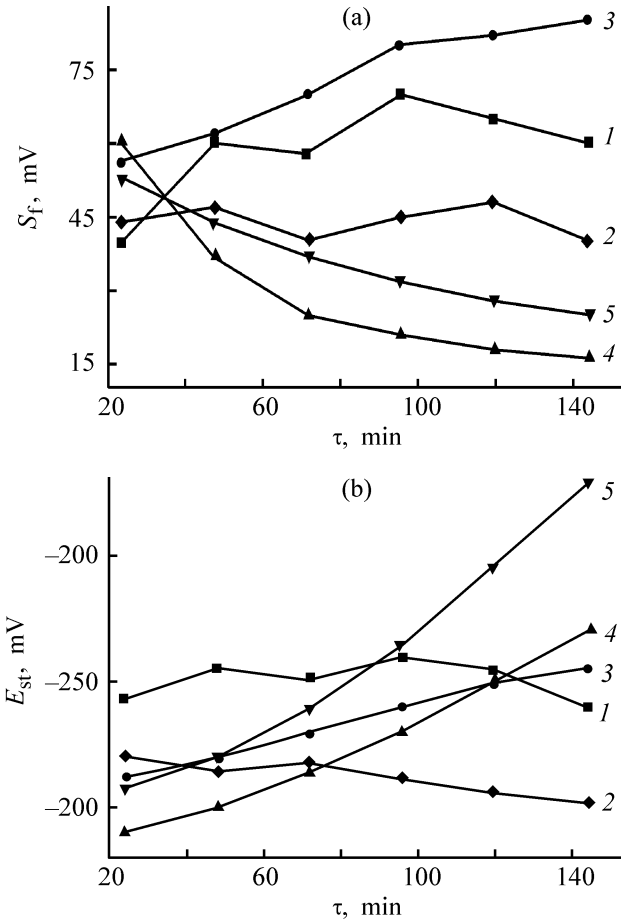


Fig. 4. (a) Changes with time τ in the sensitivity S_f of the molybdenum electrode at various compositions of the forming solution and (b) drift of the stationary potential E_{st} of the molybdenum electrode in the carbonate–bicarbonate buffer with a CO_2 content of 1.18×10^{-4} M after formation of the sensor layer in solutions. Solution composition, M: (*1*) 0.1 NaOH (S1), (*2*) 0.01 NaOH, (*3*) S1 + 0.1 $KMnO_4$, (*4*) S1 + 0.1 $K_3Fe(CN)_6$, and (*5*) S1 + 0.1 $KClO_4$.

the operation solutions for preparing sensitive layers on the electrode surface. In this solution, the electrode surface was coated with a black film. As additional components we used oxidants ($KMnO_4$, $K_2Cr_2O_7$, $KClO_4$), complexes ($K_4Fe(CN)_6$, $K_3Fe(CN)_6$, Na–EDTA), and sodium salts of carboxylic acids (such as aminoacetic, acetylsalicylic, tartaric, malic, oxalic, and citric acids).

The sensor electrodes (SEs) change their properties on being keept in the forming solution in the presence of oxidants, such as $KMnO_4$, $K_2Cr_2O_7$, $KClO_4$, or $K_3Fe(CN)_6$.

Visual monitoring of the films was performed with an SBS-04 optical microscope (×56 magnification). We examined the uniformity of the film and its adhesion to the electrode surface.

We found that the properties of the surface films are determined by the nature of oxidant and its concentration. In the supporting electrolyte containing 0.1 M $K_2Cr_2O_7$, the electrode surface was etched due to the intense dissolution of molybdenum, whereas in 0.01 M $K_2Cr_2O_7$, the electrode surface was coated with a thin semitransparent film, which dissolved in several days.

The variation of the function of the resulting electrodes $dE/d\log[CO_2]$ with time and the shift of the voltage of the open circuit Ag, AgCl, KCl/solution/molybdenum sensor electrode are shown in Fig. 3. The E_{st} values were recorded after keeping the formed electrodes in CBCB (pH 9.4) + KCl (0.001 M) with a CO_2 content of 1.18×10^{-4} M.

The sensor electrodes formed in solutions in the presence of $KMnO_4$, $KClO_4$, and $K_3Fe(CN)_6$ exhibit a linear dependence E_{st}–$\log[CO_2]$ at carbon dioxide concentrations of 10^{-6} to 4×10^{-4} M.

In a 0.1 M $KMnO_4$ solution, the face of the molybdenum electrode was coated with a shining black film. The sensitivity measurements showed that the slope of the E_{st}–$\log[CO_2]$ function is 56 ± 2 mV per tenfold change in the CO_2 concentration (Fig. 4b). Upon a continuous operation of the electrode for 6 days, the slope increases to 80 mV and E_{st} shifts by +40 mV (Fig. 4a); after further keeping, two portions were observed, with slopes of 162 and 80 mV in the CO_2 concentration ranges 3.9×10^{-4}–1.87×10^{-4} and 1.18×10^{-5}–3.13×10^{-6} M, respectively. After keeping for 2 weeks, no film was observed on the electrode surface.

A deeply black film was formed in 0.1 $KClO_4$ solution. In the course of 6-day operation, the slope of the electrode function of the resulting electrodes gradually decreased from 53 to 25 mV (Fig. 4a), and E_{st} shifted by +120 mV, with the film appearance remaining unchanged (Fig. 4b).

In the case of $K_3Fe(CN)_6$, the formation of the film on the electrode surface strongly depends on the concentration of the iron complex. No film was formed in the saturated $K_3Fe(CN)_6$ solution, and the electrode surface was etched in a 1 M solution. Only a thin brownish film was formed in 0.01 M $K_3Fe(CN)_6$, but it disappeared already during the first day of tests. Only in 0.1 M $K_3Fe(CN)_6$ we obtained a black film on the electrode surface, which moved deeper inside the glass holder as the keeping time was made longer. This was to dissolution of the edge surface of the molybdenum electrode. After immersion of the molybdenum electrode in 0.1 M NaOH + 0.1 M $K_3Fe(CN)_6$ solution, the opencircuit voltage in the first two minutes shifted to negative values (Fig. 2, curve *3*) due to the dissolution of the electrode surface, and then the voltage became more positive owing to passivation. A constant $E_{st} = -290$ mV was attained after keeping for 15 min.

The function $dE/d\log[CO_2]$ of the electrodes prepared in 0.1 M $K_3Fe(CN)_6$ solution in the first operation day was 60 mV, and after continuous operation for 6 days it decreased to 20 mV per tenfold change in the CO_2 concentration (Fig. 4a). Measurements of the sensitivity of the resulting electrodes in CBCB showed that, during this period, the stationary potential shifted to the positive values by +70 mV (Fig. 4b).

As can be seen, the sensitivity of the sensor electrodes prepared in solutions containing oxidants [$KMnO_4$, $KClO_4$, and $K_3Fe(CN)_6$] in first operation days was 56 ± 4 mV per tenfold change in the CO_2 concentration. However, in prolonged operation of the sensor electrodes, E_{st} shifts toward positive values (Fig. 4b) with simultaneous changes in the slope of the electrode function (Fig. 4a).

An analysis of our experimental data demonstrated that the electrodes formed in the presence of oxidants show an exponential shift of the output signal with time, which is accompanied by a decrease in the sensitivity to CO_2, whereas in the case of the thin films formed in the presence of $KMnO_4$, E_{st} decreases linearly. This fact is attributable to gradual dissolution of the film coating. For molybdenum electrodes prepared with various oxidants, the exponential drift of E_{st} differs in the characteristic times τ: 110.2 and 141.3 h for $KClO_4$ and $K_3Fe(CN)_6$, respectively. The sensitivity of the electrodes $S_f = dE_{st}/d\log[CO_2]$ also exponentially decreases with a characteristic time τ of 86.2 and 33.7 h for $KClO_4$ and $K_3Fe(CN)_6$, respectively.

The influence exerted by complex compounds used in electroplating to prepare finely crystalline and uniform coatings on the formation of the electrodes and their properties was studied after keeping the molybdenum electrodes in two-component solutions: supporting electrolyte + Na–EDTA and supporting electrolyte + $K_4Fe(CN)_6$. It is known that complex electrolytes enhance the adhesion of the coatings.

In a 1 M Na–EDTA solution, the electrode surface was coated with a black film. The sensor electrodes prepared in the presence of Na–EDTA exhibit linear dependences E–$\log[CO_2]$ with significant differences in E_{st} (±30 mV) and sensitivity $S = 74 \pm 12$ mV (determined for a set of 20 electrodes). A study of the variation of the potentiometric response with time revealed an irregular drift of E_{st} and changes in the electrode sensitivity from 62 to 84 mV. After operation for 2 days, an inflection appeared: at a CO_2 content of 3.9×10^{-4}–1.18×10^{-4} M the electrode sensitivity was 50 ± 3 mV, and at 10^{-4}–3.13×10^{-6} M, 80 ± 5 mV, which is close to the super-Nernst value. Probably, the surface properties of the sensor electrodes change in the course of operation in CBCB.

Keeping in the supporting electrolyte containing 1 M $K_4Fe(CN)_6$ causes formation of the strong black film on the edge surface of the electrode. Upon immersion of the electrodes in 1 M $K_4Fe(CN)_6$ for 20 min, the opencircuit voltage became negative (Fig. 2, curve *4*); however, after keeping for 30 min, it shifted toward positive values, suggesting that the passivation is predominant. The resulting electrodes exhibit linear dependences E–$\log[CO_2]$ with a sensitivity of 64 ± 1 mV per tenfold change in the CO_2 concentration. Changes in E_{st} with time can be described by the dependence $E_{st} = E_1 + A_E \exp(-t/\tau)$ with $\tau = 46.2$ h (Fig. 5a), and the electrode function $dE/d\log[CO_2]$ varied at a rate of +4 mV day^{-1} (Fig. 5b, curve *1*).

The properties of the sensor surface of the molybdenum electrodes as influenced by the organic cations were studied in a 0.1 NaOH + 1.0 $K_4Fe(CN)_6$ supporting electrolyte (S2). The complex $K_4Fe(CN)_6$ is used in electroplating [17] because, when added to the electrolyte, it enhances its throwing power and allows preparation of finely crystalline precipitates.

As can be seen from the dynamic voltammograms, the passivation current of molybdenum electrodes decreases in the presence of $K_4Fe(CN)_6$ and the passivation potential shifts toward negative values (Fig. 1).

The values of E_{st} (Fig. 5a) and S_f of the sensor electrodes formed in the ternary systems containing anions of polybasic hydroxy acids [18] are more reproducible. The open-circuit voltage after immersion of the electrodes into a solution containing S2 + 0.1 M sodium citrate attains stationary potential in approximately 3 h (Fig. 2, curves *5*, *5'*); and passivation becomes predominant after 17-min keeping in the above solution.

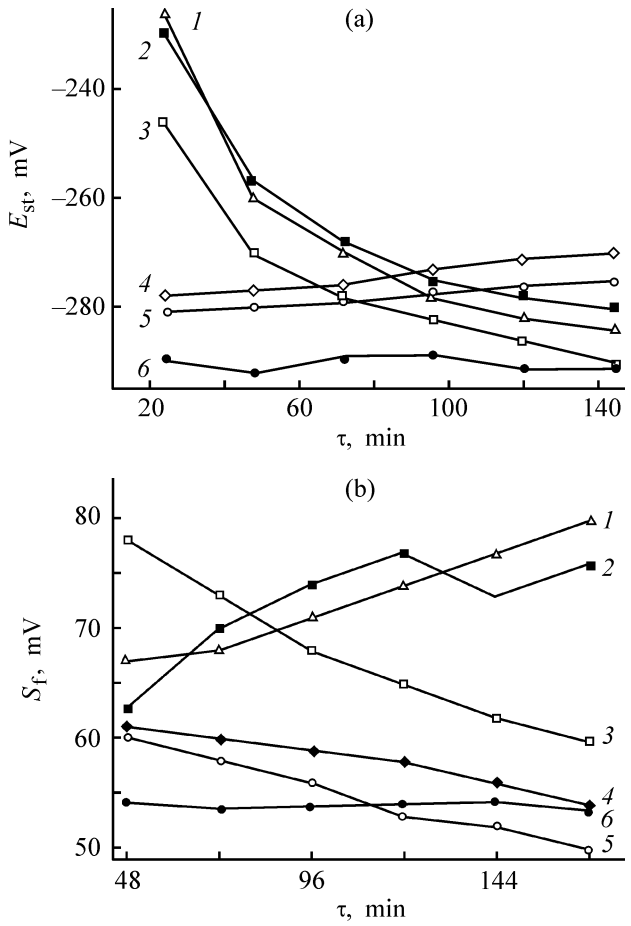


Fig. 5. (a) Drift of the stationary potential E_{st} of the molybdenum electrode in the carbonate-bicarbonate buffer with a CO_2 content of 1.18×10^{-4} M after formation of the sensor layer in given solutions and (b) variation of the sensitivity S_f of the molybdenum electrode at various compositions of the forming solutions with time τ. Solution composition, M: (*1*) 0.1 NaOH + 1.0 $K_4Fe(CN)_6$ (S2) , (*2*) S2 + 0.1 sodium aminoacetate, (*3*) S2 + 0.1 sodium acetylsalycilate, (*4*) S2 + 0.1 sodium oxalate, (*5*) S2 + sodium succinate, and (*6*) S2 + sodium citrate.

A distinctive feature of the sensor electrodes formed in the presence of sodium salts of aminoacetic, acetylsalicylic, malic, oxalic, and citric acids is the linearity of the E–$\log[CO_2]$ dependence in a wider range of CO_2 concentrations. The slopes of the curves depend on the anion (Fig. 5b) and vary from 78 (super-Nernst) to 54 mV per tenfold change in the CO_2 concentra-

Table 1. Statistical analysis of the E_{st} values of the sensor electrodes

Parameters of statistical analysis	Composition of the working solution, M						
	1.0 $K_4[Fe(CN)_6]$ + 0.1 NaOH (S2)	S2 + 0.1 glycine	S2 + 0.1 sodium acetylsalycilate	S2 + 0.1 sodium aminoacetate	S2 + 0.1 sodium succinate	S2 + 0.1 sodium oxalate	S2 + 0.1 sodium citrate
$x = -E_{st}$, mV (average) $f = 29$	282.0	274.1	289.2	264.7	280.1	278.0	249.3
S^*	18.875	11.458	9.764	6.416	4.281	2.600	3.258
$\sigma \cong \sqrt{\overline{S}^2}$	3.446	2.092	1.783	1.171	0.782	0.475	0.595
$G_{max}(exp)^*$	0.539	0.430	0.548	0.523	0.488	0.788	0.553
G_{max} (tab.), significance level 0.01	0.23	0.27	0.31	0.36	0.43	0.74	0.55

* $S = \sqrt{\frac{1}{n-1}\sum_{i=1}^{i}(x_1 - x)^2}$, $G_{max}(exp) = \frac{S^2_{max}}{\sum_{i=1}^{n} S_i^2}$, the same for table 2.

Table 2. Statistical analysis of the S_f values of the sensor electrodes

Parameters of statistical analysis	Composition of the working solution, M						
	1.0 $K_4[Fe(CN)_6]$ + 0.1 NaOH (S2)	S2 + 0.1 glycine	S2 + 0.1 sodium acetylsalycilate	S2 + 0.1 sodium aminoacetate	S2 + 0.1 sodium succinate	S2 + 0.1 sodium oxalate	S2 + 0.1 sodium citrate
$\overline{Z} = \Delta E/\Delta p(CO_2)$, mV, $f = 19$	68.05	63.85	78.2	60.65	59.8	62.05	55.35
S	3.967	4.234	5.782	5.294	3.458	2.762	2.059
$\sigma \cong \sqrt{\overline{S}^2}$	0.887	0.947	1.293	1.184	0.773	0.618	0.460
$G_{max}(exp)$	0.132	0.156	0.280	0.375	0.178	0.074	0.086
G_{max} (tab.), signicance level 0.01	0.27	0.30	0.34	0.39	0.78	0.47	0.59

tion for electrodes formed in electrolytes S2 + 0.1 M acetylsalicylate and S2 + 0.1 M sodium citrate, respectively. The stationary potentials of the sensor electrodes relative to the EVL-1M silver chloride reference electrode in the pH 8.5–10.5 range (corresponding to the CO_2 concentration from 10^{-3} to 10^{-6} M) can be described by the following equations:

$$E = (0.223 \pm 0.018) - (0.078 \pm 0.006)\text{pH},$$
S2 + sodium acetylsalicylate,

$$E = (0.260 \pm 0.010) - (0.054 \pm 0.002)\text{pH},$$
S2 + sodium citrate.

However, as can be seen from Fig. 5a, the drift of the stationary potential of the electrodes formed in the presence of sodium oxalate, succinate, and citrate is significantly smaller than that for the electrodes formed in solutions containing sodium acetylsalicylate or aminoacetate. The CO_2 function of the sensor electrodes formed in solutions of sodium oxalate, succinate, and citrate is also more stable in the course of time (Fig. 5b).

A statistical analysis of the experimental results was performed to check whether changes observed on varying the electrolyte composition are significant (Tables 1, 2). The results of this analysis by the Cochran test show that the properties of the sensor electrods (stationary potential and sensitivity) regularly change as the electrolyte composition is varied.

Our prolonged studies of the sensitivity of the sensor electrodes to dissolved CO_2 showed that the sta-

tionary potential of the electrode formed in the oxalic acid solution shifts in two months by +70 mV (Fig. 6a) and the slope of the CO_2 function increases to 100 mV per tenfold change in the CO_2 concentration (Fig. 6b). The most stable operation parameters (output signal and sensitivity) were found for sensor electrodes formed in solutions containing sodium citrate, used in electroplating to prepare finely dispersed dense metallic coating strongly adherent to the electrode surface. The trends in the potentiometric response to CO_2 of the sensor electrodes formed in the model solutions of carboxylic acid anions may be due to the formation on their surface of passive films exhibiting a proton conductivity, as in the case of solid solutions.

The stability of the resulting sensor surface is determined by the mechanism of ion transfer in the film in the course of its formation.

It is known that layers covering metallic electrodes contain bound water and its amount increases with pH; the OH^-/O^{2-} ratio in the surface layer is greater than that in the film bulk. Water bound in the form of both H_2O and OH^- groups is a source of highly mobile protons, and, thus, hydrogen ions can penetrate from solution into the crystalline structure of the passivating film. Organic acid anions present in the electrolyte, which control the stoichiometry of the transition metal oxygen in the film and thus affect the film properties, can be also involved in the formation of the structure of the passivating film:

$$H_xMoO_n + pA^- = H_xMO_{n-p}A_p + p/2\,O^{2-},$$

$$H_xMoO_{n-p}A_p + mH^+ + me = H_{x+m}MO_{n-p}A_p.$$

Considering $H_xMoO_{n-p}A_p$ as a solid solution of protons, we can calculate the potential as follows:

$$E = E_{st} + (2.3RT/F)\log a(H^+) - (2.3RT/F)\log a(H_s).$$

This equation suggests the Nernst response to the content of H^+ ions in the aqueous phase at a constant activity of hydrogen atoms in the phase of the solid solution.

CONCLUSIONS

(1) Molybdenum-based electrodes sensitive to dissolved CO_2 were formed in multicomponent solutions. The dependences of the stationary potential on time, sensitivity with respect to CO_2, and operation life of the indicator electrodes are determined by the conditions under which the surface films are formed.

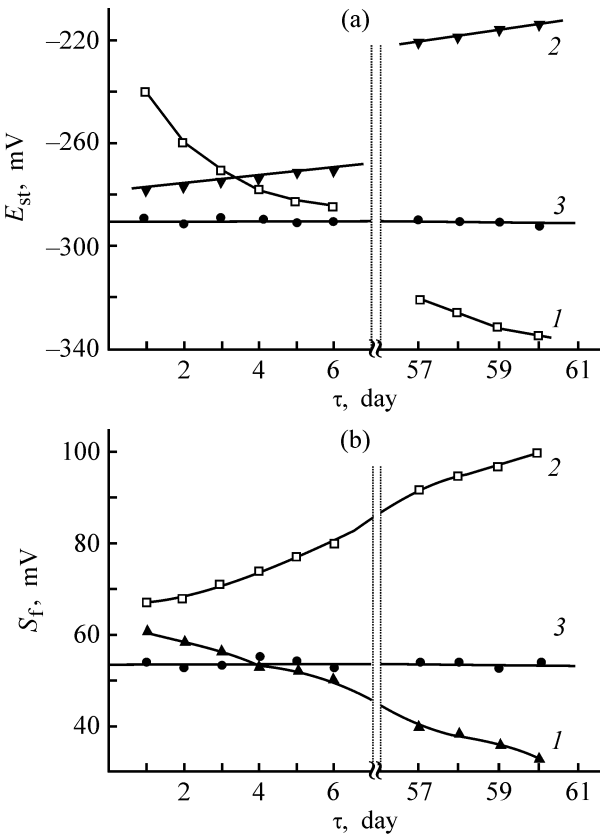


Fig. 6. (a) Drift of the stationary potential E_{st} of the molybdenum electrode in the carbonate-bicarbonate buffer with a CO_2 content of 1.18×10^{-4} M after formation of the sensor layer in given solutions and (b) variation of the sensitivity S_f of the molybdenum electrode at various compositions of the forming solutions with time τ. Solution composition, M: (*1*) S2, (*2*) S2 + 0.1 sodium oxalate, and (*3*) S2 + sodium citrate.

Organic acid anions, being added in the electrolyte, stabilize the operation properties of the electrodes.

(2) The electrolytes containing citrate anions allow preparation of a prototype sensor for dissolved CO_2, which exhibits the Nernst dependence for the open-circuit voltage in the 2×10^{-6}–1.18×10^{-3} M concentration range of carbon dioxide and the output signal remains reproducible for 65 days.

REFERENCES

1. Hanstein, S. and de Beer, D., *Sensors Actuators, Ser. B*, 2001, vol. 81, no. 1, pp. 107–114.
2. Zhou, Z.B., Liu, W.J., and Liu, C.-C., *Sensors Actuators, Ser. B*, 2000, vol. 65, no. 1, pp. 35–38.
3. Severinghaus, J. W., Ann. N.Y. *Acad. Sci.*, 1968, vol. 148, no. 1, pp. 115–132.
4. Mokhallalati, A.O. and Virtosu, D., *Rev. Chim. (RSR)*, 1984, vol. 11, no. 5, pp. 1040–1043.

5. Tarlov, M.J., Semancik, S., and Kreider, K.G., *Sensors Actuators, Ser. B*, 1990, vol. 1, nos. 1–6, pp. 293–297.
6. Kinoshita, K. and Madou, M. J., *J. Electrochem. Soc.*, 1984, vol. 131, no. 5, pp. 1089–1094.
7. Rechnitz, G. A., *Israel J. Chem.*, 1985, vol. 26, no. 1, pp. 35–39.
8. Opdycke, W. N., Parks, S.J., and Meyerhoff, M.E., *Anal. Chim. Acta*, 1983, vol. 155, no. 1, pp. 11–20.
9. Meyerhoff, M.E. and Fraticelli, Y.M., *Clin. Chem. (Winston-Salem)*, 1982, vol. 28, no. 9, pp. 1973–1978.
10. Olthuis, W., Robben, M.A.M., Bergveld, P., Boss, M., Linden, W.E van der, *Sensors Actuators, Ser. B*, 1990, vol. 1, nos. 1–6, pp. 247–256.
11. Issa, M. and Khalifa, H., *Anal. Chim. Acta*, 1954, vol. 10, no. 6, pp. 567–574.
12. Kolotyrkin, Ya.M., *Metall i korroziya* (Metal and Corrosion), Moscow: Metallurgiya, 1985.
13. Sukhotin, A.M., Pozdeeva, A.A., and Antonovskaya, E.I., in *Molibden: Passivnost' i korroziya metallov* (Passivity and Corrosion of Metals), Sukhotin, A.M., Ed., Leningrad: Khimiya, 1971, pp. 12–17.
14. Chukalovskaya, T.V., Tomashov, N.D., and Manskaya, V.D., *Zashch. Met.*, 1984, vol. 20, no. 6, pp. 864–871.
15. *Spravochnik po elektrokhimii* (Handbook on Electrochemistry), Sukhotin, A.M., Ed., Leningrad: Khimiya, 1981.
16. Grodzinskii, A.M. and Grodzinskii, D.M., *Kratkii spravochnik po fiziologii rastenii* (Brief Handbook on Plant Physiology), Kiev: Naukova Dumka, 1973.
17. Yampol'skii, A.M. and Il'in, V.A., *Kratkii spravochnik gal'vanotekhnika* (Brief Handbook of Electroplater), Moscow: Mashgiz, 1962.
18. Tarasenkova, I.V. and Turaeva, M.S., Abstracts of Papers, *Vserossiiskaya konferentsiya s inostrannym uchastiem: Sensory i mikroskhemy* (Sensors and Chips: Russian Conf. with Foreign Participation), St. Petersburg, June 21–23, 2000, p. 112.

Russian Journal of Applied Chemistry, Vol. 78, No. 12, 2005, pp. 1961–1969. Translated from Zhurnal Prikladnoi Khimii, Vol. 78, No. 12, 2005, pp. 1993–2001.
Original Russian Text Copyright © 2005 by Tsygankova, Vigdorovich, Kim, Kichigin, Boldyrev.

APPLIED ELECTROCHEMISTRY AND CORROSION PROTECTION OF METALS

Inhibition of Corrosion and Hydrogenation of Carbon Steel with a Number of Inhibitors in Weakly Acid Media Containing H_2S and CO_2

L. E. Tsygankova, V. I. Vigdorovich, Ya. R. Kim, V. I. Kichigin, and A. V. Boldyrev

Derzhavin State University, Tambov, Russia
Natural-Science Institute, Perm, Russia
AMDOR Private Company, St. Petersburg, Russia

Received June 15, 2005

Abstract—The inhibitive power of AMDOR IK-7 formulation, homologous mixture of alkyl ammonium acetates C_{10}–C_{14} in a specific solvent, and PKU-6 toward corrosion of St. 3 steel in weakly acid media containing 5.8 g l^{-1} NaCl, H_2S, and CO_2 was studied. The influence exerted by the inhibitors on the kinetics of partial electrode reactions and on the hydrogenation of steel was examined. Impedance spectra were recorded and analyzed.

The intensive extraction of oil containing no less than 500 mg l^{-1} hydrogen sulfide [1] makes the protection of building materials against hydrogen sulfide corrosion a matter of current interest. In solving this problem, an important role belongs to corrosion inhibitors. A steadily increasing number of new forms of these inhibitors is being synthesized, because oil companies need inhibitors that would be effective at low concentrations not exceeding 100–200 mg l^{-1}, with the cost of anticorrosion protection thereby reduced and the competitiveness enhanced. It is advisable to develop versatile inhibitors that could retard hydrogen sulfide and carbon dioxide corrosion and hydrogenation of building materials. Such an approach makes it possible to tackle with the presently existing shortage of protective materials, to enlarge the domestic resources of raw materials, and to search for ways to diminish the required amount of imported materials.

This communication presents the results obtained in a comparative study of the efficiency of new corrosion inhibitors for St. 3 steel (AMDOR IK-7 and a formulation composed of alkyl ammonium acetates C_{10}–C_{14} in a specific solvent) and of the known PKU-6 inhibitor (laboratory sample) [2], as versatile inhibitors of the carbon dioxide and hydrogen sulfide corrosion and hydrogenation.

EXPERIMENTAL

The corrosion resistance of St. 3 steel was studied gravimetrically at room temperature on polished samples ($20 \times 12 \times 2$ mm) in solutions containing 5.8 g l^{-1} NaCl, acidified with HCl to pH 2.0–6.0, in the presence of CO_2 and H_2S. Hydrogen sulfide was obtained in the reaction medium by the method reported in [3]. An excess pressure of CO_2 (0.5–2.0 atm) was produced in plastic vessels equipped with nipple valves, as in [4]. CO_2 was pumped from the cylinders, with pressure monitored with a manometer. The exposure time of the electrodes was 24 h. The conventional procedure was used in corrosion tests. The degree of protection, Z (%), by an inhibitor was calculated by the formula:

$$Z = (K_0 - K_{inh})/K_0,$$

where K_0 and K_{inh} are the corrosion rates in a solution with and without inhibitor, respectively.

The following corrosion inhibitors were used: AMDOR IK-7 formulation (c_{inh} = 5–200 mg l^{-1}), which is a 10% solution of higher amines C_{10}–C_{16} in a mixture of aprotic solvents; a formulation composed of alkyl ammonium acetates (AA) C_{10}–C_{14} in a specific solvent; and PKU-6, a product formed

1070-4272/05/7812-1961 © 2005 Pleiades Publishing, Inc.

Table 1. Degree Z of steel protection by inhibitors (c_{inh} = 200 mg l^{-1}) in solutions containing 5.8 g l^{-1} NaCl with and without CO_2 and H_2S at pH 2.0–6.0

pH	Additive	K_0, g m^{-2} h^{-1}	Z, %		
			ANDOR IK-7	AA C_{10}–C_{14}	PKU-6
2.0	–	0.306	64	47	88
4.0	–	0.189	63	43	76
6.0	–	0.081	61	39	52
2.0	CO_2, P = 1 atm	0.261	69	54	48
4.0	CO_2, P = 1 atm	0.162	79	49	51
6.0	CO_2, P = 1 atm	0.181	81	44	52
2.0	H_2S, c = 400 mg l^{-1}	1.4	87	94	87
4.0	H_2S, c = 400 mg l^{-1}	1.2	88	91	90
6.0	H_2S, c = 400 mg l^{-1}	0.59	85	88	89
2.0	H_2S + CO_2, c = 200 mg l^{-1}, P = 1 atm	0.861	91	81	96
4.0	H_2S + CO_2, c = 200 mg l^{-1}, P = 1 atm	0.543	88	79	99
6.0	H_2S + CO_2, c = 200 mg l^{-1}, P = 1 atm	0.423	87	75	84

in condensation of urotropin with alkyl chloride C_{12}–C_{15}.

The potentiostatic polarization of the steel was studied with a P-5827M potentiostat in a three-electrode cell with separated anode and cathode spaces, with a 30-s exposure at each potential. A saturated silver chloride electrode served as reference, and Pt, as an auxiliary electrode. The potentials are given relative to a standard hydrogen electrode. The electrochemical measurements under an excess pressure of CO_2 were made using the method described in [5].

The rate of the hydrogen mass-transfer in steel was estimated as in [6], using a Devanathan two-compartment cell (Pyrex) divided in two by a vertical 300-μm-thick steel membrane [7]. Changes in the hydrogen diffusion flux across the membrane were characterized by the coefficient $\gamma_H = i_0/i$, where i_0 and i are the diffusion currents in the supporting solution and in the solution containing additives, respectively.

The mechanism of the inhibiting effect was analyzed by the impedance spectroscopy. The electrochemical impedance of the steel electrodes was studied at frequencies ($\omega/2\pi$) in the range 60 kHz–10 MHz at the amplitude of the ac voltage of 10 mV, using the Solartron system (UK). The working electrode (St. 3 steel, S_{el} = 0.785 cm^2) and auxiliary electrode (Pt, S_{Pt} = 54 cm^2) were coaxial. A silver chloride electrode was used as reference. The potentials were recalculated to the standard hydrogen scale. The samples were polished, degreased, and cathodically activated (ΔE from E_{cor} equal to 0.2 V) for 10–15 min to remove the air-oxide film. After the polarization was switched off, the electrodes were kept in the solution for 10–15 min, until the quasi-stationary potential was attained. The results of the impedance measurement were processed using the software[1] that enabled calculations for any equivalent circuit with up to 12 elements [8]. The program uses complex (real and imaginary) values of the resistance of the electrochemical system and the corresponding frequencies. Preliminarily, arbitrarily chosen initial values are set for all the elements of the equivalent circuit. The calculation is based on a simplex search for an extremum of a function of several variables. To avoid finding a local minimum of the function, the calculation was repeated many times with different initial values of the elements of the circuit. As a criterion for assessment of the circuits was used the root-mean-square deviation s. An equivalent circuit was considered satisfactory at $s \le 5\%$.[2]

In the supporting solutions without gaseous additives, the protective effect of the inhibitors is low. It increases with the solution acidity and inhibitor concentration, to reach the maximum value at c_{inh} = 200 mg l^{-1} (Table 1).

Introduction of CO_2 into the solutions makes K_0 of the steel lower at pH 2.0 and 4.0, in agreement with published data [9, 10], and higher at pH 6.0. Simultaneously, Z of AMDOR IK-7 and AA C_{10}–C_{14} increases in the presence of CO_2, whereas that of PKU-6 decreases (Table 1).

[1] IBM PC compatible software developed at the Institute of Physical Chemistry, Russian Academy of Sciences.

[2] The authors thank Yu.I. Kuznetsov for the opportunity to perform measurements, and D.B. Vershok and S.V. Oleinik for their assistance in measurements.

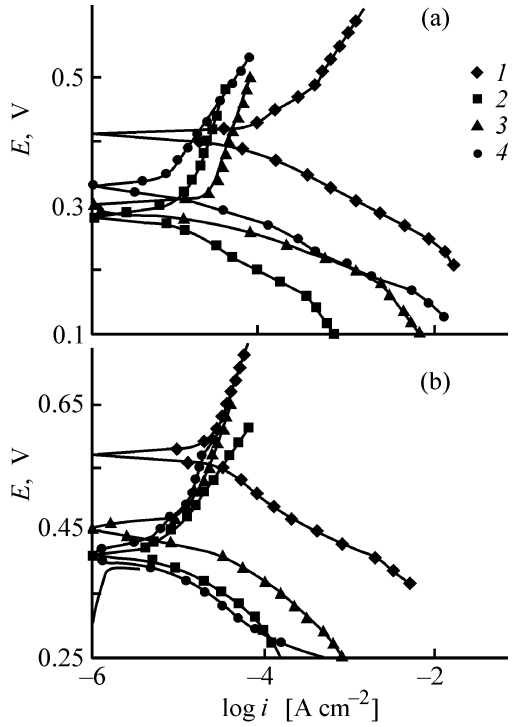


Fig. 1. Potentiostatic polarization curves measured on St. 3 steel at pH (a) 2.0 and (b) 6.0 in weakly acid solutions containing 400 mg l^{-1} H_2S (*1*) without and (*2–4*) in the presence of inhibitors c_{inh} = 200 mg l^{-1}; the same for Figs. 2, 3. (*E*) Corrosion potential and (*i*) current density; the same for Fig. 2. Inhibitor: (*2*) AMDOR IK-7, (*3*) AA C_{10}–C_{14}, and (*4*) PKU-6; the same for Fig. 2.

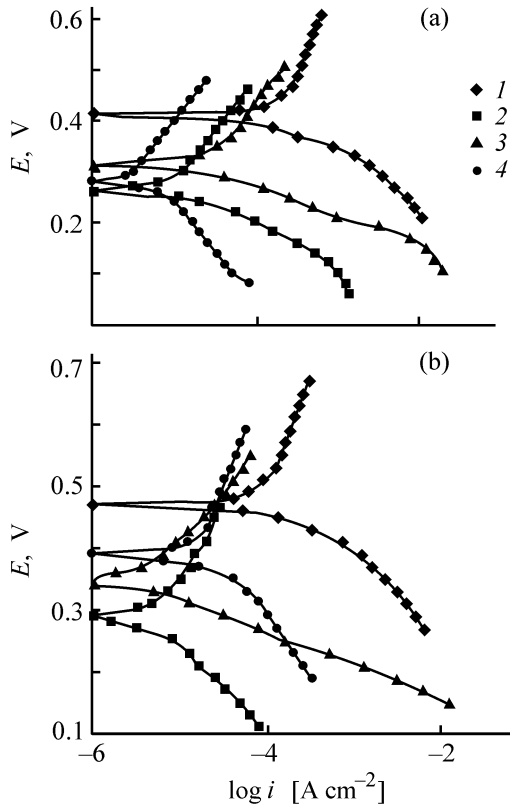


Fig. 2. Potentiostatic polarization curves measured on St. 3 steel at pH (a) 2.0 and (b) 6.0 in weakly acid solutions containing 200 mg l^{-1} H_2S and CO_2 (1 atm) (*1*) without and (*2–4*) in the presence of the inhibitors.

Introduction of H_2S into the supporting solutions makes higher the corrosion rate of the steel and enhances the protective effect of the inhibitors, which depends on pH only slightly (Table 1). However, raising the c_{H_2S} leads to a rise in the corrosion rate K_0 in uninhibited solutions and to an increase in Z at all pH values only to c_{H_2S} = 400 mg l^{-1}. Introduction of an additional amount of H_2S makes K_0 and Z lower. If H_2S and CO_2 are present simultaneously, the corrosion rate increases in comparison with that in solutions containing no hydrogen sulfide or carbon dioxide, and decreases in comparison with purely hydrogen sulfide solutions. The inhibitors produce the most pronounced protective effect at c_{H_2S} = 200 mg l^{-1} and P_{CO_2} = 1 atm (Table 1).

The cathodic polarization curves (CPC) obtained in supporting solutions containing no CO_2 and H_2S show two linear portions with slopes b_c close to 120 and 220 mV. A higher value of b_c indicates that H_3O^+ is reduced at high cathode potentials in the diffusion-kinetic region. The anodic polarization curves (APC) exhibit short linear initial portions with b_a = 60 mV, followed by the region of a higher variable slope.

The presence of CO_2 (P = 1 atm) in the supporting solutions at pH 2.0 and 4.0 inhibits the cathodic process and facilitates the anodic process. The first effect apparently predominates because the corrosion rate K of the steel decreases. In the solutions with an initial pH value of 6.0, both the electrode processes on the steel are accelerated in the presence of CO_2, with pH simultaneously decreasing to 3.9 [11] and K increasing.

Introduction of hydrogen sulfide into the supporting solution at pH 2.0–6.0 and the subsequent rise in its concentration accelerate both the cathodic and the anodic processes, and it is this process that is responsible for the overall increase in the corrosion rate. By contrast, the cathodic reaction at c_{H_2S} = 1000 mg l^{-1} becomes slower in solutions with pH 2.0, and at pH 4.0 and 6.0 the same occurs with the anodic reaction.

The joint introduction of H_2S and CO_2 (P = 0.5, 1 atm) into supporting solutions at pH 2.0 facilitates the cathodic and anodic processes (c_{H_2S} = 200 mg l^{-1}). In the presence of 1000 mg l^{-1} H_2S, the cathodic process is inhibited, whereas the anodic process is stimulated. At pH 4.0 and 6.0, both the processes are

Table 2. Effect of inhibitors on the current i_H of hydrogen diffusion across a steel membrane in a supporting solution (i_H^0) and in inhibited weakly acid solutions containing 5.8 g l^{-1} NaCl (τ = 2 h, T = 20°C)

pH	Additive to supporting solution	i_H^0, A m^{-2}	i_H, A m^{-2}, in the presence of indicated inhibitor		
			ANDOR IK-7	AA C_{10}–C_{14}	PKU-6
2.0	–	0.19	0.23	0.07	0.26
	1.7 g l^{-1} CO_2	0.25	0.23	0.21	0.15
	200 mg l^{-1} H_2S	0.36	0.38	0.3	0.21
	200 mg l^{-1} H_2S + 1.7 g l^{-1} CO_2	0.33	0.30	0.17	0.15
4.0	–	0.16	0.30	0.13	0.23
	1.7 g l^{-1} CO_2	0.26	0.12	0.19	0.19
	200 mg l^{-1} H_2S	0.35	0.26	0.25	0.11
	200 mg l^{-1} H_2S + 1.7 g l^{-1} CO_2	0.30	0.11	0.27	0.29
6.0	–	0.13	0.12	0.12	0.27
	1.7 g l^{-1} CO_2	0.24	0.31	0.25	0.11
	200 mg l^{-1} H_2S	0.30	0.24	0.16	0.13
	200 mg l^{-1} H_2S + 1.7 g l^{-1} CO_2	0.26	0.11	0.17	0.19

accelerated, and the cathodic curves show short linear portions with b_c = 120 mV in the kinetic region, which rapidly pass into the region of the limiting current.

Introduction of inhibitors into the supporting solutions in the absence of gases and the subsequent increase in c_{inh} lead to a rise in E_{cor}. At all pH values, the cathodic process is accelerated, and the anodic process, decelerated. The same pattern is observed in the presence of CO_2. The inhibitors under study decelerate both the electrode processes in a solution with c_{H_2S} < 1000 mg l^{-1} at pH 2.0 (Fig. 1a) and facilitate the cathodic reaction in a solution with c_{H_2S} = 1000 mg l^{-1}. In the inhibited solutions with pH 4.0 and 6.0, only the ionization of iron is decelerated (Fig. 1b).The joint presence of H_2S and CO_2 in the inhibited solutions decelerates of both the electrode processes at pH 2.0 (Fig. 2a). At pH 4.0 and 6.0, only the anodic reaction is decelerated (Fig. 2b). A study of the diffusion of hydrogen across a steel membrane (Table 2) confirmed the known evidence [10, 12] that H_2S and CO_2 produce a stimulating effect. The decrease in the current i_H of hydrogen diffusion across a membrane upon introduction of CO_2 into a solution containing hydrogen sulfide is presumably due to the concurrent adsorption of CO_2, which is a less efficient stimulant of hydrogenation, compared with H_2S.

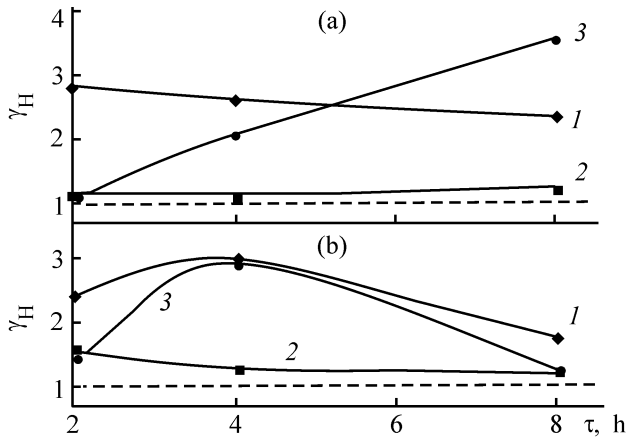


Fig. 3. Effect of the duration τ of an experiment on the coefficient γ_H of change in hydrogen diffusion into a steel in solutions at pH (a) 4.0 and (b) 6.0 containing 200 mg l^{-1} H_2S and 1.7 g l^{-1} CO_2. Inhibitor: (*1*) ANDOR IK-7, (*2*) AA formulation C_{10}–C_{14}, and (*3*) PKU-6.

Raising the duration of an experiment to 4.8 h in the presence of H_2S and CO_2 leads, in virtually all cases, to a decrease in i_H.

According to the results of 2-h tests, AA C_{10}–C_{14} inhibits hydrogenation in the supporting solutions without H_2S and CO_2, whereas ANDOR IK-7 and PKU-6, by contrast, stimulates this process (Table 2). When stimulants are present both separately and simultaneously, the inhibitors decelerate, on the whole, the diffusion of hydrogen into the steel. In this case, i_H is suppressed to the greatest extent by the inhibitors AA and PKU-6 in solutions with pH 2.0, and by ANDOR IK-7 at pH 4.0 and 6.0.

Figure 3 shows how the duration of an experiment affects the coefficient of change in the diffusion of hydrogen into the steel. The dashed line corresponds to γ_H = 1. Above and below this line lie the inhibition and stimulation regions, respectively. Although γ_H

Table 3. Kinetic parameters of hydrogen evolution at the cathode in the solutions studied at different pH values

Inhibitor	Additive to supporting solution	$n_{H^+} = (\partial \log i_c / \partial \log c_{H^+})_E$	$b_c = (\partial E / \partial \log i_c)$, mV	$(\partial E / \partial \log c_{H^+})_i$, mV
ANDOR IK-7	–	0.4*/0.3	120/116	62/40
	1 atm CO_2	0.9/0.5	124/200	112/96
	200 mg l^{-1} H_2S	1.0/0.6	110/120	90/72
	200 mg l^{-1} H_2S + 1 atm CO_2	0.7/0.5	260/180	186/86
AA C_{10}–C_{14}	–	0.4/0.7	120/140	62/42
	1 atm CO_2	0.9/0.3	124/–	112/80
	200 mg l^{-1} H_2S	1.0/0.4	110/154	90/62
	200 mg l^{-1} H_2S + 1 atm CO_2	0.7/0.5	260/180	186/86
PKU-6	–	0.4/0.4	120/134	62/60
	1 atm CO_2	0.9/0.50	124/180	112/96
	200 mg l^{-1} H_2S	1.0/0.55	110/92	90/55
	200 mg l^{-1} H_2S + 1 atm CO_2	0.7/0.35	260/160	186/50

* Without (numerator) and with (denominator) 200 mg l^{-1} inhibitors.

decreases with time, its value remains rather high after 8 h, especially in the presence of ANDOR IK-7 and PKU-6 (γ_H = 1.7 and 1.2, respectively, at pH 6.0 and 2.3 and 2.7 at pH 4.0).

The reason why addition of gases and inhibitors affects the change in the hydrogen diffusion into the steel can be ascertained by analyzing the data in Table 3, which lists selected kinetic parameters of the reaction of hydrogen evolution (RHE) in the solutions under study at pH 2.0–6.0, calculated from the cathodic polarization curves.

The parameters of RHE are considerably smaller than the values corresponding to the delayed discharge theory. This suggests that the discharge is not the limiting stage of the process. Introduction of H_2S and CO_2 into the solutions somewhat increases the kinetic parameters of RHE, with their values approaching those required by this theory. Apparently, the observed increase in i_H is not due to deceleration of the stage of recombination of adsorbed hydrogen or to an increase in γ_H.

The presence of an inhibitor in virtually any of the solutions somewhat decreases the kinetic parameters of RHE, making them approach the values required by the recombination theory, which is inconsistent with the decrease in the hydrogen diffusion flux into the steel. Apparently, the change of the nature of the limiting stage of RHE does not affect the solid-phase diffusion of hydrogen.

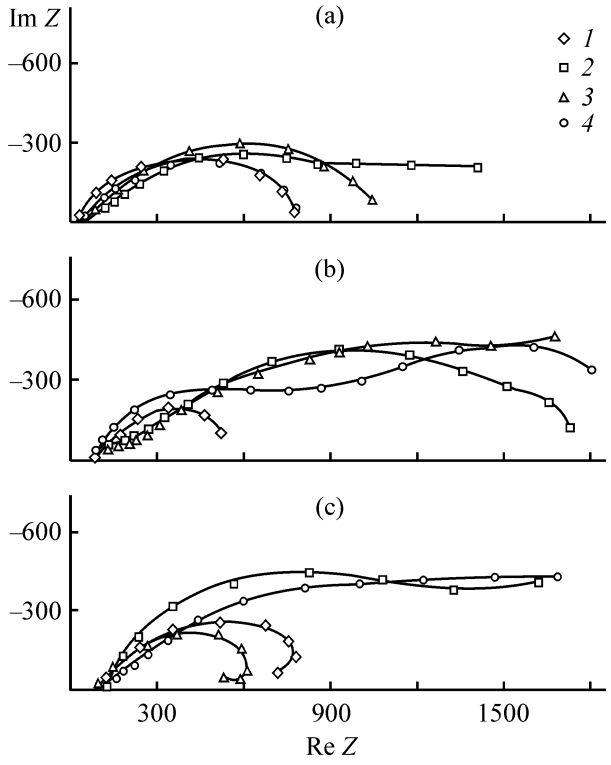


Fig. 4. Nyquist diagrams for steel in weakly acid solutions (a) at pH 2.0, (b) at pH 4.0 in the presence of 50 mg l^{-1} H_2S and (c) at pH 6.0 in the presence of 400 mg l^{-1} H_2S. (*Dots*) experimental data, (*solid lines*) calculation for the equivalent circuit used. (*1*) Supporting solution; inhibitor (200 mg l^{-1}): (*2*) AA C_{10}–C_{14}, (*3*) ANDOR IK-7, and (*4*) PKU-6.

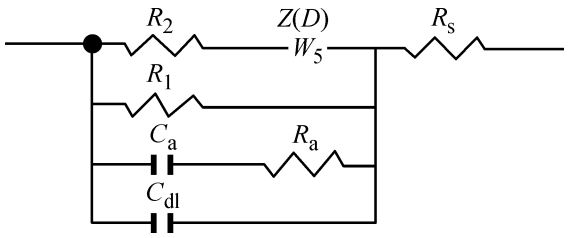


Fig. 5. Extended equivalent circuit for a corroding steel electrode in weakly acid solution. R_1 and R_2 are the charge-transfer resistance in the anodic and in the cathodic reaction of O_2 reduction, respectively; $Z_D = R_D th(j\omega\tau)^p/(j\omega\tau)^p$ is the final form of the generalized diffusion impedance; $R_D = RT\sigma/(n^2F^2c_{x=0}D)$, mass-transfer resistance; $\tau = \delta^2/D$, characteristic time of diffusion; δ, thickness of the diffusion layer; D, diffusion coefficient of depolarizer; $c_{x=0}$, the surface concentration of electroactive species; $0 < p < 1$; C_{dl}, capacitance of the double electric layer (DEL); and R_s, solution resistance. The R_a–C_a circuit determines the adsorption of intermediate products (of the anodic process).

On steel and a number of other metals, chemisorbed hydrogen exists in two equilibrium forms, suprasurface (H^r) and subsurface (H^s) [13]:

$$H^r_{ads} \rightleftarrows H^s_{ads}. \quad (1)$$

Therefore, it may be suggested, with account taken of the fact that H^s_{ads} is responsible for the solid-phase diffusion [14], that the increase in $i_{H_{ads}}$ in the presence of H_2S and CO_2 is due to a shift of equilibrium (1) to the right [14]. By contrast, the adsorption of inhibitor onto the steel surface shifts equilibrium (1) to the left.

Nyquist diagrams plotted on a complex plane for steel in weakly acid solutions with different pH values, with and without H_2S and in the presence and absence of an inhibitor, are shown in Fig. 4. Commonly, the hodographs have two overlapping arcs in the capacitance half-plane. The equivalent electrical circuit (EC) was obtained using that suggested in [15] for a corroding electrode made of low-carbon steel (neutral medium) (Fig. 5).

It is noteworthy that the EC in [15] contains no elements R_a and C_a, and $p = 0.5$.

The EC is suitable for description of the impedance spectra of steel electrodes [16] in model stratal water, which is virtually neutral. It can also be used in weakly acid solutions, because here, as in neutral media, oxygen reduction is a major cathodic process at pH 6.0. At pH 2.0, the hydrogen over-voltage is due to the deceleration of the electrochemical or heterogeneous chemical stage, rather than being the diffusion overvoltage [17]. To a first approximation, RHE can be modeled with a resistance connected in parallel with the impedance of O_2 reduction and with that of the anodic process. In this case, the resistance associated with charge transfer in RHE is combined with that associated with charge transfer in the anodic reaction into a single resistance R_1, i.e., an EC is obtained (Fig. 5). Only at pH 4.0 it may be expected that the above EC will describe experimental data with poorer precision, because, in this case, the concentration polarization caused by the low rate of delivery of H^+ ions to the electrode cannot be neglected. However, the data processing demonstrated that, as regards the criterion of a weighted sum of root-mean-square deviations, the experimental impedance graphs at pH 4.0 are described in terms of the chosen model with a precision that is not worse than that at pH 2.0 and 6.0.

The EC in Fig. 5 satisfactorily describes the experimentally observed impedance spectra in weacly

Table 4. Numerical values of the parameters of the EC (Fig. 5) in weakly acid HCl solutions containing 5.8 g l^{-1} NaCl without and with H_2S in the presence of ANDOR IK-7 inhibitor

c_{inh}, mg l^{-1}	R_2, Ω	R_D, Ω	τ, s	p	R_1, Ω	C_a, μF	R_a, Ω	C_{dl}, μF
pH 2.0								
–	86.1	5094	0.56	0.56	789.8	82.6	5420	41.0
25	4.32	2986	1.98	0.51	1987	0.96	4521	1.24
200	2.35	2584	0.55	0.48	1714	0.56	3216	1.03
pH 2.0 + 50 mg l^{-1} H_2S								
–	82.27	3413	0.19	0.51	652.4	38.6	1564	72.4
25	145.4	18564	6.1	0.52	1076	0.62	452.3	1.05
200	139.1	16551	9.21	0.56	2321	0.31	376.2	0.72
pH 2.0 + 400 mg l^{-1} H_2S								
–	15.45	1376	19.81	0.57	693.8	28.6	72.31	39.4
25	92.3	18073	13.52	0.34	1501	0.21	153.62	0.85
200	118.2	14171	19.49	0.57	526.4	0.38	257.5	0.59
pH 4.0								
–	21.13	28939	24.3	0.57	951.2	42.0	1077	25.6
25	2.64	12879	35.61	0.42	2654	0.99	154.6	0.79
200	3.54	11789	29.64	0.48	1689	0.55	384.6	0.81
pH 4.0 + 50 mg l^{-1} H_2S								
–	16.35	21771	37.8	0.61	610.2	70.8	168.6	24.6
25	75.3	17854	36.52	0.59	1325	0.62	231.8	0.96
200	52.74	12795	47.31	0.62	1454	0.57	181.3	0.65
pH 4.0 + 400 mg l^{-1} H_2S								
–	12.36	18038	55.64	0.63	812.3	10.3	189.2	20.9
25	85.1	14123	23.6	0.54	1159	2.3	352.7	0.69
200	55.3	18785	28.32	0.55	1392	2.05	214.32	0.60
pH 6.0								
–	11.2	32021	53.22	0.49	2299	40	40.89	23.2
25	121.7	12554	371.3	0.28	3187.8	0.20	842.3	0.57
200	94.73	17091	183.7	0.32	7556	0.15	1896	0.54
pH 6.0 + 50 mg l^{-1} H_2S								
–	10.5	16790	52.12	0.52	530.1	64.8	94.2	81.1
25	17.32	10523	6.42	0.57	1563	13.2	265.3	4.25
200	36.1	14578	5.32	0.52	1235	11.2	529.7	3.21
pH 6.0 + 400 mg l^{-1} H_2S								
–	4.2	18592	14.41	0.55	738.1	67.1	108.5	28.1
25	35.2	23654	39.5	0.59	876.5	4.65	289.3	6.54
200	45.3	19254	25.7	0.57	1236.3	7.36	369.5	2.65

acid solutions inhibited and uninhibited with ANDOR IK-7, AA, PKU-6, and (or) hydrogen sulfide. The values of the EC elements, obtained by data processing, are listed in Table 4.

The effect of inhibitors on the kinetics of the cathodic and anodic reactions is manifested upon adsorption of their molecules onto the electrode surface. As in the case of neutral solutions [16], the inhibitors

Table 5. Values of *Z*, obtained from impedance data

Inhibitor	c_{H_2S}, mg l^{-1}	*Z*, %, at indicated pH		
		2.0	4.0	6.0
ANDOR IK-7	0	54	44	69
	50	72	58	57
	400	–	41	41
AA C_{10}–C_{14}	0	53	43	39
	50	86	65	63
	400	40	44	–
PKU-6	0	52	52	52
	50	70	89	82
	400	44	56	71

under study are adsorbed in a weakly acid medium onto the steel electrode, thereby lowering C_{dl} by one and a half or two orders of magnitude (at an inhibitor concentration of 200 mg l^{-1}) both in the absence and in the presence of H_2S. Presumably, the fact that $C_{dl} < 1$ μmF cm^{-2} in some cases indicates that there occurs a multilayer adsorption of the inhibitor.

As the pH of the supporting solutions (without H_2S and inhibitors) is raised, R_2, C_a, R_a, and C_{dl} decrease, R_1, R_D, and τ increase, and *p* remains approximately constant. The closest correlation with *K* is observed for R_1. Its increase with the solution pH corresponds to a decrease in the corrosion rate, in agreement with the results of gravimetric measurements (Table 1). In supporting solutions with pH in the range 2.0–6.0, $\partial \log R_2/\partial \mathrm{pH} \approx -0.2$. Iron without an oxide film belongs to the group of electrode materials for which $\partial E/\partial \mathrm{pH} \approx -2.3RT)/F$ in the region of oxygen reduction [18], and the derivative $\partial \log R_2/\partial \mathrm{pH}$ must have a value on the order of unity. The value $\partial \log R_2/\partial \mathrm{pH} < 0$ is apparently due to a shift of E_{cor} into the negative region on raising the pH. Therefore, the following two factors affect R_2: (1) an increase in R_2, in accordance with [18], and (2) a decrease in R_2, caused by the lowering of the corrosion potential. Presumably, the effect of the second factor predominates in the solutions studied, with the result that negative values of $\partial \log R_2/\partial \mathrm{pH}$ are also obtained in H_2S-containing solutions (both with and without inhibitors). The only exception are solutions containing inhibitors in the absence of H_2S, in which R_2 increases as pH decreases.

As the pH of the supporting solutions is raised, the parameters of the diffusion impedance vary in the following manner: on passing from pH 2.0 to pH 6.0, the characteristic time $\tau = \delta^2/D$ increases to the greatest extent, and the resistance R_D, which is proportional to $\delta/(c_{x=0}D)$, to the least extent. The extent to which the τ/R_D ratio, which is proportional to $c_{x=0}\delta$, increases is intermediate between those for τ and R_D. Hence follows that, as the pH of the supporting solution increases, $c_{x=0}$ and δ grow, with the increase in δ presumably exceeding that for $c_{x=0}$.

As the hydrogen sulfide concentration in the uninhibited solution increases, R_2 and R_D decrease at all pH values (with R_D decreasing to the greatest extent at pH 2.0), *p* somewhat increases, and R_1 decreases (to a greater extent at pH 6.0). C_{dl} depends on c_{H_2S} only slightly. Thus, H_2S somewhat accelerates the cathodic and anodic reactions, in a qualitative agreement with the results of polarization measurements. The action of H_2S on the surface of a steel electrode results in the development of its surface profile, as indicated by an increase in *p*.

It is noteworthy that, as the concentration of the inhibitors grows, the impedance parameters increase in a manner common to all the inhibitors. In the absence of H_2S, R_2 decreases at pH 2.0 and increases at pH 6.0, and the resistance R_1 grows. The value of *p* tends to decrease (which reflects a partial activation of the electrode surface [16]). R_D decreases solely in the presence of ANDOR IK-7; R_D changes insignificantly in the case of PKU-6 and somewhat increases in the presence of AA. In the presence of H_2S, R_1, R_2, and R_D increase, and p = const.

The degree of protection (%) by the inhibitor can be calculated by substituting the impedance data into the relation [19]:

$$Z = \frac{R_{1,\,\mathrm{inh}} - R_{1,\,\mathrm{sup}}}{R_{1,\,\mathrm{inh}}} \times 100.$$

The results of this calculation (Table 5) are in a qualitative agreement with the gravimetric data. For example, the results of impedance measurement show that the protective effect is weak in solutions without H_2S and becomes stronger as the solution pH and inhibitor concentration increase. Introduction of H_2S enhances the protective effect. The values of *Z* are at a maximum at $c_{H_2S} = 50$ mg l^{-1}. However, the values of *Z*, calculated from the impedance data, are, as a rule, lower than those obtained from gravimetric measurements. This is apparently due to the different times of exposure of the samples to a solution.

CONCLUSIONS

(1) A high efficiency of protection of St. 3 steel by such inhibitors as ANDOR IK-7, homologous mixture

of alkyl ammonium acetates C_{10}–C_{14}, and PKU-6 in chloride solutions containing H_2S and CO_2 (pH 2.0–6.0) was demonstrated. The protection efficiency increases as the pH value is raised and H_2S and CO_2 are introduced.

(2) The inhibitors studied effectively suppress the hydrogen diffusion into steel in solutions containing H_2S and CO_2.

(3) The inhibitors decelerate the anodic reaction of iron ionization in solutions with pH 4.0 and 6.0 and cause retardation of both the electrode processes at pH 2.0.

(4) An equivalent electrical circuit is suggested for describing the impedance spectra of a corroding steel electrode in weakly acid solutions in both absence and presence of inhibitors and (or) hydrogen sulfide. The influence exerted by inhibitors and H_2S on the corrosion rate and on the kinetics of the anodic and cathodic reactions is considered in terms of this model.

REFERENCES

1. Markin, A.N., *Zashch. Met.*, 1996, vol. 32, no. 5, pp. 497–503.
2. Podobaev, N.I. and Shalygin, S.P., *Zashch. Met.*, 1985, no. 3, pp. 414–418.
3. Nashchekina, Ya.R., Oshe, E.K., and Tsygankova, L.E., *Khim. Khim. Tekhn.*, 2005, vol. 48, no. 1, pp. 112–115.
4. Kuznetsov, Yu.I. and Vagapov, R.K., *Zashch. Met.*, 2000, vol. 36, no. 5, pp. 520–526.
5. Kuznetsov, Yu.I., Andreev, N.N., and Ibatullin, K.A., *Zashch. Met.*, 1999, vol. 35, no. 6, pp. 586–591.
6. Kardash, N.V., and Batrakov, V.V., *Zashch. Met.*, 1995, vol. 31, pp. 441–444.
7. Tsygankova, L.E., Mozharov, A.V., Ivanishchenkov, S.S., *et al.*, *Praktika Protivokorroz. Zashch.*, 2003, no. 2 (28), pp. 25–29.
8. Oleinik, S.V., Kuznetsov, Yu.I, Veselyi, S.S., and Komakhidze, M.G., *Elektrokhimiya*, 1992, vol. 28, no. 6, pp. 856–861.
9. Sinyutina, S.E., Tsygankova, L.E., Vigdorovich, V.I., *et al.*, *Zh. Prikl. Khim.*, 1997, vol. 70, no. 3, pp. 430–436.
10. Uhlig, G.G. and Revie, R.W., *Corrosion and Corrosion Control: An Introduction to Corrosion Science and Engineering*, New York: Wiley, 1985.
11. *Spravochnik khimika* (Chemist's Handbook), Nikol'skii, B.P., Ed., Moscow: Khimiya, 1964, vol. 3.
12. Vagapov, R.K., Frolova, L.V., and Kuznetsov, Yu.I., *Zashch. Met.*, 2002, vol. 38, no. 1, pp. 32–37.
13. Horiuti, D. and Toya, T., *Solid State Surface Science*, Green, M., Ed., New York: Dekker, 1969.
14. Vigdorovich, V.I., D'yachkova, T.P., Pupkova, O.L., and Tsygankova, L.E., *Elektrokhimiya*, 2001, vol. 37, no. 12, pp. 1437–1445.
15. Bonnel, A., Dabosi, F., Deslouis, C., *et al.*, *J. Electrochem. Soc.*, 1989, vol. 130, no. 4, pp. 753–761.
16. Kim, Ya.P., Tsygankova, L.E., and Kichigin, V.I., *Korroziya: Mater., Zashch.*, 2005, no. 9, pp. 30–36.
17. Shatalov, A. Ya., *Elektrokhimicheskie osnovy teorii korrozii metallov* (Electrochemical Foundations of the Metal Corrosion Theory), Voronezh: Voronezh. Gos. Univer., 1971.
18. Tarasevich, M.P., Khrushcheva, E.I., *Kinetika slozhnykh elektrokhimicheskikh reaktsii* (Kinetics of Complex Electrochemical Reactions), Moscow: Nauka, 1981, pp. 104–165.
19. Reinhard, G., and Rammelt, U., *Corrosion*, 1984, vol. 15, no. 4, pp. 175–193.

Russian Journal of Applied Chemistry, Vol. 78, No. 12, 2005, pp. 1970–1976. Translated from Zhurnal Prikladnoi Khimii, Vol. 78, No. 12, 2005, pp. 2002–2007.
Original Russian Text Copyright © 2005 by Mil'chenko, Domanskii, Vorob'ev-Desyatovskii.

PROCESSES AND EQUIPMENT OF CHEMICAL INDUSTRY

Design of Large-Volume Agitators for Polydisperse Suspensions

A. I. Mil'chenko, I. V. Domanskii, and N. V. Vorob'ev-Desyatovskii

St. Petersburg State Technological Institute, St. Petersburg, Russia
POLIMETALL INZhINIRING (Polymetal Engineering) Private Company, St. Petersburg, Russia

Received July 7, 2005

Abstract—Specific features of designing of large-volume agitators for mechanical agitation of concentrated polydisperse suspensions are considered. Mathematical models and results of model experiments are applied to obtain calculational relations that can be use to determine technical parameters of industrial agitators. The designing procedure is confirmed by the experience of industrial use of agitators with a capacity of up to 1000 m^3.

Processes of mechanical agitation in fluid–solid and fluid–solid–gas systems are widely employed in chemical and mining-and-smelting industries. As examples of processes of this kind can serve leaching-out of gold and silver from ores with sodium cyanide and of sodium aluminate from bauxites with an alkali, biooxidation of sulfide ores, manufacture of extraction phosphoric acid in sulfuric acid treatment of apatite, and many others. It should be noted that many processes are not only large-tonnage, but also require a long time (up to 4 days). All these factors make necessary development of cascaded agitators or chains of agitators working in the rotary mode. The capacity of single agitators in such cascades or chains has reached a value of 5000 m^3 [1]. A specific feature of agitators of this kind is also that the solid phase is a polydisperse medium (Fig. 1), whose particle size, as a rule, does not exceed 200 μm, and the agitation process is performed at a nearly zero excess pressure in the agitators.

Designing of such unconventional large-volume agitators meets certain difficulties, which have been insufficiently discussed in the special literature [2–4].

The influence exerted by centrifugal forces on the distribution of the solid phase along the agitators radius in agitation of finely dispersed suspensions is insignificant. Therefore, it is advisable to use for this purpose low-energy-intensive smooth-walled agitators. The scheme of the agitators we recommend, with account of the minimum expenditure for its fabrication and use, is shown in Fig. 2. This is an ap-

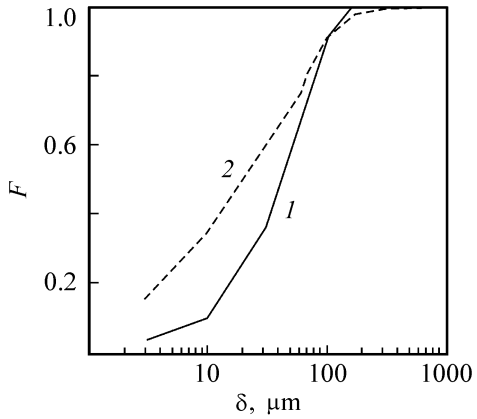


Fig. 1. Integral dispersion composition of the ore (*1*) before and (*2*) after leaching. (*d*) Particle diameter.

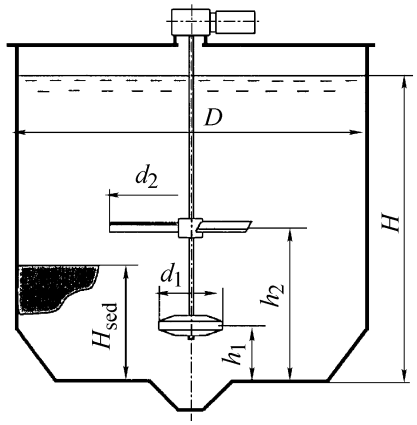


Fig. 2. Design of a large-volume agitators.

1070-4272/05/7812-1970 © 2005 Pleiades Publishing, Inc.

paratus with flat cover and bottom. The latter has a conical fillet along its perimeter for eliminating the stagnant zone and a small collector with a pipe for discharging the suspension at the center, with the height H of agitators filling approximately equal to its diameter D.

A preferable type of impeller is that of the standard three-blade design with a diameter d_2 and angle of blade inclination of 24°–30° [3], which provides an intense three-dimensional motion of the slurry throughout the working volume of the agitators. The size of such a impeller and the height at which it is mounted, to ensure economical and accident-free operation, is calculated from the inequality

$$\Gamma_{D_2} = D/d_2 = 2.5\ldots4, \quad H_{sed} < h_2 \le d_2. \qquad (1)$$

As shown by studies and industrial tests of the agitators used for the purpose in question [5–7], the rotor of the mechanical agitating devices (MAD) should be supplemented [especially in those cases when $H_{sed} = (0.2–0.5)H$] with another standard impeller, a closed turbine of diameter d_1 [3], for which

$$\Gamma_{D_1} = D/d_1 = 6\ldots7, \quad h_1 = 0.5d_1. \qquad (2)$$

This impeller rapidly suspends the sediment formed after a prolonged standstill of an MAD and provides a nearly complete discharge of the solid phase from the agitators, after the suspension level becomes lower than the impeller d_2.

In the stationary mode, i.e., in prolonged operation, when all the technological parameters have stabilized, the power expended for agitation can be calculated by the formula [2–4]

$$N = K_N \rho_{susp} n^3 d_2^5, \qquad (3)$$

where K_N is the power factor; n rotation rate of the impeller; and ρ_{susp}, suspension density.

To diminish the power consumption, it is necessary to perform the agitation process at the lowest (determining) rotation rate n_0, which ensures that, on the bottom, there is no sediment of particles whose diameter is chosen in accordance with the inequality

$$\delta \le \delta_{lim}, \qquad (a)$$

where δ_{lim} is the diameter of the limiting grain, whose being suspended in agitation of a polydisperse suspension is guaranteed.

It is planned beforehand that, to save energy, a minor fraction of particles (1–2%) (Fig. 1) with diameters

$$\delta > \delta_{lim}, \qquad (b)$$

is to be precipitated and collected in the central collector, with their subsequent delivery to additional grinding.

The problem of finding the value of n_0 has been studied extensively [8–11]. However, the solutions obtained are only for particular cases, because they refer to a limited range of variation of variables and fail to take into account in full measure the effect of design features of an agitators, concentration and granulometric composition of the dispersed solid phase, shape of particles, and their tendency to cake.

Therefore, the most reliable way to design and calculate such unique industrial agitators is scaling [12] based on physical modeling. The method consists in the following. A model installation geometrically similar to the agitators being designed is used to experimentally find the determining rotation rate n_m and power N_m, which correspond to the instant of when the whole sediment of the solid phase of the industrial slurry becomes suspended. The resulting n_m and N_m can be used to calculate with a sufficient accuracy n_P and N_P for the industrial agitators being designed. For this purpose, it is necessary to preliminarily determine how the agitators diameter D_m affects the rotation rate n_m by using a mathematical description of the model of suspension of solid particles.

It follows from [13] that the shear model [14] can be adopted as such a mathematical model of particle suspension from the sediment surface or from the horizontal surface of the agitators bottom. In accordance with [14], the condition for the onset of suspension of a monolayer of particles in a turbulent flow can be written as

$$\tau_b = (\rho_s - \rho_{fl}) g \delta_{lim} (1 - \varepsilon_{sed}) f, \qquad (4)$$

where f and ε_{sed} are the experimentally found friction factor and porosity of the sediment.

Condition (4) for a smooth-walled agitators with a flat bottom can be represented [14] as

$$n = 10.4 \frac{D}{d_2^2} \left[\frac{(\rho_s - \rho_{fl}) \delta_{lim} (1 - \varepsilon_{sed}) f \Gamma_{D_2}}{\rho_{susp} K_N} \right]^{0.5}. \qquad (5)$$

As shown in [14], the shear model is well confirmed by experimental data of numerous domestic and foreign researchers [11, 15].

Thus, the similarity condition (τ_b = idem), which characterizes the onset of particle motion over the bottom, can be written, with account of the invariability of suspension properties and the geometrical similar-

ity of the model and industrial agitators and in accordance with Eq. (5), as

$$nDK_N^{0.5} = \text{idem.} \quad (6)$$

In the turbulent mode of mixing, the power factor in equality (6) can be represented as a power monomial

$$K_N = a_2\left(\frac{\rho_{susp} n d_2^2}{\mu_{susp}}\right)^{-a_1}, \quad (7)$$

in which, e.g., $a_1 = 0.18$ and $a_2 = 1.5$ for a three-blade impeller at $\Gamma_{D_2} = 2.4$ [3]. The viscosity of low-concentrated Newtonian suspensions (at $\varphi < 0.1$) can be found using the known equality [4]:

$$\mu_{susp} = \mu_{fl}(1 + 2.5\varphi). \quad (8)$$

If, however, $\varphi \geq 0.1$, the suspension frequently has the form of a non-Newtonian fluid, whose behavior depends on the shear rate $\dot{\gamma}$ and can be described by Ostwald's power rheological equation [3]:

$$\tau = K\dot{\gamma}^m, \quad (9)$$

In this case, the effective viscosity is calculated by the equation

$$\mu_{susp} = K\dot{\gamma}^{m-1}, \quad (10)$$

with the constants K and m found experimentally [16].

For example, $K = 0.46$ and $m = 0.14$ were obtained on a rotation viscometer for an aqueous suspension with $\delta = 74$ μm, $\rho_s = 2640$ kg m^{-3}, and $\varphi = 0.16$.

In scaling of agitators of non-Newtonian suspensions, it is necessary, to ensure that particles are suspended in accordance with the shear model, to create tangential stresses equal to the stresses in the model agitators at the bottom of the industrial agitators. With account of Eqs. (9) and (10), this is equivalent to equality of the shear rates and effective viscosities at the bottom of the model agitators and that being designed. It is also noteworthy that, in the case of a developed turbulent agitation and turbulent flow around the blades, the viscosity only slightly affects the resistance characteristics of the impeller. Therefore, the scaling of agitators in a turbulent mode of mixing of non-Newtonian suspensions should be performed following the same recommendations as in the case of agitation of Newtonian suspensions.

Substituting (7)–(10) into condition (6) and excluding from consideration the invariable parameters of the suspension, we obtain the first condition for scaling of the industrial agitators

$$nD^b = n_m D_m^b = n_P D_P^b = \text{idem}, \quad (11)$$

with the exponent b found using the formula

$$b = \frac{1 - a_1}{1 - 0.5a_1}. \quad (12)$$

In a particular case of agitation with three-blade impellers ($a_1 = 0.18$), the exponent $b = 0.9$, in accordance with formula (12), and the rule (11) takes the form

$$nD^{0.9} = \text{idem}. \quad (13)$$

The other three scaling conditions, which are frequently used in the special literature [8–11] for calculating the power N, specific power $P = N/V$, and specific torque $T = M/V$, can be readily derived from (11) with account of formula (3):

$$N/D^{3-b} = \text{idem}, \quad (14)$$

$$PD^b = \text{idem}, \quad (15)$$

$$TD^0 = T = \text{const}. \quad (16)$$

The last rule (16) was noted previously in a study [17] of specific features of agitation of highly concentrated suspensions: the thick sediment of aluminum hydroxide particles was completely suspended at one and the same specific torque T for three-blade impellers with different diameters and rotation rates. It is also noteworthy that, when studying the dissolution of oxalic acid fixed in the form of a bulky pellet at the flat bottom of an agitators with changeable rabbles, professor Gzovskii found [18] that its dissolution rate is the same at T = const (for 12 different types and sizes of impellers). As the mass-transfer coefficient in a turbulent flow of a fluid is proportional to the dynamic velocity $U_* = \sqrt{\tau_b/\rho_f}$ [19], we can conclude that the tangential stresses at the bottom remained constant in these experiments, irrespective of the type and size of a impeller. This circumstance indirectly confirms the applicability of the shear model to a wide variety of impeller designs.

In impeller operation in the stationary mode, the quality of agitation is commonly evaluated by the deviation of the running concentration φ at a height z

($z = 0$ at the bottom and $z = H$ at the slurry surface) from its prescribed average value φ_{av}. As is known [12], this distribution follows from a solution to the equation of the circulation-diffusion model and has the form

$$\frac{\varphi}{\varphi_{av}} = \frac{\mathrm{Pe}\exp\left(-\mathrm{Pe}\dfrac{z}{H}\right)}{1-\exp(-\mathrm{Pe})}. \quad (17)$$

This equation contains a single generalized coefficient, the Peclet number

$$\mathrm{Pe} = w_i H/D_s, \quad (18)$$

where w_i is the velocity of hindered sedimentation of particles with diameter δ_i.

The similarity condition for concentration fields in agitators scaling has the form

$$\mathrm{Pe} = \text{idem}. \quad (19)$$

It is recommended [4] to calculate the longitudinal diffusion coefficient D_s in formula (18), averaged along the agitators height, using the semiempirical dependence

$$D_s \sim nD^2. \quad (20)$$

Substitution of (20) into (18) and (19) yields (with account of H/D = const and invariability of w_i in the model and industrial agitators) the following scaling condition

$$nD = \text{idem} \quad (21)$$

and, accordingly,

$$ND^{(a_1-2)} = \text{idem}, \quad PD^{(1+a_1)} = \text{idem}, \quad TD^{a_1} = \text{idem}. \quad (22)$$

For example, for the above-mentioned three-blade impeller, i.e., at $a_1 = 0.18$, the scaling conditions take the form

$$nD = \text{idem},\ N/D^{1.82} = \text{idem},\ PD^{1.18} = \text{idem},\ TD^{0.18} = \text{idem}.$$

As follows from the solution (17), deviations of the running concentration from its average value become well practically acceptable (15% and less) already at Pe = 0.3.

Equation (17) makes it also possible to evaluate the average residence time of the solid phase, compared with the average residence time of the suspension in the agitators,

$$\tau_s = (\varphi_{out}/\varphi_{av})\tau_{susp}, \quad (23)$$

where

$$\tau_{susp} = V/Q_{susp}, \quad (24)$$

φ_{out}, concentration of particles in the agitators at the height of the suspension outlet point [Eq. (17)]; and Q_{susp} is the volumetric flow rate of the suspension through the agitators.

Thus, to evaluate the agitation quality in accordance with formula (17) and the residence time of particles in the agitators in accordance with formula (23), it is necessary to know the velocity w_i of hindered sedimentation of solid particles with a prescribed limiting diameter δ_{lim} in the suspension.

The velocities w_i for each fraction δ_i of the polydisperse suspension can be calculated using the equation derived in terms of the model of mutually penetrating continuums [19]

$$\left[\left(\frac{2\delta_i S_{susp}}{\varphi_{fl}} + \frac{3}{\zeta}\right)\mathrm{Re}_i^{-1} + 0.45(\mathrm{Re}_i\zeta)^{-4/9} + 0.042\right]\frac{w_i^2}{g\delta_i} = \frac{(\rho_s-\rho_{fl})\rho_{fl}}{6\rho_{fl}\zeta^3}. \quad (25)$$

In Eq. (25), which takes into account the interaction forces of all the particle fractions with the fluid, the following designations are used:

$$\mathrm{Re}_i = \frac{\delta_i w_i \rho_{fl}}{\mu_{fl}},\ S_{susp} = \sum_{i=1}^{m}\frac{6\varphi_i}{\delta_i},\ \zeta = 1 + \left(\frac{\pi}{2}-1\right)\varphi_{fl}.$$

The volume fraction of the solid phase and the fluid are related by apparent expressions

$$\varphi_s = \sum_{i=1}^{m}\varphi_i,\ \varphi_s + \varphi_{fl} = 1.$$

Figure 1 shows the dispersion composition of solid particles of an ore in an industrial suspension before and after leaching-out of silver, and Fig. 3 presents the sought-for dependences $w_i = f(\delta_i)$ for the dispersion composition in Fig. 1, divided into 100 fractions. As shown by special-purpose experiments, the accuracy of calculation of the velocities of hindered sedimentation of particles is within 4.2–7.4%.

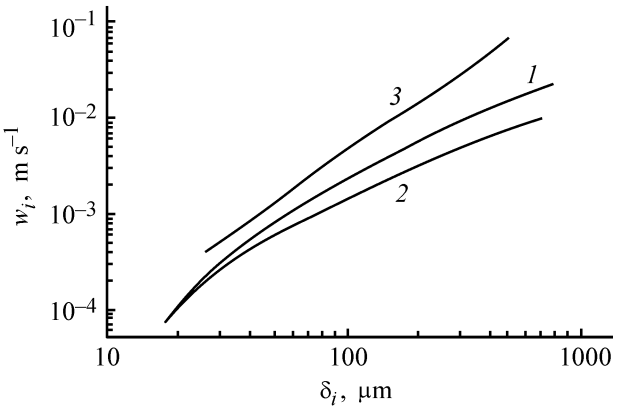


Fig. 3. Velocities w_i of hindered sedimentation vs. particle diameter δ_i. (*1*) Before leaching {Eq. (25)], (*2*) after leaching [Eq. (25)], and (*3*) before leaching (calculation by the Todes formula [13]).

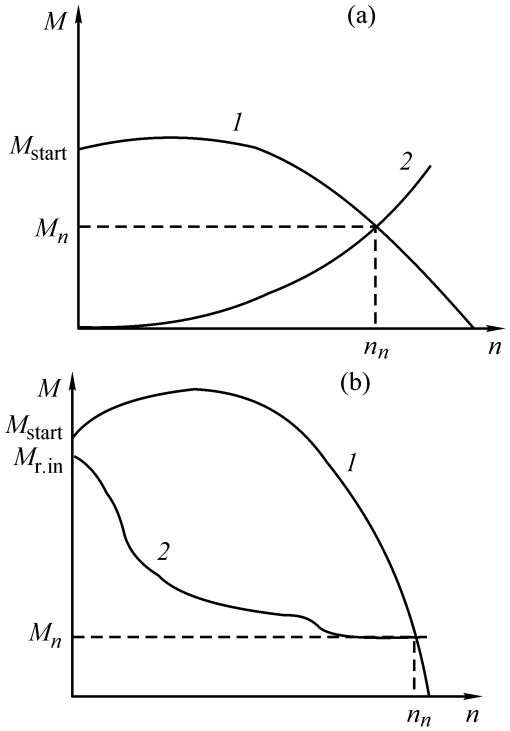


Fig. 4. Experimental dependence of the moment M of resistance of the medium on the rotation rate n of the impeller for a two-stage MAD. (n_n) Nominal rotation rate of the impeller. Rotation: (a) in water and (b) in the sediment from the suspension. $M(n)$ dependence: (*1*) for motor-gearbox and (*2*) for impeller [20].

Figure 3 shows for comparison data on the velocities of hindered sedimentation of monodisperse particles, calculated using the Todes formula [13], which is frequently used in practice. This comparison shows that the velocities of hindered sedimentation of particles of mono- and polydisperse suspensions are strongly different.

Of particular interest is the nonstationary operation mode of a two-stage MAD, e.g., that when the MAD is started after a shutdown and subsequent sedimentation of the slurry to form a many-ton sediment layer (Fig. 2). To prevent failure of rotor elements under an overload, we use the experimental dependence of the resistance momentum of the medium for a two-stage MAD (Fig. 4b):

$$M_{r.in} < M_{start}, \quad (26)$$

where M_{start} is the starting (passport) drive shaft torque, and $M_{r.in}$ is the initial momentum of the force of resistance by the sediment to the turbine rotation during 2–3 s after the switch-on of the drive.

In the course of time, the resistance momentum of the sediment falls from $M_{r.in}$ to M_n because of the fast dilution of the sediment by the pure fluid pumped in by the impeller of the second stage (Fig. 4b). As shown by tests on pilot stands and industrial agitators [5–7, 20], the value of $M_{r.in}$ for the standard turbine impeller can be found using the following formula:

$$M_{r.in} = 0.29\tau d_1^3, \quad (27)$$

in which the tangential stresses in the sediment are determined by Coulomb's law for the shear resistance of water-saturated soils

$$\tau = \tau_0 + \sigma_0 \tan\phi = \tau_0 + (\rho_s - \rho_{fl})(1 - \varepsilon_{sed})(H_{sed} - h_1)gf. \quad (28)$$

The constants τ_0, ε_{sed}, and f can be determined for a particular sediment experimentally, using the standard procedures of engineering geology [21]. Then, the power consumed for agitation will be as follows:

(i) in the starting period, in accordance with formula (27):

$$N_{start} = M_{r.in} 2\pi n = 1.8\tau n d_1^3, \quad (29)$$

(ii) in the stationary mode:

$$N_{st} = K_{N1}\rho_{susp} n^3 d_1^5 + K_{N2}\rho_{susp} n^3 d_2^5, \quad (30)$$

where K_{N1} and K_{N2} are found as in [2–4].

Using the results of calculation by formulas (11)–(16) and (28–30), we can choose the rotation rate and power of the standard motor-gearbox, which, in addition, should satisfy the inequality

$$N_{m\text{-}g} \geq \max(N_{start}, N). \quad (31)$$

To conclude, we present the results of a practical verification of the specific features of calculation of large-volume agitators, described above.

A cascade of seven 1000-m^3 agitators (Fig. 2), designed for the first time in accordance with [2–4], but having no central collector of coarse particles for leaching-out of precious metals from hydrometallurgical slurries [22] has been in industrial exploitation for more than four years. Numerous measurements of electrical parameters, laboratory analyses of a multitude of samples of the suspensions and sediment, observation of how the cascade operates, and, finally, special-purpose model experiments revealed the following.

(1) The agitators of the cascade mostly fulfill their technological purpose. At the same time, their design and technical and economical parameters can be markedly improved using the design procedures described above.

(2) The principles of scale-up of the results of model tests to industrial agitators according to relations (11)–(16) are correct at a scaling factor $D_p/D_m \leq 35$.

(3) The agitators require an expensive periodic cleaning, because they are filled, even though slowly, by settling particles whose size approximately corresponds to inequality (b) at $\delta_{lim} = 160$ μm. The working rotation rate of MAD is lower by 20% than that required by condition (13). The experimentally measured power consumed for agitation exceeds that given by the design by 50% and more. This is due to the friction of the lower impeller against the sediment, which is indicated by the erosion wear of its elements and of the central part of the bottom.

(4) The experimentally measured particle distribution nonuniformity at depths of 9 and 1 m is within 4%. This is considerably better than the value of 21% in the design calculation and shows a good agreement with relations (17)–(22) of the circulation-diffusion model based on the results of measurements and calculations of the velocity of hindered sedimentation of real polydisperse particles (Fig. 3).

(5) The average residence time of the solid phase in the cascade, with account of the sediment accumulated by the instant of measurement, is about 62 h, instead of 72 h in accordance with the design, which corresponds to the results of calculations by formula (23).

(6) Even after a prolonged sedimentation of the slurry (19 h) the agitators can be safely started, which has been tested as yet only at a halved rotation rate of the MAD rotor. This quantitatively verifies the procedure used to calculate the startup power and the method for evaluation of the physicomechanical properties of the sediment [formulas (26)–(29)].

Successful tests of a similar agitators with a volume of 400 m^3 (Fig. 2), which confirmed the above-suggested calculation procedure for a suspension of aluminum hydroxide, were previously reported in [7].

CONCLUSIONS

(1) An integrated method for design of large-volume agitators for mechanical agitation of concentrated polydisperse suspensions was developed.

(2) The method is based on the following: a new shear model which makes it possible to lift the particles from the agitator's bottom, confirmed by published data; known circulation-diffusion model based on the experimentally confirmed new procedure for calculation of the velocity of hindered sedimentation of particles of the polydisperse suspension; and model of washing-off of the sediment at MAD startup, based on new experimental data of physicomechanical parameters of sediments formed from ore slurries.

(3) The method is verified by experimental data obtained in industrial exploitation of agitators with a volume of up to 1000 m^3.

REFERENCES

1. Kotlyar, Yu.A. and Meretukov, M.A., *Metallurgiya blagorodnykh metallov* (Metallurgy of Precious Metals), Moscow: Izd. ASMI, 2002.
2. Braginskii, L.N., Begachev, V.I., and Barabash, V.M., *Peremeshivanie v zhidkikh sredakh* (Agitation in Fluid Media), Leningrad: Khimiya, 1984.
3. Vasil'tsov, E.A. and Ushakov, V.G., *Apparaty dlya peremeshivaniya zhidkikh sred: Spravochnoe posobie* (Agitators for Agitation of Fluid Media: Reference Book), Leningrad: Mashinostroenie, 1979.
4. *GD* (Guiding Document) *26-01-90–85. Mechanical Agitating Devices. Calculation Methods*. Moscow: Minkhimmash, 1985.
5. Mil'chenko, A.I., Mikhalev, M.F., Lebedev, V.V., *et al., Vtoraya Vsesoyuznaya konferentsiya, Cherkassy 29 maya 1973 g.* (Second All-Union Conf., Cherkassy, May 29, 1973), Moscow: NIITEKhIM, 1973, pp. 291–297.
6. Mil'chenko, A.I., Sidorovich, P.A., and Serdyuk, V.I., *Khim. Neft. Mashinostr.*, 1986, no. 2, pp. 15–16.
7. Sidorovich, P.A., Mil'chenko, A.I., Borovinskii, V.P., and Davydov, I.V., *Vsesoyuznaya nauchnaya konferentsiya, Kharkov, 10 sentyabrya 1985 g.* (All-Union

Conf., Kharkov, September 10, 1985), Kharkov, 1985, pp. 109–110.

8. Oldshue, J.Y., *Fluid Mixing Technology*, New York: McGraw-Hill, 1983.
9. Zlokarnik, M., *Ruhrtechnik: Theorie Praxis*, Berlin: Springer, 1999.
10. *Mixing: Theory and Practice*, New York: Academie, 1986, vol. 3.
11. Einenkel, W.D., *Chem. Ing. Tech.*, 1979, vol. 51, no. 7, pp. 697–704.
12. Kafarov, V.V., *Metody kibernetiki v khimii i khimicheskoi tekhnologii* (Methods of Cybernetics in Chemistry and Chemical Technology), Moscow: Khimiya, 1976.
13. Ostrovskii, G.M., *Prikladnaya mekhanika neodnorodnykh sred* (Applied Mechanics of Heterogeneous Media), St. Petersburg: Nauka, 2000.
14. Domanskii, I.V. and Mil'chenko, A.I., *Khim. Prom–st.*, 2003, vol. 80, no. 12, pp. 18–24.
15. Barabash, V.M., Braginskii, L.N., and Kozlova, E.G., *Teor. Osn. Khim. Tekhnol.*, 1990, vol. 24, no. 1, pp. 63–68.
16. *Reometriya pishchevogo syr'ya i produktov: Spravochnik* (Rheometry of Raw Materials and Products in Food Industry: Reference Book), Machikhin, Yu.A., Ed., Moscow: Agropromizdat, 1990.
17. Migunov, V.V., Mil'chenko, A.I., and Borisov, V.Z., *Issledovanie, konstruirovanie i raschet elementov khimicheskikh mashin i apparatov: Mezhvuzovskii sbornik trudov* (Study, Design, and Calculation of Elements of Chemical Machines and Agitators, Intercollegiate Coll. of Works), Leningrad: Len. Tekhnol. Inst. im. Lensoveta, 1976, issue 1, pp. 52–58.
18. Gzovskii, S.Ya. and Planovskii, A.N., *Vestn. Tekhn. Ekonom. Inform.*, 1959, no. 5, pp. 19–24.
19. *Novyi spravochnik khimika i tekhnologa: Protsessy i apparaty khimicheskikh tekhnologii* (New Handbook of a Chemist and Technologist: Processes and Apparatus of Chemical Technology), Ostrovskii, G.M., Ed., St. Petersburg: Professional, part 1, 2004.
20. Sidorovich, P.A., Mil'chenko, A.I., and Shebatin, V.G., *Khim. Neft. Mashinostr.*, 1985, no. 3, pp. 11–12.
21. *GOST* (State Standard), *20276–99. Soils: Methods for in-the-Field Determination of Strength and Deformability*, 1999.
22. Barabash, V.M., Begachev, V.I., Belevitskaya, M.A., *et al.*, *Tsvetn. Met.*, 2002, no. 7, pp. 41–42.

Russian Journal of Applied Chemistry, Vol. 78, No. 12, 2005, pp. 1977–1980. Translated from Zhurnal Prikladnoi Khimii, Vol. 78, No. 12, 2005, pp. 2008–2010.
Original Russian Text Copyright © 2005 by Sudarushkin, Pavlyuk, Makhov.

PROCESSES AND EQUIPMENT OF CHEMICAL INDUSTRY

Convective-Infrared Drying of a Polyamide-based Composite in a Fluidized Bed

Yu. K. Sudarushkin, V. V. Pavlyuk, and A. N. Makhov

Saratov State University, Saratov, Russia

Received April 28, 2005

Abstract—The effect of convective-infrared drying of a glass-filled polyamide in a fluidized bed on the diffusion properties of the material and physicomechanical properties of the articles obtained is considered.

An increasingly wide use in fabrication of articles for construction, electric insulation, and special purposes is found by the following polyamide-based thermoplastic cast composites possessing a set of valuable mechanical, thermal, and dielectric properties [1, 2]: PA 6-210KS [OST (All-Union Standard) 6-11-498–79], PA 6-210-DS (OST 6-11-498–79), PA 6-211-KS (OST 6-11-498–79), PA 6-211-DS (OST 6-11-498–79), PA SV-30-2T (2243-015-11378612–97), PA SV-30-3M (2243-015-11378612–97).

The wide-scale introduction of the progressive polyamide-based composites requires a further improvement of the technology of their processing, in which one of the most important stages is drying. This stage affects formation of bubbles, "silver" cracks, delaminations, and inclusions (in products of thermooxidative destruction of polymers) in construction articles made of polyamide.

In the course of drying of thermoplastics, a humid body tends to attain equilibrium with the environment, and, therefore, its moisture content Δ and temperature T depend on time and the coordinates of a point of the body (x, y, z):

$$\Delta(x, y, z, \tau), \quad (1)$$

$$T = T(x, y, z, \tau). \quad (2)$$

The time dependence of temperature can be disregarded if the temperature of a material reaches equilibrium considerably faster than its moisture content does.

The above dependences describe the dynamics of drying and heating of a material. According to [3–5], the variation with time of the average (over the body volume) moisture content Δ and temperature characterizes the kinetics of drying and heating of thermoplastics:

$$\Delta = \Delta(\tau), \quad (3)$$

$$T = T(\tau), \quad (4)$$

$$\Delta = \iiint_V \Delta(x, y, z, \tau)\,dx\,dy\,dz, \quad (5)$$

$$T = \iiint_V T(x, y, z, \tau)\,dx\,dy\,dz. \quad (6)$$

The strongest influence on the drying process is exerted by factors defining the thermoplastic being dried as an object of drying. To these factors belong the microstructure of the materials, their thermal properties and geometric dimensions (grains, beads, crumb), and the content and nature of a filler.

The process of drying of thermoplastics is also affected by parameters of the heat-carrying agent: temperature, pressure, relative humidity, flow velocity of air and motion velocity of the material, and also the possible use of radiant energy.

The presently used method of drying of thermoplastics in shelf-type drying ovens (SNOL, VG-0.35A, VSh-0.05, ShSSU, VN-5805, ShSV-16-KU, and TShch-903), both evacuated and not, involves a considerable expenditure of time (up to 36 h) and is not always effective.

Drying of thermoplastics in a fluidized bed with the use of a USPE installation [6, 7] fails to always provide the residual humidity required by regulations (State Standard, All-Union Standard, Technical Spe-

1070-4272/05/7812-1977 © 2005 Pleiades Publishing, Inc.

Table 1. Parameters of the drying process at T = 80°C

Parameter	Convective drying	Convective-infrared drying	Convective-infrared drying in a fluidized bed
Optimal time of drying, h	9	6.5	4
Residual humidity, %	0.1	0.1	0.085
Particle radius, m	0.00185	0.00185	0.00185
tan α	0.46	0.75	0.90
Molecular diffusion coefficient, $m^2\ s^{-1}$	0.44×10^{-11}	0.72×10^{-11}	0.86×10^{-11}
Turbulent diffusion coefficient, $m^2\ s^{-1}$	–	–	0.14×10^{-11}
Diffusion flux, mol $m^{-2}\ s^{-1}$	–	–	-0.998×10^{-6}

cifications). This is due to the fact that, in convective-radiant heat exchange, moisture is only removed from the surface layer of the fractions of the material (grains or beads) that are processed.

In order to improve and intensify the technological process, a procedure for drying a material in a fluidized bed, with a simultaneous infrared irradiation, on a TIS installation has been developed [8–10]. The use of temperatures elevated to 100°C and of infrared light ensured a rapid, and uniform throughout the volume, removal of the residual moisture from the thermoplastics being processed, which are in the state of continuous circulation and fluidization.

For unfilled thermoplastics, the use of convective-infrared drying in a fluidized bed made it possible to intensify the technological process by a factor of 9–11 (compared with convective drying in a fixed bed) or 1.35–1.5 (compared with convective drying in a moving bed). Moreover, use of IR irradiation precludes overheating of thermoplastic grains and thereby diminishes the destruction of the material [11].

EXPERIMENTAL

Experiments on drying of a glass-filled polyamide of PA 6-210-KS brand (OST 6-11-498–79) were performed in a TShch-903 shelf-type drying oven and a TIS-50 installation at a varied temperature and time of drying (at fixed air pressure of 0.3–0.4 MPa). Thus, the group of variable parameters P_c includes temperature T and treatment time τ:

$$P_c = f(T, \tau). \quad (7)$$

For the glass-filled polyamide mentioned above, the effect of various drying technologies on the rate of moisture removal, diffusion coefficients (molecular and turbulent), diffusion flux, and main physicomechanical parameters was studied.

The molecular diffusion coefficient D was determined experimentally, using the relation

$$D = \frac{r^2 \tan \alpha}{\pi^2}, \quad (8)$$

where r is the radius of grains of the material; tan α, slope ratio of the dependence $\ln(1 - M_t/M_\infty) = f(t)$; M_t, amount of moisture in polyamide at instant of time t; and M_∞, that in equilibrium [12].

The turbulent diffusion coefficient E_m can be found from

$$E_m = E_t - D, \quad (9)$$

where E_t is the total diffusion coefficient [12].

The diffusion flux J is given by

$$J = -E_t \frac{dc_A}{dy}, \quad (10)$$

where dc_A is a change in water concentration in a time t (mol dm^{-3}), and dy is the pathway of the flow in a grain (m).

The calculated values of the parameters are listed in Tables 1–3.

It can be seen from Tables 1–3 that the convective-infrared drying of the PA 6-210-KS polyamide in a fluidized bed intensifies the drying process by a factor of 2.14–2.5, compared with convective drying in a fixed bed.

The following physicomechanical parameters were studied for a material dried at 100°C: tensile strength, relative elongation at break, bending stress at fracture,

Table 2. Parameters of the drying process at T = 90°C

Parameter	Convective drying	Convective-infrared drying	Convective-infrared drying in a fluidized bed
Optimal time of drying, h	7.5	5.5	3.5
Residual humidity, %	0.11	0.1	0.062
Particle radius, m	0.00185	0.00185	0.00185
tan α	0.6	0.91	1.18
Molecular diffusion coefficient, $m^2\ s^{-1}$	0.58×10^{-11}	0.87×10^{-11}	1.13×10^{-11}
Turbulent diffusion coefficient, $m^2\ s^{-1}$	–	–	0.26×10^{-11}
Diffusion flux, mol $m^{-2}\ s^{-1}$	–	–	-1.34×10^{-6}

Table 3. Parameters of the drying process at T = 100°C

Parameter	Convective drying	Convective-infrared drying	Convective-infrared drying in a fluidized bed
Optimal time of drying, h	6	3.5	2.5
Residual humidity, %	0.11	0.1	0.006
Particle radius, m	0.00185	0.00185	0.00185
tan α	0.85	1.1	1.48
Molecular diffusion coefficient, $m^2\ s^{-1}$	0.82×10^{-11}	1.06×10^{-11}	1.42×10^{-11}
Turbulent diffusion coefficient, $m^2\ s^{-1}$	–	–	0.36×10^{-11}
Diffusion flux, mol $m^{-2}\ s^{-1}$	–	–	-1.7×10^{-6}

Table 4. Physicomechanical parameters of articles fabricated from PA 6-210-KS polyamide with the use of various drying technologies

Parameter	Required by regulations	Convective drying	Convective-infrared drying	Convective-infrared drying in a fluidized bed
Tensile strength, MPa	118–122	119–123	122–124	136–138
Relative elongation at break, %	3–4	3.4–3.5	3.3–3.4	4.2–4.4
Bending stress at fracture, MPa	167–170	166–170	142–146	172–178
Impact viscosity, kJ m^{-2}	24.5–27.0	25–26	25–27	34–35

and impact viscosity without notch. The results obtained are listed in Table 4.

CONCLUSIONS

(1) Use of convective-infrared drying of a glass-filled polyamide leads to an increase in its bending stress at fracture, tensile strength, relative elongation at break, and impact viscosity.

(2) Making the time of drying shorter diminishes the thermo-oxidative destruction of a material. The residual internal stresses are lowered, which improves the longevity of articles. Formation of bubbles, "silver" cracks, delaminations, and inclusions is totally precluded.

(3) Thus, the developed drying technology with convective-radiant heat exchange on a TIS-50 installation eliminates the basic defects, improves the performance and mechanical parameters of the articles fabricated, and intensifies the technological process.

REFERENCES

1. *Poliamidy: Katalog* (Polyamides: Catalogue), Cherkassy: NIITEHIM, 1983.
2. *Konstruktsionnye i termostoikie plastmassy: Kata-*

log (Construction and Thermally Stable Plastics: Catalogue), Cherkassy: NIITEHIM, 1988.

3. Lykov, A.V., *Teoriya teploprovodnosti* (Theory of Heat Conductivity), Moscow: Vysshaya shkola, 1967.
4. Lykov, A.V., *Teoriya sushki* (Theory of Drying), Moscow: Energiya, 1968.
5. Sazhin, B.S., *Osnovy tehniki sushki* (Fundamentals of the Drying Technology), Moscow: Khimiya, 1984.
6. Sudarushkin, Yu.K., *Obmen proizvodstvenno-tehnicheskim opytom* (Exchange of Industrial-Technological Experience), Moscow: NIIEIR, 1990, issue 8, pp. 38–41.
7. Sudarushkin, Yu.K., *Plast. Massy*, 1992, no. 1, pp. 43–45.
8. Sudarushkin, Yu.K., *Radiopromyshlennost'* (Radio Industry), Moscow: NIIEIR, 1992, issue 4, pp. 28–32.
9. RF Patent 2094717.
10. RF Patent 2128813.
11. Sudarushkin, Yu.K., Shipovskaya, D.S., Romanov, D.S., and Sokolov, M.Yu., *Plast. Massy*, 2000, no. 4, pp. 35–38.
12. Malkin, A.Ya. and Chalykh, A.E., *Diffuziya i vyazkost' v polimerah: Metody izmereniya* (Diffusion and Viscosity in Polymers: Measurement Techniques), Moscow: Khimiya, 1979.
13. Reynolds, A.J., *Turbulent Flow in Engineering*, New York: Wiley, 1974.

Russian Journal of Applied Chemistry, Vol. 78, No. 12, 2005, pp. 1981–1986. Translated from Zhurnal Prikladnoi Khimii, Vol. 78, No. 12, 2005, pp. 2011–2016.
Original Russian Text Copyright © 2005 by Nazarova, Nuretdinov, Slita, Pavlov, Evlampieva, Litvinova, Gubskaya, Fazleeva, Berezhnaya, Pronina, Kiselev, Panarin.

MACROMOLECULAR CHEMISTRY AND POLYMERIC MATERIALS

Water-Soluble Polymeric Methanofullerene and Fulleropyrrolidine Derivatives

O. V. Nazarova, I. A. Nuretdinov, A. V. Slita, G. M. Pavlov, N. P. Evlampieva, L. S. Litvinova, V. P. Gubskaya, G. M. Fazleeva, L. Sh. Berezhnaya, A. P. Pronina, O. I. Kiselev, and E. F. Panarin

Institute of Macromolecular Compounds, Russian Academy of Sciences, St. Petersburg, Russia

Arbuzov Institute of Organic and Physical Chemistry, Russian Academy of Sciences, Kazan, Tatarstan, Russia

Research Institute of Influenza, Russian Academy of Medical Sciences, St. Petersburg, Russia

Fock Research Institute of Physics, St. Petersburg State University, St. Petersburg, Russia

Received November 11, 2005

Abstract—Water-soluble methanofullerene and fulleropyrrolidine derivatives were synthesized by the reactions of methanofullerenes (MFs) and fulleropyrrolidines (FPs) with poly(*N*-vinylpyrrolidone) (PVP) bearing one terminal amino group. The products contain MF or FP covalently bound to the polymer, corresponding polymeric complexes, and unreacted PVP. Large aggregates of the polymeric MF and FP derivatives are found in aqueous solutions. The electrooptical properties of the products differ considerably from those of the initial polymer. The phosphorus-containing MF and FP derivatives are capable of cleaving the molecule of plasmid DNA.

Water-soluble fullerene derivatives are of great interest for biomedical use [1].

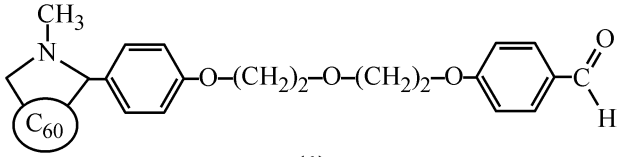
Previously, we have synthesized water-soluble star-like polymeric fullerene (C_{60}) derivatives of PVP bearing one terminal amino group (PVP–NH_2) and examined their molecular-weight and electrooptical characteristics [2–5].

In this study, starting from PVP–NH_2, we synthesized a series of metallofullerene (MF) and fulleropyrrolidine (FP) derivatives and examined their physicochemical properties. The products were also characterized by their ability to interact with biopolymers, such as DNA.

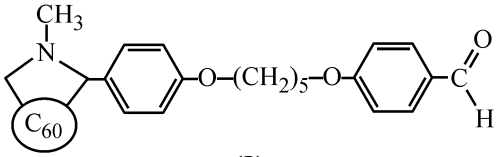
EXPERIMENTAL

MFs and FPs are stable monoadducts of fullerene C_{60}. They are readily soluble in many organic solvents, and their physical and chemical properties are reported in [6–9]. The structures of MFs and FPs used for modification of PVP–NH_2 are shown in Fig. 1.

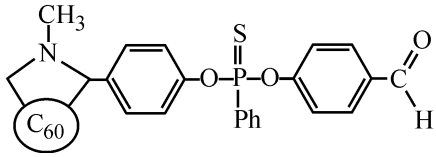
The starting PVP–NH_2 was prepared by radical polymerization of *N*-vinylpyrrolidone in the presence of an amino derivative of mercaptan, cysteamine hydrochloride [10]. The reactions of PVP–NH_2 with MFs or FPs were carried out at $[NH_2]:[MF(or\ FP)] = 6:1$ molar ratio in a DMF/toluene mixed solvent for



(1)



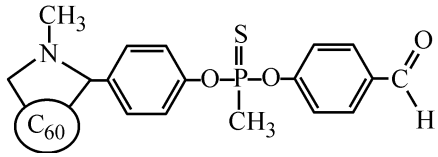
(2)



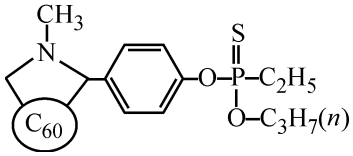
(3)

Fig. 1. Structures of MFs and FPs.

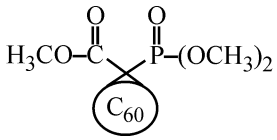
1070-4272/05/7812-1981 © 2005 Pleiades Publishing, Inc.



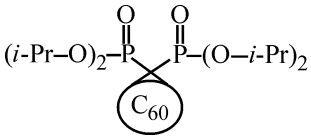
(4)



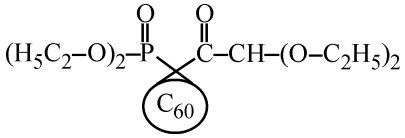
(5)



(6)



(7)



(8)

Fig. 1. (Contd.)

24 h. The reaction mixture was then filtered and concentrated in a vacuum. The dry residue was dissolved in water and filtered. The products were isolated by freeze drying.

The products were characterized by gradient step TLC on Sorbfil plates, PTSKh-AF-B-UF (Sorbpolimer, Krasnodar, Russia), with toluene, chloroform, and CCl_4 as eluents. To develop the chromatograms we used UV light (254 nm) or iodine vapor.

The sedimentation velocity of the polymer solutions was studied in 0.2 M NaCl on a Beckman XL-I analytical ultracentrifuge at a rotor speed of 42 000 rpm and, in the case of fast sedimentation, at 10 000 rpm. The interference and absorption (λ = 250 nm) scans were performed to monitor the sedimentation boundary mostly at the concentration $c = 0.17 \times 10^{-2}$ g cm^{-3}. For some of the samples we studied the concentration dependence over the range $(0.02–0.2) \times 10^{-2}$ g cm^{-3}. In these experiments we observed no significant concentration effects.

To study the electrooptical properties of the fullerene derivatives of PVP, we measured the electrooptical Kerr effect in a rectangular-pulse electrical field. The experiments were carried out in chloroform at 21°C. The experimental setup and conditions were reported elsewhere [5]. The Kerr constant K was estimated by the relation

$$K = \lim_{E \to 0} {}_{c \to 0} (\Delta n - \Delta n_0)/E^2 c,$$

where $(\Delta n - \Delta n_0)$ is the difference between the optical birefringence under the electric field in the test solution with a concentration c and in the solvent, and E, the electric field strength.

The interaction of the polymeric MF and FP derivatives with DNA was studied as follows. Aqueous polymer solutions (c = 0.4–10 mg ml^{-1}, V = 10 μl) were mixed with a solution of plasmid DNA pUC 19 (0.1 mg ml^{-1}, 2 μl). The interaction was evaluated by using electrophoresis in 0.8% agarose gel at a current of 90 mA.

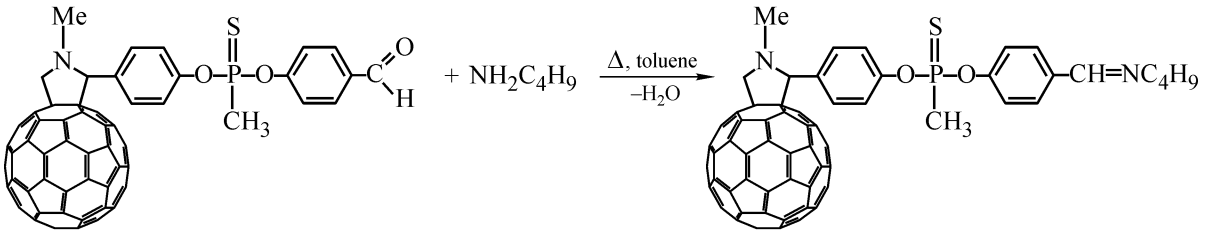
The products of the reactions of compounds **1**–**8** with PVP–NH_2 (PVP-1–PVP-8) are soluble in water. However, in contrast to the initial polymer PVP–NH_2, they are brown. The UV spectra of PVP-1–PVP-8, like those of the initial MFs and FPs, have the form of steadily descending curves with weak features near 260 nm, which is typical of covalently bound C_{60} [11, 12].

The formation of polymeric derivatives with the MF and FP covalently bound to the polymer matrix was confirmed by TLC. In chromatography on Sorbfil silica gel plates, the eluent (toluene, chloroform, CCl_4), C_{60}, MFs, and FPs move along with the solvent front, while PVP–NH_2 is irreversibly adsorbed, remaining at the start zone. Under these conditions, the complex of C_{60} with PVP decomposes [2, 3], and two zones are observed in the chromatograms, namely, those of C_{60} and PVP. In the cases of previously described covalent C_{60} derivatives of PVP–NH_2 (PVP–C_{60}) [2, 3], C_{60} is not eluted, and the only colored zone at the start is observed. This zone shows absorption in the UV(254) range and also dark brown fluorescence in the UV(366) range, which is atypical of the initial PVP–NH_2 samples and can be attributed only to the presence of covalently bound C_{60} [2, 3].

Similarly to PVP–C_{60}, in the cases of PVP-1–PVP-8 products, the zones of the corresponding PVP–MF or PVP–FP derivatives is found at the start. How-

ever, for PVP-1–PVP-8, in contrast to PVP–C_{60}, the zones of the initial MFs or FPs are also observed in the chromatograms. As mentioned above, all the products obtained are water-soluble, unlike the initial MFs and FPs. Evidently, the products also contain, along with the covalent derivatives PVP–MF (or FP), water-soluble complexes of MFs or FPs with PVP.

To confirm the structure of the polymeric MF and FP derivatives, we studied the reaction of the aldehyde-containing compound with a model low-molecular-weight amine, *n*-butylamine. It was found that this reaction yields the corresponding Schiff bases. For example, a mixture of **4** and *n*-bytylamine (1 : 1 molar ratio) was refluxed in toluene for 7 h with a Dean–Stark trap. The precipitated compound **4'** was dried and characterized by the mass and IR spectra. The filtrate contained minor amounts of unreacted compound **4**, as demonstrated by HPLC. The yield of **4'** was 77.8% (recalculated to the reacted fulleropyrrolidine **4**).

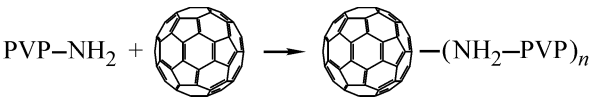


(4) **(4')**

The mass spectra of **4'** show a peak of the molecular ion with *m*/*z* 1121.95 (calculated *m*/*z* 1122.81). No absorption band of the aldehyde group of the initial compound **4** at 1700 cm^{-1} was found in the IR spectrum, but the characteristic band of the C=N bond appears at 1648 cm^{-1}.

Therefore, in the case of fulleropyrrolidine **4**, the addition of PVP–NH_2 occurs essentially at the aldehyde group.

At the same time, it is known that both low-molecular-weight amines and polymers containing primary amino groups are capable of readily reacting with the fullerene core [11, 12]. In this case, if macromolecules of the polymer contain a single terminal amino group, star-like derivatives with the fullerene molecule as a branching site are formed [2, 3].



Evidently, this is the case for the reactions of MFs and FPs containing no aldehyde group with PVP–NH_2. As noted above, in the case of aldehyde-containing compounds, the addition of PVP–NH_2 occurs essentially at the aldehyde group.

For compounds **3**–**8**, the addition of PVP–NH_2 could occur via the phosphorus atom to give salt-like structures [16].

The sedimentation data were processed using Sedfit software [17] by direct fitting with numerical solutions of the Lamm equation for the sedimentation velocity in a dilute solution of ideally sedimenting macromolecules.

The sedimentation velocity data obtained using the interference optics show that the initial PVP–NH_2 shows a peak at 1.0 Sv, which corresponds to MW 10 000 [18]. The sedimentation coefficient distributions of the fullerene derivatives show the peak practically coinciding with the sedimentation coefficient of the initial PVP–NH_2, i.e., these samples contain a considerable fraction of the unreacted initial polymer. The sedimentation analysis allows estimation of the composition of PVP-1–PVO-8. The fraction of the fullerene-containing macromolecules in PVP-1, PVP-2, PVP-5–PVP-8 is 19 ± 2 wt %, whereas that in PVP-3 and PVP-4 is less than 10 wt % (see table).

The interference scan system of a Beckman XL-I analytical ultracentrifuge provides the sedimentation coefficient distribution for the sample as a whole, while the absorption scan system records the fullerene-containing fraction of the sample, as the only

Sedimentation coefficients of MF and FP polymeric derivatives in 0.2 M NaCl, estimated using Sedfit software from the sedimentograms obtained on a Beckman XL-I analytical ultracentrifuge

Polymeric derivative	s_b,* Sv	Fast interference peak (FI), s_f, Sv	FI fraction,** %	Main absorption peak (MAP), s_f, Sv	MAP fraction,*** %	V_f/V_b
Initial PVP–NH_2	1.0	–	0	–	–	1
PVP-1	1.0	19	21	15	40	60
PVP-2	1.0	20	20	20	80	90
PVP-3	1.0	>30	4	74	58	640
PVP-4	1.0	12	8	11	56	40
PVP-5	1.1	11	18	8.7	33	20
PVP-6	1.0	11	16	2.6; 15.5	33; 23	4; 60
PVP-7	1.0	15	24	12	47	40
PVP-8	0.8	33	17	70	96	800

* Interference peak corresponding to the initial linear PVP.

** (FI) Fraction of species with higher sedimentation coefficients as compared to the initial polymer (obtained using interference optics). It corresponds to the fullerene-containing fraction of the sample.

*** (MAP) Main part of the fullerene-containing fraction of the sample (obtained using absorption optics) (% of the total fullerene-containing fraction).

fraction having UV absorption. Comparison of the sedimentograms obtained with both recording systems (Fig. 2) shows that the absorption optics reveals higher sedimentation coefficients, providing a clear evidence in favor of the fact that larger fullerene derivatives are formed as compared to the initial polymers. The results show that the fullerene fraction of the samples is nonuniform. It contains fullerene-containing macromolecules whose sedimentation coefficients are higher on the average, by an order of magnitude, than those of the initial PVP–NH_2, and also still larger water-soluble molecular aggregates. The occurrence of such aggregates has been reported previously for other fullerene-containing polymers [3, 15].

Let us estimate from the experimental sedimentation data the extent to which the volume occupied by the fullerene-containing macromolecules/clusters in the solution is larger than that occupied by the initial PVP macromolecule, using the equivalent hydrodynamic sphere model and taking into account that the measured partial specific volumes of the initial PVP–NH_2 and fullerene derivatives are similar. It may be demonstrated that, in our case, $V_f/V_b = (s_f/s_b)^{3/2}$, where V_b and s_b, and V_f and s_f are the volumes and

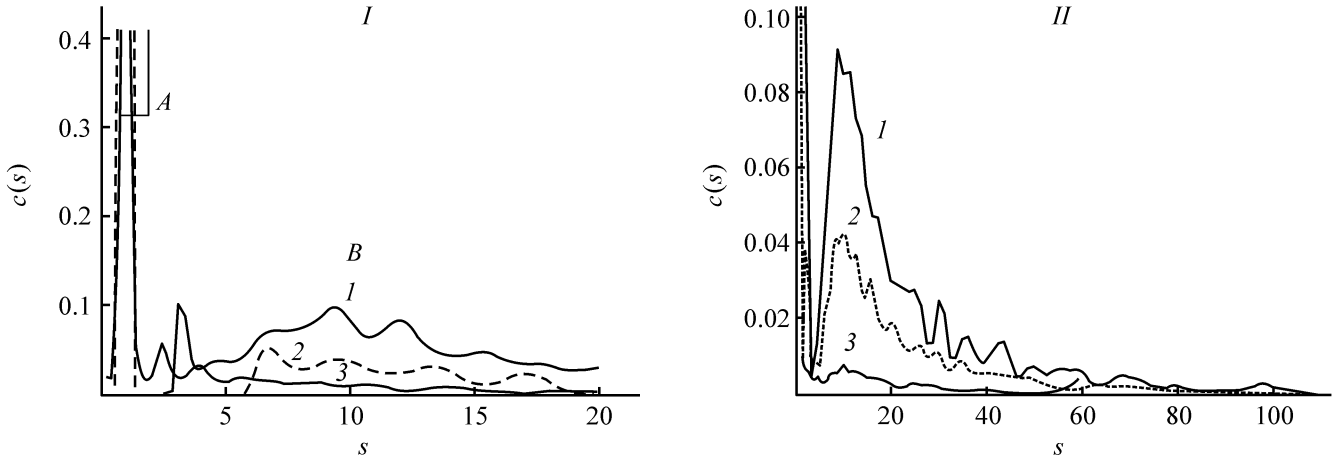


Fig. 2. Sedimentation coefficient distribution for PVP-7 at various solution concentrations ($c \times 10^{-2}$ g cm^{-3}): (*1*) 0.199, (*2*) 0.099, and (*3*) 0.019. (*I*) Distributions obtained using the interference optics: (*A*) slow sedimentation range corresponding to the sedimentation coefficient of the initial linear PVP (see table) and (*B*) fast sedimentation range corresponding to the fullerene-containing fraction of the sample. (*II*) Distributions obtained using the absorption optics, corresponding to the fullerene-containing fraction of the sample.

sedimentation coefficients of the initial PVP macromolecule and fullerene-containing macromolecules/clusters, respectively. The estimates listed in the table suggest that the volume occupied by the fullerene-containing macromolecules/clusters is, as a rule, larger by an order of magnitude than that occupied by the PVP macromolecule corresponding to a branch of the star-like dendrimer.

One of the fulleropyrrolidines (compound **2**) has been studied previously [20]. It was demonstrated that, in contrast to the nonpolar and optically isotropic (by virtue of high symmetry) fullerene C_{60}, the molecules of **2** form polar nanoparticles with high dipole moment (μ = 5.4 D) and optical anisotropy ($\Delta a \sim 20 \times 10^{-24}$ cm^3). Their Kerr coefficient in chloroform was found to be $\pm 5.3 \times 10^{-10}$ cm^5 g^{-1} (300 V)$^{-2}$. Covalent or coordination incorporation into PVP macromolecules of polar carbon nanoparticles having different polarization, dielectric, and optical characteristics, compared to the polymer, alters significantly the properties of the polymer, as we have been previously demonstrated for the example of star-like PVP-based dendrimers with C_{60} as a branching site [4, 5].

Figure 3 shows the results of a comparative study of the electrooptical Kerr effect in chloroform for samples of starting compounds **2** and PVP–NH_2 and also for the synthetic derivative PVP-2. The solutions of PVP-2 and PVP-1 in chloroform, in contrast to PVP-3–PVP-7, were molecular-disperse, which was reflected in that the optical birefringence Δn was a linear function of the squared electric field strength, E^2. For products PVP-3–PVP-7, such a dependence was distinctly nonlinear. Furthermore, they demonstrated considerable difference in Δn (by two orders of magnitude and more) as compared to the initial PVP, which is typical of the cases when charged aggregates or strongly polarizable molecular species are present in a solution. As clearly seen from Fig. 3, PVP-2 exhibits strongly different behavior as compared to the initial polymer. Its Kerr coefficient K differs significantly by the sign and absolute value from the initial PVP, exceeding that of the fullerene adduct, even though the weight fraction of the latter in the polymer is small. Generally, the above-mentioned alterations of the molecular properties of PVP-2 are consistent with the previous results obtained for the pairs constituted by a star-like PVP–C_{60} and linear PVP having similar molecular weight [4, 5].

As is known [1, 21, 22], some fullerene derivatives exert a destructive influence on DNA molecules. Therefore, we studied the interaction of the MF and FP polymeric derivatives (PVP-1–PVP-7) and also of

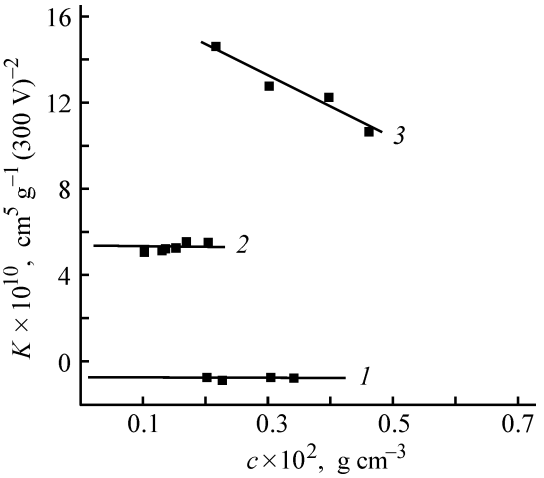


Fig. 3. Concentration dependences of the electrooptical Kerr coefficient K for (*1*) initial PVP–NH_2, (*2*) compound **2**, and (*3*) PVP-2.

the previously described PVP–C_{60} [2–5] with plasmid DNA pUC 19. The destructive effect was evaluated by the change in the DNA component ratio, using electrophoresis in agarose gel. In the reference electrophoregram of the initial DNA we found two bands corresponding to circular and supercoiled DNA conformations [21]. For PVP–C_{60}, PVP-1, and PVP-2, we obtained similar electrophoregrams. In the cases of PVP-3–PVP-7, the fraction of the circular conformation increased with the polymer : DNA ratio at the expense of the supercoiled conformation, the effect being particularly clearly pronounced for PVP-3 and PVP-7. For these samples, the band of the supercoiled DNA vanished at the polymer concentration of 2 mg ml^{-1} and higher. Furthermore, in the case of PVP-7, this effect was accompanied by the appearance of the band of linear DNA. These results suggest that DNA molecules are cleaved under the action of PVP-3–PVP-7 by the single-strand cleavage mechanism, which results in DNA conversion from the supercoiled to circular form [21]. In the case of PVP-7, the appearance of the band of linear DNA can be attributed to two-strand cleavage.

The toxicity of the MF and FP polymeric derivatives synthesized in this study was examined using the microtetrazolium test (MTT) [23]. The results showed that, when taken in concentrations of up to 100 mg ml^{-1}, these fullerene derivatives are not cytotoxic with respect to T 98G cells.

CONCLUSIONS

(1) Water-soluble polymeric derivatives of a series of methanofullerenes (MFs) and fulleropyrrolidines

(FPs) were synthesized starting from poly(*N*-vinylpyrrolidone) with a terminal amino group.

(2) It was established that the resulting products are multicomponent. They contain the initial polymer, MF or FP covalently bound to the polymer, complexes polymer–MF (or FP), and also large aggregates.

(3) It was shown that the electrooptical properties of the products differ significantly from those of the initial PVP–NH_2 by virtue of the presence of chemically bound polar and optically anisotropic FPs or MFs.

(4) It was demonstrated that incorporation of phosphorus-containing MF and FP derivatives in PVP enhances the capability of the PVP–MF(or FP) derivatives to cleave plasmid DNA pUC 19.

ACKNOWLEDGMENTS

The authors are grateful to C. Ebel (Grenoble, France) for furnishing an opportunity to perform the sedimentation experiments in her lab, and also to the Federal Agency of Science and Innovations (grant NSh 1823.2003.3), Russian Foundation for Basic Research (grant 05-03-32633), and Academy of Sciences of Tatarstan for financial support.

REFERENCES

1. Da Ros, T., Spalluto, G., and Prato, M., *Croat. Chem. Acta*, 2001, vol. 74, no. 4, pp. 743–755.
2. Nazarova, O.V., Pavlov, G.M., Bokov, S.N., *et al., Dokl. Ross. Akad. Nauk*, 2003, vol. 391, no. 2, pp. 212–214.
3. Pavlov, G.M., Nazarova, O.V., Ebel, C., *et al., Zh. Prikl. Khim.*, 2005, vol. 78, no. 1, pp. 132–138.
4. Ryumtsev, E.I., Evlampieva, N.P., Nazarova, O.V., *et al., Dokl. Ross. Akad. Nauk*, 2003, vol. 392, no. 2, pp. 212–216.
5. Evlampieva, N.P., Nazarova, O.V., Bokov, S.N., *et al., Vysokomol. Soedin.*, 2004, vol. 46, no. 5, pp. 822–829.
6. Gubskaya, V.P., Fazleeva, G.M., Nodov, K.L., *et al.*, Abstracts of Papers, *XIV Conf. on the Chemistry of Phosphorus Compounds, Kazan, Tatarstan (Russia), June 27–July 1, 2005*, Kazan, 2005, p. 105.
7. Gubskaya, V.P., Sibgatullina, F.G., Yanilkin, V.V., *et al., Izv. Ross. Akad. Nauk, Ser. Khim.*, 2005, no. 6, pp. 1424–1429.
8. Nuretdinov, I.A., Gubskaya, V.P., Berezhnaya, L.Sh., *et al., Izv. Ross. Akad. Nauk, Ser. Khim.*, 2000, no. 12, pp. 2083–2086.
9. Nuretdinov, I.A., Gubskaya, V.P., Shishkina, N.I., *et al., Izv. Ross. Akad. Nauk, Ser. Khim.*, 2002, no. 2, pp. 317–320.
10. Nazarova, O.V., Afanas'eva, E.V., Panarin, E.F., and Ivanova, N.P., *Zh. Prikl. Khim.*, 2000, vol. 73, no. 12, pp. 2060–2062.
11. Vinogradova, L.V., Melenevskaya, E.Yu., Khachaturov, A.S., *et al., Vysokomol. Soedin., Ser. A*, 1998, vol. 40, no. 11, pp. 1854–1862.
12. Andreev, S.M., Babakhin, A.A., Petrukhina, A.O., *et al., Dokl. Ross. Akad. Nauk*, 2000, vol. 370, no. 2, pp. 261–264.
13. Wudl, F., Hirsch, A., Khemani, K.C., *et al., Fullerenes, Synthesis, Properties, and Chemistry of Large Carbon Clusters*, Hammond, G.S. and Kuck, V.J., Eds., Washington, 1992, p. 161.
14. Janaki, J., Premila, M., Gopalan, P., *et al., Thermochim. Acta*, 2000, vol. 356, pp. 109–116.
15. Li, F.-M., *Makromol. Symp.*, 1996, vol. 101, pp. 227–236.
16. Panarina, A.E., Dogadina, A.V., and Ionin, B.I., *Zh. Obshch. Khim.*, 2003, vol. 73, no. 11, pp. 1826–1834.
17. Schuck, P., *Biophys. J.*, 2000, vol. 78, no. 3, pp. 606–619.
18. Pavlov, G.M., Panarin, E.F., Korneeva, E.V., *et al., Vysokomol. Soedin., Ser. A*, 1990, vol. 32, no. 6, pp. 1190–1196.
19. Lebedev, V.T., Torok, D., Klyubin, V.V., *et al., Vysokomol. Soedin., Ser. A*, 2004, vol. 46, no. 5, pp. 875–881.
20. Evlampieva, N.P., Zverev, V.V., Dmitrieva, T.V., *et al., Zh. Fiz. Khim.*, 2005, vol. 79, no. 5, pp. 489–495.
21. Ikeda, A., Hatano, T., Kawaguchi, M., *et al., Chem. Commun.*, 1999, pp. 1431–1434.
22. Zhang, Y., Yang, S., Liu, C., *et al., New J. Chem.*, 2002, vol. 26, pp. 617–620.
23. Mossmann, T.J., *Immunol. Meth.*, 1983, vol. 65, pp. 55–63.

Russian Journal of Applied Chemistry, Vol. 78, No. 12, 2005, pp. 1987–1992. Translated from Zhurnal Prikladnoi Khimii, Vol. 78, No. 12, 2005, pp. 2017–2022.
Original Russian Text Copyright © 2005 by Pavlyuchenko, Primachenko, Sorochinskaya, Ivanchev.

MACROMOLECULAR CHEMISTRY AND POLYMERIC MATERIALS

New Possibilities for Controlling the Morphology of Core–Shell Latex Particles During Emulsion Polymerization

V. N. Pavlyuchenko, O. N. Primachenko, O. V. Sorochinskaya, and S. S. Ivanchev

Boreskov Institute of Catalysis (St. Petersburg Branch), Siberian Division, Russian Academy of Sciences, St. Petersburg, Russia

Received November 14, 2005

Abstract—A simple technology is described for preparing latexes with core–shell particles, in which the composition of the shell copolymer regularly varies from the inner layers of the shell to the particle periphery. Equations are suggested for calculating the instantaneous and integrated compositions of the shell copolymer and for analyzing how the composition of the copolymer varies along the particle radius. Specific examples of synthesis of emulsion copolymers intended for preparing plastisols and latexes with hollow particles demonstrate the benefits from application of the technology suggested.

The principles of formation of polymeric latex particles with complex morphology are widely used now in development of processes for preparation and application of synthetic latexes and emulsion copolymers [1, 2]. We restrict the consideration to particles with the core–shell morphology, implying that the interior and exterior of the polymer sphere are built of different, typically thermodynamically incompatible, (co)polymers. This approach has a number of advantages over the technologies utilizing latexes with homogeneous particles. One of them consists in that the same monomer raw material can be used for preparation of various polymeric materials, sometimes with opposite properties. As an example can serve ABS emulsion plastics (with butadiene (co)-polymer as the core and random acrylonitrile–styrene copolymer as the shell) and reinforced elastomers (a polybutadiene shell and a core formed from a rigid polymer, e.g., polystyrene). The shell on the core particles imparts novel properties to the material. This principle is applied, e.g., in preparing polymer powders whose particles do not stick together during spray drying and in storage [3]. Also, many applied problems can be solved by introducing functional groups into the shell polymer, and, in this case, functionalization requires a substantially smaller amount of typically expensive components. As an example can serve antistatic coatings prepared from latexes whose particles contain amine monomer units in their shells [4, 5].

The technology of preparing latexes with core–shell particles seems fairly simple. First, a latex is synthesized by emulsion polymerization of monomer **1**. Next, monomer **2** is introduced into the latex acting as seed and is polymerized. However, implementation of this technology is troublesome because of the specific thermodynamic and kinetic features of preparation of the core–shell latex particles. If the process is run under close-to-equilibrium conditions, the structure of the resulting particles is characterized by the lowest surface free energy. Since water typically serves as the dispersion medium, formation of particles with the shell composed of a more hydrophilic polymer seems the most probable. In some cases, this structure is formed even with hydrophilic particles as seeds, since hydrophobic monomer diffuses into the bulk of the seed particles [6]. The situation is improved to a certain extent when the process is carried out under nonequilibrium conditions, i.e., when monomer **2** is introduced into the seed latex at a rate not exceeding that of its polymerization ("monomer starvation") [7]. However, complications may arise in this case as well if the core and shell polymers differ too strongly in their thermodynamic properties; the resulting particles may have a hemispherical structure, with the shell polymer incompletely covering the core polymer [8]. This problem can be solved by creating an intermediate shell exhibiting affinity for both the core polymer and the shell polymer [9, 10].

1070-4272/05/7812-1987 © 2005 Pleiades Publishing, Inc.

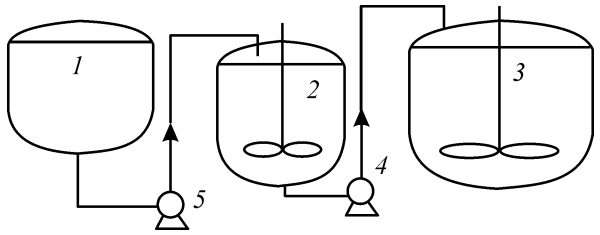


Fig. 1. Flowsheet of dosing of the monomer mixture with variable composition into the reactor. (*1*) Tank for monomers, (*2*) intermediate tank, (*3*) reactor, and (*4*, *5*) pumps.

It should be noted that this technique complicates the entire technology. At the same time, a polymer equally compatible with thermodynamically dissimilar polymers is hardly conceivable.

In this paper, we describe a simple technology for making compatible the core and shell polymers by gradually varying the chemical composition of the shell when going from the core–shell interface to the particle periphery. The properties of the inner layers of the shell are chosen in such a way that the core and the shell polymers exhibit the greatest affinity for each other.

EXPERIMENTAL

The technology described was implemented by dosing into the seed latex a monomer mixture with variable composition. At the initial moment, the monomer mixture being dosed forms a polymer having a high thermodynamic affinity for the core polymer. In an ideal case, the shell and core polymers can have identical compositions in this stage of the process. Gradual variation of the composition of the monomer mixture being dosed radically modifies the properties of the peripheral layers of the shell, thereby ensuring the desired properties of the latex.

Two requirements should be satisfied in implementation of the process. First, the monomer mixture being dosed into the seed latex should not be accumulated, i.e., the process should be run under monomer starvation conditions. Under these conditions, the instantaneous composition of the monomer mixture is identical to that of the copolymer being formed. Second, the monomers being dosed into the reaction mixture should be polymerized only on the seed particles, with formation of new particles precluded. This requirement is easily satisfied when there is no free surfactant in the dispersion medium. In other words, the seed latex should have adsorption-unsaturated particles.

As is known, the adsorption saturation is calculated on the basis of the characteristics of the latex (particle diameter and content of the polymer in the latex) and the parameters of the surfactant used (area occupied by one surfactant molecule in the saturated adsorption layer and the critical micelle concentration). The adsorption saturation can be experimentally monitored by measuring the surface tension of the latex being formed. It should be noted that the probability of particle formation by the homogeneous mechanism is sharply reduced when the dispersion medium contains seed particles [11]. As the volume of the particles increases, their adsorption saturation is reduced, and if the latex stability is endangered, it is necessary to add additional amounts of the surfactant during the process, taking into account that the increase in the total surface area of the particles is proportional to their growing volume raised to power 2/3.

Figure 1 presents the flowsheet of the process, which provides dosing of the monomer mixture with variable composition into the reactor containing the seed latex and, if the above-stated requirements are satisfied, ensures formation of particles whose chemical composition regularly varies along the shell thickness. We consider the simplest version of this process, when monomer **1** (M_1) contained in tank *1* is transferred by pump *5* into intermediate tank *2* containing monomer **2** (M_2) at a flow rate w_1, and the resulting monomer mixture $M_1 + M_2$ is dosed into reactor *3* by pump *4* at a flow rate w_2. The change in the amount of M_1, mass units, in tank *2* can be expressed by the differential equation

$$dq_1 = w_1\rho_1 dt - w_2\frac{q_1}{V}dt. \quad (1)$$

Here, ρ_1 is the density of M_1, and V, volume of $M_1 + M_2$ in tank *2* at the instant of time t.

Since the volume of the monomer mixture in tank *2* and its change are determined by the difference in the dosing rates w_1 and w_2,

$$V = V_0 + w_1 t - w_2 t, \quad (2)$$

holds. Here, V_0 is the volume of M_2 in tank *2* at $t = 0$, and

$$dV = (w_1 - w_2)dt. \quad (3)$$

The amount of M_1, occurring at any moment in tank *2*, is described by the equation

$$q_1 = [M_1]V. \quad (4)$$

Here, $[M_1]$ is the running concentration of M_1 in tank *2*, expressed as the mass of the monomer per unit volume. Then

$$dq_1 = d[M_1]V + Vd[M_1]. \quad (5)$$

By combining (1)–(5), we obtain the equation

$$\frac{1}{w_1}\int_0^{[M_1]}\frac{d[M_1]}{[M_1]-\rho_1} = \frac{1}{w_2-w_1}\int_0^t\frac{dt}{t-\frac{V_0}{w_2-w_1}}, \quad (6)$$

whose solution yields the running concentration $[M_1]$

$$[M_1] = \rho_1 - \rho_1\left(1 - \frac{w_2-w_1}{V_0}t\right)^{\frac{w_1}{w_2-w_1}}. \quad (7)$$

A simplified version of this flowsheet can be implemented at $w_1 = w_2$. We practically implemented it by eliminating pump *4* from the flow sheet and filling tank *2* to full capacity ($V = V_0$). Solution of Eq. (1) under these conditions yields

$$[M_1] = \rho_1[1 - \exp(w_1/V_0)]. \quad (8)$$

Thus, the instantaneous composition of the monomer mixture in tank *2* and, hence, the instantaneous composition of the copolymer formed in reactor *3* can be controlled by varying the dosing rates, the initial volume of M_2 or, in the simplified version, the volume of the intermediate tank.

Taking into account the need for running the process under the monomer starvation conditions, there can be only limited possibilities for varying the dosing rates. As to the intermediate tank, it is not always expedient to replace it on a pilot or commercial plant in order to change V_0. It is more convenient to vary the composition of the monomer mixtures in tanks *1* and *2* by introducing into them both monomers and varying their concentration ratio to achieve a desired distribution of the components in the shell of a particle. Basically, the reaction system can contain any amount of the monomers. Then Eqs. (7) and (8) for monomer M_i can be represented as:

$$[M_i] = c_i + \left([M_i]_0 - c_i\right)\left(1 - \frac{w_2-w_1}{V_0}t\right)^{\frac{w_1}{w_2-w_1}}, \quad (9)$$

$$[M_i] = c_i + \left([M_i]_0 - c_i\right)\exp[-(w/V_0)t] + c_i. \quad (10)$$

In Eqs. (9) and (10), the density of the monomer is replaced with its concentration in tank *1*, c_i, and integration is carried out for the concentration going from the initial concentration of M_1 in tank *2*, $[M_i]_0$, rather than from 0. The instantaneous content of the units of M_1 in the copolymer containing n types of monomer units is described by the expression

$$m_i = \frac{[M_i]}{\sum_{i=1}^{n}[M_i]}. \quad (11)$$

To calculate the integrated composition of the shell copolymer at any instant of time t, it is necessary to determine the amounts of each of the monomers Q_i, charged into the reactor by this instant of time, by solving the equation

$$\int_0^{Q_1} dQ_i = \int_0^t w_2[M_i]\,dt. \quad (12)$$

In this equation, we substitute $[M_i]$ from Eqs. (9) or (10), depending on the chosen version of the process. At $w_1 \neq w_2$,

$$Q_i = c_i w_2 t + \left([M_i]_0 - c_i\right)V_0\left[1 - \left(1 - \frac{w_2-w_1}{V_0}t\right)^{\frac{w_1}{w_2-w_1}}\right]. \quad (13)$$

At $w_1 = w_2 = w$,

$$Q_i = (c_iV_0 - [M_i]_0V_0)\exp[-(w/V_0)t] + c_iwt + [M_i]_0V_0 - c_iV_0. \quad (14)$$

As a result, the content of the M_i units in the shell copolymer, accumulated by the instant of time t, is described by the expression

$$q_i = \frac{Q_i}{\sum_{i=1}^{n}Q_i}. \quad (15)$$

The equations presented above show that, in the shell of the particle, both ascending and descending gradient of the content of the monomer units of the given type along the particle radius can be basically obtained. The nature of this gradient can be changed by varying the monomer concentrations in tanks *1* and *2* and the dosing rates w_1 and w_2. Figure 2 presents the calculated plots describing the variation of the content of monomer 1 along the particle radius for a hypothetical case of copolymerization of two monomers M_1 and M_2. The initial composition of the monomers in tank *2* precisely corresponded to the composition of the core copolymer. When constructing the plots, we calculated the shell radius r_s in various stages of the process by the equation

$$r_s = \left(r_c^3 + \frac{3kw_2t}{4\pi N}\right)^{1/3}. \quad (16)$$

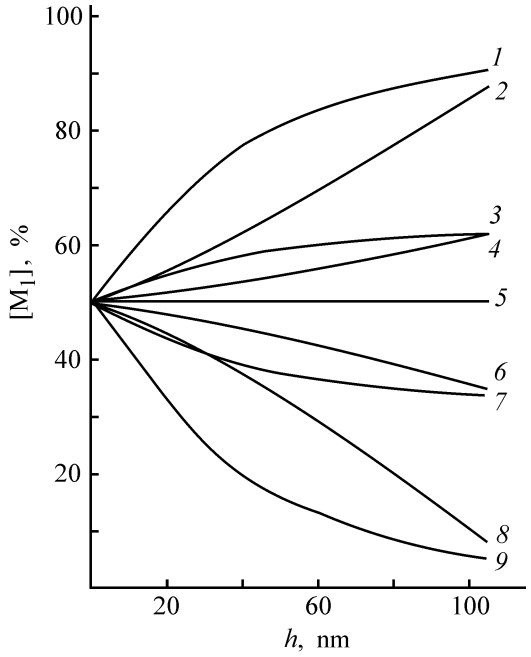


Fig. 2. Calculated plots describing the variation of the composition of the shell copolymer along its thickness *h*, expressed via the content of the M_1 monomer units for a hypothetical copolymerization of two monomers M_1 and M_2. Copolymerization conditions: core, $M_1 + M_2$ (50 : 50 wt %) copolymer; $N = 2.386 \times 10^{16}$, $r_c = 100$ nm; parameters of the monomers: $\rho_1 = 0.9$, $\rho_2 = 1.0$ g cm^{-3}, $k = 0.85$; tank *2*: $V_0 = 500$ cm^3, $[M_1]_0 = [M_2]_0 = 0.474$ g cm^{-3} (mass ratio $M_1 : M_2 = 50 : 50$), $w_2 = 3$ cm^3 min^{-1}; copolymerization time 300 min. c_1, g cm^{-3}: (*1, 2*) 0.9; (*3, 4*) 0.6; (*5*) 0.474; (*6, 7*) 0.3; and (*8, 9*) 0. w_1, cm^3 min^{-1}: (*1, 3, 7, 9*) 9 and (*2, 4–6, 8*) 2.

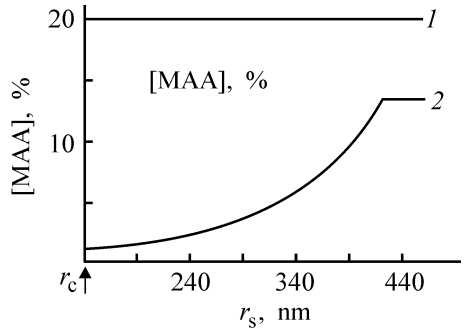


Fig. 3. Calculated plots describing the variation of the content of the MAA units in the shell copolymer along the particle radius r_s in synthesis of the emulsion copolymer for plastisols. Copolymerization at (*1*) constant and (*2*) variable composition of the monomer mixture dosed; the same for Fig. 4. For copolymerization conditions, see Table 1.

Here, r_c is the core particle radius; *k*, coefficient describing the decrease in the volume of the reaction system, associated with conversion of the monomers into the copolymer; and *N*, total number of the particles in the reaction system.

Our data suggest that the surface zone of the particles of the final latex can contain approximately the same number of the M_1 units, and the integrated composition of the copolymer can be varied within fairly wide limits by varying w_1 only.

Let us consider two specific cases of preparation of latexes with core–shell particles by the procedure we suggest. The first example concerns preparation of emulsion polymers for plastisols, i.e., dispersions of polymer particles in a plasticizer. One of the major problems in preparation and application of plastisols stems from their low stability in storage. Fast premature gelation is due to thermodynamic instability of plastisols even under ordinary conditions. It is known [12] that dissolution of the polymer particles in a plasticizer can be decelerated by coating the polymeric particles with a shell composed of a polymer having a lower thermodynamic affinity for the plasticizer that the core polymer. We synthesized latexes with particles of such type. The core of the particles was formed from a styrene–methyl methacrylate (ST–MMA) copolymer, and the shell copolymer included, along with the monomer units mentioned, methacrylic acid (MAA) units. We used two versions: In the first version, the shell copolymer had a homogeneous composition, and in the second, there was an ascending gradient of the concentration of the MAA units from the core copolymer–shell copolymer interface to the periphery of the particle.

Table 1 lists the formulations and preparation conditions of the latexes, as well as the characteristics of the plastisols thereof. Figure 3 shows how the concentration of the MAA units varies along the particle radius. It is seen that the technology we suggest makes it possible to reduce the total amount of the functional monomer, but, at the same time, provides a high content of the MAA units in the surface zone of the shell of the particle and, eventually, stable plastisols.

The second example concerns preparing latexes with hollow polymer particles. These particles, owing to a high light-scattering power, are applied as white pigment in preparation of coatings and paint and varnish materials [13]. The most promising technology of synthesis of latexes with hollow particles includes the following stages: (1) preparation of latexes with highly hydrophilic particles, e.g., consisting of weakly cross-linked MMA–MAA copolymers; (2) creation of core–shell particles by emulsion seed (co)polymerization of ST or others monomers; and (3) neutralization of the carboxy groups of the core at a temperature close to T_g of the shell (co)polymer, accompanied by ionization of the functional groups, sharp enhance-

Table 1. Conditions of synthesis of the latex and the characteristics of the plastisol (initiator, potassium persulfate, 0.875 g; emulsifier, sodium alkyl (C_{14}–C_{16}) sulfonate, 0.45 g; water 410 g; core, MMA : ST = 67.4 : 32 : 6 (wt %); copolymer; core : shell mass ratio = 1.0 : 18.6; temperature 70°C; plasticizer butyl benzyl phthalate)

Synthesis version	Formulation, g						w_1	w_2	V_0, cm^3	t_1, min
	tank *1*			tank *2*			$cm^3\ g^{-1}$			
	MMA	ST	MAA	MMA	ST	MAA				
1	77.40	68.98	36.59	–	–	–	0.882	–	–	220
2	–	–	12.18	72.51	81.45	1.53	0.075	0.882	168.9	220

Synthesis version	MAA content, wt %		Plastisol, copolymer : plasticizer = 50 : 50	
	total	in surface layer	viscosity, cP, at a shear rate of 100 s^{-1}	time of gelation onset of at 20°C, days
1	20.0	20.0	15 900	35
2	8.2	13.4	15 100	100

Table 2. Conditions of synthesis (stage 2) and characteristics of the latex with hollow particles (initiator, potassium persulfate, 2.46 g; emulsifier, sodium dodecylbenzenesulfonate, 2.24 g; water 540 g; core, MMA : MAA : ethylene glycol dimethacrylate = 70 : 29.5 : 0.5 (wt %); core : shell mass ratio = 1 : 10; copolymerization temperature 80°C; temperature of neutralization of MAA with ammonia 100°C)

Synthesis version	Formulation, g						w, $cm^3\ g^{-1}$	V_0, cm^3	t_1, min
	tank *1*			tank *2*					
	ST	AN	DVB	ST	AN	DVB			
1	217.10	72.80	1.45	–	–	–	2.55	–	130
2	298.50	–	1.50	91.01	22.80	0.99	2.55	130	130

Synthesis version	AN content, wt %		Properties of latex		
	total	at the core–shell interface	dry residue, wt %	particle diameter, nm	contrast factor of the coating
1	25.7	25.0	36.0	540	0.97
2	7.0	19.9	36.1	530	0.98

ment of their hydration, swelling of the core copolymer, and expansion of the shell, which is responsible for formation of cavities in the particles.

The most difficult-to-implement is stage 2 involving creation of particles with the hydrophilic core/hydrophobic shell morphology, which is extremely unfavorable from the thermodynamic viewpoint. We succeeded in solving this problem by enhancing the hydrophilicity of the shell copolymer through introduction of acrylonitrile (AN) units into its composition [14]. The desired effect is achieved by introducing no less than 25 wt % AN units into the copolymer. However, creation of a descending gradient of the concentration of the AN units (we used a simplified version, $w_1 = w_2$) from the surface of the core to the periphery of the particle (Fig. 4) decreases the AN content in the shell copolymer to 7 wt% without deteriorating the properties of the resulting latexes, characterized by the contrast factor of the coatings prepared using hollow pigments (Table 2). A probable reason is that, at a high content of the AN units in the inner layers of

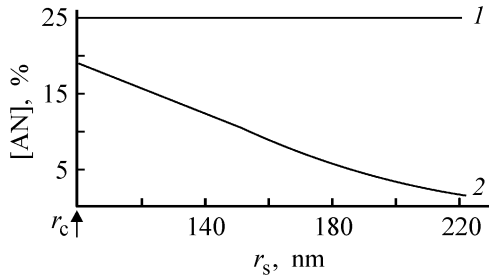


Fig. 4. Calculated plots describing the variation of the content of the AN units in the shell copolymer along the particle radius r_s in stage 2 of the synthesis of the latex with hollow particles. For copolymerization conditions, see Table 2.

the shell, adjacent to the core copolymer, conditions making compatible the core and shell copolymers are preserved or even improved.

For techniques of synthesis of the latexes and their characteristics, as well as for the properties of the plastisols and coatings, see [14–16].

CONCLUSIONS

(1) Specific examples demonstrated that it is expedient to synthesize latexes with core–shell particles in which the chemical composition of the shell varies along the particle radius. The content of the units of the functional monomer in the shell copolymer, which provides the desired properties of the latex, can be reduced severalfold without deteriorating the characteristics of the resulting products.

(2) The variable composition of the shell copolymer is provided by a very simple procedure. It can be recommended for preparation of synthetic latexes, especially with the use of highly reactive monomers whose emulsion polymerization by semicontinuous technologies, i.e., in the monomer dosing mode, is a common practice at the present time.

(3) To implement the processes that we suggest, it is sufficient to insert, between the dosing tank with the monomer mixture and the reactor in the conventional flowsheet, an intermediate tank containing a monomer mixture whose composition differs from that of the monomer mixture in the dosing tank. The equations that we derived allow the required composition of the monomer mixtures and monomer dosing modes to be easily calculated.

REFERENCES

1. Dimonie, V.L., Daniels, E.S., Shaffer, O.L., and El-Aasser, M.S., *Emulsion Polymerization and Emulsion Polymers*, Lovell, P. and El-Aasser, M.S., Eds., Chichester: Wiley, 1997, p. 293.
2. Athey Jr., *Emulsion Polymer Technology*, New York: Marcel Dekker, 1991, p. 74.
3. US Patent 2005203247.
4. Primachenko, O.N., Pavlyuchenko, V.N., Gagarina, K.A., *et al.*, *Zh. Prikl. Khim.*, 2000, vol. 73, no. 10, pp. 1713–1719.
5. RF Patent 2128671.
6. Eliseeva, V.I., *Progr. Org. Coat.*, 1985, vol. 13, pp. 195–221.
7. Cook, D.G., Rudin, A., and Plumtree, A., *J. Appl. Polym. Sci.*, 1992, vol. 46, no. 8, pp. 1387–1393.
8. Chen, Y.-C., Dimonie, V.L., and El-Aasser, M.S., *J. Appl. Polym. Sci.*, 1991, vol. 42, no. 4, pp. 1049–1063.
9. Vanderhoff, J.W. and El-Aasser, M.S., *Polymer Latexes: Preparation, Characterization and Application*, Daniels, E.S., Sudol, E.D., and El-Aasser, M.S., Eds., Washington: Am. Chem. Soc. Symp. Ser., 1992, vol. 492, pp. 272–281.
10. Vanderhoff, J.W., Park J.M., and El-Aasser, M.S., *Polym. Mater. Sci. Eng.*, 1991, vol. 64, pp. 345–346.
11. Schorlemmer, C., *Macromol. Chem. Macromol. Symp.*, 1990, vol. 31, p. 123.
12. Eur. Patent 624606.
13. Pavlyuchenko, V.N., *Vysokomol. Soedin., Ser. C*, 2004, vol. 46, no. 12, pp. 2140–2171.
14. Pavlyuchenko, V.N., Sorochinskaya, O.V., Ivanchev, S.S., *et al.*, *J. Polym. Sci., Polym. Chem. Ed.*, 2001, vol. 39, no. 9, pp. 1435–1449.
15. Pavlyuchenko, V.N., Primachenko, O.N., Nyholm, P., and Ivanchev, S.S., *Eur. Polymer Congr.*, 2005, Moscow, 2005, p. 126.
16. Pavlyuchenko, V.N., Sorochinskaya, O.V., Primachenko, O.N., and Ivanchev, S.S., *Macromol. Symp.*, 2005, vol. 226, pp. 213–226.

Russian Journal of Applied Chemistry, Vol. 78, No. 12, 2005, pp. 1993–2001. Translated from Zhurnal Prikladnoi Khimii, Vol. 78, No. 12, 2005, pp. 2023–2032.
Original Russian Text Copyright © 2005 by Smirnov, Kuryndin, Nikitin, Sidorovich, Sazanov, Kudasheva, Bukošek, Khokhlov, Elyashevich.

MACROMOLECULAR CHEMISTRY AND POLYMERIC MATERIALS

Properties of Conducting Composite Systems Containing Polypyrrole Layers on Porous Polyethylene Films

M. A. Smirnov, I. S. Kuryndin, L. N. Nikitin, A. V. Sidorovich, Yu. N. Sazanov, O. V. Kudasheva, V. Bukošek, A. R. Khokhlov, and G. K. Elyashevich

Institute of Macromolecular Compounds, Russian Academy of Sciences, St. Petersburg, Russia
Nesmeyanov Institute of Organoelement Compounds, Russian Academy of Sciences, Moscow, Russia
Ljubljana University, Ljubljana, Slovenia

Received November 1, 2005

Abstract—Conducting composite systems containing polypyrrole layers were prepared by *in situ* polymerization of pyrrole on the surface of porous polyethylene films. The polymerization was performed in the gas phase, in a monomer solution, and in supercritical CO_2. The chemical structures, electrical conductivities, and mechanical, thermodeformational, and morphological characteristics of the composites obtained were compared.

Conducting polymers, such as polypyrrole (PPyr), polyaniline, polythiophene, and their derivatives, have been extensively studied recently because of the wide prospects for their application. Thanks to a combination of electrical, magnetic, optical, and electrochemical properties, these polymers are widely used as membranes, electrochemical sensors, electrode materials, etc. [1, 2]. Among conducting polymers, polypyrrole attracts particular attention owing to its relatively high chemical stability [3]. However, this polymer has a low mechanical strength and is very brittle, which substantially restricts its potential applications. One of the best ways to solve this problem is to prepare composite systems in which an elastic support would provide the required mechanical properties and the conducting polymer would be the active component.

We have shown previously [4–6] that porous polyethylene (PE) films can be efficiently used as supports for PPyr layers. These films exhibit high adhesion to various coatings, including layers of conducting polymers. We found that the high adhesion is due to the developed profile of the film surface and to the presence of a large amount of through flow channels, providing a tight fixation of the coating.

Numerous procedures for preparing PPyr are known [7]. As the structure and, hence, the properties of a conducting polymer largely depend on the procedure and conditions of its preparation [8, 9], it is of particular interest to compare the characteristics of conducting composite systems with the active component prepared by different procedures.

In this paper, we compare the electrical, mechanical, thermodeformational, and morphological properties of PE/PPyr composite systems prepared by both well-known and new procedures, one of which is the polymerization in supercritical CO_2. The last procedure is also attractive from the environmental viewpoint, as involving no toxic solvents and initiators.

The porous films were prepared from HDPE with $M_w = 1.4 \times 10^5$, $M_w/M_n = 6–8$, and $T_m = 132°C$. The porous structure was formed by uniaxial extension of films prepared by the melt extrusion followed by annealing [10, 11]. The film thickness was 12 μm, and the overall porosity, 48%. The porous films contained through flow channels of size 180–500 nm [11].

An important feature of these films is the strongly developed surface profile (Fig. 1) produced by uniaxial extension of annealed films at the stage of pore formation. The profile scale increases with the degree of orientation of the support, ranging in the interval examined from 0.2 to 0.8 μm.

To prepare PPyr by polymerization of the monomer in solution and in the gas phase, we used pyrrole (Fluka), $FeCl_3$ (Vekton) as oxidant, and methanol (Vekton). For the synthesis in supercritical CO_2, we used 99.998% pure CO_2 [BKZ Linde Gas AGA, Balashikha; GOST (State Standard) 8050–85] and pyrrole-2-carboxylic acid (Aldrich).

1070-4272/05/7812-1993 © 2005 Pleiades Publishing, Inc.

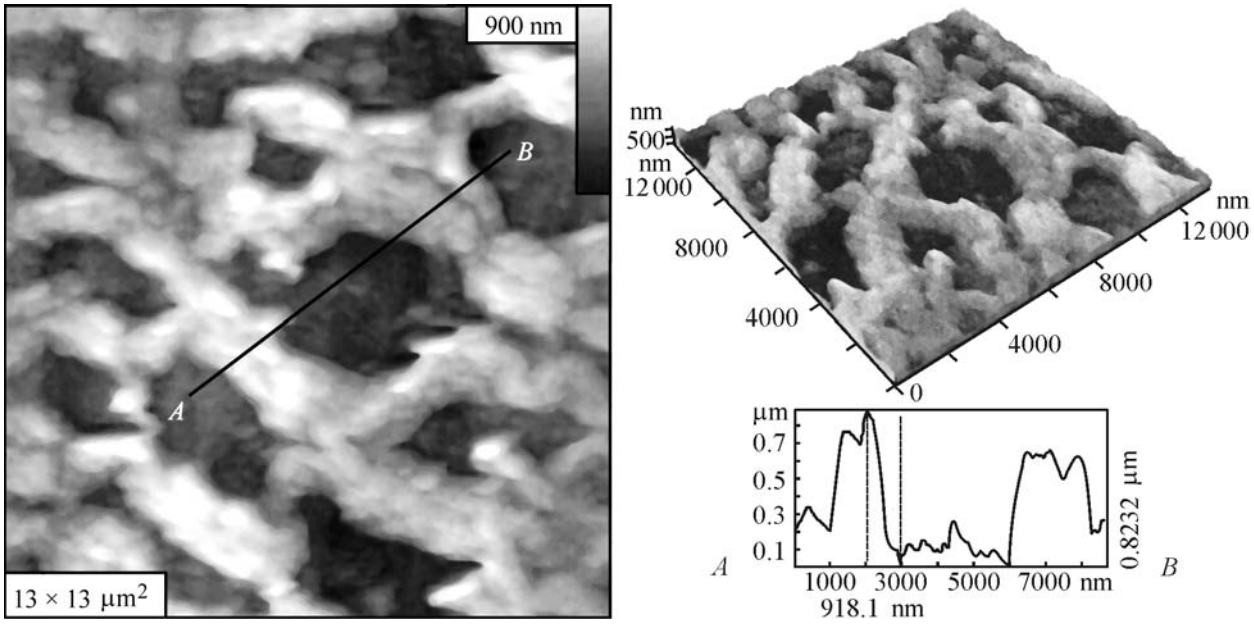


Fig. 1. AFM patterns of the surface of a porous PE film.

Composite PE/PPyr systems were prepared by, *in situ* polymerization directly on the porous PE film from the monomer gas phase [4], from a monomer solution [12], or in supercritical CO_2 [13]; the products obtained are denoted as PE/PPyr(g), PE/PPyr(s), and PE/PPyr(c), respectively.

To prepare PE/PPyr(g) systems, porous PE films impregnated with a 1 M solution of $FeCl_3$ in methanol were exposed to a pyrrole vapor. After a PPyr layer was formed (the reaction was performed for 1 day), the resulting composite material was washed with methanol and dried in air at room temperature.

Systems PE/PPyr(s) were prepared as follows. A porous support was placed in a solution of pyrrole in methanol, and an aqueous solution of $FeCl_3$ was added. The concentrations of pyrrole and the oxidant were 0.2 and 0.5 M, respectively. The polymerization was performed at 0°C; the methanol : water ratio in the reaction mixture was 3 : 7. The reaction was performed for 1 h, after which the film was withdrawn, cleaned to remove excess PPyr, washed with water, and dried in air.

To prepare PE/PPyr(c) samples, a porous PE film impregnated with a 0.5 M solution of $FeCl_3$ in methanol was placed, together with a weighed portion of pyrrole-2-carboxylic acid, in a stainless steel vessel filled with CO_2. The CO_2 was brought to the supercritical state (20 MPa, 75°C) with a pressure generator (Company for Production of High-Pressure Equipment, the United States) and a thermostat. Under these conditions, pyrrole-2-carboxylic acid decomposed to give pyrrole, which polymerized when contacting with $FeCl_3$ on the surface of the porous PE film. The samples thus prepared were also washed with methanol and dried in air.

The content of PPyr in the samples was determined gravimetrically.

The surface conductivity of the composite systems (conductivity in the direction parallel to the film surface) was measured by the standard four-probe method, and the bulk conductivity (between the surfaces), by the two-disk method.

The mechanical properties of porous PE films and composite systems were studied with an R-5 tensile-testing machine (Ivanovo). The strength, elastic modulus, and relative elongation at break were determined from the stress–strain curves in the course of uniaxial extension of 30 × 2-mm specimens at a rate of 100% min^{-1}. The strength was calculated as the ultimate (breaking) force per initial cross section of the specimen. The elastic modulus was determined at a 0.5% strain.

Thermomechanical tests were performed in the uniaxial extension mode at a heating rate of 10 deg min^{-1} and applied loads of 0.02 to 0.2 MPa. The tests were performed in a vacuum to prevent oxidation.

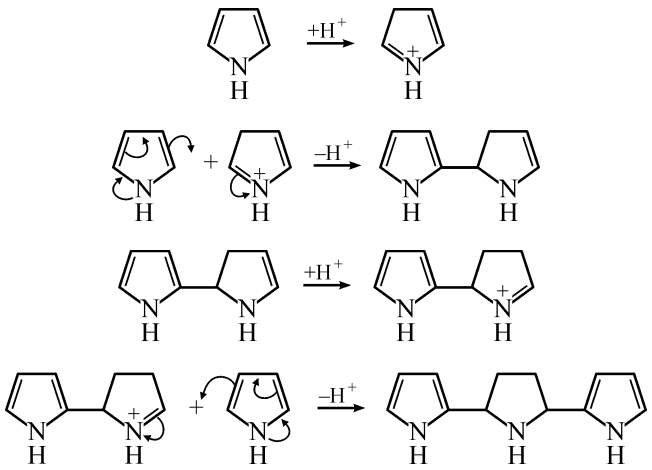
The elemental analysis was performed with a Vario El elemental analyzer (Germany).

The IR spectra were recorded on a Nicolet Impact 400 FTIR spectrometer in the attenuated total internal reflection mode.

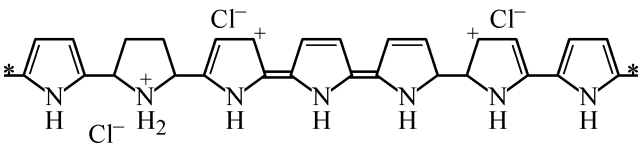
The TG and DTA curves were recorded with a C-1500 derivatograph (Hungary) in the course of heating of 50-mg samples in a self-generated atmosphere at a rate of 10 deg min^{-1}.

Chemical structure of PE/PPyr composite systems. Polymerization of pyrrole is a complex multistep process accompanied by a set of side reactions. Both the chemical and supramolecular structure of PPyr depends on many parameters, such as the synthesis temperature, composition of the polymerization medium, type and concentration of the oxidant, etc. Hence, the service properties of the polymer, such as the electrical conductivity and mechanical characteristics, will also depend on the polymerization conditions.

Published data [2, 3, 14–16] show that PPyr is chemically and structurally nonuniform, which is due to the occurrence of side reactions in the course of the polymerization. One of the most known reactions is that leading to incorporation of pyrrolidine rings into the conjugated polypyrrole chain. It has been found [14–16] that, under the action of Brønsted acids, pyrrole undergoes transformations yielding products that show no conductivity because of the lack of the conjugation system. The acid-catalyzed formation of nonconjugated compounds from pyrrole can be described by the following scheme:



This process is also possible under common conditions of the oxidative synthesis of PPyr, because Fe(III) salts frequently used as oxidants are strongly susceptible to hydrolysis with the formation of basic salts [$Fe(OH)_nCl_{3-n}$, where n = 1, 2] and rise in the solution acidity [14, 17]. Thus, because the main process (oxidative polymerization) is usually accompanied by the side reaction, PPyr contains a certain amount of saturated units making lower the electrical conductivity of the polymer. The scheme below shows how a saturated unit breaks the conjugation chain in polypyrrole:



The content of saturated units can be estimated, in particular, by elemental analysis from the C : H atomic ratio. In the "ideal" PPyr, this ratio should be 4.00 : 3.00, and incorporation of saturated rings should cause the relative content of hydrogen to increase. In PPyr prepared in a monomer solution, the C : H atomic ratio (4.00 : 3.17) was the closest to the ideal value; in the sample prepared from the gas phase it was 4.00 : 3.23, and in the sample prepared in supercritical CO_2, 4.00 : 3.80.

The differences in the chemical structure of the composite systems prepared by different methods are also manifested in the IR spectra (Fig. 2). Comparison of the IR spectra of the PE/PPyr(g) and PE/PPyr(c) samples shows that both these samples contain PPyr. The spectra exhibit all the bands characteristic of PPyr (Table 1) [18, 19]. However, some other bands are also present. The spectra of the systems PE/PPyr(g) and PE/PPyr(c) contain a weak band at ~1700 cm^{-1}, assignable to C=O vibrations. The peak position of this band is different for PE/PPyr(c) (1705 cm^{-1}) and PE/PPyr(g) (1680 cm^{-1}). This pattern suggests that the ketones are conjugated with a double bond in PE/PPyr(g), being not conjugated in PE/PPyr(c). Both the spectra also contain bands at about 1100 cm^{-1}, assignable to the C–O stretching vibrations in enols,

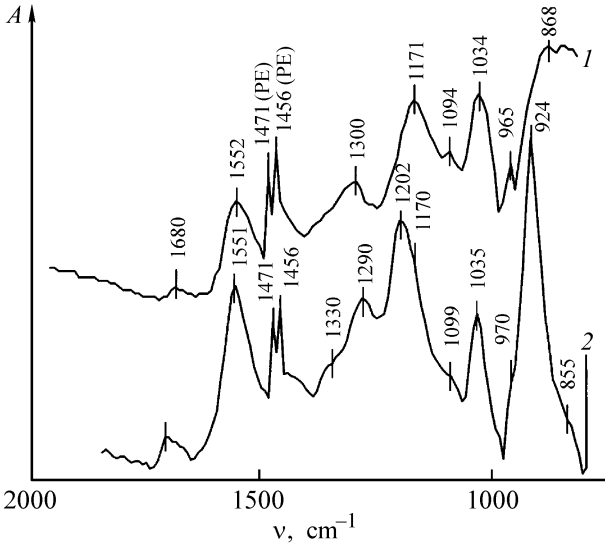


Fig. 2. IR spectra of composites (*1*) PE/PPyr(g) and (*2*) PE/PPyr(c). (*A*) Absorption and (ν) wave number.

Table 1. Assignment of the absorption bands in the IR spectra of PE/PPyr composites

PE/PPyr(g)	PE/PPyr(c)	Assignment of PPyr bands [18, 19]
1680	1702	
1552	1551	1545, stretching vibrations of C=C bonds in the ring and between rings
1471 PE	1471 PE	C–C skeleton vibrations in PE chain
1456	1456	1460, superposition of skeleton vibrations of C–C bonds in PE chain and of C=C, C–C, and C–N stretching vibrations in PPyr ring
	1330 sh	
1300	1282	1300, C–H and N–H bending vibrations
	1202	
1171	1170 sh	1170, vibrations of oxidized PPyr ring
1094	1099 sh	
1034	1035	1040, bending vibrations of C–H bonds
965	972 sh	960, vibrations in terminal rings and PPyr rings linked to adjacent rings by α–β bond
	924	
868	855 sh	860, bending vibrations of C–H bonds

which occur in equilibrium with C=O [20]. Presumably, these groups are formed by a nucleophilic attack of water molecules at cations in the chain of oxidized PPyr, which occurs both in the course of polymerization and during the subsequent storage of the composite in air. Also, the spectrum of PE/PPyr(c) contains a number of peaks absent in the spectrum of PE/PPyr(g): 1330, 1202, and 920 cm^{-1}, which can be assigned to the C–C skeleton vibrations in saturated fragments [16]; the presence of such fragments follows from the elemental analysis.

The PE/PPyr(s) sample shows 100% absorption throughout the examined IR range. Such a pattern is characteristic of substances in which electronic transitions between the valence and conduction bands have a low energy (i.e., in which the band gap is narrow). In PPyr, the band gap depends on the length of the conjugation chain. The longer the conjugation chain, the lower the electronic transition energy and the larger the wavelength of light that can be absorbed. In the PE/PPyr(g) and PE/PPyr(c) samples, the conjugation chain length is sufficient for absorption of the visible light (all these samples are black) but insufficient for the IR absorption. At the same time, the PE/PPyr(s) sample strongly absorbs the IR radiation, i.e., the conjugation chain in this sample is longer than that in the other samples; accordingly, its electrical conductivity is higher.

Thus, in the order PE/PPyr(s)–PE/PPyr(g)–PE/PPyr(c), the content of incorporated saturated rings increases, and hence the length of the conjugation chain decreases. This trend is caused by different relative rates of the side reaction under different synthesis conditions.

The side reactions occur to the least extent in solution, which is due to the optimal reactant ratio and to their uniform distribution in the reaction volume. In the gas-phase synthesis, first an oxidant solution is applied to a porous PE film, and then the monomer is gradually supplied to the film surface. In this case, $FeCl_3$ with the residual solvent is in excess relative to the monomer. The acid formed by hydrolysis of $FeCl_3$ is also in excess, which results in an increased content of the saturated units.

A similar pattern is observed in the synthesis in supercritical CO_2, but, along with the presence of excess oxidant in the reaction zone, there is another negative factor: elevated temperature (75°C), which accelerates both the formation of saturated fragments and other side reactions (e.g., deamination [14] and overoxidation of polypyrrole). Furthermore, the source of pyrrole in the polymerization in supercritical CO_2, is pyrrole-2-carboxylic acid, which also favors acceleration of the acid-catalyzed side reaction.

Morphological features of PE/PPyr composites. To reveal morphological features of the composites prepared by different methods, we examined the structure of their surface by electron microscopy (Fig. 3). As reported previously [4], in formation of composites by gas-phase polymerization of the monomer, the PPyr layer "inherits" the specific character of the surface of the porous PE support (Fig. 3a). When the polymerization is performed in a monomer solution, the PPyr layer has its own morphology, but with the preserved character and orientation of the support surface (Fig. 3b). In polymerization in supercritical

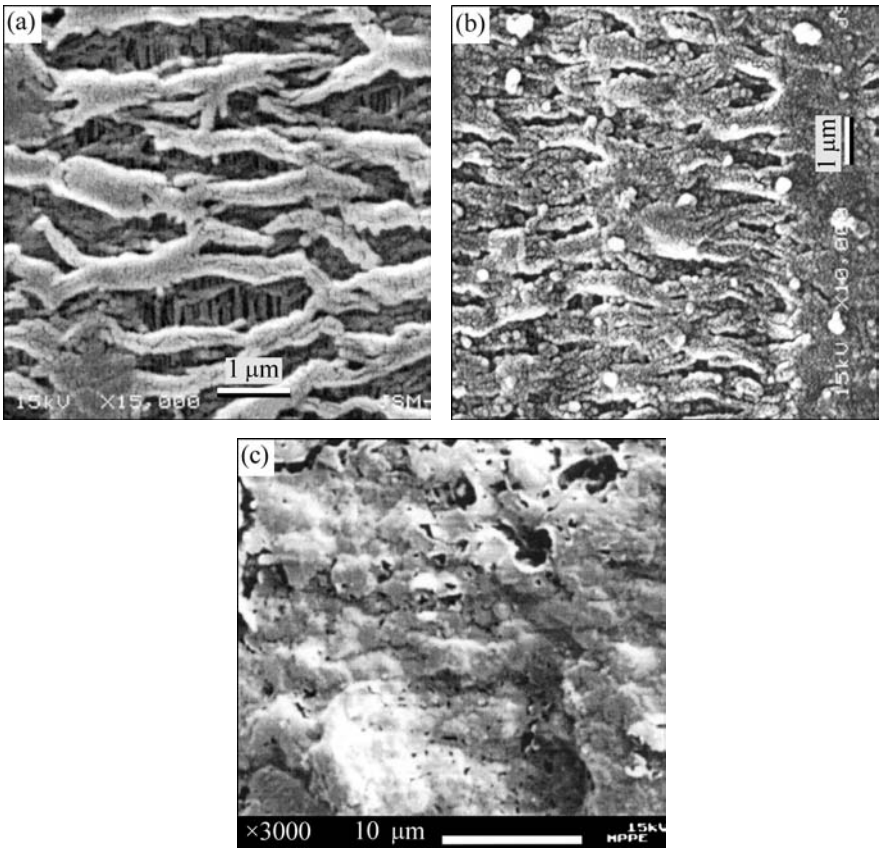


Fig. 3. Electron micrographs of the surface of (a) porous PE support, (b) PE/PPyr(s) composite, and (c) PE/PPyr(c) composite.

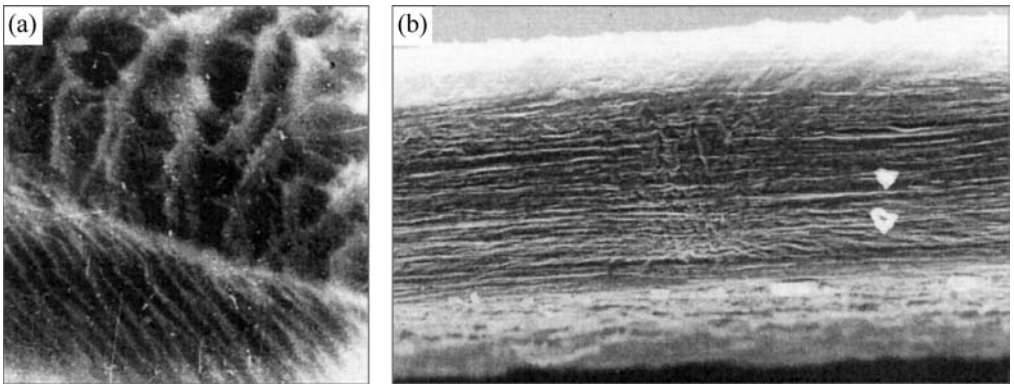


Fig. 4. Cross-sectional electron micrographs of (a) porous PE film and (b) PE/PPyr composite prepared by gas-phase polymerization.

CO_2, the layer of the conducting polymer fully masks the structure of the support surface, which can be traced only in certain areas (Fig. 3c); the structure of the PPyr layer exhibits no orientation characteristic of the PE support. Figure 3c also shows that the polymerization at high pressure yields a smoother and less structured polypyrrole layer, compared to the PE/PPyr(g) and PE/PPyr(s) samples prepared under atmospheric pressure, but this layer has visible defects disturbing its continuity.

Electrical characteristics of the composites. In the synthesis of PPyr on porous supports, the polymerization is preceded by penetration of reactant molecules into the support, and PPyr is formed not only on the film surface but also in pores and intercrystallite areas, which results in that a spatially continuous conducting phase of PPyr is formed both on the surface and in the bulk of the support. This is seen from the images of the cross sections of the porous support and composite (Fig. 4). It is seen that the

Table 2. Electrical conductivity of PE/PPyr composites (thickness of the porous support 12 μm)

Sample	Thickness, μm	PPyr content, %	Surface conductivity, S cm^{-1}	Bulk conductivity, S cm^{-1}
PE/PPyr(g)	14	40	10^0	10^{-6}
PE/PPyr(s)	14	40	10^2	10^{-3}
PE/PPyr(c)	13	18	10^{-3}	10^{-8}

Table 3. Mechanical characteristics of porous PE films and PE/PPyr composites*

Sample	Breaking strength, MPa	Elastic modulus, MPa	Elongation at break, %
Porous PE film	150	700	50
PE/PPyr(g)	143	1400	40
PE/PPyr(s)	147	2000	48
PE/PPyr(c)	145	800	47

* The mechanical characteristics were determined in the direction of orientation of the porous support.

whole volume of the support is filled with the conducting polymer, fully masking the porous structure of the support. Such a spatial structure of the conducting phase allows the composites obtained to be characterized by the sheet and volume conductivity (Fig. 2). The essential difference between these quantities is due to the fact that the volume conductivity is determined by the amount of through channels filled with the conducting polymer.

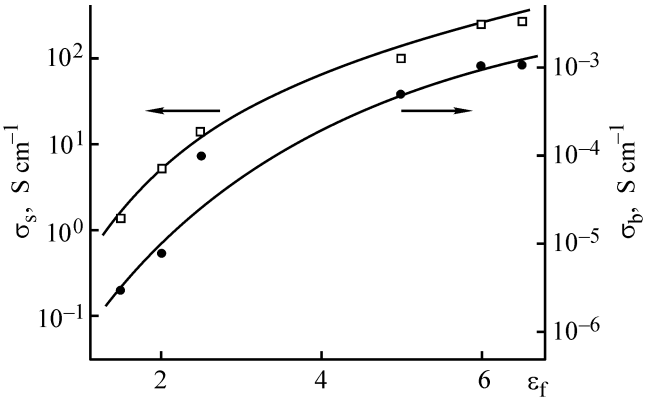


Fig. 5. Surface conductivity σ_s and bulk conductivity σ_b of PE/PPyr(s) samples vs. degree of orientation of the support ε_f.

Table 2 shows that the electrical conductivity of the samples correlates with the length of the conjugation chain in PPyr. Even despite high pressures in the synthesis in supercritical CO_2, which may favor closer packing of the PPyr chains and hence increase the conductivity, the measured conductivity of the samples prepared under these conditions is very low, because of the large content of the incorporated saturated rings. An additional factor decreasing the conductivity of these samples is the above-mentioned lack of orientation in the polypyrrole layer.

At the same time, according to our measurements (Fig. 5), the conductivity substantially increases with the degree of orientation; this also follows from the considerably higher conductivity of the PE/PPyr(g) and PE/PPyr(s) composites containing the PPyr layers with an oriented structure, compared to the PE/PPyr(c) samples.

It should be noted that the conductivities that we attained with PE/PPyr(s) are the highest among the values reported for composites and are close to the conductivity of pure PPyr.

Mechanical properties. Introduction of PPyr into a composite, as a rule, decreases its strength and results in the loss of elasticity. Therefore, we examined the mechanical properties of PE/PPyr samples (Table 3). All the samples exhibited high deformation and strength characteristics: The strength and elasticity of all the composites were comparable with those of the porous PE supports.

Table 3 shows that the mechanical properties of the composites depend on their preparation procedure: The sample prepared by polymerization in solution shows the best properties. Its electrical conductivity is also the highest (Table 2). Furthermore, the elastic modulus of PE/PPyr(g) and PE/PPyr(s) is higher than that of the support by a factor of 2 and 3, respectively, whereas the elastic modulus of PE/PPyr(c) is only slightly higher than that of the support. The increased elastic modulus of the composites is due to the appearance of a spatially continuous phase of the conducting rigid-chain polymer, which is formed on the stretched support and "inherits" its oriented character. Figure 3 shows that the degree of orientation of the PE/PPyr(c) samples is considerably lower than that of the PE/PPyr(g) and PE/PPyr(s) samples, which may be due to the fact that the conditions of the all-round compression at high pressure prevent arrangement of the forming PPyr molecules in one preferential direction. Thus, the elastic modulus of the PE/PPyr(g) and PE/PPyr(s) samples is determined by the oriented structure of the rigid-chain PPyr layer in which the degree of ori-

entation of the molecules can be higher than that in the PE support (flexible-chain polymer), whereas the PE/PPyr(c) samples contain a weakly oriented polypyrrole phase, and their elastic modulus is determined by the support.

Thermal stability. The thermal stability of the PE/PPyr composites and their components was studied by TGA and DTA. Heating of PE films to 200–250°C is not accompanied by any noticeable weight loss (Fig. 6a, curve *1*). The endothermic peak at 132°C (Fig. 5b, curve *1*) corresponds to PE melting, and the thermal effects at about 200°C, as shown in [21], to its oxidation. Active weight loss starts at 200–250°C; it is caused by the release of volatile thermal degradation products and is accompanied by exothermic effects (Fig. 6b, curve *1*).

PPyr shows weight loss from the very beginning of the heating (Fig. 6a, curve *2*); the weight loss is uniform throughout the examined temperature range. At 800°C, when the sample transforms into a carbonized residue, the weight loss is about 65% [22].

The TGA curves (Fig. 6a) show that the degradation patterns of the PE/PPyr composites are intermediate between those of the pure components and differ from each other insignificantly. Similarly to the PE support, the PE/PPyr composites show a sharp weight loss above 400°C, but it is considerably less pronounced because of the fixing effect of the PPyr layer.

The DTA curves of PE (Fig. 6b, curve *1*) exhibit pronounced thermal effects caused by melting, oxidation, and thermal degradation. The thermal degradation of PPyr is not accompanied by thermal effects; its heat capacity first steadily increases and then, above 300°C, steadily decreases (Fig. 6b, curve *2*). The DTA curves of the composites (Fig. 6b, curves *3*, *4*) mainly reflect the transformations of the PE support, but the effects are less pronounced, compared to the straight support, because of the effect of the rigid-chain component, polypyrrole. The three-dimensional PPyr framework is "fused" into the bulk of PE, which loses the porous structure upon melting, and this rigid framework prevents complete melting of PE (the heat of melting of the composites is considerably lower than that of PE [22]), restricting the motion of its chains. Thus, PPyr affects all the structural changes occurring above T_m of PE.

Thermodeformational behavior of PE/PPyr composites. We have shown previously [6, 22] that the oriented structure of the porous PE support is responsible for the shrinkage of the composite systems

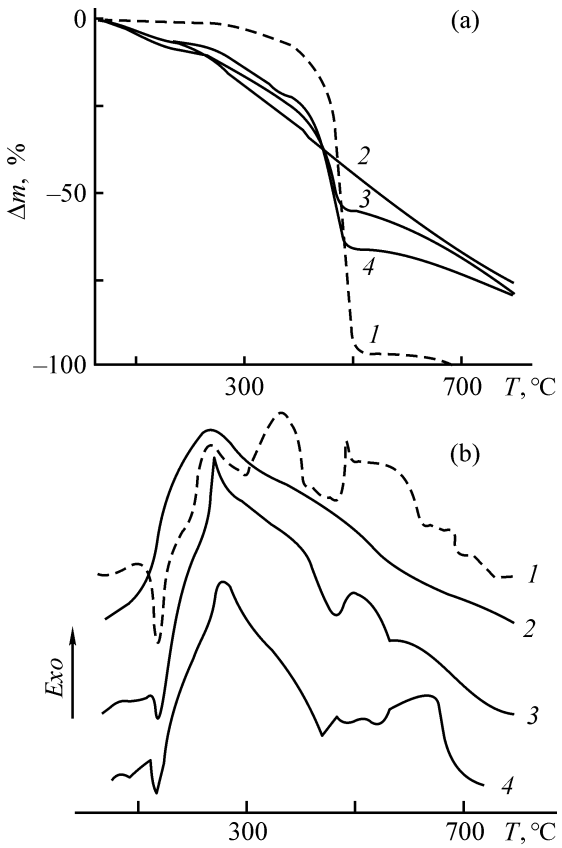


Fig. 6. (a) TGA and (b) DTA curves of (*1*) PE film, (*2*) PPyr prepared by gas-phase polymerization, (*3*) PE/PPyr(g) composite, and (*4*) PE/PPyr(s) composite. (Δ*m*) Weight loss and (*T*) temperature.

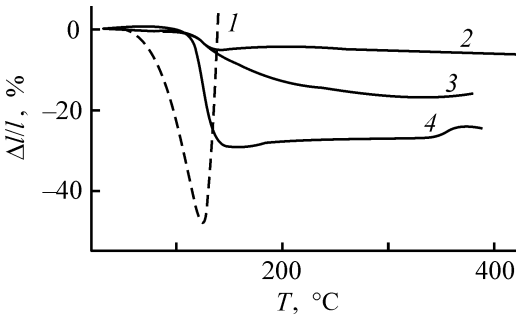


Fig. 7. Deformation Δ*l*/*l* vs. temperature *T* (thermomechanical curves) for (*1*) porous PE films and composites (*2*) PE/PPyr(s), (*3*) PE/PPyr(g), and (*4*) PE/PPyr(c). Load 0.02 MPa.

on heating. The thermomechanical curves of porous PE films (Fig. 7, curve *1*) are typical of oriented systems of flexible-chain polymers: In the vicinity of T_m of PE, the shrinkage is maximal, and above this temperature the film undergoes sharp elongation followed by break. The thermomechanical curves of the composite systems are strongly different (Fig. 7,

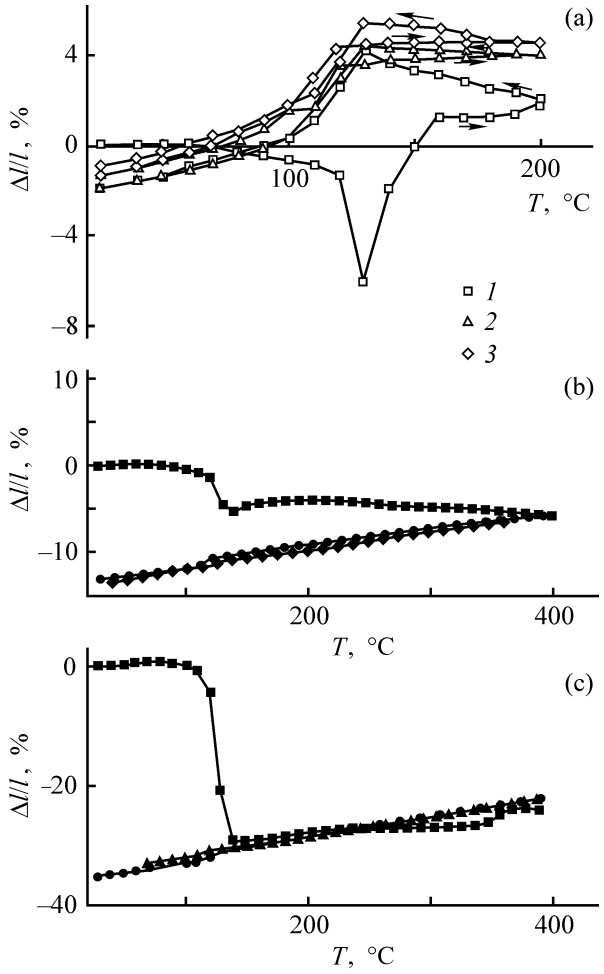


Fig. 8. Deformation $\Delta l/l$ vs. temperature T (thermomechanical curves) for PE/PPyr composites in cyclic heating. System, load (MPa): (a) PE/PPyr(g), 0.2; (b) PE/PPyr(s), 0.02; and (c) PE/PPyr(c), 0.02: Cycle: (*1*) first, (*2*) second, and (*3*) third.

curves *2*–*4*). Their major feature is a plateau in a wide temperature range above T_m of PE. In this range, the samples not only keep a load, but even do not change size on heating. It is important that the composite systems studied preserve their integrity on heating up to 400°C, i.e., to temperatures much higher than T_m of PE. This result is caused by the fact that, in these systems, the load is taken over by the three-dimensional framework of the rigid-chain conducting PPyr, rather than by the PE support.

Figure 7 illustrates noticeable differences in the behavior of PE/PPyr samples prepared by different methods. All these samples undergo shrinkage in the vicinity of the PE melting point, but the extent of this shrinkage is varies: about 30% for PE/PPyr(c) and only 5% for PE/PPyr(g) and PE/PPyr(s). As the temperature is raised further, the smallest changes in size are observed with the PE/PPyr(s) composite. Thus, the strongest fixation of the porous structure of the support by the PPyr layer is ensured by preparing this layer from the monomer solution, owing to the denser structure of the PPyr layer thus obtained. Indeed, measurements of the density of the composites by hydrostatic weighing gave the following results (g cm^{-3}): PE/PPyr(s), 1.102; PE/PPyr(g), 1.088; and PE/PPyr(c), 1.009 (the density of PE is 0.950 g cm^{-3}). The density of the PPyr component can be estimated taking into account its content in the composites; in PE/PPyr(s), PE/PPyr(g), and PE/PPyr(c), it is 1.33, 1.30, and 1.29 g cm^{-3}, respectively.

The limiting temperatures above which the samples fail are also somewhat different. The PE/PPyr(s) composites under the conditions of the thermomechanical experiment fail at temperatures exceeding 420°C, whereas the PE/PPyr(g) and PE/PPyr(c) samples do so at 380–400°C. This is due to the fact that the PPyr layer formed from the monomer solution contains less structural defects (cracks, inhomogeneities) and is considerably more oriented and ordered than the layers prepared by gas-phase polymerization or in supercritical CO_2.

To reveal changes that occur in PE/PPyr samples on heating in a vacuum, we performed repeated heating–cooling cycles under the same conditions (Fig. 8). It is seen that all the samples undergo irreversible changes in the first cycle of heating, as indicated by different runs of the heating and cooling curves; the run of the cooling curve is typical of cross-linked systems.

In the repeated cycles, the heating and cooling curves are fully reproduced for all the samples, i.e., the structural changes are complete in the first cycle. This fact can be accounted for by the cross-linking of polypyrrole at about 200°C, as found by mechanical relaxation studies [23]. As a result, the mechanical properties of the composites change after the first cycle: The elastic modulus increases, and the elongation at break decreases, although the samples preserve certain elasticity. Gas permeability measurements show that the samples become considerably denser after heating (the gas permeability decreases by more than two orders of magnitude, compared to the initial samples), which is due to collapse of pores in the support upon melting and to cross-linking of the polypyrrole layer.

CONCLUSIONS

(1) New composites were prepared by polymerization of pyrrole in solution, in the gas phase, and

in supercritical CO_2 on porous polyethylene films. The polymerization in solution yields the conducting polymer phase of a more uniform chemical structure, compared to the products obtained by polymerization in the gas phase and in suprecritical CO_2.

(2) In the composites obtained, the conducting properties of polypyrrole are combined with the high mechanical characteristics of the porous support.

(3) The composites prepared by polymerization in the monomer solution show a higher conductivity, compared to the samples prepared by polymerization in the gas phase and in supercritical CO_2.

(4) Preparation of conducting composite systems in an environmentally safe medium (supercritical CO_2) is, in principle, possible.

(5) At temperatures considerably exceeding the melting point of polyethylene, the composite systems preserve mechanical stability owing to the presence of a spatially continuous rigid framework of the conducting polymer.

ACKNOWLEDGMENTS

The study was financially supported by the Russian Foundation for Basic Research (project no. 04-03-32229) and Program for Basic Research of the Division of Chemistry and Materials Science, Russian Academy of Sciences, project "Synthesis and Study of New Polymer Systems Containing Polyconjugated Polymers and Exhibiting Semiconducting and Conducting Properties," research area "Conducting and Electroactive Polymers."

REFERENCES

1. MacDiarmid, A.G., *Synth. Met.*, 2002, vol. 125, pp. 11–22.
2. *Handbook of Organic Conductive Molecules and Polymers*, Nalwa, H.S., Ed., Chichester, 1997, vol. 2.
3. Vernitskaya, T.V. and Efimov, O.N., *Usp. Khim.*, 1997, vol. 66, no. 5, pp. 489–505.
4. Rosova, E.Yu., Polotskaya, G.A., Kozlov, A.G., *et al.*, *Vysokomol. Soedin., Ser. A*, 1998, vol. 40, no. 6, pp. 914–920.
5. Elyashevich, G.K., Kalyuzhnaya, L.M., Rosova, E.Yu., and Wolinska-Grabczyk, A., *Vysokomol. Soedin., Ser. A*, 2003, vol. 45, no. 10, pp. 1653–1658.
6. Elyashevich, G.K., Kuryndin, I.S., and Rosova, E.Yu., *Polym. Adv. Technol.*, 2002, vol. 13, pp. 725–736.
7. Malinauskas, A., *Polymer*, 2001, vol. 42, pp. 3957–3972.
8. Rapi, S., Bocchi, V., and Gardini, G.P., *Synth. Met.*, 1988, vol. 24, pp. 217–221.
9. Machida, S., Miyata, S., and Techagumpuch, A., *Synth. Met.*, 1989, vol. 31, pp. 311–318.
10. Elyashevich, G.K., Karpov, E.A., and Kozlov, A.G., *Macromol. Symp. "Mechanical Behavior of Polymeric Materials,"* Kahovec, J., Ed., 1999, vol. 147, pp. 91–101.
11. Elyashevich, G.K., Kozlov, A.G., and Rosova, E.Yu., *Vysokomol. Soedin., Ser. A*, 1998, vol. 40, no. 6, pp. 956–953.
12. Smirnov, M.A., Bobrova, N.V., Pientka, Z., and Elyashevich, G.K., *Vysokomol. Soedin., Ser. B*, 2005, vol. 47, no. 7, pp. 1231–1236.
13. Nikitin, L.N., Elyashevich, G.K., Rosova, E.Yu., *et al.*, Abstracts of Papers, *III Vserossiiskaya Karginskaya konf. "Polimery-2004"* (III Russian Kargin Conf. "Polymers-2004"), Moscow, 2004, vol. 2, p. 133.
14. Hawkins, S.J. and Ratcliffe, N.M., *J. Mater. Chem.*, 2000, vol. 10, pp. 2057–2062.
15. Potts, H.A. and Smith, G.F., *J. Chem. Soc.*, 1957, nos. 9–10, pp. 4018–4021.
16. Lamb, B.S. and Kovacic, P., *J. Polym. Sci.*, 1980, pp. 1759–1770.
17. Schoor, R.C.G.M. van der, Leur, R.H.M. van de, and Wit, J.H.W. de, *Synth. Met.*, 1999, vol. 99, pp. 17–20.
18. Davidson, R.G. and Turner, T.G., *Synth. Met.*, 1995, vol. 72, pp. 121–128.
19. Tian, B. and Zerbi, G., *J. Chem. Phys.*, 1990, vol. 92, no. 6, pp. 3886–3890.
20. Hong Xie, Manming Yan, and Zhiyu Jiang, *Electrochim. Acta*, 1997, vol. 42, no. 15, pp. 2361–2367.
21. Sazanov, Yu.N., Ugolkov, V.L., Praslova, O.E., *et al.*, *Zh. Prikl. Khim.*, 2003, vol. 76, no. 7, pp. 1167–1171.
22. Elyashevich, G.K., Sazanov, Yu.N., Rosova, E.Yu., *et al.*, *Vysokomol. Soedin., Ser. A*, 2001, vol. 43, no. 9, pp. 1548–1554.
23. Lesuer, D. and Alberola, N.D., *Synth. Met.*, 1997, vol. 88, pp. 133–138.

Russian Journal of Applied Chemistry, Vol. 78, No. 12, 2005, pp. 2002–2005. Translated from Zhurnal Prikladnoi Khimii, Vol. 78, No. 12, 2005, pp. 2033–2036.
Original Russian Text Copyright © 2005 by Galibeev, Mukhametzyanova, Kochnev, Arkhireev, Yakimov.

MACROMOLECULAR CHEMISTRY AND POLYMERIC MATERIALS

Anionic Copolymerization of γ-Butyrolactone and 2,4-Toluene Diisocyanate in the Presence of Triethylamine

S. S. Galibeev, E. A. Mukhametzyanova, A. M. Kochnev, V. P. Arkhireev, and R. V. Yakimov

Kazan State Technological University, Kazan, Tatarstan, Russia

Received May 25, 2005

Abstract—Anionic copolymerization of 2,4-toluene diisocyanate with γ-butyrolactone in the presence of triethylamine was performed. The chemical structure of the copolymer obtained was determined by IR and ^{1}H NMR spectroscopy, and some kinetic features of the process were revealed.

Lactones are valuable monomers for preparing polyesters with unique properties, showing promise both as structural materials and as biologically active substances in medicine [1–3].

The capability of various lactones to undergo polymerization strongly depends essentially on the ring strain. In particular, β-propiolactone spontaneously polymerizes under mild conditions [4]; ε-caprolactone undergoes ring opening under the action of organometallic catalysts at 60–80°C; γ-butyrolactone (γ-BL) does not undergo homopolymerization even in the presence of Ziegler–Natta catalysts but copolymerizes with a wide variety of monomers (vinyl monomers, cyclic acetals, amines, amides, ketenes, carboxy hydrides of amino acids) [5].

In this study, we examined the possibility of copolymerization of γ-BL with 2,4-toluene diisocyanate (TDI) in the presence of triethylamine (TEA). The choice of TDI as comonomer was governed by the fact that, in the presence of TEA, it can induce ring opening of some heterocyclic compounds [6–8] that do not undergo homopolymerization under these conditions.

EXPERIMENTAL

The copolymers were prepared in a solvent (acetone) at 20°C. The catalyst (TEA) concentration was 0.02 mol %. The amount of the unchanged monomer was determined by extraction with acetone in a Soxhlet apparatus for 8 h.

The reaction of TDI with γ-BL was studied by ^{1}H NMR spectroscopy with a Tesla-100 spectrometer operating at 100 MHz. Acetone-d_6 was used as solvent and reference. The mid-IR spectra of the copolymers were recorded on a Bruker FT-IR spectrophotometer. Samples were pelletized with KBr, using a hydraulic press. The molecular mobility of the polymers was studied by pulsed NMR spectroscopy on a relaxometer operating at 20 MHz.

The thermal analysis was performed with a Q-1500 derivatograph (MOM, Hungary) at a heating rate of 3 deg min^{-1}.

To determine the physicomechanical characteristics, we obtained films of TDI–γ-BL copolymers from acetone solutions by casting. The breaking stress σ_b was determined on an MR-500T-2 tensile-testing machine at 20 ± 2°C. The velocity of mobile clamps was 100 mm min^{-1}.

The reaction rate constants were determined as described in [10].

The IR spectra of TDI–γ-BL copolymers contained new bands absent in the spectra of the starting monomers (Fig. 1): at 3490–3400 (N–H stretching vibra-

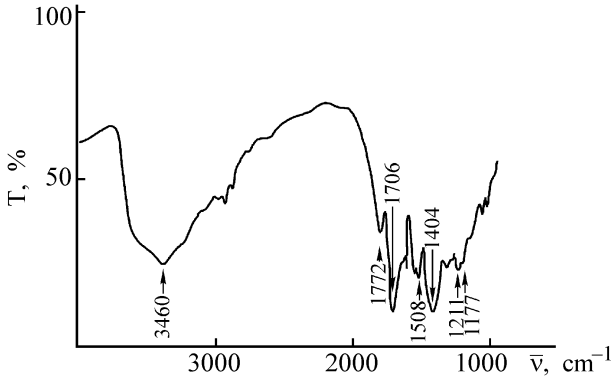


Fig. 1. IR spectrum of 2,4-TDI–γ-BL copolymer. Reactant molar ratio 1 : 1. (T) Transmission and ($\bar{\nu}$) wave number.

1070-4272/05/7812-2002 © 2005 Pleiades Publishing, Inc.

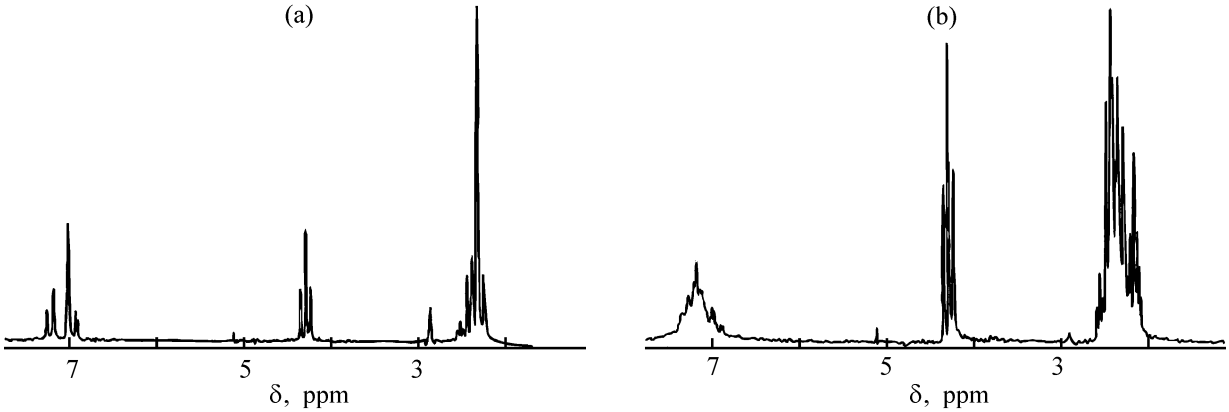


Fig. 2. ^{1}H NMR spectrum of the system γ-BL–TDI (a) before and (b) after the reaction performed for 30 min at 25°C. Solvent acetone-d_6; equimolar ratio of the monomers. (δ) Chemical shift.

tions in secondary amides and O–H stretching vibrations), 1706 (C=O stretching vibrations in tertiary amides), 1508 (N–C stretching vibrations in secondary amides), ~1404 (C–N stretching vibrations), and 1211 cm^{-1} (ester stretching vibrations). The bands at 2860 and 2920 cm^{-1} (stretching vibrations of methylene groups) are indicative of the presence of γ-BL units [10].

The chemical transformations in the system can also be monitored by ^{1}H NMR spectroscopy (Fig. 2).

The copolymerization in acetone-d_6 for 30 min results in an appreciable broadening of the aromatic proton signals at 7.2–6.9 ppm, suggesting growth of the molecular weight; the singlet at 2.8–2.7 ppm (TEA protons) virtually disappears. The signals at 2.5–2.0 ppm belonging to the protons of the TDI methyl group and methylene groups of the lactone ring get appreciably broadened, i.e., the environment of these protons changes.

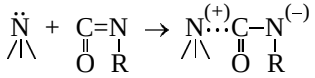
Using near-IR spectroscopy, we calculated from the absorption at 5310 cm^{-1} (vibrations of the isocyanate group) the reaction rate constant k and the rate of consumption of isocyanate groups V in the course of the copolymerization at various monomer ratios (Table 1). It is seen that the consumption rate is the highest at the equimolar ratio of the comonomers in the starting mixture.

This result suggests that, taking into account that γ-BL does not undergo homopolymerization under the synthesis conditions, the reaction of γ-BL with TDI may involve formation of an alternating copolymer in the initial steps. With an excess of the isocyanate component, it may subsequently depolymerize at active anionic centers. The IR spectra show that only γ-BL remains unchanged, and TDI is converted virtually completely at any comonomer ratios.

This suggestion is confirmed by the fact that the copolymer yield decreases with an increase in the γ-BL content in the starting mixture.

Our results suggest the following mechanism of the reaction of TDI with γ-BL.

(1) As γ-BL itself is incapable of ring opening, the first step apparently involves nucleophilic addition of the tertiary amine to the electrophilic center of the isocyanate groups to give a quasiammonium complex:



(2) The chain propagation in this case can occur via nucleophilic addition of either TDI or γ-BL to the anion formed by opening of the isocyanate group:

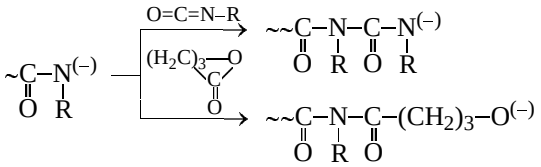


Table 1. Rate of consumption of isocyanate groups and rate constants of the reaction of TDI with γ-BL

γ-BL/TDI molar ratio	$V \times 10^6$, mol l^{-1} s^{-1}	$k \times 10^2$, l mol^{-1} s^{-1}
1.0/5.0	0.81	1.0
1.0/3.0	1.13	2.2
1.0/1.0	4.11	25.0
1.0/0.5	2.29	2.4
1.0/0.4	1.72	0.6
1.0/0.2	1.67	0.2
1.0/0.1	1.58	0.1

Table 2. Spin–lattice relaxation time T_1 of TDI–γ-BL copolymers

γ-BL/TDI molar ratio	T_1, ms
1.0/20.00	116
1.0/4.00	122
1.0/0.25	132
1.0/0.20	142
1.0/0.10	151

Table 3. Heat resistance of TDI–γ-BL copolymers (DTA data)

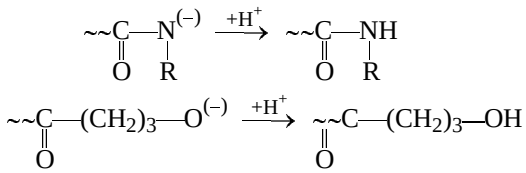
γ-BL/TDI molar ratio	$T_{\Delta m = 5\%}$, °C
1.0/3.0	310
1.0/1.0	292
1.0/0.3	284
1.0/0.1	270

Table 4. Breaking tensile stress σ_b of TDI–γ-BL copolymers

γ-BL/TDI molar ratio	σ_b, MPa
1.0/0.62	37.3
1.0/0.42	35.0
1.0/0.34	33.1
1.0/0.25	22.6
1.0/0.17	5.7

With excess isocyanates, the chain end can contain tertiary amide blocks.

(3) The termination in such polymerizing systems may occur [11] via exchange reactions of the propagating macroanions with compounds containing a labile hydrogen atom or by the chain transfer to the monomer; both hydroxy and amino groups can be formed, depending on the nature of the active center:



It is also necessary to take into account the possible presence of triisocyanurate and uretidinedione rings in the polymer, as it is known [12] that isocyanates can form such structures in the presence of tertiary amines, and certain heterocyclic compounds (oxiranes, lactones) activate the dimerization and cyclotrimerization reactions.

We examined some physicomechanical, processing, and service properties of the copolymers.

In particular, we found that they dissolve only in strongly polar organic solvents (formic acid, dimethylformamide, dimethyl sulfoxide) at high temperatures. The solubility decreases with an increase in the TDI content in the starting monomer mixture.

Such a behavior may be associated with enhanced branching and cross-linking of the macromolecules due to the bifunctional structure of TDI. This is confirmed by the NMR relaxation data (Table 2).

The copolyamido esters obtained have a high $T_{\Delta m =}$ 5% (temperature of 5% weight loss, Table 3), decreasing with an increase in the γ-BL content, which indicates that the tertiary polyamide fragments are more stable than the polyester fragments.

From the starting mixture containing excess γ-BL, we prepared polymer films by casting. The breaking stress σ_b of these films appeared to be essentially dependent on the monomer ratio, varying from 5 to 37 MPa (Table 4).

The materials obtained with excess TDI were very brittle, apparently because of the high degree of cross-linking (due to the bifunctional structure of TDI) and of the presence of polycyclic triisocyanurate structures. A decrease in σ_b with decreasing content of TDI in the starting mixture is due to the presence of a large amount of the unchanged lactone, adversely affecting the strength of the material.

CONCLUSIONS

(1) 2,4-Toluene diisocyanate undergoes anionic copolymerization with γ-butyrolactone in the presence of triethylamine. The reaction mechanism is suggested.

(2) The copolyamido esters obtained exhibit high strength, reaching a maximum at a certain excess of γ-butyrolactone in the starting mixture.

REFERENCES

1. Zhong, Z., Dijkstra, P.J., and Feijen, J., *Macromol. Chem. Phys.*, 2000, no. 201, pp. 1329–1333.
2. Stevels, W.M., Ankone, M.J.K., and Dijkstra, P.J., *Macromol. Symp.*, 1996, no. 102, pp. 107–113.
3. Vauchskii, Yu.P. and Zamchuk, Z.S., *Plast. Massy*, 1987, no. 6, pp. 6–9.

4. Sazanov, Yu.N., *Usp. Khim.*, 1968, vol. 37, no. 6, pp. 1084–1095.
5. *Entsiklopediya polimerov* (Polymer Encyclopedia), Kabanov, V.A., Ed., Moscow: Sov. Entsiklopediya, 1974, vol. 2, p. 33.
6. Spiridonova, R.R. and Galibeev, S.S., *Zh. Prikl. Khim.*, 2003, vol. 26, no. 2, pp. 298–300.
7. Galibeev, S.S., Kochnev, A.M., Spiridonova, R.R., and Gafarov, A.M., in *Materialy XVII Mendeleevskogo s'ezda po obshchei i prikladnoi khimii* (Proc. XVII Mendeleev Congr. on General and Applied Chemistry), Kazan, September 21–26, 2003, vol. 3, p. 88.
8. Spiridonova, R.R., Binary Systems Based on Isocyanates and Epoxides as Modifiers for Polyolefins, *Cand. Sci. Dissertation*, Kazan, 2003.
9. Sutyagin, V.M., *Eksperimental'nye metody issledovaniya polimerizatsii i sopolimerizatsii* (Experimental Methods for Studying Polymerization and Copolymerization), Tomsk: Tomsk. Politekh. Inst. im. S.M. Kirova, 1988.
10. Kuptsov, A.Kh. and Zhizhin, G.N., *Fur'e-KR i Fur'e-IK spektry polimerov* (Fourier Raman and Fourier IR Spectra of Polymers), Moscow: Fizmatlit, 2001.
11. Galibeev, S.S., Influence of Small Additions of Chemically Active Compounds on the Efficiency of Modification of Polyolefins, *Cand. Sci. Dissertation*, Kazan, 2000.
12. Tiger, R.P., Sarynina, L.I., and Entelis, S.G., *Usp. Khim.*, 1972, vol. 41, no. 9, pp. 1672–1695.

Russian Journal of Applied Chemistry, Vol. 78, No. 12, 2005, pp. 2006–2009. Translated from Zhurnal Prikladnoi Khimii, Vol. 78, No. 12, 2005, pp. 2037–2040.
Original Russian Text Copyright © 2005 by Konovalova, Stepanova.

MACROMOLECULAR CHEMISTRY AND POLYMERIC MATERIALS

Influence of Natural Polysaccharides on Aggregation of Aqueous Protein Dispersions

I. N. Konovalova and N. V. Stepanova

Murmansk State Technical University, Murmansk, Russia

Received January 26, 2005; in final form, April 6, 2005

Abstract—The kinetics of aggregation of aqueous protein dispersions under the action of flocculants, natural polysaccharides (cationic chitosan and anionic sodium alginate), were studied turbidimetrically in relation to the protein : polysaccharides ratio in the solution and the pH value. Sodium alginate and chitosan were tested in treatment of wastewater from the flotation processing of hydrobiontics.

Anionic and cationic macromolecular flocculants are widely used to intensify treatment of natural water and industrial wastewater to remove colloid and dispersed substances [1, 2]. One of the methods to remove organic pollutants and, in particular, proteins from water is flotation preceded by aggregation of protein particles with inorganic electrolytes and synthetic macromolecular flocculants. Inorganic flocculants have a number of drawbacks and, above all, large consumption and enhancement of the corrosion activity of water. Synthetic macromolecular flocculants hinder further utilization of the organic waste as nutritive additives. Inorganic electrolytes and synthetic macromolecular flocculants can be replaced in exhaustive treatment of water to remove protein substances with nontoxic biodegradable natural macromolecular polyelectrolytes (PEs), sodium alginate and chitosan.

EXPERIMENTAL

We examined natural macromolecular PEs, cationic chitosan and anionic sodium alginate (AlgNa). Chitosan had the degree of deacetylation of 66% {TU (Technical Specifications) 6-9-5591 [3]}. Sodium alginate was of medical grade {FS (Pharmacopoeia Item) 42-3383–97 [4]}. Food gelatin [GOST (State Standard) 11293–89)], a water-soluble degradation product of collagen, as well as an aqueous extract from a fish tissue, served as the protein component. Solutions of AlgNa and gelatin were prepared by preliminary swelling and dissolution in water. Chitosan solutions were prepared using 1% acetic acid. To prepare an aqueous extract of fish, a weighed portion of the tissue was shredded and left for 30 min in a small volume (20–25 ml) of distilled water for extraction of water-soluble components. The resulting solution was twice filtered to remove suspended matter. Flotation treatment of the wastewater was carried out on a pilot pressure-flotation setup.

The concentration of the protein substances, c_{protein}, in the extract and in the wastewater was estimated turbidimetrically, by the modified Lawry method [5].

The aggregation power of the PEs was estimated turbidimetrically [6, 7]. We constructed plots of the optical density of the solution against the time of addition and the concentration of the aggregating substances. The aggregation rate was calculated as the change in the optical density D per unit time τ in the initial linear portion of the $D = f(\tau)$ plot. The optimal flocculating concentration of the polysaccharides (OFC) was determined as the minimal concentration of the polysaccharides, required for achieving the maximal flocculation rate of the protein substances.

The conformation of the polysaccharide and gelatin macromolecules in solution was determined by plotting the pH dependences of the relative viscosity of the corresponding solutions [8]. Based on the viscometric data, we graphically estimated the intrinsic viscosity and calculated the hydrodynamic volume of the macromolecules [9], which made it possible to estimate the degree of their "folding." Using the Mark–Kuhn–Houwink equation, we calculated the viscosity-average molecular weight of the PEs under study by the procedure described in [10, 11]. The viscosity-average molecular weight of chitosan and sodium alginate was 40 000 and 4500, respectively.

1070-4272/05/7812-2006 © 2005 Pleiades Publishing, Inc.

Table 1 lists the gelatin aggregation rates at various concentrations of the PEs in solution.

Table 1 shows that, in the case of sodium alginate, the gelatin aggregation rate attains a maximum at 0.75 g_{PE}/g_{gel}. The flocculation activity of chitosan corresponds to 0.0005 g_{PE}/g_{gel}. The fact that the gelatin aggregation rate is higher in the presence of sodium alginate is most likely due to the electrostatic interaction of alginate with positively charged functional groups of gelatin, predominantly situated at the ends of the protein macromolecule chains [12]. This interaction is responsible for conformational transformations of the macromolecular chains of gelatin, which decreases the degree of ordering, as noted in [13, 14]. The negatively charged functional groups of gelatin are predominantly situated in the middle of the macromolecular chain and are less easily accessible to cationic flocculant; in this case, gelatin aggregation follows mostly the bridging mechanism.

Figure 1 (curves *1*, *2*) shows the OFC of chitosan and sodium alginate as dependent on the gelatin concentration. It is seen that, in the concentration range examined, this dependence is virtually linear. Baran [15] and Vincent [16] noted that such a dependence is typically observed in the case when the reagent added is fully involved in the interaction with the dispersed phase.

The mechanism of aggregation of dispersions containing solid negatively charged particles with synthetic cationic flocculants is discussed in [17–20]. In this case, aggregation is due to neutralization of the surface charge of the dispersed phase, which decreases the aggregation resistance, thus leading to aggregation of the particles. Also, interaction of the PE macromolecule with the surface of several particles yields a kind of "bridges" between individual particles of the dispersed phase.

This mechanism seems to be applicable to aggregation of protein macromolecules with polysaccharides, since the protein macromolecules contain both positively and negatively charged functional groups. In this case, however, we have to take into account the conformation of the macromolecules and their hydrophilic-hydrophobic properties. Evidently, the factors enhancing the hydrophobicity of the protein macromolecules via conformational changes should intensify their flotation and extraction from aqueous dispersions [21]. These factors include, above all, pH of the solution, strongly affecting the conformation of both the PE and protein macromolecules. A study of the conformation of the substances as influenced by pH is also of interest, since the protein-

Table 1. Gelatin aggregation rate g_{PE}/g_{gel} at various concentrations of the PEs in solution (c_{gel} = 100 mg l^{-1}, pH 5.5–6.0)

Polysaccharide	g_{PE}/g_{gel} at indicated PE concentration			
	0.0005	0.5	0.75	1
Sodium alginate	0	1.38	3.50	3.50
Chitosan	1.2	0	0	0

containing process wastewater delivered to flotation treatment should be neutral. Even a minor shift of pH toward acid or alkaline region can interfere with aggregation, thus deteriorating the water treatment quality [11].

Figure 2 and Table 2 show how the conformation of the polysaccharide macromolecules varies with pH.

Figure 2 shows that, at pH > 8, the viscosity of the chitosan solution is at a minimum. Most likely, the PE macromolecules occur as dense coils, irrespective of pH. In an acidic medium (pH < 4), the viscosity of the solution significantly increases, evidently, due to "unfolding" of the macromolecular coils. Sodium alginate shows an opposite trend: The degree of fold-

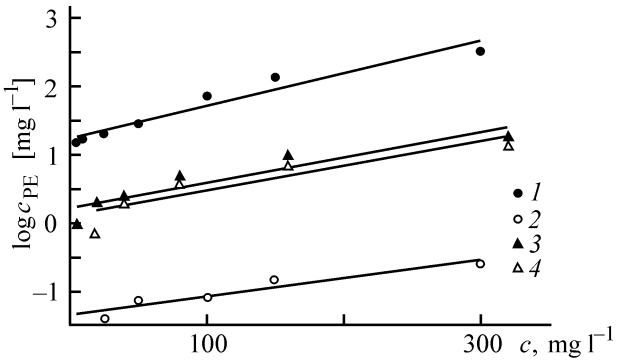


Fig. 1. Optimal flocculation concentration c_{PE} of (*1*, *3*) sodium alginate and (*2*, *4*) chitosan vs. concentration c of (*1*, *2*) gelatin and (*3*, *4*) protein substances. pH 5.5–6.

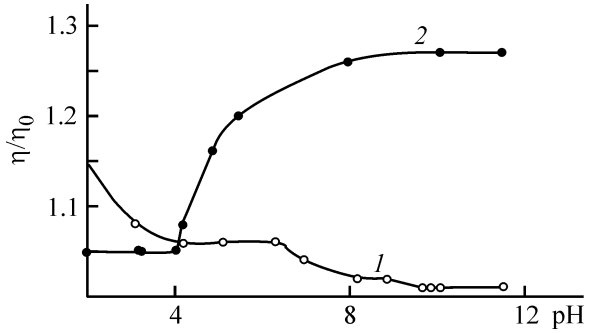


Fig. 2. (*1*, *2*) Relative viscosity η/η_0 of solution of (*1*) chitosan and (*2*) sodium alginate vs. pH of the solution. c_{PE} = 2.5 mg l^{-1}.

Table 2. Hydrodynamic volume of the PE macromolecules $V_0 \times 10^6$, $cm^3\ mol^{-1}$, at different pH of the solution

Polysaccharide	Hydrodynamic volume of PE macromolecules $V_0 \times 10^6$, $cm^3\ mol^{-1}$, at indicated pH of the solution		
	1.5	5.5	12.0
Sodium alginate	0.003	0.005	0.012
Chitosan	48.7	47.9	15.6

Table 3. Aggregation rate of the protein particles $g_{PE}/g_{protein}$ from the aqueous extract from fish at different concentrations of PE in the aqueous dispersion ($c_{protein}$ = 320 mg l^{-1}, pH 5.5–6.0)

Polysaccharide	$g_{PE}/g_{protein}$ at indicated PE concentration			
	0.01	0.03	0.07	0.13
Sodium alginate	0.005	0	0	0
Chitosan	0	3.16	42.65	7.94

Table 4. Removal of protein substances from wastewater by flotation as influenced by pretreatment of the wastewater with sodium alginate and chotisan (pH 5.6–6.5, $c_{protein}$ before flotation 139–147 mg l^{-1}, c_{PE} = 25 mg l^{-1})

Efficiency of removal of protein substances from wastewater (% of the initial protein content)		
No pretreatment	Pretreatment with	
with PE	sodium alginate	chitosan
19.4 ± 2.3	89.6 ± 3.4	50.8 ± 2.8

ing of the macromolecules decreases in alkaline medium (pH > 8), and compact structures are formed in the acidic medium (pH < 4), in agreement with the nature of the PEs under study [22].

Table 2 shows how the hydrodynamic radius of the polysaccharides under study varies with pH.

Table 2 shows that chitosan forms larger structures compared to sodium alginate, which can be due to a higher molecular weight of this PE. The hydrodynamic volume V_0 of the macromolecules of ionic PEs varies, as the pH of solution increases, in accordance with the chemical nature of the macromolecular substances. Figure 2 and Table 2 suggest that, at pH 5.5, the hydrodynamic volume of the macromolecules of both sodium alginate and chitosan is intermediate between that at pH at which the functional groups of the PE are ionized and the macromolecules are "unfolded" to the greatest extent, and that at pH at which ionization of the functional groups is completely suppressed, and the macromolecules have the conformation of compact structures. Such an intermediate state of the PE macromolecules is, most likely, the most favorable for aggregation of the protein particles.

Flocculation of the protein particles by polyelectrolytes can be regarded as a result of aggregation of the protein particles occurring in a close-to-isoelectric state (under the experimental conditions, pH was 5.5–6) owing to neutralization of the functional groups of the protein macromolecules and to the "bridging" mechanism of binding of the protein particles by the polysaccharide macromolecules. These processes, evidently, result in the formation of peculiar interpolymeric hydrophobic complexes, composed of protein particles bound by polymeric bridges of polysaccharide macromolecules. Evidently, such complexing makes the protein macromolecules more hydrophobic, which facilitates their aggregation and subsequent flotation [11].

Table 3 and Fig. 1 (curves *3*, *4*) show how sodium alginate and chitosan affect the aggregation of the protein substances contained in the aqueous extract from the fish.

A preliminary microelectrophoretic study [7] showed that the aqueous extract from the fish contained virtually identical amounts of positively and negatively charged particles.

Table 3 shows that, under the experimental conditions, aggregation of the protein substances with sodium alginate is observed at an alginate concentration of 0.01 $g_{PE}/g_{protein}$. The maximal rate of aggregation of the protein particles with chitosan is observed at a chitosan concentration of 0.07 $g_{PE}/g_{protein}$, which significantly exceeds both the aggregation rate of protein particles with sodium alginate and the rate of gelatin aggregation with PE throughout the PE concentration range studied. In aggregation of the fish extract, chitosan performs better than alginate: Table 3 shows that a high aggregation rate is observed in a wide range of the aggregating concentrations of chitosan. In this case, the aggregation is most likely affected by lipids that are structurally related to the protein macromolecules and react with the chitosan macromolecules [23].

In aggregation of the proteins extracted from fish, the OFCs of the PEs under study are virtually identical throughout the examined concentration range of the protein substances (Fig. 1, curves *3*, *4*). This is

evidently due to the presence of both positively and negatively charged particles in the dispersion. Similar to aggregation of gelatin, the OFC-vs.-$c_{protein}$ dependence is nearly linear, which suggests that the PE has completely reacted with particles of the dispersed phase [15, 16].

The data presented below show how the removal of the protein substances by flotation is influenced by the wastewater pretreatment with sodium alginate and chitosan (Table 4).

As is known, the wastewaters from hydrobiontic processing is a complex dispersed system consisting mainly of protein substances, lipids, and inorganic electrolytes. Table 4 confirms that sodium alginate and chitosan favor removal of protein substances from wastewater: In the case of sodium alginate and chitosan, the treatment efficiency is 89.6 ± 3.4 and $50.8 \pm 2.8\%$, respectively, against $19.4 \pm 2.3\%$ in water treatment without polysaccharides.

CONCLUSION

Natural polyelectrolytes sodium alginate and chitosan exhibit an aggregation power with respect to protein substances. They favor removal of protein substances from wastewater resulting from flotation processing of hydrobiontics. The efficiency of removal of the protein substances (in percent relative to the initial content of protein) after wastewater pretreatment with sodium alginate or chitosan was 89.6 ± 3.4 and 50.8 ± 2.8, respectively.

REFERENCES

1. Abramova, L.I., Baiburdov, T.A., Grigoryan, E.P., *et al.*, *Poliakrilamid* (Polyacrylamide), Kurenkov, V.F., Ed., Moscow: Khimiya, 1992.
2. Myagchenkov, V.A., Baran, A.A., Berkturov, E.A., and Bulidorova, G.V., *Poliakrilamidnye flokulyanty* (Polyacrylamide Flocculants), Kazan: Kazan. Gos. Tekh. Univ., 1998.
3. *TU* (Technical Specifications) *6-9-5591: High-Viscosity Chitosan, introduced August 1, 1991*, Murmansk: Sevrybtekhnotsentr, 1991.
4. *FS* (Pharmacopoeia Item) *42-3383–97, Sodium Alginate (for Medical Purposes)*.
5. Ovchinnikova, S.I., *Praktikum po biologicheskoi khimii* (Practical Course of Biological Chemistry), Murmansk: Murmansk. Gos. Tekh. Univ., 1997.
6. Baran, A. A. and Teslenko, A.Ya., *Flokulyanty v biotekhnologii* (Flocculants in Biotechnology), Leningrad: Khimiya, 1990.
7. Neiman, R.E., *Praktikum po kolloidnoi khimii (kolloidnaya khimiya lateksov i poverkhnostno-aktivnykh veshchestv)* (Practical Course of Colloid Chemistry: Colloid Chemistry of Latexes and Surfactants), Neiman, R.E., Ed., Moscow: Vysshaya Shkola, 1971.
8. *A Laboratory Manual of Analytical Methods of Protein Chemistry*, vol. 1–3, Alexander, P. and Blok, R.I., Eds., London: Pergamon, 1960–1961.
9. Tsvetkov, V.N., Eskin, V.E., and Frenkel, S.Ya., *Struktura makromolekul v rastvorakh* (Structure of Macromolecules in Solutions), Moscow: Nauka, 1964.
10. Tverdokhlebova, I.I., *Konformatsiya makromolekul* (Conformation of Macromolecules), Moscow: Vysshaya Shkola, 1981.
11. Frolov, Yu.G., *Kurs kolloidnoi khimii. Poverkhnostnye yavleniya i dispersnye sistemy* (Course of Colloid Chemistry. Surface Phenomena and Disperse Systems), Moscow: Vysshaya Shkola, 1989.
12. Wustnek, R., Zastrow, L., and Kraetschmar, G., *Kolloidn. Zh.*, 1987, vol. 49, no. 1, pp. 10–16.
13. Derkach, S.P., Rheological Properties of Adsorption Layers and Films of Binary Gelatin–Surfactant Solutions at the Solution–Air Interface and Stability of Foams, *Cand. Sci. Dissertation*, Murmansk, 1991.
14. Wustnek, R., Buder, E., Wetzel, R., and Hermel, H., *Colloid Polymer Sci.*, 1988, vol. 267, no. 6, pp. 516–519.
15. Baran, A.A., *Polimer-soderzhashchie dispersnye sistemy* (Polymer-Containing Disperse Systems), Kiev: Naukova Dumka, 1986.
16. Vincent, B., *Adv. Colloid Interface Sci.*, 1974, vol. 4, no. 213, pp. 196–277.
17. Baran, A.A. and Solomentseva, I.M., *Khim. Tekhnol. Vody*, 1983, vol. 5, no. 2, pp. 120–137.
18. Navrotskii, A.V., Dryabina, S.S., Malysheva, Zh.N., *et al.*, *Zh. Prikl. Khim.*, 2000, vol. 73, no. 12, pp. 1940–1944.
19. Proskuryakov, V.A. and Shmidt, L.I., *Ochistra stochnykh vod v khimicheskoi promyshlennosti* (Wastewater Treatment in Chemical Industry), Leningrad: Khimiya, 1977.
20. Izvozchikova, V.A., Pastukhova, N.V., and Ryabov, S.A., *Zh. Prikl. Khim.*, 2003, vol. 76, no. 11, pp. 1834–1836.
21. Stepanova, N.V., Konovalova, I.N., Vasilevskii, P.B., *et al.*, *Voda Ekol.*, 2001, no. 1, pp. 34–39.
22. Shur, A.M., *Vysokomolekulyarnye soedineniya* (Macromolecular Compounds), Moscow: Vysschaya Shkola, 1981.
23. Stepanova, N.V., Konovalova, I.N., Novikov, V.Yu., and Reut, K.V., *Zh. Prikl. Khim.*, 2004, vol. 77, no. 2, pp. 259–264.

Russian Journal of Applied Chemistry, Vol. 78, No. 12, 2005, pp. 2010–2013. Translated from Zhurnal Prikladnoi Khimii, Vol. 78, No. 12, 2005, pp. 2041–2044.
Original Russian Text Copyright © 2005 by Shoinbekova, Nikitina, Moldagazyeva, Mukhitdinova, Ergozhin.

MACROMOLECULAR CHEMISTRY AND POLYMERIC MATERIALS

Radical Copolymerization of Allyl and Vinyl Monomers Derived from 1,4-Benzoquinone with Acrylic Acid

S. A. Shoinbekova, A. I. Nikitina, Zh. Y. Moldagazyeva, B. A. Mukhitdinova, and E. E. Ergozhin

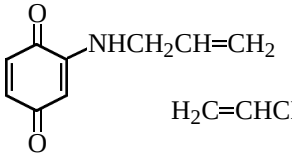
Bekturov Institute of Chemical Sciences, Ministry of Education and Science of the Republic of Kazakhstan, Almaty, Kazakhstan

Received March 16, 2005

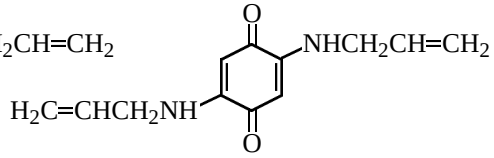
Abstract—Radical copolymerization of allyl and vinyl redox monomers derived from 1,4-benzoquinone with acrylic acid in dimethylformamide was studied.

Allyl compounds are difficultly polymerizing monomers; therefore, they are mostly used as comonomers in combination with other vinyl monomers [1]. Monoethanolamine vinyl ether (MEAVE) also polymerizes under rigorous conditions [2]. Copolymerization with carboxyl-containing monomers and, in particular, acrylic acid acquires growing importance for modification of polymeric materials as a way to enhance their heat resistance, hydrophilicity, adhesion, and also thermoreactive, ion-exchange, and other properties.

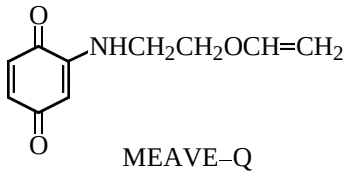
The reactions of allylamine (AlA) and MEAVE with 1,4-benzoquinone (Q) yield both mono- and disubstituted derivatives of the following structures [3, 4]:



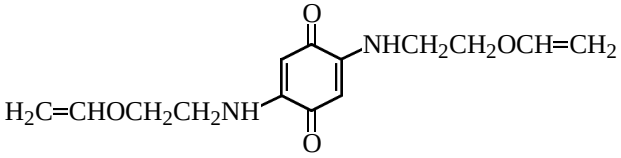
AlA–Q



AlA–Q–AlA



MEAVE–Q



MEAVE–Q–MEAVE

Owing to the presence of a quinoid ring responsible for the redox properties and to activation of the double bond, these compounds can be used for preparing redox ion exchangers. Their copolymerization with acrylic acid (AcA) allows, thanks to introduction of carboxy groups, preparation of resins combining the redox, ion-exchange, and adsorption properties. The choice of AcA as comonomer is governed by its ready copolymerization with monomers of all kinds, including even monomers whose homopolymerization is difficult [5].

In this study, we examined the radical copolymerization of mono- and disubstituted quinoid derivatives of allylamine and MEAVE with acrylic acid.

EXPERIMENTAL

Allylamine and MEAVE derivatives of 1,4-benzoquinone were prepared according to [3, 4]. Dimethylformamide (DMF) was purified by the standard procedure [6]. Benzoyl peroxide (BP) and azobis(isobutyronitrile) (AIBN) were recrystallized from absolute methanol [7], mp 106–108 and 102–103°C, respectively. Acrylic acid was purified by vacumm distillation, bp 64°C (25 mm Hg), ρ 1.062, n_D^{20} 1.421.

Copolymerization of redox monomers was performed by the ampule method in DMF in the course of 0.5 h. Copolymerization conditions: allyl derivatives, 7 wt % BP, 87°C; vinyl derivatives, 6 wt % AIBN, 68°C. The copolymerization was studied in the range of monomer ratios from 80 : 20 to 20 : 80, at a redox monomer concentration of 20 g l^{-1}. The degree of conversion was judged from the variation of

1070-4272/05/7812-2010 © 2005 Pleiades Publishing, Inc.

Table 1. Copolymerization constants and Alfrey–Price parameters of redox monomers (M_1) in copolymerization with AcA (M_2)

Redox monomer	p	r_1	r_2	r_1r_2	$1/r_1$	$1/r_2$	Q_1	e_1	Δe
AlA–Q	–1.320	1.53	0.60	0.920	0.65	1.67	2.19	0.49	0.28
AlA–Q–AlA	–0.580	0.65	1.61	1.050	1.54	0.62	0.66	0.56	0.21
MEAVE–Q	–1.143	1.49	0.57	0.849	0.67	1.75	1.48	0.37	0.40
MEAVE–Q–MEAVE	–0.983	1.58	0.41	0.647	0.63	2.44	1.69	0.11	0.66

the monomer concentrations, determined polarographically (redox monomers) and by titration (AcA).

The polarograms were recorded with a phosphate buffer solution (pH 7.4) as supporting electrolyte in 25% DMF in a temperature-controlled cell at 25 ± 0.5°C on a PU-1 polarograph, using a mercury dropping electrode (capillary characteristic at open circuit $m^{2/3}t^{1/6}$ = 4.38 $mg^{2/3}\,s^{-1/2}$ (m, mercury outflow rate, mg s^{-1}; t, dropping period, s). As reference electrode we used saturated calomel electrode. The solutions were deoxygenated by bubbling with argon.

The reactivity of the mono- and disubstituted quinoid monomers derived from AlA and MEAVE was evaluated toward a well-known and extensively studied monomer, AcA.

The copolymerization constants r_1 and r_2 of AlA–Q, AlA–Q–AlA, MEAVE–Q, and MEAVE–Q–MEAVE with AcA were calculated by the Shtraikhman graphical method based on the Mayo–Lewis integral equation [8]. From these constants, we determined the intrinsic specific activities (Q_1) and polarities (e_1) of the new redox monomers (for AcA, we took Q_2 = 1.15 and e_2 = 0.77 from [5]). The results of the calculation are listed in Table 1.

In the systems AlA–Q/AcA, MEAVE–Q/AcA, and MEAVE–Q–MEAVE/AcA, $r_1 > 1$ (Table 1), i.e., the polymeric radicals of the redox monomers react with the "own" monomers faster than with AcA; in the system AlA–Q–AlA/AcA, the pattern is the opposite. All the monomer pairs show a weak tendency toward alternation of units, since the product $r_1r_2 \approx 1$, which is usually characteristic of ideal copolymerization yielding a random copolymer. This is also suggested by small differences in polarity (Δe) between the redox monomers and AcA.

The reactivity of a monomer in copolymerization mainly depends on the polarity of the double bond, stability of the free radical formed by addition of this monomer to the propagating chain, and steric hindrance in the transition state [5]. The parameter Q is the measure of the reactivity determined by the resonance stabilization of the radical, whereas the quantity e characterizes the polarity of the double bond in the monomer. The conjugation in allyl compounds is insignificant; in most of them, Q is within 0.011–0.052 [9]. In the monosubstituted derivative AlA–Q, Q_1 increases by two orders of magnitude (Q_1 = 2.19) owing to the electron density redistribution caused by introduction of Q into the AlA molecule; therefore, this monomer should be more reactive. Its reactivity is higher than that of AlA–Q–AlA (Q_1 = 0.66). The mono- and disubstituted deriva-tives AlA–Q and AlA–Q–AlA appreciably differ in the activity in copolymerization with AcA, whereas the difference in the reactivities of MEAVE–Q and MEAVE–Q–MEAVE is less significant, with the disubstituted derivative being somewhat more reactive.

Another significant factor in copolymerization, along with the resonance factor Q, is the polarity of the monomers, determined by the electron-donor or electron-acceptor power of substituents at the double bond. The quinoid derivatives of AlA and MEAVE are considerably more reactive than the initial compounds because of the influence exerted by the quinone on the electron density in the allyl and vinyl groups which are good electron donors but weak electron acceptors [5]. Quinones are, by contrast, good electron acceptors [10]. Their high electron affinity is due to the low LUMO energy.

The homo- or copolymerization rate is influenced by the activities of both the monomer and the polymeric radical. Since the reactivity of the monomer grows and that of the polymeric radical decreases with an increase in the polarization e [11], the increase in the relative activity of the redox monomers ($1/r_2$) in their copolymerization with AcA, observed with a decrease in e, shows that the process is mainly governed by the properties of the polymeric radical, rather than of the monomer molecule. The $1/r_2$ values (Table 1) show that the vinyl compounds are appreciably more active than the allyl compounds. The reactivity of

Table 2. Composition and microstructure of copolymers obtained by copolymerization of allyl and vinyl redox monomers with AcA at their various ratios in the starting mixture

Redox monomer (M_1)	Composition of starting mixture, mol %		Copolymer composition, mol %		Microstructure of copolymers				
	M_1	M_2	m_1	m_2	$f_{M_1-M_1}$	$f_{M_1-M_2}$	$f_{M_2-M_2}$	$L^*_{M_1}$	$L^*_{M_2}$
AlA–Q	80	20	86.67	13.33	0.735	0.123	0.019	6.98	1.1
	60	40	76.47	23.53	0.481	0.215	0.088	3.24	1.4
	50	50	65.91	34.09	0.358	0.244	0.153	2.47	1.6
	40	60	46.15	53.85	0.256	0.255	0.233	2.00	1.9
	20	80	23.08	76.92	0.079	0.208	0.504	1.38	3.4
AlA–Q–AlA	79	21	80.68	19.32	0.510	0.203	0.084	3.51	1.4
	59	41	61.39	38.61	0.238	0.247	0.268	1.96	2.0
	50	50	43.05	56.95	0.155	0.235	0.375	1.66	2.6
	38	62	46.75	53.25	0.078	0.198	0.525	1.39	3.6
	20	80	16.16	83.84	0.019	0.117	0.746	1.16	7.3
MEAVE–Q	80	20	77.97	12.03	0.734	0.124	0.018	6.90	1.1
	60	40	70.95	29.05	0.482	0.217	0.083	3.22	1.3
	49	51	65.09	34.91	0.351	0.249	0.150	2.41	1.6
	30	70	43.76	56.24	0.157	0.252	0.339	1.62	2.3
	22	78	30.95	69.05	0.090	0.223	0.464	1.40	3.0
MEAVE–Q–MEAVE	79	21	84.12	15.88	0.732	0.127	0.014	6.76	1.1
	59	41	73.42	26.58	0.482	0.225	0.068	3.14	1.3
	52	48	71.45	28.55	0.408	0.247	0.097	2.65	1.3
	39	61	56.68	43.32	0.272	0.274	0.179	1.99	1.6
	21	79	36.65	63.35	0.096	0.246	0.411	1.39	2.6

* Data from [12].

the redox monomers studied toward the AcA radical decreases in the following order:

MEAVE–Q–MEAVE > MEAVE–Q > AlA–Q > AlA–Q–AlA

e	0.11	0.37	0.49	0.56
$1/r_2$	2.44	1.75	1.67	0.62

Thus, we demonstrated the possibility of copolymerization of the new redox monomers with AcA and found that the structure of the redox monomer affects its reactivity.

Then we studied how the activities and ratio of the comonomers affect the distribution of the monomeric units in the copolymer macromolecules. From the copolymerization constants found and data on the content of both monomers M_1 and M_2 in the starting mixture (Tables 1, 2), we calculated the probability of formation of various diads ($f_{M_1-M_1}$, $f_{M_1-M_2}$, $f_{M_2-M_2}$), mean block lengths (L_{M_1}, L_{M_2}), and Harwood parameters of the block structure R [12, 13]. Using these parameters (Table 2), one can estimate the distribution of units in the macromolecular chain, which determines the properties of the copolymers.

As can be seen from Table 2, the mean block lengths L_{M_1} and L_{M_2}, calculated by different methods [12, 13], essentially coincide. The largest block length is observed with an excess of one of the monomers. The Harwood parameter R is maximal when the copolymer consists of short blocks, i.e., copolymers of more regular structure are formed at the largest R. By choosing appropriate compositions of monomer mixtures, it is possible to control the microstructure of the forming copolymers, which is one of the most promising ways to modify their properties.

CONCLUSIONS

(1) Radical copolymerization of mono- and disubstituted allyl and vinyl redox monomers with acrylic acid was studied. The copolymerization constants and Alfrey–Price Q–e parameters of the redox monomers were determined; the microstructural characteristics of the copolymers obtained were calculated.

(2) It was found that the monosubstituted derivative of 1,4-benzoquinone and allylamine is involved in the radical copolymerization with acrylic acid more readily than the disubstituted redox monomer. By contrast, the disubstituted derivative MEAVE–Q–MEAVE is more reactive than the monosubstituted monomer MEAVE–Q. The copolymers show no tendency toward alternation of the monomeric units.

ACKNOWLEDGMENTS

The study was supported by ISTC (project K-604).

REFERENCES

1. Volodina, V.I., Tarasov, A.I., and Spasskii, S.S., *Usp. Khim.*, 1970, vol. 39, no. 2, pp. 276–303.
2. Shostakovskii, M.F., *Prostye vinilovye efiry* (Vinyl Ethers), Moscow: Akad. Nauk SSSR, 1952.
3. Kazakhstan Prepatent 9729.
4. Kazakhstan Patent 8813.
5. *Copolymerization*, Ham, G.E., Ed., New York: Interscience, 1964.
6. Weissberger, A. and Proskauer, E.S., *Organic Solvents. Physical Properties and Methods of Purification*, Riddick, J.A. and Toops, E.E., Eds., New York: Interscience, 1955.
7. Toroptseva, A.M., Belogorodskaya, K.V., and Bondarenko, V.M., *Laboratornyi praktikum po khimii i tekhnologii vysokomolekulyarnykh soedinenii* (Laboratory Course of Chemistry and Technology of Macromolecular Compounds), Leningrad: Khimiya, 1972.
8. Shtraikhman, G.A., Vanshteidt, A.A., and Petrova, G.A., *Zh. Fiz. Khim.*, 1958, vol. 32, no. 3, pp. 512–519.
9. Alfrey, T., Bohrer, J.J., and Mark, H., *Copolymerization*, New York: Interscience, 1952.
10. Pullman, B. and Pullman, A., *Quantum Biochemistry*, New York: Interscience, 1963.
11. Chernobai, A.V., *Vysokomol. Soedin., Ser. A*, 1968, vol. 10, no. 8, pp. 1716–1720.
12. Ushakov, S.N., Mitsengendler, S.P., and Shtraikhman, G.A., *Usp. Khim.*, 1950, vol. 19, no. 3, pp. 265–291.
13. Zil'berman, E.N., *Vysokomol. Soedin., Ser. B*, 1979, vol. 21, no. 1, pp. 33–36.

Russian Journal of Applied Chemistry, Vol. 78, No. 12, 2005, pp. 2014–2018. Translated from Zhurnal Prikladnoi Khimii, Vol. 78, No. 12, 2005, pp. 2045–2049.
Original Russian Text Copyright © 2005 by Kutsenko, Bochek, Vlasova, Volchek.

MACROMOLECULAR CHEMISTRY AND POLYMERIC MATERIALS

Synthesis of Carboxymethyl Cellulose Based on Short Fibers and Lignified Part of Flax Pedicels (Boon)

L. I. Kutsenko, A. M. Bochek, E. N. Vlasova, and B. Z. Volchek

Institute of Macromolecular Compounds, Russian Academy of Sciences, St. Petersburg, Russia

Received October 12, 2005

Abstract—The conditions under which carboxymethyl ethers of cellulose with various degrees of substitution can be prepared from wastes formed in production of flax fibers were studied. The structure of the cellulose ethers synthesized was studied by IR Fourier spectroscopy and physicochemical methods.

The rise in production of textile materials based on flax fibers, observed in recent years, is accompanied by an increase in the amount of wastes formed in flax production, such as short fibers and lignified part of flax pedicels (boon). In comparison with cotton goods, textile materials based on flax fibers have higher consumers', hygienic, and sanitary characteristics, which is caused by specific features of the fine structure of fibers, their morphology, and chemical composition.

The present-day environmental problems require development of a waste-free process for flax utilization. Flax fibers differ in their chemical composition from cotton by smaller content of cellulose, and flax pedicels are close in their composition to coniferous wood. At present, there is no procedure of waste-free utilization of the lignocarbohydrate complex of flax, including short flax fibers and flax pedicels. The possibilities of using short flax fibers and boon as a raw material, instead of cotton linter and purified wood pulp, for synthesis of sorbents and cellulose ethers are being examined [1, 2].

Among cellulose derivatives, its water-soluble ethers are used the most widely: for drilling muds in oil industry; in production of varnishes, paints, and detergents in textile industry; and also in food industry, cosmetics, and perfumery. These cellulose derivatives are methyl cellulose (MC), hydroxypropyl cellulose (HPC), hydroxypropyl methyl cellulose (HPMC), methyl ethyl cellulose (MEC), and other cellulose ethers.

Among cellulose ethers containing carboxy groups, carboxymethyl cellulose (CMC) produced in the form of a sodium salt (NaCMC) is the most widely used in practice. CMC exhibits properties typical of polyelectrolytes [3, 4]. Of scientific and practical interest is synthesis of NaCMC from large-capacity wastes formed in flax production: short fibers and boon.

This study is aimed to examine the conditions under which NaCMC can be prepared from short flax fibers and lignified part of flax pedicels and also to analyze the factors affecting the kinetics of carboxymethylation of flax cellulose.

EXPERIMENTAL

As a starting material we used short fibers and the lignified part of flax pedicels from the Nevel plant. The degree of polymerization (DP) of cellulose in the initial short flax fibers was 3000. The degree of polymerization of cellulose in flax pedicels was determined viscometrically from the viscosity of cellulose nitrate in acetone solutions (Mitchell method) [5]. The DP of cellulose in flax pedicels was 2600. Samples of flax fibers and pedicels were tentatively characterized by the component composition (Table 1). The chem-

Table 1. Chemical composition of flax fibers and pedicels

Component	Content, wt %	
	flax straw (flax pedicels)	short fibers
Ash	2.1	1.3
Fats, waxes	2.0	1.2
Lignin	31.6	4.9
Nitrogen	Not determined	0.3
Cellulose	47.2	72.1
Pectins	2.5	1.2
Other hemicelluloses	7.8	13.8
Moisture content	6.4	5.2

1070-4272/05/7812-2014 © 2005 Pleiades Publishing, Inc.

Table 2. Synthesis conditions of carboxymethyl cellulose based on short flax fibers and boon (lignified part of flax pedicels)

Run no.	Reaction conditions						Fraction of soluble part, %	Water-soluble part	
	number of moles of reagents per mole of cellulose			activation time, h	*T*, °C	reaction time, h		Amount of COOH groups	DS of CMC
	NaOH	MCAA	isopropanol						
				Short flax fibers					
				Solid-phase procedure					
1	4	2	–	3.0	55	3.5	60.0	13.0	0.56
2	4	2	–	3.0	55	24.0	99.4	21.5	1.07
				Suspension procedure					
3	4	2	25	0.5	55	3.5	30.0	7.9	0.32
4	4	2	25	3.0	20	24.0	98.0	18.0	0.84
5	4	2	25	3.0	55	24.0	99.0	20.7	1.02
6	20	12	25	3.0	20	24.0	99.5	24.2	1.27
				Boon					
				Solid-phase procedure					
7	4	2	–	3.0	55	3.5	30.0	8.8	0.36
8	4	2	–	3.0	55	24.0	50.0	24.2	1.27
				Suspension procedure					
9	4	2	25	0.5	20	24.0	40.0	8.9	0.36
10	4	2	25	3.0	55	24.0	50.0	22.2	1.12
11	20	12	25	3.0	20	24.0	60.0	18.8	0.89

ical composition of the samples was determined using the procedures described in [6].

In contrast to cotton, flax fibers contain a larger amount of fats, waxes, pectins, and hemicelluloses, which affect the rate of cellulose carboxymethylation. Therefore, the starting materials were prepurified to remove concomitant substances: fats, waxes, and pectins. The flax fibers were treated by the procedure described in [7]. Fats and waxes were removed by treatment with a benzene–ethanol mixture in a Soxhlet apparatus. Pectins were removed by treatment of degreased fibers with aqueous solutions of HCl and ammonium citrate [8]. Flax boon was preliminarily milled in a knife mill. CMC was synthesized by two commercially used procedures: of solid-phase and suspension types [9, 10].

The solid-phase carboxymethylation of flax fibers and boon involved treatment of the starting material with 30% aqueous sodium hydroxide at room temperature for 3 h. After the alkaline treatment, the sample was squeezed to threefold weight and mixed with monochloroacetic acid (MCAA). The carboxymethylation was performed at 55°C with stirring of the reaction mixture for various periods of time. The reaction products were purified with 70% ethanol, with 90% acetic acid added to neutralize excess alkali. The final product was extracted with 70% ethanol to remove sodium chloride and sodium acetate, washed with methanol, and dried at 60°C, after which the product yield and its solubility in water were determined.

The suspension carboxymethylation of flax fibers and boon was performed as follows. The cellulose material was stirred with isopropanol for 30 min. Then, 30% aqueous sodium hydroxide was added to the reaction mixture with stirring for various periods of time. After stirring at room temperature, a calculated amount of MCAA was added. The reaction with MCAA was performed at 20 and 55°C for various periods of time. The subsequent work-up procedure was similar to that in the solid-phase carboxymethylation.

The degree of substitution (DS) of the NaCMC samples synthesized was determined from the content of carboxy groups by the formula

$$DS = 162m/(4500 - 58m), \quad (1)$$

where m is the content of carboxy groups (wt %).

The content of carboxy groups was determined by conductometric titration of the samples with 0.1 N NaOH.

The IR spectra of cellulose ethers were recorded in KBr pellets on a Bruker FS-88 IR Fourier spectrometer.

The conditions of carboxymethylation of flax fibers and boon are presented in Table 2. It is seen

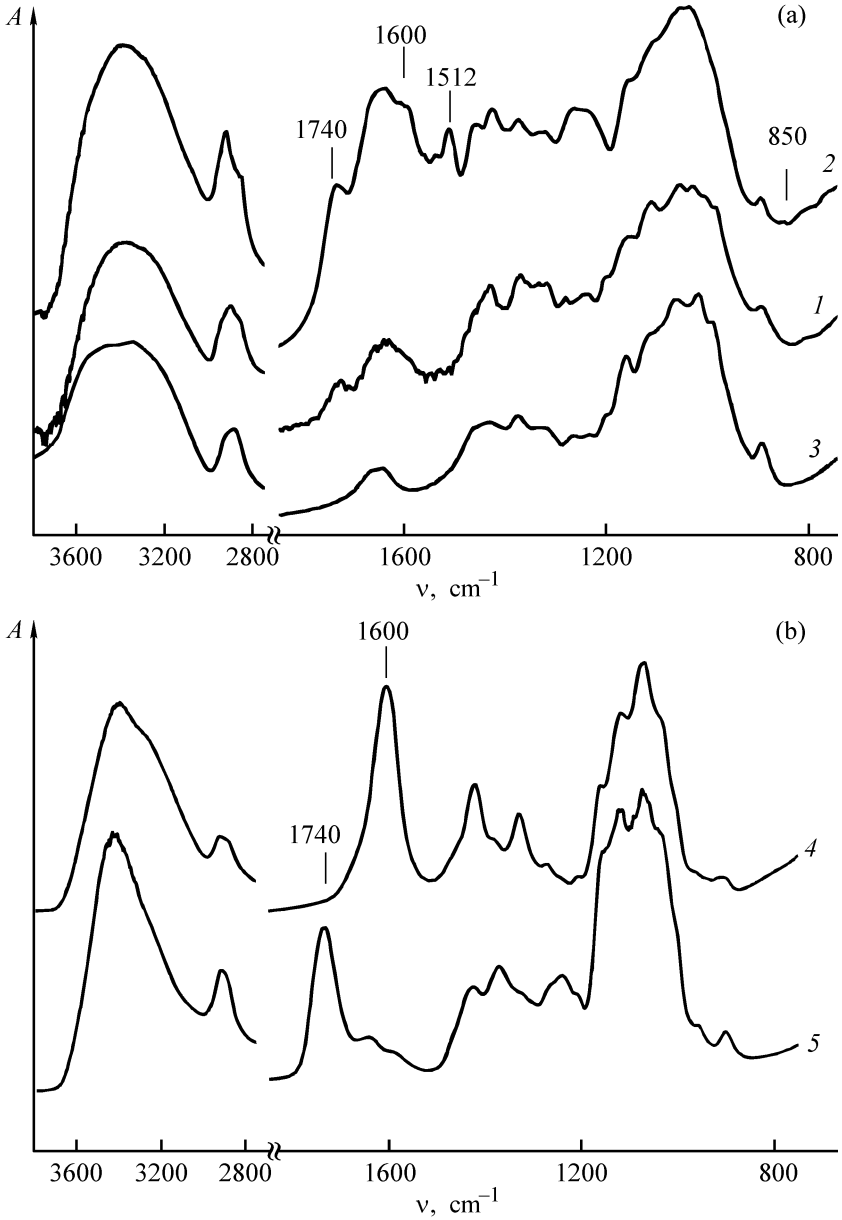


Fig. 1. IR Fourier spectra of (a) (*1*) initial flax fibers, (*2*) boon, (*3*) cotton linter, (b) (*4*) NaCMC, and (*5*) HCMC prepared from short flax fibers. (*A*) Absorption and (*ν*) wave number.

that the solid-phase and suspension procedures allow preparation of CMC partially or completely soluble in water.

To qualitatively confirm the structure of the resulting cellulose derivatives, we recorded IR spectra of the carboxymethylation products. The IR Fourier spectra of the initial short flax fibers and boon and of the resulting cellulose ethers are shown in Figs. 1a and 1b. For comparison, the IR spectrum of purified (bleached) cotton linter is shown in Fig. 1a.

The following absorption bands are typical of purified cotton cellulose: a broad band in the range 3000–3700 cm^{-1} belonging to free and H-bonded OH groups of the polymer and the band in the region of 2900 cm^{-1} corresponding to vibrations of the CH_2 and CH groups of the polymer. The absorption band at 2900 cm^{-1} in the spectrum of free cellulose is virtually symmetrical [11].

The IR spectra of crude wood pulp contain characteristic absorption bands at 1600, 1500, and 850 cm^{-1}, which are assigned to lignin [11]. Figure 1a shows that the IR spectrum of the lignified part of flax pedicels contains an absorption band appearing as a shoulder at 1600 cm^{-1}, which suggests that lignin is present

in the sample of flax pedicels (boon) in an amount comparable that in wood pulp (Table 1). In the IR spectrum of boon, there is also an absorption band in the region of 1512 cm^{-1}, typical of the aromatic structures of lignin. This band is absent in the IR spectrum of flax fibers, which may be due to a significantly smaller amount of lignin.

The characteristic bands of pectins are those at 1740 (free COOH groups of polygalacturonic acid), 1615, and 1410 cm^{-1} (symmetric and antisymmetric vibrations of ionized COO^- groups). In the range 2850–2950 cm^{-1}, there is one broad band or two bands assignable to CH_2 and CH groups [12]. It is seen that in the initial samples there is an absorption band of carboxy groups of pectin substances at 1740 cm^{-1} (Fig. 1a).

In activation of cellulose with alkali solution and carboxymethylation, hemicelluloses, pectin substances, and lignin partially dissolve, i.e., cellulose is whitened and refined. It has been shown previously [13] that, with removal of fats and pectin substances from the surface of flax fibers, the intensity of the absorption band corresponding to carboxy groups of pectins decreases. After treatment of flax fibers with a surfactant solution, the absorption band virtually desappears.

In the IR spectra of NaCMC prepared on the basis of flax fibers (Fig. 1b), there is a band in the range 1597–1605 cm^{-1}, assigned to antisymmetric vibrations of ionized carboxy groups COO [11]. In passing from NaCMC to its H form, the absorption band of COOH groups appears in the spectrum at 1740 cm^{-1}; its intensity is comparable to that of the band of residual unsubstituted OH groups of the polymer (2700–3200 cm^{-1}). In addition, in passing from ionized form to H form of CMC, an absorption band appears in the range 1200–1300 cm^{-1}, which is due to changes in the system of hydrogen bonds in the polymer [11].

It should be noted that a significant amount of lignin remains in the CMC samples synthesized on the basis of boon, which is suggested by the absorption band at 1512 cm^{-1}, observed in the spectrum of the carboxymethylated sample, as in the case of the initial sample (Fig. 1a). The presence of the residual lignin results in incomplete solubility of the CMC samples with high DP in water.

The IR data are confirmed by the results of a quantitative determination of carboxy groups in the samples by conductometric titration.

The content of carboxy groups in the water-soluble fraction of the resulting products depends on the activation time of the initial material with an alkali solution and also on the reaction time and temperature. A longer solid-phase synthesis of CMC results in an increased amount of carboxy groups and a higher DS in the resulting products. A similar trend is observed for the CMC samples synthesized by the suspension procedure. With increasing reaction temperature, the DS of the samples grows from 0.84 to 1.02 for short fibers (Table 2, run nos. 4 and 5) and from 0.36 to 1.12 for boon (run nos. 9 and 10). An increase in the amount of reagents per mole of cellulose also results in acceleration of carboxymethylation (run nos. 5, 6, 9, and 11). It should be noted that the suspension synthesis of CMC yields products with a more uniform distribution of carboxy groups in polymer macromolecules.

It is well known that NaCMC with DS ≥ 0.45–0.50 is completely soluble in water [4, 10]. Table 2 shows that the content of the water-soluble fraction in the samples synthesized by the solidphase procedure at DP = 0.56 is 60.0% (run no. 1, short fibers). The incomplete dissolution of the sample in water is due to nonuniform carboxymethylation of cellulose, caused by the presence of lignin and other concomitant substances in cellulose (Table 1). The effect of impurities (other components) on the solubility of the synthesized products is manifested to a greater extent for boon. The presence of significant amounts of lignin results in that, even at a high DS the solubility in water does not exceed 60.0%, which correlates well with the amount of lignin in the initial sample.

For a comparative estimation of how the DP of cellulose varies in carboxymethylation of flax fiber we determined the intrinsic viscosity of the NaCMC samples in 6% aqueous sodium hydroxide and evaluated the DPs of the cellulose ethers. The DP of carboxymethyl cellulose was evaluated by the expression [10]

$$[\eta] = 7.3 \times 10^3 DP^{0.93}. \quad (2)$$

It was found that, in synthesis of NaCMC from short flax fibers, the DP of the polymer decreases by 30–50%, which is caused by oxidative degradation of polymer macrochains in alkaline medium.

Thus, according to IR Fourier spectroscopy and analysis by physicochemical methods (conductometry), carboxymethyl ethers of cellulose with various degrees of substitution were synthesized from short flax fibers and lignified part of flax pedicels (boon).

CONCLUSIONS

(1) Experiments on synthesis of carboxymethyl ethers of cellulose with various degrees of substitution

from wastes formed in production of flax fibers demonstrated that the degree of substitution of the resulting cellulose ethers and their solubility depend on the activation time of the initial materials with alkali solution, temperature and duration of carboxymethylation, molar ratio of the reactants, and presence of lignin in the starting lignin materials.

(2) The study confirmed the possibility of using wastes from flax production to prepare carboxymethyl cellulose.

ACKNOWLEDGMENT

This study was supported by the Program of the Division of Chemistry and Material Science, Russian Academy of Sciences, "Scientific Foundation of Resource and Energy Saving in Recovery of Mineral, Manmade, and Renewable Raw Materials."

REFERENCES

1. Bazarnova, N.T., Tokareva, I.V., and Galochkin, A.I., Abstracts of Papers, *III Vserossiiskoe soveschanie "Lesokhimiya i organicheskii sintez"* (III All-Russian Meet. "Dendrochemistry and Organic Synthesis"), Syktyvkar, September 28–October 2, 1998, p. 55.
2. Emets, L.V., Levit, R.M., Strukova, I.M., *et al.*, *Khim. Volokna*, 1996, no. 6, pp. 20–22.
3. Yusupova, L.D., Bochek, A.M., and Petropavlovskii, G.A., *Zh. Prikl. Khim.*, 1994, vol. 67, no. 7, pp. 1187–1191.
4. Bochek, A.M., Yusupova, A.M., Zabivalova, N.M., *et al.*, *Zh. Prikl. Khim.*, 2002, vol. 75, no. 7, pp. 659–663.
5. Nikitin, N.I., *Khimiya drevesiny i tsellyulozy* (Chemistry of Wood and Cellulose), Moscow: Akad. Nauk SSSR, 1962.
6. Bochek, A.M., Shevchuk, I.L., and Lavrent'ev, V.N., *Zh. Prikl. Khim.*, 2003, vol. 76, no. 10, pp. 1725–1728.
7. *Spravochnik khimicheskoi tekhnologii obrabotki l'nyanykh tkanei* (Handbook on Chemical Technology of Treatment of Flax Fabrics), Fridlyand, G.I., Ed., Moscow: Legkaya Industriya, 1973.
8. Bochek, A.M., Zabivalova, N.M., Shamolina, I.I., *et al.*, *Zh. Prikl. Khim.*, 2002, vol. 75, no. 9, pp. 1549–1554.
9. Bytenskii, V.Ya. and Kuznetsova, E.N., *Proizvodstvo efirov of tsellyulozy* (Production of Cellulose Ethers), Leningrad: Khimiya, 1974.
10. Petropavlovskii, G.A., *Gidrofil'nye, chastichno zameshchennye efiry tsellyulozy i ikh modifikatsiya putem khimicheskogo sshivaniya* (Hydrophilic Partially Substituted Ethers of Cellulose and Their Modification by Chemical Cross-Linking), Leningrad: Nauka, 1988.
11. Zhbankov, R.G., *Infrakrasnye spektry tsellyulozy i ee proizvodnykh* (IR Spectra of Cellulose and Its Derivatives), Minsk: Nauka i Tekhnika, 1964.
12. Aimukhammedova, G.B., Alieva, Dzh.E., and Shelukhina, N.P., *Svoistva i primenenie pektinovykh sorbentov* (Characteristics and Use of Pectin Sorbents), Frunze: Ilim, 1984.
13. Shamolina, I.I., Bochek, A.M., Zabivalova, N.M., *et al.*, *Fibers Textiles East. Eur.*, 2003, vol. 11, no. 1(40), pp. 33–36.

Russian Journal of Applied Chemistry, Vol. 78, No. 12, 2005, pp. 2019–2021. Translated from Zhurnal Prikladnoi Khimii, Vol. 78, No. 12, 2005, pp. 2050–2053.
Original Russian Text Copyright © 2005 by Alekseev, Arapov, Polovtsev, Charykov, Izotova, Potalitsin.

BRIEF COMMUNICATIONS

Methods for Purification of Carbon Nanotubes Obtained from Fullerene Production Deposits

N. I. Alekseev, O. V. Arapov, S. V. Polovtsev, N. A. Charykov, S. G. Izotova, and M. G. Potalitsin

Innovations of Leningrad Institutes and Enterprises Closed Joint-Stock Company, St. Petersburg, Russia

Ioffe Physicotechnical Institute, Russian Academy of Sciences, St. Petersburg, Russia

St. Petersburg State University, St. Petersburg, Russia

State Institute of Applied Chemistry, St. Petersburg, Russia

Received June 2, 2005

Abstract—Methods of preparation and purification of nanocarbon materials (nanotubes, nanobarrels, nanobulbs) from deposits formed in fullerene production were developed.

Since the beginning of extensive studies of carbon nanotubes (CNTs) and other nanostructures in 1991 [1, 2], the separation of CNTs from concomitant products (amorphous carbon, graphite, and sometimes catalyst metal particles) has become an increasingly topical problem, strongly affecting the CNT cost.

At present, the purest CNTs (< 90%) are prepared by their CVD growth in the presence of catalysts on special supports [3, 4]. In this case, the amount of amorphous carbon is relatively small, graphite is virtually absent, and catalyst metal particles can be eliminated by comparatively brief treatment with an acid. Various pathways of purification of CNTs prepared by CVD are described in [5–7] and depend on CNT type (single- or multiwalled). However, only small CNT amounts can be prepared by CVD, and, therefore, this method is not widely used today. Nevertheless, a CVD method for preparation of single-walled nanotubes containing no impurities was described in [8].

The HIPCO method [9], which is essentially similar to CVD and involves preliminary synthesis of catalyst particles in the gas phase, gives CNTs with a high content of excess catalyst, which requires a complex purification procedure [10].

Very complex treatment is required for CNT-containing raw material obtained by electric arc synthesis, which is the most productive now [11, 12]. According to [13], the purification procedure in the arc synthesis of single-walled CNT with a catalyst must be multistep. However, this method (arc + catalyst) is also inefficient and is claimed only when just single-walled CNTs are required.

When multiwalled CNTs with varied size and orientation are applicable (e.g., as catalysts, hydrogen accumulators, etc.), a common noncatalytic arc method of CNT preparation is used [11]. In this case, a deposit formed on the cathode during recrystallization of the carbon evaporated from the anode surface is the source of CNTs. An apparatus for fullerene generation, produces during continuous work for one day, up to 1 kg of soot and 200–300 g of a deposit containing up to 10 g of CNTs [14].

These amounts of the deposit require that strongly different treatment procedures should be used to separate amorphous carbon and graphite constituents. For example, it was shown in [15] that selective oxidation in air at 700°C proceeds slowly. The deposit ground to 50–100-nm particles loses no more than 50% of the initial weight upon a 12-h treatment. Other gaseous oxidants were also ineffective. Rotation of the working volume of a tubular furnace substantially accelerates the treatment of the ground deposit [13]. However, this technology is suitable only for a small volume of the material treated. Treatment with acids [16] is only efficient at continuous addition of fresh portions of the acid and small amounts of the deposit (a few grams per 100 ml of working volume). Treatment of larger amounts is possible in a countercurrent

1070-4272/05/7812-2019 © 2005 Pleiades Publishing, Inc.

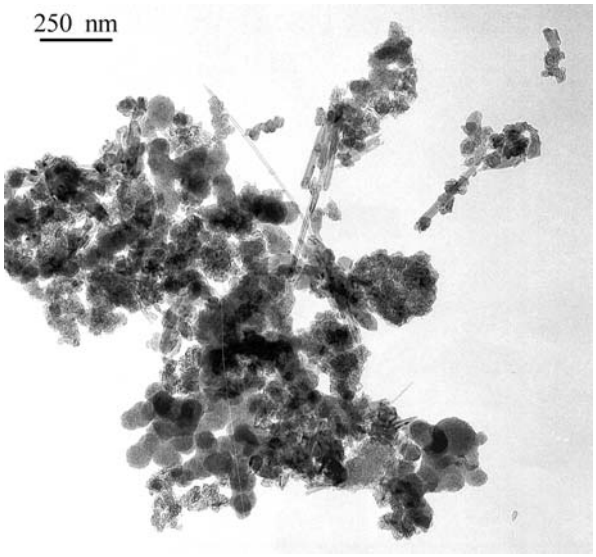


Fig. 1. Electron micrograph of the ground initial deposit.

Soxhlet apparatus. However, the acid is rapidly deactivated in this case. In our experiments, boiling of 10 g of the deposit in a tenfold excess $HClO_4$ under atmospheric pressure decreases the deposit weight by no more than 20% in the first 3 h, and then the weight loss stops completely (5 h of treatment). Oxidation through intercalation of the graphite component of the deposit with a KCl + $CuCl_2$ aqueous solution described in [17] is also time consuming (4–6 days). A hydrothermal method of CNT purification has also been described [18]. It is known that superheated steam exhibits fairly strong oxidizing properties at the near-critical pressures (~400 atm) [19, 20]. Unfortunately, the required high-pressure apparatus is very complex, and, as it follows from [18], the weight of the material being treated cannot be large (no more than 1 g per 100 ml).

Here we describe several simple and unconventional methods for purification of the cathodic deposit containing CNTs, which are based on selective decomposition of its amorphous and graphite constituents.

The initial cathodic deposit was obtained as a by-product in the synthesis of a fullerene-containing soot on a device developed at Innovations of Leningrad Institutes and Enterprises Closed Joint-Stock Company, described in [14, 21]. This device is mainly intended for fullerene production (up to 4.5 kg of fullerene-containing soot per day; content of fullerene mixture in soot 12–15 wt %). The conditions were not optimal with respect to production of the deposit and CNTs: the pressure in the working chamber was lower than optimal 300 torr and the current density was about 320 A cm^{-2}. The device productivity for the deposit is 800–1200 g per day, and the content of the carbon nanostructures in the deposit (various nanotubes, nanobarrels, and nanobulbs) is 3–5 wt %. A typical electron micrograph of the ground deposit, obtained on a JEM-100S transmission electron microscope (JEOL, Japan) at a 10^4–10^5 magnification, is shown in Fig. 1. Spheroid particles of nanocarbon phases, single- and multiwalled nanotubes nanobarrels, and nanobulbs, soldered in nonnanocarbon structures, are seen.

The cathodic deposit ground in a ball mill (50–100-μm fraction) was soaked in 20 wt % aqueous solution of $(NH_4)_2MoO_4$. Carbon particles were well wetted with this solution and formed a stable suspension. A further study showed that the same result, complete wetting of the cathodic deposit, is attained in aqueous solutions of NH_4NO_3 and NH_4Cl. However, these solutions were less technologically effective. The suspension was treated (up to 3 times) as follows: freezing in a Peltier refrigerator to –35°C and thawing at 20°C in order to cleave graphitic layers in the graphite component of the deposit through expansion of the ice formed, after which the deposit was washed in water to neutral pH and dried at 100°C. This material is oxidized more readily than the initial deposit. The material obtained was oxidized with atmospheric oxygen at 700–800°C. Annealing in air for 3–5 h gave a weight loss of 50 to 95% relative to the initial deposit. The residue contained nanostructures (mainly multiwalled nanotubes and a small amount of single-walled nanotubes, nanobarrels, and nanobulbs). The content of nanostructures increased by an order of magnitude and reached 50 to 90 wt %. An electron micrograph of a sample enriched with CNT after oxidation in a furnace of 80% of the initial deposit is shown in Fig. 2. The content of the sum of nanomaterials was about 60 wt % (40% multiwalled CNT and 60% nanobarrels and nanobulbs; single-walled nanotubes were virtually absent).

Along with intercalation (and subsequent oxidation) of the graphite constituent of the deposit, selective dissolution can be used. Similarly to intercalation, the latter should initially dissolve,during reaction with the liquid oxidant, the more reactive part of the deposit, graphitic and amorphous carbon, and only then structurally regular nanotubes, nanobarrels, and nanobulbs. The oxidant can be taken in deficiency with account of the relative content of nanotubes in the deposit. This idea was implementeded with two efficient solvents of carbon: a mixture of $KClO_3$ (10 wt %) with concentrated nitric acid (65 wt %) and a mixture of CrO_3 (5 wt %) with concentrated sulfuric acid (70 wt %). During treatment of the ground deposit

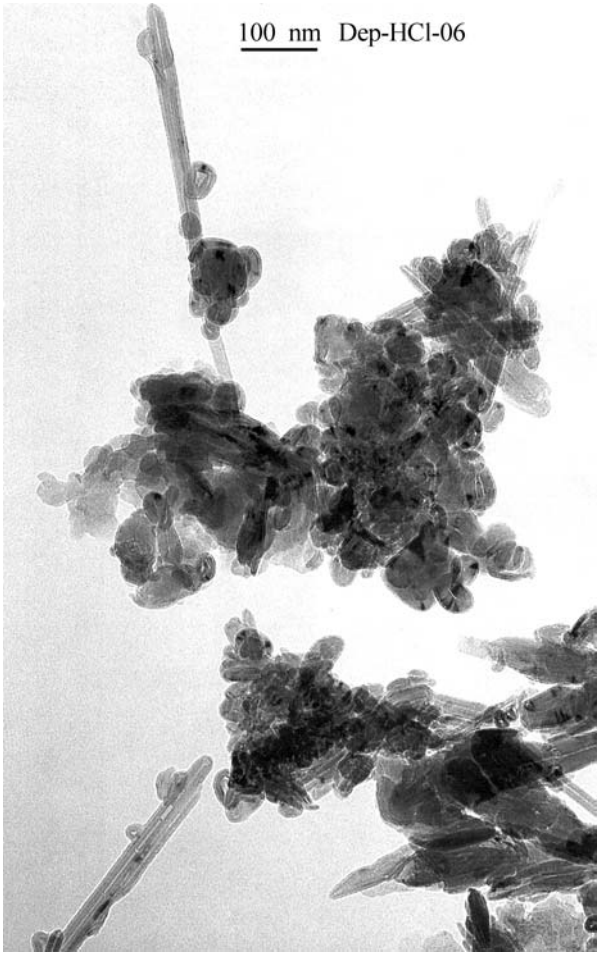


Fig. 2. Electron micrograph of the deposit prepared by intercalation of the graphite constituent with water followed by gas-phase oxidation with air.

with the above oxidants at 80–85°C, the nonnanocarbon part of the deposit is oxidized to carbon monoxide and is eliminated from the reaction zone. Despite that a small part of nanocarbon material is also decomposed (mainly the most brittle single-walled CNTs), the deposit material is substantially enriched with carbon nanostructures. The enrichment level is close to that obtained by intercalation followed by gas-phase oxidation, and the method is somewhat more technologically effective. Electron micrographs of samples prepared by this method are virtually the same as that in Fig. 2.

REFERENCES

1. Iijuma, S., *Nature*, 1991, vol. 354, pp. 56–61.
2. Iijuma, S., Ichihashi, T, and Ando, Y., *Nature*, 1992, vol. 356, pp. 776–780.
3. Li, W.Z., Xie, S.S., Qain, L.X., *et al.*, *Science*, 1996, vol. 274, pp. 1701–1703.
4. Fan, S., Chapline, M.G., and Franklin, N.R., *Science*, 1996, vol. 283, pp. 512–516.
5. Feng, Y., Zhou, G., Wang, G., *et al.*, *Chem. Phys. Lett.*, 2003, vol. 375, pp. 645–648.
6. Kim, Y.A., Hayashi, T., Osawa, R., *et al.*, *Chem. Phys. Lett.*, 2003, vol. 380, pp. 319–324.
7. Chiang, I.W., Brinson, B.E., Smalley, R.E., *et al.*, *J. Chem. Phys. B*, 2001, vol. 105, pp. 1157–1161.
8. Maruyama, S., Kojima, R., Miyauchi, *et al.*, *Chem. Phys. Lett.*, 2002, vol. 360, pp. 229–234.
9. Dai, H., Rinzler, A.G., Nicolaev, P., *et al.*, *Chem. Phys. Lett.*, 1996, vol. 262, pp. 161–166.
10. Chiang, I.W., Brinson, B.E., and Huang, A.Y., *J. Chem. Phys. B*, 2001, vol. 105, pp. 8297–8301.
11. Ebbesen, T.W. and Ajayan, P.M., *Nature*, 1992, vol. 358, pp. 220–224.
12. Journet, C., Maser, W.K., Bernier, P., *et al.*, *Nature*, 1997, vol. 388, pp. 756–759.
13. Park, Y.S., Choi,Y.C., Kim, K.S., *et al.*, *Carbon*, 2001, vol. 39, pp. 655–661.
14. Dyuzhev, G.A., Basargin, I.V., Filippov, B.M., Alekseyev, N.I., *et al.*, *Int. Appl. Publ. under PCT*, WO 02/096800, PCTRU02/00083.
15. Ajayan, P.M., Ebbesen, T.W., Ichihashi, T, *et al.*, *Nature*, 1993, vol. 362, pp. 522–526.
16. Tsang, S.C., Chen, Y.K., Harris, P.J., and Green, M.L., *Nature*, 1994, vol. 372, pp. 159–164.
17. Ikazaki, F., Ohshima, S., Ushida, K., *et al.*, *Carbon*, 1994, vol. 32, pp. 1539–1550.
18. Moreno, C.J. and Yoshimura, M., *J. Am. Chem. Soc.*, 2001, vol. 123, pp. 741–745.
19. Chang, J.Y., Chang, A.G., Tzing, S.H., and Ling, Y.C., *Chem. Phys. Lett.*, 2002, vol. 363, pp. 583–590.
20. RF Patent 39129.

Russian Journal of Applied Chemistry, Vol. 78, No. 12, 2005, pp. 2022–2023. Translated from Zhurnal Prikladnoi Khimii, Vol. 78, No. 12, 2005, pp. 2054–2055.
Original Russian Text Copyright © 2005 by Khamaganova, Oshorova.

BRIEF COMMUNICATIONS

$Ba_{3-x}Sr_xSm(BO_3)_3$ Solid Solutions ($0 < x < 3$)

T. N. Khamaganova and V. K. Oshorova

Baikal Institute of Nature Management, Siberian Division, Russian Academy of Sciences, Ulan-Ude, Buryatia, Russia

Geological Institute, Siberian Division, Russian Academy of Sciences, Ulan-Ude, Buryatia, Russia

Received August 24, 2005

Abstract—Samples of a continuous series of $Ba_{3-x}Sr_xSm(BO_3)_3$ solid solutions ($0 < x < 3$), crystallizing in the trigonal crystal (system, space group $R\bar{3}$) were synthesized by solid-phase reactions. Formation of a continuous series of solid solutions in the system was confirmed by X-ray phase analysis. The X-ray characteristics of phases of variable composition were determined.

Complex borates $M_3R(BO_3)$, where M is alkaline-earth element Ba or Sr and R is rare-earth element (REE) [1–6], are of interest as materials for microelectronics and nonlinear optics. Variation of the cationic composition allows purposeful synthesis of phases and makes it possible to elucidate the influence exerted by the composition and structure on their characteristics. Since double borates $Ba_3Sm(BO_3)_3$ and $Sr_3Sm(BO_3)_3$ crystallize in the same structural type [3, 4], formation of a continuous series of solid solutions would be expected.

In this study, we examined the possibility of formation of solid solutions based on double borates of alkaline-earth elements and samarium, with the composition $Ba_{3-x}Sr_xSm(BO_3)_3$, by isovalent substitution of Sr^{2+} for Ba^{2+}. The x value was varied from 0 to 3 with a step of 0.5.

EXPERIMENTAL

Polycrystalline samples were synthesized by solid-phase reactions from Sm_2O_3 (content of the main component no less than 99.99%), $BaCO_3$ and $SrCO_3$ of ultrapure grade, and H_3BO_3 of chemically pure grade. Mixtures of stoichiometric amounts of the initial reagents were calcined in platinum crucibles in air with repeated intermediate grindings. Barium and strontium carbonates were preliminarily annealed at 400°C, and samarium oxide, at 800°C, for 5 h. The synthesis temperature was gradually raised from 600°C to 1000°C, with a step of 100°C, over a period of 70–80 h. Single-phase samples were prepared by annealing at 1000°C for 20–25°C. The phase composition of the compounds studied and the attainment of equilibrium were monitored by X-ray phase analysis (Bruker D8 Advance diffractometer, Cu_{K_α} radiation, graphite monochromator).

The X-ray patterns diffraction of all the compounds obtained (Fig. 1) are similar in the positions and rela-

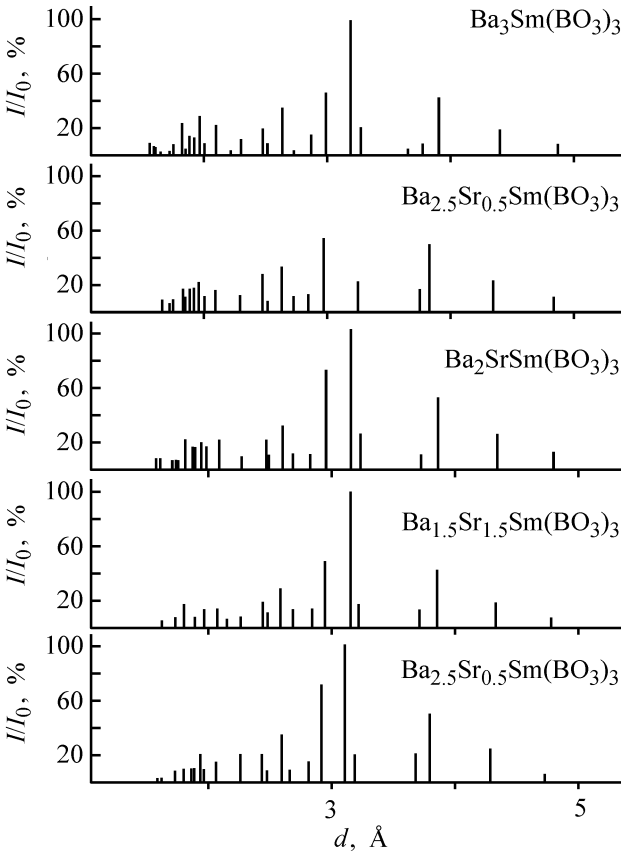


Fig. 1. X-ray diffraction patterns of the compounds. (I/I_0) Relative intensity and (d) interplanar spacing.

1070-4272/05/7812-2022 © 2005 Pleiades Publishing, Inc.

Indexing of a powder X-ray pattern of $Ba_{1.5}Sr_{1.5}Sm(BO_3)_3$ (space group $R\bar{3}$, $Z = 6$)

I/I_0	d, °C	$10^8/d^2_{exp}$	hkl	$10^4/D^2_{calc}$
8	4.79	434	021	437
20	4.32	535	012	535
45	3.85	674	211	679
15	3.71	727	030	728
18	3.218	965	220	970
100	3.136	1016	122	1020
50	2.935	1160	131	1165
15	2.814	1262	113	1265
15	2.667	1405	401	1408
30	2.578	1505	312	1506
12	2.464	1647	321	1651
20	2.426	1699	140, 410	1699
10	2.242	1989	223	1992
8	2.132	2200	330	2194
15	2.053	2373	241	2379
15	1.953	2622	511	2622
20	1.918	2718	143, 413	2718
10	1.869	2863	134	2867
15	1.841	2950	152	2957
18	1.782	3149	250, 520	3155
8	1.713	3408	125	3408
8	1.704	3444	342	3448
5	1.595	3931	603, 063	3935

tive intensities of the reflections. The powder X-ray patterns of the variable-composition phases were indexed using X-ray data for $Ba_3Sm(BO_3)_3$ (trigonal crystal system, space group $R\bar{3}$) [3] on the assumption that these phases are isostructural. The results of indexing of the powder X-ray pattern of $Ba_{1.5}Sr_{1.5}Sm(BO_3)_3$ are presented in the table. The unit cell parameters were refined by the least-squares method in the range of angles 2θ 10°–60°, using the LATTIC software.

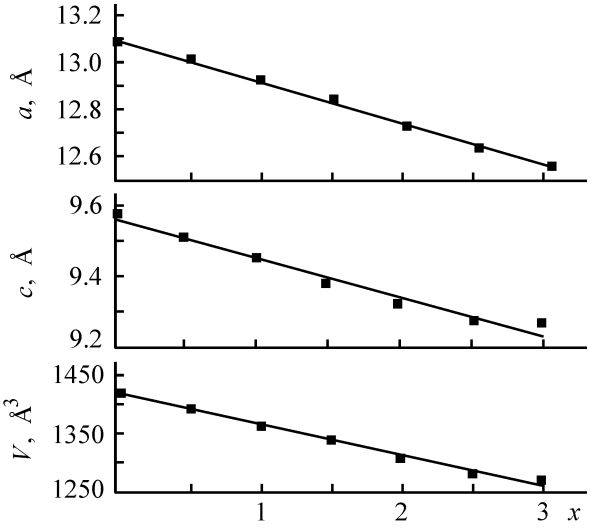


Fig. 2. Parameters a and c and unit cell volume V vs. the degree of Sr substitution for Ba, x, in $Ba_{3-x}Sr_xSm(BO_3)_3$ ($0 < x < 3$).

According to published data [7], the ionic radii of bivalent cations Ba^{2+} and Sr^{2+} for the coordination number 9 realized in this structural type are 1.47 and 1.31 Å, respectively. Analysis shows that the triple phases obtained are substitutional solid solutions based on the double borate $Ba_3Sm(BO_3)_3$ crystallizing in the trigonal crystal system (space group $R\bar{3}$). The concentration dependences of parameters a and c of the rhombohedral units and also unit cell volumes V for $Ba_{3-x}Sr_xSm(BO_3)_3$ are shown in Fig 2.[1] It is seen that, with increasing degree of Sr substitution for Ba, x, in the solid solutions studied, parameters a, c, and V decrease linearly.

The similarity of the X-ray diffraction patterns of all the samples and linear dependences of the unit cell parameters on the composition suggest that a continuous series of solid solutions is formed.

CONCLUSIONS

(1) Previously unknown phases of variable composition, $Ba_{3-x}Sr_xSm(BO_3)_3$ ($0 < x < 3$), were synthesized by solid-phase reactions from barium and strontium carbonates, samarium oxide, and boric acid.

(2) An X-ray phase analysis showed that the resulting ternary phases are isostructural and form a continuous series of substitutional solid solutions.

REFERENCES

1. Khamaganova, T.N., *Cand. Sci. Dissertation*, Moscow, 1990.
2. Khamaganova, T.N. and Trunov, V.K., *Zh. Neorg. Khim.*, 1993, vol. 38, pp. 1792–1793.
3. Khamaganova, T.N., Kuperman, N.M., and Bazarova, Zh.G., *J. Solid State Chem.*, 1999, vol. 145, pp. 33–36.
4. Khamaganova, T.N., Kuperman, N.M., and Bazarova, Zh.G., *Zh. Neorg. Khim.*, 1999, vol. 44, no. 10, pp. 1625–1626.
5. Khamaganova, T.N. and Tushinova, Yu.L., *Zh. Prikl. Khim.*, 2000, vol. 73, no. 12, pp. 2046–2048.
6. Stefanovich, S.Yu. and Khamaganova, T.N., *Izv. Ross. Akad. Nauk, Neorg. Mater.*, 2002, vol. 38, no. 1, pp. 78–80.
7. Shannon, R.D., *Acta Crystallogr., Sect. A*, 1976, vol. 32, pp. 751–767.

[1] The powder X-ray diffraction patterns of the sample were recorded on an FR-552 focusing camera-monochromator (Cu_{K_α} radiation, Ge internal reference) [3].

Russian Journal of Applied Chemistry, Vol. 78, No. 12, 2005, pp. 2024–2025. Translated from Zhurnal Prikladnoi Khimii, Vol. 78, No. 12, 2005, pp. 2056–2058.
Original Russian Text Copyright © 2005 by Kozyreva, Kolesnikova, Glukhareva, Lebedeva.

BRIEF COMMUNICATIONS

Oxidative Degradation of Neonol AF 9-12

Yu. N. Kozyreva, E. N. Kolesnikova, N.A. Glukhareva, and O.E. Lebedeva

Belgorod State University, Belgorod, Russia

Received August 22, 2005

Abstract—The oxidative degradation of a difficultly degradable surfactant, oxyethylated isononylphenol (Neonol AF 9-12), with aqueous hydrogen peroxide containing iron(III) chloride was studied tensimetrically.

The wide application of surfactants, primarily, household chemicals, leads to wastewater pollution with these agents. As a rule, surfactant-containing municipal wastes of large cities are treated at wastewater treatment plants in combination with some industrial wastes. However, biodegradation of some surfactants is not sufficiently fast to decrease their content in decontaminated wastewater to the level of the maximum permissible concentration (MPC). Oxyethylated alkylphenols, the only type of nonionic surfactants produced in Russia, belong to extremely slowly degradable "biologically hard" surfactants. To remove these surfactants from wastewater, local treatment facilities and specific physicochemical technique are required [1].

Published methods for water treatment to remove oxyethylated alkyphenols are few. The degradation of Igepal CA 520 commercial product mainly consisting of oxyethylated octylphenol with varied degree of oxyethylation was studied in [2]. It was found that UV light (365 nm) decomposes this surfactant in the presence of iron(III).

The oxidative degradation of oxyethylated alkylphenols shows much promise in view of the fact that this procedure has been successfully used for degradation of other chemically resistant xenobiotics. The Fenton reagent [mixture of hydrogen peroxide with iron(II) or iron(III) salts] is one of the most efficient oxidants [3]. The iron cations present in this reagent induce the hydrogen peroxide decay by a radical mechanism.

The oxidative degradation of oxyethylated isononylphenol with hydrogen peroxide in the presence of iron(III) was studied in [4]. It was found that this surfactant is effectively decomposed by hydrogen peroxide. In this study, with Neonol AF-9-12 as an example, we attempted to evaluate the extent of its oxidative degradation under the action hydrogen peroxide and to find the optimal conditions of this process.

EXPERIMENTAL

In our experiments, we used oxyethylated isononylphenol with an average degree of oxyethylation of 12 (Neonol AF 9-12, Neonol) produced by Nizhnekamskneftekhim Limited Liability Company in accordance with TU (Technical Specifications) 38.507-63-300–93.

Neonol was subjected to oxidative degradation by its treatment with aqueous hydrogen peroxide in the presence of iron(III) at varied concentrations of these reagents. The oxidant solutions were prepared in twice-distilled water.

The Neonol oxidation was monitored by surface tension measured by the ring detachment technique on a Kruss tensimeter at room temperature (23°C).

In all the experiments, the Neonol concentration was 6.7×10^{-5} M. This value is lower than the critical micelle concentration (CMC) of Neonol. Therefore, even minor variations in the Neonol concentration give rise to noticeable changes in the surface tension. In contrast, at the surfactant concentration exceeding CMC, the surface tension is insensitive to the surfactant concentration.

The surface tension at the initial Neonol concentration was 38 mN m^{-1}. On adding hydrogen peroxide to aqueous Neonol, the surface tension did not change significantly: the surface tension was 37.5 mN m^{-1} in 1 h, and 34 mN m^{-1} after 1 day. On keeping aqueous Neonol without adding hydrogen peroxide for 1 day, the surface tension decreases to a similar extent owing to attainment of the equilibrium sorption of Neonol at the interface between the aqueous surfactant and air.

A different pattern is observed after adding H_2O_2 in combination with a Fe(III) salt to aqueous Neonol. In this mixture, the surface tension noticeably increases after 15 min (see Fig. 1a), and this increase

1070-4272/05/7812-2024 © 2005 Pleiades Publishing, Inc.

reaches a maximum after approximately 1 h. We believe that this increase in the surface tension is caused by a decrease in Neonol concentration due to its oxidative degradation.

In the initial experiments, the iron(III) chloride concentration was kept constant (10 mM), while the hydrogen peroxide concentration was varied. Figure 1a shows that the maximum surface tension substantially depends on the H_2O_2 concentration. At a H_2O_2 concentration of 16.5 mM, Neonol degrades only partially. At a H_2O_2 concentration 66.0 mM, the surface tension reaches 67–68 mN m^{-1}, suggesting a high degree of Neonol degradation.

Further studies showed that the degree of Neonol degradation is also influenced by the Fe(III) concentration. Figure 1b demonstrates how the surface tension changes in the system with a constant H_2O_2 concentration (56 mM) and variable Fe(III) content.

We found that the initial rate of Neonol oxidation increases with the iron(III) content. After the completion of the experiment, the surface tension of the final solution was 71 mN m^{-1}. Comparison of this value with the surface tension of twice-distilled water (72.5 mN m^{-1}) shows that, in our experiments, the Neonol degradation was virtually complete, because, otherwise, the surface tension whould decrease.

With increasing iron(III) concentration, the initial rate of Neonol oxidation grows but the surface tension of the solution decreases after the completion of the experiment (see Fig. 1b). It is possible that the Neonol oxidation was incomplete under these conditions.

It is known that, in oxidation of Neonol with H_2O_2 in the presence of Fe(III), radicals are generated by the reaction

$$Fe^{3+} + H_2O_2 = Fe^{2+} + HOO^{\cdot} + H^+.$$

In accordance with the stoichiometry of this reaction, the most efficient oxidation of Neonol should be reached at an approximately equimolar ratio of H_2O_2 and Fe(III) in the reaction mixture. In the first step of Neonol oxidation, the $HOO^{\cdot}$ radical ruptures one of bonds in the Neonol molecule by the scheme

$$HOO^{\cdot} + RH \rightarrow H_2O_2 + R.$$

To reach complete oxidation of oxyethylated nonylphenol, a large amount of these radicals is required.

CONCLUSIONS

(1) The oxidative degradation of Neonol with hydrogen peroxide in the presence of Fe(III) allows efficient removal of this surfactant from wastewater.

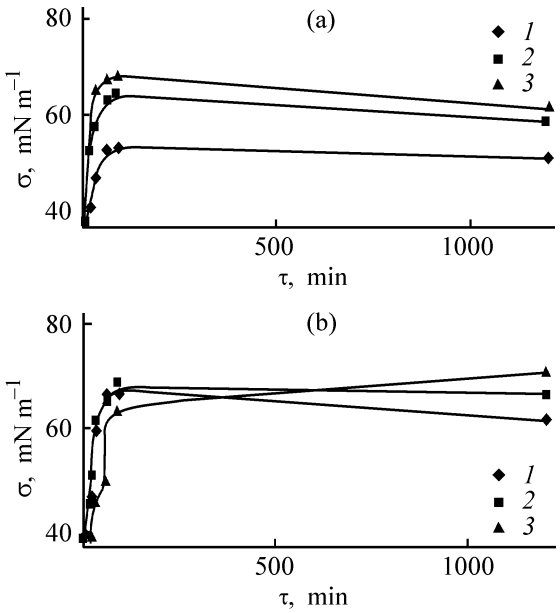


Fig. 1. Variation of surface tension σ with time τ in the course of oxidative degradation of Neonol. (a) $FeCl_3$ concentration 10 mM; H_2O_2 concentration, mM: (*1*) 16.5, (*2*) 33, and (*3*) 66. (b) H_2O_2 concentration 56 mM; $FeCl_3$ concentration, mM: (*1*) 10, (*2*) 2.5, and (*3*) 1.25.

(2) The rate and completeness of surfactant oxidation can be controlled by varying the oxidant content. At optimal ratio of hydrogen peroxide and iron(III) chloride, the surface tension of solution contaminated with the surfactant becomes approximately equal to that of twice-distilled water, which indicates that the surfactant degradation is virtually complete.

(3) Oxidative degradation of surfactants can be used instead of biodegradation technique or in combination with it to rupture the strongest bonds in the surfactant molecules. The development of an efficient technique for water treatment to remove Neonol can prolong the commercial use of surfactants of this kind until new softer nonionic surfactants is developed.

REFERENCES

1. Bocharov, V.V., *Byt. Khim.*, 2002, no. 8, pp. 4–8.
2. Brand, N., Mailhot, G., and Bolte, M., *Environ. Sci. Technol.*, 1998, vol. 32, no. 18, pp. 2715–2720.
3. Rudakov, E.S., *Reaktsii alkanov s okislitelyami, metallokompleksami i radikalami v rastvorakh* (Reactions of Alkanes with Oxidants, Metal Complexes and Radicals in Solutions), Kiev: Naukova Dumka, 1985.
4. Lebedeva, O.E., Glukhareva, N.A., Zheltyakova, N.E., *et al.*, *Izv. Vyssh. Uchebn. Zaved., Khim. Khim. Tekhnol.*, 2004, vol. 47, no. 8, pp. 14–17.

Russian Journal of Applied Chemistry, Vol. 78, No. 12, 2005, pp. 2026–2028. Translated from Zhurnal Prikladnoi Khimii, Vol. 78, No. 12, 2005, pp. 2059–2061.
Original Russian Text Copyright © 2005 by Gasanov, Allakhverdiev.

BRIEF COMMUNICATIONS

Synthesis of 1-Alkoxy-3-*N*-succinimido-2-propanols

R. A. Gasanov and M. A. Allakhverdiev

Institute of Chemistry of Additives, National Academy of Sciences of Azerbaijan, Baku, Azerbaijan

Received June 22, 2004; in final form, October 2005

Abstract—Procedures for preparing 1-alkoxy-3-chloro-2-propanols, with their subsequent transformation to 1-alkoxy-*N*-succinimido-2-propanols, were developed.

N-Substituted succinimides show a wide spectrum of pharmacological properties [1, 2]. They are effective against convulsions caused by Metrazole and electric shocks; some of them have also proved to be effective against epilepsy. Many *N*-aryl-substituted succinimides have been tested for activity and toxicity; among these compounds, *N*-*p*-xylylsuccinimide is the most promising as anticonvulsant [1–3]. 2-Ethyl-3-methyl-3-phenylsuccinimide exhibits sedative, anticonvulsive, and tetragenic properties [4]. Other nontoxic highly active anticonvlusants for treating apoplectic shocks are *N*-methyl-2-phenyl-2-ethylsuccinimide and *N*-methyl-2-phenyl-3-methylsuccinimide [5]. *N*-Methyl-2-phenylsuccinimide (Milontin) is an antiepileptic drug and is used as a reference for comparing the anticonvulsive activities [6].

In this context, synthesis of *N*-substituted succinimides by the reaction of sodium succinimide with 1-alkoxy-3-chloro-2-propanols is a topical problem. The first step is to prepare sodium succinimide **III** by the reaction of sodium isopropylate **I** with succinimide **II**:

$$\underset{\mathbf{I}}{(CH_3)_2CHONa} + \underset{\mathbf{II}}{\begin{matrix}CH_2—CO\\|\\CH_2—CO\end{matrix}>NH} \xrightarrow{-(CH_3)_2CHOH} \underset{\mathbf{III}}{\begin{matrix}CH_2—CO\\|\\CH_2—CO\end{matrix}>NNa.}$$

Reactions of sodium succinimide with 1-alkoxy-3-chloro-2-propanols **IV**–**IX** are carried out at 70–75°C in the course of 3 h and yield the corresponding *N*-substituted succinimides **X**–**XV** (see table):

$$\underset{}{\begin{matrix}CH_2—CO\\|\\CH_2—CO\end{matrix}>NNa} + \underset{\mathbf{IV}–\mathbf{IX}}{ClCH_2CH(OH)CH_2OR} \xrightarrow{-NaCl} \underset{\mathbf{X}–\mathbf{XV}}{\begin{matrix}CH_2—CO\\|\\CH_2—CO\end{matrix}>NCH_2CH(OH)CH_2OR,}$$

where R = CH_3 (**IV**, **X**); C_2H_5 (**V**, **XI**); C_3H_7 (**VI**, **XII**); C_4H_9 (**VII**, **XIII**); C_5H_{11} (**VIII**, **XIV**); C_6H_{13} (**IX**, **XV**).

Yields, boiling points, refractive indices, and elemental analyses of substituted succinimides **X**–**XV**

Compound	Yield %	bp, °C (P, mm Hg)	n_D^{20}	Found, %/Calculated, %			Formula
				C	H	N	
X	60	149–150 (0.7)	1.4922	51.15/51.33	7.03/7.00	7.73/7.48	$C_8H_{13}NO_4$
XI	55	154–155 (0.6)	1.4894	53.65/53.72	8.07/7.51	6.93/6.96	$C_9H_{15}NO_4$
XII	53	168 (1.0)	1.4847	55.39/55.80	8.13/7.96	6.52/6.51	$C_{10}H_{17}NO_4$
XIII	50	160 (0.6)	1.4836	57.12/57.62	8.79/8.35	6.47/6.11	$C_{11}H_{19}NO_4$
XIV	48	176 (1.0)	1.4825	58.78/59.24	8.62/8.70	5.94/5.76	$C_{12}H_{21}NO_4$
XV	49	179–180 (0.7)	1.4060	60.95/60.68	9.28/9.01	5.16/5.44	$C_{13}H_{23}NO_4$

1070-4272/05/7812-2026 © 2005 Pleiades Publishing, Inc.

The starting 1-alkoxy-3-chloro-2-propanols **IV**–**IX** were prepared by reactions of epichlorohydrin with aliphatic alcohols in the presence of $ZnCl_2$ (yield 80–90%). It should be noted that alternative procedures are also known [7, 8]. In particular, Floress Gallardo and Pollard [7] reacted epichlorohydrin with aliphatic alcohols in the presence of H_2SO_4; the yield of the target products did not exceed 55%. With $BF_3 \cdot OEt_2$ used as acid catalyst [8], the yield of the target products did not exceed 55%, either.

In both the studies cited, the yield of the target product was relatively low, and one of the reactants was taken in a large excess (threefold or sixfold excess of aliphatic alcohol, or sixfold excess of epichlorohydrin). Furthermore, $BF_3 \cdot OEt_2$ used in [8] is expensive and toxic.

We tested as acid catalysts in the reactions of epichlorohydrin with aliphatic alcohols both Brønsted (H_2SO_4, $HClO_4$) and aprotic Lewis acids ($AlCl_3$, $SnCl_4$, $ZnCl_2$). The best result was obtained with $ZnCl_2$. When the reaction was performed at the equimolar ratio of the alcohol and epichlorohydrin in the presence of 1.2 wt % $ZnCl_2$ (relative to the sum of the reactants) at the boiling point of the alcohol for 2.5–3 h, the yield of 1-alkoxy-3-chloro-2-propanols **IV**–**IX** reached 80–90%. Thus, the procedure is improved by eliminating the excess of one of the components, using a cheaper catalyst, and making shorter the reaction time.

The reaction course and the accumulation of 1-alkoxy-3-chloro-2-propanols were monitored by gas–liquid chromatography on a Tsvet-104 device (flame ionization detector; 200×0.03-cm column packed with 5% polyethylene glycol adipate on Porapak; sample volume 0.1 μl; P_{He} 0.8 kg cm^{-2}; paper feed velocity 240 mm h^{-1}; column temperature 140°C; vaporizer temperature 200°C).

The composition and structure of substituted succinimides **X**–**XV** were confirmed by elemental analysis, IR and NMR (^{1}H, ^{13}C) spectroscopy, and TLC.

The IR spectra of substituted succinimides **X**–**XV** contain bands at 3604–3598 (free OH groups), 3537–3532 (intramolecular hydrogen bond), and 1715–1705 cm^{-1} (C=O).

The highest-field signal in the ^{1}H NMR spectra of **X**–**XV** is the triplet of the terminal methyl group (3H) at 0.9–1.0 ppm. The OCH_2 protons give a multiplet at about 2.9 ppm. A broad singlet centered at 4.15–4.20 ppm belongs to the hydroxyl proton. The methine proton appears as a multiplet at about 3.71 ppm. Two methylene groups of the succinimide ring give a singlet at 4.8–5.7 ppm. In the ^{13}C NMR spectrum, the C=O signals are observed at 178–237 ppm.

EXPERIMENTAL

The ^{1}H NMR spectra were measured on a Bruker spectrometer operating at 300 MHz, and the IR spectra, on a Specord 75-IR spectrophotometer (thin films).

The purity of the products and the reaction progress were monitored by TLC on Silufol UV-254 plates, with isopropyl alcohol–heptane (1 : 5) as eluent.

1-Propoxy-3-chloro-2-propanol. A three-necked flask was charged with 6 g of 1-propanol, 9.3 g of epichlorohydrin, and 0.2 g of $ZnCl_2$. The mixture was heated at 90–95°C for 3 h, after which the product was cooled and vacuum-distilled. Yield 13 g (85%), bp 95–96°C (20 mm Hg), n_D^{20} 1.4391. Published data [7]: bp 97–98°C (20 mm Hg), n_D^{20} 1.4378.

Other 1-alkoxy-3-chloro-2-propanols **IV**–**IX** were prepared similarly; their constants agree with published data [7, 8].

1-Propoxy-3-*N*-succinimido-2-propanol XII. A three-necked flask equipped with a reflux condenser, dropping funnel, thermometer, and stirrer was charged with 50 ml of 2 propanol, after which 4.6 g of finely divided sodium metal was added with vigorous stirring. When the whole amount of sodium dissolved, the mixture was cooled, 19.8 g of succinimide was added, and the mixture was stirred on a water bath at 70–75°C for 1 h. After that, 1-propoxy-3-chloro-2-propanol was added dropwise over a period of 20 min. The resulting mixture was heated on a water bath at 90°C for 3 h and then cooled; the NaCl precipitate was filtered off. The 2-propanol was distilled off in a water-jet-pump vacuum, and the product was vacuum-distilled. Yield of the substituted succinimide 23 g (53%), bp 168°C (20 mm Hg), n_D^{20} 1.4847.

Found, %: C 55.39, H 8.13, N 6.52.
$C_{10}H_{17}NO_4$.
Calculated, %: C 55.80, H 7.96, N 6.51.

N-Substituted succinimides **X**–**XV** were prepared similarly.

CONCLUSIONS

(1) The optimal conditions of the reaction of epichlorohydrin with aliphatic alcohols in the presence of

$ZnCl_2$ were found, and 1-alkoxy-3-chloro-2-propanols were obtained in 80–90% yields.

(2) A procedure was developed for preparing 1-alkoxy-3-*N*-succinimido-2-propanols in 48–60% yield from 1-alkoxy-3-chloro-2-propanols and sodium succinimide.

REFERENCES

1. Chen, G., Rodman, P., Ensor, C.R., and Bratton, C.R., *J. Pharm. Exp. Ther.*, 1951, vol. 103, no. 1, pp. 54–58.
2. Muller, C.A. and Lang, L.M., *J. Am. Chem. Soc.*, 1951, vol. 73, no. 10, pp. 4895–4899.
3. Namsawa, J., Shihala, S., and Yamada, H., *Nippon Yakurigaku Zasshi*, 1957, vol. 53, no. 1, pp. 165–167.
4. Rosnati, V. and Bighami, G., *Farmaco. Ed. Sci.*, 1965, vol. 20, no. 1, p. 3.
5. US Patent 2643257, *Chem. Abstr.*, 1954, vol. 48, p. 5885.
6. Davidson, D.T. and Lambroso, C., *New Eng. J. Med.*, 1954, vol. 251, no. 5, pp. 853–859.
7. Floress Gallardo, H. and Pollard, C.B., *J. Org. Chem.*, 1947, vol. 12, no. 6, pp. 831–833.
8. Ponomarev, F.G., *Tr. Voronezh. Univ.*, 1956, vol. 40, no. 1, pp. 151–154.

Russian Journal of Applied Chemistry, Vol. 78, No. 12, 2005, pp. 2029–2031. Translated from Zhurnal Prikladnoi Khimii, Vol. 78, No. 12, 2005, pp. 2062–2064.
Original Russian Text Copyright © 2005 by Kasenov, Tukhmetova, Kasenova, Adekenov, Gazaliev, Fazylov, Nukhuly, Boldashevskii.

BRIEF COMMUNICATIONS

Thermodynamic Properties of Salsoline Salsolinodithiocarbamate

B. K. Kasenov, Zh. K. Tukhmetova, Sh. B. Kasenova, S. M. Adekenov, A. M. Gazaliev, S. D. Fazylov, A. Nukhuly, and A. V. Boldashevskii

Institute of Phytochemistry, Ministry of Education and Science of the Republic of Kazakhstan, Karaganda, Kazakhstan

Institute of Organic Synthesis and Coal Fuel Chemistry, Karaganda, Kazakhstan

Pavlodar State University, Pavlodar, Kazakhstan

Received September 9, 2005

Abstract—Heat of solution of salsoline salsolinodithiocarbamate (SS) at 1 : 18000, 1 : 36000, and 1 : 72000 dilution (mol per mol H_2O) was determined on a DAK-I-IA calorimeter, and the standard heat of solution at infinite dilution was estimated. The temperature dependence of the heat capacity of SS was studied over the range 173–348 K. The heats of combustion and fusion, and the standard heat of formation of liquid (molten) and crystalline SS were estimated by indirect methods.

Sulfur-containing alkaloids, among them dithiocarbamates, are of practical interest for developing highly effective domestic drug preparations from plant raw materials [1–4].

Determination of the fundamental thermodynamic characteristics of natural alkaloids and their synthetic derivatives is of considerable theoretical and practical interest for physicochemical simulation of their reactions and for standardization of drug substances on their basis.

Therefore, the goal of this study, was to measure by calorimetry the heat of solution of salsoline salsolinodithiocarbamate (SS) in water, to examine the temperature dependence of its heat capacity over the range 173–348 K, and to characterize its thermodynamic properties.

The heat of SS solution was measured on a DAK-I-IA automatic differential isothermal calorimeter at 25°C. The theory and procedure of the calorimetric experiment were described in detail in [5–8]. The performance characteristics of the calorimeter were as follows: temperature range 25–200°C, ampule volume 8 ml, sensitivity in the direct mode of measurement of the thermoelectric voltage less than 0.012 μV, and uncertainty of the measured thermal effects within 2.0%. Thermal effects were recorded on a KSP-4 potentiometer and then quantified using an IP-4 high-precision integrator. The preliminary thermostating time was 2 h. The sample was placed into a metallic ampule, which was inserted in a metallic cylinder with a solvent.

The system was tested by measuring the heat of solution of triple-recrystallized KCl at dilutions of 1 : 1600, 1 : 2400, and 1 : 3200 (mol per mol H_2O). The value we measured, $\Delta H_s = 17780 \pm 262$ J mol^{-1} (25°C), is well consistent with that recommended in [9, 10].

The errors of the experiments and the homogeneity of their variances were estimated using the Student and Bartlett tests [11].

The heat capacity of SS was measured over the range 173–348 K on an IT-S-400 dynamic calorimeter. It took about 2.5 h to carry out measurements over the entire experimental temperature range and to process the data. According to the equipment certificate, the upper limit of the error of the calorimeter is 10%. To calibrate the calorimeter, we measured its thermal conductivity K_T [12, 13]. For this purpose, we carried out a series of blank experiments with a copper sample and empty ampule. The thermal conductivity was estimated by Eq. (1)

$$K_T = C_{Cu}/(\bar{\tau}_{Cu} - \bar{\tau}^0), \quad (1)$$

1070-4272/05/7812-2029 © 2005 Pleiades Publishing, Inc.

Table 1. Heat of solution of salsoline salsolinodithiocarbamate $C_{23}H_{30}N_2O_4S_2$ (MW 462.6194) in water at various dilutions

Dilution (mol : mol H_2O)	Sample weight, g	ΔH_s, J	ΔH_s^m, kJ mol^{-1}
1 : 18 000	0.0073	3.977	252.03
	0.0071	3.991	260.04
	0.0071	4.053	264.08
	0.0070	3.761	258.56
	0.0071	3.958	257.89
		$\Delta\bar{H}_1^m$ =	258.52 ± 5.41
1 : 36 000	0.0037	1.740	217.56
	0.0035	1.665	220.07
	0.0035	1.630	215.45
	0.0035	1.654	218.62
	0.0035	1.640	216.77
		$\Delta\bar{H}_2^m$ =	217.69 ± 2.19
1 : 72 000	0.0019	0.935	178.45
	0.0018	0.681	175.02
	0.0018	0.700	179.91
	0.0018	0.698	179.39
	0.0018	0.680	174.77
		$\Delta\bar{H}_3^m$ =	177.51 ± 3.04

Table 2. Experimental heat capacity of salsoline salsolinodithiocarbamate

T, K	$C_p \pm \bar{\delta}$, J g^{-1} K^{-1}	$C_p^0 \pm \mathring{\Delta}$, J mol^{-1} K^{-1}
173	0.9278 ± 0.0209	429 ± 28
198	1.0279 ± 0.0291	475 ± 31
223	1.1301 ± 0.0213	522 ± 35
248	1.1749 ± 0.0323	543 ± 36
273	1.2019 ± 0.249	555 ± 37
298.15	1.2143 ± 0.0289	561 ± 37
323	1.2818 ± 0.0239	592 ± 39
348	1.3085 ± 0.0392	605 ± 40

where C_{Cu} is the total heat capacity of the copper sample (J mol^{-1} K^{-1}); $\bar{\tau}_{Cu}$, mean delay time of the calorimeter in the blank experiments (s); and $\bar{\tau}^0$, mean time.

The specific heat capacity was measured at 25 K intervals.

The sample was placed in a metallic ampule of the measuring cell and heated by a continuous heat flux through the calorimeter. The time delay of the sample temperature relative to the base temperature was measured at 25 K intervals.

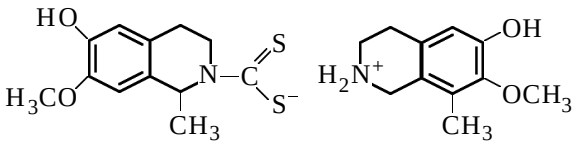
As in the case of calibration, five replicate runs were carried out with the samples investigated, and the experimental data were processed statistically [8].

At each temperature, we estimated the root-mean-square deviation $\bar{\delta}$, for the averaged specific heat capacity and the random error $\mathring{\Delta}$ for molar heat capacity.

The combustion heat was estimated by the Karash–Frost method [14], and the enthalpy of melting, by the equation recommended in [15]. The enthalpy of SS formation, $\Delta_f H^0_{298.15}$, was estimated using the Hess cycle from ΔH^0_{comb} and reference data on the heats of formation of the reagents.

EXPERIMENTAL

The crystals of SS ($C_{23}H_{30}N_2O_4S_2$) were prepared at the Institute of Organic Synthesis and Coal Fuel Chemistry (Karaganda, Kazakhstan). The quality of the product corresponded to chemically pure grade (mp 160°C). The structural formula of SS is given below.



A calorimetric determination of the heat of solution of SS was carried out in water at the 1 : 18 000, 1 : 36 000, and 1 : 72 000 dilutions (mol per mol H_2O). The results are listed in Table 1.

From the averaged data on the enthalpies of SS solution at various dilutions ($\Delta\bar{H}_1^m$, $\Delta\bar{H}_2^m$, $\Delta\bar{H}_3^m$), using the known relationship $\Delta H_s^m = f\sqrt{m}$ (m is the molal concentration), we derived Eq. (2) [16]:

$$\Delta H_s^m = 98.58 + 2918.5\sqrt{m},\ \text{kJ mol}^{-1}. \quad (2)$$

From this linear expression we determined the standard enthalpy of SS solution at infinite dilution (98.58 ± 1.48 kJ mol^{-1}). It should be pointed out that the enthalpy of solution decreases linearly with increasing dilution. As mentioned above, the heat capacity of SS was measured on an IT-S-400 calorimeter over the range 173–323 K, since the melting point of SS is 433 K. As a coolant we used liquid nitrogen.

The experimental specific and molar heat capacities are listed in Table 2.

From these data we derived a polynomial expression for the temperature dependence of the heat capacity (J mol^{-1} K^{-1}):

$$C_p^0 = (604 \pm 40) + (144 \pm 9) \times 10^{-3}T - (60.1 \pm 4.0) \times 10^5 T^{-2}. \quad (3)$$

To determine the standard enthalpy of formation of $C_{23}H_{30}N_2O_4S_2$, we estimated the heats of combustion and fusion, using the empirical methods [14, 15]. The mean heat of combustion, estimated by the Karash and Frost equations [14], is $\Delta H^0_{comb} = -12\,889 \pm 395$ kJ mol^{-1}. The standard enthalpy of SS formation in the liquid (molten) state was determined by Eq. (4) using the $\Delta_f H^0_{298.15}$ values for $CO_{2(g)}$, $H_2O_{(l)}$, and $SO_{2(g)}$ from [17].

$$C_{23}H_{30}N_2O_4S_{2(l)} + 53.5O_{2(g)} = 23CO_{2(g)} + 15H_2O_{(l)} + N_{2(g)} + 2SO_{2(g)} - \Delta H^0_{comb}. \quad (4)$$

To determine $\Delta_f H^0_{298.15}$ of crystalline SS, we estimated its heat of fusion ΔH_m, using the Gambill equation [15] (283.0 kJ mol^{-1}).

$$\Delta_f H^0_{298.15,\, C_{23}H_{30}N_2O_4S_{2(cr)}} = \Delta_f H^0_{298.15,\, C_{23}H_{30}N_2O_4S_{2(l)}} - \Delta H_m. \quad (5)$$

The standard enthalpy of formation of crystalline SS, estimated by Eq. (5), is –1330.0 kJ mol^{-1}.

CONCLUSIONS

(1) The first calorimetric study of the alkaloid derivative, salsoline salsolinodithiocarbamate, was made to determine the standard heat of solution in water at infinite dilution, heats of combustion and melting, and also the standard heats of formation of $C_{23}H_{30}N_2O_4S_2$ in the liquid (molten) and crystalline states.

(2) The temperature dependence of the heat capacity of $C_{23}H_{30}N_2O_4S_2$ was studied over the range 173–348 K. The C_p^0(298.15 K) was determined and an equation for the temperature dependence was derived.

REFERENCES

1. Terent'ev, A.P., Rukhadze, E.G., Dunina, V.V., and Drobyshevskaya, E.V., *Zh. Obshch. Khim.*, 1968, vol. 38, pp. 745–749.
2. Dinzhumanova, R.T., Synthesis of Piperidine, Tetrahydropyridine-, and 1,4-Dihydropyridine Derivatives as New Potentially Bioactive Compounds, *Cand. Sci. Dissertation*, Almaty, 1997.
3. Nazarov, I.N., *Izbrannye trudy* (Selected Works), Moscow: Akad. Nauk SSSR, 1961, pp. 593–600.
4. Boldyrev, B.G., *et al.*, in *Biopovrezhdenie v promyshlennosti: Mezvuzovskii sbornik* (Biodamage in Industry: An Intercollegiate Collection of Works), Gorki, 1983, pp. 44–51.
5. Skuratov, S.M., Kolesov, V.P., and Vorob'ev, A.F., *Termokhimiya* (Thermochemistry), Moscow: Mosk. Gos. Univ., 1964, vol. 1.
6. Calvet, E. and Prat, H., *Recent Progress in Microcalorimetry*, New York: Macmillan, 1963.
7. Topor, N.D. and Suponitskii, Yu.L., *Usp. Khim.*, 1984, no. 9, pp. 1425–1462.
8. Recent Progress in Microcalorimetry, *Zh. Fiz. Khim.*, 1959, no. 6, pp. 1161–1175.
9. Mishchenko, K.P. and Poltoratskii, G.M., *Termodinamika i stroenie vodnykh i nevodnykh rastvorov elektrolitov* (Thermodynamics and Structure of Aqueous and Nonaqueous Electrolyte Solutions), Leningrad: Khimiya, 1976.
10. *Termicheskie konstanty veshchestv: Spravochnik* (Thermal Constants of Substances: A Reference Book), Glushko, V.P., Ed., Moscow: Nauka, 1982, issue 10, part 2.
11. Spiridonov, V.P. and Lopatkin, A.A., *Matematicheskaya obrabotka eksperimental'nykh dannykh* (Mathematical Processing of Experimental Data), Moscow: Mosk. Gos. Univ., 1970.
12. Platunov, E.S., *Teplofizicheskie izmereniya v rezhime* (On-Line Thermal Measurements), Moscow: Energiya, 1973.
13. *Tekhnicheskoe opisanie i instruktsii po ekspluatatsii IT-S-400* (Design Description and Manual Directions for Use of IT-S-400 Calorimeter), Aktyubinsk: Etalon, 1986.
14. Kazanskaya, A.S. and Skoblo, V.A., *Raschety khimicheskikh ravnovesii* (Calculation of Chemical Equilibria), Moscow: Vysshaya Shkola, 1974.
15. Viktorov, V.V., *Metody vychisleniya fiziko-khimicheskikh velichin i prikladnye raschety* (Methods for Physicochemical Calculations and Their Applications), Moscow: Khimiya, 1977.
16. Krestov, G.A., *Termodinamika ionnykh peotsessov v rastvorakh* (Thermodynamics of Ionic Processes in Solutions), Leningrad: Khimiya, 1977.
17. Ryabin, V.A., Ostroumov, M.A., and Svit, T.F., *Termodinamicheskie svoistva veshchestv: Spravochnik* (Thermodynamic Characteristics of Substances: A Handbook), Leningrad: Khimiya, 1977.

Russian Journal of Applied Chemistry, Vol. 78, No. 12, 2005, pp. 2032–2034. Translated from Zhurnal Prikladnoi Khimii, Vol. 78, No. 12, 2005, pp. 2065–2066.
Original Russian Text Copyright © 2005 by Lebedev.

BRIEF COMMUNICATIONS

Separation of Titanium from Niobium and Tantalum via Complexation of Titanium with Fluoride Ions

V. N. Lebedev

Tananaev Institute of Chemistry and Technology of Rare Elements and Mineral Raw Materials, Kola Scientific Center, Russian Academy of Sciences, Apatity, Murmansk oblast, Russia

Received March 25, 2005

Abstract—Conditions in which niobium and tantalum can be separated in the presence of fluoride ions from titanium-containing products formed in processing of loparite were studied.

In decomposition of a loparite concentrate with nitric or hydrochloric acid, titanium(IV), niobium(V), and tantalum(V) are recovered into a combined concentrate, which is for the most part a hydrated cake [1–3]. In the sulfuric acid technology of loparite, titanium(IV) is recovered as a binary salt and, in the extraction separation of niobium(V) and tantalum(V), a fluoride is expended virtually only for these elements. At the same time, in processing of the overall product, the fluoride is also required for formation of fluorotitanic(IV) acid, which results in an increased expenditure of hydrofluoric acid and a stronger operating load on the equipment.

Previously, the possibility of recovering titanium(IV) by its selective transfer to solution upon introduction of fluoride ions has been considered [4–6]. A prerequisite in this case is that niobium(V) and tantalum(V) form readily soluble stable complexes with titanium(IV), which decompose in the presence of fluoride ions, because titanium(IV) is a stronger fluoride-acceptor [7]. The destruction of the complexes results in precipitation of the less soluble niobium(V) and tantalum(V). Positive results were obtained in [4] in selective hydrolytic precipitation of niobium(V) and tantalum(V) from model sulfate solutions in the presence of 2 mol of fluoride ions per 1 mol of TiO_2. A poorer separation of titanium(IV) and niobium(V) was achieved in [5], with the optimal results obtained at the molar ratio F^-:Ti(IV) = 3. There is a US patent [6] on selective leaching-out of titanium(IV) from precipitated hydroxides by introduction of fluoride ions.

The separation of titanium from technological products obtained in large-scale experiments with various versions of the hydrochloride technology of loparite was studied in [2, 3].

EXPERIMENTAL

A hydrated cake (74, 14.8, and 1.1 wt % TiO_2, Nb_2O_5, and Ta_2O_5, respectively) and acid chloride solution (40.8, 5.8 and 0.27 g l^{-1} of TiO_2, Nb_2O_5, and Ta_2O_5, respectively) were used in the experiments. The chloride solution was a re-extract obtained in separating the sum of titanium(IV), niobium(V), and tantalum(V) from rare-earth elements by extraction with octanol. The proportion of the components points to loss of niobium(V) and, to a greater extent, tantalum(V) during the extraction.

The hydrated cake was treated with various acids in fluoroplastic beakers under reflux at 85°C for 3 h. The precipitates formed were separated on a vacuum filter and analyzed by the X-ray fluorescence method. The data obtained are listed in Table 1. It follows

Table 1. Leaching-out of titanium(IV) from hydrated cake

Acid concentration, M	F^-:TiO_2 mole ratio	Recovery into a precipitate, %		
		Ti	Nb	Ta
HCl:				
1	2.5	56	76	88
3	2	53	81	90.6
3*	2	52.6	84.1	89.2
3	2.5	46	72	84
3	3	35.6	71.5	79
3	3.5	34.7	51.4	53.2
5	2.5	47.2	84.1	83
H_2SO_4:				
3	2.5	47	82	88
3	3.5	19.7	36	52
HNO_3:				
1*	2.5	58	74.7	88.2
3	2.5	52.5	76	89.6

* Gradual introduction of NaF.

1070-4272/05/7812-2032 © 2005 Pleiades Publishing, Inc.

Table 2. Hydrolytic recovery of niobium(V) and tantanium(V) from sulfate solutions

H_2SO_4 concentration, M	$F^-:TiO_2$ mole ratio	Recovery into a precipitate, %			H_2SO_4 concentration, M	$F^-:TiO_2$ mole ratio	Recovery into a precipitate, %		
		Ti(IV)	Nb(V)	Ta(V)			Ti(IV)	Nb(V)	Ta(V)
1	2.5	43.0	92.6	99.0	1.5	2.5	21.0	96.3	98.9
1	3	25.4	89.4	99.0	1.5	3	17.9	87.2	97.5
1.5	2	46.5	95.6	99.1	2	3	10.8	79.9	86.9

Table 3. Precipitation of niobium(V) and tantalum(V) from acid chloride solutions

$F^-:TiO_2$ mole ratio	Phase	Content of the sum of Ti, Nb, and Ta oxides, g	HCl concentration, M	Content of indicated oxide, wt %, in the phases		Recovery, %	
				TiO_2	Nb_2O_5	TiO_2	Nb_2O_5
2.0	Solution	1.9	1.9	61.6	1.7	29.0	5.3
	Precipitate	3.9		74.8	13.9	71.0	94.7
2.5	Solution	3.9	2.75	88.0	0.5	85.5	3.9
	Precipitate	1.15		50.8	43.5	14.5	96.1
3.0	Solution	4.1	2.7	87.0	1.08	87.5	6.9
	Precipitate	1.19		42.7	45.4	12.5	93.1

from the experimental results that, under all the conditions tested, the leaching-out of titanium(IV) from the hydrated precipitate is insufficiently complete and selective. Apparently, this occurs because of the low solubility of hydrated oxides.

The solubility of the hydrated cake increases upon addition of fluoride ions, and niobium(V) and tantalum(V) pass into solution owing to the excess of these ions, since the amount added is calculated for the entire sample weight. A gradual introduction of fluoride ions has virtually no effect on the selectivity of isolation.

The acid sulfate solution was prepared by decomposition of the hydrated cake with a 93% acid at 220°C, with the subsequent leaching of the sulfate mass with water. The total concentration of titanium(IV), niobium(V), and tantalum(V) was 75 g l^{-1} (in terms of oxides). A calculated amount of NaF was added to the solutions, which were heated until the onset of hydrolysis. The results obtained in hydrolysis of the sulfate solution are listed in Table 2.

It follows from Table 2 that the separation of titanium(IV) from niobium(V) and tantalum(V) is not complete; however, hydrolysis in the presence of 2.5 mol of F^- per 1 mol of TiO_2 makes it possible to diminish the mass of the precipitate being processed by nearly a factor of 3, with insignificant loss of niobium. As the solution acidity increases, niobium(V) and tantalum(V) are precipitated more selectively.

Similar results were obtained in hydrolysis of chloride solutions (Table 3). The optimal norm of fluoride ions for both the sulfate and chloride solutions is the mole ratio $F^-:TiO_2 = 2.5$. In all the cases, tantalum is contained almost completely in a precipitate.

CONCLUSIONS

(1) A study of the separation of niobium(V) and tantalum(V) from titanium(IV) by their precipitation in the presence of fluoride ions from products formed in processing of loparite demonstrated that the dissolution of hydrated oxides is nonselective, irrespective of the type and amount of an acid and the amount of fluoride ions.

(2) It is possible to isolate 96% of niobium(V) and 99% of tantalum(V) with coprecipitation of 14.5–20% of titanium(IV) by hydrolysis from solutions with the mole ratio $F^- : TiO_2 = 2.5$. The best separation is achieved at an acidity of 2–3 mol-equiv l^{-1}.

REFERENCES

1. Skorovarov, D.I., Pchelkin, V.A., Anufriev, I.I., and Sviridov, A.N., *Khimicheskaya tekhnologiya loparitovogo kontsentrata* (Chemical Technology of Loparite Concentrate), Apatity: KNTs AN SSSR (Kola Scientific Center of the Academy of Sciences of USSR), 1991, pp. 21–28.
2. Petrov, V.B., Nikolaev, A.I., Zots, N.N., *et al.*, *Khim. Tekhnol.*, 2003, no. 5, pp. 29–32.
3. Skiba, G.S., Voskoboinikov, N.B., Solov'ev, A.V., *et al.*, *Zh. Prikl. Khim.*, 2003, vol. 76, no. 10, pp. 1738–1739.
4. Petrova, N.B., Kolenkova, M.A., Koz'min, V.A., *et al.*, *Izv. Vyssh. Uchebn. Zaved., Tsvet. Metall.*, 1972, no. 5, pp. 52–56.
5. Belokoskov, V.I., Malnatskaya, E.N., and Akhmetova, T.V., *Gidrometallurgiya i khimiya redkikh elementov* (Hydrometallurgy and Chemistry of Rare Elements), Apatity: KNTs AN SSSR (Kola Scientific Center of the Academy of Sciences of USSR), 1991, pp. 75–78.
6. US Patent 2 895 792.
7. Goroshchenko, Ya.G., *Khimiya niobiya i tantala* (Chemistry of Niobium and Tantalum), Kiev: Naukova Dumka, 1965.

Russian Journal of Applied Chemistry, Vol. 78, No. 12, 2005, pp. 2035–2037. Translated from Zhurnal Prikladnoi Khimii, Vol. 78, No. 12, 2005, pp. 2067–2069.
Original Russian Text Copyright © 2005 by Podolina, Korenman, Kharitonova.

BRIEF COMMUNICATIONS

Extraction-Chromatographic Determination of Phenol in Polar Binary Organic Extracts

E. A. Podolina, Ya. I. Korenman, and L. A. Kharitonova

Elektrostal Polytechnic Institute, Moscow Institute of Steel and Alloys, Electrostal, Moscow oblast, Russia
Voronezh State Technological Academy, Voronezh, Russia

Received November 29, 2004; in final form, October 2005

Abstract—Extraction of phenol from aqueous solutions containing NaCl, K_2CO_3, and $(NH_4)_2SO_4$ as salting-out agents with hexane–2-propanol binary mixtures was studied, and conditions of determining the phenol concentration in the organic phase were optimized.

Organic solvents are widely used for extracting phenols from aqueous solutions [1]. Extractive preconcentration of phenols is performed with organic solvents of various polarities, used in high-performance liquid chromatography as mobile liquid phases [2].

In this study, we examined the extraction of phenol from aqueous sodium chloride, potassium carbonate, and ammonium sulfate with binary polar organic mixtures. An extraction-chromatographic technique for determining phenol in binary organic extracts was developed.

EXPERIMENTAL

In experiments, we used phenol (pure grade) and prepurified extractants hexane and 2-propanol [3]. The extraction power of the binary mixture was estimated by its total polarity [4]. The polarity of hexane–2-propanol binary organic mixtures was evaluated using the rational polarity criterion P_i^0, which takes into account the normalized Snyder polarity index, Hildebrand criterion, and solvatochromic Dimroth-Reichardt parameter [5]. The total polarity of the binary mixture was calculated by the equation

$$P_{tot}^0 = \Sigma \varphi_i P_i^0,$$

where φ_i is the volume fraction of the solvent of *i*th kind.

Since 2-propanol is unlimitedly miscible with water [6], the extraction of phenol was performed in the presence of salts. The phenol concentration in the equilibrium phases was determined spectrophotometrically on an SF-46 spectrophotometer. The fields of a two-phase equilibrium in the ternary system water–salting-out agent–2-propanol were found by constructing its phase diagram [7]. Taking into account that the solubility of the salting-out agent is temperature-dependent, we performed all the experiments at $22 \pm 2°C$.

The phenol content was determined on a Milikhrom-4 liquid chromatograph under the following conditions: eluent (hexane–2-propanol mixture with hexane to 2-propanol volume ratio 92.5 : 7.5); eluent flow rate 100 μl min^{-1}; Silasorb 600 sorbent with grain size of 7 μm; column size 2 × 64 mm; analytical wavelength λ = 270 nm; and phenol retention time 2.75 min.

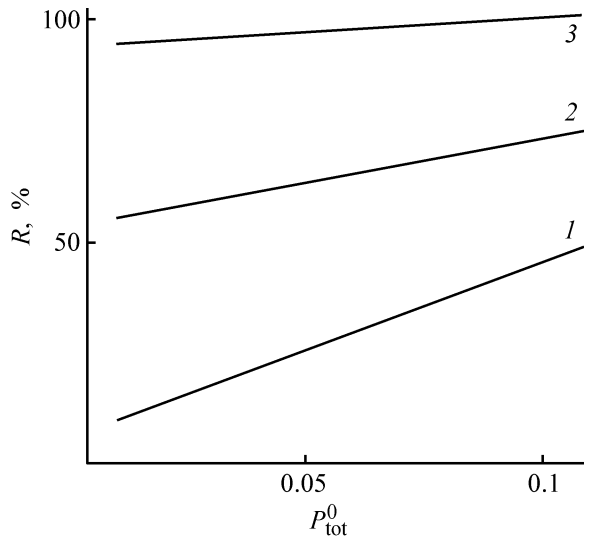
The efficiency of extractive recovery of phenol with the binary solvent was evaluated using the distribution factor *D* of phenol and its degree of recovery *R*, %. Table 1 shows that the distribution factor of

Table 1. Distribution factors of phenol in systems constituted by a binary organic mixture and a saturated aqueous solution of salt (n^* = 5, P = 0.95, and V_{aq}/V_o = 10)

P_{tot}^0	*D*		
	NaCl	K_2CO_3	$(NH_4)_2SO_4$
0.0158	1.63 ± 0.15	16.32 ± 1.50	160 ± 13
0.022	2.05 ± 0.20	17.88 ± 1.65	170 ± 16
0.027	2.62 ± 0.30	20.30 ± 1.95	200 ± 20
0.0295	3.33 ± 0.25	22.79 ± 2.05	240 ± 21
0.0396	4.29 ± 0.45	25.09 ± 2.67	300 ± 24
0.047	5.15 ± 0.37	28.46 ± 2.35	360 ± 32
0.117	7.24 ± 0.81	34.44 ± 2.96	500 ± 46

* *n* is the number of replicate experiments, and *P*, the confidence level.

1070-4272/05/7812-2035 © 2005 Pleiades Publishing, Inc.



Degree of extraction of phenol, *R*, from aqueous solutions containing (*1*) NaCl, (*2*) K_2CO_3, and (*3*) $(NH_4)_2SO_4$ with the binary organic mixture vs. its total polarity P^0_{tot}.

phenol increases with the total polarity of the binary solvent at a constant volume ratio of the organic (V_o) and aqueous (V_{aq}) phases.

The salting-out power of salts is dependent not only on the cation and anion but also on the solubility of a salt in water [6]. The mostl soluble in water is K_2CO_3. However, the solution of this salt has pH ~10, which considerably hinders transfer of phenol from the salt solution to the organic phase. As a result, the efficiency of extraction of phenol from aqueous K_2CO_3 is considerably lower than that in the presence of $(NH_4)_2SO_4$ (Table 1).

The interaction of organic solvents with phenol occurs via van der Waals forces and hydrogen bonding [8]. It is known that extraction of phenol from aqueous solution with hexane occurs at the interface [1]. In our experiments, the content of the hydrophilic solvent 2-propanol in the binary organic mixtures was varied. The higher was the total polarity of a binary extractant, the more probable was the transfer of phenol to the organic phase not only across the macroscopic interface, but also in the bulk across the interfaces of numerous small bubbles at their nucleation. In extraction of phenol with binary mixtures, its molecules are solvated not only with organic molecules, but also with water to form hydrate solvates. The figure shows that the maximum extractive recovery of phenol is reached at the total polarity of the binary extractant equal to 0.117.

Table 2. Determination of phenol extracted from aqueous solution containing $(NH_4)_2SO_4$ with hexane–2-propanol mixture (n = 5, P = 0.95)

Added	Found	$S_R \times 10^{-2}$	W, %
μM			
1.0	0.99 ± 0.075	3.2	7.6
10.0	9.80 ± 0.234	9.1	2.4
100.0	99.95 ± 1.530	59.5	1.5

The phenol concentration in the aqueous solution was determined as follows. A phenol-containing water sample (500 ml) to be analyzed for phenol was placed in a separatory funnel and acidified with H_2SO_4 to pH ~2. Thereafter, solid $(NH_4)_2SO_4$ was added in an amount sufficient to form an approximately saturated solution, and then the binary organic extractant hexane–2-propanol (5 ml) was added. The resulting mixture was shaken on a vibromixer for 15 min. After the phase separation, the organic phase was separated and its chromatogram was obtained on a Milikhrom-4 liquid chromatograph. The phenol content in water was calculated from the chromatogram by the formula

$$c_{aq} = c_o \times 100/Rr,$$

where c_{aq} is the chromatographically determined phenol concentration in the organic extract (g cm^{-3}); R, degree of phenol recovery in the system constituted by an aqueous salt solution and binary organic mixture (%); and r, the volume ratio of equilibrium organic and aqueous phases.

The statistically processed results of phenol determination in aqueous solutions are listed in Table 2, where S_R is the standard deviation, and W, relative total error, %.

The error in determination of phenol in aqueous solutions by our express extraction-chromatographic technique does not exceed 10%.

CONCLUSION

The distribution factors of phenol in the systems constituted by a hexane–2-propanol mixture and an aqueous solution of salting-out agents [$(NH_4)_2SO_4$, NaCl, K_2CO_3] were determined. The maximal distribution factor (500 ± 46) and the maximal degree of recovery (~98%) of phenol were reached with the binary organic mixture with a total polarity of 0.117. An express extraction-chromatographic technique for determining phenol in binary organic extracts on a Milikhrom-4 chromatograph was developed. The total determination error of phenol does not exceed 10%.

REFERENCES

1. Korenman, Ya.I., *Koeffitsienty raspredeleniya organicheskikh soedinenii: Spravochnik* (Distribution Factors of Organic Substances): Handbook, Voronezh: Voronezh. Gos. Univ., 1992.
2. Styskin, E.P., Itsikson, L.B., and Braude, E.V., *Prakticheskaya vysokoeffektivnaya zhidkostnaya khromatografiya* (Practical High-Performance Liquid Chromatography), Moscow: Khimiya, 1985.
3. Korostylev, P.P., *Reaktivy i rastvory v metallurgicheskom analize* (Chemicals and Solutions in Metallurgical Analysis), Moscow: Metallurgiya, 1977.
4. Rudakov, O.B., *Rastvoritel' kak sredstvo upravleniya protsessom v zhidkostnoi khromatografii* (Solvent as Means for Controlling Liquid Chromatography), Voronezh: Voronezh Gos. Univ., 2003.
5. Reichardt, Ch., *Solvents and Solvent Effects in Organic Chemistry*, Weinheim: VCH, 1988.
6. *Novyi spravochnik khimika i tekhnologa: Analiticheskaya khimiya*, (New Handbook for Chemists and Production Engineers: Analytical Chemistry), St. Petersburg: Mir i Sem'ya, 2002, part 2.
7. Korenman, Ya.I., Ermolova, T.N., and Mishina, A.V., *Izv. Vyssh. Uchebn. Zaved., Khim. Khim. Tekhnol.*, 1994, vol. 37, no. 4–6, pp. 36–40.
8. Reid, K.F., *Properties and Reactions of Bonds in Organic Molecules*, London: Longmans, Green and Co, 1968.

Russian Journal of Applied Chemistry, Vol. 78, No. 12, 2005, pp. 2038–2039. Translated from Zhurnal Prikladnoi Khimii, Vol. 78, No. 12, 2005, pp. 2070–2071.
Original Russian Text Copyright © 2005 by Morachevskii.

Professor Nikolai Nikolaevich Baraboshkin (To 125th Anniversary of His Birthday)

Nikolai Nikolaevich Baraboshkin is widely known as one of founders of the domestic platinum industry. He also made a major contribution to the organization of higher-school metallurgical education in Sverdlovsk (Yekaterinburg) and to the development of a number of branches of nonferrous metallurgy in the Urals.

N.N. Baraboshkin was born on October 24 (November 6), 1880. He descended from peasants of Moscow province. Having finished a village school, he educated at nonclassical secondary schools at towns of Syzran' and Samara. In 1899, he finished his secondary education and entered the Mining Institute in St. Petersburg. In view of the financial difficulties and the necessity to maintain his family, his education at the institute was prolonged and repeatedly interrupted, and was complete only in April 1915. A detailed list of a diversity of works in which Baraboshkin took part during his education at the Mining Institute can be found in the scientist's biography, prepared by S.S. Naboichenko [1]. Particularly noteworthy are geological expeditions that surveyed the gold-fields and platinum deposits in the Urals (1906, 1907), umpire analysis of raw platinum from Ural deposits (1911), development and improvement of methods for platinum refining (1914, 1915), and works at plants of nonferrous metallurgy (1908, 1910, 1912). Baraboshkin, in particular, took part in an inspection of Ural copper plants, which was commenced in 1914 by the decision of the Scientific Council of the Mining Institute.

Among Baraboshkin's teachers at the Mining Institute, who should be primarily mentioned, are chemists I.F. Shreder (1857–1918) and N.S. Kurnakov (1860–1941, academician since 1913), and metallurgist N.P. Aseev (1871–1952). Other teachers also included quite a number of known scientists: crystallographer E.F. Fedorov (1853–1919), mathematician I.P. Dolbnya (1853–1912), and metallurgist V.N. Lipin (1858–1930). Already in 1901, Baraboshkin started to work at Shreder's chemical laboratory; in 1902, he moved to the analytical laboratory headed by Kurnakov and worked there till 1913, with an interruption in 1908–1910. In 1913–1914, Baraboshkin was a not-on-the-staff assistant of professor Aseev.



When working at the laboratory headed by Kurnakov, together with Kurnakov's closest associate N.I. Podkopaev (1872–1930), Baraboshkin did a great deal in the field of analytical chemistry of platinum metals. A known Russian chemist-analyst, chairman of the Analytical Commission of the Institute of General and Inorganic Chemistry (Academy of Sciences of the USSR), B.G. Karpov (1870–1940) highly appreciated Baraboshkin's activities and regarded him as "... one of the most outstanding representatives of Kurnakov's analytical school" [2].

At the beginning of 1915, Baraboshkin graduated with success from the institute to become a mining engineer. He presented as his graduation thesis the results obtained in a study of the phase diagram of the binary system constituted by antimony oxide and antimony sulfide. Later, this study was awarded the prize named after Professor K.I. Lisenko (1836–1903) [1, 3]. Simultaneously, a design of a plant for processing of copper ore was presented. Having graduated from the Mining Institute, Baraboshkin continued to work there as an assistant.

In 1914, Russia's Government made a concession contract with the joint-stock company of the Nikolae-Pavdinskii mining district in the Urals for construc-

1070-4272/05/7812-2038 © 2005 Pleiades Publishing, Inc.

tion of Russia's first plant for refining of raw platinum and manufacture of platinum articles. Baraboshkin was invited to supervise the construction process. The technology to be used in platinum purification was based on the method that had been suggested by Russian inorganic chemist K.K. Klaus (1796–1864) and was modified by Baraboshkin and Podkopaev. In November 1915. Baraboshkin took the office of director of the plant being constructed.

At the beginning of 1916, a temporary laboratory for refining and production of spongy platinum started to work in Yekaterinburg. In October of the same year, the construction of the plant was, for the most part, complete. The commonly accepted official data of its starting is October 10 (23), 1916, when the Ministry of commerce and industry approved a special instruction regulating all aspects of operation of the new plant. From November 1916 till November 1917, 900 kg of platinum was refined [4]; by the beginning of 1918, the monthly output capacity reached a value of 400 kg and continued to gradually increase. However, the plant was nationalized on February 6 (19) and closed soon after. During the Civil war, the work on refining of platinum was suspended, but the plant was not evacuated and the equipment was intact. Baraboshkin's public and political activities were considered in detail in [1].

In the spring of 1920, the refining plant resumed its work, largely due to Baraboshkin's efforts, and soon started to manufacture, in addition to platinum, other metals: palladium (1922), iridium (1923), rhodium (1925), osmium (1927), and ruthenium (1930). Manufacture of platinum of extra brand was organized in 1928, platinum was smelted into ingots beginning in 1923; platinum alloys and articles made of platinum and its alloys started to be manufactured in 1928. The purity of the resulting platinum and its accessories was as good as, and in some cases considerably exceeded, that of the metals produced by foreign companies [5, 6].

Beginning in 1915, Baraboshkin was engaged in the development of higher-school metallurgical education in Yekaterinburg. Being an organizer of the Ural Mining Institute, he was elected a docent (1913), professor (1919), and dean of the metallurgical faculty at this institute. He was a professor of the Ural University in 1922–1925 and a professor of the Ural Polytechnic Institute in 1925–1935. The permanent reorganizations of higher-school institutions, faculties, chairs, and research institutions, which were characteristic of that time, give no way of briefly describing Baraboshkin's diverse pedagogical and scientific activities during this period. The Refining plant remained the scientist's main working place, where he was a technical director till 1930, and a scientific advisor later. As noted in Baraboshkin's biography [1], he was directly involved in the organization of the chairs of metallurgy of precious and nonferrous metals and theory of metallurgical processes at the Ural Polytechnic Institute and headed these chairs during several years.

Baraboshkin was among the organizers of the first in the Urals research institute of nonferrous metallurgy (1930) and was a deputy director for research work at this institute.

On July 27, 1935, when taking a rest, Baraboshkin tragically lost his life under unclear circumstances. The Russian science was deprived of one of the most talented representatives: an engineer, researcher, pedagogue, and organizer and head of industrial and research collectives. Papers devoted to Baraboshkin's memory have been published by his colleagues and pupils [5, 7, 8].

REFERENCES

1. Naboichenko, S.S., *Metallurg Nikolai Baraboshkin* (Metallurgist Nikolai Baraboshkin), Glavatskii, M.E., Ed., Yekaterinburg: Ural'sk. Univ., 2001.
2. Karpov, B.G., *Usp. Khim.*, 1936, vol. 5, nos. 7–8, pp. 1153–1159.
3. Fedorenko, N.V., *Razvitie issledovanii platinovykh metallov v Rossii* (Development of Studies of Platinum Metals in Russia), Moscow: Nauka, 1985.
4. Morachevskii, A.G., *Ocherki ob uchenykh-khimikakh Sankt-Peterburga. XIX vek i pervaya polovina XX veka* (Essays about Scientists Chemists of St. Petersburg, XIX Century and First Half of the XX Century), St. Petersburg: Politekhn. Univ., 2004.
5. Zvyagintsev, O.E., *Izv. Sektora Izuch. Platiny, Inst. Obshch. Neorg. Khim., Akad. Nauk SSSR*, 1936, no. 13, pp. 5–7.
6. Zvyagintsev, O.E., *Materialy po istorii otechestvennoi khimii: Sbornik dokladov na Vtorom Vsesouyznom soveshchanii po istorii otechestvennoi khimii* (Materials on History of Domestic Chemistry: Proc. 2nd All-Union Symp. on History of Domestic Chemistry), Moscow: Akad. Nauk SSSR, 1953, pp. 142–158.
7. Deryagin, P.I., *Tsvetn. Met.*, 1967, no. 10, pp. 102–104.
8. Derevyankin, V.A. and Deryagin, P.I., *Izv. Vyssh. Uchebn. Zaved., Tsvetn. Metall.*, 1980, no. 6, pp. 89–90.

A. G. Morachevskii

Russian Journal of Applied Chemistry, Vol. 78, No. 12, 2005, pp. 2040–2041. Translated from Zhurnal Prikladnoi Khimii, Vol. 78, No. 12, 2005, pp. 2072–2073.
Original Russian Text Copyright © 2005 by Morachevskii.

BOOK REVIEWS

Stromberg Armin Genrikhovich (1910–2004): Materialy k biografii. Vospominaniya uchenikov [Stromberg Armin Genrikhovich (1910–2004): Materials for Biography, Recollections of Pupils],

Mikheeva, N.P. and Zakharova, E.A., Compilers, Bakibaev, A.A., Ed., Tomsk: Tomsk. Politekhn. Univ., 2005, 104 pp.

Stromberg Armin Genrikhovich (1910–2004), Bibliograficheskii ukazatel' trudov [Stromberg Armin Genrikhovich (1910–2004), Bibliography of Works],

Kubrakova, N.I. and Vasil'eva, O.M., Compilers, Gagarin, A.V. and Zibareva, I.V., Foreword, Bakibaev, A.A., Ed., Tomsk: Tomsk. Politekhn. Univ., 2005, 76 pp.

Istoriya kafedry fizicheskoi i analiticheskoi khimii (1900–2004) [History of the Chair of Physical and Analytical Chemistry (1900–2004)],

Bakibaev, A.A., Ed., Tomsk: Tomsk. Politekhn. Univ., 2005, 67 pp.

All the three publications are devoted to 95th birthday of a prominent Russian scientist, founder of a large scientific school in the field of electroanalytical chemistry, honored professor of Tomsk Polytechnic University, Honored Chemist of the Russian Federation, honored Soros professor, and doctor of chemical science, Armin Genrikhovich Stromberg. One of the oldest Russian electrochemists, Stromberg was the first in our country who widely used polarographic methods in studies of various objects, in research work, and in industrial conditions. A particular prominent contribution was made by the scientist to the theory and practice of amalgam polarography. In 1951, he defended his doctoral (chem. sci.) dissertation "Theory and Practice of Polarography, and Amalgam Polarography in Particular." In 1956, Stromberg was elected head of the chair of physical and colloid chemistry at Tomsk Polytechnic Institute. In 1962, he initiated the organization of "Problem-solving laboratory for physicochemical of microimpurities in semiconductors and high-purity materials." Stromberg's talent not only as a theoretician, experimenter, and pedagogue, but also as a head and organizer of a large research team, was displayed in full measure at the chair and the problem-solving laboratory. The laboratory was directly headed by Stromberg during 24 years, after which he remained there as a scientific advisor. All the staff members of the laboratory, who included teachers of the chair, research workers, and postgraduate students, were engaged in comprehensive development of the method of inversion voltammetry: the theory of the method, development of apparatus and practical procedures for determination of microimpurities. During the 40 years of existence of the problem-solving laboratory under Stromberg's supervision, near 100 candidate dissertations were defended and a number of his pupils became doctors of science and headed research teams in other cities of the country.

The main results obtained at the problem-solving laboratory were summarized in the previously pub-

1070-4272/05/7812-2040 © 2005 Pleiades Publishing, Inc.

lished collection of works *Tomskoi elektrokhimicheskoi shkole i problemnoi laboratorii mikroprimesei sorok let. 1962–2002* (Tomsk Electrochemical School and Problem-solving Laboratory of Microimpurities Are Forty, 1962–2002) (Tomsk, 2004). In recollections of Stromberg's pupils, they emphasize his talent and self-discipline, remarkable working capacity, and devotedness to science.

The bibliography of Stromberg's works presents the results of a detailed sciencemetric analysis of the activities of the Tomsk electrochemical school and its head. The analysis was based on the databases Science Citation Index and Chemical Abstracts. In the ranked list of 20 world's most active authors in the field of voltammetry, Stromberg is the third, with three of his pupils also appearing in this list. According to the Chemical Abstracts database, Stromberg is an author of 372 publications that have appeared since 1935, 92% of these being journal articles. All the publications are in Russian in domestic journals and books. It should be noted that, together with being actively engaged in works in the field of voltammetry, Stromberg paid a considerable attention to sciencemetric studies and was the first in our country who understood their importance. The bibliographic list gives 471 references to scientist's works carried out in 1930–2005.

Stromberg (together with D.P. Semchenko) is the author of the textbook *Fizicheskaya khimiya* (Physical Chemistry) for higher-school institutions, which has already run into five editions. The three last of these (in 1999, 2001, and 2003) were supplemented by Stromberg with new important sections: "Introduction to the Theory of Self-Organization of Matter. Elements of Synergetics" and "Introduction to the Theory of Fractals." In 1999 was published an original textbook *Sinergetika. Primenenie v khimii* (Synergetics. Application to Chemistry), written by Stromberg.

The third of the books discussed is devoted to the history of the chair of physical and analytical chemistry. Studies at the chemical department of the Tomsk Polytechnic Institute (now Tomsk Polytechnic University) commenced in 1900. However, independent chairs of analytical chemistry and of physical and colloid chemistry appeared much later, in 1930 and 1934, respectively. In 1999, these chairs were amalgamated into the chair of physical and analytical chemistry. The book presents evidence concerning the teaching staff and research areas from their organization to amalgamation, and further until the present.

All the three small publications are of interest for a wide audience of readers interested in the development of science and higher-school education in our country.

A. G. Morachevskii

Russian Journal of Applied Chemistry, Vol. 78, No. 12, 2005, pp. 2042–2043. Translated from Zhurnal Prikladnoi Khimii, Vol. 78, No. 12, 2005, pp. 2074–2075.
Original Russian Text Copyright © 2005 by Zaikov, Artsis, Madyuskina.

INFORMATION

21st Annual Meeting of the Polymer Processing Society, 2005

The 21st Annual Meeting of the Polymer Processing Society was held in Leipzig (Germany) on June 19–23, 2005. The first such conference was organized seventeen years ago and held in Germany, too.

The participants of the Conference were about 500 scientists from 230 research centers of 41 countries. Leipzig was selected as a place for holding the Conference because the region of Germany around this city is characterized by a concentration of chemical industry and research centers specialized in processing of polymers.

The Conference Program included seven plenary lectures, fifteen symposia, and a workshop.

The first plenary lecture entitled Innovative Methods of Injection Molding for Automotive Components was presented by H. Eckardt (Meinerzhagen, Germany). In the second lecture, L.J. Lee (Columbus, the United States) reported on polymer processing at the micro/nanoscale. The third lecture was devoted to modeling of extrusion chain processes [H. Potente (Paderborn, Germany)]. P.D. Coates (Bradford, the United Kingdom) presented his concept of metrology as a science. The following plenary lectures were devoted to indicator products as a new tool for prediction of long-term properties of degradable polymers [A.-C. Albertsson (Stockholm, Sweden)]; extrusion, injection molding, and technological parameters of fibers reinforced with composites [P. Oswald (Munich, Germany]; and recent advances in silicon-containing polymeric nanocomposites [Maurice Lambada Award Lecture, M. Okamoto (Nagoya, Japan)].

The scientists participated in the Workshop "Rheology and Processing of Polymers" and discussed practical aspects of polymer processing.

Recent data covering various areas of polymer research were presented in fifteen Symposia.

Symposium 1. Extrusion and Coating (Chairmen: W. Michaeli, C. Rauwendaal, and T. Sakai). The following topics were considered: microwave-mediated plasticizing of PVC, effects of various catalysts on the reaction of 1,3-acetidine-2,4-dione with hydroxy groups, UV study of the kinetics of radical polymerization of methylmethacrylate with azobisisobutyronitrile and benzoyl peroxide in toluene, and extrusion of polyolefins.

Furthermore, there were presented results on blow extrusion to give a foam of polyesterimide used as a low-molecular-weight thermoplastic substrate, effect of extrusion on mechanical properties of polyethylene, and interfacial instabilities that occur in preparation of multilayer films.

Symposium 2. Injection Molding and Molds (S.-J. Liu, G. Mennig, and G. Titomanlio). Problems concerning the development of new injection molding machines, in particular, those for manufacture of hybrid Microsystems were considered. It was demonstrated that mechanical stress occurring in injection molding affects the mechanical characteristics of the products.

Symposium 3. Blow and Rotational Molding and Thermoforming (E. Harkin-Jones, J. Vlachopoulos, and J. Wortberg). Two presentations were made: (1) Thermomechanical Analysis of Protective Coating for Automotive Parts, Prepared by Thermoforming and Polymer-Polymer Diffusion, and (2) Interfacial Reactions in Multilayer Moldings.

Symposium 4. Reactive Processing (E. Haberstroh, M. van Duin, and M. Xanthos) (eight reports). Among others, such topics were discussed as oxidation of molten polypropylene, preparation and properties of high-performance ion-exchange acryl fibers, continuous process for production of polyurethane-based adhesives by reactive extrusion, and properties of reactive polypropylene for use as an elastomer in manufacture of rubber powders.

Symposium 5. Mixing and Compounding (M. Bousmina, T. Osswald, and C.L. Tucker, III). Four reports were delivered; they concerned determination of the electrical conductivity as a method for study of mixing processes that occur in carbon black rubbers, conditions for the attainment of homogeneity through a decrease in the number of ingredients, and stabilization of mechanical characteristics of low-density polyethylene with cyclohexylphosphonic acid.

Symposium 6. Rheology and Rheometry (E. Mitsoulis, P. Moldenaers, and M. Wagner). Among the

1070-4272/05/7812-2042 © 2005 Pleiades Publishing, Inc.

topics were the effect of acrylate polymers on properties of asphalt, deformation and fluidity of long-chain branched polypropylene prepared by the reaction of propylene with nonconjugated dienes, comparison of parameters obtained in studying the fluidity by vibrational and extrusion methods, fluidity of filled polymers, and analysis of the deformation and fluidity of paper fibers.

Symposium 7. Process Modeling (A. Hrymak, T. Kajiwara, and I. Manas-Zloczower). In this section, such questions were considered as processes in segmented polyurethane fibers, adhesion in layers, simulation of fiber break in textile materials, and quantitative *3D* simulation of processing.

Symposium 8. Morphology and Structure Development (J.-M. Haudin, S.C. Kim, and H. Muenstedt). The following topics were discussed: supramolecular structure of isotactic polypropylene obtained by the thermal reaction, X-ray study of the morphology and structure, anion-exchange resins, formation of solid phases, glassy and crystalline states in various polymers, and morphology and its correlation with mechanical properties of polymers.

Symposium 9. Polymer Blends and Composites (W. Hufenbach, H.E.H. Meijer, and R.D. Paul): synthesis and properties of polymer blends and composites; effect of various, particularly nanoscale fillers; optimization of the component proportion in preparation of composites; effect of pressure on the thermal conductivity in filled and unfilled powdered polymers; thermal and rheological characteristics of various polymers and polymer articles; and chemorheological study of phase separation and gelation.

Symposium 10. Natural Based and Biodegradable Polymers (A.-C. Albertsson, A. Bledzki, and A. Cunha): kinetics and mechanism of biodegradation of a wide variety of natural-based biodegradable polymers and sorption/desorption of water and saline solutions on these polymers.

Symposium 11. Elastomers and Elastomer Processing (A. Limper, W. Rzymski, and S. Thomas): morphology of elastomers and elastomer chains with and without fillers, and also of elastomers obtained from natural renewable raw materials. A special attention was paid to the injection molding and the construction of molding machines. Furthermore, synergistic and antagonistic effects in elastomer processing were considered, including vulcanization.

Symposium 12. Nano-Structured Materials (V. Altstaedt, S. Bhattacharya, and L.J. Lee). This section attracted special interest of the participants, particularly as regards flame retardants. It was demonstrated that nanocomposite flame retardants show promise for considerable decrease in the flammability of polymer and composite materials; they also reduce the volume of toxic compounds formed in pyrolysis and combustion of various polymers. Use of these nanocomposites allows alteration of the pyrolysis route toward formation of low-toxic products.

Symposium 13. Process Monitoring, Control, and Sensors (P.D. Coates, M. Stephan, and H. Yokoi). In this section, special attention was paid to small-angle scattering methods.

Symposium 14. Sustainable Development, Reprocessing, and Recycling (M. Kozlowski, C.D. Papaspyrides, and R. Renz). In this section, the main topics were environmental protection and collection, grading, and recycling of polymer wastes to obtain polymer blends and composites with acceptable properties.

Symposium 15. Foams, Novel Processes, and Applications (P. Eyerer, C.B. Park, and P. Saha). This section was devoted to foamed polymers, new processes for their preparation and processing, and practical applications. Part of the foams were prepared on the basis of rubbers, using nanocomposites. Particular attention was paid to blowing agents, foam extrusion, and polymer foams. Of special interest were reports on the development of bioactive foams and biocompatibility.

In addition to oral reports, the Symposia included more than 100 poster presentations.

The Conference showed how theoretically and practically important is the problem of polymer processing.

The next, 22nd Conference will be held in Yamagata (Japan) on July 2–6, 2006, and the 23rd Conference, in Salvador (Brasil) on May 27–31, 2007. It is anticipated that about 700–800 researchers and industry representatives from 50 countries will participate in these Conferences.

G.E. Zaikov, M.I. Artsis, and L.L. Madyuskina